with styrene and substituted styrenes did occur, it was hampered by competing 5-*exo*-*trig* cyclizations, which took place upon the consecutive palladium-catalyzed alkenylation of the intermediate *o*-bromostyrene subunits on the central benzene ring.[5] This led to a variety of benzylideneindane and benzylindene by-products that were isomeric with and, therefore, not easily separable from the hexastyrylbenzenes.[6]

Both multiple coupling of vicinal oligohalobenzene derivatives[7] and the subsequent five-membered ring closing reactions[5] are favored only under modified Jeffery conditions[8] for the Heck reaction.[9] We were, therefore, intrigued to find out whether other types of palladium-catalyzed cross-coupling reactions, such as Suzuki[10] and Stille couplings,[11] might be feasable for preparing hexaalkenylbenzene derivatives.[12, 13]

Sixfold Suzuki alkenylation of hexabromobenzene (**1**) with **2a**, prepared by hydroboration of 3,3-dimethyl-1-butyne (*tert*-butylacetylene) with catecholborane,[14] under typical conditions ($[PdCl_2(PPh_3)_2]$, NaOH, toluene/THF 1/1) gave hexakis(3,3-dimethyl-1-butenyl)benzene (**3a**) as a colorless crystalline material [Eq. (1); Table 1]. Under the same conditions, reaction

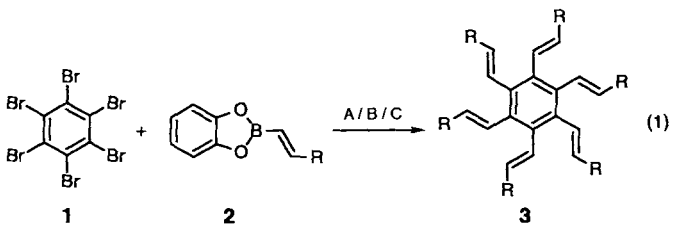

1 **2** **3**

Table 1. Yields and conditions for the sixfold coupling of hexabromobenzene (**1**) with alkenyl boronates **2**.

2	R	Conditions[a]	Yield of **3**[%]
a	*t*Bu	A	73
b	nC_7H_{15}	A/B	0[b]
c	Ad	C	6[c]

[a] A: $[PdCl_2(PPh_3)_2]$, NaOH, toluene/THF (1/1), 100 °C, 24 h; B: $[PdCl_2(dppf)]$, NaOH, toluene/DMF (1/1), 80 °C, 24 h; C: [*trans*-di(*μ*-acetato)bis[(di-*o*-tolylphosphano)benzyl]palladium(II)] [15], NaOH, toluene, 110 °C, 2 d; dppf = 1,1′-bis(diphenylphosphanyl)ferrocene. [b] Mixture of debrominated oligononenylbenzenes. [c] Additional 6% pentakis(adamantylethenyl)benzene.

of **1** with **2b** did not yield the sixfold coupling product **3b**, not even with $[Pd(dppf)Cl_2]$ as catalyst, which is known to accelerate reductive elimination in R_2Pd intermediates (R = alkyl, aryl).[16] Surprisingly, the bulky adamantyl derivative **2c** gave the highly congested **3c** (albeit in only 6% yield) when the palladacycle prepared from $Pd(OAc)_2$ and tris(*o*-tolyl)phosphane[15] was applied as the catalyst.

Since hydroboration of trimethylsilylacetylene (**4d**) with catecholborane led to a practically inseparable mixture of α- and β-(trimethylsilylethenyl)borole, the Suzuki coupling was not favorable for accessing the trimethylsilyl-substituted analog of **3a**. However, **5d**[17] could be readily prepared by hydrostannylation of **4d** (97% yield, *E*:*Z* = 9:1) and coupled to **1** six times in the presence of a palladacycle catalyst[15] to give hexakis(trimethylsilylethenyl)benzene (**3d**) in 41% yield (Table 2). This sixfold Stille coupling[11] was also successful with (*E*)-(2-*tert*-butylethenyl)tributylstannane, but the yield of **3a** (35%) was lower than for the sixfold Suzuki coupling.

Crystal structure analysis of **3a** and its trimethylsilyl analog **3d**[18] gave a clue as to why only these highly crowded molecules are formed in good yields. Both molecules exhibit approximate

Table 2. Yields and conditions for the sixfold coupling of **1** with alkenylstannanes **5** prepared from alkynylstannanes **4**.

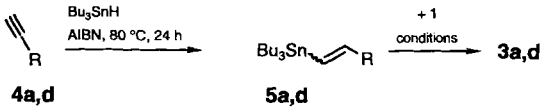

4a,d **5a,d**

4	R	Yield of **5**[%]	*E*:*Z*	Conditions[a]	Yield of **3**[%]
a	*t*Bu	72	9:1	D, 120 °C, 4 d	35
c	Ad	91	9:1	D, 110 °C, 3 d	[b]
d	$SiMe_3$	97	9:1	D, 100 °C, 1 d	41

[a] D: [*trans*-di(*μ*-acetato)bis[(di-*o*-tolylphosphano)benzyl]dipalladium(II) [15], toluene. [b] According to the ^1H NMR spectrum the crude product contained **3c** and pentakis[2-(1′-adamantyl)ethenyl]benzene; purification attempts failed.

C_6 symmetry in the crystal, and all six alkenyl groups are arranged on one side of the central ring like the blades of a propeller (Figure 1).[19] In **3a** the torsional angles of the six alkenyl groups out of the central plane vary from 47.2(4) to 57.2(3)°

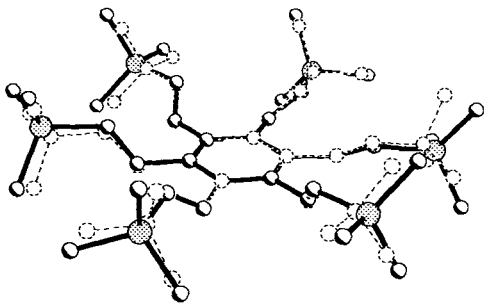

Figure 1. Crystal structures of **3a** and **3d** as superimposed ball-and-stick plots to show the differences; shaded balls represent Si atoms, and the rest carbon [18].

with an average of 51(3)°. In **3d** this angle is slightly smaller [44.3(4)–54.9(4), av 49(4)°], which is in accord with the longer bond length between the ethenyl C and Si atoms. The shortest nonbonding distances between hydrogen atoms on two adjacent *tert*-butyl or trimethylsilyl groups in **3a** and **3d** are around 2.5 and 2.6 Å, respectively, which are close to the sum of two van der Waals radii of hydrogen.[21] This suggests that an attractive van der Waals interaction might be operating as a self-organization principle during the six-step coupling sequence and, thus, favor the formation of the highly ordered molecules. The C_6-symmetrical arrangement of all six ethenyl groups around the ring is also a feature of the parent hexaethenylbenzene in the crystal;[12a] this indicates that there may be an additional π-stacking effect favoring the one-sided orientation. According to molecular mechanics calculations (MM2-ERW and MM3 programs) for **3a**, the *all-syn* conformation is 5.5 kcal mol^{-1} more favorable than one in which alternating groups are rotated above and below the ring.[22] With six *t*-butyl groups, **3a** adopts an interesting bowl shape, which may enable it to form host–guest complexes with appropriate substrates (Figure 2).

The major absorption in the UV spectrum of **3a** at λ = 262.3 nm (ε = 53600) is almost the same as that of the parent compound.[23] The oxidation potential E^0_{Ar} = 0.81 V vs. ferrocene/Fe^+ (corresponding to E^0_{Ar} = 1.21 V vs. NHE) as measured by cyclic voltammetry[24] is considerably lower than that of hexaethylbenzene.[25] Treatment of **3a** with $[Cr(NH_3)_3(CO)_3]$ in dioxane at 100 °C resulted in the bright yellow tricarbonylchromium complex **6** (62%).

 © VCH Verlagsgesellschaft mbH, D-69451 Weinheim, 1997 0570-0833/97/3612-1290 $ 17.50+.50/0

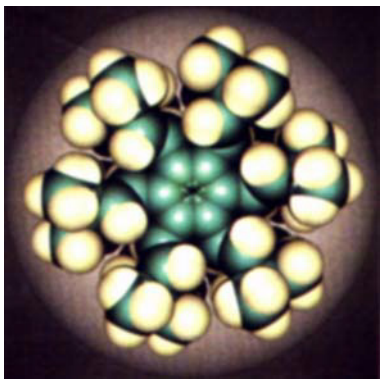

Figure 2. Space-filling model of hexakis(3,3-dimethyl-1-butenyl)benzene (**3a**).

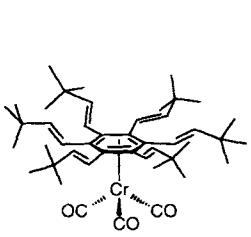

6

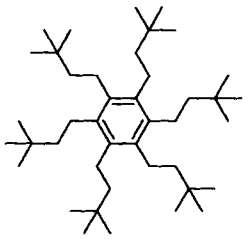

7

Catalytic hydrogenation of **3a** in hexane over Pd/C proceeds smoothly to hexakis(3,3-dimethylbutyl)benzene (**7**, 89% yield). This indicates that, at least in solution, the six unsaturated arms in **3a** have more conformational flexibility than the crystal structure suggests. Otherwise they could not be properly attached to the catalyst surface and accessible to the activated hydrogen molecules. Interestingly, **7** has approximate D_{3d} symmetry in the crystal, and the six saturated *tert*-butylethyl groups are alternatingly above and below the central plane (Figure 3).[19] This is typical for hexaalkylbenzene derivatives[1] and reproduced by molecular mechanics calculations, which indicate an energetic preference of 12.3 kcal mol^{-1} for this conformation over that with all groups on one side of the ring.[22] In the crystal **7** packs in columns, and the *tert*-butylethyl groups of each two adjacent molecules are staggered. Whether this leads to interesting charge-transfer phenomena in doped crystals remains to be seen.

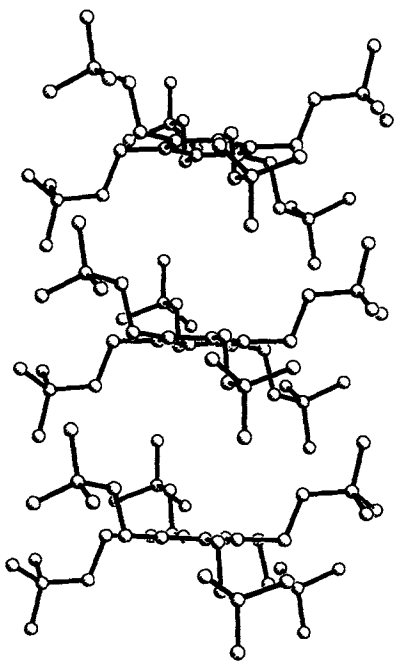

Figure 3. Structure of **7** and packing of the molecules in the crystal [19]; hydrogen atoms have been omitted.

Experimental Section

3a: A solution of **1** (1.00 g, 1.81 mmol) in a mixture of anhydrous toluene and anhydrous THF (50 mL each), which had been flushed with argon for 5 min, was treated with $[PdCl_2(PPh_3)_2]$ (0.36 g, 0.51 mmol), **2a** [14] (2.45 g, 12.1 mmol), and powdered NaOH (1.30 g, 32.5 mmol) and heated under an argon atmosphere at 100 °C for 24 h. After the mixture had cooled to room temperature, it was treated with 3 M NaOH (16 mL) and 30% hydrogen peroxide (2 mL) and stirred at room temperature for 1 h. The organic layer was then separated, washed with 3 M NaOH (5 × 10 mL), and dried ($MgSO_4$). The solvent was removed under reduced pressure, and the residue purified by chromatography on silica gel with pentane as eluent. Recrystallization from hexane/ethanol afforded **3a** (0.761 g, 73%) as colorless crystals, m.p. = 202 °C. ^{1}H NMR (250 MHz, $CDCl_3$): δ = 6.47 (d, J = 16.5 Hz, 6H), 5.73 (d, J = 16.5 Hz, 6H), 1.18 (s, 54H); ^{13}C NMR (75.5 MHz, $CDCl_3$, additional DEPT): δ = 145.48 (+), 134.83 (C_{quat}), 124.72 (+), 33.79 (C_{quat}), 29.65 (+).

3d: Colorless solid, m.p. = 227–230 °C. ^{1}H NMR (250 MHz, $CDCl_3$): δ = 6.86 (d, J = 19.6 Hz, 6H), 5.63 (d, J = 19.6 Hz, 6H), 0.12 (s, 54H); ^{13}C NMR (75.5 MHz, $CDCl_3$, additional DEPT): δ = 143.91 (+), 137.05 (+), 135.79 (C_{quat}), −1.10 (+).

Received: November 7, 1996 [Z 9759 IE]
German version: *Angew. Chem.* **1997**, *109*, 1343–1346

Keywords: arenes · homogeneous catalysis · palladium

[1] H.-W. Marx, F. Moulines, T. Wagner, D. Astruc, *Angew. Chem.* **1996**, *108*, 1842–1845; *Angew. Chem. Int. Ed. Engl.* **1996**, *35*, 1701–1704, and references therein.

[2] a) E. Weber, F. Vögtle, *Angew. Chem.* **1979**, *91*, 813–837; *Angew. Chem. Int. Ed. Engl.* **1979**, *18*, 753–776; b) D. D. MacNicol, J. J. McKendrick, D. R. Wilson, *Chem. Soc. Rev.* **1978**, *7*, 65–87; c) U. Rosenthal, W. Schulz, *J. Prakt. Chem.* **1986**, *328*, 335–341; d) K. Praefcke, B. Kohne, D. Singer, *Angew. Chem.* **1990**, *102*, 200–202; *Angew. Chem. Int. Ed. Engl.* **1990**, *29*, 177–179, and references therein.

[3] D. Astruc, *Acc. Chem. Res.* **1986**, *19*, 377–383; *Top. Curr. Chem.* **1992**, *160*, 47–95.

[4] a) R. Diercks, J. C. Armstrong, R. Boese, K. P. C. Vollhardt, *Angew. Chem.* **1986**, *98*, 270–271; *Angew. Chem. Int. Ed. Engl.* **1986**, *25*, 268–269; b) R. Boese, J. R. Green, J. Mittendorf, D. L. Mahler, K. P. C. Vollhardt, *ibid.* **1992**, *104*, 1643–1645 and **1992**, *31*, 1643–1645.

[5] S. Bräse, J. Rümper, K. Voigt, S. Albecq, G. Thurau, R. Villard, B. Waegell, A. de Meijere, *Liebigs Ann.* **1997**, in press.

[6] a) A. Lansky, Ph.D. thesis, Universität Göttingen, **1992**; b) A. de Meijere, F. E. Meyer, *Angew. Chem.* **1994**, *106*, 2473–2506; *Angew. Chem. Int. Ed. Engl.* **1994**, *33*, 2379–2411; c) see also ref. [11] in: B. König, H. Zieg, P. Bubenitschek, P. G. Jones, *Chem. Ber.* **1994**, *127*, 1811–1813.

[7] Up to threefold vicinal couplings of 1,2,3-trihaloarenes and even fourfold couplings with 1,2,4,5-tetrahaloarenes with styrenes have been achieved under Jeffery conditions [8]: a) A. Lansky, O. Reiser, A. de Meijere, *Synlett* **1990**, 405–407; b) K. Voigt, A. Lansky, M. Noltemeyer, A. de Meijere, *Liebigs Ann.* **1996**, 899–911. Such multiple couplings did not proceed under traditional Heck conditions: W. Tao, S. Nesbitt, R. F. Heck, *J. Org. Chem.* **1990**, *55*, 63–69.

[8] a) T. Jeffery, *Tetrahedron Lett.* **1985**, *26*, 2667; b) *J. Chem. Soc. Chem. Commun.* **1984**, 1287–1289.

[9] a) R. F. Heck, J. P. Nolley, Jr., *J. Org. Chem.* **1972**, *37*, 2320–2322; b) R. F. Heck, *Acc. Chem. Res.* **1979**, *12*, 146–151; c) *Palladium Reagents in Organic Syntheses*, Academic Press, London, **1985**; d) for recent reviews see ref. [6b] and S. Bräse, A. de Meijere in *Cross Coupling Reactions* (Eds.: F. Diederich, P. Stang), Wiley-VCH, Weinheim, **1997**.

[10] N. Miyaura, A. Suzuki, *J. Chem. Soc. Chem. Commun.* **1979**, 866–867; recent review: N. Miyaura, A. Suzuki, *Chem. Rev.* **1995**, *95*, 2457–2483.

[11] a) D. Milstein, J. K. Stille, *J. Am. Chem. Soc.* **1979**, *101*, 4992–4998; reviews: b) J. K. Stille, *Angew. Chem.* **1986**, *98*, 504–519; *Angew. Chem. Int. Ed. Engl.* **1986**, *25*, 508–524; c) T. N. Mitchell, *Synthesis* **1992**, 803–815.

[12] a) The unsubstituted hexaethenylbenzene was prepared by conventional sixfold dehydrobromination of hexakis(1′-bromoethyl)benzene: C. Krüger, M. Yalpani, *Chem. Ber.* **1983**, *116*, 3359–3365. b) Hexaisopropenylbenzene was obtained in only 4% yield by cobalt-mediated trimerization of diisopropenylacetylene: E. M. Arnett, J. M. Bollinger, J. C. Sanda, *J. Am. Chem. Soc.* **1965**, *87*, 2050–2051.

 © VCH Verlagsgesellschaft mbH, D-69451 Weinheim, 1997 0570-0833/97/3612-1291 $ 17.50+.50/0

[13] Hexastyrylbenzene and substituted hexastyrylbenzenes were prepared starting from the threefold coupling product of 1,3,5-tribromo-2,4,6-trimethylbenzene and styrene: H. Meier, N. Hanold, H. Kalbitz, *Synthesis* **1997**, 276.
[14] H. C. Brown, S. K. Gupta, *J. Am. Chem. Soc.* **1972**, *94*, 4370–4371.
[15] W. A. Hermann, C. Broßmer, K. Öfele, C.-P. Reisinger, T. Priermeier, M. Beller, H. Fischer, *Angew. Chem.* **1995**, *107*, 1989–1992; *Angew. Chem. Int. Ed. Engl.* **1995**, *34*, 1844–1848.
[16] T. Hayashi, M. Konishi, Y. Kobori, M. Kumada, T. Higuchi, K. Hirotsu, *J. Am. Chem. Soc.* **1984**, *106*, 158–163.
[17] R. F. Cunico, F. J. Clayton, *J. Org. Chem.* **1976**, *41*, 1480–1482.
[18] Good-quality crystals of **3a** and **3d** were obtained by letting ethanol slowly diffuse into a saturated solution of **3a** in hexane and **3d** in hexane/ethanol.
[19] Crystal structure analyses: **3a**: Nicolet R3m/V four-circle diffractometer, $Mo_{K\alpha}$ (graphite monochromator, $\lambda = 0.71069$ Å), $T = 125$ K; crystal dimensions $0.52 \times 0.31 \times 0.45$ mm^3; $C_{42}H_{66}$, $M_r = 570.99$; $a = 10.691(3)$, $b = 14.697(3)$, $c = 14.714(4)$ Å, $\alpha = 60.29(2)$, $\beta = 77.78(2)$, $\gamma = 73.35(2)^\circ$, $V = 1917.2(8)$ Å^3; triclinic, space group $P\bar{1}$, $Z = 2$, $\rho_{calcd} = 0.98$ g cm^{-3}, $\mu = 0.05$ mm^{-1}; 5015 independent reflections with $3 \le 2\theta \le 45^\circ$, 3872 observed with $F_0 \le 4\sigma(F)$; $R(F) = 0.0491$, $R_w(F) = 0.0573$ [20]. **3d**: STOE-AED2 diffractometer, $Mo_{K\alpha}$ ($\lambda = 0.71069$ Å), $T = 153$ K; crystal dimensions $0.4 \times 0.2 \times 0.2$ mm^3; $C_{36}H_{66}Si_6$, $M_r = 667.43$; $a = 13.288(6)$, $b = 14.039(6)$, $c = 14.760(6)$ Å, $\alpha = 66.44(3)$, $\beta = 67.88(3)$, $\gamma = 68.95(3)^\circ$, $V = 2267(2)$ Å^3, triclinic, space group $P\bar{1}$, $Z = 2$, $\rho_{calcd} = 0.978$ g cm^{-3}, $\mu = 0.204$ mm^{-1}; 7959 independent reflections with $7 \le 2\theta \le 50^\circ$; 5811 observed with $F_0 \le 4\sigma(F)$; $R(F) = 0.0616$, $R_w(F) = 0.1436$ [20]. **7**: STOE-AED2 diffractometer, $Mo_{K\alpha}$ ($\lambda = 0.71069$ Å), $T = 153$ K; crystal dimensions $0.6 \times 0.6 \times 0.5$ mm^3; $C_{42}H_{78}$, $M_r = 583.04$; $a = 23.819(3)$, $b = 23.819(3)$, $c = 6.1908(12)$ Å, $\alpha = 90$, $\beta = 90$, $\gamma = 120^\circ$; $V = 3041.8(9)$ Å^3; rhombohedral, space group $R\bar{3}$, $Z = 3$, $\rho_{calcd} = 0.955$ g cm^{-3}, $\mu = 0.052$ mm^{-1}; 894 independent reflections with $7 \le 2\theta \le 45^\circ$; 695 observed with $F_0 \le 4\sigma(F)$; $R(F) = 0.0450$, $R_w(F) = 0.1040$ [20]. Crystallographic data (excluding structure factors) for the structures reported in this paper have been deposited with the Cambridge Crystallographic Data Centre as supplementary publication nos. CCDC-100015 and -100016. Copies of the data can be obtained free of charge on application to The Director, CCDC, 12 Union Road, Cambridge CB2 1EZ, UK (fax: int. code +(1223)336-033; e-mail: deposit@chemcrys.cam.ac.uk).
[20] SHELXTL-PLUS (Program System for Crystal Structure Solution and Refinement, Universität Göttingen).
[21] A. Bondi, *J. Phys. Chem.* **1964**, *68*, 441–451.
[22] *W. R. Roth, Universität Bochum (Germany)*, personal communication. We are indebted to Professor Roth for carrying out the calculations with his MM2-ERW program.
[23] J. M. Bollinger, J. J. Burke, E. M. Arnett, *J. Org. Chem.* **1966**, *31*, 1310.
[24] The cyclic voltammogram was kindly measured by Prof. Dr. S. Bäuerle and Dipl.-Chem. M. Emge, Universität Ulm (Germany)
[25] J. O. Howell, J. M. Goncalves, C. Amatore, L. Klansinc, R. M. Wightman, J. K. Kochi, *J. Am. Chem. Soc.* **1984**, *106*, 3968–3976.

First Structural Characterization of a Benzophenone Ketyl Complex**

Zhaomin Hou,* Xueshun Jia, Mikio Hoshino, and Yasuo Wakatsuki

Although the formation of ketyls by one-electron reduction of ketones has been known for more than a hundred years,[1, 2] structurally characterized examples of this important class of highly reactive species remain very rare and are still limited solely to the fluorenone ketyl species that were recently isolated in our laboratories.[3] Isolation and structural characterization of new ketyl complexes continue to be of great importance and interest. Benzophenone ketyl is among the best known and most widely used ketyls.[1, 2, 4] Previous attempts to isolate a benzophenone ketyl species by utilization of low-valent titanium and lanthanide reducing agents were not successful.[4–6] Reaction of $[CpTiCl_2]$ with benzophenone in THF/ether was reported to give rapidly the corresponding pinacol-coupling product.[6] The use of a sterically demanding titanium(III) reductant such as $[Ti(OSitBu_3)_3]$ suppressed the pinacol-coupling reaction, but benzophenone dimerized by coupling of the *para*-carbon atom of a phenyl group with the carbonyl carbon of another molecule.[5f] Reactions of benzophenone with sterically demanding lanthanide reducing agents such as $[Ln(OAr_2(L)_n]$ (Ln = Sm, Yb; Ar = 2,6-tBu_2-4-MeC_6H_2); L = thf, hmpa),[3a, b] $[R_2Sm]$ (R = BH(3,5-dimethylpyrazolyl)$_3$),[7] or Ln/hmpa[3d] did not afford structurally characterizable benzophenone ketyl species either, but resulted in hydrogen abstraction in some cases, although many of these reducing agents have been successfully used for the isolation of fluorenone ketyl complexes.[3] All these results show that benzophenone ketyl species are extremely reactive and much more unstable than the corresponding fluorenone ketyl species. After the survey of several different types of reducing agents, we successfully isolated structurally characterizable benzophenone ketyl species by binding them to a calcium(II) ion containing hmpa ligands. In this communication, we report the isolation and structural characterization of a bis(benzophenone ketyl)calcium complex, which constitutes the first structurally characterized benzophenone ketyl complex, as well as the first structurally characterized complex of an alkaline earth metal with a ketyl.[8, 9] Its reaction with 2-propanol is also described.

In the presence of three equivalents of hexamethylphosphoric triamide (HMPA), reaction of fresh calcium chips with two equivalents of benzophenone in THF gradually gave a blue solution, which after filtration, concentration, and addition of hexane, afforded blue blocks of **1** in 77% yield of isolated product (Scheme 1). The UV/Vis ($\lambda = 635$ nm, $\varepsilon = 3.8 \times 10^3$ M^{-1} cm^{-1})[5c] and ESR ($g = 2.0028$) spectra of **1** in THF are very similar to those reported for the benzophenone ketyl species generated in situ.[5]

An X-ray analysis has shown that **1** is a bis(benzophenone ketyl)calcium(II) complex, which possesses a distorted trigonal-bipyramidal structure with one hmpa and two ketyl ligands in equatorial and two hmpa ligands in apical positions (Figure 1).[10] The two ketyl ligands form an O-Ca-O angle of 114.2(4)°, and the distance between the two radical carbon atoms (C(1) and C(14)) is 5.99 Å. The overall structure of **1** is similar to that of the calcium(II) aryloxide complex $[Ca(OAr)_2(thf)_3]$ (Ar = 2,6-tBu_2-4-MeC_6H_2).[11] The bond lengths of the Ca–O(ketyl) bonds in **1** (av 2.20(1) Å) are also similar to those of the Ca–OAr bonds in $[Ca(OAr)_2(thf)_3]$ (av 2.206(6) Å).[11, 12] The C–O bonds of the benzophenone ketyl ligands in **1** are significantly longer (av 1.31(2) Å) than that of free benzophenone (1.23(1) Å),[13] but comparable with those of fluorenone ketyls (1.27–1.31 Å).[3] As in fluorenone ketyls, the radical carbon atoms C(1) and C(14) in **1** are nearly coplanar with the atoms around them (d_{max} from the best least-squares plane smaller than 0.03 Å) and are still sp^2-hybridized. However, the planes defined by O(1)-C(1)-C(2)-C(8) and O(2)-C(14)-C(15)-C(21) are not coplanar with any of the phenyl rings. The dihedral angles formed by the O(1)-C(1)-C(2)-C(8) plane and the C(2)–C(7) and C(8)–C(13) phenyl rings are 16° and 30°, respectively, and those formed by the O(2)-C(14)-C(15)-C(21) plane and the C(15)–C(20) and C(21)–C(26) phenyl rings are 20° and 30°, respectively. This is in sharp contrast to fluorenone ketyl in which all the atoms lie in the same plane.[3] The lack of planarity in the whole benzophenone ketyl

[*] Dr. Z. Hou, Dr. X. Jia, Dr. M. Hoshino, Dr. Y. Wakatsuki
The Institute of Physical and Chemical Research (RIKEN)
Hirosawa 2-1, Wako, Saitama 351-01 (Japan)
Fax: Int. code +(48)462-4665
e-mail: houz@postman.riken.go.jp

[**] This work was partly supported by a grant-in-aid from the Ministry of Education, Science, and Culture of Japan.

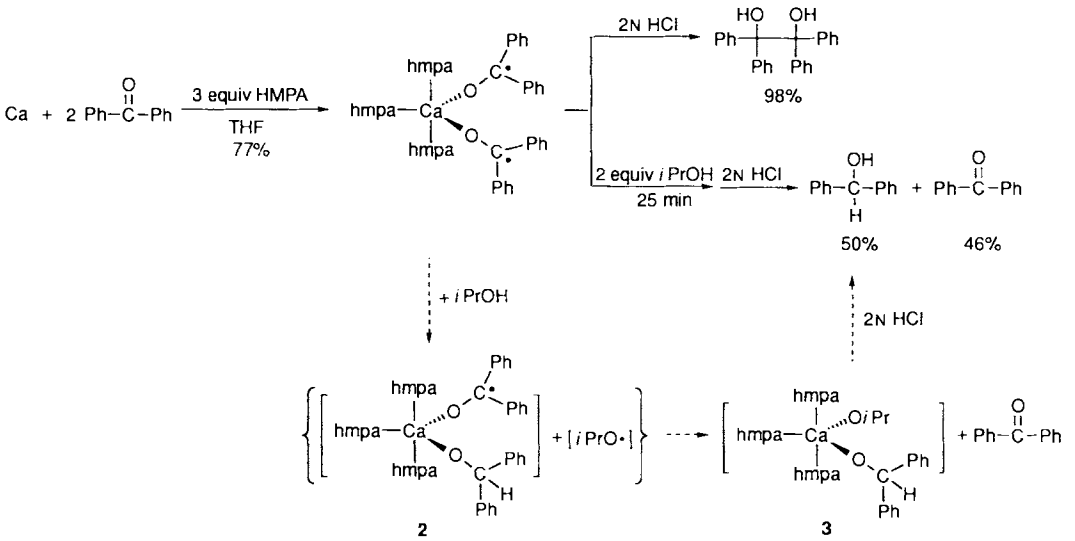

Scheme 1. Synthesis of **1** and mechanism of its reaction with 2-propanol.

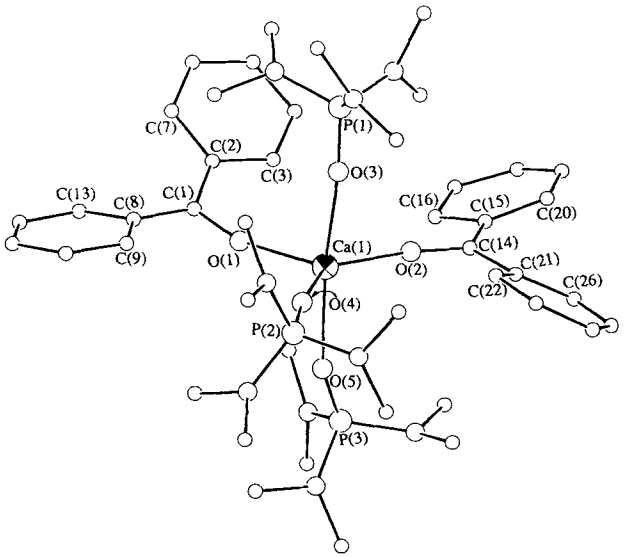

Figure 1. X-ray structure of **1**. Selected bond lengths (Å) and angles (°): Ca(1)–O(1) 2.187(9), Ca(1)–O(2) 2.206(10), Ca(1)–O(3) 2.315(9), Ca(1)–O(4) 2.286(8), Ca(1)–O(5) 2.314(10), O(1)–C(1) 1.31(1), O(2)–C(14) 1.31(2); O(1)-Ca(1)-O(2) 114.2(4), O(1)-Ca(1)-O(3) 95.0(4), O(1)-Ca(1)-O(4), 110.2(4), O(1)-Ca(1)-O(5) 94.5(4), O(2)-Ca(1)-O(3) 89.4(4), O(2)-Ca(1)-O(4) 135.6(4), O(2)-Ca(1)-O(5) 90.0(4), O(3)-Ca(1)-O(4) 86.2(3), O(3)-Ca(1)-O(5) 169.8(4), O(4)-Ca(1)-O(5) 87.1(4), Ca(1)-O(1)-C(1) 162.5(8), Ca(1)-O(2)-C(14) 160.0(10).

unit makes it difficult to stabilize the radical through $p_z-\pi$ orbital interactions with the phenyl groups, and thus explains why benzophenone ketyl is much more reactive than fluorenone ketyl.

Hydrolysis of **1** gave the coupling product, benzopinacol, almost quantitatively (Scheme 1). However, reaction of **1** with two equivalents of 2-propanol in THF followed by hydrolysis afforded benzhydrol and benzophenone in 50% and 46% yields, respectively (Scheme 1). This reaction could be explained by the mechanism shown in Scheme 1. Hydrogen radical abstraction by one of the two ketyls in **1** from 2-propanol[14] gives the ketyl/diphenylmethoxide **2** and the radical *i*PrO•. The subsequent rapid oxidation of the ketyl **2** by the inner-sphere radical *i*PrO• affords benzophenone and **3**, which yields benzhydrol after hydrolysis.

Experimental Section

Typical procedure for the synthesis of **1**: Under argon atmosphere, calcium chips (28 mg, 0.7 mmol) were stirred with CH_2I_2 (2 mol%) in THF (1 mL) for 2 h to activate the metal surface. Hexamethylphosphoric triamide (hmpa; 0.36 mL, 2.1 mmol) was then added by syringe. Addition of a THF solution of benzophenone (255 mg, 1.4 mmol) yielded a blue mixture within a few minutes. After being stirred at room temperature overnight, the blue solution was filtered and concentrated under reduced pressure. Addition of hexane precipitated the benzophenone ketyl complex **1** as blue blocks (510 mg, 0.54 mmol, 77% yield). Anal. calcd for $C_{44}H_{74}N_9O_5P_3Ca$: C 56.09, H 7.92, N 13.38; found: C 55.81, H 8.03, N 13.33.

Received: January 21, 1997 [Z 10014 IE]
German version: *Angew. Chem.* **1997**, *109*, 1348–1350

Keywords: arenes · calcium · radicals · reductions · structure elucidation

[1] For early examples of the formation of ketyl species, see a) F. Bechman, T. Paul, *Justus Ann. Chem.* **1891**, *266*, 1; b) W. Schlenk, T. Weichel, *Ber. Dtsch. Chem. Ges.* **1911**, *44*, 1182; c) W. Schlenk, A. Thal, *ibid.* **1913**, *46*, 2840.

[2] For reviews on metal ketyl mediated organic synthesis, see a) A. Fürstner, B. Bogdanovic, *Angew. Chem.* **1996**, *108*, 2582; *Angew. Chem. Int. Ed. Engl.* **1996**, *35*, 2442; b) T. Wirth, *ibid.* **1996**, *35*, 61 and **1996**, *108*, 65; c) J. W. Huffman in *Comprehensive Organic Synthesis, Vol. 8* (Eds.: B. M. Trost, I. Fleming), Pergamon, Oxford, **1991**, p. 104; d) G. M. Robertson in *Comprehensive Organic Synthesis, Vol. 3* (Eds. B. M. Trost, I. Fleming, G. Pattenden), Pergamon, Oxford, **1991**, p. 563; e) J. E. McMurry, *Chem. Rev.* **1989**, *89*, 1513; f) B. E. Kahn, R. T. Riecke, *ibid.* **1988**, *88*, 733; g) S. K. Pradhan, *Tetrahedron* **1986**, *42*, 6351; h) J. W. Huffman, *Acc. Chem. Res.* **1983**, *16*, 399; i) J. E. McMurry, *ibid.* **1983**, *16*, 405; *ibid.* **1974**, *7*, 281; j) H. O. House, *Modern Synthetic Reactions*, 2nd ed., W. A. Benjamin, Menlo Park, CA, **1972**, p. 145.

[3] a) Z. Hou, T. Miyano, H. Yamazaki, Y. Wakatsuki, *J. Am. Chem. Soc.* **1995**, *117*, 4421; b) Z. Hou, Y. Wakatsuki, *J. Synth. Org. Chem. Jpn.* **1995**, *53*, 906; c) Z. Hou, A. Fujita, H. Yamazaki, Y. Wakatsuki, *J. Am. Chem. Soc.* **1996**, *118*, 2503; d) *ibid.* **1996**, *118*, 7843; e) Z. Hou, Y. Wakatsuki, *Chem. Eur. J.* **1997**, *3*, 1005.

[4] For example, sodium benzophenone ketyl has been used by almost every chemist in the dehydration and deoxygenation of etheral solvents.

[5] For examples of spectroscopic studies on benzophenone ketyl species, see a) P. H. Rieger, G. K. Fraenkel, *J. Chem. Phys.* **1962**, *37*, 2811; b) P. B. Ayscough, R. Wilson, *J. Chem. Soc.* **1963**, 5412; c) N. Hirota, S. I. Weissman, *J. Am. Chem. Soc.* **1964**, *86*, 2538; d) N. Hirota, *ibid.* **1967**, *89*, 32; e) R. Dams, M. Malinowski, I. Westdorp, H. Y. Geise, *J. Org. Chem.* **1982**, *47*, 248; f) K. J. Covert, P. T. Wolczanski, S. A. Hill, P. J. Krusic, *Inorg. Chem.* **1992**, *31*, 66.

[6] R. S. P. Coutts, P. C. Wailes, R. L. Martin, *J. Organomet. Chem.* **1971**, *50*, 145.

[7] J. Takats, *J. Alloys Compnds*, in press.

[8] Only the structures of sodium and samarium ketyl complexes have been reported [3].

[9] For examples of spectroscopic studies on alkaline earth metal ketyl species, see a) S. W. Mao, N. Hirota, *Chem. Phys. Lett.* **1973**, *22*, 26; b) S. W. Mao, K. Nakamura, N. Hirota, *J. Am. Chem. Soc.* **1974**, *96*, 5341; see also ref. [5c].

 © *VCH Verlagsgesellschaft mbH, D-69451 Weinheim, 1997* *0570-0833/97/3612-1293 $ 17.50+.50/0*

[10] Crystal structure data of **1**: $C_{44}H_{74}N_9O_5P_3Ca$, $M_r = 942.14$, triclinic, space group $P\bar{1}$ (No. 2), $a = 10.953(2)$, $b = 11.812(2)$, $c = 22.360(5)$ Å, $\alpha = 93.09(2)$, $\beta = 93.36(2)$, $\gamma = 108.90(2)$ Å, $V = 2724(1)$ Å^3, $Z = 2$, $\rho_{calcd} = 1.15$ g cm^{-3}, $\mu(Mo_{K\alpha}) = 2.432$ cm^{-1}, 10383 measured reflections, of which 9566 independent ($R_{int} = 0.06$), empirical absorption correction (max.: 0.997, min.: 0.896), $R = 0.0867$ ($R_w = 0.890$) for 3929 reflections with $I > 2\sigma(I)$ and 559 refined on $|F|$, max. residual electron density: 0.66. The crystal was sealed in a thin-walled glass capillary under N_2. Data were collected on a Mac Science MXC3K diffractometer (20 °C, $Mo_{K\alpha}$ radiation, graphite monochromator, $\lambda = 0.71073$ Å, ω-2θ mode, $1.5 \leq \theta \leq 27.5°$) and were corrected for Lorentzian and polarization effects. The structure was solved by direct methods with SIR92 in the CRYSTAN-GM software package. Refinements were performed anisotropically for all non-hydrogen atoms by the block-diagonal least-squares method. Attempts to locate the hydrogen atoms were not made. The function minimized in the least-squares refinements was $(\sum(|F_o| - |F_c|)^2$. Crystallographic data (excluding structure factors) for the structures reported in this paper have been deposited with the Cambridge Crystallographic Data Centre as supplementary publication no. CCDC-100217. Copies of the data can be obtained free of charge on application to The Director, CCDC, 12 Union Road, Cambridge CB21EZ, UK (fax: int. code +(1223)336-033; e-mail: deposit@chemcrys.cam.ac.uk).

[11] P. B. Hitchcock, M. F. Lappert, G. A. Lawless, B. Royo, *J. Chem. Soc. Chem. Commun.* **1990**, 1141.

[12] The similarity in length between M–O(fluorenone ketyl) bonds and M–OAr bonds was previously observed; see ref. [3].

[13] E. B. Fleischer, N. Sung, S. Hawkinson, *J. Phys. Chem.* **1968**, *72*, 4311.

[14] Abstraction of a hydrogen atom from an alcohol by a fluorenone ketyl was previously observed; see ref. [3d].

Multicomponent Self-Assembly: Generation and Crystal Structure of a Trimetallic [4]Pseudorotaxane

Paul N. W. Baxter, Hanadi Sleiman, Jean-Marie Lehn,* and Kari Rissanen

The generation of threaded molecular entities such as pseudorotaxanes, rotaxanes, and catenanes is currently the subject of considerable interest owing to the intriguing synthetic and structural issues posed by such systems.[1, 2] Recent developments in this field include potential applications for materials science and the design of supramolecular devices[3] such as novel polymer composites[4] and simple mechanical molecular processes.[5] In the case of rotaxanes initial synthetic strategies focused on statistical methods of preparation, but more recently supramolecular approaches utilizing intermolecular interactions—such as aromatic attractive forces,[2, 6] hydrogen bonding,[7] and metal ion coordination[2, 8]—have been found to be most efficient for threaded molecules. Rotaxanes and pseudorotaxanes that incorporate metal ions represent a particularly interesting class of supramolecular species that might display a rich variety of physicochemical properties such as redox, optical, and magnetic behavior. Metal ion directed threading may also be used for constructing linear arrays of metal ions with precisely defined interionic distances, for example, inorganic rack-type architectures.[9] This approach may additionally provide access to self-assembled pseudorotaxane racks that incorporate linear strings of metal ions in oxidation states not normally accessible in the presence of nonmacrocyclic ligand analogues due to dissociative instability.

We here report the high-yield formation (Scheme 1) and X-ray crystallographic investigation of the trinuclear [4]pseudorotaxane rack **1**. In previous work on metallorotaxanes incorporating linear oligobipyridines as the central unit,[10] the metal ions were alternately situated on opposite sides of the ligand rack in a *trans* conformation in the solid state. In contrast,

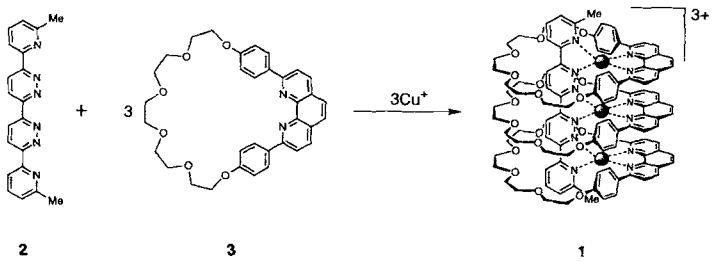

Scheme 1. Self-assembly of the tricopper pseudorotaxane [3]rack **1**.

2, which incorporates pyridazine metal ion bridging units, is expected to yield a pseudorotaxane rack in which the metal ions are situated on the same side, that is, an all *syn* relationship with shorter internuclear separations. This structural modification may increase electronic communication between the metal centers and render these systems more attractive candidates for molecular-device components.

Mixture of **2**, **3**, and $[Cu(MeCN)_4]PF_6$ in a 1:3:3 stoichiometric ratio in CH_2Cl_2/MeCN (1/1) resulted in the formation of **1** in greater than 80% yield. The rigid-rod ligand **2** and the macrocyclic ligand **3** were prepared as previously reported.[11, 12] The identity of the reaction product was established with ^1H and ^{13}C NMR spectroscopy, FAB-MS (Table 1), and X-ray crystallography. The ^1H NMR spectrum was particularly informative and showed **3** to be in two different chemical environments. For example, the *ortho* and *meta* phenyl-ring

Table 1. Physical and spectroscopic data for $\mathbf{1}(PF_6)_3$.

^1H NMR (CD_3NO_2, 500 MHz, 20 °C): $\delta = 9.212$ (d, J(H3′,H4′) = 9.3 Hz, **2**-H3′), 9.159 (d, J(H4′,H3′) = 9.3 Hz, **2**-H4′), 8.527 (d, J(H3,H4) = 8.1 Hz, **2**-H3), 8.192 (d, J(H4,H3) = J(H7,H8) = 8.3 Hz, $\mathbf{3}_{outer}$-H4/7), 8.153 (t, J(H3,H4,H5) = 7.9 Hz, **2**-H4), 8.096 (d, J(H4,H3) = J(H7,H8) = 8.4 Hz, $\mathbf{3}_{inner}$-H4/7), 7.908 (s, $\mathbf{3}_{inner}$-H5/6), 7.812 (s, $\mathbf{3}_{outer}$-H5/6), 7.498 (d, J(H3,H4) = J(H8,H7) = 8.3 Hz, $\mathbf{3}_{outer}$, H3/8), 7.444 (d, J(H5,H4) = 7.7 Hz, **2**-H5), 7.284 (d, J(H3,H4) = J(H8,H7) = 8.3 Hz, $\mathbf{3}_{inner}$-H3/8), 6.678 (d, J(*ortho*-H,*meta*-H) = 8.6 Hz, $\mathbf{3}_{outer}$-*ortho*-H), 6.422 (d, J(*ortho*-H,*meta*-H) = 8.7 Hz, $\mathbf{3}_{inner}$-*ortho*-H), 6.215 (d, J(*meta*-H,*ortho*-H) = 8.8 Hz, $\mathbf{3}_{inner}$-*meta*-H), 6.171 (d, J(*meta*-H,*ortho*-H) = 8.7 Hz, $\mathbf{3}_{outer}$-*meta*-H), 4.125–3.600 (m, $\mathbf{3}_{inner/outer}$-$H(CH_2)$), 1.711 (s, **2**-CH_3). All CH_3 and ring proton signals for **2** in the ^1H NMR spectrum of **1** represent magnetically and chemically equivalent pairs of protons on the ligand; ^{13}C NMR (CD_3NO_2, 75 MHz, 20 °C): δ = 165.839, 165.346, 163.068, 162.577, 162.289, 161.219, 157.959, 152.301, 147.940, 147.499, 144.381, 143.766, 143.249, 136.826, 135.345, 134.143, 133.980, 133.936, 133.752, 133.597, 133.074, 132.944, 132.241, 131.643, 129.630, 129.293, 127.772, 119.691, 119.220 (aromatic C atoms); 75.690, 75.608, 75.457, 75.346, 75.268, 74.617, 74.141, 73.496 (CH_2); 28.496 (CH_3); FAB-MS (CH_2Cl_2): *m/z* (relative intensity in %) = 2520.6 (0.5) $[Cu_3(\mathbf{2})(\mathbf{3})_3](PF_6)_2^+$, 2375.6 (0.7) $[Cu_3(\mathbf{2})(\mathbf{3})_3](PF_6)^{\cdot+}$, 2230.6 (0.1) $[Cu_3(\mathbf{2})(\mathbf{3})_3]^{\cdot+}$, 1745.4 (2.3) $[Cu_2(\mathbf{2})(\mathbf{3})_2](PF_6)^+$, 1600.5 (1.1) $[Cu_2(\mathbf{2})(\mathbf{3})_2]^{2+}$, 1115.3 (1.2) $[Cu_3(\mathbf{2})(\mathbf{3})_3]^{2+}$, 969.3 (12.0) $[Cu(\mathbf{2})(\mathbf{3})]^+$, 629.2 (100) $[Cu(\mathbf{3})]^+$; UV/Vis (CH_2Cl_2): λ (ε in mol^{-1} dm^3 cm^{-1}) = 286.0 (81320), 321.0 (102480), 478.0 nm (8073); elemental analysis calcd for $C_{122}H_{118}Cu_3F_{18}N_{12}O_{18}P_3$: C 54.97, H 4.46, N 6.30; found: C 54.79, H 4.33, N 6.24.

[*] Prof. Dr. J.-M. Lehn, Dr. P. N. W. Baxter
Laboratoire de Chimie Supramoléculaire, Institut Le Bel
Université Louis Pasteur
4, rue Blaise Pascal
F-67000 Strasbourg (France)
CNRS URA 422
Fax: Int. code +(3)8841-1020
e-mail: lehn@chimie.u-strasbg.fr
Dr. H. Sleiman
Department of Chemistry, American University of Beirut (Lebanon)
Dr. K. Rissanen
Department of Chemistry
University of Jyväskylä (Finland)

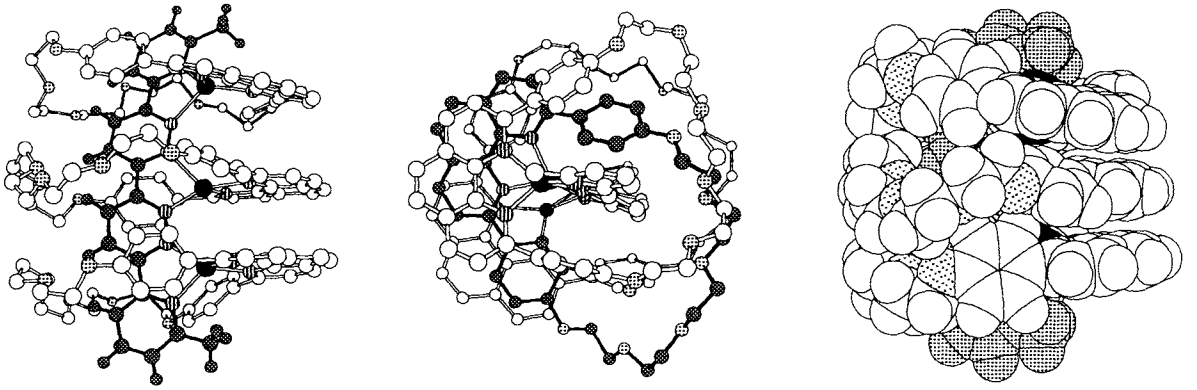

Figure 1. Crystal structure of **1**. Left: Side view; the central ligand **2** is highlighted in black (hydrogen atoms of ligands **3** removed for clarity). Center: Ball-and-stick representation as viewed down the long axis of **2**; the inner macrocycle **3** is highlighted in black (all hydrogen atoms removed for clarity). Right: CPK representation, side view. Labeling of atoms in the structure on the left from bottom to top: Cu1 to Cu3, N_1 to N_6, C–C bonds C_6–C_7, C_{10}–C_{11}, and C_{14}–C_{15} between successive rings.

protons of **3**, which appeared as two doublets, were split into two groups in a 2:1 ratio. Also the signals corresponding to the phenanthroline-ring protons (H3,8; H4,7; H5,6) were each divided into two sets in a 2:1 ratio. This corresponds to two outer and one inner units of **3**. The *ortho* phenyl-ring protons of the inner ligand **3** experience the greatest shielding, as expected for protons buried deepest within the interior of **1**. The protons of **2** on the other hand appear as a set of five signals, which indicates that **2** is in a single chemical environment. This then provides a ligand ratio $\mathbf{2}$:$\mathbf{3}_{outer}$:$\mathbf{3}_{inner}$ of 1:2:1. The FAB-MS of a CH_2Cl_2 solution of the reaction product displayed three peaks at $m/z = 2520.6$, 2375.6, and 2230.6 corresponding to the cations $\{[Cu_3(\mathbf{2})(\mathbf{3})_3](PF_6)_2\}^+$, $\{[Cu_3(\mathbf{2})(\mathbf{3})_3](PF_6)\}^+$, and $\{[Cu_3(\mathbf{2})(\mathbf{3})_3]\}^+$. No peaks higher than $m/z = 2520.6$ were observed, but bands at lower values that are characteristic of partially dethreaded species were present.

An X-ray crystallographic investigation of **1** confirmed that its structure was that of a trinuclear [4]pseudorotaxane rack (Figure 1).[13] As defined by its van der Waals surface, the cation is approximately a cube of dimensions 16 × 16 × 15.5 Å. Three macrocyclic ligands **3** are threaded onto a single ligand **2**, which passes centrally through the internal cavity of each macrocycle. The array of three Cu^+ ions, each coordinated to **2** and a unit of **3**, is curved (Cu1-Cu2-Cu3 160.69°) as a result of the curvature of **2** itself.[16]

The pseudometallorotaxane **1** self-assembles by correct association of seven particles by a metal ion mediated threading of three units of **3** onto **2**. Ten aromatic edge-to-face and face-to-face attractive interactions also help to stabilize the resulting superstructure. Further evidence for the stability of **1** was provided by UV/Vis spectroscopic dilution experiments, which demonstrated that **1** showed no appreciable dethreading in ten days down to a concentration of 10^{-4} M in CH_2Cl_2. To establish whether it was possible to generate a rack of composition $[Cu_3(\mathbf{2})(\mathbf{4})_3](PF_6)_3$, a control experiment was performed in which **2**, **4**, and $[Cu(MeCN)_4]PF_6$ (1:3:3) were combined under conditions identical to those for the preparation of **1**. The ^1H NMR spectrum of the reaction mixture after 96 h showed it to consist of $[Cu(\mathbf{4})_2]^+$ and a complex mixture of species comprising **2**, **4**, and Cu^+. This demonstrates that pseudorotaxane self-assembly is essential for the formation of multinuclear Cu^I racks.

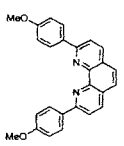

4

The successful generation of a trimetallic rack incorporating metal ions in close proximity has been achieved. This design principle should be extendable to the preparation of multimetallic racks that are inaccessible by sequential synthesis (although this is possible for ruthenium(II) [2]- and [3]racks)[9] or by self-assembly from mixtures of nonmacrocyclic ligand components. Metallopseudorotaxane racks such as **1** may display novel electro-, photo-, and surface chemical properties, and their incorporation into more complex supramolecular assemblies may be envisioned.

Experimental Section

CH_2Cl_2 (2 mL) was added with a syringe to a mixture of **2** (5.0 mg, 1.47×10^{-5} mol), **3** (25.0 mg, 4.41×10^{-5} mol), and $[Cu(MeCN)_4]PF_6$ (16.5 mg, 4.42×10^{-5} mol) under an argon atmosphere, and the dark brown solution stirred at ambient temperature for 3 h. MeCN (2 mL) was then added with a syringe, and the reaction mixture heated at 60 °C with stirring for a further 96 h. After the mixture had cooled to room temperature, all solvent was removed under vacuum, and the residue redissolved in CH_2Cl_2 (3 ml), filtered through a microporous filter, and the solvent again removed under vacuum to give a dark brown, glassy solid. A ^1H NMR spectrum (CD_3NO_2) of the product showed it to be $\mathbf{1}(PF_6)_3$ (≥80% yield) [17]. Final purification was achieved by recrystallization from $MeNO_2$/benzene by liquid–liquid diffusion. The crystals that formed over a three-month period were isolated by vacuum filtration, washed with benzene, and dried in the air and then at 90 °C/2×10^{-6} mm Hg for 48 h. Yield: 0.019 g (49%) $\mathbf{1}(PF_6)_3$ as small, dark brown-red cubes.

Received: January 16, 1997 [Z10001IE]
German version: *Angew. Chem.* **1997**, *109*, 1350–1352

Keywords: copper · pseudorotaxanes · self-assembly · supramolecular chemistry

[1] D. M. Walba, *Tetrahedron* **1985**, *41*, 3161; H. Ogino, *New. J. Chem.* **1993**, *17*, 683.
[2] J.-C. Chambron, C. O. Dietrich-Buchecker, J.-P. Sauvage in *Comprehensive Supramolecular Chemistry, Vol. 9*, Elsevier, UK, **1996**, chap. 2; D. B. Amabilino, F. M. Raymo, J. F. Stoddart in *ibid.*, chap. 4.
[3] J.-M. Lehn, *Supramolecular Chemistry, Concepts and Perspectives*, VCH, Weinheim, **1995**, chap. 8.
[4] H. W. Gibson, S. Liu, P. Lecavalier, C. Wu, Y. X. Shen, *J. Am. Chem. Soc.* **1995**, *117*, 852; I. Yamaguchi, K. Osakada, T. Yamamoto, *ibid.* **1996**, *118*, 1811.
[5] A. Livoreil, C. O. Dietrich-Buchecker, J.-P. Sauvage, *J. Am. Chem. Soc.* **1994**, *116*, 9399; M. Asakawa, S. Iqbal, J. F. Stoddart, N. D. Tinker, *Angew. Chem.* **1996**, *108*, 1054; *Angew. Chem. Int. Ed. Engl.* **1996**, *35*, 976; R. Ballardini, V. Balzani, A. Credi, M. T. Gandolfi, S. J. Langford, S. Menzer, L. Prodi, J. F. Stoddart, M. Venturi, D. J. Williams, *ibid.* **1996**, *108*, 1056 and **1996**, *35*, 978, and references therein.
[6] D. Philp, J. F. Stoddart, *Angew. Chem.* **1996**, *108*, 1242; *Angew. Chem. Int. Ed. Engl.* **1996**, *35*, 1155, section 4.4.
[7] F. Vögtle, R. Jäger, M. Händel, S. Ottens-Hildebrandt, W. Schmidt, *Synthesis* **1996**, 353; P. T. Glink, C. Schiavo, J. F. Stoddart, D. J. Williams, *J. Chem. Soc. Chem. Commun.* **1996**, 1483; M. Asakawa, P. R. Ashton, G. R. Brown, W. Hayes, S. Menzer, J. F. Stoddart, A. J. P. White, D. J. Williams, *Adv. Mater.* **1996**, *8*, 37.
[8] J.-C. Chambron, C. O. Dietrich-Buchecker, J.-F. Nierengarten, J.-P. Sauvage, *J. Chem. Soc. Chem. Commun.* **1993**, 801; J.-C. Chambron, C. O. Dietrich-Buchecker, J.-F. Nierengarten, J.-P. Sauvage, N. Solladié, A.-M. Albrecht-

Gary, M. Meyer, *New J. Chem.* **1995**, *19*, 409; J.-C. Chambron, S.-Chardon-Noblat, A. Harriman, V. Heitz, J.-P. Sauvage, *Pure Appl. Chem.* **1993**, *65*, 2343; N. Solladié, J.-C. Chambron, C. O. Dietrich-Buchecker, J.-P. Sauvage, *Angew. Chem.* **1996**, *108*, 957; *Angew. Chem. Int. Ed. Engl.* **1996**, *35*, 906.

[9] G. S. Hanan, C. R. Arana, J.-M. Lehn, D. Fenske, *Angew. Chem.* **1995**, *107*, 1191; *Angew. Chem. Int. Ed. Engl.* **1995**, *34*, 1122; G. S. Hanan, C. R. Arana, J.-M. Lehn, G. Baum, D. Fenske, *Chem. Eur. J.* **1996**, *2*, 1292.

[10] H. Sleiman, P. N. W. Baxter, J.-M. Lehn, K. Rissanen, *J. Chem. Soc. Chem. Commun.* **1995**, 715.

[11] P. N. W. Baxter, J.-M. Lehn, J. Fischer, M.-T. Youinou, *Angew. Chem.* **1994**, *106*, 2432; *Angew. Chem. Int. Ed. Engl.* **1994**, *33*, 2284.

[12] C. O. Dietrich-Buchecker, J.-P. Sauvage, *Tetrahedron* **1990**, *46*, 503.

[13] Crystal structure data for $[\mathbf{1}(H_2O)](PF_6)_3 \cdot 3C_6H_6 \cdot CH_3NO_2$, $M_r = 2979.346$ (the crystallographically determined value for M_r was 2977.24, since the positions of the H atoms of the included water molecules could not be located or calculated), triclinic, space group $P\bar{1}$ (no. 2), $a = 18.239(3)$, $b = 19.766(2)$, $c = 20.572(2)$ Å, $\alpha = 69.53(1)$, $\beta = 83.85(1)$, $\gamma = 85.22(1)^\circ$, $V = 6915(2)$ Å^3, $Z = 2$, $\rho_{calcd} = 1.433$ g cm^{-3}, $F(000) = 3079$, $T = 296 \pm 1$ K. Crystals of **1** were grown by slow diffusion of benzene into a CH_3NO_2 solution of the complex at 293 K. Data was collected on a crystal of dimensions $0.40 \times 0.40 \times 0.50$ mm (Enraf-Nonius CAD4 diffractometer, $\lambda(Mo_{K\alpha}) = 0.7107$ Å, graphite monochromator). Of 17515 collected reflections 16859 were unique ($R_{int} = 0.007$), $\omega/2\theta$-scan mode, $2\theta = 44^\circ$ (h: $0 \rightarrow 19$, k: $-20 \rightarrow 20$, l: $-21 \rightarrow 21$); 10912 reflections with $I > 3\sigma I$ were used for refinement. Lp and absorption corrections based on psi scans were applied, $\mu(Mo_{K\alpha}) = 0.585$ mm^{-1}. The structure was solved by direct methods (SHELXS) [14] and subjected to block-matrix refinement in seven blocks [15]. The H atoms were calculated at theoretical positions (C–H 1.0 Å, isotropic temperature factor 8.0 Å^2) and included in the final structure-factor calculations but not refined; F_0-parameter ratio = 6.09, final R value 0.055, $R_w = 0.064$ for 1793 parameters: $w = w'[1.0 - (\Delta F/6\sigma F)^2]^2$, where w' is the Chebychev polynomial for F_c with three coefficients (12.9, −2.42, and 10.4); $S = 1.15$, convergence, max. shift/error < 0.08. The final difference map displayed no electron density higher than 0.77 e Å^{-3}. Crystallographic data (excluding structure factors) for the structures reported in this paper have been deposited with the Cambridge Crystallographic Data Centre as supplementary publication no. CCDC-100241. Copies of the data can be obtained free of charge on application to The Director, CCDC, 12 Union Road, Cambridge CB21EZ, UK (fax: int. code +(1223)336-033; e-mail: deposit@chemcrys.cam.ac.uk).

[14] G. M. Sheldrick in *Crystallographic Computing, Vol. 3* (Eds.: G. M. Sheldrick, C. Krüger, R. Goddard), Oxford University Press, Oxford, England, **1985**, p. 175.

[15] D. Watkin, J. R. Carruthers, P. W. Betteridge, *CRYSTALS*, Chemical Crystallography Laboratory, Oxford (UK), **1990**.

[16] The deviation of the array of three Cu^+ ions from linearity arises from the curvature of **2**, which in turn results from the summed effects of two types of distortions. Firstly, when viewed perpendicular to its mean plane, the six nitrogen atoms of **2** describe a shallow arc, which stems from the fact that the pyridazine ring is not a regular hexagon but contracted along the N=N bond. Secondly, the aromatic rings of **2** are bent and rotated with respect to each other through each interring bond, which causes **2** to adopt a twisted crescent shape when viewed along the ligand mean plane perpendicular to its long axis (torsion angles N1-C6-C7-N2 14.36, N3-C10-C11-N4 12.84, N5-C14-C15-N6 19.44°). A striking feature of the complex is the relative arrangement of the phenanthroline moieties along **2** (Figure 1b). The three phenanthrolines from **3** are not eclipsed, but substantially staggered with respect to each other (torsional angles D1-Cu1-Cu2-D2 35.56, D2-Cu2-Cu3-D3 76.90, D1-Cu1-Cu3-D3 39.07°; D1, D2, and D3 are the centroids of the central fused C_6 rings in the phenanthrolines coordinated to Cu1, Cu2, and Cu3 respectively). When viewed along the long axis of **2**, one outer (coordinated to Cu3) and the inner phenanthroline units lie on opposite sides of the mean plane through **2**, whereas the remaining outer phenanthroline sits approximately centrally. Due to the relatively short distances between the copper ions (Cu1–Cu2 3.597, Cu2–Cu3 4.268, Cu1–Cu3 7.753 Å), the phenyl rings of the three ligands **3** cannot lie simultaneously coplanar to **2**. The relative staggering of the macrocyclic ligands about **2** is therefore a possible way of minimizing steric congestion between the phenyl rings. The relative displacements of **3** additionally introduce five stabilizing face-to-face contacts between **2** and the phenyl rings of **3**, and a further two face-to-face and three edge-to-face interactions (that is, within 3.4 Å) between the phenyl rings themselves. The highly dissymmetric environment of **3** is however not observed in the ^{1}H NMR sprectrum of **1**, presumably because of averaging by rapid rotational oscillations at room temperature. The wide range of N(ligand **2**)-Cu-N(ligand **3**) bond angles (108.1(2)–134.9(2)°) indicates that the Cu^+ ions are located in a highly distorted tetrahedral coordination polyhedron, and results mainly from the staggering of ligands **3** along **2**. On the other hand, the Cu–N bond lengths (1.973(4)–2.169(4) Å) are unexceptional. A single water molecule is captured within the cation and hydrogen bonded to three of the oxygen atoms of the central macrocyclic ligand **3**, ($O(H_2O)$–O(**3**) 2.95–3.06 Å).

[17] Attempted further purification by column chromatography on silica gel or alumina with a variety of eluant systems resulted in rapid dethreading and extensive decomposition of $\mathbf{1}(PF_6)_3$.

Cyclic Metal Complexes of Nucleobases and Other Heterocycles: Molecular Boxes, Rectangles, and Hexagons**

Holger Rauter, Ilpo Mutikainen,* Merja Blomberg, Colin J. L. Lock, Pilar Amo-Ochoa, Eva Freisinger, Lucio Randaccio,* Ennio Zangrando, Elisabetta Chiarparin, and Bernhard Lippert*

In memory of Colin J. L. Lock

Spontaneous self-assembly of cyclic metal complexes with right angles at their corners ("molecular squares", "molecular boxes") represents an area of great current interest.[1–4] In general, the metal unit provides the right-angular component, whereas four bifunctional organic ligands, for example 4,4'-bipyridine, form the sides (Scheme 1a).[5] In principle, it is possible to reverse this situation by placing the organic ligands at the corners and the metal units along the edges.[6, 7] This leads to "squares" in the strict sense (Scheme 1b).[8] Use of six-membered heterocycles with angles of 120° at the ligands and linear metal units provides molecular hexagons instead of squares.

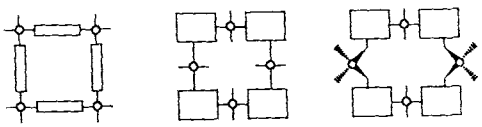

Scheme 1. Schematic representation of the basic structural types of molecular squares.

Variations of this principle with simultaneous use of different metal moities (such as *cis*-MX_2 and *trans*-MX_2 with M = Pt^{II}, Pd^{II}; X = NH_3, H_2O, NO_3^-, etc.) are also feasible (Scheme 1c). Here we report on relevant principles of this strategy utilizing the two nucleobases uracil (U) and 1-methylcytosine (1-MeC) as well as 2-aminopyridine (Hampy; Scheme 2).

We recently described a "molecular box" (open at the top and bottom) consisting of four Pt^{II}(en) units (en = 1,2-diaminoethane) and four bridging uracil nucleobases.[9] The cation **1** (UH_{-1} = monoanion from uracil) resembles calix[4]arenes as

[*] Dr. I. Mutikainen
Department of Chemistry
University of Helsinki
SF-00100 Helsinki (Finland)
Prof. Dr. L. Randaccio, Dr. E. Zangrando, Dr. E. Chiarparin
Dipartimento di Scienze Chimiche
Università di Trieste
I-34127 Trieste (Italy)
Fax: Int. code +(40)676-3903
Prof. Dr. B. Lippert, Dr. H. Rauter, Dr. P. Amo-Ochoa,
Dipl.-Chem. E. Freisinger
Fachbereich Chemie der Universität
D-44221 Dortmund (Germany)
Fax: Int. code +(231)755-3797
Dr. M. Blomberg
Department of Physics, University of Helsinki

[**] This work is in memory of Prof. Dr. C. J. L. Lock (Laboratories of Inorganic Medicine, Chemistry and Pathology, McMaster University, Hamilton, Ontario L8S4M1, Canada) who contributed to it but passed away too early. We gratefully acknowledge financial support of the Deutsche Forschungsgemeinschaft, the Fonds der Chemischen Industrie, and MURST and CNR (Rome, Italy). We thank Prof. Dr. W. S. Sheldrick and Mrs H. Mayer-Figge (Bochum, Germany) for their help with the structure determination of Pt_2Hg_6. This research was a part of HCM and COST projects.

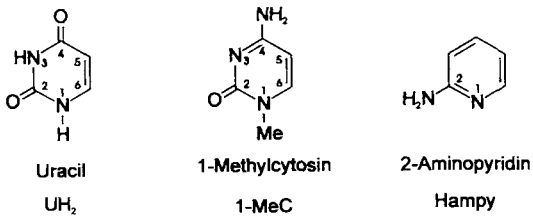

Scheme 2. The ligands uracil, 1-methylcytosine, and 2-aminopyridine.

far as its structure and solution dynamics are concerned. This analogy also includes the propensity of calix[4]arenes to complex metals.[10, 11] For example, after deprotonation of U to the uracil dianion (UH_{-2}), **1** binds additional divalent cations to yield octanuclear complexes **2** (M = *cis*-$Pt^{II}(NH_3)_2$ (**2a**), Pt^{II}(en) (**2b**), $Ni^{II}(H_2O)_3$ (**2c**), Pd^{II}(en) (**2d**), Cu^{II} (**2e**)). With M = Ag^{I}

$[\{Pt(en)(UH_{-1}\text{-}N1,N3)\}_4]^{4+}$ **1**

$[\{Pt(en)M(UH_{-2})\}_4]^{8+}$ **2a–2e**

$[\{Pt(en)Ag(UH_{-1})\}_4]^{8+}$ (**2f**) is obtained. In all of the octanuclear compounds the basic structure of the open box **1** is retained, but, instead of a single Pt^{II}(en) residue, two metal units (Pt^{II}(en) and M) represent the corners of the boxes (Scheme 3).

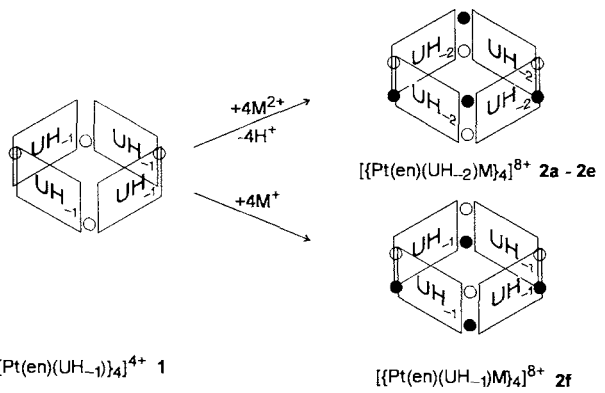

Scheme 3. Schematic representation of the molecular boxes **1** and **2**.

The complex cations were isolated as their nitrate salts, and crystals suitable for X-ray crystallography were obtained for **2a–2c** and **2f**. Although the octanuclear composition of the cation was established in all cases, a complete crystallographic analysis was only possible for **2a**.[12a] For **2b**,[12b] **2c**,[12c] and **2f**[9a] disorder of the NO_3^- anions and water molecules was so severe that, despite repeated attempts and data collection at low temperature, no satisfactory refinement was achieved.[12b,c]

The structure of the cation in **2a** is depicted in Figure 1. The basic feature of **1**, the 1,3-*alternate* arrangement of the four uracil nucleobases, is evident. The acidic protons of the UH_{-1} ligands in **1**, located between the O(2) and O(4) atoms of adjacent nucleobases, have been replaced with *cis*-$Pt^{II}(NH_3)_2$ units in **2a**. As a consequence, each uracil ring carries a metal ion at four positions (N(1), N(3), O(2), O(4)). Compared to the free base[13] and platinum complexes coordinated at N(1) and N(3),[9, 14] there are no significant changes in the ring geometry. The Pt(1)(en) units, which link the N(1) and N(3) positions, display normal geometries, as do the *cis*-$Pt^{II}(NH_3)_2$ moities. The Pt–Pt distances are Pt(1)–Pt(1c) 8.31, Pt(1)–Pt(2a) 7.51, Pt(1)–Pt(1b) 5.88, Pt(1)–Pt(2b) 4.75, and Pt(1)–Pt(2)

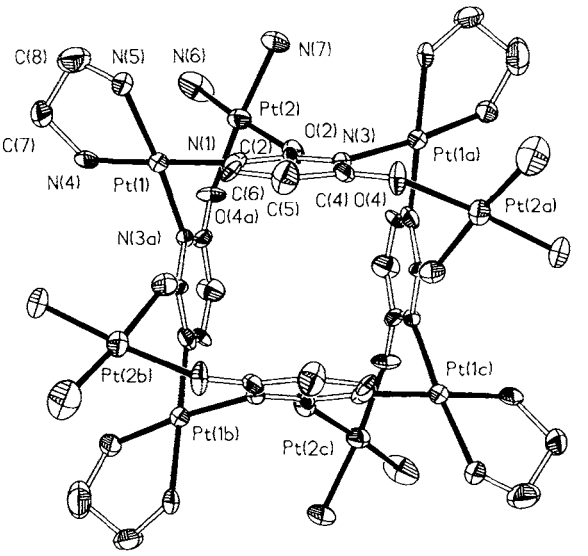

Figure 1. Crystal structure of the cation **2a** of the cyclic uracil complex $[\{Pt(en)\}_4(C_4H_2N_2O_2)_4\{Pt(NH_3)_2\}_4](NO_3)_4 \cdot 4H_2O$.

3.036(2) Å. Therefore, the shortest Pt–Pt separation is about 0.1 Å longer than that in related dinuclear complexes *cis*-$[Pt(a)_2L_2Pt(a)_2]^{2+}$ (a = NH_3; head-to-head orientation of bridging uracil nucleobases L).[15] The dihedral angle between the planes of the Pt(en) and *cis*-$Pt(NH_3)_2$ moities (Pt(1) and Pt(2)) is also rather large (40.9(6)°). Uracil rings at opposite sides of the box are not exactly parallel, which leads to different O(2)–O(2c) and C(5)–C(5c) distances (5.92 and 4.27 Å, respectively). Considering the spatial requirements of the π electron clouds of the uracil rings, the openings of the box at the top and bottom, which are rotated by 90° with respect to each other, are about 1×2.5 Å. There are no significant intermolecular Pt···Pt contacts, as frequently seen for dinuclear *cis*-$[Pt^{II}(a)_2L_2Pt^{II}(a)_2]^{2+}$ cations (L = UH_{-2} or cyclic amidate).[9, 16]

The composition of **2b** (M = Pt^{II}(en))[12b] is analogous to that of **2a**. Within the Pt_2 pairs, metal–metal separations differ slightly: 2.998(2) and 3.023(3) Å. The cations of the Pt_4Ni_4 compound **2c**[12c] is also of similar composition, but the Ni^{II} centers display distorted octahedral coordination spheres of five oxygen atoms (O(4), O(2), and three OH_2 groups) and a Pt atom. All four Pt–Ni distances within **2c** vary slightly (2.652(2)–2.700(5) Å). The structure of the Pt_4Ag_4 complex **2f** proves that the *cone* conformation can also be stabilized by metal ions and demonstrates that the 1,3-*alternate* → *cone* rearrangement can take place even in strongly acidic medium with the help of a suitable metal ion. Considering the close structural similarities of related di- and trinuclear PtM and Pt_2M complexes (M = Pt^{II}, Pd^{II}, Cu^{II}) with uracil nucleobases,[15] we propose that the compositions of the Pt_4Pd_4 and Pt_4Cu_4 cations **2d** and **2e** are analogous to those of **2a–2c**.

Cations **2a** and **2b** are inert in D_2O (see Experimental Section) and only decompose at pH* = 0. In the presence of excess NaCl, loss of the Pt units bound to O(4) and O(2) takes place over a period of several days at 40 °C. The cations react with excess CN^- within minutes to give **1** and $[Pt(CN)_4]^{2-}$. In a slow secondary reaction (1 d, 22 °C) an equilibration of 1,3-*alternate* and *cone* forms of **1** occurs (see *Experimental Section*). These findings confirm earlier observations that, despite the high thermodynamic stability of $[Pt(CN)_4]^{2-}$, N(3)-platinated uracil (and thymine) is inert with respect to CN^-.[17] Only those Pt residues bound to the exocyclic oxygens are readily displaced. The reaction $\mathbf{1} + 4M^{n+} \rightarrow \mathbf{2}$ can, therefore, be reversed; this fur-

 © VCH Verlagsgesellschaft mbH, D-69451 Weinheim, 1997 0570-0833/97/3612-1297 $ 17.50+.50/0

ther corroborates the analogy with the metal-coordinating properties of suitably modified calix[4]arenes.

The crystal structure determinations of **2a** and of its precursor **1** demonstrate that, irrespective of the 120° angle between the Pt–N1 and Pt–N3 vectors, molecular boxes are formed as long as the metal units are of *cis* geometry. As shown for **6**

$[\{Pt(CH_3NH_2)_2(1\text{-}MeCH_{-2})_2Hg_3(OH)\}_2](NO_3)_6 \cdot 4H_2O$ **6**

(1-$MeCH_{-2}$ = dianion of 1-MeC) *trans* geometry at the metal units leads to formation of a molecular hexagon (Scheme 4). To suppress formation of open-chain oligomers, fixation of the two cytosine nucleobases in **3**[18, 19] in a head-to-head arrangement is advantageous. This can be accomplished by metal binding at the deprotonated exocyclic amino groups[18] by, among others, Hg^{II}.[19]

Electrophilic attack of excess $Hg(NO_3)_2$ or $Hg(OAc)_2$ at the C5 positions of the two cytosine ligands in **4** leads, presumably via **5**, to **6** (Scheme 4). Metalation reactions at C5 are known for

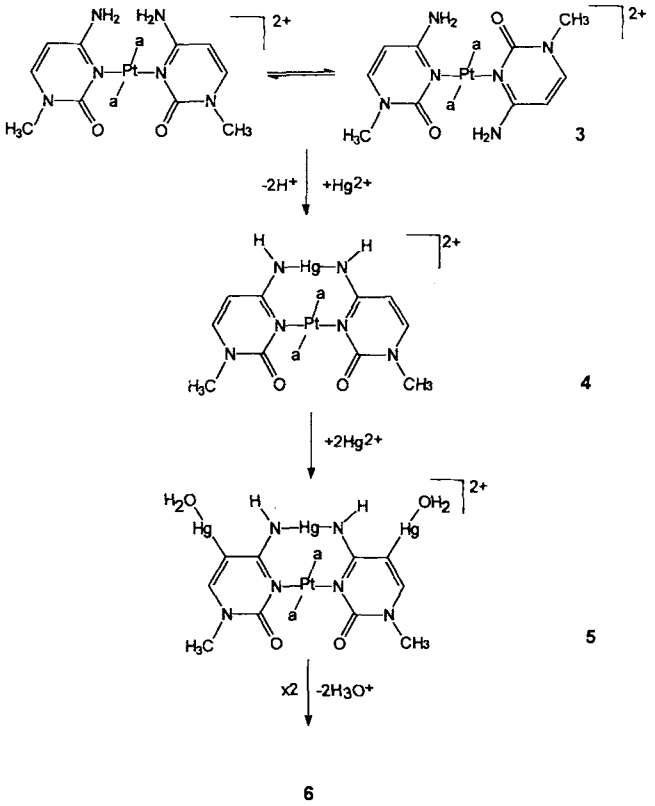

Scheme 4. Synthesis of **6**.

free cytosine[20] and various uracil derivatives.[21] Following the formation of **6** by ^1H NMR spectroscopy indicates that reaction of the head-to-head rotamer[22] of **3** via an intermediate (**5**?) takes place with a drop in pH. Compound **6** was isolated from acidic solutions (pH = 1.8–3) and characterized by elemental analysis, X-ray crystal structure determination,[23] and NMR spectroscopy.

Figure 2 shows the structure and Figure 3 schematic views of the cyclic cation $[\{Pt(CH_3NH_2)_2(C_5H_3N_3O)_2Hg_3(OH)(NO_3)\}_2]^{4+}$ of **6**. The basic form of the centrosymmetric cation is that of a compressed hexagon (sides 7 and 5.5 Å) with four Hg^{II} and two Pt^{II} atoms at the edges, and four nucleobases and two OH groups representing the corners. Two additional Hg^{II}

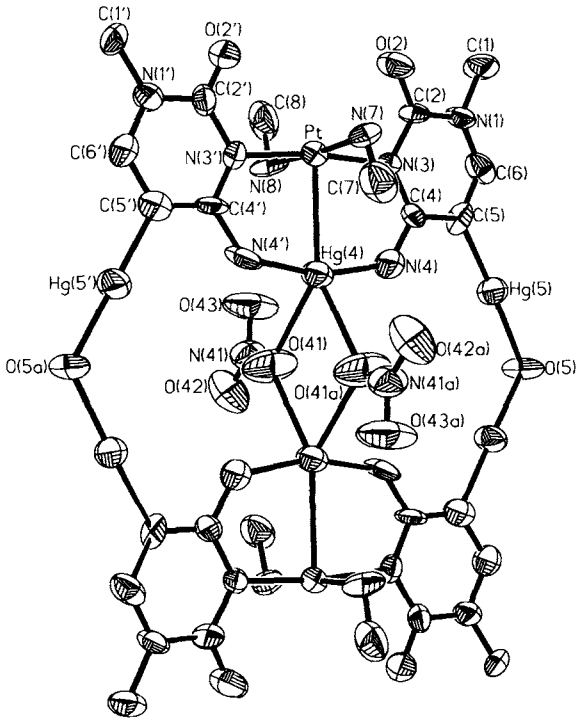

Figure 2. View of the cation $[\{Pt(CH_3NH_2)_2(C_5H_3N_3O)_2Hg_3(OH)(NO_3)\}_2]^{4+}$ in **6**. Selected bond lengths [Å] and angles [°]: Pt–N(3) 2.05(2), Pt–N(3') 2.07(2), Hg(4)–N(4) 2.08(2), Hg(4)–N(4') 2.08(2), C(5)–Hg(5) 2.05(2), Hg(5)–O(5) 2.09(1), C(5')–Hg(5') 2.04(2), Hg(5')–O(5') 2.06(1); N(3)-Pt-N(3') 172.8(5), N(4)-Hg(4)-N(4') 162.3(6), C(5)-Hg(5)-O(5) 175.0(6). For intermetallic distances see Figure 3.

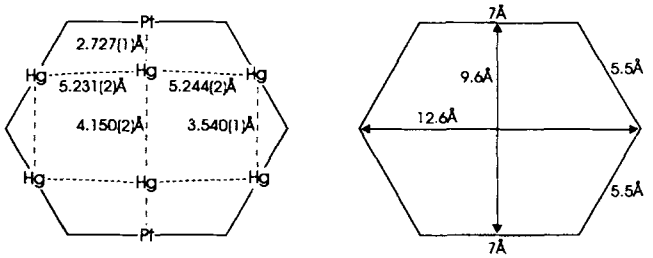

Figure 3. Dimensions and intermetallic distances in the cation of **6**.

ions, which bridge pairs of deprotonated exocyclic N(4) groups of the cytosine bases, are located along the Pt–Pt vector. All metal ions and OH groups are almost coplanar. The cation of **6** is made up of two units of **4**, which are linked by two Hg-OH-Hg units. Apart from the Pt–Hg(4) distances (2.727(1) Å in **6**, 2.785(1) Å in **4**) and the additional Hg(5) ions, there are no major differences between the structures of **4** and **6**. Even the NO_3^- groups bridging the dinuclear PtHg units in **6** are present.

In the crystal Pt_2Hg_6 cations form infinite, interlacing staircases. Thus the four O(2) oxygen atoms of the cytosine bases each form pairs of two hydrogen bonds with the amino protons of the CH_3NH_2 groups of the adjacent cations (O–N 2.85(2) and 2.89(2) Å). The intermolecular separation between the Pt ions is 4.929(2) Å. The steps in the second direction are formed by two intermolecular OH···OH hydrogen bonds (O(5)–O(5)' 2.773(23) Å) and four weak intermolecular Hg–ONO_2 bonds between the bridging nitrate groups and the Hg(5) or Hg(5') center of the adjacent cations (Hg–O 2.68(2)–2.94(2) Å). The Hg ions located at the sides of the hexagon exhibit different coordination geometries.

 © VCH Verlagsgesellschaft mbH, D-69451 Weinheim, 1997 0570-0833/97/3612-1298 $ 17.50+.50/0

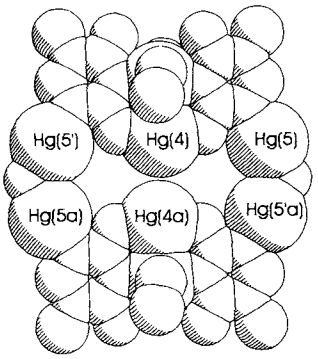

Figure 4. Space-filling model of the cation in **6**; bridging NO_3^- groups have been omitted.

A special structural feature of **6** is the arrangement of the six Hg^{II} ions (Figure 4). It is feasible that in solution, as in the solid state with weakly bonded nitrate anions and water molecules, interactions between the Lewis acidic Hg centers and nucleophiles occur, which could lead to specific substrate binding and catalysis.[26, 27] This arrangement bears some resemblance to the surface of a metal salt.[28]

Reaction of Hampy with first *trans*-$[Pt^{II}(CH_3NH_2)_2(H_2O)_2](NO_3)_2$ and then $[PdCl_4]^{2-}/AgNO_3$ leads to a species that can be considered as a hybrid between a rectangle and an open box containing both *trans*-MX_2 and *cis*-MX_2 units. Complex **9** was obtained from **7** upon reaction with $K_2[PdCl_4]$ and excess $AgNO_3$. Initially **7** reacts with K_2PdCl_4 with a drop in pH to give a poorly soluble orange product (**8**), which redissolves with red coloring upon addition of $AgNO_3$. Dark red cubes of **9**

trans-$[Pt(CH_3NH_2)_2(Hampy)_2](NO_3)_2$ **7**

$[\{Pt(CH_3NH_2)_2(ampy)_2\}_2Pd_4(NO_3)_6(H_2O)_2](NO_3)_2 \cdot 3.5H_2O$ **9**

crystallize from the solution. X-ray structure analysis[29] reveals that **9** consists of two crystallographically independent hexanuclear cations (A and B), nitrate anions, and water of crystallization. The two cations have a crystallographic C_2 axis, which passes through the two Pt centers in the case of A and is perpendicular to the Pt–Pt vector in B. Consequently, adjacent cations are mutually perpendicular in the crystal lattice. Cation A is depicted in Figure 5. Each *trans*-$[Pt(CH_3NH_2)_2]$ unit carries two coplanar aminopyridonate rings that are bound to Pt through the endocyclic ring N atoms and adopt, unlike in **7**, a head-to-head orientation. The two Pd_2 units each bridge the four deprotonated exocyclic amide nitrogen atoms to give a μ_3-η^2 coordination pattern for the ampy ligands.[31] All four Pd ions have *cis* geometries: the four remaining coordination sites are occupied by oxygen atoms (three from NO_3^- and one from H_2O). The resulting Pd_2N_2 rings are folded along the N···N vectors, which leads to short Pd–Pd distances (2.877(2) and 2.855(2) Å). In planar Pd_2N_2 rings, metal–metal distances are usually much longer (3.0633(9) Å).[32] The edges of the two cations are 4.07 (N1···N1') by 7.18 (N1···N4) (A) and 7.23 Å (B), respectively. Pt···Pt distances are 6.949(1) (A) and 6.990(1) Å (B), and the separations between the midpoints between the pairs of oppositely placed Pd_2 units are 6.276(1) (A) and 6.270(1) Å (B). In both cations the two $Pt(ampy)_2$ units are slightly twisted (Figure 6). The roughly coplanar orientation of the four NH protons of the exocyclic amide groups could be of interest with respect to receptor properties.

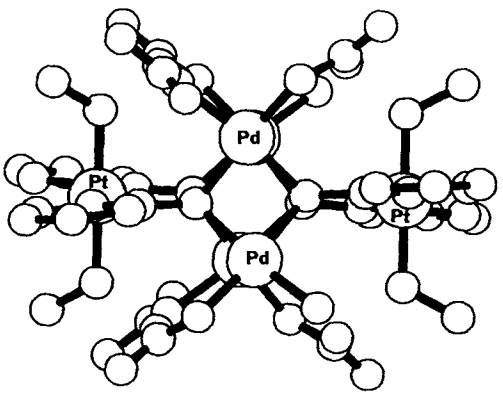

Figure 6. Side view of cation A in **9**. The two $Pt(ampy)_2$ units are slightly twisted with respect to each other.

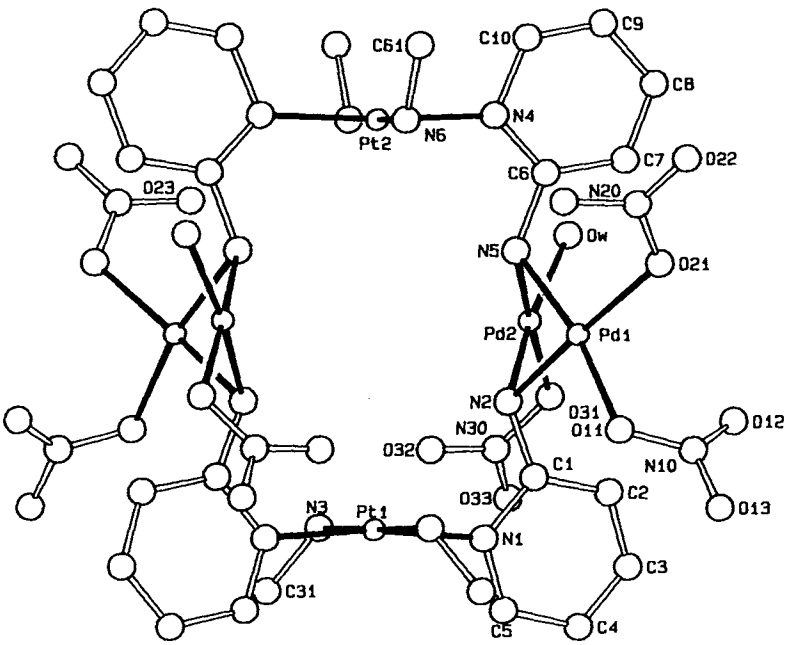

Figure 5. Structure of the crystallographically independent cation A in **9**. Selected bond lengths [Å] and angles [°]: Pt1–N1 2.04(1), Pt2–N4 2.01(2), Pd1–N2 2.03(2), Pd1–N5 2.03(1), Pd2–N2 2.07(1), Pd2–N5 2.08(1); N1-Pt1-N1' 172.0(6), N4-Pt2-N4' 175.1(7), Pd1-N2-Pd2 89.2(6), Pd1-N5-Pd2, 88.9(6), N2-Pd1-N5 77.4(6), N2-Pd2-N5 75.4(5).

Experimental Section

2: In a typical experiment, **1** (0.058 mmol) was dissolved in 15 mL of an aqueous solution of the respective metal salt ($Ni(NO_3)_2$, $Cu(NO_3)_2$, $AgNO_3$, *cis*-$[M(a)_2(H_2O)_2]^{2+}$ with $M = Pt^{II}$, Pd^{II}; four- to tenfold excess). The solution was concentrated under vacuum to about 5 mL and then exposed to air. The pH values of the solutions were typically between 1.5 and 2.5. In the case of the Ag compound **2f** the pH was adjusted to 0 with HNO_3. Within 2–7 d yellow (**2a**, **2b**, **2e**), green/yellow (**2c**), orange (**2d**), or colorless (**2f**) crystals formed, which were isolated by filtration, washed with a minimum amount of water, and dried in air. Yields 15–30%. Higher yields were not possible since further concentration resulted in cocrystallization of the metal-salt reagent. Satisfactory elemental analyses (C, H, N) were obtained for $[(C_2H_8N_2)_4(NH_3)_8Pt_8(C_4H_2N_2O_2)_4](NO_3)_8 \cdot 4H_2O$ (**2a**), $[(C_2H_8N_2)_8Pt_8(C_4H_2N_2O_2)_4](NO_3)_8 \cdot 4H_2O$ (**2b**), $[(C_2H_8N_2)_4Pt_4(C_4H_2N_2O_2)_4Ni_4(H_2O)_{12}](NO_3)_8 \cdot 1.5H_2O$ (**2c**), $[(C_2H_8N_2)_8Pt_4(C_4H_2N_2O_2)_4Pd_4](NO_3)_8$ (**2d**), $[(C_2H_8N_2)_4Pt_4(C_4H_2N_2O_2)_4Cu_4](NO_3)_8(H_2O)_8$ (**2e**), and $[(C_2H_8N_2)_4Pt_4(C_4H_3N_2O_2)_4Ag_4](NO_3)_8(H_2O)_4$ (**2f**).

2a: ^1H NMR (200 MHz, D_2O, TSP, pH* = 1.5–7): $\delta = 8.01$ (d, $J = 7.4$ Hz, H6), 5.90 (d, H5), 2.8 (en).

2b: ^1H NMR (200 MHz, D_2O, TSP, pH* = 1.5–7): $\delta = 7.95$ (d, $J = 7.4$ Hz, H6), 5.87 (d, H5), 2.7 (en). ^{195}Pt NMR (D_2O, pD = 4): $\delta = -2484$ (PtN_4), -1570 (Pt_2O_2); immediately after addition of CN^- (20 equiv per Pt atom, pD = 12): $\delta = -2613$ (**1**, PtN_4, 1,3-*alternate*), -4720 ($[Pt(CN)_4]^{2-}$); after 6–18 h: $\delta = -2613$ (**1**, PtN_4, 1,3-*alternate*), -2647 (**1**, PtN_4, *cone*), -4720 ($[Pt(CN)_4]^{2-}$). Assignment of the conformers of **1** by comparison of ^{195}Pt and ^1H NMR spectra [9a] of **1** in the presence of CN^- (pD = 8.2).

6: Method 1: $Hg(NO_3)_2$ (324 mg, 0.95 mmol) was added to a solution of *trans*-$[Pt(CH_3NH_2)_2(1\text{-}MeC)_2](NO_3)_2$ (**3**) [18] (200 mg, 0.32 mmol) in water (13 mL), and the solution stirred at 22 °C. After 7 h a colorless precipitate was isolated by filtration, washed with a minimum amount of H_2O and MeOH, and dried in the air. Colorless crystals of **6** form in the filtrate (pH = 2–2.5) within 3 d. The precipitate and the single crystals are identical (IR and ^1H NMR spectroscopy). Yield 223 mg (51%). Method 2: $Hg(NO_3)_2$ (53 mg, 0.15 mmol) was added to a solution of *trans*-$[Pt(CH_3NH_2)_2(1\text{-}MeC_{-1})_2Hg](NO_3)_2$ (**4**) [19] (64 mg, 0.07 mmol) in water (13 mL), and the solution stirred at 22 °C. Precipitation of **6** started after 4 h. The yield of the isolated product after 19 h is 18% and increases to that of Method 1 with higher concentrations (NMR). Elemental analysis data (C, H, N) agree with the composition determined by X-ray analysis. ^1H NMR (200 MHz, D_2O, NMe_4^+ internal standard, TSP) $\delta = 7.25$ (s, H(6); ^{199}Hg satellites: $^3J = 196$ Hz), 7.47, 7.56, 7.61 (three weak singlets; intensities increase with time and after addition of DNO_3 (pD = 1.7) at the expense of the signal at $\delta = 7.25$). ^{195}Pt NMR (D_2O, $[PtCl_6]^{2-}$): $\delta = -2195$.

7: Reaction of *trans*-$[Pt(CH_3NH_2)_2Cl_2]$ with Hampy (2 equiv) in the presence of $AgNO_3$ (2 equiv) in H_2O (pH = 7, 1 d, 50 °C), removal of AgCl and little Pt^0 by filtration, and crystallization results in colorless cubes of **7** in 84% yield. Satisfactory elemental analysis (C, H, N). ^{195}Pt NMR (42.95 MHz, $[PtCl_6]^{2-}$): $\delta = -2681$; ^1H NMR (200 MHz, D_2O, pD = 7, TSP): $\delta = 8.40$ (m, H6; ^{195}Pt satellites: $^3J \approx 34$ Hz), 7.66 (m, H4), 6.82 (m, H5, H3), 2.14 (s, CH_3; ^{195}Pt satellites: $^3J \approx 43$ Hz). Derivative **7′** was prepared analogously with $AgClO_4$ instead of $AgNO_3$. IR (KBr, cm^{-1}): $\tilde{\nu}$ = 3500 s, 3380 s, 3260, 3220, 3160 s, 1680 s, 1650 s, 1615 s, 1555 s, 1500 s, 1380 vs, 1310 m, 1220 m, 1140 m, 1060 m, 810 s, 650 m, 565 s, 510 m, 480 m. Crystal structure analyses of **7** and **7′** confirmed the compositions.

8: Compound **7** (0.5 mmol) was dissolved in H_2O (20 mL), and the pH value of the solution (6.3) adjusted to 12.2 with NaOH. $K_2[PdCl_4]$ (1 mmol) dissolved in water (5 mL) was added dropwise with stirring. Precipitation of red-orange **8** started immediately. The pH value of the solution, which dropped to 4, was repeatedly adjusted to 7 until it remained constant. After the solution had been stirred for 1 h at 22 °C, the precipitate was isolated by filtration, washed with water, and dried at 40 °C. Elemental analysis (C, H, N, Cl) approximately corresponded to $[Pt(CH_3NH_2)_2(C_5H_5N_2)_2(PdCl_2)_2]\cdot 4H_2O$. Yield 90%. IR (KBr, cm^{-1}): $\tilde{\nu}$ = 3530 s, b, 3280 s, 1680 s, 1660 s, 1610 s, 1520 s, 1490 s, 1330 m, 1230 m, 1250 m, 1150 m, 1140 m, 820 m, 500 m, 360 m, b.

9: Excess $AgNO_3$ (8–10 equiv) was added in small portions to a suspension of **8** (0.133 mmol) in H_2O (5 mL) until **8** had completely dissolved. The now dark red solution was filtered to remove AgCl and concentrated at 22 °C. Within two weeks, dark red cubes of **9** formed. Only the first fraction (10–15% yield) was not contaminated with $AgNO_3$ and other products. Elemental analysis (C, H, N) of a freshly isolated sample was in agreement with a septa- or octahydrate (Pt:Pd = 1:2 (scanning electron microscopy)). The X-ray structure analysis indicated six positions for water molecules, five of which display occupancies of only 0.5. ^{195}Pt NMR (D_2O): $\delta = -2594$; ^1H NMR (D_2O, pD = 3.7): $\delta = 9.09$ (d, 1H), 9.02 (d, 1H), 8.20 (t, 1H), 7.53 (t, 1H), 2.02 (s, 3H). The signals for the aromatic protons could not be unambiguous assigned, even with a ^1H–^1H COSY experiment; coupling constants were determined from the 2-D, *J*-resolved NMR spectrum ($^3J \approx 6-7$, $^4J \approx 1.3-1.4$ Hz); IR (KBr, cm^{-1}): $\tilde{\nu}$ = 3500 s, vb, 3160 s, 1615 s, sp, 1565 s, sp, 1480 vs, 1440 vs, 1380 vs, 1270 vs, 1245 s, 1200 s, 1160 m, 1100, 1090 m, 1000 s, b, 850 m, 825 m, sp, 790 m; UV/Vis (H_2O): λ[nm] (ε[mol L^{-1} cm^{-1}]) = 218 (43790), 275 (sh), 300 (32720), 380 (6106), 437 (7514).

Received: November 7, 1996 [Z9740, Z9741, Z9740IE]
German version: *Angew. Chem.* **1997**, *109*, 1353–1357

Keywords: macrocycles · nanostructures · nucleobases · platinum · supramolecular chemistry

[1] Reviews: D. Philp, J. F. Stoddart, *Angew. Chem.* **1996**, *108*, 1243; *Angew. Chem. Int. Ed. Engl.* **1996**, *35*, 1154; C. A. Hunter, *ibid.* **1995**, *107*, 1181 and **1995**, *34*, 1079.

[2] M. Fujita, J. Yazaki, K. Ogura, *J. Am. Chem. Soc.* **1990**, *112*, 5645; *Chem. Lett.* **1991**, 1031.

[3] P. J. Stang, D. H. Cao, *J. Am. Chem. Soc.* **1994**, *116*, 4981; P. J. Stang, D. H. Cao, S. Saito, A. M. Arif, *ibid.* **1995**, *117*, 6273; P. J. Stang, B. Olenyuk, *Angew. Chem.* **1996**, *108*, 798; *Angew. Chem. Int. Ed. Engl.* **1996**, *35*, 732.

[4] Additional examples: R. W. Saalfrank, O. Struck, D. Danion, J. Hassa, L. Toupet, *Materials* **1994**, *6*, 1432; W. S. Sheldrick, H. S. Hagen-Eckhard, S. Heeb, *Inorg. Chim. Acta* **1993**, *206*, 15; X. Chi, A. J. Guerin, R. A. Haycock, C. A. Hunter, L. D. Sarson, *J. Chem. Soc. Chem. Commun.* **1995**, 2567; M. Ohba, H. Okawa, T. Ito, A. Ohto, *ibid.* **1995**, 1545; T. Kajiwara, T. Ito, *ibid.* **1994**, 1773; P. Chaudhuri, I. Karpenstein, M. Winter, M. Lengen, C. Butzlaff, E. Bill, A. X. Trautwein, U. Flörke, H.-J. Haupt, *Inorg. Chem.* **1993**, *32*, 888.

[5] The term "molecular square" [3] is somewhat misleading in that it ignores the three-dimensional structure (with the organic ligand perpendicular to the plane created by the metal ions). Therefore, the term "open box" is better.

[6] A. Schreiber, E. C. Hillgeris, B. Lippert, *Z. Naturforsch. B* **1993**, *48*, 1603.

[7] C. M. Drain, J.-M. Lehn, *J. Chem. Soc. Chem. Commun.* **1994**, 2313; *ibid.* **1995**, 503.

[8] Coplanar arrangement of the organic ligand and metal center.

[9] a) H. Rauter, E. C. Hillgeris, A. Erxleben, B. Lippert, *J. Am. Chem. Soc.* **1994**, *116*, 616; b) H. Rauter, E. C. Hillgeris, B. Lippert, *J. Chem. Soc. Chem. Commun.* **1992**, 1385.

[10] Review: V. Böhmer, *Angew. Chem.* **1995**, *107*, 785; *Angew. Chem. Int. Ed. Engl.* **1995**, *34*, 713.

[11] Other examples of multiply metalated species: W. Xu, J. P. Rourke, J. J. Vittal, R. J. Puddephatt, *Inorg. Chem.* **1995**, *34*, 329; X. Delaigne, J. McB. Harrowfield, M. W. Hosseini, A. De Cian, J. Fischer, N. Kyritsakas, *J. Chem. Soc. Chem. Commun.* **1994**, 1579; E. Solari, W. Lesueur, A. Klose, K. Schenk, C. Floriani, A. Chiesi-Villa, C. Rizzoli, *Chem. Commun.* **1996**, 807.

[12] Crystal structure analyses: a) **2a**: $C_{24}H_{72}N_{32}O_{36}Pt_8$ (M_r = 2945.86); tetragonal, space group $I4_1/a$ (no. 88), $a = b = 28.356(5)$, $c = 8.630(5)$ Å, V = 6939(4) Å^3, $Z = 4$, $\rho_{calcd} = 2.82$ g cm^{-3}; $F(000) = 5408$; 2168 observed reflections with $I > 2\sigma(I)$; R1 = 0.0698; Rigaku ACF-7S diffractometer, $Mo_{K\alpha}$ radiation ($\lambda = 0.71069$ Å), $T = 193$ K; the structure was refined with full-matrix, least-squares methods [30]. b) **2b**: monoclinic, space group $C2/c$, $a = 33.728(7)$, $b = 8.941(2)$, $c = 30.140(6)$ Å, $\beta = 125.90(3)°$, $V = 7363(3)$ Å^3, $Z = 4$. c) **2c**: monoclinic, space group $P2(1)/n$, $a = 8.578(5)$, $b = 24.278(10)$, $c = 32.186(12)$ Å, $\beta = 92.24(4)°$, $V = 6698(5)$ Å^3, $Z = 4$.

[13] R. F. Stewart, L. H. Jensen, *Acta Crystallogr.* **1967**, *23*, 1102; G. S. Parry, *ibid.* **1954**, *7*, 313.

[14] R. Faggiani, B. Lippert, C. J. L. Lock, *Inorg. Chem.* **1980**, *19*, 295.

[15] B. Lippert, *Prog. Inorg. Chem.* **1989**, *37*, 1; E, Zangrando, F. Pichierri, L. Randaccio, B. Lippert, *Coord. Chem. Rev.* **1996**, *156*, 275.

[16] H. Schöllhorn, U. Thewalt, B. Lippert, *Inorg. Chim. Acta* **1984**, *93*, 19, and references therein; L. S. Hollis, S. J. Lippard, *Inorg. Chem.* **1983**, *22*, 2600; J.-P. Laurent, P. Lepage, F. Dahan, *J. Am. Chem. Soc.* **1982**, *104*, 7335.

[17] G. Raudaschl-Sieber, B. Lippert, *Inorg. Chem.* **1985**, *24*, 2426; G. Frommer, B. Lippert, *ibid.* **1990**, *29*, 3259; M. Schmülling, B. Lippert, R. van Eldik, *ibid.* **1994**, *33*, 3276.

[18] M. Krumm, E. Zangrando, L. Randaccio, S. Menzer, B. Lippert, *Inorg. Chem.* **1993**, *32*, 700; D. Holthenrich, M. Krumm, E. Zangrando, F. Pichierri, L. Randaccio, B. Lippert, *J. Chem. Soc. Dalton Trans.* **1995**, 3275; G. Fusch, E. C. Fusch, A. Erxleben, J. Hüttermann, H. J. Scholl, B. Lippert, *Inorg. Chim. Acta* **1996**, *252*, 167.

[19] M. Krumm, E. Zangrando, L. Randaccio, S. Menzer, A. Danzmann, D. Holthenrich, B. Lippert, *Inorg. Chem.* **1993**, *32*, 2183.

[20] R. M. K. Dale, E. Martin, D. C. Livingston, D. C. Ward, *Biochemistry* **1995**, *14*, 2447.

[21] P. H. Toma, I. M. Dalla Riva Toma, D. E. Bergstrom, *Acta Crystallogr. Sect. C* **1993**, *49*, 2047; M. Höpp, A. Erxleben, I. Rombeck, B. Lippert, *Inorg. Chem.* **1996**, *35*, 397; F. Zamora, M. Sabat, B. Lippert, *ibid.* **1996**, *35*, 4858.

[22] D. Holthenrich, I. Sóvágó, G. Fusch, A. Erxleben, E. C. Fusch, I. Rombeck, B. Lippert, *Z. Naturforsch. B* **1995**, *50*, 1767.

[23] Crystal structure analysis of **6**: Siemens P4 four-circle diffractometer, $Mo_{K\alpha}$ radiation, room temperature, $[C_{12}H_{21}N_{11}O_{12}PtHg_3\cdot 2H_2O]_2$, M_r = 2688.58, triclinic, space group $P\bar{1}$, $a = 7.712(2)$, $b = 13.369(3)$, $c = 13.749(3)$ Å, $\alpha = 84.02(3)$, $\beta = 78.77(3)$, $\gamma = 83.65(3)°$, $V = 1376.9(6)$ Å^3, $Z = 1$, ρ_{calcd} = 3.242 g cm^{-3}, $F(000) = 1208$, $\mu(Mo_{K\alpha}) = 21.821$ mm^{-1}, ω-scan with $4 \le 2\theta \le 42.5°$, absorption correction: ψ-scan/DIFABS, of 3320 reflections measured 3034 were independent, and 2253 observed ($F_o \ge 4\sigma(F_o)$), max./min. residual electron density = 1.20 and −1.21 e Å^{-3}, $R_1 = 0.0435$ and wR_2 = 0.0965 (observed reflections), $R_1 = 0.0647$ and $wR_2 = 0.1095$ (all reflections). The structure was solved with Patterson and Fourier methods (SHELXS-86) [24] and refined with least-squares methods (SHELXL-93) [25]. Anisotropic temperature factors were used for all non-hydrogen atoms except disordered nitrate oxygen atoms (O61, O61A, O63, O63A). The dimer is on a crystallographic inversion center, and two anions and two water molecules are independent. Two nitrate oxygens are disordered with occupancies of 0.25 and 0.75 (O61, O61A) and 0.5 (O63, O63A) [30].

[24] G. M. Sheldrick, *SHELXS-86*, Universität Göttingen, **1990**.

[25] G. M. Sheldrick, *SHELXS-93*, Universität Göttingen, **1993**.

[26] The fact that 3-(trimethylsilyl)-1-propanesulfonate (TSP) cannot be used as a ^1H NMR standard is possibly due to such an interaction.

[27] Multidentate Lewis acids: Z. Zheng, C. B. Knobler, M. F. Hawthorne, *J. Am. Chem. Soc.* **1995**, *117*, 5105; X. Yang, C. B. Knobler, Z. Zheng, M. F. Hawthorne, *ibid.* **1994**, *116*, 7142; M. Simard, J. Vaugeois, J. D. Wuest, *ibid.* **1993**, *115*, 370; X. Yang, S. E. Johnson, S. I. Khan, M. F. Hawthorne, *Angew. Chem.* **1992**, *104*, 886; *Angew. Chem. Int. Ed. Engl.* **1992**, *31*, 893.

[28] R. G. Raptis, J. P. Fackler, Jr., *Inorg. Chem.* **1988**, *27*, 4179.

[29] Crystal structure analysis of **9**: $C_{24}H_{44}N_{20}O_{26}Pd_4Pt_2\cdot 3.5H_2O$ (M_r = 1907.57); monoclinic, space group $C2/c$; $a = 21.722(2)$, $b = 22.013(5)$, $c = 23.909(4)$ Å, $\beta = 100.576(9)°$, $V = 11238(7)$ Å^3, $Z = 4$; $\rho_{calcd} = 2.25$ g cm^{-3}; $R = 0.052$, $R_w = 0.061$ [for 4571 reflections with $I > 3\sigma(I)$]; Enraf-Nonius-CAD4 diffractometer, $Mo_{K\alpha}$ radiation ($\lambda = 0.71069$ Å), graphite monochromator. The structure was solved by a combination of direct methods and Fourier techniques and refined with full matrix, least-squares methods. The metal ions were anisotropically refined, and contributions of H atoms were included at calculated positions in the refinement (except of H_2O molecules); Pd_2 units in cation A are disordered (0.85 : 0.15) [30].

[30] Crystallographic data (excluding structure factors) for the structures reported in this paper have been deposited with the Cambridge Crystallographic Data Centre as supplementary publication no. CCDC-100021 (**2a**), -100020 (**6**), and -100025 (**9**). Copies of the data can be obtained free of charge on application to The Director, CCDC, 12 Union Road, Cambridge CB21EZ, UK (fax: int. code +(1223)336-033; e-mail: deposit@chemcrys.cam.ac.uk).

[31] For other examples of this binding pattern, see P. L. Andreu, J. A. Cabeza, A. Llamazares, V. Riera, S. Garcia-Granda, J. F. van der Maelen, *J. Organomet. Chem.* **1992**, *434*, 123; A. J. Deeming, R. Peters, M. B. Hursthouse, J. D. Backer-Dirks, *J. Chem. Soc. Dalton Trans.* **1982**, 1205.

[32] M. Kita, M. Nonoyama, *Polyhedron* **1993**, *12*, 1027.

Quasi-Complete Solvation of Organic Molecules in the Crystalline State**

Alexander Shivanyuk, Erich F. Paulus, Volker Böhmer,* and Walter Vogt

The solvation of biologically important molecules with water has been intensively studied by X-ray diffraction. The structural information obtained from such studies provides valuable insights into the role of solute–solvent interactions for crucial processes like protein folding or DNA double helix formation.[1] Examples of crystal structures of more simple compounds like cyclodextrins[2] and calixarenes[3] containing many water molecules per unit cell are also known. In the latter case bilayers of the sulfonated calixarene anion held together by hydrophobic forces are separated by water-rich layers containing the cations. However, these structures, dubbed "organic clays", provide little or no information on the solvation of the single molecules in solution. Here we describe the quasi-complete solvation of resorcarene **1**[4, 5] by dimethyl sulfoxide (DMSO) and pyridine (Pyr) in the crystalline state.

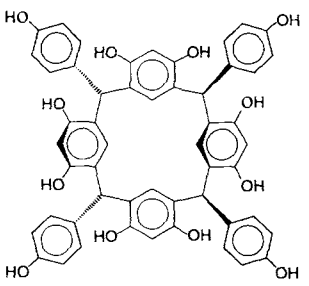

1

Acid-catalyzed condensation of resorcinol with 4-hydroxybenzaldehyde in EtOH at room temperature led to a mixture[6] from which the *rctt* isomer **1**[7] could be isolated simply by repeated recrystallization. The rigidity of its macrocyclic skeleton completely excludes the formation of intramolecular hydrogen bonds between hydroxy groups, contrary to the *rccc* isomer.[8] We therefore expected that **1** would form supramolecular structures in the crystalline state, held together by intermolecular hydrogen bonds between different resorcarene molecules.[9]

Slow recrystallization of **1** from DMSO at room temperature (20–23 °C) gave colorless crystals of the composition **1**·18 DMSO which, although extremely unstable without solvent, were suitable for X-ray structure analysis.[10] These crystals (containing 62.2% DMSO) proved to be stable in the presence of the mother liquor at higher temperatures and could be completely redissolved only at 80–100 °C.

The resorcarene **1** indeed adopts the C_{2h} symmetrical chair conformation (Figure 1)[11] in which two opposite aryl rings of the macrocyclic framework are almost coplanar (the deviation

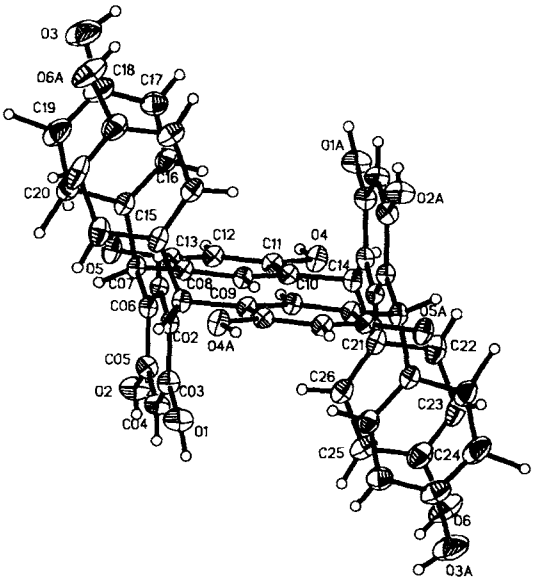

Figure 1. Molecular conformation and numbering scheme of resorcarene **1** (20% thermal elipsoids are shown).

between their planes is 0.35 Å) and two others are nearly perpendicular to this plane (dihedral angle: 85.9°) with their hydroxy groups pointing in opposite directions. (Since molecule **1** has a crystallographic inversion center, opposite aryl rings must be parallel.) The phenolic rings connected to the bridging carbon atoms assume the axial positions; two of them point up and two down leading to dihedral angles of 83.0 and 88.8° with the coplanar resorcinol rings. These pairs of *cis*-oriented phenolic rings are almost parallel (dihedral angle: 8.4°), and their hydroxy groups (O3H and O6AH) together with those of the vertically oriented resorcinol ring (O1H and O2H) form a polar "cap" of the molecule.

The distances between neighboring oxygen atoms of the resorcinol rings (O1–O4A = 4.00 and O2–O5 = 4.02 Å) and of the *cis*-oriented phenolic moieties (O6–O3A = 4.54 Å) are too long to allow intramolecular hydrogen bonding and therefore twelve intermolecular hydrogen bonds pointing in all directions are formed to twelve DMSO molecules. Six additional DMSO molecules fill voids in the crystal lattice (Figure 2). The distances between the oxygen atoms of hydroxy groups and the hydrogen-bonded DMSO molecules are between 2.58–2.81 Å. Both the shortest and the longest distances were found for the *para*-hydroxy groups O3H and O6H.

All 18 (nine crystallographically independent) DMSO molecules are located at definite positions; however, their sulfur atoms are disordered between two sites above and below the triangle formed by the oxygen and the two carbon atoms (Figure 2 top). The site occupation probabilities for those two positions could be exactly determined for each sulfur atom. They vary between 0.51 and 0.93. Four of them are within 0.51–0.57 (S1, S3, S6, S7), suggesting that there is almost no preference for any position. Values between 0.73 and 0.93 for S9, S8, S2, S4, and S5 demonstrate an increasing preference for one site.

[*] Dr. V. Böhmer, Dr. A. Shivanyuk, Prof. Dr. W. Vogt
Institut für Organische Chemie der Universität
J.-J.-Becher-Weg 3 SB1, D-55099 Mainz (Germany)
Fax: Int. code +(6131)395419
e-mail: vboehmer@mzdmza.zdv.uni-mainz.de
Dr. E. F. Paulus
Hoechst AG, D-65926 Frankfurt/Main (Germany)

[**] This work was supported by the Deutsche Forschungsgemeinschaft and by the European Community.

 © VCH Verlagsgesellschaft mbH, D-69451 Weinheim, 1997 0570-0833/97/3612-1301 $ 17.50+.50/0

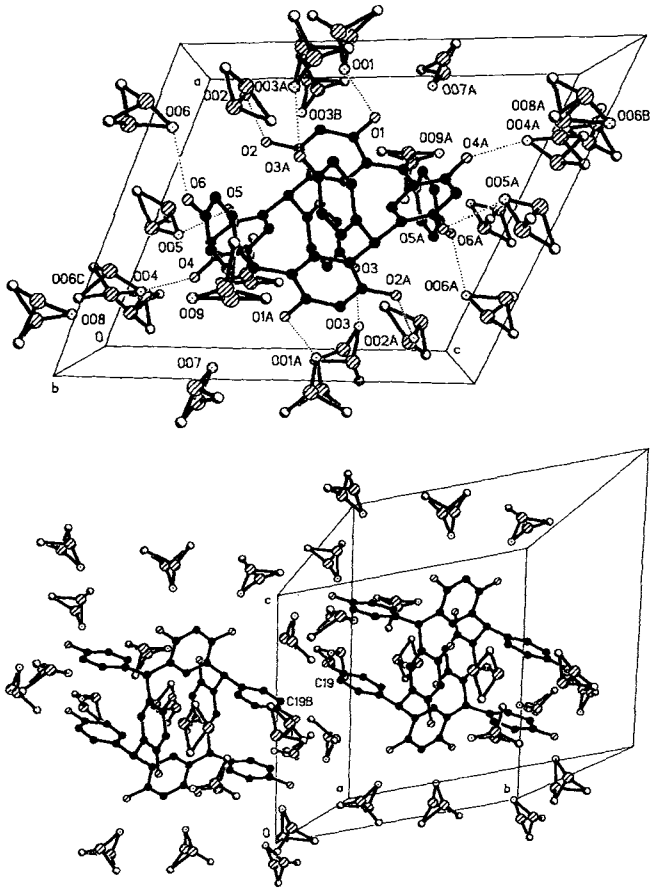

Figure 2. Packing and quasi-complete solvation of **1**·18 DMSO (hydrogen atoms are omitted and carbon atoms of **1** darkened for clarity). Top: The embedding of molecule **1** by DMSO seen along the crystallographic *b* axis. For each DMSO molecule the two positions of the sulfur atoms are shown. Hydrogen bond lengths [Å]: O1–O01 2.688(4), O2–O02 2.777(4), O3–O03 2.584(4), O4–O04 2,652(4), O5–O05 2.662(4), O6–O06 2.805(4). Bottom: "Corner-to-corner" contact between molecules of **1**; shortest intermolecular distance: C19–C19B 3.705(5) Å).

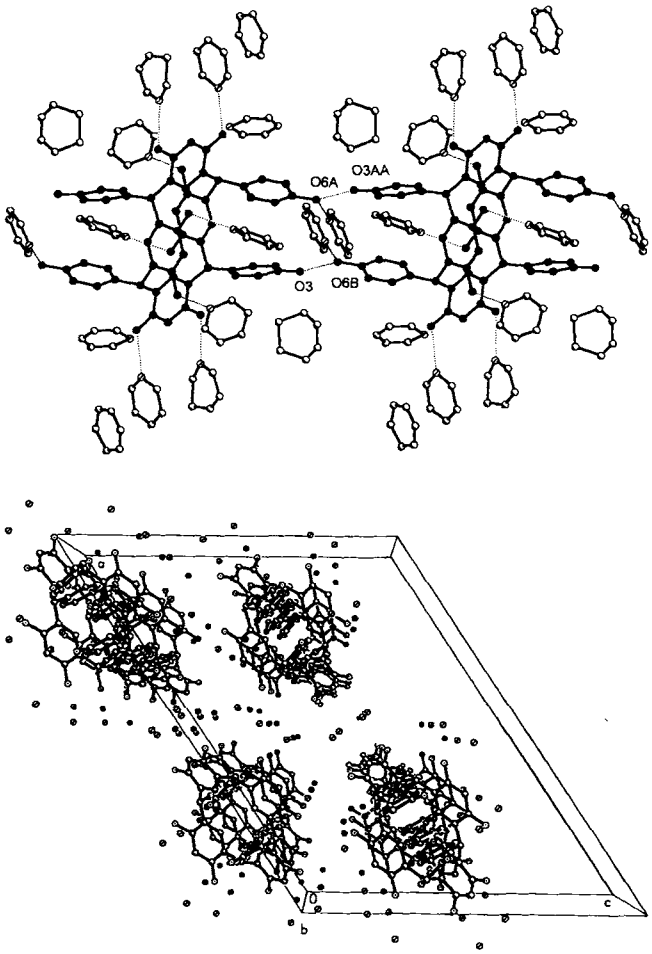

Figure 3. Crystal packing of **1**·14 Pyr. Top: Two molecules of **1** (darkened for clarity) from the infinite hydrogen-bonded column entirely wrapped by pyridine. The intermolecular hydrogen OH···OH···NC_5H_5 bonds are clearly shown (O3–O6B 2.78(1) Å, O6–N6 2.68(1) Å). Bottom: Hydrogen-bonded columns of **1** seen along their axes (only nitrogen atoms of pyridine molecules are shown for clarity).

The packing of **1**·18 DMSO can be also deduced from Figure 2. In the directions of the crystallographic axes *a* and *c* the molecules **1** are completely separated from each other by layers of DMSO, thus preventing any direct intermolecular contacts (Figure 2 top). Only the two carbon atoms C19 and C19A protrude out of this "solvent box" and form "corner-to-corner" van der Waals contacts between the molecules **1** along the axis *b* (Figure 2 bottom). The shortest intermolecular distance (C19–C19B = 3.70 Å) rules out any strong interaction also in this case.

In conclusion, the molecule **1** is almost entirely surrounded by solvent in the crystal and can be considered as "completely solvated", since hydrogen bonding gives by far the highest contribution to the solvation enthalpy. The volume of the unit cell ($V = 2949$ Å^3) corresponds to a concentration of 0.563 mol dm^{-3} for this "quasi-solution". In a slightly simplified description, the crystal of **1**·18 DMSO is formed by molecules **1** together with their first and most ordered solvation shell. The structural information described above can be compared, for instance, with molecular dynamics simulations for molecule **1** in solution.

Recrystallization of **1** from pyridine gave transparent, pink crystals (composition **1**·14 Pyr) that were of perfect size and shape for X-ray structure analysis (Figure 3),[10] although they were again quite unstable without the solvent. As in the previous case, the crystals were very stable in the presence of the mother liquor, and could be redissolved only by boiling.

The conformation of **1** in **1**·14 Pyr is almost the same as for the adduct **1**·18 DMSO. (root mean square = 0.083 Å for the macrocyclic skeleton). Of the fourteen (seven crystallographically independent) partly disordered pyridine molecules, ten are hydrogen bonded by ten hydroxy groups (N–O distances 2.68–2.78 Å). The remaining four, which fill voids in the crystal lattice, also assume definite positions, although in two cases the nitrogen atom cannot be located.

In contrast to **1**·18 DMSO the molecules of **1** are connected by two intermolecular hydrogen bonds that are formed on each side between the phenolic hydroxy groups O3H and O6H. One molecule of pyridine is involved as acceptor (O6H···Pyr) in this intermolecular contact, making O6H a strong acceptor for the intermolecular hydrogen bond O3-H···O6B-H. In this way, hydrogen-bonded molecules **1** are arranged to infinite columns, which are entirely wrapped (solvated) by layers of pyridine, and therefore, completely isolated from each other (Figure 3).

Highly solvated structures were observed also for resorcarenes prepared with 3- and 2-hydroxybenzaldehyde, showing the generality of the phenomenon described above. Intensive crys-

 © VCH Verlagsgesellschaft mbH, D-69451 Weinheim, 1997 0570-0833/97/3612-1302 $ 17.50+.50/0

tallographic and molecular dynamics studies of these unusual supramolecular systems are currently in progress.

Received: October 4, 1996 [Z9611IE]
German version: *Angew. Chem.* **1997**, *109*, 1358–1360

Keywords: calixarenes · hydrogen bonds · solvation · supramolecular chemistry

[1] a) T. F. Burling, W. I. Weis, K. M. Flaherty, A. T. Brünger, *Science* **1996**, *271*, 72–77; b) M. Egli, *Angew. Chem.* **1996**, *108*, 2020–2036; *Angew. Chem. Int. Ed. Engl.* **1996**, *35*, 1894–1909; c) F. Guarnieri, M. Mezei, *J. Am. Chem. Soc.* **1996**, *118*, 8493–8494.

[2] a) P. Klüfers, J. Schuhmacher, *Angew. Chem.* **1994**, *106*, 1925–1927; *Angew. Chem. Int. Ed. Engl.* **1994**, *33*, 1863–1865; b) I. Nicolis, A. W. Coleman, P. Charpin, C. de Rango, *Acta Crystallogr. Sect. B* **1996**, *52*, 122; c) for a crystal structure of β-cyclodextrin solvated with eight pyridine and three water molecules see: C. de Rango, P. Charpin, J. Navaza, N. Keller, I. Nicolis, F. Villian, A. W. Coleman, *J. Am. Chem. Soc.* **1992**, *114*, 5475–5476.

[3] a) A. W. Coleman, S. G. Bott, S. D. Morley, M. C. Means, K. D. Robinson, H. Zhang, J. L. Atwood, *Angew. Chem.* **1988**, *100*, 1412–1413; *Angew. Chem. Int. Ed. Engl.* **1988**, *27*, 1361–1363; b) J. L. Atwood, A. W. Coleman, H. Zhang, S. J. Bott, . *J. Incl. Phen.* **1989**, *7*, 203–207; c) C. P. Jonson, J. L. Atwood, *Inorg. Chem* . **1996**, *35*, 2602–2607; d) J. W. Steed, C. P. Jonson, C. L Barnes, R. K. Juneja, J. L. Atwood, S. Reilly, R. L. Hollis, H. P. Smith, D. L. Clark, *J. Am. Chem. Soc.* **1995**, *117*, 11426–11433.

[4] Resorcarenes are readily synthesized in multigram quantities by acid-catalyzed condensation of resorcinol with different aldehydes. Among four possible stereoisomers only two are easily available, namely the *rccc* isomer that exists in a C_{4v} symmetrical *crown* conformation and the *rctt* isomer that assumes a C_{2h} symmetrical *chair* conformation. The *rccc* isomers having intramolecular cavities were widely used [5] for the complexation of polyols like sugars and steroids through an interplay of cooperative hydrogen bonds and CH-π interactions and for the construction of even more sophisticated receptors such as cavitands, carcerands, and hemicarcerands. However, the *rctt* isomers have not yet attracted much attention.

[5] a) D. J. Cram, J. M. Cram, *Container Molecules and Their Guests* in *Monographs in Supramolecular Chemistry* (Ed.: J. F. Stoddart), The Royal Society of Chemistry, Cambridge, **1994**; b) P. Timmerman, W. Verboom, D. N. Reinhoudt, *Tetrahedron* **1996**, *52*, 2663–2704; c) V. Böhmer, *Angew. Chem.* **1995**, *107*, 785–818; *Angew. Chem. Int. Ed. Engl.* **1995**, *34*, 713–745.

[6] This mixture was characterized by ^{1}H NMR spectroscopy, however, the individual compounds were not isolated: F. Weinelt, H.-J. Schneider, *J. Org. Chem.* **1991**, *56*, 5527–5535.

[7] M.p. > 300 °C; ^{1}H NMR (200 MHz, [D$_6$]DMSO, 25 °C, TMS): δ = 8.65 (s, 4H, OH), 8.39 (s, 4H, OH), 8.34 (s, 4H, OH), 6.55–6.18 (m, 20H, CH), 6.08 (s, 2H, CH), 5.90 (s, 2H, CH), 5.41 (s, 4H, CH); FD-MS *m/z* (%): 856.3 (100) [*M*$^+$].

[8] a) L. M. Tunstad, J. A. Tucker, E. Dalcanale, J. Weiser, J. A. Bryant, J. C. Sherman, R. C. Helgeson, C. B. Knobler, D. J. Cram, *J. Org. Chem.* **1989**, *54*, 1305–1312; b) T. Lippmann, H. Wilde, M. Pink, A. Schafer, M. Hesse, G. Mann, *Angew. Chem.* **1993**, *105*, 1258–1260; *Angew. Chem. Int. Ed. Engl.* **1993**, *32*, 1195–1197; c) G. Mann, L. Hennig, F. Weinelt, K. Müller, R. Meusinger, G. Zahn, T. Lippmann, *Supramol. Chem.* **1994**, *3*, 101–113.

[9] Anthracene derivatives, bearing two divergent resorcinol residues, have been used to design hydrogen-bonded solid-state networks: Y. Aoyama, K. Endo, T. Anzai, Y. Yamaguchi, T. Sawaki, K. Kobayashi, N. Kanehisa, H. Hashimoto, Y. Kai, H. Masuda, *J. Am. Chem. Soc.* **1996**, *118*, 5562–5571.

[10] Crystallographic data for **1**·18 DMSO and **1**·14 Pyr. The unstable crystals were sealed in a Lindemann glass capillary containing the mother liquor. Measurement at 21 °C with a Siemens three-circle diffractometer with CCD, Siemens-rotating anode X-ray generator (50 kV, 120 mA), $Mo_{K\alpha}$ radiation (graphite monochromated, λ = 0.7107 Å). LP correction, empirical absorption corrections. Direct methods (G. M. Sheldrick, *Acta Crystallogr. Sect. A* **1990**, *46*, 467), refinement with full matrix versus F^2 (G. M. Sheldrick, SHELXL-93, Program for the Refinement of Crystal Structures. Universität Göttingen, Germany, **1993**). **1**·18 DMSO: crystal size 0.75 × 0.6 × 0.3 mm^3, triclinic, space group $P\bar{1}$, a = 14.168(1), b = 15.596(1), c = 15.970(1) Å, α = 78.97(1), β = 64.69(1), γ = 67.68(1)°, V = 2949.0(3) Å^3, ρ_{calcd} = 1.274(1) g cm^{-3}, $2\theta_{max}$ = 51.1°, μ = 4.001 cm^{-1}, 798 parameters, R = 0.0748 (for 6236 reflections $I > 2\sigma(I)$), $wR(F^2)$ = 0.2475 (for all 8830 unique reflections), S = 1.077, σ(C–C) = 0.003 Å; **1**·14 Pyr: crystal size 0.5 × 0.5 × 0.3 mm^3, monoclinic, space group $C2/c$, a = 32.534(1), b = 16.504(1), c = 24.510(1) Å, β = 124.07(1)°, V = 10901.8(3) Å^3, Z = 4, 686 parameters, ρ_{calcd} = 1.197(1) g cm^{-3}, $2\theta_{max}$ = 44.0°, μ = 0.80 cm^{-1}, R = 0.0533 (for 4870 reflections $I > 2\sigma(I)$), $wR(F^2)$ = 0.1675 (for all 6649 unique reflections), S = 1.03, σ(C–C) = 0.003 Å. Crystallographic data (excluding structure factors) for the structures reported in this paper have been deposited with the Cambridge Crystallographic Data Centre as supplementary publication no. CCDC-100224. Copies of the data can be obtained free of charge on application to The Director, CCDC, 12 Union Road, Cambridge CB2 1EZ, UK (fax: int. code +(1223) 336-033; e-mail deposit@chemcrys.cam.ac.uk).

[11] Only the crystal structure of a completely acylated *rctt* resorcarene has been described: K. J. Palmer, P. Y. Wong, L. Jurd, K. Stevens, *Acta Crystallogr. Sect. B* **1976**, *32*, 847.

PS Ligands as Building Blocks of Chiral Dimetallatetrahedranes with a Common Vertex**

Otto J. Scherer,* Clemens Vondung, and Gotthelf Wolmershäuser

Dedicated to Professor Hans Bürger on the occasion of his 60th birthday

The preparation of the first complex with a PO ligand[1] was rapidly followed by several further examples.[2] A few isolated examples of compounds with a PS ligand were described earlier[3a, b] as well as more recently;[3c, d] however, to date **1** is the only crystallographically characterized example.[3d]

$[\{CpFe(CO)_2\}\{\mu\text{-}CO[CpFe(CO)]_2\}PS]$ **1**

The trinuclear complex **3** with two μ_3-P=S ligands can be obtained in good yields from **2**[1] (Scheme 1) by oxidation with S_8 at room temperature. When **3** is heated to 100 °C for about

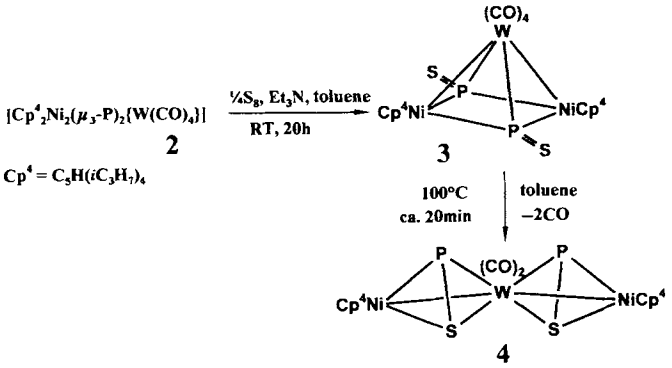

Scheme 1.

20 min, the unusual cluster **4** is formed under CO elimination (^{31}P NMR, monitoring by IR). The two tetrahedra in **4**, which each contain four different framework atoms (two transition metals and two main group elements), are linked to each other through a common tungsten vertex. Complex **3**[4] forms red-

[*] Prof. Dr. O. J. Scherer, Dipl.-Chem. C. Vondung, Dr. G. Wolmershäuser[+]
Fachbereich Chemie der Universität
Erwin-Schrödinger-Strasse, D-67663 Kaiserslautern (Germany)
Fax: Int. code +(631)205-2187

[+] Crystal structure analysis.

[**] This work was supported by the Fonds der Chemischen Industrie and by the Graduiertenkolleg "phosphorus chemistry as a link between different chemical disciplines".

brown crystals, and complex **4**[4] red crystals, the solubilities of which are moderate to good in hexane and good to very good in toluene.

The most important structural features in the tetragonal-pyramidal complex **3** are its μ_3-PS ligands (Figure 1). The P–S

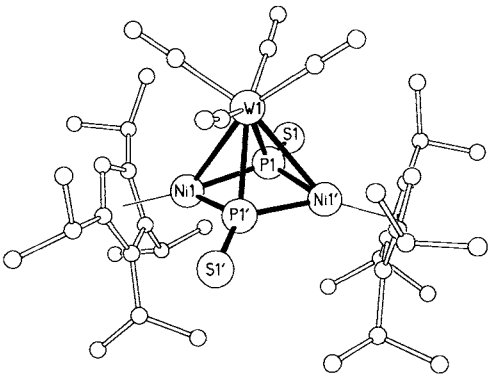

Figure 1. Crystal structure of **3** [5]. Selected bond lengths [Å] and angles [°]: Ni1–W1 2.8578(7), W1–P1 2.5219(13), Ni1–P1 2.1635(14), Ni1–P1′ 2.173(2), P1–S1 1.952(2), Ni1 ··· Ni1′ 3.37, P1 ··· P1′ 2.70; Ni1-P1-Ni1′ 102.04(6), P1-Ni1-P1′ 77.16(6), dihedral angle (Ni1-P1-P1′)/(Ni1′-P1-′P1) 192.1.

distance is 1.952(2) Å, which is almost identical with that for the P–S bonds in the triangulated dodecahedron compound $[Cp_4Fe_4(P_2S_2)_2]$;[6] the P–S bond length in **1** is 2.008 Å.[3d] For the PS radical, which was prepared by the discharge of a $PSCl_3$/helium mixture,[7a] a value of 1.8977 Å was established by laser spectroscopy; the theoretically[7b] calculated value is slightly larger.

A "simple" PS-side-on coordination was proposed for the compound **5** formed in the photolysis of **1**.[3d] The "five-membered ring middle deck" of **6**[8] consists of a P_3 and one PS ligand (d(P–S) = 2.023(5) Å).[8] The P–S distances in the tetrahedrane framework of **4** are as expected slightly longer than those in **3** (2.092(2) Å, Figure 2). The Ni–W (2.86 and 2.69 Å) and P–W distances (2.52 and 2.45 Å) in the tetragonal-pyramidal Ni_2P_2W framework of **3** are significantly longer than the respective distances in the tetrahedra of **4**; in contrast, the Ni–P bond lengths differ only slightly (**3**: 2.17, **4**: 2.20 Å).

$[\{CpFe(CO)\}(\mu\text{-}\eta^2\text{-PS})\{\mu\text{-CO}[CpFe(CO)]_2\}]$ **5**

$[Cp^*_2Mo_2\{\mu_3\text{-}\eta^3\text{:}\eta^3\text{-P}_3[Cr(CO)_5]\}(\mu\text{-}\eta^2\text{:}\eta^2\text{-PS})]$ **6**

With 54 valence electrons (VE) the μ_3-P=S complex **3** corresponds to a *nido* octahedron. The cluster **4** has 62 VE, which

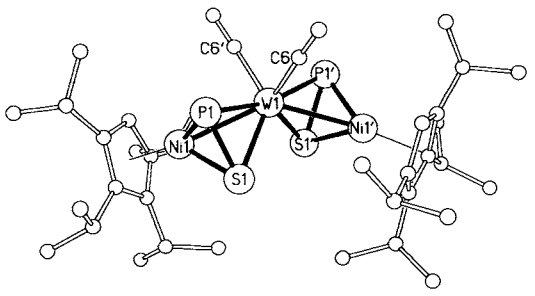

Figure 2. Crystal structure of **4** [5]. Selected bond lengths [Å] and angles [°]: Ni1–W1 2.6911(4), W1–P1 2.4506(11), W1–S1 2.4526(10), Ni1–S1 2.1837(12), Ni1–P1 2.2040(12), P1–S1 2.092(2); Ni1-W1-Ni1′ 137.87(2), P1-W1-P1′ 166.56(6), S1-W1-S1′ 94.58(5), C6-W1-C6′ 87.5(3).

according to the Wade–Mingos rules[9] is the number required for two tetrahedra sharing a common vertex; to our knowledge this structural type is very rare. Examples with two sandwichlike oriented three-membered rings $(M'L_n)_3$ with a common corner M occur in the $[M\{(M'L_n)_3\}_2]^{n+}$ class of substances;[10] in $[H_2Os_5(CO)_{14}(\mu_3\text{-}S)_2]$[11] the two Os triangles of the Os_5 bow tie substructure exhibit a dihedral angle of 56.3°. The triangular planes Ni1-P1-S1 and Ni1′-P1′-S1′ in the two tetrahedrane frameworks in **4** display an $(Ni1\text{-}P1\text{-}S1)_{centroid}$-W1-$(Ni1'\text{-}P1'\text{-}S1')_{centroid}$ angle of 138.5° and thus deviate significantly from a parallel orientation (Figure 2). Cluster **4**, which exists as a racemate in the crystal,[5] is to our knowledge the first compound in which two chiral tetrahedranes,[12] each containing two main group and two transition metal fragments, are additionally linked to each other through a common vertex. ^1H and ^{31}P NMR spectroscopic studies provided no evidence for an additional isomer of **4**.

Experimental Section

3: **2** (45 mg, 0.047 mmol), S_8 (3 mg, 0.0117 mmol), and triethylamine (0.8 mL) were added to toluene (10 mL) and stirred for 20 h at room temperature. The solution changed color from green to red-brown. After removal of the solvent under vacuum, the residue was taken up in a small amount of petroleum ether and transferred to a column (30 × 1.5 cm) packed with silica gel (activity grade II). A red-brown fraction was eluted with petroleum ether/toluene (5/1), from which **3** was obtained as a black-brown powder (38 mg, 77%). Recrystallization from hexane at −18 to 6 °C gave red-brown crystals

4: **3** (25 mg, 0.024 mmol), dissolved in toluene (15 mL), was warmed to 100 °C for about 20 min, and this caused the solution to change from red-brown to dark green (monitored by IR); work-up as for **3**. A dark, black-green fraction was eluted with petroleum ether/toluene (10/1) (column 15 × 0.6 cm), from which **4** (11 mg, 46%) was isolated as a black-green solid. Recrystallization from hexane at room temperature afforded dark red crystals.

Received: December 5, 1996 [Z9855IE]
German version: *Angew. Chem.* **1997**, *109*, 1360–1362

Keywords: chirality · clusters · P ligands · S ligands · tungsten

[1] O. J. Scherer, J. Braun, P. Walther, G. Heckmann, G. Wolmershäuser, *Angew. Chem.* **1991**, *103*, 861–863; *Angew. Chem. Int. Ed. Engl.* **1991**, *30*, 852–854. In the meantime we have established that **2** can be oxidized to the PO complex very simply with oxygen (see ref. [2c]). Experimental procedure: O_2 (0.2 bar, purity 99.8%) was passed through a tube (3 mm diameter) into a solution of **2** (45 mg, 0.047 mmol) in hexane (30 mL) for at least 1 min. The color of the solution changed from green to red brown. The solvent was removed under vacuum, and the residue was purified by column chromatography (silica gel, activity grade II, column 30 × 1.5 cm, petroleum ether/ether 7/1). $[Cp^4_2Ni_2(\mu_3\text{-}PO)_2\{W(CO)_4\}]$ (11 mg, 23.4%) was isolated from a dark red fraction; $\tilde{\nu}$(PO) = 1159 cm^{-1} (m, in hexane) and not—as in ref. [1]—1260 cm^{-1}.

[2] a) J. F. Corrigan, S. Doherty, N. J. Taylor, A. J. Carty, *J. Am. Chem. Soc.* **1994**, *116*, 9799–9800; b) W. Wang, J. F. Corrigan, S. Doherty, G. D. Enright, N. J. Taylor, A. J. Carty, *Organometallics* **1996**, *15*, 2770–2776; c) J. Foerstner, F. Olbrich, H. Butenschön, *Angew. Chem.* **1996**, *108*, 1323–1325; *Angew. Chem. Int. Ed. Engl.* **1996**, *35*, 1234–1237.

[3] a) A. Vizi-Orosz, G. Pályi, L. Markó, *J. Organomet. Chem.* **1973**, *60*, C25–C26; b) V. Grossbruchhaus, D. Rehder, *Inorg. Chim. Acta* **1988**, 141, 9–10; c) C. E. Laplaza, W. M. Davis, C. C. Cummins, *Angew. Chem.* **1995**, *107*, 2181–2183; *Angew. Chem. Int. Ed. Engl.* **1995**, *34*, 2042–2044; d) I.-P. Lorenz, W. Pohl, K. Polborn, *Chem. Ber.* **1996**, *129*, 11–13.

[4] ^1H NMR (400 MHz, C_6D_6, C_6D_5H as internal standard): δ(CH) = 4.50 (s, 2H) **3**, 4.76 (s, 2H) **4**; ^1H NMR (200 MHz, $CDCl_3$): $\delta(CHMe_2)$ = 3.22 (br sept., 4H), 3.08 (sept., 4H, ^3J(H,H) = 6.7 Hz) **3**, 2.81–2.65 (4 superimposed sept., 8H) **4**; $\delta(CHMe_2)$ = 1.51 (br d, 12H), 1.39 (superimposed d, 24H, ^3J(H,H) = 6.6 Hz), 0.86 (d, 12H, ^3J(H,H) = 6.6 Hz) **3**, 1.36 (d, 6H, ^3J(H,H) = 7.1 Hz), 1.29 (d, 6H, ^3J(H,H) = 7.2 Hz), 1.28 (d, 6H, ^3J(H,H) = 7.3 Hz), 1,23 (d, 6H, ^3J(H,H) = 7.2 Hz), 1.14 (d, 6H, ^3J(H,H) = 6.8 Hz), 1.06 (d, 6H, ^3J(H,H) = 6.6 Hz), 1.04 (d, 6H, ^3J(H,H) = 6.4 Hz), 1.00 (d, 6H, ^3J(H,H) = 6.3 Hz); $^{31}P\{^1H\}$ NMR (81 MHz, C_6D_6, 85% H_3PO_4 external): δ(P) = 381.9 (s) **3**, 150.1 (s, ^1J(W,P) = 23.0 Hz) **4**, for **3** the value of ^1J(W,P) could not be determined; IR (in hexane): $\tilde{\nu}$(CO) = 2044 (s), 1980 (s), 1966 (w), 1929 (m) **3**, 1958 (s), 1898 (s) **4**, IR(KBr disk): $\tilde{\nu}$(PS) = 663 (m) **3** (in cm^{-1}).

[5] Crystal structure data of complex **3** [**4**]: $C_{38}H_{58}Ni_2O_4P_2S_2W$, monoclinic, M_r = 1006.17, $C2/c$ [$C_{36}H_{58}Ni_2O_2P_2S_2W$, orthorhombic, M_r = 950.15, $Pbcn$], a = 9.6261(8) [23.039(2)], b = 18.544(2) [10.3272(8)], c = 23.374(3)

[17.265(2) Å], $\alpha = \gamma = 90$, $\beta = 92.580(8)$ [90°], $Z = 4$ [4], $V = 4168.0(8)$ [4107.8(6) Å^3], $\rho_{calcd} = 1.603$ [1.536 Mgm^{-3}], $T = 183(2)$ [293(2) K]; θ-range: 2.20–27.49 [2.36–25.87°], measured reflections: 5605 [22331], independent reflections: 4540 ($R_{int} = 0.0409$) [3955 ($R_{int} = 0.0536$)], R values ($I > 2\sigma I$): $R1 = 0.0411$ [0.0262], $wR2 = 0.0752$ [0.0524], all data: $R1 = 0.0645$ [0.0491], $wR2 = 0.0838$ [0.0592]. Diffractometer: Siemens P4 [Stoe IPDS]. Structure solution with direct methods. Program for structure solution: Siemens SHELXTL [SHELXS-86 (G. Sheldrick, 1990)], structure refinement: Full-matrix least-squares methods against F^2; 230 [373] parameters, 6 [150] restraints. Crystallographic data (excluding structure factors) for the structures reported in this paper have been deposited with the Cambridge Crystallographic Data Centre as supplementary publication no. CCDC-100046. Copies of the data can be obtained free of charge on application to The Director, CCDC, 12 Union Road, Cambridge CB2 1EZ, UK (fax: Int. code +(1223) 336-033; e-mail deposit(a) chemcrys.cam.ac.uk).

[6] O. J. Scherer, G. Kemény, G. Wolmershäuser, *Chem. Ber.* **1995**, *128*, 1145–1148.

[7] a) K. Kawaguchi, E. Hirota, M. Ohishi, H. Suzuki, S. Takano, S. Yamamoto, S. Saito, *J. Mol. Spectrosc.* **1988**, *130*, 81–85; b) D. P. Chong, *Chem. Phys. Lett.* **1994**, *220*, 102–108; D. E. Woon, T. H. Dunning, Jr., *J. Chem. Phys.* **1994**, *101*, 8877–8893.

[8] H. Brunner, U. Klement, W. Meier, J. Wachter, O. Serhadle, M. L. Ziegler, *J. Organomet. Chem.* **1987**, *335*, 339–352; H. Brunner, H. Kauermann, U. Klement, J. Wachter, T. Zahn, M. L. Ziegler, *Angew. Chem.* **1985**, *97*, 122; *Angew. Chem. Int. Ed. Engl.* **1985**, *24*, 132.

[9] D. M. P. Mingos, D. J. Wales, *Introduction to Cluster Chemistry*, Prentice-Hall, **1990**, p. 249ff.

[10] a) M = Hg, M'L_n = Pt(μ-CNR)(CNR), $n = 0$: Y. Yamamoto, H. Yamazaki, T. Akurai, *J. Am. Chem. Soc.* **1982**, *104*, 2329–2330; b) M = Ag, M'L_n = Pt(μ-CO)(PR_3), $n = 1$: A. Albinati, K.-H. Dahmen, A. Togni, L. M. Venanzi, *Angew. Chem.* **1985**, *97*, 760–761; *Angew. Chem. Int. Ed. Engl.* **1985**, *24*, 766–767; c) M = Cu, Au; M' = Pt(μ-CO)(PPh_3), $n = 1$: M. F. Hallam, D. M. P. Mingos, T. Adatia, M. McPartlin, *J. Chem. Soc. Dalton Trans.* **1988**, 335–340.

[11] R. D. Adams, I. T. Horváth, L.-W. Yang, *Organometallics* **1983**, *2*, 1257–1258.

[12] H. Vahrenkamp, *Adv. Organomet. Chem.* **1983**, *22*, 169–208, and references therein; *J. Organomet. Chem.* **1989**, *370*, 65–73, and references therein; F. G. A. Stone, *Pure Appl. Chem.* **1986**, *58*, 529–536, and references therein.

Effective Low-Temperature Aromatization of Ethane over H-Galloaluminosilicate(MFI) Zeolites in the Presence of Higher Alkanes or Olefins**

Vasant R. Choudhary*, Anil K. Kinage, and Tushar V. Choudhary

Over the last seven to eight years, aromatization of lower alkanes (C_3 and C_4) over Ga-modified zeolites of type ZSM-5 has been widely investigated,[1–3] and commercial processes for aromatizing propane and higher alkanes have been developed.[1] Natural gas contains an appreciable amount of ethane (upto about 10 mol%). In addition, ethane can be produced in large quantities by oxidative coupling of methane, but, because of its low concentration, separation of ethane from the product stream by conventional means is difficult or uneconomical.[4] Ethane is also formed to an appreciable extent in the Cyclar LPG aromatization process as an undesirable by-product.[1] Its conversion into arenes would, therefore, be of great practical importance. However, because of its very low reactivity[5–7] and high thermodynamic barrier to aromatization,[6, 8] ethane can be converted and yields of arenes that are of practical significance obtained only at high temperatures (≥600 °C).[8] Conversion of ethane into arenes with high yield and selectivity at lower temperatures would not only be of scientific interest but also have a great impact on the natural gas conversion technology. Here we show that the thermodynamic barrier can be overcome and that the conversion and yield of arenes in the aromatization of ethane over H-galloalluminosilicate of ZSM-5 type (H-GaAlMFI) zeolite at lower temperatures (400–500 °C) can be increased manyfold (4–80×) by adding olefins or higher alkanes to the feed. Furthermore, we show that the ethane–ethylene conversion mechanism is changed in the presence of olefins or higher alkanes; the large enhancement in the reactivity of ethane results from a hydrogen-transfer reaction between ethane and higher (C_{3+}) olefins.

Results showing a large increase in the conversion of ethane by aromatization over H-GaAlMFI zeolite due to the presence of various additives A—such as ethylene, propylene, *n*-butylene, propane, and *n*-hexane—at different A/C_2H_6 mole ratios in the feed are presented in Table 1 and Figures 1 and 2. The increase

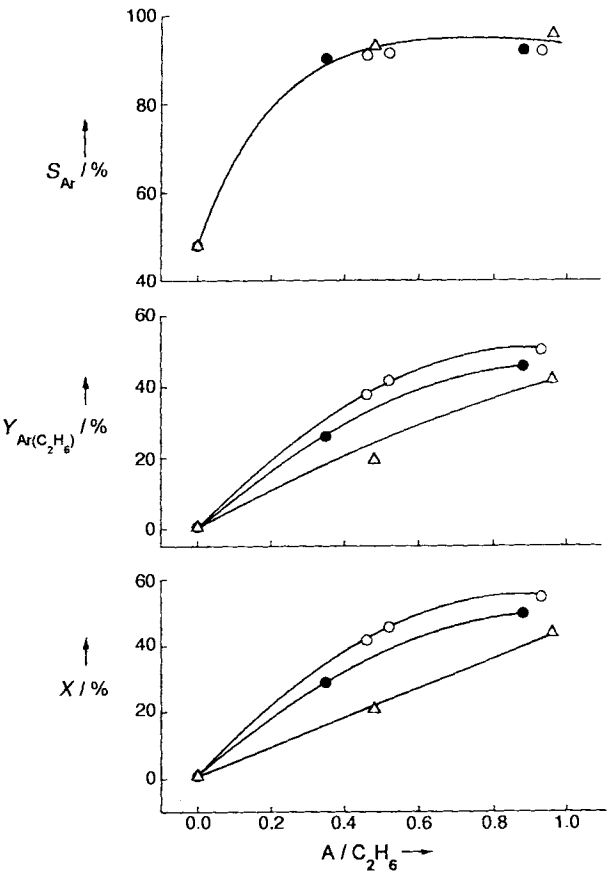

Figure 1. Enhancement in ethane conversion X and yield of arene based on ethane conversion ($Y_{Ar(C_2H_6)}$) over H-GaAlMFI zeolite at 500 °C in the presence of *n*-butylene (○), propylene (●), and ethylene (△) as additives in the feed at different A/C_2H_6 ratios. S_{Ar} = aromatics selectivity in the overall aromatization of ethane and additive; conversion of the olefin additives = 98±2%.

in ethane conversion is higher when the A/C_2H_6 ratio is larger and for additives containing a greater number of carbon atoms. It is interesting that arene selectivity in the simultaneous aromatization of ethane and any of the additives is higher than that in the aromatization of the additives in the absence of ethane (Table 1). The ethane conversions and yields of arenes (based on

[*] Dr. V. R. Choudhary, A. K. Kinage, T. V. Choudhary
Chemical Engineering Division
National Chemical Laboratory
Pune-411 008 (India)
Fax: Int. code +(212)33-3941, 33-0233, 33-4761
e-mail: vrc(a) ems.ncl.res.in

[**] A. K. K is grateful to the Council of Scientific and Industrial Research, New Delhi for the award of senior research fellowship. Editorial note: for a similar study with propane in place of ethane see V. R. Choudhary, A. K. Kinage, T. V. Choudhary, *Chem. Commun.* **1996**, 2545–2546.

 © VCH Verlagsgesellschaft mbH, D-69451 Weinheim, 1997 0570-0833/97/3612-1305 $ 17.50+.50/0

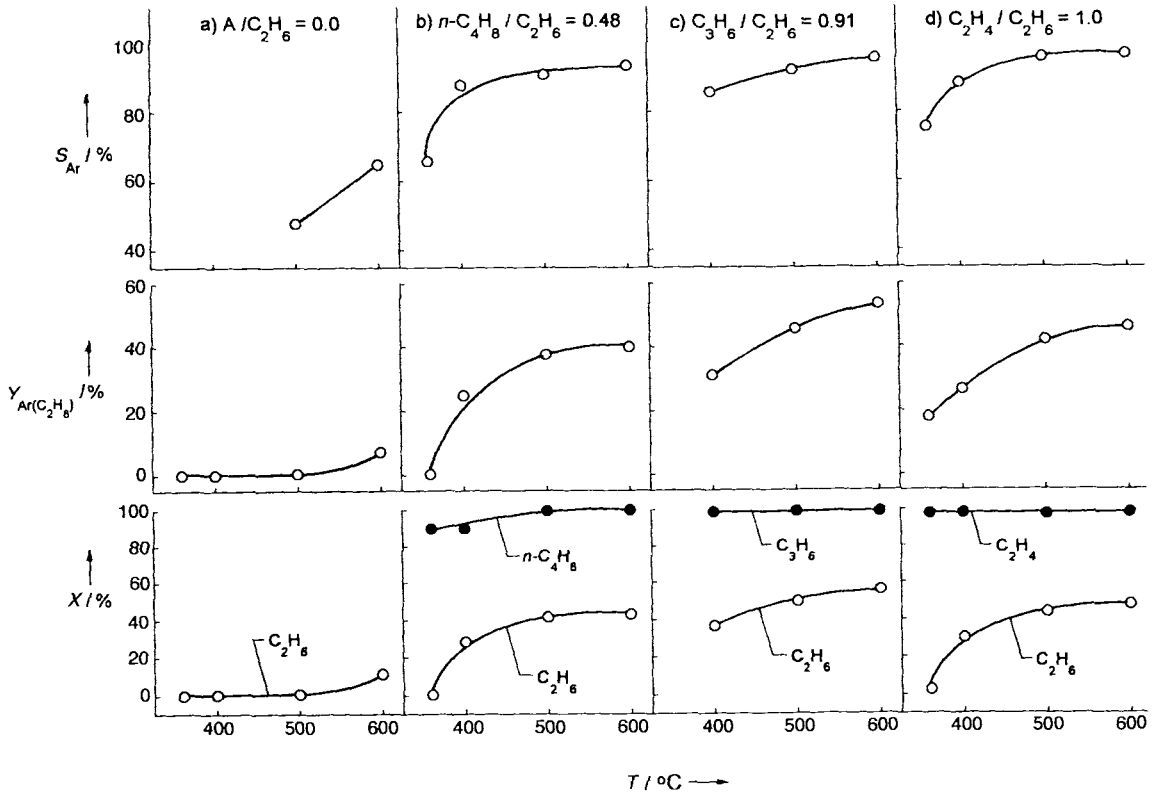

Figure 2. Influence of temperature on the enhancement of ethane conversion X and yield of arenes based on ethane conversion ($Y_{Ar(C_2H_6)}$) over H-GaAlMFI zeolite in the presence of olefin additives A in the feed.

Table 1. Results of aromatization of ethane in the presence and absence of olefin or higher alkane additive and aromatization of pure additive over a H-GaAlMFI zeolite (space velocity 6100 $cm^3 g^{-1} h^{-1}$).

T[°C]	Feed	X[%] Ethane	Additive A	S_{Ar}[%]	$Y_{Ar(C_2H_6)}$[%][a]
500	ethane (33.3%) + N_2	0.94	–	47.9	0.45
500	*n*-butylene (31.0%) + N_2	–	100	88.9	–
500	ethane (33.3%) + *n*-butylene (31.0%) + N_2	54.6	100	92.1	50.3
500	propylene (29.3%) + N_2	–	100	85.1	–
500	ethane (33.3%) + propylene (29.3%) + N_2	49.6	99.2	92.2	45.7
500	ethylene (32.0%) + N_2	–	94.9	90.7	–
500	ethane (33.3%) + ethylene (32.0%) + N_2	43.7	97.1	95.9	41.9
600	ethane (33.3%) + N_2	11.2	–	65.0	7.3
600	*n*-hexane (16.3%) + N_2	–	100	71.5	–
600	ethane (33.3%) + *n*-hexane (16.3%) + N_2	53.0	100	88.6	47.0
600	*propane* (25.0%) + N_2	–	90.3	83.6	–
600	ethane (33.3%) + propane (25.0%) + N_2	41.1	93.9	86.6	35.6

[a] Yield of arene based on the ethane conversion X.

ethane conversion) obtained are much higher than those reported earlier (Table 2). The present results and their comparison with earlier ones[5, 8, 9] clearly show a highly beneficial effect for the addition of olefins or higher alkanes to the feed. Because of the additives, both the limitations—high thermodynamic barrier and very low reactivity of ethane for its aromatization at lower temperatures—are overcome.

The change in free energy (ΔG_r) for ethane aromatization, which is positive below 575 °C, approaches zero and becomes negative (even at lower temperatures, Table 3) with increasing concentrations of the additives. This makes the process thermodynamically more and more feasible. The increase in the ethane conversion with higher A/C_2H_6 ratio (Figure 1) and temperature (Figure 2) is consistent with the decrease in ΔG_r (Table 3).

Table 2. Earlier results of ethane aromatization over Ga-modified zeolites of type ZSM-5 without addition of alkenes or higher alkanes.

Catalyst	T[°C]	v[a]	X[%]	$Y_{Ar(C_2H_6)}$ [%]	Ref.
Ga/H-ZSM-5	600	4500	15.0	8.0	[9]
Ga/H-ZSM-5 (Si/Al = 34)	550	1300	–	< 1.0	[8]
Ga/H-ZSM-5 (Si/Al = 34)	600	1300	–	3.0	[8]
Ga/H-ZSM-5 (Si/Al = 34)	700	1300	21.0	13.0	[8]
Ga/H-ZSM-5 (Si/Al = 15)	600	1160	28.2	16.2	[8]
Pt/Ga silicate	500	2000	14.0	5.8	[5]

[a] Recalculated value (in $cm^3 g^{-1} h^{-1}$) in all but the last case.

 © VCH Verlagsgesellschaft mbH, D-69451 Weinheim, 1997 0570-0833/97/3612-1306 $ 17.50+.50/0

Table 3. Change in free energy (ΔG_r) for the simultaneous aromatization of ethane and alkene or higher alkane.

Reaction	A/C_2H_6	ΔG_r[kcal mol^{-1}]$_{benzene}$ 400 °C	500 °C	600 °C
$3C_2H_6 \rightarrow C_6H_6 + 6H_2$	0.0	17.6	7.2	−3.5
$2C_2H_6 + C_2H_4 \rightarrow C_6H_6 + 5H_2$	0.5	5.1	−2.2	–
$3C_2H_6 + 3C_2H_4 \rightarrow 2C_6H_6 + 9H_2$	1.0	−1.2	−6.9	–
$3C_2H_6 + 2C_3H_6 \rightarrow 2C_6H_6 + 9H_2$	0.67	2.8	−4.4	–
$6C_2H_6 + 6C_3H_6 \rightarrow 5C_6H_6 + 21H_2$	1.0	−0.16	−6.7	–
$4C_2H_6 + C_4H_8 \rightarrow 2C_6H_6 + 10H_2$	0.25	7.1	−1.8	–
$C_2H_6 + C_4H_8 \rightarrow C_6H_6 + 4H_2$	1.0	−3.5	−10.8	–
$3C_2H_6 + 2C_3H_8 \rightarrow 2C_6H_6 + 11H_2$	0.67	–	0.7	−10.0
$3C_2H_6 + n\text{-}C_6H_{14} \rightarrow 2C_6H_6 + 10H_2$	0.33	–	−5.2	−15.8

The intrinsic reactivity of ethane is much lower than that of the higher alkanes.[5–7] The observed enhancement in the ethane reactivity due to the presence of C_3 and C_4 olefins results from their hydrogen-transfer reaction with ethane [Eq. (a)]. Since ethylene and propane or butane are much more reactive than ethane, they are further converted into arenes over the zeolite according to Equations (b) and (c).

$$C_2H_6 + C_nH_{2n} \longrightarrow C_2H_4 + C_nH_{2n+2} \quad (a)$$

$$C_nH_{2n+2} \longrightarrow C_nH_{2n} + H_2 \quad (b)$$

$$C_nH_{2n} \longrightarrow C_{6+} \text{ olefins} \longrightarrow \text{arenes} \quad (c)$$

However, the enhancement in the ethane conversion due to the presence of ethylene in the feed was expected due to the hydrogen-transfer reaction of its dimer butylene, which is formed by ethylene dimerization over the zeolite. In the case of higher-alkane addition, the enhancement also results from the hydrogen-transfer reaction of ethane with the olefin formed from the alkanes by dehydrogenation over the zeolite [Eq (b)], which is a bifunctional catalyst with both dehydrogenation and acid functions.

The reactivity of the olefins in the hydrogen-transfer reaction is higher for that with a larger number of carbon atoms.[10] Therefore, the observed larger enhancement due to the longer carbon chain in the additive and the higher A/C_2H_6 ratio (Figure 1) is consistent with the above-mentioned hypothesis. It is also consistent with the fact that the pentasil zeolites of ZSM-5-type show high activity for the hydrogen-transfer reaction between alkane and olefin, even at 400 °C.[10, 11]

A path and elementary reaction steps for ethane aromatization over the zeolite, which contains both Lewis (extraframework Ga sites) and Brønsted (zeolitic protons) acid sites, are proposed here for explaining the beneficial effect of the additive. In the absence of additive, dehydrogenation of ethane is expected to occur by interaction with the Lewis acid site G located close to the zeolitic proton; this is similar to that proposed for dehydrogenation of propane.[12–15] The steps involve C–H bond cleavage (which is facilitated in the presence of a proton) and abstraction of H^- by the Lewis acid site [Eq. (d)], regeneration of the Lewis acid site by interaction with the nearby proton and H_2 desorption [Eq. (e)], and finally desorption of ethylene by the release of proton from the carbonium ion [Eq. (f)].

$$C_2H_6 + G \rightleftharpoons C_2H_5^+ + GH^- \quad (d)$$

$$GH^- + H^+ \rightleftharpoons G + H_2 \quad (e)$$

$$C_2H_5^+ \rightleftharpoons C_2H_4 + H^+ \quad (f)$$

Because of the very low reactivity of ethane, the activation of ethane by reaction (d) is slow and, hence, limits its conversion. However, the enhancement in ethane conversion in the presence of higher (C_{3+}) olefins results from a change in the mechanism of ethane activation. First, the olefin is activated by interaction with a zeolitic proton to form a carbonium ion by the equilibrium reaction (g). The carbonium ion then undergoes a hydrogen-transfer reaction with ethane [Eq. (h)]. The ethyl carbonium ion undergoes reaction according to Equation (f) to form

$$C_nH_{2n} + H^+ \rightleftharpoons (C_nH_{2n+1})^+ \quad (g)$$

$$C_2H_6 + (C_nH_{2n+1})^+ \rightleftharpoons C_2H_5^+ + C_nH_{2n+2} \quad (h)$$

ethylene with the release of a proton. The activation of ethane according to Equation (h) is much faster than that by Equation (d). Because of its high reactivity, the higher alkane formed in reaction (h) is converted back into the olefin by reactions similar to that in the ethane–ethylene conversion in the absence of olefin additive [Eqs. (d)–(f)].

Ethylene and higher olefins are converted into arenes on the Brønsted acid sites by oligomerization [Eq (i), $N = 6–10$]. Successive dehydrogenation of the carbonium ions[16] by reaction (j) results in formation of the arenes, release of protons, and adsorbed H atoms that remain unchanged.

$$C_2H_4 \text{ or } (C_nH_{2n}) + C_2H_5^+ \text{ [or } (C_nH_{2n+1})^+] \rightleftharpoons (C_NH_{2N+1})^- \quad (i)$$

$$(C_NH_{2N+1})^+ \rightleftharpoons C_NH_{2N-6} \text{ (arenes)} + H^+ + 6H_{ad} \quad (j)$$

The desorption of H_{ad} atoms from the zeolite surface as molecular hydrogen, which controls the formation of aromatics and hence the aromatics selectivity,[17] is facilitated by their spillover to the Ga sites followed by recombinative desorption [Eqs. (k) and (l)].[16, 17] The very high arene selectivity observed

$$H_{ad} + G \rightleftharpoons H\text{–}G \quad (k)$$

$$2H\text{–}G \rightleftharpoons H_2 + 2G \quad (l)$$

is, therefore, attributed to the presence of well-dispersed nonframework Ga sites in the zeolite channels in a close vicinity of the zeolitic protons.

Since the aromatization of ethylene is exothermic and the ethane dehydrogenation or overall ethane aromatization is endothermic, there is a coupling of exothermic and endothermic reactions in the simultaneous aromatization of ethane and ethylene. This makes the process most energy efficient, which is similar to the case of the methane–syngas[18] and ethane–ethylene[19] conversion processes.

This investigation clearly shows that ethane, which has very low reactivity (compared to higher hydrocarbons), can be converted into arenes with high conversion, yield, selectivity, and productivity (because of the high space velocity) at low temperatures (400–500 °C) if enough olefins or higher alkanes are present in the feed. This concept would have great practical implications, particularly for the conversion of ethane from natural gas, which contains appreciable amount of higher hydrocarbons along with methane and ethane, and from the OCM (*o*xidative *c*oupling of *m*ethane) product stream, which contains comparable amounts of ethane and ethylene along with smaller amounts of higher hydrocarbons.

Experimental Section

H-GaAlMFI zeolite [framework (FW) Si/Ga 49.9, FW Si/Al 40.3, non-FW Ga 2.2 wt%, Na/(Al+Ga) 0.03, crystal shape spherical hexagonal, and crystal size 5.5 ± 1.5 μm] was prepared and characterized by methods described earlier [20]. The zeolite was pretreated in a flow of hydrogen (space velocity 1030 $cm^3 g^{-1} h^{-1}$) at 600 °C for 1 h and then in air for 0.5 h. The number of strong acid sites (in terms of the pyridine chemisorption at 400 °C) in the zeolite is 0.46 mmol g^{-1}. The ethane aromatization reaction over the zeolite was carried out under steady-state conditions at atmospheric pressure in a continuous-flow quartz reactor with a mixture of

ethane (33.3 mol%) and nitrogen, with or without any additive (higher alkanes or olefins), as the feed at a space velocity of $6100 \pm 100\ cm^3 g^{-1} h^{-1}$ with a square-pulse technique described earlier [21]. The space velocity was measured at 0 °C and 1 atm. Conversion X in %, S_{A_r} in %, and yield of arene based on ethane conversion ($Y_{Ar(C_2H_6)}$ in %) were determined as follows: $X = [\{(wt\%\ of\ reactant\ in\ the\ feed\ hydrocarbons) - (wt\%\ of\ reactant\ in\ the\ product\ hydrocarbons)\}/(wt\%\ of\ reactant\ in\ the\ feed\ hydrocarbons)] \times 100$; $S_{A_r} = [(wt\%\ of\ arenes\ in\ the\ hydrocarbon\ products)/\{100 - wt\%\ of\ reactant(s)\ in\ the\ hydrocarbon\ products\}] \times 100$; $Y_{Ar(C_2H_6)} = (X S_{A_r})/100$.

Received: December 3, 1996 [Z 9849 IE]
German version: *Angew. Chem.* **1997**, *109*, 1362–1365

Keywords: arenes · cyclizations · ethane · heterogeneous catalysis · zeolites

[1] M. Guisnet, N. S. Gnep, F. Alario, *Appl. Catal. A: Gen.* **1992**, *89*, 1–30.
[2] Y. Ono, *Catal. Rev. Sci. Eng.* **1992**, *34*, 179–226.
[3] G. Giannetto, R. Monque, R. Galliasso, *Catal. Rev. Sci. Eng.* **1994**, *36*, 271–304.
[4] M. S. Scurrell, *Appl. Catal.* **1987**, *32*, 1–22.
[5] T. Inui, Y. Makino, F. Okazumi, S. Nagano, A. Miyamoto, *Ind. Eng. Chem. Res.* **1987**, *26*, 647–652.
[6] M. S. Scurrell, *Appl. Catal.* **1988**, *41*, 89–98.
[7] M. Guisnet, N. S. Gnep, D. Aittaleb, Y. J. Doyemet, *Appl. Catal. A: Gen.* **1992**, *87*, 255–270.
[8] P. Schulz, M. Baerns, *Appl. Catal.* **1991**, *78*, 15–29.
[9] Y. Ono, H. Nakatani, H. Kitagawa, E. Suzuki, *Stud. Surf. Sci. catal.* **1989**, *44*, 279–290.
[10] D. B. Lukynov, *J. Catal.* **1994**, *147*, 494–499.
[11] D. B. Lukynov, *J. Catal.* **1994**, *145*, 54–57.
[12] C. R. Bayense, A. J. H. P. van der Pol, J. H. C. van Hooff, *Appl. Catal.* **1991**, *72*, 81–98.
[13] P. Meriaudeu, C. Naccache, *J. Mol. Catal.* **1991**, *59*, L31–L38.
[14] G. Buckles, G. J. Hutchings, C. D. Williams, *Catal. Lett.* **1991**, *11*, 89–94.
[15] B. S. Kwak, W. M. H. Sachter, *J. Catal.* **1994**, *145*, 456–463.
[16] O. P. Keipert, D. Wolf, P. Schulz, M. Baerns, *Appl. Catal. A: Gen* **1995**, *131*, 347–365.
[17] E. Iglesia, J. E. Baumgartner, G. L. Price, *J. Catal.* **1992**, *134*, 549–571.
[18] V. R. Choudhary, A. M. Rajput, B. Prabhakar, *Angew. Chem.* **1994**, *106*, 2179–2181; *Angew. Chem. Int. Ed. Engl.* **1994**, *33*, 2104–2106; *Catal. Lett.* **1995**, *32*, 391–396.
[19] V. R. Choudhary, B. S. Uphade, S. A. R. Mulla, *Angew Chem.* **1995**, *107*, 721–723; *Angew. Chem. Int. Ed. Engl.* **1995**, *34*, 665–666.
[20] V. R. Choudhary, A. K. Kinage, C. Sivadinarayana, M. Guisnet, *J. Catal.* **1996**, *158*, 23–33.
[21] V. R. Choudhary, A. K. Kinage, C. Sivadinarayana, P. Devadas, S. D. Sansare, M. Guisnet, *J. Catal.* **1996**, *158*, 34–50.

High-Yield Synthesis of [2]Catenanes by Intramolecular Ring-Closing Metathesis**

Bernhard Mohr, Marcus Weck, Jean-Pierre Sauvage,* and Robert H. Grubbs*

The development of effective approaches to interlocked molecular rings, catenanes, constitutes a great challenge in preparative chemistry,[1] especially in light of their role in DNA structure and related molecules of biological relevance.[2] Following the pioneering work of Schill and Wasserman,[3] template-directed strategies that used transition metal complexation,[4, 5] π-donor–acceptor interactions,[6] and hydrogen bonding[7] have not only made the synthesis of interlocking rings more accessible but have also allowed the introduction of various functional groups. In most cases, the cyclization reaction is restricted to the formation of ether and amide bonds or quaternary ammonium salts by an intermolecular pathway.

Ring-closing metathesis (RCM) has been established as an efficient approach to macrocyclic systems with intramolecular formation of carbon–carbon double bonds.[8, 9] The ruthenium benzylidene catalyst **1** (Cy = cyclohexyl) is particularly attractive in these reactions, due to its high activity and tolerance to an array of functional groups.[8, 10] Although RCM was initially applied in the synthesis of small five- to eight-membered rings,[11] this methodology has recently been extended to larger ring systems incorporating up to 38 atoms.[12]

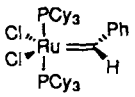

1

The approach presented here utilizes a combination of a transition metal based template strategy and RCM to provide access to [2]catenanes (Figure 1). The building blocks are the 30-membered macrocycle **2**, bearing a 2,9-diphenyl-1,10-phenanthroline (dpp) bidentate chelate in its backbone, and the acyclic ligands **3** and **4**, in which the dpp moiety is symmetrically substituted with ethylene oxide groups with a terminal olefin (Scheme 1a).[13] The threaded complexes **5** and **6** were formed quantitatively by the reaction of **2** with a stoichiometric amount of $[Cu(MeCN)_4]PF_6$ in CH_2Cl_2/MeCN followed by addition of diolefins **3** and **4**, respectively. Analogously, the intertwined

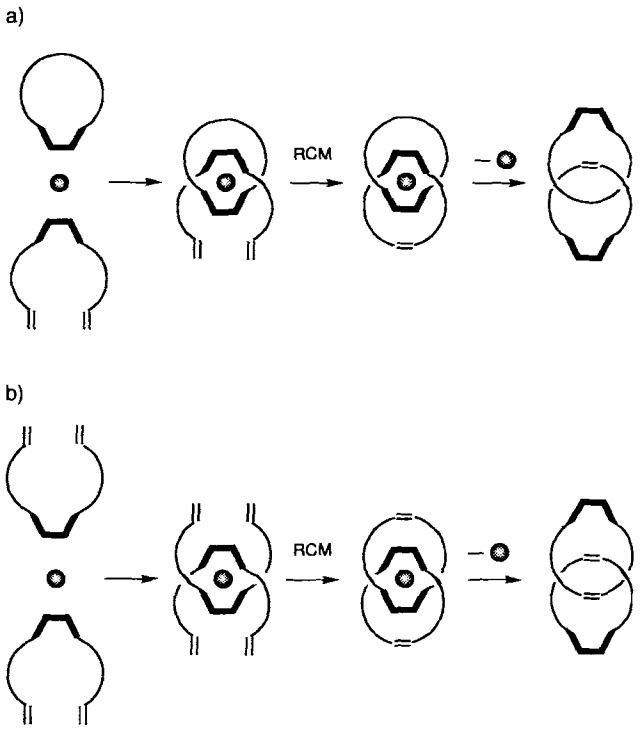

Figure 1. Schematic drawing of the approach utilizing a combination of a transition metal based template strategy and RCM to provide access to [2]catenanes: a) formation of a threaded complex followed by RCM and decomplexation; b) formation of an intertwined complex followed by twofold RCM and decomplexation. The black circle represents the transition metal ion.

[*] Dr. J.-P. Sauvage, Dr. B. Mohr
Laboratoire de Chimie Organo-Minérale, UA 422 au CNRS
Faculté de Chimie
Université Louis Pasteur
4, rue Blaise Pascal, F-67070 Strasbourg (France)
Fax: Int. code +(388)607-312
e-mail: sauvage@chimie.u-strasbg.fr
Prof. R. H. Grubbs, M. Weck
Arnold and Mabel Beckman Laboratories of Chemical Synthesis
Division of Chemistry and Chemical Engineering
California Institute of Technology
Pasadena, CA 91125 (USA)
Fax: Int. code +(818)564-9297
e-mail: rhg@starbase1.caltech.edu

[**] This work was supported by a postdoctoral fellowship from the European Community and by the United States Air Force.

 © VCH Verlagsgesellschaft mbH, D-69451 Weinheim, 1997 0570-0833/97/3612-1308 $ 17.50+.50/0

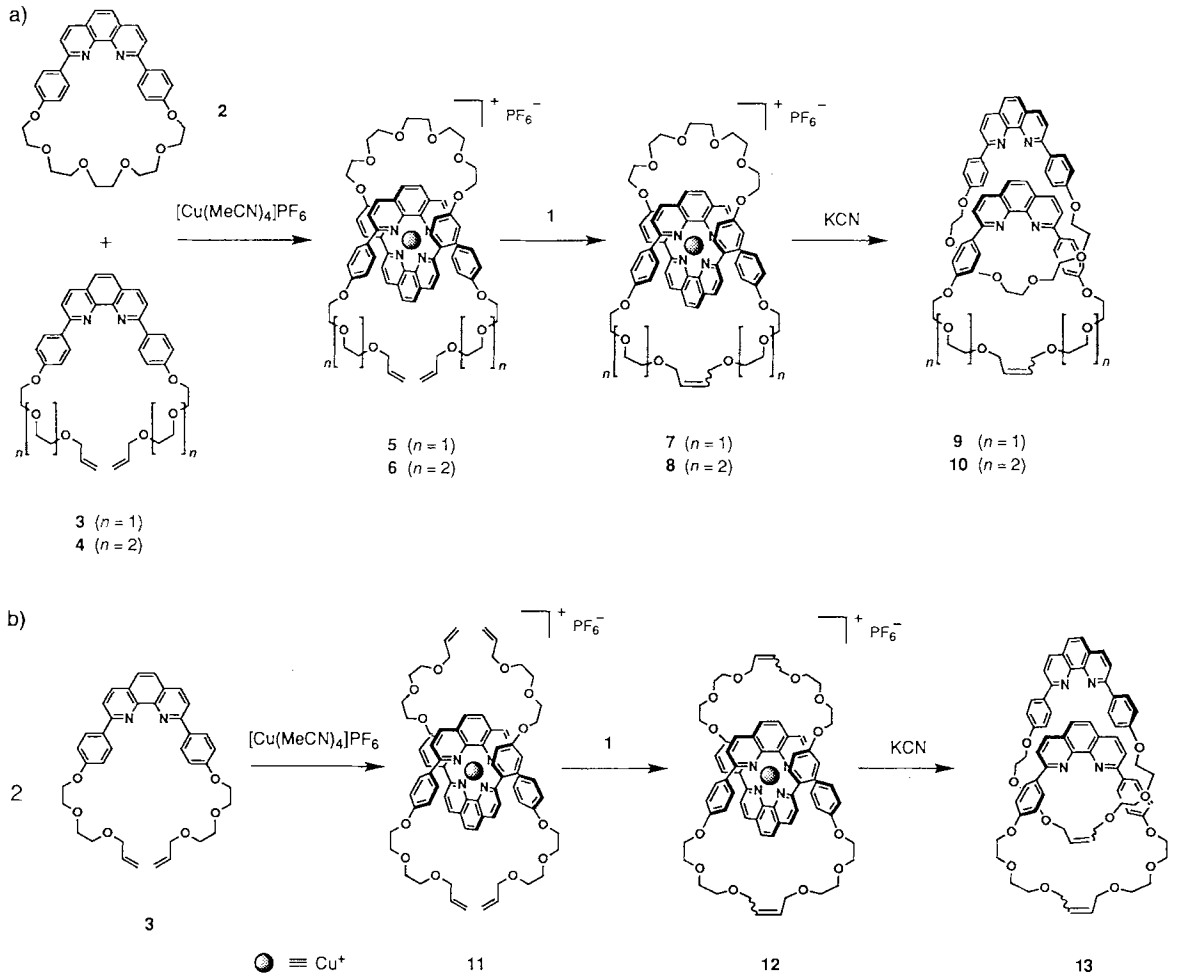

Scheme 1. Synthesis of the [2]catenanes **9**, **10**,and **13**. a) RCM of the threaded complexes **5** and **6** resulting in a 32- and 38-membered ring, respectively. b) RCM of the intertwined complex **11** resulting in two 32-membered rings.

complex **11** was obtained in quantitative yields by complexation of two equivalents of **3** with $[Cu(MeCN)_4]PF_6$ (Scheme 1b). Complexes **5**, **6**, and **11** were then subjected to intramolecular RCM with catalyst **1** to yield the corresponding catenates **7**, **8**, and **12** by formation of 32- (**7**, **12**) and 38-membered (**8**) rings. Twofold RCM of **11** led exclusively to the system with two interlocked rings; the twisted product (formed by the intramolecular reaction between the olefins of different ligands) did not form, as unequivocally concluded by ^1H NMR spectroscopy, FAB-MS (FAB = Fast Atom Bombardment), and the topology of the demetalated species. The yields obtained in these cyclization reactions (Table 1) exceed those for most other medium or even large rings, where hydrogen bonding,[8, 12] the presence of conformational constraints, or template effects[14] are present to facilitate RCM. We believe that the remarkable efficiency of this RCM reaction stems, at least in part, from a preorganization of the olefins due to electrostatic interactions between the oxygen atoms and the phenanthroline system,[15] in combination with a locked conformation of the phenyl rings (π donor) and phenanthroline system (π acceptor).[16] This is supported by the exclusive formation of the interlocked species in the RCM of **11** and the observation that RCM of the free ligands **3** and **4** proceeds in lower yields (73%). For all catenates, the energetically favored *trans* configuration at the double bond prevails.

Table 1. Results of the ring-closing metathesis and demetalation reaction.

Catenate	Yield[%][a]	*trans*/*cis*[b]	Catenand	Yield[%][a]
7	92	97/3	**9**	92
8	88	95/5	**10**	93
12	92	98/2	**13**	90

[a] Yield of isolated product. [b] Determined by integration of the ^1H NMR signals of the isomeric olefin protons.

Demetalation of the catenates **7**, **8**, and **12** with potassium cyanide in aqueous MeCN afforded the [2]catenands **9**, **10**, and **13** in almost quantitative yields (Scheme 1, Table 1). Their composition was confirmed by FAB-MS (see Figure 2 for **13**). All spectra display the characteristic pattern for catenated species, in particular the absence of peaks between the molecular ion peak and the peaks corresponding to the individual macrocycles.[17] The FAB-MS of **13** provides further proof for the exclusive formation of the interlocked species **12** in the RCM step.

In conclusion, RCM has been established as a highly efficient protocol for the synthesis of [2]catenanes by intramolecular cyclization. This methodology provides a versatile approach for the efficient synthesis of [*n*]catenanes, knots, and topologically related species.

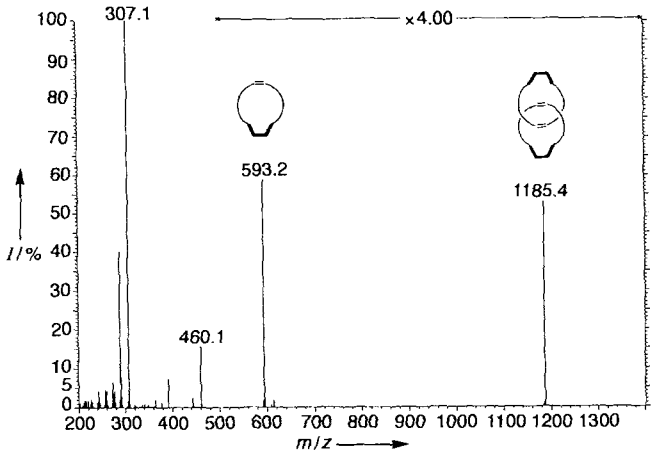

Figure 2. Positive FAB-MS spectrum of catenane **13** in a *p*-nitrobenzyl alcohol matrix (display from $m/z = 200$ to 1400; peaks at $m/z = 307.1$ and 460.1 result from the alcohol matrix). The peak at $m/z = 1185.4$ corresponds to [catenane $- H^+$], and at $m/z = 593.2$ to [macrocycle $- H^+$]. The absence of peaks between the molecular ion peak and the the peak corresponding to the individual macrocycle is characteristic for catenated species [16].

Experimental Section

General procedure for ruthenium benzylidene catalyzed RCM: Under exclusion from air and moisture, **1** (5 mol%) in CH_2Cl_2 was added to a 0.01 M solution of the diolefin (typically 200 to 900 mg) in CH_2Cl_2. After the mixture was stirred for 6 h at room temperature, additional catalyst (5 mol%) was added, and stirring continued for 6 h. The solvent was then removed under reduced pressure, and the crude reaction mixture purified by repeated column chromatography (silica gel, CH_2Cl_2/MeOH 96/4 v/v) to yield the [2]catenates as burgundy solids. All compounds were characterized by NMR spectrscopy, FAB-MS, and elemental analysis.

Received: December 23, 1996 [Z9924IE]
German version: *Angew. Chem.* **1997**, *109*, 1365–1367

Keywords: catenanes · cyclizations · metathesis · ruthenium · template synthesis

[1] Recent reviews on catenanes and related compounds: a) J.-P. Sauvage, C. O. Dietrich-Buchecker, J.-C. Chambron in *Comprehensive Supramolecular Chemistry, Vol. 9* (Ed.: J.-M. Lehn), Pergamon Press, Oxford, **1996**, p. 43; b) special issue of the *New J. Chem.* (Ed.: J.-P. Sauvage) **1993**, *17*; c) D. B. Amabilino, J. F. Stoddart, *Chem. Rev.* **1995**, *95*, 2725; d) D. P. Philip, J. F. Stoddart, *Angew. Chem.* **1996**, *108*, 1242; *Angew. Chem. Int. Ed. Engl.* **1996**, *35*, 1154.

[2] a) A. D. Bates, A. Maxwell, *DNA Topology*, Oxford University Press, New York, **1993**; b) S. D. Levene, C. Donahue, T. C. Boles, N. R. Cozzarelli, *Biophys. J.* **1995**, *69*, 1036.

[3] a) E. J. Wasserman, *J. Am. Chem. Soc.* **1960**, *82*, 4433; b) H. L. Frisch, E. J. Wasserman, *ibid.* **1960**, *82*, 4433; c) G. Schill, *Catenanes, Rotaxanes and Knots*, Academic Press, New York, **1971**.

[4] a) C. O. Dietrich-Buchecker, J.-P. Sauvage, *Tetrahedron Lett.* **1983**, *24*, 5091; b) C. O. Dietrich-Buchecker, J.-P. Sauvage, *Bioorganic Chemistry Frontiers*, *Vol. 2*, Springer, Berlin, **1991**, pp. 195–248.

[5] Catenanes whose rings incorporate transition metal atoms: M. Fujita, K. Ogura, *Coord. Chem. Rev.* **1996**, *148*, 249.

[6] a) J. Y. Ortholand, A. M. Z. Slawin, N. Spencer, J. F. Stoddart, D. J. Williams, *Angew. Chem.* **1989**, *101*, 1404; *Angew. Chem. Int. Ed. Engl.* **1989**, *28*, 1394; b) D. B. Amabilino, P.-L. Anelli, P. R. Aston, G. R. Brown, E. Cordova, L. A. Godinez, W. Hayes, A. E. Kaifer, D. Philip, A. M. Z. Slawin, N. Spencer, M. S. Tolley, D. J. Williams, F. J. Stoddart, *J. Am. Chem. Soc.* **1995**, *117*, 11142.

[7] a) F. Vögtle, S. Meier, R. Hoss, *Angew. Chem.* **1992**, *104*, 1628; *Angew. Chem. Int. Ed. Engl.* **1992**, *31*, 1619; b) F. Vögtle, T. Dünnwald, T. Schmidt, *Acc. Chem. Res.* **1996**, *29*, 451; c) C. A. Hunter, *J. Am. Chem. Soc.* **1992**, *114*, 5303; d) A. G. Johnston, D. A. Leigh, R. J. Pritchard, M. D. Deegan, *Angew. Chem.* **1995**, *107*, 1324; *Angew. Chem. Int. Ed. Engl.* **1995**, *34*, 1209.

[8] Recent reviews on RCM: a) R. H. Grubbs, S. J. Miller, G. C. Fu, *Acc. Chem. Res.* **1995**, *28*, 446; b) H.-G. Schmalz, *Angew. Chem.* **1995**, *107*, 1981; *Angew. Chem. Int. Ed. Engl.* **1995**, *34*, 1833.

[9] Early attempts to synthesize catenanes with RCM: a) R. Wolovsky, *J. Am. Chem. Soc.* **1970**, *92*, 2132; b) D. A. Ben-Efraim, C. Batich, E. Wasserman, *ibid.* **1970**, *92*, 2133.

[10] P. Schwab, R. H. Grubbs, J. W. Ziller, *J. Am. Chem. Soc.* **1996**, *118*, 100.

[11] a) G. C. Fu, R. H. Grubbs, *J. Am. Chem. Soc.* **1992**, *114*, 5426; b) M. D. E. Forbes, J. T. Patton, T. L. Myers, H. D. Maynard, D. W. Smith, G. R. Schulz, K. B. Wagener, *ibid.* **1992**, *114*, 10978, c) S. J. Miller, S. H. Kim, Z. R. Chen, R. H. Grubbs, *ibid.* **1995**, *117*, 2108.

[12] a) S. J. Miller, H. E. Blackwell, R. H. Grubbs, *J. Am. Chem. Soc.* **1996**, *118*, 9606; b) A. Fürstner, K. Langemann, *J. Org. Chem.* **1996**, *61*, 3942; c) T. D. Clark, M. R. Ghadiri, *J. Am. Chem. Soc.* **1995**, *117*, 12364; d) B. König, C. Horn, *Synlett* **1996**, 1013; e) A. Fürstner, N. Kindler, *Tetrahedron Lett.* **1996**, *37*, 7005; f) P. Bertinato, E. J. Sorensen, D. Meng, S. J. Danishefsky, *J. Org. Chem.* **1996**, *61*, 8000; g) Z. Xu, C. H. Johannes, S. S. Salman, A. H. Hoveyda, *J. Am. Chem. Soc.* **1996**, *118*, 10926; h) K. C. Nicolaou, Y. He, D. Vourloumis, H. Vallberg, Z. Yang, *Angew. Chem.* **1996**, *108*, 2554; *Angew. Chem. Int. Ed. Engl.* **1996**, *35*, 2399.

[13] Macrocycle **2** was prepared as described: C. Dietrich-Buchecker, J.-P. Sauvage, *Tetrahedron* **1990**, *46*, 503; acyclic ligands **3** and **4** were prepared from dpp with 2-(2-chloroethoxy)ethanol/Na_2CO_3 and 2-[2-(2-chloroethoxy)ethoxy]ethanol/Na_2CO_3, respectively, in *N*,*N*-dimethylformamide (DMF) and subsequent alkylation with allylbromide/NaH in DMF.

[14] M. J. Marsella, H. D. Maynard, R. H. Grubbs, *Angew. Chem.* **1997**, *109*, 1147; *Angew. Chem. Int. Ed. Engl.* **1997**, *36*, 1101.

[15] a) G. R. Desiraju, *Angew. Chem.* **1995**, *107*, 2541; *Angew. Chem. Int. Ed. Engl.* **1995**, *34*, 2311; b) for a comprehensive survey on π-donor/π-acceptor interactions in related supramolecular assemblies see also ref. [1d].

[16] These interactions have been observed in the solid state for a structurally related [2]catenate: a) M. Cesario, C. O. Dietrich-Buchecker, G. Guilhelm, C. Pascard, J.-P. Sauvage, *J. Chem. Soc. Chem. Commun.* **1985**, 244; b) C. O. Dietrich-Buchecker, G. Guilhelm, J.-M. Kern, C. Pascard, J.-P. Sauvage, *Inorg. Chem.* **1994**, *33*, 3498.

[17] C. O. Dietrich-Buchecker, E. Leize, J.-F. Nierengarten, J.-P. Sauvage, A. Van Dorsselar, *J. Chem. Soc. Chem. Commun.* **1994**, 2257, and references therein.

Azo-Dye Rotaxanes

Sally Anderson,* Tim D. W. Claridge, and Harry L. Anderson*

Azo dyes are the largest and most commercially important class of synthetic colorants.[1] Their interaction with cyclodextrins (CDs) has been investigated as a method of controlling their stability, solubility, and aggregation.[2] Rotaxane formation offers a way of converting these labile inclusion complexes into robust encapsulated chromophores, with the dye permanently protected inside the cavity of the CD. There seem to be no previous reports of rotaxanes of this type.[3] We have synthesized a range of water-soluble azo-dye rotaxanes using the hydrophobic effect to direct rotaxane formation (Scheme 1).[4]

When azobenzene diazonium salt **1a** is added to an aqueous solution of β-naphthol **2** in the presence of either α-CD **3a** or β-CD **3b** at 0–5 °C, the solution immediately turns deep purple. Paper chromatography reveals the formation of the fast-running rotaxanes **4a**⊂**3a** or **4a**⊂**3b**, respectively, as well as the less mobile non-rotaxanated dye **4a**, which is rather insoluble in water and can be separated from the rotaxanes by centrifugation. Rotaxanes **4a**⊂**3a** and **4a**⊂**3b** were purified by paper chromatography and recrystallization, and isolated in 12 and 15% yields, respectively. The tolidine diazonium salt **1b** also gave a

[*] Dr. S. Anderson, Dr. H. L. Anderson, Dr. T. D. W. Claridge
University of Oxford
Dyson Perrins Laboratory
South Parks Road, Oxford OX1 3QY (UK)
Fax: Int. code +(1865)275-674
e-mail: harry.anderson@dyson.ox.ac.uk

[**] This work was supported by the Engineering and Physical Sciences Research Council and an Award to Newly Appointed Science Lecturers from the Nuffield Foundation. S. A. gratefully acknowledges a Research Fellowship and generous support from Trinity College, Cambridge (UK).

 © VCH Verlagsgesellschaft mbH, D-69451 Weinheim, 1997 0570-0833/97/3612-1310 $ 17.50+.50/0

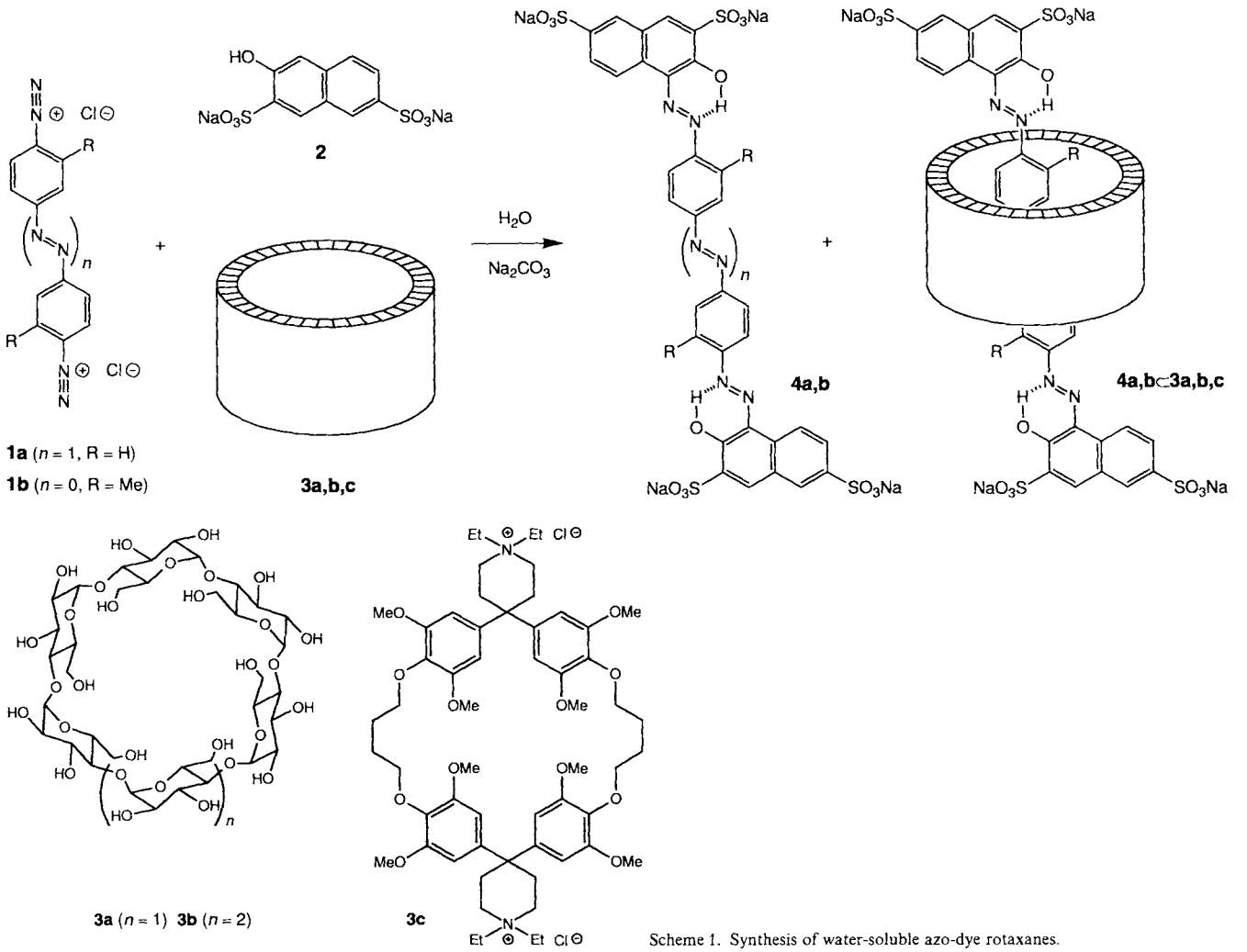

Scheme 1. Synthesis of water-soluble azo-dye rotaxanes.

rotaxane with **3b** when allowed to react with **2** under similar conditions, but it failed to give any rotaxane with **3a**. Diazonium salt **1b** is evidently too large to bind in the cavity of **3a**. Rotaxane **4b⊂3b** was isolated in 6% yield.

All three rotaxanes were fully characterized by ^{1}H and ^{13}C NMR spectroscopy and ESI-MS (Table 1).[5] In all mass spectra the most abundant molecular ion corresponds to the tetraanion formed by loss of four sodium cations. The NMR spectra show that the symmetry of the CD is imposed on the azo dye, making its two ends nonequivalent, whereas the symmetry of the CD is maintained, since it rotates rapidly around its guest on the NMR timescale. When ^{1}H NMR spectra are recorded in [D$_6$]DMSO, all the signals for hydroxyl groups are sharp and well-resolved. Two signals appear at about $\delta = 17$ due to the hydrogen-bonded phenolic OH groups at each end of the rotaxanes. The ^{1}H NMR spectrum of **4b⊂3b** was assigned by 1-D-NOESY and 2-D-COSY NMR techniques. Long-range weak NOEs are observed with 1-D double-pulsed field-gradient spin-echo (DPFGSE) NOESY experiments.[6] A separate and complementary set of NOEs is seen from each rim of the CD (Scheme 2). For example, the naphthalene proton H_A shows NOEs to hydroxyl protons OH-2 and OH-3 as well as to the proximate internal CD proton H-3, whereas H_A shows NOEs to OH-6 and H-6, which are situated on the opposite rim of the CD. Both protons $H_{G'}$ and H_I show NOEs to CD H-5 and H-3 on the inner surface of the CD. This shows that the central portion of the dye is encapsulated by the CD.

Table 1. Selected physical and spectroscopic data for **4a⊂3b**, **4a⊂3b**, and **4a** [a].

4a⊂3b: ^{1}H NMR: $\delta = 16.79$ (s, 1H; $H_{E'}$), 16.47 (s, 1H; H_E), 8.51 (d, $J = 8$ Hz, 1H; $H_{A'}$), 8.44 (d, $J = 8$ Hz, 1H; H_A), 8.28 (s, 1H; $H_{D/D'}$), 8.26 (s, 1H; $H_{D/D'}$), 8.14 (d, $J = 9$ Hz, 2H; $H_{G'}$), 8.02 (d, $J = 9$ Hz, 2H; H_G), 8.0–7.9 (m, 7H; $H_{C'}$, H_C, H_F, $H_{F'}$, $H_{B'}$), 7.87 (d, $J = 9$ Hz, 1H; H_B), 5.70 (d, $J = 7$ Hz, 7H; OH-2), 5.60 (brs, 7H; OH-3), 4.79 (d, $J = 3$ Hz, 7H; H-1), 4.49 (t, $J = 5$ Hz, 7H; OH-6), 3.7–3.1 (m, 42H; H-2, H-3, H-4, H-5, H-6); ^{13}C NMR: $\delta = 174.13$, 173.53, 150.37, 150.25, 146.94, 146.77, 144.81, 144.56, 141.14, 140.74, 139.80, 139.52, 133.29, 133.14, 130.87, 130.54, 128.35, 127.83, 126.77, 126.58, 125.76, 125.49, 124.57, 124.47, 122.22, 121.37, 118.06[b], 101.85, 81.11, 73.01, 72.39, 71.88, 59.61; UV/Vis: $\lambda_{max}(\lg\varepsilon) = 567$ nm (4.75); negative-ion ESI-MS: $m/z = 493.3$ $[M - 4Na^+ + H^+]^{4-}$, 658.1 $[M - 4Na^+ + H^+]^{3-}$, 987.7 $[M - 4Na^+ + 2H^+]^{2-}$, correct for $C_{74}H_{88}N_6Na_4O_{49}S_4$.

4a⊂3c: ^{1}H NMR: $\delta = 16.19$ (s, 2H; H_E), 8.32 (d, $J = 8$ Hz, 2H; H_A), 8.29 (s, 2H; H_D), 7.96 (s, 2H; H_C), 7.93 (d, $J = 8$ Hz, 2H; H_B), 6.99 (ABq, $J = 8$ Hz, 8H; $H_{F/G}$), 6.93 (s, 8H; cyclophane arenes), 3.64 (s, 24H; OMe), 3.5–2.6 (m, 32H; N^+CH_2, $N^+CH_2CH_2$, and OCH_2), 1.32 (m, 8H; OCH_2CH_2), 1.17 (t, $J = 7$ Hz, 12H; $N^+CH_2CH_3$); ^{13}C NMR: $\delta = 171.07$, 152.86[b], 149.67, 146.94, 144.66, 141.46, 138.14, 135.26, 132.43, 130.35, 127.08, 126.28, 125.74, 123.57, 120.53, 117.63, 104.01, 70.97[b], 55.86, 54.92, 42.68, 28.01, 25.05, 6.67; UV/Vis: $\lambda_{max}(\lg\varepsilon) = 567$ nm (4.82); negative-ion ESI-MS: $m/z = 920.4$ $[M - 2Na^+]^{2-}$, correct for $C_{90}H_{102}N_8Na_2O_{26}S_4$.

4a: ^{1}H NMR: $\delta = 16.18$ (s, 2H; H_E), 8.42 (d, $J = 8$ Hz, 2H; H_A), 8.26 (s, 2H; H_D), 8.06 (ABq, $J = 9$ Hz, 8H; H_G, H_F), 7.91 (brs, 2H; H_C), 7.83 (d, $J = 8$ Hz, 2H; H_B); UV/Vis: $\lambda_{max}(\lg\varepsilon) = 562$ nm (4.71); negative-ion ESI-MS: $m/z = 209.6$ $[M - 4Na^+]^{4-}$, 279.9 $[M - 4Na^+ + H^+]^{3-}$, 420.2 $[M - 4Na^+ + 2H^+]^{2-}$, correct for $C_{32}H_{18}N_6Na_4O_{14}S_4$.

[a] ^{1}H (500 MHz) and ^{13}C (125 MHz) NMR spectra were recorded in [D$_6$]DMSO, and UV/Vis spectra in DMSO unless otherwise stated. [b] Two coincident signals.

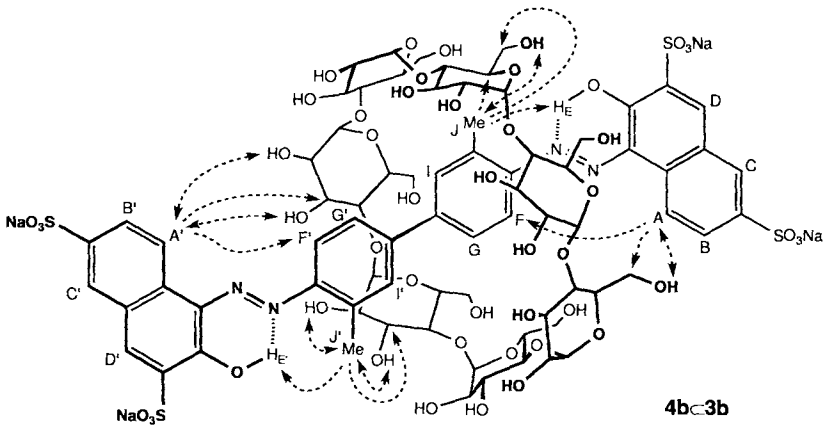

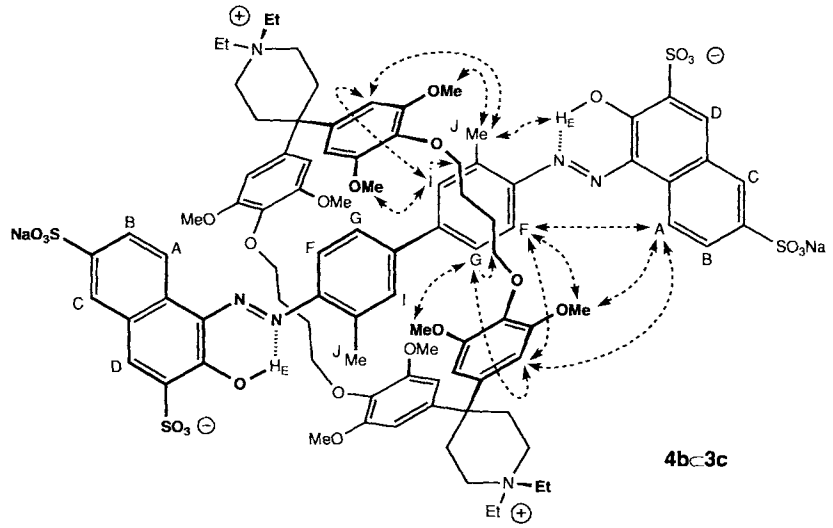

Scheme 2. Structures of **4b**⊂**3b** and **4b**⊂**3c** as well as some of the NOEs observed (double-headed arrows indicate NOEs in both directions).

We also synthesized azo-dye rotaxanes with cyclophane **3c**.[7] In the presence of **3c**, **1a** and **1b** couple with **2** to give rotaxanes **4a**⊂**3c** or **4b**⊂**3c** as the exclusive azo-dye product; no non-rotaxanated dye **4a** or **4b** is formed, although some by-products are produced due to dediazotization. The rotaxanes were isolated as their sodium salts in 46 and 40% yields, respectively. They precipitate from the reaction mixtures as $[\mathbf{4a}\subset\mathbf{3c}]^{2-}\cdot[\mathbf{3c}]^{2+}$ and $[\mathbf{4b}\subset\mathbf{3c}]^{2-}\cdot[\mathbf{3c}]^{2+}$ salts; they were filtered off and purified by column chromatography, then ion-exchanged to the sodium salts. The ^{1}H NMR spectra of these cyclophane rotaxanes are considerably simpler than those of their CD analogues due to both the higher symmetry of the cyclophane and to the cyclophane's aromatic ring current, which disperses the signals of the guest. For example, for **4b**⊂**3c** H_F, H_G, Me_J, and H_I are shifted upfield by $\Delta\delta = 0.90$, 2.08, 0.51, and 1.75, respectively, showing that these protons reside inside the cyclophane. DPFGSE NOESY experiments confirmed that the central portion of the dye is buried inside the cyclophane's cavity. Some of the observed NOEs are illustrated in Scheme 2.

We have shown that the hydrophobic effect can be used to direct the synthesis of azo-dye rotaxanes with both CD and cyclophane macrocycles. The cyclophane rotaxanes are formed in higher yield and are easier to characterize spectroscopically. All of these rotaxanes are more soluble (in most solvents) than the non-rotaxanated dyes. They also aggregate less than their non-rotaxanated analogues; for example, **4a** forms stable bimolecular aggregates in water ($K = 2\times10^3\,\mathrm{M}^{-1}$), whereas **4b**⊂**3b** does not ($K<20\,\mathrm{M}^{-1}$).[8] We plan to explore the effects of rotaxane encapsulation on the stability and photochemistry[9] of these dyes.

Experimental Section

4a⊂**3b:** $NaNO_2$ (41 mg, 0.59 mmol) was added to 4,4′-diaminoazobenzene (60 mg, 0.28 mmol) in aqueous HCl (0.1 M, 10 mL, 1.1 mmol) at 0–5 °C. The solution was stirred for 1 h, aqueous **3b** (11.4 mM, 70 mL, 0.80 mmol) added, and the mixture again stirred at 0–5 °C for 30 min. This solution was added to a mixture of **2** (200 mg, 0.56 mmol) and Na_2CO_3 (99 mg, 0.93 mmol) in water (8 mL) and stirred for 3 h at 20 °C. NaOAc (15 g) was added, and the mixture heated to 80 °C. The precipitate (**4a**) was separated from the supernatant by centrifugation. The product was then precipitated from the supernatant with acetone, washed with hot ethanol, dissolved in water, recrystallized by addition of ethanol, purified by chromatography on paper plates (Whatman 3MM) eluting with $MeCN/H_2O$ (1/1), and recrystallized from $DMSO/H_2O$ (1/1) by addition of acetone. Yield: 89 mg (15%).

4a⊂**3c:** $NaNO_2$ (20 mg, 0.29 mmol) was added to 4,4′-diaminoazobenzene (30 mg, 0.14 mmol) in aqueous HCl (0.19 M, 3 mL, 0.58 mmol) at 0–5 °C. The solution was stirred for 1 h, aqueous **3c** (21 mM, 20 mL, 0.42 mmol) added, and the mixture again stirred at 0–5 °C for 30 min. This solution was added to a mixture of **2** (98 mg, 0.28 mmol) and Na_2CO_3 (50 mg, 0.47 mmol) in water (2 mL) and stirred for 1 h. The solid was collected by centrifugation and purified by flash column chromatography on silica eluting with $MeOH/2\,\mathrm{M}\ NH_4CHO_2/MeNO_2$ (16/2/1). Concentration of the solution to 10% of its original volume resulted in precipitation of the rotaxane, which was isolated by filtration, washed with a minimum of water, and dried in vacuo at 100 °C/0.01 mm Hg to remove traces of ammonium formate. Cation exchange was carried out with Na^+ Dowex 50WX8-400 (10 g), and recrystallization from 1:1 $DMSO/H_2O$ by addition of ethanol. Yield: 122 mg (46%).

Received: January 2, 1997 [Z9955IE]
German version: *Angew. Chem.* **1997**, *109*, 1367–1370

Keywords: azo compounds · cyclodextrins · cyclophanes · rotaxanes · supramolecular chemistry

[1] H. Zollinger, *Color Chemistry*, 2nd ed., VCH, Weinheim, **1991**.
[2] a) N. Yoshida, *J. Chem. Soc. Perkin Trans. 2* **1995**, 2249–2256; b) P. Bortolus, S. Monti, *J. Phys. Chem.* **1987**, *91*, 5046–5050; c) A. M. Sanchez, R. H. de Rossi, *J. Org. Chem.* **1996**, *61*, 3446–3451; d) M. Suzuki, H. Takai, K. Tanaka, K. Narita, H. Fujiwara, H. Ohmori, *Carbohydrate Res.* **1996**, *288*, 75–84; e) J. H. Jung, C. Takehisa, Y. Sakata, T. Kaneda, *Chem. Lett.* **1996**, 147–148; f) H. Hirai, N. Toshima, S. Uenoyama, *Bull. Chem. Soc. Jpn.* **1985**, *58*, 1156–1164.
[3] Cram et al. and Gokel et al. unsuccessfully attempted to prepare azo-dye rotaxanes from crown ether/diazonium salt complexes: G. W. Gokel, D. J. Cram, *J. Chem. Soc. Chem. Commun.* **1973**, 481–482; J. R. Beadle, D. M. Dishong, R. K. Khanna, G. W. Gokel, *Tetrahedron* **1984**, *40*, 3935–3944.
[4] Hydrophobic binding has been used to prepare rotaxanes: a) S. Anderson, H. L. Anderson, *Angew. Chem.* **1996**, *108*, 2075–2078; *Angew. Chem. Int. Ed. Engl.* **1996**, *35*, 1956–1959; b) G. Wenz, *ibid.* **1994**, *106*, 851–870 and **1994**, *33*, 803–822; c) A. Harada, J. Li, M. Kamachi, *J. Am. Chem. Soc.* **1994**, *116*, 3192–3196; *Nature* **1992**, *356*, 325–327; d) M. Kunitake, K. Kotoo, O. Manabe, T. Muramatsu, N. Nakashima, *Chem. Lett.* **1993**, 1033–1036; e) G. Wenz, B. Keller, *Angew. Chem.* **1992**, *104*, 201–204; *Angew. Chem. Int. Ed. Engl.* **1992**, *31*, 197–199; f) R. S. Wylie, D. H. Macartney, *J. Am. Chem. Soc.* **1992**, *114*, 3136–3138; g) R. Isnin, A. E. Kaifer, *ibid.* **1991**, *113*, 8188–8190; h) H. Ogino, *ibid.* **1981**, *103*, 1303–1304.
[5] Negative-ion ESI-MS measurements were carried out on a VG-Bio Q instrument. We are grateful to Dr R. T. Aplin for recording these mass spectra.
[6] J. Stonehouse, P. Adell, J. Keeler, A. J. Shaka, *J. Am. Chem. Soc.* **1994**, *116*, 6037–6038; K. Stott, J. Stonehouse, J. Keeler, T.-L. Hwang, A. J. Shaka, *ibid.* **1995**, *117*, 4199–4200. The selective DPFGSE sequence made use of a 180° Gaussian pulse of 40 or 80 ms duration and 1 ms gradient of 5:5:8:8 Gcm^{-1}. Mixing times of up to 200 ms were used, and all observed NOEs were negative.

[7] Cyclophane **3c** was synthesized according to Diederich et al.: S. B. Ferguson, E. M. Sanford, E. M. Seward, F. Diederich, *J. Am. Chem. Soc.* **1991**, *113*, 5410–5419.

[8] Aggregation constants were determined by ^{1}H NMR spectroscopy in D_2O at 298 K in the concentration range 10^{-2}–10^{-5} M.

[9] Several photochemically interesting rotaxanes have been investigated: a) D. B. Amabilino, P. R. Ashton, V. Balzani, C. L. Brown, A. Credi, J. M. J. Fréchet, J. W. Leon, F. M. Raymo, N. Spencer, J. F. Stoddart, M. Venturi, *J. Am. Chem. Soc.* **1996**, *118*, 12012–12020; b) N. Solladié, J.-C. Chambron, C. O. Dietrich-Buchecker, J.-P. Sauvage, *Angew. Chem.* **1996**, *108*, 957–960; *Angew. Chem. Int. Ed. Engl.* **1996**, *35*, 906–909; c) A. C. Benniston, A. Harriman, V. M. Lynch, *J. Am. Chem. Soc.* **1995**, *117*, 5275–5291; d) J.-C. Chambron, A. Harriman, V. Heitz, J.-P. Sauvage, *ibid.* **1993**, *115*, 6109–6114; e) P. L. Anelli, P. R. Ashton, R. Ballardini, V. Balzani, M. Delgado, M. T. Gandolfi, T. T. Goodnow, A. E. Kaifer, D. Philp, M. Pietraszkiewicz, L. Prodi, M. V. Reddington, A. M. Z. Slawin, N. Spencer, J. F. Stoddart, C. Vicent, D. J. Williams, *ibid.* **1992**, *114*, 193–218.

Friedel–Crafts β-Silylvinylations**

Masahiko Yamaguchi,* Yoshiyuki Kido, Akio Hayashi, and Masahiro Hirama

The Friedel–Crafts reaction is a fundamental method for converting aromatic C–H bonds to C–C bonds. Although Friedel–Crafts alkylations and acylations are often used in organic synthesis, the corresponding vinylations have not been successful. Attempts at vinylation using either ethyne or vinyl halides have given polymeric substances and 1,1-diarylethanes, even when the arenes are present in large excess.[1] This is due to the instability of the vinylated products under the reaction conditions. Even 2-propenylations gave very low yields, and formed various by-products.[2] Low efficiency in generating the electrophilic species may be another reason why the electrophilic vinylations failed. We report here the Friedel–Crafts (*E*)-β-silylvinylation of aromatic hydrocarbons promoted by $GaCl_3$. This reaction is a direct C_2-olefination of arenes[3] that proceeds via novel organogallium intermediates.

An aromatic hydrocarbon (1 equiv) and trimethylsilylacetylene (3 equiv) were treated with $GaCl_3$ (3 equiv) in a mixture of methylene chloride and methylcyclohexane at −78 °C. After 30 min, methyllithium (9 equiv) in ether was added, and the (*E*)-[(β-trimethylsilyl)vinyl]arene was obtained by aqueous workup (Scheme 1). The C–C bond was formed at the β-carbon atom of the silylacetylene, and the (*E*)-configuration of the product was determined by ^{1}H NMR spectroscopy. When only one equivalent of silylacetylene and $GaCl_3$ were used the yield was much lower. The regioselectivity of the aromatic substitution indicates an electrophilic mechanism,[4] and is consistent with the low reactivity of chlorobenzene, which can be used as solvent. Steric factors are also important. For example, 2,6-dimethylnaphthalene reacted at C-4 rather than at the most reactive position (C-1), and a considerable amount of 2-vinylated product was obtained from naphthalene. The electrophilic species involved in this reaction appears to be considerably

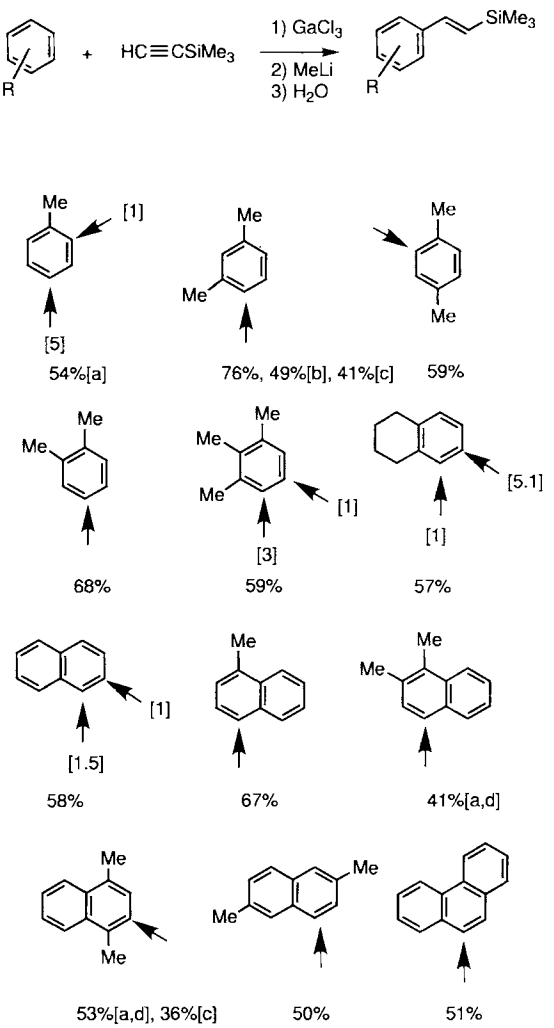

Scheme 1. $GaCl_3$-promoted β-silylvinylations of arenes. The reaction sites on the starting materials are marked with arrows; the relative regioselectivity in each case is given in square brackets. [a] Yield determined by gas chromatography. [b] Reaction in chlorobenzene. [c] Molar ratio $GaCl_3$:acetylene:arene = 1.0:1.0:1.0. [d] Molar ratio $GaCl_3$:acetylene:arene = 2.0:2.0:1.0.

bulky. Unlike previously reported Friedel–Crafts vinylations and alkenylations,[1, 2] this reaction does not require excess arene. Therefore, nonvolatile polycyclic arenes can be β-silylvinylated without the necessity to carry out the tedious separation of a large amount of unconverted starting materials. There was very little divinylation and isomer formation under the present reaction conditions. Triethylsilyl- and *tert*-butyldimethylsilylacetylene reacted analogously with *m*-xylene to give the corresponding products in yields of 54 and 52%, respectively. When 1-methylnaphthalene was treated with $GaCl_3$ and ethyne at −78 °C, the arene was consumed within 30 min to give a polymeric compound. Thus, the silyl group prevents the olefin group on the products from undergoing side reactions.

The (β-silylvinyl)arenes are useful synthetic intermediates for a variety of aromatic compounds (Scheme 2). For example, the trimethylsilyl group can be removed by trifluoroacetic acid to give the parent vinylarene, and epoxidation followed by treatment with an acid gives an arylacetaldehyde,[5] which can be reduced to an arylethanol.

The use of $GaCl_3$[6] in these β-silylvinylations is critical; other Lewis acids ($AlCl_3$, $GaBr_3$, $InCl_3$, $SnCl_4$, $SbCl_5$, SbF_5), protic acids (CF_3SO_3H, HCl), and heterogeneous acids (Na-Mont-

[*] Prof. Dr. M. Yamaguchi, Y. Kido
Faculty of Pharmaceutical Sciences, Tohoku University
Aoba, Sendai 980-77 (Japan)
Fax: Int. code +(22)217-6811
Dr. A. Hayashi, Prof. Dr. M. Hirama
Department of Chemistry, Graduate School of Science
Tohoku University, Sendai (Japan)

[**] This work was supported by a Grant-in-Aid for Scientific Research from the Ministry of Education, Science, Sports and Culture, Japan (no. 07554065 and 08404050). We also thank the Shin-Etsu Chemicals Co. Ltd for the generous gifts of silicon reagents.

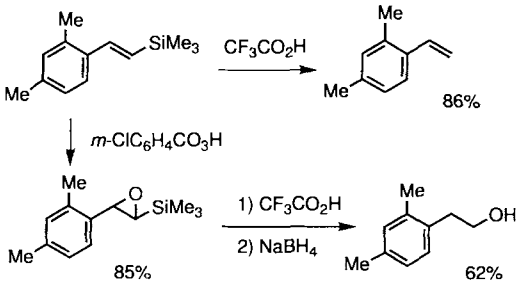

Scheme 2. Examples of reactions of (β-silylvinyl)arenes.

morillonite, Sn-Montmorillonite, Montmorillonite K10) were not effective. Methylene chloride and chlorobenzene are the preferred solvents, since they dissolve arenes at low temperatures. The methyllithium added prior to the aqueous quench can be replaced by methylmagnesium bromide or diethylzinc. However, the yields vary substantially with subtle changes in the workup procedures if the treatment with the organometallic compound is omitted. When D_2O was added after methyllithium, the (β-silylvinyl)arene was deuterated at the olefinic β-carbon atom (Scheme 3). Such deuteration did not take place when

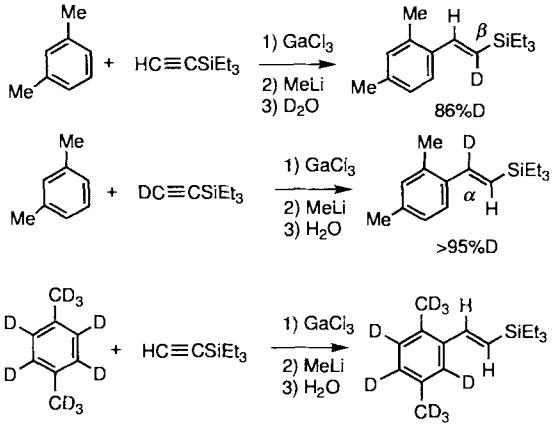

Scheme 3. $GaCl_3$-promoted β-silylvinylations of arenes with deuterated starting materials or reagents.

the olefinic product was treated with methyllithium followed by D_2O either in the presence or in the absence of $GaCl_3$. These observations can be explained by formation of a (β-gallio-β-silylvinyl)arene. Methyllithium probably converts the $GaCl_n$ group to a $GaMe_n$ group, which facilitates the protonation of the organogallium intermediate. When a deuterated silylacetylene was used, the α-carbon atom was deuterated. The olefin group was not deuterated with [D_{10}]*p*-xylene as substrate.

The high reactivity of the electrophilic vinylating reagent is clearly evident from the rapid reaction at a low temperature without the use of excess arenes. We assume that a $GaCl_3$-complexed silylacetylene is formed. The formation of a vinyl cation by protonation of the silylacetylene with $HGaCl_4$ does not explain the results of the deuteration experiments. Furthermore, the addition of 2,6-di(*tert*-butyl)-4-methylpyridine (0.3 equiv) did not interfere with the reaction. Therefore, the mechanism may be summarized as followed (Scheme 4): The activated silylacetylene, presumably either the open vinyl cation **A** or the bridged cation **B**, is attacked by *m*-xylene at the β-carbon atom. The resulting organogallium intermediate, the β-gallio-(β-silylvinyl)arenium cation **C** or the (β-gallio-β-silylvinyl)arene **D**,

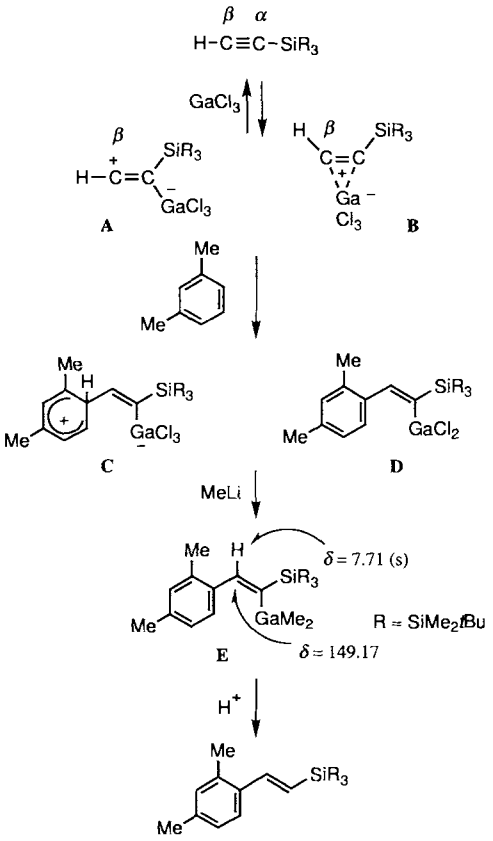

Scheme 4. Proposed mechanism of the $GaCl_3$-promoted β-silylvinylation of *m*-xylene.

is then methylated, and the (β-silylvinyl)arene is obtained by protonation. The intermediate **E** was detected by NMR spectroscopy ([D_8]THF): the olefin proton appeared as a singlet at $\delta = 7.71$, which disappeared on the addition of water. Its (*Z*)-configuration was deduced by NOE studies.

$GaCl_3$ promotes alkenylation as well as β-silylvinylation. For instance, when *tert*-butylacetylene was treated with *m*-xylene and $GaCl_3$ followed by methyllithium and D_2O, a β-deuterated α-(*tert*-butyl)styrene derivative was obtained (Scheme 5). Since

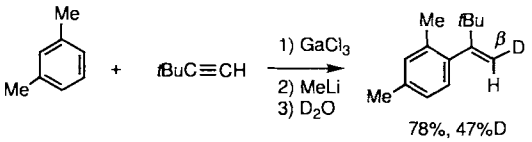

Scheme 5. $GaCl_3$-promoted alkenylation of *m*-xylene with *tert*-butylacetylene.

the reaction with [D_{10}]*p*-xylene did not lead to deuteration of the olefin moiety, the mechanism of the alkenylation must be similar to that of the β-silylvinylation. The regioselectivity can be ascribed to the ability of the substituents to stabilize the cations in the electrophilic intermediates rather than to steric reasons. Stabilization of the β-cation by the silyl group[7] is substantial in the intermediate **A** and **B**, while the *tert*-butyl group stabilizes the α-cation. Notably, *trans*-addition occurred with *tert*-butylacetylene, and *cis*-addition with silylacetylene, although the origin of the stereoselectivity is unclear at present. Vinyl cations stabilized by a β-silicon group have attracted a great deal of interest over the last few years.[8] However, their reactivity, particularly C–C bond-forming reactions, has received little atten-

 © VCH Verlagsgesellschaft mbH, D-69451 Weinheim, 1997 0570-0833/97/3612-1314 $ 17.50+.50/0

tion because of the very rapid desilylation to give acetylenic compounds. The electrophilic activation of silylacetylenes generally results in substitution.[7] It is therefore notable that the formation of a C–C bond at the β-silicon-stabilized vinyl cation can take place giving addition products. Thus, the chemistry of this extremely reactive electrophilic vinylating reagent promises to be very interesting.

In summary $GaCl_3$ promotes the C_2-olefination of aromatic hydrocarbons with silylacetylene via novel organogallium intermediates. Organogallium compounds have received much less attention in organic synthesis than organoaluminum compounds,[9] although both contain an element from group 13. Thus, the strong activation of π compounds by $GaCl_3$ is a new very promising approach to organogallium chemistry.

Experimental Section

Under an argon atmosphere, a 1.0 M stock solution of $GaCl_3$ in methylcyclohexane (3.0 mL) was added to a solution of *m*-xylene (107 mg, 1.0 mmol) in CH_2Cl_2 (10 mL) at −78 °C. Trimethylsilylacetylene (295 mg, 3.0 mmol) in methylcyclohexane (1.0 mL) was then added, and the mixture was stirred for 30 min. Methyllithium (1.4 M solution in diethyl ether, 6.5 mL) was added, and the mixture was stirred for another 30 min at −78 °C. Aqueous workup gave (*E*)-1-(2-trimethylsilylethenyl)-2,4-dimethylbenzene (155 mg, 76%).

Received: November 11, 1996
Revised version: February 17, 1997 [Z9752IE]
German version: *Angew. Chem.* **1997**, *109*, 1370–1372

Keywords: Friedel–Crafts reactions · gallium · silicon

[1] R. Anschütz, *Ann. Chem.* **1886**, *235*, 150, 299; O. W. Cook, V. J. Chambers, *J. Am. Chem. Soc.* **1921**, *43*, 334; J. S. Reichert, J. A. Nieuwland, *ibid.* **1923**, *45*, 3090; J. A. Reilly, J. A. Nieuwland, *ibid.* **1928**, *50*, 2564; I. P. Tsukervanik, K. Y. Yuldashev, *J. Gen. Chem. USSR* **1961**, *31*, 790.

[2] I. P. Tsukervanik, K. Y. Yuldashev, *J. Gen. Chem. USSR* **1963**, *33*, 3429; A. G. Martinez, R. M. Alvarez, A. G. Fraile, M. Hanack, L. R. Subramanian, *Chem. Ber.* **1987**, *120*, 1255.

[3] We recently reported the direct vinylation reaction of phenols: M. Yamaguchi, A. Hayashi, M. Hirama, *J. Am. Chem. Soc.* **1995**, *117*, 1151.

[4] See for example: C. C. Price, *Org. React.* **1946**, *3*, 1; E. Berliner, *ibid.* **1949**, *5*, 229; J. B. Kim, C. Chen, J. K. Krieger, K. R. Judd, C. C. Simpson, E. Berliner, *J. Am. Chem. Soc.* **1970**, *92*, 910.

[5] G. Stork, E. Colvin, *J. Am. Chem. Soc.* **1971**, *93*, 2080.

[6] $GaCl_3$ has been used in some Friedel–Crafts alkylations: F. P. Dehaan, H. C. Brown, *J. Am. Chem. Soc.* **1969**, *91*, 4844; F. P. Dehaan, H. C. Brown, J. C. Hill, *ibid.* **1969**, *91*, 4850.

[7] See for example: "Activating and directive effects of silicon": A. R. Bassindale, P. G. Taylor in *The Chemistry of Organic Silicon Compounds* (Eds.: S. Patai, Z. Rappoport), **1989**, Wiley, chapter 14, p. 893.

[8] H.-U. Siehl, F.-P. Kaufmann, Y. Apeloig, V. Braude, D. Danovich, A. Berndt, N. Stamatis, *Angew. Chem.* **1991**, *103*, 1546; *Angew. Chem. Int. Ed. Engl.* **1991**, *30*, 1479; G. K. S. Prakash, V. P. Reddy, G. Rasul, J. Casanova, G. A. Olah, *J. Am. Chem. Soc.* **1992**, *114*, 3076; C. Dallaire, M. A. Brook, *Organometallics* **1993**, *12*, 2332; V. Gabelica, A. J. Kresge, *J. Am. Chem. Soc.* **1996**, *118*, 3838, and references therein.

[9] J. J. Eisch, *J. Am. Chem. Soc.* **1962**, *84*, 3830.

Liquid-Crystal Templates for Nanostructured Metals**

George S. Attard,* Christine G. Göltner,* Judith M. Corker, Susanne Henke, and Richard H. Templer

A rapidly developing new trend in materials science is the transfer of structure from surfactant aggregates to inorganic solids.[1–3] In water, surfactants aggregate into micelles or, at higher concentrations, into lyotropic liquid-crystalline phases. Despite their beauty, lyotropic mesophases have so far not been utilized for their structure, but only for their properties (for example in shampoos), because these ordered aggregates readily undergo phase changes as a result of dynamic exchange processes.

Surfactant aggregates are, however, useful templates for the synthesis of inorganic nanostructures. For example, the synthesis of ordered mesoporous ceramic oxides involves the use of ionic surfactants as structure-directing additives in precipitation processes.[4] A more recent approach to mesoporous ceramic oxides makes use of lyotropic liquid crystals as structure-directing bulk media.[5] Here the sol–gel synthesis of inorganic ceramic oxides (for example silicates) is conducted in the aqueous domains of the microphase-separated medium; hence a cast of the liquid-crystalline phase is produced. In this way, different nanostructures have been obtained from the H_I, Ia3d, and L_x mesophase.[6] The generation of nanostructures from bulk lyotropic mesophases is not restricted to sol–gel processes such as the production of silicates; precipitation processes can also be carried out without loss of long-range order.[7] Pileni et al. have reported the generation of metal nanoparticles in surfactant solutions or lamellar lyotropic liquid crystals. Here metal particles are produced with a high degree of control over shape and size,[8] but the particle morphology cannot be correlated with the ordered structure of the liquid-crystalline phase.

Our aim was to apply the bulk liquid-crystal template method to the generation of ordered, porous metal nanostructures and to show that lyotropic liquid crystalline phases are versatile media for nanostructure design. A mesoporous metal can be expected to have advantages over classical metal colloids with respect to stability and handling. In particular we show that the reduction of platinum salts dissolved within the aqueous domains of a hexagonal (H_I) mesophase leads to platinum whose nanostructure is a cast of the liquid-crystalline phase architecture.

We employed hexachloroplatinic acid (HCPA) and ammonium tetrachloroplatinate (ATCP) as the platinum source. The lyotropic liquid-crystalline phases were prepared from $C_{16}(EO)_8$ (octaethyleneglycol monohexadecyl ether), because

[*] Dr. G. S. Attard, Dr. J. M. Corker
Department of Chemistry
University of Southampton
Southampton SO17 1BJ (UK)
Fax: Int. code +(1703)593781
e-mail: gza@soton.ac.uk

Dr. C. G. Göltner, Dipl.-Chem. S. Henke
Max-Planck-Institut für Kolloide und Grenzflächen
Kantstrasse 55, D-14513 Teltow (Germany)
Fax: Int. code +(3328)46204
e-mail: goeltner@mpikg-teltow.mpg.de

Dr. R. H. Templer
Department of Chemistry, Imperial College
London SW7 2AZ (UK)

[**] We are indebted to the Director of the Daresbury Laboratory for access to facilities. We also thank Dr. E. Schaaf for carrying out the TGA measurements. This work was supported by the UK Engineering and Physical Sciences Research Council.

this surfactant forms a wide hexagonal mesophase that is stable at room temperature.[9] The liquid-crystalline nature of the ternary mixtures of platinum salt, surfactant, and water was confirmed by polarized-light optical microscopy. HCPA was reduced by adding large pieces (>3 mm) of less noble metals (Fe, Zn, Mg) and allowing the mixture to stand at room temperature for 24 h, after which the mixture had become black. ATCP was reduced by bringing a ternary mixture of surfactant, water, and hydrazine hydrate (mixture A) into contact with a ternary system containing the metal salt (mixture B). Optical microscopy revealed that both mixtures A and B were hexagonal mesophases when brought into contact. Immediate reaction caused the system to turn black. To obtain platinum free from reagents (platinum salts, surfactant, and reducing agent), the solid products of the reaction were treated successively with acetone, water, 6 M hydrochloric acid, water, and acetone. Thermogravimetric analysis (TGA) of the resulting metal powders revealed that virtually all the surfactant could be removed by extraction, as a weight loss of 2% only was detected up to to 600 °C (in air). Scanning electron microscopy (SEM; see Figure 1, top) of the dried powder showed that the product comprised particles 90–500 nm in diameter.

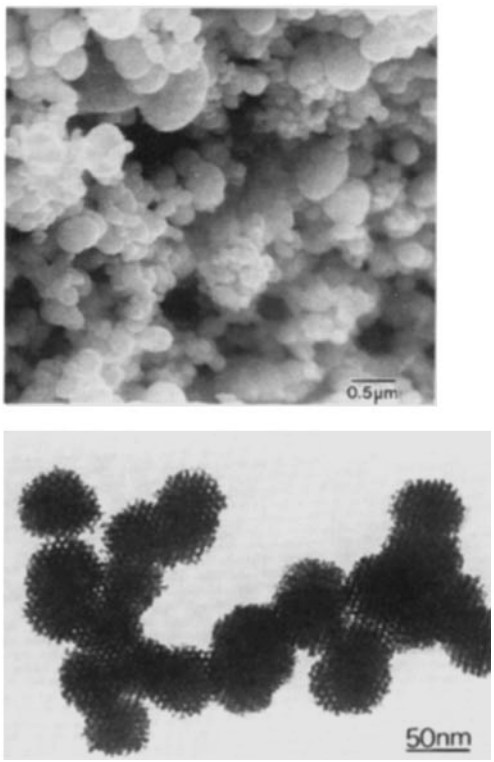

Figure 1. SEM image of a washed sample of mesoporous platinum (top) and TEM image of H_I-platinum (bottom). The material was suspended in acetone, sonicated for 5 min and applied to a carbon-coated copper grid.

Transmission electron microscopy (TEM; see Figure 1, bottom) revealed that these particles (termed H_I-Pt) have a hexagonal nanostructure consisting of cylindrical (30 Å diameter) pores separated by platinum walls 30 Å thick, with an average pore-to-pore distance of 60 Å. TEM studies of ultramicrotomed samples confirmed that this internal nanostructure was also present in larger particles. The wall thickness of the nanostructured metal H_I-Pt appears to be larger than that of the corresponding H_I-silica (where it is typically 12 Å).

X-ray diffractograms (Figure 2) of H_I-Pt show only one diffraction peak in the small-angle region, with a lattice parameter

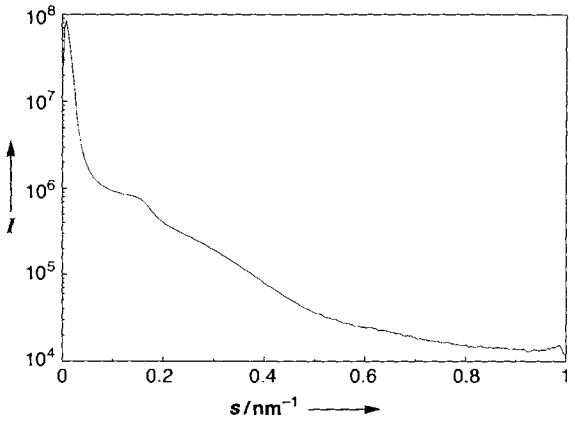

Figure 2. Small-angle X-ray diffractogram of H_I-platinum I = intensity (arbitrary units).

of 65 Å, which is in good agreement with the TEM results. The low-angle scattering and broadening of the diffraction peak indicates a degree of disorder, which is borne out by the TEM image. The presence of only one scattering peak in the diffractogram is probably due to a low degree of long-range order, which could be caused by nonuniform wall thickness. Wide-angle X-ray diffractograms showed the material to be polycrystalline with a face-centered cubic (fcc) structure.

The extended X-ray absorption fine structure (EXAFS[10]) data obtained for the platinum L_{III} edge of the nanostructured material (see Figure 3) are entirely consistent with the presence of pure platinum metal. Backscattering shells due to platinum are observed out to about 5.5 Å in the Fourier transform of the spectrum.

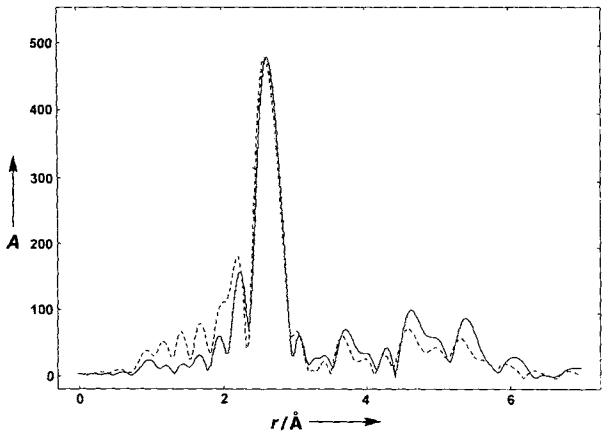

Figure 3. Comparison of the Fourier transforms of the L_{III} edge EXAFS for platinum foil (solid) and H_I-platinum. For clarity, the amplitude of the curve for platinum foil has been scaled down by a factor of 2.8. A = amplitude [13].

The absence of oxygen backscattering shells rules out the presence of platinum oxide. The best fit to the EXAFS data was achieved with four shells of platinum atoms at 2.75, 3.89, 4.79, and 5.47 Å (Table 1). These distances compare well with those observed for bulk platinum metal. Furthermore, the coordination numbers of 7, 3, 13, and 7 for the four shells indicate an fcc structure, which is in good agreement with the wide-angle X-ray diffraction results. The Fourier transforms of the EXAFS spectrum[11] for platinum foil and the nanostructured metal are almost identical, although a significantly lower amplitude is observed in the latter spectrum. The lower amplitude and the

 © VCH Verlagsgesellschaft mbH, D-69451 Weinheim, 1997 0570-0833/97/3612-1316 $ 17.50+.50/0

Table 1. Structural parameters for H_I-platinum and platinum foil. CN = coordination number.

	Shell	CN	Dist. R [Å]	$2\sigma^2$ [Å^2]	R factor [%]
H_I-Pt	Pt	7.0(1)	2.749(1)	0.0126(1)	24.2
	Pt	2.9(3)	3.893(6)	0.0177(9)	
	Pt	13.3(8)	4.795(4)	0.0220(7)	
	Pt	7.3(7)	5.466(5)	0.026(1)	
Pt foil	Pt	12	2.764(1)	0.0091(1)	22.0
	Pt	6	3.915(3)	0.0125(5)	
	Pt	24	4.808(2)	0.0143(3)	
	Pt	12	5.509(4)	0.0180(6)	

associated decrease in coordination numbers can be attributed to the presence of a high proportion of surface atoms. An additional effect of the larger number of surface atoms is an apparent shortening of the metal–metal bonds relative to those of the bulk metal.

A separate series of experiments employed lower surfactant concentrations in order to demonstrate that the structure of nanostructured H_I-Pt is a result of the liquid-crystalline phase acting as a template. Treating micellar solutions of $C_{16}(EO)_8$ [or cetyltrimethylammonium bromide (CTAB) as a cationic surfactant] and HCPA with iron as described above gave dense, unstructured particles. These results confirm that the template mechanism responsible for formation of M41S at low surfactant concentrations does not operate here.

The preparation of H_I-Pt is strongly dependent on the reducing agent. Hydrogenation (25 bar, 12 h) afforded only dendritic crystals, as revealed by TEM. Hydrogenation of the platinum salt is slower than reduction with iron or hydrazine and therefore allows the liquid-crystalline phase to reorganize, and large crystals to grow.

However, the confinement of the polar metal salt within the aqueous domains of the lyotropic phase does not imply that the same liquid-crystal template mechanism that is observed for the production of siliceous ceramic oxides[1,2] is responsible for the development of the metal nanostructure. The primary product of the reduction, a cluster of platinum(0) atoms, cannot be stabilized by the liquid-crystalline environment in the same way as the oligomeric silicic acid precursor of silica, which is able to undergo hydrogen bonding. Furthermore, a large reduction in the product's volume relative to that of the low-density (with respect to Pt) precursor ion, has to be accounted for. This is also the reason why no monolithic material is formed during the reduction. As the lyotropic phase nevertheless acts as a structure-directing medium, it seems reasonable to assume that the metal is stabilized at the interface between the hydrophobic and the hydrophilic domains of the microphase-separated environment. Reduction of the platinum salt affords small colloidal primary particles at this interface. Subsequently, these primary particles agglomerate and coalesce, until a wall thickness is reached at which the structure is mechanically stable. The proposed mechanism can also explain why only fast reduction is able to generate a metal nanostructure; only then can the nanostructure be generated before the LC phase is able to rearrange. Metal nanoparticles stabilized at this interface in micellar block copolymer solutions have been observed before.[13]

Our experiments demonstrate that lyotropic liquid-crystalline phases provide versatile reaction media for the synthesis of nanostructured mesoporous platinum. The inherent nanostructure of the porous material provides a high surface area, which is advantageous for catalytic applications. The large absolute particle size (relative to classical metal colloids) might allow for greater ease of catalyst without compromising the surface area. The combination of high surface area with a tailored nanoarchitecture consisting of regular pores and a continuous electron-conduction pathway would be expected to be advantageous in fuel cells, batteries, or sensors, whose performance is determined by mass transport and interfacial processes.

Received: October 17, 1996 [Z9662IE]
German version: *Angew. Chem.* **1997**, *109*, 1372–1374

Keywords: mesoporosity · nanostructures · platinum · template synthesis

[1] P. Behrens, *Adv. Mater.* **1993**, *5*, 127.
[2] D. Antonelli, J. Ying, *Curr. Opin. Colloid Surf. Sci.* **1996**, *1*, 523.
[3] C. G. Göltner, M. Antonietti, *Adv. Mater.* **1997**, *9*, 431.
[4] a) C. T. Kresge, M. E. Leonowicz, W. J. Roth, J. C. Vartuli, J. S. Beck, *Nature* **1992**, *359*, 710–712; b) J. S. Beck, J. C. Vartuli, W. J. Roth, M. E. Leonowicz, C. T. Kresge, K. D. Schmitt; C. T. W. Chu, D. H. Olson, E. W. Sheppard, S. B. McCullen, J. B. Higgins, J. L. Schlenker, *J. Am. Chem. Soc.* **1992**, *114*, 10834–10843; c) Q. Huo, D. I. Margolese, U. Ciesla, P. Feng, T. E. Gier, P. Sieger, R. Leon, P. M. Petroff, F. Schüth, G. D. Stucky, *Nature* **1994**, *368*, 317–320; d) C.-F. Cheng, Z. Luan, J. Klinowski, *Langmuir* **1995**, *11*, 2815–2819; e) J. Liu, A. Y. Kim, J. W. Virden, B. C. Bunker, *ibid.* **1995**, *11*, 689–692.
[5] G. S. Attard, J. C. Glyde, C. G. Göltner, *Nature* **1995**, *378*, 366–368.
[6] G. S. Attard, M. Edgar, C. G. Göltner, *Acta Mater.*, in press.
[7] P. V. Braun, P. Osenar, S. I. Stupp, *Nature* **1996**, *380*, 325–328.
[8] J. Tanori, N. Duxin, C. Petit, I. Lisiecki, P. Veillet, M. P. Pileni, *Colloid Polym. Sci.* **1995**, *273*, 886–892.
[9] D. J. Mitchell, G. J. Tiddy, L. Waring, T. Bostock, M. P. McDonald, *J. Chem. Soc. Faraday Trans.* **1983**, *79*, 975–1000.
[10] The X-ray absorption spectra were recorded on Station 9.2 of the Synchrotron Radiation Source at the Daresbury Laboratory (operating at 2 GeV with an average current of ca. 180 mA, equipped with a Si(220) order-sorting monochromator. H_I-Pt samples were mixed with boron nitride prior to EXAFS measurements to ensure a suitable edge jump of between 1 and 3. Spectra were acquired at room temperature in transmission by using thin aluminum cells equipped with Kapton windows.
[11] Background-subtracted EXAFS data were obtained by using the program PAXAS (N. Binsted, PAXAS—*p*rogramme for the analysis of *X*-ray *a*bsorption *s*pectra, University of Southampton). A second-order polynomial was used in the pre-edge background subtraction, and the post-edge background was subtracted by fitting this region with coupled polynomials of the order 7 or 8 to remove low-frequency contributions.
[12] G. S. Attard, M. Edgar, J. W. Emsley, C. G. Göltner, *Mater. Res. Soc. Symp. Proc.* **1996**, *425*, 179.
[13] M. Antonietti, L. Bronstein, O. Platonova, unpublished.

Asymmetric Aziridination over Ylides: Highly Stereoselective Synthesis of Acetylenyl-*N*-sulfonylaziridines**

An-Hu Li, Yong-Gui Zhou, Li-Xin Dai,* Xue-Long Hou, Li-Jun Xia, and Lin Lin

Although chiral aziridines have found numerous applications in the synthesis of many kinds of biologically important substances,[1] development of simple but efficient methods for preparing them, especially the functionalized aziridines, is still a

[*] Prof. L.-X. Dai, Dr. A.-H. Li, Y.-G. Zhou, Dr. X.-L. Hou
Laboratory of Organometallic Chemistry
Shanghai Institute of Organic Chemistry
Chinese Academy of Sciences
354 Fenglin Lu, Shanghai 200032 (China)
Fax: Int. code +(21)64166128
e-mail: dailx@pub.sioc.ac.cn
Prof. L.-J. Xia, L. Lin
The Analytic Chemistry Department
Shanghai Institute of Organic Chemistry
Chinese Academy of Sciences, Shanghai

[**] Financial support from the National Natural Foundation of China and Chinese Academy of Sciences is gratefully acknowledged.

great challenge. By retrosynthetic analysis, there are two direct pathways for constructing the nitrogen-containing three-membered ring: reaction of a nitrene with a prochiral C=C bond[2-4] and of a carbene (or its equivalent carbanion or ylide) with a prochiral C=N bond.[5-7] In contrast to the extensively studied and overwhelmingly successful asymmetric epoxidation[8] and asymmetric cyclopropanation,[9] asymmetric aziridination is much less explored. Most examples appeared in the 1990s.[10] Evans et al.[2a] and Jacobsen et al.[2b] reported two excellent asymmetric aziridinations of a prochiral C=C bond with a nitrene in the presence of a chiral catalyst. Due to the intrinsic high reactivity of nitrenes, no aliphatic substrate was used in these reactions.[11] By the other route, Jacobsen et al.[5] realized the first asymmetric aziridination of a prochiral C=N bond with a carbene, and obtained a *cis/trans* mixture of chiral aziridines in low yields and moderate *ee* values. A substrate-controlled asymmetric aza-Darzens reaction with good *de* values was reported by Davis et al.[6a]. Very recently, Aggarwal et al.[12] disclosed an efficient, asymmetric benzylidene transfer to a prochiral C=N bond by a catalytic ylide aziridination. Optically active aziridines were also prepared by methylene transfer from $Me_2S^+CH_2^-$ or $Me_2S(O)^+CH_2^-$ to chiral sulfinimines.[6c-e] We found that the ylide pathway provides very efficient entry to vinylaziridines[13] and chiral epoxides.[14] For vinylaziridines, a mixture of *cis/trans* isomers was always obtained. After numerous investigations, exclusive *cis* selectivity was achieved by the reaction of *N*-sulfonylimines with propargylic sulfonium ylides under phase-transfer conditions. This may be explained by an intermediate formed by the [2+2] cycloaddition of the imine and the ylide (Scheme 1). This is similar to the epoxidation reaction of carbonyl compounds with propargylic telluronium ylides.[15] The high stereoselectivity enables as to realize a reagent-controlled asymmetric aziridination by a ylide route. We here disclose the preliminary results for preparing optically active acetylenylaziridines **1** in high yields and moderate to high *ee* values (Scheme 2).

Several results from the reaction of *N*-sulfonylimines **2** and sulfonium ylides—produced in situ from chiral sulfonium salts **3**, **4**, or **5**—under solid–liquid phase-transfer conditions are summarized in Table 1. This reaction proceeds smoothly with various kinds of substrates, including aryl- and heteroarylaldimines (reactions 4, 10, and 13), α,β-unsaturated

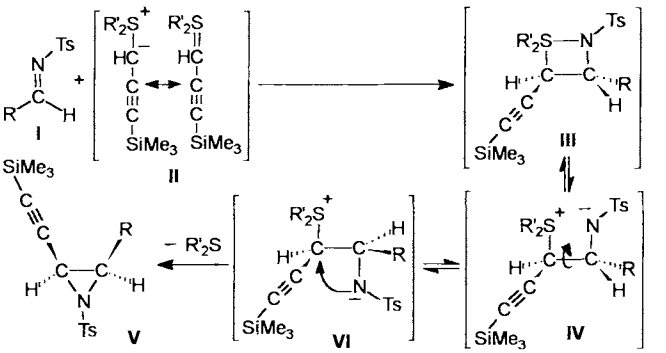

Scheme 1. Mechanism of the aziridination with propargylic sulfonium ylides. The [2+2] cycloaddition (**II** → **III**) is the rate-determining step. Due to steric hindrance, only the *trans* product forms.

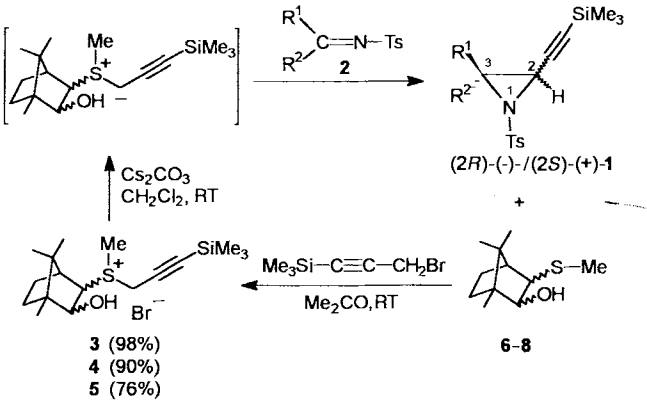

Scheme 2. Asymmetric aziridination with chiral sulfonium propargylides (yields are given in parentheses). Compounds **6**–**8** were retrieved after the reaction; **3**, **6** *exo*-S, *exo*-OH; **4**, **7** *endo*-S, *endo*-OH; **5**, **8** *endo*-S, *exo*-OH.

aldimines (reaction 5), aliphatic aldimines (reactions 6, 7, 11, and 14), and even relatively unreactive ketimine (reaction 8). It is especially noteworthy that aziridination succeeded in aliphatic aldimine and ketimine systems, which is not possible with the nitrene or carbene methods (see above).

There is one example of a chiral, sulfide-catalyzed asymmetric ylide aziridination.[12] Although it gives high *ee* values and pro-

Table 1. Synthesis of chiral **1** by asymmetric aziridination of *N*-sulfonylimines **2** with sulfonium salts **3**, **4**, and **5**—derived from D-(+)-camphor—under phase-transfer conditions [a].

Reaction	R^1	R^2	Yield [%][b]	*cis/trans*[c]	$[\alpha]_D^{20}$ [°] (acetone)	*ee* [%][d]	Config. at C2[g]
1	phenyl	H	85[h]	>99/1	−17.2 (c = 1.16)	50.5	*R*[f]
2	*p*-acetoxyphenyl	H	87[h]	>99/1	−12.0 (c = 1.20)	50.0	(*R*)
3	*p*-fluorophenyl	H	89[h]	>99/1	−28.4 (c = 1.07)	69.5(96.6[e])	(*R*)
4	3-pyridinyl	H	85[h]	>99/1	−20 (c = 1.35)	77.5(99.1[e])	(*R*)
5	*trans*-PhCH=CH	H	88[h]	>99/1	−13.7 (c = 1.00)	44.3	(*R*)
6	cyclohexyl	H	81[h]	>99/1	−21.1 (c = 0.67)	84.9	(*R*)
7	*tert*-butyl	H	92[h]	>99/1	−23.6 (c = 1.25)	40.8	(*R*)
8	Me	Me	95[h]	–	−79 (c = 1.04)	67.4	(*R*)
9	Phenyl	H	88[i]	>99/1	+8.8 (c = 1.00)	25.7	*S*[f]
10	3-pyridinyl	H	85[i]	>99/1	+13.3 (c = 0.80)	56.3	(*S*)
11	cyclohexyl	H	90[i]	>99/1	+10.6 (c = 0.40)	51.9	(*S*)
12	phenyl	H	89[j]	>99/1	+4.2 (c = 1.10)	14.0	(*S*)
13	3-pyridinyl	H	82[j]	>99/1	+8.8 (c = 0.80)	41.9	(*S*)
14	cyclohexyl	H	89[j]	>99/1	+8.7 (c = 0.50)	39.2	(*S*)

[a] All reactions were carried out with a imine:sulfonium salt:Cs_2CO_3 ratio of 1:1.2:1.2 on a 0.5 mmol scale in CH_2Cl_2 at room temperature. In all cases, chiral sulfides **6**, **7**, or **8** were recovered in >80% yields without loss of optical purity after work-up. [b] Yields of isolated products based on imines. [c] Determined by 300 MHz ^1H NMR analysis and/or HPLC. [d] Determined by chiral HPLC on a Chiralcel OD column or a Chiralpak AD column. [e] The *ee* values refer to those after single recrystallization. [f] Determined for one of the aziridine carbons connected to the acetylenyl group by transforming the product into a compound whose configuration was known: *cis*-2-methoxycarbonyl-3-phenyl-*N*-tosylaziridine [6a]. [g] The configuration in parentheses was estimated by comparison with the corresponding phenyl analog. [h] Salt **3**. [i] Salt **4**. [j] Salt **5**.

 © VCH Verlagsgesellschaft mbH, D-69451 Weinheim, 1997 0570-0833/97/3612-1318 $ 17.50+.50/0

ceeds in a catalytic mode, it requires strict reaction conditions and suffers from low *trans/cis* selectivity ($\approx 3/1$). The present asymmetric aziridination is a stoichiometric reaction but may represent a promising general[16] and practical approach to optically active functionalized aziridines due to its compatibility to a wide range of substrates, high yields, and very mild reaction conditions. Furthermore, the ylide precursors (chiral sulfides) could be easily recovered in higher than 80% yields without loss of optical purity and reused. Though the *ee* value of the product is not very high (maximum 84.9%, reaction 6), it can be efficiently improved by a single recrystallization from *n*-hexane; this may offer a practical utility of these products. For example, the *ee* values of the products from reactions 3 and 4 can be increased from 69.5% to 96.6% and from 77.5% to 99.1% for yields of 58% and 52%, respectively. The opposite asymmetric induction was achieved with sulfonium salts containing *exo*-sulfido groups (**3**, reactions 1-8) to provide (2*R*)-(−)-aziridines and *endo*-sulfido groups[17] (**4** and **5**, reactions 9-14) to provide (2*S*)-(+)-aziridines. Chiral acetylenylaziridines are very difficult to prepare by the two direct approaches based on carbene, nitrene, or aza-Darzens reaction.[18]

Experimental Section

General procedure for aziridination: **2** (0.5 mmol), the chiral sulfonium salt **3**, **4**, or **5** (0.6 mmol), and Cs_2CO_3 (0.6 mmol) were mixed and stirred in CH_2Cl_2 (3 mL, reagent grade, used directly without drying) at room temperature in air. After the reaction was completed (TLC, 2–5 h), the reaction mixture was filtered through a short silica-gel column to remove inorganic salts. The filtrate was concentrated and purified by chromatography on a silica-gel column with petroleum ether(60–90 °C) and ethyl acetate (4:1) as the eluent to give pure (-)- or (+)- *N*-sulfonyl acetylenylaziridines **1**. Chiral sulfides **6**, **7**, or **8** were also recovered (>80% yields).

3, **4**, or **5**: A mixture of a chiral sulfide[14] **6**, **7**, or **8** (2.004 g, 10 mmol) and 3-trimethylsilylpropargyl bromide[19] (2.294 g, 12 mmol) in acetone (3 mL) was stirred at room temperature for 6–48 h. Most of acetone was removed under reduced pressure, and the residue collected by filtration, washed with dry ether (3 × 40 mL), and dried under vacuum at room temperature to give the desired sulfonium salt as a white solid. It was used directly without further purification.

Received: December 16, 1996 [Z 9893 IE]
German version: *Angew. Chem.* **1997**, *109*, 1375–1376

Keywords: asymmetric synthesis · aziridines · sulfur · ylides

[1] a) D. Tanner, *Angew. Chem.* **1994**, *106*, 625; *Angew. Chem. Int. Ed. Engl.* **1994**, *33*, 599; b) *Pure Appl. Chem.* **1993**, *65*, 1319; c) T. Hudlicky, G. Seoane, J. D. Price, K. G. Gadamasetti, *Synlett* **1990**, 433.

[2] a) D. A. Evans, M. M. Faul, M. T. Bilodeau, B. A. Anderson, D. M. Barnes, *J. Am. Chem. Soc.* **1993**, *115*, 5328; b) Z. Li, K. R. Conser, E. N. Jacobsen, *ibid.* **1993**, *115*, 5326.

[3] a) R. S. Atkinson, W. T. Gattrell, A. P. Ayscough, T. M. Raynham, *Chem. Commun.* **1996**, 1935; b) R. S. Atkinson, M. P. Coogan, I. S. T. Lochrie, *Tetrahedron Lett.* **1996**, *37*, 5179; c) J. T. Kapron, B. D. Santarsiero, J. C. Vederas, *J. Chem. Soc. Chem. Commun.* **1993**, 1074; d) J. Aires-de-Sousa, A. M. Lobo, S. Prabhakar, *Tetrahedron Lett.* **1996**, *37*, 3183.

[4] N. Furukawa, T. Yoshimura, M. Ohtsu, T. Akasaka, S. Oae, *Tetrahedron* **1980**, *36*, 73.

[5] K. B. Hansen, N. S. Finney, E. N. Jacobsen, *Angew. Chem.* **1995**, *107*, 750; *Angew. Chem. Int. Ed. Engl.* **1995**, *34*, 676.

[6] a) F. A. Davis, P. Zhou, G. V. Reddy, *J. Org. Chem.* **1994**, *59*, 3243; b) F. A. Davis, H. Liu, G. V. Reddy, *Tetrahedron Lett.* **1996**, *37*, 5473; c) J. L. G. Ruano, I. Fernandez, C. Hamdouchi, *ibid.* **1995**, *36*, 295; d) F. A. Davis, P. Zhou, C.-H. Liang, R. E. Reddy, *Tetrahedron: Asymmetry* **1995**, *6*, 1511; e) J. L. G. Ruano, I. Fernandez, M. D. P. Catalina, A. A. Cruz, *ibid.* **1996**, *7*, 3407.

[7] T. Satoh, T. Sato, T. Oohara, K. Yamakawa, *J. Org. Chem.* **1989**, *54*, 3973.

[8] Asymmetric epoxidation: a) D. Yang, Y.-C. Yip, M.-W. Tang, M.-K. Wong, J.-H. Zheng, K.-K. Cheung, *J. Am. Chem. Soc.* **1996**, *118*, 491; b) V. K. Aggarwal, M. F. Wang, *Chem. Commun.* **1996**, 191; c) Y. Tu, Z.-X. Wang, Y. Shi, *J. Am. Chem. Soc.* **1996**, *118*, 9806.

[9] M. P. Doyle in *Catalytic Asymmetric Synthesis* (Ed.: I. Ojima), VCH, Weinheim, **1993**, p. 63.

[10] Review on asymmetric aziridination: A.-H. Li, L.-X. Dai, *Chemistry (The Chinese Chem. Soc., Taipei)* **1996**, *54*, 157 (Chinese).

[11] Insertion of nitrene into an allylic C–H bond was observed by the reaction with an aliphatic alkene: P. Müller, C. Baud, Y. Jacquier, *Tetrahedron* **1996**, *52*, 1543, and references therein.

[12] V. K. Aggarwal, A. Thompson, R. V. H. Jones, M. C. H. Standen, *J. Org. Chem.* **1996**, *61*, 8368; for a corresponding epoxidation, see V. K. Aggarwal, J. G. Ford, A. Thompson, R. V. H. Jones, M. C. H. Standen, *J. Am. Chem. Soc.* **1996**, *118*, 7004.

[13] a) A.-H. Li, L.-X. Dai, X.-L. Hou, *Chem. Commun.* **1996**, 491; b) *J. Chem. Soc. Perkin Trans. 1* **1996**, 867; c) A.-H. Li, L.-X. Dai, X.-L. Hou, M.-B. Chen, *J. Org. Chem.* **1996**, *61*, 4641; d) A.-H. Li, L.-X. Dai, X.-L. Hou, *J. Chem. Soc. Perkin Trans. 1* **1996**, 2725.

[14] A.-H. Li, L.-X. Dai, X.-L. Hou, Y.-Z. Huang, F.-W. Li, *J. Org. Chem.* **1996**, *61*, 489.

[15] Z.-L. Zhou, Y.-Z. Huang, L.-L. Shi, J. Hu, *J. Org. Chem.* **1992**, *57*, 6598.

[16] We have shown that *N*-sulfonylimine-based aziridination is applicable to either semistable (including allylic, propargylic, and benzylic), reactive (simple alkyl ylides), and stabilized ylides (substituted with electron-withdrawing groups). Other reactive imines and activation methods of common imines also undergo this aziridination reaction.

[17] Prepared according to literature methods: a) R. J. Goodridge, T. W. Hambley, R. K. Haynes, D. D. Ridley, *J. Org. Chem.* **1988**, *53*, 2881; b) see also ref. [14].

[18] Rearrangement of an acetylenyl-substituted vinylaziridine by a multistep sequence: a) N. Manisse, J. Chuche, *Tetrahedron* **1977**, *33*, 2399; b) *J. Am. Chem. Soc.* **1977**, *99*, 1272.

[19] T. K. Jones, S. E. Denmark, *Org. Synth.* **1990**, *7*, 524.

Synthesis of Taxoid Ring Systems: AC → ABC Approach by Way of Intramolecular Alkylation**

Takashi Takahashi,* Hajime Iwamoto, Kensuke Nagashima, Tadashi Okabe, and Takayuki Doi

Taxol (**1**) is an attractive molecular target both in terms of its biological activity and its synthetic complexity, which includes a conformationally restricted ABCD ring system bearing many stereogenic centers with interesting functional groups.[1–3] We have focused on the development of a method for constructing the B ring of the taxoid system.[4] There are several methods for the preparation of medium-membered rings, however, it has been difficult to effect direct cyclization of eight-membered rings due to entropic and enthalpic effects.[5] This is especially true, if the conformation of the desired cyclic molecule is restricted in a highly strained conformation, such as in the taxoid system, thereby making the preparation of the ring from a strain-free acyclic compound even more difficult. We have previously reported several methods for overcoming this problem; for example, the contraction of large-membered ring molecules and the intramolecular alkylation of cyanohydrin ethers with alkyl iodides, tosylates, and allylic halides, efficiently form 10-

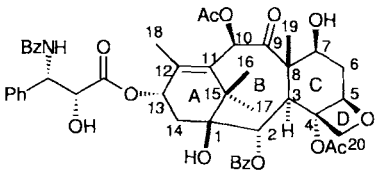

1

[*] Prof. T. Takahashi, H. Iwamoto, K. Nagashima, T. Okabe, Dr. T. Doi
Tokyo Institute of Technology, Department of Chemical Engineering
2-12-2 Ookayama, Meguro, Tokyo 152 (Japan)
Fax: Int. code +(3)5734-2884
e-mail: ttakashi@o.cc.titech.ac.jp

[**] We thank a support from the Ministry of Education, Science, Sports and Culture, Japan (Grant-in-aid No. 08245103). The X-ray crystallographic analysis was carried out by Prof. Yoshimasa Fukazawa and Prof. Shuji Usui (Hiroshima University).

 © VCH Verlagsgesellschaft mbH, D-69451 Weinheim, 1997 0570-0833/97/3612-1319 $ 17.50+.50/0

to 15-membered rings.[6, 7] Herein, we report the efficient formation of the eight-membered B ring of the taxoid system by the latter method.

Scheme 1 summarizes our initial study on the formation of the B ring of the taxoid system, in which the CD rings are

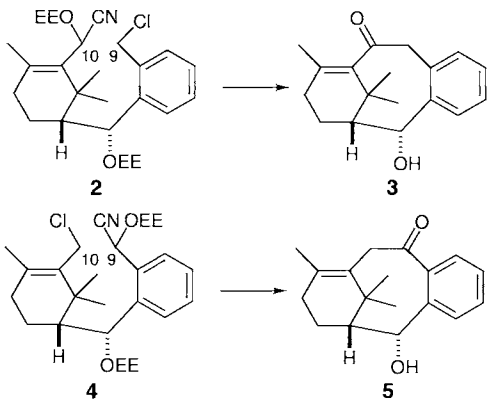

Scheme 1. Construction of the B ring in an aromatic taxoid system by intramolecular cyclization. EE = ethoxyethyl.

replaced with an aromatic ring. We planned to cyclize the B ring at positions C9 and C10 by applying an intramolecular cyanohydrin alkylation. In this respect, it was important to determine the feasibility of the alkylation of C10 in **2** by C9 and that of C9 in **4** by C10, which should lead to **3** and **5**, respectively. The syntheses of **2** and **4** are shown in Scheme 2. The

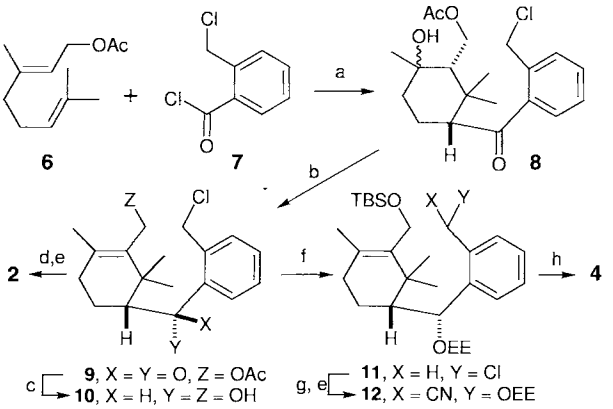

Scheme 2. a) $AlCl_3$, CH_2Cl_2, 0 °C, 5 h, 61%; b) $HC(OMe)_3$, *p*-TsOH, 25 °C, 5 h, 51% + 31% (isomer); c) diisobutyl aluminum hydride (DIBAL), CH_2Cl_2, −78 °C, 30 min, 91%; d) MnO_2, PhH, 25 °C, 44% (recovery of starting material: 40%); e) TMS(CN), [18]crown-6 KCN; 1N HCl, THF; *p*-TsOH, ethylvinyl ether (EVE), 84–88% in three steps; f) TBSCl, DMF, imidazole; PPTS, EVE, CH_2Cl_2-PhH, 91% (two steps); g) DMSO, $NaHCO_3$, 110 °C, 10 h, 77%; h) TBAF, THF; MsCl, NEt_3, CH_2Cl_2; LiCl, THF, 79% (two steps).

Friedel–Crafts reaction of geranyl acetate (**6**) with *ortho*-(chloromethyl)benzoyl chloride (**7**) gave a diastereomer mixture of **8** by acid-catalyzed olefin cyclization.[8] Dehydration of the tertiary alcohol in **8** provided tetrasubstituted alkene **9** in 51% yield, together with an *endo* isomeric alkene (30%). Stereoselective reduction of the ketone in **9** and deprotection of the acetate using DIBAL furnished diol **10** in 91% yield. Selective oxidation of the allylic alcohol gave the enal, which was converted to the protected cyanohydrin ether **2** in three steps (84% overall yield). The cyclization precursor **4** was also prepared from **10**: Selective protection of the primary alcohol of **10** with *tert*-butyldimethylsilyl chloride (TBSCl), followed by protection of the secondary alcohol with EVE gave **11** in 91% yield. Oxidation of **11** with DMSO afforded the aldehyde, which was converted to the protected cyanohydrin ether **12** as previously described. Deprotection of the TBS group in **12**, followed by chlorination afforded the cyclization precursor **4** in 79% overall yield.

The closure of the eight-membered ring in **2** and **4** was achieved by intramolecular alkylation (Scheme 1). Treatment of **2** or **4** with $LiN(SiMe_3)_2$ in THF at 80 °C immediately produced the cyclized products in 93 and 89% yields, respectively. The products underwent sequential hydrolysis with acid and base leading to the desired cyclic ketones **3** and **5** in 80% and 95% yields, respectively.[9] The structure of **3** was unambiguously determined by X-ray crystallographic analysis.[10] Thus, we have found that intramolecular alkylation of cyanohydrin ethers can form the eight-membered ring in both directions (C10 → C9, C9 → C10) leading to ABC taxoids with an aromatic C ring.

We then examined whether this method could be applied to the formation of taxoid system **14** with a nonaromatic C ring (Scheme 3). The cyclization of **13** must overcome the transannular interactions of the dimethyl groups (17-Me and 19-Me) which are close during the construction of the B ring. We prepared the cyclization precursor **13** as follows (Scheme 4): According to the reported method,[11, 12] the epoxide **15** was obtained by the coupling reaction of a vinyllithium species

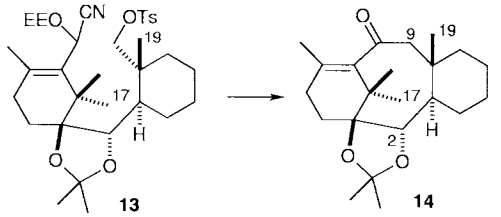

Scheme 3. Construction of the B ring in a nonaromatic taxoid system by intramolecular cyclization.

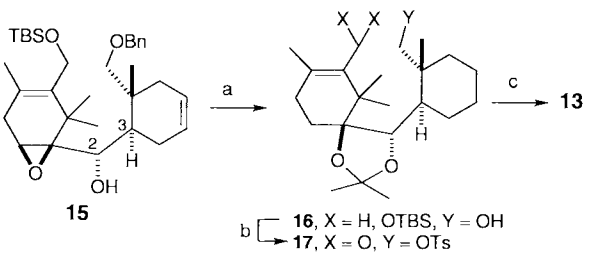

Scheme 4. a) $LiAlH_4$, ether, 25 °C, 82%; isopropenyl methyl ether, camphorsulfonic acid (CSA), CH_2Cl_2, 0 °C, quant.; $Pd(OH)_2$, H_2, AcOEt, 25 °C, 16 h, 89%; b) TsCl, Py, 25 °C, 14 h, quant.; tetrabutylammonium fluoride (TBAF), THF, 25 °C, 18 h, 93%; tetrapropylammonium perruthenate (TPAP), 4-methylmorpholine *N*-oxide (NMO), 25 °C, 5 h, 76%; c) TMS(CN), [18]crown-6 KCN; 1N HCl, THF; *p*-TsOH, EVE, CH_2Cl_2, 59% (three steps).

corresponding the A ring moiety with *trans*-6-benzyloxylmethyl-6-methyl-3-cyclohexenecarboxaldehyde.[13] Reduction of **15** with $LiAlH_4$,[11] followed by protection of the resulting 1,2-diol, gave the corresponding acetonide, whose hydrogenation and concomitant deprotection of the benzyl ether furnished alcohol **16**. Tosylation of the neopentyl function in **16**, followed by deprotection of TBS provided the allylic alcohol, which was oxidized by TPAP[14] to afford enal **17** in 71% overall yield. The cyanohydrin ether **13** was prepared from **17** analogous to step

(e) in Scheme 2. Intramolecular alkylation of **13** proceeded in 70% yield by using $LiN(SiMe_3)_2$ in refluxing dioxane (Scheme 3). Treatment of the cyclized products with acid followed by base gave the desired cyclic enone **14** in 58% overall yield (based on **13**). The stereochemistry of **14** was fully consistent with the NMR data and was confirmed unequivocally by NOE difference spectroscopy.[15] It is noteworthy that the intramolecular alkylation using cyanohydrin anions overcame not only the transannular interactions in the formation of the taxoid B ring but also the steric hindrance in the alkylation at the neopentyl position.

In summary, we have demonstrated that the intramolecular alkylations of the cyanohydrin ethers are effective for the formation of the B ring of the taxoid systems with not only aromatic but also nonaromatic C rings.

Received: December 26, 1996 [Z9918IE]
German version: *Angew. Chem.* **1997**, *109*, 1377–1378

Keywords: alkylations · cyanohydrins · cyclizations · eight-membered rings · taxol

[1] M. C. Wani, H. L. Taylor, M. E. Wall, P. Coggon, A. T. McPhail, *J. Am. Chem. Soc.* **1971**, *93*, 2325–2327.

[2] R. A. Holton, C. Somoza, H.-B. Kim, F. Liang, R. J. Biediger, P. D. Boatman, M. Shindo, C. C. Smith, S. Kim, H. Nadizadeh, Y. Suzuki, C. Tao, P. Vu, S. Tang, P. Zhang, K. K. Murthi, L. N. Gentile, J. H. Liu, *J. Am. Chem. Soc.* **1994**, *116*, 1597–1598; R. A. Holton, H.-B. Kim, C. Somoza, F. Liang, R. J. Biediger, P. D. Boatman, M. Shindo, C. C. Smith, S. Kim, H. Nadizadeh, Y. Suzuki, C. Tao, P. Vu, S. Tang, P. Zhang, K. K. Murthi, L. N. Gentile, J. H. Liu, *ibid.* **1994**, *116*, 1599–1600; K. C. Nicolaou, Z. Yang, J.-J. Liu, H. Ueno, P. G. Nantermet, R. K. Guy, C. F. Claiborne, J. Renaud, E. A. Couladouros, K. Paulvannan, E. J. Sorensen, *Nature* **1994**, *367*, 630–634; J. J. Masters, J. T. Link, L. B. Snyder, W. B. Young, S. J. Danishefsky, *Angew. Chem.* **1995**, *107*, 1886–1888; *Angew. Chem. Int. Ed. Engl.* **1995**, *34*, 1723–1726.

[3] C. S. Swindell, *Studies in Natural Products Chemistry, Vol. 12*, Elsevier, New York, **1993**, pp. 179–231; K. C. Nicolaou, W. M. Dai, R. K. Guy, *Angew. Chem.* **1994**, *106*, 38–69; *Angew. Chem. Int. Ed. Engl.* **1994**, *33*, 15–44.

[4] Routes to taxoid B ring: A. S. Kende, S. Johnson, P. Sanfilippo, J. C. Hodges, L. N. Jungheim, *J. Am. Chem. Soc.* **1986**, *108*, 3513–3515; M. H. Kress, R. Ruel, W. H. Mijjer, Y. Kishi, *Tetrahedron Lett.* **1993**, *34*, 5999–6002; J. J. Masters, D. K. Jung, W. G. Bornmann, S. J. Danishefsky, *ibid.* **1993**, *34*, 7253–7256; C. S. Swindell, W. Fan, *ibid.* **1996**, *37*, 2321–2324; R. Hara, T. Furukawa, Y. Horiguchi, I. Kuwajima, *J. Am. Chem. Soc.* **1996**, *118*, 9186–9187.

[5] For the synthesis of carbocyclic eight-membered rings see N. A. Petasis, M. A. Patane, *Tetrahedron* **1992**, *48*, 5757–5821.

[6] T. Doi, T. Takahashi, *J. Org. Chem.* **1991**, *56*, 3465–3467.

[7] T. Takahashi, H. Nemoto, J. Tsuji, *Tetrahedron Lett.* **1983**, *24*, 2005–2008; T. Takahashi, T. Nagashima, J. Tsuji, *ibid.* **1981**, *22*, 1359–1362; G. Stork, J. C. Depezay, J. d'Angelo, *ibid.* **1975**, 389–392.

[8] T. Kumagai, F. Ise, T. Uyehara, T. Kato, *Chem. Lett.* **1981**, 25–28; T. Kato, H. Takayanagi, T. Suzuki, T. Uyehara, *Tetrahedron Lett.* **1978**, 1201–1204.

[9] Spectral data in agreement with the reported structures were obtained for all compounds in this paper.

[10] Crystallographic data (excluding structure factors) for the structure reported in this paper have been deposited with the Cambridge Crystallographic Data Centre as supplementary publication no. CCDC-100231. Copies of the data can be obtained free of charge on application to The Director, CCDC, 12 Union Road, Cambridge CB2 1EZ, UK (fax: int. code +(1223) 336-033; e-mail deposit@chemcrys.cam.ac.uk).

[11] K. C. Nicolaou, Z. Yang, E. J. Sorensen, M. Nakada, *J. Chem. Soc. Chem. Commun.* **1993**, 1024–1026; K. C. Nicolaou, C. F. Claiborne, P. G. Nantermet, E. A. Couladouros, E. J. Sorensen, *J. Am. Chem. Soc.* **1994**, *116*, 1591–1592.

[12] M. J. D. Grandi, D. K. Jung, W. J. Krol, S. J. Danishefsky, *J. Org. Chem.* **1993**, *58*, 4989–4492.

[13] The less polar **15** was isolated from a 4:1 mixture of diastereomers produced by the coupling reaction by chromatography on silica gel. The stercochemistry at the 2 position was determined after cyclization.

[14] W. P. Griffith, S. V. Ley, *Aldrichimica Acta* **1990**, *23*, 13.

[15] **14**: ^{1}H NMR (270 MHz, $CDCl_3$): δ = 3.93 (1H, d, J = 5.0 Hz), 2.6–2.8 (1H, m), 2.76 (1H, d, J = 16.2 Hz), 2.21 (1H, d, J = 16.2 Hz), 1.9–2.2 (2H, m), 1.0–1.8 (10H, m), 1.75 (3H, d, J = 1.0 Hz), 1.41 (3H, s), 1.34 (3H, s), 1.29 (3H, s), 1.19 (3H, s), 0.92 (3H, s); ^{13}C-NMR (67.5 MHz, $CDCl_3$): δ = 204.3, 145.1, 137.8, 105.6, 87.1, 58.9, 41.5, 39.8, 39.0, 38.0, 31.2, 29.7, 28.1, 26.81, 26.78, 26.4, 26.2, 23.6, 22.1, 21.9, 21.5, 20.8; IR (neat): $\tilde{\nu}$ = 2922, 1671 cm^{-1}; high-resolution MS (EI): calcd for $C_{22}H_{34}O_3$ 346.2508 (M^+), found 346.2493; NOEs: 19-Me↔H-2, H-2↔17-Me, 19-Me↔H-9/H-9′.

Cofactor-Assisted Self-Cleavage in DNA Libraries with a 3′–5′-Phosphoramidate Bond**

Jens Burmeister, Günter von Kiedrowski,* and Andrew D. Ellington

Dedicated to Dr. Leslie E. Orgel on the occasion of his 70th birthday

The technique of directed molecular evolution[1] is a powerful tool in the emerging field of evolutive biotechnology. In vitro selections have been carried out to isolate RNA aptamers directed against various molecular targets[2] and to develop artificial ribozymes with stunning catalytic properties.[3] Preliminary results with DNA indicate that artificial deoxyribozymes exhibiting interesting catalytic functions can be achieved as well.[4] Directed molecular evolution may also prove useful in the search for an exponential self-replicating system based on oligodeoxynucleotide analogs.[5] Our objective was to select a 5′-aminooligodeoxynucleotide that can catalyze the carbodiimide-dependent condensation of the trideoxynucleotides CCGp and pCGG to yield the hexameric 3′–5′-pyrophosphate CCGppCGG.[6] Such an aminooligodeoxynucleotide could act as a nucleophilic catalyst, that is, a leaving group, for phosphoryl transfer (Figure 1). Similar transphosphorylations involving phosphoramidates and pyrophosphates occur in reactions catalyzed by T7-DNA ligase.[7]

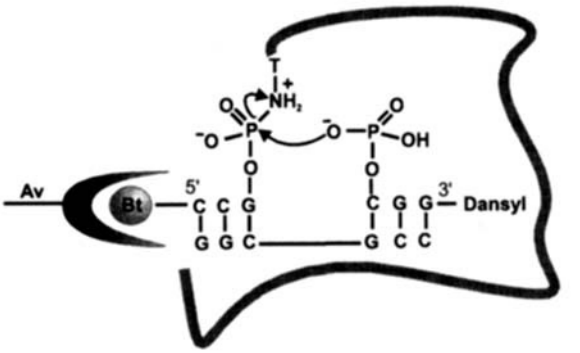

Figure 1. Schematic representation of the template-directed transphosphorylation reaction (Av = Avidine, Bt = Biotin).

To better understand the proposed transphosphorylation, we studied uncatalyzed reactions between N3-CCGpnT (**1**) and pCGG-dansyl (**2**) with HPLC (UV and fluorescence detection).[8] Even after long reaction times (up to two months) no fluorescent hexadeoxynucleotide N3-CCGppCGG-dansyl resulting from phosphoryl transfer could be detected. Hydrolysis of the 3′–5′-phosphoramidate bond (pn bond) was the only reaction observed, and the logarithm of the rate of hydrolysis is linearly dependent on the pH of the aqueous solvent. Between pH = 3 and 7,[9] the pseudo-first-order rate constants follow Equation (1).

$$\lg(k/h^{-1}) = 1.2 - 0.97 \times pH \qquad (1)$$

[*] Prof. Dr. G. von Kiedrowski, Dipl.-Chem. J. Burmeister
Lehrstuhl für Organische Chemie I der Universität
Universitätsstrasse 150, D-44801 Bochum (Germany)
Fax: Int code +(234) 709-4355
e-mail: kiedro@ernie.orch.ruhr-uni-bochum.de
Prof. Dr. A. D. Ellington
Department of Chemistry, Indiana University, Bloomington, IN (USA)

[**] This work was supported by the Deutsche Forschungsgemeinschaft and NATO. We thank D. Bartel for the generous gift of the N72-pool.

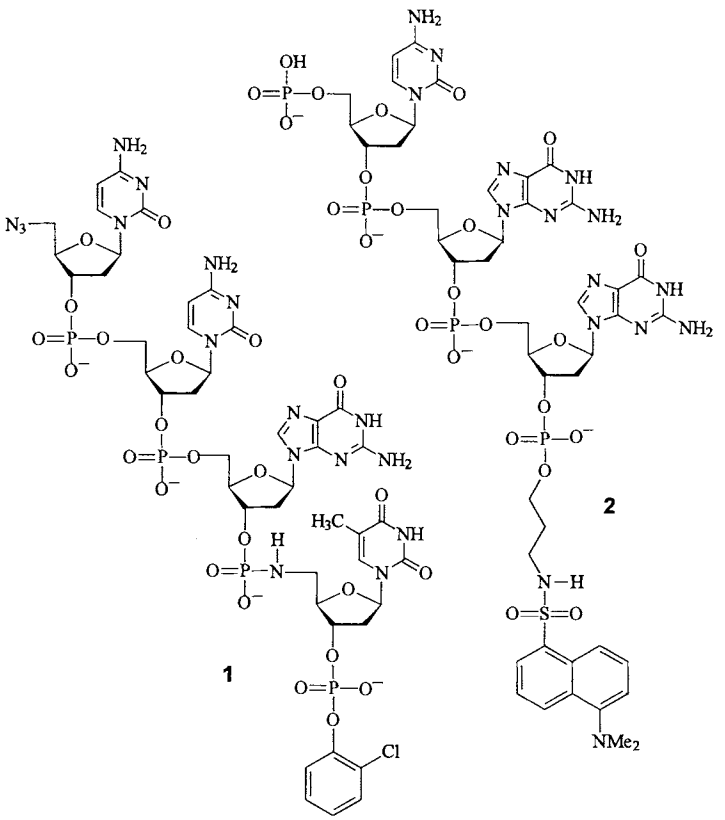

Based on these results, we expected to find nucleic-acid sequences that could catalyze cleavage of the pn bond and possibly enhance the rate of pyrophosphate ligation as well. For the in vitro selection studies we synthesized a modified primer bearing a 5′-terminal biotin moiety and an internal pn bond following the leader sequence CCG as well as an umodified primer for the second primer-binding site.[10] These primers were used to amplify a DNA pool containing 72 randomized positions embedded in two constant sequences by means of a polymerase chain reaction (PCR, Figure 2). Immobilization of the double-stranded pool on streptavidin-coated paramagnetic beads (Promega) and subsequent removal of the nonbiotinylated strand by denaturation resulted in a single-stranded DNA pool immobilized on the beads. The in vitro selection was performed on the beads by adding an excess of trimer **2** (5 μM) and the hexameric template CCGCGG (5 μM) in a magnesium-containing buffer with a high salt concentration. Prior to selection the mixture was warmed to 50 °C for 5 min to allow proper folding of the single-stranded pool and inclusion of **2** and the template.

In rounds 1–6, selection was performed for 30 h at room temperature. The 5′-aminooligomers released from the beads were amplified by PCR to form the starting pool for the next round. Starting with the seventh round we increased the stringency of selection to end up with an incubation time of 1 h in the tenth round. In addition, negative selection—that is, removal of those DNA sequences that were released from

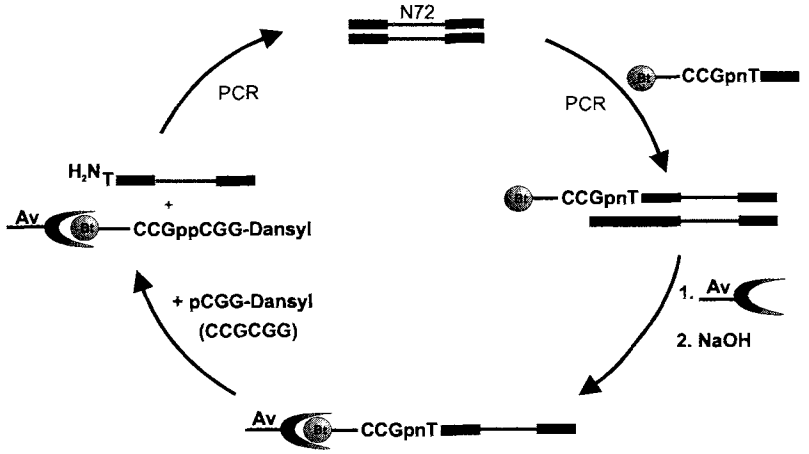

Figure 2. The selection cycle. The N72-pool had the following composition: 5′-GGAACACTATC-CGACTGGCACC-N72-CCTTGGTCATTAGGATCCCG-3′. Primers for PCR amplification: 5′-Bt-CCGpnTGGATCCTAA-TGACCAAGG-3′ (primer A) and 5′-AACACTATCCGACTGGCACC-3′ (primer B). PCR was performed in 30 individual reactions under the following conditions: primer A (80 pmol), primer B (80 pmol), $MgCl_2$ (300 nmol), dNTPs (40 nmol), template (100 ng), PCR buffer (20 μL, 10×; Promega), and Taq DNA-polymerase (0.05 U μL^{-1}) in 200 μL of solution. Gradient: 45 s at $T = 94$ °C, 1 min at $T = 52$ °C, 2 min at $T = 72$ °C, additional 5 min at $T = 72$ °C after 6 cycles. Immobilization was achieved by incubation of the lyophilized pool sequences for 20 min in PBS buffer (pH = 8, 0.690 M NaCl, 0.010 M KCl, 0.045 M Na_2HPO_4, 0.008 M KH_2PO_4) over streptavidin-coated (2 mg) paramagnetic beads (Promega). Denaturation was performed by incubation of the beads in 0.2 M NaOH for 15 min. For the selection the beads were incubated in 2-(*N*-morpholino)ethanesulfonic acid (MES) buffer (0.1 M, sodium salt (pH = 6.1), 0.05 M $MgCl_2$, 0.50 M NaCl, 0.50 M KCl) with pCGG-dansyl (5 μM) and CCGCGG (5 μM) at $T = 23$ °C after an initial warming at $T = 50$ °C for 5 min. The released aminooligomers were precipitated with ethanol and subsequently amplified by PCR with *n* cycles with primer B and 5′-CGGGATCCTAATGACCAAGG-3′ (primer C) under the conditions described above.

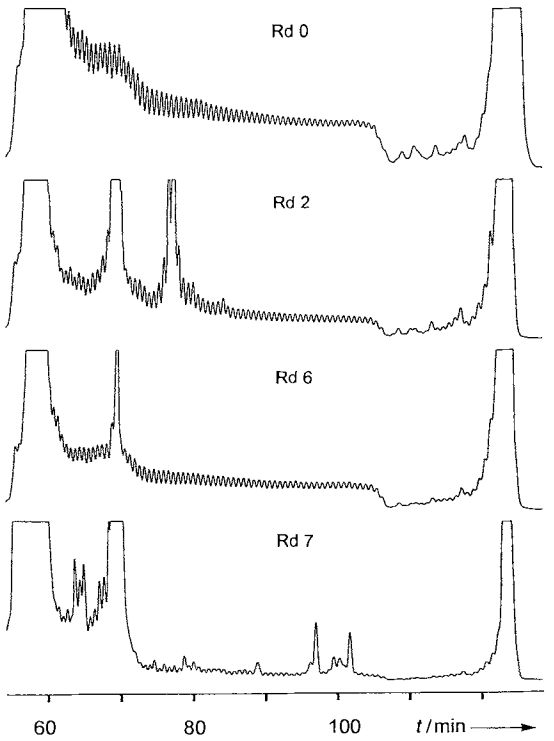

Figure 3. Analysis of pool diversity. DNA from each round (Rd) was amplified by PCR with the CY5-labeled primer 5′-CY5-CGGGATCCTAATGACCAAGG-3′ (primer D, Pharmacia) and primer B under the conditions described above (see legend for Figure 2). PCR products (4 μg) were digested with a combination of AluI, TaqI, and Tru9I (each 10 U enyzme in 10 mM Tris-HCl (pH = 7.9), 10 mM $MgCl_2$, 50 mM NaCl, and 1 mM 1,4-dimercapto-2,3-butanediol, DTT). Fragment analysis was performed on an ALFexpress automated sequencer (Pharmacia). The peak at 130 min corresponds to a full-length pool; the primer is detected at 58 min. The selected clone does not contain a restriction site, and the peak at 70 min probably corresponds to a Tru9I site in the second isolated clone randomized.

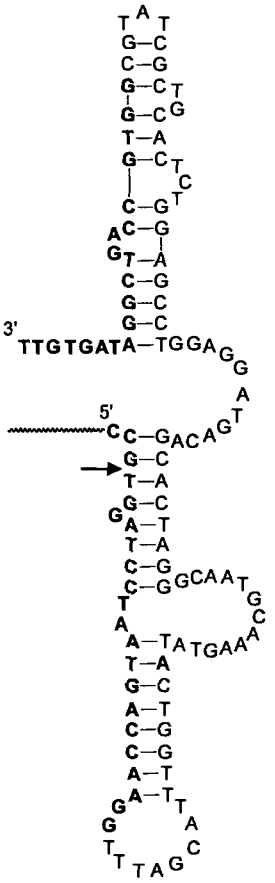

Figure 4. Proposed secondary structure for the selected clone as calculated by DNA *mfold* [15] for $T = 23\,^{\circ}C$. Primer sequences are written in boldface, and the arrow indicates the position of the pn bond. Cloning was performed with the TA-cloning kit (Invitrogen), and sequencing reactions were analyzed on an *A.L.Fexpress* automated sequencer (Pharmacia).

the beads by hydrolysis in the absence of **2** and the template—was used in rounds 7–10.[11] The progress of the in vitro selection was monitored with restriction digestion[3a] and bulk-pool sequencing.[12] Initial changes in sequence space were visible in the second round, and negative selection exhibited a dramatic influence on pool diversity (Figure 3). Our experience shows that an automated DNA sequencer is a useful tool for bulk-pool sequencing and restriction-digestion assays, as it allows rapid monitoring of the progress of an in vitro selection and can potentially quantify pool diversity.[13] Cloning and sequencing of PCR products from the last rounds revealed a single dominating clone in ten of eleven colonies.[14] The secondary structure calculated by the computer program DNA *mfold* from Zuker et al.[15] shows tight folding around the constant primer regions (Figure 4). To elucidate the catalytic activity in the selected pools, activity assays were performed on the beads as well as in solution. For solid-phase assays d-α-^{32}P-ATP was incorporated during PCR of the selected pools. Isotopic labeling facilitated the sensitive analysis of all column eluates with gel electrophoresis and autoradiography (Table 1).

The results indicate that 1) incubation of selected pools in the presence of **2** results in elution of 5′-aminooligomers that are not detectable during incubation of the initial pool under the same conditions, 2) the elution process does not depend on the presence of the hexadeoxynucleotide CCGCGG but rather on the sequence of the trimer, 3) the 5′-phosphate group of the trimer is essential, 4) phosphate itself does not assist cleavage, and 5) activity drops in the absence of magnesium.

We developed a solution phase assay to answer the question of whether the cleavage of 5′-aminooligomers results from hydrolysis of the pn bond or from phosphoryltransfer. It was necessary to extend the 5′ end of the DNA library to distinguish between the product of hydrolysis and the product of phosphoryl transfer with electrophoresis. Therefore, a modified primer was synthesized with the sequence ATGCTGCCGpnT instead of CCGpnT. Based on the proposed secondary structure of the selected clone (Figure 4), we concluded that this variation would not considerably disturb the system. Selected pools were amplified by PCR with the modified primer and a second primer containing a 5′-lengthener–terminator sequence.[16] Single-stranded DNA was purified with gel electrophoresis and subsequently radiolabeled with T4-polynucleotide kinase and γ-^{32}P-ATP. No ligation product could be detected upon incubation of the selected pools in the presence of **2** with and without hexamer. In contrast, a product whose length corresponds to that of the fragment formed by hydrolysis was observed.

We conclude that in vitro selection yielded a novel oligodeoxynucleotide that catalyzes the hydrolysis of an internal 3′–5′-phosphoramidate bond in the presence of the trideoxynucleotide **2** as a cofactor. Cofactor-assisted hydrolysis is at least three orders of magnitude faster than background hydrolysis when comparing the estimated pseudo-first-order rate constant with the kinetics of hydrolysizing model compound **1**.[17] Our present results underline the catalytic potential of DNA and give the first example of a cofactor-assisted deoxyribozyme.

Received: December 12, 1996 [Z9896IE]
German version: *Angew. Chem.* **1997**, *109*, 1379–1381

Keywords: combinatorial chemistry · DNA cleavage · ribozymes

Table 1. Results of the solid-phase activity assays. Selected pools were amplified by PCR with primer A (8 pmol), primer B (8 pmol), $MgCl_2$ (16 nmol), dNTPs (0.4 nmol), d-α-^{32}P-ATP (25 μCi), template (10 ng), Taq DNA-polymerase (0.05 U μL^{-1}), PCR buffer (2 μL, 10×; Promega) in 20 μL of solution. Immobilization, denaturation, and selection were performed under the same conditions as described for the in vitro selection (see legend of Figure 2). Column eluates were collected and analyzed by electrophoresis on 10% polyacrylamide/7 M urea gels.

Round	Mg^{2+} (50 mM)	Cofactors (5 μM)	Activity [a]
0/1	+	pCGG and CCGCGG	–
8	+	pCGG and CCGCGG	++
8	–	pCGG and CCGCGG	+
8	+	pCGG	++
8	+	CCGCGG	–
0/8	+	–	–
8	+	pCGT	–
8	+	pATT	–
8	+	HOCGG	–
0/8	+	1 mM phosphate (pH = 6)	–

[a] Semiquantitative measure for the amount of eluate after 16 h incubation as compared to the amount of denatured strand: ++: about 50% eluate; +: about 20% eluate; –: < –5% eluate.

[1] a) C. Tuerk, L. Gold, *Science* **1990**, *249*, 505–510; b) A. D. Ellington, J. W. Szostak, *Nature* **1990**, *346*, 812–822; c) A. A. Beaudry, G. F. Joyce, *Science* **1992**, *257*, 635–641.

[2] Reviews: a) R. C. Conrad, L. Giver, Y. Tian, A. D. Ellington, *Methods Enzymol.* **1996**, *267*, 336–367; b) J. R. Lorsch, J. W. Szostak, *Acc. Chem. Res.* **1996**, *29*, 103–110; c) M. Famulok, J. W. Szostak, *Angew. Chem.* **1992**, *104*, 1001–1011; *Angew. Chem. Int. Ed. Engl.* **1992**, *31*, 979–988.

[3] a) D. P. Bartel, J. W. Szostak, *Science* **1993**, *261*, 1411–1418. Review: b) P. Burgstaller, M. Famulok, *Angew. Chem.* **1995**, *107*, 1303–1307; *Angew. Chem. Int Ed. Engl.* **1995**, *34*, 1189–1193.

[4] a) R. R. Breaker, G. F. Joyce, *Chem. Biol.* **1994**, *1*, 223–229; b) B. Cuenod, J. W. Szostak, *Nature* **1995**, *375*, 611–614; c) R. R. Breaker, G. F. Joyce, *Chem. Biol.* **1995**, *2*, 665–660, d) Y. Li, D. Sen, *Nature Struct. Biol.* **1996**, *3*, 743–747, e) D. Faulhammer, M. Famulok, *Angew. Chem.* **1996**, *108*, 2984–2988; *Angew. Chem. Int. Ed. Engl.* **1996**, *35*, 2837–2841. f) N. Carmi, L. A. Shultz, R. R. Breaker, *Chem. Biol.* **1996**, *3*, 1039–1046.

[5] B. G. Bag, G. von Kiedrowski, *Pure and Appl. Chem.* **1996**, *68*, 2145–2152.

[6] G. von Kiedrowski, B. Wlotzka, J. Helbing, *Angew. Chem.* **1989**, *101*, 1259–1261; *Angew. Chem. Int. Ed. Engl.* **1989**, *28*, 1235–1237.

[7] J. D. Watson, N. H. Hopkins, J. W. Roberts, J. A. Steitz, A. M. Weiner, *Molecular Biology of the Gene*, 4th ed., Benjamin/Cummings, New York, **1987**.

[8] N3-CCGpnT (**1**) and pCGG-dansyl (**2**) were synthesized in solution by the standard phosphotriester method.

[9] Reactions ($T = 23\,^{\circ}C$, 1 mM N3-CCGpnT (**1**), 50 mM $MgCl_2$) were followed in a 0.1 M solution of the following buffers: sodium citrate (pH = 3, 4, and 5); 2-(*N*-morpholino)ethanesulfonic acid, sodium salt (pH = 6); *N*-(2-hydroxyethyl)piperazine-*N*′-(2-ethanesulfonic acid), sodium salt (pH = 7).

[10] a) The modified primer B was prepared on an Applied Biosystems 391 DNA Syntheziser with the phosphoramidite biotin TEG (Glen Research) and the phosphoramidite of 5′-*N*-(4-monomethoxytrityl)amino-2′,5′-dideoxythymidine; b) M. Mag, J. W. Engels, *Nucl. Acids Res.* **1989**, *17*, 5973–5977.

 © VCH Verlagsgesellschaft mbH, D-69451 Weinheim, 1997 0570-0833/97/3612-1323 $ 17.50+.50/0

[11] Negative selection was performed by incubation of the immobilized single-stranded pool in the selection buffer for 2.5 h in round 7 and 1 h in rounds 8–10. Following incubation the beads were washed several times with bidistilled water to remove released aminooligomers. Positive selection was performed according to the conditions described above (see legend of Figure 2).
[12] T. Fitzwater, B. Polisky, *Methods Enzym.* **1996**, *267*, 275–301.
[13] The pool diversity D is a statistical estimate that can be derived as the product of the positional diversities d_i for N positions according to $D = \prod_{i=1}^{N} d_i$. The positional diversity d_i can be estimated from the ratio of the peak integrals of the fragments $a_i:c_i:t_i:g_i$ in the normalized lanes by dividing the single integrals $x_{ij}(j = 1-4)$ by the largest of the four integrals x_{imax} and summing the quotients: $d_i = \sum_{j=1}^{4} x_{ij}/x_{jmax}$. For example, if the ratio $a_i:c_i:t_i:g_i$ is 100:0:0:0, x_{imax} is 100 and $d_i = 1$. For $a_i:c_i:t_i:g_i = 50:50:0:0$ $x_{imax} = 50$ and $d_i = 2$. In general the positional diversity d_i is a rational number between 1 and 4, and the pool diversity D is a rational number between 1 and 4^N.
[14] The second clone had the following sequence:
5′-CCGpnTGGATCCTAATGACCAAGGCATAGCCTTTTAATGGATC-CTCAGAAGGGGCTTGGTCCCGCCTGCGTCTAAACAACACGC-TACGGCTATTTCGGTGCCAGTCGGATAGTGTT-3′
[15] The program was invoked with the World Wide Web at http://www.ibc.wustl.edu/~zuker/dna/form1.cgi.
[16] K. P. Williams, D. P. Bartel, *Nucl. Acids Res.* **1995**, *23*, 4420–4221.
[17] At pH = 6 the pseudo-first-order rate constant for the hydrolysis of **1** is $k = 2 \times 10^{-5}\,h^{-1}$. Upon incubation of selected pools in the presence of **2** and the template at pH = 6, more than 50% hydrolyzed product was detected after 16 h. Under the assumption that the whole pool can be hydrolyzed we conclude that the catalyzed reaction is about three orders of magnitude faster than uncatalyzed hydrolysis.

$^1_\infty[P_3Se_4^-]$: A Novel Polyanion in $K_3RuP_5Se_{10}$; Formation of Ru–P Bonds in a Molten Polyselenophosphate Flux

Konstantinos Chondroudis and Mercouri G. Kanatzidis*

Recent advances in the polychalcophosphate flux technique has resulted in many novel quaternary chalcophosphate compounds.[1] The in situ fusion of A_2Q_x and P_2Q_5 (Q = S, Se), yields various $[P_yQ_z]^{n-}$ units. These highly anionic ligands, in the presence of metal ions, coordinate through the Q atoms in an astonishing number of ways forming new materials.[1] By fine-tuning the flux composition various ligands have been stabilized, such as $[PQ_4]^{3-}$, $[PSe_5]^{3-}$, $[P_2Q_6]^{4-}$, $[P_2Q_7]^{4-}$, and $[P_2Se_9]^{4-}$,[1-11] which have become the building blocks of various polymeric, solid-state, or even molecular structures.[8] Examples of compounds synthesized this way include $ABiP_2S_7$ (A = K,Rb),[2] $A_3M(PS_4)_2$ (A = Rb, Cs; M = Sb, Bi),[3] $A_2M_2P_2Se_6$ (A = K, Cs; M = Cu, Ag),[1] KMP_2Se_6 (M = Sb, Bi),[4] $Cs_8M_4(P_2Se_6)_5$ (M = Sb, Bi),[5] $APbPSe_4$,[6] $Rb_4Ti_2(P_2Se_9)_2(P_2Se_7)$,[7] $A_5Sn(PSe_5)_3$ (A = K, Rb),[8], $Rb_2AuP_2Se_6$,[9] $K_2UP_3Se_9$,[10] and $K(Ln)P_2Se_6$ (Ln = Y, La, Ce, Pr, Gd).[11] An inspection of the entire class of chalcophosphate compounds reveals a conspicuous absence of any ruthenium-containing members, even though several iron compounds are known. Furthermore, in all compounds the metal atoms form exclusively M–Q bonds. Given that Ru belongs to the noble metal group it seemed that the highly reactive polychalcogenide fluxes would serve as an excellent tool to access its chemistry. Here we report on the first structurally characterized ruthenium selenophosphate compound, $K_3RuP_5Se_{10}$, which surprisingly, shows a significant departure from the chemistry of any other metal studied in the P/Q systems.

$K_3RuP_5Se_{10}$[12] has an one-dimensional structure with Ru in the 2+ oxidation state (Figure 1). The compound contains

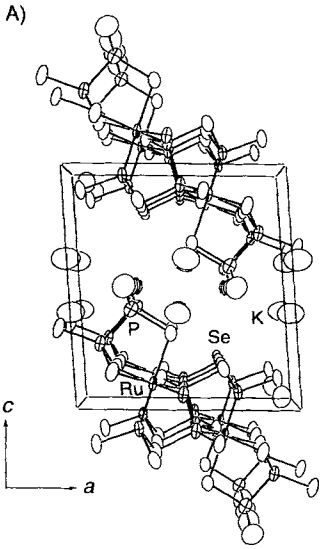

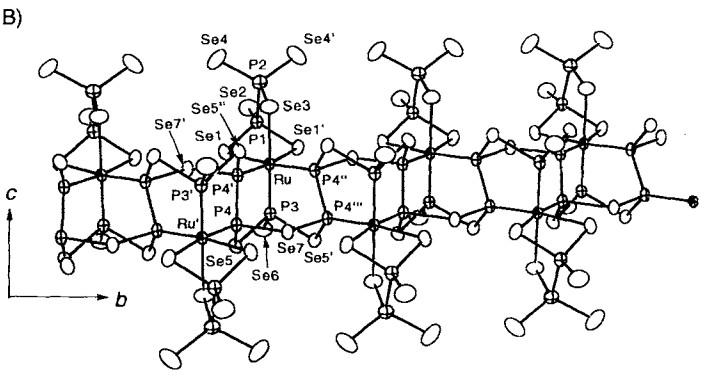

Figure 1. ORTEP representations of the unit cell viewed down the *b* axis (A) and of a section of the infinite $[Ru(P_2Se_6)(P_3Se_4)]^{3n-}_n$ chain with atom labeling (B). Selected distances [Å] and angles [°]: Ru–Se1 2.601(1), Ru–Se3 2.601(1), Ru–P3 2.288(3), Ru–P4′ 2.262(2), P1–Se1 2.202(2), P1–Se2 2.130(3), P1–P2 2.241(4), P2–Se3 2.240(3), P2–Se4 2.144(2), P3–Se5 2.326(2), P3–Se6 2.161(3), P4–Se5 2.240(2), P4–Se7 2.297(2), P4–P4′ 2.206(4); Se1-Ru-Se1′ 79.48(4), Se1-Ru-Se3 89.83(4), Se1-Ru-P4′ 92.23(5), Se1-Ru-P4″ 171.29(6), Se1-Ru-P3 91.346, angles around P range from 98.1(1) to 127.3(1)°.

$[P_2Se_6]^{4-}$ and $^1_\infty[P_3Se_4^-]$ ions and can thus be described as $K_3^+Ru^{2+}(P_2Se_6)^{4-}(P_3Se_4)^-$. Two unprecedented features in this compound are 1) the mixed P/Se coordination of the Ru centers and 2) the stabilization of a novel polymeric $^1_\infty[P_3Se_4^-]$ ion with P atoms in two different oxidation states (P^{2+}, P^{3+}), and which binds to Ru exclusively through P atoms. Hitherto in all the known polychalcophosphates, the $[P_yQ_z]^{n-}$ units coordinate to the metal centers through the negatively charged Q atoms (Q = S, Se). $K_3RuP_5Se_{10}$ is the first polychalcophosphate with bonding between the metal center and the P atoms of the $[P_yQ_z]^{n-}$ units. The strong preference of Ru^{2+} ions for binding to phosphorus is reminiscent of the coordination of ruthenium centers by phosphanes (R_3P) in organometallic complexes.

[*] Prof. Dr. M. G. Kanatzidis, K. Chondroudis
Department of Chemistry, Michigan State University
East Lansing, MI, 48823 (USA)
e-mail: kanatzidis@cemvax.cem.msu.edu
Fax: Int. code +(517)353-1793

[**] This work was supported by the National Science Foundation DMR-9527347. The authors are grateful to the X-ray Crystallographic Laboratory of the University of Minnesota and to Dr. Victor G. Young Jr. for collecting the single-crystal X-ray data set.

The selection of phosphorus from a "sea" of selenide anions for bonding is remarkable and, at first unexpected. It can be rationalized by soft acid/soft base arguments, if we assign a softer basic character to the bound phosphorus centers than to the Se atoms of the $[P_2Se_6]^{4-}$ ions.

The $^1_\infty[Ru(P_2Se_6)(P_3Se_4)^-]$ chain structure is essentially based upon the $^1_\infty[P_3Se_4^-]$ unit, a novel, infinitely long, anionic ligand. Formally, it can be viewed as resulting from the polymerization of the cyclic $[P_3Se_4]$ unit (Scheme 1). The conformation of the

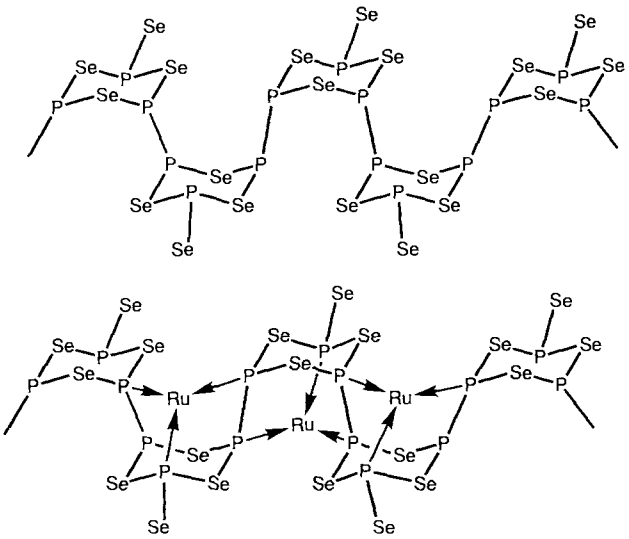

Scheme 1. The $^1_\infty[Ru(P_2Se_6)(P_3Se_4)^-]$ chain structure (bottom) in $K_3RuP_5Se_{10}$ based on the $^1_\infty[P_3Se_4^-]$ unit (top).

chain presents triangular binding pockets made of P atoms which accomodate the Ru centers. The formal oxidation states can be assigned as P^{2+} for the P–P bonded pair of atoms (e.g. P4) and P^{3+} for the remaining atom (e.g. P3). Both the P^{2+} and P^{3+} atoms in the chain are bound to Ru through their lone pairs of electrons. Therefore, they are electronically more similar to the phosphorus atoms in phosphane ligands which are so abundant in Ru coordination chemistry. The coordination sphere of Ru is completed by a tridentate $[P_2Se_6]^{4-}$ unit.

It is noteworthy, that the 2+ and 3+ oxidation states for P are among the lowest yet observed in chalcophosphate chemistry. The infinite "ladder" structure of the $^1_\infty[Ru(P_3Se_4)^+]$ unit that is formed by the coordination of the $^1_\infty[P_3Se_4^-]$ unit to the Ru centers is the backbone of the one-dimensional structure of $K_3RuP_5Se_{10}$ and propagates along [010]. The $^1_\infty[P_3Se_4^-]$ can be considered as an infinite chelating ligand which creates a cage structure around each Ru center. These cages are formed by the fusion of two five- and two six-membered rings and consists of one Ru, five P, and three Se atoms. Every Ru^{2+} center is in an octahedral coordination environment with three Se and three P atoms in a *fac* configuration (Scheme 2). The Ru–P bonds in $K_3RuP_5Se_{10}$ are very short [Ru–P(3) 2.288(3), Ru–P(4') 2.262(2) Å], and comparable only to the shortest distances found in some Ru phosphides

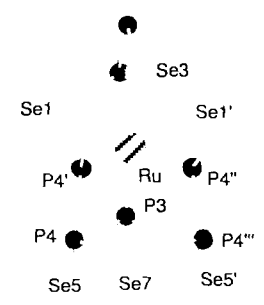

Scheme 2. Coordination sphere of Ru^{2+} in $K_3RuP_5Se_{10}$.

such as RuP_3,[13] and RuP_4,[14] and the shortest distances found in phosphane complexes such as *mer*-$[Ru(PEt_2Ph)_3Cl_3]^-$.[15]

The chains are separated by three, crystallographically independent, K cations (Figure 1). The ion K1 has an unusually high coordination environment with 11 Se atoms and one P atom in its coordination sphere; the average K1–Se distance is 3.59 Å and the K1–P distance is 3.526(4) Å. The K2 ion is eight-coordinate [av K2–Se 3.62 Å], and K3 is nine-coordinate with eight Se [av K3–Se 3.61 Å] and one P atom [K3–P 3.613(4) Å].

$K_3RuP_5Se_{10}$ melts incongruently at 661 °C yielding a mixture of amorphous $K_xP_ySe_z$ glass and residual $K_3RuP_5Se_{10}$. Some $RuSe_2$ or RuP_x should also be formed but they are either amorphous or in concentrations and particle sizes undetectable by our X-ray diffraction analysis. We have been unable to prepare $K_3RuP_5Se_{10}$ by a direct stoichiometric reaction for several days at 560 °C.

That metal centers can choose their own coordination sphere and even dictate the final structure of a compound is well known, but seldom in flux reaction chemistry do they play a prominent role in determining which ligand will form. This is mostly determined by the composition of the reactive flux, the reaction temperature, and the nature of the counterion. In $K_3RuP_5Se_{10}$ we observe an extreme case, in which the Ru exhibits a protagonistic role in stabilizing a ligand, which otherwise is unstable under the experimental conditions, to suit its coordination chemistry needs. The exclusively P-bound $[P_3Se_4]$ ligand with its low oxidation state phosphorus atoms seems tailor-made for binding to ruthenium centers.

Experimental Section

$K_3RuP_5Se_{10}$ was synthesized from a mixture of Ru (0.15 mmol), P_2Se_5 (0.45 mmol), K_2Se (0.225 mmol), and Se (1.5 mmol) that was sealed under vacuum in a Pyrex tube and heated to 490 °C for 10 d, and then cooled (2 °C per h) to 50 °C. The excess $K_xP_ySe_z$ flux was removed with DMF under N_2 atmosphere. The product was washed with tri-*n*-butylphosphane to remove residual elemental Se, and then with ether. Black, rodlike crystals were obtained (75% yield based on Ru). The crystals appear air- and water-stable. Semiquantitative microprobe analysis on single crystals gave $K_{2.8}RuP_{4.9}Se_{9.7}$ (average value from four analyses).

Received: December 16, 1996 [Z98951E]
German version: *Angew. Chem.* **1997**, *109*, 1382–1383

Keywords: chalcogens · phosphorus · ruthenium · selenium

[1] a) T. J. McCarthy, M. G. Kanatzidis, *Inorg. Chem.* **1995**, *34*, 1257–1267, and references therein; b) A. Sutorik, M. G. Kanatzidis, *Progr. Inorg. Chem.* **1995**, *43*, 151–265.
[2] T. J. McCarthy, T. Hogan, C. R. Kannewurf, M. G. Kanatzidis, *Chem. Mater.* **1994**, *6*, 1072–1079.
[3] T. J. McCarthy, M. G. Kanatzidis, *J. Alloys Comp.* **1996**, 236, 70–85.
[4] T. J. McCarthy, M. G. Kanatzidis, *J. Chem. Soc. Chem. Commun.* **1994**, 1089–1090.
[5] T. J. McCarthy, M. G. Kanatzidis, *Chem. Mater.* **1993**, *5*, 1061–1063.
[6] K. Chondroudis, T. J. McCarthy, M. G. Kanatzidis, *Inorg. Chem.* **1996**, *35*, 840–844.
[7] K. Chondroudis, M. G. Kanatzidis, *Inorg. Chem.* **1995**, *34*, 5401–5402.
[8] K. Chondroudis, M. G. Kanatzidis, *Chem. Commun.* **1996**, 1371–1372.
[9] K. Chondroudis, T. J. McCarthy, M. G. Kanatzidis, *Inorg. Chem.* **1996**, *35*, 3451–3452.
[10] K. Chondroudis, M. G. Kanatzidis, *C. R. Acad. Sci. Paris Ser. B* **1996**, *322*, 887–894.
[11] a) J. H. Chen, P. K. Dorhout, *Inorg. Chem.* **1995**, *34*, 5705–5706; b) J. H. Chen, P. K. Dorhout, J. E. Ostenson, *ibid.* **1996**, *35*, 5627–5633.
[12] a) A Siemens SMART Platform CCD diffractometer was used to collect data from a crystal of 0.28 × 0.04 × 0.04 mm dimensions; $Mo_{K\alpha}$ (λ = 0.71073 Å) radiation; Lorentz polarization effects correction and an empirical absorption correction [12b] were applied to the data (min./max. transmission = 0.519). The structure was solved by direct methods with SHELXS-86 [12c] and refined by full-matrix least-squares techniques of the TEXSAN [12d] package of crystallographic programs. Crystal data at 23 °C: a = 11.2099(2), b = 7.2868(1), c = 12.3474(2) Å, β = 93.958(1), V = 1006.18(2) Å^3, Z = 2, ρ_{calcd} =

 © VCH Verlagsgesellschaft mbH, D-69451 Weinheim, 1997 0570-0833/97/3612-1325 $ 17.50+.50/0

3.838 g cm^{-3}, space group $P2_1/m$ (no. 11), $\mu(Mo_{K\alpha}) = 198.70$ cm^{-1}, $1.65 \le \theta \le 25.40°$, index ranges: $-13 \le h \le 13$, $0 \le k \le 8$, $0 \le l \le 14$; 8462 measured reflections; 1966 unique reflections ($R_{int} = 0.044$); 1575 reflections with $F_o^2 > 3\sigma(F_o^2)$. No. of variables: 104. Final $R = 0.034$ $Rw = 0.036$ (refined on $|F|$), GOF = 1.87; largest Difference peak and hole: 1.04/ −1.10 e Å^{-3}. Further details of the crystal structure investigation may be obtained from the Fachinformationszentrum Karlsruhe, D-76344 Eggenstein-Leopoldshafen (Germany), on quoting the depository number CSD-406200. b) R. H. Blessing, *Acta Crystallogr. A* **1995**, *51*, 33–38. c) G. M. Sheldrick, in *Crystallographic Computing 3*; (Eds.: G. M. Sheldrick, C. Kruger, R. Doddard), Oxford University Press, Oxford, England, **1985**, p. 175–189. d) TEXSAN: Single Crystal Structure Analysis Software (**1981 & 1992**). Molecular Structure Corporation, The Woodlands, TX 77381 (USA). e) IR: $\tilde{\nu}$ = 515, 453, 441, 401, and 360 cm^{-1} ($^1_\infty[P_3Se_4^-]$ unit), as well as 486 and 313 cm^{-1} ($[P_2Se_6]^{4-}$ group).

[13] W. Hönle, R. Kremer, H. G. von Schnering, *Z. Kristallogr.* **1987**, *179*, 443–453.

[14] V. D. J. Braun, W. Jeitschko, *Z. Anorg. Allg. Chem.* **1978**, *445*, 157–166.

[15] E. A. Seddon, K. R. Seddon, *The Chemistry of Ruthenium*, Elsevier, New York, **1984**, pp. 503–511.

$R_2Si{=}P{-}SiR_2F$: 1,3-Sigmatropic Migration of Fluorine in a 2-Phospha-1,3-disilaallyl Derivative Capable of Conjugation and Its Conversion to Phosphadisilacyclopropanes**

Matthias Driess,* Stefan Rell, Hans Pritzkow, and Rudolf Janoschek*

Dedicated to Professor Gottfried Huttner on the occasion of his 60th birthday

Although stable compounds with isolated Si=E bonds (E = C, Si, N, P, As, S), which have an enormous synthetic potential at their disposal, have been prepared and even structurally characterized over the last few years,[1, 2] only very little is known about heteronuclear conjugated Si–E π systems, and nothing is known about corresponding homonuclear Si–Si π systems. Until now, only the 1,3-diphospha- and 1,3-diaza-2-silaallyl anionic derivatives **A**[3] and **B**[4] have been experimentally studied. We have been investigating the synthesis of stable conjugated Si–P π systems **C** (allyl, butadiene, and benzene analogues), whose stepwise formation can be achieved with salt-condensation reactions, as, for example, in the preparation of phosphasilenes (Si=P compounds).[2]

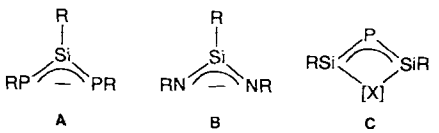

A **B** **C**

[*] Prof. Dr. M. Driess,[+] S. Rell, Dr. H. Pritzkow
Anorganisch-chemisches Institut der Universität
Im Neuenheimer Feld 270, D-69120 Heidelberg (Germany)
Prof. Dr. R. Janoschek
Institut für Theoretische Chemie der Universität
Strassoldogasse 10, A-8010 Graz (Austria)
Fax: Int. code +(316)38 21 30
e-mail: janoschek@bkfug.kfunigraz.ac.at

[+] New address:
Lehrstuhl für Anorganische Chemie I, Fakultät für Chemie
Universitätsstrasse 150, D-44801 Bochum (Germany)
Fax: Int. code +(243)709-4378
e-mail: driess@ibm.anch.ruhr-uni-bochum.de

[**] This work was supported by the Deutsche Forschungsgemeinschaft (SFB 247) and the Fonds der Chemischen Industrie. We thank Messer Griesheim GmbH for donation of chemicals.

Here we report the first 2-phospha-1,3-disilaallyl fluoride derivative **1**, which undergoes a 1,3-sigmatropic shift (fluctional behavior) of the fluorine atom above 40 °C. Ab initio calculations on $H_2Si{=}P{-}SiH_2F$ are in agreement with this. Reduction of **1** with lithium leads to the elimination of LiF and, surprisingly, formation of the *P*-lithium phosphadisilacyclopropanide **2**. Compound **2**, which is most likely formed as a reactive intermediate via its valence isomer **5**, readily reacts to form neutral **3**.

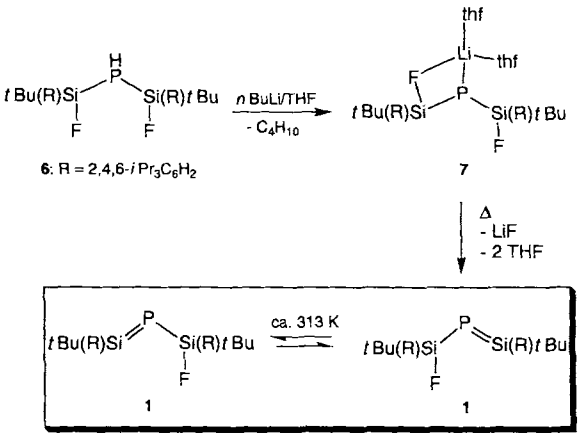

The synthesis of **1** was carried out in a stepwise manner starting from the bulkily substituted bis(fluorosilyl)phosphane **6**,[5] which was converted to the lithium phosphanide **7** (a precursor of **1**) by reaction with lithium. The lithium center in **7** is coordinated by two THF molecules and is, as expected, dissociated in toluene at 25 °C (Table 1). The compound crystallized as a monomer and, surprisingly, enantiomerically pure in the space group $P2_12_12_1$ (Figure 1).[6]

The Li center is fourfold coordinated by two THF molecules, the phosphorus atom, and the fluorine atom. In contrast, the

Table 1. Selected NMR and MS data of **1**, **3**, **4**, **7**, and **8**. Is = 2,4,6-*i*Pr$_3$C$_6$H$_2$.

1: ^{1}H NMR (300 MHz, C_6D_6, 298 K): δ = 1.18 (d, 12H, J(H,H) = 6.8 Hz, *p*-CH*Me*$_2$), 1.26 (s, 9H, *t*Bu), 1.32 (s, 9H, *t*Bu), 1.33–1.60 (m, 24H, *o*-CH*Me*$_2$), 2.72 (sept, 2H, J(H,H) = 6.8 Hz, *p*-C*H*Me$_2$), 3.35 (m, 2H, *o*-C*H*Me$_2$), 3.62 (sept, 1H, J(H,H) = 6.9 Hz, *o*-C*H*Me$_2$), 3.78 (sept, 1H, J(H,H) = 6.9 Hz, *o*-C*H*Me$_2$), 6.92 (s, 2H, arom. H), 7.14 (s, 2H, arom. H); ^{19}F-NMR (84.7 MHz, C_6D_6, 298 K, $CFCl_3$ ext. standard): δ = −140.7 (d, ^2J(F,P) = 44 Hz); ^{31}P NMR (81 MHz, C_6D_6, 298 K): δ = −33.0 (d, ^2J(P,F) = 44 Hz); MS (EI): m/z = 626 [M^+, 8%], 569 [(M − *t*Bu)$^+$, 15%], 307 [(*t*BuIsSiF)$^+$, 90%], 288 [(*t*BuIsSi)$^+$, 100%]; correct C,H analysis

3: ^{1}H NMR (200 MHz, C_6D_6, 298 K): δ = 1.05 (s, 18H, *t*Bu), 1.25 (d, 12H, J(H,H) = 6.9 Hz, *p*-CH*Me*$_2$), 1.30–1.80 (m, 24H, *o*-CH*Me*$_2$), 2.78 (sept, 2H, J(H,H) = 6.9 Hz, *p*-C*H*Me$_2$), 4.10 (sept, 2H, J(H,H) = 6.9 Hz, *o*-C*H*Me$_2$), 4.60 (sept, 1H, J(H,H) = 6.9 Hz, *o*-C*H*Me$_2$), 7.21 (s, 4H, arom. H); ^{31}P NMR (81 MHz, C_6D_6, 298 K): δ = −325.0 (d, ^1J(P,H) = 161 Hz); ^{29}Si NMR (36 MHz, C_6D_6, 298 K): δ = −43.6 (d, ^1J(Si,P) = 36 Hz), −44.5 (d, ^1J(Si,P) = 36 Hz); MS (EI): m/z = 608 [M^+, 85%], 551 [(M − *t*Bu)$^+$, 93%], 288 [(*t*BuIsSi)$^+$, 85%], 231 [(IsSi)$^+$, 100%]

4: ^{19}F NMR (84.7 MHz, THF, $CFCl_3$ ext. standard): δ = −132.5 (d, ^2J(F,P) = 38 Hz); ^{31}P NMR (36 MHz, THF): δ = −306.0 (d, ^2J(P,F) = 38 Hz)

7: ^{1}H NMR (300 MHz, C_6D_6, 298 K): δ = 1.24 (d, 12H, J(H,H) = 6.8 Hz, *p*-CH*Me*$_2$), 1.26 (m, 8H, THF), 1.31 (d, 6H, J(H,H) = 6.8 Hz, *o*-CH*Me*$_2$), 1.37 (d, 6H, J(H,H) = 6.8 Hz, *o*-CH*Me*$_2$), 1.41 (d, 6H, J(H,H) = 6.8 Hz, *o*-CH*Me*$_2$), 1.49 (s, 18H, *t*Bu), 1.59 (d, 6H, J(H,H) = 6.8 Hz, *o*-CH*Me*$_2$), 2.79 (sept, 2H, J(H,H) = 6.8 Hz, *p*-C*H*Me$_2$), 3.33 (m, 8H, THF), 3.85 (sept, 2H, J(H,H) = 6.8 Hz, *o*-C*H*Me$_2$), 4.33 (sept, 2H, J(H,H) = 6.8 Hz, *o*-C*H*Me$_2$), 7.15 (s, 4H, arom. H); ^{19}F NMR (84.7 MHz, C_6D_6, 298 K, $CFCl_3$ ext. standard): δ = −130.7 (s); ^{31}P NMR (81 MHz, C_6D_6, 298 K): δ = −288.8 (s)

8: ^{31}P NMR (81 MHz, C_6D_6, 298 K): δ = −221.6 (d, ^1J(P,H) = 170.2 Hz); ^{29}Si NMR (36 MHz, C_6D_6, 298 K): δ = 23.5 (d, ^1J(Si,P) = 15 Hz), 24.2 (d, ^1J(Si,P) = 15 Hz); MS (EI): m/z = 624 [M^+, 9%], 567 [(M − *t*Bu)$^+$, 64%], 510 [(M − 2*t*Bu)$^+$, 17%], 247 [(IsSiO)$^+$, 60%]

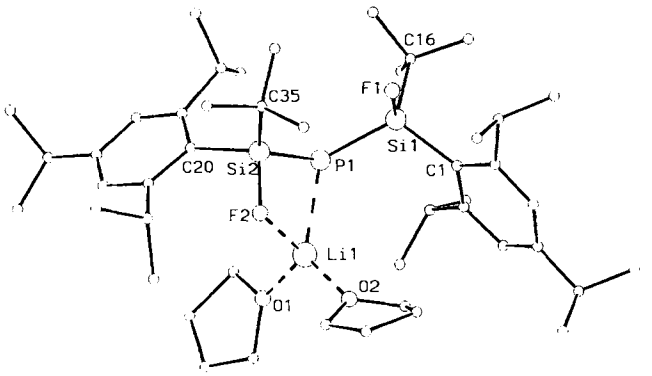

Figure 1. Crystal structure of 7. Selected distances [Å] and angles [°]: P1–Si1 2.199(2), P1–Si2 2.195(2), Si1–F1 1.619(3), Si2–F2 1.666(3), Li1–P1 2.538(9), Li1–F2 1.998(9), Li1–O1 1.955(10), Li1–O2 1.895(10), Si1–C1 1.914(4), Si2–C20 1.920(4), Si1–C16 1.918(5), Si2–C35 1.915(4); Si1-P1-Si2 113.56(7), Si1-P1-Li1 118.5(2), Si2-P1-Li1 74.5(2), F2-Li1-P1 81.1(3), P1-Si2-F2 99.9(1), P1-Si1-F1 110.4(1).

Li center in the analogous bis(di-*tert*-butylfluorosilyl)phosphanide[7] is not coordinated by the phosphorous atom, but by the two fluorine atoms in a chelating fashion. The substituents in **7** are apparently bulkier, and the observed arrangement provides efficient space filling. The Li1–F2 distance is 1.998(9) Å, and the Si2–F2 bond length (1.666(3) Å) is, as expected, longer than that of Si1–F1 (1.619(3) Å). However, this has no effect on the Si–P bond lengths (2.195 and 2.199(2) Å), which are in the range observed in related fluorosilylphosphanides.[8]

Heating a solution of **7** to 70 °C results in loss of LiF and formation of the desired 2-phospha-1,3-disilaallyl fluoride **1**, which crystallizes from hot toluene(!) as pale yellow cubes. The ^{31}P NMR spectrum of **1** (Table 1) shows a doublet ($\delta = -33.0$, $^2J(P,F) = 44$ Hz), which is at relatively high field for phosphasilenes. This indicates greater σ-donor character of the fluorodiorganosilyl group with respect to the triorganosilyl group.[2] All of the structures calculated by ab initio methods and the "thermally corrected" relative free energies were determined at the MP2/6-31G* level.[9] The calculated Si=P bond length in the parent compound **D** is 2.070 Å (Scheme 1), and the Si–P bond length in **D** is 2.235 Å. The crystal structure analysis of **1**,[6] which is unfortunately disordered in the crystal, gave similar distances. In addition, it showed that the fluorine atom is located in a position *trans* to the *tert*-butyl group. An isolated Si=P bond is present, and there are no intramolecular or intermolecular Si-F-Si contacts (Figure 2).

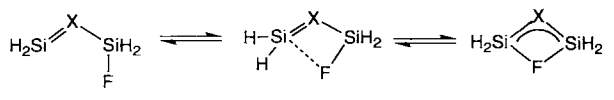

D **E** **F**

Relative free energy (298 K) ΔG [kcal mol^{-1}]

	D (C_s, min.)	E (C_1, TS)	F (C_s, min.)
X = P	0.0	14.7	12.5
X = CH	0.0	24.2	23.9
distances [Å]			
Si=P/Si-F	2.070/1.628	2.100/1.725[a]	2.147/1.852
Si=C/Si-F	1.719/1.626	1.747/1.804[b]	1.759/1.871

[a] Si···F 2.193 Å; [b] Si···F 1.980 Å

Scheme 1. Ab initio calculated migration of fluorine in **D** with the transition states **E** and **F**; X = P, CH. ΔG is the difference in the Gibbs free energy [kcal mol^{-1}] at 298.15 K, min = minimum, TS = transition state.

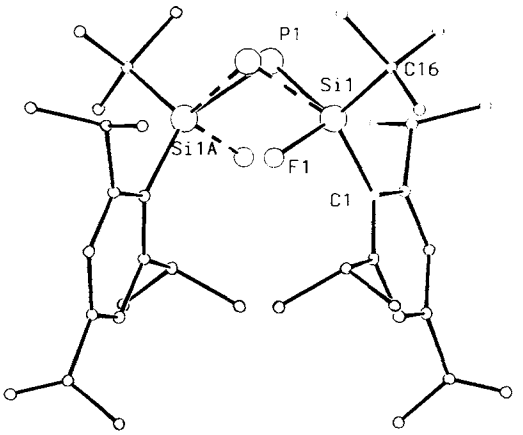

Figure 2. Crystal structure of **1**, which is disordered (two sites for both the P and F atoms). Selected distances [Å] and angles [°]: P1–Si1A 2.053(2), P1–Si1 2.207(2), Si1–F1 1.764(3), Si1–C16 1.895(4), Si1–C1 1.879(4); Si1A-P1-Si1 104.60(9), P1-Si1-F1 74.1(1), P1-Si1A-C16 105.4(1), P1-Si1A-C1 139.7(1), C1-Si1A-C16 114.1(2).

The ^1H NMR spectrum of **1** shows two types of anisochronic *tert*-butyl groups and aryl protons, and confirms that the isolated Si=P bond is retained in solution at 25 °C. Equilibration of the *tert*-butyl groups and thus fluctuation of the fluorine atom (suprafacial [1,3]-sigmatropic shift) is first observed at about 40 °C in [D_8]toluene. Therefore, this process has a Gibbs activation energy of about 16 kcal mol^{-1}. Until now, such fluctional behavior had only been observed in the silaethene $Me_2Si{=}C(SiMe_3)_2$.[10] We studied the reaction pathway of the [1,3]-fluorine shift in **D** with the fragments X = P (2-phospha-1,3-disilaallylfluoride) and X = CH (1,3-disilaallylfluoride) with ab initio calculations.[9] The transition state approximately corresponds to the expected structure **F**, with a symmetrically bridging fluorine atom between the silicon centers, only in the case of X = CH, whereas the transition state for X = P is described by **E** (Scheme 1). The experimentally verified migration of the methyl group of $Me_2Si{=}C(SiMe_3)_2$ occurs via a transition state with a structure analogous to that of **F** (as for **D** when X = CH).[10] For X = P, the calculated barrier of 14.7 kcal mol^{-1} agrees well with the experimental value of 16 kcal mol^{-1} for **1**. The barrier for $H_2Si = CH(SiH_2F)$, which is approximately 10 kcal mol^{-1} higher and results from the relatively high ring strain of **F**, is noteworthy.

We then carried out studies to investigate whether **1** could be converted to **4** by addition of lithium to the Si=P bond, and whether the lithium 1,3-disila-2-phosphaallyl anion **5** could be obtained by subsequent elimination of LiF. Addition of lithium to **1** does indeed occur at room temperature in THF, and **4** is formed as an extremely reactive intermediate.

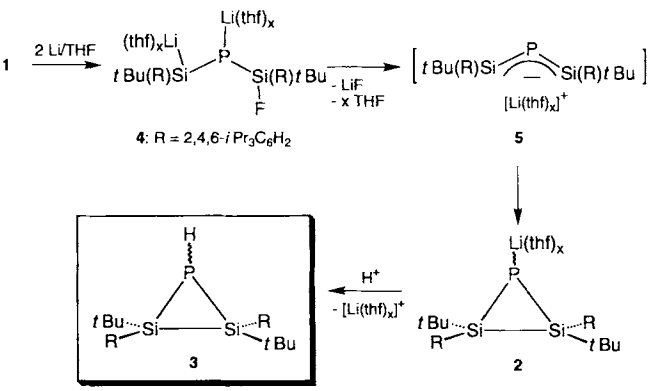

We were only recently able to prepare compounds of the type **4** from other phosphasilenes.[11] Because of its very high reactivity, it was only possible to characterize **4** by means of ^{31}P NMR spectroscopy, which shows a doublet at very high field ($\delta = -306$, $^2J(P,F) = 38$ Hz) at 25 °C (Table 1). However, gentle warming of **4** to 40 °C in THF or hexane initially leads to strongly basic **2** by elimination of LiF. This in turn is protonated (partially under the reaction conditions and completely upon work-up in anhydrous hexane) to form **3**. The hydrogen atom on the phosphorus atom in **3** originates from the THF ligands that initially solvate the lithium center in **2** and are then partially cleaved due to the strong basicity of the phosphanide (ether cleavage). The conversion of **4** into the ring compound **2** with elimination of LiF most likely occurs via **5**. The shift from **5** to **2** would be a particularly interesting parallel to the isomerization of bis(methylene)phosphoranes to phosphacyclopropanes.[12] Since the electrons in the HOMO of allyl anions are localized at the 1,3 positions and this structure is very unfavorable for the electropositive Si centers, the formation of a Si–Si bond proves very effective. In contrast, and as expected, no cyclization is observed for the "inverse" 1,3-diphospha-2-silaallyl anions **A** with more electronegative phosphorus atoms at the 1,3 positions.[3]

The composition of **3** was confirmed by mass spectrometry, and its structure determined by NMR spectroscopy (Table 1) and crystallography.[6] The ^{31}P NMR spectrum shows a doublet with ^{29}Si satellites at high field ($\delta = -325$), as expected for phosphasilacyclopropanes,[14] with a relatively small coupling constant of $^1J(P,H) = 161$ Hz. Furthermore, the $^1J(P,Si)$ coupling constant of 36 Hz is much smaller than that for other phosphacyclopropanes ($^1J(P,Si) = 72.5-121.7$ Hz).[13] The high degree of p character of the P–Si bonds apparently lowers ring strain. Geometry optimization of the derivative **3*** was carried out with the density-function method by Becke (B3LYP/6-31G*), and the ^{31}P and ^{29}Si NMR chemical shifts were calculated at the GIAO/6-311++G(2d,2p) level.[9] The $\delta(^{31}P)$ and $\delta(^{29}Si)$ values for **3*** (−344 and −48.4, respectively) agree well with the experimental values for **3** (−325 and −43.6/−44.5).

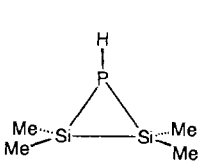

3*

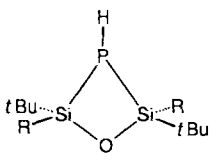

8: R = 2,4,6-*i*Pr$_3$C$_6$H$_2$

The *two* doublet signals at high field ($\delta = -43.6$ and -44.5, $^1J(Si,P) = 36$ Hz) in the ^{29}Si NMR spectrum of **3** are characteristic for silacyclopropanes[14] and show unequivocally that the two silicon atoms are not chemically equivalent. These data are only consistent with the *trans* configuration of the *tert*-butyl groups on silicon and pyramidal coordination of the phosphorus atom, as confirmed by crystal-structure analysis (Figure 3).[6]

Until now, single crystals were only obtained of a mixture of **3** and the novel four-membered PSi_2O heterocycle **8** (ratio about 7:1). As a result of this "disorder", a discussion of the geometrical parameters is not meaningful. Surprisingly, **8** is formed as a side product (about 10 %, ^{31}P NMR) in the reaction of **1** with lithium in THF. The oxygen atom in **8** most likely originates from THF. We can exclude both unintentional entry of air and the presence of surface oxide/hydroxide on the lithium powder as possible sources of oxygen from control experiments. These

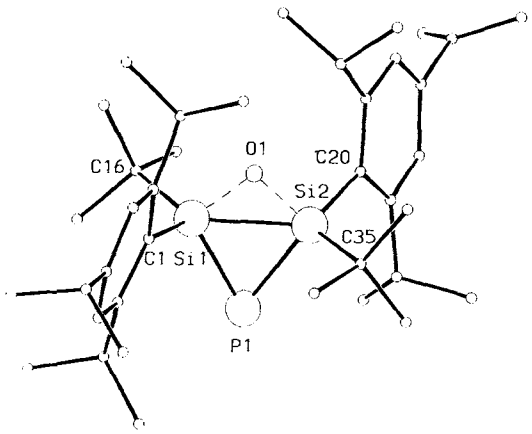

Figure 3. Overlap of the crystal structures of **3** and **8** (ratio about 7:1). Selected distances [Å] and angles [Å]: Si1–Si2 2.357(3), Si1–P1 2.292(3), Si2–P1 2.282(2), Si1–O1 1.56(2), Si2–O1 1.57(2); Si1-P1-Si2 62.04(8), P1-Si1-Si2 58.76(8), P1-Si2-Si1 59.20(7), C1-Si1-C16 114.7(2), C35-Si2-C20 115.0(2).

showed that **1** is inert to suspensions of Li_2O/LiOH in THF and that solutions of **3** and **8** do not react with oxygen in the air at room temperature.

The calculated Si–P (2.318 Å) and Si–Si (2.285 Å) distances as well as the endocyclic angles on phosphorus (59.06°) and silicon (60.47°) in **3*** show no principle differences to the corresponding experimental values of other heterodisilacyclopropanes with a Si_2X framework (X = O, S, Te, C, Ge, N, W).[14] In contrast, the calculated Si–Si distance in *P*-metallated phosphadisilacyclopropane derivatives of **3*** varies considerably depending on the nature of the metal center (s-, p-, and d-block metals), because the Si–Si bond can act as a σ and/or a π donor towards the metal centers. We are currently attempting to synthesize a heteroallyl π complex with the Si_2P framework.

Experimental Section

7: **6** (5.0 g, 7.74 mmol) in THF (50 mL) was allowed to react with *n*-BuLi (0.49 g, 7.74 mmol, 2.5 M solution in hexane) at −78 °C. The clear yellow solution was warmed slowly to 25 °C, and the solvent removed under vacuum (10^{-2} Torr). The residue was dissolved in a little hexane, and colorless, air-sensitive **7** crystallized at 25 °C. Yield: 5.3 g (6.6 mmol, 86 %).

1: **7** (5.3 g, 6.6 mmol) was stirred in toluene (50 mL) for 8 h at 70 °C. On cooling, poorly soluble **1** was obtained as extremely air-sensitive, pale yellow crystals. Yield: 3.7 g (5.9 mmol, 88 %).

3: **1** (2.0 g, 3.2 mmol) was stirred with Li powder (about 100 mg) in THF (30 mL) at 25 °C. Compound **4** was formed within 2–4 h (^{31}P NMR). The solvent was removed, and the yellow residue dissolved in hexane. Excess lithium powder was filtered off. The colorless solution was concentrated under reduced pressure (10^{-2} Torr) at 25 °C, and colorless crystals were formed (about 90 % **3** and 10 % **8**; ^{31}P NMR). Yield: 1.5 g (2.5 mmol, 78 %).

Received: August 5, 1996 [Z9425IE]
German version: *Angew. Chem.* **1997**, *109*, 1384–1387

Keywords: allyl compounds · heterocycles · lithium · phosphorus · silicon

[1] Recent review on Si=C: A. G. Brook, M. A. Brook, *Adv. Organomet. Chem.* **1996**, *39*, 71; Si=Si: R. Okazaki, R. West, *ibid.*, 232; Si=N: I. Hemme, U. Klingebiel, *ibid.*, 159; Si=S: H. Suzuki, N. Tokitoh, S. Nagase, R. Okazaki, *J. Am. Chem. Soc.* **1994**, *116*, 11578.

[2] Recent review on Si=P and Si=As: M. Driess, *Adv. Organomet. Chem.* **1996**, *39*, 193, and references therein; *Coord. Chem. Rev.* **1995**, *145*, 1; M. Driess, H. Pritzkow, S. Rell, U. Winkler, *Organometallics* **1996**, *39*, 193.

[3] E. Niecke, E. Klein, M. Nieger, *Angew. Chem.* **1989**, *101*, 792; *Angew. Chem. Int. Ed. Engl.* **1989**, *28*, 751.

[4] G. E. Underiner, R. P. Tan, D. R. Powell, R. West, *J. Am. Chem. Soc.* **1991**, *113*, 8437.

 © VCH Verlagsgesellschaft mbH, D-69451 Weinheim, 1997 0570-0833/97/3612-1328 $ 17.50+.50/0

[5] M. Driess, H. Pritzkow, S. Rell, unpublished results. Compound **6** is formed by salt condensation from Is(*t*Bu)Si(F)–PHLi with Is(*t*Bu)SiFCl. Is = 2,4,6-iPr$_3$C$_6$H$_2$.

[6] Crystal structure analyses: All intensity measurements were carried out on a Siemens-Stoe AED2 diffractometer at −70 °C. The H atoms were placed in calculated positions, and the other atoms refined anisotropically [15]. **7**: rhombic, space group $P2_12_12_1$, $a = 15.392(8)$, $b = 17.995(9)$, $c = 18.026(9)$ Å, $V = 4993$ Å^3, $Z = 4$, 4880 independent reflections ($Mo_{K\alpha}$ radiation, ω scans, $2\theta_{max} = 50°$), $R1 = 0.047$ (observed reflections, $I > 2\sigma(I)$), $wR2 = 0.126$ (all reflections) [15b]. The THF molecules are disordered. **1**: monoclinic, space group $C2/c$, $a = 27.94(2)$, $b = 9.905(6)$, $c = 21.443(14)$ Å, $\beta = 138.34(3)°$, $V = 3945$ Å^3, $Z = 4$, 3883 independent reflections ($Mo_{K\alpha}$ radiation, ω scans, $2\theta_{max} = 54°$), $R1 = 0.063$ (observed reflections, $I > 2\sigma(I)$), $wR2 = 0.169$ (all reflections) [15b]. The molecule is disordered; two sites are half occupied by a phosphorus and fluorine atom, respectively. Moreover, the *tert*-butyl groups and the aryl substituents show rotational disorder. **3**: triclinic, space group $P\bar{1}$, $a = 9.312(8)$, $b = 10.300(8)$, $c = 11.673(9)$ Å, $\alpha = 74.35(6)$, $\beta = 78.38(6)$, $\gamma = 65.63(6)°$, $V = 976.8$ Å^3, $Z = 1$, 5591 independent reflections ($Mo_{K\alpha}$ radiation, ω scans, $2\theta_{max} = 60°$), $R1 = 0.056$ (observed reflections, $I > 2\sigma(I)$), $wR2 = 0.137$ (all reflections) [15b]. The crystals contain about 14 % of **8** as an impurity. The observed structure is an overlap of both structures. Crystallographic data (excluding structure factors) for the structures reported in this paper have been deposited with the Cambridge Crystallographic Data Centre as supplementary publication no. CCDC-100141. Copies of the data can be obtained free of charge on application to The Director, CCDC, 12 Union Road, Cambridge CB21EZ, UK (fax: int. code +(1223)336-033; e-mail: deposit@chemcrys.cam.ac.uk).

[7] U. Klingebiel, M. Meyer, U. Pieper, D. Stalke, *J. Organomet. Chem.* **1991**, *408*, 19.

[8] M. Driess, U. Winkler, W. Imhof, L. Zsolnai, G. Huttner, *Chem. Ber.* **1994**, *127*, 1031, and references therein.

[9] GAUSSIAN 94, Revision B. 3., M. J. Frisch, G. W. Trucks, H. B. Schlegel, P. M. W. Gill, B. G. Johnson, M. A. Robb, J. R. Cheeseman, T. Keith, G. A. Petersson, J. A. Montgomery, K. Raghavachari, M. A. Al-Laham, V. G. Zakrzewski, J. V. Oritz, J. B. Foresman, C. Y. Peng, P. Y. Ayala, W. Chen, M. W. Wong, J. L. Andres, E. S. Replogle, R. Gomperts, R. L. Martin, D. J. Fox, J. S. Binkley, D. J. Defrees, J. Baker, J. P. Stewart, M. Head-Gordon, C. Gonzalez, J. A. Pople, Gaussian, Inc., Pittsburgh PA, **1995**.

[10] N. Wiberg, H. Köpf, *Chem. Ber.* **1987**, *120*, 653.

[11] M. Driess, H. Pritzkow, *Z. Anorg. Allg. Chem.* **1996**, *622*, 858.

[12] W. W. Schoeller, T. Busch, *J. Chem. Soc. Chem. Commun.* **1989**, 234.

[13] M. Baudler, H. Jongebloed, *Z. Anorg. Allg. Chem.* **1979**, *458*, 9; M. Weidenbruch, M. Herrndorf, A. Schaefer, K. Peters, H. G. von Schnering, *J. Organomet. Chem.* **1985**, *295*, 7; M. Baudler, T. Pontzen, *Z. Anorg. Allg. Chem.* **1982**, *491*, 27; M. Driess, H. Pritzkow, *Angew. Chem.* **1992**, *104*, 775; *Angew. Chem. Int. Ed. Engl.* **1992**, *31*, 751; M. Driess, H. Pritzkow, M. Reisgys, *Chem. Ber.* **1991**, *124*, 1923.

[14] Recent review on Si_2X three-membered rings: M. Weidenbruch, *Chem. Rev.* **1995**, *95*, 1489, and references therein.

[15] a) G. M. Sheldrick, *SHELXS86*, Universität Göttingen (Germany), **1986**; b) G. M. Sheldrick, *SHELXL93*, Universität Göttingen, **1993**.

Hexaphenylethane Derivatives Exhibiting Novel Electrochromic Behavior**

Takanori Suzuki,* Jun-ich Nishida, and Takashi Tsuji

9,9,10,10-Tetraphenyl-9,10-dihydrophenanthrene (**3**) is a stable molecule[1] whose central C–C bond is predicted to be the longest among "clamped" hexaphenylethane derivatives.[2] Although this weakened bond is resistant to homolytic rupture, the activation energy for its scission can be lowered by electron transfer,[3] especially when suitable substituents are introduced. Bearing this in mind, we have now designed a new redox system in which reversible C–C bond breaking and bond making occur upon two-electron transfer (Scheme 1). This system has the following interesting features: 1) the four dimethylamino and methoxy substituents in **1a** and **1b**, respectively, should facilitate the removal of electrons from these molecules, thereby activating the scissile bond; 2) the central bond in **1** like that in **3** is still expected to be sufficiently stable against homolysis taking into consideration that the aromatic substituents have little effect on the Gibbs activation energy of the homolytic cleavage $\Delta G^{\neq}_{homolysis}$ in 1,2-diarylethanes;[3,4] 3) the dications $\mathbf{2}^{2+}$ formed by the oxidation of **1** should be stabilized by delocalization of each positive charge over half of the molecule and due to the presence of the triarylmethylenium chromophores these cations are intensely colored; 4) the interconversions between **1** and $\mathbf{2}^{2+}$ should proceed very cleanly because they are intramolecular processes. Here we report the preparation, properties, and structures of these novel redox couples.

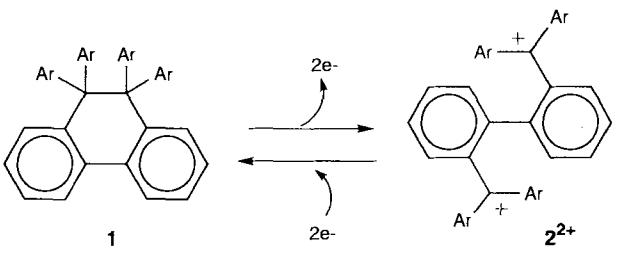

a: Ar = *p*-$Me_2NC_6H_4$; **b**: Ar = *p*-$MeOC_6H_4$

Scheme 1. Dynamic redox behavior of **1** and $\mathbf{2}^{2+}$.

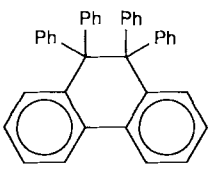

3

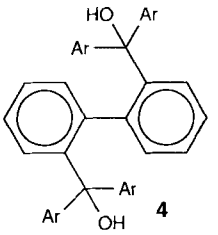

4

The dication salts $\mathbf{2a}^{2+}(BF_4^-)_2$ and $\mathbf{2b}^{2+}(BF_4^-)_2$ were obtained in 98 and 93% yield by treating the diols **4a**[5] and **4b**, respectively, with HBF_4. Reduction of these salts with Mg in MeCN gave ethanes **1a** and **1b** as stable solids in 86 and 93% yield, respectuvely. On the other hand, oxidation of **1a** and **1b** with two equivalents of $(p\text{-}BrC_6H_4)_3N^{+\bullet}SbCl_6^-$ in CH_2Cl_2 led to the regeneration of the dications $\mathbf{2a}^{2+}$ and $\mathbf{2b}^{2+}$, which were isolated as $SbCl_6^-$ salts in 85 and 97% yield, respectively. The high-yield interconversions between **1** and $\mathbf{2}^{2+}$ indicate that they constitute "reversible" redox couples, although the bond breaking and making are induced by electron transfer.

The sharp contrast in the UV/Vis spectra of these couples is noteworthy. Ethanes **1** show absorption only in the UV region, whereas intense absorption bands in the visible region occur for the dications $\mathbf{2a}^{2+}$ [λ_{max} (MeCN): 661 (lgε 4.92), 604 nm (5.05)] and $\mathbf{2b}^{2+}$ [539 sh (4.72), 514 (4.87)]. Thus, electrochromic systems with color changes from colorless to deep blue and colorless to deep red could be constructed by using *p*-dimethylamino

[*] Prof. T. Suzuki, J. Nishida, Prof. T. Tsuji
Division of Chemistry, Graduate School of Science
Hokkaido University, Sapporo 060 (Japan)
Fax: Int. code +(11)746-2557
e-mail: taku@science.hokudai.ac.jp

[**] This work was supported by the Ministry of Education, Science, and Culture of Japan (Grant No. 06640675 and 08640664) and by Hokscitec Foundation. We thank Prof. Tamotsu Inabe (Hokkaido University) for the use of facilities to analyze the X-ray structures.

 © VCH Verlagsgesellschaft mbH, D-69451 Weinheim, 1997 0570-0833/97/3612-1329 $ 17.50+.50/0

and *p*-methoxy derivatives, respectively. Spectrophotometric monitoring of the electrochemical reduction of $\mathbf{2}^{2+}$ to **1** revealed the presence of several isosbestic points in both cases (Figure 1), indicating the quantitative conversion as well as the negligible steady-state concentration of the intermediary cation radicals.

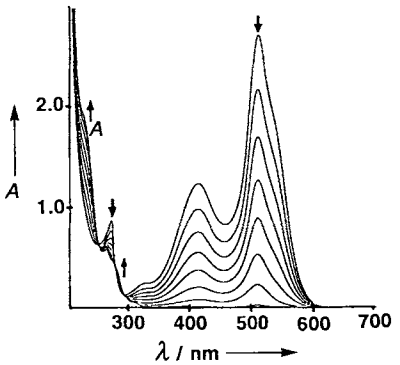

Figure 1. Change in UV/Vis spectrum of $\mathbf{2b}^{2+}(BF_4^-)_2$ (3.6×10^{-5} mol dm^{-3}, 2 mL) upon electrochemical reduction (10 μA) at 3 min intervals. The coulometric analysis indicates that the interconversion is a two-electron process.

Not only the color but also the geometry change drastically during the interconversion, as determined by the X-ray structure analyses.[6] While the biphenyl skeleton of **1b** is nearly planar (Figure 2a), the two molecular halves in $\mathbf{2a}^{2+}$ are twisted by 69° around the biphenyl axis; the distance between the two methylenium carbon atoms is 3.66(2) Å (Figure 2b). Such a dynamic change in structure causes the hysteretic redox properties of **1** and $\mathbf{2}^{2+}$ (Figure 3). Thus, **1a** and **1b** undergo electrochemical oxidation at peak potentials of +0.77 and +1.47 V vs. SCE in CH_2Cl_2, respectively. These processes are irreversible in the sense that the corresponding cathodic peaks were absent in the cyclic voltammograms (scan rate: 100–500 mV s^{-1}). Instead, new peaks appeared in the far cathodic region (−0.45 and +0.18 V, respectively), which were assigned to the reduction potentials of $\mathbf{2a}^{2+}$ and $\mathbf{2b}^{2+}$. This assignment was confirmed by separate measurements on $\mathbf{2}^{2+}(BF_4^-)_2$ salts under the same conditions. Again, quite similar hysteretic behavior was observed in the voltammograms of $\mathbf{2}^{2+}$, which showed new anodic peaks corresponding to the oxidation potentials of **1**.

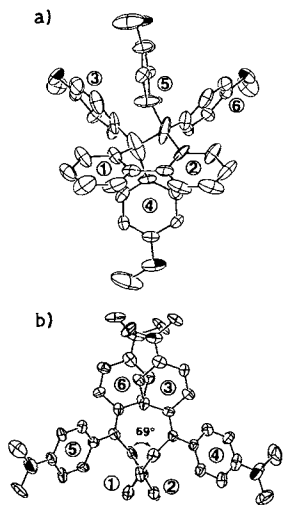

Figure 2. a) Molecular geometry of **1b** determined by X-ray structure analysis on the **1b**·THF solvate crystal. Two aryl groups (3 and 6) are equatorial and the other two (4 and 5) are axial substituents in the pseudo-half-chair six-membered ring. b) Molecular geometry of $\mathbf{2a}^{2+}$ determined by X-ray structure analysis on the $\mathbf{2a}^{2+}(SbCl_6^-)_2$ salt. The dication has pseudo-C_2 symmetry. Two aryl groups (3 and 6) overlap each other in a face-to-face manner (interplanar distance, 3.37 Å; dihedral angle 11.5°), indicating the π–π interaction between these rings.

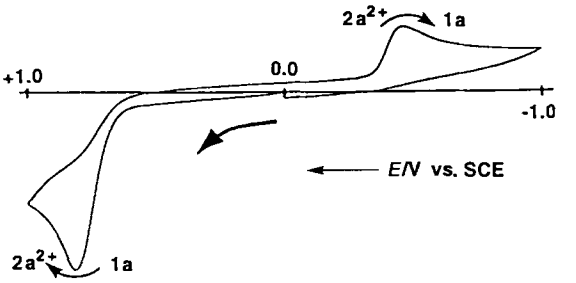

Figure 3. Cyclic voltammogram of **1a** in CH_2Cl_2 (0.1 M nBu$_4$NBF$_4$, Pt electrode, scan rate 500 mV s^{-1}). The reduction peak at −0.45 V was absent when the voltammogram was first scanned to the cathode.

Such separation of redox potentials is characteristic of "dynamic redox systems" that undergo reversible and drastic structural change during electron transfer, as in the present case.[7] In the region between the reduction potential and the oxidation potential, both the reduced form (**1**) and the oxidized form ($\mathbf{2}^{2+}$) can coexist in any ratio. By combining **1** with a suitable electron acceptor, it may be possible to apply this unique feature to the construction of novel redox-type photochromic systems in which the back reactions in the dark become endothermic due to the large shift of redox potentials.

Experimental Section

4b: The reaction of 4,4′-dimethoxybenzophenone and 2,2′-dilithiobiphenyl in THF afforded **4b** as a colorless powder in 47%. M.p. 226–228 °C; ^{1}H NMR (90 MHz, $CDCl_3$): δ = 6.97–7.13 (m, 10H), 6.71–6.89 (m, 12H), 6.05–6.15 (m, 2H), 4.35 (s, 2H), 3.82 (s, 6H), 3.78 (s, 6H).

$\mathbf{2}^{2+}(BF_4^-)_2$: To a solution of diol **4a** (5.65 g, 8.18 mmol) in THF (100 mL) was added 42% HBF_4 (2.60 mL, 17.4 mmol) over 10 min at 0 °C. After the mixture had been stirred for 18 h at room temperature, deep-blue microcrystals of $\mathbf{2a}^{2+}(BF_4^-)_2$ (6.64 g, 98%) were filtered, and washed with THF and ether, m.p. 316–317 °C (decomp); ^{1}H NMR (400 MHz, $CDCl_3$, 25 °C): δ = 7.60 (br., 2H), 7.23 (ddd, J = 7.6, 7.6, 1.5 Hz, 2H), 7.17 (ddd, J = 7.6, 7.6, 1.5 Hz, 2H), 7.13 (br. AA′XX′, 4H), 7.05 (dd, J = 7.6, 1.5 Hz, 2H), 6.98 (dd, J = 7.6, 1.5 Hz, 2H), 6.92–7.02 (br., 6H), 6.77 (br. AA′XX′, 4H), 3.37 (s, 12H), 3.20 (s, 12H); ^{13}C NMR (100 MHz, CD_3CN): δ = 174.65, 158.21, 157.26, 143.86, 141.99, 140.38, 139.67, 133.93, 133.61, 131.29, 128.16, 128.04, 127.85, 114.81, 114.08, 41.50, 41.04; UV/Vis (MeCN): λ_{max} (lgε) = 661 (4.92), 604 (5.05), 431 (4.50), 408 (4.41), 319 nm (4.50). Diol **4b** was similarly treated with 42% HBF_4 in propionic anhydride, and $\mathbf{2b}^{2+}(BF_4^-)_2$ was obtained as a red powder in 93% yield, m.p. 200.5–202 °C (decomp); ^{13}C NMR (100 MHz, CD_3CN): δ = 192.63, 175.39, 172.50, 146.8 (br.), 144.39, 143.02, 140.93, 136.63, 134.48, 134.42, 134.04, 132.56, 128.62, 118.47, 117.71, 59.09, 58.20; UV/Vis (MeCN): λ_{max} (lgε) = 539 sh (4.72), 514 (4.87), 416 (4.54), 335 (3.83), 274 nm (4.36).

1: A suspension of $\mathbf{2b}^{2+}(BF_4^-)_2$ (173 mg, 0.222 mmol) and Mg turnings (740 mg, 30.4 mmol) in dry MeCN (10 mL) was stirred for 22 h at room temperature. The solvent was evaporated, and the residue was triturated with benzene. Chromatographic separation on Al_2O_3 (benzene) afforded **1b** (126 mg, 93%) as a colorless solid, m.p. 270–272 °C (decomp); ^{1}H NMR (400 MHz, $CDCl_3$, 50 °C): δ = 7.68 (dd, J = 7.8, 1.5 Hz, 2H), 7.23 (ddd, J = 7.8, 7.8, 1.5 Hz, 2H), 7.16 (dd, J = 7.8, 1.5 Hz, 2H), 7.11 (ddd, J = 7.8, 7.8, 1.5 Hz, 2H), 6.93 (br., 8H), 6.48 (br., 8H), 3.70 (s, 12H); UV/Vis (MeCN): λ_{max} (lgε) = 287 (4.13), 274 nm (4.25). Similarly **1a** was obtained as a colorless solid in 86% yield by Mg reduction of $\mathbf{2a}^{2+}(BF_4^-)_2$, m.p. 315–317 °C (decomp); ^{1}H NMR (400 MHz, $CDCl_3$, 50 °C): δ = 7.65 (dd, J = 7.8, 1.0 Hz, 2H), 7.21 (dd, J = 7.8, 1.0 Hz, 2H), 7.18 (ddd, J = 7.8, 7.8, 1.0 Hz, 2H), 7.07 (ddd, J = 7.8, 7.8, 1.0 Hz, 2H), 6.91 (br. AA′XX′, 8H), 6.31 (br. AA′XX′, 8H), 2.83 (s, 24H); UV/Vis (MeCN): λ_{max} (lgε) = 268 nm (4.87).

$\mathbf{2}^{2+}(SbCl_6^-)_2$: To a solution of **1a** (35 mg, 0.053 mmol) in CH_2Cl_2 (10 mL) was added (p-$BrC_6H_4)_3N^+SbCl_6^-$ (90 mg, 0.110 mmol), and the mixture was stirred for 1.5 h at room temperature. Deep blue precipitates of $\mathbf{2a}^{2+}(SbCl_6^-)_2$ (60 mg, 85%) were filtered, and washed with CH_2Cl_2, m.p. 300–320 °C (decomp). Similar oxidation of **1b** afforded $\mathbf{2b}^{2+}(SbCl_6^-)_2$ in 97% yield, m.p. 174.5–177 °C (decomp); ^{1}H NMR (400 MHz, CD_3CN, 24 °C): δ = 7.46 (ddd, J = 7.3, 7.3, 1.5 Hz, 2H), 7.41 (ddd, J = 7.3, 7.3, 1.5 Hz, 2H), 7.33 (dd, J = 7.3, 1.5 Hz, 2H), 7.23-7.33 (br. AA′XX′, 8H), 7.17 (dd, J = 7.3, 1.5 Hz, 2H), 7.09-7.15 (br. AA′XX′, 8H), 4.09 (br. s, 6H), 4.07 (br. s, 6H).

All the new compounds gave satisfactory analytical data, and IR and mass spectra.

Received: November 4, 1996 [Z9726IE]
German version: *Angew. Chem.* **1997**, *109*, 1387–1389

Keywords: carbocations · dyes · electrochemistry · redox chemistry

[1] G. Wittig, H. Petri, *Justus Liebigs Ann. Chem.* **1933**, *505*, 17.
[2] W. D. Hounshell, D. A. Dougherty, J. P. Hummel, K. Mislow, *J. Am. Chem. Soc.* **1977**, *99*, 1916.
[3] P. Maslak, J. N. Narvaez, T. M. Vallombroso, Jr., *J. Am. Chem. Soc.*, **1995** *117*, 12373; P. Maslak, W. H. Chapman, Jr., T. M. Vallombroso, Jr., B. A. Watson, *ibid.* **1995**, *117*, 12380.
[4] G. Kratt, H. -D. Beckhaus, C. Rüchardt, *Chem. Ber.* **1984**, *117*, 1748.
[5] G. Wittig, W. Herwig, *Chem. Ber.* **1954**, *87*, 1511.
[6] **1b**·THF: $C_{42}H_{36}O_4 \cdot C_4H_8O$, orthorhombic $Pna2_1$, $a = 8.277(2)$, $b = 34.15(1)$, $c = 13.025(5)$ Å, $V = 3681(2)$ Å^3, ρ_{calcd} ($Z = 4$) = 1.222 g cm^{-1}, $R = 0.086$. The structural parameters of **1b** are not reliable enough to allow a comparison with those of calculated **3** due to the low quality of the data for the structural determination (large thermal motion and positional disorder). **2a**$^{2+}$$(SbCl_6^-)_2$ salt: $C_{46}H_{48}Cl_{12}N_4Sb_2$, monoclinic $C2/c$, $a = 34.187(6)$, $b = 12.638(6)$, $c = 30.664(6)$ Å, $\beta = 119.98(1)^\circ$, $V = 11475(6)$ Å^3, ρ_{calcd} ($Z = 8$) = 1.535 g cm^{-1}, $R = 0.079$. Crystallographic data (excluding structure factors) for the structures reported in this paper have been deposited with the Cambridge Crystallographic Data Centre as supplementary publication no. CCDC-100006. Copies of the data can be obtained free of charge on application to The Director, CCDC, 12 Union Road, Cambridge CB2 1EZ, UK (fax: int. code +(1223) 336-033; e-mail deposit@chemcrys.cam.ac.uk).
[7] Similar potential separation was also observed in 1,3-dimethylenecyclobutanes or bicyclic trichalcogenides which undergo structural change accompanied with transannular bonding upon two-electron oxidation: M. Horner, S. Hünig, *J. Am. Chem. Soc.* **1977**, *99*, 6122; H. Fujihara, H. Mima, T. Erata, N. Furukawa, *ibid.* **1992**, *114*, 3117. Linkage isomerism in the transition metal complexes also leads to molecular hysteresis of this kind: M. Sano, H. Taube, *ibid.* **1991**, *113*, 2327; A. Livoreil, C. O. Dietrich-Buchecker, J. -P. Sauvage, *ibid.* **1994**, *116*, 9399.

Perfectly Staggered and Twisted Difluoromethylene Groups in Perfluoroalkyl Chains: Structure of M[$C_4F_9SO_2NSO_2C_4F_9$] (M = Na, K)**

Lixin Xue, Darryl D. DesMarteau,* and William T. Pennington*

In contrast to the perfectly all-staggered conformation observed for *n*-alkanes, the generally accepted structure of a perfluorinated *n*-alkane involves a helical conformation of the carbon backbone.[1] This is presumably due to the larger van der Waals radius of fluorine relative to that of hydrogen; rotation about the carbon–carbon chain bonds occurs to increase the distance between fluorine atoms on carbon atoms separated by one CF_3 group.[2]

Polytetrafluoroethylene possesses a helical structure at ambient conditions, but undergoes a solid–solid phase transition to a planar zigzag conformation under increased pressure.[3, 4] A similar transition occurs for perfluoro-*n*-alkanes, but at considerably lower pressure.[5] In a recent article it has been suggested that short perfluorinated carbon chains take on a planar zigzag structure rather than a helical one at ambient pressure, when closely packed on the surface of a substrate.[6] In that report, the structures of thin films of perfluorodecanoic acid deposited on glass were investigated by a combination of low-angle X-ray diffraction, X-ray grazing-incidence diffraction and molecular modeling. The compound was found to be present as two phases, and for both phases the best model had carbon chains that were untwisted. We have obtained more direct evidence, based on single-crystal X-ray diffraction analysis, of similar behavior for the perfluoro-*n*-alkyl side chains of the sodium salts **1**–**3** of bis[(perfluoroalkyl)sulfonyl] imides.

Na[$C_mF_{2m+1}SO_2NSO_2C_nF_{2n+1}$]

1, $m = n = 4$; **2**, $m = n = 6$; **3**, $m = 4$, $n = 6$

In this communication, we report the crystal structure of **1**,[7] a representative member of the series, and contrast its structure with that of a potassium derivative of **1** (compound **4**, $m = n = 4$).[8] A more thorough discussion of all of these compounds will appear later.[9]

The remarkable acidity of bis[(perfluoroalkyl)sulfonyl] imides[10, 11] is due, in part, to the resonance stabilization of the conjugate base anions of the acids. Extensive delocalization of charge over the SO_2-N-SO_2 framework allows these anions to serve as multidentate ligands that bond to multiple metal centers to maximize electrostatic interaction.[12] These interactions result in the formation of ionic hydrophilic regions and perfluoro hydrophobic regions, which typically associate into layers consisting of an ionic core and perfluoro surfaces.[13, 14] This behavior is observed in **1**; the sodium ion (Figure 1, left) interacts strongly with the nitrogen atom of the anion (interatomic distance 2.531(7) Å) and is chelated by a pair of sulfonyl oxygen atoms (Na1–O1b,O1c 2.331(5) Å) of an anion related by translation along the **b** axis to form ion-pair chains; chains related by inversion symmetry (1/2, 0, 0) are connected by additional interactions between the sodium ion and sulfonyl oxygen atoms (Na1–O2d,O2e 2.356(4) Å) to form layers, which stack along the *a* axis (Figure 1, right). Due to the strong interactions in-

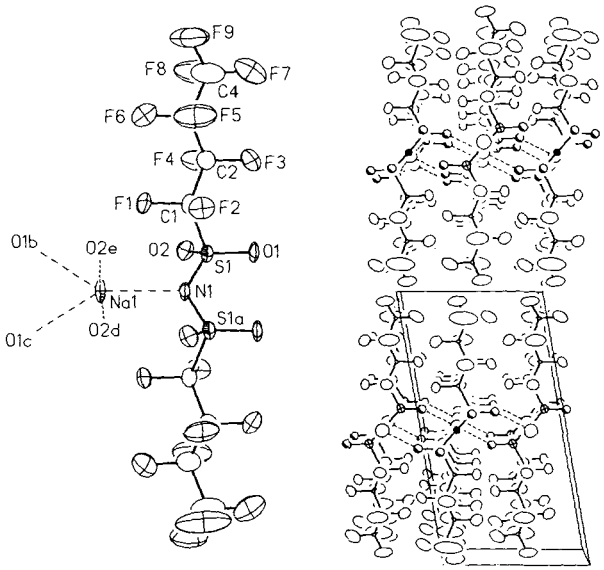

Figure 1. a) Left: Crystal structure of **1** *(thermal ellipsoids at 50% probability), showing the interionic contacts and the atom labeling scheme used. Atoms containing a lower case character in their labels were generated by the following symmetry operations: a) $1-x, y, 1/2-z$; b) $x, y-1, z$; c) $1-x, y-1, 1/2-z$; d) $1-x, -y, -z$; e) $x, -y, 1/2+z$. Right: crystal packing of* **1** *viewed down the b axis. The origin is the lower left rear corner; $+x$ is up, $+y$ is out and $+z$ is to the right. The sulfur atoms are represented as hatched ellipsoids, the sodium ions as large open circles, the fluorine atoms as boundary ellipsoids, the oxygen atoms as shaded circles, the nitrogen atoms as solid circles, and the carbon atoms as small open circles.*

[*] Dr. D. D. DesMarteau, Dr. W. T. Pennington, L. Xue
Department of Chemistry, Hunter Research Laboratory
Clemson University
Clemson, SC 29634-1905 (USA)
Fax: Int. code +(864)656-6613
e-mail: bill.pennington@ces.clemson.edu

[**] Support of this work by the National Science Foundation (CHE-9133028, CHE-9207230, and OSR-9108772) and the Department of Energy (Cooperative Agreement DE-FC02-91ER-75666, "DOE/EPSCoR Research Implementation Plan") is gratefully acknowledged.

 © VCH Verlagsgesellschaft mbH, D-69451 Weinheim, 1997 0570-0833/97/3612-1331 $ 17.50+.50/0

volving the sodium ions, the perfluoroalkyl chains extending out from the hydrophilic core are too closely packed to allow helical twisting (Figure 2, left). The chains have a nearly ideal, planar, all-staggered conformation (range of largest F-C-C-F torsion angles along the chain range: 174.3–178.1°). By contrast, although the structure of **4** is also layered with an ionic core and perfluoroalkyl surfaces, the layers are much more complex. The perfluoroalkyl chains in **4** are more loosely packed on the hydrophilic core because of the significantly longer contacts to the potassium ions (K···O range: 2.624(12)–2.970(12) Å; average 2.8(1) Å). In contrast to those in **1**, many of these chains assume a twisted conformation (Figure 2, right)— the largest

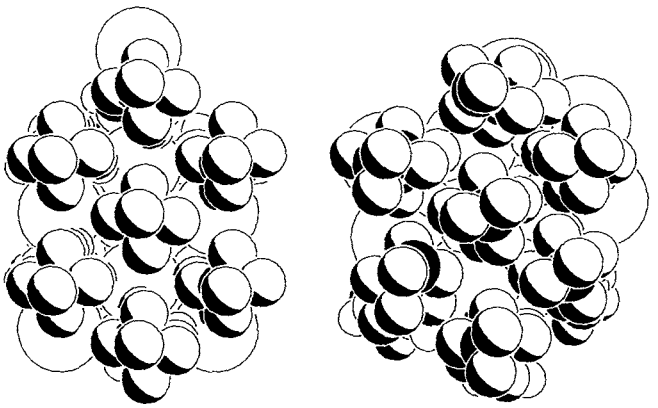

Figure 2. Left: space-filling drawing of **1** viewed normal to the layer. Right: space-filling drawing of **4** viewed normal to the layer.

F-C-C-F torsion angles along the chains range from 156.5 to 179.9°.[15] As with other compounds containing perfluoroalkyl groups, the repulsion between fluorine atoms is also alleviated by expansion of the C-C-C bond angle in the chain (average value of 117.8(8)° for **1** and 119(4)° for **4**).

Another interesting difference between the structures of **1** and **4** is the conformation of the anion. In **1**, it assumes a *trans* conformation—the two perfluoroalkyl chains extend to opposite sides of the hydrophilic core of the layer. In **4**, two of the anions in the asymmetric unit have a similar *trans* conformation, but the other two have *cis* conformation in which the perfluoroalkyl chains of a given anion extend away from the hydrophilic core to the same side of the layer. We have structurally characterized a wide variety of salts of the related anion $[CF_3SO_2NSO_2CF_3]^-$: this anion typically possesses a *cis* conformation when complexed to a cation, but more often has a *trans* conformation when uncomplexed.[16]

One of the interests in compounds such as those reported here is their potential usefulness as structural models for perfluorinated ionomeric membranes, which are important because of their outstanding performance in chlor-alkali and fuel cells.[17] These materials consist of three phases: a crystalline phase that results from ordered packing of the perfluorinated backbone, ionic regions typically referred to as clusters, which result from strong Coulombic associations of the polar side groups, and an amorphous phase.[18] Ion transport properties of these membranes critically depend on the clustering phenomenon. Many descriptions of clustering in hydrocarbon ionomers have been proposed, including a model consisting of spherical clusters in a paracrystalline lattice,[19] a shell core model,[20] and a lamellar model.[21] There is no consensus about which best describes clustering in hydrocarbon ionomers, and the situation in perfluorinated ionomers is even more complicated.[22] However, any model that successfully describes this phenomenon will have to take into account effects such as the steric restrictions imposed on and by the packing of the perfluorinated backbone of the polymer chain that are reported herein.

Received: September 10, 1996 [Z9546IE]
German version: *Angew. Chem.* **1997**, *109*, 1389–1391

Keywords: alkanes · conformation analysis · fluorine · ionomers · solid-state structures

[1] C. W. Bunn, E. R. Howell, *Nature* **1954**, *174*, 549.
[2] However, as pointed out in reference [1], the rotation about the carbon–carbon bond that occurs is not sufficient to move a given fluorine atom to a point equidistant from the fluorines atoms on the next-but-one carbon atom. In addition to rotation, steric interaction between fluorine atoms is accommodated by expansion of the C-C-C bond angle.
[3] H. D. Flack, *J. Polym. Sci. Polym. Phys Ed.* **1972**, *10*, 1799.
[4] C. K. Wu, M. Nichol, *Chem. Phys. Lett.* **1973**, *21*, 153.
[5] K. Song, V. M. Hallmark, J. F. Rabolt, *J. Chem. Phys.* **1991**, *95*, 2862.
[6] G. Knochenhauer, J. Reiche, L. Brehmer, T. Barberka, M. Woolley, R. Tredgold, P. Hodge, *J. Chem. Soc. Chem. Commun.* **1995**, 1619.
[7] Crystal data for **1** ($C_8NO_4F_{18}NaS_2$, $M_r = 603.20$): crystal dimensions: $0.10 \times 0.29 \times 0.40$ mm, monoclinic, space group $P2/c$, $a = 16.469(9)$, $b = 6.492(2)$, $c = 8.637(4)$ Å, $\beta = 99.62(4)°$, $V = 910.5(7)$ Å^3, $Z = 2$ (formula unit possesses crystallographic twofold rotation symmetry; atoms Na1 and N1 lie on the twofold rotation axis (1/2, *y*, 1/4), $\rho_{calcd} = 2.200$ g cm^{-3}. Intensity measurements were made at 295 ± 1 K on a Nicolet R3 mV diffractometer with graphite-monochromated $Mo_{K\alpha}$ radiation ($\lambda = 0.71073$ Å), scan rate 2–15° min^{-1} (in ω), scan range $3.5 < 2\theta < 45.0°$, $\mu = 0.52$ mm^{-1}, transmission coefficients (empirical absorption correction): 0.64–1.00, 2409 reflections measured, 1201 unique ($R_{int.} = 0.046$). Solution by direct methods; full-matrix least-squares refinement on *F* (SHELXTL-Plus, version 4. 2.1) of 155 parameters based on 842 reflections with $I > 3\sigma(I)$ converged to final residuals of $R = 0.050$, $R_w = 0.061$ and maximum residual electron density of 0.47 e Å^{-3} [8].
[8] Crystal data for **4** ($C_8NO_4F_{18}S_2K$, $M_r = 619.31$): crystal dimensions: $0.10 \times 0.28 \times 0.37$ mm, monoclinic, space group $P2_1/n$, $a = 19.310(5)$, $b = 17.999(5)$, $c = 22.800(6)$ Å, $\beta = 110.34(2)°$, $V = 7431(4)$ Å^3, $Z = 16$ (four independent formula units), $\rho_{calcd} = 2.214$ g cm^{-3}. Intensity measurements were made at 203 ± 1 K on a Rigaku AFC7R diffractometer with graphite-monochromated $Mo_{K\alpha}$ radiation ($\lambda = 0.71073$ Å), scan rate 8.00° min^{-1} (in ω) with up to three rescans to improve counting statistics, scan range $3.5 < 2\theta < 45.0°$, $\mu = 0.71$ mm^{-1}, transmission coefficients (empirical absorption correction): 0.56–1.00, 10447 reflections measured, 10033 unique ($R_{int.} = 0.046$). Solution by direct methods, full-matrix least-squares refinement on *F* (SHELXTL-Plus, version 4.2.1) of 551 parameters (due to the large size of the asymmetric unit, the refinement was carried out in blocks consisting of the potassium cations and alternating combinations of two anions per block) based on 4551 reflections with $I > 3\sigma(I)$ converged to final residuals of $R = 0.084$, $R_w = 0.098$ and maximum residual electron density of 0.86 e Å^{-3}. Crystallographic data (excluding structure factors) for the structures reported in this paper have been deposited with the Cambridge Crystallographic Data Centre as supplementary publication no. CCDC-179-176. Copies of the data can be obtained free of charge on application to The Director, CCDC, 12 Union Road, Cambridge CB2 1EZ, UK (fax: int. code +(1223)336-033; e-mail: deposit@chemcrys.cam.ac.uk).
[9] D. D. DesMarteau, W. T. Pennington, L. Xue, unpublished results.
[10] I. A. Koppel, R. W. Taft, F. Anvia, S.-Z. Shu, L.-Q. Hu, K.-S. Sung, D. D. DesMarteau, L. M. Yagupolskii, Y. L. Yagupolskii, N. V. Ignat'ev, N. V. Kondratenko, A. Y. Volkonskii, V. M. Vlasov, R. Notario, P.-C. Maria, *J. Am. Chem. Soc.* **1994**, *116*, 3047.
[11] D. D. DesMarteau, *J. Fluorine Chem.* **1995**, *72*, 203.
[12] D. D. Desmarteau, S. Zhu, W. T. Pennington, Y. Gotoh, M. Witz, S. Zuberi, S. Singh, *J. Fluorine Chem.* **1989**, *45*, 24.
[13] D. D. Desmarteau, W. T. Pennington, K.-S. Sung, S.-Z. Zhu, R. Scott, *Eur. J. Solid State Inorg. Chem.* **1991**, *28*, 905.
[14] D. D. DesMarteau, S. S. Zuberi, W. T. Pennington, B. B. Randolph, *Eur. J. Solid State Inorg. Chem.* **1992**, *29*, 777.
[15] Two of the eight independent perfluoroalkyl chains within the asymmetric unit of **4** have planar all-staggered conformations with chain torsion angles of 177.2 and 178.3°. This is presumably due to local packing forces that result in close-packing of these chains similar to those in **1**. If these values are excluded, the range of torsion angle values for **4** is 154.7–173.7°.
[16] D. D. DesMarteau, W. T. Pennington, L. Xue, unpublished results.
[17] *Perfluorinated Ionomer Membranes* (Eds.: A. Eisenberg, H. L. Yeager) (*ACS Symp. Ser.* **1982**, *180*).

 © VCH Verlagsgesellschaft mbH, D-69451 Weinheim, 1997 0570-0833/97/3612-1332 $ 17.50+.50/0

[18] M. R. Tant, K. P. Darst, K. D. Lee, C. W. Martin in *Multiphase Polymer Materials: Blends, Ionomers and Interpenetrating Networks* (Eds.: L. A. Utracki, R. A. Weiss) (ACS Symp. Ser. **1989**, *395*, pp. 370–400.
[19] C. L. Marx, D. F. Caulfield, S. L. Cooper, *Macromolecules* **1973**, *6*, 344.
[20] W. J. MacKnight, W. P. Taggert, R. S. Stein, *J. Polym. Sci. Polym. Symp.* **1974**, *45*, 113.
[21] E. J. Roche, R. S. Stein, T. P. Russell, W. J. MacKnight, *J. Polym. Sci. Polym. Phys. Ed.* **1980**, *18*, 1497.
[22] T. D. Gierke, G. E. Munn, F. C. Wilson in *Perfluorinated Ionomer Membranes* (Eds.: A. Eisenberg, H. L. Yeager) (*ACS Symp. Ser.* **1982**, *180*, 195–216).

Electrogenerated Chemiluminescence and Proton-Dependent Switching of Fluorescence: Functionalized Difluoroboradiaza-*s*-indacenes**

Matthias Kollmannsberger, Thomas Gareis, Stefan Heinl, Josef Breu, and Jörg Daub*

Dedicated to Fabian Gerson

Functional fluorescent dyes are of central importance as active components for light and electron transfer induced processes, mainly in the field of materials science and analysis.[1] Especially a combination of reversible electron transfer and of efficient light absorption/emission is essential for those processes playing the crucial role in photovoltaic/photoelectrochemical devices.[2] Due to their high absorption coefficients as well as high quantum yields of emission, difloroboradiaza-*s*-indacenes have very favorable photonic qualities.[3] To our knowledge, investigations concerning the electron transfer properties of these dyes have not yet been reported. In this communication we present tailor-made compounds that on one hand are highly fluorescent and on the other form stable radical cations and radical anions. The aim of these investigations is to obtain electrochemiluminescent compounds that can be incorporated as active components into organic light-emitting diodes (OLEDs).[4] During the course of this work we also synthesized a donor-substituted derivative whose fluorescence is quenched by photoinduced electron transfer.[5] This compound can be used for efficient proton-driven fluorescent switching.

Simple difluoroboradiaza-*s*-indacenes like **1** proved to be unsuitable for optoelectrochemical applications, because they do not form stable radical ions. To examine the possibility of stabilizing the radical ions by different substitution patterns at the chromophore, we synthesized compounds **2**–**4**. The synthesis started with pyrroles, which were condensed with appropriate aldehydes to form dipyrromethanes. These were then oxidized and treated with $BF_3 \cdot Et_2O$ to form the target compounds.[6]

For stabilizing the radical anions the *meso*-position of the indacene framework is of crucial importance, because of the expected strong spin localization at this carbon atom. In cyclic voltammetric (CV) experiments compound **1** shows an irreversible reduction, which under thin-layer conditions forms a chemically reversible cycle with a separation of the peak potentials of more than 900 mV. This shift of the reoxidation to significantly more positive potentials indicates a fast, subsequent chemical reaction of the primarily formed radical anions, presumably a dimerization at the *meso* position. If this position is blocked with phenyl substituents, the radical anions are stable under aprotic conditions. Spectroelectrochemical measurements show an absorption of the radical anions at 560–630 nm that is red shifted relative to that of the neutral compounds, whereas the spectrum of the reduction product of **1** lacks this characteristic peak and is therefore in agreement with a dimeric dianion species (Table 1). The values of the reduction potentials depend in a characteristic manner on the type of substituents and their position at the chromophore and thus can be varied in a defined way. The substituents in α-position to the nitrogen atom are increasingly electron-withdrawing from **2a** to **2c** and lead to a strong anodic shift of the reduction potentials, whereas comparing **2a** with **4b**, the presence of the additional electron-releasing ethyl groups at the β-position causes only a smaller cathodic shift (Table 1).

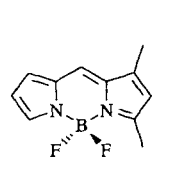

1

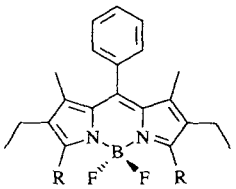

2a: R=Me
2b: R=H
2c: R=CO_2Et

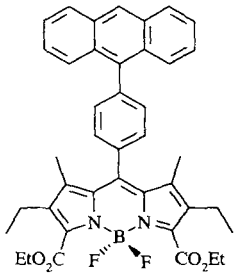

3

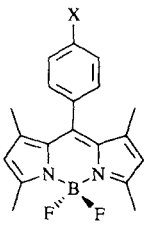

4a: X=NMe_2
4b: X=H

Table 1. Optical and electrochemical data of **1**–**4**.

	λ_{max}[nm] (lg ε)	λ_{em} [nm]	$E_{red.\,1/2}$[mV] (vs. FOC)	$E_{ox.\,1/2}$[mV] (vs. FOC)	$\lambda_{max}(R^{\cdot-})$ [nm]
1	491 (4.71)	509	−1420/ −460[a]	–	239[b]
2a	525 (4.86)	541	−1630	620	584
2b	519 (4.68)	539	−1410	910[c]	560
2c	535 (4.70)	560	−1050 −2140[c]	–	630
3	536 (4.69)	562	−1030 −2090[c] −2270(anthracene)	–	630
4a	496 (4.88)	–	−1610	520(NMe_2) 840	563
4b	496 (4.90)	514	−1570	760	569
4a-H$^+$	501 (4.88)	518	–[d]	840	–

[a] Peak potentials of reduction and reoxidation at 25 mVs^{-1} scan rate under thin-layer conditions. [b] Product of dimerization. [c] Irreversible, peak potentials given. [d] Cannot be measured because of hydrogen evolution in the acidic solution.

[*] Prof. J. Daub, Dipl.-Chem. M. Kollmannsberger, Dr. T. Gareis, S. Heinl
Institut für Organische Chemie der Universität
Universitätsstrasse 31, D-93040 Regensburg (Germany)
Fax: Int. code +(941)943-4984
e-mail: joerg.daub@chemie.uni-regensburg.de
Dr. J. Breu
Institut für Anorganische Chemie der Universität Regensburg

[**] This work was supported by the Bundesministerium für Bildung und Forschung (03N1004C6) and the Bayerische Staatsregierung (Sonderprogramm für Infrastrukturmassnahmen). J. B. is grateful to Prof. Dr. K.-J. Range for financial support.

 © VCH Verlagsgesellschaft mbH, D-69451 Weinheim, 1997 0570-0833/97/3612-1333 $ 17.50+.50/0

Stabilization of the radical cations can also be achieved by suitable substitution. Compound **1** cannot be oxidized at potentials accessible in common solvents. For a detectable electrochemical oxidation the electron density in the indacene ring has to be increased. This higher electron density, which is illustrated by the increasing values of the reduction potentials from **2c** to **2a**, runs parallel to the behavior upon oxidation. While **2c** like **1** cannot be oxidized, the radical cation of **2b** is unstable whereas **2a** can be oxidized at a lower potential and yields a stable radical cation. During oxidation the intense peak of the neutral compound decreases and a new absorption at shorter wavelengths (about 400 nm) appears.

The two reversible redox processes of **2a** are illustrated in Figure 1a. The difference of the potentials between the two redox processes is sufficiently high to populate excited singlet states upon recombination of radical cations and radical anions, which then emit photons. This electrogenerated chemiluminescence (ECL) matches the fluorescence spectrum obtained by photonic excitation (Figure 1b, for conditions see *Experimental Section*). The relatively narrow emission band and the stability of the radical ions makes this compound particularly interesting for applications in OLEDs.[7]

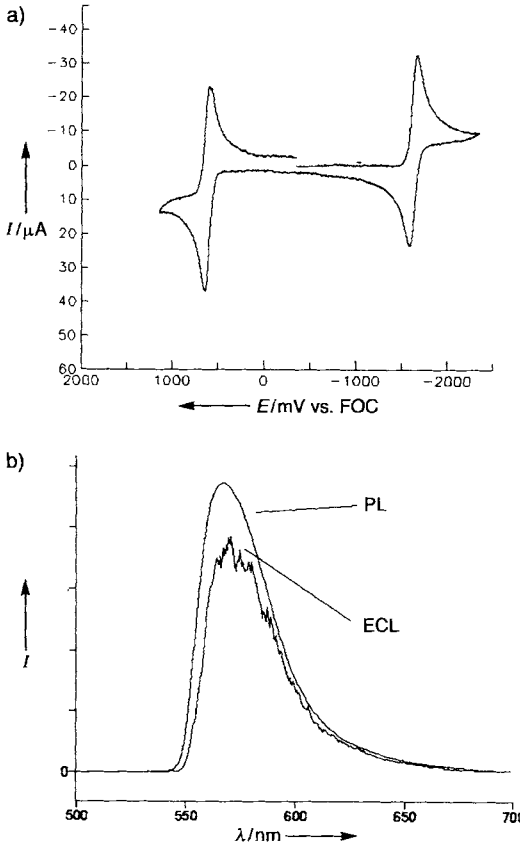

Figure 1. a) Cyclic voltammogram of **2a** in acetonitrile, scan rate 100 mVs^{-1}; b) comparison of the ECL spectrum of **2a** (bottom) with the photoluminescence at equal concentrations (top, excitation at 530 nm), both in CH_2Cl_2.

The attempt to stabilize the radical cations by donor substitution at the phenyl ring leads to an interesting result. The electron-accepting properties of the chromophore can be used for the construction of a proton-sensitive fluorescent switch. Compound **4a** shows practically no emission in its neutral state: fluorescence is probably quenched by an intramolecular electron transfer in the excited state from the dimethylamino group to the indacene chromophore.[8] Addition of trifluoroacetic acid protonates **4a**, and the bright green fluorescence typical of this class of compounds[3] appears (Figure 2). The ratios of the fluorescence quantum yields of the free base and of the protonated form in chloroform are about 1:200, whereas the UV spectra show only a slight difference. Owing to the complete quenching of the emission in the neutral form, this system should be suitable as a fluorescent pH-sensor.[9]

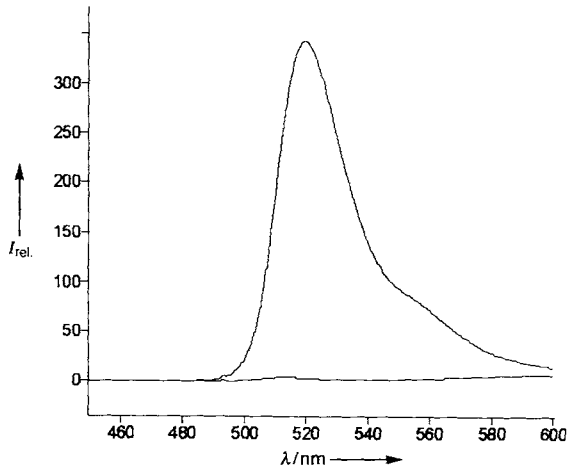

Figure 2. Fluorescence spectra of **4a** before (bottom) and after (top) protonation of the dimethylamino group with trifluoroacetic acid in $CHCl_3$ (excitation at 495 nm).

On- and off-switching of the fluorescence of **4a** is not based on a change of the electronic structure of the chromophore due to conjugation. The kind of interaction between the substituents at the phenyl ring and the chromophore is determined by the steric conditions at the bridging atom of the indacene framework, as shown by the X-ray structure of **3** (Figure 3).[10] The

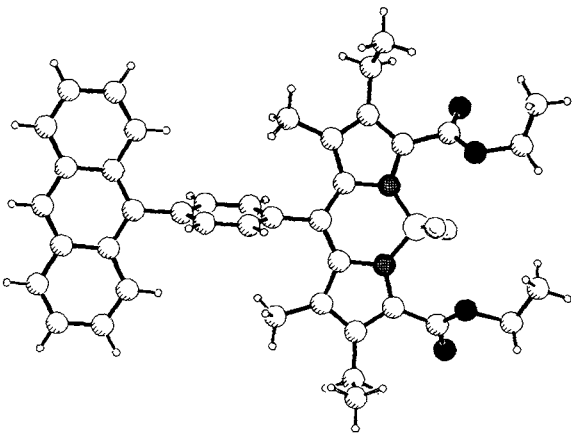

Figure 3. Crystal structure of **3**. The anthracene and the phenyl ring are twisted by 78°, the phenyl and the indacene ring by 75°.

twisting of the phenyl ring out of the plane of the indacene chromophore caused by the methyl groups interrupts the conjugation of the substructures. The UV spectrum of **3** is composed additively of the spectra of its subchromophores, which follows from a comparison with **2c**. Also **4a** and **4b** do not differ in their absorption maxima. In addition to the first reversible reduction signal, cyclic voltammetry of **3** shows a second irreversible re-

 © VCH Verlagsgesellschaft mbH, D-69451 Weinheim, 1997 0570-0833/97/3612-1334 $ 17.50+.50/0

duction indicating destruction of the indacene structure. At an even higher negative potential reversible reduction of the phenylanthracene substructure can be observed. Apparently the substructures are electrochemically independent, too.

Cyclic voltammetry of **4a** indicated that the oxidation of the dimethylamino group appears between the oxidation and the reduction of the indacene framework. This suggests that the lone electron pair at the amino group is energetically located between the HOMO and the LUMO of the indacene chromophore. The oxidation potential of the protonated dimethylamino group is considerably higher than that of the free base and beyond the accessible potentials in acetonitrile, which is reflected in the CV upon protonation by the disappearance of this peak. This increase of the oxidation potential makes a nonradiative deactivation process like the one described above impossible. The oxidation of the indacene chromophore in the protonated form occurs at the same potential as in the neutral form, where it appears as the second oxidation step. Apparently the indacene chromophore is influenced inductively by a positive charge on the dimethylamino group in the same way no matter how the charge is created, by protonation or oxidation.

We have showed that by specific functionalization the electron donor and acceptor properties of the difluoroboradiaza-*s*-indacene chromophore can be directed in a way that leads to electrogenerated luminescence or proton-dependent fluorescence. Presently we aim to incorporate the described dye compounds as active components in OLEDs and to test analytical applications in sensor chemistry.

Experimental Section

Cyclic voltammetry: Solvent acetonitrile; potentials reported [mV] vs ferrocene (FOC) as internal standard. Experimental conditions: reversible half-wave potentials $E_{1/2}$, room temperature, scan rate 250 mVs^{-1}, platinum disc working electrode, Ag/AgCl pseudo-reference electrode, platinum counterelectrode, supporting electrolyte 0.1 M tetrabutylammonium hexafluorophosphate.

Spectroelectrochemistry: Solvent acetonitrile, transmission cell with a gold minigrid working electrode or reflection cell with a platinum disc working electrode.

Optical spectra: Concentrations 10^{-5} M to 10^{-6} M in chloroform filtered over basic alumina before use. Emission spectra are corrected.

ECL-measurements: The ECL spectrum was recorded by applying an alternating square wave with redox potentials determined by cyclic voltammetry (switching time 20 ms, solvent dichloromethane). Concentration: 10^{-3} M, supporting electrolyte: 0.1 M tetrabutylammonium hexafluorophosphate. The emission is red-shifted because of reabsorption in more highly concentrated solutions.

Received: December 12, 1996
Revised version: February 14, 1997 [Z9877IE]
German version: *Angew. Chem.* **1997**, *109*, 1391–1393

Keywords: boron · cyclic voltammetry · dyes · luminescence · sensors

[1] *Third International Symposium on Functional Dyes* (Eds.: D. O. Cowan) in *Pure Appl. Chem.* **1996**, *68*, 1355–1478.

[2] D. Wöhrle, D. Meissner, *Adv. Mater.* **1991**, *3*, 129–138; K.-Y. Law, *Chem. Rev.* **1993**, *93*, 449–486; B. M. Krasowitskii, *Organic Luminescent Materials*, VCH, Weinheim, **1988**; J. Salbeck, *Ber. Bunsenges. Phys. Chem.* **1996**, *100*, 1667–1677.

[3] E. Vos de Wal, J. A. Pardoen, J. A. van Knoeveringe, J. Lugtenburg, *Recl. Trav. Chim. Pays-Bas* **1977**, *96*, 306–309; J. Karolin, L. B.-A. Johansson, L. Strandberg, T. Ny, *J. Am. Chem. Soc.* **1994**, *116*, 7801–7806; R. W. Wagner, J. Lindsey, *ibid.* **1996**, *118*, 3996–3997.

[4] J. H. Burroughes, D. D. C. Bradley, H. R. Brown, R. N. Marks, K. Mackay, R. H. Friend, P. L. Burns, A. B. Holmes, *Nature* **1990**, *347*, 539–41; J. Pommerehne, H. Vestweber, W. Guss, R. F. Mahrt, H. Bässler, M. Porsch, J. Daub, *Adv. Mater.* **1995**, *7*, 551–554.

[5] *Photoinduced electron transfer*, *Vol. A–D* (Eds.: M. A. Fox, M. Chanon), Elsevier, Amsterdam, **1988**; *Top. Curr. Chem.* **1990**, *156*, *158*; *ibid.* **1991**, *159*; *ibid.* **1992**, *163*; *ibid.* **1993**, *168*.

[6] **2a** and **4a/b**: modified method similar to R. W. Wagner, J. S. Lindsey, *P. Appl. Chem.* **1996**, *68*, 1373-1380; for **2b/c** and **3** dipyrromethanes were synthesized as in C. K. Chang, I. Abdalmuhdi, *J. Org. Chem.* **1983**, *48*, 5388-5390; *p*-anthracenylbenzaldehyde: H. Spreitzer, J. Daub, *Liebigs Ann.* **1995**, 1637-1642.

[7] K. Kelnhofer, A. Knorr, Y.-H. Tak, H. Bässler, J. Daub, *Acta Polym.* **1997**, *48*, 188–192; J. Daub, J. Kelnhofer, J. Gareis, A. Knorr, M. Kollmannsberger, Y.-H. Tak, H. Bässler, *Polym. Prepr.* **1997**, *38*, 339–340.

[8] Fluorescent pH indicators: R. A. Bissell, A. P. de Silva, H. Q. N. Gunaratne, P. L. M. Lynch, G. E. M. Maguire, K. R. A. S. Sandanayake, *Chem. Soc. Rev.* **1992**, *21*, 187–195.

[9] In the meantime this has been proved in solution as well as by immobilization in a hydrogel matrix: T. Werner, C. Huber, S. Heinl, M. Kollmannsberger, J. Daub, O. S. Wolfbeis, *Fresenius J. Anal. Chem.*, submitted.

[10] Crystal structure data ($C_{82}H_{78}B_2F_4N_4O_8$; two independent molecules in the asymmetric unit): $M_r = 1345.10$, triclinic, space group $P\bar{1}$, $a = 7.5242(9)$, $b = 19.996(3)$, $c = 23.172(3)$ Å, $\alpha = 88.021(11)$, $\beta = 89.408(11)$, $\gamma = 83.433(10)^\circ$, $V = 3461.3(8)$ Å^3, $Z = 2$, $\rho_{calcd} = 1.291$ Mg m^{-3}, $Mo_{K\alpha}$ radiation ($\lambda = 0.71069$ Å), graphite monochromator, $\mu = 0.09$ mm^{-1}, $F(000) = 1416$, $T = 150$ K, orange needles ($0.640 \times 0.130 \times 0.070$ mm). Data collection: Stoe IPDS Diffractometer, 19742 measured reflections, 9871 independent reflections, $R_{int} = 0.0369$, 6834 observed reflections [$> 2\sigma(I)$] $2\theta_{max} = 47.42$, $-8 \le h \le 8$, $-22 \le k \le 22$, $-26 \le l \le 26$; refinement: full-matrix least-squares refinement of F^2, $\omega R(F^2) = 0.1597$, $R = 0.0774$, $S = 1.473$, 9871 reflections used for refinement, 913 parameters, $(\Delta/\sigma)_{max} = 0.000$, H atoms "riding", $\Delta\rho_{max} = 0.402$ e Å^{-3}, $\Delta\rho_{min} = -0.330$ e Å^{-3}, SIR92 program used for structure solution [11], SHELXL93 used for structure refinement [12], PLUTON graphics [13]. Crystallographic data (excluding structure factors) for the structure reported in this paper have been deposited with the Cambridge Crystallographic Data Centre as supplementary publication no. CCDC-100031. Copies of the data can be obtained free of charge on application to The Director, CCDC, 12 Union Road, Cambridge CB21EZ (Fax: Int. code +(1223)336-033; e-mail: deposit@chemcrys.cam.ac.uk).

[11] A. Altomare, G. Cascarano, C. Giacovazzo, A. Guagliardi, *J. Appl. Crystallogr.* **1993**, *26*, 343–350

[12] G. M. Sheldrick, *SHELXL93*, Universität Göttingen, **1993**.

[13] A. L. Spek, *Acta Crystallogr. Sect. A* **1990**, *46*, C34.

Protonation of a Linear Oxo-Bridged Diiron Unit without Rehybridization of the Bridging Oxygen: Structure of the (μ-Hydroxo)bis-(tetraphenylporphyrinato)iron(III) Cation**

Daniel R. Evans, Rajeev S. Mathur, Kristel Heerwegh, Christopher A. Reed,* and Zuowei Xie

The recognition that oxo- and hydroxo-bridged diiron active sites are widespread biological units has led to intense activity in defining their chemistry.[1] The transformation of an oxo to a hydroxo bridge is an obligatory or proposed step in the reaction pathways of a great variety of iron and copper redox enzymes, particularly the oxidases,[2] and is even a part of the more simple process of dioxygen binding in hemerythrin.[3] Structural responses, changes in spin coupling,[4] pK_a values, and rates of protonation[5] are all of particular interest. Structurally, singly bridged M-O-M units tend towards linearity because of π bonding and steric effects.[6] Upon protonation, they become more bent as the oxygen atom rehybridizes.[7] We now report a

[*] Prof. C. A. Reed, Dr. D. R. Evans, R. S. Mathur, Dr. K. Heerwegh
Department of Chemistry
University of Southern California
Los Angeles, CA 90089-0744 (USA)
Fax: Int. code +(213)740-0930
e-mail: careed@usc.edu
Prof. Z. Xie
Department of Chemistry
The Chinese University of Hong Kong
Shatin, N. T., Hong Kong

[**] This work was supported by the National Institutes of Health (GM 23851) and the National Science Foundation (CHE 9407284).

 © VCH Verlagsgesellschaft mbH, D-69451 Weinheim, 1997 0570-0833/97/3612-1335 $ 17.50+.50/0

diiron(III) complex in which this does not occur. Protonation of the nearly linear μ-oxo bridge in [(tpp)Fe–O–Fe(tpp)] (tpp = tetraphenylporphyrinate) leaves the bridge angle essentially unchanged. The resulting μ-hydroxo-bridged cation, $[(tpp)Fe–O(H)–Fe(tpp)]^+$, provides only the second known example of a diiron complex with a single hydroxo bridge unsupported by ancillary ligands.[7] Two additional features are notable. Antiferromagnetic coupling is greatly attenuated and the self-exchange rate of proton transfer for this strong acid is slow on the NMR timescale.

The synthesis of the hydroxo-bridged cation $[(tpp)Fe–O(H)–Fe(tpp)]^+$ by protonation of the μ-oxo precursor requires a strong Brønsted acid with a very weakly coordinating counterion. The inadequacy of anhydrous acids such as teflic acid ($HOTeF_5$) in this regard is illustrated by the formation of species with coordinated anions, such as $[Fe(OTeF_5)(tpp)]$.[8] The formation of bis(solvent) complexes such as $[Fe(H_2O)_2(tpp)][ClO_4]$ from aqueous perchloric acid[9] illustrates the additional problem of finding reaction conditions that exclude coordinating solvents. Current best choices for the least coordinating anion are hexahalo carboranes of the type $CB_{11}H_6X_6^-$ (X = Cl, Br, I),[10] and the tetraphenylborate ion with perfluorinated phenyl groups $[F_{20}\text{-}BPh_4]^-$.[11] For the case of the carborane anions, the isolable acids $[H_9O_4^+][CB_{11}H_6X_6^-]$[12] can be used to protonate [(tpp)Fe–O–Fe(tpp)] in haloarene solvents. Alternatively, strong Brønsted acidity is readily generated by hydrolysis of the strongly Lewis acidic "bare" $[Fe(tpp)]^+$ ion[13] in arene solvents. In practice, excellent yields of the μ-hydroxo dimer can be obtained by recrystallization of salts of this arene-solvated cation from toluene wetted with one equivalent of water. Single crystals suitable for high-quality X-ray diffraction were obtained with both the hexachloro carborane counterion to give **1** and with the $[F_{20}\text{-}BPh_4]^-$ counterion to give **2**.[14] Figure 1 shows a perspective view of the μ-hydroxo cation in **1**.

$[(tpp)Fe–O(H)–Fe(tpp)][CB_{11}H_6Cl_6]\cdot$toluene **1**

$[(tpp)Fe–O(H)–Fe(tpp)][F_{20}\text{-}BPh_4]\cdot 3$ toluene **2**

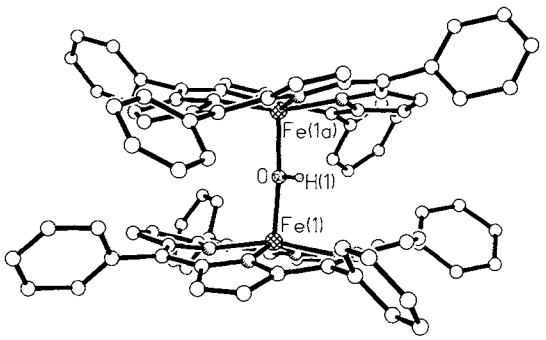

Figure 1. Perspective view of the μ-hydroxo-bridged cation $[(tpp)Fe–O(H)–Fe(tpp)]^+$ in the crystal structure of the $CB_{11}H_6Cl_6^-$ salt **1**.

The salient structural features of the μ-hydroxo cation from the two independent determinations are compared to those of the analogous μ-oxo compound in Table 1. Remarkably, the Fe–O–Fe bridge angle of 176.1(2)° in the μ-oxo dimer[15] is insignificantly changed by 3° upon protonation in **1** and is only 7° smaller in **2**. In the only other reported singly bridged μ-hydroxo iron(III) dimer, $[(oep)Fe–O(H)–Fe(oep)]^+$ (oep = octaethylporphyrinate), the Fe–O(H)–Fe angle is about 30° more acute (146.2(2)°).[7] The origin of this effect must be the steric bulkiness of the tpp phenyl rings. Although conformationally

Table 1. Comparison of properties of μ-oxo and μ-hydroxo iron(III) tetraphenylporphyrin dimers.

	[(tpp)Fe–O–Fe(tpp)]	**1**	**2**
Fe-O-Fe [°]	176.1(2)	173.6(5)	169.2(1)
FeO [Å]	1.759(1)	1.92(3)	1.821(8)
FeN [Å] [a]	2.081(3)	2.000(17)	2.047(5)
Fe···Ctp [Å]	0.54	0.36(1)	0.40(2)
spin state(s)	$S = 5/2$	$S = 3/2, 5/2$	$S = 3/2, 5/2$
$\delta\ ^1H_{pyr}$ ([D$_8$]toluene) [b]	13.8	−42	−42
J [cm^{-1}]	−135	0±3	0±3

[a] Average values. [b] pyr = pyrrole ring.

staggered (Figure 2), the porphyrin rings have little room to splay if a short Fe–O(H)–Fe linkage is to be maintained. In the corresponding manganese complex, the separation of the porphyrin rings is greater and the bridge angle is 160.4(8)°.[16] The Fe–O bond lengths undergo an expected extension from 1.759(1) Å in the μ-oxo complex to an average of 1.87(6) Å in the μ-hydroxo complex. Offsetting this, however, the out-of-plane displacements of the Fe atoms from the 24-membered porphyrin core (Fe···Ct_p) have contracted by 0.13–0.19 Å so that overall, the separation of the porphyrin planes is little changed. The change in iron atom displacement can be understood in terms of a change from a high to an admixed-intermediate spin state upon protonation. The shorter Fe–N and Fe···Ct_p distances of the hydroxo species (see Table 1), as well as the value for δ_{pyr} at −42 upfield in the ^{1}H NMR spectrum and large quadrupole splitting in the Mössbauer spectra ($\Delta E_q = 3.29 \pm 0.06$ mm s^{-1} for **1**) at room temperature, unambiguously identify the hydroxo spin state(s) as admixed-intermediate ($S = 3/2,5/2$).[17, 18] A suitable structural comparison is with other five-coordinate derivatives such as the perrhenate complex $[Fe(OReO_3)(tpp)]$, where an admixed-intermediate spin state is observed and the Fe–N and Fe···Ct_p distances are 2.059 and 0.48 Å, respectively.[19] The lower values of these parameters in **1** and **2** indicate somewhat more $S = 3/2$ spin character. Evidently, the hydroxo bridge provides a weaker axial ligand field than the oxo bridge. One consequence of the longer Fe–O bonds and the change of spin state is that the strong antiferromagnetic coupling in the μ-oxo dimer ($J \approx -135$ cm^{-1})[20] is attenuated to nearly zero in the μ-hydroxo species. The magnetic susceptibility data between 4 and 300 K for **1** and **2** yield plots of μ_{eff} versus temperature that do not contain points of inflection and have magnitudes very similar to monomeric admixed $S = 3/2, 5/2$ spin species. This places an upper limit of a few cm^{-1} on the magnitude of the magnetic coupling constant $|J|$.[21]

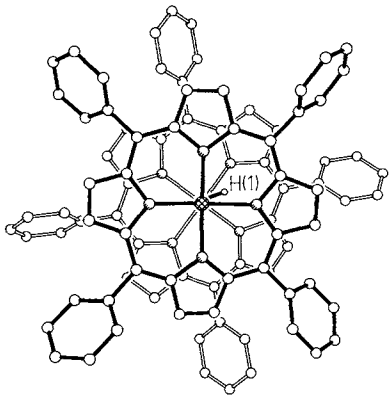

Figure 2. View of the μ-hydroxo-bridged cation $[(tpp)Fe–O(H)–Fe(tpp)]^+$ in **1** down the Fe–O(H)–Fe linkage. A similar staggered arrangement of the tpp rings and location of the H atom is seen in **2**.

The proton on the hydroxo bridge was located in both X-ray structure analyses with O–H distances of about 0.97 Å and Fe-O-H angles close to 90°. The location is apparently determined by steric considerations although weak hydrogen bond-

 © VCH Verlagsgesellschaft mbH, D-69451 Weinheim, 1997 0570-0833/97/3612-1336 $ 17.50+.50/0

ing to the porphyrinato-N atoms may also play a role (N···H = 2.48–2.51 Å; Figure 2).

Trapped deeply in a hydrophobic environment and bonded to an unusually hybridized oxygen atom, the acidity of the μ-hydroxo proton is of both thermodynamic and kinetic interest. There is a conceptual parallel to acidic protons buried in protein structures. Obtaining a pK_a value in a suitable solvent for such measurements (e.g., CH_3CN, dimethyl sulfoxide (DMSO)) is complicated by the tendency of such solvents to act as ligands. The chemical shift of the ^2H NMR signal of the hydroxo group proton of **1** or **2** ($\delta = 11.6$) in bromobenzene solvent cannot be used as a criterion of acidity because of chemical shift contributions from the paramagnetism of iron. Nevertheless, the acidity can be bracketed by $H_9O_4^+$ in dry arene solvents (which protonates the μ-oxo conjugate base) and a two-phase arene/aqueous H^+ system. Addition of a drop of water to a solution of the μ-hydroxo species in bromobenzene causes deprotonation.

Kinetically, the lack of angular change at the oxygen atom upon protonation/deprotonation should contribute to a fast rate of proton transfer.[5] On the other hand, the iron atoms must move about 0.15 Å upon proton transfer and this will contribute to a slowing of the rate. Experimentally, there is no proton exchange between the μ-oxo and μ-hydroxo species on the ^1H NMR timescale. In [D_5]bromobenzene at 25 °C, separate pyrrole resonances are observed in a mixture of the two species and the chemical shifts are unchanged from those of single component measurements ($\delta = 13.8$ and -42, respectively). This probably reflects the steric impossibility of close approach of the protonated Fe–O(H)–Fe moiety to the unprotonated Fe–O–Fe moiety. Traces of smaller proton carriers such as hydronium ions, which must inevitably be present even in dried solvents, are apparently also ineffective at mediating proton exchange on the NMR timescale. This experiment suggests that the nature of the proton carrier and the accessibility of the base must be considered along with structural and electronic reorganizational barriers when rationalizing slow proton transfer rates. Given the interest currently being paid to proton transfer rates in bioinorganic chemistry,[22, 23] and the possibility that systems such as [(tpp)Fe–O(H)–Fe(tpp)]$^+$ may be useful in partitioning the various contributions to these rates, these aspects warrant more detailed study.

Received: November 18, 1996
Revised version: February 24, 1997 [Z97861E]
German version: *Angew. Chem.* **1997**, *109*, 1394–1396

Keywords: acidity · bioinorganic chemistry · carboranes · O ligands · porphyrinoids

[1] D. M. Kurtz, Jr. *Chem. Rev.* **1990**, *90*, 585–606; L. Que, Jr., A. E. True, *Prog. Inorg. Chem.* **1990**, *38*, 97–200; U. Bossek, H. Hummel, T. Weghermüller, E. Bill, K. Wieghardt, *Angew. Chem.* **1995**, *107*, 2885–2888; *Angew. Chem. Int. Ed. Engl.* **1995**, *34*, 2642–2645.
[2] M. J. Scott, H. H. Zhang, S. C. Lee, B. Hedman, K. O. Hodgson, R. H. Holm, *J. Am. Chem. Soc.* **1995**, *117*, 568–569; S. Fox, A. Nanthakumar, M. Wikström, K. D. Karlin, N. J. Blackburn, *ibid.* **1996**, *118*, 24–34.
[3] R. E. Stenkamp, L. C. Sieker, L. H. Jensen, J. D. McCallum, J. Sanders-Loehr, *Proc. Natl. Acad. Sci. USA* **1985**, *82*, 713–716.
[4] P. Knopp, K. Wieghardt, *Inorg. Chem.* **1991**, *30*, 4061–4066.
[5] K. W. Kramarz, J. R. Norton, *Prog. Inorg. Chem* **1994**, *42*, 1–65.
[6] K. S. Murray, *Coord. Chem. Rev.* **1974**, *12*, 1–35.
[7] W. R. Scheidt, B. Cheng, M. K. Safo, F. Cukiernik, J.-C. Marchon, P. G. Debrunner, *J. Am. Chem. Soc.* **1992**, *114*, 4420–4421.
[8] P. J. Kellett, M. J. Pawlik, L. F. Taylor, R. G. Thompson, M. A. Levstik, O. P. Anderson, S. H. Strauss, *Inorg. Chem.* **1989**, *28*, 440–447.
[9] M. E. Kastner, W. R. Scheidt, T. Mashiko, C. A. Reed, *J. Am. Chem. Soc.* **1978**, *100*, 666–667.
[10] a) Z. Xie, T. Jelínek, R. Bau, C. A. Reed, *J. Am. Chem. Soc.* **1994**, *116*, 1907–1913; b) Z. Xie, J. Manning, R. W. Reed, R. Mathur, P. D. W. Boyd, A. Benesi, C. A. Reed, *ibid.* **1996**, *118*, 2922–2928.
[11] K. Seppelt, *Angew. Chem.* **1993**, *105*, 1074–1076; *Angew. Chem. Int. Ed. Engl.* **1993**, *32*, 1025–1027.
[12] Z. Xie, R. Bau, C. A. Reed, *Inorg. Chem.* **1995**, *34*, 5403–5404.
[13] Z. Xie, R. Bau, C. A. Reed, *Angew. Chem.* **1994**, *106*, 2566–2567; *Angew. Chem. Int. Ed. Engl.* **1994**, *33*, 2433–2434.
[14] Crystal data **1** (**2**): purple (purple), $0.3 \times 0.3 \times 0.4$ mm^3 ($0.4 \times 0.3 \times 0.4$ mm^3), monoclinic $P2(1)/c$ (triclinic ($P\bar{1}$), $a = 17.550(4)$, $b = 23.381(7)$, $c = 22.372(6)$ Å ($a = 16.491(2)$, $b = 17.928(3)$, $c = 20.601(3)$ Å), $\beta = 110.69(2)°$ ($\alpha = 109.52(1)$, $\beta = 105.45(1)$, $\gamma = 104.12(1)°$), $V = 8588(4)$ Å^3 ($V = 5148(2)$ Å^3), $\rho_{calcd} = 1.389$ g cm^{-3} for $Z = 4$ ($\rho_{calcd} = 1.490$ g cm^{-3} for $Z = 2$), $\mu = 4.856$ mm^{-1} (3.096 mm^{-1}). Data collection: $Cu_{K\alpha}$, 1.54178 Å, scan mode: ω (ω), 153 K (173 K), $2\theta_{max} = 104.5°$ ($2\theta_{max} = 104.0°$), 10624 (12256) measured reflections, 9332 (10766) independent reflections. Full-matrix least-squares refinement on $|F^2|$ with 4223 (8390) reflections having $I > 2\sigma(I)$ (SHELXL-93). Direct methods and difference Fourier techniques (SHELXL PLUS), 662 (818) parameters, absorption correction (psi scans) max 1.000 (0.8275), min 0.105 (0.4923), residual electron density max 0.599 (0.912) -0.454 (-0.486) e Å^{-3}, $R_1 = 0.010$ (0.068) $wR_2 = 0.020$ (0.015). All H atoms were idealized except the hydroxo-H atom whose coordinates and temperature factors were refined by full-matrix least-squares methods. The hexachlorocarborane anion in **1** was disordered over two sets of positions which was successfully modeled as a 0.88:0.12 disorder. Further details of the crystal structure investigations may be obtained from the Fachinformationszentrum Karlsruhe, D-76344 Eggenstein-Leopoldshafen (Germany), on quoting the depository numbers CSD-406151 and CSD-406152.
[15] P. N. Swepston, J. A. Ibers, *Acta Crystallogr. Sect. C Cryst. Struct. Commun.* **1985**, *41*, 671.
[16] B. Cheng, P. H. Fries, J.-C. Marchon, W. R. Scheidt, *Inorg. Chem.* **1996**, *35*, 1024–1032.
[17] W. R. Scheidt, C. A. Reed, *Chem. Rev.* **1981**, *81*, 543–555.
[18] C. A. Reed, F. Guiset, *J. Am. Chem. Soc.* **1996**, *118*, 3281–3282.
[19] L.-N. Ohlhausen, D. Cockrum, J. Register, K. Roberts, G. J. Long, G. L. Powell, B. B. Hutchinson, *Inorg. Chem.* **1990**, *29*, 4886–4891.
[20] S. H. Strauss, M. J. Pawlik, J. Skowyra, J. R. Kennedy, O. P. Anderson, K. Spartalian, J. L. Dye, *Inorg. Chem.* **1987**, *26*, 724–730, and references therein.
[21] G. P. Gupta, G. Lang, C. A. Reed, K. Shelly, W. R. Scheidt, *J. Chem. Phys.* **1987**, *86*, 5288–5293.
[22] J. M. Carroll, J. R. Norton, *J. Am. Chem. Soc.* **1992**, *114*, 8744–8745.
[23] T. La, G. M. Miskelly, *J. Am. Chem. Soc.* **1995**, *117*, 3613–3614.

Tetraphosphasemibullvalene: First Valence Isomerizations in the Phosphaalkyne Cyclotetramer System**

Andreas Mack, Bernhard Breit, Thomas Wettling, Uwe Bergsträsser, Stefan Leininger, and Manfred Regitz*

Dedicated to Professor Michael Hanack on the occasion of his 65th birthday

Thermal or metal-induced cyclooligomerizations of phosphaalkynes in many cases provide a surprisingly simple access to polycyclic phosphorus–carbon cage compounds.[1, 2] The phosphaalkyne cyclotetramers have been investigated in most detail and are available in good yields by specific syntheses. Thus, for example, the tetraphosphacubane **1**,[3] the tetraphosphatricyclooctadiene **2**,[4] and the tetraphosphabarrelene **3**[5] may be considered as milestones along this road.

[*] Prof. Dr. M. Regitz, Dipl.-Chem. A. Mack, Dr. B. Breit, Dr. T. Wettling, Dr. U. Bergsträsser, Dr. S. Leininger
Fachbereich Chemie der Universität
Erwin Schrödinger Strasse, D-67663 Kaiserslautern (Germany)
Fax: Int. code +(631)205-3921

[**] Phosphorus Compounds; Part 110. This work was supported by the Deutsche Forschungsgemeinschaft (Graduiertenkolleg "Phosphorchemie als Bindeglied verschiedener chemischer Disziplinen"), the Fonds der Chemischen Industrie, and the Landesregierung von Rheinland-Pfalz. Part 109: L. Nyulaszi, P. Varnai, W. Eisfeld, M. Regitz, *J. Comput. Chem.* **1997**, *18*, 609.

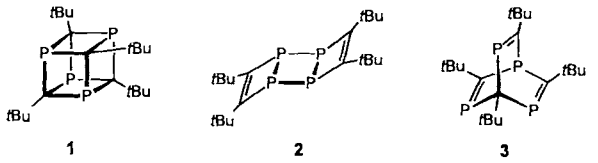

1 2 3

We now report on a new phosphaalkyne cyclotetramer, the tetraphosphasemibullvalene **7**. Although no valence isomerizations have yet been described for **1**–**3**, compound **7** can be both final and starting product for reactions of this type.

First evidence for the formation of the tetraphosphasemibullvalene **7** during the thermal cyclotetramerization of the phosphaalkynes **4** was surprisingly found in the reaction of **4** with tropone (**5**) at 95 °C, in which the diphosphatetracyclodienone **6** was formed by a sequence of Diels–Alder and homo-Diels–Alder reactions (Scheme 1).[6]

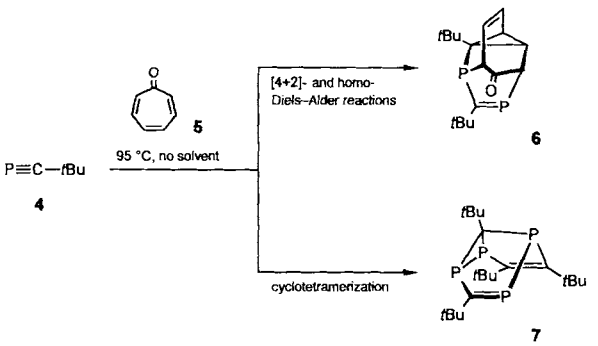

Scheme 1.

Work-up of the reaction mixture by column chromatography at −30 °C gave in addition to **6** the tetraphosphasemibullvalene **7** as an orange-red oil that was still contaminated with ≤5% (by ^{31}P NMR spectroscopy) of a further novel phosphaalkyne cyclotetramer. The latter was assigned the tetracyclic structure **13** on the basis of its NMR data (see Scheme 3).

The presence of tropone (**5**) has a significant but not yet understood influence on the course of the reaction. This is evident from the fact that the thermolysis of pure **4** at 95 °C[7] leads to the formation of a different cyclotetrameric distribution: after 8 h the main product is the tetraphosphatetracyclooctene **13**,[8] formed together with **7** and **12**[3c] in a ratio of 55:25:20 (by ^{31}P NMR spectroscopy).

Although semibullvalene itself undergoes a rapid, degenerate Cope rearrangement at −110 °C,[9] a Cope rearrangement for the tetraphosphasemibullvalene **7** cannot be detected even at room temperature. Higher temperatures cannot be used on account of thermal isomerization of **7** to furnish **12** (see Scheme 3). The constitution of **7** is confirmed by its NMR spectroscopic data. In the ^{31}P NMR spectrum the four phosphorus nuclei give rise to signals at $\delta = -49.0$ (P-7), −14.9 (P-1), 127.7 (P-4), and 332.0 (P-3); in the ^{13}C NMR spectrum the P=C and C=C units are characterized by signals at $\delta = 156.8$ (C-6), 170.5 (C-5), and 208.8 (C-2), while, as expected, the signal for C-8 is shifted markedly to high field ($\delta = 57.9$). The coupling patterns as well as the P,C coupling constants (Table 1) are in accord with the proposed structure.

Compound **7** reacts with [W(CO)$_5$·thf] by extrusion of tetrahydrofuran to furnish exclusively the dark-red complex **8** (Scheme 2), which is thermally more stable than the noncomplexed molecule. A skeletal rearrangement to afford the

Table 1. Selected spectroscopic data for the tetraphosphapolycyclic compounds **7**–**9** [a].

7: ^{1}H NMR (400 MHz): $\delta = 0.87$ (s, 9H; C(CH$_3$)$_3$), 1.29 (d, ^4J(P,H) = 1.6 Hz, 9H; C(CH$_3$)$_3$), 1.45 (d, ^4J(P,H) = 1.6 Hz, 9H; C(CH$_3$)$_3$), 1.47 (d, ^4J(P,H) = 1.8 Hz, 9H; C(CH$_3$)$_3$); ^{13}C NMR (100.64 MHz): $\delta = 29.4$ (m; C(*C*H$_3$)$_3$), 34.7 (d, ^3J(P,C) = 14.4 Hz; C(*C*H$_3$)$_3$), 34.9 (dd, ^3J(P,C) = 12.3 and 9.3 Hz; C(*C*H$_3$)$_3$), 35.0 (*C*(CH$_3$)$_3$), 35.6 (d, ^3J(P,C) = 11.9 Hz; C(*C*H$_3$)$_3$), 38.4 (d, ^2J(P,C) = 28.8 Hz; *C*(CH$_3$)$_3$), 39.5 (d, ^2J(P,C) = 21.2 Hz; *C*(CH$_3$)$_3$), 42.1 (dd, ^2J(P,C) = 22.0 Hz, ^3J(P,C) = 12.7 Hz; *C*(CH$_3$)$_3$), 57.9 (ddd, ^1J(P,C) = 49.0 and 42.2 Hz (2×); C-8), 156.8 (d, ^1J(P,C) = 65.5 Hz; C-6), 170.5 (d, ^1J(P,C) = 34.2 Hz; C-5), 208.8 (pseudo-t, ^1J(P,C) = 79.7 Hz; C-2); ^{31}P NMR (161.98 MHz): $\delta = -49.0$ (dd, ^1J(P,P) = 167.9 Hz, ^2J(P,P) = 22.9 Hz; P-7), −14.9 (ddd, ^1J(P,P) = 167.9 Hz, ^2J(P,P) = 22.9 and 15.3 Hz; P-1), 127.7 (ddd, ^1J(P,P) = 259.4 Hz, ^2J(P,P) = 22.9 and 15.3 Hz; P-4), 332.0 (dd, ^1J(P,P) = 259.4 Hz, ^2J(P,P) = 22.9 Hz; P-3); MS (EI, 70 eV): *m*/*z* (%): 400 (52) [*M*$^+$], 343 (3) [*M*$^+$ − *t*Bu], 300 (4) [*M*$^+$ − *t*BuCP], 262 (89) [*M*$^+$ − (*t*BuC)$_2$], 247 (8) [*M*$^+$ − (*t*BuC)$_2$ − CH$_3$)], 200 (9) [*M*$^+$ − 2*t*BuCP], 169 (100) [P(*t*BuC)$_2^+$], 131 (29) [P$_2$(*t*BuC)$^+$], 100 (11) [*t*BuCP$^+$], 57 (47) [*t*Bu$^+$].

8: ^{1}H NMR (400 MHz): $\delta = 0.87$, 1.28, 1.46 (each s, 9H; C(CH$_3$)$_3$), 1.47 (d, ^4J(P,H) = 2.6 Hz, 9H; C(CH$_3$)$_3$); ^{13}C NMR (100.64 MHz, skeletal carbon atoms only): $\delta = 55.2$ (ddd, ^1J(P,C) = 44.1 and 37.2 Hz (2×); C-8), 159.4 (d, ^1J(P,C) = 59.4 Hz; C-6), 167.5 (dd, ^1J(P,C) = 35.6 Hz, ^2J(P,C) = 10.2 Hz; C-5), 196.9 (d, ^2J(P,C) = 6.8 Hz, ^1J(W,C) = 125.5 Hz; *C*O-eq.), 200.6 (d, ^2J(P,C) = 27.2 Hz; *C*O-ax.), 210.6 (dd, ^1J(P,C) = 89.9 and 25.4 Hz; C-2); ^{31}P NMR (161.98 MHz): $\delta = -61.9$ (ddd, ^1J(P,P) = 188.2 Hz, ^2J(P,P) = 15.3 Hz (2×); P-7), 9.2 (ddd, ^1J(P,P) = 188.2 Hz, ^2J(P,P) = 15.3 Hz (2×); P-1), 144.2 (ddd, ^1J(P,P) = 305.2 Hz, ^2J(P,P) = 15.3 Hz (2×); P-4), 312.6 (d, ^1J(P,P) = 305.2 Hz, ^1J(W,P) = 218.7 Hz; P-3).

9: ^{1}H NMR (400 MHz): $\delta = 1.15$ (d, ^4J(P,H) = 2.0 Hz, 9H; C(CH$_3$)$_3$), 1.18, 1.38, 1.48 (each s, 9H; C(CH$_3$)$_3$), 2.04 (s, 3H; 4-CH$_3$), 2.52 (s, 6H; 2,2′-CH$_3$), 6.70 (s, 2H; 3,3′-CH$_3$); ^{13}C NMR (100.64 MHz): $\delta = 20.9$ (s; 4-*C*H$_3$), 22.0 (d, ^4J(P,C) = 5.7 Hz; 2,2′-*C*H$_3$), 29.0 (dd, ^3J(P,C) = 7.2 Hz (2×); C(*C*H$_3$)$_3$), 30.8 (s; C(*C*H$_3$)$_3$), 34.1 (dd, ^3J(P,C) = 14.0 Hz, ^4J(P,C) = 2.7 Hz; C(*C*H$_3$)$_3$), 34.4 (d, ^3J(P,C) = 13.6 Hz; C(*C*H$_3$)$_3$), 35.5 (m, *C*(CH$_3$)$_3$), 38.8, 38.9 (each s, *C*(CH$_3$)$_3$), 40.0 (dd, ^2J(P,C) = 21.9 and 17.8 Hz; *C*(CH$_3$)$_3$), 56.2 (ddd, ^1J(P,C) = 49.9 and 37.8 Hz (2×); C-1), 125.9 (dd, ^1J(P,C) = 71.2 and 53.8 Hz; C-3), 127.2 (d, ^2J(P,C) = 16.1 Hz; C-1 arom.), 129.6 (s; C-3,3′ arom.), 137.6 (s; C-2,2′ arom.), 138.3 (s; C-4 arom.), 150.2 (dd, ^1J(P,C) = 63.4 Hz, ^2J(P,C) = 15.2 Hz; C-10), 158.9 (dd, ^1J(P,C) = 48.2 Hz, ^2J(P,C) = 8.0 Hz; C-6), 164.3 (dd, ^1J(P,C) = 20.3 Hz, ^2J(P,C) = 9.3 Hz; C-9); ^{31}P NMR (161.98 MHz): $\delta = -2.8$ (ddd, ^1J(P,P) = 219.1 Hz, ^2J(P,P) = 16.3 and 9.1 Hz; P-2), 2.7 (dd, ^1J(P,P) = 219.1 Hz, ^2J(P,P) = 21.4 Hz; P-11), 62.5 (dd, ^1J(P,P) = 272.0 Hz, ^2J(P,P) = 9.1 Hz; P-7), 154.1 (ddd, ^1J(P,P) = 272.0 Hz, ^2J(P,P) = 21.4 and 16.3 Hz; P-8); MS (CI, 200 eV): *m*/*z* (%): 562 (2) [*M*$^+$ + H]; MS (EI, 70 eV): *m*/*z* (%): 561 (0.02) [*M*$^+$], 504 (2) [*M*$^+$ − *t*Bu], 416 (12) [*M*$^+$ − MesCN], 400 (5) [*M*$^+$ − MesCNO], 300 (2) [*M*$^+$ − MesCNO, −*t*BuCP], 262 (18) [*M*$^+$ − MesCNO, −(*t*BuC)$_2$], 169 (100) [P(*t*BuC)$_2^+$], 131 (11) [P$_2$(*t*BuC)$^+$], 119 (4) [Mes$^+$], 57 (51) [*t*Bu$^+$].

[a] NMR: Bruker AMX-400, ^{1}H and ^{13}C NMR in C_6D_6; ^{31}P NMR in C_6D_6 with 85% H_3PO_4 as external reference, all spectra recorded at $T = 25$ °C; MS: Finnigan MAT 90.

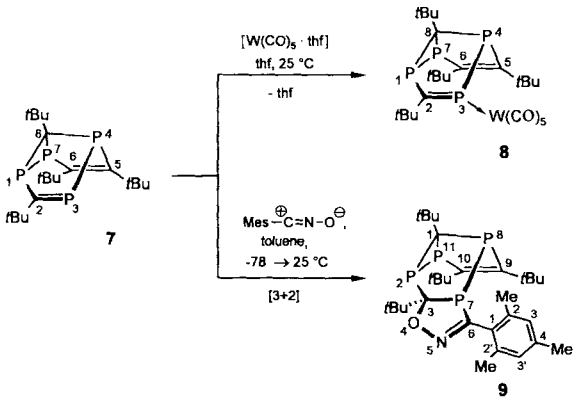

Scheme 2.

W(CO)$_5$ complex of the structure **12** does not occur either in the solid state or in solution. Coordination of the metal fragment at P-3, the signal of which is shifted only slightly to higher field ($\delta = 312.6$), is confirmed by the ^{183}W satellites [^1J(P,W) = 218.7 Hz] (for further NMR data, see Table 1).

Mesityl nitrile oxide undergoes rapid addition to the phosphaalkene unit of **7** in toluene to furnish the crystalline, polycyclic product **9** (Scheme 2), which is isolated in 92% yield after work-up by column chromatography. The NMR data unequivocally demonstrate the cycloaddition to the P–C double bond as well as the regiochemistry of the reaction. The signals for both reaction centers in **7** are shifted significantly to higher field: P-7 from $\delta = 332.0$ to $\delta = 62.5$, C-3 from $\delta = 208.8$ to $\delta = 125.9$. The unusual lowfield position of the signal for C-3 is reasonable when the oxygen of the dipole is bonded at this position. The remaining question of the stereochemistry of the cycloadduct **9** was resolved in favor of an *exo*-arrangement of the newly formed five-membered ring by a crystal structure analysis (Figure 1); an *endo* attack of the dipole is apparently prevented by the *tert*-butyl substituents at the C–C double bond. At the same time the structure of this novel phosphaalkyne cyclotetramer is confirmed.[10]

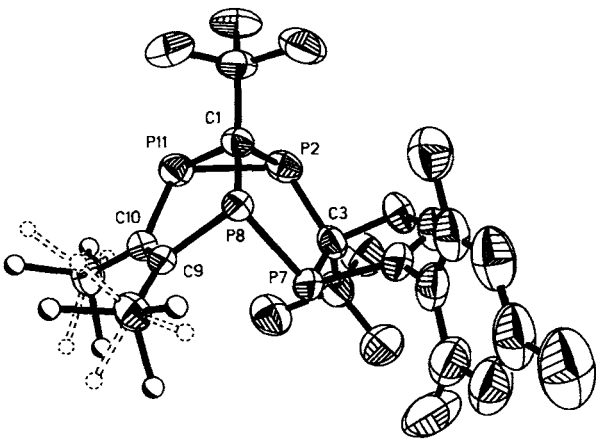

Figure 1. Structure of **9** in the crystal (XP-Plot, thermal ellipsoids drawn at 50% probability level). Selected bond lengths [Å] and angles [°]: P2–P11 2.2185(13), P7–P8 2.2095(12), P7–C3 1.865(3), P2–C3 1.892(3), P8–C9 1.869(3), P2–C1 1.855(3), P8–C1 1.845(3), P11–C1 1.836(3), P11–C10 1.851(3), C10–C9 1.357(4); C1-P2-P11 52.65(10), C1-P2-C3 103.49(14), C3-P2-P11 116.12(10), C1-P11-C10 100.21(14), C1-P11-P2 53.45(10), C10-P11-P2 115.66(11), P11-C1-P8 108.0(2), P11-C1-P2 73.89(12), P8-C1-P2 116.9(2).

The P–C single bond lengths in the tricyclic phosphorus–carbon skeleton of **9** are between 1.836 and 1.892 Å (average value 1.856 Å) and thus in good agreement with those of other polycyclic compounds.[11] The P2–P11 bond length of 2.219 Å lies at the upper limit for diphosphiranes.[12] In accord with this, the angle P2-C1-P11 in the three-membered ring is larger (73.9°) and the angles C1-P11-P2 (53.5°) and C1-P2-P11 (52.7°) are smaller than those in other polycyclic systems containing a diphosphirane element.[13]

Valence isomerizations in phosphaalkyne cyclotetramer systems were previously unknown. We report here on reactions of this type that also make the tetraphosphasemibullvalene **7** accessible from the polycyclic systems **10**–**13** (Scheme 3).

The compounds **10** and **11** are known[13a,14] and coexist as a 1:1 equilibrium mixture (by ^{31}P NMR spectroscopy) upon irradiation of the one or the other in C_6D_6 (mercury high-pressure lamp Phillips, HPK 125W, Duran-50 filter). When each of the two isomers is heated separately at 150 °C, compound **12** (100 and 48%, respectively) is formed by a skeletal rearrangement; the latter product is also accessible directly from the thermal cyclotetramerization of the phosphaalkyne **4** at 180 °C.[3c] When **12** is photolyzed under the conditions mentioned for the equilibrium **10**⇌**11**, the valence isomer **7** is formed (up to 75%);

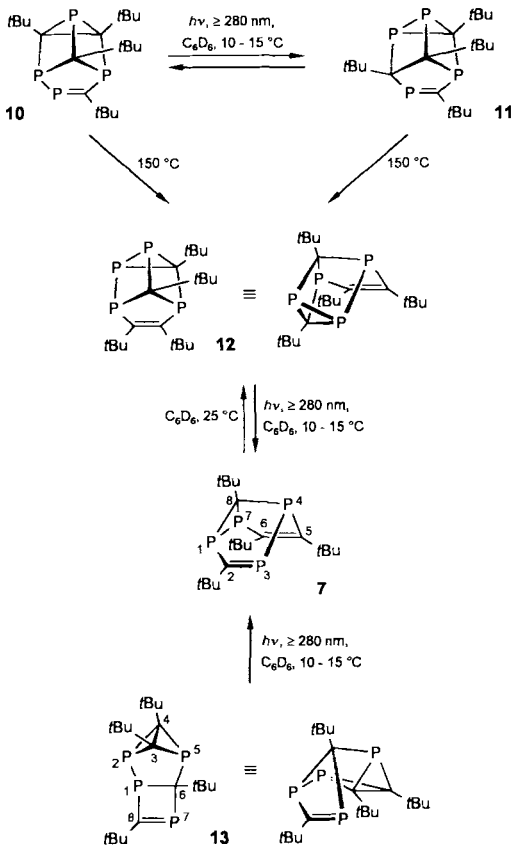

Scheme 3.

the reverse isomerization of **7** occurs relatively slowly at 25 °C in C_6D_6 (ca. 20% **12** after 7 d, both by ^{31}P NMR spectroscopy). Finally, **13** can undergo complete photochemical isomerization to furnish an isomeric mixture of **7** and **12** (80:20).

Experimental Section

7: In a 15-mL-pressure Schlenk tube, tropone (**5**) (0.14 g, 1.3 mmol) was added to phosphaalkyne **4** [15] and the two-phase system was heated with magnetic stirring under argon pressure (5 bar) for 17 h at 95 °C. After the mixture had cooled to 25 °C, unconverted phosphaalkyne **4** (2.15 g, 21.5 mmol) was recovered by condensation (0.003 mbar, received −192 °C). Column chromatography (1.4 × 30 cm) on silica gel (63–200 μm, baked for 16 h at 175 °C and 10^{-3} mbar and deactivated with 4% argon-saturated water) at −30 °C afforded the following in sequence: a) elution with *n*-pentane (500 mL) gave after evaporation of the solvent at 10^{-3} mbar/25 °C the orange-red, oily **7**. Yield: 32 mg (4.9%, with respect to converted **4**); stored at −25 °C; b) elution with *n*-pentane/diethyl ether 10/1 (50 mL) gave a dark orange-red, unidentified "polymer"; c) elution with *n*-pentane/diethyl ether 5/1 (70 mL) gave the pale yellow, oily tetracyclic product **6**.

8: Compound **7** (70 mg, 0.17 mmol) in tetrahydrofuran (5 mL) was added to a solution of [W(CO)$_5$·thf],[16] prepared by irradiation of [W(CO)$_6$] (92.3 mg, 0.26 mmol) in tetrahydrofuran (60 mL). After 17 h the solvent was evaporated at 25 °C/10^{-3} mbar, the oily residue was eluted with *n*-pentane (20 mL) and subjected to chromatography on silica gel (column: 1.8 × 37 cm) with *n*-pentane. Yield: 85.5 mg (69%) dark red oil, which could be crystallized from *n*-pentane at −80 °C. M.p. 8–13 °C (in thawing cold bath).

9: Mesityl nitrile oxide (40 mg, 0.25 mmol) in toluene (3 mL) was added dropwise with stirring at −78 °C to the tetraphosphasemibullvalene **7** (100 mg, 0.25 mmol) in toluene (3 mL), and the mixture was stirred for further 3 h at 25 °C. After evaporation (25 °C/10^{-3} mbar), dissolution in *n*-pentane (1.5 mL), and chromatography on silica gel (as described for **7**, but with water-cooling) the following were obtained in sequence: a) elution with *n*-pentane (80 mL) gave after evaporation about 5 mg of **12** formed by isomerization of **7**; identification by a comparison of the NMR spectrum with that of an authentic sample [3c]; b) elution with *n*-pentane/diethyl ether 25/1 (50 mL) gave the pale yellow cycloadduct **9**. Yield: 129 mg (92%), m.p. 123 °C (from *n*-pentane at −20 °C).

Received: November 18, 1996 [Z97901E]
German version: *Angew. Chem.* **1997**, *109*, 1396–1398

Keywords: cyclizations · cycloadditions · isomerizations · phosphaalkynes · phosphorus

[1] Brief summary: R. Streubel, *Angew. Chem.* **1995**, *107*, 478–480; *Angew. Chem. Int. Ed. Engl.* **1995**, *34*, 436–438.

[2] Reviews: M. Regitz, A. Hoffmann, U. Bergsträsser, *Chem. Rev.* **1997**, *97*, in press; M. Regitz, A. Hoffmann, U. Bergsträsser in *Modern Acetylene Chemistry* (Eds.: P. J. Stang, F. Diederich), VCH, Weinheim, **1995**, p. 173.

[3] a) T. Wettling, J. Schneider, O. Wagner, C. G. Kreiter, M. Regitz, *Angew. Chem.* **1989**, *101*, 1035–1037; *Angew. Chem. Int. Ed. Engl.* **1989**, *28*, 1013–1014; b) T. Wettling, B. Geissler, R. Schneider, S. Barth, P. Binger, M. Regitz, *ibid* **1992**, *104*, 761–762 and **1992**, *31*, 758–759; c) B. Geissler, T. Wettling, S. Barth, P. Binger, M. Regitz, *Synthesis* **1994**, 1337–1343.

[4] B. Geissler, S. Barth, U. Bergsträsser, M. Slany, J. Durkin, P. B. Hitchcock, M. Hofmann, P. Binger, J. F. Nixon, P. von R. Schleyer, M. Regitz, *Angew. Chem.* **1995**, *107*, 485–488; *Angew. Chem. Int. Ed. Engl.* **1995**, *34*, 484–487.

[5] P. Binger, G. Glaser, B. Gabor, R. Mynott; *Angew. Chem.* **1995**, *107*, 114–116; *Angew. Chem. Int. Ed. Engl.* **1995**, *34*, 81–83.

[6] M. Julino, U. Bergsträsser, M. Regitz, *J. Org. Chem.* **1995**, *60*, 5884–5890.

[7] Previously only thermolyses at $T \geq 130\,^{\circ}C$ had been investigated [3a,c].

[8] The spectroscopic characterization of **13** was carried out in an admixture with **7** and **12**; the assignments of the skeletal atoms were based on the values for the corresponding 1-adamantyl compound, which was isolated in the pure state. ^1H NMR (400 MHz): $\delta = 1.15$ (s, 9H; $C(CH_3)_3$), 1.17 (d, $^4J(P,H) = 1.6$ Hz, 9H; $C(CH_3)_3$), 1.34 (s, 9H; $C(CH_3)_3$), 1.48 (s, 9H; $C(CH_3)_3$); ^{13}C NMR (100.64 MHz): $\delta = 77.4$ (ddd, $^1J(P,C) = 51.6$, 45.1 and 6.2 Hz; C-6), 234.4 (dd, $^1J(P,C) = 57.3$ and 35.0 Hz; C-8), the remaining skeletal carbon atoms could not be assigned because of signal overlap; ^{31}P NMR (161.98): $\delta = 0.9$ (ddd, $^2J(P,P) = 35.2$, 26.9 and 25.6 Hz; P-5), 4.4 (dd, $^1J(P,P) = 282.3$ Hz, $^2J(P,P) = 26.9$ Hz; P-2), 107.0 (ddd, $^1J(P,P) = 282.3$ Hz, $^2J(P,P) = 28.3$ and 25.6 Hz; P-1), 348.5 (dd, $^2J(P,P) = 35.2$ and 28.2 Hz; P-7).

[9] H. E. Zimmermann, R. W. Binkley, R. S. Givens, G. L. Grunewald, M. A. Sherwin, *J. Am. Chem. Soc.* **1969**, *91*, 3316–3323.

[10] Data collection with a Siemens P4 diffractometer, $Mo_{K\alpha}$ radiation, $\lambda = 0.71073$ Å with a graphite monochromator; $C_{30}H_{47}NOP_4$, $M = 561.57\ g\,mol^{-1}$, monoclinic space group $P2_1/n$, $a = 9.9470(10)$, $b = 20.689(2)$, $c = 15.776(3)$ Å, $\beta = 94.29(3)^{\circ}$, $Z = 4$; $V = 3237.5(8)$ Å^3, $\rho_{calcd} = 1.152\ g\,cm^{-3}$, $\mu = 2.55\ cm^{-1}$, $F(000) = 1208$; 5040 ($R_{int} = 0.0368$) independent reflections were recorded, of which 4563 with $I \geq 2\sigma(I)$ were considered in the structure refinement to F^2 (SHELXL-93) [17]. The *tert*-butyl groups at C9 and C10 exhibit disorder with regard to the methyl groups. The anisotropic refinement of split positions (occupation factors were also refined) for the methyl-C atoms led to a marked improvement of the structure model. This converged with $R1 = 0.0546$, $wR2 = 0.1052$ ($R1 = 0.903$, $wR2 = 0.1280$ for all data). The final differential Fourier analysis showed a maximum of $0.249\ e\,Å^{-3}$ and a minimum of $-0.247\ e\,Å^{-3}$. Further details of the crystal structure investigation may be obtained from the Fachinformationszentrum Karlsruhe, D-76344 Eggenstein-Leopoldshafen (Germany), on quoting the depository number CSD-406473.

[11] D. Hu, H. Schäufele, H. Pritzkow, U. Zenneck, *Angew. Chem.* **1989**, *101*, 929–931; *Angew. Chem. Int. Ed. Engl.* **1989**, *28*, 900–902.

[12] F. Mathey, *Chem. Rev.* **1990**, *90*, 997–1025.

[13] a) B. Breit, U. Bergsträsser, G. Maas, M. Regitz, *Angew. Chem.* **1992**, *104*, 1043–1046; *Angew. Chem. Int. Ed. Engl.* **1992**, *31*, 1055–1058; b) M. Julino, M. Slany, U. Bergsträsser, F. Mercier, F. Mathey, M. Regitz, *Chem. Ber.* **1995**, *128*, 991–997.

[14] B. Breit, M. Regitz, *Chem. Ber.* **1995**, *129*, 489-494.

[15] G. Becker, G. Gresser, W. Uhl, *Z. Naturforsch. B* **1981**, *36*, 16–19; improved procedure: W. Rösch, U. Hees, M. Regitz, *Chem. Ber.* **1987**, *120*, 1645–1652.

[16] W. Strohmeier, F.-J. Müller, *Chem. Ber.* **1969**, *102*, 3608–3612.

[17] G. M. Sheldrick, SHELXL93 Program for crystal structure refinement, University of Göttingen.

Rotational Spectroscopy of Mixtures of Trimethylamine and Fluorine: Identification of the Ion Pair $[(CH_3)_3NF]^+ \cdots F^-$ in the Gas Phase**

Hannelore I. Bloemink, Stephen A. Cooke, John H. Holloway, and A. C. Legon*

Reactions of elemental fluorine with organic compounds are notorious for their violence. They are assumed usually to proceed by a chain mechanism that is initiated by the facile homolytic dissociation of F_2 into atoms. The next step (propagation) is presumably the abstraction of an H atom from a CH_n group to give $\cdot CH_{n-1}$ and HF, which is strongly exothermic and makes the reaction difficult to control. Consequently, the products are often predominantly HF, CF_4, and carbon. The large value for the energy of heterolytic dissociation $F_2 = F^+ + F^-$ ($1370\ kJ\,mol^{-1}$)[1] means that reactions in the gas phase involving the F^+ ion are unlikely to be common. Are there reactions of F_2 in which heterolysis of the diatomic molecule needs to be invoked?

We report herein the identification and characterization of a complex formed by trimethylamine with F_2 in the gas phase. Interpretation of spectroscopic constants derived from analyses of the rotational spectra of three isotopomers leads to the conclusion that the observed species is best described as a Mulliken complex $[(CH_3)_3NF]^+ \cdots F^-$ of the inner type, that is, one in which the F^+ ion has been transferred from F_2 to the Lewis base. This is a surprising result, not only because of the reluctance of F_2 to dissociate heterolytically but also because, for all complexes $B \cdots F_2$ previously investigated ($B = NH_3$,[2] HCN,[3] CH_3CN,[4] H_2S,[5] and H_2O[6]), the interaction between the Lewis base and F_2 is very weak.

The rotational spectrum of the complex $[(CH_3)_3N, F_2]$ was observed by using a pulsed-nozzle, Fourier-transform microwave spectrometer[7] fitted with a fast-mixing nozzle.[8] This latter device consists of two concentric, nearly coterminal tubes and ensures that the two components (trimethylamine flowing continuously through the inner tube and F_2/Ar mixture pulsed down the outer tube) do not mix until they expand simultaneously into the evacuated Fabry–Pérot cavity of the spectrometer. The reasons why the fast-mixing nozzle is effective in inhibiting the production of F atoms, and therefore in precluding violent chain reactions of the type alluded to earlier, have been discussed elsewhere.[6]

The ground-state rotational spectrum of the isotopomer $[(CH_3)_3{}^{14}N, F_2]$ is characteristic of a symmetric-top molecule carrying a ^{14}N ($I = 1$) nucleus on the unique axis. Analysis of the ^{14}N nuclear quadrupole hyperfine structure in the $J = 2 \leftarrow 1$, $3 \leftarrow 2$, $4 \leftarrow 3$, and $5 \leftarrow 4$ transitions yielded the rotational constant B_0, the centrifugal distortion constants D_J and D_{JK}, and the ^{14}N-nuclear quadrupole coupling constant $\chi(^{14}N)$ (Table 1). A partially resolved substructure, arising from coupling of the various $I = 1/2$ (H and F) nuclei, together with the small magnitudes of $\chi(^{14}N)$ and D_{JK}, resulted in a complex and congested

[*] Prof. A. C. Legon, Dr. H. I. Bloemink, S. A. Cooke
Department of Chemistry, University of Exeter
Stocker Road, Exeter EX4 4QD (UK)
Fax: Int. code +(1392) 263434
e-mail: ACLegon@exeter.ac.uk

Prof. J. H. Holloway
Department of Chemistry, University of Leicester
University Road, Leicester LE1 7RH (UK)

[**] This work was supported by a research grant and a research studentship (for S. A. C.) from the Engineering and Physical Science Research Council.

Table 1. Ground-state spectroscopic constants of isotopomers of $[(CH_3)_3N, F_2]$.

	$[(CH_3)_3{}^{14}N,F_2]$	$[(CH_3)_3{}^{15}N,F_2]$	$[(CD_3)_3{}^{14}N,F_2]$ [a]	$(CH_3)_3{}^{14}N\cdots F_2$ [b]
B_0 [MHz]	1736.7453(7)	1731.9475(5)	1550.045(2)	1274.5
D_J [kHz]	0.288(13)	0.295(13)	0.21(3)	2.0
D_{JK} [kHz]	6.38(8)	6.16(5)	–	–
$\chi(^{14}N)$ [MHz]	−1.73(1)	–	–	≈ −5.0

[a] Only $K = 0$ transitions fitted to give B_0 and D_J. See text for discussion. [b] Values in this column are estimated for the weak binding model $(CH_3)_3N\cdots F_2$, as described in the text, but the species observed is the ion pair $[(CH_3)_3NF]^+\cdots F^-$. See text for discussion.

spectrum. For each ^{14}N nuclear quadrupole component, the center frequency of the partially resolved substructure was used in the analysis. The determined spectroscopic constants of $[(CH_3)_3{}^{15}N, F_2]$ and $[(CD_3)_3{}^{14}N,F_2]$ are also given in Table 1. For the latter isotopomer, the spectral complexity arising from the nine D ($I = 1$) quadrupolar nuclei precluded a detailed analysis and only the highest frequency component belonging to each $K = 0$ transition was fitted to give the reported B_0 and D_J values.

To establish the nature of the detected species $[(CH_3)_3N, F_2]$, we first compare its observed spectroscopic constants (Table 1) with those predicted from the model $(CH_3)_3N\cdots F_2$ of the complex in which the intermolecular binding is weak. The intermolecular stretching force constant k_σ for each $B\cdots F_2$ complex so far investigated[2–6] is small. For example, the largest value is $k_\sigma = 4.70(3)\ N m^{-1}$ for $H_3N\cdots F_2$ and this is similar in magnitude to those of $Rg\cdots HX$ complexes, where Rg is an inert gas atom.[9] The centrifugal distortion constant D_J for a weakly bound symmetric-top complex $B\cdots F_2$ composed of rigid, unperturbed subunits is related to k_σ by Equation (a),[10] where

$$D_J = (16\pi^2\mu B_0^3/k_\sigma)\{1 - (B_0/B_B) - (B_0/B_{F_2})\} \quad (a)$$

B_0, B_B, and B_{F_2} are rotational constants of the complex and the molecules B[11] and F_2,[12] respectively, and $\mu = m_B m_{F_2}/(m_B + m_{F_2})$. Using the estimated B_0 value for the weak binding model $(CH_3)_3N\cdots F_2$ from Table 1 and assuming $k_\sigma \approx 5\ N m^{-1}$, we obtain $D_J^{calcd} \approx 2.0$ kHz. The observed value of D_J is about seven times smaller and indicates that the detected complex is much more strongly bound than expected.

The value of $r(B\cdots F)$ for each $B\cdots F_2$ complex previously investigated[2–6] is close to the sum of the van der Waals radii $(\sigma(F) + \sigma(B))$ of F and the acceptor atom in B, a result also consistent with weak binding. If we assume $r(N\cdots F) = 2.65$ Å, (that is a distance slightly shorter than that of 2.71(1) Å in $H_3N\cdots F_2$[2]) and unperturbed geometries for $(CH_3)_3N$[11] and F_2,[12] we obtain the calculated value of B_0 recorded in Table 1 for the model $(CH_3)_3{}^{14}N\cdots F_2$. Comparison of the calculated value B_0^{calcd} and the observed value B_0 indicates that the complex has a much smaller moment of inertia than expected. Indeed, to fit B_0 with the weak binding model requires $r(N\cdots F) = 1.97$ Å, which is 0.9 Å shorter than $\sigma(N) + \sigma(F)$.

Additionally, the ^{14}N nuclear quadrupole coupling constant of the model complex $(CH_3)_3{}^{14}N\cdots F_2$ should be slightly less than the value of $\chi_0(^{14}N) = -5.502(3)$ MHz of the free molecule,[13] mainly as a result of the zero-point angular oscillation of the subunit $(CH_3)_3N$ in the complex. For example, the value $\chi(^{14}N) = -4.918(3)$ MHz was measured in the weakly bound complex $(CH_3)_3N\cdots HCCH$ ($k_\sigma = 5.86(2)\ N m^{-1}$),[14] and a similar value is expected for $(CH_3)_3N\cdots F_2$. The observed change $\Delta\chi = \chi(^{14}N) - \chi_0(^{14}N) = 3.77$ MHz is much larger (see Table 1).

Clearly, the comparisons of B_0, D_J, and $\chi(^{14}N)$ (Table 1) indicate that the detected complex is not the weakly bound species $(CH_3)_3N\cdots F_2$. However, the observed values can all be understood if we assume that the preponderant contribution to a valence-bond description of the complex is the ion pair $[(CH_3)_3NF]^+\cdots F^-$. Then k_σ would have a value appropriate to an ion pair. Typical values are $k_\sigma = 82$ and $67\ N m^{-1}$ for $[(CH_3)_3NH]^+\cdots Br^-$ and $[(CH_3)_3NH]^+\cdots I^-$, both obtained from D_J.[15] The version of Equation (a) relevant to the ion-pair structure $[(CH_3)_3NF]^+\cdots F^-$ is Equation (b), where B_+ is the

$$D_J = (16\pi^2\mu B_0^3/k_\sigma)\{1 - B_0/B_+\} \quad (b)$$

rotational constant of the cation and can be estimated to have the value 5035 MHz if the cation is modeled by placing F^+ on the C_3 axis of an unperturbed $(CH_3)_3N$ molecule at the distance $r(N-F) = 1.365$ Å, as in NF_3.[16] When $k_\sigma \approx 70\ N m^{-1}$ is used in Equation (b), the result is $D_J \approx 0.2$ kHz, which is much closer to the observed quantity than that estimated for $(CH_3)_3N\cdots F_2$ (see Table 1).

The difference $\Delta\chi(^{14}N) = \chi(^{14}N) - \chi_0(^{14}N) = 3.77$ MHz for $[(CH_3)_3{}^{14}N, F_2]$ is even larger than those observed in the vapor phase for the trimethylammonium halides $[(CH_3)_3N, HX]$, where X = Cl, Br, and I. The fractional contribution f of the ion-pair structure $[(CH_3)_3NH]^+\cdots X^-$ was estimated[15] from the X-nuclear quadrupole coupling constant for the complexes $[(CH_3)_3NH]^+\cdots X^-$, and Figure 1 shows a plot of $\Delta\chi(^{14}N)$ versus f for this series. The value of $\Delta\chi(^{14}N)$ for $[(CH_3)_3{}^{14}N, F_2]$ is shown as a horizontal dashed line in Figure 1 and corresponds to a f value of approximately 1. Hence, the $\Delta\chi(^{14}N)$ value is consistent with the observation of the ion pair $[(CH_3)_3NF]^+\cdots F^-$.

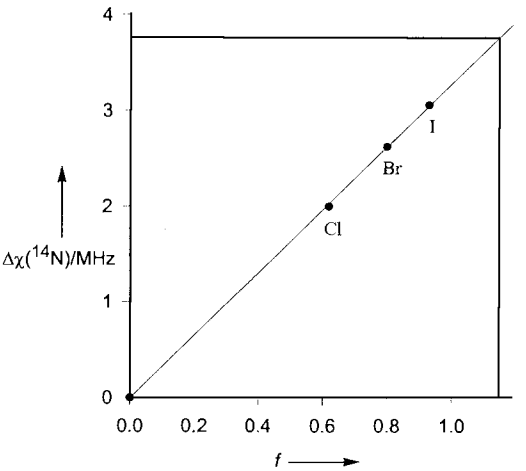

Figure 1. Plot of $\Delta\chi(^{14}N) = \chi(^{14}N) - \chi_0(^{14}N)$ against f (fractional ionic character) for some trimethylammonium halides. The horizontal dashed line indicates the value of $\Delta\chi(^{14}N)$ for $[(CH_3)_3N, F_2]$.

The ion pair $[(CH_3)_3NF]^+\cdots F^-$ should have a large electric dipole moment μ. Flygare et al.[17] demonstrated that a time-domain emission signal from a pulsed-nozzle, Fourier-transform microwave spectrometer passes through a maximum value as the input power P_{in} increases and that at the maximum $P_{in}^{1/2}\kappa\tau_p$ is a constant, where τ_p is the microwave pulse length and $\kappa = \langle J'K'F'|\mu|J''K''F''\rangle$ is the rotational transition moment. By comparing the P_{in} values that give maximum signals in transitions of $H_3N\cdots F_2$ and $[(CH_3)_3NF]^+\cdots F^-$, we find that the electric dipole moments of these two species are in the approxi-

mate ratio of 1:6. If the electric dipole moment μ for $H_3N\cdots F_2$ is assumed to be about 1.6 D (that is slightly in excess of that of the free NH_3), the implied electric dipole moment of $[(CH_3)_3NF]^+\cdots F^-$ is roughly 10 D.

Finally, the observed moments of inertia of the three isotopomers of the complex (Table 1) can be fitted to give the distances $r(N\cdots F_i)$ and $r(F_i\cdots F_o)$ (i = inner; o = outer) under the assumption that the geometry of the $(CH_3)_3N$ subunit is unchanged when F_2 approaches along the C_3 axis to produce $[(CH_3)_3NF]^+\cdots F^-$. The results of the least squares fit are $r(N\cdots F_i) = 1.29(4)$ Å and $r(F_i\cdots F_o) = 2.32(4)$ Å. Although the errors are large because these distances are highly correlated, it is significant that $r(N\cdots F_i)$ and $r(F_i\cdots F_o)$ are, respectively, similar to and much larger than the quantities $r(N-F) = 1.365$ Å in NF_3[16] and $r(F-F) = 1.41744(6)$ Å in F_2.[12] The bond lengths $r(N\cdots F_i)$ and $r(F_i\cdots F_o)$ are evidently also consistent with the conclusion from the other evidence adduced here: that is that F_2 is heterolyzed as it approaches the nitrogen atom along the C_3 axis of the $(CH_3)_3N$ unit to form a N–F bond and the ion pair $[(CH_3)_3NF]^+\cdots F^-$.

A possible mechanism for formation of the ion pair is shown in Scheme 1, in which the weak, outer complex (as observed for

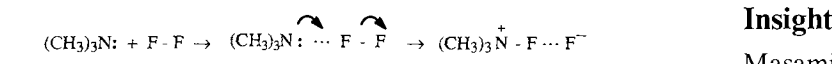

Scheme 1.

$H_3N\cdots F_2$[2]) is formed first but nucleophilic attack on F_2 then occurs, accompanied by synchronous charge transfer. The present investigation is noncommittal about the existence of the outer complex at a minimum in the potential energy surface. The transfer of F^+ from F_2 to $(CH_3)_3N$ implies that the F^+ affinity (the analogue of proton affinity) of trimethylamine is large. We note that the mechanism in Scheme 1 is identical to that which would be written for formation of the isoelectronic molecule $(CH_3)_3CH_3\cdots F^-$ from trimethylamine and methyl fluoride.

Experimental Section

Rotational spectra of the complexes $[(CH_3)_3N, F_2]$ were observed by using a pulsed-nozzle, Fourier-transform microwave spectrometer [7] fitted with a fast-mixing nozzle [8]. A mixture of approximately 2% of fluorine (99.8% pure, Distillers M. G.) in argon was pulsed down the outer of the two concentric tubes that constitute the fast-mixing nozzle at a rate of 2 Hz from a stagnation pressure of 3 bar. Trimethylamine vapor (Aldrich) was flowed continuously from the inner (glass, 0.3 mm internal diameter) tube to yield a nominal pressure of 8×10^{-5} mbar in the evacuated Fabry–Pérot cavity of the spectrometer. Gas pulses produced in this way were rotationally polarized and the subsequent free induction decay at rotational transition frequencies collected and processed as described elsewhere [8]. Samples of [^{15}N]trimethylamine (99 atom%) and [D_9]trimethylamine (99.9 atom%) were supplied by CK Gas Products Ltd.

Received: January 20, 1997 [Z10011IE]
German version: *Angew. Chem.* **1997**, *109*, 1399–1401

Keywords: fluorine · gas-phase chemistry · intermediates · ion pairs · rotational spectroscopy

[1] The dissociation energy for the process $F_2 = F^+ + F^-$ is given by $D_0 + IP - EA$, where D_0 is the zero-point dissociation energy for $F_2 = 2F$, and IP and EA are the first ionization energy and electron affinity of F, respectively. The values $D_0 = 154.4(4)$ kJ mol^{-1}, IP = 1513.5(6) kJ mol^{-1} and EA = 297(10) kJ mol^{-1} are given in: *Gmelin Handbuch der Anorganischen Chemie*, 8th ed., *Fluorine, Supplement Volume 2*, Springer, Berlin, **1980**, pp. 57–69.

[2] H. I. Bloemink, K. Hinds, J. H. Holloway, A. C. Legon, *Chem. Phys. Lett.* **1995**, *245*, 598–604.
[3] S. A. Cooke, G. Cotti, C. M. Evans, J. H. Holloway, A. C. Legon, *Chem. Phys. Lett.* **1996**, *262*, 308–314.
[4] S. A. Cooke, G. Cotti, C. M. Evans, J. H. Holloway, A. C. Legon, *Chem. Phys. Lett.* **1996**, *260*, 388–394.
[5] G. Cotti, C. M. Evans, J. H. Holloway, A. C. Legon, *Chem. Phys. Lett.* **1997**, *264*, 513–521.
[6] S. A. Cooke, G. Cotti, J. H. Holloway, A. C. Legon, *Angew. Chem.* **1997**, *109*, 81–83; *Angew. Chem. Int. Ed. Engl.* **1997**, *36*, 129–130.
[7] A. C. Legon in *Atomic and Molecular Beam Methods, Vol. 2* (Ed.: G. Scoles) Oxford University Press, Oxford, **1992**, Chapter 9, p. 289.
[8] A. C. Legon, C. A. Rego, *J. Chem. Soc. Faraday Trans.* **1990**, *86*, 1915–1921.
[9] See, for example, L. W. Buxton, E. J. Campbell, M. R. Keenan, T. J. Balle, W. H. Flygare, *Chem. Phys.* **1981**, *54*, 173–181.
[10] D. J. Millen, *Can. J. Chem.* **1985**, *63*, 1477–1479.
[11] J. E. Wollrab and V. W. Laurie, *J. Chem. Phys.* **1969**, *51*, 1580.
[12] H. G. M. Edwards, E. A. M. Good, D. A. Long, *J. Chem. Soc. Faraday Trans. 2* **1976**, *72*, 984–987.
[13] C. A. Rego, R. A. Batten, A. C. Legon, *J. Chem. Phys.* **1988**, *89*, 696–702.
[14] A. C. Legon, C. A. Rego, *J. Mol. Struct.* **1988**, *189*, 137–152.
[15] A. C. Legon, *Chem. Soc. Reviews*, **1993**, *22*, 153–163.
[16] M. Otake, C. Matsumura, Y. Morino, *J. Mol. Spectrosc.* **1968**, *28*, 316.
[17] E. J. Campbell, L. W. Buxton, T. J. Balle, W. H. Flygare, *J. Chem. Phys.* **1981**, *74*, 813–828.

Biomimetic Extradiol Cleavage of Catechols: Insights into the Enzyme Mechanism**

Masami Ito and Lawrence Que, Jr.*

The catechol dioxygenases are a class of nonheme iron enzymes that catalyze the oxidative cleavage of catechols as part of nature's biodegradation pathway for aromatic molecules.[1] These enzymes can be divided into two subclasses: intradiol-cleaving enzymes, which break the catechol C1–C2 bond, and extradiol-cleaving enzymes, which break the C2–C3 bond (Scheme 1).[2, 3]

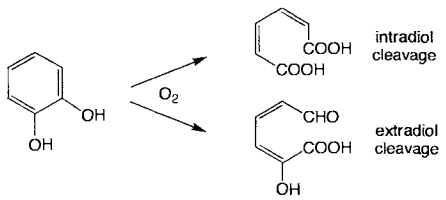

Scheme 1. The two modes of oxidative cleavage of catechols in nature.

The intradiol-cleaving enzymes require Fe^{III} and are the more extensively characterized. The persistence of the Fe^{III} oxidation state in the reaction cycle has led to a proposed mechanism in which the substrate catechol is activated by coordination to the Fe^{III} center for direct electrophilic attack by O_2.[4, 5] In contrast, the extradiol-cleaving enzymes, which typically require Fe^{II}, are proposed to utilize an oxygen activation mechanism,[2, 6] though this mechanism is not as well understood. Interestingly, extradiol-cleavage can also be elicited by catechol 1,2-dioxygenase with some substrate analogues,[7, 8] which demonstrates that even an Fe^{III} enzyme can carry out this chemistry.

[*] Prof. Dr. L. Que, Jr., Dr. M. Ito
Department of Chemistry and Center for Metals in Biocatalysis
University of Minnesota
207 Pleasant St. SE, Minneapolis, MN 55455 (USA)
Fax: Int. code +(612)624-7029
e-mail: que@chem.umn.edu

[**] This work was supported by a grant from the National Institutes of Health (GM-33162, L. Q.) and a fellowship from the Japan Society for the Promotion of Science (M. I.).

Biomimetic [Fe^{III}(L)dbc] complexes (L = tetradentate tripodal ligand; dbc = 3,5-di-*tert*-butylcatecholate dianion) react with O_2 to afford excellent yields of intradiol cleavage product.[5, 9] These complexes have played an important role in supporting and refining the novel substrate activation mechanism for intradiol cleavage. We have thus embarked on an analogous effort to elicit extradiol cleavage from a metal catecholate. Thus far, there are only two reported examples of extradiol cleavage by synthetic iron complexes. Funabiki et al. found that $FeCl_2$ in THF/H_2O cleaves $dbcH_2$ to extradiol cleavage products in 40% yield,[10] but the relevant reactive species was not identified. On the other hand, Dei et al. found that the complex [Fe^{III}(tacn)Cl(dbc)] (**1**, tacn = 1,4,7-triazacyclononane) afforded extradiol cleavage product upon exposure to O_2 in 35% yield.[11] Neither of these studies featured a systematic investigation that shed light on the extradiol cleavage mechanism. We have thus followed up on the study by Dei et al. and report in this paper conditions under which extradiol cleavage of the coordinated catecholate in **1** can be achieved quantitatively. Our observations provide the basis for a proposed mechanism for extradiol cleavage and the principles underlying the regioselectivity of catechol cleavage.

[Fe^{III}(tacn)Cl(dbc)] (**1**, Scheme 2) is a six-coordinate complex with a structure akin to that recently reported for [Fe^{III}(tacn)N_3(Cl_4cat)] (Cl_4catH_2, tetrachlorocatechol).[12] When exposed to O_2 in CH_3CN, **1** afforded three products: 3,5-di-*tert*-butylquinone (**2**) in 50% yield, and the two isomeric di-*tert*-butyl-2-pyrones (**3** and **4**) in 29% combined yield (Table 1). The pyrones **3** and **4** derive from the extradiol cleavage of dbc with insertion of one oxygen atom into either the C1–C6 or the C2–C3 bond followed by loss of CO.[10, 13, 14] In pyridine solvent the complex afforded a comparable yield of extradiol cleavage products, though the isomer ratio differs. In both cases 3,5-di-*tert*-butylmuconic acid anhydride, the intradiol cleavage product, was observed in only trace amounts, confirming the proclivity of this complex towards extradiol cleavage.

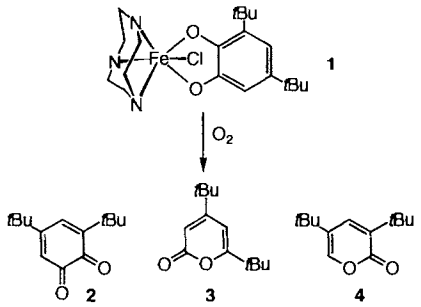

Scheme 2. The reaction of **1** with O_2 gives **2**–**4**.

Complex **1** differs from the [Fe(L)dbc] complexes that afford intradiol cleavage products in having a tridentate tacn ligand (instead of a tetradentate L) plus an additional chloride. Dei et al. have suggested that the presence of the labile chloride in **1** may be the essential factor for achieving extradiol cleavage.[11] We have thus investigated the reactivity properties of **1** in the presence of silver salts to remove the chloride (Table 1). No extradiol cleavage products were formed upon addition of an equivalent of AgOAc; instead about a 40% yield of quinone **2** was obtained in both CH_3CN and pyridine. However the use of $AgBF_4$ significantly favored the oxidative cleavage reaction; indeed, the conversion was 90% in pyridine. The contrasting effects of AgOAc and $AgBF_4$ on the oxidation of the coordinated catecholate suggest that the availability of a coordination site on the metal center plays a key role in the extradiol cleavage mechanism. Extradiol cleavage is inhibited in the presence of a coordinating anion such as acetate but favored in the presence of a noncoordinating anion such as BF_4.

Table 1. Product distributions for the reaction of complex **1** with O_2 [a].

Solvent	Reagent	**2**	**3**	**4**
CH_3CN	–	50	24	5
	1 equiv AgOAc	38	trace	trace
	1 equiv $AgBF_4$	1	35	20
C_5H_5N	–	–	16	12
	1 equiv AgOAc	36	trace	trace
	1 equiv $AgBF_4$	8	76	15
CH_2Cl_2	–	13	2	1
	1 equiv AgOAc	35	2	1
	1 equiv $AgBF_4$	82	2	1
	1 equiv $AgBF_4$, 20 equiv pyridine	trace	67	11
	1 equiv $AgBF_4$, 20 equiv 2-methylpyridine	trace	70	16
	1 equiv $AgBF_4$, 20 equiv 4-methylpyridine	trace	78	20
	1 equiv $AgBF_4$, 20 equiv *N*-methylimidazole	trace	68	30
	1 equiv $AgBF_4$, 20 equiv 2,6-dimethylpyridine	trace	8	2

[a] Reaction time $t = 12$ h, ca. 25 °C. In all cases, only trace amounts (< 1% yield) of the intradiol cleavage product, 3,5-di-*tert*-butylmuconic anhydride, could be detected. Numbers reported are the average of three runs. For the reactions with low product yields, the balance is unchanged starting complex.

The reaction of **1** with O_2 was also investigated in CH_2Cl_2 to determine whether the coordinating solvents used thus far may play a role in extradiol cleavage. The major product observed in the presence of $AgBF_4$ was the quinone **2** (82% yield, Table 1). In the presence of $AgBF_4$ and 20 equiv pyridine, only trace amounts of quinone **2** were found, and the major products were the two isomeric pyrones **3** and **4** (78% yield). Under these conditions, ^{18}O labeling studies showed that the extradiol cleavage products formed had incorporated one atom of ^{18}O. The prominent ions at m/z 208 [M^+], 193 [$(M - CH_3)^+$], and 180 [$(M - CO)^+$] in the mass spectra of the two pyrone isomers shifted by two mass units in the corresponding ^{18}O-labeled products. Comparison of their intensities with the residual ^{16}O peaks indicated that the pyrone ring oxygen atoms of the products were approximately 90% labeled.

Interestingly, the use of stronger Lewis bases such as 2-methylpyridine, 4-methylpyridine, or N-methylimidazole afforded even higher conversions; indeed the latter two gave nearly quantitative (98%) extradiol cleavage of the bound catecholate, which suggests that coordination of this base to the metal center is an important feature of the mechanism. In accord with this observation, use of a sterically hindered pyridine such as 2,6-dimethylpyridine afforded a low yield of extradiol cleavage products. Thus, extradiol cleavage is elicited in the absence of chloride and in the presence of an additional coordinating aromatic nitrogen ligand.

The nearly quantitative extradiol cleavage elicited from the dbc complex **1** with tridentate tacn stands in striking contrast to the quantitative intradiol cleavage observed for the complexes with tetradentate ligands.[5, 9] This difference suggests that the key to the extradiol cleavage mechanism lies in the availability of a coordination site. While intradiol cleavage must involve the direct attack of an electrophilic O_2 molecule on the enediolate moiety of the coordinated catecholate,[4, 5] in extradiol cleavage

the initial C–O bond-forming step must occur at the carbon adjacent to the enediolate moiety. This distinct regiochemistry can only be achieved by a different mode of attack, which we propose to be that of a nucleophilic superoxide on an electrophilic site on the aromatic ring (Scheme 3). The superoxide would be generated from the binding of O_2 to the five-coordinate iron center.

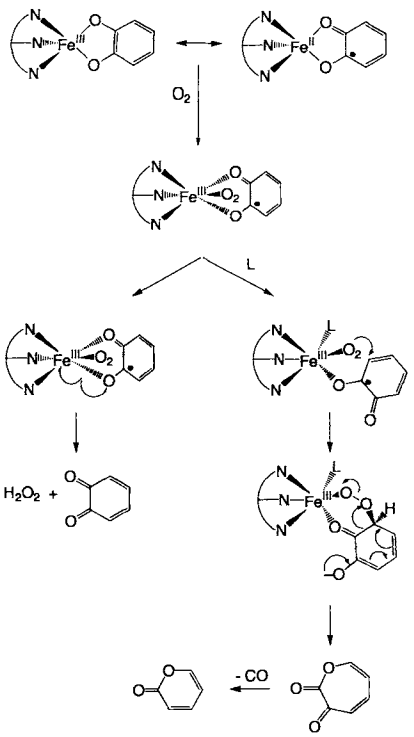

Scheme 3. Proposed mechanism for the reaction of **1** with O_2. The first step, the freeing of a coordination site on cleavage of the chloride ligand from **1**, is not shown.

Such a mechanistic scheme raises an important question: how does O_2 bind to an Fe^{III} center? We propose that the Fe^{III}–catecholate complex is in resonance with its Fe^{II}–semiquinone form, as proposed for the intradiol cleavage mechanism.[5] The loss of the halide ligand from **1** enhances the covalency of the Fe^{III}–catecholate interaction, which increases the Fe^{II} character of the metal center. The availability of an iron coordination site allows O_2 to bind to the iron center, thereby forming an Fe^{III}–superoxide complex. In the absence of the added pyridine, electron transfer occurs between the semiquinone and the superoxide through the iron center to produce quinone, as observed in CH_2Cl_2. When present, the pyridine binds to the metal–O_2 adduct by displacing the more weakly bound carbonyl oxygen of the semiquinone. The conversion of the semiquinone into a monodentate ligand brings the bound superoxide in close proximity to a ring carbon adjacent to the enediol unit. The nucleophilic superoxide can then attack the ring at this carbon to effect a Michael addition on the dienone function; subsequent decomposition of the resultant peroxide affords the observed pyrone products. The regiospecificity of oxidative cleavage is thus determined by the nature of the dioxygen species that attacks the bound catechol: nucleophilic attack by superoxide for extradiol cleavage versus electrophilic attack by O_2 for intradiol cleavage.[5]

The emerging details of the active site of extradiol-cleaving dioxygenases derived from spectroscopy [6, 15] and X-ray crystallography,[16–18] show that the enzyme–substrate complex has a five-coordinate iron active site with a bidentate catecholate. This result supports the conclusions from our biomimetic studies.

Experimental Section

1 was synthesized as previously described [11]. The oxygenation reactions were carried out with 50 mg (0.1 mmol) of **1** in 10 mL solvent under O_2 over 12 h. The products were then extracted in ether and subjected to GC analysis (Hewlett Packard 5890 Series II gas chromatograph fitted with a J & W Scientific DB-1 column; injection temperature 250 °C; initial column temperature 200 °C for 1 min, then increasing at a rate of 2 °C min^{-1} to 260 °C, which was maintained for 10 min); retention times: 7.5 min for **3**, 8.4 min for **4**, 9.7 min for 3,5-di-*tert*-butylmuconic acid anhydride, and 10.8 min for **2**. The 3,5-isomer **4** was identified by independent synthesis [13]; the 4,6-isomer **3** exhibited similar NMR and mass spectra but could be distinguished from the 3,5-isomer by comparison of their GC retention times. Mass spectral analysis was carried out on a Hewlett-Packard Model 5989B mass spectrometer.

Received: January 21, 1997 [Z 10015 IE]
German version: *Angew. Chem.* **1997**, *109*, 1401–1403

Keywords: bioinorganic chemistry · biomimetic synthesis · dioxygenases · extradiol cleavage · iron

[1] *Microbial Degradation of Organic Molecules* (Ed.: D. T. Gibson), Marcel Dekker, New York, **1984**.
[2] J. D. Lipscomb, A. M. Orville, *Metal Ions Biol. Syst.* **1992**, *28*, 243–298.
[3] L. Que, Jr., in *Iron Carriers and Iron Proteins* (Ed.: T. M. Loehr,), VCH, New York, **1989**, pp. 467–524.
[4] L. Que, Jr., J. D. Lipscomb, E. Münck, J. M. Wood, *Biochim. Biophys. Acta* **1977**, *485*, 60–74.
[5] a) H. G. Jang, D. D. Cox, L. Que, Jr., *J. Am. Chem. Soc.* **1991**, *113*, 9200–9204; b) D. D. Cox, L. Que, Jr., *ibid.* **1988**, *110*, 8085–8092.
[6] L. Shu, Y.-M. Chiou, A. M. Orville, M. A. Miller, J. D. Lipscomb, L. Que, Jr., *Biochemistry* **1995**, *34*, 6649–6659.
[7] M. Fujiwara, L. A. Golovleva, Y. Saeki, M. Nozaki, O. Hayaishi, *J. Biol. Chem.* **1975**, *250*, 4848–4855.
[8] L. Que, Jr., *Biochem. Biophys. Res. Commun.* **1978**, *84*, 60–66.
[9] W. O. Koch, H.-J. Krüger, *Angew. Chem.* **1995**, *107*, 2928–2931; *Angew. Chem. Int. Ed. Engl.* **1995**, *34*, 2671–2674.
[10] T. Funabiki, A. Mizoguchi, T. Sugimoto, S. Tada, M. Tsuji, H. Sakamoto, S. Yoshida, *J. Am. Chem. Soc.* **1986**, *108*, 2921–2932.
[11] A. Dei, D. Gatteschi, L. Pardi, *Inorg. Chem.* **1993**, *32*, 1389–1395.
[12] T. Jüstel, T. Weyhermüller, K. Wieghardt, E. Bill, M. Lengen, A. X. Trautwein, P. Hildebrandt, *Angew. Chem.* **1995**, *107*, 744–747; *Angew. Chem. Int. Ed. Engl.* **1995**, *34*, 669–672.
[13] Y. Tatsuno, M. Tatsuda, S. Otsuka, *J. Chem. Soc. Chem. Commun.* **1982**, 1100–1101.
[14] M. Matsumoto, K. Kuroda, *J. Am. Chem. Soc.* **1982**, *104*, 1433–1434.
[15] P. A. Mabrouk, A. M. Orville, J. D. Lipscomb, E. I. Solomon, *J. Am. Chem. Soc.* **1991**, *113*, 4053–4061.
[16] S. Han, L. D. Eltis, K. N. Timmis, S. W. Muchmore, J. T. Bolin, *Science* **1995**, *270*, 976–980.
[17] K. Sugiyama, T. Senda, H. Narita, T. Yamamoto, K. Kimbara, M. Fukuda, K. Yano, Y. Mitsui, *Proc. Japan Acad.* **1995**, *70*, 32–35.
[18] T. Senda, K. Sugiyama, H. Narita, T. Yamamoto, K. Kimbara, M. Fukuda, M. Sato, K. Yano, Y. Mitsui, *J. Mol. Biol.* **1996**, *255*, 735–752.

 © VCH Verlagsgesellschaft mbH, D-69451 Weinheim, 1997 0570-0833/97/3612-1344 $ 17.50+.50/0

The Most Iodine-Rich Polyiodide Yet: Fc_3I_{29}**

Karl-Friedrich Tebbe* and Rita Buchem

Polyiodide ions of the general formula I_{2m+n}^{n-} (or $I_{1+2i+2l'/n}^{-}$, where i, l', and n are integers, $0 \le i, 0 < l' \le n$; n is the ionic charge, l' represents an independent series of compounds with the given ionic charge, i is a compound within such a series, and m the excess iodine) are generated by the addition of m iodine molecules and n iodide ions.[1] The number of known compounds with low or medium iodine content, particularly triiodides, is considerable: there are 329 entries in the crystallographic data bases.[2] On the other hand, the occurrence of iodine-rich compounds, which are distinguished by diverse cross-linking patterns, as the anions I_x^- for $x > 3$ (to date x = 8/2, 13/3, 5, 22/4, 12/2, 26/4, 7, 16/2, 9)[3] is increasingly rare because of decreased stability.

The ferrocenium ion $[(C_5H_5)_2Fe]^+$ or Fc^+ is capable of forming a series of crystalline polyiodides. Shortly after the discovery of ferrocene, the polyiodides FcI_x ($3 \le x \le 15$) were reported[4] although their structures, with the exception of the triiodide FcI_3, were not characterized. Surprisingly, the simple ferrocenium iodide FcI has not been found. FcI_3 can be described in the space group $R\bar{3}m$ with a rotational disorder of the cyclopentadienyl rings.[5]

We recently investigated the completely ordered heptaiodide FcI_7[6] as well as the hexadecaiodide Fc_2I_{16},[7] which has a stacking disorder of the cations. We report here the synthesis of presumably the most iodine-rich compound of this series, Fc_3I_{29}, whose iodine content with $I_{9.67}^-$ is even greater than that of the rare nonaiodide I_9^-.[8] Furthermore, the formula I_{29}^{3-} indicates that this compound is the first example from the series of ions I_{6i-1}^{3-}, which has a formal threefold charge, with $i = 5$. In contrast the series of ions I_{6i+1}^{3-} contains the known compounds $[Co(NH_3)_6]I_7$,[9] with $i = 1$ as well as $(Me_2Ph_2N)_3I_{13}$,[10] and $[\{Pb(phen)_2\}_2I]I_{13}$ with $i = 2$ (phen = 1,10-phenanthroline).[11] $FcI_{9.67}$ was obtained as single crystals from the reaction of FcI_3, synthesized by oxidation of ferrocene with iodine in ethanol, with excess iodine (molar ratio 1:45) in acetonitrile. The surface of the black, initially shiny polyhedrons quickly dulls in air due to loss of iodine. The composition was confirmed by elemental analysis,[12] and validated by comparing the X-ray powder diffractograms (Debye-Scherrer, $Cu_{K\alpha}$) with the diagram calculated from structural data.[13] The vibrational spectra are not meaningful, due to the high iodine content and the complicated network structure of the compound.[14] According to the crystal-structure analysis[15] the salt consists of complex cations and an anionic, three-dimensional network of iodine atoms, which exhibits typical structural features (Figure 1).

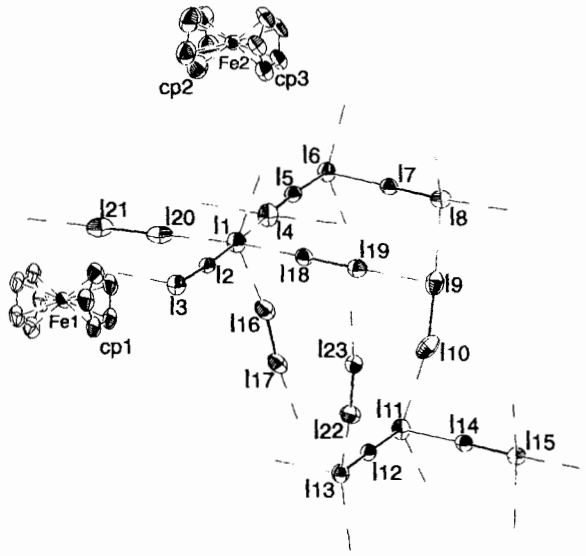

Figure 1. Fc_3I_{29}: ORTEP representation (with ellipsoids at the 50% probability level) of the structure with numbering scheme for the atoms. The hydrogen atoms of the cation have been omitted for clarity.

Bond lengths and angles within the anionic substructures of the polyiodides are often characteristic. For example, the distances of "extended" iodine molecules, which are mostly present in cross-linking iodine bridges, are 270 to 280 pm, whereas those of the stretched-symmetrical triiodide unit I_3^- are about 292 pm. A V-shaped pentaiodide unit I_5^- is often composed of a distorted triiodide ion and an iodine molecule, which are bonded with a distance of about 320 pm. Cross-linking secondary interactions[16] cover the range up to the van der Waals distance of 430 pm for the iodine atom with less sharp maxima at 340, 360, and 380 pm. The bond angles are preferentially around 90 and 180°, however, deviations can increase with longer bond lengths. Accordingly, the highly cross-linked polyiodide ion I_{29}^{3-} can be built up from triiodide and pentaiodide units as well as bridging iodine molecules.

The rather confusing structure of the anion is composed of iodine atoms that lie on and between the mirror planes with $y = 1/4$ and 3/4. In one mirror plane there is a $^1_\infty(I_5^-)$ chain that is built up of pentaiodide units (I11 to I15) and zigzags according to [100] (Figure 2a). This substructure is known for $(C_{10}H_{10}N)I_5$,[17] $(C_{20}H_{27}O_4N_2)I_5$,[18] and $(C_{34}H_{28}Br_2Fe_3)I_5$.[19] An iodine band $^1_\infty(I_{12}^{2-})$ with the composition of a dodecaiodide, which is built up in a manner similar to that of staggered dominos tiles, is parallel to the chain. This novel design contains a stretched asymmetrical triiodide ion (I1, I2, and I3), which is linked to the end of one leg (I4) of the V-shaped pentaiodide unit (I4 to I8). This produces a unique hook-shaped octaiodide unit that resembles an ice-hockey stick. Adjacent octaiodide hooks are bridged by two iodine molecules (I18–I19 and I20–I21) to form the novel dodecaiodide band. The pentaiodide chain is cross-linked over an iodine molecule (I22–I23) lying between the mirror planes to form a layer (Figure 2b). A further iodine bridge (I16–I17) lies between the mirror planes and connects the bands between I1 and I6 to form a layer parallel to that above. This produces the unique sixfold coordination at I1 (Figure 2c), which until now has only been reported for $^1_\infty[\{Ag([18]aneS_6)\}I_7]$ ([18]aneS$_6$ = 1,4,7,10,13,16-hexathiacyclooctadecane).[20] The chain and the band are joined together by a third iodine bridge (I9–I10) (Figure 2d) to form a three-dimensional network with the characteristics of an anionic cage structure $(I_5^- \cdot I_{12}^{2-})_{1/2} \cdot 3I_2$ or more precisely $[\{(I_5^-)_{1/2} \cdot I_2\} \cdot \{(I_{12}^{2-})_{1/2} \cdot I_2\} \cdot I_2]$. The completely ordered cations are intercalated within the cavities of the cage (Figure 3).

There are two crystallographically independent ferrocenium ions Fc^+ with point symmetry $\bar{1}$ and 1. Since the inversion center leads to a parallel arrangement of the two ligands, there is excellent convergence to D_{5d} symmetry. The ligands of the second cation, which is tilted towards the first by 14.70°, are almost parallel (deviation 1.52°). The ligands are in a staggered

[*] Prof. Dr. K.-F. Tebbe, Dipl.-Chem. R. Buchem
Institut für Anorganische Chemie der Universität
Greinstrasse 6, D-50939 Köln (Germany)
Fax: Int. code +(221)470-5196
e-mail: tebbe@rrz.uni-koeln.de

[**] Studies of Polyhalides, Part 29. This work was carried out within the framework of the Graduiertenkolleg "Klassifizierung von Phasenumwandlungen kristalliner Stoffe aufgrund struktureller und physikalischer Anomalien" and was supported by the Fonds der Chemischen Industrie. Part 28: H. Stegemann, A. Oprea, K. Nagel, K.-F. Tebbe, *Z. Anorg. Allg. Chem.* **1996**, *622*, 89.

 © VCH Verlagsgesellschaft mbH, D-69451 Weinheim, 1997 0570-0833/97/3612-1345 $ 17.50+.50/0

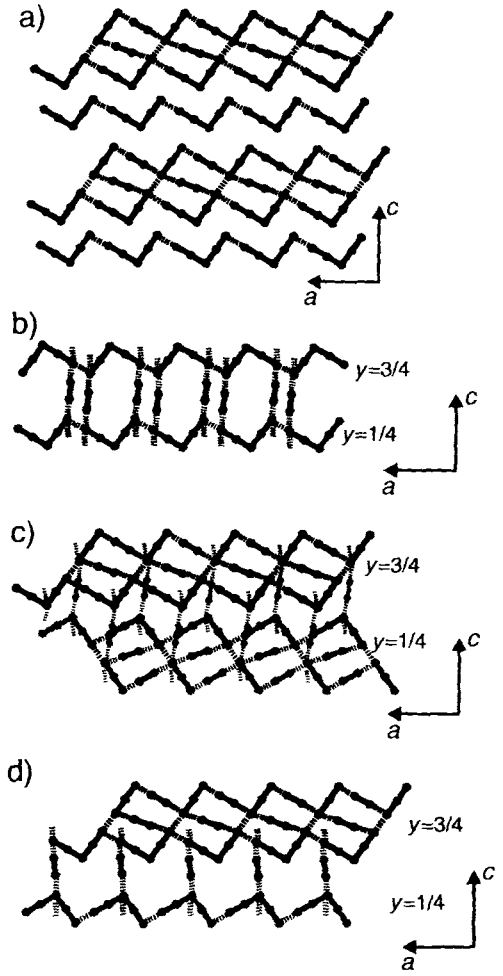

Figure 2. Fc_3I_{29}: Pattern of the cross-linking within the iodide partial structure. a) Pentaiodide chain and dodecaiodide band; b) Linkage of the pentaiodide chain to a heptaiodide network; c) Linkage of the dodecaiodide band to a hexadecaiodide layer; d) Three-dimensional cross-linking between the pentaiodide chain and the dodecaiodide band.

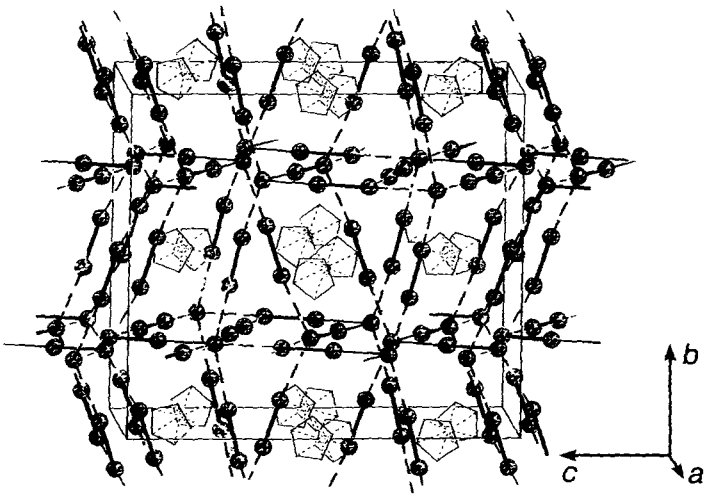

Figure 3. Unit cell of Fc_3I_{29} as viewed (almost) along the mirror planes; anionic iodide network (dark shading) and the intercalated cation complexes (dashed lines).

arrangement with a twist of about 15°. The distances between the carbon atoms within the rings and to the iron atom are as expected. Less important interactions within the anionic substructure and with the cation exhibit distances of $d(I\cdots H)$ = 309, $d(I\cdots C)$ = 378, and $d(I\cdots I)$ = 405.7 pm. The displacement parameters of all the atoms appear to be normal.

Experimental Section

A mixture of FcI_3 (1.2 g, 2.1 mmol) and I_2 (11.2 g, 88 mmol) was dissolved in CH_3CN (≈80 mL) at 50–60 °C with stirring (3–4 h). After the solution had cooled to RT, and solvent was partially removed by evaporation, black polyhedrons were obtained (m.p. 352 K). The compound is soluble in nitromethane and acetone. Only the iodine-poorer phases, Fc_2I_{16} or FcI_7, are retrieved upon recrystallization.

Received: June 27, 1996 [Z9261IE]
German version: *Angew. Chem.* **1997**, *109*, 1403–1405

Keywords: cage compounds · iodine · iron · polyanions · sandwich complexes

[1] K.-F. Tebbe, *Z. Kristallogr. Suppl.* **1996**, *11*, 52.
[2] F. H. Allen, O. Kennard, R. Taylor, *Acc. Chem. Res.* **1983**, *31*, 187; G. Bergerhoff, R. Hundt, R. Sievers, I. D. Brown, *J. Chem. Inf. Comput. Sci.* **1983**, *23*, 66.
[3] K.-F. Tebbe in *Rings, Chains and Macromolecules of Main-Group Elements* (Ed.: A. L. Rheingold), Elsevier, Amsterdam, **1977**, p. 551; K.-F. Tebbe, B. Freckmann, *Z. Naturforsch. B* **1982**, *37*, 542; K.-F. Tebbe, W. Lindenthal, T. Farida, *Z. Kristallogr. Suppl.* **1991**, *4*, 203; K.-F. Tebbe, A. Kavoosian, *Z. Naturforsch. B* **1993**, *48*, 438; K.-F. Tebbe, T. Gilles, *Acta Crystallogr. Sect. C* **1993**, *49*, 2042; K.-F. Tebbe, T. Farida, *Z. Naturforsch. B* **1995**, *50*, 1440; *ibid.* **1995**, *50*, 1685; K.-F. Tebbe, M. Bittner, *Z. Anorg. Allg. Chem.* **1995**, *621*, 218; H. Stegemann, K.-F. Tebbe, L. A. Bengtsson, *ibid.* **1995**, *621*, 165.
[4] S. A. Miller, J. A. Tebboth, J. F. Tremain, *J. Chem. Soc.* **1952**, 632; T. J. Kearly, P. L. Pauson, *Nature* **1950**, *168*, 1039; A. N. Nesmeyanov, E. G. Perevalova, N. Nesmeyanova, *Dokl. Akad. Nauk SSSR* **1955**, *100*, 1099; E. W. Neuse, M. S. Loonat, *J. Organomet. Chem.* **1985**, *286*, 329; K.-F. Tebbe, R. Buchem, *Z. Kristallogr. Suppl.* **1995**, 9, 353.
[5] T. Bernstein, F. H. Herbstein, *Acta Crystallogr. Sect. B* **1968**, *24*, 1640.
[6] K.-F. Tebbe, R. Buchem, *Z. Kristallogr.* **1995**, *210*, 438.
[7] K.-F. Tebbe, R. Buchem, *Z. Kristallogr.* **1996**, *211*, 689.
[8] W. J. James, R. J. Hach, D. French, R. E. Rundle, *Acta Crystallogr.* **1955**, *8*, 814; K.-F. Tebbe, *Z. Kristallogr.* **1988**, *185*, 496.
[9] K.-F. Tebbe, *Acta Crystallogr. Sect. C* **1983**, *39*, 154.
[10] K.-F. Tebbe, T. Gilles, *Z. Anorg. Allg. Chem.* **1996**, *622*, 138.
[11] W. Crump, K.-F. Tebbe, *Z. Kristallogr. Suppl.* **1991**, *3*, 44.
[12] Elemental analysis (calcd) for Fc_3I_{29}: I 84.25 (86.83), argentometric titration after reduction with zinc powder in acetic acid (Mettler, Greifensee, Switzerland, 1978); C 8.59 (8.50), H 0.79 (0.71), combustion analysis (Leybold-Heraeus, Hanau, Germany); Fe 3.99 (3.95), AAS (Varian).
[13] K. Yvon, W. Jeitschko, E. Parthé, *J. Appl. Crystallogr.* **1977**, *10*, 73.
[14] FT-IR: $\tilde{\nu}$ = 139 (s), 133 (s), 106 (s), 87 (s) cm^{-1} (Nicolet); Raman: $\tilde{\nu}$ = 428.5 (w), 213 (w), 172.5 (m), 115.5 (m), 74 (s) cm^{-1} (Spectr Physics, λ = 514.5 nm).
[15] Crystallographic data for Fc_3I_{29}: M_r = 4238.19 $g\,mol^{-1}$, monoclinic, space group $P2_1/m$, a = 1063.1(5), b = 1816.3(3), c = 2037.7(3) pm, β = 91.31(3)°, V = 3.933(2) nm^3 (24 reflections with $5.68 \le \theta \le 13.49°$), λ = 71.069 pm, T = 293 K, Z = 2, ρ_{calcd} = 3.578 $Mg\,m^{-3}$, $\mu(Mo_{K\alpha})$ = 11.949 mm^{-1}. Black polyhedrons (0.20 × 0.18 × 0.11 mm) with formation of decomposition pressure by additional substance within the glass tube. The 8866 reflections were corrected by LP and ψ-scans ($2.00 \le \theta \le 24.97°$, max./min. transmission: 62.62/99.92%) with max. loss of intensity of 0.4% in 81.3 h, 7142 symmetry-independent reflections (R_{int} = 0.0483); R_1 = 0.0595 (3005 reflections with $|F_o| \ge 4\sigma|F_o|$), wR_2 = 0.0808 ($|F|^2$, all reflections), $S(|F|^2)$ = 1.136 (306 parameters), residual electron density 0.991 $e\,Å^{-3}$; Enraf-Nonius-CAD4 diffractometer; solution of the iodide structure by direct methods (SHELXS-86) [21]; refined against $|F|^2$, iron and carbon atoms: difference electron density with SHELXL-93 [22]; I, Fe: anisotropic displacement parameters, C: ISOR, H: calculated with HFIX. Shorter distances within the iodide anion [pm]: I13–I15 365.1, I1–I4 364.3, I1–I20 342.7, I1–I18 344.9, I3–I19 347.7, I4–I21 371.1, I4–I8 369.9, I1–I16 357.1, I6–I17 341.7, I13–I22 377.9, I15–I23 351.9, I8–I9 363.0. The crystallographic data (excluding structure factors) for the structure reported in this paper have been deposited with the Cambridge Crystallographic Data Centre as supplementary publication no. CCDC-100216. Copies of the data can be obtained free of charge on application to The Director, CCDC, 12 Union Road, Cambridge CB21EZ (fax: int. code +(1223)336-033; e-mail: deposit@chemcrys.cam.ac.uk).
[16] N. Alcock, *Adv. Inorg. Chem. Radiochem.* **1972**, *15*, 1.
[17] F. H. Herbstein, G. M. Reisner, W. Schwotzer, *J. Inclusion Phenom.* **1985**, *3*, 173.
[18] F. H. Herbstein, M. Kapon, *Philos. Trans. R. Soc. London A* **1979**, *291*, 199.
[19] T.-Y. Dong, C.-C. Schei, M.-Y. Hwang, T.-Y. Lee, S.-K. Yeh, Y.-S. Wen, *Organometallics* **1992**, *11*, 573.
[20] A. J. Blake, R. O. Gould, S. Parsons, C. Radek, M. Schröder, *Angew. Chem.* **1995**, *107*, 2563; *Angew. Chem. Int. Ed. Engl.* **1995**, *34*, 2374.
[21] G. M. Sheldrick, *Acta Crystallogr. Sect. A* **1990**, *46*, 467.
[22] G. M. Sheldrick, Universität Göttingen (Germany), **1993**, unpublished.

 © VCH Verlagsgesellschaft mbH, D-69451 Weinheim, 1997 0570-0833/97/3612-1346 $ 17.50+.50/0

o-Benzyne: Strained Alkyne or Cumulene?—NMR Characterization in a Molecular Container**

Ralf Warmuth*

Since the concept of *o*-benzyne (**1**) as an unstable intermediate in nucleophilic aromatic substitutions was developed by Georg Wittig,[1] and its existence later proven indirectly with ^{14}C-labeling experiments by John D. Roberts and Diels–Alder trapping by Wittig,[2, 3] much effort has been made to characterize this highly reactive, short-lived species, which exists as a stable molecule only under cryogenic conditions in an inert gas matrix.[4] UV/Vis and IR spectra of **1** trapped below 77 K in an argon matrix and, most recently, a solid-state ^{13}C dipolar NMR spectrum of **1** at 20 K were recorded.[4f, 4g, 5, 6] However, detailed solution NMR spectroscopic characterization of **1** was not possible.

We made use of guest incarceration inside a molecular container to stabilize **1** in solution. The inner phase of molecular container compounds, developed and introduced to the scientific world by Donald J. Cram,[7] is particularly suitable for stabilizing reactive species. This was demonstrated by the generation of cyclobutadiene in the inner cavity of a hemicarcerand.[8] Protected by the surrounding host shell from self-destruction or reaction with reactants too large to enter the inner cavity through one of the host portals, cyclobutadiene was stable at room temperature and characterized in solution by ^{1}H NMR spectroscopy. Here we report the successful photochemical generation of **1** inside the known hemicarcerand **2**[9] as well as its ^{1}H and ^{13}C NMR spectra in solution.

We chose benzocyclobutenedione (**3**), whose photolysis has been studied at 77 K in an argon matrix,[4a, f, 10a, b] as the precursor to **1**. Upon illumination of **3** ($\lambda > 400$ nm) the highly strained benzocyclopropenone (**4**) is generated selectively.[10a, b] Simon et al. recorded ^{1}H and ^{13}C NMR spectra of **4** as a mixture with its decomposition products in [D$_6$]acetone at $-80\,^\circ$C.[10a] Upon further photolysis ($\lambda < 297$ nm) at 77 K **4** converts into **1**.[4f]

Hemicarcerand **2** was selected as the host for two reasons. Firstly, CPK model studies show that **2** has a cavity large enough to accommodate **3** but prevents **1** from exiting through one of the four equatorial host portals at ambient temperature. Secondly, the sharp decrease of the UV absorption of **2** above 275 nm allows photolysis of guest molecules at larger wavelengths.

Heating empty **2** in molten **3** at 145 °C in the absence of moisture gave the hemicarceplex **2**·**3** in 30–35% yield after column chromatographic separation from empty **2**.[11] Photolysis of a degassed solution of **2**·**3** in $CDCl_3$, sealed in a pyrex

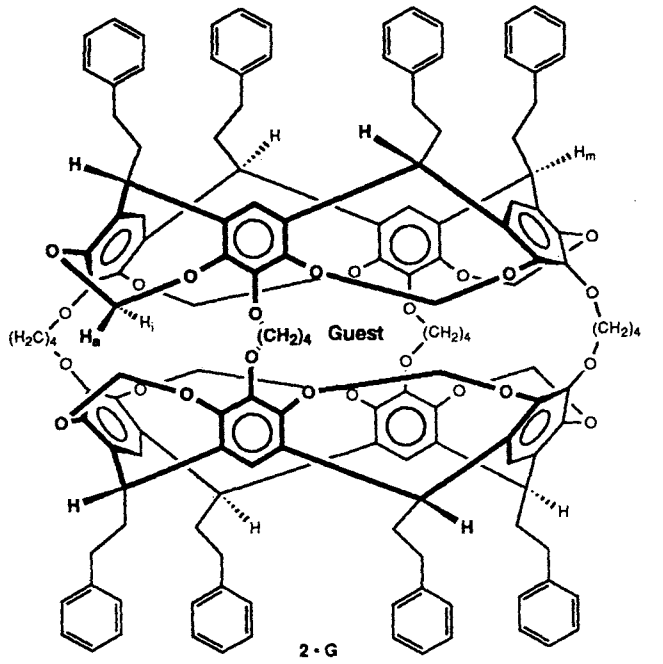

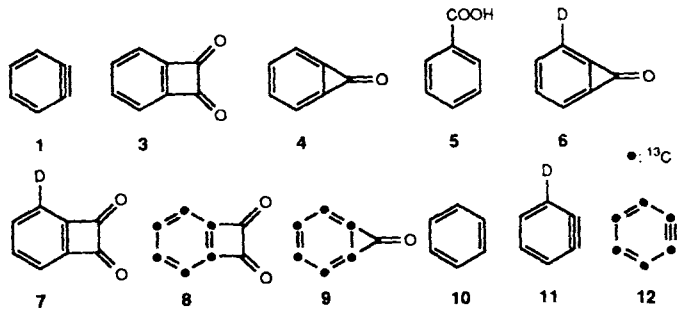

NMR tube, at 77 K with ($\lambda > 400$ nm) gave **2**·**4** as the only product. This new hemicarceplex is stable at room temperature in solution. In water-saturated $CHCl_3$ at 25 °C, the incarcerated guest reacted very slowly within several days to form the benzoic acid hemicarceplex **2**·**5**, which was identified by comparison with an authentic sample.[12] Furthermore, **2**·**5** forms instantaneously upon contact of **2**·**4** with silica gel. This and the good agreement of the observed guest ^{13}C chemical shifts (Figure 1a and Table 1) with those published for free **4** at $-80\,^\circ$C strongly suggest that this new guest is **4**.[10a, b] The solid-state structure was confirmed by an X-ray crystal structure analysis.[10c] In general, guest ^{13}C signals are shifted upfield by about $\Delta\delta = 1$–4 upon incarceration, as seen by comparing the ^{13}C chemical shifts of free and incarcerated **3** (Figure 1b and Table 1).

The room-temperature ^{1}H NMR spectrum of **4** shows the expected AA′XX′ spin system for the guest protons (Figure 2). Assignment of the guest ^{1}H and ^{13}C NMR signals of **3** and **4** was possible with ^{1}H NMR spectra of deuterated **2**·**6** and **2**·**7** as well as heteronuclear ^{1}H–^{13}C COSY spectra of ^{13}C-enriched benzocyclobutenedione (**8**; 99% ^{13}C at C2, C2′, C3, C3′, C4, C4′) and its hemicarceplex **2**·**8**, and ^{13}C-enriched benzocyclopropenone hemicarceplex **2**·**9** (99% ^{13}C at carbon C2, C2′, C3, C3′, C4, C4′).[13]

To photochemically generate **1** from **4** encapsulated in hemicarcerand **2**, a solution of **2**·**4** in [D$_8$]THF (3 mM) was degassed, sealed in a quartz NMR tube, and irradiated at 77 K for 88 h with a 300 W xenon arc lamp, whose radiation was filtered through a water filter (15 cm) and an interference filter (maximum transmission of 17% at 280 nm; width at half maximum

[*] Dr. R. Warmuth
Department of Chemistry and Biochemistry
University of California
Los Angeles, CA 90095-1569 (USA)
Fax: Int. code +(310)825-7213
e-mail: warmuth@xenon.chem.ucla.edu

[**] The IUPAC name for *o*-benzyne is 1,2-didehydrobenzene. The author extends special thanks to Prof. Dr. D. J. Cram, in whose research group this work was conducted. I am very grateful for his many helpful, critical, and stimulating discussions. Furthermore, I thank Prof. Dr. F. A. L. Anet, Prof. Dr. K. N. Houk, and Dr. R. C. Helgeson for helpful discussions, Dr. J. M. Strouse for assisting the NMR and EPR experiments, and the Alexander von Humboldt Foundation for a Feodor-Lynen fellowship. Also, I am indebted to Prof. Dr. F. A. L. Anet for providing the programs MIMIR and IGOR. I warmly thank the U. S. Public Health Service for a supporting grant for D. J. Cram (no. GM-12640).

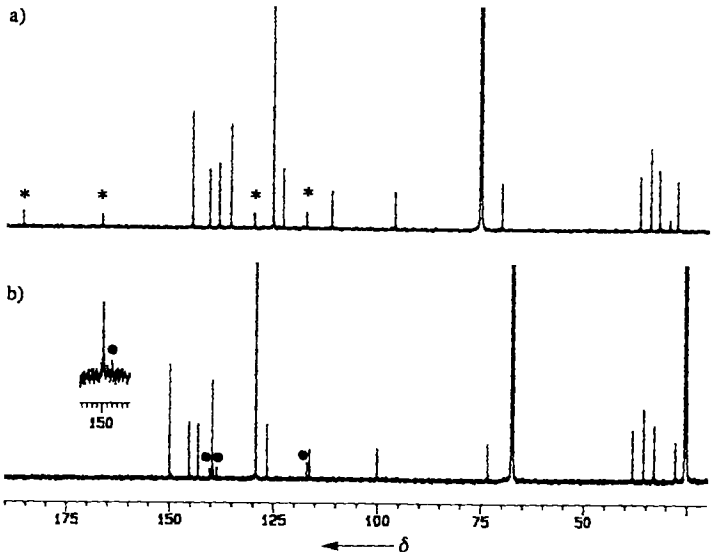

Figure 1. ^{13}C NMR spectra (125.76 MHz, 25 °C): a) hemicarceplex **2·3** (in $CDCl_3$); b) the photolysis product of **2·3** (in $[D_8]THF$). The ^{13}C signals of incarcerated guests are marked with an asterisk or a black dot.

Table 1. ^1H and ^{13}C chemical shifts [δ values] and chemical shift differences $\Delta\delta = \delta$(free) $- \delta$(incarcerated) of free and incarcerated benzocyclobutenedione **3** and benzocyclopropenone **4**.

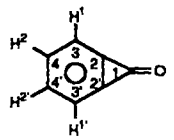

3

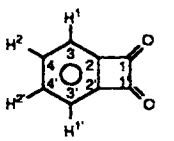

4

	incarcerated	free		incarcerated	free	
	δ [a]	δ [b, d]	$\Delta\delta$	δ [c]	δ [c]	$\Delta\delta$
H1	7.05	8.28	1.23	5.76	8.05	2.29
H2	4.34	7.82	3.48	5.27	7.79	2.52
C1/C1′	149.74	154.90	5.16	190.76	194.68	3.92
C2/C2′	140.20	141.72	1.52	170.83	173.35	2.52
C3/C3′	116.89	117.89	1.00	120.13	122.50	2.37
C4/C4′	138.52	139.33	0.81	133.14	135.49	2.35

[a] In $[D_8]THF$ at 25 °C. [b] In $[D_6]$acetone at −80 °C [10a]. [c] In $CDCl_3$ at 25 °C. [d] Simon et al. assigned δ of C2/C2′ to C3, C3′, δ of C3/C3′ to C4/C4′, and δ of C4/C4′ to C2/C2′ [10a].

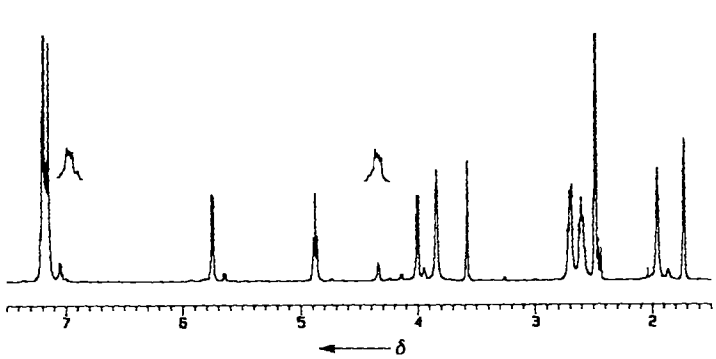

Figure 2. ^1H NMR spectrum (500.133 MHz, $[D_8]THF$; 25 °C) of the photolysis product of **2·3**.

intensity 10 ± 2 nm). Based on argon-matrix studies, photolysis of **4** under these conditions should lead to >95% **1**.[4f] The frozen sample was warmed to −97 °C for 2 min every 11 h to thoroughly mix the solution to maximize photo conversion. After photolysis the solution was warmed to −75 °C in the precooled probe of a 500 MHz NMR spectrometer, and its ^1H NMR spectrum recorded immediately (Figure 3a).

A second ^1H NMR spectrum was recorded 30 min later at −75 °C (Figure 3b), which clearly differs from the first. Additional spectra recorded still later showed no further change.

Figure 3. ^1H NMR spectra (500.133 MHz, $[D_8]THF$, −75 °C): a) a photolyzed solution of **2·4** immediately after warming from −196 °C to −75 °C; b) after 30 minutes at −75 °C; c) *o*-benzyne hemicarceplex **2·1**; d) benzene hemicarceplex **2·10**. Peaks marked with a black dot and an asterisk indicate the ^1H nuclei of incarcerated **1** and benzene, repectively.

Most likely **1** underwent reaction to form a new compound, which shows no carbonyl stretch between 1650–1900 cm^{-1} in the FT-IR spectrum and gives only one single FAB-MS peak for **2·1** at the expected mass ($[M+3] = 2327$). These results coupled with the absence of a FAB-MS signal for empty **2** (usually observed for hemicarceplexes of **2**) clearly demonstrate that **1** was formed and reacted with the host to form an addition product.[14]

These results clearly show that the ^1H NMR spectrum recorded at −75 °C (Figure 3a) is a superposition of the spectra of **2·1** and its hemicarcerand addition product. The spectrum of incarcerated **1** was obtained by spectral subtraction (Figure 3c). The proton signals assigned to **1** are at $\delta = 4.99$ and 4.31. The expected line pattern of the AA′MM′ spin system could not be verified due to strong line broadening. However, both signals were partially resolved in some runs and appear as doublets ($\Delta\delta = 5.20$ Hz). The strong line broadening, which is also observed for all proton signals of **2**, does not result from a triplet ground state for **1** but rather from the slow tumbling rate of **2·1** at low temperature. For comparison, the ^1H NMR spectrum of the benzene hemicarceplex **2·10** was recorded at the same temperature (Figure 3d). Both spectra show a remarkable similarity (comparable line shape and broadening) for the signals assigned

 © VCH Verlagsgesellschaft mbH, D-69451 Weinheim, 1997 0570-0833/97/3612-1348 $ 17.50+.50/0 Angew. Chem. Int. Ed. Engl. 1997, 36, No. 12

to **2**. The signal for incarcerated benzene at $\delta = 4.67$ appears between the two proton signals of **1**. The spin state of **1** was confirmed by EPR studies at $-100\,^{\circ}C$ in THF; no EPR signal for incarcerated **1** was observed. A singlet ground state has been predicted from the measured singlet–triplet gap of $E_{ST} = 37.7$ kcal mol^{-1}.[15]

Assignment of the signals for **1** was made with the ^{1}H NMR spectrum of deuterated **2**·**11**, which was generated photochemically from **2**·**6**. In this spectrum (not shown), an intensity ratio of 1:2 for the signals for **1** at $\delta = 4.99$ and 4.31 was observed. Hence, the first signal was assigned to H1/H1′, and the latter H2/H2′. The lifetime of **1** inside the hemicarcerand **2** at $-75\,^{\circ}C$ was determined from the decay of the intensity of the signal at $\delta = 4.99$. The rather short lifetime ($t_{1/2} = 205$ s) reflects the high reactivity of **1**.

Even stronger evidence for incarcerated **1** was obtained from its ^{13}C NMR spectrum. Preliminary experiments at lower temperature[14] show that the lifetime of **1** just above the melting point of [D$_8$]THF ($-108\,^{\circ}C$) is several hours, which is sufficient for recording a ^{13}C NMR spectrum. The ^{13}C-enriched incarcerated *o*-benzyne (99% ^{13}C at all positions) **2**·**12** was prepared from **2**·**9**. The ^{13}C NMR spectrum was recorded at $-98\,^{\circ}C$ in [D$_8$]THF. A pure ^{13}C NMR spectrum of $^{13}C_6$-**1** was obtained by subtracting the spectra of unphotolysed starting material **2**·**9** from the addition product between **12** and **2**, which formed during the accumulation (Figure 4).

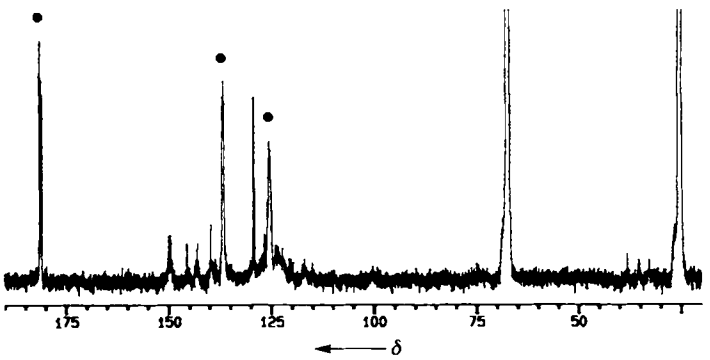

Figure 4. ^{13}C NMR spectrum (125.757 MHz, [D$_8$]THF, $-98\,^{\circ}C$) of the [$^{13}C_6$]1 hemicarceplex **2**·**12**. Carbon signals of incarcerated **12** are marked with a black dot.

Three carbon signals for **1** were found, as expected for this AA′MM′XX′ spin system (Table 2). The exact assignment was made by line pattern analysis and confirmed by ^{1}H–^{13}C heteronuclear decoupling experiments.

We estimated the chemical shifts of free **1** in solution by assuming that the protons and carbon atoms of **1** and benzene, which are of similar shape and size, experience the same shielding by the surrounding host **2**. We further assumed that, on the time average, the two different protons in **1** must be located equally in the shielding area of the polar regions of **2**. The same must be true for the three different carbon atoms of **1**. Taking the chemical shift differences $\Delta\delta$(H) and $\Delta\delta$(C) of incarcerated benzene (**2**·**10**) as a measure for the host shielding and adding them to the observed chemical shifts of incarcerated **1** gives an estimate for the chemical shifts of free **1** in solution (Table 2). These predictions are tainted with uncertainty, since only empirical models for estimating host-shielding effects are available.

The chemical shifts of C2/C2′ and C3/C3′ are in the range of aromatic or olefinic nuclei; the signals for C2/C2′ are the most similar to those for benzene. The rather high chemical shift of

Table 2. ^{1}H and ^{13}C chemical shifts [δ_{exp}] of incarcerated guests in **2**·**1**, **2**·**10**, and of **10** as well as predicted chemical shifts [δ_{pred}] for free **1**.

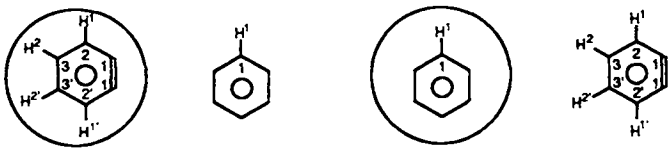

2·**1** **10** **2**·**10** **1**

	δ_{exp}	δ_{exp}	δ_{exp} ($\Delta\delta$) [c]	δ_{pred} [d]
H1/H1′	4.99 [a]	7.34 [a]	4.64 (2.70) [a]	7.69 [a]
H2/H2′	4.31 [a]			7.01 [a]
C1/C1′	181.33 [b]	129.19 [b]	127.81 (1.38) [b]	182.71 [b]
C2/C2′	125.45 [b]			126.86 [b]
C3/C3′	136.80 [b]			138.18 [b]

[a] At $-75\,^{\circ}C$ in [D$_8$]THF. [b] At $-98\,^{\circ}C$ in [D$_8$]THF. [c] $\Delta\delta = \delta_{exp}$(**10**) $- \delta_{exp}$(**2**·**10**). [d] $\delta_{pred} = \delta_{exp}$(**2**·**1**) $+ \Delta\delta$.

C1/C1′ is in good accordance with the average of the three chemical shift tensor principle values $\delta_{calcd} = 193 \pm 15$ of matrix-isolated, ^{13}C-enriched **1** at 20 K in argon. The latter was determined by Grant et al.[6] by dipolar ^{13}C NMR spectroscopy. The difference might be partially due to the temperature difference, a medium effect, or the lower accuracy of the chemical shift tensors. However, the average of the three chemical shift tensors $\delta_{calcd} = 183$, obtained by Grant et al.[6] by DFT (density functional theory) calculations with the fully optimized MP2/TZ2P geometry of **1**, approximates very well our experimental value for incarcerated **1** and almost exactly duplicates the chemical shift predicted for free **1**. The good agreement of experimental and theoretical chemical shifts not only supports our prediction but also leaves little doubt that the observed spectrum is due to **2**·**1**.

The line pattern of all three multiplets was analyzed for information about the ^{13}C–^{13}C coupling constants. A modified version of the program MIMER[16] was used to simulate the spectrum. Due to the line broadening only the stronger one-bond couplings could be calculated with sufficient precision. Figure 5a–c shows the simulated best fit overlaid on the individual multiplets (see also Table 3).

The line frequencies of the calculated spectrum of **1** give excellent agreement with those of the experimental spectrum. However, some line intensities of the experimental spectrum, especially obvious in the multiplet for C1/C1′ (Figure 5a), deviate from the calculated intensities. This is possibly due to some

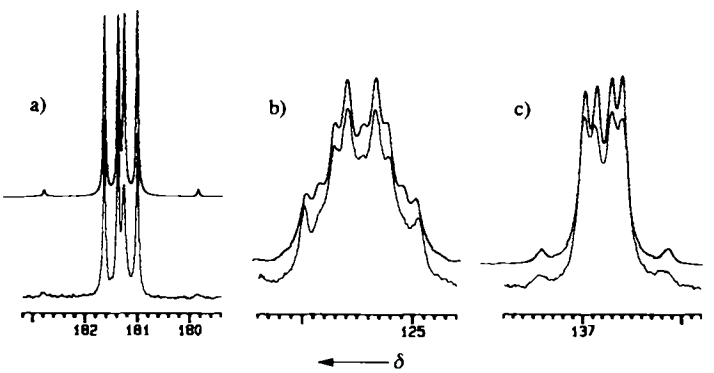

Figure 5. Part of a ^{13}C NMR spectrum (125.757 MHz, [D$_8$]THF, $-98\,^{\circ}C$) of **2**·**12**. The ^{13}C multiplets are given with the best fit (upper trace): a) C1/C1′, b) C2/C2′, and c) C3/C3′.

Table 3. $^{13}C-^{13}C$ coupling constants $^1J_{C,C}$ [Hz] of incarcerated [$^{13}C_6$]1 at −98 °C.

	C1–C1′	C1–C2/C1′–C2′	C2–C3/C2′–C3′	C3–C3′
$^1J_{C,C}$ [a]	177.9 (±0.7)	75.7 (±0.9)	50.9 (±0.8)	71.0 (±0.8)

[a] The 95%-confidence limits are given in parentheses.

interference effect between chemical shift anisotropy and dipole–dipole relaxation.[17]

The coupling constant $J_{C1,C1'}$ is in the frequency range expected for C–C triple bonds: for example, $J_{C1,C2} = 185$ Hz for diphenyl acetylene **13**, and $J_{C1,C2} = J_{C1',C2'}$ for **1** is smaller than the sp-C–sp^2-C coupling in **13** ($J_{C1,C3} = 91$ Hz).[18] We attribute the difference to the ring strain, which increases the p character of the hybridization of C1 and C1′ in **1** relative to **13**.

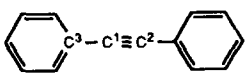

13

However, $^1J_{C3,C3'}$ is of the order of an olefinic bond (for example $^1J_{C3,C4} = 70.0$ Hz for *cis*-hexa-1,3-diene),[19] and $^1J_{C2,C3}$ and $^1J_{C2',C3'}$ are comparable with the coupling constants between two sp^2-hybridized carbon atoms connected through a single bond as in buta-1,3-diene ($J_{C2,C3} = 53.7$ Hz).[20] These comparisons and the fact that δ(C2,C3) = 170.3 for butatriene is only slightly smaller than the measured δ(C1/C1′) for **1** can be interpreted as follows: **1** has cumulenic character and is dominated by the mesomeric structure **1b**.[21]

1a **1b**

Such a hypothesis requires significant bond length alternation, which conflicts with recent ab initio calculations even at the highest level of theory.[6, 22] The problem is the lack of suitable model compounds for comparing their NMR spectra with those of **1** and the large uncertainty of structural predictions based on empirical correlations. The exact influence of the main factors that determine the value of the coupling constants is not fully understood.[23] However, the experimental NMR spectra of **1** reported here, in connection with ab initio methods that simulate the observed NMR spectrum with high precision, are valuable for making reliable predictions of the geometry and the electronic properties of this interesting molecule.[22g]

We have demonstrated that **1** can be stabilized in solution by incarceration in the unique protective inner cavity of a molecular container and characterized by NMR spectroscopy in solution. Additional compounds with highly strained multiple bonds and other reactive intermediates should be stabilized, and their structural and electronical properties examined.

Received: October 11, 1996 [Z 9647 IE]
Publication delayed at author's request
German version: *Angew. Chem.* **1997**, *109*, 1406–1409

Keywords: 1,2-didehydrobenzene · hemicarcerands · host–guest chemistry · NMR spectroscopy · photolysis

[1] G. Wittig, *Naturwissenschaften* **1942**, *30*, 696.
[2] J. D. Roberts, H. E. Simmons, Jr., L. A. Carlsmith, C. W. Vaughaun, *J. Am. Chem. Soc.* **1953**, *75*, 3290.
[3] G. Wittig, L. Pohmer, *Angew. Chem.* **1955**, *67*, 348.
[4] a) O. L. Chapman, K. Mattes, C. L. McIntosh, J. Pacansky, G. V. Calder, G. Orr, *J. Am. Chem. Soc.* **1973**, *95*, 6134; b) O. L. Chapman, C.-C. Chang, J. Kolc, N. R. Rosenquist, H. Tomioka, *ibid.* **1975**, *97*, 6586; c) C. Wentrup, R. Blanch, H. Briehl, G. Gross, *ibid.* **1988**, *110*, 1874; d) I. R. Dunkin, J. G. MacDonald, *J. Chem. Soc. Chem. Commun.* **1979**, 772; e) H.-H. Nam, G. E. Leroi, *J. Mol. Struct.* **1987**, *157*, 301; f) J. G. G. Simon, N. Münzel, A. Schweig, *Chem. Phys. Letters* **1990**, *170*, 187; g) J. G. Radziszewski, B. A. Hess, Jr., R. Zahradnik, *J. Am. Chem. Soc.* **1992**, *114*, 52.
[5] N. Münzel, A. Schweig, *Chem. Phys. Letters* **1988**, *147*, 192.
[6] A. M. Oerndt, J. C. Facelli, J. G. Radziszewski, W. J. Horton, D. M. Grant, J. Michl, *J. Am. Chem. Soc.* **1996**, *118*, 846.
[7] a) D. J. Cram, *Science* **1983**, *219*, 1177; b) D. J. Cram, S. Karbach, Y. H. Kim, L. Baczynskyj, G. W. Kalleymeyn, *J. Am. Chem. Soc.* **1985**, *107*, 2575; c) D. J. Cram, J. M. Cram, *Container Molecules and Their Guests*, Royal Society of Chemistry, Cambridge (UK), **1994**.
[8] D. J. Cram, M. E. Tanner, R. Thomas, *Angew. Chem.* **1991**, *103*, 1048; *Angew. Chem. Int. Ed. Engl.* **1991**, *30*, 1024.
[9] T. Robbins, C. B. Knobler, D. Bellew, D. J. Cram, *J. Am. Chem. Soc.* **1994**, *116*, 111.
[10] a) J. G. G. Simon, N. Münzel, A. Schweig, *Chem. Phys. Letters* **1993**, *201*, 377. b) J. G. G. Simon, A. Schweig, Y. Xie, H. F. Schaefer III, *ibid.* **1992**, *200*, 631. c) R. Warmuth, C. B. Knobler, unpublished results.
[11] All new compounds gave correct C and H elemental analyses, M^+ *m/z* signals of substantial intensity in their FAB-MS, and ^{1}H NMR and ^{13}C NMR spectra consistent with their structure.
[12] Hemicarceplex **2·5** was prepared by heating empty **2** and benzoic acid in diphenyl ether at 185 °C for 4 d (90% yield).
[13] Compound **2·6** was prepared as follows: Repetitive *ortho*-lithination/D_2O-quench of N-BOC-aniline gave 2,6-d_2-BOC-aniline [24], which was converted into **7** by literature procedures (7.25% overall yield) [25, 26]. 2-d-Benzocyclobutenedione **7** was incarcerated into **2** as described (20% yield). Hemicarceplex **2·7** was converted photochemically into **2·6** as described for **2·3** → **2·4**. Compound **8** was prepared in 32% yield from commercially available $^{13}C_6$-aniline (99% ^{13}C-enriched, Cambridge Isotope Laboratoties) by literature procedures [24–26].
[14] R. Warmuth, *Chem. Commun.* **1997**, submitted.
[15] D. G. Leopold, A. E. S. Miller, W. C. Lineberger, *J. Am. Chem. Soc.* **1986**, *108*, 1379.
[16] A version of the program MIMER (O. H. Manschen, J. P. Jacobsen, K. Schaumburg, QCPE, Indiana University, Bloomington IN (USA), Program 394), which was modified by Prof. F. A. L. Anet to interface with the IGOR display program for Macintosh, was used.
[17] a) F. A. L. Anet, *J. Am. Chem. Soc.* **1986**, *108*, 7102; b) T. C. Farrar, B. R. Adams, G. C. Grey, R. A. Quintero-Arcaya, Q. Zuo, *ibid.* **1986**, *108*, 8190.
[18] P. E. Hansen, O. K. Poulsen, A. Berg, *Org. Magn. Reson.* **1975**, *7*, 405.
[19] R. Huebers, M. Klessinger, K. Wilhelm, *Magn. Reson. Chem.* **1986**, *24*, 1016.
[20] G. Becher, W. Luettke, G. Schrumpf, *Angew. Chem.* **1973**, *85*, 357; *Angew. Chem. Int. Ed.* **1973**, *12*, 339.
[21] V. Bilinski, A. S. Dreiding, H. Hollenstein, *Helv. Chim. Acta* **1983**, *66*, 2322.
[22] a) A. C. Scheiner, H. F. Schaefer III, B. Liu, *J. Am. Chem. Soc.* **1989**, *111*, 3118. b) R. Liu, X. Zhou, P. Pulay, *J. Phys. Chem.* **1992**, *96*, 8336. c) P. B. Karadakov, J. Gerratt, G. Raos, D. L. Cooper, M. Raimondi, *Israel J. Chem.* **1993**, *33*, 253. d) A. Hinchliffe, H. J. Soscún Machado, *J. Mol. Struct. (Theochem)* **1994**, *313*, 265. e) E. Kraka, D. Cremer, *J. Am. Chem. Soc.* **1994**, *116*, 4929. f) R. Lindh, T. J. Lee, A. Bernhardsson, B. J. Persson, G. Karlström, *ibid.* **1995**, *117*, 7186. g) H. Jiao, P. von R. Schleyer, B. R. Beno, K. N. Houk, R. Warmuth, *Angew. Chem.* **1997**, submitted.
[23] L. B. Krivdin, G. A. Kalabin, *Progress in NMR Spectroscopy* **1989**, *21*, 293.
[24] J. M. Muchowski, M. C. Venuti, *J. Org. Chem.* **1980**, *45*, 4798.
[25] H. Duerr, H. Nickels, L. A. Pacala, M. Jones, Jr., *J. Org. Chem.* **1980**, *45*, 973.
[26] M. P. Cava, D. Mangold, K. Muth, *J. Org. Chem.* **1964**, *29*, 2947.

The Anions $[W(CH_3)_7]^-$ and $[Re(CH_3)_8]^{2-}$ **

Valérie Pfennig, Neil Robertson, and Konrad Seppelt*

Dedicated to Professor Gottfried Huttner on the occasion of his 60th birthday

The compounds $[W(CH_3)_6]$ and $[Re(CH_3)_6]$ were first prepared by G. Wilkinson et al.[1–5] Theoretical models predicted a nonoctahedral structure for six-coordinate d^0 complexes with pure σ ligands;[6–11] $[Zr(CH_3)_6]^{2-}$ has a trigonal prismatic

[*] Prof. Dr. K. Seppelt, Dipl.-Chem. V. Pfennig
Institut für Anorganische und Analytische Chemie der Freien Universität
Fabeckstrasse 34–36, D-14195 Berlin (Germany)
Fax: Int. code +(30)838-3310
e-mail: seppelt@chemie.fu-berlin.de
Dr. N. Robertson
Department of Chemistry, University College of North Wales, Bangor (UK)

[**] This work was supported by the Deutsche Forschungsgemeinschaft and by the Fonds der Chemischen Industrie.

structure.[12] Recently the structures of $[W(CH_3)_6]$ and $[Re(CH_3)_6]$ were elucidated:[13] $[W(CH_3)_6]$ is a trigonal prism that is strongly distorted along the C_{3v} axis. It contains three long W–C bonds to methyl groups that form small angles with each other and three short W–C bonds to methyl groups that form large angles with each other. In contrast, crystalline $[Re(CH_3)_6]$ has an almost perfect trigonal-prismatic structure.

Recent theoretical calculations support the unusual structure of $[W(CH_3)_6]$.[14] It has also been established that $[Ta(CH_3)_5]$ is built like a square pyramid, and not like a trigonal bipyramid (as is $Sb(CH_3)_5$).[15, 16] Therefore, we wondered if d^0 complexes with pure σ ligands and coordination numbers larger than six would also show structural anomalies. Since neutral compounds of this type (for example $[Re(CH_3)_7]$) are apparently unknown, we looked for corresponding anions. G. Wilkinson et al. prepared $Li_2[W(CH_3)_8]$ and $Li_2[Re(CH_3)_8]$.[3–5] According to its ESR spectra, the $[Re(CH_3)_8]^{2-}$ anion probably has a square-antiprismatic structure.[17]

Our attempts to obtain a compound containing $[W(CH_3)_8]^{2-}$ failed. However, we could prepare salts of $[W(CH_3)_7]^-$ with various cations and investigate their structures by X-ray crystallography (Figure 1). $[W(CH_3)_7]^-$ is built like a capped octahedron. In the case of $[Li\{(CH_3)_3N\}][W(CH_3)_7]$ the C_{3v} structure is strictly obeyed because of the cubic crystal symmetry. The compounds appear as ion pairs with the lithium atom attached to the basal methyl groups; the W–C bonds to these methyl groups are markedly lengthened.

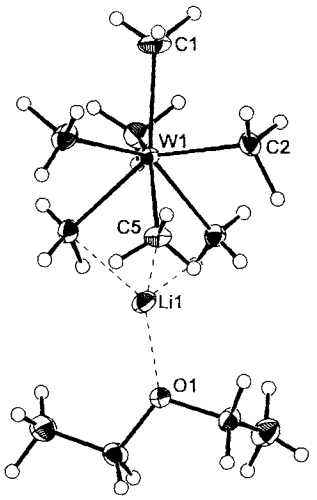

Figure 1. Crystal structure of $[Li(Et_2O)][W(CH_3)_7]$ at −153 °C (ORTEP, ellipsoids at 50% probability). Bond lengths [pm] and angles [°]: W–C1 218.4(6), W–C2 214.7(6), W–C3 215.8(5), W–C4 215.2(6), W–C5 227.8(5), W–C6 228.9(6) W–C7 228.2(5), Li–C5 212.4(11), Li–C6 213.5(11), Li–C7 216.4(11); C1-W-C2 81.2(3), C1-W-C3 80.9(3), C1-W-C4 80.3(3), C1-W-C5 132.2(3), C1-W-C6 132.5(3), C1-W-C7 131.5(3). The structure of the anion in $[Li\{(CH_3)_3N\}][W(CH_3)_7]$ is nearly identical. Bond lengths [pm] and angles [°]: $W-C_{apical}$ 216.9(13), $W-C_{equatorial}$ 215.4(6), $W-C_{basal}$ 228.3(5), $Li-C_{basal}$ 211.8(13); C_{apical}-W-C_{basal} 131.5(2), C_{apical}-W-$C_{equatorial}$ 80.2(2).

In the case of coordination number seven, the capped octahedron is the geometry with the least ligand-repulsion energy (followed by the capped trigonal prism and the pentagonal bipyramid) and is also found for $[WF_7]^-$ and $[MoF_7]^-$, independent of the type of cation.[18] Therefore, a structure anomaly due to the pure σ ligands is not observed for $[W(CH_3)_7]^-$. The building principle for similar main-group compounds is the pentagonal bipyramid (IF_7,[19, 20] $[TeF_7]^-$,[21, 22] $[ROTeF_6]^-$, $[(RO)_2TeF_5]^{2-}$, $[IOF_6]^-$[22]). The capped octahedral configuration of seven fluorine atoms is only observed in the presence of a "nonbonding" electron pair, such as in $[XeF_7]^-$.[23] $[Th(CH_3)_7]^-$, the sole homoleptic f-atom complex of this type, has also a capped octahedral structure.[24]

The structure of a mixed-substituted complex with tungsten(v) is also capped octahedral. Organometallic reactions with WF_6 are always difficult to control, although it is more stable and has lower oxidation power than WCl_6. The structure of $[WF(CH_3)_4(CH_3CN)_2]$ is shown in Figure 2. In accord with the ligand-repulsion model, the fluorine atom and the two acetonitrile ligands occupy positions that are characterized by longer bonds in $[WF_7]^-$ and $[W(CH_3)_7]^-$.

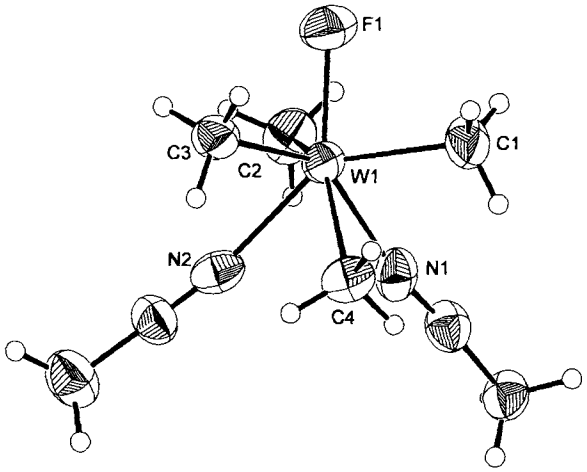

Figure 2. Crystal structure of $[WF(CH_3)_4(CH_3CN)_2]$ in $[WF(CH_3)_4(CH_3CN)_2]\cdot WF_6$ (ORTEP, ellipsoids at 50% probability). Bond lengths [pm] and angles [°]: W1–F1 189.0(10), W1–C1 210.4(19) W1–C2 212.8(19) W1–C3 212.8(18), W1–C4 225.5(16), W1–N1 220.7(16), W1–N2 217.0 (16); F1-W1-C1 78.8(7), F1-W1-C2 86.2(7), F1-W1-C3 79.3(7), F1-W1-C4 130.6(6), F1-W1-N1 137.4(5) F1-W1-N2 138.3(5).

Preparation and crystal growth of a compound with the $[Re(CH_3)_8]^{2-}$ anion is straightforward; apparently $[Re(CH_3)_6]$ is prepared via $[Re(CH_3)_8]^{2-}$. The structure of the deep red-brown compound $[Li(Et_2O)]_2[Re(CH_3)_8]$ is shown in Figures 3 and 4.

Disregarding the $[Li(Et_2O)]^+$ cations, which each cap four methyl groups, the structure of the anion is regular square antiprismatic, as predicted by G. Wilkinson et al. based on the ESR spectra.[17] This structure is also observed in the fluoro-anion $[ReF_8]^{2-}$,[25, 26] independent of the counterion, as well as in $[WF_8]^{2-}$, $[IF_8]^{2-}$, and $[XeF_8]^{2-}$.[26] The square antiprism seems to be the building principle for complexes with coordination number eight. Again, in contrast to $[W(CH_3)_6]$ and $[Re(CH_3)_6]$, no structure anomaly is observed.

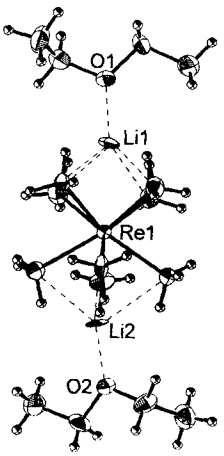

Figure 3. Crystal structure of $[Li(Et_2O)]_2[Re(CH_3)_8]$ (ORTEP, ellipsoids at 50% probability). Bond lengths [pm]: Re1–C1–8 223.1(14)–225.6(13), Li1–C5–8 233.9(24)–245.9(28), Li2–C1–4 233.5(25)–235.9(26).

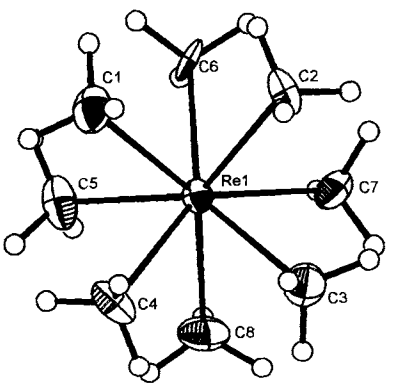

Figure 4. Structure of the $[Re(CH_3)_8]^{2-}$ anion in $[Li(Et_2O)]_2[Re(CH_3)_8]$ as viewed along the almost perfect S_8 axis (ORTEP, ellipsoids at 50% probability).

A preliminary bond-theory result is that the structures of $[M(CH_3)_7]^-$ and $[M(CH_3)_8]^{2-}$ are dominated by ligand repulsion. Furthermore, a 180° positioning of two ligands is avoided: in the case of $[W(CH_3)_7]^-$, the capped octahedron is favored over the pentagonal bipyramid. If the ligand sphere is less crowded, the principle of avoiding 180° orientations dominates: $[W(CH_3)_6]$ and $[Re(CH_3)_6]$ have C_{3v} structures, whereas $[Te(CH_3)_6]$ has an octahedral structure,[27] and $[Ta(CH_3)_5]$ has a C_{4v} structure, whereas $Sb(CH_3)_5$ has a D_{3h} structure. The root of this second principle can only be found by analysis of very precise ab initio calculations; these are not yet available for $[W(CH_3)_7]^-$ and $[Re(CH_3)_8]^{2-}$. Nevertheless, simplified models do exist. A ligand induces an extra electron density opposite to itself in the easily polarizable electron density of the heavy atoms W and Re. This prevents a second ligand from positioning there.[28] According to the Pauling bond theory s–d hybrid orbitals are not suitable for 180° ligand orientations, because s and d orbitals are gerade functions.[11]

In main-group chemistry an opposite principle is observed. Coordination geometries with ligand orientations of 180° are favored (trigonal bipyramid over tetragonal pyramid, octahedron over trigonal prism, and pentagonal bipyramid versus over capped octahedron). This is easily explained with the dominating p character of the central atom–ligand bonding.

Experimental Section

All procedures were carried out under argon or in vacuum in order to exclude, especially, oxygen. Solvents and Me_3N were dried by known procedures.

$[W(CH_3)_7]^-$: WCl_6 (500 g, 1.26 mmol) in isopentane (5 mL) was allowed to react in a Schlenk tube at −78 °C with trimethylaluminium (0.75 mL, 7,8 mmol) in isopentane (5 mL). The red solution was briefly warmed to room temperature and then cooled to −78 °C. Excess Me_3N was slowly added, and the voluminous adduct $Al(CH_3)_2Cl{\cdot}N(CH_3)_3$ removed by filtration at −77 °C. The solvent was removed in vacuo at −78 °C, and Et_2O (10 mL) added by condensation. CH_3Li (6 mL, 9.6 mmol, 1.6 M in Et_2O) was added dropwise; the solution turned yellow-brown. Removing solvent and adding isopentane yielded yellow platelets of $[Li(Et_2O)][W(CH_3)_7]$ upon cooling to −95 °C. Removing solvent at −10° and recrystallizing from isopentane at −95 °C afforded light yellow needles of $[Li\{(CH_3)_3N\}][W(CH_3)_7]$.

Crystal structure analyses: $[Li(Et_2O)][W(CH_3)_7]$: A suitable crystal ($0.2 \times 0.2 \times 0.2$ mm, yellow) was mounted at −120 °C under nitrogen on an Enraf Nonius CAD 4 four-circle diffractometer and measured at −153 °C; $a = 690.31(6)$, $b = 1274.92(8)$, $c = 1726.57(22)$ pm, $V = 1519.5(3) \times 10^6$ pm^3, space group $Pbc2_1$ (no. 29), $Z = 4$, $2\theta_{max} = 70°$, $Mo_{K\alpha}$, $\lambda = 71.063$ pm, ω scan. Of 3183 reflections measured, 3033 were independent and used for the calculation; Lorentzian-polarization and Ψ-scan absorption corrections, $\mu = 7.58$ mm^{-1}, min./max. correction = 0.91/0.99, no extinction correction. The structure was solved with SHELXS 86 [29] and refined with SHELXS 93 [30], 217 parameters, all atoms except hydrogen were treated anisotropically, $R_1 = 0.022$, $R_{w2} = 0.050$.

$[Li\{N(CH_3)_3\}][W(CH_3)_7]$: A suitable crystal ($0.3 \times 0.3 \times 0.3$, yellow) was mounted and measured as described above; $a = 1147.6(4)$ pm, $V = 1511.4(7) \times 10^6$ pm^3, −153 °C, space group $P2_13$ (no. 198), $Z = 4$, $2\theta_{max} = 52°$, $Mo_{K\alpha}$, $\lambda = 71.029$ pm, ω scan. Of 3439 reflections measured (including Friedel pairs), 994 were independent, and 961 reflections used for the calculation; Lorentzian-polarization and Ψ-scan absorption corrections, $\mu = 7.61$ min^{-1}, min./max. correction = 0.85/0.99, 71 parameters, all atoms except hydrogen were treated anisotropically, $R_1 = 0.021$, $R_{w2} = 0.044$.

$[WF(CH_3)_4(CH_3CN)_2]{\cdot}WF_6$: $Zn(CH_3)_2$ (100 mg 1.05 mmol) was dissolved in CH_3CN (2 mL) in a glass tube, and WF_6 (400 mg, 1.34 mmol) added by condensation. The solution was kept at room temperature. After 0.5 h the color was red, and large amounts of a brown deposit formed after 2 h, which were removed by centrifugation. Storing the mother liquor at −4 °C for weeks afforded yellow-brown crystals. ^{19}F NMR: $\delta = 144.3$. a suitable crystal ($0.2 \times 0.2 \times 0.2$ mm) was mounted and measured as described above; $a = 1185.5(5)$, $b = 1133.7(5)$, $c = 1202.0(5)$ pm, $\beta = 99.98(2)°$, $V = 1590.9 \times 10^6$ pm^3, −143 °C, space group $P2_1/n$ (no. 14), $Z = 4$, $2\theta_{max} = 50°$, $Mo_{K\alpha}$, 71.069 pm, ω scan. Of 2836 reflections measured, 2619 were independent and used for the calculation; Lorentzian-polarization and difabs absorption corrections [31], $\mu = 14.53$ mm^{-1}, max./min. correction = 0.79/0.99, 227 parameters, all atoms except hydrogen were treated anisotropically. $R_1 = 0.049$, $R_{w2} = 0.137$.

$[Li(Et_2O)]_2[Re(CH_3)_8]$: By varying the known procedure [5] $ReOCl_4$ (0.342 g) was dissolved in Et_2O (10 mL), and CH_3Li (6 mL, 9.6 mmol, 1.6 M in Et_2O) slowly added at −78 °C. The dark red solution turned orange-brown. The solvent was removed in vacuo at −10 °C, and the solid residue extracted with *n*-pentane at 0 °C. crystallization from the dark red solution occured at −18 °C. A suitable crystal ($0.3 \times 0.3 \times 0.3$ mm, brown) was measured as described above; $a = 1104.0(8)$, $b = 1958.2(8)$, $c = 1100.0(4)$, $\beta = 117.72(3)°$, $V = 2105.1(17)$, −153 °C, space group $P2_1/n$, $Z = 4$, $2\theta_{max} = 50°$, $Mo_{K\alpha}$, $\lambda = 70.069$ pm, ω-scan. Of 3245 reflections measured, 3040 were independent and used for the calculation; Lorentzian-polarization and Ψ-scan absorption corrections, $\mu = 5.77$ mm^{-1}, min./max. correction = 0.92/0.99, 323 parameters, all atoms except hydrogen were treated anisotropically, $R_1 = 0.047$, $R_{w2} = 0.113$.

Crystallographic data (excluding structure factors) for the structures reported in this paper have been deposited with the Cambridge Crystallographic Data Centre as supplementary publication no. CCDC-100080. Copies of the data can be obtained free of charge on application to The Director, CCDC, 12 Union Road, Cambridge CB21EZ, UK (fax: int. code +(1223)336-033; e-mail: deposit@chemcrys.cam.ac.uk).

Received: December 13, 1996 [Z9884IE]
German version: *Angew. Chem.* **1997**, *109*, 1410–1412

Keywords: methyl compounds · rhenium · structure elucidation · tungsten

[1] A. J. Shortland, G. Wilkinson, *J. Chem. Soc. Dalton Trans.* **1973**, 872–876.
[2] L. Galyer, K. Mertis, G. Wilkinson, *J. Organomet. Chem.* **1975**, *85*, C37–C38
[3] L. Galyer, G. Wilkinson, *J. Chem. Soc. Dalton Trans.* **1976**, 2235–2238.
[4] K. Mertis, G. Wilkinson, *J. Chem. Soc. Dalton Trans.* **1976**, 1488–1492.
[5] P. G. Edwards, G. Wilkinson, M. B. Hursthouse, K. M. A. Malik, *J. Chem. Soc. Dalton Trans.* **1980**, 2467–2475.
[6] R. Hoffmann, J. M. Howell, A. G. Rossi, *J. Am. Chem. Soc.* **1976**, *98*, 2484–2492.
[7] A. Demolliens, Y. Jean, O. Eisenstein, *Organometallics* **1986**, *5*, 1457–1464.
[8] S. K. Kang, T. A. Albright, O. Eisenstein, *Inorg. Chem.* **1989**, 28, 1611–1613.
[9] M. Shen, H. F. Schaefer III, H. Partridge, *J. Chem. Phys.* **1993**, *98*, 508–521.
[10] S. K. Kang, H. Tang, T. A. Albright, *J. Am. Chem. Soc.* **1993**, *115*, 1971–1981.
[11] C. R. Landis, T. Cleveland, T. K. Firman, *J. Am. Chem. Soc.* **1995**, *117*, 1859–1860.
[12] P. M. Morse, G. S. Girolami, *J. Am. Chem. Soc.* **1989**, *121*, 4114–4116.
[13] V. Pfennig, K. Seppelt, *Science* **1996**, *271*, 626–628. According to electron diffraction data $[W(CH_3)_6]$ has a trigonal prismatic structure in the gaseous state. However, a distortion into a C_{3v} structure, as found in the crystalline state, cannot be excluded: A. Haaland, A. Hammel, K. Rypdal, H. V. Volden, *J. Am. Chem. Soc.* **1990**, *112*, 4547–4549; A. Haaland, personal communication.
[14] M. Kaupp, *J. Am. Chem. Soc.* **1996**, *118*, 3018–3024.
[15] C. Pulham, A. Haaland, A. Hammel, K. Rypdal, H. P. Verne, H. V. Volden, *Angew. Chem.* **1992**, *104*, 1534–1537; *Angew. Chem. Int. Ed. Engl.* **1992**, *31*, 1464–1467.
[16] T. A. Albright, H. Tang, *Angew. Chem.* **1992** *104*, 1532–1534; *Angew. Chem. Int. Ed. Engl.* **1992**, *31*, 1462–1464.
[17] J. F. Gibson, G. Lack, K. Mertis, G. Wilkinson, *J. Chem. Soc. Dalton Trans.* **1976**, 1492–1495.
[18] S. Giese, K. Seppelt, *Angew. Chem.* **1994**, *106*, 473–475; *Angew. Chem. Int. Ed. Engl.* **1994**, *33*, 461–463.
[19] K. O. Christe, E. C. Curtis, D. A. Dixon, *J. Am. Chem. Soc.* **1993**, *115*, 1520–1526.
[20] R. Marx, A.-R. Mahjoub, K. Seppelt, R. M. Ibberson, *J. Chem. Phys.* **1994**, *101*, 585–593.
[21] X. Zhang, K. Seppelt, *Z. Anorg. Allg. Chem.* **1997**, *623*, 491–500.
[22] A.-R. Mahjoub, T. Drews, K. Seppelt, *Angew. Chem.* **1992**, *104*, 1047–1050; *Angew. Chem. Int. Ed. Engl.* **1992**, *104*, 1036–1038.
[23] A. Ellern, A.-R. Mahjoub, K. Seppelt, *Angew. Chem.* **1996**, *108*, 1198–1200; *Angew. Chem. Int. Ed. Engl.* **1996**, *35*, 1123–1125.
[24] H. Lauke, P. J. Swepston, T. Marks, *J. Am. Chem. Soc.* **1984** *106*, 6841–6843. The authors describe the anion as a distorted capped trigonal prism. The almost regular capped octahedral structure is obtained by choosing C7 as the capping atom.
[25] N. S. Nikolaev, E. G. Ipolitov, *Dokl. Akad. Nauk* **1961**, *136*, 111–113; **1961**, *140*, 129–132.
[26] S. Adam, A. Ellern, K. Seppelt, *Chem. Eur. J.* **1996**, *2*, 398–402.
[27] A. Haaland, H. P. Verne, H. V. Volden, J. A. Morrison, *J. Am. Chem. Soc.* **1995**, *117*, 7554–7555.
[28] R. J. Gillespie, E. A. Robinson, *Angew. Chem.* **1996**, 108, 539–560; *Angew. Chem. Int. Ed. Engl.* **1996**, *35*, 477–494.
[29] G. M. Sheldrick, *Program for Crystal Structure Solution*, Universität Göttingen (Germany), **1986**.
[30] G. M. Sheldrick, *Program for Crystal Structure Refinement*, Universität Göttingen (Germany), **1993**.
[31] N. Walker, D. Stuart, *Acta Crystallogr. Sect. A.* **1983**, *39*, 158–166.

Abstracts on CD-ROM—The New Age?

Crystal Structures. I: Patterns and Symmetry. By *M. O'Keeffe* and *B. G. Hyde*. Mineralogical Society of America, Washington, DC, 1996. 453 pp., hardcover $ 36.00.—ISBN 0-939950-40-5

The contents of this book are: "Preface and Note to the Reader" (6 pp.), "Symmetry in Two Dimensions" (27 pp.), "Three-Dimensional Point Groups" (30 pp.), "Three-Dimensional Space Groups" (41 pp.), "Lattice Geometry" (33 pp.), "Polyhedra and Tilings" (66 pp.), "Sphere and Cylinder Packings" (81 pp.), "Nets and Infinite Polyhedra" (92 pp.), Appendices (64 pp.), Book List (2 pp.), and Indices (7 pp.). The appendices as well as notes and exercises at the end of each of the chapters provide additional material for study. The scope of the book is narrower than the title would suggest. It deals with inorganic crystal structures of interest to the solid state chemist.

Crystallography has been too successful recently. If you can raise a few hundred thousand dollars you can buy a black box (an automatic single crystal diffractometer). At the push of a button most crystal structures can be solved without any deeper understanding of the scientific background involved. This results in a flood of published crystal structure data that tell us how atoms arrange in space. Unfortunately these data cannot be assimilated without (according to the preface) "...learning the methods appropriate to describing infinite periodic objects. These methods are generally unfamiliar to those who are not professional crystallographers (a fact that greatly hinders the development of solid state chemistry) and one of the aims of this book is to provide a usable introduction to them." The volume is meant by the authors "as a textbook for courses and as a general reference". The necessary basic tools of crystallography are introduced in the first four chapters. That covers the symmetry part of the subtitle. The remaining three chapters deal with the patterns of inorganic crystal structures, that is with polyhedra, tilings, packings, and nets, and they contain some new material. The short book list is well annotated, but even with the few references interspersed throughout the text it is insufficient as a guide for further study. One electronic data base is listed (Inorganic Crystal Structure Data) and is judged as rather imperfect, but still as excellent value for money. However, the equally important data base for metals, CRYSTMET, is omitted (a pity since intermetallics figure prominently in this volume). The incomplete indices are woefully inadequate and will unfortunately hamper the use of the volume as a general reference source. Thus, a notation is introduced for "coordination numbers" (p. vi), the term is used in the text (e.g., between pp. 208 and 255), but it is not entered in the subject index. The related topic of filling of interstices comes up in the text, but cannot be located via the subject index under "filling", "stuffing" or "interstices". The term "rutile" has four references in the index, but in fact shows up at least four more times (on pages vi, 82, 220, and 321).

The attempt to cover many aspects of basic crystallography and the tools of crystal chemistry within one book (the authors call this the "split personality" of the volume) means that both goals suffer from a lack of the space necessary for a thorough exposition. As a textbook for self-study by neophytes it seems to be too concise. It might be useful as ancillary reading in courses on solid state chemistry and the like. For experienced workers it will be fun, much appreciated, and very instructive in its last three chapters (which cover more than one half of the book). There they will find, after some searching (which should be entertaining in itself), many a nugget of information out of the rich store of the authors' knowledge. The fun part comes also from the idiosyncratic nature of the book and from the less-than-pompous language used by the authors ("why, for heaven's sake" on p. 270, when questioning the popular view on the reason for the occurrence of close packed structures). At its price, *Crystal Structures* is certainly a good buy.

Werner H. Baur
Institut für Kristallographie
der Universität
Frankfurt am Main (Germany)

Electronic Conference on Trends in Organic Chemistry, ECTOC 1. Edited by *H. S. Rzepa, C. Leach* and *J. M. Goodman*. Royal Society of Chemistry, London, 1996. CD-ROM £ 50.00.—ISBN 0-85404-899-5

So, the virtual conference has finally arrived. No more long trips to Tokyo, Rome, or Jerusalem to discuss new ideas with other scientists working in the same field. By using the Internet via a laptop we can now take part in conferences from the work-desk or even from home. Actually, of course, it has not quite reached that point yet, so do not worry. Although the expression "Electronic Conference" may at first conjure up an image of such a situation resulting from the use of new media, the reality is slightly different. As will become clear below, the purpose of an electronic conference is essentially to complement and report on an actual conference.

The growth of interest in electronic conferences in the last few years has largely been due to developments in the Internet, which has changed from being a text-orientated medium based on services such as e-mail, telnet, and ftp, to a multimedia network (the Worldwide Web, www). This transformation has opened up new possibilities for handling information, especially in the natural sciences. Lectures, posters, and discussion sessions taking place at a conference can now be recorded fully in electronic form, and transmitted without any loss of information in HTML format (hypertext markup language).

Three-dimensional molecular models embedded within the text can be moved and rotated on the monitor screen. Dynamic processes can be shown as animat-

This section contains book reviews and a list of new books received by the editor. Book reviews are written by invitation from the editor. Suggestions for books to be reviewed and for book reviewers are welcome. Publishers should send brochures or (better) books to the editorial office: Redaktion Angewandte Chemie, Postfach 101161, D-69451 Weinheim, Germany. The editor reserves the right of selecting which books will be reviewed. Uninvited books not chosen for review will not be returned.

ed images, spectra can be compressed, stretched, or edited in other ways, and so on. By using the hypertext transfer protocol (HTTP), documents from any computer can be loaded onto the Internet, regardless of the operating system that they use or the computer platform. The only requirement for all these operations is that the client browser's plug-in is capable of recognizing the standardized data structure of the application concerned.

The first Electronic Conference on Trends in Organic Chemistry, ECTOC 1, was organized by one of the pioneers in the field of standardization of chemical information, Henry S. Rzepa of Imperial College, London, together with his colleague Christopher Leach, and Jonathan M. Goodman (Department of Chemistry, Cambridge University), and is published in a CD-ROM version by the Royal Society of Chemistry.

The conference proceedings consist of six "keynote papers" and 71 articles, which present recent results (up to mid-1995) in the areas of synthetic, mechanistic, and biological chemistry. The authors are from 13 countries. On reading the keynote papers one immediately appreciates the advantages of the HTML format. A mouse-click on one of the two-dimensional valence bond formulas that are displayed brings up a three-dimensional image of the molecule that can be rotated at will, an extremely useful facility for complicated structures. These 3D structures are filed as cartesian coordinates in the format of the Brookhaven Protein Database (*.pdb files).

Taking as an example the contribution "A New Synthetic Route to the Illudin and Pterosin Family of Sesquiterpenes", by Albert Padwa, Erin A. Curtis, and Vincent P. Sandanayaka (Department of Chemistry, Emory University, Atlanta), the key structure can be viewed from any direction and in many different representations (wire model, stick model, stick-and-ball model, space-filling model, etc.). The coordinates (from an X-ray crystallographic analysis) on which this is based are those of a precursor of illudin, which already has all the five benzene ring substituents of the later products, with the correct regiochemistry. Moreover, a novel feature of the HTTP approach is that one can then go on from this 3D presentation to edit the data. Once the coordinates from the X-ray data have been stored locally on the hard disk of one's PC, the way is clear for further data processing such as energy calculations.

In the contribution "Studying Perturbation Theory with Explorer EyeChem and VRML", by Guillermo A. Suner, Omer Casher, and Henry S. Rzepa, the imaging of structures is taken a step further. These authors have translated the semiempirical (AM1) calculated transition state structures for a large number of Diels–Alder reactions into the VRML format (virtual reality modeling language). This allows one to move around in the virtual space of the calculated structures and study the overlapping of the frontier orbitals. This technique opens up new perspectives, in the truest sense of the word, and has great possibilities for use in teaching.

Most of the other contributions use only HTML text and graphics in the GIF format. They range over many different areas of organic chemistry, from new syntheses of natural products and enantioselective catalytic reactions, via the chemistry of fullerenes (where, incidentally, pdb coordinates would have been ideal), to new nonlinear optical materials and to purely theoretical studies. The work includes a full list of contributions to the discussions of the individual presentations and a list of participants (with photographs in some cases), making altogether a very successful CD-ROM. Within the next five years we may witness the disappearance of the conventional printed "book of abstracts".

Jörg Grunenberg
Institut für Organische Chemie
der Technischen Universität
Braunschweig (Germany)

pH and Buffer Theory – A New Approach. (Series: Solution Chemistry, Vol. 1.) By *H. Rilbe*. John Wiley & Sons, Chichester, 1996. 192 pp., hardcover £ 40.00.—ISBN 0-471-96735-1

This subject has traditionally been a favorite area of research for Scandinavian chemists, and H. Rilbe is on familiar ground in this book. The author's claim to present a "new approach" refers essentially to a general procedure for treating all types of problems in this field. According to this, all the quantities that occur in pH and buffer theory, such as concentrations and equilibrium constants, are converted into dimensionless logarithmic numbers, so as to benefit from the well-known mathematical simplifications associated with the use of logarithmic relationships. Despite this, however, as the arguments are developed in greater depth the equations quickly become very complicated. Consequently the author's presentation comes over as rather dry and leaden on the whole, although that is partly due to the nature of the subject. Another disadvantage of the author's new approach is that, because of the special expressions that are used, one cannot simply begin reading at a chosen place in a chapter or section of interest; instead one must first search back in the book to work out the definitions. Many of the results have been published before by the author in specialist journals, and thus the book is a summary and consolidation of that work.

Chapter 1 begins by introducing the concepts of pH and the relevant equilibrium constants. For each of the aspects that are treated from a stoichiometric standpoint the author then goes on to discuss the thermodynamic relationships involved. Buffer solutions consisting of a single-proton weak acid combined with a strong base, or a weak base with a strong acid, are considered next. Here the reader meets the difficulty already mentioned above, as one needs to be familiar with the author's definitions in order to fully understand the curves that are shown.

Chapter 2 deals with two-proton protolytes and their salts with strong acids and bases. Here the ionic strength of buffer solutions is also considered.

In Chapter 3 the author guides the reader through the Scylla and Charybdis of mixtures of weak acids and weak bases, offering first an approximate solution to the problem and then a more rigorous analysis. Here, as in the other chapters, he mentions alternative approaches used by other authors and considers the strengths and weaknesses of the different methods.

Chapter 4 treats acids with three or more protons and their salts. Special attention is devoted to the differences between the K-values and how these affect the buffer properties. The main topic of Chapter 5 is the Debye–Hückel theory for strong electrolytes and its application to the calculation of activity coefficients. Chapter 6 is entirely devoted to the buffer properties of water and the associated titration curves. This is followed by a chapter on experimental methods for determining pK- and ΔpK-values and isoprotic (or isoelectric) points. Finally there is an appendix containing some computer programs for determining isoprotic points.

This book, written by a well-recognized expert in the field, is intended for the specialist rather than for the student, as indicated by the absence of exercise problems, and not least by its price. It takes up from the point where the usual introductions to quantitative analysis leave off, and assumes that one is already familiar with ordinary buffer theory. The question of whether one can begin to accept the nota-

 © VCH Verlagsgesellschaft mbH, D-69451 Weinheim, 1997 0570-0833/97/3612-1354 $ 17.50+.50/0

tion used in the book is for the reader to decide. It remains to be seen to what extent the proposed new approach will be taken up in research and teaching.

Bernhard Neumüller
Fachbereich Chemie der Universität
Marburg (Germany)

Introduction to Theoretical Organic Chemistry and Molecular Modeling. By *W. B. Smith*. VCH Publishers, New York, 1996. 192 pp., hardcover DM 89.00.—ISBN 1-56081-937-5

Computer programs for quantum-chemical calculations are becoming increasingly user-friendly, and consequently chemists with limited theoretical knowledge are using them more and more often. It is all too easy for non-theoreticians to be misled by the suggestive power of the attractive graphics, so that they overvalue the information content of the results that the black box turns out with so little effort. For these users there are only three possible ways out of this dilemma: 1. leave well alone; 2. work in collaboration with colleagues; or 3. acquire the necessary theoretical knowledge by private study. This book by W. B. Smith is intended to help with the third alternative.

It is certainly a welcome development when an attempt is made to present theoretical organic chemistry at such a level that it can be understood by most non-specialists. Although there are many excellent books on the quantum-mechanical fundamentals of chemistry, few of these offer help in the practical application of theoretical methods. In accordance with the title of this book, the author's idea is first to introduce the reader to the theoretical fundamentals of quantum chemistry (qualitative MO theory), then in the second part (from Chapter 7 onward) to treat the most commonly used theoretical methods, and this approach is undoubtedly correct.

However, it must be said at the outset that neither the first nor the second part is suitable as a student textbook. The choice of subject matter and the strong emphasis placed on the Hückel theory give cause for concern. It is true that in a treatment of such a complex topic as this within a mere 192 pages, one has to be prepared to accept some compromises. Nevertheless, the mathematical derivations must be error-free, understandable, and entirely consistent. This book contains so many errors, loose and careless statements, and lapses from rigor in the physical arguments, that a newcomer to the subject is at risk of failing to follow the discussion or getting an incomplete picture. A few examples will illustrate this. The first is the derivation of the Schrödinger equation in a few steps on pages 2 and 3. The transition from classical mechanics to quantum mechanics is made, without further explanation, by replacing the momentum in the classical expression for the total energy by the corresponding quantum-mechanical operator, then multiplying the expression by a wave function which appears from nowhere. Arguments of this kind do not help towards an understanding of the quantum theory. The symbols used for variables are not always consistent. On page 3 the symbol ψ is used for the total wave-function, whereas on page 4 it represents the basis orbitals. Later we find that Ψ is used for molecular orbitals, whereas in the description of the SCF methods (p. 109) Ψ represents the total wave-function and ψ a molecular orbital. As the text contains no mention of the changes in meaning, the reader unfamiliar with the theory will inevitably be confused. In the mathematical formulas, vectors are never clearly distinguished as such, and operators and matrices only occasionally. The lack of care in the text also appears in statements that are difficult to understand or even misleading. On page 30 alone we find that a summation index is missing from each of the equations (2.17) to (2.22), a bracket is missing in the example of butadiene, and in Equation (2.22) the indices on the two sides of the equation do not agree. Often the symbols in the figures and equations do not correspond to those in the text; for example, on pages 32 and 33 the coefficients are denoted by 'a' in the figure but by a in the text, and on page 95 the symbol for the basis orbitals is ϕ in Equation (6.23) but φ in the text immediately below. On page 119 the method described here for minimizing the energy has little to do with the Newton–Raphson method to which the author refers. Also the general discussion about mathematical methods for energy minimization is scarcely understandable and will convey little to the reader. The explanation of CISD in Section 7.4 is simply incorrect. "CI-singles,doubles" is not, as stated here, a linear combination of the ground state Slater determinants and the first and second excited states.

There are also many mistakes in the non-mathematical part of the book. In Chapter 6 (pericyclic reactions, etc.) even the first reaction equation (6.1) defining pericyclic reactions is incorrect. In the Claisen rearrangement shown here, allylphenyl ether rearranges to give *o*-hydroxystyrene. In Equation (6.2) the second reaction arrow has below it *nv* instead of *hv*, and *hv* is missing from Equation (6.3). The claim that "... no stable ring systems containing an odd number of changes in β can exist ..." is presumably a guess. Again, it is incorrect and misleading to state (on page 91) that for a qualitative treatment of the stereochemistry of photochemical reactions it is unimportant whether a singlet or a triplet state is present. The list of errors and examples of slipshod writing could be continued.

The poor quality of the figures is evident even on first opening the book (the Möbius strip on p. 88 and the energy hypersurface on p. 150 are two interesting examples). Leaving aside esthetic considerations, many of the figures are not very suitable for explaining the matters to which they relate. For example, the connection between the orbital diagram (6.20) and the reaction equation (6.18) would only be apparent to a specialist.

Due to the large number of mistakes and examples of careless writing, the absence of any indications as to the previous knowledge assumed, and the disjointed and unclear style in which the arguments are presented, the reader unfamiliar with the subject is unlikely to learn much from the book. Moreover, the price seems unjustifiably high for a textbook of 192 pages. Perhaps the printing error on the first page—"testbook" in place of textbook—is no ordinary mistake but a Freudian slip.

Rainer Herges
Institut für Organische Chemie
der Technischen Universität
Braunschweig (Germany)

 © *VCH Verlagsgesellschaft mbH, D-69451 Weinheim, 1997* *0570-0833/97/3612-1355 $ 17.50+.50/0*

The inhibition of $\alpha_v\beta_3$ integrin, which plays a special role among the cell–cell and cell–matrix surface receptors, is important for the treatment of various diseases such as cancer, osteoporosis, acute renal failure, and retinopathy. Most novel is the suppression of tumor-induced angiogenesis and thus "starving" of the cancer metastasis. The picture shows the superposition of the structures of a high-affinity and selective peptide $\alpha_v\beta_3$ inhibitor (light spheres) as well as a non-peptidic active substance whose development was influenced by the peptide conformation (dark spheres).

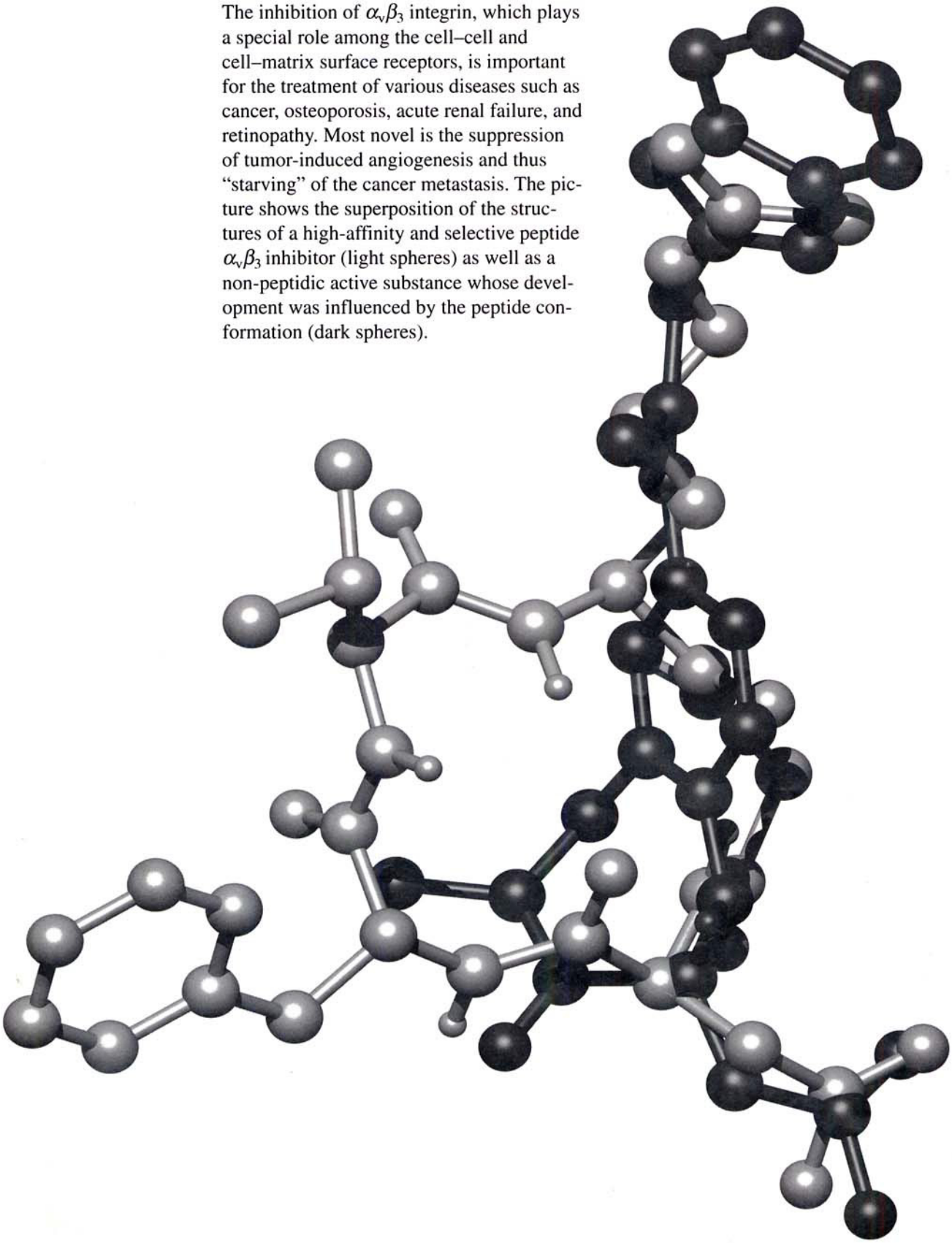

Stereoisomeric Peptide Libraries and Peptidomimetics for Designing Selective Inhibitors of the $\alpha_V\beta_3$ Integrin for a New Cancer Therapy

Roland Haubner, Dirk Finsinger, and Horst Kessler*

Cell–cell and cell–matrix interactions play a major role in biology. An important class of surface receptors are the integrins, which exist in a number of subtypes and are involved in many biological processes, for example embryonic development, blood coagulation, osteoporosis, cancer, and regulation of the balance between proliferation and death (apoptosis) of a cell. Therefore, selective inhibition of specific integrin subtypes is of great pharmaceutical interest. It is possible to develop highly selective and active inhibitors of integrins, especially the $\alpha_V\beta_3$ subtype, by the novel procedure of spatial screening. The resulting $\alpha_V\beta_3$ antagonists exhibit activity in the nanomolar range and suppress tumor-induced angiogenesis (formation of new blood vessels). Tissues with intact blood vessels are not influenced. This opens a promising new way for cancer therapy.

Keywords: cyclic peptides · integrins · receptors · structure–activity relationships

1. Introduction

Physiological processes such as embryogenesis, cell differentiation, hemostasis, wound healing, and immune response are strongly influenced by cell–cell and cell–matrix interactions. Already in the early stage of embryonal development adhesion between cells, and between cells and the extracellular matrix, contribute to the determination of morphological development. Interaction of platelets with proteins of the extracellular matrix supports wound healing after injuries by forming blood clots, which stop bleeding.[1–5]

To maintain the efficiency of the immune system leukocytes have to move freely in the body to find infectuous organisms but must also be able to adhere to different cells and proteins of the extracellular matrix. This function is necessary to penetrate endothelial barriers and basal membranes, to reach the location of the infection, and to bind to cells presenting foreign antigenes. Different cell-adhesion receptors are involved in the interplay of adhesion and free mobility.[6, 7]

To get a feeling for the complexity of these processes one should recognize that the earliest signs of unicellular life on earth are more than two billion years old, whereas the first traces of multicellular life appeared only 600 milion years ago. A complicated network for the transfer of information, specialization, and functional interplay was necessary to organize this new form of life.[8] Recently it has been found that cell adhesion plays an important role in signal transduction and, thus, is involved in information transfer between cells.[9] However, binding of the cell to the extracellular matrix also signals into the cytoplasma and leads to the reorientation of the cytoskeleton as well as functional changes in cellular behavior,[10, 11] for example prevention of apoptosis[12–14] (progammed cell death) or stimulation of cell proliferation.

Elucidation of these interactions at the molecular level is an exciting yet, to a large extent, unknown chapter of modern cellular biology and medicine. Malfunctions in these highly complex regulatory processes between cellular adhesion and migration express themselves in pathological degeneration. For example, an uncontrolled coagulation of thrombocytes may cause stroke, emboly, or cardial infarction.[4, 15–18] During metastasis the tumor cells undergo a number of different adhesive interactions.[19, 20] In connection with osteoporosis[21–24] and several other diseases that involve uncontrolled formation of blood vessels[25–27]—such as arthritis, different malfunctions of the eye,[28] and tumor growth[29, 30]—a therapy by inhibition of adhesion has been discussed.

There are four major classes of receptors involved in cell–cell and cell–matrix interactions: cadherins, selectins, receptors of the immunoglobuline superfamily, and integrins. In the following chapter the integrins, in particular the $\alpha_V\beta_3$ receptor and its role in different diseases, are discussed. This is followed by a description of the development of selective antagonists using stereoisomeric libraries (spatial screening) and investigations on conformationally controlled structure–activity relationships (SAR). Finally the development of non-peptidic inhibitors is discussed.

[*] Prof. Dr. H. Kessler, Dipl.-Chem. D. Finsinger
Institut für Organische Chemie und Biochemie
der Technischen Universität München
Lichtenbergstrasse 4, D-85747 Garching (Germany)
Fax: Int. code +(89)289-13210
e-mail: kessler@artus.org.chemie.tu-muenchen.de
Dr. R. Haubner
Nuklearmedizinische Klinik und Polyklinik
der Technischen Universität München

 © *VCH Verlagsgesellschaft mbH, D-69451 Weinheim, 1997* *0570-0833/97/3613-1375 $ 17.50+.50/0*

2. The Integrins

Integrins are heterodimeric transmembrane glycoproteins consisting of an α and a β subunit. The larger α subunit (approximately 1100 residues) is often processed to form two disulfide-bridged chains of different length. The extracellular part of the α subunit is characterized by three to four regions near the N terminus that contain 12 to 15 amino acid residues capable of binding bivalent cations (Ca^{2+}, Mg^{2+}). These regions exhibit sequence homology to the EF hand, a calcium-binding motif found in other proteins such as calmodulin.[31] Five of the six octahedral binding sites in the EF hand are conserved in the integrin sequence.[32] Only glutamic acid 104 ($-Z$ in Scheme 1)[34] is replaced by a lipophilic amino acid residue that cannot interact with the metal ion. It is assumed that the Asp side chain of the RGD sequence (see below) occupies this binding site in the complex.[33]

		X	Y	Z	-y	-X	-Z	
EF (3CLN):	90 -R-V-F-	D	K	D	G	N	G	Y-I-S-A-A-E-L-R-H-Y-
α_{IIb}:	363 -P-L-G-	D	L	D	R	D	G	Y-N-D-I-A-V-A-A-P-Y-
α_v:	346 -P-L-G-	D	L	D	Q	D	G	F-N-D-I-A-I-A-A-P-Y-
α_5:	357 -P-L-G-	D	L	D	Q	D	G	Y-N-D-V-A-I-G-A-P-F-

Scheme 1. Sequence comparison of the calmodulin (3CLN) EF-hand and three single calcium-binding repeating units of integrin α subunits [34].

X-ray structure investigations[35, 36] of the A domain of the α subunit also indicate the importance of the metal-binding sites for ligand binding. This is confirmed by observations[37–40] that show that integrins depend on the presence of bivalent metal ions and that addition of Mn^{2+} can increase the binding affinity of ligands.

The β subunit typically has about 800 amino acid residues, with the exception of β_4[41] (about 1750 amino acids). It contains four highly conserved cysteine-rich regions of 40 residues proximal to the transmembrane domain and a large loop at the N-terminus of the extracellular part. Both the α and β subunits contain a short transmembrane (20–30 residues) and an intracellular region (20–50 residues), and participate in ligand binding through contact regions next to the N-termini.[1, 42–45]

The C-terminus of the β subunit[2, 42] connects the integrin with actin filaments of the cytoskeleton[11] through intracellular proteins such as talin,[46] vinculin,[47, 48] and α-actinin.[49] This allows attachment of cells to the extracellular matrix as well as signal transduction into the cell (Figure 1).

There are many different integrins. Eight separate β and 15 α subunits are known (Scheme 2). Some α subunits (for example

R. Haubner D. Finsinger H. Kessler

Horst Kessler (right), born in 1940 in Suhl, Thüringen (Germany), studied chemistry in Leipzig and Tübingen, and finished his Ph.D. with Eugen Müller in preparative organic chemistry. In his habilitation (1969), he used NMR spectroscopy to find evidence for innermolecular mobility. In 1971 he became a full professor for organic chemistry at the Frankfurter Universität, and in 1989 moved to the Technische Universität München. He is a member of the Bayerische Akademie der Wissenschaften. In 1986 he received the Otto-Bayer-Preis, in 1988 the Max-Bergmann-Medaille für Peptidchemie, and 1997 the Emil-Fischer-Medaille from the Gesellschaft Deutscher Chemiker. He has been a guest professor in Halifax (Canada), Tokyo (Japan), Madison (USA), Haifa (Israel), and Austin (USA). His research interests include rational drug design on the basis of conformation, synthesis of peptides, sugars, and peptidomimetics, as well as development and application of NMR techniques and calculational methods for determination of peptides and proteins.

Roland Haubner (left), born in 1962 in Munich (Germany), studied chemistry from 1985 to 1991 as a recipient of the Bayerische Begabtenförderung at the Technische Universität München. He finished his Ph.D. with Horst Kessler in 1995 on the design, synthesis, and conformational analysis of high-affinity and selective $\alpha_v\beta_3$ antagonists. Since 1995 he has been developing new PET tracers for tumor diagnostic and therapy control at the Nuklearmedizinischen Klinik und Poliklinik des Klinikums at the Technische Universität München.

Dirk Finsinger (middle), born in 1968 in Munich, studied chemistry at the Technische Universität München. His Diplomarbeit in the research group of Horst Kessler dealt with the synthesis and structural characterization of thiopeptides. His current doctoral work concerns $\alpha_v\beta_3$-integrin antagonists and peptidomimetics.

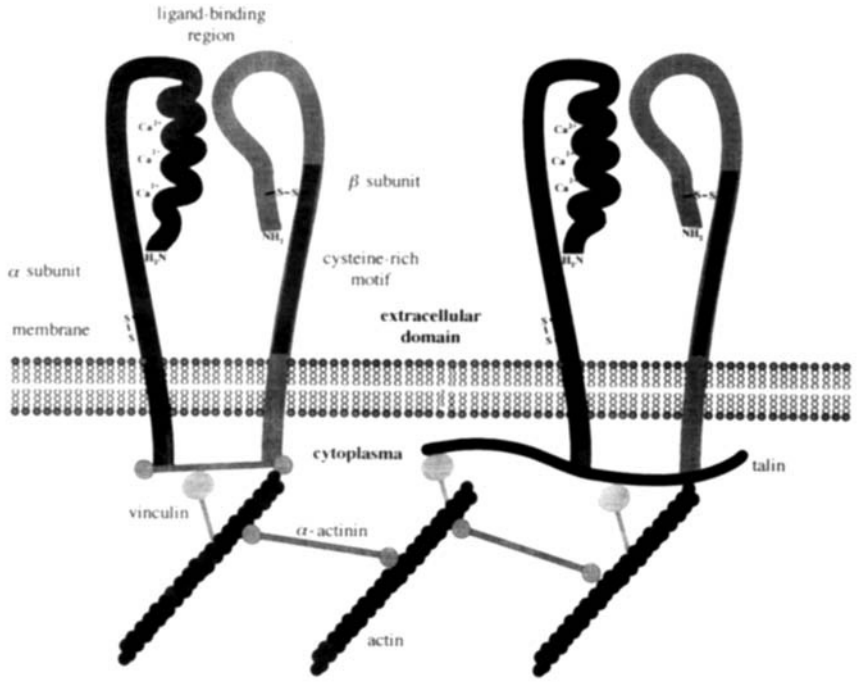

Figure 1. Schematic illustration of integrins and their interactions with proteins of the cytoskeleton.

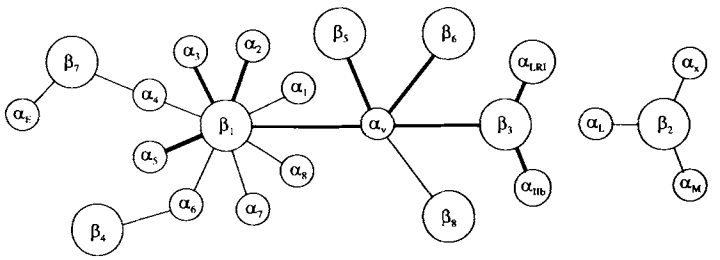

Scheme 2. The members of the distinct integrin subfamilies. Each integrin consists of an α and a β subunit (Figure 1). Different subtypes show distinct protein sequences. The bold lines indicate the integrins that bind their ligands through the RGD sequence.

α_V) can associate with a range of β subunits. The integrins are classified in three main families: β_1, β_2, and the β_3 subfamily.[2, 3, 6, 42]

The members of the widely distributed β_1-integrin family play a central role in tissue organization. They participate in the binding of different cells to extracellular matrix proteins in muscles, the nervous system, as well as the endothelial and epithelial layers, and are often found at the surface of leukocytes. Some β_1 integrins (for example $\alpha_1\beta_1$ and $\alpha_2\beta_1$) are expressed only after activation of the T lymphocytes by antigens, and, hence, are called very late activation antigens (VLA). They are important in inflammatory processes and control the localization of leukocytes after permeation of the endothelial layer.[2, 6, 50]

The β_2 integrins, also called leukocyte cell adhesion molecules (LeuCAM), are mainly found on leukocytes and microglia cells of neuronal tissue. Receptors of this type (Scheme 2) play an important role in the immune system.[2, 51, 52]

The family of β_3 integrins contains three receptors: the $\alpha_{IIb}\beta_3$ receptor ("platelet receptor"), the vitronectin receptor $\alpha_V\beta_3$, and the $\alpha_X\beta_3$ receptor[50] (which has not yet been fully characterized). The $\alpha_{IIb}\beta_3$ receptor,[53] also called GPIIb/IIIa, is probably the most investigated integrin receptor of the β_3 subfamily. Although it is expressed mainly on megakaryocyte-derived cells such as platelets, it was also found on melanoma cells.[54, 55] The $\alpha_{IIb}\beta_3$ receptor binds with different affinity to a great number of extracellular matrix proteins (for example fibrinogen, fibronectin, vitronectin, von Willebrand factor, and thrombospondin).[1, 2, 6, 56]

This receptor is involved in primary and secondary hemostasis. It allows aggregation of platelets at sites of vascular injuries by binding to the collagen filaments in the connective tissue at the lip of wounds. Aggregation of platelets by fibrinogen then forms a blood clot and seals the injured tissue. Defective formation of these clots may lead to embolies, stroke, or myocardinal infarction.[57–59]

The $\alpha_V\beta_3$ integrin is expressed on a considerably higher number of cell types than $\alpha_{IIb}\beta_3$.[60] Its function is discussed in the following.

3. The Role of $\alpha_V\beta_3$ Integrins in Diseases

The $\alpha_V\beta_3$ integrin, also known as the vitronectin receptor, can be found on almost all cells originating from the mesenchyme.[2] The complete amino acid sequence of the α_V subunit was obtained from cDNA studies,[61] and shows the typical structure for integrins as described in Section 2. It binds to a number of different ligands including the above-mentioned matrix proteins that also bind to $\alpha_{IIb}\beta_3$, tenascin, denaturated collagen type I, and osteopontin.[50] The vitronectin receptor is involved in many cell-adhesion processes. For example, it plays a role in angiogenesis,[25, 62] at different levels of tumor metastasis,[29] in phagocytosis of cells undergoing apoptosis,[63] in bone remodeling,[21, 23] and in acute renal failure.[101] There is also a relationship between $\alpha_V\beta_3$ integrin and the expression of the urokinase receptor (uPAR = urokinase-type plasminogen-activator receptor), which is involved in proteolytic processes, in metastatic melanoma cells.[64] Moreover, regulation of the integrin function by uPAR has been discussed.[65]

Tumor metastasis involves a number of different cell–cell and cell–matrix interactions (Figure 2), for example during release from the primary tumor, migration of tumor cells in the lymphatic system or blood vessels, anchoring in the capillary system of the target organ, and extravasation.[3, 66–70] Numerous investigations of integrin expression on tumor cells forming metastasis have demonstrated that those integrins that are responsible for stable contact in the tissue are down-regulated.[71–75] In contrast, those that are involved in migration are overexpressed. In particular $\alpha_V\beta_3$, which is responsible for binding to extracellular matrix proteins, is highly expressed on many tumor cells[76] such as osteosarcomas, neuroblastomas, carcinomas of the lung, breast, prostata, and bladder, as well as gliobastomas[77] and invasive melanomas.[78–80]

The formation of new capillary blood vessels from endothelial cells is essential to organ development, wound healing, and

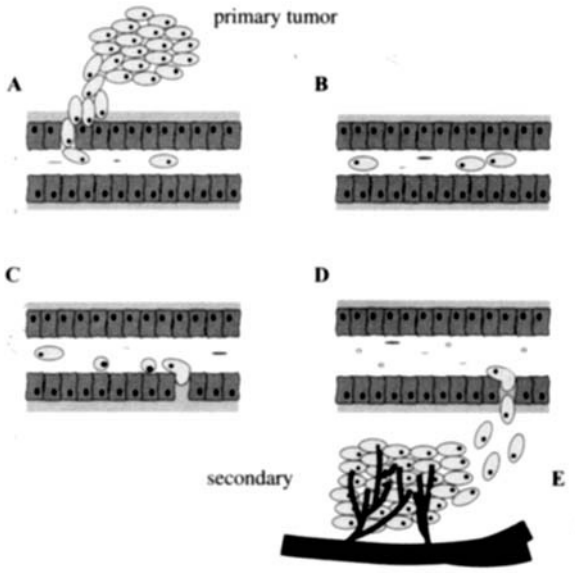

Figure 2. Metastatic cascade. A) Detachment of cancer cells from the primary tumor and invasion. B) Circulation in the blood or lymphatic system. C) Arrest in the venous or capillary bed. D) Extravasation. E) Development of metastatic colonies and tumor-induced angiogenesis.

inflammatory processes. The required adhesive events are strongly regulated; they are limited to affected cells, activated only for a relatively short period of time (several days), and suppressed completely afterwards. Cytokines and growth factors such as bFGF (basic fibroblast growth factor), VEGF (vascular endothelial growth factor), TNF-α (tumor-necrosis factor), and angiogenin activate the involved endothelial cells and regulate the formation of new capillaries.[81] The stimulated endothelial cells express proteases that decompose the basal membrane. This allows the endothelial cells to migrate into the tissue towards the stimulus.[29] The chemotactic and haptotactic behavior is controlled by cell-adhesion receptors.[82, 83] Moreover, it has been discussed[84] that lack of specific cell–matrix interactions induces an apoptotic signal in endothelial cells involved in angiogenesis and thus prevents neovascularization.

However, formation of new blood vessels is also involved in many diseases in which angiogenesis is misregulated. For example, in rheumatic arthritis the cartilage of joints is destroyed by invasion of new blood vessels. In diabetes blood vessels grow into the retina and the vitreous body (retinopathy), and lead to bleedings and, as a consequence, blindness.[26, 84]

The involvement of $\alpha_v\beta_3$ in neovascularization of the retina was demonstrated in a hypoxic-mouse model.[85] Expression of the $\alpha_v\beta_3$ and/or $\alpha_v\beta_5$ integrins can also be induced by growth factors.[86] In both cases the $\alpha_v\beta_3$-antagonistic peptides developed in our group (see below and ref. [87, 88]) drastically reduce capillary proliferation in retinal tissue.

Brooks et al.[82, 84] demonstrated that the integrin $\alpha_v\beta_3$ is present on cells of blood vessels of granulation tissue but not that of normal tissue. Expression of $\alpha_v\beta_3$ integrin is stimulated by angiogenetic factors such as bFGF and TNF-α.[89] Specific antibodies against $\alpha_v\beta_3$, for example LM 609 and our cyclic peptide *cyclo*(-Arg-Gly-Asp-D-Phe-Val-),[87] block the bFGF-induced angiogenesis but do not affect existing blood vessels. Tumors require angiogenesis to provide sufficient nutrition for the rapidly proliferating cancer cells.[26, 29, 90] Furthermore, the newly formed blood vessels are often used as a pathway for cancer cells to enter the blood circulation.

Tumor-induced angiogenesis is inhibited by the above-mentioned $\alpha_v\beta_3$ antagonists (Figure 3). For these experiments melanoma cell lines (human M21-L) that do not express $\alpha_v\beta_3$ integrins were chosen to demonstrate that blocking of angiogenesis can act directly through antagonism of cells of the blood vessels.[89] Investigations of human $\alpha_v\beta_3$ negative breast tumor tissue in a chimeric human/mouse model indicate reduction of tumor-supporting blood vessels and distinct reduction of tumor-cell proliferation by $\alpha_v\beta_3$-specific antibodies.[91] Therefore, blocking tumor-induced angiogenesis by inhibition of the $\alpha_v\beta_3$ receptor is an attractive target for fighting metastasis formation and tumor growth.[92]

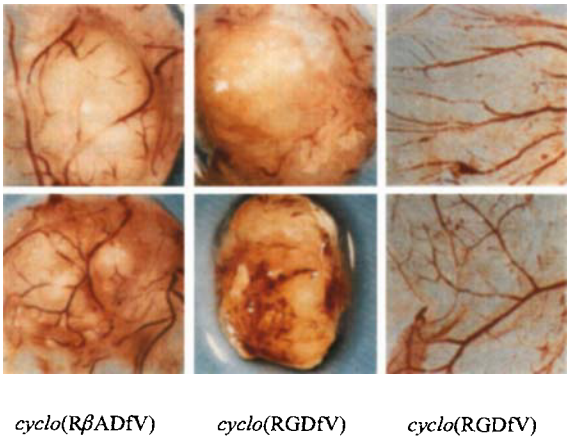

Figure 3. Inhibition of tumor-induced angiogenesis by *cyclo*(-RGDfV-)(middle). The picture on the left shows that the inactive peptide *cyclo*(-RβADfV-) with a similar amino acid sequence cannot inhibit angiogenesis of tumors implanted in chick embryos. The adjacent, normal CAM (chick chorioallantoic membrane) with blood vessels is not harmed by these peptides (right).

Another area where integrin-transmitted cell adhesion plays an important role is the turnover of bone mass. Docking of osteoclasts to extracellular bone-matrix proteins such as osteopontin or bone sialoprotein requires $\alpha_v\beta_3$ integrin.[93] This integrin is expressed in significant amounts on the cell surface of human osteoclasts as well as on those of rat or chicken.[94] In addition, in vitro studies with synthetic peptides containing the Arg-Gly-Asp sequence have demonstrated that bone resorption by isolated osteoclasts can be inhibited.[21, 95] The β_3-selective disintegrin echistatin exhibits the same effect on bone resorption in rats.[96] Therefore, $\alpha_v\beta_3$ antagonists also represent a promising therapeutic approach to preventing increased bone resorption.[24, 97]

Pathophysiological adhesion phenomena are also involved in acute renal failure. Isolated, detached necrotic endothelial cells cause ischemia in the tubular lumen.[98, 99] More recent investigations have found viable epithelial cells in the urine of kidney patients. This suggests that exfoliation of epithelial cells plays a role in the formation of vasoconstriction.[100] Analogous investigations have demonstrated that integrin receptors are involved in detachment of animal epithelial cells.[101, 102] Regeneration time after renal failure has been shortened drastically by directly injecting the peptidic $\alpha_v\beta_3$ antagonist *cyclo*(-Arg-Gly-Asp-D-Phe-Val-) into the renal artery.[103, 104]

4. The RGD Sequence

Many extracellular matrix proteins are involved in interactions with integrins. For example, the basal membrane—the border between epithelial and connective tissue underneath—partially consists of these proteins.[105] Structure-forming collagen as well as the glycoproteins laminin[106,107] and fibronectin are found there.[108-112] Extracellular matrix proteins in the plasma that are involved in blood clotting are fibrinogen,[113,114] thrombospondin,[115,116] and the von Willebrand factor.[117,118] The glycoprotein vitronectin[119-121] is observed in plasma as well as in connective tissue. Osteopontin and bone sialoprotein, which are involved in osteoporosis,[23,122] and tenascin[123,124] are also ligands for the $\alpha_v\beta_3$ receptor. These extracellular matrix proteins contain different motifs that are potential cell-binding regions.[50] One of the most frequent cell-recognition motifs is the amino acid sequence Arg-Gly-Asp (RGD; Scheme 3), the "universal cell-recognition site"[1,6,44,119,125] (Table 1). Fibrinogen also binds to the $\alpha_{IIb}\beta_3$ receptor through the GGAKQAGDV sequence of the γ chain.[126]

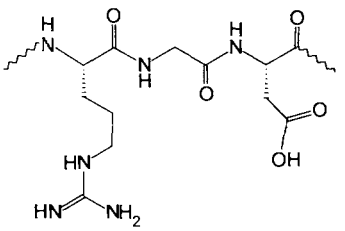

Arg Gly Asp

Scheme 3. The RGD sequence.

The RGD sequence is the basis for the development of different antagonists, specifically for the prevention of platelet aggregation. However, antagonists based on this sequence can also be used to inhibit the $\alpha_v\beta_3$ receptor.

The reason for the high selectivity of certain integrins for distinct adhesion proteins, in spite of their common RGD-recognition site, is still not understood completely. Additional binding sites as well as different conformations of the RGD sequence in different proteins have been discussed.[1] We will demonstrate here that conformationally restricted peptides can show high receptor selectivity and affinity.

So far investigations on the conformation of natural matrix proteins have concentrated on fibronectin,[127] in particular the type III modules. The tenth type III module that contains the RGD sequence was studied by NMR spectroscopy[128,129] and X-ray crystallography.[130] An X-ray structure[124] from the third fibronectin type III domain of tenascin also exists. In both structures the RGD motif is located in a βII' turn between two β sheets extending from the protein core. It is assumed that this loop is flexible in solution, and, hence, it is not possible to draw a conclusion about its conformation on the integrin receptor. More recent X-ray[131] and NMR[132] investigations of a larger fibronectin segment (domains seven to ten) did not yield any additional information about the conformation of the RGD motif.

The RGD motif is also found in several snake venoms. Most of these disintegrins are toxins that interfere in the blood-coagulation cascade. They induce bleeding, which causes heart failure and circulatory collapse.[133] Disintegrins are efficient inhibitors of platelet aggregation.[50] Three-dimensional structures have been obtained for kistrin,[134,135] echistatin,[136-141] and flavoridin.[142] In addition, secondary structural elements are known in the case of albolabrin.[143] In all structures the RGD sequence is found at the apex of a flexible loop without a distinctly prefered conformation.

Dendroaspin,[144] also called mambin,[145] is found in snakes of the family *Elapidae* and also contains the RGD sequence. This is unusual, since the snakes of this family do not form hemotoxins but rather neurotoxins. Although dentroaspin exhibits a folding pattern typical for neurotoxins, it is not a neurotoxin. The RGD sequence, which is atypical for neurotoxins, is again located at the top of a flexible loop and allows inhibition of platelet aggregation similar to hemotoxins.

Polypeptides that inhibit blood coagulation are also found in leeches. Hirudin, for example, inhibits thrombin. On the other hand, ornatin and decorsin block binding of $\alpha_{IIb}\beta_3$ to fibrinogen and, thus, inhibit platelet aggregation. The RGD sequence in decorsin is also found in a loop region, but, in contrast to the structures mentioned above, this loop is well-defined. The RGD sequence exhibits an extended conformation in which the pharmacophoric groups are oriented in opposite directions. Since decorsin shows high affinity for $\alpha_{IIb}\beta_3$ and $\alpha_v\beta_3$ integrins, we have to assume that the RGD sequence in this well-defined structure is still flexible enough to bind to both receptors.[146]

These structural studies indicate that the high activity of the disintegrins is based on the structural adaptability of the RGD sequence. Hence, the structures of these flexible compounds do not allow conclusions about the receptor-bound conformation, although knowledge of this conformation is necessary for rationally designing new bioactive compounds.

Table 1. Binding sites of various integrins[50].

Integrin	Ligand	Binding sequence
$\alpha_2\beta_1$	collagen	DGEA/RGD
	laminin	?
$\alpha_3\beta_1$	laminin	KQNCLSSRASFRGCVRNLRLSR
	collagen I; epiligrin	?
	fibronectin	RGD
$\alpha_4\beta_1$	fibronectin	IDAPS/LDV/REDV/X-D-Y
	VCAM-1	?
$\alpha_5\beta_1$	fibronectin	RGD
$\alpha_v\beta_1$	fibronectin, vitronectin	RGD
$\alpha_L\beta_2$	ICAM-1	KELLLPGNNRKV
	ICAM-2, ICAM-3	?
$\alpha_M\beta_2$	fibrinogen	GGAKQAGDV
	complement 3bi	?
$\alpha_X\beta_2$	fibrinogen	GPRP
$\alpha_{IIb}\beta_3$	fibrinogen	GGAKQAGDV/RGD
	fibronectin, vitronectin, vWF, thrombospondin	RGD
$\alpha_v\beta_3$	vitronectin, fibronectin, fibrinogen, collagen, thrombospondin, thrombin, osteopontin, bone sialoprotein, tenascin	RGD
$\alpha_{LRI}\beta_3$	entactin	RGD
$\alpha_v\beta_5$	vitronectin	RGD
$\alpha_v\beta_6$	fibronectin	RGD

5. Design of Selective $\alpha_V\beta_3$-Integrin Antagonists

The development of antagonists for peptidic ligands normally starts with the search for the recognition site. In our case the active sequence was identified by sequence comparison of integrin-binding proteins.[147-149] Recently biologically or chemically synthesized peptide libraries were screened to obtain the same information. It was possible to confirm the RGD sequence by screening a phage-display library[150] and to identify adjacent amino acids that increase affinity for the receptor.[151] However, new developments focus on non-peptidic libraries to yield lead structures for drug development.[152]

At the beginning of our work the RGD sequence was known,[153] and it was clear that small modifications such as replacement of Asp with Glu or Gly with D-Ala or L-Ala result in total loss of binding activity.[154, 155] Therefore, our goal was to gain high activity and selectivity by fixing the spatial conformation.[156] Since the receptor-bound conformation, the "bioactive conformation", was not known, we synthesized stereoisomeric, constrained cyclic peptide libraries to define the optimal structure required for distinct receptor subtypes (spatial screening). We had already demonstrated that cyclization yields high affinity and selectivity if the conformation of the constrained structure is close to the bioactive conformation (matched case). This approach was also successful in the case of the RGD peptides.[157] Comparison of the activity of *cyclo*(-Arg-Gly-Asp-D-Phe-Val-) with that of the linear sequences -D-Phe-Val-Arg-Gly-Asp-, -Val-Arg-Gly-Asp-D-Phe-, and -Arg-Gly-Asp-D-Phe-Val- exhibits drastically reduced activities and selectivities for the linear peptides (Scheme 4).

The use of cyclic peptides for the elucidation of the bioactive conformation and the generation of drug leads is now commonly accepted. However, cyclization may often fix a molecule in a conformation that is not bioactive. This results in a compound with drastically reduced activity (mismatched case). Searching for the best conformational restraints is still difficult and does not always lead to success.

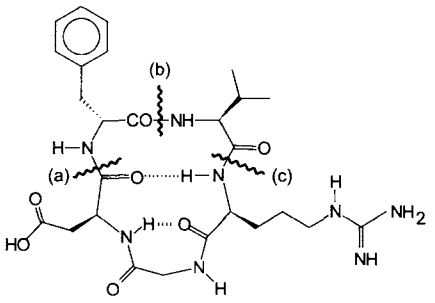

	IC_{50}	$\alpha_{IIb}\beta_3/\alpha_v\beta_3$
cyclo(-RGDfV-)	0.002	415
(a) Ac-fVRGD-NH_2	0.03	3.0
(b) Ac-VRGDf-NH_2	0.04	38.0
(c) Ac-RGDfV-NH_2	0.19	8.0

Scheme 4. Comparison of the activity (IC_{50} [μmol]) and selectivity (ratio of activity on the platelet and the vitronectin receptor) of the $\alpha_V\beta_3$-selective peptide *cyclo*(-Arg-Gly-Asp-D-Phe-Val-) and its linear analogues. (Data for the linear peptides were provided by G. Hölzemann, Merck KGaA.)

5.1. Stereoisomeric Peptide Libraries

5.1.1. Choice of Basic Structures

A stereoisomeric peptide library has to lock the bioactive sequence in different conformations without changing its constitution. This is achieved with a rigid basic template such as a cyclic peptide, which should be as small as possible to induce sufficient restraints but large enough to include all pharmacophoric groups. Therefore, we chose cyclic penta- and hexapeptides, since larger cyclic peptides already exhibit greater flexibility.[158]

In the case of homodetic cyclic peptides the conformation is dominated by the chirality of the amino acid residues. Interactions of functional groups of the side chains with the peptide backbone— known, for example, for Ser and Thr in the *i* position of β turns[159] or for Asn[160]—as well as the influence of β branching are less important. We synthesized all possible cyclic penta- and hexapeptides with L-Ala and/or D-Ala and investigated their conformations in solution by NMR spectroscopy and molecular dynamics (MD) calculations (Scheme 5).[161] In addition, we introduced glycine (the only α amino acid without a side chain) and D- or L-Pro. Proline exhibits steric restraints of the ψ angle and keeps the ϕ angle between $+60$ and $-60°$.

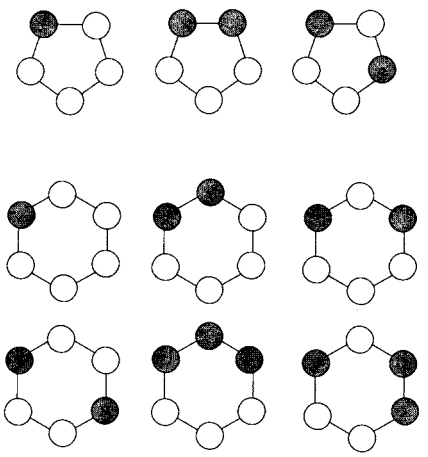

Scheme 5. Cyclic penta- and hexapeptides consisting of D- (grey circle) and L-alanine. Cyclopeptides with more units of D-Ala than L-Ala, for example *cyclo*(L-Ala-D-Ala_4), are enantiomers of the shown compounds.

Some of the cyclic peptides prefer a single conformation, whereas others show evidence for fast equilibria of energetically similar conformations.[156] If one distinct conformation is preferred, often inappropriatly called a "rigid conformation", it can be used as a template for spatial screening. An example is given in the following:

Cyclic hexapeptides normally prefer a conformation with two β turns.[162] A cyclic hexapeptide containing only L-amino acids and a bioactive sequence ABC can adopt three different conformations in a fast equilibrium in which the sequence is found in different positions of the ring (Scheme 6a). However, a D-amino acid residue, especially D-Pro, strongly prefers the $i+1$ position of a βII′ turn. Therefore, we can now fix our ABC sequence in three different positions depending on which of the remaining

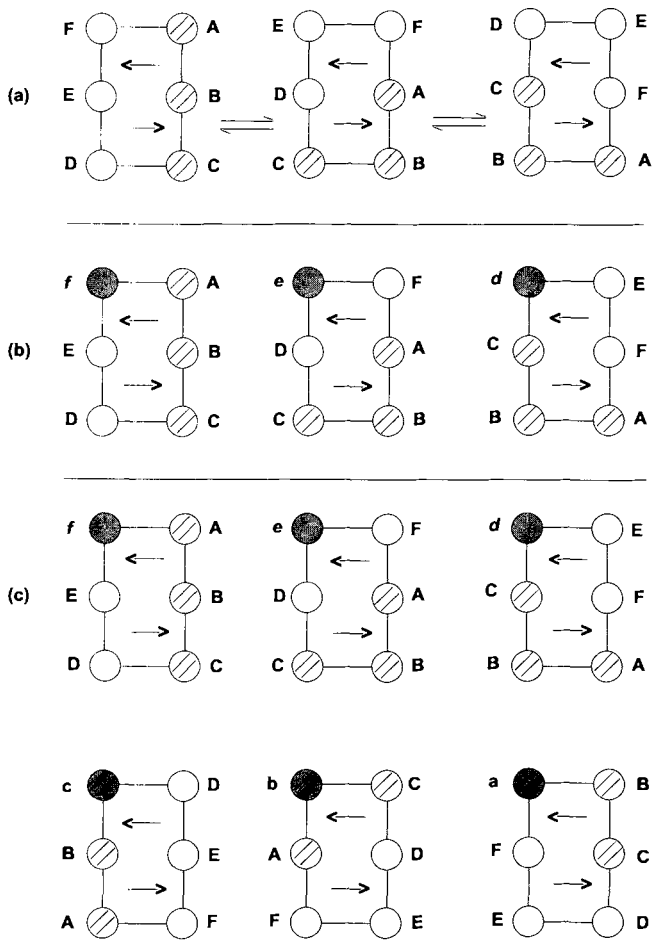

Scheme 6. Arrangement of an assumed bioactive amino acid sequence ABC (hatched circles) in cyclic hexapeptides. The arrows show the orientation of the hydrogen bonds in the β turns. a) The prefered β,β-conformation of hexapeptides allows a nearly equal population of three conformations if only L-amino acids are present. b) The bioactive sequence ABC is fixed in three different positions by a structure-inducing amino acid (D-Xaa or proline). c) Prefered conformations of six possible hexapeptides with an amino acid sequence ABCDEF with one D-amino acid each. The active sequence is shifted around the basis template by structural induction of the D-amino acid (grey circle) in the $i+1$ position of a βII′ turn.

three residues D, E, and F in the hexapeptide is D-configurated (Scheme 6b). We already used this method to design the bioactive conformation of the binding loop of tendamistat, an α-amylase inhibitor.[163, 164] If the bioactive conformation is not known one can synthesize six cyclic hexapeptides, each with D-configuration at one of the six amino acids. The D-amino acid residue prefers the above-mentioned distinct position and forces the essential sequence (ABC) into different spatial arrangements (Scheme 6c). The constitution, that is, all connectivities, remain constant in all six peptides. A correlation of their biological activities then identifies the required conformation.

5.1.2. *Stereoisomeric RGD Peptide Library*

In our search for selective and active inhibitors of integrins we started with the RGD sequence flanked by the hydrophobic amino acid phenylalanine at the C-terminus (based on sequence comparison of different natural RGD proteins). We synthesized different cyclic penta- and hexapeptides by systematically varying the chirality of the residues. We assume that in the first approximation the resulting conformations correspond to those of the equivalent alanine peptides. As shown in Figure 4, the conformations of *cyclo*(-D-Ala-Ala_4-) and *cyclo*(-Arg-Gly-Asp-D-Phe-Val-) are in fact similar to a large extent. The cyclopeptide conformations are controlled by the amino acid residues D-Ala and D-Phe, respectively.

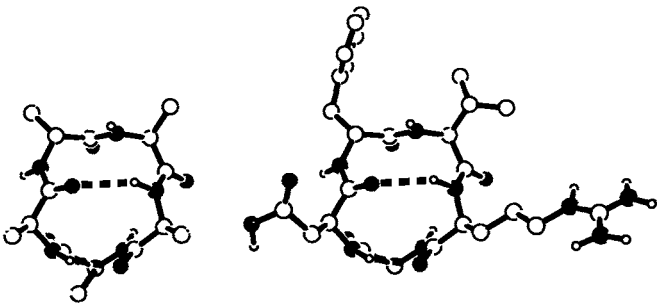

Figure 4. Conformations of *cyclo*(-D-Ala-Ala_4-) and *cyclo*(-Arg-Gly-Asp-D-Phe-Val-) in DMSO; the time-averaged trajectory of a rMD simulation (restrained molecular dynamics) based on NMR data is shown.

However, the glycine residue of the RGD sequence complicates the procedure, since glycine may serve as a D- or L-amino acid and allows greater flexibility due to the lack of steric hindrance from a side chain. Since the conformations of the RGD cyclic peptides were not completely predictable, we determined the structure by NMR spectroscopy in combination with distance geometry and/or molecular dynamics calculations.

Using this approach we indeed found cyclic hexapeptides with drastically increased affinity for the platelet receptor $\alpha_{IIb}\beta_3$.[157, 165] However, highly potent peptidic[166, 167] and non-peptidic[168–173] compounds for this receptor are already in clinical testing as antithrombolytica. In our most active hexapeptides[87] (for example *cyclo*(-Arg-Gly-Asp-D-Phe-Leu-Gly-) $IC_{50}(\alpha_{IIb}\beta_3/Fb) = 3\,\mu M$) the RGD sequence is located in a βII turn with C^{α}(Arg)–C^{α}(Asp) distances of about 560 pm and corresponding C^{β}(Arg)–C^{β}(Asp) distances of 700–780 pm. Peishoff et al.[174–176] observed comparable activities in homodetic proline-containing hexapeptides. In this case, the RGD sequence is in a similar kinked β turn. However, more active peptide analogues with IC_{50} values in the nanomolar range exhibit an extended conformation of the RGD sequence.[177–183] It is particularly interesting that some cyclic pentapeptides exhibit higher activities and selectivities for the $\alpha_v\beta_3$ integrin overexpressed on cancer cells (Scheme 7).[87]

Investigation of our stereoisomeric peptide library yielded two highly potent inhibitors of vitronectin binding to $\alpha_v\beta_3$: *cyclo*(-Arg-Gly-Asp-D-Phe-Val-) and *cyclo*(-Arg-Gly-Asp-Phe-D-Val-).[165, 184] These pentapeptides prevent adhesion of different human cell lines (fibrosarcoma HT 1080, melanoma A 375, breast epithelial cells HBL 100)[87, 88, 184] and show IC_{50} values for the isolated, immobilized $\alpha_v\beta_3$ receptor in the nanomolar range.[165] This opens the possibility to affect tumor metastasis with this receptor selectively. Of particular interest was the inhibition of tumor-induced angiogenesis (see above). Furthermore, endothelial cells may receive an apoptotic signal from these cyclic pentapeptides. This can probably be attributed to

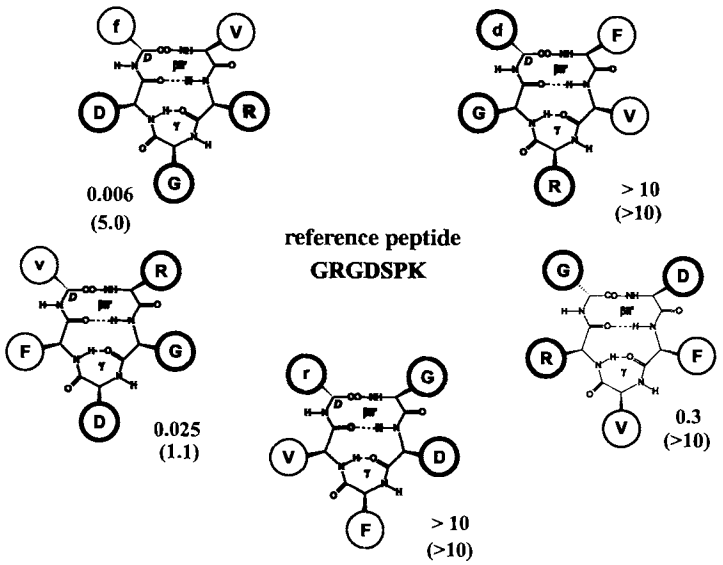

Scheme 7. Relative inhibition of cell adhesion, $Q = IC_{50}/IC_{50ref}$, by cyclic RGD pentapeptides. The values are based on the $\alpha_v\beta_3$ receptor; those referring to the platelet receptor ($\alpha_{IIb}\beta_3$) are given in parentheses. Lower values indicate higher biological activity (and lower concentration of the peptide that induces 50% inhibition).

the blocking of $\alpha_v\beta_3$ integrins, which prevents formation of focal adhesion points. All these properties qualify these peptides as promising candidates for a new class of anti-tumor drugs.[185-189]

5.1.3. Three-Dimensional Structure, Dynamics, and Retro-Inverso Peptides

Structure-activity studies have shown that high $\alpha_v\beta_3$ selectivity is obtained if glycine is in the $i+1$ position of a γ turn.[157] The sequence RGD has a strong kink in $\alpha_v\beta_3$-selective ligands whereas it is elongated in those selective for $\alpha_{IIb}\beta_3$. Usually the relative orientation of $C^\alpha-C^\beta$ bond vectors are considered to be the crucial parameter for describing the side-chain conformation of a peptide or protein (for example, the program CAVEAT[190] is based on this assumption). In cyclic pentapeptides these vectors for Asp and Arg point almost parallel to the same side of the ring. A similar arrangement is found for $\alpha_{IIb}\beta_3$-active peptides, but the distances between the C^α atoms of Arg and Asp (547 pm) and of the corresponding C^β atoms (668 pm) in $\alpha_v\beta_3$-selective compounds are significantly shorter.[191, 192]

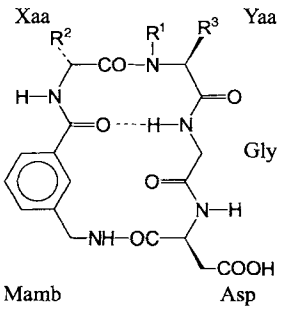

Scheme 8. Constitution of the cyclopeptide *cyclo*(-Yaa-Gly-Asp-Mamb-Xaa-); Mamb = *meta*-aminomethylbenzoic acid.

Recently Bach et al.[191, 192] investigated different peptide analogues of the sequence *cyclo*(-Xaa-Yaa-Gly-Asp-Mamb-); Xaa = D-Ala, L-Ala, Aib, Pro, D-Abu; Yaa = *N*-Me-Arg, Arg; Mamb = *meta*-aminomethyl benzoic acid (Scheme 8). They demonstrated that peptides containing the sequence D-Xaa-*N*-Me-Arg are highly active $\alpha_{IIb}\beta_3$ antagonists, whereas the corresponding L-Xaa-Arg analogues are selective $\alpha_v\beta_3$ antagonists. The two structures differ mainly in the β loop formed by the dipeptide unit. The former compounds form a βII' turn with the D-amino acid residue in the $i+1$ position, and the latter a βI turn with the L-amino acid residue in the $i+1$ position. The βI-turn arrangement allows the formation of a γ turn about Gly similar to that discussed above with *cyclo*(-Arg-Gly-Asp-D-Phe-Val-). In close analogy to the cyclic pentapeptide[157] the C^β(Arg)$-C^\beta$(Asp) distance (630-660 pm) is smaller than that in the $\alpha_{IIb}\beta_3$ antagonist. In addition, Burgess et al.[193] observed a conformation with Gly in the $i+1$ position of a γ turn in the $\alpha_v\beta_3$-selective *cyclo*(-Arg-Gly-Asp-Arg-Gly-Asp-).

To elucidate the stereochemical requirements in more detail we synthesized almost all the stereoisomers of the pentapeptide *cyclo*(-Arg-Gly-Asp-D-Phe-Val-) and its retrosequence *cyclo*(-Val-Phe-Asp-Gly-Arg-).[194] The use of the retrosequence is based on the observation of Prelog, Gerlach, and Owtschinnikow,[195, 196] who showed that a reverse amino acid sequence should be accompanied by an inversion of all amino acids to allow the side chains to adopt the same orientation as in the original peptide. Numerous publications describe this concept for obtaining enzymatic stability by partial substitution of natural sequences with retrosequences containing D-amino acids. Frequently this approach results in biologically active retro-inverso peptides.[194] However, it is easy to show that the assumption of similar conformation of retro-inverso peptides and their parent peptides is only valid if the backbone conformation is neglected.[194, 197] In fact, the retro-inverso compound of the highly potent *cyclo*(-Arg-Gly-Asp-D-Phe-Val-) is four to five orders of magnitude less active (Figure 5). On the other hand, among the stereoisomeric retrosequences one compound shows surprisingly high activity, although the D-configuration of the Asp residue is normally accompanied by a total loss of affinity. Since this peptide shows high flexibility, we refrain from discussing its conformation. Nevertheless, there is considerable flexibility in the γ turn of *cyclo*(-Arg-Gly-Asp-D-Phe-Val-).[198]

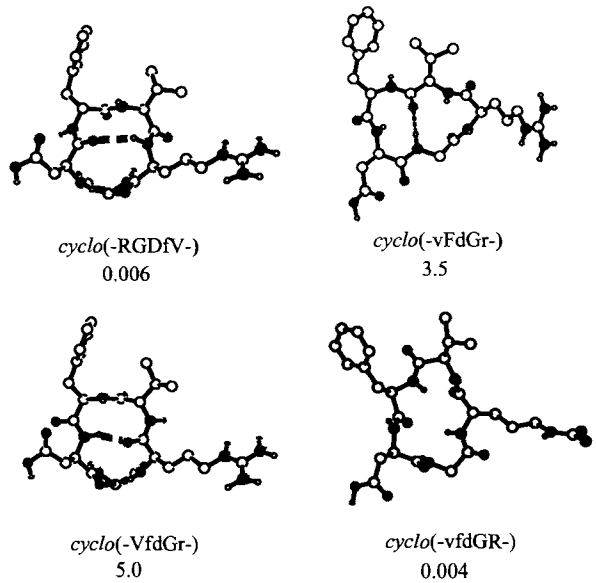

Figure 5. Steroisomers and retrostereoisomers of the pentapeptide *cyclo*(-RGDfV-). The relative inhibition of cell adhesion $Q = IC_{50}/IC_{50ref}$ (based on the linear reference peptide GRGDSPK) on the $\alpha_v\beta_3$-integrin receptor is given. Top left: parent peptide. Top right: retro-inverso peptide. Bottom left: retro-peptide with the same orientation of side chains, but opposite peptide-bond orientation. Bottom right: highly active retro-peptide (see Section 5.3.1).

According to ensemble calculations especially the peptide bonds between Arg and Gly as well as between Gly and Asp exhibit different orientations in which the external geometry of the γ turn is more or less unchanged, but the internal hydrogen bridge of Asp–NH to Arg–CO is broken.[199]

The dynamics of cyclopentapeptide conformations can be explained with a model that reduces the cyclopentapeptide structure to the structure of a cyclopentane.[200] For that purpose, each *trans* peptide bond is transformed into a (*E*)-ethylene unit, and each *cis* peptide bond into a (*Z*)-ethylene unit. In the next step, according to Dunitz and Waser,[201] the (*E*)-ethylene unit is replaced by a "long" bond, and the (*Z*)-ethylene by a "phantom" CH_2 group. For a cyclic peptide with all-*trans* peptide bonds this results in the corresponding cycloalkane when only the α carbon atoms of the amino acids are considered as relevant. According to this concept, we expect to find a cyclic pentapeptide in an envelope conformation (four α carbons in one plane and one above or below), which shows rapid pseudorotation. This was indeed confirmed by X-ray crystallography.[202]

In a similar way the conformations of other cyclic peptides can be compared with those of cycloalkanes.[200, 231] As in cycloalkanes, 1,3-diaxial positions or ecliptic arrangements of the C^{α} atoms are avoided. This is surprizing at a first glance considering the large distance between α carbon atoms across the peptide bond. However, it can be explained by allylic strain, which is minimized in the arrangement shown in Scheme 9. This allows transmission of the steric effects at the α atoms across the peptide bonds (see also the discussion of conformational aspects of peptides in ref. [230]). In addition to this basic, sterically induced conformational behavior, hydrogen bonds may also play a role (although to a lesser degree[204]). We therefore expect that cyclopentapeptides adopt many low-energy conformations in fast equilibrium and cyclic hexapeptides, with all-*trans* peptide bonds, a cyclohexane-like conformation.

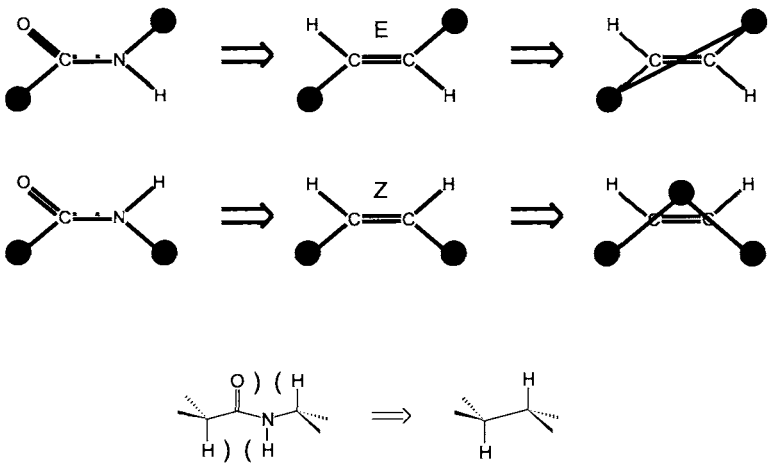

Scheme 9. Schematic illustration of the Dunitz–Waser concept and its application to amide bonds in peptides. Minimization of allylic strain leads to transmission of steric effects across the double bond.

5.2. Conformationally Controlled SAR

The peptides *cyclo*(-Arg-Gly-Asp-D-Phe-Val-) and *cyclo*(-Arg-Gly-Asp-Phe-D-Val-) of the first generation were used to investigate the effect of the amino acids flanking the RGD sequence.[205, 206] These structure–activity studies were performed under conformational control;[207] the investigation of the influence of side-chain variation on biological activity was simultaneously accompanied by NMR spectroscopic structure determination to guarantee that the change in constitution did not change the conformation as well. Any change in biological activity can then be attributed to the change in side-chain functionality. The importance of this control was shown for the replacement of one of the amide bonds by thioamide or reduced amide bonds, which induces a total conformational change.[208] It is, therefore, not possible to decide if the drastic reduction in activity is due to the change in constitution or conformation (see below). A hydrophobic amino acid residue following the aspartic acid increases the affinity for the $\alpha_v\beta_3$ receptor, whereas the position preceeding the arginine residue can be varied without a reduction in affinity.

Mullen et al.[209] investigated a number of disulfide-bridged cyclic RGD peptides. The $\alpha_v\beta_3$-selective cyclic peptide Gly-Pen-Arg^{-2}-Ala^{-1}-Arg^{1}-Gly^{2}-Asp^{3}-Asp^{4}-Val^{5}-Cys-Ala exhibits a conformation in which the RGD sequence is involved in an undefined β turn adjacent to the Asp-Asp-Val sequence in a β sheet. It seems that here the RGD sequence is also in a bent conformation. In addition, a lipophilic β-branched amino acid next to the RGD sequence enhances the activity, although it is not in the same position as in the cyclic pentapeptides.

Screening of phage-display libraries for the sequence Cys-Xaa_6-Cys and Cys-Xaa_7-Cys confirm that the $\alpha_v\beta_3$ integrin has a hydrophobic binding pocket.[150] Several $\alpha_v\beta_3$-binding ligands contain Ser or Thr next to Asp followed by a hydrophobic amino acid residue such as Phe, Leu, or Ile. Phage-display libraries have also been used by Healy et al.[151] to screen for $\alpha_v\beta_3$ ligands. Although no unambiguous correlation between affinity and flanking residues could be derived from the qualitative data, sequences in which the RGD motif was flanked by two cystein residues bound most strongly. These results confirm that conformationally constrained peptides have a high affinity for the $\alpha_v\beta_3$ integrin if they can adopt a bent conformation as in a γ-turn arrangement.

5.3. Peptidomimetics

Substitution of one or more peptide bonds by thioamide groups, ketomethylene groups, or reduced peptide bonds and other modifications can be used to determine structural requirements for biological activity. This allows an investigation of the importance of distinct structural elements (for example a peptide bond in the active sequence) for receptor–ligand interactions. However, it is critical to confirm that the overall conformation of the peptide is not changed upon substitution. Only then can the observed effect be attributed to changes in constitution rather than changes in conformation.[207]

5.3.1. Influence of Peptide Bonds

There are different ways to investigate the importance of a distinct peptide bond for biological activity: for example, substitution by a peptide-bond isoster,[210] elimination of the amide

proton by N-alkylation,[211] or the use of retro–inverso peptides in which the orientation of the amide bond is inverted.[212] Replacement of the peptide bond between Asp and Gly by a thioamide[213, 214] (C(S)NH) and introduction of a reduced amide bond[208] (CH_2NH) between Phe and Val in the lead structure *cyclo*(-Arg-Gly-Asp-D-Phe-Val-) led in both cases to a drastic reduction in affinity. However, it was not possible to assess whether this reduced activity is based on changes in the constitution of the cyclopeptide, because these modifications also induced conformational changes in the peptide backbone.[214]

Methylation of the different amide bonds in *cyclo*(-Arg-Gly-Asp-D-Phe-Val-) results in five compounds. From this series, *cyclo*(-Arg-Gly-Asp-D-Phe-*N*-Me-Val-) exhibits high affinity as well as specificity.[189, 215] The other four cyclic peptides show only low affinity. N-Methylation induces structural changes in all five cyclic pentapeptides. For example, the *N*-Me-Val peptide exhibits a distinctly expanded βII′ loop centered around the N-methylated amide bond, which, however, does not influence the conformation of the RGD sequence. Conformational analysis for the other four peptides is not yet completed, and the reason for the reduced activity remains to be found.

Investigation of the retro–inverso peptides demonstrated that at least one of the peptide bonds of the cyclic pentapeptide participates in binding to the receptor (see above and ref. [194, 214]). One of the stereoisomeric retro-peptides (*cyclo*-(-Val-D-Phe-D-Asp-Gly-D-Arg-)) adopts a conformation in which all side chains assume the same orientation as in the lead compound (Figure 5). Nevertheless, the activity of the retro-peptide was four orders of magnitude lower.[194] Since all amide bonds in the retro-peptide are inverted, the difference in activity has to be attributed to a nonoptimal orientation of at least one of the peptide bonds.

5.3.2. *Further Reduction in Flexibility*

Rational drug design requires a maximum of information about the structures of the ligand and the receptor as well as their interactions. If the three-dimensional structure of the receptor or the receptor–ligand complex is unknown, only indirect conclusions can be drawn based on the structure of the ligand. Therefore, rigid ligands are required for structure–activity studies.[156] Although cyclic pentapeptides are already relatively restricted in mobility,[157] the cyclic peptides described above show considerable conformational interconversions,[206, 216] especially in the γ-turn region.[198, 206] Ensemble calculations revealed that the two peptide bonds in the γ turn flip around the adjacent ϕ and ψ angles.[199, 217]

Turn mimetics[218, 219] were incorporated into the lead structure *cyclo*(-Arg-Gly-Asp-D-Phe-Val-) to further reduce the flexibility of the pentapeptides.[220] Since structural changes in the RGD motif greatly influence the biological activity,[154, 155, 157] the mimetics were introduced in place of the D-Phe-Val dipeptide unit (Scheme 10). The mimetics were expected to stabilize the βII′ turn and simultaneously reduce flexibility in the γ-turn region.

Only the (*S*,*S*)-spiro-Pro-Leu moiety lead to the expected conformation with the turn mimetics in the $i+1$ and $i+2$ positions of the βII′ turn. The other peptide analogues *cyclo*(-Arg-Gly-Asp-(*S*)-ANC-), *cyclo*(-Arg-Gly-Asp-(*R*)-ANC-), and *cyclo*(-Arg-Gly-Asp-BTD-) contain the β-turn mimetics in the γ-turn region, and Gly is found in the $i+1$ position of a βII′ turn (the achiral Gly residue can act as D-amino acid residue). On the other hand, these investigations resulted in one of the most potent $\alpha_V\beta_3$ inhibitors, *cyclo*(-Arg-Gly-Asp-(*R*)-ANC-) with $IC_{50}(\alpha_V\beta_3/Vn) = 0.8$ nM.

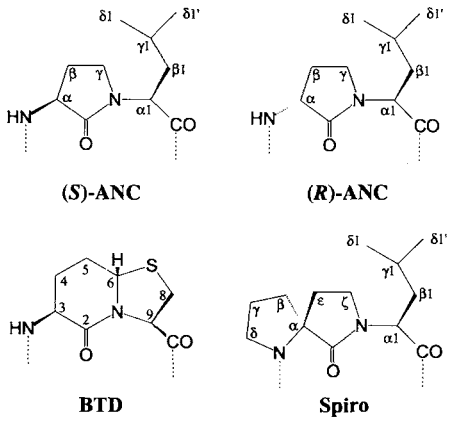

Scheme 10. β-Turn mimetics. Building blocks shown were introduced into the β turn of the parent peptide *cyclo*(-RGDfV-) instead of the dipeptide -D-Phe-Val-.

Turn mimetics not only restrict flexibility but can also change the accessible conformational space. For this purpose 5-aminomethyl-2-thiophene acetic acid (Ate), a turn mimetic from Feigel et al.[221] was incorporated.[188, 222] In contrast to the D-Phe-Val unit this moiety provides seven atoms for the peptide backbone. The resulting cyclic peptide exhibited very high affinity ($IC_{50}(\alpha_V\beta_3/Vn) = 2$ nM) and specificity ($IC_{50}(\alpha_{IIb}\beta_3/Fb) = 3300$ nM) for $\alpha_V\beta_3$.

In many cases increased rigidity of the ligand reduces biological activity. This is often taken as an indication for the importance of molecular mobility in the binding process. In our opinion, the optimal fit is simply not reached in most of these rigid molecules. It should be possible to further increase the activity by more closely approximating the structure of the natural ligand. In most cases—an exception is, for example, the binding of cyclosporin to cyclophilin[223]—the biological activity is controlled by the *thermodynamic stability* of the receptor–ligand complex and not by the *kinetics of complex formation*. Hence, it is advisable to search for rigid molecules that present the pharmacophoric groups in an optimal spatial orientation to maximize biological activity.

6. Non-Peptidic $\alpha_V\beta_3$-Integrin Antagonists

The transition from peptidic lead structures to non-peptidic, orally administrable drugs is an important goal in medicinal chemistry. Peptides often have nonideal properties; for example, they are easily degraded in vivo by proteases. However, in the case of cyclic pentapeptides this was not an issue, since, due to the fixation in the cyclic structure, exo- and endopeptidases do not cleave these peptides. The stability is further increased with a retro–inverso peptide, as the high content of D-amino acids prevents cleavage. Aside from cyclization, introduction of peptidomimetics could also lead to higher proteolytic

stability. Another aspect to be considered in the development of pharmacologically active compounds is the rapid excretion of compounds with molecular weights of 500–1000. Depending on their hydrophilic–lipophilic profile, they are rapidly excreted through the kidney or the liver/bile pathway. Hence, small non-peptide molecules are usually prefered goals in the development of drugs. However, orally administrable drugs can also lead to problems due to individual differences in resorption rates by the gastrointestinal tract. In the case of life-threatening diseases intravenous, intraperitoneal, or subcutaneous injection is acceptable. Peptides may even be the drugs of choice, especially when extracellular receptors are targeted, and cellular membranes do not have to be passed.

The development of non-peptidic drugs can be successful if structure–activity studies of a stereoisomeric cyclic peptide library indicate which side-chain functionalities in a defined spatial orientation are essential for activity. Of course, other pharmacophors such as individual peptide bonds can also be incorporated in non-peptidic structures.

Investigations on the $\alpha_{IIb}\beta_3$ integrin have shown that the distance between the pharmacophors (the carboxyl group of Asp and the guanidino group of Arg) is crucial for activity and specificity.[224] This in principle allows an arbitrary choice of template to present these pharmacophors in the required spatial orientation. Direct de novo design is extremely difficult, even if the three-dimensional structure of the receptor is known. However, it is facilitated if the structure of a lead compound is known. For example, a suitable new non-peptidic template can be designed by studying the three-dimensional structure of a constrained peptide.[190] This should already have a reasonably rigid structure to guarantee selectivity by orienting the pharmacophors in distinct positions.

With the $\alpha_{IIb}\beta_3$-integrin inhibitors the transition from peptides to non-peptides has already been made, and there are several orally administrable integrin antagonists with sufficient activity and selectivity.[168, 173, 225] Most of these compounds contain an N-terminal guanidino or benzamidino group and a carboxyl group, which are separated by a defined distance.

Conformational investigations have shown that a cupped conformation for a potential template molecule is important for the correct presentation of the RGD sequence.[173, 177] This conformation mimics the peptidic loop. This conformation, as well as reduced flexibility, is achieved with substituted benzodiazepines, which present the RGD-like pharmacophors in the correct position.

The development of selective $\alpha_v\beta_3$ integrin antagonists has not yet advanced to a similar stage. Several compounds have been derived from the known $\alpha_{IIb}\beta_3$ selective benzodiazepines. The $\alpha_v\beta_3$ antagonists that should be employed as drugs for the treatment of osteoporosis were developed by varying the carboxyl and guanidino functional groups.[226, 227] This resulted in compounds that are active at the micromolar range. As shown in Scheme 11, variation in the guanidino group led to the largest increase in $\alpha_v\beta_3$ selectivity. Upon changing the benzamidine function into an aminopyridine, activity increased by one order of magnitude, and α_v selectivity raised by a factor of 300.

An important advancement was the recent introduction of the benzimidazole residue as an arginine mimic.[228] The resulting benzodiazepine derivative (Scheme 12) showed $\alpha_v\beta_3$ affinity in the nanomolar range, which was 15000 times higher than for $\alpha_{IIb}\beta_3$.

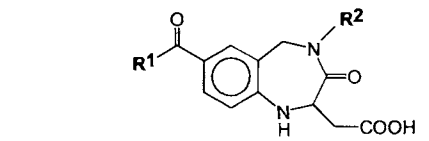

$\alpha_{IIb}\beta_3$ selective

R1	R2	μmol	$\alpha_v\beta_3/\alpha_{IIb}\beta_3$
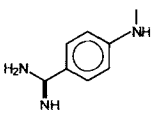	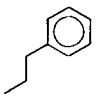	0.0028	–
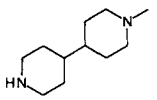	CH_3	0.0025	4136

$\alpha_v\beta_3$ selective

R1	R2	μmol	$\alpha_{IIb}\beta_3/\alpha_v\beta_3$
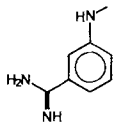	CH_3	1.50	3.4
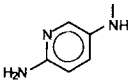	CH_3	9.18	12.0
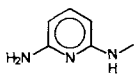	CH_3	0.15	1067

Scheme 11. Non-peptide $\alpha_v\beta_3$- and $\alpha_{IIb}\beta_3$-integrin antagonists with benzodiazepine structure. Activities (lower values indicate higher activities) and selectivities (quotient of activities) related to the isolated $\alpha_v\beta_3$ and $\alpha_{IIb}\beta_3$ receptors are given for selected compounds.

The superposition of the three-dimensional structures of the cyclic peptide *cyclo*(-Arg-Gly-Asp-D-Phe-Val-) and the 3-oxo-1,4-benzodiazepine derivative (see full-page picture on page 1374) shows that the distances between the arginine mimic and the carboxy group are very similar in both compounds.[229] This distance is distinctly shorter than in $\alpha_{IIb}\beta_3$ antagonists, which supports the hypothesis that the γ turn is crucial for $\alpha_v\beta_3$ antagonists.[88] A comparison of the functionalities of α_{IIb}- and α_v-

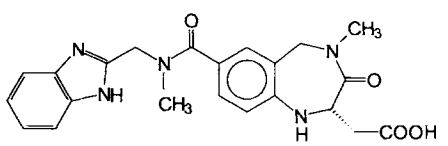

Scheme 12. Non-peptide $\alpha_v\beta_3$-integrin antagonists. Introduction of a benzimidazole side chain leads to activity in the nanomolar range: $IC_{50} = 0.002$ μmol ($\alpha_{IIb}\beta_3/\alpha_v\beta_3 = 15000$).

selective antagonists imply that a side-on interaction of two nitrogen atoms is important for strong binding to $\alpha_V\beta_3$.

Another class of $\alpha_V\beta_3$ antagonists is aimed at similar processes such as restenosis, osteoporosis, and tumor metastasis. These compounds are based on a *p*-hydroxybenzamide structure,[230] which allows a wide range of variation in the substituent R (Scheme 13).

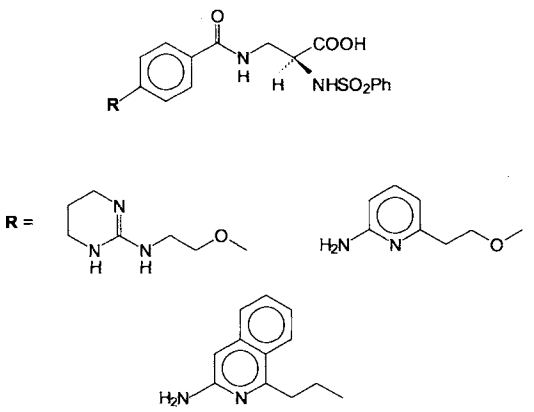

Scheme 13. Non-peptide $\alpha_V\beta_3$-integrin antagonists with *para*-hydroxybenzoic acid amide structure. Biological data are not available.

The next step from non-peptidic, orally administrable, selective, highly potent $\alpha_V\beta_3$ antagonists to useful therapeutic agents appears feasible. Several of these compounds are already at the level of toxicological or clinical trials. This explains why they are mainly described in patents. It is difficult to directly compare their biological activities, bioavailabilities, and metabolic stabilities at the present stage.

7. Summary

Selective manipulation of cellular-adhesion processes should allow us to influence many physiological and pathological processes. The biochemistry of cell adhesion and signal transduction is currently of great interest. The approach described here represents a new way of identifying bioactive compounds in a semi-rational way, even if the three-dimensional structure of the receptor or the receptor–substrate complex is not known. Information derived by comparing protein sequences or from peptide libraries can be used to design a library of peptides in which the pharmacophors are presented in distinct, well-defined spatial orientations. This allows for an optimization of activity and specificity.

Compounds with high activity and selectivity for the integrin $\alpha_V\beta_3$ exhibit a shorter distance between carboxyl and guanidino groups than $\alpha_{IIb}\beta_3$ inhibitors. In peptidic structures this is achieved by a kinked conformation around glycine (γ turn). Moreover, a hydrophobic residue next to the RGD sequence is important for activity and selectivity. Bulky substitutions in the region of Gly are not tolerated.

The presented approach should also be applicable to other integrins to gain a more detailed understanding of the role of the different integrins in the organism. However, a prerequisite is the isolation of receptor subtypes for the biological assays. The cyclic pentapeptides and benzodiazepine derivatives, which have meanwhile been developed, are highly active and selective $\alpha_V\beta_3$ antagonists and may be used in the treatment of restinosis, osteoporosis, acute renal failure, and retinopathy as well as to inhibit cancer metastasis by blocking angiogenesis.

Many members of our group have been involved in these studies. We would especially like to emphasize the initial work of Dr. M. Gurrath and Dr. G. Müller. Also involved were (in alphabetic order) M. Dechantsreiter, Dr. A. Geyer, Dr. M. Kranz, Dr. E. Graf von Roedern, J. Schmitt, and Dr. J. Wermuth. For the initial biological investigations we thank Prof. R. Timpl (Max-Planck-Institut, Martinsried, Germany) and Prof. J. Engel (Biozentrum Basel, Switzerland). Since 1992 all work has been performed in close collaboration with Merck KGaA (Darmstadt, Germany). Our special thanks go to Dr. A. Jonczyk, Dr. S. L. Goodman and Dr. G. Hölzemann. The conformational studies were done by Prof. D. Mierke (now at Clarke University, Worcester, MA, USA), Dr. W. Schmitt, and R. Gratias. We also thank Dr. R. Geiger, Dr. J. Knolle, and Dr. W. König (Hoechst AG) for stimulating discussions. Financial support was provided by Merck KGaA (Darmstadt), the Deutsche Forschungsgemeinschaft, and the Fonds der Chemischen Industrie. Nephrological studies were performed by Prof. M. S. Goligorski (Stoney Brook, NY, USA).

Received: December 20, 1996 [A 198 IE]
German version: *Angew. Chem.* **1997**, *109*, 1440–1456

[1] E. Ruoslahti, M. D. Pierschbacher, *Science* **1987**, *238*, 491–497.
[2] S. M. Albelda, C. A. Buck, *FASEB J.* **1990**, *4*, 2868–2880.
[3] R. O. Hynes, A. D. Lander, *Cell* **1992**, *68*, 303–322.
[4] J. Travis, *Science* **1993**, *260*, 906–908.
[5] G. Wagner, D. F. Wyss, *Curr. Opin. Struct. Biol.* **1994**, *4*, 841–851.
[6] T. A. Springer, *Nature* **1990**, *346*, 425–434.
[7] T. L. Collins, P. D. Kassner, B. E. Bierer, S. J. Burakoff, *Curr. Opin. Immun.* **1994**, *6*, 385–393.
[8] A. J. Bridges, *Chemtracts: Org. Chem.* **1995**, *8*, 73–107.
[9] S. J. Singer, *Science* **1992**, *255*, 1671–1677.
[10] C. H. Damsky, M. Bernfield, *Curr. Opin. Cell Biol.* **1990**, *2*, 813–814.
[11] A. P. Gilmore, K. Burridge, *Structure* **1996**, *4*, 647–651.
[12] A. M. P. Montgomery, R. A. Reisfeld, D. A. Cheresh, *Proc. Natl. Acad. Sci. USA* **1994**, *91*, 8856–8860.
[13] E. Ruoslahti, J. C. Reed, *Cell* **1994**, *77*, 477–478.
[14] C. B. Thompson, *Science* **1995**, *267*, 1456–1462.
[15] D. C. Levin, J. T. Fallon, *Circulation* **1982**, *66*, 316–320.
[16] M. J. Davies, A. C. Thomas, *Br. Heart J.* **1985**, *53*, 363–373.
[17] E. Falk, *Circulation* **1985**, *71*, 699–708.
[18] F. E. Ali, J. M. Samanen, R. J. Shebuski (Smith Kline, Beechham), EP-A 341915-A2, **1989** [*Chem. Abstr.* **1990**, *112*, 158983p].
[19] S. M. Albelda, *Lab. Invest.* **1993**, *68*, 4–17.
[20] F. G. Giancotti, F. Mainiero, *Biochim. Biophys. Acta* **1994**, *1198*, 47–64.
[21] M. A. Horton, M. L. Taylor, T. R. Arnett, M. H. Helfrich, *Exp. Cell Res.* **1991**, *195*, 368–375.
[22] D. T. Denhardt, X. Guo, *FASEB J.* **1993**, *7*, 1475–1482.
[23] M. Grano, P. Zigrino, S. Colucci, G. Zambonin, L. Trusolino, M. Serra, N. Baldini, A. Teti, P. C. Marchisio, A. Zambonin Zallone, *Exp. Cell Res.* **1994**, *212*, 209–218.
[24] M. Chorev, R. Dresnerpollak, Y. Eshel, M. Rosenblatt, *Biopolymers* **1995**, *37*, 367–375.
[25] P. A. D'Amore, R. W. Thompson, *Annu. Rev. Physiol.* **1987**, *49*, 453–464.
[26] J. Folkman, Y. Shing, *J. Biol. Chem.* **1992**, *267*, 10931–10934.
[27] J. Folkman, *Nature Medicine* **1995**, *1*, 27–31.
[28] G. C. Brown, R. H. Brown, M. M. Brown, *Int. Ophthalmol.* **1987**, *11*, 41–50.
[29] L. A. Liotta, P. S. Steeg, W. G. Stetler-Stevenson, *Cell* **1991**, *64*, 327–336.
[30] D. Weinstat-Saslow, P. S. Steeg, *FASEB J.* **1994**, *8*, 401–407.
[31] A. P. Mould, A. Komoriya, K. M. Yamada, M. J. Humphries, *J. Biol. Chem.* **1991**, *266*, 3579–3585.
[32] D. S. Tuckwell, A. Brass, M. J. Humphries, *Biochem. J.* **1992**, *285*, 325–331.
[33] M. H. Ginsberg, X. P. Du, T. E. O'Toole, J. C. Loftus, E. F. Plow, *Thromb. Haemostasis* **1993**, *70*, 87–93.
[34] J. W. Smith, D. A. Cheresh, *J. Biol. Chem.* **1990**, *265*, 2169–2172.
[35] J.-O. Lee, P. Rieu, M. A. Arnaout, R. Liddington, *Cell* **1995**, *80*, 631–638.

[36] J.-O. Lee, P. Rieu, L. A. Bankston, M. A. Arnaout, R. Liddington, *Structure* **1995**, *3*, 1333–1340.
[37] D. C. Altieri, *J. Immunol.* **1991**, *147*, 1891–1898.
[38] T. Yanai, T. Shimooka, I. Ii, *Cell Struct. Funct.* **1991**, *16*, 149–156.
[39] M. Busk, R. Pytela, D. Sheppard, *J. Biol. Chem.* **1992**, *267*, 5790–5796.
[40] I. Dransfield, C. Cabanas, A. Craig, N. Hogg, *J. Cell Biol.* **1992**, *116*, 219–226.
[41] S. Suzuki, Y. Naitho, *EMBO J.* **1990**, *9*, 757–763.
[42] R. O. Hynes, *Cell* **1987**, *48*, 549–554.
[43] C. A. Buck, A. F. Horwitz, *Annu. Rev. Cell Biol.* **1987**, *3*, 179–205.
[44] S. E. D'Souza, M. H. Ginsberg, E. F. Plow, *Trends Biochem. Sci.* **1991**, *16*, 246–250.
[45] R. O. Hynes, *Cell* **1992**, *69*, 11–25.
[46] D. J. Rees, S. E. Ades, S. J. Singer, R. O. Hynes, *Nature* **1990**, *347*, 685–689.
[47] A. P. Gilmore, K. Burridge, *Nature* **1995**, *373*, 197.
[48] R. P. Johnson, S. W. Craig, *Nature* **1995**, *373*, 261–264.
[49] C. A. Otey, F. M. Pavalko, K. Burridge, *J. Cell Biol.* **1990**, *111*, 721–729.
[50] D. Cox, T. Akoi, J. Seki, Y. Motoyama, K. Yoshida, *Med. Res. Rev.* **1994**, *14*, 195–228.
[51] M. A. Arnaout, *Blood* **1990**, *75*, 1037–1050.
[52] T. K. Kishimoto, R. S. Larson, A. L. Corbi, M. L. Dustin, D. E. Staunton, T. A. Springer, *Adv. Immunol.* **1989**, *46*, 149–182.
[53] D. R. Phillips, I. F. Charo, R. M. Scarborough, *Cell* **1991**, *65*, 359–362.
[54] Y. Q. Chen, X. Gao, J. Timar, D. Tang, I. M. Grossi, M. Chelladurai, T. J. Kunicki, S. E. G. Fligiel, J. D. Taylor, K. V. Honn, *J. Biol. Chem.* **1992**, *267*, 17314–17320.
[55] K. V. Honn, Y. Q. Chen, J. Timar, J. M. Onoda, J. S. Hatfield, S. E. G. Fligiel, B. W. Steinert, C. A. Diglio, I. M. Grossi, K. K. Nelson, J. D. Taylor, *Exp. Cell Res.* **1992**, *201*, 23–32.
[56] T. Weller, L. Alig, M. Hürzeler-Müller, W. C. Kouns, B. Steiner, *Drugs Future* **1994**, *19*, 461–476.
[57] W. Forth, D. Henschler, W. Rummel, *Allgemeine und spezielle Pharmakologie und Toxikologie*, *Bd. I*, 5th ed., Wissenschaftsverlag, Mannheim, **1987**, pp 311–331.
[58] R. J. Gould, *Perspect. Drug Discovery Des.* **1994**, *1*, 537–548.
[59] N. S. Cook, G. Kottirsch, H.-G. Zerwes, *Drugs Future* **1994**, *19*, 135–159.
[60] B. Felding-Habermann, *Biospektrum* **1996**, *2*, 25–29.
[61] S. Suzuki, W. S. Argraves, H. Arai, L. R. Languino, M. D. Pierschbacher, E. Ruoslahti, *J. Biol. Chem.* **1987**, *262*, 4080–4085.
[62] S. Strömblad, D. A. Cheresh, *Chem. Biol.* **1996**, *3*, 881–885.
[63] J. Savill, I. Dransfield, N. Hogg, C. Haslett, *Nature* **1990**, *343*, 170–173.
[64] J. Nip, S. A. Rabbani, H. R. Shibata, P. Brodt, *J. Clin. Invest.* **1995**, *95*, 2096–2103.
[65] Y. Wei, M. Lukashev, D. I. Simon, S. C. Bodary, S. Rosenberg, M. V. Doyle, H. A. Chapman, *Science* **1996**, *273*, 1551–1555.
[66] G. Poste, I. J. Fidler, *Nature* **1980**, *283*, 139–146.
[67] G. L. Nicholson, *Biochim. Biophys. Acta* **1982**, *695*, 113–176.
[68] L. A. Liotta, *Cancer Res.* **1986**, *46*, 1–7.
[69] L. A. Liotta, C. N. Rao, U. M. Wewer, *Annu. Rev. Biochem.* **1986**, *55*, 1037–1057.
[70] V. P. Terranova, E. S. Hujanen, G. R. Martin, *J. Natl. Cancer Inst.* **1986**, *77*, 311–316.
[71] M. M. Zutter, G. Mazoujian, S. A. Santoro, *Am. J. Pathol.* **1990**, *137*, 863–870.
[72] K. Koretz, P. Schlag, L. Boumsell, P. Moller, *Am. J. Pathol.* **1991**, *138*, 741–750.
[73] P. G. Natali, M. R. Nicotra, C. Botti, M. Mottolese, A. Bigotti, O. Segatto, *Br. J. Cancer* **1992**, *66*, 318–322.
[74] L. Damjanovich, S. M. Albelda, S. A. Mette, C. A. Buck *Am. J. Respir. Cell Mol. Biol.* **1992**, *6*, 197–206.
[75] J. E. Bridges, P. Englefield, I. E. Boyd, W. R. Roche, E. J. Thomas, *Int. J. Gynecol. Cancer* **1995**, *5*, 187–192.
[76] R. M. Lafrenie, S. Gallo, T. J. Podor, M. R. Buchanan, F. W. Orr, *Eur. J. Cancer Clin. Oncol.* **1994**, *30A*, 2151–2158.
[77] C. L. Gladson, D. A. Cheresh, *J. Clin. Invest.* **1991**, *88*, 1924–1932.
[78] S. M. Albelda, S. B. Mette, B. E. Elder, R. M. Stewart, L. Damjanovich, M. Herlyn, C. A. Buck, *Cancer Res.* **1990**, *50*, 6752–6764.
[79] J. F. Marshall, S. A. Nesbitt, M. H. Helfrich, M. A. Horton, K. Palakova, I. R. Hart, *Int. J. Cancer* **1991**, *49*, 924–931.
[80] B. Felding-Habermann, B. M. Mueller, C. A. Romerdahl, D. A. Cheresh, *J. Clin. Invest.* **1992**, *89*, 2018–2022.
[81] J. Folkman, M. Klagsbrun, *Science* **1987**, *235*, 442–447.
[82] P. C. Brooks, R. A. F. Clark, D. A. Cheresh, *Science* **1994**, *264*, 569–571.
[83] S. Aznavoorian, M. L. Stracke, J. Parsons, J. McClanahan, L. A. Liotta, *J. Biol. Chem.* **1996**, *271*, 3247–3254.
[84] P. C. Brooks, A. M. P. Montgomery, M. Rosenfeld, R. A. Reisfeld, T. Hu, G. Klier, D. A. Cheresh, *Cell* **1994**, *79*, 1157–1164.
[85] H.-P. Hammes, M. Brownlee, A. Jonczyk, A. Sutter, K. T. Preissner, *Nature Medicine*, **1996**, *2*, 529–533.
[86] M. Friedlander, C. L. Theesfeld, M. Sugita, M. Fruttiger, M. A. Thomas, S. Chang, D. A. Cheresh, *Proc. Natl. Acad. Sci. USA* **1996**, *93*, 9764–9769.
[87] M. Aumailley, M. Gurrath, G. Müller, J. Calvete, R. Timpl, H. Kessler, *FEBS Lett.* **1991**, *291*, 50–54.
[88] M. Gurrath, G. Müller, H. Kessler, M. Aumailley, R. Timpl, *Eur. J. Biochem.* **1992**, *210*, 911–921.
[89] M. Friedlander, P. C. Brooks, R. W. Shaffer, C. M. Kincaid, J. A. Varner, D. A. Cheresh, *Science* **1995**, *270*, 1500–1502.
[90] J. Folkman, K. Watson, D. Ingeber, D. Hanahan, *Nature* **1989**, *339*, 58–61.
[91] P. C. Brooks, S. Strömblad, R. Klemke, D. Visscher, F. H. Sarkar, D. A. Cheresh *J. Clin. Invest.* **1995**, *96*, 1815–1822.
[92] A. Giannis, F. Rübsam, *Angew. Chem.* **1997**, *109*, 606–609; *Angew. Chem. Int. Ed. Engl.* **1997**, *36*, 588–590.
[93] A. Miyauchi, J. Alvarez, E. M. Greenfield, A. Teti, M. Grano, S. Colucci, A. Zambonin-Zallone, F. P. Ross, S. L. Teitelbaum, D. A. Cheresh, K. A. Hruska, *J. Biol. Chem.* **1991**, *266*, 369–374.
[94] A. Zambonin-Zallone, A. Teti, M. Grano, A. Rubinacci, M. Abbadini, M. Gaboli, P. C. Marchisio, *Exp. Cell Res.* **1989**, *182*, 645–652.
[95] G. Shankar, T. R. Gadek, D. J. Burdick, I. Davison, W. T. Mason, M. A. Horton, *Exp. Cell Res.* **1995**, *219*, 364–371.
[96] J. E. Fisher, M. P. Caulfield, M. Sato, H. A. Quartuccio, R. J. Gould, V. M. Garsky, G. A. Rodan, M. Rosenblatt, *Endocrinology* **1993**, *132*, 1411–1413.
[97] R. Dresnerpollak, M. Rosenblatt, *J. Cell. Biochem.* **1994**, *56*, 323–330.
[98] G. A. Tanner, M. Steinhausen, *Am. J. Physiol.* **1976**, *230*, 1173–1181.
[99] W. J. Arendshorst, W. F. Finn, C. W. Gottschalk, H. K. Lucas, *Kidney Int.* **1976**, *10*, 100–105.
[100] M. Graber, B. Lane, R. Lamia, E. Pastoriza-Munoz, *J. Am. Soc. Nephrol.* **1991**, *1*, 999–1004.
[101] E. Noiri, J. Gailit, D. Sheth, H. Magazine, M. Gurrath, G. Müller, H. Kessler, M. S. Goligorsky, *Kidney Int.* **1994**, *46*, 1050–1058.
[102] J. Gailit, D. Colflesh, I. Rabiner, J. Simone, M. S. Goligorsky, *Am. J. Physiol.* **1993**, *264*, 149–157.
[103] M. S. Goligorsky, G. F. Dibona, *Proc. Natl. Acad. Sci. USA* **1993**, *90*, 5700–5704.
[104] E. Noiri, V. Romanov, T. Forest, J. Gailit, G. F. Dibona, F. Miller, P. Som, Z. H. Oster, M. S. Goligorsky, *Kidney Int.* **1995**, *48*, 1375–1385.
[105] M. Paulsson, *Crit. Rev. Biochem. Mol. Biol.* **1992**, *27*, 93–127.
[106] G. R. Martin, R. Timpl, *Annu. Rev. Cell Biol.* **1987**, *3*, 57–85.
[107] J. Engel, *Biochemistry* **1992**, *31*, 10643–10651.
[108] M. D. Pierschbacher, E. Ruoslahti, J. Sundelin, P. Lind, P. A. Peterson, *J. Biol. Chem.* **1982**, *257*, 9593–9595.
[109] E. Ruoslahti, *Annu. Rev. Biochem.* **1988**, *57*, 375–413.
[110] S. Dufour, J.-L. Duband, A. R. Kornblihtt, J. P. Thiery, *Trends Genet.* **1988**, *4*, 198–203.
[111] R. O. Hynes, *Annu. Rev. Cell Biol.* **1985**, *1*, 67–90.
[112] R. O. Hynes, *Fibronectins*, Springer, New York, **1990**.
[113] J. M. Gardner, R. O. Hynes, *Cell* **1985**, *42*, 439–448.
[114] R. F. Doolittle, *Annu. Rev. Biochem.* **1984**, *53*, 195–229.
[115] J. Lawler, R. Weinstein, R. O. Hynes, *J. Cell Biol.* **1988**, *107*, 2351–2361.
[116] D. F. Mosher, *Annu. Rev. Med.* **1990**, *41*, 85–97.
[117] J. E. Stadler, *J. Biol. Chem.* **1991**, *266*, 22777–22780.
[118] G. Piétu, A.-S. Ribba, G. Chérel, D. Meyer, *Biochem. J.* **1992**, *284*, 711–715.
[119] B. R. Tomasini, D. F. Mosher, *Prog. Hemostasis Thromb.* **1990**, *10*, 269–305.
[120] K. T. Preissner, *Annu. Rev. Cell Biol.* **1991**, *7*, 275–310.
[121] N. Nakashima, K. Miyazaki, M. Ishikawa, T. Yatohgo, H. Ogawa, H. Uchibori, I. Matsumoto, N. Seno, M. Hayashi, *Biochim. Biophys. Acta* **1992**, *1120*, 1–10.
[122] M. H. Helfrich, S. A. Nesbitt, E. L. Dorey, M. A. Horton, *J. Bone Miner. Res.* **1992**, *7*, 335–343
[123] H. P. Erickson, M. A. Bourdon, *Annu. Rev. Cell Biol.* **1989**, *5*, 71–92.
[124] D. J. Leahy, W. A. Hendrickson, I. Aukjil, H. P. Erickson, *Science* **1992**, *258*, 987–991.
[125] E. Ruoslahti, M. D. Pierschbacher, *Cell* **1986**, *44*, 517–518.
[126] H. Mohri, T. Ohkubo, *Peptides* **1993**, *14*, 353–357.
[127] J. R. Potts, I. D. Campbell, *Curr. Opin. Cell Biol.* **1994**, *6*, 648–655.
[128] A. L. Main, T. S. Harvey, M. Baron, J. Boyd, I. D. Campbell, *Cell* **1992**, *71*, 671–678.
[129] M. Baron, A. L. Main, P. C. Driscoll, H. J. Mardon, J. Boyd, I. D. Campbell, *Biochemistry* **1992**, *31*, 2068–2073.
[130] C. D. Dickinson, B. Veerapandian, X. P. Dai, R. C. Hamlin, N. H. Xuong, E. Ruoslathi, K. R. Ely, *J. Mol. Biol.* **1994**, *236*, 1079–1092.
[131] D. J. Leahy, I. Aukhil, H. P. Erickson, *Cell* **1996**, *84*, 155–164.
[132] I. D. Campbell, presented at the XVII International Conference of Magnetic Resonance in Biological Systems, Keystone, CO (USA), **1996**.
[133] A. Stockmann, S. Hess, P. Declerk, R. Timpl, K. T. Preissner, *J. Biol. Chem.* **1993**, *268*, 22874–22882.
[134] M. Adler, R. A. Lazarus, M. S. Dennis, G. Wagner, *Science* **1991**, *253*, 445–448.
[135] M. Adler, P. Carter, R. A. Lazarus, G. Wagner, *Biochemistry* **1993**, *32*, 282–289.
[136] C. Dalvit, H. Widmer, G. Bovermann, R. Breckenridge, R. Metternich, *Eur. J. Biochem.* **1991**, *202*, 315–321.

[137] R. M. Cooke, B. G. Carter, D. M. A. Martin, P. Murray-Rust, M. P. Weir, *Eur. J. Biochem.* **1991**, *202*, 323–328.
[138] V. Saudek, R. A. Atkinson, P. Lepage, J. T. Pelton, *Eur. J. Biochem.* **1991**, *202*, 329–338.
[139] V. Saudek, R. A. Atkinson, J. T. Pelton, *Biochemistry.* **1991**, *30*, 7369–7372.
[140] Y. Chen, S. M. Pitzenberger, V. M. Garsky, P. K. Lumma, G. Sanyal, J. Baum, *Biochemistry* **1991**, *30*, 1625–1636.
[141] R. A. Atkinson, V. Saudek, J. T. Pelton, *Int. J. Pept. Protein Res.* **1994**, *43*, 563–572.
[142] H. Senn, W. Klaus, *J. Mol. Biol.* **1993**, *232*, 907–925.
[143] M. Jeseja, K. J. Smith, X. Lu, J. A. Williams, H. Trayer, I. P. Trayer, E. I. Hyde, *Eur. J. Biochem.* **1993**, *218*, 853–860.
[144] M. J. Sutcliffe, M. Jeseja, E. I. Hyde, X. Lu, J. A. Williams, *Struct. Biol.* **1994**, *1*, 802–807.
[145] R. S. McDowell, M. S. Dennis, A. Louie, M. Shuster, M. G. Mulkerrin, R. A. Lazarus, *Biochemistry* **1992**, *31*, 4766–4772.
[146] A. M. Krezel, G. Wagner, J. Seymour-Ulmer, R. A. Lazarus, *Science* **1994**, *264*, 1944–1947.
[147] M. D. Pierschbacher, E. Ruoslahti, *Nature* **1984**, *309*, 30–33.
[148] M. D. Pierschbacher, E. Ruoslahti, *Proc. Natl. Acad. Sci. USA* **1984**, *81*, 5985–5988.
[149] K. N. Yamada, D. W. Kennedy, *J. Cell Biol.* **1984**, *99*, 29–36.
[150] E. Koivunen, B. Wang, E. Ruoslahti, *Bio/Technology* **1995**, *13*, 265–270.
[151] J. M. Healy, O. Murayama, T. Maeda, K. Yoshino, K. Sekiguchi, M. Kikuchi, *Biochemistry* **1995**, *34*, 3948–3955.
[152] F. Balkenhohl, C. von dem Bussche-Hünnefeld, A. Lansky, C. Zechel, *Angew. Chem.* **1996**, *108*, 2436–2487; *Angew. Chem. Int. Ed. Engl.* **1996**, *35*, 2288–2337.
[153] M. D. Pierschbacher, E. Ruoslahti, *J. Biol. Chem.* **1987**, *262*, 7294–7298.
[154] R. F. Nutt, S. F. Brady, J. T. Sisko, T. M. Ciccarone, C. D. Colton, M. R. Levy, R. J. Gould, G. Zhang, P. A. Freidman, D. F. Veber, *Pept. Proc. Eur. Pept. Symp. 21th 1990* **1991**, 784–786.
[155] F. E. Ali, R. Calvo, T. Romoff, J. Samanen, A. Nichols, B. Store in *Peptides: Chemistry, Structure and Biology* (Eds.: J. E. Rivier, G. R. Marshall), ESCOM Science, Leiden (The Netherlands), **1990**, pp. 94–96.
[156] H. Kessler, *Angew. Chem.* **1982**, *94*, 509–520; *Angew. Chem. Int. Ed. Engl.* **1982**, *21*, 512–523.
[157] G. Müller, M. Gurrath, H. Kessler, *J. Comput. Aided Mol. Des.* **1994**, *8*, 709–730.
[158] A classical example is the cyclic undecapeptide cyclosporin. It exhibits different structures in varying solvents, in crystal and, on binding to the natural receptor cyclophilin.
[159] H. Matter, G. Gemmecker, H. Kessler, *Int. J. Pept. Protein Res.* **1995**, *45*, 430–440.
[160] J. S. Richardson, *Adv. Protein Chem.* **1981**, *34*, 167–339.
[161] M. Kurz, Ph.D. thesis, Technische Universität München, **1991**.
[162] R. Schwyzer, P. Sieber, B. Gorup, *Chimia* **1958**, *12*, 90–91.
[163] H. Kessler, H. Matter, G. Gemmecker, A. Kling, M. Kottenhahn, *J. Am. Chem. Soc.* **1991**, *113*, 7550–7563.
[164] H. Kessler, H. Matter, G. Gemmecker, M. Kottenhahn, J. W. Bats, *J. Am. Chem. Soc.* **1992**, *114*, 4805–4818.
[165] M. Pfaff, K. Tangemann, B. Müller, M. Gurrath, G. Müller, H. Kessler, R. Timpl, J. Engel, *J. Biol. Chem.* **1994**, 269, 20233–20238.
[166] S. Cheng, W. S. Craig, D. Mullen, J. F. Tschopp, D. Dixon, M. D. Pierschbacher, *J. Med. Chem.* **1994**, *37*, 1–8.
[167] K. D. Kopple, P. W. Baures, J. W. Bean, C. A. D'Ambrosio, J. L. Hughes, C. E. Peishoff, D. S. Eggleston, *J. Am. Chem. Soc.* **1992**, *114*, 9615–9623.
[168] L.-H. Zhang, L. Anzalone, P. Ma, G. S. Kaufmann, L. Storace, R. Ward, *Tetrahedron Lett.* **1996**, *37*, 4455–4458.
[169] W. H. Miller, T. W. Ku, F. E. Ali, W. E. Bondinell, R. R. Calvo, L. D. Davis, K. F. Erhard, L. B. Hall, W. F. Huffman, R. M. Keenan, C. Kwon, K. A. Newlander, S. T. Ross, J. M. Samanen, D. T. Takata, C.-K. Yuan, *Tetrahedron Lett.* **1995**, *36*, 9433–9436.
[170] M. E. Duggan, A. M. Naylor-Olsen, J. J. Perkins, P. S. Anderson, C. T.-C. Chang, J. J. Cook, R. J. Gould, N. C. Ihle, G. D. Hartman, J. J. Lynch, R. J. Lynch, P. D. Manno, L. W. Schaffer, R. L. Smith, *J. Med. Chem.* **1995**, *38*, 3332–3341.
[171] P. R. Bovy, F. S. Tjoeng, J. G. Rico, T. E. Rogers, R. J. Lindmark, J. A. Zablocki, R. B. Garland, D. E. McMackins, H. Dayringer, M. V. Tóth, M. E. Zupec, S. Rao, S. G. Panzer-Knodle, N. S. Nicholson, A. Salyers, B. B. Taite, M. Herin, M. Miyano, L. P. Feigen, S. P. Adams, *Bioorg. Med. Chem.* **1994**, *2*, 881–895.
[172] R. S. McDowell, B. K. Blackburn, T. R. Gadek, L. R. McGee, T. Rawson, M. E. Reynolds, K. D. Robarge, T. C. Somers, E. D. Thorsett, M. Tischler, R. R. Webb II, M. C. Venuti, *J. Am. Chem. Soc.* **1994**, *116*, 5077–5083.
[173] R. S. McDowell, T. R. Gadek, P. L. Barker, D. J. Burdick, K. S. Chan, C. L. Quan, N. Skelton, M. Struble, E. D. Thorsett, M. Tischler, J. Y. K. Tom, T. R. Webb, J. P. Burnier, *J. Am. Chem. Soc.* **1994**, *116*, 5069–5076.
[174] C. E. Peishoff, F. E. Ali, J. W. Bean, R. Calvo, C. A. D'Ambrosio, D. S. Eggleston, S. M. Hwang, T. P. Kline, P. F. Koster, A. Nichols, D. Powers, T. Romoff, J. Samanen, J. Stadel, J. A. Vasko, K. D. Kopple, *J. Med. Chem.* **1992**, *35*, 3962–3969.
[175] J. W. Bean, K. D. Kopple, C. E. Peishoff, *J. Am. Chem. Soc.* **1992**, *114*, 5328–5334.
[176] W. J. Hoekstra, P. J. Sanfilippo, *Chemtracts: Org. Chem.* **1993**, *6*, 104–107.
[177] R. S. McDowell, T. R. Gadek, *J. Am. Chem. Soc.* **1992**, *114*, 9245–9253.
[178] J. W. Bean, K. D. Kopple, C. E. Peishoff, *Pept. Proc. Eur. Pept. Symp. 22th 1990* **1993**, 547–548.
[179] P. N. Sanderson, R. C. Glen, A. W. R. Payne, B. D. Hudson, C. Heide, G. E. Tranter, P. M. Doyle, C. J. Harris, *Int. J. Pept. Protein Res.* **1994**, *43*, 588–596.
[180] S. Jackson, W. F. DeGrado, A. Dwivedi, A. Parthasarathy, A. Higley, J. Krywko, A. Rockwell, J. Markwalder, G. Wells, R. Wexler, S. Mousa, R. Harlow, *J. Am. Chem. Soc.* **1994**, *116*, 3220–3230.
[181] L.-H. Zhang, P. Ma, *Tetrahedron Lett.* **1994**, *35*, 5765–5768.
[182] C.-B. Xue, W. F. DeGrado, *J. Org. Chem.* **1995**, *60*, 946–952.
[183] A. C. Bach II, C. J. Eyermann, J. D. Gross, M. J. Bower, R. L. Harlow, P. C. Weber, W. F. DeGrado, *J. Am. Chem. Soc.* **1994**, *116*, 3207–3219.
[184] R. Haubner, M. Gurrath, G. Müller, M. Aumailley, H. Kessler in *Prospects in Diagnosis and Treatment of Breast Cancer, Excerpta Medica International Congress Series* (Eds.: M. Schmitt, H. Greaff, G. Kindermann), Elsevier, Amsterdam, **1994**, pp. 133–144.
[185] A. Jonczyk, G. Hölzemann, B. Felding-Habermann, G. Melzer, B. Diefenbach, D. A. Cheresh, H. Kessler, M. Gurrath, G. Müller (Merck), EP-A 578083-A2, **1993** [*Chem. Abstr.* **1994**, *120*, 144169f].
[186] A. Jonczyk, G. Hölzemann, B. Felding-Habermann, F. Rippmann, G. Melzer, B. Diefenbach, H. Kessler, R. Haubner, J. Wermuth (Merck), EP-A 596350-A1, **1992** [*Chem. Abstr.* **1995**, *122*, 161376e].
[187] A. Jonczyk, G. Hölzemann, B. Felding-Habermann, F. Rippmann, B. Diefenbach, H. Kessler, R. Haubner, J. Wermuth (Merck), DE-A 4310643-A1, **1994** [*Chem. Abstr.* **1995**, *122*, 188171f].
[188] A. Jonczyk, G. Hölzemann, S. L. Goodman, H. Kessler, R. Haubner, J. Wermuth (Merck), DE-A 4415310-A1, **1994** [*Chem. Abstr.* **1996**, *124*, 118006f].
[189] A. Jonczyk, B. Diefenbach, S. L. Goodman, A. Sutter, H. Kessler, M. A. Dechantsreiter (Merck), DE-A 19534177-A1, **1997**.
[190] P. A. Bartlett, G. T. Shea, S. J. Telfer, S. Waterman in *Molecular Recognition: Chemical and Biochemical Problems* (Ed.: S. M. Roberts), Royal Society, Cambridge, **1989**, pp. 182–196.
[191] A. C. Bach II, J. R. Espina, S. A. Jachson, P. F. W. Stouten, J. L. Duke, S. A. Mousa, W. F. DeGrado, *J. Am. Chem. Soc.* **1996**, *118*, 293–294.
[192] G. Müller, *Angew. Chem.* **1996**, *108*, 2941–2943; *Angew. Chem. Int. Ed. Engl.* **1996**, *35*, 2767–2769.
[193] K. Burgess, D. Lim, S. A. Mousa, *J. Med. Chem.* **1996**, *39*, 4520–4526.
[194] J. Wermuth, S. L. Goodman, A. Jonczyk, H. Kessler, *J. Am. Chem. Soc.* **1997**, *119*, 1328–1335.
[195] V. Prelog, H. Gerlach, *Helv. Chim. Acta* **1964**, *47*, 2288–2294.
[196] H. Gerlach, J. A. Owtschinnikow, V. Prelog, *Helv. Chim. Acta* **1964**, *47*, 2294–2302.
[197] R. M. Freidinger, D. F. Veber, *J. Am. Chem. Soc.* **1979**, *101*, 6129–6131.
[198] D. F. Mierke, M. Kurz, H. Kessler, *J. Am. Chem. Soc.* **1994**, *116*, 1042–1049.
[199] M. Koppitz, M Huenges, R. Gratias, H. Kessler, S. L. Goodman, A. Jonczyk, *Helv. Chim. Acta* **1997**, *80*, 1280–1300.
[200] H. Kessler, R. Gratias, G. Hessler, M. Gurrath, M. Müller, *Pure Appl. Chem.* **1996**, *68*, 1201–1205.
[201] J. D. Dunitz, J. Waser, *J. Am. Chem. Soc.* **1972**, *94*, 5645–5650.
[202] I. L. Karle, *Int. J. Pept. Protein Res.* **1986**, *28*, 420–427.
[203] G. Quinkert, E. Egert, C. Griesinger, *Aspekte der Organischen Chemie*, VCH, Weinheim, **1995**, pp. 203–226.
[204] J. P. Snyder, *J. Am. Chem. Soc.* **1984**, *106*, 2393–2400.
[205] R. Haubner, R. Gratias, S. L. Goodman, H. Kessler in *Peptides: Chemistry, Structure and Biology* (Eds.: T. P. Kaumaya, R. S. Hodges), Mayflower, Kingswinford, **1996**, pp. 205–206.
[206] R. Haubner, R. Gratias, B. Diefenbach, S. L. Goodman, A. Jonczyk, H. Kessler, *J. Am. Chem. Soc.* **1996**, *118*, 7461–7472.
[207] H. Kessler, G. Gemmecker, A. Haupt, M. Klein, K. Wagner, M. Will, *Tetrahedron* **1988**, *44*, 745–759.
[208] A. Geyer, G. Müller, H. Kessler, *J. Am. Chem. Soc.* **1994**, *116*, 7735–7743.
[209] D. G. Mullen, S. Cheng, S. Ahmed, J. M. Blevitt, D. Bonnin, W. S. Craig, R. T. Ingram, C. Mazur, R. Minasyan, J. O. Tolley, J. F. Tschopp, M. D. Pierschbacher in *Peptides: Chemistry, Structure and Biology* (Eds.: T. P. Kaumaya, R. S. Hodges), Mayflower, Kingswinford, **1996**, pp. 207–208.
[210] M. K. Anwer, D. B. Sherman, A. F. Spatola, *Int. J. Pept. Protein Res.* **1990**, *36*, 392–399.
[211] M. Marraud, V. Dupont, V. Grand, S. Zerkout, A. Lecoq, G. Boussard, J. Vidal, A. Collet, A. Aubry, *Biopolymers* **1993**, *33*, 1135–1148.
[212] S. J. Richman, M. Goodman, T. M.-D. Nguyen, P. W. Schiller, *Int. J. Pept. Protein Res.* **1985**, *25*, 648–662.

[213] A. Geyer, D. F. Mierke, C. Unverzagt, H. Kessler in *Peptides 1992* (Eds.: C. H. Schneider, A. N. Eberle), ESCOM Science, Leiden (The Netherlands), **1993**, pp. 599–600.
[214] H. Kessler, B. Diefenbach, D. Finsinger, A. Geyer, M. Gurrath, S. L. Goodman, G. Hölzemann, R. Haubner, A. Jonczyk, G. Müller, E. Graf von Roedern, J. Wermuth, *Lett. Pept. Sci.* **1995**, *2*, 155–160.
[215] M. A. Dechantsreiter, B. Mathä, A. Jonczyk, S. L. Goodman, H. Kessler, presented at the 24th European Peptide Symposium, Edinburgh (UK), **1996**.
[216] G. Müller, M. Gurrath, H. Kessler, R. Timpl, *Angew. Chem.* **1992**, *104*, 341–343; *Angew. Chem. Int. Ed. Engl.* **1992**, *31*, 326–328.
[217] The terms "rigid" and "flexible" are often used in conformational studies in an imprecise manner. Rotations around peptide bonds, defined by the ϕ and ψ angles, normally show a low energy barrier, which means that the rotations are not hindered. If one conformation is energetically prefered among the conformations typical for peptides, that is, it dominates the equilibrium, the term "the conformation" is used. If it is clearly dominant it is called the "rigid conformation".
[218] G. Hölzemann, *Kontakte (Darmstadt)* **1991**, *1*, 3–12.
[219] G. Hölzemann, *Kontakte (Darmstadt)* **1991**, *2*, 55–63.
[220] R. Haubner, W. Schmitt, G. Hölzemann, S. L. Goodman, A. Jonczyk, H. Kessler, *J. Am. Chem. Soc.* **1996**, *118*, 7881–7891.
[221] M. Feigel, G. Lugert, M. Bremer, *Liebigs Ann. Chem.* **1987**, 367–373.
[222] R. Haubner, Ph.D. thesis, Technische Universität München, **1995**.
[223] J. L. Kofron, P. Kumic, V. Kishore, G. Gemmecker, S. W. Fesik, D. H. Rich, *J. Am. Chem. Soc.* **1992**, *114*, 2670–2675.
[224] N. Greenspoon, R. Hershkoviz, R. Alon, D. Varon, B. Shenkman, G. Marx, S. Federman, G. Kapustina, O. Lider, *Biochemistry* **1993**, *32*, 1001–1008.
[225] J. Samanen, *Annu. Rep. Med. Chem.* **1996**, *31*, 91–100.
[226] R. D. Cousins, R. M. Keenan, W. H. Miller (SmithKline Beecham), WO-A 96/00574-A1, **1995** [*Chem. Abstr.* **1996**, *124*, 289585f].
[227] F. Ali, W. Bondinell, W. F. Huffman, M. A. Lago, R. M. Keenan, C. Kwon, W. H. Miller, T. Nguyen, D. T. Takata (SmithKline Beecham), WO-A 96/00730-A1, **1996** [*Chem. Abstr.* **1996**, *124*, 289584e].
[228] R. Keenan, W. Miller, F. Ali, L. Barton, B. Bondinell, J. Burgess, J. Callahan, R. Calvo, R. Cousins, M. Gowen, W. Huffman, S. Hwang, D. Jakas, T. Ku, C. Kwon, A. Lago, V. Momouyran, T. Hguyen, S. Ross, J. Samanen, D. Takata, I. Uzinskas, J. Venslavsky, A. Wong, T. Yellin, C. Yuan, *Abstr. Pap. 211th ACS National Meeting* (New Orleans, LA, USA) **1996**, MEDI 236.
[229] J. Samanen, personal communication (**1996**).
[230] G. D. Hartman, M. E. Duggan, N. C. Ihle (Merck & Co, Inc.), WO-A 95/32710-A1, **1995** [*Chem. Abstr.* **1996**, *124*, 232066h].
[231] O. Mechnich, G. Hessler, H. Kessler, M. Bernd, B. Kutscher, *Helv. Chim. Acta* **1997**, in press.

Deposition of Data from X-Ray Structure Analyses

In order to make life easier for authors and referees the Cambridge Crystallographic Data Centre (CCDC) and the Fachinformationszentrum Karlsruhe (FIZ) have unified their procedures for the deposition of data from single-crystal X-ray structure analyses.

Prior to submitting your manuscripts please deposit the data for your compound(s) **electronically** at the appropriate data base, that is, at the CCDC for organic and organometallic compounds and at the FIZ for inorganic compounds. Both data bases will be pleased to provide help (see our *Notice to Authors* in the first issue of this year). In general, you will receive a depository number from the data base within two working days after electronic deposition; please include this number with the appropriate standard text (see our *Notice to Authors*) in your manuscript. This will enable the referees to retrieve the structure data quickly and efficiently if they need this information to reach their decision.

This is now the uniform procedure for manuscripts submitted to the journals *Advanced Materials, Angewandte Chemie, Chemische Berichte/Recueil, Chemistry—A European Journal*, and *Liebigs Annalen/Recueil*.

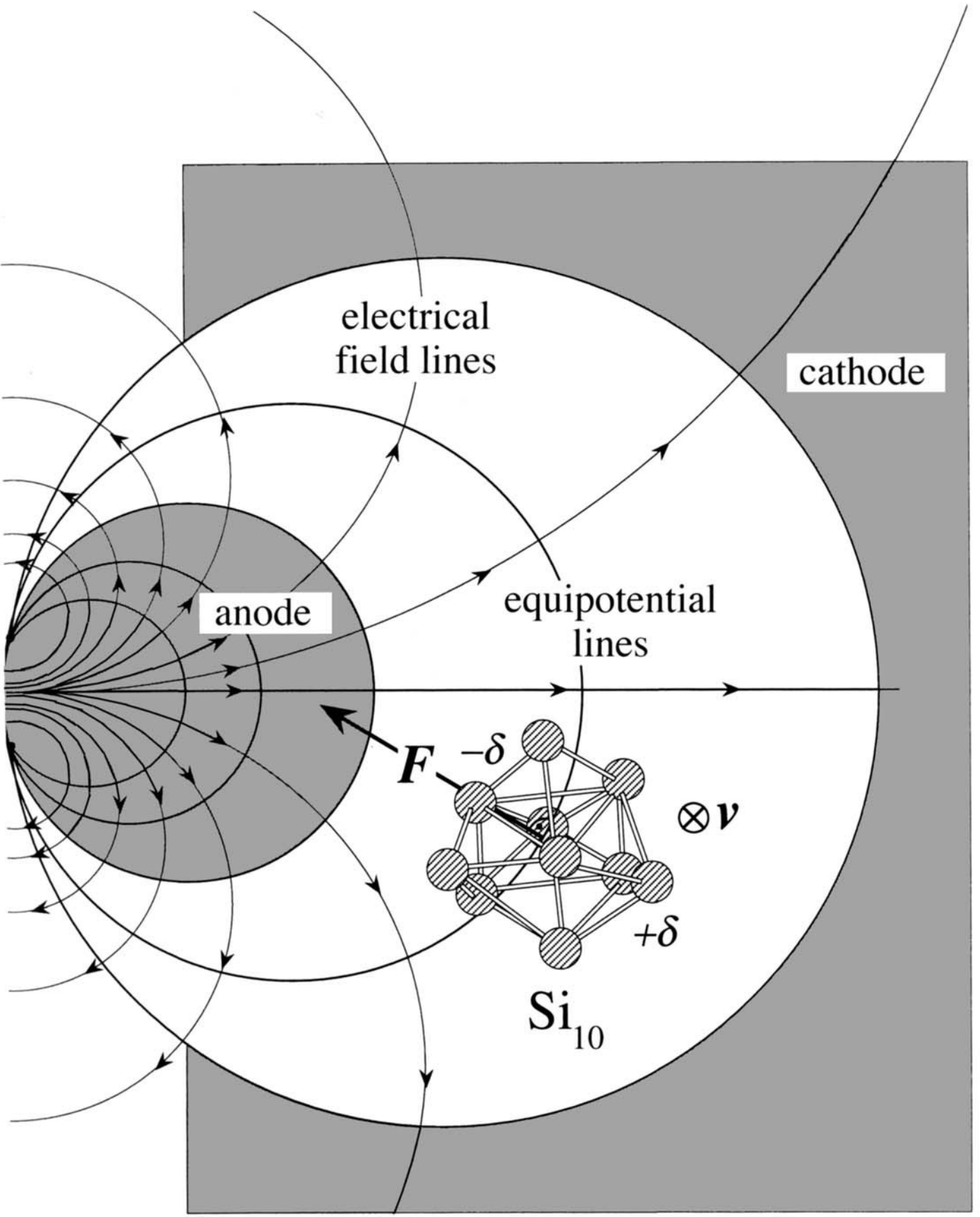

Schematic representation of a semiconductor cluster isolated in the molecular beam during the flight though an electric Stern–Gerlach field. The cluster flies with a velocity v parallel to the cylindrical bent electrode surfaces, which can be seen in the cross section. The field induces a dipole moment in the cluster that is proportional to the polarizability. Owing to the well-defined inhomogeneity of the field a somewhat larger force is exerted on the negative partial charge than on the positive. The resulting force $\boldsymbol{F}$ and the polarizability can be determined in the molecular beam experiment from the deflection of the cluster from the linear flight path.

Molecular Beam Studies on Semiconductor Clusters: Polarizabilities and Chemical Bonding

Jörg August Becker*

This article discusses experiments that measure polarizabilities, permanent dipole moments, and absorption spectra of semiconductor clusters such as Si_N, Ga_NAs_M, and Ge_NTe_M isolated in a molecular beam. The experiments show that the transition from the typical optoelectronic properties of macroscopic semiconductor crystals to the molecular properties of small polyhedral semiconductor molecules occurs in several steps. The bonding in nanometer-sized semiconductor colloids with approximately 10^3-10^5 atoms is similar to that in the solid state. The bonding orbitals of the semiconductor crystals, which extend over a nanometer range, are, however, somewhat more strongly localized in these clusters and are therefore already slightly modified. Over the size range from 10^3 to 10 atoms, a gradual transition occurs from localized solid-state-like bonds to molecule-like bonds. Interestingly, quantum size effects are found even in relatively small particles with about 10^2 atoms. These effects can be observed in the form of unusually small static polarizabilities of Si_N clusters or in the absorption bands of Ga_NAs_M clusters, which are strongly blue-shifted relative to those of the solid state. For smaller clusters, these effects disappear over the size range 10^2-10 atoms, which is manifested by an increasing red-shift of the absorption bands with decreasing cluster size.

Keywords: clusters · colloids · MO models · polarizability · semiconductors

1. Introduction

When a semiconductor crystal made of, for example, Si or GaAs, is divided into ever smaller pieces, one comes upon an interesting problem once the agglomeration numbers X in the fragments have been reduced to about 10^3. The average particle diameter D is then only about 3 nm, which can be estimated from the formula $R = X^{1/3}\bar{r}$ for a spherical particle of radius $R = D/2$ (r is the mean atomic radius in the solid state, Wigner–Seitz radii $\bar{r}_{Si} = 1.68$ Å, $\bar{r}_{GaAs} = 1.75$ Å). The nanometer-sized particles with $X > 10^3$ still contain enough atoms to maintain a bonding structure similar to that in the solid state, which can be observed in semiconductor colloids with an electron microscope.[1]

On the other hand, very small, ligand-free semiconductor particles having 5–10 atoms ($R < 0.4$ nm) exhibit typical molecular polyhedral structures, which have been demonstrated in a matrix for Si_6 and Si_7 by Raman spectroscopy and which are also found by ab initio calculations of quantum chemistry.[2] These structures differ significantly from the typical diamond or zinc blende structures of the solid. The quantum-chemical calculations[2] show that solid-state fragments such as the adamantane structure shown in Figure 1a are unstable for the Si_{10} cluster. Similarly, silicon cubane molecules,[3] which resemble a fragment of a simple cubic crystal (Figure 1b), can only be stabilized by means of ligands. According to quantum-chemical calculations, the adamantane structure shown in Figure 1a will relax into the structure of a tetracapped trigonal prism shown in Figure 1c,[2] thereby increasing its binding energy by 5 eV. These small polyhedral clusters are fairly well understood on a quantum-chemical level. There have even been calculations of isomeric structures (cf. Figure 1d) and their electronic properties.[2,4]

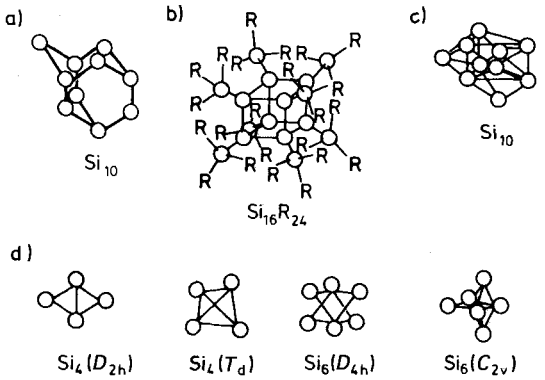

Figure 1. Possible structures for small Si clusters. a) Adamantane structure, b) silacubane molecule[3], c) quantum-chemically calculated structure of the free Si_{10} cluster [12], d) two isomeric structures of Si_4 and Si_6 [4].

[*] Priv.-Doz. Dr. J. A. Becker
Institut für Physikalische Chemie und Wissenschaftliches Zentrum für Materialwissenschaften der Universität
Hans-Meerwein-Straße, D-35032 Marburg (Germany)
Fax: Int. +6421/28-8916
e-mail: beckerj@mailer.uni-marburg.de

 © VCH Verlagsgesellschaft mbH, D-69451 Weinheim, 1997 0570-0833/97/3613-1391 $ 17.50+.50/0

The question remains, however, which changes occur in the chemical bonding[5] upon the transition from the solid-state-like semiconductor structures in particles with $X > 10^3$ to the molecule-like structures of small clusters with 5 to 10 atoms. This question does not arise for salt clusters[6] such as Na_NF_N or metal clusters such as Na_N, as the bonding in those species can be described in similar terms as the one in the solid state, even for very small aggregates. Salt clusters can be envisioned as packed anions and cations held together by Coulomb forces. In the case of metal clusters, the simplest model is a closest packing of atomic cores, bonded together by an electron gas. These two models can explain many properties of metal and salt clusters.[6, 7] In particular, properties of alkali metal clusters are often interpreted in terms of an electron gas model (jellium model).[7] For these clusters it is envisioned that the valence electrons are located within a hollow sphere of cluster radius R in which they move through an evenly distributed positive charge density.

According to the Mott criterium,[8] semiconductors can be transformed into metals even with small, doped electron or hole concentrations. In addition to the initially posed question on size-dependent bonding in semiconductor clusters, it is also necessary to deal with the influence of defect-type electrons on the chemical bonding. These effects will be discussed in this article with reference to the system $Ga_NAs_{N\pm1}$ as example.[8, 9]

Apart from the fundamental questions in chemistry about the chemical bonding, materials science also has an interest in small semiconductor particles. Because of the so-called size quantization effects, the optoelectronic and physical chemistry properties of semiconductor particles can be specifically varied based on the particle size. These effects can be observed in nanometer-sized semiconductor colloids,[1] and also play an important role for semiconductor crystallites.[11] A detailed and clear description of these size quantization effects can be found, for example, in the review article by H. Weller.[1]

The solid-state-like bonding in the semiconductor colloids allows optoelectronic excitations like those in the macroscopic semiconductor.[12a] The excitations lead from the valence band over the band gap $E_{G,F}$ into the conduction band and are often described as photochemical processes.[1, 12a, 13] During the excitation, a photon with the energy $\hbar\omega \geq E_{G,F}$ is absorbed and a positive as well as a negative particle is created. These particles are termed 'hole' (h) and 'electron' (e). The term 'hole' is meant to indicate that the positive charge is not localized on a certain atom, but that it can migrate through the crystal.[12a, 13] This migration of a positive charge is made possible by the exchange of bonding electrons between the atoms, which leads to the compensation of the positive charge on one atom and its reappearance on a neighboring atom. The electron–hole model is based on a theoretical study of the electron orbitals φ in crystalline solids by G. H. Wannier.[14] Even though this terminology may initially appear rather abstract, the electron–hole model allows the development of clear notions about the Wannier orbitals φ on the basis of known equations from physical chemistry. To this end, equations from electron spectroscopy and Born's theory of solvation are combined, because the properties of two charged particles in a dielectric medium (semiconductor) must be described. The orbital $\varphi(\boldsymbol{r})$ determines the probability density $|\varphi(\boldsymbol{r})|^2$ that the electron and hole are a distance $\boldsymbol{r}$ apart. As in electrolyte solutions, the Coulomb attraction is reduced by the polarizability of the medium.[12b, 13] This is also termed the shielding of the Coulomb potential due to the dielectric constant ε of the semiconductor. In addition, the relative motion of electron and hole are governed by a reduced effective mass m_{eff}, which is calculated, in analogy to the hydrogen problem known from gas-phase spectroscopy,[15] according to the formula $m_{eff} = m_{eff,e}m_{eff,h}/(m_{eff,e} + m_{eff,h})$. The terms $m_{eff,e}$ and $m_{eff,h}$ stand for the effective masses of electron and hole, respectively. An example is solid GaAs[16] with $E_{G,F} = 1.5$ eV, $\varepsilon = 11$, and the effective masses $m_{eff,e} = 0.07\, m_0$ and $m_{eff,h} = 0.5\, m_0$, where m_0 is the rest mass of the electron in a vacuum. As the mass of the hole is nearly ten times the mass of the electron, one can make the approximation that the electron moves towards a stationary hole and $m_{eff} \approx m_{eff,e} = 0.07\, m_0$.

Just as in the hydrogen problem, there are bound states in which the electron orbits a hole and the center of mass of the two particles moves in a straight line through the crystal. These so-called exciton states are therefore described by hydrogen-like orbital functions. The lowest excited electronic state in a semiconductor is expressed by a Wannier orbital function[13, 14] of the form $\varphi_1(\boldsymbol{r}) \propto \exp(-|\boldsymbol{r}|/a)$ with the exciton Bohr radius a [Eq. (1)].

$$a = \varepsilon\hbar^2/m_{eff}e^2 \qquad (1)$$

For GaAs the orbital radius of $a = 8$ nm obtained is very large, owing to the large dielectric constant and the small effective mass. If this orbital is supposed to fit into a small GaAs particle with a radius R of only a few nanometers, it must be compressed. The corresponding compression energy E_c must be

Jörg August Becker was born on September 15, 1962 in Kusel/Palatinate, Germany. After his studies at the Technische Universität Karlsruhe from 1982 to 1988 he completed his Diplom thesis on theoretical thermodynamics under the direction of G. Falk. He moved to Marburg to join the research group of F. Hensel and worked in the field of photoelectron spectroscopy. After completing his dissertation in 1991, he moved to the ETH Lausanne and worked, until 1993, with W. A. de Heer on Stern–Gerlach experiments on ferromagnetic metal clusters. Back in Marburg he began to study semiconductor clusters in molecular beams. In 1995 he completed his habilitation in physical chemistry and is currently Privatdozent. His area of research is the physical chemistry of inorganic clusters, colloids, and nanoparticles. He is particularly interested in the development of new techniques and the further development of existing experimental methods to examine the electronic, magnetic, and chemical properties of these particles.

accounted for in the excitation energy according to Equation (2). According to L. E. Brus[17] the compression energy

$$E_{\varphi 1} = E_{G,F} + E_c \tag{2}$$

can be approximated by $E_c = E_L + E_S$, where E_L [Eq. 3]

$$E_L = \frac{\pi\hbar^2}{2R^2}\frac{1}{m_{eff}} \tag{3}$$

represents the localization energy and E_S the solvation energy of the electron–hole pair in the dielectric medium. The latter is of the magnitude $E_S \approx -e^2/\varepsilon R$.[17,18] The high dielectric constant of GaAs means that the solvation energy is negligibly small in Equation (2), while the small effective mass leads to very high localization energies [Eq. (3)]. One could say that in colloids additional compression work has to be performed to form the electron–hole pairs. This pressure–volume work forms the basis for the size quantization effects. It causes the lowest electronic excitation energy $E_{\varphi 1}$ of a colloid to increase according to Equations (2) and (3) with decreasing particle radius R.

The constants ε, $m_{eff,e}$ and $m_{eff,h}$ are only at first glance electrical and mechanical in nature. In fact, they describe material properties that can be derived from the chemical bonding in the semiconductor with, for example, Hückel theory.[19a] This description makes it possible to understand many electronic properties of macroscopic semiconductors as well as the size quantization effects in the colloids with solid-state-like structures. However, now a question from physical chemistry arises. The concept of a macroscopic crystalline medium for the electron–hole excitations is based on a solid-state bonding model, which has to be replaced somehow with a model for a more molecular-type bonding upon decreasing cluster size. The electron–hole excitations have to disappear over the size range 10^3–10 atoms and be replaced by molecular-type electronic excitations. This example clearly shows that the changes in the chemical bonding lead to significant changes in the electronic properties of the semiconductor cluster. From a physical chemistry viewpoint, a description is therefore needed in which the chemical bonding does not yield a prescribed, fixed medium for the electronic excitations, but in which the bonding can be treated as an additional degree of freedom. This degree of freedom should manifest itself in such a way as to change the constants ε and m_{eff} into variables for the new description. Corresponding changes should occur when the solid-state-like chemical bonding is altered over the range 10^3–10 atoms. In this context, it must be considered, which molecular electronic properties of the clusters are reflected in the macroscopic electronic properties ε and m_{eff}.

I will first discuss the dielectric constant ε.[12d] Alternatively, one can use the electric susceptibility $\chi = (\varepsilon - 1)/4\pi$. Both properties can be generalized for a solid body in alternating electric fields. The frequency dependence of the dielectric function $\varepsilon(\omega)$ reflects in particular the band gap $E_{G,F}$ of the semiconductor. For frequencies $\omega < E_{G,F}/\hbar$, $\varepsilon(\omega)$ is constant and begins to increase when $\omega \approx E_{G,F}/\hbar$, similar to the electric conductivity $\sigma(\omega)$, which vanishes for $\omega < E_{G,F}/\hbar$ and increases above $\omega = E_{G,F}/\hbar$.[16] It is not useful to define the conductivity or susceptibility of a small semiconductor particle with fewer than 10^3 atoms. In addition, it would be impossible to measure these properties for clusters in the same way as for the solid state. An isolated semiconductor particle with only 10^2 atoms does not allow the attachment of metal contacts for conductivity measurements without significantly disturbing the chemical bonds within the entire cluster. The electrical polarizability $\alpha(\omega)$ however, does represent a suitable molecular property that can take on the role of $\chi(\omega)$ in clusters and can be measured without physically touching the semiconductor cluster. This can be explained by using the example of a small molecular semiconductor cluster such as Si_3. One envisions the effects on a cluster of a static homogeneous electric field of field strength $\boldsymbol{E}_0$, which is generated by two external electrodes far removed from the cluster. The effect of field-induced changes in the valence electron density $\rho(r)$ of a Si_3 cluster is depicted in Figure 2.[20] The changes in the valence electron density caused by the electric field $\boldsymbol{E}_0$ can be attributed to the shifts of the twelve valence electrons in the chemical bonds of Si_3. The thus created dipole moment $\boldsymbol{\mu}$ depends in the first approximation in a linear fashion on the strength of the applied electric field $\boldsymbol{E}_0$ according to $\boldsymbol{\mu} = \hat{\alpha}\boldsymbol{E}_0$, where the matrix $\hat{\alpha}$ stands for the static polarizability of the cluster. The polarizability matrix $\hat{\alpha}$ can be diagonalized by a suitable choice of coordinate system. The polarizability of a cluster is therefore most readily expressed by its primary axis polarizabilities α_{xx}, α_{yy}, and α_{zz}. For many questions in physical chemistry, the mean polarizability $\alpha_C = (\alpha_{xx} + \alpha_{yy} + \alpha_{zz})/3$ is of interest, as it determines the mean induced dipole moment of statistically oriented clusters. On average, a dipole moment of the value $\mu = \alpha_C|\boldsymbol{E}_0|$ is induced in the direction of the applied field. In the description of the experiments I will show that this dipole moment can be measured for a given field and that the polarizability of a cluster can thus be determined. This measurement therefore allows conclusions about the charge shifts in the cluster, rather like in the study of the dielectric polarization of a solid. As the charge cannot flow through the cluster via contacts, however, this method does not yield information analogous to the conductivity $\sigma(\omega)$. A parameter already a little closer to a conductivity measurement is obtained when the cluster is exposed to a high-frequency alternating electric field. The charge in the cluster is then moved back and forth, and direct contacts to the cluster become unnecessary. For a field that alternates with the periodic frequency ω, a corresponding expression $\mu_\omega = \alpha_C(\omega)\boldsymbol{E}_\omega$ can be found relating the amplitude of the field $\boldsymbol{E}_\omega$ to the amplitude of the dipole moment μ_ω. The proportionality constant $\alpha_C(\omega)$ is called the frequency-dependent or dynamic polarizability of the cluster and is closely related to the absorption spectrum of the cluster.

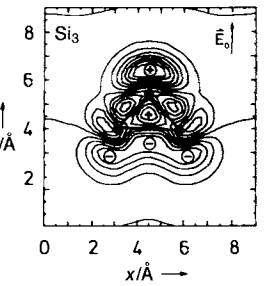

Figure 2. Contour diagram of the field-induced changes in the valence electron density ρ of the Si_3 cluster [20].

These analogies between the dielectric constant $\varepsilon(\omega)$ of a solid and the polarizability $\alpha_C(\omega)$ of a cluster can be expanded into a unified physical chemistry description of clusters and solids by reducing these two physical quantities to a common property of the chemical bonding. I will demonstrate that within a molecular orbital model the polarizability $\alpha(\omega)$ of a cluster comprises the sum of the contributions of the separate bonds in the cluster.

The average of these polarizabilities therefore describes, on one hand, the mean bond polarizability $\bar{\alpha}_B$ of the molecular cluster, and on the other hand, through the Clausius–Mosotti relation [Eq. (4)] the dielectric constant ε of the solid and of solid-like colloids in which the chemical bonds are present with the density $\hat{n}_B$.

$$\left(\frac{\varepsilon-1}{\varepsilon+2}\right)=\frac{4\pi\hat{n}_B}{3}\bar{\alpha}_B \qquad (4)$$

There is no physical chemistry approach as elegant as the Clausius–Mosotti relation for the reduction of the effective mass to a property of the chemical bonding in clusters and solids. The phenomenological description using the effective mass of the electron[12c] takes into account not only the kinetic energy of the conducting electron but also the quantum-chemical interactions with other electrons and the atomic cores in the zinc blende structure of the GaAs crystal. From the standpoint of physical chemistry, the small effective electron mass $m_{eff} = 0.07\, m_0$ implies that the conducting electrons in the semiconductor are present in a chemical environment in which they have a very low inertia and, hence, a high mobility. In this manner, the chemical environment affects the localization energy [Eq. (3)]. As it is possible to retain the concept of an electron in a chemical environment for clusters, the effective mass could be perceived as a characteristic of this environment by defining it by means of the localization energy according to $m_{eff} = \pi\hbar^2/2R^2E_L$. This is also useful from the standpoint of molecular theory, because Equation (3), in a similar form, applies approximately to the model of an electron in a spherical potential well when the effective mass m_{eff} is replaced by the rest mass m_0 of an electron in a vacuum. It is known that the model of an electron in a box can serve as a model for many molecules.[21] It should therefore also be applicable to the polyhedral structures of small semiconductor clusters, as these represent approximately spherical cages in which the molecular orbitals form. This simple picture is in accordance with quantum-chemical ab initio calculations for the clusters Ga_2As_3 and Ga_3As_2.[22] According to these calculations, in Ga_2As_3 (D_{3h}) there is a radical electron located in a molecular orbital inside the trigonal bipyramidal cage. This result is consistent with ESR signals of matrix-isolated Ga_NAs_M clusters, which have been assigned to the radical electron in Ga_2As_3.[23] Even though the electron localization model [Eq. (3)] can only yield a rough description of the molecule-like structures, it should be possible to apply it to the analysis of the critical changes during the transition from molecular to solid-state-like bonding. These changes should be rather large, as it can be assumed that, upon a decrease in the particle radius R, the parameter m_{eff} will change from its solid-state value of $m_{eff,F} = 0.07\, m_0$ into the electron rest mass m_0, an increase of more than one order of magnitude.

To study the questions posed here, a suitable experimental method is required to create semiconductor clusters containing 5 to 10^3 atoms and to measure the polarizability as well as the absorption spectrum as a function of cluster size. In the size range of interest of fewer than 10^3 atoms ($R < 1.7$ nm for GaAs or Si), colloid-chemical methods[1] only generate samples with a broad particle size distribution. The size determination for colloids containing fewer than 10^2 atoms with high-resolution electron microscopy is no longer feasible. The controlled stepwise preparation of ligand-stabilized clusters with 10, 12, 13,... atoms[1] by molecular chemistry is also exceedingly difficult. In addition, the bonding in clusters with fewer than 10^2 atoms is significantly affected by the presence of ligands. We have therefore modified molecular beam methods of metal cluster physics[7] to generate very intense molecular beams composed of ligand-free Si_N or Ga_NAs_M clusters with between 5 and 10^3 atoms and to allow their subsequent study. In these beams, the polarizabilities and the absorption spectra of the semiconductor clusters can be measured under collision-free conditions. The experiments are performed in combination with mass spectrometry, thus permitting the size-selective study of properties of isolated clusters. In this article, initial results are reported for polarizabilities and absorption spectra for clusters of 5 to typically 10^2 atoms. Size-selective measurements on clusters in the range of 10^2–10^3 atoms will have to await further developments of experimental techniques.

It should be noted that we were able to utilize the invaluable work of other research groups on colloids and small clusters already at the outset of this study.[24–26] In particular, we chose the system Ga_NAs_M for the spectroscopic studies, because the absorption spectra of GaAs colloids[25] and of the GaAs molecule[26] are known. In addition, the ionization potentials,[27] electron affinities,[28] and quantum-chemical structural calculations[29] of small Ga_NAs_M clusters have been reported.

2. Isolated Semiconductor Clusters: Preparation, Experiments and Physical Chemistry Models

The molecular beam technique offers an opportunity to study clusters under collision-free conditions.[7, 30] The semiconductor clusters are generated by laser evaporation of semiconductor crystals in a helium atmosphere.[27] The appropriate cluster source is located in the high-vacuum chamber (A) of the molecular beam apparatus, which is shown schematically in Figure 3. The sketch of the Marburg cluster source is shown in Figure 4.

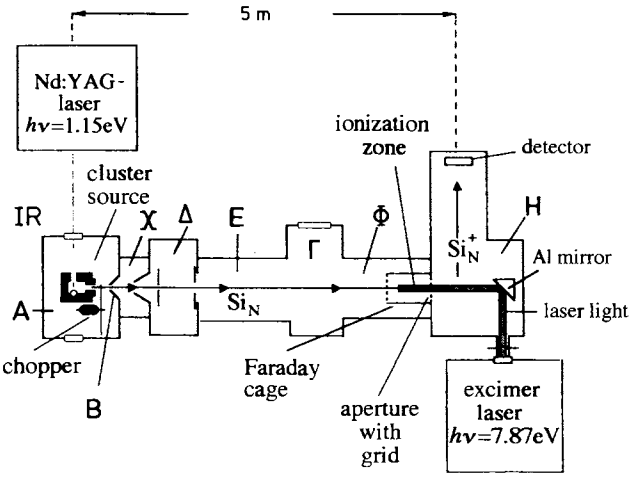

Figure 3. Schematic representation of the cluster beam apparatus. A = vacuum chamber, B = skimmer, X, Δ = differential pressure stages, E, Φ = flight tubes, Γ = experimentation chamber, H = mass spectrometry chamber.

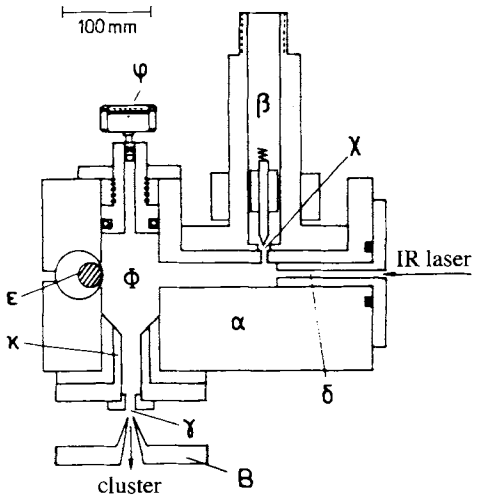

Figure 4. Molecular beam source for intense, pulsed beams of semiconductor clusters. α = housing, β = magnetic valve, χ = valve channel, δ = light introduction channel, γ = nozzle, ε = semiconductor rod, ϕ = condensation region, φ = pressure sensor, κ = nozzle channel, and B = skimmer. For operation, see text.

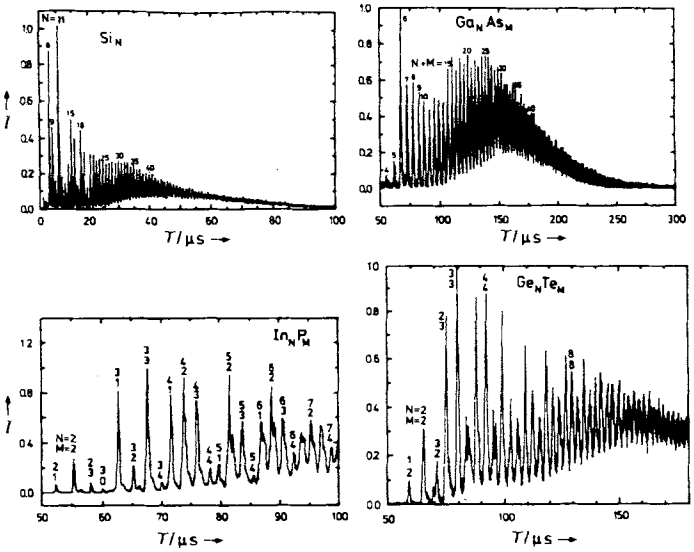

Figure 5. Mass spectra of semiconductor clusters prepared by pulsed laser evaporation of Si, GaAs, InP, and GeTe crystals in a stream of helium. The time of flight T in the flight tube of the mass spectrometer allows the calculation of the cluster mass ($M_C \propto T^2$), which in turn allows the determination of cluster sizes $X = N+M$ and compositions $N:M$.

In the housing (α), the helium carrier gas can enter the source through the pulsed magnetic valve (β) and the valve channel (χ). The pulsed IR laser beam, entering through the light introduction channel (δ), evaporates a little of the material from the slowly rotating semiconductor rod (ε). The short IR laser pulse, typically 15 ns long, contains a high pulse energy of typically 1 J and evaporates about 10^{-8} mol of the semiconductor material. In region (ϕ), the vapor condenses in the helium atmosphere ($p_{He} \approx 10$ mbar) to form clusters. The He density in the source can be monitored with the pressure sensor (φ), and the cluster distribution in the beam can be optimized. The clusters, dispersed in the carrier gas, flow through the nozzle channel (κ), leave the source through the nozzle (γ), and expand together with the helium into the vacuum chamber (A) (cf. Figure 3). The thus generated cluster beam passes through the first skimmer (B) and enters the differential pressure stages (X) and (Δ). It then passes through the flight tubes (E) and (Φ) as well as through the chamber (Γ), where the clusters can be studied under collision-free conditions. The clusters then pass into the chamber (H), where they are detected by a time-of-flight mass spectrometer. Typical mass spectra of semiconductor clusters are depicted in Figure 5. The time of flight T of the clusters in the flight tube of the mass spectrometer, a measure for the cluster mass M_C, is plotted on the x axis. The velocity v of the clusters and their residence time τ in the cluster source can be measured by using a rotating chopper. Typically one finds values of $v = 400-1200\ m\,s^{-1}$ and $\tau = 700-1200\ \mu s$.

2.1. Measurement of Permanent and Induced Dipole Moments in Molecular Beams

The dipole moment $\boldsymbol{\mu}$ of a particle isolated in a molecular beam can be determined through the force exerted on it by an inhomogeneous static electric field $\boldsymbol{E}_0$ (see Figure 6).[9, 10, 31, 32] The force that acts upon the cluster in an inhomogeneous electric field with z component $(\boldsymbol{E}_0)_z$ and corresponding field gradient $\partial(\boldsymbol{E}_0)_z/\partial z$ is given by $(\boldsymbol{F})_z = \mu\partial(\boldsymbol{E}_0)_z/\partial z$.[31] In order to examine this force, a collimated cluster beam is passed through an inhomogeneous electric field and the deflection of the beam due to the field's effect is measured after a given length of flight. The experimental setup of the deflection plates is schematically shown in Figure 6a. The clusters pass through the inhomogeneous electric field, which is located between the two bent brass

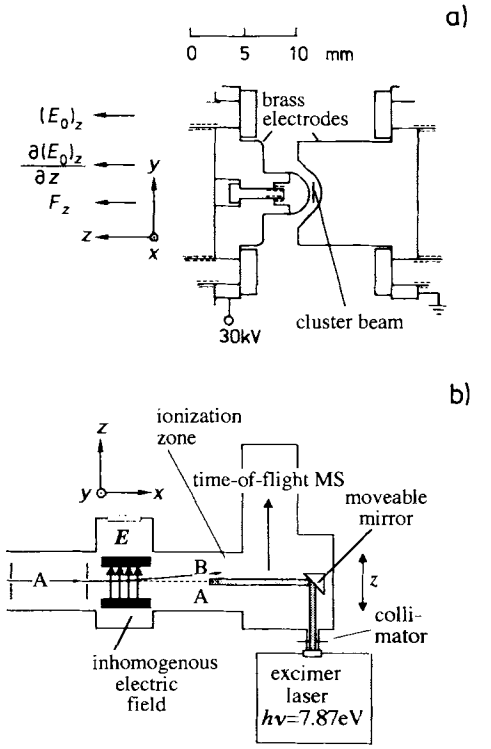

Figure 6. Experimental set-up of the apparatus for the measurement of static polarizabilities. a) Configuration of the high-voltage electrodes for the generation of the inhomogeneous electric deflection field. b) The clusters fly along beam A and are diverted in the inhomogeneous field E to direction B. The resulting beam B is sampled by the collimated ionization laser beam.

electrodes. The typical potential difference between the two electrodes is 30 kV. The deflections of the cluster beam generated in this way can be studied with a collimated pulsed ionization laser beam ($\lambda = 157$ nm, that is, a photon energy of $\hbar\omega = 7.89$ eV). The collimated ionization laser beam is directed into the Faraday cage of the mass spectrometer by means of an aluminum mirror. In the Faraday cage, the ionization of the clusters can occur in the absence of potentially interfering stray electric fields. The mirror can be moved along the z direction by step motors (Figure 6b). The UV laser beam can thus be shifted perpendicular to the molecular beam in the ionization zone. In this way, the cluster beam can be probed with laser light. The number of ionized clusters of a given size observed in the mass spectrum is proportional to their density in the sampled volume element of the Faraday cage. The mass spectra for the individual sampling positions are recorded with a multichannel analyzer and then stored. During the subsequent analysis, the intensity of a given mass can be determined for a given sampling position z. This way, an intensity profile can be measured for all cluster sizes. For particles with a permanent dipole moment, the two possible orientations of the dipole moment (parallel and antiparallel to the field) lead to a broadening of the molecular beam and, hence, to a decrease in the intensity along the beam axis.[9] Figure 7a demonstrates this effect for a Ge_2Te cluster. This

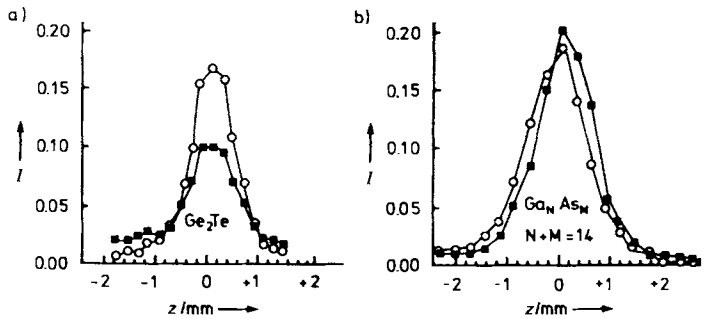

Figure 7. a) Comparison of a typical intensity profile of the undeflected beam A of Ge_2Te clusters with the field $\boldsymbol{E}$ turned off (circles) with that of the deflected beam B with the field $\boldsymbol{E}$ turned on (squares) (cf. Figure 6). b) The corresponding comparison for Ga_NAs_M clusters with $N+M=14$ and $N \approx M$. The sampling position z is varied by moving the Al mirror shown in Figure 6b.

broadening allows the determination of the permanent dipole moment of a cluster on using certain simplifying assumptions about the rotation of the cluster.[9, 33] The dipole moments obtained thus for Ge_2Te is $\mu = (1.4 \pm 0.2)$ Debye and for Ge_2Te_2 is $\mu = (1.1 \pm 0.1)$ D. This indicates C_{2v} symmetry for both Ge_2Te and Ge_2Te_2. In contrast to Ge_2Te and Ge_2Te_2, no measurable dipole moment is found for $GeTe_2$. This indicates that $GeTe_2$ possesses a linear structure, like its homologue CO_2. These symmetry considerations are supported by infrared spectra of Si_2S_2, a homologue of Ge_2Te_2, in a matrix[34] and recent quantum-chemical calculations of structures and dipole moments of small Ge_NTe_M clusters.[35] For those readers interested in theoretical quantum chemistry it should be noted that high-resolution molecular beam experiments to measure dipole moments of molecules are not only suitable for the study of molecular symmetries. These days, they are again employed to test the validity of more general symmetry principles in the theory of the electron.[36]

No effects attributable to permanent dipole moments are found for all larger Ge_NTe_M clusters studied ($4 < N + M < 25$). The same is true for the Ga_NAs_M and Si_N clusters studied.[9, 10] In this case, a shift of the molecular beam profile shown in Figure 7b for Ga_NAs_M clusters with $N+M=14$ and $N \approx M$ is observed. Due to the free rotation of the particles in the molecular beam, this experiment permits the measurement of the induced dipole moment $\boldsymbol{\mu} = \alpha_C(\boldsymbol{E}_0)_z$ and thereby the mean polarizability α_C of the clusters.

2.1.1. *Polarizability, Chemical Bonding, and Radical Electrons in Ga_NAs_M Clusters*

For Ga_NAs_M clusters, the polarizabilities were studied as a function of the cluster size $X = N+M$. To each cluster size $N+M$ observed in the mass spectrum in Figure 5 belongs a distribution of $N:M$ compositions with a maximum at $N \approx M$. Figure 8 shows that the mean polarizability per atom $\bar{\alpha}_C = \alpha_C/X$ exhibits regular oscillations as a function of the cluster size X.

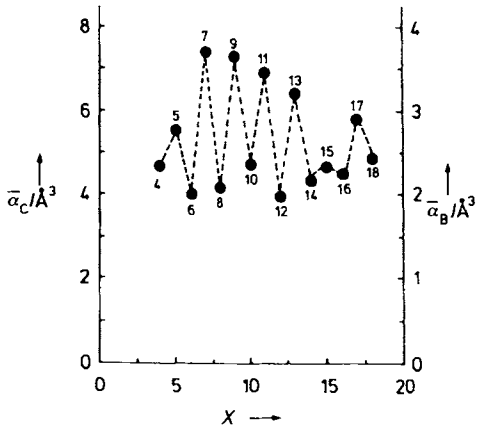

Figure 8. Measured polarizability for Ga_NAs_M clusters given as polarizability per atom $\bar{\alpha}_C$ (left ordinate) and as mean bond polarizability $\bar{\alpha}_B$ (right ordinate) as a function of the cluster size X.

The polarizability of clusters of an odd value for X is significantly larger than for those clusters with an even value for X. The values observed for odd-numbered clusters are rather high and are otherwise only found for typical metal clusters such as Na_N or K_N.[7, 37] The high polarizabilities for clusters with odd X values also affect the van der Waals forces between the Ga_NAs_M clusters and the inert gas atoms.[38] Similar odd–even effects have been observed for the ionization potentials (IPs)[27] and the electron affinities[28] of Ga_NAs_M clusters. One finds high ionization barriers for clusters with even X and low ones for odd X, and vice versa for the electron affinities. Figure 9 shows a simple MO scheme that explains this effect. The cluster Ga_3As_4 possesses an odd number of valence electrons and thus has an open-shell system of valence electrons. The unpaired (radical) electron also explains the high polarizabilities of these clusters. This electron is readily polarizable as it is not confined to a bond with another electron. It turns out, however, that even the contribution of the bonding electrons to the polarizability is affect-

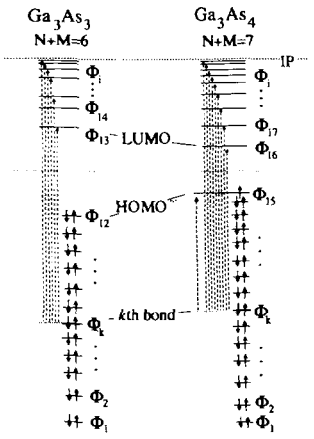

Figure 9. MO model for Ga_NAs_M clusters. Each occupied MO Φ_k can be assigned a bond or radical electron polarizability. The value of this bond or radical electron polarizability is calculated from the dipole-allowed transitions (dashed arrows), which lead from the occupied MO Φ_k into the higher-lying MOs Φ_i.

ed by the radical electron. This statement is supported by the correlation between polarizability and the chemical bonding. This correlation can be formulated with the MO model shown in Figure 9. Corrections to this approach, as well as the quantitative theoretical analysis of polarizabilities will not be discussed here, as they belong to the domain of theoretical quantum chemistry.[39]

From a chemical standpoint, the following model is appropriate: A Ga_NAs_M cluster with an even number of valence electrons $3N+5M$ (such as Ga_3As_3 in Figure 9) has $s=(3N+5M)/2$ ground-state MOs $\Phi_1, \Phi_2, \ldots, \Phi_k, \ldots, \Phi_s$ and infinitely many excited-state MOs $\Phi_{s+1}, \Phi_{s+2}, \ldots, \Phi_i, \ldots$. The energy of the cluster is calculated by adding the corresponding MO energies $E_1 \le E_2 \le E_3 \le \ldots$ according to $E = n_1E_1 + n_2E_2 + \ldots$, where $n_1, n_2, n_3, \ldots$ represent the occupation of the MOs $\Phi_1, \Phi_2, \Phi_3, \ldots$. In any given electronic state of a cluster, the occupation number n_t ($t = 1, 2, 3, \ldots$) takes on one of the values 0, 1, or 2. In the ground-state configuration of the cluster, shown on the left in Figure 9, the occupation numbers of the ground-state MOs are $n_k = 2$ and those of the excited-state MOs $n_i = 0$. Configurations for electronically excited states can be generated from this ground state by moving an electron from a ground-state MO Φ_k into an excited-state MO Φ_i (that is, by the transition $\Phi_k \rightarrow \Phi_i$). Such one-electron transitions can be used to generate all excited states (configurations) of the cluster from the ground state.

In the context of this description, the occupation of a ground-state MO Φ_k by $n_k = 2$ electrons means that a chemical bond is formed that stabilizes the cluster. The ground-state energy of the cluster can thereby be taken as the sum $E = 2E_1 + 2E_2 + \ldots + 2E_s$ of the energies $2E_k$ of all chemical bonds in the cluster. On this basis, the polarizability of a cluster can be correlated with its chemical bonds. One envisions that the chemical bonds are polarized in the z direction by the action of an infinitesimally small electric field $d(\boldsymbol{E}_0)_z$. The force of this applied electric field then leads to a small probability that the bonding electrons occupy the excited-state MOs Φ_i. This would lead to a change in the electron density in the bonds. If the transition dipole moment $M_{ki} = \int \Phi_k^* \hat{\mu}_z \Phi_i d\tau$ is not equal to zero, this change in the electron density generates an induced dipole moment and thereby a polarization of the bond. The basis for this polarization is that a change of $d(\boldsymbol{\mu})_z = \alpha d(\boldsymbol{E}_0)_z$ in the induced dipole moment $(\boldsymbol{\mu})_z$ leads to a reduction of the ground-state energy E by an amount $dE = d\boldsymbol{\mu}_z(\boldsymbol{E}_{0z})$. When this energy gain is integrated, one obtains for the decrease in the ground-state energy $\Delta E = -\alpha_C(\boldsymbol{E}_0)_z^2/2$. Hence, the polarizability is related to the second derivative of the ground-state energy with respect to the electric field $(\boldsymbol{E}_0)_z$ by the formula $\alpha_C = -d^2E/d(\boldsymbol{E}_0)_z^2$. As the energy E of the cluster comprises the sum of the energies $2E_k$ of its chemical bonds, the polarizability, too, is composed of the sum $\alpha_C = \alpha_1 + \alpha_2 + \ldots + \alpha_s$ of the polarizabilities of its constituent chemical bonds $\alpha_k = 2d^2E_k/d(\boldsymbol{E}_0)_z$. The additivity of the bond polarizabilities does not mean, however, that the bonds are independent of each other. Each chemical bond is situated within the chemical environment of the other bonds. This means that each bond can only be polarized by small electron shifts into unoccupied MOs, while shifts of electrons into the occupied MOs of the other bonds are forbidden by the Pauli principle. Quantum theory has a surprisingly simple formalism with which to describe this behavior. Using quantum-mechanical perturbation theory,[5] one can derive the formula for the bond polarizability: $\alpha_k = \sum_{i=s+1}^{\infty} 4|M_{ki}|^2/(E_i - E_k)$.[40] The summation takes into account all transitions $\Phi_k \rightarrow \Phi_i$, which can contribute to the polarization of the bond, because $M_{ki} \neq 0$. Usually one replaces the transition dipole moments M_{ki} by the oscillator strengths $f_{ki} = 2|M_{ki}|^2 m_0(E_i - E_k)/e^2\hbar^2$ known from spectroscopy, where m_0 is the rest mass of the electron in a vacuum. One thus obtains the formula (5),

$$\alpha_k = \sum_{i=s+1}^{\infty} 2\frac{e^2\hbar^2}{m_0}\frac{f_{ki}}{(E_i - E_k)^2} \qquad (5)$$

which describes the close relationship between spectroscopic properties of the cluster and the polarizable chemical bonds it contains. Every single bond polarizability α_k can therefore be correlated with excited-state MOs Φ_i, which are connected to the bonding MO Φ_k by dipole-allowed transitions ($f_{ki} > 0$). These transitions are shown schematically (dashed arrows) in Figure 9 for a selected bonding MO Φ_k. Each of these transitions contributes to the bond polarizability. Transitions into the ionization continuum need to be taken into account as well.

For clusters with an odd number of valence electrons, one obtains $s - 1 = ((3N+5M) - 1)/2$ bond polarizabilities and the polarizability $\alpha_s = \sum_{i=s+1}^{\infty} e^2\hbar^2 f_{si}/(E_i - E_s)^2 m_0$ of the radical electron. This additional polarizability of the radical electron is not the sole unusual characteristic of the open-shell clusters. The open shell allows the additional transitions $\Phi_k \rightarrow \Phi_s$ into the singly occupied HOMO. These transitions increase the bond polarizabilities by the amount $\Delta\alpha_k = (e^2\hbar^2/m_0)f_{ks}/(E_s - E_k)^2$.

For closed-shell clusters, the polarizabilities per atom shown in Figure 8 can be converted into mean bond polarizabilities by simply calculating the polarizability per electron pair, that is, $\bar{\alpha}_B = \alpha_C/((3N+5M)/2) \approx \alpha_C/2(N+M)$. Figure 8 indicates that the bond polarizability for closed-shell clusters is about 2.3 Å^3. If the radical electron is formally considered "half" a bond, the mean bond polarizability for open-shell clusters typically increases by 1 Å^3. This makes clear how a single defect electron can affect the chemical bonds and change a semiconductor cluster with up to 18 atoms into a metal-like cluster.[40] This is probably due to the strong shielding of the Coulomb potentials by the readily polarizable radical electron. The electrons are then not as strongly localized at the atomic cores or between atomic centers. Consequently, the bond polarizabilities increase, which in turn causes a further weakening of the Coulomb potentials. This transition from more strongly localized cova-

lent bonding to more delocalized metallic bonding yields the proper conditions for the earlier mentioned electron gas model (jellium model)[7] for metal clusters. It is, however, unrealistic to expect a perfect Coulomb shielding and free electron movement with the electron rest mass in a vacuum m_0. In fact, a correction is necessary for the alkali metals and is achieved by introducing an effective electron mass. The sequence of values for the alkali metals is enlightening. For Li $m_{eff}/m_0 = 1.33$, for Na 0.965, for K 0.86, for Rb 0.78, and for Cs 0.73: that is, for Na m_{eff} is approximately equal to m_0. A more detailed analysis[41,42] shows this to be due to a coincidental compensation of several effects. Nevertheless, Na_N clusters are considered ideal model systems for metal clusters, as solid state and cluster physicists[7,12] are more interested in the motion of electrons in fixed chemical environments. The main task of a description for physical chemistry must be to treat the cluster-size dependence of the chemical bonding as an additional variable and to study the consequences of this treatment on the electronic properties of the clusters. Hückel theory is a suitable starting point for this task. It can be employed effectively to describe orbital interactions of solid-state-like[19b,43,44] and molecular[45] chemical bonds.

2.1.2. *Bond Polarizabilities in Solid Si and Si_N Clusters with $N \approx 100$ Atoms*

Figure 10 shows the polarizabilities per atom $\bar{\alpha}_C = \alpha_C/N$ measured for silicon clusters. It is apparent that the bond polarizabilities of clusters with $N+M \approx 100$ are significantly smaller

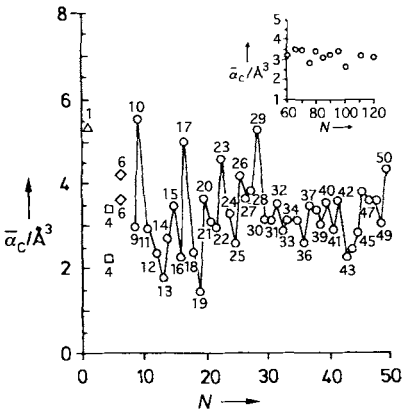

Figure 10. Polarizabilities per atom $\bar{\alpha}_C$ of Si_N clusters (circles). Inset: values for large Si_N clusters. Squares and diamonds: polarizabilities calculated from theory according to Rubio et al. [4] for the two isomers of Si_4 and Si_6 from Figure 1d). The two upper values belong to D_{2h} and D_{4h} symmetry of the two clusters Si_4 and Si_6, respectively. Triangle: theoretical values for the atom [31].

than those found for the solid state. The mean bond polarizability $\bar{\alpha}_{B,C}$ in the cluster is determined by dividing the experimentally found polarizability by the number of bonds present. The bond polarizabilities of large silicon clusters with $N \approx 100$ and $R \approx 0.8$ nm lie around 1.6 Å^3 and are therefore significantly smaller than the bond polarizability $\bar{\alpha}_{B,F} = 1.85$ Å^3 of the chemical bonds in the solid state, which can be calculated from the Clausius–Mosotti relationship [Eq. (4)] and the dielectric constant $\varepsilon = 12$. On first glance, it could be assumed that the changed bond polarizability mirrors the transition from the solid-state-like bonding structure to a more molecular bonding. A more detailed consideration, however, shows that this conclusion must be somewhat modified. The simple spatial confinement of a solid-state-like network of chemical bonds is sufficient to explain the observed bond polarizability: first one considers how the dielectric properties of a semiconductor can be derived from its chemical bonds. The electric susceptibility χ of a solid is defined by the linear relationship $\boldsymbol{P} = (\chi/4\pi)\boldsymbol{E}$ between the induced dipole density $\boldsymbol{P}$ and the electric field strength $\boldsymbol{E}$.[12d] The induced dipole moments stem from the polarizable chemical bonds between the semiconductor atoms. To quantify this bond polarization,[19c] each bond between two neighboring Si atoms μ and ν is assigned a valence bond orbital (VB) $\boldsymbol{\Phi}_k = (\phi_\mu + \phi_\nu)/\sqrt{2}$, which is formed by two overlapping sp^3 hybrid orbitals ϕ_ν and ϕ_μ. The antibonding orbital (VAB) is constructed analogously as $\boldsymbol{\Phi}_i = (\phi_\mu - \phi_\nu)/\sqrt{2}$. For each of the $s = 2N$ valence bonds between pairs of atoms in the crystal one thus obtains one VB and one VAB. The s VBs $\boldsymbol{\Phi}_1, \boldsymbol{\Phi}_2, \ldots, \boldsymbol{\Phi}_s$ and s VABs $\boldsymbol{\Phi}_{s+1}, \boldsymbol{\Phi}_{s+2}, \ldots, \boldsymbol{\Phi}_{2s}$ form a basis for an approximate description of the bonding in the solid state. If the overlap of the VB of one bond with the VBs and VABs of all other bonds is neglected, the bond polarizability is only described by the two electrons in the VB in question and their transitions into the VAB. In this purely local description, the VBs all have the same energy $E_1 = E_2 = \ldots = E_s$, as do the VABs ($E_{s+1} = E_{s+2} \ldots = E_{2s}$). The difference between the VAB and VB energies, which stems from the orbital interaction of the two sp^3 orbitals ϕ_ν and ϕ_μ, is termed $2E_{B,loc}$. With this approximation for the chemical bond, an expression for the static electric susceptibility can be derived,[19d] which can be written as $\chi_{B,loc}(0) = \hat{n}_B e^2 g^2/6E_{B,loc}$. Here, $\hat{n}_B$ stands for the density of the bonds, and g for the lattice constant. For silicon, the values obtained are $E_{B,loc} = 2.98$ eV, $g = 2.35$ Å^3, $\hat{n}_B = 1 \times 10^{23}$ cm^{-3}, and $\chi_{B,loc} = 0.45$; that is, $\varepsilon_{loc} = 1 + 4\pi\chi_{B,loc} = 6.58$.[19e] The value calculated thus for $\varepsilon_{B,loc} = 6.58$ is much smaller than the experimental value (12). Apparently, a more detailed theoretical treatment of this problem is required. The next best approximation takes into account the transitions and orbital interactions between VB and neighboring VABs. Within perturbation theory, the VB–VAB interaction with adjacent and once-removed bonds must be considered. One thus calculates a new corrected, partially delocalized VB, that has been termed an extended bond orbital.[19f] The occupation probability density for this partially delocalized VB is shown schematically in Figure 11a. The partial delocalization is reflected in a sort of corona, which has formed around the center of the bond. In the same fashion, one can obtain a corrected extended VAB. The calculation of these corrections requires a quantum-mechanical perturbation calculation and yields a correction factor for the susceptibility. In solid-state theory, this factor is usually represented by a number $\gamma^2 > 1$. I will use the same nomenclature and correlate the high experimental susceptibility of silicon with the partial delocalization of the chemical bonding in the solid. The susceptibility can be written as $\chi_{B,deloc} = \gamma^2_{deloc}\hat{n}_B e^2 g^2/6E_{B,loc}$, where the number γ^2_{deloc} acts as the correction factor. For silicon, the values for the experimental dielectric constant $\varepsilon = 12$ and $\varepsilon_{loc} = 6.6$ leads to a value for γ_{deloc} of $((\varepsilon-1)/(\varepsilon_{loc}-1))^{1/2} = 1.4$. For other semicon-

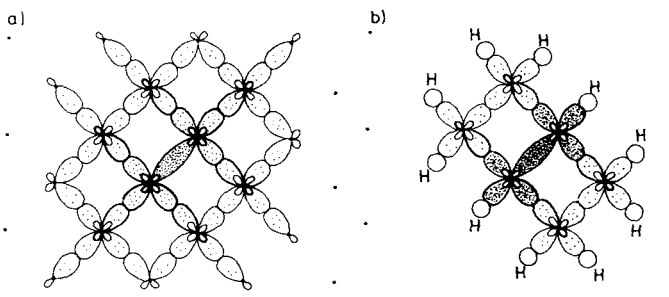

Figure 11. a) Schematic representation of the environment of a Si–Si bond in the solid state. The density of the dots represents the probability of locating the bonding electrons at any given point. These electrons can also occupy the VABs of neighboring bonds. The corresponding probability for an immediately neighboring VAB is about 3%, and still about 1% for a once-removed VAB. b) The extent of the chemical bond is significantly reduced in nanocrystallites.

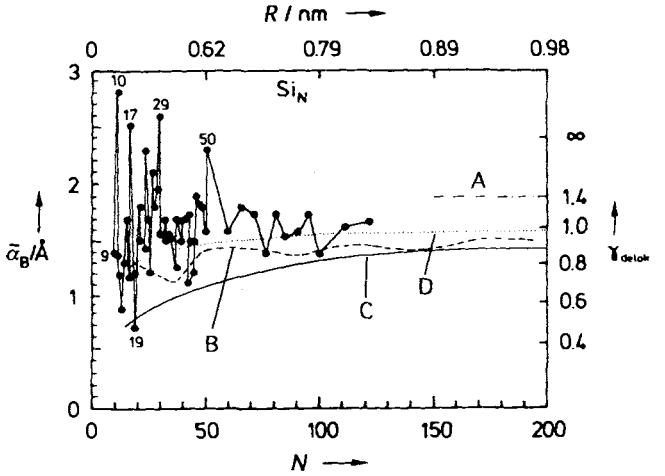

Figure 12. Comparison of the mean bond polarizabilities $\bar{\alpha}_B$ of free Si_N clusters (black dots) with the value for the solid state according to ref. [4] (A, ·····) and the theoretical results for the nanocrystallites: Hückel theory [46] (B, – – –), quantum well model I [48] (—), and quantum well model II [49] (· · · · ·).

ductors, the values fall typically within the range between $\gamma_{deloc} = 1.13$ for diamond and 1.85 for indium antimonide.[19c] These values imply a weaker delocalization for the bonding in diamond and a more strongly delocalized bonding in indium antimonide. The polarizability $\bar{\alpha}_{B,F}$ is connected to the dielectric constant by the expression of Clausius and Mosotti [Eq. (4)]. The value $\varepsilon = 12$ (that is, $\gamma_{deloc} = 1.4$) corresponds to a mean bond polarizability of $\bar{\alpha}_{B,F} = 1.85$ Å^3. The value for $\bar{\alpha}_{B,F,loc}$ of 1.61 Å^3 (valid for $\varepsilon = 6.58$, which represents the idealized, purely localized bonding with $\gamma_{deloc} = 1.0$) is correspondingly smaller. Interestingly, this value is in very good agreement with the experimental value $\bar{\alpha}_{B,F,loc} = 1.6$ Å^3 found for large clusters of $N \approx 100$ atoms. This agreement can be understood within the framework of the concepts of chemical bonds and their polarizabilities that have been developed here, as the partial delocalization of the chemical bonds must decrease together with the cluster size. This situation can be visualized by imagining a cluster that has been "cut" out of the solid-state bonding structure shown in Figure 11a. As simplification the broken local Si–Si bonds are taken to be saturated, for example with H atoms, to stabilize the structure. This is shown schematically in Figure 11 b. In this way, a small Si_NH_M crystallite has been generated.[46] The average number of nearest and next-nearest neighboring Si–Si bonds is reduced in this crystallite relative to the solid state. Consequently the delocalization parameter is reduced from the solid-state value of $\gamma_{deloc} = 1.4$ to, in extreme cases, $\gamma_{deloc} = 1.0$ in the cluster. Exactly this modification for the cluster explains the approximate agreement between $\bar{\alpha}_{B,C}$ and $\bar{\alpha}_{B,F,loc}$. The same result is obtained from a detailed Hückel calculation for Si_NH_M nanocrystallites.[46] The corresponding bond polarizabilities are shown in Figure 12. It is clear that they agree well with the experimental results for the large silicon clusters and that they correspond to a delocalization parameter γ_{deloc} of about 1.0 in our simple bonding model.

It is important to note that the changes in the bond polarizability discussed above are correlated to the known size quantization effect in the absorption spectrum. Those readers versed in the electrodynamics of continua will realize that this correlation stems from the Kramers–Kronig theorem,[12b] which relates static and dynamic polarizabilities or susceptibilities. For the experimental scientist it is helpful to develop this correlation with reference to an actual model. In the solid state, the energies $E(\boldsymbol{k})$ of the electron wave MOs having the wave vector $\boldsymbol{k}$ are so close to each other that one does not speak of energy levels but of energy bands.[44] In semiconductors, all valence band MOs are occupied by two electrons, while the conduction band MOs are empty (Figure 13a). The lower edge of the conduction band $E_c(\boldsymbol{k})$ is separated from the upper edge of the valence band $E_v(\boldsymbol{k})$

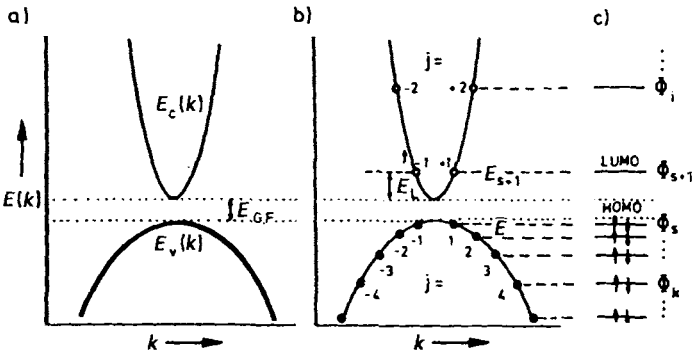

Figure 13. a) Two-band model of an infinitely extended semiconductor with conduction $E_c(k)$ and valence bands $E_v(k)$. b) Simple model for the quantization of the radial wave vector k and the energies for a spherical semiconductor cluster. One can associate each discrete value of k_j with standing spherical waves of radial wavelengths $\lambda_j = 2\pi/k_j$, which represent the MOs in c).

by the band gap (HOMO–LUMO gap), $E_{G,F}$. In solid state theory, an approximate expression for the course of a band in an isotropic semiconductor can be obtained by expanding the function $E(k) = E(|\boldsymbol{k}|)$ into a Taylor series according to Equation (6) for the magnitude of the wave vector $\boldsymbol{k} = |\boldsymbol{k}|$ around

$$E(k) = E(k)_{k=0} + (1/2!)(\partial^2 E(\boldsymbol{k})/\partial k^2)_{k=0} k^2 + \ldots \quad (6)$$

$k = 0$ and terminating the series after the quadratic term. The curvature of the band at $k = 0$ defines an effective mass. The curvature of the conduction band defines the electron mass $m_{eff,e} = \hbar^2/|\partial^2 E_c(\boldsymbol{k})/\partial \boldsymbol{k}^2|_{k=0}$, while that of the valence band defines the mass of the hole $m_{eff,h} = \hbar^2/|\partial^2 E_v(\boldsymbol{k})/\partial \boldsymbol{k}^2|_{k=0}$. On use of the two-band model, the static susceptibility of the semi-

conductor can be calculated according to D. R. Penn.[47] The electric susceptibility of the solid is expressed as $\chi = 2\hbar^2 e^2 \hat{n}_B / m_0 E^2_{G,Penn}$ and is therefore indirectly proportional to the square of the excitation energy $E_{G,Penn}$ required to generate excited electron waves within the semiconductor. The band gap $E_{G,Penn}$ can be empirically determined by the energy $\hbar\omega_{G,Penn}$, which describes the center of the absorption spectrum of the Si crystal.[47] This approach takes into account that the complicated band structure of the semiconductor is approximated by only two bands. For silicon, the literature cites values for $E_{G,Penn}$ of 4.7 eV, significantly above the regular band gap for Si of $E_{G,F} = 1.2$ eV. It is possible to transfer the two-band model for the electric susceptibility of semiconductors to clusters as well.[48] To do this, one envisions the electron waves in a spherical potential well of radius R and with infinitely high walls. The wave functions are standing spherical waves, which have a node at the edge of the potential well and vanish outside this edge. This is possible only for certain discrete values for the radial wave vector $\boldsymbol{k}_j = j\pi/2R$ where $j = \pm 1, \pm 2, \pm 3, \ldots$, and those energies $E(\boldsymbol{k}_j)$ that are marked by dots or circles in Figure 13b. An exact three-dimensional analysis[17] of the state with $j = 1$ in the conduction band yields the localization energy E_L of Equation (3). The corresponding MO scheme in Figure 13c shows, in addition, that with increasing localization energy E_L, the difference in energy $E_{G,C} = E_{s+1} - E_s$ between the HOMO $\boldsymbol{\Phi}_s$ and the LUMO $\boldsymbol{\Phi}_{s+1}$ also increases as R decreases (that is, as k_1 increases). This energy difference can become significantly bigger than the solid-state value of $E_{G,F}$. The susceptibility therefore decreases sharply with a decrease in R (see quantum well model I in Figure 12). This tendency causes a blue shift of the absorption edge as $R \rightarrow 0$ and a decrease in the static bond polarizability according to Clausius and Mosotti [Eq. (4)]. The decrease in the susceptibility caused by the localization of the molecular orbitals in the potential well is also observed in a more detailed model (cf. quantum well model II in Figure 13).[49]

The size quantization effect in the bond polarizabilities observed in the molecular beam is also of technological interest as it affects the defect conductivity in nanostructured semiconductors.[46, 49] For this reason it is particularly important for the electrochemistry during etching of semiconductor structures, for example in the electrochemical preparation of nanostructured porous silicon.[50]

2.1.3 *Small Si_N Clusters with Individual Bond Polarizabilities*

In the case of smaller clusters, other effects on the bond polarizabilities become noticeable. The polarizabilities of these clusters are very specifically dependent on the cluster size and cannot be correlated with size quantization effects. In particular, these polarizabilities can also not be related to those of diamond-like structures. This statement is supported by quantum-chemical calculations for the clusters Si_4 and Si_6.[4] The polarizabilities for the two pairs of isomers shown in Figure 1d were calculated. The values obtained thus for the polarizabilities are included in Figure 10 and fit well into the curve for the measured values for $N > 8$. This shows how sensitively the polarizability depends on the chemical bonding in the cluster. The chemical bonding must change with the cluster size to stabilize the individual geometric structure for each new cluster size. As the size quantization effects in the static polarizability vanish with decreasing cluster size, it is interesting to study the corresponding change in the absorption spectra of the clusters. These experiments were performed on Ga_NAs_M clusters,[51, 52] because the corresponding cluster beams exhibit an unusually high intensity stability.

2.2. Absorption Spectroscopy of Isolated Semiconductor Clusters

The absorption spectra reflect the eigenvibrations of the dipole moment, which can be excited by the oscillating electric field of light. If the excitation frequency satisfies the condition $\hbar\omega = E_i - E_k$ for a dipole-allowed transition $\boldsymbol{\Phi}_k \rightarrow \boldsymbol{\Phi}_i$, the induced dipole moment vibrates in resonance with the oscillating electric field. One can imagine that every chemical bond has a specific, frequency-dependent polarizability $\alpha_k(\omega)$, which determines how strongly the bond can be polarized by the excitation frequency ω. Similar arguments are valid for the radical electron polarizability of open-shell clusters. However, with clusters a problem arises: even the absorption of a single quantum of light leads to a photodissociation.[24, 51, 52] This problem is related to the fact that the electronic transition occurs from a bonding into an antibonding orbital, which therefore destabilizes the cluster. The deflections of the cluster fragments (B and C in Figure 14) that are generated in such a photoinduced dissociation are very large, due to the kinetic energy released. As the probability of the fragments' reaching the narrow detection zone is negligible, only a weakening of the cluster signal along the beam axis is observed. However, this photodissociation enables size-selective absorption spectroscopy on the clusters under study.

2.2.1. *Absorption Spectra and Radical Electrons in Small Ga_NAs_M Clusters*

Figure 14 shows the experimental setup for the measurement of the photon absorption cross sections. The absorption of a photon leads to the photodissociation of the cluster. The cluster fragments B and C depart from the beam axis A upon dissociation, and an attenuation of the original intensity in the mass

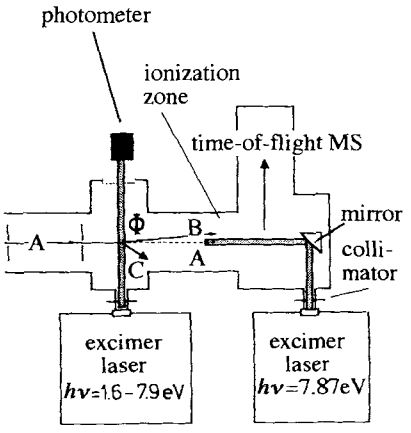

Figure 14. Experimental set-up for the measurement of absolute absorption cross sections of Ga_NAs_M clusters. The clusters fly along path A, fragment into the pieces B and C after absorption of a photon and miss the collimated ionization laser beam.

spectrum is observed when the excitation laser is turned on. This effect allows the determination of the absolute cross section $\sigma_{abs}(X)$ for the photodissociation of a cluster of size X. First the cluster beam intensities $I(X)$ and $I_0(X)$ are determined for the experiment with and without incident laser light. According to the quantum theory of absorption processes,[43, 51] the absolute cross section is calculated according to $\sigma_{abs} = (1 - I(X)/I_0(X))/\Phi$. The photon flux Φ in the interaction zone can be measured by photometer (Figure 14). The five absorption energies $\hbar\omega = 1.6, 3.5, 4.0, 5.0, 6.4$ eV are accessible in this experiment. For a photon energy of $\hbar\omega = 6.4$ eV, the photoionization cross section must be taken into account as well. This can be done by turning off the ionization laser and counting the cluster cations generated by the excitation laser. The measured photoionization yields for the isolated clusters can be a factor of 100 higher than those found for the solid state.[51] In contrast, the fluorescence yields are very low. The fluorescence of a range of clusters with between 3 and about 100 atoms was examined as a possible third reaction pathway.[51, 52] The fluorescence yields in the entire wavelength region from 400 to 900 nm are smaller than 3% and therefore much smaller than that found for GaAs crystals, which show yields of up to 99%. They are also significantly smaller than the yields for semiconductor colloids[1] and ligand-stabilized polyhedral semiconductor molecules.[53] The different chemical bonding in the isolated semiconductor clusters apparently permits a nonradiative relaxation. This conclusion is also supported by theoretically calculated potential curve schemes for electronically excited states of very small semiconductor clusters such as In_2Sb.[54]

The absorption cross sections per atom $\bar{\sigma}_{abs,C} = \sigma_{abs}/X$ for small clusters are depicted in Figure 15a for three cluster sizes and for a range of discrete photon energies. The dipole-allowed transitions shown in Figure 9, which contribute to the bond and radical electron polarizability, become noticeable in these absorption spectra. It is striking that the intensity of the absorption changes significantly with the cluster size. One observes that the absorption by the radical electron for all clusters with $X = 5$ to 11 (shown in Figure 15 for 5–7) is enhanced over the entire energy range. There are no bands in the spectra, however, that could be directly assigned to the radical electron. Such bands can be observed, for example, in salt clusters with an excess electron, such as $Na_{N+1}F_N$.[6] This leads us back to the concept, developed in Section 2.1.1, that the radical electron in the Ga_NAs_M clusters can effect a transition to a more metallike bonding. In this metallic bonding, the radical electron polarizability α_s does not only contribute directly to the polarizability of the cluster, but also enhances the bond polarizabilities α_k by increasing the corresponding oscillator strengths f_{ki} according Equation (5).

2.2.2. Optical HOMO-LUMO Band Gaps of Large Ga_NAs_M Clusters with About 80 Atoms and of Colloids

Figure 15b shows the absorption spectrum of Ga_NAs_M clusters with 80 atoms. For comparison, a spectrum calculated from the solid-state dielectric constant $\varepsilon(\omega)$ with Mie theory is shown as well.[51, 52] It is apparent that the increase in the absorption is blue-shifted relative to the edge expected from the solid, as expected from the size quantization effect (cf. Figure 13). For

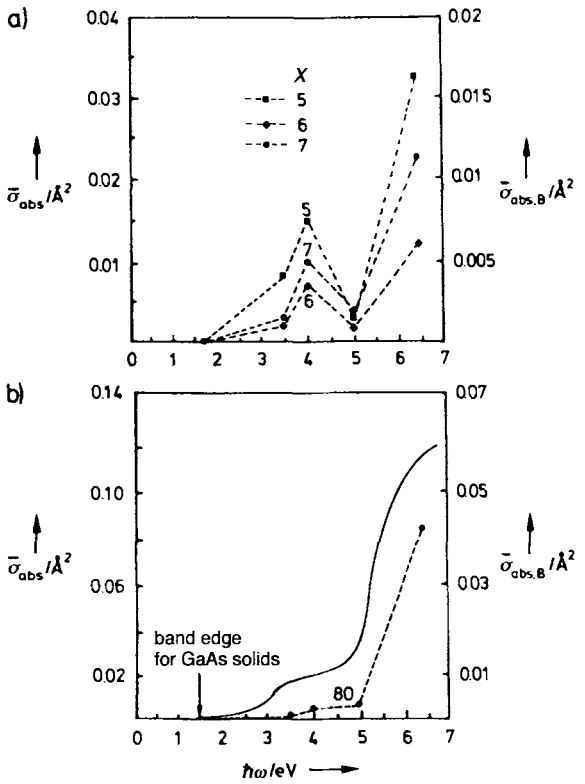

Figure 15. Mean UV/Vis absorption cross sections per atom $\bar{\sigma}_{abs}$ and per bond $\bar{\sigma}_{abs,B}$ for three small Ga_NAs_M clusters ($X = N+M$) (a) and for large clusters with $X = 80$ atoms (circles and dashed line). For comparison, the absorption spectrum of a solid-state-like GaAs sphere composed of 80 atoms, as calculated with Mie theory [51], is shown as well (solid line).

semiconductor colloids it is customary to estimate an effective optical HOMO–LUMO gap $E_{G,C}$ from optical spectra and plot it as a function of the colloid diameter, in order to quantify the observed blue shifts. The result of such an estimate of the effective optical HOMO–LUMO energy is plotted in Figure 16 for isolated clusters, GaAs colloids,[25] and for a GaAs molecule.[26] The detailed analysis is given in reference [51]. For the small clusters with a radical electron, one observes a reduced effective HOMO–LUMO gap. The theoretical calculations[22] mentioned earlier yield excited states for the clusters Ga_2As_3 and

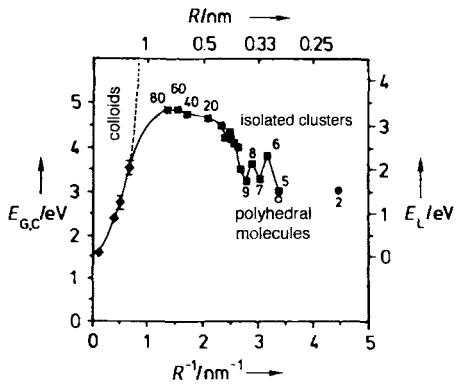

Figure 16. The size $E_{G,C}$ of the effective optical HOMO–LUMO band gap of Ga_NAs_M clusters as function of the cluster size $X = N+M$. The parabolic curve (dashed line) for the band gap energy according to the quantum well model by L. E. Brus [17] is shown for comparison. The calculated value for Ga_2As_3 [22], as discussed in the text, is also shown (circle at $X = 5$).

Ga_3As_2 with D_{3h} symmetry between 0.3 and 2.9 eV above the ground-state energy. In this calculation the most intense transition for Ga_2As_3,[22] for example, is found at $\hbar\omega = 2.8$ eV. One observes that the estimated effective optical HOMO–LUMO gap for $X = 5$ agrees fairly well with the theoretical value[22] for the intense transition at $\hbar\omega = 2.8$ eV.

The localization model [Eq. (3)] describes the results for larger colloids very well, when the solid-state value for the effective mass m_{eff} of $0.07\,m_0$ is used. For smaller particles, there are deviations from the simple localization model. Based on the usual Hückel models with size-independent parameters the HOMO–LUMO gap of a solid-state-like colloid is expected to rise steadily due to the decrease of the average bonding coordinates with a decrease in the radius R. Even though the HOMO–LUMO gaps of the larger clusters follow the values found for colloids fairly well, for clusters with less than 60 atoms the opposite behavior is observed. Hence, the Hückel parameters, and dependent on them the chemical bonding, must change markedly with the cluster size.

2.2.3. Optical HOMO–LUMO Band Gaps and the Transition from Solid-State-Like to Molecular Clusters

It has already been shown that the effective mass of the electrons in a solid can be viewed as a property of the chemical bonding. An approximate expression for the effective mass for electrons in the conduction band is given by the Hückel theory of the solid state[19a] [Eq. (7), in which the influence of the bond

$$m_{eff} = [1 + (2\gamma^2_{deloc} m_0 g^2 E^2_{B,loc}/\hbar^2 E_{L,F})]^{-1} m_0 \qquad (7)$$

polarity has been neglected as it is not relevant to the discussion below]. The formula shows that the effective mass can only be a constant for very large crystallites. It was shown when static polarizabilities were discussed that the solid-state-like bonding is already slightly modified by localization in the cluster. According to the bonding model developed in Section 2.1.2, a decrease in the radius R causes the parameter γ_{deloc} to change from the solid-state value γ_{deloc} for GaAs of 1.6 to 1.0. This slight change in the solid-state-like chemical bonding alone can lead, according to Equation (7), to a change in the effective mass upon a decrease in the cluster radius R. It is therefore useful to study how the effective mass m_{eff} in Equation (3) must be modified to yield agreement with experimental results. It must also be noted that with decreasing cluster radius R, the two-band model in Figure 13 is no longer valid in its strict theoretical solid-state definition. The values for the wave vector k_j become too large to be accounted for by the quadratic term of the Taylor series [Eq. (6)]. Thus, the effective mass of the electron can no longer be defined as the curvature of the conduction band $E_c(k)$ of a solid. Based on the foregoing discussion, however, we are particularly interested whether the concept of a localization energy can be maintained for small clusters by interpreting Equation (3) in the context of the quantum-chemical model of an electron in a box. The result of the adaptation of Equation (3) to fit the experimental results in Figure 16 is shown in Figure 17. The effective mass remains initially constant at the value for the solid state and then slowly increases with decreasing cluster radius R. For the smallest clusters, the effective mass m_{eff} reaches the value of the rest mass of the electron in a vacuum m_0. In the microscopic range, $m_{eff} \approx m_0$, as was initially assumed based on the polyhedral structures present. In the transitional range, m_{eff} follows a simple exponential expression [Eq. (8), where

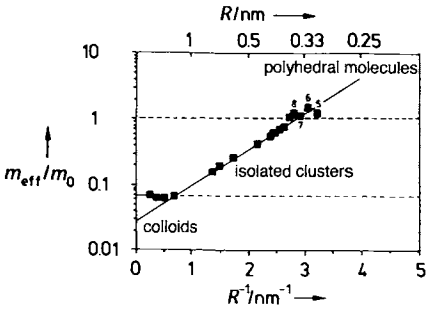

Figure 17. Effective mass based on the analysis of the experimental data of the effective optical HOMO–LUMO band gap $E_{G,C}$.

$$m_{eff} = m_U \exp(R_U/R) \qquad (8)$$

$m_U = 0.033\,m_0$ represents a characteristic mass and $R_U = 1.24$ nm a characteristic length] with a high degree of accuracy.

Based on these considerations it can be seen how the size quantization effects disappear together with the solid-state-like bonds. A small effective mass of the electron causes the most distinct size quantization effects for nanoparticles, based on Equations (2) and (3), and then leads to very significant changes in the smaller clusters so that the HOMO–LUMO gap can decrease to reach typical molecular values. A small effective mass is guaranteed by extended chemical bonds and strong orbital interactions in the semiconductor, that is, by large values of γ_{deloc} and $E_{B,loc}$. This forms the basis for the strongly increasing energy of the excited-state MOs upon increasing localization in the nanometer-sized clusters. This high localization energy cannot leave the chemical bonding unaffected as excited-state MOs and ground-state MOs are inexorably linked by quantum theory. This becomes particularly clear by the description in terms of extended VBs and VABs (see Section 2.2.1). In Hückel theory, the extended VABs take on the role of the Wannier orbitals φ.[19f,g] It was shown in Section 2.1.2 that not only the Wannier orbitals φ or the extended VABs in the cluster become localized, but that the localization also applies to the extended VB orbitals. This description makes it particularly clear that the spatial extent of an excited-state orbital is directly linked by quantum theory to the ground-state orbitals. When the excited-state orbital becomes more localized, the chemical bond is affected as well. The modification of the chemical bonding by the localization is already noticeable in the bond polarizabilities of nanometer-sized silicon clusters. Once sizes fall below the nanometer range, these modifications become so strong that the chemical bonding in its original form becomes unstable and different types of bonding arise. Quantum-mechanical simulations[55] on Si_N clusters with 20 to 45 atoms, for example, yield spherical structures (Figure 18) that resemble neither the solid-state-like structures of colloids nor the simple polyhedral structures of small clusters. They therefore support the concept developed here.

The high localization energy of the excited-state MOs can be reduced by changes in the chemical bonding upon a decrease in

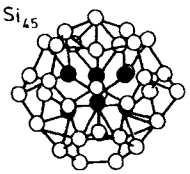

Figure 18. Suggested structure for a cluster composed of 45 silicon atoms [55]. For clarity, atoms in the interior of the cluster are depicted in black, while those on the surface are shown in white.

cluster size. This can be observed in the form of a red shift for the smaller clusters of 10 to 60 atoms (Figure 16). The strong decrease of the localization energy and the disappearance of the size quantization effects have been formally connected with the exponential increase of the effective mass. This enables a smooth transition $m_{eff} \rightarrow m_0$ with decreasing R in the relatively small interval $1.7\ nm > R > 0.4\ nm$.

3. Summary

The results of the experiments and the physical chemistry considerations can be graphically depicted by the diagram shown in Figure 19. It shows a comparison between the characteristic orbital radius a according to Equation (1) and the cluster

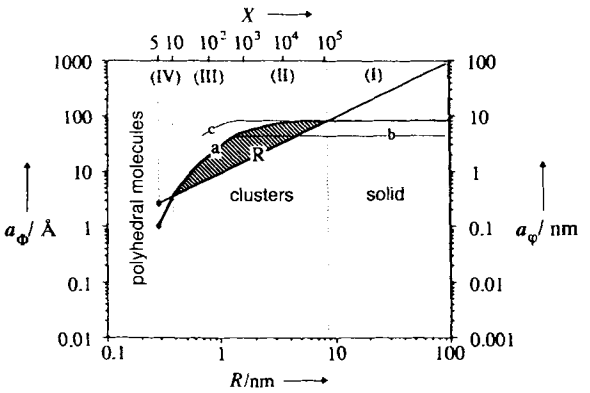

Figure 19. a) The characteristic electron orbital radius a as a function of the reciprocal cluster radius R. The corrections discussed in the text for the size dependence of the effective mass according to Figure 17 and of the dielectric constant as outlined in Section 2.1.2 were taken into account in Equation (1). For comparison, curve c shows the dependence of the Bohr radius on changes in the effective mass alone for the values $\varepsilon = \varepsilon_\infty = 11$, whereas curve b shows the corresponding effect for $\varepsilon = \varepsilon_{\infty,bulk} = 5$. In the transitional range between molecule and solid state structures, $a < R$ (hatched region), and size quantization effects occur. On the left edge, a takes on the typical extent of an excited-state orbital Φ (about 1–3 Å). On the right edge, as expected from its definition, a approaches the exciton Bohr radius of the Wannier orbital φ_1 (approximately 8 nm).

radius R for the GaAs system. In region (I), where $X > 10^5$ ($R > 8$ nm), the typical partially delocalized bonds of the macroscopic semiconductor with $\gamma_{deloc} = 1.6$ are found. This bonding yields the solid-state values $m_{eff} = 0.07\ m_0$ and $\varepsilon = 11$. One obtains $a < R$ and, hence, no significant localization energy E_L. This changes upon moving to region (II) where $10^5 > X > 10^3$ ($8\ nm > R > 1.7\ nm$). The extended chemical bonds of the semiconductor are slightly modified by localization in the cluster. The delocalization parameter γ_{deloc} decreases from right to left in region (II) from $\gamma_{deloc} = 1.6$ to about 1.0. This causes a decrease of ε from 11 to about 5. Although the solvation energy E_S in Equation (3) increases by a factor 11/5, it remains negligible with respect to the localization energy E_L. The effective mass remains at its solid-state value of $m_{eff} = 0.07\ m_0$. Under these conditions, one finds particularly strong size quantization effects, as $a \gg R$. This implies a large localization energy because the orbitals φ must be strongly compressed to fit into the cluster. In region (III), where $10^3 > X > 10$ ($1.7\ nm > R > 0.4\ nm$), the transition from the localized, solid-state-like bonding to a molecule-type bonding takes place. This leads to the exponential growth [Eq. (8)] of $m_{eff} = 0.07\ m_0$ to $m_{eff} \approx m_0$. The chemical environment of the excited electron changes so strongly, that the inertia of the electron increases by an order of magnitude, while the localization energy decreases correspondingly. One can envision a more electrophilic chemical environment for the electron, which is in agreement with the observed increase in electron affinity.[28] This change in the chemical environment accompanies an exponential decrease of the orbital radius a, so that for $X \approx 10$ ($R = 0.4$ nm), the orbital radius a [Eq. (1)] again becomes smaller than R, and size quantization effects disappear in region (IV) for polyhedral molecules with $10 > X \geq 5$. In this manner, it becomes possible to understand the transformation of the Wannier orbitals φ of the crystalline semiconductor into the excited-state molecular orbitals Φ in the polyhedral semiconductor clusters.

I wish to thank Prof. Dr. F. Hensel for his generous support of my work and for many discussions about chemical bonding in metals and semiconductors. Prof. W. A. de Heer is acknowledged for my time with him at the ETH Lausanne, where I learned about metal clusters. I thank Prof. Dr. H. Weller for the discussions about quantum size effects. I am particularly indebted to my students Dr. M. Weibels, Dr. J. Woenckhaus, Dr. R. Schäfer, S. Schlecht, S. Pokrant, my post-doctoral fellows Dr. E. Marceca, Dr. M. Sakurai, Dr. T. Hihara, as well as to our technician A. Rödig for their numerous contributions to the work presented here. The Deutsche Forschungsgemeinschaft (DFG) is acknowledged for a research stipend and the support of our work (SFB 383 'Disorder in Solids on Mesoscopic Scales' and the project 'Specific Phenomena in the Chemistry of Si'). The Fonds der Chemischen Industrie is also acknowledged for support. The Wacker-Chemitronic company (Burghausen) is acknowledged for the gift of a silicon crystal. I also thank the Klein & Becker company (Idar-Oberstein) for the free preparation of high-precision ceramic and crystal structural units.

Received: October 14, 1996 [A 192 IE]
German version: *Angew. Chem.* **1997**, *109*, 1458–1473

[1] H. Weller, *Angew. Chem.* **1993**, *105*, 43; *Angew. Chem. Int. Ed. Engl.* **1993**, *32*, 41.
[2] E. C. Honea, A. Ogura, C. A. Murray, K. Raghavachari, W. O. Spengler, M. F. Jarrold, W. L. Brown, *Nature* **1993**, *366*, 42; K. Raghavachari, C. M. Rohlfing, *J. Chem. Phys.* **1988**, 89, 2219; K. Raghavachari, *ibid.* **1986**, *84*, 5672; P. Ballone, W. Andreoni, R. Car, M. Parrinello, *Phys. Rev. Lett.* **1988**, *60*, 271.
[3] H. Bock, *Angew. Chem.* **1989**, *101*, 1659; *Angew. Chem. Int. Ed. Engl.* **1989**, *28*, 1627.
[4] A. Rubio, J. A. Alonso, X. Blase, L. C. Balbas, S. G. Louie, *Phys. Rev. Lett.* **1996**, *77*, 247.
[5] W. Kutzelnigg, *Einführung in die Theoretische Chemie, Bd. 2, Die chemische Bindung*, Verlag Chemie, Weinheim, **1975**.
[6] G. Rajagopal, R. N. Barnett, A. Nitzan, U. Landmann, E. C. Honea, P. Labastie, M. L. Homer, R. L. Whetten, *Phys. Rev. Lett.* **1990**, *64*, 2933.
[7] W. A. de Heer, *Rev. Mod. Phys.* **1993**, *65*, 611. Many of these experiments on clusters are the results of a long chain of developments that originated in the molecular beam experiments on atoms and molecules by Otto Stern in Hamburg in the 1920s. This is particularly true for the measurements of electric and magnetic dipole moments. See, for example, N. F. Ramsey, *Molecular Beams*, Oxford University Press, **1956**; *Atomic and Molecular Beams, Vol. 1 and 2*, (Eds.: G. Scoles, U. Buck), Oxford University Press, **1992**.

[8] N. F. Mott, *Rev. Mod. Phys.* **1968**, *40*, 677.
[9] R. Schäfer, S. Schlecht, J. Woenckhaus, J. A. Becker, *Phys. Rev. Lett.* **1996**, *76*, 471.
[10] S. Schlecht, R. Schäfer, J. Woenckhaus, J. A. Becker, *Chem. Phys. Lett.* **1995**, *246*, 315.
[11] S. Schuppler, S. L. Friedmann, M. A. Marcus, D. L. Adler, Y.-H. Xie, F. M. Ross, T. D. Harris, W. L. Brown, Y. J. Chabal, L. E. Brus, P. H. Citrin, *Phys. Rev. Lett.* **1994**, *72*, 2648.
[12] C. Kittel, *Einführung in die Festkörperphysik*, 8th ed., Oldenbourg, München, **1986**; a) Chap. 8; b) Chap. 11; c) p. 233; d) Chap. 13.
[13] N. Peyghambarian, S. W. Koch, A. Mysysowicz, *Introduction to Semiconductor Optics*, Prentice-Hall, Englewood, NJ, **1993**, Chap. 4 and p. 253.
[14] G. H. Wannier, *Phys. Rev.* **1937**, *52*, 191.
[15] W. Kutzelnigg, *Einführung in die Theoretische Chemie, Bd. 1, Quantenmechanische Grundlagen*, Verlag Chemie, Weinheim, **1975**, Chap. 4.
[16] G. A. Samara, *Phys. Rev. B: Condens. Matter* **1983**, *27*, 3494.
[17] L. E. Brus, *J. Chem. Phys.* **1983**, *79*, 5566; *ibid.* **1984**, *80*, 4403; R. Rosetti, R. Hull, J. M. Gibson, L. E. Brus, *ibid.* **1985**, *83*, 1406; L. E. Brus, *J. Phys. Chem.* **1986**, *90*, 2555.
[18] M. V. Rama Krishna, R. A. Friesner, *J. Chem. Phys.* **1991**, *95*, 8309; Y. Wang, A. Suna, W. Mahler, R. Kasowski, *ibid.* **1987**, *87*, 7315.
[19] W. A. Harrison, *Electronic Structure and Properties of Solids*, Freeman, San Francisco, **1980**; a) Chap. 6D; b) Chap. 2D; c) Chap. 4D; d) p. 113; e) Table 4.1; f) Chap. 3D; g) p. 87.
[20] K. Watanabe, T. Abe, T. Ogino, S. Takeda, *Sur. Rev. Lett.* **1996**, *3*, 389.
[21] H.-D. Försterling, H. Kuhn, *Moleküle und Molekülanhäufungen*, Springer, Berlin, **1983**, Chap. 6 and 7; S. Flügge, *Rechenmethoden der Quantentheorie*, 4th ed., Springer, Berlin, **1990**, Chap. 4, problem 41. The energy in Equation (3) corresponds to the localization energy for the problem of an electron in a hollow sphere with radius R and $m_{eff} = m_0$.
[22] M. Z. Liao, D. Dai, K. Balasubramanian, *Chem. Phys. Lett.* **1995**, *239*, 124.
[23] R. J. van Zee, S. Li, W. Weltner, Jr., *J. Chem. Phys.* **1993**, *98*, 4335.
[24] K.-D. Rinnen, K. D. Kolenbrander, A. M. DeSantolo, M. L. Mandich, *J. Chem. Phys.* **1992**, *96*, 4088.
[25] L. Butler, G. Redmond, D. Fitzmaurice, *J. Phys. Chem.* **1993**, *97*, 10750.
[26] G. W. Lemire, G. A. Bishea, S. A. Heidecke, M. D. Morse, *J. Chem. Phys.* **1990**, *92*, 121.
[27] S. C. O'Brien, Y. Liu, Q. Zhang, J. R. Heath, F. K. Tittel, R. F. Curl, R. E. Smalley, *J. Chem. Phys.* **1986**, *84*, 4074.
[28] C. Jin, K. J. Taylor, J. Conceicao, R. E. Smalley, *Chem. Phys. Lett.* **1990**, *175*, 17.
[29] M. A. Al-Laham, K. Raghavachari, *Chem. Phys. Lett.* **1991**, *187*, 13; L. Lou, P. Nordlander, R. E. Smalley, *J. Chem. Phys.* **1992**, *97*, 1858.
[30] T. P. Martin, *Angew. Chem.* **1986**, *98*, 197; *Angew. Chem. Int. Ed. Engl.* **1986**, *25*, 197.
[31] T. M. Miller, B. Bederson, *Adv. At. Mol. Phys.* **1977**, *13*, 1; T. M. Miller in *Atomic and Molecular Polarizabilities, CRC Handbook of Chemistry and Physics*, (Ed.: R. Lide), CRC, Boston, **1992**.
[32] V. V. Kresin, *Phys. Rep.* **1992**, *220*, 1.
[33] H. Scheffers, *Phys. Z. Sowjetunion* **1940**, *41*, 89.
[34] R. Köppe, Dissertation, Ludwigs-Maximilians-Universität, München, **1992**.
[35] a) *Z. Phys. D: At. Mol. Clusters* (*Proceedings of the ISSPIC8* **1996**, Copenhagen) **1997**, in press. b) L. C. Balbas, A. Rubio, J. L. Martins in [35a].
[36] N. F. Ramsey, A. Weis, *Phys. Bl.* **1996**, *52*, 859.
[37] W. D. Knight, K. Clemenger, W. A. de Heer, W. A. Saunders, *Phys. Rev. B: Conden. Matter* **1985**, *31*, 2539.
[38] M. Sakurai, S. Schlecht, J. Woenckhaus, R. Schäfer, J. A. Becker, *Z. Phys. Chem. (München)* **1996**, *193*, 109.
[39] H. J. Werner, W. Meyer, *Mol. Phys.* **1976**, *31*, 855.
[40] R. Schäfer, J. A. Becker, *Z. Phys. Chem. (München)* **1997**, in press.
[41] C. Kittel, C. Y. Fong, *Quantentheorie der Festkörper*, 3rd ed., Oldenbourg, München, **1989**, p. 203.
[42] F. S. Ham, *Phys. Rev.* **1962**, *128*, 2524.
[43] a) J. Berkowitz, *Photoabsorption, Photoionization and Photoelectron Spectroscopy*, Academic Press, New York, **1979**; b) J. C. Phillips, *Bonds and Bands in Semiconductors*, Academic Press, New York, **1973**.
[44] R. Hoffmann, *Angew. Chem.* **1987**, *99*, 871; *Angew. Chem. Int. Ed. Engl.* **1987**, *26*, 846.
[45] T. A. Albright, J. K. Burdett, M.-H. Whangbo, *Orbital Interactions in Chemistry*, Wiley-Interscience, New York, **1985**.
[46] M. Lannoo, C. Delerue, G. Allan, *Phys. Rev. Lett.* **1995**, *74*, 3415.
[47] D. R. Penn, *Phys. Rev.* **1962**, *128*, 2093.
[48] R. Tsu, L. Iroatti, J. F. Harvey, H. Shen, R. A. Lux, *Mat. Res. Soc. Symp. Proc.* **1993**, *283*, 437.
[49] L.-W. Wang, A. Zunger, *Phys. Rev. Lett.* **1994**, *73*, 1039.
[50] L. T. Canham, *Appl. Phys. Lett.* **1990**, *57*, 1046; V. Lehmann, U. Gösele, *ibid.* **1991**, *58*, 856.
[51] R. Schäfer, J. A. Becker, *Phys. Rev. B: Conden. Matter* **1996**, *54*, 10296.
[52] R. Schäfer, J. A. Becker, in [35a].
[53] Y. Kanemitsu, K. Suzuki, M. Kondo, H. Matsumoto, *Solid State Commun.* **1994**, *89*, 619; K. Furukawa, M. Fujino, N. Matsumoto, *Appl. Phys. Lett.* **1992**, *60*, 2744.
[54] K. K. Das, K. Balasubramanian, *J. Chem. Phys.* **1991**, *94*, 6620.
[55] U. Röthlisberger, W. Andreoni, M. Parrinello, *Phys. Rev. Lett.* **1994**, *72*, 665.

Although thus far disregarded, H-atom transfer between molecules is a key step in many dehydrogenations and hydrogenations, and may also take place in biochemical reactions with NADH/NADPH .

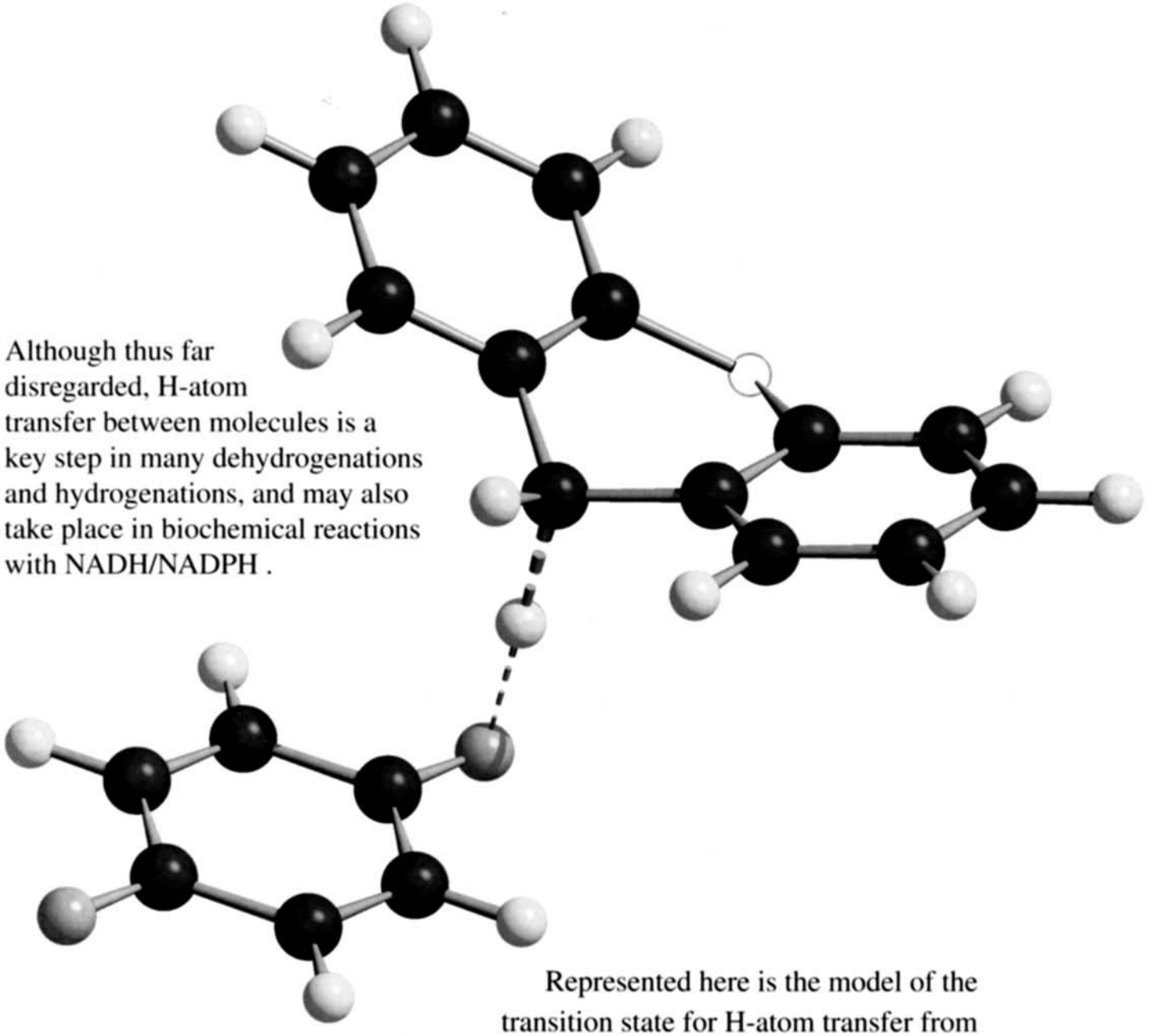

Represented here is the model of the transition state for H-atom transfer from 9,10-dihydroanthracene (X = CH_2), xanthene (X = O), or acridan (X = NH) to benzoquinone [Eq. (1)].

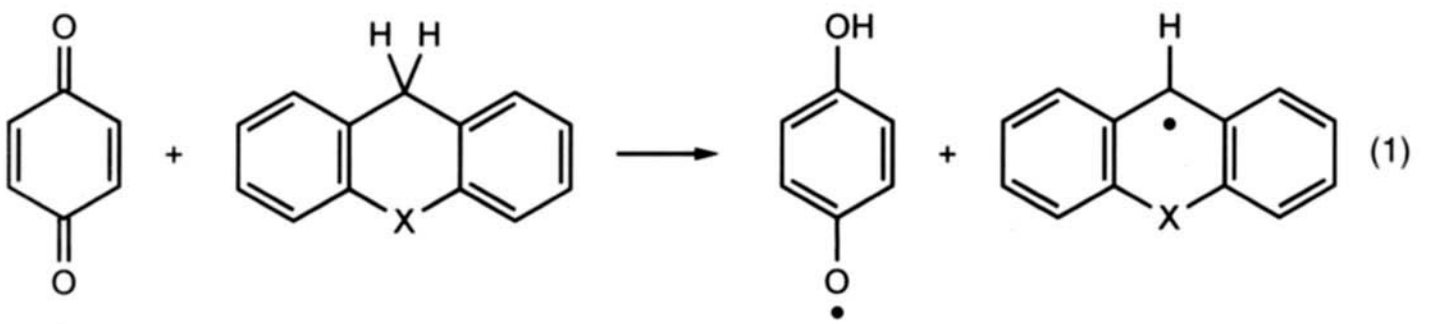

(1)

X = CH_2, O, NH

Uncatalyzed Transfer Hydrogenation and Transfer Hydrogenolysis: Two Novel Types of Hydrogen-Transfer Reactions

Christoph Rüchardt,* Matthias Gerst, and Jochen Ebenhoch

Dedicated to Professor Paul D. Bartlett on the occasion of his 90th birthday

Uncatalyzed transfer hydrogenations are H_2-transfer reactions in which donors that contain weakly bound hydrogen atoms undergo an H-atom transfer (retrodisproportionation) onto an acceptor containing unsaturated bonds such as C=C, C=O, C=N, N=N, or N=O. Transfer hydrogenolyses are reactions in which σ bonds are cleaved upon addition of H_2. These hydrogenations are terminated by H• transfer; they do not follow a radical-chain mechanism. The initial steps of both types of reactions, H-atom transfer, complement the bimolecular formation of 1,4-diradicals from alkenes or heteroalkenes within the scope of bimolecular radical formations (Molecule-Induced Radical Formation, MIRF). The title reactions play an important role in coal liquefaction, aromatization reactions with nitroarenes or quinones, and possibly biochemical dehydrogenations. This review focuses on mechanistic studies, structure–reactivity relationships, and current applications of these reactions.

Keywords: arenes · coal liquefaction · hydrogenations · radical reactions · reaction mechanisms

1. Introduction

In early 1992 while studying homolytic, thermal C–C cleavage reactions,[1, 2] we observed two unknown reactions, uncatalyzed transfer hydrogenation (1) and transfer hydrogenolysis (2). Both reactions are characterized by almost quantitative hydrogen transfer from 9,10-dihydroanthracene (DHA, **2**) to the respective substrate.

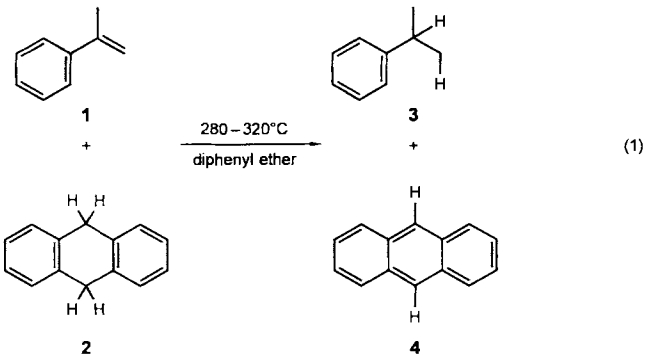

(1)

Whereas in reaction (1)[3] hydrogen is added across the π bond of α-methylstyrene (**1**), in reaction (2) a novel type of

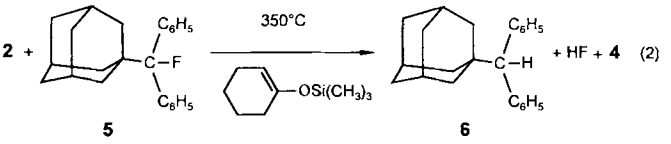

(2)

hydrogenolytic cleavage of a C–F bond leads to the formation of HF.[4] Control experiments to determine the thermal stability of **2** showed that it remains stable under the reaction conditions. Therefore, reactions (1) and (2) do not proceed by elimination and addition of elemental hydrogen,[5] but by a different pathway.

2. Transfer Hydrogenation

2.1. Mechanism

Various mechanistic possibilities exist for the uncatalyzed transfer hydrogenation (1) of α-methylstyrene (**1**, ≈0.1 M) with DHA (**2**, ≈1.0 M). In analogy to the dyotropic transfer reactions,[6, 7] the three pericyclic mechanisms (3)–(5) are theoreti-

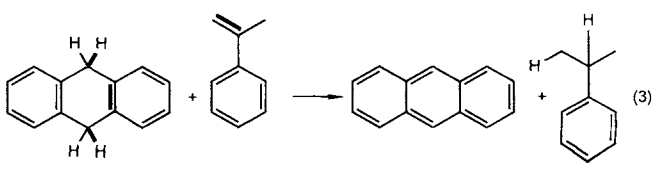

(3)

$[_\sigma 2_s + _\pi 2_s + _\sigma 2_s + _\pi 2_s]$-type

[*] Prof. Dr. C. Rüchardt, Dr. M. Gerst,[+] Dr. J. Ebenhoch[++]
Institut für Organische Chemie und Biochemie der Universität
Albertstrasse 21, D-79104 Freiburg (Germany).
Fax: Int. code +(761)203-5987

[+] New address: BASF AG, Kunststofflaboratorium, Ludwigshafen (Germany)

[++] New address: Wacker-Chemie, GmbH, S-R-G, Burghausen (Germany)

 © VCH Verlagsgesellschaft mbH, D-69451 Weinheim, 1997 0570-0833/97/3613-1407 $ 17.50+.50/0

cally possible.[6] The bonds involved in these pericyclic processes are accentuated in Equations (3)–(5).

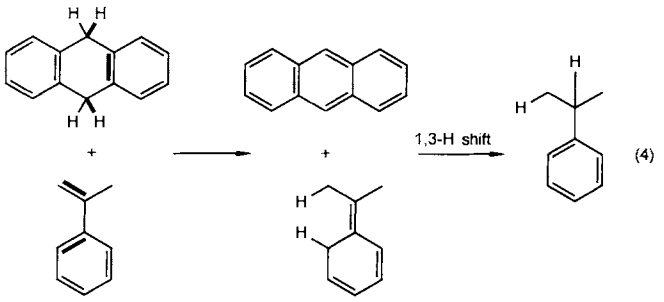

$[_{\sigma}2_s + {}_{\pi}2_s + {}_{\sigma}2_s + {}_{\pi}4_s]$-type

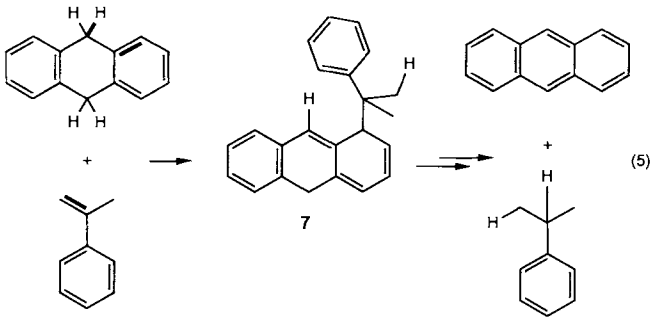

$[_{\sigma}2_s + {}_{\pi}2_s + {}_{\sigma}2_s]$-type (ene reaction)

According to the Woodward–Hoffmann rules, thermal reaction (3) between the ${}_{\pi}2_s$-bond of **1** and the $[_{\sigma}2_s + {}_{\pi}2_s + {}_{\sigma}2_s]$ bonds of **2** is symmetry forbidden. Reaction (4) between the ${}_{\pi}4_s$ bonds of **1** and the $[_{\sigma}2_s + {}_{\pi}2_s + {}_{\sigma}2_s]$ bonds of **2** is disfavored by approximately 15 kcal mol^{-1} compared to a multistep process and, therefore, does not need to be considered.[6, 8] The third pericyclic possibility is the ene reaction (5); **2** represents the ene component, and **1** functions as the enophile. Participation of a benzoidal C=C π bond postulated for this reaction type has not yet been observed. Furthermore, **1** is not a good enophile.[9] Since no ene products **7** were detected, it can be assumed that under the applied reaction conditions a rapid secondary reaction follows in which **7** undergoes quantitative homolytic decomposition to the 2-phenyl-2-propyl radical (**8**) and the 9-hydroanthryl radical (**9**), followed by their disproportionation. Enthalpically, the ene reaction should be disfavored over the retrodisproportionation.[9] As shown in control experiments methyl groups in positions 1, 4, 5, and 8 of **2** have only a small effect on the activation parameters such as, in particular, the entropy of activation.[10] This is atypical for the ene reaction, which is notoriously sensitive towards steric effects.[9] Consequently, the ene reaction can be ruled out as well.

It is also possible that the hydrogen transfer proceeds by a two-step mechanism, either as hydride transfer (6), which was first proposed by Braude and Linstead et al. for quinone dehydrogenations[11] and appears to be commonly accepted,[12] or as a radical retrodisproportionation (7) by transfer of an H atom leading to the formation of **8** and **9**.[3] The latter reaction pathway, which we prefer as a working hypothesis,[3] has occasionally been proposed for reactions for coal liquefaction[13] as well as the initiating step of chain reactions.[14, 15] However, it

C. Rüchardt

M. Gerst

J. Ebenhoch

Christoph Rüchardt, born in 1929, studied chemistry at the Universität München and the University of Georgia (M. S. degree), and completed his Ph.D. under Professor R. Huisgen in 1956 with studies on aliphatic diazoesters. Afterwards, he spent two years as a postdoctoral fellow at Harvard University with Professor P. D. Bartlett and at the California Institute of Technology with Professor J. D. Roberts. In 1963 he completed his habilitation studying radical-rearrangement reactions at the Universität München. In 1968 he accepted a position at the Universität Münster, and in 1972 at the Universität Freiburg, where he was rector from 1987 to 1991. His research interests include reaction mechanisms, in particular radical chemistry. He received the Adolf-von-Baeyer-Denkmünze from the Gesellschaft Deutscher Chemiker in 1983. He is a member of several academies and a recipient of the Bundesverdienstkreuz 1. Klasse.

Matthias Gerst, born in 1965, studied chemistry at the Universität Heidelberg and the Universität Freiburg, and received his Ph.D. in 1994 under Professor C. Rüchardt with the thesis Retrodisproportionation—A Novel Method of Radical Formation. In 1991 he worked at the Max-Planck-Institute für Polymerforschung in Mainz, and in 1992 joined the Kunststofflaboratorium at BASF AG. He has received stipends from the Fritzter-Meer-Stiftung, the Fonds der Chemischen Industrie, and the Verband der Chemischen Industrie as well as a prize from the Stifteverband fyr die Deutsche Wissenschaft and the Goedecke research award.

Jochen Ebenhoch, born in 1966, studied chemistry at the Universität Tübingen and the Universität Freiburg, and received his Ph.D. in 1996 under Professor C. Rüchardt with the thesis Transfer-Hydrogenations with 9,10-Dihydroanthracene. He joined Wacker-Chemie, GmbH in 1997.

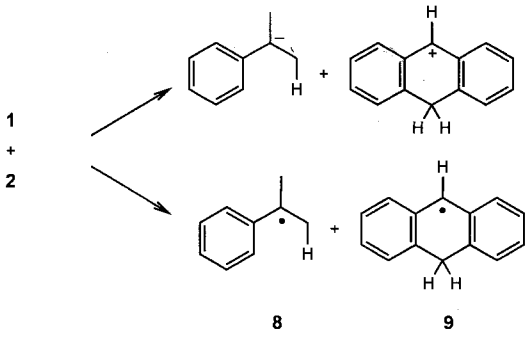

has not been experimentally proven nor defined in its application range. This reaction constitutes the reverse reaction of the disproportionation of two radicals, and, in contrast to the reverse reaction of the radical dimerization, thermal bond dissociation;[1] it is hardly known as an elemental reaction. For this reason, we prefer the name "retrodisproportionation" for this reaction over "molecular disproportionation", as it has been occasionally called.[16] The reaction is an example of the bimolecular radical-formation reactions that Pryor[16] referred to as "Molecule-Induced Homolysis", and others as "Molecule-Induced Radical Formation" (MIRF).[17]

This new reaction type in which weakly bound alkane hydrogen atoms are transferred to alkenes became primarily known by the spontaneous initiation of styrene polymerization (8) in

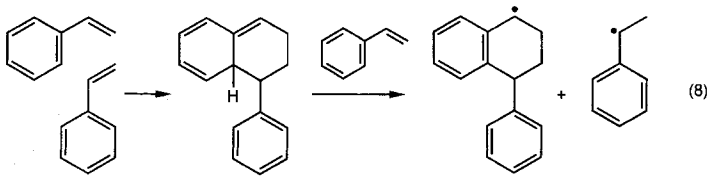

(8)

the absence of an initiator.[14] Retrodisproportionations have also been proposed for other reactions[18] such as the disproportionation of **2** and 2-ethylanthracene[19] or as the initiating reaction of the addition of alkanes to alkenes at elevated temperatures (ane reaction).[15] A reaction of great importance is the H-atom transfer of transition metal hydrides to alkenes, as first shown by Halpern et al.[20] Benson convincingly interpreted the transfer hydrogenation of ethene with cyclopentene at 380–500 °C in the gas phase as a two-step process with retrodisproportionation (9) as the initial step.[21] This suggestion was sup-

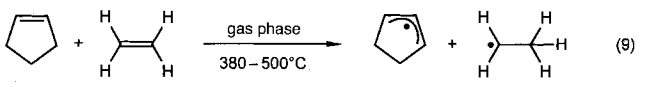

(9)

ported by the good agreement of the enthalpy of activation of $\Delta H^{\neq} = 42.8\ \mathrm{kcal\,mol^{-1}}$ with the thermochemically calculated reaction enthalpy ΔH_R of the first step (thermochemical kinetics),[21] as well as the entropy of activation $\Delta S^{\neq} = -15\ \mathrm{cal\,K^{-1}\,mol^{-1}}$. The calculated reaction enthalpy of $44.9\ \mathrm{kcal\,mol^{-1}}$ determined by Benson for reaction (9) from thermochemical data increases to $53.4\ \mathrm{kcal\,mol^{-1}}$ when the new, commonly accepted C–H bond energies and radical-stabilization energies are considered.[21c] Strictly speaking, the enthalpies must be compared at the same temperature. This surprising discrepancy of approximately $8\ \mathrm{kcal\,mol^{-1}}$ between ΔH^0 and $\Delta H^{\neq}$, and particularly the observation that $\Delta H^0 > \Delta H^{\neq}$, appear contradictory and do not seem to be consistent with the requirements of thermochemical kinetics.[21b] However, upon closer examination, and this is a direct result of our mechanistic studies of the retrodisproportionations, this observation becomes less contradictory.

A further point of discussion is whether the oxidation reactions of *tert*-benzylic hydrogen atoms with chromic acid,[22a] chromyl chloride,[22b] and permanganate[22c] or enzymatic H-activations[22b, d, e] can be included in this category from a mechanistic point of view. The relationship between the termination reactions of free radicals (dimerization and disproportionation) and the radical-forming reactions (homolytic bond dissociation and retrodisproportionation) is discussed here with the example of two ethyl radicals.[23]

The high rate constants of the dimerization and disproportionation steps, which are partially determined by the rate of diffusion of the reactants, influence the lifetime of free radicals. For the most part it is assumed that these termination reactions proceed without requiring any enthalpy of activation $\Delta H^{\neq}$.[25] This means that for the homolytic bond dissociation on the one hand and the retrodisproportionation on the other, the enthalpy of activation $\Delta H^{\neq}$ should be equal to the reaction enthalpy ΔH_R. The dotted line in Figure 1 B depicts the reaction coordinate of enthalpy ΔH in the case of two ethyl radicals. Entropically, the two radical-forming reactions are fundamentally different, because the change in number of particles is not the same for both reactions. This is demonstrated in Figure 1 A with the entropic reaction coordinate ΔS. In both reactions a radical pair is primarily formed; the dissociation of butane has a positive, and the retrodisproportionation a negative entropy. The dissociation of the radical pair to form free ethyl radicals proceeds with $\Delta S = +25\ \mathrm{cal\,K^{-1}\,mol^{-1}}$. The entropic reaction coordinate can also be reversed, starting with the ethyl radicals in the direction of the dimerization and disproportionation. Thus, it is apparent that the selectivity of the dimerization/disproportionation is generally controlled by entropy.[1, 24] For entropic reasons, the reaction coordinate of the free enthalpy ΔG (Figure 1 B) contains local maxima (transition states) for both the dimerization and the disproportionation, the geometric coordinates of which correlate to the entropy minimum.[24b] In principle the experimental enthalpies of activation $\Delta H^{\neq}$ of both termination reactions of alkyl radicals can be smaller than the respective reaction enthalpies ΔH_R.[26]

In the uncatalyzed transfer hydrogenation (1) of **1** ($\approx$0.1 M) with **2** ($\approx$1.0 M), which proceeds in greater than 98% yield at 280–300 °C (1),[27] retrodisproportionation (10) is very selectively followed by two known radical reaction steps. These include H transfer onto the cumyl radical **8** and disproportionation of two hydroanthryl radicals **9** (reactions (11) and (12) in Scheme 1).

Since these experiments are performed above the ceiling temperature, polymerization does not occur. The selectivity is dictated by the presence of the well-stabilized radicals **9**.[28] The reaction order with respect to **1** and **2** was one; therefore, the reaction does not represent a chain reaction with **9** as the chain carrier.[27] Moreover, increasing the concentration of **9** by

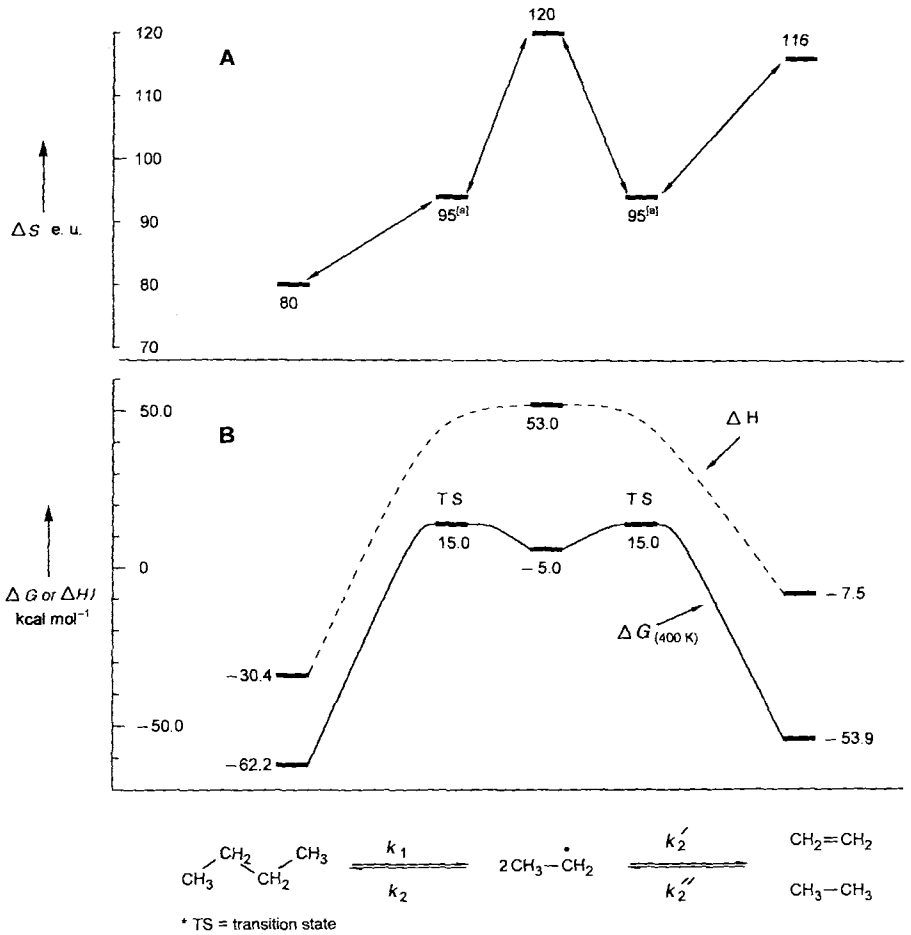

Figure 1. Reaction coordinate of entropy S (A) and of enthalpy H and free enthalpy G_{400K} (B) for the dimerization and disproportionation of ethyl radicals and the dissociation of butane, respectively, as well as the retrodisproportionation of ethane and ethene (calculated values) [23]; TS = transition state of radical-pair formation, e. u.: entropy units = 4.184 $JK^{-1}mol^{-1}$). [a] No conclusion should be drawn from this Figure concerning the selectivity of radical dimerization over disproportionation.

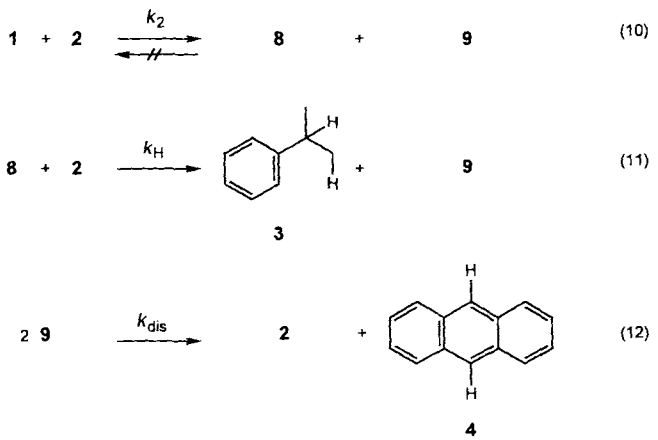

Scheme 1. Reaction mechanism of the retrodisproportionation of **1** (1.0 M) with **2** (1.0 M). The reaction was investigated in diphenyl ether at 270–320 °C.

adding either bifluorene[3] or anthracene (**4**)[19] did not result in a rate acceleration as expected for a chain reaction. Consequently, transfer hydrogenation proceeds stoichiometrically.

With 9,9,10,10-tetradeutero-9,10-dihydroanthracene ([D_4]-**2**) the H transfer with rate constant k_2 could be identified as the rate-determining step. [D_2]-cumene ([D_2]-**3**) was exclusively formed. When the reaction was stopped after approximately 80% conversion, no deuterium could be detected in the remaining **1**.[27] This observation proves that the retrodisproportionation is irreversible under these reaction conditions, and k_2 alone is rate-determining.[29]

Treating **1** with a tenfold excess of an equimolar mixture of **2** and [D_4]-**2** not only formed cumene (**3**, 48%) and [D_2]-**3** (11%) but also [D_1]-cumene ([D_1]-**3**, 41%) after 20% conversion (Scheme 2). Incompatible with the above-mentioned pericyclic mechanisms, this result is consistent with a radical mechanism. Accordingly, [D_1]-**3** was formed either from the cumyl radicals **8** with [D_4]-**2** as the radical scavenger or from [D_1]-**8** with **2** as the radical scavenger. Nondeuterated as well as mono- and dideuterated anthracene were identified as further reaction products, which excludes the possibility that **2** transfers both H atoms consecutively in one radical pair. At 300 °C, the primary kinetic isotope effect is $k_{2(H)}/k_{2(D)} = 2.1$ (see Table 4). Figure 1 B suggests that the transition state of the retrodisproportionation does not geometrically correlate to the free radicals or the radical pair, although the respective enthalpies of activation and reaction must be very similar. The H atom to be transferred is located between the participating C atoms; due to the small enthalpy difference between the radical pair and the transition state (TS, Figure 1 B) its exact location cannot be determined.[30] This explains that a primary kinetic isotope effect was determined with a value close to the highest possible expectation value, and, furthermore, that a linear alignment of the C−H···C axis should be expected.[30]

The difference of the enthalpies of activation $\delta\Delta H^{\neq}$ for the transfer hydrogenation and the transfer deuteration was experimentally determined to be 1.0 kcal mol^{-1} (see Table 4 and ref. [27]). With this value and an approximation equation the maximum kinetic isotope effect at 300 °C can be calculated to be $k_{2(H)}/k_{2(D)} = 2.7$,[31a] which correlates well with the experimental value. The activation parameters of the transfer hydrogenation and the transfer deuteration of **1** by **2** or [D_4]-**2** (see Table 4) provide the temperature dependency of the isotope effect. As expected the isotope effect of 2.5 at 250 °C is slightly higher than that of 2.2 at 350 °C.

Using approximately 20 rate constants k_2 for the reaction of **1** with **2** in a temperature range 250 to 320 °C, the activation parameters were calculated to be $\Delta H^{\neq} = 31.8$ kcal mol^{-1}, $\Delta S^{\neq} = -21.5$ cal $K^{-1}mol^{-1}$, and $\Delta G^{\neq}_{300\,°C} = 44.1$ kcal mol^{-1} (see Table 4).[3, 31b] The negative entropy of activation is in

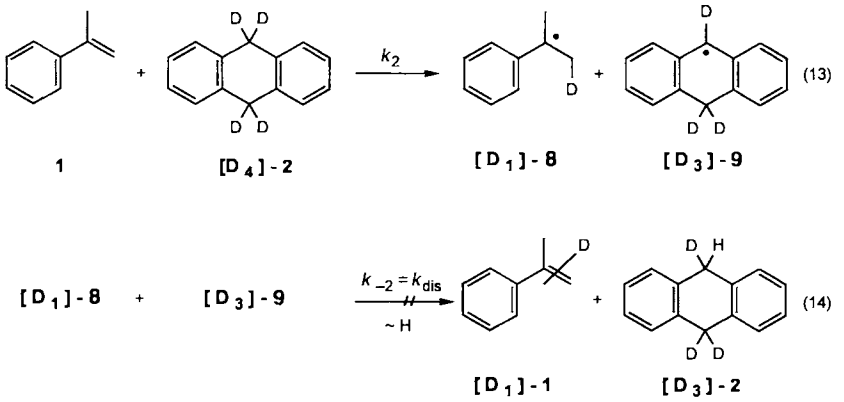

Scheme 2. Deuteration experiment as an analytical probe for the reverse reaction (v_{-2}).

agreement with the prediction of a second-order reaction. The enthalpy of activation of 31.8 kcal mol^{-1} agrees fairly well with the reaction enthalpy of $\Delta H_R = 38.7$ kcal mol^{-1} (298 K; see Table 4),[32] but this is another example of the above-mentioned unexpected phenomenon that ΔH^0 is larger than $\Delta H^{\neq}$. This supports the rate-determining character of H transfer from **2** to **1** as well as the postulated radical mechanism. The unexpected observation that $\Delta H^{\neq}$is smaller than ΔH_R, which was confirmed to varying extent in most of the retrodisproportionation reactions investigated to date (see also ref. [2a]), has also been verified for the thermolysis of bibenzyl[32d] and is consistent with the influence of entropy on the location of the transition states ($\Delta G^{\neq}$; Figure 1, Section 2.2.3). This phenomenon is probably partly due to the fact that the thermochemical reaction enthalpies were calculated for the gas phase at 25 °C, whereas the activation enthalpies were measured in solution at elevated temperatures. The equilibration of **2** and **4**, which was observed earlier by Stein et al.,[19] also follows an H-transfer mechanism and apparently does not have an impact on the reaction kinetics.

Attempts to prove the existence of a radical by ESR spectroscopy under the same reaction conditions remained unsuccessful. Due to the high rate constant of disproportionation (12), the stationary concentration of radicals **9** is apparently too low for this method. However, the ESR experiment was successful with xanthene (**10**) as the H donor (reaction (15) in Scheme 3),[33] since the xanthyl radicals **11** are unable to disproportionate.

At 280–310 °C, **1** was also hydrogenated by **10** to give cumene (**3**) in nearly quantitative yield, leading to the formation of dimer **12**, which in the given temperature range is in equilibrium with radicals **11** [Eq. (17)].[34] The stong ESR signal of **11** can therefore be observed throughout the entire reaction. The relatively high concentration of **11** is also responsible for the fact that retrodisproportionation (15) is partially reversible. This can be shown by incorporating deuterium into **1** with 9,9′-[D_2]-xanthene ([D_2]-**10**) in diphenyl ether. The deuterium content in **1** increases from 1% after 10% conversion to 13% after 64% conversion. Deuterium incorporation can be totally suppressed with the effective H donor tetraline as the solvent without significantly affecting the rate of reaction. Without **10** no hydrogenation of **1** occurs under these conditions.

To prove the existence of the radicals formed from the H acceptor, we performed a qualitative radical-clock experiment[35, 36] with α-cyclopropylstyrene (**13**) as the model compound (Scheme 4).[37] Due to the thermolability of **13**, the reaction temperature was not allowed to exceed 230 °C; therefore, we used the H donor 7*H*-benz[*de*]anthracene (**30**), which is more reactive than **2**. The intermediate radical **14** was indirectly identified

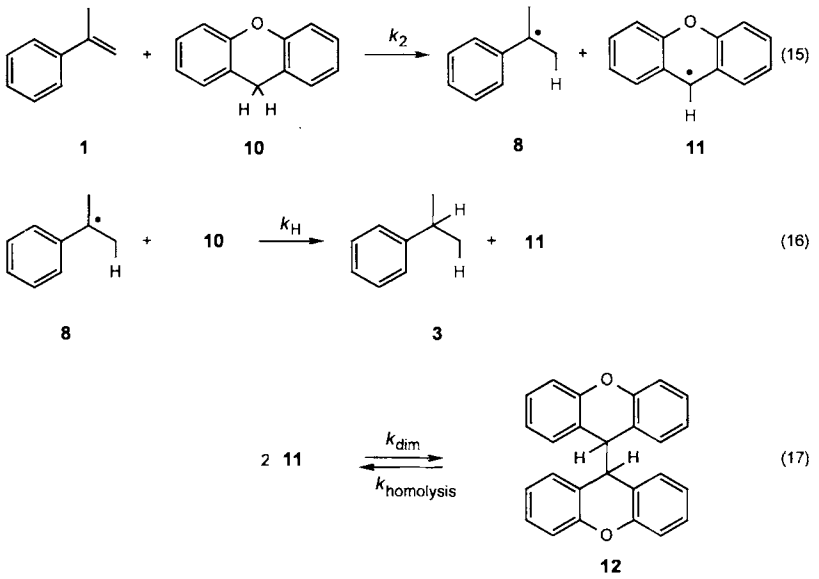

Scheme 3. Retrodisproportionation of **1** with xanthene (**10**).

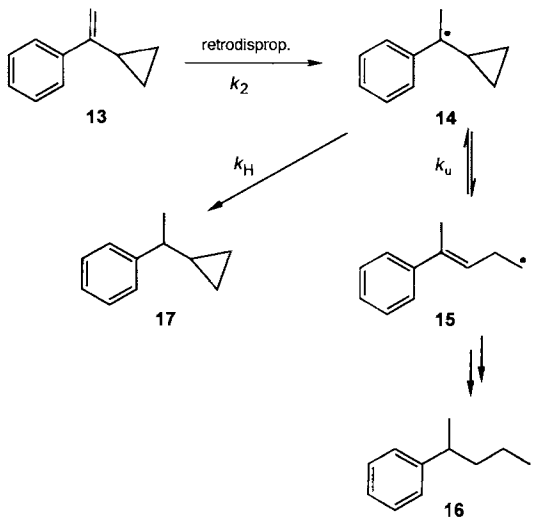

Scheme 4. Radical-clock experiment to identify the intermediate radicals of the H acceptor in the retrodisproportionation.

by the presence of the typical secondary product **16**.[36] 1-(Phenylethyl)cyclopropane (**17**) was formed as an H-trapping product.

Typical radical side and secondary reactions can also be observed in the transfer hydrogenation of **1** with *cis*-9,10-dimethyl-9,10-dihydroanthracene (*cis*-**18**).[38] Figure 2 shows product

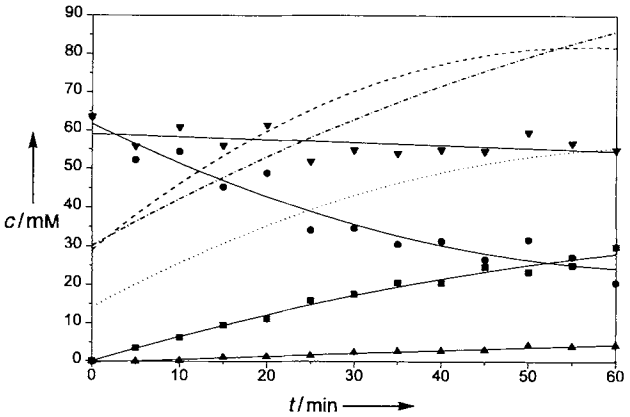

Figure 2. Transfer hydrogenation of α-methylstyrene (**1**, 0.1 M) with *cis*-9,10-dimethyl-9,10-dihydroanthracene (*cis*-**18**, 1.0 M) in diphenyl ether at 320 °C; ● **1**, ■ cumene (**3**), ▲ 2-phenylbutane (**19**), ··· *trans*-9,10-dimethyl-9,10-dihydroanthracene (*trans*-**18**), - - - - - 9-methylanthracene (**20**), — 9,10-dimethylanthracene (**21**), ▼ mass balance (total of **1**, **3**, and **19**)

formation as a function of reaction time. As the concentration of **1** decreases, the concentration of **3** and *sec*-butylbenzene (**19**) increases with a fairly constant mass balance. In addition, more than stoichiometric amounts of *trans*-**18**, 9-methylanthracene (**20**), and 9,10-dimethylanthracene (**21**) were formed. This result

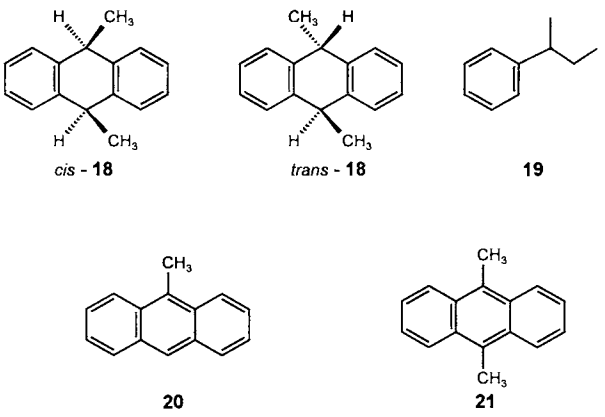

confirms a radical reaction mechanism. 9,10-dimethyl-9-hydroanthryl radicals (**22**), which formed during initial retrodisproportionation (18) in Scheme 5 and subsequent formation of **3** by H transfer [Eq. (19)], either disproportionate by reaction (20) to form **21** and *cis*/*trans*-**18** or suffer loss of methyl radicals by reaction (21) to give **20**. By adding onto **1** [Eq. (22)] the latter are responsible for the formation of *sec*-butylbenzene [**19**, Eq. (23)]. They also trigger a short radical chain reaction [Eqs. (21), (24)], which explains the overstoichiometric formation of radicals **22**, and thus products *trans*-**18**, **20**, and **21**.

To differentiate between a hydride transfer[11] and an H-atom transfer (retrodisproportionation), polar substituent[39] and solvent effects[40] were investigated with respect to the reaction kinetics. The reactivity difference between **2**, **10**, and acridan

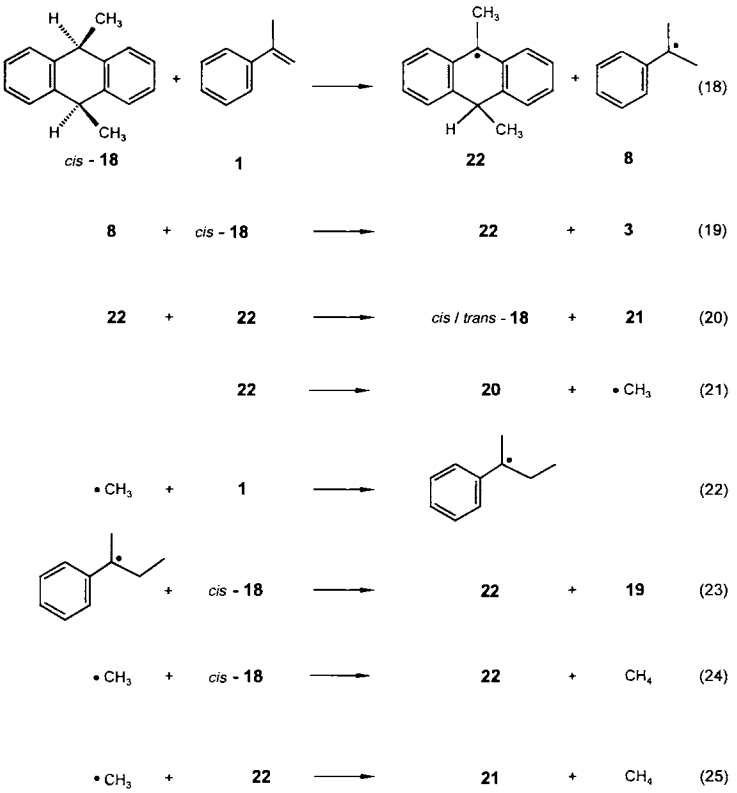

Scheme 5. Interpretation of the reaction of *cis*-9,10-dimethyl-9,10-dihydroanthracene (*cis*-**18**) and **1** at 310 °C in diphenyl ether.

(**23**)[39] in the transfer hydrogenation of **1** was small (Table 1), as is expected for the rate-determining retrodisproportionation (27) but not for the hydride-transfer step (26). Due to par-

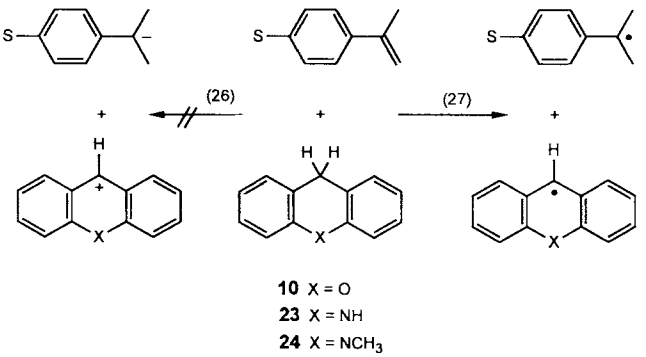

ticipation of the oxonium and ammonium structures $\mathbf{10}^+$ and $\mathbf{23}^+$ the reactivity should significantly increase in the order $\mathbf{2} < \mathbf{10} < \mathbf{23}$ for a hydride-transfer mechanism.[41]

In the transfer hydrogenation of *N*-methylacridan (**24**), the ESR spectrum of the 10-methyl-9-hydroacridyl radicals **25**

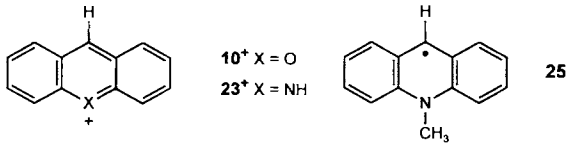

Table 1. Activation parameters and primary kinetic isotope effects for the transfer hydrogenation of α-methylstyrene (**1**) with 9,10-dihydroanthracene (**2**), xanthene (**10**), acridan (**23**), and *N*-methylacridan (**24**) [39] in solvents of varying polarity [40].

H Donor	Solvent	$E_T(30)$ [40] [kcal mol^{-1}]	$\Delta G^{\neq}$ [a] [kcal mol^{-1}]	$\Delta H^{\neq}$ [a] [kcal mol^{-1}]	$\Delta S^{\neq}$ [b] [cal K^{-1} mol^{-1}]	k_H/k_D (300 °C)
2	diphenyl ether	35.3	44.1	31.8	−21.5	2.1
10	diphenyl ether	35.3	44.3	25.0	−33.7	-
10	sec-butylbenzene	33.7 [c]	44.3	26.8	−30.6	1.7
23 [d]	triglyme	38.9	42.5	29.0	−23.5	2.0
23	pyridine	40.5	42.6	27.5	−26.2	-
23	NMA [e]	52.0	42.3	27.3	−26.2	-
24	pyridine	40.5	42.4	26.5	−27.7	-

[a] About ±0.6 kcal mol^{-1}. [b] About ±1.0 cal K^{-1} mol^{-1}. [c] E_T value for *tert*-butylbenzene given [45]. [d] The rate constants were only 18% higher in a mixture of triglyme and acetic acid (0.6:1). [e] NMA = *N*-methylacetamide.

could be observed.[39] The similarity of the isotope effects listed in Table 1 further supports a uniform mechanism. Finally, the small substituent effect on the activation parameters of the transfer hydrogenation of the substituted styrenes **26** with **2**, **10**,

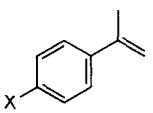

X = *p*-OCH$_3$ **26a**
X = *p*-*t*Bu **26b**
X = Cl **26c**
X = CN **26d**

or **23** (Table 2) clearly disfavors a hydride-transfer mechanism.[42] These reaction characteristics are expected for a hydrogenation proceeding by H-atom transfer under formation of substituted cumyl radicals **27**.[43]

Table 2. Activation parameters for the transfer hydrogenation of substituted α-methylstyrenes with 9,10-dihydroanthracene (**2**) in diphenyl ether, xanthene (**10**) in *sec*-butylbenzene, and acridan (**23**) in triglyme [39].

	$\Delta G^{\neq}_{300\,C)}$ [kcal mol^{-1}]			ΔH [kcal mol^{-1}]			$\Delta S^{\neq}$ [cal K^{-1} mol^{-1}]		
	2	**10**	**23**	**2**	**10**	**23**	**2**	**10**	**23**
26a	44.3	44.0	42.6 [a]	29.5	29.2	27.9 [a]	−25.8	−26.0	−25.7 [a]
26b	44.3	44.6	42.4	30.8	31.9	29.4	−23.5	−22.3	−22.6
1	44.1	44.3	42.5	31.8	26.8	29.0	−21.5	−30.6	−23.5
26c	43.9	43.5	41.8	29.4	26.8	27.5	−25.3	−29.2	−25.0
26d	43.1	41.6	40.5	27.1	25.0	25.2	−28.0	−28.9	−26.6

[a] In pyridine.

The influence of solvent polarity on the transfer hydrogenation of **1** was determined for eight different H donors (Table 3).[3] The solvent pair *N*-methylacetamide (NMA) and diphenyl ether (DPE) were compared preferably but not exclusively, because the dielectric constant for NMA is available for the temperature range used and differs significantly from that of DPE.[40] The ratio of the rate constants k_2(NMA)/k_2(DPE)varies only slightly within the range 0.7 to 1.4, which also contradicts a hydride-transfer mechanism.

Table 3. Solvent effects of the retrodisproportionation of H donors (see Figure 3) with α-methylstyrene (**1**) in diphenyl ether (DPE) and the more polar *N*-methylacetamide (NMA) [40, 44].

H Donor	T [°C]	k_{rel} [a]
9,10-dihydroanthracene **2**	320	0.7
xanthene [b] **10**	300	0.7
fluorene **28**	300	1.4
phenalene [c] **29**	250	1.1
[7*H*]benz[*de*]anthracene [d] **30**	250	1.1
1,4-dihydronaphthaline **31**	290	0.9
1,2-dihydronaphthaline **32**	350	0.9
acridan [e] **23**	280	1.3

[a] $k_{rel} = k$(NMA)/k(DPE); for the E_T values of the solvents see ref. [45]. [b] $k_{rel} = 1.2$ in *tert*-butylbenzene; $k_{rel} = 0.6$ in benzonitrile. [c] $k_{rel} = 1.5$ in *o*-dichlorobenzene. [d] $k_{rel} = 1.2$ in *o*-dichlorobenzene. [E] k(NMA)/k(pyridine) = 1.3; k(triglyme)/k(pyridine) = 1.0.

2.2 Relationship between Structure and Reactivity

The reactivity of the transfer hydrogenation is determined by both an enthalpic and an entropic term. Whereas the entropic factor is difficult to estimate and is further complicated by the phenomenon of an isokinetic relationship (see Section 2.2.3.), a direct relationship between the enthalpy of activation $\Delta H^{\neq}$ and the reaction enthalpy ΔH_R is expected and found according to Benson et al.[21] Based on the discussion above, it cannot be expected that both of these enthalpies are identical, but rather that $\Delta H^{\neq}$ is about 5 kcal mol^{-1} smaller than ΔH_R. However, it can be expected that the change of both parameters follows the same trend and, furthermore, that they correlate with one another.

Equation (a) can be formulated with the standard enthalpies of formation ΔH_f^0(g) of the starting materials **1** and **2** as well as the products **8** and **9**;[32] ΔH_R represents the reaction enthalpy at 25 °C.[21b]

$$\Delta H^{\neq} \approx \Delta H_R = \Delta H_f^0(g)[\mathbf{8}] + \Delta H_f^0(g)[\mathbf{9}] - \Delta H_f^0(g)[\mathbf{1}] - \Delta H_f^0(g)[\mathbf{2}] \quad (a)$$

For any given H donor/H acceptor pair, the corresponding standard enthalpies of formation ΔH_f^0(g) can be used to calculate the reaction enthalpies ΔH_R of the respective retrodisproportionation. It is also possible to derive a relationship [Eq. (b)]

$$\Delta H_{diss}(C{-}H) = \Delta H_f^0(g)[H^{\bullet}] + \Delta H_f^0(g)[\mathbf{9}] - \Delta H_f^0(g)[\mathbf{2}] \quad (b)$$

between the reaction enthalpy ΔH_R or the experimental enthalpy of activation $\Delta H^{\neq}$ and the C–H bond enthalpy ΔH_{diss}(C–H) of the H donor (see reaction (28)). The term $(\Delta H_f^0(g)[\mathbf{9}] - \Delta H_f^0(g)[\mathbf{2}])$ is also present in Equation (a). Under the assump-

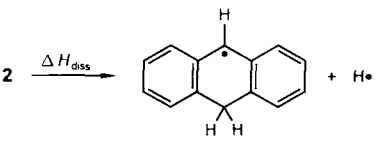

9

tion that $\Delta H^{\neq} \approx \Delta H_R$, combining Equations (a) and (b) allows one to derive a relationship between the C–H bond enthalpies ΔH_{diss}(C–H) of the H donors and the enthalpies of activation $\Delta H^{\neq}$ of the transfer hydrogenation with, for instance, **1** [Eq. (c)].

$$\begin{aligned}\Delta H_{diss}(C-H) &\approx \Delta H^{\neq} + \Delta H_f^0(g)[H^{\cdot}] + \Delta H_f^0(g)[\mathbf{1}] - \Delta H_f^0(g)[\mathbf{8}] \\ &\approx \Delta H^{\neq} + 52.1 + 28.5^{[46]} - 36.3^{[32]} \\ &\approx \Delta H^{\neq} + 44.3\ \text{kcal mol}^{-1}\end{aligned} \quad (c)$$

Thus, the C–H bond enthalpies ΔH_{diss}(C–H) can be approximated from the enthalpies of activation for the transfer hydrogenation and vice versa. Moreover, the influence of the H donor on the reactivity of the retrodisproportionation can be predicted prior to the experiment (Section 2.2.1). Predictions with respect to the reactivity can also be made from the difference in the enthalpies of formation of the H acceptor (for example **1**) and the radicals formed by H addition (for example **8**, Section 2.2.2). All this forms the basis for a discussion of the relationship between structure and reactivity of a given system.

2.2.1. Variation of the H Donor

To establish the influence of the H donor on the reactivity of the retrodisproportionation with α-methylstyrene (**1**) as the H acceptor, a series of compounds with especially low C–H bond enthalpies ΔH_{diss}(C–H) was chosen (Scheme 6).[50] Mech-

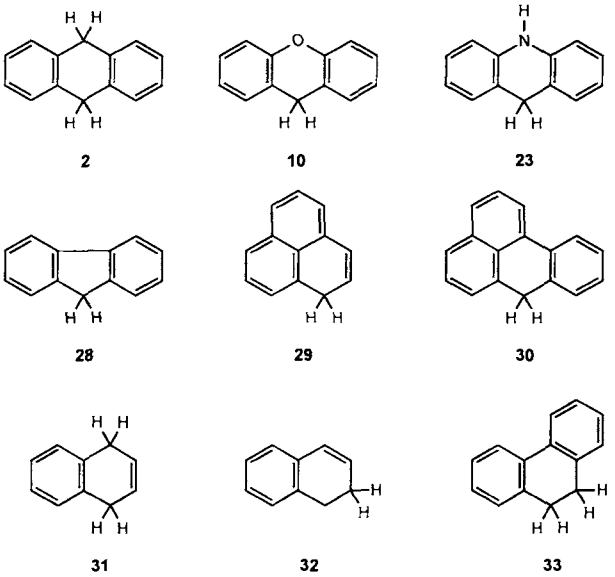

Scheme 6. H donors that react with **1** under retrodisproportionation [50] (for bond enthalpies ΔH_{diss}(C–H) see Table 4).

anistic studies were performed for each compound to confirm the radical mechanism.[48,49] In the case of the H donors xanthene (**10**), phenalene (**29**), and 7*H*-benz[*de*]anthracene (**30**), the initially formed H-donor radicals were detected by ESR spectroscopy.[33]

Among the selected H donors **10**, **29**, **30**, fluorene (**28**), and anthrone (**44**) represent special substrates, since the radicals formed by cleavage of the C–H bonds cannot disproportionate but instead only dimerize. Compared to **2**, this particular behavior can lead to a different kinetic situation if the dimer forms a dissociation equilibrium with the radicals under high-temperature conditions (200–350 °C).[34,49] In this case, the retrodisproportionation step becomes reversible, as shown by isotopic-labeling experiments. If the extent of the reversibility is small (< 10%), it can be accounted for with a kinetic correction factor.[27,49] However, it would be better in such cases to use an H-donor solvent such as mesitylene, *sec*-butylbenzene, or tetraline to trap the radicals formed in equilibrium. Even if the rate constants k_{obs} thereby change slightly, better activation parameters are obtained, since the extent of reversibility is apparently temperature-dependent.

Since the H donors **29** and 1,2-dihydronaphthalene (**32**) contain styrene-like double bonds, they can also function as H acceptors, giving them the ability to function both as an H acceptor and as an H donor.[48] This phenomenon was especially apparent with **29**,[51,48] the methylene group of which has an especially low C–H bond enthalpy (ΔH_{diss}(C–H) = 74.0 kcal mol^{-1}; Table 4). Retrodisproportionation (29) of two

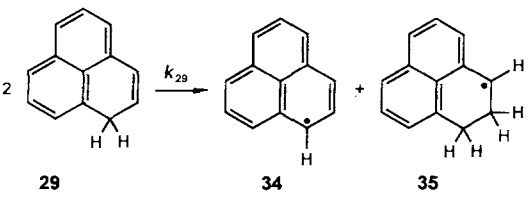

(29)

molecules of **29** led to the formation of the phenalenyl radical **34** and the dihydrophenalenyl radical **35**. This step might be responsible for the exceptionally fast autoxidation of **29** at 25 °C as well as its thermolability at temperatures above approximately 180 °C.[51]

To ensure that these radicals do not react to form known complex products such as dibenzo[*cd*,*lm*]perylene (peropyrene, **38**),[51] **2** is added in excess as a radical scavenger to the reaction

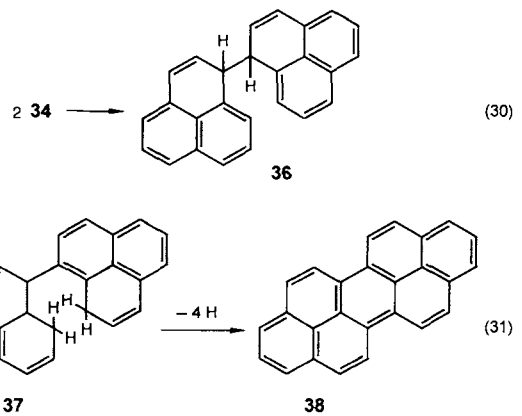

(30)

(31)

of **29** with **1**.[48] In this case, **2** serves exclusively as a radical trap in reactions (33), (35), and (36) in Scheme 7 and does not compete as a H donor. The conversion–time plots in Figure 3 show that under the given reaction conditions **1** and **29** react almost quantitatively to **3** or dihydrophenalene (**39**).

Table 4. Kinetic and thermodynamic data for the transfer hydrogenation of α-methylstyrene (**1**) with H donors.

H Donor	$\Delta G^{\neq}_{300\,°C}$ [a] [kcal mol^{-1}]	$\Delta H^{\neq}$ [a] [kcal mol^{-1}]	$\Delta S^{\neq}$ [a] [e.u.]	ΔH_{diss} (C-H) [b] [kcal mol^{-1}]	ΔH_R [c] [kcal mol^{-1}]	Solvent effect [d]	k_H/k_D [e] (300 °C)	Reverse reaction v_{-2} [%] [f]
2 [27]	44.1±1.2	31.8±1.2	−21.5±2.1	83.0	38.7	1.4 (320 °C)	2.1	0
[D4]-**2** [27]	45.0±0.9	32.8±0.9	−21.4±1.5	–	–	–	–	0
10 [39c]	44.3±1.9 [g]	26.8±1.4 [g]	−30.6±2.4 [g]	80.7	36.4	1.0 (300 °C) [g]	3.2 [a]	0
23 [39a]	42.6±0.6 [h] 42.5±0.3 [k] 42.3±0.7 [l]	27.5±0.6 [h] 29.0±0.3 [k] 27.3±0.7 [l]	−26.2±1.1 [h] −23.5±0.6 [k] −26.2±1.3 [l]	80.0	35.7	1.3 (280 °C) [i]	2.0	0
24 [39a]	42.4±0.2 [h]	26.5±0.2 [h]	−27.7±0.3 [h]	80.0	35.7	1.3 (280 °C) [i]	–	–
28 [56]	47.6±0.5 [g]	27.6±0.4 [g]	−34.9±0.5 [g]	82.6	38.3	1.4 (300 °C)	2.1	0
29 [48]	38.6±1.1 39.1±0.8 [m]	19.6±1.1 17.9±0.8	−33.1±2.1 −37.0±1.5	74.0	29.7	1.1 (250 °C)	–	15
30 [36]	39.6±2.0	24.1±2.1	−26.9±4.0	76.0	31.7	1.1 (250 °C)	2.7 (250 °C)	0
31 [27]	42.7±1.5	29.1±1.5	−23.7±2.6	83.0	38.7	0.9 (290 °C)	2.3	66
32 [27]	45.1±1.1 46.1±1.1 [n] (45.9±1.2) [o]	32.0±1.1 35.8±1.2 [n] (35.9±1.2) [o]	−22.9±1.8 −18.1±1.7 [n] (−17.5±2.0) [o]	86.0	41.7	0.9 (350 °C)	1.7 [a] 1.4 (350 °C) [n]	25
40 [38]	43.3±2.6	28.7±1.7	−25.5±2.8	83.3 [p]	39.0	1.0 [q]	1.9 (360 °C)	0
cis-**18** [38]	44.5±1.8	29.7±1.3	−25.8±2.2	81.5 [p]	37.2	1.1	–	–
trans-**41** [38]	43.7±1.2	28.0±0.8	−27.4±1.3	79.4 [p]	35.1	1.1 [q]	–	–
cis-**41**	46.0±1.5	28.2±1.0	−31.0±1.7	78.4 [p]	34.1	0.8 [q]	–	–
43 [38]	44.3±0.7	27.7±0.5	−28.9±0.7	84.5 [p]	40.2	0.9 [l]	1.9 (360 °C)	0
42 [38]	45.7±0.8	29.8±0.6	−27.7±1.0	84.9 [p]	40.6	0.9 [q]	1.3 (360 °C)	0
44 [56]	44.7±0.8 [r]	25.0±0.6 [r]	−34.4±0.8 [r]	80.2 [s]	35.9	1.7 [q]	2.5	0

[a] Solvent diphenyl ether (DPE), unless noted otherwise. [b] C–H bond-dissociation enthalpy of the donor R–H: ΔH_{diss}(Alkyl–H) [32] − RSE(R$^{\bullet}$) [63, 64]. [c] Reaction enthalpy according to Equation (c) with $\Delta H_R = \Delta H_{diss}$(R–H) − 44.3 kcal mol^{-1}. [d] Solvent effect = k_1(NMA)/k_1(DPE) at the comparison temperature given in parentheses. [e] Deuterium isotope effect. [f] The reversibility of the H transfer established from deuterium experiments was taken into consideration for the kinetics calculations [53]. [g] Solvent *sec*-butylbenzene (SBB). [h] Solvent pyridine. [i] Solvent effect = k_1(NMA)/k_1(pyridine). [k] Solvent triglyme. [l] Solvent NMA. [m] H acceptor phenalene (**29**). [n] H acceptor 1,2-dihydronaphthalene (**32**). [o] ref. [67], H acceptor **32**. [p] ΔH_{diss}(C–H) calculated relative to DHA (**2**) with semiempirical MO methods (AM1, RHF/CI), method of double difference. [q] Solvent effect = k_1(benzonitrile)/k_1(DPE). [r] Solvent tetraline [56]. [s] ΔH_{diss}(C–H) calculated with semiempirical MO methods (AM1, RHF/CI).

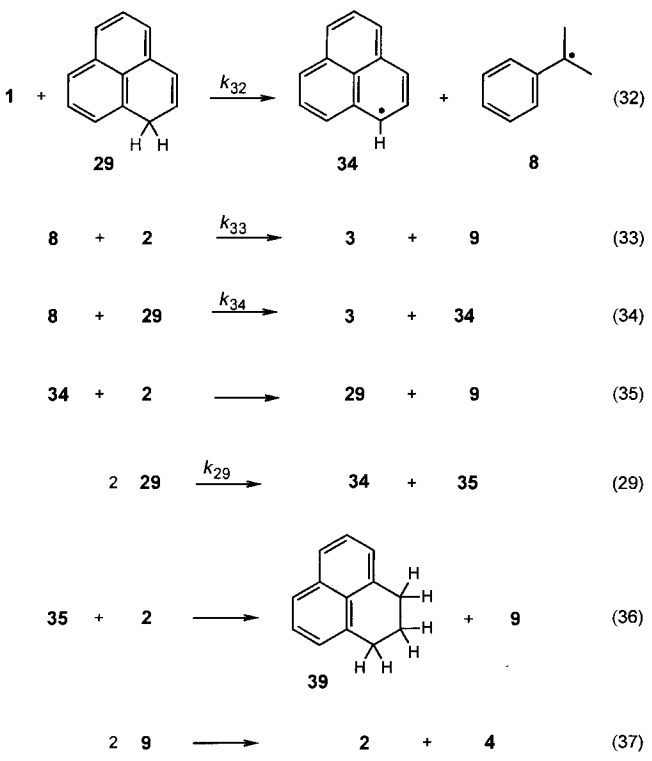

Scheme 7. Transfer hydrogenation of **1** with **2** and phenalene (**29**) as the catalyst.

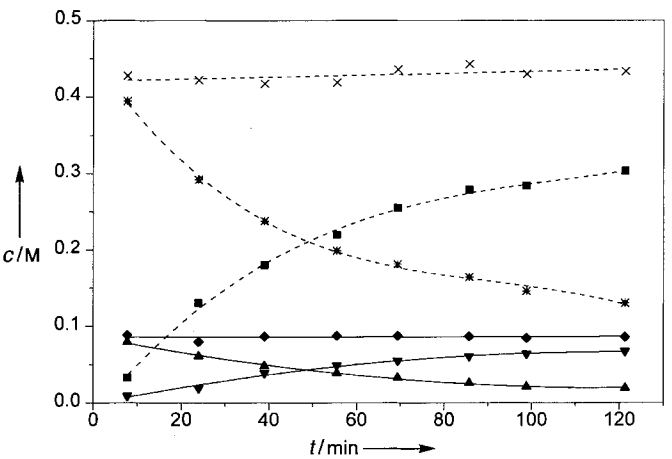

Figure 3. Conversion–time plot for the reaction of phenalene (**29**, c = 0.41 M) with α-methylstyrene (**1**, c = 0.08 M) at 227 °C in diphenyl ether. 9,10-Dihydroanthracene (**2**, 2.00 M) was added as a radical trap; ▲ **1**, ▼ **3**, ◆ **1**+**3**, * **29**, ■ **39**, × **29**+**39**.

Kinetic analysis allows one to determine both the rate constants k_{32} [Eq. (32)] and k_{29} [Eq. (33)] in the same experiment and to calculate the activation parameters from their temperature dependencies.[48] An interesting aspect of the phenalene kinetics is the fact that when **2** is added as a radical trap phenalene is reformed from the phenalenyl radicals **34** [Eq. (35)], which were detected by ESR spectroscopy. Thus, **29**

is a promotor of the transfer hydrogenation of **1** with **2**.[52] However, in reaction (29) phenalene is continuously converted so that the promotor concentration continues to decrease, and **29** is ultimately consumed.

The occurrence of the cycle (32)–(35) can be proven with [D_4]-**2**. Reactions (33) and (34) require that, in this case, **3** remains undeuterated or becomes monodeuterated but not dideuterated. At the same time, however, six or seven D atoms per molecule of **29** or **39** are being accepted in the cycle (32), (34), and (35) since the phenalenyl radical **34** contains six equivalent positions for the delocalization of the single electron.[48]

The irreversibility of reaction (29) was proven with [D_7]-phenalene ([D_7]-**29**) and [D_4]-**2**.[48] In the transfer hydrogenation of **1**, no additional deuterium was incorporated into [D_7]-**29** after 90% conversion. This observation suggests that radical [D_8]-**35**, which is formed in the reaction of [D_7]-**29** with itself,

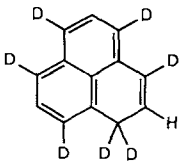

[D_7]-29

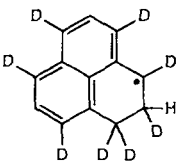

[D_8]-35

does not disproportionate back to form **29**, because then hydrogen would preferably be cleaved in this process and lead to the formation of [D_8]-**29**. Instead, [D_2]-**3**, [D_9]-**39**, and [D_2]-**4** are formed exclusively. In addition, some incorporation of deuterium (about 4–8%) could be detected in unchanged **1**, which suggests that the reverse reaction in Equation (32) does occur to a slight extent.[53] In contrast, 7*H*-Benz[*de*]anthracene (**30**) is a promotor of the transfer hydrogenation that is not consumed in the reaction (see Table 4, ΔH_{diss}(C–H) = 76.0 kcal mol^{-1}),[54] because it does not contain any styrene-like double bonds as does **29** (Figure 4).[36]

This phenomenon of acceleration by promotors containing weak C–H bonds[36, 48] appears to be an important concept

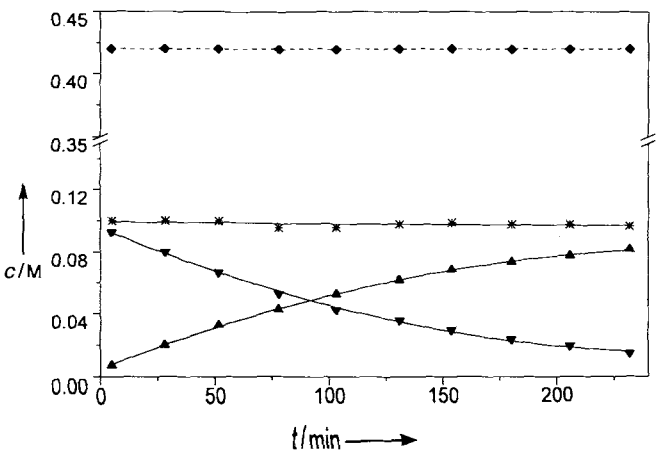

Figure 4. Conversion–time plot for the transfer hydrogenation of α-methylstyrene (**1**, c = 0.08 M) with 9,10-dihydroanthracene (**2**, 2.00 M) at 230 °C in diphenyl ether in the presence of 7*H*-benz[*de*]anthracene (**23**, 0.43 M) as a promotor; ▼ **1**, ▲ **3**, * **1** + **3**, ♦ **30**.

in coal liquefaction.[5, 13, 55] Coal, similar to phenalene structures, contains both the acceptor and donor components necessary for retrodisproportionations, and a mixture of hydroaromatic hydrocarbons is typically used in the liquefaction process. Catalysis of C–H activation by activated carbon described by Dockner[55c] can probably be explained also with this phenomenon.

The H donors fluorene (**28**),[56] 1,4-dihydronaphthalene (**31**),[27] and 1,2-dihydronaphthalene (**32**)[27] shown in Scheme 6 could also be investigated quantitatively in the retrodisproportionation with **1**. The transfer hydrogenation of **1** can also be performed in good yields with 9,10-dihydrophenanthrene (**33**) at approximately 350 °C; however, due to unwanted side reactions, the kinetic behavior of this reaction is not reliable. This can probably be attributed to the high C–H bond energy of **33** (90 kcal mol^{-1}). In the case of **32**, the same phenomenon occurred as for **29** (that of simultaneous donor and acceptor functionality). Therefore, the corresponding rate constants of both the hydrogenation of **32** and of the H transfer onto **1** as well as their activation parameters were simultaneously accessible at the same time (see Table 4).[27, 57–61] The substituted 9,10-dihydroanthracene derivatives **18**, **40**–**43** were used for investigating steric effects of the H donors in the retrodisproportionation with **1** (see Table 4).[38]

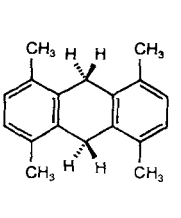

40

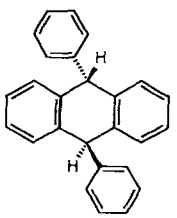

trans-**41**

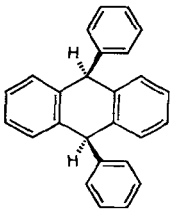

cis-**41**

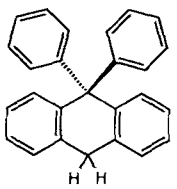

42

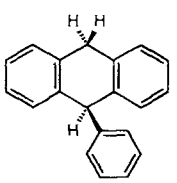

43

In the transfer hydrogenation with **41** and **42**, but not with **43**, a phenyl radical is cleaved from the initially formed substituted 9-hydroanthryl radical; this radical either phenylates with the solvent diphenyl ether or is hydrogenated to form benzene. In either case, the mass balance is greater than 95%. Surprisingly, only small differences in the rate constant k_2 can be detected in the retrodisproportionation with **1**. With 1,4,5,8-tetramethyl-9,10-dihydroanthracene (**40**) and *trans*-9,10-diphenyl-9,10-dihydroanthracene (*trans*-**41**), for instance, an acceleration relative to the reaction with **2** can be observed (k_{rel}(300 °C) = 3.1 and 2.2, respectively), whereas the other substrates react more slowly (k_{rel}(300 °C) = 2).[38] However, the activation parameters (see Table 4) are significantly different from each other (Section 2.2.3.). Steric effects in the donor molecule apparently have almost no effect on H transfer.

Although the reactivity $\Delta G^{\neq}$ of anthrone (**44**) is very similar to that of DHA, the corresponding components $\Delta H^{\neq}$ and $\Delta S^{\neq}$ differ significantly.[56] The concentration of **44** remains constant during the transfer hydrogenation since it acts as a promotor, similar to **29**. The radicals **45** are quenched by the solvent tetraline to yield **44**. In the transfer hydrogenation of **1** with the substituted dihydroanthracenes **46**, only a minor substituent effect[38] could be observed, which suggests that polar effects do not have an impact on the rate of reaction.[62]

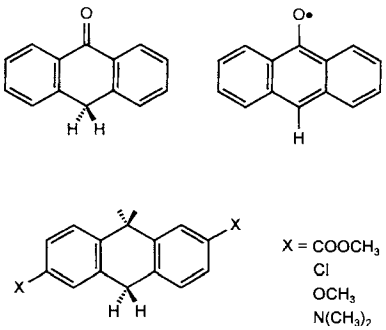

When trying to evaluate the Benson hypothesis[21] $\Delta H^{\neq} \approx \Delta H_R$ for the retrodisproportionation step using the results listed in Table 4, it can be seen that for all examples $\Delta H^{\neq}$ is 3–9 kcal mol^{-1} lower than the independently thermochemically calculated reaction enthalpies ΔH_R. This discrepancy allows the conclusion that, due to the influence of entropy, the maximum free enthalpy $\Delta G^{\neq}$ on the reaction coordinate (transition state) does not coincide with the radical products, but occurs earlier in the reaction (Figure 5).

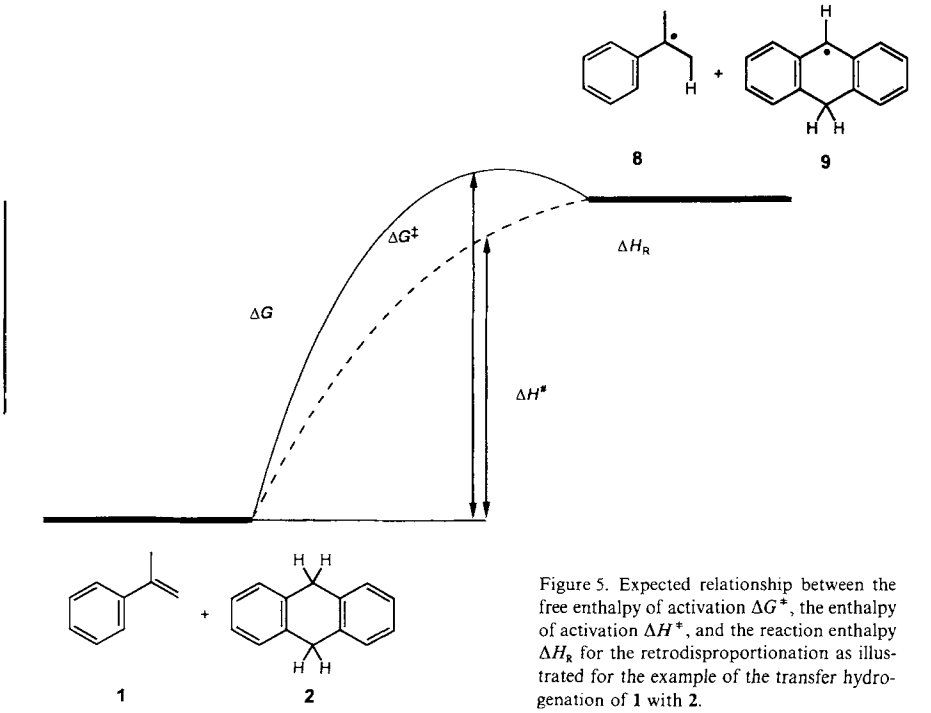

Figure 5. Expected relationship between the free enthalpy of activation $\Delta G^{\neq}$, the enthalpy of activation $\Delta H^{\neq}$, and the reaction enthalpy ΔH_R for the retrodisproportionation as illustrated for the example of the transfer hydrogenation of **1** with **2**.

(indicating that H-atom transfer from the donor to the acceptor is approximately halfway completed in the transition state. The plot of the experimental enthalpy of activation $\Delta H^{\neq}$ against the reaction enthalpy of the retrodisproportionation step for a series of H donors (Figure 6) shows that a linear correlation

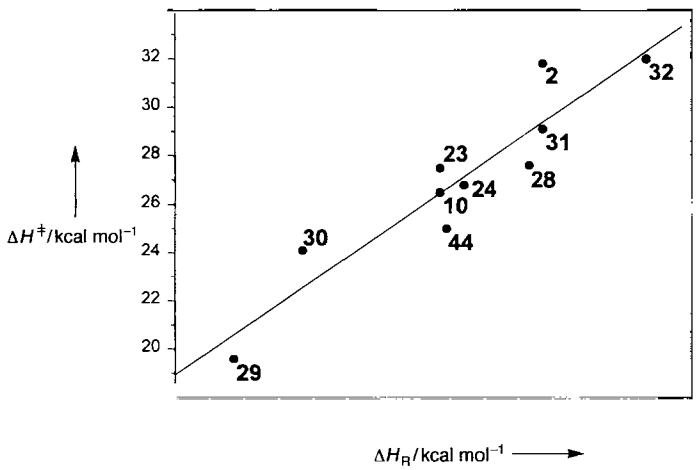

exists; the spread of the data is within experimental error. Qualitatively, the Benson criterion[21] appears fulfilled: the two parameters $\Delta H^{\neq}$ and ΔH_R follow the same trend upon structure variations. However, it should be kept in mind that ΔH_R^0 was determined in the gas phase at 25 °C, and $\Delta H^{\neq}$ in the liquid phase at higher temperatures.

The validity of Equation (c) can be demonstrated in a similar way. A linear relationship also results when the C–H bond enthalpies calculated according to Equation (c) are plotted against the thermochemical, experimentally determined or calculated bond enthalpies listed in Table 4 (Figure 7). These correlations strongly confirm that transfer of the H atom in the retrodisproportionation occurs in the rate-determining step of

2.2.2. Variation of the Olefinic H Acceptor

A variety of C=C bonds are prone to retrodisproportionation. The class of double bonds successfully investigated to date include those conjugated to double bonds, aromatic systems, or hetero double bonds (that is, C=O,[68, 70] N=O,[69a, b] and nitro

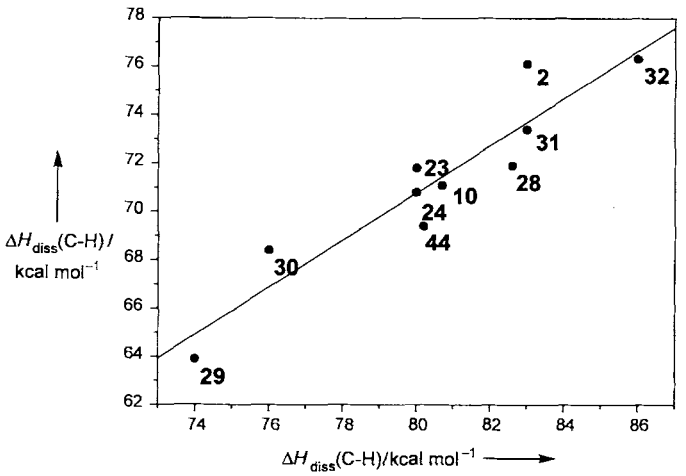

Figure 7. Correlation between the C–H bond enthalpies calculated from Equation (c) and the independently determined values from Table 4 (in kcal mol^{-1}); ΔH_{diss}(C–H) on the abscissa: from Table 4; ΔH_{diss}(C–H) on the ordinate: from Equation (c).

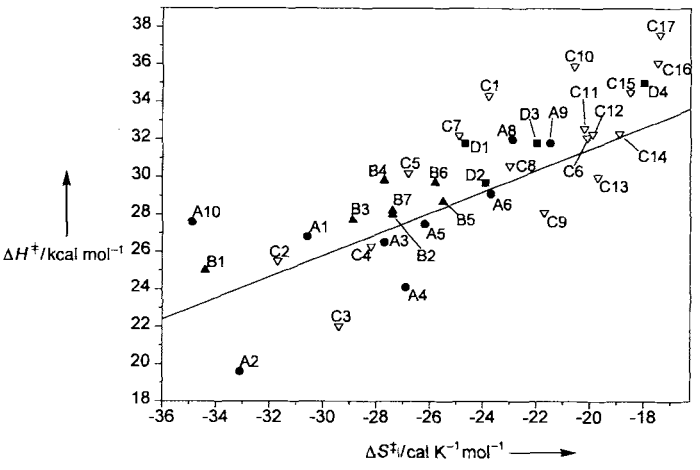

Figure 8. Correlation between the enthalpy of activation $\Delta H^{\ddagger}$ and the entropies of activation $\Delta S^{\ddagger}$ for retrodisproportionation reactions. Series A (unsubstituted H donors with **1**): A1: **10**, A2: **29**, A3: **24**, A4: **30**, A5: **23**, A6: **31**, A7: **33**, A8: **32**, A9: **2**, A10: **28**; series B (substituted dihydroanthracene derivatives with **1**): B1: **44**, B2: *cis*-**41**, B3: **43**, B4: **42**, B5: **40**, B6: *cis*-**18**, B7: *trans*-**41**; series C (H acceptors with a C=C bond and **2** as the H donor): C1: **50**, C2: **47**, C3: **55**, C4: **62**, C5: **49**, C6: **54**, C7: **51**, C8: **53**, C9: **66**, C10: **65**, C11: **57**, C12: **58**, C13: **56**, C14: **63**, C15: **48**, C16: **59**, C17: **64**; series D (additional H acceptors such as dienes and trienes with **2**): D1: **69**, D2: **67**, D:3 **68**, D4: **32**.

groups[69a, b]). Table 5 summarizes the kinetic and thermodynamic data for the retrodisproportionation of various H acceptors containing C=C bonds in the reaction with 9,10-dihydroanthracene (**2**).[36, 70]

This data shows that the reactivity ($\Delta G^{\ddagger}$ or k_{rel} in Table 5) varies only slightly with drastic structural variations of the H acceptor (maximum value of k_{rel}:2700 for **55**:**64**). For the series of H acceptors in Table 5 the reaction enthalpy $\Delta H^{\ddagger}$ is generally about 5–10 kcal mol^{-1} lower than the reaction enthalpy ΔH_R of the retrodisproportionation step. However, there is a close correlation between these two parameters. In some examples the deviation is significantly larger (in particular for **47**, **51**, **62**, **56**, and **66**). It is possible that the kinetic analysis in these examples is affected by side reactions such as reversibility or the ane reaction. Side reactions can result in errors when calculating the components $\Delta H^{\ddagger}$ and $\Delta S^{\ddagger}$ of the enthalpy of activation $\Delta G^{\ddagger}$ and create the false impression of an isokinetic relationship. Such a relationship can indeed be observed for the data in Tables 4 and 5. The reaction acceleration expected from the enthalpy data is reduced by entropy effects. Since the enthalpies of activation $\Delta H^{\ddagger}$ listed in Table 4 correlate well with the C–H bond enthalpies of the H donors (Figure 7), which deems them reliable, the isokinetic relationship (Figure 8) cannot be the exclusive result of side reactions and the experimental errors caused by them. To exclude any potential effects of this kind, the structure–reactivity relationship will be discussed under consideration of $\Delta H^{\ddagger}$.

An increase in the size of the α-alkyl substituent in the α-alkylstyrenes **1**, **48**–**50** decreases the rate only by a factor of 17. However, a clear trend cannot be determined with the enthalpies of activation $\Delta H^{\ddagger}$. The nontwisted alkenes **53**–**54** react at only a slightly faster rate.[74] 2,6-Dimethylstyrene (**51**) reacts 17 times slower than styrene (**47**), and the enthalpy of activation of **51** is 6 ± 2 kcal mol^{-1} larger than that of **47**. In the reaction of **47** with **2** [Eq. (38)] it was possible for the first time to detect the secondary product **61** [Eq. (40)] of the addition of the 9-hydroanthryl radical **9** onto the double bond of the H acceptor [Eq. (39), Scheme 8]. This product will hereafter be referred to as the ane product, as this reaction was already described earlier as the ane reaction.[15]

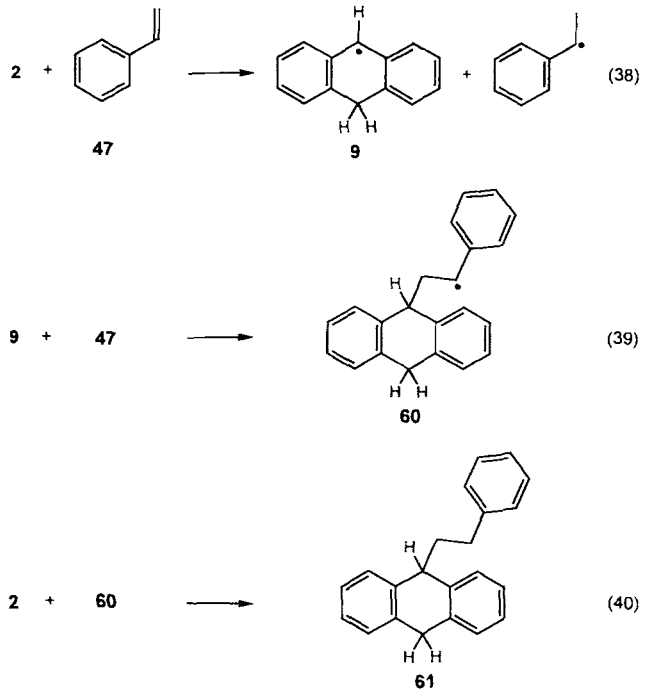

Scheme 8. Formation of the ane product **61** in the reaction of styrene (**47**) with **2**.

The formation of the ane product was later observed with other H acceptors[70] including acenaphthylene (**62**, 5%), phenylacetylene (**70**, >95%), diphenylacetylene (**71**, >30%),

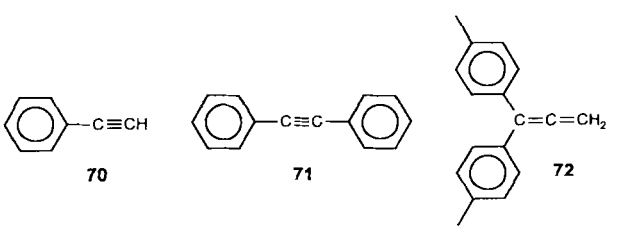

Table 5. Kinetic and thermodynamic data for the transfer hydrogenation of H acceptors containing C=C bonds with 9,10-dihydroanthracene (**2**) as the H donor [a].

H Acceptor [a]	$\Delta G^{\neq}_{300\,°C}$ [kcal mol^{-1}]	$\Delta H^{\neq}$ [kcal mol^{-1}]	$\Delta S^{\neq}$ [cal K^{-1} mol^{-1}]	ΔH_R [c] [kcal mol^{-1}]	ΔH_f° (g) (H Acceptor) [kcal mol^{-1}]	ΔH_f° (g) (Radical) [l] [kcal mol^{-1}]	Solvent effect [u]	k_H/k_D [w] (T,)	k_{rel} [x] with respect to 1 (300 °C)
47 [70]	43.6 ± 1.3	25.5 ± 1.3	−31.7 ± 2.1	40.1	35.3 [d] (35.0 [e,f])	44.5 [m]	–	–	2.7
1 [27]	44.1 ± 1.2	31.8 ± 1.2	−21.5 ± 2.1	38.7	28.5 [g]	36.3 [m]	–	–	1.0
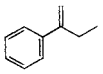 **48** [70]	45.1 ± 0.7	34.5 ± 0.7	−18.5 ± 1.1	40.4	21.9 [d]	31.4 [m]	–	–	0.4
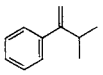 **49** [70]	45.6 ± 0.6	30.2 ± 0.6	−26.8 ± 1.1	40.1	16.3 [d]	25.5 [m]	–	2.25 (300 °C)	0.25
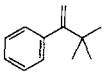 **50** [70]	47.9 ± 0.4	34.3 ± 0.3	−23.8 ± 0.4	44.7	8.5 [d]	22.3 [m]	–	2.12 (360 °C)	0.058
51 [70]	46.4 ± 0.5	32.2 ± 0.5	−24.9 ± 0.8	45.1	23.9 [e]	38.1 [m]	–	–	0.16
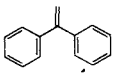 **63** [70]	43.1 ± 0.2	32.3 ± 0.2	−18.9 ± 0.4	37.3	57.9 [d] 59.8 [e]	64.3 [m]	–	–	2.7
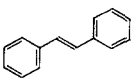 **64** [70]	47.6 ± 0.1	37.6 ± 0.1	−17.4 ± 0.2	47.1	56.5 [e])	72.7 [m]	–	–	0.045
62 [70]	42.4 ± 0.2	26.3 ± 0.2	−28.2 ± 0.3	40.8	61.6 [d]	71.5 [n]	–	2.27 (280 °C)	5.1
59 [70]	46.1 ± 2.3	36.1 ± 2.3	−17.5 ± 3.8	45.3	39.1 [d]	53.5 [m]	–	–	0.14
32 [27]	46.1 ± 1.1 [b]	35.8 ± 1.1 [b]	−18.1 ± 1.7 [b]	48.6	30.3 [h]	45.4 [o]	0.85 (350 °C)	–	–
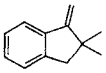 **53** [70]	43.2 ± 0.8	30.6 ± 0.8	−23.0 ± 1.5	41.7	18.4 [e]	29.2 [m]	–	2.35 (300 °C)	2.2
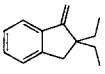 **54** [70]	43.6 ± 0.6	32.1 ± 0.6	−20.1 ± 1.1	42.0	11.4 [e]	22.5 [m]	0.76 (320 °C)	–	1.5
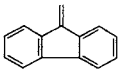 **55** [70]	38.9 ± 0.4	22.0 ± 0.4	−29.4 ± 0.9	33.6	61.1 [i]	63.8 [p]	–	–	120

Table 5. (continued).

H Acceptor [a]	$\Delta G^{\neq}_{300°C}$ [kcal mol^{-1}]	$\Delta H^{\neq}$ [kcal mol^{-1}]	$\Delta S^{\neq}$ [cal K^{-1} mol^{-1}]	ΔH_R [c] [kcal mol^{-1}]	ΔH_f° (g) (H Acceptor) [kcal mol^{-1}]	ΔH_f° (g) (Radical) [l] [kcal mol^{-1}]	Solvent effect [u]	k_H/k_D [w] (T.)	k_{rel} [x] with respect to 1 (300 °C)
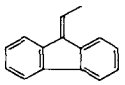 **56** [70]	41.3±0.3	30.0±0.3	−19.7±0.5	36.2	53.3 [d]	58.6 [m,q]	–	–	14
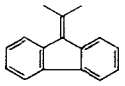 **57** [70]	44.2±0.8	32.6±0.8	−20.2±1.4	39.1	45.0 [i]	53.2 [m,q]	0.91 (300 °C)	1.64 (300 °C)	1.1
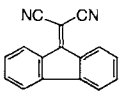 **58** [70]	43.7±0.9	32.3±0.9	−19.9±1.5	41.8	125.0 [k]	135.9 [r]	–	–	1.6
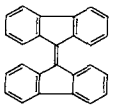 **66** [70]	40.5±2.0	28.1±2.0	−21.7±3.7	49.9	99.7 [d]	118.7 [r]	–	–	42
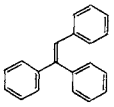 **65** [70]	47.7±0.6	35.9±0.6	−20.6±1.0	40.9	81.5 [d]	91.5 [m]	–	2.22 (320 °C)	0.051
67 [36]	43.4±0.3	29.7±0.3	−23.9±0.6	39.8	25.4 [d]	34.3 [s]	0.99 (300 °C) [v]	1.79 (300 °C)	2.1
68 [36]	44.4±1.1	31.8±1.1	−22.0±1.9	39.5	43.2 [d]	51.8 [t]	0.97 (310 °C) [v]	1.98 (310 °C)	0.77
69 [36]	45.4±0.3	31.8±1.1	−24.7±0.4	39.5	22.5 [d]	31.1 [t]	1.12 (340 °C) [v]	2.20 (340 °C)	0.40

[a] Solvent diphenyl ether (DPE); volume expansion was considered in all cases; a reverse reaction with rate k_{-1} was not detected. [b] Autohydrogenation of 1,2-dihydronaphthalene, which acts as both the H donor and the H acceptor. [c] The reaction enthalpies ΔH_R were calculated from the enthalpies of formation of the reaction partners. Except for the values shown in Table 5 for ΔH_f^0(g) of the H acceptors and the radicals fomed from them, the following values were used: ΔH_f^0(g)[**2**] = 38.2 kcal mol^{-1}, ΔH_f^0(g)[**9**] = 69.1 kcal mol^{-1}, see ref. [63, 64]. [d] Based on calorimetric measurements, see ref. [65, 70]. [e] Based on MM2-ERW force field calculations, see ref. [70]. [f] Whenever data was available from both force-field calculations and determinations of combustion enthalpies, the latter was preferably used to calculate ΔH_R. [g] See ref. [3, 48, 63]. [h] See ref. [70]. [i] Estimated from the enthalpy of formation ΔH_f^0(g) for 9-ethylidenefluorene as well as strain-free increments, see ref. [70]. [k] Based on ΔH_f^0(g) for **57** using the ΔH_f^0(g) difference of 80.0 kcal mol^{-1} obtained from AM1 calculations [66]. [l] Adduct radical formed from the H acceptor by H transfer. [m] Based on MM2-82 force-field calculations, see ref. [70]. [n] From ΔH_f^0(g) for acenaphthene (37.3 kcal mol^{-1})[65] and the estimated BDE for acenaphthene of 81.8 kcal mol^{-1} [70]. [o] Based on the resonance stabilization energy (RSE) for the 1-tetralyl radical (≈8.4 kcal mol^{-1}) and the 1,2-dihydro-2-naphthyl radical (≈13 kcal mol^{-1}). [p] Ref. [2b]. [q] The force-field method was calibrated [70] for 9-alkyl-9-fluorenyl radicals with the RSE of the 9-methyl-9-fluorenyl radical (15.3 kcal mol^{-1}) [2b]. [r] Based on ΔH_f^0(g) (9-methyl-9-fluorenyl radical) as well as strain-free increments [70]. [s] See ref. [72]. [t] The enthalpies of formation ΔH_f^0(g) of the radicals were calculated from the enthalpies of formation of the hydrogenation products and the RSE of the radicals. The following values were assumed for the latter: RSE(3-cyclohexen-1-yl) ≈ RSE(3-cyclohepten-1-yl) = −13.3 kcal mol^{-1} and RSE(3,5-cycloheptadien-1-yl) = −17.3 kcal mol^{-1}; see also ref. [73]. [u] With respect to *N*-methylacetamide (NMA) [45]: Solvent effect = k_{obs}(DPE)/k_{obs}(NMA). [v] $k_{rel} = k$(DPE)/k(benzonitrile), see also ref. [40]. [w] Kinetic isotope effect for the reaction with [D_4]-**2**. [x] $k_{rel} = k/k$(**1**).

and 1,1-bis(*p*-tolyl)allene (**72**, 50%). No kinetic data is available for the latter three cases, because the portion of the ane product is too high.

When the sterically demanding H donor 1,4,5,8-tetramethyl-9,10-dihydroanthracene (**40**) was employed, transfer hydrogenation of **47** is not accompanied by the ane reaction, so that a kinetic analysis is feasible.[70] Steric effects of α-alkyl groups influence the rate of the reaction only to a minor extent. The difference in $\Delta H^{\neq}$ for the reaction of **2** with **1** (31.8 kcal mol^{-1}) and 1,1-diphenylethene (**63**) (32.3 kcal mol^{-1}) is also surprisingly low, which can probably be attributed to the strong distortion of **63** ($\alpha = 43.5$[75]). The high reactivity of the dibenzofulvenes **55**–**58** can be explained with an increased π-electron ground-state energy of fulvenes[76] as well as with the planarity of the formed radicals.[34]

If the carbon atom that is attacked during H transfer is substituted, the rate of the transfer hydrogenation decreases, and the enthalpy of activation increases, as is known for radical addition

reactions onto alkenes.[77] This becomes very obvious in the transition from dibenzofulvene (**55**, $\Delta H^{\neq} = 22.0\ \mathrm{kcal\,mol^{-1}}$) to 9-ethylidenefluorene (**56**, $\Delta H^{\neq} = 30.0\ \mathrm{kcal\,mol^{-1}}$) and 9-isopropylidenefluorene (**57**, $\Delta H^{\neq} = 32.6\ \mathrm{kcal\,mol^{-1}}$; Table 5). This trend is presumably caused by the steric shielding of the reaction center at the attacked β-C atom, as well as by the stabilization of the C=C bond in the ground state by additional alkyl substituents. The latter effect can be observed very clearly when phenyl substituents are introduced in the β position as, for instance, in *trans*-stilbene (**64**, $\Delta H^{\neq} = 37.6\ \mathrm{kcal\,mol^{-1}}$). The slight increase in reactivity with triphenylethene (**65**, $\Delta H^{\neq} = 35.9\ \mathrm{kcal\,mol^{-1}}$) is probably also caused by distortion. The β-substituent effect is also evident in the relatively high enthalpies of activation for indene (**59**, $\Delta H^{\neq} = 36.1\ \mathrm{kcal\,mol^{-1}}$) and 1,2-dihydronaphthalene (**60**, $\Delta H^{\neq} = 35.8\ \mathrm{kcal\,mol^{-1}}$). The high reactivity of acenaphthylene (**62**, $\Delta H^{\neq} = 26.3\ \mathrm{kcal\,mol^{-1}}$) is not only caused by the increased radical stabilization in the naphthalene system,[78] but also by the *cis* stereochemistry of the double bond. At 300 °C, *trans*-crotylbenzene reacts approximately ten times slower than **1**.

Neither the rate constants nor the activation parameters change significantly when both methyl groups in **57** are replaced with two cyano groups to give 9-fluorenylidenemalononitrile (**58**). This observation is consistent only with a radical reaction mechanism and indicates a slightly polarized transition state. The solvent effect of 0.91 established for **57** at 300 °C in the transition from diphenyl ether to *N*-methylacetamide supports this hypothesis even though dibenzofulvenes possess notable dipolar character.[76] This character is probably strongly reduced in **58**, since both the dicyanomethylene and the fluorenylidene substituents can stabilize anionic but not cationic charges. Therefore, no decrease in the rate of reaction is observed by conjugation in the ground state. It is noteworthy that **57** and **58** are the only tetrasubstituted alkenes to date for which kinetic data have been established for the H-transfer reaction. Although tetraphenylethene reacts with **2** to yield the dihydro product, even at 380 °C, the reaction is very slow, and side reactions such as the decomposition of 9,10-dihydroanthracene (**2**) to tetrahydroanthracene [**73**, Eq. (41)] are so pronounced that activation parameters could not be obtained.[79]

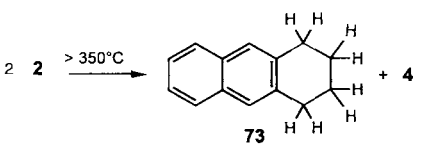

(41)

H acceptors containing conjugated C=C bonds such as 1,3-cyclohexadiene (**67**), cycloheptadiene (**68**), and cycloheptatriene (**69**)[36] are also subject to retrodisproportionation with **2** as the H donor (Table 5). Once again, $\Delta H^{\neq}$ and ΔH_R correlate within the expected values, and the other common criteria support a radical mechanism of the transfer hydrogenation.

Especially interesting is the transfer hydrogenation of azulene (**74**). Under mild conditions at 260–310 °C with **30** as the H donor, a mixture consisting of two isomeric octahydroazulenes is formed in almost quantitative yield (Scheme 9).[38b] However, when this reaction is performed at 330–380 °C and with **2** as the H donor, only 40% of the isomeric octahydroazulenes **75a**/**75b** is obtained along with 32% naphthalene and 17% tetraline. Azulene (**74**) by itself is stable under these reaction conditions. These observations support the mechanism of the thermal azulene–naphthalene rearrangement (42) at 400 °C as proposed by Scott et al.[80] Accordingly, the H-atom adducts of azulene are responsible for the isomerization. The purely

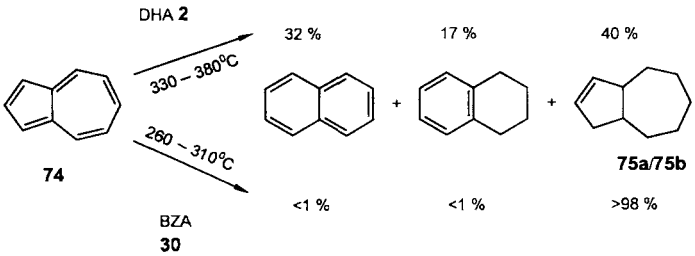

Scheme 9. Product distribution of the transfer hydrogenation of azulene (**78**) with DHA (**2**) at 330–380 °C, and with BZA (**30**) at 260–310 °C in diphenyl ether [38]; **75a,b**: two constitutional isomers.

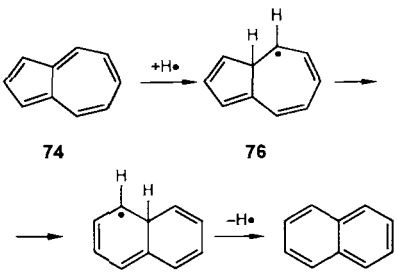

(42)

thermal azulene–naphthalene rearrangement suffers from the fact that no suitable H donor is available. Therefore, the rearrangement occurs in the presence of **2** or **30** at milder reaction conditions. The different course of reaction upon the use of **2** or **30** can be explained by the high donor reactivity of the latter upon trapping of the intermediate radical **76**.

Among aromatic π systems the rate of reaction with **2** increases in the order anthracene (**4**),[19] tetracene (**77**),[71] and pentacene (**78**) to form the corresponding dihydro derivatives. Depending on the reaction conditions even the unsaturated fullerenes C_{60} and C_{70} can be hydrogenated to $C_{60}H_{36}$, $C_{60}H_{18}$, or $C_{70}H_{36}$ (Scheme 10).[81]

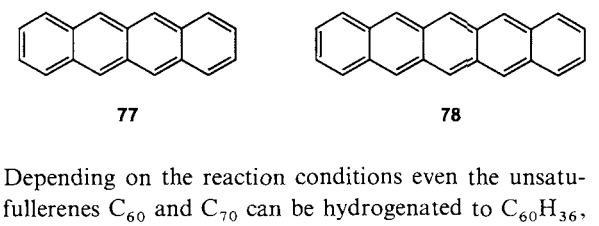

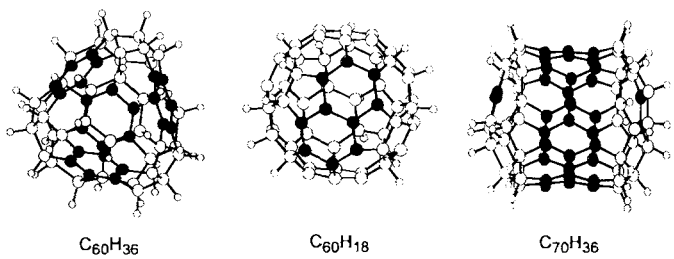

Scheme 10. Proposed structures for $C_{60}H_{36}$, $C_{60}H_{18}$, and $C_{70}H_{36}$. The sp^2-hybridized carbon atoms are partially filled for a better overview [80, 81].

Upon heating to 550 °C, the isolated hydrogenated fullerenes eliminate hydrogen to reform the parent fullerenes. This observation prompted investigations targeted towards the use of fullerenes as H-transfer promotors.[82]

2.2.3. Isokinetic Relationship

Comparison of the activation parameters of the investigated H donor/H acceptor pairs upon variation of the H donor and H acceptor clearly showed a parallel course of the enthalpy of activation $\Delta H^{\neq}$ and the entropy of activation $\Delta S^{\neq}$, which is a general trend. Smaller values of $\Delta H^{\neq}$ are accompanied by smaller values of $\Delta S^{\neq}$ and vice versa. Therefore, the entropy of activation $\Delta S^{\neq}$ acts as an antagonist to the enthalpy of activation $\Delta H^{\neq}$ when ranking the reactivities of the rate constants. Such a correlation between $\Delta H^{\neq}$ and $\Delta S^{\neq}$ for a given series of reactions is referred to as an "isokinetic relationship",[83] and is shown in Figure 8 for the results from Tables 4 and 5 (see also ref. [22b]). The slope of the best-fit curve β (in K) is the isokinetic temperature [Eq. (d)].[84] The value of β represents the tem-

$$\Delta H^{\neq} = \Delta H_0^{\neq} + \beta \Delta S^{\neq} \qquad \text{(d)}$$

perature at which all reactions of a given series should occur with the same rate constant. The isokinetic relationship can also be deduced from the temperature dependency of the rate constants of the various H-transfer reactions.[36] For the retrodisproportionation reactions shown in Figure 8 β is greater than 1000 K, which indicates that all the reactions presented here proceed at temperatures significantly below the isokinetic temperature.

In many cases it cannot be unambiguously determined if an isokinetic relationship is indeed significant. Statistical uncertainties of a kinetic analysis[84, 85] and systematic errors can create the impression of such a relationship, since, according to the Eyring relationship, $\Delta H^{\neq}$ and $\Delta S^{\neq}$ are interdependent parameters. In the current series of experiments, the statistical experimental errors of $\Delta H^{\neq}$ (2–3 kcal mol^{-1}) are small compared to the expanded range of the isokinetic relationship ($\Delta H^{\neq}$ = 19.6 kcal mol^{-1} for A2 and 37.6 kcal mol^{-1} for C17 in Figure 8). Systematic errors, especially the reversibility of the retrodisproportionation step, were also excluded when possible. The significance of the $\Delta H^{\neq}$ values are supported by their good correlation to the reaction enthalpies ΔH_R or the C–H bond enthalpies, respectively, in Figures 7 and 8.

A structure variation of the starting materials that causes a more pronounced interaction in the transition state ($\Delta G^{\neq}$) leading to a decrease in $\Delta H^{\neq}$ probably results in a shorter C–H–C distance in the transition state and, thus, in a parallel decrease in $\Delta S^{\neq}$.[83b] The main portion of the entropy loss occurs upon formation of the activation complex from the starting materials and, therefore, depends on the varying attraction of the starting materials in the activation complex (ΔS_0 activation complex) as well as on the requirements for the orientation of the starting materials to each other during the formation of the activation complex. The transition state is loacted between the activation complex and the radical pair on the ΔG reaction coordinate (Figure 1). The H-atom transfer occurs in this section under formation of the radical pair, which should be located close to the maximum of ΔG. The strong variation of $\Delta S^{\neq}$ within the reaction series suggests that the structures of the transition states vary depending on the starting materials. According to the Hammond principle, the smaller the reaction enthalpy of the retrodisproportionation step, the shorter the C–H–C distance in the transition state and the lower the entropy could be (Figure 9).

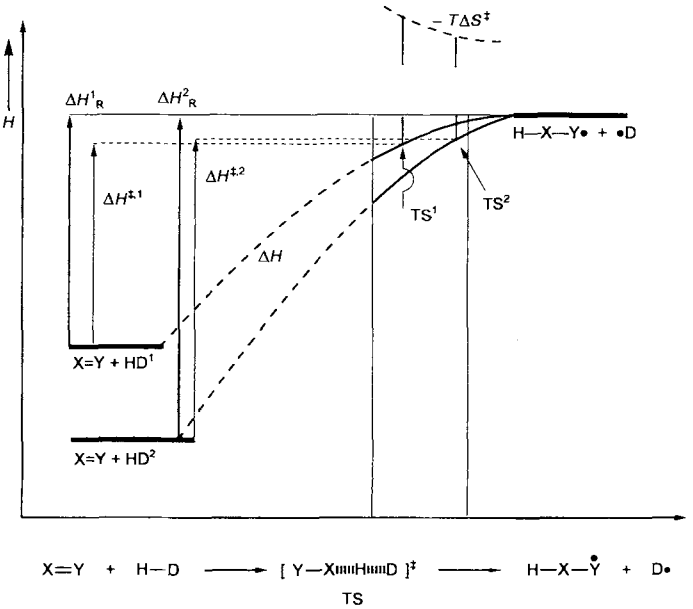

Figure 9. Shift of the transition state TS along the reaction coordinate for reactions with various reaction enthalpies; starting materials: X=Y and H–D; free radicals: H–X–Y• and D•.

Accordingly, $\Delta S^{\neq}$ would decrease parallel to $\Delta H^{\neq}$ or ΔH_R (for a similar demonstration see also ref. [86]). The fact that the actual H transfer takes place in the transition state ($\Delta G^{\neq} = \Delta G_{max}$) when the radical formation has not yet been completed explains the observation of H/D isotope effects close to the theoretical maximum on the reaction rates. It also becomes apparent why the measured enthalpy of activation $\Delta H^{\neq}$ is generally smaller than the reaction enthalpy ΔH_R.

2.2.4. Transfer Hydrogenations of C=X and X=X

Retrodisproportionation is not limited to H acceptors containing C=C bonds. However, carbonyl groups are less reactive, probably due to their high bond enthalpies. α,β-Unsaturated carbonyl compounds were selectively hydrogenated at the C=C bond,[56c] whereas ketones were only slowly hydrogenated under the same reaction conditions (activated charcoal, white mineral oil).[56c] The reduction of fluorenone (**79**) with DHA and other H donors to form fluorene (**28**) occured only above 400 °C.[68] The reduction of benzophenone (**80**) with tetraline starts with a radical transfer hydrogenation [see Eq. (43) in Scheme 11]; benzhydryl ether (**81**) is presumably formed in a secondary reaction [Eq. (44)] and further reduced to diphenylmethane (**82**) in a radical-chain reaction [Eq. (45)].[68] The complex nature of this reaction could be confirmed in our laboratory.[87]

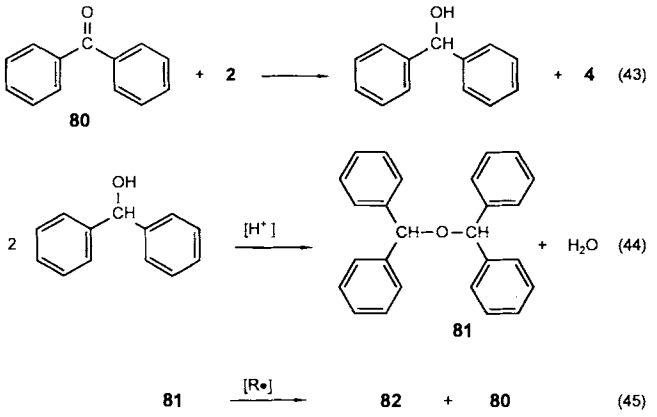

Scheme 11. Transfer hydrogenation of benzophenone with DHA (2).

The C=N bond in benzylideneaniline (**83**) could be readily hydrogenated to *N*-benzylaniline (**84**) upon heating with **2** or, for example, with 2,6-dimethoxy-9,10-dihydroanthracene to 280–320 °C in diphenyl ether [Eq. (46)]. Activation data and

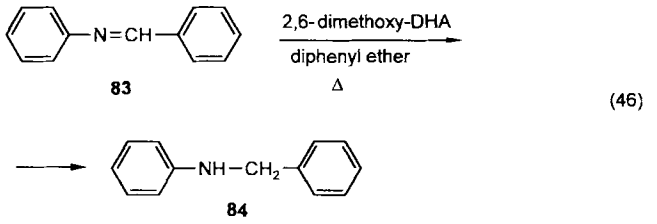

kinetic isotope effects (Table 6) again support an initial retrodisproportionation with subsequent H transfer in which, according to AM1 calculations, the hydrogen primarily adds onto the nitrogen and not the carbon atom.[36c]

Table 6. Kinetic and thermodynamic data for the transfer hydrogenation of H acceptors containing C=X bonds with H donors in diphenyl ether (DPE). X = heteroatom.

H Acceptor	H Donor	$\Delta G^{\ddagger}_{300\,°C}$ [kcal mol^{-1}]	$\Delta H^{\ddagger}$ [kcal mol^{-1}]	$\Delta S^{\ddagger}$ [cal K^{-1} mol^{-1}]
83 [36c]	[a]	42.5±0.4 [b]	29.7±0.4	−22.3±0.6
85a [69c]	**2**	38.9±0.4 [b]	25.8±0.4	−23.0±0.7
85a [69c]	**10**	39.3±0.3	23.8±0.3	−27.1±0.7
85b [69c]	**2**	39.9±0.4	25.6±0.4	−24.2±0.7
85c [69c]	**2**	38.9±0.7	26.5±0.7	−21.9±1.4
85d [96c]	**2**	39.9±0.4	26.9±0.4	−22.6±0.7
85e [69c]	**2**	38.0±0.2	26.5±0.2	−20.0±0.4
85f [69c]	**2**	37.3±0.4	27.6±0.4	−17.0±1.0
85g [69c]	**2**	40.2±0.5	28.0±0.5	−21.2±1.0

[a] 2,6-Dimethoxy-9,10-dihydroanthracene. [b] Solvent effect [45] k_{obs}(NMA)/k_{obs}(DPE) = 2.2 (**85a**, 200 °C); k_{obs}(benzonitrile)/k_{obs}(DPE) = 2.9 (**83**, 300 °C). [c] k_H/k_D = 1.4 (**83**, 300 °C; 4.7 (**85a**, 220 °C).

At temperatures between 190 °C and 250 °C, azobenzene (**85a**) and the substituted azobenzenes **85b–g** (50 mM) also react

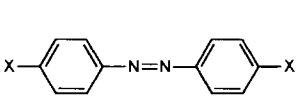

X = H **85a** X = Cl **85e**
X = CH_3 **85b** X = Br **85f**
X = *t*Bu **85c** X = NH_2 **85g**
X = OCH_3 **85d**

with **2** (1.0 M) in diphenyl ether.[69c, 88] Hydrazobenzene (**86**) could be detected by gas chromatography as an intermediate in the reaction of **85a**, ultimately leading to the formation of 68% aniline (**87a**) and 32% of a 1:1 mixture of *o*- and *p*-semidine [**88** and **89**, Eq. (47)].

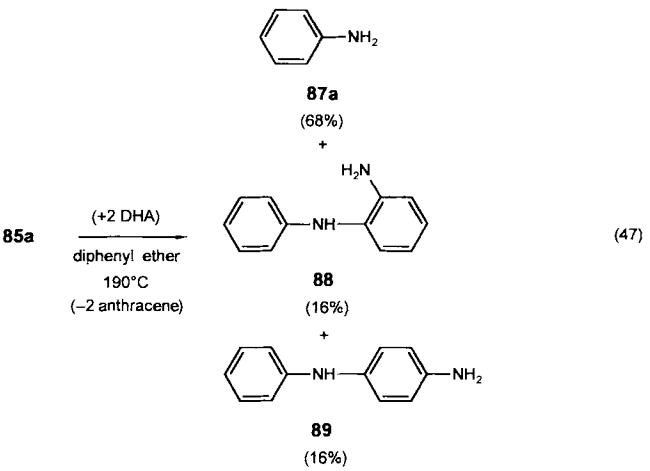

The yield of semidine decreases with higher temperatures. The yields of tetraline or *N*-methylacetamide are very similar. The reaction with *p*,*p*′-dimethylazobenzene (**85b**) at 220 °C in diphenyl ether led to the formation of *p*-toluidine (**87b**, 76%) and the corresponding *o*-semidine **88b** (20%). Similar ratios were found with **85c–f**. In contrast, *p*-phenylenediamine was formed exclusively in the transfer hydrogenation of **85g**. When performing the transfer hydrogenation of **85a** with xanthene (**10**) at 250 °C in diphenyl ether, 75% **87a**, 15% **88**/**89**, and 88% of bixanthene (**12**) formed. Dimer formation indicates the intermediate existence of the 9-xanthyl radicals **11** in the hydrazobenzene formation [see Eq. (48), (49) in Scheme 12]. Under the latter reaction conditions, **11** could also be detected by ESR spectroscopy with high resolution.

It remains unclear whether the formation of **87a** is caused by thermolysis of **86**[89] or by transfer hydrogenation [Eq. (50)]. The activation parameters for the azobenzene reduction determined by kinetic measurements confirm that the retrodisproportionation step (48) with X = O, CH_2 is rate-determining (Table 6). However, it is still not proven if this step is partially reversible under the given reaction conditions. The reaction enthalpy of 33 kcal mol^{-1} estimated from thermodynamic data at 25 °C for the retrodisproportionation of **2** (X = CH_2) with **85a** [Eq. (48)][90] corresponds well to the enthalpy of activation of 26 kcal mol^{-1} determined at 190–250 °C. Indications for a radical retrodisproportionation step, but against a possible hydride-transfer mechanism, are the small reactivity difference between **2** and **10**, (Table 6) and the small solvent effect on the rate of the transfer hydrogenation of **85a** with **2** (k(NMA)/k(DPE) = 2.2 at 200 °C).[69c] The solvent effect, which is of the same order of magnitude as for the reaction of **2** with **1**, supports a similar reaction mechanism, as does the isotope effect of k_H/k_D = 4.7 at 220 °C (Table 6).

Transfer hydrogenation of **85a** with **2** can also be considered as a dehydrogenation reaction under aromatization of **2** to anthracene (**4**). This possibility raises the question whether the

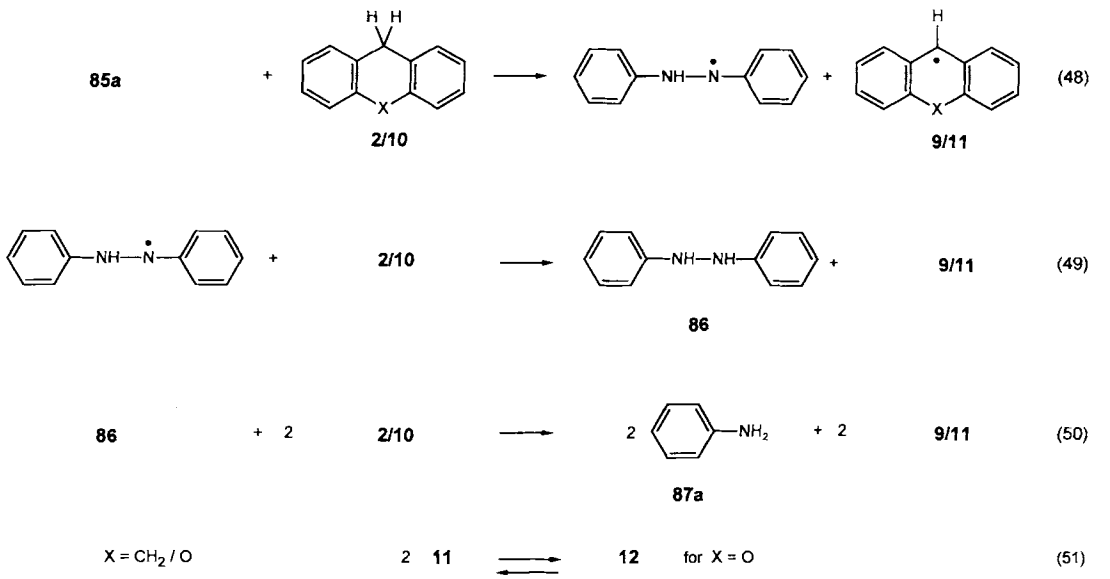

Scheme 12. Transfer hydrogenation of azobenzene (**85a**) with xanthene (**10**; X = O) or dihydroanthracene (**2**; X = CH_2) as the H donor.

stepwise H-atom transfer discussed here is mechanistically feasible for dehydrogenation reactions in general,[91] either supplementary or alternatively to the common hypothesis of a direct hydride or electron transfer.[91b] Prompted by this issue, we investigated transfer hydrogenations with aromatic nitro[91c] and nitroso compounds[91d] as well as with quinones.[11, 12] Nitrobenzene (**90**) was quantitatively reduced to aniline (**87a**) upon heating to 230–280 °C with excess **2** or **10** [Eq. (52)].[69]

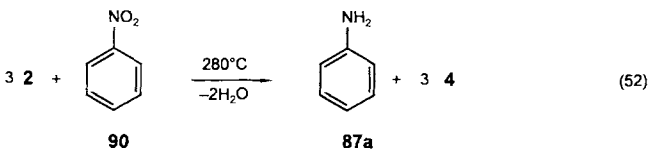

para-Substitution of **90** with methoxy, methyl, or cyano groups increased the rate of reduction with **2** by a factor up to a maximum of 7. Polar solvents do not have a significant or unambiguous influence on the rate of reduction (half-lives $t_{1/2}$; *N*-methylacetamide:diphenyl ether:*o*-dichlorobenzene:benzonitrile 2:14:56:52). The slightly increased substituent and solvent effect compared to the reaction of **2** with **1** is probably caused by the higher electronegativity of the H acceptor **90**. The kinetic isotope effect, which was determined with $[D_4]$-**2** was 2.4 (280 °C) in diphenyl ether. The reactions exhibit first-order kinetics with respect to **90**, but not precisely with respect to the H donor. This is presumably caused by the multistep process [see Eqs. (53)–(55) in Scheme 13] in which various NO radicals occur as intermediates, which can make the reaction more complicated. The experiments were therefore performed under conditions of pseudo-first-order kinetics.[69] Retrodisproportionation or an H-atom transfer is again proposed as the initial step.

Xanthene (**10**) is less reactive than **2**, which is also in contradiction to a direct hydride-transfer mechanism.[69] The observation of the strong ESR signal for the 9-xanthyl radicals **11** during the reaction supports the retrodisproportionation step. The formation of 9,9-bixanthene (**12**) as the major product shows that the radical formation does not constitute a side reaction.

Nitrosobenzene (**91**) was quantitatively converted into aniline (**87a**) and anthracene (**4**) when exposed to **2** at temperatures as low as 210 °C; azoxybenzene (**94**) and presumably phenylhydroxylamine (**92**) occur as intermediates (Scheme 13).[69b] The phenylaminyl radicals **93** were apparently trapped by excess **91**, as in spin-trapping experiments [Eq. (59)].

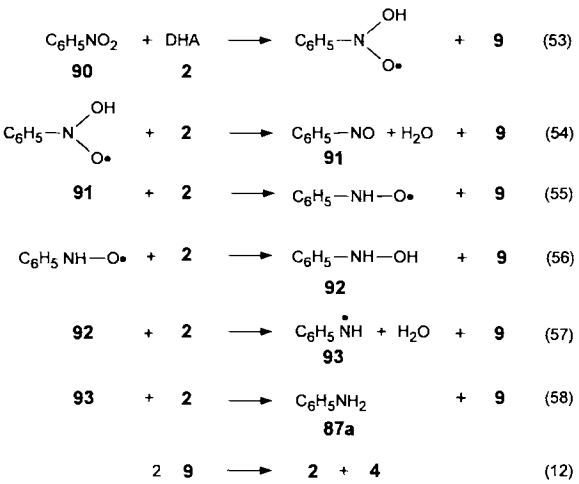

Scheme 13. Mechanism of the transfer hydrogenation of nitrobenzene (**90**) with DHA (**2**).

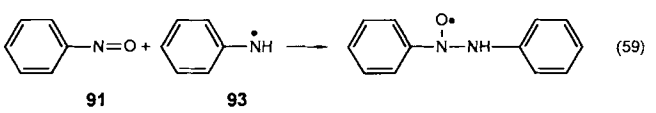

The aliphatic nitrocyclohexane (**95**) was also reduced with **2** at 280 °C to a mixture of cyclohexene and cyclohexane [Eq. (60)].[92a] The *syn* elimination of HNO_2 appears to compete with the reduction. 1- and 2-Nitroadamantane were reduced to

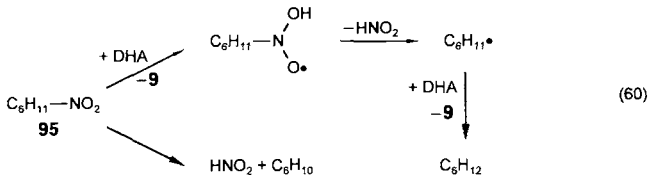

(60)

adamantane at 300 °C without any elimination.[92b] However, the homolytic cleavage of the $C-NO_2$ bond competes with the retrodisproportionation.[92a]

Reduction of phenylhydroxylamine as the intermediate [Eq. (57) in Scheme 13] presumably represents a different, novel step of a bimolecular radical formation, namely transfer hydrogenolysis (Section 3). Interest in the uncatalyzed transfer hydrogenation of nitro compounds focuses predominately on the elucidation of the reaction mechanism (retrodisproportionation versus hydride transfer) of the dehydrogenation and aromatization of cyclic alkenes by nitro compounds as, for instance, occurs in the Skraup, Doebner–Miller, or Bischler–Napieralski syntheses of quinolines.[69]

Quinones are also suitable dehydrogenation agents for the aromatization of partially hydrogenated aromatic or heteroaromatic compounds.[11, 12, 93] Scheme 14 illustrates the various mechanisms discussed for this reaction (for an overview see ref. [11, 12, 94]).

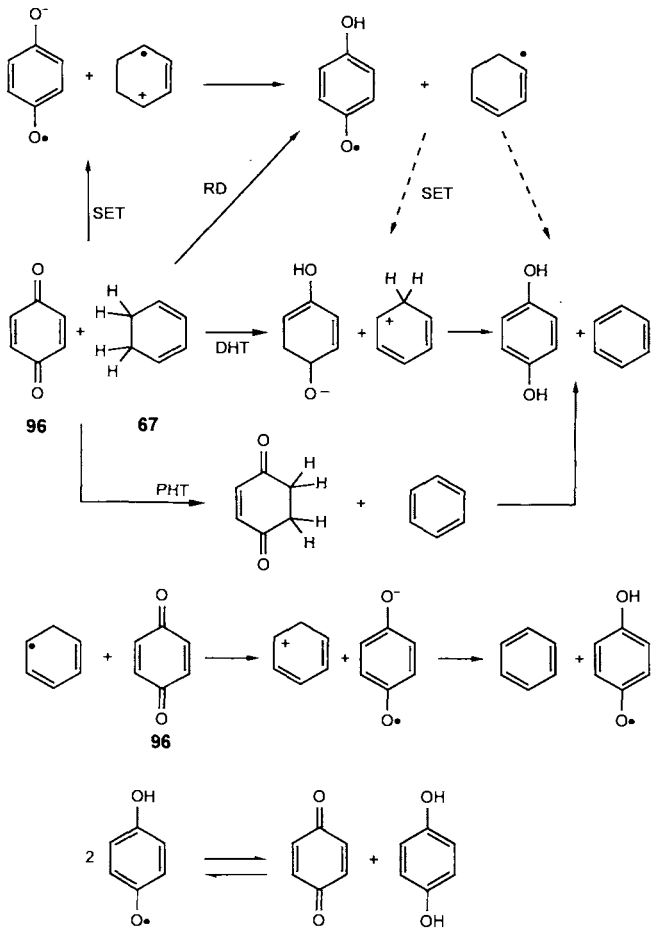

Scheme 14. Alternative pathways for the quinone dehydrogenation; single-electron transfer (SET), pericyclic H-atom transfer (PHT), direct hydride transfer (DHT), retrodisproportionation (RD).

When comparing the redox potentials of **96** and **67**, and furthermore considering the experimental enthalpy of activation $\Delta H^{\neq}$, it can be concluded that a single-electron transfer (SET) is contradictory to a dehydrogenation reaction.[94] Pericyclic H-transfer reactions (PHT) were eliminated by stereochemical isotopic labeling experiments and thermochemical arguments.[12, 94] Based on kinetic H/D isotope effects, exclusion of a radical chain mechanism, and sporadic evidence for carbenium-ion intermediates,[12] the direct hydride transfer (DHT), which was postulated by Linstead, Braude et al.,[11] is favored. However, these arguments also support a primary H-atom transfer (retrodisproportionation, RD) without any chain-reaction character, possibly followed by an electron transfer or a disproportionation. This possibility is supported by the fact that the hypothesis of increased reaction rates in polar solvents has not been convincingly proven.[12]

At 80 ° in nondried dioxane, **2** and **10** react with 2,3-dichloro-5,6-dicyano-1,4-benzoquinone (DDQ, **97**) at very similar rates and in a second-order reaction to give anthracene (**4**) or xanthone (**99**), respectively in almost quantitative yield [Eqs. (61) and (62) in Scheme 15).[94]

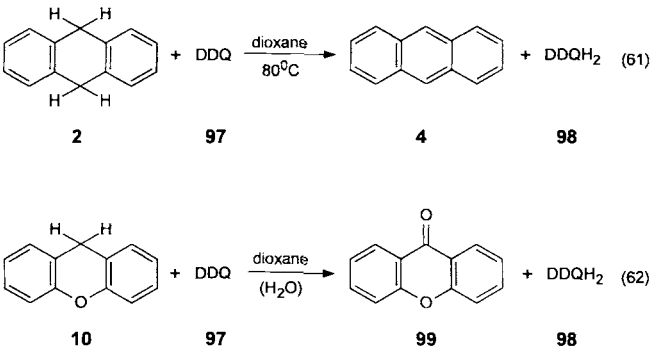

Scheme 15. Dehydrogenations of DHA (**2**) and xanthene (**10**) by DDQ (**97**).

In methanol, 18% of 9-methoxyxanthene was formed from **10** as well as 82% of **99**. Although this clearly proves the existence of the 9-xanthylium ion **100** as an intermediate, it does not provide any information as to its mechanism of formation. In the reaction of 3,5,3′,5′-tetra-*tert*-butyldiphenoquinone with xanthene in diphenyl ether at 260 °C, 35% of bixanthene (**12**) was formed, thus proving the formation of the 9-xanthyl radicals **11**.[94b] Kinetic investigations of the solvent dependency of the reaction rate were used to distinguish between the two alternatives presented in Scheme 14. The results in Table 7 show a minimal solvent effect, which is in sharp contrast to the expectations for the ionization process of the hydride transfer[40, 41] but correlates well with a primary retrodisproportionation.

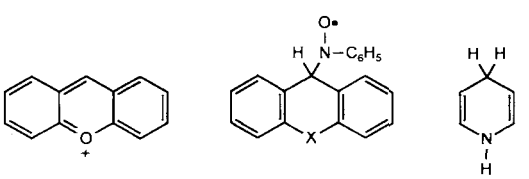

Table 7. Dehydrogenation of 9,10-dihydroanthracene (**2**, 7.2×10^{-2} M) and xanthene (**10**, 6.6×10^{-2}–1.1×10^{-1} M) by DDQ (**97**, 1.5–6.6×10^{-3} M) in various solvents at 25–65 °C.

Solvent		$E_T(30)$ [a] [kcal mol^{-1}]	k_{rel} [M^{-1} s^{-1}]	$\Delta G^{\neq}$ (25 °C) [kcal mol^{-1}]		$\Delta S^{\neq}$ [cal K^{-1} mol^{-1}]
9,10-dihydroanthracene **2**						
1	dioxane	36.0	≡1.0 [b]	20.1	11.7	−28.2
2	acetonitrile	45.6	3.6 [b]	19.4	8.3	−37.2
3	acetic acid	51.7	3.9 [b]	19.3	9.8	−32.0
4	dioxane [c]	36.0	0.12 [b]			
xanthene **10**						
5	dioxane	36.0	≡1.0 [d]	18.4	8.9	−31.8
6	acetonitrile	45.6	3.4 [d]	17.8	4.9	−43.3
7	acetic acid	51.7	3.8 [d]	17.7	9.6	−27.2
8	dioxane [e]	36.0	0.13 [b]			

[a] $E_T(30)$ parameter from ref. [40]. [b] Relative rate k_{rel} at 50 °C. [c] 9,9′,10,10′-D_4-Dihydroanthracene ([D_4]-**2**). [d] At 25 °C; $k_2(\mathbf{10})/k_2(\mathbf{2}) = 16\pm1$ at 25 °C. [e] 9,9-D_2-Xanthene ([D_2]-**10**).

The very similar rate constants of **2** and **10** are remarkable and can be explained with a primary radical formation in the 9-position (**9** and **11**, respectively), but not with the formation of carbenium ions. The oxonium stabilization of **100** should significantly accelerate the rate of reaction.[41]

Also noteworthy are the relatively low values for $\Delta H^{\neq}$ and $\Delta S^{\neq}$, which are in agreement with the isokinetic relationship established for retrodisproportionation reactions with alkenes. Unfortunately, no reliable thermodynamic data is available for the reaction enthalpies ΔH_R of this step; however, initial calculated values suggest that ΔH_R has a higher value than $\Delta H^{\neq}$.

The kinetic isotope effect $k_H/k_D = 8.0\pm0.3$ for **2** and **10** with DDQ (**97**) in dioxane at 50 °C is also astonishingly high. This value, which reaches the theoretic maximum, shows that the hydrogen transfer is completed approximately in the middle of the transition state on the ΔG reaction coordinate. This can be explained in the same way as the retrodisproportionation reactions mentioned above, however, a tunnel effect appears feasible as well.[94b, 97] Although all attempts to detect radical intermediates by ESR spectroscopy or chemically induced dynamic nuclear polarization (CIDNP)[95] failed, spin-trapping experiments with nitrosobenzene (**91**) were successful. In the reactions of DDQ with both DHA and xanthene, ESR spectra of the known adduct radicals **101** and **102** could be unequivocally identified.[94] No comparable signal could be detected without the addition of DDQ under otherwise identical reaction conditions.

The results discussed here[94] support an H-atom transfer mechanism for the quinone dehydrogenation. It is still unclear which secondary steps shown in Scheme 14 apply for the given reaction conditions. A fascinating issue is the behavior of 1,4-dihydropyridine (**103**), acridan (**23**), and *N*-methylacridan (**24**) in the reaction with quinones, since it is relevant for the mechanism of the biochemical hydride transfer with NADH or $FADH_2$.[96] Primary H-atom transfer has never been seriously considered.[96, 97] Acridan (**23**) reacts very rapidly with DDQ in acetonitrile at 40 °C to yield acridine (**104**) quantitatively.[94, 98, 99] A spin-trapping experiment with **91** provided a well-resolved ESR spectrum. Additional experiments will have to underline the significance of these results.

A related reaction, the oxidation of leuco crystal violett by chloranil (**105**) to provide cations of crystal violett was reported.[99b] The kinetics ($\Delta H^{\neq} = 8.1\pm0.5$ kcal mol^{-1}, $\Delta S^{\neq} = -19$ cal K^{-1} mol^{-1}) and the observed solvent, isotope, and pressure effects are better compatible with rate-determining H-atom transfer than the proposed electron-proton-electron transfer.[99b] The expectation that the quinone/acridan reaction also has a very low enthalpy and entropy of activation would strongly support an enzymatic mechanism in which the $\Delta S^{\neq}$ barrier is overcome in the substrate–enzyme complex (entropy protection).

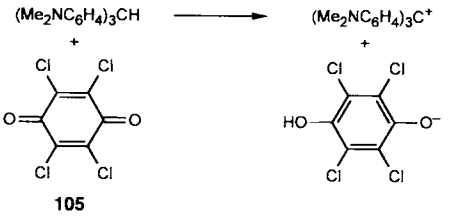

3. Transfer Hydrogenolysis

A novel type of bimolecular radical formation was found with the transfer hydrogenolysis and investigated quantitatively in the reaction of 1-adamantyldiphenylmethyl fluoride (**5**) with **2** [see Eq. (63) in Scheme 16 and Eq. (2)].[4] The reaction of **5** with

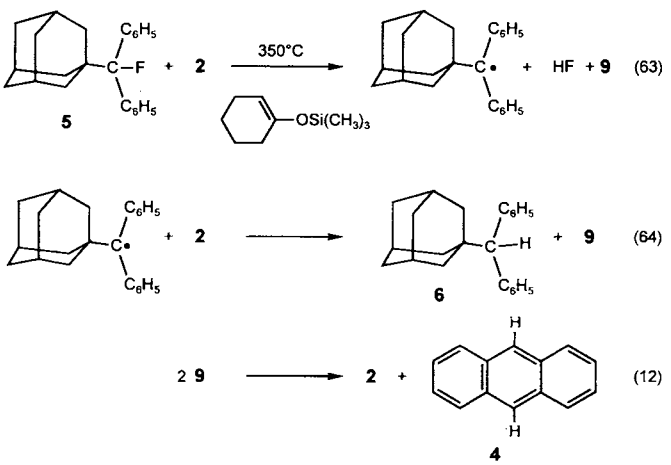

Scheme 16. Mechanism of the transfer hydrogenolysis of 1-adamantyldiphenylmethyl fluoride (**5**) with DHA (**2**) [4].

2 (tenfold molar excess) was observed between 330 °C and 375 °C with 1-(trimethylsiloxy)cyclohexene as the solvent and an efficient HF trap. The reaction products included 1-adamantyldiphenylmethane (**6**, >95% yield) as well as anthracene (**4**), cyclohexanone, and trimethylsilyl fluoride.

No example exists in the literature[4, 16, 17] for the first step (63) of this reaction sequence. The following reaction steps (64) and (12) represent a known H-trapping reaction and disproportionation. Under the given conditions, the reaction proceeds stoichiometrically rather than by a chain mechanism. The reaction mechanism illustrated in Scheme 16 was supported by selecting xanthene (**10**) and 7*H*-benz[*de*]anthracene (**30**) as H donors. In these experiments, the intermediate 9-xanthyl rad-

icals **11** and the 7*H*-benz[*de*]anthryl radicals, respectively, were detected by ESR spectroscopy with high intensity and resolution.[4] Similar to the experiments on the retrodisproportionation with **2** as the H donor, the corresponding 9-hydroanthryl radicals **9** cannot be proven by ESR due to the rapid disproportionation [Eq. (12)]. Comparison of the experimental enthalpy of activation $\Delta H^{\neq}$ with the reaction enthalpy ΔH_R (see Section 2.2) is in agreement with the postulated radical mechanism (Table 8). The comparison allows the conclusion that the transition state of this reaction is also located very close to the radicals. Deuteration experiments with [D_4]-**2** identified H transfer as the rate-determining step ($k_H/k_D(373\,^{\circ}C) = 2.4$). The reverse reaction with rate v_{-2} as a termolecular process is kinetically disfavored, hence it can be disregarded.[4]

Table 8. Kinetic and thermodynamic data for the bimolecular radical formation of 1-adamantyldiphenylmethyl fluoride (**5**) by 9,10-dihydroanthracene (**2**) [4].

$\Delta H^{\neq}$ [kcal mol^{-1}]	$\Delta S^{\neq}$ [cal K^{-1} mol^{-1}]	$\Delta G^{\neq}_{300\,K}$ [kcal mol^{-1}]	ΔH_R [kcal mol^{-1}]
37.2±0.5	−18.8±0.8	48.0±0.5	48.1±2.2

Additional experiments on the transfer hydrogenolysis showed that, in addition to triphenylfluoromethane, diphenylfluoromethane, and benzyl fluoride, 1-adamantyldiphenyl chloride also reacts with **2** with H transfer. The driving force of the transfer hydrogenolysis with fluorides is clearly the high bond enthalpy of hydrogen fluoride (136 kcal mol^{-1}).[4]

4. Summary and Outlook

Retrodisproportionation and transfer hydrogenolysis represent novel methods for forming radicals. Mechanistic investigations led to systematic and broad structural variations from which quantitative relationships were recognized and formulated, thus making retrodisproportionation very versatile. Both reactions can be classified as bimolecular radical-formation reactions of the known tetramethylene concept,[14e] which includes the intramolecular variation of the Bergman cyclization of enediynes (Scheme 17).[100]

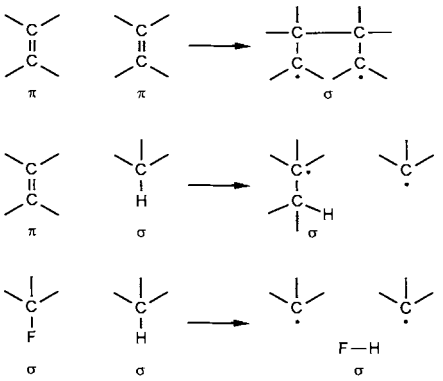

Scheme 17. Classification of bimolecular, molecule-induced radical-formation reactions: a) tetramethylene concept (that is, reaction of $F_2C{=}CF_2$ with styrene (**47**)) [14e]; b) retrodisproportionation (reaction of **1** with **2**); c) transfer hydrogenolysis (reduction of a benzylhydryl fluoride with **2**).

Instead of the established H donors containing C–H bonds, it should be feasible to employ additional H donors including, for instance, O–H, S–H, Si–H, or metal–H groups[20] as a source of H in the systematic variation of starting materials for retrodisproportionation and transfer hydrogenolysis. It is possible that some catalytic hydrogenations that proceed in the presence of metals or metal complexes with the intermediacy of metal hydrides involve retrodisproportionations.[20, 52] Broad variations are also likely for H acceptors beyond the systems known to date (conjugated or isolated olefins, ketones, polycyano alkenes, quinones, alcohols, nitro and nitroso groups, aromatic compounds, fluorides, and chlorides), which should be investigated more precisely and completely, and new systems should also be the focus of future investigations (aldehydes, ketenes, and S=O groups). Moreover, future mechanistic studies should be targeted to test, underline, or supplement the examples of retrodisproportionations that have been postulated but only qualitatively investigated.[101]

We wish to thank the following colleages who participated in the investigations reported in this review and who, both experimentally and conceptually, contributed significantly to the success of this research: Dr. Margot Nölke, Dr. Friedrich Keller, Dr. Frank Schaffer, Dipl.-Chem. Michael Cöllen, Dipl.-Chem. Christoph Höfler, Dipl.-Chem. Heike Friebolin, Dipl.-Chem. Jens Morgenthaler, Dipl.-Chem. Rolf Roers, Dipl.-Chem. Frank Wurche, and Peter Kapferer. Furthermore, we wish to thank Dr. S. P. Verevkin (thermochemistry), Dr. Manfred Keller (crystal-structure analysis), Dr. Dieter Hunkler (NMR spectroscopy), and Dr. Jürgen Wörth (mass spectrometry) and their co-workers for numerous extensive analytical investigations. Special thanks go to Dr. Hans-Dieter Beckhaus for continuous discussions and competent support (ESR spectroscopy, calculational methods, thermochemistry) as well as for a critical reading of this manuscript. We would also like to thank Prof. Dr. A. G. Davies (London) and Prof. Dr. A. L. J. Beckwith (Canberra) for many stimulating discussions and ideas. We gratefully acknowledge financial support by the Deutsche Forschungsgemeinschaft and the Fonds der Chemischen Industrie.

Received: June 19, 1996 [A 169 IE]
German version: *Angew. Chem.* **1997**, *109*, 1474–1498
Translated by Dr. Detlef Klingberg, Toledo OH (USA)

[1] C. Rüchardt, H.-D. Beckhaus, *Topics Curr. Chem.* **1985**, *130*, 1–22.
[2] a) M. Nölke, S. P. Verevkin, H.-D. Beckhaus, C. Rüchardt, *Liebigs Ann. Chem.* **1995**, 41–51, and earlier publications; b) K. Rakus, S. P. Verevkin, J. Schätzer, H.-D. Beckhaus, C. Rüchardt, *Chem. Ber.* **1994**, *127*, 1095–1103, and earlier publications.
[3] C. Rüchardt, M. Gerst, M. Nölke, *Angew. Chem.* **1992**, *104*, 1516–1518; *Angew. Chem. Int. Ed. Engl.* **1992**, *31*, 1523–1525.
[4] F. Schaffer, H.-D. Beckhaus, H.-J. Rieger, C. Rüchardt, *Chem. Ber.* **1994**, *127*, 557–563.
[5] R. D. Guthrie, B. Shi, V. Rajagopal, S. Ramakrishnan, B. H. Davis, *J. Org. Chem.* **1994**, *59*, 7426–7432.
[6] K. N. Houk, Y. Li, J. D. Evanseck, *Angew. Chem.* **1992**, *104*, 711–739; *Angew. Chem. Int. Ed. Engl.* **1992**, *31*, 682–708.
[7] a) J. A. K. Howard, K. Mackenzie, R. E. Johnson, *Tetrahedron Lett.* **1989**, *30*, 5005–5008; b) L. A. Paquette, M. A. Kesselmayer, R. D. Rogers, *J. Am. Chem. Soc.* **1990**, *112*, 284–291; L. A. Paquette, G. A. O'Doherty, R. D. Rogers, *ibid.* **1991**, *113*, 7761–7762; c) H. Geich, W. Grimme, K. Proske, *ibid.* **1992**, *114*, 1492–1493; d) W.-D. Fessner, Ph.D. thesis, Universität Freiburg, **1986**; e) J.-P. Hagenbuch, B. Stampfli, P. Vogel, *J. Am. Chem. Soc.* **1981**, *103*, 3934–3937; f) D. F. Feller, M. W. Schmidt, K. Ruedenberg, *ibid.* **1982**, *104*, 960–967; g) A. Frontera, G. A. Suñer, P. M. Deyá *J. Org. Chem.* **1992**, *57*, 6731–6735; h) K. N. Houk, Y. Li, M. A. McAlliston, G. O'Doherty, L. A. Paquette, W. Siebrand, Z. K. Smedarchina, *J. Am. Chem. Soc.* **1994**, *116*, 10895–10913; i) K. Mackenzie, J. A. K. Howard, R. Siedlecka, K. B. Astin, E. C. Gravett, C. Wilson, J. Cole, R. G. Gregory, A. S. Tomlins, *J. Chem. Soc. Perkin Trans. 2* **1996**, 1749–1760.

[8] The enthalpy of activation for the reaction of 2-butene with butadiene, a $[_\sigma 2_s + _\pi 2_s + _\sigma 2_s + _\pi 4_s]$-type reaction, was calculated to be 45 kcal mol^{-1}.[6] As it should be higher for the transfer-hydrogenation of **1** with **2**, since the aromaticity of **1** would be given up in this pericyclic reaction, it should be excluded as a mechanistic possibility. The enthalpy of activation $\Delta H^{\neq}$ of the transfer hydrogenation of **1** and **2** was experimentally determined to be 31.8 kcal mol^{-1}, approximately 15 kcal mol^{-1} lower than that of a pericyclic process.

[9] a) H. M. R. Hoffmann, *Angew. Chem.* **1969**, *89*, 597–618; *Angew. Chem. Int. Ed. Engl.* **1969**, *8*, 556–577; b) B. B. Sinder, *Acc. Chem. Res.* **1980**, *13*, 426; E. C. Keung, H. Alper, *J. Chem. Educ.* **1972**, *49*, 97; c) R. Loncharich, K. N. Houk, *J. Am. Chem. Soc.* **1987**, *109*, 6947–6952; the enthalpy of activation $\Delta H^{\neq}$ and the entropy of activation $\Delta S^{\neq}$ for the ene reaction of ethene or formaldehyde with propene are $\Delta H^{\neq} = 21.4$ kcal mol^{-1} and $\Delta S^{\neq} = -43.0$ e.u., and $\Delta H^{\neq} = 26.4$ kcal mol^{-1} and $\Delta S^{\neq} = -40.1$ e.u., respectively; the enthalpies of activation $\Delta H^{\neq}$ for the reactions of ethene with *cis*- and *trans*-2-butene are $\Delta H^{\neq} = 37.0$ kcal mol^{-1} and 36.5 kcal mol^{-1}, respectively. The entropies of activation for intermolecular ene reactions are generally between -32 and -40 e.u., and approximately -20 e.u. for intramolecular ene reactions. However, the enthalpy of activation for an ene reaction of **1** with **2** should have higher values, since the aromaticity of **2** would be perturbed.

[10] The entropy of activation changes by 4 ± 2 cal K^{-1} mol^{-1} when **40** is used as the H donor instead of **2** (see Table 4).

[11] E. A. Braude, R. P. Linstead, *J. Chem. Soc. (London)* **1954**, 3544–3547; E. A. Braude, L. M. Jackman, R. P. Linstead, *ibid.* **1954**, 3548–3568; E. A. Braude, A. G. Brook, R. P. Linstead, *ibid.* **1954**, 3569–3578.

[12] a) B. M. Trost, *J. Am. Chem. Soc.* **1967**, *89*, 1847–1851; b) F. Stoos, J. Rocek, *ibid.* **1972**, *94*, 2719–2723; c) J. March, *Advanced Organic Chemistry 4th ed.*, Wiley, New York, **1992**, p. 1163; d) L. M. Jackmann, *Adv. Org. Chem.* **1960**, *2*, 329–366.

[13] a) "New Approaches in Coal Chemistry": S. E. Stein, *ACS Symp. Ser.* **1981**, *169*, 97–129; b) M. L. Poutsma, *Energy and Fuels* **1990**, *4*, 113–131, and references therein. The thermal degradation of phenol–formaldehyde resins by tetraline probably proceeds very similarly, see D. Braun, R. Steffan, *Angew. Makromol. Chem.* **1980**, *92*, 169–189; c) L. J. J. Laarhoven, P. Mulder, *J. Phys. Chem.* **1997**, *101*, 73–77.

[14] a) L. T. Scott, W. R. Brunsvold, *J. Org. Chem.* **1979**, *44*, 641; b) W. D. Graham, J. G. Green, W. A. Pryor, *ibid.* **1979**, *44*, 907–914; c) Y. K. Chong, E. Rizzardo, D. H. Solomon, *J. Am. Chem. Soc.* **1983**, *105*, 7761–7762; d) K. R. Kopecky, M.-P. Lau, *J. Org. Chem.* **1978**, *43*, 525–526; e) H. K. Hall, *Angew. Chem.* **1983**, *95*, 448–464; *Angew. Chem. Int. Ed. Engl.* **1983**, *22*, 440–456.

[15] a) J. Hartmanns, J. O. Metzger, *Chem. Ber.* **1986**, *119*, 500–507; b) J. O. Metzger, *J. Prakt. Chem.* **1990**, *332*, 767–781; c) J. Hartmanns, K. Klenke, J. O. Metzger, *Chem. Ber.* **1986**, *119*, 488–499; d) J. O. Metzger, *Angew. Chem.* **1983**, *95*, 914–915; *Angew. Chem. Int. Ed. Engl.* **1983**, *22*, 889–890; e) *Methoden Org. Chem. (Houben-Weyl) 4th ed. 1952-*, Vol. E19a, **1986**, p. 60; f) *Angew. Chem.* **1986**, *98*, 79–80; *Angew. Chem. Int. Ed. Engl.* **1986**, *25*, 80–81; g) J. O. Metzger, F. Bangert, *Chem. Ber.* **1994**, *127*, 673–675.

[16] W. A. Pryor, *Free Radicals*, McGraw-Hill, New York, **1966**, p. 116; "Radical Formation by Interaction of Closed Shell Molecules": W. A. Pryor, *ACS Symp. Ser.* **1978**, *69*, pp. 33–62.

[17] J. A. K. Harmony in *Methods in Free Radical Chemistry, Vol. 5*, (Ed.: E. S. Huyser), Marcel Dekker, New York, **1974**, pp. 101–176.

[18] a) J. J. Gajewski, A. M. Gortva, *J. Am. Chem. Soc.* **1982**, *104*, 334–335; b) A. Schönberg, E. Singer, B. Eschenhof, *Chem. Ber.* **1979**, *112*, 1763–1768.

[19] a) R. Billmers, R. L. Brown, S. E. Stein, *Int. J. Chem. Kin.* **1989**, *21*, 375–386; b) S. E. Stein, *Acc. Chem. Res.* **1991**, *24*, 350–356; c) D. M. Camaioni, S. T. Autrey, J. A. Franz, *J. Phys. Chem.* **1993**, *97*, 5791–5792; d) R. Billmers, L. L. Griffith, S. E. Stein, *J. Phys. Chem.* **1986**, *90*, 517–523.

[20] a) H. M. Feder, J. Halpern, *J. Am. Chem. Soc.* **1975**, *97*, 7186–7188; b) R. M. Bullock, E. G. Samsel, *ibid.* **1990**, *112*, 6886–6898; c) D. C. Eisenberg, J. R. Norton, *Isr. J. Chem.* **1991**, *31*, 55–66; d) J. A. Franz, D. M. Camaioni, R. R. Beishline, D. K. Dalling, *J. Org. Chem.* **1984**, *49*, 3563–3570.

[21] a) S. W. Benson, *Int. J. Chem. Kin.* **1980**, *XII*, 755–760; b) *Thermochemical Kinetics*, 2nd ed., John Wiley, New York, **1976**; c) W. Tsang in *Energetics of Organic Free Radicals* (Ed.: J. A. M. Simões, A. Greenberg, J. F. Liebman), Blackie Academic and Professional, 1st ed., London, **1996**.

[22] a) K. B. Wiberg, G. Foster, *J. Am. Chem. Soc.* **1961**, *83*, 423–429; K. B. Wiberg, R. J. Evans, *Tetrahedron* **1960**, *8*, 313–335; b) G. K. Cook, J. M. Mayer, *J. Am. Chem. Soc.* **1994**, *116*, 1855–1868; *ibid.* **1995**, *117*, 7139–7156; c) K. B. Wiberg, R. Steward, *ibid.* **1955**, *77*, 1786–1795; K. B. Wiberg, A. S. Fox, *ibid.* **1963**, *85*, 3487–3491; K. A. Gardner, J. M. Mayer, *Science* **1995**, *269*, 1849–1851; d) J. T. Groves, *J. Chem. Educ.* **1985**, *62*, 928–931; V. W. Bowry, K. U. Ingold, *J. Am. Chem. Soc.* **1991**, *113*, 5699–5707; D. Schröder, H. Schwarz, *Angew. Chem.* **1995**, *107*, 2126–2150; *Angew. Chem. Int. Ed. Engl.* **1995**, *34*, 1973–1997; e) S.-I. Murahashi, *ibid.* **1995**, *107*, 2670–2693 and **1995**, *34*, 2443–2466; R. D. Bach, I. Mintcheva, C. M. Estévez, H. B. Schlegel, *J. Am. Chem. Soc.* **1995**, *117*, 10121–10122.

[23] Results from MM2 calculations using the Bigstrain program (QCPE 514), radical parameters in accordance with ref. [24]; H.-D. Beckhaus, personal communication.

[24] a) A. Peyman, E. Hickl, H.-D. Beckhaus, *Chem. Ber.* **1987**, *120*, 713–725; A. Peyman, H.-D. Beckhaus, *J. Comput. Chem.* **1990**, *14*, 201–210; b) D. G. Truhlar, B. C. Garrett, *Acc. Chem. Res.* **1980**, *26*, 29–40.

[25] a) I. G. Pitt, R. G. Gilbert, K. R. Ryan, *J. Phys. Chem.* **1995**, *99*, 239–247; b) N. J. Turro, A. L. Buchachenko, V. F. Tarasov, *Acc. Chem. Res.* **1995**, *28*, 69–80; c) B. Krüger, Ph.D. thesis, Universität Freiburg, **1990**; d) W. R. Roth, H. Hopf, A. de Meijere, F. Hunold, S. Börner, M. Neumann, T. Wasser, J. Szurowski, C. Mlynek, *Liebigs Ann. Chem.* **1996**, 2141–2154.

[26] See for example V. Sreedhora Rao, A. K. Chandra, *Chem. Phys.* **1995**, *192*, 247–254; T. Yu, A. M. Hebel, M. C. Lim, *J. Phys. Org. Chem.* **1995**, *8*, 47–53; ref. [21b], chap. 1.9, p. 15.

[27] M. Gerst, Ph.D. thesis, Universität Freiburg, **1994**.

[28] H. Fischer, *J. Am. Chem. Soc.* **1986**, *108*, 3925–3927; H. Fischer, H. Paul, *Acc. Chem. Res.* **1987**, *20*, 200–206.

[29] At the same time, the following reactions could be excluded with the results of the deuteration experiments. a) Disproportionation of the 2-phenyl-2-propyl radicals **8** with the 9-hydroanthryl radicals **9** to form cumene (**3**) and anthracene (**4**) [3]; b) disproportionation of **8** [27]; c) methathesis reaction of **8** with **1** or **4** [27], see also ref. [19c] and D. M. Camaioni, S. T. Autrey, T. B. Salinas, J. A. Franz, *J. Am. Chem. Soc.* **1996**, *118*, 2013–2022; I. W. C. E. Arends, P. Mulder, *Energy Fuels* **1996**, *10*, 235–242; J. P. Heuts, A. Pross, L. Radon, *J. Phys. Chem.* **1996**, *100*, 17087–17089.

[30] a) M. E. Brewster, E. Pop, M.-J. Huang, N. Bodor, *Heterocycles* **1994**, *37*, 1373–1415; b) P. A. Nielsen, S. S. Glad, F. Jensen, *J. Am. Chem. Soc.* **1996**, *118*, 10577–10583.

[31] a) The isotope effect is temperature dependent: R. W. Hoffmann, *Aufklärung von Reaktionsmechanismen*, Thieme, Stuttgart, **1976**, p. 62, Table 10. The entropies of activation of the transfer hydrogenation and the transfer deuteration have approximately the same value (see Table 4). b) The kinetics were determined with the ampoule technique under pseudo-first-order conditions (minimum of tenfold molar excess of **2** over **1**) and also accounting for the volume expansion of the reaction medium.

[32] The standard enthalpies of formation ΔH_f^0(g) for the radicals R$^{\bullet}$ were calculated according to Equation (b) in Section 2.2 from the C–H bond dissociation enthalpies ΔH_{diss}(R–H), which result from the radical stabilization enthalpies RSE(R$^{\bullet}$): ΔH_{diss}(R–H) = ΔH_{diss}(Alkyl–H) – RSE(R$^{\bullet}$). ΔH_{diss}(Alkyl–H) were used as the reference values: ΔH_{diss}[H–CH(CH$_3$)$_2$] = 98.6 [32a] and ΔH_{diss}[H–(CH$_3$)$_3$] = 95.8 [32b, c] kcal mol^{-1}. By definition, simple alkyl radicals have RSE = 0. The values for RSE(R$^{\bullet}$) were deduced from experimentally determined ΔH_{diss}(R–C) [1, 2]; among others, RSE = 10.7 [32d] for the benzyl radical and RSE = 8.4 kcal mol^{-1} [32e] for the cumyl radical. a) J. Berkowitz, G. B. Ellison, D. Gutman, *J. Phys. Chem.* **1994**, *98*, 2744–2765; b) W. Tsang, *J. Am. Chem. Soc.* **1985**, *107*, 2872–2880; see also ref. [21c]; c) J. J Russell, J. A. Seetula, R. S Timonen, D. Gutman, D. F. Nava, *ibid.* **1985**, *110*, 3084–3091; d) H. Hippler, J. Troe, *J. Phys. Chem.* **1990**, *94*, 3803–3806; e) G. Kratt, H.-D. Beckhaus, C. Rüchardt, *Chem. Ber.* **1984**, *117*, 1748.

[33] ESR-spectroscopic evidence for the corresponding H donor radicals could also be provided for the following H donor/H acceptor pairs: phenalene/α-methylstyrene, 7*H*-benz[*de*]anthracene/α-methylstyrene, and 9,10-dihydroanthracene/C_{60} [27].

[34] a) C. Herberg, H.-D. Beckhaus, C. Rüchardt, *Chem. Ber.* **1994**, *127*, 2065–2072; b) see also ref. [2b].

[35] a) D. Griller, K. U. Ingold, *Acc. Chem. Res.* **1980**, *13*, 317–323; b) R. Hollis, L. Hughes, V. W. Bowry, K. U. Ingold, *J. Org. Chem.* **1992**, *57*, 4284–4287; c) R. M. Bullock, E. G. Samsel, *J. Am. Chem. Soc.* **1987**, *109*, 6542–6544; d) R. A. Caldwell, L. Zhou, *ibid.* **1994**, *116*, 2271–2275.

[36] a) M. Gerst, J. Morgenthaler, C. Rüchardt, *Chem. Ber.* **1994**, *127*, 691–696; b) J. Morgenthaler, C. Rüchardt, *Liebigs Ann.* **1996**, 1529–1532; c) J. Morgenthaler, planned Ph.D. thesis, Universität Freiburg, **1997**.

[37] M. Newcomb, *Tetrahedron* **1993**, *49*, 1151–1176.

[38] F. Keller, Ph.D. thesis, Universität Freiburg, **1997**; F. Keller, H.-D. Beckhaus, C. Rüchardt, *Liebigs Ann./Recqueil*, submitted.

[39] a) H. Friebolin, C. Rüchardt, *Liebigs Ann.* **1995**, 1339–1341, and unpublished results; b) M. Gerst, C. Rüchardt, *Tetrahedron Lett.* **1993**, *34*, 7733–7736; c) H. Friebolin, R. Roers, J. Ebenhoch, C. Rüchardt, *Liebigs Ann.* **1996**, 385–389.

[40] C. Reichardt, *Solvents and Solvent Effects in Organic Chemistry*, 2nd ed., VCH, Weinheim **1988**, pp. 365–371; see also J. J. Gajewski, *Acc. Chem. Res.* **1997**, *30*, 219–225.

[41] H. Mayr, M. Patz, *Angew. Chem.* **1994**, *106*, 990–1010; *Angew. Chem. Int. Ed. Engl.* **1994**, *33*, 788–789.

[42] See ref. [12c], p. 278.

[43] R. A. Jackson, *NATO ASI Ser. C*, **1986**, *189*, 325–328.

[44] Landoldt-Börnstein, *Zahlenwerte und Funktionen aus Physik, Chemie, Astronomie, Geophysik und Technik* (Eds.: K. H. Hellwege, A. H. Hellwege), 6th ed., Springer, Berlin, Vol. II, part 6, **1959**, p. 618.

[45] See refs. [40, 44]: diphenyl ether: $\varepsilon(30\,^{\circ}C) = 3.7$; $E_T(25\,^{\circ}C) = 35.3$ kcal mol^{-1}; *N*-methylacetamide: $\varepsilon(30\,^{\circ}C) = 175.7$, $\varepsilon(250\,^{\circ}C) = 34.7$, E_T (25 °C) = 54.1 kcal mol^{-1}; *tert*-butylbenzene: $\varepsilon(30\,^{\circ}C) = 2.3$, $E_T(25\,^{\circ}C) = 33.7$ kcal mol^{-1}; benzonitrile: $\varepsilon(25\,^{\circ}C) = 25.2$, $E_T(25\,^{\circ}C) = 42$ kcal mol^{-1}; *o*-dichlorobenzene: $\varepsilon(25\,^{\circ}C) = 9.82$, $E_T(25\,^{\circ}C) = 38.1$ kcal mol^{-1}.

[46] The following values were used for the enthalpies of formation: $\Delta H_f^0(g)[H^{\cdot}] = 52.1$, $\Delta H_f^0(g)[\mathbf{1}] = 28.5$ [47], and $\Delta H_f^0(g)[\mathbf{2}] = 38.2$ kcal mol^{-1} [32].

[47] See Table 5, footnote [d].

[48] a) M. Gerst, C. Rüchardt, *Chem. Ber.* **1993**, *126*, 1039–1045; b) see also W. R. Roth, C. Unger, T. Wasser, *Liebigs Ann.* **1996**, 2155–2169.

[49] See ref. [31b]. Special calculation methods were used in some cases [3, 27]. The activation parameters were measured in a temperature range of at least 40 K.

[50] 1,4-Cyclohexadiene and 1,3-cyclohexadiene could also be employed as H donors with **1**. Quantitative investigations were complicated by the thermolability of 1,4-cyclohexadiene with isomerization to the 1,3-isomer, and, in the case of 1,3-cyclohexadiene, by the retrodisproportionation of two molecules, which yielded several by-products that were not further identified: S. W. Benson, R. Shaw, *J. Am. Chem. Soc.* **1967**, *89*, 5351–5354; G. R. DeMaré, G. Huybrechts, M. Toth, *J. Chem. Soc. Perkin Trans. 2* **1972**, 1256–1258; D. K. Agrafiotis, H. S. Rzepa, *J. Chem. Soc. Chem. Commun.* **1987**, 902–904; G. Huybrechts, B. V. Mele, *Int. J. Chem. Kin.* **1985**, *17*, 709–711).

[51] a) I. Murate, *Top. Nonbenzenoid Aromat. Chem.* **1973**, *1*, 159–190; b) D. H. Reid, *Quart. Rev.* **1965**, *19*, 274–302; c) W. Broser, H. Kurreck, S. Oestreich-Janzen, G. Schlömp, H.-J. Fey, B. Kirste, *Tetrahedron* **1979**, *35*, 1159–1166; d) J. E. Bennett, *Proc. Chem. Soc.* **1961**, 144–145; e) P. B. Sogo, M. Nakazaki, M. Calvin, *J. Chem. Phys.* **1957**, *26*, 1343–1345.

[52] Strictly speaking the promotor function, which can be referred to as catalysis, can presumably also be performed by other compounds that display weak C–H bond enthalpies ΔH_{diss} or by transition metal/H derivatives. The latter play an important role in the transition metal catalyzed transfer hydrogenation: a) T. E. Nalesnik, J. H. Freudenberger, M. Orchin, *J. Organomet. Chem.* **1981**, *221*, 193–197; b) R. L. Sweany, S. C. Butler, J. Halpern, *ibid.* **1981**, *213*, 487–492; c) R. L. Sweany, J. Halpern, *J. Am. Chem. Soc.* **1977**, *99*, 8335–8337; d) J. Halpern, *Pure Appl. Chem.* **1979**, *51*, 2171–2182; see also ref. [20, 35c].

[53] With a computer program the quantitative determination of deuterium incorporation into **1** by GC-MS analysis as a function of the conversion rate allows for the calculation of the percentage of the reverse reaction with rate k_{-32} of the formed 2-phenyl-2-propyl radicals **8** [27]. From these measurements, a correction factor F was introduced with which the experimental rate constants k'_{32} were multiplied to obtain the actual, slightly higher rate constants k_{32} [27]. The effect of disproportionation (for example v_{-32}) also occurs with other H donors and is usually small, so that the rate constants of the retrodisproportionation and particularly the activation parameters change only to a minor extent (see Table 4).

[54] M. J. Bausch, R. Gostowski, G. Jirka, D. Selmarten, G. Winter, *J. Org. Chem.* **1990**, *55*, 5805–5806.

[55] a) S. E. Stein, R. L. Brown, *J. Am. Chem. Soc.* **1991**, *113*, 787–793; b) see for example J. Pajak, K. R. Brower, *J. Org. Chem.* **1985**, *50*, 2210–2216, and ref. [13]; c) T. Dockner, *Angew. Chem.* **1988**, *100*, 699–702; *Angew. Chem. Int. Ed. Engl.* **1988**, *27*, 679–682.

[56] F. Wurche, Diplomarbeit, Universität Freiburg, **1997**.

[57] G. B. Gill, S. Hawkins, P. H. Gore, *J. Chem. Soc. Chem. Commun.* **1974**, 742–743.

[58] A. Heesing, W. Müller, *Chem. Ber.* **1980**, *113*, 9–18, 19–23, 24–35.

[59] D. T. Allen, G. R. Gavalas, *Int. J. Chem. Kin.* **1983**, *15*, 219–233.

[60] T. Gerres, A. Heesing, *Chem. Ber.* **1992**, *125*, 1439–1447.

[61] H.-H. King, L. M. Stock, *Fuel* **1981**, *60*, 748–749.

[62] J. Fleming, *Grenzorbitale und Reaktionen organischer Verbindungen*, 1st ed., VCH, Weinheim, **1979**, p. 217.

[63] The following values were used for the enthalpies of formation $\Delta H_f^0(g)$ [32]: [**2**]: 38.2 [65], [**8**]: 36.3 [3], [**9**]: 69.1 [64a, 34a], [**10**]: 11.6 [65], [**11**]: 40.2 [64a, 34b], $\Delta\Delta H_f^0(g)$[9-hydroacridyl radical **23**]: 24.9 [39], $\Delta\Delta H_f^0(g)$[**25** – **24**]: 29.5 [39], [**28**]: 41.8 [34b], [9-fluorenyl radical]: 72.3 [64a, 34b], $\Delta\Delta H_f^0(g)$[**34** – **29**]: 12.5 [64b], $\Delta\Delta H_f^0(g)$[7*H*-benz[*de*]anthracenyl radical **30**]: 14.5 [64b], [1-hydronaphthyl radical]: 63.8 [64c], [**31**]: 32.9 [27], [**32**]: 29.9 [27], [**33**]: 35.3 [64d], [9-hydrophenanthryl radical]: 72.8 kcal mol^{-1} [64a].

[64] a) $\Delta H_{diss}(C{-}H)[\mathbf{2}] = \Delta H_{diss}(C{-}H)[(CH_3)_2CH{-}H] - RSE[\mathbf{9}] = 98.6$ [32b] $- 15.6$ [34] $= 83.0$; $\Delta H_{diss}(C{-}H)[\mathbf{10}] = 98.6$ [32b] $- 17.9$ [34a] $= 80.7$; $\Delta H_{diss}(C{-}H)[\mathbf{28}] = 98.6$ [32b] $- 16.0$ [34b] $= 82.6$; $\Delta H_{diss}(C{-}H)[\mathbf{33}] = 98.6$ [32b] $- 9.0$ [64d] $= 89.6$; b) see ref. [54]; $\Delta H_{diss}(C{-}H)[\mathbf{29}] = 74.0$ (AM1/RHF-CI calculations) [66]; $\Delta H_{diss}(C{-}H)[\mathbf{30}] = \Delta H_{diss}(C{-}H)[\mathbf{29}] + 2.0$ [36] $= 76.0$ kcal mol^{-1}. c) The same low C–H bond enthalpy $\Delta H_{diss}(C{-}H) = 71$ kcal mol^{-1} was given for **31** and **2**: D. G. Hendry, D. Schuetzle, *J. Am. Chem. Soc.* **1975**, *97*, 7123–7127. d) By definition, the value of $\Delta H_{diss}(C{-}H) = 83.0$ kcal mol^{-1} for **2** was adopted for $\Delta H_{diss}(C{-}H)$ of **31**.

[65] J. B. Pedley, R. D. Naylor, S. P. Kirby, *Thermochemical Data of Organic Compounds*, 2nd ed., Chapman and Hall, London, **1986**, p. 460.

[66] With the program Mopac 6.0 (QCPE) with AM1/RHF-CI $\Delta H_{diss}(C{-}H)$ for DHA (**2**) was calculated to be 80.0 kcal mol^{-1}; the experimental value was 83.0 kcal mol^{-1} [2b]. All calculated results for the substituted dihydroanthracenes and the acridans (see Table 4) were calibrated accordingly.

[67] G. B. Gill, S. Hawkins, P. H. Gore, *J. Chem. Soc. Chem. Commun.* **1974**, 742–743.

[68] C. Choi, L. M. Stock, *J. Org. Chem.* **1984**, *49*, 2871–2875.

[69] a) M. Cöllen, Diplomarbeit, Universität Freiburg, **1994**; b) M. Cöllen, C. Rüchardt, *Chem. Eur. J.* **1995**, *1*, 564–567; c) M. Cöllen, planned Ph.D. thesis, Universität Freiburg, **1997**.

[70] J. Ebenhoch, Ph.D. thesis, Universität Freiburg, **1996**.

[71] J. A. Franz, D. M. Camaioni, R. R. Beishline, D. K. Dallins, *J. Org. Chem.* **1984**, *49*, 3563–3570; see ref. [20d].

[72] D. G. Hendry, D. Schuetzle, *J. Am. Chem. Soc.* **1975**, *97*, 7123–7127; see ref. [64c].

[73] Y. R. Loo, J. L. Holmes, *Chem. Phys. Lett.* **1994**, *228*, 329–333.

[74] Since the unsubstituted 1-methyleneindane (**52**) thermally isomerizes under transfer-hydrogenation conditions to yield 1-methylindene, no kinetic data could be obtained. The same applies for the monosubstituted 2-alkyl-1-methyleneindanes.

[75] Results from MM2-82 calculations supplemented with radical parameters according to ref. [25]; N. L. Allinger, H. L. Flanagan, *J. Comput. Chem.* **1983**, *4*, 399.

[76] E. D. Bergmann, *Chem. Rev.* **1968**, *68*, 41–84.

[77] B. Giese, *Angew. Chem.* **1983**, *95*, 771–782; *Angew. Chem. Int. Ed. Engl.* **1983**, *22*, 753–764, and references therein.

[78] C. Herberg, A. Peyman, M. Nölke, H.-D. Beckhaus, C. Rüchardt, *Liebigs Ann. Chem.* **1995**, 881–884.

[79] S. E. Stein, L. L. Griffith, R. Billmers, R. H. Chen, *J. Org. Chem.* **1987**, *52*, 1582–1591.

[80] L. T. Scott, *Acc. Chem. Res.* **1982**, *15*, 52–58.

[81] a) C. Rüchardt, M. Gerst, J. Ebenhoch, H.-D. Beckhaus, E. E. B. Campbell, R. Tellgmann, H. Schwarz, T. Weiske, S. Pitter, *Angew. Chem.* **1993**, *105*, 609–611; *Angew. Chem. Int. Ed. Engl.* **1993**, *32*, 584–586; b) E. E. B. Campbell, R. Tellgmann, C. Rüchardt, M. Gerst, J. Ebenhoch, H.-D. Beckhaus in *Physics & Chemistry of Fullerenes* (Ed.: K. Prassider). Kluwer Academic Publishers, **1994**, pp. 27–40; c) M. Gerst, H.-D. Beckhaus, C. Rüchardt, E. E. B. Campbell, R. Tellgmann, *Tetrahedron Lett.* **1993**, *34*, 7729–7732; M. Bühl, W. Thiel, U. Schneider, *J. Am. Chem. Soc.* **1995**, *117*, 4623–4627; S. H. Wang, S. A. Jansen, *J. Phys. Chem.* **1995**, *99*, 8556–8561; R. V. Bensasson, T. Hill, E. J. Land, S. Leach, D. McGarvey, T. G. Truscott, J. Ebenhoch, M. Gerst, C. Rüchardt, *Chem. Phys.* **1997**, *215*, 111–124.

[82] R. M. Baum, *Chem. Eng. News* **1993**, No. 22, 8–18.

[83] a) O. Exner, *Coll. Czech. Commun.* **1964**, *29*, 1094; b) N. S. Isaacs, *Phys. Org. Chem.* 1st ed., **1987**, Longman, Essex, p. 102.

[84] K. A. Conners, *Chemical Kinetics*, VCH, Weinheim, **1990**, p. 368; R. C. Peterson, J. H. Markgraf, S. D. Ross, *J. Am. Chem. Soc.* **1961**, *83*, 3819–3823; R. C. Peterson, *J. Org. Chem.* **1964**, *29*, 3133–3135; O. Exner, *Prog. Phys. Org. Chem.* **1973**, *10*, 411–483.

[85] K. Héberger, S. Kemény, T. Vidóczy, *Int. J. Chem. Kin.* **1987**, *19*, 171–181; K. Héberger, A. Lopata, *J. Chem. Soc. Perkin Trans. 2* **1995**, 91–96; K. Héberger, *J. Phys. Org. Chem.* **1994**, *7*, 244–250.

[86] a) K. N. Houk, N. G. Rondon, *J. Am. Chem. Soc.* **1984**, *106*, 4293–4294; C. Doubleday, R. N. Camp, H. F. King, J. W. Melver, D. Mullally, M. Page, *ibid.* **1984**, *106*, 447–448.

[87] In the reaction of fluorenone with **2**, fluorene and fluorenol were formed in approximately equimolar amounts. The decrease in fluorenone was not a first-order reaction, as was the case for H acceptors containing C=C bonds (see Section 2.2.2.).

[88] W. Bradley, L. J. Watkinson, *J. Chem. Soc.* **1956**, 319–327: the authors describe the hydrogenation of azobenzene (**85a**) by anthrone, which leads to the formation of hydrazobenzene and aniline.

[89] G. Koga, N. Koga, J.-P. Anselme, *The Chemistry of Hydrazo-, Azo- and Azoxygroups* (Ed.: S. Patai), 1st ed., Wiley, New York, **1975**, Vol. 1, part 2, pp. 921–922.

[90] The thermochemical calculations are based on the following standard enthalpies of formation $\Delta H_f^0(g)$ [kcal mol^{-1}]: azobenzene (**85a**): 96.6 [65]; 1,2-diphenylhydrazyl radical: 98.9, see S. Ingemann, R. H. Fokkens, N. M. M. Nibbering, *J. Org. Chem.* **1991**, *56*, 607–612; DHA (**2**): 38.2 [65]; [**9**]: 69.1, see ref. [64a, 34a].

[91] a) B. M. Trost, W. D. Ollis in *Comprehensive Organic Chemistry*, *Vol. 7* (Eds.: B. M. Trost, J. Fleming, S. V. Ley), Pergamon, Oxford, **1991**, p. 135; b) see also pp. 81–98; c) L. Golser, *Methoden der Organischen Chemie (Houben-Weyl) 4th ed. 1952-*, Vol. 4/1b, Thieme, Stuttgart, **1975**, pp. 963–987; d) T. Burger, *ibid.* pp. 953–963.

[92] a) In contrast to earlier statements [69a, b]; see also L. Blatt in *The Chemistry of Functional Groups* (Ed.: S. Patai), 1st ed., Wiley, New York, Suppl. F, part 1, **1982**, p. 434; b) P. Kapferer, unpublished results.

[93] a) D. Walker, J. D. Hiebert, *Chem. Rev.* **1967**, *67*, 153–195; b) P. P. Fu, R. G. Harvey, *Chem. Rev.* **1978**, *78*, 317–361; c) H.-D. Becker, A. B. Turner in *The Chemistry of Quinoid Compounds, Vol II* (Eds.: S. Patai, Z. Rappoport) **1988**, 1352–1384.

[94] C. Höfler, C. Rüchardt, *Liebigs Ann.* **1996**, 183–188; b) C. Höfler, unpublished results.

[95] We thank Prof. M. Goez (Halle, Germany) and Prof. A. G. Davies (London, UK) for performing these experiments.

[96] a) M. E. Brewster, E. Pop, M.-J. Huang, N. Bodor, *Heterocycles* **1994**, *37*, 1373–1415; b) W. Adam, M. Heil, R. Hutterer, *J. Org. Chem.* **1992**, *57*, 4491–4495; c) J. Gebicki, A. Marcinek, J. Adamus, P. Paneth, J. Rogowski, *J. Am. Chem. Soc.* **1996**, *118*, 691–697.

[97] a) R. B. Silverman, *Acc. Chem. Res.* **1995**, *28*, 335–342; S. Ottoboni, P. Caldera, A. Trevov, N. Castagnoli Jr., *J. Biol. Chem.* **1989**, *264*, 13684–13688; b) J. Andres, V. Moliner, V. S. Safont, L. R. Domingo, M. T. Picher, *J. Org. Chem.* **1996**, *61*, 7777–7783; c) I.-S. H. Lee, E. H. Jeoung, M. M. Kreevoy, *J. Am. Chem. Soc.* **1997**, *119*, 2722–2728. d) Calculations of the transition state by J. W. Verhoeven, W. van Gerresheim, F. M. Martern, S. M. van der Kerk, *Tetrahedron* **1986**, *42*, 975–992 suggest that the hydrogen carries only a 10% positive charge in the transition state. However, this phenomenon was also found for proton transfer between carbon atoms (C. F. Bernasconi, J. P. Wenzel, *J. Am. Chem. Soc.* **1996**, *118*, 10494–10504) and for hydride transfer of allylic hydrogen onto carbenium ions (G. Lange, H. Mayr (Munich, Germany), private communication); e) N. Moyseyev, J. Rucker, M. H. Glickmann, *J. Am. Chem. Soc.* **1997**, *119*, 3853–3867.

[98] D. H. Reid, M. Fraser, B. B. Molloy, H. A. S. Payne, R. G. Sutherland, *Tetrahedron Lett.* **1961**, 530–535.

[99] a) C. Höfler, H. Friebolin, unpublished results; see also G. Saito, A. K. Colter, *Tetrahedron Lett.* **1977**, *38*, 3325–3328; b) N. Nishimura, T. Motoyama, *Bull. Chem. Soc. Jpn.* **1985**, *58*, 1013–1018; K. M. Zaman, N. Nishimura, S. Yamamoto, Y. Sueishi, *J. Phys. Org Chem.* **1994**, *7*, 309–315.

[100] a) See ref. [6]; b) K. C. Nicolaou, A. L. Smith, *Acc. Chem. Res.* **1992**, *25*, 497–503; J. W. Grissom, T. L. Calkins, *J. Org. Chem.* **1993**, *58*, 5422–5427, and references therein; c) P. Chen, *Angew. Chem.* **1996**, *108*, 1584–1586; *Angew. Chem. Int. Ed. Engl.* **1996**, *35*, 1478–1480.

[101] a) 9,10-Dihydrophenanthrene (H donor)/anthracene (H acceptor): R. Billmers, R. L. Brown, S. E. Stein, *J. Chem. Kinet.* **1989**, *21*, 375–386; b) 9,10-dihydronaphthalene (H donor)/cyclohexadiene (H acceptor): W. von E. Doering, J. W. Rosenthal, *J. Am. Chem. Soc.* **1967**, *89*, 4534–4535; c) 1,2-dihydronaphthalene (H donor)/1,2-dihydronaphthalene (H acceptor): see ref. [13b, 58–61]; d) 1,2-dihydronaphthalene (H donor)/anthracene and phenanthrene (H acceptors): see ref. [13a]; e) 1,4-dihydronaphthalene (H donor)/arenes (H acceptor): see also c); f) tetraline (H donor)/indene, cyclohexene, and *trans*-stilbene (H acceptors): see ref. [13a]; g) tetraline (H donor)/coal (H acceptor): see ref. [55b]; K. R. Brower, *J. Org. Chem.* **1982**, *47*, 1889–1893; h) tetraline (H donor)/furan, indole, and thiophene derivatives (H acceptors): see f); i) tetraline (H donor)/ketones and aldehydes (H acceptors): see f) and B. M. Benjamin, V. F. Raaen, P. H. Maupin, L. L. Brown, C. J. Collins, *Fuel* **1978**, *57*, 269–272; j) tetraline (H donor)/quinones (9,10-phenanthrenedione, 9,10-anthraquinone; H acceptors): see f) and ref. [55b]; k) tetraline (H donor)/with nitroso derivatives and maleic esters (H acceptors): see j); l) cyclohexane (H donor)/olefins, alkynes, or carbonyl derivatives (H acceptors): see f); m) 2-propanol (H donor)/carbonyl derivatives (H acceptors): D. Malwitz, J. O. Metzger, *Chem. Ber.* **1986**, *119*, 3558–3575; n) *o*- and *p*-isotoluene (simultaneously H donor and H acceptor): ref. [18a]; W. J. Bailey, R. A. Baylouny, *J. Org. Chem.* **1962**, *27*, 3476–3478; D. Hasselmann, K. Loosen, *Angew. Chem.* **1978**, *90*, 641–642; Y. W. Andemichael, K. K. Wang, *J. Org. Chem.* **1992**, *57*, 796–798; p) dimethylaminoethyl acrylate (simultaneously H donor and H acceptor): see ref. [14e]; q) peroxides or halides with alkenes: see ref. [17].

Time is money...

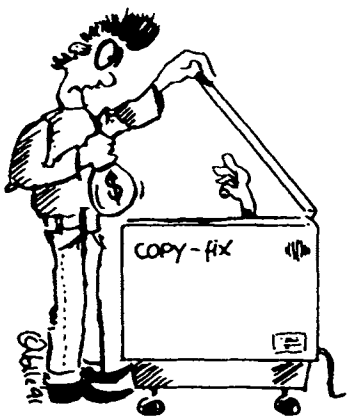

Save both by starting a personal subscription to *Angewandte Chemie*
At 9¢ per page you can't go wrong.
With your own private copy you can read the "hot" articles before they cool, and waste less time in front of the copier.

Order now!
An order form can be found on the last page of this issue.

Functional Organic Analogues of Zeolites Based on Metal–Organic Coordination Frameworks**

Christoph Janiak*

Dedicated to Professor Roald Hoffmann on the occasion of his 60th birthday

Supramolecular chemistry has reached a stage at which it is possible to select molecular building blocks that will assemble into structures with specific and desired network topologies, so that a rational design of molecular solids with potentially interesting properties is possible.[1] Recent efforts are being undertaken to generate three-dimensional (3-D) organic and metal–organic porous frameworks by the molecular building block approach. Of special interest is the search for stable microporous organic networks that exhibit reversible guest exchange and possibly selective catalytic activity. So far, no practical uses have emerged, but hopes are running high, and potential applications appear very promising. Construction of inner cavities and channels that are mainly surrounded by organic components is attractive, since the shape, size, and function of the cavity then become designable.[2] There is much interest in tailoring the geometry and the hydrophilic and hydrophobic character of the pores.[3] However, the key feature is not only the incorporation of guest molecules but also their reversible exchange. Here the present state of research concerning this crucial aspect is summarized.

Research on intercalation has concentrated largely on nanoporous inorganic materials such as aluminosilicates (zeolites), aluminophosphates, pillared clays, and graphite—all of which have been known for a long time.[4] Porous solids such as zeolites, which can now be "engineered" to some extent, are already important materials and find widespread application in adsorption (molecular sieves), shape- and size-selective heterogeneous catalysis, and ion exchange. An important aspect of zeolites is their structural stability, which allows guest concentrations to range from zero (empty host) to a maximum value (saturation).[5]

The goal in the search for organic porous frameworks is not simply to mimic inorganic materials such as zeolites by using different building blocks. Some of the properties of organic compounds, such as low thermal stability and low Lewis acidity, are inherently different. Instead it is thought that organic networks should complement the inorganic ones since they exhibit properties that are not displayed by zeolites (for example chirality). The term "zeolite analogues" in connection with organic frameworks is not meant to imply that the full functionality of zeolites should be reproduced, rather it refers to the molecular-sieve character of zeolites, reversible guest removal, and the stability of the host framework in the absence of guest molecules.

Various research projects are currently concerned with the construction of channeled organic, metal–organic, and inorganic solids with a chemical architecture and, possibly, a catalytic activity that differ from those of zeolites. One approach involves porous metal organophosphates and organophosphonates in which the organic groups cover the internal surfaces.[3, 6, 7] Another variant combines the porous framework of zeolites with the catalytic activity of transition metal complexes by encapsulating molecular transition metal complexes in the pores of zeolites. Such an immobilization of metal complexes in a zeolite matrix should mimic the active center of enzymes.[8] A particularly intriguing strategy is to use covalent coordinative bonds and organic or inorganic ligands as links between metal ions. Different metal ions, various coordination geometries (such as octahedral, tetrahedral, or square planar), and numerous ligands provide a wide range of possibilities for connecting metal ions together to construct metal–organic frameworks. Covalent metal–organic lattices offer several possible advantages over their purely organic counterparts, including greater mechanical strength and the presence of catalytically active transition metals. An attractive feature of inorganic complexes is the availability of 90° joints for constructing a polymeric framework with macrocyclic boxes[9] as well as a potentially interesting interplay of hydrophobic and hydrophilic regions and interactions.[10] The synthesis or self-organization of these coordination polymers is achieved by combining the appropriate metal salt and a tailored ligand in a suitable solvent. The reaction proceeds under mild conditions, often spontaneously. The metal centers in a coordination polymer may be thought of as an assembling and templating species for the organic (ligand) groups.

A large number of static metal–ligand frameworks and host–guest structures are known, but a reversible guest exchange or chemical transformations of the guest inside a coordination-

[*] Priv.-Doz. Dr. C. Janiak
Institut für Anorganische und Analytische Chemie der Universität
Albertstrasse 21, D-79104 Freiburg (Germany)
Fax: Int. code +(761)203-6147
e-mail: janiak@ruf.uni-freiburg.de

[**] We thank the Deutsche Forschungsgemeinschaft, the Fonds der Chemischen Industrie, and the Graduiertenkolleg "Synthetische, mechanistische und reaktionstechnische Aspekte von Metallkatalysatoren" at the TU Berlin for financial support.

 © VCH Verlagsgesellschaft mbH, D-69451 Weinheim, 1997 0570-0833/97/3613-1431 $ 17.50+.50/0

polymer framework has been described for only a few. Layered materials with channels perpendicular to the layers, such as in the first five examples, appear to be most promising as functional organic analogues of zeolites. The structural descriptions seldom include a detailed picture of the host–guest interactions, in part due to disorder. Only the building blocks will be illustrated here; for the often complicated 3-D networks see the original literature. The solid-state structure of $[Ag(TEB)CF_3SO_3]\cdot 2C_6H_6$ [(TEB = 1,3,5-tris(4-ethynylbenzonitrile)benzene, **1**) exhibits hexagonal 15 Å channels,[11] which are created in spite of the interpenetration of six independent 3-D networks. The crystals are porous to benzene exchange; storage in C_6D_6 led to the formation of the deuterosolvate, as monitored by NMR spectroscopy. Dissolution and reformation of the lattice does not occur, as shown by X-ray powder diffractometry (XRPD).[12]

The silver triflate complex with the related tridentate ligand 1,3,5-tris(3-ethynylbenzonitrile)benzene (**2**) forms a 2-D coordi-

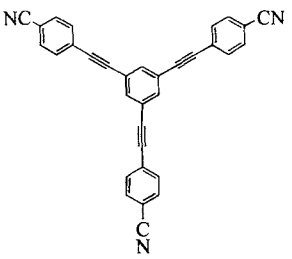

1

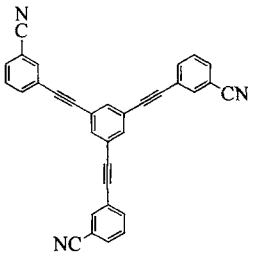

2

nation network that incorporates benzene molecules in channels running oblique to the layer plane. Of the 16 benzene molecules in the unit cell, four are lost reversibly at 110 °C (thermogravimetric analysis) without loss of crystallinity or a phase transition of the host structure, as shown by the optical transparency and XRPD. The remaining 12 benzene molecules are lost in a solid-to-solid phase transition at 145 °C, but even here subsequent cooling of the sample under a benzene atmosphere leads to the reabsorption of benzene and restoration of the original solid phase.[13]

The organic linkages can also be of smaller size, for example 4,4′-bipyridine groups. The 2-D square-network material $^2_\infty\{[Cd(4,4'\text{-bipyridine})_2](NO_3)_2\}$ (**3**), which contains microchannels perpendicular to the layers (Cd ··· Cd 11.8 Å), readily incorporates aromatic guests with high shape selectivity and catalyzes cyanosilylation of aldehydes.[2]

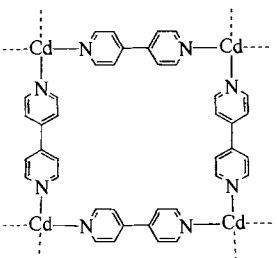

3

A porous solid of formula $M_3(BTC)_2\cdot H_2O$, which reversibly and repeatedly binds water without destruction of the framework, is obtained from divalent metal ions (such as Co^{2+}, Ni^{2+}, and Zn^{2+}) and 1,3,5-benzenetricarboxylic acid (BTC, **4**).[14] Inclusion of ammonia into the solid was also demonstrated, whereas larger molecules and those without a reactive electron lone pair were prevented from entering the channels. The 2-D metal–ligand assembly **5** with 1-D channels was proposed for the porous solid.[15] The same metal–BTC building block, but with two additional pyridine ligands at the metal center, gives the layer structure **6** in which the pyridine ligands act as

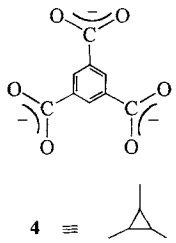

4

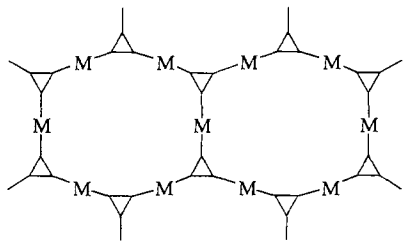

5

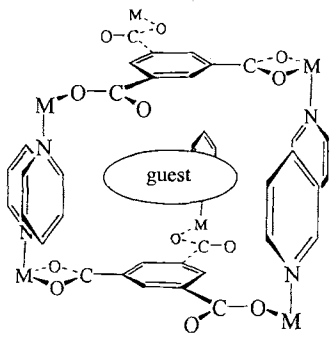

6

spacers between the layers. In the resulting 7×10 Å[11] rectangular channels, aromatic guests are accomodated and can be reversibly removed. According to optical microscopy, the single crystals retain their morphology and crystallinity upon loss of the guests. IR spectroscopy showed that aromatic molecule such as benzene, nitrobenzene, cyanobenzene, and chlorobenzene are selectively absorbed from mixtures with nonaromatic compounds. The crystal lattice is thermally stable up to 350 °C.[15]

An earlier study already showed that formation of a fully covalently interconnected 2-D or 3-D metal–organic network or coordination polymer is not a prerequisite for porosity and reversible guest exchange. The layered β-structure composed of discrete octahedral $[Ni(NCS)_2(4\text{-methylpyridine})_4]$ complexes forms inclusion compounds with aromatic guests and retains its porosity in the absence of the guest molecules. Thermodynamic and kinetic data for the uptake of different guests were collected, and sorption equilibria in systems containing two competing guests studied.[16] Furthermore, this and the next example illustrate that zeolite-type behavior of metal–organic host lattices was occasionally observed prior to the recent surge in interest: A partly reversible intercalation of ferrocene in the 3-D network of $^3_\infty[Fe^{III}(\mu\text{-CN}-SnMe_3-NC)_3]$ was described almost ten years ago. It was also demonstrated by XRPD that ferrocene can diffuse through the 6.8×6.8 Å[11] channels of the analogous network of $^3_\infty[Co^{III}(\mu\text{-CN}-SnMe_3-NC)_3]$(**7**).[17]

Not only neutral guest molecules but also lattice counterions can be removed: Crystals of $[Cu^I(\mathbf{8})]BF_4\cdot x C_6H_5NO_2$ were shown by IR spectroscopy to undergo anion exchange with PF_6^-. The metal–ligand moiety forms a diamond-related framework with no interpenetration and very large adamantane-like

 © VCH Verlagsgesellschaft mbH, D-69451 Weinheim, 1997 0570-0833/97/3613-1432 $ 17.50+.50/0

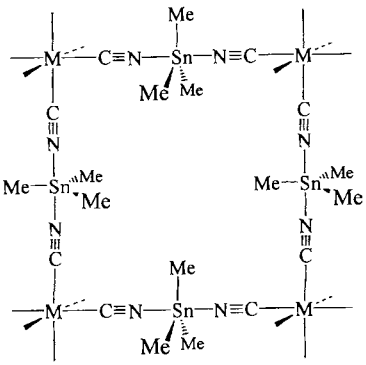

M = Fe, Co

7

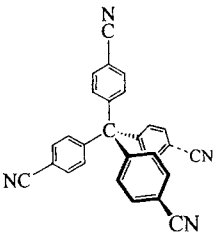

8

cavities[18] of about 1500 Å^3 (estimated from the space diagonals). The structure of [Ag(4,4′-bipyridine)NO_3] contains extended linear silver–ligand chains, which are cross-linked by Ag···Ag contacts (**9**) to give extended 23 × 6 Å[11] channels, in

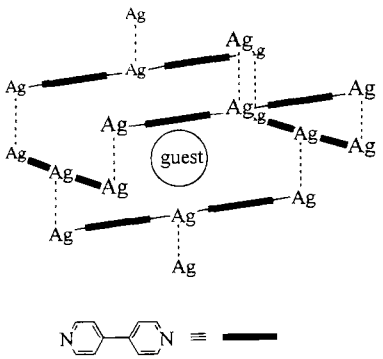

9

spite of the interpenetration of three different frameworks.[19] These channels are occupied by the nitrate "guests", which can undergo reversible exchange with PF_6^-, MoO_4^{2-}, BF_4^-, and SO_4^{2-} (monitored by IR spectroscopy and XRPD). The 4,4′-bipyridine ligand also connects Cu^I centers in a trigonal-planar geometry and thereby allows formation of the open framework **10** in [Cu(4,4′-bipyridine)$_{1.5}NO_3(H_2O)_{1.25}$]. Since six of these

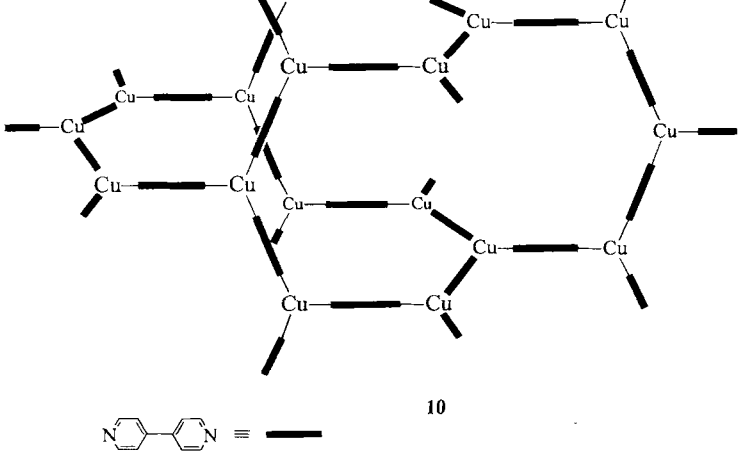

10

frameworks interpenetrate each other but do not fill all the available voids, that rectangular channels (8 × 6 and 4 × 5 Å[11]) remain. These channels are occupied by the nitrate anions, which according to IR spectroscopy and elemental analysis undergo exchange with SO_4^{2-} and BF_4^-.[20]

In the layered porous structure of $Na_2[PhMe_3N][Cr(C_2O_4)_3]_2Cl \cdot 5H_2O$, partial removal of the cationic templates ($PhMe_3N^+$) by cation exchange at room temperature and complete removal by thermal methods are apparently possible without loss of crystallinity. The $[Na_2Cr(C_2O_4)_3]^-$ moiety forms cylindrical pores of approximately 7 Å diameter and 3 Å[11] depth.[21]

From the examples given it becomes clear that nitrogen- and CN-containing ligands (nitriles) feature prominently as the organic building blocks. Building blocks for coordination networks are most often rigid bridging ligands, either linear or disk-shaped trigonal-planar; flexible ligands are used less often. Porphyrins and phthalocyanines have also been suggested as building blocks for microporous networks because of their relative rigidity and large size as well as their ready incorporation of a wide range of metal centers.[22]

Organic zeolite analogues promise a new range of applications, for example in pharmaceutical manufacture, molecular sieves, and sensors. A fascinating aspect is the potential to control the host–guest chemistry of the framework by tailoring the building blocks by including binding properties of functional organic groups that are not available in inorganic zeolites. One could imagine incorporating enantiomerically pure chiral groups to obtain microporous materials for enantiomer separation, chiral synthesis, and product-specific catalysis.[21, 23] However, before these ambitious goals can be achieved certain hurdles must be overcome. The basic problems of inclusion crystals based on an organic host lattice are that they tend to lose their crystallinity and undergo collapse of the void spaces on removal of the (reinforcing) guest molecules from the pores.[22] Furthermore, the guest may be entrapped in a clathrasil-like fashion inside the framework of the host without the possibility of diffusing through the lattice.[1] Nature tends to avoid vacuum, and identical copies interpenetrate to fill space are obtained rather than a single network.[24] Interpenetration, which arises from the necessity to fill the empty spaces inside the large cages, is the rule rather than the exception in these species. Seldom do the interpenetrating networks create large cavities.[25]

The design and synthesis of new polymeric framework materials containing cavities capable of taking up molecular substructures in a shape- and/or size-selective manner is a continuing challenge. Selective incorporation of metal ions as integral components of such frameworks offers additional factors (electron transfer) that can be exploited in stimulating substrate reactivity. The area of coordination polymers, which can also be seen as a meeting ground for the subdisciplines of molecular and solid-state inorganic chemistry, brings together synthetic techniques and analytical methods for designing and investigating extended structures with specific physical properties by low-temperature reactions.[7]

German version: *Angew. Chem.* **1997**, *109*, 1499–1502

Keywords: coordination polymers · host–guest chemistry · supramolecular chemistry · zeolites

 © VCH Verlagsgesellschaft mbH, D-69451 Weinheim, 1997 0570-0833/97/3613-1433 $ 17.50+.50/0

[1] A. Müller, H. Reuter, S. Dillinger, *Angew. Chem.* **1995**, *107*, 2505-2539; *Angew. Chem. Int. Ed. Engl.* **1995**, *34*, 2311-2327; G. R. Desiraju, *ibid.* **1995**, *107*, 2541-2558 and **1995**, *34*, 2328-2361.
[2] M. Fujita, Y. J. Kwon, S. Washizu, K. Ogura, *J. Am. Chem. Soc.* **1994**, *116*, 1151-1152.
[3] K. Maeda, J. Akimoto, Y. Kiyozumi, F. Mizukami, *Angew. Chem.* **1995**, *107*, 1313-1315; *Angew. Chem. Int. Ed. Engl.* **1995**, *34*, 1199-1201.
[4] *Progress in Intercalation Research* (Eds.: W. Müller-Warmuth, R. Schöllhorn), Kluwer, Dordrecht, **1994**.
[5] *Supramolecular Architecture* (Ed.: T. Bein), ACS Symposium Series 499, **1992**; R. Szostak, *Handbook of Molecular Sieves*, van Nostrand, New York, **1992**; F. Schüth, *Chem. Unserer Zeit* **1995**, *29*, 42-52; G. A. Ozin, A. Kuperman, A. Stein, *Angew. Chem.* **1989**, *101*, 373-390; *Angew. Chem. Int. Ed. Engl.* **1989**, *28*, 359-376; W. Hölderich, M. Hesse, F. Näumann, *ibid.* **1988**, *100*, 232-251; **1988**, *27*, 226-246; L. Puppe, *Chem. Unserer Zeit* **1986**, *20*, 117-127; P. Behrens, G. D. Stucky, *Angew. Chem.* **1993**, *105*, 729-732; *Angew. Chem. Int. Ed. Engl.* **1993**, *32*, 696-699.
[6] G. Alberti, U. Costantino, F. Marmottini, R. Vivani, P. Zappelli, *Angew. Chem.* **1993**, *105*, 1396-1398; *Angew. Chem. Int. Ed. Engl.* **1993**, *32*, 1357-1359; A. Clearfield, *Comments Inorg. Chem.* **1990**, *10*, 89-128; J. Le Bideau, C. Payen, P. Palvadeau, B. Bujoli, *Inorg. Chem.* **1994**, *33*, 4885-4890.
[7] A. Stein, S. W. Keller, T. E. Mallouk, *Science* **1993**, *259*, 1558-1564.
[8] B. M. Weckhuysen, A. A. Verberckmoes, I. P. Vannijvel, J. A. Pelgrims, P. L. Buskens, P. A. Jacobs, R. A. Schoonheydt, *Angew. Chem.* **1995**, *107*, 2868-2870; *Angew. Chem. Int. Ed. Engl.* **1995**, *34*, 2652-2654; D. E. DeVos, D. L. Vanoppen, X.-Y. Li, S. Libbrecht, Y. Bruynseraede, P. P. Knops-Gerrits, P. A. Jacobs, *Chem. Eur. J.* **1995**, *1*, 144-149.
[9] C. A. Hunter, *Angew. Chem.* **1995**, *107*, 1181-1183; *Angew. Chem. Int. Ed. Engl.* **1995**, *34*, 1079-1081.
[10] M. I. Khan, Y.-S. Lee, C. J. O'Connor, R. C. Haushalter, J. Zubieta, *Chem. Mater.* **1994**, *6*, 721-723.
[11] With respect to the channel and cavity dimensions given in the cited examples, no comment is made in the original literature as to how these dimensions were derived from the available crystal structures, that is, whether it is the distance between the nuclei or whether the van der Waals radii of the atoms were taken into account.
[12] G. B. Gardner, D. Venkataraman, J. S. Moore, S. Lee, *Nature* **1995**, *374*, 792-795.
[13] D. Venkataraman, G. B. Gardner, S. Lee, J. S. Moore, *J. Am. Chem. Soc.* **1995**, *117*, 11600-11601.
[14] O. M. Yaghi, H. Li, T. L. Groy, *J. Am. Chem. Soc.* **1996**, *118*, 9096-9101.
[15] O. M. Yaghi, G. Li, H. Li, *Nature* **1995**, *378*, 703-706.
[16] J. Lipkowski in *Inclusion Compounds, Vol. 1* (Eds.: J. L. Atwood, J. E. D. Davies, D. D. MacNicol), Academic Press, London, **1984**, pp. 59-103.
[17] P. Brandt, A. K. Brimah, R. D. Fischer, *Angew. Chem.* **1988**, *100*, 1578-1580; *Angew. Chem. Int. Ed. Engl.* **1988**, *27*, 1521-1523.
[18] B. F. Hoskins, R. Robson, *J. Am. Chem. Soc.* **1990**, *112*, 1546-1554.
[19] O. M. Yaghi, H. Li, *J. Am. Chem. Soc.* **1996**, *118*, 295-296.
[20] O. M. Yaghi, H. Li, *J. Am. Chem. Soc.* **1995**, *117*, 10401-10402.
[21] R. P. Farrell, T. W. Hambley, P. A. Lay, *Inorg. Chem.* **1995**, *34*, 757-758.
[22] B. F. Abrahams, B. F. Hoskins, D. M. Michail, R. Robson, *Nature* **1994**, *369*, 727-729.
[23] F. Toda, *Topics Curr. Chem.* **1988**, *149*, 212-238; R. F. Service, *Science* **1994**, *265*, 1363; P. Ball, *Nature* **1996**, *381*, 648-650.
[24] P. Losier, M. J. Zaworotko, *Angew. Chem.* **1996**, *108*, 2957-2960; *Angew. Chem. Int. Ed. Engl.* **1996**, *35*, 2779-2782; O. M. Yaghi, G. Li, *ibid.* **1995**, *107*, 232-234 and **1995**, *34*, 207-209; D. Venkataraman, S. Lee, J. Zhang, J. S. Moore, *Nature* **1994**, *371*, 591-593.
[25] S. R. Batten, B. F. Hoskins, R. Robson, *J. Am. Chem. Soc.* **1995**, *117*, 5385-5386; L. R. MacGillivray, S. Subramanian, M. J. Zaworotko, *J. Chem. Soc. Chem. Commun.* **1994**, 1325-1326; L. Carlucci, G. Ciani, D. M. Proserpio, A. Sironi, *ibid.* **1994**, 2755-2756.

Harmony and Dissonance in the Concert of Proton Motions

Richard L. Schowen*

The motion of a proton between donor and acceptor atoms is one of the simplest chemical reactions, and an overall reaction involving two such motions within the same molecular array represents the simplest case in which to consider the coupling of two chemical processes; do they occur simultaneously in time (concertedly) or serially in time (in a stepwise manner)?[1] Reactions in which multiple (often two) proton-transfer events among electronegative atoms such as O, N, and S accompany bonding changes in a framework of atoms heavier than H are of interest in biology as well as chemistry, for example in the action of enzymes[2] and in tautomerization reactions in nucleic-acid base pairs.[3] Several recent studies have begun to illuminate the manner in which the molecular choice between concerted and stepwise motion of the protons is made.

The history of this subject began some time ago. In 1952 Swain and Brown[4] showed that reagents with both proton-donor and proton-acceptor sites can accelerate with extraordinary power reactions that require both proton donation and proton removal. They denoted the phenomenon polyfunctional catalysis, which is exemplified by the catalysis of an elementary ring-opening step in the mutarotation of glucose (or its 2,3,4,6-tetramethyl derivative) by 2-pyridone. The ring-opening reaction of glucose derivatives involves more than the motion of the two protons. The internal C—O σ bond of the pyranose ring is cleaved, and a π bond added to the external C—O σ bond. If the formation and fission of C—O bonds (heavy-atom reorganization) were coupled to the transfer of the protons between the glucose molecule and the catalyst (which need not be true),[2] such a reaction could proceed by any of three pathways from reactant state **1** to product state **3**, which can take place via the activated complex **2** and the intermediate compounds **4** and **5**.

In reactions through **4** and **5**, the motions of the two protons between their bonding partners occur in a stepwise manner via two transition states that come before and after the intermediates along the reaction pathway. In a reaction through **2** the motions are concerted, and there is no intermediate. Swain and Brown concluded from the extraordinary catalytic activity of bifunctional compounds that the concerted pathway was preferred. This follows from the fact that 2-pyridone would function only as a very weak general base in the reaction leading to **4** and only as a very weak general acid in the reaction leading to **5**. Only in transition state **2** for the concerted reaction is the cooperative acid–base enhancement characteristic of bifunctional catalysts capable of expression. Rony and co-workers[5]

[*] Prof. R. L. Schowen
Department of Chemistry
University of Kansas
Lawrence, KS 66045-0046 (USA)
Fax: Int. code +(913)864-5349
e-mail: rschowen@caco3.chem.ukans.edu

 © VCH Verlagsgesellschaft mbH, D-69451 Weinheim, 1997 0570-0833/97/3613-1434 $ 17.50+.50/0

later showed that all highly effective bifunctional catalysts are indeed tautomeric catalysts, that is, they possess two tautomeric forms of similar energy (such as 2-pyridone and 2-hydroxypyridine) between which they interconvert in the course of bifunctional catalysis.

In 1953, the year following Swain and Brown's discovery of polyfunctional catalysis, Watson and Crick[6] proposed the best-known hydrogen-bonding scheme in all of modern science (Scheme 1). The Watson–Crick pattern that selectively binds pairs of nucleic-acid bases within the double-helical DNA structure provides for specific molecular recognition between deoxyadenylate (A) and deoxythymidylate (T) in a double hydrogen bond complex, and between deoxyguanylate (G) and deoxycytidylate (C) in a triple hydrogen bond complex. This enforces the security of the genetic code in DNA and the fidelity of the genetic code in its replication into DNA, its transcription into RNA, and its translation into a protein sequence. Watson and Crick also initiated a series of proposals, recently reviewed by Goodman[3] and by Douhal et al.,[7] according to which tautomerization within the hydrogen-bonded pairs could give rise to base pairs incorrectly matched in terms of the genetic code (see Scheme 1). Such tautomers might therefore produce genetic mutations through misreading of the DNA code during transcription into RNA or misreading of its RNA transcript during translation into a protein structure.

Like the ring-opening reaction of glucose, cooperative base-pair tautomerization in nucleic acids involves components of both proton transfer and heavy-atom reorganization. The fairly large-scale heavy-atom reorganization in glucose ring opening involves fission of a C–O σ bond and formation of a C–O π bond, whereas base-pair tautomerization produces more modest interconversions of wholly or partially single and double bonds between heavy atoms within the framework of the paired bases.

The question of whether double proton transfer in the glucose example is concerted or stepwise was addressed definitively in 1982 by Engdahl et al.[8] They measured the rate constant for mutarotation of tetramethylglucose catalyzed by 2-pyridone in benzene; the samples of sugar and catalyst had definite fractions n of deuterium replacing the protium at the two proton-bridging sites. This test for simultaneous or sequential bonding changes at two transition-state protonic sites by variation of the degree of deuteration is known as the proton-inventory ap-

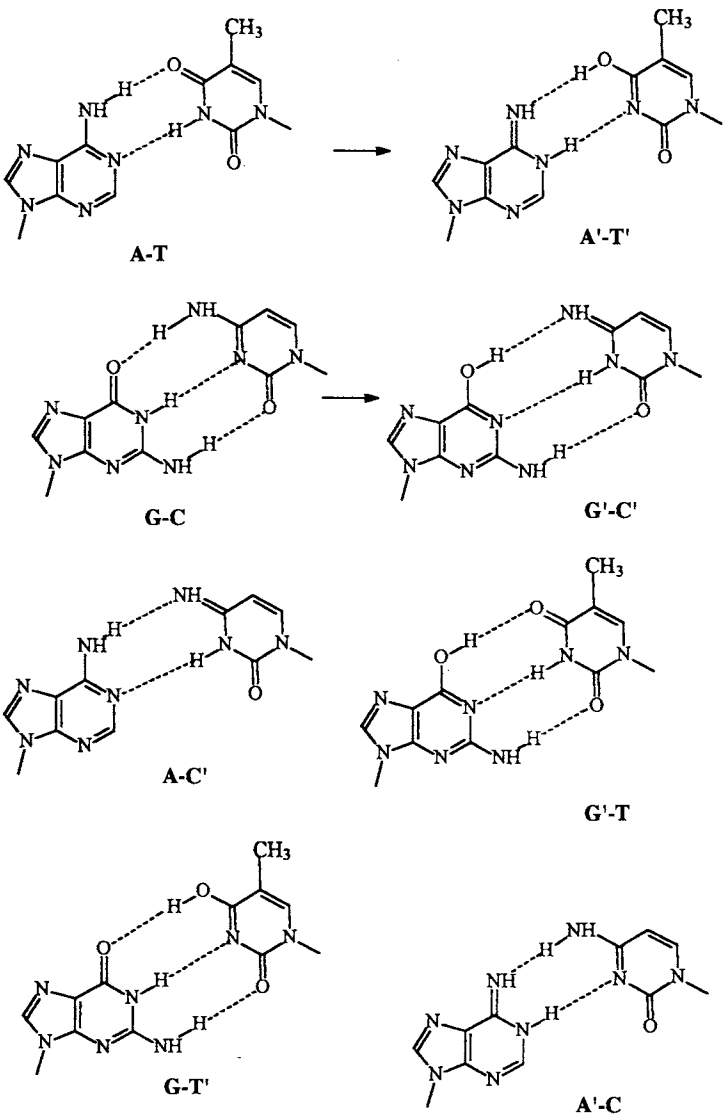

Scheme 1. Hydrogen bonding between Watson–Crick base pairs: A recognizes T (and vice versa) by the two hydrogen bond pattern (first row, left), G recognizes C (and vice versa) by the three hydrogen bond pattern (second row, left). Double proton exchange within A–T pairs can generate the tautomeric forms A′ and T′ (first row right), and double proton transfer within G–C pairs can generate the tautomeric forms G′ and C′ (second row, right). The lower half of the Scheme shows how misreading is possible by such tautomerizations. Each of the "wrong" tautomers A′, T′, G′, and C′ can successfully recognize and base pair with a "wrong" partner (C, G, T, and A, respectively).

proach.[9] A rate constant is measured as a function of the atom fraction of deuterium n in exchangeable positions from $n = 0$ (pure protium label) to $n = 1$ (pure deuterium label). A linear $k_n(n)$ indicates that the isotope effect arises from bonding changes at a single transition-state site (as in the transition states leading to or from the intermediates **4** and **5**), whereas a quadratic dependence indicates simultaneous bonding changes at two sites, as in the concerted reaction via transition state **2**. Engdahl and co-workers found a quadratic dependence with the isotope effect of about 4 arising from effects of about 2 at each of the transition-state sites. This confirms the Swain–Brown conclusion of concerted double proton transfer.

Another related isotope-effect approach to the coupling of proton motions was taken by Limbach and co-workers. From the 1970s to the present time they have been developing NMR methods for characterizing multiple hydrogen-transfer processes among tautomeric species, and have thereby elucidated the detailed dynamics of numerous tautomerization reactions in the liquid and solid states.

In very recent work, Braun and co-workers[10] examined the degenerate tautomerization of porphyrin molecules (**6**⇌**8**). This

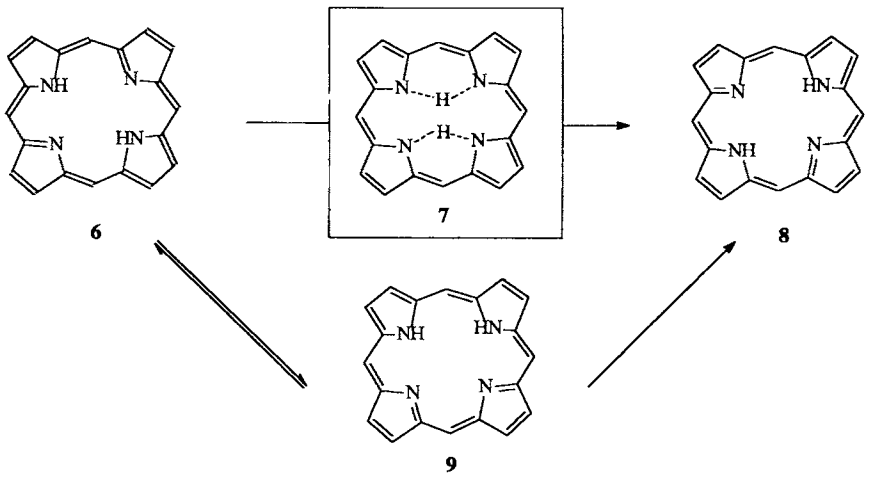

reaction may occur by simultaneous, concerted motion of the two hydrons through transition state **7**, or by two successive, stepwise motions through the "*cis* intermediate" **9**. By lineshape analysis of the ^1H, ^2H, and ^3H NMR signals of porphyrins separately labeled with the three isotopes of hydrogen (naturally necessitating precautions with the highly tritiated material), rate constants for the degenerate rearrangement of porphyrin by double proton transfer were obtained for proton and deuteron motions between 100 and 350 K as well as triton motions between 237 and 350 K. Rates and isotope effects are similar in organic solvents and in the polycrystalline state. At 298 K in dimethylformamide (DMF), the isotope effect k_{HH}/k_{DD} for simultaneous deuterium labeling at both positions is 11. The symmetry of this degenerate-rearrangement system requires the isotope effects at the two sites to be equal. If the two motions were occurring concertedly k_{HH}/k_{DD} would be equal to $(k_H/k_D)^2$, where k_H/k_D is the isotope effect at a single site. The single-site isotope effect k_{HD}/k_{DD} is then predicted to be 3.3. If the two hydrons instead move in succession, the *cis* intermediate **9** must form and then decompose through transition states of equal Gibbs free energy (because the rearrangement is degenerate). In such a case $k_{HH} = k_H$ and $k_{DD} = k_D$. In the singly deuterated species, either hydron may move first (with rate constant k_H for H or k_D for D) to generate the singly labeled intermediate. A fraction of the intermediate thus formed will proceed to product by motion of the hydron that did not previously move. The rate constant for this fraction will therefore be given by $[k_D/(k_H + k_D)]$ if H moved first and by $[k_H/(k_H + k_D)]$ if D moved first. Therefore $k_{HD} = 2k_Hk_D/(k_H + k_D)$ and k_{HD}/k_{DD} will approach 2 as k_H becomes much larger than k_D. In fact Braun et al. find that k_{HD}/k_{DD} is approximately 2 at 298 K. This is just as expected for the stepwise process, because k_H is 11 times greater than k_D on this model. This result indicates that the porphyrin rearrangement occurs by a stepwise mechanism through the low-concentration, kinetically insignificant intermediate **9**.

Along still another independent route of investigation, Petrich and his collaborators[11] examined the tautomerization of 7-azaindole in MeOH and EtOH (**10**⇌**12**). This chromophore forms the side chain of 7-azatryptophan, an unnatural amino acid introduced and applied by Petrich et al. to a wide variety of problems in peptide and protein dynamics.[12] The tautomerization of 7-azaindole occurs readily in the excited state and constitutes the major route of nonradiative relaxation; the rate constant can be measured by fluorescence decay. Compared to the rate constant for reaction in MeOH and EtOH, the decay rate constant is decreased by a factor of about 2.7 for reaction in MeOD or EtOD (since exchange at the N–H position is fast, 7-azaindole will also be deuterated in the deuterated solvents). The tautomerization reaction, which is surely mediated by at least one molecule of solvent, might occur by concerted transfer of the two hydrons through transition state **11** or by independent, stepwise hydron motions through intermediates

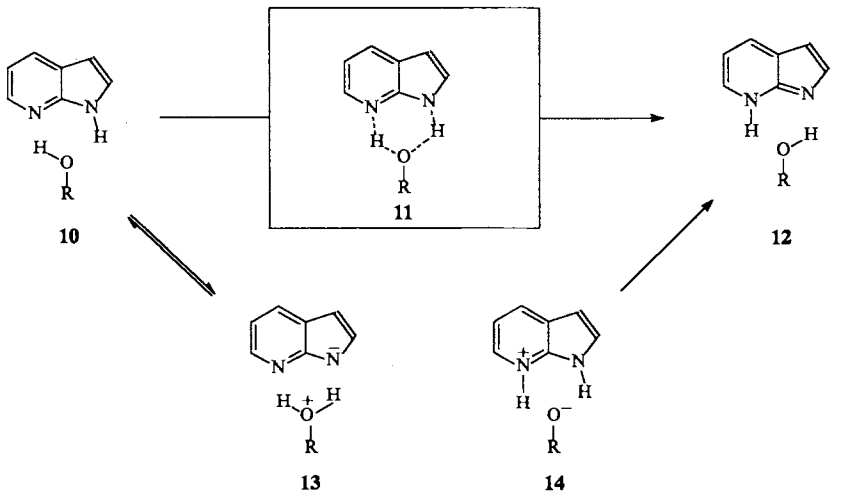

13 or **14** or both. Petrich and co-workers examined the question of concertedness in the double proton transfer by means of a proton-inventory experiment. The rate constant decreases as a quadratic function of the atom fraction of deuterium in the solvent, showing that the overall solvent isotope effect of 2.7 arises from roughly equal isotope effects of 1.6–1.7 at two sites in a single transition state such as **11**. These two sites are therefore likely to be the N–H(D) site of 7-azaindole and the O–H(D) site of the alcohol molecule mediating the tautomerization through a single transition state with concerted motion of the two protons. The alcohol molecule is thus functioning as a bifunctional catalyst.

The isomerization of excited 7-azaindole molecules also occurs in the hydrogen-bonded dimer (**15**⇌**17**), with each monomer serving as both substrate and bifunctional catalyst for the tautomerization.[13] The reaction may occur through a single transition state **16** for a concerted pathway or in a stepwise manner through intermediates such as **18** or **19**. Douhal et al.[7] examined the mechanism for this reaction in the gas

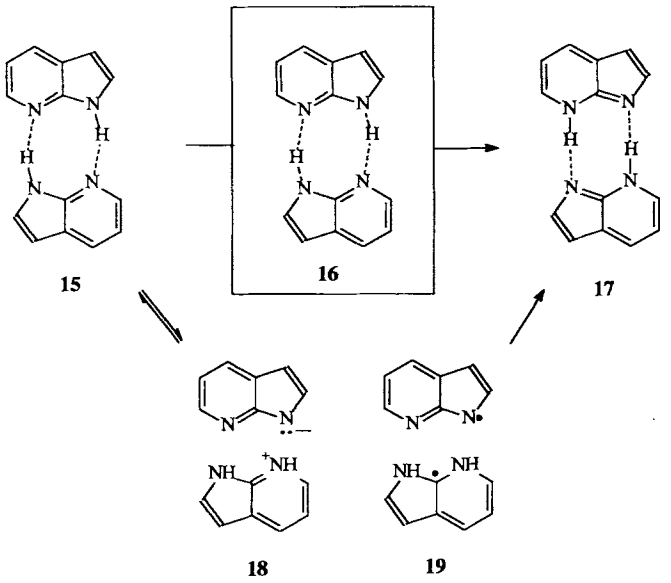

phase. They prepared dimers in a molecular beam with definite quantities of excess vibrational energy and electronically excited them with an initial 60-femtosecond laser pulse at 305–310 nm. After variable periods of up to 20 picoseconds a second pulse at 620 nm ionized the excited molecules, and the ions were drawn into the analyzer of a time-of-flight mass spectrometer. The ion signal decreased with time because the ionization cross section of the tautomer-product dimer was smaller than that of the initial 7-azaindole dimer. Furthermore, the signal decreased as a biexponential function of time, showing that an intermediate compound (of intermediate ionization cross section) formed in significant amounts in the course of the tautomerization reaction. At an excess vibrational energy of 1 kcal mol^{-1} the kinetic isotope effect $k_{HH}/k_{DD} = 10$ for the initial fast phase of the reaction and 12 for the second slower phase. This suggests that proton transfer occurs in both phases of the reaction. The most reasonable model is that single proton transfer generates the intermediate ion pair **18** or radical pair **19** or both in kinetically signficant amounts. The second proton then transfers to form the product. Thus, the gas-phase tautomerization of 7-azaindole occurs in a stepwise manner through a relatively stable intermediate.

Table 1 summarizes the results of these four studies on the question of concerted versus stepwise reaction pathways for double proton transfer accompanied by heavy-atom reorganization. The gamut of possible outcomes is observed: two reactions exhibit concerted mechanisms, one reaction occurs along a stepwise route through a high-energy, kinetically insignificant intermediate, and one reaction follows a stepwise pathway through an observable, accumulating intermediate.

It seems likely that these initially perplexing findings are in fact an expression of a principle we owe to William P. Jencks, which was summarized in 1980 in an article[14] entitled "When is an intermediate not an intermediate? Enforced mechanisms of general acid–base catalyzed, carbocation, carbanion, and ligand exchange reactions". The essence of Jencks's concept is that if an intermediate compound along a stepwise route must have a very high-energy structure, then it is likely that a lower-energy structure will be possible for the concerted-reaction transition state. If this is the case, the reaction will naturally proceed along the concerted route, a choice that Jencks describes as "enforced" by the high energy required for the alternative, stepwise process. Each of the cases we have considered obeys Jencks's principle.

The two examples that exhibit concerted mechanisms would require high-energy species as intermediates. In the mutarotation of glucose the instability of intermediates **4** and **5** enforces a concerted reaction through the transition state **2**. Similarly, in the alcohol-mediated tautomerization of 7-azaindole, the oxonium moiety of **13** and the alkoxide moiety of **14** confer instability

Table 1. Summary of the favored reaction pathways and potential intermediates for double proton transfer reactions.

Reaction	Concertedness: evidence	Potential intermediate
mutarotation of tetramethylglucose with 2-pyridone as catalyst in benzene	concerted: quadratic proton inventory indicates simultaneous bonding changes at two protonic sites	conjugate acid–base pairs for singly protonated–deprotonated sugar and catalyst (**4**·**5**)
porphyrin isomerization in DMF	stepwise: double-label isotope effect of 11, single-label isotope effect of 2 (see text)	*cis*-porphyrin **9**; steady-state intermediate not accumulating in kinetically significant amounts
alcohol-mediated isomerization of excited 7-azaindole in MeOH or EtOH	concerted: quadratic proton inventory indicates simultaneous bonding changes at two protonic sites	conjugate acid–base pairs for singly protonated–deprotonated substrate and catalyst (**13**,**14**)
isomerization of dimeric excited 7-azaindole in the gas phase	stepwise: intermediate accumulates in kinetically significant amounts; large isotope effects for both formation and decomposition of intermediate	presumably ion pair **18** or radical pair **19** or both

 © *VCH Verlagsgesellschaft mbH, D-69451 Weinheim, 1997* *0570-0833/97/3613-1437 $ 17.50+.50/0*

even if the conjugate acid and conjugate base of 7-azaindole should be relatively stable. In both cases, the high energy of the required intermediates along the potential stepwise pathway may be considered to enforce reaction by the concerted route.

The two reactions that exhibit stepwise mechanisms, as required by the Jencks principle, can employ intermediate structures that may be of some stability. The porphyrin isomerization can pass through the intermediate **9**, which maintains the cyclic conjugation of the porphyrin system. Although the energy of this intermediate is lower than that of the potential transition state **7** for the concerted reaction, the intermediate is nevertheless sufficiently unstable that it returns to the reactant state or proceeds to the product state with such rapidity that it fails to accumulate and cannot be detected in the NMR experiment. However, in the gas-phase tautomerization reaction of the electronically excited 7-azaindole dimer, the stability of the intermediate state **18**/**19** is so great that it not only surpasses the stability of the potential transition state **16** for the concerted reaction but also accumulates during the reaction, rendering the kinetics biphasic. The stability of the intermediate species in the gas phase, if its correct representation is the ion pair **18**, may seem paradoxical in comparison to the instability of intermediates **13** and **14** in the polar liquid phase. However, both ionic moieties of **18** are stabilized by charge delocalization (unlike the oxonium moiety of **13** and the alkoxide moiety of **14**), and the stability of the complex may also benefit from the polarizability of the two relatively large partners. Furthermore, intramolecular electron transfer may occur readily to generate the radical pair **19**, which could be the accumulating form of the intermediate even if a minor population of **18** is the reaction-pathway intermediate that arises from reactants and generates products.

The reactions of Table 1 occur in widely different media ranging from the gas phase through benzene to DMF and alkanols. The molecular choices made in each of the cases (concerted reactions in benzene and alkanols, stepwise reactions in the gas phase and DMF) cannot be understood in terms of coarse generalizations but instead require a more refined consideration of the structure of the intermediate and its interaction with the medium. The power of Jencks's principle thus transcends the facile simplicity of traditional thinking.

A question that has not been treated here, but will be addressed elsewhere, concerns the means by which the hydrons achieve translocation, whether along the concerted or stepwise pathway. For example, is quantum tunneling involved; or, is the hydron motion coupled into the reaction coordinate for heavy-atom reorganization? Whatever the answer to this question, the main molecular selection between concerted and stepwise pathways appears to follow from Jencks's principle of avoiding high-energy intermediates.

German version: *Angew. Chem.* **1997**, *109*, 1502–1506

Keywords: carbohydrates · heterocycles · hydrogen transfer · isotope effects · nucleic acids

[1] The terms concerted and stepwise are used here in the simplest sense of occurring via a single transition state (concerted) or different transition states (commonly with an intermediate state having a lifetime of more than one molecular-vibration period intervening between the transition states; stepwise). Considerably finer distinctions in the timing of events during chemical reactions are possible and have been reviewed: C. F. Bernasconi, *Adv. Phys. Org. Chem.* **1992**, *27*, 119–238.

[2] R. L. Schowen in *Mechanistic Principles of Enzyme Activity* (Eds.: J. F. Liebman, A. Greenberg), VCH, New York, **1988**, pp. 119–168.

[3] M. F. Goodman, *Nature* **1995**, *378*, 237–238.

[4] C. G. Swain, J. F. Brown, Jr., *J. Am. Chem. Soc.* **1952**, *74*, 2534–2537, 2538–2543.

[5] P. R. Rony, R. O. Nett, *J. Am. Chem. Soc.* **1973**, *95*, 2895–2905, and preceding papers in this series. A derivative of cytidine is a (presumably bifunctional) catalyst of the mutarotation of tetramethylglucose in benzene: C. Melander, D. A. Horne, *Tetrahedron Lett.* **1997**, *38*, 713–716.

[6] J. D. Watson, F. H. C. Crick, *Nature* **1953**, *171*, 964–967.

[7] A. Douhal, S. K. Kim, A. H. Zewail, *Nature* **1995**, *378*, 260–263.

[8] K. A. Engdahl, H. Bivehed, P. Ahlberg, W. H. Saunders, Jr., *J. Am. Chem. Soc.* **1983**, *105*, 4767–4774.

[9] K. S. Venkatasubban, R. L. Schowen, *CRC Crit. Rev. Biochem.* **1984**, *17*, 1–44.

[10] J. Braun, H.-H. Limbach, P. G. Williams, H. Morimoto, D. E. Wemmer, *J. Am. Chem. Soc.* **1996**, *118*, 7231–7232.

[11] Y. Chen, F. Gai, J. W. Petrich, *J. Am. Chem. Soc.* **1993**, *115*, 10158–10166.

[12] A. S. Smirnov, D. S. English, R. L. Rich, J. Lane, L. Teyton, A. W. Schwabacher, S. Luo, R. W. Thornburg, J. W. Petrich, *J. Phys. Chem. B* **1997**, *101*, 2758–2769.

[13] C. A. Taylor, M. A. El Bayoumi, M. Kasha, *Proc. Natl. Acad. Sci. USA* **1969**, *63*, 253–260.

[14] W. P. Jencks, *Acc. Chem. Res.* **1980**, *13*, 161–169.

 © *VCH Verlagsgesellschaft mbH, D-69451 Weinheim, 1997* *0570-0833/97/3613-1438 $ 17.50+.50/0*

Chemical order achieved from chaos: when a mixture of three different bis(catechol-amide) ligands is allowed to react with $[Ga(acac)_3]$, a highly ordered system emerges.

No mixed-ligand oligomers are observed in solution; only the discrete $[Ga_2L_3]^{6-}$-triple helical complexes form. More about this system is described by Raymond et al. on the next page.

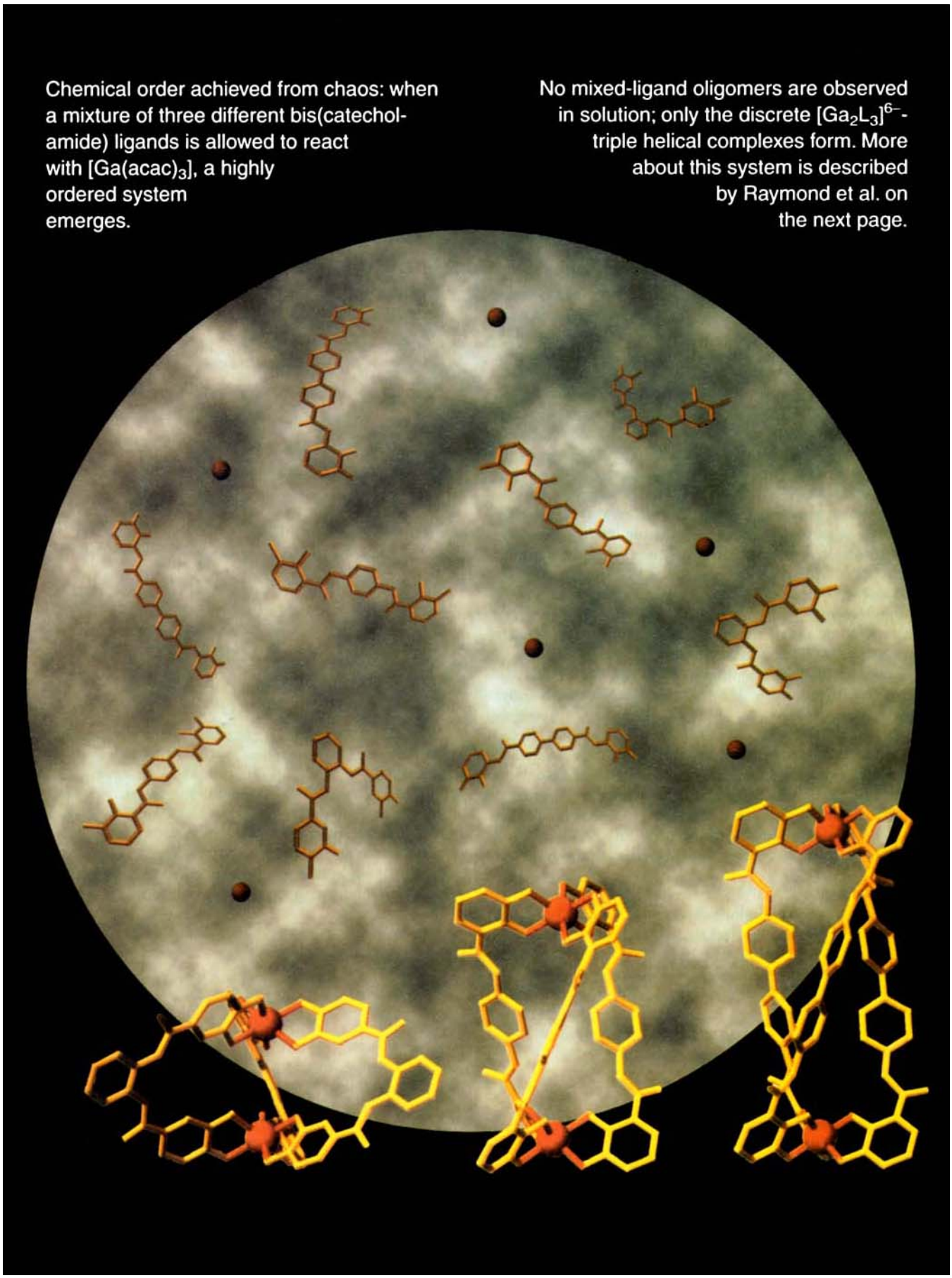

 © VCH Verlagsgesellschaft mbH, D-69451 Weinheim, 1997 *0570-0833/97/3613-1439 $ 17.50 + .50/0*

Supramolecular Self-Recognition and Self-Assembly in Gallium(III) Catecholamide Triple Helices**

Dana L. Caulder and Kenneth N. Raymond*

Supramolecular chemistry has been described as a type of molecular information science:[1] a supramolecular assembly is manufactured from the information stored in preprogrammed molecular components. In nature there are numerous examples of highly symmetric supramolecular clusters, including the 24 subunit protein ferritin (pure rotation group *O*) and the 60 subunit coat of the human rhinovirus (pure rotation group *I*).[2, 3] In an analogous process, a few metal–ligand interactions can be used in place of the many, but weaker, interactions that drive the formation of natural molecular clusters. Recently the synthesis of some highly symmetric supramolecular architectures have been reported,[4–7] and we have described a rational design of such structures based on the incommensurate coordination numbers of interacting sites of the cluster.[4, 8]

The triple helix formed by two metal centers is one of the simplest assemblies of this type. There are numerous examples of synthetic complexes with helical motifs incorporating bipyridine and benzimidazol ligands.[1, 9–11] More recently there have been examples of helical complexes with oxygen donor ligands, including catechol.[12–14] The exclusive formation of a predesigned cluster requires ligand rigidity, kinetically labile metal–ligand interactions, and thermodynamic stability. These features drive the formation of the thermodynamically favored cluster over the large number of other intermediate polymers. The complexes of catecholamides with Ga^{III} satisfy these requirements.[15, 16]

In a rational design of these self-assembling supramolecular clusters, a series of three bis(catecholamide) ligands (H_4-**1**–H_4-**3**) has been synthesized according to Scheme 1. Molecular mechanics calculations show that for all ligands the chiral helicate is lower in energy than the *meso*-$[M_2L_3]$ cluster.[17, 18] The synthesis of ligand H_4-**2** and the X-ray crystal structures of the gallium complexes of two derivatized versions of this ligand have been reported previously and confirm the helix structure.[12]

It was intended that the information stored in these rigid bis(catecholamide) ligand systems be used to overcome the intrinsic disorder of mixtures in order to produce a highly ordered system of complexes in solution. As will be shown, this has been achieved.

The three ligands H_4-**1**–H_4-**3** were designed to increase the metal–metal distance systematically in the dinuclear helicates, the goal being to probe the effect that size has on the ability of the helicates to form by self-assembly. So far a size limit has not been reached. When three equivalents of any ligand (H_4-**1**–H_4-**3**) are allowed to react with two equivalents of $[M(acac)_3]$ (M = Fe^{III}, Al^{III}, Ga^{III}; acac = acetylacetonate) and KOH in methanol at room temperature, the $K_6[M_2L_3]$ triple helical complexes can be isolated in high yield (70–80%) [Eq. (a)].

$$3\,LH_4 + 2\,[Ga(acac)_3] \xrightarrow[CH_3OH]{KOH} K_6[Ga_2L_3] \qquad \text{(a)}$$

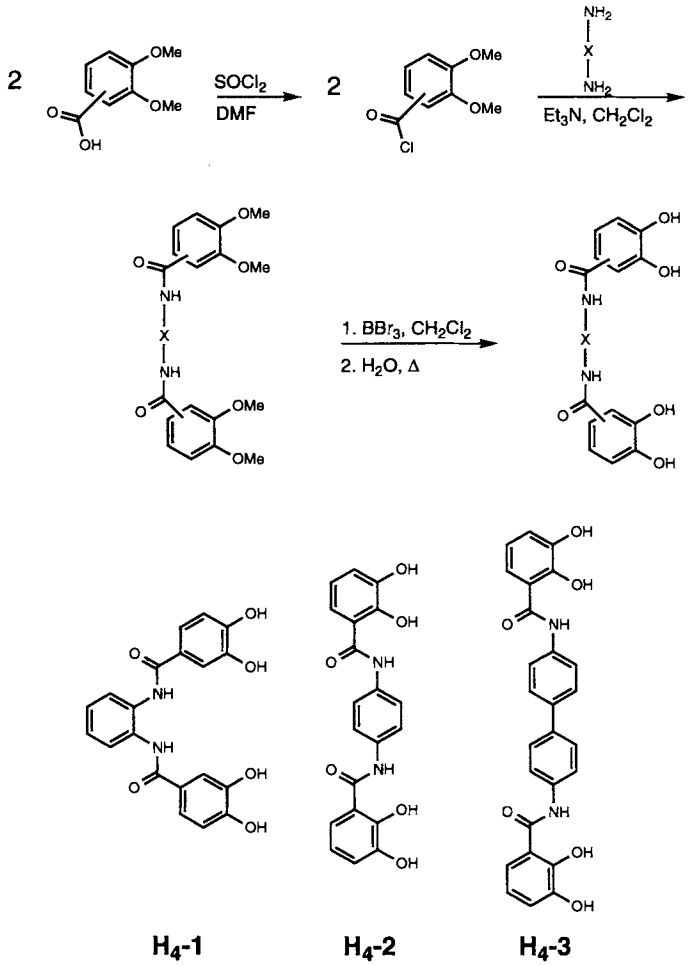

Scheme 1. Synthesis of H_4-**1**–H_4-**3**.

When the complexes are prepared in the presence of excess ligand, there is no disruption of the formation of the $[M_2L_3]$ clusters. The ^1H NMR spectrum in all cases shows two sets of peaks, one for the complex and one for the excess ligand. This cooperativity ultimately facilitates the synthesis of controlled mixtures of complexes. Remarkably, when mixtures of any two or all three of the ligands (H_4-**1**–H_4-**3**) are allowed to react with $[Ga(acac)_3]$ under the conditions described above, only complexes containing one type of ligand form (Scheme 2). No

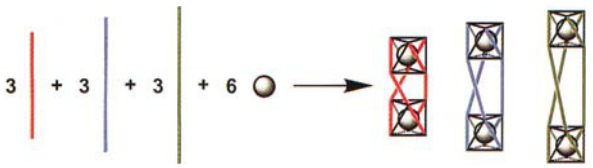

Scheme 2. Schematic representation of self-recognition of ligands in gallium catecholamide triple helices. Rods represent ligands of varying lengths and spheres represent Ga^{III} ions. Only the discrete complexes containing one type of ligand form in solution. No mixed or oligomeric species are observed.

oligomeric mixed-ligand species are observed in solution with ^1H NMR spectroscopy or with electrospray mass spectrometry (ES-MS). The ^1H NMR spectrum of the resulting solution shows a 1:1:1 mixture of the $K_6[Ga_2(\mathbf{1})_3]$, $K_6[Ga_2(\mathbf{2})_3]$, and $K_6[Ga_2(\mathbf{3})_3]$ helical complexes (Figure 1). This can be confirmed by comparing the resulting spectrum to a simulated spectrum

[*] Prof. K. N. Raymond, D. L. Caulder
Department of Chemistry
University of California
Berkeley, CA 94720-1460 (USA)
Fax: Int. code +(510)486-5283
e-mail: raymond@socrates.berkeley.edu

[**] Coordination Number Incommensurate Cluster Formation, Part 3. This research was supported in part by the National Institutes of Health (Grant DK32999). We gratefully acknowledge Ryan E. Powers for supplying the ligand H_4-**2**. Part 2: [12].

 © VCH Verlagsgesellschaft mbH, D-69451 Weinheim, 1997 0570-0833/97/3613-1440 $ 17.50+.50/0

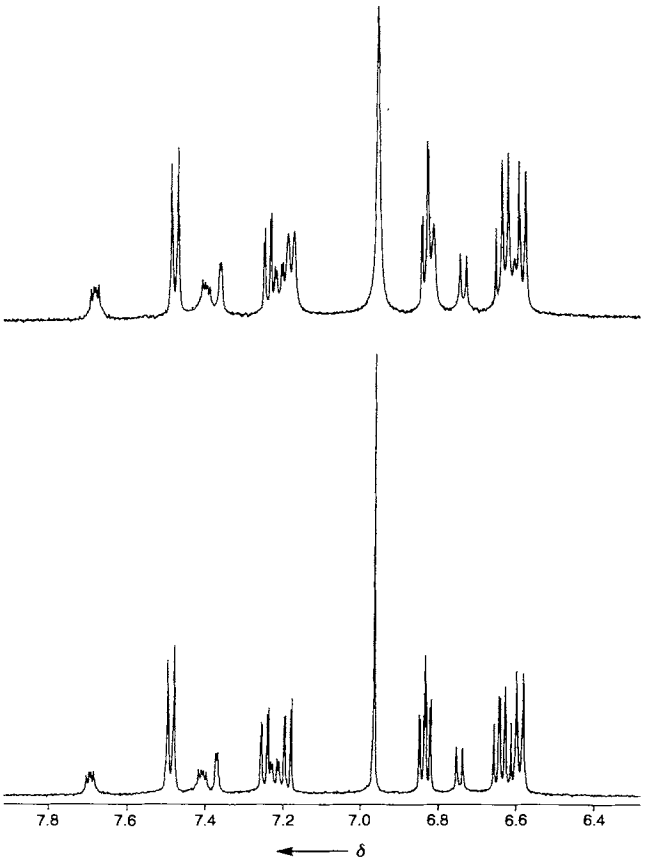

Figure 1. Bottom: ^{1}H NMR spectrum (5% K_2HPO_4, D_2O, pD = 9.2, 300 MHz) of a 3:3:3:2 mixture of **1**, **2**, **3** and [Ga(acac)$_3$] after workup. Top: simulation spectrum obtained by adding the spectra of the individually isolated gallium complexes of **1**, **2**, and **3**. No oligomeric species are observed in solution.

obtained by adding the spectra of the individual complexes. Positive-ion ES-MS (100% CH_3OH) also supports this conclusion, as no peaks from oligomeric mixed ligand species are found; only the $[Ga_2L_3]^{6-}$ complexes are observed.[19]

The driving force for the observed self-recognition is largely a concentration effect. In a closed coordination polymer (that is, all metal sites are coordinated by three catecholamide functionalities) for a simple system with one metal and one ligand, equilibrium (b) can be written. The equilibrium constant for this

$$n[M_2L_3] = [M_2L_3]_n \qquad (b)$$

equation should be approximately 1. Only if the polymer is significantly insoluble will the reaction be driven further to the right, but these species are highly charged and very soluble. Thus if $n = 4$ and the original concentration of the cluster is 2×10^{-3} M, then the polymer concentration will be approximately 10^{-11} M. This entropic driving force is also present with more complicated mixtures of ligands: the formation of mixed-ligand oligimers remains disfavored.

These ligand designs are unique, because the rigidity and different distances between the coordinating functionalities makes it geometrically impossible to form a mixed ligand $[M_2L_2L'_1]^{6-}$ complex. This steric factor makes closed polymers unattainable. Inevitably, there will be metal sites not coordinated by a catecholamide. For each mole of gallium ions coordinated by only two catecholamide functionalities, over 10 kcal of free energy is lost.[15, 16] Thus, fragments with uncoordinated ends are disfavored and removed in the equilibration of species.

In this work, a series of rigid bis(bidentate) catecholamide ligands has been designed and synthesized to form triple helicates with trivalent metal ions. As a consequence of the predesigned rigid geometry between the ligands' coordinating sites and the positive cooperativity displayed in the formation of the triple helicate systems, highly ordered systems are produced from a complex mixture of closely similar ligands upon addition of metal. Reaction of a mixture of the three bis(catecholamide) ligands (H_4-**1**–H_4-**3**) with [Ga(acac)$_3$] in methanol and KOH at room temperature yields only the individual complexes $K_6[Ga_2(\mathbf{1})_3]$, $K_6[Ga_2(\mathbf{2})_3]$, and $K_6[Ga_2(\mathbf{3})_3]$, according to both ^{1}H NMR and electrospray mass spectrometry. While similar self-recognition has been observed with mixtures of bipyridine-type ligands that differ in the number of metal coordination sites,[20] this demonstrates for the first time that molecular resolution can be achieved based solely on the distance between two metal coordination sites, cleanly separating as many as three ligand components.

Experimental Section

A solution of the appropriate diamine (3.0 mmol) and Et_3N (12 mmol) in CH_2Cl_2 (50 mL) was added dropwise to a stirred solution of the dimethoxybenzoyl chloride [21] (6.2 mmol) in CH_2Cl_2 (100 mL) at 0°C. The reaction mixture was stirred at room temperature for 2 h and then washed with distilled water, 2 N NaOH, and 2 N HCl. The CH_2Cl_2 layer was separated off, dried over $MgSO_4$, and filtered. Upon evaporation of the solvent, the methyl-protected ligands were all isolated in 85–95% yields.

BBr_3 (38 mmol) was added by syringe to a stirred solution of the methyl-protected ligand (3.1 mmol) in CH_2Cl_2 (100 mL) at −78°C. The reaction mixture was stirred at room temperature for 48 h. The volatiles were removed under vacuum, and the remaining orange-yellow solid was stirred in distilled water at 100°C. After 4 h the resulting white precipitate was collected by filtration, washed with absolute ethanol and diethyl ether, and dried under vacuum at 70°C for 12 h to yield the ligands (all in 80–95% yield). All ligands were characterized by ^{1}H NMR spectroscopy, mass spectrometry, and elemental analysis (C, H, N).

Under nitrogen, the ligand H_4L (0.39 mmol) was stirred in methanol (30 mL). A solution of KOH (0.497 N, 0.79 mmol) in methanol was added by pipet, and the reaction mixture was stirred until the ligand dissolved completely. [Ga(acac)$_3$] (0.26 mmol) was then added, and the reaction mixture was stirred at room temperature for 4 h. The volatiles were removed under vacuum, and the residue washed with acetone (2 × 10 mL). The resulting off-white residue was characterized as the $K_6[Ga_2L_3]$ complex. The complexes darken upon exposure to air.

$K_6[Ga_2(\mathbf{1})_3]$: ^{1}H NMR ([D$_6$]DMSO, 400 MHz): δ = 9.14 (s, 6H, NH), 7.76 (m, 6H), 7.26 (s, 6H), 7.10 (m, 6H), 6.99 (d, J = 7.6 Hz, 6H), 6.27 (d, J = 8.0 Hz, 6H); ^{1}H NMR (5% K_2HPO_4 in D_2O, 500 MHz): δ = 7.69 (dd, J = 3.6, 5.9 Hz, 6H), 7.40 (dd, J = 3.5, 5.9 Hz, 6H), 7.37 (d, J = 2.2 Hz, 6H), 7.21 (dd, J = 2.3, 8.1 Hz, 6H), 6.74 (d, J = 8.1, 6H). Positive-ion ES-MS: m/z: 1542[MK$^+$], 1526 [MNa$^+$], 1504 [MH$^+$] (1503 calcd. for $M = K_6Ga_2C_{60}H_{36}N_6O_{18}$).

$K_6[Ga_2(\mathbf{2})_3]$: ^{1}H NMR (5% K_2HPO_4 in D_2O, 500 MHz): δ = 7.18 (d, J = 7.8 Hz, 6H), 6.96 (s, 12H), 6.82 (d, J = 7.2 Hz, 6H), 6.62 (t, J = 7.8 Hz. 6H). Additional data as previously reported in Ref. [12].

$K_6[Ga_2(\mathbf{3})_3]$: ^{1}H NMR ([D$_6$]DMSO, 400 MHz): δ = 9.62 (s, 6H), 7.48 (d, J = 8.0 Hz, 12H), 6.83 (dd, J = 1.6, 8.0 Hz, 6H), 6.31 (dd, J = 1.6, 7.2 Hz, 6H), 6.15 (t, J = 7.2 Hz, 6H), 6.15 (d, J = 8.0 Hz, 12H); ^{1}H NMR (5% K_2HPO_4 in D_2O, 500 MHz) δ = 7.48 (d, J = 8.5 Hz, 12H), 7.25 (dd, J = 1.6, 8.2 Hz, 6H), 6.84 (dd, J = 1.6, 7.5 Hz, 6H), 6.64 (t, J = 7.9 Hz, 6H), 6.59 (d, J = 8.6, 12H); positive-ion ES-MS: m/z: 1770 [MK$^+$], 1753[MNa$^+$], 1732[MH$^+$] (1731 calcd. for $M = K_6Ga_2C_{78}H_{48}N_6O_{18}$).

Received: December 2, 1996 [Z 9840 IE]
German version: *Angew. Chem.* **1997**, *109*, 1508–1510

Keywords: cooperative effects · helical structures · self-assembly · supramolecular chemistry

[1] J.-M. Lehn, *Supramolecular Chemistry: Concepts and Perspectives*, VCH, Weinheim, **1995**.
[2] P. M. Proulxcurry, N. D. Chasteen, *Coord. Chem. Rev.* **1995**, *144*, 347.
[3] E. Arnold, M. G. Rossman, *Acta. Crystallogr. Sect. A* **1988**. *44*, 270.
[4] T. Beissel, R. E. Powers, K. N. Raymond, *Angew. Chem.* **1996**, *108*, 1166; *Angew. Chem. Int. Ed. Engl.* **1996**, *35*, 1084.
[5] R. W. Saalfrank, B. Horner, D. Stalke, J. Salbeck, *Angew. Chem.* **1993**, *105*, 1223; *Angew. Chem. Int. Ed. Engl.* **1993**, *32*, 1179.

[6] M. Fujita, D. Oguro, M. Miyazawa, H. Oka, K. Yamaguchi, K. Ogura, *Nature* **1995**, *378*, 469.
[7] S. Mann, G. Huttner, L. Zsolnai, K. Heinze, *Angew. Chem.* **1996**, *108*, 2983; *Angew. Chem. Int. Ed. Engl.* **1996**, *35*, 2808.
[8] "Coordination Number Incommensurate Cluster Formation": K. N. Raymond, D. L. Caulder, R. E. Powers, T. Beissel, M. Meyer, B. Kersting, *Proc. 40th Robert A. Welch Foundation Conf. Chem. Res.*, Houston, TX, **1996**, in press.
[9] E. C. Constable, M. J. Hannon, D. A. Tocher, *J. Chem. Soc. Dalton Trans.* **1993**, 1883.
[10] L. J. Charbonniere, G. Bernardinelli, C. Piguet, A. M. Sargeson, A. F. Williams, *J. Chem. Soc. Chem. Commun.* **1994**, 1419.
[11] D. S. Lawrence, T. Jiang, M. Levett, *Chem. Rev.* **1995**, *95*, 2229.
[12] B. Kersting, M. Meyer, R. E. Powers, K. N. Raymond, *J. Am. Chem. Soc.* **1996**, *118*, 7221.
[13] M. Albrecht, S. Kotila, *Angew. Chem.* **1995**, *107*, 2285; *Angew. Chem. Int. Ed. Engl.* **1995**, *34*, 2134.
[14] E. J. Enemark, T. D. P. Stack, *Angew. Chem.* **1995**, *107*, 2285; *Angew. Chem. Int. Ed. Engl.* **1995**, *34*, 996.
[15] M. J. Kappel, V. L. Pecoraro, K. N. Raymond, *Inorg. Chem.* **1985**, *24*, 2447.
[16] T. M. Garrett, P. W. Miller, K. N. Raymond, *Inorg. Chem.* **1989**, *28*, 128.
[17] CAChe MM2 Force Field Molecular Modeling System, V 3.6, Oxford Molecular Group Inc., Tektronix, UK, **1996**.
[18] CAChe calculations for the gallium complexes indicate that the chiral Δ,Δ- and Λ,Λ-configurated complexes are energetically favored over the *meso*-Δ,Λ-complexes by 3.7 kcal mol^{-1} ($[Ga_2(\mathbf{1})_3]^{6-}$), 12.1 kcal mol^{-1} ($[Ga_2(\mathbf{2})_3]^{6-}$), and 8.1 kcal mol^{-1} ($[Ga_2(\mathbf{3})_3]^{6-}$).
[19] Positive ion ES-MS assignments (100% MeOH) for the mixture of $K_6[Ga_2(\mathbf{1})_3]$, $K_6[Ga_2(\mathbf{2})_3]$, and $K_6[Ga_2(\mathbf{3})_3]$: *m/z*: 888 $[(K_6Ga_2\mathbf{3}_3Na_2)^{2+}]$, 896 $[(K_7Ga_2\mathbf{3}_3Na)^{2+}]$, 904 $[(K_8Ga_2\mathbf{3}_3)^{2+}]$, 1019 $[(K_8Ga_2\mathbf{3}_3)^{2+}]$, 1525 $[(K_6Ga_2\mathbf{1}_3Na)^{+}]$, $(K_6Ga_2\mathbf{2}_3Na)^{+}]$ 1542 $[(K_7Ga_2\mathbf{1}_3)^{+}]$, $(K_7Ga_2\mathbf{2}_3)^{+}]$, 1754 $[(K_6Ga_2\mathbf{3}_3Na)^{+}]$, 1770 $[(K_7Ga_2\mathbf{3}_3)^{+}]$.
[20] R. Kraemer, J.-M. Lehn, A. Marquis-Rigault, *Proc. Natl. Acad. Sci. USA* **1993**, *90*, 5394.
[21] P. F. Schuda, C. M. Botti, and M. C. Venuti, *OPPI Briefs* **1984**, *16*, 119.

A Bridged Porphyrinato(thiolato)iron(III) Complex as a Model of the Active Center of the Cytochrome P-450 Isozyme

Heinrich Volz* and Martin Holzbecher

Dedicated to Professor Leopold Horner on the occasion of his 85th birthday

The ubiquitous cytochrome P-450 isozymes are heme–thiolate enzymes, which function as oxygen-activating components in monooxygenase systems. They play a vital role both in the construction and destruction of cellular substances, catalyze the oxidative metabolism of lipophilic xenobiotics,[1] activate vitamins, and convert a range of chemical compounds into carcinogens in the course of chemical cancerogenesis.[2] Under anaerobic conditions O donors such as ROOH, RCO_3H, IO_4^-, ClO_3^-, and PhIO can be used in place of oxygen.[3]

According to crystal structure investigations of the isozyme cytochrome $P\text{-}450_{CAM}$[4] the heme group is embedded in a hydrophobic environment between the helices L and I. The heme group provides the largest hydrophobic surface for interaction with the substrate. The fifth ligand L_5 is the thiolate group of cysteine 357, which is situated in a hydrophobic pocket constructed from the amino acids Phe 350–Leu 358–Gln 360. The Fe–S bond is thus shielded to a large extent from the environment. Removal of the thiolate ligand leads to loss of monooxygenase activity.[5] Chloroperoxidase[6] and NO synthase[7] are also heme–thiolate enzymes. The chemoselectivity of these enzymes is also controlled by the heme–thiolate group.

Due to the very high molecular weight of the cytochrome P-450 isozyme (at least 45 kDa), an exact description of the mechanism of the oxidation of substrates and the nature of the iron-containing intermediates is difficult. One possible method that might cast some light on this problem is the study of chemically produced model compounds containing iron porphyrins, which resemble the natural product. To ensure that the thiolate models cannot lead to S oxidation or allow the production of μ-oxo or μ-peroxo complexes, not only the Fe–S bond but also the opposite side of the porphyrin molecule must be effectively shielded by hydrophobic groups. None of the thiolate model compounds yet described fulfills both these criteria.[8] Except for the model described by Hirobe and co-workers, these compounds were therefore not used for oxidation with O donors.[9]

We report here the synthesis of the bridged porphyrinato(thiolato)iron(III) complex **16** as a model of the active center of the cytochrome P-450 isozyme. Complex **16** was prepared from pyrrole **1** and 1,6-dibromohexane **8** in an 18-step convergent synthesis.

Pyrrole **1** was converted by known methods,[10] via 2-trichloroacetylpyrrole (**2**) and 2-chloroacetyl-4-iodopyrrole (**3**), into 2-methoxycarbonyl-4-iodopyrrole (**4**) (Scheme 1). The iodo substituent serves as protection against electrophilic attack at the 4-position in the subsequent reaction. Compound **4** is then treated with 2,6-dichlorobenzaldehyde in the presence of $BF_3 \cdot MeOH$ (20% BF_3 in MeOH) to give the dipyrromethane **5** in 57% yield. Alkaline hydrolysis of the ester followed by hydrogenolytic cleavage of the C–I bond produced the dicarboxylic acid **6** in 94% yield. This was then decarboxylated

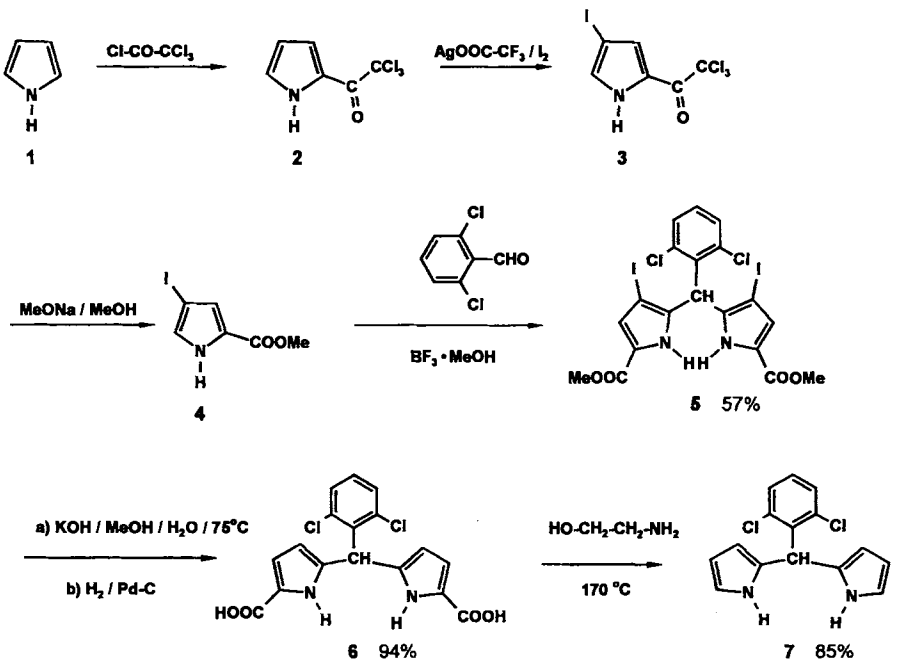

Scheme 1. Synthesis of 5-(2,6-dichlorophenyl)dipyrromethane (7).

[*] Prof. Dr. H. Volz, Dr. M. Holzbecher
Institut für Organische Chemie der Universität
Richard-Willstätter-Allee, D-76128 Karlsruhe (Germany)
Fax: Int. code +(721)69-8529

to 5-(2,6-dichlorophenyl)dipyrromethane (**7**) by heating in ethanolamine[11] (170 °C, 1.5 h).

1,6-Dibromohexane (**8**) was converted into 1,13-dibromotridecan-7-one (**9**) in four steps (Scheme 2), in analogy to the method described for 1,4-dibromobutane.[12] This was then treated with 2-hydroxy-1-naphthalenecarbaldehyde to give the dialdehyde **10**.

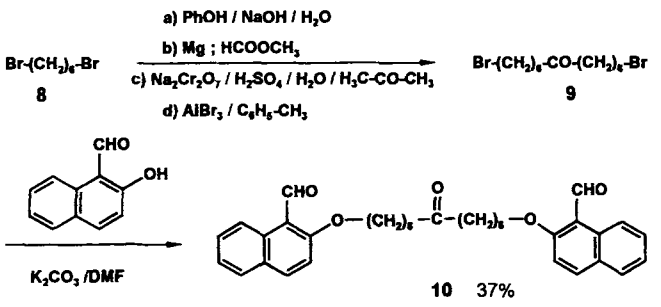

Scheme 2. Synthesis of the dialdehyde **10**.

The coupling reaction of **7** and **10** catalyzed by BF_3–methanol and the subsequent oxidation with 2,3-dichloro-5,6-dicyano-1,4-benzoquinone (DDQ) yielded the porphyrinophane **11** in 16% yield (Scheme 3). Reduction of the carbonyl group in **11** with $NaBH_4$ led to **12**, which was converted into the bromide **13** by reaction with CBr_4/Ph_3P/pyridine/THF.[13] This reacted with potassium thioacetate to give the thioester **14**.[8b] Metalation of **14** to yield the iron complex **15** was achieved with $FeBr_2$/lutidine,[14] and finally reaction with $NaOCH_3$ in $MeOH/CHCl_3$ produced the bridged porphyrinato(thiolato)iron(III) complex (**16**) in 77% yield. This crystallized together with a molecule of methanol, which is coordinated to the iron atom (Soret band at 415 nm). The methanol could be removed

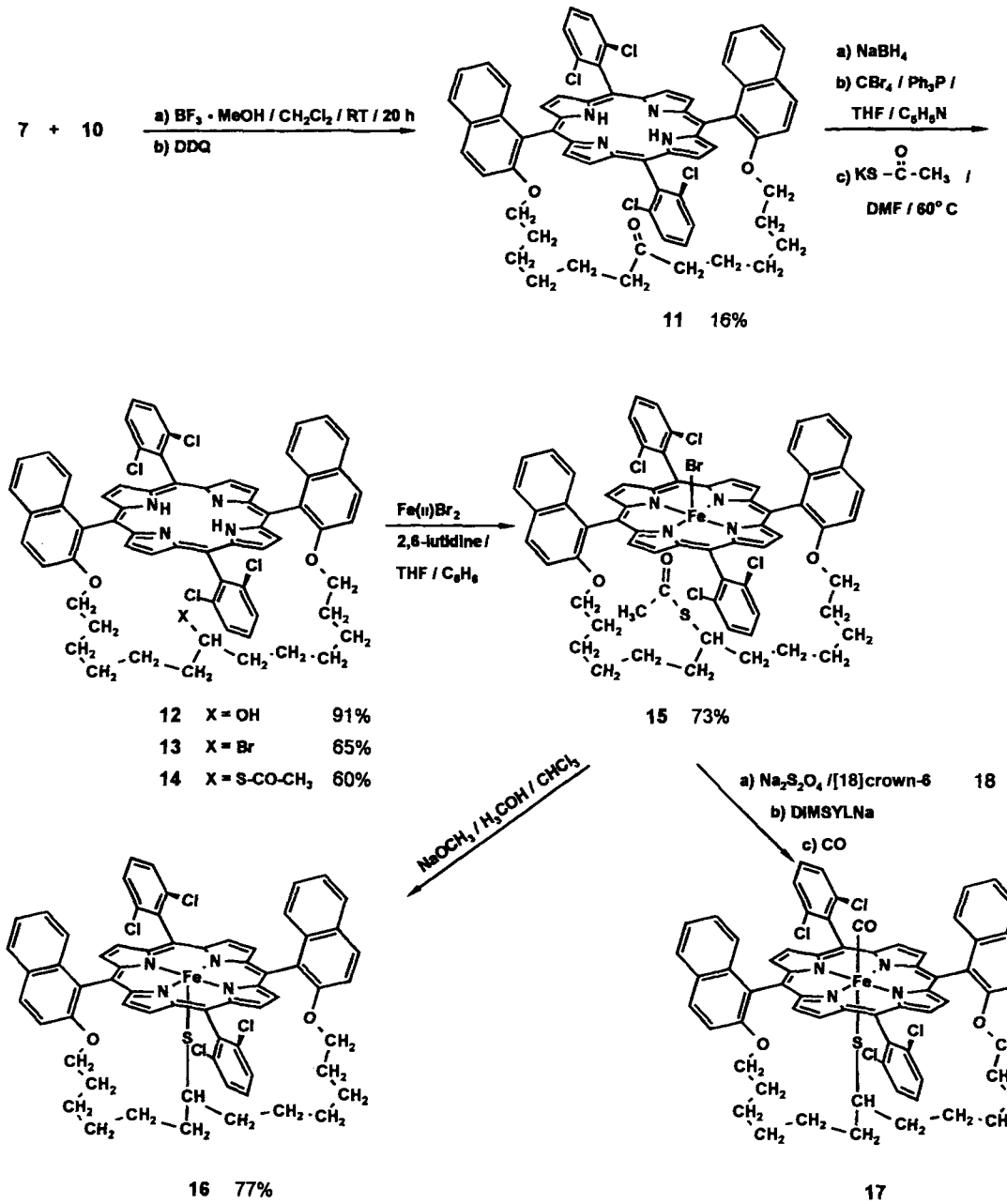

Scheme 3. The [2+2] synthesis of the porphyrinophane **11** from the components **7** and **10**, and the subsequent reaction steps from **11** to the *thiolate complex* **16**, *and the preparation of the CO-porphyrinato(thiolato)iron(II) complex* **17**.

 © *VCH Verlagsgesellschaft mbH, D-69451 Weinheim, 1997* *0570-0833/97/3613-1443 $ 17.50+.50/0*

Table 1. Selected physical and spectroscopic data for **7** and **10**–**16**

7: Isolation by column chromatography (in the dark, cooled to −78 °C, silica gel, CH_2Cl_2); m.p. 104 °C; ^{1}H NMR ($CDCl_3$): δ = 8.26 (br. s, 2H), 7.32 (d, 2H), 7.12 (t, 1H), 6.70 (m, 2H), 6.46 (s, 1H), 6.17 (m, 2H), 6.05 (m, 2H); HRMS ($C_{15}H_{12}Cl_2N_2$): calcd 290.03775, found 290.0370.

10: M.p. 90 °C; ^{1}H NMR ($CDCl_3$): δ = 10.93 (s, 2H), 9.28 (d, 2H), 8.03 (d, 2H), 7.78 (d, 2H), 7.62 (dt, 2H), 7.40 (m, 2H), 7.28 (d, 2H), 4.19 (t, 4H), 2.43 (t, 4H), 1.88 (quint., 4H), 1.60 (m, 8H), 1.41 (m, 4H); HRMS ($C_{35}H_{38}O_5$): calcd 538.2719, found 538.2734.

11: Purification by column chromatography: a) Al_2O_3, basic, activation grade I, CH_2Cl_2/Et_2O 95/5; b) silica gel, CH_2Cl_2; ^{1}H NMR ($CDCl_3$): δ = 8.60 (d, 4H), 8.55 (d, 4H) 8.30 (d, 2H), 8.03 (d, 2H), 7.70 (m, 8H), 7.27 (d, 2H), 6.88 (t, 2H), 6.50 (d, 2H), 4.18 (t, 4H), 1.16 (quint., 4H), 0.46 (m, 4H), −0.16 (m, 4H), −0.30 (m, 4H), −1.04 (t, 4H), −2.23 (s, 2H); UV/Vis (CH_2Cl_2): λ_{max} ($\varepsilon \times 10^{-3}$) = 420.8 (308), 513.8 (22.3), 545.2 (3.9), 589.4 (6.9), 645.2 nm (1.3); HRMS ($C_{65}H_{52}Cl_4N_4O_3$): calcd 1076.27935, found 1076.265.

12: Purification by column chromatography on silica gel, CH_2Cl_2; ^{1}H NMR ($CDCl_3$): δ = 8.47 (m, 8H), 8.21 (d, 2H), 7.95 (d, 2H), 7.6 (m, 8H), 7.22 (t, 2H), 6.86 (t, 2H), 6.63 (d, 2H), 4.04 (m, 4H), 0.97 (m, 5H), 0.42 (m, 4H), 0.15 (m, 4H), −0.28 (m, 4H), −0.55 (m, 4H), −2.41 (s, 2H); UV/Vis (CH_2Cl_2): λ_{max} ($\varepsilon \times 10^{-3}$) = 420.8 (294), 514.2 (21.3), 545.6 (3.8), 589.4 (6.7), 645.2 nm (1.3); HRMS ($C_{65}H_{54}Cl_4N_4O_3$): calcd 1078.2950, found 1078.311.

13: Purification by column chromatography: silica gel, CH_2Cl_2/*n*-hexane 7/3; ^{1}H NMR ($CDCl_3$): δ = 8.7 (m, 8H), 8.29 (d, 2H), 8.02 (d, 2H), 7.72 (m, 8H), 7.31 (t, 2H), 6.95 (dt, 2H), 6.71 (d, 2H), 4.12 (m, 4H), 2.30 (m, 1H), 1.05 (m, 4H), 0.51 (m, 4H), 0.22 (m, 4H), −0.05 (m, 6H), −0.31 (m, 2H), −2.28 (s, 2H); UV/Vis (CH_2Cl_2): λ_{max} ($\varepsilon \times 10^{-3}$) = 421.2 (221), 514.2 (15.8), 545.8 (2.8), 589.6 (4.9), 645.4 nm (1).

14: Purification by column chromatography: silica gel, a) CH_2Cl_2/*n*-pentane 6/4, b) CH_2Cl_2; ^{1}H NMR ($CDCl_3$): δ = 8.57 (m, 8H), 8.31 (d, 2H), 8.05 (d, 2H), 7.7 (m, 8H), 7.31 (t, 2H), 6.98 (dt, 2H), 6.80 (d, 2H), 4.06 (m, 4H), 2.01 (s, 3H), 0.98 (m, 4H), 0.40 (m, 4H), 0.21 (m, 5H), −0.02 (m, 8H), −2.81 (s, 2H); UV/Vis (CH_2Cl_2): λ_{max} ($\varepsilon \times 10^{-3}$) = 421.4 (239), 514.4 (18.1), 546.6 (3.8), 590 (5.9), 646.4 nm (1.3); IR (KBr): $\tilde{\nu}$ = 1685 cm^{-1} (C=O); ^{13}C NMR ($CDCl_3$): δ = 195.94 (C=O); HRMS ($C_{67}H_{56}Cl_4N_4O_3S$): calcd 1136.2827, found 1136.274.

15: Purification by thin-layer chromatography: Al_2O_3, basic, CH_2Cl_2; ^{1}H NMR ($CDCl_3$): δ = 80.5 (br., 8H, pyrrole-H); UV/Vis (CH_2Cl_2): λ_{max} ($\varepsilon \times 10^{-3}$) = 418 (80.3), 579 (8.5), 628 nm (2.6); IR (KBr): $\tilde{\nu}$ = 1684 cm^{-1} (C=O); magnetic susceptibility X_{mol}/magnetic moment μ_{eff} ($CDCl_3$, Ref.[19]): X_{mol} = 1.83×10^{-7} m^3 mol^{-1}; μ_{eff} = 5.85 μ_B; elemental analysis for $C_{67}H_{54}BrCl_4FeN_4O_3S$ (1272.81): calcd N 4.40, S 2.52; found N 4.17, S 2.05.

16: ^{1}H NMR ($CDCl_3$): δ = 83 (br. s, 4H, pyrrole-H), 69 (br. s, 4H, pyrrole-H); UV/Vis (CH_2Cl_2): λ_{max} ($\varepsilon \times 10^{-3}$) = 415 (82.9), 506 (11.02), 580 (4.85), 641 nm (3.07); IR (KBr): $\tilde{\nu}$ = 3057, 2955, 2924, 2853, 1621, 1592, 1556, 1530, 1509,1463, 1428, 1377,1328, 1272, 1190, 1147, 1115, 1069, 1040, 1019, 997, 981, 884, 835, 802, 791, 777, 746, 715, 697, 668, 643 cm^{-1}; EPR (pure): $g_\perp$ = 5.37 (strong signal), g = 4.18 (weak signal), g = 1.98 (weak signal); magnetic susceptibility X_{mol}/magnetic moment μ_{eff} ($CDCl_3$, Ref.[19]): X_{mol} = 1.18×10^{-7} m^{3}mol^{-1}; μ_{eff} = 4.7 μ_B; HRMS ($C_{65}H_{51}{}^{35}Cl_3{}^{37}ClFeN_4O_2S$): calcd 1149.179, found 1149.171; elemental analysis for $C_{65}H_{51}Cl_4FeN_4O_2S \cdot H_3COH$ (1181.91): calcd Fe 4.70, N 4.74, O 4.06, S 2.71; found Fe 5.17, N 4.63, O 4.44, S 3.07.

17: UV/Vis (DMSO): λ_{max} ($\varepsilon \times 10^{-3}$) = 376 (41.6), 463 (97.1), 517 (10), 555 (10.8), 609 cm^{-1} (7.6).

by drying under extreme conditions, which moved the Soret band to 399 nm (blue shift). Addition of methanol restored the original spectrum. Reduction of **15** with the $Na_2S_2O_4$-[18]crown-6 complex **18**[15] in DMSO, cleavage of the thioester with the DMSO monoanion DIMSYL-Na, and introduction of CO into the solution yielded the CO complex **17**, which displays a split Soret band (376 nm, 463 nm; hyperporphyrin). The cause of the blue- and red-shifted Soret bands in carboxycytochrome P-450 and CO-porphyrinato(thiolato)iron(II) model compounds is a charge transfer transition from an occupied p orbital on the thiolate sulfur atom (lone electron pair) to the porphyrin $e_g(\pi^*)$ orbital and the strong interaction of this transition with the transitions $a_{1u}(\pi)$,$a_{2u}(\pi) \rightarrow e_g(\pi^*)$ of the porphyrin.[16] Charge transfer transitions are quite strongly solvent dependent;[17] this is probably the reason for the slight red shift of the long wavelength Soret bands of the CO–porphyrinato(thiolato) model compounds in DMSO upon the addition of base[8a, 8e] relative to carboxycytochrome P-450.

As can be seen from molecular modeling studies[18] of **16**, the chloro substituents and the phane chain shield the thiolate group effectively from attack by oxidants (O donors). On the other side of the molecule the chloro and naphthyl substituents hinder the formation of μ-oxo and μ-peroxo complexes (Figure 1).

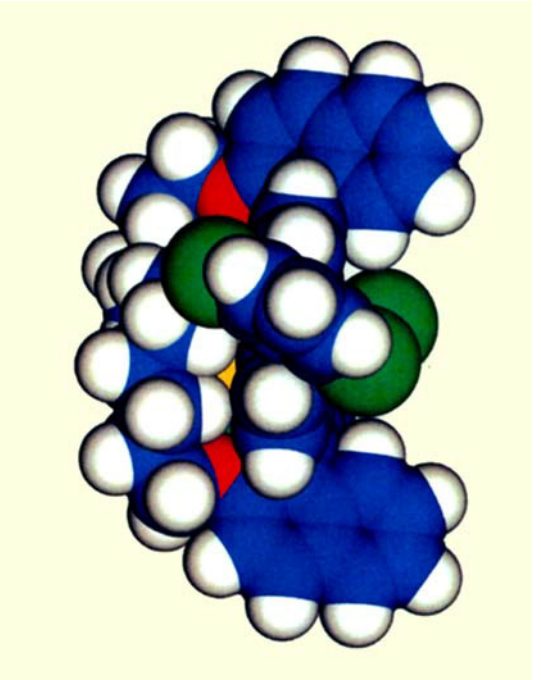

Fig. 1. Space-filling model of the porphyrinato(thiolato)iron(III) complex **16**.

Measurement of the magnetic susceptibility of **16** yields a magnetic moment μ_{eff} of 4.7 μ_B. This value is significantly smaller than the value of 5.9 μ_B expected for a high spin porphyrinatoiron(III) complex (S = 5/2) and substantially larger than that of a low spin porphyrinatoiron(III) complex (S = 1/2), where a value of 1.73 μ_B is expected. The ^{1}H NMR spectrum of **16** displays two broad signals, each of intensity 4H, at δ = 83 and 69, which we ascribe to the porphyrin protons. The porphyrin protons are not equivalent due to the unsymmetrical disposition of the phane chain and the orientation of the thiolate ligand.

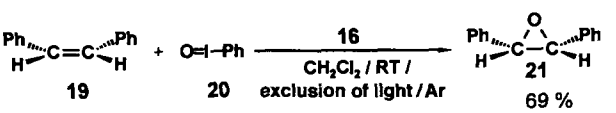

Scheme 4. Epoxidation of *cis*-stilbene to *cis*-stilbene oxide by iodosylbenzene catalyzed by **16**.

The reaction of *cis*-stilbene (**19**) with iodosylbenzene (**20**) as O donor and **16** as catalyst (room temperature, dichloromethane, exclusion of light) led to the formation of *cis*-stilbene oxide (**21**) as the single reaction product in 69% yield. This is in agreement with the conclusions drawn from molecular modeling studies and demonstrates how effectively the thiolate ligand is shielded from direct attack by the O donor iodosylbenzene.

 © VCH Verlagsgesellschaft mbH, D-69451 Weinheim, 1997 0570-0833/97/3613-1444 $ 17.50+.50/0

Experimental Section

16: To a solution of **15** (92 mg, 0.072 mmol) in chloroform/methanol 1/2 (80 mL) was added 1 M $NaOCH_3/CH_3OH$ (2 mL, 2 mmol). This was held at reflux for 4 h under argon in the dark. After removal of the solvent and drying, the residue was purified by preparative thin layer chromatography (neutral Al_2O_3, CH_2Cl_2, exclusion of light; R_f of **16** is about 1). After drying at 40 °C/10^{-2} Torr, 64 mg of **16** was obtained (0.056 mmol, 77%).

17: All reactions were carried out in a glove box under argon. Iron complex **15** (0.56 mg, 4×10^{-7} mol) and crown complex **18** (16 mg, 21.2×10^{-6} mol) were dissolved in DMSO (4 mL) and allowed to react for 30 min. After the addition of a DIMSYLNa solution (31.44 mg NaH) and a further 30 min reaction, the volume of the solution was increased to 20 mL, and CO was bubbled through the solution.

Epoxidation of *cis*-stilbene (under argon with light exclusion): *cis*-stilbene (450 mg, 2.5 mmol), **16** (28.8 mg, 0.025 mmol), and iodosylbenzene (55 mg, 0.25 mmol) were stirred in CH_2Cl_2 (6 mL) for 5 h at room temperature. After removal of the solvent (30 °C, 300 mbar), the residue was taken up in 200 mL *n*-pentane, and the catalyst removed by filtration (25–30% **16** was recovered unchanged); the solvent was then removed (30 °C, 300 mbar). Quantitative analysis of the reaction products was carried out by ^1H NMR spectroscopy with 4-chlorotoluene as internal standard.

Received: August 7, 1996
Revised version: March 12, 1997 [Z 9434 IE]
German version: *Angew. Chem.* **1997**, *109*, 1510–1513

Keywords: enzyme mimetics · iron · porphyrinoids · S ligands · synthetic methods

[1] *Cytochrome P-450* (Eds.: T. Omura, Y. Ishimura, Y. Fujii-Kuriyama), VCH, Weinheim, **1993**.
[2] *P-450 and Chemical Carcinogenesis* (Eds.: Y. Tagashira, T. Omura), Plenum, New York, **1985**.
[3] a) G. D. Nordblom, R. E. White, M. J. Coon, *Arch. Biochem. Biophys.* **1976**, *175*, 524; b) E. G. Hrycay, J.-A. Gustafsson, M. Ingelman-Sundberg, L. Ernster, *Eur. J. Biochem.* **1976**, *61*, 43; c) F. Lichtenberger, W. Nastainczyk, V. Ullrich, *Biochem. Biophys. Res. Commun.* **1976**, *70*, 939; d) R. C. Blake, M. J. Coon, *J. Biol. Chem.* **1981**, *256*, 12127; e) M. H. Gelb, D. C. Heimbrook, P. Mälkönene, S. G. Sligar, *Biochemistry* **1982**, *21*, 370.
[4] a) T. L. Poulos, B. C. Finzel, I. C. Gunsalus, G. C. Wagner, J. Kraut, *J. Biol. Chem.* **1985**, *260*, 16122; b) T. L. Poulos, B. C. Finzel, A. J. Howard, *Biochemistry*, **1986**, *25*, 5314; c) *J. Biol. Chem.* **1987**, *195*, 687; d) H. Li, S. Narasimhulu, L. M. Havran, J. D. Winkler, T. L. Poulos, *J. Am. Chem. Soc.* **1995**, *117*, 6297; e) T. L. Poulos, A. J. Howard, *Biochemistry* **1987**, *26*, 8165; f) R. Raag, T. L. Poulos, *ibid.* **1989**, *28*, 7586; g) K. G. Ravichandran, S. S. Boddupalli, C. A. Hasemann, J. A. Peterson, J. Deisenhofer, *Science* **1993**, *261*, 731.
[5] V. Ullrich, H. H. Ruf, P. Wende, *Croat. Chem. Acta* **1977**, *49*, 211.
[6] a) S. P. Cramer, J. H. Dawson, K. O. Hodgson, L. P. Hager, *J. Am. Chem. Soc.* **1978**, *100*, 7282; b) J. H. Dawson, M. Sono, *Chem. Rev.* **1987**, *87*, 1255; c) L. A. Andersson, J. H. Dawson, *Struct. Bonding* **1990**, *74*, 1.
[7] M. Sono, D. J. Stuehr, M. Ikeda-Saito, J. H. Dawson, *J. Biol. Chem.* **1995**, *270*, 19943.
[8] a) T. G. Traylor, T. C. Mincey, A. P. Berzinis, *J. Am. Chem. Soc.* **1981**, *103*, 7084; b) J. P. Collman, S. E. Groh, *ibid.* **1982**, *104*, 1391; c) A. R. Battersby, W. Howson, A. D. Hamilton, *J. Chem. Soc. Chem. Commun.* **1982**, 1266; d) B. Stäubli, H. Fetz, U. Piantini, W.-D. Woggon, *Helv. Chim. Acta* **1987**, *70*, 1173; e) T. Higuchi, S. Uzu, M. Hirobe, *J. Am. Chem. Soc.* **1990**, *112*, 7051; f) Y. Tatsuno, K. Tomita, K. Tani, *Inorg. Chim. Acta* **1988**, *152*, 5.
[9] T. Higuchi, K. Shimada, N. Murayama, M. Hirobe, *J. Am. Chem. Soc.* **1993**, *115*, 7551.
[10] a) D. M. Bailey, R. E. Johnson, N. F. Albertson, *Org. Synth.* **1971**, *51*, 100; b) D. E. Janssen, C. V. Wilson, *ibid.* **1963**, 547; c) J. W. Harbuck, H. Rapoport, *J. Org. Chem.* **1972**, *37*, 3618.
[11] H. K. Hombrecher, G. Horter, *Liebigs Ann. Chem.* **1991**, 219.
[12] a) R. F. Brown, G. H. Schmid, *J. Org. Chem.* **1962**, *27*, 1288; b) R. J. Bass, B. J. Banks, M. G. Leeming, M. Snarly, *J. Chem. Soc. Perkin Trans 1* **1981**, 124.
[13] M. Momenteau, B. Loock, C. Hull, J.-M. Lhoste, *J. Chem. Soc. Perkin Trans. 1* **1988**, 283.
[14] H. Kobayashi, T. Higuchi, Y. Kaizu, H. Osada, M. Aoki, *Bull. Chem. Soc. Jpn.* **1975**, *48*, 3137.
[15] T. Mincey, T. G. Traylor, *Bioinorg. Chem.* **1978**, *9*, 409.
[16] L. K. Hanson, W. A. Eaton, S. G. Sligar, I. C. Gunsalus, M. Gouterman, C. R. Connell, *J. Am. Chem. Soc.* **1976**, *98*, 2672.
[17] a) J. Andrews, R. M. Keefer, *Molecular complexes in organic chemistry*, Holden-Day, San Francisco, **1964**, p. 137; b) R. Foster, *Organic Charge-Transfer Complexes*, Academic Press, London, **1969**, p. 62.
[18] Model calculations: MM + Force field, HyperChem, Hypercube, Version 4.5, **1994**.
[19] D. F. Evans, *J. Chem. Soc.* **1959**, 2003.

Self-Assembly of Supramolecular Polyoxometalates: The Compact, Water-Soluble Heteropolytungstate Anion $[As^{III}_{12}Ce^{III}_{16}(H_2O)_{36}W_{148}O_{524}]^{76-}$ **

Knut Wassermann, Michael H. Dickman, and Michael T. Pope*

Dedicated to the memory of GTP (1959–1996)

The hundreds of known examples of polyoxoanions of vanadium, molybdenum, and tungsten comprise a class of inorganic complexes of unrivaled versatility and structural variation, and have applications in many fields of science.[1] Very commonly these species have structures incorporating 6, 12, or 18 metal atoms and one or more other "heteroatoms" in positive oxidation states. The Keggin tungstophosphate $[PW_{12}O_{40}]^{3-}$ is a familiar example.

There are indications that much larger polyoxometalate anions might be synthesized. The structures of complexes such as $[Mo_{36}O_{112}(H_2O)_{18}]^{8-}$[2] and $[H_7P_8W_{48}O_{148}]^{33-}$[3] incorporate smaller known polyoxoanion units ($[Mo_7O_{24}]^{6-}$ and $[H_2P_2W_{12}O_{48}]^{12-}$ respectively), and more recently a class of mixed-valent, nitrosyl-containing polymolybdates with 57 molybdenum atoms per anion has been identified and characterized.[4] Following a general polymerization–reduction–polymerization protocol that has proved to be appropriate for the latter species, Müller et al. have succeeded in synthesizing a spectacular cyclic ("big wheel") anion with 154 molybdenum atoms.[5]

We now report that polyoxometalates with 148 tungsten atoms per anion can be easily and efficiently synthesized by straightforward "self assembly" processes in aqueous solution. The title anion **1** has been isolated as an ammonium salt in a yield of roughly 35%. The new compounds are by far the largest and heaviest discrete polyoxotungstates known. Other somewhat smaller compounds with 29 and 40 tungsten atoms have also been characterized and will be reported elsewhere.[6]

The structure of **1** is illustrated in bond, polyhedral, and space-filling representations in Figures 1–3. The anion has virtual D_{2d} symmetry and incorporates twelve B-α $[As^{III}W_9O_{33}]^{9-}$ and four $[W_5O_{18}]^{6-}$ groups. The AsW_9 units are augmented by additional tungsten and cerium atoms and are linked into a *folded* cyclic structure by pairs of edge-shared WO_6 octahedra.

The anion **1** may therefore be formulated as shown below.

$[Ce_{16}(H_2O)_{36}(B\text{-}\alpha\text{-}AsW_9O_{33})_{12}(WO_2)_4(W_2O_6)_8(W_5CeO_{18})_4]^{76-}$ **1**

Details of the structural motifs are shown in Figure 4. As revealed by the space-filling representation (Figure 3) the folded structure is very compact with no large central cavity as found for Mo_{154} and other polyoxoanions of comparable size, such as $[H_7P_8W_{48}O_{148}]^{33-}$. The structure analysis suggests that the central core of **1** contains four ammonium cations and/or water molecules. In the crystal, the disc-shaped anions (diameter ap-

[*] Prof. M. T. Pope, Dr. K. Wassermann, Dr. M. H. Dickman
Department of Chemistry
Box 571227, Georgetown University, Washington, DC 20057-1227 (USA)
Fax: Int. code +(202) 687-6209
e-mail: pope@guvax.georgetown.edu

[**] Research supported in part by the U. S. Department of Energy and DAAD (postdoctoral support to K. W. through the Hochschulsonderprogramm III). We thank Georgetown University and the National Science Foundation for funding the purchase of the diffractometer and T. Matthew Cocker and Cheol Ho Choi for preparation of Figure 3.

 © VCH Verlagsgesellschaft mbH, D-69451 Weinheim, 1997 0570-0833/97/3613-1445 $ 17.50+.50/0

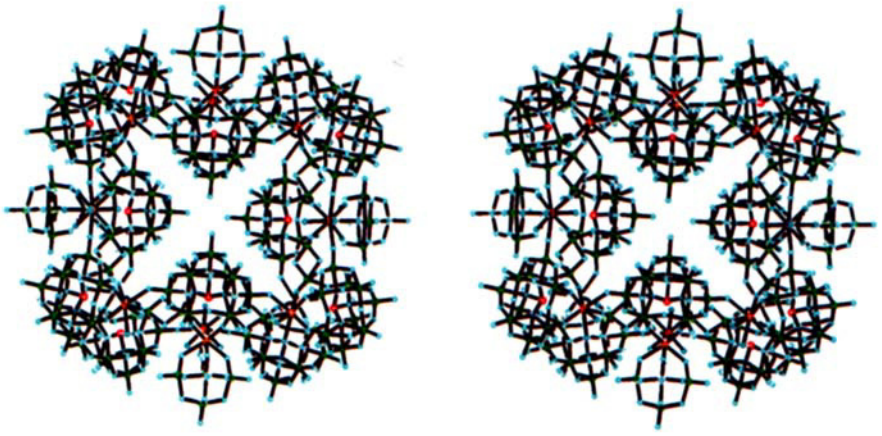

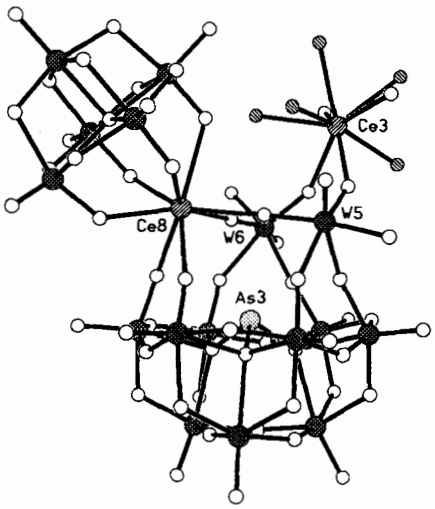

Figure 1. Stereoview of 1. Atoms are drawn with an arbitrary radius (green = W, orange = Ce, red = As, pale blue = O, dark blue = H_2O ligands).

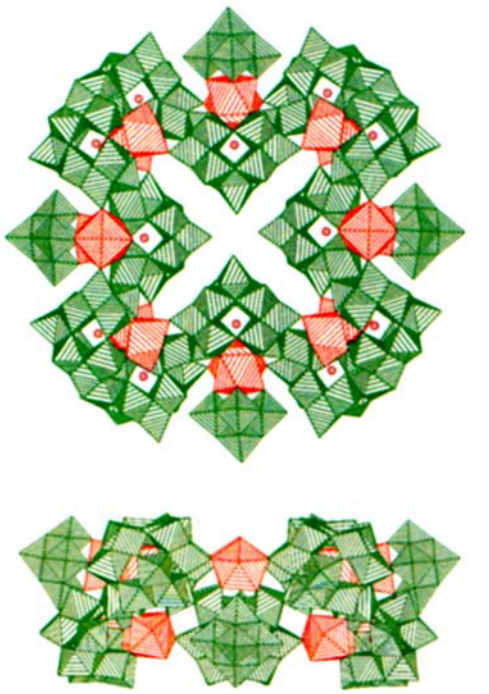

Figure 2. Polyhedral representation of 1. Top: View from the top, that is, down the unique C_2 axis of the D_{2d} molecular point group; the other two C_2 axes lie diagonally in the plane of the paper. Bottom: Side view, looking down the axis of a CeW_5 group, that is, along the bisector of the angle between the two C_2 axes (green = WO_6 octahedra, orange = CeO_x polyhedra, red = As atoms).

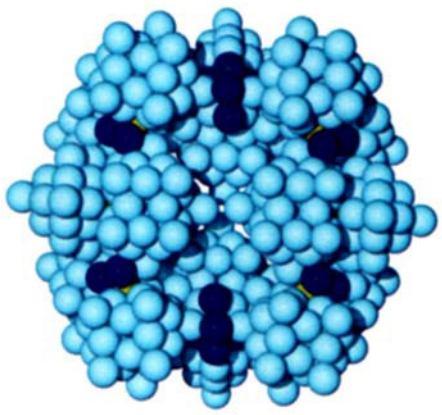

Figure 3. Space-filling view of 1 (blue = oxo oxygens, violet = water molecules coordinated to Ce; some of the Ce atoms (yellow) are visible).

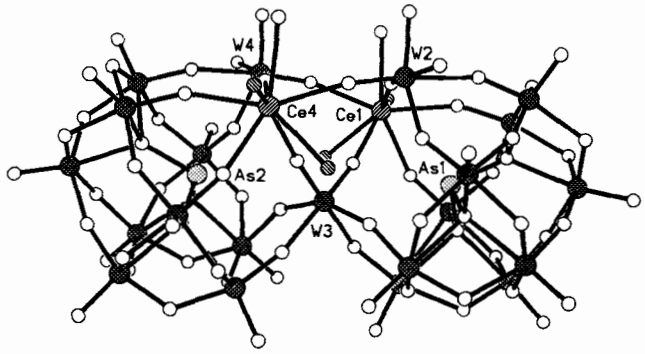

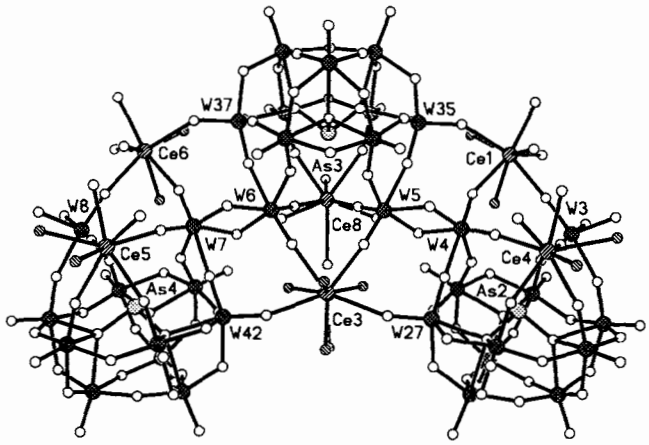

Figure 4. Details of the structure of 1 showing environments of the Ce atoms (small unnumbered hatched circles = water molecules coordinated to Ce atoms; open circles = oxygen atoms bridging Ce and W atoms. Top: Linkage of W_5 and augmented AsW_9 units through Ce8 (type *a*). Middle: Linkage of two augmented AsW_9 units through Ce1 and Ce4 (both type *b*). Bottom: Position of quadruply bridging Ce3 (type *c*). In this view the W_5 unit attached to Ce8 has been omitted for clarity.

proximately 4 nm; thickness approximately 1.8 nm) form parallel stacks along the *c* axis (see Figure 5).

There are three structural types of Ce atoms in the anion: four of type *a* are sandwiched between a W_5 and an augmented AsW_9 group (Figure 4a); eight of type *b* are shared between two AsW_9 units (Figure 4b); four of type *c* bridge three AsW_9 units (Figure 4c). Types *a* and *b* are eight-coordinate (square antiprism) and *c* is nine-coordinate (monocapped square antiprism). The Ce···Ce distances range from about 5.6 to 8.1 Å. The *b* and *c* type cerium atoms carry two and five terminal aqua ligands

 © VCH Verlagsgesellschaft mbH, D-69451 Weinheim, 1997 0570-0833/97/3613-1446 $ 17.50+.50/0

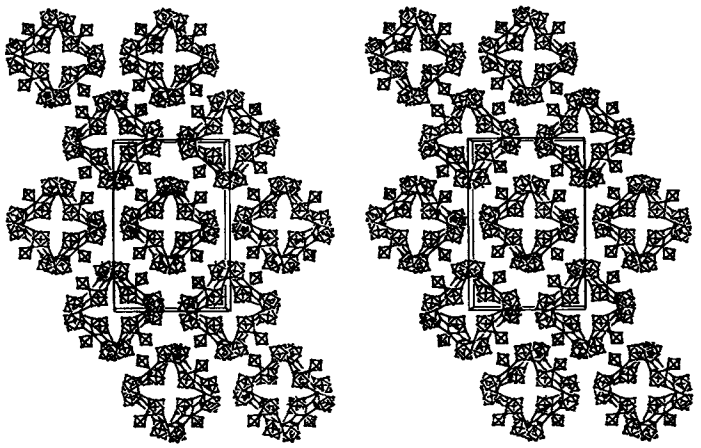

Figure 5. Stereoview of the crystal packing of **1** viewed down the crystallographic *c* axis. The *a* axis is horizontal. Only the heavy-atom skeleton is shown; lines do not represent bonds. Anions are stacked in an eclipsed fashion down the *c* axis. Alternate rows of these stacks across the *a* axis are offset by one-half of a unit cell along *c*.

respectively (see Figure 3) and offer sites for further derivatization of the heteropolyanion.

The ammonium salt of **1** can be recrystallized from water (for crystal packing structure see Figure 5) and is soluble enough to permit the observation of a well-resolved ^{183}W NMR spectrum in D_2O solution. Based on the crystal structure and assuming overall D_{2d} symmetry in solution, 21 resonances are expected, 16 of relative intensity 2 and 5 of intensity 1. Thanks to the paramagnetic Ce^{III} atoms, the spectrum (recorded at 12.5 MHz on a Bruker AM300 spectrometer) is well-dispersed: 18 of these lines are observed between $\delta = +320$ and -200. The spectrum of the diamagnetic lanthanum analogue of **1** is more congested with at least 15 lines between $\delta = -60$ and -260. Further measurements on a higher field spectrometer are planned.

That **1** can be prepared in fair yield by reaction of the stoichiometric quantities of monotungstate, arsenite, cerium cations, and protons in aqueous solution attests to its remarkable thermodynamic stability. Since the oxidation states of the components are unambiguous (As^{III}, Ce^{III}, W^{VI}), the overall anionic charge can be computed to be -76. Elemental analysis suggests that this charge is compensated by ammonium and sodium cations in the crystal, although the precision of the analysis cannot rule out the possibility of some protonation (either of the anion or of one or more lattice water molecules). The (unprotonated) anionic charge corresponds to a charge density of -0.51 per tungsten and is similar to that observed for water-stable Keggin anions such as $[H_2W_{12}O_{40}]^{6-}$ and $[Co^{II}W_{12}O_{40}]^{6-}$. Like these Keggin species, **1** is stable in solution at pH 6.5. The pH stability limits for **1** and its other physical and chemical properties are currently under investigation.

The new anion is an example of a potentially large class of isostructural heteropolyanions and may well prove to be as ubiquitous in supramolecular polyoxometalate chemistry as is the Keggin anion for "smaller" heteropolyanions. We have synthesized and collected a data set for the isomorphous lanthanum(III) derivative, and there is little doubt that other lanthanides, actinides, and other high-coordination-number cations such as Zr^{4+} can be incorporated into this structure. Moreover, since B-type XW_9O_{33} groups with $X = Sb^{III}$, Bi^{III}, Se^{IV}, and Te^{IV} are observed in other heteropolyanion structures, these could well act as building blocks for analogues of **1**. Although the two major building blocks, XW_9 and W_5 groups, are both observed in other tungstocerate heteropolyanions,[6, 7] anion **1** is a rare example where both groups are present in the same anion. To our knowledge, the only precedent for this structural feature is the tungstoeuropate $[Eu_3(H_2O)_3(SbW_9O_{33})(W_5O_{18})_3]^{18-}$ described by Yamase et al.[8]

Experimental Section

Crystals of the ammonium salt of **1** were isolated from several synthetic procedures. The following is one of the more direct approaches: $Na_2WO_4 \cdot 2H_2O$ (33.0 g, 100 mmol) and As_2O_3 (0.8 g, 4.05 mmol) were dissolved in 70 mL of boiling water. The pH of the solution was decreased from 9.0 to 7.1 by the addition of 6 M HCl (15.4 mL, 115 mmol). After 10 min a solution of $Ce(NO_3)_3 \cdot 6H_2O$ (4.69 g, 10.8 mmol) in 1.0 M acetic acid (18 mL) was added with a pipette to the vigorously stirred hot (90 °C) starting solution. The color changed to orange, and the pH decreased to 5.9. The mixture was heated for 30 min at 90 °C in a water-bath. Addition of a warm (70 °C) solution of NH_4Cl (40 g, 748 mmol) in water (150 mL) to the still hot (90 °C) transparent solution yielded a yellow-orange precipitate (about 33 g), which was recrystallized from 80 mL of warm water (70 °C, resultant pH 6.2). The recrystallized material consisted of long orange needles and a yellowish powder. The solution was stirred with a spatula so that the needles gathered at the bottom of the beaker before the milky solution was decanted. Once the precipitate in the decantate had settled, the clear supernatant (several portions of a few mL each) was poured onto the needles to extract any remaining yellowish fine powder by decantation before the needles were finally filtered off (about 17.0 g). Recrystallization of the needles from 20 mL water at 75 °C (pH 6.6) gave 10.0 g (yield: 36%) of the pure title compound. The lanthanum analogue of **1** was prepared in essentially the same way from lanthanum nitrate.

Elemental analysis calcd. (found) for $(NH_4)_{70}Na_6[(H_2O)_{36}Ce_{12}(B\text{-}\alpha\text{-}AsW_9O_{33})_{12}(WO_2)_4(W_2O_6)_8(W_5CeO_{18})_4] \cdot 175H_2O$: N 2.23 (2.17), Na 0.31 (0.30), Ce 5.10 (5.27), As 2.05 (1.82), W 61.93 (61.73), H_2O 8.65 (8.47)%. IR (KBr disk) in metal–oxygen stretching region: 950 (s), 850 (vs), 785 (vs), 700 (vs), 617 (s) cm^{-1}. Crystal structure analysis: crystal dimensions 0.28 mm × 0.28 mm × 0.36 mm, mounted under oil (to prevent water loss) on a glass fiber; $T = 173(2)$ K (nitrogen stream); Siemens SMART CCD single-crystal diffractometer equipped with a Mo anode and graphite monochromator ($\lambda = 0.71073$ Å). A hemisphere of data was collected out to a $2\theta_{max}$ value of 46° (99.65% coverage, 5.12 average redundancy); ω scans; Lorentzian and polarization corrections, empirical absorption correction based on measured intensities of equivalent reflections at different ϕ and ω values ($\mu = 22.196$ mm^{-1}; min/max transmission 0.00026/0.00644); total reflections collected: 157456; independent reflections: 54241; R(int) = 0.103, R(sig) = 0.069. Space group *Pnn*2; $a = 38.993(2)$, $b = 57.926(3)$, $c = 18.0842(11)$ Å, $V = 40847(4)$ Å^3, $Z = 2$; $\rho_{calcd} = 3.432$ $Mg\,m^{-3}$; structure solution by direct methods, refinement against $|F^2|$ over all reflections, $R_1 = 0.104$ for 49746 independent reflections with $I > 2\sigma(I)$ and 2275 parameters, $Rw_2 = 0.270$ for all reflections; highest residual electron density 4.15 e Å^3. Software used: Siemens SMART, SAINT, SHELXTL [9]. No hydrogen atoms were included. It was not possible to distinguish between H_2O and NH_4^+ due to disorder and the presence of heavy scatterers. Bond valence sum calculations [10] did not clearly indicate any protonated oxygens in the anion other than the water coordinated to cerium. Further details of the crystal structure investigation may be obtained from the Fachinformationszentrum Karlsruhe, D-76344 Eggenstein-Leopoldshafen (Germany), on quoting the depository number CSD-406326.

Received: December 20, 1996 [Z9917IE]
German version: *Angew. Chem.* **1997**, *109*, 1513–1516

Keywords: cerium · lanthanides · polyoxometalates · supramolecular chemistry · tungsten

[1] a) M. T. Pope, *Heteropoly and Isopoly Oxometalates*, Springer, Berlin, **1983**; b) V. W. Day, W. G. Klemperer, *Science* **1985**, *228*, 533–541; c) M. T. Pope, A. Müller, *Angew. Chem.* **1991**, *103*, 56–70; *Angew. Chem. Int. Ed. Engl.* **1991**, *30*, 34–48; d) *Polyoxometalates. From Platonic Solids to Anti-Retroviral Activity* (Eds.: M. T. Pope, A. Müller), Kluwer, Dordrecht, **1994**; e) M. T. Pope in *Encyclopedia of Inorganic Chemistry* (Ed.: R. B. King), Wiley, Chichester, **1994**, pp. 3361–3371; f) C. L. Hill, C. M. Prosser-McCartha, *Coord. Chem. Rev.* **1995**, *143*, 407–455; g) T. Okuhara, N. Mizuno, M. Misono, *Adv. Catal.* **1996**, *41*, 113–252.

[2] B. Krebs, I. Paulat-Böschen, *Acta Crystallogr. Sect. B* **1982**, *38*, 1710–1718.

[3] R. Contant, A. Tézé, *Inorg. Chem.* **1985**, *24*, 4610–4614; R. Contant, *Inorg. Synth.* **1990**, *27*, 104–111.

[4] a) A. Müller, E. Krickemeyer, S. Dillinger, H. Bögge, A. Proust, W. Plass, R. Rohlfing, *Naturwissenschaften* **1993**, *80*, 560–564; b) S.-W. Zhang, G.-Q. Huang, M.-C. Shao, Y. Q. Tang, *J. Chem. Soc. Chem. Commun.* **1993**, 37–38; c) G.-Q. Huang, S.-W. Zhang, M.-C. Shao, *Polyhedron* **1993**, *12*, 2067–2068; d) A. Müller, E. Krickemeyer, S. Dillinger, H. Bögge, W. Plass, A. Proust, L. Dloczik, C. Menke, J. Meyer, R. Rohlfing, *Z. anorg. allgem. Chem.* **1994**, *620*, 599–619; e) A. Müller, *J. Mol. Struct.* **1994**, *325*, 13–35; f) A. Müller, H. Bögge, E. Krickemeyer, S. Dillinger, *Bull. Acad. Sci. Pol. Chem.* **1994**, *42*,

 © VCH Verlagsgesellschaft mbH, D-69451 Weinheim, 1997 0570-0833/97/3613-1447 $ 17.50+.50/0

291–298; g) A. Müller, W. Plass, E. Krickemeyer, S. Dillinger, H. Bögge, A. Armitage, A. Proust, C. Beugholt, U. Bergmann, *Angew. Chem.* **1994**, *106*, 897–899; *Angew. Chem. Int. Ed. Engl.* **1994**, *33*, 849–851; h) A. Müller, H. Reuter, S. Dillinger, *ibid.* **1995**, *107*, 2505–2539 and **1995**, *34*, 2328–2361; i) D. Gatteschi, R. Sessoli, W. Plass, A. Müller, E. Krickemeyer, J. Meyer, D. Sölter, P. Adler, *Inorg. Chem.* **1996**, *35*, 1926–1934.

[5] a) A. Müller, E. Krickemeyer, J. Meyer, H. Bögge, F. Peters, W. Plass, E. Diemann, S. Dillinger, F. Nonnenbruch, M. Randerath, C. Menke, *Angew. Chem.* **1995**, *107*, 2293–2295; *Angew. Chem. Int. Ed. Engl.* **1995**, *34*, 2122–2124; b) A. Müller, J. Meyer, E. Krickemeyer, E. Diemann, *ibid.* **1996**, *108*, 1296–1299 and **1996**, *35*, 1206–1208; c) A. Müller, E. Diemann, B. Hollmann, H. Ratajczak, *Naturwissenschaften* **1996**, *83*, 321–322; d) A. Müller, C. Beugholt, *Nature* **1996**, *383*, 296–297.

[6] The anions $[As_3Ce_2W_{29}O_{103}]^{17-}$ and $[As_4Ce_4W_{40}O_{146}]^{28-}$ incorporate three and four AsW_9O_{33} groups, respectively.

[7] J. Iball, J. N. Low, T. J. R. Weakley, *J. Chem. Soc. Dalton Trans.* **1974**, 2021–2024.

[8] T. Yamase, H. Naruke, Y. Sasaki, *J. Chem. Soc. Dalton Trans.* **1990**, 1687–1696.

[9] G. M. Sheldrick, *Acta Crystallogr. Sect. A* **1990**, *46*, 467–473; SHELXTL Structure Determination Software Programs (1990), Siemens Analytical X-ray Instruments, Madison, Wisconsin, USA; SAINT Users Manual (1996), Version 4.050, Siemens Analytical X-ray Instruments, Madison, Wisconsin, USA.

[10] M. E. Brese, M. O'Keefe, *Acta Crystallogr. Sect. B* **1991**, *47*, 192–197; I. D. Brown, D. Altermatt, *ibid.* **1985**, *41*, 244–247.

Self-Assembly of the First Fullerene-Containing [2]Catenane**

Peter R. Ashton, François Diederich,* Marcos Gómez-López, Jean-François Nierengarten, Jon A. Preece, Françisco M. Raymo, and J. Fraser Stoddart*

Since fullerenes[1] became available[2] in macroscopic quantities during the 1990s, a wide range of chemical transformations involving these novel carbon allotropes have been developed.[3] In the last few years chemists have also exploited noncovalent bonding interactions to self-assemble[4] a number of interlocked molecules—principally catenanes and rotaxanes[5]—that display fascinating topological features.[6] The unique electronic properties of C_{60}, for example its strong electron-accepting capabilities,[3] make it an attractive candidate for incorporation into rotaxanes[7] and catenanes. We now report the self-assembly of the first C_{60}-containing catenane, thus signaling completion of the initial merger between these two contemporary areas of chemistry. Recently the Zürich wing of this collaborative venture described[8] a regio- and diastereoselective bisfunctionalization of C_{60} based on cyclization of the carbon sphere with bis(malonate) derivatives in a double Bingel[9] addition. Here we underline the versatility of this method by fusing bis(*p*-phenylene)-[34]crown-10 (**1**), which has two π electron rich hydroquinone rings, to C_{60} in a regioselective manner. Thereafter, we describe the template-directed formation of cyclobis(paraquat-*p*-phenylene)[10] around the C_{60}-appended macrocyclic polyether to give the [2]catenane, an exotic molecular compound featuring an unusual topology and sporting undeniable aesthetic appeal.

For attachment to C_{60} by a double Bingel addition, the [34]crown-10 bismalonate **7** was prepared (Scheme 1). Macrocyclization (Cs_2CO_3, MeCN) of the bis(tosylate) **2** with the hydroquinone derivative **3** to produce **4** followed by reduction

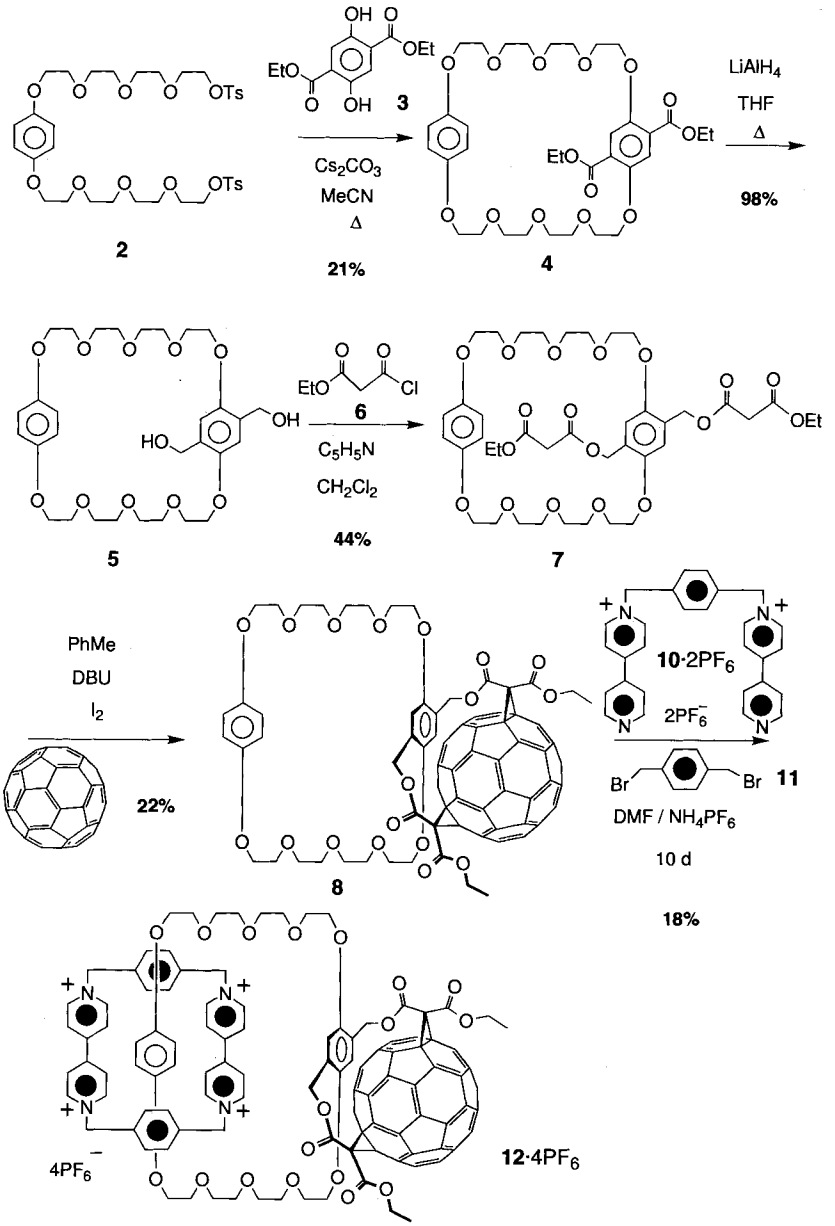

Scheme 1. Regioselective synthesis of the fullerene-containing crown ether **8** and its subsequent self-assembly into the [2]catenane $12{\cdot}4PF_6$.

[*] Prof. Dr. F. Diederich, Dr. J.-F. Nierengarten
Laboratorium für Organische Chemie, ETH-Zentrum
Universitätstrasse 16, CH-8092 Zürich (Switzerland)
Fax: Int. code +(1)632-1109
e-mail: diederich@org.chem.ethz.ch
Prof. J. F. Stoddart,[+] P. R. Ashton, M. Gómez-López,[+] Dr. J. A. Preece, Dr. F. M. Raymo[+]
School of Chemistry
University of Birmingham
Edgbaston, Birmingham B152TT (UK)
Fax: Int. code +(121)414-3531
e-mail: j.f.stoddart@bham.ac.uk

[+] Address after October 1, 1997:
Department of Chemistry and Biochemistry
University of California at Los Angeles
405 Hilgard Avenue, Los Angeles, CA 90095 (USA)

[**] This research was supported by the Swiss National Science Foundation, the Engineering and Physical Sciences Research Council in the United Kingdom, and by a predoctoral fellowship to M. G.-L. from the Eusko Jaurlaritza Unibersitate, Hizkuntza, eta Ikerketa Saila in the Basque Country, Spain. We thank Dr. M. Sebova and Dr. N. Spencer for carrying out the NMR spectroscopic measurements.

($LiAlH_4$, THF) yielded diol **5**, which was allowed to react with ethyl malonyl chloride (**6**) in the presence of pyridine to give **7**.[11] The subsequent reaction of **7** with C_{60} (I_2, 1,8-diazabicyclo[5.4.0]unde-7-ene (DBU), PhMe; Scheme 1) yielded regioselectively the macrocyclic *trans-4*-bis(adduct)[8,12] **8** in 22% yield.

The relative position of the two cyclopropane rings on the C_{60} surface in **8** was established from its ^1H and ^{13}C NMR ($CDCl_3$, 298 K) and UV/Vis spectra (CH_2Cl_2).[8,12,13] Although the intensity of the UV/Vis absorbance band of **8** is high, bands of similar intensities have been reported[12b] for other bis(adducts) of C_{60}.

Whereas the corresponding C_{60} *trans-4*-bis(adduct) produced[8] by addition of the simple, *p*-xylylene-tethered bis(ethyl malonate) [*p*-$(EtOCOCH_2CO_2CH_2)_2C_6H_4$] has C_s symmetry, and is therefore achiral, bridging of the fullerene sphere in **8** by the 2,5-disubstituted hydroquinone ring of the [34]crown-10 macrocycle introduces an element of planar chirality into the molecule, necessarily conferring upon it C_1 symmetry. As a consequence, the two sets of benzylic methylene groups, and the two protons within each group, are both, in a pairwise sense, diastereotopic, giving rise to four doublets ($J = 11$ Hz) in the 300 MHz ^1H NMR spectrum at $\delta = 4.59$, 5.30, 5.71, and 6.45. In contrast, all four benzylic methylene protons in the rapidly racemizing C_2 symmetrical enantiomers of **7** appear as the expected singlet at $\delta = 5.52$. The 125 MHz ^{13}C NMR spectrum of **8** uncovered 51 of 60 resonances expected for the fullerene C atoms. Molecular-modeling studies[14] on **8** revealed that the proximal (with respect to the carbon sphere) hydroquinone ring in **8** and one of the hexagons on the C_{60} surface undergo a nearly perfect parallel stacking at a distance of approximately 3.5 Å, implying the existence of donor(D)–acceptor(A) interactions[15] between the two rings.

Next we explored whether the fullerene-appended crown ether **8**,[16] which resembles closely **1** in its receptor portion, can act as a host for the π electron deficient guest **9**·$2PF_6$, the bis(hexafluorophosphate) salt of paraquat (*N*,*N*′-dimethyl-4,4′-bipyridinium dication).[17] In Me_2CO **1** forms a 1:1 complex ($K_a = 730\ L\,mol^{-1}$, $\Delta G° = -3.9$ kcal mol^{-1})[17] with **9**·$2PF_6$, wherein the π electron deficient bipyridinium unit is threaded through the cavity of the crown ether with its two π electron rich hydroquinone rings. On account of the low solubility of **8** in both Me_2CO and MeCN—two solvents commonly used to study this type of complexation—its affinity for **9**·$2PF_6$ was determined in $CD_3CN/CDCl_3$ (1/1). Evaluation of the complexation-induced upfield changes in chemical shift of the hydroquinone ring protons in ^1H NMR binding titrations (298 K)[18] yielded $K_a = 60 \pm 11\ L\,mol^{-1}$ ($\Delta G° = -2.44 \pm 0.1$ kcal mol^{-1}) for the 1:1 complex formed between **8** and **9**·$2PF_6$. Despite the more favorable solvent, this K_a value is considerably lower than that measured[17] for the corresponding complex with **1**. However, the ^1H NMR spectroscopic data suggest a similar, pseudorotaxane-like inclusion mode of complexation for both associations. It is not unlikely that donor–acceptor interactions between the proximal hydroquinone ring and C_{60}, as suggested by the modeling, could decrease the stabilizing donor–acceptor interactions between bound host and guest. As a result of the strong electronic absorptions of the fullerene appendage, the magnitude of the latter interactions could not be evaluated by UV/Vis spectroscopy.

Despite the low K_a value for **8**·**9**·$2PF_6$, self-assembly of the C_{60}-containing [2]catenane **12**·$4PF_6$ was attempted. A solution of **8**, the bis(pyridylpyridinium) salt **10**·$2PF_6$, *p*-xylylene dibromide (**11**), and an excess of NH_4PF_6 in DMF was stirred at 293 K for 10 d (Scheme 1). A brownish-red solid was isolated in

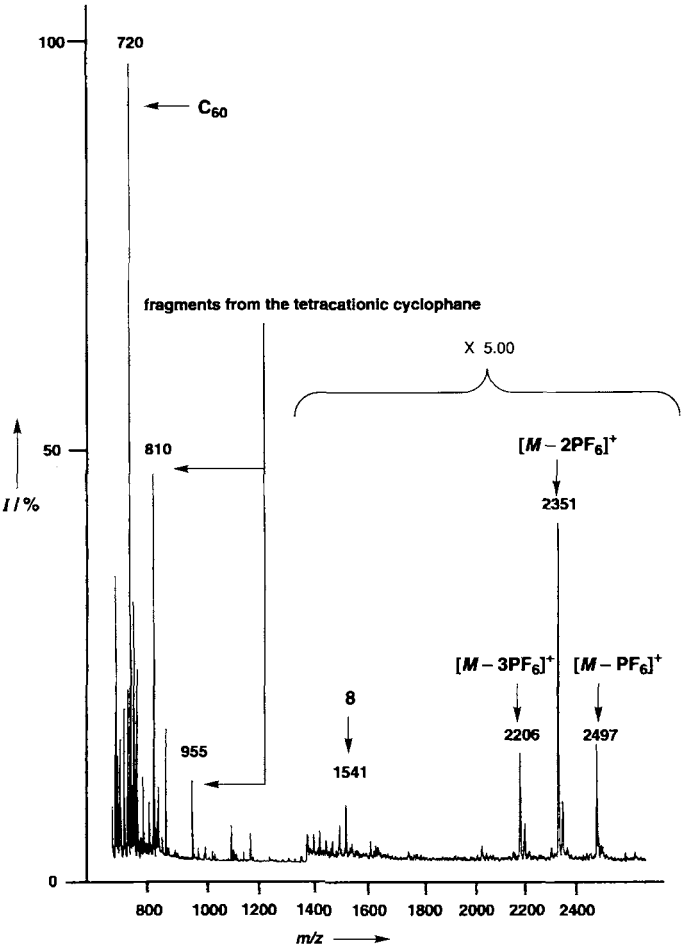

Figure 1. LSI mass spectrum of the fullerene-containing [2]catenane **12**·$4PF_6$. The *m*/*z* region from 1400 to 2600 is expanded five times for clarity.

18% yield and identified as **12**·$4PF_6$. Liquid secondary ion mass spectrometry (LSI-MS) revealed a fragmentation pattern characteristic of a catenane (Figure 1).[19] The spectrum showed peaks at $m/z = 2497$, 2351, and 2206, corresponding to the pseudomolecular ions originating from the losses of one, two, and three PF_6^- counterions from **12**·$4PF_6$, respectively. Furthermore, peaks at $m/z = 1541$, 810, and 720 arising from fragmentation of the [2]catenane were also observed: The peak at $m/z = 1541$ corresponded to the free fullerene-appended crown ether component, and the peak at $m/z = 810$ to the molecular ion of the cyclobis(paraquat-*p*-phenylene) component minus two PF_6^- counterions. A strong peak for the C_{60} fragment at $m/z = 720$ was also detected.

The ^1H NMR spectrum of **12**·$4PF_6$ (300 MHz, 298 K; Figure 2) provided further evidence for the existence of an interlocked molecular structure. A broad singlet at $\delta = 8.90$ and a broadened doublet at $\delta = 7.68$ correspond to the eight α- and eight β-bipyridinium protons, respectively, of the tetracationic cyclophane component. A singlet at $\delta = 7.79$ and a multiplet centered on $\delta = 5.67$, which integrate for eight protons, correspond to the protons on the xylyl spacers and the "corner" methylene protons, respectively, of this same component. The aromatic protons on the substituted hydroquinone ring appear as two singlets at $\delta = 6.23$ and 6.01. No signals are detected in the aromatic region for the unsubstituted hydroquinone ring. In the case of **8**, these protons resonate as a singlet at $\delta = 6.74$. However, when the hydroquinone ring is included within the

 © VCH Verlagsgesellschaft mbH, D-69451 Weinheim, 1997 0570-0833/97/3613-1449 $ 17.50+.50/0

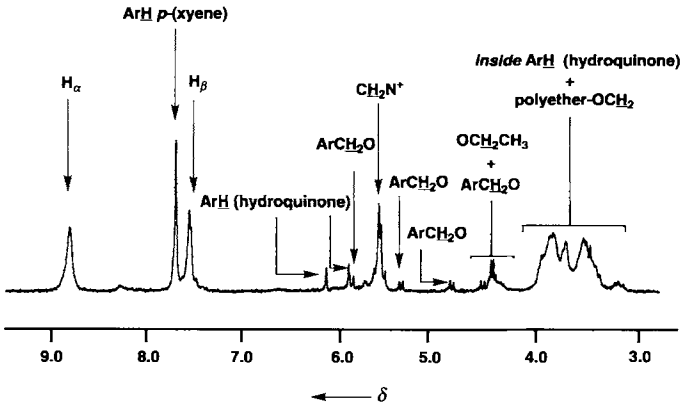

Figure 2. Section of the ^{1}H NMR spectrum (300 MHz, CD_3CN, room temperature) of **12**·4PF_6.

cavity of the cyclobis(paraquat-*p*-phenylene), its protons are shielded dramatically and shifted upfield into the region of the polyether protons.[20] Four different geminally coupled doublets are still observed at δ = 5.98, 5.45, 4.94, and 4.60 for the two pairs of *p*-(OCOCCH_2)$_2$$C_6H_4$ protons residing in diastereoisomeric environments.

Intramolecular D-A-D-A stacks involving π electron rich hydroquinone rings and π electron deficient bipyridinium units are well documented for a series of [2]catenanes.[21] However, in the case of **12**·4PF_6, the proximal substituted hydroquinone ring also acts as a π electron rich *exo* donor and undergoes additional interactions with the electron-accepting C_{60} moiety. This extra interaction builds an unprecedented intramolecular A-D-A-D-A stack into a [2]catenane, as portrayed by the space-filling molecular model of this intriguing **12**$^{4+}$ tetracation (Figure 3).

In this investigation two different branches of contemporary chemistry have been brought together to produce, by relatively new synthetic procedures including self-assembly,[4] a molecular compound that is a combination of two topologically nontrivial molecules[22]—that is, they cannot be represented by planar graphs—a macrocyclic C_{60} bis(adduct) and a catenane. The electrochemical and photophysical properties of **12**·4PF_6 are now under investigation.

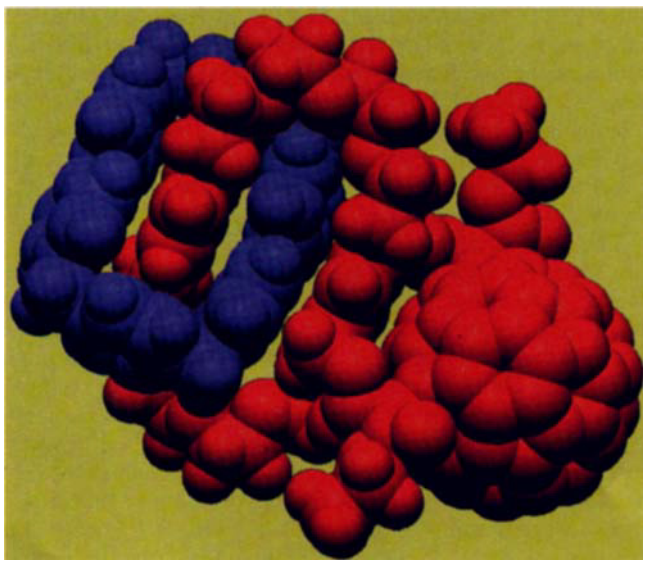

Figure 3. Molecular model of **12**$^{4+}$ revealing the intramolecular five-fold A-D-A-D-A stack.

Experimental Section

8: A solution of C_{60} (300 mg, 0.416 mmol), **7** (343 mg, 0.416 mmol), and I_2 (211 mg, 0.832 mmol) in PhMe (600 mL) was stirred under N_2. DBU (379 mg, 2.50 mmol) was added, and an instant color change from deep purple to wine red observed. The mixture was stirred overnight under N_2 before it was filtered through a plug (SiO_2) with PhMe to collect unchanged C_{60} (purple) and then with CH_2Cl_2/MeOH (98/2) to collect the product (red) of the double Bingel reaction. The solvent was removed in vacuo, and the product purified by column chromatography (SiO_2; CH_2Cl_2/MeOH, 99/1 then 98/2) to yield **8** as a brownish-red, glassy product (140 mg, 22%). IR (KBr): $\tilde{\nu}$ = 2871, 1744, 1506, 1453, 1421, 1364, 1239, 1104, 1062, 927, 862, 827, 735, 705 cm^{-1}; UV/Vis (CH_2Cl_2): λ_{max} (ε) = 280 (155000), 365 (62500), 417 (sh, 35000), 472 (25000), 635 (5000), 701 nm (3200); ^{1}H NMR (300 MHz, $CDCl_3$, 25 °C): δ = 1.50–1.55 (two coincident triplets, J = 7.1 Hz, 6H), 3.62–3.85 (m, 28H), 3.97–3.98 (m, 4H), 4.56–4.58 (m, 4H), 4.59 (d, J = 11 Hz, 1H), 5.30 (d, J = 11 Hz, 1H), 5.71 (d, J = 11 Hz, 1H), 6.45 (d, J = 11 Hz, 1H), 6.51 (s, 1H), 6.74 (s, 4H), 6.79 (s, 1H); ^{13}C NMR (125 MHz, $CDCl_3$, 25 °C): δ = 14.2, 14.3, 49.2, 49.4, 62.5, 63.5, 64.3, 68.2, 68.8, 69.2, 69.4, 69.5, 69.8, 70.4, 70.7, 70.8, 70.8, 70.9, 70.9, 72.5, 115.5, 116.2, 116.6, 125.2, 126.3, 128.0, 129.8, 131.0, 140.6, 140.8, 141.0, 141.2, 141.3, 141.4, 141.4, 141.5, 141.6, 141.9, 142.1, 142.2, 142.2, 142.7, 142.8, 142.8, 143.1, 143.2, 144.3, 144.4, 144.6, 144.8, 144.8, 145.0, 145.1, 145.1, 145.2, 145.2, 145.3, 145.3, 145.4, 145.9, 146.1, 146.3, 146.5, 146.8, 147.0, 147.0, 147.9, 148.1, 148.2, 148.4, 151.2, 152.3, 153.1, 153.1, 163.6, 164.1, 164.2, 164.3; FAB-MS (*m*-nitrobenzyl alcohol): m/z = 1541 [M + H]$^+$, 720 [C_{60}]$^+$; elemental analysis calcd for $C_{100}H_{52}O_{18}$·0.7CH_2Cl_2: C 75.55, H 3.36; found: C 75.34, H 3.70.

12·4PF_6: A solution of **8** (70 mg, 0.045 mmol), **10**·2PF_6 (32 mg, 0.045 mmol), **11** (12 mg, 0.045 mmol), and NH_4PF_6 (100 mg, 0.61 mmol) in dry DMF (10 mL) was stirred under N_2 for 10 d. The solvent was removed in vacuo to yield a brown oil, which was taken up in CH_2Cl_2 (100 mL) to produce a brownish-red precipitate and a deep red solution. The precipitate was isolated by filtration and washed with CH_2Cl_2 (50 mL), distilled H_2O (50 mL), and hot distilled H_2O (50 mL). The remaining solid was dissolved in MeCN (5 mL) and iPr_2O (about 1 mL) introduced by vapor diffusion. A white precipitate formed and was removed by filtration. Et_2O was added dropwise to the solution in MeCN until a suspension was formed. The suspension was centrifuged, and the brownish-red solution decanted. The product was purified by column chromatography (SiO_2; saturated solution of NH_4PF_6 in CH_3COCH_3). The solvent was removed in vacuo, and the remaining solid thoroughly washed with H_2O to yield **12**·4PF_6 as a brownish-red solid (20 mg, 18%). IR (NaCl): $\tilde{\nu}$ = 3327, 3135, 3048, 2920, 1743, 1636, 1508, 1404, 1232, 832, 790, 739 cm^{-1}; UV/Vis (MeCN): λ_{max} (ε) = 280 (88420), 325 (50000), 421 (21050), 463 (9200), 636 nm (3700); ^{1}H NMR (300 MHz, CD_3CN, 25 °C): δ = 1.43–1.44 (m, 6H), 3.40–4.05 (m, 36H), 4.44–4.52 (m, 4H), 4.60 (d, J = 11 Hz, 1H), 4.94 (d, J = 11 Hz, 1H), 5.45 (d, J = 11 Hz, 1H), 5.62-5.73 (m, 8H), 5.98 (d, J = 11 Hz, 1H), 6.01 (s, 1H), 6.23 (s, 1H), 7.68 (d, J = 5.9 Hz, 8H), 7.79 (s, 8H), 8.90 (br s, 8H); ^{13}C NMR (125 MHz, CD_3CN, 25 °C): δ = 14.6, 29.8, 30.0, 32.2, 62.5, 64.7, 65.8, 67.8, 69.4, 70.0, 70.2, 70.4, 70.5, 70.7, 70.9, 71.5, 71.9, 72.0, 113.0, 116.4, 117.2, 125.8, 126.3, 127.7, 128.6, 129.3, 130.4, 130.6, 131.2, 132.9, 133.1, 137.6, 139.9, 140.1, 141.1, 141.5, 141.8, 142.1, 142.2, 142.4, 142.9, 143.0, 143.2, 143.6, 143.9, 144.8, 145.2, 145.3, 145.8, 146.1, 146.3, 146.7, 147.2, 147.3, 147.6, 147.9, 148.1, 149.1, 151.2, 152.0, 164.3, 164.6, 164.7, 164.9; LSI-MS: m/z = 2642 [M + H]$^+$, 2497 [M − PF_6]$^+$, 2351 [M − 2PF_6]$^+$, 2206 [M − 3PF_6]$^+$, 1541 [**8**]$^+$, 810 [cyclobis(paraquat-*p*-phenylene) − 2PF_6]$^+$, 720 [C_{60}]$^+$.

Received: January 28, 1997 [Z10049IE]
German Version: *Angew. Chem.* **1997**, *109*, 1611–1614

Keywords: catenanes · crown compounds · donor–acceptor systems · fullerenes · supramolecular chemistry

[1] H. W. Kroto, J. R. Heath, S. C. O'Brien, R. F. Curl, R. E. Smalley, *Nature (London)* **1985**, *318*, 162–163.
[2] W. Krätschmer, L. D. Lamb, K. Fostiropoulos, D. R. Huffman, *Nature (London)* **1990**, *347*, 354–358.
[3] a) A. Hirsch, *The Chemistry of the Fullerenes*, Thieme, Stuttgart, **1994**; b) F. Diederich, C. Thilgen, *Science* **1996**, *271*, 317–323; c) "Fullerene Chemistry": *Tetrahedron Symposia-In-Print Number 60* (Ed.: A. B. Smith III) in *Tetrahedron* **1996**, *52*, 4925–5262.
[4] a) C. O. Dietrich-Buchecker, J.-P. Sauvage, *Chem. Rev.* **1987**, *87*, 795–810; b) J.-F. Nierengarten, C. O. Dietrich-Buchecker, J.-P. Sauvage, *J. Am. Chem. Soc.* **1994**, *116*, 375–376; c) D. B. Amabilino, C. O. Dietrich-Buchecker, A. Livoreil, L. Pérez-García, J.-P. Sauvage, J. F. Stoddart, *ibid.* **1996**, *118*, 3905–3913; d) P. R. Ashton, T. T. Goodnow, A. E. Kaifer, M. V. Reddington, A. M. Z. Slawin, N. Spencer, J. F. Stoddart, C. Vicent, D. J. Williams, *Angew. Chem.* **1989**, *101*, 1404–1408; *Angew. Chem. Int. Ed. Engl.* **1989**, *28*, 1396–1399; e) D. B. Amabilino, J. F. Stoddart, *Chem. Rev.* **1995**, *95*, 2725–2828; f) P. R. Ashton, P. T. Glink, J. F. Stoddart, P. A. Tasker, A. J. P. White, D. J. Williams, *Chem. Eur. J.* **1996**, *2*, 729–736; g) C. A. Hunter, *J. Am. Chem. Soc.* **1992**, *114*, 5303–5111; h) F. Vögtle, S. Meier, R. Hoss, *Angew. Chem.* **1992**, *104*, 1628–1631; *Angew. Chem. Int. Ed. Engl.* **1992**, *31*, 1619–1622; i) A. G. Johnston, D. A. Leigh, R. J. Pritchard, M. D. Deegan, *ibid.* **1995**, *107*, 1324–

1327 and **1995**, *34*, 1209–1212; j) A. G. Johnston, D. A. Leigh, A. Murphy, J. P. Smart, M. D. Deegan, *J. Am. Chem. Soc.* **1996**, *118*, 10662–10663; k) D. Whang, Y.-M. Jeon, J. Heo, K. Kim, *ibid.* **1996**, *118*, 11333–11334.

[5] G. Schill, *Catenanes, Rotaxanes and Knots*, Academic Press, New York, **1971**.

[6] a) J. S. Lindsey, *New J. Chem.* **1991**, *15*, 153–180; b) J. P. Mathias, C. T. Seto, G. M. Whitesides, *Science* **1991**, *254*, 1312–1319; c) D. Philp, J. F. Stoddart, *Angew. Chem.* **1996**, *108*, 1242–1286; *Angew. Chem. Int. Ed. Engl.* **1996**, *35*, 1154–1196.

[7] F. Diederich, C. O. Dietrich-Buchecker, J.-F. Nierengarten, J.-P. Sauvage, *J. Chem. Soc. Chem. Commun.* **1995**, 781–782.

[8] J.-F. Nierengarten, V. Gramlich, F. Cardullo, F. Diederich, *Angew. Chem.* **1996**, *108*, 2242–2244; *Angew. Chem. Int. Ed. Engl.* **1996**, *35*, 2101–2103.

[9] C. Bingel, *Chem. Ber.* **1993**, *126*, 1957–1959.

[10] M. Asakawa, W. Dehaen, G. L'abbé, S. Menzer, J. Nouwen, F. M. Raymo, J. F. Stoddart, D. J. Williams, *J. Org. Chem.* **1996**, *61*, 9591–9594 and references therein.

[11] All new compounds were fully characterized by fast atom bombardment (FAB), matrix assisted laser desorption ionization time-of-flight (MALDI-TOF), or liquid secondary ion (LSI) mass spectrometry, and by IR, UV/Vis, and ^{1}H and ^{13}C NMR spectroscopy. All precursors to **12**·4PF$_6$ were also characterized by elemental analysis.

[12] a) A. Hirsch, I. Lamparth, H. R. Karfunkel, *Angew. Chem.* **1994**, *106*, 453–455; *Angew. Chem. Int. Ed. Engl.* **1994**, *33*, 437–438; b) F. Djojo, A. Herzog, I. Lamparth, F. Hampel, A. Hirsch, *Chem. Eur. J.* **1996**, *2*, 1537–1547.

[13] Q. Lu, D. I. Schuster, S. R. Wilson, *J. Org. Chem.* **1996**, *61*, 4764–4768.

[14] a) A. Pasquarello, M. Schlüter, R. C. Haddon, *Science* **1992**, *257*, 1660–1661; b) R. Zansai, P. W. Fowler, *Chem. Phys. Lett.* **1995**, *238*, 270–280.

[15] The [2]catenane **12**·4PF$_6$ was constructed within the input mode of Macromodel 5.0 (F. Mahamadi, N. G. K. Richards, W. C. Guida, R. Liskamp, M. Lipton, D. Caufield, G. Chang, T. Hendrickson, W. C. Still, *J. Comp. Chem.* **1990**, *11*, 440–467). The geometry was subsequently optimized by energy minimization with the Polak–Ribiere Conjugate-Gradient (PRCG) method, the AMBER* force field, and the Generalized Born Surface-Accessible (GB/SA) solvation model for H_2O. The global minimum was searched for by molecular dynamics with stepwise simulated annealing performed in one step of 10 ps, followed by two steps of 20 ps in conjunction with the PRCG method, the AMBER* force field, and the GB/SA for H_2O. The simulated temperature was decreased from 300 to 150 and finally to 50 K; a bath constant of 5.0 ps was applied at all steps. The time step was maintained at 1.5 fs in the first two steps and increased to 2.0 fs in the final step.

[16] a) F. Diederich, U. Jonas, V. Gramlich, A. Herrmann, H. Ringsdorf, C. Thilgen, *Helv. Chim. Acta* **1993**, *76*, 2445–2453; b) F. Arias, Q. Xie, L. Echegoyen, Y. Wu, Q. Lu, S. R. Wilson, *J. Am. Chem. Soc.* **1994**, *116*, 6388–6394; c) F. Arias, L. A. Godínez, S. R. Wilson, A. E. Kaifer, L. Echegoyen, *ibid.* **1996**, *118*, 6086–6087.

[17] B. L. Allwood, N. Spencer, H. Shahriari-Zavareh, J. F. Stoddart, D. J. Williams, *J. Chem. Soc. Chem. Commun.* **1987**, 1064–1066.

[18] Titrations were run at $[\mathbf{8}] \approx 10^{-4}$ M and $[\mathbf{9}\cdot 2PF_6] \approx 10^{-4}-10^{-2}$ M, and K_a values were evaluated with a nonlinear curve fitting program. Maximum observed upfield shifts ($\Delta\delta_{obs,max}$) and calculated shifts for saturation binding ($\Delta\delta_{sat.}$) for the ring protons of the proximal and distal hydroquinone rings are 0.22 ($\Delta\delta_{sat.} = 0.473 \pm 0.068$) and 0.25 ($\Delta\delta_{sat.} = 0.435 \pm 0.042$), respectively.

[19] a) W. Vetter, E. Logemann, G. Schill, *Org. Mass. Spectrom.* **1977**, *12*, 351–369; b) P. R. Ashton, C. L. Brown, J. R. Chapman, R. T. Gallagher, J. F. Stoddart, *Tetrahedron Lett.* **1992**, *33*, 7771–7774; c) C. Dietrich-Buchecker, E. Leize, J.-F. Nierengarten, J.-P. Sauvage, A. van Dorsselaer, *J. Chem. Soc. Chem. Commun.* **1994**, 2257–2258.

[20] P. L. Anelli, P. R. Ashton, R. Ballardini, V. Balzani, M. T. Gandolfi, T. T. Goodnow, A. E. Kaifer, D. Philp, M. Pietraszkiewicz, L. Prodi, M. V. Reddington, A. M. Z. Slawin, N. Spencer, J. F. Stoddart, C. Vicent, D. J. Williams, *J. Am. Chem. Soc.* **1992**, *114*, 193–218.

[21] a) D. B. Amabilino, J. F. Stoddart, D. J. Williams, *Chem. Mater.* **1994**, *6*, 1159–1167; b) P. R. Ashton, C. G. Claessens, W. Hayes, S. Menzer, J. F. Stoddart, A. J. P. White, D. J. Williams, *Angew. Chem.* **1995**, *107*, 1994–1997; *Angew. Chem. Int. Ed. Engl.* **1995**, *34*, 1862–1865.

[22] J.-C. Chambron, C. O. Dietrich-Buchecker, J.-P. Sauvage, *Top. Curr. Chem.* **1993**, *165*, 131–162.

Carbohydrate Nanotubes**

Giuseppe Gattuso, Stephan Menzer, Sergey A. Nepogodiev, J. Fraser Stoddart,* and David J. Williams*

Large cyclic oligosaccharides, which can be defined as compounds incorporating more than eight monosaccharide residues in their macrorings and often possessing internal cavities of nanometer dimensions, are accessible from both natural sources[1] and from total chemical syntheses.[2] However, on account of the difficulties associated with either a) the isolation of the pure natural products or semi-synthetic compounds, or b) their availabilities in reasonable quantities from chemical syntheses, the physicochemical properties of the solid-state structures and superstructures of these large cyclic oligosaccharides have been somewhat superficially studied. It is only recently, for example, that the higher cyclodextrin (CD) homologs δ-CD,[3] ε-CD,[4] and η-CD[5] have been obtained as sufficiently pure samples to be subjected to such detailed investigations. This situation contrasts sharply with the extensive studies that have been carried out on the chief members of the CD family composed of six, seven and eight α-(1 → 4)-linked D-glucopyranose residues, namely α-CD, β-CD, and γ-CD, respectively. These compounds, as well as numerous inclusion complexes, have been throughly characterized in the solid state by X-ray and neutron diffraction methods[6] and solid-state NMR spectroscopy.[7] Amongst the large cyclic oligosaccharides, crystallographic data are available only for δ-CD[8] and ε-CD.[4] Previously, we synthesized[9, 10] a series of novel CD analogs composed of alternating D- and L-rhamnopyranose (**R**) and D- and L-mannopyranose (**M**) residues, including the first examples (**RR** and **MM** series) of achiral cyclic oligosaccharides and the largest (so far) synthetic cyclic oligosaccharide **5-RR** built up of 14 alternating D- and L-rhamnopyranose residues. The crystal structures of **1-MM** (α-CD analog) as well as **2-RM** and **2-RR** (γ-CD analogs) have been reported.[9, 10]

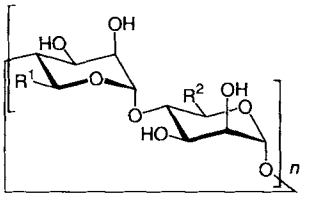

	n	R^1	R^2
1-MM	3	CH_2OH	CH_2OH
1-RM	3	Me	CH_2OH
2-RM	4	Me	CH_2OH
1-RR	3	Me	Me
2-RR	4	Me	Me
3-RR	5	Me	Me
4-RR	6	Me	Me
5-RR	7	Me	Me

X-ray crystallography reveals that, in the solid state, the cyclic octasaccharide **2-RR**[10] assembles in infinite stacks to form nanotubes of approximately 1 nm in diameter in a manner similar to that exhibited[9] by the octasaccharide **2-RM**. This stack-

[*] Prof. J. F. Stoddart, Dr. G. Gattuso, Dr. S. A. Nepogodiev
School of Chemistry
University of Birmingham
Edgbaston, Birmingham, B15 2TT (UK)
Fax: Int. code +(121)414-3531
e-mail: j.f.stoddart@bham.ac.uk

Prof. D. J. Williams, Dr. S. Menzer
Chemical Crystallography Laboratory
Department of Chemistry Imperial College
South Kensington, London, SW7 2AY (UK)
Fax: Int. code +(171)594-5804

[**] Synthetic Cyclic Oligosaccharides, Part 3. Part 2: ref. [10b].

 © VCH Verlagsgesellschaft mbH, D-69451 Weinheim, 1997 0570-0833/97/3613-1451 $ 17.50+.50/0

ing motif is closely reminiscent of the nanotubes formed by cyclic peptides composed of alternating D and L amino acids reported by Ghadiri and co-workers.[11] However, the contrast between the regular superstructures sustained by these highly symmetrical cyclic oligosaccharides and the more disordered packing exemplified by the larger members of the CD family—namely γ-CD,[12, 6c] δ-CD,[8] and ε-CD[4]—is striking. Here we report the results of X-ray crystallographic investigations on **3-RR**. This achiral cyclic decasaccharide displays quite a remarkable structure and superstructure in the solid state.

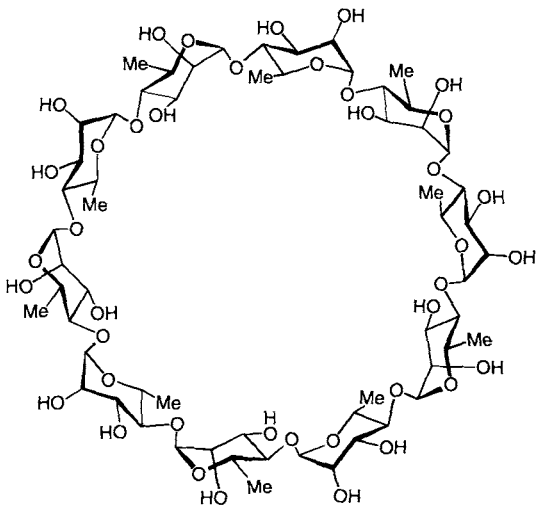

3-RR

The X-ray analysis[13] of a crystal produced by vapor diffusion of Me_2CO into an aqueous solution of the cyclic decasaccharide **3-RR** reveals a structure comprising two crystallographically independent, C_i-symmetrical macrocycles **A** and **B** (Figure 1). The two cyclic decasaccharide molecules have similar geometries, and each exhibits departures from ideal S_{10} symmetry. In **A** the radii of the polygon formed by the ten glycosidic oxygen atoms are 6.53 to 7.23 Å, whereas in **B** they are in the range of 6.73 to 7.21 Å. Although the planes of the α-D- and α-L-rhamnopyranosyl residues (those containing C2, C3, C5, and the ring O atom) are inclined approximately orthogonally to the mean plane of the macroring, as defined by the ten glycosidic oxygen atoms, they exhibit a distinct alternating pattern of inward and outward tilt angles that range between 77° and 81° in **A** and 76° and 85° in **B** (Figure 1b). The overall regularity of the molecular geometry is demonstrated by the conformation of the pseudo-ten-membered ring (Figure 2) formed by the ten glycosidic oxygen atoms, which adopts an approximately "all-*gauche*" geometry with alternating torsional twists of about ±76° about each O–O "linkage".

Inspection of the packing of the **A**- and **B**-type molecules shows each of them to be arranged in an approximately close-packed hexagonal array that extends in the crystallographic *b* and *c* directions (Figure 3). Adjacent molecules in both the *b* and *c* directions are offset by the thickness of about half a ring. However, there are no intermolecular hydrogen bonds in either case. In the *a* direction, the **A**- and **B**-type molecules form a slightly sheared alternating stack creating a nanotube-like arrangement (Figure 4). The mean interplanar separation between **A**- and **B**-type molecules is about 7.4 Å. A particular point of interest is that, within each stack, the **A**- and **B**-type molecules are not in register. Furthermore, and probably more

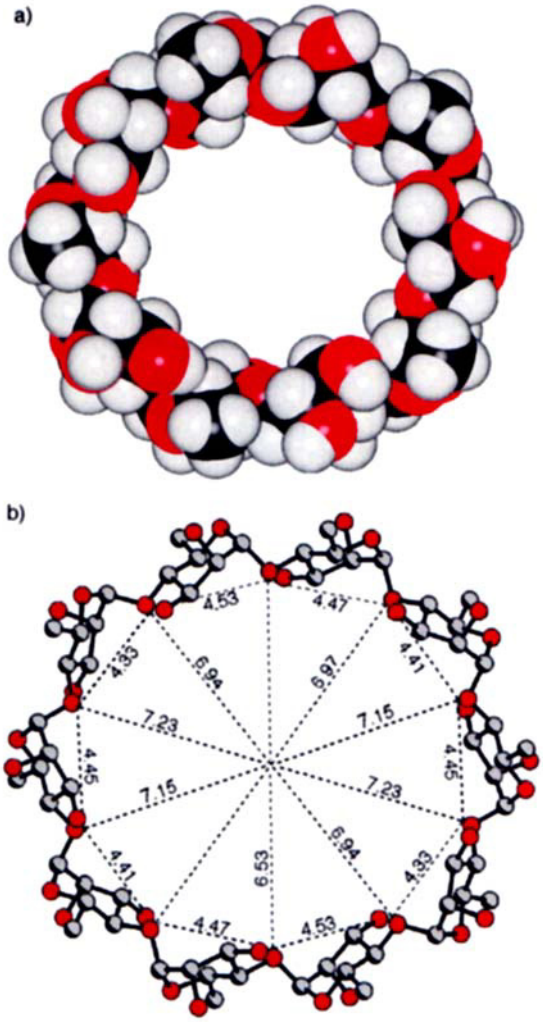

Figure 1. a) Space-filling and b) ball-and-stick representations of the C_i-symmetrical solid-state structure of **3-RR** (only molecule **A** is shown). The numbers beside the dashed lines indicate the distances [Å] between adjacent pairs of glycosydic oxygen atoms and their radial distances from the center of the cyclic decasaccharide. a) Red = O atoms; gray = C atoms; white = H atoms. b) Red = O atoms; shaded circles = C atoms.

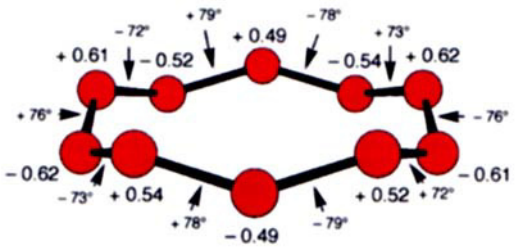

Figure 2. Polygon formed by the ten glycosidic oxygen atoms (red balls) of **3-RR** (only molecule **A** is shown). The distances [Å] from the mean plane of the molecule are shown in black beside each oxygen atom, and the "torsional angles" beside each bond.

significantly, they have different cyclic sequences for the glycosidic bonds between the α-D- and α-L-rhamnopyranosyl residues; that is, the sequence is clockwise in **A**, and counterclockwise in **B**. This disrotatory stacking is in contrast with the conrotatory arrangement present in **2-RM**[9] and **2-RR**,[10] where the molecules in each stack are in register with each other. There are no hydrogen bonds between the macrorings within each stack. Included Me_2CO and H_2O molecules lie both within and between the channels formed by the cyclic decasaccharide molecules.

 © VCH Verlagsgesellschaft mbH, D-69451 Weinheim, 1997 0570-0833/97/3613-1452 $ 17.50+.50/0

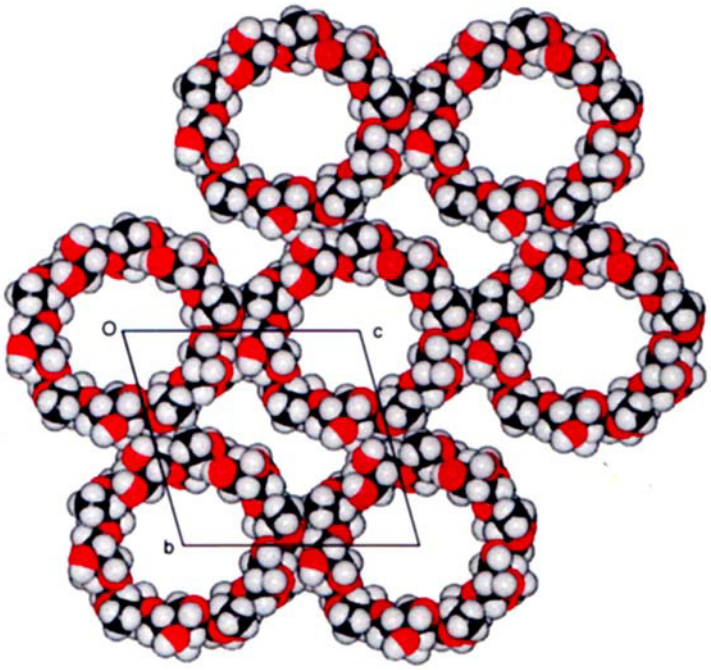

Figure 3. Distorted, close-packed hexagonal array of **3-RR** molecules (only molecule **A** is shown). Red = O atoms; grey = C atoms; white = H atoms.

Since **3-RR** crystallizes in the form of nanotubes with an internal diameter of about 1.3 nm, it adds to the two examples of cyclic octasaccharides already reported (namely, **2-RM** and **2-RR**)[9, 10] which sustain this intriguing superstructure in the solid state. Given the fact that these compounds share with the naturally occurring CDs an ability[10] to form inclusion complexes with other molecules, they could find themselves enjoying many biomedically-directed and materials-oriented applications in the future.

Received: January 28, 1997 [Z10050IE]
German version: *Angew. Chem.* **1997**, *109*, 1615–1617

Keywords: carbohydrates · cyclodextrins · oligosaccharides · supramolecular chemistry

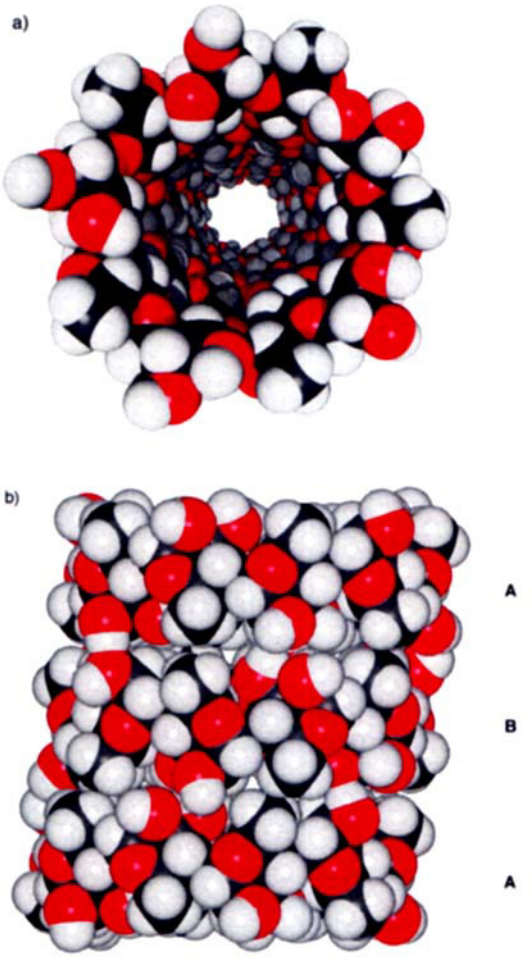

Figure 4. View of one of the discrete nanotubular stacks of **3-RR** in the solid state a) down the stackes and b) from the side (showing also the A-B-A alternation of the independent, disrotatory cyclic decasaccharides). Red = O atoms; grey = C atoms; white = H atoms.

[1] Natural and semi-synthetic examples: a) higher members of the CD family such as δ-CD, ε-CD, ξ-CD, and η-CD, which are composed of 9, 10, 11, and 12 D-glucopyranose repeating residues, respectively (D. French, A. O. Pulley, J. Effendberger, M. Rougvie, M. Abdullach, M., *Arch. Biochem. Biophys.* **1965**, *111*, 153–160); b) cyclic β-(1 → 2)-glucans incorporating 17 to 40 D-glucopyranose residues (M. W. Breedveld, K. Miller, *Microbiol. Rev.* **1994**, *58*, 145–161); c) cyclic β-(1 → 3)-glucans with 10 repeating units (P. E. Pfeffer, S. F. Osman, A. Hotchkiss, A. A. Bhagwat, D. L. Keister, K. M. Valentine, *Carbohydr. Res.* **1996**, *296*, 23–37); d) cyclic glucans with β-(1 → 3) and β-(1 → 6) types of interglycosidic linkages containing more than 11 monosaccharides (N. Iñón de Iannino, R. A. Ugalde, *Arch. Microbiol.* **1993**, *159*, 30–38); e) a unique microbial dodecasaccharide related to an enterobacterial common antigen (E. V. Vinogradov, Y. A. Knirel, J. Thomas-Oates, A. S. Shashkov, V. L. L'vov, *Carbohydr. Res.* **1994**, *258*, 223–232).

[2] Review on synthetic cyclic oligosaccharides: G. Gattuso, S. A. Nepogodiev, J. F. Stoddart, *Chem. Rev.* **1997**, submitted. A few large ring synthetic cyclic oligosaccharides have been reported: a) N. K. Kochetkov, S. A. Nepogodiev, L. V. Backinowsky, *Tetrahedron* **1990**, *46*, 139–150; b) H. Kuyama, T. Nukada, Y. Ito, Y. Nakahara, T. Ogawa, *Carbohydr. Res.* **1995**, *268*, C1–C6; c) H. Driguez, J.-P. Utille, *Carbohydr. Lett.* **1994**, *1*, 125–128.

[3] I. Miyazawa, H. Ueda, H. Nagase, T. Endo, S. Kobayashi, T. Nagai, *Eur. J. Pharm. Sci.* **1995**, *3*, 153–162.

[4] H. Ueda, T. Endo, H. Nagase, S. Kobayashi, T. Nagai in *Proceedings of the 8th International Symposium on Cyclodextrins* (Eds.: J. Szejtli, L. Szente), Kluwer, Dordrecht, **1996**, 17–20.

[5] T. Endo, H. Ueda, S. Kobayashi, T. Nagai, *Carbohydr. Res.* **1996**, *269*, 369–373.

[6] a) W. Saenger in *Inclusion Compounds, Vol. 2* (Eds.: J. L. Atwood, J. E. D. Davies, D. D. MacNicol), Academic Press, London, **1984**, pp. 231–259; b) K. Harata in *Inclusion Compounds, Vol. 5* (Eds.: J. L. Atwood, J. E. D. Davies, D. D. MacNicol), Oxford University Press, Oxford, **1991**, pp. 311–344; c) K. Harata in *Comprehensive Supramolecular Chemistry, Vol 3* (Eds.: J. Szejtli, T. Osa), Elsevier, Oxford, **1996**, pp. 279–304.

[7] P. R. Veregin, C. A. Fyfe, *Carbohydr. Res.* **1987**, *160*, 41–56.

[8] T. Fujiwara, N. Tanaka, S. Kobayashi, *Chem. Lett.* **1990**, 739–742.

[9] P. R. Ashton, C. L. Brown, S. Menzer, S. A. Nepogodiev, J. F. Stoddart, D. J. Williams, *Chem. Eur. J.* **1996**, *2*, 580–591.

[10] a) S. A. Nepogodiev, G. Gattuso, J. F. Stoddart in *Proceedings of the 8th International Symposium on Cyclodextrins* (Eds.: J. Szejtli, L. Szente), Kluwer, Dordrecht, **1996**, pp. 89–94; b) P. R. Ashton, S. J. Cantrill, G. Gattuso, S. Menzer, S. A. Nepogodiev, A. N. Shipway, J. F. Stoddart, D. J. Williams, *Chem. Eur. J.*, **1997**, *3*, 1299–1314.

[11] a) M. R. Ghadiri, K. Kobayashi, J. R. Granja, R. K. Chadha, D. E. McRee, *Angew. Chem.* **1995**, *107*, 76–78; *Angew. Chem. Int. Ed. Engl.* **1995**, *34*, 93–95; b) M. R. Ghadiri, *Adv. Mater.* **1995**, *7*, 675–677; c) M. Engels, D. Bushford, M. R. Ghadiri, *J. Am. Chem. Soc.* **1995**, *117*, 9151–9158; d) J. D. Hartgernik, J. R. Granja, R. A. Milligan, M. R. Ghadiri, *ibid.* **1996**, *118*, 43–50.

[12] a) K. Harata *Bull. Soc. Chem. Jpn.* **1987**, *60*, 2763–2767; b) J. Ding, T. Steiner, W. Saenger, *Acta Crystallogr. B* **1991**, *47*, 731–738.

[13] Crystal data for **3-RR**: $C_{60}H_{100}O_{40}\cdot 6\,Me_2CO\cdot 10\,H_2O$, $M_r = 1990.0$, triclinic, space group $P\bar{1}$, $a = 15.130(6)$, $b = 19.077(5)$, $c = 20.017(5)$ Å, $\alpha = 72.74(2)$, $\beta = 87.60(3)$, $\gamma = 88.60(3)°$, $V = 5513(3)$ Å^3, $Z = 2$ (two independent molecules, each with crystallographic C_i symmetry), $\rho_{calcd} = 1.20$ g cm^{-3}, $\mu(Cu_{K\alpha}) = 8.76$ cm^{-1}, $\lambda = 1.54178$ Å, $F(000) = 2144$. Crystal dimensions $0.33 \times 0.13 \times 0.07$ mm (plate-shaped prism), Siemens P4/RA diffractometer with $Cu_{K\alpha}$ radiation (graphite monochromated), ω scans. $T = 178$ K. The crys-

tal slowly desolvated during data collection. Of 7686 independent reflections measured ($2\theta \leq 100°$) 4846 had $I_o > (2\sigma I_o)$ and were considered to be observed. The data were corrected for Lorentz and polarization factors, but not for absorption. The structure was solved by direct methods. The Me_2CO solvent molecules were disordered over seven partially occupied positions, and the H_2O molecules over 13 positions. Hydrogen atoms within the macroring were located from ΔF maps and refined applying distance constraints with riding isotropic thermal parameters, $U(H) = 1.2\,U_{eq}(C,O)$. Anisotropic refinement of all the exocyclic atoms of the sugar moieties, the full-weight H_2O molecules and six of the Me_2CO molecules; the remainder were held isotropic. $R_1 = 0.141$ and $wR_2 = 0.379$ based on F^2. All computations were carried out with the SHELXTL 5.03 package. The crystallographic data (excluding structure factors) for the structure reported in this paper has been deposited with the Cambridge Crystallographic Data Centre as supplementary publication no. CCDC-100130. Copies of the data can be obtained free of charge on application to The Director, CCDC, 12 Union Road, Cambridge CB21EZ, UK (fax: int. code +(1223)336-033; e-mail: deposit@chemcrys.cam.ac.uk).

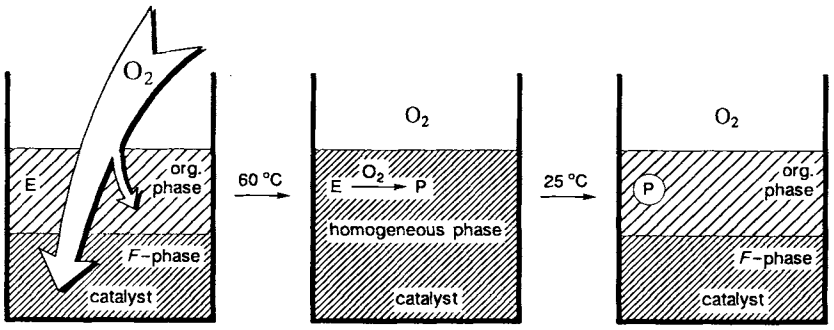

Scheme 1. Principle of the biphasic oxidations (*F*-phase = perfluorinated solvent, E = starting material, P = product).

Transition Metal Catalyzed Oxidations in Perfluorinated Solvents**

Ingo Klement, Henning Lütjens, and Paul Knochel*

Perfluorinated hydrocarbons are chemically inert compounds that have found useful applications, especially as artificial blood substitutes.[1] As a consequence of their low tendency to undergo van der Waals interactions, they solubilize well a range of gases[2] and are immiscible with many organic solvents at room temperature. However, a good miscibility with some organic solvents is observed at higher temperature.[3] These properties, which were used first for synthetic applications by Horváth and Rabai,[3] make perfluorinated hydrocarbons ideal solvents for organic reactions in which gases serve as one reactant.[3,4]

Furthermore, the temperature dependence of the miscibility of perfluorinated solvents with organic solvents can be advantageously used for enhancing the reaction rate by obtaining a monophasic system during the reaction. By cooling down the mixture at the end of the reaction, a biphasic system is formed, which allows easy separation of the reaction products and recovery of the perfluorinated solvent (Scheme 1). Recently, we have used perfluorinated solvents for oxidizing organometallic compounds, such as organozinc derivatives, to give polyfunctional hydroperoxides.[5] Under these conditions, organoboranes could be oxidized stereoselectively with oxygen to give alcohols.[6] Herein, we report a new practical method for the biphasic oxidation of aldehydes, sulfides, or olefins to give carboxylic acids, sulfoxides or sulfones, and epoxides, respectively, in good to excellent yields, which uses a transition metal catalyst (Ni, Ru) bearing perfluorinated ligands. These chemical processes combine an efficient direct oxidation with oxygen with a small or negligible leaching of the metal salts in the organic phase and a trivial product isolation by phase separation. An excellent chemoselectivity was obtained in the case of the epoxide synthesis.

The required perfluorinated ligand, the 1,3-diketone **1**, was prepared by the condensation[7] of the methyl ester **2** with the methyl ketone **3** in the presence of NaOMe (1 equiv) in diethyl ether (0 °C, 12 h, then 25 °C, 48 h, 80% yield). The reaction of the perfluorinated 1,3-diketone **1** with the appropriate metal salt MCl_2 (M = Ni, Ru) in the presence of a base furnishes the desired complexes **4a** and **4b** in 81 and 62% yield, respectively. These were readily soluble in perfluorinated solvents (Scheme 2) leading to green and purple solutions, respectively.

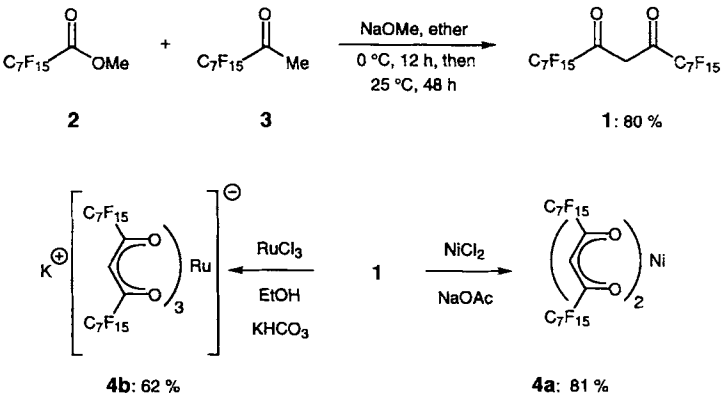

Scheme 2. Preparation of the perfluorinated complexes **4a** and **4b**.

Thus, treatment of an aldehyde of type **5** with oxygen in a monophasic solvent system (toluene/perfluorinated decalin) at 64 °C in the presence of the nickel catalyst **4a** (3 mol%) furnishes the corresponding carboxylic acid of type **6** in yields of 71–87% (Scheme 3). The reaction tolerates several functional groups (ester, chloride, tetraisopropylsilyl(TIPS)-ether) and proceeds as well with aromatic as with aliphatic aldehydes.[8]

No leaching of the catalyst is observed (Figure 1) and the catalytic system can be easily recovered (by phase separation) and reused again as shown in the case of *p*-chlorobenzaldehyde (**5a**). The yield of the reaction was still 70% after six reaction cycles (Scheme 4). Similarly, this catalytic system can be used for the oxidation of sulfides **7** to sulfoxides **8** and sulfones **9** (Figure 1, Scheme 5). The reaction required the presence of isobutyraldehyde;[9] the optimum quantities are 1.6 equiv for the oxidation to sulfoxides and 5 equiv for the oxidation to sulfones.

[*] Prof. Dr. P. Knochel, Dr. I. Klement, Dipl.-Chem. H. Lütjens
Fachbereich Chemie der Universität
Hans-Meerwein-Strasse, D-35032 Marburg (Germany)
Fax: Int. code +(6421)28-2189
e-mail: Knochel@ps1515.chemie.uni-marburg.de

[**] We thank the DFG (Schwerpunktprogramm "Peroxidchemie" and Leibniz prize) and the Fonds der Chemischen Industrie for generous financial support, and Elf-Atochem (France), Witco AG, BASF AG, Bayer AG, Chemetall GmbH, and SIPSY S. A. (France) for the generous gift of chemicals.

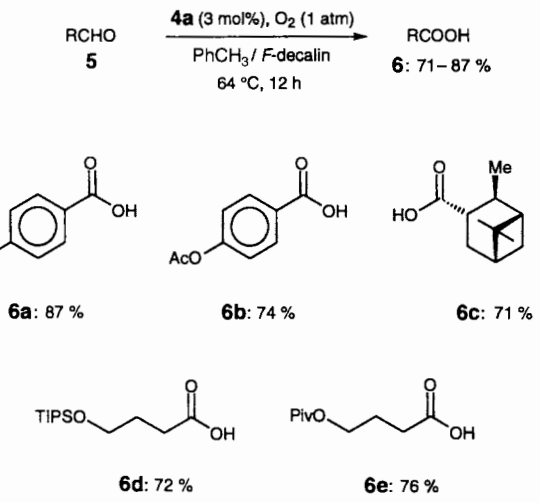

Scheme 3. Oxidation of the aldehydes **6** by oxygen with **4a** as catalyst (*F*-decalin = perfluorodecalin, TIPS = tetraisopropylsilyl).

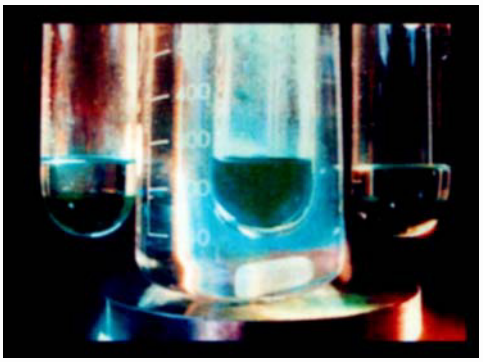

Figure 1. Oxidation of sulfides to sulfoxides in toluene/$C_8F_{17}Br$. Left: Biphasic system before the reaction. Center: Monophasic system during the reaction. Right: Biphasic system after reaction.

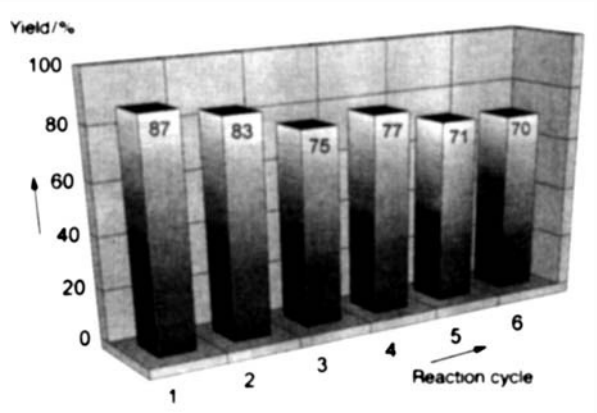

Scheme 4. Oxidation of *p*-chlorobenzaldehyde (**5a**) to give the corresponding acid **6a** (six reaction cycles with reuse of the catalyst **4a**).

Finally, whereas the nickel catalytic system is not suitable for the oxidation of olefins, we found that the ruthenium catalyst **4b** (5 mol%) allows the epoxidation of disubstituted olefins of type **10** to epoxides **11** in toluene/$C_8F_{17}Br$. The actual catalyst is a more oxidized ruthenium species, which is formed in situ and leads to a brown solution. Remarkably, only disubstituted olefins are selectively converted in good yields to the corresponding epoxide under the reaction conditions, as shown in the case of the preparation of the unsaturated epoxide **11g** (Scheme 6). Several functional groups (ester, carboxylic acid)

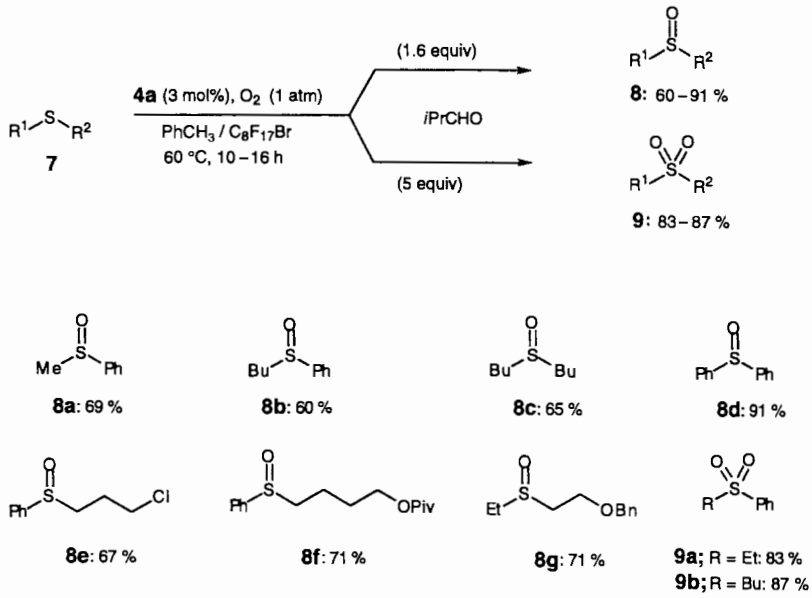

Scheme 5. Oxidation of sulfides **7**.

are tolerated in these epoxidations. The brown solution of the perfluorinated phase containing the catalyst can be used several times leading to similar yields in the epoxidation. A negligible leaching of the catalyst is observed[10] making this oxidation system suitable for large-scale reactions.[11, 12]

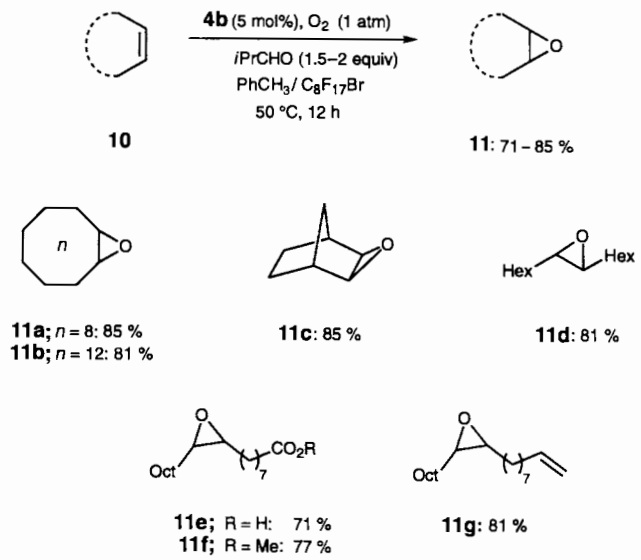

Scheme 6. Oxidation of disubstituted olefins **10**.

In summary, we have described a new metal-catalyzed oxidation method that uses perfluorinated solvents. The easy separation, nonleaching of the metal catalyst, and reuse of the catalyst make this procedure potentially interesting for industrial applications.

Experimental Section

Typical procedure for the preparation of *p*-chlorobenzoic acid (**6a**). A 150 mL Schlenk flask was charged with **4a** (250 mg, 0.15 mmol, 3 mol%) and perfluorodecalin (5 mL). A solution of *p*-chlorobenzaldehyde (0.70 g, 5 mmol) in toluene (5 mL) was added and the resulting emulsion was saturated with oxygen (15 min of bubbling at room temperature). The reaction mixture was warmed to 64 °C and the

 © VCH Verlagsgesellschaft mbH, D-69451 Weinheim, 1997 0570-0833/97/3613-1455 $ 17.50+.50/0

green solution was vigorously stirred under an oxygen overpressure (ca. 1 bar, 12 h). After allowing the mixture to cool to room temperature, phase separation of the solvent system occurred immediately. The precipitated *p*-chlorobenzoic acid (**6a**) was filtered off and recrystallized from acetonitrile affording a white solid (0.68 g, 4.3 mmol, 87% yield, mp 240–243 °C). The green perfluorinated phase containing the catalyst was separated from toluene and can be used for further experiments.

Preparation of cyclooctene oxide (**11a**). A 25 mL flask was charged with a solution of the ruthenium catalyst **4b** (640 mg, 0.25 mmol, 5 mol%) in 1-bromoperfluorooctane (2.5 mL) and a solution of cyclooctene (550 mg, 5 mmol) and isobutyraldehyde (720 mg, 10 mmol) in toluene. The biphasic system was warmed to 50 °C affording a single phase and was stirred at that temperature for 5 h under an oxygen atmosphere (oxygen balloon). The reaction mixture was cooled to 0 °C, and the phases separated. The brown perfluorinated phase containing the catalyst was separated and can be reused for further experiments. The organic phase was washed with 2M aqueous NaOH in order to remove the acid formed as by-product. The toluene was evaporated and the product was purified by flash chromatography on silica gel (eluent: hexanes/*t*BuOMe 10:1) yielding cyclooctene oxide (**11a**) (517 mg, 4.1 mmol, 82%).

Received: January 7, 1997
Revised version: March 24, 1997 [Z9973IE]
German version: *Angew. Chem.* **1997**, *109*, 1605–1607

Keywords: epoxidations · fluorine · homogeneous catalysis · oxidations · ruthenium

[1] J. G. Riess, M. Le Blanc, *Pure Appl. Chem.* **1982**, *54*, 2383; J. G. Riess, *New. J. Chem.* **1995**, *19*, 893; V. W. Sadtler, M. P. Krafft, J. G. Riess, *Angew. Chem.* **1996**, *108*, 2106; *Angew. Chem. Int. Ed. Engl.* **1996**, *35*, 1976.
[2] C. M. Sharts, H. R. Reese, *J. Fluorine Chem.* **1978**, *11*, 637 and references therein.
[3] I. T. Horváth, J. Rabai, *Science* **1994**, *266*, 72; US-A 5463082, **1995**; I. T. Horváth in *Applied Homogeneous Catalysis with Organometallic Compounds*, (Eds.: B. Cornils, W. Herrmann), VCH, **1996**, 601.
[4] For recent applications of perfluorinated solvents for the performance of organic reactions see: S. M. Pereira, G. P. Savage, G. W. Simpson, *Synth. Commun.* **1995**, *25*, 1023; R. P. Hughes, H. A. Trujillo, *Organometallics* **1996**, *15*, 286; D. P. Curran, S. Hadida, *J. Am. Chem. Soc.* **1996**, *118*, 2531; D. P. Curran, M. Hoshino, *J. Org. Chem.* **1996**, *61*, 6480.
[5] I. Klement, P. Knochel, *Synlett* **1995**, 1113.
[6] I. Klement, P. Knochel, *Synlett* **1996**, 1004.
[7] C. Massyn, R. Pastor, A. Cambon, *Bull. Soc. Chim. Fr.* **1974**, *5*, 975; A. E. Pedler, R. C. Smith, J. C. Tatlow, *J. Fluorine Chem.* **1971**, *1*, 433.
[8] Aromatic aldehydes bearing electron-withdrawing groups are not readily oxidized by oxygen in the absence of a metal catalyst (see Scheme 4).
[9] T. Yamada, T. Takai, O. Rhode, T. Mukaiyama *Chem. Lett.* **1991**, 1; T. Yamada, O. Rhode, T, Takai, T. Mukaiyama *ibid.* **1991**, 5.
[10] The ruthenium catalyst could be recovered in over 95% (by weight) from the fluorous phase after several reaction cycles.
[11] A slow autoxidation was found to occur within 60 h under the reaction conditions in the absence of the ruthenium catalyst.
[12] For a recent Mn-catalyzed epoxidation using a perfluorinated porphyrin ligand see: G. Pozzi, S. Banfi, A. Manfredi, F. Montanari, S. Quici, *Tetrahedron* **1996**, *52*, 11879.

Inter-Ring Interactions in Dimers of Magnesium π-Cation Radicals: Control by Solvent Polarity**

Kristin E. Brancato-Buentello and W. Robert Scheidt*

An important property of metalloporphyrins is the facile oxidation of the macrocyclic ligand to yield π-cation radicals, which are important in both biological oxidation chemistry and photosynthesis. Such species have been known in solution for almost three decades.[1, 2] Temperature-dependent electronic spectra indicate that sterically unhindered π-cation radicals dimerize.[2, 3] Fajer et al.[2] also noted the importance of solvent for changes in the spectra of $[Mg(oep^{\bullet})]^{+}$ (H_2oep = octaethylporphyrin) in CH_2Cl_2 and MeOH. Fuhrhop et al.[3] showed that formation of the $[Zn(oep^{\bullet})]^{+}$ radical dimer was stabilized by solvents of increasing polarity. We have been concerned with the characterization of metalloporphyrin π-cation radicals, in particular their inter-ring and spin–spin interactions. In 1989 we reported the structure of the first sterically nonbulky derivative of a π-cation radical, $[\{Zn(OH_2)(oep^{\bullet})\}_2]^{2+}$, which forms a strongly coupled, virtually eclipsed cofacial dimer with an interplanar porphyrin-ring spacing of 3.31 Å.[4] The dimers show an unprecedented complete overlap of the two π-cation radical rings in the solid state, which was subsequently found in eight other derivatives.[5]

$[Mg(oep^{\bullet})]ClO_4$ is unusual in that it displays relatively high solubility in toluene/CH_2Cl_2 (4/1). We were thus able to prepare X-ray quality single crystals of $[Mg(oep^{\bullet})]ClO_4$ derivatives from two solvent systems (Scheme 1). Both **1**[8] and **2** are dimeric in

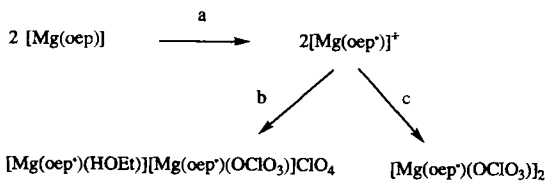

Scheme 1. Formation of dimers of π-cation radicals: a) oxidation with thianthrenium perchlorate [6] (1:1.05) in CH_2Cl_2; crystallization from b) $CH_2Cl_2/CHCl_3$ (5/1) and hexane or c) toluene/CH_2Cl_2 (4/1) and hexane. Dried solvents and flame-dried glassware must be used throughout to avoid acid-catalyzed demetalation [7].

the solid state, but their inter-ring interactions are dramatically different.[9] The structures, along with concentration-dependent electronic spectra, shed light on the effects of solvent (polarity) on the formation of radical-cation dimers.

Side and plan views of one of the identical dimeric units of **1** and that of **2** are presented in Figures 1 and 2. The π–π interaction between the rings is apparent. The two porphyrin rings of the cofacial dimer of **1** are directly above each other with no lateral shift between them. This is true for both dimeric units of **1**, even though there is no required crystallographic symmetry.

[*] Prof. W. R. Scheidt, K. E. Brancato-Buentello
Department of Chemistry and Biochemistry
University of Notre Dame
Notre Dame, IN 46556 (USA)
Fax: Int. code +(219) 631-4044
e-mail: w.r.scheidt.1@nd.edu

[**] This work was supported by the U. S. National Institutes of Health (GM-38401). K. E. B. thanks the J. Peter Grace Foundation for a doctoral fellowship.

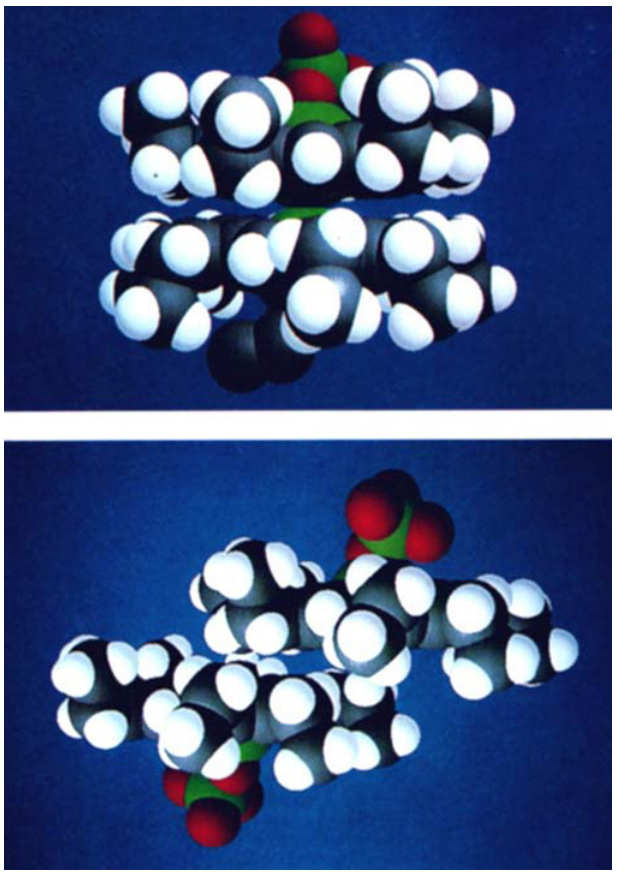

Figure 1. Space-filling diagrams showing side-on views of dimers **1** (top) and **2** (bottom), and the substantial differences in core overlaps. The interplanar spacing in **1** is 3.21 Å, and the lateral shift effectively 0 Å. In **2** the interplanar spacing is 3.46 Å, and the lateral shift 6.27 Å.

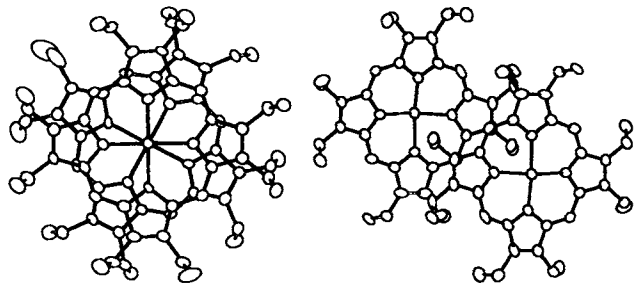

Figure 2. Plan views of the crystal structures of **1** (left) and **2** (right).

The strong interaction is consistent with a lateral shift of about 0 Å and is a feature of all previously characterized dimeric octaethylporphyrin π-cation radicals,[5] all of which were crystallized from polar solvents. The orientation of the ethyl groups in radical **1**, which all point outwards from the center, is also a characteristic feature.

The two rings of radical **2** show an apparently weaker interaction with a large lateral shift of 6.27 Å. Consistent with this, each porphyrin has four ethyl groups pointing "up" and four pointing "down" in an orientation that minimizes the inter-ring ethyl–ethyl interactions. Scheidt and Lee[11] surveyed the inter-ring geometry for all structurally characterized neutral porphyrin dimers with sterically unhindered peripheral substituents. They noted that the observed lateral shifts tend to cluster around specific values rather than displaying a continuous distribution. The lateral shift of **2** is in the range observed for the group Scheidt and Lee classified as "weak", whereas the lateral shift of about 0 Å for **1** is much smaller than that for the group they classified as "strong" (lateral shifts of 1.5 Å). However, the lateral shifts in **1** are similar to those seen in a number of other $[\{M(oep^{\bullet})\}_2]^{2+}$ dimers.[5]

All other structural features of **1** and **2** are consistent with significant differences in the inter-ring interactions in the two derivatives. The twist angle of 28.3° in **1** leads to a number of close inter-ring atomic contacts in the inner 16-membered porphyrin ring. The closest inter-ring contacts are between α-C atoms and between α-C atoms and methine C atoms. The perpendicular displacements of each atom from the 24-atom mean planes of **1** are small. Interestingly, the deviations are such that the close interatomic separations are slightly smaller than they would be if the cores were precisely planar. The two rings interlock like puzzle pieces to allow more intimate interactions. The other independent dimer in **1** shows exactly the same phenomenon with a twist angle of 28.2° and similar core conformational features. Edge-over-edge overlap in **2** is small, and the two cores, each with modest C_{4v} doming, also dome away from each other. Both features are consistent with a weak inter-ring interaction.

An alternating long–short bond-length pattern is observed in the inner 16-membered rings of **1**. The same pattern is evident in each of the four independent rings (Scheme 2).This unusual pattern was first observed in $[\{Zn(OH_2)(oep^{\bullet})\}_2]^{2+}$[4] and has subsequently been seen in a number of other dimers of π-cation radicals.[5b,c] The basis for this unusual phenomenon is not certain but appears to be associated with strongly overlapping π-cation rings. Bond lengths in the weaker dimer **2** show the normal porphyrin delocalization pattern.

Differences in the inter-ring interactions of **1** and **2** are also reflected in the geometry of the coordination groups. The axial Mg–O distances ($\bar{d}$ = 2.039(15) Å and 2.046(4) Å, respectively) fall well within the broad range seen in other five-coordinate Mg derivatives (Mg–O 2.012–2.078 Å). The mean Mg–N_p bond length in **1** is 2.073(2) Å, slightly shorter than that found in other five-coordinate Mg porphyrins (2.083–2.096 Å)[13] but within the limits observed for six-coordinate Mg porphyrins (2.068–2.078 Å).[14] The mean Mg–N_p bond length of 2.079(3) Å in **2** is slightly longer. A larger difference is found in the out-of-plane displacement of the metal. For **1** the average of 0.34(4) Å is somewhat low for five-coordinate Mg porphyrin (0.39–0.52 Å),[13] whereas the 0.50 Å displacement in **2** lies within this range. The shorter-than-normal Mg–N_p bond lengths and the smaller Mg-atom displacement of **1** are the result of the very tight face-to-face interaction,[15] whereas the weaker π–π interaction in **2** leads to the normal geometry of the five-coordinate Mg center in the porphyrin.

The dramatically different solid-state structures of **1** and **2** are reflected in significant differences in the electronic spectra of $[Mg(oep^{\bullet})]^+$ in CH_2Cl_2 and toluene/CH_2Cl_2 (4/1). At high concentration a broad, concentration-dependent, near-IR band is seen in both CH_2Cl_2 (954 nm) and toluene/CH_2Cl_2 (ca. 912 nm). These bands are similar to that arising from dimerization.[2] Most important are the striking solvent- and concentration-dependent features in the UV/Vis region. The spectra generally show the normal features for formation of π-cation radicals[1–3,12]: weaker, blue-shifted, broadened Soret bands and red-shifted, substantially broadened visible (α and β) bands along with the appearance of a new band in the visible region at about λ = 660 nm, which is characteristic of the magnesium π-cation derivative.[17]

 © VCH Verlagsgesellschaft mbH, D-69451 Weinheim, 1997 0570-0833/97/3613-1457 $ 17.50+.50/0

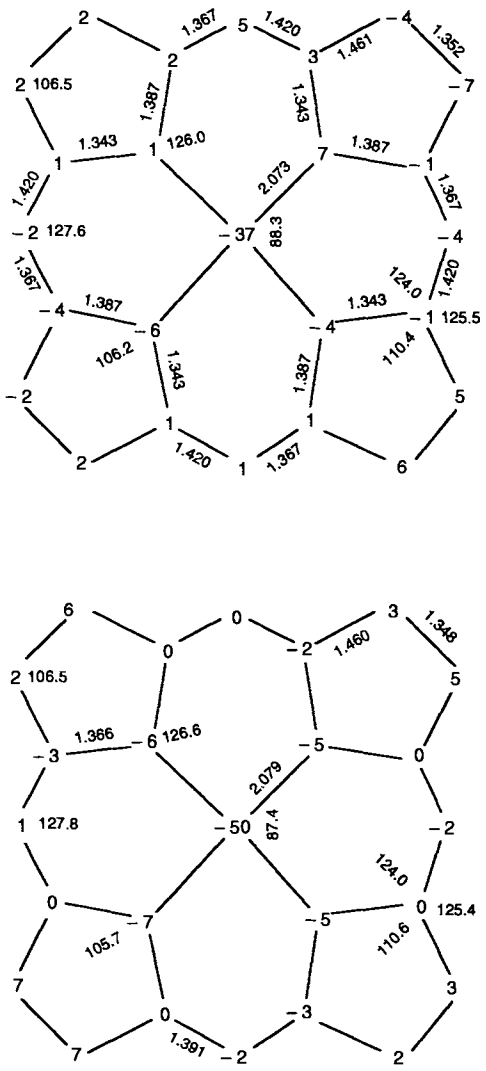

Scheme 2. Diagram of the formal porphinato cores in **1** (top) and **2** (bottom) with averaged values of bond lengths and angles. For **1** these averages are taken over the four independent rings. The values of the averaged bond distances for the inner 16-membered rings are displayed four times to illustrate the alternating bond pattern; all other averaged values are displayed only once. Also displayed are the perpendicular atomic displacements, in units of 0.01 Å, of each atom from the 24-atom mean plane of the core. Positive values of displacement are toward the center of the other ring. One of the four independent rings is shown for **1**. Estimated standard deviations for individual C–C or C–N bonds are 0.008 Å for **1** and 0.007 Å for **2**, and 0.6° and 0.5° for their angles, respectively.

Figure 3a shows the general concentration-dependent spectral changes in CH_2Cl_2 in the Soret region. At the lowest concentration shown there are bands at 394 and 408 nm; the latter is more prominent at still lower concentrations. The intensity of the band at 394 nm increases monotonically with increasing concentration at the expense of the band at 408 nm. Other blue-shifted features (shoulders at 322, 355, and 379 nm) also become more prominent. Figure 3b shows the concentration-dependent spectral changes that occur in toluene/CH_2Cl_2 (4/1). Again there is a 410 nm Soret band, whose relative intensity decreases in favor of a band at 397 nm , accompanied by other blue-shifted shoulders. Even at the highest concentrations the blue-shifted Soret band and other components are not as completely developed as in CH_2Cl_2. The blue-shifted band envelopes exhibit strong similarities in the shapes and intensities of the shoulders. However, the concentration dependence is more complex in toluene/CH_2Cl_2. The ratio of intensities of the bands at 397 and

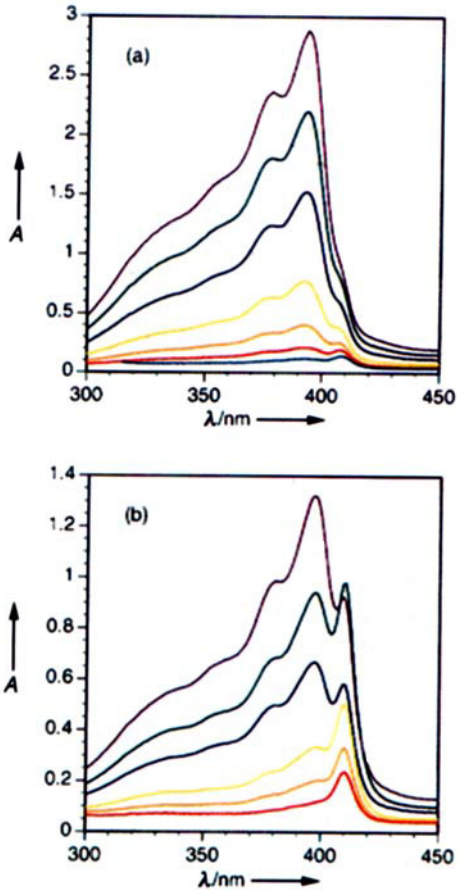

Figure 3. Electronic spectra of $[Mg(oep^{\cdot})]^+$ in a) CH_2Cl_2 and b) toluene/CH_2Cl_2. Concentrations in both solvent systems are (top to bottom) 3.00×10^{-4} M, 2.25×10^{-4} M, 1.50×10^{-4} M, 7.50×10^{-5} M, 3.75×10^{-5} M, and 1.88×10^{-5} M. The lowest concentration in a) is 9.38×10^{-6} M.

410 nm first increases, then decreases, and finally increase again. In CH_2Cl_2 the ratio of the bands at 394 and 408 nm increases monotonically.

The 408/410 nm band at low concentration almost certainly corresponds to the monomeric $[Mg(oep^{\cdot})]^+$ species, whereas the 394/397 nm Soret and other strongly blue-shifted features must correspond to the formation of an aggregated, tightly interacting dimeric species in which the in-plane x and y directions are distinct.[18] The nearly identical blue-shifted features in the two solvents suggests the presence of similar limiting species. The intensities clearly indicate differences in relative proportions in the two solvents: monomeric species are favored in toluene/CH_2Cl_2, and the species yielding the blue-shifted spectra in CH_2Cl_2. However, the presence of a significant amount of a third component, for which the intenstiy of the spectral band increases and then decreases with increasing concentration, is only seen in toluene/CH_2Cl_2. Since this (third) species appears with increasing solute concentration, it is clearly at least dimeric.

We interpret the spectral differences to be the result of differences in dimerization equilibrium constants and in the nature of the (dimeric) species in the two solvents. The differences for the two solvent systems are as expected if dimerization is more strongly favored in polar solvents, as is the case in the zinc system.[3] Although the exact nature of the solution species cannot be deduced solely from the electronic spectra, the data clearly suggest significantly different solution species in the two solvents. The dimeric solid-state structures obtained from the two solvents suggest possible structures in solution. The species yielding the strongly blue-shifted spectra could have a structure

 © VCH Verlagsgesellschaft mbH, D-69451 Weinheim, 1997 0570-0833/97/3613-1458 $ 17.50+.50/0

similar to **1**, whereas the other dimeric species in toluene/CH_2Cl_2 may be associated with a species similar to **2**.

We have reported the first solid-state analysis of five-coordinate $[Mg(oep^{\bullet})]^+$ π-cation radicals. Two distinct dimeric species have been characterized in which the inter-ring overlap is controlled by crystallization from solvents of different polarity: high polarity leads to a tightly coupled cofacial dimer, and lower polarity to a more weakly coupled cofacial dimer. The concentration- and solvent-dependent differences in the UV/Vis spectra parallel the findings in the solid state.

Received: January 14, 1997 [Z9993IE]
German version: *Angew. Chem.* **1997**, *109*, 1608–1611

Keywords: magnesium · noncovalent interactions · porphyrinoids · UV/Vis spectroscopy · $\pi-\pi$ interactions

[1] J.-H. Fuhrhop, D. Mauzerall, *J. Am. Chem. Soc.* **1969**, *91*, 4174–4181.
[2] J. Fajer, D. C. Borg, A. Forman, D. Dolphin, R. J. Felton, *J. Am. Chem. Soc.* **1970**, *92*, 3451–3459.
[3] J.-H. Fuhrhop, P. Wasser, D. Riesner, D. Mauzerall, *J. Am. Chem. Soc.* **1972**, *94*, 7996–8001.
[4] H. Song, C. A. Reed, W. R. Scheidt, *J. Am. Chem. Soc.* **1989**, *111*, 6867–6868.
[5] a) H. Song, R. D. Orosz, C. A. Reed, W. R. Scheidt, *Inorg. Chem.* **1990**, *29*, 4274–4282; b) W. R. Scheidt, H. Song, K. J. Haller, M. K. Safo, R. D. Orosz, C. A. Reed, P. G. Debrunner, C. E. Schulz, *ibid.* **1992**, *31*, 939–941; c) *ibid.* **1997**, *36*, 406–412; d) K. E. Brancato-Buentello, W. R. Scheidt, unpublished results.
[6] Y. Murata, H. J. Shine, *J. Org. Chem.* **1969**, *34*, 3368–3372.
[7] W. A. Oertling, A. Salehi, C. K. Chang, G. T. Babcock, *J. Phys. Chem.* **1987**, *91*, 3114–3116.
[8] The EtOH molecule coordinated to Mg in crystals of **1** results from from the stabilizer in commercial $CHCl_3$. Despite the importance of the EtOH in obtaining crystals, it has minimal effects on the spectra of a solution in CH_2Cl_2 at the small concentrations of the crystallization experiment.
[9] Compound **1** crystallized from $CH_2Cl_2/CHCl_3$ (ca. 5/1) layered with hexanes, and **2** from toluene/CH_2Cl_2 (4/1). A pink-purple crystal of **1** ($0.13\times0.20\times0.60$ mm) and a dark purple crystal of **2** ($0.017\times0.06\times0.17$ mm) were analyzed on an Enraf-Nonius FAST area-detector diffractometer with a Mo rotating-anode source ($\lambda = 0.71073$ Å) by procedures that were described previously (W. R. Scheidt, I. Turowska-Tyrk, *Inorg. Chem.* **1994**, *33*, 1314–1318). Crystal data for **1**: $a = 12.176(1)$, $b = 21.657(5)$, $c = 29.302(8)$ Å, $\beta = 99.94(1)^\circ$, monoclinic, $P2_1$, $V = 7610.9(3)$ Å^3, $Z = 4$ (dimers), $\rho_{calcd} = 1.291$ g cm^{-3}, $2\theta_{max} = 27.06^\circ$. Crystal data for **2**: $a = 10.280(4)$, $b = 11.681(3)$, $c = 13.939(6)$ Å, $\alpha = 83.93(2)^\circ$, $\beta = 83.63(3)^\circ$, $\gamma = 78.18(3)^\circ$, triclinic, $P\bar{1}$, $V = 1622.2(10)$ Å^3, $Z = 2$, $\rho_{calcd} = 1.344$ g cm^{-3}, $2\theta_{max} = 29.73^\circ$. All measurements were made at 124 ± 2 K. Data were corrected for Lorentzian, polarization, and absorption factors (relative transmission coefficients = 1.00–0.729 for **1** and 1.00–0.565 for **2**). Both structures were solved by direct methods (SHELXS) [10a] and refined against F^2 with SHELXL-93 [10b]. All data collected were used, and all porphyrin hydrogen atoms were idealized with the standard SHELXL-93 methods. **1**: $R_1 = 0.0746$ for 17417 observed reflections ($F_o \geq 4.0\sigma(F_o)$). $wR_2 = 0.2099$ for 24123 total unique data (1884 variables refined) including negative F^2 (residual electron density = 0.76 and -0.45 e Å^{-3}). **2**: $R_1 = 0.1030$ for 3993 observed data, $wR_2 = 0.2912$ for 8081 unique data (463 variables; residual electron density = 0.63 and -0.71 e Å^{-3}). Crystallographic data (excluding structure factors) for the structures reported in this paper have been deposited with the Cambridge Crystallographic Data Centre as supplementary publication no. CCDC-100099. Copies of the data can be obtained free of charge on application to The Director, CCDC, 12 Union Road, Cambridge CB21EZ, UK (fax: int. code +(1223)336-033; e-mail: deposit@chemcrys.cam.ac.uk).
[10] a) G. M. Sheldrick, *Acta Crystallogr. A* **1990**, *46*, 467–473; b) unpublished results.
[11] W. R. Scheidt, Y. J. Lee, *Struc. Bonding (Berlin)* **1987**, *64*, 1–70.
[12] K. E. Brancato-Buentello, S.-J. Kang, W. R. Scheidt, *J. Am. Chem. Soc.* **1997**, *119*, 2839–2846.
[13] a) K. M. Barkigia, L. D. Spaulding, J. Fajer, *Inorg. Chem.* **1983**, *22*, 349–351; b) C. C. Ong, V. McKee, G. A. Rodley, *Inorg. Chim. Acta* **1986**, *123*, L11–L14; c) V. McKee, G. A. Rodley, *ibid.* **1988**, *151*, 233–236; d) S. Yang, R. A. Jacobson, *ibid.* **1991**, *190*, 129–134.
[14] a) R. Bonnett, M. B. Hursthouse, K. M. Abdul Malik, B. Mateen, *J. Chem. Soc. Perkin Trans. 2* **1977**, 2072–2076; b) V. McKee, C. C. Ong, G. A. Rodley, *Inorg. Chem.* **1984**, *23*, 4242–4248; c) V. McKee, G. A. Rodley, *Inorg. Chim. Acta* **1988**, *151*, 233–236.
[15] The effect of π complexation or $\pi-\pi$ dimer formation on the out-of-plane position of the metal atom is that of a weakly interacting sixth ligand [4, 16].
[16] M. M. Williamson, C. L. Hill, *Inorg. Chem.* **1987**, *26*, 4155–4160.
[17] J.-H. Fuhrhop, D. Mauzerall, *J. Am. Chem. Soc.* **1968**, *90*, 3875–3876.
[18] M. Gouterman, *J. Mol. Spectrosc.* **1961**, *6*, 138–163.

Ferromagnetic Coupling in the Bis(μ-end-on-azido)iron(III) Dinuclear Complex Anion of $[Fe^{II}(bpym)_3]_2[Fe_2^{III}(N_3)_{10}]\cdot 2H_2O$**

Giovanni De Munno,* Teresa Poerio, Guillaume Viau, Miguel Julve,* and Francesc Lloret

The design of new polynuclear species exhibiting ferromagnetic coupling is one of the major challenges in magnetochemistry.[1] Three strategies have been proposed for obtaining these compounds,[2] which make use of the 1) required or 2) accidental orthogonality of the magnetic orbitals and 3) spin-polarization effects. The second case depends on structural parameters that are difficult to control during synthesis. The di-μ-hydroxo-bridged copper(II) complexes are the best example for this: Magnetic coupling is ferromagnetic for angles θ at the hydroxo bridge of less than 97.5° and antiferromagnetic for θ larger than 97.5°.[3] The remarkable ability of the end-on bridging azide ion to stabilize the triplet state in dinuclear complexes of divalent transition metal ions of the first row[4–7] is another example of accidental orthogonality. The magnitude of the ferromagnetic coupling varies between +200 (Cu^{II})[4b] and +2.4 cm^{-1} (Mn^{II}).[7]

We recently synthesized new honeycomb layered materials of formula $[M_2(bpym)(N_3)_4]$ (M = Mn^{II}, Fe^{II}, Co^{II}; bpym = 2,2′-bipyrimidine), which exhibit alternating ferro- (through double end-on azido) and antiferromagnetic (through bis(chelating) bpym) interactions.[8, 9] In our attempts to synthesize the iron(II) derivative **2**, single crystals of **1** were obtained after partial oxidation by atmospheric oxygen. Complex **1** was characterized by IR spectroscopy, variable-temperature magnetic measurements, and X-ray structural analysis.

$[Fe^{II}(bpym)_3][Fe_2^{III}(N_3)_{10}]\cdot 2H_2O$ **1**

$[Fe_2(bpym)(N_3)_4]$ **2**

The crystal structure of **1** consists of centrosymmetric double end-on azido-bridged iron(III) dinuclear anions with monodentate azide groups as terminal ligands (Figure 1, top), mononuclear tris(2,2′-bipyrimidine)iron(II) cations (Figure 1, bottom), and water molecules.

Each iron atom in the anion has a distorted octahedral coordination sphere. The metal to bridging azide bond lengths (av 2.179(5) Å) are significantly longer than those involving the metal center and the terminal azide groups (av 2.031(5) Å), as expected. The latter value compares well with that of 2.023(8) Å in the mononuclear iron(III) complex $(Et_4N)[Fe\{HB(3,5\text{-}Me_2pz)_3\}(N_3)_3]$[10] ($HB(3,5\text{-}Me_2pz)_3$ = hydrotris(3,5-dimethyl-1-pyrazolyl)borate) but is somewhat longer than the Fe–N(axial azide) bond length (1.925(7) Å) in the porphyrin iron(III) complex $[Fe(TPP)(N_3)(py)]$[11] (TPP = tetraphenylporphirinate). The occurrence of high-spin (**1** and the pyrazolylborate

[*] Prof. G. De Munno, T. Poerio
Dipartimento di Chimica
Università degli Studi della Calabria
1-87030 Arcavacata di Rende, Cosenza (Italy)
Fax: Int. code +(984)492044
Prof. M. Julve, Dr. G. Viau, Dr. F. Lloret
Departament de Química Inorgànica
Facultat de Química de la Universitat de València
Dr. Moliner 50, E-46100 Burjassot, València (Spain)
Fax: Int. code +(6)386-4322
e-mail: miguel.julve@uv.es

[**] This work was supported by the Spanish Dirección General de Investigación Científica y Técnica (DGICYT) (Project PB94-1002) and the Italian Ministero dell'Università et della Ricerca Scientifica e Tecnologica. G. V. thanks the Spanish Ministery of Education and Science for a postdoctoral fellowship.

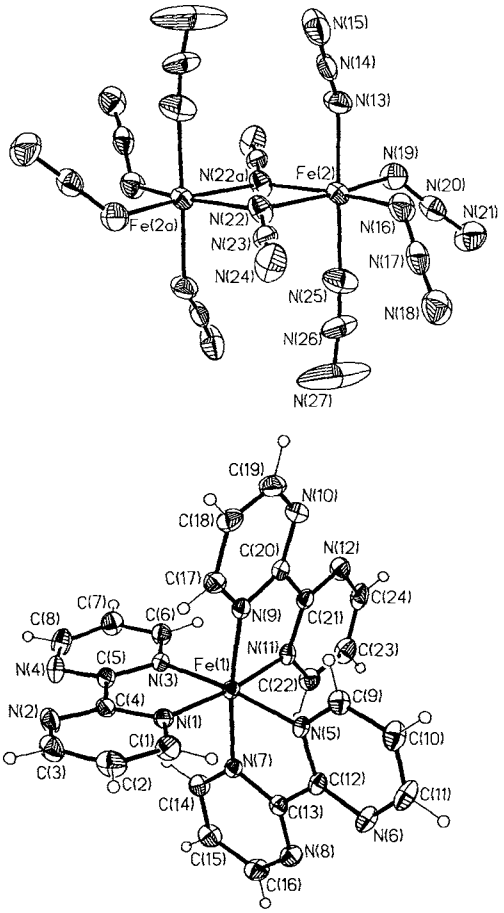

Figure 1. Top: Perspective view of the centrosymmetric $[Fe_2(N_3)_{10}]^{4-}$ dinuclear anion of **1**. Selected bond lengths [Å] and angles [°] with standard deviations in parentheses: Fe(2)–N(13) 2.027(5), Fe(2)–N(16) 2.043(5), Fe(2)–N(19) 2.039(6), Fe(2)–N(22) 2.195(5), Fe(2)–N(22a) 2.164(5), Fe(2)–N(25) 2.017(6); N(13)-Fe(2)-N(16) 90.4(2), N(13)-Fe(2)-N(19) 87.7(2), N(13)-Fe(2)-N(22) 91.7(2), N(13)-Fe(2)-N(22a) 89.9(2), N(13)-Fe(2)-N(25) 176.8(2), N(16)-Fe(2)-N(19) 101.0(2), N(16)-Fe(2)-N(22) 89.8(2), N(16)-Fe(2)-N(22a) 163.8(2), N(16)-Fe(2)-N(25) 91.4(2), N(19)-Fe(2)-N(22), 169.2(2), N(19)-Fe(2)-N(22a) 95.2(2), N(19)-Fe(2)-N(25) 89.4(2), N(22)-Fe(2)-N(22a) 74.0(2), N(22)-Fe(2)-N(25) 90.9(2), N(22a)-Fe(2)-N(25) 89.1(2), Fe(2)-N(22)-Fe(2a),106.0(2); symmetry operation a) $1-x, 1-y, 1-z$. Bottom: Perspective view of the mononuclear cation $[Fe(bpym)]^{2+}$ in **1**. Selected bond lengths [Å] and angles [°] with standard deviations in parentheses: Fe(1)–N(1), 1.971(4), Fe(1)–N(3) 1.971(4), Fe(1)–N(5) 1.976(4), Fe(1)–N(7) 1.971(4), Fe(1)–N(9) 1.965(4), Fe(1)–N(11) 1.977(4); N(1)-Fe(1)-N(3) 81.2(2), N(1)-Fe(1)-N(11) 173.8(2), N(1)-Fe(1)-N(5) 95.8(2), N(1)-Fe(1)-N(7) 91.8(2), N(1)-Fe(1)-N(9) 94.4(2), N(3)-Fe(1)-N(11) 94.1(2), N(3)-Fe(1)-N(5) 174.1(2), N(3)-Fe(1)-N(7) 93.5(2), N(3)-Fe(1)-N(9) 92.1(2), N(5)-Fe(1)-N(11) 89.2(2), N(5)-Fe(1)-N(7) 81.5(2), N(5)-Fe(1)-N(9) 93.2(2), N(7)-Fe(1)-N(9) 172.2(1), N(7)-Fe(1)-N(11) 92.5(2), N(9)-Fe(1)-N(11) 81.7(2).

compound) and low-spin (porphyrinato complex) iron(II) accounts for the shortening of the Fe–N (terminal azide) bond length in the last-mentioned compound of this series of six-coordinate iron(III) complexes. The largest deviation from the best equatorial plane around Fe(2)—defined by N(19), N(16), N(22), and N(22a)—is 0.003 Å for N(16) and only 0.007 Å for the iron center. An inversion center is present, and the Fe(2)-N(22)-Fe(2a)-N(22a) skeleton is planar. The intradimer metal–metal separation is 3.481(1) Å, and the N(22)-Fe(2)-N(22a) and Fe(2)-N(22)-Fe(2a) bond angles are 74.0(2) and 106.0(2)°. These values are very close to those reported for the high-spin dinuclear bis(μ-end-on-azido)manganese(II) complex $[Mn_2(terpy)_2(N_3)_4]\cdot 2H_2O$[7] (terpy = 2,2′:6′,2″-terpyridine). The Fe-N-N angles of the terminally bound azide groups range from 120.0(5) (N(19)) to 145.6(6)° (N(25)). The former value is typical for azido-containing metal complexes, but the latter is not; this is probably related to the short internal N(25)–N(26) and N(26)–N(27) azide bonds (1.069(9) and 1.118(13) Å, respectively). Both the bridging and terminal azido ligands are quasi-linear, and the value of the N-N-N angle varies between 178.1(7) and 175.1(6)°.

The iron atom of the tris(chelated) iron(II) unit $[Fe(bpym)_3]^{2+}$ also exhibits a distorted octahedral FeN_6 surrounding with an average Fe–N bond length of 1.972(4) Å. This value compares well with that reported for **3**[12] (1.970(5) Å) and is in the range

$[Fe(bpym)_3](ClO_4)_2\cdot 0.25H_2O$ **3**

observed for low-spin tris(chelated) iron(II) complexes.[13] The shortest separation between low- and high-spin iron centers is 7.887(2) Å for Fe(1)···Fe(2c) or Fe(2)···Fe(1c) (symmetry operation c): $1-x, -y, 1-z$), whereas that between the low-spin iron atoms is 8.069(2) Å for Fe(1)···Fe(1b) (symmetry operation b): $-x, -y, 1-z$).

The temperature dependence of $\chi_M T$, where χ_M is the magnetic susceptibility per formula unit, in the temperature range 4.2–298 K is shown in Figure 2. χ_M was measured at an applied

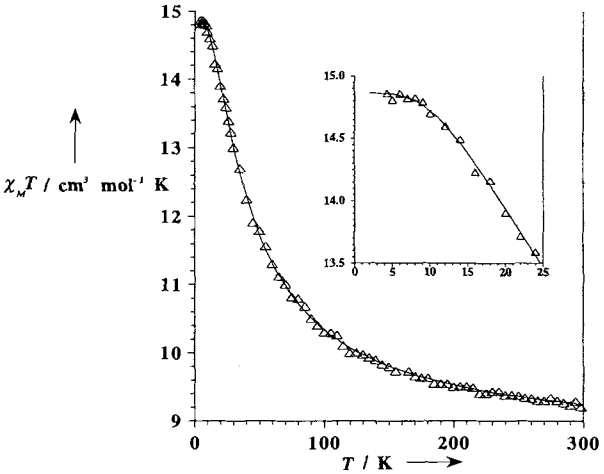

Figure 2. Plot of $\chi_M T$ versus T for complex **1**. Triangles: experimental data; line: best-fit curve (see text). The inset shows the plateau of $\chi_M T$ in the low-temperature region.

magnetic field H of 1.5 T above 50 K and 0.25 T below this temperature to avoid saturation effects. At room temperature $\chi_M T$ is 9.25 $cm^3 mol^{-1} K$, which is somewhat higher than that expected for two magnetically isolated $S = 5/2$ sextuplets. It continuously increases on cooling and reaches a plateau at $T \leq 6$ K with a maximum value of 14.86 $cm^3 mol^{-1} K$. This curve is characteristic of significant ferromagnetic coupling between two sextuplets, whereby the plateau at lower temperature corresponds to the exclusive thermal population of the low-lying $S = 5$ spin state. The fact that no further decrease occurs down to 4.2 K indicates that the zero-field splitting and/or the intermolecular magnetic interactions are very small. Therefore, the magnetic data of **1** were analyzed with the appropriate van Vleck equation for the magnetic susceptibility of a high-spin Fe^{III} dimer with the Hamiltonian operator $\hat{H} = -J\hat{S}_A\cdot\hat{S}_B$, where J is the magnetic coupling parameter and $S_A = S_B = 5/2$ (local spins). Least-squares fitting leads to $J = 4.80\ cm^{-1}$, $g = 1.99$, and $R = 1.1 \times 10^{-4}$ (R = agreement factor = $\sum_i[(\chi_m T)_{obs}(i) - (\chi_m T)_{calcd}(i)]^2/\sum_i[(\chi_M T)_{obs}(i)]^2$). The variation of the magnetization M with the field H at 4.4 K (Figure 3) follows

 © VCH Verlagsgesellschaft mbH, D-69451 Weinheim, 1997 0570-0833/97/3613-1460 $ 17.50+.50/0 Angew. Chem. Int. Ed. Engl. 1997, 36, No. 13/14

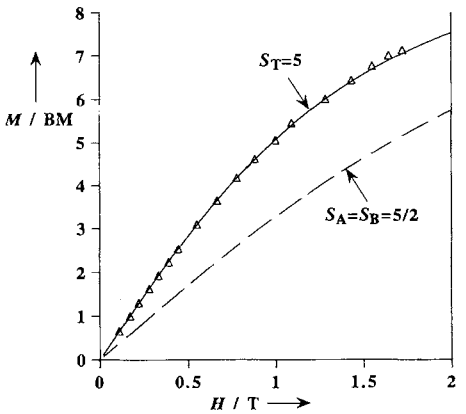

Figure 3. Dependence of the magnetization M of complex **1** on the field strength H at 4.4 K. Triangles: experimental data; solid line: Brillouin function for a spin of $S = 5$ with $g = 1.99$; dotted line: Brillouin function for two noninteracting local spins $S_A = S_B = 5/2$.

the Brillouin function for a spin of $S = 5$ with $g = 1.99$. The curve lies well above that for two independent local spins $S = 5/2$. The value of J is twice that reported for the parent bis(μ-end-on-azido)manganese(II) dimer $[Mn_2(terpy)_2(N_3)_4]\cdot 2H_2O$.[7] Because the angles at the azido bridge are similar (106.0(2)° in **1** and 104.6(1)° in the manganese(II) complex), the fact that the magnetically active 3d orbitals of Fe^{III} are lower in energy than those of Mn^{II}, and thus closer to the symmetry-adapted HOMOs of the bridging azide ligand, accounts for the greater ferromagnetic coupling in **1**. Further examples of iron(III) complexes with this structural type are needed to characterize the influence of the angle at the azido bridge on the nature and magnitude of the magnetic coupling.

Experimental Section

1: On attempting to prepare **2** by the diffusion technique described [9], polyhedral red-brown single crystals of **1** formed by slow oxidation (atmospheric oxygen) of aqueous solutions containing iron(II) chloride, bpym, and sodium azide. In the IR spectrum of **1** the $\nu_{as}(N_3)$ stretching mode appears as a very strong split band at 2040 and 2060 cm^{-1}, which is consistent with the presence of both end-on and terminal azide ligands. The ring-stretching mode of bpym appears as a quasi-symmetric doublet at 1570 and 1545 cm^{-1}, as observed in other complexes containing chelating bpym.

X-ray structure analysis of **1**: Siemens R3mV automatic diffractometer, $Mo_{K\alpha}$ radiation, $\lambda = 0.71073$ Å, graphite monochromator, 295 K. Lorentzian, polarization, and ψ-scan absorption corrections [14] were made. Data collection, solution, and refinement: ω-2θ, standard Patterson methods with subsequent Fourier recycling (SHELXTL-PLUS program) [15]. All non-hydrogen atoms were refined anisotropically. The hydrogen atoms of the water molecules were located on a ΔF map and refined with constraints. The hydrogen atoms of the bpym ligand were set in calculated positions and refined as riding atoms. They were all refined isotropically. Final geometrical calculations and graphical manipulations were performed with the PARST program [16] and the XP utility of the SHELX-PLUS system, respectively. $C_{48}H_{40}Fe_4N_{54}O_2$ ($M_r = 1628.7$), monoclinic, space group $P2_1/c$, $a = 10.644(2)$, $b = 15.026(3)$, $c = 20.549(6)$ Å, $\beta = 99.86°$, $V = 3238.0(13)$ Å^3, $Z = 2$, $\rho_{calcd} = 1.671$ g cm^{-3}, $\mu = 9.67$ cm^{-1}, $F(000) = 1652$, $3 < 2\theta < 54°$, crystal size $0.31 \times 0.27 \times 0.22$ mm. 7126 unique reflections, and 3939 assumed as observed with $I \geq 3\sigma(I)$, 487 parameters, $R = 0.050$, $R_w = 0.053$, and $s = 1.426$ with $w^{-1} = \sigma^2(F_o) + 0.0008(F_o)^2$. Crystallographic data (excluding structure factors) for the structure reported in this paper have been deposited with the Cambridge Crystallographic Data Centre as supplementary publication no. CCDC-100168. Copies of the data can be obtained free of charge on application to The Director, CCDC, 12 Union Road, Cambridge CB2 1EZ, UK (fax: int. code +(1223)336-033; e-mail: deposit@chemcrys.cam.ac.uk).

Received: January 13, 1997 [Z9982IE]
German version: *Angew. Chem.* **1997**, *109*, 1531–1534

Keywords: azides · ferromagnetism · high-spin complexes · iron · N ligands

[1] O. Kahn, *Molecular Magnetism*, VCH, Weinheim, **1993**.
[2] O. Kahn, *Comments Inorg. Chem.* **1984**, *3*, 105.
[3] W. E. Hatfield in *Magneto-Structural Correlations in Exchange-Coupled Systems* (Eds.: R. D. Willett, D. Gatteschi, O. Kahn), *NATO ASI Ser. Ser. C* **1985**, *140*, 555.
[4] a) J. Commarmond, P. Plumère, J. M. Lehn, Y. Agnus, R. Louis, R. Weiss, O. Kahn, I. Morgenstern-Badarau, *J. Am. Chem. Soc.* **1982**, *104*, 6330; b) O. Kahn, S. Sikorav, J. Gouteron, S. Jeannin, Y. Jeannin, *Inorg. Chem.* **1983**, *22*, 2877; (c) S. Sikorav, I. Bkouche-Waksman, O. Kahn, *ibid.* **1984**, *23*, 490.
[5] M. I. Arriortua, R. Cortés, L. Lezama, T. Rojo, X. Solans, M. Font Badía, *Inorg. Chim. Acta* **1990**, *174*, 263; R. Cortés, J. I. Ruiz de Larramendi, L. Lezama, T. Rojo, K. Urtiaga, M. I. Arriortua, *J. Chem. Soc. Dalton Trans.* **1992**, 2723; R. Vicente, A. Escuer, J. Ribas, M. S. El Fallah, X. Solans, M. Font-Badía, *Inorg. Chem.* **1993**, *32*, 1920; A. Escuer, R. Vicente, J. Ribas, X. Solans, *ibid.* **1995**, *34*, 1793.
[6] C. J. Harding, J. Nelson, *Inorg. Chim. Acta* **1996**, *246*, 73.
[7] R. Cortés, J. L. Pizarro, L. Lezama, M. I. Arriortua, T. Rojo, *Inorg. Chem.* **1994**, *33*, 2697.
[8] G. De Munno, M. Julve, G. Viau, F. Lloret, J. Faus, D. Viterbo, *Angew. Chem.* **1996**, 108, 1931; *Angew. Chem. Int. Ed.* **1996**, *35*, 1807.
[9] G. De Munno, T. Poerio, G. Viau, M. Julve, F. Lloret, Y. Journaux, E. Rivière, *Chem. Commun.* **1996**, 2587.
[10] H. Fukui, M. Ito, Y. Moro-oka, N. Kitajima, *Inorg. Chem.* **1990**, *29*, 2868.
[11] K. M. Adams, P. G. Rasmussen, W. R. Scheidt, K. Hatano, *Inorg. Chem.* **1979**, *18*, 1892.
[12] G. De Munno, M. Julve, J. A. Real, *Inorg. Chim. Acta* **1997**, *255*, 185.
[13] M. E. Garcia Posse, M. A. Juri, P. J. Aymoning, O. E. Piro, H. A. Negri, *Inorg. Chem.* **1984**, *23*, 948; S. Decurtins, H. W. Schmalle, P. Schneuwlly, R. Oswald, *ibid.* **1993**, *32*, 1888; L. L. Koh, Y. Xu, A. K. Hsieh, *Acta Crystallogr. Sect. C* **1994**, *50*, 884.
[14] A. C. T. North, D. C. Philips, F. S. Mathews, *Acta Crystallorgr. Sect. A* **1968**, *24*, 351.
[15] SHELXTL PLUS Version 4.21/V. Siemens Analytical X-Ray Instruments Inc., Madison, WI, **1990**.
[16] M. Nardelli, *Comput. Chem.* **1983**, *7*, 95.

Towards Artificial DNA-Repair Enzymes: Incorporation of a Flavin Amino Acid into DNA-Binding Oligopeptides**

Thomas Carell* and Jens Butenandt

UV irradiation of cells causes the formation of cyclobutane pyrimidine dimers by $[2\pi + 2\pi]$ cycloaddition of two pyrimidine bases that are adjacent to one another in the DNA double helix.[1, 2] To counteract the resulting lethal loss of genetic information, all organisms have developed sophisticated DNA-repair mechanisms to remove these DNA lesions and to restore the integrity of the genome.[3] Investigation of the inherited lethal disease *Xeroderma pigmentosum* revealed that insufficient DNA-repair capacities are directly involved in tumor genesis.[4, 5] DNA photolyases are ancient repair enzymes that are capable of specifically recognizing cyclobutane pyrimidine dimers, possibly by flipping the pyrimidine dimers out of the DNA double helix into a cage-like active site.[6] The enzymes

[*] Dr. T. Carell, Dipl.-Chem. J. Butenandt
Laboratorium für Organische Chemie
ETH-Zentrum
Universitätstrasse 16, CH-8092 Zürich (Switzerland)
Fax: Int. code +(1)632-1109
e-mail: tcarell@org.chem.ethz.ch

[**] This work was supported by the Swiss National Science Foundation, a Liebig fellowship from the Stiftung Stipendien-Fonds des Verbandes der Chemischen Industrie to T. C., and a doctoral fellowship from the Boehringer Ingelheim Fonds to J. B. We thank ASTA Medica and BASF AG for generous gifts of FMOC-protected amino acids (ASTA) as well as protected nucleotides and solid support for the oligonucleotide synthesis (BASF). We are very grateful to Prof. F. Diederich for generously supporting this research.

utilize multiple light-driven energy- and electron-transfer steps for repairing the dimer lesion. Initially, excitation of a flavin semiquinone ($FADH^{\bullet}$) yields the reduced flavin cofactor ($FADH^-$) by an electron transfer from Trp^{306}, which is more than 13 Å away from the flavin.[6] A second light-driven electron transfer from the $FADH^-$ to the bound cyclobutane pyrimidine dimer initiates monomerization (repair) of the dimer lesion. In addition to $FADH^-$ all known microbial photolyases contain a second cofactor (either a 8-hydroxy-5-deazaflavin or a methenyltetrahydrofolate), which acts as a photo antenna and transmits the required excitation energy to the flavin moiety.[6, 7]

To learn about these energy- and electron-transfer steps, we started a research program aimed at preparing small cofactor-containing model proteins that form stable and structurally well-defined complexes with DNA. These model proteins should allow rapid synthetic modification, for example incorporation of unnatural amino acids at various sites.

DNA-binding oligopeptides possessing the sequence of the DNA-binding domain of the helix-loop-helix transcription factors MyoD[8, 9] were prepared by solid-phase peptide synthesis. The DNA-repair function was included in these DNA-binding proteins by incorporation of the flavin amino acid L-**1**.[10] These

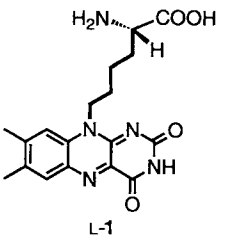

L-**1**

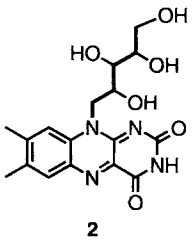

2

cofactor-modified oligopeptides were investigated for their ability to repair cyclobutane pyrimidine dimers in single-stranded DNA. A well-defined oligonucleotide containing a synthetic dimer lesion[11] was synthesized to enable quantification of the repair reaction and allow HPLC monitoring of potential side products that have been observed by irradiation of DNA in the presence of riboflavin **2**.[12]

Synthesis of L-**1** was achieved in gram quantities by the route outlined in Scheme 1. In the first two steps 4,5-dimethyl-2-nitroaniline (**3**) was oxidized with Caro's acid and hydrogen peroxide/nitric acid to yield dinitro dimethyl benzene (**4**).[13] Reaction of **4** with the chiral building block *N*-α-Boc-L-lysin (L-**5**), which was chosen with an unprotected carboxylic acid to minimize base-induced racemization at the chiral α-CH center during the *ipso*-substitution reaction, afforded nitroaniline L-**6**. The reaction conditions were varied to further reduce the risk of racemization; optimal results were finally obtained with potassium acetate as the base in water/ethanol/*n*-butanol (1/1/2). Catalytic hydrogenation of L-**6** afforded the amino acid L-**7**, which was then treated with alloxane monohydrate to yield the Boc-protected flavin amino acid L-**8**.[14] Deprotection of L-**8** and reaction of the resulting unprotected flavin amino acid L-**1** with 9-fluorenylmethoxycarbonyl-*N*-hydroxysuccinimide (FMOC-OSu) and sodium hydrogen carbonate afforded the FMOC-protected L-flavin amino acid L-**9** in an overall yield of 25%.

To determine the enantiomeric purity of L-**1**, the corresponding D-amino acid D-**1** was prepared by the same procedure from the D-lysine building block D-**5**. The racemate was obtained by

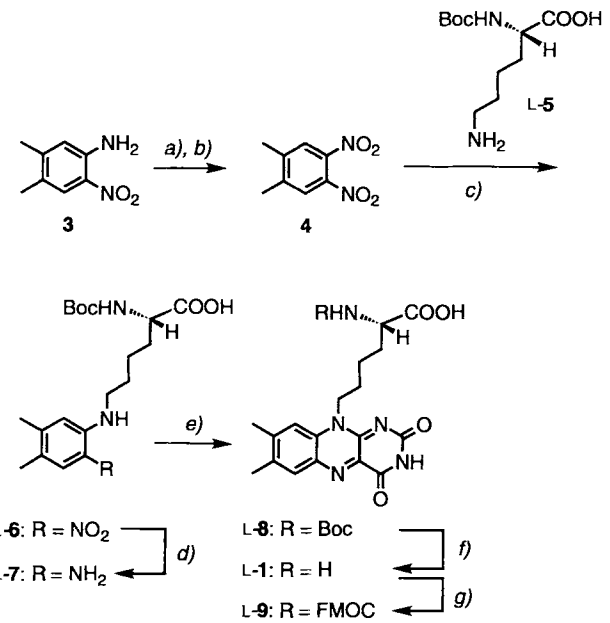

Scheme 1. Synthesis of the flavin amino acid L-**1** and the FMOC-protected amino acid L-**9**: a) H_2SO_5, room temperature (RT), 80%; b) H_2O_2, HNO_3, RT, 85%; c) KOAc, H_2O, EtOH, *n*BuOH, 80 °C, 3 d, 60%; d) H_2, Pd/C, quant; e) HOAc, $B(OH)_3$, alloxane, RT, 65%; f) TFA, RT, quant; g) FMOC-OSu, $NaCO_3$, 95%.

mixing both enantiomers. Separation of the enantiomers was accomplished by thin-layer ligand-exchange chromatography on reverse phase CHIRALPLATES.[15] A dilution experiment, in which decreasing amounts of D-**1** were added to the corresponding L-form, and subsequent scanning of the obtained TLCs established that as little as 1% D-amino acid is detectable. Since the synthetic material L-**1** yields only one spot, it was synthesized with greater than 99:1 enantiomeric purity.

A standard manual FMOC solid-phase synthesis protocol with a Rink-Amide MBHA resin as the solid support was modified for the synthesis of the oligopeptides depicted in Figure 1.[16] The X-ray crystal structure of the helix-loop-helix transcription factor MyoD complexed with double-stranded DNA was analyzed for an initial design of the flavin peptides.[17] The side chain of Leu^{121} at the C-terminal end of the basic domain points towards the major groove; Leu^{121} was therefore replaced by L-**1**. The solid-phase synthesis of the flavin oligopeptide **P1** was performed in analogy to **P2**, which does not contain flavin. However, due to the slower coupling rates of L-**9** the coupling time for this amino acid was extended from 25 to 45 min, and the coupling repeated three times with a threefold excess of L-**9**. Capping procedures (for example acetic anhydride/Hünig's base), often performed after an elongation step, were omitted when possible after incorporation of the flavin amino acid. Cleavage of the final peptide from the solid support and removal of the side-chain protection groups required larger quantities of the scavengers triisopropyl silane (2 vol%) and, in the case of the cysteine-containing peptide **P3**, ethanedithiol (2 vol%) to obtain the flavin oligopeptides **P1** and **P3** in yields and with a purity comparable to those of the non-flavin peptide **P2**.

All peptides were purified by preparative reverse-phase HPLC and characterized by analytical HPLC as well as electrospray and laser-ionization mass spectrometry.[18] The UV/Vis spectrum of the flavin peptides feature the typical flavin absorption bands around 450 and 360 nm. The fluorescence spectra show the flavin fluorescence band at 550 nm.

 © VCH Verlagsgesellschaft mbH, D-69451 Weinheim, 1997 0570-0833/97/3613-1462 $ 17.50+.50/0

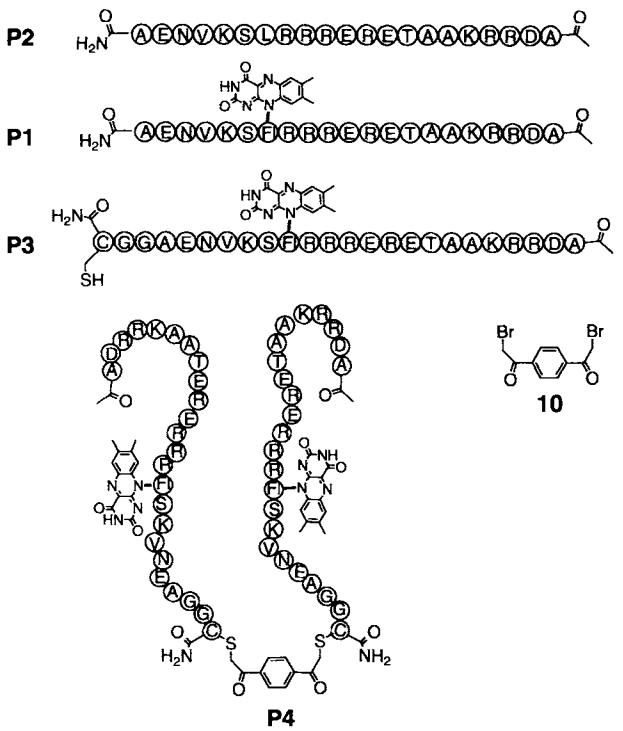

Figure 1. Sequences of the synthesized oligopeptide **P2** and the flavin-containing oligopeptides **P1** and **P3**. Presentation of the template **10** and the linked dimeric oligopeptide **P4**. Peptides were synthesized manually on Rink-Amide MBHA support (FMOC chemistry) with a HOBt/HBTU coupling protocol.

Maximizing the DNA-binding properties requires dimerization of the basic oligopeptides, for example, by linking the two peptides to a given template.[19] Such dimerized oligopeptides mimic the general feature of helix-loop-helix proteins to fold into an α-helical conformation and form stable, structurally well-defined complexes with their DNA targets.[19] To see if the novel flavin peptides are amenable to the required dimerization procedure, peptide **P3**, which possesses a Cys-Gly-Gly handle at the C-terminus, was synthesized.[19] The peptide was treated with the bis(bromo)acetyl benzene template **10**[20] under exclusion of oxygen (Figure 1) to yield a new peptide species, which was isolated by preparative reverse-phase HPLC.[18] The electro-spray mass spectrum confirmed the formation of template-linked **P4**.

To investigate if the flavin moiety within the transcription-factor fragments is a functional unit that can perform clean DNA repair, **P1** and **P4** were added to a solution containing the synthetic oligonucleotide **11**[11] (Scheme 2). The solutions were degassed with nitrogen and irradiated at 4 °C with daylight or with light of 366 nm. Ethylene diamine tetraacetic acid (EDTA)

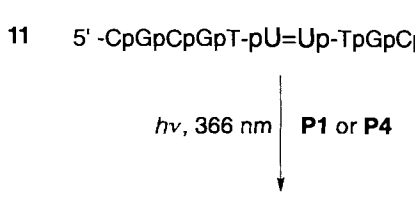

Scheme 2. Repair of the synthetic oligonucleotide **11**. A lesion model compound (U=U) of the cyclobutane uracil dimer was incorporated into a specific site [11]. *The oligonucleotide product* **12** *of the reaction was independently synthesized and* co-injected to ensure that **12** was cleanly formed.

was added to the reaction buffer to photoreduce the isoalloxazin moiety. This resulted in the in situ conversion of the flavin into the fully reduced species, which is active in photolyases. We found that **P1** is able to *completely* convert the lesion-containing **11** into the repaired oligonucleotide **12**. The irradiation times required for the complete conversion varied from one to several hours, depending on the concentration of both peptides and the oligonucleotide substrate as well as on the ion strength of the reaction buffer. This indicates that a close association between the reaction partners, presumably based on interactions between the phosphodiester and arginine or lysine, is of crucial importance. However, the formed associates are still unstructured, since similar transcription-factor elements require double-stranded DNA for the formation of structurally well-defined complexes.[21]

Nevertheless, the repaired oligonucleotide **12** is cleanly formed upon irradiation without the appearance of cleaved DNA side products, which are generally obtained after irradiation of DNA in the presence of oxidized riboflavin.[12] The results of a long irradiation experiment are depicted in Figure 2 (10 μM **11** and 20 μM **P1**). Approximately 75% conversion of the starting material **11** into **12** was recorded after 6 h of irradiation. Further irradiation resulted in almost complete conversion into **12**. Independent syntheses of **12**[11] and co-injection confirmed that the new HPLC peak belongs to **12**.

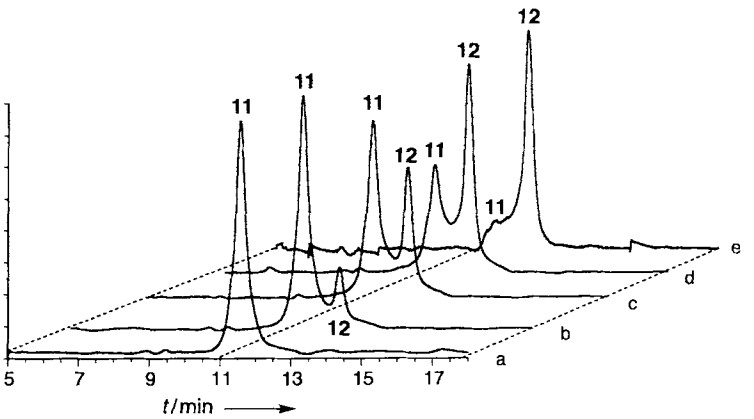

Figure 2. HPL chromatograms (a: 0 h; b: 1 h; c: 3 h, d: 6 h, e: 14 h) measured during the irradiation of a solution of oligonucleotide **11** (10 μM) in reaction buffer (12.5 mM Tris, 5 mM EDTA, 6 mM NaOH, pH 7.8) at 4 °C in the presence of **P1** (20 μM). Column: Lichrosphere C18, 100 Å, 0.4 × 250 mm. Mobile phase A: H_2O, 0.1 M NEt_3·HOAc. Mobile phase B: 80% CH_3CN, 20% H_2O, 0.1 M NEt_3·HOAc. Gradient: 0–30% B in 30 min. Injection volume: 20 μL.

Preliminary irradiation experiments with **P4** indicate that this dimeric oligopeptide performs the DNA-repair reaction faster than **P1**, even at lower substoichiometric concentrations (1–2 μM peptide, 10 μM DNA). Irradiation of DNA solutions containing either riboflavin or **P1** in the absence of EDTA caused decomposition of the oligonucleotide instead of repair. No repair was observed in the absence of the flavin peptide, in the presence of non-flavin-containing **P2**, or in the presence of reduced riboflavin under otherwise identical conditions (EDTA and damaged DNA in buffer solution). These control experiments prove that the prepared flavin-derived transcription-factor fragments **P1** and **P4** can perform primitive DNA repair. So far, reversion of pyrimidine dimers within a DNA strand has been reported with the electron-donating tripeptide Lys-Trp-Lys. Here, a maximum of 60% conversion was obtained, since the photo repair required a harmful wavelength of less than 300 nm.[22] More recently, diimine(9,10-phenanthrenequinone)-

rhodium complexes were reported to catalyze the repair of thymine dimers by electron abstraction from the DNA.[23] Therefore, the flavin oligopeptides represent the first compounds that can completely repair damaged oligonucleotides by simulating the light-driven electron-donating repair process of DNA photolyases.[24]

We have shown that the enantiomerically pure flavin-α-amino acid L-**1** is readily available in large quantities. The building block can be incorporated into oligopeptides by a slightly modified FMOC peptide synthesis protocol, and the peptides obtained are amenable to a dimerization procedure.[25, 26] Most importantly, the flavin peptides are able to cleanly repair a oligonucleotide containing a synthetic pyrimidine-dimer lesion. These results offer the possibility of constructing small, artificial DNA-binding and cofactor-containing proteins, which may help to elucidate the requirements for efficient energy- and electron-transfer reactions at the interface between proteins and DNA.

Received: January 15, 1997
Revised version: March 24, 1997 [Z10000IE]
German version: *Angew. Chem.* **1997**, *109*, 1590–1593

Keywords: DNA repair · electron transfer · flavins · nucleobases · peptides

[1] T. Lindahl, *Nature (London)* **1993**, *362*, 709–715.
[2] J.-S. Taylor, *Acc. Chem. Res.* **1994**, *27*, 76–82.
[3] E. C. Friedberg, G. W. Walker, W. Siede, *DNA Repair and Mutagenesis*, ASM Press, Washington, **1995**.
[4] H. W. Thielmann in *Recent Results in Cancer Research, Vol. 128 (Skin Carcinogenesis in Man and in Experimental Models)* (Eds.: E. Hecker, E. G. Jung, F. Marks, W. Tilgen), Springer, Heidelberg **1993**, pp. 275–297.
[5] Damaged DNA-repair factors may also be responsible for the Werner and Hutchinson–Gilford syndromes, which cause rapid aging: C.-E. Yu, J. Oshima, Y.-H. Fu, E. M. Wijaman, F. Hisama, R. Alisch, S. Matthews, J. Nakura, T. Miki, S. Ouais, G. M. Martin, J. Mulligan, G. D. Schellenberg, *Science* **1996**, *272*, 258–262.
[6] H.-W. Park, S.-T. Kim, A. Sancar, J. Deisenhofer, *Science* **1995**, *268*, 1866–1872.
[7] Recent reviews: A. Sancar, *Biochemistry* **1994**, *33*, 1–9; S.-T. Kim, A. Sancar, *Photochem. Photobiol.* **1993**, *57*, 895–904; P. F. Heelis, R. F. Hartman, S. D. Rose, *Chem. Soc. Rev.* **1994**, *27*, 394–401; T. P. Begley, *Acc. Chem. Res.* **1994**, *27*, 394–401; T. Carell, *Angew. Chem.* **1995**, *107*, 2697–2700; *Angew. Chem. Int. Ed. Engl.* **1995**, *34*, 2491–2494.
[8] D. Sassoon, G. Lyons, W. E. Wright, V. Lin, A. Lassar, H. Weintraub, M. Buckingham, *Nature (London)* **1989**, *341*, 303–307.
[9] P. Lamb, S. L. McKnight, *Trends Biochem. Sci.* **1991**, *16*, 417–422.
[10] Incorporation of other cofactor amino acids into small peptides: B. Imperiali, R. Sinha Roy, G. K. Walkup, L. Wang in *Molecular Design and Bioorganic Catalysis* (Eds.: C. S. Wilcox, A. D. Hamilton) Kluwer, Dordrecht, **1996**, pp. 35–52.
[11] The incorporated cyclobutane uracil dimer (U=U) contains an isosteric formacetal linker instead of the bridging phosphate (p). This allows synthesis of the lesion in large quantities as required for systematic sequence- and distance-dependent repair studies. The formacetal linkage is alsoan isosteric phosphodiester substitute (X-ray crystallography). The formacetal-linked dimer is a substrate for photolyases from *Neurospora crassa* and *Anacystis nidulans* (We thank Prof. Dr. A. P. M. Eker for a generous gift of both enzymes.) Synthesis of this model compound as well as its X-ray structure, incorporation into oligonucleotides, and repairability by the DNA-repair enzymes will be reported. Laser-desorption mass spectra (negative ions detected): calcd for **11**: 3548.6, found: 3549; calcd for **12**: 3548.6, found: 3548.
[12] The spectroscopic polyT assay, generally used for determining the activity of photolyases, is not applicable here since it does not allow strand breaks to be detected; irradiation experiments of DNA in the presence of riboflavin and observation of resulting strand breaks: K. Ito, S. Inoue, K. Yamamoto, S. Kawanashi, *J. Biol. Chem.* **1993**, *268*, 13221–13227; J. G. Peak, M. J. Peak, M. MacCoss, *Photochem. Photobiol.* **1984**, *39*, 713–716; with RNA: P. Burgstaller, M. Famulok, *J. Am. Chem. Soc.* **1997**, *119*, 1137–1138.
[13] E. Bamberger, R. Hübner, *Ber. Dtsch. Chem. Ges.* **1903**, *36*, 3803–3823; R. Kuhn, W. van Klaveren, *ibid.* **1938**, *71*, 779–780.
[14] R. Kuhn, F. Weygand, *Ber. Dtsch. Chem. Ges.* **1934**, *67*, 1409–1413; R. Kuhn, F. Weygand, *ibid.* **1935**, *68*, 1282–1288.
[15] CHIRALPLATES are available from Macherey & Nagel GmbH & Co. KG, D-52313 Düren (Germany); K. Günther, *J. Chromatogr.* **1988**, *448*, 11–30.
[16] R. B. Merrifield, *Adv. Enzymol.* **1969**, *32*, 221–296; G. A. Grant, *Synthetic Peptides A User's Guide*, W. H. Freeman and Company, New York, **1992**.
[17] P. C. M. Pa, M. A. Rould, H. Weintraub, C. O. Pabo, *Cell* **1994**, *77*, 451–459.
[18] Analytical HPLC column: Lichrosphere C18, 100 Å, 0.4 × 250 mm. Mobile phase A: 99.5% H_2O, 0.5% TFA. Mobile phase B: CH_3CN. Gradient: 5–40% B in 40 min. Retention times: **P2**: 19.7 min, **P3**: 19.7 min, **P4**: 21.7 min. Preparative HPLC: Vydac C18, 100 Å, 2.5 × 250 mm. Mobile phase A: 99.5% H_2O, 0.5% TFA. Mobile phase B: CH_3CN. Gradient: 10–30% B in 45 min. ESI-MS: calcd for **P1**: 2794, found: 2794; calcd for **P2**: 2554, found: 2556; calcd for **P3**: 3012, found: 3011; calcd for **P4**: 6181, found: 6181.
[19] R. V. Talanian, J. McKnight, P. S. Kim, *Science* **1990**, *249*, 769–771; M. Ueno, A. Murakami, K. Makino, T. Morii, *J. Am. Chem. Soc.* **1993**, *115*, 12575–12576; B. Cuenoud, A. Schepartz, *Science* **1993**, *259*, 510–513; C. Rodgers Palmer, L. S. Sloan, J. C. Adrian, Jr., B. Cuenoud, D. N. Paolella, A. Schepartz, *J. Am. Chem. Soc.* **1995**, *117*, 8899–8907.
[20] P. Ruggli, E. Gassenmeier, *Helv. Chim. Acta* **1939**, *22*, 496–503.
[21] Binding of bZIP peptides to their DNA targets: S. J. Metallo, A. Schepartz, *Nature Struct. Biol.* **1997**, *4*, 115–117.
[22] C. Hélène, M. Charlier, *Photochem. Photobiol.* **1977**, *25*, 429–434.
[23] Reported after acceptance of this manuscript: P. J. Dandliker, R. E. Holmlin, J. K. Barton, *Science* **1997**, *275*, 1465–1468.
[24] Repair of cyclobutane pyrimidine dimers with flavin derivatives in covalently linked model compounds: T. Carell, R. Epple, V. Gramlich, *Angew. Chem.* **1996**, *108*, 676–679; *Angew. Chem. Int. Ed. Engl.* **1996**, *35*, 620–623; R. Epple, E. U. Wallenborn, T. Carell, *J. Am. Chem. Soc.*, submitted.
[25] Recent overviews of de novo protein design: G. Tuchscherer, P. Dumy, M. Mutter, *Chimia* **1996**, *50*, 644–648; J. S. Richardson, D. C. Richardson, *Trends Biochem. Sci.* **1989**, *14*, 304–309; J. W. Bryson, S. F. Betz, H. S. Lu, D. J. Suich, H. X. Zhou, K. T. O'Neil, W. F. DeGrado, *Science*, **1995**, *270*, 935–941.
[26] Earlier reports on the modification of DNA-binding proteins and peptides: C.-H. B. Chen, D. S. Sigman, *Science* **1987**, *237*, 1197–1201; J. P. Sluka, S. J. Horvath, M. F. Bruist, M. I. Simaon, P. B. Dervan, *ibid.* **1987**, 238, 1129–1132; R. H. Ebright, Y. W. Ebright, P. S. Penergrast, A. Gunasekera, *Proc. Natl. Acad. Sci. USA*, **1990**, *87*, 2882–2886.

Solid-Phase Synthesis of the CD52 Glycopeptide Carrying an N-Linked Core Pentasaccharide Structure**

Zhong-Wu Guo, Yuko Nakahara, Yoshiaki Nakahara,* and Tomoya Ogawa*

With the increased understanding of the biological functions of glycoproteins as recognition signals for various phenomena,[1] the synthesis of glycopeptides and glycoproteins has become the focus of numerous research efforts.[2] Among the various methods that have been developed for synthesizing glycopeptides or fragments of glycoproteins, solid-phase synthesis has proven to be most suitable for larger oligomers. Thus, this method has been applied to synthesize *O*-[3] and *N*-glycopeptides,[4] usually by using acetylated oligosaccharides as building blocks. However, all reported syntheses have thus far employed relatively simple oligosaccharide moieties, whereas naturally occurring glycoproteins may contain rather compli-

[*] Dr. Yoshiaki Nakahara, Prof. Dr. T. Ogawa,[+] Dr. Z.-W. Guo, Dr. Yuko Nakahara
The Institute of Physical and Chemical Research (RIKEN)
Wako-shi, Saitama, 351-01 (Japan)
Fax: Int code +(48)462-4680
[+] Additional address: Graduate School for Agricultural and Life Sciences
The University of Tokyo, Tokyo (Japan)

[**] This work was financially supported by the Special Coordination Funds of the Science and Technology Agency of the Japanese Government and partly by the CREST program of the Japan Science and Technology Corporation. Z.-W. Guo is grateful for a RIKEN Fellowship and thanks Dr. Y. Ito for many helpful discussions. We thank Dr. S. Kurono and N. Dohmae for ESI-MS and MALDI-TOF mass spectral measurements, Dr. J. Uzawa and his staff for NMR measurements, and Ms. A. Takahashi for technical assistance.

cated oligosaccharide structures. Recently, we disclosed the synthesis of an *N*-glycopeptide with a core pentasaccharide, in which the glycoasparagine building block was synthesized with the fluorenylmethoxycarbonyl (Fmoc) method and used in solution to construct a tripeptide sequence of human chorionic gonadotropin (hCG).[5] We have now chosen to apply solid-phase synthetic methods to generating the glycopeptide part (**1**) of the CD52 antigen containing an N-linked core pentasaccharide structure.

The CD52 antigen, a GPI-anchored glycoprotein, is expressed on virtually all human lymphocytes. Monoclonal antibodies against this antigen are potent effectors of complement-mediated lysis and have been widely used in vivo and in vitro for the control of graft versus host disease and for the prevention of bone marrow transplant rejection.[6] Structural studies on the CD52 antigen revealed that it is a remarkable glycoprotein; its peptide chain is extremely short and consists of only 12 amino acid residues making it the shortest cell-surface glycoprotein known to date.[6b] The peptide structure contains only one *N*-glycosylation site and no *O*-glycosylation site, which makes it an ideal synthetic target and also a simple model for pursuing strategic studies on glycopeptide synthesis and for studying the influences of N-linked oligosaccharides on both conformation and biological functions of a glycopeptide.

For the synthesis of target compound **1**, we employed a strategy (Scheme 1) that was based on solid-phase synthesis with Fmoc-amino acids and a benzyl-protected oligosaccharide.[3u, 5] The use of the benzyl group as protective group for oligosaccharides has several advantages. First, benzylated sugars are highly reactive in glycosylation reactions, which is clearly significant for the synthesis of complex oligosaccharides. Second, the stability of benzyl groups towards basic conditions eliminates the possible side reactions during the elongation of the peptide chain, such as potential acyl exchange between acylated sugar moieties and N-terminal groups of the peptide. Third, benzyl groups can be removed easily under mild conditions, for example by catalytic hydrogenlysis. In addition, the use of benzyl protective groups can be advantageous when the synthetic target contains sialic acid.[7] Therefore, starting from D-mannose and 2-amino-2-deoxy-D-glucose, we first prepared the Asn-linked core pentasaccharide with benzyl protective groups (**2**) according to a slightly modified version of a reported procedure.[5] The peptide fragment Asp^4–Ser^{12} linked to HMP-resin (**3**) was constructed on a serine-preloaded HMP-resin with an automatic synthesizer using the supplied program and standard Fmoc method on a 0.25-mmol scale with an efficiency of 99% (monitored by ninhydrin reaction). The coupling reactions were performed by using dicyclohexyl carbodiimide/hydroxybenzotriazole (DCC/HOBt) as the activating agent in *N*-methylpyrrolidone (NMP). The amino acid side chain functionalities were protected with *tert*-butyl and trityl (Trt) groups. Deprotection of the N-terminal in **3** with 20% piperidine in NMP gave **4** (quantitative yield), which was then coupled with the Asn-linked pentasaccharide **2** manually: the mixture of **2** (2.4 equiv) activated by DCC/HOBt (2.8 equiv) and **4** (1.0 equiv) suspended in NMP was shaken on a vortex mixer overnight. This gave the glycosylated peptide fragment linked to the resin (**5**) in 98% yield. Compound **5** was applied to the automatic synthesizer again and the peptide chain elongation was carried out on a 0.1-mmol scale by using the supplied program to give **6** (94 wt%). The glycopeptide was released from the resin by treating the loaded resin **6** with a 95% aqueous trifluoroacetic acid (TFA) solution containing 2.5% 1,2-ethanedithiol; under these conditions the protective groups on the amino acid residues were also removed concomitantly. According to HPLC and MS studies, the product mixture contained only a minor quantity (< 2%) of glycopeptide carrying a degraded sugar chain, but a substantial amount of partially debenzylated glycopeptides with complete sugar chain, including mono-, di-, and tridebenzylated derivatives (according to mass spectra). After simple separation of the product mixture by high-performance gel filtration, the fractions containing the fully benzylated glycoprotein as well as its mono-, di-, and tridebenzylated derivatives were completely debenzylated by hydrogenolysis using 20% $Pd(OH)_2$ on charcoal in 50% aqueous ethanol (four days). High-performance gel filtration of the product afforded the expected glycopeptide **1**

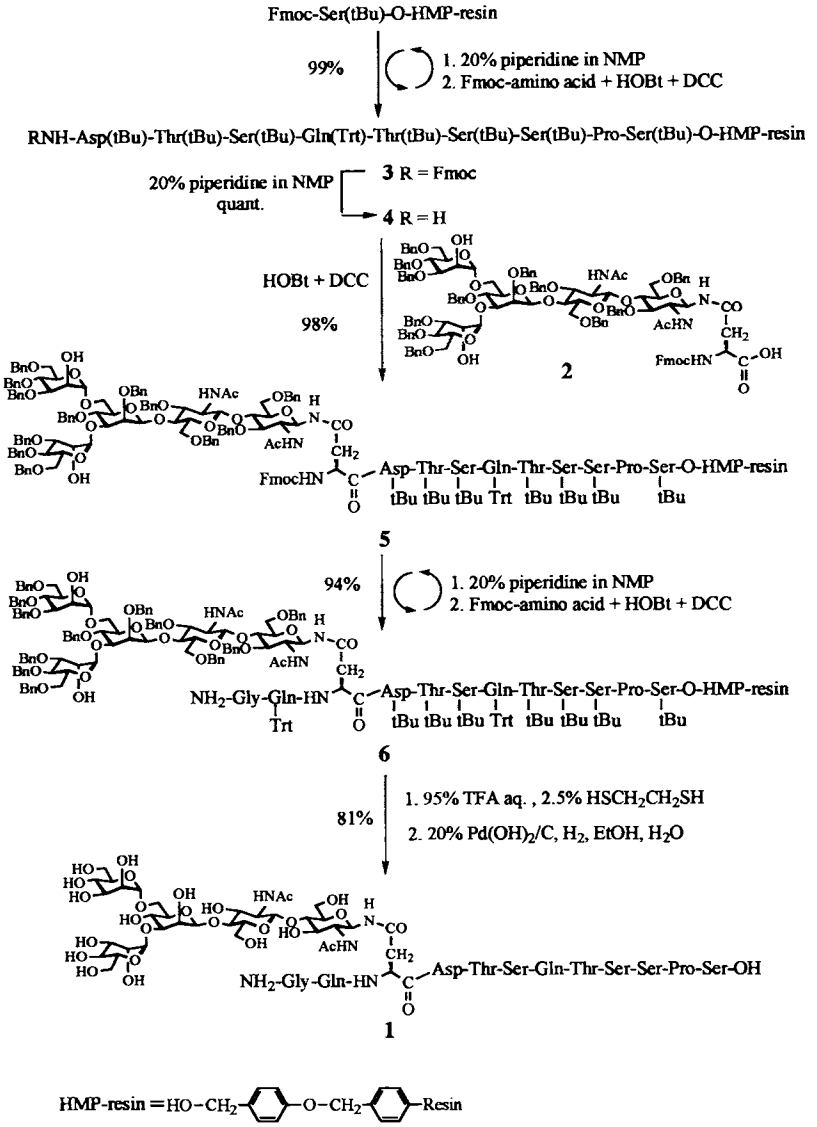

Scheme 1. Solid-phase synthesis of the glycopeptide part (**1**) of the CD52 antigen. The copolymer from 4-[4-(hydroxymethyl)phenoxymethyl]styrene and 1% divinylbenzene was used as resin.

(81% based on **6**, ≥95% purity by NMR) as a white solid,[8] which was then purifed further by reversed-phase HPLC (C18 column).

In conclusion, we have described the solid-phase synthesis of the part structure **1** of the CD52 antigen, which represents the first synthesis of an intact natural glycopeptide sequence carrying an N-linked core pentasaccharide. The results revealed that the benzylated pentasaccharide moiety does not influence the efficiencies of peptide coupling reactions in solid-phase synthesis and that the benzylated sugar moiety is sufficiently stable under the acidic conditions used to release the glycopeptide chain from the supporting resin, thus, smoothing the way to the synthesis of more complex glycopeptides containing complicated sugar structures.

Received: December 2, 1996 [Z9842IE]
German version: *Angew. Chem.* **1997**, *109*, 1527–1529

Keywords: aminosugars · glycopeptides · solid-phase synthesis

[1] A. Varki, *Glycobiology* **1993**, *3*, 97–130, and references therein.

[2] Recent reviews: a) H. Kunz, *Pure Appl. Chem.* **1993**, *65*, 1223–1232; b) M. Meldal in *Neoglycoconjugates: Preparation and Application* (Eds.: Y. C. Lee, R. T. Lee), Academic Press, Orlando, **1994**, pp. 145–198; c) H. Paulsen, *Angew. Chem.* **1990**, *102*, 851–867; *Angew. Chem. Int. Ed. Engl.* **1990**, *29*, 823–839; d) M. Meldal, *Glycoconj. J.* **1994**, *11*, 59–63.

[3] Solid-phase synthesis of *O*-glycopeptides: a) S. Lavielle, N. C. Ling, R. Saltman, R. C. Guillemin, *Carbohydr. Res.* **1981**, *89*, 229–236; b) H. Paulsen, G. Merz, U. Weichert, *Angew. Chem.* **1988**, *100*, 1425–1427; *Angew. Chem. Int. Ed. Engl.* **1988**, *27*, 1365–1367; c) B. Luning, T. Norberg, J. Tejbrant, *J. Chem. Soc. Chem. Commun.* **1989**, 1267–1268; d) M. Meldal, K. J. Jensen, *ibid.* **1990**, 483–485; e) A. M. Jansson, M. Meldal, K. Bock, *Tetrahedron Lett.* **1990**, *31*, 6991–6994; *J. Chem. Soc. Perkin Trans. 1* **1992**, 1699–1700; f) H. Paulsen, G. Merz, S. Peters, U. Weichert, *Liebigs Ann. Chem.* **1990**, 1165–1173; g) B. Luning, T. Norberg, C. Riversa-Baeza, J. Tejbrant, *Glycoconj. J.* **1991**, *8*, 450–455; h) S. Peters, T. Bielfeldt, M. Meldal, K. Bock, H. Paulsen, *Tetrahedron Lett.* **1991**, *32*, 5067–5070; i) T. Bielfeldt, S. Peters, M. Meldal, K. Bock, H. Paulsen, *Angew. Chem.* **1992**, *104*, 881–883; *Angew. Chem. Int. Ed. Engl.* **1992**, *31*, 857–859; j) S. Peters, T. Bielfeldt, M. Meldal, K. Bock, H. Paulsen, *Tetrahedron Lett.* **1992**, *33*, 6445–6448; k) R. Polt, L. Szabo, T. Treiberg, Y. Li, V. J. Hruby, *J. Am. Chem. Soc.* **1992**, *114*, 10249–10258; l) A. C. Bauman, J. S. Broderick, R. M. Dacus IV, D. A. Grover, L. S. Trzupek, *Tetrahedron Lett.* **1993**, *34*, 7019–7022; m) K. B. Reimer, M. Meldal, K. Kusumoto, K. Fukase, K. Bock, *J. Chem. Soc. Perkin Trans. 1* **1993**, 925–932; n) W. Kosch, J. Marz, H. Kunz, *React. Polym.* **1994**, *22*, 181–194; o) H. Paulsen, T. Bielfeldt, S. Peters, M. Meldal, K. Bock, *Liebigs Ann. Chem.* **1994**, 364–379, 381–387; p) M. K. Christensen, M. Meldal, K. Bock, H. Cordes, S. Mouritsen, H. Elsner, J. *Chem. Soc. Perkin Trans. 1* **1994**, 1299–1310; q) J. Rademann, R. R. Schmidt, *Carbohydr. Res.* **1995**, *269*, 217–225; r) O. Seitz, H. Kunz, *Angew. Chem.* **1995**, *107*, 901–904; *Angew. Chem. Int. Ed. Engl.* **1995**, *34*, 803–805; s) S. Rio-Anneheim, H. Paulsen, M. Meldal, K. Bock, *J. Chem. Soc. Perkin Trans. 1* **1995**, 1070–1080; t) E. Meinjohanns, A. Vargas-Berenguel, M. Meldal, H. Paulsen, K. Bock, *ibid.* **1995**, 2165–2175; u) S. Peters, T. L. Lowary, O. Hindsgaul, M. Meldal, K. Bock, *ibid.* **1995**, 3017–3022; v) Y. Nakahara, Y. Nakahara, T. Ogawa, *Carbohydr. Res.* **1996**, *292*, 71–81; w) A. M. Jansson, K. J. Jensen, M. Meldal, J. Lomako, W. M. Lomako, C. E. Olsen, K. Bock, *J. Chem. Soc. Perkin Trans. 1* **1996**, 1001–1006, x) O. Seitz, H. Kunz, *J. Org. Chem.* **1997**, *62*, 813–826.

[4] Solid-phase synthesis of *N*-glycopeptides: a) S. Lavielle, N. C. Ling, R. C. Guillemin, *Carbohydr. Res.* **1981**, *89*, 221–228; b) H. Kunz, B. Dombo, *Angew. Chem.* **1988**, *100*, 732–734; *Angew. Chem. Int. Ed. Engl.* **1988**, *27*, 711–713; c) L. Otvos, Jr., K. Wroblewski, E. Kollat, A. Perczel, M. Hollosi, G. D. Fasman, H. C. J. Retl, J. Thurin, *Peptide Res.* **1989**, *2*, 362–366; d) L. Otvos, Jr., L. Urge, M. Hollosi, K. Wroblewski, G. Graczyk, G. D. Fasman, J. Thurin, *Tetrahedron Lett.* **1990**, *31*, 5889–5892; e) M. Meldal, K. Bock, *ibid.* **1990**, *31*, 6987–6990; f) C. Unverzagt, S. Kelm, J. C. Paulsen, *Carbohydr. Res.* **1994**, *251*, 285–301; g) D. Vetter, D. Tumelty, S. K. Singh, M. A. Gallop, *Angew. Chem.* **1995**, *107*, 94–97; *Angew. Chem. Int. Ed. Engl.* **1995**, *34*, 60–63.

[5] I. Matsuo, Y. Nakahara, Y. Ito, T. Nukada, Y. Nakahara, T. Ogawa, *Biorg. Med. Chem.* **1995**, *3*, 1455–1463.

[6] a) M.-Q. Xia, M. Tone, L. Packman, G. Hale, H. Waldmann, *Eur. J. Immunol.* **1991**, *21*, 1677–1684; b) M.-Q. Xia, G. Hale, M. R. Lifely, M. A. J. Ferguson, D. Campbell, L. Packman, H. Waldmann, *Biochem. J.* **1993**, *293*, 633–640; c) A. Treumann, M. R. Lifely, P. Schneider, M. A. J. Ferguson, *J. Biol. Chem.* **1995**, *270*, 6088–6099.

[7] Y. Nakahara, H. Iijima, T. Ogawa, *Tetrahedron Lett.* **1994**, *35*, 3321–3324.

[8] **1**: $[\alpha]_D^{23} = -38.0$ ($c = 0.1$ in H_2O); HPL retention time = 9.82 min (Lichro-CART column 10 × 250 mm; eluent: 2.6% *i*PrOH in H_2O, 3 mL min^{-1}); ^{1}H NMR (600 MHz, D_2O, δ(HDO) = 4.43 as standard, 60 °C): δ = 5.10 (d, 1H, $J(1,2)$ = 1.0 Hz, H-1^4), 5.02 (d, 1H, $J(1,2)$ = 8.9 Hz, H-1^1), 4.90 (d, 1H, $J(1,2)$ = 1.7 Hz, H-1$^{4'}$), 4.80 (dd, 1H, H-α^{Asp}), 4.76 (s, 1H, H-1^3), 4.70–4.74 (m, 2H, H-$\alpha^{Asn,Ser}$), 4.61 (br. d, $J(1,2)$ = 7.6 Hz, 1H, H-1^2), 4.47–4.32 (m, 10H, H-$\alpha^{3\times Ser,\,2\times Thr,\,Pro,\,2\times Glu}$, H-$\beta^{2\times Thr}$), 4.00–3.50 (m, 42H, H-$\alpha$,$\alpha'^{Gly}$, H-$\beta$,$\beta'^{4\times Ser}$, H-$\delta$,$\delta'^{Pro}$, H-2,3,4,5,6,6′ of five sugar rings), 2.90–2.72 (m, 4H, H-β,$\beta'^{Asp,Asn}$), 2.31–2.25 (m, 5H, H-γ,$\gamma'^{2\times Gln}$,β^{Pro}), 2.20–1.99 (m, 7H, H-β,$\beta'^{2\times Gln}$,β',γ,γ'^{Pro}), 2.06 (s, 3H, Ac), 2.00 (s, 3H, Ac), 1.19 (d, 6H, J = 6.3 Hz, H-$\gamma^{2\times Thr}$); ESI-MS ($C_{79}H_{129}N_{17}O_{49}$, M_r = 2101.0): *m/z* (positive-ion mode) 1103.2 [(Na, K salt of $1+2Na)^{2+}$, calcd 1103.5], 743.3 [(Na, K salt of $1+3Na)^{3+}$, calcd 743.4]; *m/z* (negative-ion mode) 1079.6 [(K, Na salt of $1-2H)^{2-}$, calcd 1079.7]; MALDI-TOF-MS: *m/z* (positive ion mode) 2102.7 [$(M+1)^+$], 2125.7 [$(M+Na)^+$], 2141.0 [$(M+K)^+$], 2147.1 [(Na salt + Na)$^+$], 2163.3 [(K salt + Na)$^+$], 2169.4 [(2 Na salt + Na)$^+$].

Computational Binding Studies of Orthogonal Cyclosporin-Cyclophilin Pairs**

Albert C. Pierce and William L. Jorgensen*

Dedicated to Professor Dieter Seebach on the occasion of his 60th birthday

Gene therapy holds great promise for the treatment of inherited disorders, and much research is being devoted to the development of effective gene delivery systems. Control of the dosage of the gene product is a critical issue that has been addressed recently by Schreiber, Crabtree, and co-workers.[1] Their elegant method for regulation of transgenes features activation of a cellular process by association of two proteins upon the addition of a single drug molecule (Figure 1). In particular, if these proteins are the DNA binding and promoter domains of a transcriptional activator, gene expression can be induced. The receptors are chimeric proteins that include domains to bind nonoverlapping regions of the drug molecule. In the initial work, the drug-binding domains have been immunophilins such as cyclophilin (CyP) or FKBP12, with a synthetic dimer of an associated immunosuppressant drug as the chemical inducer of dimerization (CID).[1] This construct has been used successfully to provide protein synthesis both in vitro[1] and in vivo.[1c, 1d, 2] Gene expression levels may be controlled by varying the timing and quantity of drug administration.

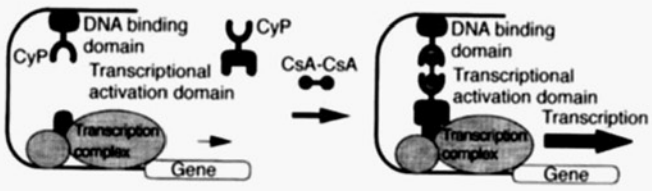

Figure 1. A typical CID scheme for regulation of protein synthesis

However, a potential problem stems from the fact that the immunophilins are expressed at high levels in many cell types.

[*] Prof. W. L. Jorgensen, A. C. Pierce
Department of Chemistry, Yale University
New Haven, CT 06520-8107 (USA)
Fax: Int. code +(203)432-6299
e-mail: bill@adrik.chem.yale.edu

[**] This research was supported by a grant from the National Institutes of Health. Gratitude is also expressed to Dr. J. Tirado-Rives and M. L. Lamb for helpful discussions and assistance.

Consequently, the drug may be absorbed by immunophilins throughout the organism with the formation of unproductive protein complexes. A solution has been provided with the idea of orthogonal receptor–ligand pairs.[3] Specifically, Schreiber and co-workers have modified cyclosporin A (CsA) with a steric

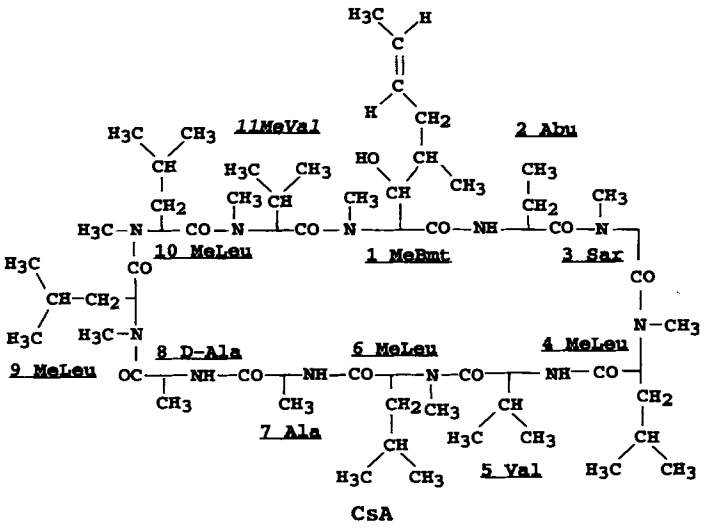

CsA

"bump"; the MeVal11 residue of the cyclic undecapeptide was changed to MeIle, which was shown to drastically reduce the binding to wild type CyP. Mutants of CyP were then expressed with accommodating "holes", such as the mutation of Phe113 to Ala (F113A), which largely restored the binding.[3] Thus, problems with drug dilution can be eliminated and, furthermore, the bumped drugs will not have the undesired property of being immunosuppressant like their parents.

Herein we demonstrate how computational methods can participate in the design and structural understanding of orthogonal receptor–ligand pairs. The thermodynamic problem centers on the free energies of binding ΔG_1–ΔG_4 for the four protein–ligand complexes in Scheme 1. These correspond to binding the reference ligand (L) and bumped ligand (bL) to the original protein (P) and holed protein (hP). Experimentally, the free energies of binding are related to the observed association constants by $\Delta G_i = -RT\ln K_i$. Then, important for comparisons are the differences $\Delta G_2 - \Delta G_1$ (the effect of the bump on binding to the original protein), $\Delta G_4 - \Delta G_1$ (the restoration of binding with the bump–hole pair), $\Delta G_3 - \Delta G_1$ (the effect of the hole

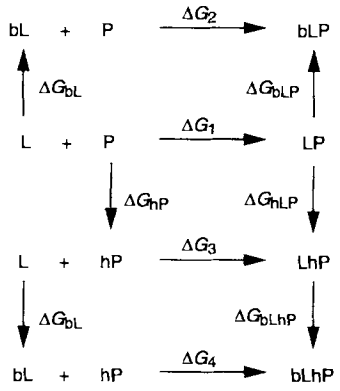

Scheme 1. Thermodynamic cycles for the study of orthogonal receptor–ligand pairs. L: reference ligand; P: original protein; bL: bumped ligand; hP: holed protein. The FEP calculations are performed for the processes with vertical arrows.

on binding the reference ligand), and $\Delta G_4 - \Delta G_3$ (the effect of the bump on binding to the holed protein). A viable bump–hole pair requires $\Delta G_2 - \Delta G_1 \gg 0$ and it is also desirable for $\Delta G_4 - \Delta G_1 \leq 0$; that is, the bump destroys the binding and the hole restores it. The latter condition would benefit from $\Delta G_3 - \Delta G_1 < 0$ and $\Delta G_4 - \Delta G_3 < 0$. Computationally, these differences are available from computer simulations using free-energy perturbation (FEP) methods.[4] It is expeditious to perform the vertical perturbations indicated in Scheme 1, where, for example, ΔG_{bL} and ΔG_{bLP} represent the free energy changes for bumping the isolated ligand and the reference protein–ligand complex, and from the thermodynamic cycle $\Delta G_2 - \Delta G_1 = \Delta G_{bLP} - \Delta G_{bL}$.

As an initial application, the aforementioned MeVal11 to MeIle11 bump for cyclosporin A and the Phe113 to Ala113 hole for cyclophilin have been considered. The ensemble configurations were generated with Monte Carlo (MC) sampling in internal coordinates as implemented in the program MCPRO.[5] Along with a study of complexes of trypsin with benzamidines,[6] these are the first reports of MC/FEP calculations for proteins. Molecular dynamics has been the standard sampling procedure for proteins; however, encouragement for trying Monte Carlo simulations has come from recent comparisons of the efficiencies of MD and MC procedures for confomational sampling[7] and from prior successes with MC/FEP calculations for organic host–guest complexes.[4, 8] The AMBER/OPLS force field was used with all atoms except for hydrogen atoms on saturated carbon atoms.[9] The nonstandard amino acids in CsA could all be described with available parameters for amides and hydrocarbons. Initial protein coordinates were based on the crystal structures of free human cyclophilin A[10] and the CsA–CyP complex.[11] For the bumping of unbound CsA, two structures were used in two separate perturbations. One structure was obtained by neutron diffraction from a crystal grown in an ethanol/oil mixture,[12] and the other was extracted from the CsA–CyP structure, which NMR studies have suggested is closer to the conformation in aqueous solution.[13] All initial structures were energy-minimized for 250–1000 steepest descent steps using a distance-dependent dielectric constant with the program AMBER.[14] For efficient treatment of the protein systems, only 107 of 165 residues within about 18 Å of the perturbed MeVal of CsA were included in the MC simulations. For CsA, the bond lengths were held fixed except for one ring-closure bond, while all bond angles and dihedral angles were sampled. For the proteins, all bond lengths were fixed, while side-chain bond angles and torsion angles except those in aryl rings were sampled for residues with any atom less than 9.5 Å from MeVal11 of CsA. The protein backbone was fixed after the energy-minimizations. Though this simplification follows from the limited backbone movement found in MD/FEP calculations of typical durations especially for small perturbations such as Val → Ile, full sampling is desirable for optimal accuracy. Presently, the structures of CsA and the protein side chains are flexible and can adjust to the addition of the bump and the hole.

Each system was solvated with an 18-Å radius sphere of TIP3P water molecules[15] based on the center of the CsA ring unbound or on the α-carbon atom of MeVal11 bound. After deletion of those water molecules with serious steric conflicts, 748 water molecules remained for the unbound system and ≈450 for the proteins and complexes. The perturbations were run at 20 °C with 9-Å radius spherical, residue-based cutoffs for all nonbonded interactions. The first window for each FEP calculation was equilibrated for 5×10^6 configurations and the final structure from each window served as the starting structure for the next window. After 3×10^6 configurations of equilibra-

tion, averaging was performed for at least 3×10^6 configurations until an additional 10^6 configurations changed the ΔG of the window by less than 0.02 kcal mol^{-1}. Most windows required $4 \times 10^6 - 6 \times 10^6$ configurations of averaging, though a few took up to 11×10^6 configurations. In all, 18–26 individual MC simulations (windows) were used for each of the five unique perturbations corresponding to the vertical arrows in Scheme 1. The resultant free energy curves are smooth (see Figures 2 and 3) and

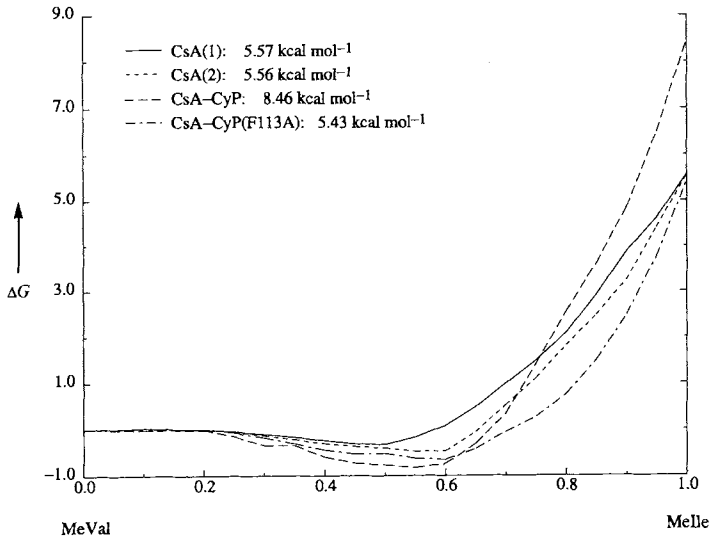

Figure 2. Computed free energy ΔG curves [kcal mol^{-1}] for the mutations of CsA to MeIle11 CsA under different conditions. The two curves for unbound CsA correspond to the two different starting geometries described in the text. The mutation was also performed with CsA bound to the protein CyP and to the mutant protein CyP(F113A). λ is the scaling parameter for the mutations.

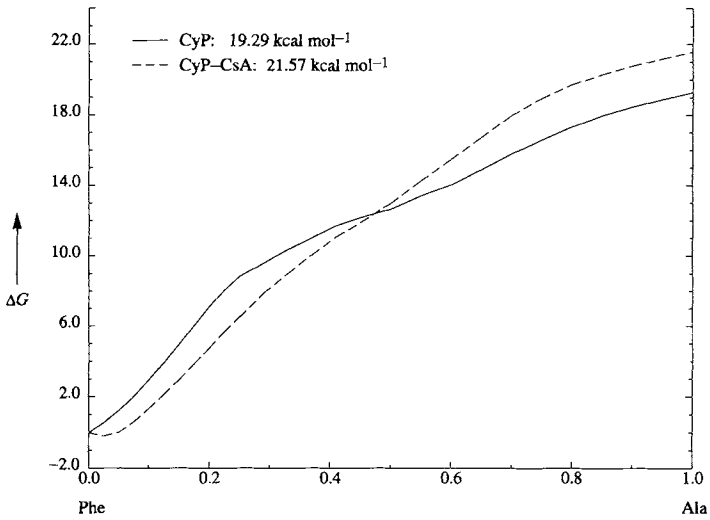

Figure 3. Computed free energy curves ΔG [kcal mol^{-1}] for the mutations of Phe113 to Ala in free cyclophilin (CyP) and in the CyP–CsA complex.

Table 1. Computed and experimental free energy differences ΔG [kcal mol^{-1}] for the processes in Scheme 1, where L = CsA, bL = MeIle11 CsA, P = CyP, and hP = CyP (F113A).

$\Delta\Delta G$	Exp. [a]	Calcd [b]
$\Delta G_2 - \Delta G_1 = \Delta G_{bLP} - \Delta G_{bL}$	>3.7	2.9±0.2
$\Delta G_4 - \Delta G_1 = \Delta G_{hLP} + \Delta G_{bLhP} - \Delta G_{bL} - \Delta G_{hP}$	1.4±0.1	2.1±0.3
$\Delta G_3 - \Delta G_1 = \Delta G_{hLP} - \Delta G_{hP}$	1.4±0.2	2.3±0.3
$\Delta G_4 - \Delta G_3 = \Delta G_{bLhP} - \Delta G_{bL}$	0.0±0.2	−0.1±0.2

[a] Ref. [3]. [b] This work.

the computed free energy differences are compared with the experimental values in Table 1. The statistical uncertainties ($\pm 1\sigma$) for the computed quantities were obtained from the fluctuations in separate averages over batches of 2×10^5 configurations. A similar protocol was applied for complexes of trypsin; high precision was also achieved including hystereses of approximately 0.3 kcal mol^{-1} for perturbations around closed cycles with three inhibitors, that is, A → B → C → A.[6]

In Figure 2, it can be seen that the net ΔG_{bL} value for the bumping of unbound CsA does not depend on which initial CsA structure was used. The Phe to Ala mutations (Figure 3) are quite large for FEP calculations; however, the MC calculations proceeded with good precision. The individual numerical results depend on the way the perturbation is performed and include contributions from, for example, the changes in intramolecular nonbonded interactions as a group is grown. The numbers become meaningful when taken as differences between bound and unbound states (see Scheme 1). It may also be noted that there is no problem at the endpoints of MC/FEP calculations when atoms appear or disappear since the forces, which can become infinite in MD simulations, are not used for MC simulations. The computed free energy differences compare favorably with the experimental results (Table 1). There are no qualitative errors and the average quantitative error is less than 1 kcal mol^{-1}. The bump is computed to substantially destabilize the complex with CyP ($\Delta G_2 - \Delta G_1$), while it has negligible effect on complexation with the holed protein ($\Delta G_4 - \Delta G_3$). The restoration of binding for the bump–hole pair, $\Delta G_4 - \Delta G_1$, is predicted to be 0.7 kcal mol^{-1} less favorable than observed.

Given the reasonable thermodynamic results, the structures from the simulations were analyzed to determine the origin of the difference of about 3 kcal mol^{-1} between the effect of the MeVal11 to MeIle11 bump on complexation for CyP and the F113A mutant. Analysis of dihedral angle distributions did not show any striking differences in conformational sampling for the ligand or protein side chains. Hydrogen-bond analyses also failed to show any salient advantage for one protein over the other. In the crystal structure, there are four hydrogen bonds between CsA and CyP: MeBmt1-O···Gln63 HN$^{\varepsilon}$, Abu2-HN···Asn102-O, MeLeu9-O···Trp121-HN$^{\varepsilon}$, MeLeu10-O···Arg55-HN$^{\eta}$. During the simulations, residues 1–3 of CsA showed considerable structural variations. The first hydrogen bond is lengthened substantially in all complexes, while the second one is also lengthened when the mutations are near the MeIle11 endpoint. However, this occurred for both proteins, so it should not provide preferential binding.

Finally, steric interactions were analyzed by determining the average distances between C$^{\delta}$ of the MeIle11 and all binding-site atoms in both proteins over 10^6 configurations. These distances were then used to calculate the average Lennard-Jones interaction energy for each pair. The most unfavorable interactions in the two binding sites are shown in Figure 4. For the wild-type protein, C$^{\delta}$ of MeIle has unfavorable interactions with C$^{\zeta}$ of Phe60, C$^{\gamma}$ of Met61, and C$^{\varepsilon}$ and C$^{\delta}$ of Phe113 (Figure 4 top); the average Lennard-Jones interactions are repulsive by 0.5–0.8 kcal mol^{-1}, and the average C–C distances are 3.3–3.5 Å. Thus, although in the original[3] and recent[16] studies only F113A and F113G mutants have been considered to provide holes for bumping MeVal11, the present results identify Phe60 and Met61 as additional candidates for size reduction. The

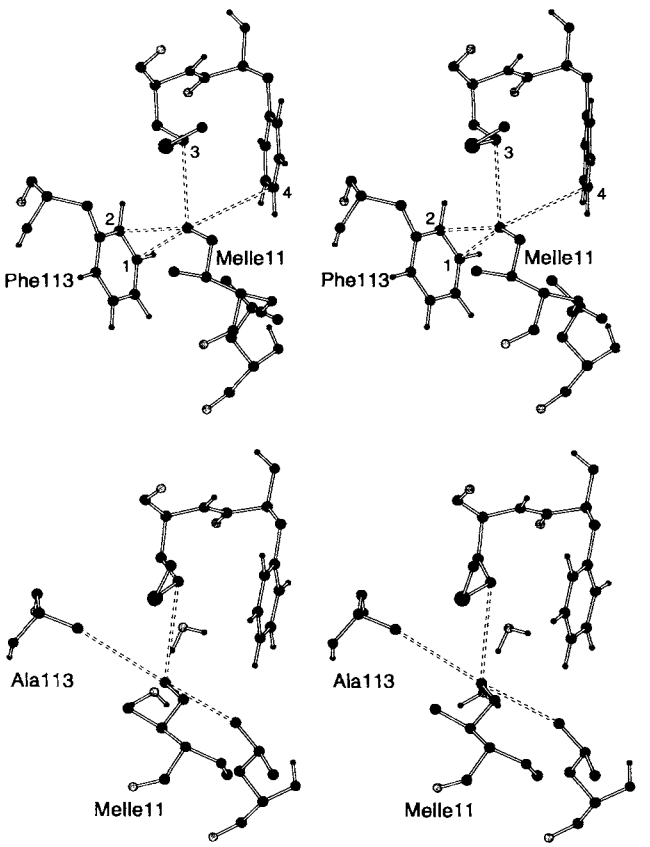

Figure 4. Stereoview of the four (top) and the three most unfavorable contacts (bottom) between the Melle11-C^{δ} atom and the binding site of CyP, and between the Melle11-C^{δ} atom and the binding site of the F113A mutant of CyP, respectively. The average values for the indicated distances and the corresponding Lennard-Jones interaction energies for the C^{δ}–CyP interaction are: to Phe113: 3.42 Å, +0.49 kcal mol^{-1} and 3.39 Å, +0.58 kcal mol^{-1}; to Met61: 3.54 Å, +0.63 kcal mol^{-1}; to Phe60: 3.33 Å, +0.84 kcal mol^{-1}; and for the C^{δ}–CyP(F113A) interaction are: to Ala113: 3.91 Å, 0.00 kcal mol^{-1}; to Met61: 3.92 Å, −0.05 kcal mol^{-1}; to Leu122: 3.80 Å, 0.14 kcal mol^{-1}.

F113A hole is larger than optimal,[3, 16] so less severe mutations are worth exploring. Turning to the F113A mutant, C^{δ} of Melle11 is now accommodated with no detrimental interactions (Figure 4 bottom). The shortest C–C contacts are 3.8–3.9 Å, and the average interaction energies are near zero. It is notable that two water molecules help fill the vacated space in the binding site of the F113A mutant. This makes the complex tolerant of the overly large hole, even in a hydrophobic pocket such as that of CyP.

The five mutations performed here provided a detailed thermodynamic and structural description of a bump–hole pair. The calculations reproduced well the observed relative binding energies, and analysis of the generated structures confirmed the steric origin of the binding differences and suggested alternative protein mutations. Though even closer quantitative accord may be expected with further enhanced sampling and use of the OPLS-AA force field,[17] these initial MC/FEP results establish the methodology as a promising tool for studying protein–ligand binding including the design and understanding of orthogonal receptor–ligand pairs.

Received: December 12, 1996 [Z9883IE]
German version: *Angew. Chem.* **1997**, *109*, 1595–1598

Keywords: cyclophilin · cyclosporin · gene technology · molecular recognition · Monte Carlo methods

[1] a) D. M. Spencer, T. J. Wandless, S. L. Schreiber, G. R. Crabtree, *Science* **1993**, *262*, 1019; b) P. J. Belshaw, S. N. Ho, G. R. Crabtree, S. L. Schreiber, *Proc. Natl. Acad. Sci. USA* **1996**, *93*, 4604; c) D. M. Spencer, P. J. Belshaw, L. Chen, S. N. Ho, F. Randazzo, G. R. Crabtree, S. L. Schreiber. *Curr. Biol.* **1996**, *1*, 839; d) S. N. Ho, S. R. Biggar, D. M. Spencer, S. L. Schreiber, G. R. Crabtree, *Nature* **1996**, *382*, 822.
[2] V. M. Rivera, T. Clackson, S. Natesan, R. Pollock, J. F. Amara, T. Keenan, S. R. Magari, T. Phillips, N. L. Courage, F. Cerasoli, Jr., D. A. Holt, M. Gilman, *Nature Med.* **1996**, *2*, 1028.
[3] P. J. Belshaw, J. G. Schoepfer, K.-Q. Liu, K. L. Morrison, S. L. Schreiber, *Angew. Chem.* **1995**, *107*, 2313; *Angew. Chem. Int. Ed. Engl.* **1995**, *34*, 2129.
[4] W. L. Jorgensen, *Chemtracts Org. Chem.* **1991**, *4*, 91; P. A. Kollman, *Chem. Rev.* **1993**, *93*, 2395.
[5] W. L. Jorgensen, MCPRO, Version 1.3, Yale University, New Haven, CT, **1995**.
[6] W. L. Jorgensen, E. M. Duffy, J. W. Essex, D. L. Severance, J. F. Blake, D. K. Jones-Hertzog, M. L. Lamb, J. Tirado-Rives, *NATO ASI Ser. Ser. C* **1997**, in press; J. W. Essex, J. Tirado-Rives, D. L. Severance, W. L. Jorgensen, *J. Phys. Chem.*, submitted.
[7] W. L. Jorgensen, J. Tirado-Rives, *J. Phys. Chem.* **1996**, *100*, 14508.
[8] See for example W. L. Jorgensen, T. B. Nguyen, *Proc. Natl. Acad. Sci. USA* **1993**, *90*, 1194; E. M. Duffy, W. L. Jorgensen, *J. Am. Chem. Soc.* **1994**, *116*, 6337.
[9] W. L. Jorgensen, J. Tirado-Rives, *J. Am. Chem. Soc.* **1988**, *110*, 1657; W. L. Jorgensen, D. L. Severance, *ibid.* **1990**, *112*, 4768.
[10] H. Ke, *J. Mol. Biol.* **1992**, *228*, 539.
[11] H. Ke, D. Mayrose, P. J. Belshaw, D. G. Alberg, S. L. Schreiber, Z. Y. Chang, F. A. Etzkorn, S. N. Ho, C. T. Walsh, *Structure* **1994**, *2*, 33.
[12] R. B. Knott, J. Schefer, B. P. Schoenborn, *Acta Crystallogr. Sect. C* **1990**, *46*, 1528.
[13] D. Altschuh, O. Vix, B. Rees, J.-C. Thierry, *Science* **1992**, *256*, 92.
[14] D. A. Pearlman, D. A. Case, J. C. Caldwell, G. L. Seibel, U. C. Singh, P. Weiner, P. A. Kollman, AMBER 4.0, University of California, San Francisco, **1991**.
[15] W. L. Jorgensen, J. Chandrasekhar, J. D. Madura, R. W. Impey, M. L. Klein, *J. Chem. Phys.* **1983**, *79*, 126.
[16] P. J. Belshaw, S. L. Schreiber, *J. Am. Chem. Soc.* **1997**, *119*, 1805.
[17] W. L. Jorgensen, D. S. Maxwell, J. Tirado-Rives, *J. Am. Chem. Soc.* **1996**, *118*, 11225.

Carbene Analogues of Boron Stabilized by Neighboring B–B Moieties: Doubly Aromatic Bishomotriboriranides**

Markus Unverzagt, Govindan Subramanian, Matthias Hofmann, Paul von Ragué Schleyer, Stefan Berger, Klaus Harms, Werner Massa, and Armin Berndt*

Dedicated to Professor Walter Siebert on the occasion of his 60th birthday

Carbenes **1** and their nitrogen analogues, nitrenium ions **2** (Scheme 1), have been characterized by crystal-structure analyses.[1, 2] However, carbene analogues of boron, borenate ions[3] **3**, have only been observed in the gas phase[4] or investigated theoretically.[4, 5] We now complete the series of isoelectronic prototypes **1**–**3** with the boron anion **7a** (see Scheme 4), a derivative of **3**. Double aromaticity,[6] delineated by computa-

[*] Prof. Dr. A. Berndt, M. Unverzagt, Prof. Dr. S. Berger. Dr. K. Harms, Prof. Dr. W. Massa
Fachbereich Chemie der Universität
D-35032 Marburg (Germany)
Fax: Int. code +(6421)28 89 17
e-mail: berndt@ps1515.chemie.uni-marburg.de
Dr. G. Subramanian, Dr. M. Hofmann, Prof. Dr. P. von R. Schleyer
Computer-Chemie-Centrum des Instituts für Organische Chemie
der Universität Erlangen-Nürnberg (Germany)

[**] This work was supported by the Deutsche Forschungsgemeinschaft and the Fonds der Chemischen Industrie. G. S. gratefully acknowledges a post-doctoral fellowship from the Alexander-von-Humboldt-Stiftung.

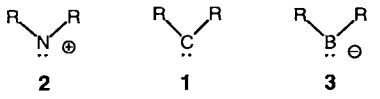

2 **1** **3**

Scheme 1. Carbene **1**, nitrenium ion **2**, and borenate ion **3**.

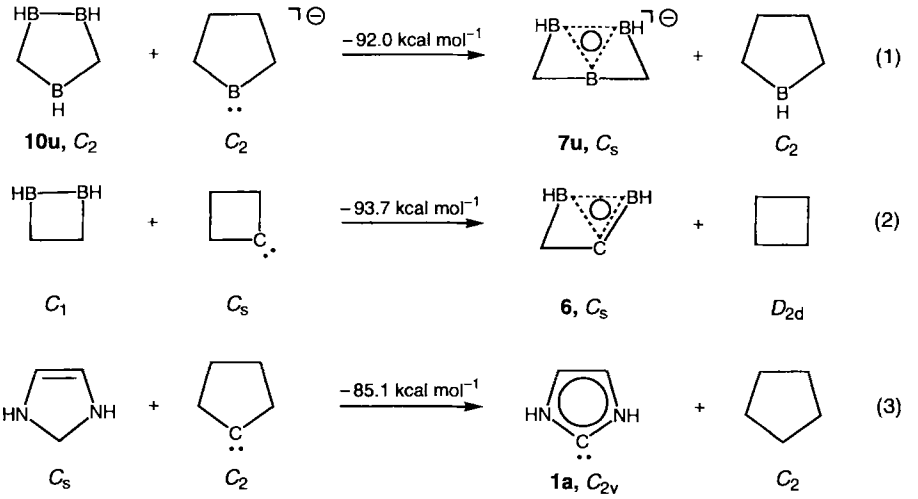

10u, C_2 C_2 **7u**, C_s C_2 (1)

C_1 C_s **6**, C_s D_{2d} (2)

C_s C_2 **1a**, C_{2v} C_2 (3)

tions for the parent compound **7u**, is the key to understanding the electronic structure of **7a,u** and related compounds.

Based on ab initio calculations and NBO analyses[7] we explained the electronic structures of carbene **4**[8] and borenate ion **5**[9] as follows.[10] In the classical representations **4*** and **5***, the electron pairs prefer the p orbitals of the carbene and borenate centers, respectively, over the hybrid orbital in the molecular plane. This "inverse" occupation allows the formation of a three-center two-electron (3c–2e) π bond involving the empty p orbitals of the neighboring B–B moiety. In addition, the formally empty hybrid orbital in **4*** and **5*** participates in a 3c–2e σ bond with the B–B σ electrons (Scheme 2).[11]

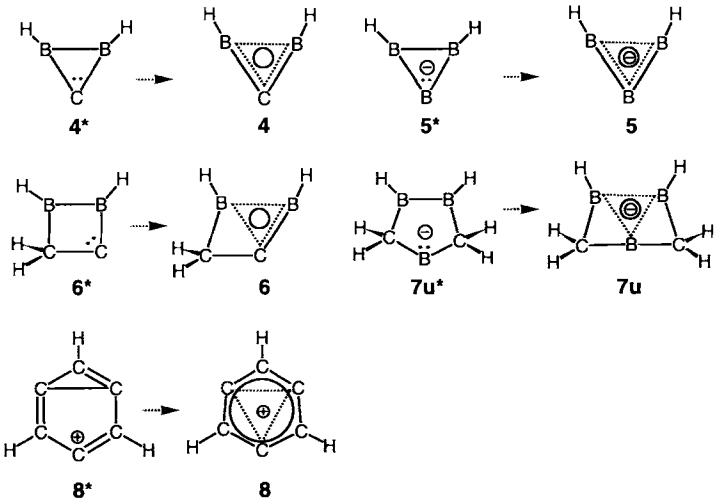

4* **4** **5*** **5**

6* **6** **7u*** **7u**

8* **8**

Scheme 2. Electronic structure of double-aromatic compounds according to theoretical investigations. An asterisk designates formal Lewis representations without π and σ delocalization, a dashed triangle a 3c–2e σ bond, and a solid circle a 3c–2e π bond (for **4**–**7**) or a 6c–6e π bond (for **8**).

Molecules with two orthogonal systems of $(4n+2)$ electrons, first described for the 3,5-dehydrophenyl cation **8**, are called doubly aromatic.[6] Derivatives of **6**, the monohomo form of **4**, are known.[8, 10] The substituted **7a** reported here is based on **7u**, the bishomo form of **5**.

An NBO analysis[7] justifies the description of **7u** with both BBB 3c–2e σ and π bonds. Along with **4**–**6** and **8**,[6] **7u** belongs to the class of doubly aromatic. The aromaticity of **7u** is demonstrated by the large magnetic-susceptibility anisotropy (> 30.3 ppm cgs) and the substantial diamagnetic-susceptibility exaltation (−18.7 ppm cgs according to Equation (1), CSGT-SCF/6-31+G*//MP2(FU)/6-31G*). The stabilization (MP2(FU)/6-31G*+0.94 ZPE) of **7u** due to the 3c–2e bonding is estimated from Equation (1) to be 92 kcal mol^{-1}.[12] The computed energy of a classical borenate geometry, arbitrarily fixed to that of **10u**, is 90 kcal mol^{-1} higher than that of **7u**. The stabilization energy for **6** computed from Equation (2) is 93.7 kcal mol^{-1}. Borenate **7u** and the nonclassical carbene **6** are stabilized just as strongly as the Arduengo-carbene prototype **1a** [Equation (3)].[13]

The classical representation **7u*** suggests that 1,2,4-triboracyclopentanes should be suitable starting materials for synthesizing derivatives of **7u**. We recently reported doubly deprotonated 1,2,4-triboracyclopentanes, the 1,2-diborata-4-boracyclopentadienes **9a,b**.[14] These dianions can be protonated by HCl in ether to give **10a,b**; surprisingly, **9a** gives only one stereoisomer **10a** with *cis* trimethylsilyl groups.[15] Compound **10a** can be converted into **10c** by reaction with BCl_3 at 0 °C (Scheme 3).

The constitution of **10a–c** is confirmed by their NMR data (Table 1) and by crystal structures for **10b,c**.[16] Attempts to optimize the geometry of the dianion of **10d**[12] converged to **7u**; the chloride ion dissociated spontaneously (Scheme 4).

Therefore, we synthesized a derivative of **7u** by reducing **10c** in THF or diethyl ether at 0 °C with lithium. This gave a rather uniform reaction product that crystallized from diethyl ether. The chemical shifts of the framework atoms ($\delta^{11}B = 24$ (2B) and 21 (1B), $\delta^{13}C = 2.1$) agree satisfactorily with the values computed for **7u** at the GIAO-MP2/tzp level[17] (25.2 (2B) and 31.4 (1B), −19.2 (C)) when substituent effects are considered. The framework carbon atoms of the new product are shielded relative to those of **10c** by at least $\Delta\delta = 58$, a remarkable effect for tetracoordinate C atoms. We calculated $\Delta\delta = 54.1$ for the corresponding difference between **10d** and **7u**.[18] Based on these results, the reduction product of **10c** is a lithium salt of anion **7a**.

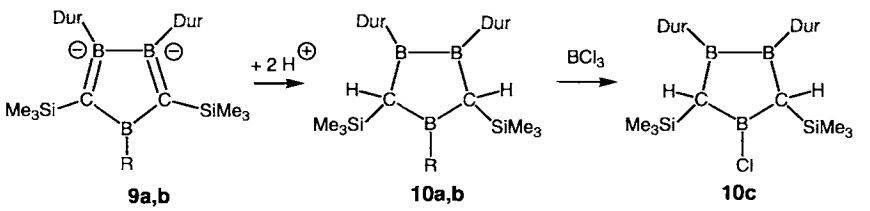

9a,b **10a,b** **10c**

Scheme 3. Protonation of **9a,b** to **10a,b**; **10a** can react further to **10c**. Dur = 2,3,5,6-tetramethylphenyl, **a**: R = OMe, **b**: R = $N(SiMe_3)_2$.

 © VCH Verlagsgesellschaft mbH, D-69451 Weinheim, 1997 0570-0833/97/3613-1470 $ 17.50+.50/0

Table 1. Selected physical and spectropscopic properties of **7a**·Li(THF)$_3$·Et$_2$O and **10a–c**.

7a·Li(THF)$_3$·Et$_2$O: yellow solid, m.p. 164 °C, yield 50%. ^{1}H NMR (500 MHz, [D$_8$]THF, −80 °C): δ = −0.14 (s, 18H, SiMe$_3$), 0.14 (s, 2H, H–CB$_2$), 1.13 (t, 6H, Et$_2$O), 1.79 (t, br, 12H, THF), 1.93, 1.97, 1.99, 2.14 (each s, each 6H, *o*- and *m*-CH$_3$), 3.36 (q, 4H, Et$_2$O), 3.64 (t, br, 12H, THF), 6.37 (s, 2H, *p*-H); ^{13}C NMR (125 MHz, ^{11}B-decoupled, [D$_8$]THF, −80 °C): δ = 2.0 (q, 6C, SiMe$_3$), 2.1 (d, br, 2C, ^1J(C,H) = 125.1 Hz, HCB$_2$), 15.6 (t, 2C, Et$_2$O), 19.5, 20.8, 20.9, 22.7 (each q, each 2C, *o*- and *m*-CH$_3$), 26.0 (t, 2C, THF), 66.2 (t, 2C, Et$_2$O), 67.9 (t, 2C, THF), 126.2 (d, 2C, *p*-C), 129.9, 130.0, 133.5, 133.8 (each s, each 2C, *o*- and *m*-C), 153.5 (s, 2C, *i*-C); ^{11}B NMR (96 MHz, [D$_8$]THF, 25 °C): δ = 24; ^{11}B NMR (96 MHz, Et$_2$O, 25 °C): δ = 22, 24 (ratio 1:2).

10a: yellow solid, m.p. 138 °C, yield 92%. ^{1}H NMR (300 MHz, CDCl$_3$, 25 °C): δ = 0.28 (s, 18H, SiMe$_3$), 1.88, 2.19, 2.23 (each s, total 24H, *o*- and *m*-CH$_3$), 2.33 (s, 2H, HCB$_2$), 3.98 (s, 3H, OCH$_3$), 6.87 (s, 2H, *p*-H); ^{13}C NMR (75 MHz, CDCl$_3$, 25 °C): δ = 3.22 (6C, SiMe$_3$), 19.0, 19.5, 21.3 (total 8C, *o*- and *m*- CH$_3$), 49.8 (2C, br., HCB$_2$), 55.0 (1C, OCH$_3$), 129.5, 129.8, 132.6, 132.9 (total 10C, *o*-, *m*- and *p*-C), 149.6 (br, 2C, *i*-C); ^{11}B NMR (96 MHz, CDCl$_3$ 25 °C): δ = 53, 94 (ratio 1:2).

10b: yellow-fluorescing solid, m.p. 156 °C, yield 38%. ^{1}H NMR (300 MHz, CDCl$_3$, 25 °C): δ = 0.30, 0.50 (each s, each 18 H, SiMe$_3$), 2.05, 2.21 (each s, each 12H, *o*- and *m*-CH$_3$), 3.13 (s, 2H, HCB$_2$), 6.89 (s, 2H, *p*-H); ^{13}C NMR (75 MHz, CDCl$_3$, 25 °C): δ = 4.5, 6.7 (each q, each 6C, SiMe$_3$), 19.4, 20.0, 20.3, 21.7 (each q, total 8C, *o*- and *m*- CH$_3$), 60.1 (d, 2C, ^1J(C,H) = 99.7 Hz, CB$_2$), 130.4, 131.8, 132.8 (total 10C, *o*-, *m*- and *p*-C), 149.0 (s, br, 2C, *i*-C); ^{11}B NMR (96 MHz, CDCl$_3$ 25 °C): δ = 59, 91 (ratio 1:2).

10c: yellow-fluorescing solid, m.p. 130–134 °C, yield 72%. ^{1}H NMR (500 MHz, CDCl$_3$, −30 C): δ = 0.22 (each s, each 18H, SiMe$_3$), 1.78, 2.10, 2.15, 2.16 (each s, each 6H, *o*- and *m*-CH$_3$), 2.73 (s, 2H, HCB$_2$), 6.83 (s, 2H, *p*-H); ^{13}C NMR (125 MHz, CDCl$_3$, −30 °C): δ = 2.8 (q, 6C, SiMe$_3$), 19.0, 19.5, 20.0, 21.4 (each q, each 2C, *o*- and *m*-CH$_3$), 60.5 (d, 2C, ^1J(C,H) = 102.2 Hz), 129.7 (d, 2C, *p*-C, ^1J(C,H) = 148.3 Hz), 129.4, 129.5, 132.6, 133.0 (each s, each 2C, *o*- and *m*-C), 148.0 (s, 2C, *i*-C); ^{11}B NMR (96 MHz, CDCl$_3$, 25 °C): δ = 74, 94 (ratio 1:2).

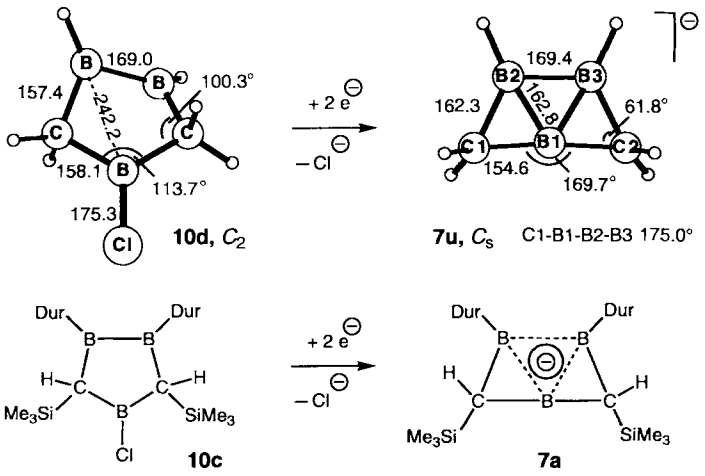

Scheme 4. Calculated formation and synthesis of bishomotriboriranides.

The definitive proof came from an X-ray structure analysis: Figure 1 shows the structure of an ion pair of this salt in the crystal.[19] The Li^+ counterion in **7a** is coordinated to one diethyl ether molecule and three THF molecules. Anion **7a** has a distorted, trapezoidal geometry with very short transannular B–B distances of 165(1) pm (predicted computationally to be 162.8 pm for **7u**).[20] The boron atoms in **7a** are nearly planar tetracoordinate: B2 and B3 deviate from the best plane of their neighbors by 4.1 and 5.9 pm, respectively, and B1 by 12.5 pm. Cation **8**[6] has three planar-tetracoordinate carbon atoms.

The borenate ion **7a**, the first carbene analogue of boron characterized in solution and in the solid state, gains its stability from 3c–2e π and σ bonding involving the borenate center and the neighboring B–B unit. Bishomotriboriranides **7** are double-aromatic compounds like the homodiboriranylidenes **6**, which

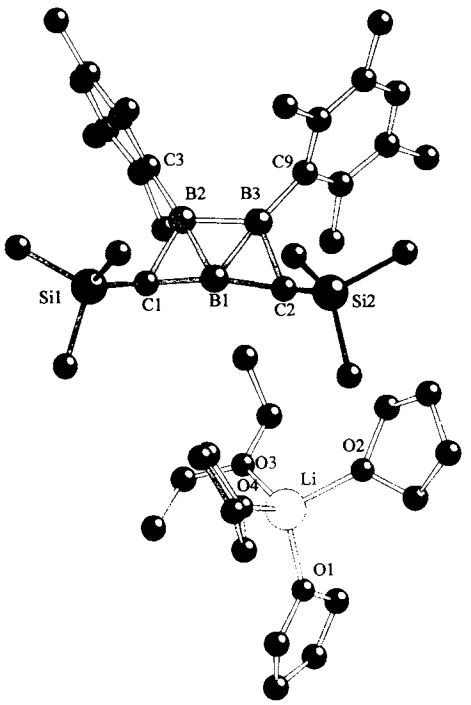

Figure. 1. Crystal structure of **7a**·Li(THF)$_3$·Et$_2$O (H atoms and alternative positions of THF at O2 are not shown). Selected interatomic distances [pm] and angles [°]: B1–B2 164.0(12), B1–B3 166.1(12), B2–B3 168.6(12), B1–C1 152.5(12), B1–C2 154.5(12), C1–B2 166.9(12), C2–B3 168.6(11), B2–C3 157.1(12), B3–C9 157.3(12), C1–Si1 182.6(8), C2–Si2 182.7(8); C1-B1-C2 167.1(8), B1-C1-B2 61.6(5), B1-C2-B3 61.7(5), C1-B2-B3 114.6(7), C2-B3-B2 113.4(7); C1-B1-B2-B3 −174.6(7).

have been characterized by NMR spectroscopy and X-ray structure analysis, and the theoretical diboriranylidenes **4** and triboriranides **5**.

Received: February 7, 1997 [Z10085IE]
German version: *Angew. Chem.* **1997**, *109*, 1567–1569

Keywords: ab initio calculations · aromaticity · boron · carbenes

[1] A. J. Arduengo III, R. L. Harlow, M. Kline, *J. Am. Chem. Soc.* **1991**, *113*, 361; A. J. Arduengo III, J. R. Goerlich, W. J. Marshall, *ibid.* **1995**, *117*, 11027, and references therein; R. W. Alder, P. R. Allen, M. Murray, A. G. Orpen, *Angew. Chem.* **1996**, *108*, 1211; *Angew. Chem. Int. Ed. Engl.* **1996**, *35*, 1121; recent review: M. Regitz, *ibid.* **1996**, *108*, 791 and **1996**, *35*, 725.

[2] G. Boche, P. Andrews, K. Harms, M. Marsch, K. S. Rangappa, M. Schimeczek, C. Willeke, *J. Am. Chem. Soc.* **1996**, *114*, 4925.

[3] We suggest the name "borenate ion" for carbene analogues of boron in analogy to "nitrenium ion" for carbene analogues of nitrogen. Upon addition of a cation R^+, a nitrene N–R forms a nitrenium ion R_2N^+, and a borene B–R becomes a borenate ion BR_2^- by adding an anion R^-.

[4] M. Krempp, R. Damrauer, C. H. DePuy, Y. Keheyan, *J. Am. Chem. Soc.* **1994**, *116*, 3629. From our point of view $B_2H_3^-$ described here is the simplest borylborenate.

[5] a) E. Kaufmann, P. von R. Schleyer, *Inorg. Chem.* **1988**, *27*, 3987; b) M. Wagner, N. J. R. van E. Hommes, H. Nöth, P. von R. Schleyer, *ibid.* **1995**, *34*, 607.

[6] P. von R. Schleyer, H. Jiao, M. N. Glukhovtsev, J. Chandrasekhar, E. Kraka, *J. Am. Chem. Soc.* **1994**, *116*, 10129; J. Chandrasekhar, E. D. Jemmis, P. von R. Schleyer, *Tetrahedron Lett.* **1979**, 3707.

[7] A. E. Reed, F. Weinhold, *Chem. Rev.* **1988**, *88*, 899.

[8] A. Berndt, *Angew. Chem.* **1993**, *105*, 1034; *Angew. Chem. Int. Ed. Engl.* **1993**, *32*, 985.

[9] Geometry of **5**: see ref. [4].

[10] A. Berndt, D. Steiner, D. Schweikart, C. Balzereit, M. Menzel, H.-J. Winkler, S. Mehle, M. Unverzagt, T. Happel, P. von R. Schleyer, G. Subramanian, M. Hofmann in *Advances in Boron Chemistry* (Ed.: W. Siebert), The Royal Society of Chemistry, Cambridge, **1997**, p. 61.

[11] In contrast to nitrogen atoms, which act as π donors and σ acceptors in amino substituents of persistent derivatives of **1** and **2**, the B–B units in **4**–**7** act as π acceptors and σ donors.
[12] MP2(FU)/6-31G* geometries computed with *Gaussian 94*; M. J. Frisch, G. W. Trucks, H. B. Schlegel, P. M. W. Gill, B. G. Johnson, M. A. Robb, J. R. Cheeseman, T. Keith, J. A. Petersson, J. A. Montgomery, K. Raghavachari, M. A. Al-Laham, V. G. Zakrzewski, J. Y. Ortiz, J. B. Foresman, J. Cioslowski, B. B. Stefanov, A. Nanayakkara, M. Challcombe, C. Y. Peng, P. Y. Ayala, W. Chen, M. W. Wong, J. L. Andres, E. S. Replogle, R. Gomperts, R. L. Martin, D. J. Fox, J. S. Blinkley, D. J. DeFrees, J. Baker, J. J. P. Stewart, M. Head-Gordon, C. Gonzalez, J. A. Pople, Gaussian, Pittsburgh, PA, **1995**.
[13] The stability of **1a** over singlet CH_2 was estimated to be 112.1 kcal mol^{-1}: C. Heinemann, T. Müller, Y. Apeloig, H. Schwarz, *J. Am. Chem. Soc.* **1996**, *118*, 2023.
[14] M. Unverzagt, H.-J. Winkler, M. Brock, M. Hofmann, P. von R. Schleyer, W. Massa, A. Berndt, *Angew. Chem.* **1997**, *109*, 879; *Angew. Chem. Int. Ed. Engl.* **1997**, *36*, 853.
[15] The *cis* configuration of **10a** unambiguously follows from the diastereotopy of the *o*- and *m*-carbon atoms and the attached methyl groups. This cannot be due to the different duryl groups, because only one signal each is seen for the *i*- and the *p*-carbon atoms.
[16] Distances in **10c** [pm]: B–B 176.1(4), BB–C 157.5(4), 158.0(4), ClB–C 155.2(3), 155.3(4), B–Cl 178.7(4), B···B (transannular) 238.0(6), 246.4(6).
[17] GIAO-MP2: a) J. Gauss, *Chem. Phys. Lett.* **1992**, *191*, 614; b) *J. Chem. Phys.* **1993**, *99*, 3629. The method was implemented in ACES11 (an ab initio program system: J. F. Stanton, J. Gauss, J. D. Watts, W. J. Lauderdale, R. J. Bartlett, *Quantum Theory Project*, University of Florida, Fl, **1991**, **1992**). The abbreviation tzp stands for triple zeta plus polarization basis set: A. Schäfer, H. Horn, R. Ahlrichs, *J. Chem. Phys.* **1992**, *97*, 2571.
[18] GIAO-SCF/6-31G* gives 20.8 (2B), 22.2 (1B), and −19.6 (C) for **7u** and 94.1 (2B), 73.0 (1B), and 34.5 (C) for **10d**.
[19] X-ray structure analysis for **7a**·Li(THF)$_3$·Et$_2$O ($C_{44}H_{80}B_3LiO_4Si_2$): A yellow crystal (ca. 0.4 × 0.2 × 0.2 mm^3) was investigated on a four-circle diffractometer (CAD4, Enraf–Nonius) with $Cu_{K\alpha}$ radiation (λ = 154.178 pm) at −60 °C. Orthorhombic, space group $P2_12_12_1$, $Z = 4$, a = 1179.6(1), b = 1931.3(1), c = 2193.7(5) pm, $V = 4997.4(12) \times 10^{-30}$ m^3, ρ_{calcd} = 1.022 g cm^{-3}. A total of 4148 independent reflections were collected with $\omega/2\theta$ scans for $2\theta = 120°$ and subjected to LP and semi-empirical absorption corrections (Ψ scans, μ = 9.04 cm^{-1}, min./max. transmission = 0.83/0.87). The structure was solved by direct methods and refined with full matrix against the F^2 data. All heavy atoms were refined with anisotropic temperature factors. All hydrogen atoms were considered riding at idealized positions in groups with common isotropic temperature factors set to 1.2 and 1.5 times (methyl groups) the U_{eq} of the corresponding carbon atom. One THF molecule showed 1:1 disorder over two alternative orientations; high anisotropic distortion parameters indicate high flexibility or disorder in the cation and for several other groups, and reduce the accuracy of the structure determination: wR_2 = 0.2298 and R = 0.073 for 2331 observed reflections ($F_o > 4\sigma(F)$), max. residual electron density 0.28 e Å^{-3}. A Flack Parameter x = −0.07(8) proves that the correct enantiomer has been refined. Crystallographic data (excluding structure factors) for the structures reported in this paper have been deposited with the Cambridge Crystallographic Data Centre as supplementary publication no. CCDC-100161. Copies of the data can be obtained free of charge on application to The Director, CCDC, 12 Union Road, Cambridge CB21EZ, UK (fax: int. code +(1223)336-033; e-mail: deposit@chemcrys.cam.ac.uk).
[20] Compare for example the distances in Scheme 4 and the Wiberg bond indices: B1–B2 0.789, B2–B3 1.000, B1–C1 0.945, B2–C1 0.829, B2–H 0.946.

Rapid Synthesis of the Enantiomers of *myo*-Inositol-1,3,4,5-tetrakisphosphate by Direct Chiral Desymmetrization of *myo*-Inositol Orthoformate**

Andrew M. Riley, Mary F. Mahon, and Barry V. L. Potter*

D-*myo*-Inositol-1,4,5-trisphosphate (Ins(1,4,5)P_3, **1**) functions as an intracellular second messenger by eliciting the release of Ca^{2+} from non-mitochondrial stores in stimulated cells.[1] In mammalian tissues phosphorylation of Ins(1,4,5)P_3 at position 3 of the inositol ring by a highly specific cytosolic 3-kinase generates D-*myo*-inositol-1,3,4,5-tetrakisphosphate (D-Ins(1,3,4,5)P_4, **2a**), a molecule whose significance is much less

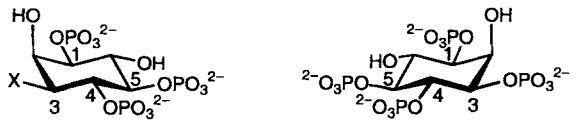

1 X = OH
2a X = OPO_3^{2-}
2b

well understood. Although binding sites for Ins(1,3,4,5)P_4 have been identified in a wide range of tissues,[2] the cellular function of Ins(1,3,4,5)P_4 remains unknown. Considerable interest has therefore followed the recent identification of an Ins(1,3,4,5)P_4-binding protein, which was purified from platelets, as a member of a family of GTPase activating proteins (GAP).[3] The high affinity of this protein (now designated GAP1^{IP4BP}) for Ins(1,3,4,5)P_4, and its extreme specificity for the 1,3,4,5 configuration of phosphate groups[4] suggest that it may be an Ins(1,3,4,5)P_4 receptor. Very recently it was reported that the interaction of Ins(1,3,4,5)P_4 with the pleckstrin homology (PH) domain of Bruton's tyrosine kinase (Btk) may be involved in B-cell activation and development.[5] Mutations in the Btk PH domain causing human X-linked agammaglobulinaemia (XLA) are associated with dramatically reduced Ins(1,3,4,5)P_4-binding activity.

The spreading interest in Ins(1,3,4,5)P_4 has created a need for an economical and rapid route to pure synthetic material.[6] Although several syntheses of D-Ins(1,3,4,5)P_4 have been published,[7] many are long or require the use of enzymes. Furthermore, the unnatural enantiomer L-Ins(1,3,4,5)P_4 (**2b**; alternative name D-Ins(1,3,5,6)P_4), for which there is only one reported synthesis,[7a] is increasingly being used as a biological tool in studies of D-Ins(1,3,4,5)P_4.[4a, 8] Here we describe a rapid and potentially useful large-scale route to both enantiomers of Ins(1,3,4,5)P_4 by desymmetrization of the well-known *myo*-inositol orthoformate **3**[9] (Scheme 1).

[*] Prof. Dr. B. V. L. Potter, Dr. A. M. Riley
School of Pharmacy and Pharmacology
University of Bath
Claverton Down, Bath, BA2 7AY (UK)
Fax: Int. code +(1225)826-114
e-mail: b.v.l.potter@bath.ac.uk
Dr. M. F. Mahon
School of Chemistry, University of Bath

[**] We thank the Wellcome Trust for Programme Grant support (045491), and Dr. P. J. Cullen (Department of Biochemistry, University of Bristol, UK) for preliminary biological evaluation of **2a** at purified GAP1^{IP4BP}.

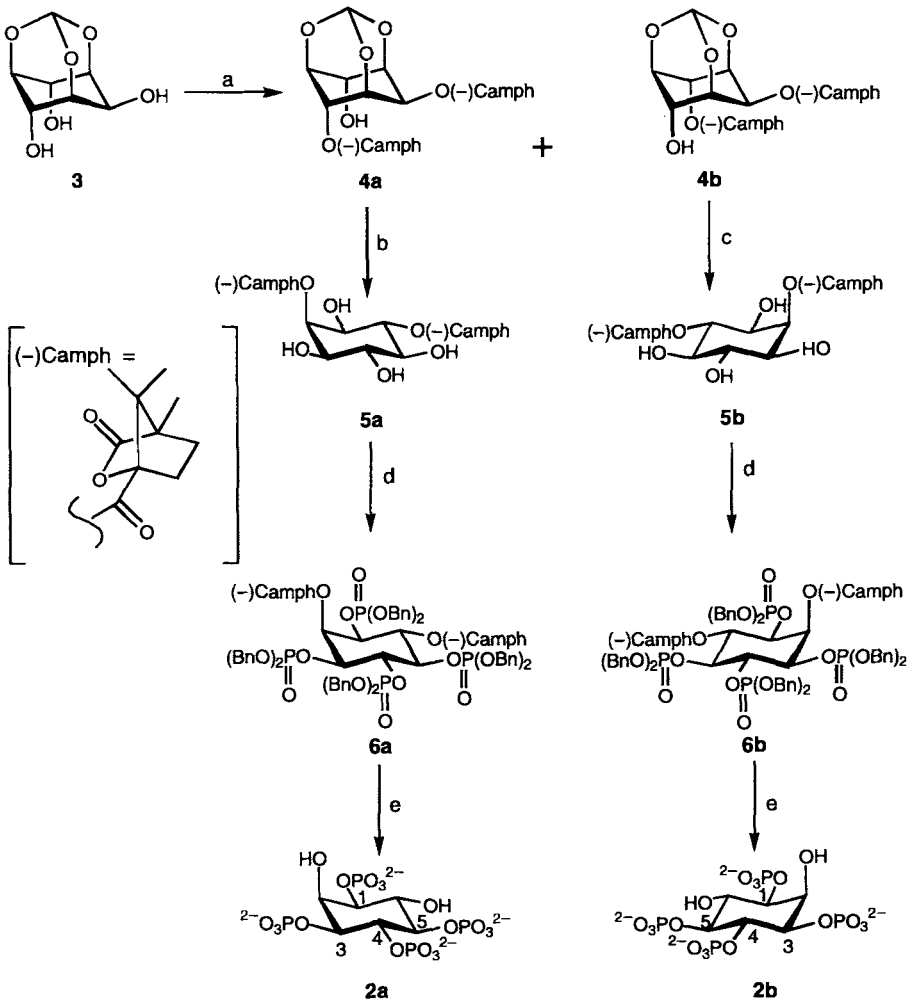

Scheme 1. Synthesis of **2a** and **2b** from *myo*-inositol orthoformate (**3**). a) (1*S*)-(−)-camphanic acid chloride (2.0 equiv), CH_2Cl_2, Et_3N, DMAP, 0 °C to room temperature (RT); b) 1 M HCl/MeOH 1/10, reflux, 6 h, 88%; c) CF_3COOH/H_2O 4/1, RT, 40 h, 85%; d) 1. $(BnO)_2PNiPr_2$, 1*H*-tetrazole, CH_2Cl_2; 2. *m*-CPBA, 78–86%; e) 1. H_2, 1 atm, Pd/C, MeOH/H_2O 19/1, RT; 2. concd aq NH_3, 60 °C, quantitative yield.

Table 1. Selected physical and spectroscopic data for **4a,b** and **2a,b**.

4a: $R_f = 0.32$ (CH_2Cl_2/ethyl acetate 3/1); $[\alpha]_D^{20} = -15.5$ ($c = 1$ in $CHCl_3$), $[\alpha]_D^{20} = -20.5$ ($c = 1$ in DMF). Crystallization from ethyl acetate/hexane, m.p. > 235 °C; elemental analysis calcd for $C_{27}H_{34}O_{12}$ (550.56): C 58.90, H 6.22; found: C 58.7, H 6.23; ^{1}H NMR (400 MHz, $CDCl_3$, TMS): $\delta = 1.00$, 1.03, 1.09, 1.10, 1.12, 1.14 (6s, 18H, camph-CH_3), 1.65–1.75 (m, 2H, camph-CH_2), 1.92–2.03 (m, 2H, camph-CH_2), 2.06–2.18 (m, 2H, camph-CH_2), 2.41–2.56 (m, 2H, camph-CH_2), 3.29 (d, $J = 6.8$ Hz, 1H, D_2O exchange, 4-OH), 4.36 (dddd, appears as dq, J = ca. 4, 2, 2, 2 Hz, 1H, C-3-H), 4.43 (dddd, appears as dq, J = ca. 4, 2, 2, 2 Hz, 1H, C-1-H), 4.55 (dddd, appears as tt, J = ca. 4, 4, 2, 2 Hz, 1H, C-5-H), 4.65–4.70 (br m, 1H, C-4-H), 5.30 (ddd, appears as partially resolved dt, J = ca. 2, 2, 1 Hz, 1H, C-2-H), 5.54 (d, $J = 0.98$ Hz, 1H, O_3CH), 5.63 (ddd, appears as dt, J = ca. 4, 4, 1.5 Hz, 1H, C-6-H); positive-ion FAB-MS: *m/z* (%) = 1101 (100) $[2M+H]^+$, 551 (80) $[M+H]^+$.

4b: $R_f = 0.23$ (CH_2Cl_2/ethyl acetate 3/1); $[\alpha]_D^{25} = +7.5$ ($c = 1$ in DMF). Crystallization from DMF/H_2O or 2-propanol, m.p. > 270 °C (decomp); elemental analysis calcd for $C_{27}H_{34}O_{12}$ (550.56): C 58.90, H 6.22; found: C 58.6, H 6.31; ^{1}H NMR (400 MHz, [D$_7$]DMF, TMS): $\delta = 0.95$, 0.96, 1.06, 1.08, 1.16, 1.17 (6s, 18H, camph-CH_3), 1.57–1.67 (m, 2H, camph-CH_2), 1.91–1.98 (m, 1H, camph-CH_2), 2.01–2.15 (m, 3H, camph-CH_2), 2.52–2.60 (m, 2H, camph-CH_2), 4.32–4.37 (m, 1H, C-1-H), 4.51–4.55 (m, 1H, C-5-H), 4.56–4.61 (m, 2H, C-3-H and C-6-H), 5.47–5.51 (m, 1H, C-2-H), 5.55–5.60 (m, 1H, C-4-H), 5.74 (d, $J = 0.91$ Hz, 1H, O_3CH), 6.21 (d, 1H, $J = 3.36$ Hz, D_2O exchange, C-6-OH); positive-ion FAB-MS: *m/z* (%) = 1101 (55) $[2M+H]^+$, 551 (100) $[M+H]^+$.

Optical rotations (cyclohexylammonium salts): **2a**: $[\alpha]_D^{22} = -2.5$ ($c = 2$ in H_2O), ref. [7a]; $[\alpha]_D^{25} = -2.5$ ($c = 1$ in H_2O); **2b**: $[\alpha]_D^{22} = 2.5$ ($c = 2$ in H_2O), ref. [7a]; $[\alpha]_D^{25} = 2.6$ ($c = 1$ in H_2O). All NMR data agree with the published values [7a, d].

Reaction of symmetrical **3** with 2.0 equivalents of (1*S*)-(−)-camphanic acid chloride gave two diastereoisomeric bis(camphanate) esters **4a** and **4b**, which were separated by flash chromatography and isolated as crystalline solids (Scheme 1, Table 1). A single-crystal X-ray crystallographic study of the less polar diastereoisomer[10] showed this compound to be 1D-2,6-di-*O*-[(−)-ω-camphanoyl]-*myo*-inositol orthoformate (**4a**, Figure 1). Diastereoisomer **4a** is therefore a synthetic precursor to D-Ins(1,3,4,5)P_4, whereas **4b** leads to L-Ins(1,3,4,5)P_4. It was possible to establish reaction conditions (see *Experimental Section*) that minimized production of the unwanted 2-monocamphanate and 2,4,6-tris(camphanate)s. Interestingly, under these conditions the reaction showed considerable diastereoselectivity in favor of **4a**, which allowed it to be isolated in up to 60% yield by careful chromatography. The more polar product **4b** was isolated in about 20% yield, and none of the possible side product 4,6-bis(camphanate) was detected.

Acid hydrolysis of the orthoformate protecting group from **4a** and **4b** gave tetraols **5a** and **5b**. Since these crystallized as hydrates, it was important that they were dried in vacuo at 60 °C before the next step. Phosphitylation with bis (benzyloxy) - *N,N* - diisopropylaminophosphine/1*H*-tetrazole followed by oxidation of the phosphites with *m*-CPBA gave the fully protected tetrakisphosphates **6a** and **6b**. As at the preced-

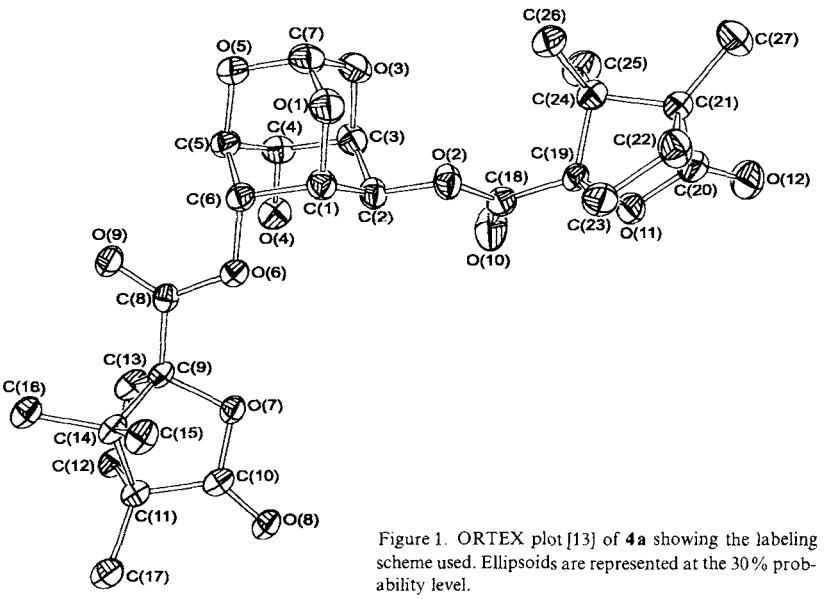

Figure 1. ORTEX plot [13] of **4a** showing the labeling scheme used. Ellipsoids are represented at the 30% probability level.

 © VCH Verlagsgesellschaft mbH, D-69451 Weinheim, 1997 0570-0833/97/3613-1473 $ 17.50+.50/0

ing stages, any diastereoisomer contamination of **6a** or **6b** would be apparent from an examination of the camphanate methyl resonances in the ^{1}H NMR spectra. At no stage was any such contamination seen. A two-step deprotection strategy involving removal of the benzyl protecting groups on phosphates by hydrogenolysis and then cleavage of camphanate esters in a concentrated solution of ammonia at 60 °C was effective with no migration of phosphate groups.[11] Tetrakis(phosphate)s **2a** and **2b** could then be isolated on a gram scale as the cyclohexylammonium[7a] or potassium[7d] salts in overall yields of 60–70% from **4a** and **4b**. The structures of **2a** and **2b** were confirmed by ^{1}H, ^{13}C, and ^{31}P NMR spectroscopy as well as high-resolution FAB-MS. We recently used bulk material prepared in this fashion to investigate the submolecular acid–base properties of Ins(1,3,4,5)P_4 by ^{31}P NMR titration experiments.[12] Alternatively, ion-exchange chromatography on Q-Sepharose Fast-Flow gave the pure tetrakisphosphates as their triethylammonium salts. A sample of **2a** was identical to biologically-derived D-Ins(1,3,4,5)P_4 with respect to its interaction with GAP1^{IP4BP}.

In conclusion, we describe rapid access to pure synthetic D- and L-Ins(1,3,4,5)P_4 from readily available starting materials by simultaneously using camphanate esters as desymmetrizing auxiliaries and protecting groups. This strategy should have wider applicability in the inositol phosphate field. Furthermore, the technique is capable of providing D-Ins(1,3,4,5)P_4 in quantities that will now be required for crystallographic and NMR studies of its interaction with the rapidly expanding range of Ins(1,3,4,5)P_4-binding proteins.

Experimental Section

4a, b: To a stirred suspension of **3** (2.00 g, 10.5 mmol) in dry CH_2Cl_2 (40 mL) at 0 °C were added Et_3N (3.3 mL, 23.7 mmol) and a catalytic amount of 4-dimethylaminopyridine (80 mg). A solution of (1*S*)-(−)-camphanic acid chloride (4.55 g, 21.0 mmol) in dry CH_2Cl_2 (10 mL) was added dropwise under an N_2 atmosphere at 0 °C. The cooling bath was removed after 30 min, and stirring continued for a further 30 min. After this time almost no solid remained, and TLC (CH_2Cl_2/ethyl acetate 3/1) showed two major products at $R_f = 0.32$ and 0.23. The solvents were removed in vacuo, and the residue was purified by flash chromatography (CH_2Cl_2/ethyl acetate 4/1) to give first **4a** (3.46 g, 6.28 mmol, 60% yield) and then **4b** (1.35 g, 2.45 mmol, 23% yield).

2a, b: A solution of **6a** or **6b** in MeOH/H_2O (19/1) was stirred vigorously with 10% Pd/C under an atmosphere of H_2 at room temperature overnight. The catalyst was removed by filtration, and the solvents in vacuo. The residue was dissolved in a concentrated solution of aq ammonia, and the solution stirred at 60 °C in a sealed Pyrex autoclavable bottle for 6 h. The solution was allowed to cool and then concentrated under reduced pressure. The residue was dissolved in deionized water, and the camphanamide removed by washing with CH_2Cl_2 (3 ×) followed by Et_2O. Purification by ion-exchange chromatography on Q-Sepharose Fast-Flow eluting with a gradient of triethylammonium bicarbonate buffer (pH 8, 0–1 M) gave the pure triethylammonium salts of **2a** or **2b**, which eluted at 730–850 mM buffer. For larger-scale production treatment with Dowex 50 H^+ resin gave solutions of the free acids of **2a** or **2b**, which were washed again with CH_2Cl_2 and Et_2O, and then converted into either the cyclohexylammonium [7a] or potassium [7d] salts in quantitative yield from **6a** or **6b**.

Received: January 31, 1997 [Z10061IE]
German version: *Angew. Chem.* **1997**, *109*, 1583–1585

Keywords: chirality · inositol phosphates · protecting groups · second messengers · signal transduction

[1] a) M. J. Berridge, *Nature (London)* **1993**, *361*, 315–325; b) M. J. Berridge, *Ann. N. Y. Acad. Sci.* **1995**, *766*, 31–43; c) recent review of the chemistry of inositol lipid mediated cellular signaling: B. V. L. Potter, D. Lampe, *Angew. Chem.* **1995**, *107*, 2085–2125; *Angew. Chem. Int. Ed. Eng.* **1995**, *34*, 1933–1972.

[2] R. F. Irvine, P. J. Cullen, *Curr. Biol.* **1993**, *3*, 540–543.

[3] P. J. Cullen, J. J. Hsuan, O. Truong, A. J. Letcher, T. R. Jackson, A. P. Dawson, R. F. Irvine, *Nature (London)* **1995**, *376*, 527–530.

[4] a) P. J. Cullen, A. P. Dawson, R. F. Irvine, *Biochem. J.* **1995**, *305*, 139–143; b) P. J. Cullen, S.-K. Chung, Y.-T. Chang, A. P. Dawson, R. F. Irvine, *FEBS Lett.* **1995**, *358*, 240–242.

[5] M. Fukuda, T. Kojima, H. Kabayama, K. Mikoshiba, *J. Biol. Chem.* **1996**, *271*, 30303–30306.

[6] There is evidence that some samples of commercially available D-Ins(1,3,4,5)P_4 are contaminated with small amounts of D-Ins(1,4,5)P_3: D. J. Gawler, B. V. L. Potter, S. R. Nahorski, *Biochem. J.* **1990**, *272*, 519–524.

[7] a) G. Baudin, B. I. Glänzer, K. S. Swaminathan, A. Vasella, *Helv. Chim. Acta* **1988**, *71*, 1367–1378; b) C. E. Dreef, R. J. Tuinman, C. J. J. Elie, G. A. van der Marel, J. H. van Boom, *Recl. Trav. Chim. Pays-Bas* **1988**, *107*, 395–397; c) Y. Watanabe, T. Fujimoto, T. Shinohara, S. Ozaki, *J. Chem. Soc. Chem. Commun.* **1991**, 428–429; d) D.-M. Gou, Y.-C. Liu, C.-S. Chen, *Carbohydr. Res.* **1992**, *234*, 51–64; e) J. R. Falck, A. Abdali, *Bioorg. Med. Chem. Lett.* **1993**, *3*, 717–720.

[8] a) R. A. Wilcox, R. A. J. Challiss, G. Baudin, A. Vasella, B. V. L. Potter, S. R. Nahorski, *Biochem. J.* **1993**, *294*, 191–194; b) J. W. Loomis-Husselbee, P. J. Cullen, U. E. Dreikhausen, R. F. Irvine, A. P. Dawson, *ibid.* **1996**, *314*, 811–816.

[9] H. W. Lee, Y. Kishi, *J. Org. Chem.* **1985**, *50*, 4402–4404.

[10] Crystal structure analysis of **4a**: Suitable crystals were grown by slow crystallization from 2-propanol (approximate crystal dimensions 0.3 × 0.3 × 0.3 mm): $C_{27}H_{34}O_{12}$, $M_r = 550.54$, monoclinic, $a = 6.755(1)$, $b = 31.139(2)$, $c = 7.035(1)$ Å, $\beta = 117.80(1)^\circ$, $V = 1309.0(3)$ Å^3, space group $P2_1$, $Z = 2$, $\rho_{calcd} = 1.397$ g cm^{-3}, $\mu(Mo_{K\alpha}) = 0.110$ mm^{-1}, $F(000) = 584$. Measurements were made at 293(2) K on a CAD4 automatic four-circle diffractometer in the range $2.61 < \theta < 21.93^\circ$. Data (1795 reflections) were corrected for Lorentzian and polarization but not for absorption effects. In the final least-squares cycles all atoms were allowed to vibrate anisotropically. Except for H1A, which was located in the penultimate difference Fourier and refined at a distance of 0.96 Å from O4, hydrogen atoms were included at calculated positions where relevant. The supramolecular structure contains a hydrogen-bonding feature. The structure was solved with SHELX86 and refined with SHELX93: based on 1326 with $F_o > 4\sigma(F_o)$ $R1 = 0.0318$ and $wR2 = 0.0755$; GOF = 1.029; max./min. residual densities 0.185/ − 0.175 e Å^{-3}. The asymmetric unit (Figure 1) and the labeling scheme were produced with ORTEX. Final fractional atomic coordinates, anisotropic temperature factors, and bond distances and angles are available as supplementary data. Crystallographic data (excluding structure factors) for the structure reported in this paper have been deposited with the Cambridge Crystallographic Data Centre as supplementary publication no. CCDC-100275. Copies of the data can be obtained free of charge on application to the Director, CCDC, 12 Union Road, Cambridge CB2 1EZ, UK (fax: int. code +(1223)336-033; e-mail: deposit@chemcrys.cam.ac.uk).

[11] An earlier strategy involving phosphitylation with bis(cyanoethyloxy)-*N*,*N*-diisopropylaminophosphine/1*H*-tetrazole and oxidation as before followed by a one-step deprotection with aqueous ammonia was not satisfactory. It gave rise to slight but detectable migration of phosphate groups at the deprotection stage.

[12] P. Guédat, E. Krempp, A. M. Riley, B. V. L. Potter, G. Schlewer, B. Spiess, *Chem. Commun.* **1997**, 625–626.

[13] P. McArdle, *J. Appl. Crystallogr.* **1994**, *27*, 438.

A New Cationic Domino Process to (±)-Uleine

Monika H. Schmitt and Siegfried Blechert*

Dedicated to Professor Ekkehard Winterfeldt on the occasion of his 65th birthday

Domino processes play an important role in organic synthesis,[1] and cation-induced processes are of great significance in both organic synthesis and biosynthesis. Herein we report on a new cationic cascade reaction (Scheme 1), which we have applied to the stereoselective synthesis of uleine. The introduced process might also be very interesting for the construction of strychnos alkaloids.

Several syntheses have been described for the alkaloids of the uleine group such as uleine (**2**), which like the strychnos alkaloids has an azocino[4,3-*b*]indole skeleton.[2] However, most concepts that employ a carbocyclization in a late step (either by formation of the C-1/C-9a or C-4/C-4a bond) lead to 3-*epi*-com-

[*] Prof. Dr. S. Blechert, Dipl.-Chem. M. H. Schmitt
Institut für Organische Chemie der Technischen Universität
Strasse des 17. Juni 135, D-10623 Berlin (Germany)
Fax: Int. code +(30)31423619
e-mail: sibl@wap0105.chem.tu-berlin.de

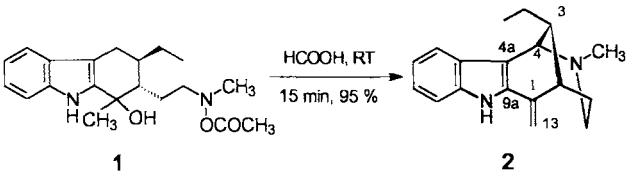

1 2

Scheme 1. Cation-induced transformations of **1** to uleine (**2**).

pounds. Therefore, for the synthesis of uleine (**2**) we envisaged a heterocyclization from the side opposite the ethyl group to form the piperidine ring. Ring closure should occur via an iminium ion of type **4** (Scheme 2) and should lead to the desired configuration at C-3. Cations of type **4** should be readily available by cleaving a suitable leaving group X from **3**, as described

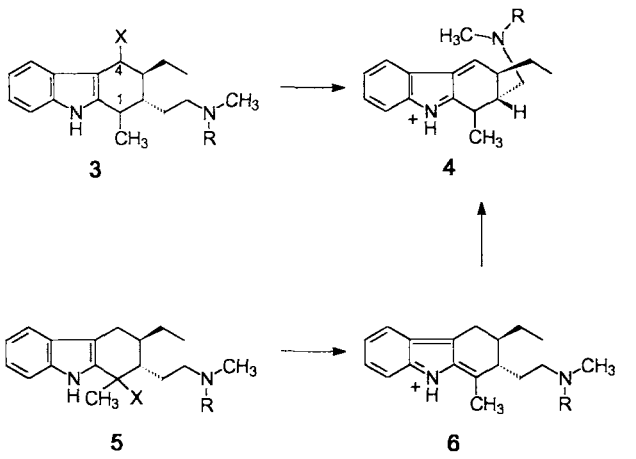

3 4 5 6

Scheme 2. Proposed routes to the vinylic iminium salt **4**.

in syntheses of similar systems.[3] We assumed that this iminium ion could also be formed by a leaving group on C-1 (uleine nomenclature). The cation **6** generated from **5** could undergo isomerization to the thermodynamically favored product **4** by a deprotonation–protonation sequence faster than addition of a nucleophile. In our concept, a positive charge generated on C-1 would activate position C-4 for nucleophilic attack. To the best of our knowledge a reaction like this has not yet been described in indole chemistry. However, the heterocyclization would give a 1,13-dihydrouleine. To construct the double bond, we planned a new cation-induced process. The *N*-acyloxyammonium ion **7** resulting from the heterocyclization step should be a suitable precursor for this reaction (Scheme 3). Because of the short distance between C-4a and the nitrogen atom of the piperidine ring and the convenient orientation of the π electrons to this nitrogen, an intramolecular substitution reaction could lead to **8**, containing a three-membered ring and an imine group. Tautomerization of **8** to **9** and subsequent removal of a proton to the vinylindole, would lead to uleine (**2**). Whereas, during the first reaction step, a carbocation on the "southern part of the molecule" should lead to a reaction in the "northern part", a cationic nitrogen center in the "northern area" should form the C-1/C-13 double bond. Generation of the ammonium ion **7** by the above-mentioned cyclization reaction serves to connect both processes.

This concept, which may seem speculative at first glance, proved viable. Thus, the *O*-acylated hydroxylamine derivative **1**, which was used as a mixture of two diastereomeres with regard to the configuration at C-1, was allowed to react with formic acid at room temperature to give uleine (**2**) in high yield (Scheme 1). The spectroscopic data of **2** are in agreement those

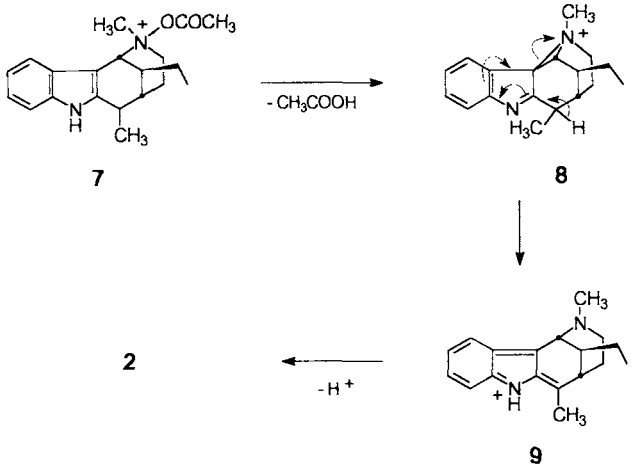

7 8 2 9

Scheme 3. Proposed mechanism for the formation of the C-1/C-13 double bond in **2** from the *N*-acyloxyammonium ion **7**.

of the natural product.[4] The structure was confirmed by comparison with an authentic sample. On the basis of our findings we propose the mechanism given in Schemes 2 and 3 for the synthesis of uleine; however, as of yet we have no definite proof. We tried to monitor the reaction by NMR spectroscopy, but we could not detect any clearly definable intermediates. Instead of tertiary alcohol **1**, the *exo*-methylene compound resulting from the removal of H_2O can be employed. We have prepared 1,13-dihydrouleine-N_b-oxide form **2** by hydrogenation with palladium and barium sulfate and subsequent conversion with *m*-chloroperbenzoic acid; its reaction with acetyl chloride at low temperature was then monitored by NMR spectroscopy. Salt **7**-Cl was formed at $-40\,^{\circ}C$ and transformed into uleine at $-30\,^{\circ}C$. Unfortunately, intermediates could not be confirmed. Several attempts at gaining indications of radical processes also proved unsuccessful. The transformation **7** → **2** is much faster than the overall process. The formation of the aziridinium ion could not be verified, but seems reasonable to us on the basis of results obtained form experiments with the *N*-acylated cationic uleine-*N*-oxide. Ions of type **7** with a double bond between C-1 and C-13 give products of a nucleophilic addition to C-13.

The devised domino process consists of the following steps: formation of a benzyl cation, multistep tautomerizations, cyclization to the piperidine derivative, formation of a three-membered ring, fragmentation, and tautomerization.

The synthesis of **1** is described in Scheme 4; each compound was fully characterized. Starting from cyclohexenone **10**, Michael addition followed by conversion of the enolate by alkylation,[5] and treatment with sodium hydride and ethylformiate yield the *trans*-configurated hydroxymethylene compound **11** in good yield.[6] A Japp–Klingemann reaction and subsequent Fischer indole synthesis give rise to the tetrahydrocarbazole **12**.[7] Unfortunately, the *trans* configuration is partially affected during the course of the Fischer indole synthesis. A complete isomerization to **12** is achieved by treatment with sodium methanolate in methanol after a reaction time of 1–2 weeks at room temperature. Evidently, the competing deprotonation of the acidic NH proton and the slight CH acidity of the vinylogous amide delay the isomerization to the thermodynamically favored *trans* product **12**. The subsequent oxidative cleavage of the double bond with a catalytic amount of osmium tetroxide and sodium periodate leads to the aldehyde, which reacts without further purification with *N*-methylhydroxylamine to give hydroxylamine **13** under reductive conditions (sodium cyanoborohydride) at pH 6. The formation of the tetrahydro-

 © VCH Verlagsgesellschaft mbH, D-69451 Weinheim, 1997 0570-0833/97/3613-1475 $ 17.50+.50/0

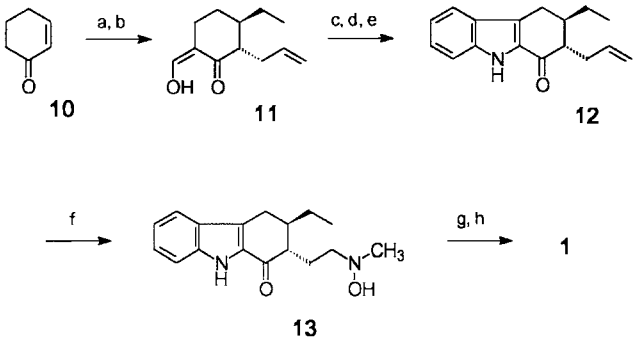

Scheme 4. a) 1. EtMgBr, CuI, Me_2S, THF; 2. $H_2C{=}CHCH_2Br$, hexamethylphosphoric acid triamide (HMPT) (60%); b) NaH, glyme, HCOOEt (95%); c) PhN_2Cl (85%); d) HCOOH (86%); e) NaOMe, MeOH, RT, 12–14 d (99%); f) 1. OsO_4, $NaIO_4$, MTBE, H_2O; 2. MeNHOH, $NaCNBH_3$, *i*PrOH, pH = 6 (85%); g) MeLi, THF, $-20\,^{\circ}C \rightarrow$ RT (98%); h) Ac_2O, pyridine, 3 h, RT (99%).

carbazole derivative **1** is achieved by the addition of methyllithium to the carbonyl function, and O-acetylization of the hydroxylamine group.[9] The conversion of **13** to uleine (**2**) can be performed in good yields without chromatographic purification of the intermediates. The novel cascade reaction allows the application of the readily obtained *trans* configuration of the tetrahydrocarbazole **13** for a concise and stereoselective synthesis of uleine. This example demonstrates once more that the application of domino processes can open more efficient and shorter synthetic pathways.

Experimental Section

2: Tetrahydrocarbazole **1** (68.8 mg, 0.2 mmol) was dissolved in formic acid (5 mL) and left at room temperature for 15 min. The solvent was evaporated under reduced pressure and the crude product was purified by preparative thin-layer chromatography (silical gel, CH_2Cl_2/MeOH, 95/5 under NH_3 atmosphere) to give (±)-uleine (**2**) (54 mg, 95%).

Received: January 22, 1997 [Z10021IE]
German version: *Angew. Chem.* **1997**, *109*, 1516–1518

Keywords: carbazoles · cations · domino reactions · total synthesis · uleine

[1] a) S. Blechert, R. Knier, H. Schroers, T. Wirth, *Synthesis* **1995**, 591; b) L. F. Tietze, U. Beifuss, *Angew. Chem.* **1993**, *105*, 137; *Angew. Chem. Int. Ed. Engl.* **1993**, *32*, 131; c) R. A. Bunce, *Tetrahedron* **1995**, *51*, 13103; d) *ibid.* **1996**, *52*, 11385.

[2] J. Gràcia, N. Casamitjana, J. Bonjoch, J. Bosch, *J. Org. Chem.* **1994**, *59*, 3939, and references therein.

[3] See for example: P. Magnus, N. L. Sear, C. S. Kim, N. Vicker, *J. Org. Chem.* **1992**, *57*, 70.

[4] Selected spectroscopic data of **2**: ^{1}H NMR (400 MHz, $CDCl_3$, [D$_4$]MeOH, TMS): δ = 8.30 (s, br., 1H, NH), 7.55 (dd, J = 8, 1 Hz, 1H, H-5), 7.35 (dd, J = 8, 1 Hz, 1H, H-8), 7.18 (ddd, J = 8, 8, 1 Hz, 1H, H-7), 7.09 (ddd, J = 8, 8, 1 Hz, 1H, H-6), 5.27 (s, 1H, H-13), 4.99 (s, 1H, H-13'), 4.10 (d, J = 2 Hz, 1H, H-4), 2.69 (dd, br., J = 7.5, 2 Hz, 1H, H-2), 2.48 (dd, J = 6.5, 2 Hz, 1H, H-11), 2.29 (s, 3H, H-12), 2.08 (m, 3H, H-3, H-10, H-11'), 1.68 (ddm, J = 10, 2 Hz, 1H, H-10'), 1.12 (dq, J = 7, 7 Hz, 2H, H-14), 0.84 (t, J = 7 Hz, 3H, H-15); ^{13}C NMR (100 MHz, $CDCl_3$): δ = 138.5 (C, C-8a), 136.6 (C, C-4b), 135.3 (C, C-9a), 129.2 (C, C-4a), 122.7 (CH, C-6), 119.9 (CH, C-5), 119.4 (CH, C-7), 110.8 (CH, C-8), 108.1 (C, C-1), 107.1 (CH$_2$, C-13), 56.6 (CH, C-4), 46.2 (CH, C-2), 45.8 (CH$_2$, C-11), 44.2 (CH$_3$, C-12), 39.3 (CH, C-3), 34.5 (CH$_2$, C-10), 24.3 (CH$_2$, C-14), 11.7 (CH$_3$, C-15); HR-MS: calcd for $C_{18}H_{22}N_2$: 266.1783, found: 266.1783.

[5] Y. Ito, M. Nakatsuka, T. Saegusa, *J. Am. Chem. Soc.* **1982**, *104*, 7609.

[6] E. J. Corey, D. E. Cane, *J. Org. Chem.* **1971**, *36*, 3070.

[7] D. P. Chakraborty, A. Islam, P. Bhattacharyya, *J. Org. Chem.* **1973**, *38*, 2728.

[8] R. Besselievre, H.-P. Husson, *Tetrahedron* **1981**, *37*, 241.

[9] Selected spectroscopic data of **1**: ^{1}H NMR (400 MHz, $CDCl_3$, TMS): δ = 7.44 (dd, J = 8 Hz, J = 1 Hz, 1H, H-5), 7.29 (dd, J = 8, 1 Hz, 1H, H-8), 7.13 (ddd, J = 8, 8, 1 Hz, 1H, H-7), 7.07 (ddd, J = 8, 8, 1 Hz, 1H, H-6), 3.15 (m, 1H, H-13), 2.99 (dd, J = 16.5, 5 Hz, 1H, H-4), 2.85 (m, 1H, H-13'), 2.77 (s, 3H, H-14), 2.22 (dd, J = 16.5, 10 Hz, 1H, H-4'), 2.05 (s, 3H, H-17), 1.76 (m, 4H, H-2, H-3, H-12, H-12'), 1.40 (s, 3H, H-15), 1.28 (m, 2H, H-10, H-10'), 0.98 (t, J = 7 Hz, 3H, H-11).

Relative Migratory Aptitude of Substituents and Stereochemistry of Dyotropic Ring Enlargements of β-Lactones

Johann Mulzer,* Karsten Hoyer, and Anke Müller-Fahrnow

Dedicated to Professor Dieter Seebach on the occasion of his 60th birthday

In a dyotropic reaction of type 1 two substituents change their positions relative to a C–C single bond (Scheme 1).[1] The mutual 1,2 shift is reversible if there is no significant energy

Scheme 1.

difference between the two tautomers. In the case of a concerted mechanism the shift follows a *syn* or *anti* stereochemistry. The latter is characterized by an inversion at C1 and C2. If, on the other hand, the 1,2 shift proceeds by a stepwise mechanism, there is no compulsory correlation between the configurations of the two centers. Apart from the stereochemistry the migratory aptitude of the substituents is a point of issue about which practically nothing is known so far.

We report here on the dyotropic ring enlargement of β-lactones to γ-lactones. These rearrangements are irreversible due to ring-strain relief (Scheme 2) and proceed by inversion at C4.[2]

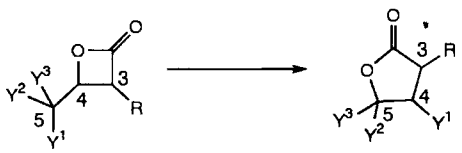

Scheme 2.

The relative migratory aptitude can be determined by placing different substituents Y^1, Y^2, and Y^3 at C5 of the β-lactone. We examined substituents with σ- (Y = alkyl), π- (Y = phenyl), and *n*- (Y = OR) donor qualities. In the last case the reaction resembles a semipinacol rearrangement.[3] The stereochemistry of the rearrangement with respect to the C4–C5 axis was studied with C3 as a stereochemical reference. The reaction can proceed by the concerted mechanism **A** or the stepwise-ionic mechanism **B** (Scheme 3).[2, 4, 5]

If mechanism **A** is involved the reaction should exclusively form γ-lactone **2** by a twofold inversion at C4 and C5. Conversely, in mechanism B a cationic species **Z-1** is generated, which may form **Z-2** by rotation about the C4–C5 axis. Intermediates **Z-1** and **Z-2** can cyclize to the epimeric γ-lactones **2** and **3**, respectively.[2] The experimental data are summarized in Table 1.

[*] Prof. Dr. J. Mulzer
Institut für Organische Chemie der Universität
Währinger Strasse 38, A-1090 Wien (Austria)
Fax: Int. code +(1)31367-2280
e-mail: mulzer@felix.orc.univie.ac.at
Dipl.-Chem. K. Hoyer
Institut für Organische Chemie der Universität Frankfurt am Main (Germany)
Dr. A. Müller-Fahrnow
Institut für Physikochemie der Schering AG, Berlin (Germany)

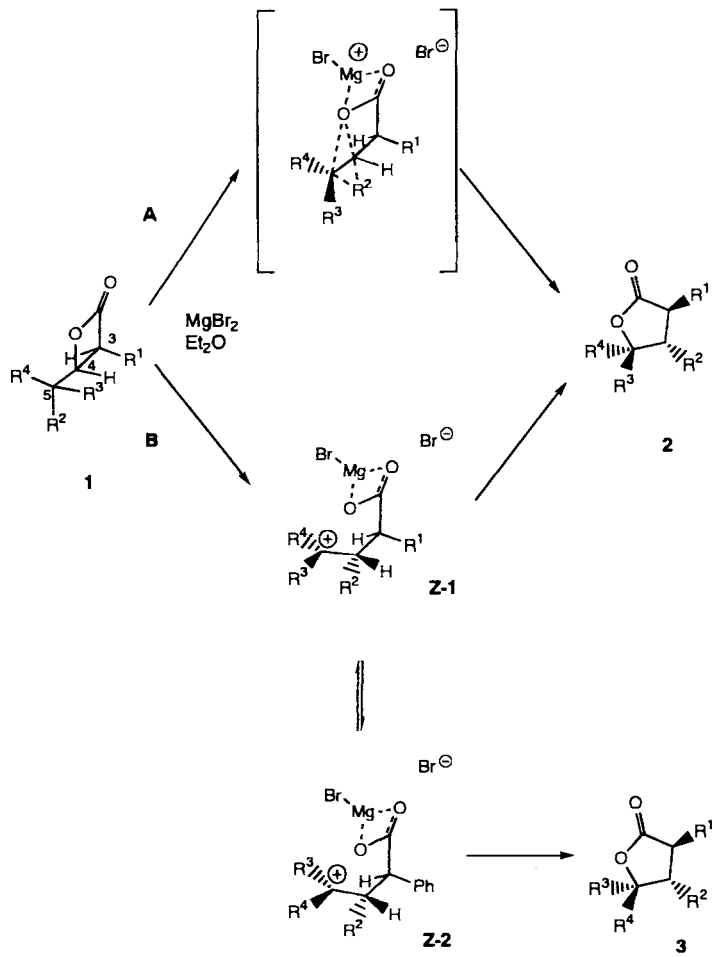

Scheme 3.

Table 1. Ratio of products **2** and **3** for the dyotropic ring enlargement of β-lactones **1**.

			β-Lactone [6]	Ratio of γ-lactones [%] [7]		Yield [2 + 3]
R^2	R^3	R^4	**1**	**2**	**3**	[%]
Ph	Me	OMe	**a**	78	22	96
Ph	OMe	Me	**b**	22	78	97
Ph	Me	H	**c**	97	3	96
Ph	H	Me	**d**	85	15	95
Ph	[a]	H	**e**	94	6	87
OBn	*t*Bu	Me	**f**	>99	<1	86
OBn	Me	Et	**g**	>99	<1	>99
OBn	Et	Me	**h**	>99	<1	>99

[a] $R^3 = (H_3C)_2C{=}CHCH_2CH_2$.

The highest migratory aptitude was observed for the phenyl group. Ring enlargement of the β-lactones **1a** and **1b** furnished the γ-lactones **2a** and **3a** or **2b** and **3b**, respectively, in practically identical ratios. This indicates that these rearrangements proceed via **Z-1**- and **Z-2**-type intermediates, which are in a fast equilibrium (Scheme 3). As ring closure of **Z-1** and **Z-2** to the corresponding γ-lactones is slower than the rotation about C4–C5, the ratio of products **2** and **3** reflects the composition of the **Z-1**⇌**Z-2** equilibrium. The rearrangement of **1c–e** also involves **Z-1** species; however, since they have secondary carbenium centers they are short-lived, and rotation about C4–C5 and ring closure are of comparable rates. In these cases the steric strain in **Z-1** determines the stereochemical pathway. If the bulky substituent (Me) is in the hindered *endo* position (R^4), as is the case for the rearrangement of **1d**, the tendency towards rotation about C4–C5 is much higher than in the case of **1c**, in which the methyl group adopts the more favorable *exo* position (R^3). This is reflected in the ratio of the products (97:3 for **2c:3c** and 85:15 for **2d:3d**, Table 1). Apparently a maximum of one rotation is allowed prior to ring closure, and phenonium species are not involved.

After the phenyl group, alkoxy substituents show the highest migratory aptitude. Within the limits of detection the rearrangement of the β-lactones **1f–h** produces the γ-lactones **2f–h** with perfect stereoselectivity. This indicates formation of the oxonium intermediate **Z-3**, which suppresses any rotation around the C4–C5 axis (Scheme 4). Diastereoselective dyotropic shifts of nitrogen residues have been reported.[8]

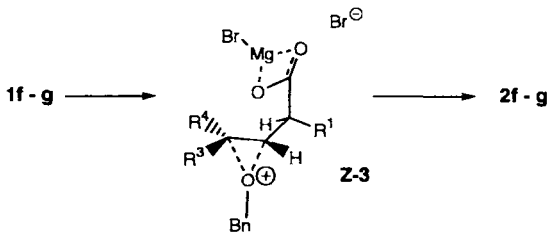

Scheme 4.

Single crystal X-ray diffraction studies of **1a–f** gave important information about the conformations around the C4–C5 axis. Assuming that the solid-state conformation remains unchanged after formation of the magnesium bromide complex in solution, the migrating substituent in **1a–e** already occupies the stereoelectronically "correct" position antiperiplanar to the C–O bond of the β-lactone. This means that in these cases the ground state and the reactive conformation are identical. Conversely, rotation about C4–C5 has to take place in **1f** to obtain the reactive conformation **1f'**, in which the Me group adopts the unfavorable *endo* position (Scheme 5).[11] For such rotations a barrier of less than 8 kJ mol^{-1} is required according to AM1-calculations, and the validity of the Curtin–Hammett principle can be assumed. This means that the ground-state conformation of β-lactones has no influence on the diastereomer ratio of the resulting γ-lactones.[12, 13]

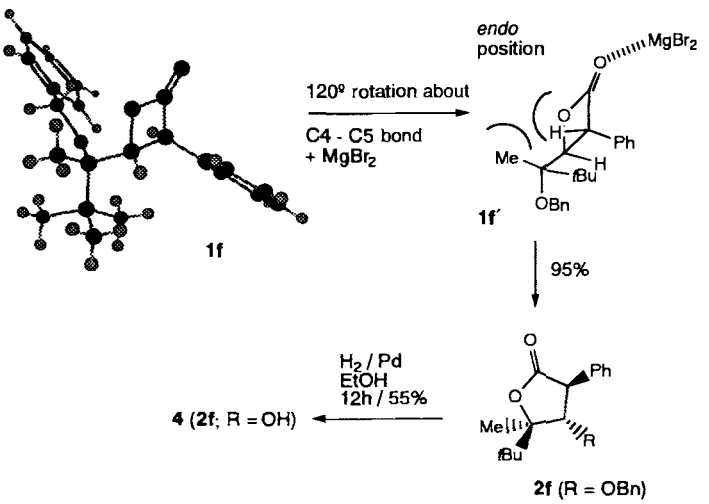

Scheme 5.

 © VCH Verlagsgesellschaft mbH, D-69451 Weinheim, 1997 0570-0833/97/3613-1477 $ 17.50+.50/0

In conclusion, dyotropic β-lactone–γ-lactone ring enlargement follows the nonconcerted mechanism **B**; the migratory aptitudes of the substituents are in the order π-donor > *n*-donor > σ-donor substituent. Migration of π-donor (and possibly also of σ-donor) substituents proceeds via intermediate **Z-1**, whose lifetime depends on carbenium stabilization. The migration of *n*-donor (oxygen) substituents involves a bridged oxonium species **Z-3**. In all rearrangements an inversion at C4 is observed without exception. The stereochemical course of the reaction is better clarified,[1] and its preparative value lies in the stereocontrolled formation of three contiguous stereogenic centers in the γ-lactones **2c, e–h**.

Received: January 3, 1997 [Z9961IE]
German version: *Angew. Chem.* **1997**, *109*, 1546–1548

Keywords: dyotropy · lactones · reaction mechanisms · rearrangements

[1] M. T. Reetz, *Angew. Chem.* **1972**, *84*, 161–162; *Angew. Chem. Int. Ed. Engl.* **1972**, *11*, 129–130; *ibid* **1979**, *91*, 185–192 and **1979**, *18*, 173–180; *Adv. Organomet. Chem.* **1977**, *16*, 33; *Tetrahedron* **1973**, *29*, 2189–2194.

[2] J. Mulzer, G. Brüntrup, *Angew. Chem.* **1979**, *91*, 840–841; *Angew. Chem. Int. Ed. Engl.* **1979**, *18*, 793–794.

[3] Review: D. J. Coveney in *Comprehensive Organic Synthesis* (Eds.: B. M. Trost, I. Fleming), *Vol. 3* (Ed.: G. Pattenden), Pergamon Press, Oxford, **1991**, p. 777.

[4] T. H. Black, J. A. Fields, *Synth. Commun.* **1988**, *18*, 125–130.

[5] T. H. Black, S. H. Eisenbeis, T. S. McDermott, S. L. Maluleka, *Tetrahedron* **1990**, *46*, 2307–2316.

[6] The synthesis of the β-lactones proceeded by carboxy-group activation with phenylsulfonyl chloride as described [9·10]. The diastereomeric β- and γ-lactones were separated by HPLC under normal-phase conditions with a Nucleosil (5–7 μm) stationary phase and *n*-hexane/ethyl-acetate as eluent.

[7] For ring enlargement the β-lactones were dissolved in anhydrous diethyl ether (10^{-1}–10^{-2} mmol mL^{-1}) and treated with 1.0 equiv of a 3.2 M solution of $MgBr_2$ in diethyl ether with ice cooling and stirring. After 12–60 h at 25–30 °C the reactions were quenched with water, and the diastereomeric γ-lactones isolated from the ether phase [2]. Cross-check experiments showed that γ-lactones **3a–e** remained unchanged under the reaction conditions.

[8] M. T. Reetz, A. Schmitz, X. Holdgrün, *Tetrahedron Lett.* **1989**, *30*, 5421–5424.

[9] J. Mulzer, A. Pointner, A. Chucholowski, G. Brüntrup, *J. Chem. Soc. Chem. Comm.* **1979**, 52–54.

[10] W. Adam, J. Baeza, J.-C. Liu, *J. Am. Chem. Soc.* **1972**, *94*, 2000–2006.

[11] X-ray crystal structure data for **1f**: 0.6 × 0.6 × 0.6 mm^3, orthorhombic, $Pca2_1$, $a = 15.624$, $b = 6.434$, $c = 37.92$ Å, $V = 3812$ Å^3, $Z = 8$, $\rho = 1.179$ g cm^{-3}, absorption coefficient 0.077 mm^{-1}, 2θ range 3.0–47.5°, $Mo_{K\alpha}$ (0.71073 Å), ω scan, $T = 294$ K. Of 3321 reflections 2892 were independent (because of a split reflex profile only the data of type $-h$, $+k$, $+l$ were used for structure determination and refinement), and 2385 observed [$F > 4\sigma(F)$]. Lorentzian and polarization corrections were carried out, but no absorption corrections. Siemens SHELXTL + was used for direct methods, and anisotropic refinement was done by the full-matrix least-squares method; 451 parameters refined. The hydrogen atoms were fitted at calculated positions and coupled to the corresponding atoms during refinement; a common isotropic displacement coefficient was refined for all hydrogen atoms. $R_{obs} = 0.1101$, $wR = 0.1020$, refinement against *I*, largest difference peak 0.33 e Å^{-3} [14].

[12] E. L. Eliel, S. H. Wilen, *Stereochemistry of Organic Compounds*, Wiley, New York, **1996**, p. 647-655.

[13] The relative configuration of **2f** was determined by hydrogenolysis to **4**, which was characterized by X-ray crystallography [14].

[14] Crystallographic data (excluding structure factors) for **1f** and **4** have been deposited with the Cambridge Crystallographic Data Centre as supplementary publication no. CCDC-179178. Copies of the data can be obtained free of charge on application to The Director, CCDC, 12 Union Road, Cambridge CB21EZ, UK (fax: int. code +(1223)336-033; e-mail: deposit@chemcrys.cam.ac.uk).

Imidazol-2-ylidene: Generation of a Missing Carbene and Its Dication by Neutralization–Reionization and Charge-Stripping Mass Spectrometry**

Graham A. McGibbon, Christoph Heinemann, David J. Lavorato, and Helmut Schwarz*

Dedicated to Professor Zvi Rappoport on the occasion of his 60th birthday

There are many simple molecules that have been studied by quantum chemical methods sufficiently often and thoroughly enough that they take on an aura of familiarity but nevertheless still manage to elude experimental observation. Among the most famous of these is O=C=C=O.[1] A more recent candidate is imidazol-2-ylidene **1**, the parent compound of a carbene family with members that proved stable enough to be isolated.[2] Although imidazolylidenes have been studied for over three decades,[3] the theoretical scrutiny of **1** has recently intensified.[4] While computational investigations have concentrated on **1**, to-date all the aminocarbenes[2, 4d–f, 5] and related compounds[4d, 6] observed in condensed phases possess non-hydrogen substituents on the nitrogen atoms. Unsubstituted aminocarbenes have been reported in the gas phase,[7] for example the acyclic carbenes H_2N-C-NH_2 and H_2N-C-OH as well as the heterocyclic tautomers of oxazole, pyridine, and thiazole were prepared and characterized by using neutralization–reionization mass spectrometry (NRMS).[8] The latter method is particularly suitable for the identification of molecules that are susceptible to intermolecular isomerization but relatively stable toward unimolecular rearrangement since the experiments are performed on solitary gaseous species. This approach may be a route to **1** and to imidazol-4-ylidene **2**, the 1,2-hydrogen shift isomers of imidazole **3**. Earlier computations predicted that neutral **1** and **3** are separated by a substantial tautomerization barrier as are their radical cations.[4h, 9] Similarly, our hybrid Hartree–Fock/density functional theory calculations (Becke3LYP/6-31G**)[10] indicate that a barrier of 36 kcal mol^{-1} restricts the exothermic (50 kcal mol^{-1}) isomerization **2** → **3** and that the apparently isoenergetic ions $\mathbf{2}^{\bullet+}$ and $\mathbf{3}^{\bullet+}$ are separated by a barrier of 56 kcal mol^{-1}.[11] In light of this, it would seem that **1** and **2** are targets suitable for generation and characterization by NRMS if precursor molecules can be found (Scheme 1).

It was presumed that the ion $\mathbf{1}^{\bullet+}$ could be generated analogously to previous gas phase syntheses of carbene radical cations by dissociative electron ionization (EI) of an appropriately substituted imidazole. Indeed, the readily available imidazole-2-carboxaldehyde **I** seemed a good initial choice since it has

[*] Prof. Dr. H. Schwarz, C. Heinemann,[+] Dr. G. A. McGibbon[++]
Institut für Organische Chemie der Technischen Universität
Strasse des 17. Juni 135, D-10623 Berlin (Germany)
Fax: Int. code +(30) 314 21102

Dr. D. J. Lavorato
Department of Chemistry, McMaster University
1228 Main Street West, Hamilton, Ontario, L8S 4M1 (Canada)

[+] New Address: Hoechst AG
D-65926 Frankfurt am Main (Germany)

[++] New Address: Barringer Research Ltd.
1730 Aimco Boulevard, Mississauga, Ontario, L4W 1V1 (Canada)

[**] The research at the TU Berlin was funded by the Deutsche Forschungsgemeinschaft and the Fonds der Chemischen Industrie. G. A. M. thanks NSERC Canada for a Post Doctoral Fellowship and the Deutscher Akademischer Austauchdienst for a Research Scholarship. Technical assistance from Prof. J. K. Terlouw (McMaster) and Dr. D. Schröder (TUB) was appreciated.

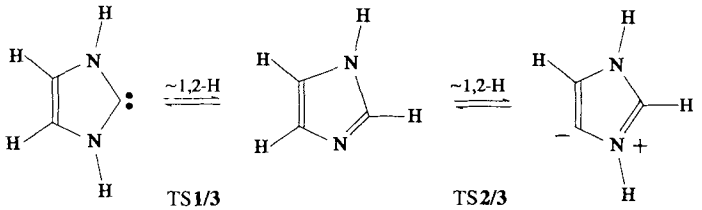

Scheme 1. Calculated (B3LYP/631G**) relative energies of imidazol-2-ylidene **1**, imidazole **3**, and imidazol-4-ylidene **2**, their interconnecting transition states and the respective radical cations.

a sizeable peak at m/z 68 (corresponding to $[C_3H_4N_2]^{\bullet+}$) in its 70 eV EI mass spectrum, which could correspond to $\mathbf{1}^{\bullet+}$ produced from the molecular ion following a formal 1,3-hydrogen shift and decarbonylation (Scheme 2). The ionized dimethyl ester of imidazole-4,5-dicarboxylic acid **II** could generate $\mathbf{2}^{\bullet+}$ by

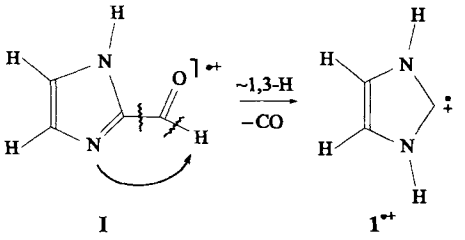

Scheme 2. Interpretation of the signal at m/z 68 in the EI (70 eV) mass spectrum of imidazole-2-carboxaldehyde **I**: $\mathbf{1}^{\bullet+}$ could form from the molecular ion by a formal 1,3 hydrogen shift and decarbonylation.

the more complicated sequence of reactions shown in Scheme 3. Radical cations $\mathbf{3}^{\bullet+}$ are obtained simply by EI (70 eV) of imidazole. Ionized imidazole has been studied extensively by mass

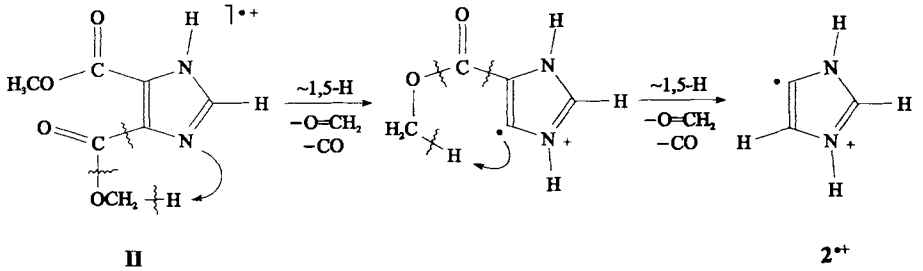

Scheme 3. Possible reaction sequence to $\mathbf{2}^{\bullet+}$ starting from the ionized dimethyl ester of imidazol-4,5-dicarboxylic acid **II**.

spectrometry.[12] The tandem mass spectrometry experiments[13] described here were performed by using the VG Analytical ZAB-R instrument at McMaster University[14] and the modified VG ZAB/HF/AMD mass spectrometer at the TU Berlin.[15]

A careful comparison of the data from the collision-induced dissociation (CID) mass spectra in Table 1 and the charge-stripping (CS) mass spectra in Table 2 reveals that two new m/z 68 $[C_3H_4N_2]^{\bullet+}$ ions, distinguishable from imidazole do exist. At first glance, the tabulated data from the CID mass spectra do not seem greatly different, which is perhaps not surprising in light of the structural similarity of the isomers and their complicated fragmentation pathways.[12] Nevertheless, the spectrum

Table 1. Data from the CID mass spectra of m/z 68 $[C_3H_4N_2]^{\bullet+}$ ions generated from **I**, **II**, and imidazole [a].

Precursor	I		II		Imidazole	
Spectrum m/z	CID Intensity	NR/CID	CID Intensity	NR/CID	CID Intensity	NR/CID
42	24	21	1	3	1	3
40	39	32	45	39	52	44
39	10	12	17	13	13	14
38	7	8	10	10	11	10
29	1	3	5	6	1	1
27	8	8	8	10	9	9
26	5	5	3	6	5	6
25	2	3	2	3	2	4
24	1	1	2	2	1	1
16	0	0	2	2	0	0
15	0	1	2	2	0	1
14	1	3	1	2	1	3
13	1	3	1	1	1	3
12	1	1	0	0	1	1

[a] Intensities based on peak heights normalized to $\Sigma = 100$. Peaks containing metastable contributions have been omitted.

(a) from precursor **I** is distinguished by an intense peak at m/z 42 (see Figure 1) that is attributed to the loss of acetylene and thus taken as a strong indication of the carbene ion structure $\mathbf{1}^{\bullet+}$. This process has been shown to occur for the closely related thiazol-2-ylidene radical cation[7e] and we surmise that in this case ionized diimide $HN{=}C{=}NH^{\bullet+}$ is the product ion. However, attempts to demonstrate this experimentally are thwarted by the fact that isomeric CH_2N_2 radical cations are very difficult to distinguish.[16] In any case, intense signals at m/z 42 are not expected from $\mathbf{2}^{\bullet+}$ and they are not present in the CID mass spectrum of the imidazole radical cation. Indeed, the m/z 68 ions from both **II** and imidazole are similar in the respect that there is almost no signal to be seen at m/z 42 and in terms of the relative abundance of the other fragments in their CID mass spectra; however, there are some notable differences between the two spectra: a considerably enhanced (5% of total CID intensity) fragment peak at m/z 29 and a weak peak at m/z 16 is observed only in the spectrum of the ions from **II**, which is an indication that these ions have a structure different from $\mathbf{1}^{\bullet+}$ or $\mathbf{3}^{\bullet+}$.

The existence of $\mathbf{1}^{\bullet+}$ and $\mathbf{2}^{\bullet+}$ is further endorsed by the CS mass spectral data in Table 2. Quite different intensity ratios for the dications at m/z 68/67/66 are observed in all three spectra and in contrast to $\mathbf{3}^{\bullet+}$ the CS peaks are much more intense than the CID peaks for both of

Table 2. Data from the charge-stripping mass spectra of m/z 68 $[C_3H_4N_2]^{\bullet+}$ ions generated from **I**, **II**, and imidazole [a].

Precursor	I		II		Imidazole	
Spectrum Dication (m/z)	CS Intensity	NR/CS[b]	CS Intensity	NR/CS[b]	CS Intensity	NR/CS[b]
68	100	100	100	100	100	94
67	5	40	9	39	33	100
66	2	10	2	5	8	30
CS-eff.[c]	0.60	0.48	1.11	1.02	0.32	0.17

[a] Relative abundance are from peak heights. [b] NR/CS refers to dications formed from neutralized ions (see text). [c] Charge-stripping efficiency as measured by the peak height ratio of m/z 68 relative to that of the nearby m/z 39 in the CID mass spectrum.

the new ions. The larger susceptibility of the ions $\mathbf{1}^{\bullet+}$ and especially $\mathbf{2}^{\bullet+}$ to charge-stripping is typical for ylide ions as compared to mundane isomers.[17] The differences in the CS and CID mass spectra of the three isomers show that ions $\mathbf{1}^{\bullet+}$ and $\mathbf{2}^{\bullet+}$ do not easily isomerize to $\mathbf{3}^{\bullet+}$. Given that the fragmentation mechanisms of even the well-known ion $\mathbf{3}^{\bullet+}$ are still largely speculative,[12] we avoid dwelling further on these differences. Thus, the three isomers can be differentiated by CID and CS mass spectrometry, therefore, it still remains to be demonstrated that the corresponding neutral molecules are stable in NRMS experiments.[18]

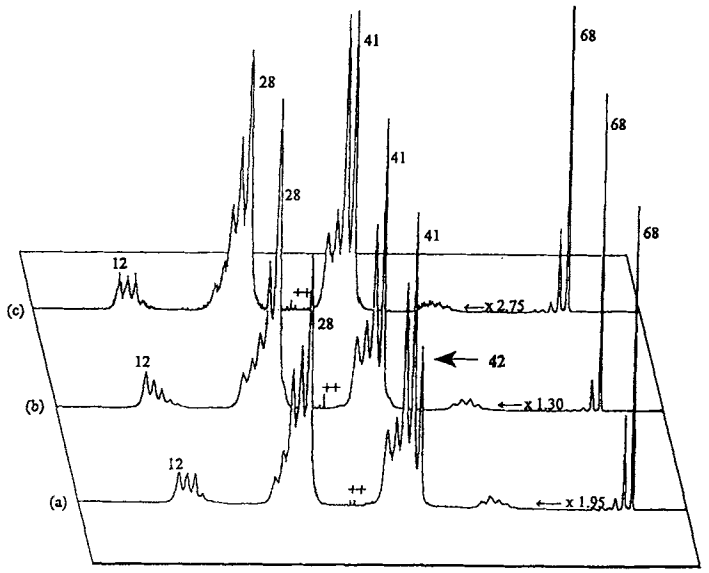

Figure 1. NR mass spectra of the m/z 68 ions generated from (a) ionized imidazole-2-carboxaldehyde **I**, (b) ionized precursor **II**, and (c) ionized imidazole.

When the individual NR mass spectra of distinguishable isomers match their respective CID mass spectra in appearance and contain observable recovery ion signals it is easy to conclude that the neutral molecules are stable. On this basis, the existence of **1** is strongly suggested since its NR mass spectrum (Figure 1 (a)) contains both the signature peak at m/z 42, and as the base peak, the recovery signal at m/z 68. The evidence is less clear-cut for **2** because the relative intensities of the peaks in the NR mass spectrum are not quite the same as in the CID mass spectrum. Note, however, that the m/z 12–16 cluster patterns are unique and the weak but observable dication peaks denoted + + in Figure 1 are very informative. The relative abundance of the dication at m/z 68 is once again most noticeable for $\mathbf{2}^{\bullet+}$ and the largest peak that is attributed to a dication at m/z 67 is again generated by $\mathbf{3}^{\bullet+}$. To probe the existence of **2** and **1** in more detail, we investigated the collision-induced dissociation behavior of the reionized species with m/z 68 (see Figure 1). This type of experiment (NR/CID)[18] requires a multisector mass spectrometer and high sensitivity.[7, 15]

To assist direct comparisons of the m/z 68 ions their NR/CID and CID mass spectra have been tabulated together in Table 1. An inspection quickly reveals the similarity of the NR/CID to the CID mass spectra for the three sets of ions, especially in regard to the key peaks at m/z 42 and 29. Scrutiny of the NR/CID mass spectra reveals that the m/z 40 peaks are likely diminished because of extensive fragmentation into smaller ions, which probably reflects a change to a higher internal energy distribution in the radical cations themselves after NR.[7b] This is consistent with the increased dissociation observed for the dications produced by charge-stripping of the m/z 68 ions (see the NR/CS mass spectra in Table 2). Taking this into account, the CS efficiencies of the recovery ions and of the ions not subjected to NR are comparable. These facts lead us to the conclusion that a significant portion of the neutral molecules **1** and **2** are able to survive structurally intact during the microsecond transit time between the neutralization and reionization cells in NRMS experiments.

In summary, the existence of imidazol-2-ylidene **1** and imidazol-4-ylidene **2**, their radical cations, and dications have been demonstrated through tandem mass spectrometry experiments.

Received: December 30, 1997 [Z9951IE]
German version: *Angew. Chem.* **1997**, *109*, 1572–1575

Keywords: carbenes · cations · imidazolylidenes · mass spectrometry

[1] For a review, see: J. A. Berson, D. A. Birney, W. P. Dailey, J. F. Liebman in *Modern models of bonding and delocalization* (Eds.: J. F. Liebman, A. Greenberg) VCH, Weinheim, **1987**. Recent attempts to identify C_2O_2 through mass spectrometry are summarized in: D. Schröder, H. Schwarz, *Int. J. Mass Spectrom. Ion Processes* **1995**, *146/147*, 183.

[2] Since the first isolation of "stable" carbenes: A. J. Arduengo III, R. L. Harlow, M. Kline, *J. Am. Chem. Soc.* **1991**, *113*, 361, the field has expanded rapidly and a précis of the "incredible renaissance" in this area can be found in: M. Regitz, *Angew. Chem. Int. Ed. Engl.* **1996**, *35*, 725; *Angew. Chem.* **1996**, *108*, 791.

[3] Reviews: a) H.-W. Wanzlick, *Angew. Chem.* **1962**, *74*, 129; *Angew. Chem. Int. Ed. Engl.* **1962**, *1*, 75; b) R. W. Hoffmann, *ibid.* **1968**, *80*, 823 and **1968**, *7*, 754; c) J. Hocker, R. Merten, *ibid.* **1972**, *84*, 1022 and **1972**, *11*, 964; d) M. Driess, H. Grützmacher, *ibid.* **1996**, *108*, 900; and **1996**, *35*, 829.

[4] a) R. Gleiter, R. Hoffmann, *J. Am. Chem. Soc.* **1968**, *90*, 5457; b) F. Geijo, F. Lopez-Calahorra, S. Olivella, *J. Heterocyclic Chem.* **1984**, *21*, 1785; c) R. Grigg, L. Wallace, J. O. Morley, *J. Chem. Soc. Perkin Trans. 2* **1990**, *51*; d) D. A. Dixon, A. J. Arduengo III, *J. Phys. Chem.* **1991**, *95*, 4180; e) A. J. Arduengo III, D. A. Dixon, D. A. Harlow, K. K. Kumashiro, C. Lee, W. P. Power, K. W. Zilm, *J. Am. Chem. Soc.* **1994**, *116*, 6361; f) A. J. Arduengo III, H. Bock, H. Chen, M. Denk, D. A. Dixon, J. C. Green, W. A. Herrmann, N. L. Jones, M. Wagner, R. West, *ibid.* **1994**, *116*, 6641; g) J. Cioslowski, *Int. J. Quant. Chem., Quant. Chem. Symp.* **1993**, *27*, 309; h) C. Heinemann, W. Thiel, *Chem. Phys. Letters* **1994**, *217*, 11; i) C. Heinemann, T. Müller, Y. Apeloig, H. Schwarz, *J. Am. Chem. Soc.* **1996**, *118*, 2023; j) C. Boehme, G. Frenking, *ibid.* **1996**, *118*, 2039; k) R. R. Sauers, *Tetrahedron Lett.* **1996**, *37*, 149; l) A. J. Arduengo III, J. R. Goerlich, W. J. Marshall, *Liebigs Ann./Receuil*, **1997**, 305.

[5] a) R. W. Alder, P. R. Allen, S. J. Williams, *J. Chem. Soc. Chem. Commun.* **1995**, 1267; b) A. J. Arduengo III, J. R. Goerlich, W. J. Marshall, *J. Am. Chem. Soc.* **1995**, *117*, 11027; c) *Methoden der Organischen Chemie* (*Houben-Weyl*), 4th ed. 1952–, Bd. E19b, **1989**.

[6] Nitrene: a) G. Boche, P. Andrews, K. Harms, M. Marsch, K. S. Rangappa, M. Schimeczek, C. Willeke, *J. Am. Chem. Soc.* **1996**, *118*, 4925; Fulvalene: b) T. A. Taton, P. Chen, *Angew. Chem.* **1996**, *108*, 10980; *Angew. Chem. Int. Ed. Engl.* **1996**, *35*, 1011.

[7] a) G. A. McGibbon, C. A. Kingsmill, J. K. Terlouw, *Chem Phys. Letters* **1994**, *222*, 129; b) G. A. McGibbon, P. C. Burgers, J. K. Terlouw, *Int. J. Mass Spectrom. Ion Processes* **1994**, *136*, 191; c) T. Wong, J. Warkentin, J. K. Terlouw, *ibid.* **1990**, *115*, 33; d) D. J. Lavorato, J. K. Terlouw, T. Dargel, W. Koch, G. A. McGibbon, H. Schwarz, *J. Am. Chem. Soc.* **1996**, *118*, 11898; e) G. A. McGibbon, J. Hrušák, D. J. Lavorato, H. Schwarz, J. K. Terlouw, *Chem. Eur. J.* **1997**, *3*, 232.

[8] For a recent review, see: N. Goldberg, H. Schwarz, *Acc. Chem. Res.* **1994**, *27*, 347.

[9] V. Q. Nguyen, F. Turecek, *J. Mass Spectrom.* **1996**, *31*, 1173.

[10] Gaussian 94 (Revision B.3), M. J. Frisch, G. W. Trucks, H. B. Schlegel, P. M. W. Gill, B. G. Johnson, M. A. Robb, J. R. Cheeseman, T. A. Keith, G. A. Petersson, J. A. Montgomery, K. Raghavachari, J. B. Foresman, J. Cioslowski, B. B. Stefanov, A. Nanayakkara, M. Challacombe, C. Y. Peng, P. Y. Ayala, W. Chen, M. W. Wong, J. L. Andres, E. S. Replogle, R. Gomperts, R. L. Martin, D. J. Fox, J. S. Binkley, D. J. DeFrees, J. Baker, J. J. P. Stewart, M. Head-Gordon, C. Gonzales, J. A. Pople, Gaussian Inc., Pittsburgh PA, **1995**.

[11] According to our calculations Frank–Condon type neutralization of the radical cations at their optimized geometries results in vibrationally excited molecules **1**–**3**, but the energy deposited (9.9, 8.7, and 11.9 kcal mol^{-1}, respectively) is insufficient to enable their interconversion.

[12] a) J. H. Bowie, R. G. Cooks, S. O. Lawesson, G. Schroll, *Aust. J. Chem.* **1967**, *20*, 1613; b) R. Hodges, M. Grimmet, *ibid.* **1968**, *21*, 1086; c) K. J. Klebe, J. J.

Houte, J. van Thuijl, *Org. Mass Spectrom.* **1971**, *5*, 1101; d) J. van Thuijl, K. J. Klebe, J. J. Houte, *ibid.* **1972**, *6*, 1363; e) G. Bouchoux, Y. Hoppilliard, *ibid.* **1977**, *12*, 196; f) J. Main-Bobo, S. Olesik, W. Gase, T. Baer, A. A. Mommers, J. L. Holmes, *J. Am. Chem. Soc.* **1986**, *108*, 106.

[13] K. L. Busch, G. L. Glish, S. A. McLuckey, *Mass Spectrometry/Mass Spectrometry. Techniques and Applications of Tandem Mass Spectrometry*, VCH, New York, **1988**.

[14] The VG Analytical ZAB-R mass spectrometer at McMaster University has a three-sector BEE (B = magnet, E = electric sector) configuration, see: H. F. van Garderen, P. J. A. Ruttink, P. C. Burgers, G. A. McGibbon, J. K. Terlouw, *Int. J. Mass Spectrom. Ion Processes* **1992**, *121*, 159.

[15] The modified VG ZAB/HF/AMD at the TU Berlin is a four-sector instrument with a BEBE configuration, see: a) R. Srinivas, D. Sülzle, T. Weiske, H. Schwarz, *Int. J. Mass Spectrom. Ion Processes* **1991**, *107*, 368; b) C. Schalley, D. Schröder, H. Schwarz, *ibid.* **1996**, *153*, 173.

[16] B. L. M. van Baar, Ph.D. Thesis, University of Utrecht, **1988**, Chapter 1.

[17] J. L. Holmes, F. P. Lossing, J. K. Terlouw, P. C. Burgers, *J. Am. Chem. Soc.* **1982**, *104*, 2931.

[18] In NRMS experiments 8 or 10 keV m/z 68 $[C_3H_4N_2]^{\bullet+}$ ions were mass-selected (by B with the ZAB-R or B_1E_1 with the ZAB/HF/AMD) and then subjected to neutralizing collisions with *N*,*N*-dimethylaniline or xenon vapor present in a small gas cell located in the field-free region. Afterward, any remaining ions were removed from the beam by deflection with a positively charged electrode so that only a beam of fast moving neutral species entered a second gas cell, therein being (dissociatively) reionized by collisions with oxygen molecules. For a NR mass spectrum, the survivor and fragment ions were analyzed by using the next available sector (B_2 in Berlin or E_1 at McMaster). Alternatively, when the recovery ions (m/z 68) were selectively transmitted by the sector and then passed through another oxygen-filled collision cell (70% transmission) the resulting CID products could be analyzed by using the last sector. The NR/CID mass spectrum so obtained is characteristic of only the species surviving neutralization and reionization. Mass spectra of doubly charged ions (NR/CS) were also obtained in the same manner. Comparative collision-induced dissociation (CID) and charge-stripping (CS) experiments were performed with the deflector electrode switched off.

Fluorescence Reporters for Phosphodiesterase Activity**

Albrecht Berkessel* and Rainer Riedl

Phosphodiesterases catalyze the hydrolysis of phosphodiester bonds [Eq. (a)].[1] Their most important biological substrates

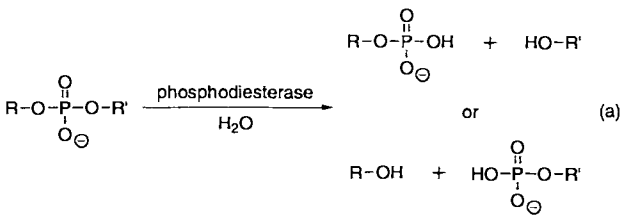

are the nucleic acids. The manipulation of genetic material ("genetic engineering") hinges on the sequence-specific cleavage of DNA by the restriction enzymes,[2] which are isolated from natural sources and, consequently, invariable with respect to their catalytic parameters and particularly their base-recognition properties (number and type of the bases recognized). Due to the extreme importance of this class of enzymes in biochemistry and biotechnology, numerous attempts have been made to design "artificial phosphodiesterases".[3] Independent of the catalytic mechanism of these systems, highly sensitive assays are needed for detecting phosphodiesterase activity. So far, UV/Vis-spectroscopical quantification of nitrophenols liberated from the corresponding phosphodiesters or ^{31}P NMR spectroscopy were used in most cases. We found it worthwhile to design a simple and much more sensitive fluorescence probe for detecting phosphodiesterase activity. Due to the high sensitivity of fluorescence assays, we reasoned that with such probes phosphodiesterase activity might also be detected in complex mixtures of biological or synthetic origin.

The mechanism of our reporter molecules is shown in Scheme 1. In compound **A**, a fluorophore and a fluorescence

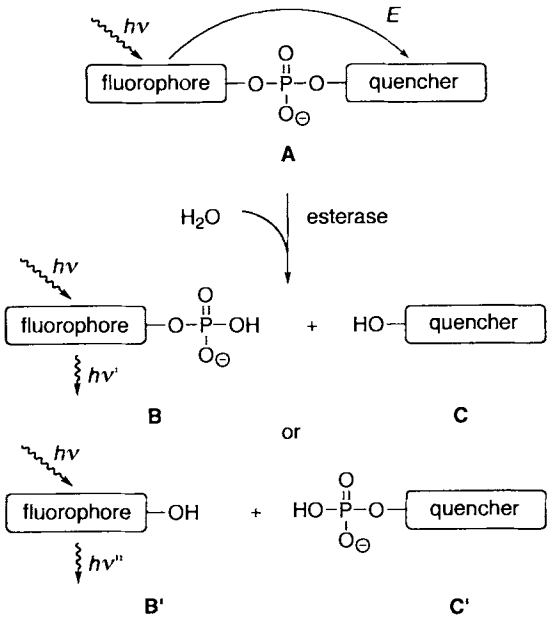

Scheme 1. Mechanism of the fluorescence reporters.

quencher are held in close proximity. The absorption spectrum of the quencher and the emission spectrum of the fluorophore should match as well as possible.[4] Upon irradiation of the fluorophore, rapid energy transfer to the quencher takes place. Therefore, this intact phosphodiester does not fluoresce.[4]

After hydrolysis of the phosphodiester group, the cleavage products **B** and **C** (or **B'** and **C'**) can diffuse away from one another, and the fluorescence is no longer quenched intramolecularly.[4] We synthesized two such fluorescence reporters, namely the phosphodiesters **1** and **2**. In these compounds a naph-

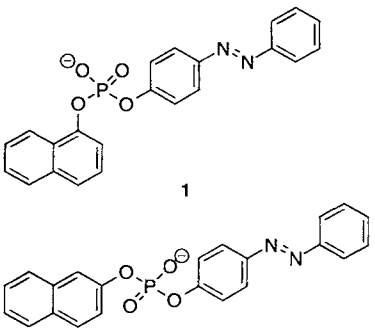

1

2

[*] Prof. Dr. A. Berkessel,[+] Dipl.-Chem. R. Riedl
Organisch-chemisches Institut der Universität
Im Neuenheimer Feld 270, D-69120 Heidelberg (Germany)

[+] New address:
Institut für Organische Chemie der Universität
Greinstrasse 4, D-50939 Köln (Germany)
Fax: Int. code +(221)470-5102
e-mail: berkessel@uni-koeln.de

[**] This work was supported by the Fonds der Chemischen Industrie.

thalene residue acts as the fluorophore, and an azobenzene moiety as the quencher. Since 4-hydroxyazobenzene (pK_s = 8.20)[5] is a better leaving group than 1-naphthol (pK_s = 9.37)[6] or 2-naphthol (pK_s = 9.49),[6] hydrolysis of **1** and **2** should result in formation of 4-hydroxyazobenzene and the corresponding naphthyl phosphates. We here report the synthesis of **1** and **2** and the activation of their fluorescence by hydrolysis.

As shown in Scheme 2 the preparation of **1** und **2** starts with the reaction of 1- or 2-naphthol with phosphoryl chloride.[7] In

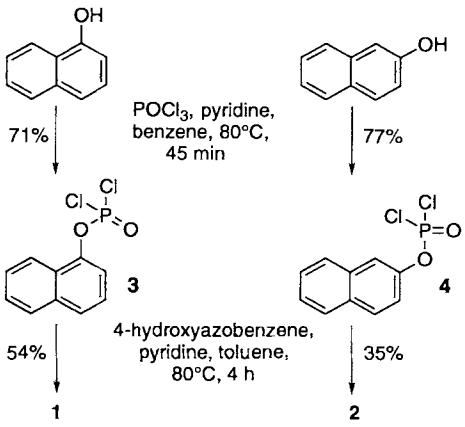

Scheme 2. Synthesis of the phosphodiesters **1** and **2**.

the second step, the azobenzene moiety is introduced. UV/Vis spectra of **1** and **2** show absorption bands for the naphthalene and azobenzene moieties (maxima at shorter and longer wavelength, respectively; Figure 1). Irradiation of the naphthalene absorption band results in virtually no fluorescence.[8]

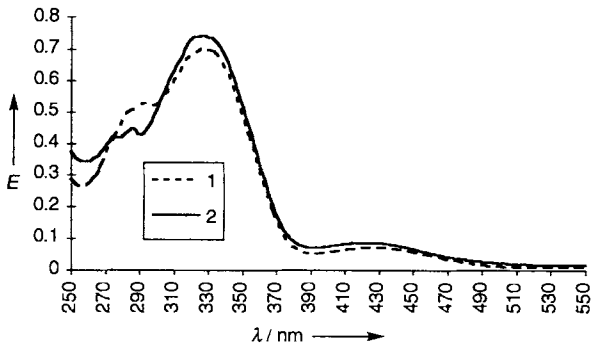

Figure 1. UV/Vis spectra of the fluorescence reporters **1** and **2** ($c = 5.0 \times 10^{-5}$ M) in AMPSO buffer (0.1 M, pH 8.8), $T = 25$ °C.

Addition of a phosphodiesterase, for example phosphodiesterase I from crotalus atrox venom,[9] to a solution of **1** in AMPSO buffer[10] results in a rapid increase in the fluorescence intensity (Figure 2). The shape of the fluorescence spectrum is identical to that of an equimolar mixture of 1-naphthyl phosphate and 4-hydroxyazobenzene. However, the intensity of the control mixture is not reached in the enzyme-catalyzed hydrolysis of **1**. Even more remarkably, the fluorescence intensity starts to decrease after about 4 h.

This unexpected observation results from a minor phosphatase activity in the commercially available enzyme preparation.[9] HPLC analysis revealed that 1-naphthyl phosphate initially liberated from **1** slowly degrades to 1-naphthol. Unlike

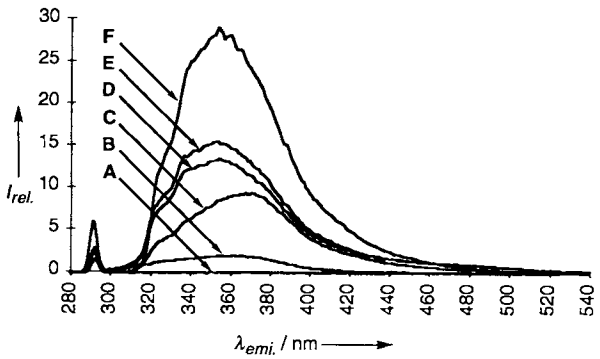

Figure 2. Fluorescence spectra of a 5.0×10^{-5} M solution of **1** in AMPSO buffer (0.1 M, pH 8.8), $T = 37$ °C, $V = 1.5$ mL. A: without enzyme; B: after addition of 0.05 u phosphodiesterase I (crotalus atrox venom); C: 30 min after addition of the enzyme; D: 360 min after addition of the enzyme; E: 240 min after addition of the enzyme; F: for comparison, 5.0×10^{-5} M 1-naphthyl phosphate $+ 5.0 \times 10^{-5}$ M 4-hydoxyazobenzene.

1-naphthyl phosphate, 1-naphthol is known[6] to show practically no fluorescence in aqueous solution at 357 nm. When we employed another commercially available[11] phosphodiesterase I (from bovine intestinal mucosa), 1-naphthyl phosphate could not be found at all as the primary hydrolysis product of **1**. HPLC analysis of the (nonfluorescent) reaction mixtures revealed immediate further degradation to 1-naphthol.

With this in mind, we subjected the 2-naphthol derivative **2** to hydrolysis catalyzed by phosphodiesterase I (from bovine intestinal mucosa). In contrast to 1-naphthol, 2-naphthol is known[6] to fluoresce strongly in aqueous solution. The results are summarized in Figure 3. Addition of the enzyme to a solu-

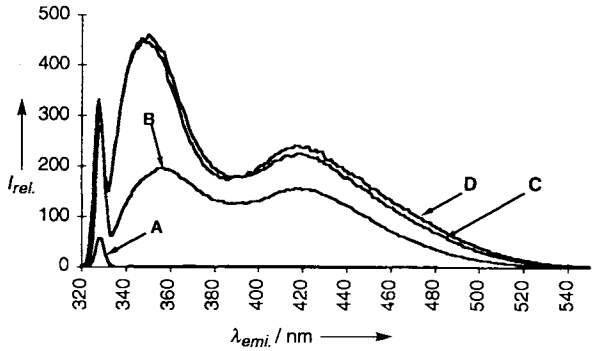

Figure 3. Fluorescence spectra of a 5.0×10^{-5} M solution of **2** in AMPSO buffer (0.1 M, pH 8.8), $T = 37$ °C, $V = 1.5$ mL. A: without enzyme; B: 40 min after addition of 0.05 u phosphodiesterase I (bovine intestinal mucosa); C: 4 h after addition of the enzyme (end of reaction); D: for comparison, 5.0×10^{-5} M 2-naphthol $+ 5.0 \times 10^{-5}$ M 4-hydoxyazobenzene

tion of **2** in AMPSO buffer[10] produced a rapid increase in the fluorescence intensity, which asymptotically approached that of an equimolar mixture of 2-naphthol and 4-hydroxyazobenzene (Figure 3). HPLC analysis of the reaction mixtures confirmed the formation of 4-hydroxyazobenzene and the secondary hydrolysis product 2-naphthol. Hydrolysis of **2** induced an at least thousandfold increase of the fluorescence intensity![12] Furthermore, the progress of the reaction was also indicated by the yellow color of the 4-hydroxyazobenzene formed (strictly speaking, of the phenolate anion, $\lambda_{max} = 421$ nm). A plot of the initial velocities versus the enzyme concentrations (addition of

0.025–0.1 u) confirmed the expected linear relationship (not shown, three experiments, $\rho = 0.9984$).

The fluorescence reporters **1** and **2** are highly sensitive probes for detecting phosphodiesterase activity. Their use as test substrates not only allows detection of phosphodiesterase activity, but also phosphatase activity.

Experimental Section

1-Naphthyl phosphoryl chloride (**3**) and 2-naphthyl phosphoryl chloride (**4**) were prepared according to ref. [7].

1: Under nitrogen **3** (2.63 g, 10.1 mmol) and 4-hydroxyazobenzene (2.00 g, 10.1 mmol, 1.0 equiv) were dissolved in abs toluene (150 mL) with heating, and abs pyridine (3.19 g, 40.4 mmol, 4.0 equiv) was added dropwise within 30 min. Stirring was continued for 4 h at 80 °C and overnight at RT. The precipitated pyridinium hydrochloride was removed by filtration, and the filtrate concentrated on a rotary evaporator to about 20 mL. The remaining oil was dissolved in pyridine/water (1/1, 20.0 mL), and the solution stirred at RT for 1 h. Afterwards 10% aqueous K_2CO_3 (100 mL) and chloroform (100 mL) were added. The biphasic mixture was shaken vigorously to induce the precipitation of the potassium salt of **1**. After 3 h the precipitate was isolated by filtration and taken up in boiling water (150 mL). The red extract was again filtered, and the filtrate adjusted to pH 1 with concd HCl. The orange precipitate was isolated by filtration and recrystallized from acetone to afford **1** as an orange crystalline powder (2.22 g, 54%).

M.p. 167 °C (acetone); IR (KBr): $\tilde{\nu} = 1222$ [s, ν(P=O)], 1204 [s, ν(C–O)], 1046, 989 [both s, ν(P–O)], 564 cm^{-1} [s, δ(P-O-Ar)]; ^1H NMR (300 MHz, [D$_6$]DMSO): $\delta = 7.34–7.51$ (m, 4H, aryl H), 7.51–7.64 (m, 5H, aryl H), 7.70–7.78 (m, 1H, aryl H), 7.81–8.00 (m, 5H, aryl H), 8.03–8.13 (m, 1H, aryl H), 11.20 (br s, 1H, OH); ^{13}C NMR (75 MHz, [D$_6$]DMSO): $\delta = 115.10$ (d, ^3J(C,P) = 2.82 Hz, aryl CH), 121.00 (d, ^3J(C,P) = 5.08 Hz, aryl CH), 121.70 (d, aryl CH), 122.64 (d, aryl CH), 124.32 (d, aryl CH), 124.38 (d, aryl CH), 125.97 (d, ^4J(C,P) = 1.70 Hz, aryl CH), 126.32 (s, ^3J(C,P) = 6.21 Hz, aryl C), 126.44 (d, aryl CH), 126.81 (d, aryl CH), 127.87 (d, aryl CH), 129.60 (d, aryl CH), 131.55 (d, aryl CH), 134.47 (s, aryl C), 147.16 (s, ^2J(C,P) = 7.35 Hz, aryl C), 148.64 (s, aryl C), 152.06 (s, aryl C), 153.96 (s, ^2J(C,P) = 6.78 Hz, aryl C); ^{31}P NMR (80 MHz, [D$_6$]DMSO): $\delta = -11.68$; LDI-MS: m/z (%) = 403.4 (100) [M^- – H], 298 (5) [$C_{16}H_{11}O_4P^-$], 197.1 (12) [$C_{12}H_9N_2O^-$], 142.9 (50) [$C_{10}H_7O^-$]; UV/Vis (H_2O): λ_{max} (ε) = 417 (1322), 330 (14910), 290 (9385), 220 nm (54300); elemental analysis calcd for $C_{22}H_{17}N_2O_4P$ (404.36): C 65.35, H 4.24, N 6.93, P 7.66; found: C 65.23, H 4.37, N 6.88, P 7.61.

2: Analogous to the preparation of **1**, abs pyridine (7.14 g, 90.4 mmol, 4.0 equiv) was added to a solution of **4** (5.90 g, 22.6 mmol) and 4-hydroxyazobenzene (4.49 g, 22.6 mmol, 1.0 equiv) in abs toluene (300 mL). The mixture was heated to 80 °C for 4 h and stirred overnight at RT. The precipitated pyridinium hydrochloride was removed by filtration, and the solvent removed on a rotary evaporator. The oily residue was stirred with pyridine/water (1/1, 20.0 mL) for 1 h at RT. The solution was then adjusted to pH 1 by adding concd HCl. A deep-red precipitate formed overnight, which was isolated by filtration and recrystallized from acetone to afford **2** as orange platelets (3.22 g, 35%).

M.p. 146 °C (acetone); FT-IR (KBr): $\tilde{\nu} = 1228$ [s, ν(P=O)], 1208 [s, ν(C–O)], 976, 946 [both s, ν(P–O)], 551 cm^{-1} [m, δ(P-O-Ar)]; ^1H NMR (300 MHz, [D$_6$]DMSO): $\delta = 5.05$ (br s, 1H, OH), 7.32–7.51 (m, 5H, aryl H), 7.52–7.63 (m, 3H, aryl H), 7.68–7.73 (br s, 1H, aryl H), 7.78–7.94 (m, 7H, aryl H); ^{13}C NMR (50 MHz, [D$_6$]DMSO): $\delta = 115.79$ (d, ^3J(C,P) = 4.58 Hz, aryl CH), 120.77 (d, ^3J(C,P) = 4.57 Hz, aryl CH), 121.08 (d, ^3J(C,P) = 5.34 Hz, aryl CH), 122.56 (d, aryl CH), 124.20 (d, aryl CH), 124.90 (d, aryl CH), 126.59 (d, aryl CH), 127.28 (d, aryl CH), 127.69 (d, aryl CH), 129.34 (d, aryl CH), 129.58 (d, aryl CH), 129.93 (s, aryl C), 131.32 (d, aryl C), 133.81 (s, aryl C), 147.91 (s, aryl C), 150.21 (s, ^2J(C,P) = 6.87 Hz, aryl C), 152.11 (s, aryl C), 155.38 (s, ^2J(C,P) = 6.87 Hz, aryl C); ^{31}P NMR (80 MHz, [D$_6$]DMSO): $\delta = -11.98$; LDI-MS: m/z (%) = 403.6 (100) [M^- – H], 298.4 (7) [$C_{16}H_{11}O_4P^-$], 197.4 (7) [$C_{12}H_9N_2O^-$]; UV/Vis (H_2O): λ_{max} (ε) = 419 (1195), 329 (15280), 286 (7480), 276 (6735), 220 nm (63090); elemental analysis calcd for $C_{22}H_{17}N_2O_4P$ (404.36): C 65.35, H 4.24, N 6.93, P 7.66; found: C 65.24, H 4.23, N 6.91, P 7.68. Hydrolyses were carried with a variable-temperature Shimadzu RF-5000 recording spectrofluorophotometer equipped with a 150 W xenon lamp.

Received: December 11, 1996 [Z 9869 IE]
German version: *Angew. Chem.* **1997**, *109*, 1518–1520

Keywords: analytical methods · enzymes · fluorescence spectroscopy

[1] N. Sträter, W. N. Lipscomb, T. Klabunde, B. Krebs, *Angew. Chem.* **1996**, *108*, 2158–2190; *Angew. Chem. Int. Ed. Engl.* **1996**, *35*, 2024–2055.

[2] a) D. M. Skinner, C. A. Holland in *Essentials of Molecular Biology, Vol. 2* (Eds.: D. Freifelder, G. M. Malacinski), Jones and Bartlett, Boston, London, **1993**, pp. 262–297; b) D. Kostrewa, F. K. Winkler, *Biochemistry* **1995**, *34*, 683–696; c) M. Newman, T. Strzelecka, L. F. Dorner, I. Schildkraut, A. K. Aggarwal, *Science* **1995**, *269*, 656–663; d) I. B. Vipond, S. E. Halford, *Mol. Microbiol.* **1993**, *9*, 225–231; e) S. E. Halford, J. D. Taylor, C. L. M. Vermote, I. B. Vipond in *Nucleic Acids and Molecular Biology, Vol. 7* (Eds.: F. Eckstein, D. M. J. Lilley), Springer, Berlin, Heidelberg, **1993**, pp. 47–69.

[3] a) D. S. Sigman, A. Mazumder, D. M. Perrin, *Chem. Rev.* **1993**, *93*, 2295–2316; b) P. B. Dervan, *Science* **1986**, *232*, 464–471; c) B. Linkletter, J. Chin, *Angew. Chem.* **1995**, *107*, 529–531; *Angew. Chem. Int. Ed. Engl.* **1995**, *34*, 472–474; d) W. H. Chapman, Jr., R. Breslow, *J. Am. Chem. Soc.* **1995**, *117*, 5462–5469; e) J. Rammo, R. Hettich, A. Roigk, H.-J. Schneider, *Chem. Commun.* **1996**, 105–107; f) M.-S. Muche, M. W. Göbel, *Angew. Chem.* **1996**, *108*, 2263–2265; *Angew. Chem. Int. Ed. Engl.* **1996**, *35*, 2126–2129.

[4] J. R. Lakowicz, *Principles of Fluorescence Spectroscopy*, Plenum, New York, London, **1983**.

[5] I. M. Klotz, H. A. Fiess, J. Y. Chen Ho, M. Mellody, *J. Am. Chem. Soc.* **1954**, *76*, 5136–5140.

[6] A. Weller, *Z. Elektrochem.* **1952**, *56*, 662–668.

[7] O. M. Friedman, A. M. Seligman, *J. Am. Chem. Soc.* **1950**, *72*, 624–625.

[8] When **2** was subjected to hydrolysis, $\lambda_{exc.} = 326$ nm was used since at this wavelength there is basically no fluorescence of the enzyme, and the fluorescence intensity of 2-naphthol is not significantly lower than that at $\lambda_{exc.} = 290$ nm. In the case of **1**, $\lambda_{exc.}$ had to be 290 nm since at this excitation wavelength the fluorescence intensity of 1-naphthyl phosphate is much higher than that at $\lambda_{exc.} = 326$ nm.

[9] Phosphodiesterase I (from crotalus atrox venom), Sigma. Definition of activity by the suppliers: 1 u hydrolyzes 1.0 μmol of bis(*p*-nitrophenyl)phosphate per min at pH 8.8 and 37 °C. Concerning the phosphodiesterase activity, the suppliers state 0.16 u mg^{-1} protein at pH 8.8 and 37 °C. The phosphatase activity is specified as less than 0.001 u mg^{-1} protein at pH 10.4 and 37 °C (substrate: *p*-nitrophenyl phosphate).

[10] AMPSO: 3-[(1,1-dimethyl-2-hydroxyethyl)amino]-2-hydroxypropanesulfonic acid.

[11] a) Phosphodiesterase I (from bovine intestinal mucosa), Sigma. Definition of activity by the suppliers: 1 u hydrolyzes 1.0 μmol of bis(*p*-nitrophenyl) phosphate per minute at pH 8.8 and 37 °C. The suppliers state "non-specific phosphatase activity" for enzyme preparation. b) In a control experiment the rapid dephosphorylation of 1- and 2-naphthyl phosphate could be shown by HPLC.

[12] Fluorescence intensity at 357 nm at the end of the reaction/fluorescence intensity at 357 nm before addition of enzyme. A higher intensity of excitation should result in an even higher increase in fluorescence intensity.

N-Bromoacetamide—A New Nitrogen Source for the Catalytic Asymmetric Aminohydroxylation of Olefins**

Milan Bruncko, Gunther Schlingloff, and K. Barry Sharpless*

The β-amino alcohol moiety is one of the most abundant structural units in biologically active compounds. Recent developments by us[1] and others[2] have led to viable metal-catalyzed routes for its asymmetric synthesis. In our recently discovered asymmetric aminohydroxylation (AA),[1] olefins are converted to nonracemic protected amino alcohols *in a single step* by using catalytic amounts of osmium(VIII) and cinchona alkaloid derivatives (Scheme 1), by a process which closely mirrors the well-established asymmetric dihydroxylation of olefins (AD).[3] We have now found conditions that allow amides to join sulfon-

[*] Prof. K. B. Sharpless, Dr. M. Bruncko, Dr. G. Schlingloff
The Scripps Research Institute
Department of Chemistry BCC 315
10550 North Torrey Pines Road, La Jolla, CA 92037 (USA)
Fax: Int. code +(619) 784-7562
e-mail: sharples@scripps.edu

[**] We thank the National Institutes of Health (GM 28384), the National Science Foundation (CHE - 9531152), the W. M. Keck Foundation, and the Skaggs Institute for Chemical Biology for financial support. G. S. is grateful for a postdoctoral fellowship granted by the Swiss National Science Foundation and the Ciba-Geigy Jubilaeums-Stiftung.

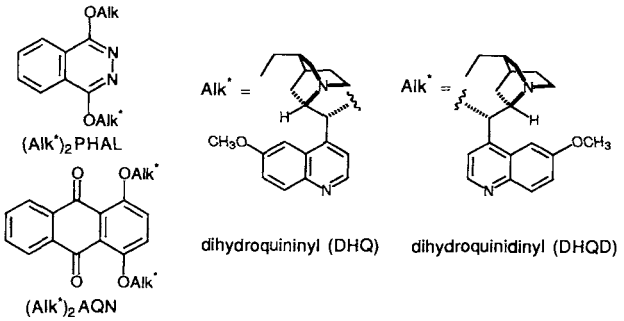

Scheme 1.

amides[1a-c] and carbamates[1d] as the nitrogen donor in this transformation.

Alkali metal salts of *N*-chloro carboxamides are well-known for their proclivity to undergo Hofmann rearrangement.[4] However, we were pleased to find that this competing reaction could be completely supressed by operating at 4 °C and using the more stable *N*-bromo derivative.[5] In the presence of 4 mol% of potassium osmate dihydrate and 5 mol% of the second generation alkaloid ligands,[3] a variety of olefins reacted smoothly with 1.1 equivalents of the oxidant/nitrogen donor to give the vicinal amino alcohols in good yield and with high enantiomeric excess (Scheme 2).

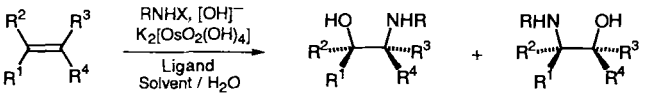

Scheme 2.

For each olefin class given in Table 1, the reaction parameters were optimized in terms of ligand, solvent, base,[6] and base/oxidant ratio, respectively. Both product enantiomers can be obtained by using either "pseudoenantiomers" of the alkaloid ligands.[3] A major advantage of this system is that only a stoichiometric amount of oxidant is needed (cf. reference [1]), which greatly simplifies isolation and purification of the product. In fact, use of excess of oxidant does not improve the reaction in any way.

As in the sulfonamide- and carbamate-based transformations,[1] cinnamates are among the best substrates (Table 1, entries 1–3).[7] While *cis*-stilbene gave mostly diol, *trans*-stilbene afforded the *threo*-amino alcohol **4** in 50% yield (together with 10% diol) and high enantiomeric excess (Table 1, entry 4). Ethyl acrylate gave rise to the isoserine derivative **5** as the major regioisomer detected by ^{1}H NMR spectroscopy (isoserine/serine > 20:1, Table 1, entry 5).

With styrenes **6** as substrates (Scheme 3), the regioselectivity is highly dependent on the choice of solvent *and* ligand. For example, alcoholic solvents resulted in a slight preference (**8**/**7** = 1.1–2.5:1) for introduction of the nitrogen substituent at the benzylic position (regioisomer **8**, Table 2), whereas acetonitrile significantly favored the other regioisomer (**7**) (**7**/**8** =

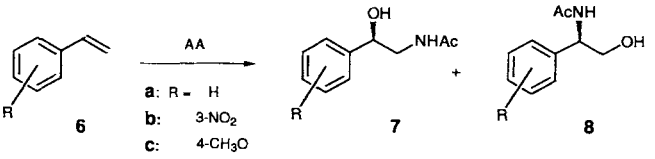

Scheme 3.

Table 1 Acetamide-based asymmetric aminohydroxylation of various olefins [a].

Entry	Substrate	Product [b]	Regio-selectivity [c]	*ee* Values [%] [d,e] (DHQ)$_2$PHAL	(DHQD)$_2$PHAL	Yield [%] [f]
1	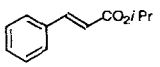	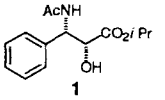 **1**	>20:1	99	−99	81
2	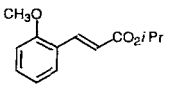	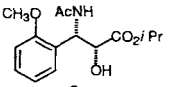 **2**	>20:1	99	−99	72
3 [g]	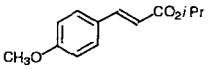	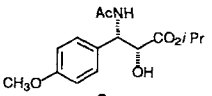 **3**	>20:1	99	−99	71
4 [h]	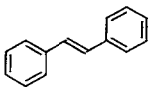	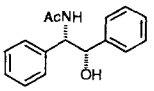 **4**	-	94	−93	50
5 [i]		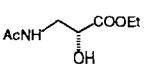 **5**	>20:1	89	−90	46

[a] Conditions: see Experimental Section. [b] From reaction catalyzed by (DHQ)$_2$PHAL. [c] Determined by ^{1}H NMR spectroscopy. [d] Determined by chiral HPLC (entries 1–4) or GC (entry 5). [e] Negative values indicate the formation of the opposite enantiomer (product from reaction catalyzed by (DHQD)$_2$PHAL). [f] Yields of the isolated pure products **1**–**5** after chromatography on silica gel. [g] *t*BuOH/water 1:1 was employed as solvent. [h] KOH as base and 1-PrOH/water 1:1 as the solvent was used. [i] CH_3CN/water 1:1 was used as the solvent.

Table 2. Improved regioselectivity of the asymmetric aminohydroxylation with styrene derivatives by using AQN ligands [a].

Entry	Olefin	Solvent	Ligand [b]	Ratio [c] 7/8	*ee* Value [d] [%] 7	8	Yield [e] [%]
1	**6a**	*n*PrOH	PHAL	1:1.1	83	91	72
2	**6a**	CH_3CN	PHAL	6.1:1	88	– [f]	55
3	**6a**	CH_3CN	*AQN*	*13:1*	*88*	– [f]	36
4	**6b**	*n*PrOH	PHAL	1:1.4	75	93	78
5	**6b**	CH_3CN	PHAL	2:1	81	86	49
6	**6b**	CH_3CN	*AQN*	*4:1*	*94*	92	54
7	**6c**	*n*PrOH	PHAL	1:2.5	62	96	83
8	**6c**	CH_3CN	PHAL	2.4:1	84	85	76
9	**6c**	CH_3CN	*AQN*	*9:1*	*86*	– [f]	58

[a] Conditions: see Experimental Section. [b] The DHQD derivative was used. [c] Determined by ^1H NMR spectroscopy. [d] Determined by chiral HPLC. [e] Yields refer to the mixtures of isomers after chromatography on silica gel. [f] Not determined.

2–13:1). In most cases, the benzylic amides were formed with higher asymmetric induction (**8**, 85–96% *ee*) than the benzylic alcohols (**7**, 62–94% *ee*), but poor regioselectivity was observed when phthalazine ligands were used. However, our recently introduced anthraquinone (AQN) ligands (see Scheme 1)[8] were much more effective, leading to good regioselectivities with this olefin class (Table 2, entries 3, 6, 9). The AA protocols now enable selective synthesis of either of the regioisomeric β-amino alcohols derived from styryl olefins. The phenyl glycinols **8** are obtained by using the carbamate AA/phthalazine ligand combination,[9] *and* the adrenaline-type regioisomers **7** are preferentially derived by using the acetamide AA/anthraquinone ligand combination.[10] Irrespective of the regiochemical outcome, the facial selectivity of these acetamide AA reactions agrees with the face selectivity rule for the AD.[3, 11] Thus, dihydroquinine-derived ligands (DHQ class) give rise to oxidation from the α face of the olefin, whereas the diastereomeric dihydroquinidine (DHQD) ligands effect attack on the β face of the double bond.

With this efficient new process in hand, we focused on its application for a large-scale synthesis of (2*R*,3*S*)-3-phenylisoserine,[12] a precursor for the side chains of the anticancer drugs Taxol and Taxotere. A 630-fold scale-up of our standard one mmol recipe was undertaken with a somewhat lower catalyst loading (1.5 mol% osmate salt and 1 mol% $(DHQ)_2PHAL$), which did not affect the outcome of the catalysis.[13] The AA product was isolated by crystallization of the crude reaction mixture from ethyl acetate/hexane, and a second crop from diethyl ether. Subsequent hydrolysis furnished the enantiomerically pure amino alcohol as the hydrochloride salt **9** in 68% yield over two steps (Scheme 4).[12]

In summary, this third modification of the AA describes the use of *N*-bromoacetamide as the nitrogen source. In the case of styrenes, the regiochemistry of amino alcohol formation is reversed from that delivered by the carbamate version of the AA.[1d, 9] An efficient large-scale synthesis of enantiomerically pure 3-phenylisoserine highlights the prodical potential of this latest advance in the osmium-catalyzed asymmetric aminohydroxylation process.

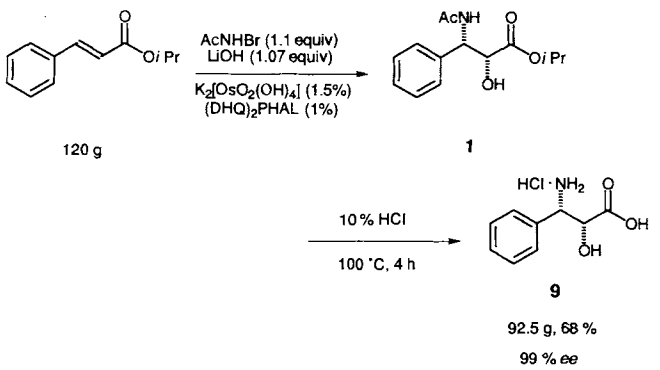

Scheme 4. Large-scale synthesis based on the acetamide-AA.

Experimental Section

General procedure (described for isopropyl cinnamate) [12]: In 3 mL of an aqueous solution of $LiOH \cdot H_2O$ (42.8 mg, 1.02 mmol), $K_2[OsO_2(OH)_4]$ (14.7 mg, 0.04 mmol, 4 mol%) was dissolved with stirring. After addition of *t*BuOH (6 mL), $(DHQ)_2PHAL$ (39 mg, 0.05 mmol, 5 mol%) was added and the mixture was stirred for 10 min to give a clear solution. Water (6 mL) was added subsequently, and the mixture was immersed in a cooling bath set to 4 °C. After addition of isopropyl cinnamate (190 mg, 1 mmol), *N*-bromoacetamide [5] (151.8 mg, 1.1 mmol) was added in one portion (which resulted in an immediate color change to green) and the mixture was vigorously stirred at the same temperature. The reaction was monitored by TLC and pH control (full conversion is indicated when the mixture reaches pH 7). After 20 h the reaction mixture was treated with Na_2SO_3 (0.5 g) and, after stirring at room temperature for 30 min, ethyl acetate (5 mL) was added. The organic layer was separated, and the water layer was extracted with ethyl acetate (3 × 10 mL). The combined organic extracts were washed with brine (5 mL), and dried over $MgSO_4$. After evaporation of the solvent, the crude product was purified by chromatography on silica gel (hexanes/ethyl acetate 1/1) to give 215 mg (81% yield, 99% *ee*) of isopropyl (2*R*,3*S*)-3-(acetylamino)-2-hydroxy-3-phenylpropanoate (**1**).

Modifications of the above procedure: see Table 1. For styryl olefins (Table 2), 1.0 equiv KOH and a 1:1 solvent/water ratio (15 mL) was employed. For reactions with anthraquinone-based ligands, $(DHQD)_2AQN$ (42.8 mg, 0.05 mmol, 5 mol%) was used instead of the PHAL ligand.

Large-scale synthesis of (2R,3S)-3-phenylisoserine hydrochloride (**9**): The above general procedure was followed by using isopropyl cinnamate (120.0 g, 0.631 mol, not corrected for purity, 96%, Lancaster), *t*BuOH (3.79 L), water (5.68 L), *N*-bromoacetamide (99.71 g, 0.694 mol, 96% pure upon titration) [5], $LiOH \cdot H_2O$ (28.32 g, 1.07 equiv, 0.675 mol) [6], $(DHQ)_2PHAL$ (4.914 g, 6.31 mmol, 1 mol%), and $K_2[OsO_2(OH)_4]$ (3.486 g, 9.08 mmol, 1.5 mol%). Reaction time: 4 h. To separate the ligand after completion of the reaction, the crude product was taken up in ethyl acetate (500 mL) and passed through a 11-cm sintered glass funnel covered with a 2.5-cm layer of silica gel. Product purification was accomplished by recrystallization from ethyl acetate/hexane 1:2 (4 mL g^{-1}). A second crop of material was obtained by trituration of the previously evaporated mother liquor with Et_2O (100 mL) and subsequent filtration. Yield 119.5 g (71% yield, 99% *ee*). Hydrolysis of this material (10% HCl, reflux, 4 h, followed by concentration and filtration) [12b] provided 92.5 g (68% over two steps) enantiomerically pure (2*R*,3*S*) **9** (m.p. 224–226 °C, $[\alpha] = -14.9$ ($c = 0.55$ in 6 N HCl, ref. −14.8) [14]; correct elemental analysis.

1: HPLC: Chiralcel ODH, 40% *i*PrOH/hexane, 0.5 mL min^{-1}, 254 nm, 8.2 min (2*S*,3*R*), 12.7 min (2*R*,3*S*) [14]. *ent*-**2**: HPLC: Chiralcel OG, 15% *i*PrOH/hexane, 1 mL min^{-1}, 254 nm, 12.6 min (2*S*,3*R*), 16.7 min (2*R*,3*S*). **3**: HPLC: Chiralcel OG, 20% *i*PrOH/hexane, 1 mL min^{-1}, 224 nm, 10.4 min (2*R*,3*S*), 14.6 min (2*S*,3*R*). *ent*-**4**: HPLC: Chiralcel ODH, 15% *i*PrOH/hexane, 0.5 mL min^{-1}, 254 nm, 21.8 min (1*R*,2*R*), 31.7 min (1*S*,2*S*) [15]. *ent*-**5** [16]: GC: Cyclodex B, J & W Scientific, initial time 5 min, initial temperature: 120 °C (5 min), rate: 0.5 °C min^{-1}, final temperature: 140 °C, 40.3 min (*R*), 41.3 min (*S*). **7a** [17]: HPLC: Chiralpak AD, 5% *i*PrOH/hexane, 1.5 mL min^{-1}, 254 nm, 12.7 min (*R*), 16.2 min (*S*). **8a** [18]: HPLC: Chiralpak AD, 5% *i*PrOH/hexane, 1.5 mL min^{-1}, 254 nm, 11.6 min (*R*), 10.1 min (*S*). **7b** HPLC: *N*,*O*-diacetate derivative: Chiralcel ODH, 7.5% *i*PrOH/hexane, 1 mL min^{-1}, 254 nm, 26.1 min (*R*), 28.8 min (*S*). **8b**: HPLC: *N*,*O*-diacetate derivative: Chiralcel ODH, 7.5% *i*PrOH/hexane, 1 mL min^{-1}, 254 nm, 36.4 min (*R*), 32.5 min (*S*). **7c** [17]: HPLC: *N*,*O*-diacetate derivative: Chiralcel ODH, 7.5% *i*PrOH/hexane, 1 mL min^{-1}, 254 nm, 19.1 min (*R*), 23.6 min (*S*). **8c** HPLC: *N*,*O*-diacetate derivative: Chiralcel ODH, 7.5% *i*PrOH/hexane, 1 mL min^{-1}, 254 nm, 26.2 min (*R*), 21.6 min (*S*).

Received: December 30, 1996 [Z 9942 1E]
German version: *Angew. Chem.* **1997**, *109*, 1580–1583

Keywords: amino alcohols · asymmetric catalysis · asymmetric aminohydroxylation · haloamides · homogeneous catalysis

[1] a) G. Li, H.-T. Chang, K. B. Sharpless, *Angew. Chem.* **1996**, *108*, 449–452; *Angew. Chem. Int. Ed. Engl.* **1996**, *35*, 451–454; b) G. Li, K. B. Sharpless, *Acta Chem. Scand.* **1996**, *50*, 649–651; c) K. B. Sharpless; J. Rudolph; P. C. Sennhenn; C. P. Vlaar, *Angew. Chem.* **1996**, *108*, 2991–2995; *Angew. Chem. Int. Ed. Engl.* **1996**, *35*, 2810–2813: Corrigendum: In the General Procedure given in the Experimental Procedure of this paper it should read $(DHQ)_2PHAL$ instead of $(DHQD)_2PHAL$; d) G. Li; H. H. Angert; K. B. Sharpless, *Angew. Chem.* **1996**, *108*, 2995–2999; *Angew. Chem. Int. Ed. Engl.* **1996**, *35*, 2813–2817: Corrigendum: In the Experimental Procedure in this paper the yield of pure (*S*)-**2** should read 0.230 g and not 0.460 g.

 © VCH Verlagsgesellschaft mbH, D-69451 Weinheim, 1997 0570-0833/97/3613-1485 $ 17.50+.50/0

[2] a) J. F. Larrow, S. E. Schaus, E. N. Jacobsen, *J. Am. Chem. Soc.* **1996**, *118*, 7420–7421; b) M. Shibasaki, H. Sasai, *Pure Appl. Chem.* **1996**, *68*, 523–530.

[3] H. C. Kolb, M. S. VanNieuwenhze, K. B. Sharpless, *Chem. Rev.* **1994**, *94*, 2483–2547.

[4] a) A. W. Hofmann, *Ber. Dtsch. Chem. Ges.* **1881**, *14*, 2725; b) E. S. Wallis, J. F. Lane, *Org. React.* **1967**, *3*, 267–306.

[5] a) *N*-bromoacetamide is commercially available (e.g. from Lancaster), but it should be recrystallized ($CHCl_3$/hexane 1/1) before use. We recommend preparation by a published procedure: E. P. Oliveto, C. Gerold, *Organic Syntheses Collective Volume IV*, 104–105. The purity of this oxidant was checked by acid–base titration: C. Bachand, H. Driguez, J. M. Paton, D. Touchard, J. Lessard, *J. Org. Chem.* **1974**, *39*, 3136–3138. b) S. C. Virgil in *Encyclopedia of Reagents for Organic Synthesis, Vol. 1* (Ed.: L. A. Paquette), Wiley, New York, **1995**, p. 691.

[6] Since the base/oxidant ratio should not exceed 1:1, the amount of hydroxide resulting from the initial oxidation of $K_2[OsO_2(OH)_4]$ to Os^{VIII}, releasing two equivalents of base, was taken into account.

[7] The use of isopropyl cinnamates instead of the methyl esters is preferable in terms of greater stability towards hydrolysis and enhanced regioselectivity under the reaction conditions. As in the case of compounds **1** and **2**, which are quite soluble in the reaction medium, the use of more than 50% (v/v) water may result in slightly increased regioselectivities.

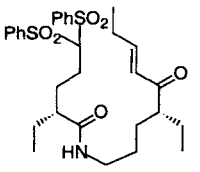

3

[8] H. Becker, K. B. Sharpless, *Angew. Chem.* **1996**, *108*, 447–449; *Angew. Chem. Int. Ed. Engl.* **1996**, *35*, 448–451: Corrigendum: The Experimental Procedure in this paper should include the following: "Asymmetric dihydoxylations of entries 1–8, and 16 in Tables 1 and 2 were run under buffered conditions in which the reaction is performed as desribed except that $NaHCO_3$ (252 mg, 3 mmol) was added at the beginning of the reaction". Also, in the syntheses of the ligands $(DHQD)_2AQN$ and $(DHQ)_2AQN$, it should be noted that the dihydroquinidine and dihydroquinine were dried over P_2O_5 under vacuum before use. Both $(DHQ)_2AQN$ and $(DHQD)_2AQN$ are commercially available (Aldrich); an improved synthesis will be reported elsewhere.

[9] K. L. Reddy, G. Li, K. B. Sharpless, unpublished results. See also ref. [1d].

[10] Preliminary experiments with other substrates indicate that a reversal of regiochemistry occurs when anthraquinone-derived ligands are used instead of phthalazines.

[11] So far, only a few exceptions to our mnemonic device for the AD have been reported: a) K. J. Hale, S. Manaviazar, S. A. Beak, *Tetrahedron Lett.* **1994**, *35*, 425–428; b) D. J. Krysan, *ibid.* **1996**, *37*, 1375–1376; c) D. L. Boger, J. A. McKie, T. Nishi, T. Ogiku, *J. Am. Chem. Soc.* **1996**, *118*, 2301–2302; d) P. Salvadori, S. Superchi, F. Minutolo, *J. Org. Chem.* **1996**, *61*, 4190–4191; e) K. P. M. Vanhessche, K. B. Sharpless, *ibid.* **1996**, *61*, 7987–7979.

[12] The yield might be further increased (5–10%) by optimizing the isolation procedure. We believe that this new amide-AA-based protocol is superior to our earlier AA- or AD-based approaches: a) Ref. [1b]; b) Z.-M. Wang, H. C. Kolb, K. B. Sharpless, *J. Org. Chem.* **1994**, *59*, 5104–5105.

[13] The fact that less ligand than osmium can be used, demonstrates once again the great advantages of a ligand-accelerated catalysis (LAC); for a review see D. J. Berrisford, C. Bolm, K. B. Sharpless, *Angew. Chem.* **1995**, *107*, 1159–1171; *Angew. Chem. Int. Ed. Engl.* **1995**, *34*, 1059–1070.

[14] a) H. Honig, P. Senfer-Wasserthal, H. Weber, *Tetrahedron* **1990**, *46*, 3841–3850; b) I. Ojima, I. Habus, M. Zhao, *J. Org. Chem.* **1991**, *56*, 1681–1683.

[15] a) G. G. Lyle, W. Lacroix, *J. Org. Chem.* **1963**, *28*, 900–901; b) K. Saigo, S. Ogawa, S. Kikuchi, A. Kasahara, H. Nohira, *Bull. Chem. Soc. Jpn.* **1982**, *55*, 1568–1573.

[16] Y. Lu, Ch. Miet, N. Kunesch, J. E. Poisson, *Tetrahedron: Asymmetry* **1993**, *4*, 893–902.

[17] T. Izumi, K. Fukaya, *Bull. Chem. Soc. Jpn.* **1993**, *66*, 1216–1221.

[18] Prepared from (*R*)-2-phenylglycinol (Aldrich).

Palladium-Catalyzed Additions of Alkenyl Epoxides to Pronucleophiles: A Synthesis of the Macrolactam Aglycone of Fluviricin B1**

Barry M. Trost,* Marco A. Ceschi, and Burkhard König

The additions of alkenyl epoxides with pronucleophiles catalyzed by palladium constitutes a promising approach for constructing complex molecules.[1–3] However, the facility by which the palladium catalysts effect epoxide rearrangements,[4] which are intramolecular processes, makes their intermolecular capture a challenge. Macrocyclizations, which resemble intermolecular reactions, illustrate the delicate balance [Eq. (1)].

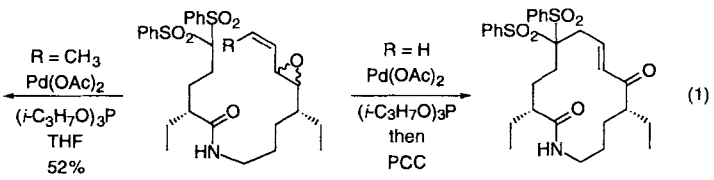

(1)

1a, R = H
1b, R = CH_3

2

Whereas, the simple vinyl epoxide **1a** cyclized smoothly to form the 14-membered ring **2**, addition of a methyl group at the terminus completely suppressed cyclization and led to isomerization of this alkenyl epoxide to the enone **3**.

The importance of such terminally substituted alkenyl epoxides stems from their use for chirality transfer to control relative configurations of distal centers. We therefore studied the characteristics of the pronucleophiles that would allow reaction with alkenyl epoxides, in order to provide a synthesis of the aglycone of fluviricin B1[5, 6] that exemplified their use in controlling stereochemistry of distal centers.

To explore the effect of substitution on the palladium-catalyzed addition of pronucleophiles to alkenyl epoxides, we chose the propenyl derivative **4** [Eq. (2)]. The unsubstituted bis(sul-

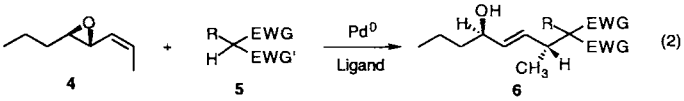

(2)

4 **5** **6**

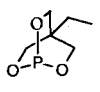

7

a, R = H, EWG = EWG' = $PhSO_2$
b, R = C_2H_5, EWG = EWG' = $PhSO_2$
c, R = H, EWG = $PhSO_2$, EWG' = CH_3CO
d, R = CH_3, EWG = $PhSO_2$, EWG' = CN
e, R = C_2H_5, EWG, EWG' =

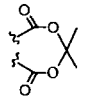

[*] Prof. Dr. B. M. Trost, Dr. M. A. Ceschi, Dr. B. König
Department of Chemistry
Stanford University
Stanford, CA 94305-5080 (USA)
Fax: Int. code +(415) 725-0259
e-mail: bmtrost@leland.stanford.edu

[**] We thank the National Science Foundation and the National Institutes of Health (NIH), General Medical Sciences Institute, for their generous support of our programs. M. A. C. and B. K. were partially supported by CAPES of Brazil and the Alexander von Humboldt Stiftung of Germany, respectively. Mass spectra were provided by the Mass Spectrometry Facility, University of California-San Francisco, supported by the NIH Division of Research Resources. Comparison spectra and data were kindly provided by Professor Amir Hoveyda, Boston. Helena Hagelin kindly performed the molecular mechanics calculations.

 © VCH Verlagsgesellschaft mbH, D-69451 Weinheim, 1997 0570-0833/97/3613-1486 $ 17.50+.50/0

fone) **5a** as pronucleophile reacted smoothly to give the desired alkylation product **6a**[7] ([$(Ph_3P)_4Pd$], THF, reflux, 62%), whereas the monoalkylated derivative **5b** gave none of its corresponding dialkylated derivative **6b**. The unsubstituted ketosulfone **5c** underwent smooth alkylation to afford **6c**[7] ([$(dba)_3Pd_2]\cdot CHCl_3$, **7**, THF, reflux, 55%). More significantly, the substituted cyanosulfone **5d** also participated quite well, yielding the monoalkylated product **6d**[7] ($Pd(OAc)_2$, (i-$C_3H_7O)_3P$, THF, reflux, 55%). The best reaction involved use of a substituted Meldrum's acid (**5e**) as the pronucleophile: alkylation proceeded at room temperature to form the alkylated product **6e**[7] ($Pd(OAc)_2$, (i-$C_3H_7O)_3P$, THF, room temperature, 75%). In each of these cases NMR analysis reveals only one diastereomer, indicating good control of chirality transfer by the palladium catalyst.

We therefore chose to use Meldrum's acid as the pronucleophile for the synthesis of fluviricin B1 aglycone **8** as outlined in Scheme 1. This target is representative of the fluviricins (macrolactams active against influenza A virus as well as against pathogenic fungi). To use the concept of stereochemical relay via π-allylpalladium species to create the proper configuration at C-5, we required macrocycle **9** as synthetic precursor: bis-decarboxylation and reduction would create **8**. Splitting **9** into **10** and **11** yields two fragments that can both be synthesized from the imidazolidinone **12**, as revealed in Schemes 2 and 3.

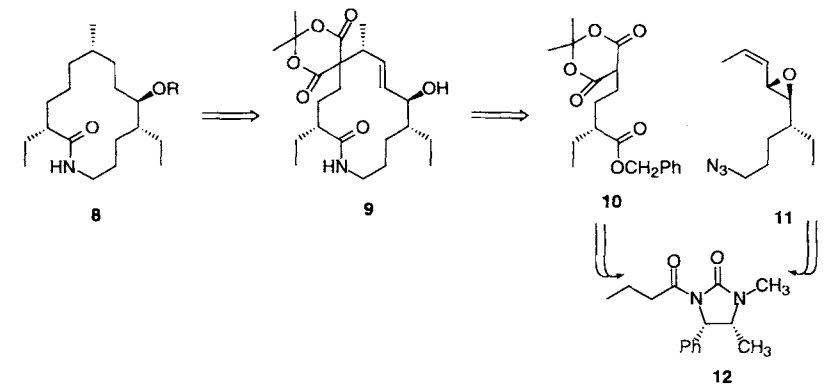

Scheme 1. Retrosynthetic analysis of fluviricin B_1 (**8**, R = H).

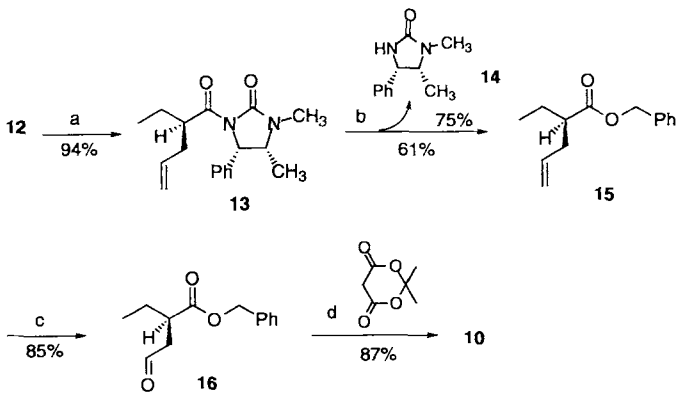

Scheme 2. Asymmetric synthesis of the pronucleophile **10**. a) Lithium diisopropylamide (LDA), THF, −78 °C, $H_2C{=}CHCH_2Br$; b) $PhCH_2OH$, n-C_4H_9Li, THF, 0 °C; c) O_3, CH_2Cl_2, −78 °C, then Ph_3P; d) NaTeH ($NaBH_4$ + Te), C_2H_5OH, piperidine, HOAc, −30 °C → room temperature.

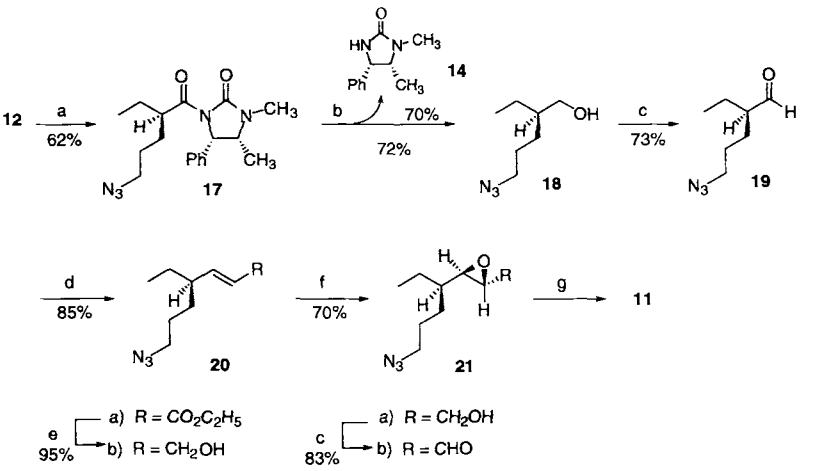

Scheme 3. Synthesis of the propenyl epoxide **11**. a) LDA, THF, −78 °C, $ICH_2CH_2CH_2N_3$; b) $LiAlH_4$, THF, 0 °C; c) $(COCl)_2$, DMSO, CH_2Cl_2, $(C_2H_5)_3N$, −78 °C; d) NaH, $(C_2H_5O)_2P(O)CH_2CO_2C_2H_5$, NaH, THF, room temperature; e) DIBAL-H, THF, −78 °C; f) 13.5 mol % Ti (Oi-$C_3H_7)_4$, 21 mol % diethyl tartrate ((−)-DET), 4 Å MS, CH_2Cl_2, 0 °C; g) $Ph_3PCH_2CH_3Br$, $KN(SiMe_3)_2$, THF, −78 °C → room temperature.

The stable imidazolidinone **12** was chosen as the chiral auxiliary because of its ease of access from ephedrine and its excellent diastereoselectivity in alkylations.[8] The alkylations to form **13**[7] and **17**[7] gave only one diastereomer detectable by NMR spectroscopy (>95% *de*). Either deacylation with lithium benzyloxide to **15**[7] or, remarkably, reduction with $LiAlH_4$ returned the chiral auxiliary **14**[7] in good yields. The monosubstituted Meldrum's acid **10** was best prepared by reductive alkylation of aldehyde **16** with sodium hydrogen telluride, generated in situ, under Knoevenagel conditions.[9]

For the azide half, direct reduction of **17** to aldehyde **19** could be accomplished with diisobutylaluminum hydride (DIBAL-H), but significant racemization accompanied the reduction—consequently, the two-step sequence via alcohol **18** was preferable. Asymmetric epoxidation[10] of the olefination product **20b** required larger amounts of catalyst for good yields, which suggests a low turnover number. On the other hand, only a single diastereomeric epoxide (**21a**) was observed. Olefination of the aldehyde **21b** under standard conditions gave a 7:1 (*Z*):(*E*) ratio of alkenes.

The key Pd-catalyzed alkylation employed a precatalyst generated by mixing [$(dba)_3Pd_2\cdot CHCl_3$] (1.5 mol%) and phosphite **7** (20 mol%) in THF. Sequential addition of equimolar quantities of the alkenyl epoxide **11** and Meldrum's acid **10** gave, after 12 h at room temperature, a 75% yield of the alkylation product **22** (Scheme 4) as a single diastereomer. Thus, chirality transfer occurred completely within experimental error. The assignment of the stereochemistry derived from mechanistic considerations[11] and the successful completion of the total synthesis.

Numerous attempts to effect both alkene hydrogenation and hydrogenolysis of the benzyl ester and azide proved futile. On the other hand, hydrogenolysis of the latter two functionalities did occur with ammonium formate in the presence of Pd/C;[12] though various protocols for the subsequent macrolactamization of the amino acid to give **23** failed, including the use of the Yamaguchi reagent,[13] bromotripyrrolidinophosphonium hexafluorophosphate[14] successfully effected macrolactamization in what may be a generally applicable procedure. The initial

 © VCH Verlagsgesellschaft mbH, D-69451 Weinheim, 1997 0570-0833/97/3613-1487 $ 17.50+.50/0

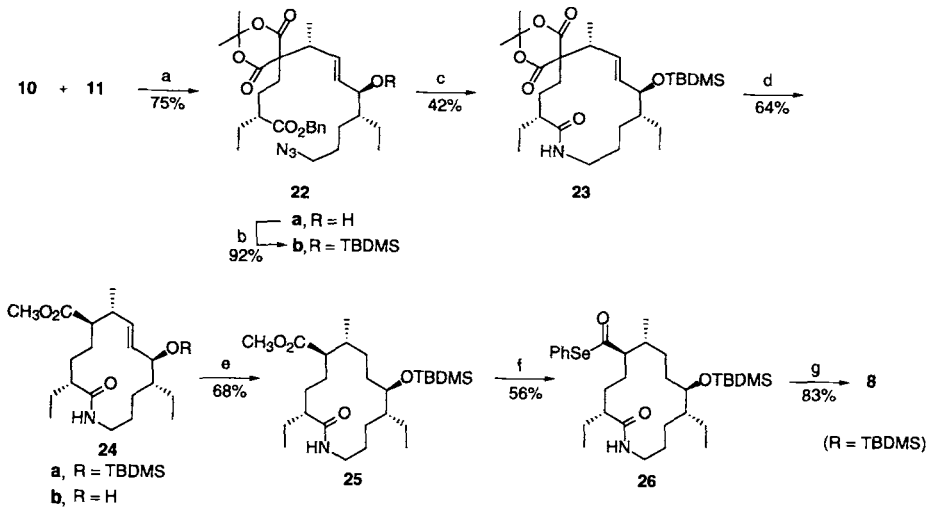

Scheme 4. Synthesis of the fluviricin B_1 aglycon **8**, R = TBDMS. a) See text; b) $TBDMSOSO_2CF_3$, 2,6-lutidine, CH_2Cl_2, 0 °C; c) 1.5% Pd/C, HCO_2NH_4, H_2O, 4 kbar, room temperature, 2. PyBroP, $(iC_3H_7)_2NC_2H_5$, 4-dimethylaminopyridine (DMAP), $PhCH_3$, 83 °C; d) LiOH, CH_3OH, H_2O, 4 kbar, room temperature, then DMSO, 120 °C; e) tetra-*n*-butylammonium fluoride (TBAF), THF, 0 → 40 °C, H_2 (1 atm), 10% Pd/C, C_2H_5OH, room temperature; $TBDMSOSO_2CF_3$, 2,6-lutidine, CH_2Cl_2, 0 °C; f) LiOH, KCN, CH_3OH, H_2O, THF, room temperature; $PhOP(O)Cl_2$, $(C_2H_5)_3N$, THF, 0 °C, then PhSeH, $(C_2H_5)_3N$, THF, 0 °C; g) $(C_4H_9)_3SnH$, azobisisobutyronitrile (AIBN), xylene, 175 °C.

decarboxylation gave a single diastereomeric monoester (**24a**, assigned based upon molecular modeling).[15] The double bond in silyl ether **24a** proved resistant to hydrogenation; however, allyl alcohol **24b** was reduced smoothly to give **25** after resilylation. Inability to form the ester from *N*-hydroxypyridine-2-thione[15] led to an alternative to decarboxylation for the removal of the remaining ester.[16] The acyl selenide **26** underwent a smooth decarbonylation[17] to the silyl ether of fluviricin B1, which was identical in every respect to an authentic sample (for physical data see Table 1). The monosilyl ether **8** (R = TBDMS) has previously been desilylated to fluviricin B1 aglycone **8** (R = H).

This reaction of terminally substituted vinyl epoxides provides a useful approach to chirality transfer. The selection of the pronucleophile is more critical than for unsubstituted vinyl epoxides. For a trisubstituted anion, steric hindrance appears to be the dominating influence as illustrated by the success of cyano-stabilized anions or those derived from Meldrum's acid. The stereochemical memory derives from its temporary storage as the π-allylpalladium species [Eq. (3)]. In this way, vicinal stereochemistry readily translates into 1,4-stereochemistry. The synthesis of the aglycone of the fluviricin family illustrates the utility of this methodology. The sequence also demonstrates some of the unusual properties of this ring system. The difficulty in hydrolyzing and decarboxylating the Meldrum's acid unit and in hydrogenating of the double bond illustrate two interesting aspects. In addition, the functionality present allows access to analogues. This convergent strategy in which the two halves are joined by a palladium-catalyzed alkylation and an amide formation may prove to be generally useful.

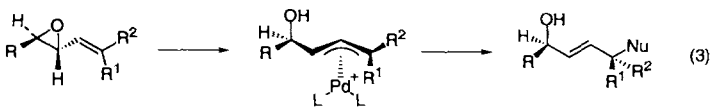

(3)

Table 1. Selected physical data of the important compounds.

8: (R = TBDMS) $[\alpha]_D^{25}$ +12 (c = 0.02, CH_2Cl_2). M.p. 187–188 °C. IR (neat): $\tilde{\nu}$ = 3448, 1633, 1553, 1463, 1381 cm^{-1}; ^1H NMR (400 Hz, C_6D_6): δ = 4.38 (dd, J = 8.7, 3.0 Hz, 1H), 3.77 (dddd, J = 23.7, 11, 4, 2 Hz, 1H), 3.51 (m, 1H), 2.44 (m, 1H), 1.98–1.10 (m, 21H), 1.04 (s, 9H), 0.97 (d, J = 7 Hz, 3H), 0.89 (t, J = 7.4 Hz, 3H), 0.82 (t, J = 7.5 Hz, 3H), 0.13 (s, 3H), 0.12 (s, 3H); ^{13}C NMR (100 MHz, C_6D_6): δ = 174.8, 73.1, 50.9, 42.9, 38.6, 34.8, 34.2, 31.5, 28.6, 27.0, 26.2, 25.9, 25.2, 24.4, 21.1, 20.9, 18.4, 12.5, 9.5, 8.1, 5.7, 4.7.

10: $[\alpha]_D^{25}$ 1.97 (c = 1.59, $CHCl_3$); IR (neat): $\tilde{\nu}$ = 1780, 1730 (broad), 1610, 1595, 1500, 1457 cm^{-1}; ^1H NMR (300 MHz, $CDCl_3$): δ = 8.43–7.30 (m, 5H), 5.18 (s, 2H), 3.53 (t, J = 9.3 Hz, 1H), 2.48–2.32 (m, 2H), 2.19–2.03 (m, 2H), 1.75 (d, J = 9.3 Hz, 6H), 1.95–1.50 (m, 2H), 0.90 (t, J = 12.2 Hz, 3H); ^{13}C NMR (75 MHz, $CDCl_3$): δ = 175.5, 165.3, 136.1, 128.3, 128.3, 105.0, 66.4, 47.1 46.1, 28.6, 26.8, 25.2, 24.1, 11.7.

11: $[\alpha]_D^{25}$ −10.5 (c = 0.74, $CHCl_2$). IR (neat): $\tilde{\nu}$ = 2096, 1650, 1480, 1380 cm^{-1}; ^1H NMR (400 MHz, $CDCl_3$): δ = 5.77 (m, 1H), 5.05 (m, 1H), 3.39 (dd, J = 7.1, 2.0 Hz, 1H), 3.27 (m, 2H), 2.61 (dd, J = 8.1, 2.2 Hz, 1H), 1.81 (dd, J = 7.0, 1.8 Hz, 3H), 1.75–1.20 (m, 7H), 0.95 (t, J = 6.0 Hz, 3H); ^{13}C NMR (75 MHz, $CDCl_3$): δ = 131.3, 128.3, 63.6, 53.9, 51.9, 42.6, 28.1, 27.0, 25.5, 13.5, 11.2.

22a: $[\alpha]_D^{25}$ +13.3 (c = 0.8, CH_2Cl_2). IR (neat): $\tilde{\nu}$ = 3528, 2099, 1770, 1737, 1456 cm^{-1}; ^1H NMR (300 MHz, $CDCl_3$): δ = 7.35 (m, 5H), 5.68–5.48 (m, 2H), 5.10 (s, 2H), 4.10 (bs, 1H), 3.25 (t, J = 7.5 Hz, 2H), 2.80 (m, H), 1.90 (m, 2H), 1.70 (s, 3H), 1.63 (s, 3H), 1.62–1.12 (m, 12H), 1.10 (d, J = 7.3 Hz, 3H), 0.88 (t, J = 7 Hz, 3H), 0.83 (t, J = 7 Hz, 3H) (J = 7 Hz, 3H); ^{13}C NMR (75 MHz, $CDCl_3$): δ = 175.2, 169.0, 168.2, 136.5, 135.3, 131.2, 129.1, 128.8, 120.8, 106.3, 74.1, 66.8, 58.7, 52.3, 47.3, 47.2, 45.6, 33.6, 31.4, 29.6, 28.2, 27.5, 27.0, 25.2, 22.7, 17.6.

23: $[\alpha]_D^{25}$ +32 (c = 0.5, CH_2Cl_2). M.p. 139 °C. IR (neat): $\tilde{\nu}$ = 1783, 1735, 1671 cm^{-1}; ^1H NMR (300 MHz, $CDCl_3$): δ = 5.52 (dd, J = 16.8, 10 Hz, 1H), 5.32 (dd, J = 16.8, 10 Hz, 1H), 5.30 (m, 1H), 3.88 (m, 1H), 3.77 (t, J = 9.6 Hz, 2H), 2.93 (m, 1H), 2.75 (m, 1H), 2.1 (dt, J = 14, 4.8 Hz), 1.72 (s, 3H), 1.75 (s, 3H), 1.40 (d, J = 7 Hz, 3H), 0.85 (s, 9H), 0.80 (m, 6H), 0.0 (s, 3H), −0.06 (s, 3H); ^{13}C NMR (75 MHz, $CDCl_3$): δ = 176.3, 172.6, 168.8, 139.9, 133.5, 108.1, 59.9, 52.8, 50.5, 46.7, 40.8, 38.3, 33.1, 31.4, 31.2, 29.1, 28.5, 27.9, 26.9, 21.6, 20.2, 19.5, 14.2, 10.4, −1.3, −2.7.

Received: January 21, 1997 [Z10013IE]
German version: *Angew. Chem.* **1997**, *109*, 1562–1564

Keywords: allylic alkylations · asymmetric synthesis · chirality transfer · macrolactamization · palladium

[1] B. M. Trost, G. A. Molander, *J. Am. Chem. Soc.* **1981**, *103*, 5969; J. Tsuji, H. Kataoka, Y. Kobayashi, *Tetrahedron Lett.* **1981**, *22*, 2575.
[2] B. M. Trost, T. S. Scanlan, *J. Am. Chem. Soc.* **1989**, *111*, 4988; A. S. Kende, I. Kaldor, R. Aslanian, *ibid.* **1988**, *110*, 6265; B. M. Trost, J. T. Hane, P. Metz, *Tetrahedron Lett.* **1986**, *27*, 5695.
[3] B. M. Trost, R. W. Warner, *J. Am. Chem. Soc.* **1983**, *105*, 5940.
[4] Suzuki, Y. Oda, R. Noyori, *J. Am. Chem. Soc.* **1979**, *101*, 1623.
[5] N. Naruse, T. Tsuno, Y. Sawada, M. Konishi, T. Oki, *J. Antibiot.* **1991**, *44*, 741; N. Naruse, M. Konishi, T. Oki *ibid.* **1991**, *44*, 756; R. V. Hegde, M. G. Patel, V. P. Gallo, M. S. Puar, *J. Chem. Soc. Chem. Commun.* **1991**, 810; R. V. Hegde, M. G. Patel, V. P. Gallo, M. S. Puar, *J. Am. Chem. Soc.* **1990**, *112*, 6403.
[6] First synthesis: A. F. Houri, Z. Xu, D. A. Cogan, A. H. Hoveyda, *J. Am. Chem. Soc.* **1995**, *117*, 2943; Z. Xu, C. W. Johannes, S. S. Salman, A. H. Hoveyda *ibid.* **1996**, *118*, 10926.
[7] This compound has been characterized spectroscopically, and the elemental composition was established by high resolution mass spectrometry and combustion analysis.
[8] G. Cardillo, A. D'Amico, M. Orena, S. Sandri, *J. Org. Chem.* **1988**, *53*, 2354.
[9] X. Huang, L. Xie, *Synth. Commun.* **1986**, *16*, 1701. For review, see: L. F. Tietze, U. Beifuss in *Comprehensive Organic Synthesis* (Eds: B. M. Trost, I. Fleming, C. H. Heathcock), Pergamon, Oxford, **1991**, Chapter 1.11, pp. 341–394.

[10] Y. Gao, M. R. Hanson, M. J. Klunder, Y. S. Ko, H. Masamune, K. B. Sharpless, *J. Am. Chem. Soc.* **1987**, *109*, 5765.
[11] B. M. Trost, T. R. Verhoeven, *Tetrahedron* **1977**, *33*, 2615; B. M. Trost, T. P. Klun, *J. Am. Chem. Soc.* **1979**, *101*, 6756.
[12] Cf. A. G. M. Barrett, N. S. Mani, *Tetrahedron Lett.* **1987**, *28*, 6133; T. G. C. Selve, J. J. Delpuech, *ibid.* **1983**, *24*, 1609; A. F. Spatola, M. K. Anwer, *Synth. Commun.* **1980**, 929; S. Ram, R. E. Ehrenkaufer, *Synthesis* **1988**, 91.
[13] M. Yamaguchi, J. Inanaga, K. Hirata, H. Saeki, T. Katsuki, *Bull. Chem. Soc. Jpn.* **1979**, *52*, 1989.
[14] J. Coste, E. Frérot, P. Jouin, *J. Org. Chem.* **1994**, *59*, 2437.
[15] Performed by Helena Hagelin in our laboratories.
[16] D. H. R. Barton, D. Crich, W. B. Motherwell, *Tetrahedron* **1985**, *41*, 3901.
[17] J. Pfenninger, G. Heuberger, W. Graf, *Helv. Chim. Acta* **1980**, *63*, 2328.

The Surprising Crystal Packing of Chlorinefluoride**

Roland Boese,* A. Daniel Boese, Dieter Bläser, Michail Yu. Antipin, Arkadi Ellern, and Konrad Seppelt

Dedicated to Professor Günter Schmid on the occasion of his 60th birthday

Interhalogen compounds are of special interest both from the synthetic and the theoretical standpoint. They are widely used as very strong oxidizing agents, and some of them, for example halogen fluorides, are typical amphoteric systems that exhibit Lewis acid Lewis base interactions in the liquid and solid states.[1, 2] As ions or neutral species they have become important objects of numerous structural investigations as they serve as model compounds in the studies of the chemical bond.[3, 4] Thus, the molecular structures of XF_3, XF_5 (X = Cl, Br, I), and some other polyhalogens are often considered as typical examples for the application of the VSEPR (Valence Shell Electron Pair Repulsion) model for describing molecular geometry.[4]

Strong intermolecular interactions between the halogen atoms (F···Cl, F···Br) were found in the crystals of neutral halogen fluorides, for example in the two polymorphic modifications of ClF_3[5] and BrF_3.[6] However, no short F···F contacts were observed in these structures. In most cases fluorine atoms act as bridging atoms, or do not participate in the intermolecular (interionic) interactions.

In general, X-ray diffraction studies of neutral interhalogen compounds are rather rare, because most of them are reactive and low-melting compounds, which causes difficulties in obtaining single crystals. Nevertheless, these studies are of great interest because they provide access to important information about the electronic nature of the intermolecular interactions between halogen atoms.

We report herein the molecular and crystal structure of the simplest interhalogen compound, chlorine monofluoride, ClF, at −188 °C. To the best of our knowledge, the solid-state structure of ClF is the only structure of the well-known family of halogen monofluorides that has ever been determined. There are a few objective reasons for this. Halogen monofluorides have very low melting and boiling points (e.g. ClF: −155.6 and −100.1 °C, respectively), and together with their very high oxidizing activity and moisture sensitivity this makes these compounds extremely difficult to handle. For example, ClF reacts readily with glass, so its storage and crystal growth in the usual thin-walled glass capillaries from the melt is very difficult. Furthermore, the crystallization point, which is essentially lower than the melting point, is almost at the limit of liquid nitrogen low-temperature devices for single-crystal diffractometers. All this was considered as a challenge to our developments in crystallization and low-temperature techniques. For the crystal packing of ClF we expected something similar to that observed for α-,[7] β-ICl[8] or IBr,[9] that is zigzag or herringbone patterns, governed by the intermolecular dipole interactions, with chlorine atoms surrounded by one or more fluorine atoms.

Surprisingly, the X-ray data show that in the crystal individual ClF molecules form infinite planar ribbons along the screw axis (space group $P2_1/c$), which are characterized by very short intermolecular Cl···Cl contacts (3.070(1) Å) between neighboring molecules (Figure 1). The ribbon planes are inclined to

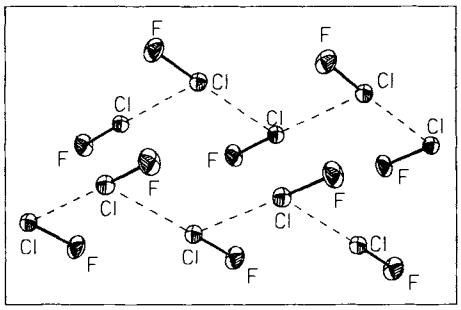

Figure 1. Perspective view of the crystal structure of ClF (ellipsoid plot (50%)), showing two rows of molecules, arranged along the screw axis.

the *a*, *b*, and *c* crystal axes by 74.7, 90, and 179.6°, respectively, and along the *c* axis they are antiparallel. In the ribbon the Cl atoms are arranged in a zigzag fashion, so each atom participates in two (symmetry equivalent) Cl···Cl contacts; the Cl···Cl···Cl angle is 87.5(1)°. One contact is directed along the prolongation of the F–Cl bond (the F–Cl···Cl angle is 178.8(1)°), and the other one is perpendicular to the same F–Cl bond (the corresponding angle is 93.5(1)°) (Figure 2). Between the ribbons there are only F···F contacts for which the shortest distance is 2.92 Å, which is a normal value for a van der Waals interaction.[10]

To our knowledge, the Cl···Cl contacts in the crystal of ClF are the shortest among the known Cl···Cl intermolecular distances in molecular crystals. In a recent study[10] a value of 3.50 Å is assumed as a typical distance for Cl···Cl contacts. In

[*] Prof. Dr. R. Boese, Dipl.-Ing. D. Bläser, Prof. Dr. M. Yu. Antipin[+]
Institut für Anorganische Chemie der Universität
Universitätsstrasse 5–7, D-45117 Essen (Germany)
Fax: Int. code +(201)1832535
e-mail: boese@structchem.uni-essen.de
A. D. Boese
Department of Chemistry, Rice University
Houston, TX 77251-1892 (USA)
Prof. Dr. K. Seppelt, Dr. A. Ellern[++]
Institut für Anorganische und Analytische Chemie der Freien Universität Berlin (Germany)
[+]Permanent address: Institute of Organoelement Compounds
Russian Academy of Sciences (INEOS), Vavilov Street 28, Moscow B-334 (Russia)
[++] Permanent address: Faculty of Chemistry, Ben Gurion University of Negev, Beer-Sheva (Israel)

[**] This work was supported by the Fonds der Chemischen Industrie (R. B.), the Deutsche Forschungsgemeinschaft (M. Y. A.), and the Alexander-von-Humboldt Foundation (A. E.). We thank Prof. G. E. Scuseria (Rice University, Houston, Texas) for his interest in the work and for providing computational recources.

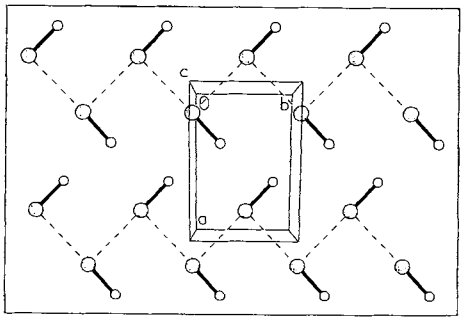

Figure 2. Packing of chlorinefluorine and the unit cell with a view down the c axis; the shaded spheres represent the chlorine atoms, the open circles the fluorine atoms.

solid chlorine, however, the intermolecular distances are 3.294(1) Å (see below).[11] The evidently strong intermolecular interactions in ClF in the solid state do not influence the Cl–F bond length of 1.628(1) Å very much, since the identical value was also obtained for ClF in the gas phase by a microwave study.[12]

We also[13] calculated the ClF monomer at MP2, B3LYP, and CCSD(T) levels of theory[14] using the 6-311 + G* basis set, which gave ClF distances of 1.673, 1.680, and 1.686 Å, respectively. These values are essentially longer than the experimentally determined data; on the other hand, the value calculated at the HF level (1.588 Å[13]) is much closer.

An approximate estimation of this distance with the Schomaker–Stevenson formula $d = R(x) + R(Y) - (0.095)\Delta(EN)$,[15] where R denotes the atomic covalent radii from the homohalogen dimers (0.710 Å for F, and 0.995 Å for Cl), and $\Delta(EN)$ is the electronegativity difference (equal to 1.0 for the pair F and Cl), results in a Cl–F distance of 1.610 Å. Taking into account that the bond lengths obtained by the X-ray method are usually longer than the data obtained in the gas phase, it is reasonable to suggest that the real internuclear Cl–F distance in the crystal should be slightly longer than 1.628 Å.

An interesting feature of the ClF crystal structure is its rather close similarity to that of chlorine,[11] where each Cl atom also forms two short intermolecular Cl···Cl contacts (3.294 Å) with nearly the same orientation as in ClF. The crystal structure of Cl_2 has planar, endless layers parallel to (100). In both structures there are zigzag chains of Cl···Cl···Cl interactions, but in ClF these chains are separated by F atoms thereby forming ribbons, whereas in Cl_2 the neighboring chains belong to one layer. The reason for this difference may be related with the inability of the F atoms to participate in bonding F···F interactions. The packing pattern in ClF also resembles that in 1,4-dichlorbenzene,[16] which exhibits T-shaped intermolecular Cl···Cl contacts. According to experimental[17] and theoretical[18] studies, the noble gas atoms in argon complexes of ClF were likewise found perpendicular to the F–Cl axis. From the molecular orbital point of view such an interaction may be regarded as involving bonding between a lone pair orbital of one Cl atom and an antibonding σ orbital of the F–Cl bond of a neighboring molecule. Modern theory on interatomic interactions, based on Bader's topological analysis of the total electron density distribution of a molecular system, describes this kind of "closed-shell interaction" as an interaction between the electron charge concentration (CC) and charge depletion (CD) areas in the electron valence shell of the interacting atoms.[19] Corresponding CC and CD areas may be related with the Lewis model of acid–base interactions, and these areas may be visualized in the Laplacian of the electron density $-\nabla^2\rho$.[20, 21]

Laplacian maps of the charge density were found to be very useful in analysis of the nature of the chemical bonds in terms of topological characteristics of the total electron density. Electron density distributions in crystals can be constructed with high accuracy from X-ray diffraction data and by using multipole models of the nonspherical atoms in the crystal (see reference [22] and references therein). In the present work we used the Hansen and Coppens multipole model[23] and the XD package programs[21] for the construction of an experimental electron density distribution in the ClF crystal and the calculation of some topological and other properties. Least-squares refinements of diffraction data with this model resulted in a strong decrease of R indexes ($R = 0.032$ and $Rw = 0.028$), and quite realistic values of multipole parameters. Values of $q(Cl) = +0.14$ and $q(F) = -0.14$ for the atomic charges, and a dipole moment of 1.2 D were calculated from the X-ray data. These values are in good agreement with the suggested polarity of ClF (Cl^+F^-, see discussions in references [24,25]), and with the experimental value of the molecular dipole moment (0.88 D[26]) as well as that obtained from theoretical calculations (1.01 D and 0.84 D in the HF and CI approximations[27, 28]).

The experimental map of the Laplacian of the electron density ($-\nabla^2\rho$) in the crystal of ClF in the plane of the interacting molecules is shown in Figure 3. It is clear that in the vicinity of

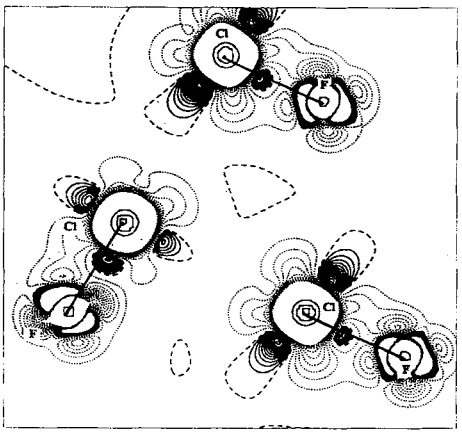

Figure 3. Laplacian of the electron density $-\nabla^2\rho(r)$ in the plane of three molecules of ClF, positive contour lines at 1, 2, 4, 6, 8... e Å^{-5} distances, zero contour lines dashed, and negative contour lines dotted.

Cl atoms the negative values of the Laplacian operator are concentrated not only in F–Cl bonds, but also in the directions perpendicular to these bonds. These peaks of the negative value of the Laplacian operator may be related with the charge concentration areas in the valence shell of the Cl atom. Each of these charge concentration peaks is directed to the neighboring Cl atoms where the Laplacian map indicates a corresponding charge depletion area along the prolongated F–Cl line. Thus, each Cl atom participates in two interactions between a Lewis base and a Lewis acid. A very similar Laplacian map, indicating the same type of interatomic interactions in the crystal, was obtained in the theoretical calculation of the topological charge density characteristics and Laplacian of the electron density in solid chlorine and its dimer.[28] For ClF (this work), the Cl_2 dimer, and Cl_2 in the crystal (see reference [28]), the (3, −1) bond critical points were found in the middles of the shortened intermolecular Cl···Cl distances (3.07 Å in ClF, 3.294 Å in solid Cl_2, and 3.37 Å in the Cl_2 dimer). The total electron density ρ and its Laplacian in these bond critical points are similar:

 © VCH Verlagsgesellschaft mbH, D-69451 Weinheim, 1997 0570-0833/97/3613-1490 $ 17.50+.50/0

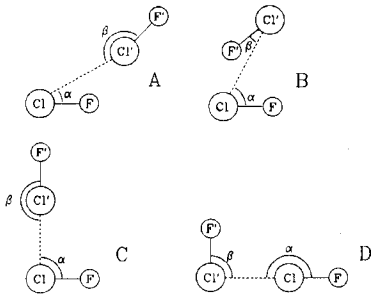

Figure 4. Orientation and angles of the ClF dimer calculated with different ab initio methods (stationary points each confirmed by frequency calculations): MP2: $\alpha = 30.7$, $\beta = 164.1°$ (A); $\alpha = 68.3$, $\beta = 10.9°$ (B); $\alpha = 179.2$, $\beta = 88.8°$ (D). B3LYP: $\alpha = 34.1$, $\beta = 160.1°$ (A); $\alpha = 177.9$, $\beta = 100.1°$ (D). CCSD(T): $\alpha = 31.2$, $\beta = 163.6°$ (A); $\alpha = 179.7$, $\beta = 85.0°$ (D) (no further angle scanning).

ρ: 0.135, 0.062, and 0.045 e Å^{-5} in ClF, Cl_2 crystal, and Cl_2 dimer, respectively; $-\nabla^2\rho$: 1.06, 0.805, and 0.713 e Å^{-5}, respectively, and the difference between the corresponding values are explained by the shortening of the Cl···Cl distances.

An ab initio energy surface scan was performed for the ClF dimer by using the 6-311 + G* basis set. The FCl···Cl′ angle α (Figure 4) was increased systematically from 0 to 180° with full optimization of the Cl···Cl′F′ angle β as well as the intra- and intermolecular distances. At the HF level of theory only one energetic minimum was detected for the linear arrangement ($\alpha = 0$, $\beta = 180°$), at the MP2 level three energy minima (A, B, and C or D, where C and D are equivalent), and with the B3LYP and the CCSD(T) method, two minima (A, D) were located. Configuration A represents the global energy minimum for all methods that include electron correlation.[29] A and B are mainly based on dipole interactions. However, the energy difference between configuration A and C (or D) decreases from 5.0 to 3.8 (MP2), 3.4 to 2.2 (B3LYP), and 4.8 to 3.8 kJ mol^{-1} (BSSE corrected).[30] The energy minimum for configuration B seems to be an artifact of basis set effects.[32] The intramolecular distances in the dimer vary from 1.672 to 1.676 (MP2), 1.676 to 1.686 Å (B3LYP), and the largest difference between both molecules ClF and Cl′F′ is represented in configuration C, in which the longer distance occurs for Cl′–F′ (reversed for D). This configuration also has the shortest Cl···Cl′ distance: 3.405 (MP2), 3.187 Å (B3LYP) and reflects the situation as found in the crystal lattice with the Cl lone pair of electrons donating into the antibonding σ-MO of Cl′–F′, thus causing a lengthening of the Cl′–F′ distance.

Although the global energy minimum of the ClF dimer was found for conformation A in the theoretical study of the dimer, the T-shaped conformation (C, D) also has a minimum which is energetically close to A, but is favored in the infinite ribbons of the crystal lattice. This demonstrates the stability of the Cl···Cl···Cl synthon.[32] The nature of the Cl···Cl interaction[33] in this polar molecule represents a cornerstone in the discussion of elliptical,[34] displaced spherical[35] van der Waals interactions. Alternatively, in simple terms, some positive charge is found in the prolongation of the F–Cl bond and some negative charge perpendicular to the bond at the chlorine atom, which holds the molecules together.

Experimental Section

Chlorine monofluoride was synthesized from ClF_3 and Cl_2 by using standard procedures [36], and purified by several low-temperature vacuum distillations in a stainless steel vacuum line. The pure ClF was kept and transported in a monel vessel with a special valve. On cooling with liquid nitrogen, a small amount of the compound was condensed several times into a thin-walled quartz capillary (diameter 0.3 mm), in order to passivate the inner surface. After the capillary had been filled, it was transferred to the diffractometer without interrupting the cooling process (to avoid bursting of the capillary) with the help of a special device, described previously elsewhere [37]. The single crystal was grown at −188 °C by applying the in situ crystallization technique using a miniature zone-melting method with an IR laser beam producing a molten zone in the capillary (Siemens-Challenge System) [38]. The data collection and structure determination were undertaken in the usual way at the same temperature [39].

Received: January 22, 1997 [Z 10020IE]
German version: *Angew. Chem.* **1997**, *109*, 1538–1541

Keywords: ab initio calculations · chlorine · fluorine · interhalogen compounds · solid-state structures

[1] J. Shamir, *Isr. J. Chem.* **1978**, *17*, 37–47.
[2] J. Shamir, *Struct. Bond.* **1979**, *37*, 143–210.
[3] R. J. Gillespie, I. Hargittai, *The VSEPR model of Molecular Geometry*, Allyn and Bacon, Boston, **1991**.
[4] R. J. Gillespie, E. A. Robinson, *Angew. Chem.* **1996**, *108*, 539–560; *Angew. Chem. Int. Ed. Engl.* **1996**, *35*, 495–514.
[5] R. D. Burbank, F. N. Bensey, *J. Chem. Phys.* **1957**, *21*, 602–603; M. Yu. Antipin, A. M. Ellern, V. F. Sukhoverkhov, Yu. T. Struchkov, *Russ. J. Inorg. Chem.* **1989**, *34*, 459–461.
[6] A. M. Ellern, M. Yu. Antipin, V. F. Sukhoverkhov, Yu. T. Struchkov, *Russ. J. Inorg. Chem.* **1991**, *36*, 792–794.
[7] K. H. Boswijk, J. van der Heide, A. Vos, E. H. Wiebenga, *Acta Crystallogr.* **1956**, *12*, 274–276.
[8] G. B. Carpenter, S. M. Richards, *Acta Crystallogr.* **1962**, *15*, 360–364.
[9] L. N. Swink, G. B. Carpenter, *Acta Crystallogr. Sect. B* **1967**, *24*, 429–433.
[10] R. S. Rowland, R. Taylor, *J. Phys. Chem.* **1996**, *100*, 7384–7391.
[11] R. L. Collin, *Acta Crystallogr.* **1956**, *5*, 431; corrigendum *ibid.* **1956**, *9*, 537; J. Donohue, S. H. Goodman, *Acta Crystallogr.* **1965**, *18*, 568–569; E. D. Stevens, *J. Mol. Phys.* **1979**, *37*, 27–45; a redetermination of solid Cl_2 was undertaken at −158 °C, with essentially the same results, $2\theta_{max} = 75°$, $R1 = 0.033$, $wR2 = 0.089$, Cl–Cl 1.985(1) Å: R. Boese, D. Bläser, unpublished results.
[12] G. Herzberg, *Spectra of Diatomic Molecules*, van Nostrand, Princeton, New York, **1950**.
[13] The former ab initio calculation was based on HF level of theory: S. Green, *J. Chem. Phys.* **1973**, *58*, 3117–3118.
[14] Gaussian 95, Development Version (Revision D2), M. J. Frisch, G. W. Trucks, H. B. Schlegel, G. E. Scuseria, M. A. Robb, J. R. Cheeseman, M. C. Strain, J. C. Burant, E. Stratmann, G. A. Petersson, J. A. Montgomery, V. G. Zakrewski, T. Keith, K. Raghavachari, M. A. Al-Laham, J. V. Ortiz, J. B. Foresman, J. Cioslowski, B. B. Stefanov, A. Nanayakkara, M. Challacombe, C. Y. Peng, P. Y. Ayala, W. Chen, M. W. Wong, J. L. Andres, E. S. Replogle, R. Gomperts, R. L. Martin, D. J. Fox, J. S. Binkley, D. J. Defrees, J. Baker, J. P. Stewart, C. Gonzales, M. Head-Gordon, P. M. W. Gill, B. G. Johnson, J. A. Pople, Gaussian, Inc., Pittsburgh PA, **1996**. Molpro 96: C. Hampel, K. Peterson, and H.-J. Werner, *Chem. Phys. Lett.* **1992**, *190*, 1.
[15] V. Schomaker, D. P. Stevenson, *J. Am. Chem. Soc.* **1941**, *63*, 37.
[16] G. R. Desiraju, *Crystal Engineering: The Design of Organic Solids*, Elsevier, Amsterdam, **1989**.
[17] J. Sadlei, G. Chałasiński, M. M. Szczęśniak, *J. Chem. Phys.* **1993**, *99*, 3700–3706.
[18] F.-M. Tao, W. Klemperer, *J. Chem. Phys.* **1992**, *97(2)*, 440–450.
[19] R. F. W. Bader, *Atoms in Molecules-a Quantum Theory*, Oxford University Press, Oxford, **1990**.
[20] R. F. W. Bader, R. J. Gillespie, P. J. MacDougall, *J. Am. Chem. Soc.* **1988**, *110*, 7329–7336.
[21] T. Koritzanszky, S. Howard, P. R. Mallinson, Z. Su, T. Richter, N. K. Hansen, *XD - Computer Program Package for Multipole Refinement and Analysis of Electron Densities from Diffraction Data*, Version **1995**.
[22] G. A. Jeffrey, J. F. Piniela, *The Application of Charge Density Research to Chemistry and Drug Desig*, (*NATO ASI Ser. Ser. B*, **1991**, *250*).
[23] N. K. Hansen, P. Coppens. *Acta Crystallogr. Sect. A* **1978**, *34*, 909–921.
[24] S. Green, *J. Chem. Phys.* **1973**, *58*, 3117–3118.
[25] K. C. Janda, W. Klemperer, S. E. Novick, *J. Chem. Phys.* **1976**, *64*, 2698–2699.
[26] R. E. Davis, J. S. Muenter, *J. Chem. Phys.* **1972**, *57*, 2836–2838.
[27] S. Green, *Adv. Chem. Phys.* **1974**, *25*, 179.
[28] V. G. Tsirelson, P. F. Zou, H.-T. Tang, R. F. W. Bader, *Acta Crystallogr. Sect. A* **1995**, *51*, 143–153.
[29] Approximately the same conformation for a ClF dimer was found in an SCF ab initio study: A. D. Buckingham, P. W. Fowler, *Can. J. Chem.* **1985**, *63*, 2018–2025.
[30] The basis set superposition error (BSSE) was determined by the counterpoise method which is essential for weakly bound complexes, see M Gutowski, J. G. C. M. van Duijneveldt-van de Rijdt, J. H. van Lenthe, F. B. van Duijneveldt, *J. Chem. Phys.* **1993**, *98*, 4728–4737.

[31] This is evident from the fact that the energy increases from 43 to 4.9 kJ mol^{-1} for configuration B by inclusion of the BSSE and even results in an endothermic binding energy for the dimer. The binding energies for configuration A and C(D) are −4.8 and −1.0 (MP2), −4.0 and 1.8 (B3LYP) and −4.4 and −0.6 kJ mol^{-1} for CCSD(T).
[32] G. R. Desiraju, *Angew. Chem.* **1995**, *107*, 2541–2558; *Angew. Chem. Int. Ed. Engl.* **1995**, *24*, 2328–2335, O. Navon, J. Bernstein, V. Khodorkovsky, *ibid.* **1997**, *109*, 640–642 and **1997**, *36*, 601–603.
[33] V. R. Pedirreddi, D. S. Reddi, B. S. Goud, D. C. Craig, D. Rae, G. R. Desiraju, *J. Chem. Soc. Perkin Trans. 2*, **1992**, 2353–2360.
[34] S. C. Nyburg, C. H. Faerman, *Acta Crystallogr. Sect. B* **1985**, *41*, 274–279.
[35] D. Kirkin, *Acta Crystallogr. Sect. B* **1987**, *43*, 405–406.
[36] G. Brauer, *Handbuch der Präparativen Anorganischen Chemie, Vol. 1*, Ferdinand Enke Verlag Stuttgart, **1975**, p. 189.
[37] R. Boese, D. Bläser, N. Niederprüm, T. Miebach in *Organic Crystal Chemistry* (Eds.: J. Garbarczyk, D. W. Jones), Oxford University Press, Oxford, **1991**, pp. 109–128.
[38] R. Boese, M. Nussbaumer, in *Correlations, Transformations, and Interactions in Organic Crystal Chemistry, In situ Cristallization Techniques, vol. 7* (Eds. D. W. Jones, A. Katrusiak) Oxford University Press, Oxford, **1994**, p. 20.
[39] Crystal system: monoclinic, space group $P2_1/c$, $Z = 4$, at −188 °C, a = 6378(1), b = 4.247(1), c = 6.425(1) Å, β = 104.55(3)°, V = 168.5(1) Å^3, ρ_{calcd} = 2.147 g cm^{-3}, μ = 1.73 mm^{-1}. Diffractometer Nicolet-Siemens R3m/V, $Mo_{K\alpha}$ radiation, graphite monochromator, λ = 0.7107 Å. A total number of 3747 reflections in the 2θ interval 2–90° were measured by using the Wyckoff scan technique (a half sphere of the reciprocal space in the interval 2θ = 2–60°, and two independent octants in the interval 2θ = 60–90°). During data collection some misalignment of the single crystal was observed (probably because of icing of the capillary at the low temperature) that resulted in relatively large variations of the intensities of the check reflections and high R_{int} value after averaging the equivalents (R_{int} = 0.130). Therefore, only one independent part of the total data set (one octant, 2θ = 2–75°) with 765 independent observable ($F_o > 4.0\sigma(F)$) reflections was used in further calculations. The structure was solved and refined (on F) in the anisotropic approximation (SHELXTL Plus programs Version 4.2) to R = 0.0357, Rw = 0.0401, and GOF = 1.73. Further details of the crystal structure investigation may be obtained from the Fachinformationszentrum Karlsruhe, D-76344 Eggenstein-Leopoldshafen (Germany), on quoting the depository number CSD-406442.

Formation of 2*H*-1,2-Azaphosphole Tungsten Complexes by Trapping Reactions of Nitrilium Phosphane Ylide Complexes**

Rainer Streubel,* Hendrik Wilkens, Annette Ostrowski, Christoph Neumann, Frank Ruthe, and Peter G. Jones

Dedicated to Professor Gottfried Huttner on the occasion of his 60th birthday

Nitrile oxides[1a] and nitrile imines[1a, 2] (**I**, E = O and E = NR, respectively; Scheme 1) are of great importance in heterocycle syntheses because of their versatility in 1,3-dipolar cycloadditions;[3] the properties of stable members of these classes of compounds have been thoroughly investigated. The synthesis of these 1,3-dipoles is usually based on readily available acyclic precursors.[1a, 2] Nitrile sulfides[4] (**I**, E = S) have until now only been identified by UV/IR spectroscopy[5] in inert matrices (e.g. PVC) at low temperature or as reactive intermediates by trapping reactions.[4] As far as we are aware, neither nitrilium phosphane ylides[6] (**I**, E = PR), nor their η^1 complexes (**II**), nor corresponding η^1 complexes of the above-mentioned nitrogen ylides are known. Our previous investigations of the thermal decomposition of a 2*H*-azaphosphirene tungsten complex in the presence of trapping reagents such as carbonyl,[7] phosphaacetylene,[8] or acetylene derivatives,[7, 9] provided evidence solely for the formation of a terminal phosphanediyl tungsten complex as a transient intermediate.[10] Here we report the synthesis and structural characterization of tungsten complexes of the novel 2*H*-1,2-azaphospholes,[11] which we explain on the basis of trapping reactions of transient nitrilium phosphane ylide tungsten complexes with dimethylacetylenedicarboxylate (DMAD; **2**).

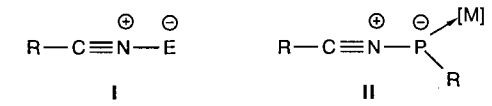

Scheme 1. Propargylic resonance structures of various nitrile ylides **I** and nitrilium phosphane ylide complexes **II** (R = alkyl, aryl; [M] = metal complex fragment).

The thermal decomposition of 2*H*-azaphosphirene tungsten complexes **1a**[12] and **1b**, **c**[13] in toluene at 75 °C in the presence of DMAD (**2**) forms the 1*H*-phosphirene tungsten complex[9] **5** as the main product, and also the 2*H*-1,2-azaphosphole tungsten complexes **6a–c** and the corresponding aryl nitriles[14] (Scheme 2). The complexes are isolated by low-temperature chromatography and crystallization. The suggested structures of the complexes **6a–c** are based on solution NMR and IR spectroscopic and MS data (Table 1), and confirmed in the case of **6b** in the solid-state by X-ray structure analysis.[15]

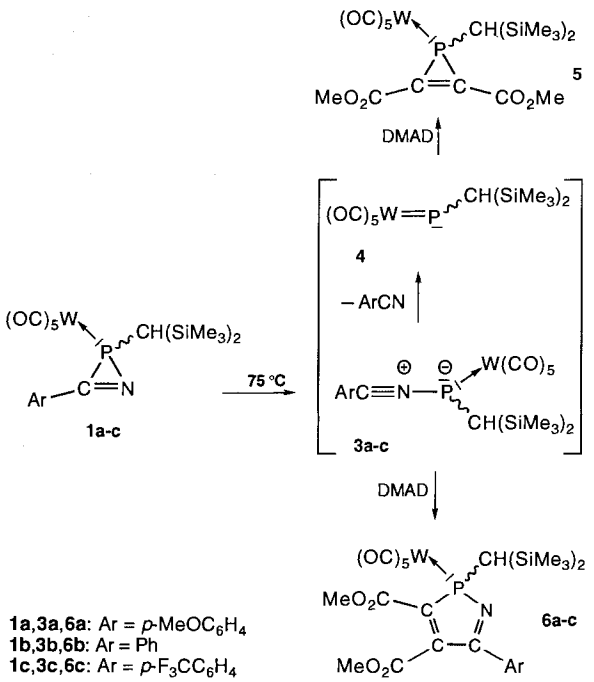

Scheme 2. Postulated reaction course for the formation of the three- and five-membered rings of the complexes **5** and **6a–c**, respectively.

As reaction mechanism we propose a thermal opening of the three-membered ring to form the ylidic complexes **3a–c**, which then decompose to the terminal phosphanediyl tungsten complex **4** and the respective aryl nitrile, and subsequent ring-form-

[*] Dr. R. Streubel, Dipl.-Chem. H. Wilkens, Dipl.-Chem. A. Ostrowski, C. Neumann, Dipl.-Chem. F. Ruthe, Prof. Dr. P. G. Jones
Institut für Anorganische und Analytische Chemie
der Technischen Universität
Postfach 3329, D-38023-Braunschweig (Germany)
Fax: Int. + code (531) 391-5387
e-mail: streubel@mvs.anchem.nat.tu-bs.de

[**] Chemistry of 2*H*-azaphosphirene complexes, Part 6. This work was supported by the Deutsche Forschungsgemeinschaft and the Fonds der Chemischen Industrie. Part 5: Ref. [10].

Table 1. Selected NMR [a] and IR spectroscopic and MS data for **6a–c** [b].

6a: $^{13}C\{^1H\}$ NMR: δ = 2.7 (d, ^3J(P,C) = 2.0 Hz, $SiMe_3$), 3.3 (d, ^3J(P,C) = 2.6 Hz, $SiMe_3$), 19.2 (s, CH), 52.8 (s, OMe), 53.3 (s, OMe), 55.5 (s, $C_6C_4OCH_3$), 114.3 (s, *o*-Ph), 126.9 (d, ^3J(P,C) = 17.2 Hz, *i*-Ph), 130.5 (s, *m*-Ph), 143.1 (d, J(P,C) = 26.5 Hz), 161.5 (d, J(P,C) = 1.6 Hz), 162.7 (s, *p*-Ph), 162.9 (d, J(P,C) = 2.2 Hz), 165.7 (d, J(P,C) = 14.3 Hz), 166.2 (d, J(P,C) = 11.6 Hz), 196.8 (d, ^2J(P,C) = 6.6 Hz, *cis*-CO), 198.4 (d, ^2J(P,C) = 22.9 Hz, *trans*-CO); ^{31}P NMR: δ = 101.0 (s, ^1J(P,^{183}W) = 238.4 Hz); IR (KBr, $\tilde{\nu}$(C=O) region): $\tilde{\nu}$ = 2072 m, 1948 vs, 1919 s, 1741 m, 1724 m cm^{-1}; MS (EI, 70 eV, ^{184}W): *m/z*: 789 [M^+].

6b: $^{13}C\{^1H\}$ NMR: δ = 2.6 (d, ^3J(P,C) = 1.9 Hz, $SiMe_3$), 3.2 (d, ^3J(P,C) = 2.4 Hz, $SiMe_3$), 18.9 (s, CH), 53.0 (s, OMe), 53.2 (s, OMe), 128.4 (s, *o*-Ph), 128.8 (s, *m*-Ph), 131.7 (s, *p*-Ph), 134.4 (d, ^3J(P,C) = 16.6 Hz, *i*-Ph), 142.7 (d, J(P,C) = 25.9 Hz), 162.0 (d, J(P,C) = 1.4 Hz), 162.7 (d, J(P,C) = 13.1 Hz), 165.1 (d, J(P,C) = 14.2 Hz), 167.2 (d, J(P,C) = 11.5 Hz), 196.7 (d, ^2J(P,C) = 6.5 Hz, *cis*-CO), 198.0 (d, ^2J(P,C) = 23.1 Hz, *trans*-CO); $^{31}P\{^1H\}$ NMR: δ = 102.8 (s, ^1J(P,^{183}W) = 237.9 Hz); IR (KBr, $\tilde{\nu}$(C=O) region): $\tilde{\nu}$ = 2073 s, 1992 m, 1953 vs, 1926 vs, 1914 vs, 1745 s, 1719 s cm^{-1}; MS (EI, 70 eV, ^{184}W): *m/z*: 759 [M^+].

6c: $^{13}C\{^1H\}$ NMR: δ = 2.7 (s, $SiMe_3$), 3.2 (s, $SiMe_3$), 18.9 (s, CH), 53.0 (s, OMe), 53.4 (s, OMe), 123.7 (q, ^1J(C,F) = 272.6 Hz, CF_3), 125.9 (q, ^3J(C,F) = 3.7 Hz, *m*-Ph), 128.8 (s, *o*-Ph), 133.2 (q, ^2J(C,F) = 33.1 Hz, *p*-Ph), 137.6 (d, ^3J(P,C) = 17.0 Hz, *i*-Ph), 141.4 (d, J(P,C) = 25.1 Hz), 162.7 (d, J(P,C) = 13.2 Hz), 163.3 (d, J(P,C) = 4.1 Hz), 164.7 (d, J(P,C) = 13.9 Hz), 166.0 (d, J(P,C) = 10.7 Hz), 196.5 (dd, ^2J(P,C) = 6.5, ^1J(C,^{183}W) = 127.2 Hz, *cis*-CO), 197.6 (d, ^2J(P,C) = 23.0 Hz, *trans*-CO); $^{31}P\{^1H\}$ NMR: δ = 104.9 (s, ^1J(P,^{183}W) = 237.4 Hz); IR (KBr, $\tilde{\nu}$(C=O) region): $\tilde{\nu}$ = 2075 s, 1994 m, 1950–1914 vs (br.), 1741 s, 1725 s cm^{-1}; MS (EI, 70 eV, ^{184}W); *m/z*: 827 [M^+].

[a] In $CDCl_3$ at 25 °C; ^{13}C NMR: 50.3, ^{31}P NMR: 81.0 MHz. The deuterated solvents were used as internal and 85% H_3PO_4 as external standards. [b] Satisfactory C,H elemental analyses were obtained for **6a–c**.

ing reaction of the reactive intermediates **3a–c** and **4** with DMAD (**2**). This is based on the following findings. 1) The three-membered heterocycles cannot be converted to five-membered heterocycles by warming the complexes in solution in the presence of the corresponding aryl nitrile (**5** → **6a–c**), but neither can a ring contraction by extrusion of aryl nitrile (**6a–c** → **5**) be observed. 2) The relative amount of 2*H*-1,2-azaphosphole complex formed depends on the electronic influence of the *para* aryl substituents, in a way that can be interpreted in terms of increased reactivity and/or lifetime of the reactive intermediates **3a–c**; similar results have been obtained for *para*-substituted aryl nitrile sulfides.[16] The complexes **6a–c** display ^{31}P resonance signals in the range δ = 102–105 and characteristic ^{13}C chemical shifts of the carbon atoms of the five-membered rings in the range δ = 135–168;[17, 18] the magnitudes of the ^1J(^{31}P,^{183}W) coupling constants are about 238 Hz (cf. Table 1).

As also observed for 1*H*-pyrazoles[18] or η^1-phosphole complexes,[19] a notable feature of the molecular structure of complex **6b** in the crystal (Figure 1) is the planar five-membered ring. The bond lengths indicate localized double bonds; the C–N double bond (129.1(6) pm) is shorter than that in 1*H*-pyrazoles,[18] 2*H*-1,2,3-diazaphospholes,[11] or a 1,2,3,4-diazadiphosphole.[20] The phosphorus center displays a distorted tetrahedral coordination; the W–P bond length is 250.45(12) pm. Further investigations of the formation and reactivity of the 2*H*-1,2-azaphosphole tungsten complexes **6a–c** are currently in progress.

Experimental Section

6a–c: **1a** (1.62 g, 2.5 mmol), **1b** (1.54 g, 2.5 mmol), or **1c** (1.71 g, 2.5 mmol) was dissolved in toluene (7.5 mL). After addition of DMAD **2** (0.5 mL, ca. 5 mmol) the reaction mixture was stirred for 2 h (**6c**: 3 h) at 75 °C. When the reaction was complete (as monitored by ^{31}P NMR spectroscopy), the solution was evaporated to dryness in vacuo (ca. 0.1 mbar), and the residue subjected to low-temperature column chromatography on silica (– 20 °C, hexane/diethyl ether 97.5/2.5). The eluates were evaporated to dryness in vacuo (ca. 0.1 mbar), and the residues recrystallized from pentane.

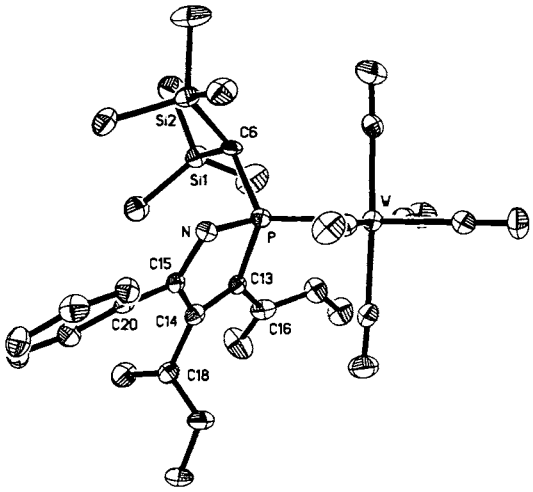

Figure 1. Molecular structure of complex **6b** in the crystal (ellipsoids represent 50% probability levels; hydrogen atoms omitted for clarity). Selected bond lengths [pm] and angles [°]: P–N 171.1(4), N–C15 129.1(6), C15–C14 149.7(6), C14–C13 134.3(6), C13–P 184.3(4); N-P-C13 91.8(2), P-C13-C14 108.2(3), C13-C14-C15 112.1(4), C14-C15-N 115.1(4), C15-N-P 112.7(3).

6a: orange powder, yield: 240 mg (12%), m.p. 132 °C (decomp); **6b**: red powder, yield: 160 mg (9%), m.p. 121 °C (decomp); **6c**: red powder, yield: 90 mg (5%), m.p. 113 °C (decomp).

Received: February 14, 1997 [Z10119IE]
German version: *Angew. Chem.* **1997**, *109*, 1549–1550

Keywords: coordination modes · heterocycles · phosphorus · tungsten · ylides

[1] a) Review: P. Caramella, P. Grünanger in ref. [1b], chapter 3; b) *1,3-Dipolar Cycloaddition Chemistry* (Ed.: A. Padwa), Wiley, New York, **1984**.
[2] Review: G. Bertrand, C. Wentrup, *Angew. Chem.* **1994**, *106*, 549; *Angew. Chem. Int. Ed. Engl.* **1994**, *33*, 527, and references therein.
[3] Reviews: a) R. Huisgen, *Angew. Chem.* **1963**, *75*, 604; *Angew. Chem. Int. Ed. Engl.* **1963**, *75*, 742; b) in ref. [1b], p. 1 ff.
[4] Review: R. M. Paton, *Chem. Soc. Rev.* **1989**, *18*, 33.
[5] a) A. Holm, N. Harrit, I. Trabjerg, *J. Chem. Soc. Perkin Trans. 1*, **1978**, 746; b) N. Harrit, A. Holm, I. R. Dunkin, M. Poliakoff, J. J. Turner, *J. Chem. Soc. Perkin Trans. 2* **1987**, 1227.
[6] To denote the zwitterionic form of the triatomic central framework of the compounds of type **I** with E = PR, and to draw attention to the relationship with other nitrogen ylides (the nitrile oxides, sulfides, and ylides), we propose the term nitrilium phosphane ylides. In recent publications we used the term phosphanitrile ylide for this reactive intermediate. Although confusion with $\sigma^3\lambda^5$-phosphanitriles (R_3PN), introduced by G. Bertrand, does not appear too evident, we decided in favor of the new term.
[7] R. Streubel, A. Kusenberg, J. Jeske, P. G. Jones, *Angew. Chem.* **1994**, *106*, 2564; *Angew. Chem. Int. Ed. Engl.* **1994**, *33*, 2427.
[8] R. Streubel, L. Ernst, J. Jeske, P. G. Jones, *J. Chem. Soc. Chem. Commun.* **1995**, 2113.
[9] A. Ostrowski, J. Jeske, P. G. Jones, R. Streubel, *J. Chem. Soc. Chem. Commun.* **1995**, 2507.
[10] We recently reported the transient formation of phosphacarbonyl ylide complexes: R. Streubel, A. Ostrowski, H. Wilkens, F. Ruthe, J. Jeske, P. G. Jones, *Angew. Chem.* **1997**, *109*, 409; *Angew. Chem. Int. Ed. Engl.* **1997**, *36*, 378.
[11] Review of azaphospholes: a) A. Schmidpeter, K. Karaghiosoff in *Multiple Bonds and Low Coordination Chemistry* (Eds.: M. Regitz, O. J. Scherer), Thieme, Stuttgart, **1990**, pp. 258 ff.; b) A. Schmidpeter in *Comprehensive Heterocyclic Chemistry II, Vol. 3*, (Eds.: A. R. Katritzky, C. W. Rees, E. F. V. Scriven), Pergamon, Oxford, **1996**, pp. 709 ff.
[12] R. Streubel, J. Jeske, P. G. Jones, R. Herbst-Irmer, *Angew. Chem.* **1994**, *106*, 115–117; *Angew. Chem. Int. Ed. Engl.* **1994**, *33*, 80–82.
[13] R. Streubel, A. Ostrowski, unpublished results.
[14] IR bands of the corresponding reaction solutions: $\tilde{\nu}_{(CN)}$ = 2227 (**1a/2**), 2229 (**1b/2**), 2234 (**1c/2**) cm^{-1}.
[15] Crystal structure analysis of complex **6b**: $C_{25}H_{30}NO_9PSi_2W$, M_r = 759.50; monoclinic, space group $P2_1/n$, a = 1050.9(2), b = 2178.5(4), c = 1359.4(2) pm, β = 103.46(2)°, V = 3.0268(9) nm^3; Z = 4, ρ_{calcd} = 1.667 $Mg\,m^{-3}$, λ = 0.71073 pm, T = 143 K. A crystal (0.54 × 0.38 × 0.20 mm) was mounted in inert oil at – 130 °C on a Stoe STADI-4 diffractometer. Inten-

 © VCH Verlagsgesellschaft mbH, D-69451 Weinheim, 1997 0570-0833/97/3613-1493 $ 17.50+.50/0

sities were registered to $2\theta = 50°$. Of 8639 reflections, 5330 were independent ($R_{int} = 0.0406$). An absorption correction based on ψ scans was applied. The structure was solved with the heavy atom method and refined against F^2 (SHELXL-93). Methyl H atoms were included by using rigid groups, all other H atoms with a riding model. Final $wR2 = 0.0732$ based on F^2 for all data, conventional $R(F)$ 0.0309, for 360 parameters and 162 restraints; max. $\Delta\rho$ 955 e nm^{-3}. Crystallographic data (excluding structure factors) for the structure reported in this paper have been deposited with the Cambridge Crystallographic Data Centre as supplementary publication no. CCDC-100177. Copies of the data can be obtained free of charge on application to The Director, CCDC, 12 Union Road, Cambridge CB2 1EZ, UK (fax: int. code +(1223) 336-033; e-mail: deposit@chemcrys.cam.ac.uk).

[16] A. Holm, J. J. Christiansen, C. Lohse, *J. Chem. Soc. Perkin Trans. 1* **1979**, 960.

[17] The ^{13}C NMR resonance signals of comparable 3-aryl-4,5-di(methyloxycarbonyl)isothiazole derivatives also fall in this range; see for example: P. A. Brownsort, R. M. Paton, *J. Chem. Soc. Perkin Trans. 1* **1987**, 2339.

[18] Review of 1*H*-pyrazoles: K. Krischke, *Methoden Org. Chem., (Houben-Weyl), 4th ed. 1952– Vol. E8b*, **1994**, pp. 399 ff.

[19] Review of 1*H*-phosphole complexes: a) F. Mathey, J. Fischer, H. J. Nelson, *Struct. Bonding (Berlin)* **1983**, *55*, 153; b) F. Mathey, *Chem. Rev.* **1988**, *88*, 429.

[20] C. Charrier, N. Maigrot, L. Ricard, P. le Floch, F. Mathey, *Angew. Chem.* **1996**, *108*, 2282; *Angew. Chem. Int. Ed. Engl.* **1996**, *35*, 2133.

Palladium-Catalyzed Amidocarbonylation—A New, Efficient Synthesis of *N*-Acyl Amino Acids**

Matthias Beller,* Markus Eckert, Frank Vollmüller, Sandra Bogdanovic, and Holger Geissler

Industrial interest in racemic *N*-acyl amino acids has led to a broad range of applications such as chelating agents, detergents, and lubrication agents for boring machines.[1] In addition, enantiomerically pure, nonnatural amino acids are important in medical chemistry as components in peptidomimetics.[2] Asymmetric synthesis of amino acid derivatives has been studied intensively in recent years,[3] but none of the known processes has yet found industrial application. The development of technically feasible multicomponent reactions with low-cost starting materials will become even more important in the future.[4] An example of a successful, efficient, three-component reaction for the synthesis of *N*-acyl-α-amino acids from aldehydes, amides, and carbon monoxide, amidocarbonylation (W-3-CR), was first described by H. Wakamatsu in 1971.[5] Amidocarbonylation is an economic improvement on the classical synthesis methods and more environmentally friendly, since low-cost starting materials can be used and the production of stoichiometric amounts of side products is avoided. For the past 25 years, amidocarbonylation has been catalyzed solely by cobalt carbonyl complexes, but harsh reaction conditions and insufficiently active catalysts often lead to poor product selectivity, which has prevented technical exploitation of the reaction.

[*] Prof. Dr. M. Beller, Dipl.-Chem. M. Eckert, Dipl.-Chem. F. Vollmüller
Anorganisch-chemisches Institut der Technischen Universität München
Lichtenbergstrasse 4, D-85747 Garching (Germany)
Fax: Int. code +(89)289-13473
e-mail: mbeller@arthur.anorg.chemie.tu-muenchen.de
Dr. S. Bogdanovic, Dr. H. Geissler
Hoechst AG, Corporate Research & Technology, Frankfurt am Main (Germany)

[**] This work was supported by the Deutsche Forschungsgemeinschaft (BE1931/1-1; BE1931/1-2). We thank Hoechst AG for the loan of a high-pressure reactor. Palladium-Catalyzed Reactions for the Synthesis of Fine Chemicals, Part 1.

Despite the well-known reasons why only cobalt carbonyl complexes should be effective,[6] we now present amidocarbonylation reactions which have been successfully catalyzed by palladium and which show significant advantages over the cobalt system (Scheme 1).

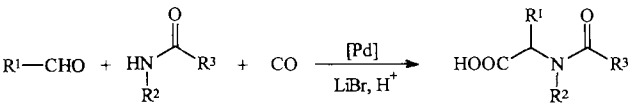

Scheme 1. Palladium-catalyzed amidocarbonylation; R^1, R^2, R^3 = H, aryl, or alkyl; [Pd] = $PdBr_2$ or $[Pd(PPh_3)_2Br_2]$, for example.

We investigated the reaction of isovaleraldehyde with acetamide and carbon monoxide in the present of different metal complexes as part of a project aimed at developing new amidocarbonylation catalysts.[7] Palladium(II) halides proved to be fundamentally capable of catalyzing the reaction in the presence of two equivalents of triphenylphosphane. Subsequently, comprehensive screening was carried out to determine the characteristic reaction parameters for palladium-catalyzed amidocarbonylation (Table 1). Surprisingly, the presence of halide ions is essential for the reaction (Table 1, no. 2, 4 and 5). The order of activity (I > Br > Cl) correlates qualitatively with the C–X bond energy. A synergistic effect, doubling the rate of reaction without lowering the selectivity, was observed when a strong acid (for example H_2SO_4) was added as a cocatalyst (Table 1, no. 6). *N*-methylpyrrolidone (NMP) was found to be a particularly suitable solvent for the palladium-catalyzed amidocarbonylation reaction. Other aprotic solvents such as *N*,*N*′-dimethylformamide (DMF), *N*,*N*-dimethylacetamide (DMAc), and dioxane can also be used. A temperature and pressure study revealed that no further improvement in the reaction rate was achieved by increasing the temperature above 130 °C and the pressure above 60 bar CO.

Table 1. Selected palladium-catalyzed amidocarbonylation experiments [a].

No.	T [°C]	t [h]	Cat. [mol %]	LiBr [mol %]	H_2SO_4 [mol %]	Yield [%] [d]
1 [b]	120	12	5	–	–	76
2 [b]	80	12	0.25	–	–	<5
3 [b]	80	12	1	5	1	76
4 [b]	80	12	0.25	5	–	20
5 [b]	80	12	0.25	35	–	45
6 [b]	80	12	0.25	35	1	92
7 [c]	80	12	0.25	35	1	85
8 [b]	120	60	0.001	35	1	25
9 [b]	120	60	0.25	35	1	99

[a] Isovaleraldehyde and acetamide (25.0 mL each of 1 M solutions in *N*-methylpyrrolidone) were treated with carbon monoxide. [b] The catalyst dibromobis(triphenylphosphane)palladium(II), was prepared in situ; 60 bar CO pressure. [c] The catalyst was palladium(II) bromide; 10 bar CO pressure. [d] Yield of isolated product.

With the new catalysts, it is now possible to carry out amidocarbonylation under the very mild conditions of 80 °C and 10 bar CO (Table 1, no. 7). Both palladium(II) (e.g., $PdBr_2$, $PdCl_2$) and palladium(0) (e.g., $[Pd_2(dba)_3]$ where dba = 1,5-diphenyl-1,4-pentadien-3-one, $[Pd(PPh_3)_4]$) compounds could be used as catalyst precursors. Palladium(II) bromide was shown to be particularly effective. This catalyst gave the highest ever turnover number (TON) of 25000 (mol product per mol Pd-cat.)

and the best-yet turnover frequency (TOF) of over 400 (mol product per mol Pd-cat. per hour) for an amidocarbonylation reaction (Table 1, no. 8).

The aldehyde and the amide components of the reaction were varied in order to illustrate the broad range of possibilities presented by the palladium-catalyzed amidocarbonylation (Table 2). Of particular interest are the good or very good yields

Table 2. Synthesis of *N*-acyl-α-amino acids by palladium-catalyzed amidocarbonylation [a].

Compound		Yield [%] [b]
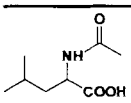	1	99
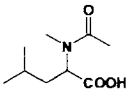	2	88
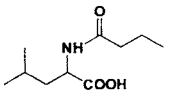	3	75
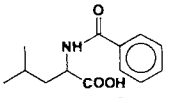	4	87
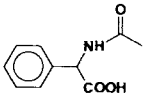	5	85
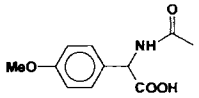	6	72
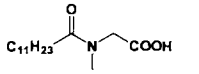	7	86
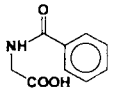	8	60
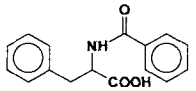	9	55

[a] Aldehyde and amide (25.0 mL each of 1 M solutions in *N*-methylpyrrolidone), 0.25 mol% dibromobis(triphenylphosphine)palladium(II), 1 mol% H_2SO_4, and 35 mol% LiBr were treated with 60 bar CO at 120 °C for 12 h. [b] Yield of isolated product.

obtained for *N*-acylarylglycine derivatives such as *N*-acetylphenylglycine (**5**)and *N*-acetyl-*p*-methoxyphenylglycine (**6**), and *N*-benzoyl-α-amino acid derivatives such as *N*-benzoylleucine (**4**), *N*-benzoylglycine (**8**), and *N*-benzoylphenylalanine (**9**). It was not previously possible to synthesize either of these groups of substances by cobalt-catalyzed amidocarbonylation![8] New synthesis strategies have therefore become available for the production of non-natural arylglycines, which are currently of great interest as components of antibiotics such as vancomycin.[9] Equally impressive are the reactions of *N*-methylamides in one-stage palladium-catalyzed amidocarbonylations to yield *N*-acetyl-*N*-methylleucine (**2**) and the sarcosine *N*-lauroyl-*N*-methylglycine (**7**). In contrast, the equivalent cobalt-catalyzed reaction, requires a two-stage synthesis procedure.[10]

Although in-depth mechanistic investigations have not yet been carried out, preliminary results show that the key steps in the palladium-catalyzed amidocarbonylation reaction mechanism are different from those in the cobalt-catalyzed reaction.[6, 11] The amidocarbonylation of benzaldehyde derivatives in the presence of palladium shows that the enamide intermediate, which is frequently discussed for the cobalt-catalyzed reaction mechanism, does not necessarily form during palladium-catalyzed reactions. The strong influence of halide and acid additives as well as the fact that both palladium(0) and palladium(II) compounds can be used as catalyst precursors add to the plausibility of the mechanism postulated in Scheme 2. Reaction

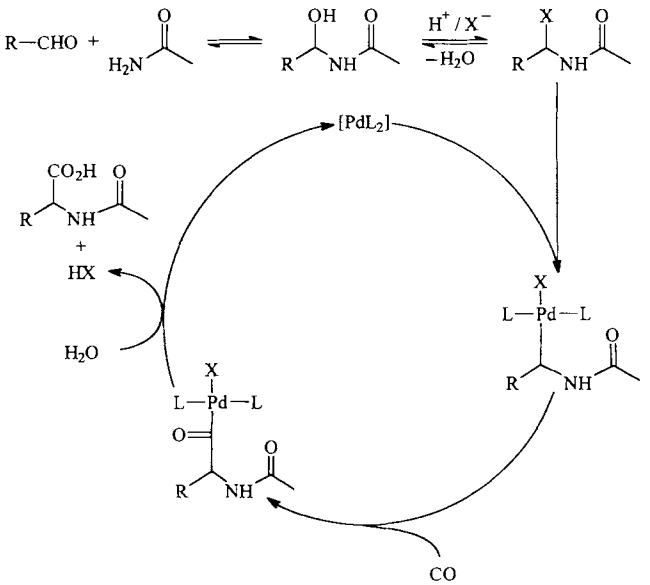

Scheme 2. Postulated mechanism for the palladium-catalyzed amidocarbonylation.

of the aldehyde with the amide leads, via a series of pre-equilibria, to the formation of an *N*-acyl hemiamidal intermediate which, after subsequent nucleophillic substitution, forms an α-haloamide. Oxidative addition inserts the Pd^0 species into the halogen–carbon bond of the α-haloamide to produce a (1-amidoalkyl)halopalladium(II) complex. After CO insertion the alkylpalladium species transforms into the corresponding acyl complex. Reductive elimination and hydrolysis of the acyl complex leads to the formation of the *N*-acyl-α-amino acid, and both the halide ion and the palladium(0) species revert to their original state. The proposed mechanism shows that amidocarbonylation takes place in the presence of CO only when catalyzed by palladium, whereas hydrogen (e.g. in synthesis gas) is also generally necessary for catalyst activation when cobalt catalysts are used. This result is a clear simplification in the process design with palladium catalysts particularly with respect to a possible continuous amidocarbonylation process.

The disadvantages of the cobalt-catalyzed amidocarbonylation, such as low catalyst activity and drastic reaction conditions, are overcome by the use of our palladium catalysts. In addition, important gaps in the range of application of this reaction have been filled. We now have catalysts available for the palladium-catalyzed amidocarbonylation reaction that can be controlled by the ligand sphere. Further investigations will show whether asymmetric amidocarbonylation can also be achieved.

Experimental Section

A 300 mL stirred reactor (No. 4561 from the Parr Company) with a magnet-driven propeller stirrer was used for the high-pressure reactions. General procedure: 25.0 mL each of 1 M solutions of the aldehyde and the amide in *N*-methylpyrrolidone (NMP), 0.25 mol% $[(PPh_3)_2PdBr_2]$, 1 mol% H_2SO_4, and

35 mol% LiBr were allowed to react under 60 bar CO at 120 °C for 12 h. The volatile components were removed under high vacuum, and the residue was taken up in a saturated aqueous solution of $NaHCO_3$ and then washed with chloroform and ethyl acetate. The aqueous phase was adjusted to pH 2 with phosphoric acid and extracted with ethyl acetate. The organic phases were then combined and dried over magnesium sulphate, and the solvent was removed under vacuum. The product was recrystallized from a suitable solvent mixture. All isolated compounds were characterized by means of NMR and IR spectroscopy and mass spectrometry. The purity of the products, as measured by HPLC, was >98%.

Received: November 2, 1996 [Z 9727 IE]
German version: *Angew. Chem.* **1997**, *109*, 1534–1536

Keywords: amino acids · carbonylations · homogeneous catalysis · multicomponent reactions · palladium

[1] a) M. Baviere, B. Durif-Varambon (Institute Français du Pétrole), DE-3514329, **1985** [*Chem. Abstr.* **1985**, 103, 8767w]; b) C. Theis, W. Latz (Hüls AG), DE-3643204, **1986** [*Chem Abstr.* **1988**, 109, 170928v]; c) J. J. Lin (Texaco Inc.), US-4720573, **1988** [*Chem Abstr.* **1988**, 109, 38240k].

[2] a) H. Kessler, *Angew. Chem.* **1993**, 105, 572; *Angew. Chem. Int. Ed. Engl.* **1993**, *32*, 543; b) J. Gante, *ibid.* **1994**, *106*, 1780–1802 and **1994**, *33*, 1699–1721; c) A. Giannis, T. Kolter, *ibid.* **1993**, *103*, 1303–1326 and **1993**, *32*, 1244.

[3] a) U. Kazmaier, *J. Org. Chem.* **1996**, *61*, 3694; b) U. Kazmaier, A. Krebs, *Angew. Chem.* **1995**, *107*, 2213; *Angew. Chem. Int. Ed. Engl.* **1995**, *34*, 2012; c) R. M. Williams, *Synthesis of Optically Active α-Amino Acids, Vol. 7* in *Organic Chemistry Series* (Eds.: J. E. Baldwin, P. D. Magnus), Pergamon, Oxford, **1989**; d) R. M. Williams, M.-N. Im, *J. Am. Chem. Soc.* **1991**, *113*, 9276.

[4] a) M. Beller, B. Cornils, C. D. Frohning, C. W. Kohlpaintner, *J. Mol. Catal.* **1995**, *104*, 17–85; b) I. Ugi, Proc. Estonian Acad. Sci. Chem. **1995**, *44*, 237–273; c) B. Cornils, W. A. Herrmann, *Quo vadis?* in *Applied Homogeneous Catalysis with Metal Complexes* (Eds.: B. Cornils, W. A. Herrmann), VCH, Weinheim, **1996**.

[5] a) H. Wakamatsu, J. Uda, N. Yamakami, *J. Chem. Soc. Chem. Commun.* **1971**, 1540; b) I. Ojima, *Chem. Rev.* **1988**, *88*, 1011; c) J. F. Knifton, *Amidocarbonylation* in *Applied Homogeneous Catalysis with Metal Complexes* (Eds.: B. Cornils, W. A. Herrmann), VCH, Weinheim, **1996**.

[6] J. Ojima, Z. Zhang, *Organometallics* **1990**, *9*, 3122–3127.

[7] We would like to thank E. Jägers (Hoechst AG) for carrying out the first amidocarbonylation trials with non-cobalt catalysts; E. Jägers, H.-P. Koll (Hoechst AG), EP-338330 **1989** [*Chem. Abstr.* **1990**, *112*, 77951z].

[8] K. Izawa, *J. Synth. Org. Chem.* **1988**, *46*, 218–231.

[9] a) D. L. Boger, R. M. Borzilleri, S. Nukui, *J. Org. Chem.* **1996**, *61*, 3561; b) K. Burgess, D. Lim, C. I. Martinez, *Angew. Chem.* **1996**, *108*, 1162; *Angew. Chem. Int. Ed. Engl.* **1996**, *35*, 1077.

[10] a) M. Beller, H. Fischer, P. Gross, T. Gerdau, H. Geissler, S. Bogdanovic (Hoechst AG), DE-4415712, **1995** [*Chem. Abstr.* **1996**, *124*, 149264a]; b) E. Drent, E. Kragtwijk (Shell), GB-2252770, **1991** [*Chem. Abstr.* **1993**, *118*, 39410p].

[11] a) J.-J. Parnaud, G. Campari, P. Pino, *J. Mol. Catal.* **1979**, *6*, 341; b) P. Magnus, M. Slater, *Tetrahedron Lett.* **1987**, *28*, 2829.

β-Silyl Diorganozinc Compounds— A New Class of Useful Zinc Reagents**

Stefan Berger, Falk Langer, Christian Lutz, Paul Knochel,* T. Andrew Mobley, and C. Kishan Reddy

Organozinc halides (RZnX) are useful organometallic intermediates for organic synthesis.[1] They are readily prepared by the direct insertion of zinc into organic halides,[2] display an exceptional functional group tolerance, and show a high reactivity toward a range of electrophiles in the presence of an appropriate transition metal catalyst.[1] Diorganozinc reagents (R_2Zn) have a significantly higher reactivity, but more importantly, they undergo highly enantioselective asymmetric additions to aldehydes to afford polyfunctional secondary alcohols.[3]

The drawback for some of these reactions[4] is that only one R group of R_2Zn is transferred. This disadvantage is especially disturbing in the case of the asymmetric addition to aldehydes when a highly functionalized, valuable R group has to be transferred, since a large excess of diorganozinc (2–3 equiv) is usually required to obtain high conversion and high enantioselectivity. Herein, we report a general solution to this problem with novel mixed β-silyl diorganozinc reagents.

Recently, Bertz et al. have shown that mixed cuprates RR'CuLi–LiX (R' is a nontransferable Me_3SiCH_2 (TMSM) group) are thermally stable but highly reactive.[5] This new class of copper reagents proves to be synthetically very useful in allowing the performance of 1,4-additions and acylations in high yields.[5] Stimulated by this work, we found that it is possible to prepare mixed diorganozinc compounds of the type R(TMSM)Zn (**1**) and to use them for Michael additions and enantioselective additions to aldehydes. The new zinc reagents **1** can be prepared by three methods: 1) by the reaction of (TMSM)Li (**2**) with an organozinc iodide, 2) by the reaction of (TMSM)ZnI (**3**) with an organolithium or -magnesium reagent, or 3) by the reaction of $(TMSM)_2Zn$ (**4**)[6] with a dialkylzinc compound (Scheme 1).

This last preparation is especially useful, because it allows the preparation of salt-free diorganozinc compounds **1**. This is of

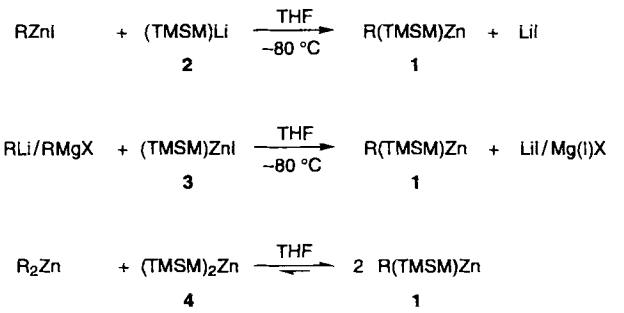

Scheme 1. Preparation of the β-silyl organozinc compounds **1**.

[*] Prof. Dr. P. Knochel, Prof. Dr. S. Berger, Dr. F. Langer, Dipl.-Chem. C. Lutz, Dr. T. A. Mobley, Dr. C. K. Reddy
Fachbereich Chemie der Universität
Hans-Meerwein-Strasse, D-35032 Marburg (Germany)
Fax: Int. code +(6421)28-2189
e-mail: Knochel@ps1515.chemie.uni-marburg.de

[**] We thank the Chemischen Industrie for generous support. C. L. thanks Chemetall GmbH Frankfurt and SIPSY S.A. (Avrillé, France) for a fellowship, C. K. R. thanks the Alexander-von-Humboldt Foundation for a fellowship. We are grateful to Witco (Bergkamen) for generous gift of chemicals.

prime importance for achieving high enantioselectivities in the asymmetric addition of diorganozinc compounds to aldehydes. The equilibrium between R_2Zn and R(TMSM)Zn as well as the evidence supporting the existence of the mixed diorganozinc compound **1** was studied in more detail with modern NMR techniques. The mixing of nearly equimolar amounts of $i Pr_2Zn$ and $(TMSM)_2Zn$ (**4**) ($\delta(CH_2) = -0.93$ and $\delta(CH_2) = -3.0$) in a ratio of 47:53 in [D_8]THF at $-20\,^{\circ}C$ leads to the appearance of a new set of signals attributed to the mixed species *i*Pr(TMSM)Zn (**1a**) ($\delta(CH_2) = -0.99$ and $\delta(CH_2) = -3.7$). New resonances for the *i*Pr and TMS groups were also observed. The ratio between remaining **4**, $i Pr_2Zn$, and the mixed species **1a**, determined by integration of the methylene groups of the TMSM of **4** and **1a**, was 20:15:65, from which an equilibrium constant of $K_{eq} = 14$ can be calculated. To confirm the structure of **1a**, we have acquired a gradient-selected, heteronuclear, multiple bond-coherence (HMBC) spectrum.[7] In this experiment we observed a cross-peak between the methylene protons of **1a** and the α-carbon (*CH*) of the *i*Pr groups, which suggests that both substituents are covalently bound to the same zinc center.[8] By mixing a primary diorganozinc compound (Et_2Zn) with **4**, a similar result was obtained. However, the exchange between Et(TMSM)Zn (**1b**) and $(TMSM)_2Zn$ (**4**) was fast on the NMR time scale at room temperature in contrast to that between *i*Pr(TMSM)Zn (**1a**) and **4**.

The thermal behavior of **1a** and **1b** were studied by variable temperature NMR spectroscopy. In addition to a dependence of the chemical shift on temperature, an exchange process between the three species, **1b**, Et_2Zn, and **4**, in solution was observed. The spectra for the methylene region of the TMSM groups at several temperatures are shown in Figure 1. For the methylene resonances of **1b** and **4** ($\Delta\nu = 42.3$ Hz), the coalescence temperature T_c is 305 K for the sample shown (1.4 M of **1b** in [D_8]THF) with the observed rate constant at the coalescence temperature for exchange $k = 94\ s^{-1}$ and $\Delta G^{\neq} = 63.2\ kJ\,mol^{-1}$.

In contrast, a 1.0 M solution of *i*Pr(TMSM)Zn (**1a**) has a T_c of 333 K ($\Delta\tilde{\nu} = 46.5$ Hz).[9] A dependence of the exchange rate on concentration was observed upon dilution of the concentrated sample of **1a** by a factor of 4. This resulted in a T_c which was greater than the boiling point of the solvent for the NMR spectroscopy (THF). Although the rate of exchange for the case of a primary alkylzinc derivative [EtZn(TMSM) **1b**] is faster than the rate of a secondary alkylzinc compound [*i*Pr(TMSM)Zn **1a**], the rates of exchange for both **1a** and **1b** are substantially faster than the observed rate of reaction with organic substrates.

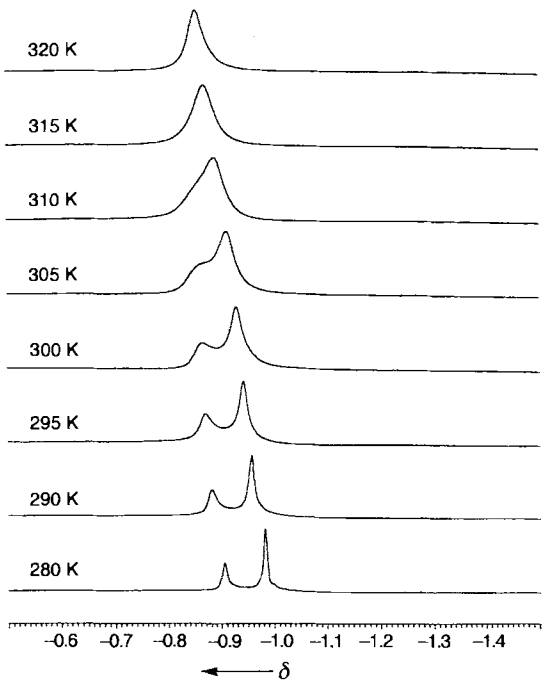

Figure 1. ^1H NMR spectra (500 MHz) for the region of methylene protons of the TMSM groups of **1b** and **4**.

Recently, we have shown that diorganozinc compounds R_2Zn add to various Michael acceptors in THF/*N*-methylpyrrolidone (NMP) (2:1).[4] As only one group R is transferred in these reactions, one R group wasted. We found that the mixed zinc reagents **1** react readily with a typical enone like cyclohexenone to afford the 1,4-addition product **5** and that this 1,4-addition requires only about 1.2 equivalents of the mixed zinc reagent **1** (Scheme 2, Experimental Section, and Table 1). The use of TMSBr[10] to promote the Michael addition instead of TMSCl gives higher yields in all cases (Table 1).

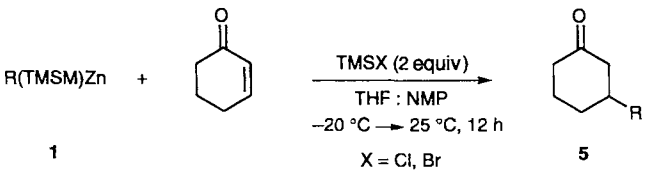

Scheme 2. Michael additions of **1** to enones.

Table 1. Michael addition of R(TMSM)Zn (**1**) to cyclohexenone in THF/NMP in the presence of TMSBr (or TMSCl).

Entry	R	Zinc reagent **1**	Product **5**	Yield [%][a, b]
1	*c*-Hex	**1c**	**5a**	83 (76)
2	Bu	**1d**	**5b**	69 (52)
3	Ph	**1e**	**5c**	82 (45)
4	*p*-MeO-C_6H_4	**1f**	**5d**	87
5	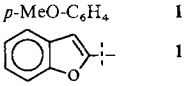	**1g**	**5e**	84
6	$PivO(CH_2)_5$	**1h**	**5f**	52 (70)[c]
7	$EtO_2C(CH_2)_3$	**1i**	**5g**	49

[a] Yields of isolated analytically pure products. [b] Yields in parentheses refer to the reaction performed in the presence of TMSCl. [c] Yield obtained for the preparation of **1h** by mixing $(PivO(CH_2)_5)_2Zn$ with **4** (1:1) and performing the reaction in the presence of TMSBr.

The addition of a functionalized primary zinc compound such as **1h** is best performed by preparing this mixed zinc derivative with method (3) by mixing equimolar amounts of $(TMSM)_2Zn$ (**4**) and $(PivO(CH_2)_5)_2Zn$ and performing the reaction in the presence of TMSBr (Table 1, entry 6). Remarkably, the enantioselective addition of a mixed zinc reagent to benzaldehyde can also be performed. Thus, mixing $Pent_2Zn$ with **4** provides the mixed zinc species Pent(TMSM)Zn (**1j**, 1.8 equiv). Its addition to benzaldehyde (1 equiv) in the presence of (1*R*·2*R*)-1,2-bis(trifluoromethanesulfonamido)cyclohexane (**6**, 15 mol%)[3c] and $Ti(OiPr)_4$ (0.6 equiv) at $-20\,^{\circ}C$ for 9 h gives the desired chiral alcohol **7** in 92% yield and 97% *ee*. The new procedure requires significantly less zinc reagent (1.8 pentyl groups compared to 4–6 pentyl groups for previously described reaction conditions[3]) and opens the way to the enantioselective transfer of highly valuable R groups to aldehydes (Scheme 3).

In summary we have developed three methods to prepare mixed β-silyl diorganozinc compounds (**1**). These novel zinc reagents were characterized by NMR studies. The TMSM

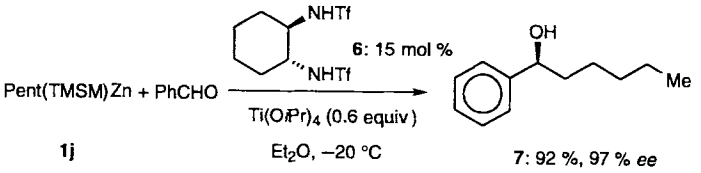

Scheme 3. Enantioselective addition of Pent(TMSM)Zn (**1j**) to benzaldehyde.

group plays the role of nontransferable ligand. The zinc reagents **1** undergo efficient 1,4-additions in NMP/THF solvent mixtures and substantially improve the highly enantioselective addition to aldehydes.

Experimental Section

Typical procedure for the 1,4-addition of **1** to enones (example of **5a**): **1c** (1.0 equiv), prepared by the reaction of *c*-HexZnI with (TMSM)Li (−80 °C to −30 °C, 0.5 h), was treated at −20 °C in THF/NMP (2:1) with cyclohexenone (about 0.7–0.8 equiv) for 5 h in the presence of trimethylsilyl chloride (TMSCl, 2.0 equiv) or TMSBr (2.0 equiv). The yield of **5a** was 76% and 83%, respectively.

Example of **5c**: A dried and argon-flushed, three-necked, 50 mL flask was charged with TMSMZnI (12 mmol, prepared by zinc insertion from TMSMI (2.5 g, 12 mmol) and zinc dust (2.6 g, 40 mmol)) in THF (6 mL). Phenyllithium (12 mmol) was slowly added at −50 °C, followed after 30 min of stirring by NMP (2 mL), cyclohexenone (0.75 g, 8 mmol), and TMSBr (2.4 g, 16 mmol) at −50 °C. The reaction mixture was allowed to warm slowly to room temperature and then stirred for 12 h. After diluting with THF (20 mL), quenching with HCl solution (10%, 20 mL) and stirring for 15 min, the reaction mixture was worked up as usual. The crude product was purified by flash chromatography (hexanes/ diethyl ether 9:1) to yield pure **5c** (1.15 g, 82%) as a colorless oil. For less reactive aryl or primary alkyl (TMSM)zinc, the reaction mixture was stirred at 25 °C for 12 h.

Typical procedure for the enantioselective addition of **1** to an aldehyde (example of the preparation of **7**): A dried and argon-flushed 50 mL Schlenk flask was charged with (1*R*,2*R*)-1,2-bis(trifluoromethanesulfonamido)cyclohexane (**6**, 0.38 mmol, 15 mol%), $Ti(OiPr)_4$ (0.45 mL, 1.5 mmol, 0.6 equiv), and diethyl ether (3 mL). This catalyst solution was cooled to −20 °C. Meanwhile $Pent_2Zn$ (0.45 g, 2.1 mmol, 0.9 equiv) and $TMSM_2Zn$ (0.56 g, 2.3 mmol, 0.9 equiv) were mixed at 25 °C in another Schlenk flask. The resulting Pent(TMSM)Zn **1j** (1.8 equiv) was slowly added to the catalyst **6**. After 10 min, benzaldehyde (0.26 g, 2.45 mmol, 1 equiv) was added. The reaction mixture was stirred at −20 °C for 9 h and worked up as usual. The crude product was purified by flash chromatography (hexanes/diethyl ether 2:1) to yield analytically pure **7** (0.40 g, 92%) with 97% *ee* (HPLC, Daicel, Chiracel OD, heptane/isopropyl alcohol 97:3). α_D^{20} −36.4 (*c* = 4.2, $CHCl_3$).

Received: January 7, 1996 [Z9972IE]
German version: *Angew. Chem.* **1997**, *109*, 1603–1605

Keywords: additions · asymmetric synthesis · NMR spectroscopy · zinc

[1] a) P. Knochel, R. D. Singer, *Chem. Rev.* **1993**, 2117–2188; b) P. Knochel, *Synlett* **1995**, 393–403.

[2] a) P. Knochel, M. P. C. Yeh, S. C. Berk, J. Talbert, *J. Org. Chem.* **1988**, *53*, 2390–2392; b) S. C. Berk, P. Knochel, M. C. P. Yeh, *ibid.* **1988**, *53*, 5789–5791; c) L. Zhu, R. M. Wehmeyer, R. D. Rieke, *ibid.* **1991**, *56*, 1445–1453.

[3] a) M. J. Rozema, S. Achyutha Rao, P. Knochel, *J. Org. Chem.* **1992**, *57*, 1956–1958; b) W. Brieden, C. Eisenberg, M. J. Rozema, *Tetrahedron Lett.* **1993**, *34*, 5881–5884; c) H. Takahashi, T. Kawakita, M. Ohno, M. Yoshioka, S. Kobayashi, *Tetrahedron* **1992**, *48*, 5691–5700; d) B. Schmidt, D. Seebach, *Angew. Chem.* **1991**, *103*, 100–102; *Angew. Chem. Ind. Ed. Engl.* **1991**, *30*, 99–101; e) D. Seebach, A. K. Beck, B. Schmidt, Y. M. Wang, *Tetrahedron* **1994**, *50*, 4363–4384; f) P. Knochel, *Chemtracts: Org. Chem.* **1995**, *8*, 205–221.

[4] C. K. Reddy, A. Devasagayaraj, P. Knochel, *Tetrahedron Lett.* **1995**, *37*, 4495–4498.

[5] a) S. H. Bertz, M. Eriksson, G. Miao, J. P. Snyder, *J. Am. Chem. Soc.* **1996**, *118*, 10906–10907; b) M. Srebnik, *Tetrahedron Lett.* **1991**, *32*, 2449–2452.

[6] Compound **4** was prepared by the reaction of (TMSM)MgBr with $ZnBr_2$ in diethyl ether, filtration under argon, and subsequent distillation of **4** (b.p. = 41 °C at 0.1 mm Hg).

[7] W. Willker, D. Leibfritz, R. Kerssebaum, W. Bermel, *Magn. Reson. Chem.* **1993**, *31*, 287–292.

[8] The corresponding cross-peak between the α-proton of the *i*Pr group and the α-carbon of the TMSM group was not observable due to coupling of the α-proton with the *i*Pr methyl groups. Attempts to acquire a selectively decoupled HMBC spectrum failed to reveal the weak couplings across the zinc center.

[9] Due to the chemical shift dependence on temperature, Δν changes as a function of temperature. Values for Δν at the coalescence temperatures were extrapolated for both the ethyl (**1b**) and isopropyl (**1a**) groups from low temperature chemical shift data. Since Δν is quite similar in the primary and secondary cases, the observed difference in fluxional behavior arises from a difference in chemical behavior.

[10] M. Bergdahl, E.-L. Lindstedt, M. Nilsson, T. Olsson, *Tetrahedron* **1989**, *45*, 535–543.

Gas-Phase Reaction of Tetraborane(10) with Allene: The Fluxional *arachno*-1-Carbapentaborane(10) Isomeric System and Derivatives 1,2- and 1,3-Me_2-1-CB_4H_8; Analogies in 1-CB_4H_{10}, MeB_5H_{10}, and $B_5H_{10}^-$**

Mark A. Fox, Robert Greatrex,* Matthias Hofmann, Paul von R. Schleyer,* and Robert E. Williams

Dedicated to Professor Walter Siebert on the occasion of his 60th birthday

Unsaturated compounds such as alkynes,[1, 2] alkenes,[3, 4] and enynes[5] react in the gas phase with boranes, for example B_4H_{10}, to give a variety of remarkable products, often in which the C–C bonds have been cleaved.[6] We now report the identification of a fluxional monocarbapentaborane isomeric system, *arachno*-1,3- (**1a**) and *arachno*-1,2-Me_2-1-CB_4H_8 (**1b**) from the quenched reaction of B_4H_{10} with $H_2C{=}C{=}CH_2$ (Scheme 1). Whereas this reaction is also a superior synthetic route to the *arachno*-carbapentaborane 1-Me-2,5-μ-CH_2-1-CB_4H_7 (**2a**),[1] there was no sign of the basket-like ethanotetraborane derivative 2,4-$(MeCHCH_2)B_4H_8$ (**3**), which is the main product under hot–cold conditions.[7] The present investigation also clarifies earlier findings on the isoelectronic compounds CB_4H_{10}[8, 9] and $B_5H_{10}^-$.[9, 10]

In 1973 Matteson and Mattschei obtained a compound, believed to be CB_4H_{10} (m/z = 65, $M-1$),[8] by the reduction of tris(dichloroboryl)methane with lithium borohydride. Although noting an "infra red spectrum somewhat resembling that of pentaborane(11)", the authors did not assign a structure. In 1976 Williams predicted that the *arachno* constitution **4** should be preferred for CB_4H_{10} (the parent compound of **1a** and **1b**, see Figure 1).[9] Although in the *absence* of bridge-

[*] Dr. R Greatrex, Dr. M. A. Fox
School of Chemistry
University of Leeds
Leeds LS29JT (UK)
Fax: Int code +(113)233-6565
e-mail: r.greatrex@chem.leeds.ac.uk
Prof. Dr. P. von R. Schleyer, Dr. M. Hofmann
Computer-Chemie-Centrum des Instituts für Organische Chemie
der Universität Erlangen-Nürnberg
Henkestrasse 42, D-91054 Erlangen (Germany)
Fax: Int code +(9131)85-9132
e-mail: pvrs@organik.uni-erlangen.de
Dr. R. E. Williams
Loker Hydrocarbon Research Institute
University of Southern California, Los Angeles (USA)

[**] This work was supported by the Engineering and Physical Sciences Research Council, the Royal Society, the Deutsche Forschungsgemeinschaft, and the Fonds der Chemischen Industrie.

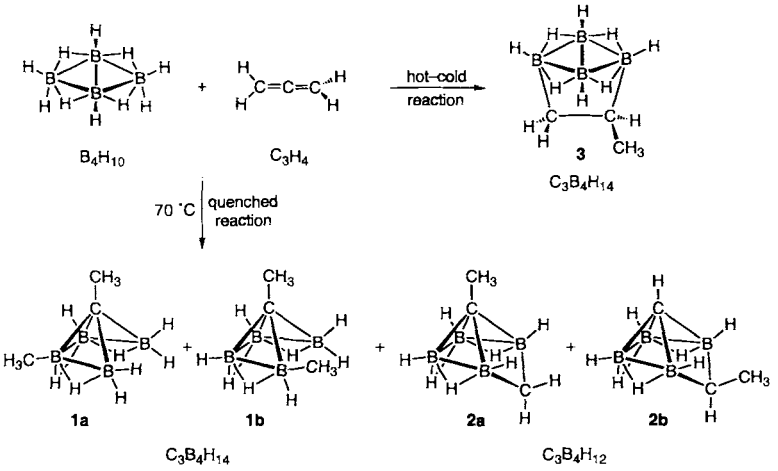

Scheme 1.

hydrogen competition carbon usually prefers a lower coordination site, 1-CB_4H_{10} (**4**) should be more favorable than alternative configurations (see below) because of the optimal locations of the three bridging hydrogen atoms.[9] About the same time Shore et al.[10] reported that isoelectronic $B_5H_{10}^-$ was produced by the reaction of hydride (KH) with pentaborane(11), and from the reaction of B_6H_{12} with NH_3. Although no structure was suggested,[10] an *arachno* arrangement like **4** also seems likely. The fluxional processes that take place in these systems are related to observations by Osborne et al. on the methylpentaborane(11) isomers.[11]

The NMR data[12] of **1** reveal two methyl groups, one attached to carbon and one to boron, and are consistent with the presence of five fluxional hydrogen atoms and single nonfluxional *exo*-terminal hydrogen atoms on three of the four boron atoms. This suggests a rapidly interconverting mixture of isomers **1a** and **1b** (see Figure 2). The mass spectrum gave a parent peak at $m/z = 93$ (corresponding to $C_3B_4H_{13}^+$, $M-1$), which, with the other experimental findings, points to a $C_3B_4H_{14}$ constitution. This was unexpected!

The rate-determining step in the reaction of B_4H_{10} with many unsaturated hydrocarbons is known to involve thermolysis, that is, elimination of H_2 to give B_4H_8 as the reactive species.[13] Addition of B_4H_8 to allene, C_3H_4, would lead to **2a** or **2b**, $C_3B_4H_{12}$. However, the formation of **1**, $C_3B_4H_{14}$, suggests that hydroboration of allene with B_4H_{10} can occur concurrently! Formally, **3** might also be formed by addition of B_4H_{10} to allene. In contrast to **1a**, **1b**, **2a**, and **2b**, **3** has C-C-C connectivity and is considerably higher in energy than **1a** (13.1 kcal mol^{-1}).

We now report the use of the ab initio/IGLO/NMR method[14] to establish the structures of **1**, CB_4H_{10}, and $B_5H_{10}^-$, and to investigate their exchange mechanisms. Relative energies as well as ^{11}B and ^{13}C NMR chemical shifts (IGLO/DZ//MP2(fc)/6 – 31G*)[15] computed[16] for the *arachno* parent compound **4** and possible isomers of its dimethyl derivative are given in Figures 1 and 2, respectively.[17] Since the computed energy of the *endo*-methyl isomer **1c** is significantly higher than that of **1a** or **1b** (Figure 2), it is not an important component in the system. (The bridging methylene groups in **2a** and **2b** are necessarily forced to be *endo*.) Experimental ^{11}B NMR chemical shifts of **1** do not compare favorably with averaged values computed for **1a** or **1b** (see Table 1). However, assuming a rapid equilibrium, averaging over **1a** and **1b** gives values closer to those from experiment. Isomer **1a** is lower in energy than **1b** and should be present to a greater extent in the mixture. Data, for example, for a 4:1 weighted average for **1a**:**1b** provide convincing support for the proposed structures.

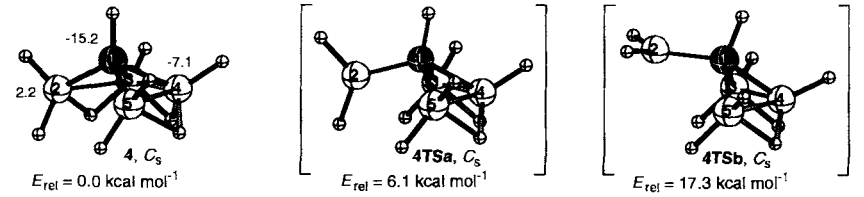

Figure 1. Computed relative energies and geometric parameters for CB_4H_{10} structures **4**, **4TSa**, and **4TSb** as well as IGLO/DZ chemical shifts for minimum **4**.

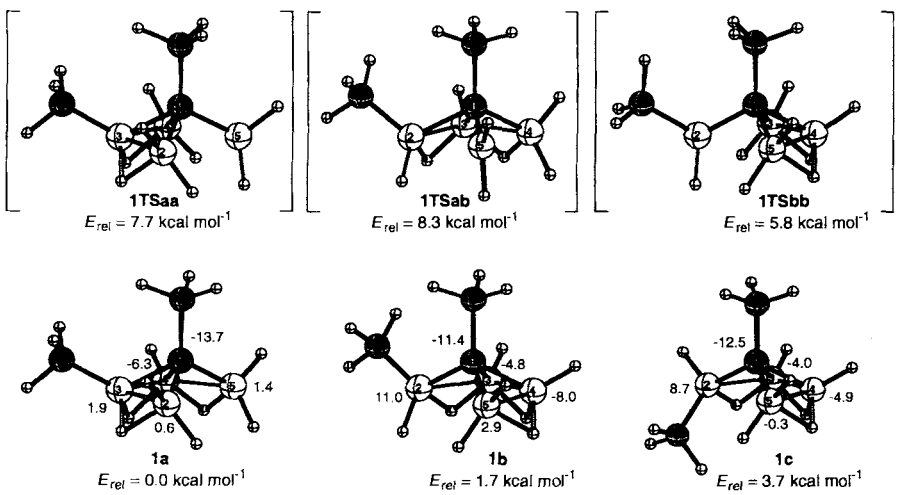

Figure 2. Computed relative energies and geometric parameters for various Me_2-1-CB_4H_8 structures as well as IGLO/DZ chemical shifts for minima **1a–c**.

With the parent compound **4** (see Figure 1) we first localized transition structures involved in the exchange of bridging and *endo* hydrogen atoms (**4TSa**, E_{rel} = 6.1 kcal mol^{-1}) as well as the exchange of *endo* and *exo* hydrogen atoms (**4TSb**, E_{rel} = 17.3 kcal mol^{-1}). In both **4TSa** and **4TSb**, a boryl group is formed at B2, and the B2–B3 bridging hydrogen becomes a terminal hydrogen atom at B3. A small rotation of the $B2H_2$ group about the C1–B2 bond leads from **4** (torsional angle H-C1-B2-H = 11.5°) to **4TSa** (H-C1-B2-H 0°) but preserves the *exo*/*endo* character. The favorably oriented (formally empty) p orbital at B2 in **4TSa** hyperconjugates effectively. In **4TSb**, $B2H_2$ is perpendicular to the plane of symmetry. The hyperconjugation in **4TSb** is not effective, and the relative energy of **4TSb** is 11.2 kcal mol^{-1} higher than that of **4TSa**. Accordingly, scrambling

Table 1. Comparison of the computed ^{11}B NMR chemical shifts for 1,3- (**1a**) and 1,2-Me_2-1-CB_4H_8 (**1b**) with the experimentally observed values.

Boron atom	**1a**	**1b**	**1a**:**1b** [a] 50:50	**1a**:**1b** [a] 80:20	exp. [b]
BMe	1.9	11.0	6.5	3.7	6.6
2BH [c]	−2.85	−0.95	−1.9	−2.4	−1.3
1BH	1.4	−8.0	−3.3	−0.5	1.6

[a] Average of the shifts for the relevant boron atom(s) in **1a** and **1b**, weighted as indicated. [b] In $CDCl_3$ at 298 K referenced externally to $BF_3 \cdot OEt_2$ ($\delta = 0.0$; see ref. [12]). [c] Average of the shifts for the boron atoms adjacent to the BMe group.

of bridge and *endo* but not of *exo* hydrogen atoms is observed for the dimethyl derivatives **1a** and **1b**. Indeed, the transition states for the degenerate rearrangements of **1a** (**1TSaa**) and **1b** (**1TSbb**) and for the conversion of **1a** into **1b** (**1TSab**, Figure 2) have relative energies comparable to that of **4TSa**. In contrast, a structure corresponding to C1,B4-dimethyl substituted **4TSb** has a much higher computed energy of 20.0 kcal mol^{-1}.

Further computations on CB_4H_{10} isomers confirm the benefits of favorable hydrogen bridging. Attempts to optimize 2- and 3-carbapentaboranes resulted in structures higher in energy than **4**.[18] The mass spectrometrically observed $CB_4H_9^+$ ion[8] has a stable B_5H_9-like *nido* structure. The same is true for the $C_3B_4H_{13}^+$ ion, which incorporates CH_3C and *exo*-CH_3B groups.

Pentaborane(11), the borane isoelectronic with **4**, is isostructural except for the additional hydrogen atom oscillating rapidly between the B1/B2 and B1/B5 bridging positions.[19] As further hydrogen scrambling does not take place, B_5H_{11} appears to have effective C_s symmetry on the NMR time scale. Consequently, the methyl derivative exists as a mixture of isomers, assigned 2-*exo*- and 3-*exo*-MeB_5H_{10}, in a temperature-dependent equilibrium.[11] A ratio of 1:2 was found from the ^{11}B NMR spectrum at −35 °C, and $\Delta H^0 = 300 \pm 30$ cal mol^{-1} was derived for a neat sample. As for the monocarboranes **1a** and **1b**, the most stable isomer has a Me-substituted basal boron atom, which is not part of the opened edge (B2/B5). According to our computations the stability of the MeB_5H_{10} isomers decreases in the order 4- ($E_{rel} = 0.0$ kcal mol^{-1}), 5-*exo*- (0.57), 2-*exo*- (0.71), 3- (0.81), 1- (2.30), 2-*endo*- (3.17), and 5-*endo*-MeB_5H_{10} (3.18).

Deprotonation of B_5H_{11} gives the fluxional $B_5H_{10}^-$ ion, for which average ^{11}B NMR chemical shifts of $\delta = -13.2$ (4B) and −52.0 (1B) were reported.[10] Structural and energetic features of the $B_5H_{10}^-$ minimum **5a** (isostructural with **4**) and transition structures **5TSa** and **5TSb** (corresponding to **4TSa** and **4TSb**, respectively, Figure 3), are analogous to those for the CB_4H_{10} system (Figure 1). However, the boron atom B1 in the apical position allows a B1−B2 hydrogen bridge. Consequently there are additional low-in-energy *arachno*-$B_5H_{10}^-$ minima: for example, **5b**, with unbridged B2−B3, and **5c**, without the B3−B4 hydrogen bridge, have energies of −0.05 and 6.3 kcal mol^{-1} relative to **5a** (MP2(fc)/6-31G* + 0.93 ZPE).[20] Barriers for the **5a**–**c** interconversion (via **5TSab**, **5TSbc**, and **5TScc**) are low, like those for the degenerate rearrangement of **5a** via **5TSa**. Averaging the individual ^{11}B NMR chemical shifts to effective C_{4v} symmetry gives $\delta = -4.2$ (4B), −57.4 (1B) for **5a** and

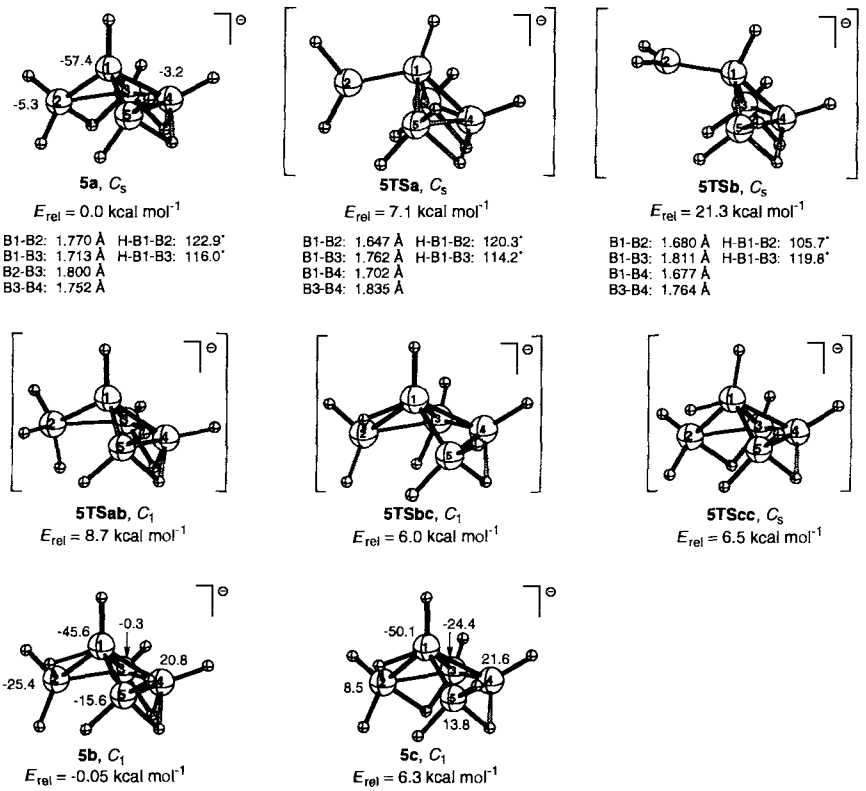

Figure 3. Computed relative energies and geometric parameters for various $B_5H_{10}^-$ structures as well as IGLO/DZ chemical shifts for minima **5a**–**c**.

−5.1 (4B), −45.6 (1B) for **5b**. The experimental NMR data should correspond to an average between **5a** and **5b**, since both have almost the same energy. The average value $\delta = -51.5$ (1B) agrees well with the experimental value of −52.0,[10] but the (4B) data do not match the reported −13.2. However, this was a typographical error;[21] the correct experimental value $\delta = -3.2$ (4B)[21] agrees well with the value of −4.5 derived theoretically. This supports the conclusion that both $B_5H_{10}^-$ structures **5a** and **5b** are present in solution.

We have isolated the smallest *arachno*-carbaborane, dimethyl-1-carbapentaborane(10), and characterized it as a mixture of rapidly interconverting isomers 1,3-Me_2-1-CB_4H_8 (**1a**) and 1,2-Me_2-1-CB_4H_8 (**1b**). The formation can be explained as the hydroboration reaction of B_4H_{10} with allene without thermolysis of the former. *Endo*-bridge hydrogen scrambling is facile due to hyperconjugative stabilization of the boryl groups that are present in the transition states. The same is true for the parent compound 1-CB_4H_{10}. Isoelectronic $B_5H_{10}^-$ is also fluxional, and the isomers with varying hydrogen-bridge positions have almost the same energy.

Experimental Section

In a typical experiment B_4H_{10} (0.5 mmol) and $H_2C{=}C{=}CH_2$ were heated for 35 min at 70 °C in a 1-L Pyrex bulb, and the reaction was quenched by pumping the volatiles into a trap immersed in liquid nitrogen. Low-temperature distillation of the combined volatiles from several reactions yielded a fraction with a main cut-off at $m/z = 92$. NMR spectroscopy showed it to consist predominantly of the methylene-bridged species **2a**, together with very small amounts of the minor isomer 2,5-μ-MeCH-1-CB_4H_8 (**2b**) and the new arachno species **1**. When this mixture was warmed to room temperature, **2** decomposed leaving **1** unchanged. Subsequent refractionation yielded a sample of **1** in an overall yield of 1% (cut-off $m/z = 93$). It is stable indefinitely at room temperature both in chloroform and in toluene.

Received: January 20, 1997 [Z 10007 IE]
German version: *Angew. Chem.* **1997**, *109*, 1542–1544

 © VCH Verlagsgesellschaft mbH, D-69451 Weinheim, 1997 0570-0833/97/3613-1500 $ 17.50+.50/0

Keywords: ab initio calculations · boron · carboranes · NMR spectroscopy

[1] J. D. Corbett, D. G. Adolphson, D. J. Merryman, P. A. Edwards, F. J. Armatis, *J. Am. Chem. Soc.* **1975**, *97*, 6267.

[2] a) C. H. E. Belin, *J. Am. Chem. Soc.* **1980**, *102*, 6036; b) J. Wolf, Dissertation, Universität Stuttgart, **1986**.

[3] a) D. Kummer, L. Diehl, *Angew. Chem.* **1970**, *82*, 881; *Angew. Chem. Int. Ed. Engl.* **1970**, *9*, 895; b) L. Diehl, K. Khodadedeh, D. Kummer, J. Strähle, *Chem. Ber.* **1976**, *109*, 3404.

[4] J. D. Corbett, *Chem. Rev.* **1985**, *85*, 383.

[5] a) E. Zintl, J. Goubeau, W. Dullenkopf, *Z. phys. Chem. Abt. A* **1931**, *154*, 1; b) E. Zintl, W. Dullenkopf, *Z. phys. Chem. Abt. B* **1932**, *16*, 183.

[6] Recent review: R. E. Williams, "Early carboranes and their structural legacy" in *Advances in Organometallic Chemistry, Vol. 36* (Eds.: F. G. A. Stone, R. West), Academic Press, New York, **1994**, *36*, pp. 1–55; earlier comprehensive review of this field: R. N. Grimes, *Carboranes*, Academic Press, New York, **1970**.

[7] T. Onak, K. Gross, T. Tse, J. Howard, *J. Chem. Soc. Dalton Trans.* **1973**, 2633.

[8] D. S. Matteson, P. K. Matschei, *Inorg. Chem.* **1973**, *12*, 2472.

[9] R. E. Williams, *Adv. Inorg. Radiochem.* **1976**, *18*, 67.

[10] R. E. Remmel, H. D. Johnson, I. S. Jaworiwsky, S. G. Shore, *J. Am. Chem. Soc.* **1975**, *97*, 5395.

[11] J. H. Osborne, R. C. P. Hill, D. M. Ritter, *Inorg. Chem.* **1986**, *25*, 372.

[12] NMR data for **1**: ^{11}B NMR ($CDCl_3$, 128 MHz, *J*/Hz): $\delta = 6.6$ (sextet, 1B, $J(B,H^{\mu/endo}) \approx 31$, BMe), 1.6 (d of sextets, 1B, $J(B,H^{t}) = 132$, $J(B,H^{\mu/endo}) \approx 33$, BH), −1.3 (d of sextets, 2B, $J(B,H^{t}) = 142$, $J(B,H^{\mu/endo}) \approx 30$, BH); $^{1}H\{^{11}B\}$ NMR ($CD_3C_6D_5$, 400 MHz): $\delta = 3.01$ (s, 1H, BH^{t}), 2.70 (s, 2H, BH^{t}), 1.43 (s, 3H, $ClCH_3$), 1.37 (s, 5H, $H^{\mu/endo}$), 0.39 (s, 3H, BCH_3).

[13] N. N. Greenwood, R. Greatrex, *Pure Appl. Chem.* **1987**, *59*, 857; R. E. Williams, F. J. Gerhart, *J. Organometal. Chem.* **1967**, *10*, 168.

[14] M. Bühl, P. von R. Schleyer, *J. Am. Chem. Soc.* **1992**, *114*, 477; M. Diaz, J. Jaballas, J. Arias, H. Lee, T. Onak, *ibid.* **1996**, *118*, 4405, and references therein.

[15] W. Kutzelnigg, *Isr. J. Chem.* **1980**, *19*, 1980; M. Schindler, W. Kutzelnigg, *J. Chem. Phys.* **1982**, *76*, 1919; W. Kutzelnigg, U. Fleischer, M. Schindler, *NMR: Basic Princ. Prog.* **1990**, *23*, 165. Huzinaga's basis sets were employed in the recommended contraction scheme (DZ = "double zeta"): S. Huzinaga, *Approximate Atomic Wave Functions*, University of Alberta, Edmonton, **1971**.

[16] Structures were optimized at the MP2(fc)/6-31G* level, and relative energies correspond to the MP2(fc)/6-31G* + 0.93 ZPE level of theory. All computations were performed with Gaussian 94, Revision C.3: M. J. Frisch, G. W. Trucks, H. B. Schlegel, P. M. W. Gill, B. G. Johnson, M. A. Robb, J. R. Cheeseman, T. Keith, G. A. Petersson, J. A. Montgomery, K. Raghavachari, M. A. Al-Laham, V. G. Zakrzewski, J. V. Ortiz, J. B. Foresman, J. Cioslowski, B. B. Stefanov, A. Nanayakkara, M. Challacombe, C. Y. Peng, P. Y. Ayala, W. Chen, M. W. Wong, J. L. Andres, E. S. Replogle, R. Gomperts, R. L. Martin, D. J. Fox, J. S. Binkley, D. J. Defrees, J. Baker, J. P. Stewart, M. Head-Gordon, C. Gonzalez, J. A. Pople, Gaussian, Inc., Pittsburgh PA, **1995**.

[17] Through a transcription error the computed chemical shifts reported for **4** are incorrect (B. Gangnus, H. Stock, W. Siebert, M. Hofmann, P. von R. Schleyer, *Angew. Chem.* **1994**, *106*, 2383; *Angew. Chem. Int. Ed. Engl.* **1994**, *33*, 2296.). The IGLO/II'//MP2(fc)/6-31G* values are C1: $\delta = -24.9$; B2,5: 3.4; B3,4: −5.3.

[18] Optimization of 2-CB_4H_{10} gave a cluster with a CH_3 group coordinated to B1 and to B3 ($E_{rel} = 13.4$ kcal mol^{-1}). A 3-CB_4H_{10} starting geometry led to a methyl-substituted B_4H_8 ($E_{rel} = 8.8$ kcal mol^{-1} with respect to **4**)

[19] P. von R. Schleyer, M. Bühl, U. Fleischer, W. Koch, *Inorg. Chem.* **1990**, *29*, 153; P. T. Brain, D. Hnyk, D. W. H. Rankin, M. Bühl, P. von R. Schleyer, *Polyhedron*, **1994**, *13*, 1453.

[20] Optimization of a $B_5H_{10}^-$ starting geometry generated by removing the B4–B5 hydrogen bridge from B_5H_{11} also gave **5b**.

[21] S. G. Shore, personal communication.

A Novel Method for Detecting Nitric Oxide (NO) by Formation of Fluorescent Products Based on Cheletropic Spin Traps

Michael Bätz, Hans-Gert Korth,* and Reiner Sustmann*

Nitrogen monoxide is an important intra- and intercellular signal molecule.[1] In recent years we have developed specific methods for detecting NO on the basis of "NOCTs" (*N*itric *O*xide *C*heletropic *T*raps, **1**), which transform NO by a formal cheletropic reaction into cyclic nitroxide radicals that can be monitored by EPR spectroscopy.[2]

This method has been successfully applied in investigations of the cytotoxicity of NO[3] and other aspects of the chemistry of NO.[2b] However, a general disadvantage of applying nitroxide radicals in biological environments lies in their markedly reduced lifetime due to facile reductive degradation to hydroxylamine derivatives.[4] We report here on a novel method based on the NOCT concept that uses fluorescence spectroscopy as a sensitive probe for detecting the trapped nitric oxide. We take advantage of the fact that aromatic π systems that are formed by reaction of NO with suitably selected NOCTs [Eq. (a)] exhibit

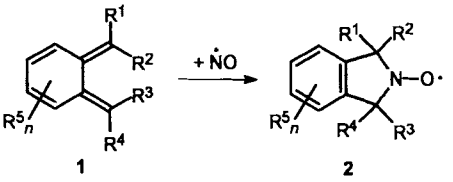

(a)

fluorescence properties. Therefore, the sensitivity is significantly increased over that of EPR spectroscopy, and the limited lifetime of the initially formed nitroxide radicals beneficially used.[5] In analogy to our current synthetic strategy, the stable cyclic *o*-quinodimethane derivatives **1**[6] were prepared as prototypes for FNOCTs [*F*luorescence *N*itric *O*xide *C*heletropic *T*raps; Eq. (b)].

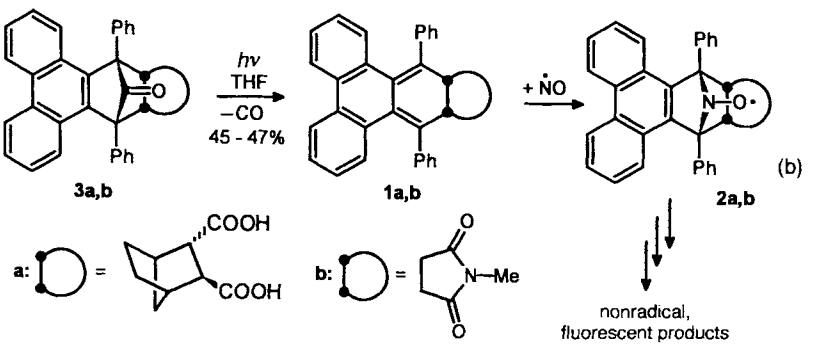

(b)

Phencyclone[7] reacts with norbornene-2,3-(*E*)-dicarboxylic acid and *N*-methylmaleinimide to yield the bridged ketones **3a** (84%, m.p. 282 °C) and **3b** (50%, m.p. 297–298 °C), respective-

[*] Dr. H.-G. Korth, Prof. R. Sustmann, Dr. M. Bätz
Institut für Organische Chemie der Universität
Universitätsstrasse 5, D-45117 Essen (Germany)
Fax: Int code +(201)183-3096
e-mail: sustmann@oc1.orgchem.uni-essen.de
hgk@oc1.orgchem.uni-essen.de

 © VCH Verlagsgesellschaft mbH, D-69451 Weinheim, 1997 0570-0833/97/3613-1501 $ 17.50+.50/0

ly.[8] Compounds **3a** and **3b** are converted by photolysis ($\lambda = 300$ nm) into **1a** and **1b** (yields of isolated products 47% and 45%, respectively).[8] The *o*-quinodimethane derivatives **1a** and **1b** are stable at room temperature in the presence of oxygen and do not decay by reactions typical for *o*-quinodimethanes.[2] The two carboxyl groups confer sufficient solubility to **1a** in buffer solution at physiological pH.

The UV/Vis spectra of **1a** (Figure 1, curve a) and **1b** are characterized by broad absorption bands at λ_{max} (ε) = 450 nm (8300;

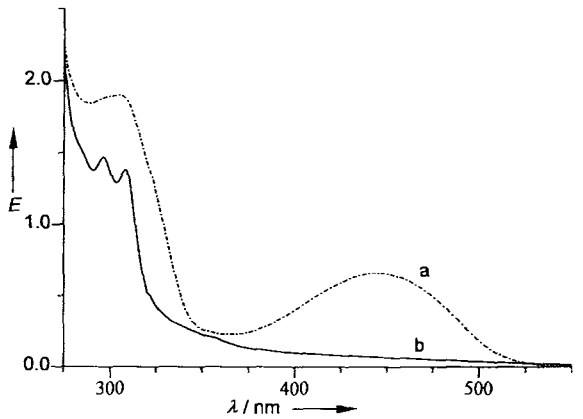

Figure 1. a) UV/Vis spectrum of **1a** (10^{-4} M) in phosphate buffer pH 7.4. b) Spectrum of a) after addition of NO (final concentration 5×10^{-4} M).

in phosphate buffer pH 7.4) and λ_{max} (ε) = 384 nm (8700; in THF), respectively, as is typical for *o*-quinodimethanes. This band is no longer detected immediately after addition of an excess of NO (in the same solvent; Figure 1, curve b). Instead, nitroxide radicals **2a** (Figure 2) and **2b** can be identified

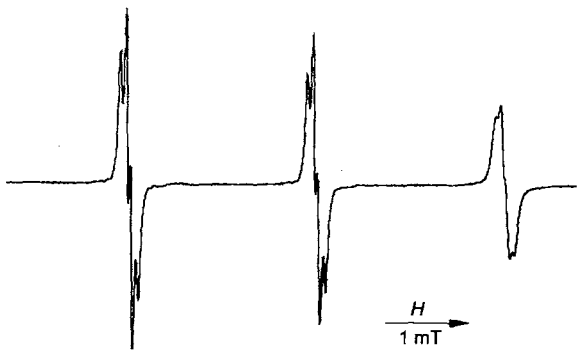

Figure 2. EPR Spectrum (9.4 GHz) of **2a** in THF at 20 °C.

by EPR spectroscopy. Based on the hyperfine splitting patterns, we assign the structures displayed in Scheme 1 to the nitroxides.

Radicals **2a** and **2b** are not very persistent and decay to nonradical products. Kinetic analysis of the time evolution of the EPR signals at 20 °C yields a half-life of about 40 min for **2a** in a buffer at pH 7.4. The lifetime of **2b** in THF is approximately five times longer.

The rate of reaction of **1a** and **1b** with NO was determined with the stopped-flow technique by following the decay of the UV/Vis absorptions at $\lambda = 450$ and 384 nm, respectively. The reaction of **1a** in phosphate buffer at pH 7.4 occurs at a rate constant of $k(\mathbf{1a}+\mathrm{NO}) = (60 \pm 8)\,\mathrm{M}^{-1}\mathrm{s}^{-1}$ at 20 °C, and that of **1b** in benzene at $k(\mathbf{1b}+\mathrm{NO}) = (134 \pm 12)\,\mathrm{M}^{-1}\mathrm{s}^{-1}$.

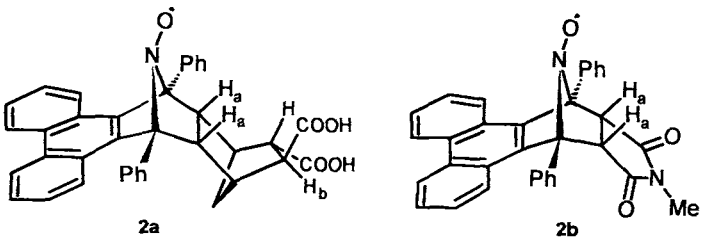

Scheme 1. Structures of **2a** and **2b** determined from ESR parameters.

Solutions of **1a** and **1b** show only a weak fluorescence at an excitation wavelength of 315 nm (Figure 3). However, upon addition of excess NO to a solution of the FNOCTs (5×10^{-5} M), the characteristic fluorescence of the phenanthrene skeleton is observed immediately.[11] The intensity of the fluorescence increases slowly with time to reach a plateau value after several hours (about 16 h for **2a** and 26 h for **2b**; Figure 3).

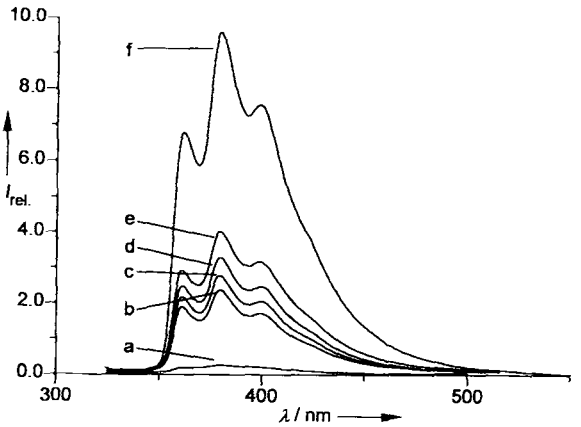

Figure 3. Fluorescence spectra of **1a** (5×10^{-5} M, phosphate buffer pH 7.4), a) before and b) 1 min, c) 35 min, d) 52 min, e) 78 min, and f) 960 min after addition of NO (final concentration 2×10^{-4} M). Excitation wavelength: 315 nm.

The time profile of the increase in fluorescence intensity correlates with the decrease in the EPR signals, that is, with the decay of the nitroxide radicals **3a** and **3b** to produce nonradical products with an intact phenanthrene fluorophore.[12] However, nitroxides can be fluorescence quenchers[13] and diminish their own fluorescence. With regard to developing a practical method for detecting NO, the fluorescence-quenching properties as well as the reduced lifetime of the nitroxides lead to a protocol by which, after formation of the nitroxide, addition of a suitable reducing agent instantaneously produces the maximum intensity of the fluorescence. Since **1a** was developed especially for biological applications, we selected ascorbic acid, which is ubiquitous in cell systems, as the reducing agent. Figure 4 demonstrates the rapid increase in fluorescence intensity to a maximum value after addition of excess ascorbic acid. Similar behavior is found for other "physiological" reductants such as glucose or Fe^{2+}.

The two FNOCTs presented here exhibit the high sensitivity towards NO necessary for biological applications. In addition to trapping from aqueous and nonaqueous nanomolar solutions of NO, good fluorescence spectra were obtained with **1a** ($c = 10^{-5}$ M) from a solution (10 nM, buffer, pH 7.4) of the NO donor compound "spermine NONOate".[14] (At these concentrations EPR signals of **2a** could no longer be detected.) The fluorescence intensity showed a strictly linear ($r^2 = 0.993$, 95%

 © VCH Verlagsgesellschaft mbH, D-69451 Weinheim, 1997 0570-0833/97/3613-1502 $ 17.50+.50/0

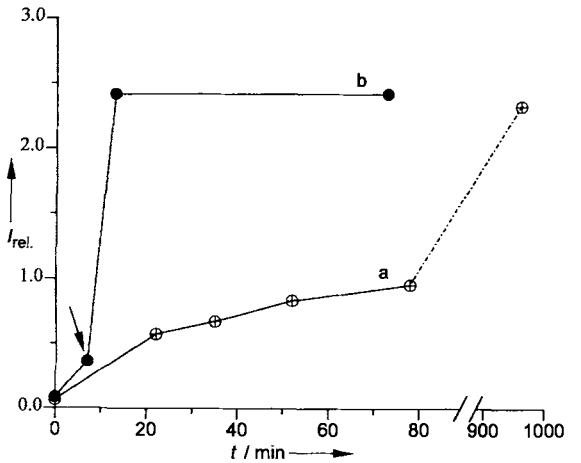

Figure 4. Time profile of the fluorescence intensity at 380 nm. a) After reaction of **1a** with NO. b) After addition of ascorbic acid (10^{-3} M). The arrow indicates when ascorbic acid was added.

confidence interval) dependency on the NO concentration between 2 nM and 4 μM.

The inertness of our FNOCTs towards reactive compounds commonly found in cell systems, in particular the "reactive oxygen species", is of special importance for their application. The influence of some typical cell ingredients on the lifetime of **1a** was tested: Figure 5 shows that the reaction with NO is by far the fastest. Compound **1a** is largely insensitive towards the buffer solution, the whole of the cell culture, glucose, superoxide, or Fe^{2+}. A slow reaction occurs with hydrogen peroxide. The Fenton system Fe^{2+}/H_2O_2, which generates OH radicals, exerts a less pronounced effect than H_2O_2 alone.

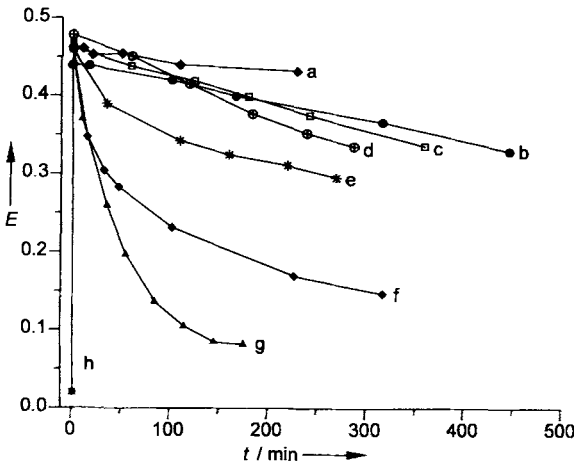

Figure 5. Time profile of the UV/Vis absorption ($\lambda = 450$ nm) of **1a** (1×10^{-4} M, phosphate buffer pH 7.4) in a) a cell culture of rat-liver endothelium cells, b) in pure phosphate buffer, and in presence of c) glucose (9×10^{-4} M), d) O_2^- (3×10^{-3} M), e) Fe^{2+} (7×10^{-4} M), f) $Fe^{2+} + H_2O_2$ (4×10^{-4} M; 1×10^{-3} M), g) H_2O_2 (2×10^{-3} M), and h) NO (2×10^{-4} M).

Our FNOCTs allow monitoring of the formation and decay of NO in chemical and biological systems with three complementary spectroscopic methods: UV/Vis, EPR, and fluorescence spectroscopy. The latter is particularly useful for the very low levels of NO found in biological environments. Synthetic modification of the *o*-quinodimethane backbone should lead to a family of custom-tailored NO traps for analyzing small amounts of NO in chemical and biochemical systems.

Received: November 13, 1996
Revised version: February 7, 1997 [Z97661E]
German version: *Angew. Chem.* **1997**, *109*, 1555–1557

Keywords: EPR spectroscopy · fluorescence spectroscopy · nitric oxides · quinodimethanes · radicals

[1] a) *The Biology of Nitric Oxide, Part 5* (Eds.: S. Moncada, J. Stamler, S. Gross, E. A. Higgs), Portland Press, London, **1996**, and preceeding volumes; b) *Methods in Nitric Oxide Research* (Eds.: M. Feelisch, J. S. Stamler), Wiley, Chichester, **1996**.

[2] a) T. Paul, M. A. Hassan, H.-G. Korth, R. Sustmann, D. V. Avila, *J. Org. Chem.* **1996**, *61*, 6835–6848, and references therein; b) H.-G. Korth, R. Sustmann, *Aspects of Nitric Oxide Chemistry* in *Free Radicals in Biology and Environment* (Ed.: F. Minisci), Klüwer, Dordrecht, **1996**, p. 63–78.

[3] a) I. Ioannidis, M. Bätz, T. Paul, H.-G. Korth, R. Sustmann, H. de Groot, *Biochem. J.* **1996**, *318*, 789–795; b) I. Ioannidis, M. Bätz, H.-G. Korth, R. Sustmann, H. de Groot, *ibid.* **1997**, submitted.

[4] a) V. Yelinova, A. Krainev, A. Savelov, I. Grigor'ev, *J. Chem. Soc. Perkin Trans 2* **1993**, 2053–2055; b) R. I. Zhdanov, I. B. Kadenatsi, L. E. Kholodov in *Bioactive Spin Labels* (Ed.: R. I. Zhdanov), Springer, Berlin, **1992**, p. 527, and references therein.

[5] This methodology is conceptually different from other applications of fluorescence spectroscopy for the detection of free radicals reported so far, see for example S. Pou, A. Bhan, U. S. Bhadti, S. Y. Wu, R. S. Hosmane, G. M. Rosen, *FASEB J.* **1995**, *9*, 1085–1090.

[6] M. Bätz, Ph.D. thesis, Universität Essen, **1997**.

[7] W. Dilthey, *J. Prakt. Chem.* **1935**, *143*, 189–210.

[8] Compounds **1a**, **1b**, **3a**, and **3b** were fully characterized by spectroscopic methods (^{1}H and ^{13}C NMR, IR, UV/Vis), mass spectrometry, and elemental analysis.

[9] The EPR spectra were completely reproduced by simulation with the following hyperfine splittings: **2a**: $a(^{14}N) = 2.284$, $a(H) = 0.077$ (2 H), $a(H) = 0.048$ mT (1 H), $g = 2.00622$; **2b**: $a(^{14}N) = 2.261$, $a(H) = 0.09$ (2 H), $a(H) = 0.027$ (3 H), $a(^{14}N_{Imid}) = 0.05$ mT, $g = 2.00628$. The magnitude of the ^{14}N splitting constants is characteristic for bridged nitroxide radicals [10]. Due to their orientation with respect to the radical center we assume that the *exo*-oriented hydrogen atoms H_a and proton H_b are responsible for the additional hyperfine splitting for **2a**, and the H_a protons, the nitrogen atom of the imide group, and the *N*-methyl group for **2b**.

[10] A. R. Forrester in *Landolt-Börnstein, New Series, Magnetic Properties of Free Radicals, Vol. 9, Part c1* (Eds.: H. Fischer, K. H. Hellwege), Springer, Berlin, **1979**, p. 524–538.

[11] G. G. Guibault, *Practical Fluorescence*, Marcel Dekker, New York, **1973**, p. 84.

[12] Preliminary product studies show that, depending on the amount of NO, several (>6) nitroso- and nitro-substituted products are formed from the nitroxides, in part by ring-opening reactions, in addition to the corresponding hydroxylamine derivatives. A detailed product study will be reported.

[13] S. A. Green, D. J. Simpson, G. Zhou, P. S. Ho, N. V. Blough, *J. Am. Chem. Soc.* **1990**, *112*, 7337–7346.

[14] (*Z*)-1-{*N*-[3-Aminopropyl]-*N*-[4-{3-aminopropylammonio)butyl]amino}-diazen-1-ium-1,2-diolate: J. A. Hrabie, J. R. Klose, D. A. Wink, L. K. Keefer, *J. Org. Chem.* **1993**, *58*, 1472–1476.

 © VCH Verlagsgesellschaft mbH, D-69451 Weinheim, 1997 0570-0833/97/3613-1503 $ 17.50+.50/0

Total Enantiotopic Discrimination between Carbon Atoms of a Double Bond in the Reaction of Diolates with *meso*-Bis(phenylsulfonyl)alkenes—Synthesis of Enantiopure Ketones**

Sergio Cossu,* Ottorino De Lucchi,* and Paolo Pasetto

Dedicated to Professor Waldemar Adam on the occasion of his 60th birthday

Enantiotopic discrimination of two functional groups in a *meso* compound is a well-established and convenient procedure for preparing enantiopure compounds, which avoids separation and disposal of the unwanted enantiomer.[1] This method, sometimes referred to as the "*meso* trick", is usually applied to diesters or other pairs of enantiotopic functional groups, and is often performed with enzymes.[2] The enantiotopic discrimination of two adjacent carbon atoms is very rare, and, other than the alkyllithium-based rearrangement of *meso* epoxides,[3] there are almost no cases in which such an extreme case of the *meso* trick was applied to an alkene.[4] Here we show that alkenes that are doubly substituted with phenylsulfonyl groups in *meso* compounds undergo reaction with the salts of alcohols and diols to afford totally dissymmetrical compounds in quantitative yields. This represents an enantiotopic discrimination[4] of the carbon atoms of a double bond. The reaction affords diastereo- and enantiopure ketones that are difficult to prepare by conventional routes, and can be utilized in the synthesis of numerous natural products,[5] antibiotics,[6] and drugs used in cancer[7] and AIDS therapy.[8]

The synthetic sequence consists of the reaction of a bis(phenylsulfonyl)alkene **1** with a chiral diol **2** followed by hydrolysis and reductive desulfonylation [Eq. (1)]. Since the reaction is totally stereoselective and affords one only of the possible diastereoisomers (**3**), a single enantiomeric ketone **4** is obtained.

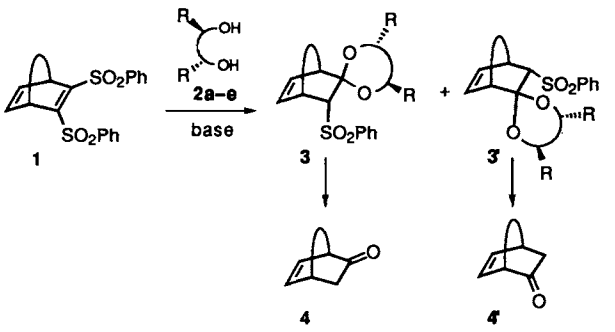

(1)

Starting **1** are readily prepared by cycloaddition of bis(phenylsulfonyl)acetylene with dienes.[9] Because this acetylene is not very stable, (*Z*)-1-chloro-1,2-bis(phenylsulfonyl)ethylene (**5**) may be used as its synthetic equivalent in the Diels–Alder reaction [Eq. (2)].[10] There are also several other routes available for preparing **1**.[11] The derivatives of **1** used in the present study

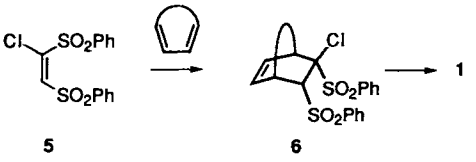

(2)

are the polycycles **7**–**9**,[12] which were chosen as representatives of the [2.2.1], [2.2.2], and cyclobutene systems.

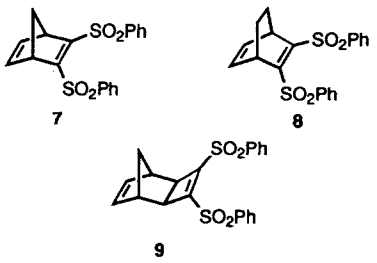

The diols used represent the classes of 1,2- (**2a**–**c**) and 1,3-diols (**2d**) with substituents of different size as well as the atropisomers 1,1'-binaphthalene-2,2'-diol (**2e**). They all possess a C_2-symmetry axis, which avoids partition of the products into further diastereoisomers. Reaction of the sodium salts of **2a**–**e** (prepared by treatment with NaH in THF) with **7**–**9** leads to the ketals **10**–**12** (Table 1).

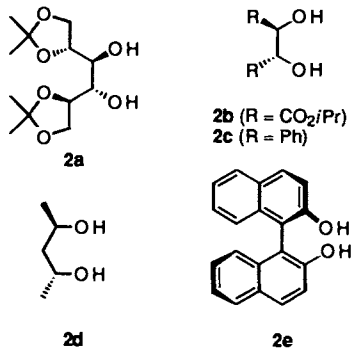

The bis(phenylsulfonyl)alkene **7** was considered as the standard substrate for testing the behavior of the different diols. Best results were obtained with (*R*,*R*)-(+)-1,2-diphenyl-1,2-ethanediol (**2c**) and **2e**, which both gave a single diastereoisomer (entries 3 and 5 in Table 1). Diol **2c** was used for desymmetrization of **8** and **9** because of the higher crystallinity of the adducts and simplicity in detecting the two diastereoisomers by NMR spectropscopy. With no exceptions **2c** gave the single diastereoisomers **11c** and **12c** (entries 7 and 9); that is, total C=C discrimination was accomplished in all cases. Diols derived from mannitol and tartaric acid **2a** and **2b** gave poorer results (entries 1, 2, and 6) with formation of both diastereoisomers. However, no attempts were made to separate the diastereoisomers. (2*R*,4*R*)-(−)-Pentanediol (**2d**) also showed little selectivity with substrates **7** and **8** (entries 4 and 8).

[*] Dr. S. Cossu, Prof. Dr. O. De Lucchi, Dr. P. Pasetto
Dipartimento di Chimica, Università Ca' Foscari di Venezia
Dorsoduro 2137, I-30123 Venezia (Italy)
Fax: Int. code +(41)529-8517
e-mail: delucchi@unive.it

[**] This work was supported by C. N. R. (Rome). We thank Prof. R. Ballini (Universitá Camerino, Italy) for helpful suggestions.

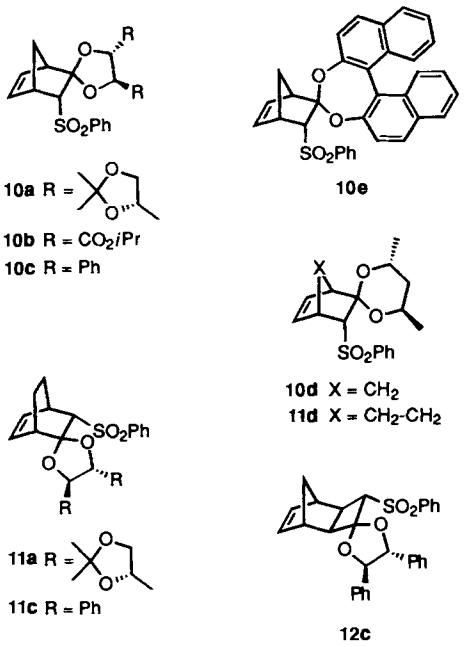

Table 1. Yields, diastereomeric ratios, and optical activity for the products of the reaction of **7**–**9** with diols **2a**–**e**.

Entry	Substrate	Diol	Product	Yield [%]	Diastereomeric ratio [a]	Optical activity [d]
1	**7**	**2a**	**10a**	97	85:15	
2		**2b**	**10b**	93	70:30	
3		**2c**	**10c**	88	[c]	+112.9 (1.7)
4		**2d**	**10d**	92	60:40	
5		**2e** [b]	**10e**	92	[c]	
6	**8**	**2a**	**11a**	72	50:50	
7		**2c**	**11c**	96	[c]	+87.9 (1.6)
8		**2d**	**11d**	90	50:50	
9	**9**	**2c**	**12c**	92	[c]	+82.2 (1.4)

[a] Determined by ^{1}H NMR spectroscopy at 200 MHz. [b] Used as a racemic mixture. [c] Only one diastereomer was obtained. [d] The concentration c is given in parentheses; the measurements were conducted in $CHCl_3$.

The stereochemistry of **10c**, **11c**, and **12c** was determined by X-ray crystallography.[13] The mechanism of formation for **10c** from **7** and **2c** requires attack of the alcoholate functionality at the vinyl carbon atom α to the sulfonyl group, elimination, and addition [Eq. (3)]. Assuming that the approach of the reagent occurs from the *exo* face of the alkene, as is usually observed in norbornenes,[14] the least encumbered trajectory is the one shown in which the phenyl group points upwards, and the alkyl chain to the side. After elimination of the phenylsulfinate anion, a second nucleophilic addition takes place to provide the observed product. The sulfonyl group in **10c** is in the *endo* position, which is in accordance with the *exo* rule of attack of the proton onto the anion.[14] The latter stereoisomer appears to be the kinetic product, because if an excess of base is present epimerization occurs with formation of only the *exo* phenylsulfonyl isomer. Similar reasoning also accounts for the stereochemistry observed for **11c** and **12c**. However, in these cases attack of the alcoholate on **8** and **9** occurs from the *endo* face, as generally observed for these systems.[15]

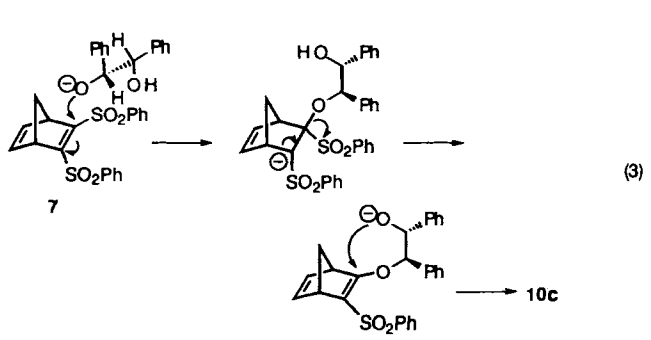

(3)

Diastereopure **10c**, **11c**, and **12c** can be hydrolyzed (Nafion H in toluene at reflux, 5 h) and desulfonylated (NaHg 6% in MeOH/$NaH_2PO_4 \cdot H_2O$, 0 °C, 2 h) to give the enantiomerically pure ketones **13**–**15**[16] in 75-90% yields with the absolute configuration shown. Deacetalization of **10c** affords

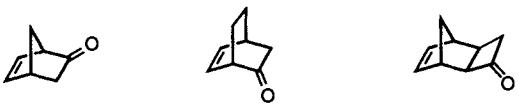

mixtures of epimers at the carbon atom α to the sulfonyl group in **16**. This scrambling apparently does not affect the enantiopurity of **13**–**15**. The α-sulfonyl ketones are also of synthetic interest and can be subjected to alkylation and further selective operations that are not dependent on the sterochemistry of the sulfone.[17] The deacetalization–desulfonylation sequence can be reversed to accomplish reductive desulfonylation[18] before hydrolysis. However, desulfonylation of α-sulfonyl ketones is easier and can be carried out with milder reducing agents.[19]

The step that is relevant for the stereochemistry of the products is the initial attack by the diolate ion on **1**. Once the alkene carbon has been chosen by the chiral diol, desymmetrization is virtually accomplished. On this basis, any monofunctionalized chiral alcoholate ion can provide desymmetrization through the enolether and, thus, the ketone. Indeed, reaction of **7** with the lithium salt of (1*R*,2*S*,5*R*)-(−)-menthol (obtained from *n*BuLi and menthol in THF) directly gives **16** in 80% yield [Eq. (4)]

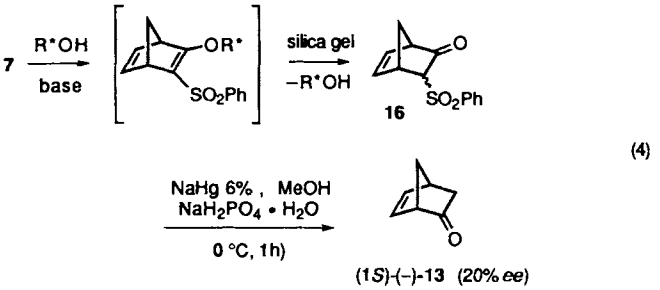

(4)

after column chromatography on silica gel. The sufonyl ketone **16** is reduced to (1*S*)-(−)-**13** with NaHg (6% in MeOH/$NaH_2PO_4 \cdot H_2O$, 0 °C, 1 h, 20% *ee*, 80% yield). This reduces the entire operation to just two steps and allows easy recovery of the chiral auxiliary.

Although this latter protocol is rapid and effective, it produces ketones with lower optical purity since it does not allow a check of the enantiomeric purity of the ketone at the diasteromeric level. We are presently defining other enantiopure alcohols capable of maximum selectivity and studying other stereoselective transformations of these and other bis(phenylsulfonyl)alkenes.

Received: December 27, 1996 [Z9936IE]
German version: *Angew. Chem.* **1997**, *109*, 1598–1601

 © VCH Verlagsgesellschaft mbH, D-69451 Weinheim, 1997 0570-0833/97/3613-1505 $ 17.50+.50/0

Keywords: asymmetric synthesis · chirality · ketones · synthetic methods

[1] E. L. Eliel, S. H. Wilen, L. N. Mander, *Stereochemistry of Organic Compounds*, Wiley, New York, **1994**, pp. 962–963.
[2] E. Schoffers, A. Golebiowski, C. R. Johnson, *Tetrahedron* **1996**, *52*, 3769–3826; L. A. Paquette, H.-C. Tsui, *J. Org. Chem.* **1996**, *61*, 142–145.
[3] N. S. Simpkins in *Advanced Asymmetric Synthesis* (Ed.: G. R. Stephenson), Chapman & Hall, London, **1996**, pp. 111–125; D. M. Hodgson, A. R. Gibbs, G. P. Lee, *Tetrahedron* **1996**, *52*, 14361–14384.
[4] Hydroboration: K. Burgess, W. A. van der Donk in *Advanced Asymmetric Synthesis* (Ed.: G. R. Stephenson), Chapman & Hall, London, **1996**, pp. 181–211; hydrosilylation: E. Campi, P. Perlmutter, *ibid.*, pp. 212–221.
[5] O. De Lucchi, W. Adam in *Comprehensive Organic Synthesis, Vol. 5* (Eds.: B. M. Trost, I. Fleming, L. A. Paquette), Pergamon, **1991**, pp. 193–214.
[6] G. Helmchen, A. Krotz, H.-P. Neumann, M. L. Ziegler, *Liebigs Ann. Chem.* **1993**, 1313–1317.
[7] M. Hono in *Anticancer Agents Based on Natural Product Models*, Academic Press, London, **1980**, p. 73.
[8] C. A. Flechter, H. Hilper, P. L. Myers, S. M. Roberts, R. J. Storer, *J. Chem. Soc. Chem. Commun.* **1989**, 1707–1709.
[9] L. Pasquato, O. De Lucchi, L. Krotz, *Tetrahedron Lett.* **1991**, *32*, 2177–2178.
[10] S. Cossu, O. De Lucchi, *Gazz. Chim. It.* **1990**, *120*, 569–576.
[11] T. Cohen, R. H. Ritter, D. Ouelette, *J. Am. Chem. Soc.* **1982**, *104*, 7142–7148; O. De Lucchi, G. Marchioro, *Phosphorus Sulfur Relat. Elem.* **1985**, *24*, 305–309; H. Landen, H.-D. Martin, A. Steigel, *Chem. Ber.* **1987**, *120*, 171–175; K. A. Herbert, M. G. Banwell, *Synth. Commun.* **1989**, *19*, 327–337; S. Cossu, O. De Lucchi, D. Fabbri, G. Licini, L. Pasquato, *Org. Prep. Proc. Int.* **1991**, *23*, 573–592; G. O'Doherty, R. D. Rogers, L. A. Paquette, *J. Am. Chem. Soc.* **1994**, *116*, 10883–10894.
[12] Preliminary experiments on several other polycyclic bis(phenylsulfonyl)-alkenes [10] show that the reaction is general.
[13] The X-ray structure analyses were carried out by Dr. Giovanni Valle (C. N. R., Centro Studi Biopolimeri, via Marzolo 1, I-35131 Padova, Italy).
[14] J. Spanget-Larsen, R. Gleiter, *Tetrahedron* **1983**, *39*, 3345–3350, and references therein.
[15] E. Müller, *Chem. Ber.* **1976**, *109*, 3793–3803; U. Azzena, S. Cossu, O. De Lucchi, G. Melloni, *Gazz. Chim. It.* **1989**, *119*, 357–358.
[16] Enantiopure **13**: J. Martynow, M. Dimitroff, A. G. Fallis, *Tetrahedron Lett.* **1993**, *34*, 8201–8204, see also ref. [6]; enantiopure **14**: M. Demuth, S. Chandrasekhar, K. Schaffner *J. Am. Chem. Soc.* **1984**, *106*, 1092–1095; D. A. Lightner, J. K. Gawronski, T. D. Bouman, *ibid.* **1980**, *102*, 5749–5754; **15**: +388.0 (*c* 3.2, in pentane).
[17] B. M. Trost, N. R. Schmuff, *J. Am. Chem. Soc.* **1985**, *107*, 396–405.
[18] N. S. Simpkins, *Sulphones in Organic Synthesis*, Pergamon, Oxford, **1993**, pp. 334–372; B. M. Trost, H. C. Arndt, P. E. Strege, T. R. Verhoeven, *Tetrahedron Lett.* **1976**, 3477–3480; H. Künzer, M. Stahnke, G. Sauer, R. Wiechert, *ibid.* **1991**, *32*, 1949–1952; G. H. Lee, E. B. Choi, E. Lee, C. S. Pak, *ibid.* **1993**, *34*, 4541–4544; E. Alonso, D. Guijarro, M. Yus, *Tetrahedron* **1995**, *51*, 2699–2708; R. Giovannini, M. Petrini, *Synlett* **1995**, 973–974.
[19] R. A. Holton, D. J. Crouse, A. D. Williams, R. M. Kennedy, *J. Org. Chem.* **1987**, *52*, 2317–2318; M. Fujii, K. Nakamura, H. Mekata, S. Oka, A. Ohno, *Bull. Chem. Soc. Jpn.* **1988**, *61*, 495–500; A. B. Smith III, K. J. Hale, J. P. McCauley, Jr., *Tetrahedron Lett.* **1989**, *30*, 5579–5582; A. R. Harris, T. J. Mason, G. R. Hannah, *J. Chem. Res. Synop.* **1990**, *7*, 218–219.

A Straightforward Solid-Phase Synthesis of Cyclic Oligodeoxyribonucleotides**

ElMostafa Alazzouzi, Nuria Escaja, Anna Grandas, and Enrique Pedroso*

Nuclease-resistant oligonucleotides have received much attention due to their potential use in antisense or antigene therapeutics.[1] Cyclic oligonucleotides (CONs) have an intrinsic resistance to degradation by exonucleases, the most active nucleases. CONs can be used as efficient templates for DNA and T7-RNA polymerases to obtain multiple copies of their sequences by the rolling-circle mechanism[2] and are excellent models for studying structures of nucleic acids.[3] In addition, some CON sequences show interesting biological properties.[4]

The synthesis of CONs is a challenging case of macrocycle formation, since each nucleotide unit contributes six atoms to the cyclic backbone. Owing to the competition between inter- and intramolecular reactions, only relatively small sequences (2- to 8-mer) have been obtained by chemical ligation of partially protected oligonucleotides in dilute solutions.[5] Larger cyclic structures (24-mer or more) have only been successfully prepared by template-directed cyclization, chemically or enzymatically, of unprotected oligonucleotides.[6] The template sequence may be either a segment of the CON, as in the ligation of nicked dumbbells,[6a] or a second oligonucleotide molecule that forms a duplex[6b] or a triplex[6c] with the linear precursor of the CON. The main drawbacks of most of these template-assisted procedures[6a,c] are that the sequence of the affordable CONs is restricted and that a lower limit is imposed on their size by the need for efficient hybridization and adequate base pairing with the template sequences.

To our knowledge, the advantages of automated solid-phase methods have been successfully used by only one group for preparing CONs.[7] In their approach, the exocyclic amino group of cytosine is attached to the solid support, where both chain elongation and cyclization are carried out. The largest sequence obtained, which of course has to contain at least one cytosine residue, is a hexadecamer in 1% yield. This shows the difficulty of the synthetic goal.

The solid-phase synthesis described here allows facile obtention of small to medium-sized CONs with no restrictions on sequence. The procedure takes advantage of two main characteristics of the solid-phase methodology: pseudo-dilution conditions for cyclization [8] and ready elimination of by-products by simple filtration.

The synthesis starts with the anchoring of the 3′-terminal nucleotide to the solid matrix through the new bifunctional linker 3-chloro-4-hydroxyphenylacetic acid (**1**, Figure 1). To obtain a homogeneously derivatized resin it is advisable to couple the nucleotide to the linker and then to anchor the resulting product to the support. Thus, the reaction between the 2,4,5-trichlorophenyl ester derivative of linker **2** and a nucleoside phosphoramidite in the presence of tetrazole followed by oxidation gives the nucleotide-linker **3** (B = T, C^{Bz}, A^{Bz}, G^{iBu}). Aminomethyl-polystyrene-*co*-1%-divinylbenzene or a poly-

[*] Prof. Dr. E. Pedroso, E. Alazzouzi, N. Escaja, Prof. Dr. A. Grandas
Departament de Química Orgànica, Facultat de Química
Universitat de Barcelona
Martí i Franquès 1–11, E-08028 Barcelona (Spain)
Fax: Int. code +(3)339-7878
e-mail: pedroso@mafalda.qui.ub.es

[**] This work was supported by funds from the DGICYT (grant nos. PB91-270 and PB94-844) and the Generalitat de Catalunya (Centre de Referència de Biotecnologia and GRQ93-1094).

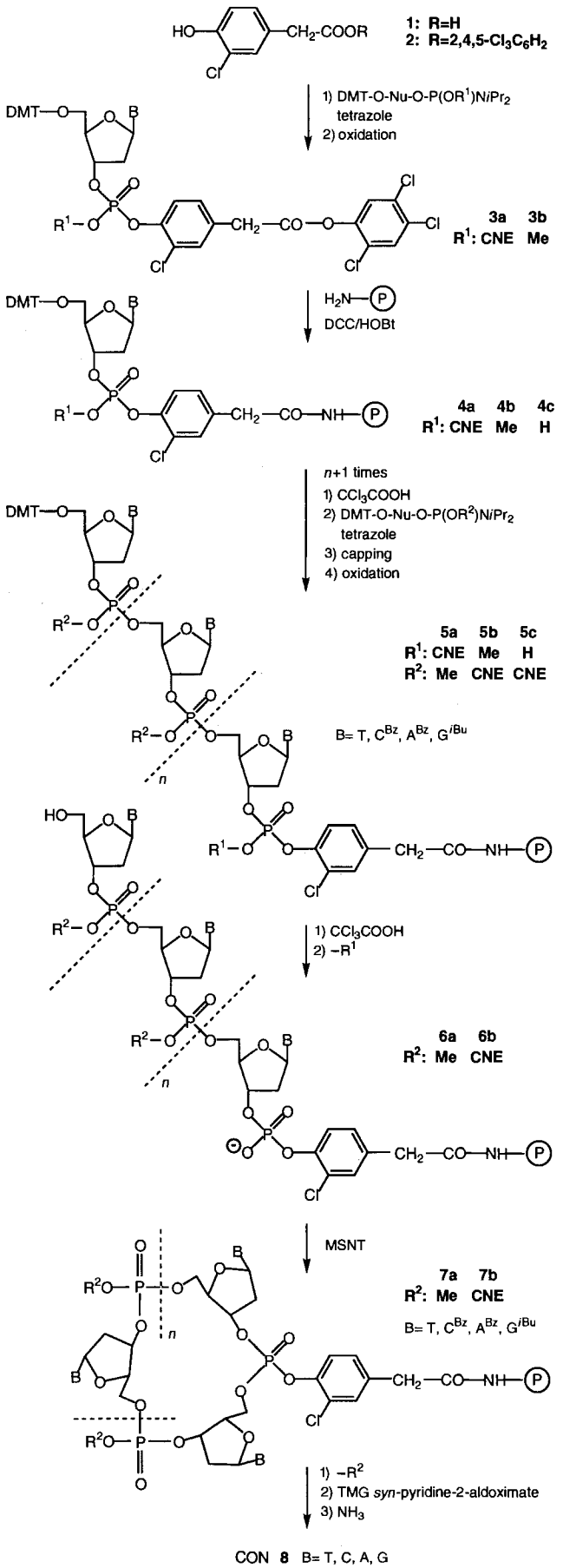

Figure 1. Synthesis of cyclic oligodeoxyribonucleotides.

ethyleneglycol-polystyrene copolymer (TentaGel-NH_2 resin) were used as solid supports, to which 6-aminohexanoic acid can be incorporated as a spacer in order to increase the flexibility of the oligonucleotide chain and facilitate the cyclization and cleavage reactions. Coupling of **3** to the amino-derivatized support affords the nucleotide-resin **4**, whose purity can be assesed by gel-phase ^{31}P NMR spectroscopy.[9] Assembly of oligonucleotide chain **5** takes place from **4** by the standard phosphite triester approach with CNE- or methylphosphoramidites of 5′-O-DMT-nucleosides (CNE = 2-cyanoethyl, DMT = dimethoxytriphenylmethyl). Removal of the 5′-OH and 3′-terminal phosphate protecting groups (if the latter was not previously removed) allows cyclization of the partially deprotected oligonucleotide **6** on the support. Finally, deprotection and cleavage of **7** affords CON **8**.

The synthetic method relies on an appropriate choice of three phosphate protecting groups. An *o*-chlorophenyl group permanently protects the 3′-terminal phosphate and anchors the oligonucleotide to the resin. This 3′-phosphate moiety is also protected with a semipermanent group R^1, which has to be selectively removed for the regioselective cyclization to take place. The remaining phosphates of the oligonucleotide chain are protected with a permanent group R^2. Various combinations of R^1 and R^2 were explored with fairly similar results. Either R^1 = CNE (**4a**), and the elongation is carried out with Me-amidites to afford **5a**, or R^1 = Me (**4b**), and CNE-amidites are used for assembling **5b**. Studies with model compounds showed that none of these approaches is completely orthogonal, since R^2 groups are partially eliminated under the conditions used for removing the semipermanent group R^1 in **5a** or **5b**. Therefore, an alternative approach was designed in which the CNE group is removed from **4a** to afford **4c**, and chain assembly to **5c** is carried out with CNE-phosphoramidites. UV monitoring of the DMT cations released in the deprotection steps shows that chain elongation proceeds normally regardless of the protecting scheme used (about 98% average yield of coupling).

Cyclization of **6** is carried out with 1-mesitylenesulfonyl-3-nitro-1,2,4-triazole (MSNT, 0.1 M in pyridine, 12–24 h). The CON **8** is obtained from **7** after deprotection of the phosphates ($PhSH/Et_3N$ if R^2 = Me or Et_3N/pyridine if R^2 = CNE), cleavage from the resin with tetramethylguanidinium *syn*-pyridine-2-aldoximate (0.1 M in dioxane/water for at least 8 h), and deprotection of the nucleoases with concentrated ammonia. After gel filtration over Sephadex G-10 or G-25, the crude CONs are analyzed, purified, and characterized with standard techniques. The sequences of some of the synthesized CONs, from dinucleotides to a 32-mer, are shown below.

d⟨pTT⟩; d⟨pGG⟩; d⟨pAG⟩; d⟨pTTT⟩; d⟨pTTTTTT⟩

d⟨pTCATTCAT⟩; d⟨p^{Br}UCAT^{Br}UCAT⟩

d⟨pTCATATCTATAT⟩; d⟨pACGCTATGCGAT⟩

d⟨pTTTCTTGCTTGATTTA⟩; d⟨pTTCACATTTTCACATT⟩

d⟨pAGGTTGGTATGGTTGGAT⟩

d⟨pTGTCGTTCGCCTTGGAGTTCTACT⟩

d⟨pTCGTCGCTTGCGCCGTTCGGAGCTTGCTACGT⟩

Yields of the crude products depend on the size of the CON and range from 40–50% for the smallest molecules (up to an 8-mer) to 4% for the largest 32-mer. The best yields were generally obtained with the TentaGel matrix, the nucleotide resin **4c**, and CNE-phosphoramidites. A positive common feature of the

HPLC profiles of all the crude oligonucleotides is a major peak (typically more than 80–90% of the total integrated area) accompanied by some small impurities. The reason for such elevated purity is that the noncyclized chains, which are anchored to the support through a phosphate diester bond, are not cleaved from the resin upon oximate treatment, whereas the cyclic molecules linked through a phosphate triester are easily removed. Furthermore, neither the capped sequences nor the polymeric products formed by interchain reactions during cyclization are detached from the polymer. As a result, the main impurities that accompany the CON on the solid support are separated in the filtration step following oximate treatment.

This reasoning accounts for the homogeneity of the crude products but also provides an argument for the cyclic character of the isolated oligonucleotides (major peaks). Moreover, their structures have been confirmed by two enzymatic digestion analyses. Complete degradation with snake-venom phosphodiesterase and alkaline phosphatase gives the expected ratio of nucleosides. On the other hand, the synthesized CONs show an increased resistance to degradation with calf-spleen phosphodiesterase under standard conditions, which is complete for the smallest sequences (up to a 12-mer) but decreases as the size of the molecule increases.[10] Most of the CONs were also analyzed by mass spectrometry, either negative electrospray or MALDI-TOF or both, and show the expected mass.

This simple procedure yields fairly pure products and, with regard to size, allows the limit under which template approaches are no longer efficient to be reached. The method is also amenable to scale-up, and, in fact, some products have been prepared on milligram scales for structural and biological studies.

Experimental Section

2: A solution of **1** (4 g) in AcOEt (130 mL) was slowly added to a solution of 2,4,5-trichlorophenol (4.7 g) and dicyclohexylcarbodiimide (DCC, 4.9 g) in CH_2Cl_2 (22 mL), and the reaction mixture stirred overnight. The filtrate was washed with aqueous $NaHCO_3$ and dried, and the solvent removed under vacuum. The resulting oil was purified by chromatography over silica gel eluting with hexanes and increasing amounts of CH_2Cl_2. After precipitation with hexanes 2.8 g of **2** were isolated (34% yield): m.p. = 78 °C; ^{1}H NMR (200 MHz, $CDCl_3$): δ = 7.53, 7.26 (Cl_3Ar), 7.35 (d), 7.20 (dd), 7.03 (d, ClAr), 5.60 (OH), 3.82 (CH_2); EI-MS: m/z = 366.

3. A solution of tetrazole (0.23 mmol) in dry CH_3CN (0.7 mL) was stirred with 5′-*O*-DMT-nucleoside phosphoramidite (0.23 mmol) and **2** (0.21 mmol) dissolved in CH_2Cl_2 (1.7 mL) under an argon atmosphere for 1 h. *t*BuOOH (0.24 mL, 3 M in toluene) was added, and 10 min later the reaction mixture diluted with CH_2Cl_2 and washed with water. The organic phase was dried, concentrated, and precipitated over hexanes. The products were isolated as white foams (65–75% yield) and used without further purification. ^{31}P NMR ($CDCl_3$): δ = ca. −7.8(**3a**), ca. −10.5 (**3b**).

4. The amino support (ca. 1 mmol NH_2 groups) was treated with *N*-Fmoc-6-aminohexanoic acid, 1-hydroxybenzotriazole (HOBt), and DCC (0.25 equiv each for PS and 1 equiv each for TentaGel) in a mixture of CH_2Cl_2/DMF (7/1) for 2 h. The unchanged amino groups were acetylated, and the Fmoc group was removed (50% piperidine in DMF). This resin (200 mg) was treated with **3**, DCC, and HOBt (1–2 equiv each based on the NH_2 groups) in CH_2Cl_2/DMF (4/1, 2 mL) for 2 h. Resins with a substitution degree ranging from 50 to 120 μmol DMT g^{-1} were obtained. The remaining amino groups were acetylated before chain elongation.

Received: December 3, 1996
Revised version: February 18, 1997 [Z 9848 IE]
German version: *Angew. Chem.* **1997**, *109*, 1564–1567

Keywords: antisense agents · macrocycles · oligonucleotides · protecting groups · solid-phase synthesis

[1] E. Uhlmann, A. Peyman, *Chem. Rev.* **1990**, *90*, 543–584.
[2] A. Fire, S.-Q. Xu, *Proc. Natl. Acad. Sci. USA* **1995**, *92*, 4641–4645; S. L. Daubendiek, K. Ryan, E. T. Kool, *J. Am. Chem. Soc.* **1995**, *117*, 7818–7819; D. Liu, S. L. Daubendiek, M. A. Zillman, K. Ryan, E. T. Kool, *ibid.* **1996**, *118*, 1587–1594.
[3] A. F. Markham, E. Nakagawa, E. Ohtsuka, M. Ikehara, *Biopolymers* **1980**, *19*, 285–296; D. E. Wemmer, A. S. Benight, *Nucleic Acids Res.* **1985**, *13*, 8611–8621; M. M. W. Mooren, S. S. Wijmenga, G. A. van der Marel, J. H. van Boom, C. W. Hilbers, *ibid.* **1994**, *22*, 2658–2666; C. A. Frederick, M. Coll, G. A. van der Marel, J. H. van Boom, A. H. J. Wang, *Biochemistry* **1988**, *27*, 8350–8361; J. H. Ippel, V. Lanzotti, A. Galeone, L. Mayol, J. E. van den Boogaart, J. A. Pikkemaat, C. Altona, *J. Biomol. Struct. Dyn.* **1992**, *9*, 821–836; see also ref [6a-c].
[4] C-Y. L. Hsu, D. Dennis, *Nucleic Acids Res.* **1982**, *10*, 5637–5647; C. Clusel, E. Ugarte, N. Enjolras, M. Vasseur, M. Blumenfeld, *ibid.* **1993**, *21*, 3405–3411; P. Ross, H. Weinhouse, Y. Aloni, D. Michaeli, P. Weinberger-Ohana, R. Mayer, S. Braun, E. de Vroom, G. A. van der Marel, J. H. van Boom, M. Benziman, *Nature* **1987**, *325*, 279–281.
[5] C.-Y. L. Hsu, D. Dennis, R. A. Jones, *Nucleosides & Nucleotides* **1985**, *4*, 377–389; E. de Vroom, H. J. G. Broxterman, L. A. J. M. Sliedregt, G. A. van der Marel, J. H. van Boom, *Nucleic Acids Res.* **1988**, *16*, 4607–4620; M. V. Rao, C. B. Reese, *ibid.* **1989**, *17*, 8221–8239; M. L. Capobianco, A. Carcuro, L. Tondelli, A. Garbesi, G. M. Bonora, *ibid.* **1990**, *18*, 2661–2669.
[6] a) D. Erie, R. A. Jones, W. K. Olson, N. K. Sinha, K. Breslauer, *Biochemistry* **1989**, *28*, 268–273; G. W. Ashley, D. M. Kushlan, *ibid.* **1991**, *30*, 2927–2933; H. Gao, N. Chidambaram, B. C. Chen, D. E. Pelham, R. Patel, M. Yang, L. Zhou, A. Cook, J. S. Cohen, *Bioconjugate Chem.* **1994**, *5*, 445–453, and references therein; b) N. G. Dolinnaya, M. Blumenfeld, I. N. Merenkova, T. S. Oretskaya, N. F. Krynetskaya, M. G. Ivanovskaya, M. Vasseur, Z. A. Shabarova, *Nucleic Acids Res.* **1993**, *21*, 5403–5407; c) S. Wang, E. T. Kool, *J. Am. Chem. Soc.* **1994**, *116*, 8857–8858; S. Rumney IV, E. T. Kool, *ibid.* **1995**, *117*, 5635–5646, and references therein.
[7] M. R. Conte, L. Mayol, D. Montesarchio, G. Piccialli, C. Santacroce, *Nucleosides & Nucleotides* **1993**, *12*, 351–358; L. De Napoli, A. Galeone, L. Mayol, A. Messere, G. Piccialli, C. Santacroce, *J. Chem. Soc. Perkin Trans. 1*, **1993**, 747–749, and references therein.
[8] S. Mazur, P. Jayalekshmy, *J. Am. Chem. Soc.* **1979**, *101*, 677–683.
[9] F. Bardella, R. Eritja, E. Pedroso, E. Giralt, *Biomed. Chem. Lett.* **1993**, *3*, 2793–2796.
[10] Thanks are given to one of the referees for suggesting that a more definitive enzymatic assay for determining the circularity would be to carry out a partial degradation of the CONs with an endonuclease, since a cyclic product will initially produce linear oligonucleotides of homogeneous length [6c].

The First 1,3-Distanna-2-platina-[3]ferrocenophane and the Pt^0-Catalyzed Addition of 1,1,2,2-Tetramethyl-1,2-distanna-[2]ferrocenophane to C≡C Bonds**

Max Herberhold,* Udo Steffl, Wolfgang Milius, and Bernd Wrackmeyer

Dedicated to Professor Cornelius G. Kreiter on the occasion of his 60th birthday

The metal-catalyzed distannylation of the C≡C bond has been known for some time.[1] The reactions were carried out mainly in the presence of $[Pd(PPh_3)_4]$ as a catalyst;[2] however, potential intermediates such as *cis*-$[(R_3Sn)_2M(PPh_3)_2]$ (M = Pd, Pt) were neither structurally characterized nor isolated. So far, a structure was proposed on the basis of ^{1}H NMR and IR data for just one platinum complex with R = Me,[3] but the reactivity towards alkynes was not studied. A somewhat better characterized platinum complex, *cis*-$[(Ph_3Sn)_2Pt(dppe)]$, with $Ph_2PCH_2CH_2PPh_2$ (dppe) instead of the two PPh_3 ligands, was

[*] Prof. Dr. M. Herberhold, Dipl.-Chem. U. Steffl, Dr. W. Milius, Prof. Dr. B. Wrackmeyer
Laboratorium für Anorganische Chemie der Universität
Postfach 101251, D-95440 Bayreuth (Germany)
Fax: Int. code +(921) 552157
e-mail: max.herberhold@uni-bayreuth.de.

[**] This work was supported by the Deutsche Forschungsgemeinschaft and the Fonds der Chemischen Industrie.

investigated by multinuclear NMR spectroscopy,[4] but information about reactions with alkynes is not available.

We have recently reported on the synthesis and molecular structure of the 1,2-distanna-[2]ferrocenophane **1**[5] for which considerable potential in the synthesis of novel ferrocenophanes can be expected.[6, 7] Here we show that **1** reacts smoothly with $[Pt(PPh_3)_2C_2H_4]$ **2** to give the 1,3-distanna-2-platina[3]ferrocenophane **3** by oxidative addition accompanied by liberation of ethene (Scheme 1, route (a)). The molecular structure of **3** is

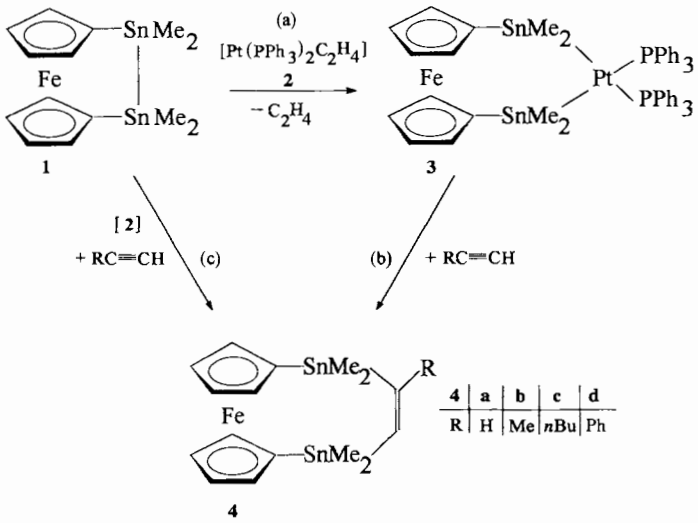

Scheme 1. Synthetic routes to **4a–d**.

shown in Figure 1.[8] A related complex, 1,3-digerma-2-platina-[3]ferrocenophane $Fe(C_5H_4GeMe_2)_2[Pt(dppe)]$, has just recently been reported.[9]

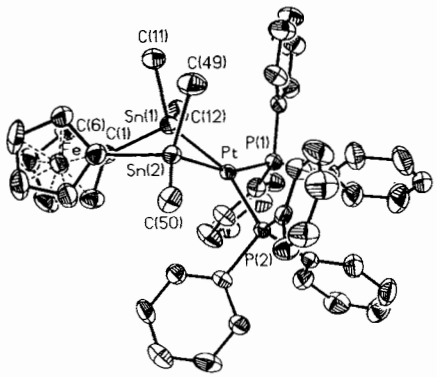

Figure 1. Molecular structure of **3**. Selected bond lengths [pm] and angles [°]: Sn(1)–Pt 264.4(1), Sn(2)–Pt 264.5(1), Sn(1)–C(1) 215.7(7), Sn(2)–C(6) 216.0(7), Sn–C(CH_3) (av) 217.0, P(1)–Pt 230.8(2), P(2)–Pt 229.9(2); Pt-Sn(1)-C(1) 112.7(2), Pt-Sn(2)-C(6) 122.7(2), Sn(1)-Pt-Sn(2) 82.3(1), Sn(1)-Pt-P(1) 88.1(1), Sn(1)-Pt-P(2) 162.9(1), Sn(2)-Pt-P(1) 160.2(1), Sn(2)-Pt-P(2) 89.2(1), P(1)-Pt-P(2) 104.2(1).

The platinum atom resides at the center of a distorted square plane of ligands; the planes P(1)-Pt-P(2) and Sn(1)-Pt-Sn(2) form an angle of 20.7°. A few examples of complexes showing such a distortion are known, for example *cis*-$[(Et_3P)_2Pt(GeMe_2Cl)_2]$.[10] However, the majority of *cis*-$[(R_3P)_2Pt(R)_2]$ complexes possess an undistorted planar coordination geometry.[11] In **3** the almost parallel cyclopentadienyl rings (tilt angle $\alpha = 2.3°$) deviate considerably from the ecliptic arrangement (twist angle $\tau = 17°$). The Sn(1)-C(1) and Sn(2)-C(6) bonds are slightly inclined from the cyclopentadienyl ring planes towards the Fe–Pt axis ($\beta = 2.2$ and 4°, respectively).

NMR spectra of **3** in solution (25 °C; CD_2Cl_2, see Experimental Section) indicate an intramolecular dynamic process (energy of activation:[12] $\Delta G^{\neq} = 41.8 \pm 2$ kJ mol^{-1}), resulting in fast site exchange of the PPh_3 ligands in *cis* and *trans* positions with respect to a particular tin atom. This is evident from the averaged coupling constant $|^2J(^{119}Sn,^{31}P)| = 680.0$ Hz in both the ^{31}P and ^{119}Sn NMR spectra. At −40 °C the $^{117/119}Sn$ satellites corresponding to $^2J(^{119}Sn,^{31}P)_{trans} = -1574.5$ Hz and $^2J(^{119}Sn,^{31}P)_{cis} = +206$ Hz are well resolved, and the comparison with the mean value proves that their signs are opposite, in agreement with the data for $[(Ph_3Sn)_2Pt(dppe)]$,[4] which, however, appears to have a rigid structure in solution. In the case of **3**, rotation of the $Pt(PPh_3)_2$ fragment about an axis bisecting an imaginary line connecting the two tin atoms can be assumed.

The dynamic properties of complexes of type **3**, observed here for the first time,[13] imply labile Pt–Sn bonds into which unsaturated units such as C≡C bonds can easily be inserted. This leads to transfer of the Sn Sn fragment, starting either from **3** in stoichiometric reactions or from **1** by using a catalytic amount of **2**. Both reactions (Scheme 1, routes (b) and (c)) give new 1,4-distanna-[4]ferrocenophanes **4** in good yield. In the case of propyne, a 1:1 mixture of **4b** and **4b′** is obtained. The Pd^0-catalyzed addition of Sn_2Me_6 to propyne affords selectively the product analogous to **4b′**.[2f] Compound **1** does not react with

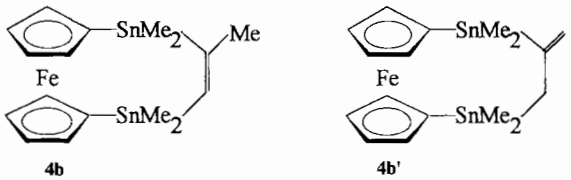

alkynes in the absence of **2**. Our attemps to add **1** to alkynes[2] in the presence of $[Pd(PPh_3)_4]$ were not successful, and we did not observe formation of the palladium complex analogous to **3**. The structure of the complexes **4** in solution follows unambiguously from the consistent set of NMR data (see Experimental Section).

The reaction between **1** and **2** enabled us to determine structural and dynamic properties of **3**, the first 1,3-distanna-2-platina[3]ferrocenophane, and the first fully characterized intermediate of a metal-catalyzed distannylation reaction. The novel 1,4-distanna[4]ferrocenophanes **4** are attractive compounds for further transformations because of their reactive Sn–C bonds.

Experimental Section

3: A solution of **1** (0.11 g, 0.22 mmol) in diethyl ether (10 mL) was slowly added to **2** (0.16 g, 0.22 mmol) in toluene (10 mL), and the mixture was stirred at room temperature for 12 h. After about 10 min a yellow product precipitated. Decanting, washing with toluene and diethyl ether, and drying gave **3** (0.19 g, 69.5%) as a yellow crystalline solid (m.p. 185 °C, decomp). ^1H NMR (CD_2Cl_2, 500 MHz, $[J(^{195}Pt,^1H)]$, $(J(^{119}Sn,^1H))$, $\{J(^{31}P,^1H)\}$): $\delta = -0.41$ (s, 12H, Me_2Sn, [6.6], (44.3)), 4.02 (m, 4H, 2,5-H, (7.6)), 4.15 (m, 4H, 3,4-H), 7.09–7.42 (m, 30H, C_6H_5); ^{13}C NMR (CD_2Cl_2, 125.8 MHz, $[J(^{195}Pt,^{13}C)]$, $(J(^{119}Sn,^{13}C))$, $\{J(^{31}P,^{13}C)\}$): $\delta = -3.0$ (Me_2Sn, [57.1], (211.7), {15.7}), 79.3 (C-1, [96.0], {4.8}), 75.4 (C-2,5, [9.5], (38.6)), 69.6 (C-3,4, [6.0], (29.1)), 128.4 (C-1), 134.3 (C-2,6, [23.0], {12.9}), 128.1 (C-3,5, [1.8], {10.1}), 129.9 (C-4); ^{31}P NMR (CD_2Cl_2, 101.2 MHz, 25 °C, $[J(^{195}Pt^{31}P)]$, $(J(^{119}Sn^{31}P))$: $\delta = 31.6$ ([2627.9],(680.0)); ^{119}Sn NMR (CD_2Cl_2, 93.3 MHz, $[J(^{195}Pt^{119}Sn)]$, $(J(^{119}Sn^{117}Sn))$: $\delta = 27.5$ ([9056], (350.0)); ^{195}Pt NMR (CD_2Cl_2, 107.1 MHz, $[J(^{195}Pt^{31}P)]$): $\delta = -762.3$ ([2640]).

4: General procedure, starting from **3**: The respective alkyne was added to a solution of **3** (0.12 g, 0.1 mmol) in THF (30 mL) and the mixture was heated for several hours at 65 °C. The solvent was removed in vacuo and the residue dissolved in

hexane. After filtration and evaporation of the hexane, chromatography on silica with hexane as eluant gave **4a–d** as orange oils.

4: General procedure, starting from **1**: A solution of **1** (0.12 g, 0.25 mmol), alkyne (0.3 mmol), and **2** (0.01 equiv.) in THF (30 mL) was heated to reflux for 72 h, workup as described above gave **4c,d**.

4a: EI MS: *m/z* (%) 508 (100) [M^+]. ^{1}H NMR (C_6D_6, 500 MHz, ($J(^{119}Sn,^1H)$): $\delta = 0.29$ (s, 12H, Me_2Sn, (54.9)), 4.06 (m, 4H, 2,5-H, (10.6)), 4.25 (m, 4H, 3,4-H, (6.1)), 7.43 (s, 2H, HC = CH, (131.8),(204.6)); ^{13}C NMR (C_6D_6, 125.8 MHz, ($J(^{119}Sn^{13}C)$): $\delta = -8.0$ (Me_2Sn, (356.2)), 66.7 (C-1, (499.7), (2.0)), 71.5 (C-3,4, (41.1)), 74.7 (C-2,5, (52.8)), 154.9 (C=C, (528.2), (31.7)); ^{119}Sn NMR (C_6D_6, 93.3 MHz, ($J(^{119}Sn^{117}Sn)$): $\delta = -71.7$ ((444.2)).

4b: EI MS: *m/z* (%) 524 (100) [M^+]. ^{1}H NMR (C_6D_6, 250 MHz, ($J(^{119}Sn^1H)$): $\delta = 0.30$ (s, 6H, Me_2Sn, (54.8)), 0.24 (s, 6H, Me_2Sn, (53.5)), 2.17 (d, 3H, Me, (49.7), (10.6), $^4J(^1H^1H) = 1.7$), 4.06 (m, 4H, 2,5-H), 4.26 (m, 4H, 3,4-H), 6.81 (q, 2H, HC=C, (204.8), (102.0), [1.7]); ^{13}C NMR (C_6D_6, 62.9 MHz, ($J(^{119}Sn^{13}C)$): $\delta = -7.7$ (Me_2Sn, (356.4)), -7.9 (Me_2Sn, (340.1)), 33.9 (Me, (113.4), (86.1)), 67.3 (C-1, (494.6), (2.0)), 67.0 (C-1, (496.4), (2.4)), 71.44 (C-3,4, (40.2)), 71.38 (C-3,4, (40.2)), 75.0 (C-2,5, (51.2)), 74.9 (C-2,5, (50.1)), 144.1 (HC=C, (556.9), (73.0)), 163.4 (HC=*C*-CH_3, (544.8), (34.8)); ^{119}Sn NMR (C_6D_6, 93.3 MHz, ($J(^{119}Sn^{117}Sn)$): $\delta = -73.1$ ((349.2)), -61.5 ((349.2)).

4b′: EI MS: *m/z* (%) 524 (100) [M^+]. ^{1}H NMR (C_6D_6, 250 MHz, ($J(^{119}Sn^1H)$): $\delta = 0.31$ (s, 6H, Me_2Sn, (53.5)), 0.29 (s, 6H, Me_2Sn, (54.2)), 2.30 (s, br., 2H, CH_2, (70.9)), 4.06 (m, 4H, 2,5-H), 4.26 (m, 4H, 3,4-H), 5.08 (d, 1H, HC=C, (80.1), (27.3), $^2J(^1H^1H) = 2.3$), 5.66 (dt, 1H, HC=C, (166.4),(25.9), $^2J(^1H^1H) = 2.3$); ^{13}C NMR (C_6D_6, 62.9 MHz, ($J(^{119}Sn^{13}C)$): $\delta = -9.1$ (Me_2Sn, (362.9)), -9.2 (Me_2Sn, (347.4)), 25.2 (CH_2, (324.6), (55.6)), 67.8 (C-1, (471.4)), 67.1 (C-1, (484.3)), 71.29 (C-3,4, (40.2)), 71.20 (C-3,4, (40.2)), 74.7 (C-2,5, (53.4)), 74.6 (C-2,5, (51.2)), 120.7 (C=CH_2, (49.0), (40.2)), 152.7 (*C*=CH_2, (518.8), (54.5)); ^{119}Sn NMR (C_6D_6, 93.3 MHz, ($J(^{119}Sn^{117}Sn)$): $\delta = -40.1$ ((96.9)), -17.9 ((96.9)).

All other compounds **4** were prepared in the analogous way.

Received: January 24, 1997 [Z10032IE]
German version: *Angew. Chem.* **1997**, *109*, 1545–1546

Keywords: alkynes · homogeneous catalysis · iron · metallocenophanes · sandwich complexes · tin

[1] a) E. J. Bulten, H. A. Budding, J. G. Noltes, *J. Organomet. Chem.* **1970**, *22*, C5–C6; b) E. J. Bulten, H. A. Budding, *ibid.* **1974**, *78*, 385–393; c) E. Piers, R. T. Skerlj, *J. Chem. Soc. Chem. Commun.* **1986**, 626–627.

[2] a) T. N. Mitchell, A. Amamria, H. Killing, D. Rutschow, *J. Organomet. Chem.* **1983**, *241*, C45–C47; b) H. Killing, T. N. Mitchell, *Organometallics* **1984**, *3*, 1917–1919; c) H. Killing, T. N. Mitchell, *ibid.* **1984**, *3*, 1318–1320; d) T. N. Mitchell, N. M. Dornseifer, A. Rahm, *J. High Pressure Res.* **1991**, *7*, 165; e) T. N. Mitchell, B. Kowall, *J. Organomet. Chem.* **1992**, *437*, 127–130; f) T. N. Mitchell, A. Amamria, H. Killing, D. Rutschow, *ibid.* **1986**, *304*, 257–265; g) T. N. Mitchell, U. Schneider, *ibid.* **1991**, *407*, 319–327; h) M. Niestroj, W. P. Neumann, T. N. Mitchell, *ibid.* **1996**, *519*, 45–68.

[3] M. Akhtar, H. C. Clark, *J. Organomet. Chem.* **1970**, *22*, 233-240.

[4] W. McFarlane, N. H. Rees, *J. Chem. Soc. Dalton. Trans.* **1990**, 3211–3214.

[5] M. Herberhold, U. Steffl, W. Milius, B. Wrackmeyer, *Angew. Chem.* **1996**, *108*, 1927–1928; *Angew. Chem. Int. Ed. Engl.* **1996**, *35*, 1803–1804.

[6] For example oxygen, sulfur, selenium, and tellurium insert into the Sn–Sn bond of **1** to give 1,3-distanna-2-chalcogena[3]ferrocenophanes: M. Herberhold, U. Steffl, W. Milius, B. Wrackmeyer, *J. Organomet. Chem.* **1997**, in press.

[7] a) M. Herberhold, "*Ferrocene Compounds containing Heteroelements*" in *Ferrocenes, Homogenous Catalysis, Organic Synthesis, Material Science* (Eds.: A. Togni, T. Hayashi), VCH Weinheim, **1995**, pp. 219–278; b) M. Herberhold, *Angew. Chem.* **1995**, *107*, 1985–1987, *Angew. Chem. Int. Ed. Engl.* **1995**, *34*, 1837–1840; c) I. Manners, *ibid.* **1996**, *108*, 1712–1731 and **1995**, *35*, 1602–1621.

[8] Crystal structure analysis of compound **3**: $C_{50}H_{50}FeP_2PtSn_2$, orange prism with dimensions $0.25 \times 0.20 \times 0.15$ mm^3; **3** crystallizes in the triclinic space group $P\bar{1}$ with the lattice parameters $a = 11.929(2)$, $b = 12.538(2)$, $c = 15.654(2)$ Å, $\alpha = 86.14(2)$, $\beta = 81.81(2)$, $\gamma = 74.85(2)°$, $Z = 2$; $\mu(Mo_{K\alpha}) = 3.981$ mm^{-1}. On a SIEMENS P4 diffractometer with $Mo_{K\alpha}$ radiation ($\lambda = 71.073$ pm, graphite monochromator) 14670 reflections were collected in the range $2° \leq 2\theta \leq 60°$ ($T = 296$ K). Solution and refinement (program SHELXTL PLUS) was done with 12944 independent and 10475 observed ($F_o \geq 2.0\sigma(F_o)$) reflections; the data were corrected empirically for absorption effects by using Ψ scans of 10 selected reflections (min./max. transmission factors: 0.3131/1.0000). All non-hydrogen atoms were refined anisotropically, the hydrogen atoms were located in calculated positions. The refinement of 506 parameters converged at R/wR values of 0.0571/0.0390 with $w^{-1} = \sigma^2(F_o)$; the max./min. residual electron density was 3.72/ -3.60 e Å^{-3}. Crystallographic data (excluding structure factors) for the structure reported in this paper have been deposited with the Cambridge Crystallographic Data Centre as supplementary publication no. CCDC-100122. Copies of the data can be obtained free of charge on application to The Director, CCDC, 12 Union Road, Cambridge CB2 1EZ, UK (fax: int. code +(1223) 336-033; e-mail: deposit@chemcrys.cam.ac.uk).

[9] J. Barrau, G. Rima, V. Cassana, J. Satgé, *Organometallics* **1995**, *14*, 5700–5703.

[10] H. Yamashita, T. Kobayashi, M. Tanaka, *Organometallics* **1992**, *11*, 2330–2333.

[11] a) G. Lesley, P. Nguyen, N. J. Taylor, T. B. Marder, A. J. Scott, W. Clegg, N. C. Norman, *Organometallics* **1996**, *15*, 5137–5154; b) T. Ishiyama, N. Matsuda, M. Murata, F. Ozawa, A. Suzuki, N. Miyaura, *ibid.* **1996**, *15*, 713–720.

[12] J. Sandström, *Dynamic NMR Spectroscopy*, Academic Press, New York, **1982**, pp. 96.

[13] a) We have prepared the known complex [$(Me_3Sn)_2Pt(PPh_3)_2$] which—in contrast to the literature [3]—possesses the *cis* configuration. Its dynamic behavior, not noted in ref. [3], is analogous to that of **3**. b) Similar dynamic behavior was reported for [$Ph_3Ge(Ph_3GeHg)Pt(PPh_3)_2$]; however, a transition state with a tetrahedrally surrounded platinum center was proposed: Yu. K. Grishin, V. A. Roznyatovsky, Yu. A. Ustynyuk, S. N. Titova, G. A. Domrachev, G. A. Razuvaev, *Polyhedron* **1983**, *2*, 895–899.

Synthesis, Structure, and Reactivity of $[Cp_2Ti(HBcat)(PMe_3)]$: A Monoborane σ Complex**

Clare N. Muhoro and John F. Hartwig*

Dedicated to Professor Walter Siebert on the occasion of his 60th birthday

Transition metal σ complexes contain an intermolecular coordination of an H–H, Si–H, or C–H bond to a transition metal center.[1–6] Dihydrogen and silane σ complexes have been isolated, but alkane σ complexes have only been detected in solution by isotopic-labeling and kinetic isotope effect measurements.[7] Until our recent report of a bis(borane) σ complex,[8] there was no direct structural information on any X–H σ complexes (X is a first-row element such as B, C, N, or O). Species with intramolecular C–H bond coordination, frequently called "agostic" complexes, have been the best models. We now report the synthesis, characterization, and reactivity of $[Cp_2Ti(PMe_3)(HBR_2)]$, a set of remarkably simple monoborane σ complexes that demonstrate the stability of borane σ complexes in the absence of any potential B–B interaction that may have stabilized the bis(borane) complex.[8]

The reaction of $[Cp_2Ti(PMe_3)_2]$ and $[Cp_2Ti(HBcat)_2]$ at 0 °C in toluene [Eq. (a)] generated a maroon solution containing

$$[Cp_2Ti(PMe_3)_2] + [Cp_2Ti(HBcat)_2] \xrightarrow[0°C,\ 1.5h]{C_7H_8} \underset{\mathbf{1}}{2\,[Cp_2Ti(HBcat)(PMe_3)]} \qquad (a)$$

$[Cp_2Ti(PMe_3)(HBcat)]$(**1**) in 75% yield (^{1}H NMR spectroscopy with an internal standard). Cooling the solution of **1** in toluene to -30 °C led to the precipitation of **1** in 47% yield as spectroscopically pure material, which was further purified by recrystallization from toluene. Complex **1** was stable as a solid under

[*] Prof. J. F. Hartwig, C. N. Muhoro
Department of Chemistry
Yale University
P. O. Box 208107, New Haven CT 06520-8107 (USA)
Fax: Int. code +(203)432-6144
e-mail: john.hartwig@yale.edu

[**] We are grateful for support from the National Science Foundation NYI Award program, the donors of the Petroleum Research Fund (administered by the American Chemical Society), the Dreyfus Foundation with a New Faculty and Camille Dreyfus Teacher–Scholar Award, DuPont with a Young Faculty Award, Union Carbide with an Innovative Recognition Award, and Yale University with a Junior Faculty Fellowship. J. F. H. is a fellow of the Alfred P. Sloan Foundation.

inert conditions at room temperature for several hours, but decomposed slowly over this time period in solution.

$[Cp_2Ti(PMe_3)(HBcat)]$ was characterized by detailed NMR studies to determine the bonding mode of the borane. Three possible structures are shown in Scheme 1. The ^{11}B NMR spectrum of **1** contained a signal at $\delta = 64.2$, which is outside of the region for borane Lewis acid–base complexes. The $^{31}P\{^1H\}$ NMR spectrum showed a singlet at $\delta = 29.3$, and the ^1H NMR spectrum a broad peak at $\delta = -9.8$, which is assigned to the borane hydrogen atom and confirmed by deuterium labeling. Typically, *cis*-boryl hydride complexes such as $[Cp_2W(H)(Bcat)]$[9] display sharp hydride signals with no broadening due to nuclear interactions through the metal center. Furthermore, hydrides of d^0-titanium complexes resonate at far lower field than that of **1**. The signal for the hydride in $[Cp^*_2TiH_2]$ appears at $\delta = 0.28$[10, 11] and that of $[(tBu_3OSi)_2(tBu_3SiNH)TiH]$ at $\delta = 8.62$.[12] A doublet at $\delta = 5.02$ ($J(H,P) = 3.0$ Hz) was observed for the Cp ligands of **1**. A single broad band at 1650 cm^{-1} was found in the IR spectrum of **1** between two bands observed previously for $[Cp_2Ti(HBcat)_2]$. The deuterated analog $[D_1]$-**1** showed no signal in this region and displayed a band at the appropriate value of 1184 cm^{-1}.

Scheme 1. Three potential structures for **1**.

Decoupling experiments revealed the connectivity of **1**. A sharp signal at $\delta = -9.8$ appeared in the $^1H\{^{11}B\}$ NMR spectrum. This contrasted the broad signal for the hydride resonance and demonstrated the presence of a B–H interaction. A sharp singlet for the cyclopentadienyl ligands was observed in the $^1H\{^{31}P\}$ NMR spectrum of **1**, demonstrating that the Cp doublet in the coupled ^1H NMR spectrum was due to phosphorus coupling as a result of PMe_3 coordination to titanium. The ^{11}B NMR chemical shift and the decoupling data are clearly inconsistent with structure **A**. In this case, structures **B** and **C** are distinguishable by the hydride chemical shift and the effect of ^{11}B decoupling on the line shape of the hydride signal. The difference in line shape between the ^1H and $^1H\{^{11}B\}$ NMR spectra demonstrates the presence of a B–H interaction, and the high-field chemical shift indicates Ti^{II} rather than Ti^{IV}.[13] The most appropriate structural description of **1** is therefore **C**.

An X-ray structure of the fluoro derivative **2** was obtained (Figure 1).[10] It is informative to make comparisons between the structure of this compound and that of $[Cp_2Ti(HBcat)_2]$ (**3**).[8] The Ti–B bond length in **2** (2.267(6) Å) is slightly shorter than that in **3** (2.335(5) Å), but is too long for a metallocene–boryl complex. The Ti–B distance in **2** is about 0.1 Å longer than the W–B distance in $[Cp_2W(BR_2)]$ complexes, despite the fact that W is 0.1 Å larger in size, and is similar to the M–B distances in Cp_2Nb and Cp_2Ta complexes, despite the fact that the Cp_2M covalent radii are 0.1 Å greater.[9, 13–21] The B–H bond length in **2** (1.35(5) Å) is longer than that in **3** (1.25(3) Å), although the difference is close to the estimated standard deviations. The Ti–H bond in **2** (1.61(5) Å) is shorter than in **3** (1.74(4) Å); again the difference may not be significant. The B-Ti-H angle in **2** is only 36(2)° and similar to the 33(1)° angle in **3**, consistent with B–H bonding in both complexes. The H-Ti-Si angle in the related $[Cp_2Ti(H_2SiPh_2)(PMe_3)]$ is 44(2)°.[22] The trends in bond length can be explained by the greater electron density on the phosphane-containing **2** than on the bis(borane) complex **3**, and perhaps by the slightly greater electrophilicity of the monofluoroborane in **2**. As a result of the increased electron density at Ti, **2** appears to be more of a full oxidative addition product than **3**. However, the decoupling data, the hydride chemical shift, the long Ti–B distance, and the small H-Ti-B angle strongly suggest that the borane has not undergone full oxidative addition in **2**.

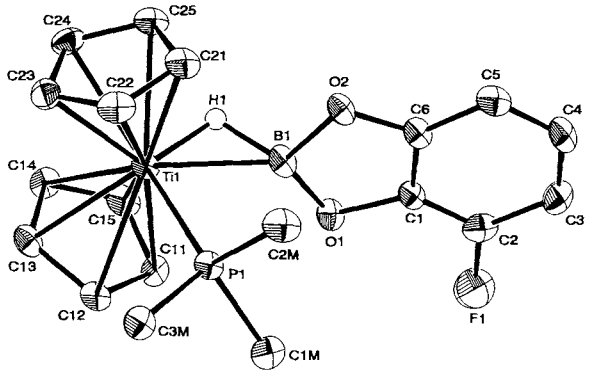

Figure 1. ORTEP drawing of **2**. Selected bond lengths [Å] and angles [°]: Ti–B 2.267(6), Ti–H 1.61(5), B–H 1.35(5), Ti–P2.522(2); B-Ti-P 74.64(14), B-Ti-H 36(2), Ti-B-H 44(2).

The chemistry of **1** was characterized by ligand-substitution reactions and addition of catecholborane across multiple bonds (Scheme 2). Reaction of triethylamine with **1** under a nitrogen atmosphere led to the displacement of catecholborane and formation of the corresponding Lewis acid–base adduct (87%) along with the titanocene dinitrogen complex $[Cp_2Ti(PMe_3)N_2]$ (23.6%).[23] Exposure of **1** to CO (2 atm) produced $[Cp_2Ti(CO)_2]$ (88%) and free catecholborane (64%). Compound **1** rapidly hydroborated *N*-methylbenzylidineamine in quantitative yield at room temperature and, furthermore, diphenylacetylene to form the vinyl boronate ester in 61% yield. In both reactions the titanium products appear to be paramagnetic and have not yet been identified.

Scheme 2. Reactivity of **1**.

Compound **1** underwent the borane and phosphane displacement reactions shown in Scheme 3: 1) [D_9]Trimethylphosphane reacted with **1** to generate a mixture of **1** and its deuterated analog [$Cp_2Ti(HBcat)\{P(CD_3)_3\}$]. 2) Addition of 3-fluorocatecholborane to **1** produced a mixture of **2** and **1**. 3) *B*-Deuteriocatecholborane reacted with **1** to form a mixture of **1** and

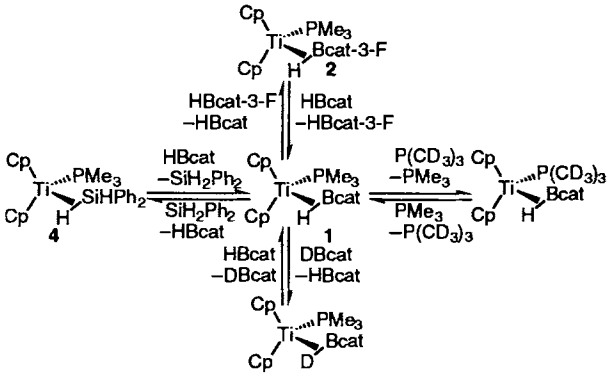

Scheme 3. Ligand-displacement equilibria for **1**.

[D_1]-**1**. 4) A similar exchange with diphenylsilane allowed comparison of the stability of **1** with that of a related titanium complex. Compound **1** reacted with diphenylsilane to form small amounts of the known [$Cp_2Ti(H_2SiPh_2)(PMe_3)$] (**4**).[22] In the reverse reaction **4** reacted with catecholborane to form **1** as the dominant species and to leave small amounts of unchanged **4**. There is clearly an equilibrium between **1** + silane and **4** + borane. This equilibrium favors the formation of **1**, but has not been measured quantitatively.

A previous theoretical study of **3** showed an important backbonding interaction from the metal into the borane p orbital, which is the LUMO.[8] A similar interaction may exist in **1**. The catecholborane LUMO is clearly different from the C–H σ^* LUMO of an alkane, but its symmetry is similar to that of an arene LUMO. It is therefore possible that arene σ complexes have structures resembling **1**. Further theoretical and experimental studies on these unusual borane σ complexes are required to better understand their structures and reactivity.

Experimental Section

1: [$Cp_2Ti(PMe_3)_2$] (395 mg, 1.20 mmol) and [$Cp_2Ti(HBcat)_2$] (500 mg, 1.20 mmol) were weighed into a sidearm flask, which was then cooled to $-30\,^{\circ}C$ and charged with cold toluene (3 mL). This solution was stirred for 90 min at $0\,^{\circ}C$. The resulting dark maroon solution was then kept at $-30\,^{\circ}C$ for 2 d, after which a dark pink solid precipitated from solution. The dark maroon supernatant was removed, and the solid dried in vacuo (46.4% yield). Further purification was achieved by recrystallization from highly concentrated solutions of **1** in toluene at $-30\,^{\circ}C$. ^1H NMR (300 MHz, [D_6]benzene, $20\,^{\circ}C$, TMS): $\delta = 7.09$ (m, 2H, CH), 6.79 (m, 2H, CH), 5.02 (d, $J(H,P) = 3.0$ Hz, Cp), 0.75 (d, $J(H,P) = 6.3$ Hz, CH_3), -9.8 (br. s, 1H, BH); ^{11}B NMR (96.38 MHz, [D_8]toluene, $20\,^{\circ}C$, $BF_3 \cdot OEt_2$): $\delta = 64.2$. $^{31}P\{^1H\}$ NMR (121.65 MHz, [D_8]toluene, $20\,^{\circ}C$, 85% H_3PO_4): $\delta = 29.3$; $^{13}C\{^1H\}$ NMR (75.48 MHz, [D_8]toluene, $-5\,^{\circ}C$, TMS) $\delta = 153.09, 120.69, 110.10, 96.69, 20.39$; IR (Nujol): $\tilde{\nu}_{BH} = 1650\ cm^{-1}$.

Received: February 4, 1997 [Z10073IE]
German version: *Angew. Chem.* **1997**, *109*, 1536–1538

Keywords: boron · coordination modes · σ complexes · titanium

[1] D. M. Heinekey, W. J. Oldham, *Chem. Rev.* **1993**, *93*, 913–926.
[2] R. H. Crabtree, *Angew. Chem.* **1993**, *105*, 828–845; *Angew. Chem. Int. Ed. Engl.* **1993**, *32*, 789–805.
[3] U. Schubert, *Adv. Organomet. Chem.* **1990**, *30*, 151–187.
[4] J. H. Morris, P. G. Jessop, *Coord. Chem. Rev.* **1992**, *121*, 155–289.
[5] M. Brookhart, M. L. H. Green, *J. Organomet. Chem.* **1983**, *250*, 395–408.
[6] R. M. Bullock in *Transition Metal Hydrides* (Ed.: A. Dedieu), VCH, New York, **1992**, pp. 263–307.
[7] C. Hall, R. N. Perutz, *Chem. Rev.* **1996**, *96*, 3125–3146; see also J. J. Schneider, *Angew. Chem.* **1996**, *108*, 1132–1139; *Angew. Chem. Int. Ed. Engl.* **1996**, *35*, 1068–1076.
[8] J. F. Hartwig, C. N. Muhoro, X. He, O. Eisenstein, R. Bosque, F. Maseras, *J. Am. Chem. Soc.* **1996**, *118*, 10936–10937.
[9] J. F. Hartwig, S. R. DeGala, *J. Am. Chem. Soc.* **1994**, *116*, 3661–3662.
[10] Crystal data for **2** ($T = 153$ K, $Mo_{K\alpha}$ rays, $\lambda = 0.71073$ Å): triclinic, $P\bar{1}$, $Z = 2$, $V = 918.91(2)$ Å^3, $\rho_{calcd} = 1.417\ g\,cm^{-3}$, $2\theta_{max} = 45°$, scan width of 0.3° in ω, of 3724 reflections 2329 were independent, $I > 2\sigma(I)$, 256 parameters, residual electron density $= 1.059\ e\,Å^{-3}$. Data corrected for Lorentzian-polarization and absorption factors (SADABS program, $\mu \times r = 0.10$, 0.564 (min) and 0.928 (max)). The structure was solved and refined with the Siemens SHELXTL (version 5.0) Software Package. Final anisotropic full-matrix least-squares refinement on F^2 converged at $R1 = 0.0638$, $wR2 = 0.1631$, and GOF = 1.024. The hydrogen atoms were located and refined isotropically. Crystallographic data (excluding structure factors) for the structure reported in this paper have been deposited with the Cambridge Crystallographic Data Centre as supplementary publication no. CCDC-100125. Copies of the data can be obtained free of charge on application to The Director, CCDC, 12 Union Road, Cambridge CB21EZ, UK (fax: int. code +(1223)336-033; e-mail: deposit@chemcrys.cam.ac.uk).
[11] J. E. Bercaw, R. H. Marvich, L. G. Bell, H. H. Brintzinger, *J. Am. Chem. Soc.* **1972**, *94*, 1219–1238.
[12] J. L. Bennett, P. T. Wolczanski, *J. Am. Chem. Soc.* **1994**, *116*, 2179–2180.
[13] D. R. Lantero, D. H. Motry, D. L. Ward, M. R. Smith, *J. Am. Chem. Soc.* **1994**, *116*, 10811–10812.
[14] J. F. Hartwig, X. He, *Angew Chem*, **1996**, *108*, 352–354; *Angew. Chem. Int. Ed. Engl.* **1996**, *35*, 315–317.
[15] The M–X bond length in [Cp^*_2TiCl] (2.363 Å) is shorter than that in [$Cp^*_2NbCl_2$] and [$Cp^*_2TaCl_2$] (2.439–2.483 Å). Despite the smaller size of Ti, the Ti–B bond length in **2** (2.267 Å) is comparable to that of tungstenocene–(2.23 Å), tantalocene–(2.263 Å), and niobocene–boryl complexes (2.295 Å), which demonstrates partial Ti–B bonding in **2** (see also Figure 1).
[16] F. M. Miao, K. Prout, *Cryst. Struct. Commun.* **1982**, *11*, 269–272.
[17] K. Prout, T. S. Cameron, R. A. Forder, S. R. Critchley, B. Denton, G. V. Rees, *Acta Crystallogr. Sect. B* **1974**, *30*, 2290–2304.
[18] H. Brunner, G. Gehart, W. Meier, J. Wachter, A. Riedel, S. Elkrami, Y. Mugnier, B. Nuber, *Organometallics* **1994**, *13*, 134–140.
[19] A. McCamley, T. J. Miller, *Acta Crystallogr. Sect C* **1994**, *50*, 33–36.
[20] L. Labella, A. Chernega, M. L. H. Green, *J. Organomet. Chem.* **1995**, *485*, C18–C21.
[21] J. W. Pattiasina, H. J. Heeres, F. van Bolhuis, A. Meetsma, J. H. Teuben, A. L. Spek, *Organometallics* **1987**, *6*, 1004–1010.
[22] E. Spaltenstein, P. Palma, K. A. Kreutzer, C. A. Willoughby, W. M. Davis, S. L. Buchwald, *J. Am. Chem. Soc.* **1994**, *116*, 10308–10309.
[23] D. H. Berry, L. J. Procopio, P. J. Carroll, *Organometallics* **1988**, *7*, 570–572.
[24] J. P. Collman, L. S. Hegedus, J. R. Norton, R. G. Finke, *Principles and Applications of Organotransition Metal Chemistry*, 1st ed., University Science Books, Mill Valley, CA, USA **1987**, pp. 300–305.

cyclo-Sb_5^{5-}: A New, Highly Charged Zintl Anion, Stabilized as an Ion Complex in the Ammoniate $[Li(NH_3)_4]_3[Li_2(NH_3)_2Sb_5] \cdot 2NH_3$

Nikolaus Korber* and Frank Richter

Dedicated to Professor Hans Georg von Schnering

There are two generally adopted approaches towards the isolation of the homoatomic polyanions of groups 14 to 16 known as Zintl anions.[1] They are obtained either by excision of preformed structural units from congruently dissolving solids (e.g. As_{11}^{3-} [2] from K_3As_{11} or Rb_3As_{11}) and by extraction of alloys (e.g. Sn_9^{4-} [3] from $NaSn_{2.5}$), or by direct reaction of an electropositive metal with the main group metal in a suitable solvent. In the past, the constitution and properties of many Zintl

[*] Dr. N. Korber, Dipl.-Chem. F. Richter
Institut für Anorganische Chemie der Universität
Gerhard-Domagk-Strasse 1, D-53121 Bonn (Germany)
Fax: Int. code +(228)735660
e-mail: korber@plumbum.chemie.uni-bonn.de

anions could be elucidated, especially by Corbett, by complexing the alkali metal counterions with cryptands and thus stabilizing the isolated polyanions in the corresponding salts.[4] However, the second method is the original one which dates back to Zintl and co-workers, who monitored the reduction of metals with sodium in liquid NH_3 by using potentiometric titrations, and gained indications of the polyanions which were subsequently named after him.[5] The characterization of salts like $[Na(NH_3)_n^+]_3Sb_7^{3-}$, which could be crystallized from these solutions, proved to be impossible with the techniques then available due to the high NH_3-decomposition pressure of these compounds. Probably for this reason, in later investigations of Zintl anions the solvent NH_3, which is the most suitable one for the direct reduction, was avoided, and ethylenediamine, in particular, was used instead, which automatically favored the excision and extraction routes. It is not clear though, whether the results thus obtained can be used to account for the observations made by Zintl and co-workers in every case; the alternative use of the chelating solvent ethylenediamine as well as the application of cryptands constitute major interferences with the systems investigated. In addition, several of the anions listed by Zintl et al. such as Sb_3^{3-} have still not been observed.[4, 5]

The methods available nowadays for performing X-ray structure analysis at low temperature allow the characterization even of very unstable ammoniates;[6] thus, it appeared appropriate to investigate the structures of the products formed by the direct reaction route. As a first example, the reactions of lithium with amorphous red phosphorus, arsenic, and antimony were chosen. The special advantage of lithium, in this context, is the relative stability of the ammine complex $[Li(NH_3)_4]^+$ (as compared to the very unstable ammine complexes of the remaining alkali metals), which is isoelectronic to the tetramethylammonium ion often used for isolating large anions.[7] In fact, the solution of lithium in liquid ammonia may be better interpreted as a solution of the "expanded metal" $Li(NH_3)_4$,[8] which forms the respective voluminous cation by oxidation, and which thus represents a simple analogy to the unknown "$N(CH_3)_4$".

The reaction of lithium with excess red phosphorus in liquid ammonia yields the compound $[Li(NH_3)_4]_4P_{14}$,[9] which contains the P_{14}^{4-} ion already synthesized by Hönle et al. by a different route.[10] The analogous reaction for arsenic yields $[Li(NH_3)_4]_3As_7 \cdot NH_3$,[11] which contains the known nortricyclane cage As_7^{3-} ion.[12] Both products form exclusively if the appropriate molar ratio is applied.

In contrast, the reaction of lithium with antimony gave a surprising result: even when high excesses of antimony are used, the product formed only contained an Li:Sb ratio of 1:1. The X-ray structure analysis[13] established the composition $Li_5Sb_5 \cdot 16\,NH_3$ for the dark red crystals, which form quantitatively if the corresponding stoichiometry is used. A better formulation, which reflects the different structural roles of the ammonia molecules, is $[Li(NH_3)_4]_3[Li_2(NH_3)_2Sb_5] \cdot 2\,NH_3$ (**1**). The main building blocks are $[Li_2(NH_3)_2Sb_5]^{3-}$ ion complexes (Figure 1), which are separated in the solid by $[Li(NH_3)_4]^+$ complexes that serve as counterion and by additional ammonia of crystallization (Figure 2). The ion complex consists of a novel *cyclo*-Sb_5^{5-} ion in an envelope conformation, which is capped by lithium cations on both sides of the ring. Each of the two lithium cations has three close contacts to antimony ($\bar{d}$(Li–Sb) = 2.82 Å); a roughly tetrahedral environment for these cations is achieved by two additionally bound ammonia molecules. This special coordination of the Sb_5 ring makes it possible to study the influence of the cations on the Sb–Sb bonds: the bonds between Sb(2), which is coordinated by two lithium cations, and its homoatomic neighbors are significantly longer (2.875 and 2.910 Å) than the mean length of the remaining Sb–Sb bonds (2.820 Å). This result agrees with the previously found bond-lengthening in polyphosphides caused by interactions with capping alkali metal cations.[14]

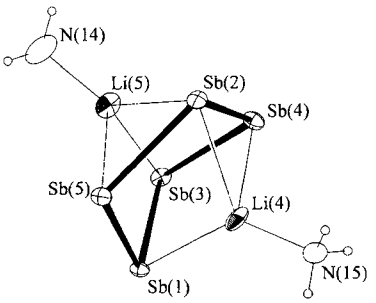

Figure 1. $[Li_2(NH_3)_2Sb_5]^{3-}$ in the crystal structure of **1** (ORTEP, 50% probability). Selected bond lengths [Å] and angles [°]: Sb(1)–Sb(5) 2.8059(10), Sb(1)–Sb(3) 2.8318(9), Sb(2)–Sb(4) 2.8751(12), Sb(2)–Sb(5) 2.9103(10), Sb(3)–Sb(4) 2.8212(12), Sb(1)–Li(4) 2.77(2), Sb(2)–Li(5) 2.80(2), Sb(2)–Li(4) 2.84(2), Sb(3)–Li(5) 2.84(2), Sb(4)–Li(4) 2.83(2), Sb(4)–Li(5) 3.28(2), Sb(5)–Li(5) 2.84(2), Sb(5)–Li(4) 3.05(2), N(14)–Li(5) 1.99(2), N(15)–Li(4) 2.02(2); Sb(5)-Sb(1)-Sb(3) 96.52(3), Sb(4)-Sb(2)-Sb(5) 101.41(3), Sb(4)-Sb(3)-Sb(1) 95.55(3), Sb(3)-Sb(4)-Sb(2) 101.97(3), Sb(1)-Sb(5)-Sb(2) 103.35(3)

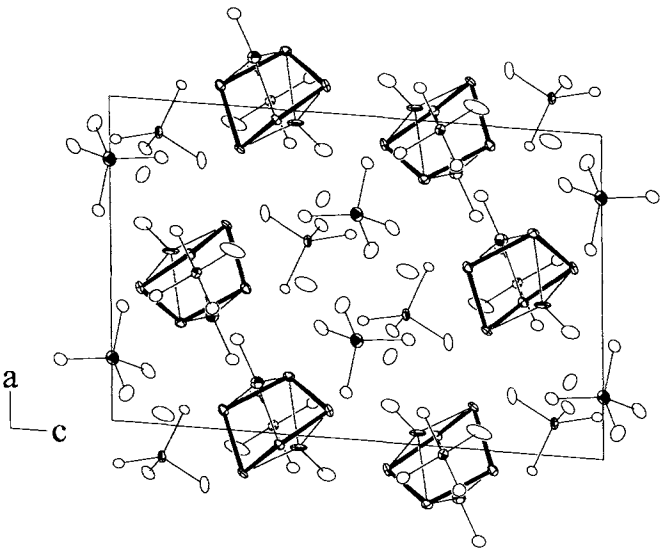

Figure 2. Projection of a unit cell of **1** in the direction [010] (ORTEP, 50% probability, designation of atom type analogous to that in Figure 1).

The dual structural role of the lithium cations in **1** demonstrates the advantages of the direct reduction with lithium in liquid ammonia for the isolation of Zintl anions: the cation coordinates directly to the highly charged anion and reduces its charge density to a value compatible with a ionic solid of this kind, and it also serves as a voluminous, noncoordinating counterion in the ammine complex $[Li(NH_3)_4]^+$, which separates the Zintl anions from each other. A cryptand fitting for lithium cations would remove the cations of the ion complex as well; a compound built from totally isolated Sb_5^{5-} and five cryptand counterions, however, would not result in a stable solid judging from past experiences. Consequently, up to now only Sb_{11}^{3-},[15] Sb_7^{3-},[16] and Sb_4^{2-}[16] were known as homoatomic antimony anions, obtained with the help of cryptands, all of which have a significantly lower charge density than Sb_5^{5-}. Group 15 cycloanions with one negative charge per atom are extremely rare, in contrast to the corresponding chains (e.g. in M^ISb, M^I = Na–Cs[17]). The most convincing example is *cyclo*-P_6^{6-} in

 © VCH Verlagsgesellschaft mbH, D-69451 Weinheim, 1997 0570-0833/97/3613-1513 $ 17.50+.50/0

Th_7P_{11},[18] while the sometimes mentioned rings Sb_4^{4-} and Bi_4^{4-} (both planar!) in $Ca_{11}Sb_{10}$ and $Ca_{11}Bi_{10}$,[19] respectively, as well as P_6^{6-} in InP_3[20] are all very much borderline cases with respect to the Zintl–Klemm–Busmann concept. More common are the respective homoatomic rings in transition metal complexes like $[Cp^*Fe(P_5)Ir_2(Co)(Cp^*)_2]$ (*cyclo*-P_5 in envelope conformation)[21] or in organo-substituted molecules like $[As(CH_3)]_5$.[22] The probably most impressive analogy to Sb_5^{5-} is found in the up to now totally singular anion $[As_8Nb]^{3-}$, which was prepared by von Schnering et al.[23] This anion contains a crown-shaped As_8^{8-} ring, the high formal charge of which is reduced by an encapsulated niobium ion.

In summary, our return to the original method of creating Zintl anions demonstrates with this first result that the possible structural diversity of homoatomic polyanions of group 15 is still not fully explored. In particular, highly charged anions, which cannot be isolated with the previously used methods, may now be obtained by the direct reduction in liquid ammonia as ion complexes and immediately characterized as ammoniates. Perhaps this approach will even be applicable for Sb_3^{3-}, which was detected by Zintl et al. in the Na-Sb-NH_3 system.[5]

Experimental Section

All manipulations were carried out under dry argon in all-glass vessels that were dried in vacuo. A piece of Li (0.011 g, 1.60 mmol; scraped off a larger block in the glove-box; Alfa), and Sb (0.195 g, 1.60 mmol; Aldrich, 99.8%), which had been dried in vacuo for three days, were placed in a Schlenk tube. NH_3 (ca. 20 mL), which had been stored over Na, was condensed into the Schlenk tube using an ethanol bath at $-78\,^{\circ}C$. The mixture was kept at $-40\,^{\circ}C$ for 10 days. The color of the solution changed from blue to deep red after one day; red crystals of **1** precipitated directly from the solution and were mounted for the X-ray structure analysis as described previously [6]. After the removal of NH_3, an X-ray amorphous, homogeneous black product of the composition LiSb remained, which retained the shape of the original crystalline ammoniate.

Received: February 7, 1997 [Z10084IE]
German version: *Angew. Chem.* **1997**, *109*, 1575–1577

Keywords: antimony · structure elucidation · Zintl anions

[1] J. D. Corbett, D. G. Adolphson, D. J. Merryman, P. A. Edwards, F. J. Armatis, *J. Am. Chem. Soc.* **1975**, *97*, 6267.
[2] a) C. H. E. Belin, *J. Am. Chem. Soc.* **1980**, *102*, 6036; b) J. Wolf, Dissertation, Universität Stuttgart, **1986**.
[3] a) D. Kummer, L. Diehl, *Angew. Chem.* **1970**, *82*, 881; *Angew. Chem. Int. Ed. Engl.* **1970**, *9*, 895; b) L. Diehl, K. Khodadedeh, D. Kummer, J. Strähle, *Chem. Ber.* **1976**, *109*, 3404.
[4] J. D. Corbett, *Chem. Rev.* **1985**, *85*, 383.
[5] a) E. Zintl, J. Goubeau, W. Dullenkopf, *Z. phys. Chem. Abt. A* **1931**, *154*, 1; b) E. Zintl, W. Dullenkopf, *Z. phys. Chem. Abt. B* **1932**, *16*, 183.
[6] a) N. Korber, J. Daniels, *J. Chem. Soc. Dalton Trans.* **1996**, 1653; b) *Polyhedron* **1996**, *15*, 2681; c) *Acta Crystallogr. Sect. C* **1996**, *52*, 2454; d) *Z. Anorg. Allg. Chem.* **1996**, *622*, 1833; e) *Helv. Chim. Acta* **1996**, *79*, 2083.
[7] N. Korber, F. Richter, *Chem. Commun.* **1996**, 2023.
[8] V. G. Young, W. S. Glaunsinger, *J. Am. Chem. Soc.* **1989**, *111*, 9260.
[9] N. Korber, F. Richter, unpublished results.
[10] W. Hönle, V. Manriquez, C. Mujica, D. Weber, H.-G. von Schnering, 29. IUPAC Congress, Köln, **1983**, Abstracts of Papers, p. 36.
[11] N. Korber, M. Grothe, unpublished results.
[12] W. Schmettow, H. G. von Schnering, *Angew. Chem.* **1977**, *89*, 895; *Angew. Chem. Int. Ed. Engl.* **1977**, *16*, 857.
[13] Crystal data and structure refinement for compound **1**: $H_{48}Li_5N_{16}Sb_5$, monoclinic, space group $P2_1/n$, $a = 12.618(5)$, $b = 13.143(3)$, $c = 19.166(6)$ Å, $\beta = 95.14(2)^{\circ}$, $V = 3166(1)$ Å^3, $\rho_{calcd} = 1.922$ g cm^{-3}, $\mu(Mo_{K\alpha}) = 4.23$ cm^{-1}, $Z = 4$. Enraf-Nonius CAD4 diffractometer with graphite-monochromated $Mo_{K\alpha}$ radiation, $\lambda = 0.71073$ Å, $T = -150\,^{\circ}C$, $\omega/2\theta$ scans, 5685 reflections measured ($1.9 < \theta < 5.0$), 5417 independent reflections, 5138 observed with $I_o > 2\sigma(I_o)$. Empirical absorption correction using Ψ scans. Structure solution by direct methods (SHELXS86), refinement on F^2 (SHELXL93), hydrogen atoms isotropic and in a riding model (with the exception of the hydrogen atoms bonded to NH_3 molecules not coordinating to Li, which were fully refined), 273 parameters, the refinment converged at $wR_2 = 0.144$ (all independent reflections), which corresponds to a conventional $R = 0.049$ using only reflections with $I_o > 2\sigma(I_o)$. Largest peak in the final difference Fourier map at 1.78 e Å^{-3} in the vicinity of Sb. Further details of the crystal structure investigation may be obtained from the Fachinformationszentrum Karlsruhe, D-76344 Eggenstein-Leopoldshafen (Germany), on quoting the depository number CSD-406510.
[14] N. Korber, H. G. von Schnering, *Chem. Ber.* **1996**, *129*, 155.
[15] U. Bolle, W. Tremel, *J. Chem. Soc. Chem. Commun.* **1992**, 91.
[16] S. C. Critchlow, J. D. Corbett, *Inorg. Chem.* **1984**, *23*, 770.
[17] a) D. T. Cromer, *Acta Crystallogr.* **1959**, *12*, 41; b) W. Hönle, H. G. von Schnering, *Z. Kristallogr.* **1981**, *155*, 307; c) H.-G. von Schnering, W. Hönle, G. Krogull, *Z. Naturforsch. B* **1979**, *34*, 1678.
[18] H.-G. von Schnering, M. Wittmann, R. Nesper, *J. Less-Common Met.* **1980**, *76*, 213.
[19] K. Deller, B. Eisenmann, *Z. Naturforsch. B* **1976**, *31*, 29.
[20] N. Kinomura, K. Terao, S. Kikkawa, H. Horiuchi, M. Koizumi, *Mater. Res. Bull.* **1983**, *18*, 53.
[21] M. Detzel, T. Mohr, O. J. Scherer, G. Wolmershäuser, *Angew. Chem.* **1994**, *106*, 1142; *Angew. Chem. Int. Ed. Engl.* **1994**, *33*, 1110.
[22] J. H. Burns, J. Waser, *J. Am. Chem. Soc.* **1957**, *79*, 859.
[23] a) H. G. von Schnering, J. Wolf, D. Weber, R. Ramirez, T. Meyer, *Angew. Chem.* **1986**, *98*, 372; *Angew. Chem. Int. Ed. Engl.* **1986**, *25*, 353; b) D. M. P. Mingos, S. Weisberger, S. Heeb, *New J. Chem.* **1993**, *17*, 531.

Probing Nanocavities with Proton-Transfer Fluorescence**

Abderrazzak Douhal,* Francisco Amat-Guerri, and A. Ulises Acuña*

The ability of cyclodextrins (CD) to encapsulate functional compounds such as emitting dyes has led to intensive studies of their inclusion complexes.[1–7] In these species proton transfer,[8, 9] energy transfer,[4, 5] and bond rotation[10] can give rise to new molecular forms of the sequestered dye with different physicochemical properties. Here we describe the light-induced tautomerism of a fluorophore encapsulated by α-, β-, or γ-CD, for which both proton transfer and conformational changes cause spectral shifts that are directly related to the size of the CD cavity. The color change of the fluorescence provides a simple way of exploring and quantifying subtle details of the induced fit and cavity diameter.

The guest 2-(2′-hydroxyphenyl)imidazo[1,2-*a*]pyridine (HPIP) is a heterocyclic dye with two groups able for forming an intramolecular hydrogen bond (**1**, Scheme 1). UV irradiation of **1** in solvents with which it does not interact induces an electronic reorganization in the excited state that provides the driving force for the shift of the proton involved in the hydrogen bond.[11] The resulting phototautomer fluorescences around 600 nm;[11] the band appears at 535 nm in a solid matrix (a thin film of poly(methyl methacrylate) (PMMA)). The fluorescence in the solid phase is due to **2**, the photoproduct of the proton-transfer reaction. In liquid media **2** gives rise to the red-emitting species **3**. In hydrogen-bonding media such as water, the spectral evidence favors solvated structures such as **4**, which emit in the near-UV region, because the intramolecular proton-transfer

[*] Prof. A. Douhal
Departamento de Química Física, Facultad de Químicas Sección de Toledo
Universidad de Castilla-La Mancha
San Lucas 3, E-45002 Toledo (Spain)
Fax: Int. code +(25)253-614
e-mail: adouhal@qui-to.uclm.es
Dr. A. U. Acuña
Instituto de Química Física Rocasolano, CSIC
Serrano 119, E-28006 Madrid (Spain)
Dr. F. Amat-Guerri
Instituto de Química Orgánica, CSIC, Madrid (Spain)

[**] This work was supported by the Dirección General de Investigación Cientifica y Tecnica of Spain (project no. PB93-0126).

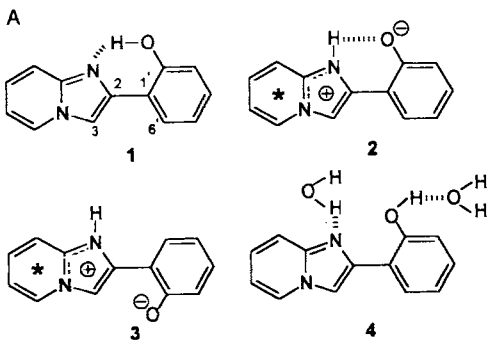

Scheme 1. A) Molecular structures of the different forms of HPIP; **2** and **3** are proton-transfer phototautomers of **1**. B) Structures of α-, β-, and γ-CD; *d* is the interior diameter.

photoreaction is prevented. The fluorescence of **4** (390 nm) and that of **3** (600 nm)[11] in liquid media, together with the weak solubility of HPIP in water and the hydrophobicity of the internal cavity of CDs, provide the experimental basis for monitoring the sequestration of the dye from water by CD and the subsequent processes.

Figure 1A shows the absorption spectra of HPIP in a nonpolar solvent (methylcyclohexane) and in water. We first investigated the influence of β-CD on the fluorescence spectrum of HPIP in water. An emission band at 550 nm grows upon addition of β-CD (Figure 1B), whereas the intensity of the fluorescence band at 390 nm decreases. The band at 550 nm can be easily understood by recalling the spectral behavior of HPIP in liquid and solid media. It is, accordingly, assigned to **2**, a proton-transfer phototautomer of **1** sequestered within the torus-shaped cavity of CD. To exclude other alternatives, such as nonencapsulating interactions, the effect of maltoheptose (MA) on the emission spectrum of HPIP in water was also analyzed. MA is a linear oligosaccharide with seven glucose units but without the characteristic conical shape of β-CD. Addition of MA (Figure 1C) only results in a slight broadening of the band at 390 nm; the yellow band observed in the presence of β-CD is indeed due to the entrapped dye. The emission band at 550 nm is very similar to that observed in dioxane,[11] and, therefore, the ground-state conformation of the entrapped dye should be close to **1**. The species emitting at 390 nm in the presence of β-CD should have a ground-state geometry similar to that of **4** according to the similarity between its excitation spectrum and the absorption spectrum of the dye in water.

A Benesi–Hildebrand (BH) plot[12] of the change in the fluorescence intensity at 550 nm as a function of β-CD concentration supports a 1:2 complex of the guest **1** with the cyclic sugar (apparent inclusion constant $K_a = 1.0 \times 10^5\ M^{-2}$; Figure 2A). This reflects the tendency of β-CD to form dimers[2, 3, 7] with a large hydrophobic cavity (Scheme 2). These complexes can be readily crystallized, and the fluorescence spectrum of the dried crystals consists of a single band at 550 nm, which is similar to that in the PMMA matrix (535 nm). Since the emission at

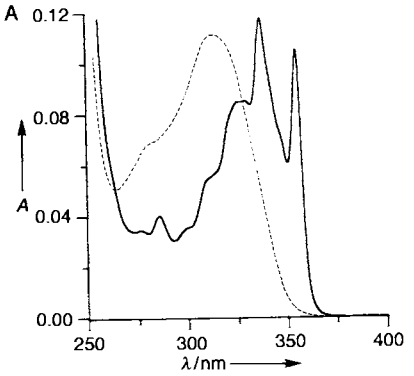

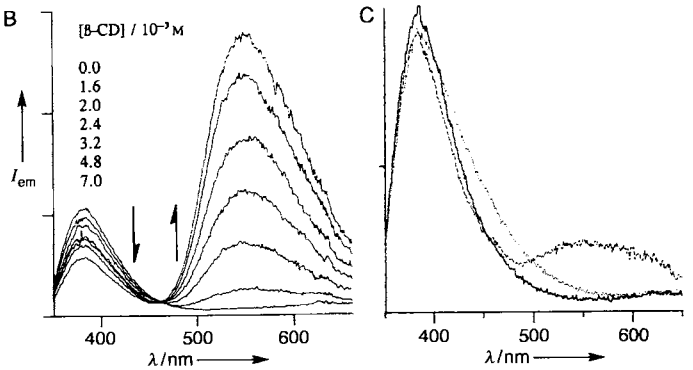

Figure 1. A) Normalized UV/Vis absorption spectra of HPIP in methylcyclohexane (solid line) and water (dashed line). *A* = absorbance. B) Fluorescence spectra (λ_{ex} = 340 nm) of HPIP (10^{-6} M) in water upon addition of β-CD. C) Fluorescence spectra (λ_{ex} = 340 nm, 300 K, pH(water) = 6.3) of HPIP in water (solid line), water plus β-CD (dashed line), and water plus maltoheptose (3×10^{-3} M; dotted line). I_{em} = intensity of the emission.

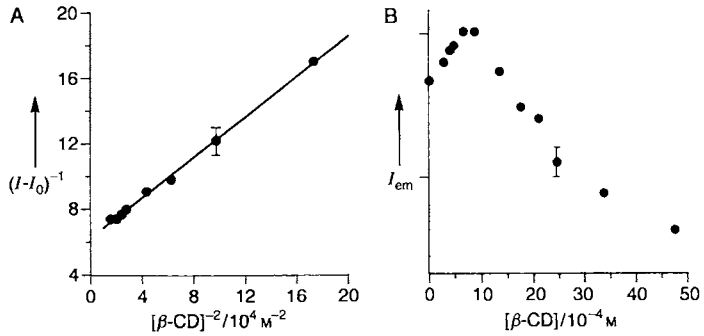

Figure 2. A) BH plot (for a 1:2 complex) of the changes in the fluorescence intensity *I* at 550 nm due to the formation of HPIP/β-CD complexes. I_0 is the fluorescence intensity in the absence of β-CD. B) Changes in the fluorescence intensity I_{em} at 390 nm upon addition of β-CD.

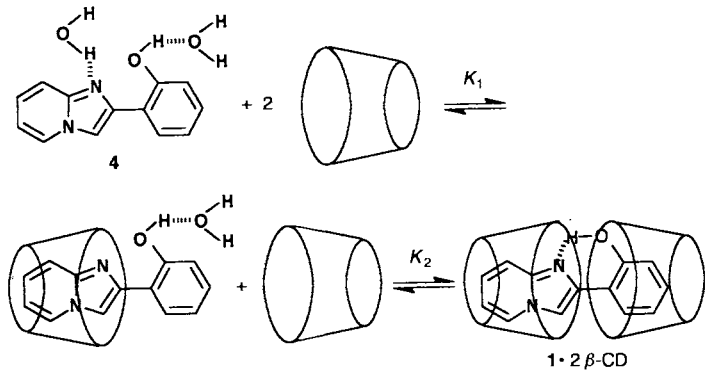

Scheme 2. Schematic view of the fitting of **4** into a β-CD cavity and the subsequent conversion into **1** in the 1:2 inclusion complex.

390 nm is absent in the crystals, the intramolecular hydrogen bond of the dye within the complex is not perturbed by the cyclic oligosaccharide host.

The dye-trapping process in aqueous solution can also be monitored by the biphasic behavior of the fluorescence intensity at 390 nm as a function of β-CD concentration. Thus, at low concentrations of β-CD the intensity of this band initially increases (Figure 2B) due to protection of the emitting fluorophore by β-CD. This trend is reversed and the intensity starts to decline upon further increase of the oligosaccharide concentration, with the simultaneous appearance of the band at 550 nm, as noted above. The BH analysis of the initial change of the intensity at 390 nm yields a 1:1 stoichiometry and a binding constant $K_1 = 500\ \text{M}^{-1}$ The equilibrium constant K_2 of the 1:2 final assembly is then $K_a(\text{apparent})/K_1 = 200\ \text{M}^{-1}$. The construction of the 1:2 assembly starts with inclusion of **4** within the hydrophobic cavity of a single β-CD molecule to form initially a 1:1 complex (see Scheme 2). Subsequent encounter of this species with a second β-CD molecule allows the binding of the two macrocycles through intermolecular hydrogen bonds and formation of the intramolecular OH···N bond, which is characteristic of HPIP in non-hydrogen-bonding environments,[11] with a partial twisting about the C2–C1′ single bond. Formation of the first inclusion complex occurs very quickly (within seconds), whereas that of the final 1:2 assembly proceeds much more slowly (within hours) and depends markedly on relative concentrations and temperature. The values of K_1 and K_2 suggest that the main driving interactions of the inclusion processes are not totally hydrophobic.[7]

UV irradiation of encapsulated **1** leads to excited **2**. The relaxation of this species to **3** by twisting about the C2–C1′ bond is restricted by the cavity formed by the two β-CD molecules (largest diameter 7.8 Å, length ca. 16 Å).[13] Therefore, formation of **3** cannot occur, and the emission must come from **2** or a very similar rotamer. The steady-state fluorescence anisotropy $\langle r \rangle$ of the band at 550 nm for the β-CD complex is 0.253 ± 0.005, which is close to that observed in PMMA ($\langle r \rangle = 0.335 \pm 0.008$ at 510 nm), where rotation is not possible. This indicates that little reorientation occurs during the lifetime (4.0 ns) of the excited phototautomer.

The spectral properties of HPIP sequestered by α- and γ-CD, which have different cavity sizes (see Scheme 1), agree with these. Thus, the maxima of the proton-transfer fluorescence bands of the α-, β-, and γ-CD inclusion complexes appear at 500, 550, and 570 nm, respectively. The red shift is due to increased twisting around the C2–C1′ bond in **2** and is, therefore, a simple and direct measure of the size (diameter) of the encapsulating cavity. Indeed, it reveals the involvement of single-bond rotation in a transient state. Recent ab initio calculations on a similar molecule are in accordance with this type of rotational process in the proton-transfer cycle.[13] Due to the dimensions of the dye (ca. $5.5 \times 11.7\ \text{Å}^2$), the cavity of the α-CD complex should provide the most constraining environment. However, since the proton motion in **1** is a direct process that takes place along the intramolecular hydrogen bond of the dye,[11, 13–15] its rate would not be substantially perturbed by these geometric restrictions. Thus the size of the bimolecular CD cavity only affects the electronic energy gap of the emitting phototautomers.

The blue to green-yellow fluorescence changes of aqueous solutions of HPIP in the presence of CDs have been found to be simply and directly related to the topology of hydrophobic cavities at the subnanometer level and to the assembly/disassembly of hydrogen-bond networks. Hence, this dye is a molecular probe for these phenomena, and we are currently investigating its use as a sensor for microdomains in biological membranes.

Received: February 18, 1997 [Z10134IE]
German version: *Angew. Chem.* **1997**, *109*, 1586–1588

Keywords: cyclodextrins · fluorescence spectroscopy · nanocavities · rotational isomerization · proton transfer

[1] a) V. Balzani, F. Scandola, *Supramolecular Photochemistry*, Ellis Horwood, London, **1995**, p. 288; V. Ramamurthy in *Photochemistry in Organized and Constrained Media* (Ed.: V. Ramamurthy), VCH Publishers, New York, **1991**, p. 319; b) P. Bortolus, S. Monti, *Adv. Photochem.* **1996**, *21*, 1–131.
[2] D. B. Amabilino, J. F. Stoddart, *Chem. Rev.* **1996**, *95*, 2725–2828.
[3] A. Harada, L. Li, M. Kamachi, *Nature* **1993**, *364*, 516–518.
[4] M. J. Pregel, L. Jullien, J.-M. Lehn, *Angew. Chem.* **1992**, *104*, 1695–1697; *Angew. Chem. Int. Ed. Engl.* **1992**, *31*, 1637–1640.
[5] L. Jullien, J. Canceill, B. Valeur, E. Bardez, J.-M. Lehn, *Angew. Chem.* **1994**, *106*, 2582–2584; *Angew. Chem. Int. Ed. Engl.* **1994**, *33*, 2438–2439.
[6] Y. Kubo, S. Maeda, S. Tokia, M. Kubo, *Nature* **1996**, *382*, 522–524.
[7] G. Wenz, *Angew. Chem.* **1994**, *106*, 851–870; *Angew. Chem. Int. Ed. Engl.* **1994**, *33*, 803-822.
[8] G. S. Cox, N. J. Turro, *J. Photochem. Photobiol.* **1984**, *40*, 185–188.
[9] E. L. Roberts, J. Dey, I. M. Warner, *J. Phys. Chem.* **1996**, *100*, 19681–19686.
[10] Y. H. Kim, *J. Phys. Chem.* **1996**, *100*, 15670–15676.
[11] A. Douhal, F. Amat-Guerri, A. U. Acuña, *J. Phys. Chem.* **1995**, *99*, 76–80.
[12] M. L. Benesi, J. H. Hildebrand, *J. Am. Chem. Soc.* **1949**, *71*, 2703–2707.
[13] V. Guallar, M. Moreno, J.-M. Lluch, F. Amat-Guerri, A. Douhal, *J. Phys. Chem.* **1996**, *100*, 19789–19794.
[14] A. Douhal, F. Lahmani, A. H. Zewail, *Chem. Phys.* **1996**, *207*, 477–498 (special issue).
[15] A. Douhal, S.-K. Kim, A. H. Zewail, *Nature* **1995**, *378*, 260–263.

Sigmatropic Shifts in Allene Oxide Rearrangements: First General Route to [3,4] Shifts in Aliphatic Systems**

Ihsan Erden,* Fu-Pei Xu, and Wei-Guo Cao

In our initial report on thermal isomerizations of saturated fulvene endoperoxides we provided the first evidence for allene oxide and cyclopropanone intermediates by means of inter- and intramolecular trapping reactions.[1] The intermediacy of allene oxides was subsequently corroborated by isolation and characterization of a stable derivative of **3** ($R^1 = t\text{Bu}$, $R^2 = \text{H}$),[2] and the mechanism of the fulvene endoperoxide/allene oxide isomerization fully elucidated (Scheme 1). We also reported synthetic applications of this rearrangement employing acid-trapping reactions[3] and intramolecular vinylcyclopropanone/cyclopentenone cyclizations.[4]

In the course of our studies on related intramolecular trapping reactions we uncovered a new facet of the endoperoxide/allene oxide methodology. Placement of a 3-butenyl group at the exocyclic double bond in the fulvene precursor and thermolysis of the corresponding saturated endoperoxide **5** in CCl_4 at 60–80 °C results in a [3,4]-sigmatropic shift of the 3-butenyl group to give the 5-oxo-6-heptenal derivatives **8.**

[*] Prof. Dr. I. Erden, Dr. F.-P. Xu, W.-G. Cao
Department of Chemistry and Biochemistry
San Francisco State University
1600 Holloway Avenue, San Francisco, CA 94132 (USA)
Fax: Int. code +(415)338-2384
e-mail: ierden@sfsu.edu

[**] This work was supported by the U. S. National Science Foundation (grant no. CHE-8904016).

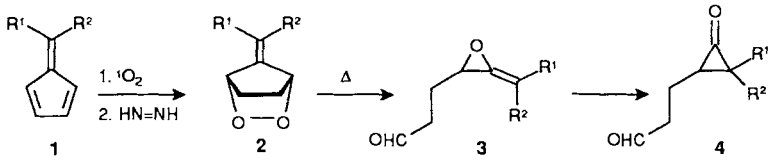

Scheme 1. Mechanism for the thermal rearrangement of saturated fulvene endoperoxides.

[3,4] Shifts were first observed by Schmid and co-workers in 1,4-cyclohexadienol/benzene rearrangements alongside competing [1,2] and [3,3] shifts.[5] Based on their failed attempts to extend these rearrangements to acyclic analogs Schmid et al. concluded that "the chances that in acyclic systems aliphatic [3s,4s] rearrangements could occur are slim".[6] Except for one isolated case, examples of [3,4]-sigmatropic shifts in aliphatic compounds are virtually unknown.[7] Dewar's prediction[8] that this type of [3,4] shift would proceed with ease if suitable systems were accessible has now been borne out in the experiments described.

Table 1[9] depicts several examples of [3,4] shifts in endoperoxides. A mechanism consistent with our results involves initial formation of the allene oxide **6**, which undergoes a [3,4] shift via the oxyallyl intermediate **7** (Scheme 2). In certain cases, and in particular with endoperoxides derived from 4-enals, intramolecular 1,3-dipolar cycloaddition[1-3] of the allene oxide/oxyallyl intermediate onto the aldehyde moiety effectively competes with the [3,4] pathway; this manifests itself in the relatively low yields of isolated [3,4]-shift products in those systems. Although we have not yet systematically explored the scope and limitations of these rearrangements, preliminary results indicate that steric hindrance in the side chain of the starting endoperoxide impedes attainment of the proper transition geometry in **7** for the [3,4]-shift pathway. In the two examples studied that exhibit no tendency for the [3,4] shift due to steric crowding at the butenyl terminus, as in **21**, or the α-carbon atom, as in **23**, the alternative intramolecular 1,3-dipolar cycloaddition dominates. In the case of **23** brief thermolysis at 80 °C allowed observation of the stable allene oxide **24** by NMR spectroscopy (Scheme 3).

Table 1. [3,4]-Sigmatropic shifts in thermal decompositions of saturated fulvene endoperoxides.

Endoperoxide	Product	Yield
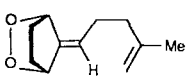 **9**	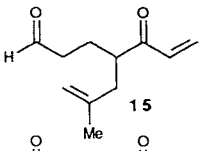 **15**	45%
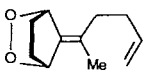 **10**	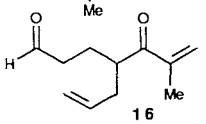 **16**	55%
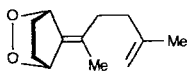 **11**	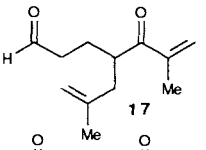 **17**	52%
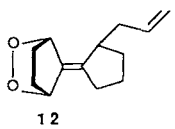 **12**	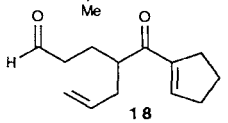 **18**	83%
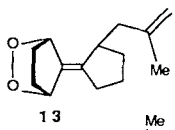 **13**	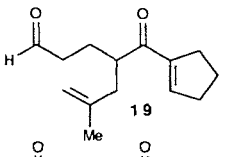 **19**	85%
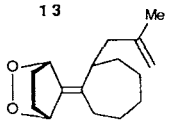 **14**	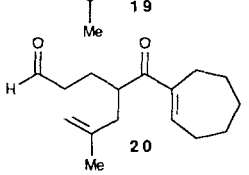 **20**	79%

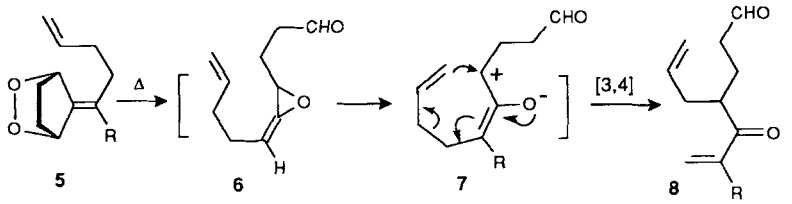

Scheme 2. Mechanism for [3,4]-sigmatropic shifts in allene oxides.

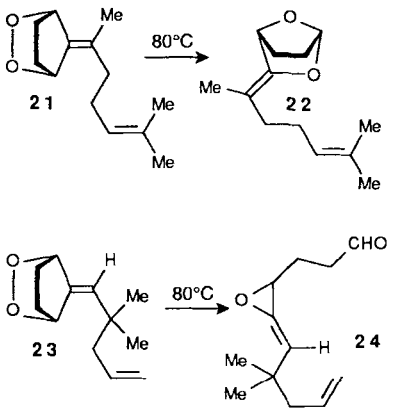

Scheme 3. Thermal rearrangements of sterically constrained systems not exhibiting [3,4] shifts.

Though a stepwise ionic or radical mechanism via cyclic intermediates might be possible for these [3,4] shifts, we favor the concerted pathway,[11-14] which is isoelectronic with its well-known [3,3] counterpart and thermally allowed by the Woodward–Hoffmann orbital-symmetry rules. In a related process, placing groups with migratory aptitude (for example SMe or Cl) at the 6-position of the starting fulvene[9b] resulted in [1,4]-sigmatropic shifts (Scheme 4). Here a stepwise mechanism involving a cyclic intermediate (**27a,b**) appears equally feasible.

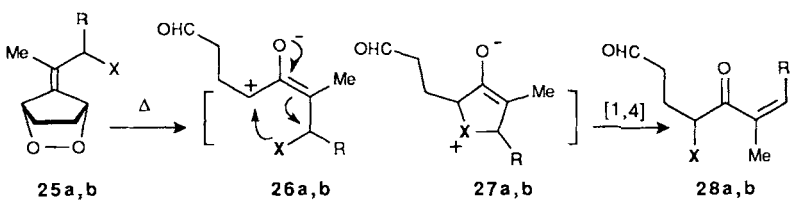

a, X = Cl, R = H (52%); **b**, X = SMe, R = Me (78%)

Scheme 4. [1,4] Shifts in allene oxides with heteroatoms.

The fulvene endoperoxide approach to allene oxides has opened the door to discovering mechanistically interesting rearrangements and synthetically useful reactions. Currently we are probing the possibility of [3,4] shifts with heteroatom variants (O, S, Se) as well as other rearrangements and intramolecular trapping reactions of functionalized allene oxide intermediates.

Received: December 5, 1996 [Z9857IE]
German version: *Angew. Chem.* **1997**, *109*, 1557–1559

Keywords: allene oxides · fulvenes · peroxides · rearrangements

[1] I. Erden, M. Amputch, *Tetrahedron Lett.* **1987**, *28*, 3779.
[2] I. Erden, J. Drummond, R. Alstad, F.-P. Xu, *Tetrahedron Lett.* **1993**, *34*, 1255.
[3] I. Erden, J. Drummond, R. Alstad F.-P. Xu, *Tetrahedron Lett.* **1993**, *34*, 2291.
[4] I. Erden, F.-P. Xu, J. Drummond, R. Alstad, *J. Org. Chem.* **1993**, *58*, 3611.
[5] a) H.-J. Hansen, B. Sutter, H. Schmid, *Helv. Chim. Acta* **1968**, *51*, 828; b) H. Heimgartner, J. Zsindeley, H.-J. Hansen, H. Schmid, *ibid.* **1972**, *55*, 1113; c) U. Widmer, H.-J. Hansen, H. Schmid, *ibid.* **1973**, *56*, 1895; see also d) K. C. Masumdar, A. T. Khan, S. K. Chattopadhyay, *J. Chem. Soc. Perkin Trans 1* **1990**, 2219.
[6] P. Viltorelli, J. Peter-Katalinic, G. Mukherjee-Myller, H.-J. Hansen, H. Schmid, *Helv. Chim. Acta* **1975**, *58*, 1379.
[7] The other example of a [3,4] shift in an aliphatic compound involves a 2-oxyallyl/Fe^{II} species that was generated from the corresponding α,α-dibromo ketone with $[Fe_2(CO)_9]$ and observed in one isolated case: M. Nishizawa, R. Noyori, *Bull. Chem. Soc. Jpn.* **1981**, *54*, 2233.
[8] M. J. S. Dewar, *Angew. Chem.* **1971**, *83*, 859; *Angew. Chem. Int. Ed. Engl.* **1971**, *10*, 761.
[9] Most of the requisite fulvenes were prepared from the corresponding carbonyl compounds and cyclopentadiene by Little's method: a) K. Stone, R. D. Little, *J. Org. Chem.* **1984**, *49*, 1849. Fulvenes **13** and **14** were obtained with NaOMe as base: b) I. Erden, F.-P. Xu, A. Sadoun, G. Sheff, M. Ossun, *J. Org. Chem.* **1995**, *60*, 813. Endoperoxides **9-14** were prepared by low-temperature photooxygenation of the respective fulvenes at $-78\,^{\circ}C$ followed by diazene reduction of the unsaturated endoperoxides at about $-40\,^{\circ}C$ [1·10].
[10] W. Adam, I. Erden, *Angew. Chem.* **1978**, **90**, 223; *Angew. Chem. Int. Ed. Engl.* **1978**, *17*, 210.
[11] R. B. Woodward, R. Hoffmann, *The Conservation of Orbital Symmetry*, Academic Press, New York, **1970**, p. 130.
[12] I. Fleming, *Frontier Orbitals and Organic Chemical Reactions*, Wiley, New York, **1975**, p. 86.
[13] T. S. Sorensen, A. Rauk, *Pericyclic Reactions, Vol. II* (Eds.: A. P. Marchand, R. E. Lehr), Academic Press, New York, **1977**, p. 64.
[14] A *homo*-Cope rearrangement via a cyclopropanone intermediate might also be considered as an alternative to the [3,4] shift: a) D. Hochstrate, F.-G. Klärner, *Liebigs. Ann.* **1995**, 745; see also b) W. R. Roth, H.-W. Lennartz, W. v. E. Doering, L. Birladeanu, C. A. Guyton, T. Kitagawa, *J. Am. Chem. Soc.* **1990**, *112*, 1723.

Synthesis and Gas-Phase Structure of Perfluoro(2,4-dimethyl-3-oxa-2,4-diazapentane), $(CF_3)_2N-O-N(CF_3)_2$

Stefan Reinemann, Rolf Minkwitz, and Heinz Oberhammer*

Although *n*-alkanes are highly stable molecules, saturated straight-chain compounds composed of other elements of the first row of the periodic table are increasingly unstable. Straight-chain molecules with more than two oxygen or nitrogen atoms could be isolated as stable species only in the presence of perfluoroalkyl groups such as CF_3. Molecular structures of bis(trifluoromethyl)trioxide, $CF_3O-O-OCF_3$,[1] and hexakis(trifluoromethyl)tetrazane, $(CF_3)_2N-NCF_3-NCF_3-N(CF_3)_2$,[2] have been reported. Their structures are influenced primarily by the interaction between electron lone pairs of adjacent atoms, which prefer a perpendicular orientation with respect to each other. In the trioxide, which possesses a C-O-O-O dihedral angle of 96(4)°, each of the two oxygen lone pairs $n_\pi(O)$ and $n_\sigma(O)$ is perpendicular to the respective lone pair of the adjacent oxygen atom. The p-shaped lone pairs of adjacent nitrogen atoms in the tetrazane are also perpendicular to each other (N-N-N-N 95(1)°). Due to their low chemical stability saturated straight-chain species composed of oxygen and nitrogen atoms are almost unknown, and no molecular structure of a compound of the type $R_2N-O-NR_2$ has yet been reported. Also in this case CF_3 groups have a strongly stabilizing effect. Perfluoro(2,4-dimethyl-3-oxa-2,4-diazapentane),[3] $(CF_3)_2N-O-N(CF_3)_2$ (**1**), was first synthesized over 30 years ago and characterized by IR, UV, and ^{19}F NMR spectroscopy as well as mass spectrometry.[4] We report here a new synthesis of **1** and its gas-phase structure.

In contrast to Haszeldine and Tipping,[4] who prepared **1** by combining the radicals $(CF_3)_2NO$ and $(CF_3)_2N$, we used OF_2 as the oxygen-carrying fluorination agent. In the presence of CsF as catalyst, OF_2 reacts with CF_3NCF_2 in the temperature range $-75/+25\,^{\circ}C$ nearly quantitatively to give **1** [Eq. (1)].[5]

$$2\,CF_3NCF_2 + OF_2 \xrightarrow{CsF\,(-70/+25\,^{\circ}C)} (CF_3)_2N-O-N(CF_3)_2 \quad \mathbf{1} \qquad (1)$$

Depending on the orientation of the electron lone pairs on the two nitrogen atoms, molecules of type $R_2N-O-NR_2$ can adopt different conformations (Scheme 1). In structure I the

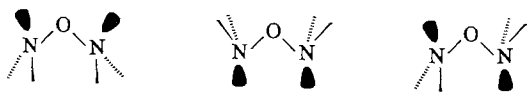

I (ap,ap) II (sp,sp) III (ap,sp)

Scheme 1.

two n(N) lone pairs are antiperiplanar with respect to the opposite O–N bonds (C_{2v} symmetry), in structure II synperiplanar (C_{2v} symmetry), and in structure III one n(N) shows antiperiplanar and the other one synperiplanar orientation (C_s symmetry). In all cases the nitrogen lone pairs are perpendicular to the p-shaped lone pair of oxygen ($n_\pi(O)$) and parallel to $n_\sigma(O)$. Structures with synclinal or anticlinal orientations of the nitrogen lone pairs (C_2 symmetry) are also feasible. No experimental structures of compounds of this kind have yet been reported. Ab initio calculations (MP2/6-31G**) on the model compound $H_2N-O-NH_2$ predict structure III to be the most stable conformer.[6]

The molecular structure of **1** was determined by gas electron diffraction (GED).[7] The radial distribution function (RDF), derived by Fourier transformation of the molecular electron diffraction intensities, is presented in Figure 1. The experimental RDF is reproduced satisfactorily only with structure II, in which both n(N) lone pairs are oriented synperiplanar with respect to the opposite O–N bonds. The geometric parameters were obtained by least-squares fitting of the molecular intensities. Local C_{3v} symmetry was assumed for the CF_3 groups with

[*] Prof. Dr. H. Oberhammer
Institut für Physikalische und Theoretische Chemie der Universität
Auf der Morgenstelle 8, D-72076 Tübingen (Germany)
Fax: Int. code +(7071)29-6910
e-mail: heinz.oberhammer@uni-tuebingen.de
Dipl.-Chem. S. Reinemann, Prof. Dr. R. Minkwitz
Institut für Anorganische Chemie der Universität Dortmund (Germany).

 © VCH Verlagsgesellschaft mbH, D-69451 Weinheim, 1997 0570-0833/97/3613-1518 $ 17.50+.50/0

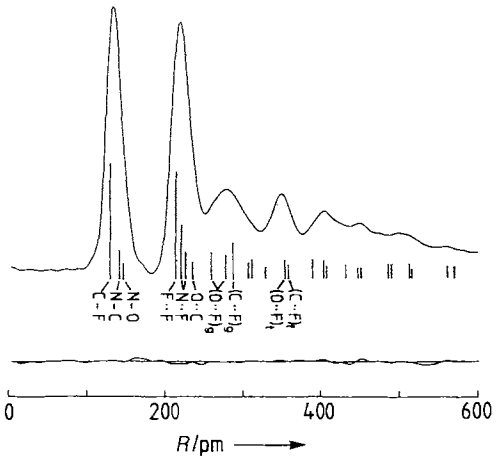

Figure 1. Experimentally determined radial distribution function and difference curve. The positions of important interatomic distances are indicated by vertical bars.

a possible tilt angle (tilt (CF_3)) in the CNC plane between the C_3 axis and the vector along N–C. The orientation of the CF_3 groups was described by a torsional angle of $\tau(CF_3)$ about the N–C bonds. For $\tau(CF_3) = 0°$ each CF_3 group exactly staggers the opposite N–C bond. The least-squares analysis results in a very small value for $\tau(CF_3)$ of 1.8(34)°, and it is not possible to determine whether adjacent CF_3 groups are rotated in the same or opposite directions. In the latter case the two $(CF_3)_2N$ entities possess local C_s symmetry, and the overall molecular symmetry is C_{2v}.

The results of this structural analysis are collected in Table 1, and the molecular model is shown in Figure 2. The fit of the

Table 1. Selected bond lengths [pm] and angles [°] from the electron diffraction analysis of **1** [a].

NO	146.2(8)	N-O-N	105.2(26)	F-C-F	109.3(2)
NC	143.5(4)	C-N-C	117.9(12)	tilt(CF_3)[b]	2.7(11)
CF	132.3(2)	O-N-C	109.3(8)	$\tau(CF_3)$[c]	1.8(23)

[a] Error limits are 3σ values and refer to the last digit. [b] Tilt angle in the CNC plane between the C_3 axis of the CF_3 group and the vector along O–N. [c] Torsional angle of the CF_3 groups about O–N bonds. For $\tau = 0°$ each CF_3 staggers the opposite N–C bond.

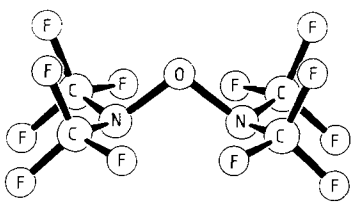

Figure 2. Molecular structure of **1**.

experimental intensities becomes worse when the two $(CF_3)_2N$ entities are rotated about the O–N bonds by more than 5°; that is, when the overall symmetry is reduced from C_{2v} to C_2. Attempts to fit the molecular intensities with structures I or III result in poor agreement, and, furthermore, in F···F or F···N contacts between the two $(CF_3)_2N$ entities of about 200 pm or shorter. Therefore, these conformations can be excluded.

The conformation determined for **1** (structure II) is different from that predicted for the model compound $H_2N–O–NH_2$ (structure III), primarily because of different steric requirements of the substituents. Replacement of H atoms by CF_3 groups leads to a strong destabilization of structures I and III due to steric repulsion between fluorine atoms and between fluorine and nitrogen atoms. The O–N bonds in **1** (146.2(8) pm) are longer than those in $(CF_3)_2N–OH$ (140(3) pm),[8] $(CF_3)_2N–OCH_3$ (142.4(28) pm),[9] or $(CF_3)_2N–ONO$ (141.0(15) pm)[10] but shorter than $O–N(sp^2)$ bonds in $O_2N–O–NO_2$ (149.2(4) pm)[11] or $(CF_3)_2NO–NO$ (157.2(21) pm). Despite the repulsion that is expected between the two nitrogen lone pairs in the *syn* orientation and between fluorine atoms of the two $(CF_3)_2N$ entities, the N–O–N angle (105.2(26)°) and the N···N nonbonded distance (232 pm) are remarkably small.

Received: February 13, 1997 [Z10111IE]
German version: *Angew. Chem.* **1997**, *109*, 1579–1580

Keywords: electron diffraction · fluorine · nitrogen · structure elucidation

[1] K. I. Gobbato, M. F. Klapdor, D. Mootz, W. Poll, S. E. Ulic, H. Willner, H. Oberhammer, *Angew. Chem.* **1995**, *107*, 2433; *Angew. Chem. Int. Ed. Engl.* **1995**, *34*, 2244.
[2] B. Krumm, A. Vij, R. J. Kirchmeier, J. M. Shreeve, H. Oberhammer, *Angew. Chem.* **1995**, *107*, 645; *Angew. Chem. Int. Ed. Engl.* **1995**, *34*, 586.
[3] IUPAC nomenclature: *N,N'*-oxobis[1,1,1-trifluoro-*N*-(trifluoromethyl)]-methanamine.
[4] R. N. Haszeldine, A. E. Tipping, *J. Chem. Soc. (C)* **1966**, 1236.
[5] CF_3NCF_2 (4 mmol) and OF_2 (2 mmol) were condensed at −196 °C into a 30-mL quartz ampoule containing activated CsF (0.5 mmol), and the ampoule sealed under vacuum. After 2 d at −78 °C the temperature was raised within 2 d to 25 °C in increments of 10 °C. After a total of 6 d the reaction mixture was seperated by fractional condensation. Compound **1** can be condensed at −60 °C in static vacuum into a glass ampoule at −196 °C. Repeating this procedure twice provided **1** in 99% purity according to IR, Raman, and ^{13}C and ^{19}F NMR spectra (yield 90%). *Caution!* If this temperature program is not followed, an uncontrolled and explosive reaction can occur. OF_2 is highly toxic and can cause lung damage. After several weeks at room temperature **1** decomposes to give violet $(CF_3)_2NO$ and $(CF_3)_2NN(CF_3)_2$, as followed by vibrational and ^{19}F NMR spectroscopy.
[6] G. Leroy, J.-P. Dewispelaere, H. Benkadour, D. Riffi Temsamani, C. Wilante, *J. Mol. Struct. (Theochem.)* **1995**, *334*, 137.
[7] Electron diffraction intensities were recorded with a gas diffractograph at nozzle-to-plate distances of 25 and 50 cm and with an accelerating voltage of about 60 kV. The temperature of the sample reservoire was −38 °C (vapor pressure about 15 mbar) and that of the gas nozzle 15 °C. The photographic plates were analyzed with the usual procedures (H. Oberhammer, W. Gombler, H. Willner, *J. Mol. Struct.* **1981**, *70*, 273). Intensities in the s-ranges 20–180 and 80–350 nm^{-1} were used for the structure analysis ($s = (4\pi/\lambda)\sin(\theta/2)$, λ = electron wavelength, θ = scattering angle).
[8] C. Glidewell, C. J. Marsden, A. G. Robiette, G. M. Sheldrick, *J. Chem Soc. Dalton Trans.* **1972**, 1735.
[9] B. Casper, J. Jakob, R. Minkwitz, H. Oberhammer, *Chem. Ber.* **1996**, *129*, 653.
[10] H. G. Ang, M. F. Klapdor, W. L. Kwik, Y. W. Lee, H. G. Mack, D. Mootz, W. Poll, H. Oberhammer, *J. Am. Chem. Soc.* **1993**, *115*, 6929.
[11] B. W. McClelland, L. Hedberg, K. Hedberg, K. Hagen. *J. Am. Chem. Soc.* **1983**, *105*, 3789.

Uridine Diphospho-α-D-*gluco*-hexodialdose: Synthesis and Kinetic Competence in the Reaction Catalyzed by UDP-Glucose Dehydrogenase**

Robert E. Campbell and Martin E. Tanner*

UDP-glucose dehydrogenase catalyzes the irreversible NAD^+-dependent oxidation of UDP-glucose to UDP-glucuronic acid (Scheme 1).[1] In mammals the product of this reaction is used in the liver to tag waste metabolites for excretion,[2] and in the biosynthesis of glycosaminoglycans such as heparin[3] and hyaluronic acid.[4] In many strains of pathogenic bacteria, such as group A streptococci[5] and *Streptococcus pneumoniae* type 3,[6] it provides glucuronic acid, which is used in the construction of an antiphagocytic capsule. This capsule allows the bacteria to evade the immune system of the host and is thus responsible for their virulence.[7–9]

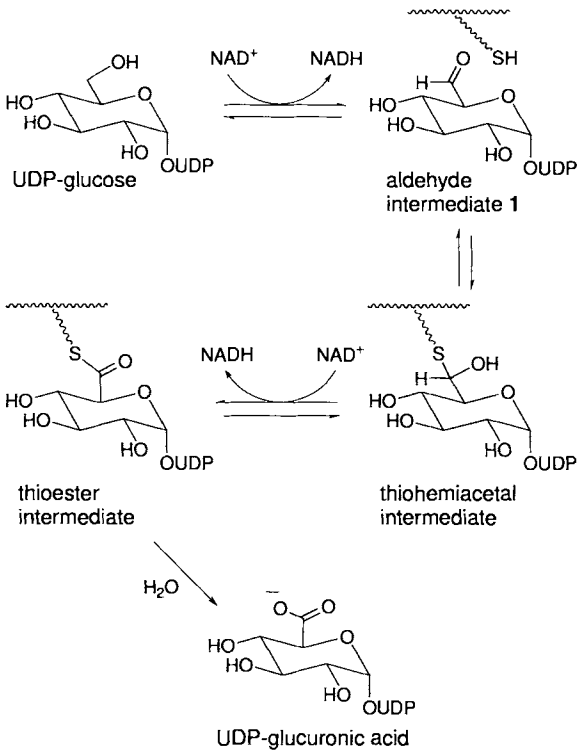

Scheme 1. Proposed mechanism for the reaction catalyzed by UDP-glucose dehydrogenase.

UDP-glucose dehydrogenase belongs to a small class of enzymes that are capable of carrying out the twofold oxidation of an alcohol to an acid without the release of an aldehyde intermediate.[1] The putative intermediate, uridine diphospho-α-D-*gluco*-hexodialdose (**1**), has therefore never been detected nor trapped with carbonyl-modifying reagents.[10–12] In previous work on the bovine liver enzyme it was suggested that the aldehyde is not an actual intermediate in the reaction and that the alcohol is converted directly to an enzyme-linked imine, which is held through a lysine side chain.[13] This is somewhat at odds with a report that only one solvent-derived oxygen atom is found in the product acid.[14] If an imine intermediate was formed one would expect both carboxylate oxygen atoms to come from solvent. In order to support the notion that **1** it is a tightly bound intermediate, we have synthesized it and measured the kinetic parameters that describe its oxidation by the enzyme.

Earlier work reported that **1** can be obtained from UDP-glucose with UDP-galactose 4-epimerase and galactose oxidase.[11, 13] This procedure tended only to work on a very small scale and required large amounts of expensive enzymes. Furthermore, the procedure neccesarily yielded an inseparable mixture of epimers at the C4 position, and no spectroscopic characterization of the product or indication of purity was reported. Therefore, we chose to carry out the stepwise synthesis of **1**.

A relatively recent paper by Müller and Schmidt[15] outlining the preparation of a dTDP-ketosugar prompted us to use an alkene as a protecting group for the sensitive aldehyde functionality (Scheme 2). The synthesis begins with an oxidation at C6 of the known tetraacetylated glucose **2**.[16] It is well documented

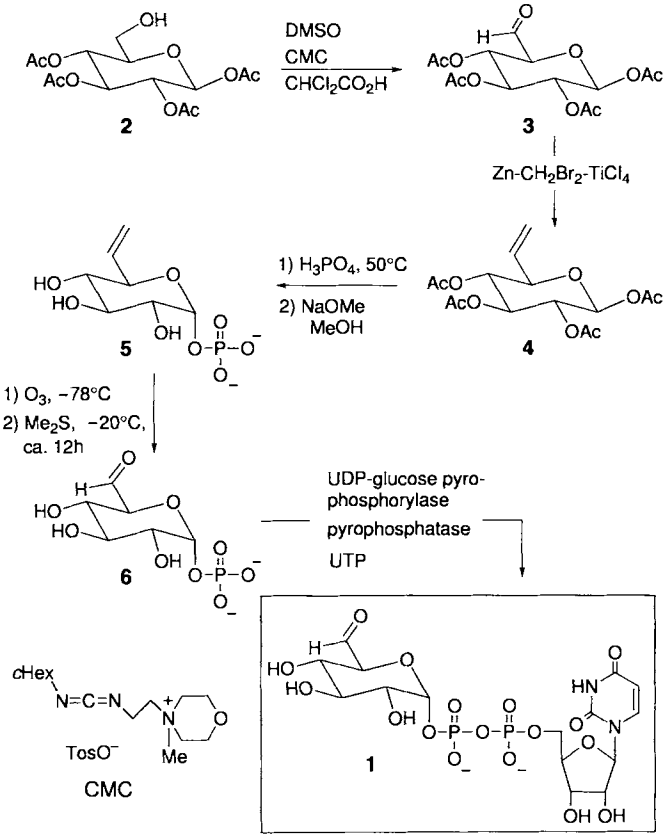

Scheme 2. Stepwise synthesis of **1** with an alkene as a protecting group for the sensitive aldehyde functionality.

that a facile β-elimination reaction occurs to give the α,β-unsaturated enone in these systems;[17] however, a Moffat oxidation is mild enough to minimize this elimination in related compounds.[18] The water-soluble coupling reagent CMC was used in place of *N*,*N*′-dicyclohexylcarbodiimide because the resulting urea derivative can easily be removed by extraction. We thus prepared aldehyde **3** and immediately used it without complete

[*] Dr. M. E. Tanner, R. E. Campbell
The University of British Columbia
Department of Chemistry
Vancouver, BC V6T 1Z1 (Canada)
Fax: Int. code +(604) 822-2847
e-mail: mtanner@chem.ubc.ca

[**] This work was supported by The Natural Sciences and Engineering Research Council of Canada.

purification. The alkene was introduced with Lombardo's reagent,[19] and **4** isolated in an overall yield of 12% based on **2** (Table 1). The α-phosphate was prepared by a modified MacDonald reaction[20] in neat phosphoric acid at 50 °C. No β-anomer was detected. The acetyl groups were removed with sodium methoxide to give **5** in 39% yield. Deprotection of **5** to give **6** was achieved by ozonolysis at −78 °C followed by an overnight treatment with dimethylsufide at −20 °C. Aldehyde **6** was used directly in an enzymatic coupling reaction with UTP, UDP-glucose pyrophosphorylase, and pyrophosphatase.[21] It was expected that **6** could replace the normal substrate glucose-α-1-phosphate in the coupling reaction, since the steric differences between them are slight. Indeed, following the reaction with ion-paired reverse-phase HPLC[22] indicated that one equivalent of UTP was cleanly converted into **1**. The product was surprisingly stable and could be isolated in 44% yield (based on **5**) by a combination of anion-exchange (DE-52 resin) and size-exclusion (Bio-Gel P-2) chromatographies. The aldehydic proton appears as a doublet at $\delta = 5.17$ in the ^{1}H NMR spectrum taken in D_2O (Figure 1, Table 1). This indicates that more than 95% of the aldehyde is present as a hydrate.[23]

Table 1. Selected physical data for **1**, **4**, and **5**.

1 (disodium salt): ^{1}H NMR (400 MHz, D_2O): $\delta = 3.51$ (m, 2H, H2″, H4″), 3.74 (dd, $J = 9.5$, 9.5 Hz, 1H, H3″), 3.83 (dd, $J = 1.3$, 10.0 Hz, 1H, H5″), 4.16–4.42 (m, 4H, H3′, H4′, H5′), 4.34 (d, $J = 3.3$ Hz, 1H, H2′), 5.17 (d, $J = 1.3$ Hz, 1H, H6″), 5.62 (dd, J(H,H) = 3.4 Hz, J(H,P) = 7.6 Hz, 1H, H1″), 5.95 (m, 2H, H1′, H5), 7.91 (d, $J = 8.2$ Hz, 1H, H6); ^{31}P NMR (300 MHz, D_2O): $\delta = -12.45$ (d, J(P,P) = 20.9 Hz, 1P), −10.82 (d, J(P,P) = 20.9 Hz, 1P); HR-LSI MS [a] calcd for $C_{15}H_{20}N_2O_{17}P_2Na$ (nonhydrated monosodium salt): 585.01349; found: 585.01370.

4: ^{1}H NMR (400 MHz, $CDCl_3$): $\delta = 1.96$, 1.98, 2.00, 2.07 (4s, 12H, 4Ac), 3.99 (dd, $J = 7.1$, 9.8 Hz, 1H, H5), 4.93 (dd, $J = 9.7$, 9.7 Hz, 1H, H4), 5.09 (dd, $J = 9.6$, 8.3 Hz, 1H, H2), 5.23 (dd, $J = 9.5$, 9.5 Hz, 1H, H3), 5.26 (d, $J = 10.5$ Hz, 1H, H7-*trans*), 5.34 (d, $J = 17.2$ Hz, 1H, H7-*cis*), 5.69 (m, 1H, H6), 5.73 (d, $J = 8.3$ Hz, 1H, H1); DCI-MS (NH_3): m/z (%) = 362 (100, $[M+NH_4]^+$); elemental analysis calcd for $C_{15}H_{20}O_9$: C 52.33, H 5.85; found: C 52.36, H 5.82.

5 (monosodium salt): ^{1}H NMR (400 MHz, D_2O): $\delta = 3.32$ (dd, $J = 9.6$, 9.7 Hz, 1H, H4), 3.57 (dt, $J = 9.8$, 2.7 Hz, 1H, H2), 3.76 (dd, $J = 9.6$, 9.5 Hz, 1H, H3), 4.25 (dd, $J = 9.4$, 8.7 Hz, 1H, H5), 5.44 (m, 3H, H1, H7-*trans*, H7-*cis*), 5.86 (m, 1H, H6); ^{31}P NMR (300 MHz, D_2O): $\delta = 0.373$; HR-LSI MS [a] calcd for $C_7H_{12}O_8P$: 255.02698; found: 255.02786.

[a] High-resolution liquid secondary-ion mass spectrometry: negative-ion mode in a glycerin matrix.

Treatment of aldehyde **1** with a saturating amount of NAD^+ (500 μM) and the *Streptococcus pyogenes* UDP-glucose dehydrogenase[10] resulted in the quantitative production of UDP-glucuronic acid and NADH, as analyzed by ion-paired reverse-phase HPLC.[22] The kinetics and stoichiometry of the reaction were followed by monitoring NADH formation with UV spectroscopy at $\lambda = 340$ nm. For each molecule of **1** that was oxidized, one molecule of NADH was generated. The oxidation of **1** at 30 °C and pH 8.7 followed Michaelis–Menten kinetics with $k_{cat} = 1.0\ s^{-1}$ and $K_M = 14\ \mu M$.[24, 25] These compare well with values obtained for UDP-glucose measured under identical conditions ($k_{cat} = 1.2\ s^{-1}$ and $K_M = 14\ \mu M$).[10, 25] The agreement in the k_{cat} values indicates that the aldehyde is kinetically competent to be an intermediate in the normal reaction pathway.

We envision two possibilities for the oxidation process. The enzyme may catalyze the oxidation of only the minor, unhydrated form of the aldehyde present in solution, leaving the hydrated form to bind nonproductively in a competitive manner. Alternatively, the enzyme may operate on the hydrated form and catalyze its dehydration prior to oxidation. It seems unlikely that the oxidation proceeds directly through the hydrate, since mounting evidence[10, 26, 27] suggests that the second oxidation proceeds via a thioester intermediate in a manner analogous to the reaction catalyzed by glyceraldehyde 3-phosphate dehydrogenase.[28, 29] The bound aldehyde is likely in equilibrium with a covalently bound thiohemiacetal intermediate that is attached to an active-site cysteine residue (see Scheme 1).

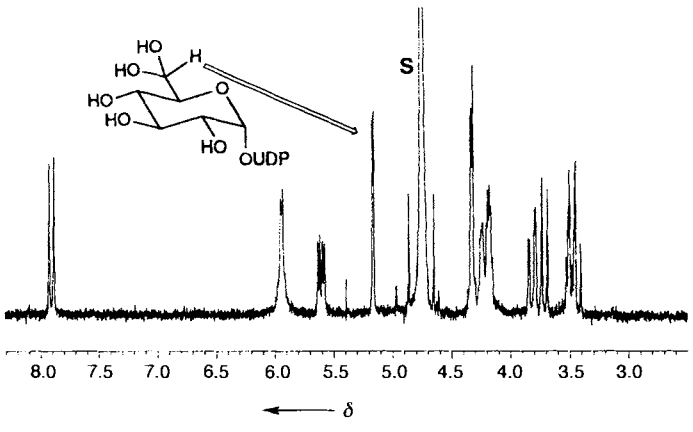

Figure 1. 200 MHz ^{1}H NMR spectrum of the hydrated form of **1** in D_2O. "S" indicates the signal for residual protiated solvent.

Received: January 7, 1997 [Z9970IE]
German version: *Angew. Chem.* **1997**, *109*, 1593–1595

Keywords: carbohydrates · enzyme catalysis · intermediates · nucleotides

[1] N. J. Oppenheimer, A. L. Handlon in *The Enzymes, Vol. 20* (Ed.: D. S. Sigman), Academic Press, San Diego, **1992**, pp. 453–504.
[2] G. J. Dutton, *Glucuronidation of Drugs and Other Compounds*, CRC Press, Boca Raton, FL, USA, **1980**.
[3] L. Kjellén, U. Lindahl, *Annu. Rev. Biochem.* **1991**, *60*, 443–475.
[4] *The Biology of Hyaluronan* (Eds.: D. Evered, J. Whelan), Wiley, Chichester, **1989**.
[5] B. A. Dougherty, I. van de Rijn, *J. Biol. Chem.* **1993**, *268*, 7118–7124.
[6] C. Arrecubieta, E. García, R. López, *J. Bacteriol.* **1996**, *178*, 2971–2974.
[7] D. A. Watson, D. M. Musher, *Infect. Immun.* **1990**, *58*, 3135–3138.
[8] E. R. Moxon, J. S. Kroll, *Curr. Top. Microbiol. Immunol.* **1990**, *150*, 65–86.
[9] M. R. Wessels, J. B. Goldberg, A. E. Moses, T. J. DiCesare, *Infect. Immun.* **1994**, *62*, 433–441.
[10] R. E. Campbell, R. F. Sala, I. van de Rijn, M. E. Tanner, *J. Biol. Chem.* **1997**, *272*, 3416–3422.
[11] G. L. Nelsestuen, S. Kirkwood, *J. Biol. Chem.* **1971**, *246*, 3828–3834.
[12] J. L. Strominger, E. S. Maxwell, J. Axelrod, H. M. Kalckar, *J. Biol. Chem.* **1957**, *224*, 79–90.
[13] A. B. Ordman, S. Kirkwood, *J. Biol. Chem.* **1977**, *252*, 1320–1326.
[14] J. G. Schiller, A. M. Bowser, D. S. Feingold, *Carbohydr. Res.* **1972**, *25*, 403–410.
[15] T. Müller, R. R. Schmidt, *Angew. Chem.* **1995**, *107*, 1467–1468; *Angew. Chem. Int. Ed. Engl.* **1995**, *34*, 1328–1329.
[16] D. D. Reynolds, W. L. Evans, *Organic Syntheses, Vol. 3* (Ed.: E. C. Horning), Wiley, New York, **1955**, pp. 432–434.
[17] R. W. Binkley, *J. Org. Chem.* **1977**, *42*, 1216–1221.
[18] D. Nicoll-Griffith, L. Weiler, *J. Chem. Soc. Chem. Commun.* **1984**, 659–661.
[19] L. Lombardo, *Tetrahedron Lett.* **1982**, *23*, 4293–4296.
[20] C. D. Warren, R. W. Jeanloz, *Biochemistry* **1973**, *12*, 5031–5037.
[21] A. N. Singh, J. S. Newborn, F. M. Raushel, *Bioorg. Chem.* **1988**, *16*, 206–214.
[22] I. Meynial, V. Paquet, D. Combes, *Anal. Chem.* **1995**, *67*, 1627–1631.
[23] D. Horton, M. Nakadate, J. M. J. Tronchet, *Carbohydr. Res.* **1968**, *7*, 56–65.
[24] Initial dismutation to an alcohol and an acid was observed during the oxidation of aldehydes by horse-liver alcohol dehydrogenase (G. T. M. Henehan, N. J. Oppenheimer, *Biochemistry* **1993**, *32*, 735–738). This does not occur with UDP-glucose dehydrogenase, since UDP-glucuronic acid, and not NADH, is released last in the kinetic mechanism [10]. No lag phase was observed during the oxidation of **1**.

 © VCH Verlagsgesellschaft mbH, D-69451 Weinheim, 1997 0570-0833/97/3613-1521 $ 17.50+.50/0

[25] The kinetic data could be fit somewhat better if corrections were made for potential weak allosteric interactions. These corrections (Hill coefficient $n = 1.5$ for UDP-glucose and $n = 1.3$ for **1**) would not change the values of k_{cat} by more than 10%.
[26] B. Franzen, C. Carrubba, D. S. Feingold, J. Ashcom, J. S. Franzen, *Biochem. J.* **1981**, *199*, 603–609.
[27] W. P. Ridley, J. P. Houchins, S. Kirkwood, *J. Biol. Chem.* **1975**, *250*, 8761–8767.
[28] C. Corbier, F. Della Seta, G. Branlant, *Biochemistry* **1992**, *31*, 12532–12535.
[29] J. I. Harris, M. Waters in *The Enzymes, Vol. 13* (Ed.: P. D. Boyer), Academic Press, New York, **1976**, pp. 1–49.

Activity of 2′,5′-Linked RNA in the Template-Directed Oligomerization of Mononucleotides**

Thazha P. Prakash, Christopher Roberts, and Christopher Switzer*

The ability of 2′,5′-linked nucleic acids to encode genetic information has been a matter of both experimental and theoretical interest. Whether 2′,5′-linked nucleic acids form helices had been debated[1] until relatively recently, when 2′,5′-linked oligonucleotides were found to associate.[2] A related issue is the possibility of forming chimeric helices. It has long been known that 2′,5′-linked oligoadenylate forms a triplex with natural oligouridylate.[3] This phenomenon has since been extended to other sequences and structures.[4] These findings raise the possibility of genetic-information transfer with 2′,5′-linked RNA or natural RNA with 2′,5′-linkage defects. Within the context of an enzymatic reaction, Lorsch et al.[5] demonstrated that reverse transcriptase reads through an RNA template bearing a 2′-linkage defect. In the context of non-enzymatic reactions, the ability of isomeric RNA to serve as a template was recently confirmed using the complex mixture of linear and cyclic 2′,5′-linked oligocytidylates that result from clay-catalyzed condensation of activated 5′-CMP.[6] Here we report the first mononucleotide oligomerizations allowing direct comparisons to be made between the properties of natural and 2′,5′-linked RNA templates.

Figure 1. Oligonucleotides used in this study. Double-underlined letters are 2′,5′-linked RNA. Single-underlined letters are 3′,5′-linked RNA. Italicized letters are 3′,5′-linked DNA.

Oligonucleotides used to explore template-directed synthesis are given in Figure 1. A schematic illustration of the template-directed reaction investigated in this work is given in Figure 2. The templates are modelled on hairpin-templates reported by Wu and Orgel.[7] As noted below and in earlier work,[7] incorporation of DNA into the stem and loop of the templates enables assay of product phosphodiester linkages (3′,5′ versus 2′,5′) with RNase. To assess whether the DNA stem perturbs the conformation of the 2′,5′-linked RNA tract in template **1**, the CD spectra of **1** and a standard for the RNA tract alone, 2′,5′-C_{12}, were compared. The standard gave an A-helix spectrum, and **1** a spectrum consistent with the superposition of B-helix and A-helix spectra. These observations are consistent with the RNA tract in **1** maintaining its conformational integrity.

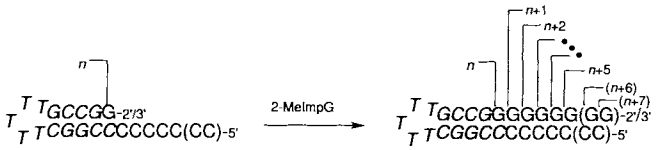

Figure 2. General scheme by which the reaction between templates **1**–**4** (Figure 1) and 2-MeImpG occurs. The GMP units sequentially add to the 2′/3′-terminus of the template (G^n). G^{n+5} is the full-length product for templates **1** and **2**, and G^{n+7} for templates **3** and **4**.

Initially the effect of different divalent metal ions on oligomerization of the 2-methylimidazolide of guanosine-5′-phosphate (2-MeImpG) was explored with templates **1** and **2** (Table 1). By far, the most effective divalent metal ion in promoting oligomerization with the 2′,5′-linked RNA bearing template **1** was magnesium. Magnesium ion was also most effective in promoting oligomerization with the 3′,5′-linked RNA template **2**, but other metal ions were also effective (notably mercury, zinc, and lead). It is not yet clear why 2′,5′-linked RNA is most active in the presence of Mg^{2+}, although it may be that the metal ion orders activated nucleotides on the template in a kinetically significant way. A representative autoradiogram showing oligomerization products obtained after eight days with **1** is given in Figure 3. On the basis of time-dependent data and comparison with the product of **2** (data not shown), the predominant product in lane 2 appears to result from incorporation of four ribonucleotides. To ensure that the observed reactions were indeed template dependent, **1** and **2** were incubated with 2-MeImpA. With this monomer no more than 10% of

Table 1. Oligomerization with templates **1** and **2** and different metal ions (100 mM in all cases) for eight days. Percentages refer to the amount of starting template remaining unconsumed by oligomerization. See the legend to Figure 3 for further details.

Metal ion	Template 1 [%]	Template 2 [%]
$MgCl_2$	27.4	1.44
$HgCl_2$	84.5	18.4
$ZnCl_2$	73.8	36.7
$CoCl_2$	76.6	61.4
$MnCl_2$	80.1	92.4
$UrO_2(NO_3)_2$	76.6	58.2
$Pb(NO_3)_2$	71.3	43.7
$Ni(NO_3)_2$	80.7	75.4

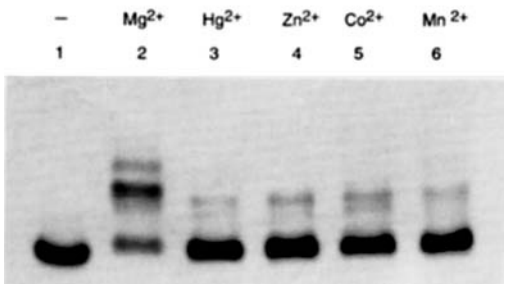

Figure 3. Autoradiogram of the products formed upon oligomerization of 2-MeImpG with template **1** in the presence of 100 mM divalent metal ion after eight days. All oligomerizations were conducted under the general conditions described by Wu and Orgel [7].

[*] Prof. C. Switzer, Dr. T. P. Prakash, C. Roberts
Department of Chemistry
University of California
Riverside, CA 92521 (USA)
Fax: Int. code +(909) 787-4713
e-mail: switzer@citrus.ucr.edu

[**] This work was supported by the National Aeronautics and Space Administration [NAGW-4184].

either template was consumed after eight days, and there were no multiple adducts.

The time dependence of oligomerization was investigated for all templates in Figure 1. These data are shown for **3** and **4** (Figure 4) after ten days and one day of incubation, respectively.

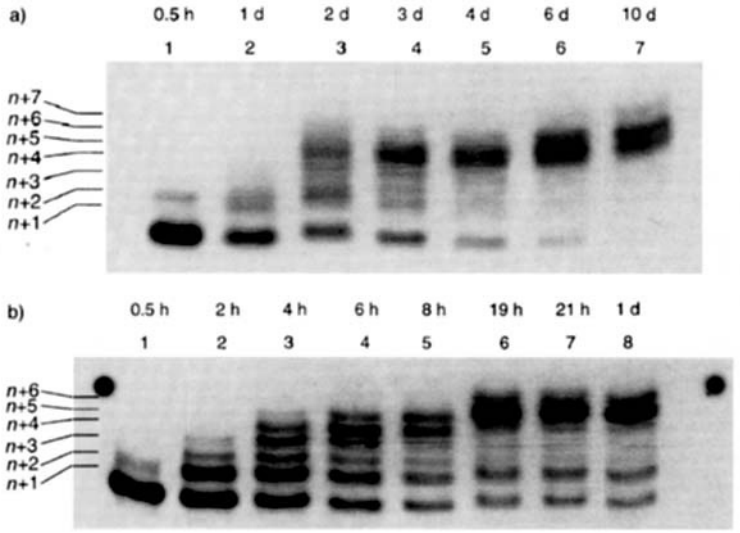

Figure 4. Results of the oligomerization of 2-MeImpG with templates **3** (a) and **4** (b) in the presence of $MgCl_2$. For each lane the time after which the reaction products were analyzed is given.

The half-lives for disappearance of templates **1**–**4** are 59, 3.4, 23, and 0.83 hours, respectively. Therefore, **3** is 28 times less efficient than 3′,5′-linked **4**, and 2′,5′-linked **1** is 17 times less efficient than 3′,5′-linked **2**. This suggests that templates **1** and **3** have roughly similar activities. 2′,5′-Linkages might well have been expected to interfere with oligomerization more dramatically, especially in **3**, which bears alternating linkages. Indeed, this is why **3** was synthesized with a more extended template region than in **1** (7-mer versus 5-mer).

Product digestions were performed with RNase T1.[7] This enzyme cleaves adjacent to *ribo*-G residues if, and only if, they are linked by a 3′,5′-phosphodiester bond. The products contain 3′-phosphate and free 5′-OH groups of the formerly adjacent nucleotides. In the present case, exhaustive RNase T1 digestion of an oligomerization product serves as an assay for the type of linkage formed between the 2′-/3′-terminal *ribo*-G residue in the hairpin templates (G^n) and the guanylate incorporated immediately adjacent to it in the product (G^{n+1}). As shown in Figure 5, lane 4, digestion of the products from 3′,5′-linked **2** yields a single major band with some faint slower-moving bands. This is consistent with the overwhelming formation of a 3′,5′-internucleotide linkage between G^n and G^{n+1} by the reaction of **2** with 2-MeImpG. As depicted in Figure 6, lanes 4–6, similar digestion of the products from 2′,5′-linked **1** yields two bands of approximately equivalent intensity. This is consistent with formation of almost equal amounts of 2′,5′- and 3′,5′-phosphodiester bonds between G^n and G^{n+1} in the oligomerization products from **1**.

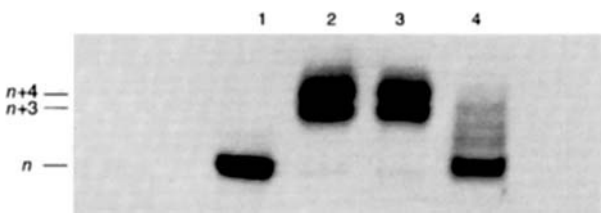

Figure 5. Digestion of the product from template **2** with RNase T_1 according to [7]. Lane 1: template **2**; lane 2: oligomerization product; lane 3: oligomerization product and buffer; lane 4: oligomerization product, buffer, and RNase T_1.

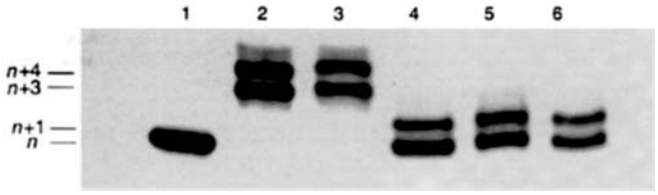

Figure 6. Digestion of the product from template **1** with RNase T_1. Lane 1: template **1**; lane 2: oligomerization product; lane 3: oligomerization product and buffer; lanes 4–6: oligomerization product, buffer, and RNase T_1 after 6, 12, and 24 hours, respectively.

In general, 2′,5′-linked RNA is more susceptible to hydrolysis than its 3′,5′-linked counterpart in a right-handed helix.[8] As noted here, diminished activity in template-directed synthesis is a further disadvantage of the 2′,5′-linkage. Consequently, there is a clear basis for supposing 3′,5′-linked oligonucleotides[9] are better adapted for the abiotic transfer of genetic information. However, there are few models for the *non-template-directed* prebiotic formation of 3′,5′-linked oligonucleotides.[10] This problem is less acute for 2′,5′-linked oligomers.[6, 11] Despite their susceptibility to hydrolysis, the present work suggests that latitude exists for the survival of 2′,5′-linked RNA. Thus, given a prebiotic bias towards non-template-directed formation of 2′,5′-linked oligomers, template-directed reactions with 2′,5′-linked RNA may have been unavoidabe to an extent. Since isomeric linkages are not per se an obstacle to template copying, 2′,5′-linked RNA (or RNA with mixed linkages) could have made a positive contribution to the evolution of modern nucleic acids.

Received: October 16, 1996
Revised version: March 20, 1997 [Z9661IE]
German version: *Angew. Chem.* **1997**, *109*, 1523–1525

Keywords: molecular evolution · molecular recognition · oligomerizations · RNA · template synthesis

[1] a) R. Parthasarathy, M. Malik, S. M. Fridey, *Proc. Natl. Acad. Sci. U. S. A.* **1982**, *79*, 7292–7296; b) M. M. Dhingra, R. H. Sarma, *Nature* **1978**, *272*, 798–801; c) A. R. Srinivasan, W. K. Olson, *Nucleic Acids Res.* **1986**, *14*, 5461–5479; d) A. Anukanth, P. K. Ponnuswamy, *Biopolymers* **1986**, *25*, 729–752.

[2] a) H. Hashimoto, C. Switzer, *J. Am. Chem. Soc.* **1992**, *114*, 6255–6256; b) K.-E. Jung, C. Switzer, *ibid.* **1994**, *116*, 6059–6061; c) H. Robinson, K.-E. Jung, C. Switzer, A. H.-J. Wang, *ibid.* **1995**, *117*, 837–838; d) J. P. Dougherty, C. J. Rizzo, R. Breslow, *ibid.* **1992**, *114*, 6254–6255; e) R. Jin, W. H. Chapman, A. R. Srinivasan, W. K. Olson, R. Breslow, K. J. Breslauer, *Proc. Natl. Acad. Sci. U. S. A.* **1993**, *90*, 10568–10572; f) R. Kierzek, L. He, D. H. Turner, *Nucleic Acids Res.* **1992**, *20*, 1685–1690; g) P. A. Giannaris, M. J. Damha, *ibid.* **1993**, *21*, 4742–4749.

[3] A. M. Michelson, C. Monny, *Biochem. Biophys. Acta* **1967**, *149*, 107–126.

[4] a) I. Hirao, Y. Ishido, K.-I. Miura, *Nucleic Acids Res. Sym. Ser.* **1983**, *12*, 193–196; b) R. Alul, G. D. Hoke, *Antisense Res. Dev.* **1995**, *5*, 3–11; c) H. Sawai, J. Seki, H. Ozaki, *J. Biomol. Struc. Dyn.* **1996**, *13*, 1043–1051; d) T. P. Prakash, K.-E. Jung, C. Switzer, *Chem. Comm.* **1996**, 1793–1794; e) T. L. Sheppard, R. Breslow, *J. Am. Chem. Soc.* **1996**, *118*, 9810–9811.

[5] J. R. Lorsch, D. P. Bartel, J. W. Szostak, *Nucleic Acids Res.* **1995**, *23*, 2811–2814.

[6] G. Ertem, J. P. Ferris, *Nature* **1996**, *379*, 238–240.

[7] T. Wu, L. E. Orgel, *J. Am. Chem. Soc.* **1992**, *114*, 317–322.

[8] D. A. Usher, A. H. McHale, *Proc. Natl. Acad. Sci. U. S. A.* **1976**, *73*, 1149–1153.

[9] a) L. E. Orgel, *Nature* **1992**, *358*, 203–209; b) G. F. Joyce, *Cold Spring Harbor Symp. on Quant. Biology* **1987**, LII, 41–51.

[10] J. P. Ferris, G. Ertem, *Science* **1992**, *257*, 1387–1389.

[11] a) R. Lohrmann, L. E. Orgel, *Tetrahedron* **1978**, *34*, 853–855; b) H. Sawai, *J. Mol. Evol.* **1988**, *27*, 181–186.

Synthesis of Nine-Membered, Masked Enediyne Analogues with DNA Intercalators and Its DNA Cleaving Activities**

Takashi Takahashi,* Hiroshi Tanaka, Haruo Yamada, Takuyuki Matsumoto, and Yukio Sugiura

Kedarcidin (KD)[1] and neocarzinostatin (NCS)[2] are members of a new class of highly potent antitumor chromoproteins whose biological activities stem from the ability of their labile nine-membered ring chromophores KD-chr (**1**) and NCS-chr (**2**) to cleave DNA via biradical intermediates. We have reported a facile approach to the nine-membered masked enediynes as analogues of **1**[3] and **2**[4] by a transannular [2,3] Wittig rearrangement. In attempts to improve the DNA cleaving activity, a number of hybrid molecules that contain a DNA-cleaving part and a DNA binder have been reported.[5] The base-[6] and sequence-[7]specificities in the cleavage of DNA by **2** have been attributed to the specific intercalation of the naphthoic acid group. However, in the cycloaromatization of **2**, intramolecular 1,5-hydrogen transfer would reduce the efficiency of double strand cleavage by quenching one of the biradical species.[8] Therefore, combination of the nine-membered KD analogue with the DNA intercalator of the NCS-chr would be expected to produce a new artificial DNA-cleaving molecule that has both high DNA-cleaving activity and base- and sequence-selectivity. In this communication, we report the synthesis and DNA-cleaving activity of the hybrid **3** possessing the KD-type DNA-cleaving moiety and the DNA intercalator of NCS-chr (Scheme 1).

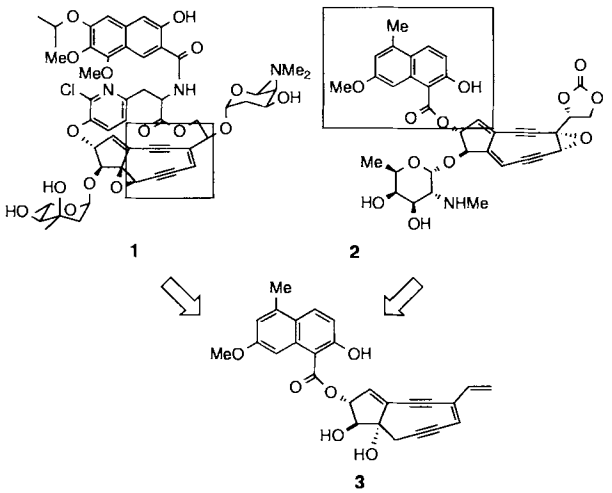

Scheme 1. Design of hybrid enediyne analogue **3**.

The masked enediyne analogues **7** were designed as a potential precursor for the KD-chr analogue **3**. Phthalic acid servers as a suitable "trigger" for controlling the stability of **7b** and generating the nine-membered enediyne **3**, which would produce the biradical species in the DNA-cleaving experiment.[9]

[*] Prof. Dr. T. Takahashi, H. Tanaka, Dr. H. Yamada
Department of Chemical Engineering
Tokyo Institute of Technology
Meguro, Tokyo 152 (Japan)
Fax: Int. code +(3)5734-2884
T. Matsumoto, Prof. Dr. Y. Sugiura
Institute for Chemical Research, Kyoto University (Japan)

[**] This work was supported by the Ministry of Education, Science, and Culture, Japan (Grant-in-Aid for Scientific Research on Priority Area No. 06240104).

The nine-membered masked enediynes **7a** and **7b** were synthesized in six steps starting from the nine-membered diyne **4** (Scheme 2).[9] Protection of the propargyl alcohol in **5** with chloroacetyl chloride at 0 °C, followed by selective removal of

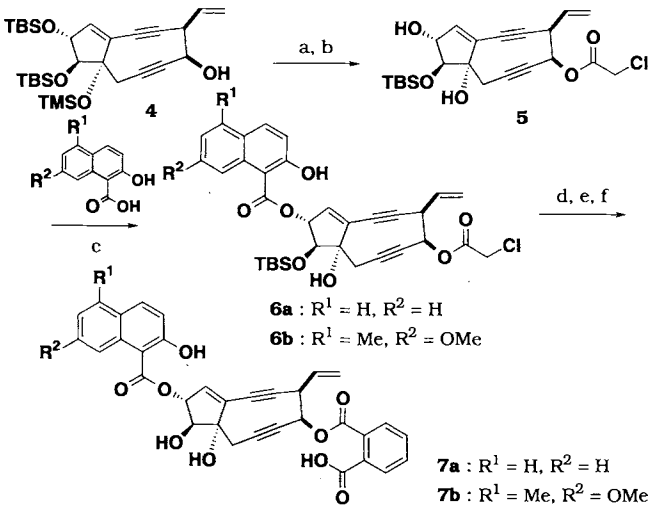

Scheme 2. Synthesis of hybrids **7a** and **7b**. a) Chloroacetyl chloride, pyridine, CH_2Cl_2; b) aqueous HF/CH_3CN (5/95), 0 °C, 76% from **4**; c) 1-ethyl-3-(3-dimethylaminopropyl)carbodiimide, CH_2Cl_2, 78%; d) aqueous NH_3, MeOH, 0 °C; e) phthalic anhydride, pyridine, DMAP, CH_2Cl_2; f) aqueous HF/CH_3CN (5/95), room temperature, **7a**: 16% from **6a**, **7b**: 24% from **5**.

the tertiary trimethylsilyl (TMS) and allylic *tert*-butyldimethylsilyl (TBS) groups with aqueous HF in CH_3CN gave diol **5** in 76% overall yield. Initially, synthesis of the model hybrid **7a** was examined. Treatment of the diol **4** with 2-hydroxy-1-naphthoic acid and 1-ethyl-3-(3-dimethylaminopropyl)carbodiimide gave ester **6a** in 78% yield. Selective removal of chloroacetyl group in **6a** with aqueous NH_3 in MeOH and treatment of the resulting alcohol with phthalic anhydride in the presence of 4-dimethylaminopyridine (DMAP) gave the diester. Deprotection by cleaving the TBS group with aqueous HF in CH_3CN afforded the desired hybrid analogue **7a**[10] in 16% overall yield from **6a**. The NCS-KD hybrid **7b** was prepared essentially as described above. The diol **5** was treated with 2-hydroxy-7-methoxy-5-methylnaphthoic acid, prepared from 5-methyl-1,3-cyclohexadione according to Hirama et al.'s procedure,[11] to give the naphthoate **6b**. The resulting ester **6b** was transformed into the **7b**[12] in 24% yield from **5**.

The DNA-cleaving activities of the hybrids **7a**, **7b**, and **8** (the triol lacking the naphthoic acid)[9] were examined under the conditions shown in Figure 1. Supercoiled pBR322 DNA was incubated with **7a** and **7b** at various concentrations (10–100 μM) in 10% MeOH in 20 mM Tris–HCl buffer (pH 7.5, Tris = tris(hydroxymethyl)aminomethane) at 37 °C for 18 h in the absence of thiol. Agarose gel electrophoresis of the DNA exposed to **7a** is shown in Figure 2 . These results clearly show that the introduction of the DNA intercalator (naphthoic acid) improved the DNA-cleaving activities of **7a** and **7b** to about ten times that of triol **8**. Remarkably, both **7a** and **7b** caused DNA cleavage with the formation of Form III even at 10 and 20 μM concentrations, respectively. The DNA-cleaving activities of the hybrid analogues **7a** and **7b** are outstanding relative to the reported enediyne analogues.[5] Studies on DNA cleavage of the 3′-labeled pBR322 fragment by **7a** and **7b** were carried out; no sequence-specificity was observed.

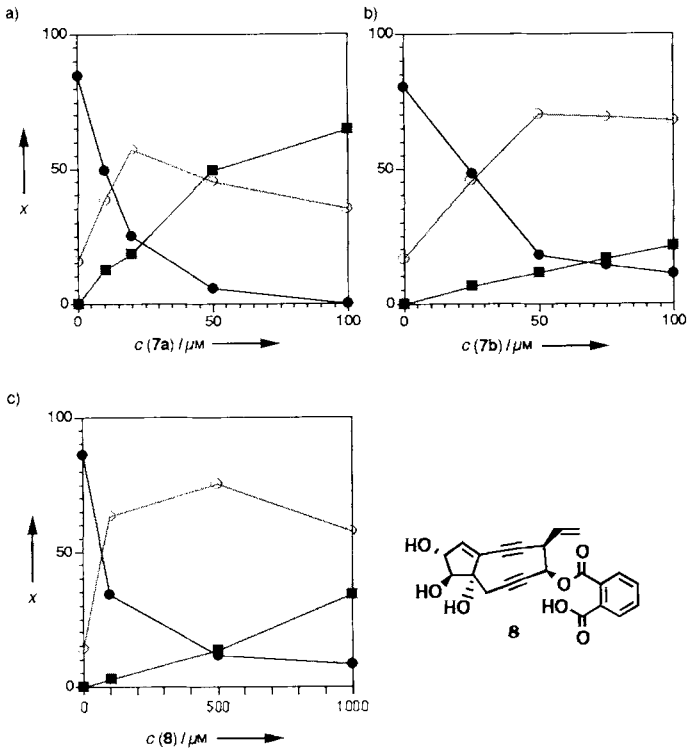

Figure 1. Percentages of the topological forms of pBR322-DNA Form I (superhelix (●)), Form II (circular DNA with one strand broken ○), and Form III (linear DNA (■)) after treatment with **7a** (a), **7b** (b), and **8** (c) at different concentrations. Reaction conditions: 10% MeOH, 20 mM Tris–HCl buffer (pH 7.5), 37 °C.

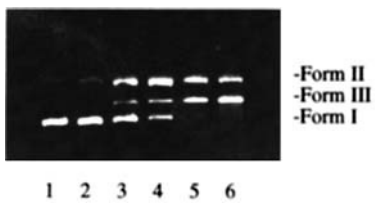

Figure 2. Dependence of the DNA-cleaving activity of **7a** on concentration: bands obtained on agarose gel by electrophoretic analysis after DNA strand cleavage. Lane 1: intact DNA; lane 2: control; lanes 3–6: fragments after DNA cleavage with 10, 20, 50, and 100 μM of **7a**.

The hybrid–DNA complex was modeled according to Schreiber et al.'s procedure[13] with the program MacroModel[14] (Figure 3). The model was developed by manually intercalating the diradical hybrid **9** (formed by activation) between A_4 and A_5 in the ten base-pair double-stranded DNA (poly-(dA-dT)). The complex was subjected to substructure minimization with the AMBER* (united atom) force field. The modeling study suggests that the hybrid analogue **3** can adopt the required conformation to facilitate double strand cleavage of DNA. The C3 radical approaches to within 3.1 Å of the C4′ hydrogen atom of A_6, and the C6 radical is also close to the C4′ hydrogen atom of T_4 (3.8 Å).

In summary, we have succeeded in designing and synthesizing nine-membered KD analogues possessing an intercalated naphthoic acid group. The biological properties of the designed analogues may provide a potential lead for the further development of DNA-cleaving molecules. Introduction of a DNA recognition site to improve base- and site-selectivities is under investigation.

Received: March 19, 1997 [Z10048IE]
German version: *Angew. Chem.* **1997**, *109*, 1570–1572

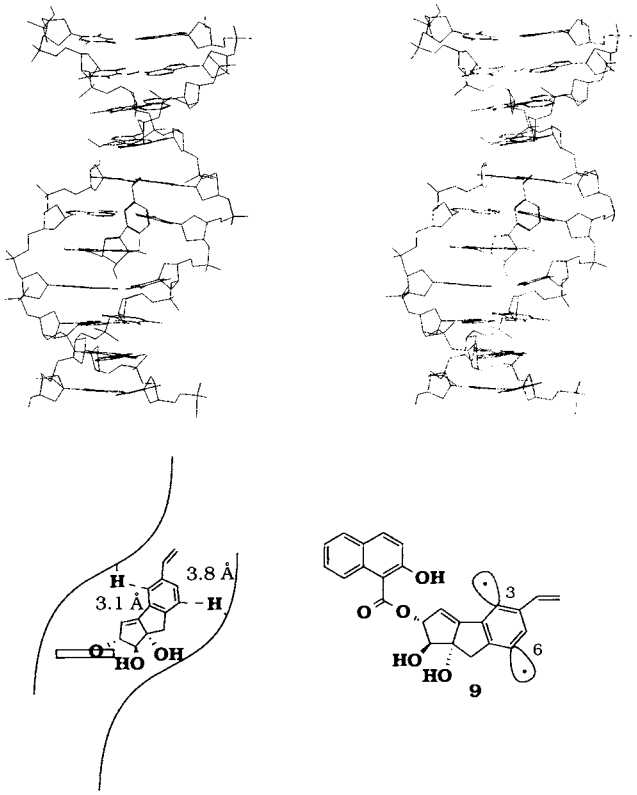

Figure 3. Top: Stereoview of the complex between the diradical hybrid **9** and DNA obtained by force field calculations. Bottom: Schematic representation of the intercalation of **9** between the DNA strands (the naphthoic acid group is symbolized by a rectangle) and the structure of **9**.

Keywords: DNA cleavage · enediynes · molecular modeling · naphthoic acid

[1] a) K. S. Lam, G. A. Hesler, D. R. Gustavson, A. R. Crosswell, J. M. Veitch, S. Forenza, K. Tomita, *J. Antibiot.* **1991**, *44*, 472–478; b) S. J. Hofstead, J. A. Matson, A. R. Malacko, H. Marquardt, *ibid.* **1992**, *45*, 1250–1254; c) J. E. Leet, D. R. Schroeder, S. J. Hofstead, J. Golik, K. L. Colson, S. Huang, S. E. Klohr, T. W. Doyle, J. A. Matson, *J. Am. Chem. Soc.* **1992**, *114*, 7946–7948; d) J. E. Leet, D. R. Schroeder, D. R. Langley, K. L. Colson, S. Huang, S. E. Klohr, M. S. Lee, J. Golik, S. J. Hofstead, T. W. Doyle, J. A. Matson, *ibid.* **1993**, *115*, 8432–8443; e) N. Zein, K. L. Colson, J. E. Leet, D. R. Schroeder, W. Solomon, T. W. Doyle, A. M. Casazza, *Proc. Natl. Acad. Sci. USA* **1993**, *90*, 2822–2826.

[2] a) Y. Koide, F. Ishii, K. Hasuda, Y. Koyama, K. Edo, S. Katamine, F. Kitame, N. Ishida, *J. Antibiot.* **1980**, *33*, 342–346; b) M. A. Napaier, B. Holmquist, D. J. Strydom, I. H. Goldberg, *Biochem. Biophys. Res. Commun.* **1979**, *89*, 635–642; c) K. Edo, M. Mizugaki, Y. Koide, H. Seto, K. Furihata, N. Otake, N. Ishida, *Tetrahedron Lett.* **1985**, *26*, 331–334; d) A. G. Myers, *ibid.* **1987**, *28*, 4493–4496; e) A. G. Myers, P. J. Proteau, T. M. Handel, *J. Am. Chem. Soc.* **1988**, *110*, 7212–7214; f) A. G. Myers, P. J. Proteau, *ibid.* **1989**, *111*, 1146–1148.

[3] T. Doi, T. Takahashi, *J. Org. Chem.* **1991**, *56*, 3465–3467.

[4] T. Takahashi, H. Tanaka, Y. Hirai, T. Doi, H. Yamada, T. Shiraki, Y. Sugiura, *Angew. Chem.* **1993**, *105*, 1719–1722; *Angew. Chem. Int. Ed. Engl.* **1993**, *32*, 1657–1659.

[5] a) M. Hirama, T. Gomibuti, K. Fujiwara, *J. Am. Chem. Soc.* **1991**, *113*, 9851–9853; b) K. C. Nicolaou, E. P. Schreiner, Y. Iwabuchi, T. Suzuki, *Angew. Chem.* **1992**, *104*, 317–319; *Angew. Chem. Int. Ed. Engl.* **1992**, *31*, 340–342; c) D. L. Boger, J. Zhou, *J. Org. Chem.* **1993**, *58*, 3018–3024; d) M. Tokuda, K. Fujiwara, T. Gomibuti, M. Hirama, M. Uesugi, Y. Sugiura, *Tetrahedron Lett.* **1993**, *34*, 669–672; e) F. Semmelhack, J. J. Gallapher, W.-D. Ding, G. Krishnamurthy, R. Babune, G. A. Ellestad, *J. Org. Chem.* **1994**, *59*, 4357–4359; f) M. D. Wittman, J. F. Kandow, R. D. Langeley, D. M. Wyas, W. C. Rose, W. Solomon, N. Zein, *Biochem. Med. Chem. Lett.* **1995**, *5*, 1049–1052; g) K. Toshima, T. Ohta, A. Ohashi, T. Nakamura, M. Nakata, K. Tatsuta, S. Matsumura, *J. Am. Chem. Soc.* **1995**, *117*, 4822–4831; h) A. G. Myers, M. Hammond, Y. Wu, J.-N. Xiang, P. M. Harrington, E. Y. Kuo, *ibid.* **1996**, *118*, 10006–10007.

[6] a) M. Takesita, L. S. Kappen, A. P. Grollman, M. Eisenberg, I. H. Goldberg, *Biochemistry* **1981**, *20*, 7599–7606; b) H. Sugiyama, H. Kawabata, T. Fujiwara, Y. Dannoue, I. Saito, *J. Am. Chem. Soc.* **1990**, *112*, 5252–5257; c) S. M. Meschwitz, I. H. Goldberg, *Proc. Natl. Acad. Sci. USA* **1991**, *88*, 3047–3051; d) B. L. Franc, L. Worth, Jr., D. F. Christner, J. W. Kozarich, J. Stubbe, L. S. Kappen, I. H. Goldberg, *J. Am. Chem. Soc.* **1991**, *113*, 2271–2275.

[7] a) S. H. Lee, I. H. Goldberg, *Biochemistry* **1989**, *28*, 1019–1026; b) A. Galat, I. H. Goldberg, *Nucleic Acids Res.* **1990**, *18*, 2093–2099; c) review on neocarzinostatin: I. H. Goldberg, *Acc. Chem. Res.* **1991**, *24*, 193–197.

[8] a) P. A. Wender, M. J. Tebbe, *Tetrahedron* **1994**, *50*, 1419–1434; b) K. Toshima, K. Yanagawa, K. Ohta, T. Kano, M. Nagatra, *Tetrahedron Lett.* **1994**, *35*, 1573–1577; c) S. Kawata, T. Oishi, M. Hirama, *ibid.* **1994**, *35*, 4595–4599.

[9] T. Takahashi, H. Tanaka, H. Yamada, T. Matsumoto, Y. Sugiura, *Angew. Chem.* **1996**, *108*, 1946–1949; *Angew. Chem. Int. Ed. Engl.* **1996**, *35*, 1835–1837.

[10] **7a**: ^{1}H NMR (270 MHz, $CDCl_3$): δ = 8.68 (d, 1H, J = 8.9 Hz, Ph), 7.94 (d, 1H, J = 8.9 Hz, Ph), 7.80–7.67 (m, 3H, Ph), 7.61–7.52 (m, 3H, Ph), 7.39 (ddd, 1H, J = 6.9, 6.9, 1.3 Hz, Ph), 7.17 (d, 1H, J = 8.9 Hz, Ph), 6.14 (d, 1H, J = 2.0 Hz, C12-H), 5.74–5.62 (m, 1H, C11-H), 5.53, (br. d, 1H, J = 5.0 Hz, C5-H), 5.39 (ddd, 1H, J = 16.8, 1.3, 1.3 Hz, vinyl), 5.18 (ddd, 1H, J = 9.9, 1.3, 1.3 Hz, vinyl), 4.52 (d, 1H, J = 3.6 Hz, C10-H), 4.07 (br. d, 1H, J = 5.3, 5.0 Hz, C4-H), 3.00 (d, 1H, J = 18.1 Hz, C8-H), 2.73 (dd, 1H, J = 18.1, 1.0 Hz, C8-H); ^{13}C NMR (67.8 MHz, $CDCl_3$): δ = 169.7, 167.3, 164.5, 137.5, 134.1, 132.1, 131.7, 131.6, 131.1, 130.8, 129.4, 129.1, 129.06, 129.0, 128.6, 127.9, 125.1, 123.9, 119.8, 119.2, 104.1, 100.2, 98.6, 94.6, 86.8, 86.3, 83.8, 83.4, 69.5, 45.9, 27.7; IR ($CHCl_3$): $\tilde{\nu}$ = 3414, 2924, 2210, 1722, 1640, 1463, 1283, 1240, 1138, 947, 831 cm^{-1}; FAB-MS: *m/z*: 563 [M^+ − H].

[11] a) K. Takahashi, T. Suzuki, M. Hirama, *Tetrahedron Lett.* **1992**, *33*, 4603–4604; b) K. Takahashi, T. Tanaka, T. Suzuki, M. Hirama, *Tetrahedron* **1994**, *50*, 1327–1340.

[12] **7b**: ^{1}H NMR (270 MHz, $CDCl_3$): δ = 8.01 (br. d, 1H, J = 8.9 Hz, Ph), 7.89 (d, 1H, J = 2.3 Hz, Ph), 7.81–7.77 (m, 1H, Ph), 7.67–7.64 (m, 1H, Ph), 7.56 (ddd, 1H, J = 7.6, 7.6, 1.7 Hz, Ph), 7.51 (ddd, 1H, J = 7.6, 7.6, 1.7 Hz, Ph), 7.00 (d, 1H, J = 8.9 Hz, Ph), 6.86 (br. d, 1H, J = 2.3 Hz, Ph), 6.08 (d, 1H, J = 2.3 Hz, C12-H), 5.68 (dd, 1H, J = 3.6, 2.3 Hz, C11-H), 5.67 (ddd, 1H, J = 16.8, 9.9, 5.9 Hz, vinyl), 5.53 (br. d, 1H, J = 5.3 Hz, C5-H), 5.39 (br. d, 1H, J = 16.8 Hz, vinyl), 5.18 (br. d, 1H, J = 9.9 Hz, vinyl), 4.52 (d, 1H, J = 3.6 Hz, C10-H), 4.40 (br. dd, 1H, J = 5.9, 5.3 Hz, C4-H), 3.84 (s, 1H, OMe), 2.98 (br. d, 1H, J = 17.8 Hz, C8-H), 2.72 (dd, 1H, J = 17.8, 1.3 Hz, C8-H), 2.56 (s, 1H, Me); ^{13}C NMR (67.8 MHz, $CDCl_3$): δ = 172.1, 169.2, 167.2, 164.0, 159.5, 136.9, 134.6, 134.0, 133.0, 132.2, 131.8, 131.2, 130.6, 130.1, 129.4, 129.2, 127.9, 123.1, 119.8, 116.6, 115.8, 104.3, 103.8, 100.4, 94.8, 87.1, 86.0, 83.7, 83.6, 83.3, 69.5, 55.2, 46.1, 27.4, 20.0; IR ($CDCl_3$): $\tilde{\nu}$ = 3410, 2924, 1724, 1634, 1614, 1464, 1412 ,1376, 1283, 1174, 1150, 1119, 991, 955 cm^{-1}; FAB-MS: *m/z*: 607 [M^+ − H], 631 [M^+ + Na].

[13] D. Elbaum, S. L. Schreiber, *Bioorg. Med. Chem. Lett.* **1994**, *4*, 309–314.

[14] F. Mohamadi, N. G. J. Richards, W. C. Guida, R. Liskamp, M. Lipton, C. Caufield, G. Chang, T. Hendrickson, W. C. Still, *J. Comput. Chem.* **1990**, *11*, 440–467.

Synthesis and Catalytic Activity of Dendritic Diphosphane Metal Complexes

Manfred T. Reetz,* Gunther Lohmer, and Renate Schwickardi

Dedicated to Professor Dieter Seebach on the occasion of his 60th birthday

The synthesis of dendrimers with defined inner and outer structural elements provides access to macromolecular materials having special properties and functions[1] that are, in principle, also useful for applications in catalysis. Although a number of metal-containing dendrimers have been described,[1, 2] they were rarely prepared for use as catalysts.[3–5] As recently delineated by van Koten et al., such catalysts can be considered to be at the interface between homogeneous and heterogeneous catalysis.[3] In the most favorable case they combine the advantages of both classes of catalysts, namely, the existence of a specific number of structurally defined, catalytically active metal centers as in traditional homogeneous catalysis as well as the possibility of simple separation and reuse of the catalyst as in heterogeneous catalysis. However, recycling has not yet been achieved for any dendritic metal catalyst.

We now report on 1) a simple synthesis of dendritic diphosphanes, 2) the preparation of the corresponding metal and bimetal complexes, 3) their application in catalysis, and 4) modes of recycling the dendritic metal catalysts.

The starting point of our synthesis is the DAB-based (DAB = 1,4-diaminobutane) polyamino dendrimer DAB-dendr-$(NH_2)_{16}$ (**1**), which can be prepared according to the method

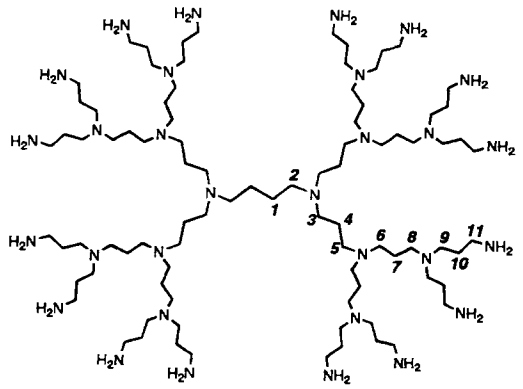

1

$CH_2O/HPPh_2$

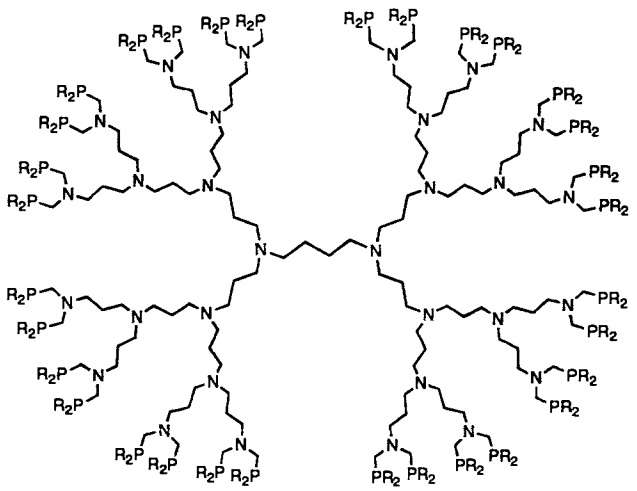

2 (R = C_6H_5)

of Vögtle et al.,[6] and which is now commercially available.[7] Double phosphinomethylation of each of the 16 primary amino endgroups, a reliable reaction type in simple cases,[8] was effected in essentially quantitative yield upon use of Ph_2PCH_2OH prepared in situ from CH_2O and $HPPh_2$. The reaction affords the dendrimer DAB-dendr-$[N(CH_2PPh_2)_2]_{16}$[9] (**2**), which has a molecular weight[10] of 8029; it was characterized by elemental

[*] Prof. Dr. M. T. Reetz, Dipl.-Chem. G. Lohmer, R. Schwickardi
Max-Planck-Institut für Kohlenforschung
Kaiser-Wilhelm-Platz 1, D-45470 Mülheim an der Ruhr (Germany)
Fax: Int. code +(208) 1 306-2985
e-mail: reetz@mpi-muelheim.mpg.de

analysis as well as IR and NMR spectroscopy. For example, during the course of the reaction the NH bands in the IR spectrum disappeared completely. The ^{13}C NMR spectra of **1** and **2** are also instructive (Figure 1). In particular, the signals at $\delta = +30.6$ and $+40.3$, corresponding to the C10 and C11

Figure 1. Portions of the ^{13}C NMR spectra of **1** (top) and of **2** (bottom).

atoms of **1**, are no longer visible in the spectrum of the phosphinomethylated compound **2**, which is a clear indication of a quantitative reaction mode. The completeness of the double phosphinomethylation is also evident by inspection of the ^{31}P NMR spectrum of **2**. It shows a sharp signal at $\delta = -28.0$ and resembles the spectrum of the parent compound n-C_3H_7-$N(CH_2PPh_2)_2$ ($\delta = -27.8$).

The dendrimer **2** with 16 bidentate ligands on the outer surface provides the possibility of specific complexation with a variety of transition metals, and loading can be complete or partial. In an initial series of experiments complete metal loading forming the metal-containing dendrimers **3**–**6** was readily accomplished under standard reactions with $[PdCl_2(PhCN)_2]$, $[Pd(CH_3)_2(tmeda)]$, $[Ir(cod)_2BF_4]$ and $[Rh(cod)_2BF_4]$. For the purpose of characterization, correct elemental analyses and particularly NMR spectroscopy were useful, especially as NMR data of the corresponding metal complexes of the parent compound n-$C_3H_7N(CH_2PPh_2)_2$ were available for comparison: the ^{31}P NMR data of the model compounds and of the dendrimers do not differ significantly ($\delta = +8.3$ for **3** and $+8.5$ for $[n$-C_3H_7-$N(CH_2PPh_2)_2PdCl_2]$; $+3.3$ for **4** and $+3.9$ for $[n$-C_3H_7-$N(CH_2PPh_2)_2Pd(CH_3)_2]$; $+7.6$ (d, $J_{P,Rh} = 141$ Hz) for **6** and $+7.8$ (d, $J_{P,Rh} = 141$ Hz) for $[n$-$C_3H_7N(CH_2PPh_2)_2$-$Rh(cod)BF_4]$).

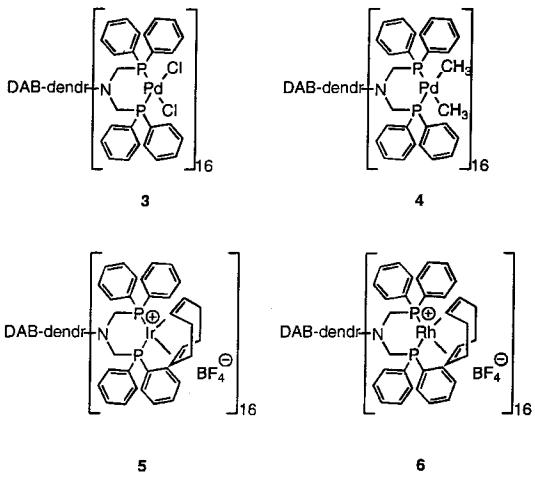

To prepare bimetallic complexes, dendrimer **2** was first loaded with $[Pd(CH_3)_2(tmeda)]$ to 50%. Due to the statistical distribution of the metal, the formation of a single defined product **7** is unlikely. The ^{31}P NMR spectrum of the crude product shows two sharp signals at $\delta = -27.8$ and $+3.5$ for the metal-free and the metal-containing ligands, respectively. Upon reacting the material with $[Ni(CH_3)_2(tmeda)]$, bimetallic dendrimers **8** were obtained. The ^{31}P NMR spectrum reveals two signals at $\delta = +3.5$ and $+18.5$.

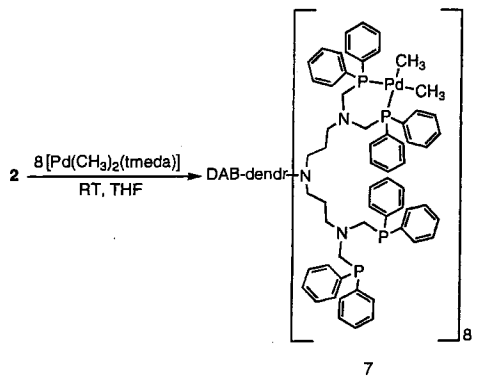

7

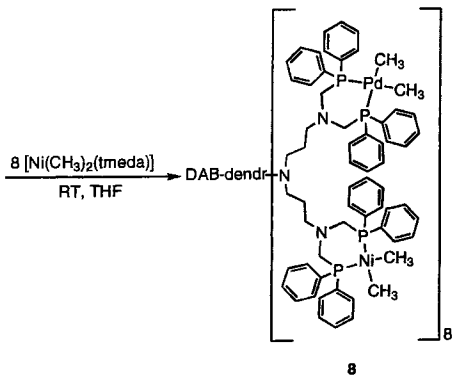

8

Initial experiments to test the metal-containing dendrimers in catalysis were successful, for example, in the Heck reaction[11] of bromobenzene **9** and styrene **10** with formation of stilbene **11**.

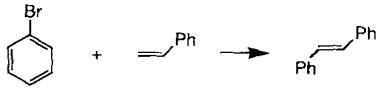

9 **10** **11**

Reactants **9** and **10** were dissolved in dimethylformamide (DMF) and heated for 3 h at 130 °C in the presence of sodium acetate as base and complex **4** (0.125 mol% corresponding to 2 mol% "Pd-monomer") as catalyst. The insoluble inorganic components were filtered from the reaction mixture, and the clear solution was diluted with diethyl ether. Addition of this relatively unpolar solvent caused essentially complete precipitation (>98%) of a Pd-containing dendrimer, the precise structure of which has not been determined.[12] The analysis of the reaction mixture by gas chromatography showed the presence of **11** (89%) and 1,1-diphenylethylene (11%) at a conversion of 85–90%. The isolated Pd-containing dendrimer was used in the same reaction once more and displayed comparable catalytic activity (91% **11** and 9% 1,1-diphenylethylene, conversion 77%). The catalytic activity of the precatalyst **7** having 50% Pd-loading was similar.

In the few previously known cases of catalysis with dendritic metal complexes, catalytic activity was shown to be slightly or significantly lower than that of the corresponding monomeric parent compounds.[3,4] In contrast, we observed in our system a significantly higher activity (typically, turnover numbers (TON) of 50 for **4** versus 16 for the parent compound $[RN(CH_2PPh_2)_2Pd(CH_3)_2]$, R = n-C_3H_7 or C_6H_5). This is attributable to the higher thermal stability of the dendritic complexes. Thus, in the case of **4** and **7** practically no undesired formation of elemental Pd was observed. In contrast, the Pd complexes of the parent compounds undergo partial decomposition with formation of Pd precipitates.

Finally, in preliminary experiments the hydroformylation[13] of 1-octene **12** was tested. Use of 0.0033 mol% (0.052 mol% "Pd-monomer") of the Rh-containing dendrimer **6** and a small excess (5%) of the free ligand **2** gave a smooth reaction with quantitative formation of the aldehydes **13** and **14** in a ratio of

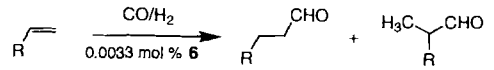

14 R = C_6H_{13} **15** **16**

60:40 (turnover frequency (TOF) = 360 h^{-1}). These data are similar to the values obtained upon using the parent compounds $[PhN(CH_2PPh_2)_2Rh(cod)BF_4]$ or $[n\text{-}C_3H_7N(CH_2PPh_2)_2Rh(cod)BF_4]$ (TOF = 240 h^{-1}; n/iso = 62:38 and TOF = 185 h^{-1}; n/iso = 61:39, respectively).[14] Although an efficient method for recycling the very small amounts of the dendritic catalyst still needs to be developed, several options are evident. The use of membrane reactors[15] is a perspective that is also of interest for the other metal-containing dendritic catalysts described herein.

The strategy that we have developed for the synthesis of dendritic diphosphanes opens a general way to prepare transition-metal-containing dendrimers for use in catalysis. Thus, dendrimer **1** was treated analogously with CH_2O/HP($cyclo$-$C_6H_{11})_2$ or CH_2O/$HP(C_2H_5)_2$ to provide the corresponding dendrimers with 16 outer cyclohexyl- or ethyl-substituted diphosphane units. The corresponding $[Pd(CH_3)_2]$ and $[Rh(cod)BF_4]$ complexes were also prepared analogously and are currently the subject of further investigations, as are diphosphane-metal complexes of the commercially available polyamino-dendrimer DAB-dendr-$(NH_2)_{64}$[7] having 64 outer amino groups.

Experimental Section

Synthesis of dendrimer **2**: Under an inert atmosphere the mixture of paraformaldehyde (0.213 g, 7.09 mmol) and diphenylphosphane (1.35 mL, 7.76 mmol) in methanol (5 mL) was heated at 65–70 °C for 10 min. The reaction mixture was cooled to room temperature and treated with a solution of **1** (0.336 g, 0.20 mmol; 3.19 mmol with respect to the amino endgroups) in methanol (3 mL). After 0.5 h stirring at room temperature, toluene (15 mL) was added, and the clear yellow solution heated at 65 °C for 0.5 h. To ensure complete reaction, the mixture was stirred for an additional 12 h at room temperature. The volume of the reaction mixture was concentrated under reduced pressure to about 3 mL, and methanol (10 mL) was added. The product precipitated in the form of a glassy colorless solid, which was dried under high vacuum for 10 h at 60–65 °C. Yield: 1.53 g (>96%). IR (KBr): $\tilde{\nu}$[cm^{-1}] = 3068 (phenyl), 3050 (phenyl), 2941 (NCH_2), 2793 (NCH_2), 1484 (phenyl), 1479 (phenyl), 1432 (phenyl), 739 (phenyl), 693 (phenyl). ^1H NMR (400 MHz, $CDCl_3$): δ = 1.45 (m, 60H, $NCH_2CH_2CH_2N$, $NCH_2CH_2CH_2CH_2N$), 2.18 (m, 52H, $CH_2NCH_2CH_2$), 2.34 (m, 32H, $NCH_2CH_2CH_2NCH_2P$), 2.80 (m, 32H, CH_2NCH_2P), 3.54 (m, 64H, NCH_2P), 7.20 (m, 192H, phenyl), 7.37 (m, 128H, phenyl). $^{13}C\{^1H\}$ NMR (101 MHz, $CDCl_3$): δ = 23.99 (s, *C10*), 24.26 (s, *C4/7*), 24.70 (s, *C1*), 51.77 (s, *C9*), 51.97 (s, *C8*), 52.47 (s, *C5/6*), 52.68 (s, *C3*), 54.67 (t, $^3J(C,P)$ = 9.5 Hz, *C11*), 58.78 (dd, $^1J(C,P)$ = 14.1 Hz, $^3J(C,P)$ = 8.6 Hz, NCH_2P), 128.29 (m, phenyl), 133.03 (d, $J(C,P)$ = 18.2 Hz, phenyl), 138.28 (d, $J(C,P)$ = 13.3 Hz, phenyl). $^{31}P\{^1H\}$ NMR (162 MHz, $CDCl_3$): δ = −28.01 (s); elemental analysis calcd. for $C_{504}H_{560}N_{30}P_{32}$: C 75.39, H 7.03, N 5.23, P 12.34; found: C 75.18, H 6.91, N 5.24, P 12.59.

Received: January 30, 1997 [Z 10057IE]
German version: *Angew. Chem.* **1997**, *109*, 1559–1562

Keywords: homogeneous catalysis · dendrimers · Heck reaction · hydroformylation · palladium · rhodium

[1] a) G. R. Newkome, C. N. Moorefield, F. Vögtle, *Dendritic Molecules: Concepts–Syntheses–Perspectives*, VCH, Weinheim, **1996**; b) D. A. Tomalia, *Sci. Am.* **1995**, *272*, 62.

[2] See, for example: a) N. Ardoin, D. Astruc, *Bull. Soc. Chim. Fr.* **1995**, *132*, 875; b) P. Lange, A. Schier, H. Schmidbaur, *Inorg. Chim. Acta* **1995**, *235*, 263; c) C. J. Hawker, J. M. J. Fréchet, *J. Chem. Soc. Perkin Trans. 1* **1992**, 2459; d) S. Achar, R. J. Puddephatt, *Angew. Chem.* **1994**, *106*, 895; *Angew. Chem. Int. Ed. Engl.* **1994**, *33*, 874; e) S. Serroni, G. Denti, S. Campagna, A. Juris, M. Ciano, V. Balzani, *ibid.* **1992**, *104*, 1540, bzw. **1992**, *31*, 1493; f) G. R. Newkome, F. Cardullo, E. C. Constable, C. N. Moorefield, A. M. W. Cargill Thompson, *J. Chem. Soc. Chem. Commun.* **1993**, 925; g) Y.-H. Liao, J. R. Moss, *ibid.* **1993**, 1774; h) M. Slany, A.-M. Caminade, J. P. Majoral, *Tetrahedron Lett.* **1996**, *37*, 9053; i) M. Bardaji, M. Kustos, A.-M. Caminade, J.-P. Majoral, B. Chaudret, *Organometallics* **1997**, *16*, 403; j) H. Brunner, S. Altmann, *Chem. Ber.* **1994**, *127*, 2285.

[3] A silane-dendrimer having 12 arylnickel(II)-bearing endgroups, a compound which catalyzes the addition of CCl_4 to methyl methacrylate in a Kharasch reaction, has been described; however, separation from the product and recyclability of the catalyst are not mentioned: J. W. J. Knapen, A. W. van der Made, J. C. de Wilde, P. W. N. M. van Leeuwen, P. Wijkens, D. M. Grove, G. van Koten, *Nature* **1994**, *372*, 659.

[4] A dendrimer with six TADDOL endgroups has been prepared and the corresponding Ti alkoxides function as catalysts (20 mol%) in the addition of Et_2Zn to benzaldehyde; separation of the metal-free ligand following aqueous workup was accomplished by column chromatography: D. Seebach, R. E. Marti, T. Hintermann, *Helv. Chim. Acta* **1996**, *79*, 1710.

[5] Branched compounds with 4 or 5 Pd-bearing triphosphane units, which catalyze the electrochemical reduction of CO_2 to CO, have been described; nothing is reported about the possible separation or reuse of the catalysts: A. Miedaner, C. J. Curtis, R. M. Barkley, D. L. DuBois, *Inorg. Chem.* **1994**, *33*, 5482.

[6] a) E. Buhleier, W. Wehner, F. Vögtle, *Synthesis* **1978**, 155; see also b) C. Wörner, R. Mülhaupt, *Angew. Chem.* **1993**, *105*, 1367; *Angew. Chem. Int. Ed. Engl.* **1993**, *32*, 1306; c) E. M. M. de Brabander-van den Berg, E. W. Meijer, *ibid.* **1993**, *105*, 1370, and **1993**, *32*, 1308.

[7] Dendrimer **1** as well as further poly(amino) dendrimers are commercially available from DSM Fine Chemicals B. V. (Heerlen/The Netherlands).

[8] a) K. Issleib, M. Lischewski, A. Zschunke, *Z. Chem.* **1974**, *14*, 243; b) K. Kellner, W. Hanke, A. Tzschach, Z. Nagy-Magos, L. Markó, *J. Organomet. Chem.* **1984**, *268*, 175; c) I. Fawcett, P. A. T. Hoye, R. D. W. Kemmitt, D. J. Law, D. R. Russell, *J. Chem. Soc. Dalton Trans.* **1993**, 2563; d) A. L. Balch, M. M. Olmstead, S. P. Rowley, *Inorg. Chim. Acta* **1990**, *168*, 255; e) K. Kellner, A. Tzschach, *Z. Chem.* **1984**, *24*, 365.

[9] Designation of **2** according to the Newkome nomenclature [1]: 32-cascade: 1,4-diaminobutane[4]:(1-azabutylidene)^3:diphenylphosphinomethane).

[10] Mass spectrometric methods such as matrix-assisted time-of-flight mass spectrometry (MALDI-TOF-MS) or electrospray mass spectrometry (ESI-MS) were not successful for the phosphinomethylated dendrimers **2** or for the corresponding metal complexes **3**–**6**.

[11] a) R. F. Heck, *Palladium Reagents in Organic Syntheses*, Academic Press, London, **1985**; b) J. Tsuji, *Palladium Reagents and Catalysts: Innovations in Organic Synthesis*, Wiley, Chichester, **1995**; c) A. de Meijere, F. E. Meyer, *Angew. Chem.* **1994**, *106*, 2473; *Angew. Chem. Int. Ed. Engl.* **1994**, *33*, 2379.

[12] Mechanistically it can be assumed that the Pd complex **4** as precatalyst undergoes a thermally induced, ethane-producing reductive elimination with formation of the corresponding 14-electron chelate [16]. This adds oxidatively to bromobenzene **9**, thereby initiating the Heck reaction. On completion of the reaction, the ^{31}P NMR spectrum of the separated solid material in [D_8]DMF shows a single signal at $\delta = +23$ as a sharp singlet. It is possibly an anionic Pd species [17].

[13] B. Cornils, W. A. Herrmann, *Applied Homogeneous Catalysis with Organometallic Compounds*, VCH, Weinheim, **1996**.

[14] S. R. Waldvogel, PhD thesis, Universität Bochum, **1996**; M. T. Reetz, S. R. Waldvogel, *Angew. Chem.* **1997**, *109*, 870; *Angew. Chem. Int. Ed. Engl.* **1997**, *36*, 865.

[15] U. Kragl, C. Dreisbach, *Angew. Chem.* **1996**, *108*, 684; *Angew. Chem. Int. Ed. Engl.* **1996**, *35*, 642.

[16] a) M. Portnoy, D. Milstein, *Organometallics* **1993**, *12*, 1665; b) M. Portnoy, D. Milstein, *ibid.* **1994**, *13*, 3465; c) W. A. Herrmann, C. Brossmer, T. Priermeier, K. Öfele, *J. Organomet. Chem.* **1994**, *481*, 97.

[17] C. Amatore, A. Jutand, M. A. M'Barki, *Organometallics* **1992**, *11*, 3009.

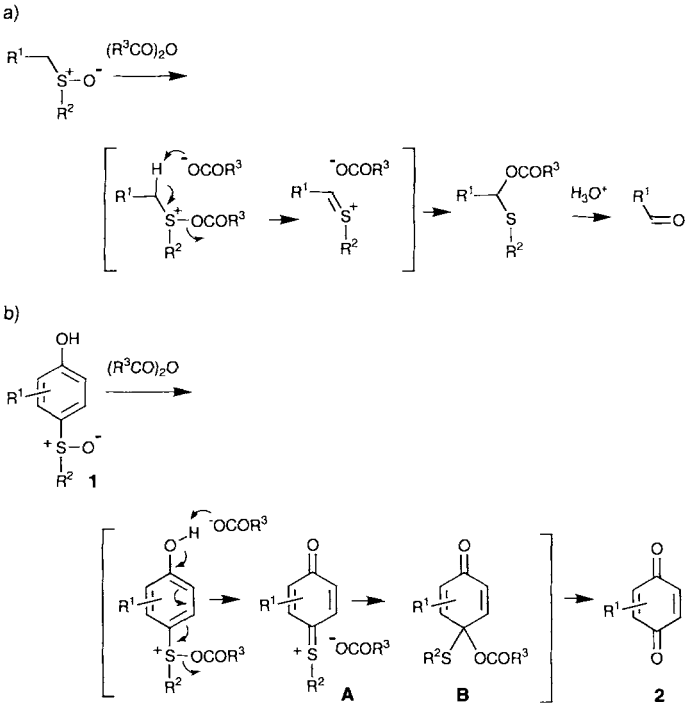

Scheme 1. a) Pummerer rearrangement of aliphatic sulfoxides; b) Pummerer-type rearrangement of aromatic sulfoxides.

Isolation of the Quinone Mono *O,S*-Acetal Intermediates of the Aromatic Pummerer-Type Rearrangement of *p*-Sulfinylphenols with 1-Ethoxyvinyl Esters**

Yasuyuki Kita,* Yoshifumi Takeda, Masato Matsugi, Kiyosei Iio, Kentoku Gotanda, Kenji Murata, and Shuji Akai

Treatment of aliphatic sulfoxides with acid anhydrides leads to a Pummerer rearrangement to give *O,S*-acetals. Because these products can be readily hydrolyzed to carbonyl compounds, these reactions have been widely utilized in a variety of organic syntheses (Scheme 1a).[1] On the other hand, similar reactions of aromatic sulfoxides have not been extensively explored. Pummerer-type rearrangements of *p*-sulfinylphenols **1** would be an effective method for the preparation of *p*-quinones **2** via the *O,S*-acetals **B** and would also be interesting from a mechanistic standpoint (Scheme 1b). King and Jung et al. have reported related studies on the reaction of acid anhydrides with 3,5-dimethyl-4-(methylsulfinyl)phenol[2] and with 4-methyl-2-(arylsulfinyl)phenols.[3,4] The main products in these reactions were obtained through conjugate addition of nucleophiles to the sulfonium ions (like **A**), while the *O,S*-acetals (like **B**) were obtained in very low yield[2] and only in very few cases.[4]

At the same time as the publications by Jung et al.,[3,4] we reported the Pummerer-type rearrangement of fully substituted *p*-sulfinylphenols **1** using trifluoroacetic anhydride (TFAA) as an effective method for preparation of *p*-quinones **2**.[5] We then extended this method to the *o*-unsubstituted *p*-sulfinylphenols **1** using TFAA and allyltrimethylsilane[6] and also to the silyl ethers of **1**, which enabled us to carry out the selective preparation of dihydroquinones.[7] Our results are noteworthy because they show novel *ipso*-substitution of sulfur functional groups into oxygen functional groups on phenol rings.

Although all of these reactions are certainly thought to proceed via the quinone mono *O,S*-acetals **B**, we were never able to isolate or even identify such acetal intermediates by spectroscopy. Difficulties in isolating **B** have been described previously[2–4] are probably due to the use of acid anhydrides as the initiator because acids or counteranions generated from the reagents would readily react with **B**.

Isolation of the acetal **B** is attractive from the view point of the utility of these compounds as useful synthons as well as the support of our proposed reaction mechanism. Here, we report the first isolation of the *O,S*-acetals **3** by employing 1-ethoxyvinyl esters **2a,b** for the Pummerer-type rearrangement of *p*-sulfinylphenols **1**.[8,9] Selective transformation of **3** into the quinones **4** and the dihydroquinone **6** was also achieved. This success is attributed to the fact that the reactions with the ketene acetal reagents **2**[10] can be carried out under nearly neutral conditions, thereby releasing neutral and stable ethyl acetate as a single side product.

We initially examined the Pummerer-type reaction of tetramethyl-4-(phenylsulfinyl)phenol (**1a**) using 1-ethoxyvinyl acetate (**2a**) (5 equiv) under various conditions. The reaction in dry MeCN or dry toluene without a catalyst proceeded very slowly and required a high temperature or a long reaction time, resulting in the formation of several products but not the *O,S*-acetal **3a**. On the other hand, use of a catalytic amount of *p*-toluenesulfonic acid (*p*-TsOH) in dry toluene sufficiently accelerated the reaction, so that **3a** could be isolated in 69% yield after stirring at 60 °C for 1 h (Table 1). This result is completely different from that obtained by a similar treatment of **1a** with acetic anhydride and a catalytic amount of *p*-TsOH in toluene at refluxing temperature: this reaction afforded the corresponding

[*] Prof. Dr. Y. Kita, Y. Takeda, M. Matsugi, K. Iio, K. Gotanda, K. Murata, Dr. S. Akai
Faculty of Pharmaceutical Sciences, Osaka University
1-6, Yamada-oka, Suita, Osaka 565 (Japan)
Fax: Int. code +(6)879-8229
e-mail: kita@phs.osaka-u.ac.jp

[**] This research was supported by a Grant-in-Aid for Scientific Research from the Ministry of Education, Science and Culture, Japan and Special Coordination Funds of the Science and Technology Agency, Japan.

acetate **5a** quantitatively, which did not react further with **2a**. Use of the chloroacetate **2b** instead of **2a** gave the acetal **3b** in 81% yield. In contrast, the more reactive trifluoroacetate **2c** did not give the *O,S*-acetal **3** but the benzoquinone **4a** (40% yield). The reactions with 1-ethoxyvinyl benzoate (R = Ph) and the *p*-nitrobenzoate (R = *p*-$NO_2C_6H_4$) were slow and gave low yields of **4a** (Scheme 2). Thus, the chloroacetate **2b** was found to be a suitable reagent for preparation of the *O,S*-acetal **3**.

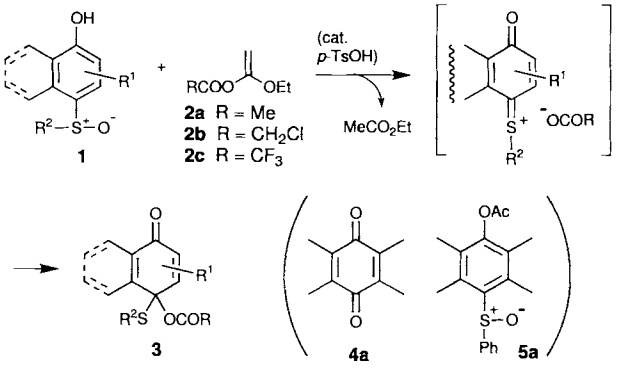

Scheme 2. Reaction of the *p*-sulfinylphenol **1** with the 1-ethoxyvinyl esters **2a–c**.

The reactions of various types of *p*-sulfinylphenols **1b–g** and naphthols **1h–j** with **2a,b** were carried out in an analogous manner to that applied for the preparation of **3a,b**, and the results are summarized in Table 1. The reactions were usually complete at room temperature or at 60 °C within several hours. Quenching the reaction mixture with Et_3N or K_2CO_3 followed by concentration and quick purification by chromatography on SiO_2 enabled us to isolate the products **3** in moderate to high yields. The compounds were identified by spectroscopy and can be stored under a nitrogen atmosphere in a refrigerator. Usually, **2b** provided **3** in higher yields. Both aliphatic and aromatic sulfinyl groups could be employed for this transformation. Allyl, ester, and hydroxyl groups are compatible with these reactions (entries 9–11). The formation of the *o*-unsubstituted products **3f,g** was also achieved in good yields (entries 6,7).

Table 1. Reactions of the *p*-sulfinylphenols **1a–j** with the 1-ethoxyvinyl esters **2a,b** to give the *O,S*-acetals **3a–l**[a].

Entry	1				2	T[°C]	t[h]	3		Yield[%]
	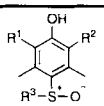							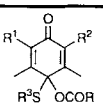		
		R^1	R^2	R^3					R	
1	**1a**	Me	Me	Ph	**2a**	60	1	**3a**	Me	69
2	**1a**	Me	Me	Ph	**2b**	60	1	**3b**	CH_2Cl	81
3	**1b**	Me	Me	Me	**2a**	20 → 60	9	**3c**	Me	86
4	**1b**	Me	Me	Me	**2b**	60	2	**3d**	CH_2Cl	80
5	**1c**	Me	Me	*t*Bu	**2b**	20	15	**3e**	CH_2Cl	74
6	**1d**	H	H	Ph	**2b**	60	2	**3f**	CH_2Cl	51
7	**1e**	Me	H	Ph	**2b**	20	2	**3g**	CH_2Cl	65
8	**1f**	Me	Et	Ph	**2b**	20	4	**3h**	CH_2Cl	81
9	**1g**	Me	allyl	Ph	**2b**	60	1	**3i**	CH_2Cl	77
	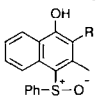							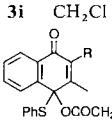		
	R									
10	**1h**	CH(OH)Me			**2b**	60	1	**3j**		80[b]
11	**1i**	CO_2Et			**2b**	20	24	**3k**		84
	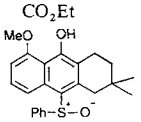							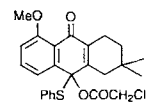		
12	**1j**				**2b**	60	3	**3l**		71

[a] *p*-TsOH (0.01–0.05 equiv) in toluene. For a typical procedure see the *Experimental Section*. [b] Obtained as a 1:1 mixture of two diastereomers.

Treatment of **3b** with aqueous $NaHCO_3$ in MeOH at room temperature caused selective saponification of the chloroacetate and the concomitant elimination of the phenylthio group to give the corresponding quinone **4a** and the disulfide PhSSPh in 94 and 90% yield, respectively. On the other hand, **3b** reacted with allyltrimethylsilane in the presence of a catalytic amount of trimethylsilyl trifluoromethanesulfonate (TMSOTf) to afford an 80% yield of the dihydroquinone **6** and allyl phenyl sulfide. Mild alkaline treatment of **3j** led to the rapid formation of quinone **4b** in 83% yield (Scheme 3). Thus, selective conversion of **3** to both quinones and dihydroquinones was achieved by the choice of the reaction conditions, which also supports the reaction mechanism for our previously reported preparation of quinones and dihydroquinones from *p*-sulfinylphenol derivatives.[5–7]

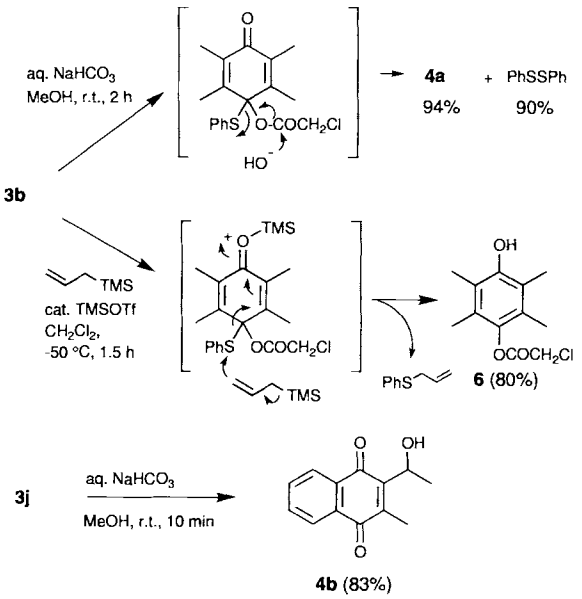

Scheme 3. Conversion of the *O,S*-acetals **3b** and **3j** to the quinones **4a** and **4b** and the dihydroquinone **6**.

The present results are of particular interest from the view point of the direct preparation of quinone monoacetals from aromatic compounds under *nonoxidative* conditions.[11] Extended studies on the utilization of the products **3** as versatile synthons are now under investigation.

Experimental Section

Typical procedure for the reaction of the *p*-sulfinylphenol **1** and 1-ethoxyvinyl esters **2a,b**: Under a nitrogen atmosphere, **2b** (0.82 g, 5.0 mmol) [9c, 10] and anhydrous *p*-toluenesulfonic acid (9 mg, 0.05 mmol) were successively added to a suspension of the *p*-sulfinylphenol **1a** (0.27 g, 1.0 mmol) in dry toluene (30 mL). The reaction mixture was stirred at 60 °C for 1 h and cooled to room temperature. Triethylamine (0.007 mL) was added and the reaction mixture was concentrated in vacuo. The residue was purified by SiO_2-flash column chromatography (hexane/ethyl acetate 8/1) to give the quinone mono *O,S*-acetal **3b**: pale yellow crystals (yield 81%); m.p. 132–133 °C (hexane/ethyl acetate); IR (KBr): $\tilde{\nu}$ = 1776, 1662, 1630 cm^{-1}; ^1H NMR (270 MHz, $CDCl_3$): δ = 1.64 (s, 6H), 2.01 (s, 6H), 4.16 (s, 2H), 7.01 (d,

$J = 7.5$ Hz, 2H), 7.21 (t, $J = 7.5$ Hz, 2H), 7.38 (t, $J = 7.5$ Hz, 1 H); MS (EI, 70 eV): m/z (%): 352 (0.6) [$M^+ + 2$], 350 (1.6) [M^+], 165 (100), 110 (57); HRMS calcd for $C_{18}H_{19}{}^{35}ClO_3S$ (M): 350.0742, found: 350.0727; elemental analysis: calcd C 61.62, H 5.46; found: C 61.61, H 5.32.

Received: January 3, 1997 [Z9959IE]
German version: *Angew. Chem.* **1997**, *109*, 1525–1527

Keywords: acetals · Pummerer rearrangement · quinones · rearrangements · sulfur

[1] Reviews: a) S. Oae, T. Numata, T. Yoshimura in *The Chemistry of the Sulphonium Group* (Eds.: C. J. M. Stirling, S. Patai), Wiley, New York, **1981**, p. 571; b) O. D. Lucchi, U. Miotti, G. Modena, *Organic Reactions*, *Vol. 40*, Wiley, New York, **1991**, chapter 3; c) D. S. Grierson, H.-P. Husson in *Comprehensive Organic Synthesis*, *Vol. 6* (Eds.: B. M. Trost, I. Fleming), Pergamon, Oxford, **1991**, p. 909; d) Y. Kita, N. Shibata, *Synlett* **1996**, 289–296. Recently published examples: e) A. Hedhli, A. Baklouti, A. Cambon, *Tetrahedron Lett.* **1994**, *37*, 6877–6878; f) A. Arnone, P. Bravo, M. Frigerio, G. Salani, F. Viani, *Tetrahedron* **1994**, *50*, 13485–13492.

[2] R. R. King, *J. Org. Chem.* **1978**, *43*, 3784–3785.

[3] M. E. Jung, C. Kim, L. von dem Bussche, *J. Org. Chem.* **1994**, *59*, 3248–3249.

[4] M. E. Jung, D. Jachiet, S. I. Khan, C. Kim, *Tetrahedron Lett.* **1995**, *36*, 361–364.

[5] S. Akai, Y. Takeda, K. Iio, Y. Yoshida, Y. Kita, *J. Chem. Soc. Chem. Commun.* **1995**, 1013–1014.

[6] S. Akai, Y. Takeda, K. Iio, K. Takahashi, N. Fukuda, Y. Kita, *J. Org. Chem.* **1997**, in press.

[7] S. Akai, K. Iio, Y. Takeda, H. Ueno, K. Yokogawa, Y. Kita, *J. Chem. Soc. Chem. Commun.* **1995**, 2319–2320; Y. Kita, Y. Takeda, K. Iio, K. Yokogawa, K. Takahashi, S. Akai, *Tetrahedron Lett.* **1996**, *37*, 7545–7548.

[8] We have elucidated a highly enantioselective Pummerer-type reaction of chiral, nonracemic aliphatic sulfoxides using *O*-silylated ketene acetals [1d], although the enantiomeric excesses for the reported asymmetric Pummerer reaction induced by acid anhydrides were low [1]. This method was efficiently applied to the asymmetric Pummerer-type cyclization of chiral, nonracemic sulfoxides and to the biomimetic conversion of Arnstein tripeptide analogs into optically active *cis* β-lactams. This synthesis resembles penicillin biosynthesis [9a]. Similar highly enantioselective Pummerer-type reactions of chiral, nonracemic aliphatic sulfoxides induced by a variety of 1-ethoxyvinyl esters including **2a,b** also gave α-acyloxy sulfides [9b,c].

[9] a) Y. Kita, N. Shibata, N. Kawano, T. Tohjo, C. Fujimori, H. Ohishi, *J. Am. Chem. Soc.* **1994**, *116*, 5116–5121; b) Y. Kita, N. Shibata, N. Kawano, S. Fukui, C. Fujimori, *Tetrahedron Lett.* **1994**, *38*, 3575–3576; c) N. Shibata, M. Matsugi, N. Kawano, S. Fukui, C. Fujimori, K. Gotanda, K. Murata, Y. Kita, *Tetrahedron: Asymmetry* **1997**, *8*, 303–310.

[10] Y. Kita, H. Maeda, K. Omori, T. Okuno, Y. Tamura, *J. Chem. Soc. Perkin Trans. 1* **1993**, 2999–3005, and references therein.

[11] Although the preparation of *p*-quinone mono *O,O*-acetal compounds has been widely explored, most of the methods that have been applied thus far are based on the oxidation of phenol or dihydroquinone derivatives: a) Y. Tamura, T. Yakura, J. Haruta, Y. Kita, *J. Org. Chem.* **1987**, *52*, 3927–3930; b) E. C. L. Gautier, N. J. Lewis, A. McKillop, R. J. K. Tayler, *Synth. Commun.* **1994**, *24*, 2989–3008, and references therein.

An Extraordinarily Twisted Polycyclic Aromatic Hydrocarbon**

Xiaoxin Qiao, Douglas M. Ho, and Robert A. Pascal, Jr.*

Among the most aesthetically pleasing chemical structures are polycyclic aromatic hydrocarbons (PAHs) that exhibit helical distortions from planarity.[1] In recent years a variety of longitudinally twisted PAHs and PAH derivatives—essentially twisted aromatic ribbons—have been prepared by the substitution of normally planar PAHs with bulky substituents.[2, 3] Thus, for example, anthracene is a planar molecule, but decaphenylanthracene exhibits an end-to-end twist of 63°.[3] In no case, however, has the overall twist of such a molecule exceeded 70°,[4] and we wondered what would be the properties of a PAH in which the twist exceeded 90°. We now report the synthesis and crystallographic characterization of 9,10,11,12,13,14,15,16-octaphenyldibenzo[*a,c*]naphthacene (**1**), a PAH with an extraordinary end-to-end twist of 105°.

The synthesis of **1** is similar to that of decaphenylanthracene;[3] the critical step is the addition of a highly substituted aryne to hexaphenylisobenzofuran[3, 5] (**2**) (Scheme 1). Thus,

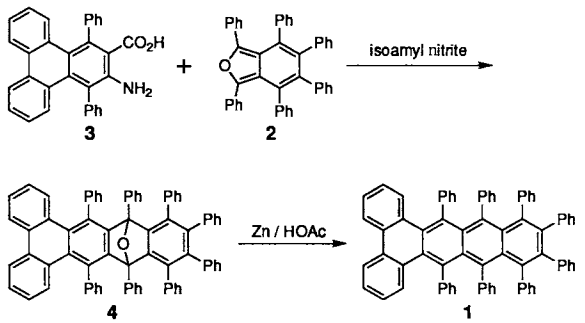

Scheme 1.

the anthranilic acid **3**[2d] was diazotized in the presence of **2**, and the resulting oxide **4** was deoxygenated with zinc in acetic acid to yield compound **1** in 1.6% overall yield. Both the cycloaddition of the aryne with isobenzofuran (15% yield) and the deoxygenation (11%) suffer from severe steric hindrance, which accounts for the low yield in an otherwise simple procedure.

Compound **1** is an orange solid that is readily soluble in a wide variety of organic solvents, in contrast with many PAHs. Orange prisms were obtained from ethanol, and X-ray structure analysis unambiguously established the structure of **1** (Figure 1).[6] The molecule lies on a crystallographic C_2 axis, thus its site symmetry is equal to its expected molecular symmetry. The central naphthacene moiety is a smoothly twisted aromatic ribbon in which the terminal bonds [C(1)–C(1′) and C(13)-C(13′)] are rotated by 105.4(8)° with respect to each other. However, the distortion is evenly distributed among the four benzene rings of the naphthacene, which contribute twists of 26.1(8)°, 28.7(8)°, 28.6(8)°, and 21.9(8)°, thus enabling good conjugation to be maintained within the aromatic π system. Indeed, the UV spectrum of **1**, with absorption maxima at 496, 470, and 364 nm, retains most of the features found in the spectrum of the parent hydrocarbon, dibenzo[*a,c*]naphthacene,[9] but shifted by about 50 nm to the red.

Compound **1** is very stable in the solid state. Crystals heated to 400 °C in an open capillary appear unchanged (apart from some cracking) by visual inspection and mass spectrometric and thin-layer chromatograpic analyses. Concentrated solutions of **1** appear to undergo slow decomposition at room temperature, but the factors governing this process are unclear. However, a dilute solution of **1** (1.8×10^{-5} M in dimethyl sulfoxide), monitored spectrophotometrically, was indefinitely stable at 50 °C even in the presence of air and added HCl, and an NMR sample (1.6×10^{-3} M in $CDCl_3$) showed no decomposition after one week at room temperature.

The preparation of **1** establishes a new record for the twisting of an aromatic π-electron system, and its end-to-end twist of

[*] Prof. R. A. Pascal, Jr., X. Qiao, Dr. D. M. Ho
Department of Chemistry
Princeton University
Princeton, NJ 08544 (USA)
Fax: Int. code +(609)2586746
e-mail: snake@chemvax.princeton.edu

[**] This work was supported by the National Science Foundation (grant CHE-9408295).

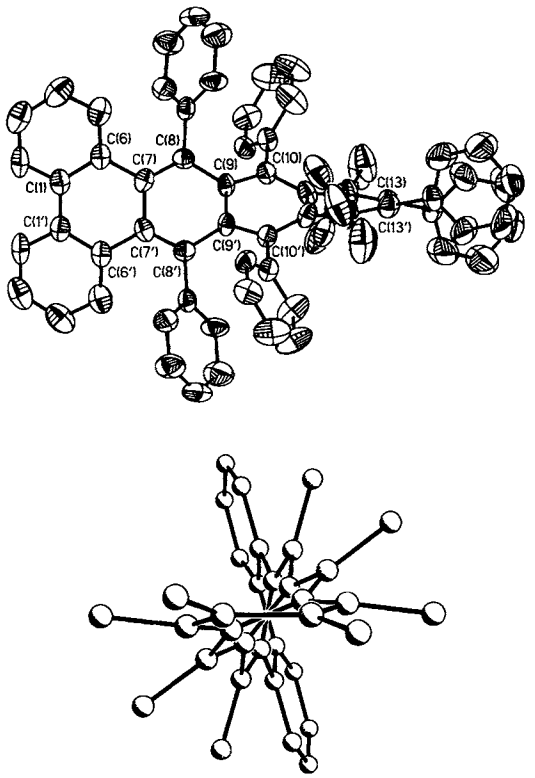

Figure 1. Molecular structure of compound **1** (thermal ellipsoids are drawn at the 50% probability level, hydrogen atoms have been omitted for clarity, and only the *ipso*-carbon atoms of the phenyl rings are shown in the lower illustration).

105° is more than 1.5 times as great as that observed in any previous PAH.[10] Looking to the future, two such molecules, fused to appropriate acenes to form a ring, would be sufficient to form a polycyclic aromatic Mobius strip. In addition, AM1 calculations,[12] which yield a geometry for **1** that is in excellent agreement with the X-ray structure, indicate that the hexacene **5** should have a twist of 178°. Such compounds are no longer unreasonable synthetic goals!

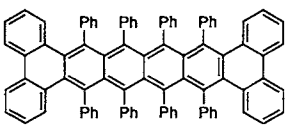

5

Experimental Section

1: A solution of **3** (0.530 g, 1.21 mmol) in 1,2-dichloroethane (80 mL) was added dropwise to a solution of **2** (1.10 g, 1.92 mmol) and isoamyl nitrite (0.5 mL) in 1,2-dichloroethane (55 mL) at reflux under argon. After 1 h, the solution was cooled, and ethanol (12 mL) and 1% NaOH (40 mL) were added. The resulting mixture was extracted with $CHCl_3$ (200 mL), and the organic extract was washed with saturated $NaHCO_3$, dried over $MgSO_4$, and concentrated to dryness. The residue was fractionated by column chromatography (silica gel; 1:1 hexanes:CH_2Cl_2, then 1:2 hexanes:CH_2Cl_2) to yield compound **4** as an off-white solid (0.174 g); ^{1}H NMR (500 MHz, $CDCl_3$): δ = 6.60–6.76 (m, 18H), 6.80 (d, J = 8 Hz, 6H), 6.86–7.03 (m, 16H), 7.09 (t, J = 8 Hz, 2H), 7.35 (t, J = 8 Hz, 2H), 7.42 (d, J = 8 Hz, 2H), 8.37 (d, J = 8 Hz, 2H); FAB MS: m/z (%) 953 (M^+ + H, 46), 849 (49), 662 (99), 575 (100). Without further purification, this material was treated with a large excess of activated Zn dust (0.3 g) in glacial acetic acid (50 mL) at reflux for 5 h. The mixture was filtered hot, and after cooling, water was added to the filtrate. The resulting orange precipitate was collected by filtration and rinsed with water. After drying, the solid was subjected to preparative TLC (silica gel; 2:1 hexanes:CH_2Cl_2) to give pure **1** as an orange solid (18.6 mg, 0.020 mmol, 1.6% yield): M.p. >400 °C; ^{1}H NMR (500 MHz, $CDCl_3$): δ = 6.19 (d, J = 8 Hz, 2H), 6.26 (t, J = 7 Hz, 2H), 6.37 (m, 4H), 6.49 (m, 12 H), 6.61–6.84 (m, 18H), 6.92 (m, 4H), 7.06 (t, J = 7 Hz, 2H), 7.20 (t, J = 8 Hz, 2H), 8.02 (d, J = 8 Hz, 2H); IR (KBr): $\tilde{\nu}$ = 3078, 3055, 3022, 1600, 1493, 1442 cm^{-1}; UV ($CHCl_3$): λ_{max} (lg ε) = 496 (3.69), 470 (3.78), 446 (sh, 3.68), 364 (4.78), 352 (sh, 4.69); FAB MS: m/z (%) 937 (M^+ + H, 100), 460 (31).

Received: January 2, 1997 [Z9954IE]
German version: *Angew. Chem.* **1997**, *109*, 1588–1589

Keywords: arenes · aromaticity · chirality · hydrocarbons · polycycles

[1] K. P. Meurer, F. Vögtle, *Top. Curr. Chem.* **1985**, *127*, 1–76.
[2] a) R. A. Pascal, Jr., W. D. McMillan, D. Van Engen, *J. Am. Chem. Soc.* **1986**, *108*, 5652–5653; b) R. A. Pascal, Jr., W. D. McMillan, D. Van Engen, R. G. Eason, *ibid.* **1987**, *109*, 4660–4665; c) P. J. Fagan, M. D. Ward, J. V. Caspar, J. C. Calabrese, P. J. Krusic, *ibid.* **1988**, *110*, 2981–2983; d) N. Smyth, D. Van Engen, R. A. Pascal, Jr., *J. Org. Chem.* **1990**, *55*, 1937–1940.
[3] X. Qiao, M. A. Padula, D. M. Ho, N. J. Vogelaar, C. E. Schutt, R. A. Pascal, Jr., *J. Am. Chem. Soc.* **1996**, *118*, 741–745.
[4] Only three polycyclic aromatic compounds have crystallographically characterized end-to-end twists (defined in note 17 of ref. [2b]) of more than 65°: 9,18-diphenyltetrabenz[*a,c,h,j*]anthracene (65.7°) [2a], its bis(trifluoromethyl) derivative (69.7°) [2b], and a tetrakis[η^5-pentamethylcyclopentadienyl)-ruthenium] complex of rubrene (67.3°) [2c].
[5] W. Ried, K. H. Bonnighausen, *Liebigs Ann. Chem.* **1961**, *639*, 61–67.
[6] An orange needle of **1**, cut to 0.06·0.08·0.40 mm, was used for the X-ray diffraction studies. Crystal data: $C_{74}H_{48}$, M = 937.12, orthorhombic, *Pbcn*, a = 16.562(2), b = 17.796(2), c = 17.641(2) Å, V = 5199.6(10) Å^3, Z = 4, ρ_{calcd} = 1.197 Mg m^{-3}. Intensity measurements were made by using graphite-monochromated $Mo_{K\alpha}$ radiation (λ = 0.71073 Å) at 298 K on a Siemens P4 diffractometer. A total of 4260 reflections were measured ($3° \le 2\theta \le 45°$, ω scan mode), of which 3406 were unique (R_{int} = 0.057), and 831 have $I > 2\sigma(I)$. Corrections were made for Lorentzian polarization but not for absorption or extinction. The structure was solved by direct methods (SHELXTL [7]) and refined by full-matrix least-squares on F^2 (SHELXL-93 [8]). All non-hydrogen atoms were refined with anisotropic displacement coefficients, and hydrogen atoms were included with a riding model and isotropic displacement coefficients [U(H) = 1.2U(C)]. The refinements converged to $R(F)$ = 0.047, $wR(F^2)$ = 0.032, and S = 1.07 for 831 reflections with $I > 2\sigma(I)$, and $R(F)$ = 0.237, $wR(F^2)$ = 0.049, and S = 0.67 for 3406 unique reflections and 334 variables. The residual electron density ranged from −0.15 to 0.17 e Å^{-3}. Crystallographic data (excluding structure factors) for the structure reported in this paper have been deposited with the Cambridge Crystallographic Data Centre as supplementary publication no. CCDC-100115. Copies of the data can be obtained free of charge on application to The Director, CCDC, 12 Union Road, Cambridge CB2 1EZ, UK (fax: int. code +(1223) 336-033; e-mail: deposit@chemcrys.cam.ac.uk).
[7] G. M. Sheldrick, SHELXTL, Version 4.2. Siemens Analytical X-ray Instruments, Madison, Wisconsin, USA, **1991**.
[8] G. M. Sheldrick, SHELXL-93. Program for the Refinement of Crystal Structures. University of Gottingen, Germany, **1993**.
[9] a) E. Clar, *Chem. Ber.* **1948**, *81*, 253–269. b) E. Clar, *Polycyclic Hydrocarbons, Vol. 1*, Academic Press, London, **1964**, p 407.
[10] An enantiomerically pure sample of compound **1** might be expected to show exceptional optical activity. No attempt has been made to resolve **1**; however, the 500 MHz ^{1}H NMR spectrum of **1** in the chiral solvent mixture *d*-trifluoromethylbenzyl alcohol/deuterochloroform (1/2) is broadened, but not cleanly split into enantiomeric subspectra, suggesting that it may have a significant barrier to racemization. Previously prepared longitudinally twisted aromatic polycycles show evidence of great conformational flexibility, possess only modest barriers to racemization, and none has been successfully resolved [2b, 3, 11].
[11] K. Shibata, A. A. Kulkarni, D. M. Ho, R. A. Pascal, Jr., *J. Org. Chem.* **1995**, *60*, 428–434.
[12] M. J. S. Dewar, E. G. Zoebisch, E. F. Healy, J. J. P. Stewart, *J. Am. Chem. Soc.* **1985**, *107*, 3902–3909.

 © VCH Verlagsgesellschaft mbH, D-69451 Weinheim, 1997 0570-0833/97/3613-1532 $ 17.50+.50/0

1,1,2,2-Tetrakis(dimethylsilyl)-1,2-ethanediyldilithium-bis(diethyl ether): Observation of a SiH–Li Agostic Interaction**

Akira Sekiguchi,* Masaaki Ichinohe, Masae Takahashi, Chizuko Kabuto, and Hideki Sakurai*

Si–H···M (M = alkali metal) agostic interactions attract considerable interest in view of the structure and bonding of organo alkali metal compounds, in particular the organolithium compounds.[1] The interaction between SiH and the lithium cation has so far only been predicted by the theoretical study of SiH_3Li.[2] The inverted C_{3v} structure is calculated to be 2.4 kcal mol^{-1} more stable than the tetrahedral C_{3v} isomer. However, the only experimental example of a SiH–Na interaction is in an oligomeric sodium alcoholate.[3]

Ab initio calculations on $LiCH_2CH_2Li$ suggest that a *trans* structure with partial or symmetrical lithium bridging is most stable, whereas the eclipsed conformation is much higher in energy than the *trans*-bridged planar structure.[4] Indeed, experimental studies of the planar or twisted lithium doubly bridged structures of ethylene dianion dilithium derivatives have been reported.[5, 6] In order to disclose SiH–Li interactions, we synthesized tetrakis(dimethylsilyl)ethylene (**1**),[7] which provides **2** upon reduction with lithium metal in ether. Here we report structural and spectroscopic evidence for a SiH–Li agostic interaction.

Reaction of **1** with excess lithium metal in dry, oxygen-free diethyl ether at ambient temperature led to a yellow solution of the dilithium derivative of **1** [Eq. (a)]. The solvent was removed

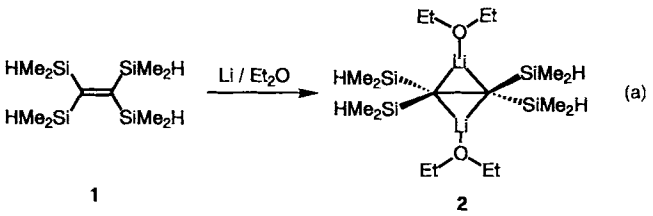

(a)

1 **2**

in vacuo, and dry, degassed pentane introduced by vacuum transfer. Crystallization from pentane afforded air- and moisture-sensitive, yellow crystals of **2**.

The structure of **2** was determined by X-ray crystallography (Figure 1).[8] The two lithium cations are bonded to two anionic

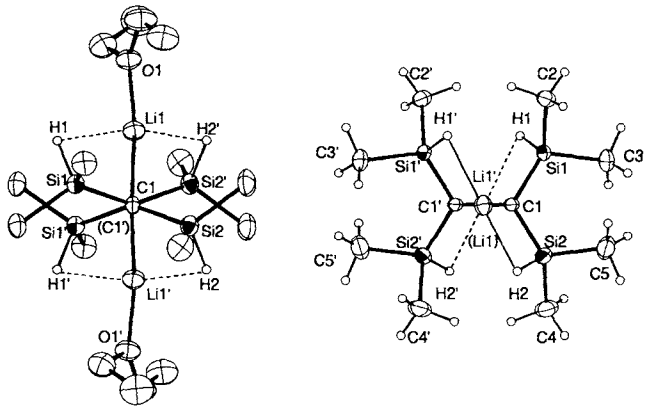

Figure 1. ORTEP representations of the crystal structure of **1a**. Left: view along the C1–C1′ bond (hydrogen atoms of CH_3 and Et_2O moieties omitted for clarity); right: top view (Et_2O omitted for clarity). Selected bond lengths [Å] and angles [°]: C1–C1′ 1.597(5), C1–Si1 1.818(4), C1–Si2 1.815(4), C1–Li1 2.125(9), C1–Li1′ 2.128(9), O1–Li1 1.908(9); Si1-C1-Si2 121.2(2), Si1-C1-C1′ 119.2(2), Si2-C1-C1′ 119.7(2), C1-Li1-C1′ 44.1(2), Li1-C1-C1′ 68.0(3), Li1-C1-Li1′ 135.9(3), Si1-C1-Si2/Si1′-C1′-Si2′ 41.0.

carbon atoms as well as to a diethyl ether moiety to produce a lithium doubly bridged structure. The central C1–C1′ bond of **2** (1.597(5) Å) is significantly longer than that of the precursor **1** (1.367(9) Å). In contrast, the Si–C(sp_2) bonds of **2** (1.818(4) and 1.815(4) Å) are shorter than those of **1** (1.901(7) Å). The dihedral angle between the Si1-C1-Si2 and Si1′-C1′-Si2′ planes is 41.0°, which is remarkably enlarged even though **1** is completely planar and gear-meshed.[7] Of particular interest are the rather short Li–H(Si) distances; the lithium–hydrogen atomic distances are 2.25(4) Å for Li1–H1 and 2.14(4) Å for Li1–H2′. These are in the range (2.00(5)–2.33(5) Å) found for Li···H–C interactions in the cyclohexyllithium hexamer.[9] Apparently the highly twisted structure of **2** can be attributed to the interaction of the hydrogen atom on the silicon atom with the lithium cations.

The SiH–Li interaction found in crystalline **2** is also observed by NMR and IR spectroscopy in solution. The NMR data are consistent with the doubly bridged structure; the signal for the anionic carbon atoms at $\delta = 14.6$ appears as a quintet due to coupling with two ^{6}Li nuclei ($I = 1$). The ^{29}Si NMR signal at $\delta = -19.7$ is shifted downfield with respect to that of **1** ($\delta = -24.4$). This is quite unusual,[10] since the ^{29}Si NMR signal of tetrakis(trialkylsilyl)ethylene dianions, which do not contain Si–H bonds, are shifted upfield.[5b–e] The ^{6}Li NMR signal of **2** is a quintet at $\delta = 0.10$ ($J = 0.49$ Hz). The splitting of the ^{6}Li signal is caused by coupling with four SiH protons, which suggests a flipping along the central C–C bond in solution. The most striking feature of **2** is the unusually small one-bond coupling (^1J(Si,H) = 141 Hz). Hydrosilanes generally display a value in the range of 160–200 Hz.[11] For example, ^1J(Si,H) = 181 Hz for **1**. The small value for **2** suggests significant SiH–Li interaction. In fact, the infrared spectrum of **2** in hexane exhibits a broad Si–H stretching band at 1937 cm^{-1}, which is at lower frequency than that for **1** (2145, 2103 cm^{-1}).

The SiH–Li interaction is also supported by a theoretical calculation of **3**. The structure of **3** with the SiH–Li interaction

$[(H_3Si)_2C{=}C(SiH_3)_2][Li(H_2O)]_2$ **3**

is calculated to be 3.93 kcal mol^{-1} more stable than the planar one without this interaction.[12] The central C–C bond is twisted by 35° due to the SiH–Li interaction. The calculated structural parameters for **3** are very similar to those experimentally

[*] Prof. Dr. A. Sekiguchi
Department of Chemistry
University of Tsukuba
Tsukuba, Ibaraki 305 (Japan)
Fax: Int. code +(298)53-4314
e-mail: sekiguch@staff.chem.tsukuba.ac.jp

Prof. Dr. H. Sakurai
Department of Industrial Chemistry, Faculty of Science and Technology
Science University of Tokyo
Noda, Chiba 278 (Japan)
Fax: Int. code +(471)23-8984
e-mail: sakurai@koura01.ci.noda.sut.ac.jp

Dr. M. Ichinohe, Dr. C. Kabuto, Graduate School of Science,
Tohoku University (Japan)

Dr. M. Takahashi, Photodynamics Research Center,
The Institute of Physical and Chemical Research (RIKEN, Japan)

[**] This work was supported by the Sumitomo Foundation (no. 960548) and a Grant-in-Aid for Specially Promoted Research (no. 02102004) and for Scientific Research on Priority Area of Reactive Organometallics (nos. 05236102 and 07454159) from the Ministry of Education, Science, and Culture.

 © VCH Verlagsgesellschaft mbH, D-69451 Weinheim, 1997 0570-0833/97/3613-1533 $ 17.50+.50/0

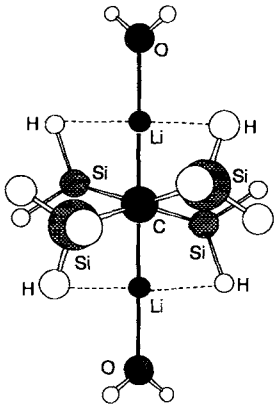

Figure 2. Optimized structure of **3** at the HF/6-31+G* level as viewed along the C–C bond. Selected bond lengths [Å] and angles [°]: C–C 1.581, C–Si 1.828, C–Li 2.105, O–Li 1.933; Si-C-Si 119.3, Si-C-C 120.4, C-Li-C 44.0, Li-C-C 67.9, Li-C-Li 136.0, Si-C-Si/Si-C-Si 35.

observed in **2** (Figure 2). The Li–H(Si) distance in **3** (2.360 Å) compares well to that in **2**.

The experimental and computational results clearly provide evidence for a SiH–Li agostic interaction. The dilithium dianion with Si–H bonds undergoes twisting due to the SiH–Li agostic interaction caused by the polarity of the $Si^{\delta+}-H^{\delta-}$ bond.[2]

Experimental Section

2: Crystalline **1** (76 mg, 0.29 mmol) and lithium metal (10 mg, 1.4 mmol) were added to a Schlenk tube with a magnetic stirrer. Degassed, dry, oxygen-free diethyl ether (≈1 mL) was introduced by vacuum transfer, and the mixture stirred at room temperature to give a yellow solution of the dianion within 1 h. The solvent was removed in vacuo, and degassed pentane introduced by vacuum transfer. The lithium metal was removed, and the solution concentrated and cooled to afford yellow crystals of **2** in quantitative yields. ^{1}H NMR ([D$_8$]toluene, TMS): $\delta = 0.45$ (d, $J = 4.0$ Hz, 24H, $SiMe_2$), 1.12 (t, $J = 7.0$ Hz, 12H, CH_3CH_2O), 3.30 (q, $J = 7.0$ Hz, 8H, CH_3CH_2O), 4.50 (br. s, 4H, SiH); ^{13}C{^{1}H} NMR ([D$_8$]toluene, TMS): $\delta = 6.3$ ($SiMe_2$), 14.6 (quint, $J(^{13}C,^6Li) = 2.3$ Hz, CLi), 15.7 (CH_3CH_2O), 66.0 (CH_3CH_2O); ^{29}Si{^{1}H} NMR ([D$_8$]toluene, TMS): $\delta = -19.7$; ^{6}Li{^{1}H} NMR ([D$_8$]toluene, LiCl in MeOH, external): $\delta = 0.10$ (quint, $J(^6Li,^1HSi) = 0.49$ Hz).

Received: September 6, 1996
Revised version: January 7, 1997 [Z Z9533 IE]
German version: *Angew. Chem.* **1997**, *109*, 1577–1579

Keywords: agostic interactions · lithium · reductions · silicon · solid-state structures

[1] Reviews: a) W. N. Setzer, P. von R. Schleyer, *Adv. Organomet. Chem.* **1985**, *24*, 353; b) C. Schade, P. von R. Schleyer, *ibid.* **1987**, *27*, 169; c) A. B. Sannigrahi, T. Kar, B. G. Niyogi, P. Hobza, P. von R. Schleyer, *Chem. Rev.* **1990**, *90*, 1061; d) H. Bock, K. Ruppert, C. Näther, Z. Havlas, H. F. Herrmann, C. Arad, I. Göbel, A. John, J. Meuret, S. Nick, A. Rauschenbach, W. Seitz, T. Vaupel, B. Solouki, *Angew. Chem.* **1992**, *104*, 564; *Angew. Chem. Int. Ed. Engl.* **1992**, *31*, 550; e) A.-M. Sapse, P. von R. Schleyer in *Lithium Chemistry: A Theoretical and Experimental Overview*, Wiley, New York, **1995**.

[2] P. von R. Schleyer, T. Clark, *J. Chem. Soc. Chem. Commun.* **1986**, 1371.

[3] H. Pritzkow, T. Lobreyer, W. Sundermeyer, N. J. R. van Eikema Hommes, P. von R. Schleyer, *Angew. Chem.* **1994**, *106*, 221; *Angew. Chem. Int. Ed. Engl.* **1994**, *33*, 216.

[4] a) A. J. Kos, E. D. Jemmis, P. von R. Schleyer, R. Gleiter, U. Fischbach, J. A. Pople, *J. Am. Chem. Soc.* **1981**, *103*, 4996; b) S. P. So, *J. Organomet. Chem.* **1989**, *361*, 283.

[5] a) M. Walczak, G. D. Stucky, *J. Am. Chem. Soc.* **1976**, *98*, 5531; b) A. Sekiguchi, T. Nakanishi, C. Kabuto, H. Sakurai, *ibid.* **1989**, *111*, 3748; c) A. Sekiguchi, M. Ichinohe, C. Kabuto, H. Sakurai, *Organometallics* **1995**, *14*, 1092; d) A. Sekiguchi, M. Ichinohe, C. Kabuto, H. Sakurai, *Bull. Chem. Soc. Jpn.* **1995**, *68*, 2981; e) A. Sekiguchi, M. Ichinohe, T. Nakanishi, C. Kabuto, H. Sakurai, *ibid.* **1995**, *68*, 3215.

[6] Ethylene dianion disodium and dicesium derivatives: a) H. Bock, K. Ruppert, D. Fenske, *Angew. Chem.* **1989**, *101*, 1717; *Angew. Chem. Int. Ed. Engl.* **1989**, *28*, 1685; b) H. Bock, T. Hauck, C. Näther, *Organometallics* **1996**, *15*, 1527.

[7] H. Sakurai, K. Ebata, K. Sakamoto, Y. Nakadaira, C. Kabuto, *Chem. Lett.* **1988**, 965.

[8] A single crystal (0.25 × 0.30 × 0.40 mm) of **2** was sealed in a capillary glass tube, and diffraction data collected at 150 K on a Rigaku Denki AFC-5R diffractometer with a rotating anode (45 kV, 200 mA) employing graphite-monochromatized $Mo_{K\alpha}$ radiation ($\lambda = 0.71069$ Å). A total of 3247 reflections ($3 < 2\theta < 55°$) were collected. Crystal data for $C_{18}H_{48}Li_2O_2Si_4$ ($M_r = 422.80$): $a = 18.551(7)$, $b = 9.890(8)$, $c = 17.183(6)$ Å, $\beta = 113.61(2)°$, $V = 2889(3)$ Å^3, monoclinic, space group $C2/c$, $Z = 4$, $\rho_{calcd} = 0.972$ g cm^{-3}. The positions of the hydrogen atoms connected to silicon atoms were determined by a difference Fourier calculation, and those of the other hydrogen atoms calculated. When the hydrogen atoms were included in the refinement, the final R factor converged at 0.0698 ($R_w = 0.0717$) for 2114 reflections with $F_o > 3\sigma(F_o)$. Further details of the crystal-structure investigation may be obtained from the Fachinformationszentrum Karlsruhe, D-76344 Eggenstein-Leopoldshafen (Germany), on quoting the depository number CSD-59427.

[9] R. Zerger, W. Rhine, G. Stucky, *J. Am. Chem. Soc.* **1974**, *96*, 6048.

[10] The GIAO calculations of **3** at the HF/6-31 + G* level suggest that the SiH–Li interaction causes the ^{29}Si NMR signal to shift downfield by $\Delta\delta = 5.62$, and the ^{6}Li NMR signal to shift upfield by $\Delta\delta = 0.46$ with respect to the corresponding signals for the planar structure without this interaction. The calculated Si–H frequency for the twisted structure of **3** is 1925 cm^{-1} (DFT/6-31 + G*). These predictions are fully consistent with the experimental observations.

[11] E. A. Williams, J. D. Cargioli in *Annual Reports on NMR Spectroscopy, Vol. 9* (Ed.: G. A. Webb), Academic Press, New York, **1979**, p. 221.

[12] The twisted structure **A** with the SiH–Li interaction is calculated to be more stable than planar **B** by 3.93 kcal mol^{-1} (**A** −1405.3569491 a.u., **B** −1405.3506778 a.u.), 3.51 kcal mol^{-1} (**A** −1405.346044 a.u., **B** −1405.3404548 a.u.), and 6.06 kcal mol^{-1} (**A** −1406.3602892 a.u., **B** −1406.350628 a.u) at the HF/6-31+G*, HF/6-31G*, and MP2/6-31G* levels, respectively.

Coordination-Mediated Optical Resolution of Carboxylic Acids with *O,O′*-Dibenzoyltartaric Acid**

András Mravik,* Zsolt Böcskei, Zoltán Katona, Imre Markovits, and Elemér Fogassy

Racemic carboxylic acids are generally resolved by optically active bases from natural or synthetic sources. Some of the naturally occurring amines (brucine, strychnine) are extremely toxic and available only in one enantiomeric form.

In contrast, tartaric acid and its derivatives are relatively cheap, nontoxic resolving agents that are available in both enantiomeric forms, even on a large scale. Although derivatives of unnatural tartaric acid are more expensive than the enantiomers, the stereoisomers of *O,O′*-dibenzoyltartaric acid can be produced by preferential crystallization at the same cost on a fully synthetic basis.[1] We report here new applications of *O,O′*-dibenzoyltartaric acid, which is used for the resolution of bases, as a resolving agent *for carboxylic acids*. Conversion of *O,O′*-dibenzoyltartaric acid into its neutral calcium salt (**2**) results in a compound of basic character that can form salts with acids. In fact, **2** readily reacts with enantiomers of suitable acids **1** to form crystallizing, mixed calcium salts **3**; this provides excellent resolution of the acids (Scheme 1).

A coordinating group attached to the chiral center has an important role in crystallization and, furthermore, in the discrimination of the enantiomers. The resolving agent **2** itself forms a bulky crystalline mass upon separation that cannot be removed by filtration. However, it readily dissolves in hot ethanol or methanol, in which it can be prepared in situ by heating dibenzoyltartaric acid and calcium oxide.

[*] A. Mravik, Z. Katona, I. Markovits, Prof. Dr. E. Fogassy
Department of Organic Chemical Technology
Technical University of Budapest
P. O. Box 91, H-1521 Budapest (Hungary)
Fax: Int. code +(1)257-7128
e-mail: mravik@oct.bme.hu
Dr. Z. Böcskei
CHINOIN Pharmaceuticals, Budapest

[**] The work at the Technical University of Budapest was supported by the Hungarian Research Fund (OTKA T 014887) and the Varga József Foundation. We thank Prof. Gy. Pokol, Budapest, for the thermoanalytical determinations.

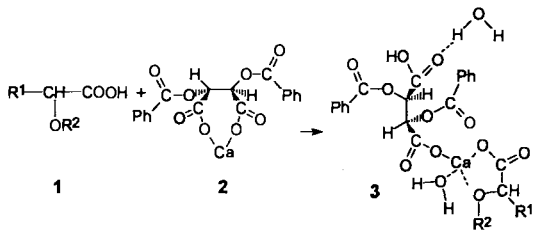

Scheme 1. Formation of a mixed calcium salt upon resolution of carboxylic acids with dibenzoyltartaric acid.

Racemic acids **1a** or **1b** and then water were added to the hot solution of **2** in the suitable alcohol. On cooling (or seeding) salts **3a** and **3b** began to separate. Thus, **1a** was resolved in aqueous ethanol, and pure (*R*)-(+)-**1a**-**2** ((*R*)-**3a**) was obtained in 51% yield after three recrystallizations (ethanol/water and methanol/water). The acid (*R*)-(+)-**1a** liberated from this salt showed a specific rotation of $[\alpha]_D^{23} = +74.5$ ($c = 1$ in methanol), $[\alpha]_D^{23} = +71.5$ (neat). (Traditional resolution of **1a** with (*S*)-(−)-1-phenylethylamine required five recrystallizations from benzene and gave a salt (63%) from which (*S*)-**1a** was obtained with $[\alpha]_D^{23} = -70.5$ (neat).[2]) Accordingly, (*S*)-(−)-**1b**-**2** ((*S*)-**3b**) was obtained (methanol/water) in 89% yield after one recrystallization, and the acid (*S*)-(−)-**1b** had $[\alpha]_D^{23} = -34.1$ ($c = 1$ in chloroform). Resolution of **1b** with brucine afforded the brucine salt (crystallization from ethyl acetate followed by two recrystallizations from acetonitrile) in 51% yield, and the isolated (*R*)-(+)-**1b** had $[\alpha]_D^{23} = +30.4$ ($c = 1.01$ in chloroform).[3] Yields were calculated based on half of the starting racemic acids.

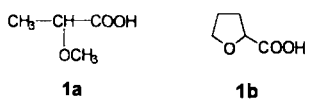

1a

1b

X-ray crystal structure analyses were carried out on (*S*)-**3b**[4] and (*R*)-**3a** to investigate the interactions controlling the optical resolution (in particular the role of coordination around the calcium atom). The molecular structure of (*S*)-**3b** is shown in Figure 1. Tetrahydrofuroic acid (**1b**) has (*S*)-(−) configuration.

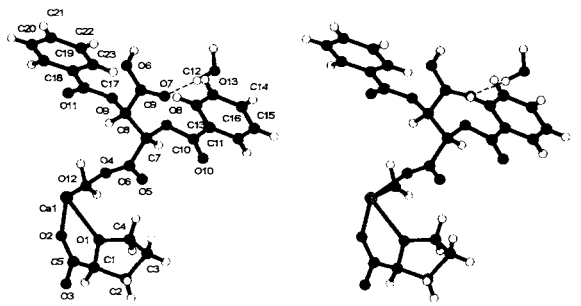

Figure 1. Stereoview of the crystal structure of (*S*)-**3b**.

A stereoview of the packing in (*S*)-**3b** is given in Figure 2. The crystal structure of (*S*)-**3b** (Figure 1) is made up of alternating hydrophobic layers, composed of the phenyl moieties of the benzoyl groups, and hydrophilic layers, composed of the Ca^{2+} ions and their coordinating ligands. The hydrophylic layers can be further divided into alternating stripes of hydrogen bonds and Ca^{2+}-coordination polyhedrons (Figure 2). The bond lengths and angles demonstrate that the coordination geometry at Ca^{2+} is distorted trigonal bipyramidal (Ca^{2+}—O 2.27–2.50 Å). The tetrahydrofurane carboxylate (THFC) ion is

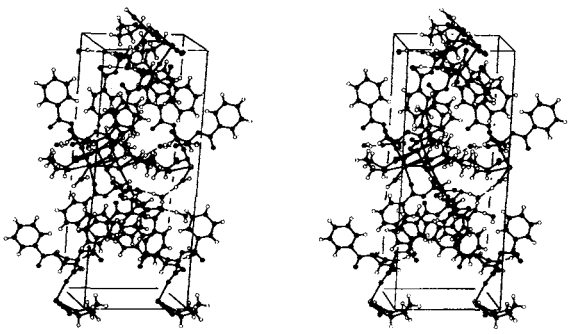

Figure 2. Stereoview of the packing of (*S*)-**3b**.

a bis(bidentate) ligand: Its carboxylate group is a bidentate Ca^{2+}-binding unit (O2···O3 nonbonding distance 2.18 Å), and one of the carboxylate oxygen atoms (O2) and the ring ether oxygen atom (O1; O1···O2 nonbonding distance 2.66 Å) form another bidentate moiety. The equatorial positions of the trigonal bipyramid are occupied by the two bidentate ligands of the THFC moiety as well as the oxygen atom O12 from water. One of the two oxygen atoms of the carboxylate groups (O2) simultaneously coordinates to two neighboring Ca^{2+} ions to form an endless Ca-O-Ca-O chain through the crystal lattice. The axial positions of the bipyramid are occupied by the carbonyl oxygen atoms of one of the two benzoyl groups (O11) and of the deprotonated carboxylate group (O4). Since the ligands at the axial positions are less bulky they are substantially closer to the Ca^{2+} ions than the equatorial ligands. The hydrogen-bonding system of the crystal also shows interesting features. The tartaric acid moieties are arranged in a head-to-tail fashion by hydrogen bonds between deprotonated and protonated carboxylate groups. Two stripes of Ca^{2+} bipyramids are interconnected by several hydrogen bonds mediated by water molecules.

Due to the crowded structure of these mixed salts, the scope of the method is limited to relatively small racemic acids. The alkyl ether functionality seems to be essential. α-Chloro acids do not form mixed salts, whereas α-hydroxy acids, due to the low solubility of their calcium complexes, separated as their simple calcium salts under the above conditions.

Because of these limitations we directed our interest to the resolution of simple derivatives of carboxylic acids (for example esters). The preparative-scale separation of an ester from the resolving acid can be easily accomplished, whereas problems might be encountered in certain cases upon separation of a free acid.

Hydroxy acids represent an important class of chiral compounds. We developed a simple, generally applicable method for resolving hydroxy acid esters (**5**, see Table 1 for examples). As the esters lack an acid functionality, salt formation should be entirely replaced by coordination bonds. The acidic calcium salt of *O*,*O*′-dibenzoyltartaric acid $Ca(HL_0)_2$ (**4**) readily coordinates hydroxy acid esters to form crystalline complex salts[5] of the general formula **6** (see Table 1).[6] This phe-

$$[Ca(L)_{n1}(A_1)_{na}(A_2)_{nw}](HL_0)_2 \quad \mathbf{6}$$

nomenon serves as a basis for the resolution of hydroxy esters, since selection between the enantiomers of **5** occurs during crystallization. In the formula for **6** L stands for **5**, and A_1 and A_2 stand for auxiliary ligands (A_1 is generally a simple ester such as ethyl or propyl acetate, and A_2 water). The complex salts formed can be divided into three major types. Type I: $n_1 = 2$; no auxiliary ligand is cocomplexed, but water may be present.

Table 1. Complex salts **6** obtained upon resolution of **5a,b** with (2*R*,3*R*)-*O*,*O*'-dibenzoyltartaric acid.

5a

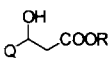

5b

	Q	R	Type	A_1 [a]	n_a [b]	n_w [c]	Yield [%][d]	*ee* [%][e]
5a	CH_3	C_2H_5	I				98	3(*S*)
5a	CH_3	C_4H_9	I				90	27(*S*)
5a	CH_3	$C_6H_5CH_2$	I				99	46(*S*)
5a	C_6H_5	CH_3	I				99	78(*R*)
5a	C_6H_5	CH_3	II	EA	1	1	84[f]	93(*S*)[g]
5a	C_6H_5	C_2H_5	II	EP	1	1	93	78(*S*)
5a	4-$CH_3OC_6H_4$	CH_3	I				90	47(*R*)
5a	$C_6H_5CH_2$	CH_3	I			2	92	51(*R*)
5a	$C_6H_5CH_2$	C_2H_5	III			2	93	65(*R*)
5a	CH_3OOCCH_2	CH_3	II	PA	0.5	1	86	40(*S*)
5a	$C_2H_5OOCCH_2$	C_2H_5	II	EA	0.5	1	85	28(*S*)
5b	CH_3	CH_3	II	EA	1	2	68	22(*S*)
5b	CH_3	C_2H_5	II	PA	1	2	63	38(*R*)

[a] EA: ethyl acetate, EP: ethyl propionate, PA: propyl acetate. [b] The number of cocomplexed auxiliary esters. [c] The number of water molecules in the complex. [d] Yield of the complex salt based on half of the starting racemic **5**. [e] Enantiomeric excess and configuration (in parentheses) of **5** obtained from the complex were determined by comparing the specific rotation value and the sign of rotation to those of the pure enantiomer. [f] Yield of the salt is based on the amount of the (*S*)-enantiomer present in the starting mixture. [g] Starting from a mixture with 76%(*S*) *ee*.

Type II: $n_1 = 1$; auxiliary ligands (generally both A_1 and A_2 when A_1 is a simple ester) are cocomplexed. Cocomplexation can be advantageous considering the remarkable influence of A_1 on the enantiomeric composition of L.[7] Type II is characteristic for medium-sized hydroxy esters. Type III: $n_1 = 1$; only water molecules are cocomplexed. This classification is valid for air-dried salts.

These methods present new aspects of optical resolution. Normally, the resolving agent should be selected to achieve better resolution. Using this second method, however, the efficiency of the resolution and, in certain cases, the configuration of the enantiomer obtained can be controlled by varying the ester function and/or the applied auxiliary ligands.

Received: April 3, 1996
Revised version: January 2, 1997 [Z 8993 IE]
German version: *Angew. Chem.* **1997**, *109*, 1529–1531

Keywords: carboxylic acids · chiral recognition · enantiomeric resolution

[1] A. Mravik, E. Fogassy, Z. Lepp, Hung. Pat. Appl. P00185 **1996**; A. Mravik, Z. Lepp, E. Fogassy, *Tetrahedron: Asymmetry* **1996**, *7*, 2387–2390.

[2] N. K. Kochetkov, A. M. Likhosherstov, V. N. Kulakov, *Tetrahedron* **1969**, *25*, 2313–2323.

[3] P. C. Bélanger, H. W. R. Williams, *Can. J. Chem.* **1983**, *61*, 1383–1386.

[4] Single crystals of (*S*)-**3b** were grown by slow concentration of a solution in methanol/water. A stereoview of (*S*)-**3b** is shown in Figure 1. $M_r = 548.50$, orthorhombic, space group $P2_12_12_1$, $a = 11.074(10)$, $b = 27.149(3)$, $c = 8.220(5)$ Å, $V = 2472(3)$ Å^3, $Z = 4$, $\rho_{calcd} = 1.474$ g cm^{-3}, $\mu = 2.806$ mm^{-1}. Data were collected on a colorless crystal (0.70 × 0.30 × 0.25 mm) at room temperature with a Rigaku AFC6S diffractometer; $\omega/2\theta$ scans with a ω scan rate of 8° min^{-1} and a scan width of $(0.89 + 0.30 \tan\theta)°$ with graphite-monochromated $Cu_{K\alpha}$ radiation. Lattice parameters were determined by least squares using 25 reflections with $46.2 < 2\theta < 55.0°$. Three standards monitored every 150 reflections indicated no significant decay. A full set of Friedel mates was collected for a total of 10292 reflections ($\theta_{max} = 75.77°$; $13 \geq h \geq -1$, $34 \geq k \geq -34$, $10 \geq l \geq -10$) of which 5109 were unique with $R_{merge} = 0.082$ (without Friedel mates). The structure was solved with the TEXSAN package (Molecular Structure Co., TEXSAN. Single Crystal Structure Analysis Package, The Woodlands, TX 77381, USA, **1992**) and refined with SHELXL-93 (G. M. Sheldrick, SHELXL-93, Program for the Refinement of Crystal Structures, University of Göttingen, **1993**) against F^2 with all unique reflections (2788 had intensities higher than $2\sigma(I)$). All non-hydrogen atoms were refined anisotropically. Most hydrogen atoms were generated based on geometrical evidence with X–H bond lengths dependant on the chemical nature of X. Some hydrogen-atom positions (for example those belonging to the two water molecules) were taken from difference-Fourier calculations and reinforced by forming hydrogen bonds with proper geometry. $R1 = 0.0602$, $wR2 = 0.1369$, GOF = 1.095 for those reflections with $I > 2\sigma(I)$. The Flack parameter $x = 0.01(2)$ confirms the absolute configuration (H. D. Flack, *Acta Crystallogr. Sect. A* **1983**, *39*, 876–881). Crystallographic data (excluding structure factors) for the structure reported in this paper have been deposited with the Cambridge Crystallographic Data Centre as supplementary publication no. CCDC-100266. Copies of the data can be obtained free of charge on application to The Director, CCDC, 12 Union Road, Cambridge CB2 1EZ, UK (fax: int. code +(1223)336-033; e-mail: deposit@chemcrys.cam.ac.uk).

[5] The previously prepared acidic calcium salt or dibenzoyltartaric acid and calcium oxide were dissolved in hot ethanol, and the racemic ester was added. In some cases crystallization can be carried out from this solution, but more frequently from a solvent mixture made by adding further solvents (such as acetone, toluene, or ethyl acetate). However, most of the complexes were separated from an ester-type solvent after the ethanol was removed by evaporation.

[6] Characterized by thermoanalytical methods (TGA, EGD), elemental analysis, and ICP-AES. The structure of the complex formed with two molecules of methyl mandelate was determined by X-ray crystallography (A. Mravik, Z. Böcskei, Z. Katona, I. Markovits, G. Pokol, D. K. Menyhárd, E. Fogassy, *Chem. Commun.* **1996**, 1983–1984.) In some cases partial decomposition occurs at slightly elevated temperatures or even at room temperature. Measurements were performed on air-dried samples, which may contain 0.5–2% of volatile impurities. Furthermore, the relatively high molecular weight may cause uncertainty in the results.

[7] The resolution of ethyl mandelate in the presence of various simple esters of C_2–C_4 alcohols afforded complex salts in which the *ee* values of the ethyl mandelate were in the range of 31–78%.

A Hydrogen-Bonding Receptor That Binds Urea with High Affinity**

Thomas W. Bell* and Zheng Hou

Urea is an important target for molecular recognition studies, both from fundamental and practical points of view. It is a small molecule having hydrogen-bonding sites of well-defined geometry. The urea moiety is present in numerous biologically relevant compounds, including barbiturates, biotin, citrulline, cytosine, thymine, uracil, and uric acid. As an end product of nitrogen metabolism, urea is found in the human blood stream in concentrations between 2 and 8 mM and is excreted in urine. The blood urea nitrogen (BUN) level is a primary indicator of kidney function[1] and compounds having high affinity for urea are potentially useful in clinical chemistry. We have synthesized an artificial receptor that fully satisfies the hydrogen-bonding capacity of urea. The resulting complex is stable even in pure DMSO, from which it can be isolated by crystallization.

The novel receptor **1** nearly encircles urea from the "bottom," that is from the side opposite the carbonyl group, as shown by the schematic structure **I** in Figure 1a. Like previously reported

[*] Prof. T. W. Bell,[+] Z. Hou
Department of Chemistry
State University of New York
Stony Brook, NY 11794-3400 (USA)

[+] Current address: Department of Chemistry, MS216
University of Nevada, Reno, NV 89557-0020 (USA)
Fax: Int. code +(702) 784-6804
e-mail: twb@unr.edu

[**] This work was partially funded by the National Institutes of Health (GM 32937).

receptor **2**,[2] **1** is capable of forming four hydrogen bonds with the amino groups of urea; the complex is apparently stabilized further by secondary electrostatic interactions between these hydrogen atoms and the nitrogen atoms of the spacer pyridine rings, as indicated by dotted lines to X in **I**. Receptor **1** also incorporates two amino groups that can form hydrogen bonds with the two remaining hydrogen-bond acceptor sites of urea, the nonbonded electron pairs of the oxygen atom. Other known hydrogen-bonding receptors bind urea or urea derivatives from the "top" end, through the carbonyl group, as shown in schematic structure **II** (Figure 1b). Complexes of type **III**[3] and

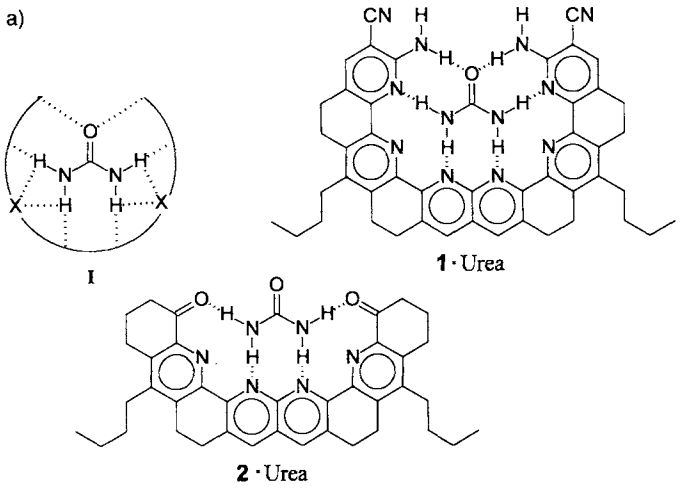

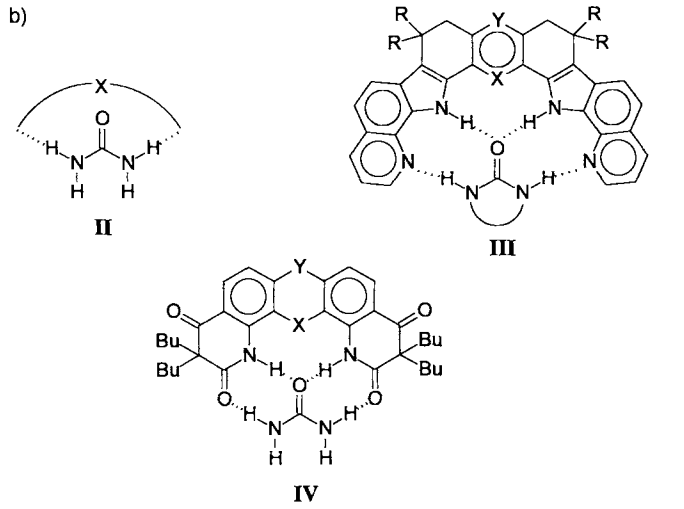

Figure 1. Representation of **1**·urea and other previously reported complexes in which hydrogen-bonding receptors bind urea a) from the bottom, that is opposite the C=O group, or b) from the top.

IV[4] bind only four of the six possible sites of urea; they lack acceptors for the two remaining NH donor groups. Therefore, we speculated that **1** would be much more selective toward urea relative to *N*-alkyl ureas. Macrocyclic polyethers capable of encircling urea are known,[5] but they do not have the high degree of conformational preorganization present in fused-ring receptors.

The choice of target structure **1** for synthesis was influenced by the known hydrogen-bond donor ability of the *o*-aminonitrile functionality[6] and the availability of the oxoaminonitrile **3**[6a] as a synthetic intermediate (Scheme 1). Friedländer condensation of **3** with 4-amino-1,3-pyrimidine-5-carboxaldehyde[7] gave **4**, which was hydrolyzed under standard conditions to give **5**, which contains both *o*-aminonitrile and *o*-aminoaldehyde functionalities. Condensation of **5** with a second equivalent of **3** was carried out in methanol/toluene, then excess urea was added to the hot reaction mixture. Cooling resulted in precipitation of receptor **1** as the complex **1**·urea, which was triturated with methanol and recrystallized from DMSO. While this complex is stable in hot DMSO, boiling in water causes the urea-free receptor to precipitate. Pure **1** was then obtained in good yield by recrystallization from dichloromethane/ethanol.[8]

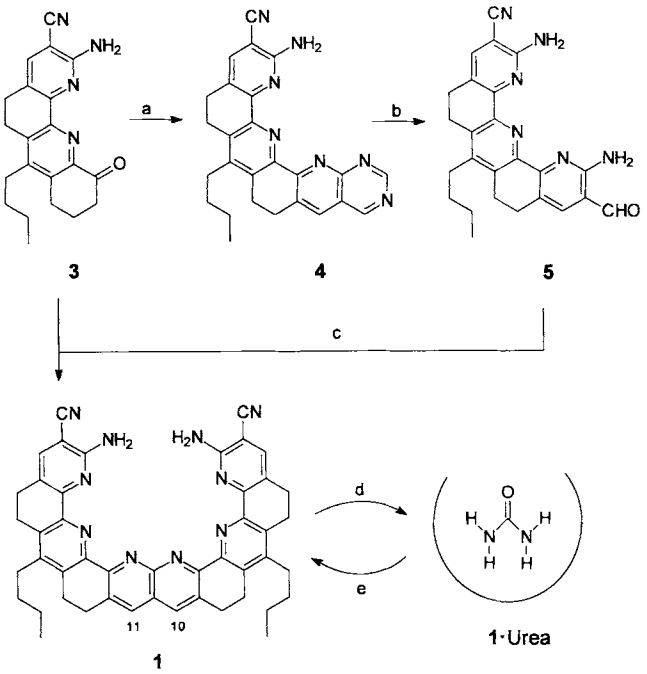

Scheme 1. Synthesis of receptor **1** and of complex **1**·urea. a) 4-Amino-1,3-pyrimidine-5-carboxaldehyde [7], KOH, CH_3OH/toluene (3/2 (v/v)), reflux, 24 h (61%); b) 0.2N HCl, reflux, 14 h (95%); c) 1,8-diazabicyclo[5.4.0]undec-7-ene (DBU), CH_3OH/toluene (6/5 (v/v)), reflux, 28 h; d) urea, DMSO, reflux, 12 h, recrystallized from DMSO (77% from **5**); e) H_2O, reflux, 4 h, recrystallized from CH_2Cl_2/ethanol (15/8 (v/v); 87%) [8].

Cocrystallization of **1** and urea from DMSO is one of several experimental results that supports the proposed formation of a 1:1 complex (**1**·urea). The IR spectrum of this complex displays a peak at 1655 cm^{-1}, corresponding to the hydrogen-bonded C=O group of urea.[5a] Binding studies in solution were limited by the low solubilities of **1** and **1**·urea in most solvents, but in a 1/1 (v/v) mixture of $CDCl_3$ and $[D_6]$DMSO a significant shift of the ^{1}H NMR signals for the naphthyridine protons (H10, H11) in the receptor is observed on complexation. This resonance signal served as a marker in titration experiments involving incremental addition of urea to a 1 mM solution of **1** in this solvent system. Figure 2a compares the resulting ^{1}H NMR shifts with a curve calculated[9] for a stability constant of $8 \times 10^3\ M^{-1}$. The assumptions in this calculation were tested by recording the ^{1}H NMR spectra of **1**·urea and **1** at various concentrations. The results are plotted in Figure 2b in comparison with the curve calculated with the parameters obtained from fitting the titration curve. Dilution causes the host resonances to shift slightly downfield rather than upfield, indicating that 1:1 binding is not the only equilibrium of importance. Aggregation of urea-free **1** is also suggested by the concentration dependence of the position of the H10,H11 signals in the 0.4–3.6 mM concentration range (Figure 2b, triangles).

 © VCH Verlagsgesellschaft mbH, D-69451 Weinheim, 1997 0570-0833/97/3613-1537 $ 17.50+.50/0

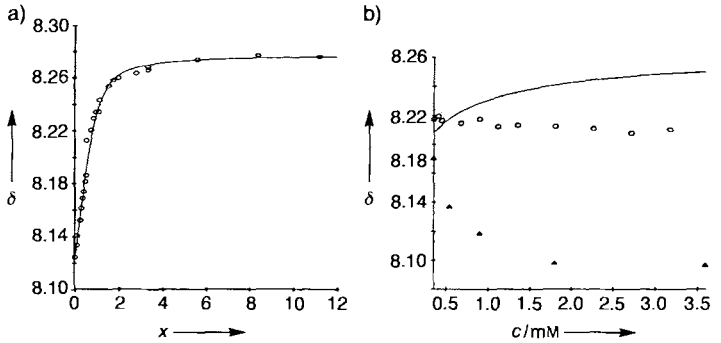

Figure 2. a) Plot of the ^{1}H NMR chemical shifts obtained for the protons H10 and H11 during the titration of a 1.07 mM solution of receptor **1** with urea ($CDCl_3$/[D_6]DMSO 1/1 (v/v), 298 K), together with the calculated curve ($K_s = 7600\,M^{-1}$)[9]. x = c(urea)/c(**1**). b) Concentration dependence of the ^{1}H NMR chemical shifts of the protons H10 and H11 for **1** (triangles) and **1**·urea (circles) in comparison with the calculated curve ($K_s = 7600\,M^{-1}$) [9].

The UV/Vis absorptions of polycyclic receptors similar to **1** undergo bathochromic shifts upon complexation of planar guests,[2a] so the effects of added urea or alkylated urea derivatives on the spectrum of **1** were compared (Figure 3). The addition of at least one equivalent of urea to a solution of receptor **1** in 1:1 $CHCl_3$/DMSO causes a shift of the longest wavelength absorption maximum from 394 nm to 410 nm (Figure 3b). *N*-Butylurea has a much smaller effect on the absorption spectrum of **1** (Figure 3b), whereas *N*,*N*′-dimethylurea and *N*,*N*-dimethylurea have negligible effects (Figures 3c,d). UV/Vis titration experiments were then conducted in which urea was added to a 22 μM solution of **1** in 1:1 $CHCl_3$/DMSO; the resulting absorbances at 410 nm are plotted in Figure 4. The stability constant of $1.4 \pm 0.2 \times 10^4\,M^{-1}$ calculated from this data[10] is larger than that obtained from NMR titration results, apparently due to suppression of competing equilibria at lower receptor concentration.

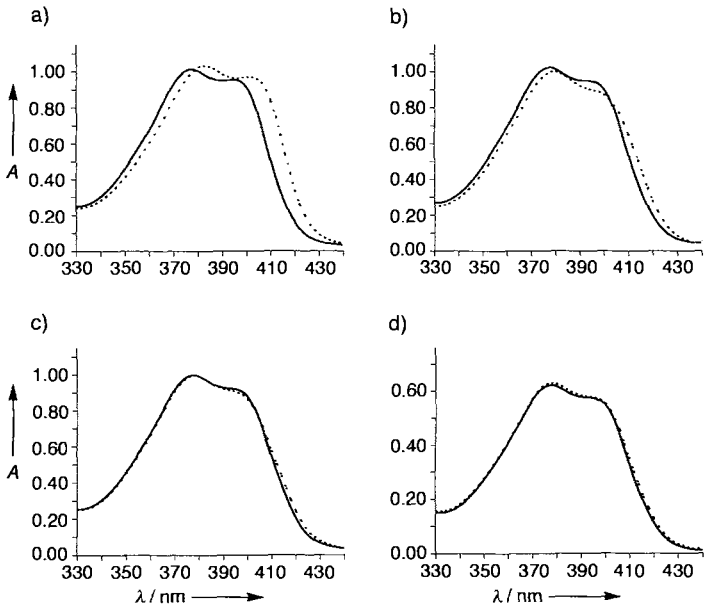

Figure 3. UV/Vis absorption spectra of receptor **1** (34.8 μM) in 1/1 (v/v) $CHCl_3$/DMSO (298 K) before (solid line) and after (dotted line) addition of a) excess urea, b) *N*-butylurea, c) *N*,*N*′-dimethylurea, or d) *N*,*N*-dimethylurea. In d) the concentration of **1** was 20.8 μM. A = absorbance.

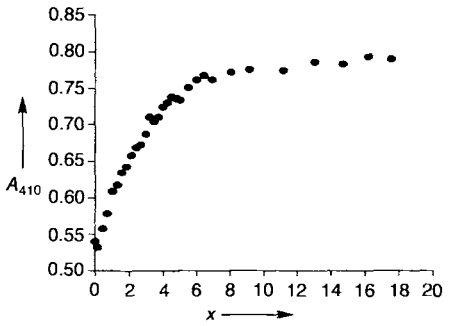

Figure 4. Absorbance changes at 410 nm during titration of receptor **1** (22.4 μM) with urea in 1/1 (v/v) $CHCl_3$/DMSO (298 K). x = c(urea)/c(**1**).

Compound **1** is the highest affinity receptor capable of binding urea solely with hydrogen bonds. Direct comparison between **1** and a uranyl complex that also forms a strong complex with urea[5c] cannot be made without performing complexation experiments under similar conditions. The observed combination of binding strength and selectivity makes **1** an attractive candidate for structural modification aimed at development of reagents and sensors[2a, 11] for urea analysis.

Received: December 16, 1996 [Z 9894 IE]
German version: *Angew. Chem.* **1997**, *109*, 1601–1603

Keywords: hydrogen bonds · molecular recognition · urea

[1] D. Johnson in *Clinical Chemistry* (Ed.: E. H. Taylor), Wiley, New York, **1989**, pp. 55–82.
[2] a) T. W. Bell, D. L. Beckles, P. J. Cragg, J. Liu, J. Maioriello, A. T. Papoulis, V. J. Santora in *Fluorescent Chemosensors for Ion and Molecule Recognition* (Ed.: A. W. Czarnik), ACS Books, Washington, DC, **1993**, pp. 85–103; b) T. W. Bell, J. Liu, *J. Am. Chem. Soc.* **1988**, *110*, 3673–3674.
[3] a) V. Hegde, C.-Y. Hung, P. Madhukar, R. Cunningham, T. Höpfner, R. P. Thummel, *J. Am. Chem. Soc.* **1993**, *115*, 872–878; b) V. Hegde, P. Madhukar, J. D. Madura, R. P. Thummel, *ibid.* **1990**, *112*, 4549–4550.
[4] M. Crego, J. J. Marugán, C. Raposo, M. J. Sanz, V. Alcázar, M. C. Caballero, J. R. Morán, *Tetrahedron Lett.* **1991**, *32*, 4185–4188.
[5] a) F. C. J. M. van Veggel, D. N. Reinhoudt in *Frontiers in Supramolecular Organic Chemistry and Photochemistry* (Eds.: H.-J. Schneider, H. Dürr), VCH, New York, **1991**, pp. 83–108; b) A. R. van Doorn, R. Schaafstra, M. Bos, S. Harkema, J. van Eerden, W. Verboom, D. N. Reinhoudt, *J. Org. Chem.* **1991**, *56*, 6083–6094; c) C. J. van Staveren, J. van Eerden, F. C. J. M. van Veggel, S. Harkema, D. N. Reinhoudt, *J. Am. Chem. Soc.* **1988**, *110*, 4994–5008; d) C. J. van Staveren, V. M. L. J. Aarts, P. D. J. Grootenhuis, W. J. H. Droppers, J. van Eerden, S. Harkema, D. N. Reinhoudt, *ibid.* **1988**, *110*, 8134–8144.
[6] a) T. W. Bell, Z. Hou, S. C. Zimmerman, P. A. Thiessen, *Angew. Chem.* **1995**, *107*, 2321–2324; *Angew. Chem. Int. Ed. Engl.* **1995**, *34*, 2163–2165; b) D. Beckles, J. Maioriello, V. J. Santora, T. W. Bell, E. Chapoteau, B. P. Czech, A. Kumar, *Tetrahedron* **1995**, *51*, 363–376.
[7] J. Baddily, B. Lythgoe, A. R. Todd, *J. Chem. Soc.* **1943**, 386–387.
[8] 2,19-Diamino-7,14-dibutyl-3,18-dicyano-5,6,8,9,12,13,15,16-octahydroquinolino[9,8-*f*]quinolino[7′,6′-*j*][1,10]phenanthrolino[2,3-*f*][1,10]phenanthroline **1**: ^{1}H NMR (300 MHz, [D_6]DMSO/$CDCl_3$ 1/1): δ = 8.11 (s, 2H, H10,11), 7.67 (s, 2H, H4,17), 6.85 (s, 4H, NH_2), 3.16–3.34 (m, 12H, H6,8,9,12,13,15), 2.97 (m, 4H, H5,16), 2.79 (m, 4H, CH_2Pr), 1.47 (m, 8H, CH_2CH_2Me), 0.95 (t, J = 7 Hz, 3H, CH_3); elemental analysis calcd for $C_{46}H_{42}N_{10}(H_2O)_{2.5}$: C 70.77, H 5.84, N 17.75%; found: C 70.84, H 6.07, N 17.96% (sample dried at 1 Torr, 80 °C, 48 h).
[9] ^{1}H NMR curves were calculated with the following chemical shifts: δ(host) = 8.123, δ(complex) = 8.277; C. S. Wilcox in *Frontiers of Supramolecular Organic Chemistry and Photochemistry* (Eds.: H.-J. Schneider, H. Dürr), VCH, New York, **1991**, pp. 123–144.
[10] The stability constant was calculated with the following molar absorptivities at 410 nm: ε(host) = 2.4×10^4, ε(complex) = $3.9 \times 10^4\,M^{-1}\,cm^{-1}$.
[11] A. W. Czarnik, *Chem. Biol.* **1995**, *2*, 423–428.

New Technology for the Synthesis of Vancomycin-Type Biaryl Ring Systems**

K. C. Nicolaou,* Xin-Jie Chu, Joshi M. Ramanjulu, Swaminathan Natarajan, Stefan Bräse, Frank Rübsam, and Christopher N. C. Boddy

Dedicated to Professor Samuel J. Danishefsky on the occasion of his 60th birthday

Due to their effective action against drug-resistant bacterial strains, the vancomycin antibiotics[1] are currently receiving unprecedented attention from chemists,[2] biologists, and clinicians.[3] As a target molecule, vancomycin[4] (**1**, Figure 1) presents several synthetic challenges, amongst which the construction of the 12-membered biaryl ring system stands, perhaps, as the most formidable. It is, therefore, not surprising that to date only one report[2a] exists for its construction. In this communication, we describe a new method for the construction of the biaryl ring system of vancomycin, which is direct and involves mild conditions. The application of the present Ni^0-mediated[5] C–C coupling strategy to the synthesis of model systems **5** and **12–14** demonstrates its generality and scope and holds promise for a solution to the vancomycin problem itself.

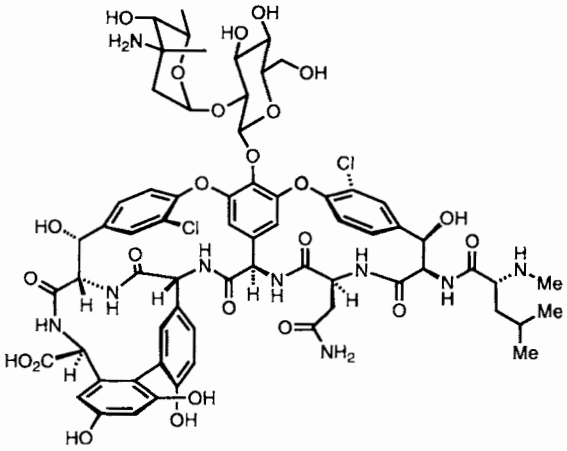

Figure 1. Molecular structure of vancomycin (**1**).

Scheme 1 summarizes the chemistry for the construction of the vancomycin model system **5**, which contains the 12-membered peptide ring. Coupling of fragments **2**[6] and **3**[6] with EDC as the coupling reagent in the presence of HOBT provided the targeted precursor **4** in 90% yield. The crucial cyclization reaction was carried out at 50 °C with tetrakis(triphenylphosphane)nickel [$(Ph_3P)_4Ni$] generated in situ in DMF (16 h) to afford the vancomycin model system **5** as a mixture of atropisomers (57% total yield). In thin-layer chromatography (TLC), compound **5** behaved as a single compound, but in the ^1H NMR spectrum ($CDCl_3$, 500 MHz, 25 °C) it exhibited splitting and broadness of signals characteristic of slow interconversion of its two atropisomers. On heating to 50 °C, the spectrum sharpened considerably, as expected (Table 1).

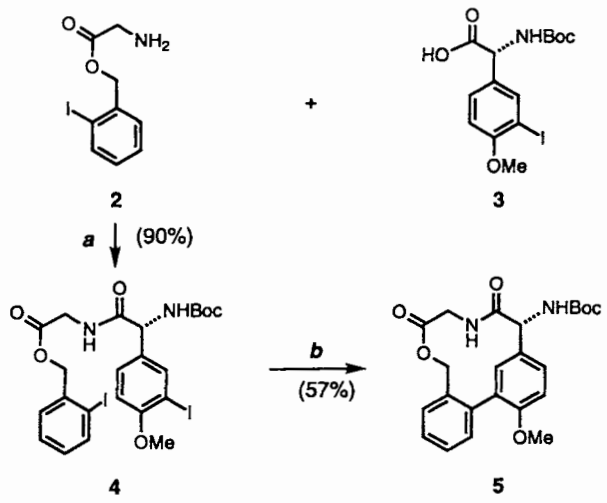

Scheme 1. Synthesis of vancomycin model system **5**: a) 1.5 equiv of EDC, 1.5 equiv of HOBT, DMF, 0 °C, 10 h; b) 1.8 equiv of $(Ph_3P)_2NiCl_2$, 1.8 equiv of Zn, 3.6 equiv of Ph_3P, DMF (0.002 M), 55 °C, 16 h. EDC = 1-(3-dimethylamino-propyl)-3-ethylcarbodiimide hydrochloride; HOBT = 1-hydroxybenzotriazole; Boc = *tert*-butoxycarbonyl, DMF = *N*,*N*-dimethylformamide.

Encouraged by this result we then attempted the construction of the more advanced systems **12–14**, which are closely related to vancomycin (Scheme 2). The required precursors **9–11**

Table 1. Selected physical properties of compounds **5**, **14a**, and **14b**.

5 (mixture of atropisomers): $R_f = 0.50$ [silica gel, 50% EtOAc in hexanes]; $[\alpha]_D^{25}$ −3.1 ($c = 0.13$ in CH_2Cl_2); IR (film): $\tilde{\nu}_{max} = 3289, 2924, 2851, 1726, 1689, 1647, 1527, 1454, 1371, 1298, 1240, 1110\ cm^{-1}$; ^1H NMR (500 MHz, $CDCl_3$) $\delta = 1.42$ (s, 9H, *t*Bu), 3.79 (s, 3H, OMe), 4.24–4.41 (m, 3H, H_1, H_4), 5.07–5.18 (m, 2H, H_7), 5.43 (bs, 1H, BocNH), 6.91 (d, $J = 4.5$ Hz, 1H, Ar_AH_c), 7.21 (bs, 1H, H_3), 7.35–7.43 (m, 6H, $Ar_AH_{a,b}$, Ar_B); ^{13}C NMR (125 MHz, $CDCl_3$): $\delta = 171.8, 171.2, 168.9, 168.4, 168.1, 167.8, 156.3, 156.2, 155.7, 155.5, 140.7, 140.4, 132.8, 132.7, 131.6, 131.5, 130.7, 130.5, 129.9, 128.6, 128.51, 128.4, 127.9, 127.6, 127.4, 127.3, 127.1, 123.7, 110.4, 107.4, 80.3, 67.0, 65.9, 56.7, 55.6, 55.5, 52.2, 42.7, 42.3, 29.6, 29.5, 28.2, 28.1, 28.0$; HRMS (FAB) calcd for $C_{23}H_{26}N_2O_6Cs$ ($M+Cs^+$) 559.0845; found 559.0828.

14a: $R_f = 0.20$ [silica, 2.5% MeOH in $CHCl_3$]; $[\alpha]_D^{25}$ −45.7 ($c = 0.37$ in CH_2Cl_2); IR (film): $\tilde{\nu}_{max}$ 3320, 2924, 1673, 1611, 1585, 1501, 1366, 1324, 1256, 1157, 1110, 1063 cm^{-1}; ^1H NMR (600 MHz, $CDCl_3$): $\delta = 1.34$ (s, 9H, *t*Bu), 3.28–3.30 (m, 1H, H_7), 3.63 (s, 6H, OMe), 3.64–3.66 (m, 1H, H_4), 3.72 (s, 3H, OMe), 3.74–3.76 (m, 1H, H_4), 3.84–3.86 (m, 1H, H_7), 4.81 (br s, 1H, H_1), 6.56 (d, $J = 2.2$ Hz, 1H, H Ar_BH_a), 6.58 (d, $J = 2.2$ Hz, 1H, Ar_BH_b), 6.85 (br s, 1H, BocNH), 6.95 (d, $J = 8.3$ Hz, 1H, Ar_AH_c), 7.08 (br s, 1H, Ar_AH_d), 7.30 (dd, $J = 8.3$, 2.1 Hz, 1H, Ar_AH_b), 7.40 (br s, 1H, N_6H), 7.82 (t, $J = 6.6$ Hz, 1H, N_3H); ^{13}C NMR (150 MHz, [D_6]DMSO) $\delta = 172.1, 170.4, 167.5, 159.5, 158.1, 156.7, 137.4, 132.9, 129.9, 127.7, 124.1, 120.8, 110.8, 107.9, 97.9, 78.3, 59.7, 55.7, 55.5, 55.3, 43.7, 43.3, 28.1$; HRMS (FAB) calcd for $C_{25}H_{31}N_3O_7Na$ ($M+Na^+$) 508.2060; found: 508.2067. **14b**: $R_f = 0.25$ [silica, 2.5% MeOH in $CHCl_3$]; $[\alpha]_D^{25}$ −18.1 ($c = 0.63$ in CH_2Cl_2); IR (film): $\tilde{\nu}_{max}$ 3314, 2924, 2853, 1677, 1581, 1504, 1459, 1366, 1320, 1262, 1160, 1110 cm^{-1}; ^1H NMR (600 MHz, [D_6]DMSO): $\delta = 1.32$ (s, 9H, *t*Bu), 3.67 (s, 3H, OMe), 3.68–3.70 (m, 1H, H_4), 3.74 (s, 3H, OMe), 3.82–3.86 (m, 1H, H_4), 3.81 (s, 3H, OMe), 4.13–4.24 (m, 2H, H_7), 5.12–5.13 (m, 1H, H_1), 6.50 (s, 2H, $Ar_BH_{a,b}$), 6.98 (d, $J = 8.6$ Hz, 1H, Ar_AH_c), 7.18 (s, 1H, Ar_AH_a), 7.36–7.38 (m, 2H, BocNH, Ar_AH_b), 8.29 (br s, 1H, N_6H), 8.57 (br s, 1H, N_3H); ^{13}C NMR (150 MHz, [D_6]DMSO) $\delta = 171.1, 168.9, 160.8, 158.4, 156.4, 155.3, 142.3, 130.2, 130.1, 129.8, 128.2, 127.8, 111.0, 105.4, 97.4, 78.7, 57.6, 56.5, 55.5, 55.1, 47.8, 42.4, 28.1$; HRMS (FAB) calcd for $C_{25}H_{31}N_3O_7Na$ ($M+Na^+$) 508.2060; found 508.2069.

[*] Prof. Dr. K. C. Nicolaou, Dr. X.-J. Chu, Dr. J. M. Ramanjulu, Dr. S. Natarajan, Dr. S. Bräse, Dr. F. Rübsam, C. N. C. Boddy
Department of Chemistry and The Skaggs Institute for Chemical Biology
The Scripps Research Institute
10550 North Torrey Pines Road, La Jolla, CA 92037 (USA)
Fax: Int. code +(619)784-2469
and
Department of Chemistry and Biochemistry
University of California, San Diego
9500 Gilman Drive, La Jolla, CA 92093 (USA)

[**] This work was financially supported by The Skaggs Institute for Chemical Biology and the U. S. National Institutes of Health (NIH). J. M. R. acknowledges the NIH, S. B. the NATO/DAAD, F. R. the Alexander-von-Humboldt-Stiftung for a post-doctoral fellowship. We thank Dr. Gary Siuzdak and Dr. Dee H. Huang for assistance with mass spectrometry and NMR spectroscopy, respectively.

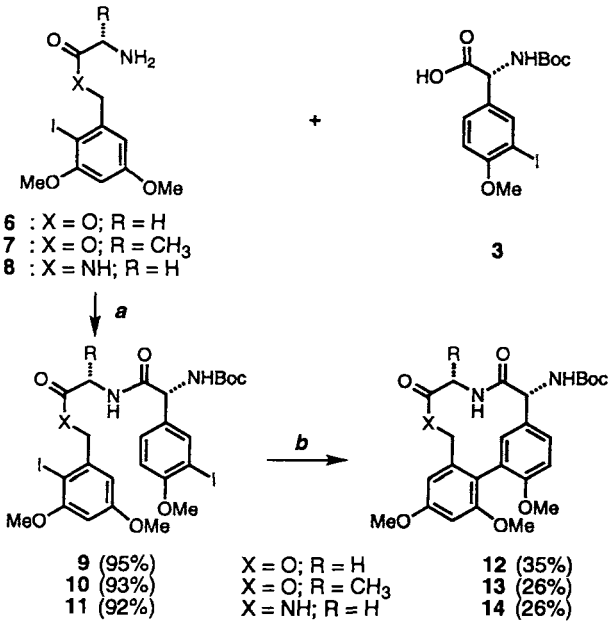

Scheme 2. Synthesis of vancomycin model systems **12**–**14**: a) 1.2 equiv of **3**, 1.3 equiv of EDC, 2.2 equiv of Et_3N, DMF, 0 °C, 12 h; b) 1.8 equiv of $(Ph_3P)_2NiCl_2$, 1.8 equiv of Zn, 3.6 equiv of Ph_3P, DMF (0.002 M), 55 °C, 16 h.

were synthesized in high yield (90–95%) by peptide coupling of the appropiate amino fragment (**6**–**8**)[6] with carboxylic acid **3**. Exposure of depsipeptides **9** and **10** with Ni^0 under the conditions of Scheme 1 gave the cyclized systems **12** and **13** in 35% and 26% yield, respectively, along with the reduced products **15** (43%) and **16** (29%) (Figure 2). Apparently, a

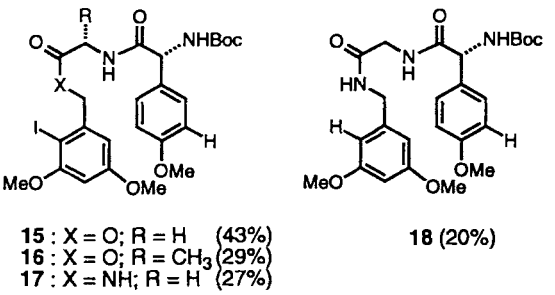

Figure 2. Reduced products from the Ni^0-mediated cyclizations of **9**–**11**.

higher degree of substitution on one of the aromatic rings slows down the intramolecular reaction, allowing the formation of reduced products. Finally, peptide **11**, upon treatment with Ni^0, resulted in the formation of biaryl system **14** in 26% yield as a mixture of two atropisomers. The two isomers (**14a** and **14b**) were separated by preparative layer chromatography [silica gel, 2.5% MeOH in $CHCl_3$, $R_f = 0.20$ (**14a**) and 0.25 (**14b**)]. NOESY experiments enabled assignment of the major atropisomer (**14a**) as indicated in Figure 3. It is noteworthy that the unnatural atropisomer **14a** prevailed as the major product in this cyclization reaction. However, removal of the methyl groups from the trimethoxybiaryl moieties of **14a** and **14b** is expected to facilitate their interconversion, as previously observed for a similar system.[2a]

The formation of dimers was also observed in all cases described above (MS, ^1H NMR). Further dilution of the reaction mixture disfavored dimerization, but increased the amount of

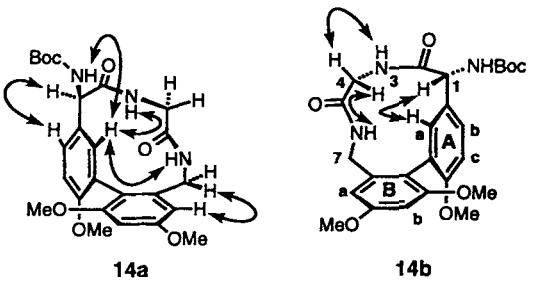

Figure 3. Structural assignment of atropisomers **14a** and **14b** based on NOESY experiments.

reduced by-products. Work is currently in progress for further optimization of these reactions and for the invention of new ones for the purposes of efficiently constructing this challenging biaryl system.

In conclusion, a mild method for the construction of the rigid 12-membered biaryl ring system of the vancomycin antibiotics has been developed. Its application to the total synthesis of natural and designed members of this class of compounds for biological studies may prove fruitful.

Received: December 23, 1996 [Z 9929 IE]
German version: *Angew. Chem.* **1997**, *109*, 1551–1552

Keywords: asymmetric synthesis · biaryls · cyclizations · peptides · vancomycin

[1] a) A. V. R. Rao, M. K. Gurjar, K. L Reddy, A. S. Rao, *Chem. Rev.* **1995**, *95*, 2135–2167 and references therein; b) *Glycopeptide Antibiotics* (Ed.: R. Nagarajan), Dekker, New York, **1994**; c) K. Burgess, D. Lim, C. I. Martinez, *Angew. Chem.* **1996**, *108*, 1162–1163; *Angew. Chem. Int. Ed. Engl.* **1996**, *35*, 1077–1078.

[2] a) D. A. Evans, C. J. Dinsmore, D. A. Evrard, K. M. De Vries, *J. Am. Chem. Soc.* **1993**, *115*, 6426–6427; b) D. A. Evans, C. J. Dinsmore, *Tetrahedron Lett.* **1993**, *34*, 6029–6032; c) A. J. Pearson, G. Bignan, *ibid.* **1996**, *37*, 735–738; d) A. J. Pearson, G. Bignan, P. Zhang, M. Celliah, *J. Org. Chem.* **1996**, *61*, 3940–3941; e) D. L. Boger, R. M. Borzilleri, S. Nukui, *Bioorg. Med. Chem. Lett.* **1995**, *5*, 3091–3096; f) D. L. Boger, J. Zhou, *J. Org. Chem.* **1996**, *61*, 3938–3939; g) R. Beugelmans, G. P. Singh, M. Bois-Choussy, J. Chastanet, J. P. Zhu, *ibid.* **1994**, *59*, 5535–5542; h) J. P. Zhu, J.-P. Bouillon, G. P. Singh, J. Chastanet, R. Beugelmans, *Tetrahedron Lett.* **1995**, *36*, 7081–7084; i) R. Beugelmans, M. Bois-Choussy, C. Vergne, J.-P. Bouillon, J. P. Zhu, *J. Chem. Soc. Chem. Commun.* **1996**, 1029–1030; j) T. Inoue, T. Sasaki, H. Takayanagi, Y. Harigaya, O. Hoshino, H. Hara, T. Inaba, *J. Org. Chem.* **1996**, *61*, 3936–3937; k) D. H. Williams, J. R. Kalman, *J. Am. Chem. Soc.* **1977**, *99*, 2768–2774; l) A. G. Brown, M. J. Crimmin, P. D. Edwards, *J. Chem. Soc. Perkin Trans 1* **1992**, 123–130; m) D. A. Evans, J. A. Ellman, K. M. De Vries, *J. Am. Chem. Soc.* **1989**, *111*, 8912–8914; n) A. V. R. Rao, T. K. Chakraborty, S. P. Joshi, *Tetrahedron Lett.* **1992**, *33*, 4045–4048; o) A. V. R. Rao, K. L. Reddy, M. M. Reddy, *ibid.* **1994**, *35*, 5039–5042; p) J. P. Zhu, R. Beugelmans, A. Bigot, G. P. Singh, M. Bois-Choussy, *ibid.* **1993**, *34*, 7401–7404; q) D. A. Evans, P. S. Watson, *ibid.* **1996**, *37*, 3251–3254; r) H. Konishi, T. Okuno, S. Nishiyama, S. Yamamura, K. Koyasu, Y. Terada, *ibid.* **1996**, *37*, 8791–8794.

[3] a) G. M. Sheldrick, P. G. Jones, O. Kennard, D. H. Williams, G. A. Smith, *Nature* **1978**, *271*, 223–225; b) C. T. Walsh, *Science* **1993**, *261*, 308–309; c) P. J. Loll, A. E. Bevivino, B. D. Korty, P. H. Axelson, *J. Am. Chem. Soc.* **1997**, *119*, 1516–1522.

[4] a) M. H. McCormick, W. M. Stark, R. C. Pittenger, G. M. McGuire, *Antibiot. Annu.* **1955–1956**, 606–611; b) R. S. Griffith, *J. Antimicrob. Chemother.* **1984**, *14 (Suppl. D)*, 1–5; c) C. M. Harris, T. M. Harris, *J. Am. Chem. Soc.* **1982**, *104*, 4293–4295; d) C. M. Harris, H. Kopecka, T. M. Harris, *ibid.* **1983**, *105*, 6915–6922.

[5] a) W. Carruthers, P. Coggins, J. B. Weston, *J. Chem. Soc. Perkin Trans. 1.* **1991**, 611–616; b) M. F. Semmelhack, P. Helquist, L. D. Jones, L. Keller, L. Mendelson, L. S. Ryono, J. G. Smith, R. D. Stauffer, *J. Am. Chem. Soc.* **1981**, *103*, 6460–6471; c) A. S. Kende, L. S. Liebeskind, D. M. Braitsch, *Tetrahedron Lett.* **1975**, 3375–3378; d) T. T. Tsou, J. K. Kochi, *J. Am. Chem. Soc.* **1979**, *101*, 7547–7560.

[6] The fragments **2**, **3**, and **6**–**8** used in this study were constructed by standard methods from readily available aromatic systems. Details will be published in a full account of this work. All new compounds exhibited satisfactory spectral and exact mass data.

Selective Inhibition of Receptor Tyrosine Kinases by Synthetic Analogues of Aeroplysinin**

Herbert Waldmann,* Klaus Hinterding, Peter Herrlich,* Hans Jobst Rahmsdorf, and Axel Knebel

Various transmembrane receptors—for example the receptors of insulin-like growth factor (IGFR), nerve growth factor (NGFR), epidermal growth factor (EGFR), and platelet-derived growth factor (PDGFR)—phosphorylate themselves on tyrosine residues in response to the binding of extracellular ligands. Thereby these receptor tyrosine kinases (RTKs) gain the ability to trigger various intracellular signaling cascades by which cell growth, proliferation, and other genetic programs are regulated.[1] Dysregulation may contribute to the generation of various diseases. For instance, enhanced activity of RTKs can promote tumor growth and has been implicated in carcinogenesis and as participant in the development of proliferative diseases such as psoriasis.[2] Therefore, these signal-transducting proteins are considered as promising targets for drug development. In addition, such drugs are likely to be useful in dissecting signaling pathways.[2, 3] Essential to the use of a RTK inhibitor in biological studies is its efficacy both in vitro and in vivo.

Whereas most compounds developed so far display IC_{50} values in the low micromolar range[2-6]—the tyrphostins[2a, b, 6] are most often used—more efficient inhibitors were recently reported.[5, 6] As these values leave substantial room for improvement, identification of new and alternative classes of RTK inhibitors is of great importance to bioorganic and medicinal chemistry.

Aeroplysinin **1**, a highly functionalized marine natural product, is cytotoxic against human breast cancer cells and inhibits the EGFR receptor in an in vitro test system.[7] Its structure differs significantly from that of the RTK inhibitors reported so far, which are almost exclusively aromatic compounds; **1** might therefore serve as a promising lead for the development of a new class of these biologically active substances. However,

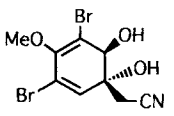

1

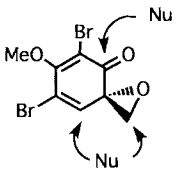

2

compounds with structural similarity to **1** have not been investigated, and data on the efficiency of **1** in vivo are lacking. To fill this gap we studied the EGFR-inhibiting activity of **1**[8] in a whole-cell assay system (see below) in which it, however, was not at all active. Since this lack of inhibition in vivo most probably has to be attributed to the inability of **1** to pass through the plasma membrane (the kinase domain of RTKs is on the cytosolic face of the membrane) due to the presence of a polar *trans*-diol unit, we designed the aeroplysinin analogue **2** as a possible RTK inhibitor for which higher membrane permeability and an enhanced inhibitory effect could be expected. In **2** the vicinal diol unit and the β-cyano alcohol are replaced by an α-spiroepoxy ketone. Thus **2** should be significantly more lipophilic than **1** and prone to nucleophilic attack at the epoxide and/or the vinylogous ketone functionality. This would lead to efficient inactivation of the receptor by covalent modification of nucleophiles in the binding site.

Ketone **2** was synthesized in a four-step sequence from the readily available aldehyde **3**[9] (Scheme 1). The methoxy group *ortho* to the aldehyde group of **3** was regioselectively cleaved by treatment with BCl_3, and the resulting phenol converted into the dibromo compound **4** with the pyridiniumhydrobromide/bromine complex.[10] Reduction of the aldehyde functionality of **4** generated the benzyl alcohol **5**, which was oxidized to **2** by a Becker–Adler oxidation.[11]

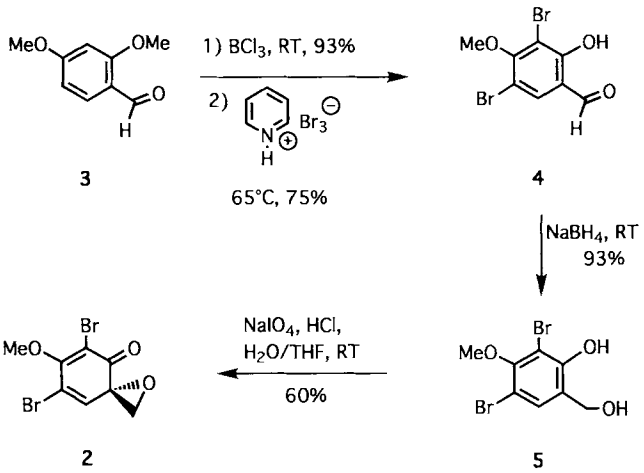

Scheme 1. Synthesis of the spiroepoxy aeroplysinin analogue **2**.

To investigate if **2** inhibits RTKs in vivo the inhibition of the receptor tyrosine kinase of the epidermal growth factor was studied first. In the assay system used, immortalized rat-1-HER cells[12] (rat fibroblasts that overexpress the human EGF receptor) were incubated with varying concentrations of inhibitor for five minutes followed by addition of EGFR to induce phosphorylation of unblocked receptor. The cells were subsequently lysed, and the proteins resolved by electrophoresis (SDS-PAGE). The extent of tyrosine phosphorylation of the EGFR was determined by phosphotyrosine immunoblotting (Figure 1).[13]

The results were very promising: **2** inhibited the kinase activity of the EGF receptor with an IC_{50} value of 10 μM (see Table 1). Preincubation of the cells for just a few minutes was sufficient to induce this effect; under the conditions of our assay inhibition of the RTK with tyrphostins required preincubation of the cells for at least several hours. These findings prove substantial in vivo activity of **2** and its sufficient lipophilicity. In a first attempt to determine whether **2** is receptor-subtype specific, the inhibition of the PDGF receptor was investigated by subjecting NIH-3T3-β-PDGFR cells to the assay conditions described above.[14] Ketone **2** did not inhibit this RTK up to a concentration of 100 μM, indicating pronounced subtype specifity.

[*] Prof. Dr. H. Waldmann, Dipl.-Chem. K. Hinterding
Institut für Organische Chemie der Universität
Richard-Willstätter-Allee 2, D-76128 Karlsruhe (Germany)
Fax: Int. code +(721)608-4825
e-mail: waldmann@ochhades.chemie.uni-karlsruhe.de
Prof. Dr. P. Herrlich, Prof. Dr. H. J. Rahmsdorf, Dipl.-Biol. A. Knebel
Institut für Genetik, Forschungszentrum Karlsruhe GmbH
D-76344 Eggenstein-Leopoldshafen (Germany)
Fax: Int. code +(7247)825-070
e-mail: genetic@igen.fzk.de

[**] This research was supported by the Deutsche Forschungsgemeinschaft and the Fonds der Chemischen Industrie.

 © VCH Verlagsgesellschaft mbH, D-69451 Weinheim, 1997 0570-0833/97/3613-1541 $ 17.50+.50/0

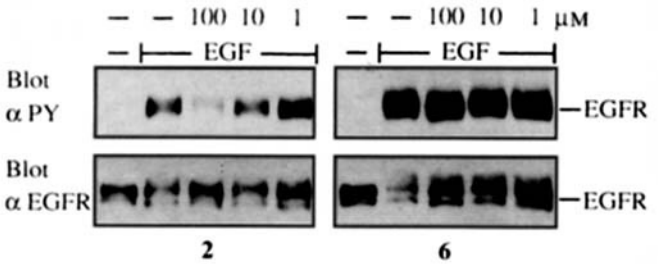

Figure 1. Determination of the IC_{50} values for the inhibition of the EGFR by immunoblotting of phosphotyrosin (αPY) and EGFR (αEGFR) to confirm that equal amounts of proteins were loaded. The aeroplysinin analogue **2**, but not *iso*-aeroplysinin **6**, inhibits the EGF-induced increase of EGF-receptor tyrosine phosphorylation in rat-1-HER cells (representative experiment). The numbers 100, 10, and 1 μM in the first row show the concentration of inhibitor for the corresponding incubation.

To delineate which structural properties are responsible for the RTK-inhibitory activity of **2**, several analogues of the spiroepoxy ketone were synthesized and investigated as possible inhibitors of the EGF and PDGF receptors in the in vivo assay systems described above. Table 1 demonstrate that neither aeroplysinin **1**[8] nor its isomer *iso*-aeroplysinin[7b] **6** inhibit the EGF or the PDGF RTK in vivo at concentrations up to 100 μM. The analogue **7**—in which the epoxide is opened, but the resulting tertiary alcohol is masked as ester—also inhibits the EGF receptor although it is less efficient than **2**. Likewise, **7** does not block the kinase activity of the PDGF receptor at all. Enhancing the polarity by saponifying the acetate (**7** → **8**) yielded a compound that is inactive under the assay conditions. This is probably due to its reduced ability to sufficiently pass through the plasma membrane of the cells within the time of assay. Interestingly the aromatic aldehydes **9**, which does not embody a methoxy group, and **4** also inhibited the EGFR (entries 6 and 7) albeit less efficiently than **2**. Furthermore, **9**, but not the methoxyaldehyde **4**, inhibited the PDGFR with an IC_{50} value of 30 μM. On the other hand neither aldehyde **3** (entry 8) nor alcohol **5** (entry 9) are inhibitors. These findings taken together suggest that the presence of the bromine atoms, probably to effect lipophilicity, and an electrophilic group are required for inhibitory activity. The nature of the electrophilic group may vary.

Table 1. Inhibition of the EGF and the PDGF receptor tyrosine kinases by aeroplysinin analogs in an in vivo assay system (see text for the description of the assay) [a].

Entry	Compound		Inhibition of the EGF receptor IC_{50} [μM]	Inhibition of the PDGF receptor IC_{50} [μM]
1	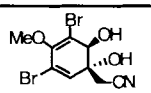	**1**	inactive	inactive
2	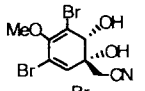	**6**	inactive	inactive
3	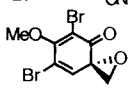	**2**	10	inactive
4	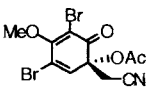	**7**	55	inactive
5	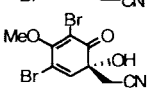	**8**	inactive	inactive
6	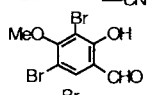	**4**	35	inactive
7	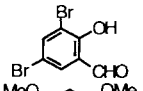	**9**	120	30
8	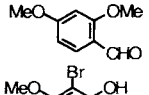	**3**	inactive	inactive
9	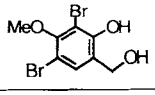	**5**	inactive	inactive

[a] Concentration at which 50% of the enzymatic activity are inhibited; "inactive" = no inhibition at <100 μM inhibitor concentration.

In conclusion we have demonstrated that α-substituted cyclohexadienones such as **2** and **7** as well as structurally related compounds inhibit RTKs. They display a marked in vivo activity and appreciable receptor-subtype specificity. Analogues of the natural product **1** are thus interesting lead compounds for the development of new drugs and tools in bioorganic and medicinal chemistry, that is, for the dissection of signal transduction pathways and the introduction of new tyrosine kinase inhibitors into medical use.

Received: January 8, 1997 [Z99751E]
German version: *Angew. Chem.* **1997**, *109*, 1553–1555

Keywords: aeroplysinin · bioorganic chemistry · enzyme inhibitors · kinases

[1] a) *Protein Phosphorylation* (Ed.: F. Marks), VCH, Weinheim, **1996**; b) *Protein Kinases* (Ed.: J. R. Woodgett), Oxford University Press, Oxford, **1994**; c) G. F. Cooper, *Oncogenes*, 2nd ed., Jones and Bartlett, Boston, **1995**.

[2] a) A. Levitzki, A. Gazit, *Science* **1995**, *267*, 1782; b) A. Levitzki, *Eur. J. Biochem.* **1994**, *226*, 1; c) A. J. Bridges, *Chemtracts Org. Chem.* **1995**, *8*, 73; d) D. W. Fry, *Annu. Rep. Med. Chem.* **1996**, *31*, 151.

[3] For the use of tyrosine kinase inhibitors in the dissection of signaling pathways, see for example ref. [2, 4a, 6] and a) H. Daub, F. U. Weiss, C. Wallasch, A. Ullrich, *Nature* **1996**, *379*, 557; b) A. Novogrodsky, A. Vanichin, M. Patya, A. Gazit, N. Osherov, A. Levitzki, *Science* **1994**, *264*, 1319; c) N. Meydan, T. Grÿnberger, H. Dadi, M. Shahar, E. Arpaia, Z. Lapidot, J. S. Leeder, M. Freedman, A. Cohen, A. Gazit, A. Levitzki, C. M. Raiffman, *Nature* **1996**, *379*, 645; d) D. T. Dudley, L. Pong, S. J. Decker, A. J. Bridges, A. R. Saltiel, *Proc. Natl. Acad. Sci. USA* **1995**, *92*, 7686; e) R. A. Lepley, F. A. Kirkpatrick, *Arch. Biochem. Biophys.* **1996**, *331*, 141.

[4] For recent studies of tyrosine kinase inhibitors, see for example a) E. Buchdunger, J. Zimmermann, H. Mett, T. Meyer, M. Myller, U. Regenass, N. B. Lydon, *Proc. Natl. Acad. Sci. USA* **1995**, *92*, 2558; b) J. Zimmermann, E. Buchdunger, H. Mett, T. Meyer, N. B. Lydon, P. Traxler, *Bioorg. Med. Chem. Lett.* **1996**, *6*, 1221; c) J. Kobayashi, T. Madono, H. Shigemoni, *Tetrahedron* **1995**, *51*, 10867; d) K. Alvi, M. C. Diaz, P. Crews, D. L. Slate, R. H. Lee, R. Moretti, *J. Org. Chem.* **1992**, *57*, 6604, and citations in ref. [5].

[5] a) G. W. Rewcastle, B. D. Palmer, A. M. Thompson, A. J. Bridges, D. R. Cody, H. Zhou, D. W. Frey, A. McMichael, W. A. Denny, *J. Med. Chem.* **1996**, *39*, 1823; b) W. Frey, A. J. Kratow, A. McMichael, L. A. Ambroso, J. M. Nelson, W. R. Leopold, R. W. Connors, A. J. Bridges, *Science* **1994**, 265, 1093; c) A. P. Spada, M. R. Myers, *Exp. Opin. Ther. Pat.* **1995**, *5*, 805; d) A. J. Bridges, H. Zhou, D. R. Cody, G. W. Rewcastle, A. McMichael, H. D. H. Showalter, D. W. Fry, A. J. Kraker, W. A. Denny, *J. Med. Chem.* **1996**, *39*, 267; e) P. Traxler, N. Lydon, *Drugs Fut.* **1995**, *20*, 1261.

[6] Review: A. Levitzki, *FASEB J.* **1992**, *6*, 3275.

[7] a) Determination of the biological activity of aeroplysinin **1**: M.-H. Kreuter, R. E. Leake, F. Rinaldi, W. Myller-Klieser, A. Maidhof, W. E. G. Müller, H. C. Schröder, *Comp. Biochem. Physiol.* **1990**, *978*, 151; b) synthesis of **1** and *iso*-aeroplysinin **6**: R. J. Andersen, D. J. Faulkner, *J. Am. Chem. Soc.* **1975**, *97*, 936

[8] (+)-Aeroplysinin was kindly supplied by Prof. Proksch, Lehrstuhl für Pharmazeutische Biologie, Universität Würzburg (Germany).

[9] Aldehyde **3** is commercially available.

[10] L. F. Fieser, M. Fieser, *Reagents for Organic Synthesis, Vol. 1*, Wiley, New York, **1967**, p. 967.

[11] H.-D. Becker, T. Bremholt, E. Adler, *Tetrahedron Lett.* **1972**, *13*, 4205. For recent applications of the Becker–Adler oxidation in natural-product synthesis, see a) E. J. Corey, J. P. Dittami, *J. Am. Chem. Soc.* **1985**, *107*, 256; b) S. Danishefsky, M. D. Shair, *J. Org. Chem.* **1996**, *61*, 16.

[12] W. J. Wasilenko, D. M. Payne, D. L. Fitzgerald, M. J. Weber, *Mol. Cell. Biol.* **1991**, *11*, 309.

[13] A. Knebel, H. J. Rahmsdorf, A. Ullrich, P. Herrlich, *EMBO J.* **1996**, *15*, 5314.

[14] The NIH-3T3-β-PDGFR cells were kindly supplied by Prof. Dr. A. Ullrich, Max-Planck-Institut für Biochemie, Martinsried (Germany).

Ion-Induced Specificity Change in Polymer-Catalyzed Solvolyses of *p*-Nitrophenyl Alkanoates**

Guang-Jia Wang and Wilmer K. Fife*

Electrostatic interactions are considered to be major contributors to protein structure and specificity of enzyme catalysis.[1] However, few investigations have explored the control of substrate specificity of enzymes with ions of different sizes and charge densities. The control of substrate specificity in enzyme catalysis by use of organic solvents is well established.[1-3] Aggregation of amphiphilic polymers in water and water/organic solvent mixtures is well-known to lead to complex supramolecular structures with multiple morphologies.[4, 5] Upon decreasing the number of generations, the aggregate morphology of polystyrene with poly(propylenimine) dendrimers in aqueous solution has been shown to change from spherical micelles through micellar rods to vesicles.[6] The same morphological changes have also been found for polystyrene-b-poly(acrylic acid) (PS-b-PAA) as poly(acrylic acid) content decreases.[7] All of these studies[4-7] suggest that an increase in hydrophobic effects of amphiphilic macromolecules upon an increase in ratio of hydrophobic to hydrophilic monomers leads to such changes of aggregate morphology. Consistent with the notion that ion-induced hydrophobic effects control aggregate morphology of amphiphiles, the morphology of aggregates of PS-b-PAA, polystyrene-b-poly(ethylene oxide) (PS-b-PEO), and PS-b-poly(4-vinylpyridinium methyl iodide) in water/organic solvent mixtures can also be changed from spheres to rods, and to vesicles by addition of salting-out agents such as NaCl and $CaCl_2$.[8]

Polymers functionalized with the 4-(dialkylamino)pyridine group have been regarded as useful model systems for investigating the origins of enzymic efficiency and selectivity.[9-12] We have reported that macromolecule **1** containing the 4-(dialkylamino)pyridine functionality and a bis(trimethylene)disiloxane backbone as a nucleophilic catalyst exhibits enzyme-like substrate selectivity for the solvolysis of **2** in aqueous and methanol/water solutions.[10, 13, 14] To our knowledge, ion-induced substrate specificity changes have not been reported previously for catalytic ester solvolysis.

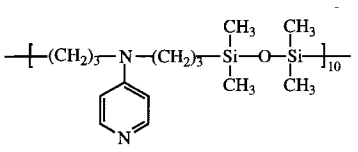

1

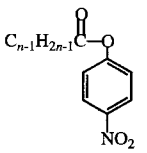

2

(n = 2, 4, 6, 8, 10, 12, 14, 16, 18)

We present here ion-induced substrate specificity changes in the **1**-catalyzed solvolysis of **2** (n = 2, 4, 6, 8, 10, 12, 14, 16, 18) in aqueous and methanol/water solutions. These results encourage more precise modeling studies of the molecular origins of catalytic efficiency and specificity in biological and chemical catalysis. Macromolecule **1** is an amphiphilic polymer that contains distinct hydrophilic and hydrophobic regions, and it dynamically associates to form macromolecular aggregates by self-assembly in aqueous or methanol/water solution.[9-11] The rate enhancements for **1**-catalyzed solvolysis of **2** have been attributed to hydrophobic association between catalyst and substrate in the reaction medium.[9-13] We have investigated the solvolysis of **2** (n = 2, 4, 6, 8, 10, 12, 14, 16, 18) catalyzed by **1** in different reaction media composed of solvent and added salts at pH 8.0 and 30 °C. Initial findings indicate that the solubility of **1** in 0.05 M aqueous tris(hydroxymethyl)methylammonium (Tris) buffer solution shows a more than tenfold increase over that in pure water as a result of salting-in effects of tris(hydroxymethyl)methylammonium ion from the Tris buffer system.[15-18] In 0.05 M aqueous phosphate or borate buffer solutions, the solubility of **1** is similar to that in pure water, and aqueous solutions of **1** show appreciable turbidity when the concentration of **1** is increased beyond 2.5×10^{-5} unit mol L^{-1}. However, a solution of **1** at 2.5×10^{-4} unit mol L^{-1} in 0.05 M aqueous Tris buffer solution remains clear even after standing for prolonged periods. These results suggest that changes of aggregate morphology of **1** at 2.5×10^{-5} unit mol L^{-1} from vesicles to rods or spheres apparently accompany changes of reaction medium from aqueous phosphate or borate to Tris buffer solutions.[7, 19]

We have measured the pseudo-first-order rate constants for **1**-catalyzed hydrolysis of **2** in 0.05 M aqueous Tris, phosphate, or borate buffer solutions (Figure 1). Without **1**, the hydrolysis rates of **2** (n = 2, 4, 6, 8, 10, 12, 14, 16) are very slow and no substrate selectivity is obtained in aqueous Tris, phosphate, or borate buffer solutions. In the presence of **1** the hydrolysis rates of **2** (n = 2, 4, 6, 8, 10, 12, 14, 16) are also very slow and differ from each other by only small factors in aqueous phosphate or borate buffer solutions, indicating that no appreciable catalysis is occurring in these systems. Increasing the alkanoate chain length in **2** causes small decreases in the hydrolysis rate and no substrate specificity is found for these systems (Table 1) in conformity with results from aqueous buffer solutions that contain

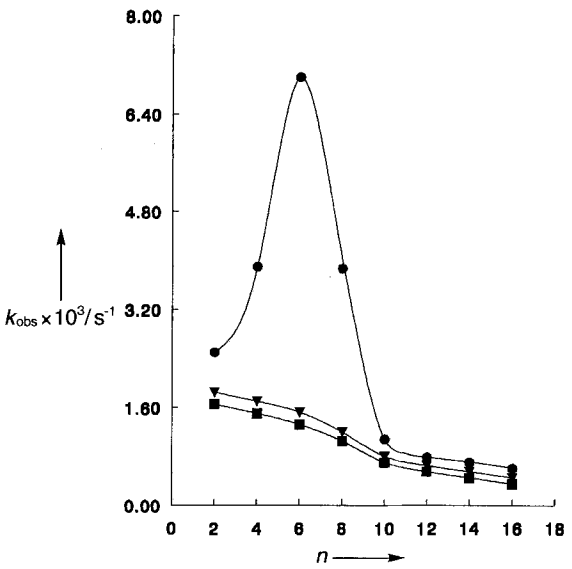

Figure 1. Pseudo-first-order rate constants (k_{obs}) for the hydrolysis of **2** (n = 2, 4, 6, 8, 10, 12, 14, 16, 5.0×10^{-5} M) catalyzed by 2.5×10^{-5} unit mol L^{-1} **1** as a function of alkanoate chain length n in 0.05 M aqueous buffer solution at pH 8.0 and 30 °C: ●: Tris buffer, ▼: phosphate buffer, ■: borate buffer.

[*] Prof. W. K. Fife, Dr. G. J. Wang
Department of Chemistry
Indiana University-Purdue University at Indianapolis
402 North Blackford Street, Indianapolis, IN 46202 (USA)
Fax: Int. code +(317)274-4701
e-mail: fife@chem.iupui.edu

[**] This work was supported by the Office of Naval Research.

Table 1. Summary of the effect of added salt concetration on the substrate specificity of 1-catalyzed solvolysis of **2** (n = 2, 4, 6, 8, 10, 12, 14, 16, 18) in aqueous and methanol/water solutions at 30 °C.

Reaction medium	Salt	c[M]	Substrate specificity
aqueous solution[a]	Tris buffer	0.05	**2** ($n = 6$)
	phosphate buffer	0.05	no
	borate buffer	0.05	no
methanol/water[b]	NaCl	0.00	**2** ($n = 14$)
	NaCl	0.01	**2** ($n = 14$)
	NaCl	0.10	**2** ($n = 14$)
	NaCl	0.25	**2** ($n = 12$)
	NaCl	0.50	**2** ($n = 12$)
	NaCl	1.00	**2** ($n = 12$)

[a] **1** (2.5×10^{-5} unit mol L^{-1}), pH 8.0. [b] **1** (5.0×10^{-6} unit mol L^{-1}), methanol/aqueous buffer (1:1, v/v; 0.05 M $H_2PO_4^-/HPO_4^{2-}$), pH 8.0.

no catalyst. However, in aqueous Tris buffer solution the rates for **1**-catalyzed hydrolysis of **2** (n = 2, 4, 6, 8) are much faster than those in aqueous phosphate or borate buffer solutions. Of added importance, macromolecule **1** demonstrates the same substrate preference for **2** (n = 6) that is observed with cholesterol esterase for the same hydrolysis reaction.[20] Under conditions where tenfold excess substrate is used in kinetic studies, the catalytic effectiveness of **1** is maintained to complete reaction.

We have also measured the effects of salting-out agent NaCl on substrate specificity for **1**-catalyzed solvolysis of **2** in 1:1 (v/v) methanol/water solution (Figure 2). Without NaCl,

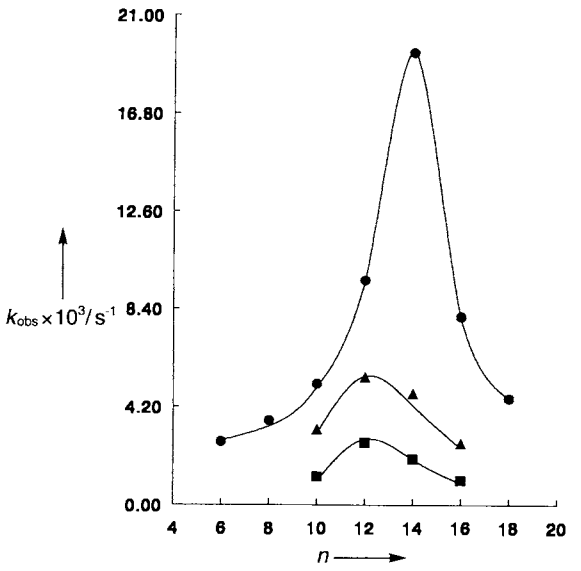

Figure 2. Effects of NaCl concentration on pseudo-first-order rate constants (k_{obs}) for the solvolysis of **2** (n = 6, 8, 10, 12, 14, 16, 18, 5.0×10^{-5} M) catalyzed by 5.0×10^{-6} unit mol L^{-1} **1** as a function of alkanoate chain length n in methanol/aqueous buffer (1:1, v/v; 0.05 M $H_2PO_4^-/HPO_4^{2-}$, pH 8.0) solution at 30 °C: ●: no NaCl; ▲: 0.25 M NaCl, ■: 1.00 M NaCl.

macromolecule **1** exhibits substrate specificity for **2** (n = 14). The solvolysis rate for **2** (n = 10, 12, 14, 16) decreases as the concentration of NaCl is increased from 0 to 1.00 M. Surprisingly, the substrate specificity is found to change from **2** (n = 14) to **2** (n = 12) when the concentration of NaCl is increased beyond 0.25 M (Table 1). Furthermore, we find that as the concentration of NaCl is increased to more than 1.00 M, the solutions of **1** at 5.0×10^{-6} unit mol L^{-1} become opalescent in 1:1 methanol/water solution. Apparently the aggregate morphology of **1** in 1:1 (v/v) methanol/water solution changes from spheres or rods to vesicles as the concentration of NaCl is increased from 0 to 1.00 M.[8, 19] We suggest that salting-out effects of NaCl induce changes of aggregate morphology of **1** in 1:1 (v/v) methanol/water solution from spheres or rods to vesicles,[15–18] while salting-in effects of the tris(hydroxymethyl)methylammonium ion induce changes of aggregate morphology of **1** in aqueous solution from vesicles to rods or spheres.[15–18] This is based on observations that added salts change aggregate morphology of small-molecule and macromolecular amphiphiles.[8, 21, 22]

Recently Zhang and Eisenberg have reported that the stretching of the hydrophobic chains in macromolecular amphiphiles is greatest in spherical micellar aggregates and decreases as the aggregate morphology changes from spheres to rods, and decreases further as vesicles are formed.[7, 19] The spherical aggregates tend to provide the strongest hydrophobic binding for lipophilic substrates in the reaction medium. We suggest that the changes of substrate specificity induced by NaCl may be attributed to changes in morphology of aggregates of **1** in 1:1 (v/v) methanol/water solution. Changes of aggregate morphology of **1** from spheres to rods or vesicles should accompany decreased hydrophobic binding for the substrates and decreased dependence of formation of complexes involving **1** and **2** on the hydrophobicity of the substrate. The substrate specificity change from **2** (n = 14) to **2** (n = 12) may result from NaCl driving a sphere to rod transition in aggregate morphology of **1** leading to hydrophobic binding that is optimum for **2** (n = 12) in 1:1 (v/v) methanol/water solution. This may be the origin of the molecular discrimination described by the term hydrophobic interactions at active sites of enzymes and catalysts for biological and chemical reactions. The behavior of **1** in aqueous Tris buffer solution may also be ascribed to spherical aggregates of **1** formed in response to the salting-in effects of tris(hydroxymethyl)methylammonium ion that contribute to efficient reaction within **1**·**2** complexes for **2** (n = 6) in aqueous solution.

These results provide the first instance in which the substrate specificity of catalytic ester solvolysis is seen to respond to the structural characteristics of aggregates of catalyst in the reaction medium, and illustrate a new approach to the control of chemical reactivity and aggregate morphology of amphiphilic macromolecules that can be useful in understanding the fundamental basis of controlling substrate specificity at the molecular level in biological and chemical catalysis. The kinetic behavior of our model system is quite similar to that of natural acyl-transfer enzymes such as chymotrypsin and cholesterol esterase for transfer of structural elements in cellular processes.

Experimental Section

Kinetic measurements: The cuvette was filled with 2.5 mL of a fresh solution containing catalyst in 0.05 M aqueous buffer solutions at pH 8.0 and the solution was equilibrated for 10 min at 30 °C in the thermostated cell compartment of a Hewlett-Packard Model 8450 spectrophotometer. The fresh catalyst solutions containing sodium chloride were prepared in methanol/aqueous buffer (1:1, v/v, 0.05 M $H_2PO_4^-/HPO_4^{2-}$, pH 8.0) solution. A stock solution (5 μL) of *p*-nitrophenyl alkanoates (2.5×10^{-2} M) in dioxane was added by microsyringe. The reaction mixture was quickly mixed by shaking and the absorbance at 400 nm was recorded as a function of time. The reactions were performed for four-to-five half-lives and the pseudo-first-order rate constants (k_{obs}) were obtained as slopes of plots of $\ln[A_\infty/(A_\infty - A_t)]$ against time, where A_∞ and A_t are the absorbance at infinite time and time t, respectively. The first-order rate constants (k_{obs}) represent the average of three runs and experimental error is less than 5%.

Received: January 28, 1997 [Z10046IE]
German version: *Angew. Chem.* **1997**, *109*, 1520–1523

Keywords: aggregates · homogeneous catalysis · polymers · solvolysis

[1] W. P. Jencks, *Catalysis in Chemistry and Enzymology*, McGraw-Hill, New York, **1969**, chapter 7.
[2] A. M. Klibanov, *Acc. Chem. Res.* **1990**, *23*, 114.
[3] T. Ke, C. R. Wescott, A. M. Klibanov, *J. Am. Chem. Soc.* **1996**, *118*, 3366.
[4] Z. Zhou, B. Chu, *Macromolecules* **1988**, *21*, 2548.
[5] K. Schillen, W. Brown, R. M. Johnsen, *Macromolecules* **1994**, *27*, 4825.
[6] J. C. M. van Hest, D. A. P. Delnoye, M. W. P. L. Baars, M. H. P. van Genderen, E. W. Meijer, *Science* **1995**, *268*, 1592.
[7] L. Zhang, A. Eisenberg, *Science* **1995**, *268*, 1728.
[8] L. Zhang, K. Yu, A. Eisenberg, *Science* **1996**, *272*, 1777.
[9] R. Vaidya, L. J. Mathias, *J. Am. Chem. Soc.* **1986**, *108*, 5514.
[10] W. K. Fife, S. Rubinsztajn, M. Zeldin, *J. Am. Chem. Soc.* **1991**, *113*, 8535.
[11] S. Rubinsztajn, M. Zeldin, W. K. Fife, *Macromolecules* **1991**, *24*, 2682.
[12] W. K. Fife, *Trends Polym. Sci.* **1995**, *3*, 214.
[13] G. J. Wang, D. Ye, W. K. Fife, *J. Am. Chem. Soc.* **1996**, *118*, 12536.
[14] G. J. Wang, W. K. Fife, *Macromolecules* **1996**, *29*, 8587.
[15] F. A. Long, W. F. McDevit, *Chem. Rev.* **1952**, *51*, 119.
[16] D. B. Wetlaufer, S. K. Malik, S. Stoller, R. L. Coffin, *J. Am. Chem. Soc.* **1964**, *86*, 508.
[17] R. Breslow, *Acc. Chem. Res.* **1991**, *24*, 159.
[18] R. Breslow, C. J. Rizzo, *J. Am. Chem. Soc.* **1991**, *113*, 4340.
[19] L. Zhang, A. Eisenberg, *J. Am. Chem. Soc.* **1996**, *118*, 3168.
[20] L. D. Sutton, J. S. Stout, D. M. Quinn, *J. Am. Chem. Soc.* **1990**, *112*, 8398.
[21] A. Sein, J. B. F. N. Engberts, *Langmuir* **1995**, *11*, 455.
[22] L. L. Brasher, K. L. Herrington, E. W. Kaler, *Langmuir* **1995**, *11*, 4267.

Chemistry at the crossroads

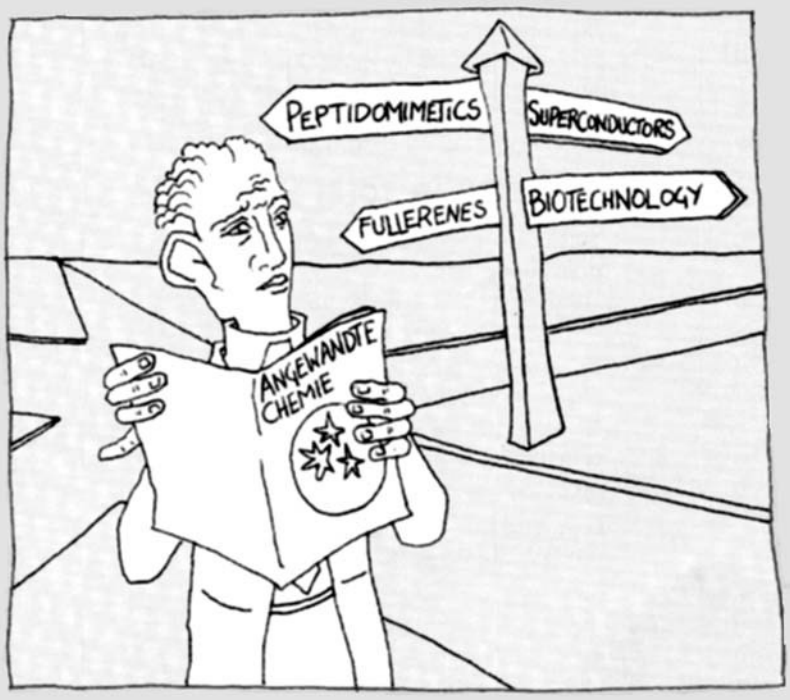

Pioneering scientists guide your way through newly charted territory with their topical reviews and discriminating highlights in **Angewandte Chemie.**

To start your own personal subscription, just fax.

An order form is provided on the last page for your convenience.

WILEY-VCH

The Success Story of Organometallic Chemistry!

Applied Homogeneous Catalysis with Organometallic Compounds. A Comprehensive Handbook. (Volumes 1 and 2). Edited by *B. Cornils* and *W. A. Herrmann*. VCH Verlagsgesellschaft, Weinheim, 1996. Vol. 1, 571 pp.; Vol. 2, 675 pp.; hardcover, two-volume set DM 748.00.—ISBN 3-527-29286-1

This handbook could be considered as the fourth component of a tetralogy on transition metal chemistry. The first three are: the classic *Principles and Applications of Organotransition Metal Chemistry*, by J. P. Collman, L. S. Hegedus, J. R. Norton, and R. G. Finke (University Science Books, Mill Valley, **1987**), the second edition of *Comprehensive Organometallic Chemistry*, edited by the late G. Wilkinson, F. G. A. Stone, and E. W. Abel (Pergamon Press, Oxford, **1996**), and *Organometallics in Synthesis. A Manual*, edited by M. Schlosser (Wiley, Chichester, **1994**). The book under review fills the gaps left by the now outdated Collman's treatment of catalytic organometallic processes and the impressive 14-volume *Encyclopedia of Organometallic Chemistry*, which contains very little on homogeneous catalysis.

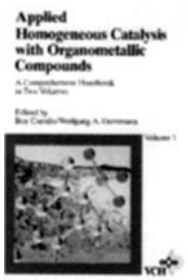

As pointed out by the editors, homogeneous catalysis is the success story of organometallic chemistry. The collaboration of an industrial research scientist and a university chemist provides an authoritative editorship for a comprehensive presentation of homogeneous catalysis in both basic and industrial aspects. The editors have assembled a team of 97 well-known authors from academia (48) and industry (49) who work in this field. The book comprises only four chapters, the central ones dealing with proven catalytic processes ("Applied Homogeneous Catalysis", Chapter 2, 542 pp.) and exploratory research ("Recent Developments in Homogeneous Catalysis", Chapter 3, 590 pp.).

In the introduction the editors give a brief account of the history of homogeneous catalysis and make the usual comparisons with heterogeneous catalysis. They stress the importance of cyclical changes in the relative popularity of the two types of catalysis as a result of progress in basic discoveries and process technologies, and changes in market requirements and feedstock availabilities, effects which are further developed in Chapter 2. They also sketch the attempts to create a symbiosis between the two types of catalysis, either at the molecular level (organometallic surface science) or at the macroscopic level (*n*-phase processes), aspects which inspire some parts of Chapter 3.

In Chapter 2 all the basic transformations using transition metal species are arranged according to either reaction types (hydrogenation, oxidation, hydrosilylation, hydroamination, asymmetric synthesis) or reactants (carbon monoxide and synthesis gas, unsaturated compounds, hydrogen cyanide, hydrocarbons).

Reactions with carbon monoxide (184 pp.) are discussed in detail by C. D. Frohning and Ch. W. Kohlpaintner (hydroformylation) and by a panel consisting mostly of industrial experts (synthesis of lower acids, carbonylation of benzyl and aryl moieties, amidocarbonylation, and oxidative carbonylation). This section provides an updated and concise survey of a domain where homogeneous catalysis has had some of its main successes. The discussions of reaction kinetics and mechanisms, commercial applications, and recent developments give the reader good insights into biphasic hydroformylation and methanol carbonylation to acetic acid, acetic anhydride, and methyl carbonate.

Reactions of unsaturated hydrocarbons are described by a panel of 16 contributors (including L. Böhm, Y. Chauvin, E. Drent, W. Kaminsky, R. Taube, and G. Wilke) who cover most of the field in 154 pages. Dimerization, codimerization, oligomerization, cyclooligomerization, polymerization of alkenes, of alkynes, and of 1,3-dienes and the corresponding cross-reactions are discussed, including industrial applications. This review of the "-ization" reactions is completed by an excellent survey of the alternating copolymerization of alkenes and carbon monoxide and a description of telomerization of olefins, although this is limited to the manufacture of 1-octanol. Finally, metathesis is reviewed, although too briefly and with little information on ring-opening polymerization.

The treatment of oxidations is mainly concernd with conversion of olefins to carbonyl compounds and with acetoxylations and other reactions promoted or catalyzed by palladium (37 pp., R. Jira), with details of the Wacker–Hoechst processes and a brief contribution on formation of aliphatic carboxylic acids via aldehyde oxidation (6 pp.), as well as reactions with aryl- and alkyl-substituted aromatic compounds (35 pp., R. W. Fischer and F. Röhrscheid). A short review (13 pp., R. A. Sheldon) on the synthesis of oxiranes with emphasis on developments for organic synthesis, especially for chiral compounds, completes this section (91 pp.), which is important because of the high selectivities towards oxygenates achieved in commercial homogeneous catalytic processes.

The shorter contributions to Chapter 2 focus primarily on recent advances in practical homogeneous catalysis. The most instructive of these is the one by R. Noyori and S. Hashiguchi, which illustrates the use of chiral molecular catalysts for the synthesis of bioactive molecules. Examples of the use of monodentate P, or more commonly bidentate N–N, N–O, P–P, P–N, and P–O ligands for the preparation of terpenes (Takasago), profens, pyrethroids, prostaglandins, secondary alcohols, amino alcohols, amino acids (Monsanto–Searle), and carbapenems (Takasago) are covered in 19 pages. The section on reactions with hydrogen cyanide also provides examples of asym-

This section contains book reviews and a list of new books received by the editor. Book reviews are written by invitation from the editor. Suggestions for books to be reviewed and for book reviewers are welcome. Publishers should send brochures or (better) books to the Redaktion Angewandte Chemie, Postfach 101161, D-69451 Weinheim, Federal Republic of Germany. The editor reserves the right of selecting which books will be reviewed. Uninvited books not chosen for review will not be returned.

metric hydrocyanation of olefins (K. Huthmacher and S. Krill, 20 pp.). The contribution on hydrosilylation and related reactions of silicon compounds (B. Marcicniec, 20 pp.) emphasizes the recent advances in dehydrogenative coupling of hydrosilanes and disproportionation of silicon-containing olefins. Finally, the lack of efficient catalysts for olefin hydroamination as reported by R. Taube (14 pp.) clearly demonstrates that homogeneous catalysis is still facing many challenges.

In Chapter 3, Volume 2, some of these challenges are discussed in the three parts devoted to development of methods (195 pp.), special catalysts and processes (224 pp.), and special products (173 pp.).

One may consider three main areas in the first section: catalyst recovery, understanding and modeling of catalytic activity, and catalytic C–C coupling reactions. Several contributions deal with the major drawback of homogeneous catalysis: catalyst recovery. Immobilization by aqueous catalysts (B. Cornils and W. A. Herrmann, 26 pp.), heterogenization by other immiscible phases (I. T. Horváth, 5 pp.), and immobilization using supports (P. Panster and S. Wieland, 19 pp.) are discussed in terms of advantages and disadvantages for industrial applications, the best example cited being the Ruhrchemie–Rhône–Poulenc two-phase hydroformylation of propene. Ligand-stabilized clusters and colloids (G. Schmid, 8 pp.) and re-immobilized catalysts (H. Bahrmann, 10 pp.) are suggested as other approaches; these introduce new technological problems for which membrane separation offers a possible solution. The understanding and modeling of catalytic activity is covered in surveys of catalytic engineering aspects (M. Baerns and P. Claus, 15 pp.) and molecular modeling (R. Klein and R. Schmid, 18 pp.). An introduction to parahydrogen labeling as a new analytical method in homogeneous catalysis (J. Bargon, 12 pp.) is also described, as an example of the development of special in-situ techniques for mechanistic studies. Finally, introductions to organometallic surface science (J.-M. Basset and G. P. Nicolai, 12 pp.), to Fischer–Tropsch synthesis (W. A. Herrmann, 16 pp.), and to multicomponent or multifunctional catalysts (D. Hesse, 13 pp.) may indicate new routes to be explored, especially at the frontier between homogeneous and heterogeneous catalysis. Catalytic C–C coupling reactions are examined from three major aspects which already provide useful applications in organic synthesis. The Heck reaction and its variants (Blaser, Jeffery, Bozell, Milstein, intramolecular ...) are concisely summarized (W. A. Herrmann, 21 pp.), together with recent improvements using palladacycles and heterocyclic-carbene complexes of palladium. A brief report on aryl–aryl coupling, Grignard cross-coupling, and phenol coupling is also provided (W. A. Herrmann, 6 pp.). Finally, recent developments in catalytic cyclopropanation (A. F. Noels and A. Demonceau, 15 pp.) mainly concern enantioselective catalysts based on copper and rhodium.

The second section of Chapter 3 covers several aspects that are not easy to classify. Some undoubtedly correspond to methods or catalysts, others to reactants or processes. In the first group are: phase-transfer catalysis and related systems (Y. Goldberg and H. Alper, 22 p.) describing mainly oxidation, carbonylation, and Heck-type reactions under phase-transfer conditions; membrane reactors (U. Kragl, C. Dreisbach, and Ch. Wandrey, 12 pp.), where membranes act as catalysts or physical barriers for bulky components such as colloids, dendrimeric structures, etc.; homogeneous electrocatalysis (D. Astruc, 14 pp.) and photocatalysis (A. Heumann and M. Chanon, 15 pp.), where electrons or photons very often participate only in the formation of the catalytic species from the precursors. In the second group dealing with catalysts, the review on biocatalysis and enzyme-analogous processes (K. Drauz, H. Waldmann, and B. Sauerbrei, 34 pp.), in addition to a survey of the uses of hydrolases, dehydrogenases, aldolases, and transferases, offers examples of commercial applications which can be compared with abiotic catalysts. A summary of the potential uses of template or host–guest relationships (F. Vögtle, R. Hoss, and M. Händel, 22 pp.) completes this contribution by introducing new concepts for homogeneous catalysis, with supramolecular control of the interactions between the catalytically active site and the reactants. The use of rare earth compounds (R. Anwander, 27 pp.) and metallocenes (F. Küber, 10 pp.) concludes this second group: the authors demonstrate that both Group 4 chiral metallocenes and organolanthanides have unique stereoelectronic properties for efficient reactions forming carbon–carbon bonds (oligomerization and polymerization, Diels–Alder reactions, aldolization, etc.) and carbon–heteroelement bonds (hydrosilylation, hydroamination, epoxidation, etc.). In the third group, specific reactants are considered, using aldehydes and keto compounds for olefin formation (W. A. Herrmann, 9 and 5 pp. respectively). The analogy between the Wittig reaction and the olefination of aldehydes with diazo compounds mediated by molybdenum and rhenium compounds is first discussed; the catalytic McMurry coupling is considered as an additional example of how to go from a stoichiometric process to a catalytic one by appropriate choice of the components involved in the mediating system. Finally, in the fourth group, specific catalytic processes such as homologation, isomerization, the water-gas shift reaction, and hydrodesulfuration processes are considered. Homologation of methanol (H. Bahrmann, 13 pp.), with comments on technical applications, completes the treatment of carbonylations (Chapter 2). The contribution on double-bond isomerization of olefins (W. A. Herrmann, 12 pp.), with special attention to reaction mechanisms, introduces recent applications such as asymmetric isomerization. The water-gas shift reaction (W. A. Herrmann, 7 pp.) is briefly described in view of its involvement in several carbonylation processes and its interest for the catalytic synthesis of isocyanates and urethanes. Hydrogenation and hydrogenolysis of thiophenic compounds (C. Bianchini and A. Meli, 11 pp.) are described in the context of attempts to design a homogeneous process for hydrodesulfuration, a reaction of great importance in petroleum refining.

The third section of Chapter 3 is also a collection of short reviews on topics similar to those of the preceding part; they roughly correspond to specific processes, reactions, and molecules. In the first group one finds enantioselective synthesis and reactions in homogeneous systems. The very thorough contribution by H.-U. Blaser, B. Pugin, and F. Spindler (33 pp.) complements the approach of R. Noyori and S. Hashiguchi by considering the technical application of homogeneous enantioselective catalysts for additions to C=C, C=O, and C=N groups. Some examples of step-growth and chain-growth polymerizations are given by B. M. Novak (10 pp.), with special attention to ROMP processes. A brief account of biomembrane hydrogenations with water-soluble hydrogenation catalysts (L. Vigh and F. Joó, 7 pp.) provides a good example of exotic applications of homogeneous catalysts.

In the second group, other areas of application are described, with specific reactions leading to special products. These reactions are related to carbon monoxide chemistry, coupling of unsaturated compounds, oxidations, and C–H bond activation. Reductive carbonylation of nitro compounds (R. Sundermann and H. J. Scholl, 9 pp.) is presented, with a pessimistic assessment of prospects for indus-

 © VCH Verlagsgesellschaft mbH, D-69451 Weinheim, 1997 0570-0833/97/3613-1548 $ 17.50+.50/0

trial production. The Pauson–Khand synthesis of cyclopentenones (V. Rautenstrauch, 10 pp.) also seems to be of doubtful value for commercial applications. The review on hydrovinylation (P. W. Jolly and G. Wilke, 25 pp.) details the catalysts, substrates, and mechanisms for this reaction, whose asymmetric counterpart would be relevant for the synthesis of bioactive molecules. Also coming from Mülheim/Ruhr is an exhaustive survey of the cyclooligomerization of alkynes (H. Bönnemann and W. Brijoux, 17 pp.), describing the formation of five- and six-membered heterocycles and six- and eight-membered carbocycles. The synthesis of diols via catalytic dihydroxylation (M. Beller and K. B. Sharpless, 16 pp.) is discussed mainly in its asymmetric version, which is of possible industrial interest for the preparation of intermediates for pharmacologically active compounds. Finally, activation of C–H bonds is discussed in two reports. New approaches to C–H activation of alkanes (A. Sen, 12 pp.) draw attention to the effectiveness of electrophilic pathways in promoting activation and functionalization of the least reactive members of the hydrocarbon family. On the other hand, intramolecular C–H carbenoid insertion offers new possibilities for the catalytic synthesis of cyclic hydrocarbons from diazoalkanes (W. A. Herrmann, 7 pp.), the challenge now being to achieve enantioselective cyclizations.

In the third group, specific molecules are considered. The use of carbon dioxide as a C_1 building block (E. Dinjus and R. Fornika, 25 pp.) is discussed, with special attention to the use of supercritical conditions which are essential for the efficient production of formic acid and dimethylformamide. The description of a new catalytic synthesis of methacrylates from propyne (E. Drent et al., 13 pp.) represents an additional example of proper design of a catalyst for highly efficient methoxycarbonylation reactions. Molecular design is also the basis of a discussion on the preparation of acrolein and acrylonitrile (W. A. Herrmann, 8 pp.).

Chapter 4, "Epilogue", focusses on the numerous scientific and industrial problems which remain to be solved, and which have been made clear to the reader in many of the conclusions reached in the general and specific reviews included in Chapters 2 and 3. The message is that there is a need for better integration of theoretical chemistry, chemical kinetics, and chemical engineering, and for stronger relationships between groups working on homogeneous and heterogeneous catalysis.

Anyone who already has some knowledge of molecular transition metal chemistry will find this book extremely useful in providing a thorough account of the state of the art in homogeneous catalysis, both in its accomplishments (Chapter 2) and current trends (Chapter 3). The organization of Chapter 3 is rather open to criticism, as it does not have a clear structure. Nevertheless, this chapter provides a series of essays which complement the topics developed in Chapter 2 and open new perspectives. The reader wishing to study topics in greater depth has access to over 5000 literature references, with some from 1996 (and 1997!). Very few errors could be found, the most noticeable one being the citation of Reppe's work on hydroxycarbonylation (p. 146), which was published in *Liebigs Annalen der Chemie*, not in *Annales de Chimie* (a computer-generated error?). This reviewer was also pleased to find on page 199 a new spelling of his name! Some drawings are incomplete, for example structure **2** on page 961. Lastly, there is a detailed index which will help in searching the literature on the basis of molecules, reactions, or processes.

To summarize, this handbook is well justified in view of the immense growth of interest in homogeneous catalysis since the "roaring sixties", and the continuing role of the subject in highlighting new fundamental problems and in presenting chemical technology with new challenges. Despite its price, it should be available in every laboratory concerned with the future of catalysis and, certainly, of organic chemistry.

Igor Tkatchenko
Institut de Recherches sur la Catalyse
CNRS
Villeurbanne Cedex (France)

Comprehensive Organic Functional Group Transformations. Volumes 1–7. Editors-in-chief: *A. R. Katritzky, O. Meth-Cohn* and *C. W. Rees*. Pergamon/Elsevier, Oxford, 1995. approx. 7800 pp., hardcover $ 4437.25.—ISBN 0-08-040604-1

As stated in the first sentence of the introduction, the objective of this monumental work is to cover the enormous field of organic synthesis by describing methods for introducing or modifying functional groups. For this huge task the editors have chosen a structural form (said to have been conceived over a glass or two of wine in a London club) that is simple, convenient, and easily memorized by the user. In this system the experimental information is arranged according to the number of attached heteroatoms, the formal valency ("coordination") of the carbon atom under consideration, the position in the Periodic Table of the heteroatom(s) directly bonded to that carbon atom, and the principle of the latest entry. Accordingly, the six main text volumes are as follows: Volume 1. Carbon atoms with no attached heteroatom; Volume 2. Carbon atoms with one heteroatom attached by a single bond; Volume 3. Carbon atoms with one heteroatom attached by a multiple bond; Volume 4. Carbon atoms with two singly bonded heteroatoms; Volume 5: Carbon atoms with two attached heteroatoms, at least one being multiply bonded; Volume 6. Carbon atoms with three and four attached heteroatoms. Volume 7 consists of an author index and a subject index for all the above volumes.

A work of this nature and size cannot be reviewed in the same way as, for example, a monograph or textbook. It can only be evaluated after working with it on practical tasks. Therefore we have concentrated here on the two volumes, namely Volumes 2 and 5, that we have already used. Our presumption that similar conclusions would apply to the other four seems well justified in view of the scientific reputations and competence of the individual authors.

In accordance with the above scheme of organization, Volume 2 begins with alkyl derivatives, followed by a second part on aryl and vinyl compounds, and finally a third part on functionalized alkynes (the unsubstituted alkynes are covered in Vol. 1).

The first 30 pages contain a concise, but complete, survey of methods for synthesizing alkyl halides. Alcohols and ethers are then treated similarly, including methods for asymmetric syntheses. This is followed by three very long chapters on the synthesis of sulfur, selenium, and tellurium compounds, and a further one on alkyl derivatives containing nitrogen or other elements of Group 5. Part 1 ends with the synthesis of alkyl-boron and alkyl-silicon compounds and an excellent chapter of 50 pages on the synthesis of organometallic alkyl compounds. This includes useful tables of Grignard reagents and titanium alkyls with methods for preparing them, so that the reader can quickly review the various possibilities.

Part 2 begins with the synthesis of vinyl and aryl halides, followed by enols, phenols, thiols, and their ethers. The important aryl- and vinyl-substituted compounds with nitrogen or phosphorus as heteroatoms are then treated at length (130 pp.). A chapter on the synthesis of

 © VCH Verlagsgesellschaft mbH, D-69451 Weinheim, 1997 0570-0833/97/3613-1549 $ 17.50+.50/0

organometallic compounds concludes Part 2.

The third and final part, consisting of nearly 90 pages, deals with the synthesis of functionalized acetylenes. As well as derivatives with halogens, nitrogen, or phosphorus as heteroatoms, followed by metal acetylides, some unusual functionalities are also included, for example in the synthesis of alkynols, the less stable tautomeric form of ketenes.

Most of the synthetic methods described are illustrated by describing at least one practical example. Each chapter is accompanied by a comprehensive bibliography giving the reader quick access to original publications and laboratory recipes.

Volume 5 is concerned with carbon compounds containing two heteroatoms, one of which has a multiple bond. In accordance with the overall scheme of this work, Part 1 covers compound classes containing a C=O group. The first few chapters deal with methods for synthesizing carboxylic acids and their derivatives: acid halides, carboxylic acids, esters, thiocarboxylic acids and derivatives, and carboxylic acid amides. The methods are classified according to their degree of general applicability, the degree of functionalization of the carboxylic acid derivative, and the types of synthetic strategies that can be used (reactions without change of oxidation state, addition reactions, oxidations). A disadvantage of this treatment is that it includes no information about the preparation of carboxylic acids from reagents such as auxiliary-bound amides, which are nowadays an essential part of the synthetic chemist's armory. The chapter by Mulzer is a concise and informative description of methods for selective esterification and lactonization, such as those based on activation of carboxyl or hydroxyl groups, and also includes addition reactions of chiral esters. Two further chapters cover synthetic routes to amides, including lactams and *N*-heterosubstituted amides. The methods, treated according to the degree of substitution of the carboxylic acid moiety, include acylation of amines, hydrolysis methods, rearrangements, and *N*-functionalization reactions. Transition-metal-catalyzed methods for synthesizing amides and lactams are also described, as too are methods based on α-oxidation of amines. Part 1 ends with synthetic routes to acylsilanes, acylgermanes, and acyl-metal compounds.

Part 2 of this volume deals with compounds containing a fragment of the form X = C–Y. Six chapters are devoted to thiono derivatives of carboxylic acids and their selenium and tellurium analogs. These are followed by a further six chapters that concentrate on routes to iminoacyl compounds (imidoyl halides, iminoethers, amidines, and α-heterodiazo compounds. Next are three chapters on the synthesis of compounds containing a carbon–heteroelement multiple bond with a second heterosubstituent at the α-position. The first of these are α-heterosubstituted phosphoranes, which are followed by α-heterosubstituted silenes, germenes, and borenes. This part ends with a detailed survey of methods for preparing Fischer carbene complexes and analogous compounds.

Part 3 is devoted to carbonic acid derivatives with sp-hybridized carbon. Synthetic strategies for preparing isocyanates, isothiocyanates, carbodiimides, cyanates, thiocyanates, cyanamides, and organometallocyanides are described in detail. Some more unusual compound classes are also included, such as silaketenes, other metallaketenes, and phosphaalkynes.

In these two volumes the editors have admirably fulfilled their purpose of providing a route into the literature for the chemist seeking synthetic methods for a particular functional group. This is helped by the clear systematic arrangement mentioned above and by the comprehensive subject index. Nevertheless, when we come to consider the index volume (Vol. 7), we can no longer avoid asking the question: "Is it still appropriate nowadays for a literature survey of this kind to be published in book form?". With regard to Volume 7 itself, the answer must be: "No". If this index volume had been replaced by a diskette, the saving in weight would have been 2.9 kg, and the required shelf space would have been reduced by 6.7 cm. However, for the main text volumes (which are, of course, more important), the question cannot be answered so simply. With these one is likely to gain at least as much from chance discoveries, when looking for something else or leafing through at random, as from focussed searches. But here again one must ask whether, in the electronic age, publishers should not hold these undoubtedly very useful compilations in the form of in-house data bases that can be updated, and offer them to users in that form. This would, at least in principle, avoid the problem that, owing to the long time needed to complete a large book project of this kind, parts of it are already outdated by the time the work is published. The effects of this time delay can be clearly seen in the bibliography, as the numbers of references fall off noticeably after 1992; for example, in Volume 5 we find over 250 citations from 1992, about 150 from 1993, less than 100 from 1994, and only 23 from 1995.

In reviews of works of this kind, it is usual to end with a verdict to the effect that no library with pretensions of being scientific can afford not to buy the work in question. However, one must also ask how the money for it can be found, at a time when more and more primary journals are having to be axed from libraries' order lists (and when the few that remain are often no longer put into bindings). In any case, it is difficult to avoid the impression that the enormous numbers of comprehensive series, encyclopedias, and lexicons appearing in the last few years could be rather like the barrage of rockets and loud bangs that comes just before the end of a firework display: one can more or less dismiss the idea that such a tour de force is about to be repeated (perhaps even in an extended form).

Henning Hopf, Burkhard König, Ullrich Jahn
Institut für Organische Chemie
der Technischen Universität
Braunschweig (Germany)

Arrhenius: From Ionic Theory to the Greenhouse Effect. (Series: Uppsala Studies in the History of Science, Volume 23.) By *E. Crawford.* Watson Publishing International, Canton, MA, 1996. XIII, 320 pp., hardcover $ 49.95.—ISBN 0-88135-166-0

According to Swedish-born historian and sociologist of science Elisabeth Crawford, senior research fellow at the Centre National de la Recherche Scientifique (CNRS) and member of the Institute for the History of Science at the Louis Pasteur University, Strasbourg, France, scientists can be divided into three categories: "'truly great men'...whose work revolutionized the scientific worldview", "'great men'...who left their mark on an entire discipline", and "those who do not fit any particular category because their work spreads over several disciplines or is carried out on the boundaries of two or more disciplines." Arrhenius, Sweden's most prominent scientist and the best-known internationally since Berzelius, belongs to the interdisciplinary category.

Book-length biographies which perpetuate the myths advanced by Arrhenius himself exist in German (Ernst Riesenfeld [Arrhenius's brother-in-law], *Svante Arrhenius*, Akademische Verlagsgesellschaft, Leipzig, **1931**) and in Russian (Yurii I. Solov'ev, *Svante Arrhenius*

 © VCH Verlagsgesellschaft mbH, D-69451 Weinheim, 1997 0570-0833/97/3613-1550 $ 17.50+.50/0

(1859–1927), Nauka, Moscow, **1990**). Crawford's biography, seven years in the making and the first in English, recreates Arrhenius's three major scientific fields, or "projects" as she prefers to call them: (1) his work in electrochemistry and physical chemistry, including specifically his most creative achievement, the theory of electrolytic dissociation, for which he was awarded the 1903 Nobel Prize in Chemistry, although he regarded himself as a physicist; (2) his cosmic physics, in which he was the first to show a quantitative link between changes in atmospheric carbon dioxide and the earth's temperature and climate and to propose a model for what is now called the "greenhouse effect"; and (3) his application of the quantitative methods of physical chemistry to biology, thus creating immunochemistry, a field which he named. Each project was shaped by different national-cultural and social contexts and occupied him for roughly a decade. Thus (1) took place in Sweden and Latvia during the 1880s, (2) in Sweden during the 1890s, and (3) belongs to German chemistry, biology, and medicine during first decade of the twentieth century. Thus Arrhenius's crossing of disciplinary boundaries was to some extent coincidental with crossing national ones. Arrhenius's important work in cosmology (volcanoes and earthquakes, auroras, magnetic storms, solar spots and flares, and the development of galaxies and nebulae), though not dealt with in the detail accorded to the three projects, is not neglected, particularly his triumph of science popularization, *Världarnas utveckling* (English translation: *Worlds in the Making*, 1908; German translation: *Werden der Welten*, 1908), which was a simplified and abbreviated version of his unsuccessful *Lehrbuch der kosmischen Physik* (1903).

According to Crawford, Arrhenius' penchant to undertake such different projects was related to his love of ideas and of controversy. His love of ideas was the major source of inspiration for his scientific achievements, which arose not from experimental work but from his imagination and wide reading of old and new scientific literature. Not being tied to a single "investigative pathway" predetermined by instrumentation or experimental materials, he was able to roam at will through those fields of science that had not yet been compartmentalized into specialties. His unusual ideas and their startling results involved him in considerable polemics, but his love of controversy, which he shared with many of his contemporaries, involved him in more conflicts than these ideas seemed to warrant. These polemics are best known to most modern chemists in his fight, together with his fellow "ionists" Wilhelm Ostwald and Jacobus Henricus van't Hoff, for the acceptance of his electrolytic dissociation theory and the emerging field of physical chemistry in Europe and the United States. However, he sought out opponents to attack even when their objections did not merit his attention. His adversarial tactics, which persisted into his middle age and became part of his scientific style, marked the last major battle of his scientific life—his conflict with Paul Ehrlich concerning toxin–antitoxin reactions, which set the agenda for several years of theoretical and experimental work.

Because of Arrhenius's adversarial view of science, Crawford was forced to find the true facts behind the highly personal and colorful but self-serving and propagandistic accounts that he gave of his battles. Thus she "decided at the outset to discount Arrhenius's own versions of events unless corroborated by other sources." For example, his claim that his ionic theory was contained in his dissertation of 1884 (whereas it did not appear until 1887, in his celebrated article in the first volume of the newly founded *Zeitschrift für physikalische Chemie*), has become part of the lore of the history of science. Crawford attributes Arrhenius's propensity for such myth-making to what his son Olof, an agricultural botanist and soil scientist, called "a wound that never healed"—the humiliation that he felt he had suffered in 1884 when the "Uppsala physicists" did not award his dissertation the highest grade, thus denying him a docentship at Uppsala.

During the late 1970s Crawford carried out the first study of the background to the awarding of the Nobel Prizes in physics and chemistry, using the recently opened archives at the Royal Swedish Academy of Sciences (*The Beginnings of the Nobel Institution: The Science Prizes, 1901–1915*, Cambridge University Press, Cambridge, **1984**; and with John L. Heilbron and Rebecca Ullrich, *The Nobel Population 1901–1937*, Office for History of Science and Technology, University of California, Berkeley, **1987**). Arrhenius had been the key figure in the creation of the Nobel Institution, and she consulted these archives and others in Sweden, Germany, Denmark, and the United States, as well as Arrhenius's extensive correspondence with scientists around the world and the primary and secondary literature. She documents in detail Arrhenius's using his influential position to block the Nobel Prize of Walther Nernst, his former friend but later Ehrlich's ally, for a decade and a half.

Crawford consistently views Arrhenius's work in the context in which it arose. For example, she provides an entire chapter, "Sweden in the 1890s", as background for his work in cosmic physics. Although she does not neglect the events in Arrhenius's personal life, her emphasis is on their relationship to his career. His brief, unhappy first marriage, to his private assistant Sofia Rudbeck, a chemistry graduate of Uppsala University, who typified the new emancipated woman, "*die Nordische Frau*", by whom he had a son, is dealt with in about a half dozen pages, while his second, longer, and happy marriage, to Maria (Maja) Johansson, by whom he had three children, is relegated to one sentence and a one-sentence footnote. In contrast, Crawford devotes a full page to Maria's brother and Arrhenius's friend, Johan Erik Johansson, Professor of Physiology (1900–1927) at the Karolinska Institute. Thus her carefully documented book containing references as late as 1994 is better characterized as a scientific rather than a personal biography. It should fulfill her hope of furthering "the comprehension of a little-understood scientist who exerted an important influence on the development of the sciences in the late nineteenth and early twentieth centuries."

George B. Kauffman
California State University
Fresno, CA (USA)

 © VCH Verlagsgesellschaft mbH, D-69451 Weinheim, 1997 0570-0833/97/3613-1551 $ 17.50+.50/0

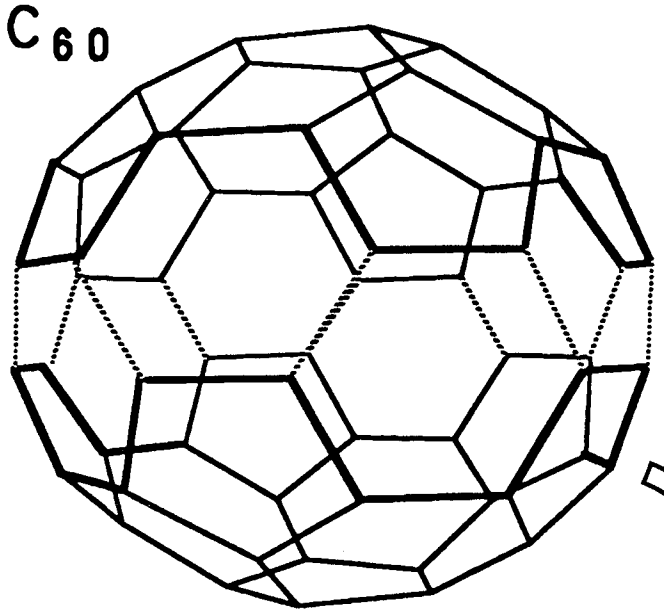

The relationship between the proposed structures of C_{60} and C_{70}: C_{60} is orientated so that pentagons are at the north and south poles.

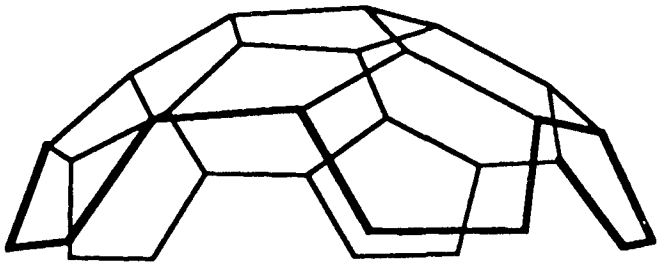

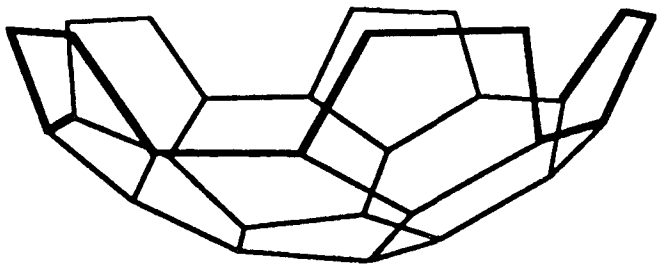

1/10 turn of the lower hemisphere

The C-C bonds connecting the northern and southern hemispheres are then cut, the hemispheres rotated with respect to each other, and ten carbon atoms introduced at the equator to provide C_{70}.

+ 10 carbon atomes

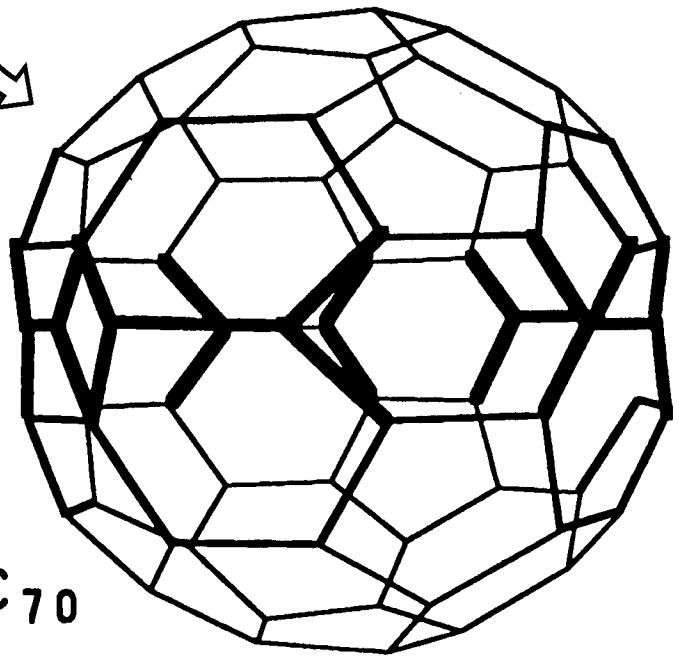

ANGEWANDTE CHEMIE ©WILEY-VCH

Dawn of the Fullerenes: Conjecture and Experiment (Nobel Lecture)**

Robert F. Curl*

Conjecture

Several individuals in widely separated parts of the world had envisioned the class of carbon cage compounds we now know as the fullerenes, in particular C_{60}, long before we began our work. The earliest reference in the area appears to be the somewhat whimsical proposal by Jones that giant carbon cage molecules, which we would now call giant fullerenes, might be synthesized by introducing defects in the graphitic sheet to allow them to curve and close.[1] He believed that such molecules should exhibit unique properties, such as having a very low density. He realized some time later that the required defects would be pentagons.[2]

Apparently the first person to imagine the truncated icosahedron isomer of C_{60} shown in Figure 1 was Osawa.[3, 4] Osawa conceived of the C_{60} structure while meditating on the structure of corannulene ($C_{20}H_{10}$), which has a central pentagon of carbon atoms surrounded by five hexagons, when he glanced at his son's soccer ball (football) and recognized the same pattern. Shortly thereafter a Hückel treatment of the π electrons was carried out in the Soviet Union[5] and repeated independently some years later in the USA as part of a larger article.[6] The Hückel calculation was repeated again by Haymet in his discussion of the stability of the molecule.[7]

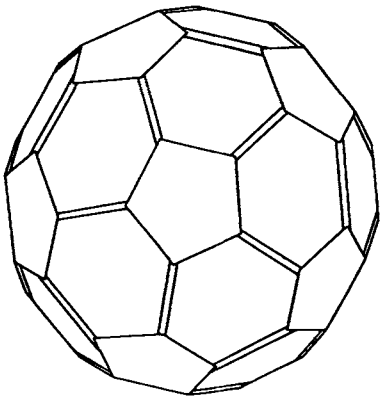

Figure 1. Truncated icosahedron C_{60} with the dominant Kekulé structure.

The synthetic organic chemist Orville Chapman took the challenge of the synthesis of truncated icosahedron C_{60} seriously in the early 1980s, obtained funding from the National Science Foundation for this purpose, and set to work with several graduate students on its total synthesis.[8] This project is indeed a tremendous challenge to the conventional methods of organic synthesis, and to date no such total synthesis of C_{60} has been completed.

These conjectures concerning C_{60} were based upon good chemical intuition backed up by approximate quantum chemical calculations. The conclusion of these conjectures was that truncated icosahedron C_{60} would be a chemically stable compound that, once prepared, could be handled much as any common substance.

Experiment

When we started our experiments on carbon clusters in late August 1985, we were completely ignorant of the conjectures just related. The purposes of our carbon-cluster project were to determine whether the sort of carbon chain compounds such as HC_7N found[9, 10] by radioastronomy in the interstellar medium could be synthesized by mixing carbon vapor with a suitable reagent such as ammonia and to find the conditions needed for a study of the low-temperature electronic spectra of carbon chain compounds using resonance-enhanced two-photon ionization. The spectroscopic work on carbon chains was motivated by the proposal made by Douglas[11] that electronic absorptions of long-chain carbon molecules, C_n ($n = 5-15$), are the source of the diffuse interstellar bands.[12] The work on formation of carbon chain compounds was ultimately published,[13, 14] but the carbon chain spectroscopy was never really begun.

I won't review in detail here the experiments we carried out in August and September of 1985 which resulted in our proposal[15] that truncated icosahedron C_{60} (buckminsterfullerene) is formed spontaneously in condensing carbon vapor. Accounts of this have been given[16, 17] by two of the five people involved and in two books on the discovery of the fullerenes.[8, 18] The authors of these books consulted all five of us and, in my opinion, made the best effort possible to use the recollections of those involved to recreate these events.

[*] Prof. R. F. Curl
Chemistry Department and Rice Quantum Institute
Rice University
Houston, TX 77005 (USA)
Fax: Int. code +(713)285-5155

[**] Copyright © The Nobel Foundation 1997. We thank the Nobel Foundation, Stockholm, for permission to print this lecture.

However, in order to understand what we did it is necessary to learn something about the apparatus[19–21] invented by Richard Smalley to investigate compounds and clusters formed from refractory elements. He and his students used it to investigate the high-resolution electronic spectra of a number of metal dimers,[20–23] copper trimer,[24] and SiC_2.[25] In 1984 Frank Tittel, Smalley, and I with our students began investigating semiconductor clusters using this apparatus.

The heart of the experiment is the laser vaporization supersonic molecular beam source. The source went through several design variations primarily to accommodate the physical form of the available sample material to be vaporized. For these experiments, it was a disk-vaporization source because the semiconductor samples that we had been investigating were more readily available in sheet form. Figure 2 shows a cross-section of

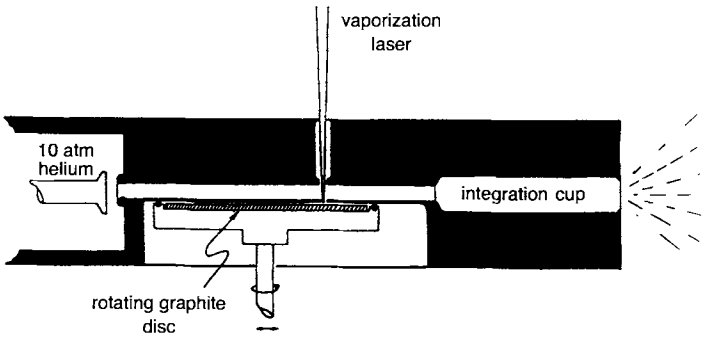

Figure 2. Laser-vaporization source for producing molecular beams of clusters of refractory materials. The integration cup can be removed. For the carbon experiments the target is a graphite disk which is rotated slowly to provide a fresh vaporization surface. The vaporization laser, a 5-ns pulse at 532 nm of about 30–40 mJ, is focused onto the surface of the graphite. The pulsed nozzle passes helium over this vaporization zone.

this pulsed molecular beam source. In operation the solenoid-actuated pulsed valve was fired to release through the 1-mm orifice a pulse of He gas over the sample lasting somewhat less than a millisecond. The backing pressure could be as high as 10 atm. At some point during the gas pulse, usually near its middle, the Q-switched frequency-doubled vaporization laser was fired generating a 5-ns-long pulse of green light (532 nm) with an energy of roughly 30–40 mJ. This laser was focused onto the rotating–translating graphite disk (to avoid digging pits into the sample) vaporizing a plume of carbon vapor into the gas stream. Multiphoton ionization and the subsequent heating of the resulting plasma limited the amount of material vaporized in a single shot and ensured that the species initially contained in it were atoms or very small molecules, such as C_2 and C_3.

Robert F. Curl, Jr. was born in 1933 in Alice, Texas (USA). He received his Ph.D. in chemistry in 1957 at the University of California, Berkeley (USA). After conducting research at Harvard University for one year he went to Rice University, where he has been a professor since 1967.

The material vaporized was caught up in the helium gas flow, mixed with it, and cooled by it. The cooling vapor then began to condense into clusters. The extent of clustering could be varied by changing the backing pressure, the timing of the firing of the vaporization laser with respect to the center of the gas pulse, and the length and geometry of the channel downstream from the vaporization point. In the configuration shown in Figure 2 an integration cup has been added to the end of the gas channel to provide more time for clustering and reaction before supersonic expansion.

After clustering, the gas pulse was expanded supersonically through a nozzle into a large vacuum chamber (Figure 3). Be-

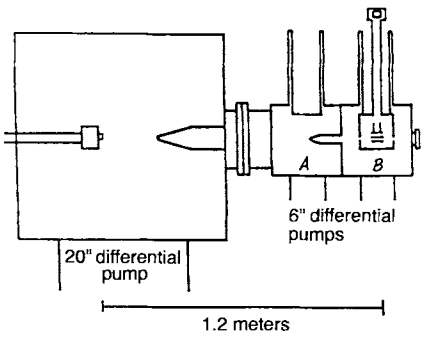

Figure 3. Molecular-beam photoionization time-of-flight (TOF) mass spectrometer.

cause this expansion is essentially an adiabatic reversible expansion, the temperature of the species in the gas drops from somewhat above room temperature to a few Kelvin. After a few dozen expansion-nozzle diameters, collisions between particles in the expansion jet cease resulting in a gas stream with a narrow, highly directional velocity distribution. The resulting jet of cold clusters can be skimmed into a molecular beam and interrogated by mass spectrometry. Mass spectrometric detection labels the species by mass, which is a particularly important consideration in the study of clusters, where a wide distribution of cluster sizes is always found. In addition, mass spectrometric detection provides high sensitivity and permits extensive control of the trajectory of the cluster ions. Consequently, a variety of methods for manipulating and probing the cluster ions were developed and used in this work. These more sophisticated methods will be described later at the appropriate point. For the present, we focus on the simplest mass spectrometry.

For mass spectrometric detection, the skimmer at the end of the large chamber forms a molecular beam from the portion of the jet moving directly away from the nozzle. This beam is passed through a differential pumping chamber and another skimmer and thence between the plates of the ion-extraction field. In the most usual experiments this field is a DC field, and ions are produced by a pulsed ionization laser (normally an ArF 193-nm excimer laser, 6.4 eV, pulse length about 10 ns). Once produced the ions are accelerated by the DC field into the drift tube of a time-of-flight (TOF) mass spectrometer. Because all ions of unit charge receive the same energy, ions of greater mass reach a final velocity that is less than that of ions of lesser mass. Therefore, the mass of the ion in the acceleration region is determined by its time of arrival at the ion detector. By plotting the ion-detector signal versus arrival time, a mass spectrum of the

cluster distribution is obtained. Often these cluster distributions are quite colorful exhibiting "magic number" cluster sizes, where a peak is more prominent than its neighbors by a factor of perhaps 2. Figure 4 shows a cluster distribution for carbon similar to that obtained previously by Rohlfing, Cox, and Kaldor in essentially the same apparatus.[26] In the Rohlfing, Cox, and Kaldor distribution C_{11}^+, C_{15}^+, C_{19}^+, and C_{60}^+ might be called magic numbers. The discovery of the fullerenes began when we found that under the right conditions, C_{60}^+ could become a super magic number that is far more prominent than its neighbors.

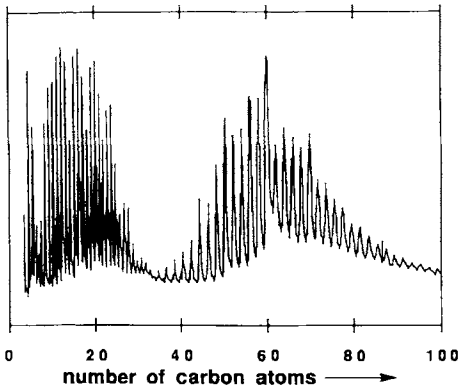

Figure 4. Carbon-cluster distribution observed under mild clustering conditions. This distribution is similar to that obtained by Rohlfing, Cox, and Kaldor; reprinted with permission [26].

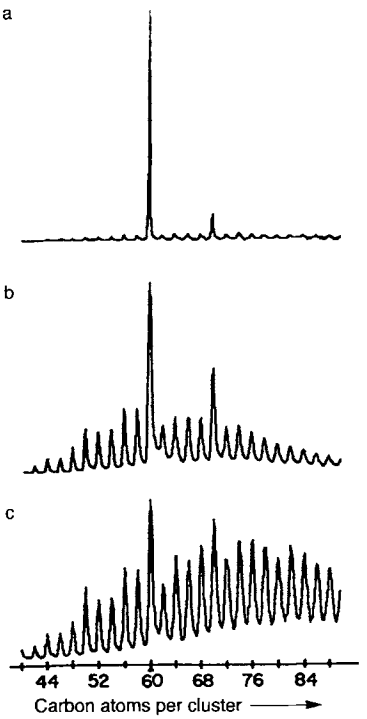

Figure 5. Series of mass spectra of the C_{60} mass region showing C_{60} peaks growing in intensity. Panel a: full helium backing pressure with integration cup. Panel b: full helium backing pressure with vaporization in the center of the gas pulse, no integration cup. Panel c: low helium backing pressure, no integration cup.

When the carbon system was investigated in September 1985, major fluctuations in the prominence of the C_{60} peak compelled us to examine this mass region more carefully under a variety of clustering conditions. It was found that the relative prominence of the C_{60} mass peak could vary from roughly twice the intensity of its nearest neighbors to about 50 times the intensity of its nearest neighbors. This led us to propose[15] that the very prominent C_{60} cluster we had observed has a closed, highly symmetric, carbon cage structure in the form of a truncated icosahedron. Since our inspiration to look for a spherical cage structure came from the geodesic domes of R. Buckminster Fuller, we dubbed this molecule buckminsterfullerene.

The buckminsterfullerene proposal rested on the single experimental observation that carbon vapor condensation conditions could be found where the intensity of the mass spectrum peak of C_{60} in the carbon-cluster beam was many times the intensity of any of its near neighbors in mass, as shown in Figure 5a. Was this proposal a lucky guess, or is this single observation taken in context sufficient to prove that the prominent C_{60} peak in Figure 5 is the truncated icosahedron isomer shown in Figure 1? Our claim has always been that the situation is much closer to proof than conjecture.

Note in Figure 5 that the relative prominence of C_{60} depends upon the clustering conditions. The C_{60} peak becomes more prominent when more time is given for high-temperature (room-temperature and above) collisions between the carbon clusters. This immediately indicates that whatever isomer(s) of C_{60} are responsible for its prominence must be "survivors" that are relatively impervious to chemical attack.

There are probably millions of plausible isomers of C_{60} that differ in chemical connectivity. Most of these millions of C_{60} isomers will be obviously chemically reactive with dangling carbon bonds and, thus, unable to survive chemical attack. The role of chemical attack is manifested in the fact that in all three distributions in Figure 5 only even carbon clusters are observed, in contrast to observations not shown here but shown in Figure 4 of the region below 25 carbon atoms where both even and odd clusters are observed with comparable intensities. It is possible to find clustering conditions where both even and odd carbon clusters are observed with comparable intensity near C_{60}; these conditions correspond to much less time for chemical reaction than for any of the mass spectra shown in Figure 5. Figure 6 (control) shows a distribution intermediate between Rohlfing, Cox, and Kaldor's and those observed with nearly equal intensity odd clusters. Thus, even in Figure 5c the observation of only clusters with even carbon numbers is evidence that already all the clusters in the region must have some special structures that are less susceptible to chemical attack than a typical dangling bond isomer. The obvious explanation from our present viewpoint is that these clusters are all closed carbon cage structures (fullerenes) also. In September 1985 we recognized, without the fullerene concept, that the even cluster distribution probably reflected isomers of reduced reactivity compared with the odd clusters.

Thus we believed that the very prominent C_{60} peak in Figure 5a could only be explained by a single isomer of C_{60} that is remarkably impervious to chemical attack. A readily imaginable alternative explanation would be in terms of a C_{60} isomer that is much easier to photoionize than its neighbors by the 6.4-eV ArF ionization laser employed. However, this explanation ignores the clear increase of the prominence in the C_{60} signal when more time is allowed for chemical reaction. Thus,

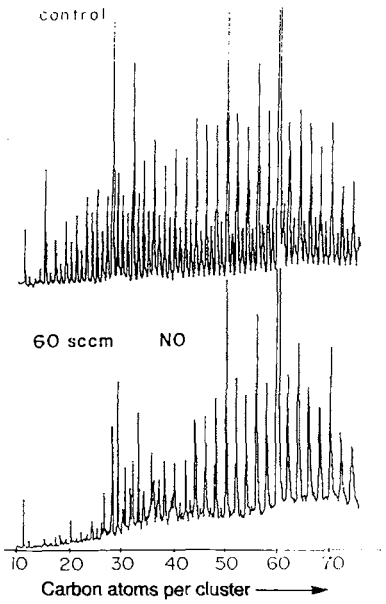

Figure 6. Reaction of carbon clusters with NO. Top: control mass spectrum obtained without added NO. Bottom: roughly 1 Torr of NO was added to the gas stream in the fast-flow reaction tube. It is clear that the odd clusters react with NO. The various products of these reactions are not resolved, but contribute to the elevated baseline.

an explanation for the prominence of C_{60} based on its easier photoionization does not take into account the obvious reduced chemical reactivity of C_{60} compared with its neighbors. Further evidence against an explanation based upon photoionization efficiency was obtained in later experiments, which demonstrated a similar prominence of C_{60}^+ upon photoionization with a 7.9-eV F_2 excimer laser.[27]

The truncated icosahedron form of C_{60} is clearly a special structure, which should be chemically very stable. It has no dangling bonds with the valences of every atom satisfied. The pattern of double and single bonds depicted in Figure 1 is just one of 12500 possible Kekulé structures[28] (but it has proved to be the dominant one). By symmetry every atom is equivalent, so there is no specific point of chemical attack. Strain is introduced in curving the intrinsically planar system of double bonds into a spherical shape, but the strain is symmetrically and uniformly distributed over the molecule thereby again avoiding a weak point for chemical attack. There is obviously no other structure with this high degree of symmetry, and very little reason to fear that another structure could be found that offers this unique combination of advantages. For these reasons, and even though it seems very counterintuitive for this high-symmetry, low-entropy molecule to form out of the chaos of carbon vapor condensing at high temperature, we have never really considered the assignment of the prominent C_{60} peak in the mass spectrum to the buckminsterfullerene structure to be a guess.

In science, more proof is always demanded. Later experiments[27, 29] demonstrated that the special prominence of C_{60} was not the result of some special preference for the C_{60}^+ ion upon photofragmentation, and that C_{60} can be made specially prominent in both the residual cations and anions (a residual ion being an ion that is formed in the vaporization plasma and survives the expansion process).

Conjecture—The Fullerene Hypothesis

We soon learned from Haymet's paper[7] of Euler's rule[30] stating that a solid figure with any even number n of 24 or more vertices could be constructed with 12 pentagons and $(n - 20)/2$ hexagons. This immediately provides an explanation in terms of such carbon cage molecules of the even cluster distribution that appears at carbon numbers above 30 in the mass spectrum, as these molecules would have no dangling bonds and would thus be relatively unreactive. These spheroidal carbon cage molecules consisting only of pentagons and hexagons were given the generic name of fullerenes.

However, in contrast with the truncated icosahedron explanation for the prominent C_{60} peak, this conclusion has always seemed to me to be much more conjecture, however plausible. The next few years of our lives were devoted to testing experimentally this fullerene hypothesis and finding that it passed every test.

Experiment—Reactivity and Photofragmentation

It is possible to inject chemical reagent gases into the cluster stream prior to the expansion and then to observe reaction-product ions in the mass spectrum.[31, 32] A reaction tube was added to the end of the cluster source and various reagents such as NO, SO_2, NH_3, H_2, CO, and O_2 were injected into the gas stream.[33] It was possible to obtain a mass distribution without added reagent that showed both odd and even carbon-number peaks with the odd carbon-number peaks about half the intensity of the even ones. When a reagent such as NO or SO_2 was added, the odd carbon-number peaks disappeared, but the even carbon-number peaks with 40 atoms or more remained unreactive as would be expected if they were fullerenes having no dangling bonds. The distributions observed in this experiment are shown in Figure 6. Note that the odd clusters which are believed to have dangling chemical bonds are much more reactive than the even clusters.

A series of photofragmentation experiments were carried out on the carbon cluster ions hypothesized to be fullerenes using a tandem time-of-flight mass spectrometer.[34] The apparatus is shown in Figure 7. In these experiments, a single carbon-cluster ion was mass selected and then interrogated by a photofragmentation laser as shown in the apparatus detail in Figure 8. It was then accelerated into a second TOF drift region, and the mass of its ionic fragments determined. The photofragmentation pattern of C_{60}^+ is shown in Figure 9. As can be seen, the fragmentation pattern corresponds to the loss of an even number of carbon atoms down to C_{32}^+ where it changes abruptly to produce ions containing about 20 atoms. We believe that C_{60}^+ is losing an even number of carbon atoms in a few-step process with the fullerene cage of the ion reclosing upon loss of the neutral even-number fragment. The abrupt change in pattern at C_{32}^+ takes place because the strained small fullerene can no longer close upon carbon loss, and instead a large neutral fragment is shaken off when the strain energy is suddenly released upon opening the cage.

The energies of many of the fullerenes have been calculated at the STO – 3G/SCF level of theory by Scuseria[35] and are

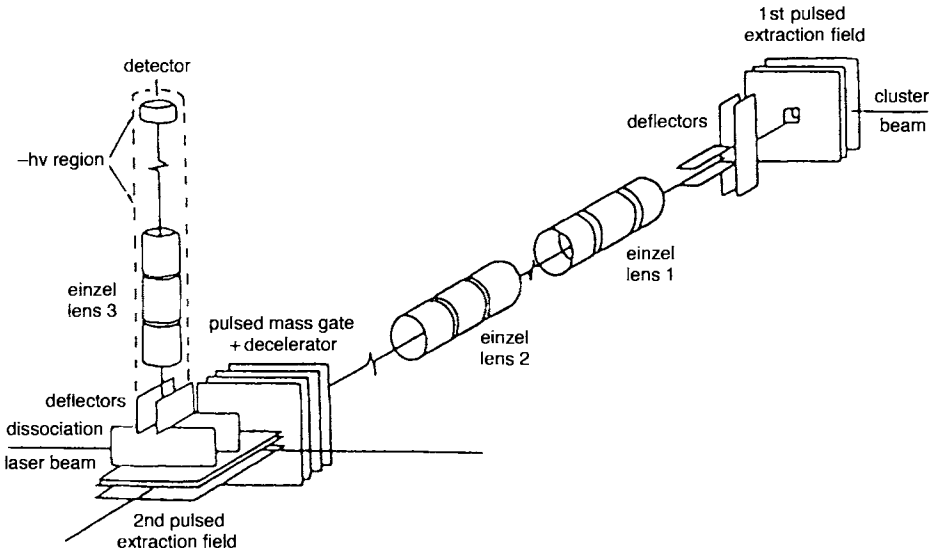

Figure 7. Tandem TOF mass spectrometer. The molecular beam containing residual ions from the vaporization plasma enters the extraction region of the primary mass spectrometer where a 2000-V pulse is applied across the grids. The deflectors remove the molecular-beam velocity. The einzel lenses focus the ion beam. Ions are selected by the mass gate, fragmented by the laser, and analyzed by the second TOF mass spectrometer.

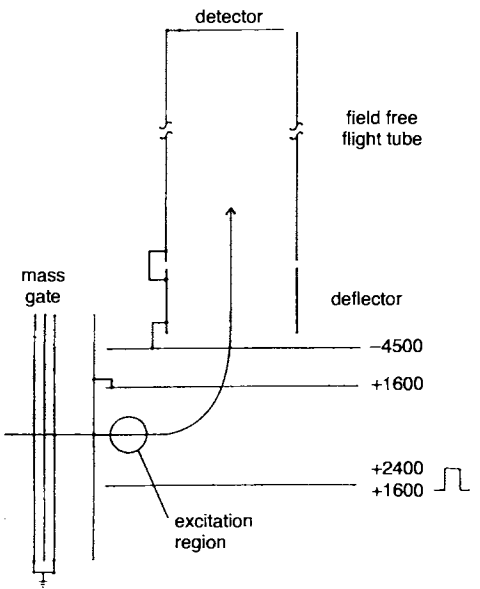

Figure 8. Detail of the photofragmentation region of the tandem TOF apparatus showing the mass gate, laser-excitation region, extraction optics, and flight tube.

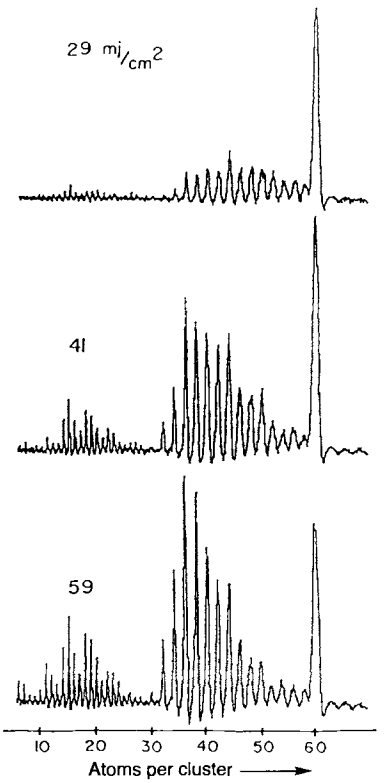

Figure 9. Photofragmentation pattern of C_{60}^+ showing loss of an even number of carbon atoms and break off at C_{32}^+.

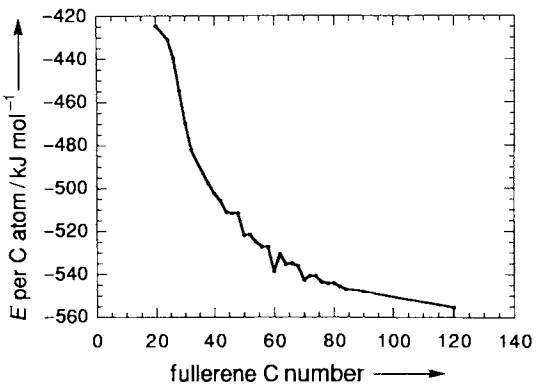

Figure 10. Energy per carbon atom relative to atomic C as a function of fullerene cluster size at the STO – 3G/SCF level at the MM3-optimized geometry for the lowest-energy fullerene structure for each size; based on calculations of R. L. Murry et al. [35].

shown in Figure 10. It should be noted that for fullerenes of size C_{28} and larger there is more than one fullerene structure for a given number of carbon atoms.[36] For example, there are 1812 fullerene isomers (that is, cages containing 12 pentagons and 20 hexagons) of C_{60} alone.[37, 38] The energies plotted in Figure 10 are for the lowest-energy fullerene isomers found. Truncated icosahedron C_{60} and D_{5h}-symmetrical C_{70}, which are respectively the lowest-energy fullerene isomers of 60 and 70 carbon atoms, are local minima in the energy curve, and this can be strikingly seen in these energetics. We label the buckminsterfullerene isomer of C_{60}, C_{60}^{BF}.

When these energies are combined with the bond dissociation energy of C_2 of 6.21 eV,[39] the overall energy change in fragmentation can be calculated. Thus the overall energy change for Equation (1) is $\Delta E = 0.7$ eV, while for the loss from C_{60}^{BF}, $\Delta E = 11.2$ eV [Eq. (2)]. The activation barrier for the fragmentation of C_{60} cannot be less than the fragmentation energy of 11.2 eV. In order to have substantial fragmentation of C_{60}^{BF+} in the few μs available in Figure 9, I estimate that about 100 eV must be deposited into the C_{60}^{BF} ion.

$$C_{62} \longrightarrow C_{60}^{BF} + C_2 \quad (1)$$

$$C_{60}^{BF} \longrightarrow C_{58} + C_2 \quad (2)$$

If the activation barriers to fragmentation follow the energetics, one would expect that the special stability of C_{60} would be apparent in the fragmentation pattern. Figure 11 shows frag-

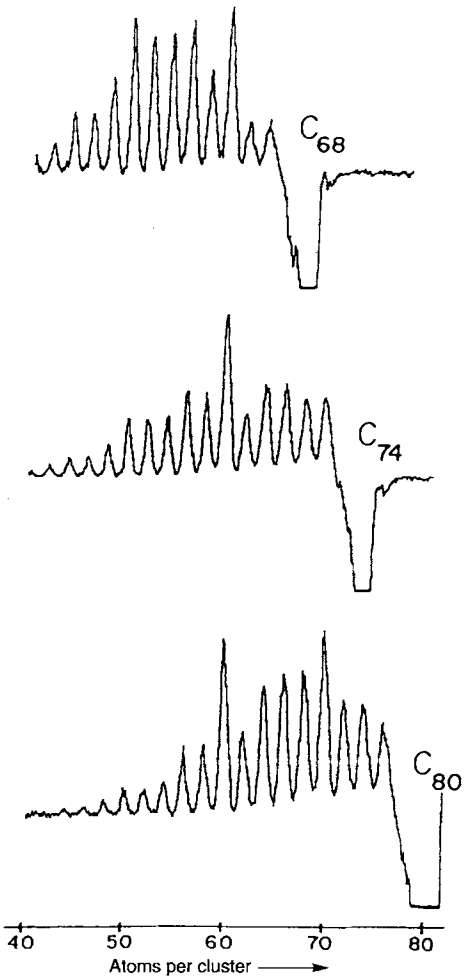

Figure 11. ArF-fragmented (15 mJ cm^{-2}), large, even carbon clusters. There is no difference in the fragmentation pattern of the large clusters. C_{60} and C_{70} are slightly favored.

mentation of some larger clusters when the sample is irradiated just before the acceleration region of the second TOF, as shown in Figure 8. Only a few μs are available for fragmentation after irradiation and before acceleration and analysis, and C_{60} and C_{70} are only slightly special fragments. However, if the irradiation is carried out in the *first* TOF extraction region just before extraction and the ions which have the right TOF for the initial species of Figure 12 are permitted through the mass gate, the pattern is much different. Here the sequence is that the large ion is irradiated and accelerated before it fragments; it then has time to fragment all the way to the second extraction region, which corresponds to a time of about 120 μs.

In Figure 12 it is clearly seen that C_{60} is quite prominent. The original ion is less energetic than is the case of the short-term fragmentation, and thus the fragmentation pattern is much more sensitive to the fragmentation energetics. The relationship between the long-time fragmentations of Figure 12, where C_{60}^+ is very prominent, to the short-time fragmentations of Figure 11, where C_{60}^+ is less prominent, can be explained if one assumes that the activation barriers to ring rearrangements on the surface of the fullerene ions are much less than the activation barrier to fragmentation of a typical fullerene ion.

Assume that a fragmentation which leads to a C_{60}^+ fullerene takes place. It is unlikely that this C_{60} ion has the buckminsterfullerene structure. Probably several rerrangements of this ion must take place before the especially stable C_{60}^{BF} structure is found. When long-time fragmentation is investigated, there is sufficient time for a number of lower activation energy ring-rearrangement processes to take place before fragmentation, because the energy deposited in the original ion is relatively small compared with the short-time fragmentation energy. These ring rearrangements find the low-energy buckminsterfullerene structure, which is very hard to fragment. With the short-time fragmentation far more energy is deposited in the original ion, and fragmentation occurs before the low-energy buckminsterfullerene structure is found.

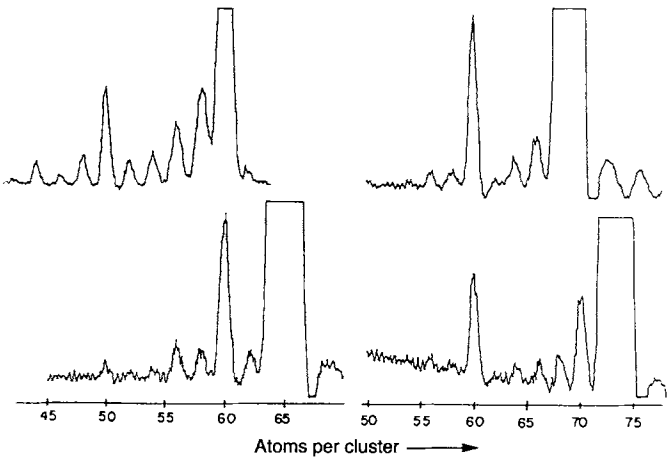

Figure 12. Metastable TOF mass spectra for 60-, 66-, 70-, and 74-atom clusters. The clusters were irradiated 1 μs before the first extraction pulse with ArF (15 mJ cm^{-2}). The ions were mass gated at the time appropriate to the parent ions listed above and analyzed in the second TOF mass spectrometer. The travel time to the second mass spectrometer was approximately 120 μs. The special prominence of C_{60} and C_{70} is clear.

Figures 9, 11, and 12 taken together provide striking evidence that cations being examined are structurally related to each other and to C_{60}^{BF}. It appears that fragmentation takes place with the preservation of the cage structure until the break-off point at C_{32} is reached.

Conjecture—The Existence of Endohedral Complexes

The fullerenes are hollow. Buckminsterfullerene has a cavity almost 4 Å in diameter that is capable of holding any atom of the periodic table. It seemed to us that it might be possible to introduce a foreign atom into the central cavity to produce an endohedral adduct. We recognized that bulk samples of such materials, if they could be obtained, might have many unusual and potentially useful properties. For this narrative, the important point is that such an endrohedral atom would be difficult to dislodge.

Experiment—Endohedral Metallofullerenes and "Shrink Wrapping"

Success in forming adducts with a single lanthanum atom was almost immediately achieved.[40] In these experiments, a low-density graphite disk was soaked in a water solution of $LaCl_3$,

dried, and used as target for laser vaporization. The mass spectrum at low-ionization laser fluence showed many peaks from both pure carbon and carbon–lanthanum adducts, but when the ionization laser power was turned up somewhat so that the least stable species would photofragment, all bare cluster peaks except for C_{60} and C_{70} disappeared, but clusters with one lanthanum atom at every even carbon number remained. There were no clusters remaining with more than one La atom. Thus, under laser fluences capable of destroying the less stable carbon clusters, one and only one lanthanum atom stuck. This is a strong indication that the lanthanum atom is inside the cage.

It was found that endohedral metallofullerenes containing the alkali metal atoms K and Cs could be readily formed. This led to a unique way to test the fullerene hypothesis by "shrink-wrapping". A series of photofragmentation experiments were carried out in a fourier transform ion cyclotron resonance cell on $C_{60}K^+$ and $C_{60}Cs^+$.[41] A supersonic beam of cluster ions is prepared as described above and injected into the ion cyclotron resonance cell where they can be trapped for several minutes. By applying a range of radio frequencies to the cell, the orbits of almost all ions but the desired one ($C_{60}K^+$ or $C_{60}Cs^+$) can be excited thereby driving the unwanted ions from the cell. Photofragmentation experiments can then be carried out on the remaining ions.

From our previous experiments on photofragmentation and $C_{60}La^+$, we expected that at low laser fluences the ions would lose C_2, C_4, and C_6 while retaining the metal. If the metal is in the cage as proposed, the cage will become increasingly strained upon loss of neutral carbon because it is shrinking down upon the resistant metal core. A point will be reached where the cage will break releasing the metal. This point will depend upon the size of the metal ion and will therefore be reached for larger clusters in the case of $C_{60}Cs^+$ than in the case of $C_{60}K^+$. Furthermore, the cage breaking point can be roughly estimated from the van der Waals radii of the alkali metal ion and the carbon atoms. Figure 13 shows the photofragmentation results. The even-carbon loss breaks off for $C_{60}K^+$ at $C_{44}K^+$ and for $C_{60}Cs^+$ at $C_{48}Cs^+$, which agrees well with predictions from the van der Waals radii. We can conceive of no explanation for these observations other than that we were observing fragmentation of endohedral fullerene complexes.

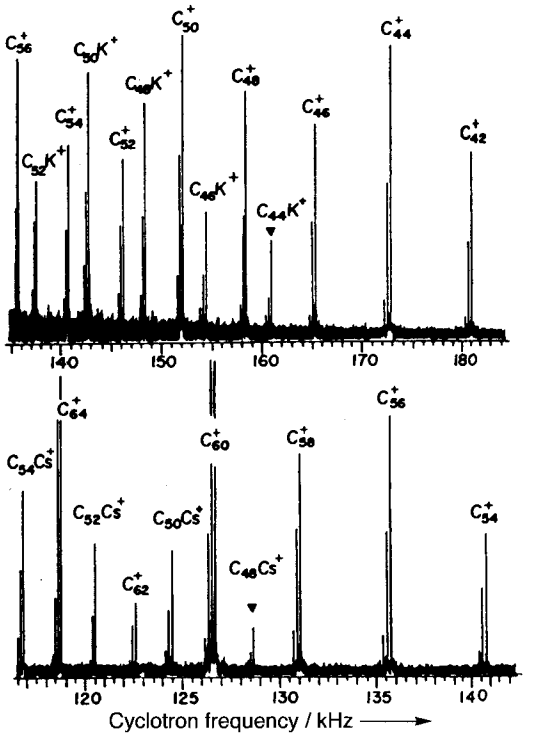

Figure 13. The low-mass portion of the fragment ions produced by intense laser excitation of $C_{60}K^+$ (A) and $C_{60}Cs^+$ (B) in the FT-ICR trap. The clusters containing carbon only seen in these spectra arise from fragmentation of empty fullerene ions simultaneously trapped with the metal species.

Conjecture—C_{70} has D_{5h} Symmetry

In almost all mass spectrometer carbon-cluster distributions where C_{60}^+ (or C_{60}^-) is prominent, C_{70}^+ (or C_{70}^-) is usually the next most prominent ion in the C_{40}–C_{90} mass range. Therefore it is likely to have a somewhat special structure. A plausible guess for the structure of C_{70} seemed to be one in which a band of five hexagons was added around the equator of C_{60}.[40] To form such a structure (Figure 14) choose an orientation of C_{60} so that pentagons are at the north and south poles; then cut the C–C bonds connecting the northern and southern hemispheres, separate them, rotate one hemisphere by a 1/10 turn with respect to the other, and add a string of 10 carbon atoms at the equator to rejoin the two hemispheres.

Both the structures of C_{60}, buckminsterfullerene, and D_{5h} C_{70} have no abutting pentagons. Haymet suggested that such connected rings would be destabilizing.[7] Shortly thereafter,

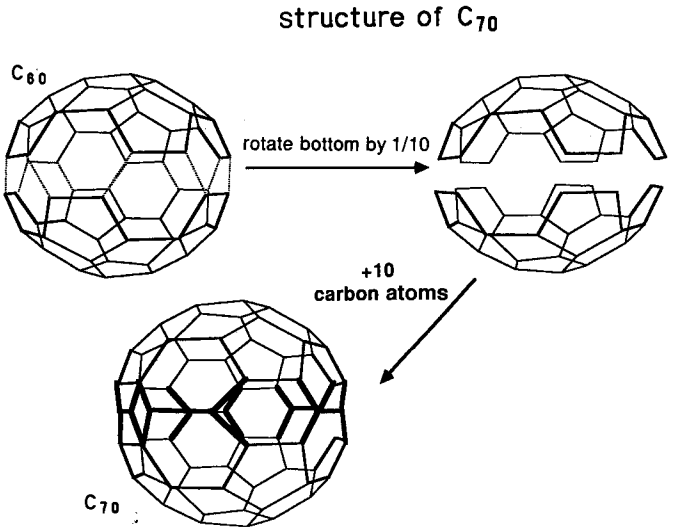

Figure 14. Relationship of the proposed structure of C_{70} to that of C_{60} (buckminsterfullerene).

Schmalz et al. pointed out that abutting pentagons necessarily involve destabilizing, antiaromatic, eight-atom, conjugated π electron circuits around the ring; this makes structures with abutting pentagons less stable.[42] Both Kroto[43] and Schmalz et al.[44] proposed that D_{5h} C_{70} is the smallest cage structure larger than C_{60}^{BF} without abutting pentagons. Both reported that they had made a diligent, but not exhaustive, search of structures between C_{60} and C_{70} for isolated pentagon cages. Subsequently, Liu et al. were able to prove this conjecture.[45] Kroto showed that the "magic number" mass spectrometer peaks containing fewer than 60 carbon atoms corresponded to structures

with the minimum number of abutting pentagons.[43] These considerations became the "isolated pentagon rule", which states that in the stable fullerenes the pentagons are isolated.

Although it was strongly supported by these theoretical considerations, the conjecture that the structure of C_{70} has D_{5h} symmetry could never be verified experimentally by molecular-beam mass spectrometry. The proof of this structure had to wait until the production[46] of macroscopic mixtures of C_{60} and C_{70} permitted the separation of C_{60} and C_{70} and the observation of the ^{13}C NMR spectrum of C_{70}.[47]

Conjecture—C_{60} Might Be the Carrier of the Diffuse Interstellar Bands

Not all conjectures can be expected to be correct. When we wrote our initial paper on C_{60}, we were inspired with wildly imaginative thoughts about the potential significance of the spontaneous formation of this remarkable molecule in all areas of chemistry and astrophysics.[15] Since we had been thinking of carbon chain molecules as possible carriers of the diffuse interstellar bands (DIBs),[11] it was natural to consider C_{60} as offering a potential explanation of the DIBs, and we proposed that as a possibility.

C_{60} seemed an attractive candidate for several reasons. First, any molecular carrier of the DIBs must be large enough so that it is not dissociated by absorbing photons of energies of up to 13.6 eV. In a large molecule such as C_{60}, when a photon is absorbed, internal conversion rapidly brings the molecule back to its ground electronic state. If there is more energy available in the photon than is needed for unimolecular dissociation, then dissociation competes with vibrational reradiation of the excess energy in the infrared. With a dissociation threshold of 11 eV and so many vibrational modes, unimolecular decay even with 13.6 eV of excitation is a very slow process and loses completely to infrared reradiation. Second, there are not many DIBs known, and, therefore, any proposed carrier must give only a few bands and should not be one of a large class of equally attractive candidates. The high symmetry of C_{60} suggests only a few bands, and, while there is a fullerene family, C_{60} is often uniquely prominent. Any carrier should consist of the more cosmically abundant elements. Lastly, the diffuseness of the bands could come from mixing of the spectroscopically active excited electronic state with ground- or lower-state levels. Subsequent to our original proposal, it became obvious that C_{60} would be likely to be photoionized or to react with H atoms so that C_{60}^+ and slightly hydrogenated derivatives of C_{60} would be more attractive.[48-50]

Experiment

Eventually it proved possible to obtain a portion of the visible electronic spectra of C_{60} and C_{70} using resonant two photon ionization,[51] and these spectra demonstrated conclusively that neither neutral C_{60} nor neutral C_{70} have absorptions that correspond to the known diffuse interstellar lines in the same region. These observations alone do not rule out C_{60}^+ or perhaps protonated C_{60} derivatives as carriers of the DIBs; however, the matrix-isolation spectrum of C_{60}^+ seems to rule it out as a DIB carrier.[52, 67]

Conjecture—Soot is Formed From Spiraling Icosahedral Carbon Shells

The control of soot formation is of enormous practical value; consequently, the nature of soot and the processes involved in its formation have been extensively studied, and this remains an active research field. Since soot consists primarily of carbon, we naturally thought about whether the chemistry involved in fullerene formation might be also applicable to soot formation. The combustion environment principally differs from condensing carbon vapor in that large quantities of hydrogen are present in combustion. Indeed, almost as many H atoms as C atoms are present in combustion soot. Combustion soot is considered to be regions of layered sheets of large polycyclic aromatic hydrocarbons joined by disorganized regions.

It seemed to us that the fullerenes were forming in a process where small carbon clusters such as C_2 and C_3 were adding to a growing, curving sheet of five- and six-membered rings. Curvature and ultimate closure into fullerenes was brought about by some sort of ring-rearrangement process that let the carbon cluster find its lowest-energy, least reactive forms. The growth of polycyclic hydrocarbons (PAH) in soot formation was thought to be by the creation of a reactive carbon atom on the periphery by H-atom abstraction from a peripheral C—H bond followed by acetylene addition to the reactive center, followed by ring closure with H-atom elimination.[53] The similarity between the process we imagined for fullerene formation and the PAH-growth process in combustion-soot formation seemed striking to us. The main difference seemed likely to be that hydrogen on the edges might interfere with the fullerene-closure processes leading to imperfect cages. Perhaps a soot particle was the result of such imperfect growth and would resemble a spiraling fullerenic shell. Thus we proposed that a soot particle would be based upon a spiraling icosahedral shell similar to the structure shown in Figure 15.

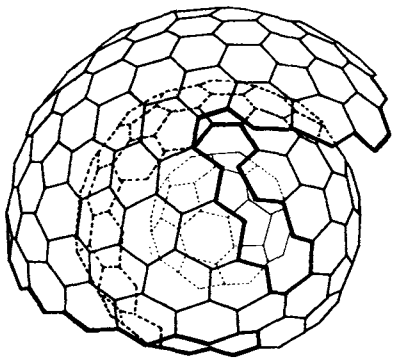

Figure 15. Spiraling icosahedral shell model of a growing soot particle. It has almost completed its second shell of growth.

Experiment

This suggestion was met with disfavor by some members of the soot community.[54-56] However, it did result in searches for fullerenes in flames by some of the leading combustion and soot scientists. Thus Homann found C_{50}^+, C_{60}^+, and C_{70}^+ prominently in hydrocarbon flames.[57] He suggested that soot particles might be supports for fullerene growth.[58] More recently

he has proposed more elaborate and detailed models for fullerene formation[59] and its relation to soot.[60] After C_{60} and C_{70} became available in bulk, soot scientists began looking for these species in combustion soots with success.[61, 62] Under optimal conditions the yield of C_{60} plus C_{70} was as much as 20% of the soot and up to 0.5% of the carbon fed making flames a practical preparation scheme for fullerenes.[63] Quite recently, electron microscope examination of nanostructures in flame soots has revealed the whole range of fullerenic structures: fullerenes, nanotubes, and the nested fullerenes resembling Russian dolls.[64] These observations are strong evidence that carbon has a strong propensity to form these structures in chemically quite different environments where elemental carbon forms are produced.

Thus some very special chemistry does not appear to be needed for fullerene formation. Howard has proposed a detailed kinetic scheme for the formation of C_{60} and C_{70} in flames, which parallels the standard mechanism for the formation of polyaromatic hydrocarbons, which are considered to be the soot precursors.[65] Nevertheless, fullerene formation and soot formation remain to him clearly distinct processes.

The soot community remains united in the belief that, while soot might produce fullerenes as an offshoot, soot formation is a different process from fullerene formation and that soot is primarily composed of PAHs and that there is no evidence for spiraling icosahedral shells. It should be noted that it is known that more than half of the soluble PAH inventory of flames contain five-membered rings and therefore curvature.[66] Whether the curvature introduced by such five-membered rings plays any role in the formation of soot particles remains an interesting, open question.

Conclusion

In science conjecture drives both experiment and theory for it is only by forming conjectures (hypotheses) that we can make the direction of our experiments and theories informed. If such and such is true, then I should be able to do this experiment and look for this particular result or I should be able to find this theoretical formulation. Conversely, experiment and theory drive conjecture. One makes a startling observation or has a sudden insight and begins to speculate on its significance and implications and to draw possible conclusions (conjecture).

However, not all conjectures are equally valid or useful. Thus the conjecture that C_{60} might be related to the diffuse interstellar bands was and remains wildly speculative. It has been one of my favorite speculations,[50] because it has many things going for it: Carbon is injected into the medium, and C_{60} forms spontaneously in condensing carbon under the right conditions; C_{60} is unique, its compounds are limited in number, and only a few species should be involved in the DIBs; C_{60}^+ could survive the UV present in the interstellar medium; the diffuseness of the bands could come from mixing of the spectroscopically active excited electronic state with ground- or lower-state levels. However, conjectures should be judged by the accumulation of evidence that supports and contradicts them. To date, there has been plentiful contradictory evidence for the C_{60} connection to the DIBs and no supporting evidence. Primarily, this conjecture has the fatal defect that it has stimulated little productive science.

The conjecture that soot may consist of spiraling spheroidal shells of carbon belongs in a slightly different category. It was based upon a hypothesis, which was somewhat vague at the time, about how fullerenes may form. Thus, it was not a wild idea in that there was some support for the speculation. In my opinion, the conjecture that soot consists of spiraling spheroidal shells is probably wrong. However, I think it likely that there is some more subtle connection between the curvature introduced by five-membered rings and soot formation. Regardless of its validity, this conjecture has turned out to be extremely valuable, because it got the soot community, in some cases somewhat grumpily, thinking about the formation of fullerenes and other carbon morphologies in flames. As a result, fullerenes were found in flames and soot. It appears that all the new carbon morphologies can be produced in flames.[64]

Turning to the central theme, the conjecture of Jones[1, 2] that carbon cage compounds might have interesting properties, and the conjecture of Osawa[3] and several others that C_{60} would be a stable, chemically interesting molecule are examples of conjectures which are correct and valuable, but which by themselves cannot be made useful. There was no way, or no easy way (remember Chapman), to proceed to further work based on the conjecture.

On the other hand, the conjecture that a new whole class of carbon cage compounds, the fullerenes, are formed spontaneously in condensing carbon vapor has led to sweeping consequences. At the time, this hypothesis seemed to be the only logical explanation of the observed carbon mass spectra distributions, but it was not self-evident. As we have seen, we tested this conjecture in a variety of experiments, which always provided evidence supporting the conjecture. This pattern of repeated confirmation of expected consequences is what is expected for a correct hypothesis. In the long run, the fullerene hypothesis has proved to be spectacularly correct and it has provided the basis for a whole new branch of organic chemistry.

Finally, I believe that the conjecture that started it all, namely that truncated icosahedron C_{60} forms spontaneously in condensing carbon, scarcely belongs in the category of conjecture. The three mass spectra in Figure 5, when coupled with the conditions under which they were obtained, demand that the species responsible for the prominent peak at C_{60} must be singularly different and chemically relatively unreactive. The human mind can conceive of no other isomer of C_{60} that better fits this requirement.

Richard Smalley and Harold Kroto are my corecipients of the Nobel prize. I must point out that we do not and cannot claim this discovery is ours alone. James Heath and Sean O'Brien have equal claim to this discovery. In addition, there are several others who were major participants in this research at an early stage: Yuan Liu, Qing-Ling Zhang, and Frank Tittel. The work of F. D. Weiss and J. L. Elkind on the shrink wrap experiments is appreciated.

Received: February 11, 1997 [A211IE]
German version: *Angew. Chem.* **1997**, *109*, 1636–1647

Keywords: carbon allotropes · fullerenes · nanostructures · Nobel lecture

[1] D. E. H. Jones, *New Scientist* **1966**, *32*, 245.
[2] D. E. H. Jones, *The Inventions of Daedalus*, Freeman, Oxford, **1982**, pp. 118–119.
[3] E. Osawa, *Kagaku (Kyoto)* **1970**, *25*, 854.
[4] Z. Yoshida, E. Osawa in *Aromaticity* (Kagakudojin, Kyoto), **1971**, pp. 174–178.
[5] D. A. Bochvar, E. G. Gal'pern, *Dokl. Akad. Nauk. SSSR* **1973**, *209*, 610.
[6] R. A. Davidson, *Theor. Chim. Acta* **1981**, *58*, 193.
[7] A. D. J. Haymet, *J. Am. Chem. Soc.* **1986**, *108*, 319.
[8] J. Baggott, *Perfect Symmetry: The Accidental Discovery of Buckminsterfullerene*, Oxford University Press, Oxford, **1994**.
[9] H. W. Kroto, C. Kirby, D. R. M. Walton, L. W. Avery, N. W. Broten, J. M. MacLeod, T. Oka, *Astrophys. J.* **1978**, *219*, L133.
[10] L. W. Avery in *Interstellar Molecules* (Ed.: B. H. Andrew), Reidel, Hingham, MA, **1979**, pp. 47–55.
[11] A. E. Douglas, *Nature* **1977**, *269*, 130.
[12] E. Herbig, *Astrophys. J.* **1975**, *196*, 129.
[13] J. R. Heath, Q. Zhang, S. C. O'Brien, R. F. Curl, H. W. Kroto, R. E. Smalley, *J. Am. Chem. Soc.* **1987**, *109*, 359.
[14] H. W. Kroto, J. R. Heath, S. C. O'Brien, R. F. Curl, R. E. Smalley, *Astrophys. J.* **1987**, *314*, 352.
[15] H. W. Kroto, J. R. Heath, S. C. O'Brien, R. F. Curl, R. E. Smalley, *Nature* **1985**, *318*, 162.
[16] R. E. Smalley, *The Sciences* **1991**, *31*, 22.
[17] H. W. Kroto, *Angew. Chem.* **1992**, *104*, 111; *Angew. Chem. Int. Ed. Engl.* **1992**, *31*, 113.
[18] H. Aldersey-Williams, *The Most Beautiful Molecule: An Adventure in Chemistry*, Aurum, London, **1995**.
[19] T. G. Dietz, M. A. Duncan, D. E. Powers, R. E. Smalley, *J. Chem. Phys.* **1981**, *74*, 6511.
[20] D. E. Powers, S. G. Hansen, M. E. Geusic, A. C. Puiu, J. B. Hopkins, T. G. Dietz, M. A. Duncan, P. R. R. Langridge-Smith, R. E. Smalley, *J. Phys. Chem.* **1982**, *86*, 2556.
[21] J. B. Hopkins, P. R. R. Langridge-Smith, M. D. Morse, R. E. Smalley, *J. Chem. Phys.* **1983**, *78*, 1627.
[22] D. L. Michalopoulos, M. E. Geusic, S. G. Hansen, D. E. Powers, R. E. Smalley, *J. Phys. Chem.* **1982**, *86*, 3914.
[23] P. R. R. Langridge-Smith, M. D. Morse, R. E. Smalley, A. J. Merer, *J. Chem. Phys.* **1984**, *80*, 593.
[24] M. D. Morse, J. B. Hopkins, P. R. R. Langridge-Smith, R. E. Smalley, *J. Chem. Phys.* **1983**, *79*, 5316.
[25] D. L. Michalopolous, M. E. Geusic, P. R. R. Langridge-Smith, R. E. Smalley, *J. Chem. Phys.* **1984**, *80*, 3556.
[26] E. A. Rohlfing, D. M. Cox, A. Kaldor, *J. Chem. Phys.* **1984**, *81*, 3322.
[27] Y. Liu, S. C. O'Brien, Q. Zhang, J. R. Heath, F. K. Tittel, R. F. Curl, H. W. Kroto, R. E. Smalley, *Chem. Phys. Lett.* **1986**, *126*, 215.
[28] D. J. Klein, T. G. Schmalz, T. G. Hite, W. A. Seitz, *J. Am. Chem. Soc.* **1986**, *108*, 1301.
[29] S. C. O'Brien, J. R. Heath, H. W. Kroto, R. F. Curl, R. E. Smalley, *Chem. Phys. Lett.* **1986**, *132*, 99.
[30] L. Euler, *Novi corumentarii academie Petropolitanae 4*, **1752/3**, *109*, 1758.
[31] M. E. Geusic, M. D. Morse, S. C. O'Brien, R. E. Smalley, *Rev. Sci. Inst.* **1985**, *56*, 2123.
[32] M. D. Morse, M. E. Geusic, J. R. Heath, R. E. Smalley, *J. Chem. Phys.* **1985**, *83*, 2293.
[33] Q. L. Zhang, S. C. O'Brien, J. R. Heath, Y. Liu, R. F. Curl, H. W. Kroto, R. E. Smalley, *J. Phys. Chem.* **1986**, *90*, 525.
[34] S. C. O'Brien, J. R. Heath, R. F. Curl, R. E. Smalley, *J. Chem. Phys.* **1988**, *88*, 220.
[35] R. L. Murry, D. L. Strout, G. E. Scuseria, *Int. J. Mass Spectrom. Ion Processes* **1994**, *138*, 113.
[36] P. W. Fowler, D. E. Manolopoulos, *An Atlas of Fullerenes*, Clarendon, Oxford, **1995**.
[37] D. E. Manolopoulos, *Chem. Phys. Lett.* **1992**, *192*, 330.
[38] X. Liu, T. G. Schmalz, D. J. Klein, *Chem. Phys. Lett.* **1992**, *192*, 331.
[39] K.-P. Huber, G. H. Herzberg, *Constants of Diatomic Molecules*, van Nostrand, New York, **1979**.
[40] J. R. Heath, S. C. O'Brien, Q. Zhang, Y. Liu, R. F. Curl, H. W. Kroto, F. K. Tittel, R. E. Smalley, *J. Am. Chem. Soc.* **1985**, *107*, 7779.
[41] F. D. Weiss, J. L. Elkind, S. C. O'Brien, R. F. Curl, R. E. Smalley, *J. Am. Chem. Soc.* **1988**, *110*, 4464.
[42] T. G. Schmalz, W. A. Seitz, D. J. Klein, G. E. Hite, *Chem. Phys. Lett.* **1986**, *130*, 203.
[43] H. W. Kroto, *Nature* **1987**, *329*, 529.
[44] T. G. Schmalz, W. A. Seitz, D. J. Klein, G. E. Hite, *J. Am. Chem. Soc.* **1988**, *110*, 1113.
[45] X. Liu, D. J. Klein, T. G. Schmalz, W. A. Seitz, *J. Comput. Chem.* **1991**, *12*, 1252.
[46] W. Krätschmer, L. D. Lamb, K. Fostiropoulos, D. R. Huffman, *Nature* **1990**, *347*, 354.
[47] R. Taylor, J. P. Hare, A. K. Abdul-Sada, H. W. Kroto, *J. Chem. Soc. Chem. Commun.* **1990**, *20*, 1423.
[48] A. Léger, L. d'Hendecourt, L. Vertraete, W. Schmidt, *Astron. Astrophys.* **1988**, *203*, 145.
[49] A. Léger, L. d'Hendecourt, L. Vertraete, W. Schmidt in *Quasicrystals, Networks, Molecules of Fivefold Symmetry* (Ed.: I. Hargattai), VCH, New York, **1990**, pp. 247–255.
[50] R. F. Curl in *Buckminsterfullerenes* (Eds.: W. E. Billups, M. A. Ciufolini), VCH, New York, **1993**, pp. 1–20.
[51] R. E. Haufler, Y. Chai, L. P. F. Chibante, M. R. Fraelich, R. B. Weisman, R. F. Curl, R. E. Smalley, *J. Chem. Phys.* **1991**, *95*, 2197.
[52] J. Fulara, M. Jakobi, J. P. Maier, *Chem. Phys. Lett.* **1993**, *211*, 227.
[53] M. Frenklach, D. W. Clary, J. W. C. Gardiner, S. E. Stein in *Twentieth Symposium (International) on Combustion*, The Combustion Institute, **1984**, pp. 887–901.
[54] M. Frenklach, L. B. Ebert, *J. Phys. Chem.* **1988**, *92*, 561.
[55] L. B. Ebert, *Science* **1990**, *247*, 1468.
[56] R. M. Baum in *Chem. Eng. News* **1990** (February 5), p. 30.
[57] P. Gerhardt, S. Löffler, K. H. Homann, *Chem. Phys. Lett.* **1987**, *137*, 306.
[58] P. Gerhardt, S. Löffler, K. H. Homann in *Twenty-Second Symposium (International) on Combustion*, The Combustion Institute, **1989**, p. 395.
[59] T. Baum, S. Löffler, P. Weilmünster, K. H. Homann in *ACS Div. Fuel Chem. Prepr., Vol. 36* **1991**, p. 1533.
[60] T. Baum, S. Löffler, P. Löffler, P. Weilmünster, K. H. Homann, *Ber. Bunsen-Ges. Phys. Chem.* **1992**, *96*, 841.
[61] J. B. Howard, J. T. McKinnon, Y. Makarovsky, A. Lafleur, M. E. Johnson, *Nature* **1991**, *352*, 139.
[62] J. T. McKinnon, W. L. Bell, R. B. Barkley, *Combust. Flame* **1992**, *88*, 102.
[63] J. B. Howard, A. L. Lafleur, Y. Makarovsky, S. Mitra, C. J. Pope, T. K. Yadav, *Carbon* **1992**, *30*, 1183.
[64] K. D. Chowdhury, J. B. Howard, J. B. VanderSande, *J. Mater. Res.* **1996**, *11*, 341.
[65] C. J. Pope, J. A. Marr, J. B. Howard, *J. Phys. Chem.* **1993**, *97*, 11001.
[66] F. W. Lam, J. P. Longwell, J. B. Howard in *Twenty-Third Symposium (International) on Combustion*, The Combustion Institute, **1991**, p. 1477.
[67] Note added in proof: Foing and Ehrenfreund have proposed that the two matrix lines observed are a good match for the DIBs observed at 9577 and 9632 Å. B. H. Foing, P. Ehrenfreund, *Astron. Astrophys.* **1997**, *317*, L59.

Not a creature from a science-fiction novel but something which has to do with the setting of many such stories—the cosmos.

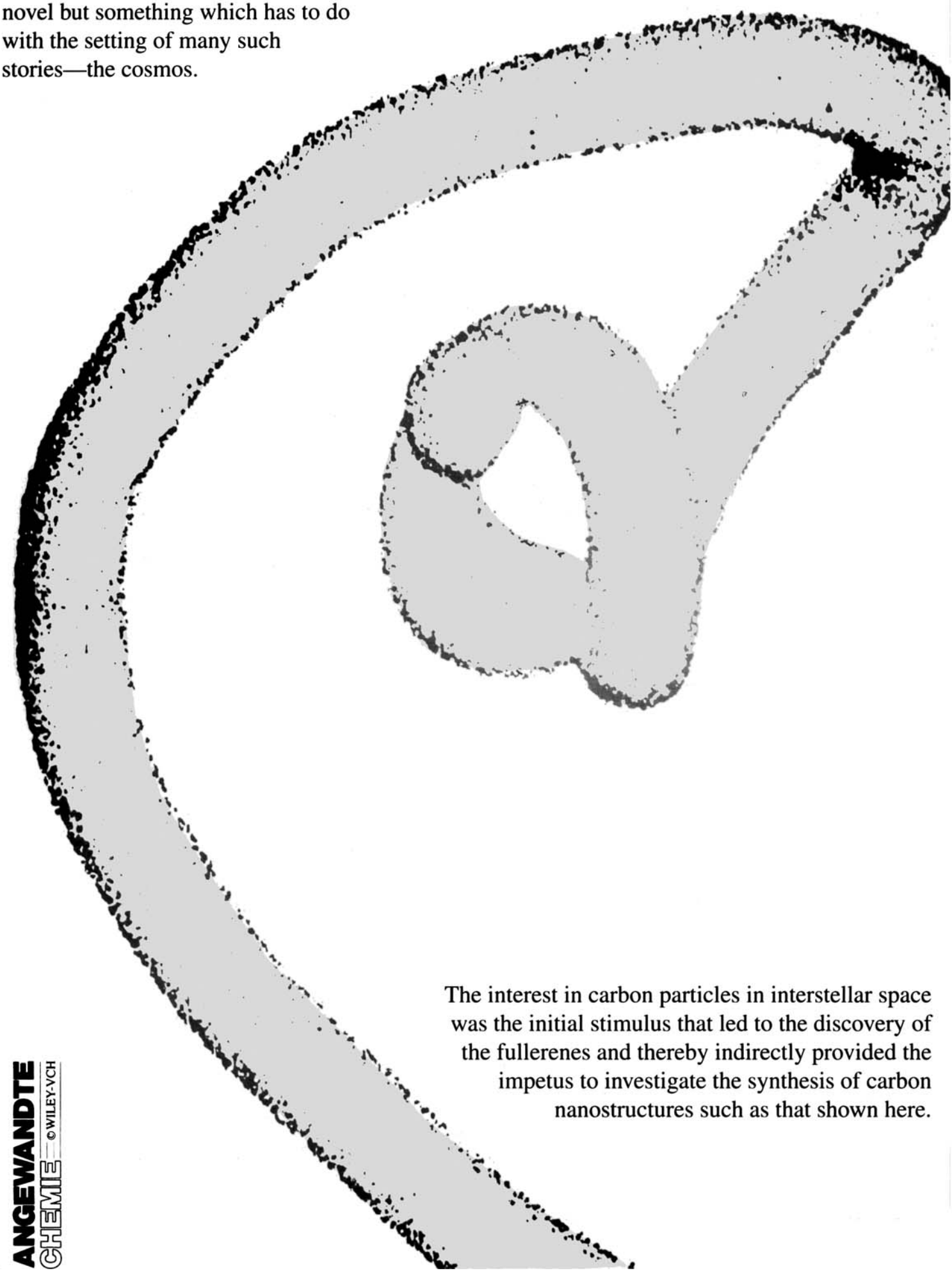

The interest in carbon particles in interstellar space was the initial stimulus that led to the discovery of the fullerenes and thereby indirectly provided the impetus to investigate the synthesis of carbon nanostructures such as that shown here.

ANGEWANDTE CHEMIE
©WILEY-VCH

Symmetry, Space, Stars, and C_{60} (Nobel Lecture)**

Harold Kroto*

Introduction: A Summary of the Key Phases in the Birth of the Fullerenes

The story of the discovery C_{60} buckminsterfullerene (Figure 1) and the birth of fullerene science consists of several disparate strands which came together over ten days in September 1985. During this period of feverish activity, working with Jim Heath, Sean O'Brien, Yuan Liu, Bob Curl, and Rick Smalley at Rice University in Texas, evidence was found that a C_{60} molecule self-assembled spontaneously from a hot nucleating carbon plasma.[1] The molecule had however a prehistory: The earliest paper that describes the C_{60} molecule is to be found in Kagaku (in Japanese) where Eiji Osawa in 1970 suggested that it should be stable[2] and the following year discussed its possible aromatic properties in more detail in a book with Yoshida.[3] Bochvar and Gal'pern published a theoretical study in 1973.[4, 5] Somewhat earlier in 1966 David Jones had conjectured that if pentagonal disclinations could be introduced among the hexagons in a graphene sheet, the sheet would close into a hollow balloon.[6, 7] We however did not know about this prehistory and none of us had ever heard of such a molecule or thought about it.

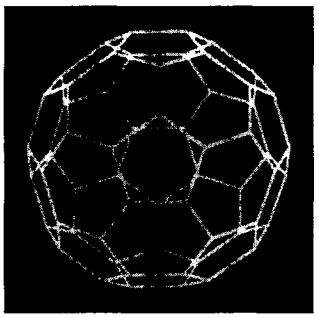

Figure 1. C_{60} buckminsterfullerene [1].

In retrospect, as far as I was concerned, I seem to have been fascinated by various peculiar aspects of carbon chemistry for much of my research career. With the perspective of hindsight my involvement can be split into five phases: At Sussex, in the late 1960s, David Walton and I initiated a synthetic/spectroscopic study (Phase I) which led directly—in the mid 1970s—to some unexpected discoveries (with colleagues at Sussex and NRC Ottawa, Canada) of long carbon chain molecules in the interstellar medium (Phase II). At about this time Don Huffman and Wolfgang Krätschmer were developing laboratory experiments which focused on the composition of the particulate carbon material which occupies the same interstellar regions—indeed the agents which caused the scattering in the dark regions and observed some intriguing new unexplainable features in the 220 nm region of their laboratory data. Also at about this time Richard Smalley was developing a range of advanced chemical physics techniques, which culminated in an ingenious apparatus that enabled small clusters of *refractory* materials to be created and probed for the first time. This was the pulsed supersonic nozzle–laser vaporization apparatus.[8] It is my view that the raison d'etre of this machine was to discover C_{60}.

It was the marriage of ideas resulting from the discoveries of carbon chains in space with the recognition that the cluster beam technique might offer laboratory support for their circumstellar origin that in 1985 resulted in the serendipitous discovery that the C_{60} molecule not only existed but that it self-assembled (Phase III).[1, 9] After this revelation it still remained for unequivocal proof of the soccerball structure to be obtained (Phase IV). Several groups made important contributions: 1) Theoreticians, who had a field day and came up with some results that ultimately proved crucial for the extraction,[10, 9] 2) the Rice group (initially in collaboration with Sussex)[11, 12, 9], 3) the Sussex Group,[13, 9] 4) the IBM group,[14] and last but not least 5) the Heidelberg/Tucson group who succeeded in the first extraction of macroscopic quantities of C_{60}.[15–17] It was this fantastic breakthrough that has made the explosive growth of fullerene science possible (Phase V). The advance made by Krätschmer and Huffman and their students is one of the most beautiful pieces of fundamental science.

In any complex story, the events can only be understood by reference to the complete set of personal subjective accounts of the participants—even purportedly objective accounts must be treated with skepticism.[18] In this case *all* the scientists—including research students—played crucial roles in the story. This article describes parts of the story to which Sussex researchers made contributions. There have now been numerous accounts ranging from the personal articles[19–22] as well as books by Baggott,[23] Aldersey-Williams,[24] Krätschmer and Schuster,[25] Dettman,[26] and Ball.[27] An excellent text focusing on the chemistry of C_{60} is that by Hirsch.[28] Several compendia have been published—some edited by or with Sussex researchers include one with a historical perspective,[29] a second from the viewpoint of carbon materials and physics,[30] and a third which concentrates on fullerene chemistry.[31] It should also be recognized that the discovery of C_{60} led to a further amazing ad-

[*] Prof. Sir H. W. Kroto
School of Chemistry, Physics and Environmental Science
University of Sussex
Brighton, BN1 9QJ (UK)
Fax: Int. code +(1273)678-097
e-mail: krotoa sussex.ac.uk

[**] Copyright The Nobel Foundation 1997. We thank the Nobel Foundation, Stockholm, for permission to print this lecture.

vance—this was the discovery by Iijima that carbon nanotubes also form at the same time as C_{60}.[32]

The story of C_{60} also cannot be recounted without reference to its beauty which results from the incredible symmetry. Another important aspect of the molecule's aura lies in the name buckminsterfullerene,[33] and the direct association it has with the geodesic domes designed by Buckminster Fuller.[34–36] It invests this elegant molecule with a charisma that has fascinated scientists, delighted lay people, and has infected children with a new enthusiasm for science, and in particular it has given chemistry a new lease of life.[37]

Prologue: Symmetry, the Key to the Theory of Everything

Symmetry appears to be fundamental to our perception of the physical world and it also plays a major role in our attempts to explain everything about it. As far as structural symmetry is concerned it goes back to ancient times, as indicated by the (pre-)Platonic structures exhibited in the Ashmolean Museum in Oxford.[38, 39] The most famous examples are of course to be found in "The Timaeus" where in the section relating to "The Elements" Plato says: "In the first place it is clear to everyone(!) that fire, earth, water, and air are bodies and all bodies are solids"(!!).[40] Plato goes on to discuss chemistry in terms of these elements and associates them with the four Platonic solids (only four at that time—until Hippasus discovered the fifth—the dodecahedron).

Although this may at first sight seem like a somewhat naive philosophy it indicates a very deep understanding of the way Nature actually functions. A curiously close contempory analogue of this ancient assumption is to be found in the historially important article by Van Vleck[41] on which almost all of modern molecular spectroscopy is based: Van Vleck says:

> "Practically everyone(!) knows that the components of total angular momentum (NB the angular momentum operator is usually denoted by the symbol $\boldsymbol{J}$ and the associated quantum number by j) of the molecule relative to the axes X,Y,Z fixed in space satisfy the commutation relation of the form
>
> $$J_X J_Y - J_Y J_X = \mathrm{i}J_Z \quad (1)$$
>
> Klein discovered the rather surprising fact that when total angular momentum is referred to axes mounted in the molecule which we will denote by x,y,z the sign of i in the commutation relation is reversed ie
>
> $$J_x J_y - J_y J_x = -iJ_z" \quad (2)$$

Does practically everyone know this?—I wondered whether to check this claim out by asking everyone on the main street in Brighton whether they did. I hardly knew—or more accurately—really understood the first relation, let alone the second. However, I did know that angular momentum was quantized and governed by the fundamental relations (3) and (4), which means that J has $2j+1$ possible orientations, and which indicates that when a transition occurs, j may only change by one unit or on occasion remain unchanged.

$$<j|\boldsymbol{J}^2|j> = \hbar^2 j(j+1) \quad (3)$$

$$M_j = -j \ldots +j \quad (4)$$

$$\Delta j = 0, \pm 1 \quad (5)$$

I knew that the row structure of Mendeleev's periodic table could be explained on the basis of these quantum properties of angular momentum, in particular the fact that a system with angular momentum j possesses $2j+1$ quantized orientations. I decided I ought to understand these and under the tutelage of Jon Hougen and Jim Watson I dived into the *Theory of Atomic Spectra* by Condon and Shortley.[42] There can surely be no more elegant printed page in the sciences or the arts than page 60 of this book (Figure 2), where Dirac's proof of the $\Delta j = \pm 1$ selection rule (it is noncommittal on $\Delta j = 0$) is presented—a perfect example of elegant and powerful use of roman typeface. One only has to look at this page to know that it must be important. As far as I was concerned it planted the desire to understand the embedded theory—the effort was (for me) considerable, but worth it and remains one of the most intellectually rewarding tasks I have undertaken. Having finally grasped the implications of these relations, I ended up writing a book called *Molecular Rotation Spectra*,[43] which deals with the way the angular momentum relations govern the rotational dynamics of molecules.

The geometric pattern of the periodic table (Figure 3) is an implicit result of the angular momentum description of atoms and electrons (together with a few odds and ends(!) such as the Pauli exclusion principle). Any intelligent life on another planet that had developed an understanding of chemistry would almost certainly recognize it. The electron angular momentum wavefunctions are described in terms of spherical harmonics—known by mathematicians long before 1925 when quantum mechanics was created and thus these symmetric mathematical functions lend an elegant beauty to the abstract description of rotational/orbital motion of atoms, molecules and, of course, electrons. Thus, we discover that symmetry principles underpin the elegant quantum mechanical description of atoms and mol-

Harold W. Kroto was born in 1939 in Wisbech, Cambridgeshire, UK. He studied at the University of Sheffield from 1958 to 1964 and received his PhD for his research in the electronic spectroscopy of free radicals with R. N. Dixon. After three years of postdoctoral research at the National Research Council in Ottawa and Bell Laboratories, he started his acedemic career in 1967 at the University of Sussex in Brighton, where he still works. In 1985 he became Professor of Chemistry there and in 1991 Royal Society Research Professor. His research interests include the spectroscopy of unstable species, carbon and metal clusters, and microparticles, as well as interstellar molecules and circumstellar dust. Graphic design is his other passion. In 1995 he was knighted for his services to chemistry.

60 ANGULAR MOMENTUM 83

Another important fact which follows immediately from 12²6 is that the scalar product of any two vectors* which satisfy this commutation rule with respect to $\boldsymbol{J}$ will commute with J_x, J_y, J_z, and hence with $\boldsymbol{J}^2$:

$$[\boldsymbol{J}, \boldsymbol{T}_1\cdot\boldsymbol{T}_2]=0, \quad [\boldsymbol{J}^2, \boldsymbol{T}_1\cdot\boldsymbol{T}_2]=0. \tag{4}$$

This is independent of whether $\boldsymbol{T}_1$ commutes with $\boldsymbol{T}_2$ or not.

We shall now consider the problem of obtaining the matrices of T_x, T_y, T_z in a representation in which $\boldsymbol{J}^2$, J_z, and a set A of observables which commute with $\boldsymbol{J}$ are diagonal. We shall first obtain a selection rule on j, i.e. a condition on $j'-j$ necessary for the non-vanishing of a matrix component connecting the states j and j'. This we may do by a method outlined by Dirac (p. 158).

Using the relation 12²6, we find that

$$\begin{aligned}[\boldsymbol{J}^2, \boldsymbol{T}]&=\boldsymbol{J}\cdot[\boldsymbol{J}, \boldsymbol{T}]-[\boldsymbol{T},\boldsymbol{J}]\cdot\boldsymbol{J}=-i\hbar(\boldsymbol{J}\cdot\boldsymbol{T}\times\mathfrak{J}-\boldsymbol{T}\times\mathfrak{J}\cdot\boldsymbol{J})\\&=-i\hbar(\boldsymbol{J}\times\boldsymbol{T}-\boldsymbol{T}\times\boldsymbol{J})=-2i\hbar(\boldsymbol{J}\times\boldsymbol{T}-i\hbar\boldsymbol{T}).\end{aligned}$$

From this we have

$$\begin{aligned}[\boldsymbol{J}^2,[\boldsymbol{J}^2, \boldsymbol{T}]]&=-2i\hbar[\boldsymbol{J}^2,(\boldsymbol{J}\times\boldsymbol{T}-i\hbar\boldsymbol{T})]=-2i\hbar\{\boldsymbol{J}\times[\boldsymbol{J}^2, \boldsymbol{T}]-i\hbar[\boldsymbol{J}^2, \boldsymbol{T}]\}\\&=-2i\hbar\{-2i\hbar\boldsymbol{J}\times(\boldsymbol{J}\times\boldsymbol{T}-i\hbar\boldsymbol{T})-i\hbar(\boldsymbol{J}^2\boldsymbol{T}-\boldsymbol{T}\boldsymbol{J}^2)\}\\&=2\hbar^2(\boldsymbol{J}^2\boldsymbol{T}+\boldsymbol{T}\boldsymbol{J}^2)-4\hbar^2\boldsymbol{J}(\boldsymbol{J}\cdot\boldsymbol{T}),\end{aligned}$$

using 12²11a to expand $\boldsymbol{J}\times(\boldsymbol{J}\times\boldsymbol{T})$. But

$$[\boldsymbol{J}^2,[\boldsymbol{J}^2, \boldsymbol{T}]]\equiv[\boldsymbol{J}^2,(\boldsymbol{J}^2\boldsymbol{T}-\boldsymbol{T}\boldsymbol{J}^2)]\equiv\boldsymbol{J}^4\boldsymbol{T}-2\boldsymbol{J}^2\boldsymbol{T}\boldsymbol{J}^2+\boldsymbol{T}\boldsymbol{J}^4.$$

Hence

$$\boldsymbol{J}^4\boldsymbol{T}-2\boldsymbol{J}^2\boldsymbol{T}\boldsymbol{J}^2+\boldsymbol{T}\boldsymbol{J}^4=2\hbar^2(\boldsymbol{J}^2\boldsymbol{T}+\boldsymbol{T}\boldsymbol{J}^2)-4\hbar^2\boldsymbol{J}(\boldsymbol{J}\cdot\boldsymbol{T}). \tag{5}$$

Take the matrix component of this equation referring to the states $\alpha\, j\, m$ and $\alpha'\, j'\, m'$, where $j'\neq j$. Since $\boldsymbol{J}\cdot\boldsymbol{T}$ commutes with $\boldsymbol{J}$ [by (4)], this component will vanish for the last term in the equation. From the rest we obtain:

$$\begin{aligned}\hbar^4[j^2(j+1)^2-2j(j+1)j'(j'+1)+j'^2(j'+1)^2](\alpha j m|\boldsymbol{T}|\alpha' j' m')\\=2\hbar^4[j(j+1)+j'(j'+1)](\alpha j m|\boldsymbol{T}|\alpha' j' m').\end{aligned}$$

The bracket on the left is

$$[j(j+1)-j'(j'+1)]^2=(j-j')^2(j+j'+1)^2,$$

while

$$2[j(j+1)+j'(j'+1)]=(j+j'+1)^2+(j-j')^2-1.$$

Hence

$$[(j-j')^2(j+j'+1)^2-(j+j'+1)^2-(j-j')^2+1](\alpha j m|\boldsymbol{T}|\alpha' j' m')=0,$$

or

$$[(j+j'+1)^2-1][(j-j')^2-1](\alpha j m|\boldsymbol{T}|\alpha' j' m')=0. \qquad (j\neq j')$$

In order to obtain a non-vanishing matrix component one of the brackets must vanish. The first cannot since $j'\neq j$ and $j, j'\geq 0$. The second vanishes only when $j'-j=\pm 1$. Hence for a non-vanishing matrix component we must have

$$j'-j=0, \pm 1. \tag{6}$$

* An important special instance of this is the square of such a vector.

Figure 2. Page 60 of Condon and Shortley's book [42] in which Dirac's elegant derivation of the fundamental selection rule for j, the angular momentum quantum number, is given (published by permission of Cambridge University Press). These relations not only describe a beautiful example of the way Nature behaves but also are an exquisite example of man's mathematical invention to describe the behavior, as well as an elegant example of typeface which visually evokes a powerful feeling for the underlying abstract concept. Buried deep in this derivation are fundamental laws of symmetry that govern the way in which light interacts with matter. These relations govern the origin of the sunlight falling on this page, the modulation of that light by the page and the print on it, as well as the way in which the receptors in your eye detect the reflected light and transforms it into perceived images in your brain. By the way, it may be worth noting that not only does this paper consist mainly of carbon but so also does the ink.

ecules in an abstract picture in which statics and dynamics are paradoxically conflated in a way that often leaves us hovering on the boundary between abstract mathematical understanding and literal physical misunderstanding. It is the existence of similar abstract aspects of symmetry that has invested the C_{60} molecule with a charismatic quality that few other molecules possess.

Phase I: Carbon, Still Crazy After All These Years

Carbon is really peculiar—in fact, the fact that there is enough carbon around in the universe to allow enough biology to occur and result in the human race at all is due to peculiarities

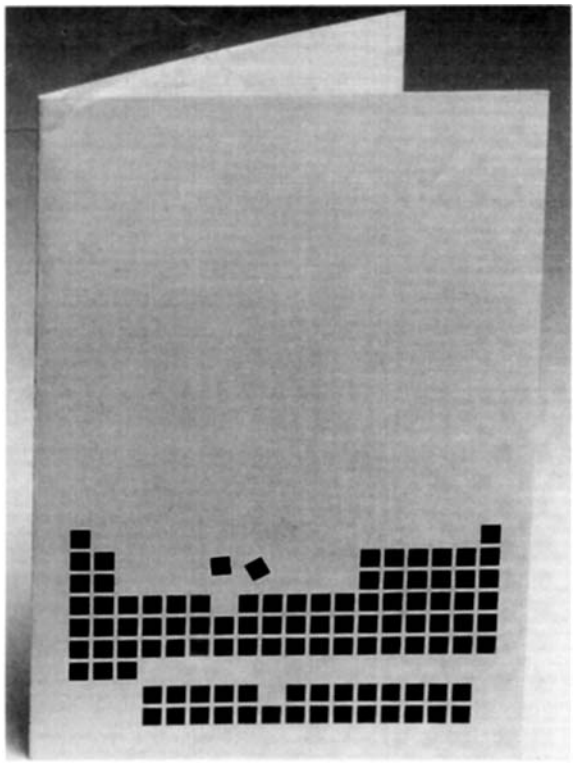

Figure 3. This item was designed by the author for a conference. It is left to the reader to deduce the topic of the conference and also the nature of item depicted. The answers may be in *The Hitchhiker's Guide to the Galaxy*.

in the nuclear chemistry of carbon. The "molecular" chemistry of carbon is no less peculiar. Even if we discount the whole of organic chemistry, the inorganic chemistry of carbon is also amazing. I worked with carbon-containing species right from the start when I was a graduate student with Richard Dixon at Sheffield. My first (successful) research project was a study of the electronic spectrum of the diatomic free radical CBr in which we also explored the intrinsic nature of the bond that the carbon atom formed with halogens.[44] Even more interesting was a preliminary (aborted) study of the fascinating molecule carbon suboxide OCCCO. The most interesting aspect of this molecule was the fact that it did not seem to know whether it wanted to be a linear or bent. The triatomic molecule C_3 was no less odd, exhibiting similar structural schizophrenia. The identification of C_3 in comets and flames, in the elegant historical study by Alec Douglas,[45] was a landmark in spectroscopy which added to the ubiquitous charismatic attraction of carbon species on earth as well as in space.

When I arrived at Sussex in 1967, after two years at NRC (Ottawa) and a year at Bell Labs (Murray Hill) I set up a microwave spectroscopy research program which aimed at the creation of new molecules that contained multiple bonds between carbon and various second or third row atoms,[46] for example sulfur (C=S, C=Se), phosphorus (C=P, C=P), and Si (C=Si). At this time the so-called double bond rule—*multiple bonds involving non first-row elements should not exist*—appeared to have some validity. However the stability of CS_2 indicated that the embargo was not total. Most importantly, as far as I was concerned, I became fascinated (while a postdoc at NRC in Canada) by the molecule HC≡P which Gier had made

in 1961.[47] I became convinced that the existence of this molecule (which incidently was produced spontaneously by a carbon arc in phosphine(!)) implied the existence of derivatives such as ClC≡P and $CH_3C{\equiv}P$. I also wondered whether these species could be used as synthons to create organic phosphorus cycloaddition products (analogues of the nitrogen heterocyclic compounds) as well as metal complexes that parallel those of the metal–nitrile complexes.

The first new molecules that we (Barry Landsberg, Krini Georgiou, Roger Suffolk, and myself) created possessed carbon–sulfur double bonds,[46] such as $CH_3CH{=}S$ (thioacetaldehyde), $CH_2{=}C{=}S$ (thioketene), and $CH_2{=}CH{-}CH{=}S$ (thioacrolein). They were created by thermolysis of custom-synthesized precursors and analyzed by both microwave and photoelectron spectroscopy. After the success with sulfur, it seemed that the same techniques might also work for phosphorus and, encouraged by Gier's HC≡P result of some dozen years previously, we tried it—and it worked like a dream![46]

With my Sussex colleague John Nixon, together with Nigel Simmons and Nick Westwood, Osamu Ohashi, Keichi Ohno and James Burkett St Laurent we produced a whole range of these species. With Colin Kirby and Terry Cooper we also produced some elegant boron–sulfur XB=S analogues.[46] $CH_2{=}PH$ was my favourite as it was the first (and simplest) molecule with a carbon–phosphorus double bond. Our first paper on $CH_2{=}PH$, $CH_2{=}PCl$, and $CF_2{=}PH$[48] and the paper by Becker, also on the creation of C=P-containing species,[49] appeared almost simultaneously. Our successful creation of $CH_3C{\equiv}P$[50] was almost equally exciting as it was the first analogue of HC≡P. It still seems amazing that Gier's 1961 result had not been recognized sooner by anyone else as a clear sign that a whole new class of compounds was just waiting to be discovered. The creation and structural determination of species such as $CH_2{=}PH$ and $CH_2{=}PCl$ (Figure 4), as well as

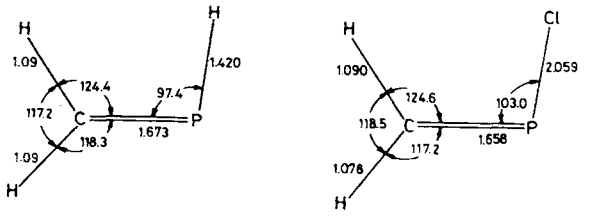

Figure 4. The structures of the first phosphaalkenes created, $CH_2{=}PH$ and $CH_2{=}PCl$, as determined by microwave spectroscopy [46, 48].

$CH_3C{\equiv}P$ and other related species, were (for me) some of our most exciting advances.[46] Since these papers were published these compounds, which we call phosphaethenes and phosphaethynes, have become the basis of some most fruitful fields of new chemistry. However, we never got to grips with the carbon–silicon double bond—a problem solved by others—as our interests led in other directions.

During this time (around 1970) my colleague David Walton was perfecting techniques for synthesizing very long linear chains of carbon atoms.[51–53] These molecules appeared like perfect test-beds for the quantum mechanical study of the dynamics of bending and rotation in simple linear systems. In 1972, as luck would have it, David and I proposed a project for the Chemistry by Thesis (CT) course at Sussex which aimed at probing such structural and dynamic behavior of moderately long carbon chains. The CT course had been initiated by Colin Eaborn[54] as a new approach to undergraduate teaching in which a BSc degree could be obtained on the basis of a thesis which the student would write on a research topic carried out under the supervision of two tutors from different chemistry disciplines (for example synthetic chemistry and spectroscopy). The course recognized that the traditional examination approach to the assessment of a student's ability—and in particular future capability—was an artificial and often unsatisfactory guide.

The course was unique to Sussex and produced a long stream of highly accomplished graduates with remarkably few who did not do well on the course. It *was* one of the numerous outstanding success stories of Chemistry at Sussex. I highlight *"was"* because the course has now been legislated out of existence by the combined efforts of Health and Safety Executive officials, lawyers, and misguided university administrators. This is an archetypal example of how a disparate mix of uncorrelated antagonists—each focused on individual goals with no perception of the true overall consequences can achieve negative results. A similar mix of advisors and officials in the secondary education sector has all but eliminated any real chemistry from the UK school curriculum. Today, students with any real chemical facility are virtually an extinct species.

Andrew Alexander was the outstanding student catalyst of the research project that aimed at the synthesis of a range of polyynes in particular HC_5N and their analysis by IR, NMR, and in particular microwave spectroscopy.[55, 46] In fact it was Alex's keeness in the first place that got the project going and his enthusiasm for the work, in the second place, which played a key role in its success. The start of the Sussex role in the story of C_{60} is really to be found in this project. It was the epitome of basic research and in these times when the mania for applied research is rampant, it is hard to imagine one less likely to gain support. There is little doubt in my mind that, had this project not been initiated, we at Sussex would not have been involved in the discovery of C_{60}.

HC_5N was the first molecule to be studied at Sussex on the newly arrived Hewlett Packard microwave spectrometer in 1974. This superb instrument enabled the rotational spectra of molecules to be measured with such ease (relative to the home-built instruments that existed in most microwave laboratories at the time). The machine enabled us to concentrate almost all our attention on the demanding chemistry involved in producing new species without worrying about how to optimize the detection parameters. There is no doubt that much of the work we did during the 1970s would have been essentially impossible without this amazing instrument.

Phase II: A Tale of Cold Black Giant Clouds and Warm Red Giant Stars

About the same time that we were creating the long-chain carbon molecules in the laboratory at Sussex, a veritable Pandora's box of molecules had been opened up by Townes and

co-workers[56] who discovered ammonia in the Orion constellation. After this discovery microwavers and radioastronomers joined forces and showed that the vast dark clouds which lie between the stars (Figure 5) harbor scores of molecules

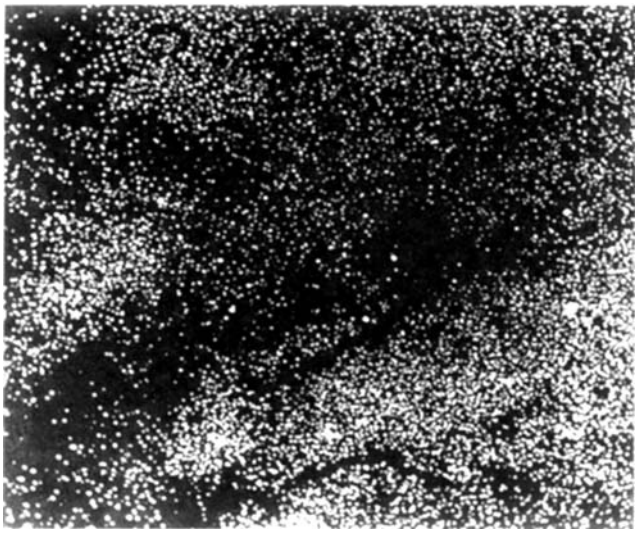

Figure 5. The dark clouds in Taurus from Barnards 1927 survey, *Atlas of Selected Regions of the Milky Way*, (Eds.: E. B. Frost, R Calvert) Carnegie Institute of Washington, **1927**. Heiles Cloud 2 is the dark area in the left-hand bottom corner.

(methanol, carbon monoxide, formaldehyde, ethanol, hydrogen cyanide, formic acid, formamide, etc)—all the molecules the galaxy could possibly need for a primordial pot of prebiotic soup.[57] Furthermore, they were all identified by the detection of their microwave rotational emission spectra using radiotelescopes. Cyanoethyne (or cyanoacetylene to we older guys) HC_3N was also detected[58] and when we made HC_5N I began to wonder whether it might also be present in interstellar space. It seemed like a very long shot at the time because an abundance *rule-of-thumb* had materialized, based on a rough correlation of available empirical data, that suggested that an additional carbon atom would reduce the abundance by approximately a factor of ten, and two extra atoms implied that HC_5N should be down by a factor of 100 from HC_3N and this meant that it would be undetectable. However my view is never to assume anything is right until it has been tested experimentally because, as often as not, assumptions are wrong and even when they are not something unexpected and interesting often happens.

However, the strong bond between laboratory spectroscopy and astrophysics, which goes back at least to Newton's time and perhaps even to antiquity, was again giving birth to yet another major new field—in this case *interstellar astrochemistry*. Molecular radioastronomy was the crucial medium in uncovering the hordes of molecules—indeed it has now shown that the molecules play a crucial role in the collapse of the clouds to form stars. As gravitational attraction causes the interstellar gas clouds to collapse and heat up, rotational transitions (mainly of CO) leak radio energy out allowing further cloud collapse to occur, ultimately to such high pressures and temperatures that new stars and planets can form.

I wrote to my friend Takeshi Oka (we had both been postdoctoral fellows at NRC during the "Golden Years" when NRC had been the outstanding National Research facility) and asked him whether he was interested in searching for HC_5N in space—he turned out to be as keen as I was. Together with NRC astronomers, Lorne Avery, Norm Broten, and John MacLeod, the molecule was detected in the giant molecular cloud SgrB2 towards the galactic center.[59] The discovery was really a surprise because the molecule turned out to be much more abundant than expected—one more example of why one should never let a theoretical assumption deter one from carrying out an experiment.

The next question was clear—was HC_7N present? David Walton worked out a synthesis and Colin Kirby set about the demanding task of synthesizing it and measuring the rotational frequencies.[60] After making it in the laboratory and searching for it in a dark cloud in Taurus (Figure 5) by using the 46-m radio dish in Algonquin Park, Canada, we found that it too was present (Figure 6)[61, 62, 57]—it scarcely seemed possible. This

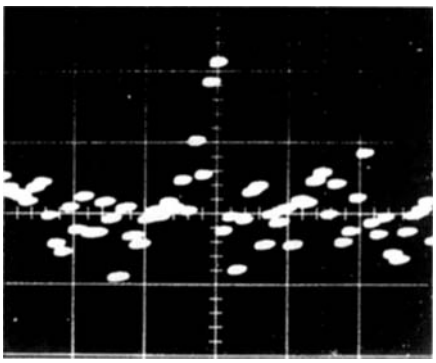

Figure 6. A photograph of the first oscilloscope trace of the radio signal emitted by interstellar HC_7N in Heiles's Cloud 2 in the constellation of Taurus (see Figure 5).

family of molecules was making total nonsense of the abundance *rule-of-thumb* that almost all other families of molecules appeared to follow. Then, just as we at Sussex were about to attempt the daunting task of synthesizing HC_9N, Takeshi found a clever way of estimating its rotational frequencies by extrapolation from the known frequencies of the set HC_nN ($n = 1,3,5,7$);[63] and we detected it as well.[64] These were then the longest and heaviest molecules conclusively detected in space—and still remain so nearly 20 years later. From these discoveries it became clear that there was a problem: The ion–molecule reaction theories of Klemperer, Herbst, Dalgarno, and Black,[65, 66] which accounted almost perfectly for almost all the other species observed were just not able to account for the high abundances such long carbon chains. It seemed to me that some alternative source was needed and fortunately a possible answer started to appear. As time progressed cool red giant carbon stars, such as the fascinating object IRC +10216,[67] were found to be pumping the chain molecules out into the interstellar medium.

Phase III: Ten Days in September 1985

During the early 1980s Robert Curl visited my laboratory at Sussex and invited me to come to Rice University in Houston at

some time in the future. During Easter 1984, just after attending the conference on molecular structure that Jim Boggs organized biennialy in Austin, I took up the invitation and visited Rice. Apart from this superb conference another good reason for going to Texas is that there are excellent "Half-Priced Bookstores" in Austin, Houston, and Dallas. When I arrived in Houston, Bob was enthusing about a very recent result that Rick Smalley and his group had just obtained. They had shown that SiC_2 was triangular[68]—a fascinating result. The way in which the Si had avoided forming a classical double bond in this species, at a stroke, explained why we had had so much difficulty observing molecules with Si=C bonds. It also fitted in nicely with the flexibility of C_3 and OC_3O which I had studied years before. I went over to Rick's laboratory where he enthusiastically described how his cluster beam machine worked. He explained how a pulsed laser, focused on a metal disc vaporized material to produce atoms which were swept up by pulses of helium which caused clustering and concomitant cooling. Then by, expansion through a nozzle into a vacuum, they are cooled further and by skimming into a pulsed beam which is analyzed by a time-of-flight mass spectrometer the cluster mass distributions can be ascertained. As Rick described the mode of operation, it reminded me of previous work on carbon clusters, particularly by Hintenberger and co-workers,[69] and I began to wonder whether, by substituting the metal target disc by a graphite one, the plasma produced by the laser might simulate the circumstellar shell of the cool red giant carbon stars such as IRC +10216 and produce the carbon chains. This would give strong support for the stellar solution to the chain problem and provide an important alternative mechanism to the ion–molecule schemes.

As that day wore on, I thought more-and-more about the idea and became more-and-more convinced that Rick's apparatus was the key to proving a circumstellar source of the chains. Furthermore the detection of the spectrum of SiC_2 suggested that the apparatus might be able to confirm the conjecture of Alec Douglas[70] that the carbon chains might be carriers of the diffuse interstellar bands (DIBs).[71] The DIBs are interstellar spectroscopic features that have puzzled astronomers and spectroscopists since the 1930s. That night I described these ideas to Bob who was keen to collaborate—particularly on the second much more difficult DIB problem. In the event, in August 1985, Bob called me at my home in the UK to say that my experiments were to be carried out at Rice imminently and asked whether I was interested in coming to Houston. I didn't need to be asked twice—I dropped everything and within three days I was in Houston.

As soon as I arrived I gave a concentrated two–three hour seminar on all aspects of interstellar molecules and their spectra. I met Jim Heath, Yuan Liu, and Sean O'Brien, the key students with whom I was to work intimately for the amazing ten-day period from September 1st to 10th, 1985. Jim Heath and I struck an instant rapport partly because we are both addicted to books and enjoy browsing in bookstores. So after long stints on the apparatus (Ap2 as Rick affectionately called his second generation cluster beam machine) Jim and I would occasionally play hooky to visit Houston book stores. We would invariably end up, often accompanied by Carmen (Jim's wife) and Sean, late in the night at the House of Pies—a Houston 24-hour coffee bar which served outstanding Dutch apple pie. Apparently (according to a recent TV program on the history of the PC) the founders of COMPAQ hatched their company at the House of Pies.

The experiments began on September 1st, and the good news is that they were successful. Almost immediately we detected the linear molecules with five to nine carbon atoms that we had observed in space,[72] and thus we got the evidence needed for the idea that the chains could easily have originated in red giant stars. The bad news is that an interloper was present. As the results emerged, our attention was quickly attracted by the precocious antics of this uninvited guest. It had 60 carbon atoms and was accompanied by a more diminutive but still fairly prominent partner with 70 carbon atoms. These characters actually had already appeared in a publication some twelve months previously by Rohlfing, Cox, and Kaldor in 1984,[73] and another group, Bloomfield et al. had also been probing their properties.[74] I had actually read the Exxon paper in some detail at the time it appeared because it described almost exactly the experiments I had proposed to the Rice group a few months previously. I had not however been moved to rub 60 brain cells together to devine what might be going on and apparently neither had anyone else. The Exxon group had made the discovery that a new family of carbon clusters with more than 30 atoms existed which appeared only to be even-numbered. Though C_{60} was definitely more prominent than its neighbors, it was not sufficiently prominent to attract any particular attention, and was certainly not dominant as it was after Jim and Sean had finally finished with it.

The stongest peak in the range between 30–100 C atoms of the mass spectrum was usually the peak for C_{60} and it was used to tee up the experimental parameters for these larger species. During these studies, conditions were discovered that gave a distribution in which C_{60} was completely off-scale (Figure 7).

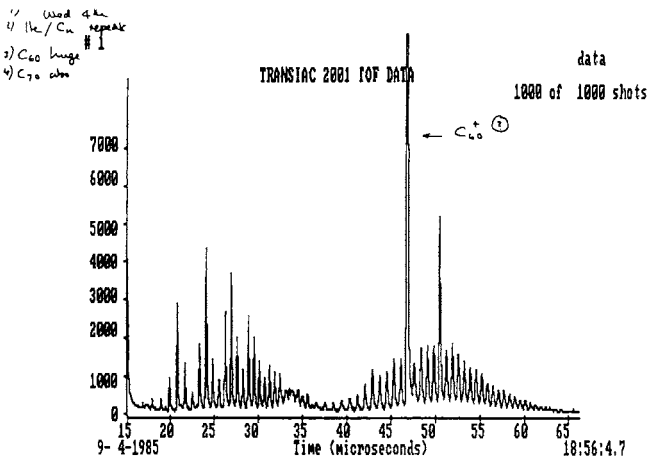

Figure 7. Annotated time-of-flight (TOF) mass spectrum of carbon clusters produced on Wednesday, September 4th, 1985 the day on which the dominance of the C_{60} signal was first recorded (see Figure 8a).

This observation was made on Wednesday, September 4th and our reactions were written up in the lab notebook by the graduate students (Figure 8). Two days later, on Friday, a group meeting took place at which Jim and Sean offered to work over the weekend to optimize conditions. Sean worked that evening

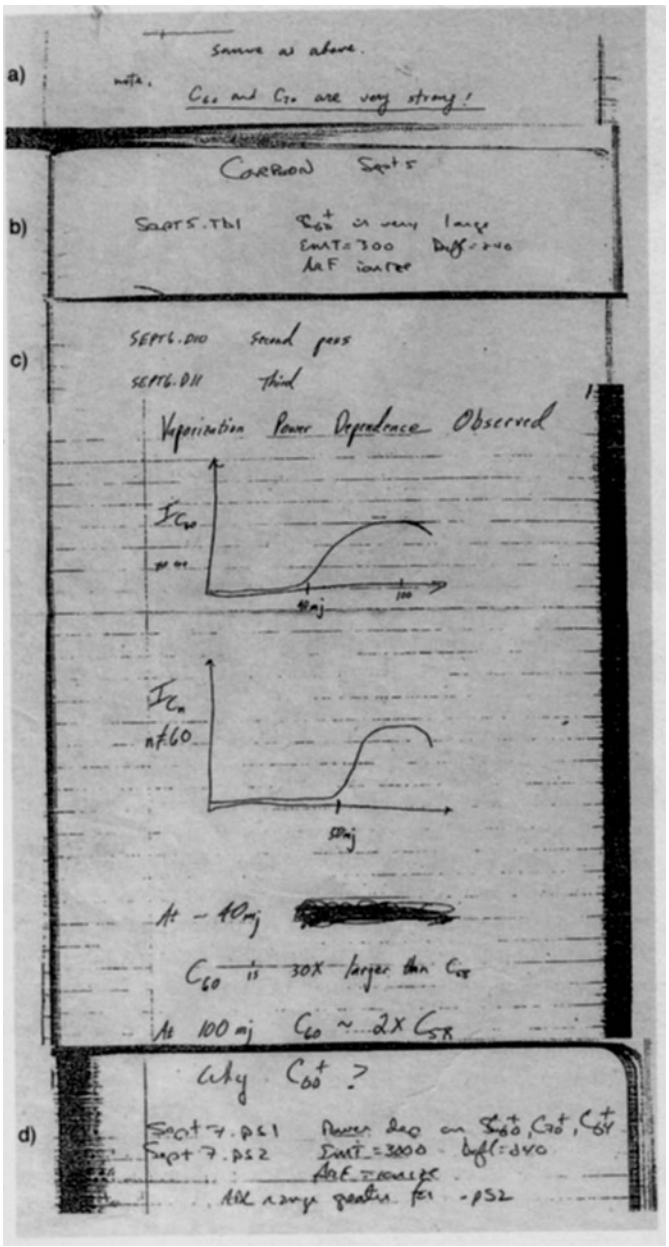

Figure 8. Entries by Heath, Liu, and O'Brien in the Rice Cluster Laboratory Notebook from the period September 4–7, 1985 when key experiments were carried out at Rice University. a) September 4th; b) September 5th; c) September 6th; d) September 7th.

and Jim took over the next day and worked all weekend on the problem of optimizing the signal. By Sunday evening (September 8th) the result was the spectrum shown in Figure 9 which exhibited almost nothing but the C_{60}; with C_{70} as a somewhat smaller but still prominent chaperone.

As C_{60} and its sidekick became the prime focus of our attentions, I began to call these peculiar *wadges* of carbon the Lone Ranger and Tonto or sometimes Don Quixote and Sancho Panza. Our deliberations came to a climax during discussions on Monday, September 9th. C_{60} appeared to be really quite unreactive, a behavior difficult to reconcile with a flat hexagonal graphene sheet—the most obvious first thought that would occur to anyone—which must have some 20 or more dangling bonds. After all, the chains had ends (two) and they added on two H atoms; thus a 60-atom flat hexagonal graphene sheet

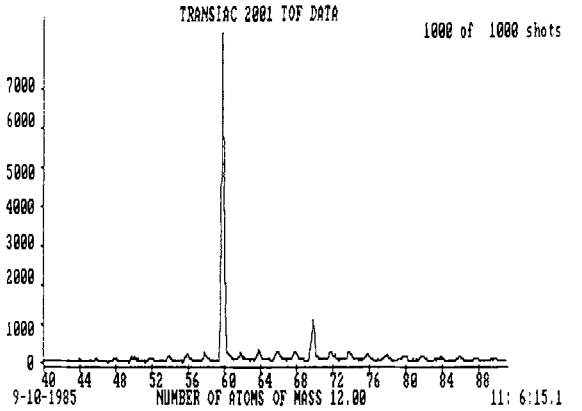

Figure 9. Time-of-flight mass spectrum of carbon clusters under the optimum conditions for the observation of a dominant C_{60} signal obtained by Jim Heath on Monday, September 9th, 1985.

should add on approximately 20 or more H atoms, but it did not. As we sought a solution, we discussed many possible structures that might explain the perplexing results.

Gradually a consensus developed that what might have happened was that flat hexagonal sheets had either formed or ablated from the surface of the graphite disc and closed into a cage, so eliminating the reactive edge. The closed hexagonal cage idea reminded me of a visit with my family to Expo67 in Montreal where Buckminster Fuller's dome had dominated the horizon. It particularly called to mind an image of the dome in an issue of Graphis magazine[75] devoted to the exhibition (Figure 10).

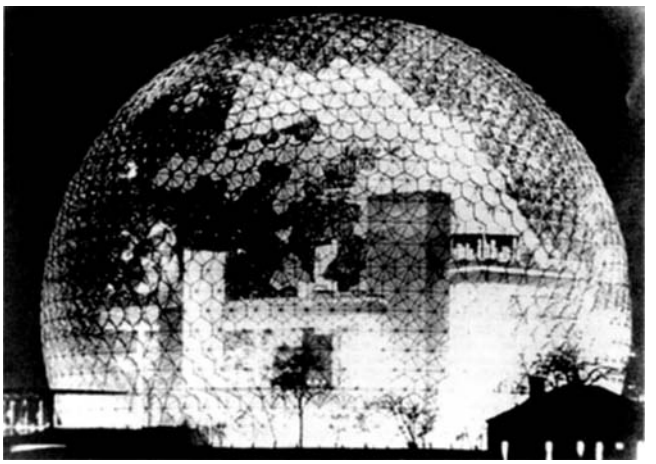

Figure 10. Photograph taken by Michel Proulx of the Geodesic Dome designed by Buckminster Fuller for the U. S. exhibit at EXPO67 in Montreal [75]. One of the pentagons necessary for closure is discernable in this photograph. The variation in the strut lengths of the hexagons in the vicinity of the pentagon, necessary to achieve a relatively smooth round surface, can also be discerned.

Rick went to the Rice Library and extracted a book about Buckminster Fuller and his inventions.[35] I also recalled a "stardome" skymap (Figure 11a), which I had built for my children some years before. I remembered that the stardome had not only hexagons but also pentagons and wondered, as Bob and I went home for lunch, whether I should call my wife at home back in England to check whether or not it had 60 vertices. As I was scheduled to leave for the UK the next day, I invited the team out for dinner at a Mexican Restaurant to celebrate the exciting

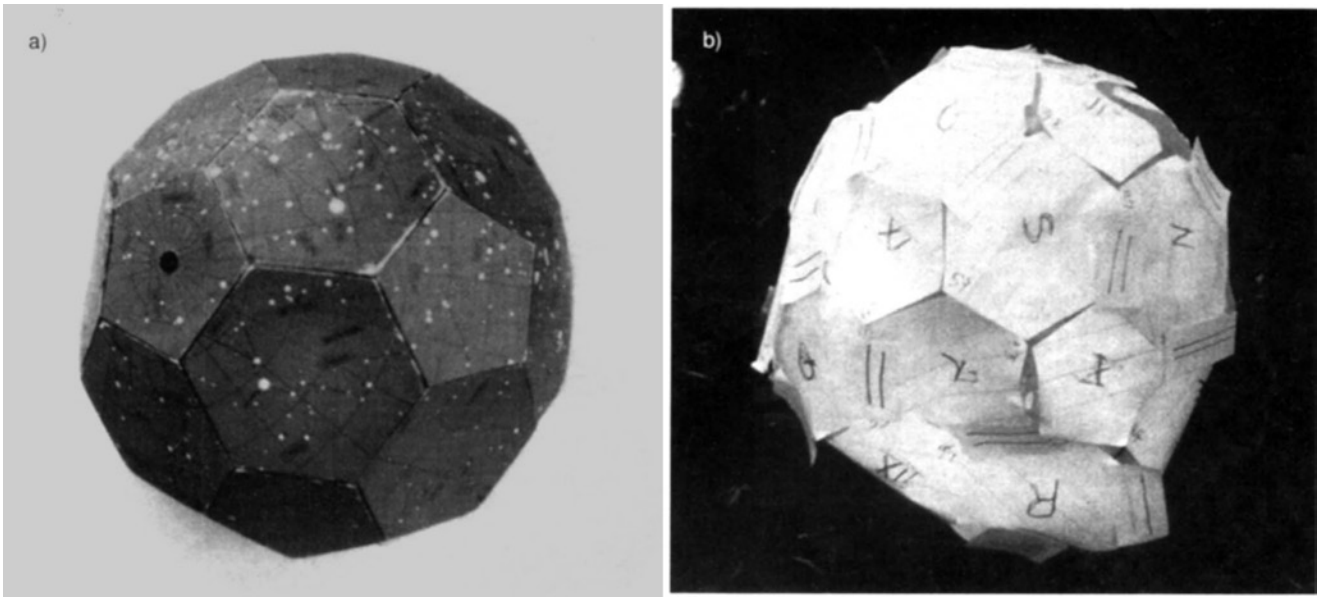

Figure 11. The two card models that played key roles in the positing of the truncated icosahedral structure of C_{60}. a) Stardome map of the sky (Buckminster Fuller patented t-icosahedral, and other polyhedral world-map projections); b) prototype C_{60} made by Smalley. Both models are truncated icosahedra with 60 vertices, 12 pentagonal and 20 hexagonal faces.

discovery. Needless to say we spent all the time at the restaurant trying to solve the puzzle.

That evening/night Rick experimented with sheets of hexagons, Jim together with Carmen experimented with toothpicks and jelly beans, and Bob and I discussed the stardome solution again. Rick could not make any progress until he remembered our discussion of the pentagons in the stardome.[19] Rick discovered that the structure started to curve into a saucer shape as soon as pentagons were included among the hexagons and finally closed as he added a twelfth pentagon. The next morning, when he revealed his paper model (Figure 11b), I remember being ecstatic. It was beautiful and looked just like the stardome (Figure 11a) as I remembered it. It is of course a truncated icosahedron and the fact that it turned out to be a football too was most appropriate. After all, the whole discovery story is an archetypal example of team effort. I remember thinking that the molecule was so beautiful that it just had to be right—and anyway even if it were not, everybody would surely love it, which they did—eventually! My suggestion that we call the molecule buckminsterfullerene (the -ene ending fitted perfectly) was, after some discussion, accepted and we sent off the paper to Nature—the date of receipt was September 13th (note: the experiments had started on September 1st).

Phase IV: Little Fullerenes, Giant Fullerenes, Red Solutions, and One-Line Solutions, or—How to Play Football Without Knowing the Rules

We decided to probe the consequences of the C_{60} discovery and experiments were initiated at Rice.[76] Jim Heath, Sean O'Brien, Yuang Liu, and Qing Ling Zhang were among the most heavily involved students. A series of experiments was also initiated at Sussex: With Tony Stace, a cluster beam machine was constructed by a highly dedicated set of students (Simon Balm, Richard Hallett, and Wahab Allaf) and we thus started to probe cluster behavior in general. With the aid of support from British Gas (through Steve Wood) we also started to probe the implications of our discovery for combustion.

One of the most charismatic things about C_{60}, and one which continually lay simmering in the back of my mind, was the fact that all the carbon atoms in C_{60} are equivalent and so the ^{13}C NMR spectrum should consist of but a single elegant line. However, how could one make enough to measure it?. That was a daunting task and I must admit that whenever my thoughts drifted onto this subject they invariably ended with the conclusion that one day some young, ingenious, upstart, synthetic organic chemist would surely observe it first. I certainly never entertained much hope of observing the line at Sussex and so it was not really an objective. It is important to understand how impossible such a task appeared at that time. My attitude to the research was to probe those aspects of the C_{60} discovery which particularly puzzled me and let the research flow whichever way it would.

A few days after the discovery I arrived back in Europe and announced our discovery and our conjectured structure at a conference in Riccione. Julie August, a former student now working at Nottingham, told Martyn Poliakoff of the discovery and he sent me a zerox copy of the idea that David Jones had had in 1966.[6, 7] Writing under the pseudonym of Daedalus in the Ariadne column of the *New Scientist* David had proposed the amazingly imaginative idea that large carbon balloons might be feasible. We also discovered that C_{60} itself had already been proposed by Osawa in a Japanese article 15 years earlier[2] and in a book with Yoshida.[3] Not only that, Bochvar and Gal'pern had even carried out a Hückel calculation and published the pattern of the molecular orbitals.[4, 5] We also discovered that Orville Chapman at UCLA (University of California at Los Angeles) had initiated a program aimed at the synthesis of the molecule (private communication). In retrospect it is rather peculiar that this charismatic molecule had not attracted the atten-

tion of the chemistry community earlier. Jones, in his articles[6, 7] introduced me to D'arcy Thompson's book *On Growth and Form*[77] and pointed out that Euler's law indicated that no sheet of hexagons could close. If however 12 pentagons were introduced into a hexagonal sheet of any size it would close. Almost everybody (who knows any organic chemistry!) knows that unsaturated molecules with adjacent pentagonal rings are extremely unstable. Thus from Jones' article it became immediately obvious that as 5×12 is 60, C_{60} had to be the smallest cage able to close without abutting pentagons. Thus the secret of C_{60}'s stability was beautifully simple. It lay in the accommodation of the two requirements: Euler's 12-pentagon closure principle and the chemical stability conferred by pentagon nonadjacency. I consider these two points to be the "2+2" of fullerene stability. Schmalz, Seitz, Klein, and Hite, using circuit theory, placed these principles on a firm theoretical basis.[78] The C_{70} peak was, as mentioned previously, also prominent and Rick found an elegant and a plausible structure, in which two C_{30} hemispherical halves were separated by a ring of ten extra C atoms. This structure was proposed in the paper describing the crucially important discovery, which Jim Heath made, that atoms (such as La) could be put inside the cage.[79] This discovery (and its refinements), that endohedral complexes could form, was perhaps the strongest empirical observation supporting the cage proposal prior to extraction in 1990.

During some moments of musing over these two stability criteria I began to wonder about the identity of the next cage (after C_{60}) that might be able to close without abutting pentagons. I started to play around with a model of C_{60} by adding atoms and before I had made much headway it suddenly struck me that perhaps closure could not occur again until C_{70} (Figure 12)—if that were the case it would explain—at a stroke—the

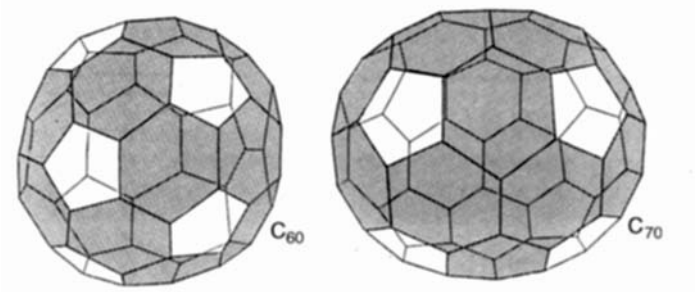

Figure 12. For species with less than 72 atoms these two structures are the only ones which can be constructed without abutting pentagons. Thus on the basis of the *pentagon isolation principle* [80,81] and geodesic considerations, C_{60} and C_{70} are predicted to be the first and second fullerene magic numbers, respectively. This result provided the simplest and most convincing circumstantial evidence in support of the closed cage concept prior to extraction.

prominence of C_{70}. That seemed to me a most unexpected and certainly not a very obvious result. Furthermore, there a subtle circular argument appeared—if it were true, closure demanded that C_{70} be strong and that would be, for me, by far the most convincing support for the fullerene proposal and I knew that there was not a hope-in-hell of an alternative explanation of *both* the 60 *and* 70 magic numbers. From that moment on I was certain that one day we would be proven right.

A call to the Galveston group to see whether they could prove the conjecture was in order. To my absolute delight Tom Schmalz told me that they had already shown that cages with 62, 64, and 66 atoms could not close without abutting pentagons and that the analysis on 68-atom cages was in mid-stream at that very moment. Thus the *pentagon isolation rule*, which governs general fullerene stability, was born.[80, 81] Another thought struck me during the phone call with Schmalz. I remembered that C_{50} was often a magic number in some of our experiments and suggested that they might check whether the 50-atom cage might be the smallest cage to close without *triplets* of abutting pentagons. Schmalz et al showed this to be the case too.[81] I wondered about a result that Sean had obtained.[82] He had found that laser irradiation of C_{60} caused it to fragment by reducing the size of the clusters more-or-less sequentially by even numbers from 60 to 58 to 56 etc... all the way down to 32. After 32 further irradiation blew the cluster into small fragments. I tried to push the pentagon multiplet isolation idea to quartets in the hope that it would explain the C_{32} result but to my amazement and delight an elegant C_{28} structure[80] formed in my hands (Figure 13). This reminded me of a result that had

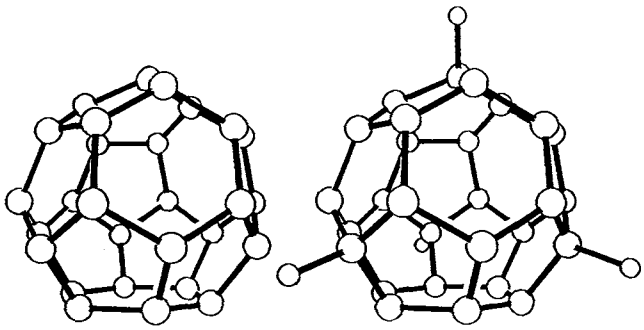

Figure 13. The tetrahedral small fullerene C_{28} (left) and the tetrahydrogenated derivative, $C_{28}H_4$ (right), which is expected to exhibit some stability [80].

puzzled us for some time—in some of our runs the 28-carbon-atom signal sometimes rivalled that of C_{60}. It also struck me that this species should be a sort of superatom cluster analogue of the carbon atom with effective tetravalency suggesting that an elegant tetrahedral $C_{28}H_4$ derivative (Figure 13) might actually be a stable molecule.[80] Indeed in some Exxon data,[83] I found just the mass spectrum distribution which confirmed that the isolation principle could be generalized to include various sizes of multiplets and account for magic numbers of smaller cages down to C_{20}.[80, 13] It not only exhibited magic numbers at 60, 50 and 28 but it stopped abruptly at 24. From Patrick Fowler I had learned that no cage could be constructed with 22 atoms.[84] Thus, there appeared to be "semistable" fullerenes (at least in beams) down to C_{20} which were predictable (Figure 14) on the basis of the cage closure concept. What more "proof" could one possibly want for the whole fullerene concept? None.

Then one day I decided that we should build our own Buckminster Fuller domes, or rather molecular models of the giant fullerenes[85] and ordered 10000 cabon atoms (molecular model atoms and bonds). Ken McKay, armed with Goldberg's paper[86] and Coxeter's book[87] set about building C_{240}, C_{540} and later C_{960} and C_{1500} with icosahedral symmetry. When Ken came in with the model of C_{540} it was beautiful but I could not quite understand its shape—the model was not round like Buck-

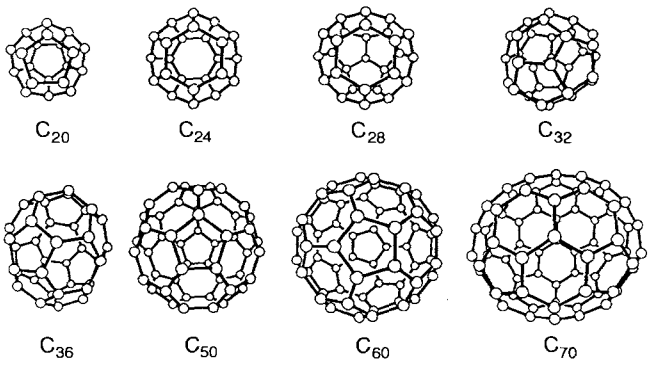

Figure 14. A set of fullerenes between C_{20} and C_{70} some of which are magic and others which are predicted to be "semi"-magic [80, 81].

minster Fuller's Montreal dome but had clear icosahedral tendancies (Figure 15).[90] Indeed Ken's model had cusps focused at the 12 pentagons and from a distance had a definite polygonal outline. Then we realized that the structure explained some very interesting results that Sumio Iijima had obtained in 1980.[89]

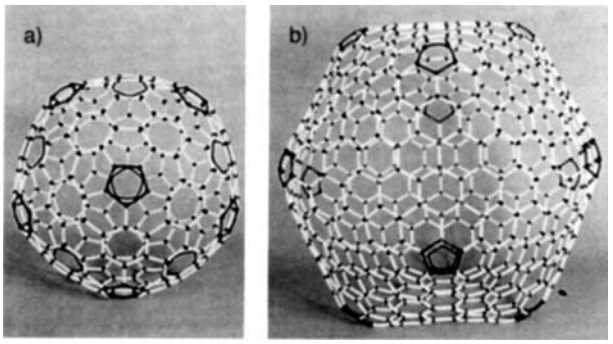

Figure 15. Photographs of molecular models of the giant fullerenes C_{240} (left) and C_{540} (right). The models turned out to possess icosahedral shapes rather than perfectly spheroidal ones similar to the geodesic domes. Each of these structures can be considered as an initially flat hexagonal network that has warped into a closed monosurface (of icosahedral symmetry) by 12 pentagonal disclinations which give rise to the cusps. The structures provided the first prediction of faceting in closed cage carbon species such as giant fullerenes and nanotubes.

He had observed concentric shell onionlike carbon particles by transmission electron microscopy. Superficially many of Iijima's particles appeared to be round, as one might assume if they were nanoscale geodesic domes. However because of this assumption I had glossed over some crucial subtle features in the micrographs—the outlines were not quite as round as they superficially appeared—they were actually polygonal.[13, 88] In fact as we looked more carefully at the infrastructure of Buckminster Fuller's domes we realized that the strut lengths in the vicinity of the pentagons had been adjusted to give them a smooth spheroidal shape (Figure 10). Thus the C_{60} discovery had led to an elegant explanation of a previously unexplained result. It showed that a cage with an icosahedral shape could be constructed *entirely* from sp^2 carbon atoms. Thus 12 pentagonal disclinations—a minimal number of defects by comparison with those found in any normal crystals—would convert a perfectly flat graphene sheet of any size into a closed cage.

There is a rather nice lesson to be drawn from this advance: There had been no premeditated research aim, the original reason for constructing the giant fullerene model was solely for the intrinsic interest and pleasure of building an elegant structure—and yet it revealed an unexpected result. The result had important consequences—for instance it was the first study of the way that the inclusion of pentagons influences the curvature of a graphene sheet—a result that was to find particular use later when elongated giant fullerenes (nanotubes) were discovered. On occasion I would wonder about our cage proposal, reassess each and every observation: 60 and 70 should be magic numbers; 50 and 28 were also explainable magic numbers; there was no clear evidence of C_{22}; the icosahedral shape of the giant fullerenes could be explained; Jim had observed metal complexes that behaved as though they were endohedral;[79] Sean had found that C_2 units were ejected,[82] and there were other supporting experimental results.[12, 19] It all fitted perfectly—there was no way we could be wrong.

I thought we should probe the Iijima result and see whether C_{60} might reveal some clues about the round particles in general. This was based on the idea we had proposed[90] that the mechanism of C_{60} production might be related to soot formation. We were able to acquire an old carbon arc evaporating unit and drill a hole in the base plate to admit He. Ken McKay monitored the structure of the carbon deposit by scanning electron microscopy as a function of He pressure. The idea was that as the He pressure increased C_{60} formation might be initiated and this would be accompanied by the creation of round carbon particles. A change in the deposit did occur as the pressure rose above 50 microns (5×10^{-2} Torr).[20] The next step *seemed* obvious—to monitor the possible production of C_{60}. However I made a fatal error. I assumed that if C_{60} were created in the arc, it would only be in minuscule quantities and only the most sensitive of detection techniques available (mass spectrometry) would work. I then tried, for the next two years (unsuccessfully), to obtain the financial support for quadrupole mass spectrometer.

I was still trying, with Geoff Cloke, to get a mass spectrometer when we learned of a study by Krätschmer, Fostiropoulos, and Huffman who had detected four IR bands (Figure 16; exactly as

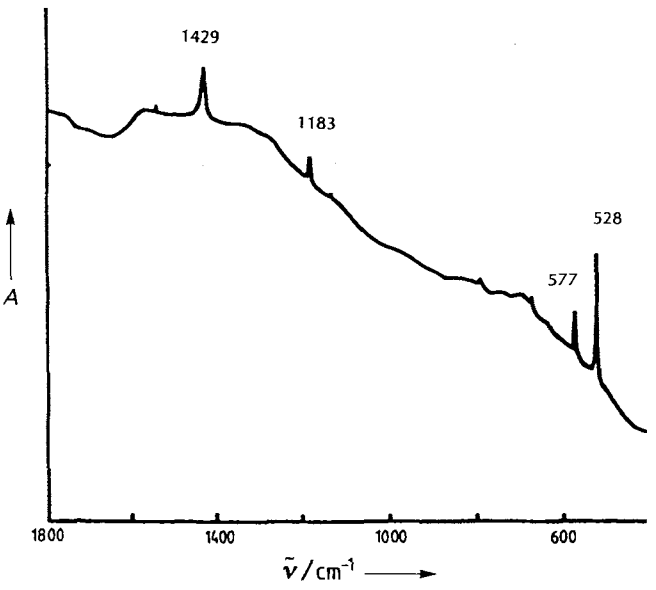

Figure 16. The four historic IR bands observed by Krätschmer, Lamb, Fostiropoulos, and Huffman, taken from reference [16].

predicted theoretically[91–93]) in a carbon deposit made in exactly the same way as ours.[16] If this were correct then their deposit (and ours also!!!) must contain at least 1% C_{60}. I could not believe it—and yet there were four sharp frequencies in the pure carbon deposit—what on earth could they be. I decided to check out this incredible (in its literal meaning) result and proposed it as as a third year project for Amit Sarkar (an undergraduate) to work with Jonathan Hare (graduate student) to see whether they could repeat it—and they did!!![20] It is difficult, today, to explain just how difficult it was to accept the Krätschmer et al. observations but it is important, for an understanding of how science advances, to try. How could C_{60} have remained undetected until the end of the 20th century if it could be produced in such a yield by this seemingly simple approach?

We then tried to see whether the deposit gave a mass spectrum and Ala'a Abdul Sada obtained a signal at m/z 720 (Figure 17 and 18a)—it still seemed impossible. I was still very suspicious,

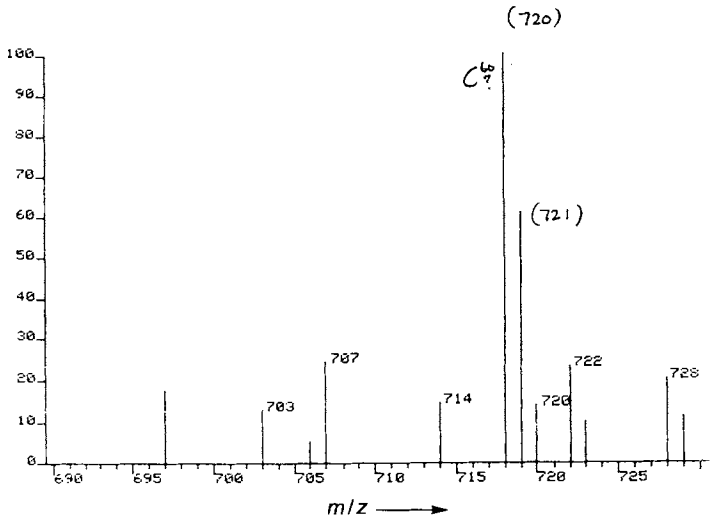

Figure 17. Fast atom bombardment (FAB) mass spectrum of a deposit of arc-processed soot obtained on July 23rd, 1990 at Sussex by Ala'a Abdul-Sada. The machine calibration is out by 2 amu; however, the isotope pattern was convincing as the peaks are close to the intensity ratio 1.0:0.66:0.22 as expected for $^{12}C_{60}$:$^{12}C_{59}{}^{13}C$:$^{12}C_{58}{}^{13}C_2$.

especially as I knew that C_{60} can be formed readily during the mass spectrometric sampling process. The mass spectrometer then broke down (Figure 18a)! Over the years we had often discussed the likely physical properties of C_{60}—some thought it would be a high melting point solid, others thought it would be a liquid or even a gas. On a Friday evening August 3rd Jonathan decided, with the unblinkered optimism that only the young possess, to test whether the species would dissolve in benzene (Figure 18b), and amazingly it produced a red solution which he placed on my desk on Monday morning (August 6th) (Figures 19 and 18c). Jonathan seemed to have no difficulty in accepting that it was C_{60} as is indicated by the fact that he called it C_{60}^{B} (see Figure 18), which was our shorthand notation for buckminsterfullerene. On the Thursday some of the solution was concentrated to see whether a deposit could be obtained which would yield a stronger signal at m/z 720—but it didn't (Figure 18d). This was exactly the right experiment and actually

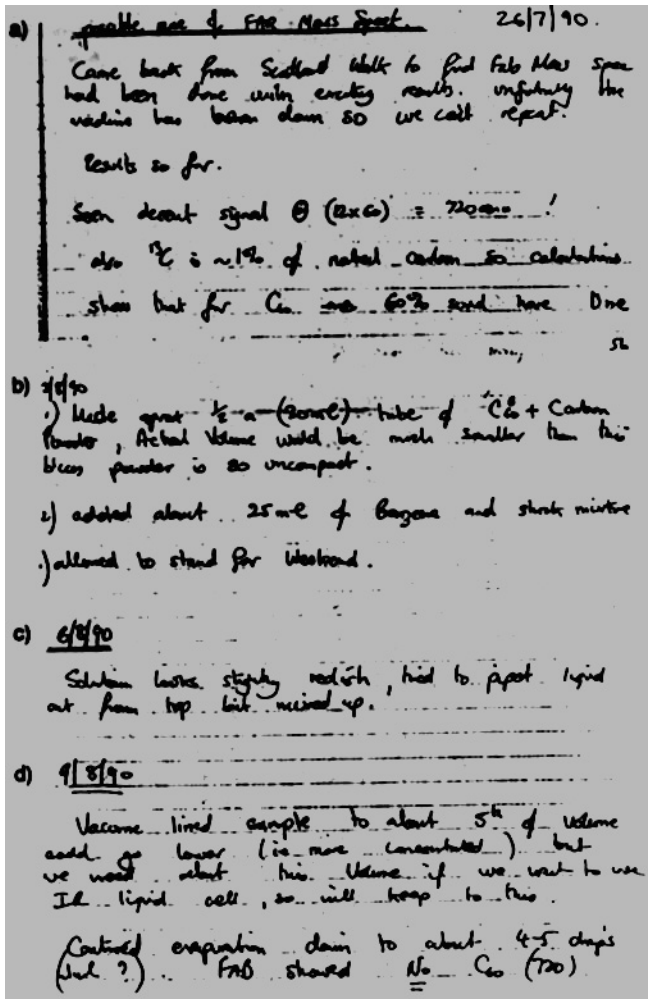

Figure 18. Entries by Jonathan Hare in his laboratory notebook: a) July 26th, 1990, b) August 3rd, 1990, c) August 6th, 1990, d) August 9th, 1990.

Figure 19. Original "reddish" extract obtained by Jonathan Hare on Monday, September 6th, 1990.

a rather difficult one for technical reasons and would almost certainly have worked the next time—*had there been one(!)*.

The next day, disaster struck—I had a call from *Nature*; Philip Ball asked whether I would referee a new paper by Krätschmer et al. When the manuscript arrived by fax at around 12 noon it was a bombshell. Krätschmer et al. had also obtained a red(!!!!) solution and what is more their solution had yielded

crystals (Figure 20), which X-ray analysis conclusively indicated consisted of arrays of spheroidal molecules exactly the right size to be C_{60}. There was absolutely no doubt about it—Wolfgang Krätschmer, Lowell Lamb, Kostas Fostiropoulos, and Don Huffman had done it.[15] It was only at that moment that I suddenly realized that we had been in a race and—we had been

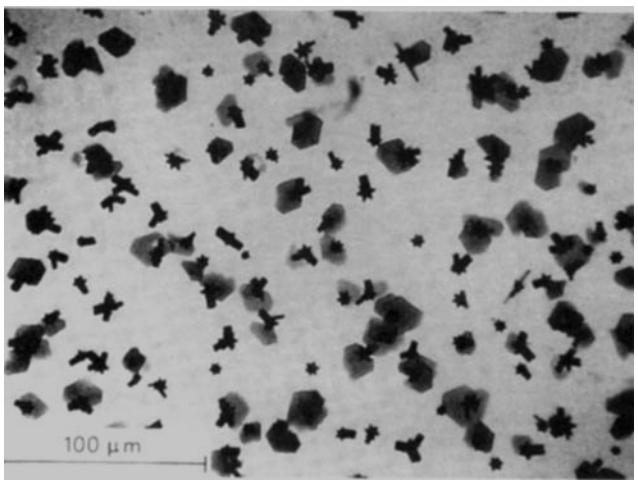

Figure 20. The astounding photograph of crystals of pure carbon which Krätschmer, Lamb, Fostiropoulos, and Huffman obtained during their breakthrough in extraction [15]. Photograph supplied by Wolfgang Krätschmer.

pipped at the post. I considered committing suicide—but decided to go for lunch instead. Over lunch I read and reread this fantastic manuscript and I doubt whether I shall ever have an experience like it again. It was a very strange mix of alternating feelings: First, exhileration from being proven right, and then disappointment from having come so close to proving it ourselves. Immediately after lunch I called Philip Ball back and told him to accept the paper immediately.

But what to do now, it was difficult to think at all let alone make any sensible decisions. However as the afternoon wore on it gradually dawned on me that although *almost* everything was lost—it was not quite all. Krätschmer et al. had analyzed their material by X-ray crystallography and not by NMR spectroscopy. So, the much-coveted single NMR line was still waiting to be observed. Thus I realized that there was just a single crumb of comfort left, but what a tasty morsel it would be and we should be able to observe it. (The NMR shift should also indicate just how aromatic the molecule was or was not. Of course the meaning of aromaticity for a species that cannot undergo substitution is debatable!) After all Jonathan had extracted the precious red solution on the Monday, four days before the extraction manuscript arrived on the Friday and we also had the confirmatory 720 amu mass spectrum. So we already had material in our hands and we were the only ones apart from Krätschmer and colleagues who had. We could also take immense intellectual satisfaction at having extracted the red solution before the arrival of the paper of Krätschmer and colleagues. I suppose that that should be enough for a scientist—but of course it never is.

In 1982 Krätschmer and Huffman had observed puzzling UV absorption features, while studying carbon dust produced by a carbon arc to simulate interstellar dust in the laboratory and measure the optical spectrum. After the publication of our discovery, and theoretical predictions of the UV spectrum such as those by Rosen and co-workers[94, 95] and others[9, 10] they conjectured that the features might be due to C_{60}. They then set about testing their idea by searching for the four telltale IR lines which theory suggested the molecule should exhibit,[91–93] (see Figure 16). When they found them they went on to make C_{60} from pure ^{13}C and show that the isotope shifts were perfectly consistent with their conjecture.[17] They then extracted crystals (Figure 20) and proved their conjecture conclusively. I look upon the conjecture that they had made C_{60} in 1982 together with the decision to test it by analyzing their deposit by IR spectroscopy as one of the most prescient pieces of science I have ever come across and as time has progressed I have come to appreciate it more and more. The role played by spectroscopy—in both the initial UV observation and in particular the crucial telltale IR fingerprinting is an archetypal example of the way spectroscopy can be used to solve important problems, in this case an historically significant one as well. To my mind there is no more amazing discovery than that there is a form of pure carbon that is soluble and the image of the carbon crystals of Krätschmer et al. (Figure 20) has to be one of the most sublime images of 20th century chemistry.

During the tea-break that afternoon I showed the paper to my colleagues. Roger Taylor, offered to help us to get the one-line solution and immediately tried to extract as much material as he could from Jonathan who was somewhat reluctant to part with the small amount of the precious material that he had. Roger then made a key discovery, he found that the red solution could be chromatographically resolved into two components, one was red and the other a beautiful delicate magenta. (Chromatography has since become the accepted way to separate all the members of the fullerene family.)

Would NMR analysis show the single line? Tony Avent who operated the NMR spectrometer produced a two(?)-line spectrum from the magenta material (Figure 21). One was a magnificent strong line, but it was benzene—quite a well-known compound. The second was a puny little blip in the base line—but Tony reckoned it was C_{60}—and he was right. To us it was the most beautiful little blip one could ever imagine. After further refinement the single line was observed as a strong signal (Figure 22a). The icing on the cake was the red material which gave five NMR lines—exactly what was expected for C_{70}[96] (Figure 22).

Thus, in summary, Krätschmer, Lamb, Fostiropoulos, and Huffman had indeed extracted C_{60} and at Sussex we had come a *very* close second. However Jonathan had extracted a red solution and Ala'a had detected a mass spectrum independently and before the Heidelberg/Tucson (*Nature*) manuscript had arrived. After this Roger had discovered the chromatographic separation of the fullerenes. Tony had detected the much coveted single line (Meijer and Bethune at IBM were also close and with Johnson also observed a single-line NMR spectrum[97]). As a certain English football manager, noted for his "eloquence", in adversity would say—"The lads dun good!"

So in September 1990 some 20 years after the molecule was conceived by Osawa and five years after we had discovered that it could self-assemble, Krätschmer et al. had extracted it and fullerene science was well and truly on its way.

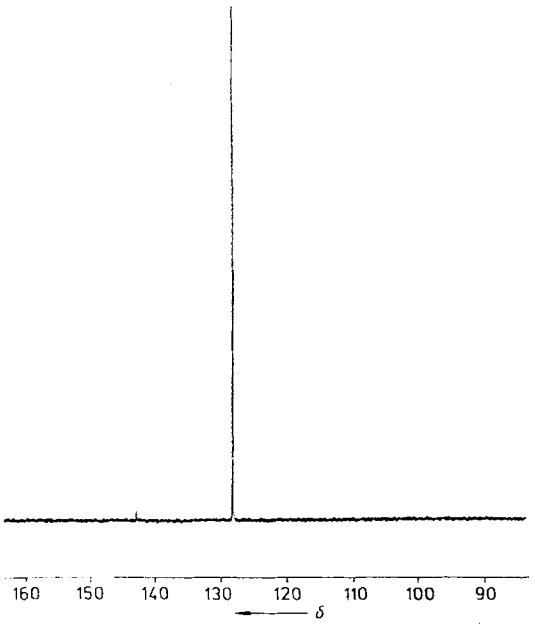

Figure 21. The first NMR trace in which the C_{60} resonance (at $\delta = 143$) was first identified (just!). The strong line at $\delta = 128$ is (rather appropriately) the resonance of benzene. The spectrum was recorded at the University of Sussex on an AMX-500 spectrometer.

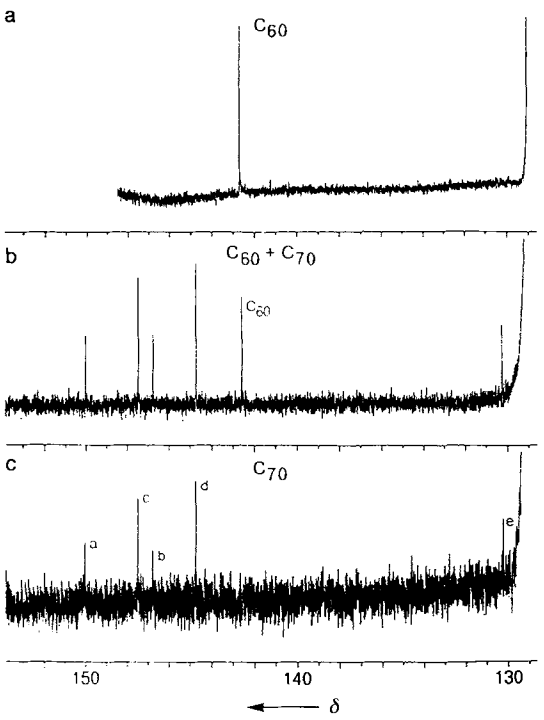

Figure 22. ^{13}C NMR spectra obtained from chromatographically purified samples of soluble material extracted from arc-processed graphite. a) Spectrum of purified C_{60} (magenta fraction), b) spectrum of mixed sample, c) spectrum of purified C_{70} (red fraction) showing five lines as expected for the symmetric egg-shaped molecule (see Figure 12).

Phase V: The New Round World of Fullerene Chemistry, Physics, and Materials Science

After the extraction breakthrough in 1990, the field of fullerene research exploded and now some thousand papers a year are published in the field. Several new research projects, designed to explore the chemical and physical behavior of the fullerenes were launched at Sussex. With Roger Taylor and David Walton fullerene synthetic chemistry became a primary aim.[98] Roger Taylor and others pioneered the extraction of higher fullerenes C_{76}, C_{78}, etc.[31] Spectroscopic studies were carried out with John Dennis and Jonathan Hare and also in collaboration with Sydney Leach and colleagues in Meudon/Orsay. Halogenation studies have turned out to be particularly important and Paul Birkett was able to show that $C_{60}Cl_6$ (Figure 23) can form.[98] These observations which may be considerd to be the fullerene equivalent of *ortho*, *meta*, and *para* direction in benzene have been followed by the creation of some key acylated derivatives. Adam Darwish has probed a wide range of reactions in particular hydrogenation and hydroxylation reactions. Interesting mixed crystalline compounds involving ferrocene and phosphorus have been made and structurally characterized by Jonathan Crane, Wyn Locke, and Peter Hitchcock.[98] Further chemical properties of C_{60} as a synthon, including for instance cycloaddition and metal complexation reactions, have been investigated by Mohammed Meidine, Brian O'Donovan, and Martin van Wijnkoop and solubilization methods have been developed by Huang Shaoming. Colin Crowley and Andy Caffyn have been investigating thermolytic routes to C_{60}. Fragmentation behavior is also being investigated with Perdita Barran, Steve Firth, and Tony Stace (in collaboration with Eleanor Cambell of the Max-Born-Institut in Berlin). These studies followed on from the work of Simon Balm, Richard Hallet, Ken McKay and Wahab Allaf. Cold fluorescence studies are being carried out with Reg Colin, Pierre Coheur, Steve Firth, Michele Carlier (in Brussels), and Eleanor Cambell (in Berlin).

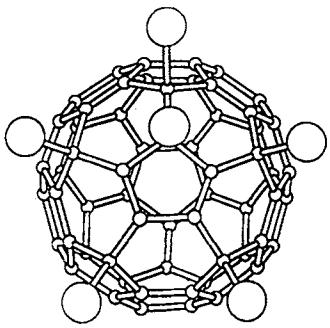

Figure 23. The structure of $C_{60}Cl_6$ [98].

A solid-state chemistry program has been initiated by Kosmas Prassides in which fascinating solid-state dynamics and phase behavior[99] as well as superconducting properties of the metal intercalation complexes have been probed.[100] With Fred Wudl's group, the elegant azafullerenes are under detailed investigation.[101]

On the nanotechnology front some fascinating advances have been made.[102] Collaboration with Morinobu Endo of Shinshu University in Japan has opened up several new avenues in the creation of nanostuctures by pyrolytic methods and possible nanotube growth mechanisms. With Mauricio Terrones, Wen Kuang Hsu, and Jon Hare, studies of the fascinating way that nanostructure creation is governed by metal cluster catalysts are being investigated (with Umberto Terrones in Mexico). Related investigations of these promising routes to nanoscale materials are under way with Thomas Müller, Doug Reid, and Nicole Grobert. Wen Kuang Hsu has observed the amazing result that nanotubes can be obtained by electrolysis.[101] Just as exciting as the new carbon structures are the boron nitride nanotubes. Some of this nanotechnology work is being carried out in collab-

oration with Tony Cheetham and Xing Ping Zhang at UCSB (University of California at Stony Brook) and Laurence Dunne at the University of the South Bank. All in all the way ahead looks exciting as is exemplified by the nanstructure shown in Figure 24, which appears very much like an extra who has escaped from the set of the film Alien II.

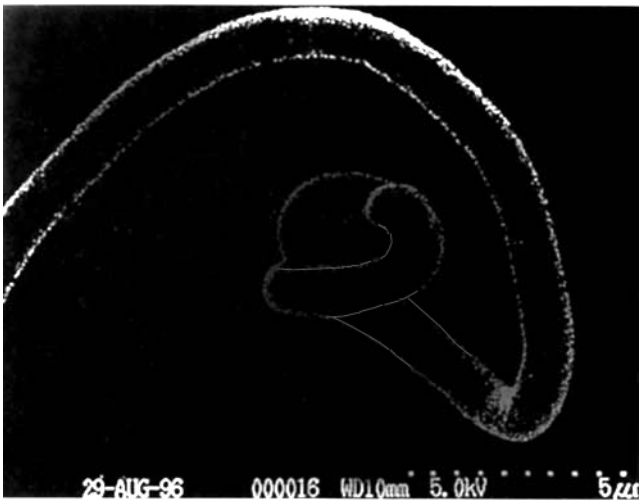

Figure 24. Thermolytically created carbon nanostructure.

Epilogue: The Cosmic and Microcosmic Charisma of the Soccerball

One cannot end any account of the discovery of C_{60} without noting that it has the same structure as a football (or soccerball) and that this led to its original conception. Thus it seems fitting to reproduce (Figure 25)[3] the image from the book by Osawa and Yoshida and point out that much of the world now plays football (or soccer). Furthermore a large number of researchers are studying the peculiar behavior of the ball on a microcosmic scale. Last but not least we should note that, perhaps, the molecules most delightful property lies in the inherent charisma[3,7] which arises from its elegantly simple and highly symmetric structure that is quite unlike any other. It is this charisma that has stimulated delight and fascination for chemistry in young and old alike. Perhaps no image captures the most important quality of C_{60} better than the photograph depicted in Figure 26. It says it all.

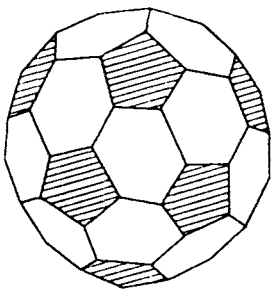

Figure 25. The first image of C_{60} ever published (Osawa and Yoshida [2,3] (taken from ref. [3]).

There are many people to whom I owe deep debts of gratitude in addition to the students, colleagues, and friends who appear in the above text. I thank in particular those students who were not directly involved with C_{60} related studies because much of their work formed a basis to which many ideas may be tenuously traced. The support over the years has come from several sources, mainly the The School of Chemistry and Molecular Sciences of the University of Sussex, SRC, SERC, EPSRC, NATO, The Royal Society, BP (John Cadogan), ICI/Zeneca (Peter Doyle, Mike Hutchinson, Neil Winterton), British Gas, and BOC (Steve Wood), and Alfred Bader.

Received: February 4, 1997 [A 207 IE]
German version: *Angew. Chem.* **1997**, *109*, 1648–1664

Keywords: carbon allotropes · fullerenes · nanostructures · Nobel lecture

Figure 26. This photograph of Ellis captures perfectly the delight that C_{60} can stimulate in youngsters of all ages (photographer: G. E. Watson, published with permission).

[1] H. W. Kroto, J. R. Heath, S. C. O'Brien, R. F. Curl, R. E. Smalley, *Nature (London)* **1985**, *318*, 162–163.
[2] E. Osawa, *Kagaku (Kyoto)* **1970**, *25*, 854–863 (in Japanese) [*Chem. Abstr.* **1971**, *74*, 75698v].
[3] Z. Yoshida, E. Osawa, *Kagaku (Kyoto)* **1971**, *28*, 174–178 (in Japanese).
[4] D. A. Bochvar, E. G. Gal'pern, *Dokl. Akad. Nauk SSSR* **1973**, *209*, 610–612; *Proc. Acad. Sci. USSR* **1973**, *209*, 239–241.
[5] I. V. Stankevich, M. V. Nikerov, D. A. Bochvar, *Russ. Chem. Rev. (Engl. Transl.)* **1984**, *53*, 640–655.
[6] D. E. H. Jones, *New Sci.* **1966**, *32*, 245.
[7] D. E. H. Jones, *The Inventions of Daedalus*, Freeman, Oxford, **1982**, pp. 118–119.
[8] T. G. Dietz, M. A. Duncan, D. E. Powers, R. E. Smalley, *J. Chem. Phys.* **1981**, *74*, 6511–6512.
[9] H. W. Kroto, W. Allaf, S. P. Balm, *Chem. Rev.* **1991**, *91*, 1213–1235.
[10] W. Weltner, Jr., R. J. Van Zee, *Chem. Rev.* **1989**, *89*, 1713–1747.
[11] J. R. Heath, S. C. O'Brien, R. F. Curl, H. W. Kroto, R. E. Smalley, *Comments Condens. Matter Phys.* **1987**, *13*, 119–141.
[12] R. F. Curl, R. E. Smalley, *Science* **1988**, *242*, 1017–1022.
[13] H. W. Kroto, *Science* **1988**, *242*, 1139–1145.
[14] G. Meijer, D. S. Bethune, *Chem. Phys. Lett.* **1990**, *175*, 1–2.
[15] W. Krätschmer, L. D. Lamb, K. Fostiropoulos, D. R. Huffman, *Nature (London)* **1990**, *347*, 354–358.
[16] W. Krätschmer, K. Fostiropoulos, D. R. Huffman, *Dusty Objects in the Universe* (Eds.: E. Bussoletti, A. A. Vittone), Kluwer, Dordrecht, **1990**.
[17] W. Krätschmer, K. Fostiropoulos, D. R. Huffman, *Chem. Phys. Lett.* **1990**, *170*, 167–170.
[18] A. Kurosawa in *Rashomon* (Eds.: D. Richie), Rutgers University Press, New Brunswick, **1987**.
[19] R. E. Smalley, *The Sciences* **1991**, March/April, 22–28.
[20] H. W. Kroto, *Angew. Chem.* **1992**, *104*, 113–133; *Angew. Chem. Int. Ed. Engl.* **1992**, *31*, 111–129.
[21] R. F. Curl, R. E. Smalley, *Sci. Am.* **1991** (10), 32–41.
[22] W. Krätschmer, D. R. Huffman in *The Fullerenes* (Eds.: H. W. Kroto, D. R. M. Walton), Cambridge University Press, **1993**, pp. 5–9.
[23] J. Baggott, *Perfect Symmetry, the Accidental Discovery of Buckminsterfullerene*, Oxford University Press, **1994**.
[24] H. Aldersey-Williams, *The Most Beautiful Molecule in Chemistry, An Adventure in Chemistry*, Aurum Press, London, **1995**.
[25] W. Krätschmer, H. Schuster, *Von Fuller bis zu Fullerenen*, Vieweg, Braunschweig, **1996**.

[26] J. Dettmann, *Fullerene – Die Buckyballs erobern die Chemie*, Birkhäuser, Basel, **1994**.
[27] P. Ball, *Designing the Molecular World*, Princeton, **1994**, pp. 13–53; *Chemie der Zukunft – Magie oder Design?*, VCH, Weinheim, **1996**.
[28] A. Hirsch, *The Chemistry of the Fullerenes*, Thieme, Stuttgart, **1994**.
[29] *The Fullerenes* (Eds.: H. W. Kroto, D. R. M. Walton), Cambridge University Press, **1993**.
[30] *The Fullerenes* (Eds.: H. W. Kroto, D. E. Cox, J. E. Fischer), Pergamon, Oxford, **1993**.
[31] *The Chemistry of the Fullerenes* (Ed.: R. Taylor), World Science, Singapore, **1995**.
[32] S. Iijima, *Nature (London)* **1991**, *354*, 58.
[33] A. Nickon, E. F. Silversmith, *Organic Chemistry—The Name Game: Modern Coined Terms and Their Origins*, Pergamon, New York, **1987**.
[34] R. B. Fuller, *Inventions—The Patented Works of Buckminster Fuller*, St. Martin's Press, New York, **1983**.
[35] R. W. Marx, *The Dymaxion World of Buckminsterfuller*, Reinhold, New York, **1960**.
[36] J. Baldwin, *Bucky Works—Buckminster Fuller's Idea for Today*, Wiley, New York, **1996**.
[37] H. W. Kroto, *MRS Bull.* **1994**, *19*, 21–22.
[38] R. Lawlor, *Sacred Geometry*, Crossroad, New York, **1982**.
[39] K. Critchlow, *Time Stands Still*, Gordon Fraser, London, **1979**.
[40] *Plato's Timaeus and Critias* (H. D. P. Lee (*Transl.*)), Penguin, Harmondsworth, UK, **1971**, p73.
[41] J. H. Van Vleck, *Rev. Mod. Phys.* **1951**, *23*, 213.
[42] E. U. Condon, G. H. Shortley, *The Theory of Atomic Spectra*, Cambridge University Press, Cambridge, **1967**.
[43] H. W. Kroto, *Molecular Rotation Spectra*, Dover, New York, **1992**; 1st ed., Wiley, Chichester, **1975**.
[44] R. N. Dixon, H. W. Kroto, *Trans. Faraday Soc.* **1963**, *59*, 1484.
[45] A. E. Douglas, *Astrophys. J.* **1951**, *114*, 466.
[46] H. W. Kroto, *Chem. Soc. Rev.* **1982**, *11*, 435–491.
[47] T. E. Gier, *J. Am. Chem. Soc.* **1961**, *83*, 1769.
[48] M. J. Hopkinson, H. W. Kroto, J. F. Nixon, N. P. C. Simmons, *J. Chem. Soc. Chem. Commun.* **1976**, 513.
[49] G. Becker, *Z. Anorg. Allg. Chem.* **1976**, *423*, 242.
[50] M. J. Hopkinson, H. W. Kroto, J. F. Nixon, N. P. C. Simmons, *Chem. Phys. Lett.* **1976**, *42*, 460.
[51] R. Eastmond, D. R. M. Walton, *Chem. Commun.* **1968**, 204.
[52] R. Eastmond, T. R. Johnson, D. R. M. Walton, *Tetrahedron* **1972**, *28*, 4601.
[53] T. R. Johnson, D. R. M. Walton, *Tetrahedron* **1972**, *28*, 5221.
[54] C. Eaborn, *Chem. Br.* **1970**, *6*, 330.
[55] A. J. Alexander, H. W. Kroto, D. R. M. Walton, *J. Mol. Spectrosc.* **1976**, *62*, 175–180.
[56] A. C. Cheung, D. M. Rank, C. H. Townes, D. D. Thornton, W. J. Welch, *Phys. Rev. Lett.* **1968**, *21*, 1701.
[57] H. W. Kroto, *Int. Rev. Phys. Chem.* **1981**, *1*, 309–376.
[58] B. E. Turner, *Astrophys. J.* **1971**, *163*, L35.
[59] L. W. Avery, N. W. Broten, J. M. MacLeod, T. Oka, H. W. Kroto, *Astrophys. J.* **1976**, *205*, L173–L175.
[60] C. Kirby, H. W. Kroto, D. R. M. Walton, *J. Mol. Spectrosc.* **1980**, *74*, 261–265.
[61] H. W. Kroto, C. Kirby, D. R. M. Walton, L. W. Avery, N. W. Broten, J. M. MacLeod, T. Oka, *Astrophys. J.* **1978**, *219*, L133–L137.
[62] H. W. Kroto, *Proc. R. Inst. GB* **1986**, *58*, 45–72.
[63] T. Oka, *J. Mol. Spectrosc.* **1978**, *72*, 172–174.
[64] N. W. Broten, T. Oka, L. W. Avery, J. M. MacLeod, H. W. Kroto, *Astrophys. J.* **1978**, *223*, L105–L107.
[65] E. Herbst, W. Klemperer, *Astrophys. J.* **1973**, *185*, 505–533.
[66] A. Dalgarno, J. H. Black, *Rep. Prog. Phys.* **1976**, *39*, 573–612.
[67] E. E. Becklin, J. A. Frogel, A. R. Hyland, J. Kristian, G. Neugebauer, *Astrophys. J.* **1969**, *158*, L133.
[68] D. L. Michalopoulos, M. E. Geusic, P. R. R. Langridge-Smith, R. E. Smalley, *J. Chem. Phys.* **1984**, *80*, 3556–3560.
[69] H. Hintenberger, J. Franzen, K. D. Schuy, *Z. Naturforsch. A* **1963**, *18*, 1236–1237.
[70] A. E. Douglas, *Nature (London)* **1977**, *269*, 130–132.
[71] G. H. Herbig, *Astrophys. J.* **1975**, *196*, 129–160.
[72] H. W. Kroto, J. R. Heath, S. C. O'Brien, R. F. Curl, R. E. Smalley, *Astrophys. J.* **1987**, *314*, 352–355.
[73] E. A. Rohlfing, D. M. Cox, A. Kaldor, *J. Chem. Phys.* **1984**, *81*, 3322–3330.
[74] L. A. Bloomfield, M. E. Geusic, R. R. Freeman, W. L. Brown, *Chem. Phys. Lett.* **1985**, *121*, 33–37.
[75] M. Proulx, *Graphis* **1967**, *132*, 379.
[76] J. R. Heath, S. C. O'Brien, R. F. Curl, H. W. Kroto, R. E. Smalley, *Comments Condens. Matter Phys.* **1987**, *13*, 119–141.
[77] D. W. Thompson, *On Growth and Form*, Cambridge University Press, **1942**.
[78] T. G. Schmalz, W. A. Seitz, D. J. Klein, G. E. Hite, *Chem. Phys. Lett.* **1986**, *130*, 203–207.
[79] J. R. Heath, S. C. O'Brien, Q. Zhang, Y. Liu, R. F. Curl, H. W. Kroto, R. E. Smalley, *J. Am. Chem. Soc.* **1985**, *107*, 7779–7780.
[80] H. W. Kroto, *Nature (London)* **1987**, *329*, 529–531.
[81] T. G. Schmalz, W. A. Seitz, D. J. Klein, G. E. Hite, *J. Am. Chem. Soc.* **1988**, *110*, 1113–1127.
[82] S. C. O'Brien, J. R. Heath, R. F. Curl, R. E. Smalley, *J. Phys. Chem.* **1988**, *88*, 220–230.
[83] D. M. Cox, K. C. Reichmann, A. Kaldor, *J. Chem. Phys.* **1988**, *88*, 1588–1597.
[84] P. W. Fowler, J. I. Steer, *J. Chem. Soc. Chem. Commun.* **1987**, 1403–1405.
[85] H. W. Kroto, *Chem. Br.* **1990**, *26*, 40–45.
[86] M. Goldberg, *Tohoku Math. J.* **1937**, *43*, 104.
[87] H. S. M. Coxeter, *Regular Polytopes*, Macmillan, New York, **1963**.
[88] H. W. Kroto, K. G. McKay, *Nature (London)*, **1988**, *331*, 328–331.
[89] S. Iijima, *J. Cryst. Growth* **1980**, *50*, 675–683.
[90] Q. L. Zhang, S. C. O'Brien, J. R. Heath, Y. Liu, R. F. Curl, H. W. Kroto, R. E. Smalley, *J. Phys. Chem.* **1986**, *90*, 525–528.
[91] M. D. Newton, R. E. Stanton, *J. Am. Chem. Soc.* **1986**, *108*, 2469–2470.
[92] Z. C. Wu, D. A. Jelski, T. F. George, *Chem. Phys. Lett.* **1987**, *137*, 291–294.
[93] R. L. Disch, J. M. Schulman, *Chem. Phys. Lett.* **1986**, *125*, 465–466.
[94] S. Larsson, A. Volosov, A. Rosen, *Chem. Phys. Lett.* **1987**, *137*, 501–504.
[95] M. Braga, S. Larsson, A. Rosen, A. Volosov, *Astron. Astrophys.* **1991**, *245*, 232–238.
[96] R. Taylor, J. P. Hare, A. K. Abdul-Sada, H. W. Kroto, *J. Chem. Soc. Chem. Commun.* **1990**, 1423–1497.
[97] R. D. Johnson, G. Meijer, D. S. Bethune, *J. Am. Chem. Soc.* **1990**, *112*, 8983–8984.
[98] A. G. Avent, P. R. Birkett, C. Christides, J. D. Crane, A. D. Darwish, P. B. Hitchcock, H. W. Kroto, M. Meidine, K. Prassides, R. Taylor, D. R. M. Walton, *J. Mol. Struct.* **1994**, *325*, 1–11.
[99] K. Prassides, C. Christides, I. M. Thomas, J. Mizuki, K. Tanigaki, I. Hirosawa, T. W. Ebbesen, *Science* **1994**, *263*, 950–954
[100] K. Prassides, K. Vavekis, K. Kordatos, K. Tanigaki, G. M. Bendele, P. W. Stephens, *J. Am. Chem. Soc.* **1997**, *119*, 834–835.
[101] K. Prassides, M. Keshavarz-K., J. C. Hummelen, W. Andreoni, P. Giannozzi, E. Beer, L. Bellavia, L. Christofolini, R. Gonzalez, A. Lappas, Y. Murata, M. Malecki, V. Srdanov, F. Wudl, *Science* **1996**, *271*, 1833–1835.
[102] H. W. Kroto, J. P. Hare, A. Sarkar, W.-K. Hsu, M. Terrones, J. R. Abeysenghe, *MRS Bull.* **1994**, *19*, 51–55.

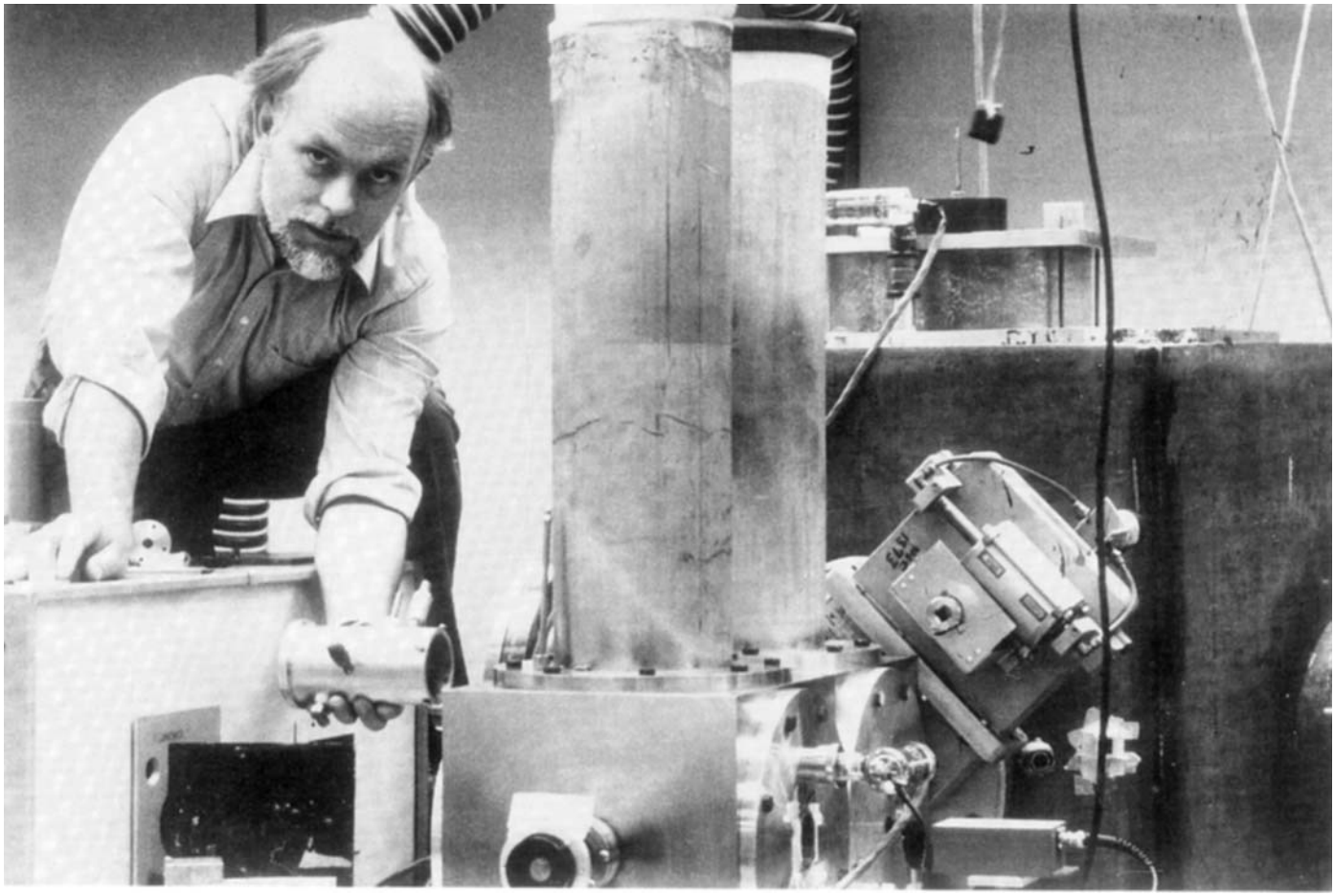

The author climbing around on top of a section of AP2, the laser-vaporization cluster beam apparatus that enabled the discovery of fullerenes.

The wide distribution of even-numbered carbon clusters is clearly evident from the mass spectrum (bottom).

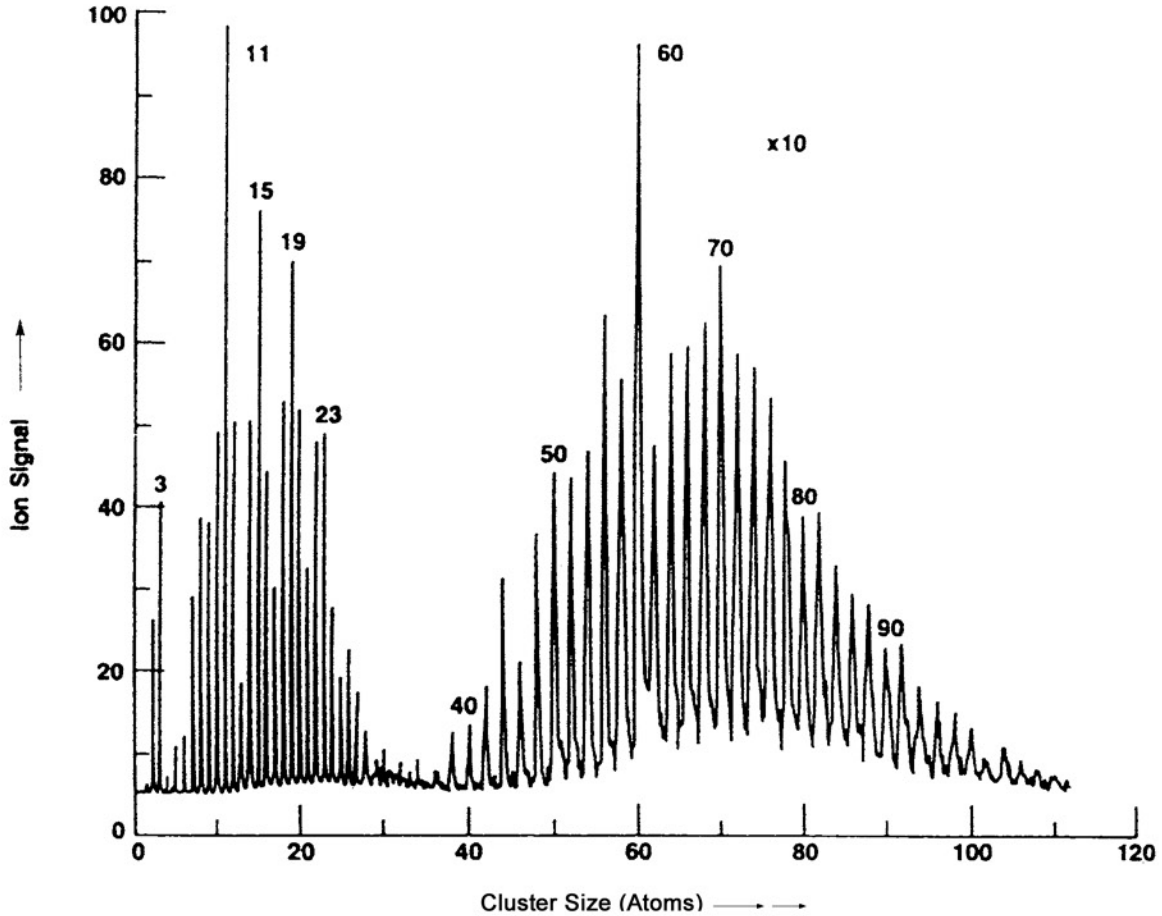

ANGEWANDTE CHEMIE © WILEY-VCH

Discovering the Fullerenes (Nobel Lecture)**

Richard E. Smalley*

It is a thrill for me to be here today and to be the first of three speakers discussing the wonders of the fullerenes, an infinite new class of carbon molecules. My colleagues in this famous photograph (Figure 1) are also thrilled to be here in Stockholm this week to see "Bucky get the Prize". This picture was taken

Figure 1. Photograph of the research group that discovered the fullerenes at Rice University in September of 1985. Standing: Curl, Kneeling in front, left to right: O'Brien, Smalley, Kroto, and Heath.

on September 11, 1985, the day before we sent off the manuscript describing the discovery of C_{60} to the editorial offices of *Nature*[1] (and only a few days after the discovery itself). Every one of the people in that photograph was critically involved in the discovery (with the exception of the one woman walking in the back – we still don't know who that mystery woman was), so you can understand that there is also some sadness in our hearts today. While the chemistry prize this year is for the discovery of the fullerenes, it is given to individuals, and this individual honor can be shared by no more than three. The Nobel committee has done as well as they possibly can with this problem. We understand. But the sadness remains.

[*] Prof. R. E. Smalley
Center of Nanoscale Science and Technology
Rice Quantum Institute, Departments of Chemistry and
Physics Rice University
Houston TX 77005 (USA)
Fax: Int. code +(713)285-5155

[**] Copyright © The Nobel Foundation 1997. We thank the Nobel Foundation, Stockholm, for permission to print this lecture.

On the other hand, there are positive aspects to the limit of three. For example, I have asked what happens in those years when there is only one person receiving an award in physics or chemistry. I was told that you just get one lecture for that prize. Now that I am beginning to appreciate the full impact of having a long lecture from each of the three winners this year in each of the two fields, physics and chemistry, all on the same day and in the same room, I can see that one must set limits somewhere.

This discovery was one of the most spiritual experiences that any of us in the original team of five have ever experienced. The main message of my talk today is that this spiritual experience, this discovery of what Nature has in store for us with carbon, is still ongoing. So the title of my talk is not "The Discovery of the Fullerenes" but rather "Discovering the Fullerenes". Fullerene researchers worldwide are still engaged in this process of discovery.

The sense in which we are still in this process has to do with what the true essence of the 1985 fullerene discovery actually turned out to be. After all, the five people in that happy photograph (Figure 1), brilliant as they all are, were not the ones who first conceived the truncated icosahedron. That was done several thousand years ago. Archimedes gets the credit for it, although one may reasonably suspect that icosahedra had been truncated long before Archimedes. Nor were we the first people to conceive that if you replaced the vertices of that pattern with carbon atoms, and let the carbon do what it wanted to do, that would be an interesting chemical object. That honor had already gone more than a decade before our discovery to E. G. Osawa,[2, 3] the Japanese physical organic chemist who had perceived that carbon in that structure would be aromatic and would therefore probably be stable. And a large part of this honor had been earned even before that by David Jones,[4] who in a wonderfully imaginative piece had conceived closed spheroidal cages made of graphene sheets somehow folded around. A little later, Jones realized that a pentagon would serve nicely as the required defect in an otherwise hexagonal lattice to produce a complex curvature.[5] The notion that C_{60} would be a closed shell molecule with a very large HOMO–LUMO gap, which is a well-appreciated signature of chemical stability, fell to Bochvar, Gal'pern,[6] and Stankevich[7] who actually did the relevant Hückel calculations in Russia well over a decade before we ever got into the game.

The conception of carbon being stable in the form of a truncated icosahedron really wasn't the discovery that is being honored this week. If that were, then Archimedes, Osawa, Jones, and/or one or more of these insightful Soviet scientists should

have gotten the prize. Instead, the discovery that garnered the Nobel Prize was the realization that carbon makes the truncated icosahedral molecule, and larger geodesic cages, all by itself. Carbon has wired within it, as part of its birthright every since the beginning of this universe, the genius for spontaneously assembling into fullerenes. We now realize that all you need to do to generate billions of billions of these objects of such wonderful symmetry is just to make a vapor of carbon atoms and to let them condense in helium. Now we are still in the process of discovering all of the other consequences of the genius that is wired into carbon atoms. It isn't just a talent to make balls. It can also make tubes such as the short section shown in Figure 2.

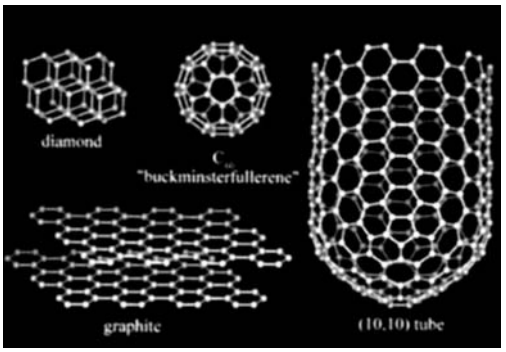

Figure 2. Four perfect crystalline forms of carbon: diamond, graphite, C_{60}, and a short length of a (10,10) fullerene nanotube showing the hemi-C_{240} end cap.

Nearly all of us have long been familiar with the earlier known forms of pure carbon: diamond and graphite. Diamond, for all it's great beauty, is not nearly as interesting as the hexagonal plane of graphite. It is not nearly as interesting because we live in a three-dimensional (3D) space, and in diamond each atom is surrounded in all three directions in space by a full coordination. Consequently, it is very difficult for an atom inside the diamond lattice to be confronted with anything else in this 3D world because all directions are already taken up. In contrast, the carbon atoms in a single hexagonal sheet of graphite (a "graphene" sheet) are completely naked above and below. In a 3D world this is not easy. I do not think we ever really thought enough about how special this is. Here you have one atom in the periodic table, which can be so statisfied with just three nearest neighbors in two dimensions, that it is largely immune to further bonding. Even if you offer it another atom to bond with from above the sheet—even a single bare carbon atom, for the matter—the only result is a mild chemisorption that with a little heat is easily undone, leaving the graphene sheet intact. Carbon has this genius of making a chemically stable two-dimensional, one-atom-thick membrane in a three-dimensional world. And that, I believe, is going to be very important in the future of chemistry and technology in general.

What we have discovered is that if you just form a vapor of carbon atoms and let them condense slowly while keeping the temperature high enough so that as the intermediate species grow they can do what it is in their nature to do, there is a path where the bulk of all the reactive kinetics follows that goes to make spheroidal fullerenes. Now it turns out that in addition to this most symmetric of all possible molecules, C_{60}, and the other fullerene balls, it is possible by adding a few percent of other atoms (nickel and cobalt) to trick the carbon into making tubes. Of all possible tubes there is one tube that is special.[8] It is the tube shown in Figure 2, the (10,10) tube. We are beginning to understand that what causes this tube to be the most favorite of all tubes is also wired within the instruction set of what it means to be a carbon atom. The propensity for bonding that causes C_{60} to be the end point of 30–40% of all the reactive kinetics, leads as well to this (10,10) tube. This detour on the road that otherwise leads to spheroidal fullerenes is taken if you somehow (with cobalt or nickel atoms) frustrate the ability of the open edge to curve in and close. The metal atoms prevent by local annealing the addition of the seventh, eighth, ninth pentagons, and insure by judicious choice of temperature and reaction rate that the growing tublet can anneal to its most energetically favored form.

The object shown in Figure 3 depicts one of the more fascinating new opportunities in the future of the fullerenes. It is a short

Figure 3. Derivatized section of a (10,10) fullerene nanotube with one end open.

piece of the (10,10) tube with chemically derivitized ends. One end is closed with a hemifullerene dome (actually one half of a very special fullerene, icosahedral C_{240}). The other end is intentionally left open. Since the closed end contains pentagons and is accordingly more reactive than the smooth, all-hexagon side of the nanotubes, there are techniques such as boiling in nitric acid[9] for eating the closed ends off of these tubes. We also know that if you take such a tube and put it in an oven and heat it to 1200 °C, it will spontaneously close back again. These ends, regardless of whether they are closed or open, are directly amenable to the formation of excellent C–O, C–N, or C–C covalent bonds[10] to attach nearly any molecule, enzyme, membrane, or surface to the end of the tube. You could attach one or several such objects (let's call them A) to the upper end and some other objects on the bottom (B). What is so stunning about this molecule, unlike any other molecule we have ever had before in chemistry, is that with this object "A" and "B" will communicate with each other by true metallic transport along the tube. The (10,10) tube is a quantum waveguide for electrons.

The band structure of graphene, the individual flat sheet of graphite, is that of a zero gap semiconductor. The valence band and conduction band meet at a point at the end of the Brillouin zone. There is a node in the density of states at Fermi energy,

and accordingly it is not a very good conductor. In my youth on first hearing that graphite was a poor conductor—more like lead than gold—I had thought that the problem must be due to some sort of original sin that the carbon had made. The valence electrons of carbon tended to be localized, and were not freely able to move from one carbon atom to another through an extended sheet. In fact that is not the problem. The π electrons are perfectly itinerant in the graphene sheet, just as they are perfectly itinerant in the aromatic ring of benzene. In fact, it is the freedom of the electrons to move around the ring that gives the special chemical stability to aromatic molecules. The trouble with the electrical conductivity is that when you calculate the band structure of the hexagonal graphene sheet, by symmetry, there is a node in the density of states at the Fermi energy. Even if you were somehow able to replace every one of the carbon atoms in the hexagonal lattice with a gold atom, the band structure would still look the same. It is the symmetry of the hexagonal lattice that is the problem, not the itinerancy of the π electrons of carbon.

But now we realize that there is one (but only one) answer to this problem of making a metal out of pure carbon. If you take the graphene sheet and cut out a thin strip, curl it along it's length to form a long cylinder, and seal up the dangling bonds together to form the (10,10) tube (Figure 2), the very symmetry that had been your enemy in preventing metallic behavior from the flat lattice, now becomes your friend. The symmetry of this tubular hexagonal lattice now insists that there will be two bands that cross at the Fermi energy, approximately two thirds of the way across the Brillouin Zone, (Figure 4). In addition, the

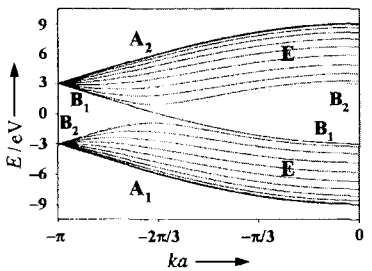

Figure 4. Electronic band structure of a (10,10) fullerene nanotube calculated with tight binding methods, using zone-folding from the band structure of an infinite two-dimensional graphene sheet [59]. The two bands that cross the Fermi energy at $ka = 2\pi/3$ have different symmetry, and guarantee that the tube will be a metallic conductor. k = crystal momentum, a = unit cell length.

cohesive rigidity of the σ-bond framework of the graphene sheet prevents the metallic π electrons from engendering a Peierls instability that normally plagues all such one-dimensional conductors.[11] The (10,10) fullerene tube, and all (n,n) tubes in general, will be a molecular wire that is simultaneously a good metallic conductor, and a good molecule, maintaining its structure and conductivity even when exposed to air and water in the real world.

I believe that in the future of chemistry, we are likely to see a vast new set of metallic fullerene molecules such as that shown in Figure 3 readily available from chemical supply houses. Imagine what the impact could be. Essentially, every technology you have ever heard of where electrons move from here to there, has the potential to be revolutionized by the availability of molecular wires made up of carbon. Organic chemists will start building devices. Molecular electronics could become reality.

This is where the fullerenes appear to be leading at the moment. One does not get a feeling that we are over with this discovery process yet. There may be many more wondrous properties of this one little atom in the periodic table than we have yet to appreciate.

Still there was a particular discovery that we celebrate this week. There was something about September of 1985. What was that? How did that happen? Since that original discovery we have been involved in a little bit of what I like to call the archeology of the buckyball: looking back in the written and oral history trying to decide what the roots of the fullerene discovery were. This discovery is principally about the way that carbon condenses, it's genius for forming clusters.

It has long been known that the carbon has a special ability to cluster in the gas phase at high temperatures. Unlike every other refractory element in the periodic table, the vapor of carbon in equilibrium with its solid at temperatures in the 3000–4000 K range is dominated by clusters, C_n, with substantial abundance of species as high as C_{15}. The first evidence of this extends back to early research on nuclear fission products by Hahn and Strassman in Germany.[12] They noticed that carbon cluster ions up to C_{15}^+ were produced in a high frequency arc with a graphite electrode, the arc being used for elemental analysis by mass spectrometry;[13] similar observations were made in the US about this same time in research associated with the Manhattan Project during the second world war.[14] By the early 1950s it was clear that there were sufficient numbers of small carbon clusters at equilibrium in the vapor to have a major affect on the measurement[15, 16] of the heat of formation of C(gas), one of the most important constants in chemical thermodynamics. In 1959 Pitzer and Clementi[17, 18] made the first serious quantum calculations of the structures responsible for this behavior in the vapor up to about 20 atoms, and concluded that they had the form of linear chains for C_2 up to about C_{10}, and above that they took the form of monocyclic rings—little 'Hula Hoops' of pure carbon.

Although it was not commented on at the time, this is quite a remarkable result. Here carbon is able to make clusters that are so stable that they are the dominant species—substantially more abundant than C_1—in the gas phase even at a temperature of 3000–4000 K, and they do this with only a coordination number of two! All other refractory elements such as platinum, tungsten, or tantalum achieve their high cohesive energy by a close packing arrangement within the bulk crystal or liquid, with coordination number of 8 to 12. Even though the clusters of these metals in the gas phase also adopt compact structures,[19] arranging as many atoms around each other in three dimensions as possible, they still do not have a sufficiently high cohesive energy to be abundant in the equilibrium vapor. Instead the vapor of these metals is almost completely monatomic. Above 1000 K the vapor in equilibrium with pure condensed phase of every element in the periodic table—except carbon—is dominantly either monatomic or diatomic. But here is carbon making so many of these large clusters that it throws off the measures of heat of formation, and in a show of chemical bonding *chutzpah*, doing this with two of it's three available dimensions for bonding "tied behind its back."

Looking back now at the data available in the literature on gas phase clusters of pure carbon up to mid 1984, it is clear that there was no suggestion in the experiments of anything more interesting going on than these one-dimensional clusters.[20, 21] All the data appeared to be well-explained by the model of linear chains and monocyclic rings, and the cluster abundance dropped off so severely by the time the clusters were in the mid-twenty-atom size that no one was led to speculate what would happen as the clusters grew larger. In light of what we now know about the fullerenes, this would have been a very fruitful line of speculation. After all, at some point as the clusters grew larger they would certainly have to start trying structures that were two- or three-dimensional. What would these look like? Consideration of the dangling bond energies could reasonably have led to the speculation that graphene sheets would form but curl up to closed cages.

But, as far as we can determine, no such speculation ever occurred. While in the mid 60's Jones[4] had the notion that graphene sheets could curl up to make "hollow molecules," Osawa[2] had already conjured up the notion of carbon in a soccer ball structure in early 1970, and Gal'pern[6] had completed the first of many Hückel calculations showing that it would be a closed shell molecule with a large HOMO–LUMO gap in 1973, but no one ever suggested these objects could form spontaneously in a condensing carbon vapor. The mystery of the buckyball was never so much that it would be a stable molecule once formed. After all, it violates no rules of organic chemistry. The secret laying there to be discovered is that part of carbon's "birth right" is the genius to form a chemically passive two-dimensional surface, to self-assemble fullerenes in general, and C_{60} in particular and in sensationally high yield, out of the chaos of a carbon vapor at thousands of degrees.

To trigger this realization, new data turned out to be necessary. Data on what happened when you allowed a carbon vapor to become supersaturated, allowed it to begin to condense, and the small clusters that were in equilibrium with the solid began to grow larger. That data had to wait for the invention of a new technique, something that would enable one to study the properties of carbon clusters in detail as they grow through the size range of 40 to 100 atoms where the dimensionality of the bonding does, in fact, increase from 1 to 2. It had to wait for the laser-vaporization cluster beam methods of the 1980s.

The laser-vaporization supersonic cluster beam technique was originally developed at Rice University in 1980–1981 as a means of studying clusters of virtually any element in the periodic table, including highly refractory metals[22–26] and semiconductors such as silicon[27] and gallium arsenide.[28] The objective of this line of research was to explore the behavior of matter intermediate in size between atoms and bulk crystals. It grew out of decades of development of atomic and molecular beams, and in particular the development of seeded supersonic molecular beams as a means of "freezing out" the vast number of rotational and vibrational excitations which otherwise preclude detailed study of polyatomic molecules.[29–32] In addition to enabling the study of common chemically stable polyatomic molecules, it was possible to generate supercold van der Waals clusters of these molecules with each other, and with other species, including at these ultralow temperatures even helium.[33] By the use of intense pulsed laser irradiation within the supersonic nozzle it was possible to study highly reactive fragments of molecules, free radicals.[34] Extension of the supersonic beam technique to seeded beams of refractory atoms and clusters was a direct outgrowth of this early work on free radicals.

Once beams of refractory clusters were available, a vast new area of research was opened, for each cluster may be thought of as a nanoscale crystalline particle that has a surface (in fact, most of it is surface). Supersonic metal cluster beams thereby provided a route to a new sort of surface science.[35] In my research group at Rice we were very heavily engaged in developing this new science. We developed and applied new methods for studying the electronic structure of the clusters by one- and two-photon laser photoionization with time-of-flight mass spectral detection,[25, 36, 37] photodissociation, and photodepletion spectroscopy,[38–40] and ultraviolet photoelectron spectroscopy.[41] In order to study the surface of the nanoscale clusters, we developed techniques using a fast flow reactor attached to the end of the supersonic nozzle.[42–44] We developed a variety of methods involving charged ions of the clusters levitated in a magnetic field and probed by ion cyclotron resonance spectroscopy,[45–47] etc. The early 1980s were a very busy, very fruitful time in this research group at Rice University, and much was learned.

The laser vaporization supersonic beam source and the associated probe techniques that we developed to study the 2–200 atom metal and semiconductor clusters was effectively a new sort of microscope. It allowed one to "see" something of the nature of nanoscopic aggregates of atoms in a way that was entirely new, and very poignant. Whatever we measured for the cluster in the supersonic beam, we knew that it was the true property of the cluster traveling free in space. We developed the technique in order to bring a sort of intellectual tension to surface science: to make measurements so fundamental that theorists stayed awake at night trying to understand them. Although we had no notion of it at the time we were engaged in this enterprise in the early 1980s, we were building the instrument and the line of research that would discover the fullerenes. All one had to do is put carbon in this new "microscope", adjust the focus a little, and "see" the fullerenes revealed plainly for the first time.

As it happened, we at Rice were not the first to put carbon into the new microscope. In 1984 a group headed by Andrew Kaldor at Exxon used such an apparatus (actually one that had been designed and built at Rice) in a study of carbon clusters that was motivated by the desire to study coke buildup on reforming catalyst. Now, in a famous mass spectrum reproduced here as Figure 5, carbon clusters were evident extending out beyond 100 atoms,[48] and it was immediately clear that a whole new world of interesting carbon clusters could exist that had never been seen before.

Three distinct regions characterized the mass spectrum: first the small clusters, containing fewer than 25 atoms, consisting of the chains and monocyclic rings[49] so well known from the earlier studies; second a new region between about 25 and 35 atoms in which few species of any sort were observed—a region that the Rice group came to call the "forbidden zone"; and, third, an even-numbered clusters distribution extending from the high 30s to well over 150 atoms. By early 1984 the laser-vaporization supersonic cluster beam technique had been

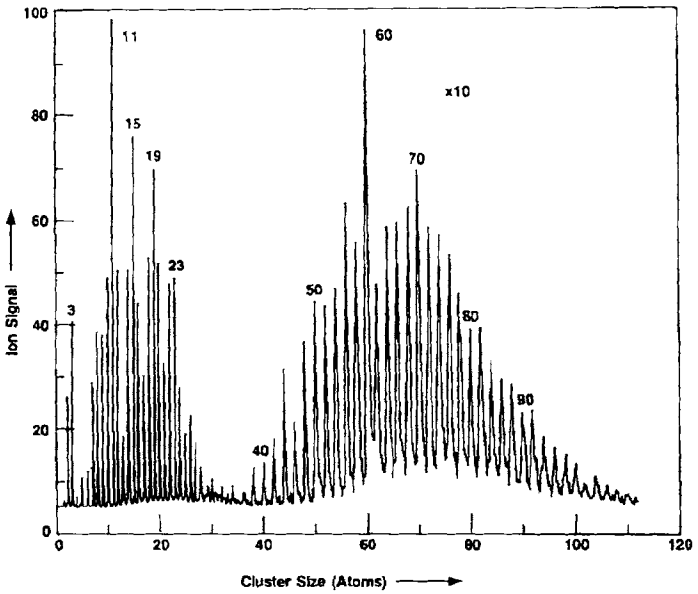

Figure 5. Mass spectrum of carbon clusters in a supersonic beam produced by laser vaporization of a carbon target in a pulsed supersonic nozzle operating with a helium carrier gas. The wide distribution of even-numbered carbon clusters starting near C_{40} and extending to over C_{100} is due the fullerenes. This was the first published experiment that revealed the fullerene cluster distribution, although it was not appreciated as such at the time. Reproduced with permission of the authors [48].

used to study clusters broadly throughout the periodic table, and many "magic number" cluster distributions had been found and studied,[35] but nothing remotely like this even-numbered distribution of carbon had ever been seen for any other element. Today this is still true: carbon is unique.

The even-numbered distribution seen by the Exxon group was due to the fullerenes. I suspect the members of that original group at Exxon still regret that they did not consider in more depth why the peak for C_{60} appeared to be about 20% more intense than its neighbors. But to be fair, at the time neither did we. This result of the Exxon group was widely known in the burgeoning metal and semiconductor cluster research world by the summer of 1984. I saw the result at a meeting, and discussed it with Andy Kaldor at some length. Bob Curl saw it. Harry Kroto saw it. Wolfgang Krätschmer and Donald Huffman saw it. None of us stopped to think just what might be the reason C_{60} was a little more prominent than the other even numbered clusters. It did not stand out sufficiently above its neighbors to attract notice. As it turned out, the Exxon group simply had not "focussed" the new cluster beam microscope carefully enough.

At nearly the same time another research group, including one of my former graduate students, Michael Geusic, had built a supersonic cluster beam apparatus as well, and was engaged in early experiments with mass-selected semiconductor cluster ions.[50] Having heard about the Exxon work, they put carbon in the apparatus, also observed the mysterious even-numbered large cluster distribution, and even selected out C_{60}^+ for a photofragmentation experiment. But they, too, failed to experiment sufficiently with the nozzle conditions to appreciate the potential preeminence of C_{60}.

The necessary "focussing" of the new supersonic cluster beam "microscope" was finally performed in my laboratory at Rice in the September of 1985.[1, 51] Now the supremacy of C_{60}, was made clear. In thinking about what this all meant, we finally saw that C_{60} must be a closed spheroidal cage. No other explanation was consistent with the observed facts. The realization that all the even-numbered carbon cluster distribution was due to carbon in the form of hollow geodesic domes—fullerenes—came within a month, as a result of reactivity studies of these clusters[52] using the fast flow reactor on the end of the supersonic nozzle. Soccer ball C_{60} quickly became a sort of "Rosetta Stone" leading to the discovery of a new world geodesic structures of pure carbon built on the nanometer scale.

This discovery episode has by now been so extensively covered in articles,[53, 54] monographs,[55, 56] and television documentaries, that there is little reason to repeat the details here. We succeeded where two other groups had failed for at least two reasons. First, we had evolved a better version of the "microscope". We had been the group to develop the supersonic cluster beam technique in the first place, and we were still leading the subsequent development and elaboration of its capabilities. The original apparatus, known affectionately by the students as "AP2" (Figure 6), was able to handle much larger gas flows,

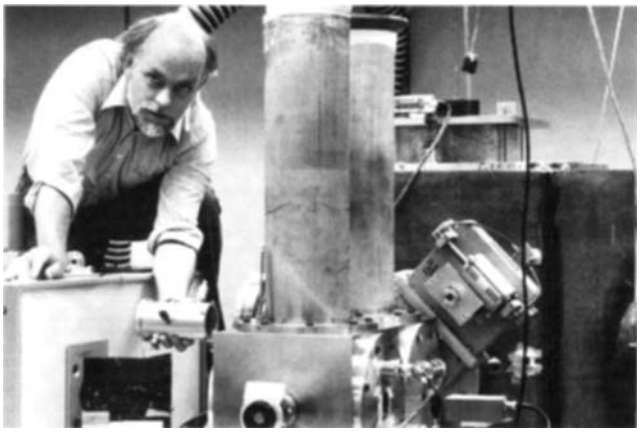

Figure 6. Photograph of the author climbing around on the top of a section of AP2, the supersonic laser-vaporization cluster beam apparatus that enabled the discovery of C_{60} and the fullerenes in the fall of 1985.

and had a more advanced supersonic nozzle design than the machines of either of the other groups. Particularly important was the development of the rotating disc design for the cluster beam source that we had just recently completed for our semiconductor cluster work with silicon, germanium,[27] and gallium arsenide.[28] As part of this project, it was necessary to anneal the semiconductor clusters in the supersonic nozzle source as much as possible. To simplify interpretation we need conditions so that the most energetically stable geometrical form would dominate the cluster distribution. For this reason the nozzle was fitted with a variety of down-stream flow restrictors to form what we called the "integrating cup" (Figure 7).

It was our experience with the extra "chemical cooking" achieved by this device that made us appreciate that it was cluster chemistry that differentiated C_{60} from the others. The relative absence of further up-clustering reactions was, we realized, what ultimately made the C_{60} peak stand out over 50 times more intensely than any other. And it was in thinking about how 60 carbon atoms could possibly avoid reactive edges, that we were led to the conclusion that C_{60} is a truncated icosahedron.

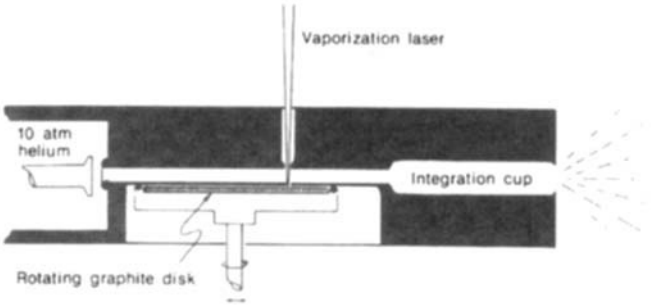

Figure 7. Schematic cross-sectional drawing of the supersonic laser-vaporization nozzle source used in the discovery of the fullerenes. Note the section labeled "integrating cup". Cluster "cooking" reactions in this zone were responsible for the C_{60} cluster becoming over 50 times more intense than any other cluster in the nearby size range. These up-clustering reactions with small carbon chains and rings reacted away nearly all clusters except for C_{60}, which because of its perfect symmetry survived.

The second reason I believe we succeeded was, in a word, karma. With Bob Curl in our collaboration on semiconductor clusters, we had evolved one of the most intellectually demanding and penetrating styles of research I have ever witnessed in any research group. Sean O'Brien had evolved just the right version of the cluster nozzle to handle the difficulties of dealing with semiconductor discs, and Jim Heath had developed an amazing talent for making "science happen" on the machine. When Harry Kroto came, his intensity and scientific background blended in perfectly. Working with the students mostly in late afternoons and at night, and in daily marathon conversations with me, he kept the focus of our minds on the results coming out of AP2, under the hot hands of Heath and O'Brien. One way or another, over the years, each member of the team had paid the dues required to deserve to be there for the discovery of the fullerenes during those wonderful days in September 1985.

Contrary to most written accounts, I do not believe the discovery of the fullerenes had much to do with questions of astrophyiscs, such as the mechanism of formation of interstellar carbon molecules. While this was certainly what brought Kroto to Texas, and this was without contest the reason we first put carbon into AP2 in preparation for his visit, in the end the connection of this line of research[57, 58] to the fullerene discovery was casual, not causal. The discovery of C_{60} and the fullerenes would have been made by AP2 or some other such instrument within a year or two in any event. Two other groups had already put carbon in a supersonic cluster beam machine for reasons that were much more mundane. At Exxon, as mentioned earlier, their principal concern was to understand carbon buildup on catalysts, while at AT & T Bell Laboratories the motivation derived from their long-term interest in semiconductors and the nanometer scale.

The notion that the discovery of the fullerenes came out of research into the nature of certain molecules in space is highly appealing to scientists. It is hard to think of any line of research that is less likely than interstellar chemistry to have some practical, technological impact back here on Earth. So if fullerenes turn out to lead to the technological wonders that some people (like me) believe are in our future, then perhaps one can argue that *any* research project could get lucky too, no matter how irrelevant to worldly problems it may currently seem. I have argued this way in the past, and I still believe there is some sense to it—but only a little. In fact, the fullerenes were discovered as a result of decades of research and development of methods to study first atoms, then polyatomic molecules, and ultimately nanometer-scale aggregates. It was well-funded research that at nearly every stage was justified by its perceived relevance to real world technological problems. To a great extent, many of these earlier bets as to the worldly significance of fundamental research actually paid off.

While it is fun to think about the wonderful role of serendipity in the story, one should also spend a bit of time comprehending the inevitability of the discovery as well. The only character of true genius in the story is carbon. Fullerenes are made wherever carbon condenses. It just took us a little while to find out.

Received: April 7, 1997 [A 220IE]
German version: *Angew. Chem.* **1997**, *109*, 1666–1673

Keywords: carbon allotropes · fullerenes · nanostructures · Nobel lecture

[1] H. W. Kroto, J. R. Heath, S. C. O'Brien, R. F. Curl, R. E. Smalley, *Nature* London **1985**, *318*, 162.
[2] E. Osawa, *Kagaku* **1970**, *25*, 854.
[3] E. Osawa, *Philos. Trans. R. Soc. London A* **1993**, *343*, 1.
[4] D. E. H. Jones, *New Sci.* **1966**, *32*, 245.
[5] D. E. H. Jones, *The Inventions of Daedalus*, Freeman, Oxford, **1982**.
[6] D. A. Bochvar, E. G. Gal'pern, *Proc. Acad. Sci. USSR* **1973**, *209*, 610.
[7] I. V. Stankevich, M. V. Nikerov, D. A. Bochvar, *Russ. Chem. Rev.* **1984**, *53*, 640.
[8] A. Thess, R. Lee, P. Nikolaev, H. Dai, P. Petit, J. Robert, C. Xu, Y. H. Lee, S. G. Kim, A. G. Rinzler, D. T. Colbert, G. E. Scuseria, D. Tománek, J. E. Fischer, R. E. Smalley, *Science* **1996**, *273*, 483.
[9] S. C. Tsang, Y. K. Chen, P. J. F. Harris, M. L. H. Green, *Nature* **1994**, *372*, 159.
[10] A. Hirsch, *Chemistry of the Fullerenes*, Thieme, New York, **1995**.
[11] J. W. Mintmire, B. I. Dunlap, C. T. White, *Phys. Rev. Lett.* **1992**, *68*, 631.
[12] O. Hahn, F. Strassmann, J. Mattauch, H. Ewald, *Naturwissenschaften* **1942**, *30*, 541.
[13] J. Mattauch, H. Ewald, O. Hahn, F. Strassmann, *Z. Phys.* **1943**, *120*, 598.
[14] L. Brewer, P. W. Gilles, F. A. Jenkins, *J. Chem. Phys.* **1948**, *16*, 797.
[15] W. A. Chupka, M. G. Inghram, *J. Chem. Phys.* **1953**, *21*, 1313.
[16] W. A. Chupka, M. G. Inghram, *J. Phys. Chem.* **1955**, *59*, 100.
[17] K. S. Pitzer, E. Clemente, *J. Am. Chem. Soc.* **1959**, *81*, 4477.
[18] S. J. Strickler, K. S. Pitzer in *Molecular Orbitals in Chemistry, Physics, and Biology* (Eds.: P. O. Lowdin, B. Pullman), Academic Press, New York, **1964**, p. 281.
[19] M. F. Jarrold, *J. Phys. Chem.* **1995**, *99*, 11.
[20] E. Dornenburg, H. Hintenberger, *Z. Naturforsch. A* **1959**, *14*, 765.
[21] E. Dornenburg, H. Hintenberger, J. Franzen, *Z. Naturforsch. A* **1961**, *16*, 532.
[22] T. G. Dietz, M. A. Duncan, D. E. Powers, R. E. Smalley, *J. Chem. Phys.* **1981**, *74*, 6511.
[23] D. L. Michalopoulos, M. E. Geusic, S. G. Hansen, D. E. Powers, R. E. Smalley, *J. Phys. Chem.* **1982**, *86*, 3914.
[24] D. E. Powers, S. G. Hansen, M. E. Geusic, A. C. Puiu, J. B. Hopkins, T. G. Dietz, M. A. Duncan, P. R. R. Langridge-Smith, R. E. Smalley, *J. Phys. Chem.* **1982**, *86*, 2556.
[25] D. E. Powers, S. G. Hansen, M. E. Geusic, D. L. Michalopoulos, R. E. Smalley, *J. Chem. Phys.* **1983**, *78*, 2866.
[26] J. B. Hopkins, P. R. R. Langridge-Smith, M. D. Morse, R. E. Smalley, *J. Chem. Phys.* **1983**, *78*, 1627.
[27] J. R. Heath, Y. Liu, S. C. O'Brien, Q.-L. Zhang, R. F. Curl, F. K. Tittel, R. E. Smalley, *J. Chem. Phys.* **1985**, *83*, 5520.
[28] S. C. O'Brien, Y. Liu, Q. Zhang, J. R. Heath, F. K. Tittel, R. F. Curl, R. E. Smalley, *J. Chem. Phys.* **1986**, *84*, 4074.
[29] R. E. Smalley, B. L. Ramakrishna, D. H. Levy, L. Wharton, *J. Chem. Phys.* **1974**, *61*, 4363.
[30] R. E. Smalley, L. Wharton, D. H. Levy, *J. Chem. Phys.* **1975**, *63*, 4977.
[31] R. E. Smalley, L. Wharton, D. H. Levy in *Chemical and Biochemical Applications of Lasers* (Ed.: C. B. Moore), Academic Press, **1977**, pp. 1-43.
[32] R. E. Smalley, L. Wharton, D. H. Levy, *Acc. Chem. Res.* **1977**, *10*, 139.
[33] R. E. Smalley, D. H. Levy, L. Wharton, *J. Chem. Phys.* **1976**, *64*, 3266.
[34] D. E. Powers, J. B. Hopkins, R. E. Smalley, *J. Phys. Chem.* **1981**, *85*, 2711.

[35] R. E. Smalley in *Comparison of Ab Inition Quantum Chemistry with Experiment for Small Molecules* (Ed.: R. J. Bartlett), Reidel, Boston, **1985**, pp. 53–65.
[36] T. G. Dietz, M. A. Duncan, M. G. Liverman, R. E. Smalley, *J. Chem. Phys.* **1980**, *73*, 4816.
[37] D. L. Michalopoulos, M. E. Geusic, P. R. R. Langridge-Smith, R. E. Smalley, *J. Chem. Phys.* **1984**, *80*, 3556.
[38] M. D. Morse, J. B. Hopkins, P. R. R. Langridge-Smith, R. E. Smalley, *J. Chem. Phys.* **1983**, *79*, 5316.
[39] P. J. Brucat, L.-S. Zheng, C. L. Pettiete, S. Yang, R. E. Smalley, *J. Chem. Phys.* **1986**, *84*, 3078.
[40] P. J. Brucat, C. L. Pettiete, S. Yang, L.-S. Zheng, M. L. Craycraft, R. E. Smalley, *J. Chem. Phys.* **1986**, *85*, 4747.
[41] O. Cheshnovsky, P. J. Brucat, C. L. Pettiette, S. Yang, M. J. Craycraft, R. E. Smalley in *Photoelectron Spectroscopy of Metal Cluster Ion Beams* (Eds.: P. Jena, S. Kanna, B. Rao) (International Symposium on the Physics and Chemistry of Small Clusters), Plenum, New York **1987**, pp. 1–13.
[42] M. D. Morse, M. E. Geusic, J. R. Heath, R. E. Smalley, *J. Chem. Phys.* **1985**, *83*, 2293.
[43] M. E. Geusic, M. D. Morse, R. E. Smalley, *J. Chem. Phys.* **1985**, *82*, 590.
[44] M. E. Geusic, M. D. Morse, S. C. O'Brien, R. E. Smalley, *Rev. Sci. Instrum.* **1985**, *56*, 2133.
[45] J. M. Alford, P. E. Williams, D. J. Trevor, R. E. Smalley, *Int. J. Mass Spectrom. Ion Processes* **1986**, *72*, 33.
[46] J. M. Alford, F. D. Weiss, R. T. Laaksonen, R. E. Smalley, *J. Phys. Chem.* **1986**, *90*, 4480.
[47] J. L. Elkind, F. D. Weiss, J. M. Alford, R. T. Laaksonen, R. E. Smalley, *J. Chem. Phys.* **1988**, *88*, 5215.
[48] E. A. Rohlfing, D. M. Cox, A. Kaldor, *J. Chem. Phys.* **1984**, *81*, 3322.
[49] S. Yang, K. J. Taylor, M. J. Craycraft, J. Conceicao, C. L. Pettiete, O. Cheshnovsky, R. E. Smalley, *Chem. Phys. Lett.* **1988**, *144*, 431.
[50] L. A. Bloomfield, M. E. Geusic, R. R. Freeman, W. L. Brown, *Chem. Phys. Lett.* **1985**, *121*, 33.
[51] R. F. Curl, R. E. Smalley, *Science* **1988**, *242*, 1017.
[52] Q.-L. Zhang, S. C. O'Brien, J. R. Heath, Y. Liu, R. F. Curl, H. W. Kroto, R. E. Smalley, *J. Phys. Chem.* **1986**, *90*, 525.
[53] *The Chemical Intelligencer, Vol. 1* (Ed.: I. Hargittai), Springer, New York **1995**, pp. 6–54.
[54] R. E. Smalley, *Sciences* **1991**, 22.
[55] J. Baggott, *Perfect Symmetry, The Accidental Discovery of Buckminsterfullerene*, Oxford University Press, Oxford, **1994**.
[56] H. Aldersey-Williams, *The Most Beautiful Molecule, The Discovery of the Buckball*, Wiley, New York, **1995**.
[57] J. R. Heath, Q.-L. Zhang, S. C. O'Brien, R. F. Curl, H. W. Kroto, R. E. Smalley, *J. Am. Chem. Soc.* **1987**, *109*, 359.
[58] H. W. Kroto, J. R. Heath, S. C. O'Brien, R. F. Curl, R. E. Smalley, *Astrophys. J.* **1987**, *314*, 352.
[59] M. S. Dresselhaus, G. Dresselhaus, P. C. Eklund, *Science of Fullerenes and Carbon Nanotubes*, Academic Press, San Diego, **1996**.

Deposition of Data from X-Ray Structure Analyses

In order to make life easier for authors and referees the Cambridge Crystallographic Data Centre (CCDC) and the Fachinformationszentrum Karlsruhe (FIZ) have unified their procedures for the deposition of data from single-crystal X-ray structure analyses.

Prior to submitting your manuscripts please deposit the data for your compound(s) **electronically** at the appropriate data base, that is, at the CCDC for organic and organometallic compounds and at the FIZ for inorganic compounds. Both data bases will be pleased to provide help (see our *Notice to Authors* in the first issue of this year). In general, you will receive a depository number from the data base within two working days after electronic deposition; please include this number with the appropriate standard text (see our *Notice to Authors*) in your manuscript. This will enable the referees to retrieve the structure data quickly and efficiently if they need this information to reach their decision.

This is now the uniform procedure for manuscripts submitted to the journals *Advanced Materials, Angewandte Chemie, Chemische Berichte/Recueil, Chemistry—A European Journal*, and *Liebigs Annalen/Recueil*.

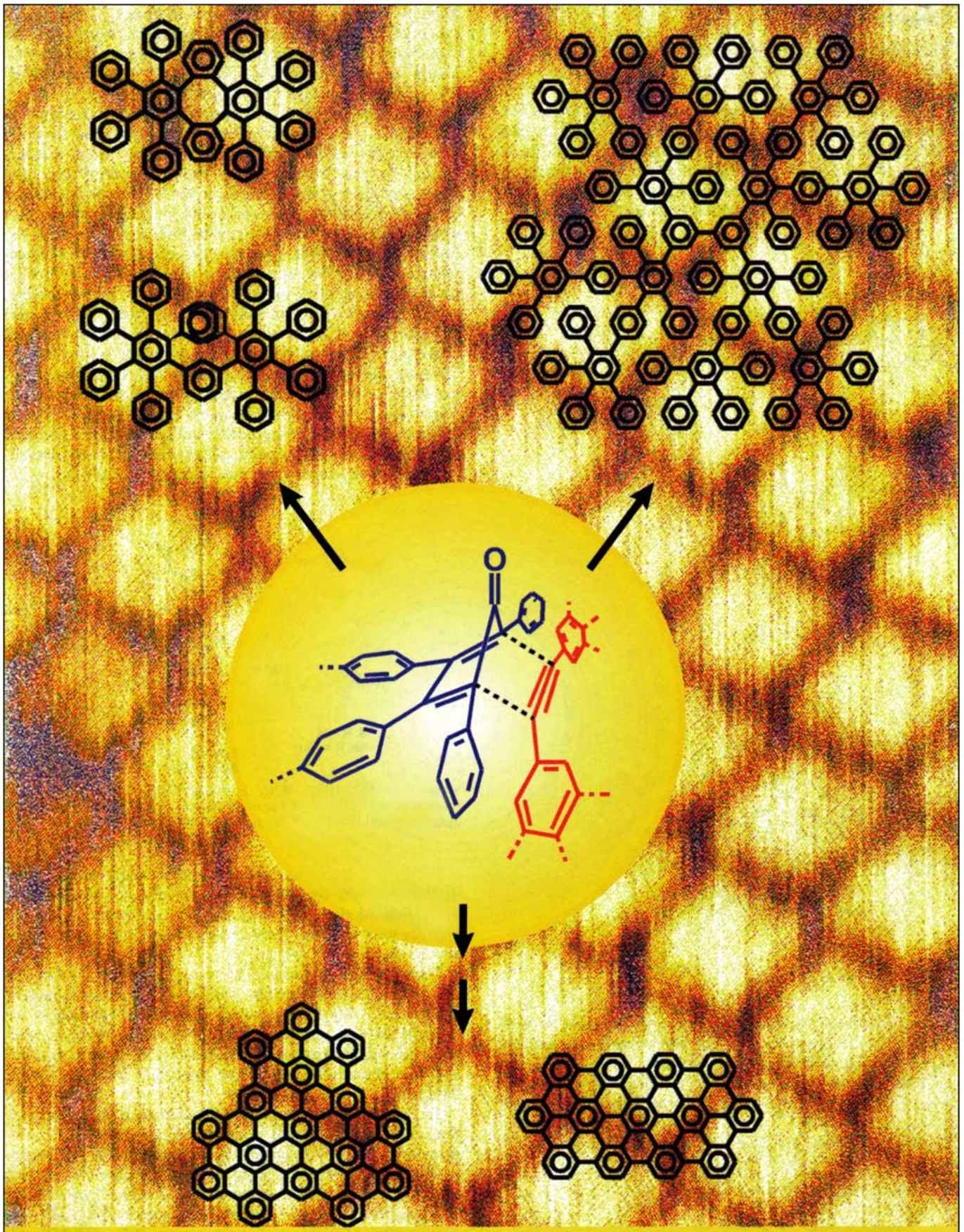

Diphenylacetylene derivatives react with tetraphenylcyclopentadienone to form oligo- and polyphenylenes (top) as well as polycyclic arenes (bottom). Background: An STM image (R. Strohmaier, Stuttgart) of a polycylic arene synthesized by this method. K. Müllen et al. report more on this "graphite chemistry" on the following pages.

 © VCH Verlagsgesellschaft mbH, D-69451 Weinheim, 1997 0570-0833/97/3607-1603 $ 17.50 + .50/0

From Hexa-*peri*-hexabenzocoronene to "Superacenes"**

Vivekanantan S. Iyer, Mike Wehmeier, J. Diedrich Brand, Menno A. Keegstra, and Klaus Müllen*

We recently synthesized soluble derivatives of hexa-*peri*-hexabenzocoronene (**1**) by cyclodehydrogenation.[1] Compounds such as **1** are building blocks for supramolecular architectures; thus **1a** shows a stable discotic mesophase with a hexagonal superstructure over a wide temperature range[2] and forms monomolecular layers on suitable substrates.[1]

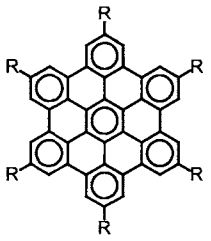

1: R = H

1a: R = *n*-$C_{12}H_{25}$

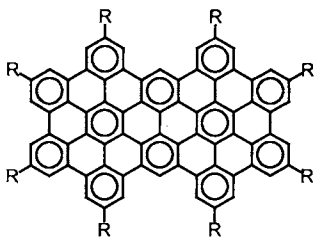

2: R = H, **2a**: R = *t*Bu

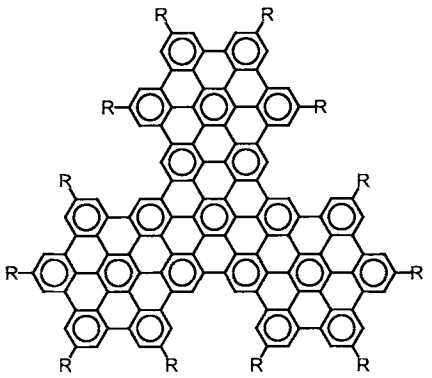

3: R = H, **3a**: R = *t*Bu

A key question concerns the change in the two- and three-dimensional superstructures upon further increasing the size and varying the periphery of the disc molecules. Their shape is particularly important when attempting to achieve densely packed layers on surfaces.[3] Here we outline a general synthetic strategy and disclose the syntheses of some extremely large polycyclic aromatic hydrocarbons (PAHs) derived from **1**. If, from a design point of view, one considers the hexagonal structure of **1** as "superbenzene", fusion reactions of **1** can lead to various homologues such as "supernaphthalene" (**2**), "supertriphenylene" (**3**), or the "phenalenyl" framework **17**.[4]

Our synthesis of PAHs is based on two steps: 1) construction of a soluble polyphenylene precursor of well-defined structure with a close spatial arrangement of the phenyl rings, which is similar to the framework of the target molecule, and 2) planarization of this precursor to the PAH by intramolecuar cyclodehydrogenation. Whereas cyclotrimerization of substituted diphenylacetylenes is restricted to PAH precursors with sixfold symmetry,[6] Diels–Alder reaction of tetraphenylcyclopentadienones with diarylacetylenes is a well-established method for the construction of polyaryl compounds.[7] By this process, each Diels–Alder reaction (followed by extrusion of CO) adds five phenyl rings to an existing alkyne in a one-pot reaction. Therefore, the task of designing the precursor is simplified to choosing the right alkyne. It appears that the known **10**[10] would be a suitable precursor to **2**. Alkyl substitution is a key step towards the synthesis of soluble PAHs. The 1,2-diketone synthesis by Mueller-Westerhoff[8] and our improved synthesis of 1,3-diarylacetones[9] expedite the synthesis of alkyl-substituted tetraphenylcyclopentadienones (Scheme 1, Table 1).

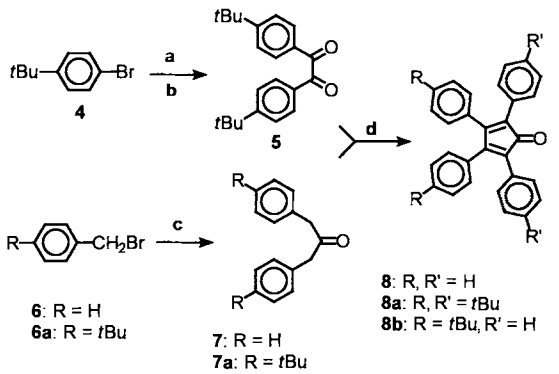

Scheme 1. a) *n*BuLi/THF/ −78 °C; b) 1,4-dimethylpiperazine-2,3-dione, 60% (two steps); c) $[Fe(CO)_5]$ (0.5 equiv)/NaOH/CH_2Cl_2/H_2O/5 mol% dodecyltrimethylammonium bromide, 65%; d) KOH/EtOH/reflux/3 h, 90–95%.

Diels–Alder reaction of alkyne **9** with two equivalents of **8** or **8a** resulted in the corresponding polyphenylene compounds **10** and **10a**, respectively, in nearly quantitative yields. Similarly, **12** and **12a** were obtained from triyne **11** and three equivalents of **8** or **8b** (Scheme 2, Table 1).

Triyne **15** was synthesized by trimerization of 3-bromoacetophenone (**13**; commercially available) with tetrachlorosilane in ethanol[11] followed by palladium-catalyzed coupling of tribromide **14** with phenylacetylene. Diels–Alder reaction of **15** with three equivalents of **8** or **8a** resulted in the precursors **16** and **16a**, respectively, in greater than 90% yield (Scheme 3, Table 1).

Similar to our results from the cyclodehydrogenation reactions of hexaarylbenzenes to give derivatives of **1**,[1,12] cyclodehydrogenation of the unsubstituted precursors **12** and **16** proceeded smoothly with copper(II) trifluoromethane sulfonate and aluminum(III) chloride to give the desired planar PAHs **17** and **3**, respectively (Scheme 4), which were identified by laser-desorption time-of-flight mass spectrometry (LD-TOF-MS; **17**: $M^+ = 1183\ g\,mol^{-1}$; **3**: $M^+ = 1633\ g\,mol^{-1}$). Cyclodehydrogenation of **10** with copper(II) chloride and aluminum(III) chlo-

[*] Prof. Dr. K. Müllen, Dr. V. S. Iyer, Dipl.-Chem. M. Wehmeier, Dipl.-Chem. J. D. Brand, Dr. M. A. Keegstra
Max-Planck-Institut für Polymerforschung
Ackermannweg 10, D-55128 Mainz (Germany)
Fax: Int. code +(6131)379-350
e-mail: muellen@mpip-mainz.mpg.de

[**] This work was supported by the Volkswagenstiftung and the Bundesministerium für Bildung und Forschung. V. S. I. thanks the Max-Planck-Gesellschaft for a fellowship.

Table 1. Selected spectroscopic data [a] of **2**, **2a**, **3**, **3a**, **10a**, **12**, **12a**, **16**, **16a**, **17**, **17a**, and **20** [15].

2: MS (LD-TOF): m/z (%) = 891 (100) [M^+] (calcd for $C_{72}H_{26}$ = 891).

2a: MS (MALDI-TOF): m/z (%) = 1340 (100) [M^+] (calcd for $C_{104}H_{90}$ = 1339.86); UV/Vis (1,1,2,2-tetrachloroethane): λ_{max} = 362, 415, 478, 505 nm.

3: MS (LD-TOF): m/z (%) = 1633.6 (100) [M^+] (calcd for $C_{132}H_{48}$ = 1633.48).

3a: MS (MALDI-TOF): m/z (%) = 2303.4 (100) [M^+] (calcd for $C_{180}H_{138}$ = 2301.08); UV/Vis (1,1,2,2-tetrachloroethane): λ_{max} = 363, 397, 424, 487, 522 nm.

10a: MS (FD, 8 kV): m/z (%) = 1364.1 (100) [M^+] (calcd for $C_{104}H_{114}$ = 1364.05); ^{13}C NMR (125 MHz, [D$_2$]1,1,2,2-tetrachloroethane, 140 °C): δ = 31.22, 31.27, 31.29, 31.33, 33.91, 33.95, 34.06, 34.16, 118.96, 125.05, 125.27, 130.67, 132.50, 133.29, 133.78, 133.91, 136.93, 137.29, 137.99, 138.14, 138.42, 138.95, 139.57, 140.63, 141.68, 142.66, 147.25, 147.48, 147.76, 147.88, 148.26, 148.30, 157.13.

12: MS (FD, 8 kV): m/z (%) = 1219.6 (100) [M^+] (calcd for $C_{96}H_{66}$ = 1219.58); ^{13}C NMR (125 MHz, [D$_2$]1,1,2,2-tetrachloroethane, 140 °C): δ = 125.2, 125.5, 125.7, 126.2, 126.5, 126.8, 127.0, 127.4, 130.2, 130.4, 131.2, 121.8, 132.0, 139.4, 140.5, 140.7, 140.8, 141.7, 142.3.

12a: MS (FD, 8 kV): m/z (%) = 1556.4 (100) [M^+] (calcd for $C_{120}H_{114}$ = 1556.23); ^{13}C NMR (125 MHz, [D$_2$]1,1,2,2-tetrachloroethane, 140 °C): δ = 31.02, 31.38, 31.76, 34.12, 123.24 123.54, 123.74, 126.99, 127.41, 127.53, 130.60, 131.20, 131.56, 131.76, 132.23, 137.64, 137.91, 139.26, 139.74, 140.49, 140.63, 140.73, 140.91, 142.19, 148.13, 148.44.

16: MS (FD, 8 kV): m/z (%) = 1676.2 (100) [M^+] (calcd for $C_{132}H_{90}$ = 1676.17); 3C NMR (125 MHz, [D$_2$]1,1,2,2-tetrachloroethane, 140 °C): δ = 123.4, 124.37, 124.44, 125.2, 125.4, 126.6, 126.8, 126.9, 129.9, 131.0, 139.5, 140.3, 140.6, 140.77, 140.84, 140.97, 141.00, 141.1, 141.3, 141.9.

16a: MS (FD, 8 kV): m/z (%) = 2343.8 (100) [M^+] (calcd for $C_{180}H_{180}$ = 2343.41); ^{13}C NMR (125 MHz, [D$_2$]1,1,2,2-tetrachloroethane, 140 °C): δ = 31.4, 34.1, 124.2, 124.3, 125.2, 131.1, 131.2, 131.9, 132.0, 138.3, 139.6, 140.0, 140.1, 140.6, 140.7, 141.1, 141.2, 141.5, 141.6, 142.0, 147.5, 148.0, 148.1.

17: MS (LD-TOF): m/z (%) = 1182.6 (100) [M^+] (calcd for $C_{96}H_{30}$ = 1183.29).

17a: MS (LD-TOF): m/z (%) = 1520.3 (100) [M^+] (calcd for $C_{120}H_{78}$ = 1519.

20: MS (FD, 8 kV): m/z (%) = 2815.4 (100) [M^+] (calcd for $C_{222}H_{150}$ = 2815.2); ^{13}C NMR (125 MHz, $CDCl_3$, 30 °C): δ = 141.78, 141.67, 140.63, 140.54, 140.45, 140.08, 140.01, 139.92, 139.12, 139.00, 138.44, 138.13, 131.65, 131.56, 131.53, 131.17, 129.96, 128.33, 127.51, 126.85, 126.74, 126.53, 126.18, 125.51, 125.26.

[a] All LD-TOF and MALDI-TOF mass specta were calibrated with C_{60} and C_{70}. 9-Nitroanthracene was used as the matrix for the MALDI-TOF measurements. MALDI = matrix-assisted laser-desorption ionization.

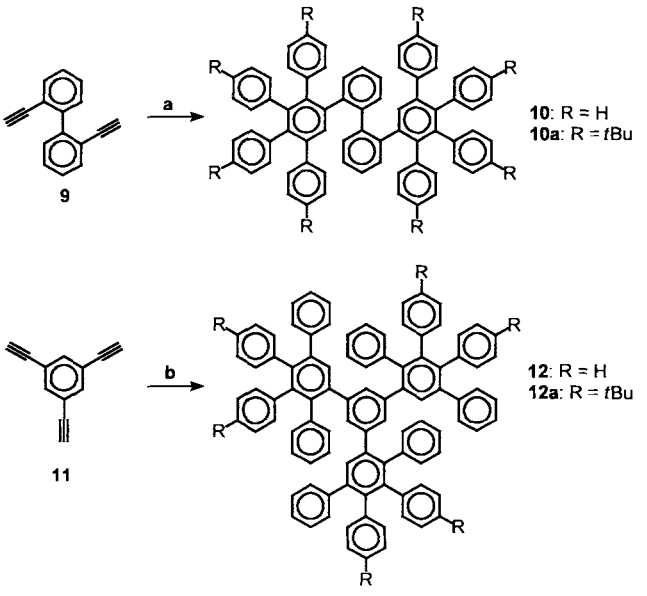

Scheme 2. a) Derivatives **8** or **8a** (2 equiv)/250 °C/Ph_2O/6–8 h, ≈100%; b) derivatives **8** or **8b** (3 equiv)/250 °C/Ph_2O/4–6 h, ≈100%.

ride led to a mixture of chlorinated derivatives of **2** (up to 26 Cl atoms by LD-TOF-MS). However, the crude mixture was successfully dechlorinated by treating the solid with an excess of *tert*-butyllithium followed by an aqueous quench. Dechlorinat-

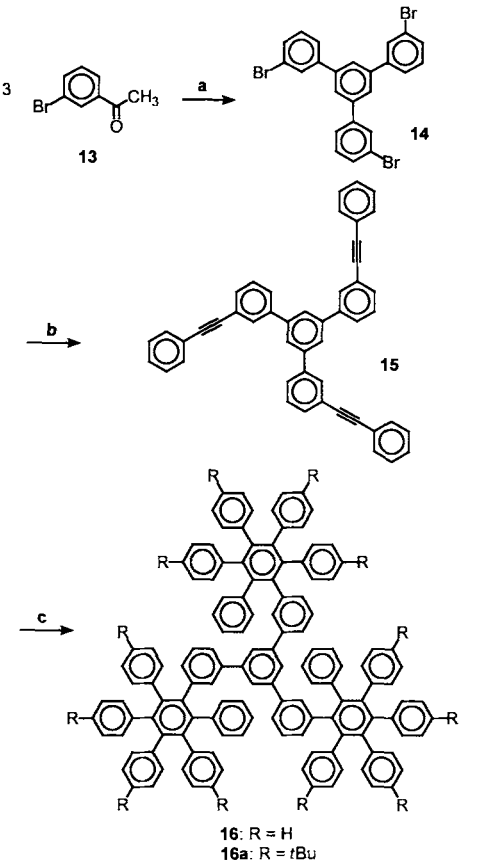

Scheme 3. a) $SiCl_4$/EtOH/25 °C/5 d, 55%; b) phenylacetylene (3.1 equiv)/piperidine/toluene/[Pd(PPh$_3$)$_4$]/CuI/80 °C, 2 d, 65%; c) derivatives **8** or **8a** (3 equiv)/250 °C/Ph_2O, 90–95%.

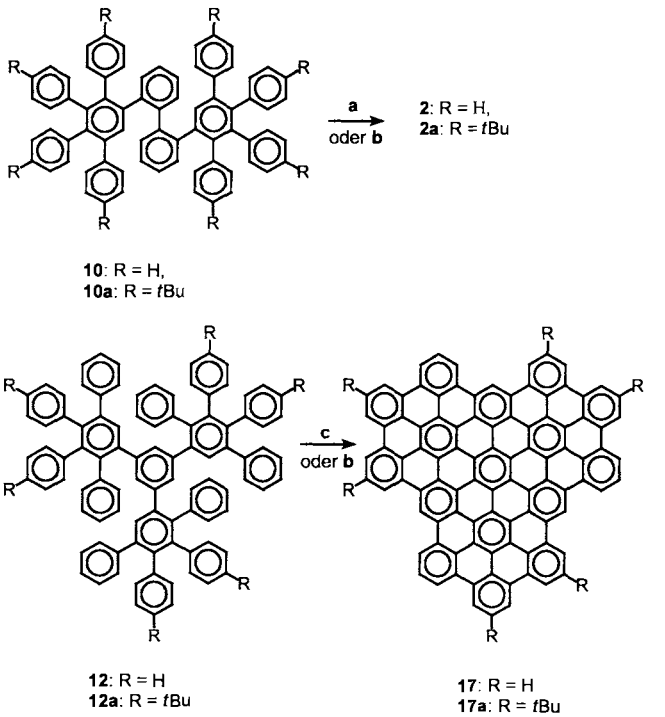

16 —c→ 3

16a —b→ 3a

Scheme 4. a) $CuCl_2$/$AlCl_3$/25 °C/CS_2, 1 d; *t*BuLi (excess), H_2O, >90%; b) $FeCl_3$/CH_2Cl_2/2–3 h, 30% (**2a**), 50% (**3a**), >80% (**17a**); c) copper(II) trifluoromethane sulfonate/$AlCl_3$/25 °C/CS_2/14 d, >90%.

ed **2** was again identified by LD-TOF-MS ($M^+ = 891\ g\,mol^{-1}$). Extensive attempts to dissolve (in high-boiling solvents or ionic liquids)[13] or sublime (under ultra-high vacuum)[14] the cyclized planar compounds for purification were unsuccessful.

To obtain soluble analogues of **2**, **3**, and **17** we prepared the *tert*-butyl precursors **10a**, **16a**, and **12a**. The latter was derived from cyclopentadienone **8b**, and **10a** and **16a** from **8a**. Cyclizations of all precursors were carried out with iron(III) chloride as the oxidizing agent. Due to the HCl formed in the course of the reaction, the expected products were invariably obtained together with chlorinated, cyclized products. Nevertheless, it was possible to isolate the non-chlorinated, fully cyclized products from these mixtures. Compound **2a** was isolated from the reaction mixture after reductive work-up (treatment with water/methanol followed by 5% aqueous Na_2SO_3) and multiple precipitation from dichloromethane (yield about 30%). Likewise, **3a** was isolated in about 50% yield.

Whereas **2a** and **3a** are slightly soluble in many solvents, **17a** is insoluble. Presumably the six *tert*-butyl groups are not enough to solubilize this large, planar PAH. UV spectra of **2a** and **3a**, recorded in tetrachloroethane, are characterized by broad absorptions from 320–500 tailing to 530 nm (Figure 1). Attempts

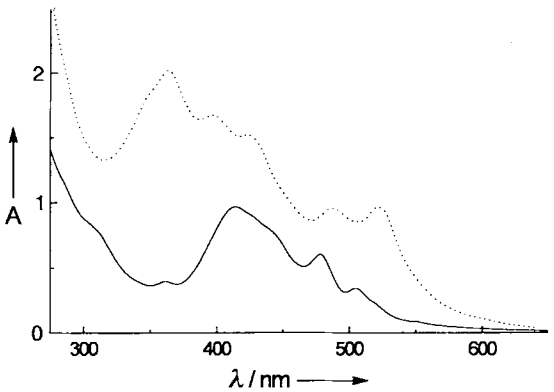

Figure 1. Absorption spectra of **2a** (solid line) and **3a** (dotted line) recorded in 1,1,2,2-tetrachloroethane.

to measure ^1H NMR spectra of **2a** and **3a** are hampered by poor solubility in a wide range of deuterated solvents. For example, **2a** has a solubility of less than 0.1 mg per 10 mL in [D_4]*o*-dichlorobenzene at 150 °C.[16]

Using the design principles presented in the introduction it is possible to envisage even larger PAH structures such as the hexagonal C_{222} hydrocarbon **21**. However, this extension meets with problems due to the lack of appropriate methods for structural proof. Triyne **18** undergoes Diels–Alder reaction with two equivalents of tetraphenylcyclopentadienone in diphenyl ether at 190° exclusively at the outer, sterically less encumbered acetylene units to give **19** (yield 66%; Scheme 5). In spite of the voluminous pentaphenyl substituents at the triple bond of **19**, its cyclotrimerization in dioxane proceeds smoothly to form **20** in 71% yield.

The soluble, fully characterized hydrocarbon **20**, which contains 37 benzene rings, serves as a precursor for the C_{222} graphite unit **21**. Treatment of **20** with aluminum(III) chloride and copper triflate in carbon disulfide affords a black solid, which is insoluble in all common solvents. Monitoring the intramolecular cyclodehydrogenation by LD-TOF-MS reflects the loss of hydrogen atoms by the formation of a broad signal in the mass range expected for **21**. However, signal broadening

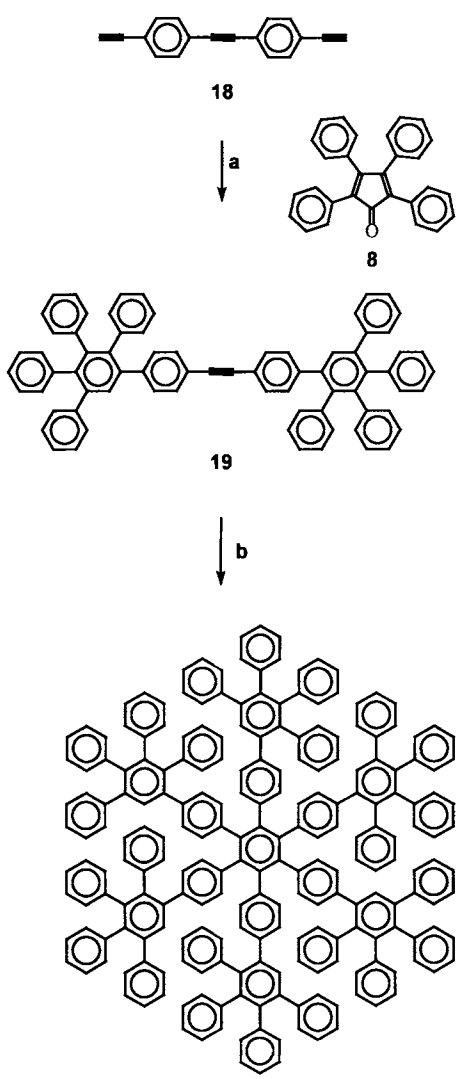

Scheme 5. a) Cyclopentadienone (2 equiv)/Ph_2O, 11 h, 190 °C, 66%; b) [$Co_2(CO)_8$]/dioxane/5 d, 100 °C, 71%.

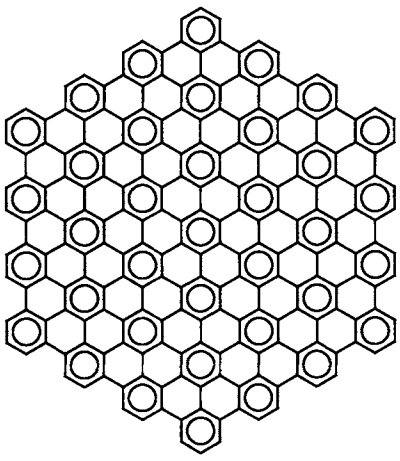

21

does not allow an exact molecular-weight determination and does not provide proof of the quantitative removal of 108 hydrogen atoms. Work directed toward the manipulation and

 © VCH Verlagsgesellschaft mbH, D-69451 Weinheim, 1997 0570-0833/97/3615-1606 $ 17.50+.50/0

characterization of extremely large PAHs ($\geq C_{222}$) is in progress.

Received: December 11, 1996 [Z9867IE]
German version: *Angew. Chem.* **1997**, *109*, 1675–1679

Keywords: arenes · cycloadditions · cyclodehydrogenations · Diels–Alder reactions · superacenes

[1] A. Stabel, P. Herwig, K. Müllen, J. P. Rabe, *Angew. Chem.* **1995**, *107*, 1768–1770; *Angew. Chem. Int. Ed. Engl.* **1995**, *34*, 1609–1611.
[2] P. Herwig, C. Kayser, H. W. Spiess, K. Müllen, *Adv. Mater.* **1996**, *8*, 510–513.
[3] G. Desiraju, A. Gavezzoti, *J. Chem. Soc. Chem. Commun.* **1989**, 621–622.
[4] The name "superbenzene" has been associated with **1** [5a] and "kekulene" [5b] in terms of possible enhanced aromaticity. We use this term simply to outline our synthetic design of the large PAHs.
[5] a) E. Clar, *The Aromatic Sextet*, Wiley, London, **1972**; b) H. A. Staab, F. Diederich, *Angew. Chem.* **1978**, *90*, 383–385; *Angew. Chem. Int. Ed. Engl.* **1978**, *17*, 372–374; H. A. Staab, F. Diederich, *Chem. Ber.* **1983**, *116*, 3487–3503; see also J. Aihara, *J. Am. Chem. Soc.* **1992**, *114*, 865–868.
[6] N. Schore in *Comprehensive Organic Synthesis, Vol. 5* (Eds.: B. M. Trost, I. Fleming), Pergamon Press, Oxford, **1991**, pp. 1129–1162.
[7] M. A. Ogliaruso, M. G. Romanelli, E. I. Becker, *Chem. Rev.* **1965**, *65*, 261–367.
[8] 1,2-Diaryl-1,2-diketones are easily accessible from the corresponding aryllithium compounds and 1,4-dimethylpiperazine-2,3-dione: U. T. Mueller-Westerhoff, M. Zhou, *J. Org. Chem.* **1994**, *59*, 4988–4992.
[9] Our improved synthesis of 1,3-diarylacetones, which gives consistent yields, is based on the following: Y. Kimura, Y. Tomito, S. Nakanishi, Y. Otsuji, *Chem. Lett.* **1979**, 321–322; H. des Abbayes, J. Clement, P.Laurent, G. Tanguy, N. Thilmont, *Organometallics* **1988**, *7*, 2293–2299.
[10] Compounds **10** and **12** are described: W. Ried, D. Freitag, *Angew. Chem.* **1968**, *80*, 932–942; *Angew. Chem. Int. Ed. Engl.* **1968**, *7*, 835–844.
[11] S. S. Elmorsy, A. Pelter, K. Smith, *Tetrahedron Lett.* **1991**, 4175–4176.
[12] M. Müller, H. Mauermann-Düll, M. Wagner, V. Enkelmann, K. Müllen, *Angew. Chem.* **1995**, *107*, 1751–1754; *Angew. Chem. Int. Ed. Engl.* **1995**, *34*, 1583–1586.
[13] We thank Dipl.-Chem. M. Müller for conducting the experiments and Prof. K. Seddon for his hospitality and providing us with 1-ethyl-3-methylimidazolium tetrachloroaluminate, the ionic liquid used in these experiments.
[14] Experiments conducted by Prof. N. Karl, Universität Stuttgart (Germany).
[15] All polyphenylene precursors show temperature-dependent NMR spectra, indicating the presence of several rotational isomers. The ^{13}C NMR chemical shifts given in Table 1 were obtained above the coalescence temperatures of these compounds.
[16] Many other high-boiling solvents were tried, but the highest solubility (which was not enough to obtain a ^1H NMR spectrum) was observed for [D_4]*o*-dichlorobenzene.

Polycyclic Aromatic Hydrocarbons by Cyclodehydrogenation and Skeletal Rearrangement of Oligophenylenes**

Markus Müller, Vivekanantan S. Iyer, Christian Kübel, Volker Enkelmann, and Klaus Müllen*

Polycyclic aromatic hydrocarbons (PAHs) are becoming increasingly important in the areas of molecular electronics and optoelectronics. They are also of theoretical interest as models for graphite.[1, 2] We showed that the oxidative cyclodehydrogenation of oligophenylene precursors, for example the cyclization of hexaphenylbenzene (HPhB, **1**) to hexa-*peri*-hexabenzocoronene (HBC, **2**; Scheme 1), can serve as a mild method for

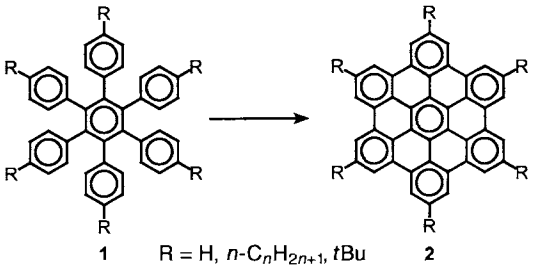

Scheme 1. Oxidative cyclodehydrogenation of hexaphenylbenzene (HPhB, **1**) to hexa-*peri*-hexabenzocoronone (HBC, **2**).

the synthesis of PAHs in high yields.[3, 4] In this case the oligophenylenes must render planarization to PAHs possible by elimination of hydrogen and formation of C–C bonds.

The work reported here involves oligophenylenes in which planarization is hindered by spatial superposition of phenyl units or by strained rings other than six-membered rings. For the intramolecular cyclodehydrogenation, surprisingly smooth skeletal rearrangements can lead to planar PAHs from "non-planarizable" oligophenylenes by removal of steric strain.

The oligophenylene derivative **6**, which is a positional isomer of oligophenylene **5**,[5] was obtained from 1,3-di(phenylethynyl)benzene (**4**) by double Diels–Alder addition with 1,2,3,4-tetraphenylcyclopenta-1,3-dienone (tetracyclone) and extrusion of carbon monoxide (Scheme 2). The crystal structure of **6** (Figure 1) shows clearly the spatial superposition of the two phenyl units directed towards the center of the molecule.[6]

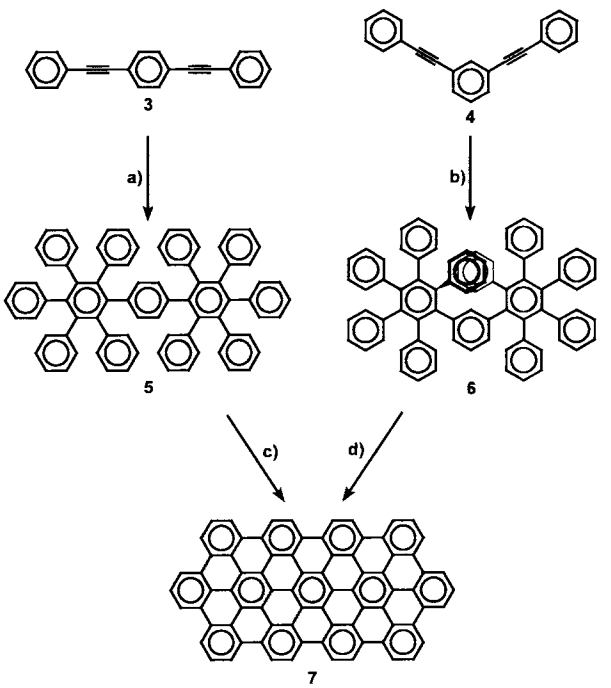

Scheme 2. a) and b) 1,2,3,4-Tetraphenylcyclopenta-1,3-dienone 220 °C/Ph_2O/2 d; a) 97%, b) 95%; c) and d) copper(II) triflate or $CuCl_2$, respectively/$AlCl_3$/RT/CS_2/2 d/quantitative yield.

[*] Prof. Dr. K. Müllen, Dipl.-Chem. M. Müller, Dr. V. S. Iyer, Dipl.-Chem. C. Kübel, Priv.-Doz. Dr. V. Enkelmann
Max-Planck-Institut für Polymerforschung
Ackermannweg 10, D-55128 Mainz (Germany)
Fax: Int. code +(6131)379-100
e-mail: muellen@mpip-mainz.mpg.de

[**] This work was supported financially by the Volkswagenstiftung and the Bundesministerium für Bildung und Forschung. We thank Dr. J. Räder and Dipl.-Chem. K. Martin for recording the LD-TOF mass spectra, and Prof. F.-G. Klärner and Dipl.-Chem. M. Kamieth for assistance with the MM3* and AM1 calculations. V. S. I. thanks the Max-Planck-Gesellschaft, and C. K. the Fonds der Chemischen Industrie for a scholarship.

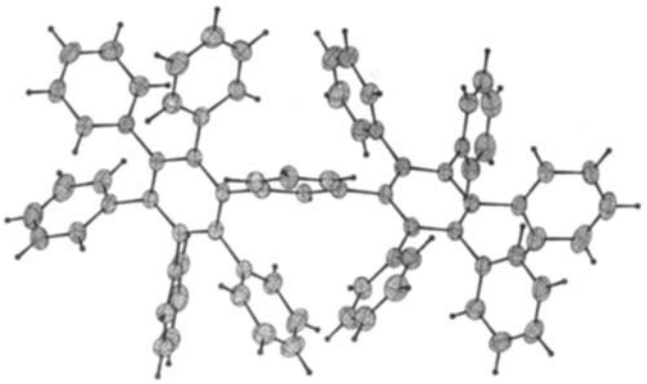

Figure 1. Crystal structure of **6**.

The polybenzenoid $C_{78}H_{26}$ hydrocarbon **7** is formed, as expected, when **5** is subjected to the mild reaction conditions of cyclodehydrogenation with copper(II) salts and aluminum(III) chloride. The quantitative yield of **7** could be demonstrated by laser-desorption time-of-flight mass spectrometry (LD-TOF-MS). Analogous cyclodehydrogenation of the *meta*-oligophenylene **6** could, in principal, permit formation of polyaromatic species with helical chirality (Figure 2).[7]

Semiempirical AM1 calculations[8] show that the products with partially cyclized hexaphenylbenzene subunits (HPhB, see **1**), which are bridged by a *meta*-phenylene structure, are higher in energy than the more extensively dehydrogenated, helical $C_{78}H_{32}$(6-5) derivative (Figure 2). (To describe the various dehdrogenation steps the number of newly formed C–C bonds is given for each of the HPhB subunits of the central, *meta*-substitued phenylene bridge, in addition to the empirical formula.) It is remarkable that **6** experiences a considerable energetic stabilization only through the complete cyclization of one HPhB subunit to HBC, whereas the partial cyclodehydrogenation of both HPhB subunits of **6** leads to products that are higher in energy.

Experiment shows that during the cyclization a quantitative 1,2-phenyl shift occurs at the central *meta*-substituted benzene ring of **6** (Figure 1) leading to formation of planar **7**, which is 30 kcal mol^{-1} more stable.[8] Although only 11 new bonds should be formed by the formation of a helical "graphite subsection" $C_{78}H_{32}$(6-5), loss of 28 hydrogen atoms with formation of 14 new C–C bonds can be demonstrated by LD-TOF-MS. Comparison of the IR spectra of the various cyclodehydrogenation products of **5** and **6** shows that the identical $C_{78}H_{26}$ hydrocarbon is involved in both cases.

By analogy to the synthesis of **6**, the doubly *meta*-bridged oligophenylene derivative **9** was obtained from the phenylethynyl compound **8** by triple Diels–Alder reaction with tetracyclone (Scheme 3). In contrast to **6**, compound **9** cannot be converted into a uniform, thermodynamically favored, planar product by cyclodehydrogenation. Consequently, intermolecular superposition of phenyl groups and fragmentation take place, which lead to formation of hydrocarbons **2** (R = H), **7**, and **13** as shown by mass spectrometry.

Octaphenyltetraphenylene **12** (Figure 3), which was synthesized as an oligopheneylene precursor with pronounced twisting, is formed from the highly strained phenylethynyl precursor **10**[9] by double Diels–Alder addition with tetracyclone (Scheme 4). Although **10** has been described as thermally unstable,[9] the double [4+2]cycloaddition could be carried out at 150 °C over 12 h in 95% yield. The crystal structure of **12** shows the boat conformation of the central eight-membered ring.[6] A molecule of carbon disulfide is deposited in the resulting cavity, as described for other tetraphenylene derivatives.[10]

Various products are formed during oxidative cyclodehydrogenation of tetraphenylene **12** depending on the temperature of reaction: copper(II) chloride/aluminum(III) chloride in carbon disulfide (30 °C) effects the quantitative cleavage of 12 hydrogen

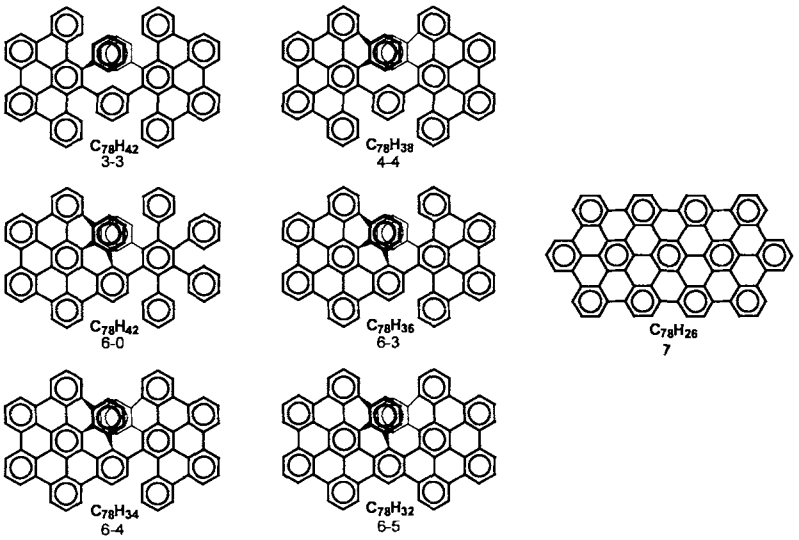

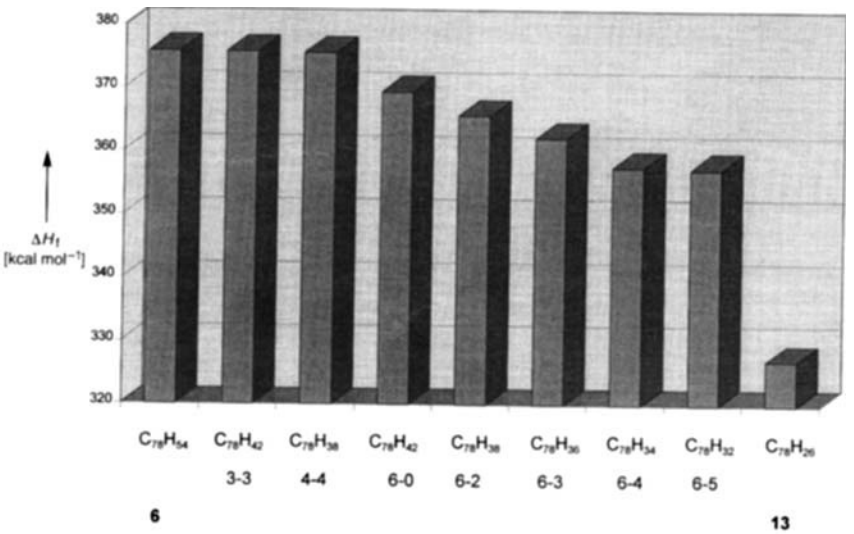

Figure 2. Theoretical cyclization products of **6** together with their relative energies [8]. To describe the various dehdrogenation steps the number of newly formed C–C bonds is given for each of the HPhB subunits of the central, *meta*-substitued phenylene bridge, in addition to the empirical formula.

 © VCH Verlagsgesellschaft mbH, D-69451 Weinheim, 1997 0570-0833/97/3615-1608 $ 17.50+.50/0

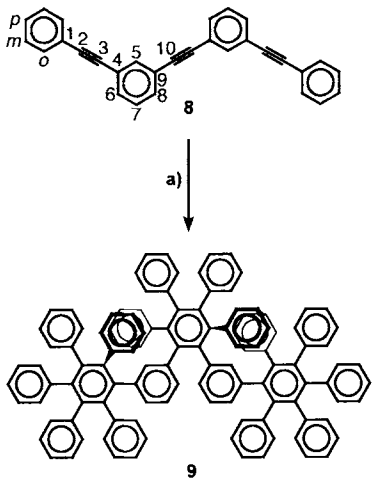

Scheme 3. a) 1,2,3,4-Tetraphenylcyclopenta-1,3-dienone(excess)/220 °C/Ph_2O/14 d/43%.

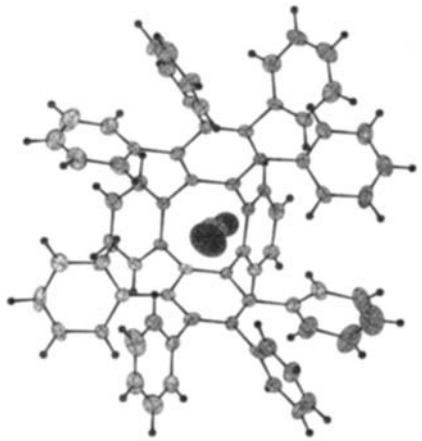

Figure 3. Crystal structure of **12**.

Table 1. Physical and spectroscopic data for **5**–**9** and **11**–**13**.

5: MS (FD, 8 kV): *m/z* (%) = 990 (100) [M^+]; ^{13}C NMR (500 MHz, [D_2]1,1,2,2-tetrachloroethane, 140 °C): δ = 141.18, 141.10, 141.07, 140.76, 140.56, 137.39, 131.86, 131.75, 131.72, 130.46, 126.69, 126.50, 126.45, 125.08, 125.01; m.p. > 462–463 °C [5].

6: MS (FD, 8 kV): *m/z* (%) = 990 (100) [M^+]; ^{13}C NMR (500 MHz, [D_2]1,1,2,2-tetrachloroethane, 140 °C): δ = 132.07, 131.76, 126.63, 126.42, 125.18, 125.06, 124.99; m.p. 285 °C.

7: MS (LD-TOF): *m/z* (%) = 962 (100) [M^+] (calibrated with C_{60} and C_{70}); IR (KBr): $\tilde{\nu}$ = 3059, 2967, 2892, 2850, 1576, 1411, 1320, 1217, 805, 751 cm^{-1}; m.p. > 300 °C.

8: MS (FD, 8 kV). *m/z* (%) = 378 (100) [M^+], 189 (7) [M^{2+}]; ^{13}C NMR (500 MHz, [D_2]1,1,2,2-tetrachloroethane, 80 °C): δ = 134.94 (C-5); 132.07, 128.89 (C-*o*, C-*m*); 131.94, 131.80, 129.10, 129.00 (C-*p*, C-6, C-7, C-8); 124.21, 123.89, 123.43 (C-1, C-4, C-9); 90.45, 89.50, 88.80 (C-2, C-3, C-10); m.p. 265 °C.

9: MS (FD, 8 kV): *m/z* (%) = 1448 (100) [M^+]; ^{13}C NMR (500 MHz, [D_2]1,1,2,2-tetrachloroethane, 140 °C): δ = 141.77, 141.26, 141.15, 140.67, 140.49, 140.30, 140.10, 139.90, 139.63, 138.63, 138.37, 132.09, 131.99, 131.75, 126.72, 126.61, 126.44, 126.37, 125.40, 125.11, 124.97; m.p. > 300 °C.

11: MS (FD, 8 kV): *m/z* (%) = 914 (100) [M^+]; ^{13}C NMR (500 MHz, [D_2]1,1,2,2-tetrachloroethane, 130 °C): δ = 142.28, 141.85, 140.83, 140.38, 140.25, 140.01, 139.58, 139.39, 133.00, 131.85, 130.39, 129.97, 127.36, 126.84, 126.47, 126.06, 125.83, 125.63, 125.21, 123.49, 119.20; m.p. 238–240 °C [5].

12: MS (FD, 8 kV): *m/z* (%) = 912 (100) [M^+]; ^{13}C NMR (500 MHz, [D_2]1,1,2,2-tetrachloroethane, 130 °C): δ = 142.59, 142.25, 142.15, 141.87, 141.30, (C-1, C-2, C-3, C-4, C-5); 139.86 (C-6); 133.82, 133.23 (C-*o*, C-*o'*); 127.75, 127.74 (C-*m*, C-*m'*); 132.15, 126.60, 126.22, 126.10, (C-*p*, C-*p'*, C-7, C-8); m.p. > 280 °C.

13: MS (LD-TOF): *m/z* (%) = 890 (100) [M^+] (calibrated with C_{60} and C_{70}); IR (KBr): $\tilde{\nu}$ = 2948, 2924, 1585, 1466, 1361, 1198, 1055, 865, 801, 746 cm^{-1}; m.p. > 300 °C.

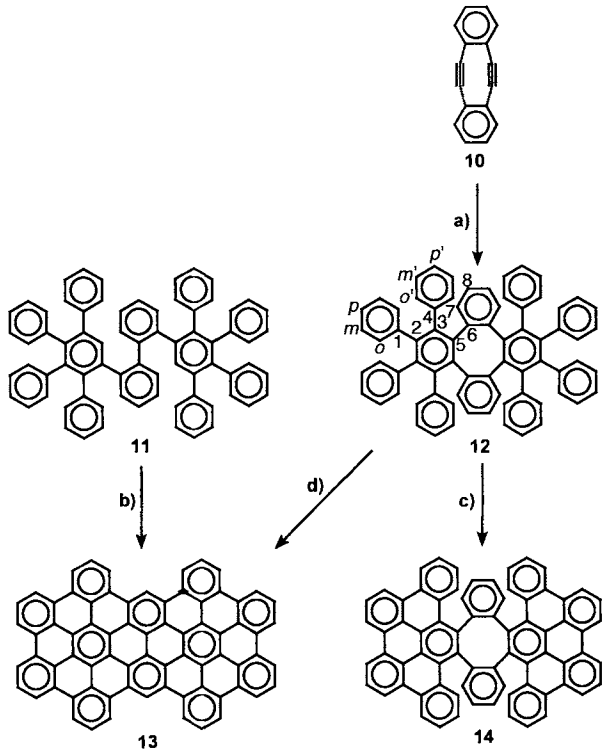

Scheme 4. a) 1,2,3,4-Tetraphenylcyclopenta-1,3-dienone/150 °C/Ph_2O/12 h/95%; b) 1) $CuCl_2/AlCl_3$/140 °C/1,1,2,2-tetrachloroethane/2 d; 2) *t*BuLi in hexane/45 °C/1 d; yield for the two steps 80%; c) $CuCl_2/AlCl_3$/30 °C/CS_2/1 d; d) $CuCl_2/AlCl_3$/80 °C/1,1,2,2-tetrachloroethane/12 h/quantitative yield.

atoms with formation of six new C–C bonds, as demonstrated by field-desorption (FD) and LD-TOF-MS. Apparently **14** is the cyclodehydrogenation product, although this could not be examined by NMR spectroscopy because of low solubility.

Cyclodehydrogenation of **12** at 80 °C in 1,1,2,2-tetrachloroethane took place quite differently. According to LD-TOF-MS 22 hydrogen atoms were removed, and 11 new bonds formed (quantitative yield). This can be explained by assuming that the central tetraphenylene unit of **12** undergoes rearrangement to a dibenzopyrene structure, together with a subsequent, complete planarization of the remaining, peripheral phenyl substituents (Scheme 4, step d).

Cyclization of oligophenylene **11**[5] with copper(II) salts, which was carried out to test this assumption, leads to the anticipated polybenzenoid $C_{72}H_{26}$ hydrocarbon **13** in 98% yield according to mass spectrometry.[11] Again, comparison of the IR spectra of the corresponding cyclodehydrogenation products of **11** and **12** showed that the same $C_{72}H_{26}$ hydrocarbon **13** is involved in both cases.

The rearrangements presented here provide evidence that the driving force for intramolecular cyclodehydrogenation is the considerable gain in energy of the planar PAHs compared to the more energetic oligopheneylene precursors or partially cyclized products. We shall shortly report on the synthesis of nonplanar PAHs formed by intramolecular cyclodehydrogenation with simultaneous formation of five-membered rings.

Received: December 11, 1996 [Z9868IE]
German version: *Angew. Chem.* **1997**, *109*, 1679–1682

Keywords: arenes · carbon allotropes · cyclodehydrogenations · graphite substructure · polycycles · rearrangements

 © *VCH Verlagsgesellschaft mbH, D-69451 Weinheim, 1997* *0570-0833/97/3615-1609 $ 17.50+.50/0*

[1] E. Clar, *Aromatische Kohlenwasserstoffe—Polycyclische Systeme*, Springer, Berlin, **1952**; E. Clar, *The Aromatic Sextet*, Wiley, London, **1972**; M. Zander, *Polycyclische Aromaten—Kohlenwasserstoffe und Fullerene*, Teubner, Stuttgart, **1995**.

[2] J. R. Dias, *Handbook of Polycyclic Hydrocarbons—Part a: Benzenoid Hydrocarbons*, Elsevier, Amsterdam, **1987**; *Top. Curr. Chem. 153* (*Advances in the Theory of Benzenoid Hydrocarbons*), **1990**.

[3] A. Stabel, P. Herwig, K. Müllen, J. P. Rabe, *Angew. Chem.* **1995**, *107*, 1768–1770; *Angew. Chem. Int. Ed. Engl.* **1995**, *34*, 1609–1611.

[4] M. Müller, H. Mauermann-Düll, M. Wagner, V. Enkelmann, K. Müllen, *Angew. Chem.* **1995**, *107*, 1751–1754; *Angew. Chem. Int. Ed. Engl.* **1995**, *34*, 1583–1586; M. Müller, J. Petersen, R. Strohmaier, C. Günther, N. Karl, K. Müllen, *ibid.* **1996**, *108*, 947–950 and **1996**, *35*, 886–888.

[5] W. Ried, K. H. Bönnighausen, *Chem. Ber.* **1960**, *93*, 1769–1773; M. A. Ogliaruso, L. A. Shadoff, E. I. Becker, *J. Org. Chem.* **1963**, *28*, 2725–2728; M. A. Ogliaruso, E. I. Becker, *J. Org. Chem.* **1965**, *30*, 3354–3360; W. Ried, D. Freitag, *Angew. Chem.* **1968**, *80*, 932–942; *Angew. Chem. Int. Ed. Engl.* **1968**, *7*, 835–844; W. Ried, V. B. Saxena, *ibid.* **1968**, *80*, 366 and **1968**, *7*, 378.

[6] X-ray crystal structure analyses were carried out with a Nonius CAD4 diffractometer with graphite-monochromatic $Cu_{K\alpha}$ irradiation ($\lambda = 1.5418$ Å) at room temperature. Lattice parameters were obtained by least-squares analysis of the angle of 25 reflections ($\theta > 25°$C). The intensities were recorded with $\theta/2\theta$ scans. The structures were solved by direct methods, C atoms refined with anisotropic deflection parameters, the H atoms taken into account with a riding model. Empirical absorption correction; applied programs: Molen, SIR92, and CRYSTALS. **6**: monoclinic, $C2/c$, $a = 24.9306(11)$, $b = .4880(7)$, $c = 30.223(1)$ Å, $\beta = 94.353(4)°$, $V = 5625.7(6)$ Å^3, $Z = 8$, $\rho_{calcd} = 1.169$ g cm^{-3}, $\mu = 4.686$ cm^{-1}, of 5915 relections 3768 were observed ($I > 3\sigma(I)$), $R = 0.045$, $R_w = 0.069$. **12**: orthorhombic, $Pna2_1$, $a = 24.131(1)$, $b = 19.702(1)$, $c = 11.7149(9)$ Å, $V = 5569.6(7)$ Å^3, $Z = 4$, $\rho_{calcd} = 1.18$ g cm^{-3}, $\mu = 11.51$ cm^{-1}, of 5159 relections 2372 were observed ($I > 3\sigma(I)$), $R = 0.075$, $R_w = 0.083$. Further details of the crystal structure investigations may be obtained from the Fachinformationszentrum Karlsruhe, D-76344 Eggenstein-Leopoldshafen (Germany), on quoting the depository numbers 406814 (**6**) and 406815 (**12**).

[7] N. D. Willmore, L. Liu, T. J. Katz, *Angew. Chem.* **1992**, *104*, 1081–1082; *Angew. Chem. Int. Ed. Engl.* **1992**, *31*, 1093–1094; H. A. Staab, M. Diehm, C. Krieger, *Tetrahedron Lett.* **1994**, *35*, 8357–8360; K. K. Laali, J. J. Houser, *J. Chem. Soc. Perkin Trans. 2* **1994**, 1303–1308.

[8] Complete geometry optimization of the molecules was carried out by using the MM3* force field in the program Macromodel 5.0 before calculating the heat of formation. Depending on the symmetry of the molecules 6–72 conformers, obtained by torsion about the central *meta*-phenylene unit by 20°, were used as starting geometries. The conformers obtained from the MM3* calculations were used as starting geometries for geometry optimization with subsequent determination of the heat of formation using AM1 calculations with the program SPARTAN. With the force-field method and the semiempirical calculations one obtains conformers with almost identical geometry. Only in the case of $C_{78}H_{42}$(6-0) does the torsional angle for the central *meta*-phenylene bond deviate by 20°.

[9] H. N. L. Wang, P. J. Garrat, F. Sondheimer, *J. Am. Chem. Soc.* **1974**, *96*, 5604–5605.

[10] N. C. Huang, T. C. W. Mak, *J. Chem. Soc. Chem. Commun.* **1982**, 543–544; H. N. C. Wong, Yuet-Ming Man, T. C. W. Mak, *Tetrahedron Lett.* **1987**, *28*, 6359–6362.

[11] V. S. Iyer, M. Wehmeier, J. D. Brand, M. A. Keegstra, K. Müllen, *Angew. Chem.* **1997**, *109*, 1675–1679; *Angew. Chem. Int. Ed. Engl.* **1997**, *36*, 1604–1607..

Transition Metal Catalysis in Fluorous Media: Practical Application of a New Immobilization Principle to Rhodium-Catalyzed Hydroboration**

Jerrick J. J. Juliette, István T. Horváth,* and J. A. Gladysz*

Catalysis pervades the incessant quest for new or improved chemical transformations. Two of the most active frontiers entail 1) nontraditional reaction media, and 2) new catalyst-immobilization or recovery strategies to facilitate reuse.[1] A conceptually new protocol, fluorous biphase catalysis, was developed in our laboratories.[2] As detailed elsewhere,[2, 3] this involves modifying catalysts with fluoroalkyl groups or "pony tails" such as $(CH_2)_y(CF_2)_xCF_3$ ($x \geq 5$). These confer high affinities for fluorous media,[2c] and the $(CH_2)_y$ spacers insulate the active sites from the electron-withdrawing fluorines. Many organic solvents give bilayers with fluorous solvents, with some systems becoming miscible above room temperature. As a result, reactions may be conducted under either biphasic or monophasic conditions. Upon workup, appropriately derivatized catalysts remain immobilized in the fluorous layer.

Although applications of fluorous biphase chemistry are rapidly appearing from many laboratories, most feature stoichiometric quantities of the fluorinated species.[4, 5] We sought to showcase this protocol in a laboratory-scale catalytic reaction of utility in fine-chemical synthesis. Our attention was drawn to the transition metal catalyzed hydroboration of alkenes, for which a variety of complexes can be employed (for example $[RhClL_3]$, $[M(cod)(L)(L')]^+$ (cod = 1,5-cyclooctadiene), $[PdCl_2L_2]$, and $[Cp_2Ti(CO)_2]$).[6, 7] However, the resulting organoboranes can be flammable and inconvenient to purify, and catalysts are destroyed by the customary oxidations to alcohol products (H_2O_2/NaOH). Therefore, we set out to prepare and evaluate a fluorous analog of Wilkinson's catalyst, $[RhCl(PPh_3)_3]$, that would be recoverable prior to any oxidation. Indeed, this strategy affords an easily recycled hydroboration catalyst that is effective at 25–40 °C and loadings of 0.01–0.25 mol%, and gives turnover numbers (TON) as high as 8500.

To synthesize the catalyst (Scheme 1) a yellow-orange solution of $[\{RhCl(cod)\}_2]$ in toluene and a colorless solution of the fluorous phosphane $P[CH_2CH_2(CF_2)_5CF_3]_3$[2] in $CF_3C_6F_{11}$ were stirred at room temperature (molar ratio 1:6). The upper toluene phase became colorless, and the $CF_3C_6F_{11}$ phase became orange. The latter was isolated, and solvent removed to give **1** as an analytically pure, orange powder in 94% yield.

$[RhCl\{P[CH_2CH_2(CF_2)_5CF_3]_3\}_3]$ **1**

DSC showed a melting point at 90 °C but no significant decomposition below 300 °C. Complex **1** is evocative of a "Teflon greaseball" and, accordingly, very soluble in $CF_3C_6F_{11}$ and $CF_3C_6H_5$,[5a] insoluble in hexane, benzene, toluene, ether,

[*] Prof. Dr. J. A. Gladysz, Dr. J. J. J. Juliette
Department of Chemistry
University of Utah
Salt Lake City, UT 84112 (USA)
Fax: Int. code +(801) 585-7807
e-mail: gladysz@rhenium.chem.utah.edu
Dr. I. T. Horváth
Corporate Research Laboratories
Exxon Research and Engineering Co.
Annandale, NJ 08801 (USA)
Fax: Int. code +(908) 730-3198
e-mail: ithorva@erenj.com

[**] We thank the U. S. National Science Foundation for support of this research.

 © VCH Verlagsgesellschaft mbH, D-69451 Weinheim, 1997 0570-0833/97/3615-1610 $ 17.50+.50/0

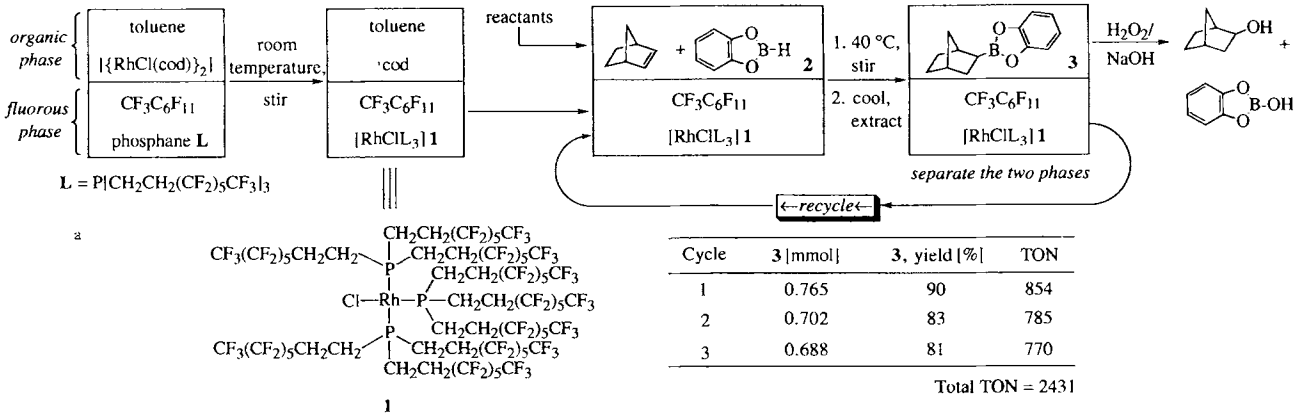

Cycle	3 [mmol]	3, yield [%]	TON
1	0.765	90	854
2	0.702	83	785
3	0.688	81	770

Total TON = 2431

Scheme 1. Fluorous biphase rhodium-catalyzed hydroboration.

$CHCl_3$, and CH_2Cl_2, and very slightly soluble in THF and acetone. For comparison, $[RhCl(PPh_3)_3]$ is insoluble in $CF_3C_6F_{11}$ and hexane, very slightly soluble in $CF_3C_6H_5$, slightly soluble in acetone, and soluble in benzene, toluene, ether, $CHCl_3$, CH_2Cl_2, and THF.

Next, alkenes and freshly distilled catecholborane (**2**) were combined in the presence of **1**. Exploratory runs with solvent mixtures ($CF_3C_6F_{11}$/THF or toluene) were sucessful. However, reactions were more rapidly and economically effected without a nonfluorous solvent. A stock solution of **1** (0.500 mL, 1.79 mM, 8.94×10^{-4} mmol, 0.10 mol%) in $CF_3C_6F_{11}$ was added to a 1:1 mixture of norbornene and **2** (0.849 mmol, 950 equiv based on Rh). The heterogeneous sample was kept for 1 h at 40 °C, and extracted with C_6D_6 (2×0.5 mL; room temperature). Then Ph_3SiMe was added to the extract; NMR analysis showed 0.765 mmol of the organoborane **3** (Scheme 1; 90%, TON 854). The $CF_3C_6F_{11}$ mother liquor was added to a second sample of norbornene and **2** (950 equiv). Identical reaction and workup gave a solution containing 0.702 mmol of **3** (83%, TON 785)in C_6D_6. A third cycle gave similar data for a combined TON of 2431 (Scheme 1). Comparable results were obtained with other alkenes. Hence, there is a very high degree of catalyst recovery.[8]

Preparative syntheses of alcohols were attempted. Thus, norbornene and **2** (1:1; 2.55 mmol) and a solution of **1** in $CF_3C_6F_{11}$ (0.03 mol%) were combined as described above. The sample was kept for 6 h at 40 °C and then extracted with THF (3×1 mL). Oxidative workup (H_2O_2/NaOH) gave *exo*-norborneol in 76% yield (TON 2170). Similar reactions were conducted with a variety of monosubstituted, disubstituted, and trisubstituted alkenes as summarized in Table 1. Some THF was added to dissolve the only solid reactant, *trans*-stilbene. With one exception reaction times ranged from 1–16 h; no special efforts were made to optimize catalyst loadings (0.03–0.25 mol%) or isolated yields (92–76%). In most cases, only one alcohol regioisomer or diastereomer was detected. These were identical to products from uncatalyzed reactions, which are commonly conducted at 100 °C.[9] However, both styrenes gave mixtures of regioisomers. The regioselectivities in rhodium-catalyzed hydroborations of styrenes can vary, and catalyst purity has been shown to be a critical factor.[6d, e] The ratios in Table 1 have been reproduced many times with different samples of **1** and **2**.[8c]

To investigate the feasibility of still higher TON values and lower catalyst loadings, the reaction of norbornene, **2**, and **1** was repeated with a 9650:9650:1 molar ratio (0.01 mol% **1**). After

Table 1. Compounds prepared under the hydroboration conditions of Scheme 1 [a].

Reactant	Product(s)	Yield [%]	1 [mol%]	TON
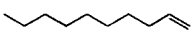	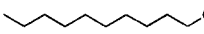	80	0.19	413
	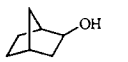	76 (88	0.03 0.01	2167 8492[b])
	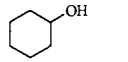	79	0.13	580
	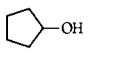	77	0.09	788[c]
	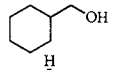	89	0.15	570
	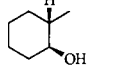	82	0.25	314
	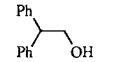	86	0.16	531
	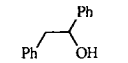	89	0.19	445
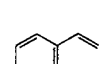	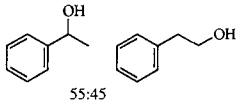	90	0.05	2022
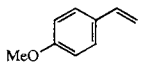	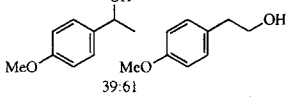	82	0.12	660
	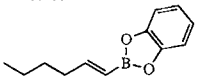	89	0.19	459
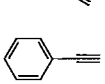	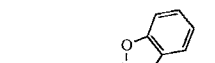	95	0.19	503

[a] 40 °C, 0.5–16 h. [b] $t = 40$ h. [c] $t = 24$ h.

 © VCH Verlagsgesellschaft mbH, D-69451 Weinheim, 1997 0570-0833/97/3615-1611 $ 17.50+.50/0

40 h workup gave *exo*-norborneol in 88% yield, which corresponds to a TON of 8492! Furthermore, as shown by the last two examples in Table 1, **1** catalyzed the addition of **2** to alkynes. These reactions were more rapid (0.5 h)[9] and gave much more stable organoboranes, which were isolated directly (89–95%). Only one regioisomer was detected. Finally, various control and comparative experiments were conducted. For example, norbornene and styrene give no detectable reaction with **2** in the absence of **1**. A single extraction with benzene or THF (1/1 v/v $CF_3C_6F_{11}$) recovers greater than 90% of the organoborane product from the $CF_3C_6F_{11}$ medium. Also, $[ClRh(PPh_3)_3]$ catalyzes the reaction of norbornene and **2** under homogeneous conditions in C_6D_6 at 40 °C at a somewhat faster rate than **1** under the heterogeneous conditions of Scheme 1. There is the attendant question of fluorous-phase versus interfacial catalysis, and studies that address these and related issues are in progress.

The protocols described offer many advantages over existing methodologies for metal-catalyzed hydroborations. Even more importantly, they demonstrate the practicality and utility of a new, more environmentally friendly approach to laboratory-scale catalytic reactions. A number of extensions can be readily visualized. For example, the organoboranes generated in Scheme 1 and Table 1 undergo various types of metal-catalyzed carbon–carbon bond forming reactions.[10] Thus, there are intriguing possibilities for liquid-phase combinatorial syntheses involving a sequence of fluorous catalysts.[11] Complex **1** also catalyzes other transformations such as hydrogenations, hydrosilylations, and hydroacylations.[12] Parallel mechanistic studies have established unique selectivity patterns for oxidative additions in $CF_3C_6F_{11}$.[13] Finally, this constitutes a highly attractive approach to enantioselective catalysis, which often involves expensive metals and ligands.

Experimental Section

1: A flask was charged with $P[CH_2CH_2(CF_2)_5CF_3]_3$ (0.643 g, 0.600 mmol) and $CF_3C_6F_{11}$ (1 mL) under N_2. Then a solution of $[\{RhCl(cod)\}_2]$ (0.049 g, 0.0994 mmol) in toluene (1 mL) was added with stirring. After 14 h the orange $CF_3C_6F_{11}$ layer was isolated and dried under vacuum to give **1** as a bright orange solid (0.620 g, 0.186 mmol, 94%). Elemental analysis calcd for $C_{72}H_{36}ClF_{117}P_3Rh$: C 25.77, H 1.08; found: C 25.85, H 1.09; ^1H NMR ($CF_3C_6F_{11}$, external C_6D_6 lock): $\delta = 2.20$ (br, 6H), 1.90 (br, 6H); $^{31}P\{^1H\}$ NMR ($CF_3C_6F_{11}$, external C_6D_6 lock): 12.9 (dd, J(P,Rh) = 136.1, J(P,P) = 39 Hz), 29.3 (dt, J(P,Rh) = 186, J(P,P) = 39 Hz).

Representative reaction: A flask was charged with norbornene (0.240 g, 2.55 mmol), **2** (0.270 mL, 0.306 g, 2.55 mmol), and a solution of **1** in $CF_3C_6F_{11}$ (0.500 mL, 1.79×10^{-3} M) under N_2. The mixture was kept at 40 °C for 6 h, cooled to room temperature, and extracted with THF (3 × 1 mL). Solvent was removed under vacuum at 0 °C to give a white solid. Then ethanol/THF (5 mL, 1/1 v/v) and NaOH (5 mL, 2 M in H_2O) were added. The mixture was cooled to 0 °C, and 30% H_2O_2 (0.5 mL, 4.4 mmol) added dropwise with stirring. After 0.5 h the mixture was warmed and extracted with ether (3 × 10 mL). The extract was washed with NaOH (10 mL, 0.5 M in H_2O), H_2O (15 mL), and brine (15 mL), and dried over $MgSO_4$. Solvent was removed by rotary evaporation to give *exo*-norborneol as a white solid (0.182 g, 1.94 mmol, 76%; TON = 2167). NMR spectra matched those reported [9].

Received: January 10, 1997 [Z9981IE]
German version: *Angew. Chem.* **1997**, *109*, 1682–1684

Keywords: fluorocarbons · hydroborations · immobilization · rhodium · two-phase catalysis

[1] a) B. Cornils, W. A. Herrmann, *Applied Homogeneous Catalysis with Organometallic Compounds*, VCH, Weinheim, **1996**; b) B. Cornils, *Angew. Chem.* **1995**, *107*, 1709; *Angew. Chem. Int. Ed. Engl.* **1995**, *34*, 1575.
[2] a) I. T. Horváth, J. Rábai, *Science* **1994**, *266*, 72; b) US-A Patent 5,463,082, **1995**. c) The term "fluorous" was introduced as an analog to "aqueous" for highly fluorinated alkane, ether, and tertiary amine solvents.
[3] J. A. Gladysz, *Science* **1994**, *266*, 55.
[4] R. P. Hughes, H. A. Trujillo, *Organometallics* **1996**, 15, 286.
[5] a) D. P. Curran, S. Hadida, *J. Am. Chem. Soc.* **1996**, *118*, 2531; b) S. G. DiMagno, P. H. Dussault, J. A. Schultz, *ibid.* **1996**, *118*, 5312; c) D. P. Curran, M. Hoshino, *J. Org. Chem.* **1996**, *61*, 6480.
[6] Rhodium catalysts: a) D. Männig, H. Nöth, *Angew. Chem.* **1985**, *97*, 854; *Angew. Chem. Int. Ed. Engl.* **1985**, *24*, 878; b) D. A. Evans, G. C. Fu, A. H. Hoveyda, *J. Am. Chem. Soc.* **1992**, *114*, 6671; c) D. A. Evans, G. C. Fu, B. A. Anderson, *ibid.* **1992**, *114*, 6679; d) S. A. Westcott, H. P. Blom, T. B. Marder, R. T. Baker, *ibid.* **1992**, *114*, 8863; e) K. Burgess, W. A. van der Donk, S. A. Westcott, T. B. Marder, R. T. Baker, J. C. Calabrese, *ibid.* **1992**, *114*, 9350; f) J. M. Brown, G. C. Lloyd-Jones, *ibid.* **1994**, *116*, 866; g) S. Pereira, M. Srebnik, *ibid.* **1996**, *118*, 909.
[7] Nonrhodium catalysts: a) K. Burgess, M. J. Ohlmeyer, *Chem. Rev.* **1991**, *91*, 1179; b) X. He, J. F. Hartwig, *J. Am. Chem. Soc.* **1996**, *118*, 1696.
[8] a) There are several possible rationales for variations in yields with cycle. For example, $[RhCl(PPh_3)_3]$ and **2** react in the absence of alkenes to give complex mixtures of rhodium hydrides and redistribution products, many of which may independently participate in or inhibit catalysis [6e]. Catalyst leaching has not been detected to date, but further studies are in progress. b) A similar five-cycle sequence with styrene (515 equiv per cycle, 8 h, room temperature) gave mixtures of branched and linear organoboranes (56:44 to 51:49) in 92, 96, 89, 58, and 77% yields (TON 471, 496, 457, 300, and 396, respectively). c) A reviewer has raised the possibility of a change in mechanism due to the fluorous solvent. One relevant observation is that **1** (in $CF_3C_6F_{11}$) and the tri-*n*-octylphosphane analog (in C_6D_6) give nearly the same isomer ratios for all styrenes.
[9] H. C. Brown, S. K. Gupta, *J. Am. Chem. Soc.* **1975**, *97*, 5249.
[10] N. Miyaura, A. Suzuki, *Chem. Rev.* **1995**, *95*, 2457.
[11] S. D. Brown, R. W. Armstrong, *J. Am. Chem. Soc.* **1996**, *118*, 6331.
[12] J. J. J. Juliette, D. Rutherford, C. Rocoboy, unpublished results.
[13] M.-A. Guillevic, A. M. Arif, I. T. Horváth, J. A. Gladysz, *Angew. Chem.* **1997**, *109*, 1685; *Angew. Chem. Int. Ed. Engl.* **1997**, *36*, 1612.

Synthesis, Structure, and Oxidative Additions of a Fluorous Analogue of Vaska's Complex, *trans*-$[IrCl(CO)\{P[CH_2CH_2(CF_2)_5CF_3]_3\}_2]$—Altered Reactivity in Fluorocarbons and Implications for Catalysis**

Marie-Andrée Guillevic, Atta M. Arif, István T. Horváth,* and J. A. Gladysz*

Although homogeneous transition metal catalysts are employed in vast numbers of bench-scale and commodity chemical transformations, there remain critical needs for improved catalyst-recovery methodologies, as well as higher or new types of selectivities.[1] Towards these ends, a conceptually new protocol, fluorous biphase catalysis, has been developed in our laboratories.[2] This entails derivatizing catalysts with fluoroalkyl groups or "pony tails" such as $(CH_2)_y(CF_2)_xCF_3$, which provide high solubility in fluorous media.[2, 3] Electronic properties can be tuned by varying the $(CH_2)_y$ spacer. Many combinations of fluorous and organic solvents give bilayers, enabling facile catalyst–product separation.

We have prepared fluorous rhodium catalysts that effect a variety of transformations and have many desirable attributes.[2, 3] Novel fluorous reagents are being developed in

[*] Prof. Dr. J. A. Gladysz, Dr. M.-A. Guillevic, Dr. A. M. Arif
Department of Chemistry
University of Utah
Salt Lake City, UT 84112 (USA)
Fax: Int. code +(801)585-7807
e-mail: gladysz@rhenium.chem.utah.edu
Dr. I. T. Horváth
Corporate Research Laboratories
Exxon Research and Engineering Co.
Annandale, NJ 08801 (USA)
Fax: Int. code +(908)730-3198
e-mail: ithorva@erenj.com

[**] We thank the U. S. Department of Energy for support of this research.

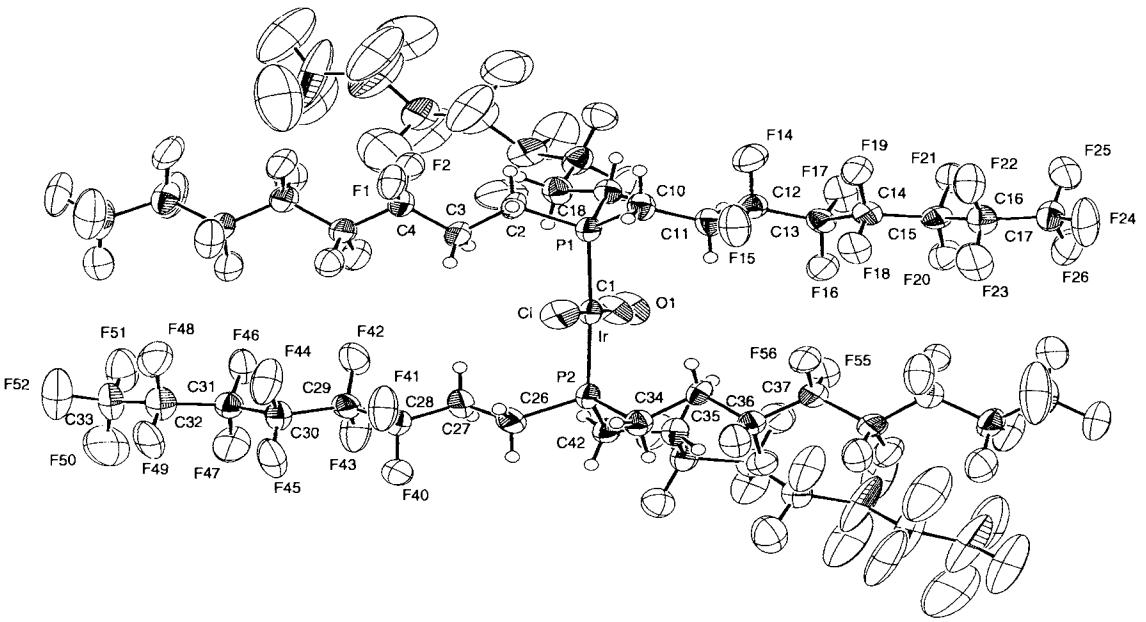

Figure 1. Molecular structure of **2**. For clarity the fluorine atoms are represented by unshaded ellipsoids, and atoms are completely numbered for only two of the $CH_2CH_2(CF_2)_5CF_3$ chains. Selected bond lengths [Å] and angles [°]: Ir–P1 2.307(2), Ir–P2 2.311(2), Ir–Cl 2.361(2), Ir–C1 1.783(7); P1-Ir-P2 172.18(6), P1-Ir-Cl 85.72(7), Cl-Ir-P2 86.46(7), P1-Ir-C1 94.4(3), Cl-Ir-C1 179.3(3), P2-Ir-C1 93.4(3).

other laboratories.[4] However, a number of fundamentally important underlying issues have yet to be addressed. For example, how are the structures of compounds with multiple pony tails best visualized? Can significant changes in selectivities occur in fluorous solvents? How is the reactivity of oxygen, which is exceptionally soluble in fluorous media, affected? Hence, we turned our attention to iridium relatives of the rhodium catalysts, seeking to make use of the large body of mechanistic and structural data involving Vaska's complex, *trans*-[IrCl(CO)-$(PPh_3)_2$] (**1**), and close congeners.[5]

$[\{IrCl(cod)\}_2]$ (cod = 1,5-cyclooctadiene) and the fluorous phosphane $P[CH_2CH_2(CF_2)_5CF_3]_3$[2] were combined in hexane/CH_2Cl_2 under CO (1 atm; see Scheme 1).[6] Workup gave **2** as an air-stable light-yellow powder in 97% yield.[7] A similar procedure with the analogous non-fluorinated phosphane $P[(CH_2)_7CH_3]_3$ gave **3** as a yellow oil in 84% yield. Complex **2**

trans-$[IrCl(CO)\{P[CH_2CH_2(CF_2)_5CF_3]_3\}_2]$ **2**

trans-$[IrCl(CO)\{P[(CH_2)_7CH_3]_3\}_2]$ **3**

is very soluble in $CF_3C_6F_{11}$, acetone, ether, and THF, but insoluble in hexane, CH_2Cl_2, and $CHCl_3$. In contrast, **3** is insoluble in $CF_3C_6F_{11}$, but soluble in all common organic solvents. Surprisingly, unlike **3** and the many fluorous phosphane complexes we have prepared to date, **2** crystallizes (yellow prisms, ether/pentane). DSC analysis (−100 to 350 °C) showed thermal decomposition above 200 °C, but only one phase transition (melting, 75 °C).

Figure 1 shows an ORTEP representation of the crystal structure of **2**.[7b] The metrical parameters are similar to those of other structurally characterized *trans*-$[IrCl(CO)(PR_3)_2]$ complexes.[8] However, data for such a perfluoroalkyl-rich species, of any composition, had previously not been available.[9] Perfluoroalkane conformations are of special interest in that *n*-C_4F_{10} exhibits three minima with C-C-C-C torsion angles of about 166, 95, and 54° (*anti*, *ortho*, and *gauche*, respectively).[10] However, the $CF_2CF_2CF_2CF_{2-3}$ segments in **2** display only the most stable *anti* conformations (torsion angles 161.7(6)–176.9(1.3)°, av 169.0(3.4)°).

The crystal structure also shows distinctive packing features. Four chains (commencing at C2, C10, C26, and C34) are essentially parallel and coplanar, defining a raft of approximately 21 × 6 Å. The two remaining chains (commencing at C18 and C42) extend on a common side of the raft. These feature *gauche* $\mathbf{CH}_2CF_2CF_2CF_2$ units and CF_2CF_3 endgroups that have larger thermal ellipsoids (20% disorder). The lattice consists of stacks of molecules, in which the rafts are paired back-to-back (Figure 2). Thus, every third layer consists of four out-of-plane

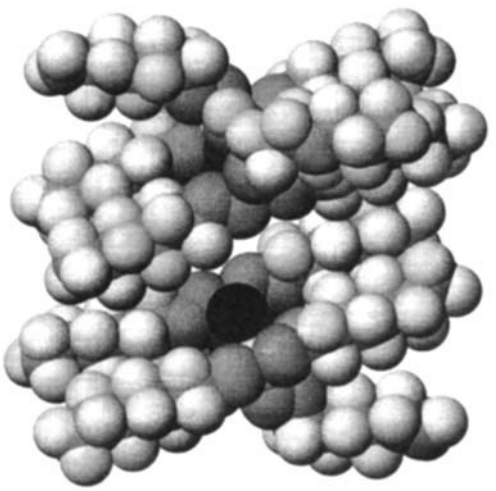

Figure 2. Packing of two molecules of **2**; non-hydrogen atoms are given at the van der Waals radii (fluorine atoms light, chlorine atoms dark). The crystal lattice consists of stacks of this repeat unit.

chains and is less densely packed. This arrangement maximizes the number of parallel perfluoroalkyl chains in every direction, in accord with the "like-dissolves-like" paradigm. However, the separations are somewhat greater than the sum of the van der Waals radii.

Reactions of **2** that model key steps in catalysis were investigated. Oxidative addition of CH_3I to **1** involves an S_N2-like

mechanism and a cationic iridium intermediate, even in benzene.[5b, 11] We thought that such pathways should be disfavored in nonpolar fluorous media. Therefore, **2** was first treated with the fluorous iodide $CF_3(CF_2)_7CH_2CH_2I$ (2 equiv) in $CF_3C_6F_{11}$ (homogeneous conditions) under anaerobic conditions. After 1 h workup gave the expected alkyl complex **4** as an analytically pure yellow oil in 84% yield (Scheme 1).[7] The ^{31}P NMR spectrum of **4** showed three peaks (73:19:8), which were presumed to represent geometric isomers. A similar reaction with CH_3I (4 equiv) in $CF_3C_6F_{11}$ (homogeneous conditions) gave the corresponding methyl complex **5** in 70% yield and greater than 97% isomeric purity. However, completion required 72 h.

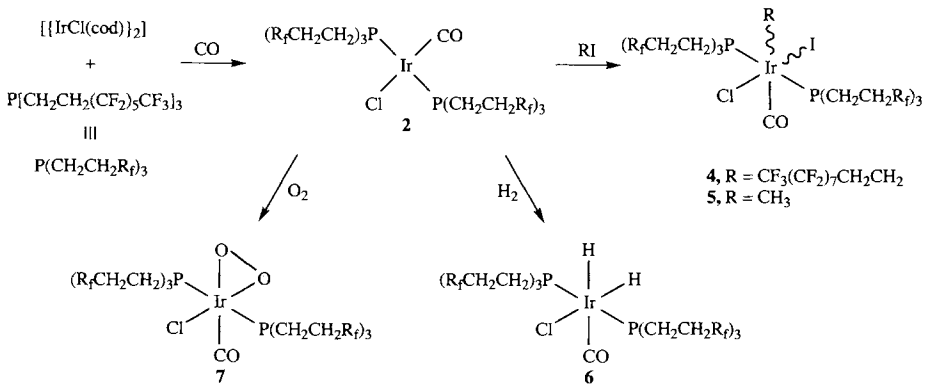

Scheme 1. Synthesis and reactivity of **2**, a fluorous analog of Vaska's complex.

Competition experiments were conducted. When **2**, $CF_3(CF_2)_7CH_2CH_2I$, and CH_3I were combined in a 1:3:3 molar ratio, only **4** formed (^1H and ^{31}P NMR). This rate trend is inconsistent with a common S_N2-like mechanism.[12] We thought it likely that one or both substrates react by a free radical chain pathway, which is well documented for **1** and secondary or tertiary alkyl halides.[13] Accordingly, **4** formed much more slowly in the dark, and much more rapidly following brief irradiation. A reaction of **2**, $CF_3(CF_2)_7CH_2CH_2I$, and CH_3I was conducted in the presence of the free-radical trap duroquinone (2:6:6:3 molar ratio; heterogeneous conditions). After 72 h, only **2** and a small amount of a previously unobserved species were detected (95:5, ^{31}P NMR). The rate of reaction of **1** and CH_3I in CH_2Cl_2 is unaffected by duroquinone and galvinoxyl.[13] Hence, the polar addition mechanism appears to be completely shut down in fluorous solvents.

Attention was turned to nonpolar substrates that add to **1** by concerted mechanisms. First, a solution of **2** in $CF_3C_6F_{11}$ was treated with H_2 (1 atm).[14] After 2.5 h workup gave the dihydride complex **6** (Scheme 1) as a spectroscopically homogeneous yellow oil in 82% yield. Two ^1H NMR signals for the hydride ligands and one ^{31}P NMR signal was observed, which is consistent with the isomer shown. Second, a similar reaction was conducted with O_2 (1 atm).[15] In view of the high solubility of oxygen in fluorous solvents, rapid addition was expected. However, the oxygen complex **7** (Scheme 1) slowly formed over the course of 72 h. Workup gave a yellow oil in 67% yield.

To help interpret this result, side-by-side reactions of **2** in $CF_3C_6F_{11}$ and in THF (both 0.006 M) with O_2 (2 atm) were periodically monitored by ^{31}P NMR spectroscopy. The first went to 20% completion after 25 h, whereas the second to 24 and 92% after 3 and 18.5 h, respectively. Hence, the fluorous solvent actually retards oxygenation, suggesting that (relative to THF) the reactants are stabilized more than the transition state. Identical experiments with **1**–**3** in THF established the order of reactivity as **3** > **1** > **2** (1.5 h: 80, 41, and 6%; 3.0 h: 95, 68, and 24%, respectively). This parallels the electron density on iridium, as approximated by the IR ν_{CO} values (Nujol: 1942, 1952, and 1975 cm^{-1}, respectively). The latter also show that the $(CH_2)_2$ spacers in **2** do not completely insulate the iridium from the electronegative fluorine atoms.[16]

These data show that oxidative-addition rates of both polar and nonpolar substrates can be strongly affected by fluorous media. This in turn provides a foundation for the design of catalysts with fundamentally new selectivities. For example, fluorous solvents should disfavor the pivotal CH_3I addition in the rhodium-catalyzed, iodide-promoted conversion of methanol and carbon monoxide into acetic acid.[17] The absence of any intra- or intermolecular carbon–fluorine bond activation reactions involving **2** is also noteworthy.[18]

Experimental Section

2: A Schlenk flask was charged with [{IrCl(cod)}$_2$] (0.069 g, 0.10 mmol), and hexane/CH_2Cl_2 (50/50, 10 mL) and P[$CH_2CH_2(CF_2)_5CF_3$]$_3$ (0.440 g, 0.412 mmol) were added with stirring. After 10 min CO (1 atm) was added, and after 15 min the volatile components were removed under vacuum. Ether was added (10 mL), the sample filtered, and solvent removed by rotary evaporation. The light yellow powder **2** was dried under vacuum (0.479 g, 0.199 mmol, 97%), m.p. 75 °C. Elemental analysis calcd for $C_{49}H_{24}ClF_{78}IrOP_2$: C 24.52, H 1.01; found: C 24.46, H 1.07; IR ($CF_3C_6F_{11}$): $\tilde{\nu}_{CO}$ [cm^{-1}] = 1975 s; ^1H NMR (acetone): δ = 2.80 (m, 6 CH_2); 2.71 (m, 6 CH_2); $^{31}P\{^1H\}$ NMR (acetone): δ = 22.52 (s).

4: A Schlenk flask was charged with **2** (0.100 g, 0.0416 mmol), and $CF_3C_6F_{11}$ (3 mL) and $CF_3(CF_2)_7CH_2CH_2I$ (0.047 g, 0.082 mmol) were added with stirring. After 1 h the volatile components were removed under vacuum. The residue was washed with CH_2Cl_2 (5 mL), dissolved in ether/pentane (50/50, 10 mL), and purified by chromatography (silica gel). Solvent was removed from a yellow band to give **4** as a yellow oil (0.100 g, 0.033 mmol, 84%). Elemental analysis calcd for $C_{56}H_{28}ClF_{95}IIrOP_2$: C 23.83, H 0.95; found: C 23.95, H 1.01; IR ($CF_3C_6F_{11}$): $\tilde{\nu}_{CO}$ [cm^{-1}] = 2035 s; ^1H NMR ($CF_3C_6F_{11}$): δ = 3.0–2.4 (m, 6 PCH_2CH_2), 2.3–2.0 (m, $IrCH_2CH_2$); $^{31}P\{^1H\}$ NMR ($CF_3C_6F_{11}$): δ = −30.50 (s, 73%), −21.35 (s, 8%), −20.23 (s, 19%).

7: A Schlenk flask was charged with **2** (0.058 g, 0.024 mmol), and $CF_3C_6F_{11}$ (4 mL) and O_2 (1 atm) were added with stirring. After 3 d the volatile components were removed under vacuum. Ether was added (10 mL), the sample filtered, and solvent removed to give **7** as a yellow oil (0.039 g, 0.016 mmol, 67%). Elemental analysis calcd for $C_{49}H_{24}ClF_{78}IrO_3P_2$: C 24.20, H 0.99; found: C 24.70, H 1.20; IR ($CF_3C_6F_{11}$): $\tilde{\nu}_{CO}$ [cm^{-1}] = 2021 s, $\tilde{\nu}_{OO}$ [cm^{-1}] = 864 m; ^1H NMR (acetone): δ = 2.82–2.66 (m, 6 PCH_2CH_2); $^{31}P\{^1H\}$ NMR (acetone): δ = 1.59 (s).

Received: January 13, 1997 [Z 9989 IE]
German version: *Angew. Chem.* **1997**, *109*, 1685–1687

Keywords: iridium · ligand effects · O–O activation · radical reactions · two-phase catalysis

[1] B. Corneils, W. A. Herrmann, *Applied Homogeneous Catalysis with Organometallic Compounds*, VCH, Weinheim, **1996**.
[2] a) I. T. Horváth, J. Rábai, *Science* **1994**, *266*, 72; b) US-A Patent 5,463,082, **1995**.
[3] J. J. J. Juliette, I. T. Horváth, J. A. Gladysz, *Angew. Chem.* **1997**, *109*, 1682–1684; *Angew. Chem. Int. Ed. Engl.* **1997**, *36*, 1610–1612.
[4] a) R. P. Hughes, H. A. Trujillo, *Organometallics* **1996**, *15*, 286; b) S. G. DiMagno, P. H. Dussault, J. A. Schultz, *J. Am. Chem. Soc.* **1996**, *118*, 5312; c) A. Studer, S. Hadida, R. Ferritto, S.-Y. Kim, P. Jeger, P. Wipf, D. P. Curran, Science **1997**, *275*, 823, and references therein.
[5] a) L. Vaska, *Science* **1963**, *140*, 809; b) P. B. Chock, J. Halpern, *J. Am. Chem. Soc.* **1966**, *88*, 3511.
[6] Prior use of related reactions: M. J. Burk, R. H. Crabtree, *Inorg. Chem.* **1986**, *25*, 931.

[7] a) All complexes were characterized by IR as well as ^{1}H and ^{31}P NMR spectroscopy. All except **2** were oils, and correct microanalyses were not always obtained. The ^{13}C NMR spectra were complicated by extensive ^{19}F couplings; b) crystallographic data for **2** ($C_{49}H_{24}ClF_{78}IrOP_2$, $M_r = 2400.27$): triclinic, $P\bar{1}$, $T = -80\,^{\circ}C$, $a = 11.277(6)$, $b = 15.094(5)$, $c = 22.595(4)$ Å, $\alpha = 84.83(2)$, $\beta = 85.85(2)$, $\gamma = 80.15(3)^{\circ}$, $V = 3768(2)$ Å^3, $Z = 2$, $\rho_{calcd} = 2.116$ g cm^{-3}, ρ_{obs} (C_6H_5Br/CH_3I, 22 °C) = 2.085 g cm^{-3}, crystal dimensions $0.34 \times 0.28 \times 0.22$ mm, $Mo_{K\alpha}$ radiation ($\lambda = 0.71073$ Å), scan mode $\theta/2\theta$, 12450 measured reflections, $0 \le h \le 12$, $-17 \le k \le 17$, $-25 \le l \le 25$, $2.00 \le \theta \le 24.03^{\circ}$, 11783 unique data, 9781 observed data ($> 2\sigma(I)$), absorption coefficient 2.082 mm^{-1}, min./max. transmission 83.6/99.9%, 1262 parameters, GOF = 1.050, $R1$ (2σ) = 0.046, $wR2 = 0.1195$, $R_{int} = 0.0324$, R indices (all data): $R1 = 0.0637$, $wR2 = 0.1442$. Crystallographic data (excluding structure factors) for the structures reported in this paper have been deposited with the Cambridge Crystallographic Data Centre as supplementary publication no. CCDC-100131. Copies of the data can be obtained free of charge on application to The Director, CCDC, 12 Union Road, Cambridge CB21EZ, UK (fax: int. code +(1223)336-033; e-mail: deposit@chemcrys.cam.ac.uk).

[8] For example, *trans*-[IrCl(CO)($P(iPr)_3$)$_2$] exhibits Ir–P, Ir–Cl, and Ir–C bond lengths of 2.347(2), 2.421(5), and 1.80(2) Å, and L-Ir-L bond angles of $(90 \pm 1)^{\circ}$ and $(180 \pm 1)^{\circ}$ at room temperature: L. Dahlenburg, A. Yardimcioglu, *J. Organomet. Chem.* **1985**, *291*, 371.

[9] The Cambridge Structural Database contains many compounds with $(CF_2)_4$ segments, but only two with $(CF_2)_{\geq 6}$ segments: a) $CF_3(CF_2)_6$-*p*-$C_6H_4CO_2$-*p*-C_6H_4CN: P. Kromm, J.-P. Bideau, M. Cotrait, C. Destrade, H. Nguyen, *Acta Cryst.* **1994**, *C50*, 112; b) [(η^5-C_9H_7)CoI(CO){$(CF_2)_5CF_3$}]: C. R. Jablonski, Z. Zhou, *Can. J. Chem.* **1992**, *70*, 2544.

[10] B. Albinsson, J. Michl, *J. Phys. Chem.* **1996**, *100*, 3418.

[11] Reviews of several distinct mechanisms by which alkyl halides can undergo oxidative addition: a) J. P. Collman, L. S. Hegedus, J. R. Norton, R. G. Finke, *Principles and Applications of Organotransition Metal Chemistry*, University Science Books, Mill Valley, California, **1987**, pp. 306–322; b) S. Henderson, R. A. Henderson, *Adv. Phys. Org. Chem.* **1987**, *23*, 1.

[12] a) PPh_3 is alkylated by CH_3I much faster than by $CF_3(CF_2)_7CH_2CH_2I$: P. Bernatis (University of Utah), unpublished results. b) A reviewer raised the question of the relative rates of radical reactions in fluorocarbons and organic solvents. One relevant observation is that **2** and $CH_3CH_2CHICH_3$ react more rapidly in $CF_3C_6F_{11}$ than THF.

[13] J. A. Labinger, J. A. Osborn, N. J. Coville, *Inorg. Chem.* **1980**, *19*, 3236.

[14] Additions of H_2 to **1**: P. P. Deutsch, R. Eisenberg, *Chem. Rev.* **1988**, *88*, 1147.

[15] Addition of $^{3}O_2$ and $^{1}O_2$ to **1**: M. Selke, W. L. Karney, S. I. Khan, C. S. Foote, *Inorg. Chem.* **1995**, *34*, 5715.

[16] Accordingly, *trans*-[IrCl(CO){$P(C_6F_5)_3$}$_2$] ($\tilde{\nu}_{CO} = 1994$ cm^{-1}) is inert to O_2: L. Vaska, L. S. Chen, *J. Chem. Soc. Chem. Commun.* **1971**, 1080.

[17] P. M. Maitlis, A. Haynes, G. J. Sunley, M. J. Howard, *J. Chem. Soc. Dalton Trans.* **1996**, 2187.

[18] a) J. L. Kiplinger, T. G. Richmond, C. E. Osterberg, *Chem. Rev.* **1994**, *94*, 373; b) M. J. Atherton, J. Fawcett, J. H. Holloway, E. G. Hope, A. Karaçar, D. R. Russell, G. C. Saunders, *J. Chem. Soc. Dalton Trans.* **1996**, 3215.

Synthesis of a Novel Stable GM_3-Lactone Analogue as Hapten for a Possible Immunization against Cancer**

Lutz F. Tietze* and Holger Keim

Dedicated to Professor Waldemar Adam on the occasion of his 60th birthday

In addition to proteins and lipids, carbohydrates—of which gangliosides constitute a large part—are essential elements of the cell surface. They are anchored to the lipid bilayer of the membrane with their ceramide portion, and the carbohydrate moiety is exposed to the outside. Gangliosides play an important role in cell–cell and cell–matrix recognition and are relevant for cellular growth since they interact with many growth receptors, for example the epidermal growth factor receptor.[1] The GM_3 ganglioside is the smallest and most widespread ganglioside in human and animal tissue. It has been found in brain and nerve cells as well as in the membranes of melanoma and liver carcinoma cells in increased concentrations.[2] However, immunization experiments with monoclonal antibodies indicate that the actual tumor-associated antigen is not the GM_3 ganglioside itself but its lactone form **1**.[3] Consequently, a greatly increased density of the GM_3 lactone was discovered in melanoma cells. Furthermore, the existence of a threshold at which the antibody recognizes the cell has been shown.[4] The GM_3 ganglioside lactone[4] and lactam[5] hitherto used to obtain antibodies are unstable towards hydrolysis under physiological conditions. Therefore, there is much interest in developing hydrolysis-resistant analogues of **1** and, thus, making a defined immunogen available for immunization. Here we describe the synthesis of the hydrolysis-stable GM_3 ganglioside lactone analogue **2** containing an ether group.

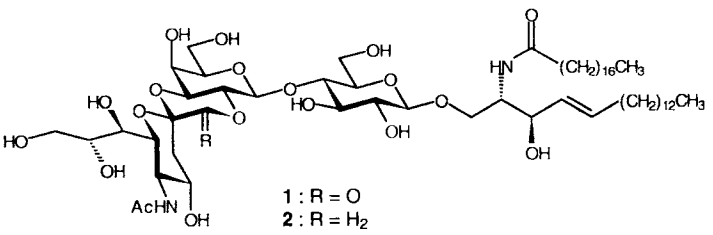

For the synthesis of **2** the cyclization of trisaccharide **3**[6]—with free hydroxy groups at C2′ and C4′ which is selectively built up from glucose, galactose and neuraminic acid by known procedures—with 1,8-diazabicyclo[5.4.0]undec-7-ene (DBU) in dichloromethane to yield the C2′-Gal lactone **5** was initially attempted (Scheme 1). However, reaction of the free hydroxy groups led to both possible lactone isomers in 86% yield as a nonseparable mixture in a ratio of 1.7:1. Conversely, the acid-catalyzed reaction of the partially deprotected trisaccharide **4**, which was already described for the isolated GM_3 ganglioside,[7] provided the desired GM_3 ganglioside lactone **5** in 57% yield.

To transform **5** into analogue **9** it was first peracetylated to give **6**; subsequent reduction of the lactone functionality led to lactol **7**, which was converted into thiohemiacetal **8**. Hydrogenolytic cleavage of the thiol moiety completed the sequence. The Red-Al derivative Na[$AlH(OCH_2CH_2OCH_3)_2$-OEt][8] proved to be the best reagent for reducing the carboxy functionality to afford **7** in 80% yield with conservation of the acetyl groups. Reaction with diisobutylaluminium hydride (DIBAL) mostly led to deacylated products; $LiBH_4$ and $NaBH_4$ yielded the corresponding, undesired diols as main products, as expected.

Conversion of the hemiacetal of **7** into the ether functionality of **9** proved extremely difficult, mainly due to the low reactivity of the hydroxy group, and almost led to failure of the entire project. The glycosidic bond at C1 was cleaved in all attempts to reductively remove the hydroxy group directly, for example with triethylsilane and boron trifluoride etherate. The obvious transformation into an *O,S*-acetal also failed initially. Activation of the hydroxy group by conversion into the acetate or trichloroacetimidate by standard procedures was achieved in very high yields. However, during the subsequent reaction with

[*] Prof. Dr. L. F. Tietze, Dr. H. Keim
Institut für Organische Chemie der Universität
Tammannstrasse 2, D-37077 Göttingen (Germany)
Fax: Int. code +(551)39-9476
e-mail: ltietze@gwdg.de

[**] This work was supported by the Deutsche Forschungsgemeinschaft (SFB 500) and the Fonds der Chemischen Industrie. H. K. thanks the latter for a doctoral scholarship.

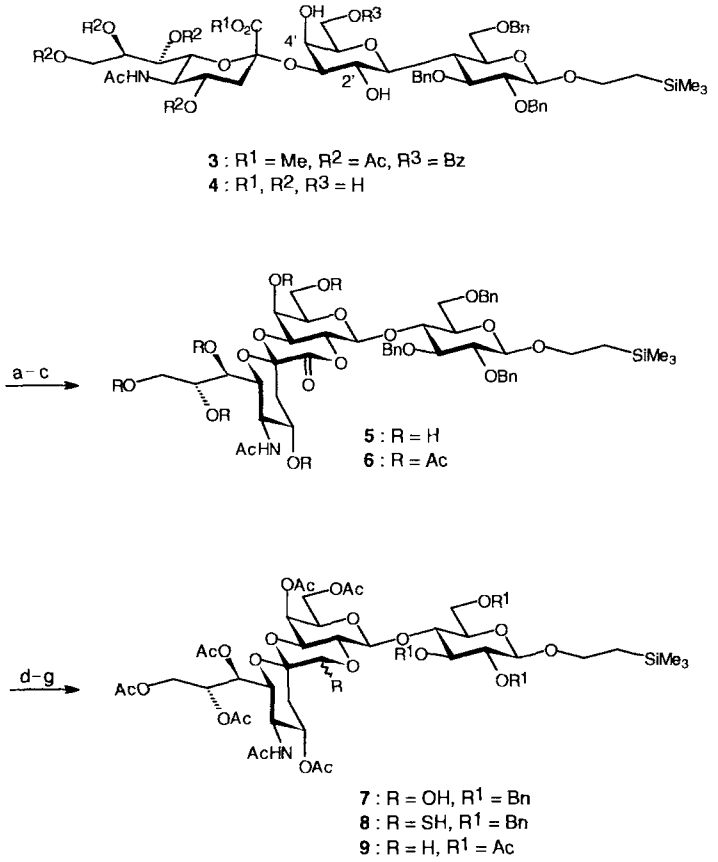

Scheme 1. a) NaOMe, MeOH, 30 h, room temperature (RT); b) HOAc, 3 d, RT, 57% (two steps); c) Ac_2O, pyridine, 4-(dimethylamino)pyridine (DMAP), 14 h, RT, 94%; d) $Na[AlH(CH_2OEt)_2OEt]$, toluene, −55 °C, 1 h, 80%; e) $(PyS)_2$ (5 equiv), nBu_3P (5 equiv), CH_2Cl_2, 3 d, RT, 6 h reflux, 71%; f) Raney nickel, EtOH, H_2 (1 atm), 30 h, RT; g) Ac_2O, pyridine, DMAP, CH_2Cl_2, 14 h, RT, 85% (two steps).

thiophenol in the presence of boron trifluoride etherate or trimethylsilyl triflate (TMSOTf), a competitive reaction took place at C1 of the glucose unit leading to the dithiophenyl glycosides. Only reaction with five equivalents each of bis(pyridinium) disulfide and *n*-tributylphosphane[9] resulted in the desired transformation of the lactol. Remarkably, the free thiohemiacetal **8** was obtained in 71% yield as a result of overreduction instead of the expected *S*-pyridyl derivative.

Subsequent conversion into the acetyl-protected GM_3-lactone analogue **9** was achieved by hydrogenation with H_2 and Raney nickel and concomitant cleavage of the benzyl groups in an excellent yield of 85%. The presence of the ether **9** was proven with NMR spectroscopy by $^1H-^1H$ correlation experiments. Two doublets at $\delta = 3.44$ and 3.89 ($^2J(H,H) = 11.5$ Hz) can be assigned to the two geminal protons at C1″.

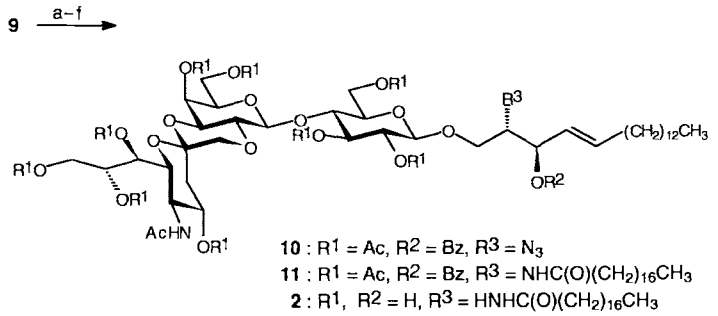

Scheme 2. a) CF_3COOH/CH_2Cl_2 (2/1), 30 min, RT; b) CCl_3CN (30 equiv), DBU, CH_2Cl_2, 1 h, 0 °C, 93% (two steps); c) CH_2Cl_2, azido sphingosine (3 equiv), $BF_3 \cdot Et_2O$ (3 equiv), 4-Å molecular sieves, 1 h, −40 °C, 66%; d) NEt_3 (5 equiv), PhSH (5 equiv), $(PhS)_2Sn$, CH_2Cl_2 (5 equiv), 4 h, RT; e) stearic acid (5 equiv), EDC (5 equiv), CH_2Cl_2, 2 h, RT, 73% (two steps); f) NaOMe, MeOH, 20 h, RT, 77%.

To convert **9** into the complete GM_3 ganglioside lactone analogue **2**, the protecting group at C1 was removed by reaction with trifluoroacetic acid in dichloromethane (Scheme 2). Unfortunately, epimerization took place at C2 of the neuraminic acid to an extent of 17% and led to the thermodynamically more stable β anomer, which fortunately was easily removed by chromatography (silica gel) at the stage of **10**. The two anomers could be distinguished by their ^1H NMR signals for 3″-H_{eq} at $\delta = 2.50$ for the α anomer and 1.96 for the β anomer. Lewis acids such as boron trifluoride etherate or zinc chloride employed to cleave the C1 protecting group effected almost complete epimerization; no reaction took place with tetrabutyl ammonium fluoride.

For the further transformation into the ganglioside **10**, reaction of the hydroxy group at C1 was carried out to lead to the trichloroacetimidate. Subsequent glycosylation with azido sphingosine at −40 °C in dichloromethane, catalyzed with boron trifluoride etherate, afforded the sphingosine derivative **10** in two hours. No further epimerization was observed under these reaction conditions. Reduction of the azido group in **10** to the corresponding amine was effected in good yields with $NHEt_3^+[(PhS)_3Sn]^-$.[12] Once again many reagents were tested—such as triphenylphosphane, 1,3-propanedithiol, and H_2S—but all led to poorer results. In the final steps of the synthesis of the free GM_3-lactone analogue **2**, the amine reacted with stearic acid upon addition of 1-ethyl-3-(3-dimethylaminopropyl)carbodiimide (EDC) to provide ceramide **11**, which was deprotected by solvolysis with sodium methanolate in methanol.

In cooperation with the Abteilung für Hämotologie und Onkologie as well as the Abteilung für Immunologie at the Universität Göttingen we are currently testing the biological activity of **2**. We are also forming conjugates with bovine serum albumin (BSA) and the keyhole-limpet hemocyanin (KLH), which are used for immunization.

Received: December 19, 1996 [Z9907IE]
German version: *Angew. Chem.* **1997**, *109*, 1704–1706

Keywords: acetals · gangliosides · glycosylations · neuraminic acids · tumor therapy

[1] Q. Zhou, S. Hakomori, K. Kitamura, Y. Igarashi, *J. Biol. Chem.* **1994**, *269*, 1959.
[2] a) W. B. Hamilton, F. Helling, K. O. Lloyd, P. O. Livingston, *Int. J. Cancer* **1993**, *53*, 566; b) C.-C. Sung, D. K. Pearl, S. W. Coons, B. W. Scheithauer, P. C. Johnson, A. J. Yates, *Cancer* **1994**, *74*, 3010.
[3] G. Magnusson, K. Ding, U. Nilsson, A. K. Ray, A. Rosén, H.-O. Sjögren in *Complex Carbohydrates in Drug Research* (Eds.: K. Bock, H. Clausen), Copenhagen, **1994** (*Alfred Benzon Symp.* **1994**, *36*, 89).
[4] G. A. Nores, T. Dohi, M. Taniguchi, S. I. Hakomori, *J. Immunol.* **1987**, *139*, 3171.
[5] M. Wilstermann, L. O. Kononov, O. Nilson, A. K. Ray, G. Magnusson, *J. Am. Chem. Soc.* **1995**, *117*, 4742.
[6] A. Hasegawa, K. Adachi, M. Yoshida, M. Kiso, *J. Carbohydr. Chem.* **1992**, *11*, 95.
[7] R. K. Yu, T. A. W. Koerner, S. Ando, H. C. Yohe, J. H. Prestegard, *J. Biochem.* **1985**, *98*, 1367.
[8] R. Kanazawa, T. Tokoroyama, *Synthesis* **1976**, 526.
[9] A. O. Stewart, R. M. Williams, *J. Am. Chem. Soc.* **1985**, *107*, 4289.
[10] ^1H NMR (500 MHz, $CDCl_3$, 25 °C, TMS): $\delta = 0.01$ (s, 9H; $SiMe_3$), 0.93 (m_c, 2H; CH_2SiMe_3), 1.87 (dd, $^3J(H,H) = 10.5$, $^2J(H,H) = 13.5$ Hz, 1H; 3″-H_{ax}), 1.90 (s, 3H; CH_3CON), 2.03, 2.06, 2.08, 2.09, 2.13, 2.15 (s, 27H; $9CH_3CO$), 2.60 (dd, $^3J(H,H) = 5.5$, $^2J(H,H) = 13.5$ Hz, 1H; 3″-H_{eq}), 3.44 (d, $^2J(H,H) = 11.5$ Hz, 1H; 1″-H_{ax}), 3.59 (dd, $^3J(H,H) = 7.5$, 10.5 Hz, 1H; 2′-H), 3.52–3.58

(m, 1H; OCH_2CH_2Si), 3.64 (dt, $^3J(H,H) = 3.5, 10.0$ Hz, 1H; 5-H), 3.71 (dd, $^3J(H,H) = 3.0, 10.5$ Hz, 1H; 3'-H), 3.81 (t, $^3J(H,H) = 9.5$ Hz, 1H; 4-H), 3.80–3.91 (m, 4H; 5'-H, 5''-H, 6'-H_a, 6''-H), 3.89 (d, $^2J(H,H) = 11.5$ Hz, 1H; 1''-H_{eq}), 3.92–3.99 (m, 1H; OCH_2CH_2Si), 4.02–4.13 (m, 2H; 6-H_a, 6'-H_b), 4.10 (dd, $^3J(H,H) = 6.0$, $^2J(H,H) = 12.0$ Hz, 1H; 9''-H_a), 4.35 (d, $^2J(H,H) = 7.5$ Hz, 1H; 1'-H), 4.38–4.43 (m, 2H; 6-H_b, 9''-H_b), 4.49 (d, $^2J(H,H) = 8.0$ Hz, 1H; 1-H), 4.88 (dd, $^3J(H,H) = 8.0, 9.5$ Hz, 1H; 2-H), 5.21 (t, $^3J(H,H) = 9.5$ Hz, 1H; 3-H), 5.15–5.23 (m, 2H; 4''-H, 8''-H), 5.25 (dd, $^3J(H,H) = 2.0, 6.5$ Hz, 1H; 7''-H), 5.29 (dd, $^3J(H,H) = 1.5, 3.0$ Hz, 1H; 4'-H), 5.32 (d, $^3J(H,H) = 9.0$ Hz, 1H; NH); $[\alpha]_D^{20} = -6.6$ ($c = 0.5$ in $CHCl_3$); MS (DCI): m/z (%) = 1098.3 (100) $[M + NH_3 + H]^+$.

[11] R. R. Schmidt, P. Zimmermann, *Angew. Chem.* **1986**, *98*, 722; *Angew. Chem. Int. Ed. Engl.* **1986**, *25*, 725.

[12] M. Bartra, F. Urpi, J. Vilarrasa, *Tetrahedron Lett.* **1987**, *28*, 5941.

Self-Assembly of a Mesogenic Polyamide: Induction and Significant Stabilization of a Liquid-Crystalline Phase through Complexation of a Phenylbenzoic Acid with a Polymer Backbone Derived from 2,6-Bis(amino)pyridine Units**

Takashi Kato,* Yasuo Kubota, Toshiyuki Uryu, and Seiji Ujiie

The use of specific interactions for the design and preparation of molecular materials such as liquid crystals has attracted attention because of their potential as dynamically functional molecular systems.[1] For liquid-crystalline polymers, specific intermolecular forces such as hydrogen bonding,[1-4] ionic,[5] and charge transfer interactions[6] have been used for several years for the formation of mesogenic structures. Thus, for instance, the first hydrogen-bonded supramolecular mesogenic polymer, which consists of different and independent molecular components, was prepared from a stilbazole and a polyacrylate containing a benzoic acid group in the side chain.[2] Two bifunctional complementary components were used for the formation of the first main-chain supramolecular mesogenic polymer.[3] Since then, a wide variety of hydrogen-bonded supramolecular polymers that exhibit mesomorphic behavior have been prepared by self-assembly processes.[4] Recently we have shown that 2,6-bis(acylamino)pyridine can be used as a molecular component for supramolecular liquid-crystalline materials through the formation of double hydrogen bonds.[7] These complexes exhibit only monotropic mesophases with relatively narrow temperature ranges. Aminopyridines have been used frequently as versatile molecular units for the control of molecular aggregation.[3, 8]

[*] Dr. T. Kato
Department of Chemistry and Biotechnology, Graduate School of Engineering
The University of Tokyo
Hongo, Bunkyo-ku, Tokyo 113 (Japan)
Fax: Int. code +(3)3818-4868
e-mail: katoα chiral.t.u-tokyo.ac.jp
Y. Kubota, Prof. T. Uryu
Institute of Industrial Science, The University of Tokyo
Roppongi, Minato-ku, Tokyo 106 (Japan)
Dr. S. Ujiie
Department of Material Science, Shimane University
Matsue, Shimane 690 (Japan)

[**] This work was supported by the Ministry of Education, Science, Sports, and Culture (Grant-in-Aid for Scientific Research in Priority Areas of "New Polymers and Their Nano-Organized Systems" (No. 277/08246101) for T. K.).

Our aim is to obtain a nylon with heterocyclic units in the backbone that is capable of molecular recognition and self-organization through the incorporation of the bifunctional pyridine, and we report here on a novel form of self-assembly of a main-chain polymer, which leads to a greatly stabilized mesophase through complexation of a phenylbenzoic acid with a 2,6-bis(amino)pyridine unit in the polymer backbone. The 2,6-bis(amino)pyridine unit was incorporated into a polymer main chain to enable the polymer to recognize hydrogen-bonding molecules on its backbone. Polyamide **1** was prepared by low-temperature polycondensation of 2,6-bis(amino)pyridine and sebacoyl chloride in solution. The polymer is nonmesogenic. On heating the polymer, glass and melting transitions were observed at 118 and 222 °C, respectively. 4-(4'-(Octyloxy)phenyl)benzoic acid (**2**) exhibits a smectic C phase between 179 and 250 °C, and a subsequent nematic phase up to 259 °C.

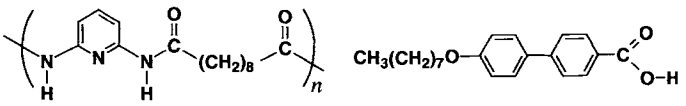

1 **2**

We expected that **1** and **2** would form a supramolecular complex.[7, 8] The 1:1 complex from **1** and **2** (equimolar amounts of aminopyridine and carboxylic acid moieties) was prepared by direct mixing in the molten state. Microscope studies and differential scanning calorimetry (DSC) measurements gave no indications of transition behavior for each of the single components, rather the complex behaved as one single macromolecular component. The complex exhibited a melting transition at 212 °C. After melting, birefringence, which suggests the existence of a mesophase, was observed under a polarizing microscope. Significantly, the mesophase was stable up to 350 °C; thereafter, the polymer slowly decomposed. The results of X-ray diffraction measurements for the complex support the existence of the mesophase. Figure 1 shows X-ray diffraction patterns of the crystalline state (A) and of the mesomorphic state (B). The peak due to the layer spacing at 31.5 Å and several peaks in the

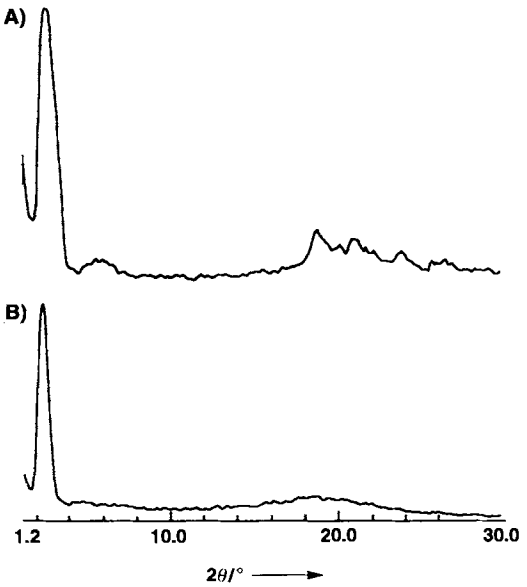

Figure 1. X-ray diffraction patterns of the complex formed from **1** and **2** at 100 °C (A) and at 290 °C (B).

 © VCH Verlagsgesellschaft mbH, D-69451 Weinheim, 1997 0570-0833/97/3615-1617 $ 17.50+.50/0

wide-angle region are observed at 100 °C (Figure 1A). The X-ray pattern at 290 °C consists of one sharp peak due to the layer spacing at 35.9 Å and one diffused halo at 4.6 Å (Figure 1B). This liquid-crystalline molecular arrangement with a layer spacing of 35.9 Å is still observed even at 350 °C, where birefringence is also clearly evident. In contrast, the single component **2** becomes isotropic at 259 °C, and polyamide **1** is completely nonmesomorphic. These results suggest that a supramolecular liquid-crystalline polyamide of type **3** is formed and that a thermally stabilized mesophase of a smectic A molecular arrangement has been induced by the self-assembly. The length of the mesogenic part from the pyridyl unit to the end of the octyl group is estimated to be 26.0 Å by molecular modeling. A proposed molecular arrangement of the molecules in the liquid-crystalline phase is shown in Figure 2.

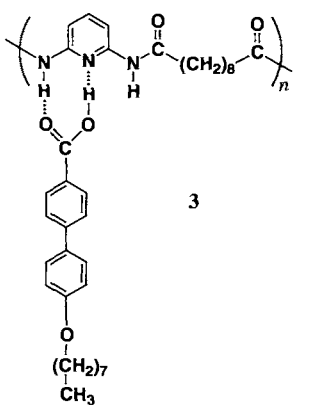

3

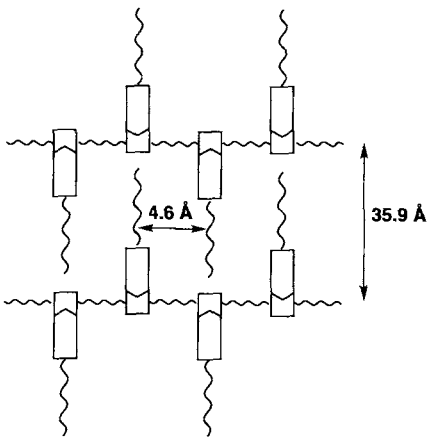

Figure 2. Schematic representation of the molecular arrangement of the supramolecular polymer complex from **1** and **2** in the liquid-crystalline state.

This polymeric structure consisting of **1** and **2** is quite unique for liquid-crystallline polymers because the mesogenic core unit is laterally connected and the structure is not simply classified into main-chain and side-chain types. Moreover, the overall structure of the supramolecular mesogenic part containing the lateral amide groups is neither simple rod nor disc shape. For a low molecular weight complex that has a similar structure but contains two rings (the biphenyl unit is replaced by a benzene ring), only a monotropic smectic B phase was observed below 100 °C,[7b] while the mesophase is observed up to 350 °C for the complex from **1** and **2**. The formation of the three-ring mesogen by the supramolecular assembly and the incorporation of the mesogen into the polyamide backbone have greatly contributed to the stabilization of the mesophase. For aromatic polyamides, high melting temperatures or no melting transitions are often encountered due to the stacking of the aromatic rings and the formation of hydrogen-bonding networks between the amide units. These interactions might also contribute to the stabilization of the mesophase. Recently a thermotropic mesogenic polyester containing a lateral pyridyl substituent was prepared to obtain hydrogen-bonded mesomorphic polymer blends;[9] however, in the present case the polymer backbone contains pyridyl groups, which, in turn, directly become part of the mesogen. The complex reported here belongs to a novel class of supramolecular mesogenic polymers, which is derived from a polyamide capable of molecular recognition on its backbone through the formation of hydrogen bonds.

Experimental Section

1: A solution of sebacoyl chloride (2.19 g, 9.16 mmol) in dry dimethylacetamide (DMAc) (5.0 mL) was added dropwise to a solution of 2,6-bis(amino)pyridine (1.00 g, 9.16 mmol) dissolved in the mixture of dry DMAc (30 mL) and LiCl (1.5 g) under argon atmosphere at room temperature. The reaction mixture was stirred for 24 h and then poured into 400 mL of acetone. The precipitate was filtered and washed with aqueous 5% Na_2CO_3, water, and finally acetone. The product was dried under vacuum at 70 °C for 24 h. Yield: 1.30 g (52%); m.p. 222 °C; $[\eta] = 0.27$ (in DMF at 30 °C). ^{1}H NMR (270 MHz, [D$_7$]DMF, 60 °C): $\delta = 9.85$ (2H; NH), 7.83 (2H; ArH *meta* to N), 7.72 (1H; ArH *para* to N), 2.47 (4H; $COCH_2$), 1.67 (4H; $COCH_2CH_2$), 1.34 (8H; $CO(CH_2)_2CH_2CH_2$); ^{13}C NMR (67.5 MHz, [D$_7$]DMF, 60 °C): $\delta = 172.9$ (CO), 151.7, 140.3, 109.3 (pyridine-C). 37.3, 25.9 (CH_2 groups). Two peaks due to the alkanediyl spacer overlapped with the peaks of DMF.

Complexation: An equimolar amount of the pyridyl unit of **1** and compound **2** was mixed and complexed in the isotropic molten state under an argon atmosphere. The sample was rapidly cooled to room temperature and used for the measurements.

Characterization: DSC thermograms were obtained on a Mettler DSC 30 apparatus at a heating rate of 10 K min^{-1} under a nitrogen atmosphere. For the polymeric materials, the temperature of the maxima of the melting endotherms and the middle point of the glass transition were taken as the transition temperatures. A polarizing microscope (Olympus BH2) equipped with a Mettler FP82HT hot stage was used for visual observation of the sample. X-ray diffraction measurements were carried out on a Rigaku X-ray Rad 2B system using Ni-filtered $Cu_{K\alpha}$ radiation. Samples placed on a Mettler FP 52 hot stage were used for the X-ray measurement.

Received: January 31, 1997 [Z 10060 IE]
German version: *Angew. Chem.* **1997**, *109*, 1687–1689

Keywords: hydrogen bonds · liquid crystals · polyamides · self-assembly · supramolecular chemistry

[1] a) T. Kato, J. M. J. Fréchet, *Macromol. Symp.* **1995**, *98*, 311–326; b) M. Paleos, D. Tsiourvas, *Angew. Chem.* **1995**, *107*, 1839–1855; *Angew. Chem. Int. Ed. Engl.* **1995**, *34*, 1696–1711; c) J.-M. Lehn, *Makromol. Chem. Macromol. Symp.* **1993**, *69*, 1–17.

[2] T. Kato, J. M. J. Fréchet, *Macromolecules* **1989**, *22*, 3818–3819; *ibid.* **1990**, *23*, 360.

[3] C. Fouquey, J.-M. Lehn, A.-M. Levelut, *Adv. Mater.* **1990**, *2*, 254–257.

[4] a) T. Kato, H. Kihara, T. Uryu, A. Fujishima, J. M. J. Fréchet, *Macromolecules* **1992**, *25*, 6836–6841; b) U. Kumar, T. Kato, J. M. J. Fréchet, *J. Am. Chem. Soc.* **1992**, *114*, 6630–6639; c) U. Kumar, J. M. J. Fréchet, T. Kato, S. Ujiie, K. Iimura, *Angew. Chem.* **1992**, *104*, 1545–1547; *Angew. Chem. Int. Ed. Engl.* **1992**, *31*, 1531–1533; d) T. Kato, H. Kihara, U. Kumar, T. Uryu, J. M. J. Fréchet, *ibid.* **1994**, *106*, 1728–1730 and **1994**, *33*, 1644–1645; e) T. Kato, N. Hirota, A. Fujishima, J. M. J. Fréchet, *J. Polym. Sci. Part A Polym. Chem.* **1996**, *34*, 57–62; f) C. G. Bazuin, F. A. Brandys, T. M. Eve, M. Plante, *Macromol. Symp.* **1994**, *84*, 183–196; g) S. Malik, P. K. Dahl, R. A. Mashelkar, *Macromolecules* **1995**, *28*, 2159–2164; h) R. V. Tal'roze, S. A. Kuptsov, T. I. Sycheva, V. S. Bezborodov, N. A. Platé, *ibid.* **1995**, *28*, 8689–8691.

[5] a) H. Ringsdorf, R. Wüstefeld, E. Zerta, M. Ebert, J. H. Wendorff, *Angew. Chem.* **1989**, *101*, 934–938; *Angew. Chem. Int. Ed. Engl.* **1989**, *28*, 914–918; b) H. Bengs, R. Renkel, H. Ringsdorf, C. Baehr, M. Ebert, J. H. Wendorff, *Makromol. Chem. Rapid Commun.* **1991**, *12*, 439–446.

[6] a) S. Ujiie, K. Iimura, *Macromolecules* **1992**, *25*, 3174–3178; b) C. G. Bazuin, A. Tork, *ibid.* **1995**, *28*, 8877–8880.

[7] a) T. Kato, M. Nakano, T. Moteki, T. Uryu, S. Ujiie, *Macromolecules* **1995**, *28*, 8875–8876; b) T. Kato, Y. Kubota, M. Nakano, T. Uryu, *Chem. Lett.* **1995**, 1127–1128.

[8] a) E. Fan, C. Vincent, S. J. Geib, A. D. Hamilton, *Chem. Mater.* **1994**, *6*, 1113–1117; b) C. Vincent, S. C. Hirst, F. Garcia-Tellado, A. D. Hamilton, *J. Am. Chem. Soc.* **1991**, *113*, 5466–5467.

[9] A. Sato, T. Kato, T. Uryu, *J. Polym. Sci. Part A Polym. Chem.* **1996**, *34*, 503–505.

 © VCH Verlagsgesellschaft mbH, D-69451 Weinheim, 1997 0570-0833/97/3615-1618 $ 17.50+.50/0

$Co_2(O_3P-CH_2-PO_3)\cdot H_2O$: A Novel Microporous Diphosphonate with an Inorganic Framework and Hydrocarbon-Lined Hydrophobic Channels**

Douglas L. Lohse and Slavi C. Sevov*

Microporous materials are of great importance as molecular sieves, catalysts, ion-exchangers, and sensor materials.[1] Extensive exploration of new systems and new methods of synthesis has led to discoveries of novel materials with controlled pore sizes, better acidity, and better thermal stability. Nevertheless, despite the large number of different microporous compounds, all of them, with only two exceptions, have hydrophilic channels. The two exceptions are the methylphosphonates of aluminum and copper.[2] Such phosphonates and diphosphonates of the transition as well as main group metals have also received much attention during the last few years.[3-6] These are built of inorganic layers or chains that are either "coated" by the phosphonate and are held together by weak intermolecular forces,[3] or are linked covalently through diphosphonate groups.[4, 5] Many of the diphosphonates[5] and one monophosphonate, an aminoethylphosphonate,[6] mimic open-framework structures with hydrophobic channels but their "frameworks" contain organic interchain or interlayer links. The Al- and Cu-methylphosphonates are the only phosphonates that are microporous, have three-dimensional inorganic-only backbones, that is composed of a metal-oxygen-phosphorus network, and contain hydrophobic channels.[2]

We describe here the synthesis and structural characterization of the first microporous diphosphonate with an inorganic backbone and hydrophobic channels. The channels in the inorganic framework have hydrophobic walls built from methylene groups. The title compound was originally made in a hydrothermal synthesis designed to produce cobalt boro(methylene)diphosphonate analogues to the recently synthesized microporous cobalt borophosphate $CoB_2P_3O_{12}(OH)\cdot(enH_2)$ (en = ethylenediamine).[7] The reaction mixture contained $Co(NH_3)_6Cl_3$, boric acid, ethylenediamine, boron trifluoride-ethylamine complex, and methylenediphosphonic acid (instead of phosphoric acid). However, the reaction produced very fine flakelike crystallites of the sky-blue compound $Co_2(O_3P-CH_2-PO_3)\cdot H_2O$. In order to grow larger single crystals we repeated the synthesis but with some of the product of previous reactions added to a very dilute mixture of the starting materials.

The structure of the compound was determined by single-crystal X-ray diffraction. The monoclinic structure is of the open-framework type with channels running along the c axis (Figure 1). It contains one tetrahedrally coordinated (Co1) and two octahedrally coordinated (Co2 and Co3) cobalt atoms (Figure 2). The octahedrally coordinated Co2 (O1, O2, O2, O3, O4, O6) and Co3 centers (O1, O1, O3, O3, O5, O5) share edges and form zigzag chains running along the b axis (in out-of-phase fashion). Each Co3 octahedron shares two parallel edges with two Co2 octahedra (O1, O3), while each Co2 octahedron shares two oblique edges with one Co2 octahedron (2 × O2) and one Co3 octahedron. In addition, the Co2 octahedra share a corner

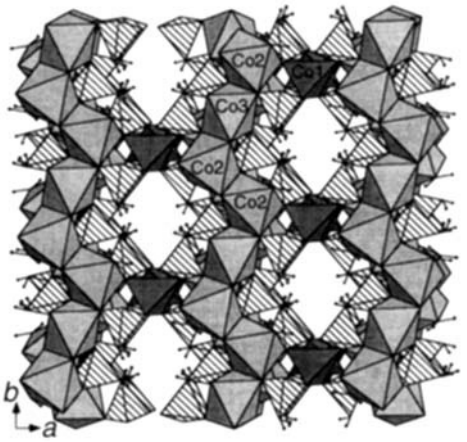

Figure 1. A view of the structure of $Co_2(O_3P-CH_2-PO_3)\cdot H_2O$ along the c axis of the monoclinic unit cell. The CoO_6 octahedra and the CoO_4 tetrahedra are shaded in light and dark gray, respectively. The tetrahedra of the O_3PC groups with a common C atom are striped. The C-H bonds of the CH_2 groups that form the walls of the hydrophobic channels are shown as well. Zigzag chains of octahedra run along the b axis; the chains are linked in sheets by the cobalt tetrahedra (see text).

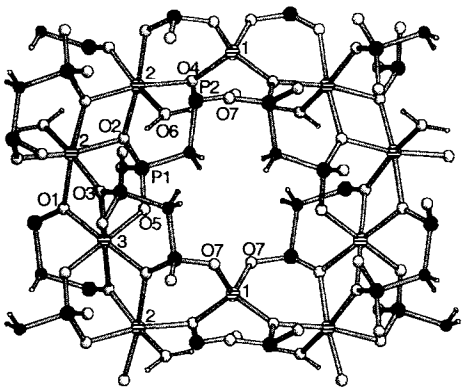

Figure 2. A detailed view of the channels along the c axis (the b axis runs vertical in the figure): C: black, P: dark gray, Co: striped, O: light gray, H: smallest circles. The "rectangular" shape of the channels is defined by CH_2 groups (the short dimension) and oxygen atoms (the long dimension). The water molecules coordinated to Co2 are also shown. The cobalt atoms are indicated by their numbers only. Pertinent (average) bond lengths [Å]: Co1-O(4×) 1.978, Co2-O(6×) 2.106, Co3-O(6×) 2.102, P1-O(3×) 1.524, P2-O(3×) 1.534, C-P(2×) 1.808, O6-H(2×) 1.00, C-H(2×) 1.02.

with the Co1 tetrahedron (O4). The remaining sixth vertex of the Co2 octahedron (O6) is occupied by a water molecule, while the two remaining vertices of the Co3 octahedron (2 × O5) are occupied by oxygen atoms from phosphonate groups. The Co1 tetrahedra link the zigzag chains at places of close approach (Figure 1) by sharing two of their vertices (2 × O4) with two Co2 octahedra from two different chains and form sheets of cobalt polyhedra (Figure 3). The remaining two vertices of the Co1 tetrahedron are occupied by atoms from phosphonate groups. The sheets of Co polyhedra are joined together to form a three-dimensional framework by oxygen-phosphorus-oxygen bonding (Figure 3); that is an inorganic-only network (backbone) is constructed. The P1 tetrahedron shares oxygen corners with two Co2 and one Co3 octahedra (O2 and O5, respectively) from one sheet, and with one Co2 and one Co3 octahedra (O1) from the adjacent one. The P2 tetrahedron shares its oxygen corners with one Co2 and one Co3 octahedra (O3) and a Co1 tetrahedron (O7) from one sheet, and with a Co2 octahedron and a Co1 tetrahedron (O4) from another one. Thus, the network of cobalt, phosphorus, and oxygen is linked quite tightly through covalent bonds.

[*] Prof. S. C. Sevov, D. L. Lohse
Department of Chemistry and Biochemistry
University of Notre Dame
Notre Dame, IN 46556 (USA)
Fax: Int. code + (219) 631-6652
e-mail: ssevov@nd.edu

[**] This work was supported by the National Science Foundation (DMR-9701550).

 © VCH Verlagsgesellschaft mbH, D-69451 Weinheim, 1997 0570-0833/97/3615-1619 $ 17.50+.50/0

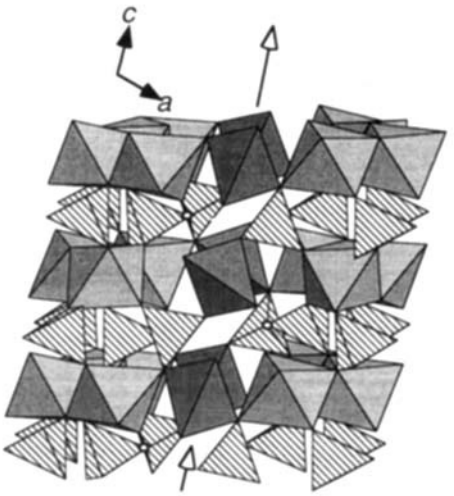

Figure 3. A view of the structure along the *b* axis showing how the layers of CoO_4 tetrahedra (dark gray) and CoO_6 octahedra (light gray) are linked by O–P–O bonds (the striped tetrahedra are of O_3PC) to give a three-dimensional inorganic framework. The carbon atoms are denoted by open circles. The open-head arrows show the general direction of the channels.

The Co–O distances are 1.963(5) and 1.992(5) Å in the tetrahedron, and range from 2.033(6) to 2.196(5) Å in the octahedra (the shortest distance is to the water molecule), all well within the expected limits. The two O_3PC tetrahedra of $[O_3P-CH_2-PO_3]^{4-}$ share the carbon atom of the methylene group; the P-C-P angle is 116.3(4)°. (The corresponding P-C-H and H-C-H angles are within the range of 101 to 116°, but as expected the uncertainties are much larger.) The P–O distances (1.513(5)–1.554(5) Å) and the two P–C distances (1.821(8) and 1.796(8) Å) are normal for phosphonates. Four of the seven different oxygen atoms are bonded to three neighboring atoms (O1, O2, O3, O4), two are bonded to two neighboring atoms (O5, O7), and one is the oxygen atom of the water molecule (O6), which is coordinated to Co2. The short distances between the oxygen atom of the water molecule and the two oxygen atoms bonded to two neighbors (2.646(9) and 2.719(9) Å for O6–O5 and O6–O7, respectively) indicate hydrogen bonding between these atoms.

The cross section of the channels has the shape of a quite elongated rectangle (Figures 1 and 2) with a short dimension of about 4.3 Å defined primarily by the methylene groups (the distance is measured from methylene group to methylene group). The compound can be considered as an inorganic microporous compound that has channels lined with hydrophobic CH_2 groups. Pointing towards the channels are also the two-bonded oxygen atoms O5 and O7, and the oxygen atom of the water molecule O6. They are located quite far from the center of the channels, about 3.5, 3.1 and 3.1 Å, respectively, and define the longer dimension of the latter. This unique arrangement of hydrophobic and hydrophilic units covering the walls of the channels may provide interesting absorption capabilities for small flat molecules with hydrophobic (hydrocarbon bodies) and hydrophilic (functional groups) regions.

Elemental analysis for carbon and hydrogen (M-H-W Laboratories) gave 4.8 and 1.19 wt%, respectively (the calculated values are 3.9 and 1.29 wt%, respectively). A diffuse reflectance spectrum of the compound shows strong absorption band in the region of 500–650 nm. Thermogravimetric measurements showed weight loss of about 4.5% above 350 °C, which is consistent with loss of most of the water in the structure (calculated value 5.8 wt%). This was confirmed by the IR spectra of the sample taken before and after the dehydration. The spectrum recorded before the heating clearly shows the characteristic P–O, C–H, and water bands in the regions 1000–1200, 2800–3000, and 3200–3600 cm^{-1}, respectively, but no water band can be seen in the IR spectrum recorded after the treatment.

The structure of the compound remains unchanged up to about 500 °C according to its X-ray diffraction pattern. The Guinier powder patterns taken of such heated samples showed relatively good crystallinity, and matched very well the powder pattern calculated from the refined structure of the compound before the dehydration. The lines were indexed with the same structure type, and the lattice parameters were only slightly smaller than those of the original unit cell. This clearly indicates that the framework of the structure remained intact at these temperatures. This, combined with the fact that the water molecules can be driven out of the structure, presumably through the channels, indicates that these channels can accommodate molecules at least the size of the water molecule. The dehydration process is irreversible and this is most likely due to the hydrophobicity of the channels.

We have shown that hydrophobic microporous compounds made of metal diphosphonates are accessible. The inorganic framework guarantees the relatively high thermal stability of the compound. The pore sizes are smaller than those in conventional microporous compounds but should be appropriate for small, flat, and hydrophobic molecules with sizes comparable to that of the water molecule such as ethylene and even benzene. Similar compounds with larger openings may be accessible by the use of appropriate hydrophobic templates in the synthesis.

Experimental Section

$Co_2(O_3PCH_2PO_3)\cdot H_2O$ was initially synthesized from a mixture of $Co(NH_3)_6Cl_3$, boric acid, methylenediphosphonic acid, ethylenediamine, $BF_3\cdot CH_3CH_2NH_2$ (all from Aldrich), and water in a molar ratio of 0.25:1:1:1:1: 50 (in an attempt to make a cobalt borophosphonate with an open-framework structure). After homogenization the mixture was loaded in teflon-lined autoclaves and heated at 190 °C for four days. Very fine blue flakes, the only solid product, were recovered and washed with water. It was determined that there was no boron in the product but the rest of the formula was not clear at this stage. A second reaction using HF instead of the boron trifluoride and without boric acid gave the same product but the flakes were again too small for single-crystal X-ray diffraction. In order to grow larger crystals, the washed product of the previous two reactions was added to a very dilute mixture of the starting materials ($Co(NH_3)_6Cl_3$, methylenediphosphonic acid, ethylenediamine, HF, and water in a molar ratio of 0.25:1:1:1:200). The idea was to use the small flakes as nuclei for larger crystals. The product had much larger crystallites indeed, and they were used for single-crystal X-ray strcuture analysis. Lastly, after the crystal structure and the stoichiometry of the compound had been determined, it was synthesized rationally from a mixture of $CoCO_3\cdot H_2O$, methylenediphosphonic acid, HF and water in a molar ratio of 2:1:1:50. The compound formed readily in high yields in acidic conditions.

Structure determination: Data were collected from a single crystal (0.1 × 0.05 × 0.01 mm) on a CAD4 single-crystal diffractometer with monochromated $Mo_{K\alpha}$ radiation at 21 °C (ω-2θ scans, $2\theta_{max} = 50°$, a hemisphere of $\pm h, k, \pm l$ was collected, 2322 measured and 1164 independent reflections with $R_{av} = 0.07$). After corrections for Lorentz and polarization effects the data set was consistent with the *C2/c* and *Cc* space groups. The Wilson plot suggested the centrosymmetric one and *C2/c* was chosen. Direct methods revealed the positions of the three cobalt and two phosphorus atoms. Subsequent least-squares refinement on F^2 followed by difference Fourier maps (using SHELXTL V5.0 package) revealed the positions of the remaining oxygen and carbon atoms. The four hydrogen atoms were refined by restraining their positions within a range of allowed O–H and C–H distances. The refinement of the cobalt, phosphorus, and oxygen atoms with anisotropic thermal parameters, and the carbon and hydrogen atoms with isotropic ones converged with $R1/wR2 = 0.0456/0.1028$ for 906 independent reflections with $I > 2\sigma_I$ and 122 parameters. (*Crystal data*: $Co_2(O_3PCH_2PO_3)\cdot H_2O$, *monoclinic*, *C2/c*, $a = 18.820(4)$, $b = 8.246(2)$, $c = 8.916(2)$ Å, $\beta = 106.68(3)°$, $V = 1325.4(5)$ Å^3 from Guinier data with Si as an internal standard and $Cu_{K\alpha 1}$ radiation, $Z = 8$, $\rho_{calcd} = 3.085$ g cm^{-3}, $\mu = 54.81$ cm^{-1}, residual electron density = + 0.85/ − 0.94 e Å^{-3} at 1.14/1.27 Å from Co3/Co1; crystal data for a sample heated at 480 °C for two days: monoclinic, *C2/c*, $a = 18.67(1)$, $b = 8.159(3)$, $c = 8.665(7)$ Å, $\beta = 106.29(3)°$ $V = 1267(1)$ Å^3 from Guinier data with Si as an internal standard and $Cu_{K\alpha 1}$ radiation). Further

 © VCH Verlagsgesellschaft mbH, D-69451 Weinheim, 1997 0570-0833/97/3615-1620 $ 17.50+.50/0

details of the crystal structure investigation may be obtained from the Fachinformationszentrum Karlsruhe, D-76344 Eggenstein-Leopoldshafen (Germany), on quoting the depository number CSD-406176.

Received: December 12, 1996
Revised version: February 17, 1997 [Z98801E]
German version: *Angew. Chem.* **1997**, *109*, 1692–1695

Keywords: cobalt · microporosity · phosphonate complexes · solid-state structures · zeolite analogues

[1] M. E. Davis, R. F. Lobo, *Chem. Mater.* **1992**, *4*, 756; C. Y. Ortiz-Avila, C. Bhardwaj, A. Clearfield, *Inorg. Chem.* **1994**, *33*, 2499; B. Z. Wan, R. G. Anthony, G. Z. Peng, A. Clearfield, *J. Catal.* **1994**, *101*, 19; J. L. Snover, M. E. Thompson, *J. Am. Chem. Soc.* **1994**, *116*, 765; G. Alberti, M. Casciola, R. Palombari, A. Peraio, *Solid State Ionics* **1992**, *58*, 339; J. L. Colon, C. Y. Yang, A. Clearfield, C. R. Martin, *J. Phys. Chem.* **1988**, *92*, 5777; G. Cao, H. Hong, T. E. Mallouk, *Acc. Chem. Res.* **1992**, *25*, 420; D. Deniaud, B. Schollorn, D. Mansuy, J. Rouxel, P. Battioni, B. Bujoli, *Chem. Mater.* **1995**, *7*, 995.

[2] K. Maeda, Y. Kiyozumi, F. Mizukami, *Angew. Chem.* **1994**, *106*, 2429; *Angew. Chem. Int. Ed. Engl.* **1994**, *33*, 2335; K. Maeda, J. Akimoto, Y. Kiyozumi, F. Mizukami, *J. Chem. Soc. Chem. Commun.* **1995**, 1033; K. Maeda, J. Akimoto, Y. Kiyozumi, F. Mizukami, *Angew. Chem.* **1995**, *107*, 1313; *Angew. Chem. Int. Ed. Engl.* **1995**, *34*, 1199; J. L. Bideau, C. Payen, P. Palvadeau, B. Bujoli, *Inorg. Chem.* **1994**, *33*, 4885.

[3] J. Zubieta, *Comments Inorg. Chem.* **1994**, *16*, 153; A. Clearfield, *ibid.* **1990**, *10*, 89; H. Byrd, A. Clearfield, D. Poojary, K. P. Reis, M. E. Thompson, *Chem. Mater.* **1996**, *8*, 2239; P. Gendraud, M E. de Roy, J. P. Besse, *Inorg. Chem.* **1996**, *35*, 6108; K. J. Martin, P. J. Squattrito, A. Clearfield, *Inorg. Chim. Acta* **1989**, *155*, 7; L. J. Sawers, V. J. Carter, A. R. Armstrong, P. G. Bruce, P. A. Wright, B. E. Gore, *J. Chem. Soc. Dalton Trans.* **1996**, 3159; A. Cabeza, M. A. G. Aranda, F. M. Cantero, D. Lozano, M. Martinez-Lara, S. Bruque, *J. Solid State Chem.* **1996**, *121*, 181; D. M. Poojary, D. Grohol, A. Clearfield, *Angew. Chem.* **1995**, *107*, 1650; *Angew. Chem. Int. Ed. Engl.* **1995**, *34*, 1508; D. M. Poojary, A. Cabeza, M. A. G. Aranda, S. Bruque, A. Clearfield, *Inorg. Chem.* **1996**, *35*, 1468.

[4] V. Soghomonian, R. Diaz, R. C. Haushalter, C. J. O'Connor, J. Zubieta, *Inorg. Chem.* **1995**, *34*, 4460.

[5] D. M. Poojary, B. Zhang, P. Bellinghausen, A. Clearfield, *Inorg. Chem.* **1996**, *35*, 5254; D. M. Poojary, B. Zhang, P. Bellinghausen, A. Clearfield, *ibid.* **1996**, *35*, 4942; V. Soghomonian, Q. Chen, R. C. Haushalter, J. Zubieta, *Angew. Chem.* **1995**, *107*, 229; *Angew. Chem. Int. Ed. Engl.* **1995**, *34*, 223; R. LaDuca, D. Rose, J. R. D. DeBord, R. Haushalter, C. J. O'Connor, J. Zubieta, *J. Solid State Chem.* **1996**, *123*, 408; G. Bonavia, R. C. Haushalter, C. J. O'Connor, J. Zubieta, *Inorg. Chem.* **1996**, *35*, 5603; G. Alberti, U. Costantino, F. Marmottini, R. Vivani, P. Zappelli, *Angew. Chem.* **1993**, *105*, 1396; *Angew. Chem. Int. Ed. Engl.* **1993**, *32*, 1357.

[6] S. Drumel, P. Janvier, B. Bujoli, *J. Chem. Soc. Chem. Commun.* **1995**, 1051.

[7] S. C. Sevov, *Angew. Chem* **1996**, *108*, 2814; *Angew. Chem. Int. Ed. Engl.* **1996**, *35*, 2630.

Enantioselective Diels–Alder Approach to Angucyclinones from (*S*)-2-(*p*-Tolylsulfinyl)-1,4-naphthoquinone and Substituted Racemic Vinylcyclohexenes**

M. Carmen Carreño,* Antonio Urbano, and Jean Fischer

Angucyclines are a large group of naturally occurring quinones of microbial origin[1] that display a broad range of biological activities.[2] This family of antibiotics shares a benz[*a*]-anthracene framework of decaketide origin,[3] as well as a methyl group at C3 and an oxygen functionality at C1. The main structural differences among the members are found in the aromatic or hydroaromatic nature of the A and/or B rings. Some examples of angucyclinone antibiotics are (+)-emycin A, SF 2315A, and SF 2315B.

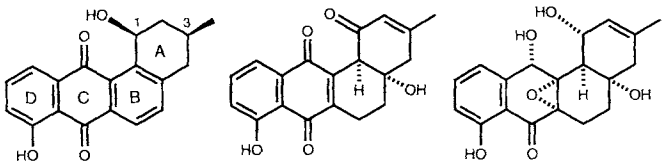

These challenging structures and their diverse biological activities have stimulated many synthetic studies of these compounds,[4] including several total syntheses.[5] The most general strategy employed for the regioselective construction of the angular tetracyclic core was the Diels–Alder reaction between a substituted naphthoquinone and a vinylcyclohexene. Efficient asymmetric syntheses were achieved by Sulikowski et al.[5d,e] from appropriately functionalized chiral dienes obtained from (−)-quinic acid, and by Larsen et al.,[5f] who used a chiral catalyst in the cycloaddition step that allowed kinetic resolution of the diene partner. To our knowledge no chiral dienophile has yet been used in asymmetric angucyclinone syntheses.

We studied the dienophilic behavior of enantiomerically pure sulfinyl quinones,[6] and found a high ability of the sulfoxide to control the regiochemistry, *endo* selectivity, and π-facial selectivity of cycloadditions with a wide range of dienes. We established the domino[7] Diels–Alder reaction/pyrolytic sulfoxide elimination as a general one-pot strategy to enantiomerically pure polycyclic dihydroquinones. This sequence could be applied to the synthesis of angucyclinones provided that substituted vinylcyclohexenes such as **2** (Scheme 1) reacted in a diastereoselective manner. We here report the first enantioselective approach to angucyclinones in which the homochiral sulfinyl quinone **1** is used to discriminate between both faces of a racemic vinylcyclohexene with a bulky alkoxy substituent at the allylic position.

A first test of this possibility was the ready reaction of (+)-**1**[8] with (±)-3-vinyl-2-cyclohexenol (**2a**;[9] Scheme 1). We isolated **3a** (28%) and **4** (51%) by flash chromatography. The stereochemistry of **3a**, which resulted from spontaneous pyrolysis of the sulfoxide in the initially formed adduct, fulfilled the expectations based on previous work with semicyclic dienes.[5c,f,10] Anthraquinone **4** was derived from **3a** in a fragmentation process[4a,5a,c] probably promoted by the free hydroxyl group and favored by the long reaction time required (3 d). The enantiomeric excess and absolute configuration of **3a** could not be determined at this stage due to its facile transformation into **4** under the experimental conditions necessary for preparing the corresponding Mosher esters.[11] To avoid the formation of **4** we thought of preparing a more stable derivative of **3a** en route to the angucyclinone functionality. Thus, treatment of **3a** with *m*-chloro peroxybenzoic acid (*m*-CPBA) afforded epoxide **5a** (90%) by the exclusive attack of the oxidant from the α face (*cis* to H12b).[12] The Mosher esters[11] of **5a** confirmed the absolute configurations shown in Scheme 1 for **3a** and **5a**. Nevertheless, the observed *ee* of 50% for **5a**[13] reflected low selectivity in the cycloaddition step.

The lability of **3a** and the low diastereoselectivity obtained with hydroxydiene **2a** prompted us to check a bulkier alkoxy substituent on the diene moiety to better differentiate the diene

[*] Dr. M. C. Carreño, Dr. A. Urbano
Departamento de Química Orgánica (C-I)
Universidad Autónoma
Cantoblanco, E-28049 Madrid (Spain)
Fax: Int. code +(1)397-3966
e-mail: carmen.carrenno@uam.es
Prof. J. Fischer
Laboratoire de Cristallochimie, UA 424
Université Louis Pasteur, Strasbourg (France)

[**] This work was supported by the Dirección General de Investigación Científica y Técnica (grant no. PB95-0174).

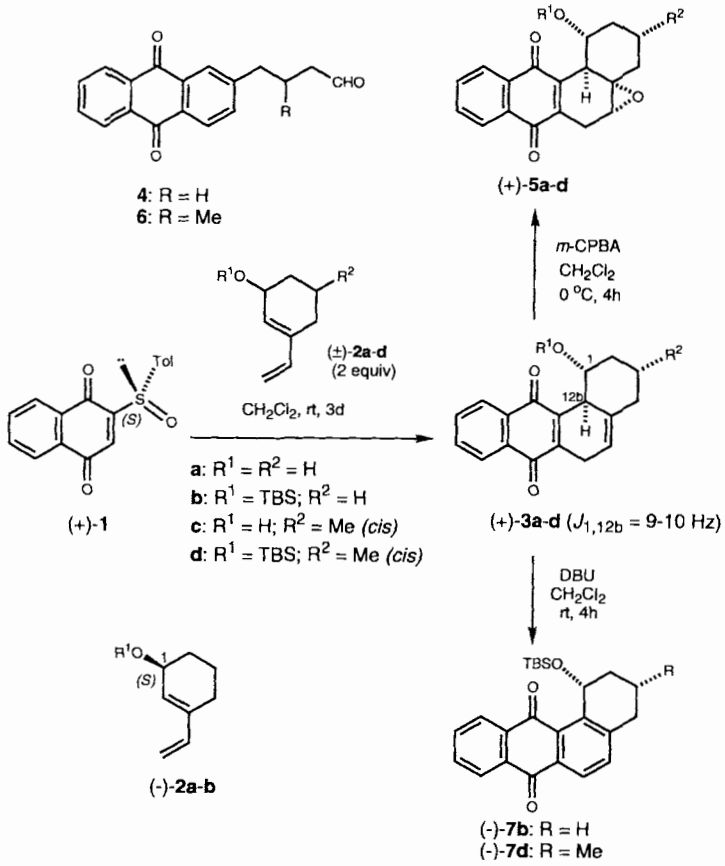

Scheme 1. DBU = 1,8-diazabicyclo[5.4.0]undec-7-ene; TBS = *tert*-butyldimethylsilyl; RT = room temperature.

faces.[9] The Diels–Alder reaction of (+)-**1** with (±)-1-*tert*-butyldimethylsilyloxy-3-vinylcyclohex-2-ene (**2b**)[9] afforded **3b** (75%) as the exclusive reaction product (Table 1) together with unchanged diene. After flash chromatography we could recover 40% of optically active (−)-**2b** ($[\alpha]_D^{20} = -38$, $c = 1$ in $CHCl_3$), showing that kinetic resolution had occurred during the cycloaddition. The *ee* value of greater than 97% for **3b**[14] indicated excellent diastereoselectivity for the Diels–Alder reaction between (+)-**1** and **2b**. The *m*-CPBA epoxidation of **3b** again gave the sole epoxide **5b** (90%). In contrast, desilylation of recovered (−)-**2b** with TBAF afforded diene (−)-**2a** ($[\alpha]_D^{20} = -47$, $c = 1$ in $CHCl_3$) whose Mosher esters showed an *ee* value of 50% and *(S)* configuration at C1 (Scheme 1).

To extend these positive results and open an easy access to the substituted A ring of several angucyclinones, we investigated the behavior of dienes *cis*-**2c** and *cis*-**2d** with a methyl group at C5. Cycloaddition of (+)-**1** with (±)-5-methyl-3-vinylcyclohex-2-enol (**2c**)[15] afforded **3c** (26%) and **6** (50%) after flash chromatography. The *m*-CPBA oxidation of **3c** gave epoxide **5c** (82%) whose Mosher esters[11] again showed the absolute configuration depicted in Scheme 1 and 50% diastereoselectivity for the initial cycloaddition.[13] On the other hand, (±)-1-*tert*-butyldimethylsilyloxy-5-methyl-3-vinylcyclohex-2-ene (**2d**), obtained from **2c**[15] (*tert*-butyldimethylsilyl chloride (TBSCl), imidazole, *N*,*N*-dimethylformamide (DMF), 87%), reacted with (+)-**1** to yield exclusively **3d** (73%), whose epoxidation afforded **5d** (86%, *ee* > 97%).[14] This high enantiomeric excess indicated total stereocontrol in both the Diels–Alder reaction and epoxidation. Moreover, the absolute configuration of **5d** was confirmed by X-ray diffraction.[16] Enantiomerically pure epoxides **5b** and **5d** could be useful synthetic intermediates for the synthesis of antibiotics SF 2315A and SF 2315B that are lacking a hydroxy group at the C8 position.

Table 1. Selected physical and spectroscopic data for **3b**, **3d**, **5b**, **5d**, **7b**, and **7d**.

3b: M.p. 141–142 °C; $[\alpha]_D^{20} = +106.4$ ($c = 0.5$ in $CHCl_3$); ^{1}H NMR (200 MHz, $CDCl_3$): $\delta = 8.06$ (m, 2H), 7.67 (m, 2H), 5.57 (ddd, $J = 1.2$, 2.7, 3.9 Hz, 1H), 3.75 (ddd, $J = 3.9$, 5.2, 9.2 Hz, 1H), 3.37 (dt, $J = 3.6$, 9.2 Hz, 1H), 3.41 (ddt, $J = 1.9$, 24.5, 3.9 Hz, 1H), 3.09 (dddd, $J = 1.7$, 2.7, 5.2, 24.5 Hz, 1H), 2.4–1.3 (m, 6H), 0.72 (s, 9H), −0.12 (s, 3H), −0.36 (s, 3H); ^{13}C NMR (50 MHz, $CDCl_3$): $\delta = 184.3$, 183.9, 144.7, 141.1, 137.8, 133.2, 132.9, 132.8, 131.6, 126.4, 125.8, 115.1, 78.0, 44.8, 36.9, 34.3, 26.1, 25.5 (3C), 25.2, 17.7, −4.9, −5.1.

3d: M.p. 189–190 °C; $[\alpha]_D^{20} = +3.5$ ($c = 0.5$ in $CHCl_3$); ^{1}H NMR (200 MHz, $CDCl_3$): $\delta = 8.04$ (m, 2H), 7.68 (m, 2H), 5.56 (t, $J = 2.9$ Hz, 1H), 3.69 (ddd, $J = 3.8$, 5.1, 9.5 Hz, 1H), 3.36 (dt, $J = 3.6$, 9.5 Hz, 1H), 3.40 (ddt, $J = 1.8$, 24.5, 3.9 Hz, 1H), 3.09 (dddd, $J = 1.5$, 2.7, 4.3, 24.5 Hz, 1H), 2.30 (m, 1H), 1.95 (m, 1H), 1.8–1.4 (m, 3H), 1.00 (d, $J = 5.7$ Hz, 3H), 0.72 (s, 9H), −0.13 (s, 3H), −0.40 (s, 3H); ^{13}C NMR (50 MHz, $CDCl_3$): $\delta = 184.3$, 183.9, 144.9, 141.1, 137.1, 133.2, 133.1, 132.9, 131.7, 126.5, 125.9, 115.4, 77.1, 45.6, 44.4, 42.7, 33.2, 25.8, 25.5 (3C), 21.8, 17.8, −4.9, −5.1.

5b: M.p. 235–236 °C; $[\alpha]_D^{20} = +47.1$ ($c = 0.7$ in $CHCl_3$); ^{1}H NMR (200 MHz, $CDCl_3$): $\delta = 8.05$ (m, 2H), 7.68 (m, 2H), 3.77 (dq, $J = 9.9$, 1.4 Hz, 1H), 3.58 (dt, $J = 20.2$, 1.9 Hz, 1H), 2.79 (dt, $J = 20.2$, 1.6 Hz, 1H), 3.47 (dt, $J = 3.8$, 9.9 Hz, 1H), 3.24 (q, $J = 1.7$ Hz, 1H), 2.1–1.3 (m, 6H), 0.65 (s, 9H), −0.11 (s, 3H), −0.43 (s, 3H); ^{13}C NMR (50 MHz, $CDCl_3$): $\delta = 184.2$, 183.1, 144.7, 137.9, 133.4, 133.1, 132.4, 131.6, 126.5, 126.0, 75.4, 61.5, 55.9, 44.5, 35.3, 32.6, 25.3 (3C), 24.6, 21.3, 17.6, −4.7, −5.3.

5d: M.p. 235–236 °C; $[\alpha]_D^{20} = +72.3$ ($c = 0.5$ in $CHCl_3$); ^{1}H NMR (200 MHz, $CDCl_3$): $\delta = 8.04$ (m, 2H), 7.67 (m, 2H), 3.72 (dq, $J = 10.0$, 1.4 Hz, 1H), 3.57 and 2.77 (2dt, $J = 20.3$, 1.6 Hz, 2H), 3.50 (dt, $J = 3.7$, 10.0 Hz, 1H), 3.23 (q, $J = 1.6$ Hz, 1H), 1.94 (m, 1H), 1.8–1.3 (m, 4H), 1.04 (d, $J = 5.9$ Hz, 3H), 0.65 (s, 9H), −0.11 (s, 3H), −0.45 (s, 3H); ^{13}C NMR (50 MHz, $CDCl_3$): $\delta = 184.3$, 183.1, 144.8, 137.9, 133.4, 133.1, 132.5, 131.7, 126.6, 126.0, 74.7, 61.0, 56.0, 44.1, 43.9, 41.1, 28.4, 25.4 (3C), 24.6, 21.7, 17.6, −4.6, −5.2.

7b: M.p. 111–112 °C; $[\alpha]_D^{20} = -62.9$ ($c = 0.5$ in $CHCl_3$); ^{1}H NMR (200 MHz, $CDCl_3$): $\delta = 8.21$ (m, 2H), 8.20 (d, $J = 8.1$ Hz, 1H), 7.74 (m, 2H), 7.47 (d, $J = 8.1$ Hz, 1H), 6.36 (dd, $J = 3.0$, 3.5 Hz, 1H), 3.06 (m, 1H), 2.84 (ddd, $J = 6.3$, 10.2, 17.2 Hz, 1H), 2.3–2.0 (m, 2H), 1.85–1.65 (m, 2H), 0.81 (s, 9H), 0.31 (s, 3H), 0.03 (s, 3H); ^{13}C NMR (50 MHz, $CDCl_3$): $\delta = 185.4$, 183.5, 145.9, 141.3, 135.4, 135.0, 133.9, 133.4, 133.2, 132.5, 131.2, 127.3, 126.5, 126.3, 63.2, 31.8, 30.7, 26.0, 18.3, 15.9, −4.3, −5.0.

7d: M.p. 125–126 °C; $[\alpha]_D^{20} = -59.0$ ($c = 0.1$ in $CHCl_3$); ^{1}H NMR (200 MHz, $CDCl_3$): $\delta = 8.20$ (m, 2H), 8.19 (d, $J = 7.9$ Hz, 1H), 7.74 (m, 2H), 7.46 (d, $J = 7.9$ Hz, 1H), 6.37 (t, $J = 5.9$ Hz, 1H), 2.86 (dd, $J = 10.8$, 15.5 Hz, 1H), 2.74 (dd, $J = 5.1$, 15.5 Hz, 1H), 2.19 (ddt, $J = 1.5$, 13.3, 5.9 Hz, 1H), 2.0–1.8 (m, 1H), 1.56 (ddd, $J = 6.2$, 8.7, 13.3 Hz, 1H), 1.18 (d, $J = 6.6$ Hz, 3H), 0.77 (s, 9H), 0.17 (s, 3H), −0.04 (s, 3H); ^{13}C NMR (50 MHz, $CDCl_3$): $\delta = 185.9$, 183.4, 148.1, 142.8, 135.4, 133.9, 133.6, 133.3, 133.2, 132.7, 131.8, 127.3, 126.5, 126.5, 66.3, 40.8, 39.0, 26.9, 26.0, 23.1, 18.1, −4.2, −4.5.

The approach to the anthraquinonic skeleton of (−)-emycin A required the aromatization of B ring of **3b** and **3d** without affecting the stereogenic moiety. Therefore, treatment of **3b** or **3d** with 1,8-diazabicyclo[5.4.0]undec-7-ene (DBU) in CH_2Cl_2 at room temperature[17] afforded anthraquinones **7b** (62%, *ee* > 97%)[14] and **7d** (58%, *ee* > 97%),[14] respectively.

According to the model proposed for (*S*)-*p*-tolylsulfinylquinone cycloadditions[6b–d] and the known behavior of dienes such as **2**,[5c,f,10] the absolute configuration of the new stereogenic centers should result from the matched *endo* approach of (*R*)-**2** from the face containing the less sterically demanding pseudoaxial substituent at the allylic position and towards the face of the quinone with the lone electron pair at sulfur in the s-*trans* conformation of **1** (Scheme 1).

We have reported the first asymmetric approach to the tetracyclic skeleton of angucyclinones from a chiral dienophile. The sulfinyl group on the quinonic framework promoted a double induction in Diels–Alder cycloadditions leading to efficient kinetic resolution of (±)-**2**. Further studies on the latter process and total syntheses of angucyclinones are in progress.

Received: January 30, 1997 [Z10052IE]
German version: *Angew. Chem.* **1997**, *109*, 1695–1697

Keywords: angucyclinones · antibiotics · asymmetric synthesis · cycloadditions · quinones

[1] a) R. H. Thomson, *Naturally Occurring Quinones IV*, 4th ed., Blackie, London, **1996**; b) J. Rohr, R. Thiericke, *Nat. Prod. Rep.* **1992**, *9*, 103–137.
[2] a) S. Kondo, S. Gomi, D. Ikeda, M. Hamada, T. Takeuchi, H. Iwai, J. Seki, H. Hoshino, *J. Antibiot.* **1991**, *44*, 1228–1236; b) M. Ogasawara, M. Hasegawa, Y. Hamagishi, H. Kamei, T. Oki, *ibid.* **1992**, *45*, 129–132.
[3] S. J. Gould, X. C. Cheng, C. Melville, *J. Am. Chem. Soc.* **1994**, *116*, 1800–1804, and references therein.
[4] Recent work: a) K. Kim, J. Reibenspies, G. Sulikowski, *J. Org. Chem.* **1992**, *57*, 5557–5559; b) K. Krohn, F. Ballwanz, W. Baltus, *Liebigs Ann. Chem.* **1993**, 911–913; c) K. Krohn, K. Khanbabaee, *ibid.* **1994**, 1109–1112; d) F. L. Andrews, D. S. Larsen, *Tetrahedron Lett.* **1994**, *35*, 8693–8696; e) K. Krohn, W. Dröge, F. Hintze, *Ann. Quim.* **1995**, *91*, 388–393; f) V. A. Boyd, J. Reibenspies, G. A. Sulikowski, *Tetrahedron Lett.* **1995**, *36*, 4001–4004; g) K. Kim, Y. Guo, G. A. Sulikowski, *J. Org. Chem.* **1995**, *60*, 6866–6871; h) D. S. Larsen, M. D. O'Shea, *ibid.* **1996**, *61*, 5681–5683.
[5] Recent work: a) D. S. Larsen, M. D. O'Shea, *Tetrahedron Lett.* **1993**, *34*, 1373–1376; b) K. Krohn, K. Khanbabaee, *Angew. Chem.* **1994**, *106*, 100–102; *Angew. Chem. Int. Ed. Engl.* **1994**, *33*, 99–100; c) D. S. Larsen, M. D. O'Shea, *J. Chem. Soc. Perkin Trans. 1* **1995**, 1019–1028; d) K. Kim, G. A. Sulikowski, *Angew. Chem.* **1995**, *107*, 2587–2589; *Angew. Chem. Int. Ed. Engl.* **1995**, *34*, 2396–2398; e) V. A. Boyd, G. A. Sulikowski, *J. Am. Chem. Soc.* **1995**, *117*, 8472–8473; f) D. S. Larsen, M. D. O'Shea, S. Brooker, *Chem. Commun.* **1996**, 203–204; g) G. Matsuo, Y. Miki, M. Nakata, S. Matsumura, K. Toshima, *ibid.* **1996**, 225–226.
[6] Overview of our work: a) M. C. Carreño, *Chem. Rev.* **1995**, *95*, 1717–1760; recent work: b) M. C. Carreño, J. L. García Ruano, M. A. Toledo, A. Urbano, V. Stefani, C. Z. Remor, J. Fischer, *J. Org. Chem.* **1996**, *61*, 503–509; c) M. C. Carreño, J. L. García Ruano, A. Urbano, M. A. Hoyos, *ibid.* **1996**, *61*, 2980–2985; d) M. C. Carreño, J. L. García Ruano, A. Urbano, M. I. López-Solera, *ibid.* **1997**, *62*, 976–981.
[7] a) L. F. Tietze, U. Beifuss, *Angew. Chem.* **1993**, *105*, 137–170; *Angew. Chem. Int. Ed. Engl.* **1993**, *32*, 131–163; b) L. F. Tietze, *Chem. Rev.* **1996**, *96*, 115–136.
[8] M. C. Carreño, J. L. García Ruano, A. Urbano, *Synthesis* **1992**, 651–653.
[9] L. Strekowski, S. Kong, M. A. Battiste, *J. Org. Chem.* **1988**, *53*, 901–904.
[10] a) M. J. Fisher, W. J. Hehre, S. D. Kahn, L. E. Overman, *J. Am. Chem. Soc.* **1988**, *110*, 4625–4633; b) S. C. Datta, R. W. Franck, R. Triphaty, G. J. Quigley, L. Huang, S. Chen, A. Sihaed, *ibid.* **1990**, *112*, 8472–8478.
[11] J. A. Dale, H. S. Mosher, *J. Am. Chem. Soc.* **1973**, *95*, 512–519.
[12] The relative configuration was established by comparison with a similar intermediate prepared by Sulikowski [5d] in the total synthesis of SF 2315A.
[13] When the cycloaddition was carried out in water the reaction was faster (completed in 12 h at room temperature) but with a lower enantiomeric excess (20%).
[14] The enantiomeric excesses were evaluated by ^{1}H NMR spectroscopy using chiral lanthanide shift reagents: [Eu(tfc)$_3$] for **3b** and **5d**, and [Yb(hfc)$_3$] for **7b** and **7d**. The required racemic compounds were obtained from racemic quinone **1** [8].
[15] S. J. Hecker, C. H. Heathcock, *J. Org. Chem.* **1985**, *50*, 5159–5166.
[16] The absolute structure was determined by comparing refinements of both configurations, and confirmed by refining Flack's *x* parameter (G. Bernardinelli, H. D. Flack, *Acta Crystallogr. Sect. A* **1987**, *43*, 75–78). Crystallographic data (excluding structure factors) for (+)-**5d** have been deposited with the Cambridge Crystallographic Data Centre as suplementary publication no. CCDC-100127. Copies of the data can be obtained free of charge on application to The Director, CCDC, 12 Union Road, Cambridge CB2 1EZ, UK (fax: int. code +(1223)336-033; e-mail: deposit@chemcrys.cam.ac.uk).
[17] These results contradict those reported by Sulikowski et al. [4g], who described no reaction for a similar system with DBU in benzene at 0 °C.

Evidence for a Stepwise Addition of Carbenes to Strained Double Bonds: Reactions of Dihalocarbenes with Cyclopropenes**

Jürgen Weber and Udo H. Brinker*

Dedicated to Professor William von Eggers Doering on the occasion of his 80th birthday

The most thoroughly investigated pathway of carbene stabilization is addition to carbon–carbon double bonds. Early studies by Skell and Woodworth[1] consider the singlet carbene addition a one-step process in which two new bonds are formed simultaneously. Even though the addition of singlet carbenes is concerted, it cannot be synchronous according to orbital symmetry considerations.[2] Jones et al.[3] suggested that the concept of nucleophilicity and electrophilicity, as applied to intermolecular additions of carbenes to alkenes, can be interpreted as the different contributions of the highest occupied and lowest unoccupied molecular orbitals (HOMOs and LUMOs). For instance, during the electrophilic attack of a dihalocarbene, charge is transferred from the olefin's HOMO to the empty p orbital of the carbene (LUMO). Calculations of activated complexes[4] for addition of dihalocarbenes to simple olefins support this direction of charge transfer. These calculations also show a shorter distance from the carbene carbon to one of the carbon atoms of the double bond.

Although addition of photochemically generated monohalocarbenes to 1,2-dimethylcyclobutene was postulated to proceed via zwitterions,[5] no conclusive evidence of their intermediacy[6] was provided.[7] We present here evidence that charge transfer during reactions of dihalocarbenes with differently substituted cyclopropenes leads to polarization of the activated complex or even to an intermediate dipolar species with complete charge separation.

Only few dihalocarbene reactions with cyclopropenes are known.[8] With the exception of perfluoro-1,3-dimethylbicyclo[1.1.0]butane,[9] geminal dihalobicyclobutanes, the addition products of dihalocarbenes, have never been isolated or unambiguously identified by spectroscopy. Instead cyclobutenes, probably formed by cationic cyclopropylallyl (CCA) rearrangements,[10] were found as the only products.

We initially reported that, for the first time, 2,3-diaryl-1,1-dihalo-1,3-butadienes were formed along with 1,3-diaryl-2,3-dihalocyclo-1-butenes by the reactions of dihalocarbenes (:CF_2, :CCl_2, :CBr_2, :CFCl, :CFBr) with 1,2-diarylcyclopropenes (Scheme 1).[11] We now present evidence for a step-wise addition of dihalocarbenes to strained double bonds of cyclopropenes. For the mechanistic studies of the formation of butadienes and cyclobutenes, three different aryl substituents were utilized. In the reactions of 1,2-diphenylcyclopropene (**1**) with dichlorocarbene, the ratios of the products, that is, of butadienes **2**[12] to cyclobutenes **5**,[12] were nearly independent of the method of carbene generation (Table 1).[13] This indicates that the same

[*] Prof. U. H. Brinker
Institut für Organische Chemie der Universität
Währinger Strasse 38, A-1090 Wien (Austria)
Fax: Int. code (1)31367-2240
e-mail: udo.brinker@univie.ac.at
Dr. J. Weber
Department of Chemistry, State University of New York at Binghamton (USA)

[**] Carbene Rearrangements, Part 47. Prof. W. M. Jones (University of Florida) and Dr. L. Xu are gratefully acknowledged for helpful discussions. Part 46: J. Weber, U. H. Brinker, *Tetrahedron* **1996**, *52*, 14641.

 © VCH Verlagsgesellschaft mbH, D-69451 Weinheim, 1997 0570-0833/97/3615-1623 $ 17.50+.50/0

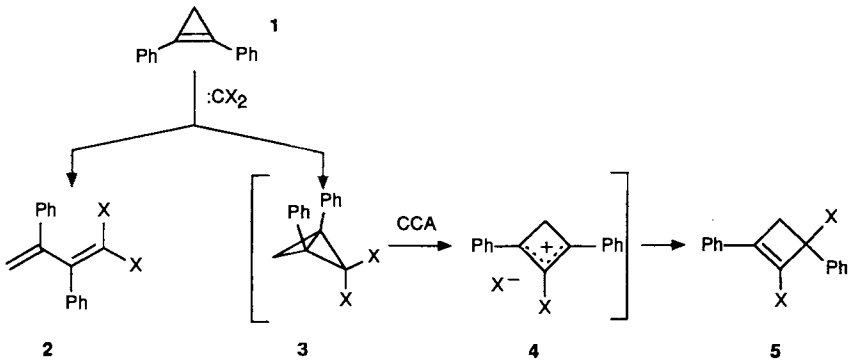

Scheme 1. Dihalocarbene addition to cyclopropene **1**: formation of 1,3-butadiene **2** and cyclobutene **5**.

Table 1. Ratios of cyclobutene **5a** to butadiene **2a** for reactions of cyclopropene **1** with the dichlorocarbene from different carbene sources.

Method	*T*	**5a**:**2a**	Yield [%] [c]
Doering–Hoffmann [13a]	−45 °C → 0 °C	79:21	20
ultrasound [a] [13b]	20 °C → 40 °C	87:13	70
Seyferth [b] [13c]	80 °C	80:20	79

[a] Catalytic phase transfer method under ultrasound conditions. [b] $PhHgCCl_2Br$. [c] 2-Chloro-1,3-diphenylcyclobut-1-en-3-ol, the hydrolysis product from **5a**, was isolated.

reactive species, that is, a dichlorocarbene(oid), was involved in the formation of both products.

Cyclobutenes **5** may be derived from intermediate bicyclobutanes **3**. Cleavage of the central bond and loss of one halide in **3** leads to the stabilized homoaromatic cyclobutenyl cation **4**. Trapping of **4** by the halide gives **5** (Figure 1). In contrast, three different pathways can be suggested for the formation of butadienes **2** (Scheme 2).

Butadienes **2** were formed when different conditions are applied for carbene generation, even at temperatures as low as −45 °C. This renders pathway C unlikely, because various substituted bicyclobutanes,[14] including several 1,3-diphenylbicyclobutanes,[15] are thermally stable at room temperature. Furthermore, attempts at an independent preparation of bicyclobutane **3b** exclude pathway C. *cis*-1-Bromo-2-chlorodifluoromethyl-1,2-diphenylcyclopropane (**8**)[12,16–18] was chosen as the precursor to **3b**. When **8** was allowed to react with methyllithium, only difluorocyclobutene **5b**, the formal CCA-rearrangement product of bicyclobutane **3b**, was found (Scheme 3). No evidence of difluorobutadiene **2b** was present. The only plausible way to explain the formation of **5b** is through **3b**. In contrast, the reaction of difluorocarbene with cyclopropene **1** affords only **2b** and no cyclobutene **5b**. That means, if **3b** were an intermediate, the formation of **5b** would also be expected.

Intermediates **6** and **7** (Scheme 2) may result from reactions of **1** with a trihalomethyl anion or a dihalocarbene (pathways A and B), respectively. However, the product ratios of the isomeric butadienes **13a** to **13b**[12] and **14a** to **14b**[12] obtained from dichlorocarbene additions to the asymmetrically substituted cyclopropenes **9**[12] and **10**[12,19], respectively, bearing an electron-withdrawing or electron-donating substituent at the *para* position of one of the phenylsubstituents support an electrophilic attack of the carbene (Scheme 2, pathway B). In contrast, butadienes **13b** and **14a**, which were expected to be the major isomers by nucleophilic attack of the trichloromethyl anion (pathway A), due to better stabilization of the negative charge, were found in lower amounts. Furthermore, direct generation of dichlorocarbene from phenyl(bromodichloromethyl)mercury without involvement of a trichloromethyl anion gave a butadiene to cyclobutene ratio of 20:80 when allowed to react with **1**. This ratio is nearly identical, within experimental error, to the ratios obtained by other methods of carbene generation (Table 1). Therefore, pathway A is not operative.

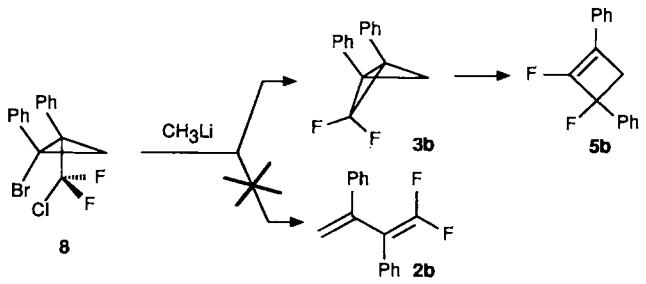

Scheme 3. Formation of cyclobutene **5b** by the ring-closing reaction of **8**.

Electrophilic attack of dichlorocarbene at the double bonds of **9** and **10** mainly gave **13a** and **14b**, which are derived from **11a** and **12b**, the intermediates that offer better charge stabilization (Scheme 4). Pathway I is more favorable for cyclopropene **9**, which has an electron-withdrawing trifluoromethyl substituent, due to better stabilization of the positive charge by the unsubstituted phenyl ring. On the other hand, for the reaction of **10** pathway II provides the better stabilization of the positive charge in **12b** through the electron-donating methoxy substituent. Comparison of the product ratios for both the butadienes substituted with *p*-methoxyphenyl or *p*-trifluoromethylphenyl shows a complete reversal of the ratios. This supports the proposed mechanism involving dipolar intermediates such as **7** (Scheme 2), **11**, and **12** (Scheme 4).[20,21] For simplicity, however, fully developed charges (zwitterions) have been depicted to explain the behavior of the reactants, even though the extent of polarization has not yet been established. Furthermore,

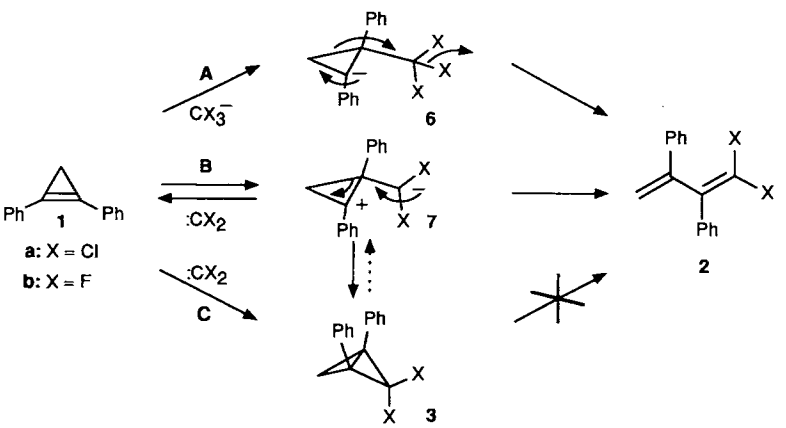

Scheme 2. Three possible reaction pathways to dihalobutadienes **2**.

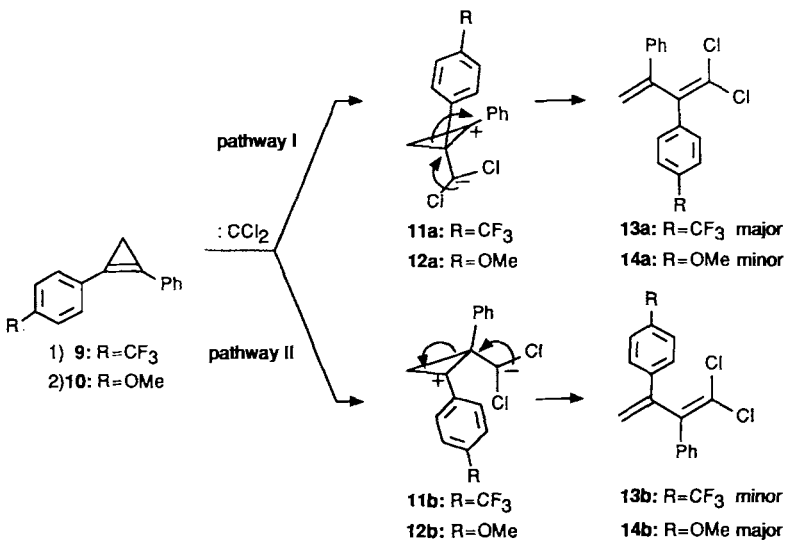

Scheme 4. Electrophilic attack of dihalocarbenes on cyclopropenes **9** and **10** followed by rearrangement. Ratios of the butadienes: a) Doering–Hoffmann method: **13a**:**13b** = 74:26 and **14a**:**14b** = 29:71; b) catalytic phase transfer method under ultrasound conditions: **13a**:**13b** = 69:31 and **14a**:**14b** = 30:70.

the reaction of **1** with dichlorocarbene gave an increased ratio of up to 50:50 of butadiene **2** to four-membered ring compounds[22] when performed in the more polar solvent acetonitrile. This also provides strong evidence for the involvement of a polar intermediate similar to **7** (Figure 2) in the addition of dichlorocarbene to the strained double bond of **1**.

The data from this study indicate that the butadienes in the reactions of cyclopropenes **1**, **9**, and **10** with dichlorocarbene are derived from zwitterionic species, whereas the cyclobutenes result from a CCA rearrangement of the intermediate geminal dihalobicyclobutanes.

Received: December 6, 1996
Revised version: March 27, 1997 [Z9861IE]
German version: *Angew. Chem.* **1997**, *109*, 1689–1692

Keywords: carbenes · cyclopropenes · rearrangements · strained molecules

[1] P. S. Skell, R. C. Woodworth, *J. Am. Chem. Soc.* **1956**, *78*, 4496; **1959**, *81*, 3383.
[2] a) R. Hoffmann, R. B. Woodward, *J. Am. Chem. Soc.* **1965**, *87*, 395; b) R. Hoffmann, R. B. Woodward, *Acc. Chem. Res.* **1968**, *1*, 17.
[3] a) W. M. Jones, R. A. LaBar, U. H. Brinker, P. H. Gebert, *J. Am. Chem. Soc.* **1977**, *99*, 6379, ref. [27]; see also W. M. Jones, U. H. Brinker in *Pericyclic Reactions, Vol. 1* (Eds.: A. P. Marchand, R. E. Lehr), Academic Press, New York, **1977**, p. 109; b) R. A. Moss, *Acc. Chem. Res.* **1989**, *22*, 15.
[4] K. N. Houk, N. G. Rondan, J. Mareda, *Tetrahedron* **1985**, *41*, 1555; see also B. Zurawski, W. Kutzelnigg, *J. Am. Chem. Soc.* **1978**, *100*, 2654.
[5] N. C. Yang, T. A. Marolewski, *J. Am. Chem. Soc.* **1968**, *90*, 5644.
[6] M. Jones, Jr., V. J. Tortorelli, P. P. Gaspar, J. B. Lambert, *Tetrahedron Lett.* **1978**, 4257.
[7] A zwitterion was proposed as an intermediate for the addition of a nucleophilic carbene to a C–C double bond: A. de Meijere, S. I. Kozhushkov, D. S. Yufit, R. Boese, T. Haumann, D. L. Pole, P. K. Sharma, J. Warkentin, *Liebigs Ann.* **1996**, 601.
[8] a) B. M. Trost, R. C. Atkins, *J. Chem. Soc. Chem. Commun.* **1971**, 1254; b) N. I. Yakushkina, L. I. Leonova, I. G. Bolesov, *Proceedings of the Second All Union Conference on the Chemistry of Carbenes and Their Analogs, Izd. Nauka*, Moscow, **1977**, p. 68; c) E. V. Dehmlow, *Tetrahedron Lett.* **1975**, 203.
[9] W. Mahler, *J. Am. Chem. Soc.* **1962**, *84*, 4600.
[10] C. H. DePuy, *Acc. Chem. Res.* **1968**, *1*, 33.
[11] J. Weber, L. Xu, U. H. Brinker, *Tetrahedron Lett.* **1992**, *33*, 4537.
[12] Selected spectroscopic data: **2a**: ^{1}H NMR (400 MHz, $CDCl_3$): δ = 7.44–7.51 (m, 4H, H-Ph), 7.25–7.37 (m, 6H, H-Ph), 5.87 (s, 1H, H-C4), 5.43 (s, 1H, H-C4); ^{13}C NMR (100.6 MHz, $CDCl_3$): δ = 146.9 (s, C3), 140.2 (s, C2), 137.5 (s), 137.4 (s), 128.8 (d), 128.5 (d), 128.12 (d), 128.09 (d), 126.2 (d), 120.6 (s, C1), 117.3 (t, C4); MS (70 eV): *m/z* (%) = 279, 277, 275 ([(*M*+1)$^+$], 0.5, 2, 5), 278, 276, 274 ([*M*$^+$], 2, 14, 21), 242, 240 ([(*M*+1)$^+$ − Cl], 3, 11), 241, 239 ([*M*$^+$ − Cl], 15, 49), 240, 238([*M*$^+$ − HCl], 11, 9), 205 ([(*M*+1)$^+$ − 2Cl], 15), 204 ([*M*$^+$ − 2Cl], 52), 203 ([*M*$^+$ − Cl − HCl], 100), 202 ([*M*$^+$ − 2HCl], 55), 178 (12), 105 (16), 101 (41), 91 ($C_7H_7^+$, 18), 77 (Ph^+, 28), 51 (21); elemental analysis calcd for $C_{16}H_{12}Cl_2$ (275.18): C 69.84, H 4.40; found: C 69.96, H 4.40.
2b: ^{1}H NMR (400 MHz, $CDCl_3$): δ = 7.36–7.42 (m, 4H, H-Ph), 7.17–7.32 (m, 6H, H-Ph), 5.87 (t, 1H, ^5J(H,F) = 1 Hz, H-C4), 5.40("s", 1H, ^5J(H,F) ≤ 0.5 Hz, H-C4); ^{13}C NMR (100.6 MHz, $CDCl_3$): δ = 154.3 (t, ^1J(C,F) = −293 Hz, C1), 140.9 (t, ^2J(C,F) = 10 Hz, C2), 138.7 (s, C3), 133.0 ("s", fine ^3J(C,F) coupling pattern, C_{Ph} at C2), 131.6 (s, C_{Ph} at C3), 128.6 (d), 128.3 (d), 127.9 (d), 127.3 (d), 126.4 (d), 118.9 (t, C4); MS (70 eV): *m/z* (%) = 243 ([*M*$^+$ + 1], 16), 242 ([*M*]$^+$, 16, 100), 241 ([*M*$^+$ − H], 33), 223 ([*M*$^+$ − F], 6), 222 ([*M*$^+$ − HF], 34), 221 ([*M*$^+$ − HF − H], 36), 220 (21), 192 (9), 178 (30), 165 ([*M*$^+$ − Ph], 19), 164 ([*M*$^+$ − PhH], 18), 127 (64), 115 (15), 112 (10), 95 (13), 77 (Ph^+, 21), 51 (16); elemental analysis calcd for $C_{16}H_{12}F_2$ (242.27): C 79.32, H 4.99; found: C 79.17, H 4.84.
5a: ^{1}H NMR (400 MHz, $CDCl_3$): δ = 7.66–7.75 (m, 4H, H-Ph), 7.36–7.50 (m, 6H, H-Ph), 3.58 (d, 1H, ^2J(H,H) = −11.5 Hz, H-C4), 3.44 (d, 1H, ^2J(H,H) = −11.5 Hz, H-C4); ^{13}C NMR (100.6 MHz, $CDCl_3$): δ = 140.1 (s), 139.5 (s), 131.0 (s, Cl), 129.7 (d), 128.6 (d), 128.4 (d), 128.3 (d), 126.9 (d), 126.1 (d), 123.4 (s, C2), 71.8 (s, C3), 47.5 (t, C4); MS (70 eV): *m/z* (%) = 278, 276, 274 ([*M*$^+$], <0.5, 2, 3), 242, 240 ([(*M*+1)$^+$ − Cl], 6, 20), 241, 239 ([*M*$^+$ − Cl], 33, 100), 240, 238 ([*M*$^+$ − HCl], 20, 6), 205 ([(*M*+1)$^+$ − 2Cl], 15), 204 ([*M*$^+$ − 2Cl], 48), 203 ([*M*$^+$ − Cl − HCl], 84), 202 ([*M*$^+$ − 2HCl], 57), 105 (19), 101 (34), 89 (10), 77 (Ph^+, 28), 65 (13), 51 (18), 39 (13), 36 (29); elemental analysis calcd for $C_{16}H_{12}Cl_2$ (275.18): C 69.84, H 4.40; found: C 69.90, H 4.46.
5b: ^{1}H NMR (360 MHz, $CDCl_3$): δ = 7.25–7.60 (m, 10H, H-Ph), 2.96 (ddd, 1H, ^2J(H,H) = −9.8 Hz, ^4J(H,F) = 11.2 Hz, ^3J(H,F) = 6.4 Hz, H-C4), 2.80 (ddd, 1H, ^2J(H,H) = −9.8 Hz, ^4J(H,F) = 15.6 Hz, ^3J(H,F) = 3.8 Hz, H-C4); ^{13}C NMR (90.6 MHz, $CDCl_3$): δ = 144.8 (dd, ^1J(C,F) = −350 Hz, ^2J(C,F) = 20 Hz, C2), 121.3 (dd, ^2J(C,F) = 17 Hz, ^3J(C,F) = 8 Hz, Cl), 97.7 (dd, ^1J(C,F) = −212 Hz, ^2J(C,F) = 24 Hz, C3), 37.6 (t"t", ^3J(C,F), ^4J(C,F) = 22 Hz, J(C,H) = 145 Hz, C4); ^{19}F NMR (282.4 MHz, $CDCl_3$ and $CFCl_3$): δ = −104.2 (ddd, 1F, ^3J(F,F) = 6.1 Hz, ^4J(H,F) = 15.6 Hz, ^3J(H,F) = 11.2 Hz, F-C2), −150.6 ("dd", 1F, ^3J(F,F) = 6.1 Hz, F-C3; from a ^{19}F–^{1}H decoupling experiment).
8: ^{1}H NMR (360 MHz, $CDCl_3$): δ = 7.27–7.24 (m, 4H), 7.13–7.00 (m, 6H), 2.58 (dd, 1H, ^2J(H,H) = −7.7 Hz, ^4J(H,F) = 3.4 Hz), 2.39 (d, 1H, ^2J(H,H) = −7.7 Hz); ^{13}C NMR (90.6 MHz, $CDCl_3$): δ = 139.3 (s), 132.8 (s), 131.1 (br. d), 128.7 (d), 128.2 (t, ^1J(C,F) = −295 Hz), 128.1 (d), 128.0 (d), 127.9 (d), 127.8 (d), 45.3 (t, ^2J(C,F) = 25 Hz), 38.4 (s), 23.5 (t, ^1J(C,H) = 164 Hz); ^{19}F NMR (282.4 MHz, $CDCl_3$ and $CFCl_3$): δ = −51.1 (d, 1F, ^2J(F,F) = −160.4 Hz, ^4J(H,F) = 2.9 Hz), −44.3 (d, 1F, ^2J(F,F) = 160.0 Hz); MS (70 eV): *m/z* (%) = 358, 356 ([*M*$^+$], 3, 2), 279, 277 ([*M*$^+$ − Br], 22, 36), 242 ([*M*$^+$ − Br − Cl], 16), 241 ([*M*$^+$ − HBr − Cl), 79), 222 ([*M*$^+$ − HBr − Cl − F], 26), 221 ([*M*$^+$ − HBr − HCl − F], 71), 220 (44), 202, 200 ([*M*$^+$ − Br − Ph], 9, 11), 201, 199 ([*M*$^+$ − HBr − Ph], 37, 100), 192 (36), 191 (41), 189 (20), 165 (22), 164 (76), 127 (31), 115 (10), 111 (10), 110 (22), 103 (14), 95 (12), 89 (16), 77 (23), 63 (13), 51 (15); elemental analysis calcd for $C_{16}H_{12}BrClF_2$ (357.62): C 53.74, H 3.38; found: C 53.80, H 3.45.
9: ^{1}H NMR (360 MHz, $CDCl_3$): δ = 7.67–7.80 (m, 6H), 7.51–7.45 (m, 2H), 7.41–7.35 (m, 1H), 1.57 (s, 2H); ^{13}C NMR (90.6 MHz, $CDCl_3$): δ = 133.6 (s), 130.0 (d), 129.8 (s), 129.6 (d), 129.0 (d), 128.8 (d), 125.6 (d"d", ^3J(C,F) = 5 Hz), 115.2 (s), 110.3 (s), 6.6 (t), the signal for the trifluoromethyl carbon atom was not found; MS (70 eV): *m/z*(%) = 261 ([*M*+1$^+$], 17), 260 ([*M*$^+$], 100), 259 ([*M*$^+$ − H], 43), 192 (16), 191 ([*M*$^+$ − CF_3], 91), 190 (22), 189 (48), 173 (18), 165 (14), 115 (14), 95 (10).
10: ^{1}H NMR (360 MHz, $CDCl_3$): δ = 7.62–7.70(m + "d", 4H, 2H on (*p*-methoxy)phenyl with J = 8.8 Hz and 2H on phenyl), 7.40–7.47 (m, 2H, H-Ph), 7.25–7.33 (m, 1H, H-Ph), 6.96–7.02 ("d", 2H, J = 8.8 Hz, other 2H on (*p*-methoxy)phenyl), 3.83 (s, 3H, H_3C-O), 1.50 (s, 2H, H_2-C3); ^{13}C NMR (90.6 MHz, $CDCl_3$): δ = 159.8 (s, C_{Ar}-O), 131.2 (d), 130.5 (s), 129.3 (d), 128.6 (d), 127.7 (d), 123.1 (s), 114.2 (d), 111.4 (s, C1/C2), 108.7 (s, C2/C1), 55.3 (q, CH_3O), 6.3 (t, ^1J(C,H) = 165.7 Hz, C3); MS (70 eV): *m/z* (%) = 223 ([(*M*+1)$^+$], 19), 222 ([*M*$^+$], 100), 221 ([*M*$^+$ − H]18), 207 ([*M*$^+$ − Me], 47), 191 ([*M*$^+$ − OMe], 15), 179 (29), 178 ([*M*$^+$ − HOMe − CH_2] 79), 176 (14), 177 (13), 152 (18), 89 (13), 76 (13), 63 (11), 40 (46); HR-MS calcd for $C_{16}H_{14}O$: 222.1045; found: 222.1025.
13a (major) and **13b** (minor) as a mixture of isomers: ^{1}H NMR (360 MHz, $CDCl_3$): δ = 7.15–7.70 (m, 18H, H-Ar), 5.89 (s, 1H, *cis* H-C4 of **13b**), 5.50 (s, 1H, *trans* H-C4 of **13b**), 5.84 (s, 1H, *cis* H-C4 of **13a**), 5.40 (s, 1H, *trans* H-C4 of **13a**); ^{13}C NMR (90.6 MHz, $CDCl_3$): δ = 119.6 (t, C4 of **13b**), 117.9 (t, C4 of **13a**).

 © VCH Verlagsgesellschaft mbH, D-69451 Weinheim, 1997 0570-0833/97/3615-1625 $ 17.50+.50/0

14a (minor) and **14b** (major) as a mixture of isomers: ^{1}H NMR (360 MHz, $CDCl_3$): δ = 7.20–7.60 (m, H-Ar), 6.80–7.00 (m, H-Ar, not assigned), 5.80 (s, 1H, H-C4 of **14a**), 5.35 (s, 1H, H-C4 of **14a**), 3.73 (s, 3H, H_3C-O); 5.70 (s, 1H, H-C4 of **14b**), 5.26 (s, 1H, H-C4 of **14b**), 3.75 (s, 3H, H_3C-O); ^{13}C NMR (90.6 MHz, $CDCl_3$): (signals of aromatic carbon atoms not assigned) **14a**: δ = 117.0 (t, C4), 113.9 (d, C3′/C5′ of Ar), 55.2 (q, CH_3); **14b**: δ = 115.2 (t, C4), 113.5 (d, C3′/C5′ of Ar), 55.2 (q, CH_3); MS (70 eV): *m/z* (%) = 306, 304 ([M^+], 16, 27), 271, 269 ([$M^+ - Cl$], 19, 52), 270 (13), 258 (20), 234 ([$M^+ - 2Cl$], 27), 233 (21), 224 (16), 223 (100), 219 (12), 208 (15), 203 (12), 192 (15), 190 (10), 189 (17), 178 (11), 145 (19), 122 (12), 116 (10), 115 (47), 91 (11); HR-MS calcd for $C_{17}H_{14}Cl_2O$: 304.0422; found: 304.0429. In addition, **14a** was independently prepared.

[13] a) W. von E. Doering, A. K. Hoffmann, *J. Am. Chem. Soc.* **1954**, *76*, 6162; b) L. Xu, F. Tao, *Synth. Commun.* **1988**, 2117; c) D. Seyferth, *Acc. Chem. Res.* **1972**, *5*, 65; d) D. Seyferth, R. Lambert, Jr., *J. Organomet. Chem.* **1969**, *16*, 21.

[14] a) G. L. Closs, P. E. Pfeffer, *J. Am. Chem. Soc.* **1968**, *90*, 2452; b) M. Christl, R. Stangl, H. Jelinek-Fink, *Chem. Ber.* **1992**, *123*, 485; c) K. A. Nguyen, M. S. Gordon, *J. Am. Chem. Soc.* **1995**, *117*, 3835.

[15] R. Jain, M. B. Sponsler, F. D. Coms, D. A. Dougherty, *J. Am. Chem. Soc.* **1988**, *110*, 1356; see also F. Allen, *Acta Crystallogr. Sect. B* **1984**, *40*, 306, and references therein.

[16] We thank Professor R. Boese, Universität Essen, Germany, for the X-ray structure determinination of **8**. Crystallographic data (excluding structure factors) for the structures reported in this paper have been deposited with the Cambridge Crystallographic Data Centre as supplementary publication no. CCDC-179-179. Copies of the data can be obtained free of charge on application to The Director, CCDC, 12 Union Road, Cambridge CB2 1EZ, UK (fax: int. code +(1223)336-033; e-mail: deposit@chemcrys.cam.ac.uk).

[17] Tetrahalocyclopropane **8** was synthesized from commercially available chlorodifluoroacetic acid: Treatment with sodium hydroxide gave the corresponding sodium salt, which reacted with phenylmagnesium bromide to afford chlorodifluoromethyl ketone [18] in 87% yield. Wittig reaction with methylenetriphenylphosphonium bromide produced α-(chlorodifluoromethyl)styrene (yield 71%). Addition of bromophenylcarbene, generated from treatment of benzal bromide with potassium *tert*-butoxide, afforded **8** and its *trans* isomer in very low yields. The isomers were purified in multiple steps and finally separated by HPLC.

[18] T. Ando, F. Namigata, M. Kataoka, K. Yachida, W. Funasaka, *Bull. Chem. Soc.* **1967**, *40*, 1275.

[19] The ratio of aryl-substituted butadienes to cyclobutenes was also found to be approximately 20:80, which is in good agreement with the previously determined ratio of **2** to **5**.

[20] Dipolar resonance structures have been proposed as intermediates in dihalocarbene additions to alkenes: P. S. Skell, A. Y. Garner, *J. Am. Chem. Soc.* **1956**, *78*, 5430; W. von E. Doering, W. A. Henderson, Jr., *J. Am. Chem. Soc.* **1958**, *80*, 5274.

[21] The strain energy probably has a major influence on the reaction of a dihalocarbene with cyclopropene **1**. Due to release of olefinic strain, an intermediate zwitterion should be lower in energy than **1**. Stabilization of the transition state can be achieved through ring opening and complete release of strain in the cyclopropane ring with concomitant formation of conjugated double bonds. On the other hand, ring closure of **7** to a geminal dichlorobicyclobutane leads to an initial increase in strain energy. However, once the bicyclic compound **3** has been formed, the CCA rearrangement inevitably proceeds, thereby releasing substantial amounts of strain energy.

[22] In addition to cyclobutene **5**, the coupling products *meso*- and (*R,S*)-2,2′-dichloro-1,1′,3,3′-tetraphenylbi[cyclobut-1-en-3-yl] were isolated.

Magnetization Studies of the Reduced Active Form of the Catalase from *Thermus thermophilus*

Lilian Jacquamet, Isabelle Michaud-Soret, Noëlle Debaecker-Petit, Vladimir V. Barynin, Jean-Luc Zimmermann, and Jean-Marc Latour*

Manganese-containing catalases[1, 2] are found in various bacteria such as *Thermus thermophilus* and *Lactobacillus plantarum*. Structural[3] and spectroscopic[4–6] evidence indicate that the enzyme from *T. thermophilus* possesses a dimanganese active site, which exists in four different redox forms. Mechanistic studies[7] have concluded that during catalysis the dimanganese center shuttles between a $Mn^{II}Mn^{II}$ and a $Mn^{III}Mn^{III}$ form. In vitro, mixed-valent forms $Mn^{II}Mn^{III}$ and $Mn^{III}Mn^{IV}$ can be generated. The latter two forms and the phosphate complex of the reduced enzyme exhibit characteristic EPR spectra, which have been extensively studied.[4–6] In particular, the temperature dependence of the EPR spectra has been used to estimate the magnetic exchange interaction J ($\mathcal{H} = -2J\boldsymbol{S}_1\boldsymbol{S}_2$) between the two manganese ions. This J value depends on the nature of the groups bridging these ions and therefore structural information may be derived from its estimation. A comparison of these values with those of structurally characterized model compounds supports the presence of a bis(μ-oxo)$Mn^{III}Mn^{IV}$ and a (μ-hydroxo)$Mn^{II}Mn^{III}$ unit in the two mixed-valent states.[5] Less conclusive results were obtained for the reduced catalase. For the phosphate derivative of the *T. thermophilus* enzyme, Khangulov et al. obtained a value of $J = -5.6\ cm^{-1}$ for the exchange interaction.[6] This value is intermediate between those observed for (μ-aqua)bis(μ-carboxylato)$Mn^{II}Mn^{II}$ centers ($-2.5\ cm^{-1} < J < -1.5\ cm^{-1}$)[8, 9] and for (μ-hydroxo)bis(μ-carboxylato)$Mn^{II}Mn^{II}$ centers ($J \approx -9\ cm^{-1}$).[10] No structural information is available for the unliganded $Mn^{II}Mn^{II}$ active form which does not have an EPR spectrum sufficiently resolved to investigate the temperature dependence.

In order to obtain structural information on the unliganded catalytically active site and on the phosphate complex of $Mn^{II}Mn^{II}$ catalase from *T. thermophilus*, we studied the field and temperature dependence of the saturation magnetization.[11] This technique is particularly suitable for evaluating the exchange interaction in dinuclear centers[12] and allowed us to get the first structural information on the active reduced state. From magnetostructural correlations we propose a (μ-aqua)(μ-carboxylato) bridging pattern in the unliganded $Mn^{II}Mn^{II}$ form of the enzyme. The same bridges are present in the phosphate derivative and the addition of a bridging phosphate is most consistent with all magnetic and biochemical observations—a fact that may have important mechanistic implications.

Figure 1 presents the magnetic properties of the reduced catalase in D_2O (curve a) and in a deuterated phosphate buffer

[*] Dr. J.-M. Latour, L. Jacquamet, Dr. I. Michaud-Soret, Dr. N. Debaecker-Petit
Département de Recherche Fondamentale sur la Matière Condensée
Service de Chimie Inorganique et Biologique
Laboratoire de Chimie de Coordination (Unité de Recherche Associée au CNRS no. 1194)
CEA-Grenoble, F-38054 Grenoble Cedex 9 (France)
Fax: Int. code +47688 5090
e-mail: jlatour@cea.fr

Dr. V. V. Barynin
Institute of Crystallography, Russian Academy of Sciences
Moscow (Russia)

Dr. J.-L. Zimmermann
Department of Molecular and Cellular Biology
CEA/Saclay (France)

 © VCH Verlagsgesellschaft mbH, D-69451 Weinheim, 1997 0570-0833/97/3615-1626 $ 17.50+.50/0

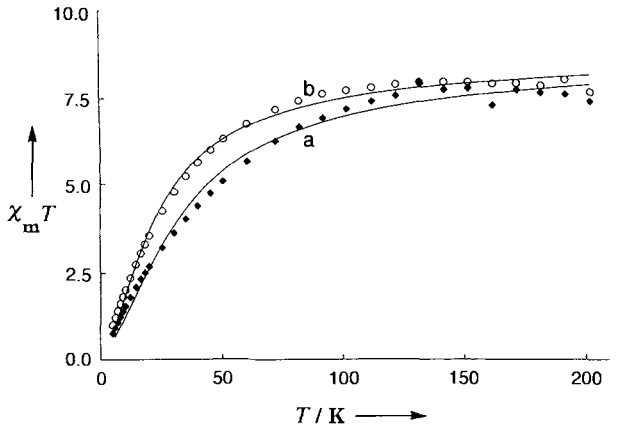

Figure 1. Temperature dependence of the product of the magnetic susceptibility and temperature (expressed in $cm^3 K mol^{-1}$) for unliganded catalase (a) and its phosphate derivative (b). Data collected at 5 Tesla. The solid lines are the theoretical curves corresponding to the best fit parameters (see text).

(curve b) as the temperature dependence of the product of the molar susceptibility and temperature. The two forms of the enzyme behave very similarly. At 200 K, $\chi_m T$ reaches about $8\ cm^3 K mol^{-1}$, a value consistent with two uncoupled spins $S = 5/2$. The product $\chi_m T$ decreases slightly over the domain between 200 and 60 K and then more strongly to become lower than $1\ cm^3 K mol^{-1}$ at 5 K. The data of both catalase forms were fitted with the Heisenberg exchange hamiltonian ($\mathcal{H} = -2J\boldsymbol{S}_1\boldsymbol{S}_2$); this gave exchange interactions J of $-2.4(2)\ cm^{-1}$ for the unliganded enzyme and $-1.7(2)\ cm^{-1}$ for the phosphate derivative. These values are very similar to each other; nevertheless, they are significantly different. Data on model systems[8, 9, 13] show that J values around $-2\ cm^{-1}$ are associated with dimanganese(II) units bridged by a water molecule and two carboxylate groups. It must be noted, however, that the number of carboxylate groups is not likely to have a strong effect on the J value provided that at least one carboxylate group is present. Thus, in contrast to EPR experiments, the magnetization data undoubtedly favor the presence of an aqua bridge in the reduced states of the enzyme.

Owing to the low absolute values of the exchange interaction it is difficult to derive firm conclusions on the phosphate binding mode. However, the decrease of $|J|$ in the presence of phosphate is in agreement with the formation of a phosphate bridge. Indeed, several examples are known in iron chemistry,[15] where introduction of a phosphate bridge in addition to or in place of a carboxylate bridge causes a decrease of the exchange interaction. The case of the diiron enzyme purple acid phosphatase (uteroferrin)[16] is enlightening in this respect. Another piece of supporting evidence for a bridging phosphate comes from our observation that phosphate binding protects the reduced center from oxidation by air or hydrogen peroxide.

The structural implications of these findings are depicted in Scheme 1. In the reduced enzyme the two manganese ions are bridged by a water molecule and one or two carboxylate groups. The presence of one or two carboxylate bridges is equally feasible. To form a bridge, the phosphate group should occupy two adjacent coordination sites of the dimanganese center. Since these sites are required for a concerted interaction of dioxygen or peroxide with the dimanganese center, a bridging phosphate would explain its inhibitory effect on the catalase reaction and the stabilization of the reduced state toward dioxygen. In turn this suggests that a single carboxylate bridge is present and that the two *syn* coordination sites of the dimanganese center are occupied by easily exchangeable ligands, namely water molecules.

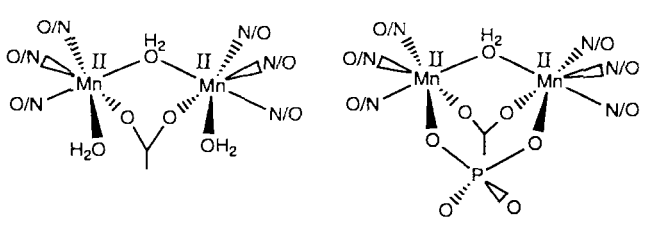

Scheme 1. Structure of the unliganded reduced catalase from *T. thermophilus* (left) and its phosphate derivative (right).

Experimental Section

All samples were checked by UV/Vis and EPR spectroscopy, which allow the traces of $Mn^{II}Mn^{III}$, $Mn^{III}Mn^{III}$, and $Mn^{III}Mn^{IV}$ forms to be quantified. [Cu(edta)] was used as EPR standard. The manganese content was measured by ICP analysis and the enzyme concentration determined as in the literature [7]. After concentration to 130–150 μL in a deuterated buffer, the samples were deaerated on a manifold argon/vacuum line and 115 μL were transferred into a quartz sample bucket within a glove box. The samples were then frozen in liquid nitrogen and introduced in the magnetometer. Two samples (0.34 mM and 2.9 mM) of the phosphate derivative were prepared by hydroxylamine reduction [7] of oxidized catalase in 10 mM phosphate buffer at pH 6.8 followed by three dilution/concentration cycles against 100 mM phosphate buffer at pH 6.8. Two samples (0.21 mM and 2.15 mM) of the unliganded form were obtained from the phosphate derivative by dilution/concentration cycles against D_2O followed by overnight incubation within a glove box and concentration.

Magnetization experiments (Figure 1) were performed with a SQUID magnetometer SHE 500 at six different fields in the range 0.5–5 Tesla in the temperature domain from 5 to 200 K on the two samples. The data were analyzed according to the procedure outlined by Day [11]. In this treatment the diamagnetic contribution of the protein is eliminated with the ferromagnetic contamination of the quartz sample holder. Owing to the extremely small field dependence of the magnetization the susceptibility data were fitted with the equation derived from the Heisenberg hamiltonian $\mathcal{H} = -2J\boldsymbol{S}_1\boldsymbol{S}_2$ appropriate for a pair of spins $S = 5/2$. The data were corrected for the presence of a small amount (sample 1: 0.5%; sample 2: 5%) of strongly antiferromagnetically coupled mixed-valent species ($S = 1/2$). The g values were fixed at 2.0.

Received: November 6, 1996
Revised version: April 2, 1997 [Z 9737 IE]
German version: *Angew. Chem.* **1997**, *109*, 1697–1699

Keywords: bridging ligands · magnetic properties · manganese · metalloenzymes

[1] J. E. Penner-Hahn, *Structural Properties of the Manganese Site in the Manganese Catalases*, VCH, New York, **1992**, p. 29.
[2] a) C. G. Dismukes in *Bioinorganic Catalysis* (Ed.: J. Reedjik), Dekker, Basel, **1993**, pp. 317–346; b) *Chem. Rev.* **1996**, *96*, 2909–2926.
[3] V. V. Barynin, A. A. Vagin, V. R. Melik-Adamyan, A. I. Grebenko, S. V. Khangulov, A. N. Popov, M. E. Andrianova, B. K. Vainshtein, *Sov. Phys. Dokl.* **1986**, *31*, 457–459.
[4] S. V. Khangulov, M. Sivaraja, V. V. Barynin, C. G. Dismukes, *Biochemistry* **1993**, *32*, 4912–4924.
[5] M. Zheng, S. V. Khangulov, C. G. Dismukes, V. V. Barynin, *Inorg. Chem.* **1994**, *33*, 382–387.
[6] S. V. Khangulov, P. J. Pesseki, V. V. Barynin, D. E. Ash, C. G. Dismukes, *Biochemistry* **1995**, *34*, 2015–2025.
[7] S. V. Khangulov, V. V. Barynin, S. V. Antonyuk-Barynina, *Biochim. Biophys. Acta* **1990**, *1020*, 25–33.
[8] A. Caneschi, F. Ferraro, D. Gatteschi, M. C. Melandri, P. Rey, R. Sessoli, *Angew. Chem.* **1989**, *101*, 1408–1410; *Angew. Chem. Int. Ed. Engl.* **1989**, *28*, 1365–1367.
[9] S. B. Yu, S. Lippard, I. Shweky, A. Bino, *Inorg. Chem.* **1992**, *31*, 3502–3504.
[10] U. Bossek, K. Wieghardt, *Inorg. Chim. Acta* **1989**, *165*, 123–129.
[11] E. P. Day, *Methods Enzymol.* **1993**, *227*, 437–463.
[12] In EPR experiments the exchange interaction is evaluated after deconvolution of the temperature-dependent experimental EPR spectra into those of the excited $S = 1$ and $S = 2$ states which allows the population of these states to be estimated and eventually fitted to the Heisenberg spin exchange equation. Owing to the larger temperature domain (ca. 200 K vs ca. 40 K) and the fact that the susceptibility is directly evaluated without an additional mathematical procedure, the magnetization techniques furnish a more reliable estimate of the magnetic exchange interaction.

 © VCH Verlagsgesellschaft mbH, D-69451 Weinheim, 1997 0570-0833/97/3615-1627 $ 17.50+.50/0

[13] Owing to its d^5 configuration the manganese(II) ion is isotropic and not very sensitive to geometrical factors. Therefore it is quite unlikely that such factors can reduce the magnetic exchange coupling mediated by a hydroxo bridge. In this respect, it is worth noting that J was also evaluated to be $-9\ cm^{-1}$ in an (μ-hydroxo)bis(μ-carboxylato)$Mn^{II}Mn^{III}$ complex [14].
[14] U. Bossek, H. Hummel, T. Weyermüller, K. Wieghardt, S. Russell, L. van der Wolf, U. Kolb, *Angew. Chem.* **1996**, *108*, 1653–1655; *Angew. Chem. Int. Ed. Engl.* **1996**, *35*, 1552–1554.
[15] W. H. Armstrong, S. J. Lippard, *J. Am. Chem. Soc.* **1985**, *107*, 3730–3731.
[16] E. P. Day, S. David, J. Peterson, W. R. Dunham, J. J. Bonvoisin, R. H. Sands, L. Que, Jr., *J. Biol. Chem.* **1988**, *263*, 15561–15567.

Perfluoroalkyl-Substituted Arylphosphanes as Ligands for Homogeneous Catalysis in Supercritical Carbon Dioxide**

Sabine Kainz, Daniel Koch, Wolfgang Baumann, and Walter Leitner*

In memory of Sir Geoffrey Wilkinson

Carbon dioxide in the supercritical state ($scCO_2$) is an interesting reaction medium that has recently been established for application in homogeneous catalysis with transition metal complexes.[1] Compared to conventional organic solvents, $scCO_2$ provides a nontoxic and ecologically benign alternative. Furthermore, $scCO_2$ is highly miscible with many gaseous reactants, thus avoiding rate limitations by diffusion processes, as is often encountered with gas/liquid-phase reactions. A possible increase in selectivity and activity through special solvent effects in the supercritical medium has also been discussed. Finally, since the solvent properties of $scCO_2$ can be tuned by variation of pressure and temperature,[2] selective separation directly from the reaction mixture seems possible.

Ironically, the solvent properties of $scCO_2$ have up to now represented the major obstacle for its wide application as a reaction medium in homogeneous catalysis. In a first approximation $scCO_2$ possesses solvent properties comparable to those of saturated hydrocarbons; this leads to severe limitations for the choice of catalysts. Especially complexes containing arylphosphane ligands (such as Ph_3P, $Ph_2P(CH_2)_nPPh_2$, 4,5-bis[(diphenylphosphanyl)methyl]-2,2-dimethyl-1,3-dioxolan (Diop), 2,2′-bis(diphenylphosphanyl)-1,1′-binaphthyl (Binap)), which have proven extremely useful in homogeneous catalysis, are often insufficiently soluble in $scCO_2$.[3] The use of complexes containing these ligands is therefore restricted to exceptional cases, for example when the substrate can act as a cosolvent.[4]

To increase the solubility of transition metal catalysts in $scCO_2$, Burk and Tumas used the lipophilic, fluorinated anion $[B\{3,5\text{-}(F_3C)_2C_6H_3\}_4]^-$ (BAr_f) for ionic catalysts with alkylphosphane ligands.[5] Jessop and Noyori suggested addition of perfluorinated alkyl alcohols to the reaction mixture for neutral complexes with Binap-type arylphosphanes.[3b] Both methods lead only to a moderate increase in solubility. The solubilizer is not directly bound to the reaction center, which results only in a weak, nonpermanent interaction. The use of the BAr_f anion is further restricted to ionic compounds, and application of additives is of course not desirable for practical reasons.

We have now developed a generally applicable methodology to increase the solubility of arylphosphanes and their metal complexes in $scCO_2$ without changing their catalytic properties. The concept is outlined in Scheme 1 for complexes containing a bidentate chelating phosphane ligand. The solubilizers (waved lines) are directly fixed at the aryl moiety in a way that keeps structural and electronic changes with respect to the unsubstituted parent complexes to a minimum. Long perfluoroalkyl chains $R = (CH_2)_2(CF_2)_yF$ ($y = 6, 8$) were chosen as solubilizers.[6]

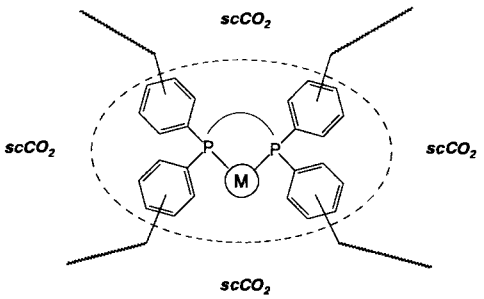

Scheme 1. Concept for the use of bis(arylphosphanes) as ligands in homogeneous catalysis in $scCO_2$. The side chains (waved lines) in the periphery of the ligands help to dissolve the insoluble parent compounds in $scCO_2$ without changing the electronic or structural properties at the catalytically active center (dashed oval).

The aryl bromides **2a–d**, which are key building blocks for the synthesis of the previously unknown arylphosphanes, were obtained by Cu^I-catalyzed coupling of the mono Grignard reagents from dibromides **1a–c** with commercially available iodides $I(CH_2)_2(CF_2)_yF$ ($y = 6, 8$; Scheme 2). Subsequent lithiation of **2a–d** and reaction with 1,2-bis(dichlorophosphino)ethane in Et_2O gave the new phosphanes **3a–d**. In a similar manner, **4** and **5** were prepared from **2b** with PCl_3 and **2c** with $(Et_2N)PCl_2/HCl$, respectively (Scheme 3).[7, 8]

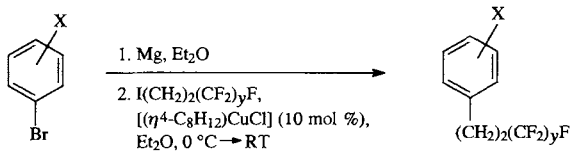

1a, X = 2-Br
1b, X = 3-Br
1c, X = 4-Br

2a, X = 2-Br, $y = 6$
2b, X = 3-Br, $y = 6$
2c, X = 4-Br, $y = 6$
2d, X = 4-Br, $y = 8$

Scheme 2. Synthesis of perfluoroalkyl-substituted aryl bromides **2a–d**.

Phosphane **5** represents a perfluoroalkyl-substituted derivative of Ph_2PCl, a starting material for the synthesis of a large variety of bis(arylphosphanes) and phosphinites including many chiral ligands. Phosphane **4** is an analogue of Ph_3P (TPP), probably the most widely used phosphane ligand in homogeneous catalysis. Phosphanes **3a–d** are derived from the well-known ligand $Ph_2P(CH_2)_2PPh_2$ (dppe). Similar to the unsubstituted

[*] Priv.-Doz. Dr. W. Leitner, S. Kainz, D. Koch
Max-Planck-Institut für Kohlenforschung
Kaiser-Wilhelm-Platz 1, D-45470 Mülheim an der Ruhr (Germany)
Fax: Int. code +(208)306-2980
e-mail: leitner@mpi-muelheim.mpg.de
Dr. W. Baumann
Research group "Komplexkatalyse" of the Max-Planck-Gesellschaft at the Universität Rostock (Germany)

[**] This work was supported by the Max-Planck-Geselischaft and the Gerhard-Hess-Programm of the Deutsche Forschungsgemeinschaft. We wish to thank Dr. K. Seevogel and M. Blumenthal (Mülheim an der Ruhr) for assistance with UV/Vis measurements. We also thank Degussa AG and Hoechst AG for generous loans of chemicals.

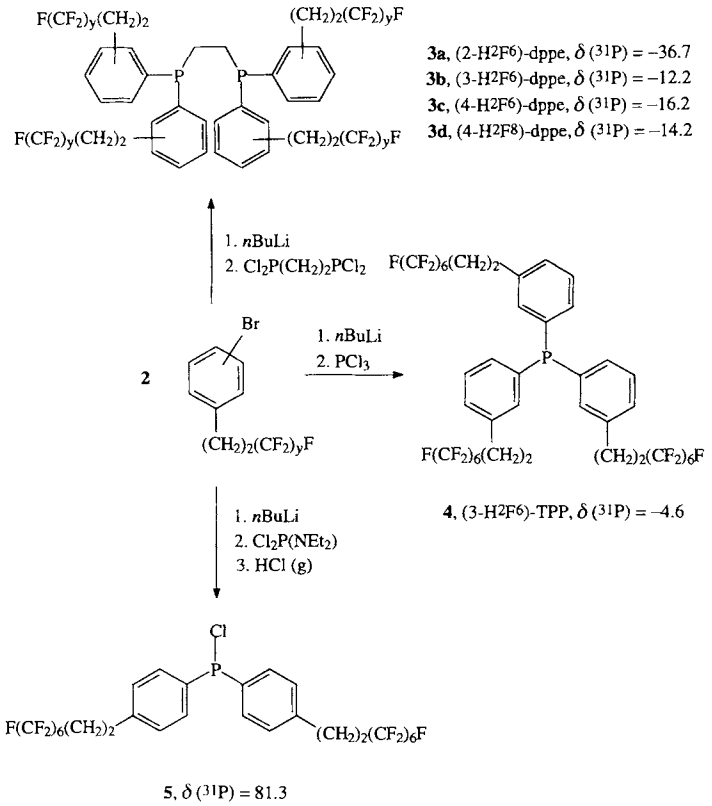

Scheme 3. Synthesis and chemical shifts δ in the $^{31}P\{^1H\}$ NMR spectra (121.5 MHz, 300 K, $CDCl_3$ or Freon/CD_2Cl_2) of new perfluoroalkyl-substituted arylphosphorus compounds **3**–**5**.

parent compounds, **3** and **4** can be employed for the synthesis of transition metal complexes by conventional methods as exemplified for **6**–**8** in Table 1. [(**4**)$_3$RhCl] (**7**) is a perfluoroalkyl-substituted analogue of Wilkinson's catalyst.

Table 1. Characteristic NMR spectroscopic data [a] for metal complexes **6**–**8** bearing perfluoroalkyl-substituted arylphosphane ligands **3** and **4**.

Complex	Formula	$\delta(^{31}P)$	J(P,Rh)[Hz]	$\delta(^{103}Rh)$[b]
6	*trans*-[$RuCl_2$(**3c**)$_2$]	43.9	–	–
7	[RhCl(**4**)$_3$]	51.1 (dt)	188, 38	[c]
		36.2 (dd)	142, 38	
8a	[Rh(hfacac)(**3a**)]	66.5 (d)	197	705
8b	[Rh(hfacac)(**3b**)]	71.8 (d)	196	461
8c	[Rh(hfacac)(**3c**)]	70.5 (d)	196	459
8d	[Rh(hfacac)(**3d**)]	70.5 (d)	196	459

[a] In [D_8]THF or $CDCl_3$ (**6**). [b] From two-dimensional $(^{31}P,^{103}Rh)\{^1H\}$ NMR experiments. [c] Not determined.

The significant enhancement of the solubility of arylphosphane complexes in $scCO_2$ upon substitution with perfluoroalkyl side chains was quantified by UV/Vis spectroscopy of saturated solutions of the colored rhodium hexafluoroacetylacetonate complexes **8**–**10**.[9, 10] The unsubstituted bis(arylphosphane) complex [Rh(hfacac)(dppe)] (**9**) is insoluble in pure $scCO_2$, even at high densities of the supercritical phase; neither a coloration of $scCO_2$ nor an absorption in the UV/Vis spectrum is observed. As expected the cyclohexyl analogue **10** is sparingly soluble. Although the supercritical phase is colorless at relatively low density ($\rho = 0.55\,g\,mL^{-1}$), it shows the typical[9b] absorption for complexes of type [Rh(hfacac)(P_2)]; the concentration was estimated to be $1.1 \times 10^{-5}\,mol\,L^{-1}$.[9] Under

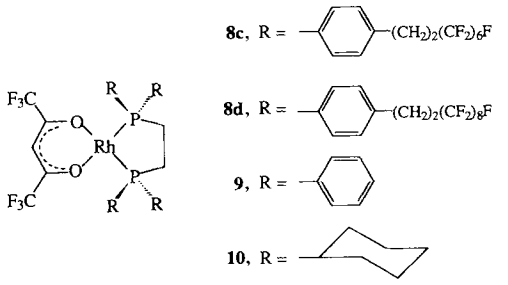

identical conditions, **8c**,**d** yield bright orange solutions with saturation concentration of $6.3 \times 10^{-5}\,mol\,L^{-1}$ (**8c**) and $7.5 \times 10^{-5}\,mol\,L^{-1}$ (**8d**), which is 5 and 7 times higher, respectively, than that of **10** (Figure 1).

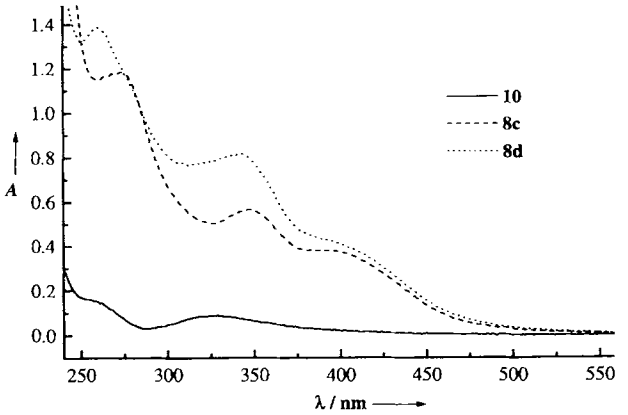

Figure 1. UV/Vis spectra of **8c**,**d** and [Rh(hfacac){$Cy_2P(CH_2)_2PCy_2$}] (**10**; Cy = cyclohexyl) in $scCO_2$ ($T = (45 \pm 5)\,°C$, $p = (90 \pm 5)$ bar, $\rho = 0.55\,g\,mL^{-1}$).

Increasing the density of the supercritical phase naturally enhances the solubility of **8**.[2] For instance, 158 mg of **8c** dissolved completely in the high-pressure cell ($V = 17.3$ mL) at a density of $\rho = 0.75\,mL^{-1}$ to yield a concentration of $4.4 \times 10^{-3}\,mol\,L^{-1}$. The solubility of **8c** in $scCO_2$ is thus at least 150 times higher than that of the alkylphosphane complex [Rh((*R*,*R*)-Et-Duphos)(η^4-C_8H_{12})][BAr_f] ((*R*,*R*)-Et-Duphos = (−)-1,2-bis[(2*R*,5*R*)-2,5-diethylphospholano]benzene), for which Burk and Tumas determined a maximum solubility of $0.03 \times 10^{-3}\,mol\,L^{-1}$ at much higher density ($T = 50\,°C$, $p = 345$ bar, $\rho = 0.89\,g\,mL^{-1}$).[5] Therefore, introduction of the perfluoroalkyl side chain not only transforms the insoluble parent compound **9** into the $scCO_2$-soluble **8**, but also results in solubilities exceeding those of known soluble catalysts by at least two orders of magnitude.

The chemical shift δ of the ^{103}Rh nucleus is a sensitive probe for structural and electronic variation at the metal center of complexes [Rh(hfacac)(P_2)].[9] The change of only a few ppm to lower field observed for the signal for **8b**–**d** compared to that for unsubstituted parent compound **9** ($\delta = 438$) shows that, as anticipated, the two CH_2 groups separate the strong electron-withdrawing effect of the long perfluorinated chains effectively from the aryl moiety (Table 1).[6a] In the case of **8a** the large perfluorinated chains in the *ortho* positions most likely lead to appreciable distortion of the coordination geometry at the rhodium center, resulting in a significant shift to lower field of $\Delta\delta \approx 270$ with respect to that of **9**.[9] This interpretation is supported by temperature-dependent ^1H and ^{31}P NMR spectra of **8a** as well as preliminary molecular modeling calculations. A simultaneous electronic influence cannot be fully excluded.

 © VCH Verlagsgesellschaft mbH, D-69451 Weinheim, 1997 0570-0833/97/3615-1629 $ 17.50+.50/0

Finally, the potential of the perfluoralkyl-substituted arylphosphanes for homogeneous catalysis in $scCO_2$ was established with the rhodium-catalyzed hydroformylation of 1-octene (**11**) to isomeric aldehydes **12a,b** (Scheme 4).[11, 12] The

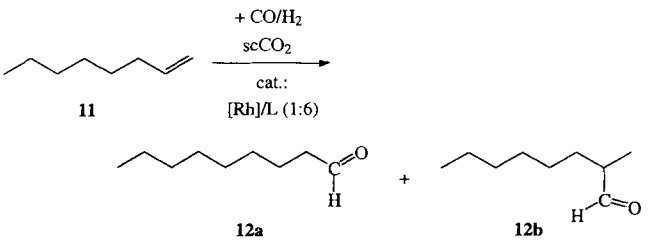

L = PPh_3 (26 % conversion) 3.5 : 1
L = **4** (92 % conversion) 4.6 : 1

Scheme 4. Rhodium-catalyzed ([Rh] = [Rh(hfacac)(η^4-C_8H_{12})]) hydroformylation of 1-octene (**11**) to nonanal (**12a**) and 2-methyloctanal (**12b**) in $scCO_2$ [12]; see text for reaction conditions.

catalytic system Rh/TPP, which is well established in organic solvents, was found to be unsuitable for application in $scCO_2$ owing to the insufficient solubility of the active species as suspected (colorless solution, 26% conversion, **12a**:**12b** = 3.5). On the other hand, a conversion of 92% and an *n*:*iso* ratio of **12a**:**12b** = 4.6 was obtained under identical but nonoptimized conditions with a catalyst formed in situ from [Rh(hfacac)(η^4-C_8H_{12})] and the TPP-analogue **4** (**11**:**4**:Rh = 200:6:1) at 60 °C and a total pressure of 220 bar ($p(CO) = p(H_2) = 30$ bar at room temperature). Side reactions such as hydrogenation or formation of further isomeric aldehydes were not observed. The intense yellow color of the homogeneous supercritical phase confirmed the solubility of the catalytically active species containing **4** during the whole course of reaction.

Our concept of homogeneous catalysis in $scCO_2$ relies on a straightforward and variable synthetic route to perfluoroalkyl substituted arylphosphanes. These ligands provide significantly higher solubility in $scCO_2$ compared to the insoluble parent compounds and to known soluble phosphane-containing catalysts. The solubilizers in the periphery of the ligand do not interfere with the electronic or structural properties of the coordinated metal center, provided that a suitable substitution pattern is maintained. Therefore, the well-known potential of arylphosphorus compounds as ligands for homogeneous catalysis is now available for applications in $scCO_2$.

Received: February 13, 1997 [Z101091E]
German version: *Angew. Chem.* **1997**, *109*, 1699–1701

Keywords: carbon dioxide · homogeneous catalysis · hydroformylations · P ligands · supercritical fluids

[1] Reviews: a) G. Kaupp, *Angew. Chem.* **1994**, *106*, 1519; *Angew. Chem. Int. Ed. Engl.* **1994**, *33*, 1452; b) M. Poliakoff, S. G. Kazarian, S. Howdle, *ibid.* **1995**, *107*, 1409 and **1995**, *34*, 1275; c) P. G. Jessop, T. Ikariya, R. Noyori, *Science* **1995**, *269*, 1065; d) D. A. Morgenstern, R. M. LeLacheur, D. K. Morita, S. L. Borkowsky, S. Feng, G. H. Brown, L. Luan, M. F. Gross, M. J. Burk, W. Tumas in *Green Chemistry* (Eds.: P. T. Anastas, T. C. Williamson), American Chemical Society, Washington DC, **1996** (*ACS Symp. Ser.* **1996**, *626*), pp. 132ff.; e) E. Dinjus, R. Fornika, M. Scholz in *Chemistry under Extreme or Non-Classical Conditions* (Eds.: R. van Eldik, C. D. Hubbard), Wiley, New York, **1996**, p. 219.

[2] K. Zosel, *Angew. Chem.* **1978**, *90*, 748; *Angew. Chem. Int. Ed. Engl.* **1978**, *17*, 702.

[3] a) P. G. Jessop, Y. Hsiao, T. Ikariya, R. Noyori, *J. Am. Chem. Soc.* **1996**, *118*, 344; b) J. Xiao, S. C. A. Nefkens, P. G. Jessop, T. Ikariya, R. Noyori, *Tetrahedron Lett.* **1996**, *37*, 2813.

[4] M. T. Reetz, W. Könen, T. Strack, *Chimia* **1993**, *47*, 493.

[5] M. J. Burk, S. Feng, M. F. Gross, W. Tumas, *J. Am. Chem. Soc.* **1995**, *117*, 8277.

[6] a) For the synthesis of phosphorus compounds with R groups connected directly to the P donor atoms and the use of these ligands in perfluorinated solvents see: I. T. Horváth, J. Rábai, *Science* **1994**, *266*, 72; F. Langer, K. Püntener, R. Stürmer, P. Knochel, *Tetrahedron: Asymmetry* **1997**, *8*, 715; b) Groups R were used independently for enhancement of solubility of tin hydrides as stoichiometric reagents for free radical reactions in $scCO_2$: S. Hadida, M. S. Super, E. J. Beckman, D. P. Curran, *J. Am. Chem. Soc.*, in press.

[7] We suggest the following general nomenclature for perfluoroalkyl-substituted arylphosphorus compounds with a known parent structure: The prefix (*z*-H^xF^y) is added in front of the established acronym, whereby *z* gives the position of the perfluorinated alkyl chain in the aryl moiety relative to the carbon bound to phosphorus, *x* gives the number of the CH_2 groups, and *y* the number of CF_2 groups.

[8] All new compounds were characterized by ^1H, ^{13}C, ^{19}F and ^{31}P NMR spectroscopy as well as mass spectrometry and/or elemental analysis.

[9] a) R. Fornika, H. Görls, B. Seemann, W. Leitner, *J. Chem. Soc. Chem. Commun.* **1995**, 1479; b) K. Angermund, W. Baumann, E. Dinjus, R. Fornika, H. Görls, M. Kessler, C. Krüger, W. Leitner, F. Lutz, *Chem. Eur. J.* **1997**, *3*, 755.

[10] UV/Vis spectra were collected in a high-pressure cell equipped with sapphire windows ($V = 17.3$ mL, $d = 12$ mm, $p_{max} = 350$ bar, $T_{max} = 150$ °C). The saturation concentrations were estimated from the Lambert–Beer equation by using extinction coefficients from calibration measurements in THF.

[11] a) For hydroformylation in $scCO_2$ with $[Co_2(CO)_8]$ as a catalyst, see J. W. Rathke, R. J. Klingler, T. R. Krause, *Organometallics* **1991**, *10*, 1350; J. W. Rathke, R. J. Klingler (Argonne Nat. Lab.), US 5,198,589, **1993** [*Chem. Abstr.* **1993**, *119*, 141597n]; b) for the influence of gaseous CO_2 on the hydroformylation in an aqueous biphasic system, see B. Cornils, W. Konkol, H. Bach, G. Dämbkes, W. Gick, E. Wiebus, H. Bahrmann (Ruhrchemie AG), DE 3415968, **1984** [*Chem. Abstr.* **1986**, *104*, 209147p].

[12] The experiments were carried out in a stainless-steel high-pressure reactor equipped with glass windows ($V = 20$ mL, $p_{max} = 300$ bar, $T_{max} = 120$ °C). The reactor was charged with the catalyst and **11** (1.50 mL, 9.60 mmol) under an inert atmosphere. The reactor was pressurized with a 1:1 mixture of CO and H_2 to 60 bar and then filled with CO_2 (13.6 g) using a compressor. After heating the reaction mixture to 60 °C for 19 h, samples were withdrawn and analyzed by GC and ^1H NMR spectroscopy.

Merocyanines as Extremely Bathochromically Absorbing Chromophores in the Halobacterial Membrane Protein Bacteriorhodopsin**

Dorothee Hoischen, Siegfried Steinmüller, Wolfgang Gärtner,* Volker Buss,* and Hans-Dieter Martin*

The binding of ligands to proteins can lead to significant changes in their physical and chemical properties. This is particularly apparent for photoisomerizable chromoproteins, for example the membrane protein bacteriorhodopsin (BR) of the halophilic archaebacterium *Halobacterium salinarium*, which contains retinal (**1**, see Scheme 1).[1, 2] Upon absorption of light, BR transports protons by a cyclic reaction sequence (the photocycle of BR lasts about 10 ms) into the outer medium, allowing

[*] Priv.-Doz. Dr. W. Gärtner
Max-Planck-Institut für Strahlenchemie
Postfach 101365, D-45413 Mülheim an der Ruhr (Germany)
Fax: Int. code +(208)306-3951
e-mail: gaertner@dsa.mpi-muelheim.mpg.de
Prof. Dr. V. Buss, Dipl.-Chem. S. Steinmüller
Fachgebiet Theoretische Chemie der Universität
Lotharstrasse 1, D-47057 Duisburg (Germany)
Fax: Int. code +(203)379-2772
Prof. Dr. H.-D. Martin, Dr. D. Hoischen
Institut für Organische Chemie und Makromolekulare Chemie der Universität
Universitätsstrasse 1, D-40225 Düsseldorf (Germany)
Fax: Int. code +(211)811-4324

[**] This work was supported by the Deutsche Forschungsgemeinschaft and the Fonds der Chemischen Industrie. W. G. thanks Prof. K. Schaffner for generous support and Prof. S. E. Braslavsky for valuable discussions. The proteins were prepared by T. Huestege, and the fluorescence spectra recorded by A. Keil-Block. D. H. and H.-D. M. wish to thank BASF AG for generous gifts of chemicals.

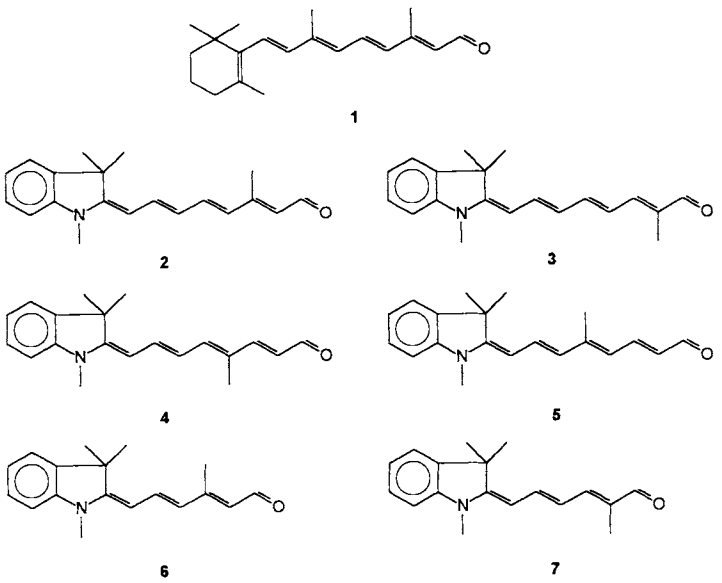

Scheme 1. Structural formulas of retinal (**1**) and the newly synthesized merocyanine dyes **2**–**7**.

the energy thus stored to be employed for further metabolic processes. During the photocycle several intermediates with clearly discernable spectral properties are formed.[3] The structural changes that the chromophore and protein undergo can be followed by a variety of spectroscopic techniques.[2, 4, 5]

Covalent attachment of all-*trans* retinal to lysine 216 through a protonated Schiff base linkage causes a strong red shift of the absorption maximum (λ_{max} = 568 nm; protonated butylamine/retinal Schiff base in ethanol: λ_{max} = 440 nm). This energy difference is called the opsin shift (OS) and amounts to 5183 cm^{-1} for BR.[6]

Three increments that concertedly cause the red-shifted absorption of BR are currently being discussed:[2, 7] the positive charge of the Schiff base, the conformational changes of the chromophore resulting from incorporation into the binding pocket of the protein, and the influence of charged and polar amino acids in the chromophore environment. To study these influences when the π-electron system is strongly delocalized, we synthesized a series of novel merocyanine dyes (Scheme 1) and studied the spectroscopic properties of the new BR derivatives obtained by reconstitution with the protein (see also ref. [8, 9]). Due to the indolylidene end group these compounds should be converted into hemicyanine chromophores that show the expected absorption spectra upon formation of a protonated Schiff base.[10] The synthetic route to these novel compounds is given for the example of **2** and **3** in Scheme 2.

Upon incubation with chromophore-depleted BR (bacterio-opsin, BO) the merocyanine dyes generate BR derivatives exhibiting remarkably bathochromic, narrow-absorption bands with large absorption coefficients (Figure 1a, Table 1). UV/Vis spectra measured throughout the incubation of **2** with BO (Figure 1a) exhibit an isosbestic point, indicating a homogeneous reaction. The reconstitution apparently leads to a stable, covalent linkage between chromophore and protein, since the subsequently added retinal does not displace the merocyanine from the binding site (Figure 1b). Likewise, addition of any of the merocyanines to native BR does not result in red-shifted absorption bands (not shown).

The most apparent structural change between the novel dyes and native retinal (besides the different substitution pattern in some of the compounds) is the replacement of the cyclohexene

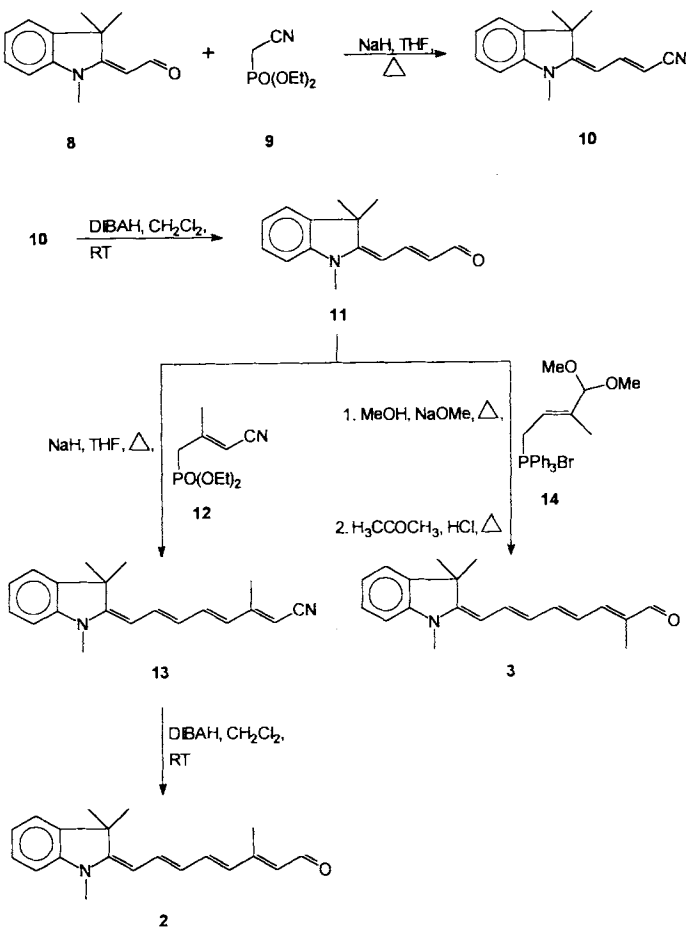

Scheme 2. Synthesis of **2** and **3** from **8**, which was kindly provided by BASF AG, Ludwigshafen, Germany (RT = room temperature). All intermediates and products exhibited the expected spectroscopic and chromatographic properties.

Table 1. Spectroscopic data of the novel merocyanine dyes and the BR derivatives obtained upon incubation with bacterio-opsin (BO).

Comp.	λ_{max} [nm]				lg ε	Δ_{OS} [c]	$\pm\Delta\varepsilon_{max,\lambda}$
	Aldehyde [a]	SB [a]	PSB [a]	BR [b]	(BR)	[cm^{-1}]	[$L\,mol^{-1}\,cm^{-1}$]
1	381	357	440	570	4.80	5183	$+21_{534}/-10_{595}$
2	487	448	666	755	5.43	1770	$+51_{737}/-30_{768}$
3	482	482	657	700	5.23	935	$+39_{685}/-3_{725}$
4	490	452	657	698	ca. 5.36 [d]	894	$+63_{672}/-20_{743}$
5	491	453	665	711 [e]	–[e]	973	$+6.6_{694}/-6_{738}$ [f]
6	463	420	578	610	ca. 5.08	908	$+13_{593}/-40_{618}$
7	456	422	567	–[g]	–	–	–

[a] In ethanol. [b] In water. [c] OS = opsin shift. [d] There are two isomers present with partially overlapping absorption bands. [e] No complete reconstitution between **5** and BO. [f] Ellipticity [mdeg]. [g] No covalent chromophore protein binding.

ring of retinal with an indolylidene group, which causes strongly red-shifted absorption maxima. Interestingly, BR derivatives also can be formed with compounds having a different methyl substitution pattern than retinal (**3**–**5**); only the correctly substituted compound forms a BR pigment upon truncation of the conjugated polyene chain (see **6** and **7** in Table 1).

A common feature of the new pigments is the formation of hypsochromic vibration band progressions.[11] The red-shifted absorption bands of the protonated Schiff bases of these compounds are already observable in ethanol and indicate a remarkable delocalization of the double bonds (see Table 1). Conse-

 © VCH Verlagsgesellschaft mbH, D-69451 Weinheim, 1997 0570-0833/97/3615-1631 $ 17.50+.50/0

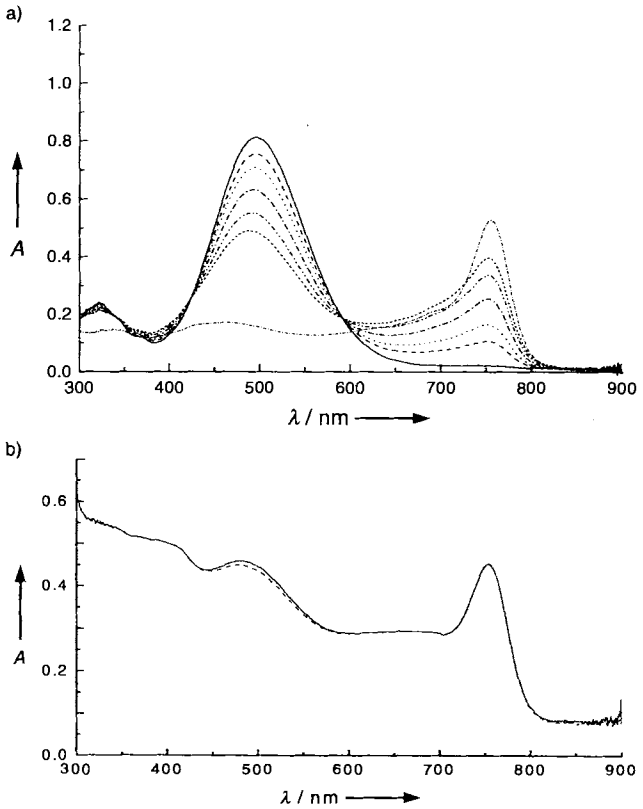

Figure 1. a) UV/Vis spectra of the reconstitution (at room temperature) of **2** with bleached bacteriorhodopsin (BO). The series of curves (growth of the absorption at 755 nm, and decrease of the absorption of the free chromophore at 500 nm) shows the course of the reconstitution starting with the spectrum recorded immediately after addition of the compound (——, λ_{max} = 500 nm) and after 40, 80, 120, 160, 200 min and 12 h (curve with largest absorption at 755 nm). The isosbestic point at about 590 nm is observed for at least 3 h and indicates a uniform reaction (incubation for 12 h—spectrum with maximal absorption at 755 nm—induces changes in the entire spectral range with loss of the isosbestic point). b) Spectrum on incubation of the fully reconstituted new pigment with all-*trans* retinal to demonstrate covalent incorporation of the merocyanine into the protein binding site.

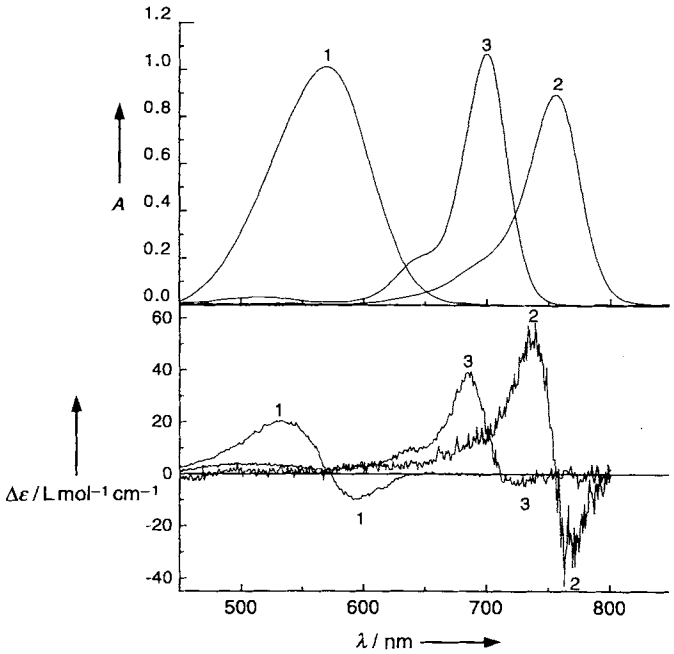

Figure 2. UV/Vis (top) and CD spectra (bottom) of BR derivatives containing **2** and **3** and the spectra of native BR (curve 1 in both panels).

quently, the influence of the protein environment on the position of the absorption maximum is only moderate, as is seen from the small values of the opsin shifts (on the order of about 900 cm^{-1}, except for **2**: 1770 cm^{-1}; see also Table 1).

Due to the strong fluorescence of the new BR pigments, direct proof of the presence of a protonated Schiff base could not be obtained from resonance Raman spectroscopy.[12] However, the CD spectra of the new BR derivatives (Figure 2) exhibit nonconservative, excitonic bands similar to those observed for native BR, and indicate incorporation of the dyes into the protein in a manner comparable to that of retinal. The CD spectra of all compounds (except for **7**, which does not react with the protein) are made up of a biphasic band with positive absorption at short and negative absorption at long wavelengths, and a cross-over wavelength identical to the absorption maximum in the UV/Vis spectrum. The nonconservative character of the CD spectra is also evident from the different $\Delta\varepsilon$ values of the extrema (Table 1). With the exception of compound **6**, the short-wavelength positive band is of greater intensity than the negative band; the ratio between them varies from 5:3 (**2**) to more than 10:3 (**3**). In line with the excitonic interpretation of the CD spectra of BR pigments,[13] all spectra can be separated into two contributions, that is, a monophasic positive contribution (negative in the case of **6**)—which correlates in shape and wavelength position with the absorption maximum, and is caused either by the chromophore that is incorporated into the protein in a twisted conformation or from chromophore–protein interactions—and a biphasic, conservative contribution resulting from the interaction between the chromophores.[14]

Laser flash induced study of the photochemical properties reveals a behavior remarkably different from that of BR. In the time range of about 100 ns to 10 ms, which covers all thermally driven kinetic processes of the BR photocycle (after photochemical generation of the intermediate K), no changes in the parent-state absorption could be detected for any of the cyanine compounds. However, the BR derivatives **4** and **5** undergo previously unreported light-induced, thermally controlled conformational changes (demonstrated for **4**, Figure 3). Narrow-band irradiation of the parent state (λ_{max} = 698 nm, curve 1) using an interference filter ($\lambda_{ex} = 654 \pm 10$ nm) for about ten minutes causes only a minimal change in the absorption for the range of absorption maximum (curve 2). A series of thermally driven conversions takes place after this photochemical reaction. On a

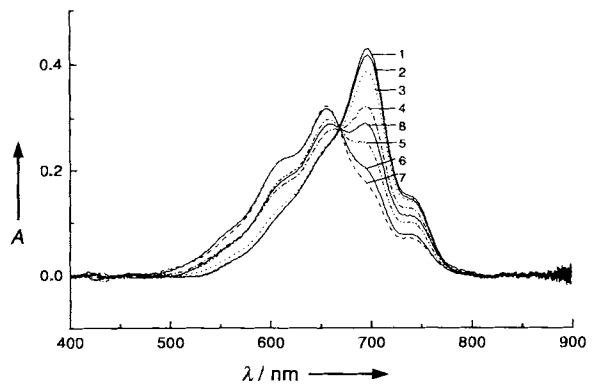

Figure 3. Photochemically induced reactions of the pigment formed from **4** and BO. Curve 1: absorption after complete reconstitution, prior to irradiation; curve 2: after irradiation for 10 min; curves 3–8: as for curve 2, but after 2, 4, 6, 7, 8, and 20 h, respectively, of incubation in the dark. Curve 8 already shows thermal reverse reaction.

 © VCH Verlagsgesellschaft mbH, D-69451 Weinheim, 1997 0570-0833/97/3615-1632 $ 17.50+.50/0

time scale of several hours, the absorption of the parent state at 698 nm declines in the dark with concomittant increase in the absorption at 654 nm (curves 3–7). This conversion exhibits an isosbestic point. Formation of the blue-shifted species does not go to completion, but is followed by an even slower process (which requires several days of incubation in the dark) by which the initial species that absorbs at 698 nm is partially restored (curve 8). These processes are definitely photo-induced; an identical sample that is not irradiated remains virtually unchanged after incubation in the dark for the same time period. This excludes thermal equilibration of present *E*,*Z* isomers as a possible origin of the observed absorption changes. As an explanation we propose a photoreaction with low quantum efficiency for these cyanine dyes that yields an isomer with nearly identical absorption properties as the parent state. This intermediate might adopt an unfavorable conformation in the binding site of the protein, thus inducing slow thermally driven reactions that generate a new species with hypsochromic absorption. This new form of the cyanine dye enters in an extremely slow kinetic equilibrium with the initial state. Further experiments to study photochemical reactions with significantly faster kinetics, as reported for other modified chromophores,[15–17] are in progress.

Received: November 4, 1996
Revised version: February 14, 1997 [Z9716IE]
German version: *Angew. Chem.* **1997**, *109*, 1702–1704

Keywords: bacteriorhodopsin · chromophores · circular dichroism · cyanines · photochemistry

[1] K. Nakanishi, *Pure Appl. Chem.* **1985**, *57*, 769.
[2] R. A. Mathies, S. W. Lin, J. B. Ames, W. T. Pollard, *Annu. Rev. Biophys. Biophys. Chem.* **1991**, *20*, 491.
[3] D. Oesterhelt, *Angew. Chem.* **1976**, *88*, 16; *Angew. Chem. Int. Ed. Engl.* **1976**, *15*, 17.
[4] K. Gerwert, G. Souvignier, B. Hess, *Proc. Natl. Acad. Sci. USA* **1990**, *87*, 9774.
[5] J. K. Lanyi, *Biochim. Biophys. Acta* **1993**, *1183*, 241.
[6] M. G. Motto, M. Sheves, K. Tsujimoto, V. Balogh-Nair, K. Nakanishi, *J. Am. Chem. Soc.* **1980**, *102*, 7947.
[7] K. Nakanishi, R. Crouch, *Isr. J. Chem.* **1995**, *35*, 253.
[8] A. E. Asato, X.-Y. Li, D. Mead, G. M. L. Patterson, R. S. H. Liu, *J. Am. Chem. Soc.* **1990**, *112*, 7398.
[9] R. S. H. Liu, E. Krogh, X.-Y. Li, D. Mead, L. U. Colmenares, J. R. Thiel, J. Ellis, D. Wong, A. E. Asato, *Photochem. Photobiol.* **1993**, *58*, 701.
[10] F. Derguini, C. G. Caldwell, M. G. Motto, V. Balogh-Nair, K. Nakanishi, *J. Am. Chem. Soc.* **1983**, *105*, 646.
[11] G. Scheibe, E. Daltrozzo, O. Wörz, J. Heiss, *Z. Phys. Chem. NF* **1969**, *64*, 97.
[12] M. Stockburger, T. Alshuth, D. Oesterhelt, W. Gärtner in *Spectroscopy of Biological Systems* (Eds.: R. J. H. Clark, R. E. Hester), Wiley, New York, **1986**, p. 483.
[13] B. Becher, T. G. Ebrey, *Biochem. Biophys. Res. Comm.* **1976**, *69*, 1.
[14] J. Y. Cassim, *Biophys. J.* **1992**, *63*, 1432.
[15] H.-J. Polland, M. A. Franz, W. Zinth, W. Kaiser, E. Kölling, D. Oesterhelt, *Biochim. Biophys. Acta* **1984**, *767*, 635.
[16] N. Friedman, M. Sheves, M. Ottolenghi, *J. Am. Chem. Soc.* **1989**, *111*, 3203.
[17] T. L. Brack, J. K. Delaney, G. H. Atkinson, A. Albeck, M. Sheves, M. Ottolenghi, *Biophys. J.* **1993**, *65*, 964.

Anomalous Shift in the Fluorescence Spectra of a High-Generation Dendrimer in Nonpolar Solvents**

Chelladurai Devadoss, P. Bharathi, and Jeffrey S. Moore*

Charge-transfer (CT) states are characterized by broad, structureless absorption and emission spectra. The peak of the emission band is usually red-shifted (bathochromic shift) with increasing polarity of the medium.[1] This phenomenon of solvatochromism, that is the shift of emission maximum with the change in polarity of the medium, has been used to probe the microenvironment of micelles,[2] the extent of cure in epoxy resins,[3] the mobility of polymer backbones,[4] the morphology of poly(ethyleneglycol) matrices,[5] and the polarity and viscosity of various biological and other heterogeneous systems.[6] Fréchet et al. attached a solvatochromic chromophore, 4-(*N*-benzyl-*N*-methylamino)-1-nitrobenzene, to the focal point of polyether dendritic macromolecules and investigated solvatochromism as a function of generation.[7] They observed a dramatic change in the absorption maximum on going from third generation to fourth generation dendrimers in solvents of low polarity and correlated this transition with the transformation from an extended to a globular structure. Such a change in shape was consistent with their studies of intrinsic and melt viscosities of these materials.[8, 9] All of these observations and earlier molecular dynamics calculations from other groups[10] indicate that the higher generation dendrimers have compact, globular structure with a transition from an open extended form beyond a certain generation. We report here an anomalous spectral shift in the fluorescence maximum of a CT state in higher generation phenylacetylene dendrimers. In particular, large spectral shifts are observed in high generation monodendrons even in nonpolar hydrocarbon solvents in much the same way as those reported for other dendritic systems. We also show that this behavior is very dependent on dendrimer generation numbers. These findings suggest significant changes in the size and shape of these dendrimers beyond the fifth generation and the observations may have important implications for the design of dendritic molecules capable of undergoing long-range intramolecular electron transfer.

We have been studying the photoinduced electron transfer in a series of dendrimers (Scheme 1) using steady-state and time-resolved fluorescence spectroscopy. In these dendrimers, the *p*-dimethoxybenzene moiety at the focal point functions as the electron donor and the tolan segments of the dendrimer as the electron acceptors. In the lower generations (e.g. in **2**), the usual bathochromic shift with increasing polarity of the solvent is observed (see Figure 1a). However, in the higher generation dendrimers, an abnormal spectral shift in the fluorescence maximum is seen in nonpolar hydrocarbon solvents. This behavior is remarkably dependent on very subtle changes in the size and shape of the hydrocarbon molecules of the solvent. Specifically, in cyclohexane the fluorescence maximum of the fifth genera-

[*] Prof. J. S. Moore, Dr. C. Devadoss, Dr. P. Bharathi
Department of Chemistry, Materials Science & Engineering
and
Beckman Institute for Advanced Science and Technology
University of Illinois at Urbana-Champaign
Urbana, IL 61801 (USA)
Fax: Int. code +(217)244 8068
e-mail: moore@aries.scs.uiuc.edu

[**] The financial support for this research by the National Science Foundation through Grant DMR 95-20402 is gratefully acknowledged.

 © VCH Verlagsgesellschaft mbH, D-69451 Weinheim, 1997 0570-0833/97/3615-1633 $ 17.50+.50/0

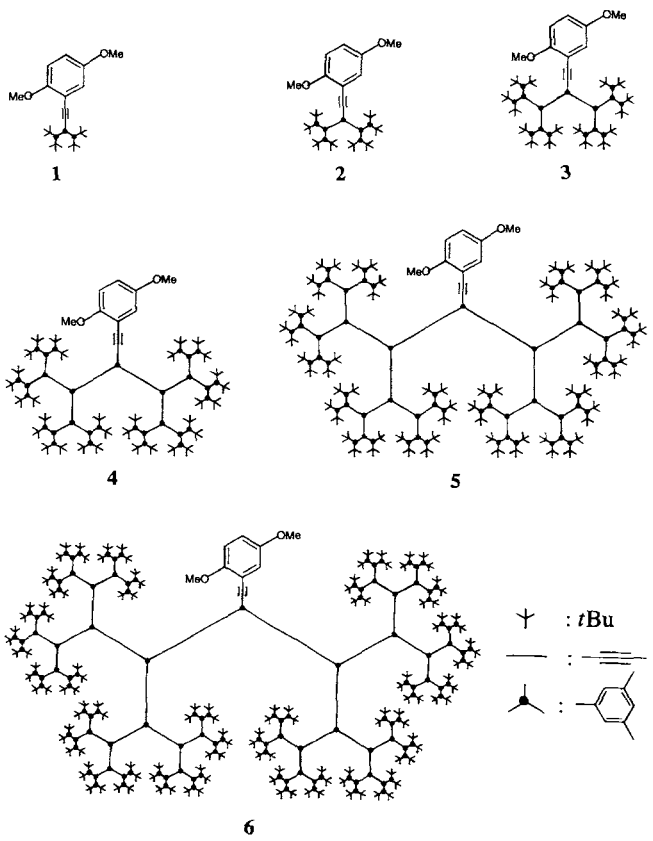

Scheme 1. Structures of the monodendrons capped with dimethoxybenzene at their focal points.

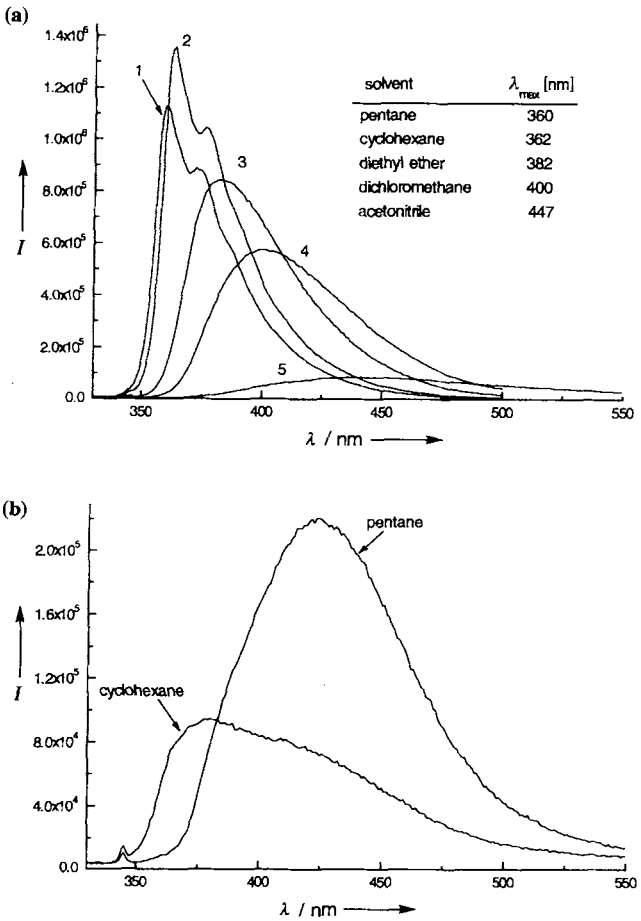

Figure 1. a) Fluorescence spectra of **2** in pentane (1), cyclohexane (2), diethyl ether (3), dichloromethane (4), and acetonitrile (5). b) Fluorescence spectra of the fifth generation (63mer) dendrimer **5** in cyclohexane and pentane. All the spectra were recorded with excitation at 310 nm and at a concentration such that they had the same absorbance at the excitation wavelength.

tion dendrimer (63mer, **5**) is 380 nm, whereas in pentane it is 421 nm (see Figure 1 b). To our knowledge, this is the first report of such a large spectral shift (41 nm) resulting from variations in the type of nonpolar solvent. Spectral parameters in other solvents are collected in Table 1. Control experiments with neat pentane and cyclohexane did not show any detectable emission upon excitation at 310 nm. The possibility of emission due to the presence of any adventitious impurities was ruled out by the matching of excitation and absorption spectra of the dendrimer. The solvents were tested for the presence of moisture using the Karl Fischer titration method and all were found to be dry (<35 ppm). It should be emphasized that the absorption spectra of this dendrimer in all nonpolar solvents are almost indistinguishable from the two-absorption maxima (293 and 310 nm) found with the tolan moiety. Moreover, this unusual behavior is observed only when the electron-donating dimethoxybenzene group is bound to the focal point (that is, when an unsubstituted phenyl group is attached to the focal point, the fluorescence maximum of the fifth generation dendrimer **5** is at 386 nm in pentane).

With increasing chain length of linear alkane solvents, the fluorescence maximum is blue-shifted (Table 1). The emission peak is at a shorter wavelength in cyclic hydrocarbon solvents than in linear ones. Moreover, branching shifts the fluorescence maximum to shorter wavelength. These results suggest that the size and shape of the solvent appears to play a major role in the magnitude of the spectral shift. There appears to be no correlation of this spectral shift with other physical parameters of the solvent like dielectric constant, viscosity, or solubility parameters.

The anomalous spectral shift is strongly dependent on dendrimer generation. As Figure 2 shows, the change in the peak of

Table 1. Fluorescence maximum λ_{max}^{fl} and quantum yield Φ_{fl} of **5** in various nonpolar solvents (dielectric constant ε, viscosity η).

Solvent	ε[a]	η[a] [10^{-3} Pa s]	λ_{max}^{fl} [nm]	Φ_{fl}
n-pentane	1.84	0.235	421	0.22
n-hexane	1.89	0.313	418	0.17
n-heptane	1.93	0.418	386	0.12
n-octane	1.95	0.545	373	0.12
cyclohexane	2.02	0.975	380	0.10
methylcyclohexane	2.02	0.734	373	0.10
methylcyclopentane	1.97[b]	0.473[b]	377	0.09
3-methylpentane	1.90	1.895	403	0.20
2,2-dimethylbutane	1.86[c]	0.33[c]	402	0.23

[a] Ref.[16]. [b] Ref.[17]. [c] Ref.[18].

the CT emission in nonpolar solvents is minimal up to the 31mer. However, there is a sudden change for the 63mer in cyclohexane as well as in pentane. This observation is similar to that reported by Fréchet et al.[7] for their polyether dendrimers and by Tomalia[11] for the poly(amidoamine) (PAMAM) dendrimers. This change in fluorescence maximum may arise from the change in size and shape of the dendrimer in the higher generations, where the shape may be compact and globular, as proposed by Fréchet et al. and Tomalia.

The fluorescence maximum, according to the Lippert–Mataga relation,[12] is influenced by three factors; namely, the polar-

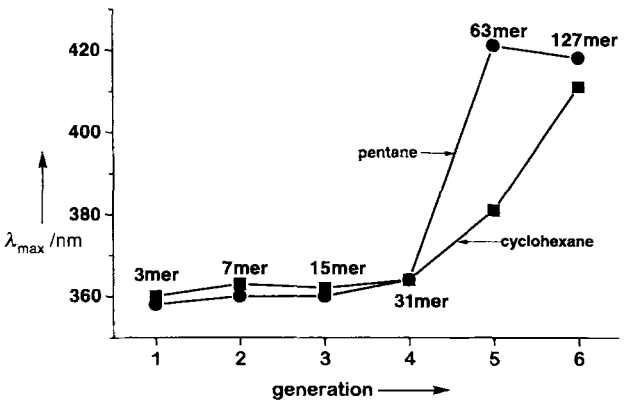

Figure 2. Plot of fluorescence maximum as a function of dendrimer generation in cyclohexane and in pentane.

ity of the solvent, the dipole moment of the CT state, and the radius of the Onsager cavity. Evidently, the polarity of the solvent does not play a major role in this spectral shift.[15] It is probable that the dipole moment of the CT state in pentane is larger than in cyclohexane due to larger distance of charge separation. This notion is supported by fluorescence lifetime measurements. The fluorescence decay of the 63mer in cyclohexane and pentane were multiexponential and the estimated lifetimes along with the percentage contributions can be described using a tri-exponential fitting function (in cyclohexane: τ[ns] (x[%]) = 11.0 (13.4), 3.1 (48.1), 0.75 (38.5); in pentane: 15.0 (61.5), 6.6 (29.7), 1.8 (8.8)). In pentane, the CT state has a longer lifetime than in cyclohexane (15 versus 11 ns), and the contribution from the long-lived component is larger. In cyclohexane, the major contributions are from short-lived components. Another possible explanation of the spectral shift is that the radius of the Onsager cavity for the dendrimer is larger in cyclohexane than in pentane. To probe for solvent-dependent size and shape changes of the dendrimer, small-angle scattering experiments (small-angle X-ray scattering (SAXS) and small-angle neutron scattering (SANS)) are underway. The preliminary SANS results indicate that the radius of gyration of **5** is smaller in cyclohexane than in pentane.[19]

Experimental Section

Unless otherwise indicated, all starting materials were obtained from commercial suppliers (Aldrich, Lancaster, Fisher, Mallinckrodt, J. T. Baker, EM Science) and were used as received. Hexane, dichloromethane, and ethyl acetate were distilled before use. All air-sensitive reactions were carried out under nitrogen by using a vacuum line or in a dry box. All monodendrons were prepared by using previously reported procedures [20, 21]. All the compounds were purified by column chromatography and characterized by ^{1}H, ^{13}C NMR spectroscopy, gel permeation chromatography (GPC), high-performance liquid chromatography (HPLC), and mass spectrometry (EI or MALDI).

1: ^{1}H NMR (400 MHz, C_6D_6): δ = 7.82 (d, J = 1.5 Hz, 2H), 7.77 (t, J = 1.5 Hz, 1H), 7.63 (d, J = 1.9 Hz, 4H) 7.50 (t, J = 1.7 Hz, 2H), 7.17 (d, J = 2.9 Hz, 1H) 6.75 (dd, J = 8.9, 3.1 Hz, 1H), 6.42 (d, J = 9.0 Hz, 1H), 3.35 (s, 3H), 3.29 (s, 3H), 1.24 (s, 36H); MS (FAB): m/z calcd for $C_{48}H_{54}O_2$: 662.9; found: 663.3.

2: ^{1}H NMR (400 MHz, C_6D_6): δ = 7.83 (t, J = 1.5 Hz, 2H), 7.79 (d, J = 1.7 Hz, 2H), 7.75 (d, J = 1.7 Hz, 4H), 7.70 (d, J = 1.7 Hz, 8H), 7.62 (t, J = 1.5 Hz, 1H), 7.53 (t, J = 1.7 Hz, 4H),7.25 (d, J = 3.1 Hz, 1H) 6.77 (dd, J = 9.0, 3.2 Hz, 1H), 6.42 (d, J = 9.0 Hz, 1H), 3.38 (s, 3H), 3.29 (s, 3H), 1.24 (s, 72H); MS (FAB): m/z calcd for $C_{96}H_{102}O_2$: 1287.8; found: 1314.

3: ^{1}H NMR (400 MHz, C_6D_6): δ = 7.88 (d, J = 1.5 Hz, 2H), 7.84 (t, J = 1.4 Hz, 4H), 7.81 (d, J = 1.5 Hz, 8H), 7.74 (t, J = 1.5 Hz, 1H), 7.71–7.66 (m, 22H), 7.52 (t, J = 1.9 Hz, 8H), 7.24 (d, J = 3.2 Hz, 1H), 6.77 (dd, J = 9.0, 3.2 Hz, 1H), 6.42 (d, J = 9.1 Hz, 1H), 3.38 (s, 3H), 3.29 (s, 3H), 1.24 (s, 144H); MS (MALDI): m/z calcd for $C_{192}H_{198}O_2$: 2537.7; found: 2535.

4: ^{1}H NMR (400 MHz, C_6D_6) : δ = 7.88 (d, J = 1.5 Hz, 2H), 7.83 (t, J = 1.4 Hz, 8H), 7.81 (d, J = 1.5 Hz, 18H), 7.77 (d, J = 1.5 Hz, 4H), 7.74–7.71 (m, 9H), 7.71–7.66 (m, 36H), 7.52 (t, J = 2 Hz, 16H), 7.22 (d, J = 3.2 Hz, 1H), 6.73 (dd, J = 9.0, 3.1 Hz, 1H), 6.41 (d, J = 9.1 Hz, 1H), 3.38 (s, 3H), 3.28 (s, 3H), 1.24 (s, 288H); MS (MALDI): m/z calcd for $C_{384}H_{390}O_2$: 5037.3; found: 5246.5.

5: ^{1}H NMR (400 MHz, C_6D_6): δ = 7.95–7.65 (m, 157H), 7.52 (t, J = 1.5 Hz, 32H), 7.21 (d, J = 3.2 Hz, 1H), 6.75 (dd, J = 9.0, 3.1 Hz, 1H), 6.73 (dd, J = 9.0, 3.1 Hz, 1H), 6.44 (d, J = 9.1 Hz, 1H), 3.38 (s, 3H), 3.28 (s, 3H), 1.24 (s, 576H); MS (MALDI): m/z calcd for $C_{768}H_{764}O_2$: 10036; found: 10213.

6: MS (MALDI): m/z calcd for $C_{1534}H_{1541}O_2$: 20010; found: 20190.

Fluorescence spectroscopy: Steady-state fluorescence spectra were recorded on a Photon Technology International (PTI) QM-1 fluorometer. The absorbance of the solution for fluorescence measurements was around 0.1 at 310 nm, the excitation wavelength. Fluorescence and excitation spectra were corrected for the wavelength dependence of detector sensitivity and excitation source output. Fluorescence quantum yields were estimated with quinine sulfate in 0.1 N H_2SO_4 as the reference (Φ_{fl} = 0.55). The spectra were recorded by using a 1-cm path length quartz cuvette in the right angle geometry at room temperature. Fluorescence lifetimes were measured on a time-correlated single photon counting fluorimeter (Edinburgh Instruments, model OB9000). The excitation source was a hydrogen flash lamp operated at 40 kHz. The emission was detected at right angle to the excitation light with a Hamamatsu R955 photomultiplier tube (PMT) which was cooled to −22 °C. The response time of the PMT was 2.2 ns. A total of 10000 counts were at the maximum channel. The samples were excited at 310 nm and the decay was monitored at the emission maximum of the respective sample.

Received: December 16, 1996
Revised version: March 3, 1997 [Z9897IE]
German version: *Angew. Chem.* **1997**, *109*, 1706–1709

Keywords: dendrimers · electron transfer · photochemistry · solvatochromism

[1] a) R. M. Hermant, N. A. C Bakker, T. Scherrer, B. Krijnen. J. W. Verhoeven, *J. Am. Chem. Soc.* **1990**, *112*, 1214; b) L. Xiu-Jin, G. S. Beddard, G. Porter, R. S. Davidson, T. D. Whelan, *J. Chem. Soc. Faraday Trans 1* **1982**, *78*, 3467.
[2] J. K. Thomas, *Chem. Rev.* **1980**, *80*, 283.
[3] C. S. P. Sung, R. Mathiesen, *Polymer* **1987**, *28*, 941.
[4] H. J. van Ramesdonk, M. Vos, J. W. Verhoeven, G. R. Möhlmann, N. A. Tissink, A. W. Meesen, *Polymer* **1987**, *28*, 951.
[5] L. W. Jenneskens, H. J. Verhey, H. J. van Ramesdonk, A. J. Witteveen, J. W. Verhoeven, *Macromolecules* **1991**, *24*, 4038.
[6] B. Valeur in *Molecular Luminescence Spectroscopy: Methods and Applications, Part III* (Ed.: S. G. Schulman), Wiley, New York, **1993**.
[7] C. J. Hawker, K. L. Wooley, J. M. J. Fréchet, *J. Am. Chem. Soc.* **1993**, *115*, 4375.
[8] T. H. Mourey, S. R. Turner, M. Rubinstein, J. M. J. Fréchet, C. J. Hawker, K. L. Wooley, *Macromolecules* **1992**, *25*, 2401.
[9] C. J. Hawker, P. J. Farrington, M. E. Mackay, K. L. Wooley, J. M. J. Fréchet, *J. Am. Chem. Soc.* **1995**, *117*, 4409.
[10] A. M. Naylor, W. A. Goddard III, G. E. Kiefer, D. A. Tomalia, *J. Am. Chem. Soc.* **1989**, *111*, 2339.
[11] G. Caminati, N. J. Turro, D. A. Tomalia, *J. Am. Chem. Soc.* **1990**, *112*, 8515.
[12] Generally, the fluorescence maximum of a CT state is estimated from the Lippert–Mataga equation (a)[13, 14], where $\tilde{\nu}_{CT}$ is the fluorescence maximum [cm^{-1}] of the CT state in a given solvent, $\tilde{\nu}_{CT}(0)$ is the fluorescence maximum in the gas phase, μ is the dipole moment of the CT state, h is the Planck's constant, c is the velocity of light in vacuum, ρ is the radius of a spherical cavity in which the molecule fits (Onsager model), and Δf is the polarity parameter which is defined by the dielectric constant (ε) and index of refraction n of the solvent as given in Equation (b).

$$\tilde{\nu}_{CT} = \tilde{\nu}_{CT}(0) - (2\mu^2/hc\rho^3)\Delta f \quad \text{(a)}$$

$$\Delta f = (\varepsilon - 1)/(2\varepsilon + 1) - (n^2 - 1)/(4n^2 + 2) \quad \text{(b)}$$

[13] E. Lippert, *Z. Naturforsch. A* **1955**, *10*, 541.
[14] N. Mataga, Y. Kaifu, M. Koizumi, *Bull. Chem. Soc. Jpn.* **1956**, *29*, 465.
[15] Δf(pentane) = 0.09, Δf(cyclohexane) = 0.10.
[16] S. L. Murov, I. Carmichael, G. L. Hug, *Handbook of Photochemistry*, 2nd ed., Marcel Dekker, New York, **1993**.
[17] N. Anno, R. De Lisi, M. Goffredi, *J. Chem. Soc. Faraday Trans. 1* **1982**, *78*, 3101.
[18] D. W. Brazier, G. R. Freeman, *Can. J. Chem.* **1969**, *47*. 893. *9*, 465.
[19] The authors thank Dr. P. Thiagarajan, Argonne National Laboratory, IL (USA), for the SANS studies. The full details of the SANS results will be published elsewhere.
[20] P. Bharathi, U. Patel, T. Kawaguchi, D. J. Pesak, J. S. Moore, *Macromolecules* **1995**, *28* , 5955.
[21] C. Devadoss, P. Bharathi, J. S. Moore, *J. Am. Chem. Soc.* **1996**, *118*, 9635.

 © VCH Verlagsgesellschaft mbH, D-69451 Weinheim, 1997 0570-0833/97/3615-1635 $ 17.50+.50/0

Columnar Liquid Crystals from Shape-Persistent Dendritic Molecules**

Douglas J. Pesak and Jeffrey S. Moore*

Dendritic molecules of well-defined structure offer special opportunities in materials chemistry.[1] In the area of self-organizing materials, correlations between molecular morphology and macroscopic symmetry are of fundamental as well as practical importance, yet this relationship is poorly understood at this time.[2] The morphology of perfectly branched dendrimers evolves from an open, extended form to a more globular shape, as generation increases.[3] Because of their globular shape, most higher generation dendrimers do not crystallize, although several reports have documented lyotropic and thermotropic liquid crystalline order. This intriguing behavior was first seen by Kim who observed lyotropic phases of hyperbranched[4] polyaramides in *N*-methylpyrrolidone (NMP) solutions.[5] Several groups have since discovered thermotropic liquid crystalline (LC) phases in dendritic materials. Percec et al. prepared a series of hyperbranched polymers based on flexible, branched mesogens that exhibited nematic LC phases resulting from the molecules ability to fold into anisotropic shapes.[6] The corresponding regular dendrimers were also found to be liquid crystalline.[7] Another type of dendritic architecture that displays liquid crystallinity involves functionalization of the periphery with mesogenic groups.[8] The flexibility of the dendritic interior in these systems allows the peripheral mesogens to acquire nematic organization. Recently, Percec et al. used benzylic ether monodendrons to prepare tapered mesogenic architectures functionalized with endo receptors or polymerizable groups at their focal points.[9] These molecules have been shown to organize into hexagonally packed columns in which a slice of the column (that is, one disc) is made of several of the wedge-shaped monodendrons. The monodendrons are suggested as being stacked in a face-to-face manner acting like the protein wedges found in the Tobacco Mosaic Virus. Another interesting recent report describes a "starlike" heptameric triphenylene derivative (a triphenylene mesogen substituted with six other triphenylene mesogens) which exhibited a discotic columnar mesophase.[10] However, the hexagonal cell edge in these materials corresponded to individual triphenylene mesogens rather than the star molecule as a whole (that is, registry of the entire molecule was not achieved).

Our group has been studying shape-persistent dendrimers,[11] which have the potential to behave like disk-shaped objects in early generations. Unlike previously reported liquid crystalline dendrimers, these molecules have the potential to be intrinsically mesogenic[12] and it is of interest to see how such behavior depends on dendrimer parameters like generation number and the type of peripheral group. Shape-persistent dendrimers may provide novel mesogenic architectures including the intriguing possibility of asymmetrically segregated columns and low-symmetry mesophases. This could be realized, for example, from a tridendron in which each of its monodendrons is terminated with three mutually incompatible segments (for example hydrocarbon, oligo(ethylene oxide), and fluorocarbon chains). Three-way demixing within the hexagonal columns might result in spontaneous symmetry reduction from *P6mm* to *P*3. Another architectural possibility unique to dendrimers would involve organizing donor and acceptor segments in concentric shells of a columnar structure. Such architectures may have unusual photoconducting properties (a molecular coaxial cable).[13] With these ideas in mind we developed a new series of columnar liquid crystalline dendrimers based on the stiff, triconnected phenylacetylene monomer.

Three generations of phenylacetylene tridendrons functionalized with isophthalic acid bis-(2-[2-(2-methoxy-ethoxy)-ethoxy]ethyl) esters on the periphery (tetramer **1**, decamer **2**, and 22mer **3**) were prepared by a convergent growth scheme.[14] All intermediates and final products were characterized by ^{1}H and ^{13}C NMR spectroscopy, mass spectrometry (FAB or MALDI[15]), and elemental analysis and shown to be devoid of significant amounts of impurities.[16] In marked contrast to the behavior of the *tert*-butyl capped dendrimers, which decompose without even undergoing a glass transition,[11a] these materials have a pastelike consistency at room temperature with **2** and **3** being more viscous than **1**. All three dendrimers show glass transition temperatures around $-55\,^{\circ}C$ (Figure 1). Two additional reversible transitions are observed for **1** and **2**, while dendrimer **3** exhibits only one reversible transition (isotropization). Molar enthalpies of isotropization increase with generation as expected (Table 1).[17]

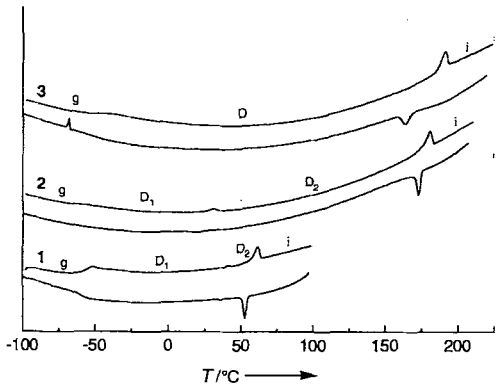

Figure 1. DSC traces recorded during the first cooling and the second heating cycle. The analyses were performed at heating and cooling rates of 20 K min^{-1}.

Optical microscopy between crossed polarizers reveals a birefringent texture up to the isotropization temperature for each dendrimer. Clearing points from both microscopy and differential scanning calorimetry (DSC) are given in Table 1. Slow cooling from the isotropic state on untreated glass reveals textures

Table 1. Transition temperatures [°C] of liquid-crystalline dendrimers **1**–**3**. Transition enthalpies [kJ mol^{-1}] are given in parentheses.

Dendrimer	*M* [kDa]	Clearing point [°C]	Thermal transitions [a] 2nd heating cycle	1st cooling cycle
1	1.520	68	g -58 D_1 41 (0.35) D_2 62 (6.02) i	i 52 D_2 36 D_1 −60 g
2	3.262	199	g -58 D_1 31 (5.52) D_2 181 (28.5) i	i 173 D_2 20 D_1 −65 g
3	6.745	209	g -52 D 191 (69.9) i	i 164 D −53 g

[a] g: glass, D_1: lower temperature discotic mesophase (**1** and **2**), D_2: higher temperature discotic mesophase (**1** and **2**), D: discotic mesophase (**3**), i: isotropic phase.

[*] Prof. J. S. Moore, D. J. Pesak
Department of Chemistry, Materials Science & Engineering
and
Beckman Institute for Advanced Science and Technology
University of Illinois at Urbana-Champaign
Urbana, IL 61801 (USA)
Fax: Int. code +(217)244 8068
e-mail: moore@aries.scs.uiuc.edu

[**] This research was supported by the National Science Foundation (Grant DMR 95-20402), the Office of Naval Research (Grant N00014-94-I-0639), and the DuPont company.

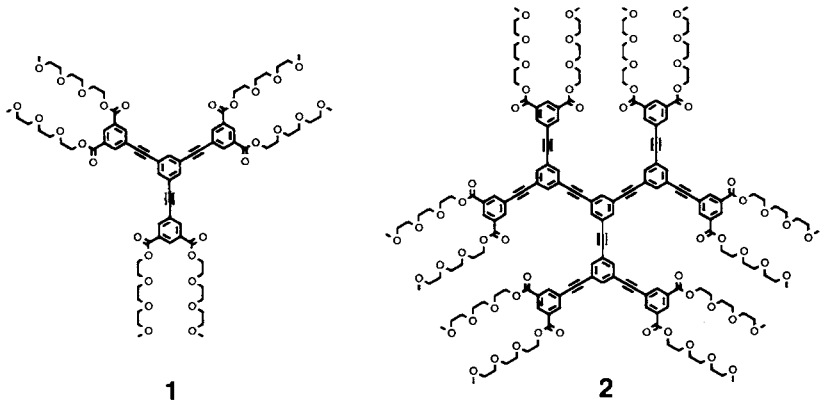

1 2

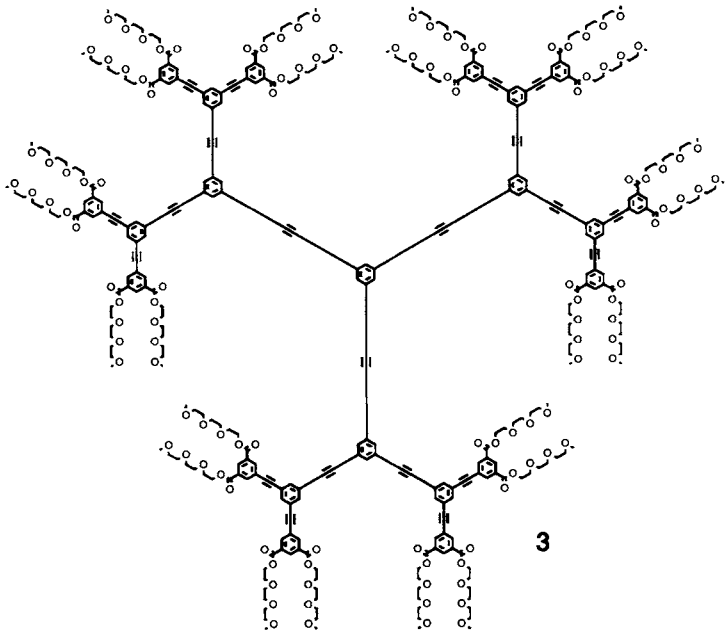

3

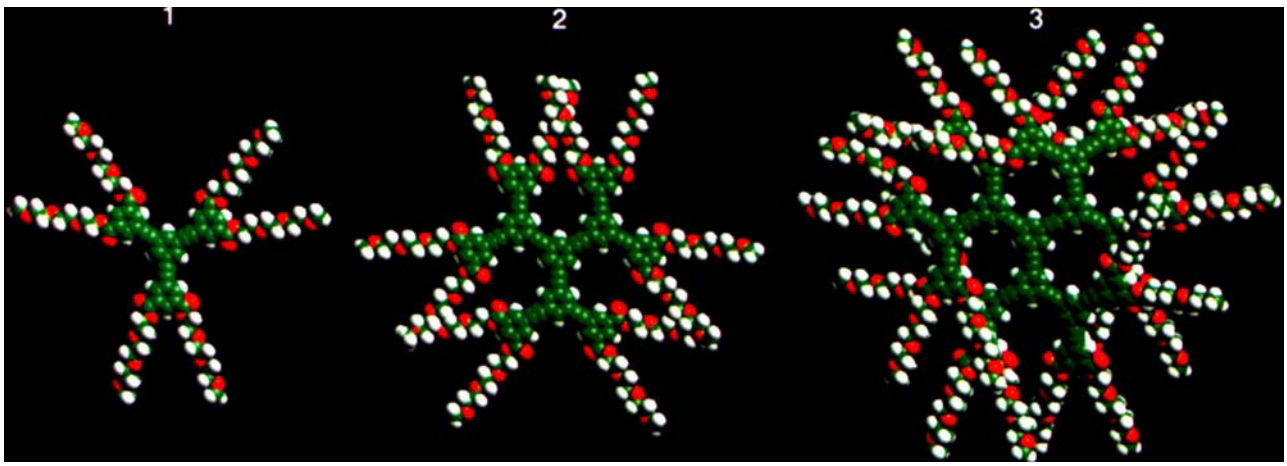

indicative of columnar discotic liquid crystalline phases. Micrographs of dendrimers **1**, **2**, and **3** are shown in Figure 2. Dendrimer **1** displays birefringent patterns of irregular shape along with homeotropically aligned regions shaped as six-pointed stars. A conoscopic image (Figure 2 top, inset) focused on a homeotropic region reveals that the material is uniaxial positive. This observation is consistent with aromatic rings whose normal axes are, on average, oriented parallel to the optic axis. It is interesting that these macroscopically aligned domains appear spontaneously on untreated glass without application of shear or other external forces.[9]

The second-generation dendrimer **2** shows birefringent "broken-fan" textures, while the third-generation dendrimer **3** shows two distinct features (Figure 2 middle and bottom, respectively). Birefringent fiberlike bundles make up most of the observable area of **3**. However, in certain regions, remarkable home-

 © *VCH Verlagsgesellschaft mbH, D-69451 Weinheim, 1997* *0570-0833/97/3615-1637 $ 17.50+.50/0*

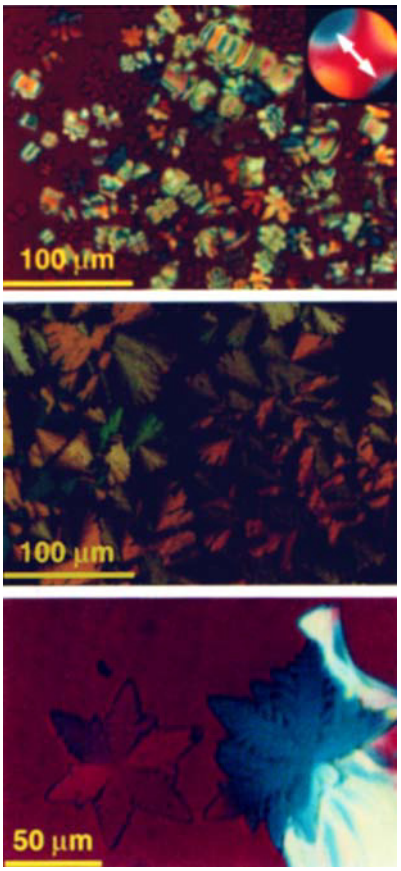

Figure 2. Optical micrographs of **1** at 65 °C (top), **2** at 196 °C (middle), and **3** at 197 °C (bottom) under crossed polarizers. All images were taken from samples slowly cooled from the isotropic melt on untreated glass slides (a cover slip was applied only to sample **3**). The inset (top right) shows a conoscopic image recorded on a homeotropically aligned domain with a quarter waveplate insert. The arrow indicates the direction of the waveplate.

otropically aligned dendritic hexagonal patterns appear that resemble snowflake morphologies. These domains are not crystalline solids as can be demonstrated by their ability to flow when sheared. Rheological studies will be required to fully characterize the fluid properties of the liquid crystilline phases. Preliminary studies on the next higher generation (46mer) indicate that it is amorphous.[18]

Wide-angle X-ray diffraction patterns of samples recorded at room temperature are shown in Figure 3 which correspond to

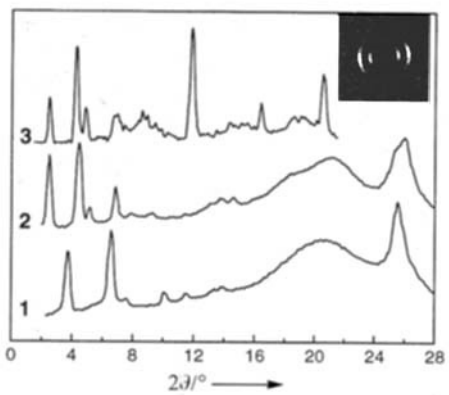

Figure 3. Wide-angle X-ray diffraction patterns of dendrimers **1**–**3** recorded at room temperature with $Cu_{K\alpha}$ X-ray radiation. The inset shows a Laue diffraction image of a melt-drawn fiber of **1**. The fiber axis is vertical.

the D_1 phases of **1** and **2**[19] and the D phase of **3**. The observed reflections can be indexed to hexagonal unit cells with a = 26.95 Å, 39.80 Å, and 41.65 Å, respectively (Table 2). These cell edges are consistent with the dimensions of **1**–**3** as calculated from molecular models (see below). The agreement between calculated and observed Bragg reflections is very good for **1** and **2**. However, for **3** the agreement is lower and additional data will be needed to rule out the possibility of lower symmetry.[20]

Table 2. Bragg reflections and corresponding calculated and observed d spacings [Å].

hkl	**1**		**2**		**3**	
	obs [a]	calcd [b] a = 26.95 Å	obs [a]	calcd [b] a = 39.80 Å	obs [a]	calcd [b] a = 41.65 Å
100	23.70	23.34	35.46	34.47	35.26	36.07
110	13.50	13.48	19.91	19.90	20.82	20.83
200	11.67	11.67	17.17	17.23	18.17	18.04
210	8.73	8.82	12.88	13.02	12.74 br	13.63
300	7.68	7.78	11.22	11.49		12.02
220	6.70	6.74			10.13 br	10.41
310	6.38	6.47				10.00

[a] All data recorded at room temperature with $Cu_{K\alpha}$ X-ray radiation. [b] Hexagonal unit cell assumed.

The sharpness of the diffraction data for **3** seems to indicate a remarkably high degree of order. Broad reflections with d spacings of approximately 3.5 Å are present in the diffraction patterns of both **1** and **2**. This is typical of van der Waals separation for π-stacked aromatic molecules. Molecular modeling suggests that both **1** and **2** can adopt completely planar conformations without experiencing unfavorable nonbonded contacts that would force the structure into a more globular shape.[21] For both **1** and **2**, the fraction of the hexagonal unit cell (c axis length of 3.5 Å) occupied by the molecule is about 0.60, consistent with that of typical liquids. In the case of **3**, however, molecular modeling suggests that a completely planar conformation is not possible. As such, one would expect the c axis length to increase to accommodate the increased thickness of the mesogen. Broad reflections are observed with d spacings of 4.3 (weak) and 7.5 Å (strong). A unit cell with a c axis length of 4.3 Å is much too small to accommodate a single molecule. The van der Waals volumes of one molecule occupies an unreasonable 93% of such a cell. In contrast, the van der Waals volumes of one molecule occupies 53% of a unit cell with a c axis length of 7.45 Å. This calculation leads us to believe the c axis elongates to accommodate the nonplanar structure. Although the X-ray diffraction data is consistent with a hexagonal lattice, we cannot rule out the possibility of other lower symmetry unit cells such as the orthorhombic or monoclinic lattices at this time. High-resolution X-ray data on oriented fibers will help resolve this issue. Preliminary diffraction data on a melt drawn fiber of **1** shows that the columnar axis aligns with the fiber direction as shown in the Laue image (Figure 3, inset).

The data presented here suggests that three generations of phenylacetylene tridendrons functionalized with isophthalic acid bis-(2-[2-(2-methoxy-ethoxy)-ethoxy]ethyl) esters on their peripheries exhibit liquid crystalline mesophases. Mesophase behavior is displayed over a wide temperature range (ca. 250 K for **2** and **3**). Optical microscopy and X-ray diffraction support a hexagonal columnar discotic phase. These compounds reveal an intriguing connection between molecular morphology and macroscopic organization. Further studies to probe the nature of the low-energy intermediate phase transitions of **1** and **2** are currently under way. We are also exploring the effect of unsym-

 © VCH Verlagsgesellschaft mbH, D-69451 Weinheim, 1997 0570-0833/97/3615-1638 $ 17.50+.50/0

metrical peripheral group substitution on mesophase behavior in order to understand the factors which govern organization of phenylacetylene dendrimers with an interest toward the preparation of low-symmetry columnar phases.

Received: January 31, 1997 [Z10062IE]
German version: *Angew. Chem.* **1997**, *109*, 1709–1712

Keywords: dendrimers · liquid crystals · mesophases · self-organization

[1] For recent reviews see: a) G. R. Newkome, C. N. Moorefield, F. Vögtle, *Dendritic Molecules: Concepts, Syntheses, Perspectives*, VCH, Weinheim, **1996**; b) J. M. J. Fréchet, C. J. Hawker, I. Gitsov, J. W. Leon, *J. Macromol. Sci. Pure Appl. Chem.* **1996**, *A33*, 1399–1425; c) D. A. Tomalia, P. R. Dvornic, *Curr. Opin. Colloid Interface Sci.* **1996**, *1*, 221–235.

[2] J. S. Moore, *Curr. Opin. Solid State Mater. Sci.* **1996**, *1*, 798–805.

[3] a) C. J. Hawker, K. L. Wooly, J. M. J. Fréchet, *J. Am. Chem. Soc.* **1993**, *115*, 4375–4376; b) A. M. Naylor, W. A. Goddard III, G. E. Kiefer, D. A. Tomalia, *ibid.* **1989**, *111*, 2339–2341. c) D. Farin, D. Avnir, *Angew. Chem.* **1991**, *103*, 1409–1410; *Angew. Chem. Int. Ed. Engl.* **1991**, *30*, 1379–1380.

[4] A hyperbranched polymer refers to a dendritic macromolecule prepared by a one-step polymerization of an AB_x monomer ($x \geq 2$).

[5] Y. H. Kim, *J. Am. Chem. Soc.* **1992**, *114*, 4947–4948.

[6] a) V. Percec, M. Kawasumi, *Macromolecules* **1992**, *25*, 3843–3850; b) V. Percec, P. Chu, M. Kawasumi, *ibid.* **1994**, *27*, 4441–4453.

[7] V. Percec, P. Chu, G. Ungar, J. Zhou, *J. Am. Chem. Soc.* **1995**, *117*, 11441–11454.

[8] a) S. A. Ponomarenko, E. A. Rebrov, A. Y. Bobrovsky, N. I. Boiko, A. M. Muzafarov, V. P. Shibaev, *Liq. Cryst.* **1996**, *21*, 1–12. b) K. Lorenz, D. Holter, B. Stuhn, R. Mülhaupt, H. Frey, *Adv. Mater.* **1996**, *8*, 414–416; c) U. Stebani, G. Lattermann, M. Wittenberg, J. H. Wendorff, *Angew. Chem.* **1996**, *108*, 1941–1943; *Angew. Chem. Int. Ed. Engl.* **1996**, *35*, 1858–1861.

[9] V. Percec, G. Johansson, G. Ungar, J. Zhou, *J. Am. Chem. Soc.* **1996**, *118*, 9855–9866, and references therein.

[10] T. Plesnivy, H. Ringsdorf, P. Schuhmacher, U. Nütz, S. Diele, *Liq. Cryst.* **1995**, *18*, 185–190.

[11] a) Z. Xu, M. Kahr, K. L. Walker, C. L. Wilkins, J. S. Moore, *J. Am. Chem. Soc.* **1994**, *116*, 4537–4550; b) T. Kawaguchi, K. L. Walker, C. L. Wilkins, J. S. Moore, *ibid.* **1995**, *117*, 2159–2165.

[12] By "intrinsically mesogenic" we mean that liquid crystallinity is a property of the molecule as a whole rather than the result of catenation of individual mesogenic monomer units.

[13] C. F. van Nostrum, *Adv. Mater.* **1996**, *8*, 1027–1030.

[14] a) C. J. Hawker, J. M. J. Fréchet, *J. Chem. Soc. Chem. Commun.* **1990**, 1010–1013. b) C. J. Hawker, J. M. J. Fréchet, *J. Am. Chem. Soc.* **1990**, *112*, 7638–7647. c) K. L. Wooly, C. J. Hawker, J. M. J. Fréchet, *J. Chem. Soc. Perkin Trans. 1* **1991**, 1059–1076; d) T. M. Miller, T. X. Neenan, *Chem. Mater.* **1990**, *2*, 346–349; e) E. W. Kwock, T. M. Miller, T. X. Neenan, *ibid.* **1991**, *3*, 775–777; f) T. M. Miller, T. X. Neenan, R. Zayas, H. E. Bair, *J. Am. Chem. Soc.* **1992**, *114*, 1018–1025; g) J. S. Moore, Z. Xu, *Macromolecules* **1991**, *24*, 5893–5894.

[15] K. L. Walker, M. S. Kahr, C. L. Wilkins, Z. Xu, J. S. Moore, *J. Am. Soc. Mass Spectrom.* **1994**, *5*, 731–739.

[16] A detailed description of the synthesis is in preparation.

[17] Enthalpies of isotropization of other discotic mesogens range from 0.8 to 20.1 kJ mol^{-1}. a) S. Chandrasekhar, B. K. Sadashiva, K. A. Suresh, *Pramana* **1977**, *9*, 471–480; b) C. Destrade, M. C. Mondon, J. Malthete, *J. Phys. (Paris), Colloq. C3* **1979**, *40*, 17–21; c) J. Billard, J. C. Dubois, H. H. Tihn, A. Zann, *Nouv. J. Chim.* **1978**, *2*, 535–540.

[18] Preliminary microscopy studies under crossed polarizers of the fourth generation (46mer) show an initial birefringent texture. When heated, the sample shows a clearing point; however, upon cooling, no birefringent texture reforms down to room temperature. The original birefringence could be caused by mechanical stress within the sample. Differential scanning calorimetry (DSC) shows no observable phase transitions. X-ray diffraction shows only amorphous characteristics. This behavior should be viewed as preliminary since the MALDI mass spectrum reveals the presence of appreciable amounts of defective dendritic species which may affect possible mesophase behavior.

[19] While compound **2** does possess a phase transition at about 30 °C, it is unlikely that the X-ray diffraction data is a composite of two phases. DSC shows that a sample of **2** heated from room temperature does undergo this phase transition, thus X-ray diffraction data is of the D_1 phase.

[20] We have initially assigned D_1 (**1** and **2**) and D (**3**) to the ordered hexagonal discotic phase (D_{ho}) and D_2 to the disordered hexagonal discotic phase (D_{hd}). X-ray diffraction data of the D_2 phase is needed, however to verify the assignment. C. Destrade, H. H. Tinh, H. Gasparoux, J. Malthete, A. M. Levelut, *Mol. Cryst. Liq. Cryst.* **1981**, *71*, 111–135.

[21] Molecular modeling was performed on a Silicon Graphics Indigo workstation using MSI's Quanta and Cerius^2 software packages.

Designing a Solid Catalyst for the Selective Low-Temperature Oxidation of Cyclohexane to Cyclohexanone**

Thomas Maschmeyer,* Richard D. Oldroyd, Gopinathan Sankar, John M. Thomas,* Ian J. Shannon, John A. Klepetko, Anthony F. Masters, James K. Beattie, and C. Richard A. Catlow

The catalytic activation, especially partial oxidation, of alkanes constitutes one of the major challenges of present-day chemistry; and the conversion of cyclohexane to cyclohexanone is among the principal target reactions since the latter is used as feedstock in several industrial processes including the production of nylon from ε-caprolactam and adipic acid. There have been numerous fundamental studies of the role of cobalt acetate as catalysts for such processes and[1] it is now recognized that cobalt(III) acetate exists as a number of distinct species,[2] both in solution and in the solid-state. Although stable alkylperoxo complexes of Co^{III} are formed in these systems there is also unmistakable evidence for free radicals such as $RO_2^{\bullet}$ and $RO^{\bullet}$ in the reaction, the occurrence of which is symptomatic of autooxidation. Homogeneous catalytic processes with $Co(OAc)_3$ suffer from the generation of significant quantities of unwanted by-products such as alkyl acetates, other ketones, cyclohexylidene diacetate, alkyl chlorides, and occasionally, cyclohexylmethanol.[1d, 3] To confer greater stability upon the homogeneous Co^{III} acetate catalyst it is also necessary to employ, for reasons that are not entirely understood, either acetic acid or trifluoro- (or trichloro-) acetic acid as solvent for the reactant mixture and bromides are often used as promoters.

With the aim of arriving at a cleaner, more efficient catalytic system for the production of cyclohexanone from cyclohexane, and also of gaining deeper insights into the nature of the catalytically active centers by in-situ EXAFS studies (EXAFS = extended X-ray absorption fine structure), we have designed a new catalyst that entails harnessing the advantages of homogeneous organometallic catalysis on the one hand and of a high-area, well-defined (MCM-41) mesoporous silica support on the other.[4]

Although there is still considerable debate[5] about the mechanism of the oxidation of cyclohexane in the presence of Co^{III}, Mn^{III}, and Ce^{IV} salts in acetic acid or other solvents, and even more about the nature of the active sites, our point of departure in this work is the earlier observation[6] that several oxo-centered trimeric cobalt(III) acetates (coordinated with pyridine)[7] exhibit much greater activity in selectively oxidizing the tertiary C–H bond in adamantane than their dimeric analogues.

[*] Dr. T. Maschmeyer, Prof. Sir J. M. Thomas, Dr. R. D. Oldroyd, Dr. G. Sankar, I. J. Shannon, Prof. C. R. A. Catlow
Davy Faraday Research Laboratory
The Royal Institution of Great Britain
21 Albemarle Street, London W1X 4BS (UK)
Fax: Int. code +(171)629-3569
e-mail: thomas@ri.ac.uk

J. A. Klepetko, Prof. A. F. Masters, Prof. J. K. Beattie
School of Chemistry, Inorganic Division
The University of Sydney
NSW 2006 (Australia)

[**] This work was supported by a ROPA award and a rolling grant from the Engineering and Physical Science Research Council (UK) and grants from the Australian Research Council and ANSTO (Australia). We thank the CLRC for the synchrotron beam time and other facilities at Daresbury Laboratory. We also gratefully acknowledge assistance with the solid-state NMR spectroscopy by Dr. Abil Aliev and useful initial discussions with Dr. Fernando Rey.

Table 1. Catalyses with the cobalt complex **1** immobilized on MCM-41.

Catalyst support	Co [wt %]	Si:Co	t [h]	Conversion [%] [a]	TOF [b]	Selectivity [%] [c]	Cyclohexanone: cyclohexanol	Life time [h]
nonderivatized	0.376	210	4	3.7	89	85	0.6	< 48
			24	7.6	63	89	0.6	
MCM 41, glycine-functionalized through bromoalkyl tethers	0.201	300	4	4.3	352	84	0.9	> 96 [d]
			24	11.9	230	89	1.5	
			4 days	38.1	216	95	3.3	

[a] Cyclohexane (9.5 mL), TBHP (10 mL), and mesitylene (0.5 mL; internal standard) at 70 °C are required for 150 mg of catalyst. [b] In mol cyclohexane/(mol catalyst per hour). [c] Based on cyclohexanone and cyclohexanol. [d] The experiment was stopped after four days.

The apertures of the MCM-41 samples prepared by us[8] are close to 30 Å (determined by high-resolution scanning transmission electron microscopy and adsorption isotherms) and readily permits ingress of the monohydroxycobalt complex **1** (known

$[Co_3(\mu_3\text{-}O)(OAc)_5(\mu_2\text{-}OH)(py)_3]PF_6$ **1**

to substitute the hydroxyl group for other ligands)[9] which we selected for immobilization inside the channels of the MCM-41 mesoporous silica.[10] It is possible to employ various routes to effect immobilization; anchoring to the surface directly or using surfaces functionalized with, for example, alkylcarboxylic acids. Each of these routes yields a catalyst for the selective oxidation of cyclohexane to cylcohexanone. However, distinct differences are observed in their respective turnover frequencies (TOF), lifetimes, and selectivities (Table 1). The catalysis reported here was effected in an essentially solvent-free fashion: the sacrificial oxidant *tert*-butyl hydroperoxide (TBHP) and the reactant cyclohexane form a miscible liquid and each is consumed to yield cyclohexanone, cyclohexanol, other minor amounts of by-products (dicyclohexyl ether, dicyclohexyl peroxide, and *tert*-butyl cyclohexyl peroxide), and *tert*-butyl alcohol (from TBHP).[11]

In our first attempt at immobilization we reacted the cobalt complex **1** with partially dehydrated siliceous MCM-41. The EXAFS spectrum after immobilization showed that there was virtually no change in the structure of the cobalt complex, indicating either substitution of the bridging hydroxide by a surface silanol or physisorption brought about by interaction of the surface with the cationic cluster. Catalytic tests showed that after 24 h 7.6% of the available cyclohexane was converted with a selectivity of about 89% to cyclohexanol and cyclohexanone. The catalyst lifetime, however, was less than 48 h (Table 1).[12] This limited lifetime is most likely due to mobility of the cobalt clusters on the surface, giving rise to cluster–cluster and other unfavorable interactions at the interior surface as well as some leaching indicated by slight discoloration of the solution.

Working on the principle that immobilization at a carboxyl-functionalized surface (that is envisaging the replacement of the bridging hydroxyl by a carboxyl group) may produce a potentially more stable catalyst, we proceeded to functionalize the MCM-41 surfaces with a 3-bromopropyltrichlorosilane tether which we then derivatized by reaction with glycine. The virtual lack of solubility of glycine in solvents other than water means that the efficiency of the reaction between the amine part of the glycine and the bromoalkyl group could be expected to be low owing to the interaction of water with the amine.[13] However, this would as a side-effect provide a means to ensure a high dispersion of the cobalt complex which might aid stability (and, hence, longevity) by reducing possible interactions between cobalt clusters. Additionally, the nonderivatized bromoalkyl groups might act as a potential promoter echoing the use of bromide in commercial processes.

Catalytic tests established that after an initial TOF of around 352 mol cyclohexane/(mol catalyst per hour) a steady TOF of around 216 could be sustained for at least four days. The true heterogeneity of the catalyst was also examined by separating it by filtration and establishing that the filtrate displayed no further activity under the same reaction conditions. Additionally, no leaching could be detected (within experimental error) when comparing the elemental analysis results of the catalyst before and after reaction. No induction period could be observed (at a time resolution of 5 min); after an initial exponential behavior, the catalyst continued to produce cyclohexanone essentially in a linear fashion. At the outset more cyclohexanol than cyclohexanone is produced, but after about six hours cyclohexanone production is predominant, an equilibrium between cyclohexanol generation and consumption to form the ketone being reached after about 12 h (Figure 1).

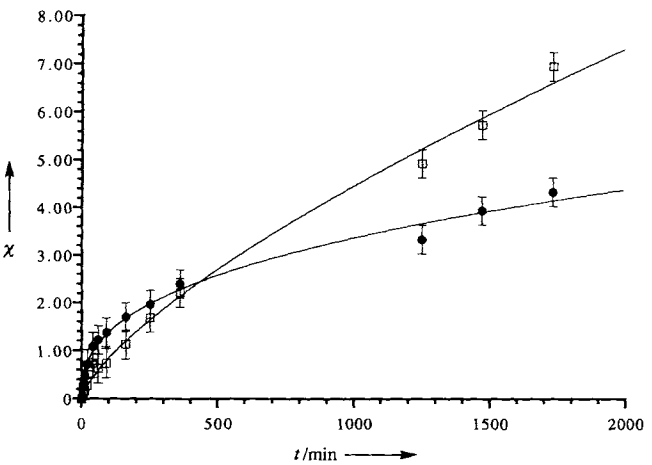

Figure 1. Plot of the percentage conversion x of cyclohexane into cyclohexanol (•) and cyclohexanone (□) against time t with 150 mg catalyst.

As expected, addition of extra TBHP after 12 h increased the oxidation rates, thus showing the potential for rate control (that is stabilization) by drip-feeding the reactants. Small amounts of the oxygenated by-products already mentioned (totalling no more than 5% of the converted cyclohexane) are also generated; however, this compares well with the 11% for the nonfunctionalized support. Hence, there is a clear advantage associated with the use of functionalized MCM-41 in terms of lifetime, TOF, and ultimate selectivity.[14] We believe this may be explained in terms of the improved isolation of the active centers achieved by the functionalization of the surface.

Additionally, in-situ X-ray absorption spectroscopy using synchrotron radiation[15a] (in what is to our knowledge the first report of such a type of experiment) enabled the detailed atomic

 © VCH Verlagsgesellschaft mbH, D-69451 Weinheim, 1997 0570-0833/97/3615-1640 $ 17.50+.50/0

environment of the active cobalt complex to be determined both prior to and during the course of the solid–liquid heterogeneous catalysis at realistic temperatures under continuous flow using a novel liquid/solid cell.[15b] The liquid collected was analyzed by GC/MS to confirm catalytic activity at the point of measurement. Figure 2 shows the EXAFS spectrum (and associated Fourier transform) of the active catalyst and Table 2 contains the relevant structural parameters.

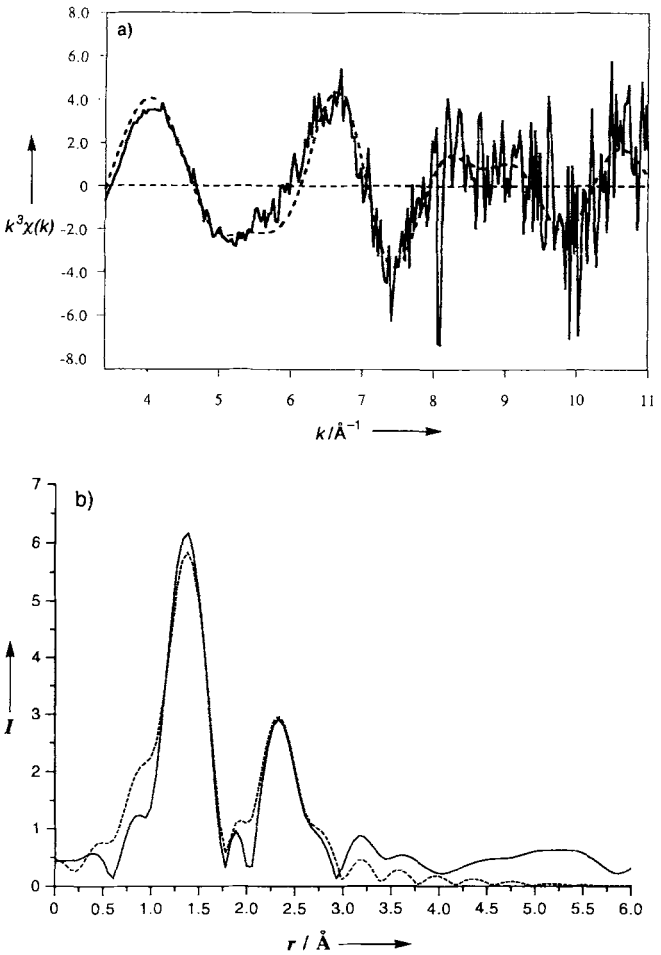

Figure 2. a) EXAFS of the active catalyst immobilized on glycine-functionalized MCM-41. b) Associated Fourier transform; solid line: experimental data, broken line: calculated data.

Upon reaction of **1** with the glycine-functionalized MCM-41, the asymmetric Co_3 unit rearranged into a symmetric one, that is the Co–Co distances changed from 2.80 Å and 3.17 Å to 3.13 Å for both Co–Co pairs (Table 2). This is readily explicable by postulating the replacement of the bridging OH group in **1** with the COOH group of the glycine tether, yielding essentially three equal coordination environments for the cobalt atoms. The structure of a homogeneous analogue has recently been determined by using single-crystal X-ray diffraction data and compares extremely well.[16]

Table 2. Local structural parameters of the complex **1** derived by Co K-edge EXAFS spectroscopy.

Cobalt cluster	Scatterer	N	r [Å]	σ^2 [Å^2]
before immobilization [a]	O [b]	6.00	1.90	0.002
	Co	0.66	2.80	0.003
	C	5.66	2.92	0.004
	Co	1.33	3.17	0.003
	O	3.33	3.26	0.004
before catalysis	O [b]	5.98	1.88	0.004
	C	6.04	2.82	0.002
	Co	1.63	3.13	0.004
	O	4.12	3.27	0.004
during catalysis	O [b]	5.37	1.87	0.007
	C	5.51	2.80	0.010
	Co	1.65	2.78	0.011
	O	3.02	3.07	0.010

[a] Deviation from distances derived from the crystal structure analysis are within experimental error (±0.03 Å). [b] Oxygen and nitrogen shells were averaged and treated as one shell.

Furthermore, in-situ EXAFS measurements during the catalysis of the glycine-immobilized catalyst revealed noteworthy structural changes (Scheme 1). The major feature is a contraction in the Co–Co distances from 3.13 Å to 2.84 Å, indicating a significant structural rearrangement in the complex. Dimitrou et al. have reported an oxo-centered trimeric cobalt acetate system that displays very similar Co–Co distances (average 2.81 Å) to the ones found in our active catalyst.[17] In their complex, however, three of the acetate groups have been displaced by bridging hydroxide groups, giving rise to the shorter distances. This may imply the presence of similarly bridging oxygen atoms in the catalytic species, which could arise from rearrangement of the μ_2-acetate groups due to the interactions with substrate molecules or, more likely, from the peroxide present in the reaction mixture (Scheme 1). The simultaneous presence of bridging hydroxide and some bridging peroxide or other organic oxide is consistent with the slightly higher than expected coordination number of the shell at 3.07 Å. For a trimer in which three of the acetate groups have been replaced by hydroxyl groups, only two oxygen atoms at around 3.1 Å would be expected; however, about three are observed. Since the distance to a carbon atom, for example in a bridging alkoxide group, is also about 3.1 Å, the larger coordination number may indicate the presence of such a species (Figure 3).

^{29}Si MAS NMR spectroscopy (MAS = magic angle spinning) revealed a significant perturbation in the ^{29}Si NMR spectrum of nonderivatized MCM-41 after immobilization of **1**, indicating a strong interaction between the complex and the surface. However, cross polarization (CP) MAS NMR spec-

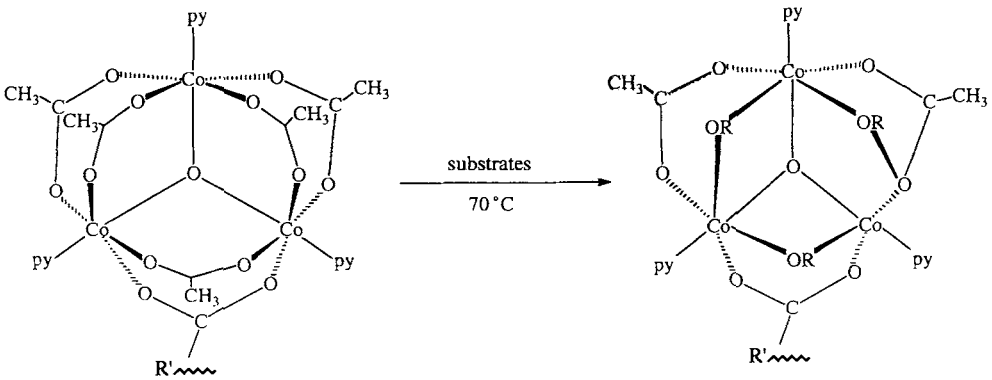

Scheme 1. Structure of the cobalt complex before catalysis (left) and of the active catalyst (right). py = pyridine, R = H, *t*BuOO, alkyl; R′ = alkyl tether.

 © VCH Verlagsgesellschaft mbH, D-69451 Weinheim, 1997 0570-0833/97/3615-1641 $ 17.50+.50/0

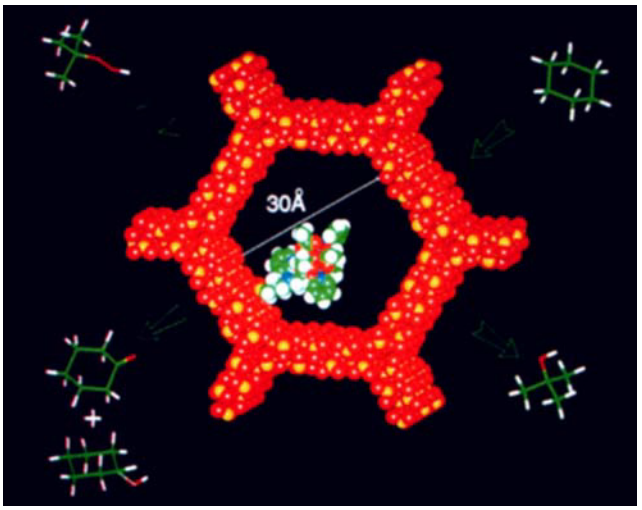

Figure 3. Proposed structure of the active catalyst (center) as well as the starting materials (top) and end products (bottom) of the oxidation of cyclohexane with *tert*-butyl hydroperoxide and Co^{III}-modified MCM41 as catalyst.

troscopy could not detect the presence of the cobalt acetate (the acetate resonances) for either catalyst, but this may well be due to a reduction of one of the diamagnetic Co^{III} centers to a paramagnetic Co^{II} center; a fact which could, incidentally, explain the fate of the PF_6^- ion.

The identification of the active trimeric cobalt allows not only further rational design of improved catalysts, but also provides a well-defined starting point for experimental and computational studies on the mechanism.

Experimental Section

Preparation of glycine-functionalized MCM-41: MCM-41 (1 g) was dehydrated under vacuum at 200 °C for 2 h and was then suspended in diethyl ether (30 mL). Me_2SiCl_2 (0.017 mL) was added and the suspension was left to stir for one hour. The solvent was then removed under vacuum. The solid was resuspended in dry chloroform (30 mL) and the suspension cooled in an isopropyl alcohol/liquid nitrogen slurry bath. $Cl_3Si(CH_2)_3Br$ (0.6 mL) was slowly added, and the mixture left to stir until it had warmed to room temperature. The resulting suspension was left to stir for a further 16 h. The solid was then separated by filtration, washed with chloroform (8 × 25 mL), suspended in 30 mL of an aqueous solution containing glycine (0.1 g) and stirred for 16 h after which it was separated by filtration, washed with water (150 mL) and then diethyl ether (100 mL).

Immobilization of 1: The same conditions were used for both supports (nonderivatized and glycine-derivatized MCM-41). The support (0.5 g) was suspended in a solution of **1** (50 mg) in dichloromethane (30 mL). The suspension was left to stir for 16 h after which the solid was separated by filtration and washed until the washings were colorless (usually around 200 mL dichloromethane). The catalysts were then washed by Soxhlet extraction in dichloromethane for 8 h.

EXAFS measurements: The EXAFS data were recorded at the Daresbury SRS facility on station 8.1 and analyzed with the XFIT (WIN95) and EXCUR V92 suites of programs [18]. The station was equipped with a Si(220) monochromator, and data were collected in fluorescence mode using a thirteen-element Canberra fluorescence detector. A powdered sample of each catalyst studied was pressed into a self-supporting wafer, and mounted into an in-situ reaction cell through which the reactant mixture (of cyclohexane and *tert*-butyl hydroperoxide) was passed by using a syringe driver. Heating to the required temperature was achieved by a jet of hot air directed onto the center of the sample. Details of the cell design have been published [15b]. Spectra were recorded both before and during the catalysis, in which the sample was heated to about 60 °C and the reactants were passed through the cell at a rate of 0.1 mL min^{-1} and the system allowed to stabilize for one hour before measurement (normal X-ray absorption spectroscopy, aquisition time per scan: 45 min). The reaction products were in all cases collected for subsequent analysis by GC/MS.

Received: September 23, 1996
Revised version: March 14, 1997 [Z9580IE]
German version: *Angew. Chem.* **1997**, *109*, 1713–1716

Keywords: cobalt · EXAFS spectroscopy · heterogeneous catalysis · mesoporosity · oxidations

[1] a) N. M. Emanuel, Z. K. Maizus, I. P. Skibida, *Angew. Chem.* **1969**, *81*, 91; *Angew. Chem. Int. Ed. Engl* **1969**, *8*, 97; b) G. W. Parshall, *Homogeneous Catalysis: The Application of Catalysis by Soluble Transition Metal Complexes*, Wiley, New York, **1980**; c) E. P. Talsi, V. D. Chinakov, V. P. Balenko, V. N. Sidelnikov, K. I. Zamaraev, *Molecular Catalysis*, Wiley, New York, **1980**; d) R. A. Sheldon, J. K. Kochi, *Metal Catalysed Oxidation of Organic Compounds*, Academic Press, New York, **1981.**

[2] a) A. B. Blake, J. R. Chipperfield, S. Lau, D. E. Webster, *J. Chem. Soc. Dalton Trans.* **1990**, 3719; b) C. F. Hendriks, H. C. A. van Beek, P. M. Heertjes, *Ind. Eng. Chem. Prod. Res. Dev.* **1979**, *18*, 43; c) W. Partenheimer, R. K. Gipe in *Catalytic Selective Oxidation* (Eds.: S. T. Oyama, J. W. Hightower), ACS Symp. Ser. 523, **1993**, 81.

[3] a) A. Onopchenko, J. G. D. Schultz, *J. Org. Chem.* **1975**, *40*, 3338; b) J. K. Kochi, *Organometallic Mechanisms and Catalysis*, Academic Press, New York, **1978**.

[4] Mesoporous materials readily permit the combination of organometallic surface chemistry with the principle of shape-selectivity generally associated with microporous zeolites and the results from this initial study of cyclohexane might possibly be extended to applications where shape-selectivity is important.

[5] a) J. K. Kochi, R. T. Tang, T. Bernath, *J. Am. Chem. Soc.* **1973**, *95*, 7114; b) P. J. Andrulis, M. J. S. Dewar, T. Dietz, R. L. Hunt, *ibid.* **1966**, *88*, 5473; c) W. S. Trahanovsky, D. W. Brixius, *ibid.* **1973**, *95*, 6778.

[6] A. F. Masters, J. K. Beattie, personal communication.

[7] S. Uemura, A. Spencer, G. Wilkinson, *J. Chem. Soc. Dalton Trans.* **1973**, 2565.

[8] F. Rey, G. Sankar, T. Maschmeyer, J. M. Thomas, R. G. Bell, G. N. Greaves, *Top. Catal.* **1996**, *3*, 121.

[9] C. E. Sumner, Jr., G. R. Steinmetz, *Inorg. Chem.* **1989**, *28*, 4290.

[10] a) J. S. Beck, J. C. Vartuli, *Curr. Opin. Solid State Mater. Sci.* **1996**, *1*, 76; b) Q. Huo, R. Leon, P. M. Petroff, G. D. Stucky, *Science* **1995**, *268*, 1324.

[11] a) This approach (results were calibrated by using mesitylene as internal standard) was deemed necessary for the in-situ X-ray absorption spectroscopy (XAS) experiments as the TOF using the flow system were anticipated to be low and appropriate chlorinated solvents interfere with the XAS measurements. b) Reaction conditions: TBHP (10 mL), cyclohexane (9.5 mL), mesitylene (0.5 mL; internal standard), catalyst (150 mg) stirred in a batch reactor at 70 °C under argon. Up to 20 aliquots of 0.1 mL were withdrawn for analysis during a catalysis run. The MCM-41 was initially exposed to a small amount of the reactive dichlorodimethylsilane with the aim of functionalizing the majority of the silanol groups on the external surface, assuming a faster rate of reaction for the external compared to the internal surface. Hence, to ensure that the catalyst was present predominantly on the inside of the MCM-41 channels, the MCM-41 was treated with the various alkyl tethers only after this pretreatment. This procedure has been shown by scanning transmission electron microscopy to yield the desired effect in related systems (unpublished results).

[12] The kinetic profile showed no detectable induction period at a resolution of 5 minute time steps and behaved in a typical exponential fashion.

[13] From the microanalysis the ratio of bromide tether to tethered cobalt is 100:1, NMR experiments aimed at trying to identify the glycine-derived tether were not sensitive enough to conclusively pick up the glycine-part, as can be expected at such low loadings.

[14] The increase in the selectivity of the catalyst system with time can be explained by the observation that the by-products dicyclohexyl peroxide and cyclohexyl *tert*-butyl peroxide might both decompose to cyclohexanone and that the by-products might react further, disappearing in the base-line. Due to the solvent-free conditions no full mass balance was attempted.

[15] a) J. M. Thomas, G. N. Greaves, *Science* **1994**, *265*, 1675; b) J. M. Thomas, I. J. Shannon, G. Sankar, T. Maschmeyer, M. Sheeky, D. Madill, A. Waller, *Catal. Lett.* **1997**, *44*, 23.

[16] J. K. Beattie, T. W. Hambley, J. A. Klepetko, A. F. Masters, P. Turner, *Polyhedron* **1996**, *15*, 2141.

[17] K. Dimitrou, K. Folting, W. E. Streib, G. Christou, *J. Am. Chem. Soc.* **1993**, *115*, 6432.

[18] a) XFIT (WIN95): P. J. Ellis, H. C. Freeman, *J. Synchrotron Radiat.* **1995**, *2*, 190; b) EXCURV92-Program: N. Binstead, J. W. Campell, S. J. Gurman, P. Stephenson, SERC Daresbury Laboratories, **1992.**

 © VCH Verlagsgesellschaft mbH, D-69451 Weinheim, 1997 0570-0833/97/3615-1642 $ 17.50+.50/0

^{13}C and ^{139}La NMR Studies of $La_2@C_{80}$: First Evidence for Circular Motion of Metal Atoms in Endohedral Dimetallofullerenes**

Takeshi Akasaka,* Shigeru Nagase,* Kaoru Kobayashi, Markus Wälchli, Kazunori Yamamoto, Hideyuki Funasaka, Masahiro Kako, Tsutomu Hoshino, and Tomoki Erata

Endohedral metallofullerenes have attracted special interest as spherical molecules with novel properties that are not expected from empty fullerenes.[1] The higher fullerenes can even encapsulate two metal atoms inside the carbon cages to form soluble and relatively air-stable endohedral dimetallofullerenes. Because of the difficulty in producing pure samples in large quantities, experimental characterization of these species has been hindered. Important progress was marked by the successful isolation and purification of endohedral dimetallofullerenes such as $Sc_2@C_{84}$[2] and $La_2@C_{80}$[3] in macroscopic quantities. This has made it possible to investigate redox properties[3] and reactivity.[4] STM[5] and TEM[6] studies were also carried out in an attempt to confirm that two metal atoms are inside the fullerene cages.

Since there are many isomers for higher fullerenes, determination of cage structures and symmetries has long been of fundamental interest in disclosing the mechanism of growth. This has been a recent subject of theoretical[4, 7, 8] and experimental studies.[9, 10] Since its first observation in 1991[11] $La_2@C_{80}$ has been widely known as a representative and abundant dimetallofullerene. Despite several attempts, its cage structure and symmetry have not yet been experimentally confirmed. In addition, it is currently of increasing interest whether encapsulated metal atoms are rigidly attached to fullerene cages or move about freely. Although rotation of a molecule within a cage is of great help in designing functional molecular devices,[12] very little has been known about the dynamic behavior of metal atoms encapsulated inside carbon cages. Based on ^{13}C and ^{139}La NMR spectra of $La_2@C_{80}$, we now report its structural determination and the first experimental evidence for circular motion of two La atoms.

[*] Prof. T. Akasaka
Graduate School of Science and Technology
Niigata University
Niigata 950-21 (Japan)
Fax: Int. code +(25)262-7390
e-mail: akasaka@gs.niigata-u.ac.jp

Prof. S. Nagase, Dr. K. Kobayashi
Department of Chemistry, Graduate School of Science
Tokyo Metropolitan University
Hachioji, Tokyo 192-03 (Japan)

Dr. M. Wälchli
Bruker Japan, Tsukuba, Ibaraki 305 (Japan)

Dr. K. Yamamoto, Dr. H. Funasaka
Nuclear Fuel Technology Development Division, Tokai Works
Power Reactor & Nuclear Fuel Development Corporation
Tokai, Ibaraki (Japan)

Dr. M. Kako
Department of Chemistry, The University of Electro-Communications Chofu, Tokyo (Japan)

Prof. T. Hoshino
Department of Applied Biochemistry, Faculty of Agriculture, Niigata University

Prof. T. Erata
Division of Molecular Chemistry, Graduate School of Engineering
Hokkaido University, Sapporo (Japan)

[**] This work was partly supported by a grant from the Uchida Energy Science Promotion Foundation and a Grant-in-Aid for Scientific Research on Priority Areas (No. 09238211) from the Ministry of Education, Science, Sports, and Culture, Japan.

For the C_{80} fullerene there are seven distinct isomers (D_2, D_{5d}, C_{2v}, $C_{2v'}$, D_3, D_{5h}, and I_h) that satisfy the isolated-pentagon rule.[13] The isomer distribution has been an open question, since C_{80} was a "missing" fullerene between C_{60} and C_{96}. By isolating C_{80} and analyzing the observed ^{13}C NMR lines, however, it was verified that the D_2 isomer is most abundantly produced (>90%).[14] It seems plausible to assume that two La atoms are encapsulated inside the D_2 isomer. However, theoretical calculations[8] have shown that encapsulation of two La atoms inside the most unstable I_h cage (about 52 kcal mol^{-1} less stable than the D_2 isomer) is most favorable (63 kcal mol^{-1} more stable than encapsulation inside the D_2 isomer). This is because the I_h-symmetrical C_{80} has only two electrons in the fourfold degenerate HOMO and can accommodate six more electrons to form the stable, closed-shell electronic state of $(La^{3+})_2C_{80}^{6-}$ with a large HOMO–LUMO gap. The most stable endohedral structure optimized with the I_h cage is shown in Figure 1. It has D_{2h} symmetry; two La atoms are located equivalently on the C_2 axis facing the hexagonal rings of C_{80} with a long La–La distance of 3.655 Å.[8]

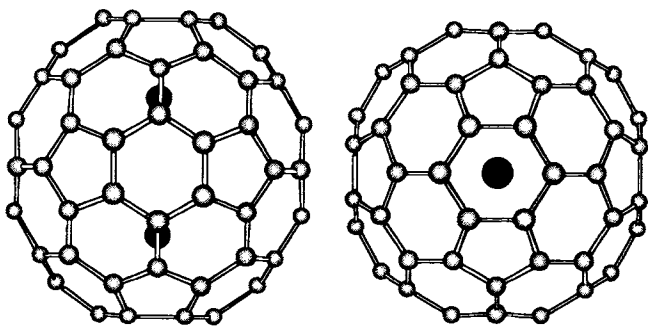

Figure 1. Two views of the optimized D_{2h}-symmetrical structure of $La_2@C_{80}$.

The ^{139}La NMR spectrum of $La_2@C_{80}$ measured at 296 K is shown in Figure 2. A single signal was observed at $\delta = -402.6$ with a linewidth of 113 Hz. This suggests that the two La atoms

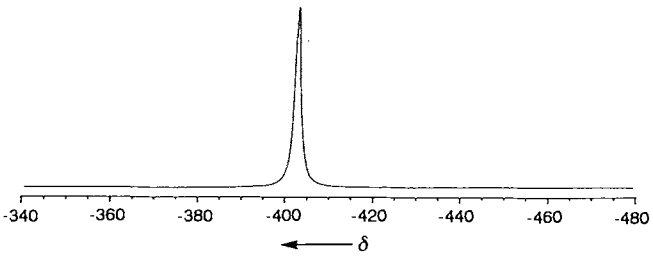

Figure 2. ^{139}La NMR spectrum of $La_2@C_{80}$ in $Cl_2C_6D_4$.

are equivalent inside the C_{80} cage. To provide insight into the cage structure the ^{13}C NMR spectrum was measured at 300 K with ^{13}C-enriched $La_2@C_{80}$ (25% ^{13}C). Although the endohedral D_{2h} structure in Figure 1 suggests a total of 13 distinct ^{13}C NMR lines for 13 nonequivalent carbon atoms, only one ^{13}C NMR line was observed at $\delta = 141.61$ with satellites due to the ^{13}C–^{13}C coupling (Figure 3). Therefore, incorporation of two La atoms into various C_{80} cages was considered. Two La atoms were placed at the highest symmetry sites possible, which nevertheless led to 20, 5, 23, 22, 14, and 6 nonequivalent carbon atoms for the D_2, D_{5d}, C_{2v}, $C_{2v'}$, D_3, and D_{5h} cages, respectively. The

 © VCH Verlagsgesellschaft mbH, D-69451 Weinheim, 1997 0570-0833/97/3615-1643 $ 17.50+.50/0

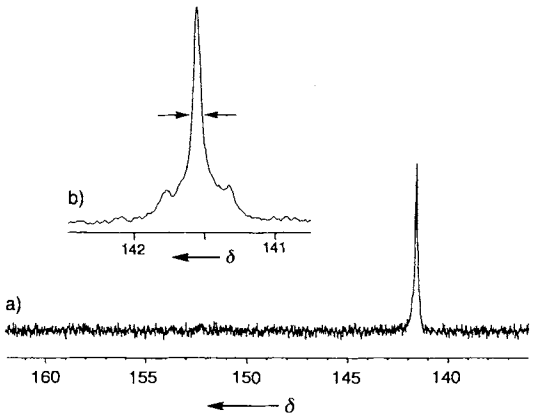

Figure 3. ^{13}C NMR spectra of $La_2@C_{80}$ in $Cl_2C_6D_4$ at (a) 150 and (b) 125 MHz. The linewidth in (b) is 0.08 ppm.

numbers of nonequivalent carbon atoms do not change, even if two La atoms are randomized uniformly. In addition, the chemical shifts should range at least over several ppm.[14] These points are not consistent with the observed ^{13}C NMR spectrum.

It is interesting that the overall symmetry is changed and increased only in the case of the I_h cage. The random motion of two La atoms inside the round I_h cage leads to two sets of slightly different carbon atoms (20 of one kind and 60 of the other). The observed linewidth of 0.08 ppm (Figure 3b) suggests that the difference in the chemical shifts is too small to be observed as two distinct lines, thereby reflecting the spherical cage. This agrees well with the small chemical shift difference of 0.07 ppm calculated for C_{80}^{6-} (I_h) at the HF – GIAO/6 – 31G// HF/6 – 31G level with the Gaussian 94 program;[15] this also supports the electronic structure of $(La^{3+})_2C_{80}^{6-}$. The presence of one or at most two lines in the ^{13}C NMR spectrum is convincing proof that two La atoms are encapsulated inside the I_h cage and circulate rapidly.

The metal motion depicted in Figure 4 is consistent with our recent calculations, which show that two La atoms can circuit the inside of the round I_h cage, since the barrier is very small (about 5 kcal mol^{-1}).[16] The presence of the barriers suggests that two La atoms can stop at the most stable positions upon a decrease in temperature. To experimentally verify this, low-temperature ^{13}C NMR measurements were carried out. At 258 K broad ^{13}C NMR signals were observed, which are ascribed to overlap of the 13 lines expected for the static D_{2h} structure (Figure 1). In addition, a single ^{139}La NMR peak, even at 258 K, supports D_{2h} symmetry for $La_2@C_{80}$ at low temperature.

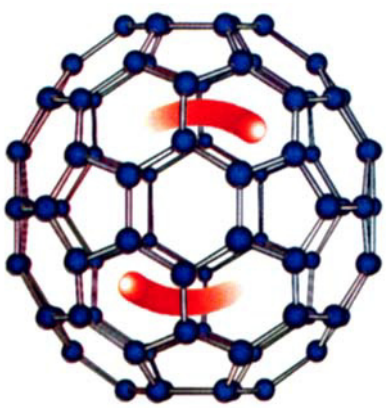

Figure 4. Circular motion of two La atoms inside the I_h cage of C_{80}.

The dynamic behavior of metal atoms should also be reflected in the ^{139}La NMR linewidth, since circulation of two La^{3+} cations produces a new magnetic field at the positions of La. Ordinarily, the interaction between La nuclear spins and the magnetic field (the spin–rotation interaction) does not contribute significantly to the relaxation time (hence, the linewidth), because molecular rotation is dominantly quenched by neighbors in solution. Since in $La_2@C_{80}$ rotation of two La atoms can be preserved due to unique cage protection, spin–rotation interaction has a drastic effect on the relaxation process and results in an increase in the linewidth upon an increase in temperature. This is quite unlike other types of relaxation.[17] Large broadening of the ^{139}La NMR linewidth was observed with increasing temperature from 305 to 363 K (Figure 5). On the other hand, narrowing of the linewidth with increasing temperature from 258 to 305 K is normal due to the overall rotation of the $La_2@C_{80}$ molecule (quadrupole-dominated relaxation).

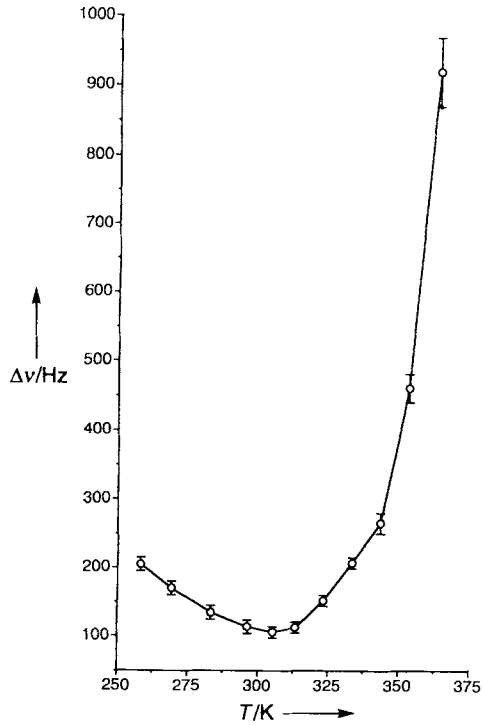

Figure 5. Linewidths $\Delta\nu$ of the ^{139}La NMR signal for $La_2@C_{80}$ as a function of temperature.

We have experimentally confirmed that two La atoms are encapsulated inside the I_h cage of C_{80}. The La atoms are not still but circulate inside the round cage even at room temperature, which is in contrast to the Sc atoms in $Sc_2@C_{84}$.[16]

Experimental Section

$La_2@C_{80}$ was synthesized and purified as reported [3]. ^{13}C-enrichment was achieved by arc-burning the lanthanum–carbon composite rods made with 90% ^{13}C-enriched amorphous carbon. $La_2@C_{80}$ (0.1 mg) was dissolved in [D_4]-*o*-dichlorobenzene under an argon atmosphere. [Cr(acac)$_3$] (acac = acetylacetonate) was added as a relaxant for the ^{13}C NMR measurements. ^{139}La NMR spectra were measured at 70.6 MHz on a Bruker DMX500 spectrometer (acquisition time 107 ms, delay time 143 ms). ^{13}C NMR spectra were obtained at 125 and 150 MHz on Varian Unity Plus 500SW, Bruker DMX500, and DMX600 spectrometers. The ^{139}La chemical shift was calibrated with 0.6 M $LaCl_3/D_2O$ as an external reference ($\delta = 0$). Chemical shifts of ^{13}C NMR were expressed downfield of the signal for the *ipso* carbon atom in *o*-dichlorobenzene as an internal standard ($\delta = 131.0$).

Received: December 9, 1996
Revised version: April 1, 1997 [Z9865IE]
German version: *Angew. Chem.* **1997**, *109*, 1716–1719

Keywords: fullerenes · lanthanum · metallofullerenes · NMR spectroscopy

[1] Recent reviews: a) D. S. Bethune, R. D. Johnson, J. R. Salem, M. S. de Vries, C. S. Yannoni, *Nature* **1993**, *366*, 123–128; b) S. Nagase, K. Kobayashi, T. Akasaka in *Recent Advances in the Chemistry and Physics of Fullerenes and Related Materials* (Eds.: K. M. Kadish, R. S. Ruoff), The Electrochemical Society, Inc., Pennington, **1995**, pp. 747–762; c) R. H. Michel, D. Fuchs, R. D. Beck, M. M. Kappes in *Physics and Chemistry of Fullerenes and Derivatives* (Eds.: H. Kuzmany, J. Fink, M. Mehring, S. Roth), World Scientific, Singapore, **1995**, pp. 89–104; d) F. T. Edelmann, *Angew. Chem.* **1995**, *107*, 1071–1074; *Angew. Chem. Int. Ed. Engl.* **1995**, *34*, 981–985; e) S. Nagase, K. Kobayashi, T. Akasaka, *Bull. Chem. Soc. Jpn* **1996**, *69*, 2131–2142; f) S. Nagase, K. Kobayashi, T. Akasaka in *Fullerenes and Fullerene Nanotubes* (Eds.: H. Kuzmany, J. Fink, M. Mehring, S. Roth), World Scientific, Singapore, **1996**, pp. 161–167; g) T. Akasaka, S. Nagase, K. Kobayashi in *Fullerenes and Fullerene Nanotubes* (Eds.: H. Kuzmany, J. Fink, M. Mehring, S. Roth), World Scientific, Singapore, **1996**, pp. 200–204; h) R. W. Saalfrank, *Nature* **1996**, *383*, 124–125; i) H. Shinohara, M. Takada, M. Sakata, T. Hashizume, T. Sakurai in *Cluster-Assembled Solids* (Ed.: K. Sattler), Transtech Publications, in press.

[2] H. Shinohara, H. Yamaguchi, N. Hayashi, H. Sato, M. Ohkohchi, Y. Ando, Y. Saito, *J. Phys. Chem.* **1993**, *97*, 4259–4261.

[3] T. Suzuki, Y. Maruyama, T. Kato, K. Kikuchi, Y. Nakao, Y. Achiba, K. Kobayashi, S. Nagase, *Angew. Chem.* **1995**, *107*, 1228–1230; *Angew. Chem. Int. Ed. Engl.* **1995**, *34*, 1094–1096.

[4] T. Akasaka, S. Nagase, K. Kobayashi, T. Suzuki, T. Kato, K. Kikuchi, Y. Achiba, K. Yamamoto, H. Funasaka, T. Takahashi, *Angew. Chem.* **1995**, *107*, 2303–2304; *Angew. Chem. Int. Ed. Engl.* **1995**, *34*, 2139–2141.

[5] H. Shinohara, N. Hayashi, H. Sato, Y. Saito, X.-D.Wang, T. Hashizume, T. Sakurai, *J. Phys. Chem.* **1993**, *97*, 13438-13440.

[6] R. Beyers, C.-H. Kiang, R. D. Johnson, J. R. Salem, M. S. de Vries, C. S. Yannoni, D. S. Bethune, H. C. Dorn, P. Burbank, K. Harich, S. Stevenson, *Nature* **1994**, *370*, 196–199.

[7] S. Nagase, K. Kobayashi, *Chem. Phys. Lett.* **1994**, *231*, 319-324.

[8] K. Kobayashi, S. Nagase, T. Akasaka, *Chem. Phys. Lett.* **1995**, *245*, 230–236.

[9] E. Yamamoto, M. Tansho, T. Tomiyama, H. Shinohara, H. Kawahara, Y. Kobayashi, *J. Am. Chem. Soc.* **1996**, *118*, 2293–2294.

[10] Y. Miyake, S. Suzuki, Y. Kojima, K. Kikuchi, K. Kobayashi, S. Nagase, M. Kainosho, Y. Achiba, Y. Maniwa, K. Fisher, *J. Phys. Chem.* **1996**, *100*, 9579–9581.

[11] M. M. Alvarez, E. G. Gillan, K. Holczer, R. B. Kaner, K. S. Min, R. L. Whetten, *J. Phys. Chem.* **1991**, *95*, 10561–10563.

[12] T. C. Bedard, J. S. Moore, *J. Am. Chem. Soc.*, **1995**, *117*, 10662–10671.

[13] P. W. Fowler, D. E. Manolopoulos in *An Atlas of Fullerenes*, Clarendon, Oxford, **1995**.

[14] F. H. Hennrich, R. H. Michel, A. Fischer, S. Richard-Schneider, S. Gilb, M. M. Kappes, D. Fuchs, M. Bürk, K. Kobayashi, S. Nagase, *Angew. Chem.* **1996**, *108*, 1839–1841; *Angew. Chem. Int. Ed. Engl.* **1996**, *35*, 1732–1734.

[15] M. J. Frisch, G. W. Trucks, H. B. Schlegel, P. M. W. Gill, B. G. Johnson, M. A. Robb, J. R. Cheeseman, T. Keith, G. A. Petersson, J. A. Montgomery, K. Raghavachari, M. A. Al-Laham, V. G. Zakrzewski, J. V. Ortiz, J. B. Foresman, J. Cioslowski, B. B. Stefanov, A. Nanayakkara, M. Challacombe, C. Y. Peng, P. Y. Ayala, W. Chen, M. W. Wong, J. L. Andres, E. S. Replogle, R. Gomperts, R. L. Martin, D. J. Fox, J. S. Binkley, D. J. Defrees, J. Baker, J. P. Stewart, M. Head-Gordon, C. Gonzalez, J. A. Pople, *Gaussian 94*, Gaussian, Inc., Pittsburgh, **1995**.

[16] K. Kobayashi, S. Nagase, T. Akasaka, *Chem. Phys. Lett.* **1996**, *261*, 502–506.

[17] For example, R. G. Kidd in *NMR of Newly Accessible Nuclei, Vol. 1* (Ed.: P. Laszlo), Academic Press, New York, **1983**, pp. 103–131.

Synthesis and Structure of Novel Mn^{III} and Mn^{V} Complexes: Development of a New, Mild Method for Forming Mn≡N Bonds**

J. Du Bois, Craig S. Tomooka, Jason Hong, Erick M. Carreira,* and Michael W. Day

The numerous reaction methods for converting alkenes to epoxides or diols are of enormous value and are commonly employed in chemical synthesis.[1, 2] In contrast, far fewer methods are available for the analogous conversion of an alkene to an aziridine or an amine, despite their great potential utility.[3, 4] We are currently exploring the development of nitridomanganese systems that may be activated for N-atom transfer to alkenes. We have reported that silyl enol ethers could be aminated with [(salen)Mn≡N] complexes (salen = *N*,*N*′-bis(salicylidene)ethylenediamine dianion) in the presence of trifluoroacetic anhydride (TFAA) to give *N*-trifluoroacetylated α-amino ketones.[5] In an effort to expand the scope of this class of reagents, we have focused on the design and synthesis of novel nitridomanganese complexes. Herein we describe the preparation and X-ray crystallographic characterization of Mn^{III} and nitridomanganese(v) complexes containing Schiff bases as ligands. The generation of such Mn^{V} nitrides (Mn≡N) (Scheme 1)

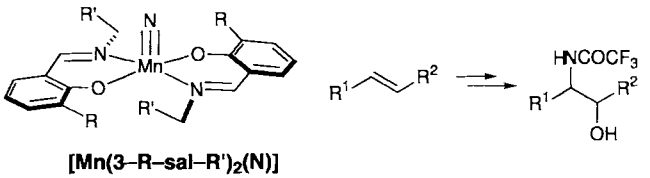

[Mn(3–R–sal–R′)$_2$(N)]

Scheme 1. Schiff base nitridomanganese(v) complexes as N-atom-transfer reagents for the aminohydroxylation of alkenes.

has required the development of a mild oxidative protocol.[6, 7] Additionally, we demonstrate the ability of these nitrides to transfer a CF_3CON unit to an unfunctionalized olefin by the successful amination of styrene, a substrate which was unreactive with previously reported Mn≡N complexes.[8]

Extensive literature exists on the coordination chemistry of manganese in its divalent and trivalent oxidation states.[9] In a majority of cases, the manganese ion is observed to form bridged, multinuclear assemblies, particularly when simple bidentate ligands (e.g. carboxylates) are used.[10, 11] We were interested in examining Mn^{III} complexes containing two Schiff base ligands as precursors for the corresponding Mn^{V} nitrides. To this end, substituted salicylimine ligands (H-3-R-sal-R′) were accessed following condensation of salicylaldehydes with primary amines (75–85% yields, Scheme 2).[12] Manganese(III)

[*] Prof. Dr. E. M. Carreira, J. Du Bois, C. S. Tomooka, J. Hong
Arnold and Mabel Beckman Laboratory for Chemical Synthesis
California Institute of Technology
Pasadena, CA 91125 (USA)
Fax: Int. code +(818)564-9297
e-mail: carreira@cco.caltech.edu

Dr. M. W. Day
Beckman Institute, X-Ray Crystallography Laboratory
California Institute of Technology
Pasadena, CA 91125 (USA)

[**] J. D. B. is grateful to the National Science Foundation for a predoctoral fellowship. J. H. thanks Pfizer for the gracious award of a Pfizer Undergraduate Summer Fellowship. This research was supported by generous grants from the David and Lucille Packard Foundation, the National Institutes of Health, the National Science Foundation, Merck, Pfizer, and Upjohn.

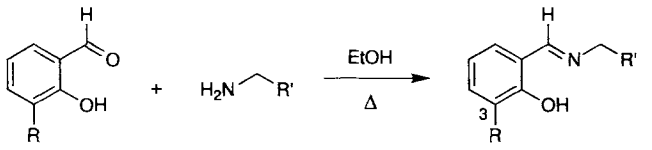

R	R'	
Ph	Me	**H-3-Ph-sal-Me**
Ph	*i*Pr	**H-3-Ph-sal-*i*Pr**
Ph	Ph	**H-3-Ph-sal-Ph**
MeO	Me	**H-3-MeO-sal-Me**
MeO	Ph	**H-3-MeO-sal-Ph**

Scheme 2. Synthesis of H-3-R-sal-R'.

adducts of the type $[Mn(3\text{-}R\text{-}sal\text{-}R')_2(X)]$ could be formed under a variety of conditions using either Mn^{II} or Mn^{III} starting materials. In the former case, reactions were conducted open to air which led to rapid oxidation of the initially formed Mn^{II} species. The effectiveness of $[Mn(acac)_2X]$ (acac = acetylacetonate; X = N_3, Br), $[Mn(acac)_3]$, $Mn(OAc)_3\cdot 2H_2O$, $MnCl_2\cdot 4H_2O$, and $Mn(OAc)_2\cdot 4H_2O$ as starting materials for the preparation of $[Mn(3\text{-}R\text{-}sal\text{-}R')_2(X)]$ complexes was examined. In a typical experiment, treatment of two equivalents of the Schiff base with one equivalent of $Mn(OAc)_2\cdot 4H_2O$ provided the $[Mn(3\text{-}R\text{-}sal\text{-}R')_2(OAc)]$ complex as a forest green solid (65–75% yields, [Eq. (a)]). Alternatively, the acetylacetonate ligands on $[Mn(acac)_2(N_3)]$ could be exchanged with two equivalents of H-3-R-sal-R' to afford the corresponding azido species [Eq. (a)]).[13]

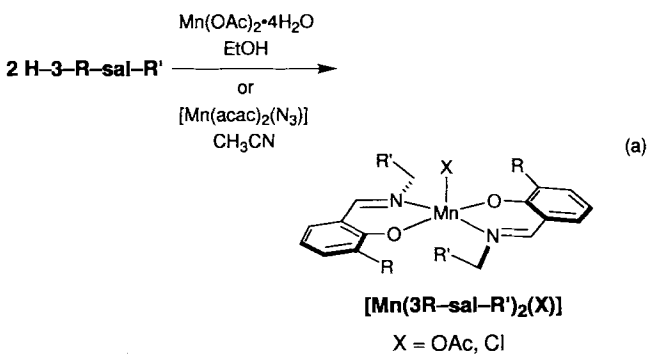

The structure of $[Mn(3\text{-}Ph\text{-}sal\text{-}i\text{Pr})_2(OAc)]$ was confirmed by single-crystal X-ray structure analysis (Figure 1).[14] The compound is monomeric with a distorted, octahedral Mn^{III} center in which the η^2-(OAc) ligand occupies two sites in the equatorial plane.[15] The salicylimine ligands fold towards one another creating a cleft lined by the appended phenyl rings. At the center of this cleft lies the acetate which sits on a crystallographically imposed C_2 axis. On the opposing face, the isopropyl moieties are disposed toward one another and appear to shield the backside of the manganese cation. Given the propensity of carboxylate ligands to form bridging complexes, the structure of $[Mn(3\text{-}Ph\text{-}sal\text{-}i\text{Pr})_2(OAc)]$ represents a rare example of bidentate carboxylate chelation to a single metal center.[9, 14, 16, 17]

Although small quantities (5–10 mg) of the desired nitridomanganese(v) complexes $[Mn(3\text{-}R\text{-}sal\text{-}R')_2(N)]$ could be generated upon irradiation (>18 h, Hg lamp) of the corresponding $Mn^{III}(N_3)$ compound, a more efficient preparative method was required.[5–8, 18] Initial attempts to form nitridomanganese(v) derivatives of $[Mn(3\text{-}R\text{-}sal\text{-}R')_2(X)]$ (X = OAc, Cl, N_3) using

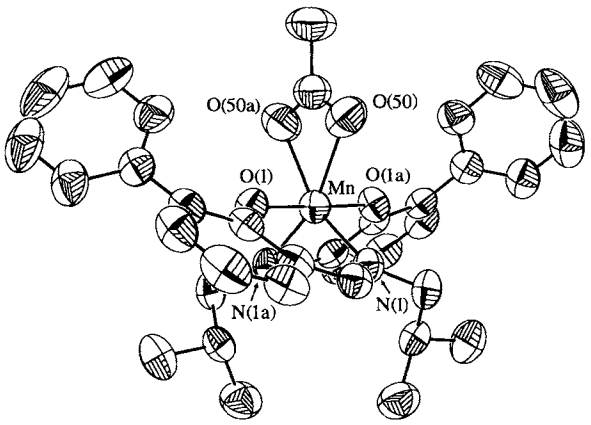

Figure 1. Crystal structure of $[Mn(3\text{-}Ph\text{-}sal\text{-}i\text{Pr})_2(OAc)]$ (ORTEP diagram displaying 50% probability ellipsoids). Selected distances [Å] and angles [°]: Mn–O(1) 1.842(12), Mn–N(1) 2.113(2), Mn–O(50) 2.212(2); O(1a)-Mn-O(1) 178.91(8), O(1)-Mn-N(1a) 91.15(6), O(1)-Mn-N(1) 89.51(6), N(1a)-Mn-N(1) 104.76(8), N(1)-Mn-O(50) 98.41(6), O(50a)-Mn-O(50) 58.43(9).

NH_4OH/Clorox bleach were, however, unsuccessful.[5, 19] We suspected that the labile Mn^{III} starting materials were not stable under the oxidizing, alkaline reaction conditions. Upon searching for a milder protocol for the synthesis of Mn≡N, we discovered that oxidation of $[Mn^{III}(3\text{-}R\text{-}sal\text{-}R')_2(OAc)]$ to $[Mn^{V}(3\text{-}R\text{-}sal\text{-}R')_2(N)]$ could be effected by using gaseous NH_3 and *N*-bromosuccinimide (NBS; 5 equiv) as the oxidant (−45 °C, CH_2Cl_2; Scheme 3).[20] At −45 °C product formation occurred

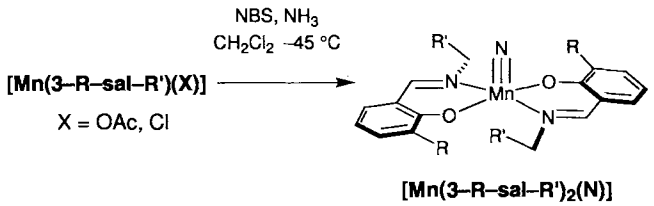

Scheme 3. Synthesis of $[Mn(H\text{-}3\text{-}R\text{-}sal\text{-}R')_2(N)]$.

immediately upon introduction of NH_3 to a solution of NBS and a Mn^{III} precursor, as noted by a slight color change. Aqueous work-up and purification using neutral Al_2O_3 (activity I) afforded the nitrido complexes as brown foams (65–70%). In all cases, single crystals were obtained by diffusing *n*-pentane into solutions of these compounds in EtOAc or benzene.

$[Mn(3\text{-}MeO\text{-}sal\text{-}Me)_2(N)]$ is one of the few crystallographically characterized nitridomanganese(v) complexes (Figure 2).[5, 6, 18, 19, 21, 22] The coordination geometry of the manganese is trigonal bipyramidal with both phenolate oxygen atoms and the nitrido ligand constituting the trigonal plane. The $Mn\text{–}N_{imine}$ bonds are substantially longer (2.02 Å) than the $Mn\text{–}O_{phenolate}$ bonds (1.87 Å) and define the two apexes of the bipyramid. Formulation of a Mn≡N bond is supported by the observed bond length of 1.54 Å as well by an IR stretch at 1047 cm^{-1}.[5, 8, 18, 19, 23]

Having developed preparative methods for the construction of nitridomanganese(v) complexes with Schiff bases as ligands, we examined these systems as nitrogen-atom-transfer reagents with unfunctionalized alkenes such as styrene **1** (Scheme 4). In a typical experiment $[Mn(3\text{-}Ph\text{-}sal\text{-}Ph)_2(N)]$ was added to a solution of TFAA and **1** (23 °C, CH_2Cl_2). The resulting unpurified reaction product was treated with an aqueous $NaHCO_3$/THF solution to afford the *N*-trifluoroacetylated amino alcohol

 © VCH Verlagsgesellschaft mbH, D-69451 Weinheim, 1997 0570-0833/97/3615-1646 $ 17.50+.50/0

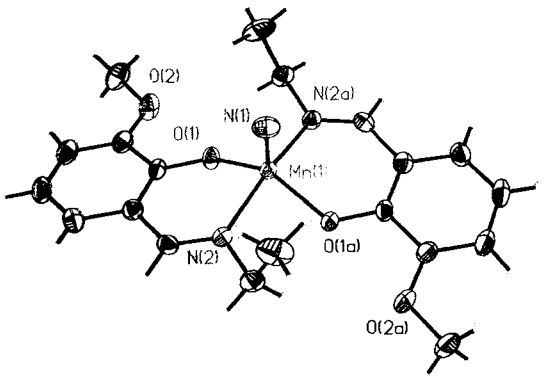

Figure 2. Crystal structure of [Mn(3-MeO-sal-Me)$_2$(N)] (ORTEP diagram displaying 50% probability ellipsoids). Selected distances [Å] and angles [°]: Mn–N(1) 1.543(4), Mn–O(1) 1.868(2), Mn–N(2) 2.023(2); N(1)-Mn-O(1) 112.51(6), O(1)-Mn-O(1a) 134.99(12), N(1)-Mn-N(2) 96.45(6), O(1)-Mn(1)-N(2) 90.46(8), O(1a)-Mn(1)-N(2) 84.61(8).

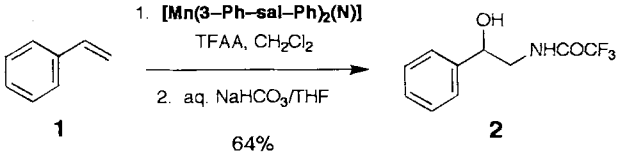

Scheme 4. Conversion of styrene **1** with [Mn(H-3-R-sal-R′)$_2$(N)] to the *N*-trifluoroacetylated amino alcohol **2**.

2. Importantly, we have found that this process can be performed with a single equivalent of styrene and one equivalent of [Mn(3-Ph-sal-Ph)$_2$(N)] to give the desired product **2** in 64% yield. The conversion of styrene to **2** with a nitridomanganese reagent is unprecedented, and thus highlights the unique reactivity which these novel systems appear to possess.

Nitridomanganese(v) complexes with Schiff bases as ligands have been prepared and demonstrated to function as potential reagents for olefin amination. Pivotal to the success of this work has been the development of new synthetic protocols for the construction of Mn^{III} Schiff base complexes and for the subsequent oxidation of these materials to the desired nitridomanganese(v) products. Extension of this methodology to encompass additional bidentate ligands and to afford alternative nitrido complexes that display greater versatility as nitrogen-atom-transfer reagents is currently under investigation.

Received: February 10, 1997 [Z100951E]
German version: *Angew. Chem.* **1997**, *109*, 1722–1724

Keywords: aminations · manganese · N ligands · nitrides · Schiff bases

[1] a) R. A. Sheldon, J. K. Kochi, *Metal-Catalyzed Oxidation of Organic Compounds*, Academic Press, New York, **1981**; b) *Organic Synthesis by Oxidation with Metal Compounds* (Eds: W. J. Mijs, C. R. H. I. de Jonge), Plenum, New York, **1986**.

[2] a) R. A. Johnson, K. B. Sharpless in *Catalytic Asymmetric Synthesis* (Ed.: I. Ojima), VCH, New York, **1993**, p. 103; b) E. N. Jacobsen, *ibid.* **1993**, p. 159; c) H. C. Kolb, M. S. VanNieuwenhze, K. B. Sharpless, *Chem. Rev.* **1994**, *94*, 2483, and references therein; d) K. A. Jørgensen, *ibid.* **1989**, *89*, 431.

[3] a) D. A. Evans, M. M. Faul, M. T. Bilodeau, *J. Am. Chem. Soc.* **1994**, *116*, 2742, and references therein; b) Z. Li, R. W. Quan, E. N. Jacobsen, *ibid.* **1995**, *117*, 5889, and references therein; c) J.-P. Mahy, G. Bedi, P. Battioni, D. Mansuy, *J. Chem. Soc. Perkin Trans. 2* **1988**, 1517.

[4] For a recent, leading reference concerning olefin aminohydroxylation, see: G. Li, H. H. Angert, K. B. Sharpless, *Angew. Chem.* **1996**, *108*, 2995; *Angew. Chem. Int. Ed. Engl.* **1996**, *35*, 2813.

[5] J. Du Bois, J. Hong, E. M. Carreira, M. W. Day, *J. Am. Chem. Soc.* **1996**, *118*, 915.

[6] For an elegant report of a 1,4,7-triazacyclononane Mn^{V} nitride see: A. Niemann, U. Bossek, G. Haselhorst, K. Wieghardt, B. Nuber, *Inorg. Chem.* **1996**, *35*, 906.

[7] For comprehensive reviews on transition metal nitrides, see: a) K. Dehnicke, J. Strähle, *Angew. Chem.* **1992**, *104*, 978; *Angew. Chem. Int. Ed. Engl.* **1992**, *31*, 955; b) W. A. Nugent, J. M. Mayer, *Metal-Ligand Multiple Bonds*, Wiley Interscience, New York, **1988**.

[8] a) T. Takahashi, Dissertation, University of Michigan, Ann Arbor, MI, **1985**; b) J. T. Groves, T. Takahashi, *J. Am. Chem. Soc.* **1983**, *105*, 2073.

[9] a) B. Chiswell, E. D. McKenzie, L. F. Lindoy in *Comprehensive Coordination Chemistry, Vol. 4* (Ed.: G. Wilkinson), Pergamon, Oxford, U. K., **1987**, p. 1; b) J. C. Vites, M. M. Lynam, *Coord. Chem. Rev.* **1995**, *146*, 167; c) V. L. Pecoraro, M. J. Baldwin, A. Gelasco, *Chem. Rev.* **1994**, *94*, 807; d) G. W. Brudvig, R. H. Crabtree, *Prog. Inorg. Chem.* **1989**, *37*, 99.

[10] a) B. C. Dave, R. S. Czernuszewicz, *New J. Chem.* **1994**, *18*, 149; b) K. Koeber, D. Schneider, *Gmelin Handbook of Inorganic Chemistry: Mn, D3* (Ed.: E. Schleitzer-Rust), Springer, Berlin, **1982**, p. 77, and references therein.

[11] Some mononuclear [Mn^{III}(Schiff base)$_2$(X)] derivatives have been documented, although reliable structural information is often lacking, see ref. [9a].

[12] H-3-R-sal-R′ is used to designate substitution on the salicylimine, as shown in Scheme 1.

[13] Other reagents and methods employing $MnCl_2 \cdot 4H_2O$/KOH, $Mn(OAc)_3 \cdot 2H_2O$, [Mn(acac)$_3$], or [Mn(acac)$_2$Br] gave variable results.

[14] Crystal data for [Mn(3-Ph-sal-*i*Pr)$_2$(OAc)]: dark green crystals were deposited by diffusing pentane into a solution of the complex in EtOAc. Crystal dimensions $0.29 \times 0.45 \times 0.48$ mm; monoclinic, space group $C2/c$, $a = 14.588(3)$, $b = 15.996(3)$, $c = 14.712(3)$ Å, $\beta = 108.62°$, $V = 3253.3(11)$ Å^3, $Z = 4$, $\rho_{calcd} = 1.263$ g cm^{-3}. A total of 6433 reflections were collected ($Mo_{K\alpha}$, $2\theta_{max} = 50°$, $-17 \le h \le 17$, $-18 \le k \le 18$, $-17 \le l \le 0$) and merged to 2859 unique reflections ($R_{merge} = 0.021$, $GOF_{merge} = 1.19$). The structure was solved by direct methods (SHELXS-86) and refined anisotropically (SHELXL-93) to an $R_1 = 0.044$, $wR_2 = 0.081$ with a GOF = 2.135. Hydrogen positions were determined from the difference Fourier map [21 b].

[15] A similar coordination geometry has been recently observed in a monoacetate Mn^{III} complex, see: K. Inamoto, M. Koikawa, M. Nakashima, T. Tokii, *Inorg. Chim. Acta* **1996**, *249*, 251.

[16] a) K. Wieghardt, *Angew. Chem.* **1994**, *106*, 765; *Angew. Chem. Int. Ed. Engl.* **1994**, *33*, 725; b) K. Wieghardt, *ibid.* **1989**, *101*, 1179 and **1989**, *28*, 1153; c) G. Christou, *Acc. Chem. Res.* **1989**, *22*, 328.

[17] a) P. Poganiuch, S. Liu, G. C. Papaefthymiou, S. J. Lippard, *J. Am. Chem. Soc.* **1991**, *113*, 4645, and references therein; b) C. J. Carrell, H. L. Carrell, J. Erlebacher, J. P. Glusker, *ibid.* **1988**, *110*, 8651.

[18] A number of elegant examples of the photolytic extrusion of N_2 from low-valent metal azides to generate nitrido metal species have been documented, see: a) T. Jüstel, T. Weyhermüller, K. Wieghardt, E. Bill, M. Lengen, A. X. Trautwein, P. Hildebrandt, *Angew. Chem.* **1995**, *107*, 744; *Angew. Chem. Int. Ed. Engl.* **1995**, *34*, 669; b) J. W. Buchler, C. Dreher, *Z. Naturforsch. B* **1984**, *39*, 222; c) S. I. Arshankow, A. L. Poznjak, *Z. Anorg. Allg. Chem.* **1981**, *481*, 201.

[19] J. W. Buchler, C. Dreher, K.-L. Lay, *Z. Naturforsch. B Anorg. Chem. Org. Chem.* **1982**, *37*, 1155.

[20] Other methods for synthesizing Mn≡N bonds with porphyrin and phthalocyanine complexes have been described, see: a) Hill, C. L.; Hollander, F. J. *J. Am. Chem. Soc.* **1982**, *104*, 7318; b) H. Grunewald, H. Homborg, *Z. Anorg. Allg. Chem.* **1992**, *608*, 81, and references therein.

[21] a) Crystal data for [Mn(3-MeO-sal-Me)$_2$(N)]: pale brown crystals were deposited by diffusing pentane into a solution of the complex in Et_2O. Crystal dimensions $0.33 \times 0.30 \times 0.26$ mm; orthorhombic, space group, $Fdd2$, $a = 14.693(2)$, $b = 23.268(3)$, $c = 11.6940(10)$ Å, $V = 3997.9(7)$ Å^3, $Z = 8$, $\rho_{calcd} = 1.413$ g cm^{-3}. A total of 1533 reflections were collected ($Mo_{K\alpha}$, $2\theta_{max} = 50°$, $0 \le h \le 17$, $0 \le k \le 27$, $0 \le l \le 13$) and merged to 931 unique reflections. The structure was solved by direct methods (SHELXTL, version 5.03) and refined anisotropically (SHELXTL, version 5.03) to an $R_1 = 0.022$, $wR_2 = 0.054$ with a GOF = 1.062. Hydrogen atoms were included at calculated positions. b) Crystallographic data (excluding structure factors) for the structures reported in this paper have been deposited with the Cambridge Crystallographic Data Centre as supplementary publication nos. CCDC-100223 and CCDC-100226 ([Mn(3-Ph-sal-*i*Pr)$_2$(OAc)] and [Mn(3-MeO-sal-Me)$_2$(N)], respectively). Copies of the data can be obtained free of charge on application to The Director, CCDC, 12 Union Road, Cambridge CB2 1EZ, UK (fax: int. code +(1223) 336-033; e-mail: deposit@chemcrys.cam.ac.uk).

[22] J. W. Buchler, C. Dreher, K.-L. Lay, Y. J. A. Lee, W. R. Scheidt, *Inorg. Chem.* **1983**, *22*, 888.

[23] Mn≡N bond lengths of 1.51 Å and IR stretching frequencies of 1050, 1036, and 1047 cm^{-1} have been observed in five-coordinate nitrido Mn^{V} porphyrin and salen complexes.

 © VCH Verlagsgesellschaft mbH, D-69451 Weinheim, 1997 0570-0833/97/3615-1647 $ 17.50+.50/0

Novel Crown Ethers with a Trithiadiazapentalene–Trithiotriuret Redox System**

Heinz Graubaum,* Franz Tittelbach, Gerhard Lutze, Karsten Gloe,* Melinda Mackrodt, Torsten Krüger, Norbert Krauss, Alfred Deege, and Heike Hinrichs

Dedicated to Professor Leonard F. Lindoy on the occasion of his 60th birthday

The host–guest chemistry of functionalized macrocycles offers much potential for special applications. For some time now special attention has been paid to macrocyclic compounds whose properties can be changed reversibly by both chemical and physical means.[1] This was achieved by introducing functional units like the reversibly isomerizable azo group[2] or the reversible dithiol–disulphide redox system[3] into the macrocycles. In this way a systematic modification of properties of the guest such as binding strength and binding selectivity offers new possibilities for complexation, separation, or detection of both valuable and toxic species.[4]

The assembly of heterocyclic trithiadiazapentalene units and diamino polyethers to form pentaleno crown compounds provides a new approach to the above-mentioned modification of macrocyclic host compounds for cations. The exceptional electronic structure of the trithiapentalenes also makes them very interesting building blocks for further synthesis, both in theory and in practice.[5]

In an earlier publication we showed that 2,5-bis(aryloxy)-3,3aλ^4,4-trithia-1,6-diazapentalenes[6a] are suitable for reaction with nucleophiles. The diphenyl derivative **1** reacts with α,ω-diaminopolyethers **2** in a 1:1 molar ratio to form bridged bispentalenes in high yields. These compounds can be used as starting materials for designing much larger cyclic molecules.[6b]

We now describe the synthesis of pentaleno crown ethers **3a–c** and their subsequent reduction to the corresponding thiourea derivatives **4a–c**. Furthermore, their complex-forming properties deduced from extraction and transport studies will also be discussed. The synthetic path way leads to a novel class of crown ethers that contains the trithiadiazapentalene–trithiotriuret redox system that can be used to control the recognition properties.

The compounds **3** were formed in reactions between **1** and **2** in a 1:2 molar ratio. Ring closure only occurred when the chain of the polyethers was long enough ($n \geq 1$). The structures of the pentaleno crown ether compounds **3a–c** have been elucidated

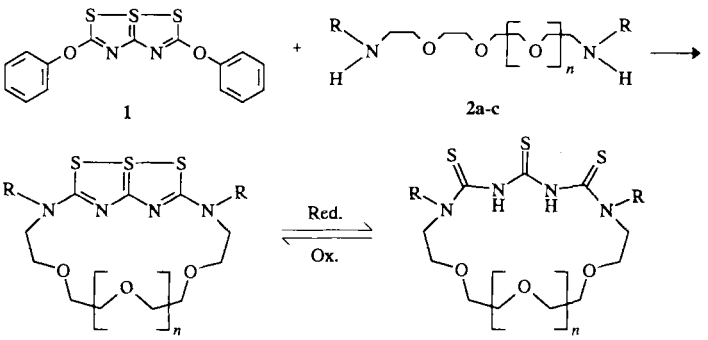

2,3,4	n	R
a	1	$CH_2C_6H_5$
b	2	CH_3
c	3	CH_3

by ^{13}C NMR spectroscopy and fast-atom-bombardment mass spectrometry (FAB-MS), and the results were confirmed by X-ray analysis[7] of compound **3b** (Figure 1).

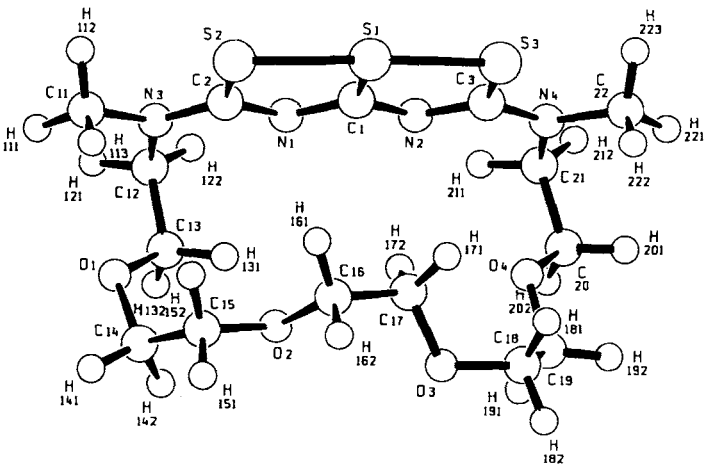

Figure 1. X-ray crystal structure of the pentaleno crown compound **3b** [7].

The macrocycles **3** can be reduced by treatment with zinc in acetic acid to form the corresponding thioureas **4**. The reoxidation is quantitative in the presence of atmospheric oxygen. As solids compounds **4** are stable in air at room temperature for several months.

Complex formation of the starting pentalene and of the new pentaleno crown compounds was investigated by liquid–liquid extraction studies with solutions of metal salt/picric acid in water and the ligand in chloroform as the liquid–liquid system.[8] The extractability of metal ions (see Figure 2 for Ag^I and Hg^{II}) by simple open-chain thiaazapentalene **1** was very low in this system. However, on introduction of **1** into a macrocyclic ring system (**3a–c**) the extractability of Ag^I and Hg^{II} increased significantly. The results for Na^I, K^I, Cs^I, Sr^{II}, Ca^{II}, Zn^{II}, Co^{II}, and Cu^{II} were comparable with that obtained in extraction studies with **1** in the same solvent extraction system. A remarkable variation in the extraction properties of the macrocyclic ring compounds **3a**, **3b**, and **3c** is observed for Ag^I and Hg^{II}. As shown in Figure 2 **3a** extracts Ag^I quantitatively into the organic phase (as picrate). In

[*] Dr. H. Graubaum, Dr. F. Tittelbach, Dr. G. Lutze
Institut für Angewandte Chemie Adlershof
Rudower Chaussee 5, D-12484 Berlin (Germany)
Fax: Int. code +(30)6392-4103
Prof. Dr. K. Gloe, M. Mackrodt, T. Krüger
Institut für Anorganische Chemie der Technischen Universität
Mommsenstrasse 13, D-01062 Dresden (Germany)
Fax: Int. code +(351)463-7287
e-mail: karsten.gloe@chemie.tu-dresden.de
Dr. N. Krauss
Institut für Kristallographie der Freie Universität Berlin (Germany)
A. Deege, H. Hinrichs
Max-Planck-Institut Kohlenforschung, Mülheim an der Ruhr (Germany)

[**] Financial support by the Akademie der Naturforscher Leopoldina (H. G.) and by the Fonds der Chemischen Industrie (H. G. and K. G.) is acknowledged. The authors wish to thank Prof. Dr. M. T. Reetz (MPI für Kohlenforschung Mühlheim) for help rendered during the transport experiments and Prof. Dr. H. Schneider (MPI für biophysikalische Chemie Göttingen) for support with the stability constant measurements. The graduate scholarship from Studienstiftung des deutschen Volkes (to M. M.) is gratefully appreciated.

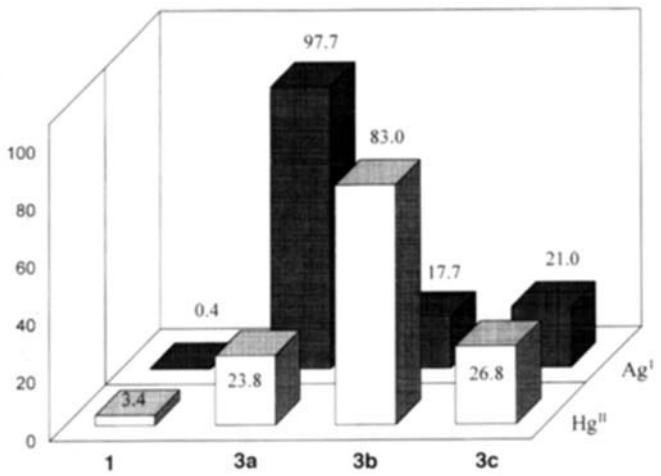

Figure 2. Liquid–liquid extraction of Ag^{I} and Hg^{II} with the open-chain trithiadiazapentalene **1** and the pentaleno crown compounds **3a–c**, $c_M = 1 \times 10^{-4}$ M ($AgNO_3$ or $HgCl_2$); $c_{HPic} = 5 \times 10^{-3}$ M; $c_L = 1 \times 10^{-3}$ M in $CHCl_3$.

contrast, only 20% extraction of Ag^{I} by the ligands **3b** and **3c** was observed.[9] The results correlate well with the order of the potentiometrically determined stability constants of the 1:1 Ag^{I} complexes with these macrocyclic ring compounds in homogeneous solutions:[10] **3a** ($\lg K_{AgL} = 6.84 \pm 0.08$) > **3b** ($4.51 \pm 0.07$) ≈ **3c** ($4.50 \pm 0.11$).

In contrast to the behavior of Ag^{I}, the Hg^{II} complex formation was optimal with the medium-sized macrocycle **3b**. In this case more than 80% of $HgCl_2$[11] was extracted. With smaller or larger macrocyclic compounds the extraction decreased significantly (25%, Figure 2).

These differences in behavior can be attributed to the different structures of the Ag^{I} and Hg^{II} complexes formed during extraction. This has been confirmed by semiempirical molecular modeling calculations of the 1:1 complexes.[12] Figure 3 shows the results of Ag^{I} and Hg^{II} complexes with compounds **3a** and **3b**. Ag^{I} formed five bonds with two nitrogen atoms of the pentalene unit and three bonds with the ether oxygen atoms of **3a**, which results in an approximately symmetrical arrangement. Since Ag^{I} forms only four longer bonds with **3b**, this complex is distinctly less favored. In the complex between **3b** and $HgCl_2$ interactions between Hg^{II} and the two nitrogen atoms of the pentalene unit and all three oxygen atoms in the macrocycle were found. In contrast, Hg^{II} coordinated with only two oxygen atoms and two nitrogen atoms of **3a**.

To determine whether bond formation with Ag^{I} and Hg^{II} depended on the oxidation state of the ligand (**3**/**4**), the macrocyclic thiourea derivatives **4** were also tested as extractants. The extraction properties of all these compounds were comparable. They extracted Ag^{I} and Hg^{II} quantitatively. This has been attributed to the change of the binding sites during complexation. Molecular modeling calculations gave some evidence that the sulfur atoms of the thiourea derivatives acted as coordination centers and that no coordination within the macrocyclic ring occurred.

In summary the new ligands uncover an interesting differentiation in the complex formation properties of Ag^{I} and Hg^{II}, which are otherwise very similar. This differentation depends on

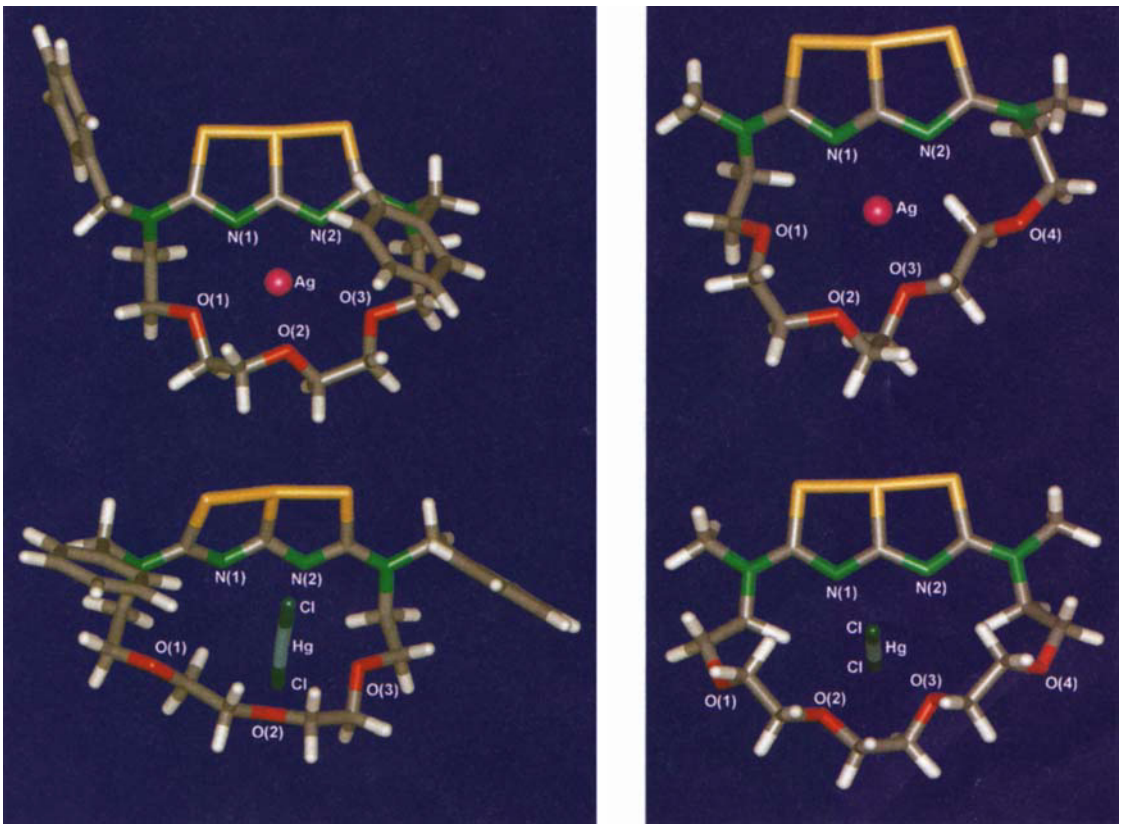

Figure 3. Structures of the complexes of Ag^{I} (top) and Hg^{II} (bottom) with **3a** (left) and **3b** (right), determined by semiempirical calculations (PM3 and ZINDO/1); selected lengths [Å]: for **3a** $Ag^{I} \cdots N(1)$ 2.25, $Ag^{I} \cdots N(2)$ 2.25, $Ag^{I} \cdots O(1)$ 2.65, $Ag^{I} \cdots O(2)$ 2.62, $Ag^{I} \cdots O(3)$ 2.80; $Hg^{II} \cdots N(1)$ 2.85, $Hg^{II} \cdots N(2)$ 2.65, $Hg^{II} \cdots O(1)$ 4.33, $Hg^{II} \cdots O(2)$ 2.31, $Hg^{II} \cdots O(3)$ 2.32; for **3b** $Ag^{I} \cdots N(1)$ 2.35, $Ag^{I} \cdots N(2)$ 2.35, $Ag^{I} \cdots O(1)$ 3.23, $Ag^{I} \cdots O(2)$ 3.01, $Ag^{I} \cdots O(3)$ 2.82, $Ag^{I} \cdots O(4)$ 4.62; $Hg^{II} \cdots N(1)$ 2.72, $Hg^{II} \cdots N(2)$ 2.76, $Hg^{II} \cdots O(1)$ 2.96, $Hg^{II} \cdots O(2)$ 2.62, $Hg^{II} \cdots O(3)$ 2.74, $Hg^{II} \cdots O(4)$ 2.97.

the size of the macrocyclic cavity and the component of the redox system. A significant change of the host selectivity is observed for the redox pairs **4b**/**3b** towards Ag^{I} and for **4a**/**3a** towards Hg^{II}. In both cases the trithiotriuret derivative binds the metal ion, but the trithiadiazapentalene does not.

Attempts to obtain crystalline complexes of the pentaleno crown ethers yielded a 1:1 complex with sodium picrate in the case of **3a** and two 1:1 complexes with ammonium rhodanide and benzylammonium perchlorate in the case of **3b**.[13] Preliminary X-ray diffraction studies on the structure of $NH_4SCN \cdot$**3b** showed that the ammonium cation is arranged symmetrically in the ring, fixed by two nitrogen atoms of the pentalene unit and four ether oxygen atoms.

Success in the synthesis and isolation of $NH_4SCN \cdot$**3b** have induced immense interest in the study of the transport properties of the compounds **3a–c** towards L-phenylalanine with the liquid membrane technique. The experimental conditions chosen were similar to those reported by Reetz et al.[14] on a system in which 3,5-bis(trifluoromethyl)benzoylboronic acid provided the synergistic effect. The results showed that the increase in the transport rates for L-phenylalanine is dependent on the cavity size of the macrocycle: **3b** ($T_R = 1037$) > **3a** ($T_R = 417.2$) > **3c** ($T_R = 74.1$).[15] The transport rate of compound **3b**, the highest among **3a–c**, is comparable with that of [18]crown-6 (T_R = 1270). Liquid–liquid extraction studies with ^{14}C-labeled L-phenylalanine have confirmed the observed trend of the transport rates of compounds **3a–c** listed above.

Experimental Section

3a–c: Pentalene **1a** (2 mmol) was stirred for 2–3 days with each of the diaminopolyethers **2a–c** (4 mmol) in chloroform (200 mL) at 25 °C. The mixture was purified by column chromatography (silica gel 60, particle size 63–100 mm, Merck) with chloroform/acetone (20/1) as eluent for phenol and chloroform/acetone (2/1) as eluent for **3a–c**. **3a**: Yield 27%, m.p. 152–154 °C; ^{13}C NMR ($CDCl_3$): δ = 49.1 (NCH_2), 56.3 127.4, 128.0, 128.8, 135.5 (benzyl-C), 66.4, 69.2, 70.2 (OCH_2), 184.0 (C-2,5), 186.8 (C-3a); FAB-MS: *m/z* (%) = 531 (48) $[M+H]^+$, 553 (48) $[M+Na]^+$. **3b**: Yield 17.5%, m.p. 135–137 °C; ^{13}C NMR ($CDCl_3$): δ = 39.2–40.2 (NCH_3), 51.1–53.8 (NCH_2), 67.0–71.9 (OCH_2), 183.4 (C-2,5), 186.0 (C-3a), FAB-MS: *m/z* (%) = 423 (48) $[M+H]^+$, 389 (14) $[M-SH]^+$. **3c**: Yield 18.8%, m.p. 66–71 °C (acetonitrile); ^{13}C NMR ($CDCl_3$): δ = 39.7–40.5 (NCH_3), 51.7–54.0 (NCH_2), 68.0–71.0 (OCH_2), 182.2, 182.8 (C-2,5), 185.7, 185.9 (C-3a); FAB-MS: *m/z* (%) = 467 (100) $[M+H]^+$, 433 (28) $[M-SH]^+$.

4a–c: Macrocycles **3a–c** (0.50 mmol) and zinc powder (150 mg) in acetic acid (5 mL) were stirred for 30 min at 25 °C under a nitrogen atmosphere. Then additional zinc powder (50 mg) was added, and the mixture stirred for 15 min. The resultant solution was neutralized with drops of a dilute solution of sodium hydrogencarbonate, extracted with chloroform, washed with water, and evaporated under vacuum. The mixture was passed through a chromatographic column (silica gel 60, particle size 63–100 mm, Merck). **4a**: Eluent heptane/acetone 1/1, yield 85%, amorphous; ^{13}C NMR ($CDCl_3$): δ = 50.3–51.7 (NCH_2), 56.7–58.5, 127.4, 128.0 128.8, 135.5 (benzyl-C), 68.2–70.8 (OCH_2), 162.4, 178.2, 180.6 (CS), FAB-MS: *m/z* (%) = 533 (62) $[M+H]^+$; **4b**: eluent heptane/acetone 4/5 to 2/5, yield 44%, m.p. 140–141 °C. ^{13}C NMR ($CDCl_3$): δ = 40.1–40.8 (NCH_3), 53.2–54.2 (NCH_2), 67.4–71.8 (OCH_2), 162.2, 179.5, 180.6 (CS), FAB-MS: *m/z* (%) = 425 (100) $[M+H]^+$; **4c**: eluent heptane/acetone 4/5 to 3/5, yield 57%, amorphous. ^{13}C NMR ($CDCl_3$): δ = 40.1–40.8 (NCH_3), 52.2–52.8 (NCH_2), 67.4–69.8 (OCH_2), 162.4, 178.2, 180.6 (CS), FAB-MS: *m/z* (%) = 469 (54) $[M+H]^+$.

Received: January 23, 1997 [Z10025IE]
German version: *Angew. Chem.* **1997**, *109*, 1719–1722

Keywords: crown compounds · host–guest chemistry · mercury · silver

[1] J.-M. Lehn, *Supramolecular Chemistry*, VCH, Weinheim, **1995**, pp. 124–138; K. Schaumburg, J.-M. Lehn, V. Goulle, S. Roth, H. Byrne, S. Hagen, J. Poplawski, K. Brunfeldt, K. Bechgaard, T. Bjornholm, P. Frederiksen, M. Jorgensen, K. Lerstrup, P. Sommer-Larsen, O. Goscinski, J.-L. Calais, L. Eriksson in *Nanostructures Based on Molecular Materials* (Eds.: W. Göpel, C. Ziegler), VCH, Weinheim, **1992**, pp. 153–173; S. L. Gilat, S. H. Kawai, J.-M. Lehn, *Chem. Eur. J.* **1995**, *1*, 275–284; S. H. Kawai, S. L. Gilat, R. Ponsinet, J.-M. Lehn, *Chem. Eur. J.* **1995**, *1*, 285–293; Z. Chen, L. Echegoyen in *Crown Compounds: Toward Future Applications* (Ed.: S. R. Cooper), VCH, Weinheim, **1992**, pp. 27–39.

[2] S. Shinkai, T. Ogawa, T. Nakaji, Y. Kusano, O. Manabe, *Tetrahedron Lett.* **1979**, 4569–4572; S. Shinkai, T. Nakaji, Y. Nishida, T. Ogawa, O. Manabe, *J. Am. Chem. Soc.* **1980**, *102*, 5860–5865.

[3] S. Shinkai, K. Inuzuka, O. Miyazaki, O. Manabe, *J. Am. Chem. Soc.* **1985**, *107*, 3950–3955; T. Nabeshima, H. Furusawa, Y. Yano, *Angew. Chem.* **1994**, *106*, 1849–1851; *Chem. Int. Ed. Engl.* **1994**, *33*, 1750–1752; H. Graubaum, F. Tittelbach, G. Lutze, K. Gloe, M. Mackrodt, *J. prakt. Chem.* **1997**, *339*, 55–58.

[4] J.-M. Lehn, *Supramolecular Chemistry*, VCH, Weinheim, **1995**, pp. 55-87.

[5] N. Lozac'h, *Adv. Heterocycl. Chem.* **1971**, *13*, 161–234; C. T. Pederson, *Sulfur Report* **1980**, 54–77; M. Yokoyama, T. Shiraishi, H. Hatanaka, K. Ogata, *J. Chem. Soc. Chem. Commun.* **1985**, 1704–1705.

[6] a) H. Graubaum, H. Seeboth, P. Zalupsky, *Monatsh. Chem.* **1989**, *120*, 997-1002; b) H. Graubaum, G. Lutze, F. Tittelbach, *Chem. Ber.* **1994**, *127*, 2209–2213.

[7] Crystallographic data (excluding structure factors) for the structure **3b** reported in this paper have been deposited with the Cambridge Crystallographic Data Centre as supplementary publication no. CCDC-100323. Copies of the data can be obtained free of charge on application to The Director, CCDC, 12 Union Road, Cambridge CB2 1EZ, UK (fax: int. code +(1223)336-033; e-mail: deposit@chemcrys.cam.ac.uk).

[8] The liquid–liquid extraction studies were carried out at 25 ± 1 °C with the radiotracer technique. The phase ratio was 1:1 and the shaking time 30 min. The concentrations are given in Figure 2. $D = c_{M(org)}/c_{M(w)}$, $E_M[\%] = D100/(D+1)$ where c_M = concentration of the metal salt in the organic (org) or aqueous (w) phase; see K. Gloe, P. Mühl, *Isotopenpraxis* **1979**, *15*, 236–239.

[9] From extraction experiments the composition of the extracted complexes can be determined with the functionality $D_M = f(c_L)$. Ag^{I} also forms $[AgL_2]^+$ complexes at higher ligand concentrations.

[10] The potentiometric titrations were performed with $AgClO_4$ and $(Et_4N)ClO_4$ (5×10^{-2} M) in acetone on a 716 DMS Titrino apparatus (Metrohm) with Ag/Ag^+-electrodes. H. J. Buschmann, *Inorg. Chim. Acta* **1992**, *195*, 51–60; B. G. Cox, H. Schneider, *Coordination and Transport Properties of Macrocyclic Compounds in Solution*, Elsevier, Amsterdam, **1992**, pp. 44–47.

[11] Hg^{II} is extracted in the form of the stable species $HgCl_2$ under the selected conditions. The results are therefore independent of the addition of picric acid.

[12] Calculations were performed with the PM3 method (program MOPAC 6.0, ligands, Hg^{II}) and the ZINDO/1 method (Hyperchem™ 4.5, Ag^{I}). T. Krüger, K. Gloe, H. Stephan, B. Habermann, K. Hollmann, E. Weber, *J. Mol. Model.* **1996**, *2*, 386–389; T. Krüger, K. Gloe, B. Habermann, M. Mühlstädt, K. Hollmann, *Z. Anorg. Allg. Chem.* **1997**, *623*, 340–346. The calculated and determined structures of **3b** are identical.

[13] Sodium picrate·**3a**: macrocycle **3a** (0.01 mmol) and sodium picrate·H_2O (0.11 mmol) were stirred for 1 h in 1 mL $CHCl_3$ at 25 °C, before filtration and addition of 1 mL of toluene; precipitation after 48 h, yield 49%, m.p. 254–256 °C; C,H,N analysis calcd. for $C_{31}H_{32}N_7O_{10}S_3Na$ (781.8): C 47.62, H 4.13, N 12.54; found C 47.74, H 4.03, N 12.56. Benzylammonium perchlorate·**3b**: macrocycle **3b** (0.02 mmol) and benzylammonium perchlorate (0.04 mmol) in $CHCl_3$ (2 mL); precipitation after 24 h, yield 32%, m.p. 160 °C (decomp.); C,H,N analysis calcd. for $C_{22}H_{36}ClN_5O_8S_3$ (630.2): C 41.93, H 5.76, N 11.11; found C 41.71, H 5.69, N 11.26. Ammonium rhodanide·**3b**: macrocycle **3b** (0.02 mmol) and NH_4SCN (0.04 mmol) were stirred for 1 h in $CHCl_3$ (2 mL) at 25 °C before filtration and addition of 2 mL of toluene; crystals after 24 h, yield 60%, m.p. 160 °C (decomp.); C,H,N analysis calcd. for $C_{16}H_{30}N_6O_4S_4$ (498.8): C 38.53, H 6.07, N 16.84, found C 38.35, H 6.13, N 16.93.

[14] M. T. Reetz, J. Huff, J. Rudolph, K. Töllner, A. Deege, R. Goddard, *J. Am. Chem. Soc.* **1994**, *116*, 11588–11589.

[15] The transport studies with L-phenylalanine were carried out in an apparatus as described by Izatt: J. D. Lamb, J. J. Christensen, S. R. Izatt, K. Bedke, M. S. Astin, R. M. Izatt, *J. Am. Chem. Soc.* **1980**, *102*, 3399–3403; results (data in mmol $L^{-1} h^{-1}$): **3a** 1210, **3b** 3007, **3c** 215, [18]crown-6 3680,[14] blank value 2.9; the relative transport rate as mentioned in the text takes into account the transport without ligand.

 © VCH Verlagsgesellschaft mbH, D-69451 Weinheim, 1997 0570-0833/97/3615-1650 $ 17.50+.50/0

Octaethylhemiporphycene: Synthesis, Molecular Structure, and Photophysics**

Emanuel Vogel,* Martin Bröring, Steven J. Weghorn, Peter Scholz, Reiner Deponte, Johann Lex, Hans Schmickler, Kurt Schaffner,* Silvia E. Braslavsky, Martin Müller, Sigrid Pörting, Christopher J. Fowler, and Jonathan L. Sessler*

Dedicated to Professor Heinz A. Staab on the occasion of his 70th birthday

Due to its role as a naturally occurring macrocyclic motif of ubiquitous importance, porphyrin, as a molecule, has inspired the conception and synthesis of numerous novel ring systems that may be regarded as structural variants of the parent cyclotetrapyrrole. One of the focal points in the current development of this new chapter in porphyrin chemistry is framed by the seven possible "nitrogen-in" structural isomers of porphyrin.[1] These first came to light with the discovery of porphycene (**1**, Figure 1),[2] or porphyrin-(2.0.2.0).

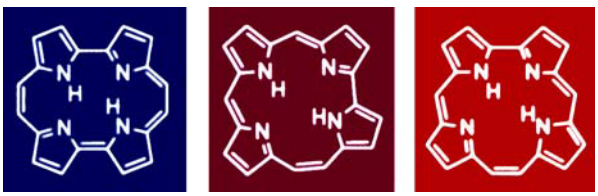

porphycene (**1**) hemiporphycene (**2**) corrphycene (**3**)

Figure 1. The three thermodynamically most stable porphyrin isomers (with an inward-pointing N_4 coordination sphere). The colors of the still unknown parent compounds **2** and **3** correspond to those of the octaethyl derivatives; the colors of porphycene (**1**) and its octaethyl derivative are indistinguishable.

Among the isomers that were still unknown at the start of the present investigations, porphyrin-(2.1.1.0) (**2**) and porphyrin-(2.1.0.1) (**3**), called hemiporphycene and corrphycene because of their structural features, were deemed to be the most promising synthetic targets. This assessment was based on retrosynthetic analyses and the prediction from PM3 calculations that **2** and **3** should have an only slightly strained planar ring system (the relative energies of **1**, **2**, and **3** with respect to porphyrin are 1.7, 8.6, and 16.0 kcal mol^{-1}, respectively).[3]

[*] Prof. Dr. E. Vogel, Dr. M. Bröring, Dr. S. J. Weghorn, P. Scholz, R. Deponte, Dr. J. Lex, Dr. H. Schmickler
Institut für Organische Chemie der Universität
Greinstrasse 4, D-50939 Köln (Germany)
Fax: Int code +(221)470-5057

Prof. Dr. K. Schaffner, Prof. Dr. S. E. Braslavsky, Dr. M. Müller, S. Pörting
Max-Planck-Institut für Strahlenchemie
Postfach 101365, D-45413 Mülheim an der Ruhr (Germany)
Fax: Int code +(208)306-3952
e-mail: schaffner@mpi-muelheim.mpg.de

Prof. Dr. J. L. Sessler, C. J. Fowler
Department of Chemistry and Biochemistry
University of Texas at Austin
Austin, TX 78712 (USA)
Fax: Int code +(512)471-7550
e-mail: sessler@mail.utexas.edu

[**] This work was funded by the Alexander von Humboldt Foundation (J. L. S. and S. J. W.), and in part by the BMBF-Verbundforschungsprojekt "Photodynamische Lasertherapie" (E. V. and K. S.) and the U. S. National Science Foundation (J. L. S.).

Recently we reported the first preparation of corrphycenes,[4a] which, despite their trapezoidal N_4 nucleus, compare favorably to the porphyrins in terms of their ability to coordinate metal ions.[4b] Since then, syntheses of corrphycenes have been reported by two other research groups.[5, 6] Therefore, the chemistry of this porphyrin isomer is apparently being studied apace. Accordingly, we focused significant attention on the synthesis of hemiporphycenes, most notably octaethylhemiporphycene (**8**) for reasons of solubility and comparability. This work had nearly been completed when H. Callot et al.[7] reported their serendipitous discovery that upon demetallation/metallation of a substituted nickel homoporphyrin two regioisomeric hemiporphycene nickel complexes were formed, one of which could be converted into the free ligand. We now present a rational synthesis of **8**, a species that has proved to be an excellent porphyrin-like tetradentate ligand.[8]

For the synthesis of **8** the tried and tested concept used for making octaalkylcorrphycenes,[4, 5] that is, generation of the tetrapyrrolic macrocycle by reductive coupling (McMurry reaction)[9] of the corresponding open-chain tetrapyrrolic α,ω-dialdehyde, in this case **6**, was followed. One possibility for preparing **6** is offered by the MacDonald condensation of 5,5′-diformyl-2,2′-bipyrrole (**5**)[10] with 5-carboxy-5′-formyl-

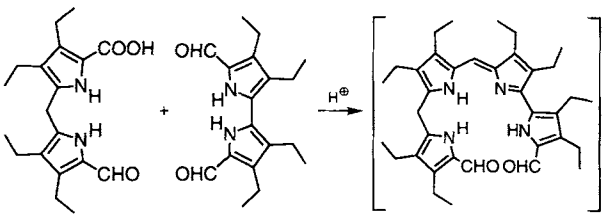

4 **5** **6**

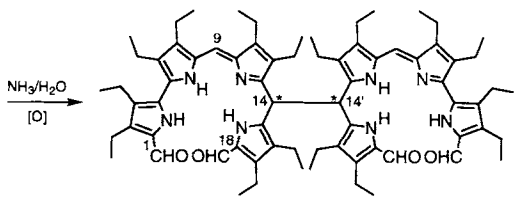

(*meso* and *rac* diastereomers)
7

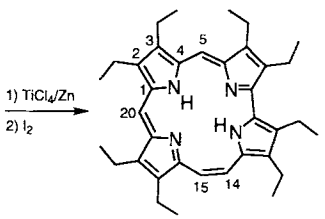

8

tetraethyl-2,2′-dipyrrylmethane (**4**). However, this approach would only be practical if side reactions, such as formation of porphyrin from two molecules of **4**,[11] could be suppressed. This may be achieved by strictly adhering to the reaction conditions outlined in the *Experimental Section*. The reaction of dialdehyde **5** with aldehydecarboxylic acid **4**, obtained by saponification of the corresponding ethyl ester,[12] in the presence of perchloric acid in THF/MeOH provided a shiny, metallic-green, lacquer-like product after chromatographic workup on silica gel with CH_2Cl_2/Et_2O (4/1) as eluent. Under the assumption that the main constituent of this product was the expected (if not identified) tetrapyrrolic dialdehyde **6**, it was subjected to reduc-

 © VCH Verlagsgesellschaft mbH, D-69451 Weinheim, 1997 0570-0833/97/3615-1651 $ 17.50+.50/0

tive coupling with titanium tetrachloride and activated zinc in THF without further purification. This approach proved to be practical, since the reaction product obtained (after oxidation with iodine or iron(III) chloride) was a solid that did contain **8** as the major component. After chromatography of this substance on silica gel with toluene as eluent and crystallization from $MeOH/CH_2Cl_2$ (5/1), pure **8** was obtained as violet cubes [m.p. 219–220 °C (20% yield)].[14] Solutions of **8** are magenta (see **2** in Figure 1) and display red fluorescence.

At a first glance one is inclined to consider the relatively facile formation of **8** by reductive coupling of the lacquer-like intermediate as indirect evidence for the existence (and presence) of dialdehyde **6**. However, as a detailed mass spectrometric analysis of the lacquer-like material showed, the bulk of the sample consisted of a compound of twice the expected molecular mass (minus two hydrogen atoms). In light of this finding the ^1H NMR spectrum, which had previously proved difficult to explain, could now be interpreted as being due to **7** (>90 %!), which exists as a mixture of the *meso* and *rac* forms. In particular the symmetrical coupling of the two halves of the molecule at the 14,14′ positions could now be readily assigned by two-dimensional NMR analysis.[15] Whereas a definitive stereochemical assignment of the diastereoisomers present in a 4:1 ratio has yet to be made, it is considered that dimer **7** most likely arises from an air-induced oxidative coupling of **6**, the presumed coupling product of **4** and **5**, in the basic reaction medium (NH_3).[16] In view of the weakness of the quadruply benzylic C14–C14′ bond in **7**, it is understandable that this bond is cleaved under the reducing conditions of the McMurry reaction, either before or after the coupling step.

Octaethylhemiporphycene (**8**) was identified as a tetrapyrrolic macrocycle that is closely related to porphyrin on the basis of structural and spectroscopic investigations, as well as its ability to complex metal ions.[8] Crystal structure analysis of **8**[17] (Figure 2) confirmed the planarity of the hemiporphycene framework inferred from PM3 calculations (maximum distance of the C and N atoms from the median plane of the framework ±0.093 Å), and clearly showed that it is an aromatic compound based on the relative bond lengths in the pyrrolic subunits ($C_\alpha-C_\beta > C_\beta-C_\beta$)[18] and the nearly complete equalization of the C–C bond lengths in the unit C⋯CH⋯C⋯CH⋯C⋯CH⋯C. The slightly increased relative energy of **8** (calculated with respect to porphyrin) is reflected by a widening of the bond angle at the *meso*-C atom C20 (131.9 versus 127.6° in octaethylporphyrin)[19] and at the C atoms of the formal double bond (134.3 and 135.5°), as well as concomitant contraction of the N2-C9-C10 and C9-C10-N3 angles (114.9 and 117.1°, respectively, versus 118.5° in octaethylporphycene).[10] Whereas the four central nitrogen atoms of porphyrins, porphycenes, and corrphycenes define squares, rectangles, and trapezoids, respectively, those in **8** describe an irregular quadrilateral in which the N⋯N distances vary between 2.627 and 3.129 Å. In the crystal the N-bonded protons can not be localized, which is in contrast to the case in solution (see NMR data below). Most likely as a result of partial disordering, these protons appear statistically distributed and show half occupancy at all four possible positions, in analogy to the behavior of porphycene.[2]

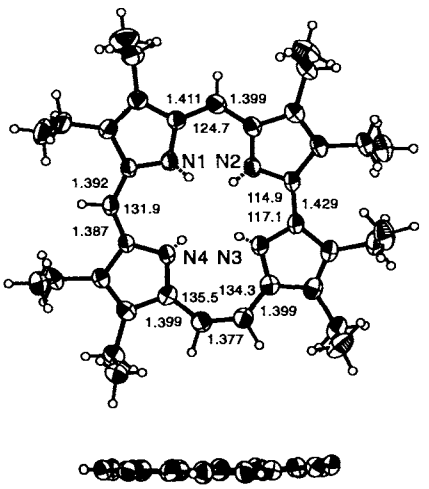

Figure 2. Crystal structure of octaethylhemiporphycene (**8**; top: view from the top; bottom: side view without ethyl substituents). Vibrational ellipsoids (40% probability) and selected bond lengths [Å] and angles [°] (standard deviations ≈0.004 Å and 0.2°); N1⋯N2 2.709, N1⋯N4 3.129, N2⋯N3 2.627, N3⋯N4 3.045 Å.

The chemical shifts in the ^1H NMR spectrum of **8** measured at room temperature (300 MHz, CD_2Cl_2/CF_2Br_2) correspond to those of porphyrin; the signals of the protons of the C_{20} perimeter appear at relatively low field (two singlets of equal intensity at $\delta = 10.11$ and 9.76, and an AB system centered at $\delta = 9.77$), whereas the signals of the N-bound protons ($\delta = -0.76$ and -2.35) appear at relatively high field. According to two-dimensional NMR experiments, octaethylhemiporphycene exists in the NH tautomeric form **8** depicted, which was shown by calculations (BLYP/3-21G and BLYP/6-31G** methods) to be the thermodynamically most stable of the six possible tautomers (one other *trans* and four *cis*).[20] The N proton that resonates at lower field is almost certainly localized on N1, since N1–H⋯N2 is expected to have a stronger hydrogen bonding interaction than N3–H⋯N4 as a result of the smaller N⋯N distance. Both NH signals are split at low temperatures into a pair of singlets (intensity ratio of the pairs 7:1), from which one can conclude that **8** is in dynamic equilibrium at room temperature with a still unidentified NH tautomer that is present in low concentration. In all likelihood **8** remains the dominant tautomer, also at low temperatures at which the equilibrium is frozen out (an unambiguous assignment of the NH singlet pairs has not yet proved possible due to instrumental limitations). The equilibrium partner of **8** is presumed to be the second *trans*-NH tautomer **8′** (Figure 3); calculations indicate

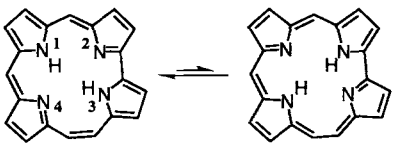

8 **8′**

Figure 3. Assumed NH tautomerism of **8** (for clarity ethyl groups have been omitted).

that this tautomer lies only 0.7–0.8 kcal mol^{-1} higher in energy than **8**, compared with the 3.5–4.5 kcal mol^{-1} energy difference between **8** and the two most stable *cis* forms.[20]

The UV/Vis spectrum of **8** shows a Soret band at $\lambda(\varepsilon) =$ 405 nm (153700), whose position (with a slightly lower extinction coefficient) almost exactly corresponds to that of octaethylporpyhrin, as well as Q bands at 484 (3900), 512 (7600), 552 (25900), 583 (9000), and 632 nm (10800).

Because of the importance of porphyrins and porphycenes in photodynamic therapy (PDT),[21, 22] it was of interest to determine the photophysical properties of **8** and to compare them with those of octaethylporphyrin (**13**), octaethylporphycene (**14**), and octaethylcorrphycene (**15**). Since **14** has a buckled ring system due to steric interactions involving the 3,6- and 13,16-ethyl groups, the planar 2,7,12,17-tetrapropylporphycene (**16**) was also considered for the sake of comparison (Table 1).

 © VCH Verlagsgesellschaft mbH, D-69451 Weinheim, 1997 0570-0833/97/3615-1652 $ 17.50+.50/0

Table 1. Photophysical parameters for octaethylhemiporphycene (**8**), octaethylporphyrin (**13**), octaethylporphycene (**14**), octaethylcorrphycene (**15**), and 2,7,12,17-tetrapropylporphycene (**16**) in toluene at room temperature (see Figure 1).

	Absorption λ_{max}/nm	Fluorescence λ_{max}/nm	ϕ_F[a] (λ_{max}/nm)	λ_{T-S}/nm[b]	ϕ_T[c]	ϕ_Δ[d]	s_Δ[e]
8	633	635	0.09 (370)	880	0.6	0.58	0.97
13[f]	619	625	0.085 (400)	790	0.8	0.62	0.78
14	665	684	0.017 (400)	- [g]	<0.1	0.06	-
15	632	635	0.03 (370)	805	0.9	0.48	0.64
16[h]	637	639	0.38 ± 0.06	980	0.4 ± 0.1	0.36 ± 0.03	0.90

[a] Fluorescence quantum yield; $A_{max} = 0.06$; exptl error ±20% unless specified; reference solution: **16** with identical A_{max} (±0.002.) [23]. [b] Triplet energy determined by stationary phosphorescence in 1-iodopropane [24]; $\lambda_{exc} > 455$ nm. [c] Triplet (intersystem crossing) quantum yield determined by laser-induced optoacoustic spectroscopy [24, 27, 28]; $\lambda_{exc} = 570$ nm; $A = 0.05-0.2$; exptl error ±30% unless specified; calorimetric reference; I_2; all solutions saturated with N_2. The upper limit for **14** is based on the finding that the prompt heat output (α) from **14** and the reference were the same. [d] Quantum yield of $O_2(^1\Delta_g)$ determined by time-resolved $O_2(^1\Delta_g)$ phosphorescence [24, 27, 29]; $\lambda_{exc} = 570$ nm; reference: **16**; $A = 0.05-0.25$; exptl error ±20% unless specified; all solutions saturated with O_2. [e] Efficiency of $O_2(^1\Delta_g)$ formation ($S_\Delta = \Phi_\Delta/\Phi_T$). [f] Reference data see ref. [30]. [g] Not measureable. [h] Reference for all measurements; for data see [23, 24].

Of the photophysical indicators that are relevant for evaluating dyes and pigments in PDT, the fluorescence quantum yield (Φ_F) and the sensitized formation of singlet oxygen $O_2(^1\Delta_g)$ by the triplet excited state of the dye (Φ_Δ) are of primary importance.[21, 22] The Φ_F values of **8**, **13**, and **15** were significantly lower than that of **16**,[23, 24] whereas the values of Φ_T (quantum yield of the S → T intersystem crossing which leads to the triplet excited state of the sensitizer) show an inverse trend. The relatively low Φ_F values of **8**, **13**, and **15** are probably due to the greater conformational flexibility of these compounds. In the case of **8** and **13** this is reflected by increases in the rates of radiationless decay and S → T intersystem crossing. However, for **15** it is manifest only in an increase in the latter.

In the case of the nonplanar **14** radiationless decay processes dominate. Although the triplet population proved too insignificant to allow these states to be detected by laser-induced optoacoustic spectroscopy, their existence was indirectly established by observing the time-resolved phosphorescence of $O_2(^1\Delta_g)$, which is formed in small amounts. In view of its properties, which are atypical for this class of compounds, **14** was not used further as a reference compound.

The efficiency of $O_2(^1\Delta_g)$ formation ($S_\Delta = \Phi_D/\Phi_T$) corresponds to that expected for **13** and **15**, since under the prerequisite that the energy relationship of the triplet sensitizers with respect to $O_2(^1\Delta_g)$ is sufficiently exothermic, the S_Δ value for aromatic systems (including porphyrinoids)[25] will be in the range of 0.7–0.8. In contrast, the S_Δ values for **8** and **16** are unusually high.[22, 26] Therefore, from a purely photophysical perspective hemiporphycene **8** and to a lesser extent, the corrphycene **15** are potential PDT sensitizers.

Experimental Section

4: Compound **11** (7.16 g, 20 mmol) was suspended in EtOH (125 mL) under an argon atmosphere and, after treatment with a solution of NaOH (4.0 g, 0.1 mol) in water (25 mL), heated at reflux for 3 h. The mixture was cooled to room temperature and poured into ice water (600 mL). Concentrated HCl (15 mL) was added with stirring, the mixture stirred for a further 10 min, and the product that separated filtered and dried under vacuum over solid KOH. The desired **4** was obtained as a violet powder (6.47 g, yield 98%) of sufficient purity (≈95%) for use in subsequent reactions. After two recrystallizations from MeOH/THF (1/1) **4** was obtained as a colorless microcrystalline powder that decomposes without melting above 220 °C (Table 2).

7: A solution of **5** (3.0 g, 10 mmol) in MeOH/THF (10/1, 330 mL) was treated sequentially at 0 °C with 70% perchloric acid (3.5 mL) and a solution of **4** (3.3 g, 10 mmol) in THF/MeOH (2/1, 450 mL), and then left at this temperature for three days. The reaction was quenched by addition of 10% ammonia (18 mL). The mixture was treated successively with Et_2O (500 mL) and water (1200 mL), and the phases were separated. The aqueous phase was then extracted with Et_2O (50 mL). After drying the combined organic phases over K_2CO_3 and removing the solvent, the residue was suspended in cold Et_2O (100 mL) and filtered to remove solids (predominantly unchanged **5**). The solvent was removed from the filtrate under vacuum after addition of silica gel (10 g), and the solid obtained purified by column chromatography (column 20 × 4 cm) with CH_2Cl_2/Et_2O (4/1) as eluent. Octaethylporphyrin (<1%) and two small fractions of unknown composition were eluted first. Recognizable by its yellow-orange fluorescence, **7** was collected as a mixture of diastereomers from the fourth fraction. The solvent was removed, and the remaining shiny, metallic-green, lacquer-like substance used in the next step without further purification (2.54 g, yield 45%, purity >90%). NMR-spectroscopically pure **7** was obtained by subjecting the crude product to renewed chromatography followed by recrystallization from a small amount of hexane/Et_2O (10/1) at −78 °C, a process that led to great loss of product. Dimer **7**, a red, microcrystalline powder with a greenish sheen (two diastereoisomers in a ratio of 4:1), decomposes without melting above 130 °C (Table 2).

8: Activated Zn (13.1 g, 200 mmol) and CuCl (2.0 g, 20 mmol) were added to THF (350 mL) and treated dropwise with $TiCl_4$ (11.0 mL, 100 mmol). The resulting

Table 2. Selected physical data for **4**, **7**, **8**, and **11**. ^{1}H NMR: 300 MHz: ^{13}C NMR: 75.5 MHz; IR: CsI.

4: Decomp >220 °C (EtOH); ^{1}H NMR ([D$_6$]DMSO): $\delta = 12.00, 11.49, 11.06, 9.46, 3.79, 2.61, 2.57, 2.32, 2.29, 1.09, 1.01, 0.85, 0.83$; ^{13}C NMR ([D$_6$]DMSO): $\delta = 176.50, 162.14, 136.40, 135.24, 131.89, 129.23, 127.12, 122.74, 121.98, 116.60, 22.13, 17.68, 17.50, 16.54, 16.54, 16.25, 16.06, 16.06, 15.75$; IR: $\tilde{\nu} = 3268, 2967, 2931, 2871, 1654, 1625, 1576, 1491, 1462, 1445, 1354, 1278, 1261, 1147, 766$ cm^{-1}; UV/Vis (DMSO): $\lambda_{max}(\varepsilon) = 278$ (19400), 316 nm (21200); MS (EI, 70 eV): *m/z* (%): 330(60) [M^{+}].

7: Decomp >130 °C (mixture of diastereomers, crude product): 1st diastereomer (main product): ^{1}H NMR ($CDCl_3$, Al_2O_3) $\delta = 11.46$ (br. s, 2H, H20,20'), 10.34 (br s, 2H, H22,22'), 10.11 (br. s, 2H, H19,19'), 9.65 (s, 2H, H1a,1a'), 9.51 (s, 2H, H18a,18a'), 6.70 (s, 2H, H9,9'), 4.70 (s, 2H, H14,14'), 2.79 (AB *and* 4H, H2a,2a'), 2.68 (q, 4H, H7a,7a'), 2.57 (q, 4H, H17a,17a'), 2.56 (AB *and* 4H, H3a,3a'), 2.51 (AB *and* 4H, H6a,6a'), 2.35 (q, 4H, H11a,11a'), 1.96 (AB part of an ABX$_3$ system, 4H, H12a,12a'), 1.61 (AB part of an ABX$_3$ system, 4H, H16a,16a'), 1.24 (X$_3$ part of an ABX$_3$ system, 6H, H2b,2b'), 1.23 (t, 6H, H7b,7b'), 1.12 (X$_3$ part of an ABX$_3$ system, 6H, H3b,3b'), 1.11 (X$_3$ part of an ABX$_3$ system, 6H, H6b,6b'), 1.08 (t, 6H, H17b,17b'), 0.96 (t, 6H, H11b,11b'), 0.59 (X$_3$ part of an ABX$_3$ system, 6H, H16b, 16b'), 0.58 (X$_3$ part of an ABX$_3$ system, 6H, H12b,12b'); ^{13}C NMR ($CDCl_3$, Al_2O_3): $\delta = 177.54, 177.20, 171.28, 146.78, 146.67, 138.48, 136.65, 136.21, 135.47, 134.86, 129.64, 129.03, 128.78, 128.27, 127.90, 126.71, 126.71, 126.19, 116.75, 43.52, 17.96, 17.88, 17.81, 17.67, 17.49, 17.45, 17.02, 16.92, 16.92, 16.77, 15.71, 15.40, 15.22, 14.82, 14.70$; 2nd diastereomer (only prominent signals): ^{1}H NMR ($CDCl_3$, Al_2O_3): $\delta = 10.95$ (br s, 2H, H20,20'), 10.95 (br s, 2H, H22,22'). 10.67 (br s, 2H, H19,19'), 9.58 (s, 2H, H1a,1a'), 9.40 (s, 2H, H18a,18a'), 6.73 (s, 2H, H9,9'), 4.67 (s, 2H, H14,14'), ^{13}C NMR ($CDCl_2$, Al_2O_3): $\delta = 177.58, 176.78, 170.02, 117.37, 43.52$. - IR: $\tilde{\nu} = 3278, 2966, 2932, 2871, 1622, 1439, 1415, 1374, 1298, 1226, 1195, 1060, 1007, 949, 818, 771$ cm^{-1}; UV/Vis (CH_2Cl_2): $\lambda_{max}(\varepsilon) = 284$ (32400), 327 (65800), 507 nm (48200); MS (FAB): *m/z* (%): 1135 (3) [$(M+1)^+$], 1134 (1) [M^{+}], 567 (100) [$(M/2)^+$]; high-resolution-MS (FAB): $C_{72}N_{94}N_8O_4$, calcd 1134.7398, found 1134.7361.

8: m.p. 219–220 °C ($MeOH/CH_2Cl_2$); ^{1}H NMR ($CDCl_3$): $\delta = 10.11$ (s, 1H, H20), 9.80 (A part of an AB system, 1H, H14), 9.76 (s, 1H, H5), 9.74 (B part of an AB system, 1H, H15, $J_{14,15} = 12.5$ Hz), 4.18 (q, 2H, H11a), 4.05 (q, 2H, H2a), 4.05 (q, 2H, H12a), 4.04 (q, 2H, H8a), 4.02 (q, 2H, H18a), 3.99 (q, 2H, H3a), 3.95 (q, 2H, H17a), 3.93 (q, 2H, H7a), 1.88 (t, 3H, H2b), 1.86 (t, 3H, H3b), 1.86 (t, 3H, H18b), 1.82 (t, 3H, H7b), 1.82 (t, 3H, H17b), 1.81 (t, 3H, H12b), 1.76 (t, 3H, H11b), 1.70 (t, 3H, H8b), −0.76 (br. s, 1H, H21), −2.35 (br. s, 1H, H23); ^{13}C NMR ($CDCl_3$): $\delta = 151.29, 146.01, 145.10, 144.79, 144.79, 143.44, 142.79, 141.04, 139.80, 139.50, 138.90, 137.42, 136.56, 134.93, 134.89, 131.88, 110.50, 108.30, 100.57, 100.28, 20.93, 20.83, 20.35, 20.28, 19.84, 19.80, 19.54, 19.48, 18.79, 18.54, 18.54, 18.54, 18.54, 18.54, 18.32, 18.22$; IR: $\tilde{\nu} = 3195, 2962, 2930, 2868, 1584, 1554, 1529, 1466, 1450, 1422, 1373, 1320, 1281, 1250, 1225, 1202, 1180, 1116, 1108, 1099, 1056, 1015, 999, 948, 845, 789, 669$ cm^{-1}; UV/Vis (CH_2Cl_2): $\lambda_{max}(\varepsilon) = 405$ (153700), 484 (3900), 512 (7600), 552 (25900), 583 (9000), 632 nm (10800); MS (EI, 70 eV): *m/z* (%): 534 (100) [M^{+}], 267 (7) [M^{2+}].

11: M.p. 145–146 °C (EtOH); ^{1}H NMR ($CDCl_3$): $\delta = 10.96, 10.19, 9.47, 4.22, 3.93, 2.71, 2.70, 2.46, 2.45, 1.25, 1.23, 1.13, 1.07, 1.06$; ^{13}C NMR ($CDCl_3$): $\delta = 176.52, 161.55, 139.87, 136.74, 133.44, 128.66, 127.77, 124.21, 123.25, 117.50, 59.58, 22.72, 18.40, 17.64, 17.22, 17.17, 16.93, 16.33, 15.89, 15.80, 14.43$; IR: $\tilde{\nu} = 3265, 2968, 2932, 2872, 1684, 1618, 1447, 1356, 1278, 1262, 1223, 1144, 1123, 1095, 1027, 780$ cm^{-1}; UV/Vis (CH_2Cl_2): $\lambda_{max}(\varepsilon) = 277$ (23800), 310 nm (19800); MS (EI, 70 eV): *m/z* (%): 358 (50) [M^{+}].

Correct elemental analyses were obtained for **4**, **8**, and **11**.

 © *VCH Verlagsgesellschaft mbH, D-69451 Weinheim, 1997* *0570-0833/97/3615-1653 $ 17.50+.50/0*

mixture was heated at reflux for 1 h and then allowed to cool to room temperature. To the titanium reagent thus prepared was added dropwise within 10 min a solution of **7** (1.13 g, 1 mmol) in THF (180 mL). The reaction mixture was then hydrolyzed with 10 % aqueous ammonia (350 mL), and the organic phase washed with aqueous NaCl until the washings were neutral. To oxidize the coupling product, the organic phase was treated with iodine (5 g) for 5 min. Excess oxidant was separated with $Na_2S_2O_3$, and the solution subjected to conventional workup. Chromatography of the residue on silica gel (column 20 × 4 cm) with toluene as eluent produced, after separation of a green, nonuniform preliminary fraction, a violet, red-fluorescent main fraction containing **8**. Recrystallization of the product from $MeOH/CH_2Cl_2$ (5/1) provided **8** as violet cubes (m.p. 219–220 °C, yield 214 mg (20 %); Table 2).

Received: January 21, 1997 [Z10012IE]
German version: *Angew. Chem.* **1997**, *109*, 1725–1728

Keywords: chirality · N ligands · photophysics · porphyrinoids · synthesis design

[1] J. Waluk, J. Michl, *J. Org. Chem.* **1991**, *56*, 2729; J. L. Sessler, *Angew. Chem.* **1994**, *106*, 1410; *Angew. Chem. Int. Ed. Engl.* **1994**, *33*, 1348.

[2] E. Vogel, M. Köcher, H. Schmickler, J. Lex, *Angew. Chem.* **1986**, *98*, 262; *Angew. Chem. Int. Ed. Engl.* **1986**, *25*, 257; E. Vogel, *Pure Appl. Chem.* **1990**, *62*, 557; *ibid.* **1993**, *65*, 143; *ibid.* **1996**, *68*, 1355.

[3] E. Vogel, M. Bröring, J. Fink, D. Rosen, H. Schmickler, J. Lex, K. W. K. Chan, Y.-D. Wu, M. Nendel, D. A. Plattner, K. N. Houk, *Angew. Chem.* **1995**, *107*, 2705; *Angew. Chem. Int. Ed. Engl.* **1995**, *34*, 2511.

[4] a) J. L. Sessler, E. A. Brucker, S. J. Weghorn, M. Kisters, M. Schäfer, J. Lex, E. Vogel, *Angew. Chem.* **1994**, *106*, 2402; *Angew. Chem. Int. Ed. Engl.* **1994**, *33*, 2308; b) E. Vogel, *J. Heterocycl. Chem.* **1996**, *33*, 1461.

[5] A French group reported a synthesis of corrphycene that was analogous to ours shortly after our publication [4a] appeared: M. A. Aukauloo, R. Guilard, *New J. Chem.* **1994**, *18*, 1205.

[6] An alternative corrphycene synthesis in which cyclization leading to the corrphycene framework is accomplished by an intramolecular Ullmann coupling of the corresponding α,ω-diiodotetrapyrrole: H. Falk, Q.-Q. Chen, *Monatsh. Chem.* **1996**, *127*, 69.

[7] H. J. Callot, A. Rohrer, T. Tschamber, B. Metz, *New J. Chem.* **1995**, *19*, 155. We are grateful to Prof. Callot for providing us with his results prior to publication.

[8] Hemiporphycene **8** affords stable complexes with numerous metals. Hemiporphycene–metal complexes with axial ligands have characteristic metal-centered chirality. Attempts to resolve the enantiomeric forms of the recently obtained complexes σ-phenyl-octaethylhemiporphycenatocobalt(III) and σ-methyl-octaethylhemiporphycenatorhodium (III) are in progress (collaboration between the groups of E. V. and J. L. S.).

[9] J. E. McMurry, *Chem. Rev.* **1989**, *89*, 1513; A. Fürstner, B. Bogdanović, *Angew. Chem.* **1996**, *108*, 2582; *Angew. Chem. Int. Ed. Engl.* **1996**, *35*, 2442.

[10] E. Vogel, P. Koch, X.-L. Hou, J. Lex, M. Lausmann, M. Kisters, M. A. Aukauloo, P. Richard, R. Guilard, *Angew. Chem.* **1993**, *105*, 1670; *Angew. Chem. Int. Ed. Engl.* **1993**, *32*, 1600.

[11] J. B. Paine III in *The Porphyrins*, *Vol. I* (Ed.: D. Dolphin), Academic Press, New York, **1978**, p. 226.

[12] 5-Ethoxycarbonyl-5′-formyl-3,3′,4,4′-tetraethyl-2,2′-dipyrrylmethane (**11**) was prepared by the acid-catalyzed condensation of 5-acetoxymethyl-2-ethoxycarbonyl-3,4-diethylpyrrole (**9**) [13a] with 3,4-diethyl-2-formylpyrrole (**10**) [13b]; colorless crystals from EtOH; m.p. 145–146 °C; yield 79 %. Reaction conditions: *para*-toluenesulfonic acid, CH_3CN, reflux, 3 h, inert atmosphere.

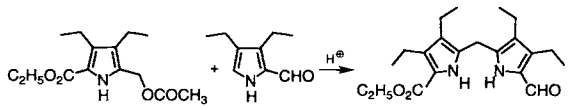

[13] a) H. H. Inhoffen, J. H. Fuhrhop, H. Voigt, H. Brockmann Jr., *Justus Liebigs Ann. Chem.* **1966**, *695*, 133; b) A. W. Johnson, I. T. Kay, *J. Chem. Soc.* **1965**, 1620.

[14] If **8** is contaminated with octaethylporphyrin, the latter can be removed by converting it and **8** into the corresponding zinc complexes (10 equiv of zinc acetate in MeOH, 1 h at reflux). Chromatography of the resulting mixture on silica gel with hexane/CH_2Cl_2 (5/2) as eluent produces two fractions. The first fraction (pink) consists of the porphyrin complex, and the second (blue-green) contains octaethylhemiporphycenatozinc(II) (violet needles from $MeOH/CH_2Cl_2$ (6/1), m.p. 260–261 °C). Liberation of **8** is achieved by treatment with concentrated H_2SO_4 (room temperature, 1 h) and conventional workup.

[15] Additional support for the structure of **7** is provided by the similarity of its NMR spectrum to that of the dibenzyl ester **12**, for which an X-ray crystal structure is available (as the *rac* diastereomer).

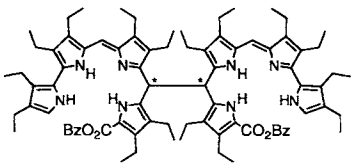

12

[16] An alternative route to **7** that avoids the tetrapyrrolic α,ω-dialdehyde **6** could involve an initial oxidative coupling of two molecules of **4** at the *meso* position with concomitant formation of a tetrapyrrylethane, followed by condensation with **5** to give **7**. Among the evidence militating against this route is the observation that in the first step a labile product can be detected by thin layer chromatography that has a color comparable to that of **7**, and from which **7** is formed only after treatment with ammonia.

[17] X-ray crystal analysis of **8**: $C_{36}H_{46}N_4$, $M = 534.77\ g\,mol^{-1}$, crystallized from CH_2Cl_2/CH_3CN; crystal dimensions $0.40 \times 0.28 \times 0.34$ mm, triclinic, space group $P\bar{1}$, $a = 8.106(2)$, $b = 10.053(3)$, $c = 20.390(6)$ Å, $\alpha = 87.05(2)$, $\beta = 83.97(2)$, $\gamma = 66.36(2)°$, $V = 1513.6$ Å^3, $Z = 2$, $\rho_{calcd} = 1.173\ g\,cm^{-3}$; $F(000) = 580$; $\mu_{Mo} = 0.69\ cm^{-1}$; of 6555 measured reflections 4020 were observed ($F_o^2 > 2\sigma F_o^2$); $\theta_{max} = 26.95°$; $R1 = 0.0618$, $wR2 = 0.1615$. Enraf-Nonius CAD4 diffractometer (room temperature, $Mo_{K\alpha}$ radiation, $\lambda = 0.71069$ Å). The structure was solved with direct methods and refined for all observed reflections against F^2 (heavy atoms with anisotropic, H atoms with isotropic temperature factors); $wR2 = [\sum w(F_o^2 - F_c^2)^2 / \sum w(F_o^2)^2]^{1/2}$. Programs used: MolEN (Enraf-Nonius) for structure calculation and SHELXL-93 (G. M. Sheldrick, Universität Göttingen, Germany) for refinement. Calculated in the Regionales Rechenzentrum der Universität zu Köln. Crystallographic data (excluding structure factors) for the structures reported in this paper have been deposited with the Cambridge Crystallographic Data Centre as supplementary publication no. CCDC-100248. Copies of the data can be obtained free of charge on application to The Director, CCDC, 12 Union Road, Cambridge CB21EZ, UK (fax: int. code +(1223)336-033; e-mail: deposit@chemcrys.cam.ac.uk).

[18] C. W. Bird, G. W. H. Cheeseman in *Comprehensive Heterocyclic Chemistry*, *Vol. 4* (Eds.: A. R. Katritzky, C. W. Rees), Pergamon Press, Oxford, **1984**, p. 4; K. M. Smith, *ibid.*, p. 386.

[19] J. W. Lauher, J. A. Ibers, *J. Am. Chem. Soc.* **1973**, *95*, 5148.

[20] We thank Prof. Y.-D. Wu (Hongkong) for the calculations.

[21] R. Bonnett, *Chem. Soc. Rev.* **1995**, *24*, 19; R. W. Boyle, D. Dolphin, *Photochem. Photobiol.* **1996**, *64*, 469.

[22] The high efficiency of the sensitized $O_2(^1\Delta_g)$ formation is of decisive importance when considering 2,7,12,17-tetrapropylporphycene (**16**) and other porphycenes as possible "second-generation" PDT photosensitizers: K. Schaffner, E. Vogel, G. Jori in *Biologic Effects of Light* (Eds.: E. G. Jung, M. Holick), de Gruyter, Berlin, **1994**, p. 312.

[23] P. F. Aramendia, R. W. Redmond, S. Nonell, W. Schuster, S. E. Braslavsky, K. Schaffner, E. Vogel, *Photochem. Photobiol.* **1986**, *44*, 555.

[24] S. Nonell, P. F. Aramendia, K. Heihoff, R. M. Negri, S. E. Braslavsky, *J. Phys. Chem.* **1990**, *94*, 5879.

[25] For example G. Rossbroich, N. A. García, S. E. Braslavsky, *J. Photochem.* **1985**, *31*, 37.

[26] Corrphycene **15** presents an as yet unsolved problem: its T-T absorption decays biexponentially in the absence of oxygen (lifetime components of 200 μs (≈30 %) and 1 ms (≈70 %)) and is completely quenched in the presence of oxygen giving rise to $O_2(^1\Delta_g)$ by a monoexponential process ($\tau_\Delta = (30 \pm 0.3)$ μs).

[27] D. O. Mártire, N. Jux, P. F. Aramendía, R. M. Negri, J. Lex, S. E. Braslavsky, K. Schaffner, E. Vogel, *J. Am. Chem. Soc.* **1992**, *114*, 9969.

[28] S. E. Braslavsky, G. E. Heibel, *Chem. Rev.* **1992**, *92*, 1381.

[29] G. Martínez, S. G. Bertolotti, O. E. Zimerman, D. O. Mártire, S. E. Braslavsky, N. A. García, *J. Photochem. Photobiol. B: Biol.* **1993**, *17*, 247.

[30] R. P. Burgner, A. M. Ponte Gonçalvez, *Chem. Phys. Lett.* **1977**, *46*, 275; B. M. Dzhagarov, G. P. Gurinovich, *Nauka* **1982**, *C.* 59; O. Ohno, Y. Kaizu, H. Kobayashi, *J. Chem. Phys.* **1985**, *82*, 1779; B. M. Dzhagarov, G. P. Gurinovich, V. E. Novichenkov, K. I. Salokhiddinov, A. M. Shul'ga, V. A. Ganzha, *Khim. Fiz.* **1987**, *6*, 1069; K. Kikuchi, J. Kurabayashi, H. Kokubun, J. Kaizu, H. Kobayashi, *J. Photochem. Photobiol. A: Chem.* **1988**, *45*, 261.

 © VCH Verlagsgesellschaft mbH, D-69451 Weinheim, 1997 0570-0833/97/3615-1654 $ 17.50+.50/0

Controversial Chemists

Linus Pauling: A Life in Science and Politics. By *T. Goertzel* and *B. Goertzel*. BasicBooks, New York, 1995. XVII, 300 pp., hardcover $ 27.50.—ISBN 0-465-00672-8

Force of Nature: The Life of Linus Pauling. By *T. Hager*. Simon & Schuster, New York, 1995. 771 pp., hardcover $ 35.00.—ISBN 0-684-80909-5

Linus Pauling in His Own Words: Selections from His Writings, Speeches, and Interviews. Edited by *B. Marinacci*. Introduction by *L. Pauling*. A Touchstone Book, Simon & Schuster, New York, 1995. 320 pp., paperback $ 15.00.—ISBN 0-684-81387-4

The life, both scientific and personal, of Linus Pauling, the only person to have received two unshared Nobel Prizes, was characterized by controversy. Even within his family, which was dedicated to his success, there was no consensus: "Linus Pauling may be the closest embodiment, in this age of uncertainty, amorality, and constant conflict, of a living universal hero."—Linus Pauling, Jr.; "My father is not the great man you think he is."—Peter Pauling (both quotations from the Goertzels' book, pp. xiii and 220, respectively). Almost everything about Pauling was larger than life. The internationally acclaimed scientist, educator, humanitarian, and political activist was characterized as one of "the twenty greatest scientists of all time, on a par with Newton, Darwin, and Einstein" (*New Scientist*); as one of the two greatest scientists of the 20th century, the other being Einstein; and as the greatest chemist since Antoine-Laurent Lavoisier, the 18th-century founder of modern chemistry. His *Nature of the Chemical Bond* (1939) is considered to be one of the most influential and frequently cited scientific books of the 20th century.

The Goertzels' book, the first biography to be published since Pauling's death at age 93, is a family effort, encompassing three generations, through the assistance of Mildred Goertzel and Victor Goertzel and with original drawings by Gwen Goertzel. In 1962, more than three decades ago, writer Mildred Goertzel and psychologist Victor Goertzel began work on this biography, with Pauling's assistance, as a continuation of their work on the childhood of eminent people (*Cradles of Eminence* and *Three Hundred Eminent Personalities*). Admiring Pauling especially for his leadership of the peace movement, they thought that this biography would be "inspirational for young people who might be thinking of a career in science or involvement in worthy causes."

Because they differed with Pauling about the focus of the book (he wanted the emphasis to be on his scientific work rather than his personality), they abandoned the project for a number of years, while continuing to follow Pauling's career. They were troubled by Pauling's crusade for megadoses of vitamin C in the prevention and treatment of the common cold and later by his treatment of the president and director of the Linus Pauling Institute of Science and Medicine, Arthur B. Robinson, whom they had interviewed extensively and had come to know personally. They again resumed work on the biography, which became "more critical, less pacifist hagiography."

The Goertzels then asked their eldest son Ted, Professor of Sociology at Rutgers University with an interest in the psychosocial roots of political beliefs, to continue the project by adding more interviews and material on Pauling's later scientific research and the controversies about orthomolecular medicine. In 1991, when they learned that Pauling had prostate cancer, they decided that Ted should prepare a final manuscript because his parents' health no longer allowed their full participation and because a complete rewrite by a single author would result in a more coherent book. Ted then asked his son, Benjamin, a mathematician and Lecturer in Cognitive Science at the University of Western Australia, to help with the chapters on Pauling's scientific work, which had come to occupy a more prominent part of the biography than originally planned.

The resulting book, like Hager's biography, deals with all aspects of Pauling's life and career from his birth in Portland, Oregon on February 28, 1901 to his death from cancer on his ranch near Big Sur on August 19, 1994—his childhood; education; study of atomic and quantum physics with Arnold Sommerfeld in Munich, Erwin Schrödinger (consistently spelled Schroedinger) in Zürich, and Niels Bohr in Copenhagen; his professorships at the California Institute of Technology, the Center for the Study of Democratic Institutions at Santa Barbara, California, the University of California, San Diego, and Stanford University; his use of one science (physics) to explain another (chemsitry); his combination of quantum mechanics and X-ray diffraction to win the 1954 Nobel Prize in Chemistry "for his research on the chemical bond and its application to the elucidation of the structure of complex substances"; his seminal contributions to chemistry, quantum mechanics, X-ray crystallography, anesthesia, electronegativity, the structure of proteins and DNA, nutrition, mineralogy, nuclear physics, and immunology; his work on molecular biology and orthomolecular medicine (a name that he coined); his work for the U.S. government during World War II; his campaign against nuclear weapons testing, which earned him the 1962 Nobel Prize for Peace; his evolution, encouraged by his wife Ava Helen, from an ivory tower scientist to an ardent and articulate public spokesman on technological issues and the social responsibility of scientists; his difficulties during the McCarthy era with government committees and the refusal of his passport application; his family life; his advocacy of megadoses of vitamin C for the common cold, cancer, and AIDS, the controversial work for which he is best known to the general public (Ted Goertzel's experience in statistical research methods was helpful here in making sense of the ongoing controversies concerning vitamins and health); and his

This section contains book reviews and a list of new books received by the editor. Book reviews are written by invitation from the editor. Suggestions for books to be reviewed and for book reviewers are welcome. Publishers should send brochures or (better) books to the editorial office: Redaktion Angewandte Chemie, Postfach 101161, D-69451 Weinheim, Germany. The editor reserves the right of selecting which books will be reviewed. Uninvited books not chosen for review will not be returned.

founding of the Pauling Institute and his feuds and lawsuits with former collaborators.

Not content to describe these and other events, the Goertzels have evaluated and interpreted them in the context of Pauling's public and private life and the state of science at the time. Because the book is intended for a general readership, they provide much background material and diagrams by Benjamin Goertzel's wife Gwen to elucidate the complexities of quantum physics, X-ray diffraction, wave mechanics, atomic and molecular orbitals (although in Fig. 7, p. 70, the p and d orbitals are mistakenly designated as s and p orbitals), resonance, protein structures, DNA, and other technical topics needed to understand the magnitude of Pauling's scientific contributions. Inasmuch as Pauling's modus operandi was largely intuitive, they devote considerable attention to his psychological profile and personality. Their book bears signs of hasty proofreading and contains a number of misspellings of scientists' names, understandable because the authors are not chemists.

In addition to primary and secondary sources, the Goertzels have made extensive use of interviews with Pauling, his relatives, friends, colleagues, and contemporaries; the diary that Pauling kept as a boy and that of his maternal grandfather, Linus Wilson Darling; the Linus and Ava Helen Pauling Papers at Oregon State University; and the results of Pauling's Rorschach inkblot tests that he had taken as one of the subjects in Anne Roe's classic study *The Making of a Scientist* (1953). (The latter results, along with their interpretations by eight psychologists to predict Pauling's personality, appear in a unique 22-page appendix—a feature that we have not seen in any other biography of Pauling. Victor Goertzel's doctoral dissertation involved use of the Rorschach test.) The Notes (5 pp.) and Selected References (2 pp.) contain items as late as 1994 and one from 1995. Sixteen illustrations of Pauling and others are provided.

Although the Goertzels began their project with Pauling's cooperation and assistance and he was reviewing the manuscript at the time of his death, their book is in no way an authorized biography. They are critical of Pauling in many ways. For example, they contrast Herman Branson's account of the discovery of the α-helix with Pauling's account; they thoroughly examine Pauling's apparent betrayal of Arthur Robinson, his closest collaborator and disciple, who had left a promising university position to cofound the Pauling Institute; and they discuss Matthias Rath's lawsuit claiming that Pauling had taken credit for his ideas on vitamin C and heart disease.

However, the overall coherent picture of Pauling that emerges from their book is an objective but empathic one. They conclude that "Linus Pauling the man was more than Pauling the chemist and, like all human beings, had flaws as well as virtues. Despite his intensely analytical mind, he was capable of being relentlessly driven by irrational emotions, a fact that became particularly obvious in the last decades of his life. In his later years, his combativeness and defensiveness increasingly triumphed over his brilliance and creativity ... In the long run, Linus Pauling the chemist will be remembered and Linus Pauling the man largely forgotten, but it was the man who made the chemist possible." With their great psychological insights, which evaluate Pauling's weaknesses as well as strengths, the Goertzels have succeeded admirably in going beyond Pauling's public persona to portray the most famous chemist of our time as an ambitious, complex, conflicted human being who spoke his own mind and lived a long life on his own terms.

Of the four biographies of Pauling that we have read (Anthony Serafini, *Linus Pauling: A Man and His Science*, Paragon House, New York, **1989**, David E. Newton, *Linus Pauling: Scientist and Advocate*, Facts on File, New York, **1994**; and the Goertzels' and Hager's books), Hager's biography, which appeared a month later and is more than twice as long as the Goertzels', is by far the most authoritative, detailed, and comprehensive. Thomas Hager, Director of Communications at the University of Oregon, freelance science writer, and former correspondent for *American Health* and the *Journal of the American Medical Association*, is, like Pauling, a native Oregonian whose intimate familiarity with many of the locales where Pauling spent much of his youth is evident from his minute descriptions tht invoke striking, realistic images that border on the poetic.

Hager's massive but eminently readable biography is the product of five years of thorough and meticulous research, involving more than forty hours of interviews with Pauling alone; scores of additional interviews with his family members, colleagues, rivals, students, and critics; personal correspondence; manuscripts; laboratory notebooks; scientific and nonscientific publications; archival materials; and government documents, including transcripts of Congressional Committee hearings and more than 3,000 pages of recently declassified FBI files, which we have not seen utilized in other Pauling biographies.

Hager uses all these sources to sort out opinion from fact and to dispel many of the misconceptions that have surrounded Pauling throughout his long life. In general, he is somewhat less critical of Pauling than the Goertzels, but he acknowledges his fierce competitiveness, litigiousness, lack of affection for colleagues, students, children, and family members – except for his wife, who was his closest friend, confidant, and political mentor – in short, all of the complexities and inconsistencies of a creative, brilliant, and outspoken human being who was neither saint nor sinner. Hager's book is uniformally excellent in its treatment of the scientific, political, and personal aspects of Pauling's life.

Hager has left no stone unturned in ferreting out information on events from the most significant to the relatively minor. Among the topics that he discusses but that the Goertzels fail to mention and that some other biographers have neglected are: J. Robert Oppenheimer's attempt in 1929 to persuade Pauling's wife to join him on a tryst in Mexico; Warren Weaver's crucial role in providing funds from the Rockefeller Foundation to support Pauling's research; Pauling's controversy with Dorothy Wrinch over the structure of proteins; his bout with life-threatening Bright's disease (nephritis); his invention of the Pauling Oxygen Analyzer to monitor oxygen levels in submarines; and Pauling's episode of being trapped on a cliff near his cabin, which produced a severe emotional reaction, a rare occurrence for Pauling, who always kept a firm grip on his feelings since his traumatic childhood.

Hager thoroughly explores Pauling's most celebrated scientific deteat, which dashed his hopes for a Nobel Prize for Physiology or Medicine – his failure to discover the structure of deoxyribonucleic acid (DNA), the physical basis of heredity, which was reported in 1953 by James D. Watson and Francis H. C. Crick. All the participants and events in this so-called "race for the double helix" are discussed, and the reasons for Pauling's loss of the race are revealed in Hager's book in great detail. Hager even cites an incorrect article on the structure of DNA by Edward Ronwin, a former CSUF chemistry professor – a paper of which no one in our department was aware.

Hager devotes considerable space to Pauling's political activities on behalf of civil rights, nuclear disarmament, and world peace. Although Pauling accomplished great and wonderful things and acquired world renown, it is indeed unfor-

 © VCH Verlagsgesellschaft mbH, D-69451 Weinheim, 1997 0570-0833/97/3615-1656 $ 17.50+.50/0

tunate that, because of these activities, he was denied research grants and his passport, was persecuted by the FBI and other governmental agencies, and was defended and supported only halfheartedly by the California Institute of Technology, to which he devoted almost four decades of his life, and snubbed by the American Chemical Society, which he had served as President in 1949. His battles with political enemies, although eventually resulting in his ultimate vindication, consumed much of his time and energy. As his wife expressed it, "It is just a shame for Linus to be wasting his talents in this way" (p. 520).

It is interesting to speculate as to what further discoveries Pauling might have made had he not been deflected from his goals by short-sighted, self-serving, mercenary, or jealous opponents. However, he never became embittered. In one of his last interviews (April 1, 1994), in response to our question as to how he was able to retain his positive outlook on life, he told us, "I suppose it's partially genetic ... actually the result of my having been pretty successful in my own career, and, of course, my feeling that we ought to be smart enough, we human beings, to solve our problems, whatever they are."

As Pauling states in his autobiographical introduction (completed only a few months before his death) to *Linus Pauling in His Own Words*, "Up to now ... there have been no general anthologies of my written words to provide lay readers with an overview of the many different interests that I have pursued during my lifetime." Fortunately, Barbara Marinacci, a consultant with the Pauling Institute who knew Pauling personally for many years, the sister of his son-in-law, and editor of his book *No More War!*, has produced a representative anthology of excerpts, about one-fifth published here for the first time, ranging from a sentence to several pages in length, from more than one hundred sources, including publications and a number of unpublished manuscripts, notes, and interviews.

Because her book is intended for a general rather than a scholarly readership, Marinacci has made minor editorial changes to reduce redundancies, added transitional words or sentences, and blended individual fragments. Although sources for specific fragments are not always identified, they are listed in chronological order for each of the 12 chapters in a separate section titled "Notes on Sources." Marinacci has provided an insightful preface and a useful four-page chronology summarizing Pauling's life and career, and she has inserted explanatory material (from a sentence to a page and in boldface type) between quotations to set the context.

The book is divided into three sections of three chapters each: I. The Path of Learning 1901–1922; II. The Structure of Matter 1922–1954; III. The Nuclear Age 1945–1994; and IV. Nutritional Medicine 1954–1994. This vivid self-portrait of an extraordinary scientist and humanist who possessed one of the greatest minds of our time makes a perfect complement to the Goertzels' and Hager's biographies discussed above. And until the long-awaited multivolume work-in-progress by chemist and science historian Robert J. Paradowski of the Rochester Institute of Technology, Pauling's official biographer and author of the 1972 doctoral dissertation, *The Structural Chemistry of Linus Pauling*, appears, Hager's book may be regarded as definitive.

George B. Kauffman
and *Laurie M. Kauffman*
California State University
Fresno, CA (USA)

Edward Frankland: Chemistry, Controversy and Conspiracy in Victorian England. By *C. A. Russell.* Cambridge University Press, Cambridge, 1996. xx + 535 pp., hardcover $ 110.00, £ 65.00.—ISBN 0-521-49636-5

Colin A. Russell, Professor Emeritus of History of Science and Technology at the Open University, spent the first half of his career as a practicing chemist. He first encountered Edward Frankland, the most eminent chemist in Victorian Britain, more than three and a half decades ago while working on his doctoral thesis (London University, 1962) on the rise and development of valency—one of the most fundamental concepts of modern chemistry and one inextricably linked with Frankland's name. This thesis formed the basis for the first in-depth study of the subject, *The History of Valency* (Leicester University Press, **1971**). Russell learned that Frankland, who is relatively unknown today, had been born a few miles from where he and his wife and frequent collaborator, Shirley Russell, were living. In the belief that Frankland's childhood and youth were his most formative years, he delved into local history, leading to the publication of *Lancastrian Chemist: the early years of Sir Edward Frankland* (Open University Press, **1986**).

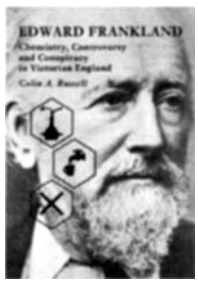

In a sense the volume under review here, the first scientific biography of Frankland, is a sequel to *Lancastrian Chemist*, but it is also complete in itself. Although Frankland himself wrote his own recollections, *Sketches from the life of Sir Edward Frankland* (privately printed, 1901; 2nd [expurgated] edition, 1902), it was incomplete and had the usual limitations inherent in any autobiography, and almost all copies of the first edition were withdrawn within months of its release. Thus the raw data for an extended biography were unavailable until Colin and Shirley Russell discovered a vast collection of Frankland papers in private hands. The Russells located and microfilmed other privately owned documents, traveling across the world in some cases. An account of their preliminary work on these and other documents that have recently come to light appeared in *Brit. J. Hist. Sci.* **1990**, *23*, 175. Not until Russell had digested this hitherto unpublished mass of material as well as primary and secondary sources from university, institutional, industrial, and governmental archives in Britain, Germany, New Zealand, and the United States, did he begin to write his latest book, which is a major new assessment not only of the life and work of "this self-made man from Lancaster alone", but also of the scientific and cultural environment in which he lived.

Edward Frankland was born on January 18, 1825 in Churchtown, Lancashire, the illegitimate son of Margaret Frankland, who had been a servant in the home of Edward Gorst, a prominent lawyer. Frankland's father was the latter's son, Edward Gorst, Jr., later also a distinguished lawyer. According to Russell, his illegitimacy, a secret that had to be suppressed, left him with a keen sense of social insecurity that contributed to his driving ambition to advance himself socially and monetarily, to be accepted by the chemical community, and to prove to himself that he had overcome his inherited disabilities, a dominant motivation throughout his life.

After attendance at eight schools and an apprenticeship in a druggist's shop in Lancaster, none of which provided him with the scientific education that he desired, at age 20 Frankland traveled to London to study systematic chemical analysis in Lyon Playfair's laboratory (a journey described with incredible attention to local color and detail in Russell's

 © VCH Verlagsgesellschaft mbH, D-69451 Weinheim, 1997 0570-0833/97/3615-1657 $ 17.50+.50/0

first chapter). The next year he followed Playfair as his Lecture Assistant to Putney College, where he met Hermann Kolbe, his first chemical collaborator and lifelong friend. With Kolbe he spent three months in 1847 in Robert Bunsen's laboratory in Marburg, where he met Sophie Fick from a German academic family, who became his wife in 1851 and by whom he had two daughters and two sons. A warm admiration for the German ideal of enlightened scholarship and the meritocracy of the intellect remained with Frankland all his life; he valued "the German division of Society into classes, which is here [Marburg] effected according to *mind* and not *money*."

After teaching at Queenwood College, a progressive private school, Frankland returned to Bunsen's laboratory in Marburg, where in 1849 he became the first Englishman to receive his Ph.D. In 1850 he succeeded Playfair as Professor at Putney College and became the first Professor of Chemistry at Owens College, Manchester (1851–1857), the forerunner of Manchester University. He became Lecturer in Chemistry at St. Bartholomew's Hospital (1857), simultaneously a Lecturer at the Royal Indian Military College at Addiscombe (1859–1861), Professor of Chemistry at the Royal Institution (1863–1865), and finally August Wilhelm von Hofmann's successor at the Royal College of Chemistry, a position which also made him official analyst for the London water supply (1865–1885). (Russell provides syllabuses of Frankland's courses, excerpts from his lectures, and detailed tables of his lectureships, appointments, and water analyses). Frankland's wife died in January 1874, and in May 1875, at the age of 50, he married 26-year-old Ellen Grenside, by whom he had two daughters. He was knighted in 1897 and died in Golaa, Norway on August 9, 1899.

Russell has chosen his subtitle "Chemistry, Controversy, and Conspiracy" advisedly. In chemistry, Frankland's discovery of zinc alkyls made him the true founder of organometallic chemistry, a field that he himself named and pioneered. These compounds not only were useful as reagents in synthetic organic chemistry, in which he was an acknowledged leader, but they also played a significant role in the creation of Cannizzaro's modern atomic weight system, and most importantly led Frankland to unite the radical and type theories into his crowning achievement in fundamental chemical theory—the idea that elements have a definite combining power, i.e., the concept of valency (1852). In 1866 he introduced the word "bond", a term universally used by today's chemists without realizing its originator. In his 1866 book, *Lecture Notes for Chemical Students*, he popularized the term along with his new structural formulas, which, along with his work as syllabus setter and trainer of teachers, made him one of the nineteenth century's great contributors to structural chemistry, chemical communication, and popular scientific education. In applied chemistry, Frankland established himself as one of Britain's leading academic consultants to industry and expert legal witnesses.

As "the greatest living authority on water supply", Frankland introduced into water analysis the entirely new concept of previous sewage contamination, which proved to be intensely controversial at a time when the ultimate cause of waterborne diseases was still speculative. For a number of reasons, the most important of which was probably the opposition of his chief rival August Kekulé, Frankland's claim to priority in the valency concept was mired in controversy, and more than two decades elapsed before his claim was publicly recognized. His involvement in "trade", i.e., his extensive consultancies and commercial activities, caused conflict with his fellow members of the shadowy, highly influential, all-male organization known as the X-Club, which included such luminaries as Crookes, Darwin, Huxley, and Tyndall. The agnosticism and anti-clericalism that had replaced his earlier religious beliefs and his participation in the X-Club, which was opposed to organized religion, served to estrange him further from his conventionally religious family, which was already opposed to his second marriage and his increasingly frequent absences. (Russell devotes considerable space to his troubled family relationships, making use of the papers, letters, and in the case of his older daughter Margaret the diary, of the children of his first marriage).

Frankland played a prominent role in the professionalization of chemistry in England, serving as president of the Chemical Society (1871–1873) and the newly founded Institute of Chemistry (1877–1880). Yet his "tendency to ride roughshod over proper democratic processes, to take short cuts, to form small groups of activists, and to manipulate individuals behind the scenes" and the Royal Society's horror of "trade" resulted in a conspiracy to deny the power-hungry Frankland its presidency. Also, following his death the Chemical Society and the Royal Society failed to publish a memorial lecture or death notice, respectively, either because the task was too difficult (to hide his illegitimacy Frankland had cloaked his private life in secrecy) or because his enemies wanted to deny him even posthumous honor.

Russell's thoroughly researched and meticulously documented book contains 52 illustrations and Frankland's original formulas along with their modern equivalents, and it is methodically organized into numbered sections and subsections. He is completely objective and devoid of hero worship and states: "A biographer does no one a service by implying that his subject has no faults." Although he does not hesitate to speculate about Frankland's motivations, he clearly distinguishes them from factual statements. His book considers in engrossing and fascinating detail every aspect of Frankland's life and career and is likely to prove to be a definitive biography. We heartily recommend it to both historians of science and chemists interested in the development of their science.

George B. Kauffman,
Laurie M. Kauffman
California State University
Fresno, CA (USA)

Laser Techniques in Chemistry. (Series: Techniques of Chemistry. Vol. 23). Edited by *A. B. Meyer* and *T. R. Rizzo*. Wiley, New York, 1995. 448 pp., hardcover $ 145.00.—ISBN 0-471-59769-4

This addition to the series *Techniques of Chemistry*, originally started by A. Weinberger, is welcome and timely in view of the continuing growth in the applications of laser spectroscopy to chemical problems, especially since no comparable survey of the field has appeared in recent years. The book contains ten articles by recognized experts, covering a selection of the most important methods. Regrettably, femtosecond spectroscopy is not included in these, but otherwise the choice of topics is excellent.

P. M. Felker contributes an article on "Fourier-Transform Nonlinear Spectroscopies". The techniques covered include stimulated emission Raman spectroscopy (SERS) with ionization detection, coherent Raman spectroscopy, and stimulated emission with fluorescence detection. The descriptions of the methods are illustrated by examples of applications to molecules and small molecular aggregates.

The article by R. E. Miller on "Near-Infrared Laser-Optothermal Techniques" gives technical details of the method and includes a good survey of the various types of detectors, with special emphasis on bolometer detectors. Examples of ap-

 © VCH Verlagsgesellschaft mbH, D-69451 Weinheim, 1997 0570-0833/97/3615-1658 $ 17.50+.50/0

plications are described, including studies of the dynamics of photochemical reactions and of energy transfer in collisions.

The article "Direct Absorption in Supersonic Free Jets", by D. S. Perry and G. A. Bethardy, contains many technical details concerning the geometry of jets for molecular beam experiments, the design of multipass absorption cells, and the processing of experimental data. The authors describe examples of electronic and vibrational spectroscopic measurements on several systems, including clusters. The contribution on "High Resolution Optical Spectroscopy in the Ultraviolet" (O. W. Pratt et al.) gives an excellent overview of the experimental aspects, followed by some very nice examples of applications to a wide variety of problems, including studies of hydrogen-bonding, van der Waals complexes, acid–base reactions, photoionization, and the dynamics of intramolecular relaxation processes.

J. W. Hepburn contributes an article entitled "Generation of Coherent Vacuum Ultraviolet Radiation: Applications to High-Resolution Photoionization and Photoelectron Spectroscopy". As well as describing the generation of tunable VUV radiation the author devotes special attention to threshold photoelectron spectroscopy. In the article "Time-Resolved Resonance Raman in the Visible and Ultraviolet: Techniques and Applications", P. A. Thompson and A. Mathies are concerned with the details of pulsed Raman spectrometers rather than with the fundamentals of Raman scattering. The examples of applications that they describe include some interesting studies of bacteriorhodopsin and of heme proteins. A. Sengupta and M. A. Foyer contribute an article on a special topic: "Local Order and Ultrafast Dynamics in Liquids: Transient Grating Optical Kerr Experiments". This is concerned with investigations of short-range order in noncrystalline systems—liquids, melts, and glasses. The method described here affords detailed insights into these systems, although it requires some knowledge of physics to be used effectively. The article "Electric Field Effects in Molecular Systems Studied via Perisistent Hole Burning" (R. I. Personov et al.) explains the basic principles of the hole-burning method and presents examples to show how it can be used to determine molecular structures and study the orientation of molecules in Langmuir–Blodgett films. The next article, "Excited Electronic State Properties from Ground State Resonance Raman Intensities", is concerned with a special application of resonance Raman spectroscopy, and describes in detail the experimental method, the theory, and the interpretation of the results.

In the last article G. C. Walter and R. M. Hochstrasser report on very recent work, under the title "Ultrafast Vibrational Spectroscopy: Methods, Theory and Applications". They describe optical pumping probe experiments on systems of biological importance, in particular heme proteins and the reaction center of the photosynthetic process.

From this brief summary of the contents it can be seen that the work covers a substantial part of the techniques of laser spectroscopy that can be used in chemical and chemically related research. In an easily readable style, each article treats the sequence from theory to experimental method to examples. Altogether the articles provide a wealth of useful information, together with extensive literature references which are carefully chosen and up-to-date. However, this is not a book for beginners, as it assumes a lot of previous knowledge. Nor is it a reference source—for that purpose a more detailed subject index would be necessary. The book can be recommended for physical chemists whose work involves the structure and dynamics of molecules, and for physicists engaged in chemistry-related areas of research. It is an essential addition to departmental libraries.

Helmut Baumgärtel
Institut für Physikalische
und Theoretische Chemie
der Freien Universität Berlin
Berlin (Germany)

 © *VCH Verlagsgesellschaft mbH, D-69451 Weinheim, 1997* *0570-0833/97/3615-1659 $ 17.50+.50/0*

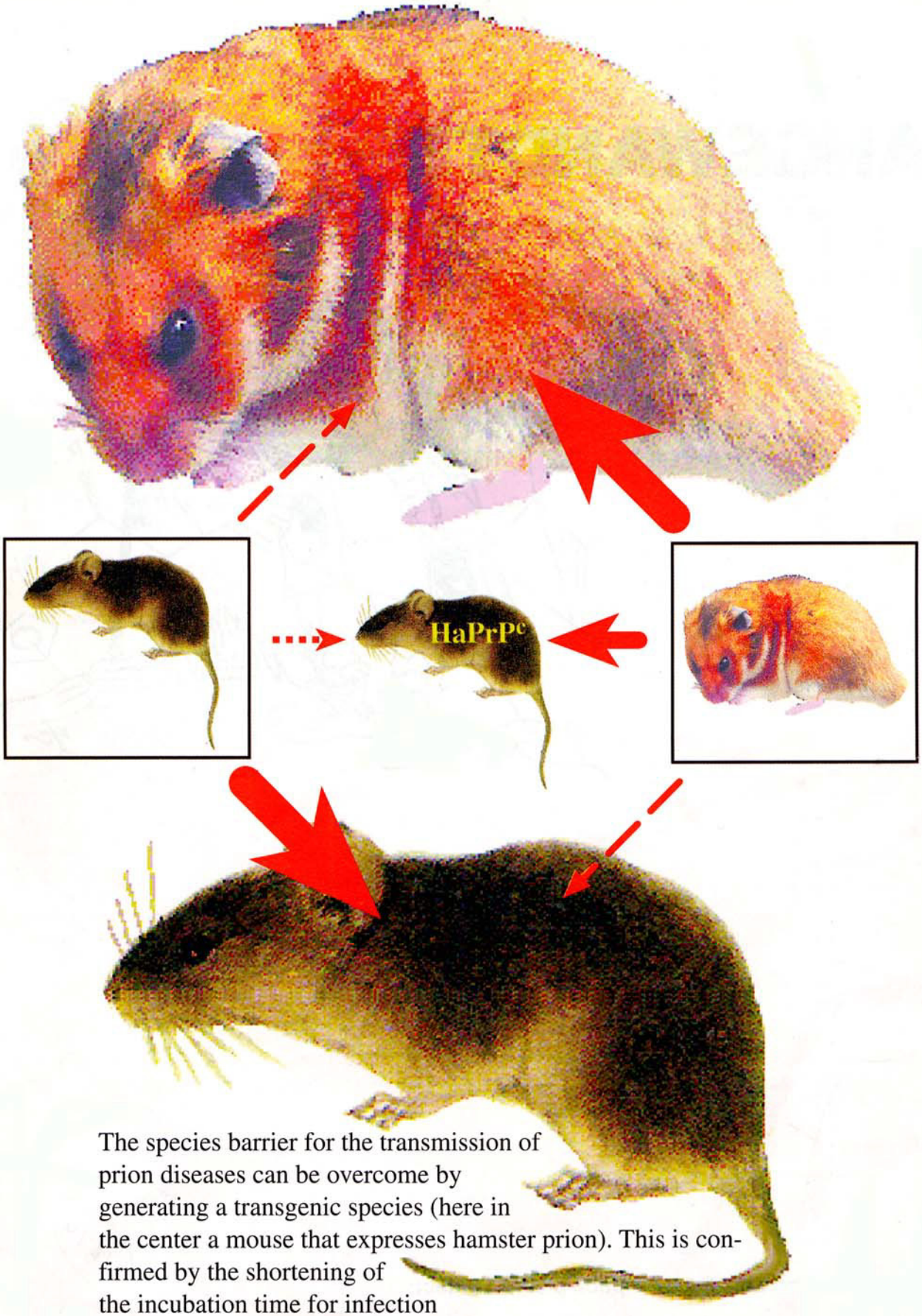

The species barrier for the transmission of prion diseases can be overcome by generating a transgenic species (here in the center a mouse that expresses hamster prion). This is confirmed by the shortening of the incubation time for infection with the prion of the foreign species: dashed arrows indicate low or no susceptibility, whereas fat arrows imply high susceptibility for prion diseases.

ANGEWANDTE CHEMIE ©WILEY-VCH

Chemistry and Molecular Biology of Transmissible Spongiform Encephalopathies**

Frank Edenhofer, Stefan Weiss, Ernst-Ludwig Winnacker,* and Michael Famulok*

Prion diseases are currently in the spotlight. Among them, the Creutzfeldt–Jakob disease in humans, scrapie in sheep, and bovine spongiform encephalopathy, or mad cow disease, are most commonly known. The term "spongiform" refers to the characteristic appearance of the lesions found in affected brains. It is likely that prion diseases originate from a causative agent that replicates independently of nucleic acids. Current research assumes that a structural isoform of prion protein, the scrapie form PrP^{Sc}, is the responsible pathogen. The three-dimensional structure, but not the amino acid sequence of the isoform differs from that of the normal cellular isoform, PrP^{c}. According to a widely accepted hypothesis, the normal isoform of the protein is converted by an autocatalytic process into the scrapie form upon contact with the latter. This hypothesis has not yet been proven. However, considerable progress has been made in the last few years, which might provide answers to many open questions about prion diseases, the subject of this review.

Keywords: Creutzfeldt–Jakob disease · gene technology · prion protein · protein-only hypothesis · protein structures

1. Introduction

The "tin pest" is a remarkable phenomenon, which shows some analogies to an even more remarkable disease, the transmissible spongiform encephalopathy (TSE). TSEs are thought to be transmitted through prions, which are infectious proteinaceous particles included in fibrillous plaques in the brains of affected species. This infectious agent is probably a structural isoform of the normal cellular form, which is expressed by the host organism. This pathogen enters the host organism upon infection, finds its way to the brain, forces the cellular isoform to change its structural conformation, and converts more and more of the physiological molecules into the deadly version. The phenomenon "tin pest" appears to proceed with striking similarity: From the molten state tin solidifies as the "normal" metallic β-tin in which every Sn atom is surrounded by six other Sn atoms to form a distorted octahedron. At temperatures below 13 °C the metallic β-tin can transform into a nonmetallic isoform, the cubic α-tin, a grey powder. Normally, this transition occurs at an infinitely slow rate. However, if the β-tin is "infected" by microscopically small particles of α-tin, the latter can act as crystal seeds for the conversion of the metallic into the powdery isoform. This damaging transformation, which in case of very valuable tinware is particularly vexatious—think only of the famous Viennese "Kapuzinergruft"—spreads like an infectious disease. The name "tin pest" thus illustrates this phenomenon quite vividly.[1]

The α-tin particles of the "tin pest" phenomenon thus resemble the prions, the pathogen of the spongiform encephalopathies. These diseases include scrapie (in sheep), bovine spongiform encephalopathy (BSE), transmissible mink encephalopathy (TME), and the human forms Creutzfeldt–Jakob disease (CJD), fatal familial insomnia (FFI), Kuru, and the Gerstmann–Sträussler–Scheinker syndrome (GSS), which all give rise to amyloid depositions in the brains of affected species from which the prions can be isolated.[2, 3] A large amount, if not all, of the infectious protein particles consists of PrP^{Sc} (abbreviation for *p*rion *p*rotein *sc*rapie). The amino acid sequence and charge distribution of PrP^{Sc} is identical to that of the noninfectious isoform of this protein, the cellular prion protein PrP^{c}.[4] A significant amount of the infectious particles consists of PrP 27–30, which is generated from the precursor PrP^{Sc} by amino-terminal proteolysis. The infectious PrP^{Sc} or PrP 27–30 is assumed to transform the cellular PrP^{c} by a yet unknown mechanism into PrP^{Sc}. In this way, PrP^{Sc} propagates and finally induces the disease. The difference between PrP^{c} and PrP^{Sc} might be reflected in different tertiary structures; PrP^{Sc} possibly acts as a "seed" for the conversion of the regular cellular form, PrP^{c}, into the scrapie isoform, PrP^{Sc}, by some unknown autocatalytic process. Prions are thus unique pathogens of an infectious disease, because their propagation functions without the information contained in a nucleic acid but rather

[*] Prof. Dr. E.-L. Winnacker, Priv.-Doz. Dr. M. Famulok,
Dipl.-Chem. F. Edenhofer, Dr. S. Weiss
Institut für Biochemie der Universität
Feodor-Lynen-Strasse 25, D-81377 München (Germany)
Fax: Int. code +(89)7401-7448

[**] The technical terms used in this publication are explained in Appendix 1.

 © WILEY-VCH Verlag GmbH, D-69451 Weinheim, 1997 0570-0833/97/3616-1675 $ 17.50+.50/0

seems to be solely determined by the amino acid sequence or tertiary structure of these proteins.

In this review we summarize the current state of prion research. The latest hypotheses concerning the replication of the pathogens of transmissible spongiform encephalopathies are presented and critically analyzed.

2. Pathology of Prion Diseases

2.1. Pathological Aberrations

The bovine spongiform encephalopathy (BSE) is the most commonly known form of transmissible spongiform encephalopathy (TSE) because of its epidemic occurrence in Britain. As a matter of fact, this kind of neurodegenerative disorder can occur in almost every mammalian species (Table 1).[5] One of the most remarkable characteristics of TSEs is the unusually long incubation period. For example, the time between infection and the first appearance of symptoms can be as long as 15 years in humans. The disease was therefore related to the "slow virus diseases" in the sixties. According to the current state of research, however, it seems unlikely that the spongiform encephalopathies are caused by viral infections (see Section 2.2.1). Because the immune system does not respond to the infection,[6] the infected organism is defenceless against the pathological changes. TSEs are neurodegenerative diseases. Consequently they display their destructive potential in the brain of the affected species. Neuropathologists diagnose TSE if the three following pathological changes are seen: 1) a spongiform change of the cortex (Figure 1), which perforates the brain, 2) a pathological proliferation of glia cells (gliosis), and 3) a loss of neuronal cells[7] linked to the deposition of an insoluble isoform of the prion protein "PrP^{Sc}". This pathological morphology in the brain of a CJD patient, for example, is accompanied by drastic disorders of body functions. In the EEG periodic anomalies are seen. After the appearance of the first symptoms such as

Table 1. Transmissible spongiform encephalopathies.

Name	Species	Origin
Scrapie	sheep, goat, mouse	infection
BSE[a]	cattle	infection
FSE[b]	cat	infection
TME[c]	mink	infection
CWD[d]	mule, deer, elk	infection
CJD[e]	human	sporadic, genetic, infection (iatrogenic)
GSS[f]	human	genetic
FFI[g]	human	genetic
Kuru	human	infection

[a] Bovine spongiform encephalopathy. [b] Feline spongiform encephalopathy. [c] Transmissable mink encephalopathy. [d] Chronic wasting disease. [e] Creutzfeldt–Jakob disease. [f] Gerstmann–Sträussler–Scheinker syndrome. [g] Fatal familial insomnia.

M. Famulok E.-L. Winnacker S. Weiss F. Edenhofer

Michael Famulok, born in Fulda in 1960, studied Chemistry at the University of Marburg, where he graduated in 1989. He carried out postdoctoral research in Cambridge, Massachusetts, and in Boston before he joined the Institute of Biochemistry at the Ludwig-Maximilians-Universität (LMU), Munich, in 1992, where he completed his habilitation in 1996. His research fields include aptamer technology, in vitro selection and in vitro evolution of ribozymes from combinatorial nucleic acid libraries, the study of nucleic acid/ligand interactions, and prion research.

Ernst-Ludwig Winnacker was born in 1941 in Frankfurt. He studied Chemistry at the ETH Zurich and graduated in 1968. Since 1980 he has held the chair of Biochemistry at the LMU, Munich. His research interests include the biochemistry of DNA repair and recombination processes, the development of vectors for gene therapy, and prions.

Stefan Weiss studied Biology at the University of Heidelberg. He graduated in the group of Roger Goody at the Max-Planck-Institut für Medizinische Forschung in Heidelberg in the field of the reconstitution of the HIV-1 initiation complex for retroviral cDNA synthesis. Since 1993 he has been working on transmissible spongiform encephalopathies at the LMU München, where he became head of the prion research group at the Genzentrum in 1995.

Frank Edenhofer was born in 1968 in Munich. He studied Chemistry at the LMU, Munich, from 1989 to 1994. In his graduate work since 1995 in the prion research group at the Genzentrum, he is working on the identification and characterization of prion cofactors and the heterologous expression of PrP^{c}.

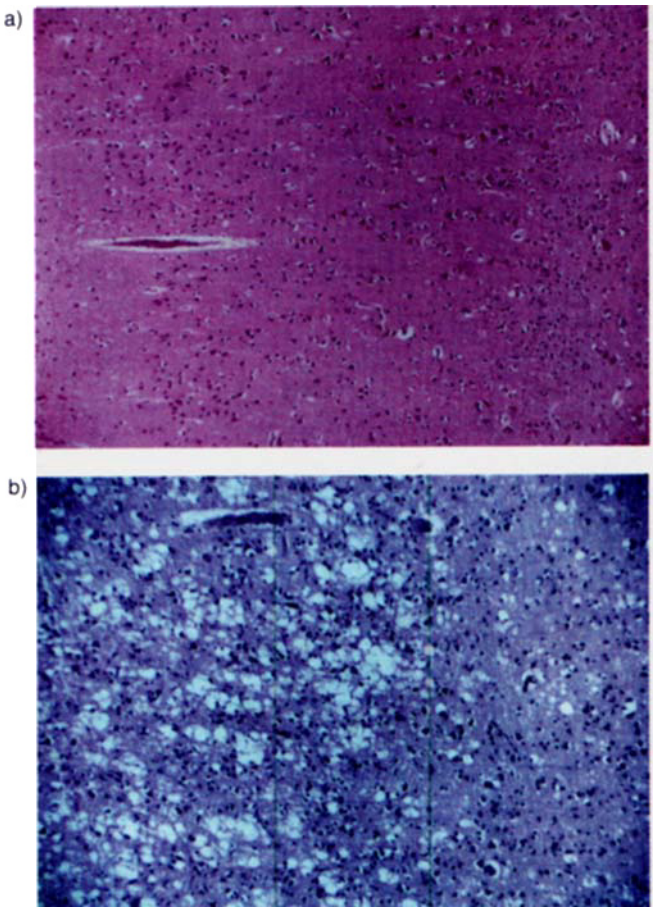

Figure 1. Thin sections of the cortex of a healthy brain (a) and of the brain of a patient who died of CJD (b). The perforation of the cortex (spongiosis means sponge-like changes) is clearly seen in this figure. We are grateful to H. A. Kretzschmar (Institute of Neuropathology, Göttingen) for providing these images.

amnesia, visual defects, and motoric malfunctions, the disease inevitably leads to death within a few months after progressive dementia. No therapeutic approaches to cure the disease exist; reliable diagnosis in a living organism is difficult.

2.2. The Pathogen

2.2.1. The Virino Hypothesis

TSEs show a number of symptoms that can be attributed to a disease caused by a viral infection. For the most commonly used mouse line C57Bl/6, for example, at least eight different TSE strains are known, which differ in specific attributes such as incubation period, nature and distribution of defects, and some other biochemical characteristics.[8, 9] The incubation periods differ when genetically identical (isogenic) mice are infected with isolated samples of different scrapie strains. These strains are passed by infection from animal to animal without loss of their specific symptoms.[10] This strain specificity within one species would argue for inheritable information and for genetic elements that contribute to the reproductive process. On the other hand, none of the experiments to isolate a virus responsible for TSE infections have yet been successful. A virus usually consists of a protein and a nucleic acid portion. The protein part protects the viral genome against external chemical and mechanical influence and in some cases helps the virus to invade the host cell. The nucleic acid represents the genetic material and therefore the infectious potential. It encodes for those proteins required for the replication of the virus in the host. Today, only a few scientists support the hypothesis of a viral transmission of TSEs (Figure 2A). For many years, the

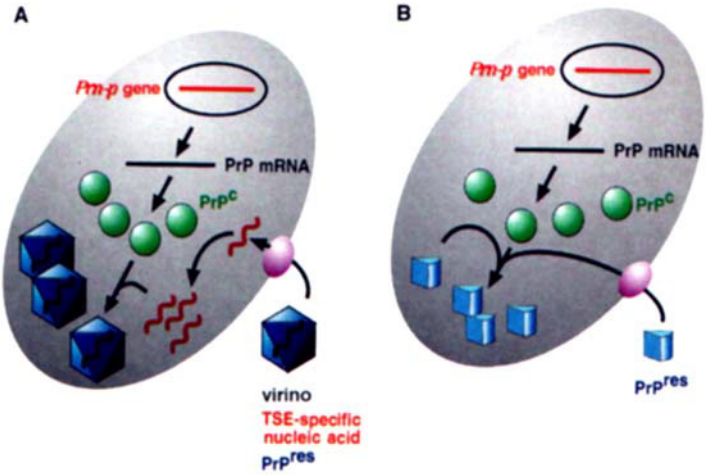

Figure 2. Models for prion propagation. A) The virino model assumes that the scrapie pathogen consists of a TSE-specific nucleic acid and the proteinase-resistant form of the prion protein PrP^{res}. The actual infectious agent, the not yet identified nucleic acid (red wavy line), is protected by packaging with PrP^{res} (blue), which has a low solubility and is extremly resistant. The virino particle invades the cell (possibly by receptor-mediated endocytosis; the putative receptor is shown in violet) and releases the nucleic acid. This nucleic acid is replicated by means of the cellular replication machinery, and the descendant molecules can associate with the cellular PrP to build new virinos. PrP^c (green spheres), which is encoded and synthesized by the host cell, is thereby converted into PrP^{res}. B) The "protein-only" model assumes that the TSE pathogen multiplies without participation of nucleic acids. The infectious particle, the prion, is identical with PrP^{res}. According to this model, exogenous PrP^{res} invades the cell (the participation of a specific receptor is likely) and converts the cellular PrP^c by direct interaction with PrP^{res}. The newly generated PrP^{res} is infectious by itself and is able to convert residual PrP^c into PrP^{res} in an autocatalytic cycle.

protagonists of the virino hypothesis—above all Laura Manuelidis (Yale Medical School) and Heino Diringer (Robert-Koch Institut, Berlin)[11]—have tried to identify such a virus without success. Diringer believes to have morphological evidence for the existence of such a virus, because in his laboratory small, symmetrical structures could be detected by electron microscopy in the brains of scrapie-infected hamsters.[12] In later experiments similar structures were indentified in the brains of deceased CJD patients.[13] These particles, which can not be detected in control tissues of healthy organisms, have a diameter of 10–12 nm. If these structures were indeed viruses, they would be much smaller than the smallest known virus, the porcine circo virus, which is 17 nm in diameter.[14]

The smallest known pathogens are viroids, small circular RNA molecules about 300 nucleotides in length, which infect plants.[15–19] The group of Detlef Riesner in Düsseldorf has carried out a systematic search for such nucleic acids in infectious scrapie samples.[20, 21] They were able to identify nucleic acids in infected preparations, but their maximum length was restricted to 80 nucleotides.[21] The genome of such a hypothetical virus or viroid would thus be considerably smaller than that of all other known viruses. Consequently, Riesner's interpreta-

tion of these results is that the existence of a scrapie-specific virus can be regarded as highly unlikely.[2, 22, 23]

2.2.2. *The "Protein-Only" Hypothesis*

The fact that no TSE virus could be detected so far is, of course, no proof that such a virus does not exist. How difficult the identification of pathogens of viral diseases can be was demonstrated, for example, by the search for a hepatitis C pathogen. It took ten years of intensive research to identify it as a virus.[24] But there is other clear evidence that nucleic acids are unlikely to be involved in the replication of TSE pathogens. Tikvah Alper et al. recognized in the sixties already that scrapie samples are resistant to nucleases and UV irradiation.[25] Usually, nucleic acids are inactivated under such conditions. Even more remarkable than these results was the fact that the scrapie pathogens lost their infectivity when they were treated with protein-denaturing agents like 8 M urea or phenol. This unusual feature of the scrapie pathogen led to the first—very cautious—speculation about the existence of infectious proteins as indicated by the title of Alper et al.'s paper:[26] "Does the scrapie agent replicate without nucleic acid?". At that time this unorthodox hypothesis could not make headway against the conventional knowledge about infectious diseases. How might an infectious agent replicate in the host without nucleic acids? Can a protein replicate itself? The classical dogma of molecular biology—the flow of genetic information from nucleic acid to protein—seems to be violated.

In 1967 J. S. Griffith was the first to suggest a possible mechanism for a self-replicating protein, which caused scrapie.[27] Stanley Prusiner of UCSF supported and extended this hypothesis by a series of experiments, which clearly showed a correlation between a protein and the observed infectivity. For example, Prusiner's group demonstrated for the first time that the infectivity of the samples increased when a specific protein contained in the samples was enriched. The concentration of this protein was found to be proportional to the titer of the infectivity in the animal.[28, 29] On the basis of these results Prusiner developed the "protein-only" hypothesis. He dubbed this new kind of pathogen as "prion", which is a short form for proteinaceous infectious particle.[30] The purification and thorough biochemical examination of this remarkable protein from the brains of affected animals was achieved by Prusiner's group after several years of intensive research. The continuing characterization of the pathogen resulted in the surprising discovery that the pathogenic protein possesses a cellular homologue. Together with the group of Charles Weissmann at the ETH Zürich they were able to clone and sequence the host gene (*Prn-p*) which encodes for PrP^c.[31, 32] This cellular prion protein, designated as PrP^c, is expressed in every normal mammal—mainly in the brain—without causing any harm to the organism. Today we know that the prion protein plays a dual biochemical role. On one hand it exists as the normal cellular form PrP^c (c for cellular); on the other hand, it can exist as a pathogenic and possibly infectious isoform PrP^{Sc} (sometimes PrP^{res}: Sc for Scrapie, res for proteinase K resistant). The PrP^{Sc} leads to death of the affected organism, whereas the biological significance of the PrP^c form is still unknown (see Section 5.3.2). A very strong argument for the protein-only hypothesis was provided by Weissmann and his co-workers, who generated transgenic mice whose *Prn-p* gene was destroyed so that they no longer expressed PrP (see Section 5.3). These so-called "PrP-knockout mice" were resistant to scrapie infections.[33] Without any doubt, the long-accepted hypothesis that the amino acid sequence of a protein is the only determinant for the biologically relevant 3D structure[34] is contradicted by the protein-only hypothesis.

Although the arguments for the protein-only hypothesis are quite compelling, a final experimental proof of the infectivity of the prion protein is still missing. The advocates of the protein-only hypothesis interpret this lack of proof as a simple preparative problem, because in purified samples only one of 10^5 PrP^{res} molecules is infectious;[22] enrichment of infectious portions is thus correspondingly difficult. Critics of the protein-only hypothesis claim that the formation of proteinase K resistant PrP^{res} is just a concomitant phenomenon, a pathological product of the infection by a not yet identified virus. This argument can be supported by experiment as well. Lasmézas et al. recently reported that mice infected with BSE samples indeed showed symptoms similar to TSE, but in 55% of the cases they could not detect proteinase K resistant PrP^{res} in the brains of the test animals.[35] These and other results show that the prion protein undoubtedly plays a central role for the pathogenesis of TSE, but until today it has not been proven that it represents the only infectious agent.

3. PrP^c and PrP^{Sc}: Differences and Common Features

The prion protein seems to be of considerable importance for the appearance of spongiform encephalopathies. In mammals as well as in some avian species the protein is expressed mainly in the brain. The prion protein is assumed to play an important biological role as is the case for many other highly conserved proteins. Various recent evidence indicates that it is important for the normal physiological function of the synapses[36] and for the long-term stability of Purkinje neurons (huge dendritic ganglial cells in the mid-layer of the cerebellum cortex),[37] as well as for the regulation of circadian rhythms and sleep patterns[38] (see Section 5.3.2. for more details).

The following statements about the composition and structure of the prion protein refer to the Syrian golden hamster, unless otherwise stated. This species is particularly suited for experimental research into TSEs, because the incubation period is only 70 days and correlates exactly with the dosage of the infectivity of the samples. According to present knowledge the characteristics of hamster PrP can be transferred with only minor modifications to PrP of other mammalian species.

3.1. Posttranslational Modifications and Infectivity

The PrP coding sequence is located entirely within an exon of the unique *Prn-p* gene.[32] Therefore, different splicing variants of PrP mRNA can be excluded. Translation of PrP mRNA leads to a PrP precursor protein of 254 amino acids in length (Figure 3). Posttranslational modification then leads to the removal of an amino-terminal signal peptide of 22 amino acids (amino

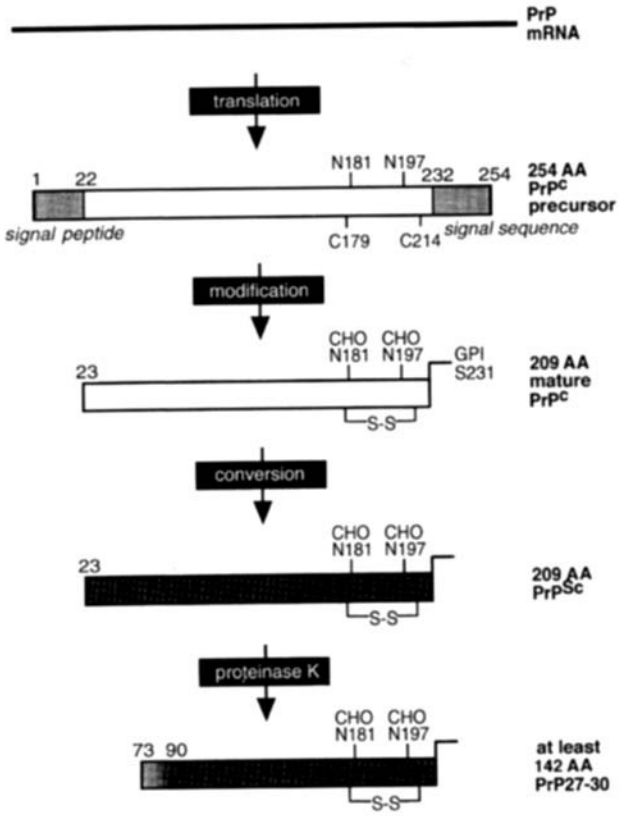

Figure 3. Maturation of PrP^c of the Syrian hamster and its conversion into the proteinase K resistant forms PrP^{Sc} and PrP 27–30. The primary structure of PrP^{Sc} does not differ from that of PrP^c. However, the two isoforms show different reactions towards proteinase K: whereas PrP^c is completely digested, PrP^{Sc} leaves a proteinase-resistant core, PrP 27–30, whose composition is not homogeneous. AA = amino acid.

acids 1–22) and of a signal sequence of 23 amino acids at the carboxy terminus (amino acids 232-254).[22] The protein contains a glycosyl phosphatidylinositol (GPI) anchor at serine 231 by which it is anchored to the cell membrane. PrP^c can be released from the cell membrane by cleavage with phosphatidylinositol-phospholipase C.[39] Characteristic for PrP is a region composed of amino acids 50–90. This region refers to five consecutive glycine- and proline-rich octapeptide sequences ("G-P repeats"). Polymorphisms within the G-P repeats have been related to hereditary forms of TSEs (see Section 4.3.2) (genetic polymorphism: differences in the genotype within a single population that cannot be explained by naturally occurring mutation rates alone). PrP is glycosylated at asparagine residues N181 and N197.[40–42] In addition, a disulfide bond forms between C179 and C214.[4, 29, 43] The resulting mature PrP, 209 amino acids in length, exists as the noninfectious form PrP^c in healthy animals. In infected hamsters the PrP^{Sc} isoform, which is generated by a yet unknown mechanism, is found as well.

Although the two isoforms PrP^c and PrP^{Sc} display the same amino acid sequence, they differ significantly from each other in many respects. As a physiological cellular protein, PrP^c does not show infectivity, whereas preparations of PrP^{Sc} do. The infectivity of prion-containing samples is maintained even in preparations treated under conditions that usually lead to inactivation of nucleic acids and most proteins; for example, incubation with formaldehyde, irradiation with UV light and X-rays, or incubation with nucleases and proteases.[31, 44, 45] The infectivity can be inhibited by heat only at temperatures above 130 °C. Infectivity is also effectively stopped by treatment with NaOH or KOH (2 N) for several hours. Incubation with proteinase K leads to the complete digestion of PrP^c, but PrP^{Sc} shows partial resistance to treatment with proteinase K.[32, 45–48] The proteinase-resistant fraction is composed of protein fragments truncated at the N-terminus and starting at amino acids between position 73 and 90. This form is also found in highly infectious preparations; it shows an electrophoretic mobility in denaturing polyacrylamide gels that corresponds to a size of 27 to 30 kDa and is therefore designated as PrP 27–30 (Figure 3). Once formed in the cell, PrP^{Sc} will not be degraded in contrast to PrP^c. The pathogenic isoform accumulates in secondary lysosomes, on the cell surface, or in the extracellular space.[49]

There is another significant physical difference between the two isoforms. PrP^c is soluble in nonionic detergents, whereas PrP^{Sc} is not. Detailed examinations of the solubility have been performed by Riesner and his group. In a recent publication they examined different ionic and nonionic detergents with respect to their ability to dissolve PrP 27–30.[50] Ultrasonication of purified infectious prion rods in the presence of 0.2–0.3% of sodium dodecylsulfate (SDS) resulted in a soluble fraction, which did not show sedimentation after ultracentrifugation for 1 h at 100000 × *g*. Relative to the infectious amyloid polymers consisting of PrP 27–30, protein in this soluble fraction contained a large number of α-helical regions and a small number of β-sheets. Furthermore, this fraction contained spherical particles with a diameter of about 10 nm and a sedimentation constant of 6 S. Each of these particles was composed of four to six PrP 27–30 molecules which, surprisingly, showed only weak or no infectivity at all. Thus, infectious preparations of soluble prion proteins could *not* be obtained in this study. When the particles were treated with 25–30% acetonitrile the α-helical regions were converted into β-sheets, as demonstrated by circular dichroism (CD) measurements. Under these conditions PrP 27–30 aggregates in nonsoluble, irregular polymers and shows partial resistance to proteinase K treatment. Insolubility and aggregation of the spheric particles treated with acetonitrile have been attributed to a conversion into β-sheets. The shape of these aggregates of PrP 27–30 clearly differs from those of the prion rods from the brains of scrapie hamsters initially used for these experiments; moreover, they did not show infectivity. As a result, protease resistance cannot necessarily be correlated with infectivity.[50]

3.2. Secondary and Tertiary Structure

The differences in the solubility of PrP^c and PrP^{Sc} might reflect differences in the secondary or tertiary structure of the two isoforms.[51] Spectroscopic data obtained by circular dichroism (CD),[52] Fourier transform infrared spectroscopy (FTIR),[53] and mass spectrometry (MS)[54] indeed provided evidence for marked differences in the secondary structure of PrP^c and PrP^{Sc}. PrP^c shows a 42% α-helical content and only 3% β-sheets, whereas PrP^{Sc} has 30% α-helical and 45% β-sheet con-

tent.[51, 52] These studies indicated that during conversion about half of the α-helical portions in PrP^c are converted into β-sheets of PrP^{Sc}.[52, 55] The mechanism by which the PrP^c is unfolded and then changed into PrP^{Sc}, however, is unknown. It is possible that the change in protein structure associated with this process requires a high activation energy.[51]

Computer models of the three-dimensional structure of the cellular PrP^c have been carried out with techniques of structure prediction such as the Chou–Fasman method or the Garnier–Osguthorpe–Robson algorithm.[56] To obtain a structural model for the Scrapie isoform, the aforementioned spectroscopic data as well as comparative analyses of the genes of various species were considered. According to this model, PrP^c contains a helix bundle of four α-helices (H1 to H4; Figure 4B, 5A).

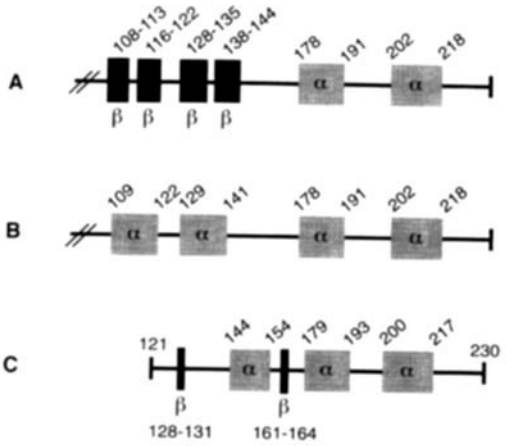

Figure 4. Secondary structures of PrP^c and PrP^{Sc}. A) Computer model of PrP^{Sc} (based on genetic data); B) computer model of PrP^c (determined by the Chou-Fasman method and the Garnier-Osguthorpe-Robson algorithm); C) schematic representation of the secondary structure determined by NMR spectroscopy. The position of the two carboxy-terminal α-helices was confirmed almost exactly by NMR spectroscopy; however the seconday structure of the domain around AA 121–178 determined by NMR spectroscopy clearly deviates from the computer model (B, C). The model proposed for PrP^{Sc} suggests a four-stranded β-sheet structure between amino acids 108 and 144 and two C-terminal helices whose position corresponds to that of PrP^c. There are no NMR data available for PrP^{Sc} due to the insolubility of the protein. (Based on data from refs. [56, 57, 61].)

H1 is formed by amino acids 109–122, H2 by amino acids 129–141, H3 by amino acids 178–191, and H4 by amino acids 202–218 (Figure 4B and 5A). The algorithm did not provide a conclusive prediction for the region comprising amino acids 23–108 in which the prion proteins contain the characteristic five octapeptide sequences in tandem orientation. For PrP^{Sc} six different structural models are suggested from a list of 10^6 initial structures. All six PrP^{Sc} models contain a four-stranded β-sheet structure which is covered by two α-helices on one side.[57] Figure 5B shows a schematic representation of these six models. Among them, model 2 correlated best with the genetic data (see Fig.4A). Accordingly, the β-sheet regions S1 to S4 are flanked by amino acids 108–113/116–122 for S1a/S1b, 128–135/138–144 for S2a/S2b, 178–184/187–191 for S3a/S3b, and 202–210/213–218 for S4a/S4b. The location of the two helices H3 and H4 corresponds to that of helices H3 and H4 in PrP^c. As suggested by this structural model, helices H1 and H2 should each convert into two

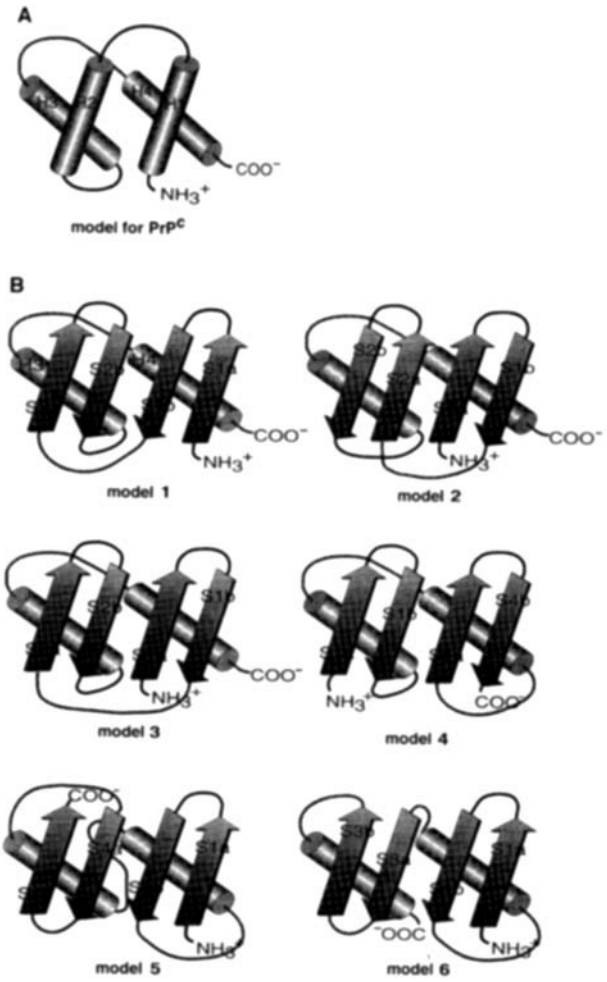

Figure 5. A) Computer-generated structural model of PrP^c modified according to ref. [57]. Two helices at a time are twisted together to form a bundle of four. B) Structural model of PrP^{Sc}. Model 2 correlates best with the genetic data of different species.

anti-parallel β-sheet structures during the structural conversion of PrP^c into PrP^{Sc}.[57]

In earlier experiments synthetic peptides of prion proteins have been examined for the aforementioned structural elements. Among four synthetic peptides which were equivalent to regions H1–H4, three exhibited only poor solubility in water. Spectroscopic data (FTIR, CD), as well as that from electron microscope images, indicated that they formed β-sheet structures and polymerized into fibrils.[58, 59] In contrast, CD and NMR experiments performed in organic solvents such as hexafluoroisopropyl alcohol (HFIP) or detergents like sodium dodecylsulfate (SDS) showed that not only H1 and H2, but also longer peptides containing these helical regions formed α-helices.[60] It therefore seems quite plausible that synthetic peptides are able to model certain aspects of the conformational differences suggested for the prion protein isoforms.

Recently the three-dimensional structure of a domain of recombinant mouse PrP^c was elucidated by NMR spectroscopy.[61] To obtain the required large amounts of protein, the mouse PrP fragment composed of amino acids 121–231 was overexpressed in the periplasm of *E. coli* cells.[62] Originally, it was attempted to express murine PrP 108–231. However, the

expression resulted in proteolytic cleavage at amino acids 112, 118, and 120. As a consequence, the protein could be obtained in stable form only from position 121. Previous studies had shown that the segment 81–231 of mouse PrP is sufficient for prion propagation in these species, indicating that the carboxy-terminal region of the protein is functionally much more important then the amino terminal region.[63] The domain PrP 121–231 used for the determination of the NMR structure lacks an extended region of the N-terminus (fragment 81–120). It is thus currently not known whether this extended region is required for the pathology of the disease or not; this domain, however, contains the majority of certain point mutations that were associated with the appearance of familial (inherited) cases of human prion diseases (see Section 4.3.2).[64]

The secondary structure of PrP121–231 determined by NMR spectroscopy is characterized by three α-helices as well as a two-stranded antiparallel β-sheet (Figure 4C). The helices are formed from amino acid residues 144–154, 179–193, and 200–217. A comparison with the structural model suggested previously[56, 57] shows that the location of H3 and H4 correlates almost exactly with that of the two C-terminal helices in the NMR studies (Figure 4). Both H2 (suggested to be formed by residues 129–141) and H1 (formed by amino acids 109–122) of the structural model are missing in the "NMR fragment". Instead, in the structure determined by NMR spectroscopy an extremely short antiparallel β-sheet structure not predicted by the structural model appeared at positions 128–131 and 161–164. This β-sheet domain in PrP^{c} might act as a seed during the conversion into PrP^{Sc}. Interestingly, the seconday structure deviates from the computer model mainly in the N-terminal region, which was heavily truncated in the fragment used for the NMR experiment (Figure 4). It remains to be seen whether the truncation of amino acids 23–120 results in significant structural changes within the N-terminus. At worst, essential elements of the prion protein may be located within this segment. The tertiary structure of PrP^{c}, determined by NMR spectroscopy, is dominated by a twisted, V-shaped arrangement of the two C-terminal helices in which the first α-helix and the β-sheet is embedded (Figure 6).

A comparison of the three-dimensional structure of PrP^{c} with a corresponding structure of the infectious PrP^{Sc} or PrP 27–30 would be interesting. However, a high-resolution, three-dimensional structure determination of the infectious prion isoforms by crystal structure or by NMR spectroscopy in solution is difficult because of the insolubility of these proteins. A technique that might lead to a structure determination of the insoluble scrapie isoform PrP^{Sc} is solid-state NMR spectroscopy. However, this requires weighable amounts of ^{13}C- or ^{15}N-labeled PrP^{Sc}, which is at present technically difficult.[65] First experiments in this direction have been carried out with a ^{13}C-enriched H1 fragment of hamster PrP, consisting of amino acids 109–122 (sequence: MKHMAGAAAAGAVV).[66] This study provided additional evidence for the ability of H1 to convert from an α-helical into a β-sheet structure. When the peptide was lyophilized from a solution of 50% acetonitrile/water, the chemical shifts in the solid-state NMR spectrum within region 112–121 were characteristic for β-sheet structures. Samples lyophilized from HFIP, on the other hand, showed chemical shifts which pointed to an α-helical secondary structure in region 113–117. A complete conversion into the α-helical form was not detected. Refolding of the α-helical into the β-sheet form was obtained after dissolving the samples in water. These results are in accordance with experimental observations that PrP can exist in different conformations. Furthermore, they correlate with structural predictions based on biological data and theoretical models which attribute to H1 an important role in determining the conformational differences between PrP^{c} and PrP^{Sc}.

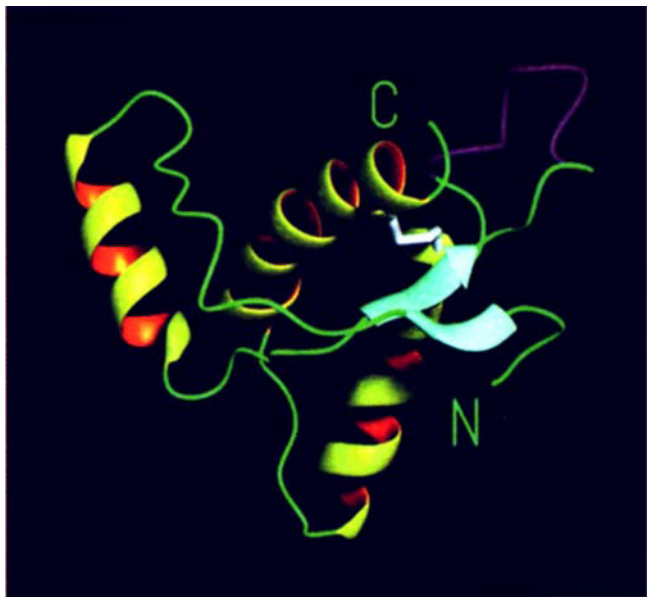

Figure 6. Structure (shown as a "ribbon diagram") of the mouse PrP^{c} fragment AA 121–231, determined by NMR spectroscopy [61]. The fragment was derived by recombinant technology from Escherichia coli. The structure contains three α-helices (yellow) and a double-stranded anti-parallel β-sheet structure (turquoise). The two C-terminal helices are mutually twisted into a V-shaped arrangement and are connected by a disulfide bond (white) between C179 (at the first turn of the second helix) and C214 (last turn of the third helix). The N-terminal helix flanked by the two β-sheet structures (turquoise) is arranged in front of this region. The short, antiparallel β-sheet structure might serve as a seed for the formation of the extensive β-sheet regions in PrP^{Sc}.

3.3. Models for the Mechanism of Prion Propagation

The next question concerns the mechanism by which the PrP^{Sc} propagates in the host cell without the involvement of nucleic acids. The protein-only hypothesis proceeds from the assumption that the PrP^{c} of the host cell is converted into PrP^{Sc} by the influence of exogenous PrP^{Sc} (which, for example, is taken in orally). The two currently competing models differ with respect to the (quaternary) structure of the infectious unit.

3.3.1. The Heterodimer Hypothesis

According to Prusiner's heterodimer hypothesis[22] PrP^{Sc}–PrP^{c} heterodimers are formed first. PrP^{c} is partially unfolded and then refolded under the influence of PrP^{Sc}, which results in the formation of a PrP^{Sc} homodimer (Figure 7A). The newly generated PrP^{Sc} can again induce the conversion of PrP^{c} in an

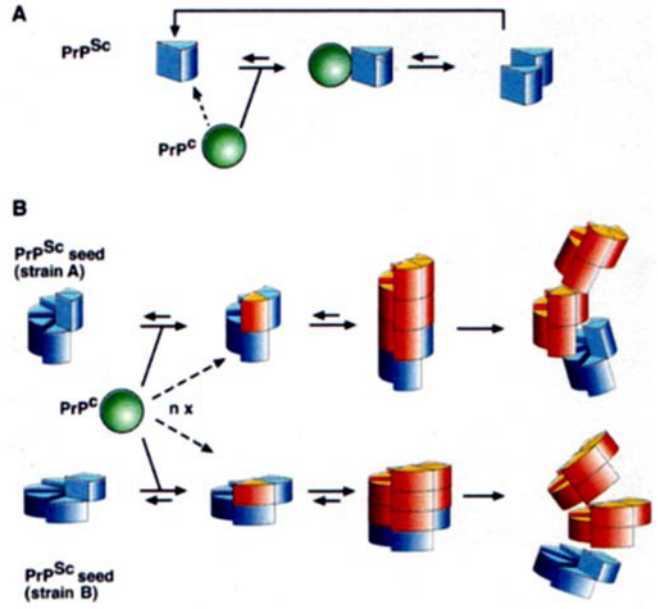

Figure 7. Models for the conversion of PrP^c into PrP^{Sc}. A) The heterodimer model [22] postulates the formation of dimers from infectious PrP^{Sc} (blue) and cellular PrP^c (green): PrP^{Sc} induces a partial unfolding of PrP^c and, subsequently, its refolding into PrP^{Sc}, which in turn can cause the formation of PrP^{Sc} in an autocatalytic process. Due to the high energy barrier of the conversion of PrP^c into PrP^{Sc} the spontaneous formation of PrP^{Sc} is very unlikely (dotted line). B) According to the model of nucleation-dependent polymerization [72, 74] the infectious unit is a PrP^{Sc}-oligomer (blue), which serves as a seed for the polymerization of PrP into fibrillous aggregates of high molecular weight. Cellular PrP (green) can successively deposit on this seed and in the process adopt its structure (red). The polymer can be separated, and the seeds generated by this process can start the nucleation-dependent polymerization again. The appearance of different scrapie strains is explained by this model as follows: every (quaternary) structure of a seed "codes" the specific characteristics of different scrapie strains (here strain A and strain B).

autocatalytic cycle. Under appropriate conditions newly formed PrP^{Sc} aggregates to furnish the fibrils or amyloid plaques that can be observed under the electron microscope. The energy barrier for the conversion of the PrP isoform is probably very high.[51] The spontaneous forms of the disease therefore only appear at an advanced age, if they appear at all (see Figure 7A; dotted line). In hereditary forms the PrP^{Sc} formation can be facilitated by specific mutations that promote the development of β-sheets. The pathological changes are probably induced either by the absence of the PrP^c form or by the massive appearance of the insoluble PrP^{Sc}.

Although this model supplies sufficient explanations for the formation of PrP^{Sc}, it leaves unanswered how *one* PrP^{Sc} can transmit *various* strains of prion diseases. As mentioned above (Section 2.2.1), even within one species different strains of PrP^{Sc} exist with clearly identifiable and inheritable characteristics.[67–70] This phenomenon argues strongly against the hypothesis that the prion propagation depends on protein factors alone without any genetic components. An explanation in this hypothesis for the hereditary propagation of the observed strain specifity without genetic information is beset with problems. Not only *two* metastable forms of the prion protein would have to exist, but also *several* PrP structures, which are each able to "code" for a specific strain. Therefore, the problem of the strain-specific transmission demanded an extension of the hypothesis and finally led to the nucleation-dependent polymerization model.

3.3.2. Nucleation-Dependent Polymerization

The idea of a seedlike growth of prion polymers was already defined in 1990 by the group of D. Carleton Gajdusek.[71] Later, Peter Lansbury et al. suggested an analogous mechanism[72, 73] and, together with Byron Caughey, developed it into the nucleation-dependent polymerization model.[74] This model differs from the heterodimer model by the assumption that an infectious unit consists of a PrP^{Sc} oligomer, which serves as a seed for the polymerization. Host PrP^c can successively deposit on this seed through a more or less unfolded transition state; on deposition it adopts the specific structure of the seed. In some kind of polymerization process, aggregated forms of PrP^{Sc} of high molecular weight are formed (Figure 7B). These aggregates can be separated again into single seeds under external influences. The main difference between this model and the previous one is that the conformation of PrP^{Sc} does not have to be an intrinsic attribute of a PrP monomer, as in the case of the heterodimer model. This difference is manifested by the experimental observation that so far no soluble, monomeric, protease-resistant, and unaggregated forms of PrP^{Sc} have been found. According to the nucleation-dependent polymerization model, the PrP^{Sc} acquires these biophysical properties only as a high molecular weight aggregate of PrP. The propagation of specific scrapie strains can be explained by this model as follows: Like in a crystal the smallest infectious unit, the nucleus, carries the information of the structure of the whole. Therefore, a PrP^{Sc} oligomer can determine the structure of the polymeric PrP aggregate (or the kinetics of its formation) by the structure of the nucleus and thereby determine the particular characteristic pathology of the various strains.

Manfred Eigen (MPI for Biophysikalische Chemie, Göttingen) recently published a detailed comparison of the two models from a kinetic point of view.[75] According to Eigen, the key difference between the models is that the nucleation-dependent polymerization model does not require a catalytic mechanism. The growth of the "crystal" is favored by the free energy, while the crystal surface gives rise to the conversion of PrP^c. In contrast, Prusiner's heterodimer model is based on an autocatalytic mechanism, but only if the dissociation of the PrP^{Sc} heterodimer is not the rate-limiting step. In the case of a slow dissociation the (auto)catalyst PrP^{Sc} would be regenerated incompletely, and the catalytic cycle would soon be terminated. A possible distinction could be the measurement of the growth rate of PrP^{Sc}; an autocatalytic mechanism would show an exponential growth, whereas the crystallization would proceed with approximately the square of time.[75]

3.4. In Vitro Conversion

In order to prove the heterodimer model, many laboratories tried hard to show a direct interaction of PrP^c with PrP^c and/or PrP^{Sc} in vitro. Proof of an in vitro conversion of PrP^c into PrP^{Sc} would confirm the protein-only hypothesis. These experiments, often designated as "key experiments" in prion research, which are based on the incubation of PrP^c with PrP^{Sc} in vitro, have failed so far. Neither was it possible to detect PrP^c/PrP^{Sc} heterodimers nor was it proven that PrP^c could be converted in

vitro by addition of PrP^{Sc}.[76] In mid 1994 Kocisko et al. reported for the first time the cell-free production of protease-resistant prion protein.[77] They used proteinase K sensitive PrP^c, radiolabeled with ^{35}S-methionine. The protein was incubated with proteinase K resistant, unlabeled PrP^{Sc}. In order to separate PrP^c from the potentially produced PrP^{Sc} the sample was treated with proteinase K. By gel electrophoresis and autoradiography they demonstrated that radioactive, proteinase K resistant PrP^{Sc} had been generated—an indication that PrP^{Sc} had emerged de novo from the labeled PrP^c (Figure 8). This experiment certainly provides necessary, but not sufficient proof for the in vitro conversion of PrP^c. That is because until now it has not been possible to show that proteinase K resistant material produced in vitro is indeed infectious. The proteinase K resistance does not necessarily correlate with the infectivity of PrP^{Sc} (see Section 3.1). In spite of this (still) missing evidence for the de novo generation of infectivity in vitro, one now has a model with which some phenomena of prion propagation can be simulated and examined. For example, even a strain-specific conversion in vitro has been demonstrated with this cell-free conversion system.[78] For that purpose, the mink-specific scrapie strains "hyper" (HY) and "drowsy" (DY) were used.[79] These TME strains were manifested originally in minks (TME = 'transmissible *m*ink *e*ncephalopathy') and can be propagated in hamsters with the particular pathology characteristic for each of them. HY- and DY-PrP^{Sc} are cleaved by proteinase K at different amino-terminal positions, from which characteristic digestion patterns of PrP fragments of variable length result, which can be detected by SDS-polyacrylamide gel electrophoresis.[79] If one uses preparations of HY-PrP^{Sc} from hamster brains for the aforementioned conversion experiments a resistant protein is produced which, after proteinase K treatment, showed a digestion pattern similar to that of HY-PrP^{Sc}. In contrast, if DY-PrP^{Sc} is used instead for the cell-free conversion of the same PrP^c-material, the characteristic DY-PrP^{Sc} pattern results.[78] These results indicate that two different conformations of the scrapie form of one prion protein can probably be forced upon a single cellular prion protein in the cell-free conversion system. These conversion experiments, therefore, serve as a model for the propagation of different scrapie strains in vitro—an important addition or alternative to the transgenic animal model.

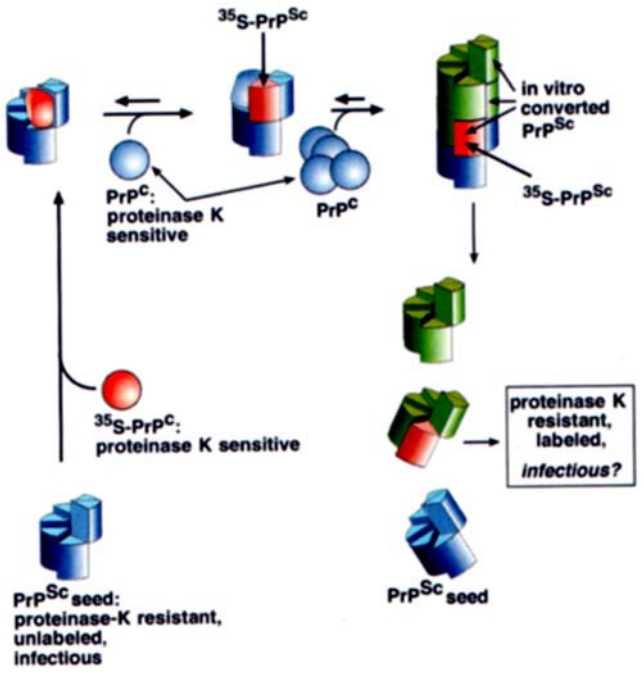

Figure 8. Cell-free production of proteinase-reistant prion protein [77, 78]. Radiolabeled PrP^c (red) is incubated with proteinase-resistant PrP^{Sc} (blue) and integrated into the polymer. In the end, a labeled, proteinase-resistant species can be detected.

3.5. More Aspects of Strain-Specific Prion Propagation

Meanwhile, experiments were carried out on transgenic mouse models[80] from which similar conclusions could be drawn to the ones of Bessen et al.,[78] who performed strain-specific in vitro conversion experiments. The mice for that experiment, abbreviated [Tg(MHu2M)],[81, 82] express a chimeric human–murine PrP gene. They were inoculated with proteinase K treated brain extracts from patients who had died from different forms of human TSE diseases. The extracts thus contained proteinase K resistant PrP^{Sc} fragments of two different human PrP strains, the sporadic Creutzfeldt–Jakob disease (sCJD) and the fatal familial insomnia (FFI; for the different human TSE forms see Section 4.3). The proteinase K treated PrP^{Sc} strains of this sort show different fragment lengths after deglycosylation: because the strain of FFI has a size of 19 kDa and the sCJD fragment 21 kDa, the two fragments can be distinguished easily by denaturing polyacrylamide gel electrophoresis. About 200 days after inoculation a PrP^{Sc} strain-specific fragment development could be observed in the mouse brains. Inoculation with the FFI strain led to the development of the 19 kDa fragment, whereas the 21 kDa fragment was obtained only after inoculation with the sCJD strain. These results led to the conclusion that the conformation of the particular PrP^{Sc} strain serves as a template for the development of PrP^{Sc} and is therefore crucial to its strain-specific characteristics. Furthermore, these experiments indicate that the diversity of the different PrP^{Sc} strains is caused by the conformation of the strain generating new PrP^{Sc}.

In a recent publication, Leslie Orgel points to another aspect that might play a role in prion propagation: "secondary nucleation".[83] Secondary nucleation can be observed, for example, in the enantiomorphic crystallization of supersaturated $NaClO_3$ solutions. If the crystallization takes place under vigorous stirring, crystals of either pure D or pure L configurations are obtained. In contrast, "undisturbed" crystallization results in almost the same amount of D and L configurated molecules in the crystals.[84] An explanation for this phenomenon is that stirring ruptures the primary crystal seed and the newly formed secondary nuclei. All developing crystals would then be "descendants" (or "clones") of the primary nucleus and would form before another primary nucleus of opposite chirality was generated. In the same way, certain details (strain specifities) of the pathology of prion diseases might be determined by secondary nucleation. Otherwise—as Orgel states—one could expect that an endogenously formed or exogenously supplied PrP^{Sc} nucleus would produce only one localized plaque. The more effective a hypothetical secondary nucleation is, the less localized the re-

sulting plaques would be. The number of developing nuclei would therefore determine the seriousness of the disease—as in the case of cancer where the severity of the disease depends on the tendency of metastasation of the primary tumor. Of course, secondary nucleation in the case of prion propagation has not yet be shown and will probably be very difficult to prove.

As discussed in greater detail later, other possibilities can explain the strain specifity of prion propagation, for example, the existence of a third component such as a strain-specific co-factor or protein X,[82] which is directly or indirectly involved in the propagation of PrP^{Sc} (see Section 5.2).

4. Epidemiology and Transmission

After close analysis of the pathogen the question arises, how are prion diseases transmitted. How could BSE in England reach epidemic proportions? What about the transmission from one species to the other? The risk of transmission of BSE to humans has, of course, important public, economic, and sanitary implications.

4.1. The Scrapie–Kuru Connection: a Historical Summary

Spongiform encephalopathies have been known since the 18th century. The oldest written record gives a description of certain peculiar behavior in sheep: at an early stage in the disease, disorientation and itching was observed in the affected animals: they scraped themselves sore at pales and trees; this is why the illness was called "scrapie" in the English speaking-world. In German-speaking countries the disease was named "Traberkrankheit", which points to the fact that affected animals progressively lose control over their body in an advanced phase, move in an uncoordinated manner ("traben"), cannot support themselves on their hind legs, and finally perish in complete paralysis. Ways of transmission of the disease and the cause of the illness remained obscure for centuries, mainly because scrapie never developed into an economic problem. The rate of infection always remained quite low—an epidemic outbreak of the disease has never been registered to date. Nowadays it has almost completely vanished in Germany, whereas only a few cases are reported in Great Britain at regular intervals.

Scientific interest arose first in this century, when William Hadlow speculated about a possible connection between the human Kuru disease and scrapie.[85] Earlier, independent of scrapie, a series of unusually slowly degenerative diseases of the central nervous system in humans such as the Creutzfeldt–Jakob disease (CJD), Gerstmann–Sträussler–Scheinker syndrome (GSS), and Kuru had been described. Kuru broke out in epidemic dimensions in the Fore, a tribe in Papua–New Guinea, and was probably transmitted by religous cannibalistic rites. D. Carleton Gajdusek succeeded in an experimental transmission of this disease to chimpanzees by injection of brain material of patients who had died of Kuru.[86] In a similar way, CJD could be transmitted to chimpanzees. The remarkably long incubation period and the pathological pattern of this neurodegeneration by spongiosis were identical in all forms of this disease. Important information about the transmissibility of scrapie resulted from experiments by J. Cuillé and P. L. Chelle, who demonstrated in the thirties that scrapie can be transmitted to healthy sheep and goats.[87] Hamsters and mice were also prone to this disease; both species are used today on a large scale for animal tests to investigate prion diseases. Nevertheless, as we will discuss later (Section 5.1), the unrestricted transmission of TSE from one species to another is not possible.

4.2. BSE—from Bonemeal to Epidemic

Because of the limited occurrence, TSE diseases in the first instance were a subject of academic interest. This changed suddenly when the first case of BSE in England was histologically confirmed in 1986.[88] Fibrils isolated from the brains of BSE-infected cattle were shown to contain a scrapie-associated protein.[89] This report was immediately followed by others. The BSE epidemic in England had its climax between 1992 and 1993 with up to 3500 new cases per month; now it has dwindled to about 500 new cases per month (Figure 9). By April 1997 a total of more than 167 300 (source: Ministry of Agriculture, Fisheries and Food [MAFF], UK) BSE cases had definitely been confirmed in England.[90] The epidemic in cattle began when in the eighties the method of meat- and bonemeal production was changed in response to economic pressures. This feed, used mainly in cattle breeding, is produced in part from sheep cadavers. In the beginning of the eighties British companies modified the sterilization temperature, lowering it from 130 °C to 110 °C. Furthermore, extractions with organic solvents were no longer performed.[91] Whether the epidemic was induced by bonemeal contaminated with scrapie (that is, the disease was transmitted from sheep to cattle) or with BSE pathogens from spontaneously affected cattle themselves (and therefore not transmitted across species) can no longer be determined with certainty. In any case the spreading of the infectious agent through feed has been confirmed as the trigger for the BSE epidemic.[91, 92] The accumulated number of BSE cases in Switzerland, which was the main importer of British bonemeal until the feed ban (July 18, 1988) on the continent, also supports this argument. BSE was detected and confirmed worldwide in 12 countries (Table 2). Besides infection through feed, even newer indications suggest that other ways of transmission, mainly from mother to calf, might be possible.[93]

A current study of the course of the BSE epidemic in Great Britain from the very beginning of the first cases to a potential epidemiological development in the future came to the conclusion that by the end of 1994 new infections by contaminated feed were almost zero, and all new cases result from horizontal (maternal) transmission.[90] Absolute numbers of new infections by this form of transmission were so small that the epidemic would vanish by the year 2001 even without slaughtering programs. In September 1996 the British government used this study as an argument to interrupt their cattle slaughtering project, which they had initiated in order to bring the epidemic under control. However, this argument neglects another important result of the study—the incubation period. It takes about five years from infection to the outbreak of the first symptoms. Since most of the cattle are killed at an age of about two years, that is, long

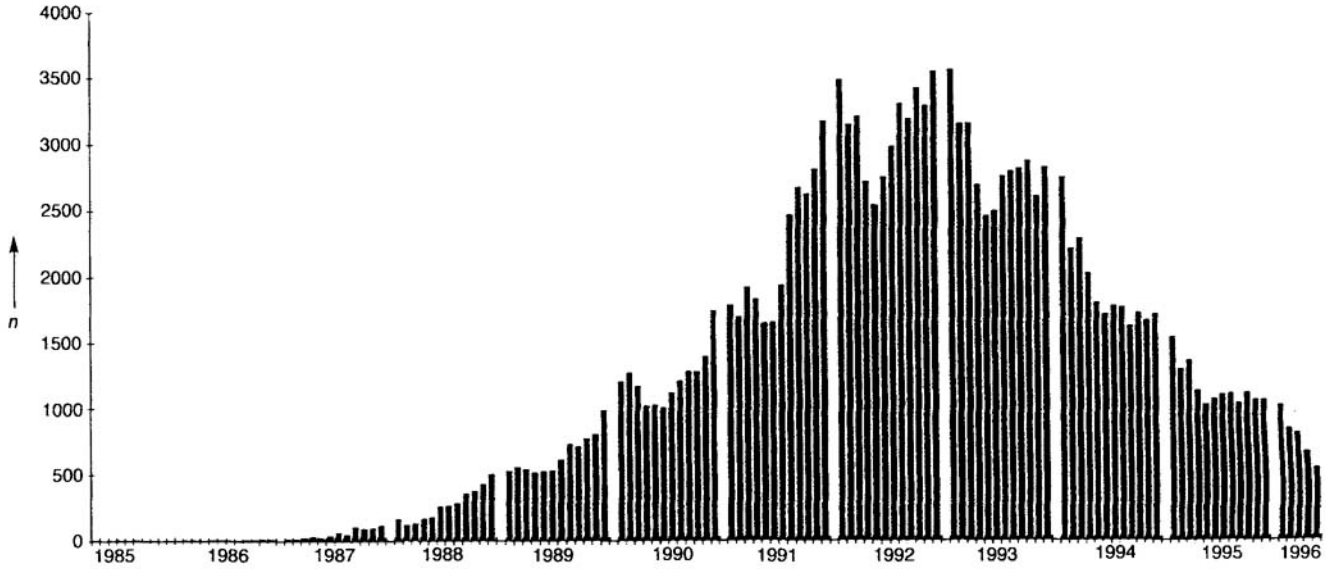

Figure 9. Confirmed cases *n* of BSE per month and year in England. The decline of the curve is traced back to the ban against meat- and bonemeal as feed and similar measures taken by the British government in 1988 and 1989. After the average incubation period of five years had passed, these measures probably led to the reduction of BSE cases.

Table 2. Appearance of BSE worldwide (data till March 1996).

Country	Number of BSE cases	Country	Number of BSE cases
Great Britain	167321 [a]	Germany	5[b]
Northern Ireland	1656	Italy	2
Switzerland	189	Oman	2
Ireland	115	Falkland Islands	1
Portugal	29	Denmark	1
France	13	Canada	1

[a] Data till April 1997. [b] Data till Januar 1997.

before the animal can be recognized as infected, infected and potentially infectious animals might get into the human food chain. Therefore absolute security can be given only if a reliable diagnosis that detects the disease long before clinical symptoms are seen is guaranteed, for example, by direct detection of the PrP^{Sc} form or the cattle prion protein (see Section 4.4).

4.3. Human Spongiform Encephalopathies

In the twenties the neurologist Hans-Gerhard Creutzfeldt[94] from Kiel, Germany, and his colleague Alfons Jakob[95] from Hamburg independently described a "strange disease of the central nervous system accompanied by remarkable anatomic findings", which led to death after an unabatable decay of brain tissue and is now known as Creutzfeldt–Jakob Disease (CJD). In the year 1936 the neuologists Josef Gerstmann and Ernst Sträussler as well as the neuropathologist I. Scheinker from Vienna observed a very similar, although rather rare, syndrome in humans.[96] They mainly observed impairments of the coordination. In contrast to CJD, in which a loss of memory and a progressive decline of intellect takes place in the beginning, the appearance of dementia in GSS patients only happens in the clinical phase. GSS is manifested by ataxia and other degeneration symptoms in the cerebellum. Histopathologically the two forms of disease, CJD and GSS, resemble each other: one could detect symptoms of degeneration connected with vacuoles (= cavities in cells with fluids like proteins or fat) as well as amyloid depositions in the brain. Such depositions are known in Alzheimer's disease as well, which, however, is not considered a prion disease. Fatal familial insomnia (FFI), another inheritable form of human prion diseases, was discovered by an American group around Pierluigi Gambetti and an Italian research group of Elio Lugaresi and Rossella Medori from the University of Bologna.[97] FFI differs from the other forms in the effect that the patients suffer from sleep disturbances in the beginning, which are followed by dementia.[98] An additional form of human prion diseases is the aforementioned Kuru disease. Among of the four human TSE forms, Kuru is the only one which is solely transmitted by infection.

4.3.1. Sporadic and Infectious Forms

Prion diseases show the remarkable characteristic that they can be caused by infections (exogenous origin) but can also originate sporadically or genetically (endogenous origin). Most cases of TSE in humans appear sporadically or are caused by transmission (for example, Kuru); however, there are cases for which genetic reasons are responsible for the outbreak of the disease as well. In humans 85% of the CJD cases occur sporadically, that is, the disease could not be traced back to a possible source of infection in these patients. A few CJD cases might be traced back to the infection with the CJD pathogen by mistake during medical treatment, for example in children who were treated with a growth hormone obtained from pituitary glands of deceased people[99, 100] (today this hormone is produced by recombinant techniques). Patients who had to undergo neurosurgery were also exposed to the risk of this iatrogenic transmission; because it was not known that the prion pathogen is extraordinarily resistant towards standard sterilization techniques (see Section 3.1), CJD was transmitted in some cases by con-

taminated instruments used in neurosurgery. Besides the iatrogenic and sporadic cases about 10% of the familial cases have a genetic dispostion, such as GSS and fatal familial insomnia (FFI).

4.3.2. *Mutations in the Prn-p Gene Locus*

Certain cases of CJD can have hereditary origin, too. Already in 1930, the physician F. Meggendorfer described hereditary cases of CJD in a family from Northern Germany. Many decades later the DNA extracted from a sample of brain tissue and conserved in celloidine was amplified by PCR and sequenced. In codon 178 within the *Prn-p* gene a GAC → AAC mutation appeared, which corresponds to an exchange of Asp178 for Asn.[101] (Figure 10).

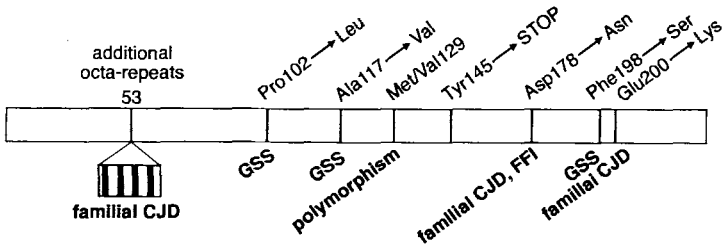

Figure 10. Mutations and polymorphisms in the human *Prn-p* gene associated with the familial form of spongiform encephalopathies. The polymorphism at position 129 seems to influence the susceptibility for vCJD, because all cases of vCJD examined so far are homozygous for Met 129.

Other mutations that were found to be associated with genetic dispositions are Glu200 → Lys, Pro102 → Leu, Ala117 → Val, and Phe198 → Ser, as well as the insertion of additional octa-repeats within the human *Prn-p* gene in position 53.[22] Position 129 appears to be of special interest as valine or methionine can appear at this site. John Collinge and his colleagues[102] from St. Mary's Hospital Medical School (London) observed a significant occurrence of Val129-homozygosity in patients who developed CJD after being treated with growth hormone from pituitary glands. At least 50% of the caucasian population is heterozygous (Met/Val) at this position. The dimerization of the prion protein, which might occur more easily in homozygous than in heterozygous patients, is possibly important for the pathogenesis of CJD. Different phenotypes of the various human TSE forms as seen, for example, in the case of CJD and FFI, seem to correlate with different genotypes. In a study in which familial TSE cases (with the exchange of Asp → Asn at position 178) were examined, it was shown that the genotype at position 129 determines the mode of pathology. Patients with Met129/Asn178 showed an FFI phenotype, whereas the Val129/Asn178 appeared in CJD patients.[103, 104] It has been suggested that the combination of the mutation in codon 178 with the polymorphism in codon 129 determines the phenotype of the disease by generating two different conformations of the prion protein.[105, 106] In the familial prion diseases the mutated forms would spontaneously adopt conformations which are determined by the mutations. A direct interaction between methionine or valine at position 129 with the asparagine at position 178 might lead to two abnormal isomers which differ in their conformation and in their pathogenic consequences. It is possible that the activation energy for the conformational change may be lowered in these mutants. Moreover, the polymorphism at position 129 also seems to be critical in a new variant of CJD, as discussed below.

The mutation Pro 102 → Leu also seems to be of great importance for the appearance of GSS. It was the first mutation identified in connection with familial prion diseases.[107, 108] Of eleven Japanese patients with GSS, all had leucine at position 102.[109] The same mutation was also found in cases of GSS in a Jewish family.[110] Interestingly, the proline at position 102 was found to be conserved in various species, which might point to an important role in the biological function of this protein (Figure 10). A rather unusual mutation within *Prn-p* was published in 1993 by a Japanese research group led by Tateishi: In one patient they found that codon 145, which normally encodes for tyrosine, was substituted by a stop-codon.[111] Accordingly, the amyloid plaques of this patient, who had initially been diagnosed for Alzheimer's disease, were analyzed to contain C-terminally truncated PrP fragments. These fragments thus lack elements of PrP thought to be important, such as glyscosylation sites, a disulfide bond, and a GPI-anchor (see Figure 3). According to recent investigations, however, it seems that the normal allele participates in the pathological process of this familial TSE form because the C-terminus of PrP could also be detected in these plaques by specific antibodies.[112]

Rather little has been published about genetic dispositions in other species. In sheep, for example, the polymorphisms at positions 136 and 171 are known to have an influence on the susceptibility to scrapie (analogously to the polymorphism at position 129 in the human gene locus). The resistance towards scrapie infection is significantly smaller in sheep with a Val136/Glu171 homozygosity than in animals with a homozygous Ala136/Arg171 genotype.[113] All these genetically determined predispositions are inheritable. With respect to the infectivity of prions, however, it is irrelevant *how* the prion disease was triggered: the prion protein from an affected brain is infectious in any case.

4.3.3. *vCJD—a Link between BSE and CJD?*

In early 1996 an English research group reported a form of CJD which had not been described until then.[114] Patients affected by the new variant ("vCJD"; by April 1997 15 patients) indeed show the usual pathological characteristics of CJD, which, however, are remarkably modified. First, with an average age of 30 years the affected patients are relatively young. Second, the average mean time from the appearance of the first symptoms to death is about 15 months, which is more than twice as long as the corresponding period in normal CJD patients. Third, the amyloid depositions or plaques show, in addition to the spongiform alterations, a characteristic morphology that had never been observed in any other case of CJD before (Figure 11). The "florid plaques" are similar to those found in Kuru patients and seem to be identical to those in Macaque apes infected with BSE.[115] These and other characteristic features (for example, lack of anomalies in the EEG of vCJD patients, homozygosity for Met129) argue for a manifestation of a new

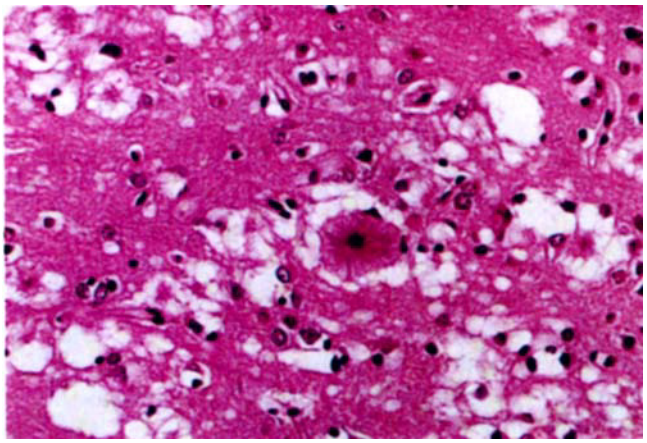

Figure 11. Thin section of the brain of a patient who died of vCJD. An especially remarkable pathological change of vCJD is the formation of florid plaques, which are surrounded by a concentric zone of spongiform changes. This picture was kindly made available by J. Ironside, University of Edinburgh.

TSE strain in humans, possibly in a direct connection with the BSE epidemic in England. Almost all vCJD patients are from England, only one patient has been reported from France.[116] It is interesting to note that France had high import quota of British beef in the relevant period; thus, certainly, a large portion of potentially infected tissue came from England to France. Recent studies confirm suspicions that BSE can be transferred to humans. Collinge and his colleagues investigated the electrophoretic mobility of PrP^{res} from preparations of different TSE cases. They looked at the fraction of proteins with different degrees of glycosylation in particular (two, one, or no glycosylation; see Figure 3) and classified these "glycoform patterns" into four groups.[117] According to this classification, type 1 and type 2 represent two different forms of sCJD. Type 3 appears only in iatrogenic cases of CJD, whereas in all vCJD cases the type 4 pattern, which had never been observed in any other CJD case, was found. BSE-affected cattle as well as macaques also showed the type 4 digestion pattern, a further indication for a causative connection between BSE and vCJD. This experimentally rather simple classification of CJD patients into four groups is, however, anything but undisputed. Parchi et al. recently reported that the method described by Collinge et al. only gave two classes of PrP^{res} in their hands.[118] Moreover, Somerville et al. could show that the "glycoform pattern" of a TSE strain described by Collinge is not necessarily stable in laboratory animals. The fraction of differently glycosylated PrP^{res} shifts upon passage of the strain from animal to animal.[119]

Closer examination of the clinical signs of vCJD raises questions about its uniqueness as well. It cannot be excluded with certainty that the striking pathological characteristics of vCJD had not already showed up before the outbreak of the BSE epidemic. Since the disease appeared so infrequently, it can be assumed that not every case of CJD was unmistakably diagnosed before the sensibilization by BSE (see Section 4.4). It is quite conceivable that there were earlier cases of vCJD that were not recognized as such, because mainly younger patients are affected. Furthermore, the appearance of florid plaques as a clear morphological criterion for the discrimination between vCJD and other CJD forms is disputable. Recently a nonfamilial case of CJD could not definitely be classified as vCJD by the aforementioned criteria; nevertheless, the autopsy of the brain of the patient revealed florid plaques. As this patient had a neurological graft of dura mater a decade before, an iatrogenic transmission could not be excluded.[120]

4.4. Diagnostic Methods

The safe diagnosis of BSE in living or symptom-free cattle is of utmost interest for economics and public health. Because of the potential threat to humans by vCJD, a diagnosis in humans is, of course, of particular importance. The aim is the development of a test to determine the status of the infection quickly, preferably by using blood or urine.

4.4.1. Present Diagnostic Methods

The early diagnosis of TSEs is restricted to the appearance of the first vague clinical symptoms or EEG anomalies, as well as the use of NMR-visualizing methods or invasive brain biopsy. In the latter method a sample of brain tissue is removed, incubated with proteinase K and then tested for the presence of proteinase-resistant PrP with an antibody. In positive cases (when the sample contains PrP^{Sc}) the brain biopsy is a relatively reliable method. To date, however, a negative diagnosis in the living organism remains difficult. A reliable diagnosis is only possible post mortem, based on the aforementioned pathological changes and immunohistological status in the brain tissue. Like in many other diagnostic systems, for example the detection of HIV, the basis of a sensitive test system would be an antibody that specifically recognizes PrP^{Sc}. It has, however, not yet been possible to develop such a pathogenic isoform-specific antibody.[121, 122] The available anti-PrP antibodies cannot distinguish between the cellular PrP form in healthy organisms and the scrapie form in the affected organism. In the immunohistochemical detection of PrP from brain slices one takes advantage of the different proteinase K sensitivities of the two protein isoforms. Proteins that can be detected by a PrP antibody after treatment with proteinase K reflect the amount of PrP^{Sc} contained in the sample. However, this test is not very sensitive; in addition, the proteinase K sensitivity does not always correlate with the infectivity of a sample (Section 3.1).

4.4.2. New Diagnostic Attempts

During the last months a number of experiments were attempted, which might constitute the basis of a diagnostic test system. We would like to discuss two of them here. A Dutch group showed that the detection of scrapie-associated PrP^{Sc} in the tonsils of sheep is possible before the first clinical symptoms appear. In the examined group of six scrapie-infected sheep they detected PrP^{Sc} at the age of 10 months, about one year before the clinical manifestation of the disease.[123] Whether this technique will work in other species is questionable. For example, in contrast to sheep, no infectivity is found in peripheric tissues in

cattle; that means that by biopsy of tonsils a detection of PrP^{Sc} would not be possible in cattle. In contrast, PrP^{Sc} was detected post mortem in the tonsils of a human vCJD case, as reported recently, although in only one case.[124]

The group of Michael Harrington does not use PrP^{Sc} itself as a diagnostic basis, but a marker protein, which is contained in the cerebrospinal fluid of CJD patients. In 1986 he and his colleagues discovered by two-dimensional gel electrophoresis that two proteins (designated p130 and p131) are found in CJD patients, which might serve as diagnostic markers. [125] Recently these proteins were indentified as degradation products of 14-3-3 proteins, and antibodies directed against them were sucessfully used in an immunoassay for CJD diagnosis.[126] Cerebrospinal fluid is taken from the spinal cord of the patients and tested for the presence of the 14-3-3 protein by SDS-gel electrophoresis and immunoblot. The required antibody can be purchased, and the test can be carried out in every biochemistry lab within a few hours. Nevertheless, this test system has a few disadvantages: the appearance of the 14-3-3 proteins is an epiphenonemon, that is, besides CJD other diseases like herpes simplex encephalopathy lead to an increased occurrence of 14-3-3 protein in the cerebrospinal fluid. The specifity in the examined group of 71 patients was therefore only 88%. The results of the application of the test in cattle were barely conclusive: only a few animals have been tested to date, and moreover, these were not infected with BSE, but with TME. This experiment revealed higher specifity concomitant with decreased sensitivity—only six of nine infected cattle were diagnosed correctly. Finally, hitherto existing data indicate that the test works only at a relatively late stage of the disease, probably not before the first clinical symptoms appear. An effective diagnostic system should respond as soon as possible after infection, so that infected cattle can, for instance, be withdrawn from the market before the epidemic can spread further.

5. Transgenic Models

In many fields of biochemisty the establishment of transgenic animal models is widely accepted for the study of molecular-biological and pathophysiological problems. Also in the case of the research into prion diseases, transgenic mouse lines led to important breakthroughs and results. One of the first animal models for prion dieseases was introduced in 1990 by Prusiner's laboratory. A mouse line was produced, into whose *Prn-p* gene a point mutation corresponding to one of the human GSS point mutations (Pro 102 → Leu; Figure 10) was introduced. As a consequence of this changed mouse genotype, it spontaneously developed neurological malfunctions, spongiform changes, and gliosis of astrocytes in the brain[127]—the three classical characteristics of transmissible encephalopathies. It had thus been possible for the first time to produce a genetically determined prion disease in mice. This neurodegeneration, induced by mutation, is hard to distinguish from experimental murine scrapie. One variation, however, is seen in these samples, which have been prepared from brains of the affected transgenic mice: they are only weakly infectious, if at all.[128] Nevertheless the transgenic "GSS mouse" not only was an important support for the protein-only hypothesis, it simultaneously opened up the exciting possibility of transfering experimental TSE studies from other species to mice. With the help of such transgenic mouse lines it is possible, for example, to examine species barriers.

5.1. Investigations of the Species Barrier

The transmission of spongiform encephalopathies from one species to the other happens, if at all, very inefficiently and with severely prolonged incubation periods. For example, when a mouse is inoculated with an infectious sample from hamster, the mouse stays alive for more than 500 days, whereas an infectious mouse sample, on average, leads to death after 140 days (Figure 12A,B). Similarly, if one tries to infect hamsters by infectious mouse preparations the hamsters survive more than 360 days, in contrast to a lifetime of 75 days after use of hamster prions (Figure 12C,D). This means that mice can be infected by hamster prions only poorly or not at all and vice versa. This species barrier seems to be caused by the different primary structures of prion proteins of the particular species;[129] the mature forms of hamster and mouse PrP, for example, differ from each other in 12 amino acids (Figure 13). In the sense of the protein-only hypothesis this means that hamster PrP^{Sc} has a much smaller influence on the conversion of mouse PrP^{c} than mouse PrP^{Sc} and vice versa. What happens if a transgenic mouse, which expresses hamster PrP^{c}, is inoculated with hamster PrP^{Sc}? The infection indeed proceeds with an incubation period of only 75 days;[130, 131] regarding scrapie susceptibility the transgenic hamster-PrP mouse responds like a hamster itself (Figure 12E).

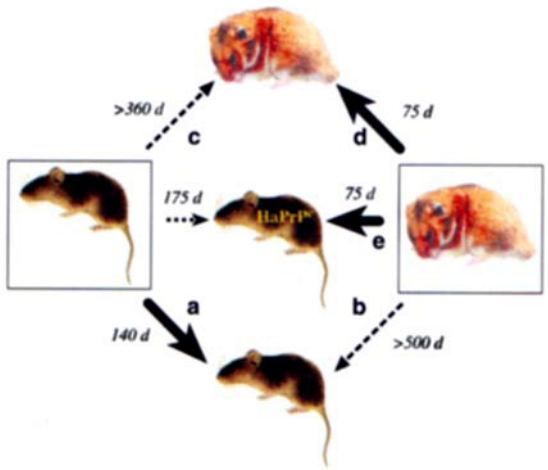

Figure 12. Species barriers and their conquest by the transgenic animal model. a) Mice inoculated with mouse-prions die, on average, after 140 days. b) Most mice survive the inoculation with hamster prions by more than 500 days in good condition. This species barrier between mouse and hamster can also be observed if hamsters are used as test animals: c) Hamsters infected by mouse prions survive, on average, longer than 360 days, whereas d) they die after 75 days if hamster prions are used for inoculation. e) The species barrier can be overcome if a transgenic mouse that expresses hamster PrP^{c} is inoculated by hamster prions. (Based on data from refs. [130, 131] and modified according to reference [150].)

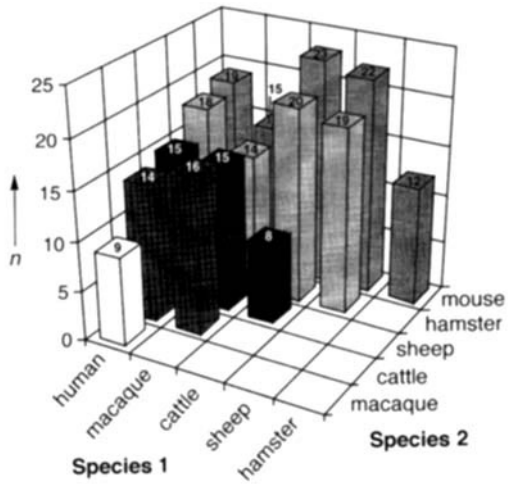

Figure 13. Deviations in the primary sequences of the mature form of PrP in selected species. The height of the columns represents the number of deviations (mutations) in the pair of species compared. The shorter a column, the more similar the PrP amino acid sequences of the two species. Whether the number of deviations between two species correlates with the extent of the species barrier is not yet clear. For clarity, the columns are drawn in different grey shades. (Based on data from ref. [129]).

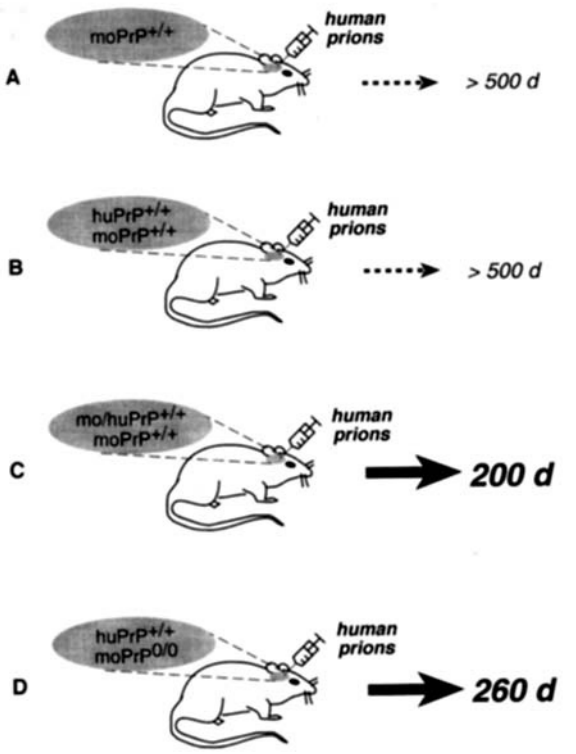

Figure 14. Inoculation experiments on transgenic mice with human prions. The genotype of the transgenic mice is symbolized by ellipses, which represent the brains: moPrP = mouse PrP, huPrP = human-PrP, mo/huPrP = PrP made of human amino acids 96–167 and the murine N- and C-terminus. A) A high species barrier exists between humans and mice: most animals survive the inoculation with human prions for more than 500 days. B) Surprisingly, the introduction of human PrP does not overcome the species barrier. C) Infection of mice by human prion material is only possible if a chimeric human–murine transgene is used. D) Mice are infected as well, if they are both transgenic for human PrP, and their mouse-PrP is switched off by knockout techniques. (Based on data from refs. [81, 82].)

5.2. The Cofactor for Prion-Propagation: Chaperoning the Prion?

Today the transgenic mouse model provides the most effective experimental possibility for analyzing species barriers in prion diseases. This model is especially suitable for examination of infection pathways to humans. Because of the species barrier, inoculation of mice with CJD material led to infection in only 5–10% of the animals after more than 500 days (Figure 14A).[81] Unexpectedly the scrapie susceptibility does not change, if transgenic human-PrP mice are used (Figure 14B). Only on introduction of a chimeric PrP, which is constructed from murine and human sequences (amino acid 96 to 167 of human, N- and C-terminus of mouse), can the transgenic mouse be made susceptible for CJD material (Figure 14C).[81] Prusiner et al. concluded from this observation that still other species-specific factors must be involved in prion propagation. This assumption was supported by the following experiment with transgenic mice: transgenic human-PrP mice can become sensitive towards CJD by knocking out the mouse-PrP (Figure 14D):[82] mice that express human PrP besides their own mouse PrP are protected against infection with human CJD material, whereas mice that express human PrP alone can be infected with CJD samples. Prusiner et al. deduced from these results the existence of a species-specific factor, which he designated as "protein X". Protein X should therefore interact preferentially with the own PrP of the species and is required for the conversion. In the transgenic mouse murine PrP competes with the human PrP^c for binding to protein X, which preferentially binds murine PrP^c, with the result that no conversion of human PrP^c is possible. Only if the mouse PrP^c is knocked out as binding partner, can protein X bind to the less preferred human PrP^c and convert it, supported by the human PrP^{Sc}.

The not yet identified protein X might act as a molecular chaperone, which lowers the activation energy for the refolding of PrP and therefore facilitates the process of conversion. Molecular chaperons are highly conserved proteins, which are involved in the folding of proteins within cells.[132] Unexpectedly, a model organism for interactions of chaperones and prion proteins was found in yeast. Although baker's yeast *Saccharomyces cerevisiae* does not express prion proteins, it contains two genetic elements that can reproduce themselves without the participation of nucleic acids: [URE3] and $[PSI^+]$.[133] $[PSI^+]$ is a prion-like aggregation of the cellular yeast protein Sup35 and replicates in yeast depending on the presence of a chaperone (Hsp104).[134] Already formed $[PSI^+]$ induces newly synthesized Sup35 to aggregate as well.[135] An attempt was made to transfer these results to prion propagation in mammals. An interaction of hamster PrP^c with a molecular chaperone (Hsp60) was indeed discoverd by applying the "Two-Hybrid" technology.[136] Experiments with scrapie-infected neuroblastoma cells in cell culture indicate that "chemical chaperones" (for example, DMSO or glycerine) might have an influence on the formation of PrP^{Sc}.[137] The final proof that a direct interaction of PrP with molecular chaperones is involved in the pathogenesis of TSE in mammals, however, is still missing.

5.3. Prion Knockout Mice

5.3.1. PrP^c is Necessary for Infection with Scrapie

The development of a mouse line in which the *Prn-p* gene is turned off was interesting in two respects. On one hand, one wanted to obtain clues for the regular biological function of PrP^c: if a specific deficiency of this $PrP^{0/0}$-mouse had been observed, conclusions might have been able to be made about the role of the missing prion protein. On the other hand, the $PrP^{0/0}$-mouse provided proof of the protein-only hypothesis. An important consequence of this hypothesis is that no propagation of PrP^{Sc} is possible in hosts which lack PrP^c and therefore the $PrP^{0/0}$-mouse would be resistant to infection with PrP^{Sc}. The $PrP^{0/0}$-mouse line developed in Weissmann's laboratory was indeed found to be resistant to scrapie infection, whereas wild-type mice under the same treatment develop the disease and die on average 140 days after inoculation.[33] In heterozygous *Prn-p*$^{0/+}$-mice the incubation period is prolonged to about 290 days; these animals are thus partially protected against scrapie infections. Therefore, the incubation period correlates with the amount of PrP^c which is expressed in the mouse brain. An important control experiment confirmed these results: the reconstitution of the *Prn-p* gene in *Prn-p*$^{0/0}$-mice led to the restoration of the susceptibility to scrapie. By introducing several copies of the *Prn-p* gene a mouse line was obtained, which overexpressed PrP^c and was, as expected, even more susceptible to scrapie infections. These mice showed a markedly reduced incubation period (60 days) relative to that of the wild-type mouse.[63]

In a collaborative effort the groups of Aguzzi and Weissmann applied another method to reintroduce the prion protein into knockout mice. Hereby, brain tissue from PrP^c-overexpressing mice was transplanted into PrP knockout mice, and these mice were used in infection studies.[138] After intracerebral inoculation with scrapie samples, the grafts showed high amounts of PrP^{Sc} together with infectivity, as well as other pathological changes characteristic for TSE. Furthermore, measurable amounts of PrP^{Sc} had gotten from the graft into the brain of the host. Nevertheless, there were no pathological changes observed in the PrP-deficient tissue—not even within the immediate surroundings of the graft. The authors concluded from these results that exogenous PrP^{Sc} does not lead to damage of the brain tissue. In contrast, PrP fragment 106–126 is toxic to neurons cultivated in vitro.[139] In the laboratory of Hans Kretzschmar, Institute for Neuropathology at the University of Göttingen, this neurotoxic effect was thoroughly analyzed. It was shown, for example, that neuronal cells of PrP-null mice did not die off in the presence of PrP 106–126.[140] This result constituted another proof that the presence of PrP^c is important for the pathogenesis of prion diseases.

5.3.2. Biological Function of PrP^c

The production of knockout cell lines has turned out to be very effective for clearing up the unknown biological function of a protein.[141] Unfortunately, the relationship between the cause (the knocked-out gene) and the effect (the phenotype) often cannot clearly be verified or has to be traced back to unspecific effects. This exactly seems to be the problem in current prion research. The PrP-knockout mouse introduced by the Weissmann group develops completely normally until the age of two years and does not show any pecularities in behavior or neurological malfunctions.[33, 142] Electrophysiological examinations performed by Collinge and co-workers led to the discovery of neuronal defects in the inhibition of synaptic $GABA_A$ receptor[36] (GABA = γ-aminobutyric acid, a neurotransmitter). This observation might explain the pathological effects resulting from the loss of functional PrP^c, but could not sufficiently be reproduced in another laboratory.[143] The reason for such a discrepancy in observation of a phenotype might be attributed to the different genetic background of the mouse strains used. Species can react to the knockout of a particular protein with increased expression of other proteins, which might compensate for the knockout under certain circumstances. The genetic background of the organism is thought to play a crucial role in such compensating effects. Different mouse sublines might therefore react differently to the knockout of PrP-expression,[144] which might explain the observed discrepancies.

In addition, another effect might have to be considered. Three research groups have reported on different phenotypes of PrP-knockout mice in the interim. Each of these knockout lines was developed by different targeting strategies. This resulted in minute differences in the genome of the knockout mouse in the vicinity of the knocked-out gene, which might be responsible for the observed deviations of the phenotype as well. For example, in the knockout mouse from the Weissmann laboratory the method chosen left part of the PrP-coding gene in. A Japanese group, on the other hand, inactivated the whole *Prn-p* gene and reported massive behavioral and neuropathological impairments in this mouse line.[37] These mice had a very insecure movements; in contrast to the wild-type they were unable to follow a straight line. The reason seemed to be the loss of Purkinje cells in the cerebellum. Purkinje cells express huge amounts of PrP and use GABA as a neurotransmitter, which might be the link to the results of the Collinge group. Tobler and co-workers recently observed a changed circadian rhythm and sleeping disorders in PrP-deficient mice.[38] This phenotype is interesting in so far as it resembles the symptoms of the human FFI (see Section 4.3). Here might be a connection to GABA as well, because GABA receptors are thought to be involved in the regulation of the circadian rhythm.[145] To confirm the specificity of the observed effects they should be neutralized by the expression of PrP^c. Moreover, isogenic mice should be used for the development of knockout lines. It therefore remains to be seen whether a clear relation between cause and effect can be found for some of the promising approaches. Because in most cases physiological effects are mediated by protein–protein interactions, the study of interaction of PrP with other cellular proteins might prove quite helpful.

6. Open Questions

According to current understanding the pathogen of the transmissible spongiform encephalopathies (TSE) is a protein

that does not require a nucleic acid for infectivity and propagation. Proof of the protein-only hypothesis by the de novo generation of infectivity in vitro after incubation of PrP^c with PrP^{Sc} is still missing. The conversion of host PrP^c into the pathogenic PrP^{Sc} seems to be the central event in the propagation of TSE. It is possible that other not yet identified cofactors take part in this process, for example a "prion receptor" or other proteins or molecules, which interact with the prion protein. It is therefore important to identify possible prion–protein interactions and to examine whether they influence the conversion of the cellular into the scrapie isoform.

Both isoforms of the prion protein differ only in their conformation as determined by CD and IR spectroscopy. Whether differences in the three-dimensional structure of different prion strains exist within one species is not clear but has to be postulated, because of the present state of knowledge, to explain certain strain-specific characteristics of prion propagation. Therefore, structural studies are in the center of research efforts to shed light into the replication mechanism of prions. The structure of a mouse PrP^c fragment identified by NMR shows the expected extended α-helical regions besides two smaller antiparallel β-sheets, which might serve as a seed for the development of β-sheet structures in PrP^{Sc}. Whether the structure of the amino-terminally truncated fragment really contains all the important domains required for the prion replication remains to be seen. Structural elucidations of PrP^{Sc} have also still not been achieved because of the difficulties connected with the low solubility of the protein.

The cell-free in vitro conversion of proteinase K sensitive PrP^c into proteinase K resistant protein material was an important step in prion research, especially with respect to the current models for prion propagation. Although the conversion is strain-specific, it proceeds relatively ineffectively and can currently be achieved only on use of a surplus of PrP^{Sc}. Whether the in vitro converted material is not only proteinase K resistant but also infectious cannot be answered yet. This question is of highest relevance for the verification of a hypothesis for prion propagation.

PrP-knockout mice are not susceptible to TSE and otherwise do not show any noticeable phenotype. The prion protein itself seems to be of no immediate benefit for the organism; the observations of the three different knockout cell lines, however, are contradictory. Maybe PrP^c participates in synaptic processes. The identification of PrP–protein interactions might suggest functional relationships in this context. The transmission of TSE is affected by species barriers, which are manifested, for example, in extended incubation periods. The reasons for the barriers are thought to be the slight differences in amino acid sequences, which result in structural differences of prion proteins of individual species. The central question whether BSE can be transferred from cattle to humans cannot be examined directly. Macaques, however, can be infected by infectious BSE material accompanied by the development of not previously observed histological characteristics. These novel pathological changes seem to be identical with those of a new variant of Creutzfeld–Jakob disease (vCJD) in humans, which appeared in England just recently. A causal relation between the BSE epidemic and this new form of TSE in humans is quite probable.

7. Concluding Remarks

"It struck me recently that one should really consider the sequence of a protein molecule, about to fold into a precise geometric form, as a line of melody written in canon form and so designed by nature to fold back upon itself, creating harmonic chords of interaction consistent with biolgical function. One might carry the analogy further by suggesting that the kinds of chords formed in a protein with scrambled disulphide bridge, ... are dissonant, but that, by giving an opportunity for rearrangement...they modulate to give the pleasing harmonics of the native molecule. Whether or not some conclusion can be drawn about the greater thermodynamic stability of Mozart's over Schönberg's music is something I will leave to the philosophers of the audience."

C. Anfinsen in *New Perspectives in Biology* (Ed.: M. Sela), Elsevier, New York, pp. 42–50.

In Anfinsen's visionary world of harmony between sequence and structure, dissonant overtones entered not only because of the results of the prion research. Experiments which were carried out with the denatured enzyme "Rubisco" (Ribulose bisphosphate carboxylase oxygenase) showed that a spontaneous renaturation into the correct structure merely by dilution with the renaturating buffer is not possible. The correct refolding can be achieved only in the presence of the chaperonin GroEL.[146] Citrate synthetase from the mitochondria of pig hearts tends to self-aggregate if the enzyme is denaturated in guanidinium hydrochloride solution and is then diluted again.[147] These and other examples show that not all proteins spontaneously fold into the thermodynamically most stable conformation, because, for example, they might be caught in a kinetic trap during the course of folding. Such proteins do indeed fold in Anfinsen's sense, but only within a protective environment.[148]

If the protein-only hypothesis is correct, the situation seems to be different for the prion protein. It can exist in at least two, maybe even more, metastable structural states.[149] The prion protein is the prototype of a structure-labile protein. By a relatively slight trigger, such as a single mutation in the *Prn-p* gene or contact with the smallest amounts of the incorrectly folded isoform, this lability is manifested in the refolding of the normal isoform. The change of one structure into the other has dramatic consequences for the organism. The understanding of "prions" and their characteristics is proceeding very rapidly—this review describes the most important progress achieved until April 1997 (a deadline we imposed on ourselves, otherwise we would not yet have completed the article because of the breathtaking development of this research field). Nevertheless, we are far from understanding the function and characteristics of this partly frightening and partly fascinating protein.

We thank H. Schätzl for critical reading of the manuscript. We are grateful to R. Glockshuber and K. Wüthrich for providing us with a picture of the NMR structure of PrP, to J. Ironside and H. Kretzschmar for the images of histological thin sections, to H. Kretzschmar and G. Ourisson for helpful discussions, and to the Deutsche Forschungsgemeinschaft and the Bundesministerium für Bildung, Forschung, Wissenschaft und Technologie (BMBF) for financial support.

Appendix 1. Glossary of the most important abbreviations and medical terms.

amyloid	pathological deposition of proteins
AA	amino acid(s)
BSE	bovine spongiform encephalopathy
CD	circular dichroism
cerebrospinal fluid	lymphoid liquid present in the medulla; secreted by the brain
chaperones	proteins that are involved in folding of cellular proteins
CJD	Creutzfeldt-Jakob disease
EEG	electroencephalogram
FFI	fatal familial insomnia
GABA	γ-aminobutyric acid
glia cells	cells of the connective tissue of the central nervous system
gliosis	pathological proliferation of glia cells
GPI	glycosyl phosphatidylinositol
GSS	Gerstmann-Sträussler-Scheinker syndrome
Octa-repeat	repeating motif of eight glycine/proline-rich AA, characeteristic for PrP
polymorphism	differences in the genotype within a single population that cannot be explained by naturally occurring mutation rates alone
prion	abbreviation for proteinaceous infectious particle
PrP	prion protein
PrP27-30	fraction of proteins truncated at the N-terminal that have an electrophoretic mobility of 27-30 kDa
PrP^{c}	cellular isoform of PrP
PrP^{Sc}, PrP^{res}	pathogenic isoforms of PrP
Purkinje cells	huge dendritic ganglial cells in the mid-layer of the cerebellum cortex
spongiosis	spongelike alteration in tissues
TSE	transmissible spongiform encephalopathy

Received: February 11, 1997 [A 210 IE]
German version: *Angew. Chem.* **1997**, *109*, 1748–1769
Translated by Claudia Famulok, Munich

[1] A. F. Hollemann, E. Wiberg, *Lehrbuch der Anorganischen Chemie*, 81st–90th ed., DeGruyter, Berlin, **1976**.
[2] S. B. Prusiner, *Science* **1982**, *216*, 136–144.
[3] S. B. Prusiner, M. P. McKinley, K. A. Bowman, D. C. Bolton, P. E. Bendheim, D. F. Groth, G. G. Glenner, *Cell* **1983**, *35*, 349–358.
[4] J. Hope, L. J. D. Morton, C. F. Farquhar, G. Multhaup, K. Beyreuther, R. H. Kimberlin, *EMBO J.* **1986**, *5*, 2591–2597.
[5] D. Westaway, G. A. Carlson, S. B. Prusiner, *Tr. Microbiol.* **1995**, *3*, 141–147.
[6] L. J. Berg, *Proc. Natl. Acad. Sci. USA* **1994**, *91*, 429–432.
[7] G. W. Roberts, J. Clinton in *Prion Disease: The Spectrum of Pathology and Diagnostic Considerations* (Eds.: S. B. Prusiner, J. Collinge, J. Powell, B. Anderton), Ellis Horwood, New York, **1992**.
[8] C. I. Lasmézas, J. P. Deslys, R. Demaimay, K. T. Adjou, J. J. Hauw, D. Dormont, *J. Gen. Virol.* **1996**, *77*, 1601–1609.
[9] M. E. Bruce, *Br. Med. Bull.* **1993**, *49*, 822–838.
[10] This phenomenon is known from viral pathogens: the pathology changes because of mutations in the viral genome, but the principal infectivity remains.
[11] H. Diringer in *Spongiforme Encephalopathien bei Tieren unter besonderer Berücksichtigung der BSE*, Band 75 (Ed.: W. Köhler), Deutsche Akademie der Naturforscher Leopoldina, Halle, **1996**, pp. 26–28. Diringer also commented on his hypothesis in a round table discussion at the Deutsche Akademie der Naturforscher Leopoldina, moderated by Prof. Rudolf Rott.
[12] M. Özel, H. Diringer, *Lancet* **1994**, *343*, 894–895.
[13] M. Özel, Y.-G. Xi, E. Baldauf, H. Diringer, M. Pocchiari, *Lancet* **1994**, *344*, 923–924.
[14] I. Tischer, H. Gelderblom, W. Vettermann, M. A. Koch, *Nature* **1982**, *295*, 64–66.
[15] T. O. Diener, R. A. Owens, R. W. Hammond, *Intervirology* **1993**, *35*, 186–195.
[16] T. O. Diener, *FASEB J.* **1991**, *5*, 2808–2813.
[17] D. Riesner, M. Colpan, T. C. Goodman, L. Nagel, J. Schumacher, G. Steger, H. Hofmann, *J. Biomol. Struct. Dyn.* **1983**, *1*, 669–688.
[18] J. Smarda, *Acta Virol. Engl. Ed.* **1987**, *31*, 506–524.
[19] T. O. Diener, *Tr. Microbiol.* **1993**, *1*, 289–294.
[20] K. Kellings, N. Meyer, C. Mirenda, S. B. Prusiner, D. Riesner, *J. Gen. Virol.* **1992**, *73*, 1025–1029.
[21] K. Kellings, S. B. Prusiner, D. Riesner, *Philos. Trans. R. Soc. London B* **1994**, *343*, 425–430.
[22] S. B. Prusiner, *Science* **1991**, *252*, 1515–1522.
[23] N. Meyer, V. Rosenbaum, B. Schmidt, K. Gilles, C. Mirenda, D. Groth, S. B. Prusiner, D. Riesner, *J. Gen. Virol.* **1991**, *72*, 37–49.
[24] R. Mestel, *Science* **1996**, *273*, 184–189.
[25] T. Alper, D. A. Haig, M. C. Clarke, *Biochem. Biophys. Res. Commun.* **1966**, *22*, 278–284.
[26] T. Alper, W. A. Cramp, D. A. Haig, M. C. Clarke, *Nature* **1967**, *214*, 764–766.
[27] J. S. Griffith, *Nature* **1967**, *215*, 1043–1044.
[28] D. C. Bolton, M. P. McKinley, S. B. Prusiner, *Science* **1982**, *218*, 1309–1311.
[29] E. Turk, D. B. Teplow, L. E. Hood, S. B. Prusiner, *Eur. J. Biochem.* **1988**, *176*, 21–30.
[30] "Prion" is a slight modification of the abbreviation "Proin".
[31] B. Oesch, D. Westaway, M. Wälchli, M. P. McKinley, S. B. H. Kent, R. Aebersold, R. A. Barry, P. Tempst, D. B. Teplow, L. E. Hood, S. B. Prusiner, C. Weissmann, *Cell* **1985**, *40*, 735–746.
[32] K. Basler, B. Oesch, M. Scott, D. Westaway, M. Wälchli, D. F. Groth, M. P. McKinley, S. B. Prusiner, C. Weissmann, *Cell* **1986**, *46*, 417–428.
[33] H. Buehler, A. Aguzzi, A. Sailer, R.-A. Greiner, P. Autenried, M. Aguet, C. Weissmann, *Cell* **1993**, *73*, 1339–1347.
[34] C. B. Anfinsen, *Science* **1973**, *181*, 223–230.
[35] C. I. Lasmézas, J.-P. Deslys, O. Robain, A. Jaegly, V. Beringue, J.-M. Peyrin, J.-G. Fournier, J.-J. Hauw, J. Rossier, D. Dormont, *Science* **1997**, *275*, 402–405.
[36] J. Collinge, M. A. Whittington, K. C. L. Sidle, C. J. Smith, M. S. Palmer, A. R. Clarke, J. G. R. Jeffreys, *Nature* **1994**, *370*, 295–297.
[37] S. Sakaguchi, S. Katamine, N. Nishida, R. Moriuchi, K. Shigematsu, T. Sugimoto, A. Nakatani, Y. Kataoka, T. Houtani, S. Shirabe, H. Okada, S. Hasegawa, T. Miyamoto, T. Noda, *Nature* **1996**, *380*, 528–531.
[38] I. Tobler, S. E. Gaus, T. Deboer, P. Achermann, M. Fischer, T. Rulicke, M. Moser, B. Oesch, P. A. McBride, J. C. Manson, *Nature* **1996**, *380*, 639–642.
[39] N. Stahl, D. R. Borchelt, K. Hsiao, S. B. Prusiner, *Cell* **1987**, *51*, 229–240.
[40] D. C. Bolton, R. K. Meyer, S. B. Prusiner, *J. Virol.* **1985**, *53*, 596–606.
[41] L. Manuelidis, S. Valley, E. E. Manuelidis, *Proc. Natl. Acad. Sci. USA* **1985**, *82*, 4263–4267.
[42] T. Endo, D. Groth, S. B. Prusiner, A. Kobata, *Biochemistry* **1989**, *28*, 8380–8388.
[43] J. Safar, W. Wang, M. P. Padgett, M. Ceroni, P. Piccardo, D. Zopf, D. C. Gajdusek, C. J. J. Gibbs, *Proc. Natl. Acad. Sci. USA.* **1990**, *87*, 6373–6377.
[44] R. A. Gibbons, G. D. Hunter, *Nature* **1967**, *215*, 1041–1043.
[45] R. K. Meyer, M. P. McKinley, K. A. Bowman, M. B. Braunfeld, R. A. Barry, S. B. Prusiner, *Proc. Natl. Acad. Sci. USA* **1986**, *83*, 2310–2314.
[46] B. Caughey, G. J. Raymond, *J. Biol. Chem.* **1991**, *266*, 18217–18223.
[47] B. Chesebro, R. Race, K. Wehrly, J. Nishio, M. Bloom, D. Lechner, S. Bergstrom, K. Robbins, L. Mayer, J. M. Keith, C. Garon, A. Haase, *Nature* **1985**, *315*, 331–333.
[48] C. Locht, B. Chesebro, R. Race, J. M. Keith, *Proc. Natl. Acad. Sci. USA* **1986**, *83*, 6372–6376.
[49] B. Caughey, *Br. Med. Bull.* **1993**, *49*, 860–872.
[50] D. Riesner, K. Kellings, K. Post, H. Wille, H. Serban, D. Groth, M. A. Baldwin, S. B. Prusiner, *J. Virol.* **1996**, *70*, 1714–1722.
[51] F. E. Cohen, K.-M. Pan, Z. Huang, M. Baldwin, R. J. Fletterick, S. B. Prusiner, *Science* **1994**, *264*, 530–531.
[52] K.-M. Pan, M. Baldwin, J. Nguyen, M. Gasset, A. Serban, D. Groth, I. Mehlhorn, Z. Huang, R. J. Fletterick, F. E. Cohen, S. B. Prusiner, *Proc. Natl. Acad. Sci USA* **1993**, *90*, 10962–10966.
[53] B. W. Caughey, A. Dong, K. S. Bhat, D. Ernst, S. F. Hayes, W. S. Caughey, *Biochemistry* **1991**, *31*, 7672–7680.
[54] N. Stahl, M. A. Baldwin, D. B. Teplow, L. Hood, B. W. Gibson, A. L. Burlingame, S. B. Prusiner, *Biochemistry* **1993**, *32*, 1991–2002.
[55] J. Safar, P. P. Roller, D. C. Gajdusek, C. J. Gibbs, Jr., *J. Biol. Chem.* **1993**, *268*, 20276–20284.
[56] Z. Huang, J.-M. Gabriel, M. A. Baldwin, R. J. Fletterick, S. B. Prusiner, F. E. Cohen, *Proc. Natl. Acad. Sci. USA* **1994**, *91*, 7139–7143.
[57] Z. Huang, S. B. Prusiner, F. E. Cohen, *Fold. Design* **1995**, *1*, 13–19.
[58] M. Gasset, M. A. Baldwin, D. Lloyd, J. M. Gabriel, D. M. Holtzmann, F. E. Cohen, R. J. Fletterick, S. B. Prusiner, *Proc. Natl. Acad. Sci. USA* **1992**, *89*, 10940–10944.
[59] J. T. Nguyen, M. A. Baldwin, F. E. Cohen, S. B. Prusiner, *Biochemistry* **1995**, *34*, 4186–4192.
[60] H. Zhang, K. Kaneko, J. T. Nguyen, T. L. Livshits, M. A. Baldwin, F. E. Cohen, T. L. James, S. B. Prusiner, *J. Mol. Biol.* **1995**, *250*, 514–526.
[61] R. Riek, S. Hornemann, G. Wider, M. Billeter, R. Glockshuber, K. Wüthrich, *Nature* **1996**, *382*, 180–182.
[62] S. Hornemann, R. Glockshuber, *J. Mol. Biol.* **1996**, *262*, 614–619.
[63] M. Fischer, T. Rülicke, A. Raeber, A. Sailer, M. Moser, B. Oesch, S. Brandner, A. Aguzzi, C. Weissmann, *EMBO J.* **1996**, *15*, 1255–1264.

[64] S. Prusiner, *Arch. Neurol.* **1993**, *50*, 1129–1153.

[65] A possible way to produce labeled PrP^{Sc} would be, for instance, the in vitro conversion of ^{13}C- and ^{15}N-labeled PrP^{c}. By in vitro or cell-free conversion, PrP^{c} is converted into PrP^{Sc} by addition of exogenous PrP^{Sc}.

[66] J. Heller, A. C. Kolbert, R. Larsen, M. Ernst, T. Bekker, M. Baldwin, S. B. Prusiner, A. Pines, D. E. Wemmer, *Protein Sci.* **1996**, *5*, 1655–1661.

[67] M. E. Bruce, A. G. Dickinson, *J. Gen. Virol.* **1987**, *68*, 79–89.

[68] R. H. Kimberlin, C. A. Walker, H. Fraser, *J. Gen. Virol.* **1989**, *70*, 2017–2025.

[69] R. I. Carp, S. M. Callahan, *J. Gen. Virol.* **1991**, *72*, 293–298.

[70] R. Hecker, A. Taraboulos, M. Scott, K. M. Pan, S. L. Yang, M. Torchia, K. Jendroska, S. J. DeArmond, S. B. Prusiner, *Genes Dev.* **1992**, *6*, 1213–1228.

[71] P. Brown, P. P. Liberski, A. Wolff, D. C. Gajdusek, *J. Infect. Dis.* **1990**, *161*, 467–472.

[72] J. H. Come, P. E. Fraser, P. T. J. Lansbury, *Proc. Natl. Acad. Sci. USA* **1993**, *90*, 5959–5963.

[73] T. T. Ashburn, P. T. Lansbury, *J. Am. Chem. Soc.* **1993**, *115*, 11012–11013.

[74] P. T. Lansbury, Jr., B. Caughey, *Chem. Biol.* **1995**, *2*, 1–5.

[75] M. Eigen, *Biophys. Chem.* **1996**, *63*, A1–A18.

[76] A. J. Raeber, D. R. Borchelt, M. Scott, S. B. Prusiner, *J. Virol.* **1992**, *66*, 6155–6163.

[77] D. A. Kocisko, J. H. Come, S. A. Priola, B. Chesebro, G. J. Raymond, P. T. Lansbury, Jr., B. Caughey, *Nature* **1994**, *370*, 471–474.

[78] R. A. Bessen, D. A. Kocisko, G. J. Raymond, S. Nandan, P. T. Lansbury, B. Caughey, *Nature* **1995**, *375*, 698–700.

[79] R. A. Bessen, R. F. Marsh, *J. Virol.* **1994**, *68*, 7859–7868.

[80] G. C. Telling, P. Parchi, S. J. DeArmond, P. Cortelli, P. Montagna, R. Gabizon, J. Mastrianni, E. Lugaresi, P. Gambetti, S. B. Prusiner, *Science* **1996**, *274*, 2079–2082.

[81] G. C. Telling, M. Scott, K. K. Hsiao, D. Foster, S.-L. Yang, M. Torchia, K. C. L. Sidle, J. Collinge, S. J. DeArmond, S. B. Prusiner, *Proc. Natl. Acad. Sci. USA* **1994**, *91*, 9936–9940.

[82] G. C. Telling, M. Scott, J. Mastrianni, R. Gabizon, M. Torchia, F. E. Cohen, S. J. DeArmond, S. B. Prusiner, *Cell* **1995**, *83*, 79–90.

[83] L. E. Orgel, *Chem. Biol.* **1996**, *3*, 413–414.

[84] D. K. Kondepudi, R. J. Kaufman, N. Singh, *Science* **1990**, *250*, 975–976.

[85] W. J. Hadlow, *Lancet* **1957**, *2*, 289–290.

[86] D. C. Gajdusek, C. J. J. Gibbs, M. Alpers, *Science* **1967**, *155*, 212–214.

[87] J. Cuillé, P. L. Chelle, *C. R. Hebd. Seances Acad. Sci. Ser. D* **1939**, *208*, 1058–1060.

[88] First reports on a putative case of scrapie in cattle go back to the 19th century[151].

[89] J. Hope, L. J. Reekie, N. Hunter, G. Multhaup, K. Beyreuther, H. White, A. C. Scott, M. J. Stack, M. Dawson, G. A. Wells, *Nature* **1988**, *336*, 390–392.

[90] R. M. Anderson, C. A. Donnelly, N. M. Ferguson, M. E. J. Woolhouse, C. J. Watt, H. J. Udy, S. MaWhinney, S. P. Dunstan, T. R. E. Southwood, J. W. Wilesmith, J. B. M. Ryan, L. J. Hoinville, J. E. Hillerton, A. R. Austin, G. A. H. Wells. *Nature* **1996**, *382*, 779–788.

[91] J. W. Wilesmith, J. B. M. Ryan, M. J. Atkinson, *Vet. Rec.* **1991**, *128*, 199–203.

[92] J. W. Wilesmith, J. B. M. Ryan, W. D. Hueston, L. J. Hoinville, *Vet. Rec.* **1992**, *130*, 90–94.

[93] J. Bradbury, *Lancet* **1996**, *348*, 393.

[94] H.-G. Creutzfeldt, *Z. Ges. Neurol. Psychiatr.* **1920**, *LVII*, 1–18.

[95] A. Jakob, *Dtsch. Z. Nervenheilkd.* **1921**, *70*, 132–146.

[96] J. Gerstmann, E. Sträussler, I. Scheinker, *Z. Ges. Neurol. Psychiatr.* **1936**, *154*, 736–762.

[97] R. Medori, H.-J. Tritschler, A. LeBlanc, F. Villare, V. Manetto, H. Y. Chen, R. Xue, S. Leal, P. Montagna, P. Cortelli, P. Tinuper, P. Avoni, M. Mochi, A. Baruzzi, J. J. Hauw, J. Ott, E. Lugaresi, L. Autilio-Gambetti, P. Gambetti, *New Eng. J. Med.* **1992**, *326*, 444–449.

[98] S. B. Prusiner, *Sci. Am.* **1995**, *272*, 48–57.

[99] C. Masson, I. Delalande, J. P. Deslys, D. Henin, C. Fallet-Banco, D. Dormont, D. Leys, *Neurology* **1994**, *44*, 179–180.

[100] A. Jaegly, F. Boussin, J. P. Deslys, D. Dormont, *Genomics* **1995**, *27*, 382–383.

[101] H. A. Kretzschmar, M. Neumann, D. Stavrou, *Acta Neuropathol.* **1995**, *89*, 96–98.

[102] J. Collinge, M. S. Palmer, A. J. Dryden, *Lancet* **1991**, *337*, 1441–1442.

[103] L. G. Goldfarb, R. B. Petersen, M. Tabaton, P. Brown, A. C. LeBlanc, P. Montagna, P. Cortelli, J. Julien, C. Vital, W. W. Pendelbury, M. Haltia, P. R. Wills, J. J. Hauw, P. E. McKeever, L. Monari, B. Schrank, G. D. Swergold, L. Autilio-Gambetti, D. C. Gajdusek, E. Lugaresi, P. Gambetti, *Science* **1992**, *258*, 806–808.

[104] L. G. Goldfarb, P. Brown, M. Haltia, F. Cathala, W. R. McCombie, J. Kovanen, L. Cervenakova, L. Goldin, A. Nieto, M. S. Godec, D. M. Asher, D. C. Gajdusek, *Ann. Neurol.* **1992**, *31*, 274–281.

[105] P. Gambetti, R. Petersen, L. Monari, M. Tabaton, L. Autilio-Gambetti, *Br. Med. Bull.* **1993**, *49*, 980–994.

[106] L. Monari, S. G. Chen, P. Brown, P. Parchi, R. B. Petersen, J. Mikol, F. Gray, P. Cortelli, P. Montagna, B. Ghetti, L. G. Goldfarb, D. C. Gajdusek, E. Lugaresi, P. Gambetti, L. Autilio-Gambetti, *Proc. Natl. Acad. Sci. USA* **1994**, *91*, 2839–2842.

[107] K. Hsiao, H. F. Baker, T. J. Crow, M. Poulter, F. Owen, J. D. Terwilliger, D. Westaway, J. Ott, S. B. Prusiner, *Nature* **1989**, *338*, 342–345.

[108] D. Goldgaber, L. G. Goldfarb, P. Brown, D. M. Asher, W. T. Brown, S. Lin, J. W. Teener, S. M. Feinstone, R. Rubenstein, R. J. Kascsak, J. W. Boelaard, D. C. Gajdusek, *Exp. Neurol.* **1989**, *106*, 204–206.

[109] K. Doh-ura, J. Tateishi, H. Sasaki, T. Kitamoto, Y. Sakaki, *Biochem. Biophys. Res. Commun.* **1989**, *163*, 974–979.

[110] Y. Goldhammer, R. Gabizon, Z. Meiner, M. Sadeh, *Neurology* **1993**, *43*, 2718–2719.

[111] T. Kitamoto, R. Iizuka, J. Tateishi, *Biochem. Biophys. Res. Commun.* **1993**, *192*, 525–531.

[112] B. Ghetti, P. Piccardo, M. G. Spillantini, Y. Ichimiya, M. Porro, F. Perini, T. Kitamoto, J. Tateishi, C. Seiler, B. Frangione, O. Bugiani, G. Giaccone, F. Prelli, M. Goedert, S. R. Dlouhy, F. Tagliavini, *Proc. Natl. Acad. Sci. USA.* **1996**, *93*, 744–748.

[113] P. Belt, I. Muileman, B. Schreuder, J. Bos de Ruijter, A. Gielkens, M. Smits, *J. Gen. Virol.* **1995**, *76*, 509–517.

[114] R. G. Will, J. W. Ironside, M. Zeidler, S. N. Cousens, K. Estibeiro, A. Alperovitch, S. Poser, M. Pocchiari, A. Hofman, P. G. Smith, *Lancet* **1996**, *347*, 921–925; this publication had ramifications beyond its scientific significance (the article was the most-cited scientific publication in 1996; source: Institute for Scientific Information, Hot Papers Database, November/December 1994–November/December 1996)—it also had political effects: in spring 1996 the British government was forced to admit for the first time that a transmission of BSE to humans cannot be excluded. At European level, the commission of the European Union introduced an export ban for British beef.

[115] C. I. Lasmézas, J.-P. Deslys, R. Demalmay, K. T. Adjou, F. Lamoury, D. Dormont, O. Robain, J. Ironside, J.-J. Hauw, *Nature* **1996**, *381*, 743–744.

[116] G. Chazot, E. Broussolle, C. I. Lapras, T. Blättler, A. Aguzzi, N. Kopp, *Lancet* **1996**, *347*, 1181.

[117] J. Collinge, K. C. L. Sidle, J. Meads, J. Ironside, A. F. Hill, *Nature* **1996**, *383*, 685–690.

[118] P. Parchi, S. Capellari, S. G. Chenn, R. B. Petersen, P. Gambetti, N. Kopp, P. Brown, T. Kitamoto, J. Tateishi, A. Giese, H. Kretzschmar, *Nature* **1997**, *386*, 232–233.

[119] R. A. Somerville, A. Chong, O. U. Mulqueen, C. R. Birkett, S. C. E. R. Wood, J. Hope, *Nature* **1997**, *386*, 564.

[120] N. Kopp, N. Streichenberger, J. Deslys, J. Laplanche, G. Chazot, *Lancet* **1996**, *348*, 1239–1240.

[121] S. B. Prusiner, D. Groth, H. Serban, R. Koehler, D. Foster, M. Torchia, D. R. Burton, S. L. Yang, S. J. DeArmond, *Proc. Natl. Acad. Sci. USA* **1993**, *90*, 10608–10612.

[122] R. A. Williamson, D. Peretz, N. Smorodinsky, R. Bastidas, H. Serban, I. Mehlhorn, S. J. DeArmond, S. B. Prusiner, D. R. Burton, *Proc. Natl. Acad. Sci. USA.* **1996**, *93*, 7279–7282.

[123] B. E. C. Schreuder, L. J. M. van Keulen, M. E. W. Vromans, J. P. M. Langeveld, M. A. Smits, *Nature* **1996**, *381*, 563.

[124] A. F. Hill, M. Zeidler, J. Ironside, J. Collinge, *Lancet* **1997**, *349*, 99–100.

[125] M. G. Harrington, C. R. Merril, D. M. Asher, D. C. Gajdusek, *New Engl. J. Med.* **1986**, *315*, 279–283.

[126] G. Hsich, K. Kenney, C. J. J. Gibbs, K. H. Lee, M. G. Harrington, *New Engl. J. Med.* **1996**, *335*, 924–930.

[127] K. K. Hsiao, M. Scott, D. Foster, D. F. Groth, S. J. DeArmond, S. B. Prusiner, *Science* **1990**, *250*, 1587–1590.

[128] K. K. Hsiao, D. Groth, M. Scott, S. L. Yang, H. Serban, D. Rapp, D. Foster, M. Torchia, S. J. DeArmond, S. B. Prusiner, *Proc. Natl. Acad. Sci. USA* **1994**, *91*, 9126–9130.

[129] H. M. Schätzl, M. Da Costa, L. Taylor, F. E. Cohen, S. B. Prusiner, *J. Mol. Biol.* **1995**, *245*, 362–374.

[130] M. Scott, D. Foster, C. Mirenda, D. Serban, F. Coutal, M. Wälchli, M. Torchia, D. Groth, G. Carlson, S. J. DeArmond, D. Westaway, S. B. Prusiner, *Cell* **1989**, *59*, 847–857.

[131] S. B. Prusiner, M. Scott, D. Foster, K.-M. Pan, D. Groth, C. Mirenda, M. Torchia, S.-L. Yang, D. Serban, G. A. Carlson, P. C. Hoppe, D. Westaway, S. J. DeArmond, *Cell* **1990**, *63*, 673–686.

[132] F. U. Hartl, J. Martin, *Curr. Opin. Struct. Biol.* **1995**, *5*, 92–102.

[133] R. B. Wickner, D. C. Masison, H. K. Edskes, *Yeast* **1995**, *11*, 1671–1685.

[134] Y. O. Chernoff, S. L. Lindquist, B.-I. Ono, S. G. Inge-Vechtomov, S. W. Liebman, *Science* **1995**, *268*, 880–884.

[135] M. M. Patino, J.-J. Liu, J. R. Glover, S. Lindquist, *Science* **1996**, *273*, 622–626.

[136] F. Edenhofer, R. Rieger, M. Famulok, W. Wendler, S. Weiss, E.-L. Winnacker, *J. Virol.* **1996**, *70*, 4724–4728.

[137] J. Tatzelt, S. B. Prusiner, W. J. Welch, *EMBO J.* **1996**, *15*, 6363–6373.

[138] S. Brandner, S. Isenmann, A. Raeber, M. Fischer, A. Sailer, Y. Kobayashi, S. Marino, C. Weissmann, A. Aguzzi, *Nature* **1996**, *379*, 339–343.

[139] G. Forloni, N. Angeretti, R. Chiesa, E. Monzani, M. Salmona, O. Bugiani, F. Tagliavini, *Nature* **1993**, *362*, 543–546.

[140] D. R. Brown, J. Herms, H. A. Kretzschmar, *NeuroReport* **1994**, *5*, 2057–2060.

[141] E. P. Brandon, R. L. Idzerda, G. S. McKnight, *Curr. Biol.* **1995**, *5*, 625–634.
[142] H. Buehler, M. Fischer, Y. Lang, H. Bluethmann, H.-P. Lipp, S. J. DeArmond, S. B. Prusiner, M. Aguet, C. Weissmann, *Nature* **1992**, *356*, 577–582.
[143] P.-M. Lledo, P. Tremblay, S. J. DeArmond, S. B. Prusiner, R. A. Nicoll, *Proc. Natl. Acad. Sci. USA* **1996**, *93*, 2403–2407.
[144] D. R. Borchelt, S. S. Sisodia, *Chem. Biol.* **1996**, *3*, 619–621.
[145] J. P. Estibeiro, *Trends Neurosci.* **1996**, *19*, 257–258.
[146] P. Goloubinoff, J. P. Christeller, A. A. Gatenby, G. C. Lorimer, *Nature* **1989**, *371*, 578–586.
[147] J. Buchner, M. Schmidt, M. Fuchs, R. Jaenicke, R. Rudolph, F. X. Schmid, T. Kiefhaber, *Biochemistry* **1991**, *30*, 1586–1591.
[148] R. John Ellis also pictorially calls this container an "Anfinsen cage" [152].
[149] This statement is valid at least in the limited sense of Prusiner's heterodimer model.
[150] C. Weissmann, *Nature* **1991**, *349*, 569–571.
[151] M. Sarradet, *Rev. Vet.* **1883**, *3*, 310–312.
[152] R. J. Ellis, *Fold. Design* **1995**, *1*, R9–R15.

Chemistry at the crossroads

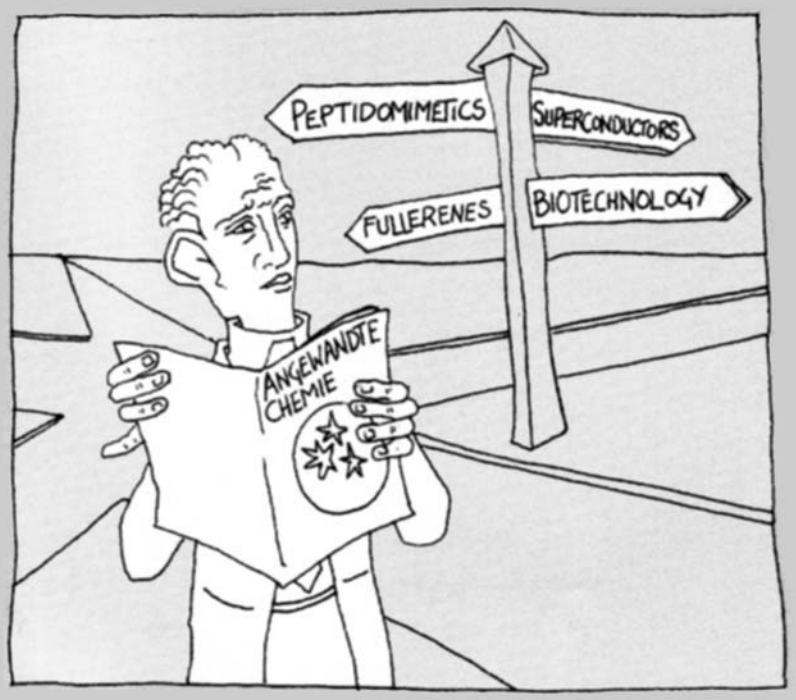

Pioneering scientists guide your way through newly charted territory with their topical reviews and discriminating highlights in **Angewandte Chemie.**

To start your own personal subscription, just fax.

An order form is provided on the last page for your convenience.

WILEY-VCH

Pentalene as a Complex Ligand: New Developments in the Chemistry of Nonalternant, Highly Unsaturated Hydrocarbons

Holger Butenschön*

Compounds with annelated five-membered rings (oligo- or polyquinanes)[1,2] have generated a great deal of interest in organic chemistry under a variety of aspects. Natural products like triquinanes,[3] coriolin, hirsutene, and pentalenes or the tetraquinanes of the crinipellin-type[4] are nowadays considered classics in the biologically orientated polyquinane chemistry, while topologically remarkable compounds like dodecahedrane,[5-8] centrohexaindane,[9] or fenestrane[10,11] fascinate many chemists, who are interested in the synthesis, structure, and properties of these unusual compounds. A special role is played by the completely unsaturated compounds like pentalene (**1**) and acepentalene (**2**), whose π-electron systems are of fundamental interest with respect to the aromaticity of nonalternant unsaturated hydrocarbons.

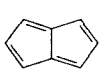

1

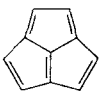

2

In accord with theoretical calculations[12-17] it was shown in the last twenty five years that **1** and **2** are unstable under normal conditions. De Mayo et al. and Hafner et al. prepared pentalene derivatives stabilized kinetically by substituents,[18-23] and in 1973 Hafner et al. were able to demonstrate the existence of the unsubstituted pentalene.[19] Recently de Meijere et al. reported on the identification of acepentalene (**2**) by mass spectrometry.[17] To stabilize the two compounds two further possibilities were considered: Firstly **1** and **2** could be stabilized as complex ligands in a similar way to the stabilization of cyclobutadiene as a tricarbonyliron complex forty years ago. Secondly the dianions formed by reduction of **1** and **2** should be more stable than the neutral compounds.[16,24] If the formation of such dianions, which were considered to be aromatic, were successful, they would be expected to readily undergo complexation.

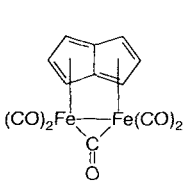

3

In 1973 Hafner et al. successfully prepared the metal complex **3** of the unsubstituted pentalene (**1**) by reaction of the [2+2] dimer of **1** with $[Fe_2(CO)_9]$.[25] A substituted derivative had been prepared earlier starting from the corresponding dihydropentalene.[26] The pentalene dianion ($\mathbf{1}^{2-}$) has been known for a longer time than pentalene (**1**) itself. It was synthesized in 1962 by Katz et al. by treatment of a dihydropentalene with butyllithium,[27,28] and was also used as a ligand in some transition metal complexes.[26,29-31] The structure determined for the $\mathbf{1}^{2-}$ is planar and is in accord with that from calculations.[24] In the previously known metal complexes pentalene acts as a bridging ligand between two late transition metals.

Now Jonas et al. have reported in two remarkable publications from the Max-Planck-Institut für Kohlenforschung in Mülheim an der Ruhr on a totally new mode of complexation of the pentalene dianion in which all eight carbon atoms are coordinated to only *one* metal atom.[32,33] The authors present thermally stable and sublimable vanadium complexes of type **4**, which were prepared by treatment of $\mathbf{1}^{2-}$ with a variety of vanadocene monohalides. As expected from earlier studies this reaction proceeds with elimination of a halide and a cyclopentadienyl ligand from the vanadocene derivative. The 10 electrons that the resulting cyclopentadienylvanadium(III) fragment requires to achieve the 18-electron configuration are provided by the pentalene dianion $\mathbf{1}^{2-}$. As expected, the mononuclear pentalene vanadium complexes are obtained in high yields as diamagnetic compounds. In addition to the unsubstituted parent compound **4** the corresponding pentamethylcyclopentadienyl and indenyl complexes were prepared as well as the complex analogous to **4** bearing the 2-methylpentalene dianion.[34]

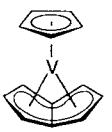

4

Some of the prepared vanadium complexes were characterized by crystal structure analyses. The outstanding feature of the three obtained structures is the folding of the pentalene ligand along the central carbon–carbon bond by 137°. Thus, the structure of the complexed ligand differs considerably from that of the planar pentalene dianion ($\mathbf{1}^{2-}$). The folding ensures that all eight coordinated carbon atoms have realistic bond lengths to the metal atom. If the ligand of the complex were planar, both central carbon atoms would be located rather closely to the vanadium atom, while the peripheral carbon atoms would be far away from it. Such a fundamental change in structure as a result of complexation to a metal is rare and impressively shows the variety of structural possibilities of cyclic π ligands.

The formation of complexes of the pentalene dianion $\mathbf{1}^{2-}$ is not restricted to the element vanadium. The authors have also

[*] Prof. Dr. H. Butenschön
Institut für Organische Chemie der Universität
Schneiderberg 1B, D-30167 Hannover (Germany)
Fax: Int. code +(511)762-4616
e-mail: holger.butenschoen@mbox.oci.uni-hannover.de

 © WILEY-VCH Verlag GmbH, D-69451 Weinheim, 1997 0570-0833/97/3616-1695 $ 17.50+.50/0

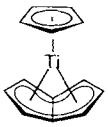

5

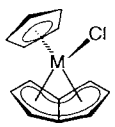

6: M = Ti
7: M = Zr

prepared interesting titanium, zirconium, and hafnium complexes starting from the corresponding cyclopentadienylchloro complexes.[33] For instance, the halide-free titanium complex **5** was prepared by reaction of $[CpTiCl_2]$ with $\mathbf{1}^{2-}$. Oxidation with 1,2-dichloroethane with loss of ethene leads to the Ti^{IV} complex **6**. The analogous zirconium complex **7** was synthesized directly by treating $\mathbf{1}^{2-}$ with zirconocene dichloride.

The homoleptic pentalene complexes **8**, which were obtained by treatment of **6**, zirconocene dichloride, or hafnocene dichloride with $\mathbf{1}^{2-}$, are of special interest. Moreover, it was possible to synthesize the corresponding dimethyl-substituted titanium complex **9**. Complexes **8** and **9**, which have still to be characterized by X-ray crystal structure analyses, are diamagnetic 20e complexes. The pseudotetrahedral coordination geometry was determined by comparative ^{13}C NMR studies of **8** and **9**. Temperature-dependent studies show that **9** has two distorted tetrahedral conformers that differ in terms of the distances between the methyl groups. In view of the 20e configuration it is evident that **8** (M = Zr) loses one of the pentalene ligands readily: Treatment with one equivalent of $[ZrCl_4(thf)_2]$ affords two equivalents of the distorted octahedrally coordinated 18e complex $[(C_8H_6)ZrCl_2(thf)_2]$ (**10**) in high yield.

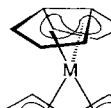

8 (M = Ti, Zr, Hf)

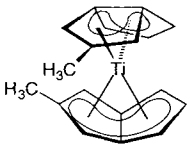

9

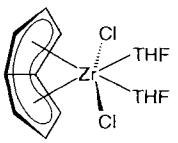

10

The fascinating results of the organometallic chemistry of pentalene (**1**) presented here lead to the question whether and to what degree does the above-mentioned acepentalene (**2**) behave analogously. Dihydroacepentalene complexes were synthesized by de Meijere et al. in 1983.[35, 36] The acepentalene dianion ($\mathbf{2}^{2-}$) was prepared by treating triquinacene in form of its potassium salt, which could not be separated from impurities, with superbases.[37] However, a short time ago the distannylated dihydroacepentalene **11** was prepared and purified by sublimation.[38] Subsequent metalation with methyllithium in dimethoxyethane (DME) at −60 °C afforded $\mathbf{2}^{2-}$ in the form of the lithium salt. The X-ray crystal structure analysis of the DME adduct shows that each DME-solvated lithium ion is located at opposite faces of the acepentalene dianion. In contrast to $\mathbf{1}^{2-}$, $\mathbf{2}^{2-}$ is not planar, but, in accord with calculations, exists in a shell-like structure with a convex and a concave surface. The chemical and structural analogy between $\mathbf{2}^{2-}$ and the ligand in the complexes **4**–**9** reported by Jonas et al. suggest that $\mathbf{2}^{2-}$ could function as ligand in transition metal complexes. Preliminary results indicate that this is indeed possible.[39]

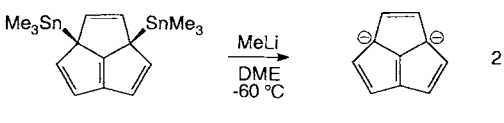

11 **2^{2-}**

The scope of the organometallic chemistry of compounds with annelated five-membered rings has been considerably broadened by the work reported here. One eagerly awaits new developments in this interesting field between organic and inorganic chemistry. Besides the synthesis and structural characterization of these complexes there is enormous interest in the chemical reactivity, especially in terms of their suitability for catalyst systems. It appears quite fitting that in the institute, in which a chapter of chemistry history was written 40 years ago with the discovery of the Ziegler catalysts, the idea of using the new pentalene complexes as zirconocene-analogous components of modern Ziegler catalyst systems is now being pursued.

German version: *Angew. Chem.* **1997**, *109*, 1771–1773

Keywords: acepentalene · coordination modes · mononuclear complexes · pentalene · structure elucidation

[1] B. M. Trost, *Chem. Soc. Rev.* **1982**, 141–170.
[2] L. A. Paquette, *Top. Curr. Chem.* **1984**, *119*, 1–158.
[3] E. J. Corey, X.-M. Cheng, *The Logic of Chemical Synthesis*, Wiley, New York, **1989**.
[4] T. Anke, J. Heim, F. Knoch, U. Mocek, B. Steffan, W. Steglich, *Angew. Chem.* **1985**, *97*, 714–716; *Angew. Chem. Int. Ed. Engl.* **1985**, *24*, 709–711.
[5] L. A. Paquette, D. W. Balogh, R. Usha, D. Kountz, G. G. Christoph, *Science* **1981**, *211*, 575–576.
[6] R. J. Ternansky, D. W. Balogh, L. A. Paquette, *J. Am. Chem. Soc.* **1982**, *104*, 4503–4503.
[7] H. Prinzbach, K. Weber, *Angew. Chem.* **1994**, *106*, 2329–2348; *Angew. Chem. Int. Ed. Engl.* **1994**, *33*, 2239–2257.
[8] M. Bertau, J. Leonhardt, A. Weiler, K. Weber, H. Prinzbach, *Chem. Eur. J.* **1996**, *2*, 570–579.
[9] D. Kuck, *Synlett* **1996**, 949–965.
[10] H. Schori, B. B. Path, R. Keese, *Tetrahedron* **1981**, *37*, 4457–4463.
[11] M. Thommen, A. L. Veretenov, R. Guidetti-Grept, R. Keese, *Helv. Chim. Acta* **1996**, *79*, 461–476.
[12] Y. Jean, *New J. Chem.* **1980**, *4*, 11–15.
[13] N. C. Baird, R. M. West, *J. Am. Chem. Soc.* **1971**, *93*, 3072–3073.
[14] K. Jug, E. J. P. Malar, *J. Mol. Struct.* **1987**, *153*, 221–226.
[15] F. Tomas, J. I. Fernandez-Alonso, *An. Quim. (Madrid)* **1976**, *72*, 122–126.
[16] A. Streitwieser, Jr., *Molecular Orbital Theory for Organic Chemists*, Wiley, New York, **1961**, pp. 290–293.
[17] R. Haag, D. Schröder, T. Zywietz, H. Jiao, H. Schwarz, P. von R. Schleyer, A. de Meijere, *Angew. Chem.* **1996**, *108*, 1413–1416; *Angew. Chem. Int. Ed. Engl.* **1996**, *35*, 1317–1319.
[18] R. Bloch, R. A. Marty, P. de Mayo, *J. Am. Chem. Soc.* **1971**, *93*, 3071–3072.
[19] K. Hafner, R. Dönges, E. Goedecke, R. Kaiser, *Angew. Chem.* **1973**, *85*, 362–364; *Angew. Chem. Int. Ed. Engl.* **1973**, *12*, 337–339.
[20] K. Hafner, H. U. Süss, *Angew. Chem.* **1973**, *85*, 626–628; *Angew. Chem. Int. Ed. Engl.* **1973**, *12*, 575–577.
[21] K. Hafner, F. Schmidt, *Angew. Chem.* **1973**, *85*, 450–451; *Angew. Chem. Int. Ed. Engl.* **1973**, *12*, 418–419.
[22] K. Hafner, M. Suda, *Angew. Chem.* **1976**, *88*, 341–342; *Angew. Chem. Int. Ed. Engl.* **1976**, *15*, 314–315.
[23] R. Dönges, K. Hafner, H. J. Lindner, *Tetrahedron Lett.* **1976**, 1345–1348.
[24] J. J. Stezowski, H. Hoier, D. Wilhelm, T. Clark, P. von R. Schleyer, *J. Chem. Soc. Chem. Commun.* **1985**, 1263–1264.
[25] W. Weidemüller, K. Hafner, *Angew. Chem.* **1973**, *85*, 958–959; *Angew. Chem. Int. Ed. Engl.* **1973**, *12*, 925.
[26] F. F. Hunt, J. W. Russell, *J. Am. Chem. Soc.* **1972**, *94*, 7198–7199.
[27] T. J. Katz, M. Rosenberger, *J. Am. Chem. Soc.* **1962**, *84*, 865–866.
[28] T. J. Katz, M. Rosenberger, R. K. O'Hara, *J. Am. Chem. Soc.* **1964**, *86*, 249–252.
[29] T. J. Katz, M. Rosenberger, *J. Am. Chem. Soc.* **1963**, *85*, 2030–2031.

 © WILEY-VCH Verlag GmbH, D-69451 Weinheim, 1997 0570-0833/97/3616-1696 $ 17.50+.50/0

[30] T. J. Katz, N. Acton, *J. Am. Chem. Soc.* **1972**, *94*, 3281–3283.
[31] D. F. Hunt, J. W. Russell, *J. Organomet. Chem.* **1972**, *46*, C22–C24.
[32] K. Jonas, B. Gabor, R. Mynott, K. Angermund, O. Heinemann, C. Krüger, *Angew. Chem.* **1997**, *109*, 1790; *Angew. Chem. Int. Ed. Engl.* **1997**, *36*, 1712.
[33] K. Jonas, P. Kolb, G. Kollbach, B. Gabor, R. Mynott, K. Angermund, O. Heinemann, C. Krüger, *Angew. Chem.* **1997**, *109*, 1793; *Angew. Chem. Int. Ed. Engl.* **1997**, *36*, 1714.
[34] According to IUPAC the anion 1^{2-} should be named dihydropentalendiide; it is obtained by double deprotonation of a dihydropentalene. The anion 1^{2-} can also be obtained from pentalene by double electron transfer and may therefore be named as pentalene dianion. In the original publications the authors prefer the graphic representation of 1^{2-} as a dianion or as a complex ligand with a formula with a closed cycle in either one of the five-membered rings. The pentalene ligand is a 10e ligand in the complexes **4**–**10**, therefore **4** should be considered as a V^{III} complex.
[35] H. Butenschön, Dissertation, Universität Hamburg, **1983**.
[36] H. Butenschön, A. de Meijere, *Tetrahedron* **1986**, *42*, 1721–1729.
[37] T. Lendvai, T. Friedl, H. Butenschön, T. Clark, A. de Meijere, *Angew. Chem.* **1986**, *98*, 734–735; *Angew. Chem. Int. Ed. Engl.* **1986**, *25*, 719–720.
[38] R. Haag, R. Fleischer, D. Stalke, A. de Meijere, *Angew. Chem.* **1995**, *107*, 1642–1644; *Angew. Chem. Int. Ed. Engl.* **1995**, *34*, 1492–1495.
[39] R. Haag, Dissertation, Universität Göttingen, **1995**.

Electron-Transfer Transition States: Bound or Unbound—That is the Question!

Hendrik Zipse*

The breathtaking advances realized in the field of computational quantum chemistry within the past two decades have made it possible to reliably predict transition state structures for most reaction types in organic chemistry. The focus of controversy has moved from the characterization of typical organic reaction mechanisms, such as pericyclic reactions,[1] to more complex issues, such as reaction mechanisms in organometallic chemistry[2] or the detailed description of solvent effects. In light of this development it is quite surprising that little structural detail is available for the most elementary reaction step in chemistry, the exchange of electrons between two reaction partners. It was only recently realized that transition states for electron-transfer reactions might also have definitive structural requirements.[3] Traditionally, electron-transfer (ET) reactions were qualitatively discussed in terms of outer-sphere and inner-sphere ET.[4] These terms were originally coined for classifying ET reactions between transition metal complexes, which either occur without breaking metal–ligand bonds (outer-sphere ET) or with concomitant cleavage/formation of metal–ligand bonds (inner-sphere ET).[5] Implicit in this categorization is the assumption that little interaction exists between the electron donor and acceptor in transition states of outer-sphere ET reactions, whereas the converse is true for inner-sphere ET reactions. Exactly this assumption was challenged by Eberson and Shaik through application of the valence-bond curve-crossing model (VBCM) to thermal ET reactions in open-shell systems.[3] According to this qualitative model transition states for dissociative electron transfer between radical anions and alkyl halides is stabilized by maximum overlap between the donor SOMO (singly occupied molecular orbital) and the alkyl halide LUMO (lowest unoccupied molecular orbital), whereas the most dominant interaction for the competing S_N2 transition state is that between the donor π HOMO (highest occupied molecular orbital) and the alkyl halide LUMO. For the combination of ketyl radical anions and alkyl halides, the corresponding orbitals are shown in Scheme 1. The most important consequences of this are the following: a) Optimization of bimolecular orbital overlap is important for transition states of formal outer-sphere electron transfer. If not prohibited by steric effects, transition states for electron transfer should be bound more strongly than either the reactant or the product complexes. b) Different selection rules apply for transition states of electron transfer and nucleophilic substitution.

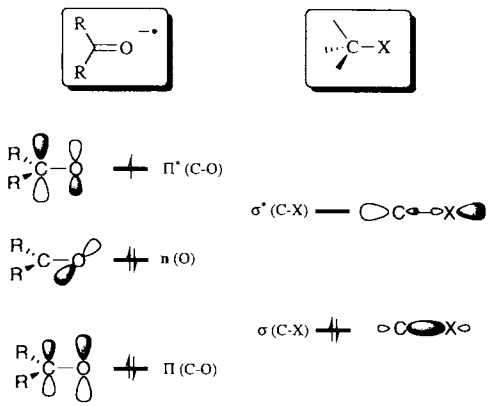

Scheme 1. Frontier molecular orbitals of ketyl radical anions and alkyl halides.

It already becomes apparent at this stage that the terms of inner- and outer-sphere electron transfer alone are not well suited for discussing mechanistic details in electron-transfer processes, as they do not describe the nature of the transition states involved. In general electron-transfer transition states might be characterized as "bound" or "unbound"; the latter describes a situation in which only weak interactions exist between the reactants, whereas for the former the electron donor and acceptor are in intimate contact in the transition state. Therefore, ET reactions might be of the unbound, outer-sphere type involving weakly bound transition states and avoiding formation of bound intermediates or products, or they might be of the bound, outer-sphere type in which formation of bound intermediates or products is again avoided, but the more compact transition state

[*] Dr. H. Zipse
Institut für Organische Chemie der Technischen Universität
Strasse der 17. Juni 135, D-10623 Berlin (Germany)
Fax: Int. code +(30)3142-1102
e-mail: zips0531@z1.chem.tu-berlin.de

 © WILEY-VCH Verlag GmbH, D-69451 Weinheim, 1997 0570-0833/97/3616-1697 $ 17.50+.50/0

has a defined structure. An upper limit of 1 kcal mol^{-1} of electronic interaction energy is commonly assumed for unbound, outer-sphere ET transition states.[3] The distinction between unbound and bound transition states is of less importance for inner-sphere ET reactions, as basically all reactions leading to bond formation will have bound transition states. This leaves us with three categories for the classification of ET transition states: "unbound, outer-sphere ET", "bound, outer-sphere ET", or "bound, inner-sphere ET".

Can the VBCM predictions of Eberson and Shaik be verified? One of the smallest model systems amenable to quantum mechanical studies is the reaction of the formaldehyde radical anion with methyl chloride (Scheme 2).[6] The results obtained are

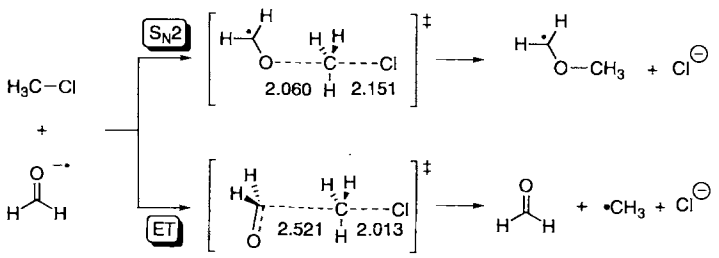

Scheme 2. Pathways for nucleophilic substitution and dissociative electron transfer in the reaction of formaldehyde radical anion and methyl chloride [UMP2(FC)/6 – 31+G*].

in complete agreement with the qualitative predictions of the VBCM model. The structure of the S_N2 transition state leading to the O-alkylation product is similar to that computed for other nucleophiles. The formaldehyde radical anion is oriented such that one of the carbonyl-group lone pairs points towards the methyl halide carbon atom. The transition state for electron transfer is distinctly different from that for the S_N2 alternative: the carbonyl carbon atom now aims towards the methyl group in CH_3Cl, and the distance between donor and acceptor is about 0.5 Å larger. The barrier for the electron-transfer process amounts to +5.3 kcal mol^{-1} relative to a complex of the reactants at the QCISD(T)/6 – 31+G(d)//UMP2/6 – 31+G(d) level of theory, and is 1.9 kcal mol^{-1} less than that for the S_N2 reaction. That both pathways involve significant binding between the two reactants is not only seen in the transition state structures but also in the activation entropies, which are negative and of comparable magnitude in both cases. These theoretical results nicely complement experimental studies by Kimura et al. on the competition of intramolecular substitution and electron-transfer processes in radical anions of benzoylhaloalkanes.[7] The product distribution obtained in these systems (Scheme 3, R = Ar) depends on the length of the chain connecting the carbonyl group and the halide carrier, the halide leaving group, and the solvent. For very short chains, such as $n = 1$, only electron transfer was observed, whereas an increase to $n = 2$ or 3 gives mainly nucleophilic substitution if chloride is the leaving group. This can readily be explained as the consequence of differing structural requirements for the transition states of the two competing processes. The connecting chain not only serves as a link between the two reactive centers, but also moderates the conformational space available for the relative orientation of these two groups. If the orientational preferences between the two groups are indeed as different as predicted by

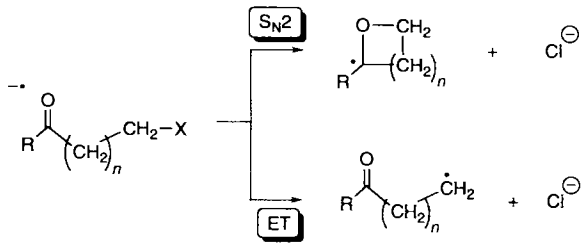

Scheme 3. Competition between intramolecular nucleophilic substitution and intramolecular dissociative electron transfer in radical anions of substituted benzoylhaloalkanes. R = H, Ar; X = Cl, Br, I; $n = 1, 2, 3$.

the theoretical model study,[6] the relative barriers for ET and substitution reactions will strongly depend on the chain length. This point was explored in more detail in another theoretical study of smaller model systems (Scheme 3, R = H, X = Cl).[8] For $n = 1$ the barrier for electron transfer is significantly lower than for nucleophilic substitution at oxygen, simply due to the fact that the ring strain is much higher in the transition state of the latter process. For $n = 2$ the S_N2 transition state can be formed much more easily, whereas the ET transition state is now burdened with excess ring strain. In agreement with experiment, the reaction now proceeds mainly by the S_N2 process. The most intriguing aspect of the experimental studies by Kimura et al. is, however, that the rate of disappearance of the initially formed ketyl radical anions correlates well with the reduction potential of the parent ketones as well as solvent polarity indicators, *irrespective* of the actual ratio between the substitution and the electron-transfer process. This observation can only be explained by assuming a *common mechanism* for both processes in the sense that fission of the C–Cl bond as well as rearrangement of the charges advance to a similar degree for both pathways.

One immediate question arising from the concept of bound outer-sphere ET transition states is whether these transition states can be bound as strongly as those of bond-forming reactions, or whether a limit exists beyond which transition state binding inevitably leads to bond formation. This question was explored in reactions of ketyl radical anion donors with methyl halide acceptors (Scheme 4).[9] Variation of the donor strength and leaving-group ability gives a series in which the reaction barrier becomes progressively larger. A mechanistic changeover from C-oriented ET to C-oriented S_N2 occurs at high barriers and short C–C distances, but all transition states can be linearly correlated with α. The parameter α is a relative measure of transition state location that, according to the Marcus equation, can be expressed as a ratio of activation- and reaction-energy contributions.[10] The clear separation between ET and S_N2 transition states illustrates that a "point of no return" exists at around 2.4 Å for the bond distance between the central carbonyl and alkyl carbon atoms. All transition states involving a C–C distance that is smaller than this limiting value lead to S_N2 products, whereas transition states with longer C–C bond distances lead to ET products. The common correlation observed for all stationary points in this study can most reasonably be explained by assuming that ET and S_N2 transition states belong to one family of related reaction mechanisms.

The discussion of bound or unbound ET transition states is, of course, not without controversy. A new theoretical study of

 © WILEY-VCH Verlag GmbH, D-69451 Weinheim, 1997 0570-0833/97/3616-1698 $ 17.50+.50/0

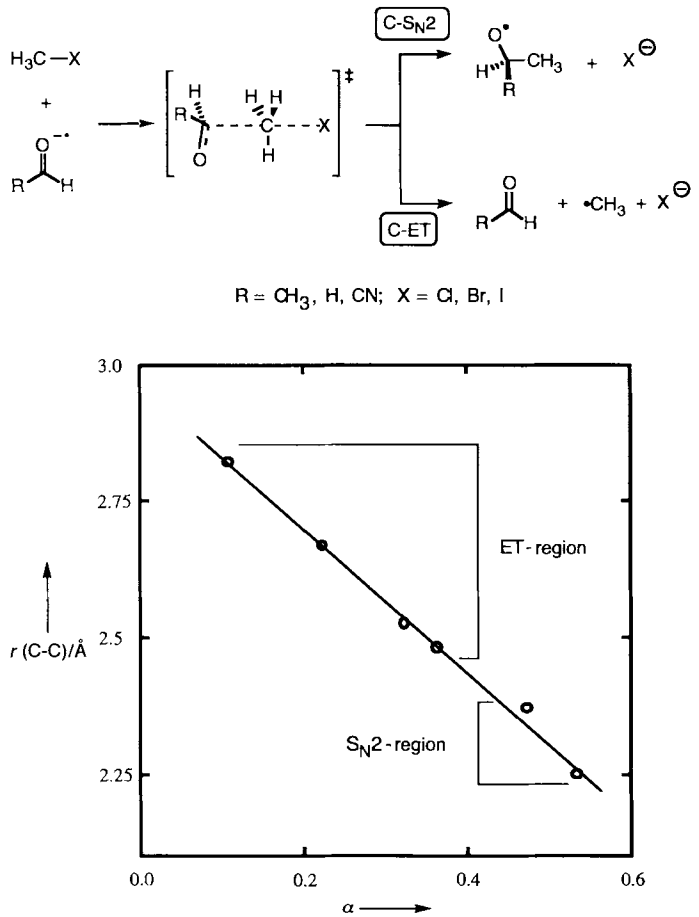

Scheme 4. Correlation of the C–C bond distance in the transition state with the Marcus parameter α.

the methyl chloride/formaldehyde radical anion system by Bertran et al.[11] reports an additional transition state for electron transfer that is close to that expected for an unbound, outer-sphere ET transition state. The distance between the reactants is significantly larger in this structure, which is energetically much less favorable than the transition state for the O-alkylation pathway. A similar stationary point was found for the ET reaction of methyl fluoride and formaldehyde radical anion. Moreover, the bound ET transition state reported earlier[6] was also found in this study. However, this reaction path led to substitution products, and this stationary point has correspondingly been designated a "C-S_N2" transition state. Indeed, the situation appears to be rather delicate in that the reaction pathway leads to different products, depending on the method chosen for following the reaction. This point was reinvestigated in more detail by Shaik et al.;[12] the ET/S_N2 reaction pathway is sensitive to the coordinate system as well as the choice of wavefunction. This controversy will eventually be settled by generating the complete potential energy surface and employing more sophisticated theoretical methods. But the results obtained so far indicate a very flat potential energy surface, in which the difference between going in one or the other direction is rather small. Certainly, the actual branching ratio between the two pathways will not only depend on the reaction energetics, but on the reaction dynamics as well.

A third mechanism for electron transfer can be found in reactions of uncharged nucleophiles with radical cations of alkenes and alkanes.[13,14] In the case of the former this involves initial nucleophilic addition to the alkene radical cation and formation of a distonic radical cation (Scheme 5, type A). Homolysis of

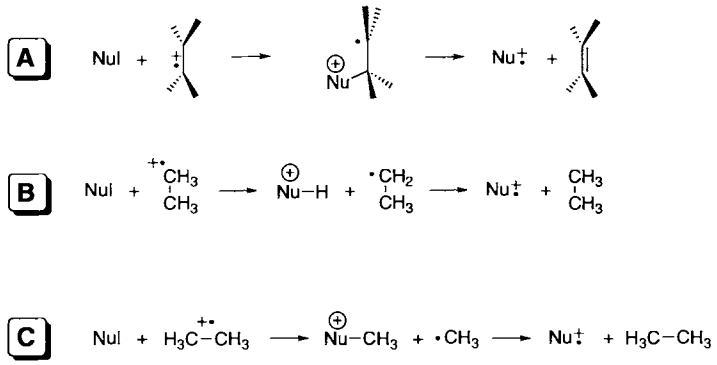

Scheme 5. Mechanisms for inner-sphere electron transfer between uncharged nucleophiles and radical cations of alkenes (type A) and alkanes (types B, C).

the newly formed bond gives the donor radical cation and the neutral alkene as products. This sequence is a classical example for inner-sphere electron transfer between organic substrates. If the radical cation of ethane, $C_2H_6^{\bullet+}$, is used as a representative model for hydrocarbon radical cations, electron transfer to uncharged nucleophiles proceeds either through bound, outer-sphere ET transition states (for PH_3 and SH_2) or by a two-step inner-sphere process that involves stepwise transfer of $H^+/H^\bullet$ (Scheme 5, type B) or $^+CH_3/^\bullet CH_3$ (type C) redox pairs. The latter two pathways are found for NH_3 and H_2O as nucleophiles. Since the initial step of inner-sphere ET processes is simply nucleophilic attack at the hydrocarbon radical cation, we can reconfirm one major conclusion reached in the studies of anionic systems: bound transition states for outer-sphere ET and nucleophilic-substitution reactions are mutually exclusive for the same system, but both belong to the same mechanistic family in the sense that they share common structural and electronic features. Irrespective of the actual choice of ET through bound transition states, an alternative pathway also exists through unbound, outer-sphere ET transition states in these systems. This option was explored for the reaction of NH_3 and PH_3 with the ethane radical cation. In both cases the unbound transition states for outer-sphere ET are energetically less favorable than the *separated* reactants, and show a much larger distance between the two reactants (>4 Å). The pathways through unbound, outer-sphere ET transition states are thus much less attractive energetically than either of the two alternatives. In matching theoretical with experimental results it is important to consider also activation entropies, which are usually more favorable for pathways involving unbound, outer-sphere ET transition states.

Ab initio studies of small model systems predict that electron transfer cannot only proceed through the traditionally anticipated pathways involving unbound, outer-sphere or bound, inner-sphere ET transition states, but that the bound, outer-sphere ET transition state is a serious contender in many cases.

 © WILEY-VCH Verlag GmbH, D-69451 Weinheim, 1997 0570-0833/97/3616-1699 S 17.50+.50/0

The latter shares some of the characteristics of transition states for bond-forming reactions, such as clear stereochemical preferences and a certain proximity of the reactants. Given the dominance of ET pathways through bound transition states emanating from the theoretical studies, it appears desirable that the interpretation of experimental results proceeds under consideration of all three reaction types. The combination of complementary experimental and theoretical methods seems to be the most promising way to achieve deeper mechanistic insight into electron-transfer processes. Promising links between theoretical and experimental studies include relative activation energies and entropies of related systems as well as kinetic-isotope effects as one of the best observable descriptors of transition state structure. Even though this highlight exclusively deals with ET processes in open-shell systems, it should be noted that recent experimental results for ET processes in closed-shell substrates[15] also suggest bound, outer-sphere ET transition states. It therefore appears that the three types of ET processes described here can be used in a more general sense to categorize ET processes.

German version: *Angew. Chem.* **1997**, *109*, 1773–1776

Keywords: ab initio calculations · electron transfer · reaction mechanisms · transition states

[1] a) K. N. Houk, J. Gonzalez, Y. Li, *Acc. Chem. Res.* **1995**, *28*, 81; b) K. N. Houk, Y. Li, J. D. Evanseck, *Angew. Chem.* **1992**, *104*, 711; *Angew. Chem. Int. Ed. Engl.* **1992**, *31*, 682.
[2] a) U. Pidun, C. Boehme, G. Frenking, *Angew. Chem.* **1996**, *108*, 3008; *Angew. Chem. Int. Ed. Engl.* **1996**, *35*, 2817; b) S. Dapprich, G. Ujaque, F. Maseras, A. Lledós, D. G. Musaev, K. Morokuma, *J. Am. Chem. Soc.* **1996**, *118*, 11660.
[3] L. Eberson, S. S. Shaik, *J. Am. Chem. Soc.* **1990**, *112*, 4484.
[4] a) L. Eberson, *Adv. Phys. Org. Chem.* **1982**, *18*, 79; b) *Electron Transfer in Organic Chemistry*, Springer, Heidelberg, **1987**; c) J.-M. Savéant, *Adv. Phys. Org. Chem.* **1990**, *26*, 1; d) B. Speiser, *Angew. Chem.* **1996**, *108*, 2623; *Angew. Chem. Int. Ed. Engl.* **1996**, *35*, 2471.
[5] a) H. Taube, *Angew. Chem.* **1984**, *96*, 315; *Angew. Chem. Int. Ed. Engl.* **1984**, *23*, 329; b) *Electron Transfer Reactions of Complex Ions in Solution*, Academic Press, New York, **1970**.
[6] G. N. Sastry, S. Shaik, *J. Am. Chem. Soc.* **1995**, *117*, 3290.
[7] a) N. Kimura, S. Takamuku, *Bull. Chem. Soc. Jpn.* **1991**, *64*, 2433; b) *J. Am. Chem. Soc.* **1994**, *116*, 4087.
[8] G. N. Sastry, A. C. Reddy, S. Shaik, *Angew. Chem.* **1995**, *107*, 1619; *Angew. Chem. Int. Ed. Engl.* **1995**, *34*, 1495.
[9] G. N. Sastry, D. Danovich, S. Shaik, *Angew. Chem.* **1996**, *108*, 1208; *Angew. Chem. Int. Ed. Engl.* **1996**, *35*, 1098.
[10] S. S. Shaik, H. B. Schlegel, S. Wolfe, *Theoretical Aspects of Physical Organic Chemistry—The S_N2 Mechanism*, Wiley, New York, **1992**.
[11] J. Bertran, I. Gallardo, M. Moreno, J.-M. Savéant, *J. Am. Chem. Soc.* **1996**, *118*, 5737.
[12] G. N. Sastry, S. Shaik, *J. Phys. Chem.* **1996**, *100*, 12241.
[13] A. C. Reddy, G. N. Sastry, S. Shaik, *J. Chem. Soc. Perkin Trans. 2* **1995**, 1717.
[14] A. C. Reddy, D. Danovich, A. Ioffe, S. Shaik, *J. Chem. Soc. Perkin Trans 2* **1995**, 1525.
[15] L. M. Tolbert, J. Bedlek, M. Terapane, J. Kowalik, *J. Am. Chem. Soc.* **1997**, *119*, 2291.

Amino Acid Derivatives by Multicomponent Reactions

Gerald Dyker*

Amino acids are one of the most important classes of naturally occurring substances and possess a variety of biological functions. The areas of application of the amino acid derivatives range from sweeteners through pharmaceuticals to crop and plant protection. Widely applicable methods for the synthesis of α-amino acids[1, 2] are of great interest especially for the construction of compound libraries by combinatorial chemistry. Multicomponent reactions as a special case of a domino process[3] are particularly fascinating since they facilitate rapid syntheses from simple building blocks.

A classic example of such a reaction is the Strecker synthesis, which has been known for almost 150 years but is still as topical as ever:[4] an aldehyde **1** (or a ketone) is condensed, using an acid catalyst, with an amine **2** and an alkali metal cyanide such as **3** to give an α-aminonitrile **4**, which can be hydrolyzed to the amino acid **5**. In recent investigations on the Strecker synthesis attempts have been made to optimize the reaction conditions[4b] and to achieve stereoselective syntheses.[4c–h] Usually chiral amines such as **7** have been employed, which can, for example, on reaction with **6** be converted to the thiophene-substituted amino acid **8**.[4c]

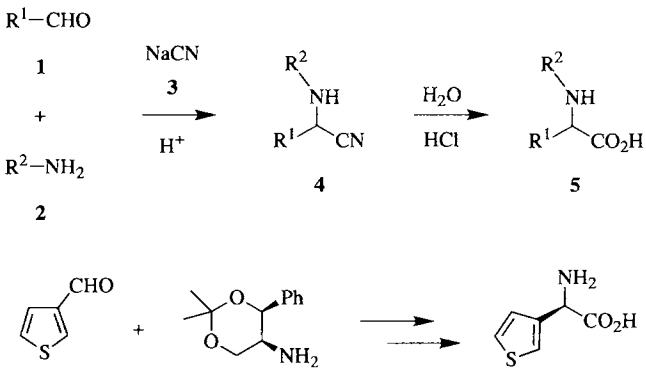

In Ugi's four-component condensation, imine formation from an aldehyde **1** and an amine **2** is likewise the initiating step;[5, 6] a carboxylic acid **9** and an isonitrile **10** are the other reaction components, which finally yield the bisamide **11**. Both for this reaction and the Strecker synthesis, the galactosylamine **12** is particularly suitable for carrying out a stereoselective reaction (synthesis of **13**).[4d, e, 5f] With an aminoglucopyranose as a chiral auxiliary the stereoselectivity of the reaction can be further increased.[5b] Amino acids as condensation components yield particularly impressive results. For instance, the iminodicarboxylic acid **17** can be synthesized from components **14**–**16**

[*] Prof. Dr. G. Dyker
Fachbereich 6, Organische/Metallorganische Chemie
der Universität-Gesamthochschule
Lotharstrasse 1, D-47048 Duisburg (Germany)
Fax: Int. code +(203)379-4192
e-mail: dyker@uni-duisburg.de

 © WILEY-VCH Verlag GmbH, D-69451 Weinheim, 1997 0570-0833/97/3616-1700 $ 17.50+.50/0

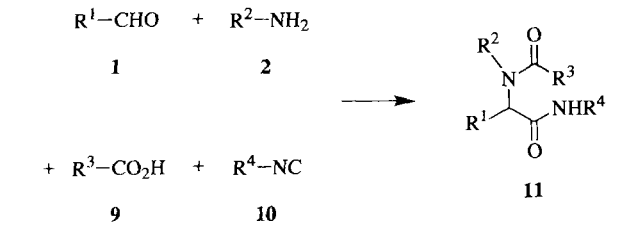

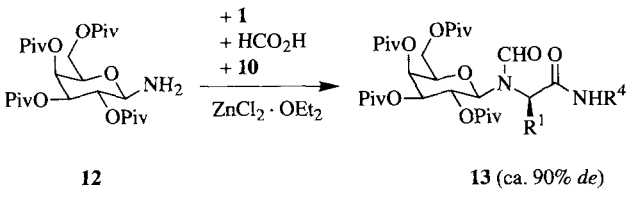

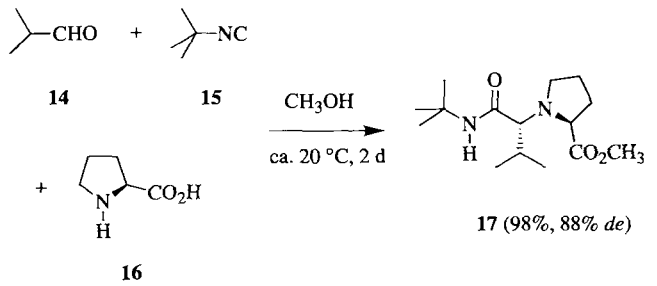

at room temperature, and obtained in excellent yield and with remarkable diastereoselectivity.[5c]

Readily available reagents were used exclusively in both the Strecker synthesis and the Ugi reaction. A convincing reaction from organometallic chemistry was a long time coming. Petasis and Zavialov now report[7a] that vinylboronic acids **18**,[7b,c] which are readily accessible and easy to handle, can participate in a three-component reaction with primary and secondary amines **19** and with α-keto acids **20**. The process, which proceeds at room temperature, leads to β,γ-unsaturated α-amino acids **21**

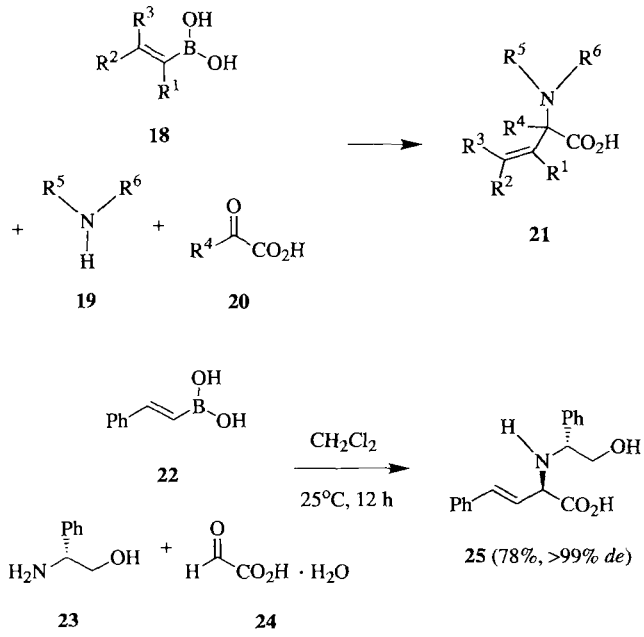

in good yields. The reaction of vinylboronic acid **22** with the chiral amino alcohol **23** and glyoxylic acid hydrate **24** illustrates that the reaction is not sensitive to air or humidity, can be carried out under mild conditions, and has impressive diastereoselectivity. Conceptually this new three-component reaction resembles the methods applied by Steglich, Enders et al.[8a] and Yamamoto et al.,[8b] who treated the preformed iminoesters **26** and **29** at low temperature with the electron-rich olefins **27** and **30**, respectively.[9] However, the use of boronic

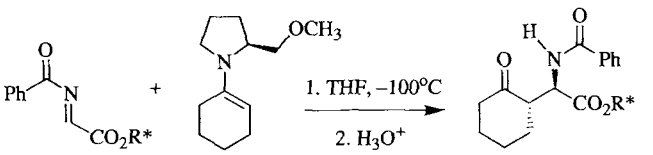

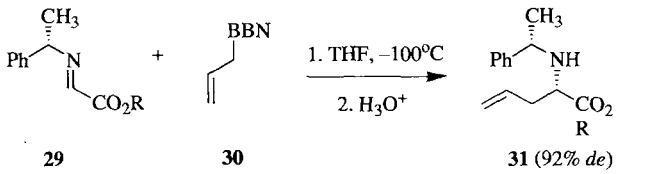

acid derivatives appears to be a versatile method with a great deal of potential. As Petasis and Zavialov note at the end of their paper unprotected amino acids and peptides, aryl boronic acids, and chiral boronates can also participate in their three-component condensation.[7a]

Transition metal catalysis also provides surprising solutions for the synthesis of amino acids by multicomponent reactions.[10] More than 25 years ago Wakamatsu et al.[11a] found that aldehyde **1** could be coupled with carboxamides **32** and carbon monoxide under pressure to give *N*-acylamino acids **33**, a process catalyzed by octacarbonyldicobalt and known as amidocarbonylation.[11b] In the presence of hydrogen the reaction conditions are suitable for hydroformylation; thus, alkenes **34** could be used in place of the aldehyde **1**.[11b] Although amidocarbonylation appears to be very favorable from an economic standpoint, it has not yet been realized in industry. The main problem concerns low catalyst efficiency, but in addition it does not appear to be possible to run the enantio/diastereoselective process with the previously applied cobalt catalysts. Beller et al. have now found[12] that amidocarbonylation of aldehydes can also be achieved by using palladium catalysts with sulfuric acid and halide ions as cocatalysts, as shown by the reaction of isovaleraldehyde **36** with acetamide **37**. This palladium-catalyzed synthesis is superior to that catalyzed by cobalt in many respects. Both the catalytic efficiency and the attainable yields are considerably higher. Several components, such as aromatic aldehydes and monoalkyl amides,[11c] which the cobalt-catalyzed method failed to convert, can now be used without any problems and, in addition, the reaction conditions required are milder: very good yields can be obtained at 80 °C and a CO pressure of only 10 bar. Most importantly, perhaps, the change

 © WILEY-VCH Verlag GmbH, D-69451 Weinheim, 1997 0570-0833/97/3616-1701 $ 17.50+.50/0

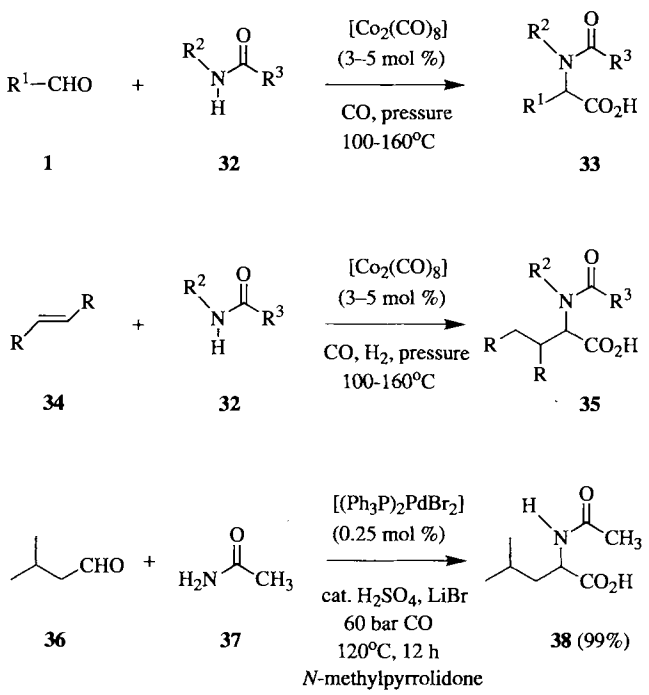

of catalyst allows the possibility of controlling the process through choice of ligand and of running an enantio/diastereoselective process.

German version: *Angew. Chem.* **1997**, *109*, 1777–1779

Keywords: amino acids · carbonylations · homogeneous catalysis · multicomponent reactions · palladium

[1] Current examples of the synthesis of α-amino acids: a) J. Mulzer, H.-J. Altenbach, M. Braun, K. Krohn, H.-U. Reissig, *Organic Synthesis Highlights*, VCH, Weinheim, **1990**, pp. 300–305; b) R. O. Duthaler, *Tetrahedron* **1994**, *50*, 1539–1650; c) U. Kazmaier, *Liebigs Ann./Recueil* **1997**, 285–295; d) M. Braun, K. Opdenbusch, *ibid.* **1997**, 141–154; e) L. S. Hegedus, *Acc. Chem. Res.* **1995**, *28*, 299–305; f) D. Enders, R. Funk, M. Klatt, G. Raabe, E. R. Hovestreydt, *Angew. Chem.* **1993**, *105*, 418–420; *Angew. Chem. Int. Ed. Engl.* **1993**, *32*, 418–420.

[2] Current examples of the synthesis of β-amino acids: a) D. Enders, J. Wiedemann, *Liebigs Ann./Recueil* **1997**, 699–706; b) J. Voigt, M. Noltemeyer, O. Reiser, *Synlett* **1997**, 202–204; c) H. Kunz, A. Burgard, D. Schanzenbach, *Angew. Chem.* **1997**, *109*, 394–396; *Angew. Chem. Int. Ed. Engl.* **1997**, *36*, 386–387; d) G. Cardillo, S. Casolari, L. Gentilucci, C. Tomasini, *ibid.* **1996**, *108*, 1939–1941 and **1996**, *35*, 1848–1849; e) J. Podlech, D. Seebach, *ibid.* **1995**, *107*, 507–509 and **1995**, *34*, 471–472; f) *Liebigs Ann.* **1995**, 1217–1228; g) P. Gmeiner, E. Hummel, C. Haubmann, *ibid.* **1995**, 1987–1992; h) J. Escalante, E. Juaristi, *Tetrahedron Lett.* **1995**, *36*, 4397–4400; i) D. C. Cole, *Tetrahedron* **1994**, *50*, 9517–9582.

[3] L. F. Tietze, U. Beifuss, *Angew. Chem.* **1993**, *105*, 137–170; *Angew. Chem. Int. Ed. Engl.* **1993**, *32*, 131–163.

[4] a) A. Strecker, *Justus Liebigs Ann. Chem.* **1850**, *75*, 27; b) M. P. Georgiadis, S. A. Haroutounian, *Synthesis* **1989**, 616–618; c) K. Weinges, H. Brachmann, P. Stahnecker, H. Rodewald, M. Nixdorf, H. Irngartinger, *Liebigs Ann.* **1985**, 566–578; d) H. Kunz, W. Sager, D. Schanzenbach, M. Decker, *ibid.* **1991**, 649–654; e) H. Kunz, K. Rück, *Angew. Chem.* **1993**, *105*, 355–377; *Angew. Chem. Int. Ed. Engl.* **1993**, *32*, 336–358; f) F. A. Davis, P. S. Portonovo, R. E. Reddy, Y. Chiu, *J. Org. Chem.* **1996**, *61*, 440–441; g) T. K. Chakraborty, K. A. Hussain, G. V. Reddy, *Tetrahedron* **1995**, *51*, 9179–9190; h) M. S. Iyer, K. M. Gigstad, N. D. Namdev, M. Lipton, *J. Am. Chem. Soc.* **1996**, *118*, 4910–4911.

[5] a) I. Ugi, *Angew. Chem.* **1982**, *94*, 826–835; *Angew. Chem. Int. Ed. Engl.* **1982**, *21*, 810–819; b) S. Lehnhoff, M. Goebel, R. M. Karl, R. Klösel, I. Ugi, *ibid.* **1995**, *107*, 1208–1211 and **1995**, *34*, 1104–1107; c) A. Demharter, W. Hörl, E. Herdtweck, I. Ugi, *ibid.* **1996**, *108*, 185–187 and **1996**, *35*, 173–175; d) A. Dömling, M. Starnecker, I. Ugi, *ibid.* **1995**, *107*, 2465–2467 and **1995**, *34*, 2238–2239; e) T. Yamada, T. Yanagi, Y. Omote, T. Miyazawa, S. Kuwata, M. Sugiura, K. Matsumoto, *J. Chem. Soc. Chem. Commun.* **1990**, 1640–1641; f) H. Kunz, W. Pfrengle, *J. Am. Chem. Soc.* **1988**, *110*, 651–652; g) P. A. Tempest, S. D. Brown, R. W. Armstrong, *Angew. Chem.* **1996**, *108*, 689–691; *Angew. Chem. Int. Ed. Engl.* **1996**, *35*, 640–642; h) T. A. Keating, R. W. Armstrong, *J. Am. Chem. Soc.* **1996**, *118*, 2574–2583; i) H. Quast, S. Aldenkortt, *Chem. Eur. J.* **1996**, *2*, 462–469.

[6] Synthesis of an amino acid derivative by using a seven-component reaction: A. Dömling, I. Ugi, *Angew. Chem.* **1993**, *105*, 634–635; *Angew. Chem. Int. Ed. Engl.* **1993**, *32*, 563–564.

[7] a) N. A. Petasis, I. A. Zavialov, *J. Am. Chem. Soc.* **1997**, *119*, 445–446; b) *Tetrahedron Lett.* **1996**, *37*, 567–570; c) N. A. Petasis, I. Akritopoulou, *ibid.* **1993**, *34*, 583–586.

[8] a) R. Kober, K. Papadopoulos, W. Miltz, D. Enders, W. Steglich, H. Reuter, H. Puff, *Tetrahedron* **1985**, *41*, 1693–1701; b) Y. Yamamoto, W. Ito, K. Maruyama, *J. Chem. Soc. Chem. Commun.* **1985**, 1131–1132.

[9] Further examples of amino acid syntheses starting with glyoxylic acid derivatives: a) P. Münster, W. Steglich, *Synthesis* **1987**, 223–225; b) M. J. O'Donnell, W. D. Bennett, *Tetrahedron* **1988**, *44*, 5389–5401; c) E. C. Roos, M. C. Lopez, M. A. Brook, H. Hiemstra, W. N. Speckamp, B. Kaptein, J. Kamphuis, H. E. Schoemaker, *J. Org. Chem.* **1993**, *58*, 3259–3268.

[10] M. Beller, B. Cornils, C. D. Frohning, C. W. Kohlpaintner, *J. Mol. Catal.* **1995**, *44*, 237–273.

[11] a) H. Wakamatsu, J. Uda, N. Yamakami, *J. Chem. Soc. Chem. Commun.* **1971**, 1540; b) "Amidocarbonylation": J. F. Knifton in *Applied Homogeneous Catalysis with Metal Complexes* (Eds.: B. Cornils, W. A. Herrmann), VCH, Weinheim, **1996**, pp. 159–168; c) P. Magnus, M. Slater, *Tetrahedron Lett.* **1987**, *28*, 2829–2832.

[12] M. Beller, M. Eckert, F. Vollmüller, S. Bogdanovic, H. Geissler, *Angew. Chem.* **1997**, *109*, 1534–1536; *Angew. Chem. Int. Ed. Engl.* **1997**, *36*, 1494–1496.

 © WILEY-VCH Verlag GmbH, D-69451 Weinheim, 1997 0570-0833/97/3616-1702 $ 17.50+.50/0

Peptidic chiral ligands screened in parallel on solid support offer exciting opportunities

for research in enantioselective catalysis (see following pages).

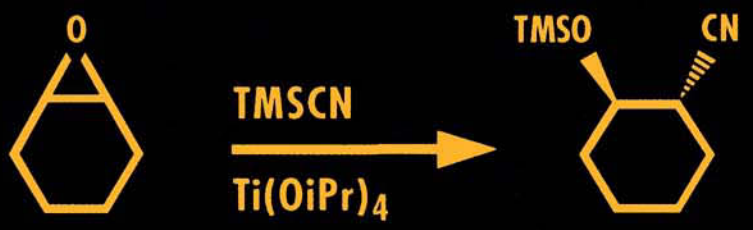

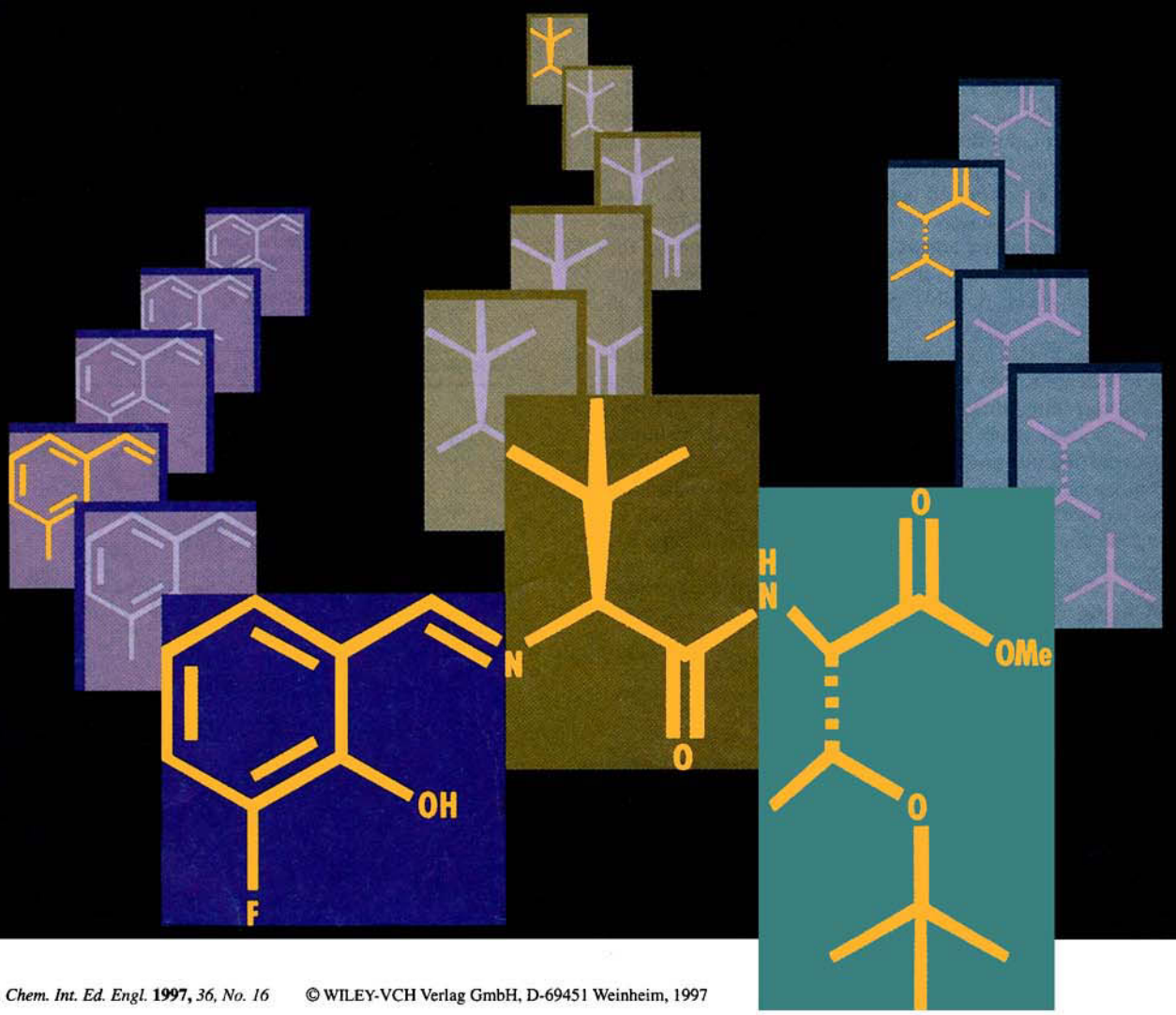

 © WILEY-VCH Verlag GmbH, D-69451 Weinheim, 1997

Search for Chiral Catalysts Through Ligand Diversity: Substrate-Specific Catalysts and Ligand Screening on Solid Phase**

Ken D. Shimizu, Bridget M. Cole, Clinton A. Krueger, Kevin W. Kuntz, Marc L. Snapper,* and Amir H. Hoveyda*

The development of new methods for discovering asymmetric catalytic transformations stands as an important and emerging objective in chemistry. In this context, we and others have reported protocols by which diversity strategies are used for an efficient search of chiral catalysts;[1-3] these procedures enhance the number of effective chiral ligands, and the rate at which they are identified. Here we report that 1) the ligand-discovery process can be carried out on solid support, significantly accelerating the search process, 2) the present protocol provides unique opportunities for the identification of substrate-specific catalysts, and 3) the diversity approach leads to the discovery of ligands that possess unusual properties and might have otherwise escaped detection.

Our initial studies focused on the addition of trimethylsilylcyanide (TMSCN) to *meso* epoxides [Eq. (1)]. Central to our

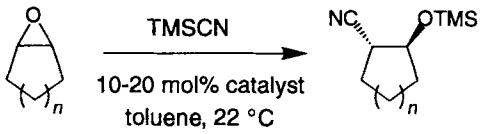

(1)

diversity-based strategy was the modular peptidic Schiff base system shown in Table 1.[4] Ligands were synthesized as described[1] in parallel on solid phase and subsequently cleaved for testing. Success of the diversity strategy is predicated by the number of dipeptide Schiff bases that can be fabricated simultaneously, and the rational and facile manner by which they are screened. Judicious selection of representative ligands for each of the variable positions allows efficient optimization of the epoxide-opening reaction in three stages without synthesizing and testing of every possible combination (see example in Table 2).[5]

At the outset of this investigation we realized that the ligand-screening scheme would be particularly efficient if ligand synthesis and screening could be performed directly on solid support. The critical issue in this regard was whether catalytic processes carried out under heterogeneous conditions (with an immobilized ligand) could be reliably extrapolated to the homogeneous variant.[7] Reactions with immobilized ligands can be problematic for a number of reasons: Various solid supports

[*] Prof. M. L. Snapper, Prof. A. H. Hoveyda, Dr. K. D. Shimizu, Dr. B. M. Cole, C. A. Krueger, K. W. Kuntz
Department of Chemistry, Merkert Chemistry Center
Boston College
Chestnut Hill, MA 02167-3860 (USA)
Fax: Int. code +(617) 552-0399
e-mail: marc.snapper@bc.edu
amir.hoveyda@bc.edu

[**] Financial support from the U. S. National Science Foundation (CHE-9632278 to A. H. H.), Johnson and Johnson (Focused Giving Grant to A. H. H.), Pfizer (Young Faculty Award to A. H. H.) and the Massachusetts Department of Public Health (Breast Cancer Scholar Award to M. L. S.) is gratefully acknowledged. We thank Pfizer for additional funds for the purchase of a GLC system. K. D. S. and B. M. C. are postdoctoral fellows of the U. S. National Institutes of Health (F32-GM-17821 and F32-GM-18209); K. W. K. is a Department of Education GAANN Fellow; A. H. H. is an NSF National Young Investigator, a Sloan Research Fellow, and a Camille Dreyfus Teacher-Scholar.

Table 1. Dipeptide Schiff base chiral ligands.

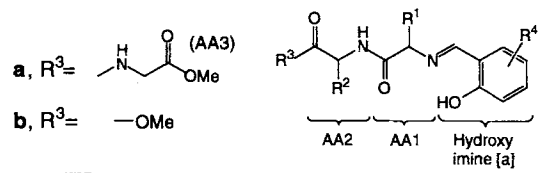

Ligand	R^2 (AA2)	R^1 (AA1)	Hydroxy imine
1	Ph		A
2	*t*BuO		A
3	Ph		A
4	*t*BuO		B
5	*t*BuO		C
6	*t*BuO		D
7	N(H)Trt		A

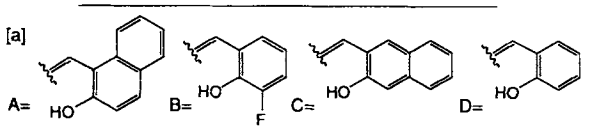

Table 2. Three-step ligand-screening strategy [6] beginning with the starting structure **1a** (generation 0). Reactions were carried out with unbound ligands that were synthesized and then cleaved from a solid support. The amino acids AA1 and AA2 as well as the hydroxy imine group were successively optimized to yield the final ligand (generation 3).

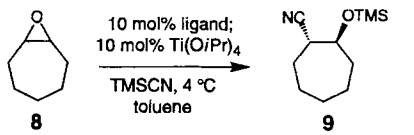

Generation	Ligand	*ee*/%
0	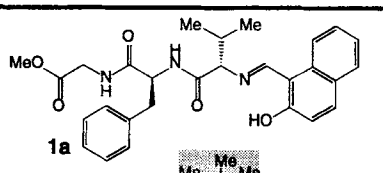	30
1	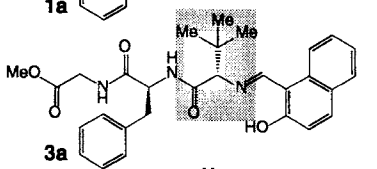	52
2	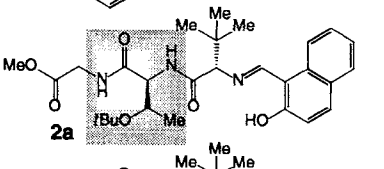	80
3	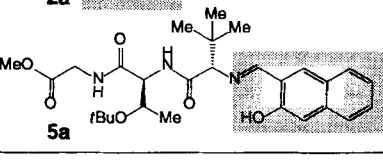	84

 © WILEY-VCH Verlag GmbH, D-69451 Weinheim, 1997 0570-0833/97/3616-1704 $ 17.50+.50/0

contain linker units with Lewis basic sites that may interact with a transition metal. Moreover, on the solid support the aggregation state of the ligand–metal complexes, and thus the reactivity and selectivity patterns they generate, may significantly deviate from those in solution. A literature survey revealed numerous examples of transformations with differing selectivities when performed on solid rather than in solution phases.[8] Therefore, it was generally unclear whether data obtained from solid-phase studies could be reliably correlated with those in solution.[2b, 9]

To address this question, we selected 20 ligands that effect the catalytic addition of TMSCN to cyclohexene oxide with varying enantioselectivities.[10] These ligands were prepared on solid support, a portion of each sample was treated under cleavage conditions, and reaction selectivities with bound and unbound ligands were compared directly for each system. Comparison of the solid- and solution-phase reactions shows a reliable correlation, particularly for the ligands that exhibit relatively higher selectivities (Figure 1); least-squares analysis affords a line that intersects the origin. Importantly, the best ligand measured in solution (89% *ee*) is the best on the solid phase (78% *ee*) as well.

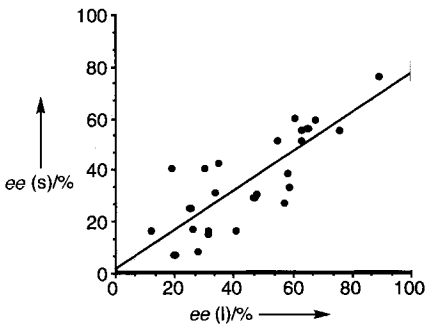

Figure 1. Correlation between solution- and solid-phase reactions (s = solid phase, l = solution phase). Each point represents a unique ligand. Reactions were run with cyclohexene oxide as the substrate (10 mol% ligand, 10 mol% $Ti(OiPr_4)$, 1 equiv of TMSCN, toluene, 4 °C).

Similar trends were observed for cyclopentene oxide (see below for further details). A correlation was measured for the selectivity pattern of 20 different ligands in the solution- and solid-phase reactions. As before, the same optimal ligand was identified when the search was carried out for both solid and solution phases. The similarity in selectivity under heterogeneous and homogeneous conditions is important as it indicates that ligand screening can be performed with immobilized ligands. This technological advance significantly facilitates the optimization procedure, since detachment of ligands from support requires several days and is the bottleneck of the process. With the latter step eliminated, peptidic Schiff bases can be prepared in six steps on solid phase in a single day, whereas the cleavage step alone requires three days. Therefore, the entire three-step screening for a substrate requires ten days on the solid phase, as opposed to one month in solution.

Our ability to examine chiral dipeptide Schiff bases on solid support leads to a notable increase in the diversity of structures that can be screened. Specifically, in our initial studies, where ligand structures were evaluated in solution, diversity was limited; amino acids with aromatic and heteroatom-containing side chains in the AA1 position proved particularly susceptible to epimerization (determined by ^{1}H NMR spectroscopy) during the cleavage process (Et_3N/DMF/MeOH 1/1/9, 3 d). Therefore, by avoiding the basic cleavage step we may access a variety of previously unavailable dipeptide Schiff bases.

The results from ligand searches on solid support bear significant implications with regard to the identity of the active Ti catalyst in the enantioselective process. In reactions performed in solution, Ti-catalyzed C–C bond formation is subject to nonlinear effects (Figure 2).[11] With cyclohexene oxide as the

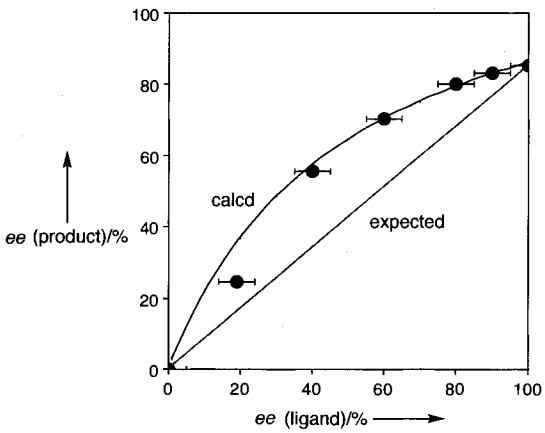

Figure 2. A positive nonlinear effect observed in the enantioselective, Ti-catalyzed addition of TMSCN to cyclohexene oxide (**12**), which was carried out with unbound ligands. The curved line is the calculated nonlinear effect [10], and the straight line the expected linear correlation.

substrate, ligand **4a** (50% optical purity) yields a product with 63% *ee* as opposed to the expected 43% *ee*. The positive nonlinear behavior suggests the existence of an equilibrium between monomeric and higher-order catalytic species.[12] Several observations suggest that the active Ti–ligand complex may be monomeric: 1) The rate of epoxide opening with ligands in solution and on a solid support are nearly the same. 2) Similar selectivities and reactivities are observed between reactions carried out in solution and on solid phase.[13]

Identification of substrate-specific catalysts differs conceptually from conventional procedures in which a single ligand–metal combination is selected and then matched to a range of substrates. As suspected from our initial studies,[1] each substrate requires a distinct ligand structure for optimal enantioselectivity when the screening protocol is applied to various *meso* epoxides (Table 3);[14] the most stereodifferentiating catalyst for one substrate is not necessarily the most desirable for all (similar to an enzyme). Whereas **4a** effects the most selective C–C bond formation for **12** (entry 2), with **10** (entry 1) peptidic Schiff base **2a** displays higher selectivity than **4a**. Chiral ligands that provide the highest level of enantiodifferentiation for seven-membered ring **8** and acyclic epoxide **14** are yet again of different constitution (entries 3 and 4). The present synthesis and screening strategy allows the search for chiral ligands to be carried out in a reasonably efficient manner, such that each individual substrate is treated as a separate case. These data raise the intriguing issue that it is perhaps unrealistic to expect that a single catalyst structure give high selectivity for the reaction of every compound of even an individual class of substrates.

Another noteworthy and unexpected feature of the results in Table 3 is that, with reactions performed in solution, ligands bearing the C-terminus Gly unit give rise to notably higher levels of selectivity.[15] This effect is particularly remarkable, since the Gly moiety (AA3) does not carry a stereogenic center, and because the original hypothesis[4] in connection with the mode of activity of these ligands primarily concerns the Schiff base unit and only the adjacent amino acid AA1. The remote and

 © WILEY-VCH Verlag GmbH, D-69451 Weinheim, 1997 0570-0833/97/3616-1705 $ 17.50+.50/0

Table 3. Catalytic, enantioselective addition of TMSCN to *meso* epoxides with the optimized ligands shown. Gly as AA 3 has a positive influence [a].

Entry	Substrate	Ligand	Product	*ee* [%][b]	Yield [%][c]	Conversion [%][d]
1	**10**	**2a (2b)**	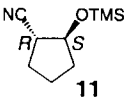 **11**	83 (63)	72	83
2	**12**	**4a (4b)**	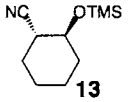 **13**	87 (86)	65	80
3	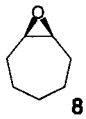 **8**	**5a (5b)**	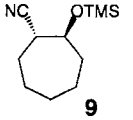 **9**	84 (69)	68	79
4	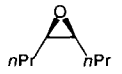 **14**	**6a (6b)**	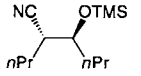 **15**	78 (58)	69	81

[a] Conditions: 20 mol% $Ti(OiPr)_4$, 20 mol% ligand, 4 °C, toluene, 6–20 h. [b] The major enantiomer was identified by comparison with authentic samples of non-racemic materials; the enantioselectivities were determined with gas–liquid chromatography (GLC; BETADEX 120 column for entries 1–3, GAMMADEX for entry 4) by comparison with authentic racemic and non-racemic samples. [c] Yields of isolated products after chromatography (silica gel). [d] Determined with GLC.

positive influence of the Gly AA 3 renders these ligand structures increasingly reminiscent of enzymatic systems. Optimization of this effect through systematic ligand screening is underway and will be followed by detailed mechanistic studies.

An advantage of the present method in catalyst identification is that it rapidly provides a wealth of structure-selectivity data. As the aforementioned case illustrates, this protocol can lead to the discovery of the unexpected. Another notable example in this regard was found in our search for the most enantioselective Ti–ligand complex for the reaction of cyclopentene oxide. Use of a ligand complex containing Asn(Trt) as AA 2 reverses reaction selectivity without a need for alteration of the absolute stereochemistry of the ligand stereogenic centers. This is in contrast to reactions initiated by the majority of chiral ligands for which the (*S*,*R*) product is formed predominantly. Therefore, a subtle variation in the constitution, but not the stereochemical identity, of one amino acid in the peptide framework can lead to a noteworthy reversal in enantioselectivity. In contrast to chiral ligand **2a**, which affords (*S*,*R*)-**11** with 84% *ee*, **7a** leads to the formation of (*R*,*S*)-**11** with 58% *ee* (Scheme 1). It merits mention that subtle modification of the AA 2 structure restores the original mode of selectivity; for example, the homologous Gln(Trt) as AA 2 affords the originally expected enantiomer with about 60% *ee*. The precise origin of the observed reversal in selectivity is under investigation; however, these observations give credence to our choice of individually synthesizing and testing each catalyst, as mixtures of catalysts can lead to racemic products. Further optimization of the unusual effect of **7a** may well lead to the evolution of an entirely different catalyst class of peptidic Schiff base ligands.

When **7a** is used with cycloheptene oxide **8** the "opposite enantiomer" (*R*,*S*)-**9** is again formed but with 23% *ee*; with cyclohexene oxide **12** the "usual enantiomer" (*S*,*R*)-**13** is formed with 29% *ee*. These data further underline the substrate-specific character of these peptidic catalysts. It is important to note that although structurally analogous substrates have disparate reactivity and selectivity properties, the present screening technology can rapidly match an appropriate ligand to each particular substrate without the necessity for any a priori mechanistic information.

The present protocol has a number of advantages over the more traditional methods for chiral-ligand discovery. 1) It can be carried out on a solid support; the search process is notably facilitated, and the ligand pool enriched. 2) It provides a method for searching for the most appropriate chiral ligand for a particular substrate; even structurally analogous *meso* epoxides can have dramatically different selectivity profiles. 3) The efficiency of the method permits collection of a plethora of experimental data within a short time. Unexpected observations can be made without the danger of missing important leads as a result of initial mechanistic bias; the selection process is instead strictly based on qualitative observations of the causality of variations in ligand structure. The technology and strategies disclosed here present new and effective pathways for the design, discovery, and development of new asymmetric catalytic methods in synthesis.

Experimental Section

The ligands were synthesized on WANG resin [16] (Advanced ChemTech, 0.7–0.85 mmol g^{-1} loading) as described, except that the final cleavage step was omitted [1]. The ligand–Wang conjugates were washed with toluene (10 × 1.0 mL) and

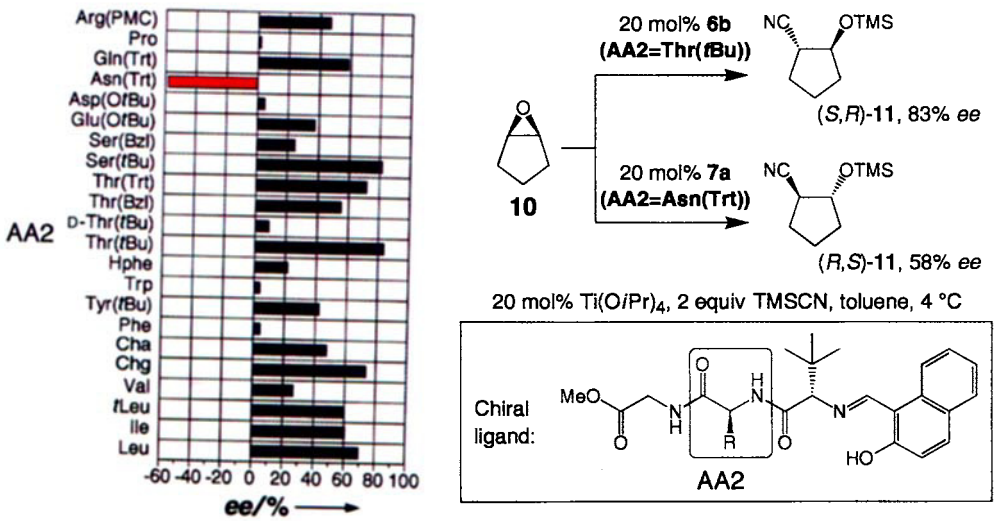

Scheme 1. Subtle variation in the functional group of chiral tripeptide Schiff bases (without altering their stereochemical identity) leads to a dramatic reversal in the enantioselectivity of the catalytic TMSCN addition to **10**. Arg(PMC) = *N*-2,2,5,7,8-pentamethylchroman-6-sulfonyl-L-arganine, Pro = L-proline, Gln(Trt) = *N*-γ-trityl-L-glutamine, Asn(Trt) = *N*-β-trityl-L-asparagine, Asp(O*t*Bu) = β-*tert*-butyl-L-asparaginate, Glu(O*t*Bu) = *O*-*tert*-butyl-L-glutamic acid, Ser(Bzl) = *O*-benzyl-L-serine, Ser(*t*Bu) = *O*-*tert*-butyl-L-serine, Thr(Trt) = *N*-trityl-L-threonine, Thr(Bzl) = *O*-benzyl-L-threonine, D-Thr(*t*Bu) = *O*-*tert*-butyl-D-threonine, Thr(*t*Bu) = *O*-*tert*-butyl-L-threonine, Hphe = L-homophenylalanine, Trp = L-tryptophan, Tyr(*t*Bu) = *tert*-butyl-L-tyrosine, Phe = L-phenylalanine, Cha = L-cyclohexylalanine, Chg = L-cyclohexylglycine, Val = L-valine, *t*Leu = *tert*-leucine, Ile = L-isoleucine, Leu = L-leucine.

 © WILEY-VCH Verlag GmbH, D-69451 Weinheim, 1997 0570-0833/97/3616-1706 $ 17.50+.50/0

dried in vacuo with toluene twice to remove any remaining solvent and water. The dried resin was weighed and used in the screening procedure. The resin-supported ligand (0.02 mmol) was placed in a dried test tube with a rubber septum under an argon atmosphere. $Ti(OiPr)_4$ (0.1 M in toluene, 200 μL, 0.02 mmol) was added and allowed to stand for 1 h. Subsequently, cyclohexene oxide (1.0 M in toluene, 200 μL, 0.2 mmol) and TMSCN (1.0 M in toluene 200 μL, 0.2 mmol) were added, and the reaction was gently agitated for 20 h (4 °C). The reaction was quenched by addition of Et_2O (1.0 mL), and the solution forced through a silica gel plug with additional Et_2O (1.0 mL). Reaction selectivity was determined by GLC analysis (BETADEX 120 chiral column).

Received: March 5, 1997 [Z10201IE]
German version: *Angew. Chem.* **1997**, *109*, 1781–1785

Keywords: asymmetric catalysis · epoxides · heterogeneous catalysis · peptides · solid-phase synthesis

[1] B. M. Cole, K. D. Shimizu, C. A. Krueger, J. P. A. Harrity, M. L. Snapper, A. H. Hoveyda, *Angew. Chem.* **1996**, *108*, 1776–1779; *Angew. Chem. Int. Ed. Engl.* **1996**, 35, 1668–1671.

[2] Recent advances in the application of combinatorial techniques in the discovery of chiral catalysts: a) F. M. Menger, A. V. Eliseev, V. A. Migulin, *J. Org. Chem.* **1995**, *60*, 6666–6667; b) G. Lin, J. A. Ellman, *ibid.* **1995**, *60*, 7712–7713; c) S. R. Gilbertson, X. Wang, *Tetrahedron Lett.* **1996**, *37*, 6475–6478; d) K. Burgess, H. Lim, A. M. Porte, G. Sulikowski, *Angew. Chem.* **1996**, *108*, 192–194; *Angew. Chem. Int. Ed. Engl.* **1996**, *35*, 220–222.

[3] F. Balkenhohl, C. von dem Bussche-Hünnefeld, A. Lansky, C. Zechel, *Angew. Chem.* **1996**, *108*, 2436–2487; *Angew. Chem. Int. Ed. Engl.* **1996**, *35*, 2288–2337.

[4] a) H. Nitta, D. Yu, M. Kudo, A. Mori, S. Inoue, *J. Am. Chem. Soc.* **1992**, *114*, 7969–7975, and references therein; b) M. Hayashi, Y. Miyamoto, T. Inoue, N. Oguni, *J. Org. Chem.* **1993**, *58*, 1515–1522.

[5] Although the synthesis of all peptide combinations is straightforward, we are currently limited in our ability to evaluate efficiently every possible ligand for asymmetric induction. Studies aimed at developing strategies that address this issue are under way.

[6] C. T. Dooley, R. A. Houghten, *Life Sciences* **1993**, *52*, 1509–1517.

[7] Our initial efforts towards carrying out ligand screening on a solid support were unsuccessful [1].

[8] R. Noyori, *Asymmetric Catalysis in Organic Chemistry*, Wiley, New York, **1994**, pp. 346–364.

[9] Although levels of selectivity on solid and in solution phases may correlate, they may not be reliable. This is particularly an issue if selectivites on solid phases are low (for example less than 15% *ee*). In such instances ranking of various catalyst systems in order of their effectiveness becomes increasingly dubious, since differences in selectivity are small.

[10] An initial analysis of various solvents (toluene, CH_2Cl_2, THF, Et_2O, and MeCN) indicated that the most selective and reproducible results were obtained in toluene.

[11] C. Bolm in *Advanced Asymmetric Synthesis* (Ed.: G. R. Stephenson), Blackie Academic and Professional, London, **1996**, pp. 9–26.

[12] The predicted nonlinear effect, based on the model in which homo- and heterodimers of the catalyst are present but dissociate at different rates to give the active monomeric catalyst, is calculated with Equation (a). (ee_{max}[%] = $ee_{calcd} = [ee_{max} \times (K \times ee_{lig})]/[K \times ee_{lig} + 1 \times (100 - ee_{lig})]$ (a)

entiomeric excess of the product with optically pure ligand, ee_{lig}[%] = enantiomeric excess of the ligand, K = ratio of the initial rates of optically pure versus racemic ligands ($K = 3$ in this case)): K. Mikami, M. Terrada, *Tetrahedron* **1992**, *48*, 5671–5680.

[13] A. Akelah, D. C. Sherrington, *Chem. Rev.* **1981**, *81*, 557–587.

[14] All reaction products in Table 3 were fully characterized by ^1H, ^{13}C NMR, and IR spectrometry, high-resolution mass spectroscopy, or combustion analysis.

[15] The effect of the glycine at AA3 was originally not appreciated and therefore went unnoted [1].

[16] FMOC-Gly-PAC resin (PerSeptive Biosystems; FMOC = 9-fluorenylmethyloxycarbonyl) may also be used to obtain similar results.

Isomers of the Elemental Composition CN_2O

Günther Maier,* Hans Peter Reisenauer, Jürgen Eckwert, Matthias Naumann, and Michael De Marco

In our search for the still unknown molecule C_2O_2,[1] we irradiated cyanogen di-*N*-oxide (**1**) in solid argon at 10 K with light of wavelength 254 nm. Nitrosyl cyanide (**3**) was formed, probably by loss of CO from the rearrangement product **2**.[2, 3]

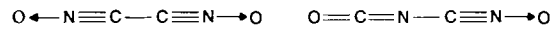

1 **2**

When an ArF laser ($\lambda = 193$ nm) was used, a new species with a strong IR absorption at 1837 cm^{-1} was generated instead of **3**. Since the position of this band could be reasonable for C_2O_2,[4] we attempted to determine its origin. A more precise study of the photochemistry of **3** in an argon matrix at 15 K showed that the above-mentioned absorption is not due to C_2O_2 but to isonitrosyl cyanide (**5**). To the best of our knowledge this isomer of **3** is the first "organic" isonitrosyl compound.[5]

Four ways of linking an NO group and a CN moiety are conceivable: not only **3**, which was synthesized in 1971,[6] but also nitrosyl isocyanide (**4**), isonitrosyl cyanide (**5**), and isonitrosyl isocyanide (**6**) are minima on the CN_2O energy hypersurface[7]. Their relative energies and structural data, calculated with the density functional theory (DFT) method BLYP/6-311+G*[8] in the Gaussian 94 package of programs,[9] are given in Scheme 1. This DFT method was chosen because MP2 cal-

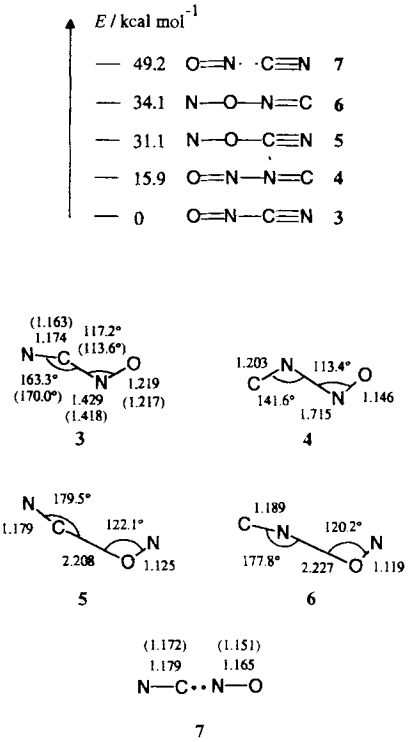

Scheme 1. Calculated relative energies and geometries (BLYP/6-311+G*) of the CN_2O isomers **3**–**6** and the radical pair **7** (distances in Å). All CN_2O isomers possess C_s symmetry. Experimental data are given in parentheses [6b, 11].

[*] Prof. Dr. G. Maier, Dr. H. P. Reisenauer, Dr. J. Eckwert, Dipl.-Chem. M. Naumann, Dipl.-Chem. M. De Marco
Institut für Organische Chemie der Universität
Heinrich-Buff-Ring 58, D-35392 Giessen (Germany)
Fax: Int. code +(641)99-34309

 © WILEY-VCH Verlag GmbH, D-69451 Weinheim, 1997 0570-0833/97/3616-1707 $ 17.50+.50/0

culations give less accurate results, especially for NO· and CN·.[10] According to the energy scheme, **4** should be even more easily accessible than **5**. Indeed, this species can also be generated and identified by matrix spectroscopy if **3** is irradiated with light of wavelengths greater than 570 nm instead of 193 nm.

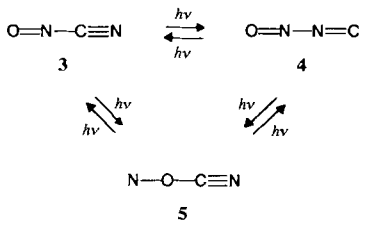

Isomers **3**, **4**, and **5** are probably linked to each other by the radical pair **7**. However, this intermediate could not be detected, presumably because it is trapped in the matrix cage and undergoes immediate recombination. In any case, all three isomers can be interconverted photochemically; the relative ratios of the components were determined by the different UV/Vis absorptions (**3**: Figure 1c, **4**: Figure 1b, **5**: Figure 1a). Compound **3** is the preferred isomer at excitation with light of wavelength $\lambda = 254$ or 405 nm, **4** at $\lambda > 570$ nm, and **5** at $\lambda = 185$ or 193 nm. No IR bands attributable to the fourth isomer **6** were detected.

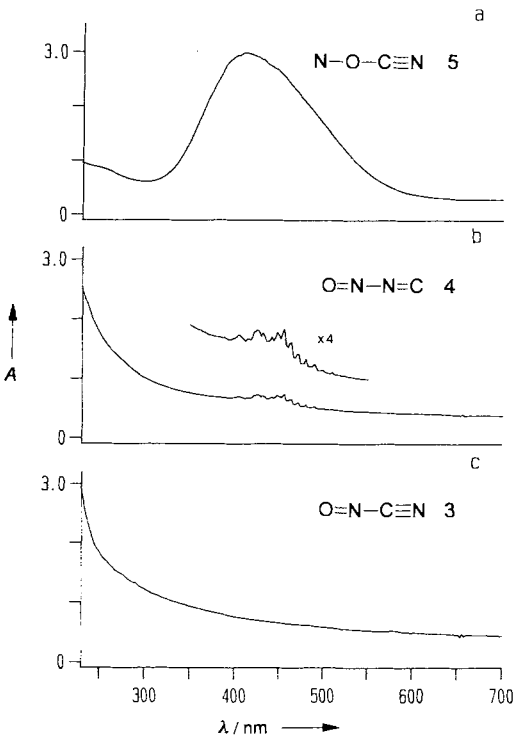

Figure 1. Experimental UV spectra of the two new isomers **5** (a) and **4** (b) as well as the starting material **3** (c) in an Ar matrix at 15 K.

For the planar molecules **3**, **4**, and **5** (C_s symmetry), six IR-active fundamental vibrations of varying intensity are expected (Tables 1–3). According to the calculation **4** should exhibit four bands in the accessible spectral range ($\tilde{\nu} > 220\ cm^{-1}$). Three of these—namely, the N–N stretching vibration at 261.0 cm^{-1}, a bending mode at 723.4 cm^{-1}, and the N–O stretching vibration at 1681.0 cm^{-1} (Figure 2b)—are readily assigned by

Table 1. Calculated vibrational spectrum of **3** (BLYP/6-311+G*) and experimentally observed IR absorptions (Ar matrix, 15 K; relative intensities are given in parentheses).

		Type [a]	$\tilde{\nu}_{calcd}/cm^{-1}$	$\tilde{\nu}_{exp}/cm^{-1}$
ν_1	A′	CN str	2126 (25.0)	2163.0 (60.2)
			^{13}C: 2079	^{13}C: 2113.4
ν_2	A′	NO str	1469 (100.0) [b]	1498.5 (100.0)
			^{13}C: 1468	^{13}C: 1497.3
			^{15}N: 1443	^{15}N: 1472.5
			^{18}O: 1430	^{18}O: 1460.2
ν_3	A′	ip	748 (31.0)	809.5 (64.8)
			^{13}C: 738	^{13}C: 798.6
ν_4	A′	ONC str	573 (29.0)	576.1 (26.6)
			^{13}C: 567	^{13}C: 570.9
ν_6	A″	oop	212 (10.0)	
ν_5	A′	ip	199 (8.0)	

[a] str = stretching vibration; ip = in-plane bending vibration; oop = out-of-plane bending vibration. [b] Absolute intensity 141 km mol^{-1}.

Table 2. Calculated vibrational spectrum of **4** (BLYP/6-311+G*) and experimentally observed IR absorptions (Ar matrix, 15 K; relative intensities are given in parentheses).

		Type [a]	$\tilde{\nu}_{calcd}/cm^{-1}$	$\tilde{\nu}_{exp}/cm^{-1}$
ν_1	A′	CN str	1944 (9.0)	1997.5 (26.1) [b]
			^{13}C: 1913	1967.1 (33.1)
				[1978.5]
				^{13}C: 1945.9
ν_2	A′	NO str	1795 (100.0) [c]	1681.0 (100.0)
			^{13}C: 1786	^{13}C: 1677.2
ν_3	A′	ip	650 (11.0)	723.4 (21.7)
			^{13}C: 649	^{13}C: 723.4
ν_4	A′	NN str	284 (19.0)	261.0 (40.5)
			^{13}C: 282	^{13}C: 259.0
ν_5	A′	ip	163 (0.4)	
ν_6	A″	oop	31 (0.0)	

Combination bands and overtones (probable assignment): 3312.2 ($2\nu_2$), 2415.1 ($\nu_2 + \nu_3$), 974.4 ($\nu_3 + \nu_4$), 539.8 ($2\nu_4$)

[a] See footnote [a] of Table 1. [b] Anharmonic resonance of ν_1 with the combination mode ($\nu_2 + \nu_4$). The band position of the fundamental tone (in parentheses) was determined from the resulting bands and their relative intensities. [c] Absolute intensity 823 km mol^{-1}.

Table 3. Calculated vibrational spectrum of **5** (BLYP/6-311+G*) and experimentally observed IR absorptions (Ar matrix, 15 K; relative intensities are given in parentheses).

		Type [a]	$\tilde{\nu}_{calcd}/cm^{-1}$	$\tilde{\nu}_{exp}/cm^{-1}$
ν_1	A′	CN str	2079 (1.3)	2086.0 (0.6)
			^{13}C: 2034	^{13}C: 2043.5
ν_2	A′	NO str	1939 (100.0) [b]	1836.9 (100.0)
			^{13}C: 1939	^{13}C: 1836.9
			^{15}N: 1904	^{15}N: 1804.9
			^{18}O: 1888	^{18}O: 1789.2
ν_3	A′	ip	469 (1.8)	485.4 (1.2)
			^{13}C: 466	^{13}C: 482.5
ν_4	A′	CO str	243 (4.2)	
ν_6	A″	oop	111 (0.05)	
ν_5	A′	ip	92 (0.05)	

Combination bands and overtones (probable assignment): 3650.7 ($2\nu_2$), 2313.0 ($\nu_2 + \nu_3$)

[a] See footnote [a] of Table 1. [b] Absolute intensity 632 km mol^{-1}.

 © WILEY-VCH Verlag GmbH, D-69451 Weinheim, 1997 0570-0833/97/3616-1708 $ 17.50+.50/0

comparison with the theoretical predictions. Instead of a single absorption for the C–N stretching mode (ν_1) we observe a pair of bands at 1997.5 and 1967.1 cm^{-1}, which arise from anharmonic resonance with the combination mode $\nu_2 + \nu_4$. This interpretation was unequivocally confirmed by a ^{13}C-labeling experiment. Due to the resulting band shifts, the accidental degeneracy of the fundamental and combination modes is removed, and only the band for the ^{13}C–N stretch appears at 1945.9 cm^{-1}.

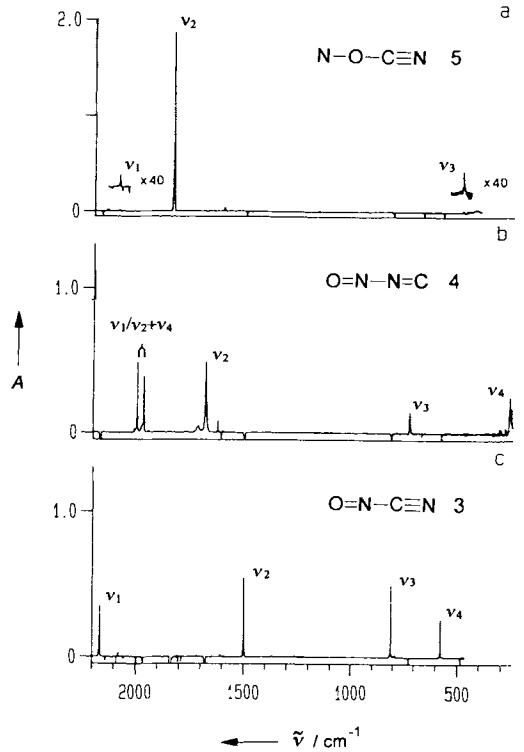

Figure 2. Experimental IR spectra of the two new isomers **5** (a) and **4** (b) as well as the starting material **3** (c) in an Ar matrix at 15 K.

The analysis of the IR spectrum of **5** (Figure 2a) is less problematic. The most intense band by far is that due to N–O stretching (ν_2) at 1836.9 cm^{-1}, the first overtone of which appears at 3650.7 cm^{-1}. The C–N stretching vibration gives rise to a weak absorption at 2086.0 cm^{-1}; the equally weak band at 485.4 cm^{-1} is due to a bending mode. We have not yet been able to definitively assign an experimental absorption to the C–O stretching transition, which should occur at the lower end of the accessible spectral range.

Two further computational results worth mentioning are the long N–N bond in **4** (1.72 Å; typical N–N single bonds are 1.4 Å) and the long O–C bond in **5** (2.21 Å; typical C–O single bonds are 1.4–1.5 Å).

It must be assumed that the conversion of **3** into an isonitrosyl isomer is not unique, but may also occur with other nitrosyl species. This is supported by the corresponding rearrangement in nitrosyl halides.[5, 12]

Received: January 23, 1997 [Z10027IE]
German version: *Angew. Chem.* **1997**, *109*, 1785–1787

Keywords: ab initio calculations · isomerizations · matrix isolation · photochemistry · radicals

[1] G. Maier, H. P. Reisenauer, B. Röther, J. Eckwert, *Liebigs Ann.* **1996**, 303–306, and references therein.
[2] G. Maier, J. H. Teles, *Angew. Chem.* **1987**, *99*, 152–153; *Angew. Chem. Int. Ed. Engl.* **1987**, *26*, 155–156.
[3] G. Maier, M. Naumann, H. P. Reisenauer, J. Eckwert, *Angew. Chem.* **1996**, *108*, 1800–1801; *Angew. Chem. Int. Ed. Engl.* **1996**, *35*, 1696–1697.
[4] Review: J. A. Berson, D. M. Birney, W. P. Dailey, III, J. F. Liebman in *Molecular Structure and Energetics*, Vol. 6 (Eds.: J. F. Liebman, A. Greenberg), VCH, New York, **1988**, pp. 391–441.
[5] The reaction of F atoms with NO leads to both possible isomers, ONF and the "inorganic" isonitrosyl compound NOF. The latter yields the thermodynamically more stable nitrosyl isomer upon irradiation in a matrix at 8 K: R. R. Smardzewski, W. B. Fox, *J. Chem. Soc. Chem. Commun.* **1974**, 241–242; *J. Chem. Phys.* **1974**, *60*, 2104–2110.
[6] a) P. Horsewood, G. W. Kirby, *J. Chem. Soc. Chem. Commun.* **1971**, 1139–1140; b) R. Dickinson, G. W. Kirby, J. G. Sweeny, J. K. Tyler, *ibid.* **1973**, 241–242; c) E. A. Dorko, L. Buelow, *J. Chem. Phys.* **1975**, *62*, 1869–1872.
[7] a) A. A. Korkin, P. von R. Schleyer, R. J. Boyd, *Chem. Phys. Lett.* **1994**, *227*, 312–320; b) B. G. Gowenlock, L. Radom, *Aust. J. Chem.* **1978**, *31*, 2349–2353.
[8] Review: L. J. Bartolotti, U. Flurchick, *Rev. Comput. Chem.* **1996**, *7*, 187–216.
[9] Gaussian 94, revision B.1: M. J. Frisch, G. W. Trucks, H. B. Schlegel, P. M. W. Gill, B. G. Johnson, M. A. Robb, J. R. Cheeseman, T. Keith, G. A.Petersson, J. A. Montgomery, K. Raghavachari, M. A. Alaham, V. G. Zakrzewski, J. V.Ortiz, J. B. Foresman, J. Cioslowski, B. B. Stefanov, A. Nanayakkara, M. Challacombe, C. Y. Peng, P. Y. Ayala, W. Chen, M. W. Wong, J. L. Andres, E. S. Replogle, R. Gomperts, R. L. Martin, D. J. Fox, J. S. Binkley, D. J. Derees, J. Baker, J. P. Stewart, M. Head-Gordon, C. Gonzalez, J. A. Pople, Gaussian Inc., Pittsburgh, PA, USA, **1995**.
[10] a) B. G. Johnson, P. M. W. Gill, J. A. Pople, *J. Chem. Phys.* **1993**, *98*, 5612–5626; b) own calculations with the Gaussian 94 program MP2/6-311+G*.
[11] G. Herzberg, *Spectra of Diatomic Molecules*, Van Nostrand, Princeton, **1950**.
[12] ONCl (N–O stretching vibration: $\tilde{\nu} = 1805$ cm^{-1}) isomerizes to NOCl (N–O stretching vibration: $\tilde{\nu} = 1842$ cm^{-1}) upon irradiation at $\lambda = 193$ nm. The reverse reaction is initiated with light of wavelength $\lambda > 310$ nm: M. De Marco, Diplomarbeit, Universität Giessen, Germany, **1996**.

2,3-Dihydrothiazol-2-ylidene

Günther Maier,* Jörg Endres, and Hans Peter Reisenauer

Dedicated to Professor Peter Welzel on the occasion of his 60th birthday

There are two main approaches for investigating species that are not isolable under normal conditions: increasing their kinetic stability by introducing sterically demanding substituents and utilizing matrix-isolation techniques. The first method was successfully applied to nucleophilic carbenes by Arduengo et al.[1a, 1c] However, it later turned out that, at least for the imidazolylidenes, steric hindrance is of secondary importance.[1b] The second method, which should be suitable for detecting unsubstituted parent compounds and allows a comparison of the experimental data with quantum-chemical calculations, was not employed for this class of compounds until now.

2,3-Dihydrothiazol-2-ylidene (**2**) was selected as the target molecule for several reasons. This ring system exemplifies the nucleophilic carbene, since, as Breslow showed almost 40 years ago,[2] it is the structural element that is responsible for the activity of vitamin B_1.[3] Additionally, the catalytic activity of the thiazolium salt/**2** system is of technical interest.[4] During the recent renaissance of nucleophilic carbenes[5] 2,3-dihydro-

[*] Prof. Dr. G. Maier, Dipl.-Chem. J. Endres, Dr. H. P. Reisenauer
Institut für Organische Chemie der Universität
Heinrich-Buff-Ring 58, D-35392 Giessen (Germany)
Fax: Int. code +(641)99-34309

 © WILEY-VCH Verlag GmbH, D-69451 Weinheim, 1997 0570-0833/97/3616-1709 $ 17.50+.50/0

thiazol-2-ylidenes only played a minor role. The new stable carbenes of the Wanzlick–Arduengo type are derivatives of imidazole,[1a, b] imidazoline,[1c] or 1,2,4-triazole.[6] Arduengo et al. only recently reported the synthesis of a stable 2,3-dihydrothiazol-2-ylidene derivative.[7]

The standard methods for generating nucleophilic carbenes (deprotonation of the corresponding H salts) are unsuitable for matrix isolation of unsubstituted **2**. On the other hand, a precursor such as thiazol-2-carboxylic acid (**1**),[8] which might directly yield **2** upon irradiation in a matrix, would be particularly suitable. Comparison of the experimental IR spectrum of matrix-isolated **1** with the calculated IR spectrum [BLYP/6-31G(d)] shows that **1** exists as a mixture of two rotamers **1a** and **1b**. According to this calculation[9] **1a** is favored over **1b** by 1.0 kcal mol^{-1}. Hence, the intensity of the bands for **1a** in the experimental spectrum is significantly higher.

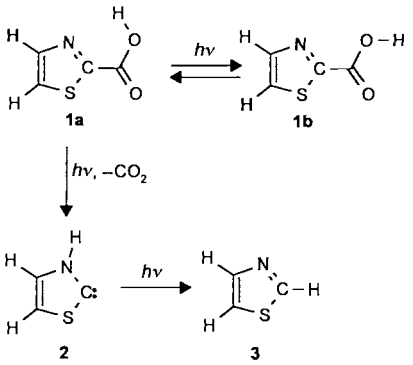

Calculations also allow an assessment of the electronic and geometric properties of the target molecule **2** and the probability of isolating it in a matrix. Whereas carbene **2** is 34.0 kcal mol^{-1} [MP4SDTQ(fc)/6-31G(d)//MP2(fc)/6-31G(d) calculation] higher in energy than the isomeric thiazole (**3**), the isomerization **2** → **3** via the transition state **4** has a considerable energy barrier of 42.3 kcal mol^{-1}. Like imidazol-2-ylidene, which was extensively analyzed by Apeloig, Schwarz et al.,[10] **2** is planar. In contrast, the nitrogen atom in the dihydro derivative **5** has a pyramidal geometry. Bond lengths and partial charges (Scheme 1) calculated for **2** (the C=C bond is longer than that in **5**, the other ring bonds are shorter, the carbene C atom bears a more negative charge, and the nitrogen and sulfur atoms bear more positive charges) indicate partial "aromatic" character, and exhibit the same trends (at least as far as the N-C-S segment is concerned) as the data obtained by Arduengo et al.[7] for highly substituted derivatives.

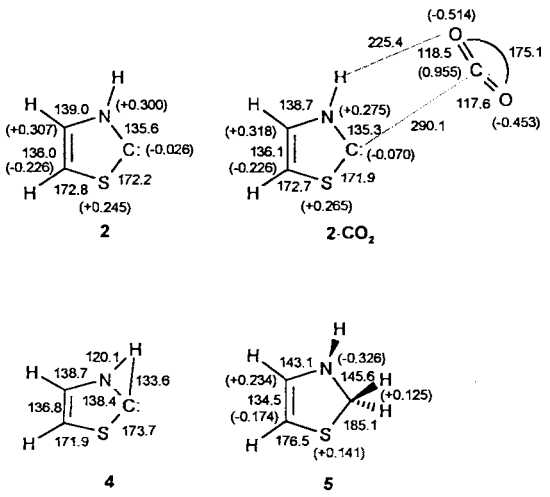

Scheme 1. Calculated [MP2(fc)/6-31G(d)] bond lengths and partial charges (according to Mulliken; atomic charges with hydrogens summed into heavy atoms) of carbene **2** (C_s), complex **2**·CO_2 (C_s), transition state **4** (C_1), and dihydrothiazole **5** (C_1).

When a mixture of **1a** and **1b** is exposed to light of wavelength 254 nm in an argon matrix at 10 K for 5–20 min, the bands for **1a** decrease in intensity, and those for **1b** increase. Upon prolonged irradiation (2 h) loss of CO_2 occurs (strong band at $\tilde{\nu}$ = 2332.6 cm^{-1}), and a new species that has an intense absorption at 3410.0 cm^{-1}, and must therefore contain an N–H group, is formed (Table 1). When deuterated **1** (CO_2D) is used this band shifts to 2521.9 cm^{-1} (Table 2), as expected. These observations leave little doubt that extrusion of CO_2 from **1** generates the desired product **2**. During prolonged photolysis with light of wavelength 250–420 nm (a total of 70 h) the absorptions of **2** diminish, and the known bands of **3** appear. The photoisomerization **2** → **3** enabled us to record the differ-

Table 1. Experimental IR absorptions (Ar matrix, 10 K; relative intensities are given in parentheses) and calculated [MP2(fc)/6-31G(d)] vibrational spectrum of **2**·CO_2. The five transitions at wavenumbers below 200 cm^{-1} are not listed.

		Type [a]	$\tilde{\nu}_{exp}$/cm^{-1} (I_{exp}) [b]	$\tilde{\nu}_{calcd}$/cm^{-1} (I_{calcd}) [c]
ν_1	A′	NH str	3410.9 (81)	3594 (100)
			^{13}C: 3410.9	^{13}C: 3594
ν_2	A′	CH str	–	3327 (1)
			–	^{13}C: 3327
ν_3	A′	CH str	–	3296 (2)
			–	^{13}C: 3296
ν_4	A′	CO_2 str	2332.6	2442
			^{13}C: 2275.2	^{13}C: 2372
ν_5	A′	NCC str	1572.8 (9)	1583 (14)
			–	^{13}C: 1583
ν_6	A′	NH (ip)	1389.7 (58)	1449 (40)
			^{13}C: 1389.2	^{13}C: 1449
ν_7	A′	NC str + NH (ip)	1301.1 (7)	1359 (7)
			^{13}C: 1300.7	^{13}C: 1359
ν_8	A′	CO_2 str	–	1332 (3)
			–	^{13}C: 1332
ν_9	A′	NC str + NH (ip)	1208.3 (20)	1289 (37)
			^{13}C: 1208.4	^{13}C: 1289
ν_{10}	A′	CH (ip)	1118.8 (7)	1136 (3)
			–	^{13}C: 1136
ν_{11}	A′	ring (ip)	1029.6 (8)	1092 (7)
			^{13}C: 1030.6	^{13}C: 1092
ν_{12}	A′	ring (ip)	876.5 (3)	908 (4)
			^{13}C: 876.3	^{13}C: 907
ν_{13}	A′	ring (ip)	833.8 (9)	875 (18)
			^{13}C: 834.1	^{13}C: 875
ν_{20}	A″	NH (oop)	751.5 (100)	831 (90)
			^{13}C: 750.9	^{13}C: 831
ν_{21}	A″	CH (oop)	–	810 (4)
			–	^{13}C: 810
ν_{14}	A′	CS str	–	756 (3)
			–	^{13}C: 756
ν_{22}	A″	CH (oop)	716.8 (95)	723 (57)
			^{13}C: 716.1	^{13}C: 723
ν_{23}	A″	CO_2 (oop)	666.1 (28)	642 (23)
			^{13}C: 646.8	^{13}C: 623
ν_{15}	A′	ring (ip) + CO_2 (ip)	626.4 (47)	639 (10)
			^{13}C: 622.5	^{13}C: 639
ν_{16}	A′	CO_2 (ip)	614.8 (42)	599 (98)
			^{13}C: 601.4	^{13}C: 584
ν_{24}	A″	ring (oop)	–	589 (3)
			–	^{13}C: 589
ν_{25}	A″	ring (oop)	473.4 (3)	483 (9)
			–	^{13}C: 483

[a] str = stretching vibration; ip = in-plane bending vibration; oop = out-of-plane bending vibration. [b] Relative to the band at 751.5 cm^{-1}. [c] Relative to the band at 3594 cm^{-1}.

 © WILEY-VCH Verlag GmbH, D-69451 Weinheim, 1997 0570-0833/97/3616-1710 $ 17.50+.50/0

Table 2. Experimental IR absorptions (Ar matrix, 10 K; relative intensities are given in parentheses) and calculated [MP2(fc)/6-31G(d)] vibrational spectrum of [D_1]**2**·CO_2. The five transitions at wavenumbers below 200 cm^{-1} are not listed.

		Type [a]	$\tilde{\nu}_{exp}/cm^{-1}$	$\tilde{\nu}_{calcd}/cm^{-1}$
ν_1	A′	CH str	–	3327
ν_2	A′	CH str	–	3296
ν_3	A′	ND str.	2521.9	2638
ν_4	A′	CO_2 str	2341.7	2441
ν_5	A′	NCC str	–	1564
ν_6	A′	CNC str	1293.9	1378
ν_7	A′	CH (ip)	1284.1	1353
ν_8	A′	CO_2 str	–	1332
ν_9	A′	CH (ip)	1093.1	1141
ν_{10}	A′	CH (ip)	1069.3	1122
ν_{11}	A′	ND (ip)	933.2	980
ν_{12}	A′	ring (ip)	868.4	900
ν_{13}	A′	ring (ip)	816.7	858
ν_{20}	A″	CH (oop)	–	811
ν_{14}	A′	CS (ip)	–	747
ν_{21}	A″	CH (oop)	716.9	723
ν_{22}	A″	CO_2 (oop) + ND (oop)	666.1	642
ν_{15}	A′	ring (ip) + CO_2 (ip)	625.6	637
ν_{23}	A″	ND (oop)	586.9	625
ν_{16}	A′	CO_2 (ip)	613.5	600
ν_{24}	A″	ring (oop)	542.6	574
ν_{25}	A″	ring (oop)	473.2	482

[a] See fotenote [a] of Table 1.

ence spectrum depicted in Figure 1a. Comparison with the MP2(fc)/6 – 31G(d) calculated IR spectrum of **2** (Figure 1c) above 700 cm^{-1} shows good agreement within the deviations of about 5%, which is typical for this theoretical method. Between 700 and 500 cm^{-1} we observed three absorptions of rather high intensity, which is in contrast to the computed spectrum. Their origin was clarified by an experiment with $^{13}CO_2H$-labeled starting material **1**. After photolysis this isotopic marker should be found exclusively in the CO_2 fragment and cause a shift of the corresponding bands. None of the bands above 700 cm^{-1} displayed an isotopic shift. Two of the bands below 700 cm^{-1} experienced a significant shift to lower wavenumber (by 19.3 and 13.4 cm^{-1}) and, hence, must be due to CO_2 bending vibrations. The position of the third transition remained almost unchanged (shift of 4 cm^{-1}). This absorption probably originates from a ring vibration that is weakly coupled with a CO_2 bending mode. The carbon dioxide molecule, trapped after photolysis in the same matrix cage as **2**, clearly forms a complex with **2**. Therefore, the doubly degenerate bending mode of free CO_2 splits into two bands: an in-plane (666.1 cm^{-1}) and an out-of-plane vibration (614.8 cm^{-1}). The interaction of CO_2 with **2** is evidently stronger than that with the final product **3**: after complete conversion into **3**, only one broad band is observed for the CO_2 bending vibration (662.2 cm^{-1}).

Calculations [MP2(fc)/6-31G(d)] gave an energy minimum for a CO_2 complex of **2** with the geometry shown in Scheme 1. The calculated IR spectrum of **2**·CO_2 satisfactorily reproduced the spectral pattern above 700 cm^{-1}, the splitting of the CO_2 bending vibration, and the ^{13}C isotopic shifts. The orientation of the CO_2 ligand relative to **2** results form hydrogen bonding as well as an interaction between the nucleophilic carbene carbon atom and the positively polarized carbon atom of CO_2. According to theory [MP2(fc)/6-31G(d)] the stabilization energy is 5.9 kcal mol^{-1}. The complex **2**·CO_2 can be regarded as a model for the catalytic activity of 2,3-dihydrothiazol-2-ylidenes in benzoin condensations of aliphatic aldehydes, since it reveals both the nucleophilic and the electrophilic properties of **2**.

The thermal decarboxylation of carboxylic acid **1** to **3** has long been known.[11, 12] In light of the relatively high calculated activation energy for the conversion of **2** into **3**, carbene **2** generated by flash-vacuum pyrolysis of **1a** might exist long enough to be detected after immediate matrix isolation. Our attempts failed, however, and we only found the final product **3**. Nonetheless, the primary product is presumably carbene **2**. We are currently investigating whether the synthetic approach for **2** can be extended to other heterocyclic carboxylic acids.[13]

In this context, it is noteworthy that photochemically generated **2** rearranges to **3** upon warming the matrix to 60 K (accompanied by complete evaporation of the argon). It must be assumed that under these conditions the isomerization **2** → **3** does not follow the intramolecular pathway via the transition state **4** (E_A = 42.3 kcal mol^{-1}) but rather proceeds by an intermolecular hydrogen shift between two molecules of **2**.

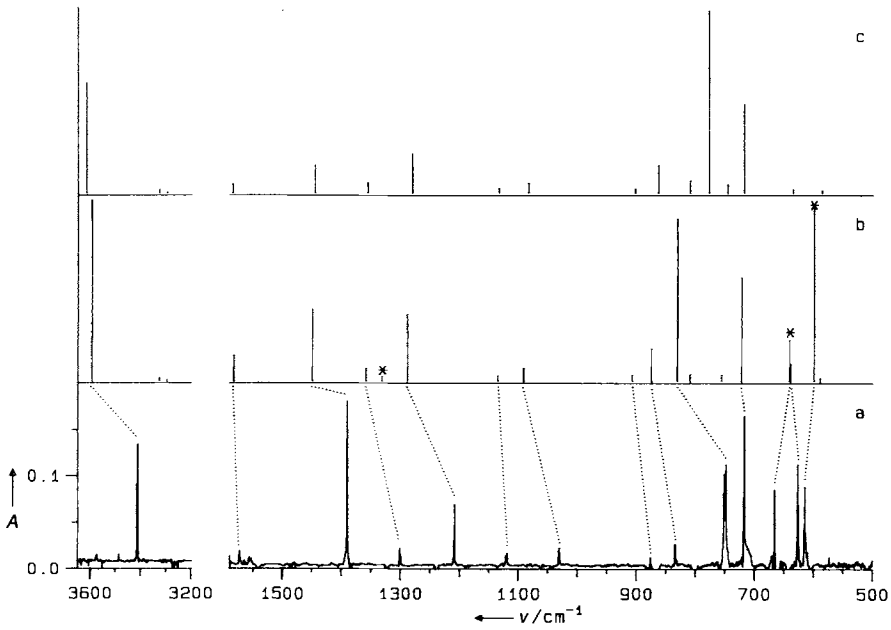

Figure 1. Calculated [MP2(fc)/6-31G(d)] spectra and experimental IR spectrum of 2,3-dihydrothiazol-2-ylidene (**2**). a) Difference spectrum (Ar matrix, 10 K) for the photochemical conversion **2** → **3**. b) Calculated spectrum of complex **2**·CO_2 (CO_2 bands are marked with an asterisk). c) Calculated spectrum of the uncomplexed carbene **2**.

Received: January 27, 1997 [Z10035IE]
German version: *Angew. Chem.* **1997**, *109*, 1788–1790

Keywords: carbenes · decarboxylation · heterocycles · matrix isolation · photochemistry

[1] a) A. J. Arduengo III, R. L. Harlow, M. Kline, *J. Am. Chem. Soc.* **1991**, *113*, 361–363; b) A. J. Arduengo III, H. V. R. Dias, R. L. Harlow, M. Kline, *ibid.* **1992**, *114*, 5530–5534; c) A. J. Arduengo III, J. R. Goerlich, W. J. Marshall, *ibid.* **1995**, *117*, 11027–11028.

[2] R. Breslow, *J. Am. Chem. Soc.* **1958**, *80*, 3719–3726.

[3] Review: R. Kluger, *Chem. Rev.* **1987**, *87*, 863–876.

[4] J. H. Teles, J.-P. Melder, K. Ebel, R. Schneider, E. Gehrer, W. Harder, S. Brode, D. Enders, K. Breuer, G. Raabe, *Helv. Chim. Acta* **1996**, *79*, 61–83. We thank Dr. Teles, BASF, Ludwigshafen, Germany, for valuable hints and discussions.

 © WILEY-VCH Verlag GmbH, D-69451 Weinheim, 1997 0570-0833/97/3616-1711 $ 17.50+.50/0

[5] Review of nucleophilic carbenes: a) H.-W. Wanzlick, *Angew. Chem.* **1962**, *74*, 129–134; *Angew. Chem. Int. Ed. Engl.* **1962**, *1*, 75–80; b) M. Regitz, *ibid.* **1991**, *103*, 691–693 and **1991**, *30*, 674–676; *ibid.* **1996**, *108*, 791–79 and **1996**, *35*, 725–728; c) C. Köcher, W. A. Herrmann, *ibid.* **1997**, *109*, in press and **1997**, *36*, in press; d) see also [6, 7], and references therein.
[6] D. Enders, K. Breuer, G. Raabe, J. Runsik, J. H. Teles, J.-P. Melder, K. Ebel, S. Brode, *Angew. Chem.* **1995**, *107*, 1119–1121; *Angew. Chem. Int. Ed. Engl.* **1995**, *34*, 1021–1023.
[7] A. J. Arduengo III, J. R. Goerlich, W. J. Marshall, *Liebigs Ann./Receuil* **1997**, 365–374, also for a review of 2,3-dihydrothiazol-2-ylidenes. We thank Dr. Arduengo for a copy of this manuscript.
[8] Synthesis: P. E. Iversen, *Acta Chem. Scand.* **1968**, *22*, 694–695.
[9] Gaussian 94, revision B.1: M. J. Frisch, G. W. Trucks, H. B. Schlegel, P. M. W. Gill, B. G. Johnson, M. A. Robb, J. R. Cheeseman, T. Keith, G. A. Petersson, J. A. Montgomery, K. Raghavachari, M. A. Alaham, V. G. Zakrzewski, J. V. Ortiz, J. B. Foresman, J. Cioslowski, B. B. Stefanov, A. Nanayakkara, M. Challacombe, C. Y. Peng, P. Y. Ayala, W. Chen, M. W. Wong, J. L. Andres, E. S. Replogle, R. Gomperts, R. L. Martin, D. J. Fox, J. S. Binkley, D. J. Derees, J. Baker, J. P. Stewart, M. Head-Gordon, C. Gonzalez, J. A. Pople, Gaussian Inc., Pittsburgh, PA, USA, **1995**.
[10] C. Heinemann, T. Müller, Y. Apeloig, H. Schwarz, *J. Am. Chem. Soc.* **1996**, *118*, 2023–2038, and references therein.
[11] H. Erlenmeyer, C. J. Morel, *Helv. Chim. Acta* **1942**, *25*, 1073–1077.
[12] H. Schenkel, M. Schenkel-Rudin, *Helv. Chim. Acta* **1948**, *31*, 924–929.
[13] Note added in proof (received on April 16, 1997): It has meanwhile been shown that **2** can be generated and detected by mass spectrometry in the gas phase (G. A. McGibbon, J. Hruscaronak, D. J. Lavarto, H. Schwarz, J. K. Terlouw, *Chem. Eur. J.* **1997**, *3*, 232–236).

Novel Mononuclear Vanadium Complexes Having Pentalene Ligands η^8-Bonded to a Single Metal Atom—A New Type of Coordination in Organometallic Chemistry

Klaus Jonas,* Barbara Gabor, Richard Mynott, Klaus Angermund, Oliver Heinemann, and Carl Krüger

More than sixty years elapsed between the discovery of the cyclopentadienide anion (**1**) by Thiele[1] and that of the bicyclic pentalene dianion (**2**), which Katz et al. prepared in 1962 as its dilithium salt (**5a**) by double deprotonation of 1,5-dihydropentalene (**3**)[2–4a] with butyllithium (Scheme 1).[4] The first transition metal complexes of pentalene were also synthesized during the early 1960s. Katz et al. showed that the ferrocene

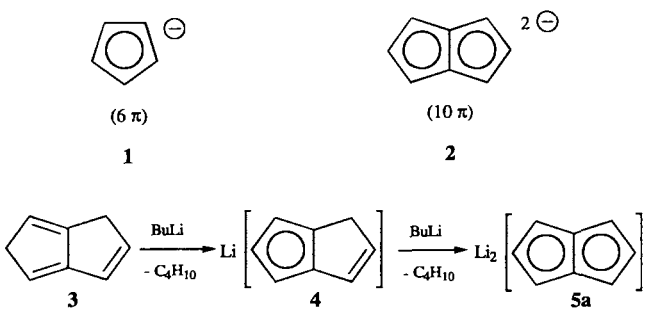

1 **2** **3** **4** **5a**

Scheme 1. Preparation of the pentalene dianion by double deprotonation of 1,5-dihydropentalene.

[*] Prof. Dr. K. Jonas, B. Gabor, Dr. R. Mynott, Dr. K. Angermund, Dr. O. Heinemann, Prof. Dr. C. Krüger
Max-Planck-Institut für Kohlenforschung
Kaiser-Wilhelm-Platz 1, D-45470 Mülheim an der Ruhr (Germany)
Fax: Int. code +(208) 306-2980
e-mail: jonas@mpi-muelheim.mpg.de

derivative bis(dihydropentalenyl)iron, synthesized from $FeCl_2$ and $Li[C_8H_7]$ (**4**), can be converted to the anionic ferrocene derivatives $Li[(C_8H_6)Fe(C_8H_7)]$ or $Li_2[(C_8H_6)_2Fe]$ by metalation with *tert*-butyllithium.[5] On the other hand, treatment of $[NiCl_2(CH_3OC_2H_4OCH_3)_2]$ or $CoCl_2$ with **5a** affords binuclear transition metal complexes with the composition $[(C_8H_6)_2M_2]$ (M = Ni, Co; yields 4–10%), for which the binuclear sandwich structure **6** has been proposed (Scheme 2).[6]

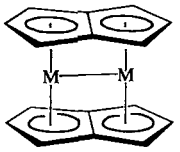

M = Ni, Co

6

Scheme 2. Proposed structure of $[(C_8H_6)_2Ni_2]$ and $[(C_8H_6)_2Co_2]$.

The structures of $[(\mu\text{-}C_8H_6)\{Ni(C_3H_5)\}_2]$,[7] the dinickel complex prepared from **5a** and allylnickel chloride, and of the binuclear complexes $[(\mu\text{-}C_8H_6)(CoCp^*)_2]$ and $[(\mu\text{-}C_8H_6)(FeCp^*)_2]$,[8] obtained by reacting **5a** with [Cp*M(acac)] (M = Fe, Co; Cp* = C_5Me_5; acac = acetylacetonate), have been confirmed by X-ray crystallography. Heterobimetallic pentalene complexes such as $[Cp^*Co(\mu\text{-}C_8H_6)Fe(\eta^5\text{-}C_8H_7)]$ and trinuclear complexes having two bridging pentalene ligands, for example $[Cp^*Fe(\mu\text{-}C_8H_6)Fe(\mu\text{-}C_8H_6)FeCp^*]$, are also known.[9] That transition metal carbonyl complexes can also be used as starting materials for the synthesis of pentalene complexes is shown by the work of Hunt et al.,[10] Hafner et al.,[11] Stone et al.,[12] and Woodward et al.[13] The pentacarbonyldiiron complex $[(\mu\text{-}C_8H_6)Fe_2(CO)_5]$ can be prepared by reacting $[Fe_2(CO)_9]$ with dihydropentalene[10a] or dimeric pentalene;[11] the reactions of the dihydropentalene derivatives C_8H_7R (R = NMe_2, C_6H_5) with $[Fe(CO)_5]$ yield $[Fe_2(CO)_5]$ complexes with substituted pentalene bridges.[10b] Stone et al.[12] employed reactions of various ruthenium carbonyl complexes with cyclooctatetraenes to form complexes having pentalene or substituted pentalene bridges. Woodward et al.[13] obtained two isomeric triruthenium complexes with $[(CH_3)_3Si]_3C_8H_3$ bridges from $[Ru_3(CO)_{12}]$ and tris(trimethylsilyl)cyclooctatriene. Thus, the only transition metal complexes that have been prepared to date that have pentalene or a derivative of pentalene as ligands are compounds of the late transition metals Ni, Co, Fe, and Ru. Without exception these are multinuclear complexes in which the bicyclic ligands, which are planar or nearly planar, act as bridges between the metal atoms (Scheme 3). We show here for

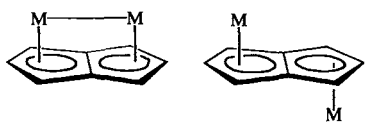

Scheme 3. Pentalene bridges in binuclear transition metal complexes as confirmed by X-ray structure analysis.

the first time that pentalene can also form complexes in which all eight carbon atoms are coordinated to a single metal atom.

The vanadium-containing starting materials used to synthesize the mononuclear vanadium pentalene complexes **8** are the vanadocene monohalides $[Cp_2VX]$ (Cp = C_5H_5; X = Cl, Br) (**7a**)[14] and their derivatives **7b** and **7c**[15] (Scheme 4). These

 © WILEY-VCH Verlag GmbH, D-69451 Weinheim, 1997 0570-0833/97/3616-1712 $ 17.50+.50/0

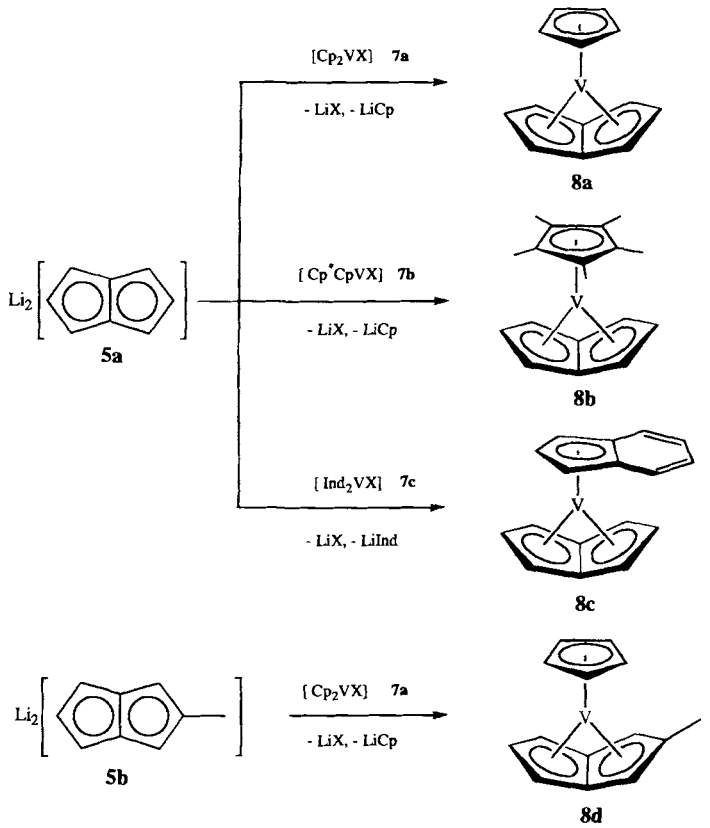

Scheme 4. Synthesis of the pentalene vanadium complexes **8**.

compounds were chosen because we knew that when the vanadium bromide compound **7a** reacts with two mole equivalents of allyllithium, the bromine atom and one of the cyclopentadienyl ligands are each replaced by an allyl group to afford the 16e complex $[CpV(\eta^3\text{-}C_3H_5)_2]$.[16] The new complexes **8**, which were prepared in high yields (80–90%) from the vanadium complexes **7** and the dilithium compounds **5a** or **5b** [17], are diamagnetic 18e complexes. They are air sensitive but can be sublimed in high vacuum at 80–100 °C without decomposition.

The compounds **8** were characterized by NMR spectroscopy and mass spectrometry (Table 1). In the ^{13}C NMR spectra of **8a–c**, three signals are observed for the pentalene ligands. The resonances appearing at highest field are those assigned to C1. Their chemical shifts (e.g., **8a**: $\delta = 84.2$) are similar to those of the Cp ligands (**8a**: $\delta = 86.9$, **8d**: $\delta = 88.4$). The signals of C2 lie to considerably lower field (e.g., **8a**: $\delta = 98.1$) and those of the bridgehead atoms C3a are found at lowest field (e.g., **8a**: $\delta = 125.9$). At 27 °C the signals of C1 (for **8d**, also of C4) and C3a are broadened for **8a–d**. The same applies to the resonances of the C atoms of the Cp ligands (**8a**, **8d**), and those of the Cp* and indenyl ligand bound to vanadium in **8b** and **8c**, respectively. For example, the line widths of these signals of **8b** are 21, 30, and 39 Hz. When the temperature is reduced the signals become narrower (9, 11, 15 Hz, respectively, −30 °C), from which follows that the line broadening is not caused by structural dynamic behavior but results from interaction with the quadrupolar vanadium nucleus. Therefore, as expected, the ^{51}V NMR spectra of these compounds are easy to measure (Table 1).

Crystals of **8a**, **8b**, and **8d** suitable for X-ray crystallography[18] were obtained by recrystallization from hexane (−30 °C). Figure 1 shows the molecular structures of the parent compound **8a**, the pentamethylcyclopentadienyl complex **8b**,

Table 1. Selected physical data of the complexes **8a–8d** [a, b]. The following numbering scheme was used for the pentalene, methylpentalene, and indenyl ligands:

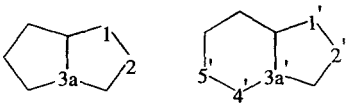

8a: ^1H NMR: $\delta = 4.47$ (s, 5H, Cp), 5.02 (t, $^3J = 2.6$ Hz, 2H, H2), 5.14 (d, $^3J = 2.6$ Hz, 4H, H1); ^{13}C NMR: $\delta = 84.2$ (d, $^1J(C,H) = 184 \pm 2$ Hz, 4C, C1), 86.9 (d, $^1J(C,H) = 175 \pm 2$ Hz, 5C, Cp), 98.1 (d, $^1J(C,H) = 168$ Hz, 2C, C2), 125.9 (s, 2C, C3a); ^{51}V NMR: $\delta = -901.9$ (line width at half height 120 Hz); MS (70 eV): *m/z* [%]: 218 (M^+) [100], 153 ($M^+ - Cp$) [27], 116 ($M^+ - C_8H_6$) [13]

8b: ^1H NMR: $\delta = 1.64$ (s, 15H, CH_3), 4.53 (t, $^3J = 2.0$ Hz, 2H, H2), 4.76 (d, $^3J = 2.0$ Hz, 4H, H1); ^{13}C NMR: $\delta = 12.7$ (q, $^1J(C,H) = 126$ Hz, 5C, CH_3), 87.7 (d, $^1J(C,H) = 181 \pm 2$ Hz, 4C, C1), 102.9 (s, 5C, Cp*), 105.6 (d, $^1J(C,H) = 160$ Hz, 2C, C2), 127.4 (s, 2C, C3a); ^{51}V NMR: $\delta = -690.7$ (line width at half height 112 Hz); MS (70 eV): *m/z* [%]: 288 (M^+) [100], 273 ($M^+ - CH_3$) [16], 153 ($M^+ - Cp^*$) [42]

8c: ^1H NMR: $\delta = 4.57$ (d, $^3J = 2.5$ Hz, 4H, H1), 4.67 (d, $^3J = 2.9$ Hz, 2H, H1'), 5.09 (s, 1H, H2'), 5.80 (t, $^3J = 2.5$ Hz, 2H, H2), 6.72 and 7.06 (AA'XX' spin system, each 2H, H4' and H5'); ^{13}C NMR: $\delta = 83.6$ (br d, ^1J = (C,H) not determined, 1C, C2'), 84.3 (d, $^1J(C,H) = 172$ Hz, 2C, C1'), 87.9 (d, $^1J(C,H) = 182 \pm 2$ Hz, 4C, C1), 101.7 (d, $^1J(C,H) = 169$ Hz, 2C, C2), 111.4 (s, 2C, C3a'), 123.0 (d, $^1J(C,H) = 158$ Hz, 2C, C5'), 126.1 (s, 2C, C3a), 128.5 (d, $^1J(C,H) = 162$ Hz, 2C, C4'); ^{51}V NMR: $\delta = -597.8$ (line width at half height 176 Hz): MS (70 eV): *m/z* [%]: 268 (M^+) [100], 153 ($M^+ - C_9H_7$) [39]

8d: ^1H NMR: $\delta = 1.86$ (s, 3H, CH_3), 4.41 (s, 5H, Cp), 4.85 (t, $^3J = 2.5$ Hz, 1H, H5), 4.99 (s, 2H, H1), 5.13 (d, $^3J = 2.5$ Hz, 2H, H4); ^{13}C NMR: $\delta = 15.6$ (q, $^1J(C,H) = 127$ Hz, 1C, CH_3), 83.6 (d, $^1J(C,H) = 182 \pm 2$ Hz, 2C, C4), 86.5 (d, $^1J(C,H) = 178 \pm 2$ Hz, 2C, C1), 88.4 (d, $^1J(C,H) = 174 \pm 2$ Hz, 5C, Cp), 96.6 (d, $^1J(C,H) = 167$ Hz, 1C, C5), 116.0 (s, 1C, C2), 126.3 (s, 2C, C3a); ^{51}V NMR: $\delta = -824.1$ (line width at half height 160 Hz); MS (70 eV): *m/z* [%]: 232 (M^+) [100], 167 ($M^+ - Cp$) [7], 166 ($M^+ - Cp - H$) [9], 116 ($M^+ - C_8H_5CH_3$) [25]

[a] ^1H NMR: 300 MHz, [D$_8$]THF, 27 °C, TMS; ^{13}C NMR: 75.6 MHz, [D$_8$]THF, 27 °C, TMS. Chemical shifts measured relative to the signals of the β-methylene groups of the solvent and converted to the TMS scale ($\delta_C^0 = 25.3$, δ_H^0 1.73). ^{51}V NMR: 157.8 MHz, [D$_8$]THF, 30 °C, $VOCl_3$ (external). [b] MS: Finnigan MAT 8200, Finnigan GmbH, Bremen.

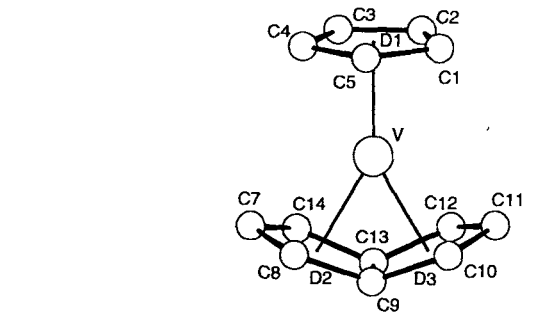

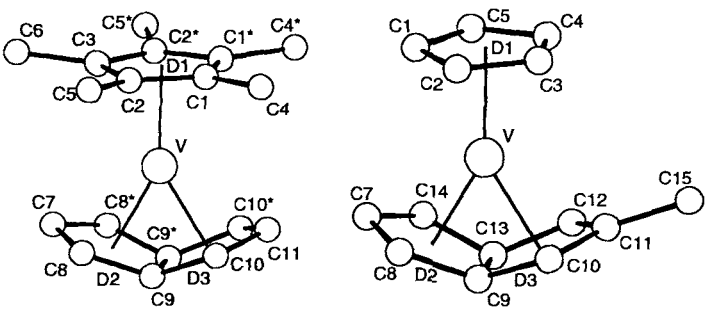

Figure 1. Molecular structures of **8a** (top), **8b** (bottom left), and **8d** (bottom right) in the crystal. Selected distances [Å] and angles [°]: **8a**: V–D1 1.886, V–D2 1.806, V–D3 1.802, V–C7 2.303(8), V–C8 2.209(6), V–C9 2.063(6), V–C10 2.216(5), V–C11 2.310(6), V–C12 2.208(5), V–C13 2.042(6), V–C14 2.218(8); D1-V-D3 149.5, D1-V-D2 150.1, D2-V-D3 60.3, C8-C9-C10 123.5(6), C12-C13-C14 125.3(6), C8-C9-C13 107.0(5), C9-C13-C14 107.2(6), C9-C13-C12 107.9(5), C10-C9-C13 107.0(5).

 © WILEY-VCH Verlag GmbH, D-69451 Weinheim, 1997 0570-0833/97/3616-1713 $ 17.50+.50/0

and the 2-methylpentalene complex **8d**. The geometrical center of the atoms C1–C5 and of C1–C3, C1*, and C2* is denoted as D1, that of C7–C9, C13, and C14 and C7–C9, C8*, and C9* as D2, and that of C9–C13 and C9–C11, C9*, and C10* as D3.

In the compounds **8a**, **8b**, and **8d** the vanadium atom has a distorted pseudo-trigonal geometry. The magnitudes of the angles D1-V-D2 and D1-V-D3 differ only slightly (148–152°), as of necessity do those of D2-V-D3 (59–61°). The V–C bond lengths within the vanadium-Cp and vanadium-Cp* moieties lie between 2.20 and 2.26 Å and in all cases V–D1 is 1.89 Å. The most prominent structural feature of the new vanadium complexes **8** is the strong folding of the pentalene or methylpentalene ligand towards the metal atom along the bond between the bridging carbon atoms. In all three vanadium complexes the angle between the plane through the atoms C7–C9, C13, and C14 (**8a**, **8d**) and C7–C9, C8*, and C9* (**8b**), respectively, and that through the plane of the atoms C9–C13 and C9–C11, C9*, and C10*, respectively, is 137°. The distances between vanadium and the C atoms of the pentalene ligands can be divided into three groups: V–C9 ≈ V–C13 (2.04–2.07 Å) < V–C8 ≈ V–C10 ≈ V–C12 ≈ V–C14 (2.20–2.23 Å) < V–C7 ≈ V–C11 (2.30–2.35 Å). The methyl substituent in **8d** causes the 2-methylpentalene ligand to be coordinated unsymmetrically to vanadium, that is within the relevant groups of bond lengths, the distances V–C14 and V–C7 in **8d** are the shortest and V–C10 and V–C11 are the longest. The methyl carbon atom C15 lies just 0.03 Å out of the mean plane of the atoms C9–C13.

We are currently carrying out further NMR studies and ab initio calculations in order to understand better the bonding situation in these novel vanadium complexes **8**.

Received: February 14, 1997 [Z10123IE]
German version: *Angew. Chem.* **1997**, *109*, 1790–1793

Keywords: coordination modes · mononuclear complexes · pentalene · structure elucidation · vanadium

[1] J. Thiele, *Chem. Ber.* **1901**, *34*, 68–71.
[2] R. Riemschneider, *Z. Naturforsch. B* **1961**, *16*, 759.
[3] A. G. Griesbeck, *Synthesis* **1990**, 144–147.
[4] a) T. J. Katz, M. Rosenberger, *J. Am. Chem. Soc.* **1962**, *84*, 865–866; T. J. Katz, M. Rosenberger, R. K. O'Hara, *ibid.* **1964**, *86*, 249–252; b) J. J. Stezowski, H. Hoier, D. Wilhelm, T. Clark, P. von R. Schleyer, *J. Chem. Soc. Chem. Commun.* **1985**, 1263–1264.
[5] T. J. Katz, M. Rosenberger, *J. Am. Chem. Soc.* **1963**, *85*, 2030–2031.
[6] T. J. Katz, N. Acton, *J. Am. Chem. Soc.* **1972**, *94*, 3281–3283; T. J. Katz, N. Acton, J. McGinnis, *ibid.* **1972**, *94*, 6205–6206.
[7] a) A. Miyake, A. Kanai, *Angew. Chem.* **1971**, *83*, 851; *Angew. Chem. Int. Ed. Engl.* **1971**, *10*, 801; b) Y. Kitano, M. Kashiwagi, Y. Kinoshita, *Bull. Chem. Soc. Jpn.* **1973**, *46*, 723–727.
[8] E. E. Bunel, L. Valle, N. L. Jones, P. J. Carrol, C. Barra, M. Gonzalez, N. Munoz, G. Visconti, A. Aizman, J. M. Manríquez, *J. Am. Chem. Soc.* **1988**, *110*, 6596–6598; J. M. Manríquez, M. D. Ward, W. M. Reiff, J. C. Calabrese, N. L. Jones, P. J. Carroll, E. E. Bunel, J. S. Miller, *ibid.* **1995**, *117*, 6182–6193.
[9] B. Oelckers, I. Chávez, J. M. Manríquez, E. Román, *Organometallics* **1993**, *12*, 3396–3397.
[10] a) D. F. Hunt, J. W. Russel, *J. Organomet. Chem.* **1976**, *104*, 373–376; b) D. F. Hunt, J. W. Russel, *J. Am. Chem. Soc.* **1972**, *94*, 7198–7199; *J. Organomet. Chem.* **1972**, *46*, C22–C24.
[11] W. Weidemüller, K. Hafner, *Angew. Chem.* **1973**, *85*, 958–959; *Angew. Chem. Int. Ed. Engl.* **1973**, *12*, 925.
[12] S. A. R. Knox, F. G. A. Stone, *Acc. Chem. Res.* **1974**, *7*, 321–328; S. A. R. Knox, R. J. McKinney, V. Riera, F. G. A. Stone, A. C. Szary, *J. Chem. Soc. Dalton Trans.* **1979**, 1801–1811.
[13] J. A. K. Howard, R. F. D. Stansfield, P. Woodward, *J. Chem. Soc. Dalton Trans.* **1979**, 1812–1818.
[14] H. J. de Liefde Meijer, M. J. Janssen, G. J. M. van der Kerk, *Recl. Trav. Chim. Pays-Bas* **1961**, *80*, 831–845.
[15] a) K. Jonas, W. Rüsseler, C. Krüger, E. Raabe, *Angew. Chem.* **1986**, *98*, 902–904; *Angew. Chem. Int. Ed. Engl.* **1986**, *25*, 925–927; b) W. Rüsseler, Dissertation, Universität Bochum, **1986**.
[16] K. Jonas, *Angew. Chem.* **1985**, *97*, 292–307; *Angew. Chem. Int. Ed. Engl.* **1985**, *24*, 295–311.
[17] The $C_8H_7CH_3$ required to synthesize $Li_2[C_8H_5CH_3]$ was prepared according to reference [3].
[18] X-ray crystallographic data for **8a**: $C_{13}H_{11}V$, $M_r = 218.2\ g\,mol^{-1}$, crystal dimensions $0.04 \times 0.53 \times 0.53\ mm^3$, $a = 7.862(1)$, $b = 10.480(2)$, $c = 11.676(1)$ Å, $V = 962.0$ Å^3, $T = 293$ K, $\rho_{calcd} = 1.51\ g\,cm^{-3}$, $\mu = 9.48\ cm^{-1}$, $F(000) = 448$ e, $Z = 4$, orthorhombic, space group $P2_12_12_1$ (no. 19), Enraf-Nonius CAD4 diffractometer, $\lambda = 0.71069$ Å, scan mode ω-2θ, 1163 measured reflections $(-h, -k, -l)$, $[(\sin\theta)/\lambda]_{max} = 0.62$ Å^{-1}, 1147 independent and 890 observed reflections, $[I > 2\sigma(I)]$, 127 refined parameters; direct methods, H atom positions calculated, $R = 0.035$, $R_w = 0.037$ $[w = 1/(\sigma^2(F_o))]$, max. residual electron density $0.40\ e\ Å^{-3}$. X-ray crystallographic data for **8b**: $C_{18}H_{21}V$, $M_r = 288.3\ g\,mol^{-1}$, crystal dimensions $0.21 \times 0.39 \times 0.39\ mm^3$, $a = 10.241(1)$, $b = 12.347(1)$, $c = 11.531(1)$ Å, $V = 1458.0$ Å^3, $T = 293$ K, $\rho_{calcd} = 1.31\ g\,cm^{-3}$, $\mu = 6.42\ cm^{-1}$, $F(000) = 608$ e, $Z = 4$, orthorhombic, space group *Pnma* (no. 62), Enraf-Nonius CAD4 diffractometer, $\lambda = 0.71069$ Å, scan mode ω-2θ, 2435 measured reflections $(-h, -k, +l)$, $[(\sin\theta)/\lambda]_{max} = 0.70$ Å^{-1}, 2216 independent and 1400 observed reflections $[I > 2\sigma(I)]$, 139 refined parameters; direct methods, H atom positions found and refined, $R = 0.042$, $R_w = 0.049$ $[w = 1/(\sigma^2(F_o))]$, max. residual electron density $0.44\ e\ Å^{-3}$. X-ray crystallographic data for **8d**: $C_{14}H_{13}V$, $M_r = 232.2\ g\,mol^{-1}$, crystal dimensions $0.24 \times 0.28 \times 0.39\ mm^3$, $a = 10.681(1)$, $b = 7.562(1)$, $c = 12.911(1)$ Å, $\beta = 90.67(1)°$, $V = 1042.7$ Å^3, $T = 203$ K, $\rho_{calcd} = 1.48\ g\,cm^{-3}$, $\mu = 8.79\ cm^{-1}$, $F(000) = 480$ e, $Z = 4$, monoclinic, space group $P2_1/c$, (no. 14), Enraf-Nonius CAD4 diffractometer, $\lambda = 0.71069$ Å, scan mode ω-2θ, 2666 measured reflections $(+h, +k, +l)$, $[(\sin\theta)/\lambda]_{max} = 0.65$ Å^{-1}, 2374 independent and 1921 observed reflections, $[I > 2\sigma(I)]$, 188 refined parameter; direct methods, H atom positions found and refined, $R = 0.045$, $R_w = 0.049$ $[w = 1/(\sigma^2(F_o))]$, max. residual electron density $0.62\ e\ Å^{-3}$. Crystallographic data (excluding structure factors) for the structures reported in this paper have been deposited with the Cambridge Crystallographic Data Centre as supplementary publication no. CCDC-100 212. Copies of the data can be obtained free of charge on application to The Director, CCDC, 12 Union Road, Cambridge CB2 1EZ, UK (fax: int. code +(1223) 336-033; e-mail: deposit@chemcrys.cam.ac.uk).

Mononuclear Pentalene and Methylpentalene Complexes of Titanium, Zirconium, and Hafnium

Klaus Jonas,* Peter Kolb, Guido Kollbach, Barbara Gabor, Richard Mynott, Klaus Angermund, Oliver Heinemann, and Carl Krüger

In organometallic complexes, cyclooctatetraene (COT) is able to contribute up to eight π electrons, the highest number for any monocyclic hydrocarbon ligand of the series $(CH)_n$ ($n = 3–8$). Therefore, the formation of complexes of the d-block transition metals in which a cyclooctatetraene ligand is η^8-coordinated to a single metal atom is confined exclusively to the early transition metals (Ti,[1, 4a] Zr,[2] Hf,[3] V,[4] Nb,[5] Ta,[5] Mo[6]). The η^8-C_8H_8 ligands in these compounds are usually planar. In addition, numerous cyclooctatetraene complexes of the rare earth metals[7a] and the actinides[7b] are known and in these compounds the η^8-COT ligands are invariably planar.

In the preceding communication[8] we reported mononuclear organovanadium complexes in which pentalene functions as an 8e ligand. The most prominent structural feature of these mononuclear complexes is the strong folding of the bicyclic ligand towards the metal along the bond between the bridgehead carbon atoms. We wish to show that this new form of

[*] Prof. Dr. K. Jonas, Dipl.-Chem. P. Kolb, Dipl.-Chem. G. Kollbach, B. Gabor, Dr. R. Mynott, Dr. K. Angermund, Dr. O. Heinemann, Prof. Dr. C. Krüger
Max-Planck-Institut für Kohlenforschung
Kaiser-Wilhelm-Platz 1, D-45470 Mülheim an der Ruhr (Germany)
Fax: Int. code +(208)306-2980
e-mail: jonas@mpi-muelheim.mpg.de

 © WILEY-VCH Verlag GmbH, D-69451 Weinheim, 1997 0570-0833/97/3616-1714 $ 17.50+.50/0

η^8-coordination can also be encountered in compounds of other transition metals and report here new mononuclear pentalene and methylpentalene complexes in which the central atom is titanium, zirconium, and hafnium.

The starting materials for the synthesis of the new titanium, zirconium, and hafnium complexes **4**–**7** are dilithiumpentalendiide (**1a**)[9] or its monomethyl derivative $Li_2[C_8H_5CH_3]$ (**1b**)[10, 11] and transition metal compounds having halide and cyclopentadienyl ligands. The metallocene dichlorides $[Cp_2MCl_2]$ (M = Ti, Zr, Hf) **2a**–**c** are commercially available and the titanium(III) complex $[CpTiCl_2]$ (**3**) is easy to prepare from $[Cp_2TiCl_2]$ (**2a**) and diisobutylaluminum chloride.[12] When $Li_2[C_8H_6]$ (**1a**) is reacted with $[CpTiCl_2]$ (**3**), both the chloro ligands are exchanged to yield the paramagnetic 17e complex **4** (Scheme 1). However, treatment of $[Cp_2ZrCl_2]$ (**2b**) with **1a** in the molar ratio 1:1 results in substitution of one chloro and one cyclopentadienyl ligand to give the 18e complex **5b**. Isostructural with this zirconium complex **5b** are the titanium compounds **5a**, which can be prepared from **4** and dichloroethane or dibromoethane, respectively (Scheme 1).

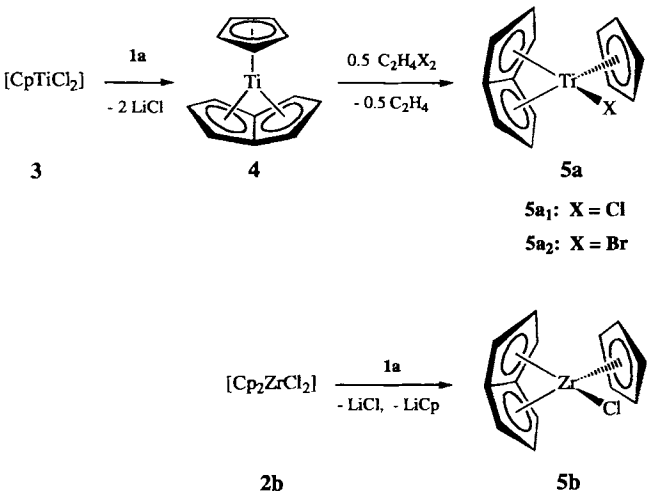

Scheme 1. Synthesis of the pentalene complexes **4**, **5a**, and **5b**.

We were able to prepare crystals of the compounds **4**, $\mathbf{5a_1}$, and **5b** suitable for X-ray crystallography.[13] The molecular structures of these compounds are depicted in Figure 1. The geometrical center of the atoms C1–C5 and of C1–C3, C1*, and C2* is denoted by D1, that of the atoms C7–C9, C13, and C14 by D2, of atoms C9–C13 by D3, and of atoms C9, C13, C7*, C8*, and C14* by D2*. In compound **4** the titanium atom has a distorted pseudo-trigonal geometry with angles at the metal of 151° (D1-Ti-D2 = D1-Ti-D3) and 58° (D2-Ti-D3). The Ti–C bond lengths, which lie between 2.33 and 2.35 Å, are typical for a $CpTi^{III}$ moiety. $[CpTi(\eta^8\text{-}C_8H_6)]$ (**4**) is isostructural with $[CpV(\eta^8\text{-}C_8H_6)]$ (**8a** in reference [8]). None of the angles at the titanium center differs by more than 2° from the corresponding one in the vanadium compound, but the metal–C distances are up to 0.12 Å longer. Here too, the distances between the metal atom and the carbon atoms of the pentalene ligand can be divided into three groups: short (Ti–C9/Ti–C13 2.08–2.13 Å), medium (Ti–C8/Ti–C10/Ti–C12/Ti–C14 2.30–2.33 Å), and long (Ti–C7/Ti–C11 2.41 Å). The angle of fold between the mean planes through each half of the pentalene ligand in **4** is 143°, which is 6° larger than in $[CpV(\eta^8\text{-}C_8H_6)]$. This angle is increased yet further by introducing an additional

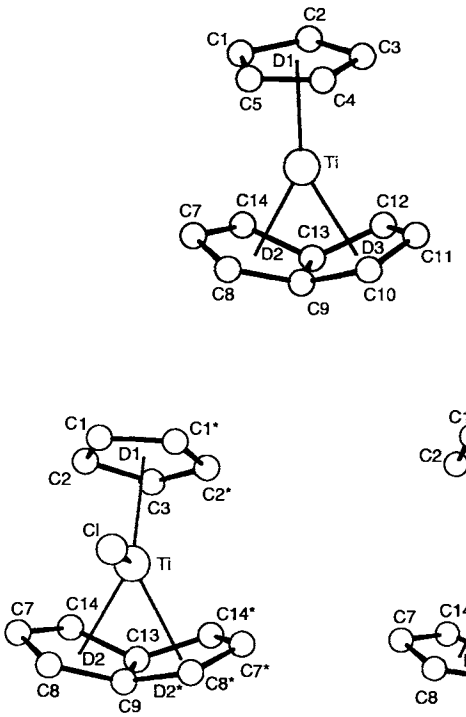

Figure 1. Molecular structure of **4**, $\mathbf{5a_1}$, and **5b** in the crystal. Selected distances [Å] and angles [°]:

	4	$\mathbf{5a_1}$	**5b**
M–D1	2.017	2.057	2.215
M–D2	1.904	1.970	2.096
M–D3	1.914	1.970	2.096
M–Cl	–	2.512(1)	2.540(1)
M–C7	2.408(7)	2.494(1)	2.586(1)
M–C8	2.295(7)	2.433(1)	2.533(1)
M–C9	2.083(8)	2.163(1)	2.287(1)
M–C10/C8*	2.33(1)	2.433(1)	2.533(1)
M–C11/C7*	2.41(1)	2.494(1)	2.586(1)
M–C12/C14*	2.310(8)	2.321(1)	2.420(1)
M–C13	2.132(7)	2.124(1)	2.256(1)
M–C14	2.312(7)	2.321(1)	2.420(1)
D1-M-D3/D2*	151.1	137.1	135.6
D1-M-D2	151.4	137.1	135.6
D2-M-D3/D2*	57.6	56.7	53.0
D1-M-Cl	–	103.7	105.2
D2-M-Cl	–	107.5	109.4
C8-C9-C13	109.2(7)	108.0(1)	107.8(1)
C9-C13-C14	105.5(7)	106.9(1)	106.4(1)
C9-C13-C12/C14*	108.0(6)	106.9(1)	106.4(1)
C10/C8*-C9-C13	107.9(7)	108.0(1)	107.8(1)
C8-C9-C10/C8*	129.7(7)	132.4(1)	133.3(1)
C12/C14*-C13-C14	127.6(7)	130.9(1)	132.1(1)

halogeno ligand; for $\mathbf{5a_1}$ an angle of 147° is found. In $\mathbf{5a_1}$ the distances between the titanium atom and the carbon atoms of the pentalene ligand are 2.12 and 2.16 Å, 2.32 and 2.43 Å, and 2.49 Å. The titanium–carbon bond lengths increase on average by about 0.05 Å in going from the Ti^{III} complex **4** to the Ti^{IV} complex $\mathbf{5a_1}$, in which the metal atom takes up a distorted pseudo-tetrahedral coordination geometry. Particularly conspicuous is the comparatively large increase in the Ti–C8 distance (**4**: 2.295(7) Å; $\mathbf{5a_1}$: 2.433(1) Å). A further striking feature is the unusually long Ti–Cl bond length of 2.512(1) Å (according to a search in the Cambridge Structure Database,[14] the average value for such bonds is 2.34 Å). The formal replacement of Ti^{IV} in $\mathbf{5a_1}$ by Zr^{IV} gives the isostructural compound **5b**. The angles at the metal center differ little from those of $\mathbf{5a_1}$ and

 © WILEY-VCH Verlag GmbH, D-69451 Weinheim, 1997 0570-0833/97/3616-1715 $ 17.50+.50/0

the angle of fold of the pentalene ligand is the same as in the titanium compound **5a**$_1$ (147°). As a result of the difference in size of the metal atoms, the metal–C distances in **5b** are about 0.1 Å greater than those in **5a**$_1$.

The pentalene ligands give rise to five signals in the ^{13}C NMR spectra of the titanium compounds **5a** and of the zirconium compound **5b** (Table 1). The carbon atoms C2 and C5 are equivalent, but the positions of the signals of the bridgehead carbon atoms C3a and C6a differ by about $\Delta\delta = 7-8$ (for numbering see Table 1). Even greater differences ($\Delta\delta \leq 18$) are observed between the signals of C1 (C6) and C3 (C4).

It is particularly noteworthy that homoleptic pentalene and methylpentalene complexes of titanium, zirconium, and hafnium can also be prepared. Bis(pentalene)titanium (**6a**) was synthesized by treating **5a** in THF with one mole equivalent of **1a**. The homologous compounds **6b** and **6c** were obtained from $[Cp_2MCl_2]$ (M = Zr, Hf (**2b** and **c**, respectively)) and two mole equivalents of **1a** (Scheme 2).

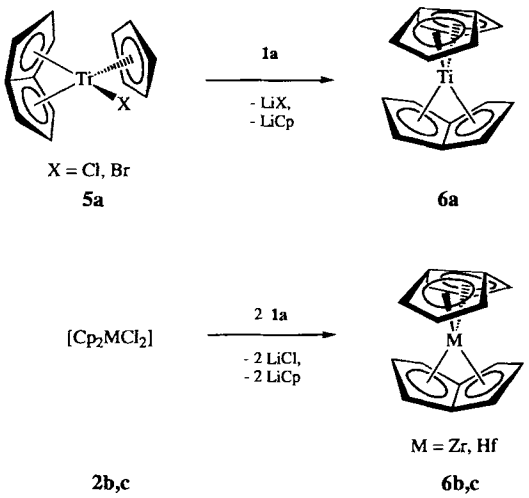

Scheme 2. Synthesis of the homoleptic pentalene complexes **6**.

The preparation of bis(2-methylpentalene)zirconium (**7b**) and bis(2-methylpentalene)hafnium (**7c**) was achieved analogously by reacting **2b** or **2c** with two mole equivalents of **1b**. To prepare the corresponding titanium compound $[(\eta^8\text{-}C_8H_5CH_3)_2Ti]$ (**7a**), it was first necessary to synthesize the methyl derivative of **4**, that is, $[(\eta^8\text{-}C_8H_5CH_3)TiCp]$, from **3** and **1b**. From $[(\eta^8\text{-}C_8H_5CH_3)TiCp]$ and dibromoethane we obtained the titanium(IV) compound $[(\eta^8\text{-}C_8H_5CH_3)TiCpBr]$, which was then converted to **7a** by treating it with one mole equivalent of **1b**. We have not yet been able to prepare crystals of **6** or **7** suitable for X-ray structure analysis.

At room temperature two signals are observed in the ^{1}H NMR spectra of **6a–6c** and three in the ^{13}C NMR spectra (Table 1). The same numbers of signals are found for the complex-bound pentalene in the NMR spectra of $[CpV(\eta^8\text{-}C_8H_6)]$.[8] Also the values of the chemical shifts and the H,H and C,H coupling constants are generally comparable. Thus the pentalene ligands are η^8-coordinated and the compounds **6a–6c** have to be classified as diamagnetic "20e complexes".[15] Information on the geometrical relationship between the pentalene ligands in these complexes can be obtained from the NMR spectra of the dimethyl derivatives **7a–7c**. In each case, there are six signals for the 2-methylpentalene ligands in the ^{1}H NMR spectra measured at room temperature. Nine signals are observed in the ^{13}C NMR spectrum of **7c** but only eight in the ^{13}C NMR spectra of **7a** and **7b** because two of the nine signals are unresolved (Table 1). Thus, the axes through the bridgeheads are not parallel but lie at an angle to each other.

Table 1. Selected physical data for the new complexes **4–8** [a, b]. The following numbering scheme was used for the complex-bound pentalene and 2-methylpentalene ligands (**5**, **6**, **8**: R = H; **7**: R = CH_3):

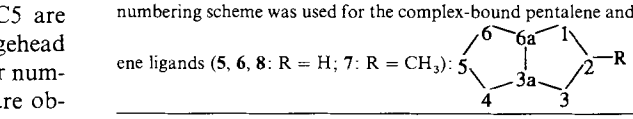

4: MS (70 eV): m/z [%]: 215 (M^+) [100], 150 ($M^+ - Cp$) [25]

5a$_1$: ^{1}H NMR: $\delta = 5.39$ and 6.21 (d, $^3J = 2.9$ and 3.7 Hz, respectively, both 2H, H1 and H3), 5.76 (s, 5H, Cp), 6.41 (dd, $^3J = 2.9$ and 3.7 Hz, 2H, H2); ^{13}C NMR: $\delta = 103.7$ and 121.5 (d, ^1J(C,H) = 180 and 183 Hz, respectively, both 2C, C1 and C3), 109.1 (d, ^1J(C,H) = 175 Hz, 5C, Cp), 112.4 (d, ^1J(C,H) = 172 Hz, 2C, C2), 124.3 and 132.5 (s, both 1C, C3a and C6a); MS (70 eV): m/z [%]: 250 (M^+) [44], 215 ($M^+ - Cl$) [14], 185 ($M^+ - Cp$) [100], 148 ($M^+ - C_8H_6$) [10]

5a$_2$: ^{1}H NMR: $\delta = 5.52$ and 6.42 (d, $^3J = 2.9$ and 3.7 Hz, respectively, both 2H, H1 and H3), 5.78 (s, 5H, Cp), 6.32 (dd, $^3J = 2.9$ and 3.7 Hz, 2H, H2); ^{13}C NMR: $\delta = 103.6$ and 120.0 (d, ^1J(C,H) = 180 Hz and 184 Hz, respectively, both 2C, C1 and C3), 108.7 (d, ^1J(C,H) = 175 Hz, 5C, Cp), 111.9 (d, ^1J(C,H) = 172 Hz, 2C, C2), 124.4 and 131.3 (s, both 1C, C3a and C6a); MS (70 eV): m/z [%]: 294 (M^+) [26], 229 ($M^+ - Cp$) [54], 215 ($M^+ - Br$) [100], 192 ($M^+ - C_8H_6$) [7], 150 ($M^+ - Cp - Br$) [30]

5b: ^{1}H NMR: $\delta = 5.25$ and 5.76 (d, $^3J = 2.9$ bzw. 3.6 Hz, both 2H, H1 and H3), 6.03 (s, 5H, Cp), 6.60 (t, $^3J = 2.9$ and 3.6 Hz, 2H, H2); ^{13}C NMR: $\delta = 95.8$ and 110.7 (d, ^1J(C,H) = 178 and 180 Hz, respectively, both 2C, C1 and C3), 109.9 (d, ^1J(C,H) = 173 Hz, 5C, Cp), 115.4 (d, ^1J(C,H) = 170 Hz, 2C, C2), 125.3 and 132.1 (s, both 2C, C3a and C6a); MS (70 eV): m/z [%]: 292 (M^+) [65], 257 ($M^+ - Cl$) [10], 227 ($M^+ - Cp$) [100]

6a: ^{1}H NMR: $\delta = 5.28$ (s, 8H, H1), 5.50 (t, $^3J = 3.2$ Hz, 4H, H2); ^{13}C NMR: $\delta = 95.9$ (d, ^1J(C,H) = 175 Hz, 8C, C1), 121.6 (d, ^1J(C,H) = 168 Hz, 4C, C2), 131.1 (s, 4C, C3a); MS (70 eV): m/z [%]: 252 (M^+) [100], 150 ($M^+ - C_8H_6$) [35]

6b: ^{1}H NMR: $\delta = 5.24$ (d, $^3J = 3.2$ Hz, 8H, H1), 5.67 (t, $^3J = 3.2$ Hz, 4H, H2); ^{13}C NMR: $\delta = 92.2$ (d, ^1J(C,H) = 174 Hz, 8C, C1), 123.4 (d, ^1J(C,H) = 167 Hz, 4C, C2), 132.9 (s, 4C, C3a); MS (70 eV): m/z [%]: 294 (M^+) [100], 192 ($M^+ - C_8H_6$) [19]

6c: ^{1}H NMR (400 MHz, [D$_8$]THF, 27 °C, TMS): $\delta = 5.16$ (d, $^3J = 3.1$ Hz, 8H, H1), 5.65 (t, $^3J = 3.1$ Hz, 4H, H2); ^{13}C NMR (100.6 MHz, [D$_8$]THF, 27 °C, TMS): $\delta = 90.2$ (d, ^1J(C,H) = 174 Hz, 8C, C1), 122.8 (d, ^1J(C,H) = 168 Hz, 4C, C2), 130.3 (s, 4C, C3a); MS (70 eV): m/z [%]: 384 (M^+) [100]

7a: ^{1}H NMR: $\delta = 1.77$ (s, 6H, CH_3), 5.03 and 5.22 (s, both 2H, H1 and H3), 5.19 and 5.26 (both 2H, H4 and H6), 5.44 (t, $^3J = 3.3$ Hz, 2H, H5); ^{13}C NMR: $\delta = 15.4$ (2C, 2-CH_3), 94.5 and 95.6 (both 2C, C4 and C6), 96.8 (2C, C1 and C3), 119.4 (2C, C5), 129.8 and 131.1 (both 2C, C3a and C6a), 137.0 (2C, C2); ^{1}H NMR (600.2 MHz, [D$_8$]THF, −80 °C, TMS): first conformer (53%): $\delta = 1.73$ (s, 6H, CH_3), 4.61 and 5.94 (d, $^3J = 3.1$ Hz, both 2H, H4 and H6), 4.99 and 5.49 (s, both 2H, H1 and H3), 5.45 (t, ^3J(H,H) = 3.1 Hz, 2H, H5); second conformer (47%): $\delta = 1.78$ (s, 6H, CH_3), 4.61 and 5.65 (s, both 2H, H1 and H3), 4.71 and 5.85 (d, $^3J = 3.2$ Hz, both 2H, H4 and H6), 5.56 (t, $^3J = 3.2$ Hz, 2H, H5); ^{13}C NMR (150.9 MHz, [D$_8$]THF, −80 °C, TMS): first conformer (53%): $\delta = 15.6$ (2C, CH_3), 91.8 and 100.5 (both 2C, C1 and C3), 93.3 and 96.2 (2C, C4 and C6), 117.0 (2C, C5), 128.9 and 131.5 (both 2C, C3a and C6a), 139.7 (2C, C2); second conformer (47%): $\delta = 15.6$ (2C, CH_3), 91.5 and 98.0 (both 2C, C4 and C6), 92.8 and 98.0 (2C, C1 and C3), 121.0 (2C, C5), 130.2 and 130.4 (both 2C, C3a and C6a), 136.0 (2C, C2); MS (70 eV): m/z [%]: 280 (M^+) [100], 265 ($M^+ - CH_3$) [14], 164 ($M^+ - C_8H_5CH_3$) [27]

7b: ^{1}H NMR: $\delta = 1.78$ (s, 6H, CH_3), 5.06 and 5.14 (s, both 2H, H1 and H3), 5.17 and 5.20 (d, $^3J = 3.3$ Hz, both 2H, H4 and H6), 5.65 (t, $^3J = 3.3$ Hz, 2H, H5); ^{13}C NMR: $\delta = 15.1$ (q, ^1J(C,H) = 127 Hz, 2C, CH_3), 92.2 and 93.0 (d, ^1J(C,H) = 173 Hz, both 2C, C4 and C6), 93.6 (d, ^1J(C,H) = 171 Hz, 4C, C1 and C3), 122.7 (d, ^1J(C,H) = 167 Hz, 2C, C5), 130.9 and 132.9 (s, both 2C, C3a and C6a), 137.6 (s, 2C, C2); MS (70 eV): m/z [%]: 322 (M^+) [100], 307 ($M^+ - CH_3$) [3], 205 ($M^+ - C_8H_5CH_3$) [7]

7c: ^{1}H NMR: $\delta = 1.82$ (s, 6H, CH_3), 4.95 and 5.08 (s, both 2H, H1 and H3), 5.09 and 5.11 (both 2H, H4 and H6), 5.64 (t, $^3J = 3.3$ Hz, 2H, H5); ^{13}C NMR: $\delta = 15.0$ (2C, CH_3), 89.9, 91.2, 91.5, 91.9 (both 2C, C1, C3, C4 and C6), 122.1 (2C, C5), 128.4 and 130.5 (2C, C3a and C6a), 137.1 (2C, C2); MS (70 eV): m/z [%]: 412 (M^+) [100]

8: ^{1}H NMR: $\delta = 5.58$ (d, $^3J = 3.4$ Hz, 4H, H1), 6.50 (t, $^3J = 3.4$ Hz, 2H, H2); ^{13}C NMR: $\delta = 103.4$ (d, ^1J(C,H) = 178 Hz, 4C, C1), 123.5 (d, ^1J(C,H) = 168 Hz, 2C, C2), 127.2 (s, 2C, C3a)

[a] ^{1}H NMR: 300 MHz, [D$_8$]THF, 27 °C, TMS; ^{13}C NMR: 75.5 MHz, [D$_8$]THF, 27 °C, TMS, unless otherwise given. The chemical shifts were measured relative to the signals of the β-methylene groups of the solvent and converted to the TMS scale ($\delta^0_C = 25.3$, $\delta^0_H = 1.73$). [b] MS: Finnigan MAT 8200.

 © WILEY-VCH Verlag GmbH, D-69451 Weinheim, 1997 0570-0833/97/3616-1716 $ 17.50+.50/0

When the temperature is lowered to −80 °C, all signals in the ^1H and ^{13}C NMR spectra of **7a**[16] with the exception of the ^{13}C NMR signal of the methyl groups split into two resonances with different intensities (Table 1). All the NMR data are consistent with the titanium complex **7a** being present as two conformers (53% and 47%; Scheme 3). These conformers **I** and **II**, both of

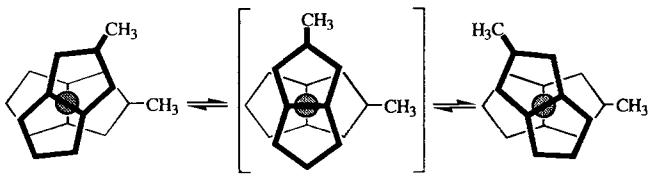

I **II**

Scheme 3. The dynamic behavior of one of the enantiomers of the C_2-symmetrical compound bis(methylpentalene)titanium (**7a**).

which have a distorted pseudo-tetrahedral coordination geometry, differ in the relative positions of the methylpentalene ligands. Conformers **I** and **II** are presumably interconverted by rotation of the ligands about the axis running through the centers of the bridges of the methylpentalene ligands and the metal atom.

When the light yellow bis(pentalene)zirconium (**6b**) is treated with $[ZrCl_4(thf)_2]$ in THF in the molar ratio 1:1, the dichloro complex **8**, which crystallizes from THF as long needles, is formed at room temperature in high yield (90%; Scheme 4).

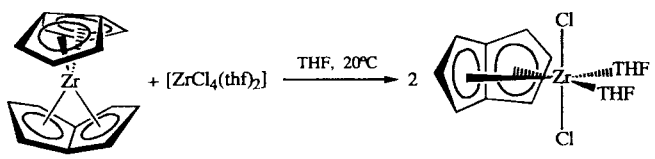

6b **8**

Scheme 4. The synthesis of the first mononuclear "half-sandwich" complex having a pentalene ligand.

Compound **8** with its two THF ligands is an 18e complex, whereas zirconocene dichloride (**2b**), which does not bind THF, is a 16e complex. The molecular structure[17] of compound **8** is illustrated in Figure 2.

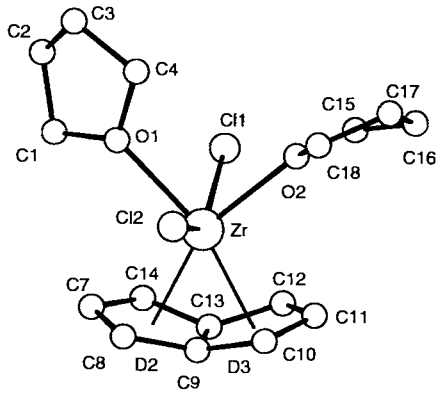

Figure 2. Molecular structure of **8** in the crystal. Selected distances [Å] and angles [°]: Zr–D2 2.107, Zr–D3 2.112, Zr–Cl1 2.595(2), Zr–Cl2 2.564(2), Zr–O1 2.303(5), Zr–O2 2.329(5), Zr–C7 2.624(9), Zr–C8 2.512(8), Zr–C9 2.261(8), Zr–C10 2.504(8), Zr–C11 2.642(9), Zr–C12 2.470(8), Zr–C13 2.257(8), Zr–C14 2.478(8); D2-Zr-O1 108.7, D2-Zr-O2 156.8, D3-Zr-O1 161.8, D3-Zr-O2 103.6, D2-Zr-Cl1 106.7(1), D2-Zr-Cl2 104.3, D3-Zr-Cl1 105.9, D3-Zr-Cl2 108.2, D2-Zr-D3 53.3, C8-C9-C10 134.4(8), C12-C13-C14 134.2(7), C8-C9-C13 107.8(7), C9-C13-C14 107.3(7), C9-C13-C12 106.0(6), C10-C9-C13 107.0(7).

In compound **8** the zirconium atom has a distorted pseudo-octahedral coordination geometry. Both axial positions are taken up by the chlorine atoms, while the equatorial sites are occupied by the geometrical centers D2 and D3 of the pentalene ligand and the oxygen atoms of the two coordinated THF molecules. D2, D3, Zr, O1, and O2 lie to a good approximation in a plane (the distances from the mean plane through Zr, D2, D3, O1, and O2 are 0.01 Å (Zr), 0.04 Å (D2), 0.04 Å (D3), 0.03 Å (O1), and 0.03 Å (O2)). This plane, which lies at an angle of 90° to that through Zr, Cl1, and Cl2, bisects the Cl1-Zr-Cl2 angle (143°). Whereas in **5b** the bond lengths Zr–C8 and Zr–C14 are markedly different, in **8** the distances between the zirconium atom and C8, C10, C12, and C14 are very similar (2.47–2.51 Å) because both sides of the pentalene ligand (that is, (C8, C9, C10 and C12, C13, C14)) lie opposite to a chlorine atom. The average value of these bond lengths is only 0.04 Å less than the Zr–C8 distance in **5b**. The angle of fold of the pentalene ligand (150°) is found to be 3° larger than that in **5b**, but the significance of this should not be overemphasized because the standard deviations of the atomic coordinates are greater (average standard deviations of the Zr–C bond lengths: 0.001 Å (**5b**), 0.008 Å (**8**)).

Some or all of the THF and chloro ligands in **8** can be replaced by various other ligands.[18] Thus, this new zirconium complex, the first mononuclear "half-sandwich" complex prepared having a pentalene ligand, plays a key role as a starting material in the newly emerging pentalene-zirconium chemistry.

Received: February 14, 1997 [Z10124IE]
German version: *Angew. Chem.* **1997**, *109*, 1793–1796

Keywords: hafnium · mononuclear complexes · pentalene · titanium · zirconium

[1] a) H. Breil, G. Wilke, *Angew. Chem.* **1966**, *78*, 942; *Angew. Chem. Int. Ed. Engl.* **1966**, *5*, 898; H. Dietrich, M. Soltwisch, *ibid.* **1969**, *81*, 785 and **1969**, *8*, 765; b) H. Lehmkuhl, K. Mehler, *J. Organomet. Chem.* **1970**, *25*, C44–C46; c) H. O. van Oven, H. J. de Liefde Meijer, *ibid.* **1969**, *19*, 373–376; P. A. Kroon, R. B. Helmholdt, *ibid.* **1970**, *25*, 451–454; d) H. R. van der Wal, F. Overzet, H. O. van Oven, J. L. de Boer, H. J. de Liefde Meijer, F. Jellinek, *ibid.* **1975**, *92*, 329–340; e) L. B. Kool, M. D. Rausch, R. D. Rogers, *ibid.* **1985**, *297*, 289–299.

[2] a) H.-J. Kablitz, G. Wilke, *J. Organomet. Chem.* **1973**, *51*, 241–271; D. J. Brauer, C. Krüger, *ibid.* **1972**, *42*, 129–137; b) *Inorg. Chem.* **1975**, *14*, 3053–3056; c) P. Berno, C. Floriani, A. Chiesi-Villa, C. Rizzoli, *J. Chem. Soc. Dalton Trans.* **1991**, 3085–3091; d) D. M. Rogers, S. R. Wilson, G. S. Girolami, *Organometallics* **1991**, *10*, 2419–2424; e) W. J. Highcock, R. M. Mills, J. L. Spencer, P. Woodward, *J. Chem. Soc. Dalton Trans.* **1986**, 821–827; f) S. Stella, M. Chiang, C. Floriani, *J. Chem. Soc. Chem. Commun.* **1987**, 161–163.

[3] a) H.-J. Kablitz, R. Kallweit, G. Wilke, *J. Organomet. Chem.* **1972**, *44*, C49–C50; b) H. Lehmkuhl, S. Kintopf, K. Mehler, *ibid.* **1972**, *46*, C1–C2; c) P. Berno, C. Floriani, A. Chiesi-Villa, C. Rizzoli, *J. Chem. Soc. Dalton Trans.* **1991**, 3093–3095.

[4] a) R. G. Swisher, E. Sinn, R. N. Grimes, *Organometallics* **1984**, *3*, 599–605; b) D. Gourier, E. Samuel, B. Bachmann, F. Hahn, J. Heck, *Inorg. Chem.* **1992**, *31*, 86–95.

[5] R. R. Schrock, L. J. Guggenberger, A. D. English, *J. Am. Chem. Soc.* **1976**, *98*, 903–913.

[6] J. A. Segal, M. L. H. Green, J.-C. Daran, K. Prout, *J. Chem. Soc. Chem. Commun.* **1976**, 766–768.

[7] a) F. T. Edelmann, *New J. Chem.* **1995**, *19*, 535–550; in ref. [7c], pp. 98–106; b) in ref. [7c], pp. 181–186; M. Ephritikhine, *New J. Chem.* **1992**, *16*, 451–469; T. J. Marks, *Science* **1982**, *217*, 989–997; c) *Comprehensive Organometallic Chemistry II, Vol. 4* (Eds.: E. W. Abel, F. G. A. Stone, G. Wilkinson), Pergamon, Oxford, **1995**.

[8] K. Jonas, B. Gabor, R. Mynott, K. Angermund, O. Heinemann, C. Krüger, *Angew. Chem.* **1997**, *109*, 1790–1793; *Angew. Chem. Int. Ed. Engl.* **1997**, *36*, 1712–1714.

[9] T. J. Katz, M. Rosenberger, *J. Am. Chem. Soc.* **1962**, *84*, 865–866; T. J. Katz, M. Rosenberger, R. K. O'Hara, *ibid.* **1964**, *86*, 249–252.

[10] Prepared in THF from 2-methyl-1,5-dihydropentalene [11] and two mole equivalents of LiC_4H_9.

[11] A. G. Griesbeck, *Synthesis* **1990**, 144–147.

[12] P. D. Bartlett, B. Seidel, *J. Am. Chem. Soc.* **1961**, *83*, 581–584.

 © WILEY-VCH Verlag GmbH, D-69451 Weinheim, 1997 0570-0833/97/3616-1717 $ 17.50+.50/0

[13] X-ray crystallographic data for **4**: $C_{13}H_{11}Ti$, $M_r = 215.1\ g\,mol^{-1}$, crystal dimensions $0.04 \times 0.56 \times 0.46\ mm^3$, $a = 8.137(1)$, $b = 10.425(1)$, $c = 11.799(1)$ Å, $V = 1000.8$ Å^3, $T = 293$ K, $\rho_{calcd} = 1.43\ g\,cm^{-3}$, $\mu = 7.97\ cm^{-1}$, $F(000) = 444$ e, $Z = 4$, orthorhombic, space group $P2_12_12_1$ (no. 19), Enraf-Nonius CAD4 diffractometer, $\lambda = 0.71069$ Å, scan mode ω-2θ, 1196 measured reflections $(-h, +k, -l)$, $[(\sin\theta)/\lambda]_{max} = 0.62$ Å^{-1}, 1181 independent and 786 observed reflections $[I > 2\sigma(I)]$, 127 refined parameters; direct methods, H atom positions calculated, $R = 0.041$, $R_w = 0.039$ $[w = 1/(\sigma^2(F_o))]$, max. residual electron density 0.24 e Å^{-3}. X-ray crystallographic data for **5a**: $C_{13}H_{11}ClTi$, $M_r = 250.6\ g\,mol^{-1}$, crystal dimensions $0.25 \times 0.39 \times 0.56\ mm^3$, $a = 10.599(1)$, $b = 13.125(1)$, $c = 7.586(1)$ Å, $V = 1055.3$ Å^3, $T = 293$ K, $\rho_{calcd} = 1.58\ g\,cm^{-3}$, $\mu = 10.16\ cm^{-1}$, $F(000) = 512$ e, $Z = 4$, orthorhombic, space group $Cmc2_1$ (no. 36), Enraf-Nonius CAD4 diffractometer, $\lambda = 0.71069$ Å, scan mode ω-2θ, 1808 measured reflections $(+h, -k, -l)$, $[(\sin\theta)/\lambda]_{max} = 0.71$ Å^{-1}, 897 independent and 854 observed reflections $[I > 2\sigma(I)]$, 98 refined parameters; direct methods, H atom positions found and refined, $R = 0.023$, $R_w = 0.030$ $[w = 1/(\sigma^2(F_o))]$, max. residual electron density 0.29 e Å^{-3}. X-ray crystallographic data for **5b**: $C_{13}H_{11}ClZr$, $M_r = 293.9\ g\,mol^{-1}$, crystal dimensions $0.23 \times 0.49 \times 0.56\ mm^3$, $a = 10.540(1)$, $b = 13.627(1)$, $c = 7.681(1)$ Å, $V = 1103.2$ Å^3, $T = 293$ K, $\rho_{calcd} = 1.77\ g\,cm^{-3}$, $\mu = 11.85\ cm^{-1}$, $F(000) = 584$ e, $Z = 4$, orthorhombic, space group $Cmc2_1$ (no. 36), Enraf-Nonius CAD4 diffractometer, $\lambda = 0.71069$ Å, scan mode ω-2θ, 940 measured reflections $(+h, +k, +l)$, $[(\sin\theta)/\lambda]_{max} = 0.70$ Å^{-1}, 905 independent and 875 observed reflections, $[I > 2\sigma(I)]$, 98 refined parameters; direct methods, H atom positions found and refined, $R = 0.020$, $R_w = 0.021$ $[w = 1/(\sigma^2(F_o))]$, max. residual electron density 0.41 e Å^{-3}.

[14] F. H. Allen, J. E. Davies, J. J. Galloy, O. Johnson, O. Kennard, C. F. Macrae, E. M. Mitchell, G. F. Mitchell, J. M. Smith, D. G. Watson, *J. Chem. Inf. Comput. Sci.* **1991**, *31*, 187–204.

[15] See, for example, references cited in ref. [2d].

[16] The signals of **7b** and **7c** are still very broad at this temperature.

[17] a) X-ray crystallographic data for **8**: $C_{16}H_{22}Cl_2O_2Zr$, $M_r = 408.5\ g\,mol^{-1}$, crystal dimensions $0.14 \times 0.46 \times 1.85\ mm^3$, $a = 7.366(1)$, $b = 27.458(3)$, $c = 8.418(1)$ Å, $\beta = 98.88(1)^\circ$, $V = 1682.2$ Å^3, $T = 293$ K, $\rho_{calcd} = 1.61\ g\,cm^{-3}$, $\mu = 9.64\ cm^{-1}$, $F(000) = 832$ e, $Z = 4$, monoclinic, space group $P2_1/a$ (no. 14), Enraf-Nonius CAD4 diffractometer, $\lambda = 0.71069$ Å, scan mode ω-2θ, 3770 measured reflections $(+h, -k, \pm l)$, $[(\sin\theta)/\lambda]_{max} = 0.62$ Å^{-1}, 3414 independent and 2530 observed reflections, $[I > 2\sigma(I)]$, 190 refined parameters; direct methods, H atom positions calculated, $R = 0.062$, $R_w = 0.076$ $[w = 1/(\sigma^2(F_o))]$, max. residual electron density 0.76 e Å^{-3}. b) Crystallographic data (excluding structure factors) for the structures reported in this paper have been deposited with the Cambridge Crystallographic Data Centre as supplementary publication no. CCDC-100213. Copies of the data can be obtained free of charge on application to The Director, CCDC, 12 Union Road, Cambridge CB2 1EZ, UK (fax: int. code +(1223) 336-033; e-mail: deposit@chemcrys.cam.ac.uk).

[18] a) P. Kolb, K. Jonas, unpublished results; b) P. Kolb, Diplomarbeit, Universität Duisburg, **1996**.

Direct Proof for O=Mn^{V}(salen) Complexes**

Derek Feichtinger and Dietmar A. Plattner*

Many first-row transition metals are able to transfer oxygen to organic substrates;[1, 2] the epoxidation of olefins is an example of particular relevance in synthesis.[3] The reactive species is usually formulated as a high-valent complex with a terminal metal–oxo multiple bond. Isolation and characterization of such complexes has been successful in only a few cases. Kochi and co-workers[4, 5] demonstrated that cationic Mn^{III} complexes of the planar tetradentate ligand salen (salen = *N*,*N*′-bis(salicylidene)ethylenediamine dianion) are highly efficient catalysts for epoxidation with a variety of terminal oxidants such as PhIO, NaOCl, MCPBA, H_2O_2, and *t*BuOOH. Based on the observed reactivities, the oxomanganese(v) complex **2** was postulated as the oxygen-transferring species. It was further suggested that the concentration of **2** is regulated by an equilibrium between the (salen)Mn^{III} complex **1** and the reactive species on one hand, and the μ-oxo bridged dimer **3** on the other. An

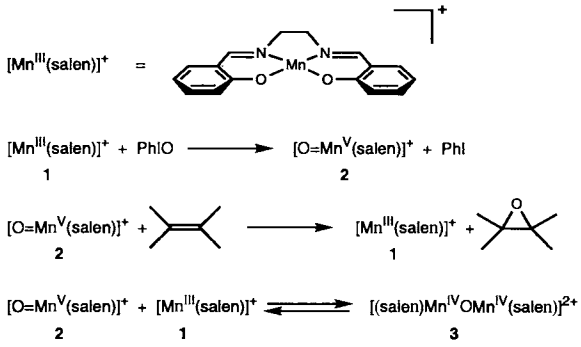

enantioselective version of the reaction was developed later by Jacobsen et al.[6] and Katsuki et al.[7] The observed enantioselectivities were explained by models based on a reactive oxomanganese(v) species,[6c, g] whose structure was taken to be similar to that of the analogous oxochromium complexes.[8] The catalyst of a Lewis acid catalyzed Diels–Alder reaction was also postulated to be a O=Mn^{V}(salen) complex.[9] However, in none of these cases was the reactive species isolated or characterized.

We recently reported the first direct observation of the reactive species in C–H activation by $[CpIr(PMe_3)CH_3]^+$ by means of electrospray (ES) tandem mass spectrometry.[10] In conducting these and the following experiments a slightly modified Finnigan MAT TSQ7000 mass spectrometer with an octopole/quadrupole/octopole/quadrupole setup behind the electrospray source was used.[11] This is especially suitable for detecting the short-lived species in question, since the complexes are ionic in nature; the electrospray technique allows direct transfer of ions from the authentic reaction mixtures to the gas phase.

Following Jacobsen's procedure[6d] (salen)Mn^{III}Cl was prepared by the reaction of the salen ligand with $Mn(OAc)_2 \cdot H_2O$ and LiCl under air oxidation. The complex cation $[(salen)Mn^{III}(NCCH_3)]^+$ (**1**·$NCCH_3$) was then obtained by abstraction of the chloride ligand with $AgClO_4$ in acetonitrile. Acetonitrile was chosen as the axial ligand, since our experience with a number of other manganese and iridium complexes shows that by varying the parameters of the electrospray source, it is possible to control the degree of dissociation of the neutral ligand from the complex. Electrospray of a dilute solution (about 10^{-5} M) of $[(salen)Mn^{III}(NCCH_3)](ClO_4)$ in acetonitrile yields $[(salen)Mn^{III}]^+$ (**1**, $m/z = 321$) in varying proportion to $[(salen)Mn^{III}(NCCH_3)]^+$ ($m/z = 362$). The degree of ligand loss depends on the potential applied to the tube in front of the first octopole. The oxidizing species were prepared by the two most common procedures: 1) addition of a solution of the complex to a suspension of iodosobenzene in acetonitrile, and 2) oxidation of the Mn^{III} complex with bleach in the two-phase system CH_2Cl_2/H_2O. It was experimentally confirmed that an epoxidizing species was formed by method 1. Cyclohexene was oxidized to cyclohexene oxide, as identified by gas chromatography with comparison to an authentic sample. Qualitative mass spectrometric analysis of the electrosprayed ions showed that the number as well as the nature of the detected species are substantially changed upon addition of the oxidant. Complexes **1** and **1**·CH_3CN are still present, however with strongly reduced in-

[*] Dr. D. A. Plattner, Dipl.-Naturwissenschaftler D. Feichtinger
Laboratorium für Organische Chemie
Eidgenössische Technische Hochschule
Universitätstrasse 16, CH-8092 Zürich (Switzerland)
Fax: Int. code +(1)632-1280
e-mail: plattner@org.chem.ethz.ch

[**] This work was supported by the ETH Zürich and the Swiss National Science Foundation. We would like to thank our mentor Prof. Peter Chen for financial support and helpful discussions.

tensities. In the case of oxidation by PhIO [(salen)Mn^{III}(OIPh)]$^+$ (**1**·PhIO) is observed in low intensity.

The appearance of species whose mass is greater than that of the above-mentioned species by 16 mass units is of particular relevance. All observations indicate that these indeed correspond to the postulated oxomanganese(v) complexes. Coordination to iodosobenzene is not surprising, as Hill and co-workers found that oxidation of a (tetraphenylporphinato)Mn complex with PhIO resulted in a dimer containing one iodosobenzene molecule per Mn atom. Spectroscopic measurements pointed to axial coordination of the iodosobenzene ligands.[13, 14] In analogy to the corresponding dimer with axially coordinated azido ligands, whose constitution was confirmed by an X-ray structure analysis, an antiferromagnetically coupled μ-oxomanganese(IV) complex with a linear Mn-O-Mn arrangement was assumed.[15] In our experiments with the salen-based systems an analogous dimeric species gave rise to a prominent peak in the mass spectrum, which is in accordance with the mechanism formulated by Kochi et al.[4, 5] The signal appears at $m/z = 549$ with isotopic peaks that are seperated by one-half mass units, as is common for doubly charged ions. Further proof for the assignment of this structure comes from the daughter ion spectrum of this species (Figure 1). The dimer **3**·2PhIO fragments to **1**·OIPh ($m/z = 541$) and the oxo complexes [(salen)Mn(O)(OIPh)]$^+$ ($m/z = 557$) and [(salen)-Mn=O]$^+$ (**2**, $m/z = 321$). Small amounts of [(salen)$Mn(O_2)$]$^+$ ($m/z = 321$), which possibly has a peroxo structure, are also formed.

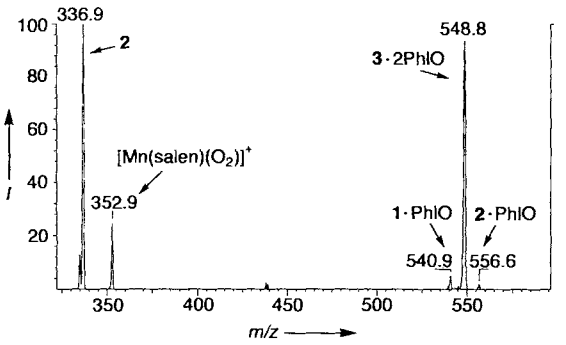

Figure 1. Daughter ion spectrum of the μ-oxo bridged, doubly charged dimer **3**·2PhIO ($m/z = 549$); I = intensity.

Strong evidence for the presence of a reactive oxomanganese(v) species is provided by collision experiments with substrates that undergo oxidation by the catalytic system in solution. When the ion corresponding to **2** is selected in the first quadrupole and then collided in the second octopole with an inert gas (about 1 mTorr of Ar) at collision energies ranging from 2 to 20 eV, no fragmentation is observed. This is in agreement with the structure of the oxo complex, because it is unlikely that all the bonds between the manganese ion and the salen ligand or the stable metal–oxo bond would fragment.[16, 17] This behavior makes it possible to establish the reactivity of the species of interest. For our oxidation experiments we chose substrates that react easily under the stated conditions in solution, that is, electron-rich olefins and sulfides.[6e] As there is no way of directly observing the oxidized products in this MS experiment, short of introducing an additional ionization step, the reactivity has to be deduced by correlating the turnover with the appearance of **1** in the daughter spectrum. At a pressure of about 0.5 mTorr of 2,3-dihydrofuran, dimethyl sulfide, or methyl phenyl sulfide in the second octopole and with collision energies of 2–5 eV, **1** was present to a considerable amount in addition to unchanged **2**. A control experiment with tetrahydrofuran as the collision gas showed no such fragmentation up to a collision energy of 20 eV.

Investigating the mechanism of the (salen)Mn-catalyzed oxidation by means of electrospray tandem mass spectrometry has proven the existence of discrete Mn^V complexes with a terminal oxo group. The reactivity of these species with respect to olefins and sulfides has been established. Moreover, a dimeric μ-oxo bridged complex could be identified as a reservoir species. Further investigations of the analogous Mn and Fe porphyrin complexes are in progress.

Received: February 18, 1997 [Z10132IE]
German version: *Angew. Chem.* **1997**, *109*, 1796–1798

Keywords: epoxidations · manganese · mass spectrometry · oxidations

[1] R. A. Sheldon, J. K. Kochi, *Metal Catalyzed Oxidations of Organic Compounds*, Academic Press, New York, **1981**.
[2] R. H. Holm, *Chem. Rev.* **1987**, *87*, 1401.
[3] K. A. Jørgensen, *Chem. Rev.* **1989**, *89*, 431.
[4] K. Srinivasan, P. Michaud, J. K. Kochi, *J. Am. Chem. Soc.* **1986**, *108*, 2309.
[5] K. Srinivasan, S. Perrier, J. K. Kochi, *J. Mol. Cat.* **1986**, *36*, 297.
[6] a) W. Zhang, J. L. Loebach, S. R. Wilson, E. N. Jacobsen, *J. Am. Chem. Soc.* **1990**, *112*, 2801; b) E. N. Jacobsen, W. Zhang, M. L. Güler, *ibid.* **1991**, *113*, 6703; c) E. N. Jacobsen, W. Zhang, A. R. Muci, J. R. Ecker, L. Deng, *ibid.* **1991**, *113*, 7063; d) W. Zhang, E. N. Jacobsen, *J. Org. Chem.* **1991**, *56*, 2296; e) M. Palucki, P. Hanson, E. N. Jacobsen, *Tetrahedron Lett.* **1992**, *33*, 7111; f) M. Palucki, P. J. Pospisil, W. Zhang, E. N. Jacobsen, *J. Am. Chem. Soc.* **1994**, *116*, 9333; g) P. J. Pospisil, D. H. Carsten, E. N. Jacobsen, *Chem. Eur. J.* **1996**, *2*, 974.
[7] R. Irie, K. Noda, Y. Ito, T. Katsuki, *Tetrahedron Lett.* **1991**, *32*, 1055.
[8] a) T. S. Siddall, N. Miyaura, J. C. Huffman, J. K. Kochi, *J. Chem. Soc. Chem. Commun.* **1983**, 1185; b) E. G. Samsel, K. Srinivasan, J. K. Kochi, *J. Am. Chem. Soc.* **1985**, *107*, 7606.
[9] Y. Yamashita, T. Katsuki, *Synlett* **1995**, 829.
[10] C. Hinderling, D. A. Plattner, P. Chen, *Angew. Chem.* **1997**, *109*, 272; *Angew. Chem. Int. Ed. Engl.* **1997**, *36*, 243.
[11] Details of the experimental setup: C. Hinderling, D. Feichtinger, D. A. Plattner, P. Chen, *J. Am. Chem. Soc.*, in press.
[12] PhIO was prepared according to H. Saltzman, J. G. Sharefkin, *Org. Synth.* **1963**, *43*, 60.
[13] B. C. Schardt, F. J. Hollander, C. L. Hill, *J. Am. Chem. Soc.* **1982**, *104*, 3964.
[14] a) J. A. Smegal, B. C. Schardt, C. L. Hill, *J. Am. Chem. Soc.* **1983**, *105*, 3510; b) J. A. Smegal, C. L. Hill, *ibid.* **1983**, *105*, 3515.
[15] For a discussion of the possible role of oxomanganese(IV) complexes in the epoxidation, see ref. [5]; the reactivity of oxomanganese(IV) species was studied thoroughly for Mn porphyrin complexes: J. T. Groves, M. K. Stern, *J. Am. Chem. Soc.* **1988**, *110*, 8628.
[16] W. A. Nugent, J. M. Mayer, *Metal–Ligand Multiple Bonds*, Wiley, New York, **1988**.
[17] Mn complexes with a terminal oxo group: a) T. J. Collins, S. W. Gordon-Wylie, *J. Am. Chem. Soc.* **1989**, *111*, 4511; b) T. J. Collins, R. D. Powell, C. Slebodnick, E. S. Uffelman, *ibid.* **1990**, *112*, 899; c) F. M. MacDonnell, N. L. P. Fackler, C. Stern, T. V. O'Halloran, *ibid.* **1994**, *116*, 7431.

 © WILEY-VCH Verlag GmbH, D-69451 Weinheim, 1997 0570-0833/97/3616-1719 $ 17.50+.50/0

On the Viability of Oxametallacyclic Intermediates in the (salen)Mn-Catalyzed Asymmetric Epoxidation**

Nathaniel S. Finney, Paul J. Pospisil, Sukbok Chang, Michael Palucki, Reed G. Konsler, Karl B. Hansen, and Eric N. Jacobsen*

The mechanism of oxygen-atom transfer from high-valent oxometal intermediates to organic substrates has stimulated great interest as a result of its relevance to a wide range of important synthetic and biological catalytic pathways.[1] Two fundamentally different proposals have been considered: direct substrate attack at the oxo ligand with concerted or sequential C–O bond formation, and substrate attack at both the metal and oxo centers to generate an oxametallacyclic intermediate.[2] For the epoxidation of conjugated olefins catalyzed by (salen)M and M porphyrin complexes (salen = *N*,*N*′-bis(salicylidene)-ethylenediamine dianion; M = Cr, Fe, Mn), a substantial body of evidence has been accumulated that supports direct attack of olefin at the oxometal (Scheme 1, path A). This model has

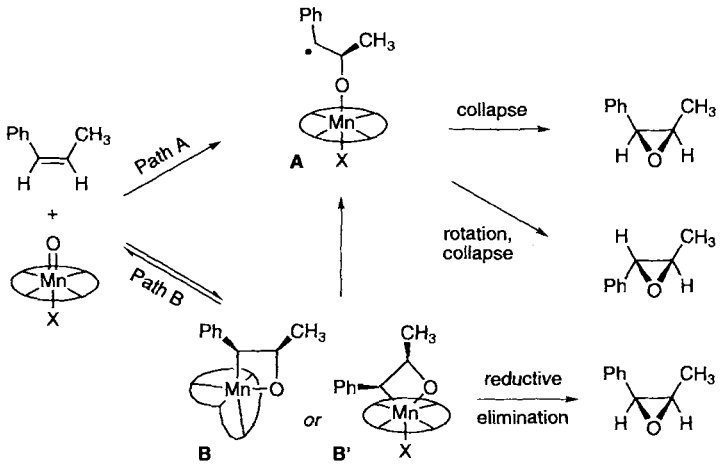

Scheme 1.

been refined on the basis of stereoselectivity data to entail a side-on approach of the olefin at the oxo center to generate a radical intermediate, which in turn partitions between collapse and rotation–collapse processes to provide the observed mixture of *cis* and *trans* epoxides.[3] Recent computational[4] and experimental[5] studies purporting to substantiate the intermediacy of oxametallacycles (path B) in the (salen)Mn-catalyzed epoxidation warrant careful scrutiny, particularly since this reaction currently stands as the most effective method for the generation of optically active epoxides by oxo transfer.[1e, 6]

Here we assess the viability of such intermediates based on an analysis of the (salen)Mn coordination environment, the observed substrate scope, a computational study of representative diastereomeric radical intermediates, and the temperature dependence of enantioselection. We conclude that the radical path A remains the simplest mechanism that is consistent with all of the available data. In contrast, the oxametallacyclic mechanism fails to accomodate several crucial experimental observations, and remains both unsubstantiated and unnecessarily complicated.

The two mechanisms in question place very different constraints on the coordination environment of the manganese center throughout the catalytic cycle. Whereas the formation of a radical intermediate requires only the presence of the apical oxo ligand, formation of the proposed oxametallacycle requires that a coordination site is available for formation of the Mn–C bond, and that this coordination site is adjacent to the oxo ligand. Two critical issues are whether the (salen)Mn intermediates possess such an open coordination site during the oxo transfer steps, as required for formation of **B**, and, if not, whether the formation of oxametallacycles can be accomodated by a 7-coordinate ligand environment as in **B′**.

The first of these questions may be addressed by analyzing the effect of amine *N*-oxide additives, which have a dramatic impact on the outcome of the epoxidation reaction. Additives such as pyridine *N*-oxide influence the rate, yield, *cis*/*trans* ratio, and enantioselectivity of the (salen)Mn-catalyzed epoxidation with a range of terminal oxidants.[7] As illustrated with *cis*-β-methylstyrene addition of *N*-oxide can more than double the *cis*/*trans*-epoxide ratio, and significantly increase the chemical yield and degree of asymmetric induction (Table 1). This clearly indicates

Table 1. Epoxidation of *cis*-β-methylstyrene with various oxidants and (*S*,*S*)-**6** as catalyst.

Oxidant	Additive [e] (equiv)	*t*[h]	Conversion [%][a]	Yield [%][a]	*cis*/*trans* ratio	ee_{fac} [%][b,c]
NaOCl(aq)	4-PPNO (0.2)	0.5	100	98	19	81
NaOCl(aq)	–	2	78	62	18	71
PhIO	4-PPNO (0.2)	8.5	81	76	3	72
PhIO	–	8.5	54	2	2	69
oxone(aq)	4-PPNO (0.4)	2	98	93	15	80
oxone(aq)	–	2	18	13	10	58
oxone/K_2CO_3	NMO (2.0)	17	100	99	27	82
oxone/K_2CO_3	–	41	24	11	4	40
*m*CPBA/K_2CO_3	NMO (10.0)	0.5	100	91	16	82
*m*CPBA/K_2CO_3	–	0.5	97	41[d]	5	7

[a] Conversion, yield, and enantiomeric excess were determined by GC (see *Experimental Section*). [b] The absolute configuration of the major *cis*-β-methylstyrene oxide enantiomer is (*1S*,*2R*), and that of the major *trans*-β-methylstyrene oxide enantiomer is (*1R*,*2R*) [3h]. [c] $ee_{fac} = (x_{cis} \times ee_{cis}) + (x_{trans} \times ee_{trans})$; x = portion of *cis* or *trans* product. [d] No epoxidation was detected under these reaction conditions in the absence of **6**. [e] 4-PPNO = 4-phenylpyridine-*N*-oxide, NMO = *N*-methylmorpholine-*N*-oxide.

that the *N*-oxide additive influences the stereoselectivity of both C–O bond forming steps. Furthermore, electrochemical studies show that the presence of *N*-oxide significantly lowers the oxidation potentials for (salen)Mn complexes (Figure 1). Since oxidation to the O=Mn^V(salen) is generally rate limiting,[8] the observed rate acceleration induced by the *N*-oxide can be attributed to association of the additive with the metal center during generation of the reactive oxo intermediate. Similarly, the increase in the turnover numbers of the catalyst in the presence of *N*-oxide was taken as evidence that the additive stabilizes the highly reactive O=Mn^V(salen) by ligation after the initial oxidation.[8]

[*] Prof. E. N. Jacobsen, N. S. Finney, P. J. Pospisil, S. Chang, M. Palucki, R. G. Konsler, K. B. Hansen
Department of Chemistry and Chemical Biology
Harvard University
12 Oxford Street, Cambridge, MA 02138 (USA)
Fax: Int. code +(617)496-1880
email: jacobsen@chemistry.harvard.edu

[**] This research was supported by the U. S. National Institutes of Health (GM43214). We thank the NIH for a postdoctoral fellowship to N. S. F. (GM16639), and the Organic Division of the American Chemical Society for a Boehringer–Ingelheim Pharmaceuticals predoctoral fellowship to K. B. H.

 © WILEY-VCH Verlag GmbH, D-69451 Weinheim, 1997 0570-0833/97/3616-1720 $ 17.50+.50/0

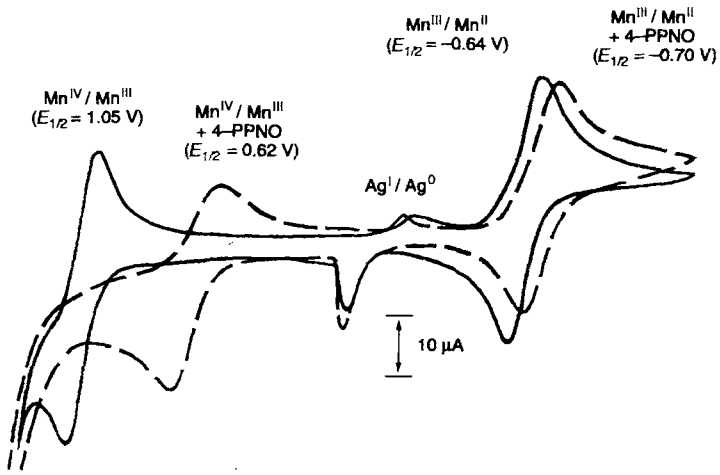

Figure 1. Cyclic voltammograms of (*R*,*R*)-**2** measured in the absence (solid line) and presence (dashed line) of 4-phenylpyridine *N*-oxide (4-PPNO, 5 equiv). Redox potentials are given relative to the saturated calomel electrode (SCE).

Further evidence that *N*-oxide additives function as axial ligands is provided by a study of catalyst **1** strapped with pyridine *N*-oxide. Figure 2 displays the X-ray crystal structure of **1** in which the tethered *N*-oxide unit is axially coordinated, as predicted, to the nearly planar (salen)Mn unit and is opposite to the chloride counterion.[9] The rate of epoxidations catalyzed by **1** is not influenced by adding 4-phenylpyridine *N*-oxide (4-PPNO; Figure 3).[10,11] For comparison, epoxidations with catalyst **2** proceed with higher conversion and at a faster rate in the presence of 4-PPNO; the combination of **2** and 4-PPNO affords results nearly identical to those obtained with catalyst **1** alone.

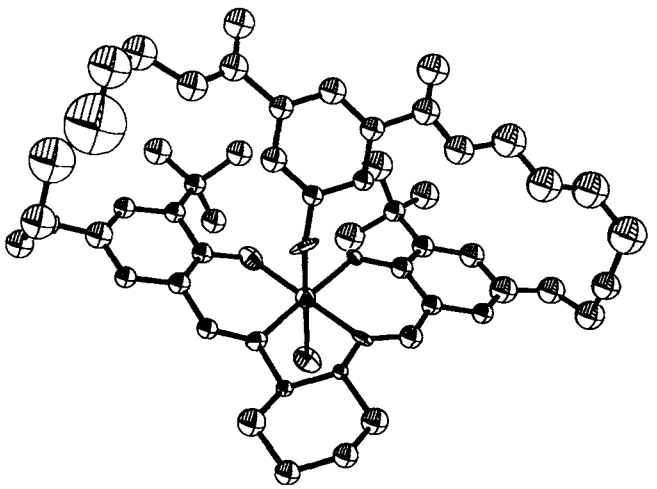

Figure 2. ORTEP representation of (*R*,*R*)-**1** (thermal ellipsoids for 50% probabilities).

These observations support a mechanism in which the *N*-oxide influences the epoxidation by axial ligation to the metal center during every step of the catalytic cycle. As a result, the relevant (salen)Mn intermediates do not possess an available coordination site for distortion of the ligand, as required for formation of intermediate **B**. Furthermore, such distortion of the (salen)Mn ligand from the square-planar disposition observed in every reported X-ray crystal structure of this class of complexes is completely unprecedented,[12] and **B** may therefore be reasonably excluded from further consideration.[13]

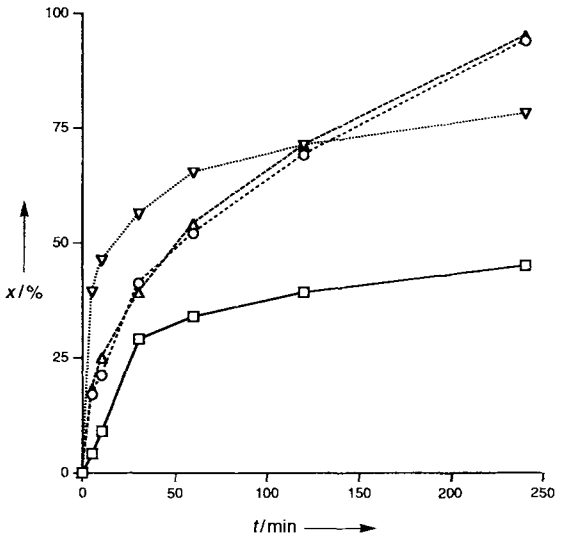

Figure 3. Plot of conversion *x* versus time *t* for the NaOCl epoxidation of styrene catalyzed by (*R*,*R*)-**1** (10 mol%; ○), (*R*,*R*)-**1** (10 mol%) and 4-PPNO (20 mol%; △), (*R*,*R*)-**2** (10 mol%; □), as well as (*R*,*R*)-**2** (10 mol%) and 4-PPNO (20 mol%; ▽).

Even cursory inspection of the alternative 7-coordinate intermediate **B′** reveals severe steric repulsions between the salen ligand and the oxametallacycle. To accomodate the observation that diastereomeric epoxides generated from acyclic *cis* olefins are epimeric at the benzylic position (see Scheme 1), the aryl-substituted olefin terminus would have to bind to the Mn center in closest proximity to the ligand plane. In light of the fact that hindered (salen)Mn catalysts such as **3** are highly active and enantioselective for the epoxidation of tri- and even certain tetrasubstituted olefins,[14] this is simply implausible.[15] The formation of oxametallacycles **B** or **B′** is thus inconsistent with a range of quantitative and qualitative experimental data, and mechanistic schemes invoking these intermediates must be regarded with skepticism.

The only experimental data presented thus far that is inconsistent with the radical mechanism is the recent report of nonlinearity in Eyring plots for the epoxidation of four olefins with a catalyst related to **2**–**5**.[5] This may indicate the presence of a reversibly formed intermediate along the reaction coordinate. However, several features complicate interpretation of this data. First, the variations in enantiomeric excess were quite small (less than 10%), rendering the changes in slope ambiguous. Second, critical experimental details—such as conversion, yield, and terminal-oxidant solubility—were missing.[16] Third, the epoxide for which the greatest effect (in terms of $\Delta\Delta G^{\neq}$) was observed, 1,2-dihydronaphthalene oxide, is known to undergo efficient kinetic resolution by a secondary oxidation pathway.[17]

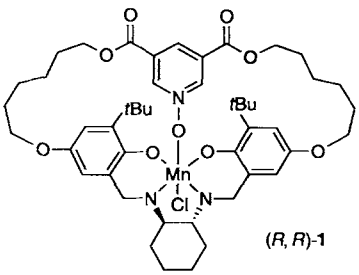

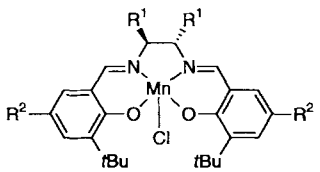

2: $R^1, R^1 = -(C_4H_8)-$, $R^2 = OCH_3$
3: $R^1, R^1 = -(C_4H_8)-$, $R^2 = tBu$
4: $R^1, R^1 = -(C_4H_8)-$, $R^2 = H$
5: $R^1 = Ph$, $R^2 = CH_3$
6: $R^1 = Ph$, $R^2 = Br$

 © WILEY-VCH Verlag GmbH, D-69451 Weinheim, 1997 0570-0833/97/3616-1721 $ 17.50+.50/0

In our earlier work on effective, homogenous epoxidation of olefins with *m*-chloro peroxybenzoic acid (*m*CPBA) catalyzed by (salen)Mn complexes,[8b] we observed a linear correlation of enantioselectivity and temperature for the epoxidation of styrene catalyzed by **5** over a wide temperature range. We carried out similar experiments with indene, dihydronaphthalene, and cyclooctadiene; the latter two (with styrene) are also substrates evaluated in the study by Katsuki et al.[5] The Eyring plot for the epoxidation of all four substrates catalyzed by **5** over a range of 100 degrees shows a completely linear correlation between asymmetric induction and temperature (Figure 4). The results from the *homogenous* epoxidation of these four olefins fail to reveal any sort of nonlinear behavior, and thus there is no reliable evidence suggesting existence of any reversibly formed intermediates.

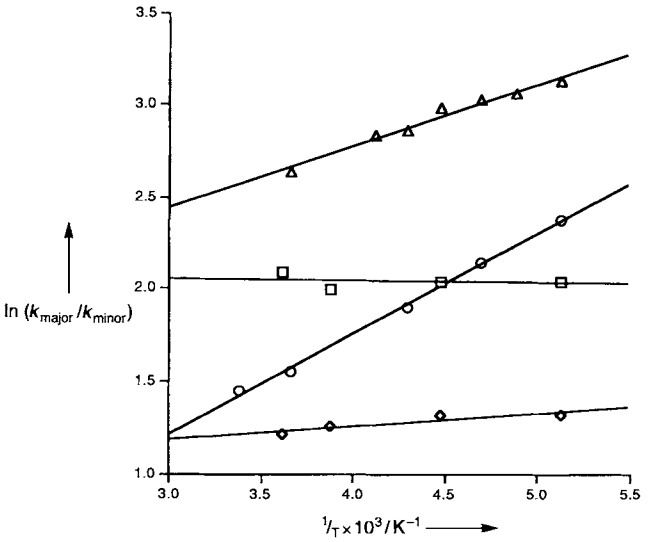

Figure 4. Eyring plots from the epoxidation of dihydronaphthalene (△), indene (□), styrene (○), and cyclooctadiene (◇) with *m*-CPBA catalyzed by (*S*,*S*)-**5**.

The simplest mechanism consistent with the observed data for (salen)Mn-catalyzed epoxidation reactions remains direct attack of olefin on an (oxo)manganese species to generate a radical intermediate, followed by ring closure to form the epoxide products. Besides adequately explaining all of the salient features of the reaction, this mechanism provides the greatest congruity with related sulfoxidation reactions[18] and biomimetic porphyrin oxidations.[3] Whereas more complicated mechanistic schemes—such as *N*-oxide ligand dissociation from the metal center during oxametallacycle formation and reassociation during epoxide formation, or the reaction of different olefins and catalysts proceeding by separate mechanisms—cannot be categorically excluded; there is no experimental evidence to support such possibilities. In what remains a fundamentally experimental discipline, it is essential to adhere to Ockham's Razor: "That which is explained with the assumption of fewer things is explained in vain by the assumption of more things."[19]

Experimental Section

Epoxidations with catalyst (*R*,*R*)-**1** were carried out following the standard biphasic epoxidation procedure [20]. Low-temperature epoxidations were conducted as described [7b], and proceeded with 20–50% conversion within 10 min; the product accounted for more than 95% of the consumed starting material. Conversion, yield, and *cis*/*trans* ratios were determined by capillary gas chromatography. Reported enantiomeric excesses are the average of at least three measurements, and were determined by either chiral capillary GC (Cyclodex-B: styrene oxide, dihydronaphthalene oxide; Gamma-TA: cyclooctadiene monoepoxide) or HPLC (Chiralcel OB: indene oxide).

Electrochemical measurements were performed at a rate of 40 mVs^{-1} on 2 mM solutions of (*R*, *R*)-**2** in CH_3CN (0.1 M Bu_4NPF_6 as the working electrolyte). The employed Pt working, Ag (vycor frit isolated) counter, and Ag/Ag^+ reference electrodes were standardized by in situ measurement of the ferrocene/ferrocenium one-electron oxidation. Redox potentials are reported relative to the saturated calomel electrode (SCE).

The semi-empirical UHF calculations described in ref. [13] were performed using the semi-empirical PM3 (tm) parameters, as implemented by the Spartan interface (Spartan version 4.0, Wavefunction, Inc., Irvine, CA (USA)). The starting catalyst conformation was derived from the crystal structure of **1** by deletion of the apical chloride and the alkyl tethers connecting the pyridine *N*-oxide to the salen aromatic rings. The phenylcyclohexanolyl fragment was appended with a fixed Mn–O bond length of 1.8 Å, and minimizations were carried out from eight different initial values for the O(salen)-Mn-O-C dihedral angle.

Received: February 19, 1997 [Z10140IE]
German version: *Angew. Chem.* **1997**, *109*, 1798–1801

Keywords: epoxidations · manganese · oxidations · radicals

[1] a) *Cytochrome P-450. Structure, Mechanism, and Biochemistry*, 2nd ed. (Ed.: P. R. Ortiz de Montellano), Plenum, New York, **1996**; b) M. K. Stern, J. T. Groves, *Manganese Redox Enzymes* (Ed.: V. L. Pecoraro), VCH, New York, **1992**, chap. 11; c) K. A. Jørgensen, *Chem. Rev.* **1989**, *89*, 431; d) R. H. Holm, *Chem. Rev.* **1987**, *87*, 1401; e) E. N. Jacobsen, *Comprehensive Organometallic Chemistry II, Vol. 12* (Eds.: G. Wilkinson, F. G. A. Stone, E. W. Abel, L. S. Hegedus), Pergamon, New York, **1995**, chap. 11.1.

[2] a) K. A. Jørgensen, B. Schiøtt, *Chem. Rev.* **1990**, *90*, 1483; b) P.-O. Norrby, H. Becker, K. B. Sharpless, *J. Am. Chem. Soc.* **1996**, *118*, 35, and references therein.

[3] Porphyrin-based catalysts: a) J. T. Groves, T. E. Nemo, R. S. Myers, *J. Am. Chem. Soc.* **1979**, *101*, 1032; b) J. T. Groves, R. S. Myers, *ibid.* **1983**, *105*, 5791; c) K. A. Jørgensen, *Chem. Rev.* **1989**, *89*, 431; d) D. Ostovic, T. C. Bruice, *Acc. Chem. Res.* **1992**, *25*, 312; e) J. P. Collman, X. Zhang, V. J. Lee, E. S. Uffelman, J. I. Brauman, *Science* **1993**, *261*, 1404; salen-based catalysts: f) E. G. Samsel, K. Srinivasan, J. K. Kochi, *J. Am. Chem. Soc.* **1985**, *107*, 7606; g) K. Srinivasan, P. Michaud, J. K. Kochi, *ibid.* **1986**, *108*, 2309; h) W. Zhang, J. L. Loebach, S. R. Wilson, E. N. Jacobsen, *ibid.* **1990**, *112*, 2801; i) E. N. Jacobsen, L. Deng, Y. Furukawa, L. E. Martínez, *Tetrahedron* **1993**, *50*, 4323; j) N. Hosoya, A. Hatayama, K. Yanai, H. Fujii, R. Irie, T. Katsuki, *Synlett* **1993**, 641.

[4] P.-O. Norrby, C. Linde, B. Åkermark, *J. Am. Chem. Soc.* **1995**, *117*, 11035.

[5] a) T. Hamada, T. Fukuda, H. Imanishi, T. Katsuki, *Tetrahedron* **1996**, *52*, 515; b) T. Katsuki, *J. Synth. Org. Chem. Jpn.* **1996**, *53*, 940.

[6] T. Katsuki, *Coord. Chem. Rev.* **1995**, *140*, 189.

[7] For previous studies of the effect of additives in (salen)M catayst sytems, see ref. [3f, g, i] and a) R. Irie, K. Noda, Y. Ito, N. Matsumoto, T. Katsuki, *Tetrahedron: Asymmetry* **1991**, *2*, 481; b) M. Palucki, P. J. Pospisil, W. Zhang, E. N. Jacobsen, *J. Am. Chem. Soc.* **1994**, *116*, 9333; c) C. H. Senanayake, G. B. Smith, J. Liu, L. E. Fredenburgh, K. M. Ryan, D. L. Hughes, R. D. Larsen, T. R. Verhoeven, P. J. Reider, *Tetrahedron Lett.* **1995**, *36*, 3993; d) C. H. Senanayake, G. B. Smith, K. M. Ryan, L. E. Fredenburgh, J. Liu, F. Roberts, D. L. Hughes, R. D. Larsen, T. R. Verhoeven, P. J. Reider, *ibid.* **1996**, *37*, 3271.

[8] A. Suárez, P. J. Pospisil, E. N. Jacobsen, unpublished results; see also ref. [7c, d].

[9] The X-ray crystal structure of a cationic O=Cr(salen) complex with an axially coordinated *N*-oxide has been reported [3f].

[10] Enantioselectivities and *cis*/*trans* ratios in epoxidations with **1** are also unaffected by added 4-PPNO.

[11] A full account of the synthesis and structural analysis of catalyst **1** will be published elsewhere: S. B. Chang, K. B. Hansen, E. N. Jacobsen, unpublished results.

[12] All known crystal structures of chiral (salen)Mn^{III} complexes contain near-planar salen moieties and axially coordinated spectator ligands and/or counterions: a) W. Zhang, J. L. Loebach, S. R. Wilson, E. N. Jacobsen, *J. Am. Chem. Soc.* **1990**, *112*, 2801; b) P. J. Pospisil, D. H. Carsten, E. N. Jacobsen, *Chem. Eur. J.* **1996**, *2*, 974; c) M. T. Rispens, A. Meetsma, B. L. Feringa, *Recl. Trav. Chim. Pays-Bas* **1994**, *113*, 413. For examples of structurally characterized achiral (salen)Mn complexes, see ref. [3g] and d) J. E. Davies, B. M. Gatehouse, *J. Chem. Soc. Dalton Trans.* **1973**, 2523; e) V. L. Pecoraro, W. M. Butler, *Acta Crystallogr. Sect. C* **1986**, *42*, 1151; f) J. W. Gohdes, W. H. Armstrong, *Inorg. Chem.* **1988**, *27*, 1841; g) X. Li, V. L. Pecoraro, *Inorg. Chem.* **1989**, *28*, 3403; h) N. Matsumoto, H. Okawa, S. Kida, T. Ogawa, A. Ohyoshi, *Bull. Chem. Soc. Jpn.* **1989**, *62*, 3812; i) M. Mikuriya, Y. Yamato, T. Tokii, *ibid.* **1992**, *65*, 1466; j) A. Garcia-Deibe, A. Sousa, M. R. Bermejo, P. P. MacRory, C. A. McAuliffe, R. G. Pritchard, M. Helliwell, *J. Chem. Soc. Chem. Commun.* **1991**, 728; k) A. R. Oki, D. J. Hodgson, *Inorg. Chim. Acta* **1990**, *170*, 65; l) W. Chiang, D. M. Ho, D. Van Engen, M. E. Thompson, *Inorg. Chem.* **1993**, *32*, 2886.

 © WILEY-VCH Verlag GmbH, D-69451 Weinheim, 1997 0570-0833/97/3616-1722 $ 17.50+.50/0

[13] One of the principal difficulties encountered in evaluating the radical mechanism is the question of how an essentially flat ligand system can impart such exquisite levels of enantioselectivity with a wide range of substrates. This has served as the impetus for the proposal by Norrby et al. [4] of the 6-coordinate oxametallacyclic intermediate **B**. Credence was lent to this pathway by calculations based on empirical force-field models, which predicted significant differences in energy between diastereomeric 6-coordinate (salen)Mn oxametallacycles. The documented effect of amine *N*-oxide derivatives on the epoxidation rules out such intermediates. Still, it is worth considering whether a similar computational analysis of the radical mechanism stands up well against available enantioselectivity data. We performed semi-empirical calculations of the diastereomeric radical intermediates for the epoxidation of phenylcyclohexene (PM3 (tm) parameters, Spartan version 4.0). This analysis indicates that the enantioselectivity of the epoxidation reaction may be readily ascribed to energetic differences between diastereomeric radical intermediates, and that the radical mechanism is perfectly consistent with enantioselective epoxide formation.

[14] For example, epoxidation of triphenylethylene catalyzed by **3** provides triphenylethylene oxide in 92% *ee* and 97% yield, and epoxidation of phenylcyclohexene proceeds in 88% *ee* and 67% yield: B. D. Brandes, E. N. Jacobsen, *J. Org. Chem.* **1994**, *59*, 4378. Similarly, epoxidation of 3′-bromo-2,2,3,4-tetramethylchromene employing **5** provides the corresponding chromene oxide in 96% *ee* and 84% yield: B. D. Brandes, E. N. Jacobsen, *Tetrahedron Lett.* **1995**, *36*, 5123.

[15] Similar steric arguments were made to exlude the formation of oxametallacycles in oxidations catalyzed by metal porphyrin complexes [3d].

[16] Iodosylbenzene, the terminal oxidant employed by Katsuki et al., is only sparingly soluble in organic solvents.

[17] J. F. Larrow, E. N. Jacobsen, *J. Am. Chem. Soc.* **1994**, *116*, 12129.

[18] The (salen)Mn-catalyzed oxidation of aryl sulfides proceeds with the same absolute sense of enantioinduction as for styrene derivatives: a) M. Palucki, P. Hanson, E. N. Jacobsen, *Tetrahedron Lett.* **1992**, *33*, 7111; b) K. Noda, N. Hosoya, Y. Yamashita, T. Katsuki, *Tetrahedron* **1994**, *50*, 9609. Sulfide oxidation clearly cannot proceed via oxametallacyclic or related intermediates.

[19] P. Boehner in *Ockham: Philosophical Writings*, Nelson, New York, **1957**, p. xxi. For a recent discussion of the role of intellectual parsimony in scientific endeavor, see R. Hoffmann, V. I. Minkin, B. K. Carpenter, *Bull. Soc. Chim. Fr.* **1996**, *133*, 117.

[20] W. Zhang, E. N. Jacobsen, *J. Org. Chem.* **1991**, *56*, 2296.

Is There a Radical Intermediate in the (salen)Mn-Catalyzed Epoxidation of Alkenes?**

Christian Linde, Moritz Arnold, Per-Ola Norrby,* and Björn Åkermark*

The mechanism for the (salen)Mn-catalyzed epoxidation of alkenes is a topic of great interest (salen = *N*,*N*′-bis(salicylidene)ethylenediamine dianion).[1] The reaction has been proposed to proceed either in a concerted manner,[2] via a radical intermediate,[1, 3] or via a manganaoxetane intermediate[4, 5] (Scheme 1). According to Jacobsen et al.[2] alkyl-substituted alkenes react concertedly (Scheme 1, pathway **A**). The *cis*/*trans* isomerization observed in the epoxidation of conjugated alkenes was taken as evidence for a radical intermediate (Scheme 1, pathway **B**).[6]

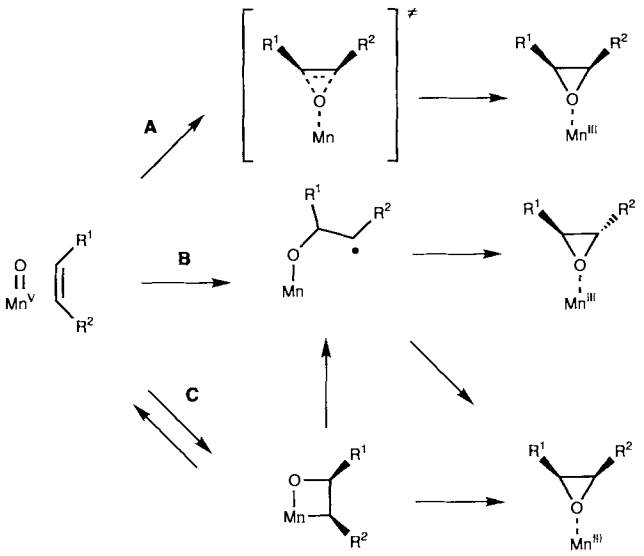

Scheme 1. Proposed mechanisms for the (salen)Mn-catalyzed epoxidation: **A**: concerted reaction ($R^1 = R^2$ = alkyl); **B**: reaction via a radical intermediate (R^1 = alkyl, R^2 = aryl, alkenyl, alkynyl); **C**: reaction via an oxetane intermediate (R^1 = alkyl, R^2 = alkyl, aryl, alkenyl, alkynyl).

Recently we suggested that the (salen)Mn-catalyzed epoxidation proceeds by reversible formation of a manganaoxetane, followed by irreversible rearrangement or ring opening, leading to the two diastereomeric products (Scheme 1, pathway **C**).[4, 7] The selectivity in the title reaction could be explained by postulating that epoxidation of conjugated alkenes mainly proceeds through an oxetane in which the conjugated carbon atom is bound to the manganese atom.[4] Katsuki et al.[5c] independently proposed a manganaoxetane intermediate to rationalize the observed nonlinear Eyring plots for relative rates of formation of the enantiomeric epoxides.[8, 9] The absence of alkene isomerization in the reaction mixture in combination with reversible formation of an intermediate suggest that any radical formation by pathway **B** (Scheme 1) is effectively *irreversible*. A concerted pathway such as **A** cannot be reconciled with the nonlinear Eyring behavior.

In the closely related epoxidations utilizing metal porphyrin complexes, strong objections were raised against the proposed metallaoxetane intermediates.[7b, 10] However, it is uncertain whether the arguments are applicable to the (salen)Mn catalysts.[11]

In analogy to the radical-probe experiments of Jacobsen et al.,[2] which were performed in a mechanistic study of the epoxidation of isolated alkenes, we investigated the catalytic epoxidation of substituted styrenes **1a**–**c**[12] to look for benzylic radicals (Scheme 2). If the mechanism of epoxidation involves a radical intermediate **4**, reaction of **1a**–**c** is expected to yield ring-opened products. A similar result is likely if a manganaoxetane intermediate **2** undergoes homolytic cleavage of the Mn–C bond. However, if **2** rearranges directly to epoxide **3** the cyclopropane unit should survive unscathed. Traps **1b** and **1c** give us the additional opportunity to study the effect of *cis*–*trans* isomerization.

For the epoxidation of **1a**–**c**, we used racemic [*N*,*N*′-bis(3,5-di-*tert*-butylsalicylidene)-1,2-cyclohexanediamine]manganese(III) chloride[13] as the catalyst. The reaction was carried out in a two-phase system of CH_2Cl_2 and a buffer solution of

[*] Prof. Dr. B. Åkermark, C. Linde, M. Arnold
Department of Chemistry, Organic Chemistry
The Royal Institute of Technology
S-10044 Stockholm (Sweden)
Fax: Int. code +(8)791-2333
e-mail: bear@orgchem.kth.se
Prof. Dr. P.-O. Norrby
Department of Medicinal Chemistry
The Royal Danish School of Pharmacy
Universitetsparken 2, DK-2100 Copenhagen (Denmark)
Fax: Int. code +(3)537-2209
e-mail: peon@medchem.dfh.dk

[**] This work was supported by The Danish Medical Research Council, The Carl Trygger Foundation, and the Swedish Research Council for Engineering Sciences. C. L. thanks the Royal Institute of Technology for a research scholarship. M. A. thanks the Universität Göttingen (Germany) and the ERASMUS program for financial support.

 © WILEY-VCH Verlag GmbH, D-69451 Weinheim, 1997 0570-0833/97/3616-1723 $ 17.50+.50/0

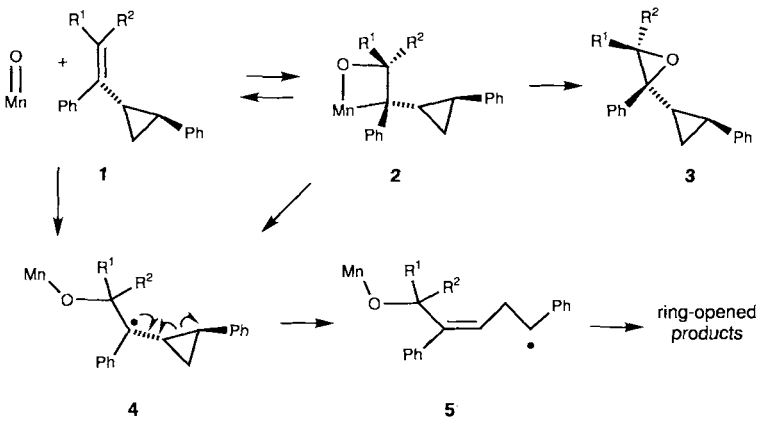

a: $R^1 = R^2 = H$; **b**: $R^1 = H$, $R^2 = Me$; **c**: $R^1 = Me$, $R^2 = H$

Scheme 2. Epoxidation of **1a–c**.

aqueous hypochlorite (I),[14] and in an iodosylbenzene/benzene system (II).[3] The crude reaction mixtures were analyzed by ^1H NMR spectroscopy (Table 1).

Table 1. Results of epoxidation.

Alkene	Product	Yield of epoxide[%][a] System I[b]	System II[c]
1a	**3a**	100	57
1b	**3b**	100	83
1c	**3c**	56	54

[a] The yield was determined by ^1H NMR spectroscopy relative to an internal standard. No epimerization or oxidative-cleavage products were detected. In non-quantitative reactions (that is, with yield <100%) products resulting from opening of the cyclopropyl ring were found. [b] NaOCl used as oxidant [14]. [c] PhIO in benzene used as oxidant [3].

In system I, reaction of **1a** exclusively yielded **3a** without any traces of ring-opened products. However, in system II the yield of **3a** was only 57%. Several substituted pentenes (products from opening of the cyclopropyl ring, Scheme 2) were observed in the crude product mixture, indicating formation of a radical intermediate. Competition experiments[15] showed that the reaction rate for the epoxidation of **1a** is comparable to that for α-methylstyrene and *cis*-stilbene.

The (*E*/*Z*)-epoxide ratios for epoxidation of *cis*-stilbene in systems I and II are 23:77 and 67:33, respectively. In system II epoxidation of the trisubstituted alkene (*Z*)-α,β-dimethylstyrene yielded an (*E*/*Z*)-epoxide ratio of 35:65 plus 20% of acetophenone resulting from oxidative cleavage. Thus, if the *cis–trans* isomerization does not proceed via a radical intermediate, either of the trisubstituted radical probes **1b** or **1c** is expected to yield substantial amounts of epimerized product. In system I the reaction rates for **1b** and **1c** were similar to that for **1a**.[15] The yield of **3b** from **1b** was quantitative, whereas that of **3c** from **1c** was only 56%. In system II **1b** yielded 83% of **3b**, and **1c** 54% of **3c**. In no experiment was the known epimeric epoxide detected. For all rections in which the alkene was not quantitatively converted into epoxide, products resulting from radicals of type **4** were observed in the crude reaction mixture. The lack of epimerization product clearly shows that the intermediate radicals prefer to react by ring opening rather than by epoxide formation, as expected from measured rates of cyclopropyl ring opening for similar probes.[16]

The results indicate that initial reversible formation of a metallaoxetane (Scheme 1, pathway **C**) is the most viable mechanism for (salen)Mn-catalyzed epoxidation. Alternative proposals (Scheme 1, pathways **A** and **B**) cannot unambiguously explain either the survival of the radical probes used here or the nonlinear Eyring effects.[5c] However, it is clear that radicals can be formed under certain conditions, and it seems likely that epimeric epoxides are formed exclusively by a radical pathway. It is still uncertain whether radicals are formed directly (Scheme 1, pathway **B**) or by homolytic cleavage of the intermediate metallaoxetane. Jacobsen et al. argued that the common trend in enantioselectivities for the epimeric products indicate that they are formed from a common intermediate.[6b] Groves and Stern[17] demonstrated that epoxidation by manganese porphyrin complexes could proceed either via an oxomanganese(V) or oxomanganese(IV) species; the former pathway is stereospecific, whereas the latter yields both epimeric epoxides by radical formation.[18] Therefore, the isomerization could be rationalized as a competition between oxomanganese(IV) and oxomanganese(V) species in solution. However, in system I (Table 1) the degree of isomerization seems to depend to a very large degree on the substrate, and in particular the quantitative yields of **3a** and **3b** indicate that epoxidation of **1a** and **1b** goes cleanly via a manganese(V) oxetane. By analogy the lower yield from **1c** would be expected to be due to homolysis in a manganaoxetane, not direct radical formation. On the other hand, the lower yields in system II might well result from the presence of oxomanganese(IV) species in the reaction mixture.

The propensity of (*Z*) alkenes to isomerize is readily rationalized by pathway **C**. The steric crowding between the two (*Z*) substituents on a metallaoxetane intermediate would be significantly relieved by homolysis of Mn–C and bond rotation, but not by rearrangement to an epoxide. This effect would not be as great for an (*E*) metallaoxetane. Steric crowding in the alkene would therefore, in general, be expected to increase epimerization in the epoxidation.

We have given strong proof that (salen)Mn-catalyzed epoxidation proceeds through a metallaoxetane intermediate, which may undergo metal–carbon bond homolysis to relieve steric crowding and form a stabilized radical. Preliminary quantum chemical investigations support this mechanism.[19]

Received: February 24, 1997 [Z10152IE]
German version: *Angew. Chem.* **1997**, *109*, 1802–1803

Keywords: epoxidations · manganese · oxetanes · oxidations · radicals

[1] Recent reviews: a) E. N. Jacobsen in *Catalytic Asymmetric Synthesis* (Ed.: I. Ojima), VCH, New York, **1993**, pp. 159–202; b) T. Katsuki, *Coord. Chem. Rev.* **1995**, *140*, 189–214; c) P. J Pospisil, D. H. Carsten, E. N. Jacobsen, *Chem. Eur. J.* **1996**, *2*, 974–980.

[2] H. Fu, G. C. Look, W. Zhang, E. N. Jacobsen, C.-H. Wong, *J. Org. Chem.* **1991**, *56*, 6497–6500.

[3] K. Srinivasan, P. Michaud, J. K. Kochi, *J. Am. Chem. Soc.* **1986**, *108*, 2309–2320.

[4] P.-O. Norrby, C. Linde, B. Åkermark, *J. Am. Chem. Soc.* **1995**, *117*, 11035–11036.

[5] a) Y. Nuguchi, R. Irie, T. Fukuda, T. Katsuki, *Tetrahedron Lett.* **1996**, *37*, 4533–4536; b) T. Fukuda, T. Katsuki, *ibid.* **1996**, *37*, 4389–4392; c) T. Hamada, T. Fukuda, H. Imanishi, T. Katsuki, *Tetrahedron* **1996**, *52*, 515–530.

[6] a) S. Chang, J. M. Galvin, E. N. Jacobsen, *J. Am. Chem. Soc.* **1994**, *116*, 6937–6938; b) W. Zhang, N. H. Lee, E. N. Jacobsen, *ibid.* **1994**, *116*, 425–426.

[7] a) K. B. Sharpless, A. Y. Teranishi, J.-E. Bäckvall, *J. Am. Chem. Soc.* **1977**, *99*, 3120–3128; b) K. A. Jørgensen, B. Schiøtt, *Chem. Rev.* **1990**, *90*, 1483–1506.

 © WILEY-VCH Verlag GmbH, D-69451 Weinheim, 1997 0570-0833/97/3616-1724 $ 17.50+.50/0

[8] H. Buschmann, H.-D. Scharf, N. Hoffmann, P. Esser, *Angew. Chem.* **1991**, *103*, 480–518; *Angew. Chem. Int. Ed. Engl.* **1991**, *30*, 477–515.
[9] a) K. J. Hale, J. R. Ridd, *J. Chem. Soc. Chem. Commun.* **1995**, 357–358; b) K. J. Hale, J. R. Ridd, *J. Chem. Soc. Perkin Trans. 2* **1995**, 1601–1605; c) P.-O. Norrby, K. P. Gable, *ibid.* **1996**, 171–178; d) A. Gypser, P.-O. Norrby, *J. Chem. Soc. Perkin Trans. 2* **1997**, 939–943.
[10] a) T. G. Traylor, A. R. Miksztal, *J. Am. Chem. Soc.* **1989**, *111*, 7443–7448; b) D. Ostovic, T. C. Bruice, *ibid.* **1989**, *111*, 6511–6517.
[11] R. Breslow, X. Zhang, R. Xu, M. Maletic, R. Merger, *J. Am. Chem. Soc.* **1996**, *118*, 11678–11679.
[12] Styrenes **1a–c** were prepared according to J. A. Donnelly, J. G. Hoey, S. O'Brien, J. O'Grady, *J. Chem. Soc. Perkin Trans. 1* **1973**, 2030–2033.
[13] The catalyst was prepared according to J. F. Larrow, E. N. Jacobsen, *J. Org. Chem.* **1994**, *59*, 1939–1942.
[14] W. Zhang, E. N. Jacobsen, *J. Org. Chem.* **1991**, *56*, 2296–2298.
[15] A 1:1 mixture of alkenes was epoxidized with 0.2 equiv of oxidant.
[16] The rate constant for ring opening of the secondary benzyl radical of 1-benzyl-*trans*-2-phenylcyclopropane was estimated to be $3.6 \times 10^8\ s^{-1}$: a) R. Hollis, L. Hughes, V. W. Bowry, K. U. Ingold, *J. Org. Chem.* **1992**, *57*, 4284–4287. Secondary and tertiary radicals of this type generally open at similar rates: b) M. Newcomb, N. Tanaka, A. Bouvier, C. Tronche, J. H. Horner, O. M. Musa, F. N. Martinez, *J. Am. Chem. Soc.* **1996**, *118*, 8505–8506; c) M. Newcomb, *Tetrahedron* **1993**, *49*, 1151–1176.
[17] J. T. Groves, M. K. Stern, *J. Am. Chem. Soc.* **1987**, *109*, 3812–3814.
[18] R. D. Arasasingham, G.-H. He, T. C. Bruice, *J. Am. Chem. Soc.* **1993**, *115*, 7985–7991.
[19] M. Svensson, C. Linde, P.-O. Norrby, B. Åkermark, unpublished results.

Three-Dimensional Framework with Channeling Cavities for Small Molecules: $\{[M_2(4,4'\text{-bpy})_3(NO_3)_4]\cdot x H_2O\}_n$ (M = Co, Ni, Zn)**

Mitsuru Kondo, Tomomichi Yoshitomi, Kenji Seki, Hiroyuki Matsuzaka, and Susumu Kitagawa*

The synthesis of coordination polymers with large channels or cavities is of great interest due to their intriguing structural diversity and their potential functions as microporous solids (including molecular adsorption, ion exchange, and heterogeneous catalysis).[1–10] The simple bis(monodentate) ligand 4,4'-bipyridine (4,4'-bpy) affords a variety of two- and three-dimensional frameworks when coordinated to various metal ions. $\{[Cd(4,4'\text{-bpy})_2(NO_3)_2]\cdot(C_6H_4Br_2)_2\}_n$,[3] $\{[Zn(4,4'\text{-bpy})_2]SiF_6\cdot x DMF\}_n$,[6] and $[\{Cu(cnge)_2\}_2(\mu\text{-}4,4'\text{-bpy})][BF_4]_2\cdot MeCN$ (cnge = 2-cyanoguanidine)[11] have assemblies of 2-D sheets, whereas $\{[Zn(4,4'\text{-bpy})_2(H_2O)_2](SiF_6)\}_n$,[12] $[Cu(4,4'\text{-bpy})Cl]_n$,[4] $\{[Cu(4,4'\text{-bpy})_{1.5}]NO_3(H_2O)_{1.5}\}_n$,[7] and $[Ag(4,4'\text{-bpy})\cdot NO_3]_n$ have 3-D interpenetrating structures.[10] Although the number of coordination polymers with new structural aspects is increasing, compounds that reveal functional properties characteristic of their cavities and channels are still lacking. The anion-exchange capability of the silver compound is one of a few recent instances of such properties.[10]

[*] Prof. Dr. S. Kitagawa, Dr. M. Kondo, T. Yoshitomi, Dr. H. Matsuzaka
Department of Chemistry, Faculty of Science
Tokyo Metropolitan University
Minami-ohsawa Hachioji, Tokyo 192-03 (Japan)
Fax: Int. code +(426)77-2525
e-mail: kitagawa-susumu@c.metro-u.ac.jp
K. Seki
Energy Conversion and Storage Technology Applied Research Center
Research and Development Department, Osaka Gas Co., Ltd.
Torishima, Konohana-ku, Osaka (Japan)

[**] This research was supported by a Grant-in-Aid for Scientific Research from the Japanese Ministry of Education, Science and Culture.

Here we report the synthesis and crystal structures of novel coordination polymers **1–3**, which have large micropores and can adsorb small gaseous molecules such as CH_4, N_2, and O_2.

$\{[M_2(4,4'\text{-bpy})_3(NO_3)_4](H_2O)_x\}_n$

1: M = Co, $x = 4$
2: M = Ni, $x = 4$
3: M = Zn, $x = 2$

Complexes **1–3** were prepared by the reaction of $M(NO_3)_2\cdot x H_2O$ (M = Co, Ni, Zn) with 4,4'-bpy in acetone/EtOH.[13] Complex **1** was characterized by X-ray crystallography, and the isomorphous structures of **1–3** were clearly demonstrated by their X-ray powder diffraction patterns.

Figure 1 shows the coordination around the Co center of **1** and the crystal structure along the *c* axis. The three nitrogen

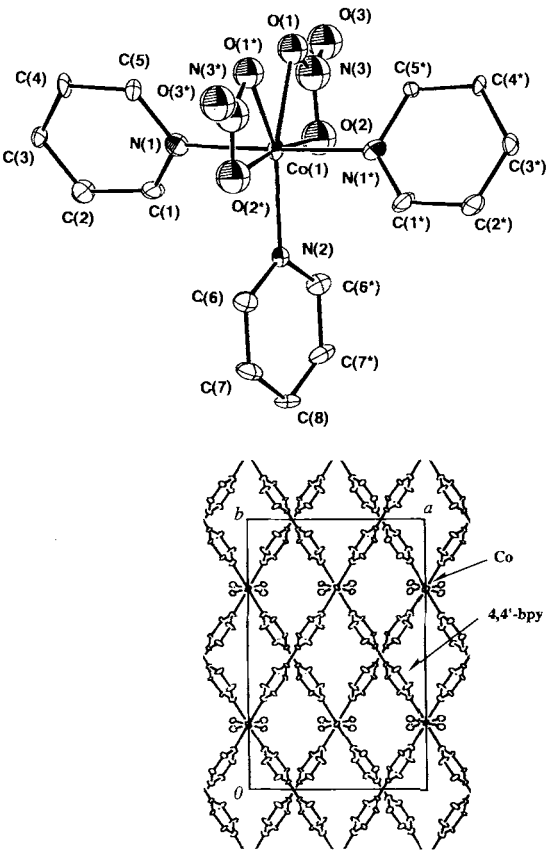

Figure 1. Top: ORTEP drawing of **1** around the Co center (ellipsoids at 20% probability); the hydrogen atoms are omitted for clarity. Selected bond distances [Å] and angles [°]: Co(1)–N(1) 2.13(1), Co(1)–N(2) 2.13(2), Co(1)–O(1) 2.23(1), Co(1)–O(2) 2.32(1); N(1)-Co(1)-N(1*) 178.2(8), N(1)-Co(1)-N(2) 90.9(4), N(1)-Co(1)-O(1) 84.5(5), N(1)-Co(1)-O(1*) 94.1(5), N(1)-Co(1)-O(2) 85.8(5), N(1)-Co(1)-O(2*) 94.3(5), N(2)-Co(1)-O(1) 140.8(4), N(2)-Co(1)-O(1*) 140.8(4), N(2)-Co(1)-O(2) 86.1(4), N(2)-Co(1)-O(2*) 86.1(4), O(1)-Co(1)-O(1*) 78.5(7), O(1)-Co(1)-O(2) 54.7(5), O(1)-Co(1)-O(2*) 133.1(6), O(2)-Co(1)-O(2*) 172.2(8). Bottom: View of the crystal structure of **1** along the *c* axis; the hydrogen atoms and nitrate anions are omitted for clarity.

atoms from the two 4,4'-bpy molecules and the four oxygen atoms from the two nitrate anions form a distorted pentagonal bipyramid around the Co^{II} atom; N(1) and N(1*) are in the axial positions. The Co^{II} centers are bridged by 4,4'-bpy to afford infinite 1-D chains in the *ab* plane in which the pyridine rings of the 4,4'-bpy units are twisted by 38.2° with respect to each other. The chains are separated by about 10.0 Å. Two sets of arrays are

 © WILEY-VCH Verlag GmbH, D-69451 Weinheim, 1997 0570-0833/97/3616-1725 $ 17.50+.50/0

observed for the 1-D chains. In one the chains are oriented at an angle of 54.8° to the *a* axis, and in the other at angle of −54.8°. The two planes that correspond to the two types of chains are designated A and B (left side of Scheme 1). The distinct planes are bound over 4,4′-bpy bridges along the *c* axis to form a double-sheet structure. The pyridine rings of the bridging 4,4′-bpy molecules are twisted by about 41.5°. Hence, each 1-D chain on the A and B planes is sterically fixed by the 4,4′-bpy unit, which acts as a pillar.

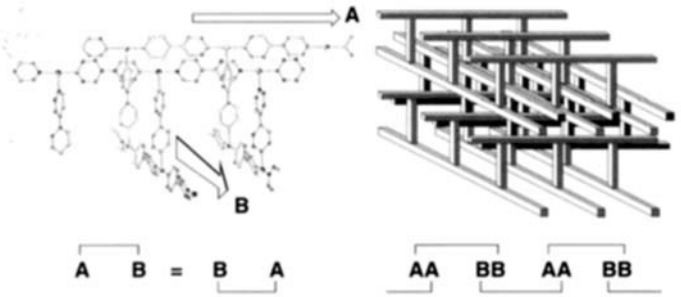

Scheme 1. Formation of the crystal structure of **1**. A section of the 3-D basic unit made up of planes A and B is shown on the left, and the result of their assembly on the right.

The assembly of these basic units is shown schematically in Scheme 1. The most characteristic feature of the resulting structure can be described as a tongue-and-groove structure (Scheme 1, right). To the best of our knowledge this type of assembly has not yet been observed in the 3-D frameworks of coordination polymers with 4,4′-bpy bridges.

The interplanar distance between A and B in the 3-D basic unit is about 11.3 Å. The nonlinked adjacent planes are separated by about 2.6 Å (A/A, B/B) and about 6.1 Å (A/B). The relatively large distance between the adjacent A and B planes creates channeling cavities along the *a* and *b* axes with dimensions of about 3 × 6 and 3 × 3 Å, respectively. These channeling cavities are occupied by water molecules, which show no significant binding interactions with the crystal framework.

The unique 3-D structures of **1**–**3** with channeling cavities prompted us to examine their gas-adsorption properties, one of the most attractive functions of microporous solids.[4, 14–16] Figure 2 shows the results of the adsorption-activity experiments of anhydrous **1**, obtained by drying under vacuum, with CH_4, N_2, and O_2. Rapid increase in the amount of adsorbed gases is shown by the increase in pressure up to 5 atm; this indicates diffusion of the gases into the cavities.[17] X-ray powder diffraction patterns confirm that there is no structural decomposition upon removal of crystal waters. Moreover, adsorption and desorption experiments with CH_4 provide the same isotherm (Figure 2), which means that there is no deformation of the crystal framework upon adsorption. The isotherms are of type I according to the IUPAC classification.[18] About 2.3 mmol of CH_4 and 0.80 mmol of N_2 or O_2 are adsorbed per 1.0 g of the anhydrous sample at a pressure of 30 atm.

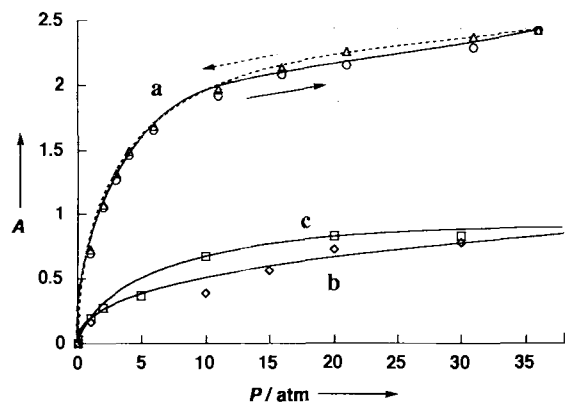

Figure 2. Isotherms for the adsorption of CH_4 (a), N_2 (b), and O_2 (c) on **1** at 298 K in the range of 1–36 atm; A = absolute adsorption in mmol of adsorbed gas per gram of anhydrous sample. In the case of CH_4 gas desorption (circles) was carried out directly after gas adsorption (triangles). Since the two isotherms are nearly identical, one can conclude that there is no structural change of the channels during gas adsorption.

An investigation of the adsorption capabilities of zeolites for several gases (CH_4, N_2, CO_2, Ar, Kr, and Xe) showed that gas affinity corresponds to cavity size.[14, 15, 19–22] Zeolites 13X and 5A show a high affinity for gases[23] and have channel dimensions of 7.4 × 7.4 Å and 4.1 × 4.1 Å, respectively, which are similar to those of **1**–**3**. In addition to structural dimensions, the specific interaction of organometallic cavity frameworks with adsorbed molecules could be controlled in the coordination polymers, which might lead to new types of adsorption properties.

Experimental Section

1: 4,4′-Bipyridine (0.82 g, 5.25 mmol) in EtOH (50 mL) was added to a solution of $Co(NO_3)_2 \cdot 6H_2O$ (0.68 g, 2.33 mmol) in acetone (50 mL), and the mixture allowed to stand for one week. The red microcrystals obtained were collected by filtration and dried in vacuo for 2 h. Elemental analysis calcd for $C_{30}H_{32}Co_2N_{10}O_{16}$: C 39.75, H 3.56, N 15.45; found: C 40.58, H 2.98, N 15.45; IR (KBr): $\tilde{\nu}$ [cm^{-1}] = 3375 (br), 1609 (s), 1536 (m), 1466 (s), 1414 (s), 1296 (s), 1219 (m), 1067 (s), 1032 (m), 1009 (m), 880 (w), 861 (w), 814 (s), 733 (m), 635 (s), 573 (m), 505 (m).

Complexes **2** and **3** were prepared analogously. **2**: Elemental analysis calcd for $C_{30}H_{32}N_{10}Ni_2O_{16}$: C 39.77, H 3.56, N 15.46; found: C 41.18, H 3.08, N 15.30; IR (KBr): $\tilde{\nu}$ [cm^{-1}] = 3385 (br), 1953 (w), 1611 (s), 1537 (m), 1494 (s), 1427 (m), 1385 (w), 1302 (s), 1224 (m), 1076 (m), 1047 (w), 1012 (m), 815 (m), 734 (w), 638 (m), 575 (w), 527 (w). **3**: Elemental analysis calcd for $C_{30}H_{28}N_{10}O_{14}Zn_2$: C 40.79, H 3.19, N 15.86; found: C 40.43, H 2.83, N 15.78; IR (KBr): $\tilde{\nu}$ [cm^{-1}] = 3406 (br), 1763 (w), 1612 (s), 1537 (m), 1415 (br), 1294 (m), 1219 (m), 1070 (m), 1030 (s), 1012 (m), 985 (w), 861 (w), 812 (s), 731 (m), 638 (m), 574 (m), 507 (m).

X-ray structure determination of **1**: All data were measured on a Rigaku AFC7R diffractometer with graphite-monochromated $Mo_{K\alpha}$ radiation and a rotating-anode generator (12 kW). The unit-cell constant was obtained from a least-squares refinement of 25 carefully centered reflections with 2θ values between 8.04 and 18.75°. The structure was solved by direct methods and refined by the block-diagonal least-squares method. Hydrogen atoms except for those of water molecules were placed at calculated positions, but their parameters were not refined. The final refinements were carried out with full-matrix least-squares techniques for non-hydrogen atoms. All calculations were performed with the TEXSAN crystallographic software package (Molecular Structure Corporation). Crystal data: $C_{30}H_{32}N_{10}Co_2O_{16}$, M_r = 906.51, orthorhombic, space group *Ccca*, a = 12.267(7), b = 19.025(7), c = 17.412(4) Å, V = 4063(2) Å^3, Z = 4, ρ_{calcd} = 1.482 g cm^{-3}, $\lambda(Mo_{K\alpha})$ = 0.71069 Å, $F(000)$ = 1856, $\mu(Mo_{K\alpha})$ = 8.96 cm^{-1}, T = 25 °C, $2\theta_{max}$ = 55.2°, of 2324 reflections measured 528 were observed ($I > 2.00\sigma(I)$), 108 parameters; R = 0.086, R_w = 0.095. Crystallographic data (excluding structure factors) for the structures reported in this paper have been deposited with the Cambridge Crystallographic Data Centre as supplementary publication no. CCDC-100382. Copies of the data can be obtained free of charge on application to The Director, CCDC, 12 Union Road, Cambridge CB21EZ, UK (fax: int. code + (1223) 336-033; e-mail: deposit@chemcrys.cam.ac.uk).

Gas-adsorption measurements for **1**: The adsorption isotherms of CH_4, N_2, and O_2 were measured by reported procedures [14, 15]. The apparatus was equipped with a Cahn R-100 electrobalance contained within a SUS steel pressure chamber that was connected with two separate lines for evacuation and adsorbate gas pressurization. Prior to adsorption measurement, to remove the solvated waters, **1** (63.1 mg, 0.074 mmol) was dried under reduced pressure at 25 °C until additional weight loss was not observed. The adsorbate gases (CH_4, N_2, O_2) were dosed into the adsorption chamber, then the change of the weight of the sample was monitored. The entire adsorption isotherms were determined by increasing the adsorbate gas pressure to a maximum of 36 atm. Gas-adsorption measurements for **2** and **3** were carried out by a similar procedure. The desorption isotherm was also obtained for CH_4 adsorption on **1**.

Received: November 5, 1996
Supplemented version: April 21, 1997 [Z9731IE]
German version: *Angew. Chem.* **1997**, *109*, 1844–1846

 © WILEY-VCH Verlag GmbH, D-69451 Weinheim, 1997 0570-0833/97/3616-1726 $ 17.50+.50/0

Keywords: cobalt · crystal engineering · inclusion compounds · microporosity · N ligands

[1] B. F. Hoskins, R. Robson, *J. Am. Chem. Soc.* **1990**, *112*, 1564–1554.
[2] A. Stein, S. W. Keller, T. E. Mallouk, *Science* **1993**, *259*, 1558–1564.
[3] M. Fujita, Y. J. Kwon, S. Washizu, K. Ogura, *J. Am. Chem. Soc.* **1994**, *116*, 1151–1152.
[4] O. M. Yaghi, G. Li, *Angew. Chem.* **1995**, *107*, 232; *Angew. Chem. Int. Ed. Engl.* **1995**, *34*, 207–209.
[5] L. Carlucce, G. Ciani, D. M. Proserpio, A. Sironi, *Angew. Chem.* **1995**, *107*, 2045–2047; *Angew. Chem. Int. Ed. Engl.* **1995**, *34*, 1895–1898.
[6] S. Subramanian, M. J. Zaworotko, *Angew. Chem.* **1995**, *107*, 2295–2297; *Angew. Chem. Int. Ed. Engl.* **1995**, *34*, 2127–2129.
[7] O. M. Yaghi, H. Li, *J. Am. Chem. Soc.* **1995**, *117*, 10401–10402.
[8] C.-G. Wu, D. C. DeGroot, H. O. Marcy, J. L. Schindler, C. R. Kannewurf, T. Bakas, V. Papaefthymiou, W. Hirpo, J. P. Yesinowski, Y.-J. Liu, M. G. Kanatzidis, *J. Am. Chem. Soc.* **1995**, *117*, 9229–9242.
[9] G. B. Gardner, D. Venkataraman, J. S. Moore, J. S. Lee, *Nature* **1995**, *374*, 792–795.
[10] O. M. Yaghi, H. Li, *J. Am. Chem. Soc.* **1996**, *118*, 295–296.
[11] A. S. Batsanov, M. J. Begley, P. Hubberstey, J. Stroud, *J. Chem. Soc. Dalton Trans.* **1996**, 1947–1957.
[12] R. W. Gable, B. F. Hosins, R. Robson, *J. Chem. Soc. Chem. Commun.* **1990**, 1677–1678.
[13] Similar coordination polymers were reported for the reaction of $M(NO_3)_2$ with 4,4′-bpy: I. S. Ahuja, R. Singh, C. P. Rai, *J. Inorg. Nucl. Chem.* **1978**, *40*, 924–926; the authors state that these are 1:2, $[M(4,4'\text{-bpy})_2(NO_3)_2]_n$ (M = Co, Ni), and 1:1 complexes, $[M(4,4'\text{-bpy})(NO_3)_2]_n$ (M = Zn, Cd, Ag), on the basis of IR spectra and elemental analysis.
[14] J. L. Zuech, A. L. Hines, E. D. Sloan, *Ind. Eng. Chem. Process Des. Dev.* **1983**, *22*, 172–174.
[15] S.-Y. Zhang, O. Talu, D. T. Hayhurst, *J. Phys. Chem.* **1991**, *95*, 1722–1726.
[16] T. C. Golden, S. Sircar, *J. Colloid Interface Sci.* **1994**, *162*, 182–188.
[17] Dependence of gas adsorption on the particle size of **1** was examined to estimate the surface adsorption. Since the amount of adsorbed gas is less dependent on the size, adsorption mainly occurs in the channeling cavities.
[18] IUPAC *Pure. Appl. Chem.* **1985**, *57*, 603–619.
[19] R. M. Barrer, R. Papadopoulos, *Proc. R. Soc. London A* **1972**, *326*, 315–330.
[20] S. Ozawa, S. Kusumi, Y. Ogino, *J. Colloid Interface Sci.* **1976**, *56*, 83–91.
[21] L. Mentasty, A. M. Woestyn, G. Zgrablich, *Adsorpt. Sci. Technol.* **1994**, *11*, 123–133.
[22] L. Mentasty, A. M. Woestyn, E. Basaldella, A. Kikot, G. Zgravlich, *Adsorpt. Sci. Techol.* **1994**, *11*, 209–216.
[23] Zeolite 13X adsorbs 2.3 mmol g^{-1} of CH_4 and 0.8 mmol g^{-1} of N_2 or O_2 at 30 atm, and Zeolite 5A adsorbs 2.8 mmol g^{-1} of CH_4 and 0.8 mmol g^{-1} of N_2 or O_2 at 30 atm.

dent to use highly rigid building blocks and to seek means that limit the ways in which these units can be assembled.[3] Here we demonstrate the use of cavitands—rigid macrocycles that contain an enforced cavity—to form new, complex assemblies, most notably the first "bis(carceplex)".

It has been known for some time that two bowl-shaped molecules, cavitands or "bowls", can be linked in the presence of a suitable guest molecule to yield a closed-surface molecule, a carceplex. The guest is permanently incarcerated within the newly formed shell, akin to a ship in a bottle.[4] We studied the effects of guests as templates in the synthesis of carceplexes,[5] and found that formation of carceplex **2**·G (G = guest) is subject to a template effect that ranges one million fold. Moreover, the yields of **2**·G are as high as 87%. The formation of **2**·G demonstrates the efficient linkage of two cavitands to form a single, relatively small, closed-surface capsule (Scheme 1).

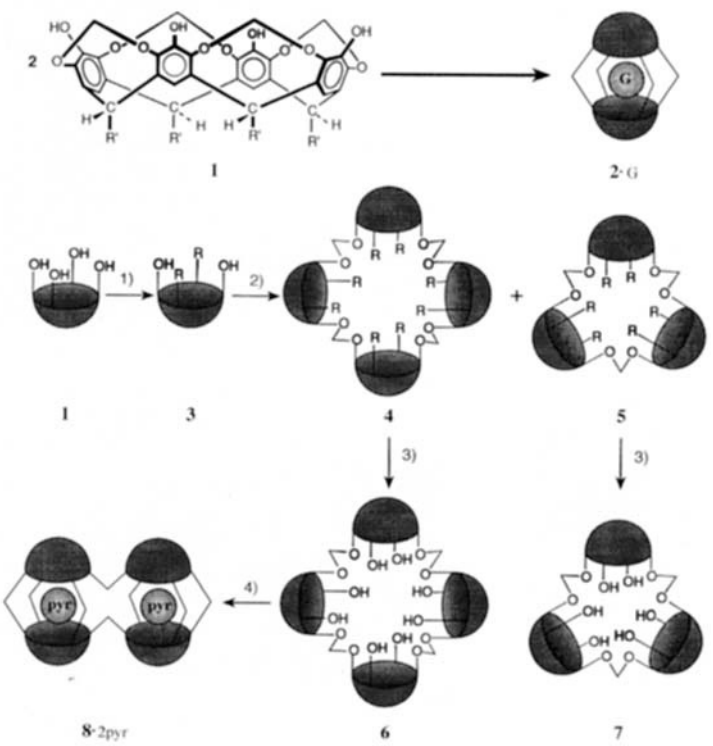

Scheme 1. Preparation of **3**–**8**. The bowls of carceplex **2**·G and bis(carceplex) **8**·2 pyr are linked through OCH_2O groups. R = $OCH_2C_6H_5$; R′ = $CH_2CH_2C_6H_5$. 1) $PhCH_2Br$, K_2CO_3, DMF, 6% yield of **3**. 2) CH_2BrCl, K_2CO_3, DMF, 15% yield of **4**, 5% yield of **5**. 3) H_2, Pd/C, 4 atm, 94% yield of **6** (based on **4**), 90% yield of **7** (based on **5**). 4) CH_2BrCl, K_2CO_3, *N*-methylpyrrolidinone, pyrazine, 74% yield of **8**·2 pyr.

A Bis(carceplex) from a Cyclic Tetramer of Cavitands**

Naveen Chopra and John C. Sherman*

One of the key goals of supramolecular chemistry is the construction of complex molecular assemblies that are composed of simple subunits or building blocks. The formation of supramolecular assemblies is common in nature and materials science, as exemplified by the braid-like structure of collagen[1] and the controlled design and engineering of crystal lattices.[2] To construct de novo assemblies of such complexity, it is prudent to use highly rigid building blocks and to seek means that limit the ways in which these units can be assembled.[3] Here we demonstrate the use of cavitands—rigid macrocycles that contain an enforced cavity—to form new, complex assemblies, most notably the first "bis(carceplex)".

Is it possible to link three or more cavitands to yield larger and/or more complex supramolecular assemblies? We report here the preparation of the first cyclic tetramer and cyclic trimer of cavitands,[6] which are potentially novel host molecules and precursors for new host molecules. To illustrate the potential of these cyclic oligomers, we also report the first bis(carceplex), which was prepared from the tetramer.

Tetrol **1** is the starting material for carceplex **2**·G and can be easily prepared in multi-gram quantities.[7] To efficiently link three or more cavitands in a cyclic array, one must limit the number of reactive sites on **1** and preclude formation of **2**·G. Both can be achieved by protecting two OH groups on opposing sides of **1**. We chose benzyl as the protecting group because of its size (it is large enough to inhibit carceplex formation), stability (the linkage remains intact upon subsequent acetal forma-

[*] Dr. J. C. Sherman, N. Chopra
Department of Chemistry
University of British Columbia
2036 Main Mall, Vancouver, BC V6T1Z1 (Canada)
Fax: Int. code + (604) 822-2847
e-mail: sherman@chem.ubc.ca

[**] We gratefully acknowledge financial support from the National Science and Engineering Research Council of Canada. We thank A. S. Causton for insightful discussions.

 © WILEY-VCH Verlag GmbH, D-69451 Weinheim, 1997 0570-0833/97/3616-1727 $ 17.50+.50/0

tion with $K_2CO_3/CH_2ClBr/DMF/60\,^{\circ}C$), ease of removal (by hydrogenolysis over Pd/C), and orthogonality to the acetal functionality (the acetal linkages are stable against hydrogenolysis). Treatment of **1** with 2.2 equivalents of benzyl bromide and excess K_2CO_3 in DMF gave a mixture of benzyl ethers, from which the desired bis(benzyloxy) diol **3** was isolated in 6% yield (Scheme 1). The remainder of the product mixture was subjected to hydrogenolysis over Pd/C to regenerate **1**. With this recycling method we obtained nearly quantitative conversion of tetrol **1** into diol **3**. The latter was cyclized with CH_2BrCl as a linking agent to yield a mixture of cyclic oligomers from which a cyclic tetramer of cavitands, **4**, and a cyclic trimer of cavitands, **5**, were isolated. These two cyclic oligomers were then debenzylated over Pd/C to yield tetramer **6** and trimer **7**; the latter will be discussed elsewhere.

According to the CPK space-filling molecular models, tetramer **6** has a large cavity that is complementary to molecules the size of C_{60}.[8] It could potentially form stacked arrays,[9] which could act as channels,[10] or be capped on the top and bottom with a molecule of tetrol **1** to yield a very large carceplex. Alternatively, **6** is flexible enough that the molecule can fold upon itself as described below.

Tetramer **6** was subjected to optimum conditions for the formation of carceplex **2**·G (Figure 1).[5] This includes using pyrazine as the guest, as we have found that it is the best template molecule for the formation of **2**·G.[5] The reaction proceeded smoothly to produce bis(carceplex) **8**·2pyr (pyr = pyrazine) in 74% yield. This new compound was characterized by elemental analysis, a MALDI-TOF mass spectrum (which

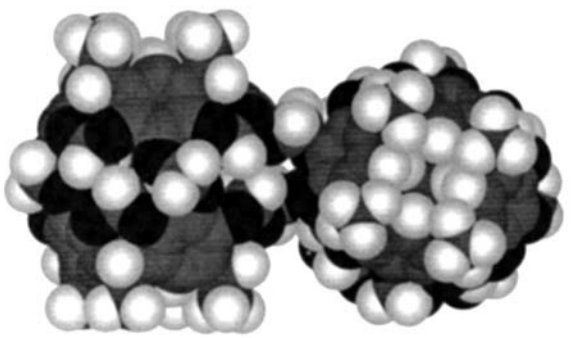

Figure 1. MM2-minimized space-filling drawing of **8**·2pyr. For clarity and simplification of the calculation, the phenylethyl pendent groups were replaced by methyl groups.

exclusively contains signals for the Na^+ and K^+ adducts), and a ^1H NMR spectrum. The latter is remarkably simple, given the size and complexity of **8**·2pyr (see *Experimental Section*). The peaks for the host were easily assigned, as was the signal for the entrapped pyrazine molecules. Integration confirms that there are two units of pyrazine per host molecule. The chemical shift of the two pyrazine molecules is shifted upfield by 4.3 ppm from its normal position in $CDCl_3$; this is typical for incarcerated pyrazine.[5, 12] Bis(carceplex) **8**·2pyr was dissolved in 1,2,4-trichlorobenzene and heated at reflux for 84 h at 214 °C with no loss of pyrazine, which demonstrates that the guests are "permanently" incarcerated. As with **2**·G the largest portal of **8**·2pyr is at the bottom of the bowls (Figure 1).[11]

MM2 molecular mechanics calculations were performed on **8**·2pyr; a space-filling drawing is shown in Figure 1. Each opposing pair of bowls was twisted by 21° with respect to one another prior to minimization, in accord with the crystal structure of **2**·G.[12] MM2 minimization of **8**·2pyr revealed a 90° twist between the two capsules.[13] Further experimental and computational studies of **8**·2pyr are currently underway, as the conformation of **8**·2G could have ramifications for intercapsule guest communication, which could be important in the development of switching devices.

Experimental Section

DMF (Fisher), HPLC-grade EtOAc (Fisher), and MeOH (Fisher) were used without further purification. *N*-methylpyrrolidinone (Aldrich) was distilled from BaO and stored over 4-Å molecular sieves, and benzene (Fisher) was dried over 4-Å molecular sieves. ^1H NMR spectra were run on a Bruker WH-400 spectrometer in $CDCl_3$ at ambient temperature using the residual $CHCl_3$ signal as a reference unless noted otherwise. "Acetal" in the NMR assignments refers to the OCH_2O linkages between the bowls; H_{in} and H_{out} refer to the diastereotopic OCH_2O linkages. Mass spectra were recorded on a Bruker Reflex MALDI-TOF (matrix assisted laser desorption ionization/time of flight) instrument in the reflectron mode. The samples were prepared by mixing the substance (5 μL of 1 mM solutions in $CHCl_3$) with the dihydroxybenzoic acid matrix (5 μL of 80 mM solutions in THF; Aldrich). A portion (0.5 μL) was applied to a MALDI-TOF target disc and allowed to dry in air for a minimum of 10 min prior to the measurement. Errors in mass accuracy are ±0.1%. Calculated molecular weights are averaged and not exact due to limited resolution. Melting points (uncorrected) were measured on a Thomas–Hoover apparatus; all compounds melt above 250 °C unless noted otherwise. Silica gel (BDH, 230–400) was used for column chromatography. Silica gel thin-layer chromatography was performed on Aldrich glass-backed plates (silica gel 60, F_{254}, 0.25 mm).

3: Tetrol **1** (3 g, 2.95 mmol), benzyl bromide (772 μL, 6.5 mmol, 2.2 equiv), and K_2CO_3 (4 g, 29 mmol, 10 equiv) were added to DMF (250 mL), and the mixture was stirred under an N_2 atmosphere for 24 h at 25 °C. The solvent was removed under vacuum and 2 M HCl (150 mL) was added to the residue. The aqueous layer was extracted with EtOAc (3 × 50 mL), and the combined EtOAc fractions were dried over $MgSO_4$ and filtered. The solvent was removed to give a viscous yellow oil, which was loaded onto a dry silica gel column. Gradient elution with EtOAc/hexanes (1/4) followed by EtOAc/hexanes (1/3), and recrystallization of the residue from $CHCl_3$/hexanes gave diol **3** (200.4 mg, 0.167 mmol, 6%) as a white solid. M.p. 157–159 °C; ^1H NMR: $\delta = 2.47$ (m, 8H, $CH_2CH_2C_6H_5$), 2.67 (m, 8H, $CH_2CH_2C_6H_5$), 4.44 (d, $J = 7.0$ Hz, 4H, H_{in}), 4.82 (t, $J = 7.9$ Hz, 4H, $H_{methine}$), 4.97 (s, 4H, $OCH_2C_6H_5$), 5.35 (s, 2H, OH), 5.86 (d, $J = 7.0$ Hz, 4H, H_{out}), 6.65 (s, 2H, *para*-H_{OH}), 6.87 (s, 2H, *para*-H_{OBn}), 7.10–7.30 (br m, $OCH_2C_6H_5$, $CH_2CH_2C_6H_5$, $CHCl_3$); MS: $m/z = 1219$ (100%) $[M + Na^+]$, 1220 calcd for $C_{78}H_{68}O_{12} + Na^+$; elemental analysis calcd for $C_{78}H_{68}O_{12} \cdot H_2O$: C 77.08, H 5.81; found: C 76.98, H 5.61.

4 and **5:** Diol **3** (297.3 mg, 0.248 mmol), CH_2ClBr (81 μL, 1.25 mmol, 5 equiv), and K_2CO_3 (261.5 mg, 1.89 mmol, 8 equiv) were added to DMF (150 mL), and the mixture was stirred under an N_2 atmosphere for 24 h at 60 °C. The solvent was removed unter vacuum, and 2 M HCl (120 mL) added to the residue. The aqueous layer was extracted with $CHCl_3$ (3 × 40 mL), and the combined $CHCl_3$ fractions were dried over $MgSO_4$ and filtered. The solvent was removed to give a viscous yellow oil, which was filtered through a pad of silica gel with $CHCl_3$. The solvent was removed under vacuum, EtOAc (50 mL) added, and the solution heated to reflux for 20 min. The suspension in EtOAc was cooled and filtered to yield tetramer **4** (45.8 mg, 0.00947 mmol, 15%). The EtOAc filtrate was then loaded onto a dry silica gel column and eluted with $CHCl_3$/hexanes (3/1). The solvent was removed, and the resulting solid recrystallized from $CHCl_3$/hexanes to give trimer **5** (15.1 mg, 0.00416 mmol, 5%).

4: ^1H NMR ([D_6]DMSO, 120 °C): $\delta = 2.50$ (br, 32H, $CH_2CH_2C_6H_5$), 2.65 (br, 32H, $CH_2CH_2C_6H_5$), 4.37 (d, $J = 7.4$ Hz, 16H, H_{in}), 4.76 (br, 16H, $H_{methine}$), 4.93 (s, 16H, $OCH_2C_6H_5$), 5.37 (s, 8H, H_{acetal}), 5.70 (d, $J = 7.4$ Hz, 16H, H_{out}), 7.36 (s, 8H, *para*-H_{acetal} or *para*-H_{OBn}), 7.38 (s, 8H, *para*-H_{acetal} or *para*-H_{OBn}); MS: $m/z = 4865$ (100%) $[M + Na^+]$, 4861 calcd for $C_{316}H_{272}O_{48} + Na^+$; elemental analysis calcd for $C_{316}H_{272}O_{48}$: C 78.46, H 5.67; found: C 78.38, H 5.60.

5: ^1H NMR: $\delta = 2.47$ (m, 24H, $CH_2CH_2C_6H_5$), 2.65 (m, 24H, $CH_2CH_2C_6H_5$), 4.36 (d, $J = 7.2$ Hz, 12H, H_{in}), 4.82 (t, $J = 7.9$ Hz, 12H, $H_{methine}$), 4.84 (s, 12H, $OCH_2C_6H_5$), 5.59 (s, 6H, H_{acetal}), 5.87 (d, $J = 7.1$ Hz, 12H, H_{out}), 6.81 (s, 6H, *para*-H_{acetal} or *para*-H_{OBn}), 6.85 (s, 6H, *para*-H_{acetal} or *para*-H_{OBn}), 7.10-7.30 (br m, $CH_2CH_2C_6H_5$, $CH_2C_6H_5$, $CHCl_3$); MS: $m/z = 3651$ (100%) $[M + Na^+]$, 3651 calcd for $C_{237}H_{204}O_{36} + Na^+$; elemental analysis calcd for $C_{237}H_{204}O_{36}$: C 78.46, H 5.67; found: C 78.20, H 5.60.

6: Tetramer **4** (98.2 mg, 0.0203 mmol) was dissolved in benzene (50 mL), MeOH (2.5 mL), and acetone (2.5 mL) in a glass bomb, and 10% Pd/C (98 mg) added. The glass bomb was subjected to high-pressure hydrogenolysis, and purification carried out as for **7** to yield tetramer **6** (78.4 mg, 0.0190 mmol, 94%). ^1H NMR ($CDCl_3$/CD_3OD 20/1): $\delta = 2.40$ (m, 32H, $CH_2CH_2C_6H_5$), 2.59 (m, 32H, $CH_2CH_2C_6H_5$), 4.31 (d, $J = 7.1$ Hz, 16H, H_{in}), 4.75 (t, $J = 7.8$ Hz, 16H, $H_{methine}$), 5.50 (s, 8H, H_{acetal}), 5.85 (d, $J = 7.2$ Hz, 16H, H_{out}), 6.58 (s, 8H, *para*-H_{OH}), 6.85 (s, 8H, *para*-H_{acetal}), 7.10–7.30 (br m, $CH_2CH_2C_6H_5$, $CH_2C_6H_5$, $CHCl_3$); MS: $m/z = 4136$ (100%) $[M + Na^+]$, 4140 calcd for $C_{260}H_{224}O_{48} + Na^+$; elemental analysis calcd for $C_{260}H_{224}O_{48}$: C 75.86, H 5.48; found: C 76.10, H 5.68.

 © WILEY-VCH Verlag GmbH, D-69451 Weinheim, 1997 0570-0833/97/3616-1728 $ 17.50+.50/0

7: Trimer **5** (65.7 mg, 0.0181 mmol) was dissolved in benzene (30 mL), MeOH (1.5 mL), and acetone (1.5 mL) in a glass bomb, and 10% Pd/C (66 mg) added. The bomb was subjected to three freeze–thaw cycles under vacuum, then cooled to −196 °C and opened to H_2 (1 atm) for 15 min, closed, and stirred for 48 h at 25 °C. The bomb was then cooled to −196 °C, and opened to air. The reaction mixture was thawed, added to a pad of Celite, and rinsed with THF. The solvent was removed from the filtrate under vacuum to give an off-white residue, which was recrystallized from $CHCl_3$/MeOH to give trimer **7** (50.1 mg, 0.0162 mmol, 90%). ^{1}H NMR ($CDCl_3/CD_3OD$ 20/1): δ = 2.41 (m, 24H, $CH_2CH_2C_6H_5$), 2.59 (m, 24H, $CH_2CH_2C_6H_5$), 4.31 (d, J = 7.1 Hz, 12H, H_{in}), 4.76 (t, J = 7.8 Hz, 12H, $H_{methine}$), 5.69 (s, 6H, H_{acetal}), 5.85 (d, J = 7.1 Hz, 12H, H_{out},), 6.59 (s, 6H, *para*-H_{OH}), 6.79 (s, 6H, *para*-H_{acetal}), 7.10–7.30 (br m, $CH_2CH_2C_6H_5$, $CH_2C_6H_5$, $CHCl_3$); MS: m/z = 3111 (100%) [M+Na^+], 3110 calcd for $C_{195}H_{168}O_{36}$+Na^+; elemental analysis calcd for $C_{195}H_{168}O_{36}\cdot H_2O$: C 75.42, H 5.52; found: C 75.18, H 5.66.

8·2pyr: Tetramer **6** (32.8 mg, 0.00797 mmol), K_2CO_3 (150 mg, 1.08 mmol, 135 equiv), CH_2ClBr (2.7 μL, 0.0415 mmol, 5 equiv), and 5 mol% pyrazine (626 mg, 982 equiv) were added to *N*-methylpyrrolidinone (15 mL). The reaction mixture was stirred under an N_2 atmosphere for 24 h at 25 °C and then for 24 h at 60 °C. Additional CH_2ClBr (2.7 μL) was added after the first day. The solvent was removed under vacuum, and 2 M HCl (30 mL) added to the residue. The aqueous layer was extracted with $CHCl_3$ (3 × 10 mL), and the combined $CHCl_3$ fractions were dried over $MgSO_4$ and filtered. The solvent was removed under vacuum. The residue was filtered through a pad of silica gel with $CHCl_3$ and recrystallized from $CHCl_3$/EtOAc to give bis(carceplex) **8**·2pyr (25.4 mg, 0.00587 mmol, 74%). ^{1}H NMR: δ = 2.51 (m, 32H, $CH_2CH_2C_6H_5$), 2.67 (m, 32H, $CH_2CH_2C_6H_5$), 4.07 (d, J = 7.6 Hz, 8H, H_{in}), 4.25 (d, J = 7.4 Hz, 8H, H_{in}), 4.30 (s, 8H, encapsulated pyrazine), 4.77 (t, J = 7.6 Hz, 8H, $H_{methine}$), 4.92 (t, J = 7.9 Hz, 8H, $H_{methine}$), 5.63 (s, 4H, H_{acetal}), 6.03 (d, J = 7.6 Hz, 16H, H_{out}), 6.06 (d, J = 5.8 Hz, 4H, H_{acetal}), 6.26 (d, J = 5.8 Hz, 4H, H_{acetal}), 6.51 (s, 4H, H_{acetal}), 6.87 (s, 4H, *para*-H_{acetal}), 6.91 (s, 8H, *para*-H_{acetal}), 7.02 (s, 4H, *para*-H_{acetal}), 7.10–7.30 (br m, $CH_2CH_2C_6H_5$, $CH_2C_6H_5$, $CHCl_3$); MS: m/z = 4345 (100%) [M+Na^+], 4348 calcd for $C_{264}H_{224}O_{48}\cdot(C_4H_4N_2)_2$+$Na^+$; elemental analysis calcd for $C_{264}H_{224}O_{48}\cdot(C_4H_4N_2)_2$: C 75.45, H 5.41, N 1.30; found: C 75.33, H 5.32, N 1.19.

Received: January 21, 1997 [Z10018IE]
German version: *Angew. Chem.* **1997**, *109*, 1828–1830

Keywords: carceplexes · cavitands · host–guest chemistry · self-assembly · supramolecular chemistry

[1] M. Goodman, Y. Feng, G. Melacini, J. P. Taulane, *J. Am. Chem. Soc.* **1996**, *118*, 5156.
[2] G. R. Desiraju, *Angew. Chem.* **1995**, *107*, 2541; *Angew. Chem. Int. Ed. Engl.* **1995**, *34*, 2311.
[3] G. M. Whitesides, E. E. Simanek, J. P. Mathias, C. T. Seto, D. N. Chin, M. Mammen, D. M. Gordon, *Acc. Chem. Res.* **1995**, *28*, 37.
[4] a) D. J. Cram, *Nature* **1992**, *356*, 29; b) J. C. Sherman, *Tetrahedron* **1995**, *51*, 3395; c) A. Müller, E. Diemann, E. Krickemeyer, S. Che, *Naturwissenschaften* **1993**, *80*, 77; d) B.-H. Huisman, D. M. Rudkevich, F. C. J. M. van Veggel, D. N. Reinhoudt, *J. Am. Chem. Soc.* **1996**, *118*, 3523.
[5] R. G. Chapman, N. Chopra, E. D. Cochien, J. C. Sherman, *J. Am. Chem. Soc.* **1994**, *116*, 369; template effect of hemicarceplex formation: N. Chopra, J. C. Sherman, *Supramol. Chem.* **1995**, *5*, 31.
[6] a) Cyclic array of two cavitands and two calixarenes: P. Timmerman, W. Verboom, F. C. J. M. van Veggel, W. P. van Hoorn, D. N. Reinhoudt, *Angew. Chem.* **1994**, *106*, 1313; *Angew. Chem. Int. Ed. Engl.* **1994**, *33*, 1292; cyclic array of 3–8 calixarenes: b) P. D. Beer, A. D. Keefe, A. M. Z. Slawin, D. J. Williams, *J. Chem. Soc. Dalton Trans.* **1990**, 3675; c) D. Kraft, J.-D. van Loon, M. Owens, W. Verboom, W. Vogt, M. A. McKervey, V. Böhmer, D. N. Reinhoudt, *Tetrahedron Lett.* **1990**, *31*, 4941; d) P. Lhoták, M. Kawaguchi, A. Ikeda, S. Shinkai, *Tetrahedron* **1996**, *52*, 12399.
[7] J. C. Sherman, C. B. Knobler, D. J. Cram, *J. Am. Chem. Soc.* **1991**, *113*, 2194.
[8] For other hosts that contain a large cavity, see ref. [6] and a) J. H. Small, D. J. McCord, J. Greaves, K. J. Shea, *J. Am. Chem. Soc.* **1995**, *117*, 11588; b) M. Fujita, D. Oguro, M. Miyazawa, H. Oka, K. Yamaguchi, K. Ogura, *Nature* **1995**, *378*, 469; c) J. W. Steed, C. P. Johnson, C. L. Barnes, R. K. Juneja, J. L. Atwood, S. Reilly, R. L. Hollis, P. H. Smith, D. L. Clark, *J. Am. Chem. Soc.* **1995**, *117*, 11426; d) S. Watanabe, K. Goto, T. Kawashima, R. Okazaki, *Tetrahedron Lett.* **1995**, *36*, 7677; e) K. Araki, K. Akao, A. Ikeda, T. Suzuki, S. Shinkai, *ibid.* **1996**, *37*, 73; f) A. Arduini, A. Pochini, A. Secchi, R. Ungaro, *J. Chem. Soc. Chem. Commun.* **1995**, 879; g) P. A. Brady, R. P. Bonar-Law, S. J. Rowan, C. J. Suckling, J. K. M. Sunders, *Chem. Commun.* **1996**, 319.
[9] We recently reported a reversible complex between two molecules of tetrol **1** in which the bowls are linked by four charged hydrogen bonds ($ArO^-\cdots HOAr$): R. G. Chapman, J. C. Sherman, *J. Am. Chem. Soc.* **1995**, *117*, 1081. Tetramer **6** can potentially oligomerize into channels over such linkages; investigations are currently underway.
[10] a) A. Harada, J. Li, M. Kamachi, *Nature* **1994**, *370*, 126; b) C. Wu, T. Bein, *Science* **1994**, *266*, 1013; c) M. R. Ghadiri, J. R. Granja, L. K. Buehler, *Nature* **1994**, *369*, 301; d) J.-A. Pérez-Adelmar, H. Abraham, C. Sánchez, K. Rissanen, P. Prados, J. de Mendoza, *Angew. Chem.* **1996**, *108*, 1088; *Angew. Chem. Int. Ed. Engl.* **1996**, *35*, 1009.
[11] The "gating" mechanism for egress of guests from carceplexes and hemicarceplexes: a) K. N. Houk, K. Nakamura, C. Sheu, A. E. Keating, *Science* **1996**, *273*, 627; b) C. Sheu, K. N. Houk, *J. Am. Chem. Soc.* **1996**, *118*, 8056; c) K. Nakamura, K. N. Houk, *ibid.* **1995**, *117*, 1853.
[12] J. R. Fraser, B. Borecka, J. Trotter, J. C. Sherman, *J. Org. Chem.* **1995**, *60*, 1207.
[13] a) CS Chem 3D, CambridgeSoft Corp., Cambridge, MA, USA, **1995**; b) U. Burkert, N. L. Allinger, *Molecular Mechanics*, American Chemical Society, Washington, DC, USA, **1982**.

Gas-Phase Enantiodifferentiation of Chiral Molecules: Chiral Recognition of 1-Phenyl-1-propanol/2-Butanol Clusters by Resonance Enhanced Multiphoton Ionization Spectroscopy**

Susanna Piccirillo, Cesare Bosman, Daniela Toja, Anna Giardini-Guidoni, Marco Pierini, Anna Troiani, and Maurizio Speranza*

Enantioselective complexation is a basic tool for molecular recognition. In the condensed phase chiral molecules (M) may establish short-range electrostatic, orbital, and steric interactions with suitable chiral partners (C) to form diastereomeric molecular complexes (MC), which are discriminable by virtue of their different physical and chemical properties. Determination of melting point and solubility, vapor-pressure measurements, as well as X-ray analysis[1] are commonly used to discriminate diastereomeric MC crystals. In solution calorimetric, colorimetric,[2] spectroscopic, and transport-rate measurements can be used, although the presence of the solvent may sometimes hinder their differentiation.[2, 3]

A way to eliminate this undesired interference and to evaluate the intrinsic interactions in diastereomeric MC is to extend their study to the gas phase; this, however, is by no means an easy task. Mass spectrometry has been occasionally employed to enantiodifferentiate chiral ions by complexation with suitable chiral hosts.[4] The inherent limitation of mass spetrometry to discriminate between diastereomeric or enantiomeric species demands the frequent use of isotopic markers, which may somewhat alter the relative stability of diastereomeric ion-neutral complexes.

[*] Prof. M. Speranza, Dr. M. Pierini, Dr. A. Troiani
Facoltà di Farmacia
Dipartimento di Studi di Chimica e Tecnologia delle Sostanze Biologicamente Attive
Università di Roma "La Sapienza"
P.le A. Moro 5, I-00185 Rome (Italy)
Fax: Int. code +(6)4991-3602
e-mail: speranza@axrma.uniroma1.it
Dr. S. Piccirillo, Dr. C. Bosman
Istituto Materiali Speciali, CNR, Tito Scalo (Italy)
Dr. D. Toja, Prof. A. Giardini-Guidoni
Dipartimento di Chimica, Università di Roma "La Sapienza"

[**] This work was supported by the Ministero della Università e della Ricerca Scientifica e Tecnologica (MURST) and the Consiglio Nazionale delle Ricerche (CNR). Help and advice from Professor F. Cacace, Professor F. Gasparrini, and Dr. M. Aschi are gratefully acknowledged.

 © WILEY-VCH Verlag GmbH, D-69451 Weinheim, 1997 0570-0833/97/3616-1729 $ 17.50+.50/0

Enantiodifferentiation of neutral chiral molecules in the gas phase can be obtained by high-resolution molecular spectroscopy of their MC complexes with chiral partners. So far there has only been one study on the laser induced fluorescence (LIF) excitation spectra of a single jet-cooled van der Waals diastereomeric MC pair.[5] Here we illustrate the first application of resonant multiphoton ionization spectroscopy (REMPI),[6] combined with time-of-flight (TOF) mass spectrometry,[7] to discriminate supersonically expanded van der Waals diastereomeric MC complexes, and to study their fundamental properties at the microscopic level. The complexes were obtained by combining a chiral chromophore, in this case (*R*)-(+)-1-phenyl-1-propanol ($\mathbf{P_R}$), with the enantiomers of 2-butanol ($\mathbf{B_R}$ or $\mathbf{B_S}$). Their MC complexes ($\mathbf{P_RB_R}$ or $\mathbf{P_RB_S}$) are expected to display different spectral signatures with respect to the electronic band origin of each pair, their appearance potential, and their vibronic bands, in particular those due to intermolecular vibrations of $\mathbf{P_R}$ with the partner ($\mathbf{B_R}$ or $\mathbf{B_S}$).[8]

The $\mathbf{P_RB_R}$ and $\mathbf{P_RB_S}$ clusters were discriminated by one-color resonance enhanced multiphoton ionization (1cREMPI) experiments, in which the complex is excited to a discrete S_1 state by absorption of one photon of frequency ν_1, and then to the continuum by absorption of several other photons with the same frequency ν_1. The 1cREMPI excitation spectra are taken by recording the TOF mass spectra of $\mathbf{P_RB_R}$ (or $\mathbf{P_RB_S}$) as a function of ν_1. The appearance potential of pure $\mathbf{P_R}$ is measured by two-color resonance enhanced two photon ionization (2cR2PI) experiments, in which the molecule is excited to a discrete S_1 state by one photon of a fixed frequency ν_1, and then ionized by a second photon of variable frequency ν_2. A value of 9.01 ± 0.01 eV is obtained for pure $\mathbf{P_R}$, which compares well with the ionization potential of 8.9 eV for benzyl alcohol at room temperature.[9]

The 1cREMPI excitation spectrum of pure $\mathbf{P_R}$ is characterized by the electronic band origin of the $S_1 \leftarrow S_0$ transition of the molecule placed at 37577 cm^{-1} and followed by two intense peaks that are shifted by 41 and 47 cm^{-1}. Other strong vibronic transitions are observed at 530, 575, 581, 629, 772, and 976 cm^{-1} from the origin. The low-frequency modes are assigned to torsional motion of the ring substituents. The other intense features are at frequencies typical for motion of the aromatic ring and ethyl or OH groups, and were not completely identified.[10]

Figure 1 reports the 1cREMPI excitation spectra of the diasteromeric pairs $\mathbf{P_RB_R}$ and $\mathbf{P_RB_S}$ around their electronic band origin. Both clusters display a complex vibronic spectrum due to numerous van der Waals vibrations, which may be coupled with low-frequency modes of the partners.[11, 12] The spectra are red shifted relative to the $S_1 \leftarrow S_0$ origin of the isolated $\mathbf{P_R}$ molecule, indicating an enhancement of binding energy for the clusters in the S_1 state relative to the S_0 state. The shifts of the most intense bands, assigned to the electronic band origin of the corresponding clusters, differ by 13 cm^{-1} as a result of a $\mathbf{P_RB_R}$-band shift of -79 cm^{-1} and of a $\mathbf{P_RB_S}$-band shift of -92 cm^{-1}. This reflects an $S_1 \leftarrow S_0$ energy gap for $\mathbf{P_RB_S}$ that is smaller than that for $\mathbf{P_RB_R}$.

The 1cREMPI excitation spectrum of the mixture with $[\mathbf{P_RB_R}]/[\mathbf{P_RB_S}] = 1$, obtained by clustering $\mathbf{P_R}$ with 2-butanol racemate, essentially corresponds to the superimposed spectra of the separate $\mathbf{P_RB_R}$ and $\mathbf{P_RB_S}$ clusters. However, when equilibration between $\mathbf{P_RB_R}$ and $\mathbf{P_RB_S}$ is favored by increasing the stagnation pressure from 2 to 5×10^5 Pa, the relative intensity of the $\mathbf{P_RB_R}$ bands increases, and that of the $\mathbf{P_RB_S}$ bands decreases by about 7%.[13] These findings corroborate molecular mechanics calculations[14] that predict that the ground-state homochiral $\mathbf{P_RB_R}$ adduct is more stable than the heterochiral $\mathbf{P_RB_S}$ adduct. Therefore, the decrease in the $S_1 \leftarrow S_0$ energy gap in going from $\mathbf{P_RB_R}$ to $\mathbf{P_RB_S}$ points to an excited state in which the stability difference of the clusters tends to be cancelled out or even reversed relative to the ground state.

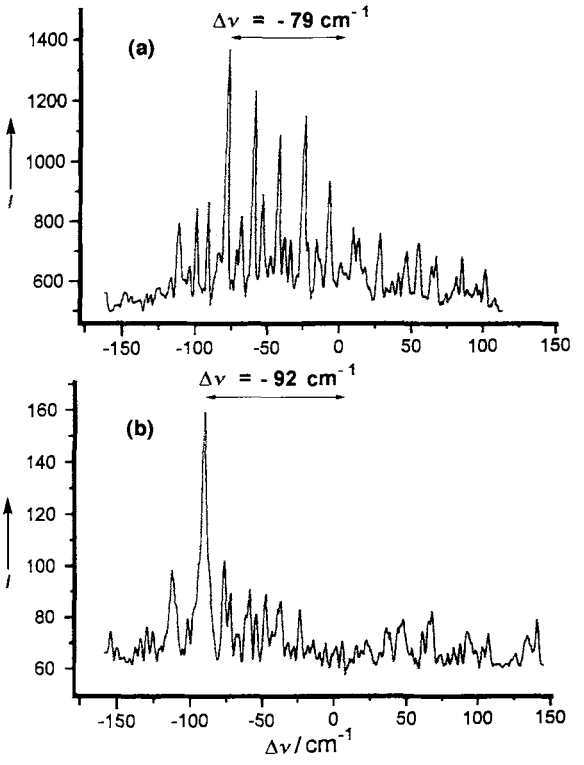

Figure 1. 1cREMPI excitation spectra of diasteromeric $\mathbf{P_RB_R}$ (a) and $\mathbf{P_RB_S}$ (b) clusters measured at $m/z = 210$ and a total stagnation pressure of 2×10^5 Pa. The origin of the frequency scale is relative to the electronic band origin of the $S_1 \leftarrow S_0$ transition of $\mathbf{P_R}$ at 37577 cm^{-1}. I = intensity (arbitrary units).

Figure 2 displays the highly reproducible 1cREMPI/TOF mass spectra of diastereomeric $\mathbf{P_RB_R}$ (Figure 2a) and $\mathbf{P_RB_S}$ (Figure 2b) complexes taken at a fixed frequency, namely at the electronic origin frequency of the corresponding cluster (Figure 1). In addition to the parent ion $[\mathbf{P_RB_R}]^+$ (or $[\mathbf{P_RB_S}]^+$) at $m/z = 210$ the spectra show the formation of fragments $[\mathbf{P_R}]^+$ ($m/z = 136$), $[\mathbf{P_RB_R} - C_2H_5]^+$ (or $[\mathbf{P_RB_S} - C_2H_5]^+$; $m/z = 181$), and $[\mathbf{P_R} - C_2H_5]^+$ ($m/z = 107$). That all these species and $[\mathbf{P_RB_R}]^+$ (or $[\mathbf{P_RB_S}]^+$) actually have the same origin is testified by their identical 1cREMPI excitation patterns.

The distinct difference between the 1cREMPI/TOF mass spectra of the diastereomers $\mathbf{P_RB_R}$ and $\mathbf{P_RB_S}$ (Figure 2a, b) provides a further tool for their discrimination. In particular the spectrum of the homochiral cluster $\mathbf{P_RB_R}$ (Figure 2a) shows a distribution of $[\mathbf{P_R}]^+ : [\mathbf{P_RB_R} - C_2H_5]^+ : [\mathbf{P_R} - C_2H_5]^+ : [\mathbf{P_RB_R}]^+ = 0.6 : 2.5 : 0.7 : 1.0$, which clearly diverges from that of the heterochiral cluster $\mathbf{P_RB_S}$ ($[\mathbf{P_R}]^+ : [\mathbf{P_RB_S} - C_2H_5]^+ : [\mathbf{P_R} - C_2H_5]^+ : [\mathbf{P_RB_S}]^+ = 1.4 : 9.7 : 3.2 : 1.0$; Figure 2b). The more extensive fragmentation observed in the spectrum of $\mathbf{P_RB_S}$ (93% ($\mathbf{P_RB_S}$) versus 79% ($\mathbf{P_RB_R}$)) is responsible for the comparatively low intensity of its 1cREMPI excitation spectrum (see Figure 1a, b), and suggests that, despite the slightly higher energy absorbed by $\mathbf{P_RB_R}$,[15] higher-energy dissociative states are more populated in heterochiral $\mathbf{P_RB_S}$ than in homochiral $\mathbf{P_RB_R}$ for the same 1cREMPI process.

The REMPI/TOF technique has been applied for the first time to enantiodifferentiate neutral chiral molecules in the gas phase. Chiral recognition is based on highly reproducible differ-

 © WILEY-VCH Verlag GmbH, D-69451 Weinheim, 1997 0570-0833/97/3616-1730 $ 17.50+.50/0

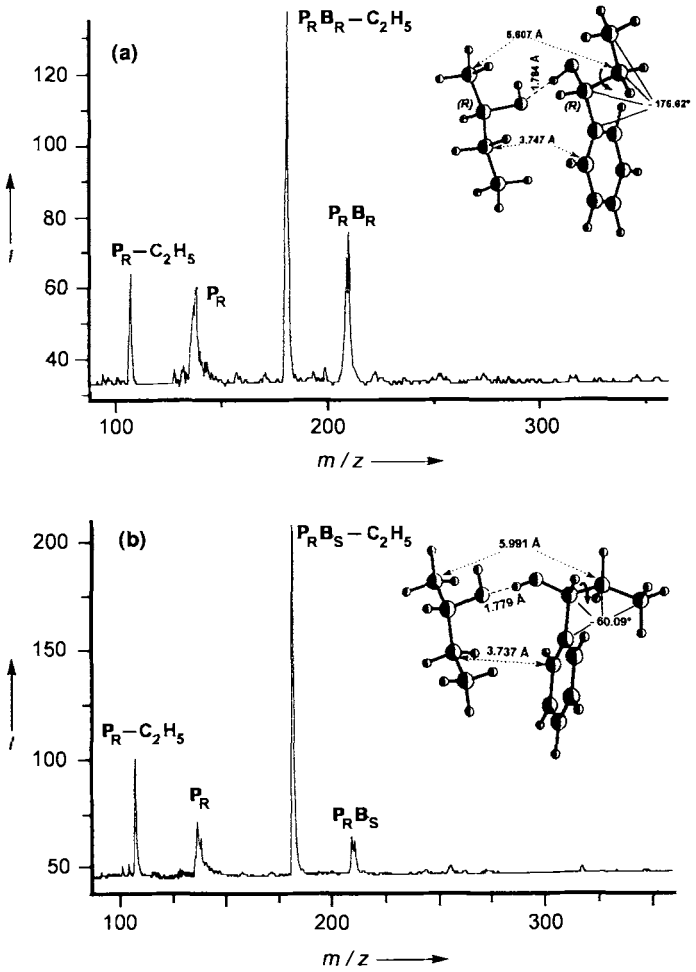

Figure 2. 1cREMPI/TOF spectra of diasteromeric P_RB_R at $\lambda = 266.68$ nm (a) and P_RB_S clusters at $\lambda = 266.77$ nm (b) at a total stagnation pressure of 2×10^5 Pa. The structures of the ground state P_RB_R and P_RB_S clusters, calculated with modified molecular mechanics (MMX), are given in (a) and (b), respectively.

ences in the photoionization fragmentation pattern of the diastereomeric clusters obtained from complexation of the chiral molecule with suitable chiral partners, and on the different bathochromic shifts of their electronic band origin relative to that of the pure chromophore. The latter indicates that attractive interactions within the clusters are more pronounced in the excited than in the ground state. Under consideration of the order of stability in the ground state, $P_RB_R > P_RB_S$, a greater stabilization of the P_RB_S cluster in the S_1 state relative to that of P_RB_R tends to cancel the stability order in the excited state. Differences in the absorption frequencies of gaseous jet-cooled species were recently used for isotope-enrichment procedures.[16] This study demonstrates that the same approach can be applied to jet-cooled diastereomeric clusters to enantiomerically enrich a racemate.

Experimental Section

The experimental setup for the generation of van der Waals clusters and their REMPI/TOF analysis was previously described [7, 11, 17]. Diastereomeric pairs P_RB_R and P_RB_S were obtained by in a supersonic beam by adiabatic expansion of a carrier gas (Ar) seeded with the corresponding alcohols (Aldrich) through a pulsed 400-μm nozzle kept at 85 °C. The molecular beam was allowed to pass through a 1-mm skimmer into a second chamber equipped with a TOF spectrometer. The laser system consisted of a frequency-doubled Nd:YAG laser ($\lambda = 532$ nm), which pumps two dye lasers. The dye frequencies were doubled and, when necessary, mixed with residual 1064-nm radiation. The ions formed by REMPI ionization in the TOF source were mass discriminated and detected by a channeltron after a 50-cm flight path.

Received: December 18, 1996
Revised version: March 27, 1997 [Z9911IE]
German version: *Angew. Chem.* **1997**, *109*, 1816–1818

Keywords: chirality · enantiomeric resolution · laser spectroscopy · mass spectrometry · molecular recognition

[1] A. Findlay, A. N. Campbell, *The Phase Rule and Its Applications*, Dover, New York, **1945**, pp. 136, 256.
[2] Y. Kubo, S. Maeda, S. Tokita, M. Kubo, *Nature* **1996**, *382*, 522.
[3] See for instance E. M. Arnett, S. P. Zingg, *J. Am. Chem. Soc.* **1981**, *103*, 1221.
[4] M. Sawada, Y. Takai, H. Yamada, S. Hirayama, T. Kaneda, T. Tanaka, K. Kamada, T. Mizooku, S. Takeuchi, K. Ueno, K. Hirose, Y. Tobe, K. Naemura, *J. Am. Chem. Soc.* **1995**, *117*, 7726, and references therein.
[5] A. R. Al-Rabaa, E. Bréhéret, F. Lahmani, A. Zehnacker, *Chem. Phys. Lett.* **1995**, *237*, 480.
[6] B. Brutschy, *Chem. Rev.* **1992**, *92*, 1567.
[7] S. Piccirillo, M. Coreno, A. Giardini-Guidoni, G. Pizzella, M. Snels, R. Teghil, *J. Mol. Struct.* **1993**, *293*, 197.
[8] S. Piccirillo, D. Consalvo, M. Coreno, A. Giardini-Guidoni, S. Duin, P. Parneix, P. Brechignac, *Chem. Phys.* **1994**, *187*, 97.
[9] R. E. Ballard, J. Jones, E. Sutherland, D. Read, A. Inchley, *Chem. Phys. Lett.* **1986**, *126*, 311.
[10] S. Piccirillo, A. Giardini-Guidoni, unpublished results.
[11] D. Consalvo, A. van der Avoird, S. Piccirillo, M. Coreno, A. Giardini-Guidoni, A. Mele, M. Snels, *J. Chem. Phys.* **1993**, *99*, 8398.
[12] Careful adjustment of the expansion parameters allowed us to maximize the concentration of two-body P_RB_R and P_RB_S clusters relative to that of larger adducts.
[13] M. D. Brookes, D. J. Hughes, B. J. Howard, *J. Chem. Phys.* **1996**, *104*, 5391.
[14] Molecular mechanics calculations were performed by using "automatic and systematic quasi-flexible docking processing" (S. Alcaro, F. Gasparrini, O. Incani, M. Pierini, C. Villani, *J. Comput. Chem.*, submitted) and applying MMX force field, as implemented in the PC-model software (PC Model Molecular Modeling Software, Serena Software, P. O. Box 3076, Bloomington, IN 17102–3076 (USA)).
[15] The energy absorbed by P_RB_R exceeds that absorbed by P_RB_S by $n13\,cm^{-1}$, where n is the number of absorbed photons, and 13 cm^{-1} the red shift between the two clusters.
[16] A. Giardini-Guidoni, E. Borsella, R. Fantoni, *Europhys. News* **1985**, *16*, 2.
[17] M. Coreno, S. Piccirillo, A. Giardini-Guidoni, A. Mele, A. Palleschi, P. Brechignac, P. Parneix, *Chem. Phys. Lett.* **1995**, *236*, 580.

Multipolymer-Supported Substrate and Ligand Approach to the Sharpless Asymmetric Dihydroxylation**

Hyunsoo Han and Kim D. Janda*

Since the initial solid-phase synthesis of oligopeptides by Merrifield[1] the use of polymers as supports, reagents or even catalysts for various reactions has increased.[2] Recently a high level of activity has been devoted to this field due to the application of combinatorial chemistry to drug discovery.[3] Although a resurgence of interest in polymers for organic synthesis has been seen, little effort has been paid to defining the structural

[*] Prof. K. D. Janda, Dr. H. Han
The Scripps Research Institute
Department of Chemistry and
The Skaggs Institute for Chemical Biology
10550 N. Torrey Pines Road, La Jolla, CA 92037 (USA)
Fax: Int. code + (619) 784-2595
e-mail: kdjanda@scripps.edu

[**] This research was supported by the R. W. Johnson Pharmaceutical Institute and The Skaggs Institute for Chemical Biology.

 © WILEY-VCH Verlag GmbH, D-69451 Weinheim, 1997 0570-0833/97/3616-1731 $ 17.50+.50/0

parameters of the supports. This is most evident for automated organic synthesis.

We demonstrated how a chiral ligand can be integrated onto a soluble polymeric species so that ligand-accelerated catalysis (LAC) can operate in an unhindered manner.[4] However, the converse case in which a small organic moiety is attached to a polymeric matrix has yet to be investigated. The implication of the combination of these two scenarios—immobilization of the ligand and the substrate—is that a multipolymer LAC reaction may be a feasible. We studied the influence of the structure of solid- and liquid-phase polymers on the Sharpless asymmetric dihydroxylation (AD) reaction. The outgrowth of these findings allowed us to successfully run a multipolymer Sharpless AD reaction.

A variety of supports have been used in organic synthesis.[5] Typically, they may be grouped into three categories: 1) minimal cross-linked supports that form well-solvated gels,[6] 2) porous but rigid supports with a high degree of cross-linking,[7] and 3) linear, soluble polymers that are also known as liquid-phase supports.[8] Three supports belonging to the first category, two low divinylbenzene-cross-linked polystyrene beads (Merrifield and Wang resin) and the graft copolymer polystyrene polyethylene glycol (Tentagel), were utilized. The choice of these resins was based on their fundamental differences. Merrifield and Wang resins are relatively hydrophobic matrices, whereas Tentagel is considered to be a hydrophilic tentacle polymer with more "solution-like" characteristics.[8b] The support used from the third category was polyethylene glycol (PEG). This homopolymer was enlisted because it fulfills the criteria for a third-group polymer, and its chemical reactivity differences contrasted that of Tentagel.

trans-Cinnamic acid was immobilized on the four polymeric supports (Figure 1). This ensured that the olefin was tethered as

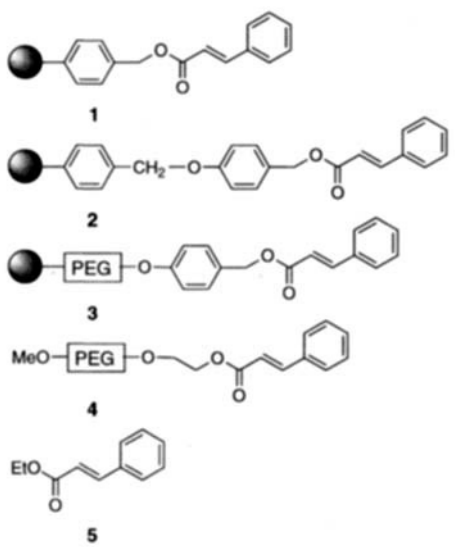

Figure 1. Polymer-bound *trans*-cinnamate esters **1**–**4** used in the Sharpless AD reaction as well as non-polymer counterpart **5**.

an ester on all supports, and that the overall reactivity was determined only by composition of the polymer. Because the AD reactivity of ethyl *trans*-cinnamate (**5**) using the ligand 1,4-phthalazinediyl diether hydroquinidine [$(DHQD)_2PHAL$, **7**] has been documented,[9] a direct correlation could be made between the solution and polymeric reactions [Eq. (1)].

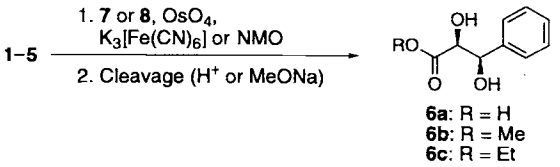

(1)

Table 1 shows the results of the AD reaction of the four polymer-bound *trans*-cinnamate esters **1**–**4** using ligands **7** and **8**.

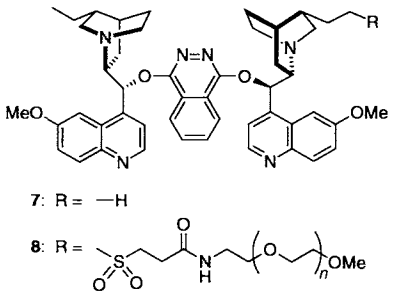

The amount of metal/ligand used, reaction time required for product conversion, and enantiomeric excess observed vary greatly depending on the support. The non-cross-linked liquid-phase resin **4** (Table 1, entries 6 and 10) provides the best overall results when considering reaction time and metal/ligand ratio. These results compare favorably with those from the reaction of the simple ethyl ester **5** (entry 11).

Table 1. AD reactions conducted with *trans*-cinnamate esters using ligands **7** and **8**.

Entry	Olefin	*t* [h]	OsO_4 [a]	Method [b]	Conversion [%] [c]	*ee* [%] [d]
1	**1**	72	0.01	A	–	–
2	**2**	72	0.01	A	–	–
3	**3**	24	0.01	A	3	99
4	**3**	24	0.02	A	63	98
5	**3**	24	0.10	A	96	99
6	**4**	0.5	0.10	A	100	99
7	**1**	24	0.01	B	100	88
8	**2**	24	0.01	B	100	90
9	**3**	24	0.01	B	100	87
10	**4**	24	0.008	A	80	97
11	**5**	24	0.008	A	100	97
12 [e]	**3**	24	0.02	A	60	98
13 [e]	**3**	24	0.10	A	98	98

[a] Equivalents of OsO_4 based on olefin. [ligand]/[OsO_4] = 2.5. [b] Method A: $K_3[Fe(CN)_6]$ and *t*-BuOH/water (1/1) at room temperature. Method B: NMO and acetone/water (10/1) at 4 °C. [c] Determined from the ratio of the signals of diol protons to that of the remaining olefin in the ^1H NMR spectrum. Absolute yields (entries 4–13) were between 25–85%. [d] Determined by NMR analysis of the derived bis(Mosher) ester of the diol. [e] Polymer-bound ligand **8** was used as the catalyst source ([**8**]/[OsO_4] = 2.5).

Among the three insoluble supports Tentagel (**3**) outperformed the Wang (**2**) and Merrifield resins (**1**) with $K_3[Fe(CN)_6]$ as oxidant (entries 1–5). However, the cross-linked polystyrene suppports **2** and **3** can provide a suitable environment for LAC when *N*-methylmorpholine *N*-oxide (NMO) is applied as the oxidant and acetone/water as the solvent (entries 7 and 8). It may be that supports **1** and **2** show an overall inability to support the AD reaction with $K_3[Fe(CN)_6]$ due to poor swelling properties in *t*-BuOH/water as solvent.[6] The consequences of poor swelling include limited chain mobility, which could com-

 © WILEY-VCH Verlag GmbH, D-69451 Weinheim, 1997 0570-0833/97/3616-1732 $ 17.50+.50/0

promise the location and distribution of catalyst and olefin within these matrices.

Somewhat unexpected was the large amount of metal and ligand that was required for the Tentagel resin (**3**) to provide a reasonable reaction time, degree of conversion, and enantioselectivity (compare entries 3–5). Interestingly, there appears to be a threshold of catalyst amount that is required for any conversion into diol to be seen (compare entries 3 and 4). We investigated this aspect further. In reaction 4 (Table 1), fresh, unbound olefin **5** (0.125 mmol) was added after 24 h along with OsO_4 (0.02 equiv based on olefin), K_2CO_3 (3.0 equiv), and $K_3[Fe(CN)_6]$ (3.0 equiv). There was only 10 % conversion of **5** into **6c** after a further 10 h. If unbound olefin **5** was used throughout the entire reaction, recharging the mixture with more **5** provided complete conversion into **6c** within 2.5 h. These results suggest that the catalyst becomes entangled in the insoluble support, thereby limiting its availability. Although resin **3** is more hydrophilic than **1** and **2**, it still must be considered as a "quasi-homgeneous" matrix that is subject to some of the same limitations as insoluble resins.

In evaluating these results we recognized that a correct combination of soluble and insoluble polymers (that is, a multipolymeric reaction) could, in principle, be suitable for AD reactions. The use of more than a single polymeric reagent and catalyst either simultaneously or consecutively was accomplished, but its exploitation has been limited to date.[10] The combination of Tentagel resin (**3**) and MeO-PEG-[$(DHQD)_2PHAL$] (**8**)[4, 11] was investigated as the multipolymer components. Entries 12 and 13 in Table 1 show that this combination of polymers can successfully support LAC. Although these two polymers are physically quite different, the outgrowth of this methodology translates into facile product separation and ligand reisolation. The significance of such technology should have direct applications to the automation of synthetic processes.[3, 12]

Experimental Section

Dichloromethane and methanol were dried over CaH_2 and powdered magnesium, respectively. Polyethylene glycol monomethyl ether (Aldrich, MeO-PEG, M_r = 5000) was dried over P_2O_5 under vacuum before use; Merrifield, Wang, and Tentagel resins were bought from Novabiochem. All other solvents and chemicals were obtained from commercial sources, and used without further purification unless stated otherwise. NMR spectra were measured on a Bruker AM-300 spectrometer.

1–4: *trans*-Cinnamic acid was coupled to each resin with the aid of coupling agents 1-(3-dimethylaminopropyl)-3-ethylcarbodiimide hydrochloride (EDC)/*N*,*N*-dimethyl 4-pyridinamine (DMAP) in CH_2Cl_2. For the soluble polymer MeO-PEG, a dicyclohexylcarbodiimide (DCC)/DMAP combination was used for preparing **4**. Upon completion of reaction the urea formed was removed by filtration. Diethyl ether was added to the filtrate, and **4** separated as a white solid from the mixture. The degree of loading for each polymer was greater than 98%, determined by measuring the release of cinnamic acid and its methyl ester from the polymers with trifluoroacetic acid (TFA)/CH_2Cl_2 (v/v 95/5) and NaOMe in MeOH, respectively.

Asymmetric dihydroxylation: method A: A small aliquot of OsO_4 in *t*-BuOH (2.5% solution (wt%), see Table 1 for the amount used in each reaction) was added to a mixture of the ligand (see Table 1), $K_3[Fe(CN)_6]$ (0.250 g, 6 equiv based on olefin), K_2CO_3 (0.052 g, 3 equiv), and methanesulfonamide (0.012 g, 1 equiv) in *t*-BuOH/water (4 mL, v/v 1/1) at room temperature. After the reaction mixture was stirred for 10 min, the polymer-bound olefin (0.125 mmol, 1 equiv) was added in one portion, and the mixture further stirred for 24 h. Solid $Na_2S_2O_5$ was added(0.400 g), and the mixture stirred for an additional 5 min, filtered, and successively washed with acetone and CH_2Cl_2. The resin was dried over Na_2SO_4 under vacuum. The results of the reaction were determined by two methods: 1) The resin was suspended in TFA/CH_2Cl_2 (v/v 95/5) for 30 min. The resin was removed by filtration, and then solvent removed from the filtrate. The degree of conversion of the olefin into the dihydroxylated product was determined by NMR spectroscopy. 2) The resin was suspended in a solution of NaOMe in MeOH. The mixture was stirred for 2 h at room temperature, and the solvent removed under vacuum. The desired diol-methylester was isolated by column chromatography (silica gel; ethyl acetate/hexane 1/1). The enantiomeric excess of this product was determined by NMR analysis of the derived bis(Mosher) ester. Method B: A similar procedure to Method A was followed except acetone/water as solvent and NMO were used. The reaction mixture contained a small amount of OsO_4 in *t*-BuOH (2.5% solution, 13 μL, 0.01 equiv based on olefin), the ligand (0.0025 g, 0.025 equiv), NMO (0.022 g, 1.5 equiv), and tetraethylammonium acetate tetrahydrate (0.033 g, 1.0 equiv) in acetone/water (4 mL, 10/1 v/v) at 4 °C.

Received: December 12, 1996
Revised version: March 12, 1997 [Z9881IE]
German version: *Angew. Chem.* **1997**, *109*, 1835–1837

Keywords: asymmetric synthesis · dihydroxylations · osmium · oxidations · solid-phase synthesis

[1] R. B. Merrifield, *J. Am. Chem. Soc.* **1963**, *85*, 2149–2154.
[2] a) J. L. Crowley, H. Rappoport, *Acc. Chem. Res.* **1976**, *9*, 135–144; b) C. C. Leznoff, *Acc. Chem. Res.* **1978**, *11*, 327–333; c) G. Manecke, W. Storck, *Angew. Chem.* **1978**, *90*, 691–704; *Angew. Chem. Int. Ed. Engl.* **1978**, *17*, 657–670; d) J. M. J. Frechet *Tetrahedron* **1981**, *37*, 663–688; e) P. Hodge in *Synthesis and Seperations Using Functional Polymers* (Eds.: D. C. Sherrington, P. Hodge), Wiley, New York, **1988**, p. 43.
[3] a) *Molecular Diversity and Combinatorial Chemistry* (Eds.: I. M. Chaiken, K. D. Janda) American Chemical Society, Washington, D. C., USA, **1996**; b) J. S. Fruchtel, G. Jung, *Angew. Chem.* **1996**, *108*, 19–46; *Angew. Chem. Int. Ed. Engl.* **1996**, *35*, 17–42; c) F. Balkenhohl, C. von dem Bussche-Hünnefeld, A. Lansky, C. Zechel, *ibid.* **1996**, *108*, 2436–2487 and **1996**. *35*, 2288–2337; d) K. D. Janda, *Proc. Natl. Acad. Sci. USA* **1994**, *91*, 10779–10785.
[4] H. Han, K. D. Janda, *J. Am. Chem. Soc.* **1996**, *118*, 7632–7633.
[5] a) N. K. Terrett, M. Gardner, D. W. Gordon, R. J. Kobylecki, J. Steel, *Tetrahedron* **1995**, *51*, 8135–8173; b) L. A. Thompson, J. A. Ellman, *Chem. Rev.* **1996**, 555–600; c) P. H. H. Hermkens, H. C. J. Ottenheijm, D. Rees, *Tetrahedron* **1996**, *52*, 4527–4554.
[6] R. B. Merrifield, *Angew. Chem.* **1985**, *97*, 801–812; *Angew. Chem. Int. Ed. Engl.* **1985**, *24*, 799–810.
[7] A. Gugot, M. Bartholin, *Prog. Polym. Sci.* **1982**, *8*, 277–332.
[8] a) K. E. Geckeler, *Adv. Polym. Sci.* 1995, *121*, 31–79; b) E. Bayer, *Angew Chem.* **1991**, *103*, 117–133; *Angew. Chem. Int. Ed. Engl.* **1991**, *30*, 113–129; c) D. E. Bergbreiter in *Proc. 6th Annu. IUCCP Symp. Functional Polymers* (Eds.: D. E. Bergbreiter, C. R. Martin), Plenum Press, New York, **1989**, p. 143.
[9] K. B. Sharpless, W. Amberg, Y. L. Bennan, G. A. Crispino, J. Hartung, K.-S. Jeong, H.-L. Kwong, K. Morikawa, Z.-M Wang, D. Xu, X.-L Zhang, *J. Org. Chem.* **1992**, *57*, 2768–2771.
[10] Examples of peptide syntheses: a) G. Heusel, G. Bovermann, W. Göhring, G. Jung, *Angew. Chem.* **1977**, *89*, 681–682; *Angew. Chem. Int. Ed. Engl.* **1977**, *16*, 642–643; b) H. Frank, H. Hagenmaier, *Experentia* **1975**, *31*, 131–133; examples other than peptides: c) B. J. Cohen, M. A. Kraus, A. Patchornik, *J. Am. Chem. Soc.* **1977**, *99*, 4165–4167; d) C. V. Pittman, L. R. Smith, *ibid.* **1975**, *97*, 1749–1754; e) J. P. Collman, K. M. Kosydar, M. Bressan, W. Lamanna, T. Garrett, *ibid.* **1984**, *106*, 2569–2579; f) D. E. Bergbreiter, R. Chandran, *ibid.* **1987**, *109*, 174–179; g) *ibid.* **1985**, *107*, 4792–4793; h) J. J. Parlow, *Tetrahedron Lett.* **1995**, *36*, 1395–1396; i) F. Svec, J. M. J. Frechet, *Science* **1996**, *273*, 205–211; detection of highly reactive intermediates with two polymeric reagents ("three-phase test"): J. Rebek, *Tetrahedron* **1979**, *35*, 723–731, and references therein.
[11] H. Han, K. D. Janda, *Tetrahedron Lett.* **1997**, *38*, 977–980.
[12] a) A. R. Frisbee, M. H. Nantz, G. W. Kramer, P. L. Fuchs, *J. Am. Chem. Soc.* **1984**, *106*, 7143–7145; b) S. H. Dewitt, A. W. Czarnik, *Curr. Biol.*, **1995**, *6*, 640–645; c) G. W. Kramer, P. L. Fuchs, *Chemtech* **1989**, *19*, 682–688; d) S. Hobbs Dewitt, A. W. Czarnik, *Acc. Chem. Res.* **1996**, *29*, 114–122.

 © WILEY-VCH Verlag GmbH, D-69451 Weinheim, 1997 0570-0833/97/3616-1733 $ 17.50+.50/0

Stabilization of Iron Centers in High Oxidation State in the Mononuclear Complex [Fe^{V}(I)('N$_2$S$_2$')]**

Dieter Sellmann,* Susanne Emig, and Frank W. Heinemann

Complexes containing iron centers in oxidation states higher than +III are intermediates in numerous biological oxidation processes[1] and of interest as potential catalysts for homogeneous oxidations. Discrete molecular complexes of Fe^{IV} are, however, rare,[2] and the even higher oxidation states Fe^{V} and Fe^{VI} have so far been established only for the solid-state structures of polynuclear tetraoxo ferrates such as $K_3[Fe^{V}O_4]$ and $K_2[Fe^{VI}O_4]$.[3] We have now found that Fe^{V} can be stabilized by the tetraanionic thiolate amido ligand 'N$_2$S$_2$'$^{4-}$ [=1,2-ethanediamide-*N*,*N*'-bis(2-benzenethiolate)(4 −)].

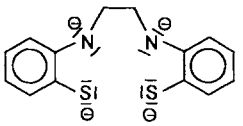

'N$_2$S$_2$'$^{4-}$

Oxidation of the readily accessible Fe^{IV} complex **1**[2a] with elemental iodine according to Equation (a) yielded **2**, which, to the best of our knowledge, is the first isolable molecular Fe^{V} complex. The lustrous crystals of **2** were dark black-brown and could be fully characterized.

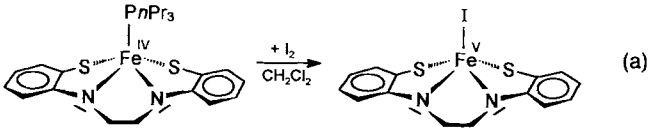

1 **2** (a)

Figure 1 shows the molecular structure of **2** determined by X-ray structure analysis.[4] The crystal of **2** is composed of discrete molecules. Like the Fe^{IV} precursor complex **1**, **2** also exhibits a distorted tetragonal pyramidal structure. N and S donors form the base, and the iodo ligand occupies the apical position. All H atoms could be located, including the four H atoms of the C16–C26 bridge. This, the C16–N1 and C26–N2 distances that correspond to C–N single bonds, and the angle sums around the N atoms (N1: 360°, N2: 360.1°) confirm that the 'N$_2$S$_2$'$^{4-}$ ligand has remained intact and not undergone (oxidative) dehydrogenation to form the Schiff-base 'gma'$^{2-}$ [= glyoxal-bis(2-mercaptoanil)(2 −)].[5]

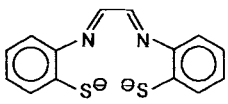

'gma'$^{2-}$

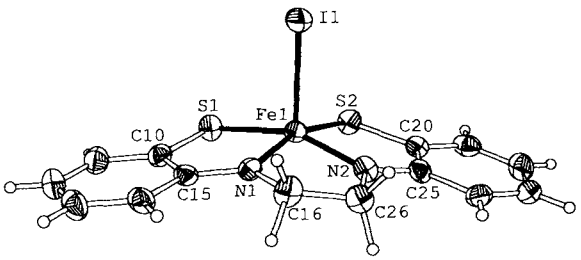

Figure 1. Molecular structure of **2**. Selected distances [pm]: Fe1–I1 255.52(9), Fe1–N1 184.2(4), Fe1–N2 185.1(5), Fe1–S1 218.1(2), Fe1–S2 218.8(2), N1–C16 146.0(6), N2–C26 145.6(6), C16–C26 150.6(8), N1–C15 133.4(7), N2–C25 134.7(7), S1–C10 171.5(5), S2–C20 172.1(6).

The Fe–S and Fe–N distances in **2** are very short and indicate S(thiolate)–Fe and N(amide)–Fe π donor bonds. Table 1 shows that the oxidation **1** → **2** does not change the [Fe('N$_2$S$_2$')] core distances, which are identical within the 3σ criterion. The Fe–I distance in **2** [255.52(9) pm] is short relative to Fe–I distances in Fe^{IV} complexes such as [Fe^{IV}(I)(L^{3-})] [259.3(2) pm; L^{3-} = pentane-2,4-dione-bis(*S*-alkylisothiosemicarbazonate)(3 −)].[2g]

Table 1. [Fe('N$_2$S$_2$')] core distances in [Fe^{IV}(P*n*Pr$_3$)('N$_2$S$_2$')] (**1**) and [Fe^{V}(I)('N$_2$S$_2$')] (**2**) [pm].

Bond	**2**	**1**[a]
Fe–N	184.7(5)[b]	184.0(6)
Fe–S	218.5(2)[b]	218.5(2)
N–C$_{aliphatic}$	145.8(6)[b]	147.2(7)
N–C$_{aromatic}$	134.1(7)[b]	134.8(8)
C–C$_{aliphatic}$	150.6(8)	154.3(13)
S–C	171.8(6)[b]	171.1(7)

[a] Complex **1** possesses crystallographically imposed C_s symmetry. [b] Averaged distances.

Complex **2** is paramagnetic. Its μ_{eff} value of 2.19 m_B at 296 K is compatible with one unpaired electron and a spin state of $S = 1/2$ and markedly distinguishes **2** from the Fe^{IV} precursor complex **1** (μ_{eff} = 2.76 m_B, $S = 1$, 295 K). The EPR spectrum of **2** shows an isotropic signal [g = 2.134, THF, 295 K; Figure 2a)], which splits anisotropically at 150 K [g_1 = 2.206, g_2 = 2.125, g_3 = 2.063; Figure 2b)]. The g value of **2** distinctly differs from that of organic radicals and is consistent with a Fe-centered unpaired electron.

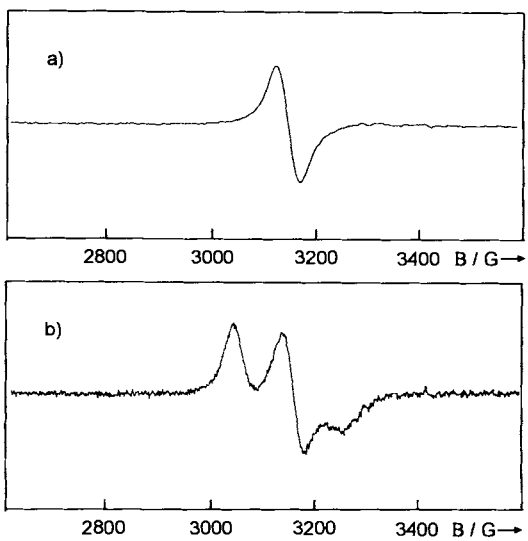

Figure 2. EPR spectra of **2** in THF at a) 295 K (g = 2.134) and b) 150 K (g_1 = 2.206, g_2 = 2.125, g_3 = 2.063).

[*] Prof. Dr. D. Sellmann, Dipl.-Chem. S. Emig, Dr. F. W. Heinemann
Institut für Anorganische Chemie der Universität Erlangen-Nürnberg
Egerlandstrasse 1, D-91058 Erlangen (Germany)
Fax: Int. code +(9131)85-7367
e-mail: sellmann@anorganik.chemie.uni-erlangen.de

[**] Transition-Metal Complexes with Sulfur Ligands, Part 126. We thank Dr. F. Tuzcek, Dipl.-Chem. N. Lehnert, and Dipl. Chem. A. Elvers for Mössbauer and EPR measurements and Prof. H. Kisch and Prof. U. Zenneck for helpful discussions. Part 125: D. Sellmann, G. H. Rackelmann, F. W. Heinemann, F. Knoch, M. Moll, *Inorg. Chim. Acta*, in press. ['N$_2$S$_2$'$^{4-}$ = 1,2-ethanediamide-*N*,*N*'-bis(2-benzenethiolate)(4 −)].

 © WILEY-VCH Verlag GmbH, D-69451 Weinheim, 1997 0570-0833/97/3616-1734 $ 17.50+.50/0

The intense violet color of the solutions of **2** is due to a strong band at 550 nm ($\varepsilon = 33000\ L\ mol^{-1}\ cm^{-1}$, CH_2Cl_2) in the electronic spectrum of **2** (Figure 3). This band is slightly more intense than the corresponding band of **1**, but distinctly shifted to shorter wavelengths.

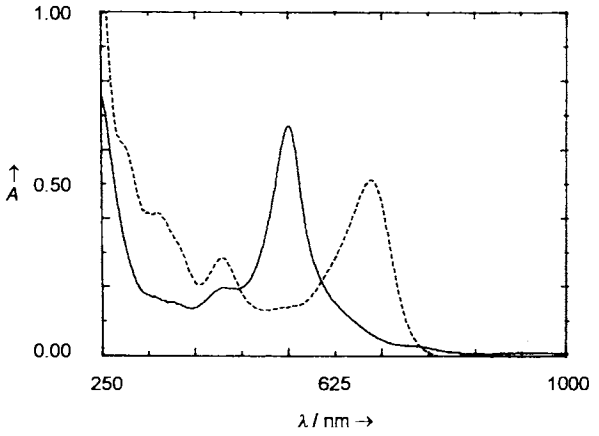

Figure 3. Electronic spectra of **2** (—) and **1** (···) in CH_2Cl_2 ($0.2\ 10^{-4}$ M, 295 K). A = absorption (arbitrary units).

The Mössbauer spectrum of **2** shows one symmetrical doublet (Figure 4). The isomeric shift of **2** [$\delta = 0.111(2)\ mm\,s^{-1}$, 4.2 K] is low, unexpectedly slightly larger than that of **1** [$\delta = 0.0396(2)\ mm\ s^{-1}$, 4.2 K], but outside the range observed

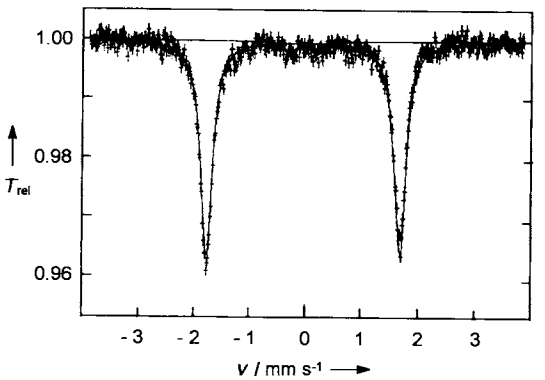

Figure 4. Mössbauer spectrum of polycrystalline **2** at 4.2 K (isomeric shift $\delta = 0.111(2)$ relative to α-Fe at 295 K, quadrupole splitting $\Delta E_Q = 3.41(5)$, line width $\Gamma = 0.125(3)$ in $mm\,s^{-1}$).

for square pyramidal $Fe^{III}(S = 1/2)$ complexes ($\delta = 0.16$–$0.38\ mm\,s^{-1}$).[6] The quadrupole splittings of both **2** [$\Delta E_Q = 3.41(5)\ mm\,s^{-1}$] and **1** [$\Delta E_Q = 3.1596(3)\ mm\,s^{-1}$] lie in the same range. Thus, the Mössbauer data do not allow an unambiguous differentiation between the oxidation states of the precursor complex **1** and the oxidation product **2**. This was rendered possible by the cyclic voltammograms. While **1** shows only two redox waves (+ 0.04, −0.86 V vs. the normal hydrogen electrode (NHE), CH_2Cl_2, 295 K), complex **2** shows three cathodic redox waves and, in addition, one anodic wave (+1.01, −0.22, −0.48, −0.77 V vs. NHE, CH_2Cl_2, 295 K, $50\ mV\,s^{-1}$; Figure 5). The cathodic waves are tentatively assigned to the redox couples Fe^V/Fe^{IV} (− 0.22 V), Fe^{IV}/Fe^{III} (− 0.48 V) and Fe^{III}/Fe^{II} (− 0.77 V). The reduction $Fe^V \rightarrow Fe^{IV}$ is irreversible, because it probably leads to release of the iodo

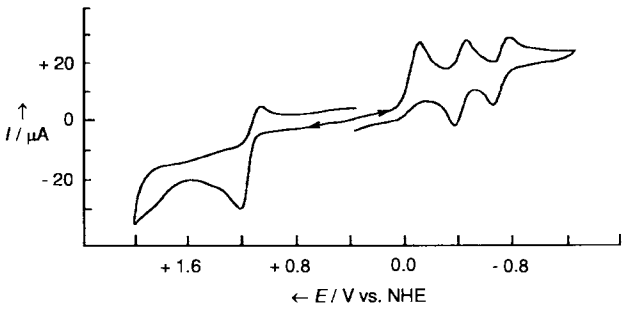

Figure 5. Cyclic voltammogram of **2** in CH_2Cl_2 (1×10^{-3} M, 0.1 M $NnBu_4PF_6$, 295 K, $50\ mV\,s^{-1}$).

ligand. In fact, the $[Fe^{IV}('N_2S_2')]$ fragment adds PR_3, $P(OR)_3$, and CN^-, but it does not add iodide.[2a, 7] The irreversible anodic oxidation wave of **2** suggests that even Fe^{VI} complexes with $[Fe^{VI}('N_2S_2')]$ cores may be accessible.

The results show that thiolate and amide donors are well suited to stabilize high oxidation states of iron. The oxidation state + v of the iron center in **2** follows from the charges of the tetraanionic $'N_2S_2'^{4-}$ and monoanionic I^- ligands. The assignment of the oxidation state is further supported by the method of preparation, the molecular structure, the magnetism, the electronic spectrum (when compared with that of **1**), and the electrochemical properties of **2**.

Iodide is a surprising ligand to find in a Fe^V complex, because FeI_3 is already unstable and instantaneously decomposes to give FeI_2 and I_2.[8] However, Fe^{IV} complexes with iodo ligands are known,[2g, h] and an important aspect to bear in mind is that the assignment of oxidation states, in a strict sense, requires completely ionic compounds. The complexes described here are covalent molecules, in which the removal of electron density from the iron center can be partially compensated by stronger iron–ligand interactions. In this regard, thiolate and amide donors with their lone pairs are perfectly suited to stabilize electron-deficient metal centers by π donation.

One question remains to be answered: why does the Mössbauer isomeric shift δ not decrease but rather slightly increase when **1** is oxidized to give **2**. The isomeric shift of complexes containing π ligands depends considerably less on changes in metal oxidation state than that of rather ionic complexes. $K_4[Fe^{II}(CN)_6]$ and $K_3[Fe^{III}(CN)_6]$, for instance, exhibit very similar δ values.[9] Furthermore, even Fe^{II} complexes such as $[AsPh_4][Fe(CN)_2(L^-)]$ [$\delta = 0.08\ mm\,s^{-1}$, 4.2 K; L^- = pentane-2,4-dione-bis(S-alkylisothiosemicarbazonate)(1 −)][2g] can exhibit isomeric shifts that are commonly observed only for Fe^{IV} complexes. Thus, the δ values of **2** and **1** can be rationalized on the qualitative basis that the isomeric shifts mainly depend on the shielding of the Fe center's s electrons. Replacing the phosphane ligand in **1** by the iodo ligand in **2**, however, is equivalent to the substitution of a π acceptor by a π donor ligand. Thus, increasing the shielding of the Fe center's s electrons in **2** by I → Fe π donation may counterbalance the removal of one d electron from the iron center in **1**.

Experimental Section

All operations were carried out under N_2 at room temperature by using standard Schlenk techniques. Solvents were dried and distilled before use. Fe^{IV} complex **1** was prepared according to literature methods [2a]. **2**: I_2 (265 mg, 1.04 mmol) was added to a green solution of **1** (510 mg, 1.04 mmol) in 20 mL of CH_2Cl_2. Black-brown microcrystals precipitated from the resultant red-violet reaction mixture. They were separated after 24 h, washed with 20 mL of CH_2Cl_2 and 30 mL of Et_2O and dried in vacuo for 1 day. Yield: 320 mg (67%). Elemental analysis calcd for $C_{14}FeH_{12}IN_2S_2$: C 36.95, H 2.66, N 6.15, S 14.09; found C 36.68, H 2.53, N 6.01,

 © WILEY-VCH Verlag GmbH, D-69451 Weinheim, 1997 0570-0833/97/3616-1735 $ 17.50+.50/0

S 14.16. MS (field desorption, CH_2Cl_2): $m/z = 455$ $[2]^+$. UV/vis (CH_2Cl_2, 295 K): λ_{max} (ε) = 447 (9800), 550 (33000). IR (KBr, [cm^{-1}]): 1570 (w), 1521 (m), 1427 (m), 1312 (w), 1158 (m), 1147 (m), 1074 (m), 1055 (m), 749 (s), 717 (s), 635 (m).

Received: March 3, 1997 [Z 10187 IE]
German version: *Angew. Chem.* **1997**, *109*, 1808–1810

Keywords: iron · magnetic properties · Moessbauer spectroscopy · N ligands · S ligands

[1] See, for instance, a) P. R. Ortiz de Montellano, *Cytochrome P-450: Structure, Mechanism and Biochemistry*, Plenum, New York, **1986**, p. 217–271; b) A. L. Feig, S. J. Lippard, *Chem. Rev.* **1994**, *94*, 759–805; c) B. Meunier, *ibid.* **1992**, *92*, 1411–1456; d) H. K. Baek, H. E. Van Wart, *J. Am. Chem. Soc.* **1992**, *114*, 718–725; e) J. E. Penner-Hahn, K. Smith Eble, T. J. McMurry, M. Renner, A. L. Balch, J. R. Groves, J. H. Dawson, K. O. Hodgson, *ibid.* **1986**, *108*, 7819–7825; f) B. G. Fox, J. G. Borneman, L. P. Wackett, J. D. Lipscomb, *Biochemistry* **1990**, *29*, 6419–6427; g) C. E. Cooper, J. C. Salerno, *J. Biol. Chem.* **1992**, *267*, 280–285; h) B. G. Fox, W. A. Froland, J. E. Dege, J. D. Lipscomb, *ibid.* **1989**, *264*, 10023–10033.

[2] See, for instance a) D. Sellmann, S. Emig, F. W. Heinemann, F. Knoch, *Angew. Chem.* **1997**, *109*, 1250–1252; *Angew. Chem. Int. Ed. Engl.* **1997**, *36*, 1203–1205; b) E. Van Caemelbecke, S. Will, M. Autret, V. A. Adamian, J. Lex, J.-P. Gisselbrecht, M. Gross, E. Vogel, K. M. Kadish, *Inorg. Chem.* **1996**, 35, 184–192; c) T. Jüstel, T. Weyhermüller, K. Wieghardt, E. Bill, M. Lengen, A. X. Trautwein, P. Hildebrandt, *Angew. Chem.* **1995**, *107*, 744–747; *Angew. Chem. Int. Ed. Engl.* **1995**, *34*, 669–672; d) C. C. Cummins, R. R. Schrock, *Inorg. Chem.* **1994**, *33*, 395–396; e) E. Vogel, S. Will, A. Schulze Tilling, L. Neumann, J. Lex, E. Bill, A. X. Trautwein, K. Wieghardt, *Angew. Chem.* **1994**, *106*, 771–775; *Angew. Chem. Int. Ed. Engl.* **1994**, *33*, 731–735; f) K. L. Kostka, B. G. Fox, M. P. Hendrich, T. J. Collins, C. E. F. Rickard, L. J. Wright, E. Münck, *J. Am. Chem. Soc.* **1993**, *115*, 6746–6757; g) U. Knof, T. Weyhermüller, T. Wolter, K. Wieghardt, E. Bill, C. Butzlaff, A. W. Trautwein, *Angew. Chem.* **1993**, *105*, 1701–1704; *Angew. Chem. Int. Ed. Engl.* **1993**, *32*, 1635–1638; h) N. V. Gerbeleu, Y. A. Simonov, V. B. Arion, V. M. Leovac, K. I. Turta, K. M. Indrichan, D. I. Gradinaru, V. E. Zavodnik, T. I. Malinovskii, *Inorg. Chem.* **1992**, *31*, 3264–3268; i) D. Sellmann, M. Geck, F. Knoch, G. Ritter, J. Dengler, *J. Am. Chem. Soc.* **1991**, *113*, 3819–3828.

[3] a) R. J. Audette, J. W. Quail, *Inorg. Chem.* **1972**, *11*, 1904–1908; b) R. Scholder, H. von Bunsen, F. Kindervater, W. Zeiss, *Z. Anorg. Allg. Chem.* **1956**, *282*, 268–279; c) W. Klemm, R. Scholder, *Angew. Chem.* **1954**, *66*, 461–474; d) F. M. Nelson in *Comprehensive Coordination Chemistry, Vol. 4* (Eds.: G. Wilkinson, R. G. Guillard, J. A. McCleverty), Pergamon, Oxford, **1987**, p. 217–271.

[4] X-ray crystal structure analysis of **2**: single crystals of **2** were obtained by diffusion of a dilute solution of I_2 in CH_2Cl_2 into a dilute solution of **1** in CH_2Cl_2 at 295 K. $C_{14}H_{12}FeIN_2S_2$, orthorhombic, space group *Pbca*, $a = 1506.0(3)$, $b = 1279.2(2)$, $c = 1529.3(3)$ pm, $V = 2.9462(9)$ nm^3, $Z = 8$, $\rho_{calcd} = 2.052$ $g\,cm^{-1}$, $\mu(Mo_{K\alpha}) = 3.39$ mm^{-1}, Siemens P4 four-circle diffractometer, graphite monochromator, $Mo_{K\alpha}$ radiation ($\lambda = 71.073$ pm), $T = 200$ K, ω scans (3.0–30.0° min^{-1}); 5621 measured reflections ($4.0° < 2\theta < 54.0°$), 3203 independent reflections, 2312 observed reflections [$F_o > 4.0\sigma(F_o)$], structure solved by direct methods (SHELXTL 5.03), refined on F^2 (SHELXTL 5.03), all nonhydrogen atoms refined anisotropically, all hydrogen atoms were located in the difference Fourier map and refined isotropically, 230 parameter, $wR_2 = 0.1231$, $R_1 = 0.0433$ [$F_o > 4.0\sigma(F_o)$]. Crystallographic data (without structural factors) of the X-ray structure analysis described here were deposited as supplementary publication no. CCDC-100229 in the Cambridge Crystallographic Data Centre. Free copies of the data can be obtained from The Director, CCDC, 12 Union Road, Cambridge CBZ 1EZ (fax: int. code +(1223) 336-033; e-mail: deposit@chemcrys.cam.ac.uk).

[5] a) D. Sellmann, M. Hannakam, F. Knoch, M. Moll, *Z. Naturforsch. B* **1992**, *47*, 1545–1549; b) D. Sellmann, R. Ruf, F. Knoch, M. Moll, *Inorg. Chem.* **1994**, *34*, 4745–4755.

[6] P. Gütlich, *Mössbauer Spectroscopy* in *Topics in Applied Physics, Vol. 5* (Ed.: U. Gonser), Springer, Berlin, **1975**.

[7] D. Sellmann, S. Emig, F. Knoch, F. W. Heinemann, unpublished results.

[8] D. Nicholls in *Comprehensive Inorganic Chemistry, Vol. 3* (Eds.: J. C. Bailar, H. J. Emeléus, S. R. Nyholm, A. F. Trotman-Dickenson), Pergamon, **1973**, p. 1038.

[9] J. Danon in *Chemical Applications of Mössbauer Spectroscopy* (Eds.: V. I. Goldanskii, R. H. Herber), Academic Press, **1968**, p. 166.

Intra-Cavity Inclusion of $[CpFe^{II}(arene)]^+$ Guests by Cyclotriveratrylene**

K. Travis Holman, Jonathan W. Steed, and Jerry L. Atwood*

The trimeric, saucer-shaped molecule cyclotriveratrylene (CTV, **1**) forms the skeleton of the cryptophanes, a family of molecules that displays an impressive range of host–guest complexation behavior involving inclusion of neutral and cationic guest molecules within their elliptical cavities.[1] CTV itself has also been known for many years to form inclusion complexes incorporating a range of neutral guest molecules.[2] These solvates are almost invariably of the channel variety, however, in which the CTV units pack in a columnar fashion in the solid state along the crystallographic *b* axis, while guest species reside only in lattice voids caused by the inefficient packing of these columns.[3] Two distinct classes of CTV inclusion compounds have been identified based upon variations in the length of the crystallographic *b* axis and in the solid-state infrared spectra of the compounds. We have recently rationalized their differences on the basis of the hydrogen-bond-accepting properties of included guest species.[4] As a consequence of the columnar packing mode, conventional inclusion complexes of CTV are generally not as interesting as those of some derivatives (for example, CTC = cyclotricatechylene),[2] since they do not exploit the molecular cavity of this host.

We have recently demonstrated, however, that in the presence of an unusual guest, namely buckminsterfullerene, CTV may form the inclusion compounds $(C_{60} \subset CTV) \cdot 0.5\,C_{60} \cdot 0.5\,C_6H_5CH_3$[5] and $(C_{60} \subset CTV)$,[6] which are not of the column variety. Instead, the CTV cavity is occupied by a C_{60} molecule in such as way as to maximize noncovalent interactions between the electron-rich host and electron-poor fullerene. We have also reported the inclusion of both anionic and neutral guests within the cavities of organometallic CTV derivatives such as $[\{Ru(\eta^6\text{-}p\text{-cymene})\}_2(\eta^6\text{:}\eta^6\text{-CTV})]X_4$ ($X = CF_3SO_3$, ReO_4).[7] CTV has also very recently been shown to form complexes with carboranes in the solid state by formation of intermolecular CH···arene hydrogen bonds.[8]

Given the highly unusual solid-state structures observed with C_{60}, it was anticipated that this new type of inclusion within the bowl of a complex may well be observed for other relatively electron-poor guest molecules with planar π electron systems. In this regard, there is strong precedence for donor–acceptor (D–A) type interactions between appropriate organic species and organometallic sandwich complexes,[9] and these interactions often emanate as infinite one-dimensional D–A–D–A stacked arrangements in the solid state. With this as our supramolecular synthon,[10] we anticipated that a similar motif involving CTV and the appropriately chosen guest would result in a polar, one-dimensional (1D) architecture with each CTV "saucer" partially aligned. We report herein the preliminary results of a study of the solid-state inclusion of organometallic

[*] Prof. J. L. Atwood, K. T. Holman
Department of Chemistry, University of Missouri-Columbia
Columbia, MO 65211 (USA)
Fax: (573) 884-9606
e-mail: chemja@showme.missouri.edu
Dr. J. W. Steed
Department of Chemistry, King's College London
London, WC2R 2LS (UK)

[**] We are grateful for sponsorship from the National Science Foundation. Cyclotriveratrylene = 2,3,7,8,12,13-hexamethoxy-5,10-dihydro-15*H*-tribenzo-[*a*,*d*,*g*]cyclononene.

 © WILEY-VCH Verlag GmbH, D-69451 Weinheim, 1997 0570-0833/97/3616-1736 $ 17.50+.50/0

salts of the type $[CpFe^{II}(arene)][PF_6]$ ($Cp = C_5H_5$) by CTV (Scheme 1).

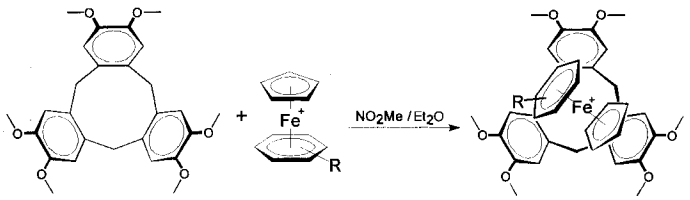

Scheme 1. Synthesis of the inclusion compounds **2**–**5**. R = Cl, *o*-Cl_2, *m*-Me_2, or 1,3,5-Me_3. Counterion: $[PF_6]^-$.

Diethyl ether was allowed to diffuse into solutions of CTV and $[CpFe^{II}(arene)][PF_6]$ (molar ratio 1:1) in nitromethane to afford, over a period of three weeks, large crystals of host–guest complexes **2**–**5** in excellent yields.[11] All crystallizations were performed in the dark to avoid photolysis of the arene.[12]

$[CpFe(C_6H_5Cl) \subset CTV][PF_6]$ **2**

$[CpFe(o\text{-}C_6H_4Cl_2) \subset CTV][PF_6]$ **3**

$[CpFe(m\text{-}C_6H_4Me_2) \subset CTV][PF_6]$ **4**

$[CpFe(1,3,5\text{-}C_6H_3Me_3) \subset CTV][PF_6]$ **5**

Complexes **2**–**4** are essentially isostructural and crystallize in the noncentrosymmetric space group $Cmc2_1$. The predominant feature of these structures is the formation of a 2D polar framework in the crystallographic *ac* plane based upon π-donor/π-acceptor-like interactions between the guest cation and the electron-rich arene faces of the CTV molecule (Figure 1). In each

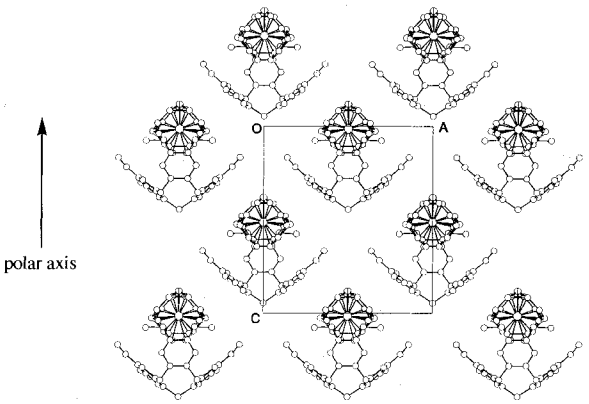

Figure 1. The polar 2D sheet structure in **2**–**4** that arises from disorder of the guest cations. Anions and arene substituents have been removed for clarity.

case the included cation is incorporated into the CTV cavity and appears to be statistically disordered across a mirror plane with the cyclopentadienyl ligands stacked against the inner ring faces of the CTV cavity. The arene portion of the cation is directed out of the cavity and interacts with the outer face of another CTV molecule in the *ac* plane. A disorder-resolved view of each included cation is shown in Figure 2a. It is this bridging function of the cation that induces the polarity along the sheet in which all of the CTV molecules are aligned in a canted fashion. The sheets then pack offset and parallel in the third dimension resulting in an overall noncentrosymmetric structure. This feature is particularly noteworthy in that a polar axis is a topological requirement for the observation of technologically useful physical properties such as second harmonic generation, piezo-, pyro-, and ferroelectric effects.[13]

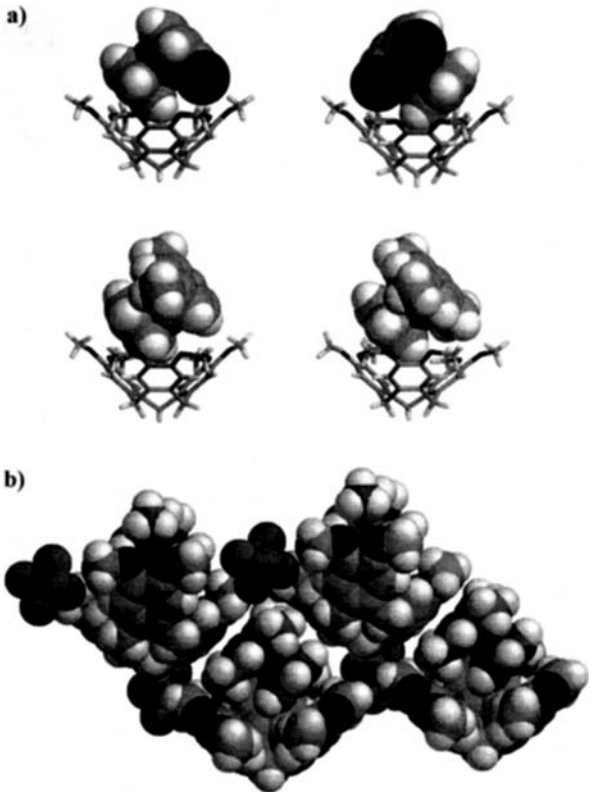

Figure 2. a) A disorder-resolved view of the host–guest complexes in **2**–**5**. b) A space-filling model of the 1D stacked arrangement in **5**. The non-hydrogen atoms of the $[CpFe(mesitylene)]^+$ guest cation have been shaded dark for clarity.

The disorder of the guest cations provide the extra dimension to the stacking array in **2**–**4**, deviating from the anticipated 1D format. The 1D architecture was realized, however, in **5**, which crystallizes in the very closely related monoclinic spacegroup *Cc*, with a β angle of only 92.0°. In this case the only difference is that the extra methyl group in $[CpFe(mesitylene)]^+$ ($[CpFe(m\text{-xylene})]^+$ has only two methyl groups) causes the arene–CTV interaction to be significantly offset relative to the corresponding interaction of the others. This is highlighted by the β angle and the longer distance between the centroids of the arene and the CTV ring (4.45 Å in **5**, 3.90–4.06 Å in **2**–**4**). Notably, the closest carbon–carbon contacts between the two C_6 rings are still of similar magnitude (Table 1). It is unclear whether this offset is due to the optimization of favorable electronic interactions between the two rings, or whether it arises in order to

Table 1. Salient structural features of the stacking interactions in complexes **2**–**5**.

	2	**3**	**4**	**5**
Cp-CTV[Å][a]	4.06	3.78	3.92	4.07
θ(Cp,CTV) [°][b]	10.9	8.4	8.8	6.8
C_5-C_6[Å][c]	3.50	3.36	3.44	3.66
arene-CTV[Å][a]	4.04	4.06	3.90	4.45
θ(arene,CTV)[°][b]	14.3	12.6	10.5	14.6
C_6-C_6[Å][c]	3.44	3.59	3.49	3.53

[a] Distance between the two ring centroids. [b] Dihedral angle between the planes defined by the ring carbon atoms. [c] Closest interatomic contact between ring carbon atoms.

 © WILEY-VCH Verlag GmbH, D-69451 Weinheim, 1997 0570-0833/97/3616-1737 $ 17.50+.50/0

minimize steric repulsions between the extra methyl group of the mesitylene fragment and the methylenic portion of the CTV molecule. The result, in any case, is loss of the cation disorder and propagation of the interaction along the predicted 1D stack (Figure 2b), rather than 2D format observed in **2**–**4**.

The host and guest seem to have little affinity in polar solvents. The visible absorption spectrum of the [CpFe(arene)][PF_6] salts in CH_3CN shows essentially no change upon the addition of up to a 50-fold excess of CTV. Furthermore, no chemical shift changes are observed for either CTV or the guest cation in the ^{1}H NMR spectrum upon the addition of up to a tenfold excess of [CpFe(ClC_6H_5)][PF_6].[14] This is not surprising considering that the association constant of various electron-rich arenes with [(mesitylene)$_2$Fe]$^{2+}$[15] are less than 2.5 M^{-1} in acetonitrile solution.[9]

The present work demonstrates a very significant extension of supramolecular chemistry involving the cavity of CTV. The formation of this type of inclusion species with electron-poor guests, in contrast to the well-known channel complexes, suggests possible applications in the engineering of crystalline materials with interesting physical properties, and in separation science. These areas are currently under investigation.[16]

Received: February 3, 1997 [Z10067IE]
German version: *Angew. Chem.* **1997**, *109*, 1840–1842

Keywords: cryptophane · host–guest chemistry · inclusion compounds · molecular recognition · sandwich complexes

[1] A. Collet, *Tetrahedron* **1987**, *43*, 5725; in *Inclusion Compounds, Vol. 2* (Eds.: J. L. Atwood, J. E. D. Davies, D. D. MacNicol), Academic Press, London, **1984**, pp. 97–121; A. Collet, J.-P. Dutasta, B. Lozach, J. Canceill, *Top. Curr. Chem.* **1993**, *165*, 103.

[2] Recent reviews on these compounds: A. Collet in *Comprehensive Supramolecular Chemistry, Vol. 6* (Eds.: D. D. MacNicol, F. Toda, R. Bishop), Pergamon, Oxford, **1996**, pp. 281–303.

[3] H. Zhang, J. L. Atwood, *J. Crystallogr. Spec. Res.* **1990**, *20*, 465; G. I. Birnbaum, D. D. Klug, J. A. Ripmeester, J. S. Tse, *Can. J. Chem.* **1985**, *63*, 3258; S. Cerrini, E. Giglio, F. Mazza, N. Pavel, *Acta Crystallogr. Sect. B* **1979**, *35*, 2605.

[4] J. W. Steed, H. Zhang, J. L. Atwood, *Supramol. Chem.* **1996**, *7*, 37.

[5] J. W. Steed, P. C. Junk, R. S. Burkhalter, J. L. Atwood, M. J. Barnes, C. L. Raston, *J. Am. Chem. Soc.* **1994**, *116*, 10346.

[6] J. L. Atwood, M. J. Barnes, M. G. Gardiner, C. L. Raston, *Chem. Commun.* **1996**, 1449.

[7] K. T. Holman, M. M. Halihan, J. W. Steed, S. S. Jurisson, J. L. Atwood, *J. Am. Chem. Soc.* **1995**, *117*, 7848; K. T. Holman, M. M. Halihan, S. S. Jurisson, J. L. Atwood, R. S. Burkhalter, A. R. Mitchell, J. W. Steed, *ibid.* **1996**, *118*, 9567; J. L. Atwood, K. T. Holman, J. W. Steed, *Chem. Commun.* **1996**, 1401.

[8] R. J. Blanch, M. Williams, G. D. Fallon, M. G. Gardiner, R. Kaddour, C. L. Raston, *Angew. Chem.* **1997**, *109*, 520; *Angew. Chem. Int. Ed. Engl.* **1997**, *36*, 504.

[9] Of the abundance of literature concerning 18-electron iron-containing sandwich complexes, see, for example: R. E. Lehmann, J. K. Kochi, *J. Am. Chem. Soc.* **1991**, *113*, 501.

[10] G. R. Desiraju, *Angew. Chem.* **1995**, *107*, 2541; *Angew. Chem. Int. Ed. Engl.* **1995**, *34*, 2311.

[11] Data were collected on an Enraf-Nonius CAD-4 diffractometer with a graphite monochromator and $Mo_{K\alpha}$ radiation ($\lambda = 0.71069$ Å) in $\omega/2\theta$ scan mode. Data were corrected for Lorentz polarization and absorption (**2**, **3**). Structures were solved by direct methods (SHELXS) [17a] and refined with full-matrix least-squares based on F^2 (SHELXL93) [17b]. Absolute configurations were assigned by refinement of the Flack parameter χ, but confidence is limited by the lack of significant data at higher angles. This problem, coupled with that fact that the structures are noncentrosymmetric, is also responsible for the low data:parameter ratios. X-ray data for **2**: orthorhombic, $Cmc2_1$ (no. 36), $a = 14.2398(9)$, $b = 17.302(2)$, $c = 15.194(1)$, $Z = 8$, $V = 3743.5(5)$ Å^3, $\rho_{calc} = 1.47$ g cm^{-3}, $\mu = 0.592$ mm^{-1}, $3 < 2\theta < 46°$, $T = 298$ K. Final refinement converged with $R = 0.0672$ and $wR2 = 0.1793$ for 1133 ($I > 2\sigma[I]$) of 1423 unique reflections and 259 parameters. X-ray data for **3**: orthorhombic, $Cmc2_1$ (no. 36), $a = 14.174(1)$, $b = 17.914(2)$, $c = 15.001(2)$, $Z = 8$, $V = 3808.9(7)$ Å^3, $\rho_{calc} = 1.51$ g cm^{-3}, $\mu = 0.653$ mm^{-1}, $3 < 2\theta < 46°$, $T = 298$ K. Final refinement converged with $R = 0.0658$ and $wR2 = 0.1775$ for 1198 ($I > 2\sigma[I]$) of 1453 unique reflections and 235 parameters. X-ray data for **4**: orthorhombic, $Cmc2_1$ (no. 36), $a = 13.7717(8)$, $b = 18.305(1)$, $c = 15.203(1)$, $Z = 8$, $V = 3832.7(5)$ Å^3, $\rho_{calc} = 1.43$ g cm^{-3}, $\mu = 0.511$ mm^{-1}, $3 < 2\theta < 46°$, $T = 298$ K. Final refinement converged with $R = 0.0591$ and $wR2 = 0.1551$ for 1216 ($I > 2\sigma[I]$) of 1456 unique reflections and 284 parameters. X-ray data for **5**: Monoclinic, Cc (no. 9), $a = 14.073(3)$, $b = 18.226(1)$, $c = 15.514(3)$, $\beta = 92.043(9)$, $Z = 8$, $V = 3977(1)$ Å^3, $\rho_{calc} = 1.40$ g cm^{-3}, $\mu = 0.493$ mm^{-1}, $3 < 2\theta < 46°$, $T = 298$ K. Final refinement converged with $R = 0.1009$ and $wR2 = 0.2651$ for 2196 ($I > 2\sigma[I]$) of 2884 unique reflections and 438 parameters. Crystallographic data (excluding structure factors) for these structures reported in this paper have been deposited to the Cambridge Crystallographic Data Centre as supplementary publication no. CCDC-100191. Copies of the data can be obtained free of charge on application to the Director, CCDC, 12 Union Road, Cambridge CB21EZ, UK (fax: int. code +(1223)336-033; e-mail: teched@chemcrys.cam.ac.uk).

[12] The deligation reaction mediated by visible light may proceed very efficiently, with high quantum yields, depending on the arene, temperature, solvent, and anion: A. M. McNair, J. L. Schrenk, K. R. Mann, *Inorg. Chem.* **1984**, *23*, 2633.

[13] D. Y. Curtin, I. C. Paul, *Chem. Rev.* **1981**, *81*, 525.

[14] ^{1}H NMR experiments were performed in CD_3NO_2. The concentration of CTV was held constant at about 0.03 M while varying the concentration of added guest from 0–0.3 M.

[15] [Fe(arene)$_2$]$^{2+}$ cations are expected to form stronger complexes with arenes, since they are much more susceptible to reduction than their [CpFe(arene)]$^+$ counterparts. For [(mesitylene)$_2$Fe]$^{2+}$, $E_1^0 = -0.06$ V [9] whereas for [CpFe(mesitylene)]$^+$, $E^0 = -1.55$ V (potentials vs. the saturated calomel electrode). For reference to this data, and that of similar compounds, see D. Astruc, *Electron Transfer and Radical Processes in Transition-Metal Chemistry*, VCH, New York, **1995**, pp. 148.

[16] J. L. Atwood, G. A. Koutsantonis, C. L. Raston, *Nature* **1994**, *368*, 229.

[17] a) G. M. Sheldrick, *Acta Crystallogr. Sect. A* **1990**, *46*, 467; b) *SHELXL-93*, Universität Göttingen, **1993**.

Solvent-Anchored Supported Liquid Phase Catalysis: Polyoxometalate-Catalyzed Oxidations**

Ronny Neumann* and Michal Cohen

An important desired refinement of homogeneous transition metal catalyzed reactions is the heterogenization of the catalysts to achieve facile recovery and recycling of the catalyst. Two basic approaches have been used. The first is immobilization by covalent binding or adsorption of catalysts on supports.[1] This generally leads to loss of activity and selectivity with respect to the original homogeneous analog. For catalytic oxidations the polar products and oxidants react with the binding units, resulting in leaching of the metal; recent reports describe improved supported catalysts.[2] Loss of catalytic species in oxidations has been prevented by confinement within zeolites[3] or dissolution in nonvolatile siloxanes.[4] The second approach is to carry out the reaction with two liquid phases; the catalyst is dissolved in one phase (water[5] or fluorinated hydrocarbon[6]), and the product is separated into the other. Rates of such reactions are often limited by slow mass transfer.

Supported liquid phase (SPL) or supported aqueous phase (SAP) catalysis[7] combines two-phase catalysis with the use of a solid support. This hybrid technique calls for dissolution of a catalyst in a hydrophilic phase (water, ethylene glycol, or polyethylene glycol), which is then adsorbed onto a support. Although the catalyst is immobilized on a solid surface, the reaction takes place at the liquid–liquid interface. Hydroformyl-

[*] Prof. Dr. R. Neumann, M. Cohen
Casali Institute of Applied Chemistry, Graduate School of Applied Science
The Hebrew University of Jerusalem
Jerusalem, 91904 (Israel)
Fax: Int. code +(2)6528-250
e-mail: ronny@vms.huji.ac.il

[**] This research was supported by the United States–Israel Binational Science Foundation (BSF), Jerusalem, Israel (grant no. 95-00076).

 © WILEY-VCH Verlag GmbH, D-69451 Weinheim, 1997 0570-0833/97/3616-1738 $ 17.50+.50/0

ations,[8] Wacker-type oxidations,[9] and enantioselective hydrogenations[10] have been described.

Here we report on a new immobilization technique for homogeneous catalysts, solvent-anchored supported liquid phase catalysis. In the present application polyethers are covalently attached to silica surfaces. The bound polyether acts as a solvent and/or a complexing agent for the oxidation catalyst, in this case polyoxometalates (POM). Two different reaction modes have been described (Figure 1). In the first case the bound phase with

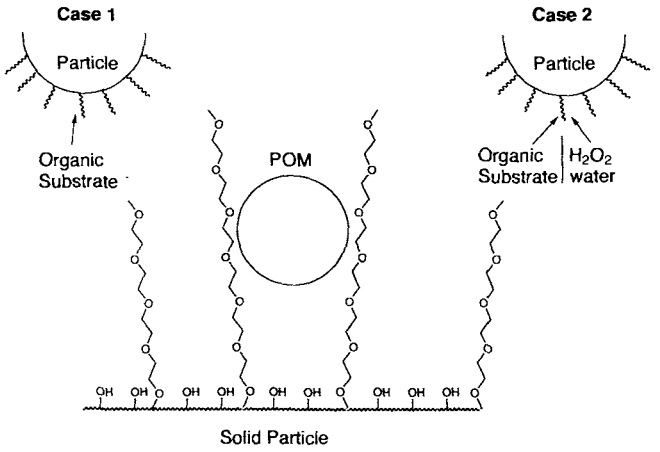

Figure 1. Illustration of the solvent-anchored supported liquid phase catalytic system. POM = polyoxometalate.

polyether (polyethylene oxide (PEO)) catalyst is in contact with a single liquid phase containing substrate. As opposed to SPL and SPA catalysis, the liquid phase here is miscible with the bound polyether, and reaction takes place within the polyether phase, thus minimizing mass-transfer constraints. The mixture appears homogeneous upon stirring but separates upon settling. In the second case the bound polyether catalyst phase is in contact with two imiscible liquid phases; one contains the oxidant, and the other the organic substrate. The supported catalyst phase is at the interphase where both reactants are soluble and meet to react.

The catalyst particles were prepared in three stages. First $(CH_3O)_3SiPhCH_2Cl$ was allowed to react with polyethylene glycol monomethyl ether (PEGME, MW = 350) or polypropylene glycol monomethyl ether (PPGME, MW = 200) to form $(CH_3O)_3SiPhCH_2O(CH_2CHRO)_nCH_3$ (**1a**: R = H; **1b**: R = Me). Then the monomer **1** was copolymerized with $Si(OCH_2CH_3)_4$ by the sol-gel method with dibutyltin dilaurate as catalyst. Finally the xerogel obtained was impregnated with the polyoxometalate catalysts to form the final catalyst assembly.

Examples that demonstrate the first reaction mode are the dehydrogenation of 9,10-dihydroanthracene with $H_5PV_2Mo_{10}O_{40}$ as catalyst[11] and 70% *tert*-butylhydroperoxide (TBHP) as oxidant [Eq. (a)],[12] and the epoxidation of cyclooctene with the same catalyst and aldehyde/O_2 as oxidant [Eq. (b)].[13]

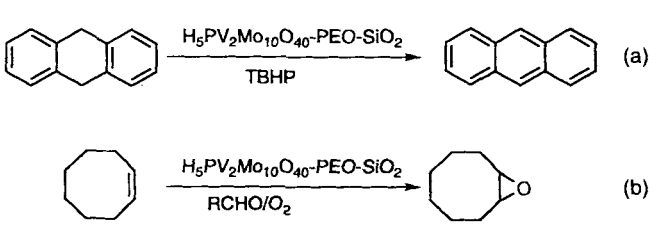

Dehydrogenation of dihydroanthracene was carried out by mixing dihydroanthracene (0.2 mmol) in toluene (0.1 mL), 70% TBHP (0.4 mmol), and catalyst (15 mg) containing 0.002 mmol of $H_5PV_2Mo_{10}O_{40}$ at room temperature for 24 h. The silica used was 25% PEO–SiO_2. Analysis of the reaction mixture showed that the reaction was quantitative, yielding 96% anthracene and 4% anthraquinone. The catalyst was recycled without loss of activity, and no catalyst leaching or decomposition was measured by UV/Vis spectroscopy or atomic absorption, respectively. This is perhaps not surprising considering that such acidic Keggin compounds are strongly complexed by diethyl ether.[14] Therefore, the $H_5PV_2Mo_{10}O_{40}$ polyoxometalate is most likely complexed rather than simply dissolved within the PEO phase. Nonsupported $H_5PV_2Mo_{10}O_{40}$ was less effective (87% conversion) and less selective (77% selectivity with respect to anthracene). Using simply unsupported or unattached $H_5PV_2Mo_{10}O_{40}$ tetraglyme as controls did not yield a true heterogenous system, but rather a catalyst dissolved in the organic phase.

The $H_5PV_2Mo_{10}O_{40}$/PEO–SiO_2 catalyst assembly was further tested with the reaction shown in Equation (b). In typical reaction cyclooctene (5 mmol) was allowed to react with isobutyraldehyde (IBA, 10 mmol) in 1,2-dichloroethane (4 mL); the reaction was catalyzed by $H_5PV_2Mo_{10}O_{40}$/25% PEO–SiO_2 (150 mg) containing 0.0075 mmol of the POM at 23 °C under O_2 (1 atm). Figure 2 gives the reaction profile for the supported

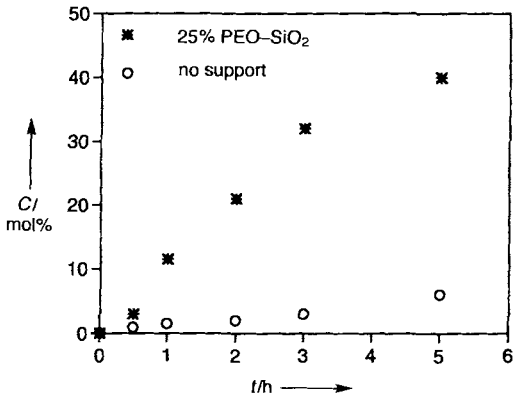

Figure 2. Oxidation of cyclooctene with isobutyraldehyde (IBA)/O_2 with supported $H_5PV_2Mo_{10}O_{40}$. Reaction conditions: cyclooctene (5 mmol), IBA (10 mmol), $H_5PV_2Mo_{10}O_{40}$/25% PEO–SiO_2 (150 mg) containing 0.0075 mmol of the POM in 1,2-dichloroethane (4 mL) at 23 °C and under O_2 (1 atm). Cyclooctene oxide was the sole product. *C* = conversion.

catalyst and the control experiment with the nonsupported catalyst. The advantage of using the supported catalyst is clear. Furthermore, loading of $H_5PV_2Mo_{10}O_{40}$ on the catalyst particle (constant weight) has little effect on the reaction profile. Use of other aldehydes showed the following relative reactivity normalized to IBA: $(CH_3)_3CCHO$ (2.2) > $(CH_3)_2CHCHO$ (1) > $CH_3(CH_2)_3CHO$ (0.2) ≈ $CH_3CH{=}CHCHO$ (0.015) > C_6H_5CHO (≈0). As in the previous case, the catalyst was recycled without loss of activity, and no catalyst leaching or decomposition was measurable.

The utility of solvent-anchored supported liquid phase catalysis in the second reaction mode was demonstrated by the epoxidation of cyclooctene with aqueous hydrogen peroxide with $Q_3PO_4[W(O)(O_2)]_4$ as the catalyst [Q = tetrahexylammonium; Eq. (c)].[15] In a typical reaction cyclooctene (1 mmol) and 30% H_2O_2 (2 mmol) were mixed with the catalyst (100 mg) at room temperature. The latter consisted of $Q_3PO_4[W(O)(O_2)]_4$ (0.005 mmol) on 20% PEO/PPO–SiO_2. This reaction was per-

 © WILEY-VCH Verlag GmbH, D-69451 Weinheim, 1997 0570-0833/97/3616-1739 $ 17.50+.50/0

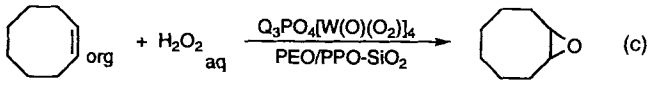

formed without an organic solvent, an important ecological advantage. In this case the functionalization of the silica with the correct balance of polyethers is critical (Figure 3). Use of hydrophilic PEO yielded only low rates and conversions. Non-

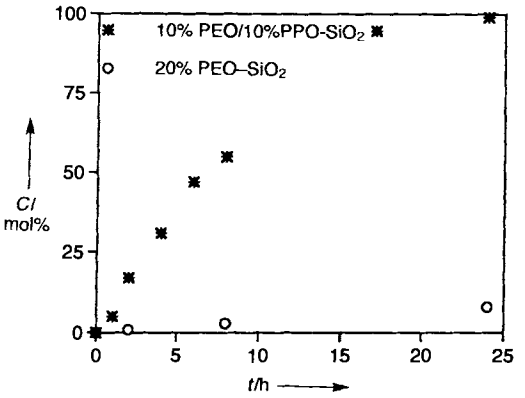

Figure 3. Oxidation of cyclooctene with 30% H_2O_2 catalyzed by supported $Q_3PO_4[W(O)(O_2)]_4$. Reaction conditions: cyclooctene (1 mmol), 30% H_2O_2 (2 mmol), $Q_3PO_4[W(O)(O_2)]_4$/20% PEO/PPO-SiO_2 (100 mg) containing 0.005 mmol of the POM at 23 °C. Cyclooctene oxide was the sole product. C = conversion.

supported $Q_3PO_4[W(O)(O_2)]_4$, that is, solid POM that is slightly dissolved in cyclooctene, was also inactive. On the other hand, a mixture of 10% PEO and 10% PPO-SiO_2 gave the optimal catalyst particle. The hydrophilic-hydrophobic balance of the catalyst particle must be adjusted to optimize the solubility of both cyclooctene and hydrogen peroxide in the polyether-bound phase. The catalyst 20% PPO-SiO_2 was almost as effective, but further increases in PPO content reduced the activity. The catalyst particle was recycled five times without loss of catalytic activity. Use of a reaction filtrate showed no catalytic species and no catalytic activity.

The new concept of solvent-anchored supported liquid phase catalysis has been introduced and demonstrated for oxidation reactions catalyzed by polyoxometalates. These new catalytic systems are more active and selective than analogous nonsupported systems, and catalytic activity is retained after recycling. Use of this technique will be expanded to other reactions and catalysts.

Experimental Section

Monomers **1** were prepared by allowing $(CH_3O)_3SiPhCH_2Cl$ (25 mmol) to react with $CH_3(OCH_2CH_2)OH$ (MW = 350; 25 mmol) or $CH_3(OCH(CH_3)CH_2)OH$ (MW = 200; 25 mmol) in acetone (100 mL) in the presence of solid K_2CO_3 (125 mmol) at reflux for 18 h. The solid salts were removed by centrifugation, and the solvent removed under vacuum. No further purification was carried out at this point. The functionalized xerogels were prepared by dissolving appropriate amounts of **1** and $Si(OEt)_4$ (in total 5 mmol) in acetone (20 mL). Water (10 equiv) and dibutyltin dilaurate (0.01 equiv) were added to initiate polymerization. The reaction mixture was held at 60 °C for three hours and left to concentrate by evaporation of solvent for two days at room temperature. The functionalized silica particles were carefully washed twice with water and ethanol and dried under vacuum. Final catalytic assembles were prepared by impregnating the polyoxometalates onto the silicates as follows: For the reaction in Equation (a) $H_5PV_2Mo_{10}O_{40}\cdot xH_2O$ (440 mg, 0.2 mmol) was dissolved in acetone (10 mL) and added to 20% PEO-SiO_2 (1.5 g), and the solvent removed. The silicate was then dried overnight under vacuum at room temperature. The procedure was identical for the reaction in Equation (b) except that $H_5PV_2Mo_{10}O_{40}\cdot xH_2O$ (165 mg, 0.075 mmol) was used. For the reaction in Equation (c) $[(C_6H_{13})_4N]_3PO_4[W(O)(O_2)]_4$ (1.04 g, 0.5 mmol) was dissolved in $CHCl_3$ (20 mL) and added to 20% PEO/PPO-SiO_2. The mixture was then treated as above.

Typical oxidations were carried out in 5-mL, magnetically stirred vials. Material quantities and reaction conditions are given in the text. The reaction mixtures were analyzed by GLC (HP 5890) with a RTX-1 column (30 m, 0.32 mm ID, 0.25 μm methylsilicone coating). The catalyst was recovered by filtration followed by washing to remove reaction remnants and drying.

Received: December 16, 1996
Revised version: March 12, 1997 [Z9892IE]
German version: *Angew. Chem.* **1997**, *109*, 1810–1812

Keywords: heterogeneous catalysis · homogeneous catalysis · oxidations · polyoxometalates

[1] F. R. Hartley, *Supported Metal Complexes*, Reidal, Dordrecht, **1985**; R. A. Sheldon, *Curr. Opin. Solid State Mater. Sci.* **1996**, *1*, 101–106.
[2] A. Corma, A. Feurte, M. Iglesias, F. Sanchez, *J. Mol. Catal. A* **1996**, *107*, 225–234; F. Minutolo, D. Oini, P. Salvadori, *Tetrahedron Lett.* **1996**, *37*, 3375–3378; A. J. Butterworth, J. H. Clark, P. H. Walton, S. J. Barlow, *Chem. Commun.* **1996**, 1859–1860; P. Battioni, E. Cardin, M. Louloudi, B. Schöllhorn, G. A. Spyroulias, D. Mansuy, T. G. Traylor, *ibid.* **1996**, 2037–2038; R. Neumann, H. Miller, *J. Chem. Soc. Chem. Commun.* **1995**, 2277–2278.
[3] P. P. Knops-Gerrits, D. E. Vos, F. Thibault-Starzyk, P. A. Jacobs, *Nature* **1994**, *369*, 543–546; R. F. Parton, I. F. J. Vankelecom, M. J. A. Casselman, C. P. Bezoukhanova, J. B. Uytterhoeven, P. A. Jacobs, *Nature* **1994**, *370*, 541–544.
[4] I. F. J. Vankelecom, D. Tas, R. F. Parton, V. Van de Vyver, P. A. Jacobs, *Angew. Chem.* **1996**, *108*, 1445–1447; *Angew. Chem. Int. Ed. Engl.* **1996**, *35*, 1346–1348.
[5] E. Wiebus, B. Cornils, *Chem. Ing. Tech.* **1994**, *66*, 916–923; B. Cornils, E. Wiebus, *Chemtech* **1995**, 33–38; R. V. Chaudhari, B. M. Bhanage, R. M. Deshpande, H. Delmas, *Nature* **1995**, *373*, 501–503; R. V. Chaudhari, A. Bhattachyna, B. M. Bhanage, *Catal. Today* **1995**, *24*, 123–133.
[6] I. T. Horvath, J. Rabai, *Science* **1994**, *266*, 72–75.
[7] P. E. Rony, *J. Mol. Catal.* **1975**, *1*, 13–25; M. E. Davis, *Chemtech* **1992**, 498–502.
[8] J. P. Arhancet, M. E. Davis, B. E. Hanson, *J. Catal.* **1990**, *121*, 327–339; J. P. Arhancet, M. E. Davis, B. E. Hanson, *ibid.* **1990**, *129*, 94–99, 100–105; M. J. Naughton, R. S. Drago, *ibid.* **1995**, *155*, 383–389.
[9] J. P. Arhancet, M. E. Davis, B. E. Hanson, *Catal. Lett.* **1991**, *11*, 129–136.
[10] K. T. Wan, M. E. Davis, *Nature* **1994**, *370*, 449–450.
[11] R. Neumann, M. Lissel, *J. Org. Chem.* **1989**, *54*, 4607–4610.
[12] R. D. Gall, M. Faraj, C. L. Hill, *Inorg. Chem.* **1994**, *33*, 5448–5455.
[13] M. Hamamoto, K. Nakayama, Y. Nishiyama, Y. Ishii, *J. Org. Chem.* **1993**, *58*, 6421–6425.
[14] G. A. Tsigdinos, C. J. Hallada, *Inorg. Chem.* **1968**, *7*, 437–441.
[15] C. Venturello, R. D'Aloisio, J. C. J. Bart, M. Ricci, *J. Mol. Catal.* **1985**, *32*, 107–110.

Palladium-Catalyzed Regioselective Mono- and Diarylation Reactions of 2-Phenylphenols and Naphthols with Aryl Halides**

Tetsuya Satoh, Yuichiro Kawamura, Masahiro Miura,* and Masakatsu Nomura

The palladium-catalyzed substitution reactions of aryl halides and their synthetic equivalents such as aryl triflates are highly useful for the preparation of substituted aromatic compounds. In these reactions arylpalladium(II) complexes occur as common intermediates which react with various reagents including alkenes, alkynes, and a number of organometallic species to give the corresponding products.[1] While aryl halides may also react

[*] Prof. Dr. M. Miura, T. Satoh, Y. Kawamura, Prof. Dr. M. Nomura
Department of Applied Chemistry, Faculty of Engineering
Osaka University, Suita, Osaka 565 (Japan)
Fax: Int. code + (6) 879-7362
e-mail: miura@ap.chem.eng.osaka-u.ac.jp

[**] We thank Ms. Y. Miyaji of the Instrumental Analysis Center, Osaka University, for helpful assistance in obtaining NMR spectra.

 © WILEY-VCH Verlag GmbH, D-69451 Weinheim, 1997 0570-0833/97/3616-1740 $ 17.50+.50/0

with aromatic compounds accompanied by cleavage of an aromatic C–H bond to give biaryls, only intramolecular cases are known to be generally effective.[2] Meanwhile, in the course of our study of palladium-catalyzed reactions with phenolic substrates,[3] we observed that the intermolecular cross-coupling of 2-hydroxybenzaldehydes with aryl iodides proceeded smoothly when the catalyst system $PdCl_2$/LiCl was used in the presence of sodium carbonate as base. Since the products are 2-aroylphenols, the reaction appears to involve activation of the aldehyde C–H bond.[3a] The phenolic function seems to act as a good anchor for this reaction, which suggests that arylation of other phenolic substrates should also be possible. Indeed, phenylation of 2-phenylphenol with iodobenzene was found to proceed to some extent, giving a terphenyl derivative; however, the reaction was very sluggish.[3a] We now report our new findings that when an appropriate base is employed, not only monoarylation, but also diarylation of 2-phenylphenols can take place effectively and regioselectively to afford sterically crowded 1,2,3-triarylbenzene derivatives;[4] and 1- and 2-naphthols can also be arylated.

When iodobenzene (**1a**; 1.2 mmol) was treated with 2-phenylphenol (**2**; 1.0 mmol) in the presence of $Pd(OAc)_2$ (0.05 mmol) with Cs_2CO_3 as base, a phenyl group was selectively introduced onto the 2′-position of **2** to produce 1,1′:2′,1″-terphenyl-2-ol (**6a**) in 76% yield (Scheme 1, Table 1). Other alkaline bases such as K_2CO_3 and Na_2CO_3 were much less effective than Cs_2CO_3 (25 and 13% yield, respectively, under the same conditions). When $PdCl_2$ was used in place of $Pd(OAc)_2$ the yield of **6a** was 66%. Increasing the amount of both **1a** and the base to 4 mmol led to further arylation to afford the corresponding diarylated product **10a** in 62% yield along with a minor amount of **6a** (25%). The results for the reactions of 4-iodoanisole (**1b**) with **2** and of **1a** with 2-(4-methylphenyl)phenol (**3**) demonstrate the generality of the present diarylation as well as monoarylation. In the reactions of 3′-substituted 2-phenylphenols **4** and **5** with **1a**, however, only the monoarylated products **8a** and **9a**, respectively, were formed even when an excess of **1a** was employed.

The monoarylation of **2** serves as an example in a possible mechanism illustrated in Scheme 2 (neutral ligands are omitted). Oxidative addition of aryl iodide to a palladium(0) species generated in situ followed by reaction with the phenolate forms aryl(aryloxy)palladium intermediate **A**. Then, **A** may be transformed into diarylpalladium species **B**, and the subsequent reductive elimination occurs to give the monoarylated product.[5] Coordination of the phenolic oxygen to the palladium center in **A**, similar to that in the coupling of 2-hydroxybenzaldehydes with aryl iodides,[3a] is thus considered to be the key to the effective, regioselective C–H bond activation. The second arylation may proceed by the same mechanism. The results of the reactions of **1a** with **4** and **5** suggest that a) the existence of a substituent at the 3′-position of **2** prevents the second arylation for steric reasons, and b) the transformation of **A** into **B** is feasible even when the substituent is strongly electron-withdrawing or electron-releasing.[6]

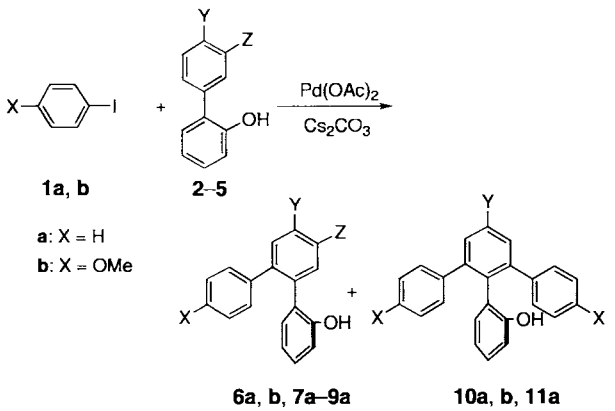

Scheme 1. Cross-coupling of **1a**, **b** with **2**–**5** (see also Table 1).

Table 1. Mono- and diarylation reactions of 2-phenylphenols with aryl iodides **1a,b**. Reaction conditions: A) **1** (1.2 mmol), ArOH (1 mmol), $Pd(OAc)_2$ (0.05 mmol), Cs_2CO_3 (1.2 mmol), molecular sieves 4 Å (200 mg), DMF (5 mL), 100 °C; B) **1** (4 mmol), ArOH (1 mmol), $PdCl_2$ (0.05 mmol), Cs_2CO_3 (4 mmol), DMF (5 mL), 100 °C.

Entry	Starting materials					Conditions	Time [h]	Product, yield [%] [a]
	X	Y	Z	1	ArOH			
1	H	H	H	**1a**	**2**	A	22	**6a**, 76 (63)
2	H	H	H	**1a**	**2**	B	44	**10a**, 62 (56)
3	H	Me	H	**1a**	**3**	A	22	**7a**, 76 (60)
4	H	Me	H	**1a**	**3**	B	22	**11a**, (63)
5	H	H	OMe	**1a**	**4**	A[b]	7	**8a**, 88 (73)
6	H	H	NO_2	**1a**	**5**	A[b]	44	**9a**, 87 (72)
7	OMe	H	H	**1b**	**2**	A	22	**6b**, (70)
8	OMe	H	H	**1b**	**2**	B	44	**10b**, (57)

[a] Determined by gas chromatography based on ArOH used. Value in parentheses indicates yield after isolation. [b] Iodobenzene (**1a**; 2 mmol) and Cs_2CO_3 (2 mmol) were used.

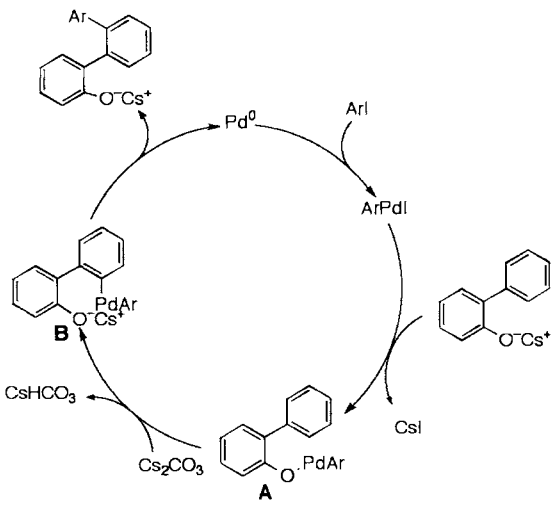

Scheme 2. Possible reaction mechanism for the cross-coupling of aryl iodides with 2-phenylphenol (**2**) to afford the corresponding monoarylation product.

With the present catalytic system 1-naphthol (**12**) was monophenylated to give 8-phenylnaphthol (**13**) selectively (Scheme 3). The use of Cs_2CO_3 was also essential for the catalytic reaction to take place smoothly. It was also of considerable interest that when 2-naphthol (**14**) was treated with two equivalents of bromobenzene (**1c**) and $Pd(OAc)_2/PPh_3$, formally diphenylated compound **15** was obtained as the predominant

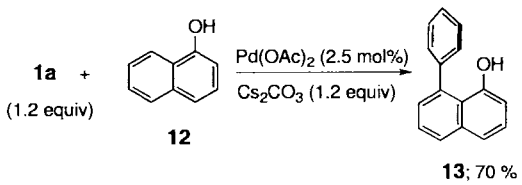

Scheme 3. Cross-coupling of **1a** with **12**: DMF, N_2, 110 °C, 10 h.

 © WILEY-VCH Verlag GmbH, D-69451 Weinheim, 1997 0570-0833/97/3616-1741 $ 17.50+.50/0

Table 2. Selected physical and spectroscopic data [a] for compounds **6b**, **7a–9a**, **10a**, **10b**, **11a**, and **15**.

6b: M.p. 88 °C, ^{1}H NMR: δ = 3.76 (s, 3H, OMe), 4.77 (s, 1H, OH), 6.75 (dt, J = 8.8, 2.0 Hz, 2H, H-3″), 6.80 (dd, J = 1.0, 7.8 Hz, 1H, H-3), 6.87 (dt, J = 1.0, 7.3 Hz, 1H, H-5), 7.07 (dd, J = 1.5, 7.3 Hz, 1H, H-6), 7.09 (dt, J = 8.8, 2.0 Hz, 2H, H-2″), 7.17 (dt, J = 1.5, 7.8 Hz, 1H, H-4), 7.37–7.49 (m, 4H)

7a: M.p. 64 °C, ^{1}H NMR: δ = 2.45 (s, 3H), 4.81 (s, 1H), 6.78 (dd, J = 1.0, 8.3 Hz, 1H), 6.81 (dt, J = 1.0, 7.3 Hz, 1H), 7.01 (dd, J = 1.9, 7.3 Hz, 1H), 7.11–7.22 (m, 6H), 7.25–7.33 (m, 3H)

8a: M.p. 136–137 °C, ^{1}H NMR: δ = 3.84 (s, 3H), 4.87 (s, 1H), 6.78 (dd, J = 1.0, 8.3 Hz, 1H), 6.84 (dt, J = 1.0, 7.3 Hz, 1H), 6.93 (d, J = 2.4 Hz, 1H), 7.03 (dd, J = 2.4, 8.3 Hz, 1H), 7.06 (dd, J = 1.5, 7.3 Hz, 1H), 7.10–7.21 (m, 6H), 7.43 (d, J = 8.3 Hz, 1H)

9a: M.p. 144–145 °C, ^{1}H NMR: δ = 4.65 (s, 1H), 6.75 (dd, J = 1.0, 8.3 Hz, 1H), 6.90 (dt, J = 1.0, 7.3 Hz, 1H), 7.07 (dd, J = 1.5, 7.3 Hz, 1H), 7.17–7.28 (m, 6H), 7.64 (dd, J = 1.5, 8.8 Hz, 1H), 8.30 (dd, J = 2.4, 8.8 Hz, 1H), 8.31 (s, 1H)

10a: M.p. 150–151 °C, ^{1}H NMR: δ = 4.66 (s, 1H), 6.54 (dd, J = 1.0, 8.3 Hz, 1H), 6.58 (dt, J = 1.0, 7.3 Hz, 1H), 6.76 (dd, J = 1.5, 7.3 Hz, 1H), 6.94 (dt, J = 1.5, 7.3 Hz, 1H), 7.09–7.18 (m, 10H), 7.45–7.53 (m, 3H)

10b: M.p. 153–154 °C, ^{1}H NMR: δ = 3.74 (s, 6H, OMe), 4.63 (s, 1H, OH), 6.61 (dd, J = 1.0, 8.3 Hz, 1H, H-3), 6.64 (dt, J = 1.0, 7.3 Hz, 1H, H-5), 6.71 (dt, J = 8.8, 2.0 Hz, 4H, H-3″), 6.77 (dd, J = 1.5, 7.3 Hz, 1H, H-6), 6.99 (dt, J = 1.5, 8.3 Hz, 1H, H-4), 7.04 (dt, J = 8.8, 2.0 Hz, 4H, H-2″), 7.42–7.52 (m, 3H)

11a: M.p. 122.5–123.5 °C, ^{1}H NMR: δ = 2.49 (s, 3H), 4.63 (s, 1H), 6.57 (dd, J = 1.0, 7.3 Hz, 1H), 6.60 (dt, J = 1.0, 7.3 Hz, 1H), 6.76 (dd, J = 1.5, 7.3 Hz, 1H), 6.96 (dt, J = 1.5, 7.3 Hz, 1H), 7.11–7.18 (m, 10H), 7.31 (s, 2H)

15: M.p. 117–118 °C, ^{1}H NMR: δ = 4.93 (s, 1H, OH), 7.02–7.10 (m, 6H), 7.27 (dt, J = 1.5, 8.1 Hz, 1H, H-6), 7.31 (dt, J = 1.5, 8.1 Hz, 1H, H-7), 7.36 (d, J = 8.1 Hz, 1H, H-8), 7.41 (d, J = 7.3 Hz, 1H, H-3′), 7.54 (dt, J = 2.2, 7.3 Hz, 1H, H-4′), 7.59 (dt, J = 1.5, 7.3 Hz, 1H, H-5′), 7.62 (dd, J = 2.2, 7.3 Hz, 1H, H-6′), 7.69 (d, J = 8.8 Hz, 1H, H-4), 7.73 (d, J = 8.1 Hz, 1H, H-5)

[a] ^{1}H NMR: 400 MHz, $CDCl_3$, TMS.

product (Scheme 4). The first step of this reaction, monophenylation at the 1-position of **14**, may involve nucleophilic attack of the corresponding naphtholate on a phenylpalladium(II) species generated in situ. Note that while palladium-catalyzed intramolecular coupling of aryl halides with enolates including phenolates is known,[7] the corresponding intermolecular version has been limited to only few reactions in which nitriles function as carbon nucleophiles.[8] Nevertheless, the present procedure was found to bring about the intermolecular cross-coupling of **1a** with 1,3-diphenyl-2-propanone (**16**) to give 1,1,3,3-tetraphenyl-2-propanone (**17**; Scheme 5).

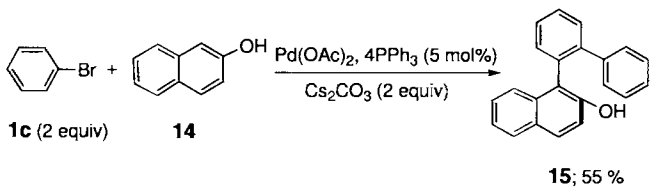

Scheme 4. Cross-coupling of **1c** with **14**: DMF, N_2, 150 °C, 1.5 h.

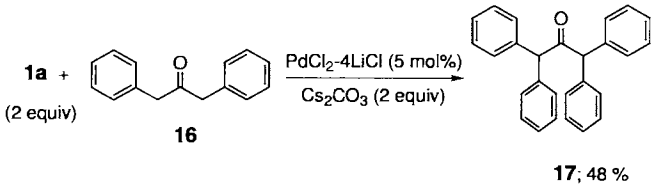

Scheme 5. Cross-coupling of **1a** with **16**: DMF, N_2, 100 °C, 5 h.

Experimental Section

A mixture of **1** (1.2–4 mmol), ArOH **2–5**, **12**, or **14** (1 mmol), a palladium catalyst (0.025–0.05 mmol), Cs_2CO_3 (1.2–4 mmol), and DMF (5 mL) was stirred in the presence or absence of molecular sieves 4 Å (200 mg) under nitrogen at 100–150 °C for 1.5–44 h. After cooling, the reaction mixture was poured into dilute hydrochloric acid, extracted with ether, and dried over sodium sulfate. The product was isolated by column chromatography on silica gel using hexane/dichloromethane or hexane/ethyl acetate as eluent.

Selected data for the new products obtained are listed in Table 2. The structures were determined with the aid of ^{1}H NMR, NOE, COSY, and HOHAHA experiments. Satisfactory combustion analysis data were also obtained. Compounds **6a**[9], **13**[10], and **17**[11] are known.

Received: March 4, 1997 [Z10194IE]
German version: *Angew. Chem.* **1997**, *109*, 1820–1822

Keywords: biaryls · C–C coupling · homogeneous catalysis · O ligands · palladium

[1] a) R. F. Heck, *Palladium Reagents in Organic Syntheses*, Academic Press, New York, **1985**, pp. 179–321; b) A. de Meijere, F. E. Meyer, *Angew. Chem.* **1994**, *106*, 2473–2506; *Angew. Chem. Int. Ed. Engl.* **1994**, *33*, 2379–2411; c) J. Tsuji, *Palladium Reagents and Catalysts*, Wiley, Chichester, **1995**, pp. 125–290.

[2] Recently, the following novel palladium-catalyzed reactions involving C–H bond activation have been reported: di-[2a,b] and triarylations[2c,d] of norbornene, and di-[2e] and trimerizations[2f] of aryl halides. a) M. Catellani, G. P. Chiusoli, *J. Organomet. Chem.* **1985**, *286*, C13–C16; b) *ibid.* **1991**, *407*, C30–C33; c) O. Reiser, M. Weber, A. de Meijere, *Angew. Chem.* **1989**, *101*, 1071–1072; *Angew. Chem. Int. Ed. Engl.* **1989**, *28*, 1037–1038; d) K. Albrecht, O. Reiser, M. Weber, B. Knieriem, A. de Meijere, *Tetrahedron* **1994**, *50*, 383–401; e) G. Dyker, *Angew. Chem.* **1992**, *104*, 1079–1081; *Angew. Chem. Int. Ed. Engl.* **1992**, *31*, 1023–1025; f) *ibid.* **1994**, *106*, 117–119 and **1994**, *33*, 103–105.

[3] a) T. Satoh, T. Itaya, M. Miura, M. Nomura, *Chem. Lett.* **1996**, 823–824; b) T. Satoh, T. Tsuda, Y. Kushino, M. Miura, M. Nomura, *J. Org. Chem.* **1996**, *61*, 6476–6477; c) T. Satoh, M. Ikeda, M. Miura, M. Nomura, *J. Mol. Catal. A* **1996**, *111*, 25–31; d) T. Satoh, K. Kokubo, M. Miura, M. Nomura, *Organometallics* **1994**, *13*, 4431–4436.

[4] Previous syntheses of 1,2,3-triarylbenzenes required multistep reactions: e.g. a) T. Sato, S. Shimada, K. Hata, *Bull. Chem. Soc. Jpn.* **1971**, *44*, 2484–2490; b) S. Ozasa, Y. Fujioka, J. Kikutake, E. Ibuki, *Chem. Pharm. Bull.* **1983**, *31*, 1572–1581.

[5] Participation of another sequence in which cyclopalladation of **2** by Pd^{II} is followed by oxidative addition of **1** to give a Pd^{IV} intermediate cannot be excluded, especially at an early stage of the reaction[2]. During the preparation of this manuscript, the palladium-catalyzed 2,6-dialkylation of aryl iodides with alkyl iodides, which seems to proceed via Pd^{IV} species, was also reported: M. Catellani, F. Frignani, A. Rangoni, *Angew. Chem.* **1997**, *109*, 142–145; *Angew. Chem. Int. Ed. Engl.* **1997**, *36*, 119–122.

[6] Stoichiometric palladation of a nitrobenzylamine: J. Vicente, I. Saura-Llamas, M. G. Palin, P. G. Jones, *J. Chem. Soc. Dalton Trans.* **1995**, 2535–2539.

[7] a) D. D. Hennings, S. Iwasa, V. H. Rawal, *J. Org. Chem.* **1997**, *62*, 2–3; b) M. A. Cuifolini, M. E. Browne, *Tetrahedron Lett.* **1987**, *28*, 171–174; c) M. A. Cuifolini, H. B. Qi, M. E. Browne, *J. Org. Chem.* **1988**, *53*, 4149–4151.

[8] M. Uno, K. Seto, W. Ueda, M. Masuda, S. Takahashi, *Synthesis* **1985**, 506–508.

[9] T. Keumi, C. Murata, Y. Sasaki, K. Ogasawara, H. Kitajima, *Nippon Kagaku Kaishi* **1981**, 259–264 [*Chem. Abstr.* **1981**, *95*, 42537x].

[10] D. G. Batt, D. G. Jones, S. L. Greca, *J. Org. Chem.* **1991**, *56*, 6704–6708.

[11] F. G. Bordwell, J. E. Bares, J. E. Bartmess, G. J. McCollum, M. V. Puy, N. R. Vanier, W. S. Matthews, *J. Org. Chem.* **1977**, *42*, 321–325.

 © WILEY-VCH Verlag GmbH, D-69451 Weinheim, 1997 0570-0833/97/3616-1742 $ 17.50+.50/0

Catalytic Three-Component Synthesis of Conjugated Dienes from Alkynes via Pd^0, Pd^{II}, and Pd^{IV} Intermediates Containing 1,2-Diimine**

Ruud van Belzen, Helmut Hoffmann, and Cornelis J. Elsevier*

The direct synthesis of conjugated dienes from alkynes is highly desirable for forming valuable synthetic intermediates.[1] A number of methods are available for the stereoselective preparation of dienes from acetylenes,[2] but these either rely on the use of a stoichiometric amount of a reactive organometallic species (precluding the presence of sensitive substituents),[3] require more than one reaction step,[4] or start from pure stereoisomers of alkenyl compounds in cross-coupling reactions.[5] A high-yield, selective catalytic procedure for preparing conjugated "open-chain" dienes directly from acetylenes has not been described.[6]

As part of our continuing studies on carbon–carbon and carbon–heteroatom cross-coupling reactions[7] mediated by palladium compounds with ancillary, rigid, bidentate nitrogen ligands (Scheme 1), instead of the usual phosphanes, we report a new catalytic three-component synthesis of conjugated dienes by coupling of alkynes with an organic halide and tetramethyltin. Mechanistic details have been elucidated that reveal that stereospecific oxidative addition and reductive elimination at carbopalladacyclic compounds occurs, and that intermediate Pd^0, Pd^{II}, and Pd^{IV} species are involved in the catalytic cycle.

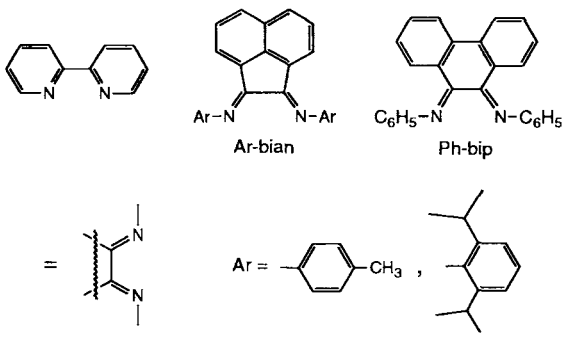

Scheme 1. Bidentate N ligands.

Palladacycles **1**[8] react with one equivalent of an organic halide (for example benzyl bromide, methyl iodide, or iodobenzene) in dichloromethane at 20 °C to give dienyl(NN-κ^2-*N*,*N*)palladium(II) halides **2**[9] (Scheme 2; NN = bis (arylimino)acenaphthene (Ar-bian), bis(phenylimino)phenanthrene (Ph-bip),[10] or 2,2′-bipyridine (bpy)). Compounds **2** are formed by a sequence of oxidative addition and reductive elimination at palladium via triorgano(NN-κ^2*N*,*N*)palladium(IV) halides **A**.[11] Reaction of **2a–c** with tetramethyltin in DMF at 60–85 °C leads to the selective formation of 2,5-difunctionalized 2,4-hexadienoates **3a–c**. Sequential addition of methyl iodide and one equivalent of Br_2 to **1** in dichloromethane results in the 2-bromo-5-methyl derivative **3x**.

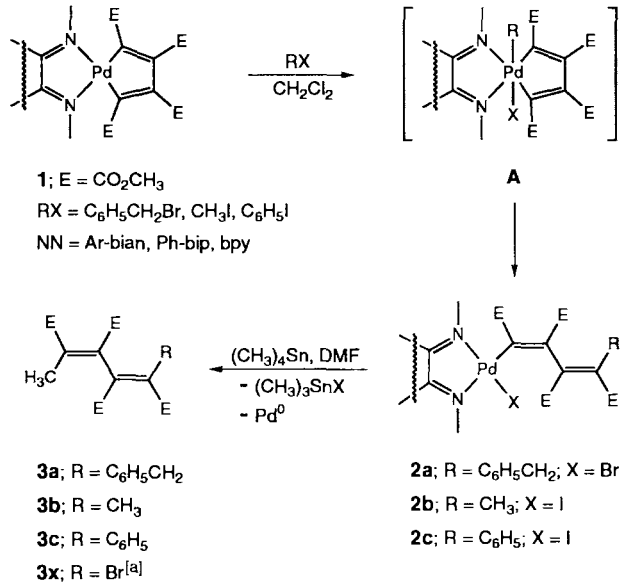

Scheme 2. Stoichiometric reaction of palladacyclopentadienes **1** with organic halides and Me_4Sn. [a] With addition of Br_2 (instead of Me_4Sn) to **2b** in CH_2Cl_2 directly after its formation.

Since formation of palladacycles **1** from $[Pd(dba)_2]$ (dba = dibenzylideneacetone) and electron-poor alkynes is much faster than oxidative addition of benzyl bromide to zero-valent Pd species, and insertion of a third molecule of acetylene in **1** is slower than reaction of the organic halide with **1** to give **2**, we anticipated that a catalytic procedure for the synthesis of dienes **3** (Scheme 3), consisting of the single steps shown above, was feasible. Indeed, employing **1** as the precatalyst (or $[Pd(dba)_2]$ and an equimolar amount of Ar-bian or Ph-bip) with

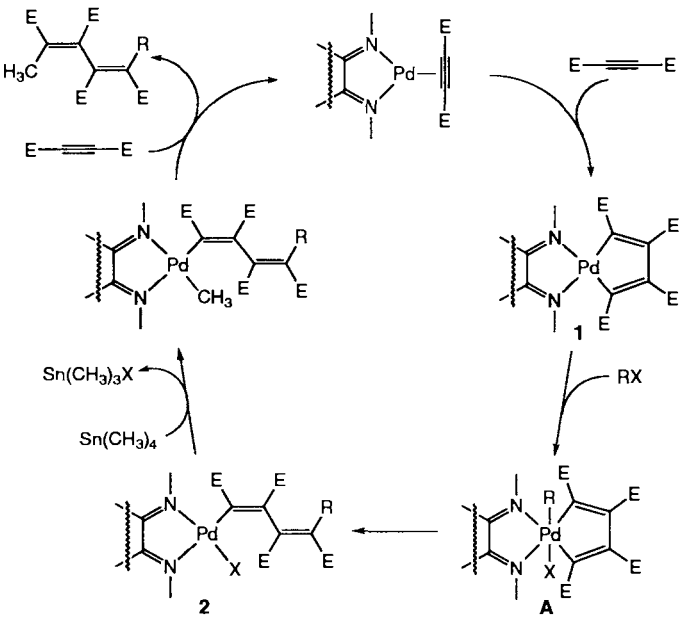

Scheme 3. Proposed cycle for the three-component synthesis of conjugated dienes from alkynes, RX, and Me_4Sn catalyzed by palladium/N ligand. E = CO_2CH_3; RX = $C_6H_5CH_2Br$, CH_3I, C_6H_5I.

[*] Prof. Dr. C. J. Elsevier, Dr. R. van Belzen, Dr. H. Hoffmann
J. H. van't Hoff Research Instituut, Anorganisch Chemisch Laboratorium
Universiteit van Amsterdam
Nieuwe Achtergracht 166, 1018 WV Amsterdam (The Netherlands)
Fax: Int. code +(20) 525-6456
e-mail: else4@anorg.chem.uva.nl

[**] Rigid Bidentate Nitrogen Ligands in Organometallic Chemistry and Homogeneous Catalysis. Part 12. Part 11: R. van Asselt, C. J. Elsevier, C. Amatore, A. Jutand, *Organometallics* **1997**, *16*, 317. This work was supported in part (H. H.) by the Netherlands Foundation for Chemical Research (SON) with financial aid from the Netherlands Organization for Scientific Research (NWO).

 © WILEY-VCH Verlag GmbH, D-69451 Weinheim, 1997 0570-0833/97/3616-1743 $ 17.50+.50/0

100 equivalents of dimethyl butynedioate, 50 equivalents of tetramethyltin; and 50–200 equivalents of benzyl bromide, methyl iodide; or iodobenzene in DMF at 65 °C resulted after 8–16 h in the complete conversion of the alkyne into conjugated dienes **3a–c**. DMF was selected as the solvent to obtain convenient rates, as reactions in acetonitrile and THF are sluggish, probably because transmetalation is the rate-determining step. The best results were obtained when employing [Pd(Ar-bian)] compounds as the catalyst (71–85% yields of isolated **3a–c**). 1-Dimethylamino-1,2-di(methoxycarbonyl)ethene formed as a secondary product in approximately 10% yield due to base- or palladium-catalyzed decarbonylative addition of DMF to coordinated dimethyl butynedioate.[12] This, in conjunction with the fact that the latter reaction does not occur in the absence of palladium species, points to the occurrence of zero-valent palladium species in the catalytic cycle. In the case of **3c** small amounts of the cyclotrimerization product hexamethylmellitate (4%) and 1-phenyl-1,2-di(methoxycarbonyl)-1-propene (7%)[13] formed as well. Importantly, no direct cross-coupling between the organic halide and tetramethyltin took place. We obtained palladacycles **1** containing mono- and bidentate nitrogen ligands for dimethyl butynedioate (E = CO_2Me) and hexafluoro-2-butyne (E = CF_3), but stoichiometric or catalytic reactions of methylpropynoate, phenylacetylene, and 1-octyne were unsuccessful so far.

Reactions of **1** with two equivalents of Br_2 in dichloromethane at 20 °C afforded (2*E*,4*E*)-2,5-dibromo-2,4-hexadienoates **5y** and [$PdBr_2$(NN-κ^2N,N)] (Scheme 4). Intermediate **B**, a diorganopalladium(IV) dihalide,[14] formed instantaneously and quantitatively at 200 K in CD_2Cl_2, as demonstrated by in situ ^{1}H NMR spectroscopy for NN = bis(2,6-diisopropylphenyl)bian or Ph-bip; the signals for the methoxycarbonyl groups adjacent to palladium in **B** are shifted to higher frequency by about 0.8 ppm.[15] The C_{2v} symmetry of **B** was apparent from the pair-wise equivalence of protons on the backbone of the NN ligand, the palladacyclopentadiene moiety, and the two (perpendicular) *N*-aryl groups, and from the fact that only two

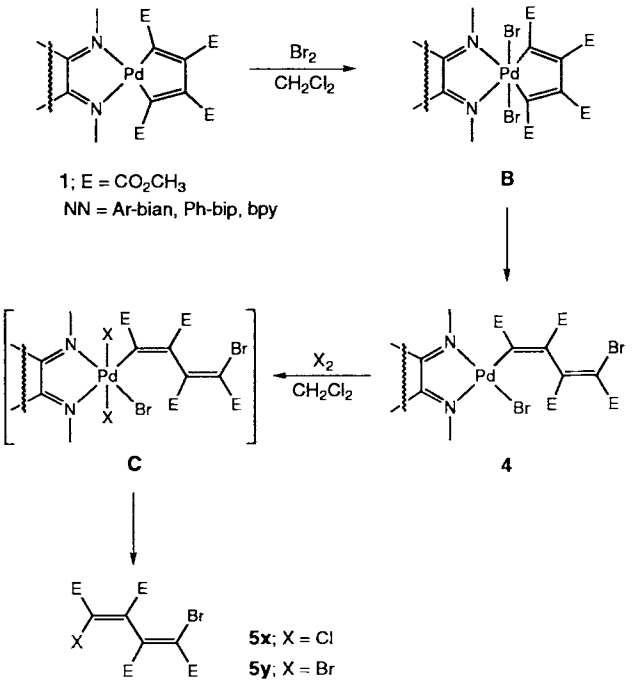

Scheme 4. Stoichiometric reactions of palladacycles **1** with molecular halogen to give 1,4-dihalo-1,3-dienes via diorganopalladium(IV) dihalides **B** and organopalladium(IV) trihalides **C**.

doublets were observed for the four CH(CH_3)$_2$ groups of the bis(*N*-2,6-diisopropylphenyl)bian derivative.[16] Reductive elimination from **B** to give **4**, which could be isolated,[17] was completed in 10–15 min at 200 K.

Reaction of **4** with Br_2 gave **5y** and [$PdBr_2$(NN-κ^2N,N)], and that of **4** with PhI·Cl2 led to the chemoselective formation of 2-bromo-5-chloro-2,4-hexadienoates **5x**. The 5-chloro-2,4-hexadienylpalladium(II) chloride analogue of **4** also reacted with Br_2 to give exclusively **5x**. These results, taken together with the fact that no elimination of dibromodienes was observed from the reaction of **4** with ICl and, moreover, that such reactions could not be effected with palladium–phosphane analogues of **4**, strongly indicate the occurrence of intermediate organopalladium(IV) trihalide species **C**, from which stereospecific reductive elimination of one of the apical halogens and the dienyl moiety takes place.

Interestingly, three oxidation states of palladium are involved in the catalytic cycle. This merits further attention, especially in view of the current interest in catalytic reactions (presumably) involving palladium in high oxidation states.[11a, 14b, c, 18] Phosphane ligands are not compatible; they either react with the alkyne, or the palladium–phosphane species involved exhibit no catalytic activity whatsoever under the conditions described.

To our knowledge the procedure described here represents the first straightforward, regioselective, three-component protocol for the synthesis of conjugated dienes involving alkynes, which are themselves sensitive to nucleophilic attack. Dienes **3** and **5** obtained by this procedure may serve as building blocks, for instance in conjugate-addition, Diels–Alder, and (for **3x** and **5**) catalytic C–C coupling reactions, for example with vinyltin and boron reagents to obtain conjugated trienes and tetraenes. The drawback of the limited scope of the reaction (as far as the alkyne is concerned) may partly be overcome by modification of the substituents, including dealkoxycarbonylation.

The results obtained thus far prompt us to undertake a more detailed investigation regarding the generality and the mechanism of this convenient protocol for the catalytic synthesis of conjugated dienes from readily available starting materials.

Experimental Section

Typical procedure for the catalytic synthesis of **3**: A solution of [Pd(*p*-tolbian){C(CO_2Me)=C(CO_2Me)C(CO_2Me)=C(CO_2Me)}] (15 mg, 0.02 mmol), dimethyl butynedioate (245 μL, 2.0 mmol), Me_4Sn (180 mg, 1.0 mmol), and methyl iodide (0.6 mL, 10 mmol) in DMF (10 mL) was stirred under a nitrogen atmosphere in a closed Schlenk tube for 16 h at 65 °C. In the case of benzyl bromide or iodobenzene 1.0 mmol of the organic halide was added, and the reaction temperature kept at 85 °C. The crude reaction mixture was dissolved in dichloromethane (100 mL), washed with water (3 × 150 mL), and dried. After removal of the solvent under vacuum, a sticky solid remained, from which the organic product was extracted with diethyl ether. After chromatographic purification on silica gel (hexanes/diethyl ether 9/1) **3a** was isolated in 71%, **3b** in 85%, and **3c** in 76% yield.

Received: February 12, 1997 [Z10104IE]
German version: *Angew. Chem.* **1997**, *109*, 1833–1835

Keywords: C–C coupling · dienes · multicomponent reactions · N ligands · palladium

[1] J. M. Klunder, G. H. Posner in *Comprehensive Organic Synthesis, Vol. 3* (Eds.: B. M. Trost, I. Fleming), Pergamon, Oxford, **1991**, p. 217.
[2] a) E. Negishi in *Comprehensive Organic Synthesis, Vol. 5* (Eds.: B. M. Trost, I. Fleming), Pergamon, Oxford, **1991**, p. 1163; b) P. F. Hudrlik, A. M. Hudrlik in *The Chemistry of the Carbon-Carbon Triple Bond* (Ed.: S. Patai), Wiley, New York, **1978**, pp. 199–273.
[3] P. Knochel in *Comprehensive Organic Synthesis, Vol. 4* (Eds.: B. M. Trost, I. Fleming), Pergamon, Oxford, **1991**, p. 865.
[4] B. M. Trost, C. Li, *Synthesis* **1994**, 1267.
[5] a) E. Negishi, *Acc. Chem. Res.* **1982**, *15*, 340; b) J. K. Stille, B. L. Groh, *J. Am. Chem. Soc.* **1987**, *109*, 813; c) E. Negishi, T. Takahashi, S. Baba, D. E. van Horn, N. Okukado, *ibid* **1987**, *109*, 2393; d) B. Jiang, Y. Xu, *Tetrahedron Lett.* **1992**, *33*, 511.

 © WILEY-VCH Verlag GmbH, D-69451 Weinheim, 1997 0570-0833/97/3616-1744 $ 17.50+.50/0

[6] Titanium and zirconium-catalyzed cyclization of diynes to exocyclic conjugated dienes: a) W. A. Nugent, J. C. Calabrese, *J. Am. Chem. Soc.* **1984**, *106*, 6422; b) E. Negishi, S. J. Holm, J. M. Tour, J. A. Miller, F. E. Cederbaum, D. R. Swanson, T. Takahashi, *ibid.* **1989**, *111*, 3336.
[7] a) R. van Asselt, C. J. Elsevier, *Organometallics* **1992**, *11*, 1999; b) *Tetrahedron* **1994**, *50*, 323.
[8] a) K. Moseley, P. M. Maitlis, *J. Chem. Soc. Chem. Commun.* **1971**, 1604; b) T. Ito, Y. Takahashi, Y. Ishii, *ibid.* **1972**, 629; c) H. tom Dieck, C. Munz, C. Müller, *J. Organomet. Chem.* **1990**, *384*, 243; d) R. van Asselt, C. J. Elsevier, W. J. J. Smeets, A. L. Spek, *Inorg. Chem.* **1994**, *33*, 1521.
[9] Satisfactory spectral and analytical data were obtained for **2**; the configurations around double bonds of the dienyl moiety were corroborated by an X-ray crystal structure determination (unpublished results).
[10] a) R. van Asselt, C. J. Elsevier, W. J. J. Smeets, A. L. Spek, R. Benedix, *Recl. Trav. Chim. Pays-Bas* **1994**, *113*, 88; b) R. van Belzen, R. A. Klein, W. J. J. Smeets, A. L. Spek, R. Benedix, C. J. Elsevier, *ibid.* **1996**, *115*, 275.
[11] a) A. J. Canty, *Acc. Chem. Res.* **1992**, *25*, 83; b) P. K. Beyers, A. J. Canty, B. W. Skelton, A. H. White, *J. Chem. Soc. Chem. Commun.* **1986**, 1722; c) M. Catellani, G. P. Chiusoli, *J. Organomet. Chem.* **1988**, *346*, C27; d) W. de Graaf, J. Boersma, D. Grove, A. L. Spek, G. van Koten, *Recl. Trav. Chim. Pays-Bas* **1988**, *107*, 299.
[12] $[Pd^0(NN)(MeO_2CC{\equiv}CCO_2Me)]$ was observed by ^1H and ^{13}C NMR spectroscopy (about 20% steady state) in reactions of $[Pd(dba)_2]$ with Ph-bip and dimethyl butynedioate to give **1**. Inadvertant (partly) dissociated NN ligands may catalytically decompose DMF.
[13] Probably formed by transmetalation of the adduct resulting from phenylpalladation of $[Pd^0(NN)(MeO_2CC{\equiv}CCO_2Me)]$.
[14] a) R. Usón, J. Forniés, R. Navarro, *J. Organomet. Chem.* **1975**, *96*, 307; b) R. van Asselt, E. Rijnberg, C. J. Elsevier, *Organometallics* **1994**, *13*, 706; c) R. van Asselt, C. J. Elsevier, *ibid.* **1994**, *13*, 1972.
[15] ^1H NMR data for $PdC(CO_2CH_3)$ and $PdC{=}C(CO_2CH_3)$ groups in $CDCl_3$: **B** (223 K): $\delta = 3.61$ and 3.57 (iPr_2-bian derivative), 3.72 and 3.58 (Ph-bip derivative); **1**: (223 K): $\delta = 2.66$ and 3.46 (iPr_2-bian derivative), 2.93 and 3.65 ppm (Ph-bip derivative).
[16] ^1H NMR data for the $(CH_3)_2CH$ groups of the 2,6-iPr_2-bian derivative in $CDCl_3$: **B** (200 K): $\delta = 1.26$ (d) and 0.52 (d); **1**: (200 K): $\delta = 1.32$ and 0.54; **4**: (223 K): $\delta = 1.39$ (d), 1.27 (d), 1.09 (d) and 0.60 (d; no C_s plane perpendicular to the $Pd(X)CN_2$ plane for **4**).
[17] Satisfactory spectral and analytical data were obtained for **4**; an X-ray crystal structure analysis of the iodo analogue of **4** (NN = bpy) was carried out (unpublished results).
[18] a) D. Milstein, J. K. Stille, *J. Am. Chem. Soc.* **1979**, *101*, 4981; b) B. M. Trost, A. S. K. Hashmi, *Angew. Chem.* **1993**, *105*, 1130; *Angew. Chem. Int. Ed. Engl.* **1993**, *32*, 1085; c) G. Dyker, *ibid.* **1994**, *106*, 117 and **1994**, *33*, 103; d) M. Beller, H. Fischer, W. A. Herrmann, K. Öfele, C. Brossmer, *ibid.* **1995**, *107*, 1992 and **1995**, *34*, 1848; e) M. Catellani, L. Ferioli, *Synthesis* **1996**, 769; f) M. Catellani, F. Frignani, A. Rangoni, *Angew. Chem.* **1997**, *109*, 142; *Angew. Chem. Int. Ed. Engl.* **1997**, *36*, 119.

Conformation Design of a Fully Flexible βII-Hairpin Analogue**

Ulrich Schopfer, Martin Stahl, Trixi Brandl, and Reinhard W. Hoffmann*

Isosteric, non-hydrolyzable analogues of secondary-structure elements of peptides are of high current interest in medicinal chemistry and serve as peptidomimetics. Such structural units yield important information on complex structure–activity relationships and are neccessary for a rational design of low molecular weight, non-peptide pharmaceutical agents.[1] Moreover, such analogues of peptide structures may be important for inducing α-helix or β-turn structures in adjacent peptide sequences.[2] Far less is known about the prerequisites for the induction of β-sheet structures, in which tertiary interactions play a decisive role. Gellman et al. pointed out that good model systems for studying the formation of β-hairpin structures are lacking.[3]

We are interested in a rational conformation design of open-chain hydrocarbon backbones that possess a strong conformational bias and yet maintain full flexibility.[4] We therefore tried to apply the principles of nature's conformation design, demonstrated in polyketide natural products, to designing new molecular backbones. We demonstrate here the value of such an approach with the design of a fully flexible β-hairpin analogue.

A β hairpin is the simplest form of an antiparallel β-sheet conformation, and is defined by a β-turn region flanked by two antiparallel peptide strands that are hydrogen bonded through the corresponding backbone CO and NH groups. Different structural types of β turns are characterized by the ϕ and ψ dihedral angles of the peptide backbone.[5] Figure 1 shows the structure of a βII-type hairpin with $\phi_1 = -60°$, $\psi_1 = 120°$, $\phi_2 = 90°$, and $\psi_2 = 0°$. The requirements that a mimic must meet are 1) a reversal in the peptide-chain direction and 2) the promotion of intramolecular hydrogen-bond formation.[2] In addition, our approach allows preservation of conformational flexibilty similar to that of the natural prototype.

Our design is based on 2,4-dimethylpentane units such as the ones nature uses in its conformation design of polyketide natural products.[4] 2,4-Dimethylpentane (**1**) is biconformational, and equally populates, to greater than 90%, two enantiomorphous and, hence, isoenergetic low-energy conformations **1a** and **1b**.

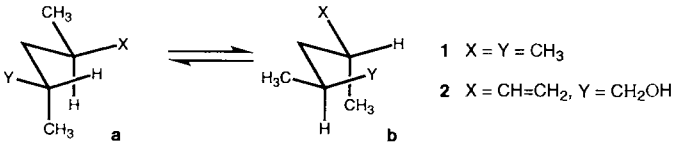

The position of the conformer equilibrium could be biased to one side by varying the substituents X and Y. In **2a** X suffers an additional *gauche* interaction, which Y does not have, and is therefore in the sterically more encumbered position. When X in **2** is a less sterically demanding vinyl group and Y a hydroxymethyl group, conformation **2a** should be preferentially populated. In fact, an equilibrium ratio **a**:**b** of about 3.5:1 was found for **2** in $CDCl_3$ solution. Therefore, **2** represents a backbone segment with a conformational preference. It can be combined with itself or other building blocks to yield larger molecular frameworks. The combination of two segments of **2** results in structure **3**, which should have a U-shaped molecular backbone that is similar to β-turn und β-hairpin moieties of peptides.

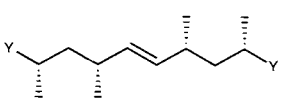

3 Y = CH_2OH **4** Y = CH_3

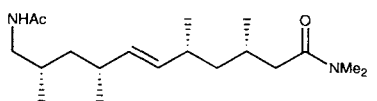

5

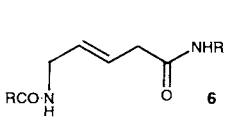

6

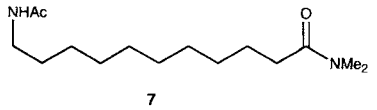

7

[*] Prof. Dr. R. W. Hoffmann, Dipl.-Chem. U. Schopfer, Dipl.-Chem. M. Stahl, T. Brandl
Fachbereich Chemie der Universität
Hans-Meerwein-Strasse, D-35032 Marburg (Germany)
Fax: Int. code +(6421)288-917
e-mail: rwho@ps1515.uni-marburg.de

[**] This work was supported by the Volkswagenstiftung. We thank the Fonds der Chemischen Industrie for a doctoral fellowship (U. S.) and a Kekulé fellowship (M. S.). We thank F. Schmock for IR measurements, and G. Häde for NMR measurements (both in Marburg).

 © WILEY-VCH Verlag GmbH, D-69451 Weinheim, 1997 0570-0833/97/3616-1745 $ 17.50+.50/0

Simple modeling (MM3*)[6] showed that the most stable conformation of the bis(amide) **5** derived from **3** matches the shape of a βII-hairpin **8** very well (Figure 1).

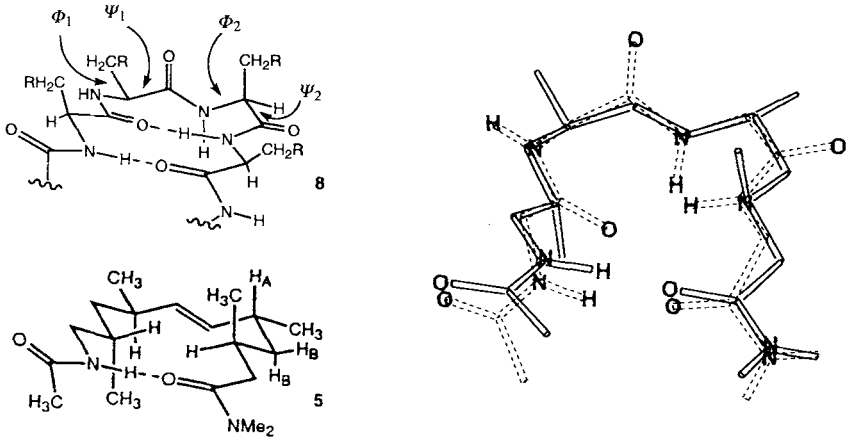

Figure 1. Superposition of the most stable conformation of **5** with a βII-hairpin **8**.

To find out whether **5** is a conformationally flexible βII-hairpin analogue, we synthesized **5** from optically active **9** (Scheme 1).[7] Compound **9** was transformed on the one hand in four conventional steps into sulfone **11**, and on the other hand in eight steps into aldehyde **10**. Julia olefination of the two components yielded alkene **12**, from which bis(amide) **5** could be obtained in four further steps.

IR and NMR spectroscopy was used to analyze the conformational properties of **5** in solution. The former is especially suited for studying intramolecular hydrogen bonds, because the transformation of hydrogen-bonded into non-hydrogen-bonded conformations is slow on the IR time scale. Both states can therefore be distinguished by separate N–H streching frequencies in nonpolar solvents. In contrast, this transformation is fast on the NMR time scale, so that the observed resonances are weighted averages of hydrogen-bonded and non-hydrogen-bonded states.

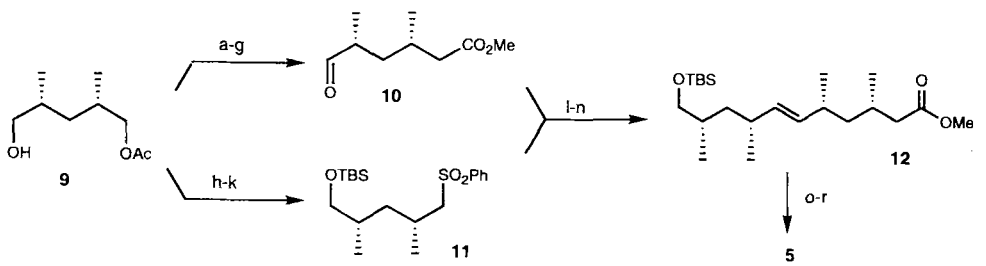

Scheme 1. a) Triisopropylsilyl chloride (TIPSCl), imidazole, 4-dimethylamino pyridine (DMAP), DMF, 50 °C, 96%; b) K_2CO_3, CH_3OH, 25 °C, 94%; c) CH_3SO_2Cl, NEt_3, CH_2Cl_2, −40 °C; LiBr, THF, 25 °C, 98%; d) NaCN, DMSO, 25 °C, 95%; e) NaOH, EtOH, 80 °C, 84%; f) CH_2N_2, Et_2O, 0 °C, 90%; g) pyridinium chlorochromate (PCC), CH_2Cl_2, SiO_2; h) I_2, PPh_3, imidazole, THF, 25 °C, 90%; i) $PhSO_2Na$, polyethylene glycol (PEG) 400, 130 °C, 91%; j) K_2CO_3, CH_3OH, 25 C, 91%; k) *tert*-butyldimethylsilyl chloride (TBSCl), imidazole, DMAP, DMF, 50 °C, 99%; l) sulfone **11**, *n*BuLi, THF, −78 °C, aldehyde **10**, 97%; m) Ac_2O, pyridine, 25 °C, 90%; n) 6% Na/Hg, CH_3OH, AcOEt, NaH_2PO_4, −30 °C, 88%; o) ClAl(Me)NMe_2, benzene, 80 °C, 95%; p) nBu_4NF, THF, 25 °C, 96%; q) CH_3SO_2Cl, NEt_3, CH_2Cl_2, −40 °C; NaN_3, DMF, 50 °C, 85%; r) PPh_3, THF, trace H_2O; Ac_2O, 25 °C, 96%.

The IR spectrum of **5** (10^{-3} M in CCl_4) shows only one sharp band, the wavenumber of which (3360 cm^{-1}) is characteristic for the N–H streching vibration of hydrogen-bonded amide protons.[8] That the preorganization of the amide groups in **5** by the hydrocarbon backbone is the origin of the predominance of the hydrogen-bonded state can be seen by a comparison with the IR spectrum of the simple ω-acetamidocarboxamide **7**. The latter shows, in addition to two bands for hydrogen-bonded NH-groups, an intensive absorption due to non-hydrogen-bonded amide protons (Figure 2). The concentration dependence of the amide proton ^1H NMR chemical shift of **5** was then determined to exclude aggregation as the cause of hydrogen bonding. From the constant value in solutions of varying concentration (10^{-1}–10^{-4} M, CCl_4) it can be unequivocally deduced that **5** is intra- rather than intermolecularly hydrogen bonded (Figure 3). In contrast, **7** exhibits a pronounced concentration dependence of the amide-proton chemical shift, which corresponds to the behavior of *N*-methylacetamide. The data clearly show that no aggregation occurs in a 10^{-3} M solution, the concentration at which the IR spectra were obtained.

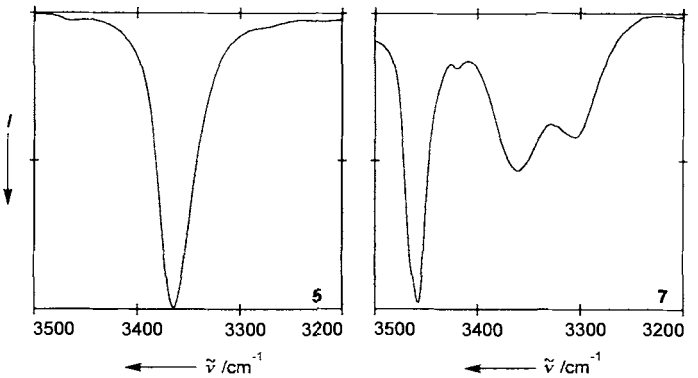

Figure 2. IR spectra (transmittance) of the bis(amide)s **5** and **7** (1 mM in CCl_4, d = 3.5 cm, NaCl): **5**, maximum at 3365 cm^{-1}; **7**, maxima at 3458, 3361 and 3305 cm^{-1}.

The conformational preference of the hydrocarbon backbone of **5** can be deduced from the vicinial ^1H–^1H NMR coupling constants. The divergence of the diagnostic[9] ^1H NMR coupling constants between H_A (Figure 1) and the two protons H_B (2.9 Hz and 10.5 Hz, $CDCl_3$) proves a pronounced conformational preference of the hydrocarbon backbone of **5**. This preference, however, is not a consequence of conformational constraints induced by the hydrogen bond: MM3* calculations show that the most stable conformation of **4** is virtually identical to that of the bis(amide) **5** (Figure 4). Therefore, the backbone conformation of **4** is already ideally suited to preorient the amide groups of **5** for formation of an intramolecular hydrogen bond. Clearly, conformation design of **5** is the origin of the spontaneous formation of the 14-membered cyclic conformation, as multiconformational **7** is converted into an essentially monoconformational

 © WILEY-VCH Verlag GmbH, D-69451 Weinheim, 1997 0570-0833/97/3616-1746 $ 17.50+.50/0

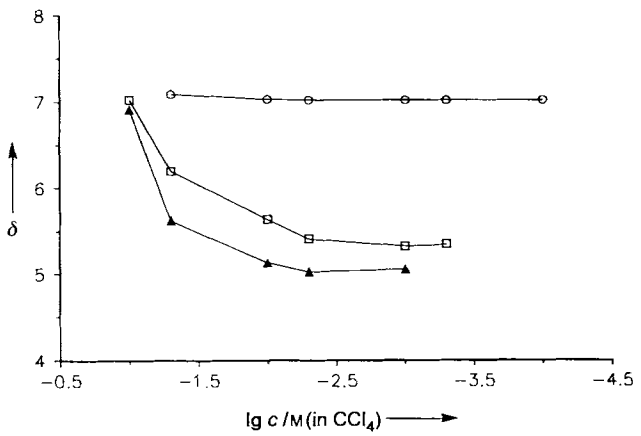

Figure 3. NMR chemical shift of the amide protons in CCl_4 at 300 K as a function of the logarithm of concentration: **5** (○), **7** (□), *N*-methylacetamide (▲).

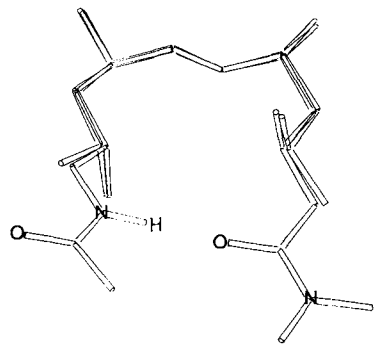

Figure 4. Superposition of the most stable conformation of **5** with that of **4**.

unit **5** by rational introduction of a *trans* double bond *and* four methyl groups. Simple introduction of a double bond into an ω-amido-alkyl-carboxamide does not suffice to induce a β-turn conformation, as Gellman et al.[10] showed with **6**.[11] Conclusion: **5** is not only isostructural with a βII hairpin, but also retains the conformational flexibility that is typical for peptides.

Received: March 5, 1997 [Z10200IE]
German version: *Angew. Chem.* **1997**, *109*, 1805–1807

Keywords: conformation analysis · hydrogen bonds · peptidomimetics

[1] a) R. Hirschmann, *Angew. Chem.* **1991**, *103*, 1305–1330; *Angew. Chem. Int. Ed. Engl.* **1991**, *30*, 1278–1301; b) G. Müller, *ibid.* **1996**, *108*, 2941–2943 and **1996**, *35*, 2767–2769.

[2] a) J. P. Schneider, J. W. Kelly, *Chem. Rev.* **1995**, *95*, 2169–2187; b) M. Kahn, *Synlett* **1993**, 821–826.

[3] T. S. Haque, J. C. Little, S. H. Gellman, *J. Am. Chem. Soc.* **1994**, *116*, 4105–4106, and references therein.

[4] R. W. Hoffmann, *Angew. Chem.* **1992**, *104*, 1147–1157; *Angew. Chem. Int. Ed. Engl.* **1992**, *31*, 1124–1134.

[5] J. B. Ball, R. A. Hughes, P. F. Alewood, P. R. Andrews, *Tetrahedron* **1993**, *49*, 3467–3478.

[6] Macromodel 4.5, Department of Chemistry, Columbia University, New York, NY 10027 (USA).

[7] J. C. Anderson, S. V. Ley, S. P. Marsden, *Tetrahedron Lett.* **1994**, *35*, 2087–2090.

[8] For the interpretation of IR and NMR data, see for example a) S. H. Gellman, G. P. Dado, G.-B. Liang, B. R. Adams, *J. Am. Chem. Soc.* **1991**, *113*, 1164–1173; b) G.-B. Liang, J. M. Desper, S. H. Gellman, *ibid.* **1993**, *115*, 925–938.

[9] R. Göttlich, B. C. Kahrs, J. Krüger, R. W. Hoffmann, *Chem. Commun.* **1997**, 247–251.

[10] R. R. Gardner, G.-B. Liang, S. H. Gellman, *J. Am. Chem. Soc.* **1995**, *117*, 3280–3281.

[11] With two methyl substituents at the double bond of **6**, a conformation corresponding to a β turn can be induced due to 1,3-allylic strain [10].

NADH-Induced Changes of the Nickel Coordination within the Active Site of the Soluble Hydrogenase from *Alcaligenes eutrophus*: XAFS Investigations on Three States Distinguishable by EPR Spectroscopy**

Arnd Müller, Andreas Erkens, Klaus Schneider, Achim Müller, Hans-Friedrich Nolting, Vicente Armando Solé, and Gerald Henkel*

Dedicated to Professor Günter Schmid on the occasion of his 60th birthday

Hydrogenases are enzymes that catalyse the reversible activation of molecular hydrogen in numerous aerobic and anaerobic microorganisms.[1] This capability has attracted increasing interest especially in view of possible applications of the catalytic principle in industrial processes or as source for "biological hydrogen" (hydrogen technology).[2]

Most of the hydrogenases known today are metalloenzymes that contain nickel and iron as essential constituents (NiFe hydrogenases) in distinction to the less widespread "iron-only" species.[1] The nickel binding site of these enzymes shows characteristic EPR signals in specific stages of the catalytic cycle indicating an uncommon redox chemistry. Thus, the nickel center is considered the site of hydrogen activation. The NiFe hydrogenase from *Desulfovibrio gigas* has recently been the focus of special attention since the crystal structure of this enzyme revealed the presence of a binuclear Ni/Fe center with cysteine sulfur bridges.[3]

The soluble NAD^+-reducing hydrogenase from the aerobic H_2-oxidizing bacterium *Alcaligenes eutrophus* H16 (E. C. 1.12.1.2) is a heterotetrameric enzyme. Composed of two heterodimeric proteins of different function ($\beta\delta$ and $\alpha\gamma$), this enzyme is of higher complexity than the "typical" heterodimeric hydrogenases.[4] In addition to the nickel center, the O_2-insensitive holoenzyme contains different iron–sulfur clusters (2Fe-2S, 3Fe-4S, 4Fe-4S) and a flavine residue (FMN) as redox-active prosthetic groups.

In this context, we were interested to learn whether and how the coordination of nickel changes upon reductive activation of the enzyme and, at the same time to tackle the question of possible structural relationships between the nickel centers of the hydrogenases from *A. eutrophus* and from *D. gigas*. To this end, high-resolution X-ray absorption spectroscopy (XAFS) was chosen as the method of choice. This technique was developed to determine the structure in the vicinity of excited atoms, and, in contrast to diffraction methods, can also be used to investigate noncrystalline systems. Thus, we characterized the soluble hydrogenase from *A. eutrophus* by XAFS analysis in three different states distuingishable by EPR spectroscopy.[5] Herein we report on the evaluation of the X-ray absorption near-edge structure (XANES) and extended X-ray absorption

[*] Prof. Dr. G. Henkel, Dipl.-Chem. A. Müller
Fachgebiet Anorganische Chemie der Universität
Lotharstrasse 1, D-47048 Duisburg (Germany)
Fax: Int. code +(203)3792110
e-mail: biohenkel@uni-duisburg.de
Dr. A. Erkens, Dr. K. Schneider, Prof. Dr. A. Müller
Fakultät für Chemie der Universität Bielefeld (Germany)
Dr. H.-F. Nolting, Dr. V. A. Solé
European Molecular Biology Laboratory
Outstation Hamburg (Germany)

[**] This work was supported by the Deutsche Forschungsgemeinschaft (DFG), the Bundesministerium für Bildung, Wissenschaft, Forschung und Technologie (BMBF), and the Fonds der Chemischen Industrie.

 © WILEY-VCH Verlag GmbH, D-69451 Weinheim, 1997 0570-0833/97/3616-1747 $ 17.50+.50/0

fine structure (EXAFS) regions of the Ni-K edge spectra and show for the first time that the individual states differ especially in the number of sulfur atoms bound to nickel, and thereby also chemically.

Starting point of the investigation is the aerobically isolated enzyme (form 1), the nickel center of which shows no EPR signal. Treatment with NADH leads to a reduced form (form 2), which shows an EPR signal characteristic for the active enzyme ("Ni-C"). By way of contrast, the reduction of the enzyme with sodium dithionite produces a state (form 3), which possesses the EPR signals associated with reduced Fe-S clusters, but—like the oxidized form—no Ni signal.[4] The normalized X-ray absorption spectra in the region of the Ni-K edge are depicted in Figure 1, and Table 1 summarizes the results of the XANES analyses. Figure 2 shows the experimentally determined EXAFS functions.

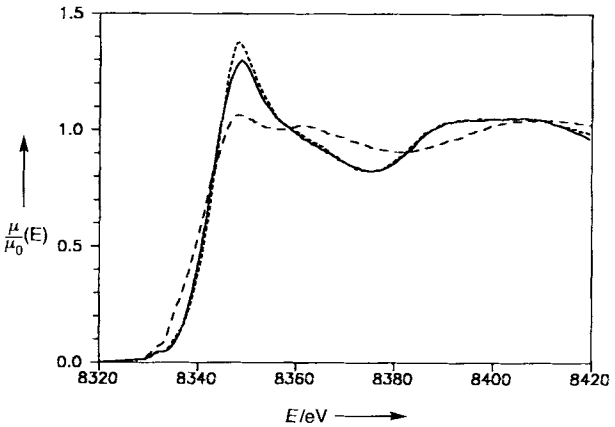

Figure 1. Normalized X-ray absorption spectra in the region of the Ni-K edge (solid line: air-oxidized; dashed line: NADH-reduced; dotted line: dithionite-reduced).

Table 1. Parameters of the normalized X-ray absorption spectra in the range of the Ni-K edge (XANES).

Enzyme form [a]	$E_{1/2}$ [eV] [b]	I_{max} [c]	A [eV] [d]
air-oxidized	8340.7	1.30	0.029
NADH-reduced	8339.6	1.07	0.035
Dithionite-reduced	8341.1	1.38	0.025

[a] See text. [b] Energy of the edge at a normalized intensity of 0.5. [c] Maximum edge intensity. [d] Integrated area of pre-edge peak.

All three investigated forms of the enzyme feature pre-edge peaks in accordance with nickel in a distorted octahedral ligand environment.[6] The edge structures of all three hydrogenase spectra also indicate an octahedral coordination of nickel. Furthermore, they suggest that nickel is predominantly coordinated by sulfur ligands after reduction with NADH (form 2), while the first coordination sphere of nickel is mainly composed of lighter atoms like nitrogen or oxygen in the other states (form 1 and form 3).

In the first step of the curve-fitting analyses based on Fourier-filtered EXAFS functions (Figure 3, $r' = 0.9-3.1$ Å), the ligand spheres of nickel were modeled by combinations of oxygen and sulfur donor functions taking into account integral occupation numbers with coordination numbers from four to six. The results confirm the characteristic differences derived from the XANES spectra in a convincing manner: while in forms 1 and 3 besides four oxygen atoms only two sulfur atoms contribute to

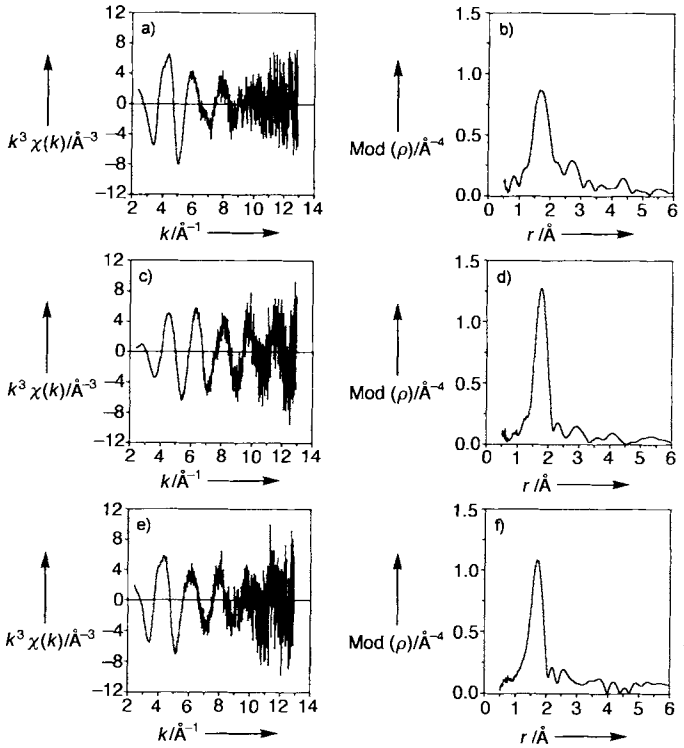

Figure 2. Experimental nickel EXAFS (k^3-weighted, left) and corresponding Fourier transform (right); top: air-oxidized; middle: NADH-reduced; bottom: dithionite-reduced.

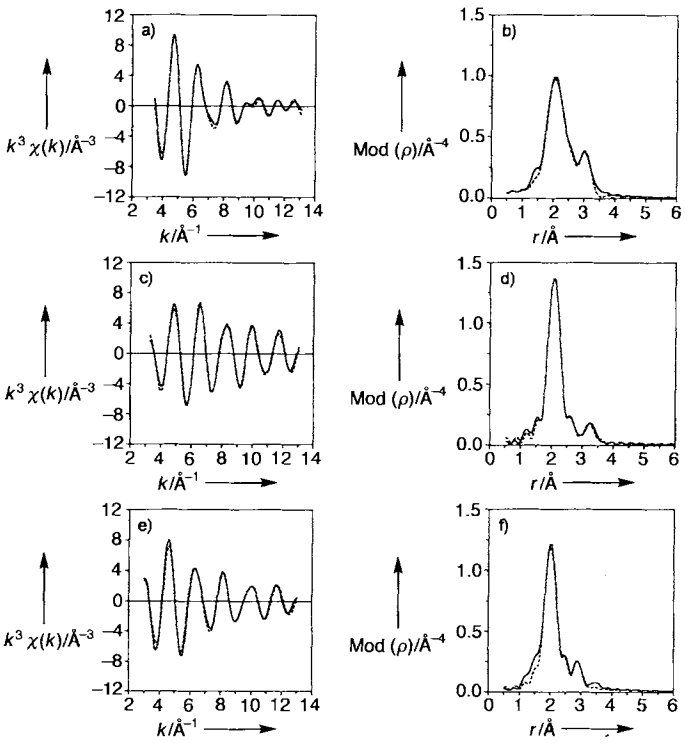

Figure 3. Left: Fourier-filtered nickel EXAFS (solid line) and theoretically fitted curve (dashed line); right: corresponding Fourier transform (solid line: experiment; dashed line: model); top: air-oxidized; middle: NADH-reduced; bottom: dithionite-reduced.

the binding of nickel, a coordination sphere composed of four sulfur and two oxygen atoms must be assigned to form 2.

In the further course of the structure determination, we included additional coordination shells in the curve-fitting proce-

 © WILEY-VCH Verlag GmbH, D-69451 Weinheim, 1997 0570-0833/97/3616-1748 $ 17.50+.50/0

dures. In the case of the NADH-treated hydrogenase (form 2, Figure 3c, d), a significant improvement of the fit is achieved by distributing the directly bound sulfur atoms in a 3:1 ratio over two shells with distances of 2.20 and 2.38 Å (fit index 0.45; the fit with solely sulfur atoms yields a fit index of 0.64). The fit is further improved by adding a scatterer from the series of electron-rich 3d metals at a distance of 3.07 Å from Ni to the model (fit index 0.29). This atom is most probably an iron atom (see below). The final results of the structure refinement are listed in Table 2.[7]

Table 2. Results of the curve-fitting analysis for the Fourier-filtered EXAFS functions ($r' = 0.9-3.1$ Å).

Enzyme form [a]	N [b]	Shell	Distance [Å] [c]	$2\sigma^2$ [Å^2] [d]	Fit index
air-oxidized	4	Ni-O	2.03	0.014	0.41
	2	Ni-S	2.33	0.016	
	1	Ni-Fe	2.71	0.013	
	2	Ni-S	3.02	0.008	
NADH-reduced	2	Ni-O	2.06	0.007	0.29
	3	Ni-S	2.20	0.013	
	1	Ni-S	2.38	0.010	
	1	Ni-Fe	3.07	0.021	
dithionite-reduced	4	Ni-O	2.05	0.011	0.51
	2	Ni-S	2.39	0.029	
	1	Ni-Fe	2.88	0.020	

[a] See text. [b] Coordination number. [c] Estimated error: 0.03 Å.
[d] Debye Waller parameter.

In contrast, the EXAFS function of the aerobically isolated hydrogenase (form 1, Figure 3a) shows features of considerably higher complexity. The strong damping behavior indicates the presence of several shells of different backscatterer atoms, which define the relatively large peak of the Fourier transform at about 3 Å (Figure 3b). Their contributions to the EXAFS are best modeled with two additional sulfur atoms at a distance of 3.02 Å and one additional metal atom 2.71 Å away from the nickel (fit index 0.41).[8] The qualitative improvement of the structural model emerges unequivocally from the development of the fit index, which amounts to 2.04 before and to 0.86 after introduction of the additional sulfur atoms. The results of the final curve-fitting analysis are summarized in Table 2.[7]

The EXAFS function of the dithionite-reduced hydrogenase (form 3, Figure 3e) resembles that of the aerobically isolated enzyme (form 1, Figure 3a). The initial two-shell model (fit index 0.89) is likewise improved by a metal atom at a distance of 2.88 Å from the nickel (fit index 0.51). However, no additional sulfur shell of physical significance comparable to that observed in form 1 can be derived from the EXAFS data. The results of the final structure refinement are listed in Table 2.[7]

Based on the results of the curve-fitting analyses, certain fundamental statements concerning the coordination of the nickel atom of the hydrogenase can be derived for all three enzyme forms, which are depicted in Figure 4. In all three cases, six ligand atoms are most likely present in a distorted octahedral arrangement around the nickel atom.

We begin the interpretation of our results with the structural model derived for the NADH-treated enzyme (form 2, Figure 4b). Here the nickel atom is surrounded by four sulfur ligands, of which three form slightly shorter bonds to the nickel than the fourth. They are supposed to be the thiolate functions of the four conserved cysteine residues of the β-subunit of the enzyme.[9] The remaining positions of the coordination octahedron are occupied by lighter atoms, which might be the oxygen atoms of bonded water molecules. The distance of 3.07 Å to the second metal atom of the active site indicates that this atom should be linked to the nickel by two bridging thiolate functions. This metal atom is assumed to be iron, since the hydrogenase from *A. eutrophus* contains—according to chemical analysis—no 3d metal other than nickel and iron.[4] Regarding the number of bridging and exogenous sulfur atoms, our proposed structure (Figure 4b) is in good agreement with the coordination of nickel in the crystallized hydrogenase from *D. gigas*. This result is especially surprising, since the crystallographically examined hydrogenase is an aerobically isolated and enzymatically inactive enzyme,[3] which shows—compared to the hydrogenase from *A. eutrophus* in its NADH-activated state—significantly different electrochemical and spectroscopic properties.[1,4]

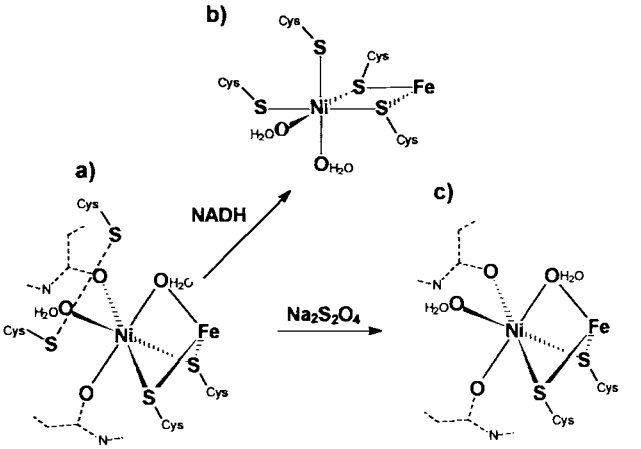

Figure 4. Schematic representations of the models for the nickel center of the hydrogenase from *A. eutrophus*: a) air-oxidized; b) NADH-reduced; c) dithionite-reduced; the assingments of O-donor functions shown here are arbitrarily chosen (see text).

In the aerobically isolated hydrogenase (form 1, Figure 4a) as well as in the preparation treated with sodium dithionite (form 3, Figure 4c), only two sulfur atoms contribute to the nickel binding. The remaining ligands are presumably nitrogen or oxygen atoms. Apart from water molecules and/or functional amino acid residues, the amide groups of the protein chains might be considered the source of these atoms.[8] In both forms the iron is 2.71 Å (form 1, Figure 4a) and 2.88 Å (form 3, Figure 4c), respectively, away from the nickel. The distinct shortening of the nickel–iron distance found here in comparison with that in form 2 (Figure 4b) strongly indicates an additional third bridge within the heterobimetallic center of the enzyme.

The contribution of a hydrogen atom to the coordination of nickel in all three enzyme forms cannot be completely ruled out by EXAFS spectroscopy, since the corresponding structural models, in which the hydrogen is modeled by an unoccupied coordination site, are still of physical significance. However, such a contribution meets the fit criteria worse than the binding situation proposed by us. The same is true for an unoccupied coordination site.

The origin of the additional cysteine sulfur atoms that contribute to the direct binding of nickel in the EPR-active state (form 2, Figure 4b) is of considerable interest. In the case of the aerobically isolated hydrogenase with only two directly bonded sulfur ligands (form 1, Figure 4a), we observe two additional sulfur atoms at a distance of 3.02 Å from the nickel, which might belong to a cystine residue. A possible reason for the ligand change within the coordination sphere of nickel upon treatment of the enzyme with NADH would be the generation of two

additional cysteine groups by reductive cleavage of the S–S bond within the cystine residue (form 2, Figure 4b; see also ref. [4d]).

According to our results the reorganization of the nickel center induced by NADH does not take place upon treatment with dithionite. This might be due to the lacking substrate properties of dithionite, which is not compatible with the NAD^+/NADH-specific binding site of the enzyme from *A. eutrophus*.

In summary, we have demonstrated that the active site of the NAD-reducing hydrogenase of *A. eutrophus* is a heterobinuclear complex with two cysteine bridges. In this respect, there are striking chemical similarities with the NiFe center of the hydrogenase from *D. gigas*. Furthermore, it was possible for the first time to detect a substantial change of the coordination of nickel upon reductive activation of a NiFe hydrogenase. Whether this property, which is characteristic for *A. eutrophus*, is also detectable in hydrogenases of other origin requires further investigations.[16] However, it should be noted that in earlier work a mechanism for the reductive activation of the hydrogenase from *A. eutrophus* specifically triggered by NADH has been proposed, which differs significantly from that of other hydrogenases.[4]

Experimental Section

Cells of *A. eutrophus* H16 (ATCC 17699; DSM 428) were heterotrophically cultivated, and the soluble hydrogenase (form 1) was isolated as described in reference [4]. The protein concentration was determined by the method described by Lowry, and the metal content was analyzed by ICP-MS. For the transformation into form 2, two independently prepared samples of the aerobically isolated hydrogenase were treated with NADH under an argon atmosphere (final concentration 15 and 30 mM NADH, respectively) and shock frozen after 10 min. Form 3 was obtained by analogous treatment with a fivefold excess of $Na_2S_2O_4$. These enzyme preparations were characterized by EPR spectra prior to the XAFS measurements (for experimental details see ref. [4b]).

The enzyme solutions used for the X-ray absorption spectroscopic investigations were concentrated by ultra-filtration in Amicon Diaflo cells (YM 100 membrane) to a concentration of about 1 mM. Inspection of the specific activity (starting activity: 80 μM reduced NAD per minute and mg enzyme; this corresponds to the 20-fold value of the in vivo activity) after the concentration step indicated no damage [4]. The samples were shock frozen and kept in a helium cryostate at 20 K during the measurements. The X-ray absorption spectra in the region of the nickel K-edge were recorded with the EXAFS spectrometer [11, 12] of EMBL (HASYLAB at DESY, Hamburg; storage ring DORIS II, 4.5 G eV, average beam current 80 mA, Si(111) double-crystal monochromator, focussing toroidal mirror, absolute calibration of the energy axis with simultaneously recorded Bragg reflections of a silicium crystal) according to reference [10].

The spectra were recorded by measuring the fluorescence radiation in a range from 8210 to 9100 eV with a 13-element solid-state detector (Canberra). The measuring time was 1–2 s per point with about 1400 points per spectrum. A total of 41 (form 1), 27 (form 2), and 28 (form 3) single scans, respectively, were averaged after individual energy calibration. Since the individual spectra did not change during the corresponding measuring sequences, we can exclude radiation damage. The EXAFS functions were isolated from the averaged spectra by literature procedures, and the determination of the background was achieved with a spline function [13]. Data evaluation was carried out with the program packages EXPROG (energy calibration and data reduction) [14] and EXCURV88 (curve-fitting procedures employing theoretical amplitude and phase functions) [15].

Received: November 19, 1996 [Z9782IE]
German version: *Angew. Chem.* **1997**, *109*, 1812–1816

Keywords: enzymes · EXAFS spectroscopy · hydrogenases · iron · nickel

[1] a) *The Bioinorganic Chemistry of Nickel*, (Ed.: J. R. Lancaster Jr.), VCH, Weinheim, **1988**; b) R. Cammack, *Adv. Inorg. Chem.* **1988**, *32*, 297; c) R. P. Hausinger, *Biochemistry of Nickel*, Plenum, New York **1993**; d) S. P. J. Albracht, *Biochim. Biophys. Acta* **1994**, *1188*, 167, and references therein.

[2] R. Cammack, *Nature* **1995**, *373*, 556.

[3] A. Volbeda, M.-H. Charon, C. Piras, E. C. Hatchikian, M. Frey, J. C. Fontecilla-Camps, *Nature* **1995**, *373*, 580.

[4] a) K. Schneider, A. Erkens, A. Müller, *Naturwissenschaften* **1996**, *83*, 78; b) A. Erkens, K. Schneider, A. Müller, *J. Biol. Inorg. Chem.* **1996**, *1*, 99; c) K. Schneider, R. Cammack, H. G. Schlegel, *Eur. J. Biochem.* **1984**, *142*, 75; d) K. Schneider, H. G. Schlegel, *Biochim. Biophys. Acta* **1976**, *452*, 66.

[5] a) G. Henkel, J. Kreutzberg, A. Müller, A. Müller, K. Schneider, C. Hermes, H.-F. Nolting, HASYLAB Annual Report, Hamburg **1993**, 679; b) A. Müller, A. Erkens, K. Schneider, A. Müller, H.-F. Nolting, G. Henkel, *J. Inorg. Biochem.* **1995**, *59*, 643; c) A. Müller, A. Erkens, K. Schneider, A. Müller, H.-F. Nolting, V. A. Solé, G. Henkel, HASYLAB Annual Report, Hamburg **1995**, *vol. II*, 917.

[6] a) G. J. Colpas, M. J. Maroney, C. Bagyinka, M. Kumar, W. S. Willis, S. L. Suib, N. Baidya, P. K. Mascharak, *Inorg. Chem.* **1991**, *30*, 920; b) M. Köckerling, Dissertation, Duisburg, **1992**.

[7] During the final cycles of the structure refinement, the occupation numbers were kept at constant values, while a common value for E_0, the distances of the individual shells from the central atom, and the Debye–Waller parameters were refined.

[8] Recently diatomic molecules with triple-bond systems were postulated as additional ligands bound to nickel in the hydrogenase from *Alcaligenes eutrophus* on the basis of FT-IR investigations (T. M. van der Spek, A. F. Arendsen, R. P. Happe, S. Yun, K. A. Bagley, D. J. Stufkens, W. R. Hagen, S. P. J. Albracht, *Eur. J. Biochem.* **1996**, *237*, 629). A diatomic molecule in a linear arrengement (e.g. CN^- or CO), which was tentatively introduced to the structural model for that reason, did not yield any results of physical significance in the curve-fitting analysis.

[9] A. Tran-Betcke, U. Warnecke, C. Böcker, C. Zaborosch, B. Friedrich, *J. Bacteriol.* **1990**, *172*, 2920.

[10] G. Henkel, A. Müller, S. Weißgräber, G. Buse, T. Soulimane, G. C. M. Steffens, H.-F. Nolting, *Angew. Chem.* **1995**, *107*, 1615; *Angew. Chem. Int. Ed. Engl.* **1995**, *34*, 1488.

[11] C. Hermes, E. Gilberg, M. H. J. Koch, *Nucl. Instr. Meth.* **1984**, *222*, 207.

[12] R. F. Pettifer, C. Hermes, *J. Appl. Crystallogr.* **1985**, *18*, 404.

[13] B. K. Teo, *EXAFS: Basic Principles and Data Analysis*, Springer, Berlin **1986**.

[14] H.-F. Nolting, C. Hermes, EXPROG: EMBL EXAFS Data Analysis and Evaluation Program Package, Hamburg, **1992**.

[15] N. Binsted, S. J. Gurman, J. W. Campbell, SERC Daresbury Laboratory EXCURV88 Program, Daresbury, UK, **1988**.

[16] Note added in proof (received on July 14, 1997): A recent XAFS investigation (Z. Gu, J. Dong, C. B. Allan, S. B. Choudhury, R. Franco, J. J. G. Moura, I. Moura, J. LeGall, A. E. Przybyla, W. Roseboom, S. P. J. Albracht, M. J. Axley, R. A. Scott, M. J. Maroney, *J. Am. Chem. Soc.* **1996**, *118*, 11155) shows that the hydrogenase from *A. eutrophus* differs from other enzymes with respect to its behavior described here.

A Facile Cycloisomerization for the Formation of Medium and Large Rings via Allenes

Barry M. Trost,* Pierre-Yves Michellys, and Vincent J. Gerusz

The importance of macrocycles is readily apparent by the large number of biologically significant molecules that possess such a core, be it a carbocycle or heterocycle.[1, 2] Such ring systems may be thought to represent a compromise in the attempt to introduce conformational rigidity into acyclic structures in order to enhance biological potency. In small and normal-sized rings, the limits on flexibility mean that a ligand must be just right for the receptor, otherwise it will not fit properly. Medium and large rings have well-defined conformations also; however, a number of conformations frequently will lie close in energy to the global minimum. Thus, if the design is not perfect, the molecule may still be able to adapt itself to fit the receptor without an inordinate cost in energy. Such a strategy for enhancing biopotency may be more routinely used if the methods

[*] Prof. Dr. B. M. Trost, Dr. P.-Y. Michellys, Dr. V. J. Gerusz
Department of Chemistry
Stanford University
Stanford, CA 94305-5080 (USA)
Fax: Int. code + (415) 725-0259
e-mail: bmtrost@leland.stanford.edu

[**] We thank the National Science Foundation and the General Medical Sciences Institute of the National Institutes of Health (NIH) for their generous support of our programs. We also thank the Bourse Lavoisier and Rhône–Poulenc for partial support for PYM and VJG, respectively. Mass spectra were provided by the Mass Spectrometry Facility, University of California San Francisco, supported by the NIH Division of Research Resources.

 © WILEY-VCH Verlag GmbH, D-69451 Weinheim, 1997 0570-0833/97/3616-1750 $ 17.50+.50/0

for forming such difficult-to-access ring systems were more readily available.[3] In conjunction with our interest in designing simple addition reactions, we have developed a protocol that effects addition of a pronucleophile to an allene[4, 5] in which macrocarbocycles and macrolactones ranging in size from nine to seventeen members are formed without the requirement of the usual high dilution techniques to minimize polymerization.[6]

Our initial studies examined cyclization of the allene **1**, which is easily accessed according to Equation (1). The use of the allene as a proelectrophile for the Pd^0-catalyzed reaction provides easy differentiation with other electrophilic functional groups as illustrated in this case: the allenyl iodide functions as a chemodifferentiated bis-electrophile in alkylations. In the initial efforts, we exposed **1** to a catalyst generated from 5 mol% of π-allylpalladium chloride dimer (**2**) and 12.5 mol% 1,3-bis-(diphenylphosphino)propane (**3**) in the presence of a base in THF at 100 °C (sealed tube). The choice of a bidentate ligand stemmed from earlier observations in the reactions of 1,3-dienes that monodentate ligands led to oligomerization.[7] Initial results showed that methanolic sodium methoxide (50–100 mol%) was more efficacious than potassium *tert*-butoxide. For a 0.01 M solution of the substrate in a batch reaction (that is, no slow addition), a remarkable 60–68% yield of the seventeen-membered ring **4a**[8] as a single isomer was obtained (see Table 1). The 15.5 Hz coupling of the vinyl protons (δ = 5.97 and 5.32) in the ^{1}H NMR spectrum indicates an *E* geometry. Use of 1,3-bis(2-methoxyphenylphosphino)propane as ligand gave, under similar conditions, a 47% yield of the macrocycle **4a** from **1a**.

Unfortunately, application of these conditions to other substrates proved disappointing. For example, allene **1b** gave only trace amounts of macrocycle with mainly unchanged starting material. Replacing methanolic methoxide with catalytic potassium *tert*-butoxide (1 equiv based on Pd) and 2-dimethylaminopyridine (2-DMAP, 1 equiv) had a dramatic effect on the reaction; the sixteen-membered macrocycle **4b**[8] was produced in 53% yield. Switching to 4-DMAP improved the yield to 68%. The catalytic amount of potassium *tert*-butoxide proved superfluous; the reaction proceeded similarly in its absence (method A, 2.5–5.0 mol% **2**, 6.25–12.5 mol% **3**, and 1 equiv 4-DMAP in THF at 100 °C). A full equivalent of 4-DMAP was not necessarily required. For example, cyanosulfone **1c** cyclized to **4c**[8] in 67% yield (73% based on recovered starting material (brsm)) in the presence of 3 mol% **2**, 7.5 mol% **3**, and 15 mol% 4-DMAP at a concentration of substrate **1c** of 0.01 M (method B, 2.5–5.0 mol% **2**, 6.25–12.5 mol% **3**, and 15–20 mol% 4-DMAP in THF at 100 °C).

While the last set of conditions proved to be reasonably general, we still encountered difficulties when the ring size was decreased as in substrate **1d** [Eq. (1)]. Cyclization of the latter by method B produced a 28% yield of the fifteen-membered ring **4d**.[8] Keeping in mind that *both* a proton donor and a proton acceptor are required, we added an amount of a proton donor (acetic acid, 1 equiv based on the dibasic amine DMAP; method C) and saw the yield of **4d** increase to 56%. Decreasing the ring size to twelve members still led to good yields of macrocyclization product [Eq. (2)]. In this case, the yield of **5**[8] increased

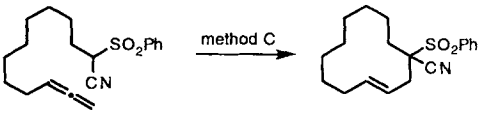

(2)

5

from 43% to 55% by running the reaction at 0.005 M rather than 0.01 M. This result suggests that, with the smaller ring size, oligomerization started to become a problem in these simple carbocycles. Only a single isomer of **5** is obtained; the 14.3 Hz coupling constant of the vinyl protons (δ = 5.68 and 5.48) suggests *trans* geometry.

The importance of macrolactones led to exploration of this cyclization for their synthesis [Eq. (3)]. Substrates for the

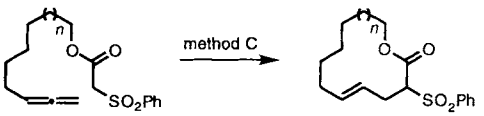

(3)

6

a: n = 6, **b**: n = 5, **c**: n = 1

macrocyclization are easily available by esterification of the requisite allenic alcohol [dicyclohexylcarbodiimide (DCC), 4-DMAP, CH_2Cl_2, room temperature (RT), 91–97% yields]. With method C, the seventeen- (**6a**[8]) and sixteen-membered rings (**6b**[8]) formed in 67% and 57% yields, respectively. The twelve-membered ring **6c**[8] also formed in a satisfactory yield of 62%. In all three cases, the single isomer formed was in the *trans* configuration, as established by proton NMR spectroscopy.

Medium-sized macrolactones pose a special problem because of their enhanced strain due to transannular effects. Interestingly, the ten-membered ring **7**[8] formed in a somewhat higher yield (82%) than the larger rings [Eq. (4)]. Unlike with the

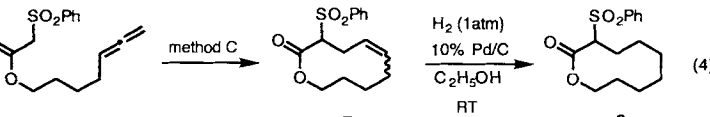

(4)

7 8

larger rings, a 1:1 mixture of two isomers was formed. That the source of the isomerism was olefin geometry was indicated by catalytic hydrogenation (87% yield) to a single macrocycle **8**[8] (m.p. 132 °C). Cyclization of **9** represents a specially interesting example, since either seven- or nine-membered rings can form [Eq. (5)]. The fact that the thermodynamically preferred *syn*-**10**

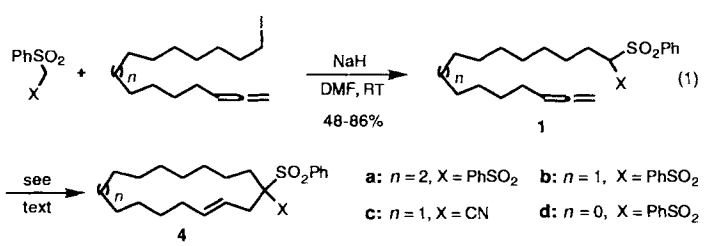

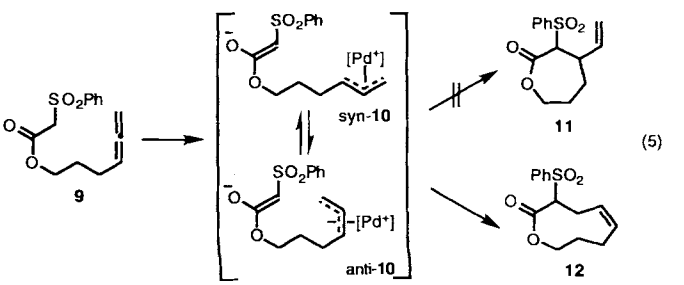

 © WILEY-VCH Verlag GmbH, D-69451 Weinheim, 1997 0570-0833/97/3616-1751 $ 17.50+.50/0

should strongly favor seven-membered ring formation due to the strain of a *trans* double bond in a nine-membered ring,[9] combined with the normal kinetic preference for seven-membered ring formation,[10] would lead to the expectation that **11** should dominate.[11] Counter to this expectation, only the nine-membered ring **12** (m.p. 119 °C) formed in 65% yield, even at 0.01 M concentration of substrate. Not surprisingly, only the *Z* geometry of the product was detected as indicated by the 10.8 Hz coupling constant of the vinyl protons (δ = 5.65 and 5.37).

The efficiency by which nine- and ten-membered rings formed induced us to explore the formation of a ten-membered macrolactam as a result of a recent report of **14** as an endopeptidase inhibitor.[12] This ring system was formed by a Pd^0-catalyzed cyclization of **13** [Eq. (6)], although not without some complications. Ironically, the substrate **13** derived from an allene! As shown in Equation 7, the macrocyclization substrate **15** is readily available in a manner analogous to that of Johnson et al.[12] Subjecting a 0.01 M solution of allene **15** to what has become our "standard" conditions (method C) gave an 86% yield of macrolactam **16**[8] as a 1:1 mixture of isomers. Catalytic hydrogenation gave a single compound **17**[8] (m.p. 104–105 °C), in 85% yield. Thus, the allene cyclization not only appears to be more straightforward than that of a related allylic acetate while saving an expensive silver-promoted conversion of an allene to an allylic acetate, but does all of this in even higher yield.

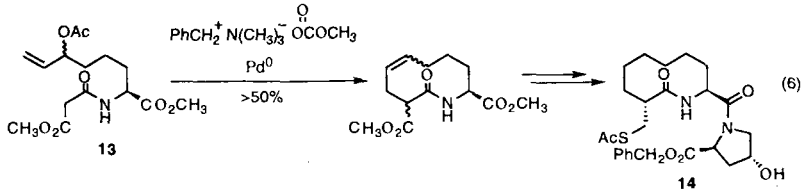

(6)

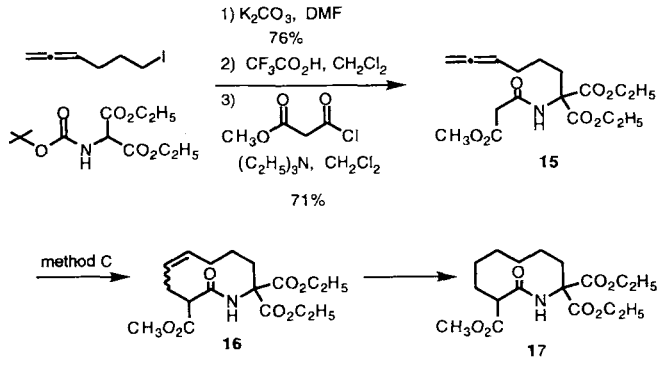

(7)

Macrocyclization with allenes as pronucleophiles appears to be a very effective way to generate normally difficult-to-form rings. The attractiveness of the methodology stems, in part, from the ease of constructing substrates because of the inertness of the allene to many standard synthetic reactions. The example of the macrolactam in which the allene served as the precursor to the allyl ester highlights this point. The remarkable efficiency by which medium-sized rings form is noteworthy. In most reactions, a plot of yield versus ring size normally has a minimum at the nine-membered ring. That is clearly not the case here. The source of the efficiency of this protocol remains to be established. It is interesting to speculate whether a bifunctional catalysis as illustrated in Equation 8 may be implicated. In any event,

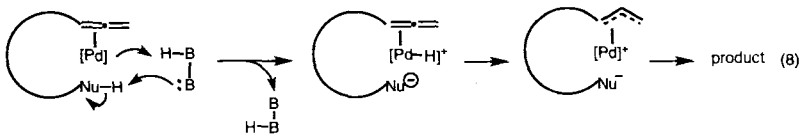

(8)

this method has proven useful for carbocycles, macrolactones, and macrolactams containing from nine- to seventeen-ring members.

Received: February 17, 1997 [Z 10129 IE]
German version: *Angew. Chem.* **1997**, *109*, 1837–1839

Keywords: cyclizations · lactams · lactones · macrocycles · palladium

Table 1. Spectroscopic data of **4a**, **6a**, **12**, and **17**.

4a: M.p. 126–127 °C (ether–hexane); IR (neat): $\tilde{\nu}$ = 1600, 1328, 1146 cm^{-1}; ^1H NMR (300 MHz, $CDCl_3$): δ = 8.20 (m, 4H), 7.03 (m, 6H), 5.96 (dt, *J* = 14.2, 5.2 Hz, 1H), 5.31 (dt, *J* = 14.2, 5.8 Hz, 1H), 3.23 (bd, *J* = 5.8 Hz, 2H), 2.39 (m, 2H), 1.91 (m, 4H), 1.18 (m, 20H); ^1H NMR (400 MHz, $CDCl_3$): δ = 8.05 (d, *J* = 7.3 Hz, 4H), 7.71 (t, *J* = 7.4 Hz, 2H), 7.59 (t, *J* = 7.8 Hz, 4H), 5.65–5.62 (m, 2H), 3.02 (d, *J* = 4 Hz, 2H), 2.21–2.16 (m, 2H), 2.11–2.04 (m, 2H), 1.75–1.66 (m, 2H), 1.39–1.20 (m, 20H); ^{13}C NMR (75 MHz, $CDCl_3$): δ = 137.1 (2C), 136.4 (2C), 134.5, 131.4 (4C), 128.5 (4C), 121.7, 91.8, 31.5, 31.4, 29.6, 28.5, 27.9, 27.7, 26.5, 26.4, 26.2, 26.1, 26.0, 25.5, 24.9, 22.5; Satisfactory C,H analysis calcd for $C_{29}H_{40}O_4S_2$ (MW found 516.2358).

6a: IR (neat): $\tilde{\nu}$ = 1731, 1310, 1145 cm^{-1}; ^1H NMR (300 MHz, $CDCl_3$): δ = 7.86 (d, *J* = 7.4 Hz, 2H), 7.66 (t, *J* = 7.4 Hz, 1H), 7.55 (t, *J* = 7.4 Hz, 2H), 5.69 (dt, *J* = 14.0, 6.7 Hz, 1H), 5.19 (dt, *J* = 14.7, 7.1 Hz, 1H), 4.21 (dt, *J* = 11.1, 6.5 Hz, 1H), 3.92 (dd, *J* = 11.9, 3.3 Hz, 1H), 3.80 (dt, *J* = 11.1, 5.4 Hz, 1H), 2.66 (m, 2H), 1.93 (m, 2H), 1.38 (m, 18H); ^{13}C NMR (75 MHz, $CDCl_3$): δ = 165.9, 137.1, 135.7, 134.3, 129.4, 129.0, 123.1, 70.9, 66.1, 31.4, 29.6, 27.7, 27.6, 26.9 (2C), 26.8 (2C), 26.7, 26.1, 24.3; Satisfactory C,H,S analysis for $C_{22}H_{34}O_4S$.

12: M.p. 119 °C (hexane); IR (neat): $\tilde{\nu}$ = 1740, 1325, 1149 cm^{-1}; ^1H NMR (300 MHz, $CDCl_3$): δ = 7.94 (d, *J* = 7.4 Hz, 2H), 7.87 (t, *J* = 7.4 Hz, 1H), 7.56 (t, *J* = 7.5, 2H), 5.65 (td, *J* = 10.8, 6.7 Hz, 1H), 5.37 (td, *J* = 10.8, 6.8 Hz, 1H), 4.45 (ddd, *J* = 11.2, 7.3, 4.1 Hz, 1H), 4.13 (ddd, *J* = 11.2, 8.8, 6.8 Hz, 1H), 3.82 (dd, *J* = 11.3, 4.1 Hz, 1H), 3.09 (ttd, *J* = 11.2, 1.1 Hz, 1H), 2.58 (ddd, *J* = 12.4, 6.9, 4.4 Hz, 1H), 2.28 (m, 1H), 1.88 (m, 3H); ^{13}C NMR (75 MHz, $CDCl_3$): δ = 166.3, 137.8, 136.0, 134.4, 129.3 (2C), 129.2 (2C), 122.6, 69.1, 63.9, 26.1, 25.6, 21.6; satisfactory C,H,S analysis for $C_{14}H_{16}O_4S$.

17: M.p. 104–105 °C (ether–pentane); IR (CH_2Cl_2): $\tilde{\nu}$ = 3348, 1736, 1678, 1509; ^1H NMR (300 MHz, $CDCl_3$): δ = 4.27 (m, 2H), 4.20 (dd, *J* = 14.2, 7.1 Hz, 1H), 3.73 (s, 3H), 3.26 (dd, *J* = 7.4, 5.6 Hz, 1H), 2.51 (m, 1H), 2.16 (m, 1H), 1.99 (m, 2H), 1.40 (m, 8H); ^{13}C NMR (75 MHz, $CDCl_3$): δ = 167.6, 167.6, 167.5, 167.1, 66.3, 61.9, 62.2, 52.2, 28.3, 25.7, 24.5, 23.0, 22.2, 19.9, 13.7, 13.6; satisfactory C,H,N analysis for $C_{15}H_{20}O_4N$.

[1] Selected overviews: B. Dietrich, P. Viout, J. M. Lehn, *Macrocyclic Chemistry*, VCH, Weinheim, **1993**; *Macrolide Antibiotics, Chemistry, Biology, and Practice* (Ed.: S. Omura), Academic Press, New York, **1984**; *Proteinase Inhibitors* (Eds.: A. J. Barret, G. Salvensen), Elsevier, Amsterdam, **1986**.

[2] Recent examples: B. Greve, P. Imming, S. Laufer, *Angew. Chem.* **1996**, *108*, 1312; *Angew. Chem. Int. Ed. Engl.* **1996**, *35*, 1221; L. Zhang, J. A. Pesti, T. D. Costello, P. J. Sheeran, R. Uyeda, P. Ma, G. S. Kauffman, R. Ward, J. L. McMillan, *J. Org. Chem.* **1996**, *61*, 5180; T. L. Hendrickson, J. R. Spencer, M. Kato, B. Imperiali, *J. Am. Chem. Soc.* **1996**, *118*, 7636; R. Haubner, W. Schmitt, G. Hölzemann, S. L. Goodman, A. Jonczyk, H. Kessler, *ibid.* **1996**, *118*, 7881.

[3] Selected reviews: C. J. Roxburgh, *Tetrahedron* **1995**, *51*, 9767; H. Stach, M. Hesse, *ibid.* **1988**, *44*, 1573; M. A. Titus, *Chem. Rev.* **1988**, *88*, 719; I. Paterson, M. M. Mansuri, *Tetrahedron* **1985**, *41*, 3569. Leading reference on the use of ring-closing metathesis (RCM) for macrocyclizations: A. Fürstner, K. Langemann, *J. Org. Chem.* **1996**, *61*, 3942 and references therein (slow additions of the substrates were employed). Conformational constraints facilitate RCM and may be required in some cases: S. J. Miller, S.-H. Kim, Z. R. Chen, R. H. Grubbs, *J. Am. Chem. Soc.* **1995**, *117*, 2108.

[4] B. M. Trost, V. J. Gerusz, *J. Am. Chem. Soc.* **1995**, *117*, 5156.

 © WILEY-VCH Verlag GmbH, D-69451 Weinheim, 1997 0570-0833/97/3616-1752 $ 17.50+.50/0

[5] For related work proposing a carbapalladation mechanism, see Y. Yamamoto, M. Al-Masum, N. Asao, *J. Am. Chem. Soc.* **1994**, *116*, 6019; Y. Yamamoto, M. Al-Masum, N. Fujiwara, N. Asao, *Tetrahedron Lett.* **1995**, *36*, 2811. More recently, Yamamoto et al. have adopted our proposed hydropalladation mechanism as more consistent for some of their cases: Y. Yamamoto, M. Al-Masum, A. Takeda, *Chem. Commun.* **1996**, 831; M. Meguro, S. Kamijo, Y. Yamamoto, *Tetrahedron Lett.* **1996**, *37*, 7453.
[6] Cyclization of ω-haloallenes: S. Ma, E. Negishi, *J. Am. Chem. Soc.* **1995**, *117*, 6345.
[7] B. M. Trost, L. Zhi, *Tetrahedron Lett.* **1992**, *33*, 1831.
[8] All new compounds have been fully characterized by spectroscopy and elemental analysis (composition determined by high-resolution mass spectrometry and/or combustion analysis).
[9] A. C. Cope, P. T. Moore, W. R. Moore, *J. Am. Chem. Soc.* **1959**, *81*, 3153.
[10] C. Galli, G. Illuminati, L. Mandolini, P. Tamborra, *J. Am. Chem. Soc.* **1977**, *99*, 2591.
[11] However, cf. B. M. Trost, T. R. Verhoeven, *J. Am. Chem. Soc.* **1980**, *102*, 4743.
[12] E. P. Johnson, G.-P. Chen. K. R. Fales, B. E. Lenk, R. J. Szendroi, X.-J. Wang, J. A. Carlson, *J. Org. Chem.* **1995**, *60*, 6595.

Crystal Structure Determination of Metaperiodic Acid, HIO_4, with Combined X-Ray and Neutron Diffraction**

Thorsten Kraft and Martin Jansen*

Dedicated to Professor Dieter Seebach on the occasion of his 60th birthday

According to textbooks on inorganic chemistry the system of iodine(VII) acids consists of the monomeric orthoperiodic acid, H_5IO_6, from which a series of oligomeric compounds $H_{6+n}I_{2+n}O_{10+4n}$ can be derived by edge-sharing of the IO_6 octahedra, and, as a terminating link, polymeric metaperiodic acid, HIO_4.[1] Besides the crystal structure of H_5IO_6, which is well-established (including the hydrogen-atom positions),[2] the proposed constitutions of iodine(VII) acids are based on insufficient experimental data. For the oligomeric periodic acids the I–O substructures of their salts are assumed to be similar to those of the free acids,[3] and in the cases of HIO_4 and $H_7I_3O_{14}$ polymeric or trimeric chains, respectively, of *trans*-edge-sharing IO_6 octahedra are proposed based on Raman spectra.[4] Attempts to grow single crystals of HIO_4 failed until now, because the compound decomposes at normal pressure, already at 105 °C, releasing oxygen and water. The development of X-ray and neutron diffraction techniques for ab initio crystal structure determination has encouraged us to investigate the structure of HIO_4 with these methods.

Microcrystalline HIO_4 was prepared by carefully dehydrating H_5IO_6 with oleum in H_2SO_4 at 50 °C. Since the reaction conditions cause the product to precipitate slowly from the homogeneous solution, the samples crystallize well despite the relatively low reaction temperature, as seen from their X-ray powder diagrams (Figure 1). The crystal structure with respect to the positions of iodine and oxygen atoms could be solved from the X-ray powder diagram; the hydrogen atoms were preliminary fixed by considering crystal-chemical evidence. Because the scattering factor of iodine is considerably higher than that of oxygen and, in particular, hydrogen, neutron diffraction techniques were necessary to complement the X-ray data. Stable refinement of the position parameters of all atoms was achieved, and the agreement between the parameter sets is satisfactory (Table 1).

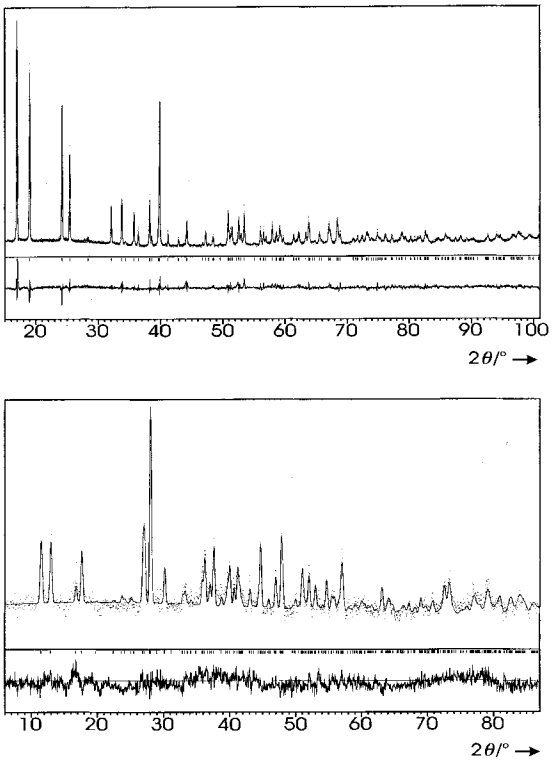

Figure 1. Observed (dotted line) and calculated (solid line) diffraction diagrams and difference profile of the Rietveld refinement (top: X-ray data; bottom: neutron data); the positions of allowed reflections are indicated by vertical lines.

Table 1. Positional parameters for HIO_4.

		x	y	z
H [a]	[b]	0.2163(28)	0.7305(47)	0.4809(67)
I	[c]	0.0	0.1432(03)	0.75
	[b]	0.0	0.1357(24)	0.75
O1	[c]	0.6335(08)	0.1654(19)	0.3988(21)
	[b]	0.6258(10)	0.1637(13)	0.3934(17)
O2	[c]	0.1116(10)	0.0946(15)	0.4479(22)
	[b]	0.1122(08)	0.0935(14)	0.4506(18)

[a] Site occupancy of 50%. [b] From neutron diffraction data. [c] From X-ray diffracion data.

In contrast to all previously proposed structures, HIO_4 consists of one-dimensional infinite chains built up of distorted, *cis*-edge-sharing IO_6 octahedra (Figure 2). The different I–O distances of the IO_6 octahedra reflect the different crystal-chemical situations of the oxygen atoms (Figure 3). The terminal oxygen atoms show, as expected, the shortest I–O distances (184 pm). The pronounced difference between the distances to the bridging oxygen atoms (191 and 201 pm) can be easily explained in terms of the *trans* effect.

[*] Prof. Dr. M. Jansen, Dr. T. Kraft
Institut für Anorganische Chemie der Universität
Gerhard-Domagk-Strasse 1, D-53121 Bonn (Germany)
Fax: Int. code +(228)735-660
e-mail: unc419@ibm.rhrz.uni-bonn.de

[**] This work was sponsored by the Deutsche Forschungsgemeinschaft, the Bundesministerium für Bildung und Forschung (PN 40469), and the Fonds der Chemischen Industrie. We thank Dr. Wolfgang Schäfer, Forschungszentrum Jülich, for measuring the neutron diagram.

 © WILEY-VCH Verlag GmbH, D-69451 Weinheim, 1997 0570-0833/97/3616-1753 $ 17.50+.50/0

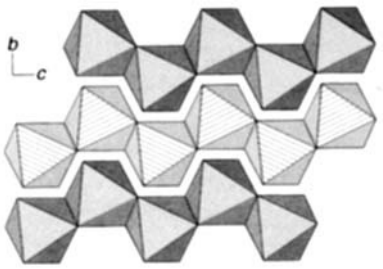

Figure 2. Chains of *cis*-edge-sharing IO_6 octahedra.

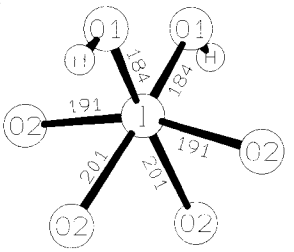

Figure 3. IO_6 octahedron; distances are given in pm.

The structural analogy to many transition metal tetrahalides, as indicated by the presence of chains of *cis*-edge-sharing octahedra, also extends on the arrangement of these structural units relative to each other. When considering the I–O substructure, isotypism to uranium tetraiodide becomes evident, that is, the oxygen atoms form a hexagonal close packing with the iodine atoms occupying a quarter of the octahedral holes.

Every polymeric chain is connected to four adjacent chains through hydrogen bonds (Figure 4; d(O···O) 269(2) pm,

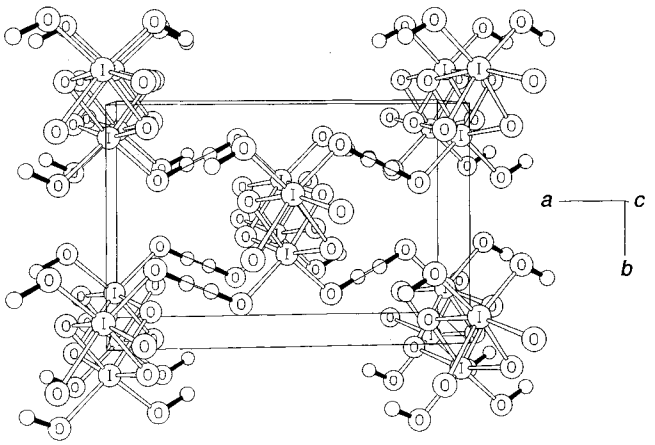

Figure 4. Connectivities between the chains through hydrogen bridges.

d(O–H) 101(3) pm, d(O···H) 169(3) pm, ∢I-O-H 112(1)°, ∢O-H···O 176(1)°). The hydrogen atoms are disordered in a double potential between the terminal oxygen atoms. This is frequently observed for linear hydrogen bonds between neutral molecules, such as in the Ih modification of ice.[7]

Until now no periodate derived from the structure of HIO_4—that is, built up by polymeric iodine–oxygen chains—is known. The structure of HIO_4 raises questions about the linkage of the iodine–oxygen polyhedra in oligomeric periodic acids. However, the crystal structure of $H_7I_3O_{14}$ does not show any new type of catenation, because this compound exists in the solid state as a stoichiometric phase containing orthoperiodic and metaperiodic acids according to the formula $H_5IO_6 \cdot 2HIO_4$.[8]

Experimental Section

HIO_4: Oleum (25%, 15 mL) was slowly added to a solution of H_5IO_6 (3 g) in concd H_2SO_4 (40 g) at 50 °C until an insoluble precipitate appeared. Upon standing for 12 h at 50 °C a voluminous precipitate separated, which was isolated by filtration under an inert-gas atmosphere. It was treated with concd H_2SO_4 (15 mL), washed with trifluoroacetic acid (5 × 15 mL) to remove traces of H_2SO_4, and finally dried in vacuo. Elemental analysis: iodine: 65.5% (calcd 66.1%), active oxygen: 27.9% (calcd 29.2%), sulfate: not detected.

Structure determination of HIO_4: After indexing [9] the X-ray powder diagram (Stoe Stadi P, $Cu_{K\alpha}$ radiation, λ = 154.051 pm) on the basis of a monoclinic system (a = 936.88(5), b = 629.59(4), c = 495.30(3) pm; β = 94.953(3)°), Cc (no. 9) and $C2/c$ (no. 15) were considered as possible space groups from the systematic absences. In both space groups the iodine- and oxygen-atom positions were determined with direct methods [10], but a crystal-chemically consistent refinement (156 reflections, 30 parameters, R = 0.0617, R_{wp} = 0.219, R_F = 0.0522 [11]) could only be achieved in the space group $C2/c$. The hydrogen bridges and, thus, the approximate positions of the hydrogen atoms were derived from crystal-chemical considerations. To verify these results optimized structure models (space group $C2/c$ with disordered H atoms and Cc with no disordering of H atoms) were refined on the basis of neutron diffraction data (λ determined to 112.704 pm [11], two-circle neutron diffractometer SV7 equipped with a linear position-sensitive JULIOS detector from the Mineralogisches Institut der Universität Bonn at the reactor FRJ2 of the KFA Jülich). The model with space group $C2/c$ was unambiguously the correct one (a = 936.60(18), b = 628.86(13), c = 495.75(19) pm; β = 94.890(15)°; 282 reflections, 27 parameters, R = 0.0185, R_{wp} = 0.336, R_F = 0.21 [11]).

Received: January 31, 1997 [Z10059IE]
German version: *Angew. Chem.* **1997**, *109*, 1842–1843

Keywords: iodine · metaperiodic acid · neutron diffraction · structure elucidation

[1] A. F. Holleman, E. Wiberg, N. Wiberg, *Lehrbuch der Anorganischen Chemie*, 101st ed., deGruyter, Berlin, **1995**, pp. 485–488.
[2] Y. D. Feikema, *Acta Crystallogr.* **1961**, *14*, 315–316; *ibid.* **1966**, *20*, 765–769.
[3] H. Siebert, *Fortschr. Chem. Forsch.* **1967**, *8*, 470–492.
[4] H. Siebert, U. Woerner, *Z. Anorg. Allg. Chem.* **1977**, *429*, 34–38.
[5] L. Paçesová, Z. Hauptman, *Z. Anorg. Allg. Chem.* **1963**, *325*, 325–333.
[6] J. H. Levy, J. C. Taylor, A. B. Waugh, *Inorg. Chem.* **1980**, *19*, 672–674.
[7] S. W. Peterson, H. A. Levy, *Acta Crystallogr.* **1957**, *10*, 70–76.
[8] T. Kraft, Dissertation, Universität Bonn (Germany), **1995**.
[9] P.-E. Werner, L. Eriksson, M. Westdahl, *J. Appl. Crystallogr.* **1985**, *18*, 367–370.
[10] Stoe & Cie, CSD V4.10, Darmstadt (Germany), **1991**.
[11] J. Rodriguez-Carvajal, *Fullprof*, Laboratoire Leon Brillouin (CEA-CNRS), Saclay, **1995**.

Ge_9^{4-}: A Deltahedral Zintl Ion Now Made in the Solid-State**

Virginie Queneau and Slavi C. Sevov*

All known main group deltahedral clusters are made either by crystallization from solution or by direct synthesis from the elements, that is by solid-state reactions. (We exclude gaseous clusters here since they are not structurally well characterized.) Members of the first group belong to the well known class of Zintl ions and include anions of group 14 (the tetrels (Tt): Tt_9^{4-},

[*] Prof. S. C. Sevov, V. Queneau
Department of Chemistry and Biochemistry
University of Notre Dame
Notre Dame, IN 46556 (USA)
Fx: Int. code +(219)631-6652
email: ssevov@nd.edu

[**] We are indebted to Dr. Victor Young (University of Minnesota) for the persistency to collect a satisfactory data set from this poorly diffracting compound. We thank Dr. Jerry Ostenson (Iowa State University) for the magnetic measurements and Dr. John D. Corbett for the Ta tubing. This research was financially supported by an award from the Camille and Henry Dreyfus foundation.

 © WILEY-VCH Verlag GmbH, D-69451 Weinheim, 1997 0570-0833/97/3616-1754 $ 17.50+.50/0

Tt_9^{3-}, Tt_5^{2-}, Tt_9^{2-}, and Tt_{10}^{2-}), of group 15 (the pnictogens (Pn): Pn_4^{2-}), and the mixed species $Tt_2Pn_2^{2-}$, $TrTt_8^{3-}$, and $TrTt_9^{3-}$ (Tr = element of group 13).[1-3] These clusters form when the corresponding alloy with Na or K (or mixtures of them) is dissolved in either liquid ammonia or ethylenediamine, often mixed with 2,2,2-crypt.[4] Most of these clusters have been characterized in terms of nuclearity and charge by NMR spectroscopy in solution.[5] Presumably, formation of the cluster takes place during the extraction with the solvent since no such clusters have been observed in the starting alloys.[2, 6] The group of clusters made by solid-state reactions is somewhat more diverse in terms of sizes and charges, and comprises primarily clusters of group 13 (the triels (Tr): Tr_{11}^{7-}, Tr_4^{8-}, Tr_5^{7-}, Tr_5^{9-}, Tr_6^{8-}, Tr_6^{6-}, Tr_6^{6-}, $Tr_{12}(Tr)^{11-}$, $Tr_{12}(Zn, Cd or Hg)^{12-}$, $Tr_{10}(Zn)^{8-}$, and $Tr_{10}(Ni, Pd or Pt)^{10-}$), but also includes a few species from groups 14 (Tt_4^{4-}), 15 (Bi_8^{2+}, Bi_5^{3+}, Bi_9^{5+}), and 16 (Se_4^{2+} and Te_4^{2+}).[2] These clusters are found in solid-state compounds with alkali metals as countercations (or $AlCl_4^-$ as counteranions), and are made by direct synthesis from the corresponding elements. Despite this big variety of deltahedral clusters in the two groups none has been made both by synthesis from solution and by solid-state reaction.

In Ge_9^{4-} we have found the first such species to bridge the two classes. Prior to this report the clusters of Ge_9^{4-} were structurally characterized only in the salt $[K^+\text{-222-crypt}]_6(Ge_9^{4-})(Ge_9^{2-})$, made by crystallization of a solution of a K-Ge alloy dissolved in ethylenediamine.[7] The tin-substituted isoelectronic clusters $[Ge_{9-x}Sn_x]^{4-}$ ($x = 1-8$) have been characterized in solution by ^{119}Sn NMR spectroscopy.[5] Transition metal derivatives of these and similar deltahedral Zintl ions are also known. They include $[Tt_9Cr(CO)_3]^{4-}$ (Tt = Sn, Pb), $[Sn_6\{Cr(CO)_5\}_6]^{2-}$, and the recently synthesized Ge-centered $[Ge_9Ni(PPh_3)]^{2-}$, all of which have been isolated with cryptated alkali metal cations and structurally characterized.[8] Similarly $[Tt_9PtL_x]^{4-}$ (Tt = Sn, Pb; L = ligand) have been characterized in solution by ^{119}Sn and ^{207}Pb NMR spectroscopy.[9]

We have now made the naked Ge_9^{4-} clusters in "neat" solids.[10] These solids are Cs_4Ge_9 and the isostructural Rb_4Ge_9, both made by direct synthesis from the corresponding elements (see *Experimental Section*). Ge_9^{4-} is the first deltahedral cluster of the tetrels in the solid state since Tt_4^{4-} was made more than forty years ago in A_4Tt_4 (A = alkali metal).[11] Our attempts to make similar A_4Ge_9 compounds with sodium or potassium proved unsuccessful. This supports the hypothesis that the precursor alloys used for the solution studies (traditionally made with the light alkali metals) do not contain the clusters.

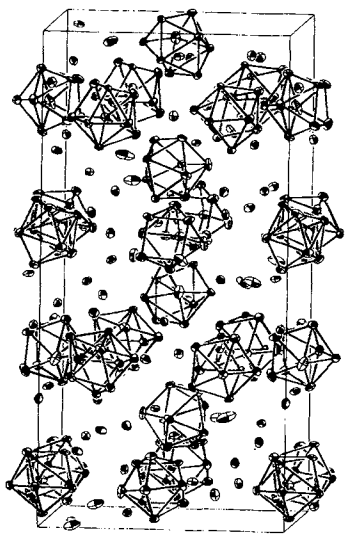

Figure 1. A general view of the tetragonal unit cell of Cs_4Ge_9 (the c axis runs vertical). Bonds are drawn between the Ge atoms of the four different Ge_9^{4-} clusters. The Cs atoms are shown isolated. All atoms are drawn with 50% thermal ellipsoids.

The structure of Cs_4Ge_9 (Figure 1) was determined by single-crystal X-ray diffraction (see *Experimental Section*). It crystallizes in the rare noncentrosymmetric $P4_1$ space group and contains four crystallographically different but otherwise very similar Ge_9 clusters A, B, C, and D. The structure can be viewed as containing quite open layers made of clusters A, B, and C, and positioned perpendicular to the c axis at $z \approx 1/12$, 4/12, 7/12, and 10/12. These layers alternate with clusters D centered along the 4_1 screw axis (the axis is at 1/2, 1/2, z) at $z \approx 5/24$, 11/24, 17/24, and 23/24. The clusters are well separated from each other by the large cesium cations positioned within and between the layers. These cations cap triangular and square faces of the clusters and also bridge some edges and "cap" some vertices. The shortest intercluster distance is 3.956(8) Å.

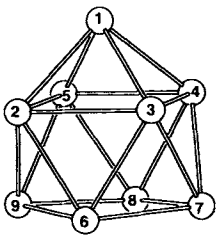

Figure 2. View of one of the four crystallographically different Ge_9^{4-} clusters (cluster A). All four clusters have the same geometry of a monocapped square antiprism. The numbering system serves for the assignment of the atoms in Table 1.

All four clusters are monocapped square antiprisms with very similar dimensions (Figure 2 and Table 1). The stoichiometry of the compounds combined with the observation that they are also electronically balanced (below), that is Zintl phases, defines the charge of each cluster as 4 − . This is also consistent with Wade's rules which predict a charge of 4 − for such *nido* species.[12] Furthermore, extended Hückel molecular orbital calculations show very similar HOMO–LUMO gaps for the four clusters at 40 electrons (2.88, 2.91, 2.91, and 3.18 eV), that is at a charge of 4 − .

Table 1. Important Ge–Ge intracluster distances for the four different clusters in Cs_4Ge_9 (at 173 K) and for Ge_9^{4-} in $[K^+\text{-222-crypt}]_6(Ge_9^{4-})(Ge_9^{2-})$ [7]. The numbering of the atoms is given in Figure 2.

Atom 1–Atom 2	Cluster A	Cluster B	Cluster C	Cluster D	Ge_9^{4-} from [7]
Ge1–Ge2	2.566(8)	2.522(8)	2.553(9)	2.585(8)	2.544(6)
Ge3	2.560(9)	2.556(8)	2.563(9)	2.591(8)	2.560(6)
Ge4	2.582(9)	2.591(9)	2.575(9)	2.575(8)	2.569(7)
Ge5	2.609(9)	2.588(9)	2.565(8)	2.577(8)	2.578(6)
Ge2–Ge3	2.876(8)	2.997(8)	3.008(11)	2.991(8)	2.962(7)
Ge5	2.777(8)	2.817(8)	2.744(9)	2.701(8)	2.703(6)
Ge6	2.556(8)	2.560(8)	2.560(9)	2.579(9)	2.585(6)
Ge9	2.604(8)	2.590(8)	2.590(9)	2.568(8)	2.538(7)
Ge3–Ge4	2.823(9)	2.770(8)	2.717(9)	2.763(8)	2.764(6)
Ge6	2.550(8)	2.584(9)	2.544(10)	2.601(9)	2.583(5)
Ge7	2.568(9)	2.586(8)	2.561(10)	2.584(9)	2.561(6)
Ge4–Ge5	2.825(9)	2.808(8)	2.866(9)	2.803(8)	2.799(6)
Ge7	2.609(9)	2.658(8)	2.637(9)	2.592(8)	2.646(6)
Ge8	2.597(9)	2.593(9)	2.581(9)	2.588(8)	2.590(5)
Ge5–Ge8	2.593(9)	2.582(9)	2.534(9)	2.590(8)	2.601(6)
Ge9	2.638(8)	2.638(8)	2.630(8)	2.631(8)	2.659(5)
Ge6–Ge7	2.609(9)	2.596(8)	2.544(10)	2.619(9)	2.561(7)
Ge9	2.618(8)	2.591(8)	2.574(9)	2.588(8)	2.557(6)
Ge7–Ge8	2.579(9)	2.591(9)	2.611(10)	2.589(8)	2.562(7)
Ge8–Ge9	2.600(8)	2.550(8)	2.571(9)	2.605(8)	2.533(7)
Ge6–Ge8	3.730(8)	3.715(8)	3.841(10)	3.802(8)	3.638(7)
Ge7–Ge9	3.624(8)	3.581(8)	3.410(10)	3.543(8)	3.580(7)

The geometry of the four clusters is virtually the same as that of the Ge clusters in the K-crypt salt.[7] The distances of the latter are listed in Table 1 for comparison. Often it is difficult to distinguish between a nine-atom *closo* species (a tricapped trigonal prism) and a nine-atom *nido* species (a monocapped square antiprism). However, the four clusters in the present compound are unambiguously *nido* polyhedra according to their distances. The diagonals of the square bases, Ge6–Ge8 and Ge7–Ge9 (Table 1), which are the potential candidates for heights in even-

 © WILEY-VCH Verlag GmbH, D-69451 Weinheim, 1997 0570-0833/97/3616-1755 $ 17.50+.50/0

tual trigonal prisms, are quite longer than the "existing" heights, Ge3–Ge4, Ge2–Ge5 and Ge2–Ge3, Ge4–Ge5, respectively. The similarities in shape and distances between the four clusters in Cs_4Ge_9 and the one in $[K^+\text{-222-crypt}]_6(Ge_9)(Ge_9)$ support the assumption that the latter is indeed Ge_9^{4-}. This is contrary to a recent suggestion that the two clusters in the crypt-salt are both Ge_9^{3-} similar to the recently discovered Sn_9^{3-} and Pb_9^{3-} in $[K^+\text{-222-crypt}]_6(Sn_9^{3-})(Sn_9^{3-})$ and $[K^+\text{-222-crypt}]_6(Pb_9^{3-})(Pb_9^{3-})$, respectively, as well as to Ge_9^{3-} in $[K^+\text{-222-crypt}]_3(PPh_3)_3(Ge_9^{3-})$ and $[K^+\text{-222-crypt}]_3(Ge_9^{3-})$.[13]

The Cs_4Ge_9 compound is a semiconductor (or an insulator) according to its magnetic susceptibility (temperature independent and near zero, see *Experimental Section*) and its appearance (semitransparent, ruby-red color).

The Cs–Ge and Rb–Ge phase diagrams are quite uncertain especially in the regions with high alkali metal content.[14] There are conflicting reports on the number of Cs–Ge and Rb–Ge compounds. Three possible stoichiometries, A_3Ge, A_3Ge_2, and AGe_4 (A = Rb or Cs), are suggested in each phase diagram, but only CsGe and RbGe have been structurally characterized. The compounds with the stoichiometries closest to A_4Ge_9 (30.8 at.% alkali-metal) would be AGe_4 (20 at% alkali metal), which melt congruently at 990 °C and 1110 °C for Cs and Rb, respectively.

The absence of large naked clusters of group 14 in the solid state may be explained by the large ratio of nuclearity to charge. According to Wade's rules deltahedral clusters of this group will have charges of 2 –, 4 –, and 6 – for *closo*, *nido*, and *arachno* species, respectively. It is important to note that these charges are independent of the nuclearity of the cluster. The charge balancing cations therefore may not be enough to efficiently keep apart (shield) large clusters. This is especially true for the smaller alkali metals such as Na and K which have been traditionally used as countercations. The effect is even more pronounced when the corresponding tetrel is among the heaviest of the group (Sn or Pb), which results in even larger clusters. In the crypt salts the large alkali metal cryptate is sufficient to separate the clusters efficiently. The new compounds are most likely the result of the combination of large cations (cesium or rubidium) and clusters of the small germanium. Despite the relatively high nuclearity and the relatively small negative charge of 4 –, the clusters are small enough that four large cations can separate them efficiently.

Experimental Section

Synthesis: Ruby-red semitransparent Cs_4Ge_9 was initially isolated and its structure determined from a reaction of Cs, Na, Al, and Ge loaded in atomic ratio of 4:1:1:10. The mixture was heated at 800 °C for five days in sealed Nb containers closed in evacuated quartz ampules. The furnace was slowly cooled to room temperature at a rate of 5 °C per hour. After the stoichiometry of the compound was determined from the single crystal work, a single-phase product of Cs_4Ge_9 (≥ 97% according to a Guinier powder pattern) was synthesized by heating a stoichiometric mixture of the elements (in Ta containers) at 800 °C for 1 h, quenching it in cold water, and then annealing it at 300 °C for 12 days. Rb_4Ge_9 (ruby-red, semitransparent, $a = 15.154(8)$ and $c = 30.82(4)$ Å from 13 measured lines, extremely weakly diffracting) was made similarly.

Structure determination: Data were collected from a single crystal (0.15 × 0.08 × 0.08 mm) on a Siemens SMART system with monochromated $Mo_{K\alpha}$ radiation at 173 K ($2\theta_{max} = 45°$), and corrected for absorption by semiempirical methods. The structure was solved by direct methods. Full-matrix least-squares refinement on F^2 of all atoms with anisotropic thermal parameters using SHELXTL V5.0 converged with $R1 = 0.064$ for 5128 independent reflections with $I > 3\sigma_I$ ($R1/wR2 = 0.093/0.189$ for 6475 independent reflections with $I > 2s_I$) and 469 parameters. Crystal data: Cs_4Ge_9, tetragonal, $P4_1$ with $a = 15.5074(5)$, $b = 31.3997(9)$ Å, $V = 7551.0(6)$ Å^3, $Z = 16$, $\rho_{calcd} = 4.17$ g cm^{-3}, $\mu = 215.73$ cm^{-1}. The compound diffracts very poorly. Data sets collected on the Siemens diffractometer from three different crystals showed very low ratios of observed to measured reflections. Further details of the crystal structure investigation may be obtained from the Fachinformationszentrum Karlsruhe, D-76344 Eggenstein-Leopoldshafen (Germany), on quoting the depository number CSD-406486.

Magnetic measurements: The magnetization of 25 mg of the Cs_4Ge_9 sample, which was obtained in near 100% yield, was measured at field of 3 T over the range of 6–295 K (Quantum Design MPMS SQUID magnetometer). The raw data, corrected for the susceptibility of the holder and the ion-core dimagnetism arising from four Cs^+ and nine Ge^{4+} ions, lay between -3.79 and -3.47×10^{-4} emu mol^{-1}. Correction for diamagnetism due to the Larmor precession of the delocalized lone pairs of electrons on cluster orbitals (-3.0×10^{-4} emu mol^{-1}) was also applied.[15] The corrected molar susceptibility is virtually zero, and fluctuates between -7.9×10^{-5} and 4.6×10^{-5} emu mol^{-1}.

Received: February 10, 1997 [Z 10096 IE]
German version: *Angew. Chem.* **1997**, *109*, 1818–1820

Keywords: caesium · clusters · germanium · solid-state structures · Zintl phases

[1] The use of triels, tetrels, and pentels or pnictogens has been suggested by the Commission of Nomenclature of Inorganic Chemistry in the Inorganic Chemistry Division of IUPAC: B. P. Block, W. H. Powell, W. C. Fernelius *Inorganic Chemical Nomenclature: Principles and Practice*, American Chemical Society, Washington, DC, **1990**, p. 24.
[2] J. D. Corbett, *Struct Bonding, (Berlin)* **1997**, *87*, 157, and references therein.
[3] J. D. Corbett, *Chem. Rev.* **1985**, *85*, 383, and references therein.
[4] 2,2,2-crypt is an abbreviation for 4,7,13,16,21,24-hexaoxa-1,10-diazabicyclo[8.8.8]hexacosane.
[5] W. L. Wilson, R. W. Rudolph, L. L. Lohr, R. C. Taylor, P. Pyykkö, *Inorg. Chem.* **1986**, *25*, 1535, and references therein.
[6] To the best of our knowledge there are no systematic studies on the precursor alloys. Kummer and Diehl (D. Kummer, L. Diehl, *Angew. Chem.* **1970**, *82*, 881; *Angew. Chem. Int. Ed. Engl.* **1970**, *9*, 895) report mixture of unidentified phases and metallic tin in a Na–Sn precursor.
[7] C. H. E. Belin, J. D. Corbett, A. Cisar, *J. Am. Chem. Soc.* **1977**, *99*, 7163.
[8] B. W. Eichhorn, R. C. Haushalter, W. T. Pennington, *J. Am. Chem. Soc.* **1988**, *110*, 8704; B. W. Eichhorn, R. C. Haushalter, *J. Chem. Soc. Chem. Commun.* **1990**, 937; B. Schiemenz, G. Huttner, *Angew. Chem.* **1993**, *105*, 295; *Angew. Chem. Int. Ed. Engl.* **1993**, *32*, 297; D. R. Gardner, J. C. Fettinger, B. W. Eichhorn, *ibid.* **1996**, *108*, 3032; *Angew. Chem. Int. Ed. Engl.* **1996**, *35*, 2852.
[9] F. Teixidor, M. L. Luetkens, Jr., R. W. Rudolph, *J. Am. Chem. Soc.* **1983**, *105*, 149.
[10] The use of "neat" here (after J. D. Corbett in ref. [2]) is to distinguish solids made by solid-state reactions from "molecular" solids crystallized from solution.
[11] R. E. Marsh, D. P. Shoemaker, *Acta Crystallogr.* **1953**, *6*, 197; On page 265 of the textbook *Advanced Inorganic Chemistry* (F. A. Cotton, G. Wilkinson, Wiley, New York, 5th ed., **1988**) it is erroneously implied that Na_4Pb_9 and Na_2Sn_5 are known and structurally characterized. The only known Pb_9^{4-} and Sn_5^{2-} ions are found in $[K^+\text{-222-crypt}]_3KPb_9$ (J. Cambell, D. A. Dixon, H. P. Mercier, G. J. Schrobilgen, *Inorg. Chem.* **1995**, *34*, 5798) and $[Na^+\text{-222-crypt}]_2Sn_5$ (P. A. Edwards, J. D. Corbett, *Inorg. Chem.* **1977**, *16*, 903), respectively.
[12] K. Wade, *Adv. Inorg. Chem. Radiochem.* **1976**, *18*, 1.
[13] T. F. Fässler, M. Hunziker, *Z. Anorg. Allg. Chem.* **1996**, *622*, 837; V. Angilella, C. Belin, *J. Chem. Soc. Faraday Trans.* **1991**, *87*, 203; C. Belin, H. Mercier, V. Angilella, *New J. Chem.* **1991**, *15*, 931; T. F. Fässler, M. Hunziker, *Inorg. Chem.* **1994**, *33*, 5380.
[14] M. E. Drits, V. F. Potemkin, L. L. Zusman, *Inorg. Mater.* **1982**, *18*, 969; A. N. Orlov, K. A. Chuntonov, L. Z. Melkhov, A. A. Semyannikov, *Russ. Metall.* **1987**, *6*, 176; In *Binary Alloy Phase Diagrams* (Ed: T. B. Massalski), ASM International, Materials Park, Ohio, **1990**) the area of uncertainty is erroneously shown at the Ge-rich side rather than the Cs-rich side.
[15] N. W. Ashcroft, D. N. Mermin, *Solid State Physics*, Holt, Reinhart and Wilson, Philadelphia, **1976**, p. 649.

 © WILEY-VCH Verlag GmbH, D-69451 Weinheim, 1997 0570-0833/97/3616-1756 $ 17.50+.50/0

[2+2] Cycloaddition Products of Tetradehydrodianthracene: Experimental and Theoretical Proof of Extraordinary Long C–C Single Bonds**

Stefan Kammermeier, Peter G. Jones, and Rainer Herges*

Dedicated to Professor George A. Olah on the occasion of his 70th birthday

C–C bonds in organic molecules can be elongated by a number of factors. Steric repulsion between bulky substituents, strain energy in polycyclic systems, and through-bond interactions are among the most important. An impressive example of extremely long C–C bonds (1.710–1.724 Å), which is the result of the interplay of several of these factors, was recently described by Toda, Tanaka, Stein, and Goldberg.[1] Other classical examples within the class of pure hydrocarbons include anthracene dimers and related compounds, in which the central C–C bonds between the anthracene units usually exceed 1.6 Å.[2] We demonstrate here with two compounds examined by both experimental and theoretical methods how the length of a C–C bond in a pure hydrocarbon can be extended to more than 1.7 Å.

The starting point for our investigations was the highly strained and reactive tetradehydrodianthracene **1**.[3] Compound **1** reacts with a number of alkenes and even with benzene in photochemical [2+2] additions to give cyclobutanes, which immediately undergo [2+2] cycloreversion yielding the product of an overall metathesis reaction.[4] The dimerizing metathesis of **1** to form a tube-shaped, conjugated hydrocarbon has also been described.[5] The driving force for the cycloreversion is the high strain energy induced by the second nonreacting bridgehead double bond in the molecular frame.

If alkynes are used as reaction partners instead of alkenes in the cycloaddition, cyclobutene derivatives are obtained as stable products. The photochemical [2+2] cycloaddition with acetylene leads to adduct **2**; the thermal addition of 1,2-dehydrobenzene gives the [2+2] adduct **3**. Electrocyclic ring opening of the cyclobutene ring in **2** and **3**, which could be expected, was not observed by spectroscopy in either case.[6] The symmetry-allowed conrotatory ring opening is probably prevented by the stiff molecular frame.[7] The reaction would have to proceed via a diradical intermediate. According to our density functional theory (DFT) calculations[8,9] at the Becke3LYP/6-31G* level,[10,11] the ring opening of **3** is thermodynamically not favored. However, in the analogous ring opening of **2** the hypothetical product **4** is only 0.3 kcal mol^{-1} less stable than **2**. We cannot exclude that small amounts of **4** may be in equilibrium with **2**, but the concentration must lie below spectroscopic detection limits. The newly formed double bonds in **4** are considerably twisted (torsion angle C2-C1-C3-C4 20°). Structure **5** is additionally disfavored by the cancellation of the aromaticity of the benzene ring. Structure **5** could not be located as a stationary point at the DFT level and probably is not a minimum on the potential energy surface.[12]

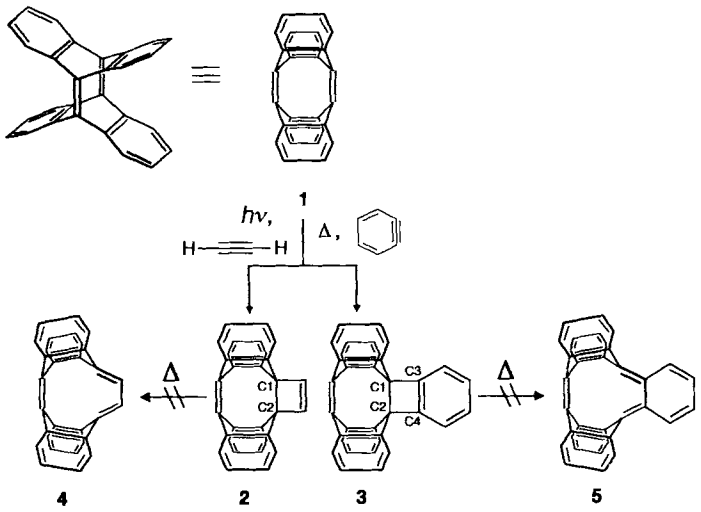

Both cycloaddition products **2** and **3** were characterized by X-ray structure analysis.[13] The central C–C single bond in the acetylene addition product **2** is 1.677(3) Å long; the corresponding bond in **3** is even longer, 1.713(2) Å (Figure 1). The remaining bond lengths and angles in the four-membered rings of **2** and

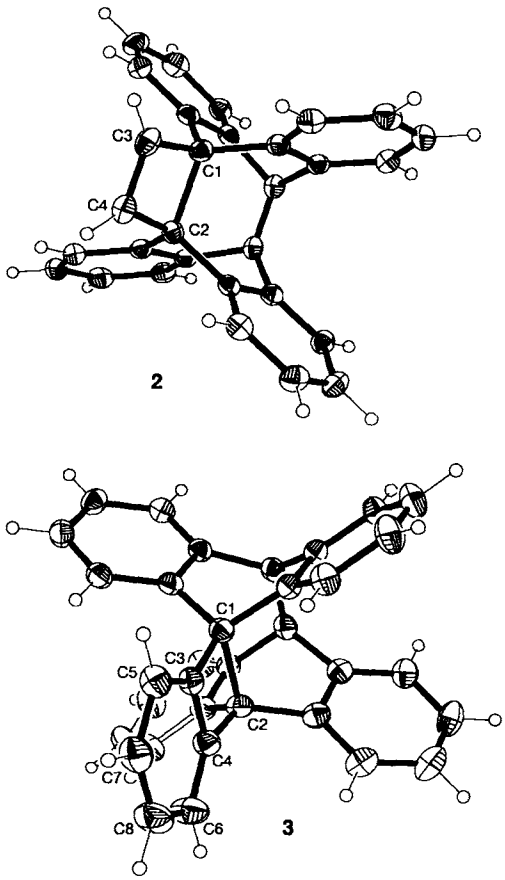

Figure 1. X-ray crystal structures of **2** and **3**. Selected bond lengths [Å] and angles [°]: **2**: C1–C2 1.667(3), C1–C3 1.512(3), C2–C4 1.511(3), C3–C4 1.329(3); C1-C2-C4 83.31(13), C3-C4-C2 96.6(2). **3**: C1–C2 1.713(2), C1–C3 1.512(2), C2–C4 1.517(2), C3–C4 1.378(2), C3–C5 1.381(2), C5–C7 1.388(2), C7–C8 1.384(3); C1-C2-C4 83.32(10), C3-C4-C2 96.56(12).

[*] Prof. Dr. R. Herges, Dipl.-Chem. S. Kammermeier
Institut für Organische Chemie der Technischen Universität
Hagenring 30, D-38106 Braunschweig (Germany)
Fax: Int. code +(531)391-5388
e-mail: r.herges@tu-bs.de

Prof. Dr. P. G. Jones
Institut für Anorganische und Analytische Chemie der
Technischen Universität Braunschweig

[**] This work was supported by the Deutsche Forschungsgemeinschaft and by the Fonds der Chemischen Industrie (scholarship for S. K.).

 © WILEY-VCH Verlag GmbH, D-69451 Weinheim, 1997 0570-0833/97/3616-1757 $ 17.50+.50/0

3 do not exhibit unusual values. This is also true for the annelated benzene ring in **3**. Neither the thermal factors nor the molecular packing display anomalies that would lead to systematic errors in bond lengths.

In a simplified scheme the extraordinary length of the C–C bonds can be explained by the interplay of three factors:

1. the through-bond interactions ($\pi-\sigma^*$) of the four benzene rings with the C–C single bond,
2. the strain induced by the facing, strongly pyramidalized double bond, and
3. the ring strain of the cyclobutene or the benzocyclobutene ring.

To study the effects of these factors we examined different anthracene derivatives, some of which are subject to only one or two of these factors (Table 1). The experimentally determined (X-ray crystal structure) and theoretically calculated (Becke-3LYP/6-31G* and PM3) bond lengths prove that the effects are almost additive. Only the $\pi-\sigma^*$ interaction[14] is operative in the anthracene dimer **6**; both the C9–C9′ and C10–C10′ bonds are already stretched to 1.624 Å by conjugation with the π-systems of the four benzene rings.[15] The annelation of two cyclobutane rings elongates the bonds in **8**[16,17] by 0.04 Å compared to those in **6**, and by 0.047 Å in **10** compared to those in **9**. The remarkably long bond in **7**[18] can be explained by through-bond conjugation with the C_3 bridge. The effect of the facing, strongly pyramidalized double bond becomes evident by comparing **6** with **9**, and **8** with **10**; the bond elongations are 0.024 and 0.028 Å, respectively. The effect of a cyclobutene ring is similar to that of a cyclobutane ring (cf. **10** and **2**), whereas the benzocyclobutene unit in **3** leads to an elongation of the already weak bond by an additional 0.036 Å (X-ray crystal structure) and by 0.021 Å (DFT calculations).

To our knowledge the C1–C2 bond in **3** is one of the longest, stable C–C bonds in an uncharged, pure hydrocarbon. The longest reported C–C bond so far (1.781 Å, X-ray crystal structure) was found by von Schnering et al. in a disilabicyclobutane.[19] Recently Toda and Goldberg et al. synthesized two tetraphenylcyclobutarenes, which are very similar in structure to compound **3** and which also have close to the same bond lengths, 1.710(5) to 1.724(5) Å.[1] Our calculations on a simplified model system (1,1,2,2-tetraphenylcyclobuta[*b*]benzene[20]) confirm the experimental bond lengths (1.720 Å, Becke3LYP/6-31G*). In these systems the four phenyl groups in conjugation with the long C–C single bond are almost freely rotating, and the $\pi-\sigma^*$ interaction therefore is less effective. Moreover, the strain induced by the pyramidalized double bond is lacking. However, this is obviously compensated by the strong steric repulsion of the phenyl groups.

One should expect unusual properties for such unusually long C–C bonds. In this context it is instructive to compare our systems with the simple model case of the C–C bond in ethane. An elongation of the C–C bond in ethane from 1.544 to 1.700 Å requires 6.53 kcal mol^{-1}. This is only 7% of the energy needed for complete bond cleavage (UBecke3LYP/6-31G*; a C–C distance of 2.1 Å is necessary before 50% of the dissociation energy is reached). At a C–C bond length of 1.7 Å the diradical character in ethane is also very low with 0.044 electrons in higher configurations (CAS(10,8)/6-31G*). Therefore C–C bonds of this length do not have unusual electronic properties.

The impact of the bond length on the bond strength, however, is considerable. According to our calculations (Becke3LYP/6-31G*[21]) the force constant of the long C–C bond in **3** (133.1 N m^{-1}) is less than one-third of the corresponding value in ethane (455.7 N m^{-1}). Because the frequency of a stretching vibration mainly depends on the force constant of the bond, the stretching vibration of the 1.713 Å-long C–C bond in **3** should appear at lower wavelengths than those of "normal" hydrocarbons. This is impressively confirmed by a Raman spectrum of compound **3** (Figure 2).[22] According to PM3 calculations[23]

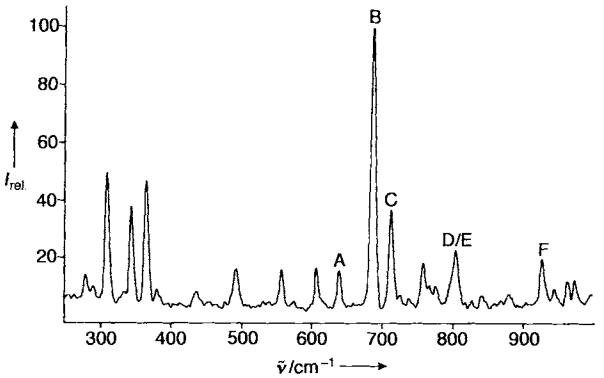

Figure 2. Experimental Raman vibrational spectrum of **3**. The labels A–F are used in the assignments in Table 2.

there are six normal modes that include the C1–C2 stretching vibration.[24] For a more reliable assignment of the theoretically calculated frequencies to the experimental Raman bands, we scaled the PM3 Raman frequencies by using a much more reliable DFT calculation (Becke3LYP/6-31G*) on a small model system.[25] The calculated frequencies of **3** were corrected by a scaling factor of 0.948. The Raman absorption with the highest intensity corresponds to the normal mode having the largest amplitude along the trajectory of our stretching vibration. According to our calculations this is also the most intensive Raman band in the region between 300 and 1000 cm^{-1}. The scaled PM3 value for the absorption is 675 cm^{-1}. Both the intensity and the wavenumber of this C–C vibration correspond well with the intense peak at 687 cm^{-1} in the experimental spectrum (Figure 2). The remaining four vibrations with A_1 symmetry can also be assigned unambiguously (Table 2). The most intense peak is thus red-shifted by more than 300 cm^{-1} relative to the Raman-active C–C stretching vibration in ethane (exp.: 995 cm^{-1}, Becke3LYP/6-31G*: 1010 cm^{-1}).

Table 1. Experimentally determined and calculated bond lengths [Å] of the central C–C single bond in selected dianthracene derivatives.

	6	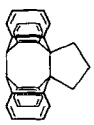 **7**	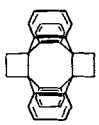 **8**	**9**	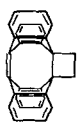 **10**	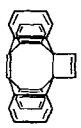 **2**	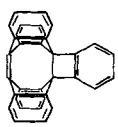 **3**
Experimental	1.624	1.669	1.648/1.663	-	-	1.677	1.713
Becke3LYP/6-31G*	1.623	1.691	1.666	1.647	1.694	1.700	1.721
PM3	1.565	1.606	1.602	1.583	1.622	1.671	1.703

 © WILEY-VCH Verlag GmbH, D-69451 Weinheim, 1997 0570-0833/97/3616-1758 $ 17.50+.50/0

Table 2. Experimentally determined and theoretically calculated absorptions in the Raman spectrum of **3**.

Vibration	Experimental $\tilde{\nu}$[cm^{-1}]	I[a]	Theoretical (PM3) $\tilde{\nu}$[cm^{-1}] unscaled	scaled[b]	I[a]
A	639	14	647	613	80
B	687	100	712	675	100
C	713	38	765	725	59
D	799	11	819	776	78
E	805	22	827	784	78
F	927	19	919	871	33

[a] Relative intensities, relative to the most intensive absorption (= 100). [b] Scaling factor: 0.948.

In agreement with our calculations the experimental data (X-ray structure analysis and Raman spectrum) show that the central C–C bonds in **2** and **3** are 1.677 and 1.713 Å long, respectively. As a consequence of the bond elongation the force constant of the bond is reduced to less than one-third of the usual value and the Raman-active C–C stretching vibration is shifted to 687 cm^{-1}. There is no reason to assume that the limit has been reached. It should be possible to stabilize even longer C–C bonds by a suitable combination of through-bond interactions, steric interactions, and ring strain, and by fixing the bond in a stiff molecular frame (to prevent subsequent reactions). Stable C–C bonds even longer than the smallest nonbonding distance of two C atoms, 1.80 Å,[26] are conceivable.

Experimental Section

2: Compound **1** (100 mg, 0.284 mmol) was suspended in acetylene-saturated benzene (120 mL) and irradiated in a quartz reactor with a high-pressure mercury lamp (150 W) for 2 h. The solvent was removed in vacuo and the residue was purified by chromatography in hexane/dichloromethane. The crude product was additionally purified by recrystallization from toluene. Compound **2** was obtained as a colorless, crystalline solid. Yield: 25 mg (31 %). M.p. 272 °C (decomp.); ^{1}H NMR (400 MHz, $CDCl_3$): δ = 7.17 (s, 2H, olefin. C=CH), 7.14 (m, 4H, arom. CH), 6.87 (m, 12H, arom. CH); ^{13}C NMR (100.6 MHz, $CDCl_3$): δ = 150.85 (R_2C=CR_2), 144.92 (C_q), 142.65 (C_q), 137.59 (olefin. C=CH), 125.77 (arom. CH), 125.55 (arom. CH), 124.22 (arom. CH), 123.96 (arom. CH), 72.59 (aliph. C_q); IR (KBr, cm^{-1}): $\tilde{\nu}$ = 3063, 3045, 3037, 1572, 1453, 753, 625; UV/Vis (CH_2Cl_2): λ_{max} (ε) = 230 (24500), 270 (2500), 280 nm (2000); MS (70 eV): m/z (%): 378 (100, M^+), 189 (8, M^{2+}); HRMS: calcd for $C_{30}H_{18}$: 378.1409, found: 378.1399.

3: A suspension of compound **1** (80 mg, 0.227 mmol) in benzene (50 mL) was charged with anthranilic acid (312 mg, 2.27 mmol) and 3-methylbutylnitrite (266 mg, 2.27 mmol), and the mixture was refluxed for 2 h. The solvent was removed in vacuo and the residue was purified by chromatography with hexane/dichloromethane over silica gel. In addition to a number of multiple addition products, which were not further characterized, **3** was obtained as a light yellow solid. Yield: 12 mg (12 %). M.p. 286 °C; ^{1}H NMR (400 MHz, $CDCl_3$): δ = 7.74 (m, 2H, arom. CH), 7.66 (m, 2H, arom. CH), 7.20 (m 4H, arom. CH), 6.91 (m, 4H, arom. CH), 6.86 (m, 4H, arom. CH), 6.78 (m, 4H, arom. CH); ^{13}C NMR (100.6 MHz, $CDCl_3$): δ = 151.09 (R_2C=CR_2), 144.79 (C_q), 142.56 (C_q), 141.87 (C_q), 129.06 (arom. CH), 126.76 (arom. CH), 125.95 (arom. CH), 125.53 (arom. CH), 124.27 (arom. CH), 124.20 (CH arom.), 76.53 (aliph. C_q); IR (KBr, cm^{-1}): $\tilde{\nu}$ = 3037, 3010, 1624, 1424, 769, 747, 722; UV/Vis (CH_2Cl_2): λ_{max} (ε) = 230 (27000), 258 (11000, sh), 270 (6000, sh), 280 nm (4200, sh); MS (70 eV): m/z (%): 428 (100, M^+), 214 (9, M^{2+}); HRMS: calcd for $C_{34}H_{20}$: 428.1565, found: 428.1564.

Received: November 18, 1996
Supplemented version: April 21, 1997 [Z 9784 IE]
German version: *Angew. Chem.* **1997**, *109*, 1825–1828

Keywords: anthracene dimers · cycloadditions · density functional calculations · Raman spectroscopy · strained molecules

[1] F. Toda, K. Tanaka, Z. Stein, I. Goldberg, *Acta Crystallogr. Sect. C* **1996**, *52*, 177–180.

[2] a) G. Kaupp, J. Boy, *Angew. Chem.* **1997**, *109*, 48–50; *Angew. Chem. Int. Ed. Engl.* **1997**, *36*, 48–49; b) D. A. Dougherty, C. S. Choi, G. Kaupp, A. B. Buda, J. M. Rudzinski, E. Osawa, *J. Chem. Soc. Perkin Trans. 2* **1986**, 1063–1070; c) E. Osawa, K. Kanematsu in *Molecular Structure and Energetics, Vol. 3* (Eds.: J. F. Liebman, A. Greenberg), VCH, Deerfield Beach, FL, USA, **1986**, Chapter 7; for more recent work see: d) G. M. Anstead, R. Srinivasan, C. S. Peterson, S. R. Wilson, J. A. Katzenellenbogen, *J. Am. Chem. Soc.* **1991**, *113*, 1378–1385; e) R. Haag, B. Ohlhorst, M. Noltemeyer, R. Fleischer, D. Stalke, A. Schuster, D. Kuck, A. de Meijere, *J. Am. Chem. Soc.* **1995**, *117*, 10474–10485.

[3] R. L. Vivattene, F. D. Greene, L. D. Cheung, R. Majeste, L. M. Trefonas, *J. Am. Chem. Soc.* **1974**, *96*, 4342–4343.

[4] S. Kammermeier, R. Herges, *Angew. Chem.* **1996**, *108*, 470–472; *Angew. Chem. Int. Ed. Engl.* **1996**, *35*, 417–419.

[5] S. Kammermeier, P. G. Jones, R. Herges, *Angew. Chem.* **1996**, *108*, 2834–2836; *Angew. Chem. Int. Ed. Engl.* **1996**, *35*, 2669–2671.

[6] Compounds **2** and **3** are stable in solution at temperatures below 80 °C. At higher temperatures slow decomposition was observed. The products were not further characterized.

[7] The same argument was used to explain the remarkable stability of the parent system didehydrodianthracene towards electrocyclic ring opening: a) R. B. Woodward, R. Hoffmann, *The Conservation of Orbital Symmetry*, Verlag Chemie, **1970**, p. 54; b) N. M. Weinshenker, F. D. Greene, *J. Am. Chem. Soc.* **1968**, *90*, 506.

[8] W. Kohn, A. D. Becke, R. G. Parr, *J. Phys. Chem.* **1996**, *100*, 12974–12980.

[9] Gaussian 92, Revision B: M. J. Frisch, G. W. Trucks, M. Head-Gordon, P. M. W. Gill, M. W. Wong, J. B. Foresman, B. G. Johnson, H. B. Schlegel, M. A. Robb, E. S. Repogle, R. Gomperts, J. L. Andres, K. Raghavachari, J. S. Binkley, C. Gonzalez, R. L. Martin, D. J. Fox, D. J. Defrees, J. Baker, J. J. P. Stewart, J. A. Pople, Gaussian, Pittsburgh PA, **1992**.

[10] A. D. Becke, *J. Chem. Phys.* **1993**, *98*, 5648–5652.

[11] C. Lee, W. Yang, R. G. Parr, *Phys. Rev. B* **1988**, *37*, 785.

[12] At the semiempirical PM3 level the ring-opened structure **5** was found as a minimum. Starting from the geometry of **5**, geometry optimization at the Becke3LYP/6-31G* level leads to structure **3**.

[13] Crystal structure analysis of compound **2**: $C_{30}H_{18}$, M_r = 378.44, triclinic, $P\bar{1}$, a = 8.0552(12), b = 9.6355(12), c = 13.184(2) Å, α = 72.871(10), β = 76.045(8), γ = 81.880(10)°, V = 946.3 Å^3, Z = 2, ρ_{calcd} = 1.328 Mg m^{-3}, $F(000)$ = 396, $\lambda(Mo_{K\alpha})$ = 71.073 pm, μ = 0.08 mm^{-1}, T = −100 °C. Colorless plate 0.75 × 0.4 × 0.1 mm, Siemens P4 diffractometer, 4547 intensities below $2\theta_{max}$ = 55°, 4288 independent (R_{int} = 0.019). Structure solved by direct methods, refinement anisotropic versus F^2 (Program SHELXL-93, G. M. Sheldrick, Universität Göttingen); H atoms with the riding model; $wR(F^2)$ = 0.116 (all reflections), $R(F)$ = 0.047 ($F > 4\sigma(F)$) for 223 parameters; max. $\Delta\rho$ = 0.26 e Å^{-3}, S = 0.85. Crystal structure analysis of compound **3**: $C_{34}H_{20}$, M_r = 428.50, triclinic, $P\bar{1}$, a = 8.2804(14), b = 9.1917(14), c = 14.951(2) Å, α = 89.334(12), β = 79.560(12), γ = 82.073(12)°, V = 1108.3 Å^3, Z = 2, ρ_{calcd} = 1.284 Mg m^{-3}, $F(000)$ = 448, μ = 0.07 mm^{-1}, T = −130 °C. Other data identical to those of **2**, except: Stoe STADI-4 diffractometer, colorless plate 0.65 × 0.4 × 0.25 mm, 4159 intensities below $2\theta_{max}$ = 50°, 3898 independent (R_{int} = 0.013), $wR(F^2)$ = 0.103, $R(F)$ = 0.040, 308 parameters, max. $\Delta\rho$ = 0.22 e Å^{-3}, S = 1.05. Crystallographic data (excluding structure factors) for the structures reported in this paper have been deposited with the Cambridge Crystallographic Data Centre as supplementary pulication no. CCDC-100012. Copies of the data can be obtained free of charge on application to The Director, CCDC, 12 Union Road, Cambridge CB21EZ. UK (fax: Int. code +(1223)336-033; e-mail: deposit@chemcrys.cam.ac.uk).

[14] a) R. Hoffmann, A. Imamura, W. J. Hehre, *J. Am. Chem. Soc.* **1968**, *90*, 1499–1509; b) D. A. Dougherty, H. B. Schlegel, R. A. Bell, K. Mislow, *Tetrahedron Lett.* **1976**, 3479–3482; c) D. A. Dougherty, H. B. Schlegel, K. Mislow, *Tetrahedron* **1978**, *34*, 1441–1446; d) K. Harano, T. Ban, M. Yasuda, E. Osawa, K. Kanematsu, *J. Am. Chem. Soc.* **1981**, *103*, 2310–2317; e) Y. Okamoto, K. Harano, M. Yasuda, E. Osawa, K. Kanematsu, *Chem. Pharm. Bull.* **1983**, *31*, 2526.

[15] C. S. Choi, P. L. Marinkas, *Acta Crystallogr. Sect. B* **1980**, *36*, 2491–2493.

[16] P. Gantzel, K. K. Baldridge, J. S. Siegel, *Tetrahedron Lett.* **1995**, *36*, 845–848.

[17] J. Harada, K. Ogawa, S. Tomoda, *Chem. Lett.* **1995**, 751–752.

[18] A. Dunand, J. Ferguson, G. B. Robertson, *Chem. Phys.* **1980**, *53*, 215–223.

[19] G. Fritz, S. Wartanessian, E. Matern, W. Hönle, H. G. von Schnering, *Z. Anorg. Allg. Chem.* **1981**, *475*, 87–108.

[20] To work with reasonable computational costs we replaced the dichloronaphthalene unit of dichloro-1,1,2,2-tetraphenylcyclobuta[*b*]naphthalene of Toda et al. by benzene. According to a PM3 calculation the bond length of the long C–C bond changes only insignificantly from 1.6778 to 1.6703 Å.

[21] Analytical gradients and numerical second derivatives of the energy to the bond length C1–C2.

[22] We thank Dr. Schiel of the Physikalisch-Technische Bundesanstalt, Braunschweig, for recording the Raman spectrum.

[23] a) J. J. P. Stewart, *J. Comput. Chem.* **1989**, *10*, 209; b) *ibid.* **1989**, *10*, 221; c) VAMP 5.0: G. Rauhut, J. Chandrasekhar, A. Alex, T. Steinke, T. Clark, Oxford Molecular Limited, **1993**.

[24] The C1–C2 stretching vibration does not exist as a "pure" normal mode, but forms linear combinations with deformation vibrations of the molecular frame having the same symmetry (A_1 of the point group C_{2v}). Therefore there are

 © WILEY-VCH Verlag GmbH, D-69451 Weinheim, 1997 0570-0833/97/3616-1759 $ 17.50+.50/0

several normal vibrations with a varying contribution of the C1–C2 stretching vibration.

[25] We chose 13,14-benzotetracyclo[4.2.2.2^{1,2}.2^{2,5}]tetradeca-3,5,7,9,11,13-hexaene as a model system. It corresponds to structure **3** in which the four benzene rings of the didehydrodianthracene framework are replaced by double bonds. A harmonic frequency analysis with the PM3 approximation and the Becke3LYP/6-31G* method was performed. A scaling factor of 0.948 for the PM3 method was determined by comparing the four normal modes with the largest contribution of the C–C stretching trajectory. The length of the corresponding C–C bond in the model system at the Becke3LYP/6-31G* level was 1.784 Å.

[26] J. L. Adock, A. A. Gakh, J. L. Pollitte, C. Woods, *J. Am. Chem. Soc.* **1992**, *114*, 3980–3981.

Self-Assembly of Convex and Concave Molecular Tectons to Form a Linear Molecular Array in the Solid State**

Frédérique Hajek, Mir Wais Hosseini,* Ernest Graf, André De Cian, and Jean Fischer

With our present level of knowledge, the complete understanding and subsequent prediction of all intermolecular interactions in the crystalline phase seems illusive. Therefore, it appears that crystal structures are not predictable.[1] However, following the statement by Jack Dunitz:[2] "A crystal is, in a sense, the supramolecule *par excellence*", one may predict some of the intermotive interactions by using proper molecular modules. The design of molecular networks in the solid state is a subject of current interest.[3] The strategy followed for the formation of molecular networks relies on a double analysis. That at the molecular level deals with the individual modules composing the solid, and the other at the supramolecular level deals with the intermotive or intermolecular interactions.[4] Obviously the latter type of analysis is more subtle. For the design and synthesis of molecular networks, the approach called molecular tectonics,[5] which is based on the self-assembly[6] of structurally defined and energetically programmed complementary tectons, seems to be viable. The most important operational concepts in molecular tectonics are molecular recognition[7] between tectons and geometrical features encoded within the framework of the tecton that allow iteration. The latter requires exoreceptor molecules possessing recognition sites that point in divergent directions.

In terms of interaction energy, hydrogen bonding[8, 9] has been used almost exclusively. However, some time ago, we proposed to use the van der Waals interactions responsible for the inclusion processes between concave and convex molecules.[10] Our approach to the preparation of linear molecular arrays (linear koilates) was based on the self-assembly of rigid and compact receptor molecules having two diametrically opposing cavities (linear koiland, from the Greek κοιλοσ, "hollow") and linear connectors with two extremities complementary to the cavities of the receptor (Scheme 1).

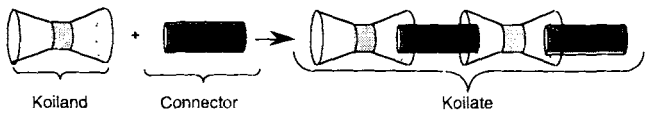

Scheme 1. Representation of a linear array (koilate) formed by connection of biconcave receptors (koilands) through convex molecules (connectors).

Calix[4]arene derivatives[11] appeared to be suitable components for our design of koilands. Indeed, they offer a preorganized hydrophobic pocket surrounded by four aryl moieties as well as four hydroxyl groups for further functionalization. Furthermore, the basket-type cavity of calix[4]arene derivatives has been shown to accommodate a variety of neutral guests in the solid state.[12] Our original design of koilands was based on the fusion of two *p-tert*-butylcalix[4]arenes **1** in *cone* conformation through two silicon atoms (**6** in Scheme 2).[10] This design was further extended to other calix[4]arene derivatives.[13] Examples of *p-tert*-butylcalix[4]arenes fused through other atoms have been also reported.[14]

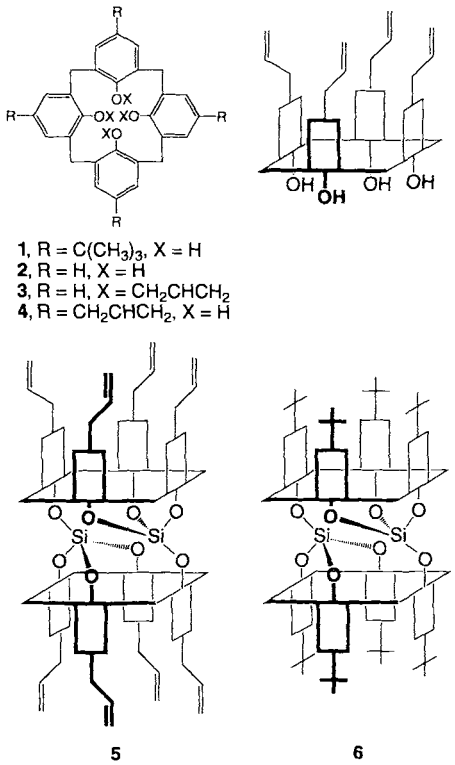

Scheme 2. Calix[4]arenes **1**–**4** (top left) and representations of *p*-allylcalix[4]arene **4** in the *cone* conformation (top right) as well as of koilands **5** and **6** (bottom).

We used compound **6** and hexadiyne to prepare the first fully characterized linear koilate in the solid state.[15] But one could argue that, due to the presence of $CHCl_3$ molecules in the lattice, the formation of the koilate was governed by solvent molecules. To preclude this possibility and to demonstrate the generality of our approach, we describe here the formation of another linear koilate in the solid state obtained without the presence of any solvent molecules.

[*] Prof. Dr. M. W. Hosseini, F. Hajek, Dr. E. Graf
Laboratoire de Chimie de Coordination Organique (URA CNRS)
Université Louis Pasteur, Institut Le Bel
4, rue Blaise Pascal, F-67000 Strasbourg (France)
Fax: Int. code +(388)416266
e-mail: hosseini@chimie.u-strasbg.fr

Dr. A. De Cian, Prof. J. Fischer
Laboratoire de Cristallochimie et Chimie Structurale (URA CNRS)
Université Louis Pasteur, Strasbourg (France)

[**] Molecular Tectonics, Part 6. We thank M. Smietana for assistance in the synthesis of compound **5** and the CNRS and the Institut Universitaire de France (IUF) for financial support. Part 5: O. Félix, M. W. Hosseini, A. De Cian, J. Fischer, *Tetrahedron Lett.* **1997**, *38*, 1933.

 © WILEY-VCH Verlag GmbH, D-69451 Weinheim, 1997 0570-0833/97/3616-1760 $ 17.50+.50/0

Calix[4]arene, in addition to the features just mentioned, presents further advantages since it can be readily modified at the *para* position with a large variety of substituents. In particular, this position may be funtionalized with allyl moieties.[16] It has been shown previously[16] that although compound **4** shows temperature-dependent conformational mobility, below room temperature it adopts a *cone* conformation. The design of the new koiland **5** possessing functional groups at both faces of the molecule was based on the double fusion of precursor **4** through two silicon atoms. The following synthetic strategy used for the preparation of compound **5**: the dealkylation of *p-tert*-butylcalix[4]arene **1**[17] afforded compound **2**, which was converted into the allyl ether **3**.[16] The latter was then transformed into the desired compound **4** by a Claisen rearrangement. The desired doubly fused compound **5** was obtained in 53% yield by treatment of compound **4** in dry THF with NaH, subsequent addition of $SiCl_4$, and column chromatography.

Since in the solid state *p*-xylene, a rigid, compact, and ditopic molecule, has been observed to form mononuclear and binuclear inclusion complexes with *p-tert*-butylcalix[4]arene[12] **1** and with the koiland **6**,[15] respectively, we investigated the formation of koilates from compound **5** as the koiland and *p*-xylene as the connector. Crystals suitable for X-ray analysis[18] were obtained from a mixture of compound **5** and *p*-xylene in excess and 2-propanol at room temperature. The crystals (space group $P\bar{1}$) are composed exclusively of **5** and *p*-xylene disposed in an alternate fashion. Both the connector and the koiland are centrosymmetric, and the latter offers two diametrically opposing cavities. The coordination geometry around the silicon atoms is tetrahedral with an average Si–O distance of 1.60 Å and an average O-Si-O angle of 109.4°. As predicted, a linear koilate forms through the interconnection of two cavities belonging to consecutive molecules of koiland **5** through the *p*-xylene molecule (Figure 1). In the crystal one can identify an assembling core, which can be defined as the inclusion of a CH_3 group of the connector within a cavity of **5**. The shortest C–C distance of 3.63 Å between the CH_3 group of the connector and one of the OH-bearing carbon atoms of the koiland at the bottom of the cavity indicates a high degree of inclusion. The formation of the α-network results from a single translation of the assembling core.

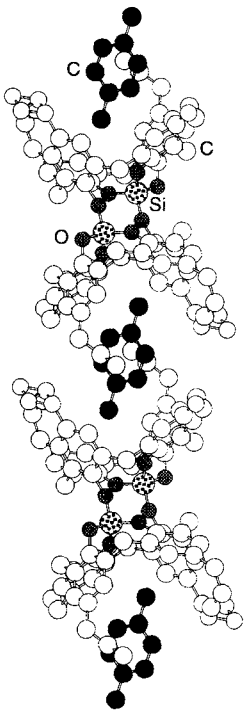

Figure 1. X-ray crystal structure of the koilate formed from compound **5** and *p*-xylene (carbon atoms in black). For clarity the hydrogen atoms are not shown.

Although the formation of the α-network was predicted, the X-ray analysis reveals another unexpected feature. Due to the high degree of rotational freedom of the allyl moieties, one cannot in fact predict their conformations in the crystal lattice. Interestingly, on examination of the lateral packing of consecutive linear koilates, we observed that among the eight allyl groups present in each koiland **5**, two of them are oriented centrosymmetrically in a peculiar manner (Figure 2). Indeed, two alkene moieties belonging to two consecutive koilands are located perfectly parallel to each other at a distance of 4.52 Å. Although this seems somewhat long, the proximity of the two double bonds suggests the possibility of interconnecting the koilates covalently by performing a [2 + 2]cycloaddition reaction in the solid state.

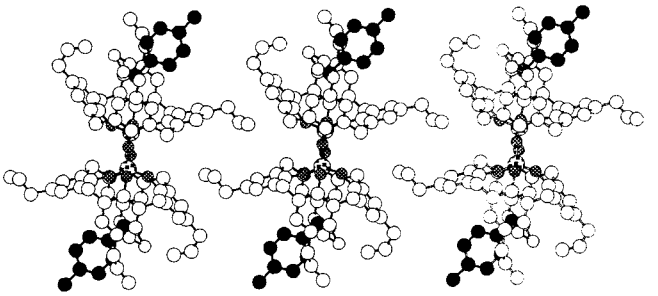

Figure 2. A section of the X-ray crystal structure of the koilate formed from **5** and *p*-xylene. The lateral packing of linear koilates leads to the parallel disposition of the allyl moieties.

In conclusion, the new koiland **5** was synthesized based on the double fusion of two *p*-allylcalix[4]arenes **4** through two silicon atoms. Koiland **5** self-assembles in the presence of *p*-xylene acting as connector to form a linear molecular array called a koilate. The formation of the koilate resulted from the encapsulation of the connector molecules by two cavities belonging to two consecutive koilands **5** and the translation of the inclusion motif.

Experimental Section

A solution of compound **4**[16] (0.42 g, 0.72 mmol) in dry THF (20 mL) was charged with NaH (0.115 g, 4.8 mmol), and the mixture was stirred under Ar for 20 h at 20 °C. $SiCl_4$ (0.1 mL, 0.87 mmol) was added in one portion, and the mixture was stirred at 20 °C for another 3 h. The solvent was removed and the solid thus obtained was purified by chromatography (SiO_2, CH_2Cl_2/hexane, 2/8) to afford **5** (0.23 g, 53%) as a white solid, which was recrystallized from $CHCl_3$/MeOH. M.p. > 300 °C, ^{1}H NMR ($CDCl_3$, 300 MHz, 20 °C): δ = 3.12 (d, $ArCH_2CH$, 4H, J = 6.7 Hz), 3.19 (d, $ArCH_2CH$, 4H, J = 6.7 Hz), 3.30 (d, $ArCH_2CH$, 8H, J = 7.2 Hz), 3.31 (d, $ArCH_2Ar$, 4H, J = 12.9 Hz), 3.37 (d, $ArCH_2Ar$, 4H, J = 13.8 Hz), 4.46 (d, $ArCH_2Ar$, 4H, J = 13.7 Hz), 4.54 (d, $ArCH_2Ar$, 4H, J = 13.4 Hz), 4.94–5.12 (m, CH_2=CH, 16H), 5.74–6.08 (m, CH=CH_2, 8H), 6.73 (s, H-Ar, 4H), 6.87 (s, H-Ar, 8H), 6.92 (d, H-Ar, 4H; J = 2 Hz); ^{13}C NMR ($CDCl_3$, 50.3 MHz, 20 °C): δ = 33.4, 34.2 (CH_2, $ArCH_2Ar$), 39.3, 39.6, 39.7 (CH_2, $ArCH_2CH$), 115.4, 115.7, 115.8 (CH_2, CH_2=CH), 128.4, 128.5 (CH-Ar), 129.7, 129.9 (CH-Ar), 129.4, 130.4, 132.8, 133.7, 134.2, 135.8 (C-Ar), 137.5, 137.7, 137.9 (CH, CH=CH_2), 145.5, 146.7, 148.9 (C-Ar, C–O); ^{29}Si NMR ($CDCl_3$, 79.49 MHz, 20 °C): δ = −112.94; FAB (*m*-nitrobenzyl alcohol matrix): *m/z* (%): 1217.4 (100) [M^+].

Received: February 5, 1997 [Z10080IE]
German version: *Angew. Chem.* **1997**, *109*, 1830–1832

Keywords: calixarenes · koilands · self-assembly · silicon

[1] A. Gavezzotti, *Acc. Chem. Res.* **1994**, *27*, 309.
[2] J. D. Dunitz, *Pure Appl. Chem.* **1991**, *63*, 177.
[3] M. C. Etter, *Acc. Chem. Res.* **1990**, *23*, 120; G. M. Whitesides, J. P. Mathias, T. Seto, *Science* **1991**, *254*, 1312; F. W. Fowler, J. W. Lauher, *J. Am. Chem. Soc.* **1993**, *115*, 5991.
[4] G. R. Desiraju, *Angew. Chem.* **1995**, *107*, 2541; *Angew. Chem. Int. Ed. Engl.* **1995**, *34*, 2311.
[5] M. Simard, D. Su, J. D. Wuest, *J. Am. Chem. Soc.* **1991**, *113*, 4696; X. Delaigue, E. Graf, F. Hajek, M. W. Hosseini, J.-M. Planeix in *Crystallography of Supramolecular Compounds, Vol. C480* (Eds.: G. Tsoucaris, J. L. Atwood, J. Lipkowski), Kluwer, Dordrecht, The Netherlands, **1996**, pp. 159–180; G. Brand, M. W. Hosseini, O. Félix, P. Schaeffer, R. Ruppert in *Magnetism a Supramolecular Function, Vol. C484* (Ed.: O. Kahn), Kluwer, Dordrecht, The Netherlands, **1996**, pp. 129–142.
[6] J. S., Lindsey, *New J. Chem.* **1991**, *15*, 153; D. S. Lawrence, T. Jiang, M. Levett, *Chem. Rev.* **1995**, *95*, 2229; D. Philp, J. F. Stoddart, *Angew. Chem.* **1996**, *108*, 1242; *Angew. Chem. Int. Ed. Engl.* **1996**, *35*, 1155.
[7] J.-M. Lehn, *Supramolecular Chemistry, Concepts and Perspectives*, VCH, Weinheim, **1995**.

 © WILEY-VCH Verlag GmbH, D-69451 Weinheim, 1997 0570-0833/97/3616-1761 $ 17.50+.50/0

[8] C. B. Aakeröy, K. R. Seddon, *Chem. Soc. Rev.* **1993**, *22*, 397; S. Subramanian, M. J. Zaworotko, *Coord. Chem. Rev.* **1994**, *137*, 357, and references therein.
[9] G. Brand, M. W. Hosseini, R. Ruppert, A. De Cian, J. Fischer, N. Kyritsakas, *New J. Chem.* **1995**, *19*, 9; M. W. Hosseini, R. Ruppert, P. Schaeffer, A. De Cian, N. Kyritsakas, J. Fischer, *J. Chem. Soc. Chem. Commun.* **1994**, 2135; M. W. Hosseini, G. Brand, P. Schaeffer, R. Ruppert, A. De Cian, J. Fischer, *Tetrahedron Lett.* **1996**, *37*, 1405; *Angew. Chem.* **1997**, *109*, 83; *Angew. Chem. Int. Ed. Engl.* **1997**, *36*, 102; O. Félix, M. W. Hosseini, A. De Cian, J. Fischer, *Tetrahedron Lett.* **1997**, *38*, 1755, 1933.
[10] X. Delaigue, M. W. Hosseini, A. De Cian, J. Fischer, E. Leize, S. Kieffer, A. Van Dorsselaer, *Tetrahedron Lett.* **1993**, *34*, 3285; X. Delaigue, M. W. Hosseini, E. Leize, S. Kieffer, A. Van Dorsselaer, *ibid.* **1993**, *34*, 7561; X. Delaigue, M. W. Hosseini, R. Graff, J.-P. Kintzinger, J. Raya, *ibid.* **1994**, *35*, 1711.
[11] C. D. Gutsche, *Calixarenes*, The Royal Society of Chemistry, London, **1989**; see also: *Calixarenes. A Versatile Class of Macrocyclic Compounds* (Eds.: J. Vicens, V. Böhmer), Kluwer, Dordrecht, The Netherlands, **1991**; V. Böhmer, *Angew. Chem.* **1995**, *107*, 785; *Angew. Chem. Int. Ed. Engl.* **1995**, *34*, 713.
[12] G. D. Andreetti, R. Ungaro, A. Pochini, *J. Chem. Soc. Chem. Commun.* **1979**, 1005; R. Ungaro, A. Pochini, G. D. Andreetti, P. Domiano, *J. Chem. Soc. Perkin Trans. 2* **1985**, 197; M. Coruzzi, G. D. Andreetti, V. Bocchi, A. Pochini, R. Ungaro, *ibid.* **1982**, 1133; M. Perrin, F. Gharnati, D. Oehler, R. Perrin, S. Lecocq, *J. Incl. Phenom. Mol. Recognit. Chem.* **1992**, *14*, 257.
[13] F. Hajek, E. Graf, M. W. Hosseini, *Tetrahedron Lett.* **1996**, *37*, 1409.
[14] M. M. Olmstead, G. Sigel, H. Hope, X. Xu, P. P. Power, *J. Am. Chem. Soc.* **1985**, *107*, 8087; F. Corazza, C. Floriani, A. Chiesi-Villa, C. Guastini, *J. Chem. Soc. Chem. Commun.* **1990**, 1083; J. L. Atwood, S. G. Bott, C. Jones, C. L. Raston, *ibid.* **1992**, 1349; J. L. Atwood, P. C. Junk, S. M. Lawrence, C. L. Raston, *Supramol. Chem.* **1996**, *7*, 15.
[15] F. Hajek, E. Graf, M. W. Hosseini, X. Delaigue, A. De Cian, J. Fischer, *Tetrahedron Lett.* **1996**, *37*, 1401.
[16] C. D. Gutsche, J. A. Levine, *J. Am. Chem. Soc.* **1982**, *104*, 2653.
[17] C. D. Gutsche, M. Iqbal, *Org. Synth.* **1989**, *68*, 234.
[18] Suitable crystals were obtained from a mixture of **5**, *p*-xylene, and 2-propanol. $C_{88}H_{82}O_8Si_2$: $M = 1323.8$, triclinic, space group $P\bar{1}$, $a = 12.0928(5)$, $b = 12.3615(7)$, $c = 14.0623(8)$ Å; $\alpha = 114.8(3)$, $\beta = 107.8(2)$, $\gamma = 91.5(3)°$, $Z = 2$, $\rho_{calc} = 1.23\ g\,cm^{-3}$, $\lambda(Mo_{K\alpha})$, 0.7107 Å (graphite monochromator). $R(F) = 0.051$. 3630 reflections with $I > 3\sigma(I)$ were used. The data were collected at 21 °C using a Enraf-Nonius-CAD4 automatic diffractometer and analyzed using the Enraf-Nonius SDP/VAX package. The structure was solved by direct methods. Crystallographic data (excluding structure factors) for the structure reported in this paper have been deposited with the Cambridge Crystallographic Data Centre as supplmentary publication no. CCDC-100399. Copies of the data can be obtained free of charge on application to the Director, CCDC, 12 Union Road, Cambridge CB21EZ, UK (fax: Int. code +(1223)336-033; e-mail: deposit@chemcrys.cam.ac.uk).

Evidence for Directed Metalation: A Structural Intermediate in the Formation of a Novel C-bound Adenine Complex of Ruthenium**

Clayton Price, Mark R. J. Elsegood, William Clegg, Nicholas H. Rees, and Andrew Houlton*

The interaction of metal ions with purine and pyrimidine nucleobases is a central theme of bioinorganic chemistry.[1-3] A key objective in this field has been to establish the preferred binding sites for the different bases and these are now generally acknowledged as the endocyclic N^7 and N^1 atoms of N^9-substituted purines and the N^3 atom and the oxygen donors of N^1-blocked pyrimidines,[1, 2] sites which are all involved in hydrogen bonding interactions in the formation of base-pairs, -triples, and -quartets.

Our interest in this area is in the design of novel metalated nucleobases, in particular, those which retain the ability for base-pairing. Such compounds may, ultimately, be used as building blocks for the assembly of supramolecular structures through interactions analogous to those seen in nucleic acid chemistry.[4] Our strategy towards this has been to develop the concept of *directed metalation*.[5] With this approach the ribose group of a nucleoside is, effectively, replaced by a multidentate chelating group forming a nucleobase–ligand conjugate[6] (Scheme 1).

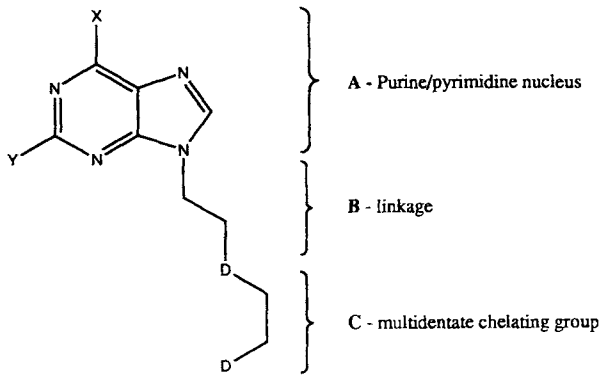

Scheme 1. Generalized structure of a nucleobase–ligand conjugate. X and Y = NH_2, =O or H. D = donor atom. For 9-[2-(2-aminoethylamino)ethyl]adenine (L), X = NH_2, Y = H; D = NH (NH_2).

With such a method each of the components, **A**, **B**, and **C**, can be varied allowing an extensive range of conjugates to be designed. It is anticipated that novel metalation reactions will result due to initial coordination through the multidentate chelating group **C**. Such chelation would then impose restrictions on the sites at which the metal ion could bind to the nucleobase. Here we report the synthesis and crystal structures of two ruthenium complexes of the adenine derivative L, which contains an ethylenediamine unit bound through an ethyl group to the nucleobase (see Scheme 1, D = NH (NH_2), X = NH_2, Y = H). These illustrate this concept and highlight the novel chemistry that may result with an unique example of a C-bound complex of a purine nucleobase.

Reaction of $[(dmso)_2H][RuCl_4(dmso)_2]$ (dmso = dimethyl sulfoxide) with L·HCl in methanol at reflux yields, after purification by column chromatography, two main products, **1a** and **1b** (Scheme 2). Monitoring the reaction by UV/Vis

$[RuCl_2(LH)(dmso)_2]Cl\cdot 4.5H_2O$ **1a**·4.5 H_2O

$[RuCl_2(L)(dmso)]\cdot H_2O$ **1b**·H_2O

spectroscopy and thin-layer chromatography confirmed the initial formation of **1a** followed by **1b**. Furthermore, refluxing a sample of **1a** in methanol leads to the formation of **1b**. Crystallization from saturated solutions in methanol in the case of **1a**, and water for **1b**, furnished single crystals which were analyzed by X-ray crystallography.[7]

Compound **1a** crystallizes with two independent molecules in the unit cell with similar metrical features (Figure 1). The metal ion is formally Ru^{II} and adopts an octahedral geometry with a donor set comprising {2Cl:2N:2S}. The nucleobase–ligand

[*] Dr. A. Houlton, C. Price, Dr. M. R. J. Elsegood, Prof. W. Clegg, Dr. N. H. Rees
Department of Chemistry
University of Newcastle upon Tyne
Newcastle upon Tyne, NE1 7RU (UK)
Fax: Int. code +(191)222 6929
e-mail: andrew.houlton@newcastle.ac.uk

[**] This work was financially supported by the University of Newcastle Research Development Fund, the Nuffield Foundation, and the Engineering and Physical Sciences Research Council. Johnson Matthey p.l.c. are thanked for the generous loan of metal salts.

 © WILEY-VCH Verlag GmbH, D-69451 Weinheim, 1997 0570-0833/97/3616-1762 $ 17.50+.50/0

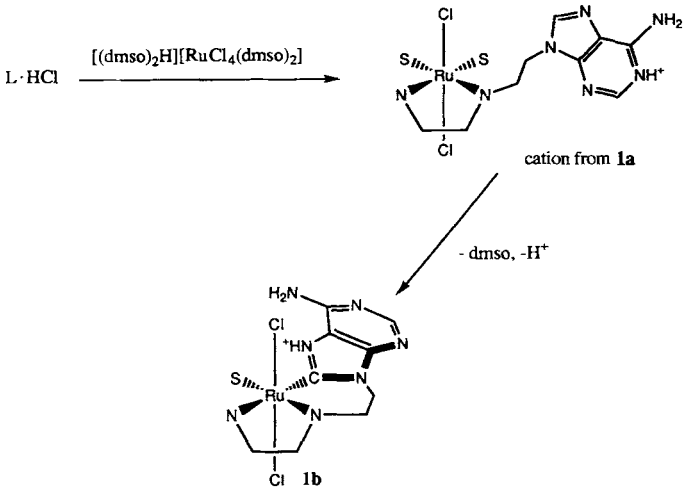

Scheme 2. Proposed reaction scheme for the formation of **1a** and **1b**. S = sulfur-bound dmso.

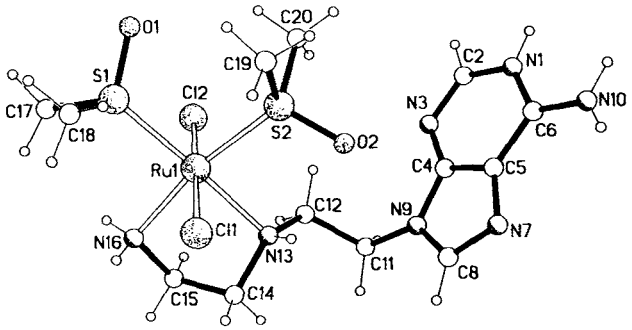

Figure 1. Molecular structure and atom labeling of the $[RuCl_2(LH)(dmso)_2]^+$ ion from **1a**. The pendant adenine lies at an angle of $\approx 65°$ to the equatorial coordination plane. Only one of the independent molecules is shown. Bond lengths [Å] around the metal, averaged over the two independent molecules, are Ru–Cl1 2.422(1), Ru–Cl2 2.415(1), Ru–N13 2.170(4), Ru–N16 2.139(4), Ru–S1 2.229(1), Ru–S2 2.237(1).

conjugate L is bound through the ethylenediamine group, leaving the adenine moiety pendant and at an average angle of $\approx 65°$ to the {2N:2S} coordination plane of the molecule. The adenine group is protonated at N^1 and participates in a variety of hydrogen bonding interactions.

In **1b** the ruthenium is similarly divalent with an octahedral coordination geometry (Figure 2). Here, however, the donor set is {2Cl:2N:S:C} with L binding in a meridional tridentate manner through the ethylenediamine group and the C^8atom of the adenine moiety. This binding mode results in five- and six-membered chelate ring formation. The adenine moiety is protonated at N^7 generating an ylide-type structure which maintains overall charge neutrality on the group.

A search of the Cambridge Crystallographic Data Base found no previous examples of $Ru-C_{(adenine)}$ complexes. A wider search for examples of purine-containing ruthenium complexes revealed a variety of binding modes; monodentate at N^7 (ethylguanine),[8] bidentate through N^7 and S^6 (mercaptopurine),[9] bridging through N^7 and N^9 (adenine),[10] and monodentate at C^8 in $[RuCl_2(NH_3)_3(caffeine)]Cl$.[11] For caffeine, N^1, N^3, and N^7 are methylated, discounting them as binding sites, while the N^3-methyl group also presents considerable steric hindrance to the large ruthenium-ammine electrophile attacking at N^9.[11, 12] *It is reasonable to assume that in this case the C^8 position* of caffeine is effectively the only available metal binding site.

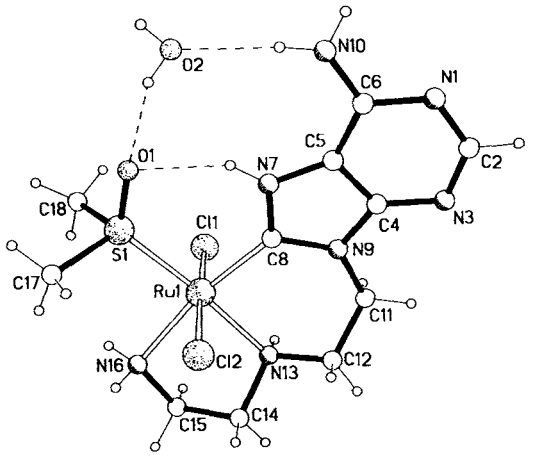

Figure 2. Molecular structure of **1b**·H_2O highlighting the five- and six-membered chelate rings. Bond lengths [Å] around the metal are Ru–Cl1 2.4181(9), Ru–Cl2 2.4209(9), Ru–S1 2.2102(9), Ru–C8 1.989(3), Ru–N16 2.208(3), Ru–N13 2.140(3).

Furthermore, despite the higher formal oxidation state of the metal, the M–C bond length is longer (2.03(1) Å) in $[RuCl_2(NH_3)_3(caffeine)]Cl$ than in **1b** (1.989(3) Å). Additional comparison can be made with the imidazolium-ylide complex *trans*-$[Ru(NH_3)_3CO(4,5\text{-dimethylimidazolium})]^{2+}$[13] which features binding analogous to that for **1b**. In this case too the Ru–C bond length is longer (2.128(4) Å). It is suggested, then, that both the metalation at C^8 and the short Ru–C bond length observed in **1b** reflect the chelating nature of ligand L and do not represent the intrinsic reactivity of adenine towards Ru^{II}.

In conclusion, the two complexes reported here highlight the role of the tethered chelating group in modifying the reactivity of nucleobases towards metal ions. The isolation of **1a** provides evidence for the principle of directed metalation and, indeed, is an intermediate in the formation of **1b**. This latter compound is the first complex to contain a C^8-metalated adenine and extends the emerging class of organometallic nucleobase derivatives that contain metal–carbon bonds derived from biomolecules,[14–16] structurally characterized examples of which, to date, have been based solely on pyrimidines.

Experimental Section

1a and **1b**: An equimolar mixture of L·HCl [5] and $[dmso_2H][trans\text{-}RuCl_4(dmso)_2]$ [17] was heated at reflux in methanol for 16 h. The reaction mixture was concentrated under reduced pressure and the crude material loaded onto a silica column. The column was eluted with methanol to give two main products **1a** (7%) and **1b** (46%) as orange and red solids, respectively. **1a**: M.p. >250 °C. UV/Vis (H_2O): λ [nm] (ε [$M^{-1}cm^{-1}$]) = 260 (8390), 300 (1160); MS: *m/z* (%): 586 (100); ^1H NMR (500 MHz, $(CD_3)_2SO$): δ = 8.20 (s, H2), 8.23 (s, H8), 7.28 (s, H10), 4.58 (ddd, H11) 4.48 (m, H11'), 3.91 (m, H12) 3.33 (m, H12') 4.48 (m, H13), 3.13 (m, H14), 2.64 (m, H14'), 2.93 (m, H15) 2.88 (m, H15') 4.47 (m, H16), 4.38 (m, H16') 3.16, 3.19, 3.22, 3.24 (s, H17–H20); ^{13}C NMR (125 MHz, $(CD_3)_2SO$): δ = 152.4 (C2), 155.8, 149.9, 118.6 (C4-C6), 140.9 (C8), 41.2 (C11), 50.6 (C12), 48.9 (C14), 42.3 (C15), 43.7, 44.0, 45.1, 45.7 (C17-C20). Crystals of **1a** suitable for single-crystal X-ray structure analysis were obtained from a saturated solution of methanol. C,H,N anal. calcd. for $C_{11}H_{28}Cl_2N_7O_2RuS$: C 26.65, H 4.82, N 16.73; found: C 27.99, H 4.73, N 16.10.

1b: M.p. >250 °C. UV/Vis (H_2O): λ [nm] (ε [$M^{-1}cm^{-1}$]) = 248 (9900), 318 (11400), 392 (350); MS *m/z* (%): 470 (100); ^1H NMR (500 MHz, $(CD_3)_2SO$): δ = 8.17 (s, H2), 13.24 (s, H7), 7.33 (s, H10), 5.03 (m, H11) 4.08 (ddd, H11'), 3.47 (m, H12) 3.36 (m, H12') 4.97 (m, H13), 3.09 (m, H14), 2.96 (m, H14'), 3.09 (m, H15), 2.65 (m, H15') 4.48 (dd, H16), 3.51 (m, H16') 3.36, 3.31 (s, H17, H18); ^{13}C NMR (125 MHz, $(CD_3)_2SO$): δ = 150.8 (C2), 151.2, 146.9, 109.5 (C4, C5, C6), 204.9 (C8), 54.4 (C11), 48.7 (C12), 52.3 (C14), 41.2 (C15), 47.5, 45.9 (C17, C18). Crystals of **1b** suitable for single-crystal X-ray structure analysis were obtained from a solution in water. C,H,N anal. calcd. for $C_{11}H_{23}Cl_2N_7O_2RuS$: C 27.00, H 4.74, N 20.03; found: C 26.79, H 4.57, N 19.79.

Received: February 28, 1997 [Z10178IE]
German version: *Angew. Chem.* **1997**, *109*, 1823–1825

 © WILEY-VCH Verlag GmbH, D-69451 Weinheim, 1997 0570-0833/97/3616-1763 $ 17.50+.50/0

Keywords: adenine · bioinorganic chemistry · N ligands · nucleobases · ruthenium

[1] *Metal Ions in Biological Systems, Vol. 32*, (Eds.: A. Sigel, H. Sigel), Marcel Dekker, New York, **1996**.

[2] B. Lippert, *Prog. Inorg. Chem.* **1989**, *37*, 1–97.

[3] S. E. Sherman, S. J. Lippard, *Chem. Rev.* **1987**, *87*, 1153–1181.

[4] *Nucleic Acids in Chemistry and Biology*, (Eds.: G. M. Blackburn, M. J. Gait), IRL Press, Oxford, **1990**.

[5] C. Price, M. R. J. Elsegood, W. Clegg, A. Houlton, *J. Chem. Soc. Chem. Commun.* **1995**, 2285–2286.

[6] Metal complexes derived from nucleobase–ligand conjugates have been prepared by ourselves and other workers; however, in these cases metal–nucleobase binding is precluded. See for example U. Koert, M. M. Harding, J.-M. Lehn, *Nature* **1990**, 346, 339–341; J. L. Sessler, C. T. Brown, R. Wang, *Inorg. Chim. Acta* **1996**, 251, 135–140; E. C. Constable, R.-A. Fallahpour, *J. Chem. Soc. Dalton Trans.* **1996**, 2389–2390; C. Price, M. Aslanglu, C. J. Isaac, M. R. J. Elsegood, W. Clegg, B. R. Horrocks, A. Houlton, *ibid.* **1996**, 4115–4120.

[7] **1a**·4.5H_2O: $C_{13}H_{28}Cl_3N_7O_2RuS_2 \cdot 4.5H_2O$, $M_r = 667.04$, crystal dimensions $0.30 \times 0.29 \times 0.06$ mm^3, triclinic, $P\bar{1}$, $a = 12.7288(11)$, $b = 14.7164(12)$, $c = 16.2058(14)$ Å, $\alpha = 93.525(2)$, $\beta = 111.256(2)$, $\gamma = 110.651(2)°$, $V = 2584.2(4)$ Å^3, $Z = 4$, $\rho_{calcd} = 1.714$ g cm^{-3}, $Mo_{K\alpha}$ ($\lambda = 0.71073$ Å), $T = 160$ K, $\mu = 1.124$ mm^{-1}. 20192 (11193 unique, $2\theta < 55°$, $R_{int} = 0.0302$) data were collected on a Siemens SMART CCD area detector diffractometer using narrow frames (0.3° steps in ω) and the absorption effects were corrected semiempirically (transmission: 0.644–0.801). The structure was solved by Patterson synthesis and refined by full-matrix least-squares on F^2 values for all data (G. M. Sheldrick, SHELXTL manual, Siemens Analytical X-Ray Instruments, Madison, WI, **1994**, version 5) to give $wR = \{\sum[w(F_o^2 - F_c^2)^2]/\sum[w(F_o^2)^2]\}^{1/2} = 0.1250$, conventional $R = 0.0525$ for F values of 8541 reflections with $F_o^2 > 2\sigma(F_o^2)$, $S = 1.055$ for 661 parameters. The asymmetric unit contains two complex cations, two chloride ions, and approximately nine molecules of water some of these disordered. All non-H atoms were refined anisotropically. Hydrogen atom coordinates were refined for N-H atoms, riding for C-H atoms, and not included for O-H; a riding model was used for all U_{iso}(H). The residual electron density extremes were 1.09 and -0.93 e Å^{-3}. **1b**·H_2O: $C_{11}H_{21}Cl_2N_7ORuS.H_2O$, $M_r = 489.39$, crystal dimensions $0.22 \times 0.17 \times 0.04$, monoclinic, $P2_1/c$, $a = 9.2067(6)$, $b = 17.1639(11)$, $c = 12.0162(8)$ Å, $\beta = 105.421(2)°$, $V = 1830.5(2)$ Å^3, $Z = 4$, $\rho_{calcd} = 1.776$ g cm^{-3}, $\mu = 1.283$ mm^{-1}; 11279 (4148 unique, $2\theta < 55°$, $R_{int} = 0.0356$) data, transmission: 0.815–0.962. The structure was solved by direct methods. $wR = 0.0991$, $R = 0.0382$ (3295 F values), $S = 1.117$ for 232 parameters. Coordinates of H atoms on N7, N10, and O2 were freely refined, all others were riding. Crystallographic data (excluding structure factors) for the structures reported in this paper have been deposited with the Cambridge Crystallographic Data Centre as supplementary publication no. CCDC-100265. Copies of the data can be obtained free of charge on application to The Director, CCDC, 12 Union Road, Cambridge, CB2 1EZ, UK (fax: int. code +(1223)336-033; e-mail: deposit@chemcrys.cam.ac.uk).

[8] W. S. Sheldrick, S. Heeb, *Inorg. Chim. Acta* **1990**, *168*, 93–100; P. M. Van Vliet, J. G. Haasnoot, J. Reedijk, *Inorg. Chem.* **1994**, *33*, 1934–1939.

[9] W. S. Sheldrick, H. S. Hagen-Eckhard, S. Heeb, *Inorg. Chim. Acta* **1993**, *206*, 15–21.

[10] R. Cini, A. Cinquantini, M. Sabat, L. G. Marzilli, *Inorg. Chem.* **1985**, *24*, 3903–3908; R. Cini, R. Bozzi, A. Karaulov, M. B. Hursthouse, A. M. Calafat, L. G. Marzilli, *J. Chem. Soc., Chem. Commun.* **1993**, 899–901.

[11] H. J. Krentzien, M. J. Clarke, H. Taube, *Bioinorg. Chem.* **1975**, *4*, 143–151.

[12] M. J. Clarke, H. Taube, *J. Am. Chem. Soc.* **1975**, *97*, 1397-1403.

[13] R. J. Sundberg, R. F. Bryan, I. F. Taylor, Jr., H. Taube, *J. Am. Chem. Soc.* **1974**, *96*, 381–392.

[14] H. Schöllhorn, U. Thewalt, B. Lippert, *J. Chem. Soc. Chem. Commun.* **1986**, 258–260.

[15] M. Hopp, A. Erxleben, I. Rombeck, B. Lippert, *Inorg. Chem.* **1996**, *35*, 397–403.

[16] F. Zamora, M. Sabat, B. Lippert, *Inorg. Chem.* **1996**, *35*, 4858–4864.

[17] E. Alessio, G. Balducci, M. Calligaris, G. Costa, W. M. Attia, G. Mestroni, *Inorg. Chem.* **1991**, *30*, 609–618.

Synthesis of Enantiomerically and Diastereomerically Pure Cyclopentanols by Asymmetric Cyclocarbolithiation of 5-Alkenyl Carbamates**

Michael J. Woltering, Roland Fröhlich, and Dieter Hoppe*

Dedicated to Professor Hans J. Schäfer on the occasion of his 60th birthday

The intramolecular carbolithiation of 5-alkenyllithium compounds has become an important alternative to cyclizations of 5-alkenyl radicals (Scheme 1) due to the high 5-*exo-trig* selectivity and the facility of further functionalization of the resulting cyclopentylmethyl anion. Recently Marek, Normant et al. described an asymmetric variant of an intermolecular carbolithiation with cinnamyl alkoxides. Enantiofacial differentiation at the attacked double bond is achieved by the (−)-sparteine-mediated addition of non-stereogenic alkyllithium compounds.[3] However, the known methods do not allow control of the absolute configuration of the attacking nucleophilic carbon center. On the other hand, a wide variety of (*S*)-configurated (α-carbamoyloxy)alkyllithium derivatives are accessible by (−)-sparteine-mediated deprotonation.[4] Despite the presence of the reactive styrene moiety, we supposed that 6-phenyl-5-hexenyl carbamates would be lithiated regioselectively at the 1-position and then undergo stereoselective nucleophilic cycloalkylation to form the appropriate cyclopentanol derivatives.

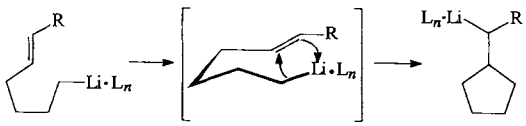

Scheme 1. Intramolecular 5-*exo-trig*-carbolithiation [1, 2]. R = H or electron-withdrawing group; L = OEt_2.

Precursors **1a** and **1b** were prepared by Wittig olefination.[5, 6] They were deprotonated with *sec*-butyllithium/(−)-sparteine (**6**) in diethyl ether at −78 °C, the reaction mixture was stirred for 20 to 30 h at this temperature, and water or an electrophilic reagent was subsequently added (Scheme 2). With exception of the carboxylic acid ester **5g**, the diastereomerically and enantiomerically pure cyclization products **5** were obtained (Table 1). Decarbamoylation of **5a** provided (1*R*,2*S*)-2-benzylcyclopentanol;[11] the collected data correspond well to that in reference [12].

Substitution at the carbamate proceeds, as expected, with retention of configuration at the carbanionic center. The cyclization shows complete 5-*exo-trig* selectivity and leads with high diastereoselectivity to the *trans*-substituted cyclopentane **5** via intermediate **4**. Electrophilic attack at the benzylic carbanionic center also proceeds with high diastereoselectivity. The absolute configuration [1*R*,2*S*,2(1*S*)] was determined from the X-ray crystal structure of diol **8**, which was generated from **5e**

[*] Prof. Dr. D. Hoppe, Dipl.-Chem. M. J. Woltering, Dr. R. Fröhlich[+]
Organisch-Chemisches Institut der Universität
Corrensstrasse 40, D-48149 Münster (Germany)
Fax: Int. code +(251)833-9772

[+] X-ray crystal structure determination

[**] This work was supported by the Deutsche Forschungsgemeinschaft and the Fonds der Chemischen Industrie.

 © WILEY-VCH Verlag GmbH, D-69451 Weinheim, 1997 0570-0833/97/3616-1764 $ 17.50+.50/0

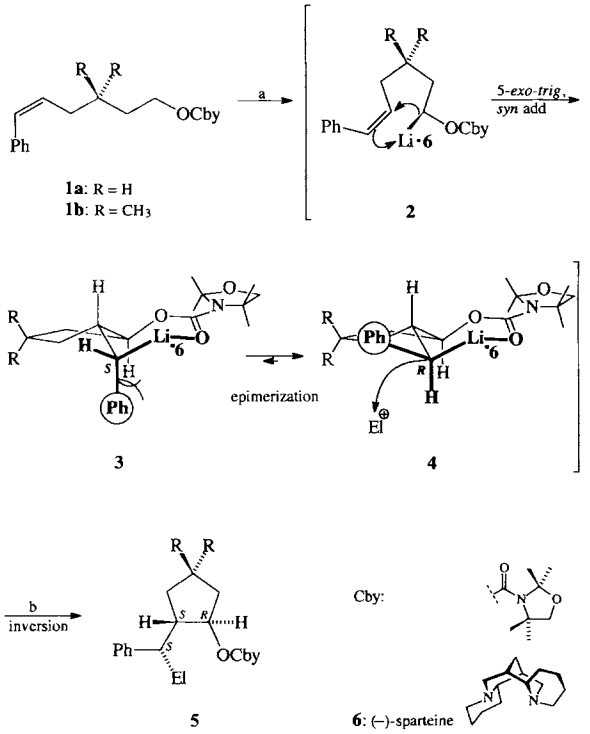

Scheme 2. Cyclocarbolithiation of **1** and scavenging reaction. a) *s*BuLi (1.5 equiv)/(–)-sparteine (**6**), Et_2O, –78 °C, 20–30 h; b) EIX, –78 °C → RT.

Table 1. Synthesis of cyclopentanol derivatives **5**.

Reagent	*t*[h]	EIX	Product[a]	Yield[%]	$[\alpha]_D^{20}$[b]	d.r.[f]
1a	20	HOH	**5a**	30	–20.9	>98:2
1a	26	Me_3SiCl	**5b**	32	–66.2	>98:2
1a	4	Bu_3SnCl	**5c**	14	–80.7	>98:2
1a	23	Me_3SnCl	**5d**[c]	17	–[g]	>98:2
1a	24	$PhMe_2SiCl$	**5e**	38	–79.7	>98:2
1b	23	HOH	**5f**	51	–29.0	>98:2
1b	23	CO_2	**5g**[d]	43	+19.2	92:8
1b	24	Bu_3SnCl	**5h**	30	–79.4	>98:2
1b	26	Me_3SiCl	**5i**[e]	38	–[g]	>98:2
1b	24	$PhMe_2SiCl$	**5j**	48	–59.4	>98:2

[a] Correct elemental analyses were obtained for all isolated products (C ±0.32, H ±0.26, N ±0.35 %). [b] $c = 0.96–1.01$ in CH_2Cl_2. [c] Mixture with **5a**. [d] Isolated as the methyl ester. [e] Mixture with **1b** and **5f**. [f] Determined by gas chromatography and ^1H NMR spectroscopy. [g] Not determined.

by deprotection of the hydroxy group and subsequent hydroxydesilylation (Scheme 3).[13, 14]

As stannylation, silylation, and carbonylation of several benzyllithium compounds occur with inversion of the configuration,[15–18] this can also be expected in our case. Therefore, the lithiated precursor **4** should have 2(1*R*) configuration. Since *syn* addition to the *cis* double bond leads to the primary adduct **3** with 2(1*S*) configuration, subsequent epimerization at the benzylic center is highly probable. The resulting epimer **4** is presumably thermodynamically more stable due to the equatorial position of the phenyl substituent within the bicyclic chelate. This is supported by the fact that the sequences of reactions starting from (*E*)-**1a**,**b** lead to the same diastereomers.

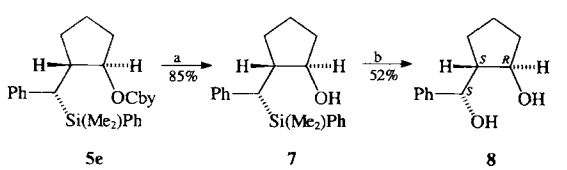

Scheme 3. Conversion of **5e** into diol **8**. a) $MeSO_3H$ (4 equiv), MeOH, reflux, 3 h, then K_2CO_3 (8 equiv), reflux, 20 h. b) $HBF_4 \cdot OEt_2$ (2 equiv), CH_2Cl_2, 0 °C, 10 min, then KF (2 equiv), $KHCO_3$ (10 equiv), 30% H_2O_2 (11 equiv), THF/MeOH, RT, 4.5 h.

The method described here allows the stereoselective formation of two C–C bonds and, therefore, three vicinal stereocenters of defined absolute configuration. The method might be interesting for the synthesis of cyclopentanoid natural products.[19]

Experimental Section

General procedure for cyclocarbolithiation: To **1a** or **1b** (0.5 mmol) and (–)-sparteine (0.75 mmol) in diethyl ether (3 mL) was added *s*BuLi (0.75 mmol) in cyclohexane/hexane at –78 °C, and the solution stirred for 20 to 30 h at –78 °C. The electrophile (0.75 mmol) was then added, and the reaction mixture warmed to room temperature over night. Water (3 mL) was added, the layers were separated, and the aqueous phase was extracted three times with ether. The combined organic fractions were dried over $MgSO_4$, the salts were filtered off, and the solvent removed from the filtrate in vacuo. The crude product was purified by flash chromatography on silica gel with ether/pentane.

Received: February 26, 1997 [Z 10161 IE]
German version: *Angew. Chem.* **1997**, *109*, 1804–1805

Keywords: asymmetric synthesis · carbanions · carbolithiations · cyclopentanols · (–)-sparteine

[1] Reviews: a) R. L. Subramanian, *Methoden Org. Chem. (Houben-Weyl), 4th ed. 1952–*, Vol. E19d, **1993**, pp. 744–754; b) P. Knochel in *Comprehensive Organic Synthesis, Vol. 4* (Eds.: B. M. Trost, I. Fleming), Pergamon, New York, **1991**, p. 865; c) J.-F. Normant, *Chemtracts: Org. Chem.* **1994**, *7*, 59–73.

[2] a) V. N. Drozd, U. A. Ustynyuk, M. A. Tsel'eva, L. B. Dmitriev, *J. Gen. Chem. USSR* **1968**, *38*, 2047; *Zh. Obsch. Khim.* **1968**, *38*, 2144; b) W. F. Bailey, T. T. Nurmi, J. J. Patricia, W. Wang, *J. Am. Chem. Soc.* **1987**, *109*, 2442–2448; c) W. F. Bailey, K. V. Gavaskar, *Tetrahedron* **1994**, *50*, 5957–5970, and references therein; d) A. Krief, J. Bousbaa, *Synlett* **1996**, 1007–1009, and references therein.

[3] S. Klein, I. Marek, J.-F. Poisson, J.-F. Normant, *J. Am. Chem. Soc.* **1995**, *117*, 8853–8854.

[4] a) D. Hoppe, F. Hintze, P. Tebben, *Angew. Chem.* **1990**, *102*, 1457–1459; *Angew. Chem. Int. Ed. Eng.* **1990**, *29*, 1422–1423; b) short review: D. Hoppe, F. Hintze, P. Tebben, M. Paetow, H. Ahrens, J. Schwerdtfeger, P. Sommerfeld, J. Haller, W. Guarnieri, S. Kolczewski, T. Hense, I. Hoppe. *Pure Appl. Chem.* **1994**, *66*, 1479–1486.

[5] Synthesis of **1a** from $Br(CH_2)_5OCby$: a) PPh_3 (1.05 equiv), neat, 100 °C, 4 h; phosphonium salt: 95%; b) $NaN(SiMe_3)_2$ (NaHMDS) (1.05 equiv) in THF, RT, then PhCHO (1.0 equiv), –40 °C; **1a**: 87% (*Z*:*E* = 96:4). Synthesis of **1b** from $OHCCH_2C(CH_3)_2(CH_2)_2OCby$: $PhCH_2PPh_3Br$ (1.3 equiv), KO*t*Bu (1.2 equiv), Et_2O, reflux, 1 h, then aldehyde [6], RT, 15 h, **1b**: 81% (*Z*:*E* = 46:54).

[6] L. Fitjer, U. Quabeck, *Synth. Commun.* **1985**, *15*, 855–864.

[7] [1*R*,2*S*,2(1*S*)]-2-[1-(Dimethylphenylsilyl)-1-phenylmethyl]cyclopentyl-2,2,4,4-tetramethyl-1,3-oxazolidin-3-carboxylate (**5e**): $R_f = 0.28$ (petroleum ether/Et_2O, 5/1); $[\alpha]_D^{20} = -79.7$ ($c = 0.97$ in CH_2Cl_2); ^1H NMR (300 MHz, $CDCl_3$): $\delta = 0.08$, 0.32 (s, 6H), 1.26 [1.31] (s, 6H), 1.41 [1.45] (s, 6H), 1.50–1.72, 1.90 (m, 6H), 2.19 (d, $^3J = 11.0$ Hz, 1H), 2.57 (m, 1H), 3.64 (s, 2H), 4.81 (m, 1H), 6.96–7.15 (m, 5H), 7.26–7.44 (m, 5H); ^{13}C NMR (75 MHz, $CDCl_3$): $\delta = -4.2$ (s), –1.9 (s), 25.3 [24.1] (s), 25.3 [26.7] (s), 23.6 (d), 32.0 (d), 32.2 (d), 41.1 (t), 47.2 (t), 59.2 [60.5] (q), 76.4 [76.1] (d), 81.5 (t), 96.1 [94.6] (q), 124.9 (t), 128.1 (t), 128.7 (t), 127.6 (t), 128.9 (t), 134.0 (t), 138.7 (q), 142.7 (q), 152.1 (q); the data of the minor amide *E*/*Z* isomer are given in brackets; IR (film): $\tilde{\nu} = 1685$ cm^{-1} (NC=O); elemental analysis calcd for $C_{28}H_{39}NO_3Si$ (465.709): C 72.21, H 8.44, N 3.01; found: C 72.29, H 8.49, N 3.26.

[8] The crude carboxylic acid was converted into the methyl ester **5g** by treatment with diazomethane. A small amount of the carboxylate presumably epimerizes under the work-up conditions.

[9] The diastereomeric excesses of products **5** were determined by ^1H NMR spectroscopy and gas chromatography to be greater than 98%. After decarbamoylation of **5a** and acetylation of the resulting alcohol, the enantiomeric excess was determined by ^1H NMR shift experiments with tris[3-heptafluoropropylhydroxymethylene)camphorato]europium ([Eu(hfc)$_3$], 21 mol%) in $CDCl_3$ to be greater than 95%.

 © WILEY-VCH Verlag GmbH, D-69451 Weinheim, 1997 0570-0833/97/3616-1765 $ 17.50+.50/0

[10] The by-products of the reactions of **1a** were the corresponding open-chain substitution product and the cyclopropane derivative resulting from intramolecular 1,3-elimination of the carbamate group. Reactions of **1b** delivered the cyclopropane derivative as well as the substrate. Therefore, in case of **1a** the yields are limited either by the rate of cyclization or the unfavorable equilibrium constant, whereas for **1b** the slow deprotonation step plays a crucial role. Other by-products were not identified.
[11] R. Seemayer, M. P. Schneider, *Recl. Trav. Chim. Pays-Bas* **1991**, *110*, 171–174, and references therein.
[12] $[\alpha]_D^{20} = -43.1$ ($c = 1.09$ in MeOH) ($[\alpha]_D^{20} = -46.8$ ($c = 1.10$ in MeOH)[11]).
[13] a) K. Tamao, N. Ishida, T. Tanaka, M. Kumuda, *Organometallics* **1983**, *2*, 1694–1696; b) K. Tamao, T. Tanaka, T. Nakajima, R. Sumiya, H. Arai, Y. Ito, *Tetrahedron Lett.* **1986**, *27*, 3370–3380; c) W. Bernhard, I. Fleming, D. Waterson, *J. Chem. Soc. Chem. Commun.* **1984**, 28–29; d) I. Fleming, R. Henning, D. C. Parker, H. E. Plaut, P. E. J. Sanderson, *J. Chem. Soc. Perkin Trans. 1* **1995**, 317–337; e) Y. Matsumoto, T. Hayashi, Y. Ito, *Tetrahedron* **1994**, *50*, 335–346, and references therein.
[14] Crystallographic data (excluding structure factors) for the structures reported in this paper have been deposited with the Cambridge Crystallographic Data Centre as supplementary publication no. CCDC-100367. Copies of the data can be obtained free of charge on application to The Director, CCDC, 12 Union Road, Cambridge CB21EZ, UK (fax: int. code +(1223)336-033; e-mail: deposit@chemcrys.cam.ac.uk).
[15] a) D. Hoppe, A. Carstens, T. Krämer, *Angew. Chem.* **1990**, *102*, 1455–1456; *Angew. Chem. Int. Ed. Eng.* **1990**, *29*, 1424–1425; b) C. Derwing, D. Hoppe, *Synthesis* **1996**, 149–154.
[16] However, protonations occur under retention of configuration [15, 17]. Therefore, for El = H the other benzylic epimer must be generated. As this is not of any significance for the examples described in here, the structure of *1'-epi-5* is not shown.
[17] F. Hammerschmidt, A. Hanninger, *Chem. Ber.* **1995**, *128*, 1069–1077.
[18] P. Beak, A. Basu, D. J. Gallagher, Y. S. Park, S. Thayumanavan, *Acc. Chem. Res.* **1996**, *29*, 552–560.
[19] L. A. Paquette, *Top. Curr. Chem.* **1984**, *119*, 1–158.

Activation of Ti–F Bonds in $[\{(C_5Me_5)TiOF\}_4]$ and $[\{(C_5Me_4Et)TiOF\}_4]$ with $AlMe_3$

Peihua Yu, Herbert W. Roesky,* Alojz Demsar, Thomas Albers, Hans-Georg Schmidt, and Mathias Noltemeyer

Dedicated to Professor Roald Hoffmann on the occasion of his 60th birthday

Substitution reactions proceed according to an S_N1 or S_N2 mechanism. For sterically shielded centers only an S_N1 mechanism is possible. It is assumed that in the latter the exit of the nucleophile can be electrophilically supported. This markedly facilitates the dissociation. Thus, C–F,[1] Si–F,[2] or P–F activations[3] have mainly been described with alkali metal and alkaline earth metal ions. Metallocenes of group 4 have been particularly intensively investigated in the last few years.[4, 5] Herein we report on the first step of a reaction of titanium fluoride oxide with $AlMe_3$.

As starting materials we chose the compounds $[\{(C_5Me_5)TiOF\}_4]$ (**1**) and $[\{(C_5Me_4Et)TiOF\}_4]$ (**2**),[6, 7] which each contain only one fluorine atom bound to each metal center. Compounds **1** and **2** were prepared by metathesis reactions from the corresponding chloride derivatives with Me_3SnF. When **1** and **2** are each allowed to react with four equivalents of $AlMe_3$ in toluene and hexane (1:1) at −10 °C, an immediate color change takes place from yellow to bright red. The solutions were stored at −20 °C, which led to red crystals of **3** and orange crystals of **4**, respectively. In the case of **4**, an intermediate is initially obtained (**4a**), which rearranges under dissociation to give **4** (Scheme 1). Both the color of the solution and that of the crystals is an indicator for the Ti–F activation in **3** and **4**.

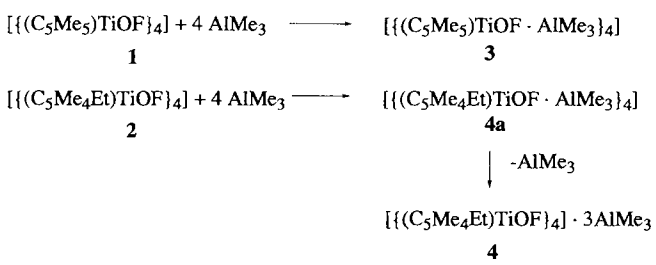

Scheme 1.

The thermal decompositions of **3** and **4** do not afford $[\{(C_5Me_5)TiOMe\}_4]$ and $[\{(C_5Me_4Et)TiOMe\}_4]$, respectively. These compounds are only obtained when a slight excess of $AlMe_3$ is used.[8] Moreover, $(FAlMe_2)_3$ is formed. NMR and mass spectra reveal that the decomposition of **3** and **4** leads to mixtures of products containing fluorine atoms and methyl groups (MS: *m/z* 845 $[(C_5Me_5)_4Ti_4O_4FMe_2]$ and 901 $[(C_5Me_4Et)_4Ti_4O_4FMe_2]$). This confirms the lability of **3** and **4**.

The structure of **3** is shown in Figure 1. The four oxygen atoms and the four titanium atoms in this compound lie almost

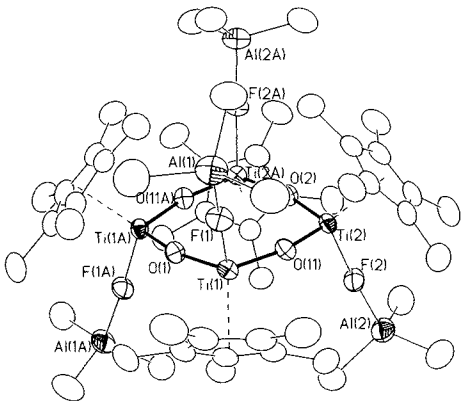

Figure 1. Crystal structure of **3**·3 toluene. Selected bond lengths [Å] and angles [°]: Ti(1)–F(1) 1.9593(13), Ti(2)–F(2) 1.9728(13), F(1)–Al(1) 1.8960(14), F(2)–Al(2) 1.8894(14), Ti(1)–O(1) 1.8282(7), Ti(1)–O(11) 1.8330(15), Ti(2)–O(11) 1.8245(15), Ti(2)–O(2) 1.8292(7); O(1)-Ti(1)-O(11) 105.24(8), O(1)-Ti(1)-F(1) 103.11(5), Ti(2)-O(11)-Ti(1) 164.67(9), Al(1)-F(1)-Ti(1) 175.90(8), Al(2)-F(2)-Ti(2) 175.62(8). The solvent molecules are not shown.

in a plane (deviation 0.02 Å). As expected the Ti–F bond lengths in **3** (av 1.965 Å) are considerably longer than those in the starting material[6] (av Ti–F 1.845 Å). Furthermore, the Ti-F-Al bond lengths (Ti–F 1.959, Al–F 1.896 Å) can be compared with the corresponding distances in $[\{(C_5H_4Me)_2TiF_2\}_3Al]$[9] (Ti–F 2.095, Al–F 1.812 Å).[10] These comparisons of the bond lengths clearly indicate that the coordinating effect of $AlMe_3$ leads to the extension of the Ti–F bonds. Moreover, the Al-F-Ti bonds are nearly linear (av 175.7°). The single-crystal structure analysis of **4** (Figure 2) shows that only three fluorine

[*] Prof. Dr. H. W. Roesky, P. Yu, Dr. A. Demsar, T. Albers, H.-G. Schmidt, Dr. M. Noltemeyer
Institut für Anorganische Chemie der Universität
Tammannstrasse 4, D-37077 Göttingen (Germany)
Fax: Int. code +(551)393373
e-mail: hroesky@gwdg.de

[**] This work was supported by the Deutsche Forschungsgemeinschaft and the Bundesministerium für Bildung, Wissenschaft, Forschung und Technologie. We thank WITCO GmbH, Bergkamen, Germany, for a sample of $AlMe_3$.

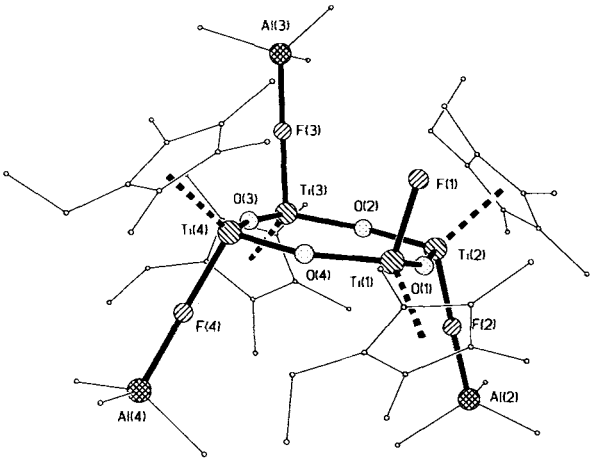

Figure 2. Crystal structure of **4**·*n*-hexane. Selected bond lengths [Å] and angles [°]: Ti(1)–O(1) 1.846(2), Ti(1)–O(4) 1.839(2), Ti(1)–F(1) 1.868(2), Ti(2)–F(2) 1.956(2), Ti(2)–O(2) 1.838(2), Ti(2)–O(1) 1.796(2), Ti(3)–O(3) 1.819(2), Ti(3)–O(2) 1.818(2), Ti(4)–O(4) 1.797(2), Ti(4)–O(3) 1.833(2), Ti(3)–F(3) 1.960(2), Ti(4)–F(4) 1.955(2), Al(2)–F(2) 1.874(2), Al(3)–F(3) 1.902(2), Al(14)–F(4) 1.876(2); Al(2)-F(2)-Ti(2) 177.55(13), Al(3)-F(3)-Ti(3) 174.58(12), Al(4)-F(4)-Ti(4) 175.48(13), O(1)-Ti(1)-O(4) 105.48(10), O(1)-Ti(1)-F(1) 103.74(10), O(4)-Ti(4)-O(3) 105.65(10), O(4)-Ti(4)-F(4) 102.11(10), O(1)-Ti(2)-F(2) 101.69(10). The *n*-hexane molecule is not shown.

atoms of the starting material **2** form coordinative bonds with three molecules of $AlMe_3$.[10] One fluorine atom (terminal) is not coordinated to $AlMe_3$ (Ti–F 1.868(2) Å), and the Ti–F bond length is correspondingly shorter than the Ti–F bond lengths with the fluorine atom in the bridging position (av Ti–F 1.95 Å). Noteworthy are the different Al–F bond lengths. Similar bond lengths are observed on one side of the ring plane (Al(2)–F(2) 1.874(2), Al(4)–F(4) 1.876(2) Å), whereas Al(3)–F(3) (1.902(3) Å) is slightly longer. Additional bond lengths and angles of **3** and **4** are given in the legends to Figures 1 and 2.

^{19}F NMR studies in solution were performed in $[D_8]$toluene at −20 °C. Initially **1** (0.1 mmol) (or **2**) was placed in an NMR tube and dissolved in $[D_8]$toluene, cooled to −20 °C, and $AlMe_3$ (0.4 mmol) was added to this solution with a syringe. The signals of the starting materials (**1**: $\delta = 64.6$, **2**: $\delta = 63.3$) disappear; they are replaced in each case by two sharp signals (intensity 1:1) that are shifted to high field, which we assign to the compounds **3** ($\delta = -132.6, -136.5$) and **4a** ($\delta = -128.2, -131.0$). These results show that the compounds are not planar in solution, as already suggested by the crystal structure analyses. Furthermore, they confirm that **4a** is initially formed in the reaction with **2**. The formation of **4** cannot be monitored by NMR spectroscopy; evidently, this compound forms by crystallization in a nonequilibrium reaction.

In summary we have shown for the first time that Ti–F bonds can be activated with $AlMe_3$. The experimental results allow conclusions and predictions for similar reactions. Furthermore, the pathways of such reactions can be readily examined by ^{19}F NMR spectroscopy.

Experimental Section

3: $AlMe_3$ (2 mL, 4 mmol, 2 M solution in *n*-hexane) was added dropwise to a stirred solution of **1** (0.87 g, 1 mmol) in toluene (30 mL) in a Schlenk tube at −10 °C. The mixture was subsequently stirred for 5 min and the tube was stored at −20 °C. Compound **3** precipitated in the form of red crystals. The mother liquor was removed with a syringe, to leave **3** (0.6 g) in 52% yield. Compound **3** is unstable at room temperature and decomposed rapidly under the formation of a yellow solid.

4: Compound **4** was prepared analogously to **3** by reacting **2** (0.93 g, 1 mmol) with $AlMe_3$ (4 mmol). The solution changed color from yellow to bright red during the addition. The solution was stored at −20 °C. This led to the formation of orange crystals, and the solution slowly changed color from red to orange. Compound **4** was obtained in 45% yield (0.51 g); it decomposed within 5 min at room temperature under an inert gas atmosphere.

Received: February 6, 1997 [Z10081IE]
German version: *Angew. Chem.* **1997**, *109*, 1846–1847

Keywords: aluminum · fluorine · titanium

[1] H. Plenio, R. Diodone, *J. Am. Chem. Soc.* **1996**, *118*, 356, contains numerous references on C-F-metal ion contacts.
[2] S. Walter, U. Klingebiel, *Coord. Chem. Rev.* **1994**, *130*, 481.
[3] M. Driess, U. Winkler, W. Imhof, L. Zsolnai, G. Huttner, *Chem. Ber.* **1994**, *127*, 1031.
[4] H.-H. Brintzinger, D. Fischer, R. Mülhaupt, B. Rieger, R. Waymouth, *Angew. Chem.* **1995**, *107*, 1255; *Angew. Chem. Int. Ed. Engl.* **1995**, *34*, 1143.
[5] Y.-X. Chen, C. L. Stern, S. Yang, T. J. Marks, *J. Am. Chem. Soc.* **1996**, *118*, 12451.
[6] H. W. Roesky, I. Leichtweis, M. Noltemeyer, *Inorg. Chem.* **1993**, *32*, 5102.
[7] A. Herzog, F.-Q. Liu, H. W. Roesky, A. Demsar, K. Keller, M. Noltemeyer, F. Pauer, *Organometallics* **1994**, *13*, 1257.
[8] R. Andrés, M. V. Galakhov, A. Martín, M. Mena, C. Santamaria, *Organometallics* **1994**, *13*, 2159; P. Gómez-Sal, A. Martin, M. Mena, C. Yélamos, *Inorg. Chem.* **1996**, *35*, 242.
[9] F.-Q. Liu, H. Gornitzka, D. Stalke, H. W. Roesky, *Angew. Chem.* **1993**, *105*, 447; *Angew. Chem. Int. Ed. Engl.* **1993**, *32*, 442.
[10] Structure analysis of **3**·3toluene: monoclinic, *I2/a*, $a = 21.982(4)$, $b = 16.339(3)$, $c = 23.490(5)$ Å, $\beta = 103.73(3)°$, $V = 8196(3)$ Å^3, $Z = 4$, $\rho_{calcd} = 1.165$ Mgm^{-3}, $\lambda(Mo_{K\alpha}) = 0.71073$ Å, $T = 193$ K. 8391 independent reflections were used for the structure solution and refinement. $R = 0.0422$, $wR = 0.1073$. Stucture analysis of **4**·*n*-hexane: triclinic, $P\bar{1}$, $a = 13.858(13)$, $b = 14.328(3)$, $c = 18.581(5)$ Å, $\alpha = 76.69(2)$, $\beta = 89.673(10)$, $\gamma = 72.791(10)°$, $V = 3448(14)$ Å^3, $Z = 2$, $\rho_{calcd} = 1.195$ Mgm^{-3}, $\lambda(Mo_{K\alpha}) = 0.71073$ Å, $T = 203$ K. 8936 independent reflections were used for the structure solution and refinement. $R = 0.0423$, $wR = 0.0966$. Crystallographic data (excluding structure factors) for the structures reported in this paper have been deposited with the Cambridge Crystallographic Data Centre as supplementary publication no. CCDC-100134. Copies of the data can be obtained free of charge on application to The Director, CCDC, 12 Union Road, Cambridge CB2 1EZ, UK (fax: int. code +(1223) 336-033; e-mail: deposit@chemcrys.cam.ac.uk).

 © WILEY-VCH Verlag GmbH, D-69451 Weinheim, 1997 0570-0833/97/3616-1767 $ 17.50+.50/0

Tips and Trends in Synthesis

Organotin Chemistry. By *A. G. Davies*. VCH Verlagsgesellschaft, Weinheim, 1997. 327 pp. plus diskette, hardcover DM 248.00.—ISBN 3-527-29049-4

In the last few decades the chemistry of the heavy elements of Main Group 4 has undergone a remarkable renaissance. This has been stimulated by a growth in the use of these elements in organic synthesis, and by the discovery of many new compounds with silicon, germanium, tin, or lead (in low or high coordination states) as the central atom. These developments have been described in many monographs and review articles on organosilicon and organotin chemistry, and in two substantial works in the Wiley series *The Chemistry of Functional Groups* edited by Patai: the two-volume work on organosilicon chemistry published in 1989, and the volume on organogermanium, organotin, and organolead chemistry, which appeared in 1995 and should cover the literature up to the end of 1994. Against this background one must ask whether it is worth buying another book on organotin chemistry, whose only obvious advantage is that it is slightly more up-to-date. However, on comparing the contents with those of the recent monographs and the Patai volume mentioned above, one soon discovers that its aim is different. Whereas the other works mostly deal with a variety of individual topics, this book is essentially devoted to the preparation of organotin compounds and their reactive properties, while also covering some aspects of their use as substrates in synthetic organic chemistry.

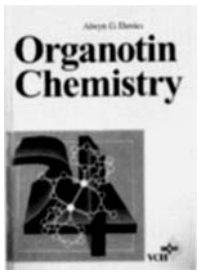

The monograph begins by discussing physical methods of characterization and listing data. Reactions leading to the formation of compounds with tin–carbon bonds are then described, arranged in the conventional way according to the various classes of organic groups. This is followed by chapters on functionalized organotin compounds with Sn–halogen, Sn–O, Sn–N, Sn–S, Sn–Sn, and Sn–metal bonds. These derivatives occupy almost half the book, reflecting the special area of interest of the author (a professor at University College, London), whose research in the field of organotin chemistry extends over more than 30 years. The book ends with two short chapters, one on organotin radicals and radical ions and the other on tin compounds with low coordination numbers.

The author gives relatively little information about toxicological aspects or the technological applications of organotin compounds. This is a conventional book in the best sense, with a firm emphasis on the synthesis, structures, and reactive properties of organotin compounds. It has a comprehensive subject index, and an author index which enables one to quickly link each literature reference to the relevant chapter. However, the diskette that is also supplied with the book seems to me a rather pointless gimmick, since unless one has special software it yields hardly any information that is not already provided by the indexes. Perhaps the younger generation will see things differently.

The book contains few errors or inconsistencies. Occasionally the positions of alkyl substituents in aryl groups have been inadvertently interchanged. A more annoying fault is the author's tendency to cite conference reports that are virtually unobtainable, even in cases where the work has also been published in well-known journals in the same year. On the other hand, there are some passages which are more likely to raise a smile, as in the explanation of nomenclature rules in the introduction where, after reading that "... the names of the attached ligands are given in alphabetical order ...", the first example cited is "dimethyldichlorostannane". The treatment of stannaimines (more correctly: stannanimines) and stannaphosphenes in two different chapters is not consistent.

However, these minor criticisms do not detract significantly from the very positive overall impression. The book gives an excellent (although not exhaustive) overview of the synthetic aspects of organotin chemistry, based on a survey of about 1400 literature references. The standard of production is very good, with well-structured tables and an abundance of clear formula schemes, which enable the reader to quickly grasp the essence of the text. Therefore I have no hesitation in recommending this book for all organic and organometallic chemists engaged in synthetic work. It is just reasonably priced for a monograph of this kind, a point to bear in mind when deciding whether to buy it.

Manfred Weidenbruch
Fachbereich Chemie
der Universität Oldenburg (Germany)

Hypervalent Iodine in Organic Synthesis. By *A. Varvoglis*. Academic Press, San Diego, 1996. 223 pp., hardcover £ 55.00.—ISBN 0-127-14975-9

During the last 15 years there has been a renaissance in the chemistry of hypervalent iodine compounds with oxidation states +3 or +5, resulting in a dramatic increase in the number of publications appearing. One of the main causes of this is the availability of a variety of new reagents of this type, some of which have unique chemical properties. Nevertheless, apart from a few exceptions such as the Dess–Martin reagent, hypervalent iodine compounds have not yet been able to cast off their image as belonging to a very specialized area of chemistry.

Many reviews and monographs on this subject have appeared in the last few years, and one must therefore ask whether the publication of one more book is an important event. The answer is undoubtedly yes! This book, which raises high ex-

This section contains book reviews and a list of new books received by the editor. Book reviews are written by invitation from the editor. Suggestions for books to be reviewed and for book reviewers are welcome. Publishers should send brochures or (better) books to the editorial office: Redaktion Angewandte Chemie, Postfach 101161, D-69451 Weinheim, Germany. The editor reserves the right of selecting which books will be reviewed. Uninvited books not chosen for review will not be returned.

 © WILEY-VCH Verlag GmbH, D-69451 Weinheim, 1997 0570-0833/97/3616-1769 $ 17.50+.50/0

pectations in view of the reputation of the Academic Press series *Best Synthetic Methods*, treats the chemistry of hypervalent iodine compounds from the standpoint of the reagents. In a masterly fashion the author presents this class of iodine compounds, often seen as a difficult and confusing subject, in a way that can be readily understood by nonspecialists. The emphasis is on the synthetic potential of hypervalent iodine compounds, with relatively little attention to the reaction mechanisms and the analytical aspects.

After a brief and succinct introduction in Chapter 1, the second chapter describes the most commonly used hypervalent iodine reagents, such as diacyloxyiodobenzene, iodosobenzene, and the iodine(V) compounds, including methods for preparing them (with detailed laboratory recipes) and some general information about their reactive properties and handling characteristics. Chapters 3–7 then describe in detail the reactions of each of the hypervalent reagents introduced in Chapter 2, subdivided according to substrates and reaction types. These cover, for example, reactions with alkenes, carbonyl compounds, and alcohols, as well as chlorination reactions and acetoxylation reactions. The most important applications are accompanied by laboratory recipes.

Chapters 8–10 cover iodine(III) compounds which formally contain two iodine–carbon bonds, with their reactions subdivided in the same way as above. The reagents described include, for example, diaryliodonium salts and phenyliodonium zwitterions. It is also pointed out here that iodine(III) intermediates can serve as substrates for C–C bond-forming reactions catalyzed by transition metals.

Chapter 11 is devoted to a brief description of the chemistry of iodine(V) compounds, with special attention to the important Dess–Martin reagent and related compounds. Finally, in Chapter 12 the author collects together an assortment of widely different reagents which he believes have the potential for being promoted to the first league of the iodine(III) compounds. Some of these, such as *o*-iodosylbenzoic acid and its derivatives, and the oxygen-bridged iodine(III) reagents, are already close to fulfilling that prediction.

The special qualities of this monograph arise from the wealth of practical advice and critical comparisons of the various hypervalent iodine reagents, with regard to their reactivities, convenience of handling, solubilities, stabilities, storage characteristics, etc. Almost every chapter contains tips and trends of a kind that are rarely found in the original publications, based on the author's detailed knowledge and years of practical experience in this field.

For the synthetic chemist, reagents emerge from the twilight into day-to-day use only when they show good chemoselectivity and have proved their capabilities in reactions involving complex multifunctional natural products or intermediates. Although the author describes some good examples of oxidation reactions for steroids, it would have been useful to devote more space to this and related aspects. Finally, one brief suggestion: The many useful laboratory recipes included in the book could have been improved still further by highlighting them with a distinctive typeface.

To summarize, the book can be thoroughly recommended as an introduction to hypervalent iodine reagents, with a strong emphasis on applications. It should be available in every chemistry department library and in laboratories engaged in synthesis.

Andreas Kirschning
Institut für Organische Chemie
der Technischen Universität
Clausthal (Germany)

Macrocycle Synthesis. A Practical Approach. (Series: Practical Approach in Chemistry.) Edited by *D. Parker*. Oxford University Press, Oxford, 1996. 252 pp., paperback £ 29.95/hardcover £ 50.00.—ISBN 0-19-855840-6/0-19-855841-4

The idea of collecting together in a single book laboratory recipes for preparing the most important macrocycles is a good one. Supramolecular chemistry is a very active area of research which generates many short communications with a claim to be highlighted, and there is usually insufficient space to include experimental details. This book consists of nine chapters containing laboratory recipes that are designed to enable even chemists with limited preparative experience to synthesize the most important macrocycles. Most of the compounds described are important key products with a variety of uses. In supramolecular chemistry especially, success often depends on combining synthetic building blocks from different areas of investigation, and therefore this book will certainly also be very useful for chemists already engaged in research on host/guest chemistry. For these readers the fact that the editor has necessarily restricted the subject matter to a limited selection of macrocycles will be no disadvantage.

The first four chapters are concerned with the synthesis of both "classical" crown ethers and hetero-crown compounds. By introducing the most important cyclization methods they prepare the reader for the three chapters on cryptands, torands, and calixarenes that follow. Next Chapter 8 deals with spherands, hemispherands, and calixospherands, thus showing how one can link together various macrocyclic building blocks. The last chapter leads to supramolecular structures by describing syntheses of catenanes and rotaxanes which use transition-element templates.

Each chapter begins with a brief introduction. This is followed by a detailed experimental part consisting of a number of procedures varying from 6 to 19. Finally there is a short bibliography, which makes no claim to be exhaustive. Each laboratory recipe is preceded by short introductory survey or linking paragraph. The sequence of the various procedures corresponds to that of the reaction stages, thus offering a direct invitation to carry out the synthesis. All the procedures originate from well-respected groups engaged in research in the areas concerned, a fact that gives the compilation an additional appeal. Furthermore, if one is using the ring-binder version, the pages—like those of a good cook-book—stay conveniently open on the laboratory bench!

Detailed safety notes and a list of the required apparatus and materials are given at the beginning of every experimental procedure. The reactions involved are set out in clear formula schemes. The operations are described in a step-by-step manner, a style which perhaps not everyone will find ideal. Many helpful details and hints are included, but unfortunately the form of presentation leads to much unnecessary repetition. For example, a note in the first paragraph about the need to dry glassware in an electric oven appears in 39 of the 99 procedures described, varying only in the recommended temperature (from 105 to 150 °C) and time (from 30 minutes to "overnight"). Some of the paragraphs included in the experimental procedures seem unduly meticulous or unnecessary, even when one considers the fact that the book is intended for students. Thus, on page 191 it is mentioned twice (in paragraphs 14 and 18) that before the solution is concentrated in the rotary evaporator it must be transferred to a single-neck round-bottom flask. It is not until paragraph 19 that the reader, by being left to choose suitable glassware, is credited with having received a reasonably good

 © WILEY-VCH Verlag GmbH, D-69451 Weinheim, 1997 0570-0833/97/3616-1770 $ 17.50+.50/0

general chemical training. Again, we find that although a "rotary evaporator with vacuum pump" (p. 97, paragraph 6) is used in nearly every case, it appears repeatedly in the list of apparatus for several of the procedures. It would have been better to include a short chapter collecting together general information about laboratory practice, which could have been placed immediately before the list of suppliers at the end of the book. The space thereby released would perhaps make it possible to list the most important spectroscopic data for the compounds described, or at least to give the relevant literature references, as is provided, for example, in *Organic Syntheses*.

However, despite these minor shortcomings, this is a very useful compilation of important synthetic methods for macrocycles, which is clearly set out and convenient to use. The detailed laboratory recipes will be helpful for organic chemists and for those working in the area of coordination chemistry, and they will undoubtedly give inspiration for the synthesis of new and interesting compounds.

Helmut Sonnenschein
Institut für Angewandte Chemie
Berlin-Adlershof e. V. (Germany)

Stable Carbocation Chemistry. Edited by *G. K. S. Prakash* and *P. von R. Schleyer*. Wiley, New York, 1997. 587 pp., hardcover £ 65.00.—ISBN 0-471-59462-8

Carbocations persist under conditions where the absence of nucleophiles ensures that no intermolecular reactions can occur, and the energy minimum is deep enough to prevent isomerizations. This book on such "stable" cations is based on a symposium held to mark the 65th birthday of G. A. Olah, and contains 17 articles by leading researchers in the field.

In Chapter 1 George Olah describes his pioneering work on carbocations, the importance of which was recognized by the award of a Nobel Prize in 1994. Some more recent results from Olah's laboratory, including the latest work, are reported in Chapter 4 by G. K. Surya Prakash. These include studies of carbocations with silyl groups or very bulky substituents, and of cations and dications derived from pagodane. Olah's recipe for success can be summarized very briefly as "superacids and NMR". The superacids concerned have remained virtually unchanged since the beginning (usually SbF_5 and/or FSO_3H, sometimes diluted with SO_2ClF), whereas the range of NMR instruments and techniques has greatly expanded. The isotopic-perturbation method enables one to distinguish between static and equilibrating carbocations (M. Saunders et al., Ch. 9). Similar information is obtainable by CPMAS solid-state NMR spectroscopy in amorphous SbF_5, which allows measurements down to temperatures as low as 5 K (P. C. Myrhe and C. S. Yannoni, Ch. 10). Measurements of intrinsic isotope shifts can be used for structural and conformational analysis (D. Forsyth, Ch. 9). Theoretical calculations of NMR chemical shifts (using IGLO and GIAO methods) can be used to verify proposed structural models. Theoretically calculated vibration frequencies were found to be essential for interpreting infrared spectra of carbocations in SbF_5 matrices (D. E. Sunko, Ch. 11). Such calculations have been made possible through the development of better and faster quantum-chemical methods, which yield exact structures even for quite large carbocations (P. von R. Schleyer et al., Ch. 2). The only experimental method that can give information of comparable quality is X-ray crystallography (T. Laube, Ch. 14), but unfortunately its scope is limited by the extreme difficulty of growing single crystals of carbocation salts. Calorimetric and electrochemical measurements have yielded important thermodynamic data for carbocations (E. M. Arnett and R. A. Flowers, Ch. 8). An interesting approach is the use of X-ray photoelectron spectroscopy to study carbocations at interfaces, but the account of this work is somewhat disappointing as it gives little definite information (D. T. Clark, Ch. 13).

In addition to these chapters that concentrate on methods, there are others that deal with special types of carbocations. Chapter 3 (T. S. Sorensen) is devoted to carbocations with μ-hydride bridges, Chapter 5 (H.-U. Siehl) to vinyl cations, and Chapter 6 (P. Ahlberg) to 9-barbaralyl cations ($C_9H_9^+$) and isomers thereof. Some important reactions of stable cations are also treated. These include rearrangements, especially of arenonium ions (V. G. Shubin and G. I. Borodkin, Ch. 7), alkane carbonylation reactions (J. Sommer, Ch. 15), and electrophilic substitutions of arenes (K. Shudo and T. Ohwada, Ch. 16). A topic that deserves particular attention is the enormous variety of highly selective reactions that can be performed on natural products (especially terpenes and steroids) in superacids (J.-C. Jacquesy, Ch. 17). Most of the reactions described in Chapters 15–17 do not directly involve the carbocations as such but their protonated forms or Lewis acid adducts ("superelectrophiles"). Thus even the chemistry in superacids involves reactive intermediates that can only be detected indirectly; here dications have a role similar to that of simple carbocations in nucleophilic media.

The editors have managed to avoid significant overlapping of subject matter between the contributions, and the work of the authors (and of the publishers) is of a high quality. The presentation is excellent, and there are very few misleading errors. (Examples: **26b**/p. 148, **9**/p. 167, **15**/p. 204, **2**/p. 550; in Fig. 11.7 the experimental data are missing, and in Fig. 15.5 the numbering of the curves should be interchanged.) The book gives the reader "at first hand" a comprehensive and up-to-date survey of this fascinating and highly productive area of physical-organic chemistry; the literature coverage extends up to 1995 in most cases. The ideas and methods described here also have the potential to contribute to advances in other fields. The book should be of interest to a wide readership.

Wolfgang Kirmse
Lehrstuhl für Organische Chemie
der Universität Bochum (Germany)

 © WILEY-VCH Verlag GmbH, D-69451 Weinheim, 1997 0570-0833/97/3616-1771 $ 17.50+.50/0

+k↑
−k↓

Superconductivity and Chemistry

Arndt Simon*

Dedicated to Hans Georg von Schnering

The microscopic theory of superconductivity worked out by Bardeen, Cooper, and Schrieffer led to a fundamental understanding of the phenomenon. However, this theory does not provide a materials aspect. Starting from the special situation of chemical bonding in carbides and carbide halides of the rare earth metals a general view of the origin of superconductivity is developed, based on a tendency for (pairwise) localization of conduction electrons. This approach is tested in terms of special features in the electronic band structure and compared with existing physical models of electron pairing in real space. Its applicability to high-temperature superconductors discovered during the last decade is discussed.

Keywords: band structure · carbides · cuprates · lanthanoids · superconductivity

1. Introduction

In 1911, three years after successfully liquifying the last remaining "permanent" gas, helium, and thus opening a new dimension of low-temperature research, Kamerlingh-Onnes in Leiden discovered the phenomenon of superconductivity.[1] He found that the electrical conductivity of mercury below 4.2 K decreased to an unmeasurably low value within an interval of a few hundreds of a degree Kelvin. The resistance actually disappears completely. Experiments show that the induced current in a superconducting ring will still be flowing after 10^5 years.[2] One such ring can be thought of as a macroscopic analogy to the Bohr model of the atom, as the charge carriers that provide superconductivity all occupy a single quantum state and are free to move without energy loss.

A superconductor is characterized by a further property that differentiates it from a metal with zero direct current resistance: the exclusion of magnetic fields from the interior. If a superconductor is cooled in a magnetic field below its critical temperature, T_c, it will become an ideal diamagnet (Meissner–Ochsenfeld effect). Under suitable conditions a superconductor levitates above a magnet and vice versa. Only if the magnetic field exceeds the value of a critical field strength will it penetrate the superconductor, thus forcing the transition to the normal conducting state. Both the measurement of the electrical conductivity and the behavior in a magnetic field are necessary for the basic characterization of a superconductor.

[*] Prof. Dr. A. Simon
Max-Planck-Institut für Festkörperforschung
Heisenbergstrasse 1, D-70569 Stuttgart (Germany)
Fax: Int. code +(711)689-1642

For decades superconductivity occurred only at such low temperatures that cooling with liquid helium was necessary. Not until the production of metastable superconducting Nb_3Ge films (critical temperatures of 22.3 K[3] or 23.2 K[4]) more than sixty years after the discovery of the phenomenon did it become possible to enter the region of liquid hydrogen cooling. The work of Bednorz and Müller[5] in 1986 on the basis of oxocuprates started the discovery of a rapidly increasing number of superconductors, whose critical temperatures lie above the boiling point of liquid nitrogen. The current record is held by $HgBa_2Ca_2Cu_3O_{8-\delta}$, which has a critical temperature T_c of 164 K under pressure.[6]

How does current microscopic theory provide an understanding of the phenomenon of superconductivity?

2. Theory of Superconductivity

In normal metals and also superconductors in the normal conducting state above T_c the charge carriers are single electrons. These repel each other because of the Coulomb interaction between their charges. Due to structural defects as well as an exchange interaction between the electrons and lattice vibrations (electron–phonon scattering) a metal exhibits electrical resistance, which increases with temperature. It has been demonstrated simultaneously experimentally[7, 8] and theoretically[9, 10] that lattice vibrations are also important for superconductivity. The experimental proof was obtained from the variation of the critical temperature of Hg by isotope substitution.

Electron–phonon interaction under certain circumstances can cause the pairwise coupling of conduction electrons—that

 © WILEY-VCH Verlag GmbH, D-69451 Weinheim, 1997 0570-0833/97/3617-1789 $ 17.50+.50/0

is, it sets up another type of charge carrier. While conduction electrons in the normal state obey Fermi statistics, and all take different quantum states, electron pairs with a total spin $S = 0$ are bosons, and must obey Bose–Einstein statistics. Therefore, they can all occupy a single quantum state. Interestingly, it was the chemist Ogg who first had the idea (prompted by the work of London[11] who interpreted the superfluidity of helium through Bose–Einstein condensation) that electron pairs are the charge carriers in superconductivity.[12, 13]

The pairing of electrons in real space is sometimes visualized in greatly simplified models[18] such as the mechanical analogy of two metal balls that roll towards one another when placed upon an elastic membrane, or, more realistically, as the dynamic polarization of the lattice by a moving electron that catches the movement of a second electron in the polarization track of the first. But even the second comparison cannot begin to describe the necessary prerequisites for superconductivity in terms of specific chemical bonding.

The microscopic theory of superconductivity[19] developed by Bardeen, Cooper, and Schrieffer (BCS theory) does not establish a relationship with real chemical systems either. The essence of this theory is shown graphically in Figure 1. An electron characterized by its wave vector $\boldsymbol{k}_1$ interacts with the lattice of positively charged ions and is scattered (new wave vector $\boldsymbol{k}_1'$), thus changing the vibrational state of the lattice. A second electron ($\boldsymbol{k}_2$) produces the initial vibration state again, and through the exchange of a virtual phonon the electrons $\boldsymbol{k}_1'$ and $\boldsymbol{k}_2'$ are coupled. The state of lowest energy corresponds to a collective state of electron pairs (Cooper pairs) formed from electrons having opposite spins and directions of their wave vectors: $+\boldsymbol{k}\uparrow\ -\boldsymbol{k}\downarrow$.

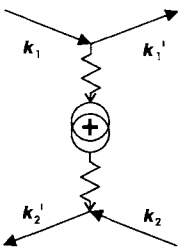

Figure 1. Schematic representation of the electron-electron interaction by the exchange of a virtual phonon. The electrons are represented by their wave vectors $\boldsymbol{k}_i$. The exchange interaction via the lattice of positively charged atomic cores is through the emission and absorption of a phonon (see text).

In the superconducting state an energy gap opens between the BCS ground state, which is derived from the paired electrons, and the excited state of the quasi free electrons ("quasiparticles"). The energy gap corresponds to a pair-breaking energy, which in BCS theory at 0 K has a magnitude of $2\Delta(0) = 3.52 k_B T_c$, where k_B is the Boltzmann constant. For the superconducting critical temperature, the following relationship is derived from BCS theory:

$$T_c = 1.14 \frac{\hbar\omega_D}{k_B} e^{-1/N(E_F)V}$$

where $\hbar = h/2\pi$, where h is Planck's constant, ω_D the Debye frequency, $N(E_F)$ the density of states at the Fermi level E_F (that is, the highest energy level of the electrons in the normal state (at 0 K)), and V the electron–phonon interaction parameter.

The results reflect the extremely simplified model that lies at the heart of BCS theory. The electronic behavior is described as isotropic, that is, the energy gap $2\Delta(0)$ is constant in all directions. Shortly after the appearance of the BCS work, it was demonstrated that many superconductors have several energy gaps, or, put in another way, are highly anisotropic. There are probably interesting consequences of this fact (see Section 7). The assumption of a Debye-type phonon spectrum as well as the restriction to weak electron–phonon coupling are also simplifications in the model that lead to many deviations between experiment and theory even with classical superconductors. Later, important extensions to the theory were made, especially those by Eliashberg[21] and McMillan,[22] which gave a better correspondence between experiment and prediction. Until now, however, BCS theory has lost nothing of its fundamental importance, as becomes clear from the fact that a new superconductor will be termed BCS-like or not. When the deviations from BCS-type behavior are large, as is the case with high-temperature superconductors, new "exotic" mechanisms are looked for. But even for this class of materials the participation of lattice vibrations on the pair exchange interaction has meanwhile been clearly shown by experiment.[23, 24]

The question arises whether the general statements of BCS theory can be associated with specific bonding situations, and whether an understanding of the physical phenomenon of superconductivity can be developed from the viewpoint of chemistry. This will be attempted in this review.

So far the electron has been described as a plane wave characterized by the wave vector $\boldsymbol{k}$, perpendicular to the wave front, as $|\boldsymbol{k}| = 2\pi/\lambda$. The electron is also a particle with momentum $\boldsymbol{p}$ and according to de Broglie $\boldsymbol{p} = \hbar\boldsymbol{k}$.

Arndt Simon was born in Dresden 1940, started his studies in chemistry at Münster University in 1960 and finished his thesis with Harald Schäfer in 1966. Since 1974 he has been director at the "Max-Planck-Institut für Festkörperforschung" in Stuttgart and, since 1975, honorary professor at the local university. His scientific interests include the investigation of metal-rich compounds (e.g. alkali metal suboxides; subnitrides of the alkaline earth metals; halides of rare earth metals with inclusions of H, B, C, N; metal clusters; concept of cluster condensation), intermetallic phases (Pauling–Simon rule), structure property relations (photoemission, magnetism, superconductivity), and structures and phase transitions of molecular crystals. These activities include apparatus development (Guinier–Simon camera). He is member of numerous academies and has received several awards (e.g., the Klemm prize 1985, Bayer prize 1987, and Leibniz prize 1990).

The Cooper pair, which corresponds to two electrons with opposite spins and momenta (that is, total momentum zero) resembles something that is known to the chemist: An electron pair, commonly symbolized by a line between two atoms in a chemical bond, depicts an "approximation" of the Cooper pair. However, there are two principle problems with such a comparison. Firstly, the Cooper pair, as part of a highly correlated state, is free to move through the lattice, in contrast to a localized electron pair. Secondly, in BCS theory the pairing of electrons occurs in momentum space,[25] a space defined reciprocally to real space ($|\boldsymbol{p}| \propto 1/\lambda$), and the Cooper pair cannot be described locally. The coherence length can be several thousand Angstroms.

Regardless of the problems just outlined, many theoretical models are derived from the assumption of real space pairing in superconductors. Schafroth,[26] in particular, followed this course in the time before Bardeen, Cooper, and Schrieffer offered their comprehensive theory. With the discovery of high-temperature superconductors, whose coherence lengths correspond to a few atomic radii, local approaches have again become more relevant.[27–29] Later a few of these ideas will be examined.

The normal state of a metal becomes unstable when an attractive exchange interaction occurs between the conduction electrons.[30, 31] Understanding the origins of the attraction in terms of chemical bonding therefore opens the door to learning about the chemical prerequisites for superconductivity. In the following chapters the C–C bond that is so familiar to every chemist will be chosen to demonstrate that an attractive exchange interaction can originate from a tendency for pairwise localization of conduction electrons ("virtual localization").

3. C_2 Units as Traps for Electron Pairs

The carbide halides of rare earth metals with the general formula $(RE)_2X_2C_2$, discovered by us some years ago,[32, 33] form layered crystals with double layers of close-packed metal atoms sandwiched between layers of halogen atoms. C_2 units are found inside the octahedral voids between metal atoms. Figure 2 shows the stacking of these layer packages, which are bonded through van der Waals forces between the halogen atoms. Two variants of the stacking sequence are known, which are identified as 1s or 3s depending upon the number of layers needed until the identity is reached.

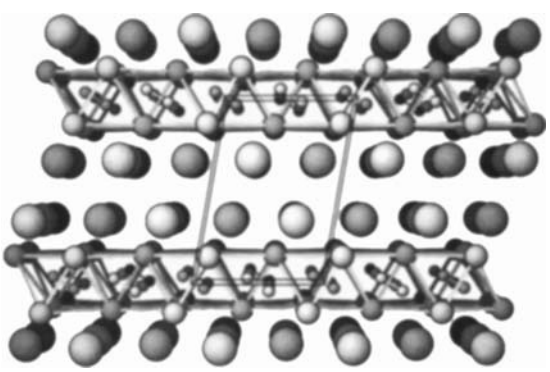

Figure 2. Projection of the monoclinic unit cell of the (1s)-layered structure of $(RE)_2X_2C_2$ in the direction of the *b* axis (*a* horizontal). The atoms, X, RE, and C are shown with decreasing size.

C_2 units have been known for a long time to occur in ionic structures. Calcium carbide is the best known example.[34] The short C–C distance of 120 pm in calcium carbide identifies the compound structurally as a derivative of ethyne in agreement with its chemical behavior. The separation distance of 128 pm[36] found in the carbide halide $Y_2Br_2C_2$ corresponds rather to that of an ethenide.[37] This classification is in accord with the ionic formulation in the Zintl-Klemm concept: $CaC_2 = Ca^{2+}(C_2)^{2-}$ and $Y_2Br_2C_2 = (Y^{3+})_2(Br^-)_2(C_2)^{4-}$. The MO examination for the C_2 units (Figure 3) shows the occupation of all the bonding MOs corresponding to a triple bond for CaC_2 and the occupation of the first antibonding MO for $Y_2Br_2C_2$. In this last case the degeneracy of the π^* levels is lost due to the monoclinic crystal symmetry and the broad spectrum of Y–Y distances (340 to 395 pm)[36] in the Y_6 octahedron that surrounds the C_2 unit.

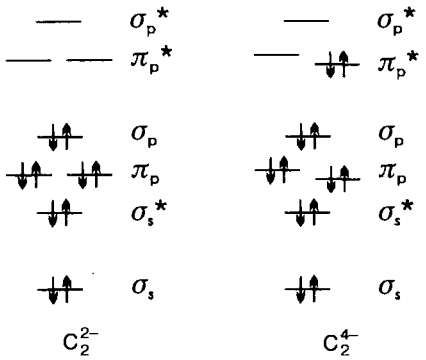

Figure 3. Schematic MO diagram of the $(C_2)^{2-}$ and $(C_2)^{4-}$ ions as found in CaC_2 and (to a first approximation) in $(RE)_2X_2C_2$, respectively. The degeneracy of the π^* levels is removed through the monoclinic crystal symmetry.

CaC_2 is an ionic crystal and insulator. The same properties could be expected for $Y_2Br_2C_2$. The compound is, however, metallic in two dimensions. As is suggested by the shortened C–C double-bond distance, backbonding from the occupied π^* MO into the empty d states of the metal atoms occurs, which in the case of the extended solid can be discerned directly from the electronic delocalization. This assumption is verified through the band structure calculations for the magnetic compound $Gd_2Cl_2C_2$.[39] The nonmagnetic compound, $Y_2Br_2C_2$, is not only metallic with a resistance in the mΩ range, but becomes superconducting at 5 K.[36, 40, 41] Superconductivity occurs similarly for the corresponding compounds, $Y_2X_2C_2$ (X = Cl, Br, I) and $La_2X_2C_2$ (X = Cl, Br).[36, 42, 43] Figure 4 shows the characteristic changes in the electric and magnetic behavior of $Y_2I_2C_2$ that occur with the transition to the superconducting state at $T_c \approx 10$ K.

The simplified discussion within the Zintl–Klemm concept portrays $Y_2Br_2C_2$ as a simple valence compound, which is only coincidentally metallic due to the covalence in the Y–C bond. The closeness to electronic localization is evident. The quasi-molecular C_2-π^* states lie near to the Fermi level, E_F. In the following, these states will be addressed as π^* states for sake of simplicity in spite of considerable π–d mixing. From our hypothesis,[41] a tendency towards a pairwise occupation of these states is the reason for attractive interactions between the conduction electrons. The phases $(RE)_2X_2C_2$ allow this assumption to be tested in a variety of ways, both experimentally and theoretically.

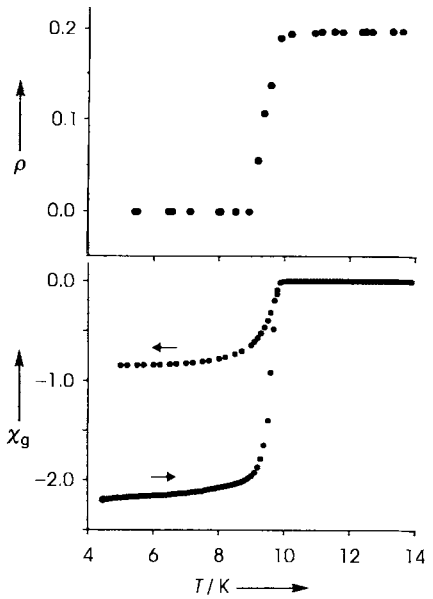

Figure 4. Transition to superconductivity in a $Y_2I_2C_2$ crystal. Top: The disappearance of the electrical resistance ρ (mΩcm); bottom: magnetization results (measured at 10 G; field cooled curve (←) shows Meissner effect; zero field cooled curve (→) displays shielding)[40]. Mass susceptibility χ_g in 10^{-2} emu g^{-1}.)

3.1. Covalence and Electron Count

From the above considerations, the mixture of C_2-π^* and metal d states is seen to be responsible for the electronic delocalization (consequence: metallic conductivity), and the presence of the C_2-π^* "MOs" at E_F is seen as the cause of the tendency for a (pairwise) localization (consequence: superconductivity). Examination of the structure in Figure 2 shows that the balance between the two effects can be easily varied by chemical means. One way is by changing the size and shape of the void for the C_2 units by exchanging halogen atoms, and thus changing the metal carbon covalence. Another way is to increase the energy of the Fermi level through the intercalation of alkali metals into the van der Waals region between the layers. In this way a direct influence on the energy of the π^* level relative to E_F is possible.

3.1.1. Halogen Exchange

Figure 5 shows the results of halogen atom substitutions for the system $Y_2(XX')_2C_2$. The substitution of Cl by I leads to approximately five percent stretching of all distances parallel to the layers, and in mixed crystals a Vegard-type behavior is found. The ratio X:X′ enables a mean halogen radius $\bar{r}_x$ to be calculated, which relates to a systematic variation in transition temperature.[36] This is equally valid if $\bar{r}_x$ is adjusted through a Cl/Br, Cl/I, or Br/I mixture. The transition temperature is $T_c = 2.30$ K for $Y_2Cl_2C_2$, and it increases monotonically through $T_c = 5.05$ K for $Y_2Br_2C_2$, to a maximum of $T_c = 11.6$ K for $Y_2I_{1.6}Br_{0.4}C_2$, decreasing again to $T_c \approx 9.7$ K for the pure iodide phase.[46] The transition temperature for the pure bromide is very sharp and reproducible, whereas T_c varies for different iodide samples, probably due to small carbon deficiencies resulting in the replacement of C_2 units with single C atoms.[43]

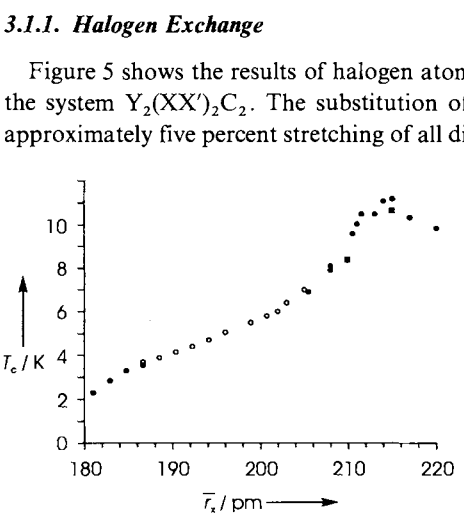

Figure 5. Critical temperature T_c for mixed crystals $Y_2Cl_{2-x}Br_xC_2$ and $Y_2Br_{2-x}I_xC_2$ (circles) as well as $Y_2Cl_{2-x}I_xC_2$ (squares), plotted against the mean halide ion radius, $\bar{r}_x$. Open and filled symbols represent 1s and 3s stacking, respectively[40].

It is interesting to note that the monotonic increase in T_c towards larger $\bar{r}_x$ values does not reflect the structural change from 1s to 3s stacking at $\bar{r}_x \approx 187$ pm, and a return to the 1s structure at $\bar{r}_x \approx 205$ pm. The difference in the layer stacking has no effect on the superconducting transition. This is a clear indication that the origin of superconductivity is to be found within the individual layers.

As shown by the change in T_c with $\bar{r}_x$ in Figure 5, the metrics in the $Y_2(X,X')_2C_2$ system can be optimized with respect to superconductivity. The maximum in T_c possibly has an interesting interpretation[46] that, however, needs substantiating. According to this interpretation the π^* level due to the bonding Y–C interaction will lie increasingly lower in energy as the Y–C separation decreases, and with the X/X′ variation the level is shifted continuously relative to E_F. Possibly the electron density of states at E_F is scanned by variation of T_c (see Section 3.4).

3.1.2. Intercalation of Alkali Metal Atoms

The consequences of the intercalation of sodium between the halogen atom layers of $Y_2Br_2C_2$ seem more clearly apparent.[47] What at first looks to be a simple increase of the Fermi level through the addition of injected electrons in the layers is nonetheless a rather complicated change. First, the intercalation reaction changes the structure from 3s to 1s stacking. This should, according to Figure 5, have no effect on the magnitude of T_c. Moreover, the intercalation leads to slight changes in the band structure, and not only the energy of the Fermi level but also that of the π^* level varies. The transition temperature increases nearly linearly with sodium content in $Na_xY_2Br_2C_2$, starting from $T_c = 5.05$ K for $x = 0$, to $T_c = 6.20$ K, the highest achievable value, for $x = 0.46$.[47] The optimal electron count per C_2 unit with regard to superconductivity lies above four electrons to be transferred from the surrounding framework. This result is interesting when compared with the optimal condition found in the carbides of the rare earth metals.

3.2. A Small Step

The explanation of the metallic properties of $Y_2Br_2C_2$ and the hypothesis concerning the origin of superconductivity for this compound is easy to test chemically on the basis of the comparison in Figure 3. If one succeeds in partially occupying C_2-π^* MOs in CaC_2, the result should be a metal, which becomes superconducting at low temperatures. The occupation is easily possible through the simple replacement of Ca^{2+} with Y^{3+}. And indeed, the golden colored, isotypic YC_2 is metallic and

becomes superconducting at approximately 4 K. This result is not new, however. The superconductivity of YC_2 was discovered in the course of extended studies on superconductivity in rare earth metal carbides.[48] In the 1970s a wealth of results was produced from compounds of the general composition $((RE)_{1-x}M_x)C_y$,[49, 50] which now can be analyzed in the light of the ideas presented here. In order to do so the given formulae have to be rewritten as $((RE)_{1-x}M_x)_{2/y}C_y$, and the number of electrons $\sum n_i$ that participate in a complete charge transfer from the metal atom framework to the C_2 unit is calculated. This number n_i is 3 for RE, 2 for Ca, 4 for Th etc. Without knowledge of the structure one already discovers important clues from the electron count. In the case of $\sum n_i \geq 8$ superconductivity will not be observed with any rare earth metal carbide. In this case the number of electrons transferred to two C atoms is sufficiently large to occupy all the antibonding MOs of a C_2 unit, and therefore only single C atoms (C^{4-}) are allowed in the structure.

In the carbides of the rare earth metals superconductivity is obviously connected to the presence of C_2 units[51] and appears only with correspondingly low electron concentrations. Plotting T_cs vs. $\sum n_i$ values for a large number of analytically well-characterized phases results in the characteristic relationships seen in Figure 6.[52] At values around $\sum n_i/C_2 \approx 4$ high critical tempera-

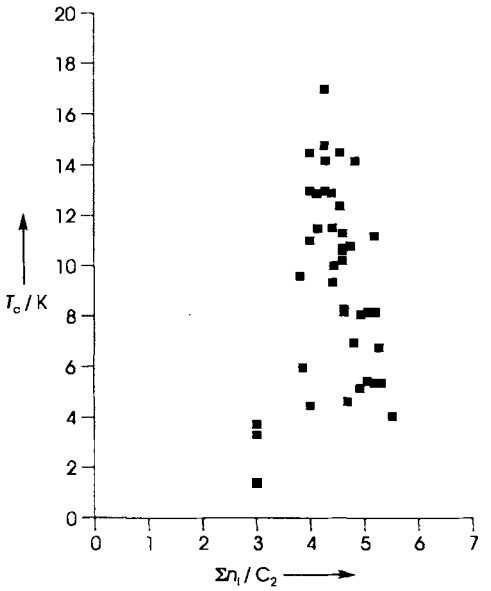

Figure 6. Critical temperature T_c for carbides of the general formula $((RE)_{1-x}M_x)_{2/y}C_2$. The abscissa represents the number of valence electrons $\sum n_i$ that are accessible to be transferred from the framework of the metal atoms to two C atoms[52].

tures appear frequently. The corresponding phases all belong to the composition $(RE)_2C_3 \equiv (RE)_4(C_2)_3$, and they crystallize in the Pu_2C_3 structure type. The maximum T_c (17.0 K) is found for the sample $Y_{0.7}Th_{0.3}C_{1.55}$, that is, with $\sum n_i/C_2 = 4.26$.[53] The characteristic electron count found for the superconductivity in the structurally completely different compound classes $(RE)_2X_2C_2$ and $(RE)_yC_2$ ($y = 1.00$ and 1.25) gives evidence for a dominant role of the C_2-π^* states in the formation of Cooper pairs in these phases.

The relationship shown in Figure 6 is reminiscent of the well-known Matthias rule,[54] although this follows a different, less chemically based electron counting procedure. The rule states that the arithmetic mean of the number of valence electrons in a superconductor is of crucial importance to the value of T_c. For mixed crystals of the transition metals, the maximum in T_c is seen to occur at approximately 4.7 and 6.5 valence electrons per atom.

The T_c dependence on the mean number of valence electrons of the A15 phases is particularly impressive. The earlier mentioned superconductor Nb_3Ge belongs to them. For this compound the valence electron concentration (VEC) is calculated as follows: VEC = $(3 \times 5 + 4)/4 = 4.75$. Through (partial) substitution of the transition metal, or alternatively, the p element, by elements with other valence electron numbers, numerous phases that show superconductivity at varying T_c values can be obtained. Figure 7 indicates that superconductors with high T_c

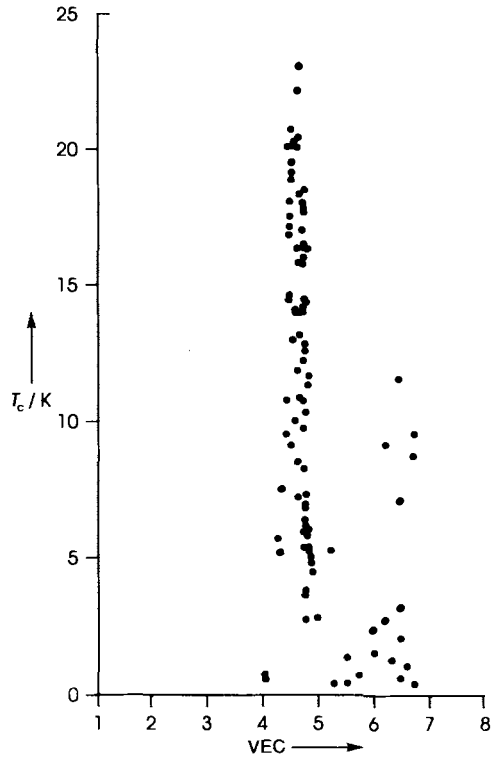

Figure 7. Critical temperature T_c as a function of the valence electron concentration (VEC) for M_3Z compounds of the A15 type (Matthias rule)[54].

values occur for VECs between 4 and 5, or alternatively, between 6 and 7. Again, the values of the valence electron concentration between the two maxima differ by about 2. A15 superconductors with high T_c values collect in rather narrow VEC ranges. The wider spread of high T_c values in Figure 6 is not that surprising when the different structural types are taken into account. One question remains open: is the shown accumulation of high T_c values for the carbides of the rare earth elements followed by a second area after a distance of two electrons/C_2 group, corresponding to the occupation of the next C_2-π^* MO in ethanides?

3.3. Similarities and Differences

The structure of α-YC_2, isotypic with CaC_2, is derived from the sodium chloride structural type by replacing the single atom anions by parallel C_2 units with $d(C-C) = 127$ pm. If layers are cut out of this structure, as is shown in Figure 8, and the broken

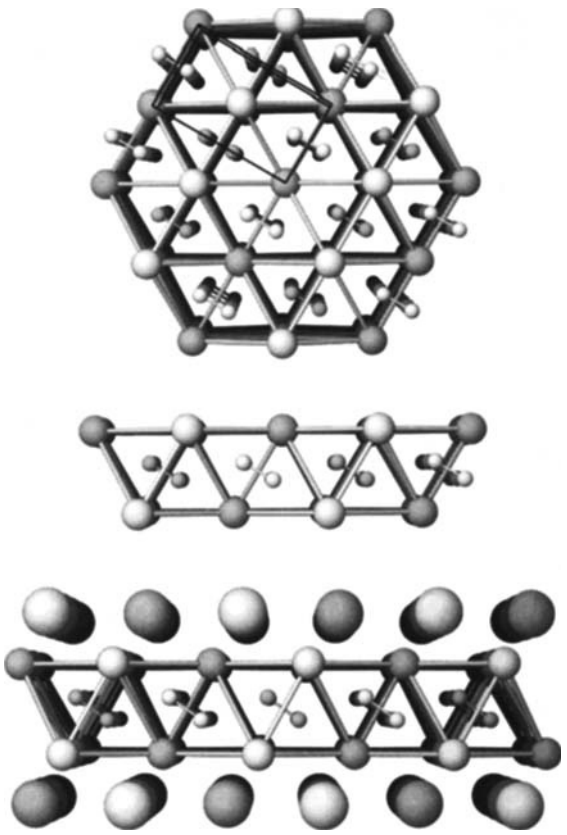

Figure 8. Topological relationship between the YC_2 and $Y_2X_2C_2$ structures. Projection of the tetragonal YC_2 structure along the a axis (top); two-dimensional layer cut from the YC_2 structure (center), which, when separated by halogen atoms, X, gives the $Y_2X_2C_2$ structure (bottom). (X, Y, C are depicted in decreasing size).

bonds replaced through Y–Br bonds, then the result is the characteristic layered structure of $Y_2Br_2C_2$.

There are close similarities between the two systems, both topologically and with regard to the assumed importance of the C_2-π^* MOs for superconductivity, but there are also large differences. Firstly, different numbers of electrons are available to be transferred from the framework to the C_2 unit, a maximum of three in the case of YC_2 and four in $Y_2Br_2C_2$. Secondly, the expected Y–Y separation is shorter in $Y_2Br_2C_2$ than in YC_2 (383 pm relative to 391 pm in α-YC_2) and, as a consequence, the practically identical C–C distance yields a shortened Y–C separation in $Y_2Br_2C_2$ (256 pm against 262 pm). An essential difference between the two compounds lies in the three-dimensional electron delocalization in YC_2, and the two-dimensional metallic character of $Y_2Br_2C_2$.

Our current knowledge of the physical properties of the two compounds will be summarized in the following. The thermodynamic properties in the superconducting state, as taken from magnetic measurements (Section 3.3.1) and heat capacity measurements (Section 3.3.2) show major differences between the two compounds. The question arises whether these differences and also the different isotope effects (Section 3.3.3) are due to the difference in dimensionality.

3.3.1. Magnetization

As mentioned earlier, superconductivity can be suppressed through a sufficiently high magnetic field. There are two types of behavior. Soft superconductors (type I) are ideal diamagnets. The magnetic field remains fully excluded from an infinitely long cylinder until a critical value H_c is reached. At H_c the magnetic field penetrates the superconductor completely, returning it to the normal conducting state. In the case of hard superconductors (type II) an increasing amount of magnetic flux penetrates the superconductor above a critical field H_{c1} and a mixed state (Shubnikov phase) develops. At H_{c2} the superconductivity within the sample is lost. The remaining superconductivity in a surface layer disappears at H_{c3}. Soft superconductivity appears for very pure elements; they display full reversibility of the magnetization. The technically important superconductors such as Nb_3Sn belong to type II.

The magnetic isotherms for YC_2[56] and $Y_2Br_2C_2$[57] measured in the superconducting state are contrasted in Figure 9. The negative magnetic polarization $-J$ decreases with increasing temperature and disappears at T_c. The curves follow very different courses for each compound. At first glance YC_2 appears to be a type I superconductor (Figure 9, top). The irreversibility of the magnetization curve after divergence from the initial line, however, is an indication of type II behavior with small and close H_{c1} and H_{c2} values.[58] The measurements on $_2Br_2C_2$ (Figure 9, bottom) show unambiguously type II behavior, with an upper critical field strength lying far above the shown measurement range. The value for H_{c2} is fifty times larger than that for YC_2.[58]

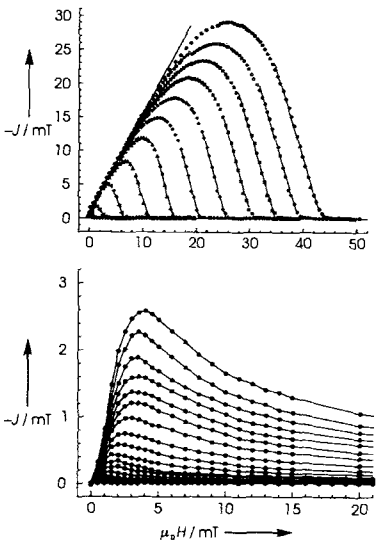

Figure 9. Isotherms of magnetization, measured on a spherical polycrystalline YC_2 sample (top, temperature from 2 K (maximum magnetization) to 4 K in steps of 0.2 K) and a compressed powder pellet of $Y_2Br_2C_2$ (bottom, $2\,K < T < 5\,K$)[56, 57].

Distinctive type II behavior is characteristic for layered superconductors and is related to the strong pinning of the magnetic flux lines between the layers.[59] By tilting a $Y_2I_2C_2$ single crystal in a magnetic field one finds the typical cusplike dependence of T_c as a function of the tilt angle, as is well known from measurements on other layered superconductors like $NbSe_2$[60] or high-temperature superconductors such as $YBa_2Cu_3O_{6.6}$.[61] Also, the magnitude of the anisotropy $H_{C2(\parallel)}/H_{C2(\perp)} \approx 5$ is comparable. The drastic change in the characteristics of the type II behavior between YC_2 and $Y_2X_2C_2$ representatives is due to the difference in dimensionality.

3.3.2. Heat Capacity

The specific heat capacity of a (nonmagnetic) metal is composed of contributions from lattice vibrations (phonons) and electrons. The lattice contribution at low temperature is usually described by the Debye T^3 law, which is derived from the

assumption of a normal spectrum of lattice vibrations within the limiting frequency ω_D. Such behavior is readily observed in the temperature range $T < 0.1\theta_D$, where the Debye temperature θ_D is defined as $\hbar\omega_D/k_B$. The contribution of the conduction electrons increases linearly with temperature; the proportionality factor γ (Sommerfeld coefficient) depends on the number of the electrons and their effective mass. With the transition to superconductivity, an ordered state is established, and the loss in entropy is evident in the well-known anomaly in the specific heat capacity. In Figure 10 the anomalies in the specific heat capacity due to superconductivity in YC_2 and $Y_2Br_2C_2$ are contrasted. The measured data are already corrected for the normal state contributions, which are readily attainable by suppression of the superconductivity by an external magnetic field.

Again large differences in the properties of YC_2 and $Y_2Br_2C_2$ arise. The specific heat capacity for the YC_2 sample (Figure 10, top)[56, 62] is a textbook example of BCS behavior with weak coupling. The fitted curve shows the expected theoretical behavior.[63] The energy gap has been calculated from experimental data, which yield $2\Delta(0) = 3.58(5)k_BT_c$, identical with the BCS value within experimental error. For $Y_2Br_2C_2$ the extrapolated Debye temperature lies at $\theta_D = 240(10)$ K. This value is considerably lower than for the hard and brittle YC_2 ($\theta_D \approx 420$ K)[63] with the three-dimensional interconnection in its crystal structure. Approaching the transition from the low-temperature side the specific heat capacity corrected for the normal state contributions increases steeply as it nears T_c, and it is only very insufficiently described by BCS weak coupling theory (Figure 10, bottom). In contrast, an excellent agreement with the predicted results of the (empirical) two fluid model[64] for (moderately) strong electron–phonon coupling is found, as is shown by the fitted curve.[57]

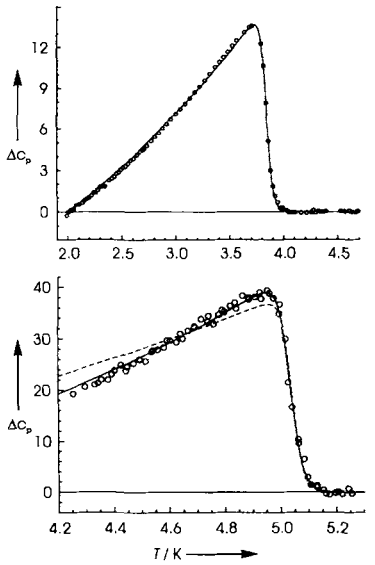

Figure 10. Difference in the specific heat capacity, $\Delta C_p(T)$ between the normal and superconducting states in mJ mol^{-1}K^{-1} as function of the temperature for YC_2 (top) and $Y_2Br_2C_2$ (bottom). While YC_2 shows nearly perfect BCS behavior (solid line), the measured points for $Y_2Br_2C_2$ deviate markedly from the fitted BCS curve (broken line) and are well fitted to the two fluid model (solid line)[40, 56, 57].

3.3.3. *Isotope Effect*

The most obvious differences in the superconducting properties of YC_2 and $Y_2Br_2C_2$ concerns the isotope effect. As is discussed in Section 2, the involvement of phonons in superconductivity was first demonstrated experimentally by the change in T_c with atomic mass through isotope substitution in Hg. With $\omega_D \propto M^{-1/2}$ the BCS theory predicts $T_c \propto M^{-1/2}$.

Because of the large atomic mass of mercury, the expected changes in T_c are rather marginal. For an average atomic mass of 199.7 the transition temperature was found at $T_c = 4.161$ K, for $M = 203.4$ it was 4.126 K. In the case of YC_2 and $Y_2Br_2C_2$ the experimental conditions are much more favorable. Assuming that the C_2 groups are crucial for the occurrence of superconductivity, one expects a change in T_c of $\Delta T_c = -0.17$ K for YC_2 and -0.20 K for $Y_2Br_2C_2$ upon substitution of ^{13}C for ^{12}C. The results[46, 62, 66] are given in Figure 11. The decrease in T_c of 0.14 K for $Y^{13}C_2$ lies near to the BCS value and demonstrates the participation of the C_2 units and their vibrations in the formation of Cooper pairs. In contrast, $Y_2Br_2C_2$ shows no isotope effect within experimental error limits. The measurements rather demonstrate the good reproducibility of the preparation (see Section 3.4).

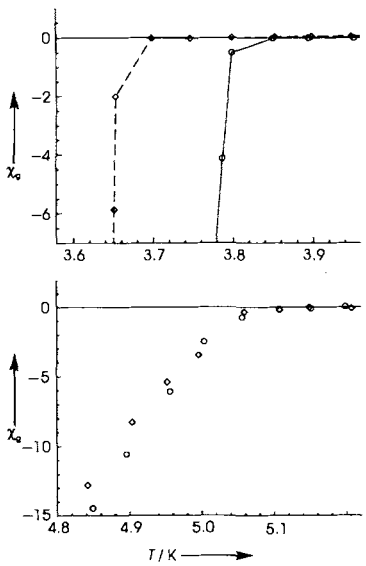

Figure 11. Isotope effects for YC_2 (top) and $Y_2Br_2C_2$ (bottom). Diamonds indicate measurements on ^{13}C samples. Circles represent measurements with the natural ^{12}C isotope mixture[46]. χ_g in 10^{-4} emu g^{-1}.

Despite the large differences between YC_2 and $Y_2Br_2C_2$ in the superconducting state, there is much evidence for a common origin of superconductivity in the two compounds. One may conclude that the special physical properties of the superconducting state are apparently of secondary importance in the search for a general connection between superconductivity and its chemical prepositions.

3.4. Chemical Bonding

The description of chemical bonding for the C_2 units in carbides and carbide halides, as outlined in Figure 3, refers to discrete molecular entities. In the solid the interaction of a multitude of these units in connection with the corresponding covalence of the carbon–metal bonds (p–d mixing) produces a band-type broadening of the energy levels. It needs to be tested whether in a detailed description of the bonding the crux of the hypothesis is retained, namely, that band states with quasi-molecular C_2-π^* character at the Fermi surface can cause a tendency for pairwise localization of conduction electrons. With regard to the validity of band structure arguments, a misunderstanding should be avoided right away. A metal in the superconducting state represents a highly correlated, many-electron system, which, by its nature, excludes any description with one-electron approximations. In the following the emphasis is merely to search the band structure in the normal state for special features that set the conditions for superconductivity at low temperature. In order to be able to follow the arguments the

essentials for the description of the chemical bonding in a solid will be introduced first. There are many sources that explain the electronic band structure to the chemist, and only a few can be mentioned here.[67-69]

If we stay with carbon and consider π bonding in the hydrocarbons ethene, the cyclopropenyl cation, cyclobutadiene, the cyclopentadienide ion, benzene etc., the number of MOs is equal to the number of C atoms. A hypothetical ring composed of 10^{23} carbon atoms, that is, a quasi-infinite chain, is characterized by a sequence of extremely closely spaced levels, that is, an electron band. The combination of the atomic wave functions for the lowest energy state is all-bonding, the highest all-antibonding in character. As Figure 12 indicates, the density of states $N(E)$ increases towards both the top and the bottom of the band.

The all-antibonding combination of the atomic wave functions with alternating sign can be described with the shortest possible wavelength, $\lambda = 2a$ (a = atomic spacing), and the all-bonding combination is described with an infinitely long wavelength. The wave vector $\boldsymbol{k}$ is therefore the positional parameter for an electron in the band of allowed states. With $|\boldsymbol{k}| = 2\pi/\lambda$, k changing from 0 to π/a, the band has a characteristic dispersion, as shown in Figure 12. The more states in an energy interval the flatter the band becomes, as is seen when $k \rightarrow 0$ (zone center or Γ point) and $k \rightarrow \pi/a$ (zone boundary). In the chosen example the band is filled with two electrons per C atom, and it is therefore half filled in the case of the chain $(CH)_{n\rightarrow\infty}$.[70]

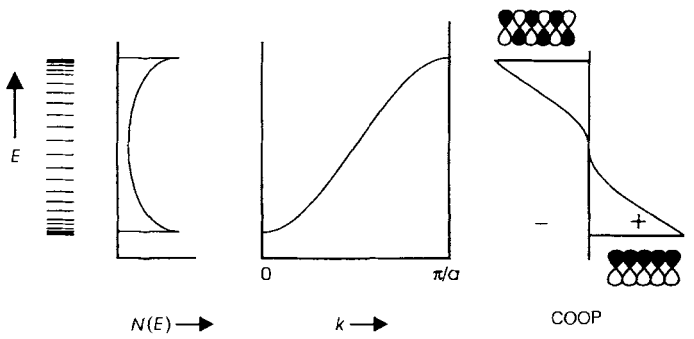

Figure 12. Schematic representation (from left to right) of the MO sequence for the π-like interaction in a polyene, the density of states $N(E)$, the dispersion k of the electronic band, and the chemical characterization of the band states with regard to the interaction between nearest neighbors ("crystal orbital overlap population", COOP). The bottom of the band corresponds to all-bonding, the top to all-antibonding combinations of the AOs[68].

The slope of the band at the Fermi level is a measure of the velocity v of the conduction electrons. Using the equations $E = mv^2/2$ and $p = mv$, one obtains $E = p^2/2m = \hbar^2k^2/2m$, and through differentiation one gets $dE/dk = \hbar^2k/2m = \hbar v$. A large slope of the conduction band at E_F corresponds to a high velocity of the conduction electrons,[71] and a horizontal band at E_F corresponds to a Fermi velocity $v_F \rightarrow 0$ in the special direction of k.

The electronic band structure describes the chemical bonding in momentum space (reciprocal space). A useful aid for the transformation of this description into real space is provided by the COOP formalism (crystal orbital overlap population),[72] which allows the analysis of the band character with respect to bonding, nonbonding, or antibonding interactions between selected atoms. According to the above discussion, the band character in the chosen example of π-type interaction between adjacent C atoms develops from bonding via nonbonding to antibonding with increasing energy (Figure 12).

The discussion of the bonding in a chain with the additional restriction to a single electronic band serves well as an introduction to the concepts and ideas. Band structures of three-dimensional crystals are naturally much more complicated. Normally they are portrayed in the form of the density of states $N(E)$ as a projection of all the band states on the energy axis. The dispersion of the bands is only shown in certain symmetry directions, and the specific zone boundaries are labeled with letters.

In Figure 13 the electronic density of states for $Y_2Br_2C_2$ as calculated with the Extended Hückel method[73, 74] is shown

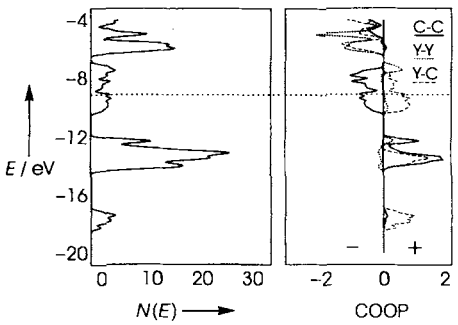

Figure 13. Band structure calculation for $Y_2Br_2C_2$ in the Extended Hückel approximation. On the left the total density of states $N(E)$ (also known as DOS) is given; right is the COOP analysis for the C–C (solid line), Y–C (dotted line), and Y–Y (dashed line) exchange interaction between nearest neighbors. The dotted horizontal line corresponds to E_F.

together with the COOP analysis for C–C and C–Y interactions between nearest neighbors. Concentrating on the energy range around the Fermi level, the structure at E_F is recognized as having antibonding C–C and bonding C–Y character. In accord with earlier results of band structure calculations on $Gd_2Cl_2C_2$[39] and newer ones on further $(RE)_2X_2C_2$ representatives,[75] the structure at E_F can be assigned to the C_2-π^* states which mix strongly with the Y-d states. At E_F a local maximum in the density of states appears, giving evidence of a flat band. The individual bands with their dispersions give a clue about the origin of this maximum.

In Figure 14 the results of self-consistent band structure calculations in various directions are presented.[76, 77] The results have already been described and discussed in more detail.[36] Here, only the character of the band states of the conduction electrons is of interest. The conduction bands cross E_F several times, partly with large gradients corresponding to high conduction electron velocity, and partly very flat at E_F, that is, a Fermi velocity that tends towards zero. The small dispersion in the direction from Γ to A (perpendicular to the layers) is a trivial consequence of the two-dimensionality of the structure of $Y_2Br_2C_2$. However, the special situation is due to the fact that the flat band occurs exactly at the Fermi level.

The orbital character of each of the two conduction bands in the so called "fat band" representation is given in Figure 14. The line width is proportional to the indicated orbital contribution. Because the contribution of the C_2-π^* is of particular inter-

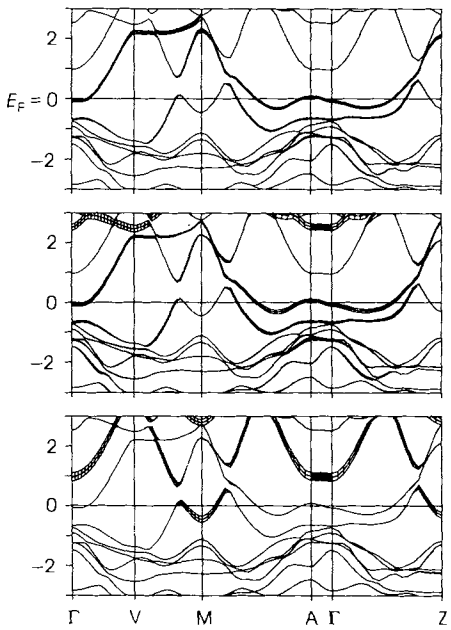

Figure 14. Representation of the dispersion of the bands for $Y_2Br_2C_2$ in the energy range close to the Fermi level, calculated self-consistently according to the TB-LMTO-ASA method ($E_F = 0$ eV). The prominent orbital contributions to the band structure are indicated in the form of "fat bands" (from top to bottom: C_2-π^*_{xz}, Y-d_{xz}, Y-$d_{x^2-y^2}$)[36].

est here, the linear combinations of the atomic orbitals in the C_2 unit were formed with z pointing in the direction of the C–C axis. It is obvious that the steeply crossing band at M and Z (zone boundaries in the plane of the layers) has strong $Yd_{x^2-y^2}$ character, while the C_2-π^* contribution mixed with Yd_{zx} determines the flat band. These results corroborate the naive approach that a tendency towards pairwise localization of conduction electrons should be connected to the C_2-π^* MOs.

The special course of the flat band is interesting, because a saddle point at the Γ point is formed. The band rises in the direction of A and falls (almost) perpendicularly towards Z.[36] Saddle points at E_F are well known from the classical layered superconductors, like niobium and tantalum dichalcogenides,[78] and also from the layered high T_c superconductors found with oxocuprates.[79] The existence of such saddle points—van Hove singularities[80]—was repeatedly discussed in connection with the origin of superconductivity in these layered compounds.[81–85] With the appearance of a van Hove singularity, the critical temperature follows an expression similar to that from BCS theory; however, the Debye temperature, $\theta_D = \hbar\omega_D/k_B$, is replaced by the Fermi temperature, $\theta_F = E_F/k_B$. Electron–phonon coupling therefore looses its importance for electron pairing, and because of the large value of θ_F in comparison with θ_D (and because of the higher density of states at E_F) higher critical temperatures are possible than in the BCS scenario. Therefore, van Hove singularities are possibly of particular relevance for high-temperature superconductivity (see Section 7). The replacement of θ_D with θ_F in $Y_2Br_2C_2$ should make the isotope effect disappear, as is actually observed in the case of this compound.

Despite the missing carbon isotope effect in $Y_2Br_2C_2$, it can be demonstrated unambiguously that vibrations of the C_2 units couple to the conduction electrons in a special way. In "frozen phonon" calculations the band structure is calculated for a slightly deformed lattice. The static distortion corresponds to a snapshot of the dynamic displacements of the atoms caused by a lattice vibration. As is obvious from Figure 15, small changes

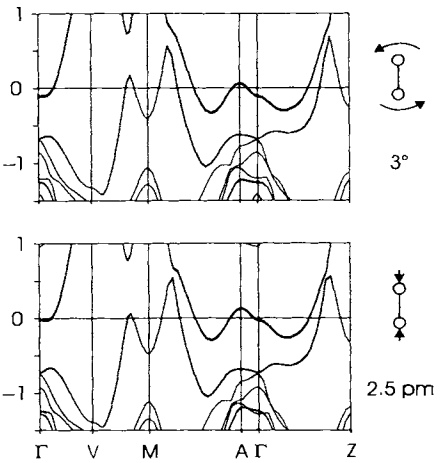

Figure 15. "Frozen phonon" calculations for the band structure changes in $Y_2Br_2C_2$. The changes in position and size of the C_2 units are shown to the right (fat band representation for the C_2-π^*_{xz} part, $E_F = 0$ eV)[36].

in the C atom positions influence the position of the flat C_2-π^* bands relative to E_F significantly. The band structure has been calculated for Γ phonons, that is, identical changes to all C_2 units. These changes are an increase of the C–C distance by 2.5 pm and a tilt of the C_2 units by 3° in the *ac* plane. As expected, the expansion of the C_2 unit weakens the antibonding interaction, and the π^* level decreases in energy. However, the rotation of the C_2 unit also leads to a drastic change due to the change in C–Y covalence. The C_2 units obviously form a charge reservoir that experiences a permanent dynamic alternation.

The carbides MC_2, with M = Ca, RE, Th, were the repeated subject of band structure calculations,[86–89] which aimed at understanding the transition from CaC_2 to ThC_2 type structure as well as explaining the stability of the CaC_2 type itself.[35] As expected, the self-consistently calculated band structure of YC_2[90] (Figure 16) showed no bands flat through the entire zone as in the case of the layered compound $Y_2Br_2C_2$. The density of states at E_F has again C-p and Y-d character, and it is high, but still does not show a maximum. Nevertheless, special features are closely related to those found for $Y_2Br_2C_2$. Because of the tetragonal symmetry of YC_2, the C_2-π^* bands become degenerate. They have a large amount of Y-$d_{xy,yz}$ character, and they approach E_F horizontally at the zone boundary. These bands are only flat at the zone boundary and otherwise cross the Fermi level steeply in the neighborhood of the center Γ. The pure Y-$d_{x^2-y^2}$ band, too, is steep at E_F. The three-dimensional YC_2 therefore also shows the characteristic juxtaposition of different kinds of conduction electrons as seen before: those which are highly mobile (itinerant), and those which have a disappearing Fermi velocity. The latter fill band states that come from the C_2-π^* MOs.

If one stays within the frame of BCS theory, the density of states $N(E_F)$ and the coupling constant V enter the exponent of the expression for T_c as the decisive parameters. Figure 15 illus-

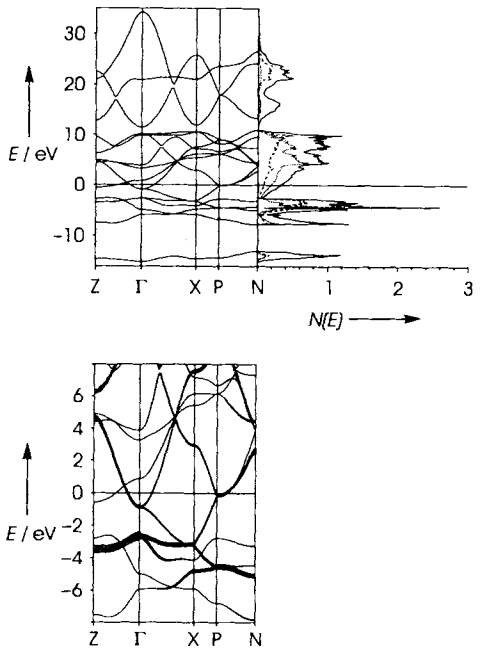

Figure 16. Self-consistently calculated band structure of YC_2 (top left), projected and total density of states (dashed: C-p, dotted: Y-d; top right, $N(E)$ in (eV·spin·formula unit)$^{-1}$), and fat band representation of the C_2-π^* part of the band around $E_F = 0$ eV (bottom)[90].

trates the coupling between vibrations of the C_2 units and the conduction electrons in the superconductors discussed here, and a high density of states results in flat bands at E_F. The example of YC_2 indicates that these bands may be highly dispersive and only need to be flat at E_F within a small interval Δk. In this context a long known fact should be remembered, namely, that a high density of states at the Fermi level leads to structural instability. A lattice that distorts statically implies localization of charge carriers. Structural instability and superconductivity compete.

4. Itinerant Electrons and Local Pairs

According to our hypothesis the origin of superconductivity is related to a tendency for a pairwise localization of some of the conduction electrons, without causing a structural phase transformation. The band structure is characterized by the simultaneous presence of steep bands and extremely flat band portions at the Fermi level, and the pairwise attractive interaction between conduction electrons results from a local attraction caused by special atomic arrangements, such as those of the C_2 units in the carbides and carbide halides of the rare earth metals. This local approach is somehow in contrast to the present general opinion, and particularly the large coherence lengths in the superconducting state are used as a main argument against it.

As already mentioned, the theory of superconductivity on the basis of local exchange interactions has regained some popularity due to the discovery of high-temperature superconductivity and the short coherence lengths that are observed there. Particularly revealing is a physical modeling and extension[27, 91–93] of the chemical view presented here, which is based on an interaction of local pairs with itinerant electrons. The model rests on a two band picture with one broad band **a** that is populated with single electrons (fermions) as in a normal metal and one very narrow band **b** that contains locally paired electrons (bosons).

The electrons in band **a** shield the far-reaching Coulomb interaction between the pairs in band **b** and suppress any structural phase transition. The superconductivity in this model system involves the electrons of the broad band **a** in the long-range pair interaction of an indirect nature, and the microscopic mechanism of superconductivity depends on the relative position of bands **b** and **a**, that is, on their relative degree of occupation. If **b** lies below **a** (or rather E_F?), band **b** is occupied by local pairs, which can move by virtual excitation of pairs of electrons with opposite momenta and spins in band **a**. The mechanism resembles the exchange interaction between local magnetic moments by polarization of the electron gas put forward by Rudermann, Kittel, Kasuya, and Yosida (RKKY).[94]

The maximum values for T_c are obtained when band **b** lies exactly at the Fermi level. The exchange interaction between the local pairs in the narrow band and the itinerant electrons in the broad band also couples the electrons in **a** to form Cooper pairs. The condensation of all pairs produces the superconducting state. If band **b** lies above the Fermi surface, electrons in **a** with opposite momenta and spins couple through the virtual transition to local pair states of the empty band **b**. This case leads to BCS-type behavior and $2\Delta(0) = 3.52 k_B T_c$.[27]

5. Prediction

The special features in the electronic band structures of carbides and carbide halides of the rare earth metals are viewed as a characteristic "fingerprint" for superconductivity. Because of its qualitative character and the restriction to electronic criteria only, quantitative predictions cannot be expected. Using the fingerprint in the search for new superconductors is, however, also of great enough interest. A new superconductor[95] discovered in the chemical neighborhood of the compounds discussed before serves as an example.

During extensive phase studies on boride carbide halides of the rare earth metals[96, 97] we obtained the new compound $Ce_9Br_5(CBC)_3$. The structure is shown in Figure 17. The chemical bonding can be described in a simplified way as $(Ce^{3+})_9(Br^-)_5(CBC^{7-})_3e^-$ according to the Zintl-Klemm concept. The bent CBC units, which occur as discrete anions, are electronically isovalent with SO_2. From much experience with other rare earth metal compounds the electron surplus is expected to

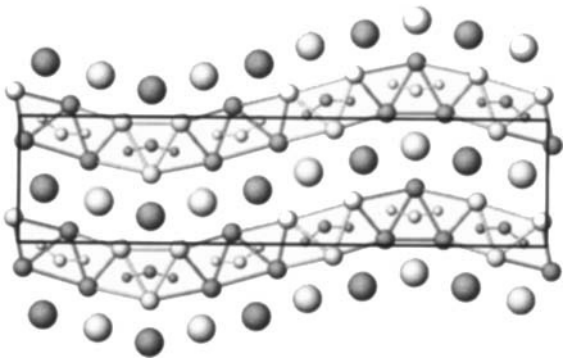

Figure 17. Projection of the orthorhombic structure of $Ce_9Br_5(CBC)_3$ in the direction of the b axis (a horizontal). The atoms Br, Ce, B, and C are shown with decreasing size[95].

be used for metal–metal bonding. Because of the partial occupancy of a M–M bonding band a "true" metal should result.

The results of Extended-Hückel calculations (Figure 18) are in agreement with this simplified view of chemical bonding as

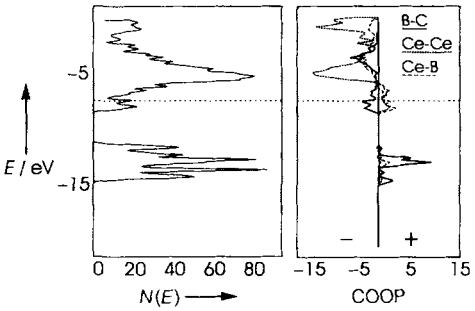

Figure 18. Band structure of $Ce_9Br_5(CBC)_3$ calculated in the Extended Hückel approximation (left: total density of states, right: COOP for the indicated interactions between nearest neighbors; dotted horizontal line: E_F).

well as with the resulting metallic properties. One finds a maximum of the density of states at the Fermi level, and the COOP analysis shows the bands at E_F to be of Ce–Ce and B–Ce bonding character on one side and of B–C antibonding character on the other. The local maximum at E_F gives evidence for the existence of a flat band with effectively nonbonding character due to the backbonding from occupied antibonding states of the molecular anion into the metal d states. With the exception of significant M–M bonding, there are many similarities in the bonding between $Ce_9Br_5(CBC)_3$ and $Y_2Br_2C_2$, and one is tempted to search for the existence of superconductivity. Of course, a superconducting transition is not expected for the magnetic compound of cerium containing Ce^{3+} ions ($4f^1$ configuration). Luckily the nonmagnetic isotypic La compound can also be prepared; moreover, the band structure exhibits the same characteristic feature at E_F despite the differences in the electronic energy levels of Ce and La, and the slightly different lattice parameters. $La_9Br_5(CBC)_3$ is a superconductor, as is demonstrated by the disappearance of resistance at 6 K, and the simultaneous change to diamagnetism.

The self-consistently calculated band structure of $La_9Br_5(CBC)_3$ is shown in Figure 19. The Fermi level is crossed by a multitude of steep bands. One of the degenerate bands at E_F is again almost dispersionless. As expected, the direction from S to R where the band is flat corresponds to the *c* direction. The flat band has both BC_2-π^* and La-$d_{xz,yz}$ character. As in the case of the C_2 units, the conduction electrons also couple with specific "molecular" vibrations of the CBC unit. The bending vibrations, especially, change the position of the flat band greatly and should therefore be of importance to the superconductivity.

In contrast to the recently discovered boride carbide halides, the boride carbides of the rare earth elements have been known for a long time. The compound $La_5C_2(CBC)_2$ is particularly interesting here. It can be formulated, according to the Zintl-Klemm concept, as $(La^{3+})_5(C_2)^{4-}(CBC^{5-})_2e^-$, and it contains C_2 units beside linear CBC units which are isoelectronic to CO_2.[98] The compound is superconducting at 6.9 K.[99] This is the parallel to the much studied superconductor $(RE)Ni_2B_2C$[100, 101] with (also linear) BCB units. An examination of the electronic structure must show whether the presence of the C_2 units, or possibly, the CBC groups is important for the appearance of superconductivity in the d-metal-free compound $La_5C_2(CBC)_2$.

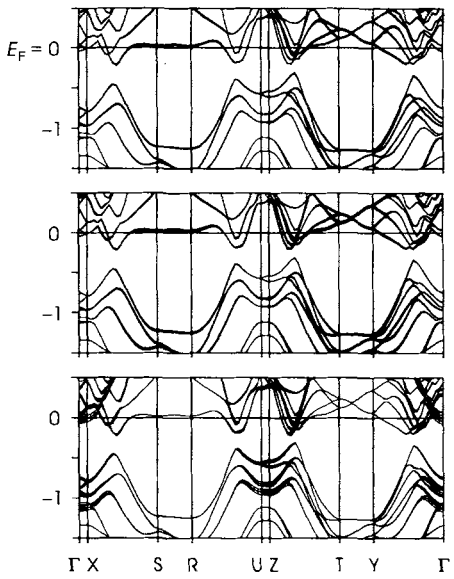

Figure 19. Self-consistently calculated band structure of $La_9Br_5(CBC)_3$ for the bands lying around the Fermi level at $E_F = 0$ eV. From top to bottom the contributions of the BC_2-MOs (approximate π^*), the La-$d_{xz,yz}$, and La-$d_{x^2-y^2}$ orbitals are emphasized in the fat band representation [95].

6. Orbital Topology

When the fingerprint of superconductivity is reduced to the condition of "steep bands beside parts of bands with vanishing slope at the Fermi level", the consideration of specific bonding conditions, which has been distinctly addressed for the systems discussed so far, is lost. The question of the symmetry of the band states, as is necessary for superconductivity, remains open. What kind of atomic orbitals in which combinations produce the condition for superconductivity?

Krebs sought an answer to this question in a series of papers, first addressing the question selectively,[102] and later more generally.[103, 104] He was of the opinion that the prerequisite for superconductivity must be a partially occupied band formed by the atomic orbitals in such a way that the electrons can move in at least one direction without finding planar or conelike nodes.[102] Such systems are δ-bonded linear chains of d-metal atoms, as in Nb_3Sn (compare Section 7). The all-bonding combination—the argument has at its basis a representation of the bands at the Γ point—creates tubes along the chain with the same sign of the atomic wave functions (ψ_+ and ψ_-) in each. Absence of nodes in the total function naturally characterizes bonding with s electrons, and one would therefore expect superconductivity to occur with alkali metals. However, these show no superconductivity under normal pressure, where they are s metals. Nevertheless, the s electrons, in spite of their large radial extension and the resulting width of the bands and consequently low density of states, were assumed to be of special importance for superconductivity. The idea found no acceptance, and the publication of the last manuscript was rejected. In a theory developed ten years later,[105] essentials of the idea were applied.

The starting point of the considerations was the idea of Weisskopf,[106] who, in order to visualize the Cooper pair, put forward the real space model of a moving conduction electron that leaves a polarization trace behind it, which produces an interaction with a conduction electron moving in the opposite direction. The polarization trace ("long thin tube"), according to Johnsson and Messmer,[105] is produced in adjacent tubes or layers with alternating positive and negative sign of the wave function, which as regions of p–π bonding or bonding through d_{z^2} orbitals in a layer as well as d–δ bonding in a chain can be identified with the node-free areas of the total function according to Krebs. For the d–δ bonded chain, for example, this produces tubes from the Ψ_+ and Ψ_- contributions of the atomic wave functions, which each construct bonding systems of mutually antibonding character adjacent to one another. The electrons in each are assigned spin ↑ and spin ↓. This "antiferromagnetism" of the conduction electrons[107] describes the bonding state for the singlet electron pair. The description corresponds to the original suggestion by Schafroth of characterizing Cooper pairs as "quasi-molecules".[108, 109]

The occurrence of such tubes is not restricted to explicitly one-dimensional structures. As an illustration of the basic idea[105] the construction of the tubes for a body-centered cubic lattice of a transition metal, plotted as the Γ point configuration with the all-bonding δ interaction along the *z* axis is shown in Figure 20. Niobium, the metal with the highest critical temperature of all the element superconductors ($T_c = 9.3$ K), crystallizes in this structure, and interestingly, the concentration of the electrons is just large enough to provide a near coincidence of the triply degenerate $d_{xy,xz,yz}$ band at the Γ point with the Fermi level.[110] By definition, the band has zero slope at Γ.

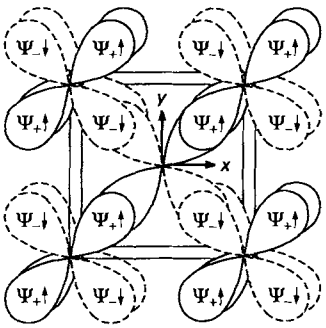

Figure 20. Depiction of the δ bonding in the body-centered cubic crystal of niobium. The combination of the d_{xy}, d_{xz}, and d_{yz} orbitals give a triply degenerate band, which nearly coincides with the Fermi level at the Γ point. The figure is taken from ref. [105] where the regions of different sign of the wave function are associated with opposite spins.

The band degeneracy at the Fermi level is the cause of a Jahn–Teller or pseudo Jahn–Teller effect: the conduction electrons couple with atomic displacements to remove the degeneracy. The dynamic Jahn–Teller coupling between conduction electrons and lattice lead to formulas for T_c and other superconductivity parameters that resemble those derived from the BCS theory. The model thus represents a real space analogue to coupling of electrons through virtual phonons. In the quantitative formulation of the theory, the degree of the dynamic displacement of the atoms is a function of two parameters, which quantify, on one hand, the distance between the tubes or layers with differing signs of the wave function, and on the other hand, the strength of the bonding in the tubes and layers. These parameters set the field for structural phase transformations (with static Jahn–Teller effect) and superconductivity (if the Jahn-Teller effect stays dynamic). Critical temperatures and isotope effects are predicted for simple elemental and compound superconductors with an impressive accuracy.[105]

When one applies the theory qualitatively to the carbides and carbide halides of the rare earth metals, one meets fundamental problems. For $Y_2Br_2C_2$ node-free tubes parallel to the *b* axis are easily constructed. These are made of, on one side, bonding combinations of C-p_x and Y-d_{xz} orbitals, and on the other side, very weak δ bonding involving the Y-d_{xz} orbitals.[88] This configuration corresponds to that of the Γ point, and it is indeed part of the flat, although not degenerate, band at E_F in the band structure. In contrast, the corresponding construction for YC_2 does not correlate with the band structure, because no electronic states at E_F lie at the Γ point, and it is only at the zone edge in the 111-direction (P point) that the conduction band becomes flat and touches the Fermi level. The example, as many more, demonstrates the difficulties in connecting this interesting real space model with the description of chemical bonding in momentum space. We are working on an extension of the model to general points in momentum space.

7. To Higher Temperatures

Superconductivity is known to exist in more than ten thousand materials. Here the term material refers to the complete spectrum of pure metals, structurally and analytically defined chemical compounds, mixed crystals, alloys, and phase mixtures. So there are many different materials on which to test the presented ideas about the necessary prerequisites in chemical bonding for superconductivity to occur. Perhaps the most investigated compounds are the technically important A15 phases, which before 1986 were termed high-temperature superconductors.

The cubic structure is characterized by three nonpenetrating linear chains of transition metals, all mutually orthogonal (Figure 21). With decreasing temperature, the equivalence of the

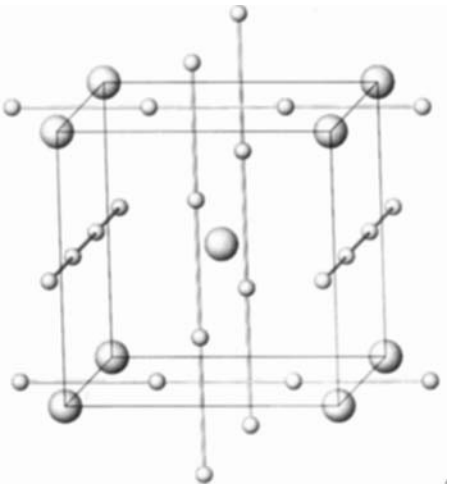

Figure 21. Unit cell of Nb_3Sn (A15 type). The linear chains, orthogonally oriented to one another, of Nb atoms are emphasized.

chains is lost through structural phase transformations before superconductivity appears. The band structure[111, 112] for the tetragonal Nb_3Sn (Figure 22) shows a degenerate extended flat band at the Fermi level around the Γ point corresponding to δ-type interaction in the chain, which is closely related to the bonding in discrete complexes with multiple metal–metal bonds known to every chemist.[113]

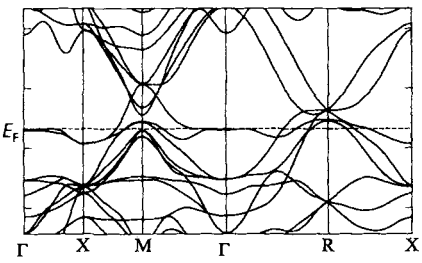

Figure 22. Band structure of tetragonal Nb_3Sn with an extended flat band at the Fermi level[112].

In the past decade, three classes of superconductors were discovered; the critical temperatures of some of them are way above the critical temperatures of conventional superconductors that had been optimized over decades. These are oxobismuthates, fullerides (sometimes called fullerites), and oxocuprates. The high critical temperatures gave physicists hope that new mechanisms would be discovered, or at least that a better understanding would be gained of the nature of electron–electron coupling in these systems where it must be very pronounced. For some chemists the proximity to normal valence compounds, different from metallic elements and intermetallic phases, was of interest as it allows the use of familiar terms and notions like oxidation number, coordination, etc. in discussing superconductivity.

7.1. Oxobismuthate Superconductors

The superconducting bismuth oxides crystallize in the perovskite structure, or in structures closely related to it. The arrangement of the atoms in this very simple structure is depicted in Figure 23. In the compound $BaBiO_3$, Bi has the unusual oxidation state +IV. At room temperature the unit cell is doubled

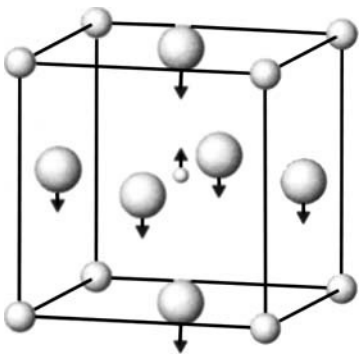

Figure 23. Unit cell of the perovskite-type structure. The arrows show the Γ point displacements for the ferroelectric mode in $BaTiO_3$. The O, Ba, and Ti are depicted in decreasing size.

and distorted to monoclinic. It contains two types of Bi atoms in differently sized coordination polyhedra.[114] As the compound is a semiconductor the bonding can be described by the formula $(Ba^{2+})_2(Bi^{3+})(Bi^{5+})(O^{2-})_6$, and the complicated static distortion can be easily related to the localization of two electrons at the Bi^{3+} ion with the "lone pair" configuration. Such an interpretation remains contradictory, though. From band structure calculations[115] there is hardly any difference between the charges of the Bi atoms ($\approx 3.9+$ and $\approx 4.1+$). The naive assignment of integral oxidation numbers leads to the argument that the specific deformation of the structure resulting in nonequivalent Bi atoms—corresponding to a charge density wave (CDW)—can be suppressed through the partial replacement of Bi with Pb as Pb^{4+}, since its closed electron configuration prefers a regular coordination octahedron, which would stabilize the structure. In fact, the (tetragonal) mixed crystal $BaPb_{0.75}Bi_{0.25}O_{3-\delta}$ shows no CDW transition; it is metallic and becomes superconducting below 13 K.[117] The compound should be seen as an important predecessor of the actual high-temperature superconductors. In an analogous way, the stabilization of the undistorted structure is obtained through an increase of the relative amount of Bi^{5+} ions, which again have a closed shell ($5d^{10}6s^06p^0$) configuration. This is achieved, accompanied by a change in the charge carrier concentration, by partial replacement of Ba with K. Cubic $Ba_{0.6}K_{0.4}BiO_3$ shows superconductivity at $T_c \approx 30$ K.[118]

The proximity of these superconductors to ferroelectrics, for example, the technically important $BaTiO_3$, is evident. The characteristic lattice vibration shown in Figure 23, which becomes soft in the zone center, is responsible for the ferroelectric behavior of barium titanate. The resulting static deformation—chemically it is due to a distortion in the direction of a titanyl cation, TiO^{2+}—produces parallel dipole moments in all unit cells. These moments can be reversed by an external electric field, in analogy to the magnetic moment in a ferromagnet. The instability of the cubic structure is due to the configurational instability of the O^{2-} ion,[119, 120] which is reflected in its nonlinear atomic polarizability. It is reasonable to associate a (dynamic) deformation of the same type as in $BaTiO_3$ with the superconductivity in oxobismuthates.[121, 122] In contrast to the valence-stable Ti^{4+}, the intermediate valence system Bi^{3+}/Bi^{5+} can react sensitively with a tendency to pair localization with a pseudooctahedral environment.[123] Thus, to the configurational instability of the O^{2-} ion is added a vibronic coupling due to the presence of a lone pair at Bi^{3+}. In a lattice dynamics model[124, 125] the common origin of ferroelectricity and superconductivity in these systems, which has also been empirically recognized,[126] has been demonstrated.

The superconducting oxobismuthates are looked upon as representative examples for systems that are composed of local pairs next to itinerant electrons as considered in Section 4.[127] Indeed the band structure calculated for the approximate composition $Ba_{0.5}K_{0.5}BiO_3$ (Figure 24)[128] shows a broad conduction band formed from Bi-6s and O-2p orbitals, which becomes very flat with the formation of a saddle point at E_F in X.

The element bismuth itself could serve as a very obvious example of the role of local pairs in superconductivity. Under ambient conditions it has a structure[129] formed from corrugated layers of hexagons, where each Bi atom has three nearest

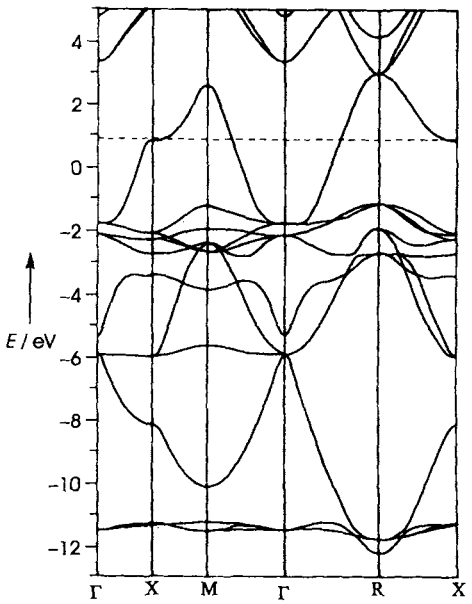

Figure 24. Band structure of $Ba_{0.5}K_{0.5}BiO_3$ with flat Bi-6s/O-2p bands at E_F (dashed horizontal line) at point X [128].

neighbors in its own layer (307 pm) and three in an adjacent layer (353 pm). Its noncentric position in the trigonal antiprism can be interpreted in terms of a localization of the stereoactive nonbonding electron pairs, in agreement with the semimetallic properties, which classifies Bi close to a (degenerate) semiconductor. Under pressure the structure becomes highly symmetrical—first cubic primitive, then body-centered cubic. The charge carrier concentration is many times larger than in the ambient pressure form, that is, the localization of the nonbonding electron pairs is lost in the high-pressure forms. However, the tendency towards localization through dynamic deformation of the atomic surroundings apparently still remains, and leads to superconductivity with critical temperatures up to $T_c = 8.5$ K.[130] Also, deposition of Bi from the gas phase on a cold substrate at 4 K yields a film that is superconducting up to 6 K.[131] The film recystallizes upon warming to 20 K and no longer shows superconductivity when cooled again. Obviously, the "locking in" of the electron pairs is apparently avoided in the case of amorphous Bi. This last example once again stresses the relevance of local effects to superconductivity, as do several other amorphous superconductors.[132]

7.2. Fulleride Superconductors

Graphite becomes superconducting on intercalation of alkali metals. The critical temperatures are, however, very low ($T_c \approx 0.5$ K for C_8K).[133] In contrast, the intercalation of alkali metals in the other allotrope of carbon, fullerene C_{60}, produces critical temperatures of over 30 K.

C_{60} is a semiconductor. After reaction with alkali metals, poorly conducting metals are obtained, and at the composition A_3C_{60}, superconductivity appears. This was first discovered in K_3C_{60} (critical temperature $T_c \approx 18$ K)[134] The critical temperature increases with the size of the alkali metal atoms. Rb_3C_{60} and Cs_2RbC_{60} are superconducting at 29 K and 33 K, respectively.[135] Higher values such as $T_c = 45$ K[136] for the combination $Rb_{2.7}Tl_{2.2}C_{60}$ have still to be reproduced. The maximum alkali metal content is reached at A_6C_{60}, and it produces, along with A_4C_{60}, semiconducting behavior.

The phase relations and the structures of the alkali metal fullerides are complicated. The structure of the A_3C_{60} phases appear relatively simple at first sight. The molecules show a cubic close packing, with an occupation of both the octahedral and tetrahedral voids by the cations ($BiLi_3$-type structure). However, because of an orientational disorder of the quasi-spherical anions, the structure is still unknown in detail.[137-139]

The band structure of C_{60} looks like that typical of a molecular crystal. The broadening of the MOs to bands is only slight, and groups of bands are therefore well separated by large forbidden gaps. The valence bands correlate with the HOMO with h_u character, and the conduction bands are derived from the LUMO with t_{1u} character. Upon intercalation, the electrons of the alkali metal atoms are transferred almost completely to the C_{60} molecules to form triply charged anions; the Fermi level is thereby raised, and the LUMO consequently becomes partially occupied. The MO diagram of the C_{60} molecule[140] is very exactly known. However, as the relative orientations of the molecules in the solid cannot be determined unambiguously because of orientational disorder, the specific interaction of the molecules are not exactly known, and the band structure that results therefore remains uncertain. Calculations have been performed for different ordered structural models, assuming one single orientation of all anions, or two or four different orientations.[140-142] It is tempting to show the best fitting result, which is characterized by steeply crossing bands beside an extended flat band at E_F. However, it would have no evidential value.

Despite this lack of detailed knowledge of the crystal structures and the resulting problems of describing the bonding in the solid, there seems to be agreement that the superconductivity in fullerides can be understood within the framework of conventional theories.[143, 144] Such a statement can not be made for the oxocuprate superconductors.

7.3. Oxocuprate Superconductors

Experiments and theories of high-temperature superconductivity are described in tens of thousands of original papers and in a number of books. The problems in understanding the superconductivity of oxocuprates begins with the exact chemical compositions. The first high-T_c superconductor found was based on La_2CuO_4, made metallic and superconducting by the substitution of cations in $La_{1.85}Ba_{0.15}CuO_4$.[5, 145] Later it was shown that with an excess of oxygen of the order of one percent, superconductivity occurs also in the unsubstituted compound $La_2CuO_{4.04}$.[146, 147] The oxygen content, in particular, is frequently unknown in the investigated multicomponent phases. The second problem affects the crystal structures, that even at room temperature can often be described only approximately, because they are modulated with long periodicities as in (EA)-Bi-Cu-O and (EA)-Tl-Cu-O systems (EA = alkali earth metal)[148, 149] and, like the previously described fullerides,

elude an exact description in terms of the band structure. Even in homogeneous single crystals structural and electronic phase separations are observed at low temperatures.[149-153] These produce extremely complicated features in the real structure that are puzzling with respect to their importance for superconductivity. From the point of view of physics, the oxocuprates differ from the oxobismuthates in the presence of magnetic ions. Antiferromagnetic interactions between the Cu^{2+} ions might therefore be involved in the emergence of superconductivity in these materials.

$YBa_2Cu_3O_{7-\delta}$ is possibly the most completely characterizable and best examined high-T_c superconductor.[154, 155] The unit cell of $YBa_2Cu_3O_7$ is shown in Figure 25. It is characterized

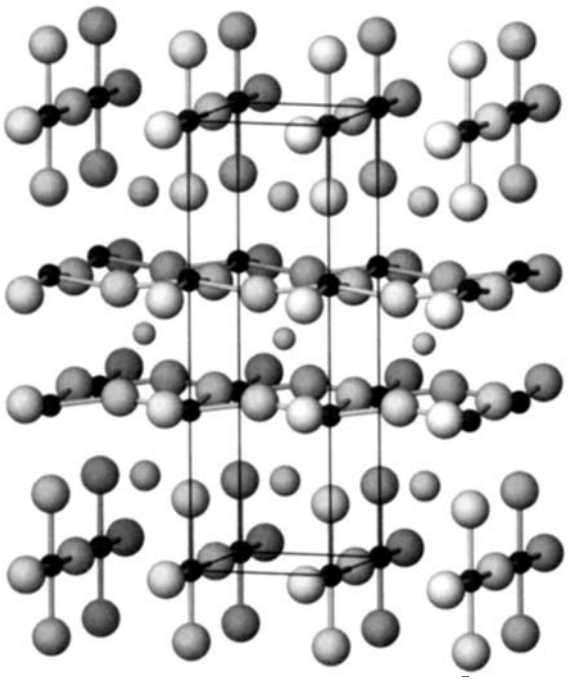

Figure 25. Unit cell of $YBa_2Cu_3O_7$. The CuO_2 layers around the Y atoms, and the CuO_3 chains next to the Ba atoms are highlighted (dark small spheres Cu, the others Y, Ba, O with increasing size).

by the CuO_2 layers with their typical deviation from planarity, which enclose the Y^{3+} ions, and the CuO_3 chains between the layers next to the Ba^{2+} ions.[156] Starting from an assignment of Cu^{2+} in the layers and Cu^{3+} in the chains,[158] one arrives at an intermediate valence and metallic conductivity through a partial charge compensation between layers and chains.

The O atoms between the Cu atoms in the chains can be easily removed. By complete removal ($\delta = 1$) the chain is left with CuO_2 dumbbells containing Cu^+. The composition would suggest all copper in $YBa_2Cu_3O_{6.5}$ to be Cu^{2+}; however, this is not true as indicated by the metallic conductivity of this phase. Given enough time, a crystal develops an ordered array of alternating filled CuO_3 and depleted CuO_2 chains accompanied by a doubling of the a axis.[159, 160] With the formula $YBa_2Cu_3O_{6.67}$, the order is two filled following one empty chain with a tripling of the a axis.[161] The seemingly simple chemical compound $YBa_2Cu_3O_{6.5}$ is therefore a mixed valence phase[162] with crystallographic ordering in different coordinations for Cu in the +I, +II, and +III oxidation states. Beyond this, an intermediate valence adds to the mixed valence and leads to the electronic delocalization by charge transfer. With the successive removal of the oxygen atoms, the critical temperature decreases from $T_c = 93$ K for $\delta = 0.1$ to an extended plateau around 60 K for $0.3 \leq \delta \leq 0.5$ and reaches 0 K for $\delta = 0.6$.[163] At this value the phase becomes semiconducting. Antiferromagnetism, first occurring at $\delta = 0.75$, has a maximum ordering temperature T_N of 500 K at $\delta = 0$.[164]

Mixed valence with the special feature of involving oxidation states differing by 2 and antiferromagnetism in a system with strong correlations indicate quite different kinds of electron localization. Whether one of them, or both, are responsible for the formation of Cooper pairs is still an open question.[165] Interestingly, a valence change from Cu^+/O^{2-} to Cu^{3+}/O^{2-} (or $(CuO)^+$)[158] can be compared to the situation with the carbide examples. In the carbides the metal-d bands interact with the filled antibonding π^* MOs of the anion, and in the doped oxocuprates the reverse interaction of the empty antibonding $d_{x^2-y^2}$ level of Cu^{3+} with the filled oxygen p band exists.

As is shown in Figure 26 for two special sections of the band structure of $YBa_2Cu_3O_7$, the electronic structure is again characterized by bands with large dispersion besides very flat band portions at E_F.[79, 167-169] This structure differs from those of the examples discussed before in the multiple occurrence of both types of band. The saddle point close to X has also been verified experimentally[170] by angle-dependent photoemission studies, and it is the basis for arguments that explain the high critical temperature within the theory of the van Hove singulari-

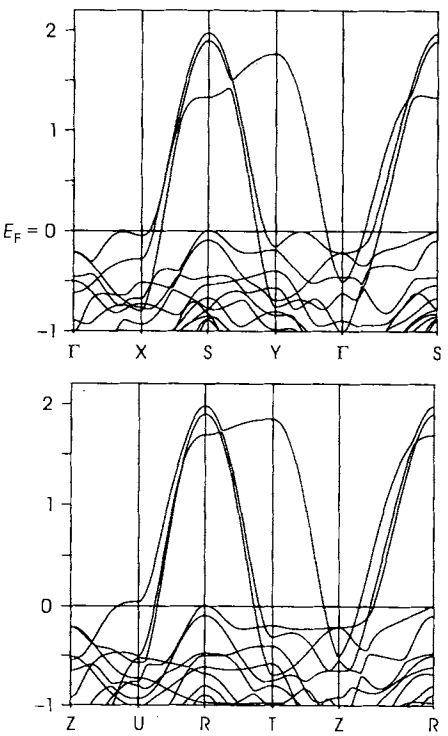

Figure 26. Band structure of $YBa_2Cu_3O_7$. Planes are parallel to the layers passing through the zone center (top) and through the zone edge (bottom)[168]. The band maximum at $E_F = 0$ eV at point S has essential contributions from O-2p and Cu-d_{xz} orbitals from those atoms forming the CuO_3 chains. Obviously, the chains do not only represent charge reservoirs but participate in the formation of Cooper pairs.

ty.[84, 171] One can also argue in terms of an interplay of the electrons in different flat bands at E_F, which increases the critical temperature. The energy gap in the superconducting state is very anisotropic.[172–175] If one represents it through a spectrum of discrete values taken from IR reflectivity measurements, the observed critical temperature can be derived without the assumption of an unconventional mechanism.[176] Perhaps one complicates matters when searching for a chemical understanding of superconductivity in high-temperature superconductors. Maybe what Hans Georg von Schnering called "virtual valence instability" in a paper on new superconductors[177] is easier to grasp in the simpler low-T_c superconductors.

8. Concluding Remarks

The understanding of superconductivity from a chemical point of view, as developed from special examples, leads to the conclusion that a tendency to pairwise localization of conduction electrons must occur. The prerequisite is the occurrence of steep electronic bands at the Fermi level as well as bands that display maxima, minima, points of inflection, or saddle points at E_F in order to provide a vanishing Fermi velocity to part of the conduction electrons. This condition is obviously necessary, though not sufficient, as clearly shown by the competition between superconductivity and structural phase transformation or magnetism.

Hardly any physical phenomenon has had so much work dedicated to it as the disappearance of the electrical resistance in a metal—in fact, even decades before the final (accidental) discovery of superconductivity. Probably every thought that one may now develop about the phenomenon of superconductivity has already been considered and written down somewhere. The earlier cited work of London from 1938[11] about Bose–Einstein condensation, which refers to superfluidity and superconductivity serves as a good example of this statement. "The well known formula for the electrical conductivity $\sigma \approx (l/v)_{Av}$ would yield the value $\sigma \approx \infty$ in the case where a finite fraction of all particles has zero velocity. . . .In general (particularly in the case of Fermi statistics, and also in the case $T > T_0$ for the Bose statistics) one is accustomed and entitled to disregard the few particles. . . In the case of Bose degeneracy ($T < T_0$), however, we are not allowed to neglect the *finite fraction* of particles with $v = 0$. . . One may say the 'conductivity' viz. the *fluidity*. . . becomes infinite. . ., and this abruptly, as soon as $T < T_0$." The large spatial extension of these "particles" is a consequence of their vanishing momentum.

In this work the introduced ideas are born from chemistry and carried some way into physics. Entirely independent of the topic superconductivity, one meets an interesting aspect. The term "tailor-made" is frequently used in modern chemistry when we put into use our knowledge of structures and structural increments in real space, to build molecules, supramolecular assemblies, and solids with desired properties. A "tailoring" in momentum space up till now is restricted to a few questions raised about chemically trivial materials, such as how to make the indirect band gap semiconductor silicon a direct one. Could it be that there is a large open field of research for chemists in constructing desired band structure features?

My group contributed numerous results to the work reported here. In particular, I would like to thank Peter Adler, Kyungsoo Ahn, Michael Bäcker, Annette Bussmann-Holder, Shuiquan Deng, Claudia Felser, Thomas Gulden, Rüdiger Henn, Jürgen Köhler , Reinhard Kremer, and Hansjürgen Mattausch for their contributions and many helpful discussions. The help of Claudia Kamella with the drawings and of Brendan Gibson in the translation of the text is gratefully acknowledged.

Received: February 3, 1997 [A 205 IE]
German version: *Angew. Chem.* **1997**, *109*, 1879–1891

[1] H. Kamerlingh-Onnes, *Akad. van Wetenschappen* **1911**, *14*, 113, 818.
[2] J. File, R. G. Mills, *Phys. Rev. Lett.* **1963**, *10*, 93.
[3] J. R. Gavaler, *Appl. Phys. Lett.* **1973**, *23*, 480.
[4] L. R. Testardi, J. H. Wernick, W. A. Royer, *Solid State Commun.* **1974**, *15*, 1.
[5] J. G. Bednorz, K. A. Müller, *Z. Phys. B* **1986**, *64*, 189.
[6] L. Gao, Y. Y. Xue, F. Chen, Q. Ziong, R. L. Meng, D. Ramirez, C. W. Chu, J. H. Eggert, H. K. Mao, *Phys. Rev. B* **1994**, *50*, 4260.
[7] E. Maxwell, *Phys. Rev.* **1950**, *78*, 477.
[8] C. A. Reynolds, B. Serin, W. H. Wright, L. B. Nesbitt, *Phys. Rev.* **1950**, *78*, 487.
[9] H. Fröhlich, *Phys. Rev.* **1950**, *79*, 845.
[10] J. Bardeen, *Phys. Rev.* **1950**, *80*, 567.
[11] F. London, *Phys. Rev.* **1938**, *54*, 947.
[12] J. M. Blatt, *Theory of Superconductivity*, Academic Press, New York, **1964**, preface.
[13] Richard Andrew Ogg, Jr., (1909–1962), experimental chemist at Stanford University, California, had proved the stability of electron pairs in solutions of alkali metals in ammonia [14]. Starting from that finding he performed experiments on quenched Na–NH_3 solutions, which hinted at superconductivity up to 190 K [15,16], but the results could not be reproduced by other authors.[17] A little poem by George Gamow says: "In Ogg's theory it was his intent That the current keep flowing, once sent; So to save himself trouble, He put them in double, And instead of stopping, it went." My thanks are due to Professor Peter P. Edwards, Birmingham, for detailed information.
[14] R. A. Ogg, Jr., *J. Chem. Phys.* **1946**, *14*, 114.
[15] R. A. Ogg, Jr., *Phys. Rev.* **1946**, *69*, 243, 668.
[16] R. A. Ogg, Jr., *Phys. Rev.* **1946**, *70*, 93.
[17] H. A. Boorse, D. B. Cook, R. B. Pontius, M. W. Zemansky, *Phys. Rev.* **1946**, *70*, 92.
[18] W. Buckel, *Supraleitung*, VCH, Weinheim, **1990**.
[19] J. Bardeen, L. N. Cooper, J. R. Schrieffer, *Phys. Rev.* **1957**, *108*, 175.
[20] H. Suhl, B. T. Matthias, L. R. Walker, *Phys. Rev. Lett.* **1959**, *3*, 552.
[21] G. M. Eliashberg, *Sov. Phys. JETP Engl. Trans.* **1960**, *11*, 696.
[22] W. L. McMillan, *Phys. Rev.* **1967**, *167*, 331.
[23] J. P. Frank in *Physical Properties of High-Temperature Superconductors IV* (Ed.: D. M. Ginsberg), World Scientific, Singapore, **1994**, p. 189.
[24] H. A. Mook, M. Mostoller, J. A. Harvey, N. W. Hill, B. C. Chakoumakos, B. C. Sales, *Phys. Rev. Lett.* **1990**, *65*, 2717.
[25] Pairing is described in momentum space. Momentum space and real space transform into one another, as is obvious to a chemist from X-ray scattering. There is the visual approach in real space with only limited power of prediction (lattice planes acting as mirrors, Bragg equation) and the much more abstract but comprehensive approach in momentum space (reciprocal lattice, Laue equations).
[26] R. M. Schafroth, *Phys. Rev.* **1955**, *100*, 463.
[27] R. Micnas, J. Ranninger, S. Robaszkiewicz, *Rev. Mod. Phys.* **1990**, *62*, 113.
[28] A. S. Alexandrov, N. F. Mott, *Int. J. Mod. Phys. B* **1994**, *8*, 2075.
[29] B. N. F. Mott, *Z. Phys. Chem. München* **1994**, *184*, 1.
[30] L. N. Cooper, *Phys. Rev.* **1956**, *104*, 1189.
[31] P. G. de Gennes, *Superconductivity of Metals and Alloys*, Benjamin, New York, **1966**, reissued, Addison-Wesley, Reading, MA, **1989**, p. 93.
[32] U. Schwanitz-Schüller, A. Simon, *Z. Naturforsch. B* **1985**, *40*, 710.
[33] A. Simon, H. Mattausch, G. J. Miller, W. Bauhofer, R. K. Kremer in *Handbook on the Physics and Chemistry of Rare Earths, Vol. 15* (Eds.: K. A. Gschneidner, Jr., L. Eyring), Elsevier, Amsterdam, **1991**, p. 191.
[34] M. von Stackelberg, *Z. Phys. Chem. B* **1930**, *9*, 437. The tetragonal form of CaC_2 is possibly only stable through the inclusion of impurities[35].
[35] N. G. Vannenberg, *Acta Chem. Scand.* **1961**, *15*, 769; *ibid.* **1962**, *16*, 1212.
[36] A. Simon, A. Yoshiasa, M. Bäcker, R. W. Henn, C. Felser, R. K. Kremer, H. Mattausch, *Z. Anorg. Allg. Chem.* **1996**, *622*, 123.
[37] Whereas the hydrolysis reaction of CaC_2 is known to produce ethyne, the corresponding reaction of the metallic phase $Y_2X_2C_2$ releases hydrogen and a mixture of hydrocarbons (C_1 to C_4)[38].
[38] C. Schwarz, Dissertation, Technische Universität Stuttgart, **1987**.
[39] G. J. Miller, J. K. Burdett, C. Schwarz, A. Simon, *Inorg. Chem.* **1986**, *25*, 4437.

[40] R. W. Henn, W. Schnelle, R. K. Kremer, A. Simon, *Phys. Rev. Lett.* **1996**, *77*, 374.

[41] A. Simon, H. Mattausch, R. Eger, R. K. Kremer, *Angew. Chem.* **1991**, *103*, 1210; *Angew. Chem. Int. Ed. Engl.* **1991**, *30*, 1188.

[42] K. Ahn, H. Mattausch, A. Simon, *Z. Anorg. Allg. Chem.* **1997**, *623*, 619.

[43] The (spurious) superconductivity mentioned in ref. [41] of $Lu_2Cl_2C_{2-x}$ could not be reproduced. It is due to impurities; see also ref. [44]. With luthetium the phase Lu_2Cl_2C, which contains no C_2 units, is the only accessible product [45]. $Y_2I_2C_2$ always yields smaller T_c values when prepared from educts in the stoichiometric ratio [46], as a part of the carbon apparently reacts with the Ta ampoule.

[44] J. Y. Chan, S. M. Kauzlarich, *Chem. Mater.* **1997**, in press.

[45] T. Schleid, G. Meyer, *Z. Anorg. Allg. Chem.* **1987**, *552*, 90.

[46] R. W. Henn, Dissertation, Universität Karlsruhe (TH), **1996**.

[47] M. Bäcker, A. Simon, R. K. Kremer, H. Mattausch, R. Dronskowski, J. Rouxel, *Angew. Chem.* **1996**, *108*, 837; *Angew. Chem. Int. Ed. Engl.* **1996**, *35*, 752. The Na content given in Table 1 of this paper should be doubled.

[48] A. L. Giorgi, E. G. Szklarz, M. C. Krupka, T. C. Wallace, N. H. Krikorian, *J. Less-Common Met.* **1968**, *14*, 247.

[49] M. C. Krupka, A. L. Giorgi, E. G. Szklarz, *J. Less-Common Met.* **1973**, *30*, 217.

[50] G. Adachi, N. Imanaka, Z. Fuzhong in *Handbook on the Physics and Chemistry of Rare Earths, Vol. 15* (Eds.: K. A. Gschneidner, Jr., L. Eyring), Elsevier, Amsterdam, **1991**, p. 61.

[51] This remark refers to the carbides of the electropositive rare earth metals and is not transferable to the superconducting transition metal carbides of the NaCl type, for example NbC, which exhibit different bonding.

[52] A. Simon, J. G. Smith, R. K. Kremer, **1992**, unpublished. Data taken from: B. W. Roberts, *J. Phys. Chem. Ref. Data* **1976**, *5*, 581.

[53] M. C. Krupka, A. L. Giorgi, N. H. Krikorian, E. G. Szklarz, *J. Less-Common Met.* **1969**, *19*, 113.

[54] B. T. Matthias, *Phys. Rev.* **1955**, *97*, 74.

[55] M. Atoji, *J. Chem. Phys.* **1961**, *35*, 1950.

[56] R. W. Henn, T. Gulden, W. Schnelle, R. K. Kremer, A. Simon, *Proc. Int. Conf. Low Temp. Phys. 21th* **1996**; *Czech. J. Phys.* **1996**, *46-S3*, 641.

[57] R. W. Henn, W. Schnelle, R. K. Kremer, A. Simon, *Proc. Int. Conf. Low Temp. Phys. 21th* **1996**; *Czech. J. Phys.* **1996**, *46-S3*, 865.

[58] For YC_2 at 0 K the values $\mu_0 H_{c1}(0) < 30$ mT and $\mu_0 H_{c2}(0) \approx 60$ mT are estimated. For $Y_2Br_2C_2$ $\mu_0 H_{c1}(0) < 1.5$ mT, $\mu_0 H_{c2}(0) \approx 3.0$ T and for $Y_2I_2C_2$ the value (11.8 T) is even higher [46].

[59] E. H. Brandt, *Rep. Prog. Phys.* **1996**, *58*, 1465.

[60] P. P. Garoche, *J. Low Temp. Phys.* **1978**, *30*, 323.

[61] W. Bauhofer, W. Biberacher, B. Gegenheimer, W. Joss, R. K. Kremer, H. Mattausch, A. Müller, A. Simon, *Phys. Rev. Lett.* **1989**, *63*, 2520.

[62] T. Gulden, Dissertation, Technische Universität Stuttgart, **1997.**

[63] B. Mühlschlegel, *Z. Phys.* **1959**, *155*, 313. The refinement is done with fitting parameters of $\gamma = 2.75(3)$ mJ mol^{-1} K^{-2}, $T_c = 3.84(1)$ K, and width $\Delta T_c = 0.008$ K. The γ value is in quantitative agreement with the direct determination in the normal state, which further yields $\Theta_D = 418(1)$ K.

[64] C. J. Gorter, H. B. G. Casimir, *Phys. Z.* **1934**, *35*, 963. The agreement with the so called α-model for strong coupling [65] is slightly better. The analysis gives $T_c = 5.04(1)$ K, $\Delta T_c = 0.008$ K. For the energy gap one obtains $2\Delta(0) = 4.6(1) k_B T_c$ [46]. In addition, the values of the energy gap determined from the specific heat measurements agree within experimental error with those derived from critical field measurements.

[65] H. Padamsee, J. Neighbor, C. A. Shifman, *J. Low Temp. Phys.* **1973**, *12*, 387.

[66] The experiment with ^{12}C refer to those with the natural abundance of ^{12}C (98.89%).

[67] R. Hoffmann, *Angew. Chem.* **1987**, *99*, 871; *Angew. Chem. Int. Ed. Engl.* **1987**, *26*, 846.

[68] R. Hoffmann, *Solids and Surfaces: A Chemist's View of Bonding in Extended Structures*, VCH, Weinheim, **1988.**

[69] J. K. Burdett, *Chemical Bonding in Solids*, Oxford University Press, **1995**.

[70] The one-dimensional metallic system is unstable. A Peierls distortion leads to the formation of atom pairs, that is, to a chain with alternating double bonds.

[71] The curvature of the conduction band minimum is much larger for GaAs than for Si. The conduction electrons introduced through doping are therefore faster in GaAs, which is the reason why high-power computing developed on the basis of this material.

[72] T. Hughbanks, R. Hoffmann, *J. Am. Chem. Soc.* **1983**, *105*, 3528.

[73] J. H. Ammeter, H.-B. Bürgi, J. C. Thebault, R. Hoffmann, *J. Am. Chem. Soc.* **1978**, *100*, 3686.

[74] M.-H. Whangbo, R. Hoffmann, R. B. Woodward, *Proc. R. Soc. A* **1979**, *366*, 23.

[75] G. J. Miller in *The Chemistry of Transition Metal Carbides and Nitrides* (Ed.: S. T. Oyama), Chapman & Hall, London **1995**, p. 134.

[76] O. K. Andersen, *Phys. Rev. B* **1975**, *12*, 3060.

[77] O. K. Andersen, *Phys. Rev. Lett.* **1984**, 53, 2571.

[78] L. N. Bulaevskii, *Sov. Phys. Usp. Engl. Transl.* **1976**, *18*, 514.

[79] O. K. Andersen, O. Jepsen, A. I. Liechtenstein, I. I. Mazin, *Phys. Rev. B* **1994**, *49*, 4145.

[80] L. van Hove, *Phys. Rev.* **1953**, *89*, 1189. This work treats the singularities encountered in the spectrum of vibrational frequencies of layered crystals, with only a short comment on the transferability to electronic density of states.

[81] J. E. Hirsch, D. J. Scalapino, *Phys. Rev. Lett.* **1986**, *56*, 2732.

[82] J. Labbé, J. Bok, *Europhys. Lett.* **1987**, *3*, 1225.

[83] J. Friedel, *J. Phys.* **1988**, *49*, 1435.

[84] D. M. Newns, H. R. Krishnamurthy, P. C. Pattniak, C. C. Tsui, C. C. Chi, C. L. Kane, *Phys. Status Solidi B* **1993**, *186-188*, 801.

[85] T. Yokoya, A. Chianani, T. Takahashi, H. Katayama-Yoshida, M. Kasai, Y. Tokura, *Phys. Rev. Lett.* **1996**, *76*, 3009.

[86] J. R. Long, R. Hoffmann, H.-J. Meyer, *Inorg. Chem.* **1992**, *31*, 1734.

[87] J. R. Long, J.-F. Halet, R. Hoffmann, H.-J. Meyer, J.-Y. Saillard, *New J. Chem.* **1992**, *16*, 839.

[88] G. J. Miller, *J. Am. Chem. Soc.* **1994**, *116*, 6332.

[89] E. Ruiz, P. Alemany, *J. Phys. Chem.* **1995**, *99*, 3114.

[90] C. Felser, reported in ref. [46].

[91] J. Ranninger, S. Robaszkiewicz, *Phys. Status Solidi B* **1985**, *135*, 468.

[92] J. Ranninger, J. M. Robin, M. Eschrig, *Phys. Rev. Lett.* **1995**, *74*, 4027.

[93] J. Ranninger, J. M. Robin, *Physica C* **1995**, *253*, 279.

[94] C. Kittel, *Solid State Phys.* **1968**, *22*, 1.

[95] H. Mattausch, A. Simon, C. Felser, R. Dronskowski, *Angew. Chem.* **1996**, *108*, 1805; *Angew. Chem. Int. Ed. Engl.* **1996**, *35*, 1685.

[96] H. Mattausch, A. Simon, *Angew. Chem.* **1995**, *107*, 1764; *Angew. Chem. Int. Ed. Engl.* **1995**, *34*, 1633.

[97] H. Mattausch, A. Simon, C. Felser, *J. Phys. Chem.*, in press.

[98] J. Bauer, O. Bars, *J. Less-Common Met.* **1983**, *95*, 267.

[99] J. Bauer, O. Bars, *Proc. Conf. Supercond. in f- and d-Band Met. 4th*, Karlsruhe **1982**; (*J. Less-Common Met.* **1982**, *88*, 267).

[100] T. Siegrist, H. W. Zandbergen, R. J. Cava, J. J. Krajewski, W. F. Peck, *Nature* **1994**, *367*, 254.

[101] J.-F. Halet, *Inorg. Chem.* **1994**, *33*, 4173.

[102] H. Krebs, *Z. Naturforsch. A* **1968**, *23*, 332; *ibid.* **1969**, *24*, 848.

[103] H. Krebs, *Z. Naturforsch. A* **1972**, *27*, 236.

[104] H. Krebs, *Prog. Solid State Chem.* **1975**, *9*, 269.

[105] K. H. Johnson, R. P. Messmer, *Synth. Met.* **1983**, *5*, 151.

[106] V. F. Weisskopf, *Contemp. Phys.* **1981**, *22*, 375.

[107] S. N. Ekbote, A. V. Narlikar, *Mater. Res. Bull.* **1980**, *15*, 827.

[108] M. R. Schafroth, J. M. Blatt, S. T. Butler, *Helv. Phys. Acta* **1957**, *30*, 93.

[109] M. R. Schafroth, *Phys. Rev.* **1958**, *130*, 1244.

[110] S. G. Louie, K.-M. Ho, M. L. Cohen, *Phys. Rev. B* **1979**, *19*, 1774. The energy of the band at the Γ point varies. According to our self-consistent calculations, the band lies approximately 0.7 eV above E_F.

[111] B. M. Klein, L. L. Boyer, D. A. Papaconstantopoulus, L. F. Mattheiss, *Phys. Rev. B* **1978**, *18*, 6411.

[112] W. Weber, L. F. Mattheiss, *Phys. Rev. B* **1982**, *25*, 2270.

[113] F. A. Cotton, R. A. Walton, *Multiple Bonds between Metal Atoms*, Wiley, New York, **1982**.

[114] D. E. Cox, A. W. Sleight, *Acta Crystallogr. Sec. B* **1979**, *35*, 1.

[115] P. Blaha, K. Schwarz, G. Vielsack, W. Weber in *Electronic Properties of High-T_c Superconductors and Related Compounds*, (Eds.: H. Kuzmany, M. Mehring, J. Fink), Springer, Berlin, **1990**, p. 343. When counting electrons inside the fixed atomic sphere of Bi, the difference between metal-centered nonbonding electrons and those in covalent Bi–O bonds is lost. The conclusion that "oxygen breathing neutralizes the charge transfer due to the disproportionation" [116] has to be understood in this context.

[116] I. I. Mazin, A. I. Liechtenstein, O. V. Ivanov, *Ferroelectrics* **1995**, *164*, 169.

[117] A. W. Sleight, J. J. Gillson, P. E. Bierstedt, *Solid State Commun.* **1975**, *17*, 27.

[118] R. J. Cava, B. Batlogg, J. J. Krajewski, R. Farrow, L. W. Rupp, A. E. White, K. Short, W. F. Peck, T. Kometani, *Nature*, **1988**, *332*, 814.

[119] R. Migoni, H. Bilz, D. Bäuerle, *Phys. Rev. Lett.* **1978**, *37*, 1155.

[120] H. Bilz, G. Benedek, A. Bussmann-Holder, *Phys. Rev. B* **1987**, *35*, 4840.

[121] A. Simon, *Angew. Chem.* **1987**, *99*, 602; *Angew. Chem. Int. Ed. Engl.* **1987**, *26*, 579.

[122] A. Simon, *Chem. Unserer Zeit* **1988**, *22*, 1.

[123] Mott [29] talks of bosons ("Bi^{3+} that is moving in a sea of Bi^{5+}") that are stabilized by polaron formation (as two electrons are attached to Bi^{3+} rather bipolaron formation), that is, by local distortions.

[124] A. Bussmann-Holder, A. Simon, H. Büttner, *Phys. Rev B* **1989**, *39*, 207.

[125] A. Bussmann-Holder, H. Büttner, A. Simon, V. Waas, *Z. Phys. B* **1990**, *79*, 445.

[126] P. Villars, J. C. Philips, *Phys. Rev. B* **1988**, *37*, 2345.

[127] S. Robaszkiewicz, R. Micnas, J. Ranninger, *Phys. Rev. B* **1987**, *37*, 180.

[128] L. F. Mattheiss, D. R. Hamann, *Phys. Rev. Lett.* **1988**, *60*, 2681.

[129] A. F. Wells, *Structural Inorganic Chemistry*, Clarendon, Oxford, **1986**, p. 876.

[130] A. Eichler, J. Wittig, *Z. Angew. Phys.* **1968**, *25*, 319.

[131] W. Buckel, R. Hilsch, *Z. Phys.* **1952**, *132*, 420.

[132] The band structure concept breaks down here because of the lack of translational symmetry. The argument "tendency to localization" remains nevertheless correct if dispersionless electron states lie at the Fermi level.

[133] N. B. Hannay, T. H. Geballe, B. T. Matthias, K. Andres, P. Schmidt, D. Macnair, *Phys. Rev. Lett.* **1965**, *14*, 225.
[134] A. F. Hebard, M. J. Rosseinski, R. C. Haddon, D. W. Murphy, S. H. Glarum, T. T. M. Palstra, A. P. Ramirez, A. R. Kortan, *Nature* **1991**, *350*, 600.
[135] R. C. Haddon, *Acc. Chem. Res.* **1992**, *25*, 127.
[136] D. L. Novikov, V. A. Gubanov, A. J. Freeman, *Phys. Status Solidi C* **1992**, *191*, 399.
[137] P. W. Stephens, L. Mihaly, P. L. Lee, R. L. Whetten, S.-M. Huang, R. Kaner, F. Deiderich, K. Holczer, *Nature* **1991**, *351*, 632.
[138] S. E. Barrett, R. Tycko, *Phys. Rev. Lett.* **1992**, *69*, 3754.
[139] R. E. Walstedt, D. W. Murphy, M. Rosseinsky, *Nature* **1993**, *362*, 611.
[140] N. Laouini, O. K. Andersen, O. Gunnarson, *Phys. Rev. B* **1995**, *51*, 17446.
[141] J. L. Martins, N. Troullier, *Phys. Rev. B* **1992**, *46*, 1766.
[142] S. Satpathy, V. P. Antropov, O. K. Andersen, O. Jepsen, O. Gunnarson, A. I. Liechtenstein, *Phys. Rev. B* **1992**, *46*, 1773.
[143] O. V. Dolgov, I. I. Mazin, *Solid State Commun.* **1992**, *81*, 935.
[144] O. Gunnarson, Rev. *Mod. Phys.* **1997**, *69*, 57.
[145] J. G. Bednorz, K. A. Müller, *Angew. Chem.* **1988**, *100*, 757; *Angew. Chem. Int. Ed. Engl.* **1988**, *27*, 735.
[146] J. Beille, R. Cabanal, C. Chaillout, B. Chevalier, G. Demazeau, F. Deslandes, J. Etourneau, P. Lejay, C. Michel, J. Provost, B. Raveau, A. Suplice, J.-L. Tholence, R. Tournier, *C. R. Acad. Sci. Ser. 2* **1987**, *304 (II)*, 1097.
[147] J. C. Grenier, N. Lagueyte, A. Wattiaux, J. P. Doumerc, P. Dordor, J. Etournaux, M. Pouchard, J. B. Goodenough, J. S. Zhou, *Phys. Status Solidi C* **1992**, *202*, 209.
[148] C. Michel, M. Hervieu, M. M. Borel, A. Grandin, F. Deslandes, J. Provost, B. Raveau, *Z. Phys. B* **1987**, *68*, 421.
[149] M. A. Subramanian, J. C. Calabrese, C. C. Torardi, J. Gopalakrishnan, T. R. Askew, R. B. Flippen, K. J. Morrissey, U. Chowdhry, A. W. Sleight, *Nature* **1988**, *332*, 420.
[150] *Phase Separations in Cuprate Superconductors* (Eds.: E. Sigmund, K. A. Müller), Springer, Berlin, **1994**.
[151] R. K. Kremer, E. Sigmund, V. Hizhnyakov, F. Hentsch, A. Simon, K. A. Müller, *Z. Phys. B* **1992**, *86*, 319.
[152] J. M. Tranquada, B. J. Sternlieb, J. D. Axe, Y. Nakamura, S. Uchida, *Nature* **1995**, *375*, 561.
[153] A. Bianconi, N. L. Saini, A. Lanzara, M. Missori, T. Rossetti, H. Oyanagi, H. Yamaguchi, K. Oka, T. Ito, *Phys. Rev. Lett.* **1996**, *76*, 3412.
[154] M. K. Wu, J. R. Ashburn, C. J. Torug, P. H. Hor, R. L. Meng, L. Goa, Z. J. Huang, Y. Q. Wang, C. W. Chu, *Phys. Rev. Lett.* **1987**, *58*, 908.
[155] J. D. Jorgensen, M. A. Beno, D. G. Hinks, L. Soderholm, K. J. Volin, R. L. Hitterman, J. D. Grace, I. K. Schuller, C. U. Segre, K. Zhang, M. S. Kleefisch, *Phys. Rev. B* **1987**, *36*, 3608.
[156] Single crystals notoriously tend to twin, especially when Al impurities enter from the alumina reaction crucible. By using SnO_2 crucibles untwinned crystals were obtained, which from an X-ray structure investigation exhibit an oxygen deficiency in the chains, corresponding to the formula $YBa_2Cu_3O_{6.93}$[157].
[157] A. Simon, J. Köhler, H. Borrmann, B. Gegenheimer, R. Kremer, *J. Solid State Chem.* **1988**, *77*, 200.
[158] Using the formulation $(CuO)^+$ instead of Cu^{3+}, one avoids the long discussion on whether the electron holes are found on the oxygen atom (O^-).
[159] C. Chaillout, M. A. Alario-Franco, J. J. Cappon, J. Chevenas, P. Strobel, M. Marezio, *Solid State Commun.* **1988**, *65*, 283.
[160] A. Simon, K. Trübenbach, H. Borrmann, *J. Solid State Chem.* **1993**, *106*, 128.
[161] K. Ruck, H. Borrmann, A. Simon, *Solid State Commun.* **1995**, *93*, 865.
[162] N. B. Robin, P. Day, *Adv. Inorg. Chem. Radiochem.* **1967**, *10*, 248.
[163] R. J. Cava, B. Batlogg, C. H. Chen, E. A. Rietman, S. M. Zahurak, D. Werder, *Phys. Rev. B* **1987**, *36*, 5719.
[164] J. M. Tranquada, D. E. Cox, W. Kunnmann, H. Moudden, G. Shirane, M. Suenaga, P. Zolliker, D. Vaknin, S. K. Sinha, M. S. Alvarez, A. J. Jacobson, D. C. Johnston, *Phys. Rev. Lett.* **1988**, *60*, 156.
[165] With spin-polarized neutrons and polarization analysis the absence of local moments in normal state $YBa_2Cu_3O_{6.95}$ is clearly demonstrated. The observed paramagnetic scattering cross-section corresponds to less than 3.2% of the Cu atoms carrying a spin $\frac{1}{2}$[166].
[166] T. J. Smith, K. H. Anderson, U. Beck, H. Capellmann, R. K. Kremer, K.-U. Neumann, O. Schärpf, A. Simon, K. R. A. Ziebeck, Proc. ICM **1997**, in press; see also H. F. Fong, B. Keimer, D. L. Milius, I. A. Aksay, *Phys. Rev. Lett.* **1997**, *78*, 713.
[167] W. E. Pickett, R. E. Cohen, H. Krakauer, *Phys. Rev B* **1990**, *42*, 8764.
[168] O. K. Andersen, A. I. Liechtenstein, O. Jepsen, F. Paulsen, *J. Phys. Chem. Solids* **1995**, *56*, 1573.
[169] The figure indicates that the total Fermi surface must be searched for flat bands. The representation in selected symmetry directions is not sufficient.
[170] A. A. Abrikosov, J. C. Campuzano, K. Gofron, *Phys. Status Solidi C* **1993**, *214*, 73.
[171] D. M. Newns, C. C. Tsuei, P. C. Pattniak, *Phys. Rev. B* **1995**, *52*, 13611.
[172] S. Chakravarty, A. Sudboe, P. W. Anderson, S. Strong, *Science* **1993**, *261*, 337.
[173] Z.-X. Shen, W. E. Spicer, D. M. King, D. S. Dessau, B. O. Wells, *Science* **1995**, *267*, 343.
[174] A. T. Boothroyd, A. Mukherjee, *Phys. Rev. Lett.* **1996**, *77*, 1600.
[175] W. M. Temmerman, Z. Szotek, B. L. Gyorffy, O. K. Andersen, O. Jepsen, *Phys. Rev. Lett.* **1996**, *76*, 307.
[176] A. Bussmann-Holder, L. Genzel, A. Simon, A. R. Bishop, *Z. Phys. B* **1993**, *92*, 149.
[177] H. G. von Schnering, L. Walz, M. Schwarz, M. Hartweg, T. Popp, B. Hettich, P. Müller, *Angew. Chem.* **1988**, *100*, 604; *Angew. Chem. Int. Ed. Engl.* **1988**, *27*, 574.

The three-dimensional representation of the ELF isosurface for methyl acetate (top) and sections corresponding to the planes drawn as well as to those parallel to the plane through the carbonyl group uncover many details about the distribution of electron density and can therefore contribute to supporting qualitative concepts and models. This is true not only for molecules but also for solids.

ELF: The Electron Localization Function**

Andreas Savin,* Reinhard Nesper,* Steffen Wengert, and Thomas F. Fässler

Dedicated to Professor Hans Georg von Schnering

The chemical bond is always considered from different points of view, depending on the classes of compounds or on the chemical and physical aspects to be examined. In both cases, descriptions of the chemical bond are chosen that are appropriate for the particular research or application. Therefore, there are significant differences in the understanding as what constitutes chemical bonding. This is acceptable in practice but proves to be a hindrance for true interdisciplinarity. The concept of the chemical bond offers a firm basis upon which to forge links not only within chemistry but also to all related sciences. The general desire and the growing necessity for interdisciplinary collaboration requires a careful treatment of these concepts and, if possible, a tightening and standardization to a level that is widely acceptable and beneficial. In the age of tremendously fast development of computers and computer science, we believe that the electron localization function (ELF) provides a new description of the chemical bond for almost all classes of compounds. Its graphical language earns it the ultimate qualification for enhanced interdisciplinarity.

Keywords: bond theory · electron localization function · structure elucidation

1. The Electron Localization Function—ELF

Chemistry—as we know it—without the Pauli principle is inconceivable. This principle is deeply rooted in so many chemical concepts that the connection is frequently neglected; for instance, the systematics of the periodic table, steric hindrance, and the covalent bond. The Pauli principle itself is also presented in various ways. In books on quantum mechanics it is often described as a property of the wave function, which needs to be antisymmetric with respect to interchange of electrons. From textbooks on chemistry one recalls mostly the fact that orbitals can be occupied by at most two electrons. The Pauli principle is reflected in the expression for the total energy of a system both in an energy-lowering part (the exchange term) and a larger energy-raising contribution, which can be found indirectly in the kinetic energy. The following explanation is usually used: The energetically higher canonical orbitals occupy the same space as the ones lower in energy but they must have additional nodal planes (in order to meet the criterion of orthogonality) and therefore a steeper behavior. Their appearance strongly resembles a growing precipitous landscape. The slope is expressed mathematically by the derivative; the latter can be found in the formula for the kinetic energy T [Eq. (1)], where φ_i are the orbitals and n_i their occupation numbers.

$$T = \int \frac{1}{2} \sum_i n_i |\nabla \varphi_i|^2 d^3r \qquad (1)$$

The Pauli principle has been used as a basis for the explanation of many chemical concepts. For example, Gillespie's explanation of his rules.[1] In this article we will show that most of these chemical concepts can be described very well with the electron localization function (ELF). The relationship of ELF with older concepts will be emphasized first.

Artmann was the first to introduce a formulation similar in concept to ELF.[2] In quantum mechanics, the sum of squares of the N-particle wave function corresponds to a probability density. Therefore he searched for the maximum of this quantity and found it to occur where the chemist imagines the bonds; for instance, in the case of the methane molecule, he observed four valence electron pairs arranged tetrahedrally around the carbon atom.[*] Examinations of the sum of the squares of the wave function are quite interesting but difficult to perform in practice (see for example ref. [3]). Lennard-Jones recognized that only two electrons of equal spin and therefore only two coordinates

[*] Priv.-Doz. A. Savin
Université Pierre et Marie Curie
Tour 22, Couloir 22-23
4 Place Jussien, F-75252 Paris (France)
e-mail : Andreas.Savin@lct.jussieu.fr
Prof. Dr. R. Nesper, Dr. T. F. Fässler, Dr. S. Wengert
Laboratorium für Anorganische Chemie
Eidgenössische Technische Hochschule
Universitätstrasse 6, CH-8092 Zürich (Switzerland)
Fax.: Int. code +(1)632-1149
e-mail : nesper@inorg.chem.ethz.ch

[**] This work was supported by the Swiss National Foundation under Grant Nos. 0-20-851-94, and 0-20-288-96, and the C⁴-project of the ETH, Zürich.

[*] Artmann used an approximate valence electron wave function composed of hybrid orbitals.

 © WILEY-VCH Verlag GmbH, D-69451 Weinheim, 1997 0570-0833/97/3617-1809 $ 17.50+.50/0

are necessary for the examination of the Pauli principle, a significant simplification on the work of Artmann. Lennard-Jones found that space is divided into regions according to the Pauli principle. If an electron resides in a given region, the other stays away from that region. More precisely, if an electron resides at a place $\vec{r}$, the probability of finding an electron in the surrounding region $B(\vec{r})$ is clearly diminished. B remains practically unchanged as long as $\vec{r}$ stays in that region. The interaction of all particles under the condition of energetic stability defines the division into regions and is therefore always dependent on the system.

Even electrons with opposite spin avoid each other. This fact cannot be attributed to the Pauli principle and the effect is usually smaller by an order of magnitude. This is the reason why a given electron permits the presence of another with opposite spin in its region: the region is therefore occupied by a pair of electrons. Such a formation of pair regions corresponds exactly to the picture proposed by Kossel eighty years ago.[4]

Lennard-Jones went one step further in assigning every pair region a localized orbital. Such orbitals have only very small values outside their assigned regions. Sometimes they are denoted "chemical orbitals" because of their proximity to chemical definitions based on electron pairs (bond, lone pair of electrons) and therefore they are very useful. In addition, they can be used in the calculation of measurable quantities on equal footing with the common (delocalized, canonical) orbitals. The symmetry behavior of localized orbitals is different from that of canonical orbitals. By applying a symmetry operation, the latter (in the absence of degeneracy) always transform into themselves (except for the sign), whereas the former may be interchanged. In the ethene molecule the canonical (σ, π) orbitals are frequently considered. Their linear combination yields two equivalent localized orbitals often regarded as the C–C "banana bonds", which are interchanged upon reflection in the atomic plane.[*] The generation of localized orbitals can be problematic in symmetry groups allowing degeneracy: In practice just a minimal numeric effect can determine the localization. This can be seen, for example, in the benzene molecule[5] in which nine (six σ and three π) electron pairs are available. On the other hand it

[*] There are also localized orbitals that correspond to the C–H bonds and the 1s cores; they are interchanged for example upon inversion.

A. Savin

R. Nesper

S. Wengert

T. F. Fässler

Andreas Savin was born in 1950 in Bukarest, Romania, where he studied chemistry and received his diploma in 1973. He completed his PhD thesis in 1983 under the supervision of Professor H. Preuss at the Universität Stuttgart, where he also performed his habilitation. Between 1983 and 1993 he worked at the Universität Stuttgart, where he also lectured from 1985 onwards, and at the Max-Planck-Institut für Festkörperforschung. In 1993 he moved to the Centre National de la Recherche Scientifique in Paris. Since 1995 he has lectured at the Université Pierre et Marie Curie, Paris. His main areas of interest are density functional theory and the electron localization function as well as Monte-Carlo procedures and the application of quantum chemical methods.

Reinhard Nesper, born in Elze/Hannover, Germany, in 1949, studied chemistry at the Universität Münster and then moved to the Max-Planck-Institut für Festkörperforschung in Stuttgart where he received his PhD thesis under the supervision of Professor von Schnering. Apart from a period of research with Professor Roald Hoffmann at Cornell University in 1984, he was a member of the scientific staff at the Max-Planck-Institut Stuttgart from 1978 to 1990. In 1989 he received his habilitation at the Universität Stuttgart and in 1990 he accepted the chair of inorganic chemistry at the ETH Zürich. His main areas of interest are solid-state chemistry, structure determination, and the electronic structure of solids as well as new materials, nanostructures, structure–property relationships, and models for structure formation.

Steffen Wengert was born in Heilbronn, Germany, in 1964. He studied chemistry at the Universität Stuttgart where he also carried out his diploma thesis in theoretical chemistry. He then moved to the ETH Zürich to work with Professor Nesper and subsequently completed his PhD thesis on the topic of "experimental and theoretical solutions to fundamental problems in Zintl compounds" in spring 1997.

Thomas F. Fässler, born in Bad Waldsee/Reute, Germany, in 1959, studied chemistry and mathematics in Konstanz. In 1988 he received his PhD for work on transition metal cluster compounds under the supervision of Professor G. Huttner in Heidelberg. During a period of research at the University of Chicago with Professor J. Burdett he carried out fundamental theoretical studies on chemical bonding at metal surfaces. Since 1991 he has been carrying out work at the ETH Zürich towards his habilitation. His research interests are focused at the interface between molecular and solid-state chemistry, and involve the synthesis, structural characterization, and the study of the electronic properties of soluble Zintl ions, Zintl phases, and intermetallic compounds.

is not possible to generate nine equivalent regions on the six-membered ring (this is only compatible with three- or ninefold rotation axes, not with a sixfold axis). A similar situation arises for clusters such as the cage of $[B_6H_6]^{2-}$ in which seven pairs of electrons are available, which is incompatible with the icosahedral symmetry of the anion. Unfortunately, this problem appears frequently in solid phases.

The homogeneous electron gas represents an extreme case. Here, the pair region must also show a translational invariancy due to the translational symmetry of the Hamiltonian operator. To understand this phenomenon the analogy to resonance structures is quite helpful. Here, the best compromise is an average of the extreme cases.

Therefore, we will return to the original treatment by Lennard-Jones. He reduced the probability density of two electrons mathematically upon integrating over all coordinates of the remaining $N-2$ electrons. The resulting quantity (the pair density) is a function of the coordinates of two electrons, a six-dimensional function that is too complicated for our three-dimensional concept of the chemical bond that we want to develop here. A possible solution is to reduce the examination to a single electron, that is to consider the electron density. Its partitioning into contributions from different atomic orbitals is very common. The latter are not precise in the original formulation (Mulliken population analysis[6]) leading to a certain arbitrariness, which can be restricted by additional regulations such as those introduced by Davidson or Ahlrichs and co-workers.[7, 8] An additional variant is obtained by the use of "natural" bonding orbitals.[9] Bonding relationships are also discussed in terms of differences between molecule (or crystal) densities and those of atoms and ions. Nowadays, spherical atoms,[10] formerly used as a reference, can be substituted by nonspherical ones.[11] Finally, the elegant procedure of Bader and co-workers with no reference systems at all should be mentioned: only the density ρ as a function of the positional coordinates and their derivatives is used.[12] The Pauli principle can, of course, be found in the electron density, which is certainly different for bosons at a given potential. A clear connection is not easily discernible. For that reason we return to the pair density for the moment.

A solution, and at the same time a direct precursor to the electron localization function described in this article, was found by Luken and Culbertson.[13] They studied the modification of the region $B(\vec{r})$ upon substituting the point $\vec{r}$ by a neighboring point. It is small in the pair region, but becomes predominant on leaving the region (cf. the investigations of Lennard-Jones) and, as a consequence, these changes can serve in the determination of the borders of the pair region. An overlap integral is used to measure the change.

Becke and Edgecombe proposed the examination of the Taylor expansion.[14] They used the fact that for small distances $s = |\vec{r} - \vec{r}'|$ only the second derivative of the pair density P (spherically averaged around $\vec{r}$) for electrons of equal spin is important [Eq. (2)] and therefore the examination can be restricted to the value $C(\vec{r})$ which is dependent on $\vec{r}$.

$$P(\vec{r},s) = \frac{1}{2}s^2 C(\vec{r}) + \ldots \tag{2}$$

The simplest form of a wave function satisfying the Pauli principle, is the Slater determinant. In this case C can be expressed by Equation (3); thus, the electron density [Eq. (4)] as well as the sum $\sum_i n_i|\nabla\varphi_i|^2$ over the orbitals φ_i at $\vec{r}$ can be calculated.

$$C(\vec{r}) = \frac{1}{2}\sum_i n_i|\nabla\varphi_i|^2 - \frac{1}{8}\frac{|\nabla\rho|^2}{\rho} \tag{3}$$

$$\rho = \sum_i n_i|\varphi_i|^2 \tag{4}$$

Becke and Edgecombe proposed two additional scaling rules:
1. The homogenous electron gas is used as a reference. In this system, C depends only on the electron density [Eq. (5)].

$$C(\vec{r}) \rightarrow C_h(\vec{r}) \sim \rho^{5/3} \tag{4}$$

2. The introduction of a value which is defined between zero and one. Whereas this second scaling is convenient for comparison of numerical data, it does not play a decisive role (see Sections 2–6).

Becke and Edgecombe named the scaled function the *electron localization function* (ELF) [Eq. (6)]. ELF has its highest

$$\mathrm{ELF} = \left\{1 + \left[\frac{C(\vec{r})}{C_h(\rho(\vec{r}))}\right]^2\right\}^{-1} \tag{6}$$

value ($\rightarrow 1$) if $\vec{r}$ is within the pair region (where P does not change very much and C is small). On the other hand, ELF is small when $\vec{r}$ is close to the border between two pair regions.[15] In a homogeneous electron gas ELF has everywhere the value 1/2.

In solid-state physics the homogeneous electron gas is commonly used as a reference system. Another reason is the aforementioned average of extreme cases, which occurs in homogenous systems leading to an average picture. The value C_h can also be introduced independently from the homogeneous electron gas.[16] Instead of a Taylor expansion, Dobson proposed the integration over a small sphere,[17] leading to the number of electrons of equal spin in the surrounding of the reference electron. Thus, Equation (2) changes to give Equation (7).

$$\int_0^R \frac{1}{2}s^2 C(\vec{r}) 4\pi s^2 \,\mathrm{d}s + \ldots = \frac{1}{2}\frac{4\pi R^5}{5}C(\vec{r}) + \ldots \tag{7}$$

The radius of the spheres can be made position dependent, which keeps the number of reference electrons in a sphere with radius R unchanged. Equation (8) is valid for small spheres

$$\int_{V_{\mathrm{sphere}}} \rho(\vec{r}+\vec{s})\,\mathrm{d}^3 s \approx \rho(\vec{r})\frac{4\pi R^3}{3} + \ldots \tag{8}$$

around $\vec{r}$, where $R \sim \rho^{-1/3}$ and the number of electrons around the reference electron [see Eq. (7)] is proportional to $C(\vec{r})/\rho^{5/3}$ and $C(\vec{r})/C_h(\rho(\vec{r}))$.

It is evident from the definition of ELF in Equation 6 that the scale has been established more or less arbitrarily. This fact is irrelevant in graphical representations as the numerical scale is transformed into a (arbitrary) color scale or is shown in the form of isosurfaces (selected arbitrarily in three-dimensional representations). No information is lost as electron pairs and the chemical bond are first and foremost examined qualitatively. It must be mentioned that qualitative statements can also be described mathematically (for example the catastrophe theory of R. Thom,[18] which was used by Bader and co-workers[12] in analyzing the density). We now want to comment on this aspect in connection with ELF.[19] As we have decided to focus on the

characterization of pair regions, those regions where ELF exhibits maxima are of special interest. Mathematically, it is known that the positions of maxima may be sought by examining the first derivative of a function. For ELF they are fulfilled by the first derivatives of C/C_h; thus, for this property the second scaling rule is irrelevant. ELF can have several maxima. The positions of these maxima are denoted as *attractors*. The next step is the division of space by considering the path of steepest ascent (the gradient of ELF) from every point in space. If an attractor is found along this path, the point is assigned to it. All points in space from which this attractor is reached form its *domain* (Wirkungsbereich, WB). Thus, we obtain a more precise definition of the "pair regions".

Another way to analyze ELF is to examine the spatial region (the *f-localization domain*) in which ELF $\geq f$ is valid, where f is a constant.[19, 20] For larger values of f there is only one attractor in each of the f-localization domains. At a certain (smaller) f-value different f-localization domains come into contact at a single point (an ELF saddle point; again only the relation C/C_h is important because we are dealing with the first derivative). Smaller values of ELF lead to a merging of these localization domains: here the f-localization domain contains more than one attractor. The f-interval, where only one attractor in the f-localization domains exists (the difference of the ELF values at the maximum and the saddle point), is characteristic of the bond. The separation between the core and valence regions is more sharply defined than the separation observed within the valence shell. In particular, the separation of the regions of double-bond pairs is weak.[21]

Of course, quantitative statements can also be obtained with ELF. Quantifications of charge, volume, etc. can be determined. A total electron number can be obtained upon integration of the electron density in a certain domain (see Section 4.2). ELF yields electron numbers that are usually in agreement with chemical intuition, for example two for a region assigned to a pair of electrons. On the other hand, special electron numbers appear due to the above-mentioned overlap effects, such as $\approx 3/2$ for the C–C bond in benzene or ≈ 8 for the valence shell of the Ne atom.[22] Remarkably in ionic solids, ELF predicts electron numbers that correspond to those derived from formal charges.[23]

The precision of the determination of such electron numbers is interesting. According to the Heisenberg uncertainty principle, the above-mentioned numbers can only be considered as mean values. But it is possible to get average deviations. These deviations are relatively small when dealing with atomic cores, whereas for valence electrons they are larger.[21] More sophisticated calculations show that the partition obtained by ELF resembles the one yielding the smallest uncertainty.[24]

Although ELF is currently only obtainable from calculations, it is, in principle, possible to derive ELF from experimental data. Certainly, the evaluation of the sum of the squares of the wave function (and the pair density) according to the postulates of quantum mechanics is a possibility; but this is more difficult to realize. Therefore, we want to show how ELF can be determined from the electron density alone, and in the following we present a definition of ELF equivalent to that given before.[25]

A computational method that is successfully applicable for molecules as well as for solids is based on the (exact) density functional theory defined by Kohn and Sham.[26] Therein the ground state energy is exclusively determined from the electron density. The terms in the energy expression can either be easily calculated from the density (the classical interaction of the charge distribution), or sufficiently approximated (the exchange and correlation energy). However, the construction of the kinetic energy can cause difficulties if the Pauli principle is neglected. In the density functional theory defined by Kohn and Sham, the kinetic energy of a hypothetical system T_s with identical density but no interaction between the particles is calculated instead of the kinetic energy from Equation (1). This leads to a simplification and the ground state function is (usually) a Slater determinant so that the orbitals in Equations (1) and (4) are not singly or doubly occupied (i.e.: $n_i = 0$, 1, or 2).

If the Pauli principle is ignored, it has been shown[27] that all electrons will occupy the orbital of lowest energy, which is defined by $\varphi_i = \sqrt{\rho(\vec{r})/N}$ (N = electron number). Therefore it is possible to evaluate the increase in kinetic energy that occurs on consideration of the Pauli principle [Eq. (9)].

$$\Delta T = \int \left[\frac{1}{2} \sum_i |\nabla \varphi_i|^2 - \sum_i \left| \nabla \sqrt{\rho(\vec{r})/N} \right|^2 \right] \mathrm{d}^3 r \qquad (9)$$

Upon applying the same scalings used for ELF (electron gas, interval (0,1)), the integrand yields a local value that corresponds exactly to the expression of the ELF formula [Eq. (6) with Eqs. (3)–(5)]. These orbitals, which yield the exact density, are not easily obtained from the electron density, but this is possible with several algorithms and programs (see, for example, ref. [28]).

To investigate the role of approximations in ELF calculations, densities (and no other information) determined by exact calculations on small atoms were used. ELF values were obtained that fortunately do not differ significantly from the Hartree–Fock (HF) and density functional calculations that are routinely carried out.[29] Even rather simple methods, such as the extended Hückel method (EHMO), reveal the characteristic features of ELF.[16, 30, 31] There are other interpretations of ELF but all of them are based on the Pauli principle.

2. Fundamental Studies of the Chemical Bond

In the first publications on the practical applications of ELF, the ability of the function to generate easily understood pictures of the chemical bond for many different chemical systems was demonstrated.[32] Subsequently, many more chemical systems have been examined, all of them substantiating this result: ELF yields very meaningful, easily understandable, and visually informative patterns of the chemical bond. In this section we want to analyse some typical chemical bonding forms with ELF. We will demonstrate how ELF portrays these forms, and the similarities and differences to other existing methods will be highlighted. It has been shown that pictures obtained with ELF by using different theoretical calculation methods are qualitatively comparable (see Section 1). Here, we present results obtained by using the relatively simple extended Hückel approximation[33] and the more sophisticated ab initio linear-muffin-tin orbital method (LMTO).[36]

A single krypton atom serves as an example to explain the shell structure of atoms in the ELF pattern. Figure 1a shows

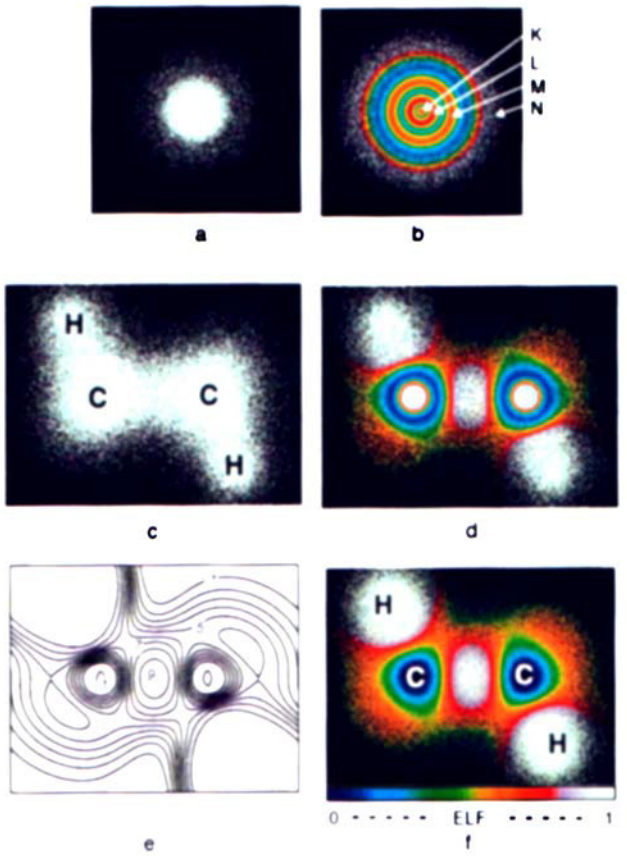

Figure 1. Distribution of electron density a) in a section through a krypton atom, c) in a section through an ethane molecule and coloring with ELF b) and d), respectively, based on HF calculations. The color scale for all such ELF representations corresponds to that given in Figure 1 f. e) and f) Representation of ELF for the EHMO valence electron calculation of ethane with contour lines and the corresponding ELF representation with colored valence electron density, respectively.

only the electron density for the free atom, whereas in Figure 1 b this point pattern is colored according to the ELF values. Thus, in such two-dimensional graphical representations the electron density (as a density of points) and the ELF values (coded in a color scale in analogy to a geographical map) are depicted simultaneously. High ELF values (approximately 0.8 to 1.0) are colored white; the series descends through brown and yellow to green for middle ELF values (ca. 0.5). The lower end of the scale is represented by blue and violet.[39] Of course, it is possible to reproduce ELF in two dimensions by using contour line diagrams. In three-dimensional representations, isosurfaces are shown for each chosen ELF value.

Four separate localization shells with varying degrees of contraction and compactness can be recognized in the krypton atom. In the course of our discussion we will focus on the regions that can be assigned to either atomic cores or to valence electrons. Figures 1 d–f depict the ELF representations for sections through the ethane molecule along the C–C bond. It is known that the electron density is poorly structured (Figure 1 c), whereas all chemical details of the structure can clearly be discerned in the ELF representation: the C atom cores and the C–C as well as the C–H bonding regions. The latter are diffuse and also show the H positions. In the EH valence electron calculation (Figure 1 f), regions of low localization appear instead of the C-atom cores. A similar result is obtained with calculations using pseudopotentials. In such calculations, the problem is restricted to the quantum mechanical treatment of valence electrons, while interactions with the core electron density are substituted by effective potentials. Figure 1 e depicts ELF in terms of a contour line diagram.

In the series ethane, ethene, and ethyne (Figure 2) differences between covalent single, double, and triple bonds are clearly seen.[40] This is valid for both representations: the two-dimensional (2D) cross sections in Figures 2 a, c, e, and g as well as the three-dimensional (3D) isosurfaces in Figures 2 b, d, f, and h. It

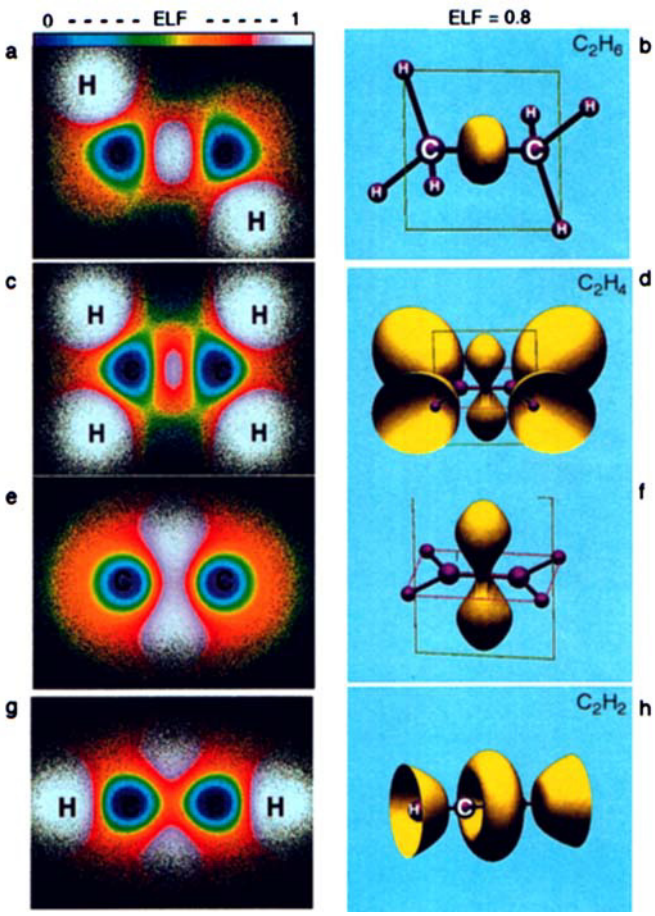

Figure 2. Left: 2D cross sections (EHMO calculations) through the molecules a) ethane, c) and e) ethene, and g) ethyne. Right: 3D representations of ELF isosurfaces with ELF = 0.8, b) ethane, d) and f) ethene, and h) ethyne. The planes around the hydrogen atoms are either not shown or only cut.

should be pointed out here that the number and form of the localization regions are strongly dependent on the choice of the isovalue. An isovalue of ELF = 0.8 has proven to be a useful standard for the classical valence compounds; this corresponds to the white-orange border in the 2D cross sections. In both representations an increasing contraction of the σ-like region along the C–C axis is observed with the increase of bond order. The 3D representation of ethyne gives the impression that only a localization torus is present. HF calculations using a double-zeta basis set and polarization functions[29] show that this is correct in principle. With both methods (EH, HF) the highest electron density is found on the core–core connecting line (Figure 2 g) but the highest ELF values are found outside (Figure

2f). The torus obtained from EH calculations is more distinctive. In conclusion, this result corroborates the formally equivalent descriptions of double bonds previously formulated by Pauling:[41] the banana or bent bonds and the σ-π-bonding model.

In electron-rich compounds, lone pairs of electrons play an important role in structure formation. Their structure-directing influences are summarized by the rules of Nyholm and Gillespie (VSEPR model[1]). These rules have been used successfully for decades and although they are more or less intuitive, only recently have quantifications been attempted.[42]

Figure 3 shows the 3D ELF isosurfaces for PF_3, SF_2, ClF_2^-, and ClF_3. As expected, the geometrical distributions of lone

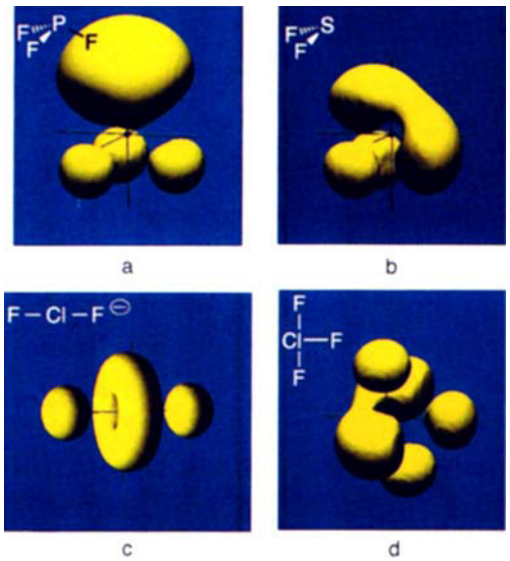

Figure 3. 3D representations of ELF isosurfaces with ELF = 0.8 for molecules differing in the number of lone pairs (based on EHMO calculations): a) PF_3; b) SF_2; c) ClF_2^-; d) ClF_3. The positions of the fluorine ligands (within the yellow ELF regions) can be taken from the given structure formulae. The central atom is located at the origin of the coordinate system shown in each figure.

pairs of electrons and bonding electron pairs and ligands correspond in principle to the VSEPR model: extended regions of lone pairs of electrons and relatively compact, almost spherical localizations around the F ligands. A closer inspection of the latter reveals a division in regions of element–F bonds and lone pairs of electrons at the F center.[16, 32] The contraction of the lone pairs of electrons is very evident in going from the relatively extended region at P in PF_3 to the compact torus at Cl in ClF_2^-.[43] The exceptional *anti*-position of the lone pairs of electrons both in SF_2 and ClF_3 is more distinctive than expected from the VSEPR model.

The topological similarity between ethyne C_2H_2 (Figure 2h) and ClF_2^- (Figure 3c, ref. [44]) is also interesting. These units are clearly distinguished by chemists but they are equivalent with respect to the attractor model (see Section 1). In other words, the attractor may be bonding (C–C bond) as well as nonbonding around the Cl atom. In this sense it is possible to deduce a hierarchical relationship even for these two simple species (ref. [121], see Section 7.2): the topology of the attractors is the same but the chemical structure realized therein is diversely complex.

In addition to the examination of the real electron space, cores, bonds, and lone pairs and their mutual interactions, become visible in simple molecules. In organic chemistry these interactions are understood by using qualitative concepts. Methyl acetate CH_3COOCH_3 serves as an example (Figure 4).[40] The three-dimensional representation of the ground

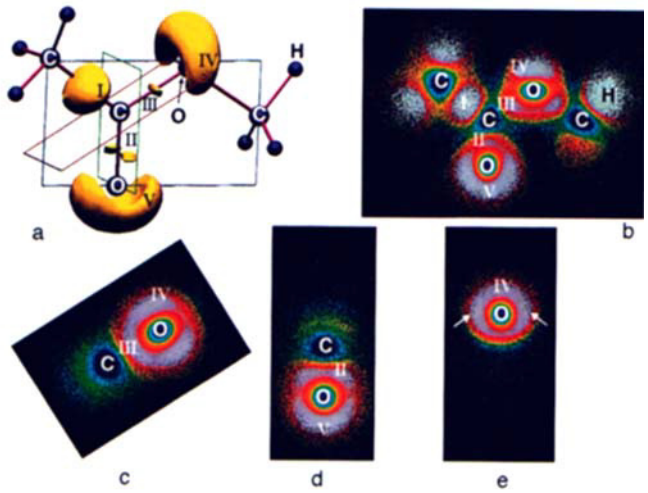

Figure 4. a) 3D representation of the ELF isosurface ELF = 0.85 (EHMO calculations) for methyl acetate. The regions around the hydrogen atoms are not included. For ELF = 0.80 the regions of the lone pairs (IV and V) are no longer separated from the neighboring C–O bonding regions (III and II, respectively). b)–e) 2D cross sections through different planes: b) through the plane drawn in blue in (a); c) through the plane drawn in red in (a); d) through the plane drawn in green in (a); e) through the plane parallel to that drawn in (d), which contains the oxygen atom of the ester.

state conformation contains an ELF isosurface showing extended localization domains for the lone pairs of the carbonyl and the oxygen atom of the ester. In addition there is a relatively extended region that includes the C–C bond (for clarity the C–H bonds were not included in the calculation of ELF). On the other hand, the regions of C–O single and double bonds are comparatively strongly contracted but show the expected distributions with respect to the core–core bond lines. ELF sections were calculated for planes through the molecule (Figures 4b–e). The cut through the C–O ester bond perpendicular to the molecular plane (Figure 4c) shows a broadening in the bond region in agreement with a double-bond contribution as given in Scheme 1A. Such an ELF analysis is helpful in the assignment of resonance formulae. Furthermore, a n-σ* anomeric effect is expected between the lone pair at the carbonyl oxygen atom and the σ bond to the ester oxygen atom (Scheme 1B). This should lead to a deformation of the ELF distribution around the oxygen atom of the carbonyl group, as can indeed be seen (Figure 4b, regions II and V merge asymmetrically). However, the n-σ* interaction in the ester bridge (Scheme 1C) is not supported by ELF, though the difference in the comparable sections through the oxygen atoms is striking (Figure 4b region V and Figure 4e region IV). The ELF distribution at the oxygen atom of the ester has a slight p-characteristic (the local maxima facing each other in region IV of Figure 4e, marked with arrows), which may be interpreted in terms of a reduction of the s part of the lone pairs (Scheme 1C).

Investigations of carbosilanes proved ELF to be a powerful tool in the comprehension of complicated bonding systems. It was shown for 1,3-disilacyclobutane that there is no (not even

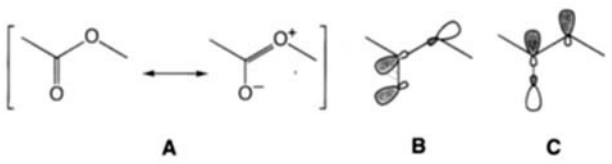

Scheme 1. Bonding features in methyl acetate.

weak) bond between the two Si centers in spite of a relatively short interatomic distance. Therefore an alternative interpretation was necessary: the Si–C bonds appear as bent bonds in the ELF analysis, and they can be interpreted in terms of a bent bond between two building blocks, which differ in size but retain tetrahedral angles at the cores. From this description it follows that the relatively short Si–Si distance is a geometrical consequence of the bent Si–C bond.[45] Analogously, the bond shortening in C_2H_4 compared with that in C_2H_6 was previously explained by Pauling with the assumption of bent bonds.[41]

2.1. Covalent versus Ionic

The division of chemical bonds into homopolar or primarily ionic bonds has proved to be very useful in the language and comprehension of chemistry. Naturally, the ideal covalent bond is simply defined in element–element bonds but, strictly speaking, only when the surroundings of both bonding partners are identical. The ideal ionic bond with a complete charge transfer does not exist. In general, a bonding interaction intermediate to ionic and covalent bonds is observed: a polar bond.[46]

The definition of the range of influence for ELF attractors permits a new formulation of ionicity in which the delimitation and mutual significance of covalent and ionic parts is simplified.[47] First, a qualitative impression is gained upon analyzing the form of the attractors. If they are more spherically distributed around the cores either a more ionic or a van der Waals interaction is present. If the covalency of a bond increases, the migration of the attractor becomes more distinctive between the centers until a totally symmetric topology is achieved in the ideal covalent case. The position of the attractor between the centers can quantitatively be used to define the extent of polarity of a chemical bond.[48] As long as the attractor lies on the line connecting the cores and can be separated from the cores themselves by a trajectory, and the attractor does not circumscribe the core, a situation is reached that is usually described as polar covalency. An ionic formulation is suitable if the attractor is close to the core region of one of the atoms and no longer on the connecting line. One must take into account that no clear separation is possible.

The combination of the division of the electron density according to Bader[12] and ELF in domains (WBs) is a second way for a complete quantitative description of the chemical bond. The actual charges of the atoms can be determined by the partition of the density in ranges of atomic influence. The covalent contribution of the bond is obtained by the number of electrons in the mutually shared electronic range of influence and attractor (partition of ELF). This is illustrated in Section 4.2 with the results of calculations on several intermetallic phases.

2.2. ELF in Simple Crystal Structures

The investigation of structure and chemical bonding is frequently carried out with a small number of ELF plots, where series of structures can visually be compared. In this way the language of ELF can be learned "simply", asking the basic question: "what happens if...?". Figure 5 illustrates ELF for sections through simple structure types with primitive cubic arrangements and their AB variant, the rock salt structure, (Figures 5a–d), as well as the diamond structure and its AB variant, the zinc blende structure (Figures 5e–h). The ELF obtained from LMTO calculations on the isoelectronic series silicon ("SiSi"), AlP, MgS, and NaCl are shown. The corresponding hypothetical modifications are given in quotation marks.

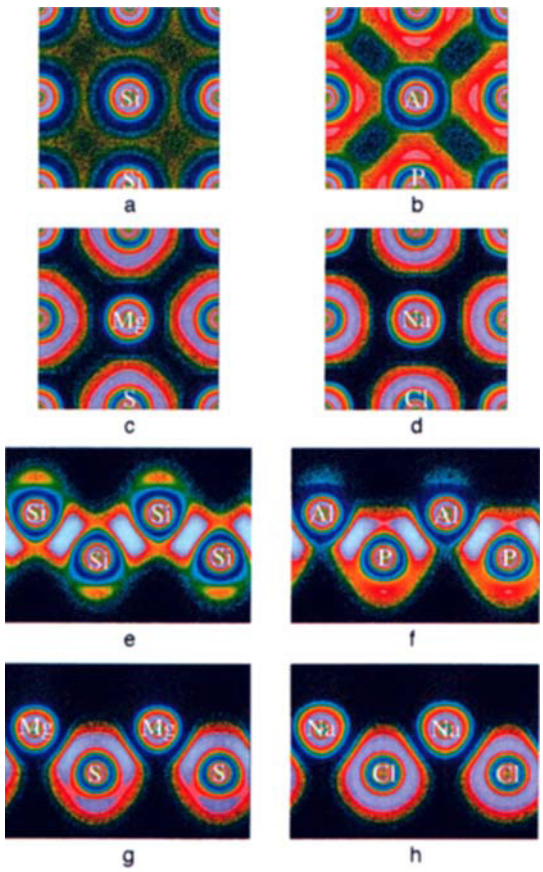

Figure 5. ELF sections (based on LMTO calculations) for the (100) surface of a) a hypothetical primitive cubic structure of silicon, as well as for the rock salt structure for b) AlP, c) MgS, and d) NaCl. The increasing concentration of regions of high ELF values on spherelike shells around the cores is evident. e)–h) Actual and hypothetical modifications of diamond structure: e) silicon, f) AlP with a clearly increased bond polarity, g) MgS with polarized "S^{2-} ions", and h) NaCl with clearly separated but still polarized anions.

"Silicon" in a primitive cubic arrangement would be really lost in a metallic state: the valence electrons are totally delocalized over that region which is not covered by the cores (Figure 5a). A localization of ELF ~ 0.7 is rather high with respect to the free electron gas (ELF = 0.5). For the corresponding "AlP" phase, ELF provides an almost perfect example of a polar bond: it increases in a wedge-shaped fashion from the Al core to the phosphorus atom, where it merges with five other

equivalent localization domains (Figure 5b). It should be mentioned that the individual localization regions can be separated by trajectories of minimal function values (orthogonal trajectories). This can be used for the division into domains (WBs) and for subsequent quantitative evaluations (see Section 4.2).

For MgS, ELF indicates a more ionic structure. The soft S^{2-} ions are polarized, resulting in an octahedral distortion of the spherical symmetry (Figure 5c). In NaCl, a region of high localization with nearly spherical symmetry is found around the anion (Figure 5d). If a corresponding division of ELF is made, no attractors can be found between the Na and Cl atom pairs. Rather an alignment of the attractors is found as expected on the basis of the VSEPR or ligand field theory.[49] The six attractors around the chloride ion are directed precisely between the Na neighbors. Whether the disappearance of the attractors from the line connecting interatomic centers is suitable for a sharp separation of polar-covalent and ionic bonds must be further investigated as very polar π or δ interactions cause similar effects.

From the general evolution of the localization in the former case it can be concluded that an increase in the localization in the vicinity of certain attractors leads simultaneously to its decrease in the interstitial regions. With respect to the free electron gas, whose density is totally uniform and revealed by the green coloring in ELF (see Section 1), a more or less distinctive localization of electrons takes place in every structure. In the primitive cubic packing of identical atoms (Figure 5a), the proximity to the electron gas is even more pronounced. For example, Savin showed a dramatic alteration of the localizations with different valence electron numbers in the fcc structure. For calcium (2e per atom) the localization regions are in the octahedral holes, whereas in aluminum (3e per atom) the regions of highest localization are always found between the Al pairs[50] (see Figure 12o). On average, the localization for silicon in the bonding region is even higher but the distribution is distinctively less structured than in the aluminum case.

In compounds exhibiting the diamond structure (Figure 5e–h), localized regions are only present in sections of ELF along the plane diagonal of the unit cell ([110]). In this series the localization maximum is again shifted stepwise along the core–core connecting line towards the more electronegative atom. The position of the ELF maximum can be used to measure the extent of the polarity of the bond. Even for "NaCl", a considerable deviation from the spherical symmetry of the anions is observed (Figure 5h). Examination of the plots reveals that AlP appears to be predominantly covalent, whereas "MgS" and "NaCl" are more ionic, because of an increasing spherical distribution of the localization around the anions. In "NaCl" the appearance of a strongly polarized anion is predominant. In AlP and MgS it is possible to clearly distinguish between the regions of localization of high ELF values. For the more ionic compounds, such distinctions are hardly or often not possible. The immediate impression gained from these ELF representations confirms those gleaned from chemical intuition.

Similar ELF investigations of the diamond structure for the elements carbon, silicon, germanium, and tin also show interesting trends; a reduction of localization in the two-electron–two-center bond, while the localization in the interstitial region increases continuously.[25] The comparison of α- with β-tin clearly verifies that in the latter a much lower localization is present than in the diamond modification.[25]

2.3. Bonds between Metals

One faces the metallic bond as if one is meeting an alien: with suspicion, lack of understanding, and a certain respect. The actual meaning of the term "metallic bond" is complex with many variations and we will examine it in more detail in Section 4. First we consider the smallest metal aggregations, biatomic clusters[16] such as $[Re_2(CO)_{10}]$, $[W_2(CO)_8]^{4-}$, and $[Mo_2Cl_8]^{4-}$. The question is: may bonds between transition metals be resolved as well as those between main group elements?

According to the 18-electron rule $[Re_2(CO)_{10}]$ and $[W_2(CO)_8]^{4-}$ should have one and two metal–metal bonds, respectively. Four metal–metal bonds are expected in $[Mo_2Cl_8]^{4-}$. Figures 6a–c present the structures of these clusters with the accompanying 3D ELF isosurfaces as calculated with the EH method. As expected, for $[Re_2(CO)_{10}]$ a rotationally symmetric localization is found between the metal centers that is relatively small compared to the localization regions around the CO ligands (Figure 6a). This holds also for the two other clusters: the corresponding localization regions are very compact in spite of the contribution of 4d and 5d states. This is generally observed

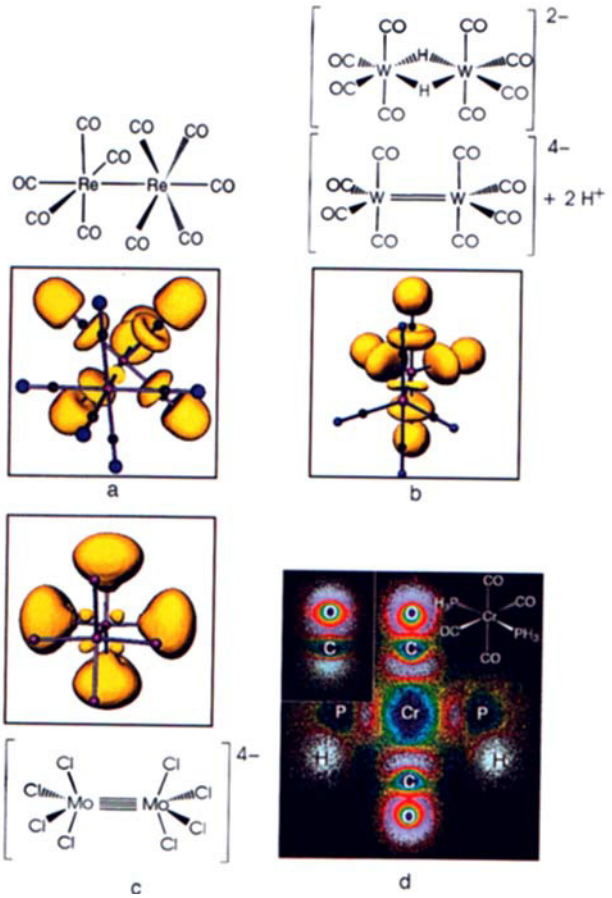

Figure 6. 3D representation of the isosurface ELF = 0.80 for molecules with a) metal–metal single, b) metal–metal double, and c) metal–metal quadruple bonds (EHMO calculations). d) 2D section through a plane in $[Cr(CO)_4(PH_3)_2]$ and 2D cross section through a free carbon monoxide molecule (insert).

in systems containing transition metals. As a rule, regions of ELF with high contributions of d states are rather small both with respect to the ELF values and the volume.

In the case of $H_2[W_2(CO)_8]^{2-}$, a π-like distribution between the metal centers is indeed observed in the deprotonated form $[W_2(CO)_8]^{4-}$ (Figure 6b). Of course, in this case the double bond is aligned in this special way only because the arrangement of the CO ligands breaks the degeneracy of the two possible π states. The two possible formulations $2H^+ + [(CO)_4W{=}W(CO)_4]^{4-}$ and $[(CO)_4W(\mu_2\text{-}H)_2W(CO)_4]^{2-}$ again show the hierarchical relationship, which is evident at the ELF attractor: the attractor is able to accommodate electrons as well as atoms and ions or multicentered groups without changing the topology of the total system.

For $[Mo_2Cl_8]^{4-}$, ELF shows four localization regions around the line connecting the M centers. This can be understood in terms of four bent bonds (Figure 6c). Taking into account that the point group D_{4h} allows only a twofold degeneracy, a principal difficulty arises, which also appears in the MO description of methane. The problem is that we do not have a "natural sense" for degeneracy caused by symmetry. At first the chemistry student is surprised at the strange partitioning of spherical symmetry into one s, three p, five d, seven f etc. representations but this is quickly accepted. It is a matter of debate whether $[Mo_2Cl_8]^{4-}$ actually "believes" its electronic structure may be reduced into irreducible representations. It must be emphasized that ELF always provides a picture that corresponds to the full symmetry of the respective group. This property is reminiscent of the symmetry-adapted hybrids of the VB theory, but it must be stressed that in contrast, ELF is always unambiguous.

Finally the ELF at the ligands is also worth mentioning. A comparison of the CO groups in Figures 6a, b reveals an extended region that surrounds the polar triple bond and the lone pair around oxygen. In $(H^+)_2[W_2(CO)_8]^{4-}$ it is smaller and more round, whereas the region between W and C atoms is more extended. Figure 6d shows the sections of ELF through an isolated CO molecule and in the octahedral complex $[Cr(CO)_4(PH_3)_2]$. Clear displacements of the localization regions are found when the free and bound CO molecules are compared. Here, the differences between a strong CO–Cr and a normal donor P–Cr bond are evident. Similar results were obtained recently by Kaupp in the analysis of two-center carbonyl clusters with terminal and bridging CO ligands.[51]

To substantiate this result we carried out EH calculations on the following series: free CO, $[CO{-}Cr(CO)_5]$, and $[CO{-}Cr(CO)(PH_3)_4]$ (Figure 7[52]). A distinct bonding effect between chromium and the CO ligand is expected and can clearly be seen by comparing the left part and the center of Figure 7. In $[CO{-}Cr(CO)_5]$ the attractor lies on the Cr–C bond axis (center), whereas in $[CO{-}Cr(CO)(PH_3)_4]$ this axis is surrounded by a torus (right), which indicates the presence of π-bonding contributions. In the first case the metal–ligand backbonding is relatively weak because the Cr center has to distribute its electrons evenly onto six ligands; thus, the σ character is dominant.

From these examples it is evident that in organic molecules (Section 2, Figure 4) as well as in complexes, weak effects such as changes in the behavior of backbonding become directly visible with ELF.

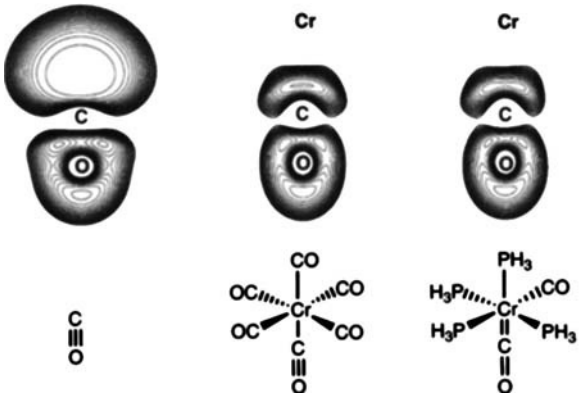

Figure 7. Contour line representations of the ELF (EHMO calculations) through a free CO molecule (left), CO complexed in $[Cr(CO)_6]$ (center), and in *cis*-$[Cr(CO)_2(PH_3)_4]$ (right) with the corresponding valence line formulae.

2.4. Clusters, Multicenter Bonds, and the Principle of Duality

The boranes, carboranes, and naked clusters (especially those of the heavier elements of group 14) form deltahedral clusters that may be understood with the aid of Wade's rules.[53] Here, terminal lone pairs and terminal bonds on the cluster are separated from the framework states as one- or two-center states. The framework bonds can be formally described as local three-center interactions in the sense of closed three-center bonds.[54] However, this leads to problems because, as a rule, there are more triangles than occupied framework states in *closo* deltahedrons. Here, a kind of inverse problem to that discussed in both the examination of multiple bonds (Section 2.3) and benzene (Section 1) arises. This forces the formulation of mesomeric structures, that is formulations coinciding with the phenomenon of delocalization (at least in the conventional sense).

What pictures are provided by ELF with regard to framework electrons and framework–ligand interactions, and how do ELF distributions change with respect to the number of framework electrons?

The first ELF examination of boron clusters revealed a pronounced duality between the polyhedral framework and the localization regions. The latter form the dual tetrahedron for the tetrahedral B_4H_4 framework, a cube for the octahedral $B_6H_6^{2-}$ ion, and a pentagonal dodecahedron for the icosahedral $B_{12}H_{12}^{2-}$ ion.[30] Recently theoretical studies based on experimental investigations were carried out on B_9X_9 (X = Cl, Br, I), the findings from which add further support to this interpretation.[55]

Figure 8c shows ELF for a $B_6H_6^{2-}$ cluster.[16] The localization regions above the planes are clearly seen and simultaneously a noticeable localization appears above the edges. A systematic study of ELF versus the number of framework electrons n_G reveals localization regions that are either spherical ($n_G = 2$, Figure 8a), concentrated above planes ($n_G = 8$, Figure 8b), distributed above planes and edges ($n_G = 20$, Figure 8d, Wade's framework electron number), or only above the edges ($n_G = 20$, Figure 8d). For main group element clusters, twenty electrons corresponds to a strongly antibonding situation. If d states are present at the metal centers up to twelve orbitals must be occupied before antibonding states are reached. The $[Mo_6Cl_8]^{4+}$ group found first in $MoCl_2$[62] has 24 framework electrons and

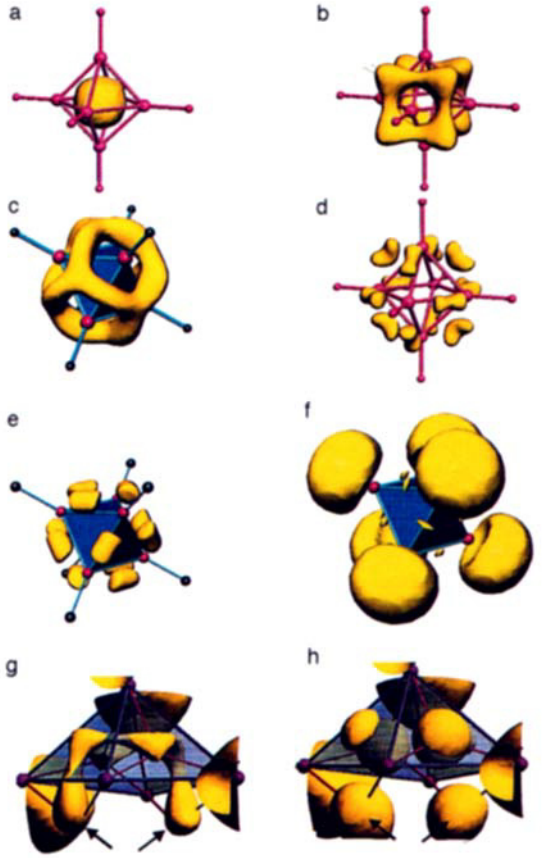

Figure 8. 3D representations of the ELF = 0.80 isosurface for different cluster molecules (EHMO calculations). a)–d) Octahedral clusters with different numbers of framework electrons n_G, each calculated with the parameters used for the calculation of $B_6H_6^{2-}$. For details see text. e) $[Sn_6H_6]^{4+}$ as a model for $[Sn_6(Cr(CO)_5)_6]^{2-}$. f) The corresponding hypothetical $[Sn_6]^{2-}$ ion without transition metals. g) and h) ELF isosurfaces of the square-pyramidal clusters $[Zr_5Cl_{12}(PMe_3)_5]^{4-}$ and $[Zr_5Cl_{12}(PMe_3)_5H_4]$, respectively, together with the structure of the Zr_5 cluster unit. The Cl and PMe_3 ligands are omitted for clarity. The arrows mark the positions of the bridging hydrogen atoms. In addition to the spherical localization regions of the four hydrogen atoms, h) shows two smaller regions that are found in the unoccupied triangular planes. The ELF isosurfaces of the isoelectronic and formally fourfold deprotonated cluster in g) are very similar: four almost equal regions above the triangular planes and two distinctive ones above the open plane of the cluster. See text for details.

is representative of the latter situation. For such systems variable numbers of framework electrons ranging from 19 to 24 have been verified experimentally.[56]

The duality relationship was already pointed out in investigations of metal carbonyl clusters[51] and for clusters in intermetallic phases.[57] Again, this is only valid for certain numbers of framework electrons, for example for main group element clusters with electron numbers close to those predicted by Wade's rules.

There are typical examples of octahedral clusters with different electron counts (Figures 8a–d) that sometimes contain condensed rather than isolated polyhedra. The ELF distribution with two framework electrons is shown in Figure 8a. The octahedral Li_6C group is an example of such a two-electron system, for which a totally symmetric lithium-centered framework state has been calculated.[58] To our knowledge, the eight-electron case (Figure 8b) has never been observed. Here, the duality between the framework structure and ELF is most evident. Wade's electron number for the octahedron is achieved with 14 electrons, whereas the 15e and 16e systems are realized in the well known clusters $[Nb_6X_{12}]^{3+}$ and $[Nb_6X_{12}]^{2+}$, respectively. Here, almost equally pronounced localization regions above planes and edges of the polyhedron are found as well, but with a slight accentuation above the planes. Clusters with 19 to 24 framework electrons like Nb_6I_{11}, HNb_6I_{11},[59,60] the Chevrel phases,[61] and $[Mo_6X_8]^{4+}$ are examples of 20e systems with very distinctive concentrations of regions of high localization above the edges of the polyhedra (Figure 8d). The shape of the localization regions in $B_6H_6^{2-}$ as well as in $[Zr_6Cl_{18}]^{8-}$ and $[Nb_6Cl_{18}]^{4-}$ (14 and 16 framework electrons, respectively) is almost identical. With regard to the framework atoms, the localization regions are located outside of the B_6 cluster, but inside of the clusters in the other two metal polyhedra.[52,66] Two possible reasons for this are: first, the different size of the polyhedra and the relation of orbital expansion to edge length, and second, the different interactions and repulsions between ligands and framework electrons.

Several examples of clusters with different numbers of valence electrons exist. For instance, $[AuPR_3]_4^{2+}$[63,64] and Li_4^{2+} contain two framework electrons, B_4Cl_4 and C_4R_4 eight, and Si_4^{4-} and P_4 twelve. A corresponding spherical distribution is found in ELF. Four localization regions above the planes and six above the edges[16] may be seen in ELF and can be interpreted in terms of bent bonds over the planes.[45,67,68] As in the dinuclear metal complexes mentioned previously (Section 2.3), the mutual distribution of ligands and localization regions of the framework is also apparent here: if the ligands are electron-rich octet systems, the ligands and localization regions avoid each other. Here, a kind of higher hierarchical level of the ligand field theory is found. The form and the number of the attractors is not only determined by the type of the occupied framework states, but also by the type of the ligands and their distribution. Therefore, it should be possible to transfer effects like the Jahn–Teller distortion and ligand-field induced changes, which are well understood for mononuclear metal complexes, to topologically related larger systems, that is on a higher hierarchical level. This was carried out many years ago on M_6 clusters such as M_6X_8 and M_6X_{12} by Simon.[56] ELF is especially suitable for the observation of such effects in real space.

Figures 8e and f show the comparison of the clusters $[Sn_6H_6]^{4+}$ and the hitherto unknown naked cluster $[Sn_6]^{2-}$; the former is used as a model for the recently published cluster $[Sn_6(Cr(CO)_5)_6]^{2-}$. It is clearly seen that electrophilic ligands are bound at the cluster vertices (Figure 8f). Further ligands would approach the localization regions of the framework. If there are ligands at the edges and vertices of the cluster, localization regions are found at the faces. This is validated experimentally. In $H_7Th_6Br_{15}$, seven of the eight planes of the octahedron are occupied statistically by H atoms. Presumably, they can easily tautomerize above the localization regions on the plane centers and would as such be carried along the localization regions by an "overhead cable".[30] Experimental and theoretical examinations carried out on the $B_6H_7^-$ ion verify such behavior.[69,70] According to quantum mechanical calculations, the two H atoms in $H_2B_9Br_9$ with *anti*-conformation are distributed over two planes of the B_9 polyhedron.[55]

Protons bound on cluster surfaces often give rise to problems in structure determination as illustrated in the following example. A compound containing octahedral Zr_6 clusters was ini-

tially published as $[Zr_6Cl_{14}(PR_3)_4]$,[71] and subsequently proven to be $[Zr_6Cl_{14}(PR_3)_4H_4]$.[72] In the structure determination of $[Zr_5Cl_{12}(PR_3)_5H_4]$, which features a square-pyramidal Zr_5 framework, the position of the protons were determined crystallographically.[73] Two of the protons are located in opposite triangular planes of the Zr_5 pyramid and two protons bridge the opposite edges of the open square plane (Figures 8g and h). Whereas the positions in the triangular planes are located in or above the center of the Zr_3 triangles for reasons of symmetry, there are more degrees of freedom for possible positions above the edges. The ELF investigation of the fourfold deprotonated cluster $[Zr_5Cl_{12}(PR_3)_5]^{4-}$ (Figure 8g) shows four local maxima in the triangular planes and two very pronounced localization regions caused by a slight asymmetrical distribution of the chlorine and phosphane ligands. Their centers correspond exactly to the crystallographically determined positions of the hydrogen atoms.[52] The localization regions are determined only by the electronic structure of the cluster framework and the remaining ligands, independently from the basis functions of the hydrogen atoms used in the calculation. More about the use of ELF in making predictions of structures is given in Section 6.

3. Zintl Phases: Semiconducting Compounds

In the semiconducting compounds M_aX_b (M = metal, X = semimetal) two fundamental chemical classes are united: metals and insulators. In this "symbiosis", the latter component dominates as is reflected in electron structures that are, nearly without exception, described in terms of localized electronic states. In fact, the majority of compounds in this enormously diverse class obey the $(8-N)$ rule, that is, only two-electron–two-center bonds and lone pairs of electrons are possible states for the valence electrons. Therefore, the electronic structure may be qualitatively determined directly from the topology. As a rule, the connection of semimetals X to give oligo- and polymeric Zintl anions $(X_m)^{n-}$ as well as the coordination of these Zintl anions, which are surrounded by M^{n+} ions through their lone pairs of electrons, may be easily understood from an electrostatic point of view.

The connection pattern is a structural solution to the average connectivity of the X atoms that results from the average valence electron number at X determined from the $(8-N)$ rule. Bonds and lone pairs form sp^3, sp^2, or sp hybrid-like arrangements around the X atoms with more or less pronounced deviations from the ideal angles as predicted by the Nyholm–Gillespie rules. If there are different structural solutions for the same stoichiometry and the number of valence electrons, the details of the electron structure and a detailed knowledge of the long-range interactions is of interest. Then, local distributions, diffusiveness or compactness, polarizability, and total expansion of local electron density may be important. Only the latter values can be qualitatively and quantitatively examined in three dimensions with ELF.

3.1. Lone Pairs of Electrons in Zintl Phases

The crystal structures of $Ca_{14}Si_{19}$ ($Ca_3Si_{4.071}$) and Ca_3Si_4 differ significantly despite having almost identical formulae and being in thermodynamic equilibrium at 1270 K.[74] Therefore, a phase transformation is not present here, but a peritectic transformation of the low-temperature (LT) phase Ca_3Si_4 into the high-temperature (HT) phase $Ca_{14}Si_{19}$.

Both compounds contain the bicyclic Si_9 unit (Figure 9a) that appears in $Ca_{14}Si_{19}$ as a sixfold connected building unit $R_6[Si_9^{14-}]$ and in Ca_3Si_4 as a threefold connected unit $R_3[Si_9^{17-}]$. It seems to be that at low temperatures a higher charge can be accumulated in individual regions than at higher temperatures; the distribution of charges and bonds in space becomes more regular at higher temperatures. The average Ca–Si bond lengths of 3.18 and 3.19 Å in the LT and HT phase, respectively, are hardly distinguishable, which is attributable to the almost equal formal overall charges. Apart from the connectivity of the Si frameworks, the Ca atoms have very similar chemical environments with respect to the lone pair electrons.

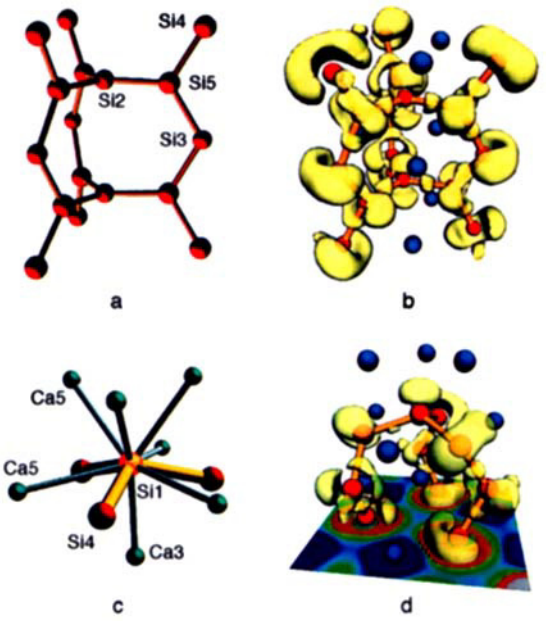

Figure 9. a) Bicyclic unit in $Ca_{14}Si_{19}$ containing the planar Si3-Si4-Si5 chain and planar three-coordinate silicon atoms (Si2, Si5). b) 3D isosurface (ELF = 0.80, based on LMTO calculations) showing very large attractor regions (yellow) for the lone pairs at the two-bonding Si centers and a p-characteristic at the three-bonding Si atoms. c) Bent cap $Si1(Si4)_3$ in Ca_3Si_4. In comparison to that in b), the Ca coordination changes slightly at the Ca5 positions and markedly at Ca3; in this case Ca3 occupies the center of the Si arrangement. d) An enlarged section of the 3D ELF isosurface shown in c) with a similar characteristic distribution of the large lone pair regions. See text for details.

Up to this point, ELF does not significantly enhance our understanding of the structural topology. What is clearly seen with ELF are the enormously extended regions for the lone pair of electrons at the two-bonding Si atoms, which fill the large void that is not occupied by the two bonding neighbors in a horseshoe geometry (Figure 9b). The mutual positions of neighbors and localization regions reveal a relatively good packing of all attractor regions, that is either atomic cores, bonding electrons, or lone pairs (see Figure 9b). In contrast, at the central Si2 atom, which adopts a trigonal-planar coordination, the lone pair clearly has p character. This is also observed at the other three-bonding Si atoms of Si5 type, but the localization regions of the three bonds and the lone pairs are not fully resolved (see Figures 9b and d). Figure 9b clearly shows that

the lone pairs aligned along the Si3-Si5-Si4 chain avoid each other. Furthermore, the lone pairs do not point directly towards the Ca cations (blue spheres) in the inner region of the fragment. A small change in position of the three-bonding Si1 in Figure 9c is accompanied by an immediate spatial change of the lone pair electron, which now shows a sp^3 geometry (Figure 9d). Therefore it can no longer take part in the coordination of Ca3. On the other hand, Ca3 polarizes the three two-bonding Si centers located at the same plane such that the localization regions of their lone pairs deviate from the usual horseshoe form. Overall, it is remarkable that the horseshoe-like lone pairs circumscribe very large spatial regions around the two-bonding Si atoms, perhaps exceeding the effect expected from VSEPR theory. In the 2D cross section of Figure 9d, the cation–polyanion interaction is clearly seen between the yellow localization region and the blue Ca center. The central region of the lone pair is directed towards the Ca atom. We believe that a more extensive spatial examination of this kind with the aid of ELF will lead to a deeper comprehension, because many attractors relevant in structural chemistry become visible in their mutual relations.

The relationship between electron localization regions and cation distribution becomes even more apparent in $Ca_7Mg_{7.25}Si_{14}$,[74–76] because there are two different cations with completely different structural and chemical functions. The compound contains isolated octet Si^{4-} anions and planar Si_{12} groups stacked in an eclipsed manner in the [001] direction (Figure 10a). The regular distribution of large Ca cations around the Si_{12} unit and of the Mg centers at terminal and isolated Si atoms is clearly seen. Despite the large interunit distance of $c = 4.40$ Å, there is a weak interaction that develops between the π states of the Si_{12} group. Such interactions have recently been verified for many polyanionic arrangements of silicon. Band structure calculations on different structures confirm these results.[31] The corresponding EH band structure of $Ca_7Mg_{7.25}Si_{14}$ shows the large dispersion of the π^* bands in the c^* direction by which the semiconducting characteristic of the bulk of the band structure is overshadowed by a one-dimensional metallic conductivity (Figure 10c, see ref. [31]). This effect is not identifiable in the form of a localized interaction in the ELF, as it is evidently a weak interaction. The quantum mechanical analysis supports a formulation that corresponds only approximately to the Zintl–Klemm formalism, namely $(Ca^{2+})_7(Mg^{2+})_{7.25}[Si^{4-}]_2[Si_{12}^{20.5-}]$. Nevertheless, all ocupied electronic states must be assigned to the silicon anions. Even the conduction band is centered at Si. Therefore, such compounds can be described as metallic Zintl phases. ELF clearly depicts those localization regions that are well understood according to the Zintl–Klemm concept.

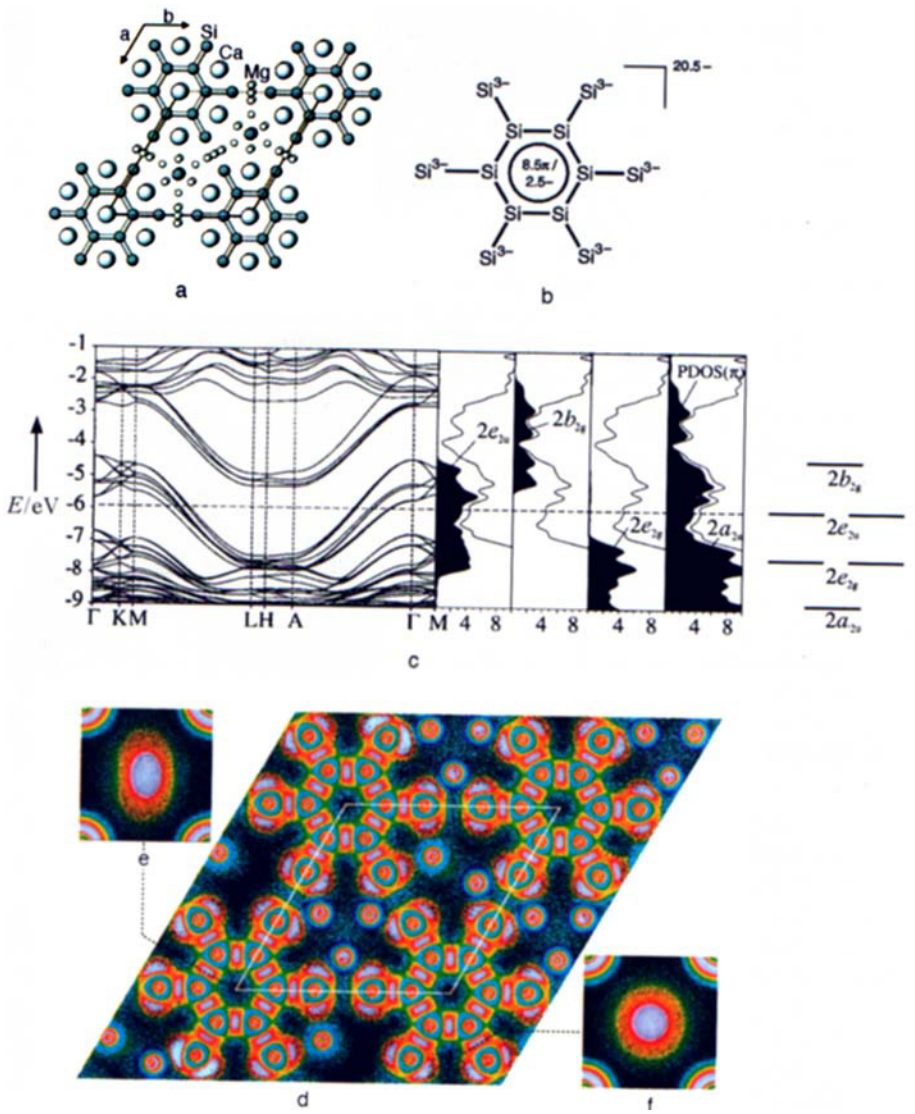

Figure 10. a) Structure of $Ca_7Mg_{7.25}Si_{14}$ containing isolated Si^{4-} anions and planar Si_{12} units. b) Schematic Lewis formula of the planar $Si_{12}^{20.5-}$ Zintl anion. c) EHMO band structure (left), density of states (DOS, center, in states per cell and eV), and MO scheme (pattern) of the π orbitals of $Ca_7Mg_{7.25}Si_{14}$ close to the Fermi level. The band structure reveals bands with large dispersion intersecting the Fermi level. These bands give rise to the metallic nature of $Ca_7Mg_{7.25}Si_{14}$ and are composed of the π^* states (e_{2u} symmetry) of the Si_6 ring (left DOS). The comparison between the total DOS (black line) and the DOS of all π states beautifully reveals that despite the metallic conductivity all occupied electronic states are centered on silicon. d) ELF (LMTO) cross section containing Si_{12} rings and several Mg centers. The plot is perpendicular to the c axis of the crystal structure. e) and f) ELF of cross sections of an intraring bond and a terminal bond, respectively, in the Si_{12} ring.

An interesting bonding structure can be found in the ELF of the highly charged oligomeric anion $Si_{12}^{20.5-}$. Figure 10d shows the pattern of the Si–Si bonds and the localized lone pairs. Remarkably, the lone pairs clearly interact with the small Mg^{2+} ions, whereas the larger Ca^{2+} ions interact more with the bonding electron pairs and the π system (not shown). This result was also observed in other structures.[31, 74] The relatively complicated band structure (Figure 10c) can thus be brought into a readily interpretable form (Figure 10d) with the aid of ELF.

The 68.5 valence electrons of the $Si_{12}^{20.5-}$ unit occupy the first twelve σ bonds and form the $6 \times 3 = 18$ lone pairs. The remaining 8.5 electron pairs occupy three π-bonding and two π*-antibonding states. The latter contribute to the conduction band (Figure 10c). Therefore, a π-bonding contribution remains that is unambiguously located in the ring as seen in the bond cross sections shown in Figures 10e and f. The intraring bonds are ecliptically distorted. A distribution of the π-bonding contribution over the whole silicon framework is also conceivable, but such a phenomenon is not observed. The planarity of the polyanions and the absence of significant distortions of the bonding structure in spite of partial occupancy of π* states is conspicuous here, and has also been observed in numerous other cases of planar Zintl anions. This is due to the relatively high formal and therefore comparatively high effective charges that can only be distributed equally when very delocalized π* states are generated.[77] Any distortion would lead to an irregular charge distribution, which evidently could not be stabilized by given cation fields.

The structure of the ternary silicide $Ba_2Mg_3Si_4$ contains Si_2 pairs and Si_6 chains.[31] The latter are in the *cis–trans* conformation and planar. The all-*trans* chain is well known for the compounds MSi (M = Ca, Si, Ba), which crystallize in the chromium boride structure type.[78–80] In $Ba_2Mg_3Si_4$ it is conceivable that the *cis* conformation is only present when Mg centers are coordinated to one of the Si centers. The Mg atoms are always in the *exo*- and the large Ba atoms in the *endo*-position to the chain (Figure 11 top). The center of the *trans* connection (of the chain) is always surrounded by four large metal atoms, whereas the highly charged terminal Si centers are always stabilized by four Mg atoms (in both cases only two of these atoms are seen in the figure). This coordination pattern is also found at the Si_2 pair (Figure 11 top). Furthermore, an ecliptic packing of Zintl anions along the *c* axis of the unit cell is present here. Even in this case it is not possible to formulate a completely saturated system with respect to charge balance: $(Ba^{2+})_4(Mg^{2+})_6(Si_2^{6-})(Si_6^{14-})$ and $(Ba^{2+})_4(Mg^{2+})_6(Si_2^{4-})(Si_6^{16-})$ represent possible formulations of $Ba_2Mg_3Si_4$. In the former case, the six-membered chain is unsaturated (e.g. $[Si-Si-Si=Si-Si-Si]^{14-}$ with 36 valence electrons), in the latter a $[Si=Si]^{4-}$ pair is proposed. Now we want to address the following questions with the aid of ELF:

1. Are there double bonds in Zintl phases and if so, where?
2. What dictates the conformation of the Si_6 chain?
3. Why is there a conspicuous accumulation of Mg centers at the terminal Si atoms?

To answer the first question ELF for a plane perpendicular to the *c* axis of the structure was analyzed (Figure 11 top). The small representations in the lower part of the figure are sections through Si–Si bonds that are correspondingly indicated in the picture above. There is a rotationally symmetric Si–Si bond in the Si_2 unit that is centered with respect to the interatomic vector (Figure 11, I). It clearly features the characteristics of a σ bond. On the other hand, the central bond in the chain shows an elliptical form and is more extended (Figure 11, II). The Ba atoms come closer to the extended bond, which leads to an enhanced coordination of the π bond. The next bond is markedly distorted towards the Mg centers and shows an elliptical shape in the central, relatively compact region (Figure 11, III). Finally, the bond to the terminal Si atom is almost rotationally symmetric and reveals hardly any π character (Figure 11, IV). This ELF analysis suggests the simplified formulation $[Si-Si\cdots Si\cdots Si\cdots Si-Si]^{14-}$ for the Si_6^{14-} ion. A more detailed analysis of the underlying band structure calculations confirms this formulation. Thus, $Ba_2Mg_3Si_4$ may be formulated $(Ba^{2+})_4(Mg^{2+})_6(Si_2^{6-})(Si_6^{14-})$.[31]

The second question can be answered in light of the geometrical arrangement of cations and lone pairs. Upon comparing the position of the Ba_2Mg_2 groups around bond III with the alignment of the participating Si centers, it is clearly seen that both lone pairs are oriented towards the Mg centers and away from the Ba centers. Therefore, a local *cis* conformation results. In the bonds exclusively coordinated by Ba cations (I, II, and IV), the lone pairs are in the *trans* position, which allows a symmetrical interaction with the cations.

Figure 11 shows that most of the lone pair electrons are oriented towards the Mg centers. It is thus the Mg and not the Ba centers that play the dominating role in dictating the coordination geometry. Therefore it is clear that assuming an equal proportion of cations to anions, the Mg^{2+} ions are able to stabilize higher charges in Zintl anions. This can be predominantly attributed to the higher Coulomb effect. It was previously shown that this structure-directing effect of the Mg cations can be used for controlling the variety of Zintl anions in the solid state.[31, 74, 81]

Finally the spherically symmetric ELF distribution around all metal centers, where only a shell-like structure is visible, should be mentioned, that is, the metal centers act almost as perfect cations. This will be further quantified in Section 4.2. The effective charges of the metal centers are smaller than $q = +2$; however, this is not important as they only stabilize the electronic states of the anions.

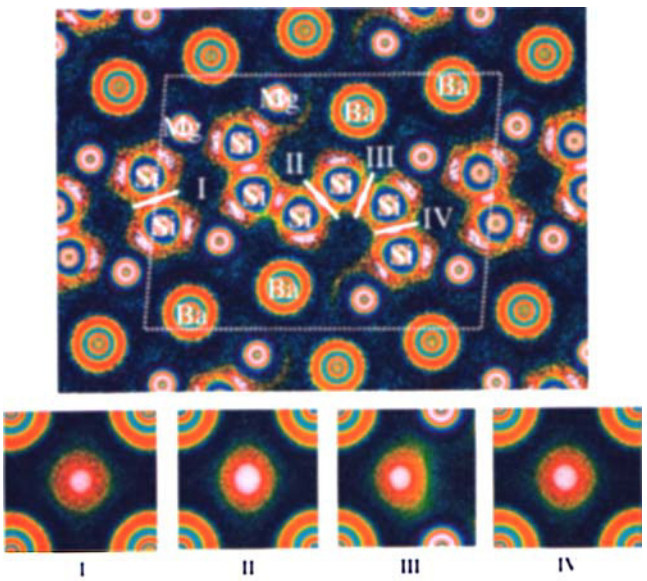

Figure 11. Top: ELF plot (LMTO) of the (010) plane in the new Zintl phase $Ba_2Mg_3Si_4$ [31] that contains Si_2 pairs and Si_6 chains. As in Figure 10, the direct relationship between the Mg centers and the lone pair electrons is demonstrated, whereas the coordination of the Ba cations at the Zintl anions is less pronounced. According to the determined stoichiometry one of the Si_n Zintl anions must contain π contributions. Bottom: The ELF cross sections of the bonds labeled above clearly show that only the six-membered chain contains π contributions. These contributions are very distinctive in the central bond II, weaker in III, and almost absent in IV.

Table 1. Classes of chemical compounds, typical building groups, and chemical interactions.

No.	Class of compound	Basic units	Type of interaction
I	van der Waals packings metal packings	atoms, molecules	van der Waals metallic
II	alloys	atoms, clusters, simple structures	covalent and delocalized
III	intermetallic phases	polyhedra, nets, partly complex structures	covalent, ionic, and delocalized
IV	Zintl phases, semiconductors	isolated, oligomeric, and polymeric ions	covalent, ionic
V	insulators	ions, valence polymers	covalent, ionic
VI	coordination compounds	molecules, complexes, and clusters	covalent, ionic
VII	H-bridging systems	polar molecules, valence polymers	covalent, ionic
VIII	composite	combinations of classes I–VI	

4. Intermetallic Compounds

In the past twenty years a great number of novel solid-state inorganic compounds have been synthesized, leading to a deeper understanding of structure–property relationships; thus, we are now able to face intermetallic compounds with new ideas and concepts. The evident conflict between more or less uniform structures of many metallic elements and their often quite complex compounds highlights complicated aspects of the chemical bond, which, however, are gradually being unraveled thanks to the development of theoretical methods. A significant difficulty in transferring classical valence concepts to compounds of classes II and III (Table 1) is their unique structural chemistry and topological form. Obvious relations exist only to boranes and clusters. The definition of intermetallic compounds as a unified family is not so simple; an encompassing theory is not at hand, especially considering the smooth transition to the semiconductors on the one hand and to the alloys on the other, the diverse expressions of the chemical bond, and the extraordinarily rich and varied structural chemistry. Older classifications such as that of B. Pearson (molar volumina, portion of the total energy in the band structure, framework or hybrid-framework structures, ref. [82]) are generally useful but definitely limited with regard to a deeper understanding of the chemical bond. Even the successful division into structure maps does not lead to true understanding.[83]

Also in this context, investigations with ELF led to completely new qualitative but also quantitative insights. We will show in the following sections how the chemical bond in intermetallic phases may be analyzed with ELF. To this end we studied two principal classes of compounds: Type A) those with more homopolar networks and type B) those with cluster-building units.

4.1. ELF in Intermetallic Phases

Figure 12 shows ELF calculations on a series of substances that reveals a transition from the semiconducting compounds to intermetallic phases and to metals in the following order: α-Si, $CaAl_2Si_2$, $SrAl_2$, $BaAl_4$, $CaAl_2$, and α-Al.[84] We assign these phases to type A. The general change in the ELF shows a development of strongly structured, contracted localization regions to distributions revealing not only distinctive structuring but considerably smaller differences between the extrema. The very high localizations (white regions) decrease proportionally and vary strongly in form and extension. Simultaneously, a change from clearly defined two-center localizations (α-Si, $CaAl_2$, $SrAl_2$) to the coexistence ($BaAl_4$) of two-center (Figure 12i, broad white spots) and multicenter bonds (Figure 12i, small white spots) as well as antibonding interactions (Figure 12j) occurs. The differences in bond lengths in $BaAl_4$, however, are not so dramatic and sometimes counterintuitive: the shortest distance is found for the five-center–six-electron bond (272.5 pm), whereas the two-electron–two-center bond is slightly longer (278.4 pm). An Al–Al distance of 305 pm is indicative of antibonding interactions (Figure 12j) and is quite close to the Al–Al distance in α-Al (286.3 pm). A discussion about bond lengths and bond strengths inevitably fails here.[85] It should be noted that even in $SrAl_2$ and $BaAl_4$ some localization regions show rather high ELF values and therefore yield corresponding integrated electron numbers (see Section 4.2).

The Laves phase $CaAl_2$ and α-Al belong to the class of substances clearly classified as metals; however, distinct localization regions are also present that may be understood in terms of covalent pair interactions even in the case of α-Al. The conspicuously complex structural chemistry of Al compounds, including quasicrystals, is expressed in the highly symmetric cubic closed packing of the metal. A similar case is found in $CaAl_2$, but only for the Al–Al interactions; the Ca–Al contacts are more ionic (Figure 12l,m). There are no Ca–Ca bonding contributions in spite of the diamond-like Ca substructure. Furthermore, all cases show a relatively spherically symmetric distribution of core and very weak valence localization (blue colored) around the large Ca, Sr, and Ba metal atoms, which indicates ionic character. This has been confirmed by quantitative analyses (see Section 4.2).

4.2. Quantitative Investigations

In structural chemistry, geometrical parameters as well as those deduced from topology and composition such as coordination numbers, bond strength, and formal charges have been used for a long time to classify compounds. With skillfully chosen division procedures, model systems are obtained that are sometimes amazingly resilient, but with well-defined limits. More precise statements about, for example, effective or partial charges, or valence electron distributions require other defini-

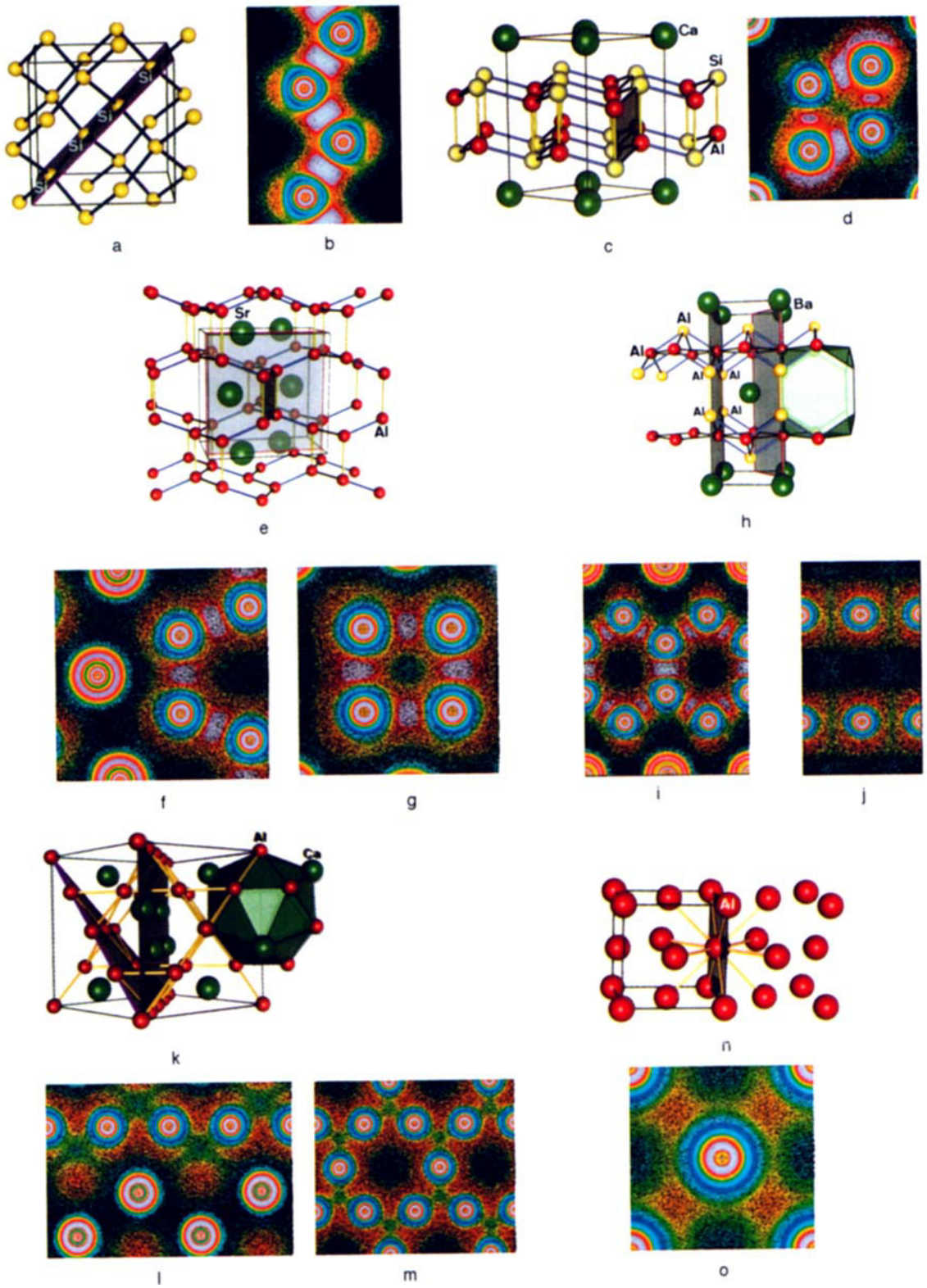

Figure 12. Structure and ELF representations (based on LMTO calculations) of selected 2D cross sections of the following structures: a), b) α-silicon, c), d) $CaAl_2Si_2$, e)–g) $SrAl_2$, h)–j) $BaAl_4$, k)–m) $CaAl_2$, n), o) α-Al. This series is representative for the transition from valence compounds to metals.

tion schemes and as such lead to different results. In principle, centers which are meaningful in structural chemistry, such as the so-called attractors (molecules, complexes, atoms, centers of bonds, etc.) and their domains (WBs) are defined.[21, 85] The most basic model is that of rigid spheres that do not completely fill the space. The simplest, and for the most part volume-preserving domain (WB) division was proposed by Voronoi and Dirichlet[86] in the 19th century and used by Niggli and Laves for crystal chemical investigations.[87, 88] The domains (WB) are restricted by the construction of convex polyhedra around the attractors. A sufficient number of planes are erected on the interatomic vectors so that the polyhedra are completely

closed. The division point on the vector can be chosen according to radius relation criteria and is critical. Even the volume-preserving power plane method[89] is not free from that arbitrariness. Furthermore, the restriction of domains (WBs) by planes is a relatively rough approximation.

As mentioned, domains (WBs) of single atoms or ions are obtained upon the division of electron density according to the method of Bader.[12] A corresponding division with ELF yields electronic domains (WBs) for atom cores (only in the case of all-electron calculations), lone pair electrons, bonds, and bonding contributions such as in cluster compounds with delocalized three-center bonds (e.g. boranes). Both the atomic and electronic domains (WBs) can be used for integration of incremental values such as partial charges, ionicity of bonds, and number of electrons per interaction center per attractor.

The domain (WB) regions for the electron density in α-Al, α-Si, and $CaAl_2$ in the form of three-dimensional envelopes are shown in Figures 13a, c, and g, respectively. Whereas a euclidean polyhedron (rhombic dodecahedron) is obtained for aluminum, the border planes for the atomic cells of α-Si and $CaAl_2$ are bent. A comparison of the edges of the polyhedra for the euclidean division (Figure 13f) and the division of orthogonal trajectories according to Bader[12] (Figure 13e) clearly reveals different results due to the restriction to planar borders in the former case.

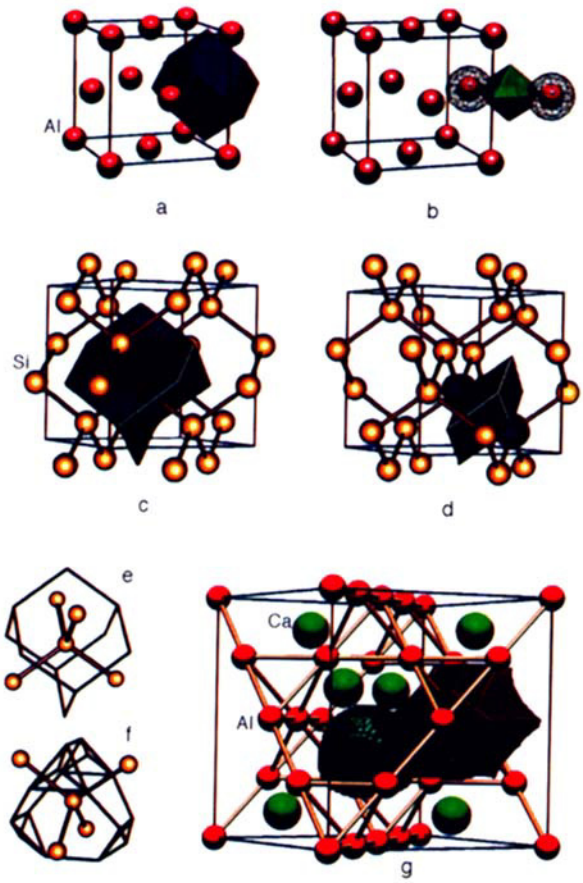

Figure 13. Domain (WB) divisions for quantitative partitioning of electron densities ρ [12] (a, c, g) and ELF (b, d). a), b) Al; c), d) Si; g) $CaAl_2$. The bonding regions in b) and d) appear either as a distorted octahedron (α-Al, green) or as a rhombus (α-Si, dark green). e) The atomic domain (WB) in α-Si may be described as a saddle polyhedron with bent boundary planes. The comparison of the topology of edges of this polyhedron with that obtained by a geometrical division method f) [89] reveals distinctive differences.

The clearly structured domain (WB) of Al in $CaAl_2$ is striking (red) (Figure 13g). It appears to be polarized by an almost spherical core region around Ca (green). This implies that significant ionic bonding contributions are present in the $CaAl_2$ Laves phase as evidenced by a relatively hard cation ($Ca^{\delta+}$) and a very soft anion ($Al_2^{\delta-}$) and thus covalent Al–Al interactions may be assumed. The quantitative investigations confirm this impression convincingly (see Table 2). Figures 13b and d show the divisions for the corresponding ELF.

Figure 14 displays the course of the trajectories in the two-dimensional sections in Figure 12; each picture shows the division of the electron density (atomic regions, top) and the division of the ELF (electronic regions, bottom). A comparison of both regions reveals a certain duality in the sense that where attractors are found in ELF, trajectories are present in the electron density and a minimum is found for the electron density at bond critical points along the interatomic vector. Furthermore, in $CaAl_2Si_2$, $SrAl_2$, $BaAl_4$, and $CaAl_2$ only one attractor is found for the alkaline earth metals and it is at the core position. This

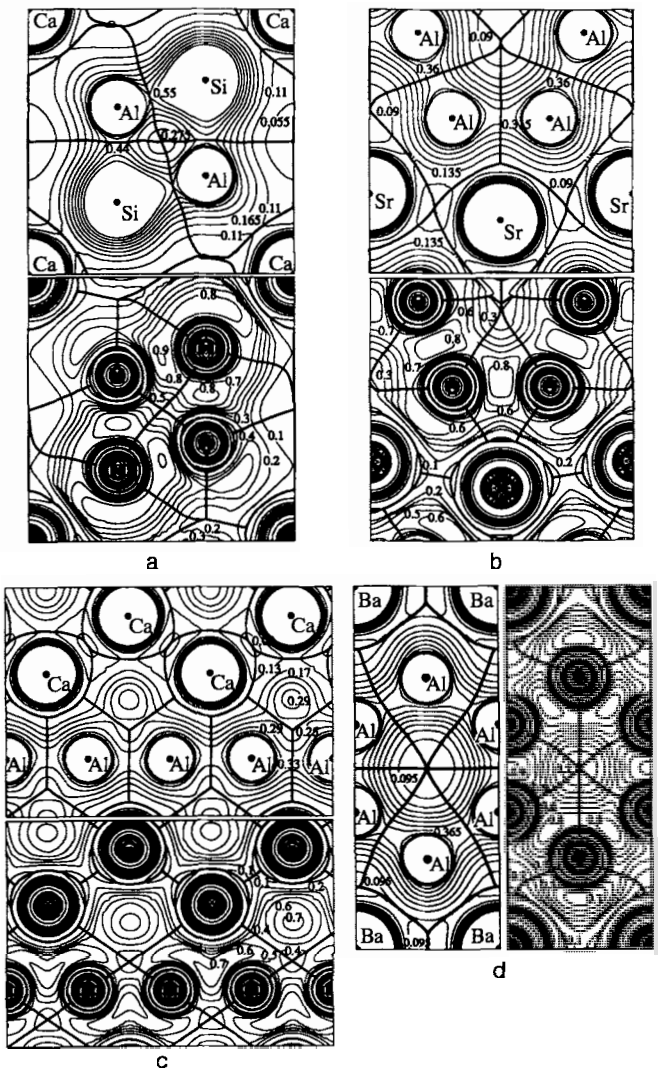

Figure 14. Contour line diagrams (thin black lines) with orthogonal trajectories that indicate the course of space divisions (thick black lines) in pairs for the electron density (top) and ELF (bottom) for a) $CaAl_2Si_2$, b) $SrAl_2$, c) $CaAl_2$, and d) $BaAl_4$ (LMTO calculations). The values given in Table 2 are obtained by separately integrating each domain (WB).

coincidence of atomic and electronic domains is indicative of the presence of quasi-ions in all cases. Furthermore, it is interesting that the domains (WB) in electron density and those of the cores in ELF are almost equal in form and extension for the electropositive metals Ca, Sr, and Ba. In Figure 14 these dual relations between ρ and ELF as well as the corelike form of the electronic domains at Ca, Sr, and Ba are emphasized.

Some quantitative values of this domain (WB) analysis are given in Table 2. The division of ρ yields partial charges q (difference between the number of valence electrons in the neutral atom and the N_e(at.) values) that are about the same with respect to the electropositive metals for the intermetallic phases $SrAl_2$ and $CaAl_2$ ($q(Ca) \approx q(Sr) \approx 1$). Suprisingly, the charge does not increase in $BaAl_4$ ($q(Ba) \approx +0.7$) although the concentration of the more electronegative component Al is doubled. As expected the calcium atom in $CaAl_2Si_2$ carries a higher charge ($q(Ca) \approx +1.3$). However, the high positive charge of aluminum ($q(Al) \approx +1.3$) in this phase is unexpected. Actually, aluminum and silicon form a network with clearly covalent bonding contributions that are expressed in the ELF in the form of separable electronic attractors (see Figure 14a). The term "polar covalency" can be used to describe $CaAl_2Si_2$ with the formulation $(Ca^{\alpha+}[Al^{\beta+}Si^{\gamma-}]_2)$, whereas the interaction between Ca centers and $[Al_2Si_2]$ has pronounced ionic character.

Table 2. Quantification of the electron density and the ELF over domain (WB) divisions: N_e(at.): Number of electrons for atomic domains (WB); N_e(al.): Number of electrons for electronic domain (WB) and ELF attractor.

Compound	atomic cell	N_e(at.)	electronic cell	N_e(el.)	distance [pm]
α-Al	Al atom	3.01	Al–Al	0.5	286.3
$CaAl_2$	Ca atom	0.99			
	Al atom	3.50	Al–Al	1.30	284.2
$SrAl_2$	Sr atom	1.01	Al–Al	2.13	279.9
	Al atom	3.51	Al–Al	2.01	278.6
			Al–Al	1.60	293.0
$BaAl_4$	Ba atom	1.33	Al–Al	2.05	278.4
	Al atom	2.57	Al–Al	1.45	272.5
	Al atom	3.75	Al–Al	-	305.2
$CaAl_2Si_2$	Ca atom	0.77	e_2-pair	1.96	
	Al atom	1.46	Al–Si	1.67	248.9
	Si atom	6.18	Al–Al	1.00	257.2
α-Si	Si atom	4.03	Si–Si	2.02	235.1

The effective electron numbers per domain (WB) reveal the influence of the corresponding attractor (bond, formula unit). Domain (WB) regions with approximately two electrons include the Si–Si bond, one of the three kinds of Al–Al bonds in $SrAl_2$, as well as the lone pair in $CaAl_2Si_2$ (Table 2). The integration of another Al–Al bond in $SrAl_2$ yields slightly more than two electrons; the cross section through this bond shows an elliptic form of the ELF. A weak π-bonding contribution seems to be present, but it does not appear to influence the bond length. Similar effects have also been found in Zintl anions of silicon.[31, 74, 75, 81] Smaller integrated electron numbers indicate multicenter bonds (see $BaAl_4$) or polar bonds with a corresponding Coulomb contribution.

The quantitative results summarized here reveal ELF to be very suitable for the examination of intermetallic phases. The function is particularly valuable because the rules of valency do not hold here and there is no other comprehensive bonding theory yet. However, according to the few ELF investigations to date it is evident that the exceptional feature of intermetallic phases is a mixture of a wide variety of bonding forms.

4.3. $CuAl_2$ and Its Variants

The $CuAl_2$ structure is the aristo structure type of a great number of intermetallic phases. Pt_3Ga_7, $PdSn_3$, $PtSn_4$, $PtPb_4$, $RhBi_4$, and $PdGa_5$ are isotypical to or derived from the $CuAl_2$ structure. All these compounds can be classified under type B (see Section 4). They feature a common building element, namely square antiprisms of main group elements E, which are interconnected[92, 93] in various ways through E–E, T–E, and T–T bonds (T = transition element). Examination of the local chemical bond with ELF reveals the development of totally different, strongly bound partial fragments especially in the E partial structure,[95] which are accompanied by a noticeable localization within the square antiprisms. In $CuAl_2$, for example, there are strong bonds between the Al pairs connecting the prisms.[96] This is reminiscent of the strong bonds between boron polyhedra and the terminal two-electron–two-center bonds in boron clusters, and of the Ga_2 pairs in the structure of α-Ga.[94] These bonds are sections of two interpenetrating graphite-like networks.[96]

The lone pairs of electrons in $PtPb_4$ and $RhBi_4$ are located on the main group elements that are oriented according to the topology of simple periodical nodal surfaces (PNSs).[95, 97] Such a surface-active behavior of inert pairs of electrons is known, for example, from the work of Andersson, Galy et al.,[98] and has also been interpreted by using PNS.[99] In $PdGa_5$, the Ga_4 squares emerge as the more strongly bound units and, according to quantitative analyses, four electrons (i.e. two bonds) are distributed over the four-membered groups.[95] Furthermore, weak Pd–Ga interactions were found described in the sense of a "real" metallic bond. It was shown here that different interactions are spatially separated and that this division can be simply visualized with the aid of a PNS.[95]

5. ELF of Surfaces

The surface structures of many substances are unknown today. The reconstruction and passivation of surfaces are crucial phenomena that determine, for example, reactivity, thermal stability, crystal growth, electrolytical, and sintering characteristics. With regard to the specific control of these phenomena and to the access to nanotechnology, mechanistic bonding and dynamic models become extremely important, particularly because the surface area becomes more important as the particles become smaller.

Scanning probe methods enable exciting new insights in surface phenomena, and with scanning tunnel microscopy (STM) it is possible to generate images of surfaces at subatomic resolution. The corresponding images cannot easily be interpreted, because they depend on many factors such as composition of the probe tip, surface covering, bias voltage, and the density of

states close to the Fermi level for the surface.[100] The latter means that only a part of the electronic structure of the surface is explored. For this reason it is interesting to carry out theoretical modeling of surfaces not only with calculations of partial electron densities (PED) alone but also with the ELF. Spatial representations that may also be calculated for surfaces are obtained with both methods and both are able to reproduce aspects of STM images.

Today, surfaces of silicon single crystals are among the most well defined and thoroughly examined surfaces. The (100) surface of silicon has been frequently and controversially discussed. It is known that a 2×1 surface reconstruction takes place, but there is no agreement as to whether the dimer formation is symmetrical or unsymmetrical (Figure 15a).[101, 102] The results of the theoretical investigations depend on the quality of the calculation and there is no consensus yet as to which model is superior. However, it is possible to draw direct topological comparisons between experiment and models with the PED and the ELF. Figure 15b shows the corresponding density of states (DOS) close to the Fermi level (E_F) of the three surface situations depicted in Figure 15a. It is clearly seen that in both cases the reconstruction (formation of dimer) leads to a decrease of the DOS at E_F. Figure 15c reveals the total valence electron densities (TEDs, top), the partial electron densities (PEDs) for unoccupied states ($E_F \leq E \leq (E_F + 3\,eV)$ center), and the PED for occupied states close to E_F ($((E_F - 3\,eV) \leq E \leq E_F$, bottom) for the same three situations. The accompanying 2D ELF cross sections calculations are presented in Figure 15d for quantum mechanical states occupied up to $E_F + 3$ eV (top) and for the states occupied up to E_F (bottom). Figure 15e shows the accompanying three-dimensional isosurface representations of ELF, whose exact form depends on the ELF value. Since ELF is always determined over all occupied states, the images obtained from the detection of the unoccupied (virtual) states (tunnel current from the tip to the surface) and occupied states (reversed tunnel current) must be simulated with the calculation of a slightly reduced or neutral system (Figure 15e bottom).

The comparison of calculated images with those measured (Figures 15f and g) for both directions of bias voltage shows interesting differences, which are discussed in reference [101]. Figure 15f shows the STM picture at positive bias voltage (electrons move from the tip to the surface) and therefore a reproduction of the unoccupied states (conduction band) of the surface.[103] This corresponds to Figures 15c center, 15d top, and 15e top. The result for the reversed bias voltage (electrons move from the surface to the tip) is presented in Figure 15g. The correlation to the calculated Figures 15c bottom, 15d bottom, and 15e bottom is clear.

At this point it must be stressed that

1. the TED is not sufficiently structured for a good explanation of these observations,
2. the PED are well structured and subtly differentiable but change significantly with small variations of the energy window $[(E_F - \Delta E), E_F]$ (like the STM pictures upon change of the bias voltage),
3. the ELF shows a situation intermediate to TED and the PED, that is it is well structured and considers all occupied states.

The advantage of ELF is that it not only provides an accurate reproduction of the spatial distribution but also a detailed image of the chemical bond and, particularly here, of dangling bonds at the surface. This is rarely possible with the other methods. Therefore ELF provides necessary and sufficient information for the analysis of STM images. It must be emphasized that there is no theoretical basis up to now for a relation between ELF and the STM experiment.

6. Localization Patterns in Interstitial Space

Nowadays, diffraction methods constitute a most important part of the determination of structure–property relationships. However, in some cases X-ray diffraction methods face nontrivial problems if, for example, super- or noncommensurate structures are to be determined, if twinning or disorder phenomena demand very sophisticated approaches, or if very light atoms must be resolved in the presence of strong X-ray scatterers.

Semiconducting compounds such as Zintl phases can in general be rationalized by the application of simple bonding concepts.[104] If, however, unusual or unexpected moieties occur it is not always certain whether they actually exist or are just an artifact of an erroneous structure determination.[105, 106] The existence of a geometrical void in such a structure is expected to arouse suspicion, but it cannot be used as a sure indicator for an overlooked atom or group of atoms. The "free" space may be generated for electronic reasons, for example as a packing space for lone pairs that are tightly bound to specific atoms, or of more or less free electrons as in electrides, intermetallic compoundss, and metals. The ELF is an extraordinarily useful sensor, especially for such problems in structure determination.[107]

Several times we have alluded to hierarchical relations in the sense that an ELF attractor also represents electrophilic particles such as protons. Mostly, these special attractors can be assigned to a part of the atomic structure. We should point out that ELF enables the visualization of patterns in interstitial space in such regions that cannot be associated with single atoms. The following four examples illustrate that such patterns, which indicate weakly bound but still spatially localized electrons, are in many cases indicative of overlooked atoms and thus may be of considerable importance for verifying the correctness of a structure.

6.1. Suboxides of Zintl Phases

To corroborate our findings concerning ELF we analyzed with LMTO band structure calculations[36] Zintl phases that contain light heteroatoms X in addition to mononuclear and oligomeric Zintl anions.

Compound Ca_4Sb_2O[108] was first described as a binary calcium antimonide Ca_2Sb[109] (Figure 16a), an assertion corrected shortly thereafter by the authors. The structure contains isolated Sb^{3-} ions and thus the compound can only be a valence compound, as expected, if an additional X^{2-} anion is present. The additional anion was identified as O^{2-} coordinated octahedrally by six calcium atoms. Surprisingly, the calculation of the ELF for Ca_4Sb_2 (without the O atom!) generates one and only

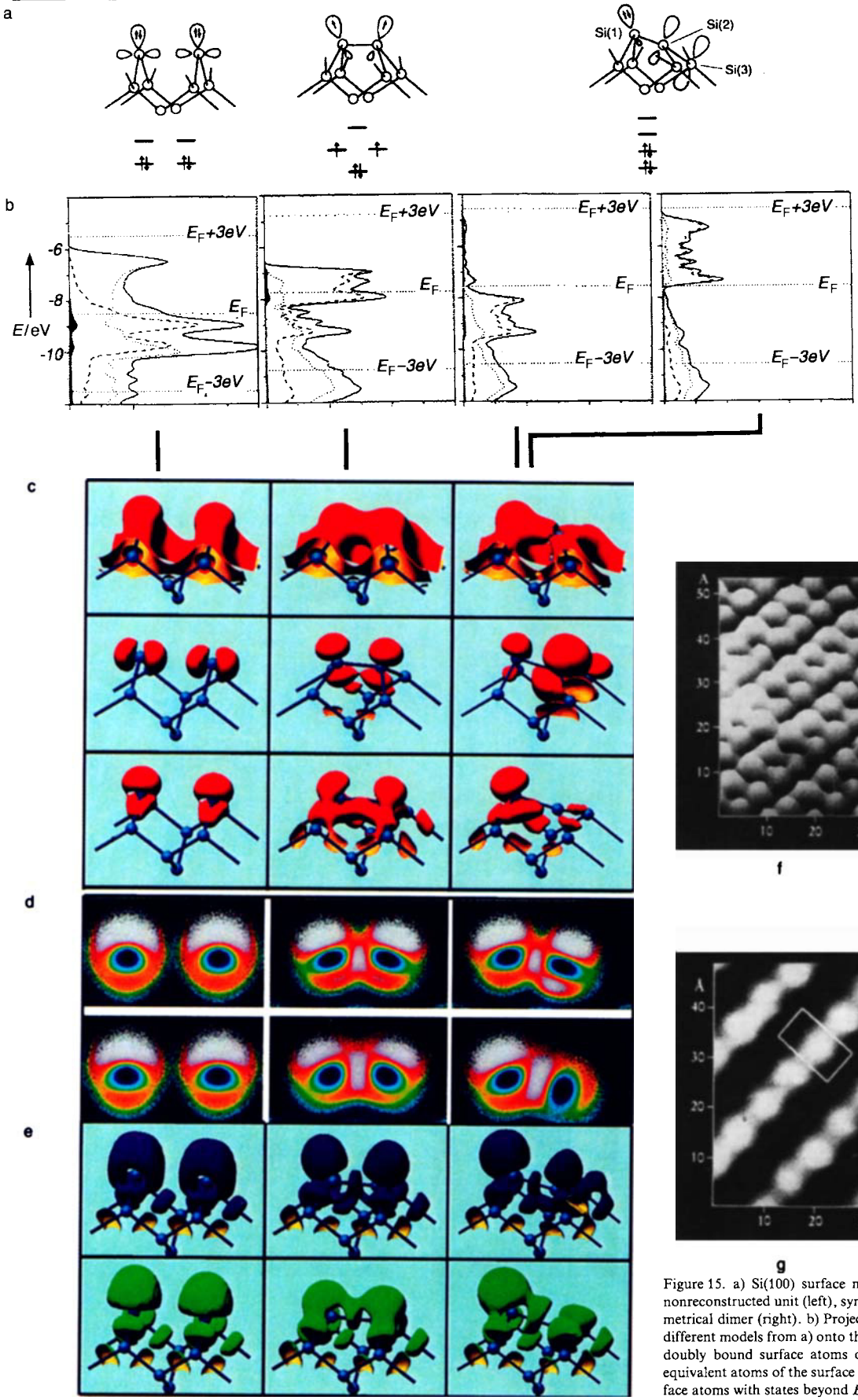

Figure 15. a) Si(100) surface models containing dangling bonds: nonreconstructed unit (left), symmetrical dimer (center), and asymmetrical dimer (right). b) Projections of the density of states of the different models from a) onto the surface atoms. From left to right: doubly bound surface atoms of the nonreconstructed unit, both equivalent atoms of the surface layer of the symmetrical dimer, surface atoms with states beyond E_F, and the atoms slightly below the surface with states above E_F. c) 3D representations of isosurfaces of TED (top row), PED of states in the energy region from E_F to $E_F + 3$ eV (second row), and PED in the region from $E_F - 3$ eV to E_F (third row). d) and e) 2D and 3D representations, respectively, of ELF with electronic occupation up to E_F (corresponding to the electron number of Si, bottom row), and with electronic occupation of the states up to $E_F + 3$ eV (corresponding to the formation of a further electron pair at the surface atoms, top row). f) STM image of the unoccupied surface states (positive bias voltage). g) STM image of the occupied surface states (negative bias voltage).

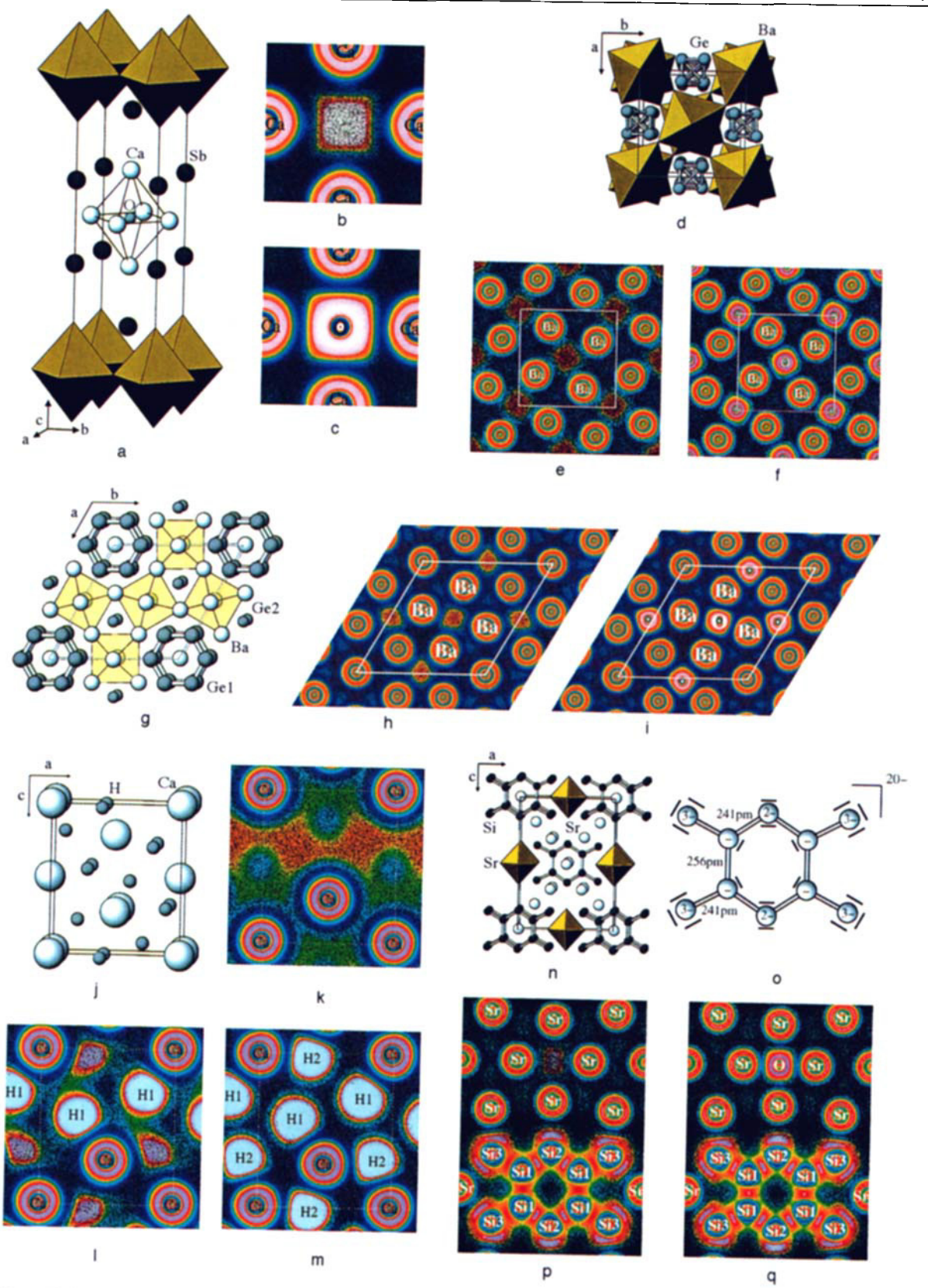

Figure 16. Structures and representative ELF (LMTO) cross sections with and without interstitial atoms (see text): a) structure of Ca_4Sb_2O, b), c) cross sections of the empty Sr_6 octahedron (ELF of the empty octahedron suggests the presence of the heteroatom) and with interstitial O atom, respectively; d) structure of Ba_3Ge_4X, e), f) cross sections of the empty Ba_6 octahedron and with interstitial O atom, respectively; g) structure of $Ba_3Ge_7O_3$ h), i) cross sections of the empty Ba_6 octahedron and with interstitial O atom, respectively; j) structure of CaH_2, k)–m) ELF of the Ca partial structure, with only one crystallographically unique H atom, and with all H atoms, respectively; n)–q) "SrSi" (second modification), n) structure with empty Sr octahedra [79], o) planar Zintl anion $[Si_{10}]^{(20-x)-}$, p) ELF cross section containing a Si_{10} unit and a Sr_6 octahedra; q) like p) but with O as a heteroatom corresponding to the $Sr_{10}Si_{10}O$ composition.

one additional localization region, which lies at the center of the Ca_6 octahedron (Figure 16b, white area). After introduction of the O atom into the calculation, an ELF is yielded that clearly displays the O atom with its core regions (Figure 16c). It is remarkable that despite the use of the different electron counts similar localization patterns are found for Ca_4Sb_2 ($\{8+10\}e$) and Ca_4Sb_2O ($\{8+10+6\}e$).

Quite recently, von Schnering et al. synthesized derivatives of barium germanides that contain Ba_6X octahedra and typical Zintl anions of germanium.[110, 111] In Ba_3Ge_4X there are Ge_4^{4-} tetrahedra (Figure 16d) and in $Ba_{10}Ge_7X$ planar Ge_6^{10-} rings occur. The ELF distributions without the heteroatoms X show localization patterns that are exactly at those positions that are occupied by X atoms or X groups. Figures 16e, f, h, i display the corresponding ELF sections through the Ba_6 octahedra without (Figures 16e, h) and with the X atoms (Figures 16f, i, X = O). The ELF displays the sites of the heteroatoms quite convincingly. According to the Zintl–Klemm concept and band structure calculations, X^{2-} units such as O^{2-}, C_2^{2-}, NH^{2-} are expected in these sites.[112]

The so-called second modification of "SrSi" (Figure 16n), which has never been confirmed experimentally, contains a very interesting Zintl anion, a planar $[Si_{10}]^{20-}$ unit with quite a peculiar variation in Si–Si bond lengths.[113] One would expect a formal charge distribution for this Zintl anion like that depicted Figure 16o. However, the Si1–Si1 bond lengths (256 pm) are so much longer than the other two (Si1–Si2 241 pm, Si1–Si3 241 pm) that this explanation seems quite suspect. A closer inspection reveals that the Sr atoms form an empty octahedron. The ELF treatment reveals a localization pattern (white spots in the structural section in Figure 16p) consistent with the assumption of σ bonds between Si1 and Si2. The lone pairs are indicated by white clouds of high ELF value located at expected positions.

The long Si1–Si1 bond has unusually low ELF values. More remarkable, however, is the center of the single Si1–Si3 bond (241 pm), for which a white region is to be expected, if the electron structure shows no peculiarities, and thus obeys the Zintl–Klemm concept (Figure 16o).[104]

Even more surprising is the large localization region between the four Sr atoms in the upper middle of Figure 16p. Two additional Sr atoms above and below that plane generate a distorted octahedron that shows a remarkable contraction compared with the neighboring Sr groups on the left and right side. Too high an accumulation of charge on the Zintl anion could lead to the formation of a cage orbital[106] in the Sr_6 octahedron. In this case, SrSi would belong to the class of electrides. The center of the octahedron, however, is an ideal position for an electronegative heteroatom such as oxygen. The corresponding distances (4×245, 2×285 pm) coincide very well with the Sr–O distances found in SrO (6×257 pm, ref. [114]) and in $SrTiO_3$ (12×276 pm, ref. [115]). The presence of a heteroatom would also explain the failed attempts to synthesize this "SrSi" modification from rigorously purified elements.[116] Neither the EH nor the LMTO investigations on the hypothetical phase $Sr_{10}Si_{10}O$ reveal a band gap at the Fermi level indicating a semiconductor. Therefore, there is no preferred valence electron number that allows for the more electronegative neighbors of oxygen, such as fluorine, nitrogen, or carbon, to act as heteroatoms.[117] In the meantime, it has been shown on numerous Zintl phases that a limited capacity for accumulation of charge in highly charged Zintl anions leads to a planar geometry and a partially occupied π system. For the binary "SrSi", there are unusually high Sr contributions to a few bands below the Fermi level. This is quite unusual according to our experience.

A LMTO calculation with oxygen in the void position leads to an ELF that shows a surprisingly smooth distribution of white bond regions in the Si_{10} framework (Figure 16q), and the Sr contribution below the Fermi level disappears. We would like to emphasize that it was not obvious at the outset that a removal of two electrons from the Si partial structure to the O^{2-} ion would generate a, by our standards, very reasonable σ-bonded structure that is understandable with the quantum mechanical ELF analysis.

6.2. Determination of Hydrogen Positions in Hydrides

The following example, CaH_2,[119, 120] is important because, in general, hydrides present a problem in structure determination. Quite frequently, such compounds are microcrystalline and thus single-crystal investigations cannot be performed. Furthermore, hydride positions may not be found by X-ray analysis because of the small scattering factor of hydrogen.

To follow the typical procedure adopted in the determination of a hydride structure, the CaH_2 structure was analyzed with the ELF starting with the pure Ca substructure. Figures 16j—m display a section of the structure that contains atom positions Ca, H1, and H2. In Figure 16k the ELF is shown for the pure Ca substructure, that is without electron pair acceptors. There is a weak but significant localization (yellow spot) that includes the position of H2. If now one H atom is added and located at that site, a new localization spot that coincides with the position of H1 becomes clearly visible (Figure 16l). Actually this second localization region is already distinct in the ELF for the Ca substructure, but only equally as strong as a neighboring position unoccupied by H. These two weaker localization regions can be clearly distinguished after an antisymmetrical introduction of the first H atom on the observed position.[119] Therefore, this second localization region is clearly observable in a subsequent ELF calculation (Figure 16l).

The ELF of the complete structure (Figure 16m) beautifully reveals the ionic character of this hydride: there are only low ELF minima between the atoms. Nevertheless, a significant polarization is visible, especially of the hydride ions but also of the Ca^{2+} ions, which includes deviations from the spherical symmetry.

We must emphasize that this new way for the determination of missing atom positions is less reliable if the substructure reveals a higher symmetry than the complete structure, because the quantum mechanical calculation represents only a given symmetry. For example, starting from the magnesium position in MgH_2, an isolated localization cloud is obtained that indicates an interstitial region.[21, 31] But this region only represents the center of a region containing two hydride ions and does not permit any further geometrical specifications. Starting with such information, further methods in optimizing geometry can successfully lead to a complete structural model.

There are many indications that ELF describes the chemical bond in molecules, clusters, and extended structures in such a differentiated way, that, in general, regions of high ELF values can be understood as nucleophilic centers. With ELF it is possible to find missing atoms in incomplete structures, and in fact, as in CaH_2, even the positions of the major component and not only of a few of overlooked atoms.

7. Outlook

7.1. The Chemical Bond in Intermetallic Phases

Quite recently, a highlight by J. C. Schön appeared in this journal dealing with the chemical bond.[90] Therein an article by Burdett et al.,[91] and especially the following statement, was critically discussed: "... that the 'metallic bond' as a separate term with equal weight to the other three traditional schemes[*] should be abandoned" and "certainly it does not have a mathematical framework distinct from the other three categories ...". Equivalently, the metallic bond does not represent a special type of chemical bond because previously known bonding types appear simultaneously in the corresponding structures and band structures should be used in the classification.[91] The rebuttal of Schön praised the usefulness of the usual forms of description of the metallic bond and criticized Burdett et al. for focussing on only one method (EH) for the calculation of band structures.

We believe that both authors are certainly correct, but the essential things that are governed by the term metallic bond are not yet fully understood. In our ELF investigations on intermetallic phases, definite localized bonding structures are found, mostly coexisting with ionic interactions, two-electron–two-center, two-electron–three-center, multielectron–multicenter bonds, as well as lone pair electrons, and conducting electrons. Here, clear separations between bonding forms, as known from valence compounds, can no longer be drawn. Furthermore, intermetallic phases sometimes show a very complicated structural chemistry. This proves that the coexistence of totally different bonding forms leads to a new structure chemical quality, where local and cooperative effects arrange themselves in very specific ways. The metallic bond might be one of the most homogeneous of all bonding classes with respect to differences in localization, but at the same time one of the most complex regarding the variety of bonding forms that are simultaneously present in a structure.

Evidently, the metallic bond may be explained by using a combination of classical bonding concepts but there is no reason to reject its definition as an independent class. It is important that an independent phenomenon is described here that is valid for many substances. The essence of a system is not simply the sum of its parts. We believe that the essence of the characteristic features of metals and intermetallic phases as an independent class is not yet clear, but ELF will contribute significantly to this end.

7.2. Hierarchy

A totally general relation in the construction of chemical and presumably all other structures emerged from the analysis of the chemical bond with the aid of ELF: there is a hierarchical correlation between structures of equal basic topology. For example, there is a correlation between the structures of diamond, cristobalite, and $Li_{10}P_4N_{10}$.[120] Every C atom in the diamond structure is substituted by a SiO_4 tetrahedron in cristobalite and by a $P_4N_{10}^{10-}$ unit in $Li_{10}P_4N_{10}$. It is important here that the correlated structures belong to the same symmetry group or correspond to group–subgroup relations. The central sites, the positions of the C atoms in the diamond structure, are invariant attractors, whereas other structural elements are located at those sites in each of the accompanying structures. The chemical correlation between the building groups may change completely, but the topology of the structure invariant attractors (the center of gravity of the structure elements) is always preserved. In the mathematical sense, it is unimportant whether distortions of the complete structure (e.g. change of the angles, change of unit cell dimensions) occur as long as the number of principle neighbors around each invariant attractor remains unchanged.

Von Schnering has demonstrated "hierarchical relationships" in a great number of such hierarchical families.[121] Now, with the aid of ELF, localization regions of electrons may be introduced in such hierarchical relationships and thereby, surprising new correlations have been found. It seems that attractor structures, which are obtained from electron distributions using ELF, are also formed by atoms, molecules, or clusters. This was already demonstrated in individual cases, for example the attachment of hydrogen atoms at attractors of transition metal complexes and boranes (see Section 2.4).

This correlation seems to be most important for the structural relations of intermetallic phases, oxides, and fluorides found by O'Keeffe and Hyde.[122] In many cases the atomic distribution in intermetallic phases is identical or very similar to the cation distribution in oxides and fluorides. In 1991, one of us pointed at the misinterpretation of this correlation by O'Keeffe and Hyde, namely in the sense of large cations.[82] At the time an explanation was given correlating the electronic domains in intermetallic phases with the anion positions of oxides and fluorides.[82] So far, ELF investigations increasingly confirm this assumption and its unexpected scope. It seems that there are correlations between localization regions of electrons and many atomic or molecular structures. Further systematic investigations are necessary for the confirmation of this statement. We were surprised that this method can be reversed for the localization of missing atoms in uncompletely determined structures.

Such correlations have been occasionally observed[121, 123, 124] but not yet amalgamated into a general concept. The calculation of the ELF may be quite useful for a classification of this kind.[21] In this respect, the observed ELF patterns provide not only compound- or structure-specific information but gain a general topological significance.

[*] This refers to ionic, covalent, and van der Waals bonding.

Received: February 18, 1997 [A 212 IE]
German version: *Angew. Chem.* **1997**, *109*, 1892–1918

[1] R. J. Gillespie, R. S. Nyholm, *Q. Rev. Chem. Soc.* **1957**, *11*, 339; R. J. Gillespie, *Molecular Geometry*, Van Nostrand Reinhold, London, **1972**.
[2] K. Artmann, *Z. Naturforsch.* **1946**, *1*, 426.
[3] R. Daudel, *Quantum Theory of the Chemical Bond*, Reidel, Dordrecht, **1974**.
[4] A. Kossel, *Ann. Phys. Chem.* **1916**, *49*, 229.
[5] W. England, L. S. Salmon, K. Ruedenberg, *Fortschr. Chem. Forsch.* **1971**, *23*, 31; W. England, *Int. J. Quantum Chem.* **1971**, *5*, 683.
[6] R. S. Mulliken, *J. Chem. Phys.* **1955**, *23*, 1833, 1841, 2338, 2343.
[7] E. R. Davidson, *J. Chem. Phys.* **1967**, *46*, 3320.
[8] R. Ahlrichs, C. Erhard, *Chem. Unserer Zeit* **1985**, *19*, 120; R. Heinzmann, R. Ahlrichs, *Theor. Chim. Acta* **1976**, *42*, 33.
[9] J. E. Carpenter, F. Weinhold, *J. Mol. Struct.* **1988**, *169*, 411.
[10] R. Daudel, citation 12 in reference [11].
[11] K. Ruedenberg, W. H. E. Schwarz, *J. Chem. Phys.* **1990**, *92*, 4956.
[12] R. W. F. Bader, *Atoms in Molecules: A Quantum Theory*, Oxford University Press, Oxford, **1990**; see R. F. W. Bader, P. L. A. Popelier, T. A. Keith, *Angew. Chem.* **1994**, *106*, 647; *Angew. Chem. Int. Ed. Engl.* **1994**, *33*, 620. A comparison of the topologies of $\nabla^2\rho$ and the ELF presented here in respect to a series of atomic interactions is found in: R. W. F. Bader, S. Johnson, T.-H. Tang, P. L. A. Popelier, *J. Phys. Chem.* **1996**, *100*, 15398.
[13] W. L. Luken, J. C. Culberson, *Int. J. Quantum Chem.* **1982**, *16*, 265.
[14] A. D. Becke, N. E. Edgecombe, *J. Chem. Phys.* **1990**, *92*, 5397.
[15] According to Equations (3) and (6) within a certain space of very low density, ELF may adapt high values that are physically meaningless. For example, in the Be atom ELF has the value one at $\rho \to 0$ ($r \to \infty$). Principally, these difficulties may be removed by the definition of an effective ELF′ as $\{1+[(C(\vec{r})+\varepsilon)/C_h(\rho(\vec{r}))]^2\}^{-1}$, where $\varepsilon = 2.87 \times 10^{-5}$ is chosen so that for $\rho \leq 10^{-3}$ bohr^{-1} ELF′ adapts smaller values than 0.5. (to this see ref. [21]).
[16] T. F. Fässler, A. Savin, *Chem. Unserer Zeit* **1997**, *31*, 110.
[17] J. F. Dobson, *J. Chem. Phys.* **1991**, *94*, 4328.
[18] R. Thom, *Stabilité Structurelle et Morphogénèse*, Intereditions, Paris, **1972**.
[19] B. Silvi, A. Savin, *Nature* **1994**, *371*, 683.
[20] For similar examinations of electron density see: P. Mezey in *Reviews in Computational Chemistry, Vol. 1*, (Ed.: K. B. Lipkowitz, D. B. Boyd), VCH, Weinheim, **1990**.
[21] A. Savin, B Silvi, F. Colonna, *Can. J. Chem.* **1996**, *74*, 1088.
[22] M. Kohout, A. Savin, *Int. J. Quantum Chem.* **1996**, *60*, 875.
[23] A. Savin, 2nd International Conference on Inorganic Chemistry, Stuttgart, **1993**.
[24] F. Colonna, A. Savin, B. Silvi, unpublished results.
[25] A. Savin, O. Jepsen, J. Flad, O. K. Andersen, H. Preuss, H. G. von Schnering, *Angew. Chem.* **1992**, *104*, 187; *Angew. Chem. Int. Ed. Engl.* **1992**, *31*, 187.
[26] W. Kohn, L. Sham, *Phys. Rev.* **1965**, *A 140*, 1133.
[27] Y. Tal, R. W. F. Bader, *Int. J. Quantum Chem. Symp.* **1978**, *12*, 153; see also R. M. Dreizler, E. K. U. Gross, *Density Functional Theory: An Approach to the Quantum Many-Body Problem*, Springer, Berlin, **1990**, p. 15.
[28] R. G. Parr, W. Yang, *Annu. Rev. Phys. Chem.* **1995**, *46*, 701.
[29] M. Kohout, A. Savin, *J. Comp. Chem.* **1997**, in press.
[30] A. Burckhardt, U. Wedig, H. G. von Schnering, A. Savin, *Z. Anorg. Allg. Chem.* **1993**, *619*, 437.
[31] S. Wengert, PhD thesis, ETH, Zürich, **1997**.
[32] A. Savin, A. D. Becke, J. Flad, R. Nesper, H. Preuss, H. G. von Schnering, *Angew. Chem.* **1991**, *103*, 421; *Angew. Chem. Int. Ed. Engl.* **1991**, *30*, 409.
[33] All Extended-Hückel calculations in this article were carried out with the program MEH-MACC [34], which allows the calculation of electron localization function, total electron density (TED), and the partial electron density (PED) and their graphical two- and three-dimensional representation based on charge self-consistent Hückel parameters H_{ii}.
[34] U. Häussermann, R. Nesper, S. Wengert, T. F. Fässler, program MEH-MACC, modified extended-Hückel version based on the QCPE program EH-MACC [35] (inquiries to mehmacc@inorg.chem.ethz.ch).
[35] Program EHMACC: M.-H. Whangbo, M. Evain, T. Hughbanks, M. Kertesz, S. Wijeyesekera, C. Wilker, C. Zheng, R. Hoffmann, R. Hoffmann, unpublished results.
[36] TB-LMTO-ASA: tight-binding linear muffin-tin orbital in the atomic sphere approximation. Program TB-LMTO: M. van Schilfgarde, T. A. Paxton, O. Jepsen, O. K. Andersen, G. Krier, Max-Planck-Institut für Festkörperforschung, Stuttgart, **1994**, unpublished results. All TB-LMTO-ASA calculations based on the LDA approximation were carried out by the use of the exchange correlation potential according to Barth and Hedin [37]. The radii of the muffin-tin spheres and sometimes necessary hollow spheres E within the framework of the ASA approximation are determined according to the method described by Jepsen and Andersen [38].
[37] U. Barth, L. Hedin, *J. Phys. C* **1972**, *5*, 1629.
[38] O. Jepsen, O. K. Andersen, *Z. Phys. B* **1995**, *97*, 35.
[39] Program GRAPA: J. Flad, F.-X. Fraschio, B. Miehlich, Institut für Theoretische Chemie der Universität, Stuttgart, **1989**.
[40] D. Seebach, H. M. Bürger, D. A. Plattner, R. Nesper, T. Fässler, *Helv. Chim. Acta* **1993**, *76*, 2581.
[41] L. Pauling, *The Nature of the Chemical Bond*, 3rd ed., Cornell University Press, **1960**, 136.
[42] R. J. Gillespie, I. Hargittai, *VSEPR Model of Molecular Geometry*, Allyn and Barton, Boston, **1991**; R. J. Gillespie, E. A. Robinson, *Angew. Chem.* **1996**, *108*, 539; *Angew. Chem. Int. Ed. Engl.* **1996**, *35*, 495.
[43] Naturally, like the electron density, ELF shows the total symmetry of the corresponding unit in contrast to the popular formulation in textbooks using localized two-electron centers with bonding lines.
[44] The presence of a torus instead of three separate attractors in the isoelectronic XeF_2 molecule was previously pointed out by S. Andersen, *Acta Crystallogr. Sect. B* **1979**, *35*, 1321.
[45] A. Savin, H. J. Flad, O. Flad, H. W. Preuss, H. G. von Schnering, *Angew. Chem.* **1992**, *104*, 185; *Angew. Chem. Int. Ed. Engl.* **1992**, *31*, 187.
[46] W. Kutzelnigg, *Angew. Chem.* **1984**, *96*, 262; *Angew. Chem. Int. Ed. Engl.* **1984**, *23*, 272.
[47] M. Kohout, A. Savin, J. Flad, H.Preuss, H. G. von Schnering, *Computer Aided Innovation of New Materials II* (Ed.: M. Doyama), Elsevier, **1997**, 261.
[48] T. F. Fässler, R. Glaser, unpublished results.
[49] H. L. Schläfer, G. Gliemann, *Einführung in die Ligandenfeldtheorie*, 2nd ed., Akademische Verlagsanstalt, Wiesbaden, **1980**.
[50] A. Savin, unpublished results.
[51] M. Kaupp, *Chem. Ber.* **1996**, *129*, 527.
[52] T. F. Fässler, unpublished results.
[53] K. Wade, *Adv. Inorg. Radiochem.* **1976**, *18*, 1.
[54] J. E. Huheey, E. A. Keiter, R. L. Keiter, *Inorganic Chemistry: Principles of Structure and Reactivity*, 2nd ed., Walter de Gruyter, Berlin **1995**.
[55] W. Hönle, Yu. Grin, U. Wedig, M. Schulthess, H. G. von Schnering, R. Kellner, H. Binder, *J. Solid State Chem.*, in press.
[56] A. Simon, *Chem. Unserer Zeit* **1976**, *10*, 9.
[57] Yu. Grin, personal communication.
[58] P. von R. Schleyer, J. Kapp, *Chem. Phys. Lett.* **1996**, *255*, 363.
[59] A. Simon, H. G. von Schnering, H. Schäfer, *Z. Anorg. Allg. Chem.* **1967**, *355*, 295; *ibid.* **1967**, *355*, 311; H. Imoto, A. Simon, *Inorg. Chem.* **1982**, *21*, 308.
[60] A. N. Fitch, S. A. Barrett, B. Fender, A. Simon, *J. Chem. Soc. Dalton Trans.* **1972**, *4*, 501.
[61] R. Chevrel in *Superconducting Materials Sciences—Metallurgy, Fabrication and Application*, (Eds.: S. Foner, B. B. Schwarz), Chapter 10, Plenum Press, New York **1981**.
[62] H. Schäfer, H. G. von Schnering, *Z. Anorg. Allg. Chem.* **1967**, *353*, 281.
[63] E. Zeller, H. Beruda, H. Schmidbaur, *Inorg. Chem.* **1993**, *24*, 3203.
[64] P. Pyykkö, N. Runeberg, *J. Chem. Soc. Chem. Commun.* **1993**, *24*, 1812.
[65] M. N. Gluhovtsev, P. von R. Schleyer, A. Stein, *J. Phys. Chem.* **1993**, *97*, 5541.
[66] A. Burkardt, PhD thesis, Universität Stuttgart, **1992**.
[67] H. G. von Schnering, W. Hönle, *Chem. Rev.* **1988**, *88*, 243.
[68] H. G. von Schnering, U. Wedig, R. Nesper, L. Schröder, R. H. Cardoso Gil, W. Carrillo-Cabrera, "Einfache Muster in komplexen Strukturen" (Simple Models in Complex Structures), *Jahrbuch der Max-Planck-Gesellschaft* **1994**, p. 390.
[69] K. A. Soltntsev, Y. A. Buslaev, N. T. Kuznetsov, *Russ. J. Inorg. Chem.* **1988**, *31*, 633.
[70] A. M. Mebel, O. P. Charkin, K. A. Soltntsev, N. T. Kuznetsov, *Russ. J. Inorg. Chem.* **1988**, *31*, 2263.
[71] F. A. Cotton, X. Feng, M. Shang, W. A. Wojtczak, *Angew. Chem.* **1992**, *104*, 1117; *Angew. Chem. Int. Ed. Engl.* **1992**, *31*, 1050.
[72] L. Chen, F. A. Cotton, W. A. Wojtzak, *Angew. Chem.* **1995**, *107*, 2050; *Angew. Chem. Int. Ed. Engl.* **1995**, *34*, 1877.
[73] F. A. Cotton, J. Lu, M. Shang, W. A. Wojtczak, *J. Am. Chem. Soc.* **1994**, *116*, 4364.
[74] A. Currao, PhD thesis, ETH Zürich, **1995**.
[75] R. Nesper, A. Currao, S.Wengert in *Organosilicon Chemistry, Vol. II, From Molecules to Materials* (Eds.: N. Auner, P. Weis), VCH, Weinheim, **1995**, p. 469.
[76] R. Nesper, A. Currao, S. Wengert, unpublished results.
[77] R. Nesper, unpublished results.
[78] W. Rieger, E. Parthé, *Acta Crystallogr.* **1967**, *22*, 919.
[79] B. Eisenmann, H. Schäfer, K. Turban, *Z. Naturforsch. B* **1974**, *29*, 464.
[80] F. Merlo, M. L. Fornasini, *J. Less-Common Met.* **1967**, *13*, 603.
[81] A. Currao, J. Curda, R. Nesper, *Z. Anorg. Allg. Chem.* **1996**, *622*, 85.
[82] R. Nesper, *Angew. Chem.* **1991**, *103*, 805; *Angew. Chem. Int. Ed. Engl.* **1991**, *30*, 789.
[83] D. G. Pettifor, *Solid State Commun.* **1984**, *51*, 37; P. Villars, *J. Less-Common Met.* **1986**, *119*, 89; P. Villars, K. Girgis, F. Hulliger, *ibid.* **1982**, *42*, 89.
[84] U. Häussermann, S. Wengert, P. Hoffmann, A. Savin, O. Jepsen, R. Nesper, *Angew. Chem.* **1994**, *106*, 2147; *Angew. Chem. Int. Ed. Engl.* **1994**, *33*, 2069.
[85] U. Häussermann, S. Wengert, R. Nesper, *Angew. Chem.* **1994**, *106*, 2151; *Angew. Chem. Int. Ed. Engl.* **1994**, *33*, 2073.
[86] G. L. Dirichlet, *J. Reine Angew. Math.* **1850**, *40*, 216; G. F. Voronoi, *ibid.* **1908**, *134*, 198.
[87] P. Niggli, *Z. Kristallogr.* **1928**, *68*, 404.
[88] F. Laves, *Z. Kristallogr.* **1931**, *78*, 208.
[89] W. Fischer, E. Koch, E. Hellner, *New Jahrb. Mineral. Monatsh.* **1971**, 227.

[90] J. C. Schön, *Angew. Chem.* **1995**, *107*, 1183; *Angew. Chem. Int. Ed. Engl.* **1995**, *34*, 1081. See also the ensuing correspondence between L. C. Allen and J. K Burdett, and J. C. Schön (*Angew. Chem.* **1995**, *107*, 2157; *Angew. Chem. Int. Ed. Engl.* **1995**, *34*, 2003).
[91] L. C. Allen, J. F. Capitani, *J. Am. Chem. Soc.* **1994**, *116*, 8810; W. P. Anderson, J. K. Burdett, P. T. Czech, *ibid.* **1994**, *116*, 8808.
[92] K. Schubert, *Kristallstrukturen zweikomponentiger Phasen*, Springer, Berlin, **1964**.
[93] Yu. Grin,, U. Wedig, H. G. von Schnering, *Jahresbericht des Max-Planck-Institut für Festkörperforschung Stuttgart*, **1995**, I-73; Poster B 14 at the Symposium for Theoretical Chemistry, Loccum, **1995**.
[94] H. G. von Schnering, R. Nesper, *Acta Chem. Scand.* **1991**, *45*, 870.
[95] Yu. Grin, U. Wedig, F. Wagner, H. G. von Schnering, A. Savin, *J. Alloys Compd.* **1997**, *255*, 203.
[96] Yu. Grin, U. Wedig, H. G. von Schnering, Poster C29 at the European Solid State Conference in Montpellier.
[97] Yu. Grin, U. Wedig, H. G. von Schnering, *Angew. Chem.* **1995**, *107*, 1318; *Angew. Chem. Int. Ed. Engl.* **1995**, *34*, 1204.
[98] J. Galy, G. Meunier, S. Andresson, A. Åström, *J. Solid State Chem.* **1975**, *9*, 92.
[99] R. Nesper, Habilitation thesis, Universität Stuttgart, **1989**; M. Oehme, PhD thesis, Universität Stuttgart, **1989**.
[100] E. Tekman, S. Cirai, *Phys. Rev. B Condens. Matter* **1989**, *40*, 10286; J. Tersoff, D. R. Hamann, *Phys. Rev. Lett.* **1983**, *50*, 1998; J. Tersoff, *ibid.* **1986**, *57*, 440; M.-H. Whangbo, S. N. Magonov, *Adv. Mater.* **1994**, *6*, 355.
[101] T. F. Fässler, U. Häußermann, R. Nesper, *Chem. Eur. J.* **1995**, *1*, 625.
[102] See also : H. N. Waldenbrug, J. T. Yates, Jr., *Chem. Rev.* **1995**, *95*, 1689.
[103] H. Neddermeyer, *Chem. Unserer Zeit* **1992**, *26*, 18; R. Kliese, B. Rüttger, D. Badt, H. Neddermeyer, *Ultramicroscopy* **1992**, *42*, 824.
[104] E. Zintl, *Angew. Chem.* **1939**, *52*, 1; E. Zintl, G. Brauer, *Z. Phys. Chem. Abt. B* **1933**, *20*, 245; E. Zintl, W. Dullenkopf, *Z. Phys. Chem. Abt. A* **1931**, *154*, 1; *Z. Phys. Chem. Abt. B* **1932**, *16*, 183; W. Klemm, *FIAT Review of German Science, Naturforschunf und Medizine in Deutschland 1939–1946, Anorganische Chemie Teil IV, 26*, 103; W. Klemm, *Trab. Reun. Int. React. Solidos 3rd* **1956**, *1*, 447; W. Klemm, *Proc. Chem. Soc. London* **1959**, 329; E. Mooser, W. B. Pearson, *Phys. Rev.* **1956**, *101*, 1608; E. Mooser, W. B. Pearson, in *Progress in Semiconductors, Vol. 5* (Eds.: G. A. Gibson, F. A. Kröger, R. E. Burgess), Heywood, London, **1960**, p. 103; W. Klemm, *Festkörperprobleme*, Vieweg, Braunschweig, **1963**; E. Busmann, *Z. Anorg. Allg. Chem.* **1961**, *313*, 90; H. Schäfer, *Angew. Chem.* **1973**, *85*, 742; *Angew. Chem. Int. Ed. Engl.* **1973**, *12*, 694.
[105] H. G. von Schnering, R. Nesper, J. Curda, K.-F. Tebbe; *Angew. Chem.* **1980**, *92*, 1070; *Angew. Chem. Int. Ed. Engl.* **1980**, *19*, 1033; M. C. Böhm, R. Ramirez, R. Nesper, H. G. von Schnering, *Phys. Rev.* **1984**, *B30*, 4870; M. C. Böhm, R. Ramirez, R. Nesper, H. G. von Schnering, *Ber. Bunsen-Ges. Phys. Chem.* **1985**, *89*, 465.
[106] R. Ramirez, R. Nesper, H. G. von Schnering, M. C. Böhm, *J. Phys. Chem. Solids* **1987**, *48*, 51.
[107] R. Nesper, S. Wengert, *Chem. Eur. J.* **1997**, *3*, 985.
[108] B. Eisenmann, H. Limartha, H. Schäfer, H. A. Graf, *Z. Naturforsch. B* **1980**, *35*, 1518.
[109] B. Eisenmann, H. Schäfer, *Z. Naturforsch. B* **1974**, *29*, 13; C. Harmon, R. Marchand, P. L'Haridon, Y. Laurant, *Acta Crystallogr. Sect. B* **1974**, *31*, 427.
[110] H. G. von Schnering, M. Somer, J. Curda, personal communication.
[111] H. G. von Schnering, U. Bolle, J. Curda, K. Peters, W. Carrillo-Cabrera, M. Somer, M. Schultheiss, U. Wedig, *Angew. Chem.* **1996**, *108*, 1062; *Angew. Chem. Int. Ed. Engl.* **1996**, *35*, 984.
[112] In Ba_3Ge_4X a split position is found for X, which can be interpreted in terms of a disordered C_2^{2-}; H. G. von Schnering, personal communication. This may be possible according to the ELF calculated for Ba_3Ge_4, but, as expected, there is no indication of an atomic distribution of lower symmetry.
[113] B. Eisenmann, H. Schäfer, K. Turban, *Z. Naturforsch. B* **1974**, *29*, 464.
[114] W. Gerlach, *Z. Phys.* **1922**, *9*, 184; W. Primak, H. Kaufmann, R. Ward, *J. Am. Chem. Soc.* **1948**, *70*, 2043.
[115] H. D. Megaw, *Proc. Phys. Soc. London* **1948**, *58*, 133; J. Hutton, R. J. Nelmes, *Acta Crystallogr. Sect. A* **1981**, *37*, 916.
[116] A. Currao, R. Nesper, unpublished results.
[117] Experience shows that EH calculations overestimate band gaps, whereas these values are systematically underestimated by LMTO analyses. If both methods reveal no band gap, the material under study is most probably metallic.
[118] B. Bergsma, B. O. Loopstra, *Acta Crystallogr.* **1962**, *15*, 92.
[119] A. F. Andresen, A. J. Maeland, D. Slotfeld-Ellingsen, *J. Solid State Chem.* **1977**, *20*, 93.
[120] W. Schnick, U. Berger, *Angew. Chem.* **1991**, *103*, 857; *Angew. Chem. Int. Ed. Engl.* **1991**, *30*, 830.
[121] H. G. von Schnering has always searched for such structural chemical interrelations. He employed the term "hierarchical relation" in various respects in the nineties, see, for example, ref. [68]; W. Carrillo-Cabrera, N. Caroca-Canales, K. Peters, H. G. von Schnering, *Z. Anorg. Allg. Chem.* **1993**, *619*, 1556; W. Carrillo-Cabrera, N. Caroca-Canales, H. G. von Schnering, *ibid.* **1994**, *620*, 247; ref. [32].
[122] M. O'Keeffe, B. G. Hyde, *Struct. Bonding (Berlin)* **1985**, *61*, 77.
[123] A. F. Wells, *Structural Inorganic Chemistry*, Clarendon Press, Oxford, **1991**.
[124] B. G. Hyde, S. Andersson, *Inorganic Crystal Structures*, Wiley, New York, **1989**.

Well-Rounded Research: Nanotubes through Self-Assembly

Burkhard König*

Tube-shaped structures with nanometer dimensions are currently being reported from completely different fields of chemistry: on one hand, carbon chemists keep surprising us with new shapes[1] and properties[2] of carbon nanotubes; on the other, synthetic chemists are introducing highly functionalized nanotubes, which are of some interest as models for biological ion channels. This account is concerned with topical developments in the latter field.

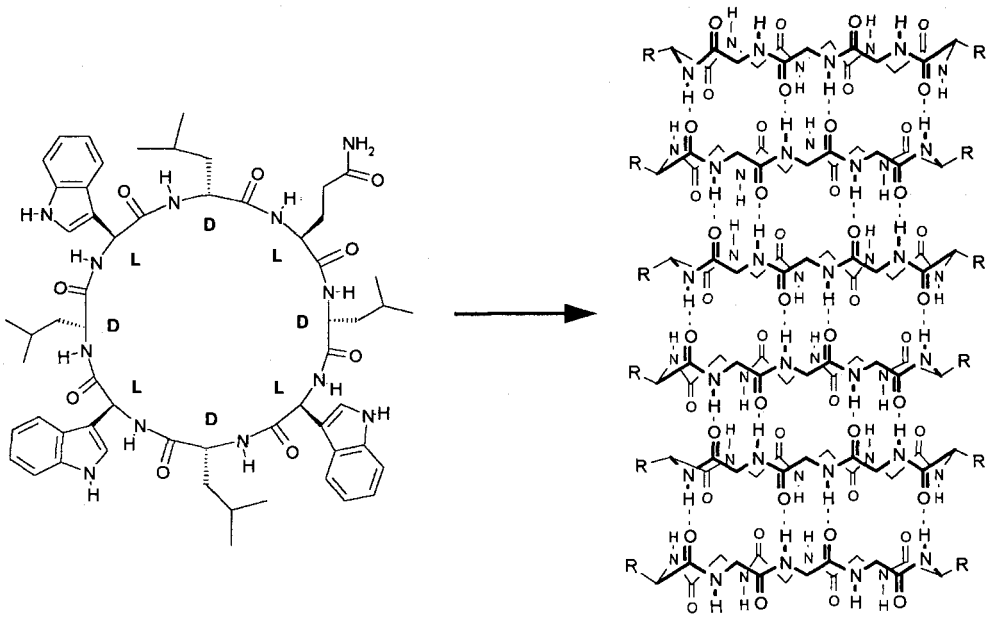

Scheme 1. Cyclic peptides of alternating chirality spontaneously form nanotubes. For reasons of clarity most side chains were omitted.

The construction of synthetic nanotubes is achieved through self-assembly of suitable subunits. Among the various possibilities for such self-alignment, stacking of macromolecules is a particularly promising starting point. As early as 1974, DeSantis and co-workers predicted a roughly planar structure for cyclopeptides made up of alternating D and L amino acids.[3] In this conformation the amide chain would be oriented at a right angle to the plane of the macrocycle; thus the carbonyl groups would be set in ideal positions for the formation of intermolecular hydrogen bonds between the stacked rings. The side chains would protrude outwards in the D/L motif to give an open channel whose diameter is determined only by the number of amino acid residues. Based on this model, Lorenzi et al. constructed cyclopeptides consisting of D- and L-valine units in 1987; however, their low solubility prevented structure investigations.[4] A breakthrough was then achieved in 1993 by Ghadiri's group with the octapeptide *cyclo*[-(D-Ala-Glu-D-Ala-Gln)$_2$-].[5] The glutamic acid residue renders this compound soluble in alkaline media; stacking to form nanotubes occurs after acidification (Scheme 1). The more hydrophobic side chains in *cyclo*[-(Trp-D-Leu)$_3$-Gln-D-Leu-] even enabled the construction of a transmembrane ion channel with a proton transport activity similar to that of gramicidin A or amphotericin B.[6] Measurements of single-channel conductivity showed fast transport of sodium and potassium; the channel's pore diameter of 7.5 Å led to weak potassium selectivity.[7]

Larger cyclopeptides yield nanotubes with a larger inner diameter.[8] Thus, macrocycles with ten to twelve amino acid residues result tubes in whose cavities molecules can be transported. The pore size of the channel leads to exclusion selectivity: A nanotube built from cyclic decapeptides with 10 Å diameter is permeable by glucose, whereas a tube of cyclic octapeptides is not.[9]

The biological activity of self-assembling transmembrane channels has now been determined by in vitro assays. These channels are antibacterially active against gram-positive strains and cytotoxic in a test with human kidney cells.[7]

Not only cyclopeptides are suitable for the construction of nanotubes. Stacked cyclodextrins[10] also form tube-shaped structures with inner diameters of up to 1.3 nm, as has just been proved by Stoddart, Williams, and co-workers through X-ray structure analysis (Figure 1).[11] The similarity of the design principles used here is striking: the cyclodextrin macrocycles

[*] Priv.-Doz. Dr. B. König
Institut für Organische Chemie der Technischen Universität
Hagenring 30, D-38106 Braunschweig (Germany)
Fax: Int. code +(531)3915-388
e-mail: b.koenig@tu-bs.de

 © WILEY-VCH Verlag GmbH, D-69451 Weinheim, 1997 0570-0833/97/3617-1833 $ 17.50+.50/0

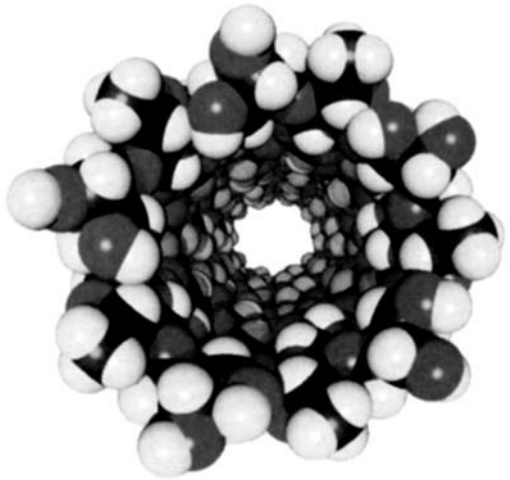

Figure 1. View into the cavity of an isolated nanotube consisting of stacked cyclodextrins **3-RR** in the solid.

consist of alternating D and L sugar units! A whole series of new cyclodextrin derivatives from alternating D and L rhamnopyranose and D and L mannopyranose units has been presented by this research group (Scheme 2). Among these are also the first

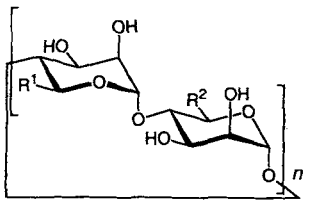

	n	R^1	R^2
1-MM	3	CH_2OH	CH_2OH
1-RM	3	Me	CH_2OH
2-RM	4	Me	CH_2OH
1-RR	3	Me	Me
2-RR	4	Me	Me
3-RR	5	Me	Me
4-RR	6	Me	Me
5-RR	7	Me	Me

Scheme 2. D/L-Cyclooligosaccharides synthesized so far. **M** = mannopyranose, **R** = rhamnopyranose.

achiral cyclic oligosaccharides (**RR** and **MM** derivatives) as well as the largest cyclooligosaccharide known to date (5-**RR**) with 14 sugar units. The synthesis of the cyclodextrin analogues **1-RM** and **2-RM** succeeded efficiently by polycondensation–cycloglycosylation of the disaccharide **1**, in which the cyanoethylidene group serves as glycosyl donor and the trityloxy function as glycosyl acceptor. The key intermediate **1** is available in 15 steps from L-rhamnose and D-mannose.

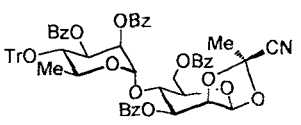

1

The results obtained by Fujita, Lichtenthaler, and coworkers show that cyclooligosaccharides with sugar units other than glucose do not necessarily have to assemble as tubes. Via the 2,3 anhydro compound as intermediate, α and β cycloaltrin were obtained from the corresponding cyclodextrins (Scheme 3).[12] The X-ray structure analysis of the α cycloaltrin revealed a highly unusual structure with alternating $^1C_4/^4C_1$ chair conformations and a cavity open on only one side. Instead of the now impossible formation of tubes, the layers lie on top of each other in a staggered way with water molecules in the gaps.

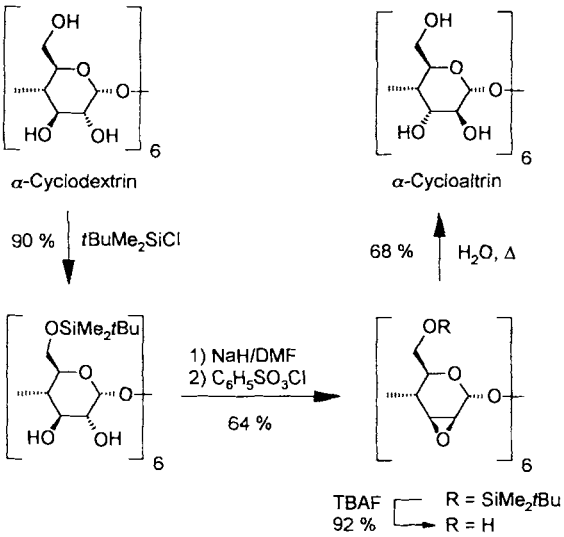

Scheme 3. Synthetic sequence leading from α-cyclodextrin to α-cycloaltrin. TBAF = tetrabutylammonium fluoride.

Other than with ion channels, it is not the inner void, but the groups pointing outwards that are crucial for the function of a tube-shaped self-replicating system[13] built up on the base of α-helical peptides (Scheme 4). For this purpose a peptide consisting of 32 amino acids whose sequence resembles the GCN4

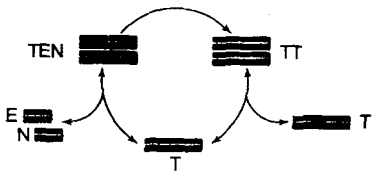

Scheme 4. Schematic representation of the minimal autocatalytic reaction cycle of a self-replicating, α-helical peptide. The peptide fragments E and N are preorientated at the template T through hydrophobic, interhelical interaction. The amide bond formation leads to an identical copy of the template, which further accelerates the peptide ligation in the autocatalytic cycle.

leucine zipper region was used. Ghadiri and co-workers showed that this compound catalyzes its own formation by accelerating amide bond formation between appropriate peptide strands. The most important interaction responsible for the specific interhelical recognition between template and reactant is the hydrophobic interaction of the leucin and valine residues, which increases due to electrostatic forces. If this interaction is interrupted, for example, through the addition of guanidinium hydrochloride or through exchange of a valine or leucine residue for alanine, the autocatalysis comes to a standstill.

The above-mentioned examples show impressively how fast the development of functional nanostructures on the base of molecular recognition is progressing.[14] Even if the complexity falls far short of that of biological self-assembly processes like the RNA-induced formation of the coat of the tobacco mosaic virus from 2130 identical proteins, the next step might already lead to applications in nano- and microtechnology.

German version: *Angew. Chem.* **1997**, 1919–1921 [H1300]

 © WILEY-VCH Verlag GmbH, D-69451 Weinheim, 1997 0570-0833/97/3617-1834 $ 17.50+.50/0

Keywords: cyclodextrins · macrocycles · peptides · self-replication · supramolecular chemistry

[1] a) H. Terrones, M. Terrones, W. K. Hsu, *Chem. Soc. Rev.* **1995**, *24*, 341–350; b) C. N. R. Rao, R. Seshardri, A. Govindaraj, R. Sen, *Mater. Sci. Eng. A* **1995**, *15*, 209–262; c) T. W. Ebbesen, *NATO ASI Ser. Ser. C* **1994**, *443*, 11–25; d) S. Iijima, T. Ishihashi, *Nature* **1993**, *363*, 603–605; e) A. Thess, *Science* **1996**, *273*, 483–487; f) R. Tenne, *Adv. Mater.* **1995**, *7*, 965–972, 989–995; g) for the synthesis and structure of a hydrocarbon picotube, see S. Kammermeier, P. G. Jones, R. Herges, *Angew. Chem.* **1996**, *108*, 2834–2838; *Angew. Chem. Int. Ed. Engl.* **1996**, *35*, 2669–2671.

[2] S. J. Tans, M. H. Devoret, H. Dai, A. Thess, R. E. Smalley, L. J. Geerligs, C. Dekker, *Nature* **1997**, *386*, 474–477.

[3] P. DeSantis, S. Morosetti, R. Rizzo, *Macromolecules* **1974**, *7*, 52–58.

[4] a) L. Tomasic, G. P. Lorenzi, *Helv. Chim. Acta* **1987**, *70*, 1012–1016; b) X. Sun, G. P. Lorenzi, *ibid.* **1994**, *77*, 1520–1526.

[5] a) J. D. Hartgernik, J. R. Granja, R. A. Milligan, M. R. Ghadiri, *J. Am. Chem. Soc.* **1996**, *118*, 43–50; b) M. R. Ghadiri, J. R. Granja, R. A. Milligan, D. E. McRee, N. Khazanovich, *Nature* **1993**, *366*, 324–327; c) M. R. Ghadiri, K. Kobayashi, J. R. Granja, R. K. Chadha, D. E. McRee, *Angew. Chem.* **1995**, *107*, 76–78; *Angew. Chem. Int. Ed. Engl.* **1995**, *34*, 93–95; d) K. Kobayashi, J. R. Granja, M. R. Ghadiri, *ibid.* **1995**, *107*, 79–81 and **1995**, *34*, 95–97. e) The structure of the nanotube was confirmed by transmission electron microscopy, electron scattering, and infrared spectroscopy.

[6] a) M. R. Ghadiri, J. R. Granja, L. K. Buehler, *Nature* **1994**, *369*, 301–304; b) R. M. Ghadiri, *Adv. Mater.* **1995**, *7*, 675–677. c) Apart from the self-assembly process of several subunits described here, working artificial ion channels have also been obtained by insertion of a single complex molecule. The synthetic requirements are less with self-assembly; however, with covalent structures the transmembrane channel stability is greater. Reviews of chemical models of transmembrane channels: U. Koert, *Chem. Unserer Zeit* **1997**, *31*, 20–26; d) G. W. Gokel, O. Murillo, *Acc. Chem. Res.* **1996**, *29*, 425–432; e) N. Kimizuka, T. Kawasaki, K. Hirata, T. Kunitake, *J. Am. Chem. Soc.* **1995**, *117*, 6360–6361; f) a modified peptide as a transmembrane channel: J.-C. Meillon, N. Voyer, *Angew. Chem.* **1997**, *109*, 1004–1006; *Angew. Chem. Int. Ed. Engl.* **1997**, *36*, 967–969; g) an ion-binding, tube-shaped calix[4]arene dimer: P. Schmitt, P. D. Beer, M. G. B. Drew, P. D. Sheen, *ibid.* **1997**, in press.

[7] Recent results show that ion conductivity changes discontinuously with the number of stacked units: M. R. Ghadiri, personal communication (1997).

[8] N. Khazanovich, J. R. Granja, D. E. McRee, R. A. Milligan, M. R. Ghadiri, *J. Am. Chem. Soc.* **1994**, *116*, 6011–6012.

[9] J. R. Granja, M. R. Ghadiri, *J. Am. Chem. Soc.* **1994**, *116*, 10785–10786.

[10] Three general types of structure have been observed in solid cyclodextrins (CD): cage structures, which are found in all CD hydrates, as well as channel and layer structures for host–guest complexes: K. Harata in *Comprehensive Supramolecular Chemistry, Vol 3* (Eds.: J. Szejtli, T. Osa), Elsevier, Oxford, **1996**, pp. 279–304.

[11] a) P. R. Ashton, C. L. Brown, S. Menzer, S. A. Nepogodiev, J. F. Stoddart, D. J. Williams, *Chem. Eur. J.* **1996**, *2*, 580–591; b) S. A. Nepogodiev, G. Gattuso, J. F. Stoddart, *Proceedings of the 8th International Cyclodextrin Symposium* (Eds.: J. Szejtli, L. Szente), Kluwer, Dordrecht, **1996**, pp. 89–94; c) P. R. Ashton, S. J. Cantrill, G. Gattuso, S. Menzer, S. A. Nepogodiev, A. N. Shipway, J. F. Stoddart, D. J. Williams, *Chem. Eur. J.* **1997**, *3*, 1299–1314; d) G. Gattuso, S. Menzer, S. A. Nepogodiev, J. F. Stoddart, D. J. Williams, *Angew. Chem.* **1997**, *109*, 1615–1617; *Angew. Chem. Int. Ed. Engl.* **1997**, *36*, 1451–1454.

[12] a) K. Fujita, H. Shimada, K. Ohta, Y. Nogami, K. Nasu, T. Koga, *Angew. Chem.* **1995**, *107*, 1783–1784; *Angew. Chem. Int. Ed. Engl.* **1995**, *34*, 1621–1622; b) Y. Nogami, K. Nasu, T. Koga, K. Ohta, K. Fujita, S. Immel, H. J. Lindner, G. E. Schmitt, F. W. Lichtenthaler, *ibid.* **1997**, *109*, 1987–1991; and **1997**, *36*, 1899–1902.

[13] a) D. H. Lee, J. R. Granja, J. A. Martinez, K. Severin, M. R. Ghadiri, *Nature* **1996**, *382*, 525–528; b) K. Severin, D. H. Lee, J. A. Martinez, M. R. Ghadiri, *Chem. Eur. J.* **1997**, *3*, 1017–1024. c) The kinetic analysis of the self-replication progress revealed parabolic growth; for other self-replication systems, see: d) D. N. Reinhoudt, D. M. Rudkevich, F. de Jong, *J. Am. Chem. Soc.* **1996**, *118*, 6880–6889 and references therein; e) G. von Kiedrowski, *Nature* **1994**, *369*, 221–224; f) A. Terfort, G. von Kiedrowski, *Angew. Chem.* **1992**, *104*, 626–628; *Angew. Chem. Int. Ed. Engl.* **1992**, *31*, 654–656.

[14] a) Recent research by Whitesides et al. shows that the strategy of spontaneous association of molecules is not restricted to nanometer dimensions, but is also suitable for the construction of aggregates of millimeter size: A. Terfort, N. Bowden, G. M. Whitesides, *Nature* **1997**, *386*, 162–164; b) N. Bowden, A. Terfort, J. Carbeck, G. M. Whitesides, *Science* **1997**, *276*, 233–235.

[15] a) K. Namba, G. Stubbs, *Science* **1986**, *231*, 1401–1406. b) The in vitro reconstitution of the intact virus from the isolated components shows impressively that the information about the supramolecular structure is stored in the subunits and that the process of self-assembly is highly cooperative: A. Klug, *Angew. Chem.* **1983**, *95*, 579–596; *Angew. Chem. Int. Ed. Engl.* **1983**, *22*, 565–582; c) H. Conrat-Fraenkel, R. C. Williams, *Proc. Natl. Acad. Sci. USA* **1955**, *41*, 690–698.

 © WILEY-VCH Verlag GmbH, D-69451 Weinheim, 1997 0570-0833/97/3617-1835 $ 17.50+.50/0

β-Peptides: Novel Secondary Structures Take Shape

Ulrich Koert*

The prerequisite for the biological function of any protein is the folding of the peptide strand composed of α-amino acid residues into the corresponding active conformation. Important intermediates during the folding process are domains having a particular secondary structure. Secondary structures of α-peptides have been studied intensively; the most common structural themes are the α-helix and the β-sheet. Is the occurrence of secondary structures limited to α-peptides only?

Recent results from the groups led by D. Seebach[1–3] and S. Gellman[4, 5] show that β-peptides[6] such as **1** and **2** also may

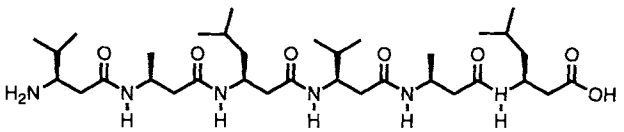

H-(β-HVal-β-HAla-β-HLeu)$_2$-OH

1

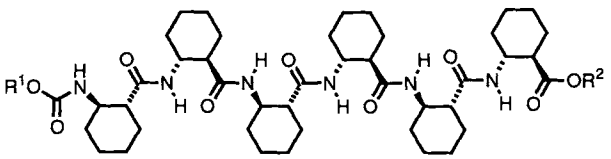

2

form well-defined, remarkably stable secondary structures. The required β-amino acid building blocks are accessible, for example, by Arndt–Eistert homologation of the corresponding α-amino acids.[1]

Seebach et al. examined β-peptides of type **1**.[1–3] NMR studies in solution (MeOH, pyridine) prove the presence of a helical secondary structure (Figure 1 A, B). An oligomer containing only six β-amino acid residues forms a stable helix! With α-peptides, a stable secondary structure usually occurs first for the 15–20-mers. Exceptions are shorter homo-α-peptides and α-peptides containing proline or 2-amino-2-methylpropanoic acid

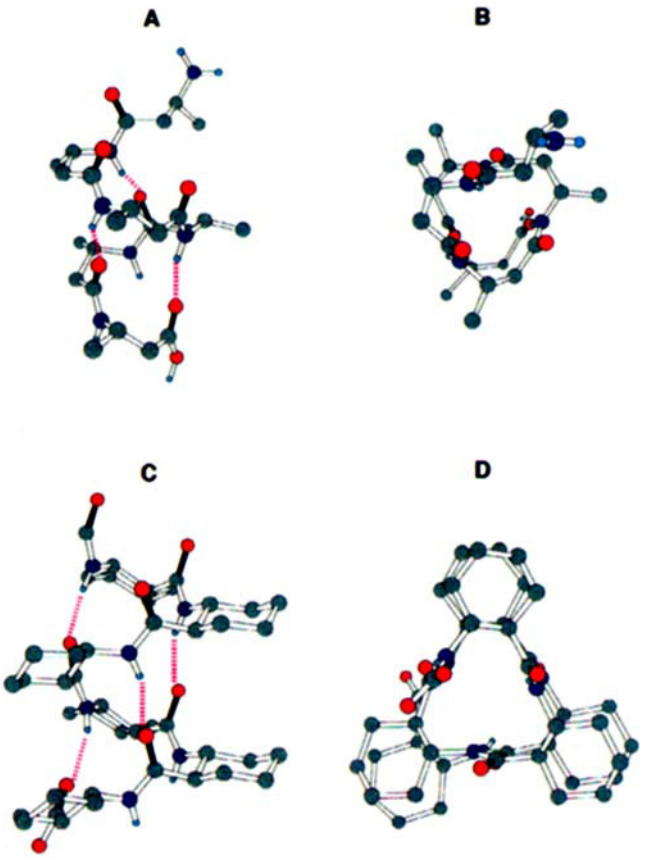

Figure 1. 3_1-Helices of the β-peptides **1** and **2**; respective side views (A and C) and views along the helix axis (B and D). The intramolecular hydrogen bonds are drawn in violet. For clarity, only one carbon atom in each side chain in A and B is shown.

(Aib). Gellman et al. proved the presence of an almost identical secondary structural motif in type **2** β-peptides by X-ray structure analysis and conformational studies in solution (Figure 1 C, D).[4] The new helical secondary structure is stabilized by hydrogen bonds forming a 14-membered ring (the α-helix contains 13-membered rings). Exactly three amino acid residues are required to form one turn of the helix. Therefore the new secondary structure is designated a 3_1-helix. The known α-helix with 3.6 α-amino acids per turn is a 3.6_1-helix.

An α-peptide composed of naturally occurring L-α-amino acids forms, with respect to its helical sense, a 3.6_1-*P*-helix. In contrast, a β-peptide like **1** made of homologated L-α-amino acids forms a 3_1-*M*-helix (Figure 2).

How much stereochemical "information" in the β-peptide is necessary to establish the new secondary structure? Gellman

[*] Prof. Dr. U. Koert
Institut für Chemie der Humboldt-Universität
Hessische Strasse 1–2, D-10115 Berlin (Germany)
Fax: Int. code +(30)2093-2766
e-mail: koert@lyapunov.chemie.hu-berlin.de

 © WILEY-VCH Verlag GmbH, D-69451 Weinheim, 1997 0570-0833/97/3617-1836 $ 17.50+.50/0

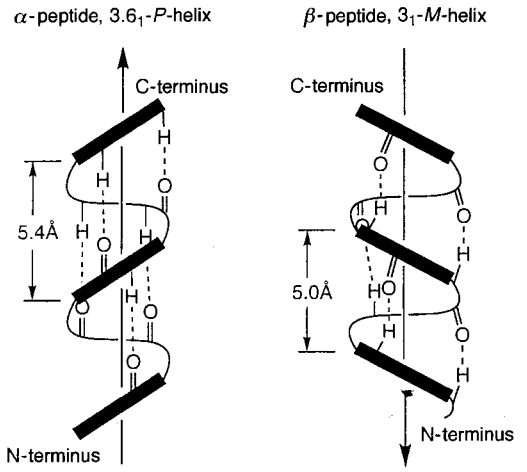

Figure 2. Schematic representation of the helix of a peptide composed of L-α-amino acids (left) and one composed of L-β-amino acids (right). The arrows follow the helix dipoles. The α-peptide is depicted as a 3.6_{13}- or α-helix (*P* configuration with 3.6 α-amino acid residues per turn and a pitch of 5.4 Å). β-peptides consisting of homologated L-α-amino acids form a 3_{14}-helix (peptide nomenclature) or 3_1-helix (crystallographic notation) of *M* configuration (3 β-amino acid residues per turn and a pitch of 5.0 Å).

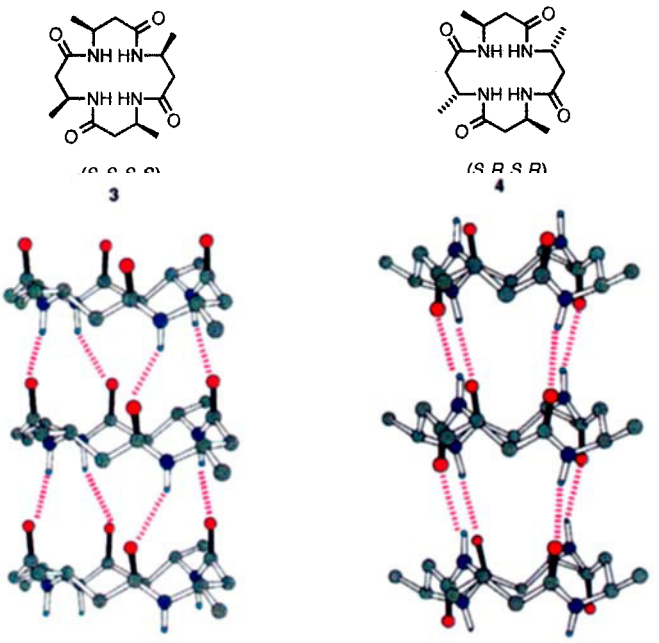

Figure 3. Side view of the solid-state structures of the cylindrical stacks made up of the cyclopeptides **3** (left) and **4** (right). The intramolecular hydrogen bonds are depicted in violet.

et al. attribute the stability of their 3_1-helix to the conformational rigidity of the cyclohexane rings.[4] Van Gunsteren and Seebach et al. used molecular dynamics calculations to show that the single stereogenic center in their β-amino acids already causes a stable folding pattern. The 3_1-helix, stable at 298 K, unfolds when heated to 350 K. Within only 200 ps the helical conformation is re-established![7] Without stereogenic centers in the β-peptide backbone, the formation of a 3_1-helix is not preferred.[1, 2]

The *trans*-substituted cyclohexane ring in Gellman's β-amino acids has a strong influence on the formation of the hydrogen bonds making up the 14-membered ring in the 3_1-helix. When the corresponding *trans*-substituted cyclopentane β-amino acid is employed, an altered helix with 12-membered-ring hydrogen bonds results.[5]

In addition to the linear β-peptides, Seebach et al. synthesized cyclic β-peptides such as **3** and **4** and studied their conformations.[8] In the solid state these cyclo-β-peptides form cylindrical stacks stabilized by hydrogen bonds (Figure 3). In the (*S*,*S*,*S*,*S*) tetramer **3**, the amide bonds are orthogonal to the ring plane and all point in the same direction. In the (*S*,*R*,*S*,*R*) tetramer **4**, the orthogonal amide bonds alternatingly point in opposite directions. These cylindrical stacks display structural similarities with the nanotubes investigated by Ghadiri et al.[9] and by Sun and Lorenzi.[10]

Summarizing the structural results, one can say that β-peptides are at least as good candidates for protein folding as their counterparts in the world of β-peptides. This fact raises the following, thrilling question: what kinds of interactions exist between the world of α-peptides and that of β-peptides? Seebach et al. report that peptides composed of β-amino acids have not yet been found to have mutagenic properties and that β-peptides are stable against various peptidases.[11] Another interesting question with respect to β-peptides concerns the evolution of life: why do we live in an α-peptide and not in a β-peptide world?

German version: *Angew. Chem.* **1997**, *109*, 1922–1923

Keywords: helical structures · hydrogen bonds · peptides · protein structures

[1] D. Seebach, M. Overhand, F. N. M. Kühnle, B. Martinoni, L. Oberer, U. Hommel, H. Widmer, *Helv. Chim. Acta* **1996**, *79*, 913–941.
[2] D. Seebach, P. E. Ciceri, M. Overhand, B. Jaun, D. Rigo, L. Oberer, U. Hommel, R. Amstutz, H. Widmer, *Helv. Chim. Acta* **1996**, *79*, 2043–2066.
[3] T. Hintermann, D. Seebach, *Synlett* **1997**, 437–438.
[4] D. H. Appella, L. A. Christianson, I. L. Karle, D. R. Powell, S. H. Gellman, *J. Am. Chem. Soc.* **1996**, *118*, 13071–13072; B. L. Iverson, *Nature* **1997**, *385*, 113–115.
[5] D. H. Apella, L. A. Christianson, D. A. Klein, D. R. Powell, X. Huang, J. J. Barchi, Jr, S. H. Gellman, *Nature* **1997**, *387*, 381–384.
[6] Earlier investigations of possible elements of secondary structures in homopolymeric β-peptides: F. Chen, G. Lepore, M. Goodman, *Macromolecules* **1974**, *7*, 779–783; H. Yuki, Y. Okamoto, Y. Doi, *J. Polym. Sci. Polym. Chem. Ed.* **1979**, *17*, 1911–1921; J. M. Fernandez-Santin, S. Munoz-Guerra, A. Rodriguez-Galan, J. Aymami, J. Lloveras, J. A. Subirana, E. Giralt, M. Ptak, *Macromolecules* **1987**, *20*, 62–68.
[7] X. Daura, W. F. van Gunsteren, D. Rigo, B. Jaun, D. Seebach, *Chem. Eur. J.*, *3*, 1410–1417.
[8] D. Seebach, J. L. Matthews, A. Meden, T. Wessels, C. Baerlocher, L. B. McCusker, *Helv. Chim. Acta* **1997**, *80*, 173–182.
[9] J. D. Hartgerink, J. R. Granja, R. A. Milligan, M. R. Ghadiri, *J. Am. Chem. Soc.* **1996**, *118*, 43.
[10] X. Sun, G. P. Lorenzi, *Helv. Chim. Acta* **1994**, *77*, 1520.
[11] T. Hintermann, D. Seebach, *Chimia* **1997**, *51*, 244.

 © WILEY-VCH Verlag GmbH, D-69451 Weinheim, 1997 0570-0833/97/3617-1837 $ 17.50+.50/0

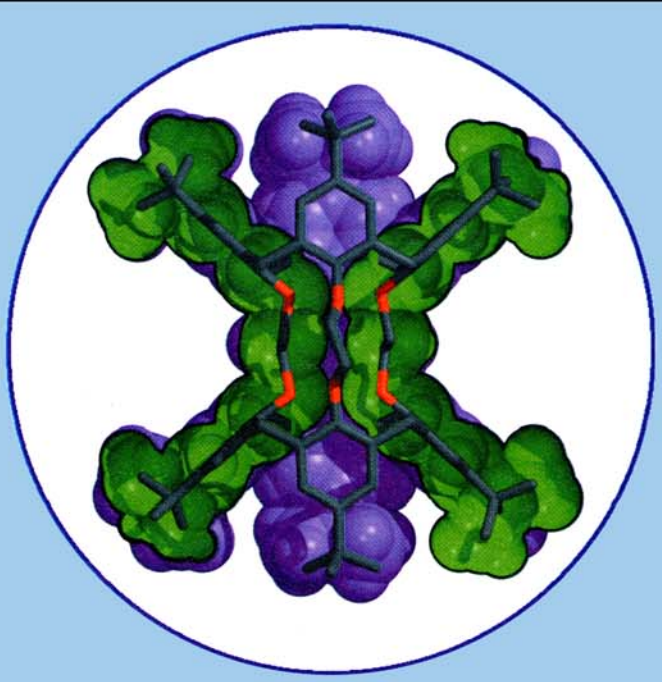

A new cage molecule possessing an eight-coordinate binding site displays a remarkable affinity for the potassium cation over any other alkali metal.

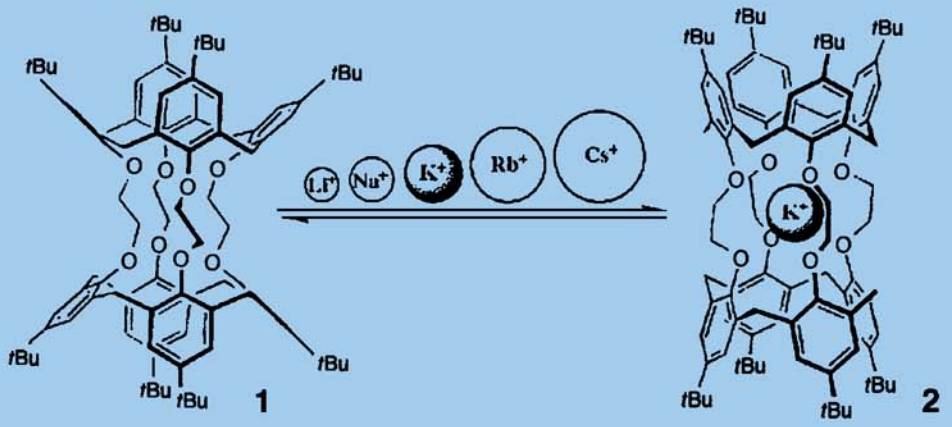

The two inserts, taken from crystal structures of **1** and **2** , illustrate the channel-like nature of the ligand and the gating of one potassium ion as it travels along the molecule's main (vertical) axis. More about **calix[4]tube** on the following pages.

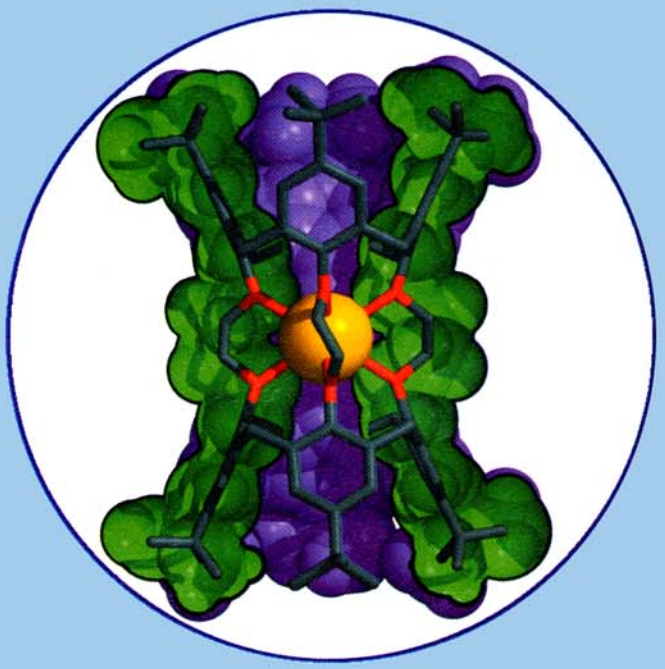

 © WILEY-VCH Verlags GmbH, D-69451 Weinheim, 1997 0570-0833/97/3617-1839 $ 17.50 + .50/0

Calix[4]tube: A Tubular Receptor with Remarkable Potassium Ion Selectivity**

Philippe Schmitt, Paul D. Beer,* Michael G. B. Drew, and Paul D. Sheen

Potassium channel proteins have been investigated intensely in the last decade and a great deal of information about their structure/function relationships has been elucidated.[1] A very exciting, and still controversial, aspect focuses on how these proteins transport potassium ions through the cell membrane at high rates and with almost perfect selectivity (K^+ transported 1000 times more efficiently than Na^+).[2] The region of the channel pore responsible for the selection of the alkali metal ion, termed the selection filter, contains a square-planar array of four converging tyrosine residues.[3] The results of experimental and ab initio studies suggest that an *en face* cation-π interaction between K^+ ions and the arene surfaces of the tyrosine residues could be determinant for such a unique selectivity pattern.[4]

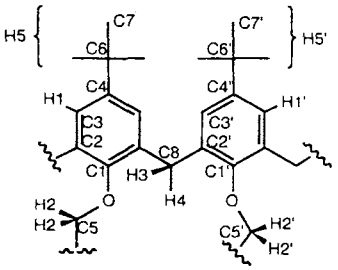

Despite the involvement of numerous research groups in the development of synthetic channels,[5, 6] it appeared to us that a biomimetic approach focusing in particular on the selection of alkali metal ions had not been fully investigated. In an effort to accredit the cation–π interaction hypothesis, we designed a novel biomimetic calix[4]arene-based tubular receptor whose access to metal cations may be controlled by filtering gates based on a square-planar array of arene surfaces.[7]

The template-driven condensation of the *p-tert*-butyl-calix[4]arene **2** with the pertosylated derivative **1**[8] in acetonitrile furnished the novel calix[4]tube **3** in fairly good yields (Scheme 1). Surprisingly this compound was found to be insoluble in all common organic solvents with the exception of chloroform and carbon tetrachloride. After crystallization from a chloroform/benzene mixture, **3** was submitted to crystal structure analysis (Figure 1) and found to exhibit C_i symmetry in the solid state.[9] The molecule contains two calix[4]arene units in a flattened, C_2-symmetrical *cone* conformation. Within the same calixarene macrocycle, each phenyl ring intersects the plane of the four methylene carbon atoms at angles of 89.6(2), 41.3(2), 87.3(2), and 43.7(2)°, respectively. It is noteworthy that the ethylene linkages alternate in two different geometries. Two of them present an *anti*-like conformation (O-C-C-O torsion angle

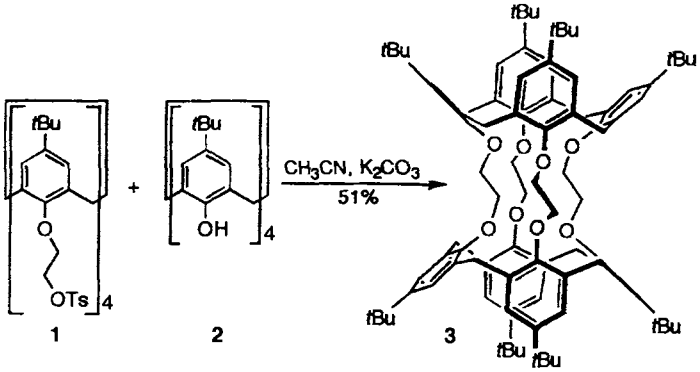

Scheme 1. Synthesis of the calix[4]tube **3**.

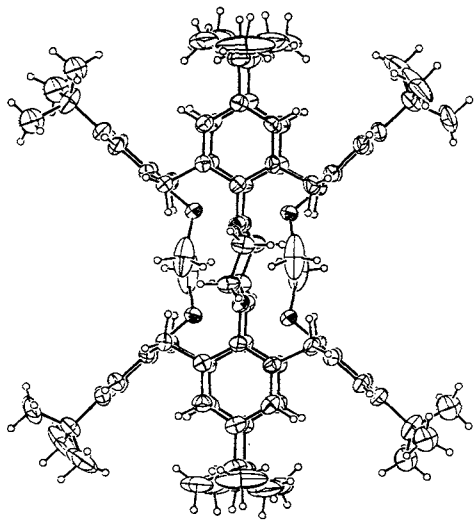

Figure 1. Crystal structure of the centrosymmetric calix[4]tube **3** in $3 \cdot 2.5\,C_6H_6$, with ellipsoids at 30% probability. Hydrogen atoms are included with small arbitrary radii. The benzene solvent molecules are not shown.

of 161.2(6)°), whereas the remaining two display a *gauche*-type conformation (O-C-C-O torsion angle of 47.8(8)°). As a consequence of this particular arrangement, the central cage composed of eight oxygen atoms is unsuitable to form an inclusion complex.

Interestingly, on the NMR time scale, this conformational symmetry is conserved in solution. The ^1H and ^{13}C NMR spectra of **3** in deuterated chloroform are consistent with the freezing of the calixarenes in a flattened *cone* conformation. All the signals, with the exception of those for the methylene groups, are split into two singlets of equal intensity. Moreover, the ^1H NMR spectra were found to be temperature independent up to 55°C. The absence of any coalescence or even peak broadening, features indicative of a time-averaged D_{4h} symmetry, suggests the calix[4]tube **3** is an extremely rigid molecule in solution.

As a consequence of the solubility limitations of **3**, a mixture of deuterated chloroform and methanol (8:2) was employed as solvent for the NMR spectroscopic investigations of the complexation of metal ions by **3**. Solid alkali metal iodide (10 μmol ($\approx$10 equiv)) was added to 1 mL of a solution of the calix[4]tube in this solvent mixture ([**3**] = 1 mM) at 25°C. The samples were sonicated briefly and ^1H NMR spectra were recorded at various times.

Compound **3** underwent a dramatic change when treated with potassium iodide. Within the first hour after mixing, the initial spectrum disappeared and was replaced by a new set of peaks suggestive of an increase of the ligand symmetry (Figure 2). The

[*] Dr. P. D. Beer, Dr. P. Schmitt
Inorganic Chemistry Laboratory, University of Oxford
South Parks Road, Oxford OX1 3QR (UK)
Fax: Int. code +(1865) 272 690
e-mail: paul.beer@icl.ox.ac.uk
Dr. M. G. B. Drew, Dr. P. D. Sheen
Department of Chemistry, University of Reading (UK)

[**] We thank the Engineering and Physical Sciences Research Council (EPSRC) for use of the mass spectrometry service at University of Swansea and, with the University of Reading, for funds for the image plate system. This work was supported by A. W. E. Aldermaston (fellowships for P. S. and P. D. S.).

 © WILEY-VCH Verlag GmbH, D-69451 Weinheim, 1997 0570-0833/97/3617-1840 $ 17.50+.50/0

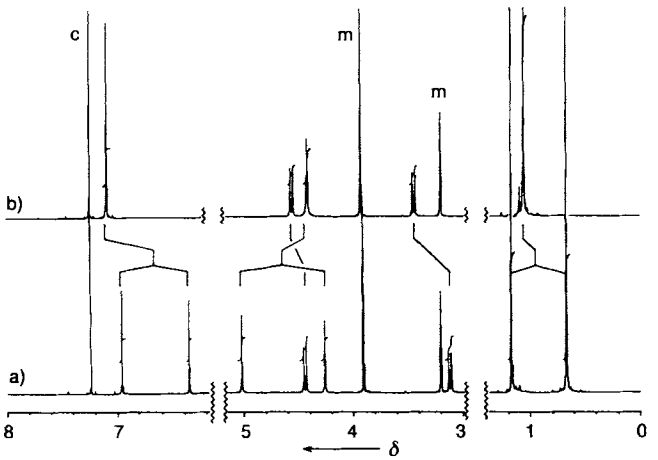

Figure 2. ^{1}H NMR spectrum of **3** [500 MHz, $CDCl_3/CD_3OD$ 4/1 (v/v)]: a) pure, b) with 10 equivalents of solid potassium iodide (c, m: solvent peaks corresponding to chloroform and methanol, respectively).

structural degeneracy of **3** after K^+ complexation, characterized by a fourfold symmetry along the molecule's main axis, is consistent with the opening of the binding cavity driven by the complexation of the potassium ion within the cage consisting of eight oxygen atoms.

Analogous experiments with other alkali metal iodides (LiI, NaI, RbI and CsI) failed to exhibit any significant cation uptake. Estimated by integration of the NMR signals, less than 7% of **3** was complexed after more than three days in presence of 10 equivalents of RbI; in the cases of LiI, NaI, and CsI the complexation after three days was less than 5% (Figure 3). Such a preference for potassium ions over any of the other alkali metal ions is remarkable for a synthetic receptor.[10]

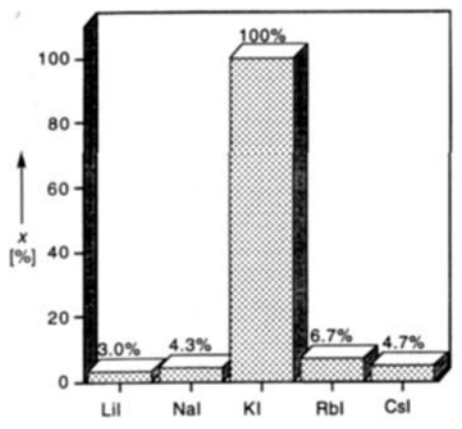

Figure 3. Uptake of alkali metal ions by **3** after treating its chloroform-methanol solution (4/1, [**3**] = 1 mM) with 10 equivalents of alkali metal iodide. The complexation ratio x was determined by integration of the ^{1}H NMR spectra after the samples had been left to stand for 90 h. In the case of KI, equilibrium was reached within an hour.

To investigate the potassium complexation process quantitatively, the uptake of 1 μmol of KI ([KI] = 10^{-3} M) by one equivalent of **3**, in homogeneous solution at 25 °C, was monitored as a function of time. After 24 h the system was evaluated to have reached equilibrium (86% of **3** was complexed), the formation of a 1:1 complex was established, and a stability constant of 4×10^4 L mol^{-1} was estimated. The complexation halftime, defined by the time necessary for the system to reach half the equilibrium conversion ratio, was measured to be 18 minutes. Although these are preliminary results, this experiment reveals the complexation process is kinetically slow and may be a consequence of an important intramolecular reorganization necessary for the cation uptake.

Comparison of the chemical shifts values of **3** and of its potassium complex (**4**), shows in general low-field shift deviations of all the calix[4]arene-related peaks ($\Delta\delta$ *t*-Bu: +0.923, Ph: +0.426, CH_2: +0.216), whilst the signals of the ethylene protons exhibit an average high-field variation (− 0.228, Figure 2). This feature is consistent with a displacement of the electron density of the ligand towards the molecule's equatorial plane caused by the close proximity of the positive charge of the complexed metal ion.

The geometry of the complex was confirmed by X-ray analysis.[11] As predicted by NMR spectroscopy, **4** is highly symmetrical and contains an approximate C_4 element of symmetry along the main axis of the molecule. All ethylene linkages present a *gauche* conformation (O-C-C-O torsion angles vary from 51.7 to 68.00°) and the potassium ion is located at the center of a slightly flattened cube; the K−O distances range from 2.759(6) to 2.809(6) Å (Figure 4). The angles of intersection of the phenyl rings with the mean plane of the four methylene carbon atoms vary between 64.6(2) and 67.9(2)°.

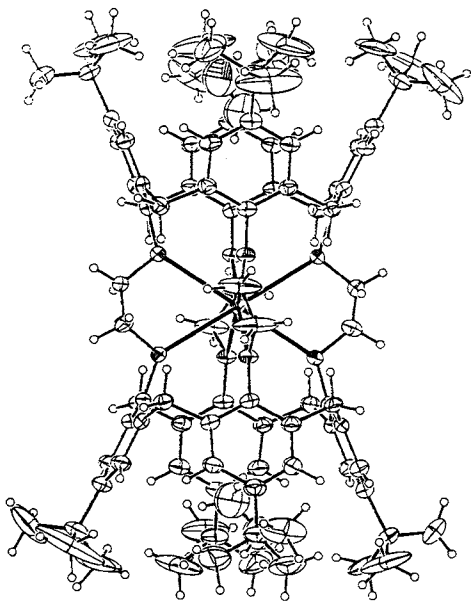

Figure 4. Structure of the K^+ complex **4** of the calix[4]tube **3** in crystals of **4**·I·3 $CHCl_3$·4 CH_3OH·H_2O. A potassium ion is located in the center of **3**, and two methanol molecules in the cone cavities. Ellipsoids are drawn at 30% probability. Hydrogen atoms are included with small arbitrary radii. The chloroform and water solvent molecules are not shown.

Of relevance to K^+ selective channel transportation, the assumption that the calixarene units provide the preferred cation-accessing gates was tested by using constrained molecular mechanics calculations.[12, 13] Preliminary calculations suggested that indeed the complexation of the potassium ion would require an activation energy about 10 kJ mol^{-1} larger by accessing the cavity across rather than along the main axis of the molecule and may involve a prior weak complexation of the cation in the calixarene cone (Scheme 2).[14] Our current efforts are directed in the collection of experimental evidence of such a behavior and in the derivatization of **3** as a potential new class of membrane-spanning compounds.

 © WILEY-VCH Verlag GmbH, D-69451 Weinheim, 1997 0570-0833/97/3617-1841 $ 17.50+.50/0

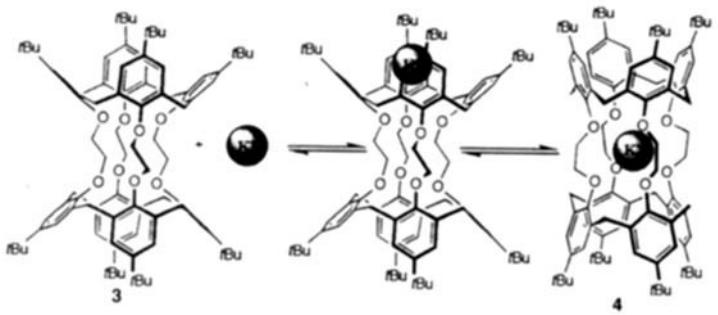

Scheme 2. Schematic representation of the uptake of K^+ ions by **3** based on molecular mechanics calculations.

Experimental Section

3: A suspension of *p-tert*-butyl-calix[4]arene (451 mg, 0.70 mmol) and potassium carbonate (480 mg, 3.5 mmol) in dry acetonitrile (100 mL) was stirred under nitrogen. After 2 h at room temperature, **1** (1 g, 0.70 mmol) was added and the reaction mixture brought to reflux for five days. The solvent was then removed in vacuo and the solid suspended in a 1:1 ethanol-water mixture. The suspension was heated to reflux overnight and hot filtered. The crude mixture was then dissolved in chloroform (50 mL) and the solution carefully paper filtered to yield a clear solution to which acetone (40 mL) was added. Filtration of the microcrystalline material obtained after the solution had been allow to stand for a few hours, followed by its drying in vacuo yielded **3** (500 mg) as an analytically pure product (51%). ^{1}H NMR (500 MHz, $CDCl_3$, 25 °C): δ = 7.09 (s, 8H; H1/H1′), 6.48 (s, 8H; H1/H1′), 5.15 (s, 8H; H2/H2′), 4.57 (d, ^3J(H,H) = 13 Hz, 8 H; H3), 4.39 (s, 8 H; H2/H2′), 3.25 (d, ^3J(H,H) = 13 Hz, 8 H; H4), 1.31 (s, 36H; H5/H5′), 0.80 (s, 36 H, H5/H5′); ^{13}C NMR (125 MHz, $CDCl_3$, 25 °C): δ = 156.0 (C1/C1′), 152.8 (C1/C1′), 144.5 (C2/C2′), 144.3 (C2/C2′), 135.1 (C4/C4′), 131.9 (C4/C4′), 125.5 (C3/C3′), 124.8 (C3/C3′), 73.0 (C5/C5′), 72.5 (C5/C5′), 34.1 (C6/C6′), 33.5 (C6/C6′), 32.4 (C8), 31.7 (C7/C7′), 31.0 (C7/C7′); C,H,Cl analysis ($C_{96}H_{120}O_8 \cdot CHCl_3$): calc.: C 76.58, H 8.02, Cl 6.99; found: C 76.32, H 8.17, Cl 8.09.

Received: February 27, 1997 [Z10172IE]
German version: *Angew. Chem.* **1997**, *109*, 1926–1928

Keywords: alkali metals · calixarenes · ion channels · potassium · supramolecular chemistry

[1] For example see: C. Miller, *Science* **1991**, *252*, 1092–1096 (review); Q. Lü, C. Miller, *ibid.* **1995**, *268*, 304–307; P. Hidalgo, R. MacKinnon, *ibid.* **1995**, *268*, 307–310; M. Stocker, C. Miller, *Proc. Natl. Acad. Sci. USA* **1994**, *91*, 9509–9513; J. C. Bradley, W. C. Richards, *Protein Eng.* **1993**, *7*, 859–862.

[2] G. Yellen, *J. Gen. Physiol.* **1984**, *84*, 157; J. Neyton, C. Miller, *ibid.* **1988**, *92*, 569.

[3] For example see: R. Ranganathan, J. H. Lewis, R. MacKinnon, *Neuron* **1996**, *16*, 131–139; L. Heginbotham, Z. Lu, T. Abramson, R. MacKinnon, *Biophys. J.* **1994**, *66*, 1061–1067; S. Bogusz, A. Boxer, D. Busath, *Protein Eng.* **1992**, *5*, 285–293.

[4] D. A. Dougherty, *Science* **1996**, *271*, 163–168; C. Miller, *ibid.* **1993**, *261*, 1692–1693; L. Heginbotham, R. MacKinnon, *Neuron* **1992**, *8*, 483–491; J. Sunner, K. Nishizawa, P. Kebarle, *J. Phys. Chem.* **1981**, *85*, 1814–1820.

[5] For reviews see: G. W. Gokel, O. Murillo, *Acc. Chem. Res.* **1996**, *29*, 425–432; K. S. Akerfeldt, J. D. Lear, Z. R. Wasserman, L. A. Chung, W. F. DeGrado, *ibid.* **1993**, *26*, 191–197.

[6] I. Tabushi, Y. Kuroda, K. Yokota, *Tetrahedron Lett.* **1982**, *23*, 4601–4604; Y. Tanaka, Y. Kobuke, M. Sokabe, *Angew. Chem.* **1995**, *107*, 717–718, *Angew. Chem. Int. Ed. Engl.* **1995**, *34*, 693–694; Y. Kokube, K. Ueda, M. Sokabe, *J. Am. Chem. Soc.* **1992**, *114*, 7618–7622; U. F. Kragten, M. F. M. Roks, R. J. M. Nolte, *J. Chem. Soc. Chem. Commun.* **1985**, 1275–1276; N. Voyer, M. Robitaille, *J. Am. Chem. Soc.* **1995**, *117*, 6599–6600; M. J. Pregel, L. Jullien, J.-M. Lehn, *Angew. Chem.* **1992**, *104*, 1695–1698, *Angew. Chem. Int. Ed. Engl.* **1992**, *31*, 1637–1640; L. Jullien, J.-M. Lehn, *Tetrahedron Lett.* **1988**, *29*, 3803–3806; T. M. Fyles, T. D. James, K. C. Kaye, *J. Am. Chem. Soc.* **1993**, *115*, 12315–12321; T. M. Fyles, T. D. James, A. Pryhitka, M. Zojaji, *J. Org. Chem.* **1993**, *58*, 7456–7468; E. Stadler, P. Dedek, K. Yamashita, S. L. Regen, *J. Am. Chem. Soc.* **1994**, *116*, 6677–6682; A. Nakano, Q. Xie, J. V. Mallen, L. Echegoyen, G. W. Gokel, *ibid.* **1990**, *112*, 1287–1289; O. Murillo, S. Watanabe, A. Nakano, G. W. Gokel, *ibid.* **1995**, *117*, 7655–7679; J. D. Lear, Z. R. Wasserman, W. F. DeGrado, *Science* **1988**, *240*, 1177–1181; N. Khazanovich, J. R. Granja, D. E. McRee, R. A. Milligan, M. R. Ghadiri, *J. Am. Chem. Soc.* **1994**, *116*, 6011–6012; M. R. Ghadiri, J. R. Granja, L. K. Buehler, *Nature* **1994**, *369*, 301–304; C. J. Stankovic, S. H. Heinemann, J. M. Delfino, F. J. Sigworth, S. L. Schreiber, *Science* **1989**, *244*, 813–817.

[7] For a general survey on calixarenes see: V. Böhmer, *Angew. Chem.* **1995**, *107*, 785–817, *Angew. Chem. Int. Ed. Engl.* **1995**, *34*, 713–745.

[8] P. L. H. M. Cobben, R. J. M. Egberink, J. G. Bomer, P. Bergveld, W. Verboom, D. N. Reinhoudt, *J. Am. Chem. Soc.* **1992**, *114*, 10573–10582.

[9] Crystal data for **3**·2.5C_6H_6: crystal dimensions: 0.25 × 0.25 × 0.20 mm, triclinic, $P\bar{1}$, a = 10.286(12), b = 14.803(14), c = 19.01(2) Å, α = 75.70(1), β = 83.66(1), γ = 64.91(1)°, V = 2541(5) Å^3, Z = 1, ρ_{calcd} = 1.044 mg m^{-3}, $2\theta_{max}$ = 50.180, $\lambda(Mo_{K\alpha})$ = 0.71073 Å, T = 293(2) K. 7510 independent reflections were measured on a MARresearch Image Plate, and data processing including Lorentzian polarization were carried out using the XDS program (W. Kabsch, *J. Appl. Crystallogr.* **1988**, *21*, 916). The structure was determined by direct methods by using the SHELX86 program (G. M. Sheldrick, Universität Göttingen, **1986**) and anisotropically refined on $|F^2|$ using the Shelxl program (G. M. Sheldrick, Universität Göttingen) with non-hydrogen atoms given anisotropic thermal parameters. Hydrogen atoms were included in calculated positions with anisotropic thermal parameters set to 1.2 times those of the atom to which they were bonded. One of the *tert*-butyl groups was disordered. Compound **3** and one of the benzene molecules (which is given 50% occupancy) had crystallographically imposed $\bar{1}$ symmetry. No absorption correction was carried out. The final R and wR^2 values are 0.0850 and 0.2387, respectively, for 3239 data with $I > 2\sigma(I)$. Largest peak and hole in the final difference were 0.588, −0.375 e Å^{-3}, respectively [11 b].

[10] For synthetic ionophores displaying high potassium selectivity see: A. Casnati, A. Pochini, R. Ungaro, C. Bocchi, F. Ugozzoli, R. J. M. Egberink, H. Struijk, R. Lugtenberg, F. de Jong, D. N. Reinhoudt, *Chem. Eur. J.* **1996**, *2*, 436–445.

[11] a) Crystal data for **4**·I·3$CHCl_3$·4CH_3OH·H_2O, crystal dimensions: 0.45 × 0.30 × 0.45 mm, yellowish color, monoclinic, $P2_1/a$, a = 24.46(2), b = 12.334(13), c = 36.65(4) Å, β = 96.902(10)°, V = 10976(19) Å^3, Z = 4, ρ_{calcd} = 1.268 mg m^{-3}, $2\theta_{max}$ = 50.260, $\lambda(Mo_{K\alpha})$ = 0.71073 Å, T = 293(2) K. 27485 reflections were measured on a MARresearch Image Plate. 17598 were independent [R(int) = 0.825]. Data analysis and refinement of structure as for **3** [9]. The iodide was disordered over two sites with occupation factors of 0.74 and 0.26, respectively. Two water molecules were refined with 50% occupancy. The final R and wR^2 values are 0.0826 and 0.2893, respectively, for 9655 data with $I > 2\sigma(I)$. Largest peak and hole in the final difference Fourier map were 1.029, −0.713 e Å^{-3}, respectively. b) Crystallographic data (excluding structure factors) for the structures reported in this paper have been deposited with the Cambridge Crystallographic Data Centre as supplementary publication no. CCDC-100240. Copies of the data can be obtained free of charge on application to The Director, CCDC, 12 Union Road, Cambridge CB2 1EZ, UK (fax: int. code + (1223) 336-033; e-mail: deposit@chemcrys.cam.ac.uk).

[12] For a reference about transannular motion of cations across calix[4]arenes see: P. Guibauld, A. Varnek, G. Wipff, *J. Am. Chem. Soc.* **1993**, *115*, 8298–8312.

[13] Cerius 2, Molecular Simulations Inc., Cambridge UK, San Diego, CA, USA.

[14] For an example of such complex see: A. Zanotti-Gerosa, E. Solari, L. Giannini, C. Floriani, A. Chiesi-Villa, C. Rizzoli, *Chem. Commun.* **1997**, 183–184.

Coordination Arrays: Tetranuclear Cobalt(II) Complexes with [2 × 2]-Grid Structure**

Garry S. Hanan, Dirk Volkmer, Ulrich S. Schubert, Jean-Marie Lehn,* Gerhard Baum, and Dieter Fenske

A major goal in inorganic supramolecular chemistry is the self-assembly of polynuclear coordination arrays through the suitable design of ligands and choice of metal ions in order to generate well-defined architectures in a controlled fashion.[1] In

[*] Prof. Dr. J.-M. Lehn, Dr. G. S. Hanan, Dr. U. S. Schubert, Dr. D. Volkmer
Laboratoire de Chimie Supramoléculaire, Institut Le Bel
Université Louis Pasteur, CNRS URA422
4, rue Blaise Pascal, F-67000 Strasbourg (France)
Fax: Int. code + (388) 41 10 20
e-mail: lehn@chimie.u-strasbg.fr

Prof. Dr. D. Fenske, G. Baum
Institut für Anorganische Chemie der Universität Karlsruhe (Germany)

[**] G. S. H. thanks the NSERC (Canada) for a doctoral fellowship. U. S. S. and D. V. thank the Fonds der Chemischen Industrie and the Alexander-von-Humboldt Foundation, respectively, for postdoctoral fellowships.

 © WILEY-VCH Verlag GmbH, D-69451 Weinheim, 1997 0570-0833/97/3617-1842 $ 17.50+.50/0

addition to the novel physicochemical properties that such entities may present, they are potentially interesting as components of functional nanostructures.

We have recently investigated three fundamental types of metal ion coordination arrays: racks $[n]R$,[2, 3] ladders $[2n]L$,[4] and grids $[m \times n]G$,[5] where the nuclearity of different species is given by $[n]$, $[2n]$, and $[m \times n]$ (n represents the rank) and where the ligand components are oriented more or less orthogonal to each other. Two-dimensional gridlike structures are of particular interest as their architectures may serve as a basis for the construction of information storage devices.[6] Such arrays of metal ions could represent ion dots that might be addressable photo- or electrochemically; they would be of still smaller size than quantum dots[7] and would form spontaneously by self-assembly—microfabrication would therefore not be required.[1]

To form "orthogonal" coordination arrays one may either combine tetrahedrally coordinated metal ions and bidentate ligands (such as 2,2′-bipyridine derivatives)[4, 5] or octahedrally coordinated metal ions and tridentate ligands (such as 2,2′:6′,2″-terpyridine units).[2, 3] For both of these combinations the ligands are arranged in a more or less perpendicular fashion as required for the construction of grid-type complexes. However, by using metal ions presenting octahedral coordination rather than those which prefer a tetrahedral[5, 8] environment, one may expect a wider variety of interesting physical and chemical properties.[9] We describe here the synthesis, characterization, and electrochemical properties of the $[2 \times 2]G$ Co^{II} complexes **1a–c** based on the bis-tridentate ligands **2a–c**.

Ligands **2a–c** were synthesized by Stille cross-coupling reactions between stannyl bipyridines and dichloropyrimidines.[10] The ligands vary in the substitution at the 2-position of the central pyrimidine ring (R = H, Me) and at the 5-position of the terminal pyridine ring (R = H, Me). The steric effect of the substituent in the pyrimidine 2-position was previously shown to influence the relative disposition of ancillary ligands in $[2]R$-diruthenium(II) complexes.[2] The 5-methyl groups on the terminal pyridine ring in **2c** were introduced to allow functionalization of the grid-type structure for incorporation into more complex systems.

Mixing equimolar amounts of cobalt acetate tetrahydrate and ligands **2a**, **2b**, or **2c** in methanol at reflux led to the assembly of the $[2 \times 2]G$ tetracobalt(II) complexes **1a–c** in high yields (typically ranging from 80 to 85% after precipitation as their PF_6^-, AsF_6^-, or SbF_6^- salts). The elemental analyses of **1a–c** indicate a 1:1 ligand-to-metal ratio.

The electrospray mass spectrum of **1b** shows only the peaks from multiply charged cationic species, due to loss of the hexafluorophosphate counteranions. It unequivocally confirms the grid structures in solution, in agreement with data from analytical ultracentrifugation studies.[11]

Slow diffusion of methanol into saturated acetonitrile solutions of the complexes gave crystalline materials. Single crystals of the complex $[Co_4(\mathbf{2b})_4](SbF_6)_8$ of sufficient quality were obtained, and its structure was determined by X-ray crystallography.[12, 13]

The asymmetric unit contains a single cation and eight SbF_6^- counteranions of which two are highly disordered (Figure 1). The complex cation is composed of four ligands **2b** and four cobalt cations arranged in a $[2 \times 2]$-grid-type structure of distorted D_{2d} symmetry. The metal ions lie almost perfectly in a plane (mean deviation of 0.13 Å) and form a slightly distorted square (angles of 88.8–91.4°) with Co,Co distances of 6.41–

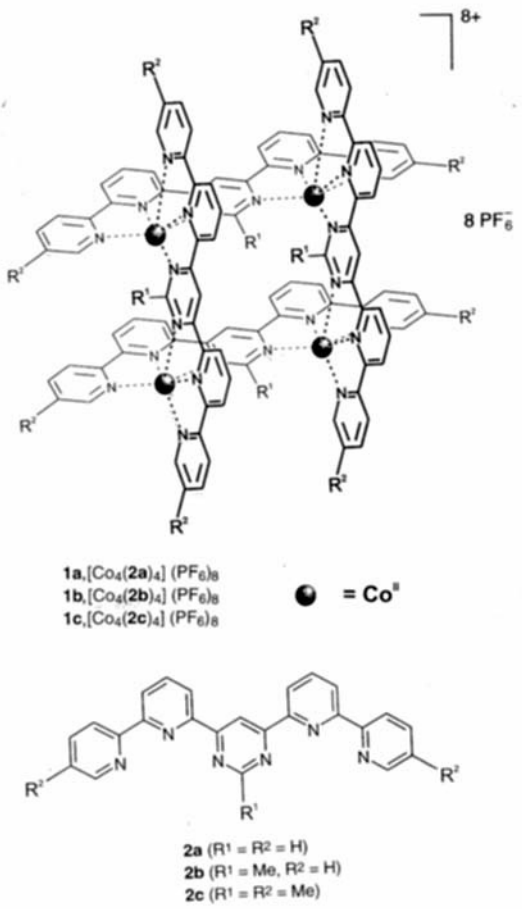

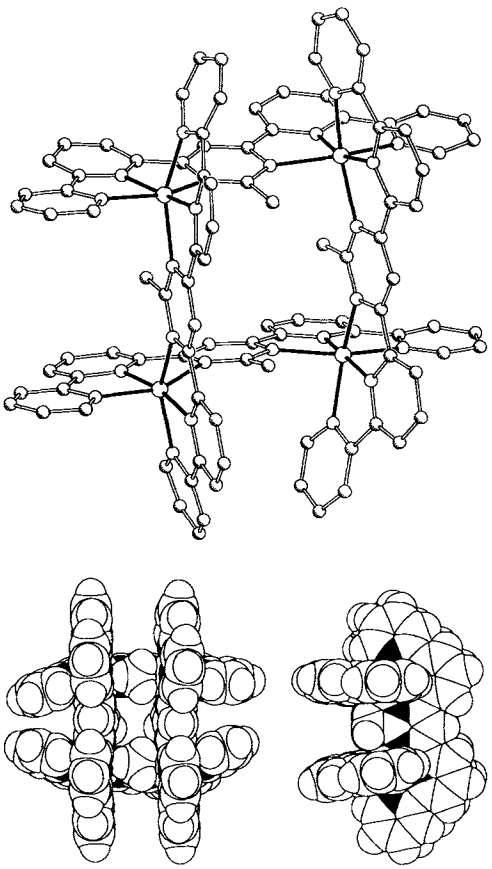

Figure 1. Crystal structure of the tetranuclear $[2 \times 2]$-grid-type complex cation $[Co_4(\mathbf{2b})_4]^{8+}$ of **1b**. Top: ball-and-stick representation (hydrogen atoms omitted for clarity); bottom: two views in space-filling representation.

 © WILEY-VCH Verlag GmbH, D-69451 Weinheim, 1997 0570-0833/97/3617-1843 $ 17.50+.50/0

6.52 Å. They display a distorted octahedral coordination to two perpendicularly oriented ligand fragments. The average Co,N distances are 2.10 (pyridine-N) and 2.23 Å (pyrimidine-N); the average Co,Co distance is 6.35 Å. The complex cation is roughly a parallelipiped with almost parallel walls and dimensions $20 \times 20 \times 14$ Å (total volume 5600 Å^3).

The self-assembly of the [2 × 2]-grids complies with the principle of "maximum coordination site occupation"[1, 14] and may further be rationalized in terms of the appropriate design of the ligand and choice of its dimensional properties, which exclusively lead to the generation of the closed grid structure instead of a coordination polymer. Indeed, the formation of the latter is hindered by the steric repulsion that would arise between the partially overlapping terminal pyridines in the polymeric structure.

The degree of metal–metal interaction in polynuclear complexes is highly dependent on the nature of the bridging ligand.[15] Ligands **2a** and **2b** were previously shown to mediate electronic interactions between the metal ions within [2]*R*-Ru^{II} rack-type complexes.[2, 3] In the present grid complexes, each Co^{II} ion is connected at a distance of 6.5 Å to its two nearest neighbors through the pyrimidine moities, whilst the Co^{II} ion at the opposite corner is farther away (Co$^{II}\cdots$Co^{II}: 9.2 Å).

Interaction between the metal ions may be indicated by the redox properties of the complexes. Complex **1a** undergoes reversible oxidations of the cobalt centers at + 0.46, + 0.66, and + 0,91 V (vs. SCE in DMF).[16] These values are more positive than those found in $[Co^{II}(terpy)_2](PF_6)_2$.[17a] The first four reductions at − 0.14, − 0.24, − 0.44, and − 0.83 V are ascribed to the Co$^{II}\rightarrow$Co^{I} reduction process and occur at a less negative potential than those of $[Co^{II}(terpy)_2](PF_6)_2$[17a] and of a related dinuclear Co^{II} complex of sexipyridine.[17b] The next four reversible one-electron reductions are ascribed to ligand-localized reductions at − 0.83, − 1.09, − 1.33, and − 1.77 V. Complexes **1b** and **1c** also undergo multiple redox processes.[13]

As a first approximation the observed trends in electrochemical behavior may be explained by the high charge of the tetranuclear Co^{II} grids, which—just for electrostatic reasons—makes these complexes easier to reduce than their mononuclear counterparts. In addition, the electronic interactions between the metal ions may make a significant contribution to the altered redox potentials of the Co^{II} ions. Magnetization studies on compound **1b** indicate an antiferromagnetic exchange interaction between the Co^{II} ions.[18]

The UV spectra of the complexes **1a–c** in acetonitrile show broad and highly intense absorption bands at 275 and 345 nm, which may be assigned to nonresolved, ligand-centered (LC) $\pi-\pi^*$ transitions. In the visible region, the broad bands centered between 440–450 nm are assigned to Co^{II}–bipyridine MLCT transitions, and the broad shoulder at about 550 nm could be due to a Co^{II}–pyrimidine MLCT transition.

The present results demonstrate the directed synthesis of [2 × 2]-grid-type coordination arrays of octahedrally coordinated metal ions by a simple, yet efficient self-assembly approach. This approach is general and has been applied to other metal ions to generate grids of Ni^{II}, Zn^{II}, Cd^{II}, and Cu^{II}.[13] The appropriate shape of the ligands ensures a rigid and discrete spacing between the metal ions. The physicochemical properties of complexes **1a–c** indicate that electronic interactions exist between the Co^{II} ions and that coordination arrays of grid type may be suitable building blocks for the construction of molecular information storage devices. For instance, single grids embedded into a highly ordered monolayer might be individualy addressable by altering their redox state with the tip of a scanning–tunneling microscope. Another strategy could be the construction of devices in which the metal ions within the coordination arrays form magnetic domains. Investigations of higher ranking racks, ladders, and grids containing different bridging groups as well as other transition metal ions are being pursued.[19]

Received: February 25, 1997 [Z 10158 IE]
German version: *Angew. Chem.* **1997**, *109*, 1929–1931

Keywords: cobalt · coordination modes · N ligands · supramolecular chemistry · tetranuclearcomplexes

[1] J.-M. Lehn, *Supramolecular Chemistry—Concepts and Perspectives*, VCH, Weinheim, **1995**, chap. 9.
[2] G. S. Hanan, C. R. Arana, J.-M. Lehn, G. Baum, D. Fenske, *Chem. Eur. J.* **1996**, *2*, 1292.
[3] G. S. Hanan, C. R. Arana, J.-M.Lehn, D. Fenske, *Angew. Chem.* **1995**, *107*, 1191; *Angew.Chem. Int. Ed. Engl.* **1995**, *34*, 1122.
[4] P. N. W. Baxter, G. S. Hanan, J.-M. Lehn, *J. Chem. Soc. Chem. Commun.* **1996**, 2019.
[5] P. N. W. Baxter, J.-M. Lehn, J. Fischer, M.-T. Youinou, *Angew. Chem.* **1994**, *106*, 2432; *Angew. Chem. Int. Ed. Engl.* **1994**, *33*, 2284.
[6] J. R. Friedman, M. P. Sarachik, J. Tejada, R. Ziolo, *Phys. Rev. Lett.* **1996**, *76*, 3830.
[7] R. C. Ashoori, *Nature* **1996**, *379*, 413; M. A. Kastner, *Rev. Mod. Phys.* **1992**, *64*, 849.
[8] M.-T. Youinou, N. Rahmouni, J. Fischer, J. A. Osborn, *Angew. Chem.* **1992**, *104*, 771; *Angew. Chem. Int. Ed. Engl.* **1992**, *31*, 733.
[9] Other square inorganic architectures: P. J. Stang, D. H. Cao, S. Saito, A. M. Arif, *J. Am. Chem. Soc.* **1995**, *117*, 6273; M. Fujita, O. Sasaki, T. Mitsuhashi, T. Fujita, J. Yasaki, K.Yamaguchi, K. Ogura, *Chem. Commun.* **1996**, 1535. For a case with octahedral metal centers, see W.-H. Leung, J. Y. K. Cheng, T. S. M. Hun, C.-M. Che, W.-T. Wong, K.-K. Cheung, *Organometallics* **1996**, *15*, 1497.
[10] G. S. Hanan, U. S. Schubert, D. Volkmer, E. Rivière, J.-M. Lehn, N. Kyritsakas, J. Fischer, *Can. J. Chem.* **1997**, *75*, 169.
[11] D. Schubert, J. A. van den Broek, B. Sell, H. Durchschlag, W. Mächtle, U. S. Schubert, J.-M. Lehn, *Progr. Colloid Polym. Sci.*, in press.
[12] Crystal structure analysis of $[Co_4(\mathbf{2b})_4](SbF_6)_8 \cdot 3H_2O \cdot 3.5CH_3CN$: monoclinic, space group $P2_1/c$, $a = 18.205(9)$, $b = 20.566(7)$, $c = 37.126(5)$ Å, $\beta = 97.65(2)^\circ$, $V = 13776(9)$ Å^3, $Z = 4$. Further information on the measurement and refinement together with a detailed structure analysis will be presented elsewhere[13]. The crystal structure of the PF_6^- salt **1b** could not be resolved due to disorder of the cationic part of the structure.
[13] G. S. Hanan, U. S. Schubert, D.Volkmer, J.-M. Lehn, G. Baum, D. Fenske, unpublished.
[14] P. N. W. Baxter, J.-M. Lehn, *Angew. Chem.* **1993**, *105*, 92; *Angew. Chem. Int. Ed. Engl.* **1993**, *32*, 69.
[15] P. J. Steel, *Coord. Chem. Rev.* **1990**, *106*, 227.
[16] The difference in peak potential (ΔE_p) of the oxidation at + 0.66 V is 110 mV, which may be attributed to the close proximity of two one-electron oxidation waves and not to its irreversibility: B. R. Serr, K. A. Andersen, C. M. Elliott, O. P. Anderson, *Inorg. Chem.* **1988**, *27*, 4499.
[17] a) A. Guadalupe, D. A. Usifer, K. T. Potts, H. C. Hurrell, A.-E. Mogstad, H. D. Abruna, *J. Am. Chem. Soc.* **1988**, *110*, 3462; b) K. T. Potts, M. Keshavarz-K., F. S. Tham, H. D. Abruna, C. R. Arana, *Inorg. Chem.* **1993**, *32*, 4436.
[18] O. Waldmann, J. Hassmann, P. Müller, G. S. Hanan, D. Volkmer, U. S. Schubert, J.-M. Lehn, *Phys. Rev. Lett.* **1997**, *78*, 3390.
[19] G. S. Hanan, Dissertation, Université Louis Pasteur, Strasbourg, **1995**; D. Bassani, P. N. W. Baxter, J. Rojo, F. Romero-Salguero, J.-M. Lehn, unpublished work.

 © WILEY-VCH Verlag GmbH, D-69451 Weinheim, 1997 0570-0833/97/3617-1844 $ 17.50+.50/0

Designed Self-Generation of an Extended Helical Structure From an Achiral Polyheterocyclic Strand**

Dario M. Bassani, Jean-Marie Lehn,* Gerhard Baum, and Dieter Fenske

The generation of helical chemical entities requires specific structural and conformational features. The helicity in the molecular chains of proteins and nucleic acids as well as in the supramolecular strands of self-assembled hydrogen-bonded polymers[1] results from the presence of an asymmetrically substituted carbon atom in the backbone components. Numerous organic molecules present helical characteristics.[2] The helicity of self-assembled metal complexes, the helicates, rests on the design of the ligands and on the choice of the coordinating metal ion.[1]

Helicity induction into a molecular or supramolecular strand thus requires encoding of structural and conformational information through suitable design of the components. This is the case for a new structural motif reported recently, that led to the formation of a helical structure from a nonchiral linear molecule.[3] It is based on the preference of 2,2′-bipyridine for a *transoid* conformation[4] and relies on the combination of three basic features: 1) an alternating sequence of pyridine and pyrimidine units, 2) the linkage of these units at specific positions, and 3) the *transoid* conformation adopted by the single bonds linking the units. The combination of these features is illustrated in **A** for a species composed of six alternating pyridine–pyrimidine heterocycles. A molecule of this type (**1**, Scheme 1) adopts a helical structure in solution and in the solid phase.[3] We now report the synthesis and structure elucidation of compound **3**, composed of thirteen alternating pyridine–pyrimidine units. Its preference for the helical conformation **3A** demonstrates the generality of the principle outlined above.

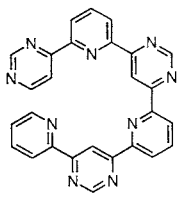

A

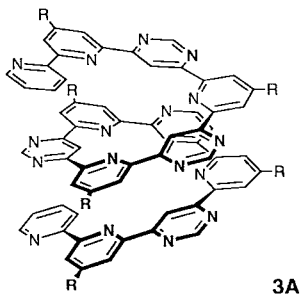

3A

The synthesis of **3** was accomplished by a combination of tin-mediated cross-coupling reactions and Potts's synthesis of 2,6-disubstituted pyridines (Scheme 1).[5] Compound **4** was prepared in three steps from 4,6-dichloropyrimidine and α-ethoxyvinyltributyltin[6] Construction of other symmetrical and unsymmetrical pyridine–pyrimidine sequences, such as **2**, is possible with different combinations of **4**, **5**, and **6**.[7]

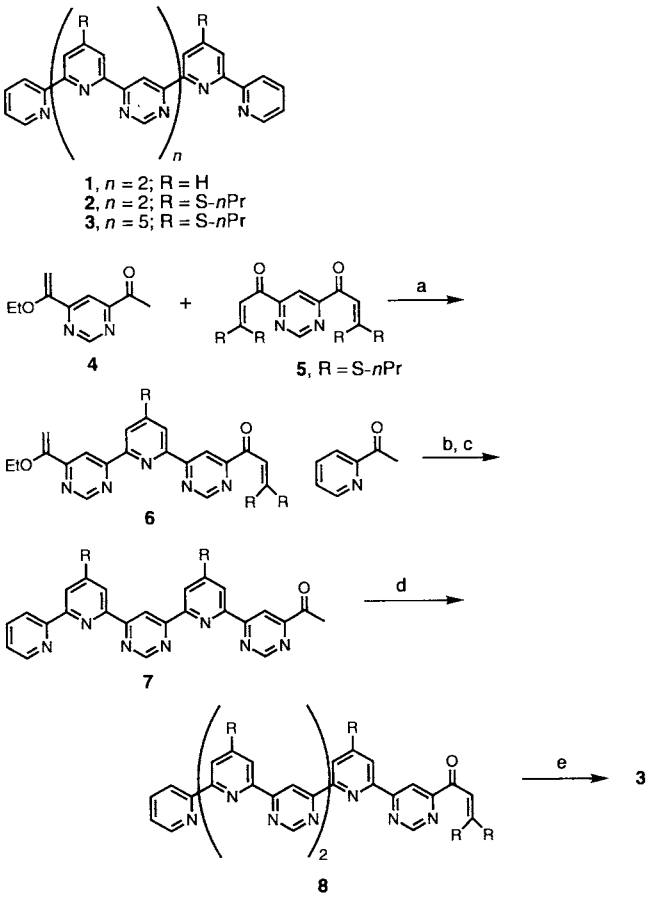

Scheme 1. a) 1. *t*BuOK, DMSO, RT; 2. NH_4OAc (44%). b) 1. *t*BuOK, **6**, THF, RT; 2. NH_4OAc (53%). c) HCl_{aq} (70%). d) 1. *t*BuOK, **5**, THF, RT; 2. NH_4OAc (46%); e) 1. *t*BuOK, **7**, THF (reflux); 2. NH_4OAc (47%).

The use of α-oxoketene dithioacetals in the preparation of **3** has the advantage over other syntheses of substituted pyridines that one of the thioalkyl groups is retained in the incipient pyridine heterocycle after ring closure. Thus, **3** incorporates six thiopropyl side chains, which contribute to its solubility in organic solvents such as chloroform. The presence of substituents in the C-4 position of the pyridines is not expected to interfere with helication, as they are oriented outwards from the helix.

The structure of **3** in solution may be deduced from ^1H NMR studies. The assignments shown in Figure 1 were determined by combining the results from COSY and ROESY NMR experiments. Nevertheless, protons corresponding to the trisubstituted pyridines (H5, H6, H9, H10, H13, and H14) could not be unambiguously assigned. The high upfield shifts observed for the terminal pyridine H2 and H3 are indicative of significant shielding by nearby heterocycles. Strong NOE interactions are observed in the ROESY NMR spectrum between H4 and H8, H8 and H12, and H12 and H16. This is consistent with a helical conformation in which the pyrimidine C5 carbon atoms point towards the interior and the thiopropyl side chains towards the exterior of the helix. The interior cavity is lined alternately with pyridine nitrogen atoms and pyrimidine C–H groups. Such a structure places H2 and H3 above a central pyridine ring, which could account for their significant upfield chemical shifts. It also corresponds to an all-*transoid* conformation about the single bonds connecting the heterocyclic subunits. It is thus assumed that, in solution, **3** adopts the helical conformation **3A** with two turns.

[*] Prof. Dr. J.-M. Lehn, Dr. D. M. Bassani
Laboratoire de Chimie Supramoléculaire, Institut Le Bel
Université Louis Pasteur, CNRS URA 422
4, rue Blaise Pascal, F-67000 Strasbourg (France)
Fax: Int. code + (388) 41 10 20
e-mail: lehn@chimie.u-strasbg.fr
Prof. Dr. D. Fenske, G. Baum
Institut für Anorganische Chemie der Universität Karlsruhe (Germany)

[**] We thank P. Maltèse for the ROESY and COSY NMR experiments. D. M. B. thanks TMR programme of the European Union for financial support.

 © WILEY-VCH Verlag GmbH, D-69451 Weinheim, 1997 0570-0833/97/3617-1845 $ 17.50+.50/0

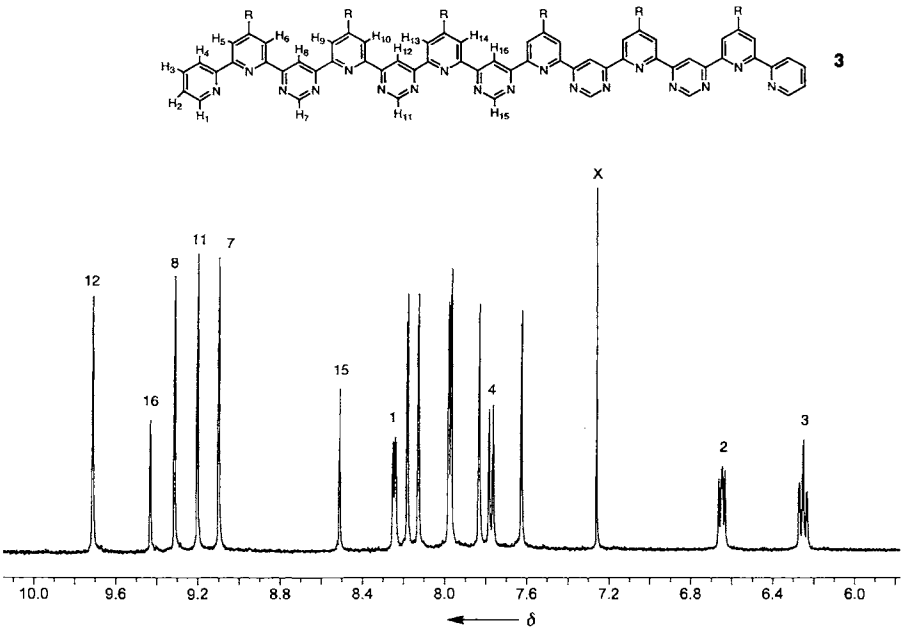

Figure 1. Portion of the 400 MHz ^{1}H NMR spectrum of **3** in $CDCl_3$ showing the signals from aromatic residues. Signal assignment is shown above the relevant peak and was deduced from COSY and ROESY NMR experiments.

Further evidence for the helical nature of **3** is provided by its fluorescence spectrum (Figure 2). The overlap of the pyridine rings gives rise to some rather unusual electronic interactions between the aromatic residues. Thus, upon excitation of dilute

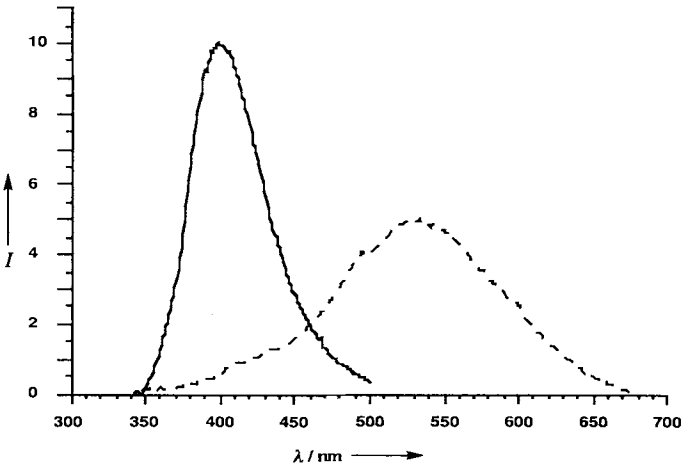

Figure 2. Fluorescence emission spectra of **2** (solid line) and **3** (dashed line) in dichloromethane upon excitation at 280 nm; I = relative intensity ($c \approx 1 \times 10^{-5}$ M).

solutions of **2** in dichloromethane at 280 nm, pyridine-like fluorescence is observed at about 400 nm. However, excitation of **3** under similar conditions results in the observation of a broad, structureless band at 540 nm and only weak residual pyridine fluorescence. The band at longer wavelengths is attributed to emission from intramolecular pyridine excited state dimers (excimers); these dimers result from the self-organized stacking of the pyridine residues in the helix. The lack of excimer fluorescence in **2** despite the overlap of the terminal pyridines may be attributed to an unfavorable geometry, or to their greater mobility because **2** only forms one turn of a helix. Fluorescence emission at 550 nm has been reported to occur in polypyridine polymers and was assigned to excimer formation.[8]

The crystal structure of **3** is shown in Figure 3 (see opposite page) and unambiguously identifies the solid-state structure as helical.[9] The unit cell is centrosymmetric and contains four molecules of **3** (two enantiomeric pairs) and eight molecules of acetonitrile. In the crystal structure the molecules are stacked one above the other along a central axis, thus forming long channels, a feature of interest for ion channel design. Each molecule possesses a twofold rotation axis passing through the central pyrimidine. The pyridine–pyrimidine torsional angles are between 8.0° and 14.0°, whereas the two terminal pyridines are offset by only 3.5°. The structure possesses an interior void of 2.6 Å diameter and a helical pitch of 3.75 Å.

Stabilization of the helical conformation **3A** may also involve favorable aromatic stacking interactions in addition to the preference for a *transoid* geometry about the single bonds.[4] The latter may be attributed to electrostatic repulsion between the nitrogen dipoles and steric repulsion between the CH groups in the *cisoid* conformation. The helical structure adopted by *m*-deciphenyl in the solid state[10] may also result from favorable stacking interactions.

The present results demonstrate the generality of the principle of helicity induction in chains of alternating pyridine–pyrimidine heterocycles. This spontaneous formation of a helical superstructure also represents a molecular self-organization process directed by the structural and conformational information encoded in the polyheterocyclic strand and operating through intramolecular nonbonded interactions, in the same way as supramolecular self-organization is based on intermolecular recognition events and noncovalent interactions.[1] One may envisage combining intra- and intermolecular interactions to induce self-organization of complex chemical architectures on both the molecular and supramolecular levels.

Received: March 3, 1997 [Z10192IE]
German version: *Angew. Chem.* **1997**, *109*, 1931–1933

Keywords: helical structures · heterocycles · self-organization

[1] J.-M. Lehn, *Supramolecular Chemistry*, VCH, Weinheim, **1995**, chap. 9.
[2] K. F. Meurer, F. Vögtle, *Top. Curr. Chem.* **1995**, *127*, 1; R. H. Martin, *Angew. Chem.* **1974**, *86*, 727; *Angew. Chem. Int. Ed. Engl.* **1974**, *13*, 649.
[3] G. S. Hanan, J.-M. Lehn, N. Krytsakas, J. Fisher, *J. Chem. Soc. Chem. Commun.* **1995**, 765.
[4] The planar *transoid* form has been calculated to be 25 kJ mol^{-1} more stable than the *cisoid* (nonplanar) form: S. T. Howard, *J. Am. Chem. Soc.* **1996**, *118*, 10269.
[5] K. T. Potts, M. J. Cipullo, P. Ralli, G. Theodoridis, *J. Org. Chem.* **1982**, *47*, 3027.
[6] A. J. Majeed, Ø. Antonses, T. Benneche, K. Undenheim, *Tetrahedron* **1989**, *45*, 993.
[7] The compounds possess ^{1}H NMR, ^{13}C NMR, and mass spectral data in accord with the structures shown. The detailed synthesis of **2** and **3** will be reported elsewhere.
[8] T. Yamamoto, T. Maruyama, T. Ikeda, M. Sisido, *J. Chem. Soc. Chem. Commun.* **1990**, 1306.

 © WILEY-VCH Verlag GmbH, D-69451 Weinheim, 1997 0570-0833/97/3617-1846 $ 17.50+.50/0

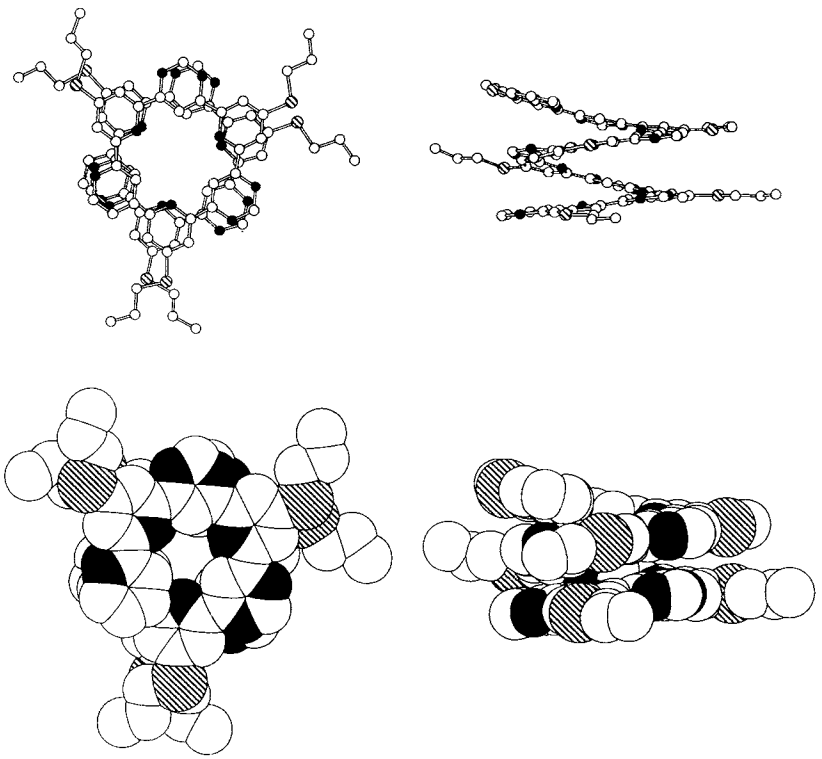

Figure 3. Ball-and-stick (top) and space-filling (bottom) representation of the crystal structure of **3** viewed along the axis (left) and from the side (right); hydrogen atoms omitted for clarity.

[9] Crystal data for **3**: $C_{78}H_{72}N_{18}S_6 \cdot 4CH_3CN$; diffractometer and data collection: STOE IPDS (200 K), graphite-monochromated $Mo_{K\alpha}$ radiation ($\lambda = 0.71073$ Å), monoclinic, space group $C2/c$, $a = 33.748(8)$, $b = 16.836(9)$, $c = 14.665(4)$ Å, $\beta = 106.52(2)°$, $V = 7988(5)$ Å^3, $Z = 4$, $\mu = 0.234$ mm^{-1}, $F(000) = 3400$, $\rho_{calcd} = 1.345$ Mg m^{-3}, $2\theta_{max} = 44°$, $-26 \le h \le 41$, $-20 \le k \le 17$, $-16 \le l \le 15$. Structure solution and refinement: A total of 6498 reflections were collected, 4391 independent [R(int) = 0.0836], of which 3799 were used to fit 413 parameters with 4 restraints. The structure was refined against F^2 (full-matrix least squares), GOF($F^2 = S$) = 1.065, $R1 = 0.1480$ [$R1 = 0.2324$ (all data)], $wR2 = 0.3860$ [$wR2 = 0.4611$ (all data)], max./min. residual density: $+0.896/-0.399$ e Å^{-3}. All atoms in rings (except for central pyrimidine ring) are calculated as pertaining to a regular hexagon. All hydrogen positions are calculated. Crystallographic data (excluding structure factors) for the structure(s) reported in this paper have been deposited with the Cambridge Crystallographic Data Centre as supplementary publication no. CCDC-100400. Copies of the data can be obtained free of charge on application to The Director, CCDC, 12 Union Road, Cambridge CB21EZ, UK (fax: int. code +(1223) 336-033; e-mail: deposit@chemcrys.cam.ac.uk).

[10] D. J. Williams, A. M. Colquhoun, C. A. O'Mahoney, *J. Chem. Soc. Chem. Commun.* **1994**, 1643.

Analysis of the Bonding in $[Ni_5(\mu_5\text{-}S)(\mu_2\text{-}SR)_5]^-$, an Unprecedented Pentanuclear Sulfide Cluster**

Fu-Wah Cheung and Zhenyang Lin*

In the past decade, much progress has been made in the synthetic chemistry of metal chalcogenide clusters.[1-6] These clusters can act as model compounds for the active sites of certain metalloproteins and metal sulfide catalysts.[7] They also exhibit many interesting structural types and bonding modes. Chalcogen atoms in metal chalcogenide clusters can occupy terminal or bridging positions (μ_n, $n = 2$–6). The existence of numerous coordination modes of chalcogenide ligands gives rise to the question whether they are part of the polyhedral framework. In other words, the electronic structures of these clusters is difficult to describe. As Dance and Fisher noted in their review,[1] the diversity of compositions and structures known for metal chalcogenide clusters makes the establishment of a relationship between the observed geometry and bonding theory a true challenge.

Such relationships have been established for boranes and metal carbonyl clusters: in the 1970s, Williams and Wade[8-9] formulated well-known $n+1$ rule, which describes the relationship between the structure of boranes and carboranes and the number of skeletal electrons. Subsequently, Wade and Mingos[9-11] recognized the similarities between the bonding in these main group clusters and that in many transition metal carbonyl clusters. Since then, the geometries of these various clusters have been systematized by a set of rules known collectively as the polyhedral skeletal electron pair theory (PSEPT), which describes the relationship between the skeletal structure and the total number of valence electrons in clusters.[11] Other rules have also been put forward to account for these structural relationships.[12,13] While these rules have proved helpful in understanding the structure and bonding of transition metal carbonyl clusters, they can not readily be extended to metal chalcogenide clusters.[14] For example, the recently synthesized pentagonal cluster **1** formally contains nickel atoms of oxidation state +1.2. A formal nickel oxidation state of +1.6 is found in $[Ni_{20}Se_{12}(SeMe)_{10}]^{2-}$,[3] although this cluster contains similar $Ni_5(\mu_5\text{-}Se)$ structural units. A simple description of the bonding in these compounds was regarded as impossible.[3]

Here we describe a simple bonding model, based on the or-

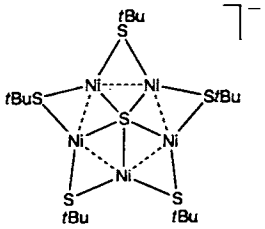

1 $[Ni_5(\mu_5\text{-}S)(\mu_2\text{-}StBu)]^-$

[*] Dr. Z. Lin, F.-W. Cheung
Department of Chemistry
The Hong Kong University of Science and Technology
Clear Water Bay, Kowloon (Hong Kong)
Fax: Int. code +2358-1594
e-mail: chzlin@usthk.ust.hk

[**] This work was supported by the Research Grants Council of Hong Kong. We would like to thank Dr. Virginia Anne Unkefer for carefully reading and checking the manuscript.

 © WILEY-VCH Verlag GmbH, D-69451 Weinheim, 1997 0570-0833/97/3617-1847 $ 17.50+.50/0

bital interaction concept,[15] for the unprecedented pentagonal cluster **1**. We hope that this analysis will serve as a foundation for a similar orbital interaction concept that will explain the bonding situation in all Ni–S and Ni–Se clusters.

On examining the structure of the $[Ni_5S(StBu)_5]^-$ cluster, one can see that each nickel metal atom is bonded to two *tert*-butyl sulfide ligands. In other words, $[Ni_5S(StBu)_5]^-$ can be regarded as being derived from five ML_2 fragments (M = Ni, L = *t*BuS ligand) and a μ_5-S capping atom. The molecular orbitals of an ML_2 fragment are shown in Figure 1a. The frontier orbitals of the fragments that are involved in the metal–metal interaction are depicted with their orbital lobes. Because of the high 3d–4p promotion energy, the contribution of the p_z orbital to the metal–metal bonding is ignored in the following discussion of the orbital interactions for the sake of simplicity. Figure 1b

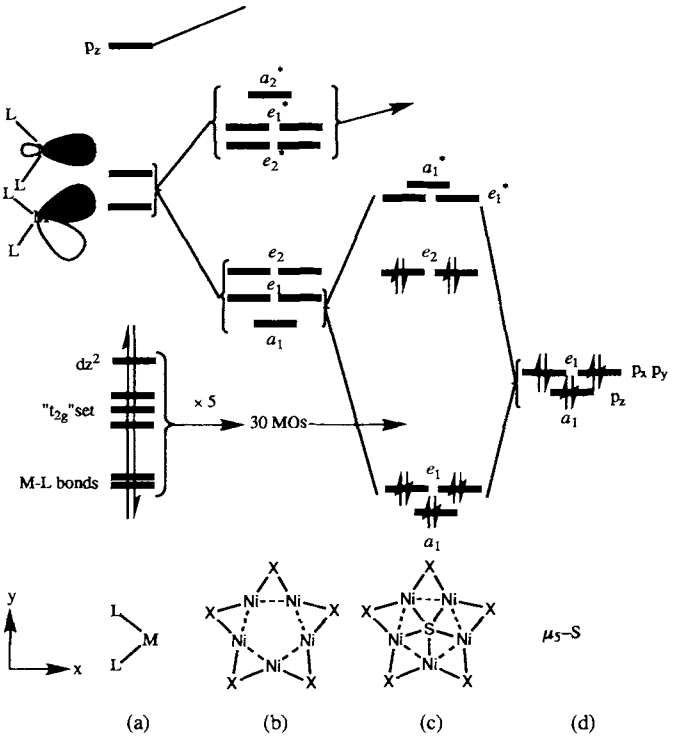

Figure 1. MO diagrams for $[Ni_5S(StBu)_5^-]$ in which *S*t*Bu* groups are represented by X. a) Frontier orbitals of an ML_2 fragment; b) orbitals of Ni_5X_5; c) orbitals of Ni_5SX_5; d) p valence orbitals of the capping μ_5 sulfur atom.

shows the energy levels of the molecular orbitals (MOs) derived from the linear combinations of five ML_2 fragment orbitals. In the lower part of the MO diagram, 30 MOs are derived mainly from the M–L σ bonds (two per fragment)and the t_{2g} and d_{z^2} orbitals. These 30 orbitals are fully occupied and, therefore, their contributions to the metal–metal bonding can be neglected. The interactions of the frontier orbitals of the five fragments gives rise to five bonding ($a_1 + e_1 + e_2$) and five antibonding ($a_2^* + e_1^* + e_2^*$) MOs. The five metal–metal bonding orbitals correspond formally to the five metal–metal edge bonds.

Figure 1c shows the resulting MO energy levels for $[Ni_5(\mu_5\text{-}S)(\mu_2\text{-}StBu)_5]^-$. In the point group C_{5v}, the orbitals of the capping sulfur atom have the transformation properties of $a_1(p_z)$ and $e_1(p_x, p_y)$ symmetries (see Figure 1d). The sulfur p_z orbital is of appropriate symmetry to interact strongly with the a_1 orbital of the pentagonal fragment. Similarly, the p_x and p_y orbitals of sulfur are of appropriate symmetry to interact strongly with the e_1 orbitals. As a result of the interaction between the pentagonal $[Ni_5(\mu_2\text{-}StBu)_5]$ fragment and the capping μ_5-sulfur atom, three ($a_1 + e_1$) of the five metal–metal bonding orbitals stabilize the three p orbitals of the capping sulfur atom, and three additional antibonding orbitals are generated (see Figure 1c). The e_2 orbitals remain nonbonding as there are no orbitals of the same symmetry on the capping atom. A preliminary MO calculation[16] on the model compound $[Ni_5(\mu_5\text{-}S)(\mu_2\text{-}StBu)_5]^-$ showed that the e_2 orbitals are indeed the HOMOs (Figure 2). The HOMO–LUMO gap is 0.28 au, which is remarkably large.

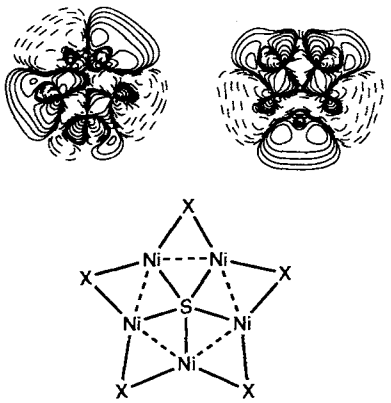

Figure 2. Contour maps of the two HOMOs (e_2) of the $[Ni_5(S(SH)_5]^-$ cluster complex. The contours of the plots decrease by a factor of 1/2, and the lowest contour is 0.000976563.

The $[Ni_5S(StBu)_5]^-$ cluster has 70 valence electrons. Figure 1b shows that the 30 molecular orbitals are completely filled with 60 electrons. These 60 electrons do not take part in $Ni\text{–}S_{capping}$ and M–M interactions. Therefore, ten valence electrons are available for $Ni\text{–}S_{capping}$ and M–M bonding. If these extra ten valence electrons are excluded, one would expect each Ni atom to have a d^8 electron configuration. When the ten valence electrons are added, six electrons are formally assigned to the capping S^{2-} ligand. The remaining four electrons, which occupy the e_2 metal–metal bonding orbitals, should be assigned to the five Ni atoms. Each nickel atom therefore has formally 8.8 d electrons ($d^{8.8}$ configuration), and a formal mean oxidation state of +1.2 can be assigned. As discussed above, because the p_z orbital of each Ni atom is hardly involved in the bonding, the $[Ni_5S(StBu)_5]^-$ cluster actually fulfills the 16-electron rule.

Based on the analysis of $[Ni_5S(StBu)_5]^-$ complex, we can now describe the bonding in the novel selenolato-bridged nickel cluster **2** (Scheme 1).[3] The central unit of the $[Ni_{20}Se_{12}(SeMe)_{10}]^{2-}$ anion is a pentagonal Ni_{10} antiprism in which the two pentagonal faces are capped by two μ_5-Se ligands. The remaining ten nickel atoms form a ten-membered ring that encompasses the pentagonal antiprism and in which the nickel atoms bridge the edges along the prismatic axis. The ten μ_4-Se ligands cap the square faces formed by the Ni_{20} metal core. Five of them are above the ten-membered ring, and the other five are below the ring (see Scheme 1). In such an arrangement, the central antiprismatic unit of the $[Ni_{20}Se_{12}(SeMe)_{10}]^{2-}$ complex can be regarded as a combination of two $[Ni_5(\mu_5\text{-}Se)(\mu_2\text{-}Se)_5]$ units, similar to the above-mentioned $[Ni_5(\mu_5\text{-}S)(\mu_2\text{-}StBu)_5]^-$ complex.

The outer Ni_{10} ring is bridged by ten μ_2-SeMe groups, and therefore each nickel atom in the Ni_{10} ring is coordinated by two $SeMe^-$ and two Se^{2-} ligands in a distorted tetrahedral fashion. If the metal–metal interaction between the two pentagonal

 © WILEY-VCH Verlag GmbH, D-69451 Weinheim, 1997 0570-0833/97/3617-1848 $ 17.50+.50/0

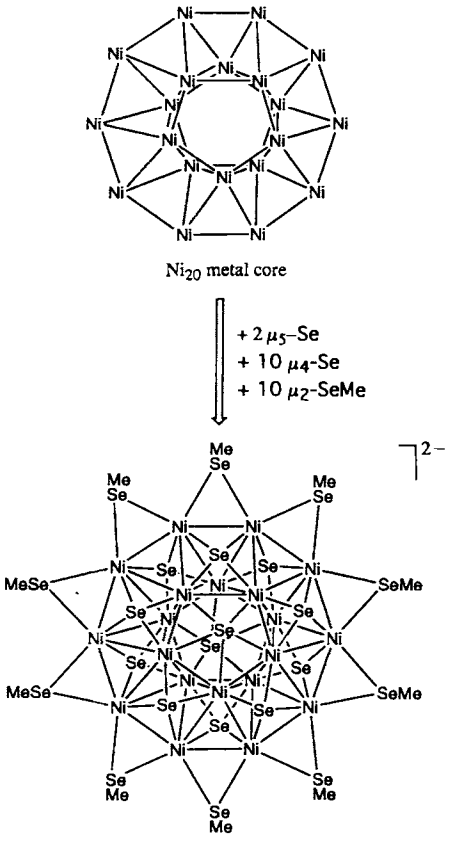

Scheme 1.

units and that between the central Ni_{10} antiprismatic unit and the encompassing ten-membered ring are weak, one would expect that the bonding in the $Ni_5(\mu_5\text{-S})$ unit in the Ni_{20} cluster should be similar to that of the $[Ni_5(\mu_5\text{-S})(\mu_2\text{-S}t\text{Bu})_5]^-$ cluster. In other words, if the three building blocks [two $Ni_5(\mu_5\text{-S})$ units and one Ni_{10} ten-membered ring] are simply connected by the ten μ_4-Se bridging ligands and no metal–metal interactions occur, an oxidation state of +1.2 can be assigned to each Ni atom of the central pentagonal antiprismatic unit. As $[Ni_{20}Se_{12}(SeMe)_{10}]^{2-}$ contains 20 Ni atoms with a total charge of +32, each Ni atom in the ten-membered ring should have a formal oxidation state of +2.0. If we examine the structure of $[Ni_{20}Se_{12}(SeMe)_{10}]^{2-}$ in detail, this bonding description seems quite plausible, as the Ni–Ni distances within each of the two pentagonal $Ni_5(\mu_5\text{-Se})$ units (ca. 2.47 Å) are much shorter than those between the two $Ni_5(\mu_5\text{-Se})$ units (ca. 2.62 Å).[3] The Ni–Ni distances within the Ni_{10} ten-membered ring (ca. 2.57 Å) and between the Ni_{10} ten-membered ring and the two pentagonal $Ni_5(\mu_5\text{-Se})$ units (ca. 2.53 Å) are also noticeably longer. The assignment of a formal oxidation state of +2.0 for each Ni atom in the ten-membered ring is also reasonable, since several trinuclear Ni clusters, for example $[Ni_3S(S\text{Bu})_3(CN)_3]^{2-}$,[6] $[Ni_3S(SMe)_6]^{2-}$,[17] $[Ni_3S(SCH_2C_6H_4CH_2S)_3)^{2-}$,[18] and $[Ni_3S(SPh)_6]^{2-}$,[19] contain tetrahedrally coordinated Ni^{II} centers.

A preliminary ab initio calculation[16] on $[Ni_{20}(\mu_5\text{-Se})_2(\mu_4\text{-Se})_{10}(\mu_2\text{-SeH})_{10}]^-$ gave net atomic charges of +0.12 and +0.23 for the inner Ni atoms [those in the two $Ni_5(\mu_5\text{-Se})$ pentagonal units] and the outer Ni atoms (those in the ten-membered ring), respectively. This result supports the above conclusion that the outer Ni atoms have a higher atomic charge than the inner ones. The bonding similarity between the two $Ni_5(\mu_5\text{-Se})$ pentagonal units of this Ni_{20} cluster and the $[Ni_5(\mu_5\text{-S})(\mu_2\text{-SR})_5]^-$ cluster is also supported by their similar net atomic charges. The net atomic charge of the Ni atoms in the latter is +0.15.

In summary, contrary to the common belief that a simple description of the bonding situation in the Ni–S(Se) clusters is not possible, we have demonstrated that the cluster $[Ni_5S(S\text{Bu})_5]^-$ can be understood in terms of a schematic MO diagram; $[Ni_5S(S\text{Bu}^t)_5]^-$ has a total number of 70 valence electrons and thus obeys the 16-electron rule. Based on the mean oxidation number of nickel atoms in $[Ni_5S(S\text{Bu})_5]^-$, $[Ni_{20}Se_{12}(SeMe)_{10}]^{2-}$ can be regarded as containing ten Ni atoms of oxidation state +1.2 and ten of oxidation state +2. We are now examining other Ni–S(Se) clusters such as $[Ni_5Se_4Cl_2(PEt_2Me)_6]$,[2] $[Ni_8S(SC_4H_9)_9]^-$[5] and $[Ni_{12}(S_2)_6S_8]^{3-}$[20] to determine whether we can find a simple bonding description for them.

Received: January 21, 1997 [Z10017IE]
German version: *Angew. Chem.* **1997**, *109*, 1933–1936

Keywords: bond theory · clusters · mixed-valent compounds · nickel · S ligands

[1] I. Dance, K. Fisher, *Progr. Inorg. Chem.* **1994**, *41*, 637.
[2] D. Fenske, H. Krautscheid, M. Müller, *Angew. Chem.* **1992**, *104*, 309; *Angew. Chem. Int. Ed. Engl.* **1992**, *31*, 321.
[3] D. Fenske, A. Fischer, *Angew. Chem.* **1995**, *107*, 340; *Angew. Chem. Int. Ed. Engl.* **1995**, *34*, 307.
[4] D. Fenske, J. Ohmer, J. Hachgenei, *Angew. Chem.* **1985**, *97*, 993; *Angew. Chem. Int. Ed. Engl.* **1985**, *24*, 993.
[5] T. Krüger, B. Krebs, G. Henkel, *Angew. Chem.* **1989**, *101*, 54; *Angew. Chem. Int. Ed. Engl.* **1989**, *28*, 61.
[6] A. Müller, G. Henkel, *Chem. Commun.* **1996**, 1005.
[7] *The Bioinorganic Chemistry of Nickel* (Ed.: J. R. Lancaster), VCH, Weinheim, **1988**.
[8] R. E. Williams, *Adv. Inorg. Chem. Radiochem.* **1976**, *18*, 67.
[9] K. Wade, *Adv. Inorg. Chem. Radiochem.* **1976**, *18*, 1.
[10] D. M. P. Mingos, *Nature (London) Phys. Sci.* **1972**, *236*, 99.
[11] a) D. M. P. Mingos, R. L. Johnston, *Struct. Bonding (Berlin)* **1987**, *68*, 29; b) D. M. P. Mingos, T. Slee, Z. Lin, *Chem. Rev.* **1990**, *90*, 383.
[12] B. K. Teo, *Inorg. Chem.* **1984**, *23*, 1251.
[13] R. B. King, *Chemical Application of Topological and Graph Theory*, Elsevier, Amsterdam, **1983**.
[14] P. Alemany, R. Hoffmann, *J. Am. Chem. Soc.* **1993**, *115*, 8290.
[15] T. A. Albright, J. K. Burdett, M. H. Whangbo, *Orbital Interactions in Chemistry*, Wiley, New York, **1985**.
[16] Single-point calculations for $[Ni_5(\mu_5\text{-S})(\mu_2\text{-SH})_5]^-$ with the experimentally determined geometry were performed at the Restricted Hartree-Fock level. The basis set used for sulfur and hydrogen atoms was 6-31G*. For the nickel atom, an effective core potential (ECP) with LANL2DZ basis set was employed. For $[Ni_{20}(\mu_5\text{-Se})_2(\mu_4\text{-Se})_{10}(\mu_2\text{-SeH})_{10}]^-$, an ECP with LANL2MB basis set was employed for both Ni and Se atoms.
[17] G. Henkel, M. Kriege, K. Matsumoto, *J. Chem. Soc. Dalton Trans.* **1988**, 657.
[18] W. Tremel, B. Krebs, G. Henkel, *Inorg. Chim. Acta* **1983**, *80*, L31.
[19] K. Matsumoto, H. Nakano, S. Ooi, *Chem. Lett.* **1988**, 828.
[20] C. L. Cahill, K. Tan, R. Novoseller, J. B. Parise, *Chem. Commun.* **1996**, 1677.

 © WILEY-VCH Verlag GmbH, D-69451 Weinheim, 1997 0570-0833/97/3617-1849 $ 17.50+.50/0

A Facile Synthesis of Unusual Liquid-Crystalline Gold(I) Dicarbene Compounds**

Kwang Ming Lee, Ching Kuan Lee, and Ivan J. B. Lin*

Self-assembly of molecules through weak forces such as hydrogen bonds and hydrophobic and electrostatic interactions to form supramolecular aggregates has become a major research area in recent years.[1] While conventional liquid crystals (LC) are one aspect of this subject,[2] metal-containing liquid crystals (metallomesogens, MLCs) provide new possibilities for varying the structure and properties such as color and polarizability.[3] Designing stable MLCs remains a challenge. Many MLCs decompose at the clearing point; their applications are therefore limited. We are interested in the chemistry of gold(I). Gold(I) compounds are used in medicine, they exhibit remarkable photophysical properties, and aurophilic interactions are important in the construction of supramolecules. The above reasons and the inherent thermal stability of metal complexes of 1,3-disubstituted imidazol-2-ylidene (imy) led us to investigate the synthesis of liquid-crystalline bis(1,3-dialkylbenzimidazol-2-ylidene)gold(I) bromide $[\{(C_nH_{2n+1})_2\text{-bimy}\}_2Au]Br$ ($n = 12, 14, 16$).

Gold(I) carbene compounds have been prepared by methods such as addition of alcohols or amines to coordinated isocyanides,[4a,b] carbene transfer from tungsten complexes,[4c] alkylation of gold(I)-2-pyridine or gold(I)-2-thiazole,[4d] and other, unexpected methods.[4e] In these methods, bases such as KO*t*Bu, NaH, or LiBu were used, solvents had to be dried, and reactions had to be carried out under a dry nitrogen atmosphere. Initially, we attempted to synthesize compounds **1** by treating salts of the 1,3-dialkylbenzimidalozolium cation $[(C_nH_{2n+1})_2\text{-bim}]^+$ with AgOAc, NaH, or LiBu in dry THF. However, yields were low, and care had to be taken to avoid extensive decomposition. In the last decade, we have used phase-transfer catalysis (PTC) techniques in the synthesis of metal ylides[5] and the hydrolysis of Pt–dppm compounds (dppm = $Ph_2PCH_2PPh_2$);[6] therefore, the idea of using PTC to synthesize **1** seemed logical. It turns out that PTC is an excellent synthetic route to **1**. Thus treatment of $Au(SMe_2)Cl$ with $[(C_nH_{2n+1})_2\text{-bim}]Br$ ($n = 12, 14, 16$) under PTC/OH^- conditions leads to the formation of **1** in greater than 80% yield.

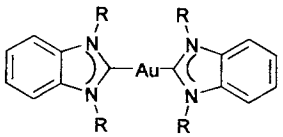

$[((R)_2\text{-bimy})_2Au]Br$ **1** ($R = C_nH_{2n+1}$, $n = 12, 14, 16$),

The structure[7] of cationic $[\{(C_{16}H_{33})_2\text{-bimy}\}_2Au]^+$ is shown in Figure 1. Each molecular cation has four alkyl chains, which are "perpendicular" to the bimy rings and which all point in the same direction. That this must not necessarily be so is illustrated by pyridinium salts[8] and a cyanine dye.[9] If the plane formed by two bimy rings and a gold atom is regarded as a table top, then the molecular geometry of the cation resembles a table with four slightly distorted legs. Each table top forms Br···O bridges, and this results in a herringbone-like arrangement in the plane. Interdigitation of two such planes, with interpenetrating alkyl chains, produces a bilayer of about 22 Å thickness; stacking of bilayers gives a lamellar structure (Figure 2) with a repeating lamellar spacing of about 26 Å and an Au···Au distance of 3.66 Å. Along the normal plane (i.e., along the *c*-axis), the table tops exhibit columnar stacking. Two of the four alkyl chains of a molecular cation are more highly distorted to allow better packing and stronger hydrophobic interations between interpenetrating chains. Structures of gold–bis(imy) com-

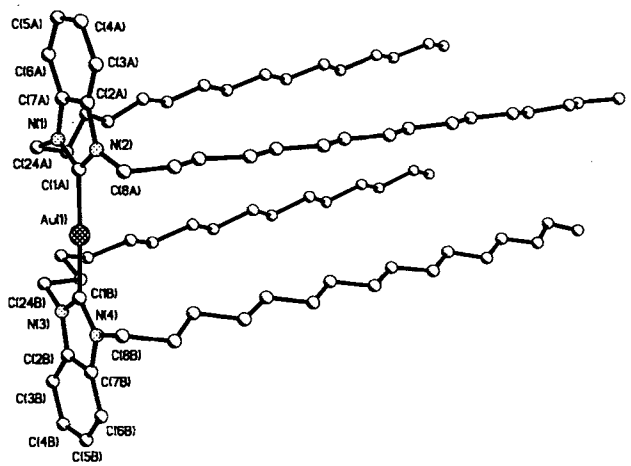

Figure 1. Structure of the cation of **1** ($n = 16$) with partial atom numbering. Hydrogen atoms of the alkyl chains have been omitted for clarity. Selected bond lengths [Å] and angles [°]: Au(1)–C(1A) 2.03(2), Au(1)–C(1B) 2.02(2), N(1)–C(1A) 1.36(2), N(1)–C(7A) 1.40(3), N(2)–C(1A) 1.36(2), N(2)–C(2A) 1.38(2), C(2A)–C(7A) 1.44(3), N(3)–C(1B) 1.35(2), N(3)–C(2B) 1.39(2), N(4)–C(1B) 1.40(2), N(4)–C(7B) 1.40(2), C(2B)–C(7B) 1.43(3); C(1A)-Au(1)-C(1B) 176.5(12), N(1)-C(1A)-N(2) 113(2), C(1A)-N1-C(7A) 101(2), C(1A)-N(2)-C(2A) 109(2), N(1)-C(7A)-C(2A) 113(2), N(2)-C(2A)-C(2A) 104(2), N(3)-C(1B)-N(4) 108(4), C(1B)-N4-C(7B) 109(2), C(1B)-N(3)-C(2B) 109(2), N(4)-C(7B)-C(2B) 105(2), N(3)-C(2B)-C(7B) 108(2)

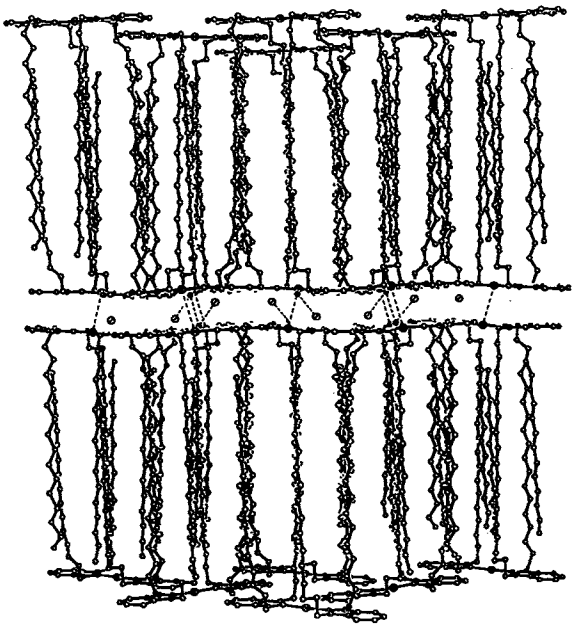

Figure 2. Stacking of the bilayered structure of **1** ($n = 16$).

[*] Prof. Dr. I. J. B. Lin, K. M. Lee, C. K. Lee
Department of Chemistry
Fu-Jen Catholic University
Hsinchuang, Taipei 242 (Taiwan)
Fax: Int. code +(2)902-3209
e-mail: chem1001@fujens.fju.edu.tw

[**] We thank the National Science Council of Taiwan for supporting this work with a research grant (NSC 86-2113-M-030-001).

 © WILEY-VCH Verlag GmbH, D-69451 Weinheim, 1997 0570-0833/97/3617-1850 $ 17.50+.50/0

pounds with short *N*-alkyl chains and Au–Au distances of 3.37 and 3.23 Å have been reported.[10]

Examples of gold(I) MLCs are rare.[11] These gold(I) MLCs require high temperatures for the transition into the liquid-crystalline phase and have narrow mesophase temperature ranges and low thermal stability. In contrast, the ionic gold dicarbenes presented here have relatively low transition temperatures (Table 1, determined by differential scanning calorimetry, DSC)

Table 1. Transition temperatures [°C] of complexes **1** ($n = 12, 14, 16$) [a]; in parentheses: ΔH [kJ mol^{-1}].

n	K		M		I
16	•	102 (118.2)	•	155 (27.1)	•
14	•	93 (100.9)	•	162 (31.1)	•
12	•	92 (48.0)	•	152 (11.4)	•

[a] K: crystalline phase; M: mesophase; I: isotropic liquid.

and high thermal stability. For example, compound **1** ($n = 14$) undergoes the transition from crystal (K) to LC phase at 93 °C (at 76 °C on cooling), and the mesophase has a range of 70 °C; decomposition occurs only above 240 °C. The mesomorphic structure of **1** ($n = 14$) was studied by X-ray diffraction (XRD) and polarized optical microscopy (POM). The XRD spectrum of a nonoriented LC sample is characterized by a series of intense reflections and another set of relatively weak reflections around a diffraction angle 2θ of 9° (Figure 3). The former set of

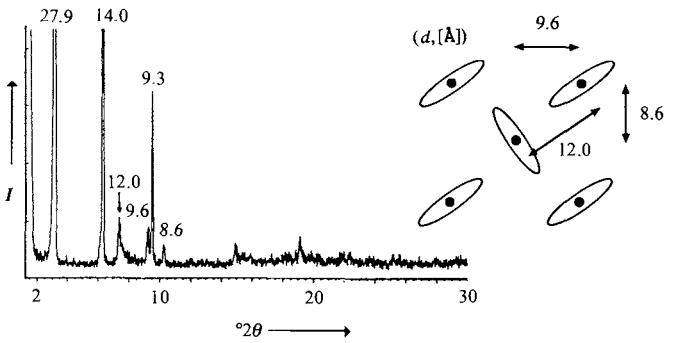

Figure 3. X-ray diffraction spectrum of **1** ($n = 14$) at 120 °C, showing the ordering of repeating layers and the order within the layers. A schematic representation of the latter is also given.

reflections is related to the stacking period of the layers, and the latter set is indicative of ordering of the molecules within the layers. The strong reflections yield a repeating layer distance of 27.9 Å. The three weak reflections at 12.0, 9.6, and 8.6 Å result from the herringbone order in the layers (Figure 3). Therefore, results of XRD investigations suggest that the mesomorphic structure of **1** ($n = 14$) is a layer structure with order in the layers; that is, a lamellar β phase. A POM investigation of the mesophase at 160 °C shows irregularly shaped dendrites, which on further cooling (140 °C) form the mosaic texture (Figure 4) typical for a lamellar β phase. The mesophase deduced from XRD and POM studies is similar to those found for 1,2,ψ,ω-*n*-alkanetetraols.[12]

We have synthesized liquid-crystalline gold dicarbenes under very mild PTC/OH$^-$ conditions. The ease of formation of gold carbene compounds suggests the possible formation of metal carbene compounds under physiological conditions. These thermally stable and highly ordered liquid-crystalline compounds are the first example of gold(I) dicarbene compounds in which a lamellar β mesophase is formed by the unusual interdigitation of long alkyl chains. The formation of this mesophase is the result of a compromise between aromatic π interactions, hydrophobic interactions of alkyl chains, and hydrogen-bonding forces between the anions and C–H hydrogen atoms. Currently we are investigating derivatives of bimy and imy salts with chiral anions or substituted *N*-alkyl chains, to produce ferroelectric systems.

Figure 4. The mosaic texture of **1** ($n = 14$) at 140 °C.

Experimental Section

1 ($n = 16$)·H_2O: $Au(SMe_2)Cl$ (0.10 g, 0.34 mmol) was added to a solution of $[(C_{16}H_{33})_2$-bim]Br (0.44 g, 0.68 mmol) in CH_2Cl_2 (30 mL), followed by cetyltrimethylammonium bromide (0.02 mmol) and aqueous NaOH (0.25 N, 4 mL). After stirring for 5 h, the CH_2Cl_2 solution was separated from water and then added to solution of LiBr (0.12 g, 0.68 mmol) in ethanol (95%, 10 mL), and the resulting mixture was stirred for an additional 30 min. The solvents were removed on a rotary evaporator. The white solid was washed with water several times. Recrystallization from CH_2Cl_2/EtOH (95%), gave a white product in >80% yield. Crystals suitable for single-crystal X-ray diffraction were obtained by slow evaporation from the above solution. Elemental analysis: $C_{78}H_{142}BrN_4OAu$: calcd C 65.67, H 10.02, N 3.92; found C 65.71, H 10.10, N 4.00. ^{1}H NMR (300 MHz, $CDCl_3$, 25 °C, TMS): $\delta = 0.8$ (t, $^3J = 7$ Hz, 12H, CH_3), 1.2–1.4 (m, 104H, CH_2), 2.0 (m, $^3J = 7$ Hz, 8H, CH_2), 4.65 (t, $^3J = 7$ Hz, 8H, CH_2), 7.50 and 7.62 (dd, $^3J = 6$ Hz, $^4J = 3$ Hz, 4H, CH).

1 ($n = 12$): Elemental analysis: $C_{62}H_{110}BrN_4OAu$: calcd C 61.83, H 9.21, N 4.65; found C 62.15, H 8.90, N 4.71. ^{1}H NMR (300 MHz, $CDCl_3$, 25 °C, TMS): $\delta = 0.86$ (t, $^3J = 7$ Hz, 12H, CH_3), 1.20–1.39 (m, 96H, CH_2), 2.0 (m, $^3J = 7$ Hz, 8H, CH_2), 4.64 (t, $^3J = 7$ Hz, 8H, CH_2), 7.49 and 7.62 (dd, $^3J = 6$ Hz, $^4J = 3$ Hz, 4H, CH). **1** ($n = 14$) Elemental analysis: $C_{70}H_{126}BrN_4OAu$: calcd C 63.86, H 9.65, N 4.26; found C 63.89, H 9.66, N 4.31%. ^{1}H NMR (300 M Hz, $CDCl_3$, 25 °C, TMS): $\delta = 0.87$ (t, $^3J = 7$ Hz, 12H, CH_3), 1.20–1.43 (m, 88H, CH_2), 2.03 (m, $^3J = 7$ Hz, 8H, CH_2), 4.65 (t, $^3J = 7$ Hz, 8H, CH_2), 7.50 and 7.61 (dd, $^3J = 6$ Hz, $^4J = 3$ Hz, 4H, CH).

Received: February 8, 1997
Revised version: April 29, 1997 [Z10088IE]
German version: *Angew. Chem.* **1997**, *109*, 1936–1938

Keywords: carbene complexes · gold · liquid crystals · phase-transfer catalysis

[1] J.-M. Lehn, *Supramolecular Chemistry*, VCH, Weinheim, **1995**.
[2] H. Ringsdorf, B. Schlarb, J. Venzmer, *Angew. Chem.* **1988**, *100*, 117; *Angew. Chem. Int. Ed. Engl.* **1988**, *27*, 113.
[3] a) S. A. Hudson, P. M. Maitlis, *Chem. Rev.* **1993**, *93*, 861; b) J. L. Serrano, *Metallomesogens*, VCH, Weinheim, **1996**; c) F. Neve, *Adv. Mater.* **1996**, *8*, 277.
[4] a) J. A. McCleverty, M. M. M. Da Mota, *J. Chem. Soc. Dalton Trans.* **1973**, 2571; b) J. E. Parks, A. L. Balch, *J. Organomet. Chem.* **1973**, *57*, C103; c) R. Aumann, E. O. Fischer, *Chem. Ber.* **1981**, *114*, 1853; d) L. G. Vaughan, *J. Am. Chem. Soc.* **1970**, 730; e) J. F. Britten, C. J. L. Lock, Z. Wang, *Acta Crystallogr. Sect. C* **1992**, *48*, 1600.
[5] a) I. J. B. Lin, C. W. Liu, L.-K. Liu, Y.-S. Wen, *Organometallics* **1992**, 1447; b) I. J. B. Lin, H. I. Shen, *J. Chin. Chem. Soc.* **1992**, 583.
[6] I. J. B. Lin, H. I. Shen, D. F. Feng, *J. Chin. Chem. Soc.* **1995**, 783.
[7] Crystallographic data of **1** ($n = 16$): crystal dimensions $0.5 \times 0.5 \times 0.3$ mm; triclinic; space group $P\bar{1}$ (no. 2); $a = 16.647(7)$, $b = 18.83(2)$, $c = 26.667(8)$ Å, $\alpha = 74.00(3)$, $\beta = 89.57(2)$, $\gamma = 88.97(6)°$, $V = 8035(10)$ Å^3, $Z = 2$, $\mu =$

 © WILEY-VCH Verlag GmbH, D-69451 Weinheim, 1997 0570-0833/97/3617-1851 $ 17.50+.50/0

2.369 mm^{-1}, ρ_{calcd} = 1.179 gcm^{-3}, $1.96 < \theta < 22.5°$. Of 21 609 measured reflections, 20 721 were unique. $R1 = 0.0899$, $wR2 = 0.1652$ (1164 parameters). Data were collected at 293(2) K on a Siemens P4 diffractometer with graphite-monochromatized $Mo_{K\alpha}$ radiation ($\lambda = 0.71073$ Å) in ω scan mode. The structure were solved by the heavy atom method and refined (based on F^2 using all independent data) by full-matrix least-squares methods (Siemens SHELXTL V. 5.03). R values are reported for $R1$ (based on observed data, $I > 2\sigma$) and $wR2$ (based on all data). Non-hydrogen atoms, apart from those of the alkyl chains, were refined with anisotropic thermal parameters. Crystallographic data (excluding structure factors) for the structure reported in this paper have been deposited with the Cambridge Crystallographic Data Centre as supplementary publication no. CCDC-100417. Copies of the data can be obtained free of charge on application to The Director, CCDC, 12 Union Road, Cambridge CB2 1EZ, UK (fax: int. code +(1223)336-033; e-mail: deposit@chemcrys.cam.ac.uk).

[8] K. Vongbupnimit, K. Noguchi, K. Okuyama, *Acta Crystallogr. Sect. C* **1995**, *51*, 1940.

[9] D. L. Smith, H. R. Luss, *Acta Crystallogr. Sect. B* **1972**, *28*, 2793.

[10] J. F. Britten, C. J. L. Lock, Z. Wang, *Acta Crystallogr. Sect. C* **1992**, *48*, 1600.

[11] a) T. Kaharu, R. Ishii, S. Takahashi, *J. Chem. Soc. Chem. Commun.* **1994**, 1349; b) R. Ishii, T. Kaharu, N. Pirio, S.-W. Zhang, S. Takahashi, *ibid.* **1995**, 1215; c) M. Benouazzane, S. Coco, P. Espinet, J. M. Martin-Alvarez, *J. Mater. Chem.* **1995**, *5*, 441; d) J. Barbera, A. Elduque, R. Gimenez, L. A. Oro, J. L. Serrano, *Angew. Chem.* **1996**, *108*, 3048; *Angew. Chem. Int. Ed. Engl.* **1996**, *35*, 2832, and references therein.

[12] F. Hentrich, S. Diele, C. Tschierske, *Liq. Cryst.* **1994**, *17*, 827.

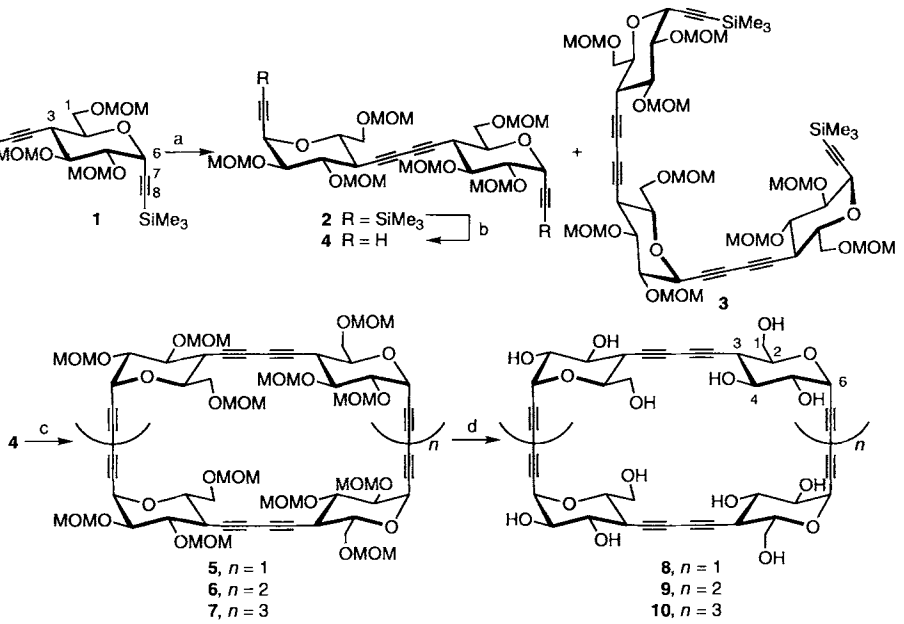

Scheme 1. Synthesis of the cyclotetramer **8**. a) CuCl, pyridine, O_2, **2** (83%), **3** (9%); b) NaOMe, MeOH, THF, 98%; c) $Cu(OAc)_2$, pyridine, **5** (68%), **6** (7%), **7** (1.8%); d) HCl, MeOH, **8** (91%); **9** (94%); **10** (81%).

Cyclic "Acetylenosaccharides"—Novel Cyclodextrin Analogues**

Roland Bürli and Andrea Vasella*

Analogues of cyclodextrins (CDs) with a designed shape, size, and electrostatic potential of the cavity are of interest as specific host molecules. An incisive change of the cavity of the CDs is attained, for example, by changing the configuration and/or the conformation of the repetitive unit.[2] Substitution of one or several of these units by non-saccharide moieties also leads to a profound change of the cavity, as demonstrated by the "glycophanes".[3]

Diethynylated carbohydrates in which the angle between the ethynyl substituents is lower than 180° are potential building blocks for the preparation of cyclic "acetylenosaccharides".[4] A large number of such monomeric building blocks is conceptually available by changing the constitution (position of the ethynyl substituents, pyranose or furanose form, mono- or oligosaccharide) and/or the configuration. Several coupling steps are required for the preparation of cyclic "acetylenosaccharides" from a given monomer; homo- and/or heterocoupling leads to constitutional isomers of a specific ring size. 1,4-*cis*-Diethynylated glucopyranose derivatives should lead to cyclodextrin analogues;[5] this monomer has the same configuration as the repetitive unit of the CDs and is connected at the same positions of the tetrahydropyrane units, albeit by butadiyne units.

An efficient synthesis of the D_2-symmetric cyclotetramer **8**, which is prepared by homocoupling the 1,4-*cis*-diethynylated glucopyranose **1**, is presented in Scheme 1. Two additional macrocycles, the D_3-symmetric cyclohexamer **9** and the D_4-symmetric cyclooctamer **10** were isolated as by-products.

The readily available[5] mono-*C*-silylated dialkyne **1**[1] was converted to the butadiyne **2** in a yield of 83% by homocoupling under Glaser conditions;[6] the trimer **3** was isolated as a by-product (9%). Base-catalyzed desilylation of the dimer **2** led to the butadiyne derivative **4**, which was added to a solution of $Cu(OAc)_2$ in pyridine over a period of 10 h; separation by chromatography of the cyclooligomers (**5** (68%), **6** (7%), and **7** (1.8%)) and subsequent deprotection with HCl in methanol led to the cyclotetramer **8**, the cyclohexamer **9**, and the cyclooctamer **10**. The ^{1}H and ^{13}C NMR spectra of the macrocycles **8**, **9**, and **10** show signals for one monomeric unit only, as expected for the D_n symmetry. The molecular weights of **8**, **9**, and **10** were determined by mass spectrometry. The NMR spectra are very similar to each other; this finding and the mass spectra data indicate that the octamer **10** is not a catenane.[7]

The chemical shift (^{1}H NMR, D_2O) for the C*H* signals of the cyclotetramer **8** does not significantly depend on the concentration (0.1 mM $< [8] <$ 1 mM), suggesting that **8** does not strongly self-assemble in water. Similarly as for the CDs, the solubility[8] of the macrocycles **8**, **9**, and **10** in water depends strongly on their size. Thus, the concentration of a saturated solution of the tetramer **8** is 3.1 mM, while that of the hexamer **9** rises to 117 mM and that of the octamer **10** drops to 2.8 mM. Remarkably, a suspension of the cyclooctamer **10** in methanol forms a gel upon ultrasonication. The smaller homologues, **8** and **9**, do not show a similar tendency towards gelation.

The cyclotetramer **8** crystallized as needles from a mixture of H_2O, methanol, and diethyl ether. In spite of the small size of the crystals, the structure of **8**, albeit only isotropically refined,

[*] Prof. Dr. A. Vasella, Dipl.-Chem. R. Bürli
Laboratorium für Organische Chemie
ETH-Zentrum
Universitätstrasse 16, CH-8092 Zürich (Switzerland)
Fax: Int. code +(1) 632 11 36
e-mail: vasella@sugar.org.chem.ethz.ch

[**] Oligosaccharide Analogues of Polysaccharides Part 13. We thank the Swiss National Science Foundation and F. Hoffmann-La Roche AG, Basel, for generous support, and Dr. B. Schweizer for the X-ray analysis. Part 12: ref. [1].

was determined by X-ray analysis.[9] The unit cell consists of two independent molecules. As expected from MM3* calculations, the butadiyne groups are not in one plane. The average distances between the four butadiyne groups (7.4 and 11.4 Å) correspond approximately to the expected values (MM3: 7.8 and 11.2 Å). There are five molecules of water in the cavity of the cyclotetramer and one outside of it. The molecules of **8** are stacked to form antiparallel tubes (Figure 1).

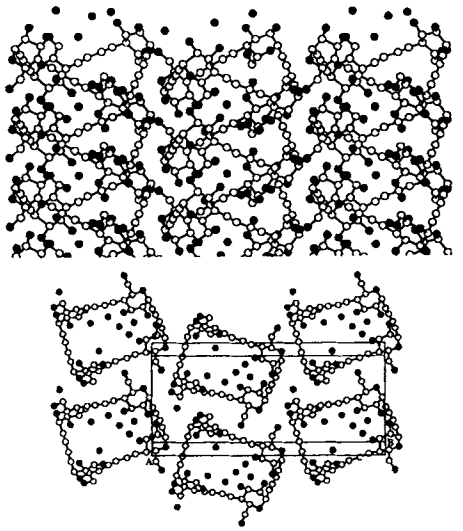

Figure 1. Crystal structure of the cyclotetramer **8**. Top: Side view; bottom: plan view.

The cyclotetramer **8** binds adenosine in aqueous solution. We determined the dissociation constants and the binding free energies of **8** with D- and L-adenosine[10] by ^{1}H NMR spectroscopic titrations in D_2O (Table 1).[11] The high-field shift of the signal of C(2)-H upon addition of adenosine suggested that the aromatic part of adenosine is bound in the cavity of **8**, while the ribosyl moiety is still solvated. This is supported by the fact that the free energies of binding for the complexes between D- and L-adenosine with **8** do not differ significantly.

Table 1. Association constants K_a and binding free energies $-\Delta G°$ from ^{1}H NMR binding titrations for 1:1 complexes of **8** with D- and L-adenosine at 296 K in D_2O [a].

Guest	K_a [L mol^{-1}]	$-\Delta G°$ [kcal mol^{-1}]	Degree of saturation [%]
D-adenosine	40	2.1	70
L-adenosine	32	2.0	66

[a] Titrations in buffered D_2O solutions (pD = 6.8, $[K_2DPO_4] = [KD_2PO_4]$ = 1.35 mM) at constant ion-strength ([NaCl] = 1.35 mM); [**8**] = 1 mM, [guest] varied. The association constants were obtained by nonlinear least-squares curve fitting of the titration data [12]. Accuracy of the K_a values is about ±12%.

Experimental Section

Treatment of **4** with $Cu(OAc)_2$ in pyridine: A solution of **4** (1.32 g, 2.01 mmol) in pyridine (10 mL) was added over a period of 10 h to a solution of $Cu(OAc)_2$ (18.3 g, 0.1 mol) in pyridine (1.45 L) at 50°C under N_2. The mixture was stirred for 19 h and then the solvent was evaporated. The residue was suspended in AcOEt and a saturated aqueous NH_4Cl solution was added. The solids were filtered off and washed with AcOEt. The aqueous layer was extracted (3 × AcOEt). The organic layers were dried ($MgSO_4$) and the solvent was evaporated. Chromatographic purification of the crude product (toluene/AcOEt 9/1 → 4/1) gave **5** (0.894 g, 68%), **6** (90 mg, 7%), and **7** (24 mg, 1.8%) as colorless solids.

5: R_f: 0.30 (toluene/AcOEt 2/3 (v/v)); m.p. 106–107.5°C; $[\alpha]_D^{25} = 152.7$ ($c = 0.48$, $CHCl_3$); ^{1}H NMR (200 MHz, $CDCl_3$; coupling constants in Hz): $\delta = 5.09$ (br. d, $J = 5.8$, 1H; H-6), 4.96 (br. d, $J = 6.7$, 1H; MeOCH), 4.85 (br. d, $J = 6.7$, 1H; MeOCH), 4.77 (br. d, $J = 7.1$, 1H; MeOCH), 4.70 (br. d, $J \approx 7.1$, 1H; MeOCH), 4.68 (s, 2H; $MeOCH_2$), 4.10 (br. ddd, $J \approx 1.8$, 4.0, 10.5, 1H; H-2), 3.93 (br. t, $J \approx 10.0$, 1H; H-4), 3.91 (br. dd, $J \approx 4.0$, 11.2, 1H; H-1), 3.81 (br. dd, $J \approx 1.8$, 11.2, 1H; H′-1), 3.55 (dd, $J = 5.8$, 9.6, 1H; H-5), 3.52 (s, 3H; CH_3O), 3.40 (s, 6H; 2 CH_3O), 2.93 (br. t, $J \approx 10.4$, 1H; H-3); ^{13}C NMR (50 MHz, $CDCl_3$): δ = 98.51, 97.97, 96.98 (3 t, 3 $MeOCH_2$), 78.80, 76.23 (2 d, C-4, C-5), 74.99, 74.80 (2 s, 2 $C\equiv C$), 73.65 (d, C-2), 72.99 (s, $C\equiv C$), 69.28 (d, C-6), 68.67 (s, $C\equiv C$), 66.74 (t, C-1), 56.45, 56.32, 55.44 (3 q, 3 CH_3O), 37.44 (d, C-3); MALDI-MS: 1327 ($[M + Na]^+$); elemental analysis: calcd for $C_{64}H_{88}O_{28}$: C 58.89, H 6.79; found: C 59.05, H 6.70.

6: R_f: 0.17 (toluene/AcOEt 3/7 (v/v)); MALDI-MS: 1979 ($[M + Na]^+$).

7: R_f: 0.17 (toluene/AcOEt 1/4 (v/v)); MALDI-MS: 2631 ($[M + Na]^+$); FAB-MS: 2609 (37, $[M + H]^+$), 2502 (41), 2426 (62), 2350 (94), 2274 (100), 2230 (72), 2198 (57), 2122 (36).

8: A solution of **5** (70 mg, 54 mmol) in 0.1 M HCl in MeOH (5 mL) was stirred at 50°C for 22 h and the solvent was then evaporated. Recrystallization (Et_2O, MeOH, H_2O) of the crude product gave **8** (40 mg, 91%) as a colorless solid. m.p. >225.0°C (decomp); ^{1}H NMR (500 MHz, [D$_6$]DMSO; coupling constants in Hz): $\delta = 5.60$ (d, $J = 4.8$, exchange with D_2O, 1H; HO-5), 5.51 (d, $J = 6.3$, exchange with D_2O, 1H; HO-4), 4.85 (t, $J = 5.5$, exchange with D_2O, 1H; HO-1), 4.84 (d, $J = 5.8$, 1H; H-6), 3.71 (ddd, $J = 1.7$, 4.6, 10.5, H-2), 3.65 (br. ddd, $J \approx 1.7$, 5.3, 11.7, addition of D_2O → br. dd, $J \approx 1.7$, 11.5, 1H; H-1), 3.55 (br. ddd, $J \approx 4.5$, 5.9, 11.6, addition of D_2O → br. dd, $J \approx 4.7$, 11.7, 1H; H′-1), 3.50 (br. dt, $J \approx 6.4$, 9.8, addition of D_2O → br. t, $J \approx 9.9$, 1H; H-4), 3.27 (br. ddd, $J \approx 4.9$, 5.9, 9.5, addition of D_2O → dd, $J = 5.7$, 9.3, 1H; H-5), 2.51 (br. t, $J \approx 10.4$, 1H; H-3); ^{13}C NMR (100 MHz, [D$_6$]DMSO): δ = 76.38, 75.94 (2 s, 2 $C\equiv C$), 75.41 (d, C-2), 71.77 (d, C-4), 71.28 (s, $C\equiv C$), 70.81 (d, C-5), 68.92 (d, C-6), 67.48 (s, $C\equiv C$), 61.82 (t, C-1), 37.73 (d, C-3); MALDI-MS: 799 ($[M + Na]^+$); elemental analysis: calcd for $C_{40}H_{40}O_{16} \cdot 2H_2O$: C 59.11, H 5.46; found: C 59.07, H 5.63.

Received: March 22, 1997 [Z 10271 IE]
German version: *Angew. Chem.* **1997**, *109*, 1945–1946

Keywords: acetylenosaccharides · alkynes · cyclodextrins · host–guest chemistry · structure elucidation

[1] R. Bürli, A. Vasella, *Helv. Chim. Acta* **1997**, *80*, 1027–1052.
[2] An overview of cyclodextrin analogues with modified cavities is given in: P. R. Ashton, C. L. Brown, S. Mezner, S. A. Nepogodiev, J. F. Stoddart, D. J. Williams, *Chem. Eur. J.* **1996**, *2*, 580–591.
[3] a) R. R. Bukownik, C. S. Wilcox, *J. Org. Chem.* **1988**, *53*, 463–471; b) S. Penadés, J. M. Coterón, *J. Chem. Soc. Chem. Commun.* **1992**, 683–684; c) J. M. Coterón, C. Vicent, C. Bosso, S. Penadés, *J. Am. Chem. Soc.* **1993**, *115*, 10066–10076.
[4] For leading references on "acetylenosaccharides": a) J. Alzeer, C. Cai, A. Vasella, *Helv. Chim. Acta* **1995**, *78*, 242–265; b) J. Alzeer, A. Vasella, *ibid.* **1995**, *78*, 177–193; c) *ibid.* **1995**, *78*, 1219–1237; d) C. Cai, A. Vasella, *ibid.* **1996**, *79*, 255–268; e) A. Ernst, A. Vasella, *ibid.* **1996**, *79*, 1279–1294.
[5] R. Bürli, A. Vasella, *Helv. Chim. Acta* **1996**, *79*, 1159–1168.
[6] C. Glaser, *Ber. Dtsch. Chem. Ges.* **1869**, *2*, 422–424.
[7] The mass spectrum (FAB) of the protected octamer **7** shows no signal at half the molecular mass.
[8] Determination of the solubility of **8**, **9**, and **10** in water. A specified volume of a saturated solution was lyophilized and dried. The residue was weighed. Accuracy of the values: about ±10%.
[9] X-ray analysis of **8**: $C_{40}H_{40}O_{16} \cdot 6H_2O$, $M_r = 884.81$, 0.07 × 0.02 × 0.02 mm, $a = 6.651(4)$, $b = 27.655(7)$, $c = 11.682(7)$ Å, $\beta = 103.50(5)°$, $V = 2090.1$ Å^3, $Z = 2$, space group $P2_1$, $\rho_{calcd} = 1.403$ g cm^{-3}, $F(000) = 932$. Data collection at $T = 293$ K with $Cu_{K\alpha}$ radiation (graphite monochromator, $\lambda = 1.54184$ Å); $\omega/2\theta$ scan; 4080 collected reflections, 3194 independent reflections, of which 1237 $> 3\sigma(I)$; $R_1 = 0.1289$, $wR_2 = 0.2869$. Refinement of the non-hydrogen atoms with the least squares method on F^2 with SHELXL-92 (G. Sheldrick, Göttingen, **1993**). Hydrogen atoms were calculated in ideal positions. The ratio of reflections to parameters did not allow an anisotropic refinement. For *one* molecule of water two positions are given.
[10] We thank Dr. S. Pitsch, Laboratorium für Organische Chemie der ETH Zürich, for a sample of L-adenosine.
[11] A Job-Plot showed, that **8** binds to D-adenosine mainly in a 1:1 complex. a) P. Job, *Ann. Chim. Ser.* **1928**, *9*, 113–134; b) M. T. Blanda, J. H. Horner, M. Newcomb, *J. Org. Chem.* **1989**, *54*, 4626–4636.
[12] B. Peterson, PhD thesis, University of California, Los Angeles, **1994**.

 © WILEY-VCH Verlag GmbH, D-69451 Weinheim, 1997 0570-0833/97/3617-1853 $ 17.50+.50/0

Organometallic Chemistry under Hydro(solvo)thermal conditions: Synthesis and X-ray structure of $(Ph_4P)_2[Mn_3(CO)_9(S_2)_2(SH)]$, $(Ph_4P)[Mn_2(CO)_6(SH)_3]$, and $(Ph_4P)_2[Mn_4(CO)_{13}(Te_2)_3]$**

Songping D. Huang,* Chunqiu P. Lai, and Charles L. Barnes

Hydrothermal, or more generally, hydro(solvo)thermal syntheses may be defined as chemical reactions carried out in superheated water or organic solvents at sub-, near, or supercritical conditions.[1-3] The rapid transport ability of the solvent under such conditions often leads directly to crystal growth of the product similar to the formation of many mineral crystals in nature.[4] Thus far, the hydro(solvo)thermal synthesis has found numerous applications in solid-state chemistry and materials science.[5-6] Use of a similar concept to carry out organometallic reactions in sealed ampoules or autoclaves at elevated pressures and temperatures has opened up a new avenue for organometallic cluster chemistry.[7-8] In this report, we describe three novel cluster compounds **1**–**3**, obtained from

$(Ph_4P)_2[Mn_3(CO)_9(S_2)_2(SH)]$ **1**

$(Ph_4P)[Mn_2(CO)_6(SH)_3]$ **2**

$(Ph_4P)_2[Mn_4(CO)_{13}(Te_2)_3]$ **3**

ethanothermal synthesis. The formation of these compounds provides insight into the reaction pathways dictated by the solvent under the solvothermal conditions.

The reaction of $[Mn_2(CO)_{10}]$ with Na_2S_2 and ethanol in the molar ratio 1:4:80 in a sealed tube at 85 °C for 1.5 h gave **1**. When the same reaction was carried out for 80 hours, **2** was obtained. Compound **3** was synthesized analogously from the reaction of $[Mn_2(CO)_{10}]$ with Na_2Te_2 and ethanol in the molar ratio 1:2:50 (Scheme 1). The structures of **1**, **2**, and **3** were determined by single-crystal X-ray analyses.[9] The $[Mn_3(CO)_9(S_2)_2(SH)]^{2-}$ anion in **1** contains a triangle of Mn atoms bridged by two disulfide S_2^{2-} and a hydrosulfide HS^- ligand (Figure 1). The two disulfide ligands adopt different coordination modes: one is μ_3-η^1,η^1,η^1-bridging and the other μ_3-η^1,η^1,η^2-bridging. The hydrosulfide acts as a μ_2-ligand. The H atom on the monosulfide could not be located from the difference Fourier electron density map of the X-ray diffraction data. Its presence is implied by other experimental evidence (vide infra). The cluster possesses idealized C_s molecular symmetry with the mirror plane through O8/C8/Mn3/S5/S4/S1/H1. Each Mn atom is coordinated to three S atoms and three *cis* CO groups in an approximately octahedral environment. The observed Mn–Mn distances [3.523(1)–4.048(1) Å] preclude any metal–metal bonding. All Mn atoms are assigned a formal oxidation state of +I. The average Mn–S bond length of 2.372(7) Å is comparable to those of 2.34–2.38 Å found in $[Mn_4(S_2)_2(CO)_{15}]$.[10] The S–S distances of 2.076(2) and 2.055(3) Å can be considered normal single bonds.[11]

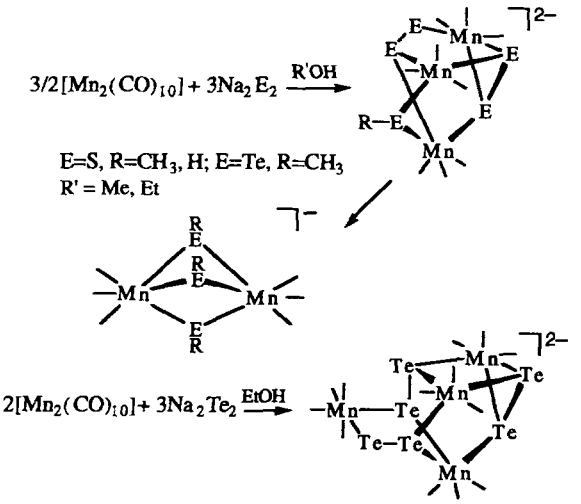

Scheme 1. Synthesis of the cluster anions 1–3.

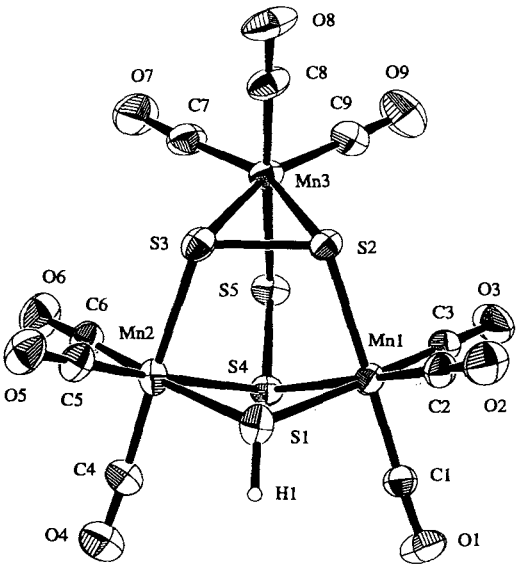

Figure 1. ORTEP representation of the structure of $[Mn_3(CO)_9(S_2)_2(SH)]^{2-}$. Selected bond lengths [Å] and bond angles [°]: Mn1–S1 2.408(2), Mn1–S1 2.402(2), Mn1–S2 2.372(2), Mn1–S4 2.349(2), S2–S3 2.076(2), S4–S5 2.055(3) Å; S1-Mn1-S2 88.10(7), S1-Mn1-S2 79.68(6), Mn1-S4-Mn2 96.82(6).

The $[Mn_2(CO)_6(SH)_3]^{2-}$ anion in **2** (Figure 2) is formed by two Mn^I centers bridged by three μ_2-HS^- ligands. The octahedral coordination of each of the Mn atoms is completed by three *cis* CO groups. Atom S1 is situated on the crystallographic twofold axis, which causes positional disorder of the attached H atom. Thanks to the high quality X-ray data collected at low temperature with the SMART diffractometer, both H1 and H2 atoms were located from the difference Fourier electron density map. The S–H bond lengths and bond angles were refined satisfactorily. Furthermore, three weak peaks at 2527, 2495, and 2478 cm^{-1} found in the FT-IR spectrum are attributable to the bridging ν(S–H) vibrations.[12] The molecule approaches D_{3h} symmetry if the H atoms are omitted. The Mn–Mn distance of

[*] Prof. S. D. Huang, C. P. Lai
Department of Chemistry
University of Puerto Rico
San Juan, PR 00931 (USA)
Fax: Int. code +(787)281-7349
e-mail: huang@zintl.chem.uprr.pr
Dr. C. L. Barnes
Department of Chemistry
University of Missouri-Columbia (USA)

[**] This work was supported by the U. S. National Science Foundation and Department of Energy Through the EPSCoR Programs (OSR-9452893 and DE-FC02-91ER75674). We thank Dr. Charles F. Campana of Siemens Analytical X-ray Instruments, Madison, WI (USA) for collecting the low-temperature X-ray diffraction data for 2.

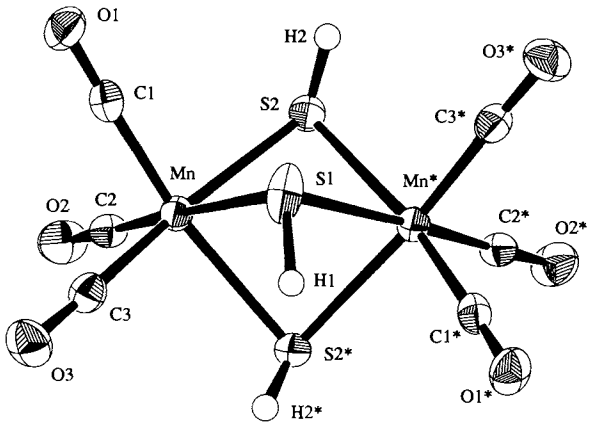

Figure 2. ORTEP representation of the structure of $[Mn_2(CO)_6(SH)_3]^-$. Selected bond lengths [Å] and bond angles [°]: Mn–S1 2.3978(9), Mn–S1 2.4091(7) or 2.4176(7), S1–H1 1.38(5), S2–H2 1.15(5) Å; S1-Mn-S2 81.51(2) or 81.33(2), S2-Mn-S2 82.47(3), Mn-S1-H1 111(2) or 99(2), Mn-S2-H2 117(2) or 99(2).

3.154(1) Å suggests no metal–metal bonding interactions. The average Mn–S bond distance of 2.408(6) Å is slightly longer than that in **1**.

Figure 3 is the ORTEP representation of the $[Mn_4(CO)_{13}(Te_2)_3]^{2-}$ anion in **3**. It consists of an $Mn(CO)_4$ and three Mn-

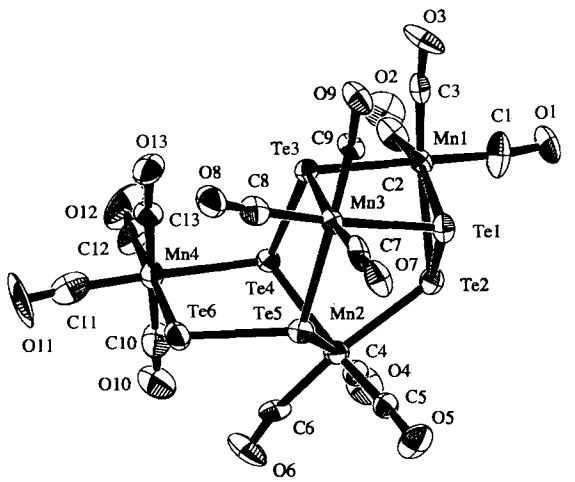

Figure 3. ORTEP representation of the structure of $[Mn_4(CO)_{13}(Te_2)_3]^{2-}$. Selected bond lengths [Å] and bond angles [°]: Te1–Mn1 2.684(4), Te3–Mn1 2.643(4), Te5–Mn2 2.662(4), Te6–Mn(4) 2.717(5), Te1–Te2 2.723(3), Te3–Te4 2.777(2); Te1-Mn1-Te2 61.1(1), Te1-Mn1-Te3 84.1(1), Te2-Mn2-Te4 89.3(1), Te2-Mn2-Te5 98.5(1), Mn1-Te1-Mn3 94.3(1), Mn2-Te4-Mn(4) 112.9(1).

$(CO)_3$ fragments bridged in an unusual fashion by three ditelluride Te_2^{2-} ligands. First, three $Mn(CO)_3$ fragments and three ditelluride Te_2^{2-} ligands define a $[Mn_3(CO)_9(Te_2)_3]^{2-}$ cluster core, reminiscent of the $[Mn_3(CO)_9(S_2)_2(SH)]^{2-}$. The minor change in bonding mode of a Te_2^{2-} unit in **3** stems from the need to accommodate another Mn center: atom Te4 is detached from Mn3 so that Te4 and Te6 can form new bonds with the $Mn(CO)_4$ fragment while Te3 is connected to Mn3 instead. Two of the ditelluride Te_2^{2-} ligands in **3** are bound to three, and the third Te_2^{2-} ligand to four Mn centers. Their coordination modes can be designated as $\mu_3,\eta^1,\eta^1,\eta^2$-bridging for $\{Te1–Te2\}^{2-}$, $\mu_4,\eta^1,\eta^1,\eta^1,\eta^1$-bridging for $\{Te3–Te4\}^{2-}$, and $\mu_3,\eta^1,\eta^1,\eta^1$-bridging for $\{Te5–Te6\}^{2-}$. All the Mn atoms can be assigned the formal oxidation state +1 and are in approximately octahedral environments with either *cis* C_{3v} or C_{2v} local symmetry. The Mn···Mn distances range from 3.91 to 5.41 Å, thus excluding any possibility of metal–metal bonding. The average Mn–Te bond lengths of 2.665(7) Å is comparable to those of 2.676(1) and 2.671(1) Å found in *cis*-{[Na([18]crown-6)]·2THF}$[Mn(CO)_4(TePh)_2]$.[13] The Te–Te bond lengths are, on average, 2.75(2) Å and can be considered normal single bonds.[14]

Attempts to use IR and ^1H NMR spectroscopy to confirm the presence of the SH^- ligand in **1** have thus far been unsuccessful. The ν(S–H) vibrational modes may be too weak to be detected.[12] On the other hand, a trace amount of acid or base in solution has been known to cause exchange broadening and collapse of the SH^- proton NMR signal in other metal hydrosulfide complexes.[15] The hydrosulfide ligand in **1** is formulated as a result of the following observations: 1) If the monosulfide ligand were not protonated, mixed valence would have to be invoked for the Mn centers in **1**. However, magnetic susceptibility measurements showed that the compound is diamagnetic, which is supportive of an assignment of the precise formal oxidation state +1 to the Mn atoms; 2) the control reactions carried out in superheated MeOH gave **4** and **5**, the methylated analogues of **1** and **2**, as confirmed by single crystal X-ray

$(Ph_4P)_2[Mn_3(CO)_9(S_2)_2(SCH_3)]$ **4**

$(Ph_4P)[Mn_2(CO)_6(SCH_3)_3]$ **5**

analyses.[16] The cluster ions $[Mn_3(CO)_9(E_2)_2(ER)]^{2-}$ (E = S, R = CH_3, H; E = Te, R = CH_3)[17] are formed by attack of the solvent (MeOH or EtOH) on the coordinated monochalcogenide ligands because of the nucleophilicity or Lewis basicity of such atoms.[7] However, tellurium is unable to follow the same course of reaction if protonation is required. This is consistent with the lower Lewis basicity of telluride relative to sulfide. Instead, the monotelluride ligand is replaced by a ditelluride ligand, and the structure expands to include an extra $Mn(CO)_4$ fragment. Therefore, we speculate that **1** and **3** are probably formed by the same pathway, but the ultimate structure is controlled by the need to satisfy the electronic requirements of the monochalcogenide ligand. This leads to either methylation, protonation, or replacement of the monochalcogenide with a dichalcogenide in this position.

Pure **1** failed to react with EtOH to give **2**. The formation of the latter may have involved, besides EtOH, some unidentified intermediate species generated in situ. We have also been unable to prepare **1**, **2**, or **3** from the refluxing ethanol solution. Kolis and co-workers have shown that the solution reaction between $[M_2(CO)_{10}]$ (M = Mn or Re) and K_2E_x (E = S, Se; x = 2–4) in DMF gives the E_4^{2-}-containing dimers $(Ph_4P)_2[M_2(E_4)_2(CO)_6]$.[18] Heating of the latter in DMF leads to the formation of homoleptic $(Ph_4P)_2[M(E_4)_2]$.[18] All this underscores the intrinsic difference of the chemistry under hydro(solvo)thermal conditions and that at ambient temperatures and pressures.

Experimental Section

Na_2S_2 and Na_2Te_2 were prepared by treating a stoichiometric amount of sulfur (or tellurium) with sodium metal in liquid ammonia. Other reagents were used as obtained. All the manipulations were carried out under a dry nitrogen atmosphere in a Labconco glovebox.

1: A sample of $[Mn_2(CO)_{10}]$ (40 mg, 0.1 mmol), Na_2S_2 (44 mg, 0.4 mmol), and Ph_4PBr (252 mg, 0.6 mmol) was ground and mixed thoroughly in a mortar with a pestle. The reagents were loaded into a thick-walled Pyrex tube (~25 cm long). After addition of EtOH (0.4 mL), the tube was frozen with liquid N_2, evacuated, and sealed with a flame. The tube was heated at 85 °C for 1.5 h to afford orange single crystals of $(Ph_4P)_2[Mn_3(CO)_9(S_2)_2(SH)]$. Analytically pure crystals can be isolated in 34% yield by washing with ethanol and diethyl ether. Mid-IR spectrum in the CO region: $\tilde{\nu}$ = 1999(sh), 1972(s), 1955(s), 1900(sh), 1878(s), and 1859(sh) cm^{-1}.

 © WILEY-VCH Verlag GmbH, D-69451 Weinheim, 1997 0570-0833/97/3617-1855 $ 17.50+.50/0

2: This compound was prepared analogously except that the sealed tube was heated at 85 °C for 80 hours. Orange-yellow, cube-shaped single crystals were isolated in 70% yield. Mid-IR spectrum in the CO region: $\tilde{\nu}$ = 1994(s), 1910(sh), 1898(s), 1884(s), and 1863(sh) cm^{-1}.

3: The sealed Pyrex tube containing $[Mn_2(CO)_{10}]$ (80 mg, 0.2 mmol), Na_2Te_2 (120 mg, 0.4 mmol), Ph_4PBr (252 mg, 0.6 mmol), and 0.4 mL EtOH was heated at 85 °C for 14 hours. After washing with ethanol and diethyl ether, black single crystals of **3** were separated by hand in about 55% yield. Mid-IR spectrum in the CO region: $\tilde{\nu}$ = 2030(s, sharp), 1962(vs, broad), 1929(s, shoulder), 1883(s, multiple) cm^{-1}. Semi-quantitative elemental analysis by SEM-EDAX: P/Mn/Te = 1/2.07/3.11.

Satisfactory C and H analyses were obtained for **1** and **2**. The phase identity and homogeneity of the three compounds was confirmed by comparing their experimental X-ray powder diffraction patterns of bulk material with those of calculated from the single crystal X-ray data.

Received: December 18, 1997
Revised version: May 2, 1997 [Z9905IE]
German version: *Angew. Chem.* **1997**, *109*, 1961–1964

Keywords: clusters · hydrothermal synthesis · manganese · sulfur · tellurium

[1] L. M. Demianets, A. N. Lobachev in *Crystallization Process under Hydrothermal Conditions* (Ed.:. N. Lobachev), Consultants Bureau, New York, **1973**.
[2] R. M. Barrer, *Hydrothermal Chemistry of Zeolites*, Academic Press, New York, **1982**.
[3] A. Rabenau, *Angew. Chem.* **1985**, *97*, 1017; *Angew. Chem. Int. Ed. Engl.* **1985**, *24*, 1026.
[4] R. A. Laudise, *Chem. Eng. News* **1987**, *65* (39), 30.
[5] a) M. I. Khan, Q. Chen, D. P. Goshorn, H. Hope, S. Parkin, J. Zubieta, *J. Am. Chem. Soc.* **1992**, *114*, 3341, and references therein; b) J. B. Parise, *Science* **1991**, *251*, 293; c) *J. Chem. Soc. Chem. Commun.* **1990**, 1553; d) R. C. Haushalter, K. G. Strohmaier, F. W. Lai, *Science* **1989**, *246*, 1289, and references therein.
[6] a) W. S. Sheldrick, *Z. Anorg. Allg. Chem.* **1988**, *562*, 23; b) W. S. Sheldrick, H.-J. Häuser, *ibid.* **1988**, *557*, 98; c) *ibid.* **1988**, *557*, 105; d) W. S. Sheldrick, J. Kaub, *ibid.* **1986**, *535*, 179.
[7] Examples of hydro(solvo)thermal synthesis of organometallic cluster compounds: a) S. Huang, M. G. Kanatzidis, *J. Am. Chem. Soc.* **1992**, *114*, 5477; b) *Inorg.Chem.* **1993**, *32*, 821–825; c) *Inorg.Chim. Acta* **1994**, *230*, 9; d) B. K. Das, M. G. Kanatzidis, *Inorg.Chem.* **1995**, *34*, 1011; e) *ibid.* **1995**, *34*, 5721; f) *J. Organomet. Chem.* **1996**, *513*, 1.
[8] a) R. Seidel, R. Kliss, S. Weissgräber, G. Henkel, *J. Chem. Soc. Chem. Commun.* **1994**, 2791; b) R. Seidel, B. Schnautz, G. Henkel, *Angew. Chem.* **1996**, *108*, 1836; *Angew. Chem. Int. Ed. Engl.* **1996**, *35*, 1710.
[9] Crystallographic data of **1**: $C_{57}H_{41}Mn_3O_9P_2S_5$, monoclinic, space group $P2_1/n$ (no. 14), a = 11.6577(6), b = 25.967(1), c = 19.286(1) Å, β = 102.880(1)°, V = 5691.3(4) Å^3, Z = 4, ρ_{calcd} = 1.467 g cm^{-3}, μ = 0.949 mm^{-1}, T = 295 K, structure solution and refinement based on 5181 reflections with $I_0 \geq 3.0\sigma(I_0)$ converged at R = 0.0516, R_w = 0.0638 and GOF = 1.65. **2**: $C_{30}H_{23}Mn_2O_6PS_3$, orthorhombic, space group $P2_12_12$ (no. 18), a = 14.1505(5), b = 16.7409(5), c = 6.4639(2) Å, V = 1531.25(7) Å^3, Z = 2, ρ_{calcd} = 1.554 g cm^{-3}, μ = 1.123 mm^{-1}, T = 153 K, structure solution and refinement based on 1867 reflections with $I_0 \geq 3.0\sigma(I_0)$ converged at R = 0.0245, R_w = 0.0408 and GOF = 1.51. **3**: $C_{61}H_{40}Mn_4O_{13}P_2Te_6$, triclinic, space group $P\bar{1}$ (no. 2), a = 12.331(1), b = 12.601(1), c = 22.846(2) Å, α = 95.64(2), β = 90.34(2), γ = 106.93(2)°, V = 3377.4(7) Å^3, Z = 2, ρ_{calcd} = 1.994 g cm^{-3}, μ = 3.376 mm^{-1}, T = 295 K, structure solution and refinement based on 3714 reflections with $I_0 \geq 3.0\sigma(I_0)$ converged at R = 0.0575, R_w = 0.0577 and GOF = 1.60. Data were collected on Siemens SMART diffractometers using $Mo_{K\alpha}$ radiation (λ = 0.71073 Å). An empirical absorption correction based on simulated c-scans was applied to each data set. Further details of the crystal structure investigations are available from the Fachinformationszentrum Karlsruhe, D-76344 Eggenstein-Leopoldshafen (Germany), on quoting the depository number CSD-406241 (**1**), -406242 (**2**), and -406559 (**3**).
[10] V. Küllmer, E. Röttinger, H. Vahrenkamp, *J. Chem. Soc. Chem. Commun.* **1977**, 782.
[11] A. Müller, W. Jaegermann, J. H. Enemark, *Coord. Chem. Rev.* **1982**, *46*, 245.
[12] W. Beck, W. Danzer, R. Höfer, *Angew. Chem.* **1973**, *85*, 87; *Angew. Chem. Int. Ed. Engl.* **1973**, *12*, 77.
[13] W.-F. Liaw, D.-S. Ou, Y.-S. Li, W.-Z. Lee, C.-Y. Chuang, Y.-P. Lee, G.-H. Lee, S.-M. Peng, *Inorg. Chem.* **1995**, *34*, 3747.
[14] a) H. D. Lutz, M. Jung, G. Waschenbach, *Z. Anorg. Allg. Chem.* **1987**, *554*, 87; b) M. Di Vaira, M. Peruzzini, P. Stoppioni, *Angew. Chem.* **1987**, *99*, 955; *Angew. Chem. Int. Ed. Engl.* **1987**, *26*, 916; c) B. W. Eichhorn, R. C. Haushalter, F. A. Cotton, B. Wilson, *Inorg. Chem.* **1988**, *27*, 4084.
[15] D. Kwon, J. Real, D. Curtis, A. Rheingold, B. S. Haggerty, *Organometallics* **1991**, *10*, 143.
[16] **4**: triclinic, space group $P\bar{1}$ (no. 2), a = 20.70(1), b = 23.40(1), c = 12.837(5) Å, α = 91.86(4), β = 90.50(4), γ = 69.84(4)°, V = 5835(9) Å^3, Z = 2; **4**: triclinic, space group $P\bar{1}$ (no. 2), a = 10.162(6), b = 11.667(7), c = 16.665(9) Å, α = 107.15(5), β = 92.75(5), γ = 113.44(4)°, V = 1701(4) Å^3, Z = 2.
[17] S. Huang, Dissertation, Michigan State University (USA), **1993**.
[18] a) S. C. O'Neal, W. T. Pennington, J. W. Kolis, *Inorg. Chem.* **1990**, *29*, 3134; b) *Can. J. Chem.* **1989**, *67*, 1980.

A Five-Atom Molecule which Enantiomerizes in a Single Step via Chiral Transition States **

Michael Mauksch and Paul von Ragué Schleyer*

Dedicate to Professor Kurt Mislow

Racemizations of chiral molecules do not necessarily involve achiral transition states or intermediates. A rubber glove, turned inside out by stripping it from the right hand, will then fit the left without going through a symmetric representation. Mislow demonstrated in 1955[1] an enantiomerization involving only chiral intermediates along the whole path (termed a "chiral path") in dissymmetric biphenyl derivatives.[2, 3]

Other enantiomerizations along chiral paths, involving one or more reaction steps, are known. The stereomutation of phosphoranes substituted with five different groups by the Berry pseudorotation mechanism,[4] which proceeds through five steps (that is, four intermediate configurations and five transition states), the enantiomerization of triarylamines ("molecular propellers") by a sequence of three two-ring flips,[5, 6] correlated rotation of "gear" systems such as appropriately substituted bis-(9-tripticyl)-methane,[7] as well as the internal rotation of Mislow's biphenyl,[1, 2] are examples with complicated, many atom molecules. A recently synthesized chiral knot from single-stranded DNA may enantiomerize without even being able to assume any achiral conformation.[8] The racemizations of a number of *o,o'*-bridged biphenyls are more recent single-step examples.[9]

The simplest possible asymmetric enantiomerization of a real molecule would require only five atoms as well as a single reaction step, that is, without an intervening minimum.[10] The goal of this research was to locate a chemically feasible possibility with a chiral path of minimum energy and a low barrier. The demonstration of such an example computationally did not prove to be easy.

As the stereomutation of methane has been computed to occur via a nonplanar transition state (a $CH_2 \cdot H_2$ complex),[11] the hypothetical chiral isotopomer CHDTMu (Mu = muonium, a hydrogen-like particle) might enantiomerize by an asymmetric path. This barrier for CH_4, although below the H_2 elimination threshold, was computed to be very high (107 ± 2 kcal mol^{-1} and 5 ± 1 kcal mol^{-1} at 0 K) above the CH dissociation energy.[11] We have not been able to find any chiral five-atom methane-based molecule (for example CHFClBr, recently dis-

[*] Prof. Dr. P. von R. Schleyer, Dipl. Chem. M. Mauksch
Computer Chemistry Center
Institut für Organische Chemie der Universitat Erlangen-Nürnberg
Henkestrasse 42, D-91054 Erlangen (Germany)
Fax: Int. code +(9131)859-132
e-mail: schleyer@organik.uni-erlangen.de

[**] This work was supported the DFG, the VW foundation, and the Fonds der Chemischen Industrie. We thank Kurt Mislow (Princeton), Paul Mezey (Saskatoon), David Avnir (Jerusalem), and Martin Quack (Zürich) for helpful discussions and suggestions as well as for permission to cite unpublished results.

 © WILEY-VCH Verlag GmbH, D-69451 Weinheim, 1997 0570-0833/97/3617-1856 $ 17.50+.50/0

cussed by Quack et al[12]) with a low barrier to chiral enantiomerization. SiH_4 (and its chiral isotopomer, SiHDTMu) has a more complex potential energy hypersurface (PES) than methane.[13] Stereomutation involves a high-lying isomer (a perpendicular $SiH_2 \cdot H_2$ complex, 50.3 kcal mol^{-1} higher in energy at BECKE3LYP/6-311++G(2d,2p)), which can rotate internally (barrier 2.2 kcal mol^{-1}) and exchange the H atoms through a parallel $SiH_2 \cdot H_2$ transition state. However, the barrier of 55.3 kcal mol^{-1} for obtaining this $SiH_2 \cdot H_2$ intermediate from the SiH_4 ground state is 2.1 kcal mol^{-1} higher than the dissociation into SiH_2 and H_2 at 0 K.[13]

Moreover, like the last example, most completely chiral enantiomerization paths in five atom systems involve more than one step.[14, 15] Four examples, representing three different connectivities, illustrate this further here: "tetrahedral" HDTSiLi (**1**), "branched" HFNOH (**2**), and HFPSH (**3**), as well as "linear" HSOOH (**4**) (see Figures **1**–**3** and also see Table **1**). The computations were carried out with the GAUSSIAN 94 program at the BECKE3LYP/6-311G** level (see Table 1).[16]

Table 1. BECKE3LYP/6-311G** total energies E/E_h, zero point energies (ZPE) and ZPE-corrected relative energies E_{rel} [kcal mol^{-1}] of stationary points on the potential energy surfaces of molecules **1**–**4**.

Structure[a]	NIMAG	Symmetry	E/E_h	ZPE	E_{rel}
1a[b]	0	C_{3v}	−298.82939	14.60	2.81
1b	0	C_{3v}	−298.83380	14.56	0.0
1c	1	C_{3v}	−298.78977	13.65	26.69
1d	1	C_1	−298.81595	13.89	10.52
1e	2	C_s	−298.81263	13.30	12.01
1f	2	C_{2v}	−298.77122	14.12	38.80
2a	0	C_1	−230.98033	20.26	0.0
2b	0	C_1	−230.97316	20.02	4.26
2c	1	C_1	−230.93469	19.24	27.60
2d	1	C_1	−230.96574	19.31	8.20
2e	1	C_1	−230.96092	19.33	11.24
2f	2	C_s	−230.91575	18.46	38.69
2g	2	C_s	−230.91139	18.50	41.47
3a	0	C_1	−840.70182	13.52	0.0
3b	0	C_1	−840.69910	13.37	1.56
3c	1	C_1	−840.61471	12.83	53.93
3d	1	C_1	−840.68855	12.81	7.61
3e	1	C_1	−840.68898	12.76	7.29
3f	2	C_s	−840.58415	12.07	72.33
3g	2	C_s	−840.58380	12.05	72.53
4a	0	C_1	−549.79002	15.85	0.0
4b	0	C_1	−549.78894	15.69	0.52
4c	1	C_1	−549.78201	15.54	4.71
4d	1	C_1	−549.77668	15.67	8.18
4e	1	C_1	−549.78885	15.54	0.42
4f	1	C_1	−549.77860	15.69	7.00
4g	2	C_s	−549.75953	15.24	18.51
4h	2	C_s	−549.77489	15.39	9.03
4i	2	C_s	−549.77407	15.35	9.50
4j	2	C_s	−549.76474	15.24	15.24

[a] See Figures 1–3. [b] H_3SiLi represents the chiral derivative HDTSiLi, which should have a similar potential energy surface.

The lithium in **1** is ionically bound, and, unlike a halogen substituent, is relatively mobile. For chiral HDTSiLi (represented in Figure 1 by H_3SiLi) SiH_3 inversion (**1a** → **1c** → **1b**) and the more facile migration of the Li^+ ligand (**1b** → **1d** → **1a**) participate in the enantiomerization.[17] The two minima **1a** and **1b** are interconnected by two transition states, **1c** and **1d**. The racemization barrier (energy difference between **1a** and **1c**) is 24.0 kcal mol^{-1}, that is, much smaller than for the methane[11] or silane[13] isotopomers, or for CHFClBr.[12]

The "branched" connectivity, considered earlier,[14, 15] is illustrated here by HFNOH (**2**, Figure 2**a**) and HFPSH (**3**, Figure **2b**). Both enantiomerizations pass through two separate

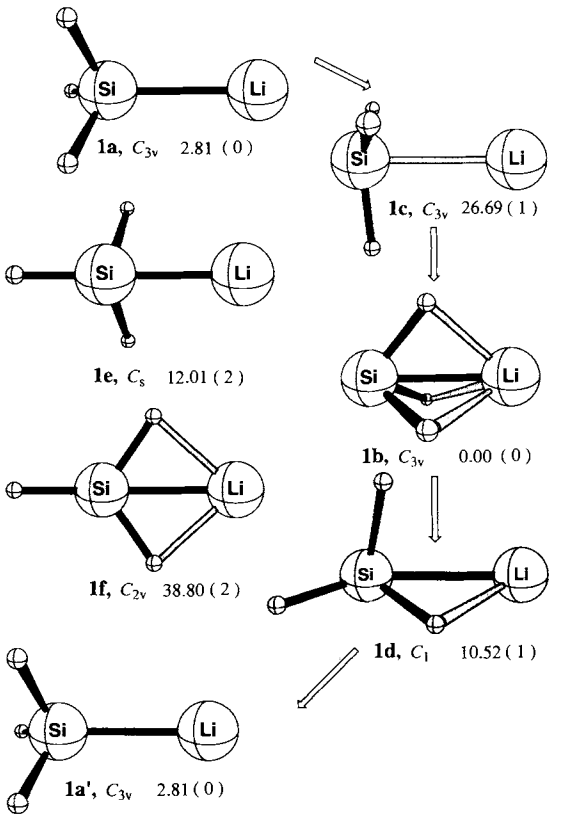

Figure 1. Schematic representation of two-step racemization of HDTSiLi, **1a**↔**1a'**, via the lower energy inverted minimum **1b**. Point groups are shown for the parent H_3SiLi species; relative energies are at B3LYP/6-311G** (Table 1) and the number of imaginary frequencies (NIMAG) are given in parenthesis. The steps involve pyramidal inversion at silicon (via transition state (TS) **1c**) and migration of Li^+ (via TS **1d**). The more symmetrical alternative (**1e**) is higher in energy and has NIMAG = 2. The planar geometry **1f** (also with NIMAG = 2) does not compete energetically. The relative energies (vs. **1a**) are given below the structures in kcal mol^{-1} (including zero point vibrational correction).

chiral transition states for the inversion at nitrogen (**2c**, barrier for the rate-determining step 27.6 kcal mol^{-1}) or phosphorus (**3c**, barrier 53.9 kcal mol^{-1}), and for the rotation around the N–O (**2d**) or the P–S bonds (**3d** (clockwise rotation) and **3e** (counterclockwise), which have nearly the same energy).[14] Both HFNOH and HFPSH have two planar conformations, but these are second-order saddle points, considerably higher in energy than the chiral inversion transition states.

The enantiomerization of the helical conformation of HOOSH, **4a** (Figure **3**) can occur by two separate rotations around the O–S and the O–O bonds and involves four chiral transition states **4c**–**f** (and their enantiomers). Of these, the transition states for O–S bond rotation are highest in energy (8.18 kcal mol^{-1} for **4d** and 7.00 kcal mol^{-1} for **4b**), but lie somewhat below the planar second-order saddle points **4h** (9.03), **4g** (8.51), **4i** (9.50) and **4j** (15.24 kcal mol^{-1}). The overall racemization barrier is thus 7.0 kcal mol^{-1} at 0 K. We assumed that this PES would be simplified if the hydrogen atoms were replaced by divalent atoms that were joined together.

Indeed, the facile interconversion ("pseudorotation") of C_2 and C_s conformations of cyclopentane,[18–21] S_5,[22] and other[18] five-membered rings suggested possible one-step enantiomerization candidates. Pentaatomic five-membered rings without any nonplanar achiral conformations require at least three different chemical elements, appropriately placed, to provide five differentiable chemical environments. *cyclo*-SeSSOS (**5**), although unknown, should fulfill this condition, as

 © WILEY-VCH Verlag GmbH, D-69451 Weinheim, 1997 0570-0833/97/3617-1857 $ 17.50+.50/0

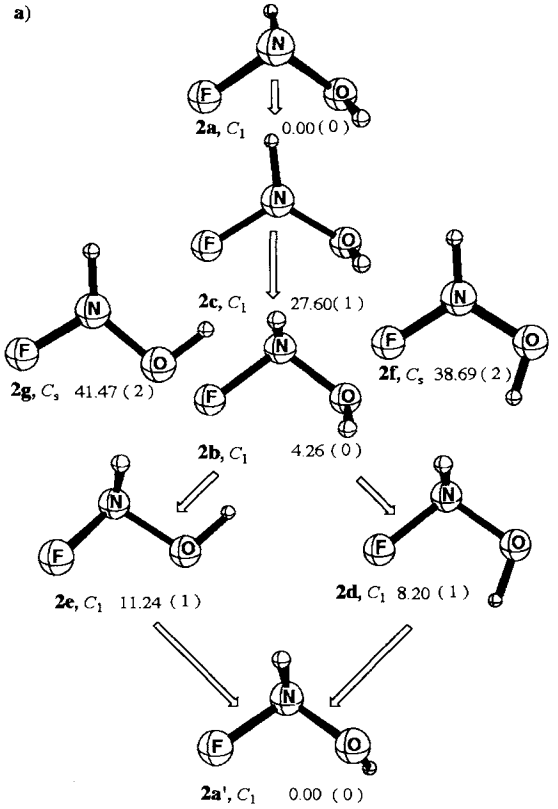

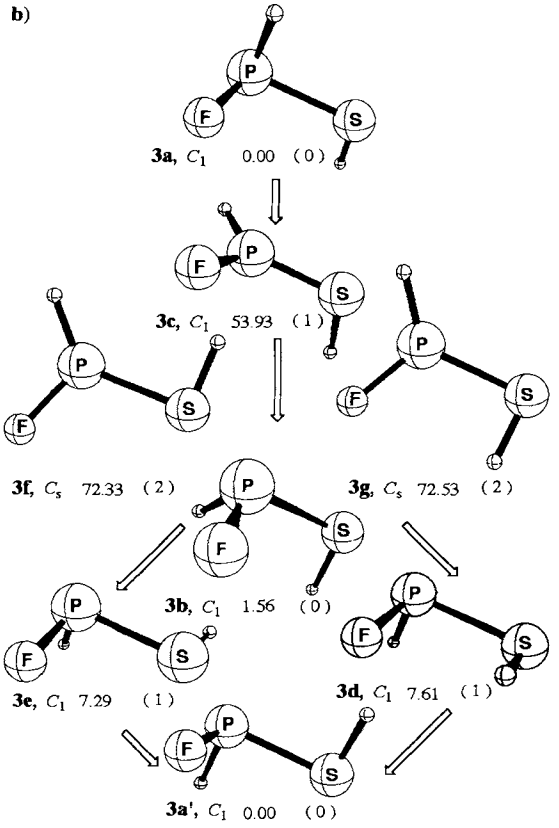

Figure 2. Two examples of another five-atom molecule connectivity: NHFOH (**2**, a) and PHFSH (**3**, b). Transition states **2c** and **3c** belong to inversion, **2d,e** and **3d,e** to rotation processes. The planar forms **2e,f** and **3e,f** do not take part in the enantiomerization. The energies given are relative to the most stable structure.

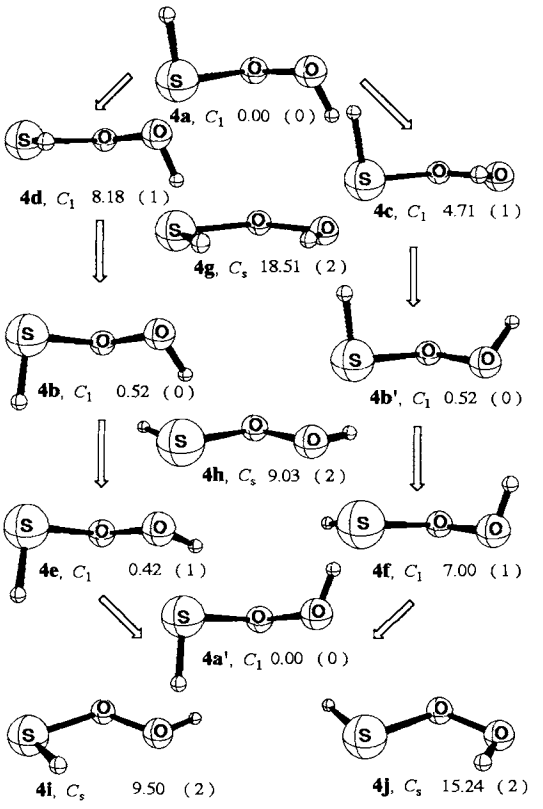

Figure 3. HOOSH (**4**) serves as example for a chiral five-atom chain. The two-step enantiomerization of the global minimum, helical **4a** (shown schematically), involves the intermediate **4b** (0.84 kcal mol^{-1} above **4a**). The two pathways involve TSs **4c**–**4f**. The four planar conformations, **4g**–**4j** (also shown) are second-order saddle points.

its enantiomerization is predicted to proceed along a completely chiral reaction path in only one step! This was demonstrated by computations at several different levels of ab initio and density functional theory (HF/3-21G*, HF/6-31G*, B3LYP/6-31G*, and B3LYP/6-311G*); all give similar geometries and relative energies (Table 2).

The enantiomers **5a**, **5a'** and the transition states **5b**/**5b'** are shown in Figure 4. The racemization barrier of *cyclo*-SeSSOS is only 6.2 kcal mol^{-1} (at BECKE3LYP/6-311G* + ZPE). In contrast, the achiral planar **5c** is a second-order saddle point with a high relative energy (31.8 kcal mol^{-1}). Hence, inversion by ring flattening should not occur. Two enantiomerically related minimum-energy reaction pathways connect the chiral structures (**5a**, **5a'**). The truly chiral character of the path is confirmed by results of HF/3-21G(*) intrinsic reaction coordinate (IRC) computations, plotted in Figure 5.[22] Full geometry optimizations, starting from the endpoints of the IRC paths, gave both enantiomers (with identical energies). The asymmetry of the energy profile results from the chirality of the transition state. Figure 5 also depicts some of the intermediate structures along one of the two enantiomeric racemization pathways.

The low-energy stereomutation pathways of the pentacyclic system **5a** contrasts, for example, with the conceivable one-step enantiomerization of chiral methane derivatives, which have high racemization barriers.[12–14] The verification of a single-step chiral inversion of a five-atom molecule is an experimental challenge.

Received: October 30, 1997
Revised version: April 14, 1997 [Z9703IE]
German version: *Angew. Chem.* **1997**, *109*, 1976–1980

 © WILEY-VCH Verlag GmbH, D-69451 Weinheim, 1997 0570-0833/97/3617-1858 $ 17.50+.50/0

Table 2. Total energies E/E_h, zero point energies (ZPE), and ZPE-corrected relative energies E_{rel} referred to the most stable isomer [kcal mol^{-1}] of cyclic SeSSOS species [kcal mol^{-1}], calculated at several levels of theory.

Structure[a]	NIMAG[b]	Symmetry		HF/3-21G*	HF/6-31G*	B3LYP/6-31G*	B3LYP/6-311+G*
5a	0	C_1	E/E_h	−3650.09099	−3664.90389	−3669.12733	−3671.39871
			ZPE	–	5.7	4.7	–
			E_{rel}	0.0	0.0	0.0	0.0
5b	1	C_1	E/E_h	−3650.08187	−3664.89755	−3669.11751	−3671.38852
			ZPE	–	5.6	4.5	–
			E_{rel}	5.7	3.9	6.0	6.2
5c	2	C_s	E/E_h		−3664.86705	−3669.07652	−3671.35083
			ZPE	–	–	4.6	–
			E_{rel}	–	23.1	31.8	29.9

[a] See Figure 4. [b] Number of imaginary frequencies.

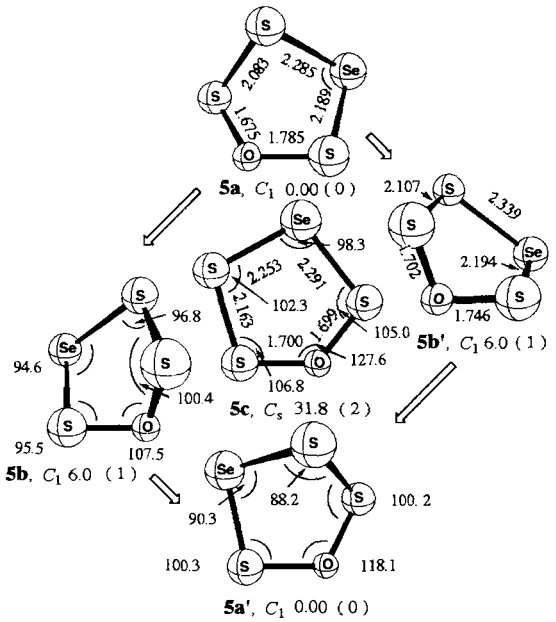

Figure 4. One-step enantiomerization by pseudorotation of *cyclo*-SeSSOS (**5**). Geometries and energies are at the ZPE-corrected BECKE3LYP/6-31G* level. The racemization barrier is 6.0 kcal mol^{-1}. Both enantiomeric minimum-energy paths with the equivalent C_1 transition states **5b**, **5b'** are indicated. The planar second-order saddle point **5c** (energy 31.8 kcal mol^{-1} relative to **5a**) is depicted in the middle.

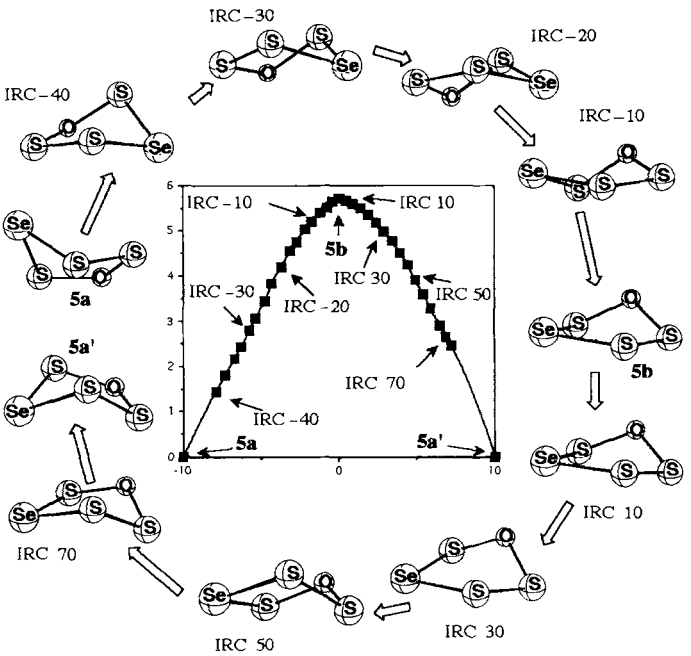

Figure 5. Intermediate structures and energy profile of an IRC HF/3-21G(*) calculation. Only one minimum-energy path is shown. The asymmetry of the energy profile results from the chirality of the transition state.

Keywords: chirality · density functional calculations · small ring systems · stereomutation · transition states

[1] a) K. Mislow, *Science* **1954**, *120*, 232; b) K. Mislow, R. Bolstad, *J. Am. Chem. Soc.* **1955**, *77*, 6712.
[2] K. Mislow, *Introduction to Stereochemistry*, W. A. Benjamin, New York, **1966**.
[3] D. M. Walba, *Tetrahedron*, **1985**, *41*, 3161.
[4] E. L. Muetterties, *Inorg. Chem.* **1967**, *6*, 635.
[5] D. Gust, K. Mislow, *J. Am. Chem. Soc.* **1973**, *95*, 1535.
[6] R. Glaser, J. F. Blount, K. Mislow, *J. Am. Chem. Soc.* **1980**, *102*, 2777.
[7] W. D. Hounshell, C. A. Johnson, A. Guenzi, F. Cozzi, K. Mislow, *Proc. Natl. Acad. Sci. USA* **1980**, *77*, 6961.
[8] E. Flapan, N. C. Seeman, *J. Chem. Soc. Chem. Commun.* **1995**, 2249.
[9] K. Müllen, W. Heinz, F.-G. Klaerner, W. R. Roth, I. Kindermann, O. Adamczak, M. Wette, J. Lex, *Chem. Ber.* **1990**, *123*, 2349.
[10] a) P. G. Mezey, *J. Math. Chem.* **1995**, *17*, 185; b) P. G. Mezey, *ibid.* **1995**, *18*, 133.
[11] a) M. S. Gordon, M. W. Schmidt, *J. Am. Chem. Soc.* **1993**, *115*, 7486; b) M. J. M. Pepper, I. Shavitt, P. von R. Schleyer, R. Janoschek, M. Quack, *J. Comput. Chem* **1995**, *16*, 208.
[12] a) A. Bauder, A. Beil, D. Luckhaus, F. Müller, M. Quack, *J. Chem. Phys.* **1997**, submitted; b) A. Beil, D. Luckhaus, M. Quack, J. Stohner, *Ber. Bunsen-Ges. Phys. Chem.* **1997**, submitted; c) A. Beil, D. Luckhaus, R. Marquardt, M. Quack, *Faraday Discuss. Chem. Soc.* **1994**, *99*, 49.
[13] a) J. Kapp, Dissertation, Erlangen, **1996**; b) C. Maerker, J. Kapp, P. von R. Schleyer in *Organosilicon Chemistry II* (Eds.: J. Auner, J. Weis), VCH, Weinheim, **1995**, p. 334.
[14] K. Mislow, in *Fuzzy Logic in Chemistry*, Academic Press, in press, and references cited therein.
[15] S. Wolfe, H. B. Schlegel, I. G. Csizmadia, F. Bernardi, *J. Am. Chem. Soc.* **1975**, *97*, 2020. These authors considered the enantiomerization of CH_2OH^- in this context. Mislow discusses HDNOH in a similar way [14].
[16] a) GAUSSIAN 94, Revision C3: J. S. Binkley, R. A. Whiteside, K. Rhagavachari, D. J. DeFrees, H. B. Schlegel, M. J. Frisch, D. J. Fox, G. W. Trucks, L. R. Kahn, R. L. Martin, C. Gonzalez, R. Seeger, P. M. W. Gill, B. G. Johnson, J. R. Cheeseman, M. A. Robb, T. Keith, J. A. Montgomery, B. B. Stefanov, M. Challacombe, C. Y. Peng, P. Y. Ayala, W. Chen, M. W. Wong, J. L. Andres, E. S. Replogle, R. Gomperts, J. Baker, J. P. Stewart, M. Head-Gordon, M. A. Al-Laham, V. G. Zakrzewski, J. Cioslowski, J. V. Ortiz, J. B. Foresman, A. Nanayakkara, G. A. Petersson, J. A. Pople, Gaussian, Inc., Pittsburgh, PA, **1995**; b) W. J. Hehre, L. Radom, P. von R. Schleyer, J. A. Pople, *Ab initio Molecular Orbital Theory*, Wiley, New York, **1986**; c) J. B. Foresman, A. Frisch, *Exploring Chemistry with Electronic Structure Methods*, 2nd ed., Gaussian Inc., Pittsburgh, PA, **1996**.
[17] P. von R. Schleyer, T. Clark, *J. Chem. Soc. Chem. Commun.* **1986**, *17*, 1371.
[18] a) H. Rosas, *J. Phys. Chem.* **1990**, *94*, 1830; b) D. Cremer, J. A. Pople, *J. Am. Chem. Soc.* **1975**, *97*, 1358; c) K. S. Pitzer, W. E. Donath, *ibid.* **1959**, *81*, 3214.

 © WILEY-VCH Verlag GmbH, D-69451 Weinheim, 1997 0570-0833/97/3617-1859 $ 17.50+.50/0

[19] L. E. Bauman, J. Laane, *J. Phys. Chem.* **1988**, *92*, 1040.
[20] L. A. Carreira, G. J. Jiang, W. B. Person, *J. Chem. Phys.* **1972**, *56*, 1440.
[21] L. Ferguson, I. Raber, *J. Am. Chem. Soc.* **1989**, *111*, 4370.
[22] The similar activation barriers (5.7 kcal mol^{-1} at HF/3-21G(*) and 6.2 kcal mol^{-1} at BECKE3LYP/6-311G*) justifies the use of the more economical HF/3-21G(*) level for the IRC calculation. Also see [23] for a similar method of evaluation. The isomeric *cyclo*-SeOSSS (the C_1 global minimum is 10.8 kcal mol^{-1} less stable than **5a** at BECKE3LYP/6-31G*) behaves similarly and will be discussed in a full paper. Trials with five-membered rings comprising other combinations of chalcogen atoms did not succeed (PES searches led to three-membered rings, for example).
[23] K. Raghavachari, C. M. Rohlfing, J. S. Binkley, *J. Chem. Phys.* **1990**, *93*, 5862.

Proton-Dependent Monomer–Oligomer Interconversion of Metal Complexes**

Naohide Matsumoto,* Yukiko Mizuguchi, Genjin Mago, Shingo Eguchi, Hitoshi Miyasaka, Toshio Nakashima, and Jean-Pierre Tuchagues*

Metal-directed self-assembly processes like formation of catenanes and helicates by spontaneous assembly of oligo-2,2′-bipyridine strands and metal ions have attracted much interest in recent years.[1] As a further development of this fascinating area of supramolecular chemistry, metal complexes capable of reversibly interconverting between monomers and self-assembled oligomers by inputting external information (afforded, for example, by protons, electrons, or photons) would be of the utmost interest. Indeed, they could afford new functional materials with a switching ability, and in more specific cases the ability to sequester/release guest molecules or ions according to the delivered external information, provided the polydentate ligand is properly designed to induce the formation of a monomeric species that exhibits the following building block characteristics:[2] a) potential donor ability at a suitable external site of the chelating ligand; b) potential acceptor ability at a vacant or substitutable metal coordination site; c) building process from monomeric into oligomeric species and reverse dismantling process both triggered by appropriate external signals; d) for the more specific case of sequestering/release of guest molecules or ions, presence of one or more cavities in the resulting oligomeric molecular structure, cooperatively determined by the steric restriction provided by the ligand frame and the coordination geometry required by the metal ion.

We are currently investigating whether polydentate ligands including an imidazole moiety can be used to synthesize metal complexes capable of exhibiting such monomer–oligomer interconversions through self-assembly.[3] We report here the pH-controlled interconversion of the Cu^{II} complex of 2-(4-imidazolyl)-ethylimino-6-methylpyridine (HL) between the protonated monomer $[Cu(HL)Cl_2]$ (**1**) and the self-assembled deprotonated cyclic hexamer $[\{Cu(L)\}_6](ClO_4)_6$ (**3**). As an example of the structural tuning afforded by the metal ion, the protonated monomeric Pd^{II} complex with the same ligand [Pd(HL)Cl]Cl (**2**) and the self-assembled deprotonated cyclic tetramer $[\{Pd(L)\}_4](ClO_4)_4$ (**4**) are also described.

Monomeric complexes **1** (light-green crystals) and **2**·H_2O (yellow needles) were synthesized by reacting $CuCl_2 \cdot 2H_2O$ and $PdCl_2 \cdot 2H_2O$, respectively, with HL (1:1 metal-to-ligand molar ratio) in methanol. When the pH value of MeOH, MeOH/H_2O, or H_2O solutions of **1** is raised by addition of NaOH, a color change from green to blue is observed. The pH dependence of the electronic spectra obtained upon dropwise addition of aqueous NaOH to the methanolic solution of **1** up to an equimolar **1**:NaOH ratio has been studied. The original spectrum of **1** (d-d absorption at 750 nm) changes to that of a unique new species (**3**, d-d absorption at 640 nm), and an isosbestic point occurs at 690 nm. Conversely, when an aqueous HCl solution is added to the resulting solution of **3** the intensity of the d-d band absorption at 640 nm decreases and that of the d-d band around 750 nm increases, while the green color is restored.[4] Although the color change of complex **2** from yellow to orange upon increase of the pH value did not afford significant spectral changes, NMR spectroscopy clearly indicates the formation of a unique new species (**4**). The complexes **3** (deep-blue crystals) and **4** (orange crystals) were quantitatively prepared as their perchlorate salts.

The crystal structures of complexes **1**–**4**[5] afforded an illuminating picture of the proton-dependent conversion between the appropriate monomer and imidazolate-bridged copper hexamer (**1**↔**3**) or palladium tetramer (**2** → **4**). The ORTEP drawings of the monomeric protonated complexes **1** and **2** and deprotonated imidazolate-bridged cyclic hexamer **3** and tetramer **4** are shown in Figures 1 and 2), respectively. Clearly, the driving force for these monomer–oligomer interconversions is the deprotonation/protonation of the imidazole moiety of the polydentate ligand that switches alternately from the protonated tridentate state to the deprotonated tetradentate one according to the proton supply (Scheme 1). Thus, the metal ion determines the nuclearity of the oligomeric species through its coordinative requirements: although the ligand environment of the metal ion is close to square planar in both oligomers, Cu^{II}, which has the flexibility to assume square planar, tetrahedral, and intermediate geometries, accommodates a cyclic hexanuclear array of $[CuL]^-$ building blocks in **3**, while Pd^{II} which has not such flexibility imposes a cyclic tetranuclear array of $[PdL]^-$ moieties in **4**.

A more detailed picture of the structural changes associated with these monomer–oligomer conversions is afforded by comparative examination of the metal coordination sphere for complexes **1**–**4**. The trigonal basal plane of the pentacoordinate Cu^{II} atom in the protonated monomeric complex **1** comprises two Cl^- ions and the central imine-nitrogen atom of the tridentate ligand, while its imidazole- and pyridine-nitrogen donors occupy the apical coordination sites. On the other hand, each Cu^{II} ion of the deprotonated imidazolate-bridged cyclic hexamer **3** essentially assumes a square-planar coordination geometry involving the three imine-nitrogen donor atoms of a tetradentate ligand and the imidazolate-nitrogen donor atom of the adjacent unit. However, the monomer–hexamer interconversion does not involve a Cu^{II} valence interconversion because the above-mentioned Cu^{II} pentacoordination is not retained when **1** is

[*] Prof. N. Matsumoto, Y. Mizuguchi, G. Mago, S. Eguchi, H. Miyasaka
Department of Chemistry, Faculty of Science, Kyushu University Hakozaki, Higashi-ku, Fukuoka 812 (Japan)
Fax: Int. code +(81)92-642 2607
e-mail: hidescc@mbox.nc.kyushu-u.ac.jp
Prof. J.-P. Tuchagues
Laboratoire de Chimie de Coordination du CNRS
UP 8241 liée par conventions à l'Université Paul Sabatier
et à l'Institut National Polytechnique
205 route de Narbonne, F-31077 Toulouse Cedex (France)
Fax: Int. code +561-553003
e-mail: tuchague@lcc-toulouse.fr
Prof. T. Nakashima
Faculty of Education, Oita University (Japan)

[**] This work was supported by the Ministry of Education, Science and Culture of Japan (Grant-in Aid for Scientific Research No 04453048).

 © WILEY-VCH Verlag GmbH, D-69451 Weinheim, 1997 0570-0833/97/3617-1860 $ 17.50+.50/0

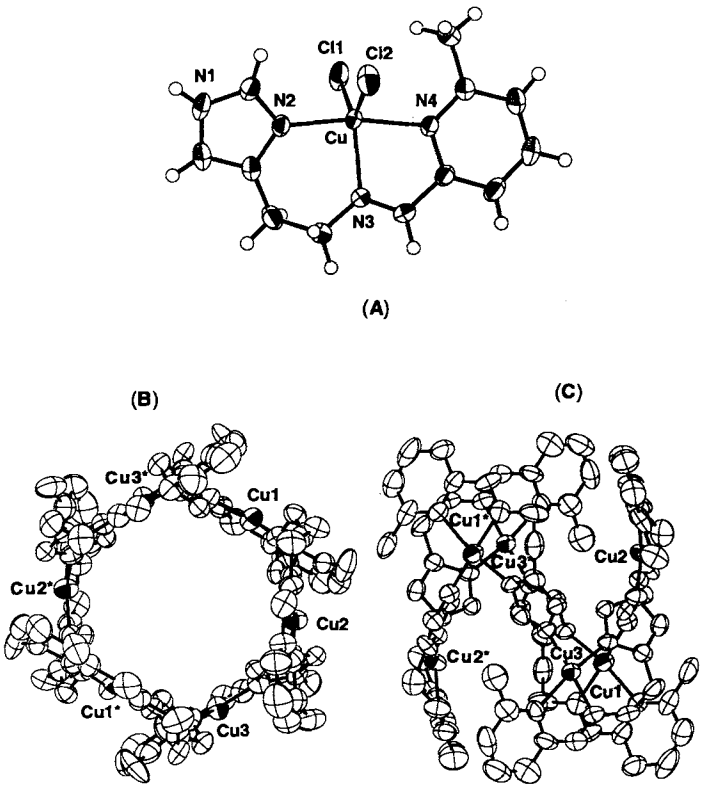

Figure 1. Perspective drawings of the Cu^{II} complex **1** (A) and the complex cation of cyclic hexamer **3** (view along (B) and perpendicular to (C) the pseudo C_3 axis). Hydrogen atoms of **3** are omitted for clarity. Selected Cu–Cu distances [Å]: imidazolate-bridged Cu atoms: Cu1 ··· Cu2 5.894(4), Cu1 ··· Cu3* 5.884(4), Cu2 ··· Cu3 5.878(3); next-nearest Cu atoms: Cu1 ··· Cu2* 6.809(4), Cu1 ··· Cu3 6.666(3), Cu2 ··· Cu3* 6.650(4).

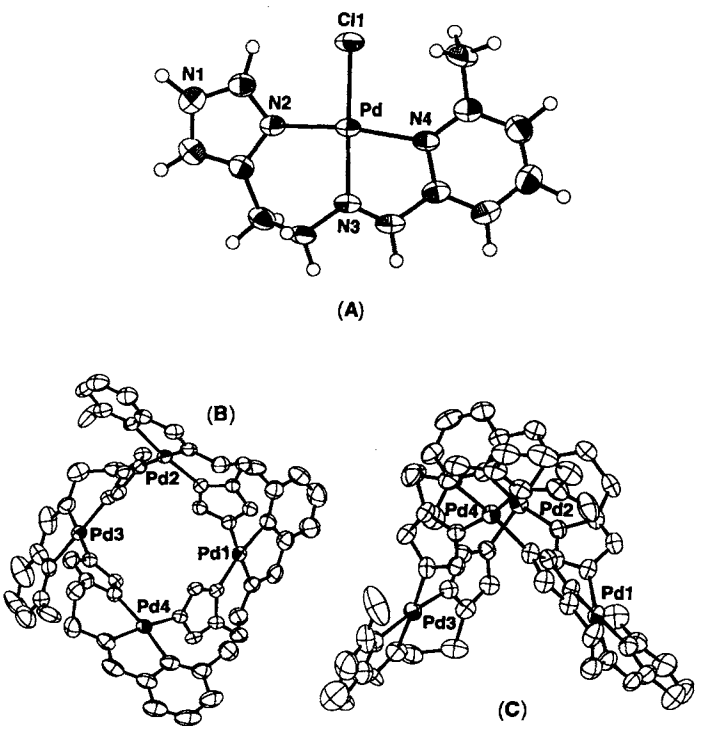

Figure 2. Perspective drawings of the Pd^{II} complex **2** (A) and the complex cation of the cyclic tetramer **4** (B, C). Hydrogen atoms of **4** are omitted for clarity. Selected Pd–Pd distances [Å]: imidazolate-bridged Pd atoms: Pd1 ··· Pd2 6.019(1), Pd2 ··· Pd3 6.019(2), Pd3 ··· Pd4 6.079(1), Pd1 ··· Pd4 6.045(2); next-nearest Pd atoms: Pd1 ··· Pd3 6.475(2), Pd2 ··· Pd4 6.999(3).

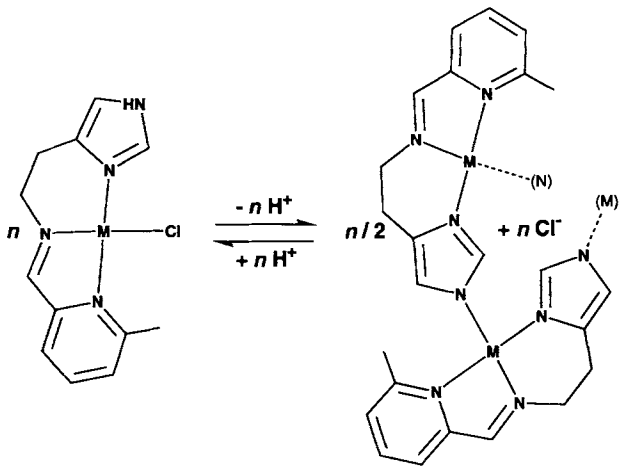

Scheme 1. Protonation and deprotonation of the imidazole moiety of the polydentate ligand L.

dissolved: electron spectroscopy reveals that the $[CuN_3Cl_2]$ chromophore observed in the solid state is converted to the $[CuN_3Cl]$ chromophore in solution.[4] Consequently, the reorganization of the coordination sphere is minimized to a Cl^-/N^- ligand exchange upon monomer–hexamer interconversion. The same is true for the monomer–tetramer interconversion of the palladium complex. The Pd^{II} coordination geometry is square planar in **2** and **4**, and the coordination sphere reorganization is identical to that described for conversion of **1** to **3**.

The reversible interconversion between **1** and **3** was confirmed by potentiometric pH titration. In water at 25 °C, the degree of proton dissociation α calculated by Bjerrum's method increases from 0 to 1 for the titration of the monomer leading to the formation of the hexamer and decreases from 1 to 0 for the reverse titration; this affords superimposable α vs pH curves. The apparent dissociation constant K_d is expressed by Equation (a), where $[Cu(L^-)]^{tot}$ is defined by Equation (b), and the pK_d value by Equation (c). A pK_d value of 8.59 ± 0.01 is obtained

$$K_d = [Cu(L^-)]^{tot}[H^+]/[Cu(HL)] \quad (a)$$

$$[Cu(L^-)]^{tot} = [Cu(L^-)] + 6[\{Cu(L^-)\}_6] \quad (b)$$

$$pK_d = lg\{[Cu(HL)]/([Cu(L^-)]^{tot}[H^+])\} \quad (c)$$

for both forward and reverse titrations. The potentiometric pH titration of the Pd^{II} monomer **2** showed different behavior. Prior to the titration of the monomer, the initial potential indicated that approximately 17% of the imidazole protons were already dissociated. In the course of the forward titration the degree of dissociation of the imidazole protons increased to $\alpha = 1$. In the reverse titration, 80% of the protons did not associate to the nitrogen atoms of the imidazole moiety, indicating that the cyclic Pd^{II} tetramer **4** does not dissociate as easily as the Cu^{II} cyclic hexamer **3**. A pK_d value of 4.50 ± 0.01 was obtained from the forward titration of the Pd^{II} monomer **2**, based on the assumption given in Equation (d).

$$[Pd(L^-)]^{tot} = [Pd(L^-)] + 4[\{Pd(L^-)\}_4] \quad (d)$$

The reversibility of the overall monomer–oligomer conversion depends on the reversibility of reactions I and II. Re-

$$M(HL) \rightleftharpoons M(L^-) + H^+ \quad (I)$$

$$nM(L^-) \rightleftharpoons \{M(L^-)\}_n \quad (II)$$

action I is an intrisically reversible ligand-dependent reaction in which the nature of the metal ion determines only the pH range of the proton dissociation. On the other hand, the reversibility

 © WILEY-VCH Verlag GmbH, D-69451 Weinheim, 1997 0570-0833/97/3617-1861 $ 17.50+.50/0

of reaction II depends exclusively on the relative stabilities of $M(L^-)$ and $\{M(L^-)\}_n$; these stabilities depend on the metal as well as on the association state n of the final oligomeric species.

The complex cation of **3** has a tubular shape with a cylindrical cavity parallel (radius ca. 4 Å) to the pseudo C_3 axis. A constriction in the middle of the cylindrical cavity delimitates two half-cavities. Each set of three copper atoms that is involved in the construction of one of these half-cylinders defines one of the two faces of a compressed copper octahedron constructed exclusively from next-nearest copper atoms. Three vacant coordination sites for each such set of three copper atoms define an approximately equilateral triangle, suggesting that a molecule or anion with three trigonally arrayed (donor) atoms may be conveniently hosted in each half-cavity. We are currently evaluating the potential use of this reversibly self-assembling cyclic hexamer in host–guest chemistry, monitoring the size of the cavity through ligand modifications, and studying the relationship between the nature of the metal atom and the nuclearity with an extensive range of metal ions.

Experimental Section

1: 6-Methyl-2-pyridinecarboxyaldehyde (242 mg, 2 mmol) in methanol (20 mL) was treated with a neutralized (1 M NaOH, 4 mL) solution of histamine dihydrochloride (368 mg, 2 mmol) in MeOH (20 mL). $CuCl_2 \cdot 2H_2O$ (340 mg, 2 mmol) in methanol (20 mL) was then treated with the solution of the ligand and the pH was adjusted to 7–8. The resulting green solution was filtered and allowed to stand for several days. The precipitated green crystals were filtered off, washed with acetone, and dried in air.

2·H_2O: Yellow needles: same synthetic procedure as for **1** except that the pH was adjusted to 3–4.

3·$4CH_3CN \cdot 2H_2O$: A 1 M NaOH solution (2 mL) and $NaClO_4$ (244 mg, 2 mmol) in methanol (10 mL) were added to a solution of **1** (2 mmol) in water-methanol. After the mixture had been allowed to stand for several days, deep blue crystals appeared, which were filtered off and dried in air. Recrystallization from CH_3CN-H_2O gave blue prismatic crystals overnight (90% yield).

4·EtOH: Orange crystals (75% yield): same procedure as for **3**.

Correct elemental analyses were obtained for all compounds.

Potentiometric pH titrations were carried out in a thermostated bath at 25 °C and under a 99.9995% N_2 atmosphere. Extra pure grade water was used (resistivity $\rho > 18.0$ MΩ). The GS-5015c electrode and the potentiometer used in these experiments were supplied from TOA Co. Ltd, Tokyo. The standard electrode potential (E_0) was first determined by Gran's plot method [6]. About 50 mL of a solution (ionic strength 0.15) containing metal complex (0.2 mmol) and sodium chloride was titrated with a solution containing 0.10 M NaOH and 0.05 M NaCl. Immediatedly after the forward titration the resulting solution was titrated back with a solution containing 0.10 M HCl and 0.05 M NaCl. The electrode potentials were converted into proton concentration scale ($-\log[H^+] = (E_0(\text{mV}) - E(\text{mV}))/59.15$) and the degree of dissociation, α, was calculated by Bjerrum's method for the forward and reverse titrations, respectively [7].

Received: October 30, 1996
Revised version: May 2, 1997 [Z9704IE]
German version: *Angew. Chem.* **1997**, *109*, 1964–1966

Keywords: copper · oligomers · palladium · self-assembly · supramolecular chemistry

[1] See for example J.-P. Sauvage, *Acc. Chem. Res.* **1990**, *23*, 319; E. C. Constable, A. J. Edwards, P. R. Raithby, J. V. Walker, *Angew. Chem.* **1993**, *105*, 1486; *Angew. Chem. Int. Ed. Engl.* **1993**, *32*, 1465.

[2] N. Matsumoto, T. Nozaki, H. Ushio, K. Motoda, M. Ohba, G. Mago, H. Okawa, *J. Chem. Soc. Dalton Trans.* **1993**, 2157; T. Nozaki, H. Ushio, G. Mago, N. Matsumoto, H. Okawa, Y. Yamakawa, T. Anno, T. Nakashima, *ibid.* **1994**, 2339.

[3] C. T. Brewer, G. Brewer, L. Mat, J. Sitar, R. Wang, *J. Chem. Soc. Dalton Trans.* **1993**, 151; Y. Nakano, W. Mori, N. Okuda, A. Nakahara, *Inorg. Chim. Acta* **1979**, *35*, 1; N. Matsumoto, M. Ohba, M. Mitsumi, K. Inoue, Y. Hashimoto, H. Okawa, *Mol. Cryst. Liq. Cryst.* **1993**, *233*, 299, and references therein.

[4] UV/Vis (reflectance spectrum): $\lambda_{max} = 841$ (**1**), 627 nm (**3**); UV/Vis (methanol): λ_{max} (ε) = 750 (190) (**1**), 640 nm (110 $dm^3 mol^{-1} cm^{-1}$) (**3**). The electronic absorption bands at 750 nm (**1**) and 640 nm (**3**) can be assigned to the d-d transition due to the $[CuN_3Cl]$ and $[CuN_4]$ chromophore, respectively. The molar electrical conductivity of **1** in methanol agrees with the 1:1 electrolyte, indicating that the species in methanol is $[Cu(HL)Cl]^+$.

[5] Crystal structure analysis of **1**: $[Cu(HL)Cl_2]$, $M_r = 348.72$, green crystal (0.3 × 0.3 × 0.25 mm), triclinic, space group $P\bar{1}$, $a = 8.052(2)$, $b = 12.777(2)$, $c = 7.615(2)$ Å, $\alpha = 102.74(1)$, $\beta = 112.52(2)$, $\gamma = 89.89(2)°$, $V = 703.0(3)$ Å^3, $Z = 2$, $\rho_{calcd} = 1.648$ g cm^{-3}, $\mu(Mo_{K\alpha}) = 19.23$ cm^{-1}, 2253 observed reflections, 229 parameters, $R = 0.024$, and $R_w = 0.022$. Crystal structure analysis of **2**·H_2O: $[Pd(HL)Cl]Cl \cdot H_2O$, $M_r = 409.59$, yellow crystal (0.2 × 0.2 × 0.2 mm), triclinic, space group $P\bar{1}$, $a = 8.526(3)$, $b = 12.291(6)$, $c = 7.838(3)$ Å, $\alpha = 102.91(3)$, $\beta = 98.58(3)$, $\gamma = 69.94(3)°$, $V = 794.7(6)$ Å^3, $Z = 2$, $\rho_{calcd} = 1.814$ g cm^{-3}, $\mu(Mo_{K\alpha}) = 15.94$ cm^{-1}, 2181 observed reflections, 246 parameters, $R = 0.028$, $R_w = 0.023$. Crystal structure analysis of **3**·$4CH_3CN \cdot 2H_2O$: $[Cu(L)]_6(ClO_4)_6 \cdot 4CH_3CN \cdot 2H_2O$, $M_r = 2383.85$, blue crystal (0.2 × 0.2 × 0.3 mm), monoclinic, space group $P2_1/n$, $a = 16.608(8)$, $b = 16.371(7)$, $c = 23.566(7)$, $\beta = 107.41(3)°$, $V = 6113(4)$ Å^3, $Z = 2$, $\rho_{calcd} = 1.335$ g cm^{-3}, $\mu(Mo_{K\alpha}) = 12.27$ cm^{-1}, 5667 observed reflections, 677 parameters, $R = 0.093$, $R_w = 0.090$. Crystal structure analysis of **4**·EtOH: $[\{Pd(L)\}_4](ClO_4)_4 \cdot EtOH$, $M_r = 1740.53$, orange crystal (0.2 × 0.2 × 0.25 mm), triclinic, space group $P\bar{1}$, $a = 15.134(3)$, $b = 15.671(4)$, $c = 14.710(5)$ Å, $\alpha = 116.99(2)$, $\beta = 98.80(2)$, $\gamma = 88.22(2)°$, $V = 3069(1)$ Å^3, $Z = 4$, $\rho_{calcd} = 1.880$ g cm^{-3}, $\mu(Mo_{K\alpha}) = 14.12$ cm^{-1}, 9022 observed reflections, 829 parameters, $R = 0.046$, $R_w = 0.060$. Crystallographic data (excluding structure factors) for the structures reported in this paper have been deposited with the Cambridge Crystallographic Data Centre as supplementary publication no. CCDC-100007. Copies of the data can be obtained free of charge on application to The Director, CCDC, 12 Union Road, Cambridge CB2 1EZ, UK Fax: Int. code +(1223)336-033; e-mail: deposit@chemcrys.cam.ac.uk).

[6] G. Gran, *Analyst* **1952**, *77*, 661.

[7] M. T. Beck, I. Nagypal, *Chemistry of Complex Equilibria*, Wiley, New York, **1990**, p. 44.

2-Thioxoethen-1-one (O=C=C=S)**

Günther Maier,* Hans Peter Reisenauer, and Raimund Ruppel

Generally, upon irradiation in an argon matrix at 10 K dioxides,[1, 2] sulfide oxides,[3] and disulfides[4] of carbon (**1**; X = O, S) decompose into the fragments **2** and **3**.[5] In the

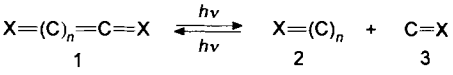

case of the sulfide oxides only CO and no CS is formed as leaving group. Since the fragments remain embedded in the matrix cage the reverse reaction **2** + **3** → **1** can also be triggered upon irradiation with light of the appropriate wavelength.[2–4] Even the photocleavage of matrix-isolated C_2S_2 (**5**) is reversible;[6] hence, we tried to synthesize the elusive C_2O_2 (**7**) in

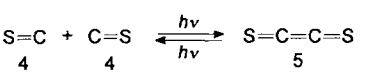

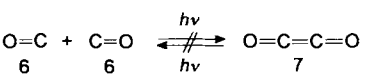

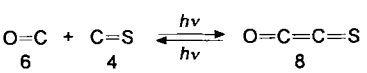

[*] Prof. Dr. G. Maier, Dr. H. P. Reisenauer, Dipl.-Chem. R. Ruppel
Institut für Organische Chemie der Universität
Heinrich-Buff-Ring 58, D-35392 Giessen (Germany)
Fax: Int. code +(641)99-34309

[**] Heterocumulenes, Part 10. This work was supported by the Fonds der Chemischen Industrie and the Deutsche Forschungsgemeinschaft. Part 9: Ref. [8].

 © WILEY-VCH Verlag GmbH, D-69451 Weinheim, 1997 0570-0833/97/3617-1862 $ 17.50+.50/0

the same manner.[7, 8] However, our attempts failed even though with diisocyanate O=C=N–N=C=O[7] we had the ideally suited precursor to produce two CO molecules in the same matrix site. Thus, since the photoaddition of two CS molecules occurs readily, whereas the corresponding dimerization of two CO does not, the behavior of the mixed pair CO/CS should be of particular interest, and herein we report our findings on this system.

The carbon monosulfide needed for the photoreaction was generated by exposing a CS_2/Ar mixture (1/100) to a microwave discharge.[9] It was deposited on a CsI window cooled to 10 K together with the same volume of a CO/Ar mixture (1/5). The concentrations applied were much higher than those necessary for a good matrix isolation; however, this is a statistical prerequisite for a significant fraction of the CS molecules to be trapped in the direct vicinity of a CO molecule. After irradiation of the resulting matrix with 254-nm light (a wavelength at which CS has a strong absorption band), several new IR absorption bands were detected and assigned to C_2OS (Figure 1). Simultaneously, the intensity of the CS band diminished by about 5%,

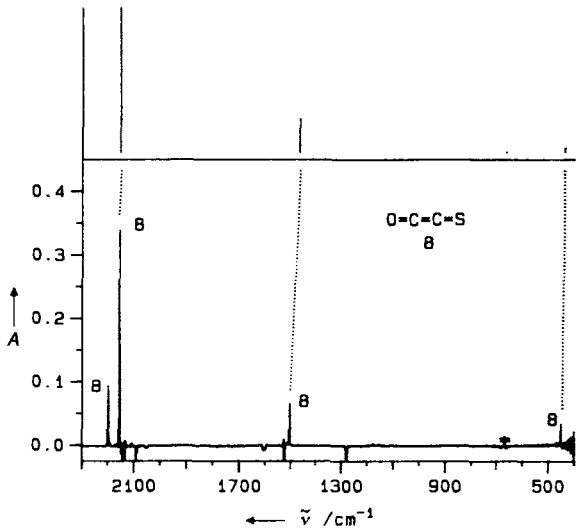

Figure 1. Calculated (BLYP/6-311+G*; top) and experimental (Ar matrix, 10 K, bottom) IR spectrum of thioxoethenone **8**. The experimental spectrum is a difference spectrum of the photoreaction **8** → **4** + **6**.

a corresponding decrease in the intensity of the CO band could not be detected due to the huge initial concentration. During a subsequent short irradiation with 313-nm light the bands of C_2OS listed in Table 1 disappeared and could be recovered again with 254-nm light. The UV spectrum recorded after exposure of a CO/CS matrix to 254-nm light showed a new absorption with vibrational fine structure in the range between 280 and 320 nm with a maximum at 306 nm. The behavior of this UV transition paralleled that of the IR bands during the reverse reaction with 313-nm light. Therefore, this absorption must be attributed to C_2OS (**8**).

In addition to the absorption bands for C_2OS, the described irradiation gave rise to bands attributable to the formation of minor quantities of C_2S_2.[4c] Lower CO concentrations led to higher yields of C_2S_2. In all experiments COS was formed as an additional by-product, presumably as a photoproduct of CO and S atoms present in the matrix.

To facilitate an assignment of the IR bands of C_2OS quantum mechanical calculations were conducted. We employed the MP2(full), MP4(full), CCD, CCSD, and CCSD(T) methods

Table 1. Calculated vibrational spectrum (harmonic approximation) of thioxoethenone **8** (BLYP/6-311+G*) and experimentally observed IR absorptions (Ar matrix, 10 K, relative intensities in parentheses).

		Mode		$\tilde{\nu}_{exp.}$ [cm^{-1}]		$\tilde{\nu}_{calcd}$ [cm^{-1}]	
$\nu_2 + 2\nu_3$	σ			2885.4	(0.1)		
$\nu_1 + \nu_3$	σ			2828.2	(0.45)		
			^{13}C:	2780.0	(0.3)		
$\nu_2 + \nu_3$	σ			2200.1	(32)		
			^{13}C:	2185.3	(6)		
ν_1	σ	OCC str		2156.0	(100)	2151	(100)[a]
			^{13}C:	2109.3	(100)	2098	(100)
ν_2	σ	OCCS str		1505.2	(20)	1464	(23)
			^{13}C:	1501.8	(22)	1461	(26)
			$^{13}C^{18}O$:	1476.5	(5)	1435	(4)
ν_3	σ	OCCS str		ca. 685[b]		662	(0.002)
			^{13}C:	ca. 679[b]		658	(0.007)
ν_4	π	bend		452.2	(9)	437	(3)
			^{13}C:	440.0	(7)	425	(3)
ν_5	π	bend				177	(0.05)
						177	(0.04)

[a] Absolute intensity: 445 km mol^{-1}. [b] Estimated from combination bands.

implemented in the GAUSSIAN 94[10] package of programs in combination with the basis set 6-31G* as well as the density functional approaches BLYP and B3LYP with the 6-31G* and 6-311+G* basis sets. In all cases the following two molecular structures were located as minima on the C_2OS hypersurface: a linear thioxoethenone in a triplet state and a transoidally bent singlet molecule with identical connectivity. ^3C_2OS was always lower in energy, the singlet–triplet gap (including zero point vibrational energies) ranged between 5.4 and 16.3 kcal mol^{-1} depending on the method. A comparison of the calculated IR spectra with those obtained experimentally showed a good correlation with respect to the position of the bands and their intensities, particularly for the linear triplet molecule. This is consistent with Hund's rule, which predicts a triplet ground state for linear C_2OS.

Three stretching vibrations and two degenerate bending modes are expected for the linear C_2OS molecule. The stretching vibrations ν_1 and ν_2 are directly observable (2156 and 1505 cm^{-1}, respectively). The ν_3 vibration could not be detected, which is consistent with the theoretical prediction of an extremely low intensity. Its approximate position (ca. 685 cm^{-1}) can be deduced from the observed combination bands. One of the bending vibrations (ν_4) appears at 452 cm^{-1}. It is essential to note for a correct assignment of the measured IR absorptions that the second strongest band at 2200 cm^{-1} originates from a combination of the fundamentals ν_2 and ν_3. An anharmonic resonance of this combination band with ν_1 leads to an increase in the intensity of the combination band.

To substantiate these findings an analogous experiment with ^{13}C-labeled carbon monoxide containing about 10% ^{18}O was conducted. In all cases, the measured isotopic shifts of the IR bands corresponded with the calculated ones for linear triplet C_2OS. The correlation was less satisfactory for the distorted singlet C_2OS. This is most apparent for the shift of the fundamental ν_2: All computations predict a shift of about 3 cm^{-1} for ^3C_2OS; the experimental value is 3.4 cm^{-1}. In contrast, this absorption band should not shift at all in the corresponding singlet molecule. The resonance of the combination vibration $\nu_2 + \nu_3$ with the fundamental ν_1 virtually disappears in O=^{13}C=C=S. Therefore, the intensity of the higher band decreases sharply.

 © WILEY-VCH Verlag GmbH, D-69451 Weinheim, 1997 0570-0833/97/3617-1863 $ 17.50+.50/0

2-Thioxoethen-1-one (**8**) can thus be generated in a photochemically induced addition of CS to CO. This reaction is reversible. C_2OS, which probably possesses a triplet ground state, is stable under matrix conditions. Our results are in accordance with the findings of Schwarz et al., who by neutralization reionization mass spectrometry identified C_2OS[11] but not C_2O_2[12] as a viable species in the gas phase.

Received: February 24, 1997 [Z10149IE]
German version: *Angew. Chem.* **1997**, *109*, 1972–1973

Keywords: ab initio calculations · cumulenes · IR spectroscopy · matrix isolation · photochemistry

[1] C_3O_2: M. E. Jacox, D. E. Milligan, N. G. Noll, W. E. Thompson, *J. Chem. Phys.* **1965**, *43*, 3734–3746.
[2] a) C_3O_2: G. Maier, H. P. Reisenauer, U. Schäfer, H. Balli, *Angew. Chem.* **1988**, *100*, 590–592; *Angew. Chem. Int. Ed. Engl.* **1988**, *27*, 566–568; b) C_4O_2: G. Maier, H. P. Reisenauer, H. Balli, W. Brandt, R. Janoschek, *ibid.* **1990**, *102*, 920–923; *ibid.* **1990**, *29*, 905–908; c) C_7O_2: G. Maier, H. P. Reisenauer, A. Ulrich, *Tetrahedron Lett.* **1991**, *32*, 4469–4472.
[3] a) C_3OS: G. Maier, J. Schrot, H. P. Reisenauer, *Chem. Ber.* **1991**, *124*, 2613–2616; b) C_4OS: G. Maier, J. Schrot, H. P. Reisenauer, R. Janoschek, *ibid.* **1991**, *124*, 2617–2622.
[4] a) C_5S_2: G. Maier, J. Schrot, H. P. Reisenauer, R. Janoschek, *Chem. Ber.* **1990**, *123*, 1753–1756; b) C_4S_2: [3b]; c) C_2S_2: G. Maier, H. P. Reisenauer, J. Schrot, R. Janoschek, *Angew. Chem.* **1990**, *102*, 1475–1477; *Angew. Chem. Int. Ed. Engl.* **1990**, *29*, 1464–1466.
[5] C_3S_2 and C_3OS are apparently photostable, that is the two fragments recombine immediately: H. P. Reisenauer, unpublished results.
[6] Ref. [4c], footnote 14.
[7] G. Maier, M. Naumann, H. P. Reisenauer, J. Eckwert, *Angew. Chem.* **1996**, *108*, 1800–1801; *Angew. Chem. Int. Ed. Engl.* **1996**, *35*, 1696–1697.
[8] The monoxime of C_2O_2 could be isolated by a completely different route and identified by matrix-isolation spectroscopy: G. Maier, H. P. Reisenauer, B. Röther, J. Eckwert, *Liebigs Ann.* **1996**, 303–306.
[9] Review: E. K. Moltzen, K. J. Klabunde, A. Senning, *Chem. Rev.* **1988**, *88*, 391–406.
[10] GAUSSIAN 94 (Revision B.1), M. J. Frisch, G. W. Trucks, H. B. Schlegel, P. M. W. Gill, B. G. Johnson, M. A. Robb, J. R. Cheeseman, T. A. Keith, G. A. Petersson, J. A. Montgomery, K. Raghavachari, M. A. Al-Laham, V. G. Zakrzewski, J. V. Ortiz, J. B. Foresman, J. Cioslowski, B. B. Stefanov, A. Nanayakkara, M. Challacombe, C. Y. Peng, P. Y. Ayala, W. Chen, M. W. Wong, J. L. Andres, E. S. Replogle, R. Gomperts, R. L. Martin, D. J. Fox, J. S. Binkley, D. J. Defrees, J. Baker, J. P. Stewart, M. Head-Gordon, C. Gonzalez, J. A. Pople, Gaussian, Inc., Pittsburgh PA, **1995**.
[11] D. Sülzle, J. K. Terlouw, H. Schwarz, *J. Am. Chem. Soc.* **1990**, *112*, 628–630.
[12] D. Sülzle, T. Weisske, H. Schwarz, *Int. J. Mass. Spectr. Ion Proc.* **1993**, *125*, 75–79.

Pyrazinedioxide–Tetracyanoethylene Arrays in the Solid State—New Donor–Acceptor Interactions for Crystal Engineering**

Melinda L. Greer, Byron J. McGee, Robin D. Rogers, and Silas C. Blackstock*

Molecular recognition forms the basis of supramolecular chemistry[1] and, in the solid state, of crystal engineering.[2] Of the intermolecular interactions commonly employed as crystal engineering synthons,[3] neutral organic donor–acceptor (DA) attractions[4] have remained relatively rare. Recent findings[5,6] of TCNE/azooxide complexes (TCNE = tetracyanoethylene) prompted our further investigation of heterocyclic *N*-oxides as donors for the preparation of dimensionally ordered organic DA crystals. The first examples, crystalline pyrazinedioxide–TCNE arrays, are reported here.

Pyridine *N*-oxides are known to give colored solutions with TCNE.[7] However, these mixtures typically decompose on standing, and no structurally characterized DA complexes in this series have previously been reported. Recently we found that mixtures of 2,3,5,6-tetramethylpyrazine-*N*,*N*′-dioxide (TMPDO)[8] and TCNE in solution yield chemically stable purple solutions (λ_{max} = 524 nm in CH_2Cl_2, 500 nm in CH_3CN) from which crystalline $(TMPDO)_2TCNE$ solids may be isolated.

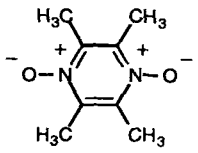

TMPDO

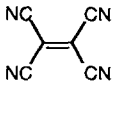

TCNE

The visible absorption of TMPDO/TCNE solutions is assigned to a charge-transfer (CT) excitation of the 1:1 DA complex. Benesi–Hildebrand analysis[9] of TMPDO/TCNE mixtures in CH_2Cl_2 yields a complex formation constant K_f of $1.4(2)\,M^{-1}$.[10]

Cooling of purple TMPDO/TCNE mixtures in CH_3CN affords deeply colored $(TMPDO)_2TCNE$ crystals. Two polymorphs of the solid crystallize and may be prepared independently as purple needles (at short times) or red prisms (at longer times). As indicated by these crystal equilibration results at 253 K, the red crystals are thermodynamically favored, and the purple crystals are a kinetic product at this temperature in CH_3CN. UV/Vis data for the $(TMPDO)_2TCNE$ solids (Nujol mulls) and for the complex in solution are shown in Figure 1.

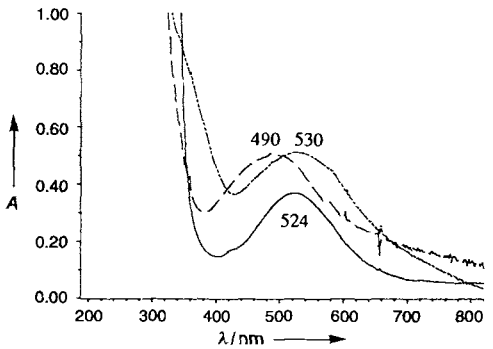

Figure 1. UV/Vis spectra of TMPDO (1.9 mM) and TCNE (51.2 mM) in CH_2Cl_2 (—), as well as of red (– – –) and purple crystals of $(TMPDO)_2TCNE$ (—·—).

The purple $(TMPDO)_2TCNE$ crystal is composed of infinite double strands in which intermolecular O–C attractions are apparent between donor and acceptor (Figure 2).[11] The O–C contacts are 2.769(2) and 2.914(2) Å, much shorter than the sum of atomic van der Waals radii[12] (3.22 Å). In this array TCNE molecules, located on inversion centers, are the rungs of a TMPDO-railed ladder. We postulate that electrostatic forces and HOMO–LUMO overlap between the TMPDO oxygen

[*] Prof. S. C. Blackstock, M. L. Greer, B. J. McGee, Prof. R. D. Rogers
Department of Chemistry
The University of Alabama
Tuscaloosa, AL 35487-0336 (USA)
Fax: Int. code +(205)348-9104
e-mail: sblackst@ua1vm.ua.edu

[**] This research was supported by the United States National Science Foundation (NSF projects CHE-9200144 and CHE-9626144) and by the University of Alabama. We thank L. M. Rogers for assistance with X-ray crystal structures. B. J. M. was supported by the NSF REU program (CHE-9531496).

 © WILEY-VCH Verlag GmbH, D-69451 Weinheim, 1997 0570-0833/97/3617-1864 $ 17.50+.50/0

atoms, and the TCNE olefin carbon atoms contribute to a weak DA "bond", which provides cohesion for the strand formation in the lattice. Accordingly, the donor oxygen atoms are positioned at the four π^* lobes of the TCNE LUMO in a rectangular "ligand field" about the electron-poor alkene. Intraladder π stacking of TMPDO donors occurs at van der Waals distance (3.4 Å from plane to plane). Slipping of the π-stacked donors by about 1.3 Å along the ladder axis creates head-to-tail NO dipolar alignment across the ladder and skews the ladder superstructure slightly. Adjacent ladders close-pack in a staggered arrangement (Figure 2).

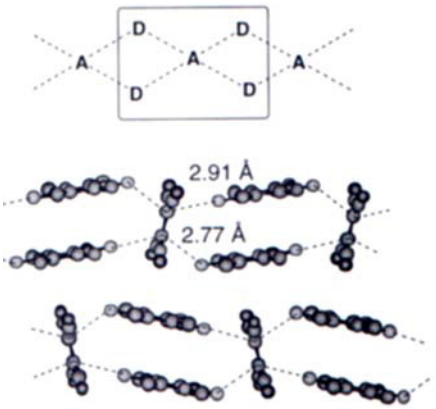

Figure 2. Schematic representation of the DA connectivity in the ladder array in purple crystals of $(TMPDO)_2TCNE$ (top) as well as a ball-and-stick drawing of two adjacent ladder chains (bottom).

Polymorphic red $(TMPDO)_2TCNE$ crystals form a topologically different DA array, which possesses 2D D–A connectivity (Figure 3).[13] Here, each TCNE "binds" four TMPDO donors (as for the purple array) and each TMPDO donor bridges a unique pair of TCNE molecules, creating a web-like D_2A "sheet". A pinwheel arrangement of four donors about each TCNE acceptor is observed. Distances between TMPDO oxygen atoms and TCNE olefinic carbon atoms are 2.849(2) and 2.764(2) Å. The web sheets are not planar but sinusoidal in profile and stack in a closest-packing arrangement. The web itself comprises fused eight-molecule rings, made of four TMPDO donors and four TCNE acceptors.

At 363–373 K red $(TMPDO)_2TCNE$ crystals change irreversibly to purple without melting.[14] Room-temperature UV/Vis spectroscopy[15] and (most convincingly) powder X-ray diffraction analysis of the crystals before and after heating verify the irreversible web to ladder supramolecular transformation.[16, 17] Representative powder X-ray diffractograms are shown in Figure 4. Topologically, the red web network may be viewed as a cross-linked ladder array, and thus the thermal process may be considered a reverse cross-linking of the lattice. Because the spacing between TCNE units [18] and the donor–oxygen positions[19] about TCNE are quite similar in the two polymorphs, a web-to-ladder transition requires only slight molecular reorientation in the solid. The mechanism for isomerization of the array minimally involves pivoting (one end migration) of half the TMPDO donors and rotation of alternate TCNE acceptors.

The NO···C interactions of azaaromatic *N*-oxides with TCNE reported here constitute a new functional group interaction in the solid state, whose potential application to crystal engineering appears promising, especially in view of the wide structural diversity of this donor group.[20, 21] A common struc-

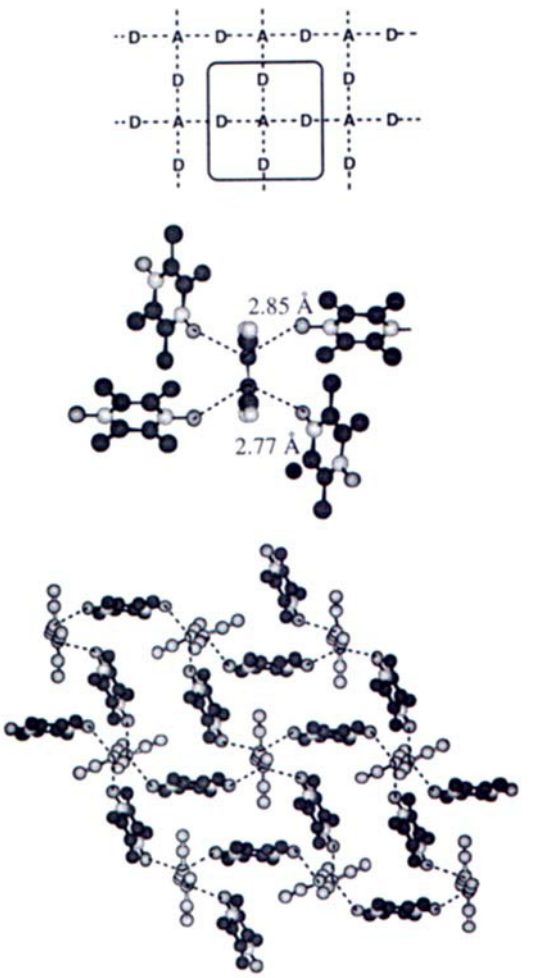

Figure 3. Schematic representation of the DA connectivity on the web array of red crystals of $(TMPDO)_2TCNE$ (top) as well as a ball-and-stick drawing of the "binding" of the TCNE molecule (middle) and the two-dimensional web molecular array (bottom).

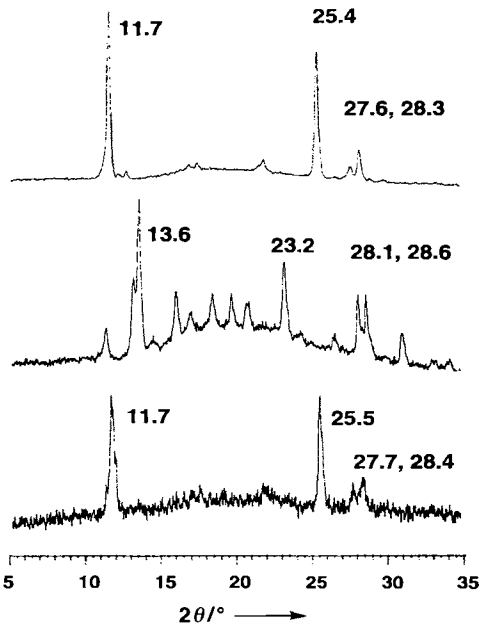

Figure 4. Powder-diffractograms of $(TMPDO)_2TCNE$ crystals: purple (top); red before (middle) and after heating (bottom).

 © WILEY-VCH Verlag GmbH, D-69451 Weinheim, 1997 0570-0833/97/3617-1865 $ 17.50+.50/0

tural feature of these $(TMPDO)_2TCNE$ arrays is rectangular four-site O–C binding at the TCNE olefinic carbon atoms, which appear to interact through their π^* lobes. The topological requirement for DA complexation at the *N*-oxide center is more flexible, allowing the formation of both ladder and web (cross-linked ladder) DA arrays in the $(TMPDO)_2TCNE$ crystals as the N-O-C angle flexes.

Experimental Section

TMPDO (2.58 g, 69%, m.p. 498 K (493 K [22])) was prepared by treatment of 2,3,5,6-tetramethylpyrazine (2.95 g, Aldrich) in CH_2Cl_2 (50 mL) with potassium peroxomonosulfate (66.6 g, 5 equiv; OXONE, Aldrich) in H_2O (400 mL) with vigorous stirring at 298 K for 24 h. TCNE (Aldrich) was purified by multiple sublimation (373 K, 0.05 mm Hg) through activated charcoal. Conditions for the Benesi–Hildebrand analysis: [TMPDO] = 1.90 mM; [TCNE] = 18.7, 34.0, 51.1, 66.4, 75.7, and 90.6 mM. Purple crystals of $(TMPDO)_2TCNE$ were prepared by cooling a mixture of TMPDO (40 mM) and TCNE (20 mM) in CH_3CN to 253 K for 2–5 h. Red prismatic crystals of $(TMPDO)_2TCNE$ were prepared analogously, after 2–3 d crystallization.

Crystal X-ray diffraction was performed on a Siemens SMART diffractometer with CCD area detection at 293 (purple [11]) and 173 K (red [13]) with monochromatic $Mo_{K\alpha}$ radiation ($\lambda = 0.71073$ Å). Solution and refinement (against $|F^2|$) were performed with SHELXTL. No absorption correction was employed. Hydrogen atoms were placed in calculated positions (0.95 Å from the methyl carbon atom with tetrahedral angles). They were given torsional freedom and their thermal parameters were set to $1.2 \times U_{eq}$ of the bonded carbon atom. Crystallographic data (excluding structure factors) for the structures reported in this paper have been deposited with the Cambridge Crystallographic Data Centre as supplementary publication no. CCDC-100438. Copies of the data can be obtained free of charge on application to The Director, CCDC, 12 Union Road, Cambridge CB2 1EZ, UK (fax: int. code + (1223) 336-033; e-mail: deposit@chemcrys.cam.ac.uk). Powder $Cu_{K\alpha}$ X-ray spectra were obtained on a Rigaku powder diffractometer.

Received: January 24, 1997 [Z 10030 IE]
German version: *Angew. Chem.* **1997**, *109*, 1973–1976

Keywords: crystal engineering · donor–acceptor systems · noncovalent interactions · polymorphism · supramolecular chemistry

[1] J.-M. Lehn, *Supramolecular Chemistry*, VCH, Weinheim, **1995**.
[2] Reviews: a) G. R. Desiraju, *Crystal Engineering: The Design of Organic Solids*, Elsevier, Amsterdam, **1989**; b) A. Gavezzotti, *Acc. Chem. Res.* **1994**, *27*, 309; c) *The Crystal as a Supramolecular Entity. Perspectives in Supramolecular Chemistry* (Ed.: G. R. Desiraju), Wiley, New York, **1996**.
[3] D. S. Reddy, Y. E. Ovchinnikov, O. V. Shishkin, Y. T. Struchkov, G. R. Desiraju, *J. Am. Chem. Soc.* **1996**, *118*, 4085, and references therein.
[4] Reviews: a) H. A. Bent, *Chem. Rev.* **1968**, *68*, 587; b) R. S. Mulliken, W. B. Person, *Molecular Complexes: A Lecture and Reprint Volume*, Wiley-Interscience, New York, **1969**; c) R. Foster, *Organic Charge-Transfer Complexes*, Academic Press, New York, **1969**, chap. 8; d) F. H. Herstein, *Perspect. Struct. Chem.* **1971**, *4*, 166.
[5] S. C. Blackstock, K. Poehling, M. L. Greer, *J. Am. Chem. Soc.* **1995**, *117*, 6617.
[6] M. L. Greer, S. C. Blackstock, *J. Org. Chem.* **1996**, *61*, 7895.
[7] a) P. Bruni, C. Conti, E. Giorgini, G. Tosi, G. Marrosu, *Spectrochim. Acta Part A* **1991**, *47*, 665; b) A. V. Ryzhakov, L. L. Rodina, *Russ. J. Heterocycl. Chem.* **1991**, *4*, 386; c) P. Bruni, G. Tosi, L. Cardellini, E. Giorgini, P. Stipa, *Spectrochim. Acta Part A* **1989**, *45*, 519; d) A. V. Ryzhakov, V. V. Vapirov, L. L. Rodina, *Zh. Org. Khim.* **1991**, *27*, 955.
[8] The standard potential of TMPDO was determined by cyclic voltammetry to be 1.61 V versus SCE (0.1 M nBu_4NBF_4 in CH_2Cl_2).
[9] H. A. Benesi, J. H. Hildebrand, *J. Am. Chem. Soc.* **1949**, *71*, 2703.
[10] This value derives from a single Benesi–Hildebrand analysis with [TCNE] ≫ [TMPDO], in which absorbances at 484, 504, 524, and 544 nm (with ε values of 1928, 2771, 2701, and 2371 $M^{-1}cm^{-1}$, respectively) were monitored to calculate K_f on the assumption of 1:1 complexation.
[11] Crystal structure data for the purple crystal: dimensions: 0.30 × 0.55 × 0.70 mm; monoclinic, space group *C*2/*c*, $a = 15.7184(5)$, $b = 10.3443(3)$, $c = 14.2302(2)$ Å, $\beta = 91.824(2)°$, $V = 2312.6(1)$, $\rho_{calcd} = 1.334\ g\,mL^{-1}$; $2.36 \le \theta \le 27.86°$; of 2738 unique data 1632 with $I > 2\sigma(I)$, 159 parameters; $R_1 = 0.054$, $wR_2 = 0.134$, GOF = 0.981. Several different purple crystals were analyzed at 293 and at 173 K. All gave the same unit cell.
[12] For van der Waals radii in crystals, see a) A. Bondi, *J. Phys. Chem.* **1964**, *68*, 441; b) R. S. Rowland, R. Taylor, *ibid* **1996**, *100*, 7384.
[13] Crystal structure data for the red crystal: dimensions: 0.40 × 0.30 × 0.25 mm; monoclinic, space group $P2_1/n$, $a = 9.2619(4)$, $b = 9.8160(4)$, $c = 12.7949(5)$ Å, $\beta = 99.590(1)°$, $V = 1146.99(8)$, $\rho_{calcd} = 1.345\ g\,mL^{-1}$; $2.53 \le \theta \le 27.91°$; of 2634 unique data 1967 with $I > 2\sigma(I)$, 159 parameters; $R = 0.054$, $wR_2 = 0.123$, GOF = 1.133. Several different red crystals were analyzed, and all gave the same unit-cell parameters.
[14] Both the red and purple solids melt at 177–180 °C with decomposition.
[15] A 40 nm shift in the visible absorption of the red crystal is observed after heating the red solid to 90 °C for 20 min.
[16] Reviews of thermal solid-state transformations: a) I. C. Paul, D. Y. Curtin, *Acc. Chem. Res.* **1973**, *6*, 217; b) J. D. Dunitz, *Pure Appl. Chem.* **1991**, *63*, 177.
[17] A differential scanning calorimetric (DSC) scan of the red polymorph shows an endotherm ($13.16\ J\,g^{-1}$) at 376 K corresponding to the lattice transition. This transition is not observed for the purple polymorph.
[18] Average intraweb (red) and intraladder (purple) TCNE–TCNE distances (olefin C-to-C) are 9.9 and 10.5 Å, respectively.
[19] Distances between TMPDO oxygen atoms at a single TCNE are 3.97 (1,2) and 4.97 Å (1,1) in the red crystal, and 3.67 and 5.19 Å in the purple crystal.
[20] Precedence for this type of NO···C interaction is found in azooxide–TCNE complexes of ref. [5, 6]. Such interactions appear to be general as indicated by their occurrence in the crystal structures of phenazine-*N*,*N*′-dioxide/TCNE and 2,3-dimethylquinoxaline-*N*,*N*′-dioxide/TCNE (to be reported elsewhere).
[21] A Cambridge Structure Database (edition December 1996) search of crystal structures with NO···C=C interactions, O–C distances of 2.0–3.0 Å and O-C-C angles of 80–140° yielded 25 structures (excluding the azooxide complexes mentioned above), all of which involve nitrate or nitro oxygen donors and (in all but one case) arene acceptors with O–C contacts of 2.89–3.00 Å. Of the 25 structures found, 14 contain metal-coordinated donor and/or acceptor groups.
[22] G. A. Tolstikov, U. M. Jemilev, V. P. Jurjev, F. B. Gershanov, S. R. Rafikov, *Tetrahedron Lett.* **1971**, *30*, 2807.

In Search of Molecular Ratchets**

T. Ross Kelly,* Imanol Tellitu, and José Pérez Sestelo

The creation and the control of movement are fundamental aspects of dynamics on both macroscopic and microscopic levels. Much current interest is focused on constructing molecular scale analogues of macroscopic devices, in part because of the intellectual challenge, but also because of their potential applications in nanotechnology.[1] We now report the results of an effort to synthesize the first molecular ratchets. The work was undertaken partly as a result of a continuing[1a] interest in molecular devices, but it also serves to demonstrate that macromechanical principles do not always transfer to the molecular scale.

In their simplest form, ratchets consist of three components (Figure 1): a) a toothed ratchet wheel, b) a pawl that prevents unintended rotation of the ratchet wheel, and c) a spring that holds the pawl in place. Both the tension of the spring and the contours of the ratchet wheel and pawl determine the ease (and direction) of rotation.

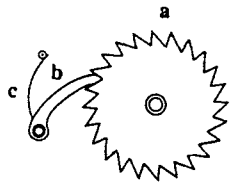

Figure 1. A simple ratchet: a) toothed wheel, b) pawl, c) spring.

In the present instance a triptycene[2] was chosen as the ratchet wheel and helicenes[3] as the pawls and springs. The two molecular "ratchets" are **1**[4] and **2**. Molecular modeling calcu-

[*] Prof. T. R. Kelly, Dr. I. Tellitu, Dr. J. P. Sestelo
E. F. Merkert Chemistry Center
Boston College
Chestnut Hill, MA 02167 (USA)
Fax: Int. code + (617) 552-2705
e-mail: ross.kelly@bc.edu

[**] J. P. S. acknowledges Xunta de Galicia and the University of Santiago de Compostela (Spain) for a postdoctoral fellowship. We thank Dr. Chun Zhou for assistance with the spin polarization transfer measurements, Dr. Matthew Bratcher and Prof. W. H. Laarhoven for valuable exchanges of information, and a referee for helpful comments.

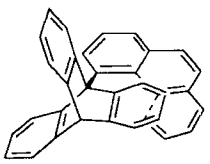

1

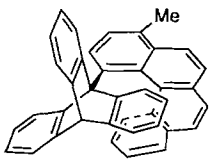

2

lations[5] indicated unexpectedly—at least to us—that the [3]helicene spring and pawl in **1** present a greater barrier to rotation (ΔH calculated to be 27 kcal mol^{-1}) than the [4]helicene in **2** ($\Delta H = 22$ kcal mol^{-1}).

Compound **1** was prepared from the known ketone **3** (Scheme 1).[6] Conversion of **3** to the enol triflate **4** and palladium-catalyzed coupling with anthracenyl stannane **5**[1a] gave **6**.[7]

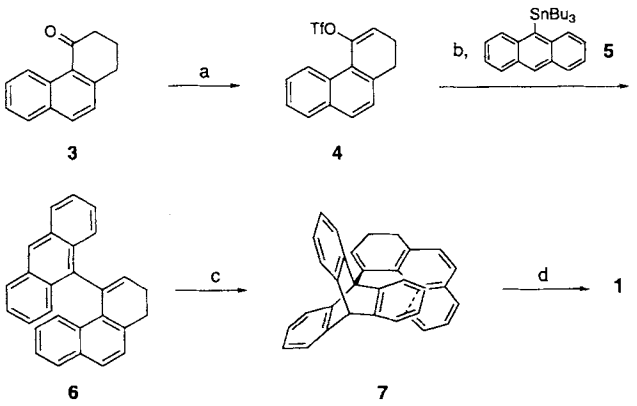

Scheme 1. a) $(F_3CSO_3)_2O$, 2,6-lutidine, CH_2Cl_2, 0 °C, 77%; b) $[Pd(PPh_3)_4]$, LiCl, dioxane, 120 °C, sealed tube, 3 d, 55%; c) benzyne, dioxane, reflux; d) 2,3-dichloro-5,6-dicyano-1,4-benzoquinone (DDQ), C_6H_6, reflux, 53% (overall yield for steps c and d).

Addition of benzyne[8] across the 9,10 positions of the anthracene in **6** generated the triptycene unit **7**; dehydrogenation[9] of **7** completed the synthesis.[10]

Compound **2** was synthesized by the route in Scheme 2. Palladium-catalyzed coupling of bromoaldehyde **8**[11] with stannane **5** gave **9**, which was converted into triptycene **10** by addition of benzyne.[8] Wittig reaction of the aldehyde group in **10** with the ylide from **11**[12] delivered an *E*/*Z* mixture of stilbenes **12**. Irradiation[3, 13, 14] through Pyrex of a benzene solution of **12** with a medium pressure (100 W) mercury lamp under argon in the presence of I_2 (1 equiv) and excess propylene oxide generated

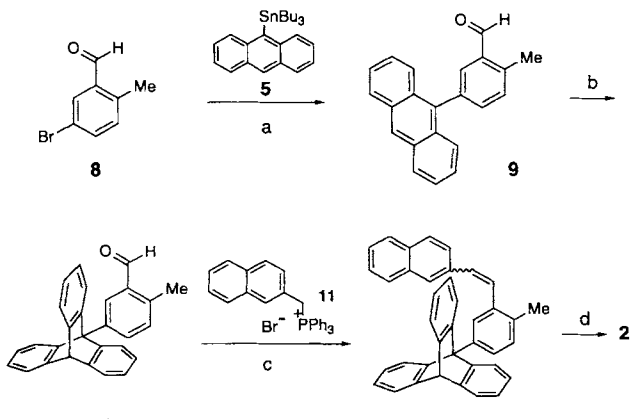

Scheme 2. a) $[Pd(PPh_3)_2]Cl_2$, dioxane, 130 °C, sealed tube, 60 h, 60%; b) benzyne, dioxane, reflux, 68%; c) *n*-BuLi, THF, −78 °C, 84%; d) *hv*, 54%.

2[15] in 54% yield. The methyl group blocks photocyclization in the undesired, but otherwise less hindered direction.

The ^{1}H NMR spectra of **1** and **2** indicate that at room temperature rotation around the triptycene/helicene bond is frozen in both compounds, but that the topology of the two is distinctly different. In particular, the ^{1}H NMR spectrum of **1** reveals a plane of symmetry; two (but not all three) of the rings of the triptycene unit are equivalent. The phenanthrene component of **1** is therefore either planar or exists as a rapidly racemizing mixture of two helical enantiomers.[4] Even at 160 °C, ^{1}H NMR spin polarization transfer experiments[16] reveal no detectable rotation within two seconds of polarization, which indicates a barrier ($\Delta G^{\neq}$) to rotation in excess of 27 kcal mol^{-1}.

The ^{1}H NMR spectrum of **2** recorded at room temperature reflects an absence of symmetry; all three rings of the triptycene are nonequivalent. At 160 °C, however, peak-broadening of triptycene (but not helicene) resonances indicates slow rotation. Extrapolation, based on analogy to our earlier work,[1a] suggests a coalescence temperature of about 220 °C, which corresponds to $\Delta G^{\neq} \approx 25$ kcal mol^{-1}, a value that is corroborated by the studies described below, and which is reassuringly close to the calculated barrier ($\Delta H^{\neq}$ not $\Delta G^{\neq}$) of 22 kcal mol^{-1}. We suggest that the barrier to rotation in **2** is smaller than in **1** because in **2** the interaction between the one-ring-longer helicene and the blade of the triptycene prevents the molecule from relaxing to as stable a ground state conformation (relative to the energy maximum) as is accessible to **1**.

The remaining question is whether **2** functions as a ratchet; that is, whether rotation of the triptycene is uni- or bidirectional. Given the helicity of the [4]helicene in **2**, it is not surprising that the calculated[5] energy diagram (Figure 2) for rotation around the triptycene/[4]helicene bond in **2** is decidedly asymmetric. Clockwise rotation ($\alpha = 0 \rightarrow 120°$) has a more gradual energetic slope than counterclockwise rotation ($\alpha = 120 \rightarrow 0°$).

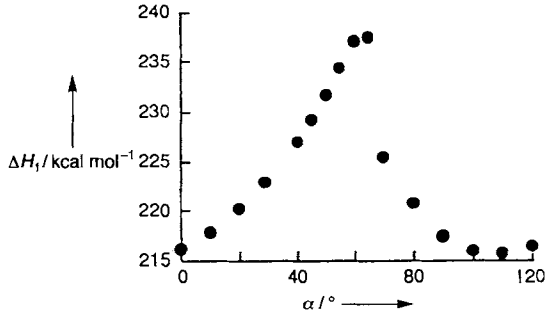

Figure 2. Calculated energy diagram (AM1 [5]) for rotation around the triptycene/[4]helicene bond. Clockwise rotation of the triptycene in **2** corresponds to a rotation from $\alpha = 0$ to $\alpha = 120°$.

One should be able to establish the direction of rotation of the triptycene in **2** by using isotopically labeled rotamers of **2**, but their synthesis, rotamer separation, and structure determination would be very laborious. Fortunately, the spin polarization transfer NMR technique[16] affords the same information at a small fraction of the effort. In short, if a system is conformationally mobile, but that mobility is slow on the NMR time scale, the spin of a slowly conformationally mobile atom can be polarized, and after an appropriate time an assay will show where (if anywhere) that polarization has moved to.

In the present case in which a single rotamer has an experimentally determined half-life of about 0.17 sec at 160 °C, the barrier ($\Delta G^{\neq}$) to rotation is approximately 24.5 kcal mol^{-1}. Thus, if one selectively polarizes one of the three H_a, H_b, and H_c protons (see **13** in Figure 3) and—after appropriate time de-

 © WILEY-VCH Verlag GmbH, D-69451 Weinheim, 1997 0570-0833/97/3617-1867 $ 17.50+.50/0

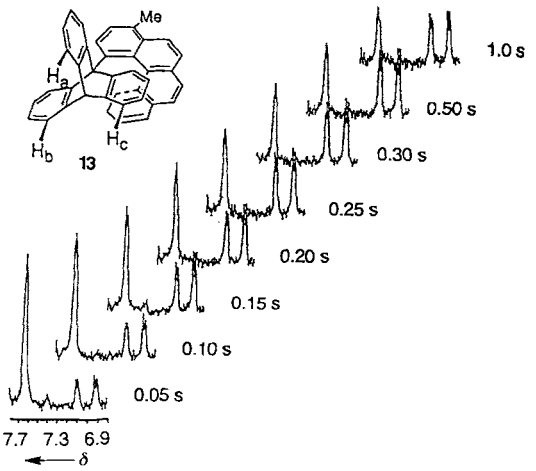

Figure 3. Results of spin polarization transfer experiment in [D$_6$]DMSO at 160 °C (calibrated temperature). The resonances for H_a, H_b, and H_c (see **13**) appear at $\delta = 7.6$, 7.1, and 6.9 (not necessarily respectively). The spin of the proton resonating at $\delta = 7.6$ was polarized, and transfer of that polarization was monitored over time.

lays—assays for the location of that polarization, a clearcut distinction between predominantly unidirectional rotation and bidirectional rotation is available. In the first case, a disproportionate share of the polarization that has moved should be transferred to a resonance for only one of the two other protons. In the second case, the polarization that moves should be transferred equally to the remaining two resonances.

Spin polarization of one (see **13**) of the three H_x protons in **2** was achieved with a selective 180°-pulse–delay–observe sequence. As is evident from Figure 3, the triptycene rotates clockwise and counterclockwise to the same extent. Control experiments polarizing the spin of each of the other two H_x protons gave equivalent results.[17] The asymmetry of the rotational energy curve in Figure 2 is thus deceptive: In contrast to mountain climbing, it is only the height of the summit, not the steepness of the terrain that matters. The chemical principle of microscopic reversibility prevails.

The current study also provides experimental corroboration of a theoretical, thermodynamic analysis of a ratchet and pawl by the physicist Richard Feynman.[18]

In conclusion, the synthesis of triptycene[4]helicene **2** successfully incorporates into a single molecule the essential components of a simple ratchet: the asymmetric combination of a ratchet wheel, a pawl, and a spring. Tantalizing as models of **2** are, the experimental demonstration that **2** rotates equally in both directions illustrates the perils of extrapolating from macroscopic to molecular scales. It follows that molecular units such as **2** cannot by themselves be used to induce unidirectional rotation in an isothermal environment. Nonetheless, their ability to modulate the barrier to free rotation should make them useful components of more complex systems such as molecular motors and machines.

Received: December 23, 1996
Revised version: May 5, 1997 [Z9932, Z9933IE]
German version: *Angew. Chem.* **1997**, *109*, 1969–1972

Keywords: helical structures · molecular devices · nanostructures · triptycenes

[1] a) For the report of a molecular brake from this laboratory see T. R. Kelly, M. C. Bowyer, K. V. Bhaskar, D. Bebbington, A. Garcia, F. Lang, M. H. Kim, M. P. Jette, *J. Am. Chem. Soc.* **1994**, *116*, 3657–3658. For leading references to other studies see b) T. C. Bedard, J. S. Moore, *ibid.* **1995**, *117*, 10662–10671; c) J. Rebek, Jr., *Acc. Chem. Res.* **1984**, *17*, 258–264; d) K. Mislow, *Chemtracts: Org. Chem.* **1989**, *2*, 151–174; e) H. Iwamura, K. Mislow, *Acc. Chem. Res.* **1988**, *21*, 175–182; f) D. H. Evans, A. Fitch, *J. Am. Chem. Soc.* **1984**, *106*, 3039–3041; g) R. Ballardini, V. Balzini, A. Credi, M. T. Ganfolfi, S. J. Langford, S. Menzer, L. Prodi, J. F. Stoddart, M. Venturi, D. J. Williams, *Angew. Chem.* **1996**, *108*, 1056–1059; *Angew. Chem. Int. Ed. Engl.* **1996**, *35*, 978–981; h) K. V. Kilway, J. S. Siegel, *J. Am. Chem. Soc.* **1991**, *113*, 2332–2333; i) N. P. M. Huck, W. F. Jager, B. de Lange, B. L. Feringa, *Science* **1996**, *273*, 1686–1688; j) M. Jorgenson, K. Lerstrup, P. Frederiksen, T. Bjornholm, P. Sommer-Larsen, K. Schaumburg, K. Brunfeldt, K. Bechgaard, *J. Org. Chem.* **1993**, *58*, 2785–2790; k) R. M. Metzger, C. A. Panetta, *New. J. Chem.* **1991**, *15*, 209–221; l) A. C. Benniston, A. Harriman, *Angew. Chem.* **1993**, *105*, 1553–1555; *Angew. Chem. Int. Ed. Engl.* **1993**,*32*, 1459–1461.

[2] Review: V. R. Skvarchenko, V. K. Shalaev, E. I. Klabunovskii, *Russ. Chem. Rev.* **1974**, *43*, 951–966.

[3] Reviews of helicene chemistry: a) R. H. Martin, *Angew. Chem.* **1974**, *86*, 627–638; *Angew. Chem. Int. Ed. Engl.* **1974** *13*, 649–660; b) W. H. Laarhoven, W. J. C. Prinsen, *Top. Curr. Chem.* **1984**, *125*, 63–130; c) K. P. Meurer, F. Vögtle, *ibid.* **1985**, *127*, 1–76. Some more recent references: d) N. D. Willmore, L. Liu, T. J. Katz, *Angew. Chem.* **1992**, *104*, 1082–1083; *Angew. Chem. Int. Ed. Engl.* **1992**, *31*, 1093–1094; e) R. H. Janke, G. Haufe, E. Würthwein, J. H. Borkent, *J. Am. Chem. Soc.* **1996**, *118*, 6031–6035.

[4] Although the parent phenanthrene itself is planar, calculations [5] indicate that the phenanthrene ring system in **1** is helical. For the discussion of another helical phenanthrene, see E. L. Eliel, S. H. Wilen, *Stereochemistry of Organic Compounds*, Wiley, New York, **1994**, p. 1163.

[5] Calculations (AM1) were carried out with the coordinate drive feature of the Spartan molecular modeling program (Wavefunction, Inc., Irvine, CA), Version 4.0, on a Silicon Graphics workstation.

[6] S. Huggenberg, M. Hesse, *Helv. Chem. Acta* **1980**, *63*, 2295–2301.

[7] J. K. Stille, *Angew. Chem.* **1986**, *98*, 504–520; *Angew. Chem. Int. Ed. Engl.* **1986**, *25*, 508–524.

[8] F. M. Logullo, A. H. Seitz, L. Friedman, *Org. Synth. Coll. Vol. 5* **1973**, 54–59.

[9] M. Tashiro, T. Yamato, K. Kobayashi, T. Arimura, *J. Org. Chem.* **1987**, *52*, 3196–3199.

[10] **1**: M.p. 316–317 °C; ^{1}H NMR ($CDCl_3$, 400 MHz): $\delta = 8.38$ (d, $J = 8.0$ Hz, 1H), 8.06 (d, $J = 8.0$ Hz, 1H), 7.87–7.80 (m, 2H), 7.75 (d, $J = 8.4$ Hz, 1H), 7.72 (d, $J = 8.0$ Hz, 1H), 7.56–7.54 (m, 1H), 7.50 (d, $J = 7.6$ Hz, 2H), 7.35–7.33 (m, 1H), 7.21 (d, $J = 8.8$ Hz, 1H), 7.17 (t, $J = 7.3$ Hz, 1H), 7.00–6.96 (m, 2H), 6.89–6.86 (m, 2H), 6.79 (d, $J = 7.6$ Hz, 2H), 6.59–6.55 (m, 2H), 6.38–6.34 (m, 1H), 5.46 (s, 1H); ^{13}C NMR ($CDCl_3$, 100 MHz): $\delta = 150.2$, 148.7, 145.3, 144.1, 134.6, 134.0, 133.7, 132.2, 131.7, 131.6, 131.5, 130.6, 128.9, 127.5, 127.1, 126.9, 125.9, 125.3, 124.9, 124.7, 124.6, 124.1, 123.5, 123.3, 122.0, 63.5, 55.2 (two peaks are coincident); LR-MS (EI, 70 eV): *m/z* (%): 431 (45, $[M+H]^+$), 430 (100, M^+), 253 (21), 252 (30); HR-MS (EI): calcd: for $C_{34}H_{22}$: 430.1721, found: 430.1721.

[11] I. Stoilov, D. S. Watt, J. P. Goodman, J. S. Pyrek, *J. Heterocycl. Chem.* **1993**, *30*, 1645–1651.

[12] J. P. Geerts, R. H. Martin, *Bull. Soc. Chim. Belg.* **1960**, *60*, 563–569.

[13] F. B. Mallory, C. W. Mallory, *Org. React.* **1984**, *30*, 1–456.

[14] L. Lui, B. Yang, T. J. Katz, M. K. Poindexter, *J. Org. Chem.* **1991**, *56*, 3769–3775.

[15] **2**: M.p. 310 °C; ^{1}H NMR ($CDCl_3$, 300 MHz): $\delta = 8.43$ (m, 1H), 8.33 (d, $J = 8.4$ Hz, 1H), 8.23 (d, $J = 7.2$ Hz, 1H), 7.96 (d, $J = 7.5$ Hz, 1H), 7.87 (t, $J = 8.4$ Hz, 2H), 7.76 (d, $J = 8.1$ Hz, 1H), 7.75 (d, $J = 8.4$ Hz, 1H), 7.57 (m, 1H), 7.35 (m, 3H), 7.05 (dd, $J = 7.2$, 1.5 Hz, 1H), 6.88 (dd, $J = 7.6$, 1.2 Hz, 1H), 6.82 (t, $J = 7.8$ Hz, 1H), 6.61 (dq, $J = 7.5$, 1.8 Hz, 2H), 6.48 (d, $J = 8.0$ Hz, 1H), 6.38 (dt, $J = 7.2$, 1.2 Hz, 1H), 5.92 (dt, $J = 7.8$, 1.2 Hz, 1H), 5.87 (d, $J = 7.8$ Hz, 1H), 5.79 (dt, $J = 7.8$, 1.2 Hz, 1H), 5.10 (s, 1H), 3.00 (s, 3H); ^{13}C NMR ($CDCl_3$, 100 MHz): $\delta = 151.9$, 150.4, 147.0, 145.2, 143.8, 143.6, 137.3, 134.9, 134.4, 133.2, 131.5, 130.9, 130.8, 130.4, 129.9, 129.7, 127.9, 127.6, 126.4, 126.2, 126.1, 126.0, 125.9, 125.6, 125.5, 124.6, 124.2, 124.0, 124.0, 123.9, 123.9, 123.7, 123.5, 123.1, 122.7, 122.2, 65.8, 55.8, 20.6; LR-MS (EI, 70 eV): *m/z* (%): 496 (M^+, 87), 252 ([M – triptycenyl]$^+$, 100); HR-MS (EI): calcd for $C_{39}H_{26}$: 494.2030, found: 494.2034; elemental analysis calcd. for $C_{39}H_{26}$: C 94.70, H 5.30; found: 94.80, 5.13.

[16] Leading references to the spin polarization transfer method: F. W. Dahlquist, K. J. Longmur, R. B. Du Vernet, *J. Magn. Reson.* **1975**, *17*, 406–410; R. Frim, G. Zilber, M. Rabinovitz, *J. Chem. Soc. Chem. Commun.* **1991**, 1202–1203; A. H. Abdourazak, A. Sygula, P. W. Rabideau, *J. Am. Chem. Soc.* **1993**, *115*, 3010–3011. For a more general review of the application of 2D NMR spectroscopy to the kinetics of exchange processes, see: C. L. Perrin, T. J. Dwyer, *Chem. Rev.* **1990**, 90, 935–967.

[17] The experiment distinguishes between rotation of the triptycene and racemization of the helicene. Racemization would not transfer polarization to both other resonances. Note that it is not necessary to resolve **2** to carry out the NMR experiments because the NMR spectra of enantiomers are identical in an achiral environment.

[18] R. P. Feynman, R. B. Leighton, M. Sands, *The Feynman Lectures on Physics, Vol. 1*, Addison-Wesley, Reading, MA, USA, **1963**, chap. 46.

 © WILEY-VCH Verlag GmbH, D-69451 Weinheim, 1997 0570-0833/97/3617-1868 $ 17.50+.50/0

The Donor-Stabilized $[PS_2]^+$ Ion**

Manfred Meisel,* Peter Lönnecke,
Arnd-Rüdiger Grimmer, and Dirk Wulff-Molder

Dedicated to Professor Roger Blachnik on the occasion of his 60th birthday

Within the scope of our investigations on donor-stabilized dithiometaphosphoric acid halides $(C_5H_5N)PS_2X$ (**1**, X = halogen) we have varied the amine donor function and/or the halogen substituents to determine the influence of these ligands on bonding and reactivity. Our attempts to synthesize the hitherto unknown iodo compound $(C_5H_5N)PS_2I$ (**1c**) surprisingly resulted in the formation of the donor-stabilized $[(C_5H_5N)_2PS_2]^+$ ion with a tetracoordinate phosphorus center.

Trimethyliodosilane and $(C_5H_5N)PS_2Cl$ (**1a**) presumably react in pyridine under the formation of $[Me_3Si(C_5H_5N)]^+$ ions[1] and strongly nucleophilic iodide ions, which are able to substitute the chloride ion in **1a**. In an equilibrium reaction the iodide of the intermediate **1c** is replaced by pyridine because of its stronger basicity, and the dipyridine(dithio)phosphonium iodide $[(C_5H_5N)_2PS_2]I$ (**2c**) is formed, which can also be synthesized by the reaction of P_4S_{10}, PI_3, and sulfur in pyridine as solvent (Scheme 1). In a similar reaction the nucleophilic degradation of P_4S_{10} with pyridine in the presence of $PSBr_3$ led to the formation of the corresponding dipyridine(dithio)phosphonium bromide $[(C_5H_5N)_2PS_2]Br$ (**2b**).

NMR investigations on **2b** and **2c** in acetonitrile indicate an equilibrium of the species **1** and **2** in solution (Scheme 1). This equilibrium shifts progressively from left to right for the series

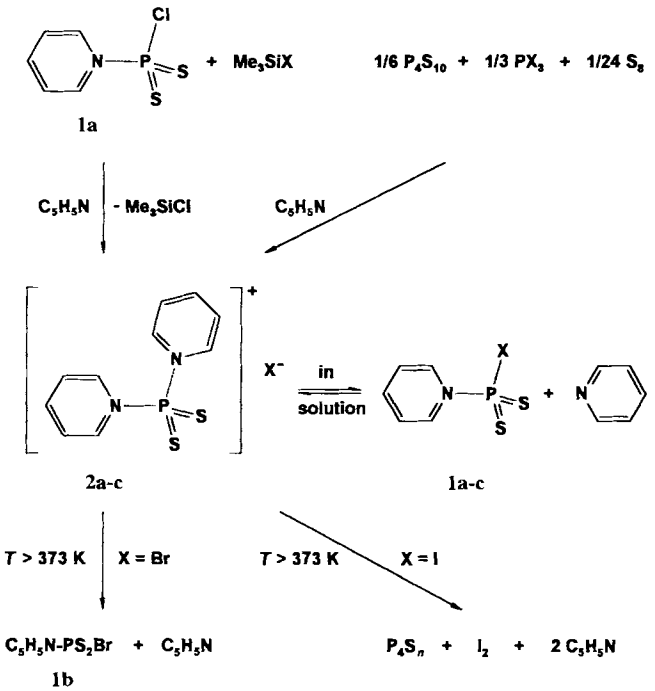

Scheme 1.

I, Br, Cl and lies for X = Cl completely on the side of **1a**, which is attributed to the decreasing basicity on going from the chloride to the iodide.

As a result of one-bond coupling of phosphorus with the ^{14}N quadrupole nucleus the ^{31}P NMR signal is split into a triplet when the compounds **1b** and **1c** are dissolved in acetonitrile.[2] Comparable spectra are recorded for $(C_5H_5N)PS_2F$ and **1a**.[3] This finding is remarkable, because the low symmetry of **1** and the great difference in the electronegativities of the halogen substituents should encourage an effective quadrupole relaxation. In contrast to this no comparable effect has been observed for the more symmetric $[(C_5H_5N)_2PS_2]^+$ ion, and only a singlet is visible in the ^{31}P NMR spectrum. The $^1J(^{31}P,^{14}N)$ coupling constants increase linearly with decreasing electronegativity of the halogen substituent X in the series $(C_5H_5N)PS_2X$ (X = F, Cl, Br, I; Figure 1). In solution[2] and in the solid state[4] the isotropic chemical shifts of **2b** and **2c** are comparable; thus, $[(C_5H_5N)_2PS_2]^+$ ions exist both in the solid state and in solution.

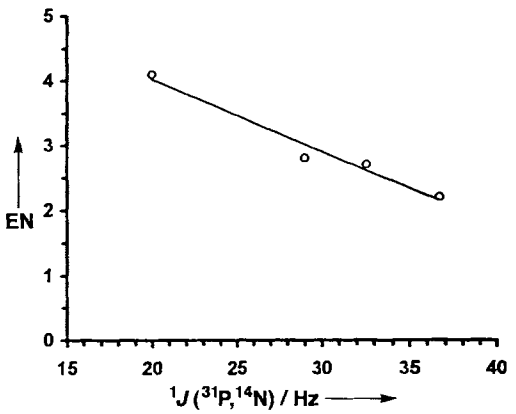

Figure 1. $^1J(^{31}P, ^{14}N)$ coupling constants of the dithiometaphosphoric acid halides $(C_5H_5N)PS_2X$ (X = F, Cl, Br, I) as a function of the electronegativity (EN) of the halogen substituents.

For the discussion of the bonding the anisotropy of the chemical shift has been taken into account.[4] A comparison of the tensor data for the iodide **2c** and the bromide **2b** shows only small differences; thus, the bonding at the phosphorus center is expected to be nearly the same in both compounds. This is in accordance with the structure parameters[5, 6] estimated for **2b** and **2c**. Both tensors show an unusual, extremely large span Ω value of approximately 500 ppm. A span of this magnitude had never been observed in noncyclic phosphorus–sulfur compounds. Evidently, the tetrahedral symmetry of the distribution of the bonds, which is realized, for example, in the $[PS_4]^{3-}$ ion, is extremely distorted. In the present case of an exactly or approximately axial tensor the orientation of the tensor axis can be given in relation to the symmetry axis of the respective molecule or ion.[7] Thus, the bisector of the S-P-S angle—as the twofold axis of the $[PS_2]^+$ cation—coincides in a good approximation with the symmetry axis of the ^{31}P shielding tensor. From the negative sign of the span it can be deduced that the direction of the strongest shielding (δ_3) as $\delta_\parallel$ coincides with the bisector of this angle; therefore, the double-bond character is concentrated in the PS_2 plane.

The single-crystal X-ray structure analysis of **2b**[5] and **2c**[6] (Figure 2) enabled us to attain deeper insights into the bonding. P–N single bonds normally range from 169 to 175 pm. For the $[(N_3)_2PS_2]^-$ ion, whose molecular geometry is similar to that of the $[(C_5H_5N)_2PS_2]^+$ ion, a normal P–N distance of 173 pm had

[*] Prof. Dr. M. Meisel, Dr. P. Lönnecke, Dr. A.-R. Grimmer, D. Wulff-Molder
Institut für Chemie der Humboldt Universität
Hessische Strasse 1-2, D-10115 Berlin (Germany)
Fax: Int. code +(30)2093-7468

[**] We thank the Wissenschaftler-Integrations-Programm (WIP) for financial support and Mrs. A. Rabis for recording the MAS-NMR spectra.

 © WILEY-VCH Verlag GmbH, D-69451 Weinheim, 1997 0570-0833/97/3617-1869 $ 17.50+.50/0

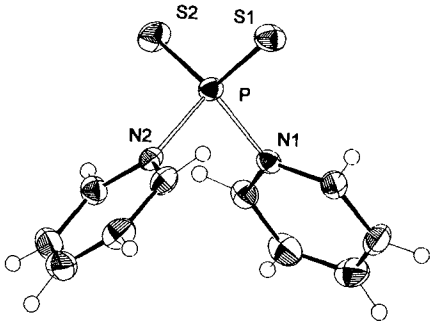

Figure 2. Structure of the $[PS_2(NC_5H_5)_2]^+$ ion (ORTEP, ellipsoides with 50% probability). Selected bond lengths [pm] and angles [°] for the bromide **2b**/iodide **2c**: P-S1 191.9(2)/191.7(2), P-S2 191.0(2)/191.1(2), P-N1 176.8(14)/183.1(3), P-N2 187.4(13)/183.1(3); S1-P-S2 123.75(9)/124.85(8), N1-P-N2 94.2(2)/93.1(2), N1-P-S1 107.6(4)/108.55(9), N1-P-S2 108.8(4)/108.56(9), N2-P-S1 109.6(5)/108.55(9), N2-P-S2 108.8(4)/108.56(9).

been determined.[8] The P–N bond lengths for **1a** (184.9 pm),[9] **2b** (177 pm and 187 pm),[5] and **2c** (both 183.1 pm)[6] lie outside this normal range and should therefore be regarded as weak coordinative P–N bonds. P–S single bonds range between 203 and 217 pm, P–S double bonds between 188 and 198 pm, and for the $[PS_2]^+$ ion calculations predict a value of 182–187 pm.[10] The P–S distances for **2b** and **2c** (191 and 192 pm) demonstrate the double-bonding character of these P–S units. The P–Br and P–I distances (490.7(2) and 503.4(2) pm, respectively) are clearly longer than the sum of the respective van der Waals radii. S-P-S bond angles of phosphorus sulfides usually lie between 100 and 115°. Initial predictions on the structure of the PS_2 species were based on the results of IR spectroscopic investigations and MNDO calculations.[10, 11] The S-P-S bond angle increases in the series $[PS_2]^-$ ion (IR: $\sphericalangle \leq 118°$), $[PS_2]^{\cdot}$ radical (IR: $\sphericalangle \leq 127°$, MNDO: $\sphericalangle \leq 143°$), and linear $[PS_2]^+$ ion. The experimentally observed S-P-S angle for the $[(C_5H_5N)_2PS_2]^+$ ion is about 124° and demonstrates the change of the bonding towards that of the free $[PS_2]^+$ ion.

Compounds **2b** and **2c** are stable at room temperature. Under vacuum **2c** decomposes above 100 °C to give pyridine, elemental iodine, and phosphorus sulfides such as P_4S_7, P_4S_9, and P_4S_{10}, which have been detected by NMR spectroscopy. In addition, this decomposition process was confirmed by mass spectrometry. In contrast, **2b** (as well as **2c**) decomposes under the same conditions, but only one mole of pyridine is split off and the compound is transformed into **1b**. This behavior can be explained on the basis of the two different P–N distances determined for **2b** (see above).[5]

Unlike **2b**, compound **2c** is not hygroscopic and is relatively stable towards dry air. Both compounds are sensitive towards moisture, and **2c** decomposes under decolorization of the bright yellow substance to yield $[(C_5H_5N)PS_2]_2O$, pyridine hydroiodide, and other, unknown decomposition products. Solutions of **2b** and **2c** are extremely sensitive towards moisture and can be handled only under an inert gas atmosphere.

$[NO_2]^+$ and $[NS_2]^+$ are stable, linear cations that occur in a number of compounds. $[PO_2]^+$ is still unknown, but $[PS_2]^+$ had been detected by mass spectrometry.[12] Since **2c** readily eliminates pyridine and iodine, it could conceivably be used as a starting material for the synthesis of compounds with isolated $[PS_2]^+$ ions.

Experimental Section

All operations were carried out under an inert gas atmosphere by using standard Schlenk techniques.

2b: $SPBr_3$ (5.1 g, 16.8 mmol) in dry pyridine (250 mL) and P_4S_{10} (3.74 g, 8.4 mmol) were heated until reflux. The hot solution was filtered and then allowed to cool to room temperature. After 15 h pale yellow crystals of **2b** could be separated from the mixture. These were washed with toluene, recrystallized from dry pyridine, and dried in vacuum. Yield: 15.5 g (92%). Elemental analysis: Calcd.: C 36.05, H 3.03, N 8.41, P 9.30, S 19.24, Br 23.98; found: C 35.47, H 3.42, N 8.28, P 8.85, S 18.04, Br 23.72.

2c: a) P_4S_{10} (2 g, 4.5 mmol), PI_3 (3.7 g, 9 mmol) and sulfur (0.29 g, 9 mmol) were dispersed in pyridine (200 mL) and heated to reflux. The hot dark red solution was filtered and allowed to cool to room temperature. Bright yellow crystals of **2c** were obtained after 48 h, which were washed with toluene and dried in vacuum. Yield: 8.3 g (81%). b) $PyPS_2Cl$ (4 g, 19 mmol) in pyridine (200 mL) was treated with Me_3SiI (3.81 g, 19 mmol) and heated until the precipitate had dissolved. The hot dark red solution was filtered and allowed to cool to room temperature to yield crystals of **2c**, which were washed with toluene and dried in vacuum. Yield: 4.1 g (58%). Elemental analysis: Calcd.: C 31.59, H 2.65, N 7.37, P 8.15, S 16.86, I 33.38; found: C 31.51, H 2.77, N 7.57, P 8.20, S 16.97, I 33.29

Received: February 7, 1997 [Z 10038 IE]
German version: *Angew. Chem.* **1997**, *109*, 1940–1942

Keywords: N ligands · NMR spectroscopy · phosphorus · solid-state structures · sulfur

[1] K. Wieghardt, K. Pohl, W. Gebert, *Angew. Chem.* **1983**, *95*, 739; *Angew. Chem. Int. Ed. Engl.* **1983**, *22*, 727; K. Hensen, R. Busch, *Z. Naturforsch. B* **1982**, *37*, 1174.

[2] ^{31}P NMR (300 MHz, lock [D$_6$]benzene (external), solvent: CH_3CN, 20 °C): $[Py_2PS_2]Br$: $\delta = 104.7$ (s); $PyPS_2Br$: $\delta = 65.5$ (t, $^1J(P^{14}N) = 32{,}6$ Hz); $[Py_2PS_2]I$: $\delta = 104.7$ (s); $PyPS_2I$: $\delta = -0.4$ (t, $^1J(P^{14}N) = 36{,}7$ Hz).

[3] B. Costisella, J. Schulz, H. Teichmann, C. Donath, M. Meisel, *Phosphorus Sulfur Silicon* **1990**, *53*, 367.

[4] MAS ^{31}P NMR: $[Py_2PS_2]Br$: $\delta_1 = 276$, $\delta_2 = 243$, $\delta_3 = -224$, $\delta_{iso} = 99.5$, $\Delta\delta = -484$, $\eta = 0.26$, $\Omega = -500$, $\chi = -0.87$; $[Py_2PS_2]I$: $\delta_1 = 281$, $\delta_2 = 245$, $\delta_3 = -229$, $\delta_{iso} = 99.5$, $\Delta\delta = -492$, $\eta = 0.28$, $\Omega = -510$, $\chi = -0.86$.

[5] a) $[Py_2PS_2]Br$: yellow crystal, crystal dimensions $0.95 \times 0.30 \times 0.27$ mm^3, orthorhombic space group *Pna*2$_1$ (no. 33), $a = 10.380(2)$, $b = 11.840(3)$, $c = 10.485(2)$ Å, $V = 1288.6(5)$ Å^3, $Z = 4$, $\rho_{calcd} = 1.718$ g cm^{-3}, $\mu(Mo_{K\alpha}) = 3.612$ mm^{-1}, $R = 0.0404$ ($wR2 = 0.0899$) for 1241 independent reflections (observed: 1248, independent: 1248) with $2\theta_{max} = 52.3°$ and $I \geq 2\sigma(I)$ for 145 parameters, residual electron density in final difference synthesis 0.814 and -0.763 e Å^{-3}. Stoe Image Plate, $Mo_{K\alpha}$ radiation, $\lambda = 0.71073$ Å, graphite monochromator, rotation, $T = 200$ K. Structure solution with direct methods (SHELXS-86), full-matrix least-squares refinement of $|F_o^2|$ with SHELXL-93 and H atoms in a riding model. b) Further details of the crystal structure investigations may be obtained from the Fachinformationszentrum Karlsruhe, D-76344 Eggenstein-Leopoldshafen (Germany), on quoting the depository number CSD-406235 ($[Py_2PS_2]Br$) and CSD-406234 ($[Py_2PS_2]I$).

[6] $[Py_2PS_2]I$: yellow crystal, crystal dimensions $0.80 \times 0.70 \times 0.20$ mm^3, orthorhombic, space group *Pnma* (no. 62), $a = 10.603(2)$, $b = 10.441(2)$, $c = 12.173(3)$ Å, $V = 1347.7(5)$ Å^3, $Z = 4$, $\rho_{calcd} = 1.874$ g cm^{-3}, $\mu(Mo_{K\alpha}) = 2.779$ mm^{-1}, $R = 0.0242$ ($wR2 = 0.0550$) for 1155 independent reflections (observed: 8127, independent: 1164) with $2\theta_{max} = 48.7°$ and $I \geq 2\sigma(I)$ for 99 parameters, residues in final difference synthesis 0.4 and -0.823 e Å^{-3}. H atoms refined freely and isotropic [5b].

[7] A.-R. Grimmer in *Nuclear Magnetic Shieldings and Molecular Structures*, (Ed.: J. A. Tossel), (*NATO ASI Ser.*, **1993**, *386*, 191).

[8] H. W. Roesky, M. N. Noltemeyer, G. M. Sheldrick, *Z. Naturforsch. B* **1986**, *41*, 803.

[9] M.-T. Averbuch-Pouchot, M. Meisel, *Acta Crystallogr. Sect. C* **1989**, *45*, 1937.

[10] P. Pyykkö, *J. Chem. Soc. Chem. Commun.* **1990**, 933.

[11] Z. Mielke, G. D. Brabson, L. Andrews, *J. Phys. Chem.* **1991**, *95*, 75.

[12] H. Keck, W. Kuchen, H. Renneberg, J. K. Terlouw, H. C. Visser, *Chem. Ber.* **1989**, *122*, 2265.

 © WILEY-VCH Verlag GmbH, D-69451 Weinheim, 1997 0570-0833/97/3617-1870 $ 17.50+.50/0

Direct Catalytic Asymmetric Aldol Reactions of Aldehydes with Unmodified Ketones

Yoichi M. A. Yamada, Naoki Yoshikawa, Hiroaki Sasai, and Masakatsu Shibasaki*

The aldol reaction is one of the most powerful of carbon–carbon bond-forming reactions, and the development of a range of catalytic asymmetric aldol-type reactions has thus proven to be a valuable contribution to asymmetric synthesis.[1] In all of these asymmetric aldol-type reactions, however, pre-conversion of the ketone moiety to a more reactive species such as an enol silyl ether, enol methyl ether, or ketene silyl acetal is an unavoidable necessity. Development of a direct catalytic asymmetric aldol reaction, starting from aldehydes and *unmodified* ketones is thus a worthwhile endeavor.[2] Such reactions are known in enzyme chemistry:[3] the fructose-1,6-bisphosphate and dihydroxyacetone phosphate (DHAP) aldolases are characteristic examples. The mechanism of these is thought to involve cocatalysis by a Zn^{2+} ion and a basic functional group in the enzyme's active site; the latter abstracts a proton in proximity to a carbonyl compound while the former functions as a Lewis acid to activate the second carbonyl component. These aldolases can thus be thought of as multifunctional catalysts displaying both Lewis acidity and Brønsted basicity, so making possible efficient catalytic asymmetric aldol reactions under typically mild in vivo conditions. An analogous cooperative mode of action can be seen in reactions mediated by any of several heterobimetallic asymmetric catalysts having both Lewis acidity and Brønsted basicity, which have been developed by our research group.[4, 5]

We speculated that it might be possible to develop a direct catalytic asymmetric aldol reaction of aldehydes with unmodified ketones by employing catalysts like **I** (Scheme 1). A

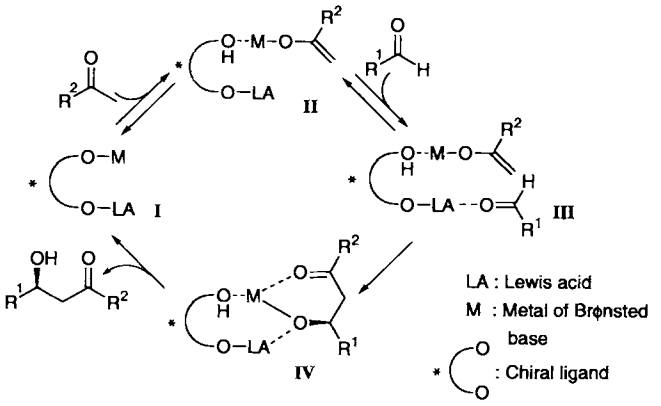

Scheme 1. Catalytic cycle of the direct catalytic asymmetric aldol reactions.

Brønsted base unit (OM) of catalyst **I** could deprotonate an α-proton of a ketone to generate the metal enolate **II**, while at the same time a Lewis acid unit (LA) could activate an aldehyde to give **III**. These reaction partners might react in the chelation-controlled, asymmetric environment to afford a β-keto metal alkoxide (**IV**). Proton exchange between the metal alkoxide moiety and a hydroxy proton of the aryl unit or an α-proton of a ketone could then generate an optically active aldol adduct with regeneration of the catalyst **I**. We now wish to report the first example of such a reaction,[6] in which we have obtained optically active aldol adducts in up to 94% *ee*.

We were initially concerned that our heterobimetallic asymmetric catalysts would be ineffective at promoting aldol reactions as a result of their rather low Brønsted basicity and were thus pleased to find that aldol reactions of the desired type proceeded quite smoothly with $LaLi_3$tris(binaphthoxide) (LLB)[4d] as catalyst (Figure 1). As shown in Table 1, when the

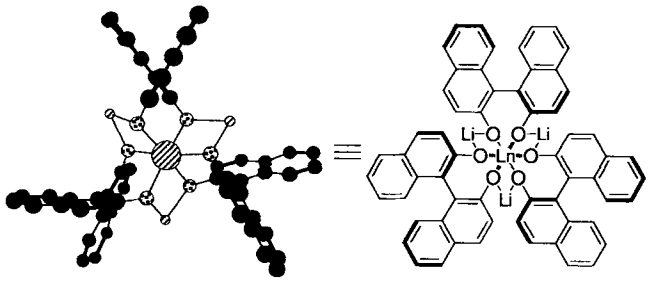

Figure 1. The structure of $LnLi_3$tris[(*R*)-binaphthoxide] ((*R*)-LnLB).

Table 1. Direct catalytic asymmetric aldol reactions promoted by (*R*)-LLB (20 mol%).

Entry	Aldehyde	Ketone (equiv)	Product	*t* [h]	Yield [%]	*ee* [%]
1 [a]	**1a**	**2a** (5)	**3a**	88	43	89
2	**1a**	**2a** (5)	**3a**	88	76	88
3	**1a**	**2a** (1.5)	**3a**	135	43	87
4	**1a**	**2a** (10)	**3a**	91	81	91
5	**1a**	**2b** (8)	**3b**	253	55	76
6	**1b**	**2a** (7.4)	**3c**	87	90	69
7	**1c**	**2a** (8)	**3d**	169	72	44
8 [b]	**1d**	**2a** (8)	**3e**	277	59	54
9	**1e**	**2a** (8)	**3f**	72	28	52
10	**1b**	**2c** (10)	**3g**	185	82	74
11	**1a**	**2c** (10)	**3h**	100	53	73
12	**1b**	**2d** (50)	**3i**	185	71	94

[a] (*R*)-LLB and addition of 1 equiv of H_2O to LLB; see ref. [10]. [b] The reaction was carried out at −30 °C.

direct catalytic asymmetric aldol reaction of pivalaldehyde (**1a**) with 5.0 equivalents of acetophenone (**2a**) was carried out in the presence of 20 mol% of (*R*)-LLB and 1.0 equivalent of H_2O (relative to LLB) in THF at −20 °C for 88 h, we obtained the desired adduct **3a**[7, 8] in 43% yield with 89% *ee* (entry 1).[9] Anhydrous LLB was more efficient than hydrated LLB, affording **3a** with 88% *ee* in 76% yield after stirring for 88 h (entry 2).[10] Furthermore, the use of 1.5 equivalents of **2a** gave **3a** with 87% *ee*, albeit in 43% yield (entry 3), and increasing the amount to 10 equivalents afforded **3a** with 91% *ee* in 81% yield after stirring for 91 h (entry 4).[11]

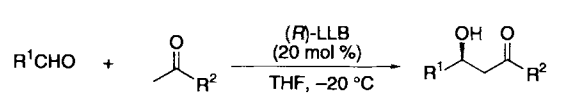

1a: R^1 = *t*Bu
1b: R^1 = $PhCH_2C(CH_3)_2$
1c: R^1 = cyclohexyl
1d: R^1 = *i*Pr
1e: R^1 = $Ph(CH_2)_2$

2a: R^2 = Ph
2b: R^2 = 1-naphthyl
2c: R^2 = CH_3
2d: R^2 = Et

3a: R^1 = *t*Bu, R^2 = Ph
3b: R^1 = *t*Bu, R^2 = 1-naphthyl
3c: R^1 = $PhCH_2C(CH_3)_2$, R^2 = Ph
3d: R^1 = cyclohexyl, R^2 = Ph
3e: R^1 = *i*Pr, R^2 = Ph
3f: R^1 = $Ph(CH_2)_2$, R^2 = Ph
3g: R^1 = $PhCH_2C(CH_3)_2$, R^2 = CH_3
3h: R^1 = *t*Bu, R^2 = CH_3
3i: R^1 = $PhCH_2C(CH_3)_2$, R^2 = Et

[*] Prof. Dr. M. Shibasaki, Y. M. A. Yamada, N. Yoshikawa, Prof. Dr. H. Sasai
Graduate School of Pharmaceutical Sciences
The University of Tokyo
Hongo, Bunkyo-ku, Tokyo 113 (Japan)
Fax: Int. code +(3)5684-5206
e-mail: mshibasa@mol.f.u-tokyo.ac.jp

 © WILEY-VCH Verlag GmbH, D-69451 Weinheim, 1997 0570-0833/97/3617-1871 $ 17.50+.50/0

Following on from these results we turned our attention to broadening the range of substrates. The reaction of **1a** with **2b** at −20 °C proceeded satisfactorily to give **3b** with 76% *ee* in 55% yield (entry 5), as did the reaction of **1b** with **2a** at −20 °C to afford the aldol adduct **3c** with 69% *ee* in 90% yield (entry 6). The achievement of efficient catalytic asymmetric aldol reactions of aldehydes with α-hydrogen atoms clearly represents a much greater challenge than for cases such as those above, since self-aldol products can easily be produced as by-products. However, the reaction of cyclohexanecarbaldehyde (**1c**) with **2a** proceeded smoothly without significant self-aldol of **1c**. Thus, after optimization, the reaction of **1c** with 8.0 equivalents of **2a** in the presence of 20 mol% of LLB gave **3d** with 44% *ee* in 72% yield, with no detectable self-condensation products of **1c** (entry 7).[12, 13] The reaction of isobutyraldehyde (**1d**) also proceeded smoothly, giving **3e** with 54% *ee* in 59% yield at −30 °C (entry 8). The reaction of hydrocinnamaldehyde (**1e**), which possesses two α-hydrogen atoms, with **2a** proved more difficult; **3f** was obtained with 52% *ee*; however, the yield was low (28%) due to the formation of self-condensation by-products (entry 9).

Aldol reactions that utilize acetone (**2c**) as a starting material are generally difficult to control. However, in this case the reaction of aldehyde (**1b**) and 10 equivalents of **2c** with LLB gave **3g** with 74% *ee* in 82% yield (entry 10), the reaction of **1a** with 10 equivalents of **2c** at −20 °C product **3h** with 73% *ee* in 53% yield (entry 11), and the reaction of **1b** and 50 equivalents of 2-butanone (**2d**) at −20 °C adduct **3i** with excellent *ee* (94%) in 71% yield (entry 12).[14, 15] Acetone and 2-butanone are widely used as solvents and are much cheaper than the corresponding enol silyl ethers and/or methyl enol ethers, which are used as substrates in the catalytic asymmetric Mukaiyama aldol reaction;[1] the use of large excesses of ketone can thus be justified in this particular case.

As outlined above (Scheme 1) in these reactions the lanthanum atom is believed to function as a Lewis acid and a lithium binaphthoxide moiety as a Brønsted base. The nature of the coordination of the aldehyde appears to be of first importance, as the accompanying activation makes possible a smooth reaction of the hypothetical LLB enolate (**II**), which on the basis of pK_a values can be expected to be present at only low concentrations, and also enables control of the orientation of the aldehyde and so facilitates the enantioselective reaction. To determine the extent of coordination between aldehydes and the lanthanum cation we carried out a ^{1}H NMR study on a mixture of $PrLi_3$tris(binaphthoxide) (PrLB)[4d] and **1a** (Figure 2).[4a] The propensity of Pr complexes to induce upfield shifts is known,[16] and in fact reaction of **1a** with **2a** in the presence of (*R*)-PrLB gave (*S*)-**3a** in 79% *ee*, indicating that Pr-containing catalysts are also a reasonable model for those containing La in terms of chemical reactivity. In the relevant ^{1}H NMR spectra the chemical shift of the formyl hydrogen of **1a** appears at $\delta = 9.37$ in THF; however, when 20 mol% of PrLB was added, an upfield shift of this signal to $\delta = 9.27$ was observed. In contrast, adding 60 mol% of the dilithium salt of (*R*)-binaphthol alone gave no detectable chemical shift of **1a**, and moreover, reaction of **1a** with **2a** catalyzed by this salt gave *rac*-**3a**. These results clearly indicate that coordination of the aldehyde to Pr is indeed occurring, allowing activation and stereocontrol to occur as proposed.[17]

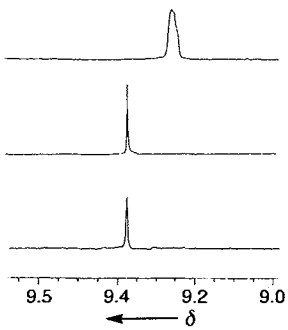

Figure 2. Chemical shift of the formyl hydrogen in **1a** in THF (bottom) as well as in the presence of 60 mol% of (*R*)-dilithium binaphthoxide (center), and 20 mol% of (*R*)-PrLB (top).

In conclusion, we have succeeded in carrying out the first catalytic asymmetric aldol reaction of aldehydes with unmodified ketones by using heterobimetallic multifunctional catalysts. Although the present catalytic asymmetric reaction is still being developed, the results reported here should provide a solid foundation for further work.

Experimental Section

General procedure: To a stirred solution of (*R*)-LLB (0.10 mmol) in THF (1.67 mL) was added 2-butanone (**2d**, 25 mmol) at −20 °C. After 30 min, 2,2-dimethyl-3-phenylpropanal (**1b**, 0.50 mmol) was added to the solution, which was then stirred for 185 h at −20 °C. The reaction was quenched by adding 2 mL of 1 N HCl and extracted with Et_2O (3 × 10 mL). The combined organic layers were washed with brine and dried over Na_2SO_4. The solvent was removed under reduced pressure, and the residue purified by flash chromatography (SiO_2, Et_2O/hexane 1/12) to give (*S*)-**3i** with 94% *ee* in 71% yield.

Received: March 4, 1997 [Z10195IE]
German version: *Angew. Chem.* **1997**, *109*, 1942–1944

Keywords: aldol reactions · asymmetric catalysis · asymmetric synthesis · homogeneous catalysis · lanthanum

[1] For recent developments, see the following papers and the references cited therein: a) S. E. Denmark, S. B. D. Winter, X. Su, K.-T. Wong, *J. Am. Chem. Soc.* **1996**, *118*, 7404–7405; b) D. A. Evans, J. A. Murry, M. C. Kozlowski, *ibid.* **1996**, *118*, 5814–5815; c) R. A. Singer, E. M. Carreira, *ibid.* **1995**, *117*, 12360–12361; d) G. E. Keck, D. Krishnamurthy, *ibid.* **1995**, *117*, 2363–2364; e) M. Sodeoka, K. Ohrai, M. Shibasaki, *J. Org. Chem.* **1995**, *60*, 2648–2649; f) K. Mikami, S. Matsukawa, *J. Am. Chem. Soc.* **1994**, *116*, 4077–4078; g) S. Kobayashi, H. Uchiro, I. Shiina, T. Mukaiyama, *Tetrahedron* **1993**, *49*, 1761–1772; h) E. J. Corey, C. L. Cywin, T. D. Roper, *Tetrahedron Lett.* **1992**, *33*, 6907–6910; i) E. R. Parmee, Y. Hong, O. Tempkin, S. Masamune, *ibid.* **1992**, *33*, 1729–1732; j) S. Kiyooka, Y. Kaneko, K. Kume, *ibid.* **1992**, *33*, 4927–4930; k) K. Furuta, T. Maruyama, H. Yamamoto, *J. Am. Chem. Soc.* **1991**, *113*, 1041–1042; l) E. R. Parmee, O. Tempkin, S. Masamune, A. Abiko, *ibid.* **1991**, *113*, 9365–9366; m) K. Uotsu, H. Sasai, M. Shibasaki, *Tetrahedron: Asymmetry* **1995**, *6*, 71–74.

[2] a) R. Noyori, *Asymmetric Catalytsis in Organic Synthesis*, Wiley, New York, **1994**; b) M. Sawamura, Y. Ito in *Catalytic Asymmetric Synthesis* (Ed.: I. Ojima), VCH, New York, **1993**, pp. 367–388.

[3] W.-D. Fessner, A. Schneider, H. Held, G. Sinerius, C. Walter, M. Hixon, J. V. Schloss, *Angew. Chem.* **1996**, *108*, 2366–2369; *Angew. Chem. Int. Ed. Engl.* **1996**, *35*, 2219–21, and references therein.

[4] a) H. Sasai, T. Arai, Y. Satow, K. N. Houk, M. Shibasaki, *J. Am. Chem. Soc.* **1995**, *117*, 6194–6198; b) T. Arai, Y. M. A. Yamada, N. Yamamoto, H. Sasai, M. Shibasaki, *Chem. Eur. J.* **1996**, *2*, 1368–1372; c) H. Sasai, S. Arai, Y. Tahara, M. Shibasaki, *J. Org. Chem.* **1995**, *60*, 6656–6657; d) H. Sasai, T. Suzuki, N. Itoh, K. Tanaka, T. Date, K. Okamura, M. Shibasaki, *J. Am. Chem. Soc.* **1993**, *115*, 10372–10373; e) H. Sasai, T. Suzuki, S, Arai, T. Arai, M. Shibasaki, *ibid.* **1992**, *114*, 4418–4420; f) For review, see; M. Shibasaki, H. Sasai, T. Arai, *Angew. Chem.* **1997**, *109*, 1290–1310; *Angew. Chem. Int. Ed. Engl.* **1997**, *36*, 1236–1256.

[5] For an excellent review, see H. Steinhagen, G Helmchen, *Angew. Chem.* **1996**, *108*, 2489–2492; *Angew. Chem. Int. Ed. Engl.* **1996**, *35*, 2339–2342.

[6] A partially successful attempt to develop a direct catalytic, asymmetric aldol reaction has been reported; however, only one reactive aldehyde and acetone were used and the *ee* value of the corresponding product was not determined: M. Nakagawa, H. Nakao, K.-I. Watanabe, *Chem. Lett.* **1985**, 391–394.

[7] The spectral data of the compounds **3a**, **3d**–**3f**, and **3h** resemble those previously reported. See ref. [8].

[8] a) K. Narasaka, T. Miwa, H. Hayashi, M. Ohta, *Chem. Lett.* **1984**, 1399–1402; b) P. V. Ramachandran, W.-C. Xu, H. C. Brown, *Tetrahedron Lett.* **1996**, *37*, 4911–4914.

[9] The enantiomeric excess of all the aldol adducts was determined by HPLC analysis with DAICEL CHIRALPAK AS, AD, or CHIRALCEL OJ; absolute configurations were determined to be (*S*)-form. Absolute configurations of **3b**, **3c**, **3g**, and **3i** were determined by Mosher's method: J. A. Dale, H. S. Mosher *J. Am. Chem. Soc.* **1973**, *95*, 512–519.

[10] To (*R*)-LLB in THF was added 1.0 equiv of H_2O in THF (1.0 M) to give hydrated (*R*)-LLB, which had been found to be a more effective catalyst for previously reported catalytic asymmetric nitroaldol reactions [4b].

[11] Results with 5 or 10 mol% of (*R*)-LLB: 42% yield, 77% *ee* and 52% yield, 88% *ee*, respectively.

 © WILEY-VCH Verlag GmbH, D-69451 Weinheim, 1997 0570-0833/97/3617-1872 $ 17.50+.50/0

[12] Results with 20 mol% of other catalysts at −20 °C: $LaNa_3$tris(binaphthoxide) (LSB)[4a] in THF (16%, 13% *ee*), LaK_3tris(binaphthoxide) (LPB)[4c] in THF (49%, 0% *ee*), AlLibis(binaphthoxide) (ALB)[4b] in THF (quite low yield), LLB in toluene (25%, 31% *ee*), LLB in CH_2Cl_2 (33%, 15% *ee*), LnLB where Ln = Pr, Sm, Gd, Dy, or Yb in THF (low *ee* values), LLB* in THF (B* = 6,6′-bis((triethylsilyl)ethynyl(binaphthoxide)) (low *ee*), 6,6′-dibromo(binaphthoxide) (low *ee*), 6,6′-dimethoxy(binaphthoxide) (low *ee*)).

[13] The moderate yield is mainly due to the low reactivity of LLB. A small amount of dehydrated product was detected.

[14] A trace amount of 4-hydroxy-3,5,5-trimethyl-6-phenyl-2-hexanone was detected.

[15] The reaction of benzaldehyde and 8 equiv of **2a** in the presence of 20 mol% of (*R*)-LLB at 198 h gave the desired aldol adduct with only 3% *ee* (*S*) in 41% yield, but the reaction under the same conditions except in the presence of $YbLi_3$tris((*R*)-binaphthoxide) ((*R*)-YbLB) instead of (*R*)-LLB gave the aldol product with 36% *ee* (*R*) in 47% yield.

[16] Review: A. F. Cockerill, L. O. Davies, R. C. Harden, D. M. Rackham, *Chem. Rev.* **1973**, *73*, 553–588, and references therein.

[17] It is unlikely, even if the aldehyde coordinates to a Li atom of the Pr complex, that proximity to the Pr or the positioning of the formyl C–H in the shielding region of the naphthyl ring could produce a shift of such magnitude, as no such chemical shift is observed in the presence of LLB.

Synthesis and Crystal Structure of Phosphorus(v) Nitride α-P_3N_5**

Stefan Horstmann, Elisabeth Irran, and Wolfgang Schnick*

Dedicated to Professor Hans Georg von Schnering

Polymeric nonmetal nitrides are of considerable interest for the development of inorganic materials.[1] Among the binary members of this class of compounds dimorphic boron nitride (BN) and silicon nitride (Si_3N_4) have gained significance. Their potential applications include use as substrate for semiconductors (Si_3N_4) and as high-temperature materials (for example crucibles made of hexagonal BN or valve tappets and turbochargers made of Si_3N_4).

Chemically and structurally related phosphorus(v) nitride P_3N_5 was assumed to be built up by a polymer network structure of connected TN_4 tetrahedra (T = B, Si, P) similar to that of cubic BN and Si_3N_4. The crystal structures of BN and Si_3N_4 have already been investigated in detail.[1] However, no structural model of P_3N_5 was available in spite of many intensive efforts,[2, 3] because neither monocrystalline nor pure polycrystalline samples of P_3N_5 had been obtained. In our recently developed synthesis of phosphorus(v) nitride [Eq. (1)] we always obtained mixtures of the polymorphs α- and β-P_3N_5, which were characterized by electron diffraction (ED), high-resolution transmission electron microscopy (HRTEM), EXAFS (extended X-ray absorption fine structure) spectroscopy, and ^{31}P and ^{15}N solid-state NMR spectroscopy.[3]

$$(PNCl_2)_3 + 2NH_4Cl \longrightarrow P_3N_5 + 8HCl \quad (1)$$

[*] Prof. Dr. W. Schnick, Dipl.-Chem. S. Horstmann, Mag. E. Irran
Laboratorium für Anorganische Chemie der Universität
D-95440 Bayreuth (Germany)
Fax: Int. code +(921)55-2788
e-mail: wolfgang.schnick@uni-bayreuth.de

[**] This work was supported by the Fonds der Chemischen Industrie, the Deutsche Forschungsgemeinschaft (project SCHN 377/2-2, and Gottfried-Wilhelm-Leibniz-Programm), the Bundesministerium für Bildung, Wissenschaft, Forschung und Technologie in the Verbundprojekt "Erforschung kondensierter Materie" (project 03-SC4 BAY), and the ESRF Grenoble. The authors thank Dr. P. Pattison (ESRF, Grenoble) for his help during the synchrotron experiment.

We have now synthesized single-phase α-P_3N_5 by thermal condensation of tetraaminophosphonium iodide $[P(NH_2)_4]I$ according to Equation (2).[4] The NH_4I atmosphere that develops during the decomposition of $[P(NH_2)_4]I$ evidently is significant for the formation of ordered α-P_3N_5, because heavily disordered P_3N_5 is formed when $[P(NH_2)_4]Cl$ is used under comparable experimental conditions. During our procedure α-P_3N_5 is formed as a microcrystalline, beige powder, which is insoluble in common solvents as well as in hot acids and alkaline solutions.

$$3[P(NH_2)_4]I \xrightarrow{825\,^\circ C} P_3N_5 + 3NH_4I + 4NH_3 \quad (2)$$

The crystal structure of α-P_3N_5 was determined and refined on the basis of powder X-ray diffraction data. Due to numerous overlapping peaks the resolution of conventional powder diffractometers (typical full width of half maximum height (FWHM) of the peaks: 0.09°) did not allow us to deconvolute the diffraction pattern of α-P_3N_5. Therefore we performed powder diffraction investigations with higher resolution by using synchrotron radiation at the European Synchrotron Radiation Facility in Grenoble (ESRF, Beamline BM1, typical FWHM: 0.03°). We could index the powder pattern obtained unambiguously (Figure 1) and the structure was determined by direct methods and refined by the Rietveld method (Table 1, see Experimental Section).

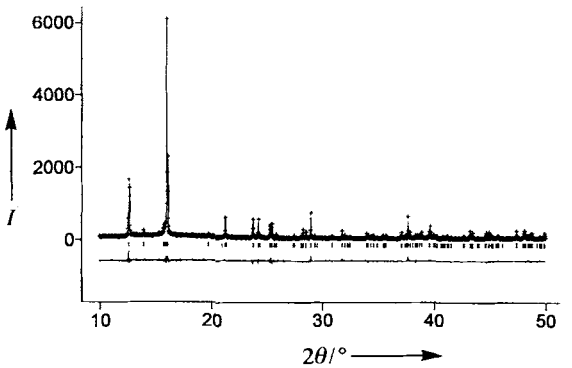

Figure 1. Observed (crosses) and calculated (line) X-ray powder diffraction pattern as well as difference profile of the Rietveld refinement of α-P_3N_5 (only section until $2\theta = 50°$ is shown). Possible positions of the peaks are marked by vertical lines. The powder pattern was obtained at the ESRF, Grenoble, on the Beamline BM1 (λ = 99.963(4) pm).

In the solid state α-P_3N_5 has a three-dimensional network structure of connected PN_4 tetrahedra (Figure 2). As a consequence of the molar ratio P:N = 3:5 two fifths of the nitrogen atoms ($N^{[3]}$) are bound to three neighboring P atoms and the remaining nitrogen atoms ($N^{[2]}$) to two P atoms according to

Table 1. Atomic coordinates and isotropic displacement factors [Å²] of α-P_3N_5.

	x/a	*y/b*	*z/c*	U_{iso} [a]
P(1)	0.0 [b]	0.5182(3)	0.0 [b]	0.0036(4)
P(2)	0.136(1)	0.2000(8)	0.309(1)	0.0036(4)
P(3)	0.365(2)	0.2924(8)	0.196(1)	0.0036(4)
N(1)	0.009(2)	−0.003(2)	0.269(1)	0.0017(7)
N(2)	0.129(1)	0.341(1)	0.450(1)	0.0017(7)
N(3)	0.370(1)	0.119(1)	0.066(1)	0.0017(7)
N(4)	0.142(2)	0.351(2)	0.147(1)	0.0017(7)
N(5)	0.356(2)	0.135(2)	0.348(1)	0.0017(7)

[a] U_{iso} is defined as $\exp(-8\pi^2 U_{iso}\sin^2\theta/\lambda)$, the displacement factors of P and N were constrained to be equal. [b] Atomic coordinations were fixed during the refinement.

 © WILEY-VCH Verlag GmbH, D-69451 Weinheim, 1997 0570-0833/97/3617-1873 $ 17.50+.50/0

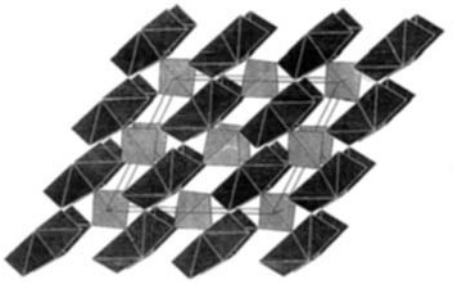

Figure 2. Crystal structure of α-P_3N_5, view along [010]. Crossing zweier single chains (black), in which the PN_4 tetrahedra are linked alternately through common corners and edges, are connected by addional PN_4 tetrahedra.

$^3_\infty[P_3^{[4]}N_3^{[2]}N_2^{[3]}]$.[*] Thus the coordination resembles that in silicon dioxide ($^3_\infty[Si^{[4]}O_2^{[2]}]$) and in silicon nitride ($^3_\infty[Si_3^{[4]}N_4^{[3]}]$). Examples of $N^{[3]}$ connections recently have been proven in P_4N_6O[5] and $K_3P_6N_{11}$,[6] while in less condensed phosphorus nitrides (molar ratio P:N $\leq$1:2) exclusively terminal $N^{[1]}$ and simple bridging $N^{[2]}$ are found.[1] On the other hand, in higher condensed nitridosilicates[7] numerous examples of $N^{[3]}$ connections between Si tetrahedral centers are known (e. g. $Ca_2Si_5N_8$, $Ce_3Si_6N_{11}$), and surprisingly even $N^{[4]}$ connections were found in nitridosilicates ($MYbSi_4N_7$, M = Sr, Ba).[8]

In α-P_3N_5 zweier single chains occur parallel to [110] and [1$\bar{1}$0], in which the PN_4 tetrahedra are connected alternately through edge- and corner-sharing. These zweier single chains are linked together through additional vertex-sharing PN_4 tetrahedra. First indications of the edge linkage of the tetrahedra already appeared during the analysis of the EXAFS spectrum of α-P_3N_5, in which an interatomic distance of about 250 pm was determined.[3] This corresponds to the transannular P$\cdots$P distance in P_2N_2 rings. In almost all known condensed phosphorus(v) nitrides the PN_4 tetrahedra are connected exclusively through common corners.

A similar connection through edge-sharing has only previously been observed in the phosphorus(v) nitride oxide P_4N_6O[5] and in the phosphorus(v) nitride imide HP_4N_7.[9] Among nitridosilicates examples of an analogous connection through edge-sharing SiN_4 tetrahedra include $Ba_5Si_2N_6$[10] and $BaSi_7N_{10}$.[11] "Fibrous" SiO_2 was assumed to contain edge-sharing SiO_4 tetrahedra;[12] however, this statement has not yet been confirmed by using modern experimental techniques.

The network structure of connected PN_4 tetrahedra in α-P_3N_5 could be characterized by analogy to condensed silicates by the specific distribution of the occurring P_nN_n ring sizes.[13] All ring sizes with the exception of $n = 3$ are found in α-P_3N_5. In contrast, analogously condensed Si_3N_3 rings often occur in highly condensed nitridosilicates (Si:N $>$1:2).[7]

The P–N bond lengths (151–174 pm) and the P-$N^{[2]}$-P bond angles (142–170°) vary in ranges typical of phosphorus(v) nitrides.[1] The sum of the angles at the $N^{[3]}$ center is 360°; therefore, these N atoms must be considered as sp^2 hybridized. According to the experience gained with nitridosilicates, P–$N^{[2]}$ distances (151–160 pm) are significantly shorter than P–$N^{[3]}$ distances (164–174 pm). However, due to the specific properties of the chemical bond between P and N the assumption of a double bond is not justified. Thus, polar character of the bond must be responsible for the observed bond shortening.[14]

α-P_3N_5 crystallizes in a new and unprecedented structure type. However, isotypic compounds of the other polymeric nonmetal nitrides built up by TN_4 tetrahedra (T = B, Si), cubic BN and Si_3N_4, exist. The crystal structure of cubic BN corresponds to the sphalerite type and Si_3N_4 crystallizes analogously to phenakite Be_2SiO_4. Hypothetical $BeSi_2O_5$ would be isoelectronic to P_3N_5. However, in the corresponding region of the quasi-binary system BeO–SiO_2 only vitreous phases and no crystalline compound of the given composition are found. Among the hitherto known binary compounds of the formula type A_3X_5 (e. g. Ti_3O_5, V_3O_5, Ta_3N_5, Si_3Mn_5, Si_3W_5) there are no examples that are isotypic to α-P_3N_5. Here higher coordination numbers of either 6 (Ti_3O_5, V_3O_5, Ta_3N_5, Si_3Mn_5) or 8 (Si_3W_5) are found for the A atoms.

On the basis of the solved crystal structure of α-P_3N_5 we are now working on the determination of structural models for β-P_3N_5 and disordered P_3N_5. The HRTEM[3] results show that similar to the situation in the polytypes of SiC[15] the different stacking variants are based on the same structural modules, which are linked in different ways.

Experimental Section

For the synthesis of α-P_3N_5 [$P(NH_2)_4$]I (200 mg, 0.9 mmol) was transferred under argon into the lower end of a quartz ampoule 30 cm in length and the opening was connected with a bubble counter filled with paraffin. Then the lower end was heated to 825 °C in a tube furnace for three days. Ammonia, which formed according to Equation (2), escaped through the bubble counter, and ammonium iodide precipitated at the wall of the ampoule. The product was obtained as a beige solid (12.0 mg) that remained at the bottom of the ampoule (yield: 24.5%). Elemental analysis by Mikroanalytisches Labor Pascher, Remagen, Germany, calc.: P 57.0, N 43.0; found: P 56.8, N 42.7%. The absence of hydrogen (N-H) was checked by IR spectroscopy.

The diffraction investigations with synchrotron radiation were carried out in Debye–Scherrer geometry. The sample was enclosed in a glass capillary (diameter 0.3 mm). A wavelength of 99.963(4) pm was selected by a Si(111) single crystal monochromator, and also a Si(111) crystal was used as analyzer. A scintillation counter was used, and the measured diffraction intensities were normalized for storage ring decay by a ionization chamber monitor. The diffraction pattern was indexed unambiguously by the programs ITO [16] and TREOR-90 [17] (de Wolff figure of merit M_{20} = 131). On the basis of the systematic absences the space groups *Cc* (No. 9) and *C2/c* (No. 15) were considered. The program EXTRA [18] was employed to extract 184 integrated intensity data and these were used as input for the program SIRPOW.92 [19] for the structure determination by direct methods. As a result all P and N could be localized immediately. The refinement (program system GSAS [20]) was carried out with the space group *Cc*. On the basis of the same topology space group *C2/c* would require unusual bond angles P-N-P of 180° and the assumption of structural disorder. P_3N_5: *Cc*, a = 812.077(4), b = 583.433(4), c = 916.005(5) pm, β = 115.809(1)°, Z = 4, $F(000)$ = 320, μ = 5.283 mm^{-1}, measured range 10° $\leq 2\theta \leq$ 97.4°, 17203 data points, 699 observed reflections, 22 positional parameter refined, wR_p = 0.113, R_p = 0.091, R_F = 0.060. At the beginning of the calculation scaling factor, lattice constants, zero point shift, and background were refined. The profile was fitted by a pseudo-Voigt function [21] and its asymmetry corrected according to reference [22]. As compared to the unit cell of α-P_3N_5 [3] derived on the basis of electron diffraction data, the here mentioned metric results from the transformation matrix (0, 0, 1/2; 0, −1, 0; 1, 0, −1/2). Further details of the crystal structure investigation may be obtained from the Fachinformationszentrum Karlsruhe, D-76344 Eggenstein-Leopoldshafen, on quoting the depository number CSD-406599.

Received: February 21, 1997 [Z10144IE]
German version: *Angew. Chem.* **1997**, *109*, 1938–1940

Keywords: nitrides · phosphorus · structure elucidation · solid-state chemistry

[*] The superscript numbers in square brackets following element symbols define their coordination numbers.

[1] W. Schnick, *Angew. Chem.* **1993**, *105*, 846; *Angew. Chem. Int. Ed. Engl.* **1993**, *32*, 806.

[2] a) A. A. Baltkaula, T. N. Miller, I. A. Puzinja, G. W. Ozolinsch, A. Ja. Wajwad, *Latv. PSR Zinat. Akad. Vestis* **1968**, *6*, 761; b) A. A. Baltkaula, T. N. Miller, *ibid.* **1971**, *4*, 389; c) G. Boden, G. Sadowski, H.-A. Lehmann, *Z. Chem.* **1971**, *11*, 114; d) J. V. Ronis, A. A. Kuzjukevic, B. J. Bondars, V. E. Avotins, A. A. Vitola, *Latv. PSR Zinat. Akad. Vestis* **1986**, *3*, 366; e) S. Vepřek, Z. Iqbal, J. Brunner, M. Schärli, *Philos. Mag. B* **1981**, *43*, 527; f) T. N. Miller, A. A. Vitola, *Neorganicheskie Soedineniya Fosfora s Azotom*, Zinatne, Riga, **1986**.

[3] W. Schnick, J. Lücke, F. Krumeich, *Chem. Mater.* **1996**, *8*, 281.

[4] a) W. Schnick, S. Horstmann, A. Schmidpeter, *Angew. Chem.* **1994**, *106*, 818; *Angew. Chem. Int. Ed. Engl.* **1994**, *33*, 785; b) S. Horstmann, W. Schnick, *Z. Naturforsch. B* **1994**, *49*, 1381; c) W. Schnick, S. Horstmann, M. Häser, *Phosphorus Sulfur* **1996**, *109/110*, 93.

 © WILEY-VCH Verlag GmbH, D-69451 Weinheim, 1997 0570-0833/97/3617-1874 $ 17.50+.50/0

[5] J. Ronis, B. Bondars, A. Vitola, T. Millers, J. Schneider, F. Frey, *J. Solid State Chem.* **1995**, *115*, 265.
[6] H. Jacobs, R. Nymwegen, *Z. Anorg. Allg. Chem.* **1997**, *623*, 429.
[7] W. Schnick, H. Huppertz, *Chem. Eur. J.* **1997**, *3*, 679.
[8] a) H. Huppertz, W. Schnick, *Angew. Chem.* **1996**, *108*, 2115; *Angew. Chem. Int. Ed. Engl.* **1996**, *35*, 1983; b) H. Huppertz, W. Schnick, *Z. Anorg. Allg. Chem.* **1997**, *623*, 212.
[9] S. Horstmann, E. Irran, W. Schnick, *Angew. Chem.* **1997**, *109*, in press; *Angew. Chem. Int. Ed. Engl.* **1997**, *36*, in press.
[10] Edge-sharing tetrahedra $[Si_2N_6]^{10-}$ are found in $Ba_5Si_2N_6$: H. Yamane, F. J. DiSalvo, *J. Alloys Compounds* **1996**, *240*, 33.
[11] Vierer single chains with alternating corner- and edge-sharing SiN_4 tetrahedra are found in $BaSi_7N_{10}$: H. Huppertz, W. Schnick, *Chem. Eur. J.* **1997**, *3*, 249.
[12] A. Weiss, A. Weiss, *Z. Anorg. Allg. Chem.* **1954**, *276*, 95.
[13] Network structures of linked TX_4 tetrahedra (T = Si, P; X = O, N) can be characterized topologically by the so-called cycle class sequences, which give the relative frequency of the T_nX_n ring sizes (for $n = 1, 2, 3 \ldots$) that occur in the unit cell. Cycle class sequence of α-P_3N_5: {-, 4, 0, 4, 16, 52, 104, 336 ..}. cf. also: a) W. E. Klee, *Z. Kristallogr.* **1987**, *179*, 67; b) A. Beukemann, W. E. Klee, *ibid.* **1994**, *209*, 709.
[14] W. Kutzelnigg, *Angew. Chem.* **1984**, *96*, 262; *Angew. Chem. Int. Ed. Engl.* **1984**, *23*, 272.
[15] P. Pirouz, J. W. Yang, *Ultramicroscopy* **1993**, *51*, 189.
[16] J. W. Visser, *J. Appl. Crystallogr.* **1969**, *2*, 89.
[17] P.-E. Werner; "TREOR 90", Trial and Error Program for Indexing of Unknown Powder Patterns, University of Stockholm, **1990**; P.-E. Werner, L. Eriksson, M. Westdahl, *J. Appl. Crystallogr.* **1985**, *18*, 367.
[18] A. Altomare, M. C. Burla, G. Cascarano, C. Giacovazzo, A. Guagliardi, A. G. G. Moliterni, G. Polidori, *J. Appl. Crystallogr.* **1995**, *28*, 842.
[19] A. Altomare, G. Cascarano, C. Giacovazzo, A. Guagliardi, M. C. Burla, G. Polidori, M. Camalli, *J. Appl. Crystallogr.* **1994**, *27*, 435.
[20] R. B. von Dreele, A. C. Larson, General Structure Analysis System, Los Alamos National Laboratory Report LAUR 86-748, **1990**.
[21] P. Thompson, D. E. Cox, J. B. Hastings, *J. Appl. Crystallogr.* **1987**, *20*, 79.
[22] L. W. Finger, D. E. Cox, A. P. Jephcoat, *J. Appl. Crystallogr.* **1994**, *27*, 892.

Preparation, NMR, and Ab Initio/IGLO/GIAO-MP2 Study of the Elusive Protonated Fluoroformic Acid and Fluorocarbonyl Cation**

George A. Olah,* Arwed Burrichter, Thomas Mathew, Yashwant D. Vankar, Golam Rasul, and G. K. Surya Prakash*

Fluoroformic acid, the monofluoro derivative of carbonic acid, is a proposed intermediate in the oxidation of fluorocarbons[1] and ozonolysis of fluoroalkenes.[2] Considerable interest has been focused on its potential role in the depletion of the ozone layer in the stratosphere.[3, 4] Fluoroformic acid has recently[5] been observed in the gas phase by neutralization–reionization mass spectrometry (NMRS). All attempts to prepare fluoroformic acid in solution have so far failed. According to a chemistry textbook,[6] fluoroformic acid cannot exist in condensed phases because of its autocatalytic decomposition to HF and CO_2 [Eq. (a)].

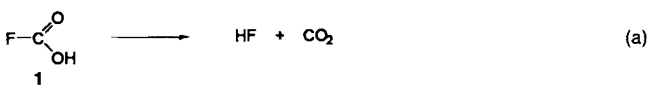

(a)

The structure and decomposition pathways of fluoroformic acid have been investigated in a number of theoretical papers.[2, 7–10] While neutral FCOOH was found to be unstable, its conjugate acid and base, protonated fluoroformic acid $[FC(OH)_2]^+$ and fluoroformate ion $[FCO_2]^-$, respectively, are expected to be considerably more stable due to resonance stabilization (Scheme 1).

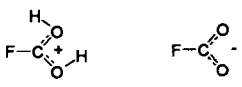

Scheme 1. Resonance stabilization of the conjugate acid and base of fluoroformic acid.

Seppelt et al. have recently[11] prepared and characterized stable salts of the fluoroformate anion by reaction of CO_2 with dry quaternary ammonium fluorides such as Me_4NF. The fluoroformate anion was found to be remarkably stable under anhydrous conditions in aprotic solvents such as dry acetonitrile and has been characterized by ^{13}C and ^{19}F NMR and IR spectroscopy.

Similar to the fluoroformate anion, protonated fluoroformic acid $[FC(OH)_2]^+$ is expected to be significantly resonance-stabilized, involving backdonation (p–p interaction) from oxygen as well as fluorine nonbonded electron pairs (Scheme 2). Wiedmann and Wesdemiotis previously obtained evidence for protonated fluoroformic acid in the gas phase through dissociative ionization of ethyl fluoroformate.[5] We now report the first preparation and characterization of protonated fluoroformic acid $[FC(OH)_2]^+$ in the condensed phase under superacid stable ion conditions, the results of ab initio calculations of its structure and energetics, and the ^{13}C and ^{19}F NMR chemical shifts calculated by IGLO[12] and GIAO-MP2[13] methods together with a comparison with the experimental NMR data.

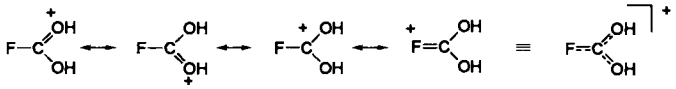

Scheme 2.

Protolytic ionization of *tert*-butyl fluoroformate in fivefold excess of FSO_3H/SbF_5 (1/1 molar solution; Magic Acid) in SO_2ClF as solvent at −78 °C resulted in a deep yellow solution [Eq. (b)]. The 75 MHz ^{13}C NMR spectrum of the solution

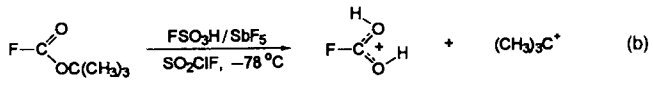

(b)

at −78 °C (Figure 1) clearly showed the formation of the *tert*-butyl cation $[(CH_3)_3C]^+$ (δ = 334.3 (C^+, *s*), 41.4 (CH_3, *q*)), as well as two well-resolved doublets at δ = 157.8 (*d*, $J_{C,F}$ = 321.0 Hz) and 117.5 (*d*, $J_{C,F}$ = 322.4 Hz). We assign the peak at δ = 157.8 to protonated fluoroformic acid $[FC(OH)_2]^+$, which is deshielded by $\Delta\delta$ = 14.6 relative to its progenitor *tert*-butyl fluoroformate [δ = 143.2 (*d*, $J_{C,F}$ = 285 Hz)]. Similar results were obtained in the even stronger fluoroantimonic acid medium (HF/SbF_5). The carboxyl carbon of $[FC(OH)_2]^+$ is shielded relative to those of protonated carbonic acid $[C(OH)_3]^+$ (δ = 165.4),[14] protonated formic acid $[HC(OH)_2]^+$ (δ = 177, 174),[15] and protonated acetic acid $[CH_3C(OH)_2]^+$ (δ = 193.0).[15]

[*] Prof. Dr. G. A. Olah, Prof. Dr. G. K. S. Prakash, Dr. A. Burrichter, Dr. T. Mathew, Prof. Dr. G. Rasul
Loker Hydrocarbon Research Institute and Department of Chemistry
University of Southern California
University Park, Los Angeles, CA 90089-1661 (USA)
Fax: Int. code +(213)740-5087
Prof. Dr. Y. D. Vankar
Department of Chemistry
Indian Institute of Technology
Kanpur 208016 (India)

[**] Onium Ions Part 49. Support of our work by the National Science Foundation is gratefully appreciated. A. B. wishes to thank the Konrad-Adenauer-Foundation for a scholarship. Part 48: G. K. S. Prakash, Q. Wang, G. Rasul, G. A. Olah, *J. Organomet. Chem.*, in press.

 © WILEY-VCH Verlag GmbH, D-69451 Weinheim, 1997 0570-0833/97/3617-1875 $ 17.50+.50/0

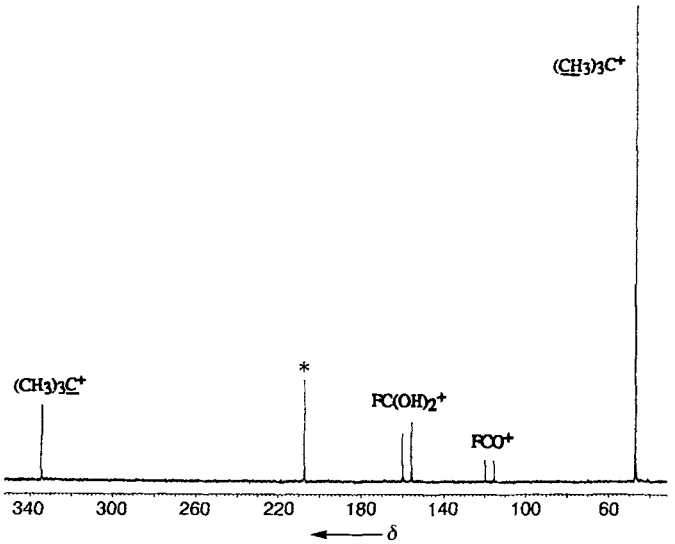

Figure 1. ^{13}C NMR spectrum (75 Hz) of the ionization of *tert*-butyl fluoroformate in FSO_3H/SbF_5 in SO_2ClF as solvent at $-78\,^{\circ}C$ (the peak marked with an asterisk is due to [D_6]acetone as external standard).

O-Protonation of fluoroformic acid could result in three different isomers of protonated fluoroformic acid (Scheme 3). However, only the *cis–trans* isomer was observed by ^1H and ^{13}C NMR spectroscopy under the experimental conditions. The 300 MHz ^1H NMR spectrum of the solution at $-78\,^{\circ}C$ exhibited two peaks at δ^1H 8.95 (*s*) and 8.88 (*s*) in a 1:1 ratio, besides the peaks resulting from the acid system [FSO_3H/SbF_5 ($\delta = 12.91$) and H_3O^+ ($\delta = 9.66$)]. The magnetic nonequivalence of the two protons is in accordance with a *cis–trans* structure and indicates the restricted rotation about the C···OH^+ bond. The ^{19}F NMR spectrum of the solution recorded at $-78\,^{\circ}C$ showed a signal at $\delta = -4.7$. This value agrees with the GIAO-MP2 calculated ^{19}F NMR chemical shift of $\delta = -0.4$ (see Table 2).

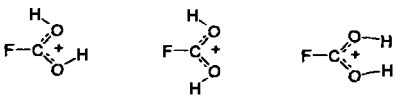

Scheme 3.

The additional doublet observed at $\delta = 117.5$ ($J_{C,F} = 322.4$ Hz) in the ^{13}C NMR spectrum is assigned to the hitherto elusive fluorocarbonyl cation $[FCO]^+$. In an attempt to dehydrate $[FC(OH)_2]^+$ further to $[FCO]^+$, the reaction mixture of protonated fluoroformic acid was allowed to warm up to $-10\,^{\circ}C$ and kept at this temperature for twelve hours. Subsequent NMR analysis of the sample at $-78\,^{\circ}C$, however, showed a substantial decrease in the intensity of both peaks at $\delta = 157.8$ and 117.5. The calculated ^{19}F NMR chemical shift for $[FCO]^+$ at GIAO-MP2 level is $\delta = -96.7$ (see Table 2). We could not conclusively locate this signal in the ^{19}F NMR spectrum, because it overlapped with strong absorptions of the acid system (FSO_3H/SbF_5), but the observed doublet in the ^{13}C NMR spectrum is clearly due to coupling with fluorine. Previous[16] attempts to obtain $[FCO]^+$ by ionization of oxalyl fluoride with SbF_5/SO_2ClF were been unsuccessful, although the other halocarbonyl cations ($[XCO]^+$, X = Cl, Br, I) were generated in this way.

As further support for the experimental observations, the structures, energies, and NMR chemical shifts of the protonated and diprotonated fluoroformic acid and fluorocarbonyl cation, and the protonated fluorocarbonyl dication $[FCOH]^{2+}$ were calculated. Structures were optimized at the MP2/6-31G** level, and improved energies were obtained at the MP4(STDQ)/6-31G**//MP2/6-31G** + ZPE level.[17] The calculated geometry of fluoroformic acid (**1**) is in agreement with previously reported results.[5] Three minimum structures (**2**–**4**) were located for O-protonated fluoroformic acid $[FC(OH)_2]^+$. In accordance with the experimental results, the *cis/trans* isomer **2** (C_s) was found to be the global minimum on the $[FCO_2H_2]^+$ potential energy surface, but only 0.5 and 6.1 kcal mol^{-1} more stable than *cis–cis* isomer **3** (C_{2v}) and *trans–trans* isomer **4** (C_{2v}), respectively (Table 1). Protonation of FCOOH (**1**) to form $[FC(OH)_2]^+$ (**2**) is calculated to be exothermic by 171.3 kcal mol^{-1}. We have also located the transition states **5** and **6** for the interconversion of structure **2** into **3** and **4**, respectively, and the rotational barriers for these conversions were calculated to be 12.1 and 13.4 kcal mol^{-1}. Therefore, interconversion of *cis–trans*, *cis–cis*, and *trans–trans* isomers does not seem feasible, despite their similar energies. The calculated C–F bond in **2** is only 0.057 Å (4.2%) shorter than in **1**, indicating very little p–p backdonation of a fluorine nonbonded electron pair (Figure 2). There seems to be no O-H-F intramolecular hydrogen bonding in **2**, as the distance between F and H is 2.342 Å.

Table 1. Energies, zero-point vibrational energies (ZPE)[a], and relative energies [b].

Cmpd	MP2/6-31G**	ZPE	MP4(SDTQ)/6-31G**	$E_{rel.}$
1	288.28841	15.9	288.31891	171.3
2	288.57014	23.3	288.60369	0.0
3	288.56931	23.1	288.60282	0.5
4	288.55987	23.1	288.59369	6.1
5 (TS)	288.54872	22.2	288.58261	12.1
6 (TS)	288.54665	22.2	288.58062	13.4
7	288.57151	28.7	288.607807	3.3
8	288.53510	26.6	288.57019	28.7
9 (TS)	288.45397	23.7	288.48742	73.4
10	212.24408	6.3	212.26699	0.0
11	212.13530	10.3	212.16176	70.0

[a] ZPE in kcal mol^{-1} at the MP2/6-G31G** level, scaled by a factor of 0.93. [b] Relative energies based on MP4(SDTQ)6-31G**//MP2/6-31G** + ZPE.

The ^{13}C and ^{19}F NMR chemical shifts were calculated by IGLO (basis set II) and correlated GIAO-MP2 (basis set tzp/dz) methods based on MP2/6-31G** geometries (Table 2).[18] The ^{13}C NMR chemical shift of protonated fluoroformic acid $[FC(OH)_2]^+$ (**2**), calculated with GIAO-MP2, is $\delta = 170.6$, which is 12.8 ppm downfield from that of the experimental data ($\delta_{exp} = 157.8$). Calculated $\delta^{13}C$ values of the other two isomers (168.9 for **3** and 170.3 for **4**) are very close to that of **2**. On the other hand, the calculated $\delta^{13}C$ shift of diprotonated fluoroformic acid (**7**, 160.5) is shifted 10.1 ppm downfield relative to the calculated value of the monoprotonated species **2**, but very close to the experimenal data of $[FC(OH)_2]^+$. The $\delta^{13}C$ signal of $[FCO]^+$ (**10**) calculated with GIAO-MP2 is 124.5, which agrees with the observed experimental shift of $\delta_{exp} = 117.5$. Interestingly, calculated $\delta^{13}C$ value of the protonated fluoroformyl dication $[FCOH]^{2+}$ (**11**) is 116.6, which is also very close to the experimenal data of $[FCO]^+$. Similar results were obtained with the IGLO program (see Table 2). However, $[FCOH]^{2+}$ is ex-

 © WILEY-VCH Verlag GmbH, D-69451 Weinheim, 1997 0570-0833/97/3617-1876 $ 17.50+.50/0

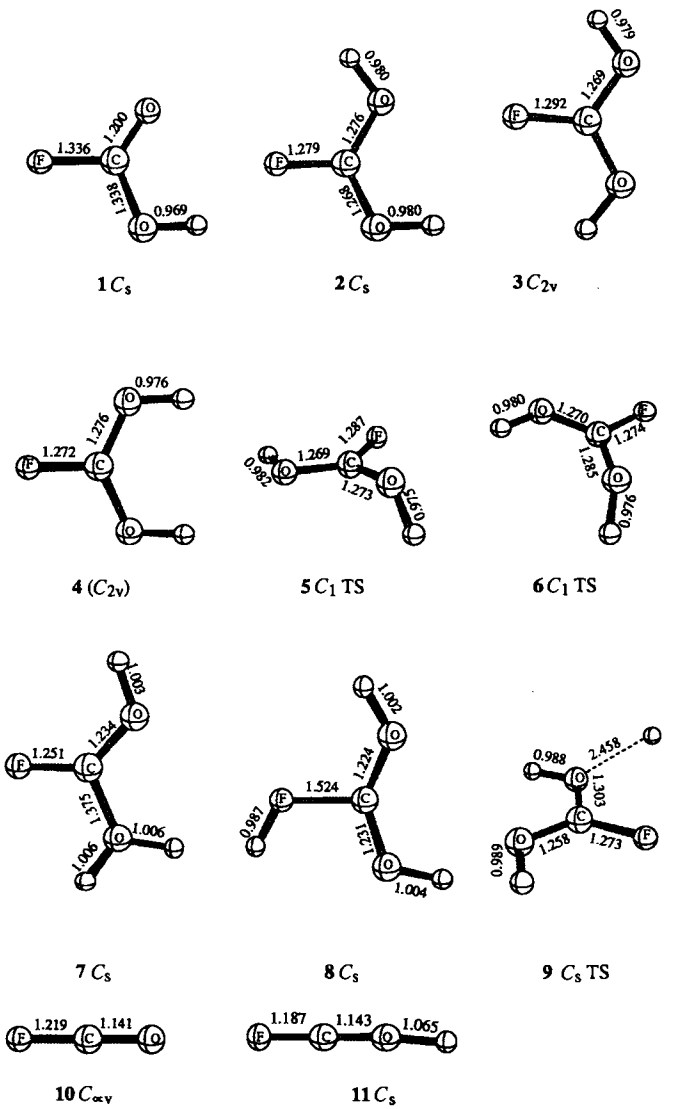

Figure 2. MP2/6-31G**-calculated structural parameters of free and protonated fluoroformic acid, as well as the fluorocarbonyl cation and its protonated forms.

pected to dissociate into $[FCO]^+$ and H^+, as it is 70 kcal mol^{-1} more unstable than these products.

The potential further protonation of **2** to diprotonated fluoroformic acid, a gitonic[19] fluorocarboxonium dication, was also investigated. Considerable interest has been focused recently on such highly electron-deficient superelectrophiles,[20] as they might play an important role in many superacid-catalyzed reactions, as well as in biological processes.[21] Based on experimental and theoretical studies, we recently[22] suggested the intermediacy of diprotonated trifluoroacetic acid $[CF_3C(OH_2)OH]^{2+}$ in the protolytic cleavage reaction of CF_3COOH with FSO_3H/SbF_5. For diprotonated fluoroformic acid, the O,O-diprotonated dication **7** was found to be the global minimum on the potential energy surface. Interestingly, O,F-diprotonated dication **8** was calculated to be a stable minimum. However, structure **8** is 25.4 kcal mol^{-1} higher in energy than structure **7**. Significantly, protonation of $[FC(OH)_2]^+$ (**2**) to form dication **7** was calculated to be endothermic by only 3.3 kcal mol^{-1}. We have also located the transition state **9** for protodissociation of **7** into **2**. Structure **9** lies 70.1 kcal mol^{-1} above structure **7**. Thus, dication **7** has a very high kinetic barrier for protodissociation. Although diprotonated fluoroformic acid could not be observed as a persistent species in NMR studies under the experimental conditions (even in fluoroantimonic acid medium), a limited diprotonation equilibrium could exist in the superacid solution. Gitonic dications (or related protosolvated cations) are energetic, reactive intermediates and should be differentiated from persistent, long-lived, relatively stable intermediates.

Table 2. Experimental and calculated ^{13}C and ^{19}F NMR chemical shifts [a].

Cmpd	Atom	δ values IGLO	GIAO-MP2	exp.
1	C	149.5	152.2	
	F	−14.8	−31.6	
2	C	166.2	170.6	157.8
	F	17.2	−0.4	
3	C	165.0	168.9	
	F	26.9	13.5	
4	C	166.4	170.3	
	F	17.0	−4.1	
7	C	157.6	160.5	
	F	51.8	37.9	
8	C	145.6	145.7	
	F	−20.4	−34.1	
10	C	131.1	124.5	117.5
	F	−53.4	−96.7	
11	C	119.3	116.4	
	F	−11.8	−58.1	

[a] The reference is tetramethylsilane for experimental and calculated ^{13}C NMR and $CFCl_3$ for calculated ^{19}F NMR chemical shifts.

Received: February 11, 1997 [Z10103IE]
German version: *Angew. Chem.* **1997**, *109*, 1958–1961

Keywords: ab initio calculations · carbocations · fluorine · fluoroformic acid · NMR spectroscopy

[1] R. J. Gordon, M. C. Lin, *Chem. Phys. Lett.* **1973**, *22*, 107.
[2] D. Cremer, *J. Am. Chem. Soc.* **1981**, *103*, 3633.
[3] J. S. Francisco, I. H. Williams, *J. Am. Chem. Soc.* **1993**, *115*, 3746.
[4] J. S. Francisco, W. A. Ghoul, *Chem. Phys.* **1991**, *157*, 89.
[5] F. A. Wiedmann, C. Wesdemiotis, *J. Am. Chem. Soc.* **1994**, *116*, 2481.
[6] F. A. Cotton, G. Wilkinson, *Advanced Inorganic Chemistry*, Wiley-Interscience, New York, **1988**.
[7] Z. Havlas, T. Kovar, R. Zahradnik, *J. Am. Chem. Soc.* **1985**, *107*, 7243.
[8] C. M. Rohlfing, L. C. Allen, R. Ditchfield, *J. Chem. Phys.* **1983**, *79*, 4958.
[9] K. E. Edgecombe, R. J. Boyd, *Can. J. Chem.* **1984**, *62*, 2881.
[10] R. Ditchfield, J. E. Del Bene, J. A. Pople, *J. Am. Chem. Soc.* **1972**, *94*, 703.
[11] X. Zhang, U. Gross, K. Seppelt, *Angew. Chem. Int. Ed. Engl.* **1995**, *34*, 1858.
[12] W. Kutzelnigg, U. Fleischer, M. Schindler, *NMR Basic Principles Prog.* **1990**, *23*, 165.
[13] J. Gauss, *Chem. Phys. Lett.* **1992**, *191*, 614.
[14] G. Rasul, V. P. Reddy, L. Z. Zdunek, G. K. S. Prakash, G. A. Olah, *J. Am. Chem. Soc.* **1993**, *115*, 2236.
[15] G. A. Olah, A. M. White, *J. Am. Chem. Soc.* **1967**, *89*, 7072.
[16] G. K. S. Prakash, J. W. Bausch, G. A. Olah, *J. Am. Chem. Soc.* **1991**, *113*, 3203.
[17] M. J. Frisch, G. W. Trucks, H. B. Schlegel, P. M. W. Gill, B. G. Johnson, M. A. Robb, J. R. Cheeseman, T. A. Keith, G. A. Peterson, J. A. Montgomery, K. Raghavachari, M. A. Al-Laham, V. G. Zakrzewski, J. V. Ortiz, J. B. Foresman, J. Cioslowski, B. B. Stefanov, A. Nanayakkara, M. Challacombe, C. Y. Peng, P. Y. Ayala, W. Chen, M. W. Wong, J. L. Andres, E. S. Replogle, R. Gomperts, R. L. Martin, D. J. Fox, J. S. Binkley, D. J. Defrees, J. Baker, J. J. P. Stewart, M. Head-Gordon, C. Gonzalez, J. A. Pople, Gaussian, Inc., Pittsburgh, PA, USA, **1995**.
[18] J. F. Stanton, J. Gauss, J. D. Watts, W. J. Lauderdale, R. J. Bartlett, *Quantum Theory Project*, University of Florida, Gainesville, Florida, USA, **1991**.
[19] G. A. Olah, N. Hartz, G. Rasul, G. K. S. Prakash, M. Burkhart, K. Lammertsma, *J. Am. Chem. Soc.* **1994**, *116*, 3187.
[20] G. A. Olah, *Angew. Chem. Int. Ed. Engl.* **1993**, *32*, 767.
[21] R. K. Thauer, A. R. Klein, G. C. Hartmann, *Chem. Rev.* **1996**, *96*, 3031.
[22] G. K. S. Prakash, G. Rasul, A. Burrichter, K. K. Laali, G. A. Olah G., *J. Org. Chem.* **1996**, *61*, 9253.

 © WILEY-VCH Verlag GmbH, D-69451 Weinheim, 1997 0570-0833/97/3617-1877 $ 17.50+.50/0

$[L_3Ni(\mu\text{-}L)_3NiL_3](AsF_6)_4$, (L = $N{\equiv}SF_2NMe_2$), a Dinuclear Nickel Complex with Bridging Thiazyl(dimethylamide)difluoride Ligands**

Ulrich Behrens, Jan Petersen, Enno Lork, Paul G. Watson, and Rüdiger Mews*

Dedicated to Professor Alois Haas on the occasion of his 65th birthday

The coordination chemistry of ligands with sulfur–nitrogen triple bonds has been investigated for a number of years, and all of the results to date show that the ligands NSX (X = F, Cl),[1–4] NS^+,[3,5] and NSF_3[6,7] coordinate "end-on" through the nitrogen atom.

Thiazyldialkylamides NSF_2NR_2 (R = Et,[8] Me,[9] R_2N = piperidine[10]) have been known since the work of Glemser, Meyer, and Haas.[8] The donor properties and coordination possibilities of the nitrogen atom of the $N{\equiv}S^{VI}$ system are dramatically improved by exchanging one of the sulfur-bound fluorine atoms of NSF_3 for the more strongly electron-donating R_2N group.[11] Thus, for example, although only two NSF_3 ligands can coordinate to the Ag^+ ion to form the unstable $[Ag(NSF_3)_2]^+$ ion,[12] a stable silver complex can be prepared by addition of three $NSF_2(NMe_2)$ ligands [Eq. (a)].[7]

$$\underset{\mathbf{1}}{Ag[AsF_6]} + 3\,\underset{\mathbf{2}}{NSF_2NMe_2} \longrightarrow \underset{\mathbf{3}}{[Ag(NSF_2NMe_2)_3][AsF_6]} \qquad (a)$$

In **5**, which can be formed from **4** and **2** according to Equation (b), the central Co^{II} atom is surrounded by a regular tetrahedron of ligands, in contrast the corresponding NSF_3 complex $[Co(NSF_3)_4(FAsF_5)_2]$ shows octahedral geometry.[7] In **7** [Eq. (c)]

$$\underset{\mathbf{4}}{[Co(OSO)_4(FAsF_5)_2]} + 4\,\mathbf{2} \longrightarrow \underset{\mathbf{5}}{[Co(NSF_2NMe_2)_4](AsF_6)_2} + 4SO_2 \qquad (b)$$

$$\underset{\mathbf{6}}{[Ni(OSO)_6][AsF_6]_2} + 6\,\mathbf{2} \longrightarrow \underset{\mathbf{7}}{[Ni(NSF_2NMe_2)_6](AsF_6)_2} + 6SO_2 \qquad (c)$$

as many as six $N{\equiv}S^{VI}$ ligands are attached to one central atom. The $[Ni(NSF_2NMe_2)_6]^{2+}$ ion has C_i symmetry as shown in Figure 1.[13]

By using the correct stoichiometry of **6** and **2**, the binuclear complex **8** can be isolated in almost quantitative yield [Eq. (d); L = $N{\equiv}SF_2NMe_2$].

$$2\,\mathbf{6} + 9\,\mathbf{2} \longrightarrow \underset{\mathbf{8}}{[L_3Ni(\mu\text{-}L)_3NiL_3](AsF_6)_4} + 12SO_2 \qquad (d)$$

Complex **8** is the first example in which the thiazyl nitrogen atom is fixed in a bridging position. Two $[Ni(NSF_2NMe_2)_6]^{2+}$ octahedra are connected by a common face formed by three nitrogen atoms of the thiazyl triple bond to give a dimeric complex $[Ni_2L_9]^{4+}$ (Figure 2). The Ni–N distances to the terminal nitrogen atoms (204.2(9)–208.6(9) pm) are significantly shorter than those to the bridging nitrogen atoms (213.2(8)–219.2(8) pm). The geometry of the terminal Ni-N-S bonds (d(SN) = 137.6(9)–141.1(9) pm, Ni-N-S angles 143.7(6)–164.9(7)°) varies slightly more than that of the bridges, in which the Ni-N-S angles range between 124.0(5) and 139.5(5)° and the S–N distances between 141.8(9)–142.9(8) pm.

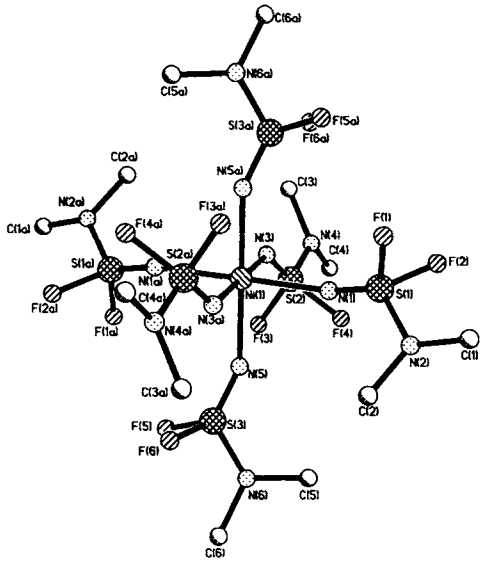

Figure 1. Structure of the cation of **7** with selected bond lengths [pm] and angles [°]: Ni–N 207.1(4)–211.5(4), (av 209.2); N≡S 139.1(4)–140.9(4), (av 139.7); S–N 155.6(4)–157.7(4), (av 156.7); S–F 153.5(3)–156.9(3), (av 156.0); Ni-N-Ni 88.2(2)–91.8(2); Ni-N≡S 138.3(2)–155.0(3), (av 147.6); N≡S-F 115.7(2)–119.4(2), (av 117.9), F-S-F 91.0(2)–92.1(3), (av 91.4); N-S-F 98.2(2)–103.6(2), (av 100.6); N≡S-N 120.4(2)–124.8(3), (av 122.5). The sums of the angles at the nitrogen atoms of the dimethyl amino group range between 353.3 and 357.8°.

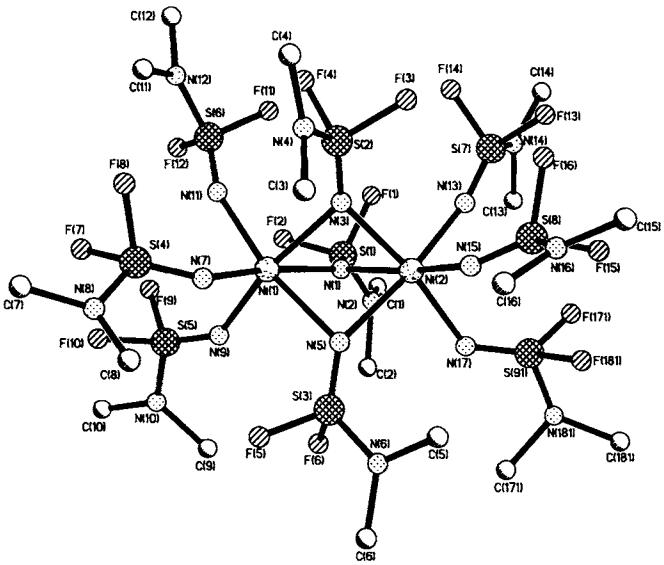

Figure 2. Structure of the cation of **8**.

Complexes of type **8** with isolated $[Ni(\mu\text{-}N)_3Ni]$ units are rare, to our knowledge only one analogous complex (with three bridging 1,1-N_3 groups) has been structurally characterized.[15] In the related $[Ni(N_3)(tmeda)]_\infty$[16] (tmeda = *N,N,N',N'*-tetramethylethylenediamine) the $[(tmeda)Ni(\mu\text{-}1,1\text{-}N_3)_3Ni(tmeda)]$ units are linked by 1,3-azido bridges, forming a polymeric structure.

The Ni_2N_3 cluster in **8** (Ni(1)-N-Ni(2) angle 86–87°, d(Ni(1)–Ni(2)) 296.7(4) pm) is very similar to the known example.[15] Complex **8** is paramagnetic at room temperature.[17]

[*] Prof. Dr. R. Mews, Dr. J. Petersen, Dr. E. Lork, Dr. P. G. Watson
Institut für Anorganische und Physikalische Chemie der Universität
Postfach 33 04 40, D-28334 Bremen (Germany)
Fax: Int. code: (421)218 4267
e-mail: mews@chemie.uni-bremen.de
Prof. Dr. U. Behrens
Institut für Anorganische und Angewandte Chemie
der Universität Hamburg (Germany)

[**] This work was supported by the Fonds der Chemischen Industrie and the FNK (Universität Bremen).

 © WILEY-VCH Verlag GmbH, D-69451 Weinheim, 1997 0570-0833/97/3617-1878 $ 17.50+.50/0

Experimental Section

7 and **8**: Freshly prepared $[Ni(SO_2)_6](AsF_6)_2$ (1–2 mmol) was dissolved in SO_2 (10 mL) in a two-legged thick-walled glass vessel at −30 °C. The stoichiometric amount of ligand, also dissolved in SO_2 (10 mL) was added. A color change to light green (**7**) and to yellow (**8**) indicated immediate reaction, and the mixture was stirred for 1 h in order to complete the reaction. The product was obtained in quantitative yield after removal of the solvent.

7: NMR ($SO_2/CD_2Cl_2/CFCl_3$/TMS/309 K): $\delta(^1H) = 7.8$ (s, br); $\delta(^{19}F) = 51.3$ (s, br, SF_2); IR: $\nu_{NS} = 1508\ cm^{-1}$ (vs, br). Elemental analysis: calcd: Ni 4.87, S 15.96; found: Ni 4.74, S 16.2.

8: NMR ($SO_2/CD_2Cl_2/CFCl_3$/TMS/309 K): $\delta(^1H) = 8.6$ (s, br), $\delta(^{19}F) = 55.1$ (s, br, SF_2); IR: ν_{NS} 1553, 1531 cm^{-1} (vs, br). Elemental analysis ($C_{18}H_{54}As_4F_{42}N_{18}Ni_2S_9$): calcd: Ni 5.79, S 14.24; found: Ni 5.84, S 14.3.

Single crystals of **7** suitable for structural analysis were obtained after removal of the solvent and pumping off of excess ligand under vacuum. Single crystals of **8** were grown by slow removal of SO_2 from a solution of the complex in SO_2/diethyl ether at ambient temperature.

Received: February 14, 1997 [Z10117IE]
German version: *Angew. Chem.* **1997**, *109*, 1951–1953

Keywords: main group elements · multiple bonds · nickel · N ligands · sulfur

[1] B. Buss, P. G. Jones, R. Mews, M. Noltemeyer, G. M. Sheldrick, *Angew. Chem.* **1979**, *91*, 253; *Angew. Chem. Int. Ed. Engl.* **1979**, *18*, 231.
[2] J. Hanich, P. Klingelhöfer, U. Müller, K. Dehnicke, *Z. Anorg. Allg. Chem.* **1983**, *506*, 68.
[3] Review: *Gmelin Handbook of Inorganic Chemistry, Sulfur-Nitrogen Compounds, Part 5*, Springer, Berlin, **1990**.
[4] Review: K. Dehnicke, U. Müller, *Comments Inorg. Chem.* **1985**, *4*, 213.
[5] Reviews: H. W. Roesky, K. K. Pandey, *Adv. Inorg. Chem. Radiochem.* **1983**, *26*, 337; K. K. Pandey, *Prog. Inorg. Chem.* **1992**, *40*, 445; M. Herberhold, *Nachr. Chem. Tech. Lab.* **1981**, *29*, 365; T. Chivers, F. Edelmann, *Polyhedron* **1986**, *5*, 1661; P. F. Kelly, F. D. Woolins, *ibid.* **1986**, *5*, 607.
[6] B. Buss, W. Clegg, G. Hartmann, P. G. Jones, R. Mews, M. Noltemeyer, G. M. Sheldrick, *J. Chem. Soc. Dalton Trans.* **1981**, 61; U. Behrens, R. Hoppenheit, W. Isenberg, E. Lork, J. Petersen, R. Mews, *Z. Naturforsch. B* **1994**, *49*, 238.
[7] J. Petersen, E. Lork, R. Mews, unpublished results.
[8] O. Glemser, H. Meyer, A. Haas, *Chem. Ber.* **1965**, *98*, 2049.
[9] O. Glemser, J. Wegener, R. Höfer, *Chem. Ber.* **1972**, *105*, 474.
[10] O. Glemser, W. Koch, *Z. Naturforsch. B* **1968**, *23*, 745.
[11] D. B. Beach, W. L. Jolly, R. Mews, A. Waterfeld, *Inorg. Chem.* **1984**, *23*, 4080.
[12] R. Mews, *J. Chem. Soc. Chem. Commun.* **1979**, 278.
[13] X-ray crystal structure analysis of **7** ($C_{12}H_{36}As_2F_{24}N_{12}NiS_6$), $M_r = 1205.44$; crystal dimensions $0.8 \times 0.4 \times 0.3\ mm^3$; orthorhombic, space group *Pbca*, $a = 1303.2(3)$, $b = 1263.5(3)$, $c = 2499.3(5)$ pm, $V = 4.115(2)\ nm^3$, $Z = 4$, $\rho_{calcd} = 1.946\ Mg\,m^{-3}$, $\mu = 2.511\ mm^{-1}$. A single-crystal suitable for X-ray analysis was fixed to a glass fiber with Kel-F oil and measured at −100 °C on a Siemens P4 four-circle diffractometer (graphite monochromator, $Mo_{K\alpha}$ radiation, $\omega/2\theta$ scan). Of the 5876 measured reflections ($2.39° < \theta < 27.5°$) 4687 independent reflections remained after averaging. The structure was solved by direct methods. The refinement calculations converged at $wR_2 = 0.1316$ (refinement against F^2) for all 4687 reflections and 267 variables ($R1 = 0.0514$ for 2851 reflections with $I > 2\sigma(I)$). Heavy atoms were assigned individual anisotropic deflection parameters. Hydrogen atoms were calculated with a riding model and common isotropic temperature factors. A difference Fourier synthesis indicated no residual electron density beyond $+730\ e\,nm^{-3}$ and $-929\ e\,nm^{-3}$. The structure solution and preparation of the drawings were performed with the SHELXTL program package [18], the refinements with the program SHELXL-93 [19·20].
[14] X-ray crystal structure analysis of **8** ($C_{18}H_{54}As_4F_{42}N_{18}Ni_2S_9$), $M_r = 2026.43$; crystal dimensions $0.6 \times 0.4 \times 0.3\ mm^3$; triclinic, space group, $a = 1190.8(2)$, $b = 1375.3(3)$, $c = 2313.7(5)$ pm, $\alpha = 77.40(3)$, $\beta = 75.51(3)$, $\gamma = 64.50(3)°$, $V = 3.2847(11)\ nm^3$, $Z = 2$, $\rho_{calcd} = 2.049\ Mg\,m^{-3}$, $\mu = 3.018\ mm^{-1}$. A single-crystal suitable for X-ray analysis was fixed to a glass fiber with Kel-F oil and measured at −100 °C on a Siemens P4 four-circle diffractometer (graphite monochromator, $Mo_{K\alpha}$ radiation, $\omega/2\theta$ scan). 12076 reflections were measured ($2.62° < \theta < 25°$). The structure was solved by direct methods. Due to twinning in the crystal, some reflections lay so close to each other that they appeared with greater than normal intensity. These reflections had to be removed from the data set before the final refinement. 912 of the 12076 reflections were deleted under the following criteria: $F_o^2 > F_c^2$ and $F_o^2 > 3\sigma(F_o^2)$. 10379 reflections were obtained after averaging of the remaining 11164 intensities. The final refinement calculations converged at $wR_2 = 0.2296$ (refinement against F^2) for 10379 reflections and 905 variables ($R1 = 0.0873$). Heavy atoms were assigned individual anisotropic deflection parameters. Hydrogen atoms were calculated with a riding model and common isotropic temperature factors. A difference Fourier synthesis indicated no residual electron density beyond $+1872\ e\,nm^{-3}$ and $-885\ e\,nm^{-3}$. The structure solution and preparation of the drawings were performed with the SHELXTL program package [18], the refinements with the program SHELXL-93 [19·20].
[15] P. D. Beer, M. G. B. Drew, P. B. Leeson, K. Lyssenko, M. I. Ogden, *J. Chem. Soc. Chem. Commun.* **1995**, 929.
[16] J. Ribas, M. Monfort, B. Kumar Ghosh, X. Solans, *Angew. Chem.* **1994**, *106*, 2177; *Angew. Chem. Int. Ed. Engl.* **1994**, *33*, 2087.
[17] **7** (294 K): $\chi_M = 3.993 \times 10^{-3}\ cm^3\,mol$; $\mu = 3.06\ \mu_B$. **8** (294 K): $\chi_M = 8.686 \times 10^{-3}\ cm^3\,mol$; $\mu = 4.51\ \mu_B$. The temperature dependence of χ_M for the complex cited in reference [15] indicates ferromagnetic behavior. There is an indication of some weak antiferromagnetic coupling at low temperatures that may be due to interdimer exchange.
[18] Siemens SHELXTL-Plus: Release for Siemens R3 Crystallographic Research Systems, Siemens Analytical X-Ray Instruments Inc., Madison, WI, **1989**.
[19] G. M. Sheldrick, SHELXL-93, Universität Göttingen, **1993**.
[20] Crystallographic data (excluding structure factors) for the structures reported in this paper have been deposited with the Cambridge Crystallographic Data Centre as supplementary publication no. CCDC-100215. Copies of the data can be obtained free of charge on application to The Director, CCDC, 12 Union Road, Cambridge CB2 1EZ, UK (fax: int. code +(1223) 336-033; e-mail: deposit@chemcrys.cam.ac.uk).

In Vitro Selection without Intervening Amplification**

Joseph Smith and Eric V. Anslyn*

Aptamers to medically important targets have potential value as drug leads.[1] Currently, aptamer selection procedures are typically limited to unmodified DNA and RNA. When modified oligomers are incorporated, the selection procedure is terminated after just one round of amplification since polymerases will not tolerate most chemically modified mononucleotides.[2] However, if the modified nucleotides are not part of the random region that is amplified by the polymerase chain reaction (PCR) after each selection, they would not disturb the amplification. Unfortunately, using such a method would require reincorporation of the modified oligomers into the library after each selection cycle, making the method quite tedious. This limitation would be circumvented if the screening process did not involve amplification during each selection cycle, but instead relied on a single amplification of the random region after the final round of selection. If the modified region was separated from the random region by a PCR primer (Scheme 1), then the successful

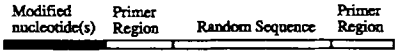

Scheme 1. Representation of the DNA aptamers found.

aptamer could be resynthesized in a manner similar to that used to produce the original library. In addition, such a recursive selection without intervening amplification should yield high-affinity aptamers in a fraction of the time required for in vitro selection. Although we do not describe the use of modified nucleotides here, we introduce three requirements for in vitro selection without intervening amplification and demonstrate its viability.

[*] Prof. E. V. Anslyn, Dr. J. Smith
The Department of Chemistry and Biochemistry
The University of Texas at Austin
Austin, TX 78712 (USA)
Fax: Int. code +(512)471-8696
e-mail: anslyn@ccwf.cc.utexas.edu

[**] We gratefully acknowledge financial support for this work from the National Science Foundation, the Texas Advanced Technology Program, Sloan and Dreyfus Foundation Awards to E. V. A., and a University of Texas Fellowship to J. S.

 © WILEY-VCH Verlag GmbH, D-69451 Weinheim, 1997 0570-0833/97/3617-1879 $ 17.50+.50/0

We envisioned three minimal conditions that must be met before in vitro screening of oligonucleotide libraries can be achieved without intervening amplification. First, the number of copies of ligand-binding sequences must be great enough to survive iterative small losses during the entire process. Second, the ratio of signal to noise (ratio of ligand-binding to nonspecific binding sequences) must increase with every round of screening until the noise is totally overwhelmed. Since the signal is not amplified, the noise must be capable of being repetitively reduced until signal strength is greater than noise level. The third condition is that the amplification after the last selection round must be sufficiently effective so that polymerases can make enough copies of the few surviving sequences for eventual identification. As an initial test of the concept, iterative screenings for aptamers to ATP were performed without amplification. We used ATP since it has been previously targeted;[3] hence we could compare our new method to the literature method for in vitro selection. Steps from the new method and the traditional method are schematically summarized in Figure 1.

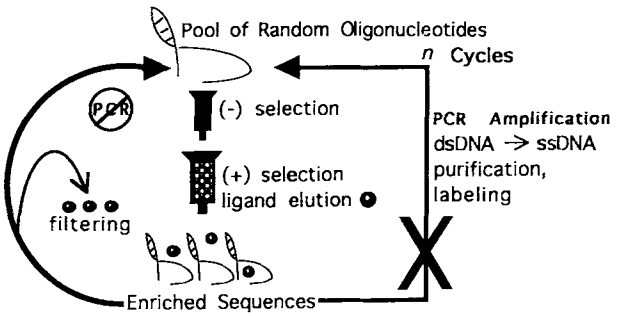

Figure 1. Schematic representation of the new and traditional in vitro selection methods. The "no PCR" sign is only meant to imply a lack of PCR during the selection cycles since a final PCR step is still required. ● = ATP, (−) selection indicates an acetate-agarose precolumn, and (+) selection indicates an ATP-agarose column. dsDNA = double-stranded DNA, ssDNA = single-stranded DNA.

The first condition of recursive selection without amplification was satisfied with the synthesis of a library of DNA oligonucleotides containing an 18-nucleotide random region,[4] which after labeling and purification yielded roughly 17800 copies per distinct sequence. Six cycles of selection were then performed without any intervening amplification (see the Experimental Section).

As mentioned in reference to the second condition, noise reduction is of paramount importance in this method. Therefore, the radioactive decay (in counts per minute (cpm)) was measured after each selection cycle to monitor the progress of the procedure (Table 1). The initial library had a total activity of 4.2×10^7 cpm. After the first selection round, the ATP-eluted oligonucleotides had an activity of near 10^5 cpm, less than 0.25% of the original quantity loaded. Since almost all the sequences lost during selection are likely oligonucleotides that do not bind the target, this serves as an estimate of noise. After the second cycle, the activity of the ATP-eluted DNA had dropped to about 600 cpm. Retained noise was again reduced over 99%. For later cycles no measurable radioactivity above background could be detected. Since the amount of signal was unknown, we could not determine at this point in the selection whether the second condition had been met.

Table 1. Review of the six cycles of selection. cv = column volumn, fb = folding buffer (300 mM KCl, 5 mM $MgCl_2$, 20 mM Tris, pH 7.5).

Cycle	DNA	cpm	Pre-column (300 µL)	ATP-agarose (2.5 mM, 800 µL)	Ligand elution
1	300 µL fb	4.2×10^7	2 cv fb	+5 cv fb	3 mL, 5 mM ATP in fb
2	10 mL 30 µM ATP in fb	1×10^5	1 cv fb	+2 cv fb	fb
3	fb	600	fb	fb	fb
4–5	fb	–	fb	fb	fb
6	fb	–	fb	fb	3 mL, 10 mM ATP in fb

The third condition was met using the "rare-DNA PCR" protocol created specifically for the amplification of DNA with a low number of copies.[5] The effective range of the optimized amplification protocol is reported to be from 1 to 20000 molecules of DNA as the initial substrates. Also, rare-DNA PCR has been used to quantitate less than ten molecules of herpes simplex viral DNA in a reaction that also had 100 ng of contaminating nonviral DNA as background.[6] Although use of a single amplification at the end of an in vitro selection protocol requires more cycles than if each selection cycle is followed by amplification, the former has the advantage that it should introduce less replication bias in the final populations than the latter.[7]

After the rare-DNA protocol was performed (see the Experimental Section), the amplified DNA was cloned and ten clones were sequenced. Three sequences had duplicates. There were obvious homologies among the three with two consensus regions. Figure 2 shows the base pairing of these sequences based on Huizenga's and Szostak's postulated general sequence[3] for an ATP DNA aptamer. Indeed, according to the number of flanking base pairs stabilizing the guanine-rich regions of the sequences, the order of ATP affinity found correlates with the predictions of Huizenga and Szostak.

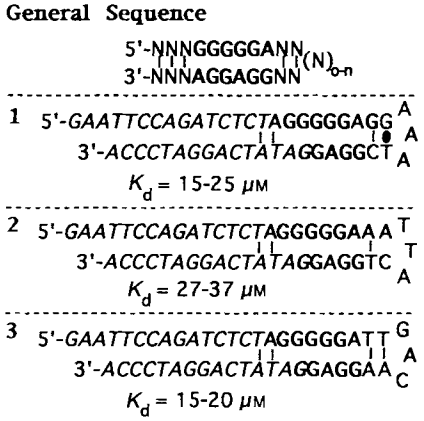

Figure 2. Base pairings based on the proposed general sequence for an ATP DNA aptamer[3]. The sequences in bold are thought to form two stacked guanine quartets. The italicized sequences are parts of the fixed primer regions. The methods of isocratic elution[8], membrane diafiltration[1b, 3], and equilibrium gel filtration[9] were used to determine the dissociation constant for the ATP–aptamer complex. ● indicates a non-Watson–Crick base pair.

The original method of Huizenga and Szostak proceeded through several rounds of screening, amplifying, isolating ssDNA, radiolabeling, and purifying before a DNA population was developed with moderate affinity to ATP.[3] After 17 clones had been sequenced, no consensus sequence was found. One clone was chosen for a series of truncation experiments wherein the ATP-binding domain was localized to a region 42 nucle-

 © WILEY-VCH Verlag GmbH, D-69451 Weinheim, 1997 0570-0833/97/3617-1880 $ 17.50+.50/0

otides in length. In vitro "evolution" was done on this region at 30% mutagenesis, and four more rounds of in vitro selection followed before this second population was cloned. From these sequences, a consensus region was discovered. Certainly though this work is a pioneering achievement in the field, it is an example of how the conventional protocol is significantly more involved than that presented here.

In summary, a novel in vitro selection protocol has been designed to take advantage of a combinatorial library of small size that has multiple copies of every distinct sequence. The method condensed the many days of a typical screening strategy to less than two days. This was a proof-of-concept experiment that showed that the new method succeeds by creating a large number of copies of individual sequences in the initial random pool, consistently reducing the level of nonspecific binding sequences per selection round, and effectively amplifying the few surviving sequences.

Since only the original synthesized sequences were used for all the screenings, the technique should allow for the iterative in vitro selection of modified oligonucleotides that previously could not undergo this powerful process.[10] Hence, this method should significantly increase the power of the in vitro selection method and is the direction that we are currently investigating.

Experimental Section

The DNA library[4] (31 mg) was labeled at the 5'-end with [γ-^{32}P]ATP, purified by gel chromatography, and suspended in 300 mL of folding buffer (300 mM KCl, 5 mM $MgCl_2$, 20 mM Tris, pH 7.5). After cooling down to room temperature following denaturation at 75 °C, the ^{32}P-labeled DNA was loaded onto an acetate-agarose precolumn (300 µL), which was attached directly to a 2.5 mM ATP-agarose column (800 µL, Sigma). The precolumn was washed with 600 µL of buffer, and the eluted DNA was allowed to equilibrate on the ATP-agarose column for 10 min. The precolumn was discarded after a single use as were all subsequent columns. After equilibration, the ATP-agarose column was washed with 4 mL of folding buffer to elute unbound or weakly bound oligonucleotides. The retained DNA was eluted with 3 mL of the ATP elution buffer (5 mM ATP in folding buffer) and collected in 500 µL fractions.

In order to perform another round of selection, the ATP had to be removed. Hence, the eluted fractions were collected directly into Microcon-3 microcentrifuge devices (3000 D cutoff, Amicon). After membrane diafiltration, about 98% of the total ATP was removed. The filtered fractions were then pooled, and folding buffer was added until a final volume of 10 mL was attained. The concentration of contaminating ATP concentration was 30 µM for the DNA sample, which was over 80 times more dilute than that of the 2.5 mM ATP-agarose column. Each cycle of selection started with a new set of stacked affinity columns, i.e. a precolumn attached to a ligand column. The screening cycles for the ATP aptamers are summarized in Table 1.

The rare-DNA PCR was performed as follows: On the last cycle the DNA was eluted from the ATP-agarose column with 3 mL of 10 mM ATP in 20 mM Tris, pH 7.5. This last fraction was precipitated twice from ethanol, and the PCR reagents (50 mM KCl, 8 mM $MgSO_4$, 10 mM $(NH_4)_2SO_4$, 20 mM Tris, pH 8.8 at 25 °C, 200 µM dNTPs, 0.1% Triton X-100, 20 units of Deep Vent (exo-) DNA polymerase, 0.5 µg 5'-primer, 0.5 µg 3'-primer) were added. Thermal cycling (94 °C for 45 s; 42 °C for 90 s; 60 °C for 45 s; 45 cycles) was done in a microcentrifuge tube that had first been irradiated with UV light. A positive control containing a dilute solution (~20000 molecules) of a 52-mer, and a negative control containing no DNA also underwent the same amplification protocol. Gel electrophoresis after amplification showed DNA in all lanes except the negative control.

Received: February 27, 1997 [Z10170IE]
German version: *Angew. Chem.* **1997**, *109*, 1956–1958

Keywords: aptamers · combinatorial chemistry · in vitro selection · nucleotides · polymerase chain reaction

[1] L. C. Bock, L. C. Griffin, J. A. Latham, E. H. Vermaas, J. J. Toole, *Nature* **1992**, *355*, 564–566; J. R. Lorsch, J. W. Szostak, *Biochemistry* **1994**, *33*, 973–982; D. Smith, G. P. Kirschenheuter, J. Charlton, D. M. Guidot, J. E. Repine, *Chem. Biol.* **1995**, *2*, 741–750; D. Jellinek, L. S. Green, C. Bell, N. Janjić, *Biochemistry* **1994**, *33*, 10450–10456; C. Tuerk, S. MacDougal, L. Gold, *Proc. Natl. Acad. Sci. USA* **1992**, *89*, 6988–6992; C. Tuerk, S. MacDougal-Waugh, *Gene* **1993**, *137*, 33–39; D. P. Bartel, M. L. Zapp, M. R. Green, J. Szostak, *Cell* **1991**, *67*, 529; C. T. Lauhon, J. W. Szostak, *J. Am. Chem. Soc.* **1995**, *117*, 1246–1257; P. Burgstaller, M. Famulok, *Angew. Chem.* **1994**, *33*, 1163–1166; *Angew. Chem. Int. Ed. Engl.* **1994**, *33*, 1084–1087; M. Famulok, J. W. Szostak, *J. Am. Chem. Soc.* **1992**, *114*, 3990–3991; M. Famulok, *ibid.* **1994**, *116*, 1698–1706; J. G. Connell, M. Illangesekare, M. Yarus, *Biochemistry* **1993**, *32*, 5497; M. Sassanfar, J. W. Szostak, *Nature* **1993**, *364*, 550–553; a) M. G. Wallis, U. von Ahsen, R. Schroeder, M. Famulok, *Chem. Biol.* **1995**, *2*, 543–552; b) R. D. Jenison, S. C. Gill, A. Pardi, B. Polisky, *Science* **1994**, *263*, 1425–1429; J. F. Milligan, M. D. Matteucci, J. C. Martin, *J. Med. Chem.* **1993**, *36*, 1923–1937; J. D. Ecker, S. T. Crooke, *Biotechnology* **1995**, *13*, 351–360.

[2] Some exceptions include 2'-amino- and 2'-fluoro substitutions on sugar (H. Aurup, D. M. Williams, F. Eckstein, *Biochemistry* **1992**, *31*, 9636–9641) and 1-pentynyl substitution on pyrimidine (J. A. Latham, R. Johnson, J. J. Toole, *Nucleic Acids Res.* **1994**, *22*, 2817–2822).

[3] D. E. Huizenga, J. W. Szostak, *Biochemistry* **1995**, *34*, 656–665.

[4] Oligonucleotides were purchased HPLC-purified from Operon. The initial sequence was 5'-GAATTCCAGATCTCT-(18N)-GATATCAGGATCCCA-3'. The two primers were 5'-GAATTCCAGATCTCT-3' and 5'-TGGGATCCT-GATATC-3'. These sequences incorporated EcoR I and BamH I digestion enzyme restriction sites.

[5] D. M. Coen in *Current Protocols in Molecular Biology* (Eds.: F. M. Ausubel, R. Brent, R. E. Kingston, D. D. Moore, J. G. Seidman, J. A. Smith, K. Struhl), Current Protocols, New York, **1994**, Chapter 15.4.

[6] J. P. Katz, E. T. Bodin, D. M. Coen, *J. Virol.* **1990**, *64*, 1690–1694.

[7] S. A. Kauffman, *The Origins of Order: Self Organization and Selection in Evolution*, Oxford University Press, New York, **1993**, Chapter 3.

[8] D. H. Freeman, *Anal. Chem.* **1972**, *44*, 117–120; B. M. Dunn, I. M. Chaiken, *Proc. Natl. Acad. Sci. USA* **1974**, *71*, 2382.

[9] J. P. Hummel, W. J. Dreyer, *Biochim. Biophys. Acta* **1962**, *63*, 530.

[10] Another method for the use of modified nucleotides in the 5'-region of a primer has been described recently: J. Burmeister, G. von Kiedrowski, A. D. Ellington, *Angew. Chem.* **1997**, *109*, 1379–1381; *Angew. Chem. Int. Ed. Engl.* **1997**, *36*, 1321–1324.

The Synthesis of Enantiopure ω-Methanoprolines and ω-Methanopipecolic Acids by a Novel Cyclopropanation Reaction: The "Flattening" of Proline**

Stephen Hanessian,* Ulrich Reinhold, and Gabriella Gentile

Proline occupies a prominent position in the hierarchy of natural amino acid constituents of mammalian proteins.[1] As part of a peptidic motif, its unique structure results in secondary amide bonds, leading to important conformational and functional consequences.[2] For example, the well-known *cis–trans* isomerism in prolylamides is associated with vitally important biological phenomena and functions, such as protein folding,[3] hormone regulation,[4] recognition,[5] and transmembrane signaling[6] to mention a few. The importance of *cis–trans* conformational changes is manifested by the role that peptidyl prolyl isomerases such as the immunophilins play in immunoregulation.[7] Proline has also figured prominently as a component of therapeutic agents,[8] in drug design,[9] and in probing enzyme activity.[10]

Conformationally constrained analogues of proline have been used extensively in connection with peptidomimetic research.[11] Although 2,3- and 3,4-methanoprolines have been

[*] Prof. Dr. S. Hanessian, Dr. U. Reinhold, G. Gentile
Department of Chemistry
Université de Montréal
C. P. 6128, Succ. Centre-ville
Montreal, QC, H3C 3J7 (Canada)
Fax: Int. code +(514)343-5728

[**] We thank NSERC for generous financial assistance through the Medicinal Chemistry Chair program. We thank Dr. Michel Simard for the X-ray analyses. U. R. acknowledges a DFG Research Fellowship from the Deutsche Forschungsgemeinschaft. G. G. thanks the University of Siena and the Italian C. N. R. for a summer fellowship.

 © WILEY-VCH Verlag GmbH, D-69451 Weinheim, 1997 0570-0833/97/3617-1881 $ 17.50+.50/0

described,[12, 13] the 4,5-methanoprolines are relatively unexplored.[14] Furthermore, structural investigations that study the consequences of introducing strain and its effects on the configuration and stability of amide linkages are not available to compare such systems to their proline counterparts.

We describe herein highly stereocontrolled syntheses of the diastereomeric 4,5-methano-L-prolines and 5,6-methano-L-pipecolic acids by a novel intramolecular cyclopropanation reaction of iminium ions and the extension of the methodology to other congeners.[15, 16]

Treatment of the readily available lactam **1**[17a] with lithium hexamethyldisilazide (LiHMDS) and Me_3SnCH_2I gave the α-alkylated products **2** ($[\alpha]_D = -15.3$, $c = 0.43$ in $CHCl_3$) and **3** ($[\alpha]_D = -16.0$, $c = 1.23$ in $CHCl_3$) in 63% and 23% yields, respectively (Scheme 1). The *syn*-isomer **3** could be easily obtained

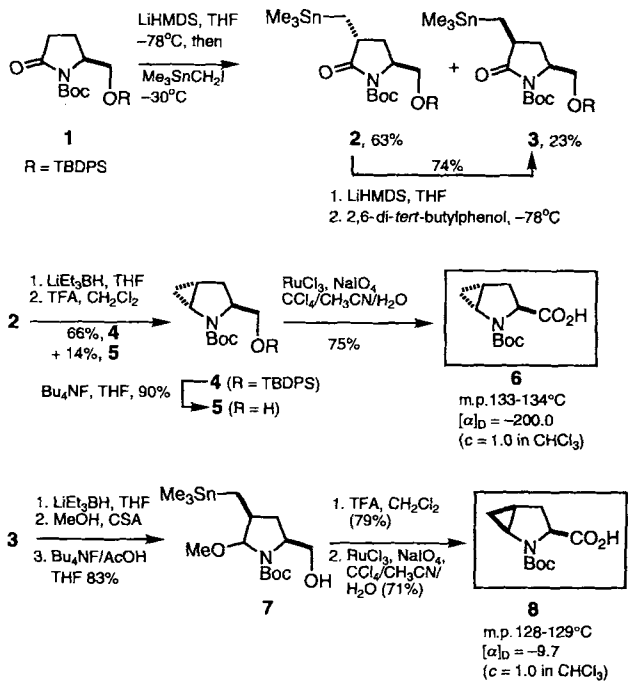

Scheme 1. TBDPS = *t*-BuPh$_2$Si, TFA = trifluoroacetic acid, Boc = *tert*-butoxycarbonyl, CSA = camphor-10-sulfonic acid.

by treatment of the enolate from **2** with the proton source 2,6-di-*tert*-butylphenol.[18, 19] Generation of the hemiaminal from **2** and treatment with TFA led to the (4*R*,5*R*)-methanopyrrolidine derivative **4** ($[\alpha]_D = -69.3$, $c = 1.41$ in $CHCl_3$), which was smoothly deprotected to **5**, and the latter oxidized to give the crystalline (4*R*,5*R*)-methano-*N*-Boc-L-proline in excellent overall yield.

Similar treatment of the *syn*-isomer **3** gave the diastereomeric crystalline acid **8** via its methylaminal derivative **7**. The structures and conformations of **6** and **8** in the solid state were unambiguously confirmed by single-crystal X-ray analysis. Table 1 lists selected torsion angles for compounds **6** and **8**, where considerable "flattening" of the pyrrolidine ring is observed relative to *N*-Boc-L-proline,[20] particularly in the case of **6**. The flattening of the pyrrolidine ring in **6** is also manifested in the root-mean-square value of 0.003 Å for the C_β and N atoms from the plane defined by C_β,C_γ,C_δ, and N (0.013 Å in **8**). The lowest deviation of 0.018 Å in the case of *N*-Boc proline was found for C_α and C_γ atoms in the plane C_α,N,C_δ,C_γ; in this case C_β was distinctly above the plane (0.521 Å). This differs substantially

Table 1. Selected torsion angles and root-mean-square deviations from fitted atoms in a given plane of X-ray crystal structures, and ^{13}C NMR chemical shifts ($CDCl_3$).

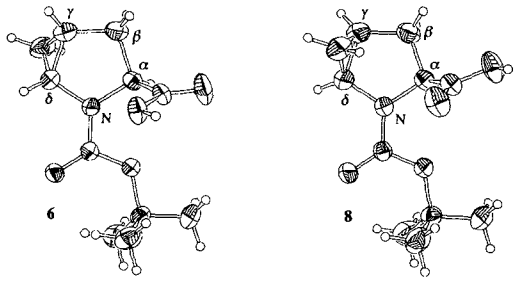

	N-Boc-L-proline [20]	**6**	**8**
τ(NC$_\alpha$)	−17	−5.6	−14.4
τ(C$_\alpha$C$_\beta$)	+31	+4.8	+15.3
τ(C$_\beta$C$_\gamma$)	−35	−2.6	−11.4
τ(C$_\gamma$C$_\delta$)	+24	−0.7	+2.9
τ(C$_\delta$N)	−4	+4.1	+7.6
τ(BocNC$_\alpha$CO$_2$H)	−72	−64.0	−67.1
rms deviation of fitted atoms	0.018 C$_\alpha$, N, C$_\delta$, C$_\gamma$	0.003 C$_\beta$, C$_\gamma$, C$_\delta$, N	0.013 C$_\beta$, C$_\gamma$, C$_\delta$, N
	δ(*cis*/*trans*)	δ(*cis*/*trans*)	δ(*cis*/*trans*)
COOH	178.35/176.60	177.7/175.5	179.1/176.1
NC=O	153.95/155.39	157.1/154	155.7/154.1
C$_\alpha$	58.8	60.8/60.1	59.5/59.1
C$_\beta$	30.75/29.53	32.0	31.5/29.1

from **6** and **8**, in which the out-of-plane carbon atom was the one bearing the carboxyl group (0.082 Å and 0.235 Å respectively).

Intermediates **2** and **3** could also be subjected to further stereocontrolled branching leading to the α-C-allyl derivative **9**, which upon controlled reduction and acid-catalyzed destannylation led to the branched 4,5-methano-L-proline precursor **10** ($[\alpha]_D = +4.3°$, $c = 0.72$ in $CHCl_3$; Scheme 2). Treatment of **2**

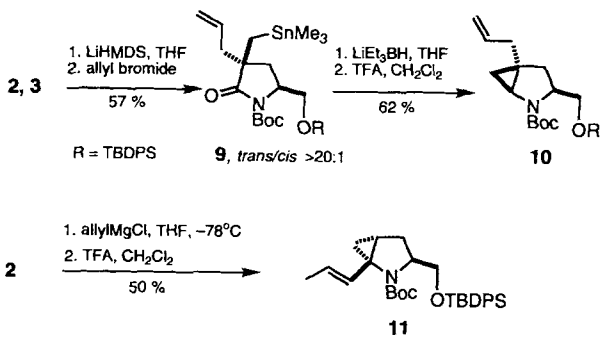

Scheme 2.

with allylmagnesium chloride, followed by trifluoroacetic acid (TFA), led to the (*S*)-5-(2-propenyl)-4,5-methano-L-proline derivative **11** ($[\alpha]_D = -27.0$, $c = 0.57$ in $CHCl_3$) on migration of the double bond. Compounds **10** and **11** represent uniquely functionalized precursors to constrained ω-methanoprolines.

The versatility and generality of the intramolecular carbocyclization reaction with appended trimethylstannylalkyl groups via incipient iminium ions can be demonstrated in the synthesis of bicyclic proline congeners (Scheme 3). These compounds are related to the antihypertensive agent ramipril.[21] A highly stereoselective allylation of the enolate from **1** gave **12** ($[\alpha]_D = -45.0$, $c = 1.0$ in $CHCl_3$), which was subjected to a photoinduced trimethylstannylation[22] to give **13** ($[\alpha]_D = -23.6$,

 © WILEY-VCH Verlag GmbH, D-69451 Weinheim, 1997 0570-0833/97/3617-1882 $ 17.50+.50/0

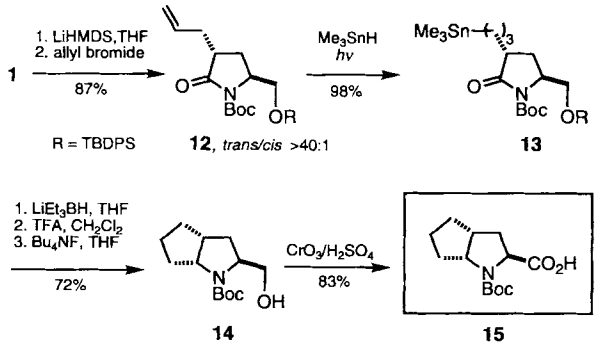

Scheme 3.

$c = 0.92$ in $CHCl_3$). Formation of the hemiaminal, followed by acid-catalyzed cyclization and deprotection, led to the bicyclic prolinol derivative **14** ($[\alpha]_D = -97.3$, $c = 1.38$ in $CHCl_3$). Finally, oxidation under Jones conditions gave the immediate precursor to the *N*-Boc-(4*R*,5R)-ramipril diastereomer **15** (m.p. 61–63 °C; $[\alpha]_D = -126.7$, $c = 0.46$ in $CHCl_3$).

It is also of interest to view compounds **6**, **8**, **10**, and **11** as precursors to constrained analogues or precursors to L-pipecolic acid. The extension of the cyclopropanation reaction to the pipecolic acid series is shown in Scheme 4. Trimethylstannylmethylation of the lithium enolate derived from the readily available **17**[23] gave the *anti*-isomer **18**. Reduction to the hemiaminal and acid-catalyzed cyclization led to **20** ($[\alpha]_D = -56.0$, $c = 1.02$ in $CHCl_3$), which was deprotected and oxidized to the crystalline (5*R*,6*S*)-methano-*N*-Boc-L-pipecolic acid **21** (m.p. 138–140 °C; $[\alpha]_D = -105.2$, $c = 1.17$ in $CHCl_3$). Epimerization of **18** to the *syn*-isomer **19** by diastereoselective protonation, followed by functional group manipulation as described above, led to the crystalline diastereomeric (5*S*,6*S*)-methano-*N*-Boc-pipecolic acid **23** (m.p. 79–81 °C; $[\alpha]_D = -126.7°$, $c = 0.40$ in $CHCl_3$). The structure of crystalline **21** was unambiguously established by X-ray analysis. It is of interest to note that while the proline derivatives **6** and **8** adopt a *cis*-*N*-Boc proline orientation in the solid state (Table 1), the corresponding 4,5-methanopipecolic acid analogue **21** exhibits a *trans* orientation (Scheme 4). The presence of *cis* and *trans* isomers of **6** and **8** in $CDCl_3$ was evidenced by the corresponding ^{13}C NMR shifts, as in the case of *N*-Boc-L-proline (Table 1).

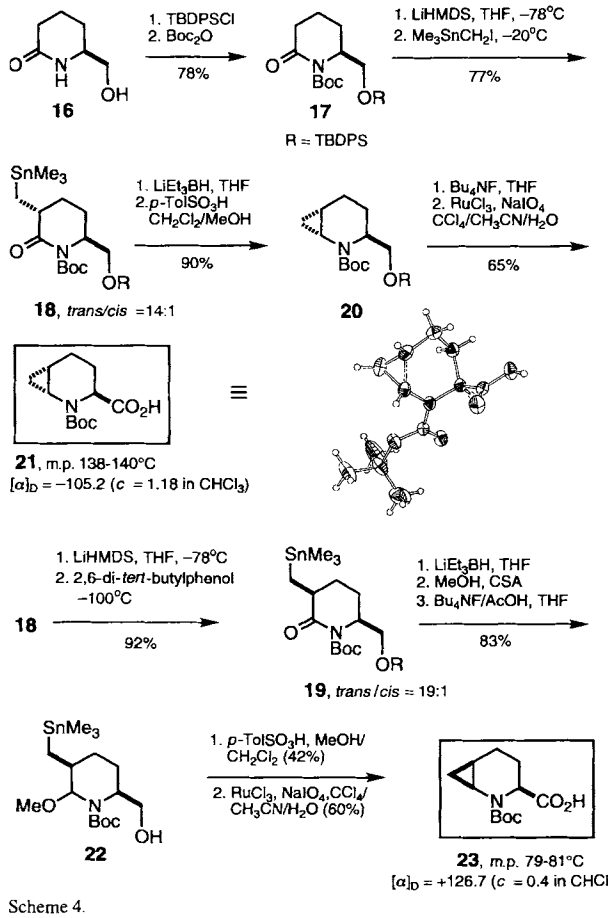

Scheme 4.

Pipecolic acid is an important constituent of the immunosuppressive agents FK-506[24] and rapamycin,[25] in which its α-ketoamide portion is intimately involved in an "active complex" with the target enzyme.[26] It is also involved in the metabolism of L-lysine, an essential amino acid for mammalian growth and development.[27] Functionalized pipecolic acids are also considered strained analogues of lysine with applications in drug design and peptidomimetic research,[28] as well as in the inhibition of L-pipecolate oxidase.[27]

It is our belief that the replacement of L-proline and L-pipecolic acid by conformationally altered ring variants represented by the methano congeners described in this work could have important consequences in biological recognition, in *cis–trans* conformational changes, in the susceptibility of the secondary amide bonds to enzymatic cleavage, and in related processes or phenomena. Studies that address these issues will be reported in due course.

Received: February 4, 1997 [Z10076IE]
German version: *Angew. Chem.* **1997**, *109*, 1953–1956

Keywords: amino acids · asymmetric synthesis · cyclizations · strained molecules

[1] Example: T. E. Creighton, *Proteins: Structures and Molecular Principles*, W. H. Freeman, New York, **1984**.
[2] a) C. M. Deber, V. Madison, E. R. Blout, *Acc. Chem. Res.* **1976**, *9*, 106–113; b) E. S. Eberhardt, S. N. Loh, R. T. Raines, *Tetrahedron Lett.* **1993**, *34*, 3055–3059; c) W. A. Houry H. A. Scheraga, *Biochemistry* **1996**, *35*, 11719–11733.
[3] a) J. F. Brandts, H. R. Halvorson, M. Brennan, *Biochemistry* **1975**, *14*, 4953–4963; for more recent references see b) K. L. Borden, F. M. Richards, *ibid.* **1990**, *29*, 3071–3077; c) F. L. Texter, D. B. Spencer, R. Rosenstein, C. R. Matthews, *ibid.* **1992**, *31*, 5687–5695; d) K. Lang, F. X. Schmid, *J. Mol. Biol.* **1990**, *212*, 185–196.
[4] a) K. A. Williams, C. M. Deber, *Biochemistry* **1991**, *30*, 8919–8923; b) J. Wess, S. Nanavati, Z. Vogel, R. Maggio, R. *EMBO J.* **1993**, *12*, 331–338; c) T. M. Suchyna, L. X. Xu, F. Gao, C. R. Fourtner, B. J. Nicholson, *Nature* **1993**, *365*, 847–849.
[5] N. G. J.Richards, M. G. Hinds, D. M. Brennand, M. J. Glennie, J. M. Welsh, J. A. Robinson, *Biochem. Pharmacol.* **1990**, *40*, 119–123.
[6] a) A. Yaron, F. Naider, F. *Crit. Rev. Biochem. Mol. Biol.* **1993**, *28*, 31–81; b) R. E. London, J. M. Stewart, J. R. Cann, *Biochem. Pharmacol.* **1990**, *40*, 41–48.
[7] a) C. J. Andres, T. L. Macdonald, T. D. Ocain, D. Longhi, *J. Org. Chem.* **1993**, *58*, 6609; b) M. K. Rosen, S. L. Schreiber, *Angew. Chem.* **1992**, *104*, 413–439; *Angew. Chem. Int. Ed. Engl.* **1992**, *31*, 384–400; c) G. Fischer, *ibid.* **1994**, *106*, 1479–1501 and **1994**, *33*, 1415–1436.
[8] D. W. Cushman, H. S. Cheung, E. F. Sabo, M. A. Ondetti, *Biochemistry* **1977**, *16*, 5484–5491.
[9] M. J. Genin, R. K. Mishra, R. L. Johnson, *J. Med. Chem.* **1993**, *36*, 3481–3483.
[10] J. T. Yli-Kauhaluoma, J. T.; J. A. Ashley, C.-H. L. Lo, J. Coakley, P. Wirsching, K. D. Janda, *J. Am. Chem. Soc.* **1996**, *118*, 5496–5497.
[11] A. Giannis, T. Kolter, *Angew. Chem.* **1993**, *105*, 1303–1325; *Angew. Chem. Int. Ed. Engl.* **1993**, *32*, 1244–1267; M. Kahn, *Synlett*, **1993**, 821–826; *Peptide Secondary Structure Mimetics, Tetrahedron Symposium-in-Print*, No. 50 (Ed.: M. Kahn), **1993**, *49*, 3433–3689; J. Gante, *Angew. Chem.* **1994**, *106*, 1780–1802; *Angew. Int. Ed. Engl.* **1994**, *33*, 1699–1720; A. E. P. Adang, P. H. H. Hermkens, J. T. M. Linders, H. C. J. Ottenheijm, C. J. van Staveren, *Recl. Trav. Chim. Pays Bas* **1994**, *113*, 63–78; see also, T. Curran, P. M. McEnancy, *Tetrahedron Lett.* **1995**, *36*, 191–194; G. Müller, M. Gurrath, M. Kurz, H. Kessler, *Proteins: Struct., Funct. and Genet.* **1993**, *15*, 235; S. Hanessian, G. McNaughton-Smith, H.-G. Lombart, W. D. Lubell, *Tetrahedron*, in press.

 © WILEY-VCH Verlag GmbH, D-69451 Weinheim, 1997 0570-0833/97/3617-1883 $ 17.50+.50/0

[12] Synthesis of racemic and enantiopure 2,3-methanoproline: a) A. Hercouet, B. Bessières, M. Le Corre, *Tetrahedron: Asymmetry* **1996**, *7*, 1267–1268; b) F. L. Switzer, H. van Halbeek, E. M. Holt, C. H. Stammer, *Tetrahedron* **1989**, *45*, 6091–6100. Recent accounts on 2,3-methanoamino acids: C. H. Stammer, *Tetrahedron* **1990**, *46*, 2231–2254; K. Burgess, K. K. Ho, D. Moyl-Sherman, *Synlett* **1994**, 575–583; K. Burgess, C.-Y. Ke, *J. Org. Chem.* **1996**, *61*, 8627–8631; J. M. Jiménez, R. M. Ortuno, *Tetrahedron: Asymmetry* **1996**, *7*, 3203–3208, and references therein.

[13] Synthesis of *cis*- and *trans*-3,4-methanoprolines: a) Y. Fujimoto, F. Irrevere, J. M. Karle, I. L. Karle, B. Witkop, *J. Am. Chem. Soc.* **1971**, *93*, 3471–3477; recent discussion of cyclopropylpyrrolidines: D. F. Harvey, D. M. Sigano, *J. Org. Chem.* **1996**, *61*, 2268–2272; K. E. Brighty, M. J. Castaldi, *Synlett* **1996**, 1097–1099.

[14] Synthesis of racemic 4,5-methanoproline amides: a) H. Urbach, R. Henning, R. Becker, DE-A 3,324,263 (Cl. C07D209/2) [*Chem. Abstr.* **1985**, 103: P 54461q]; b) related example involving mixtures of diastereomers: R. Pellicciari, L. Arenare, P. De Caprariis, B. Natalin, M. Marinozzi, A. Galli, *J. Chem. Soc. Perkin Trans. 1* **1995**, 1251–1257.

[15] a) S. Hanessian, U. Reinhold, S. Ninkovic, *Tetrahedron Lett.* **1996**, *37*, 8967–8970; b) S. Hanessian. S. Ninkovic, U. Reinhold, *ibid.* **1996**, *37*, 8971–8974.

[16] Selected examples of carbocyclizations mediated by alkyltin(IV) intermediates: T. L. Macdonald, C. M. Delahunty, K. Mead, D. E. O'Dell, *Tetrahedron Lett.* **1989**, *30*, 1573–1576; T. L. Macdonald, S. Mahalingam, D. E. O'Dell, *J. Am. Chem. Soc.* **1981**, *103*, 6767–6769; cyclopropane formation from γ-stannyl alcohols: D. D. Davis, H. T. Johnson *ibid.* **1974**, *96*, 7576–7577; H. G. Kuivila, N. M. Scarpa, *ibid.* **1970**, *92*, 6990–6991; N. Isono, M. Mori, *J. Org. Chem.* **1996**, *61*, 7867–7872; cyclopropane formation from β-stannyl ketones: T. Sato, M. Watanabe, T. Watanabe, Y. Onoda, E. Murayama, *ibid.* **1988**, *53*, 1894–1899; C. R. Johnson, J. F. Kadow, *ibid.* **1987**, *52*, 1493–1500.

[17] a) S. Hanessian, G. McNaughton-Smith, *Bioorg. Med. Chem. Lett.* **1996**, *6*, 1657–1662; see also b) S. Saijo, M. Wada, J.-I. Himizu, A. Ishida, *Chem. Pharm. Bull.* **18**, *28*, 1449; c) T. Katoh, Y. Nagata, Y. Kobayashi, K. Arai, J. Minami, S. Terashima, *Tetrahedron Lett.* **1993**, *34*, 5473–5476; d) K.-H. Altmann, *ibid.* **1993**, *34*, 7721–7724. e) J. Ackermann, M. Matthes, C. Tamm, *Helv. Chim. Acta* **1990**, *73*, 122–132.

[18] S. G. Davies, N. M. Garrido, O. Ichihara, I. A. S. Walters, *J. Chem. Soc. Chem. Commun.* **1993**, 1153–1159.

[19] All new compounds afforded satisfactory spectroscopic and analytical data (^{1}H, ^{13}C NMR, IR, LRMS, HRMS). Experimental procedures are available upon request. Crystallographic data (excluding structure factors) for the structure reported in this paper have been deposited with the Cambridge Crystallographic Data Centre as supplementary publication no. CCDC-100227. Copies of the data can be obtained free of charge on application to The Director, CCDC, 12 Union Road, Cambridge CB21EZ, UK (fax: int. code + (1223) 336-033; e-mail: deposit@chemcrys.cam.ac.uk).

[20] E. Benedetti, M. R. Ciajolo, A. Maisto, *Acta Crystallogr. Sect. B* **1974**, *30*, 1783–1788.

[21] a) V. Teetz, R. Geiger, R. Henning, H. Urbach, *Arzneim.-Forsch./Drug Res.* **1984**, *10b*, 1399; b) R. Henning, U. Lerch, H. Urbach, *Synthesis* **1989**, 265–268 and references therein.

[22] Hydrostannylation of alkenes: M. Lautens, S. Kumanovic, C. Meyer, *Angew. Chem.* **1996**, *108*, 1428–1429; *Angew. Chem. Int. Ed. Engl.* **1996**, *108*, 1428–1431, and references therein.

[23] a) S.-B. Huang, J. S. Nelson D. D. Weller, *Synth. Comm.* **1989**, *19*, 3485–3496; b) S. A. Hermitage, M. G. Moloney, *Tetrahedron: Asymmetry* **1994**, *5*, 1463–1464.

[24] J. J. Sierkierka, S. K. Y. Hung, M. Roe, C. S. Lin, N. H. Sigal, *Nature* **1989**, *341*, 755–757.

[25] a) M. W. Harding A. Galat, D. E. Uehling, S. L. Schreiber, *Nature* **1989**, *341*, 758–760; b) H. Fretz, M. W. Albers, A. Galat, R. F. Standaert, W. S. Lane, S. J. Burakoff, B. E. Bierer, S. L. Schreiber, *J. Am. Chem. Soc.* **1991**, *113*, 1409–1410.

[26] J. Liu, J. D. Farmer, W. S. Lane, J. Friedman, L. Weissman, S. L. Schreiber, *Cell* **1991**, *66*, 807–815.

[27] T. M. Zabriskie, *J. Med. Chem.* **1996**, *39*, 3046–3048, and references therein.

[28] P. J. Murray, I. D. Starkey, *Tetrahedron Lett.* **1996**, *37*, 1875–1878; A. Claesson, B.-M. Swahn, K. M. Edvinsson, H. Molin, M. Sandberg, *Bioorg. Med. Chem. Lett.* **1992**, *2*, 1247–1250.

1,8-Bis(dimethylamino)-4,5-dihydroxynaphthalene, a Neutral, Intramolecularly Protonated "Proton Sponge" with Zwitterionic Structure**

Heinz A. Staab,* Claus Krieger, Gisela Hieber, and Klaus Oberdorf

The interaction of basic groups in close proximity to each other may lead, as in the case of 1,8-bis(dimethylamino)-naphthalene (**1**), to unusually high basicities ("proton sponges").[1] The influences of gradually changed distances and orientations of the basic centers as well as of inductive, mesomeric, and steric effects on the basicity of such compounds have been thoroughly studied.[2] In comparison to the basicity of **1** [$pK_a \approx 12.1$ (H_2O); 7.5 (DMSO)],[3] that of 2,7-dimethoxy-1,8-bis(dimethylamino)naphthalene (**2**) is found to be increased by four powers of ten [$pK_a \approx 16.1$ (H_2O); 11.5 (DMSO)].[3] To separate the mesomeric effect of the two methoxy groups from their steric effect on the dimethylamino groups, we were interested in **3**, an isomer of **2** in which the two methoxy groups are not in the 2,7-positions but in the opposite *peri*-positions. In fact, 1,8-bis(dimethylamino)-4,5-dimethoxynaphthalene (**3**) is considerably less basic [$pK_a \approx 13.9$ (H_2O); 9.3 (DMSO)] than the isomer **2**, indicating that the main reason for the high basicity of **2** is the steric effect of the methoxy groups in *ortho*-positions to the dimethylamino groups. Irrespective of this primarily intended basicity comparison of **2** and **3**, the synthesis of **3** should allow the easy preparation of the corresponding 4,5-dihydroxy compound **5**, which by intramolecular proton displacement may lead to a new type of neutral, yet zwitterionic "proton sponge" (formula **6**).

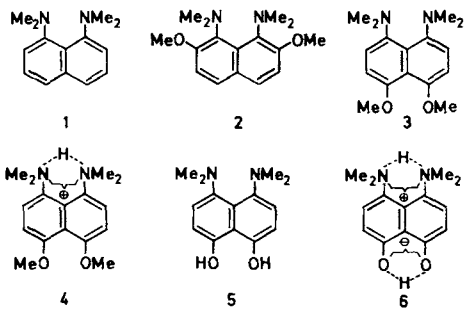

For the synthesis of **3**, 1,8-dihydroxynaphthalene[4] was methylated to give 1,8-dimethoxynaphthalene, which was nitrated (conc. nitric acid, glacial acetic acid/dichloromethane, 9:5) to yield 1,8-dimethoxy-4,5-dinitronaphthalene (39%; m.p. 278 °C); the isomeric 2,5-dinitro product (m.p. 151–153 °C) was separated by chromatography on silica gel with dichloromethane as eluent. Catalytic hydrogenation (10% Pd/C, tetrahydrofuran (THF), 20 °C) resulted in the formation of 1,8-diamino-4,5-dimethoxynaphthalene (97%; m.p. 83–95 °C, decomp), which was N-methylated according to the method of Quast et al.[5] to give **3** (71%; m.p. 75 °C, from *n*-hexane/ethyl

[*] Prof. Dr. H. A. Staab, C. Krieger, Dr. G. Hieber, Dr. K. Oberdorf
Abteilung Organische Chemie
Max-Planck-Institut für medizinische Forschung
Jahnstrasse 29, D-69120 Heidelberg (Germany)
Fax: Int.code + (6221) 486219
e-mail: staab@mixi.mpimf-heidelberg.mpg.de

[**] New "Proton Sponges", Part 12. Part 11: H. A. Staab, M. Diehm, C. Krieger, *Tetrahedron Lett.* **1996**, *36*, 2967–2970.

 © WILEY-VCH Verlag GmbH, D-69451 Weinheim, 1997 0570-0833/97/3617-1884 $ 17.50+.50/0

acetate 4:1); reaction with hydrogen bromide in ethyl acetate furnished **3**·HBr (m.p. 313 °C). Cleavage of the methoxy groups of **3** with boron tribromide in dichloromethane yielded the hydrobromide of 4,5-bis(dimethylamino)-1,8-dihydroxynaphthalene (**5**·HBr, 59%; m.p. 177–180 °C), which on treatment with the equivalent amount of lithium diisopropylamide in DMSO/cyclohexane gave **5** (83% yield; m.p. 212 °C, decomp). Analytical data and the molecular mass determined are in accord with structure **5**. In fact, however, both ^{1}H NMR and X-ray structure analysis clearly demonstrate that we did not obtain **5**, but the zwitterionic isomer **6**.

Figure 1 shows the structure of **3**, Figure 2 that of the cation **4** of the hydrobromide of **3**. Similar to the structure of the original naphthalene proton sponge **1**,[6] the naphthalene skeleton in **3** is not planar but shows a twist around the C(4a)–C(8a) axis. In **3** this twist is more pronounced than in **1**, due to the additional two methoxy groups in the *peri*-positions 4 and 5. The side view along the long axis of the naphthalene unit (Figure 1, bottom) demonstrates that in each of the two pairs of

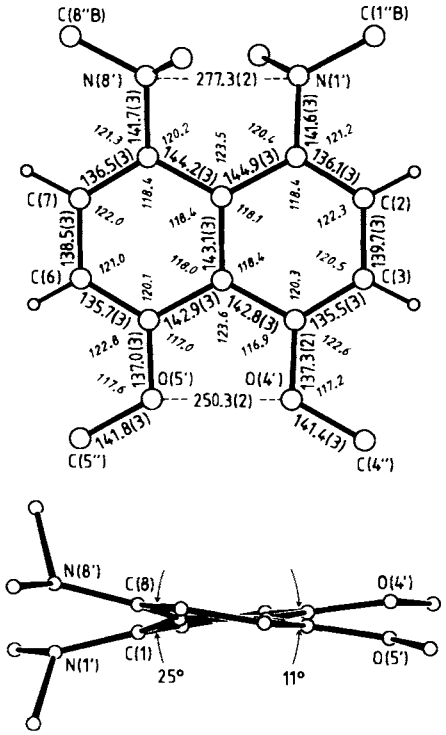

Figure 1. X-ray crystal structure of **3**; view perpendicular to the central bond of the naphthalene unit (top) and view along the long axis of the naphthalene unit (bottom).

peri-substituents the groups avoid short contacts by deviating in opposite directions. In addition, the methyl groups of the dimethylamino and methoxy substituents reduce close contacts by rotation around the bonds to the *peri*-positions. Nevertheless, the N···N distance, 277 pm, is similar to that in **1**, and the O···O distance between the methoxy groups, 250 pm, is considerably shorter than the sum of the van der Waals radii of oxygen (ca. 280 pm). The methoxy groups are oriented exactly in the plane of the neighboring naphthalene π-systems; thus, the mesomeric effect of the methoxy substituents is fully active like in **2**.

Protonation of **3** results in the formation of the strong intramolecular N···H···N hydrogen bond in **4** (Figure 2). The naphthalene system including the bonds to the four substituents

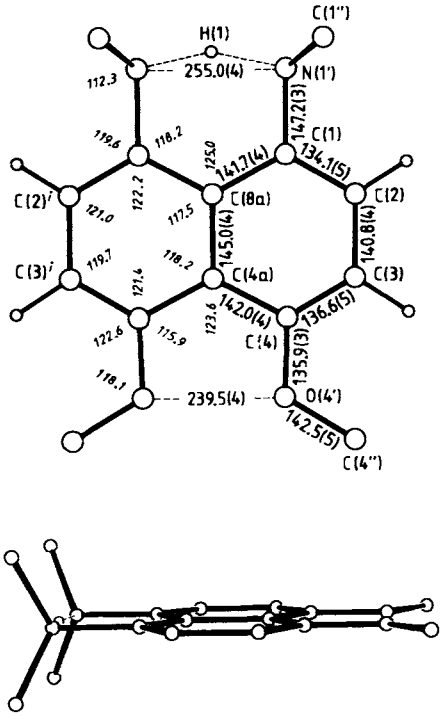

Figure 2. X-ray structure of **4** (of **3**·HBr); view perpendicular to the central bond of the naphthalene unit (top) and view along the long axis of the naphthalene unit (bottom).

is now completely planarized, leading to a shortening of the N···N and O···O distances to 255 and 239 pm, respectively.

The most interesting result of the present study, however, concerns the structure of the compound obtained from **3** by cleavage of the two methoxy groups; 1,8-bis(dimethylamino)-4,5-dihydroxynaphthalene (**5**) was expected. Both the elemental analysis and the mass spectrum (molecular ion peak $m/z = 246$ as base peak) are in full agreement with structure **5**. However, the ^{1}H NMR data (500 MHz, [D$_6$]DMSO, 303 K) disprove this structure. In addition to the signals at $\delta = 2.93$ (12 H, NMe_2), 6.06 (d, $J = 8.4$ Hz, 2 H, 2,7-H), and 7.37 (d, $J = 8.4$ Hz, 2 H, 3,6-H) there are *two* strongly downfield-shifted signals at $\delta = 18.10$ and 19.30, which each correspond to one proton. The slightly broadened signal at $\delta = 18.10$ is due to a N···H···N hydrogen bond (nuclear Overhauser effect with the NMe_2 substituents); the signal at $\delta = 19.30$, then, must be assigned to an O···H···O hydrogen bond. Apparently, cleavage of the methoxy groups in **3** does not lead to dihydroxynaphthalene **5**, but rather to the isomeric zwitterion **6**, which contains the N···H···N hydrogen bond with positive charge typical of protonated proton sponges. The signal at $\delta = 19.30$, then, corresponds to the O···H···O hydrogen bond carrying the negative charge of the zwitterion.

The result of the X-ray structure analysis of **6** shown at the top of Figure 3 confirms the presence of an intramolecularly protonated proton sponge, which due to the zwitterionic structure is an overall neutral molecule. The zwitterionic structure determines the crystal packing (Figure 3, bottom). Along the crystallographic *a*-axis the molecules of **6** are arranged in a type of belt, with the positive parts of the zwitterions facing the negative parts of their neighbors. This belt is coordinated with a corresponding second belt, in which the zwitterions are oriented in the opposite direction. In this "double belt" the positive parts of the zwitterions of one belt are roughly opposite the negative parts of the neighboring belt. Figure 4 shows in a per-

 © WILEY-VCH Verlag GmbH, D-69451 Weinheim, 1997 0570-0833/97/3617-1885 $ 17.50+.50/0

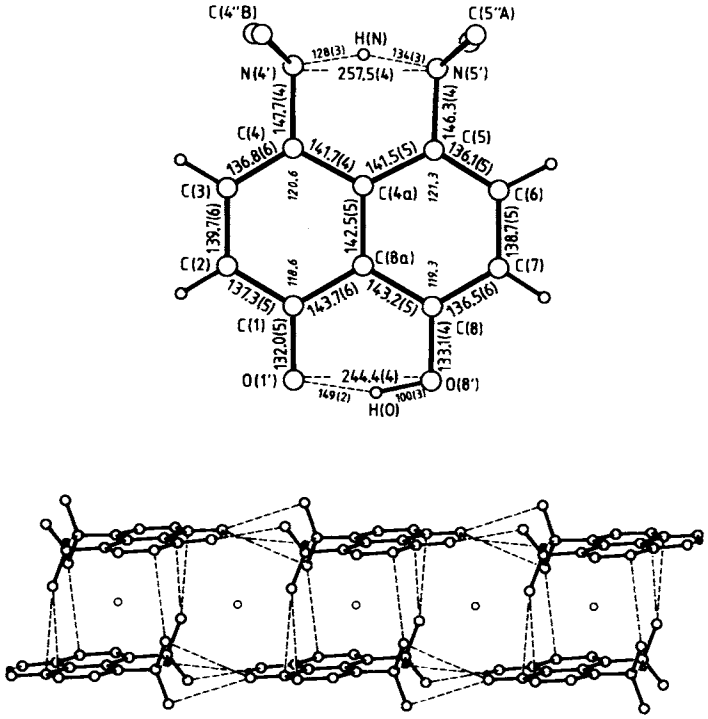

Figure 3. X-ray crystal structure of **6**; top view (top; bond lengths in pm, standard deviations in units of the last digit). The bottom view shows a section of the arrangement of **6** in a double belt (for details see text).

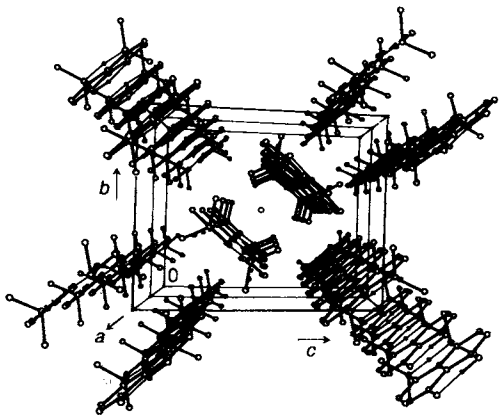

Figure 4. Crystal packing of **6** in perspective view along the crystallographic *a* axis.

spective view that an ensemble of such double belts is oriented along the *a* axis of the crystal. This very interesting crystal packing of the zwitterion **6** prompts further studies of anisotropic crystal properties.

Experimental Section

Analytical data of the synthesized compounds: 1,8-Dimethoxy-4,5-dinitronaphthalene: Correct elemental analysis; ^{1}H NMR (360 MHz, [D$_6$]DMSO, 303 K): δ = 4.05 (s, 6H, OCH_3), 7.26 (d, J = 9.0 Hz, 2H, H-2,7), 8.44 (d, J = 9.0 Hz, 2H, H-3,6). 1,8-Dimethoxy-2,5-dinitronaphthalene: Correct elemental analysis; ^{1}H NMR (360 MHz, $CDCl_3$, 303 K): δ = 4.02 (s, 3H), 4.15 (s, 3H), 7.00 (d, J = 8.9 Hz, 1H), 7.92 (d, J = 9.5 Hz, 1H), 8.41 (d, J = 8.9 Hz, 1H), 8.52 (d, J = 9.5 Hz, 1H). 1,8-Diamino-4,5-dimethoxynaphthalene: Correct high-resolution mass spectrum; ^{1}H NMR (360 MHz, [D$_6$]DMSO, 303 K): δ = 3.69 (s, 6H, OCH_3), 5.19 (br. s, 4H, NH_2), 6.55 (d, J = 8.2 Hz, 2H, H-2,7), 6.68 (d, J = 8.2 Hz, 2H, H-3,6). **3**: Correct elemental analysis; correct high-resolution mass spectrum; ^{1}H NMR (360 MHz, [D$_6$]DMSO, 303 K): δ = 2.64 (s, 12H, $N(CH_3)_2$), 3.76 (s, 6H, OCH_3), 6.82 (d, J = 8.4 Hz, 2H, H-3,6), 6.89 (d, J = 8.4 Hz, 2H, H-2,7). **5**·HBr: Correct elemental analysis; ^{1}H NMR (500 MHz, [D$_6$]DMSO, 303 K): δ = 3.04 (d, J = 2.2 Hz, 12H, $N(CH_3)_2$), 6.92 (d, J = 8.4 Hz, 2H, H-2,7), 7.86 (d, J = 8.4 Hz, 2H, H-3,6), 18.61 (br. s, 1H, N···H···N). **6**: Correct elemental analysis; correct mass spectrum; ^{1}H NMR (500 MHz, [D$_6$]DMSO, 303 K): δ = 2.93 (d, J = 2.2 Hz, 12H, $N(CH_3)_2$), 6.06 (d, J = 8.4 Hz, 2H, H-2,7), 7.37 (d, J = 8.4 Hz, 2H, H-3,6), 18.10 (br. s, 1H, N···H···N), 19.30 (s, 1H, O···H···O).

Crystal structure analyses: Enraf-Nonius CAD 4 diffractometer; graphite monochromator, $Mo_{K\alpha}$ radiation, λ = 0.071073 nm, $\omega/2\theta$ scan, 303 K), refinements on $|F|$ according to the full matrix least squares process (hydrogen atoms with isotopic displacement parameters). **3**: Colorless platelets from *n*-hexane, 0.10 × 0.20 × 0.20 mm, orthorhombic, space group *Pbca* (No. 61 Int. Tables), a = 1001.2(1), b = 1855.3(2), c = 1624.6(2) pm; $V = 3018(1) \times 10^6$ pm^3, Z = 8, ρ_{calcd} = 1.207 g cm^{-3}, μ = 0.075 mm^{-1}; 3099 symmetry-independent reflections up to $\sin\theta/\lambda$ = 6.7 nm^{-1}, of which 1881 with $I \geq 3.0\sigma(I)$ were regarded as observed; structure solution by direct method (MULTAN), R = 0.042. **3**·HBr: Colorless needles from methanol, 0.12 × 0.15 × 0.30 mm; tetragonal, space group $C\bar{4}m2_1$ (No. 113 Int. Tables), a = 1141.0(1), c = 1312.6(2) pm; $V = 1709(1) \times 10^6$ pm^3, Z = 4 (symmetry of molecule in crystal C_{2v}), ρ_{calcd} = 1.381 g cm^{-3}; 663 symmetry-independent reflections up to $\sin\theta/\lambda$ = 6.8 nm^{-1}, of which 519 with $I \geq 3.0\sigma(I)$ were regarded as observed; μ = 2.39 mm^{-1}; empirical absorption correction (ψ scan, τ_{min} = 84.91, τ_{max} = 95.62); structure solution by heavy atom method (Patterson); R = 0.026. **6**: Light yellow needles from dimethylformamide, 0.05 × 0.08 × 0.20 mm; monoclinic, space group $P2_1/n$ (No. 14 Int. Tables), a = 932.5(2), b = 1064.8(4), c = 1377.3(4) pm; β = 106.95(2)°; $V = 1308(1) \times 10^6$ pm^3, Z = 4, ρ_{calcd} = 1.251 g cm^{-3}, μ = 0.079 mm^{-1}; 2350 symmetry-independent reflections up to $\sin\theta/\lambda$ = 6.0 nm^{-1}, of which 982 with $I \geq 2.0\sigma(I)$ were regarded as observed; structure solution by direct method (SIR); R = 0.049. Crystallographic data (excluding structure factors) for the structures reported in this paper have been deposited with the Cambridge Crystallographic Data Centre as supplementary publication no. CCDC-100308. Copies of the data can be obtained free of charge on application to The Director, CCDC, 12 Union Road, Cambridge CB21EZ, UK (fax: int. code + (1223) 336-033; e-mail: deposit@chemcrys.cam.ac.uk).

Received: March 25, 1997 [Z10277IE]
German version: *Angew. Chem.* **1997**, *109*, 1946–1949

Keywords: hydrogen bonds · naphthalene derivatives · proton sponges · structure elucidation · zwitterions

[1] R. W. Alder, P. S. Bowman, W. R. S. Steele, D. R. Wintermann, *J. Chem. Soc. Chem. Commun.* **1968**, 723; R. W. Alder, M. R. Bryce, N. C. Goode, N. Miller, J. Owen, *J. Chem. Soc. Perkin Trans. 1* **1981**, 2840, and references therein.
[2] Review: H. A. Staab, T. Saupe, *Angew. Chem.* **1988**, *100*, 895; *Angew. Chem. Int. Ed. Engl.* **1988**, 27, 865.
[3] F. Hibbert, K. P. P. Hunte, *J. Chem. Soc. Perkin Trans. 2* **1983**, 1895; R. L. Benoit, D. Lefebre, M. Fréchete, *Can. J. Chem.* **1987**, *65*, 996, and references therein.
[4] N. P. Buu-Hoi, D. Lavit, *J. Chem. Soc.* **1956**, 2412; K. A. Parker, T. Iqbal, *J. Org. Chem.* **1980**, *45*, 1149.
[5] H. Quast, W. Risler, G. Döllscher, *Synthesis* **1972**, 558.
[6] H. Einspahr, J.-B. Robert, R. E. Marsh, J. D. Roberts, *Acta Crystallogr. Sect. B* **1973**, *29*, 1611; M. Peräkylä, *J. Org. Chem.* **1996**, *61*, 7420, and references therein.

Alanyl PNA: Evidence for Linear Band Structures Based on Guanine–Cytosine Base Pairs**

Ulf Diederichsen*

The stability of a DNA double strand is based on the formation of hydrogen bonds between the nucleobases guanine and cytosine, and between adenine and thymine, as well as base stacking and hydrophobic interactions.[1] In addition, the influ-

[*] Dr. U. Diederichsen
Institut für Organische Chemie und Biochemie
der Technischen Universität München
Lichtenbergstrasse 4, D-85747 Garching (Germany)
Fax: Int. code + (89) 2891-3210
e-mail: ud@linda.org.chemie.tu-muenchen.de

[**] This work was supported by the Deutsche Forschungsgemeinschaft (Di 542/2-1), the Fonds der Chemischen Industrie, and the Leonhard-Lorenz-Stiftung. I am grateful to Professor H. Kessler, Garching, for generous support.

ence of the backbone is important: the pairing mode and geometric requirements for a base pair are restricted for topological reasons, whereas charge repulsion of the phosphodiester groups seems functionally important[2] but has a destabilizing effect. The influence of the backbone on the stability of the double strand can be illustrated by comparing the UV melting temperature of the self-pairing DNA oligomer $d(GC)_3$ ($T_m = 47\,^\circ C$)[3] with that of the homo-DNA oligomer $dd(GC)_3$ ($T_m = 58\,^\circ C$);[4] the latter contains 2′,3′-dideoxyglucopyranosyl sugar moieties and pairs in approximately linear double strands. This stabilization is mainly due to entropic effects. Reduction of charge repulsion, however, should be important for the stabilization of double strands containing *N*-(2-aminoethyl)glycine peptide nucleic acids (PNAs) in the order DNA/DNA < PNA/DNA < PNA/RNA < PNA/PNA.[5] We introduced a new kind of PNA oligomer that forms linear double strands and also lacks charge repulsion (Scheme 1).[6] Alanyl amino acids with

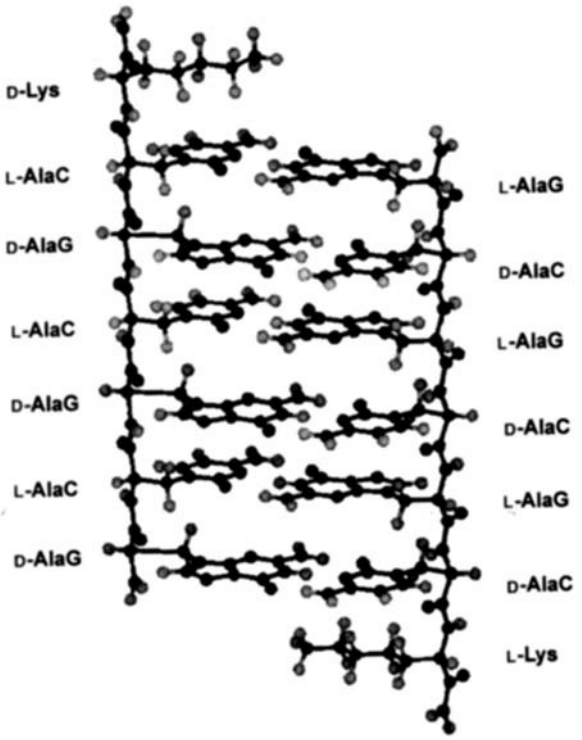

Scheme 1. Model of a linear alanyl PNA double strand (Insight II; Biosym/MSI): The regular peptide strands have alternating configuration, and thus the PNA in β-sheet conformation is repetitive in each nucleo amino acid. The Watson–Crick pairing G/C hexamer is shown with antiparallel strand orientation and nucleo amino acids with the same configuration forming a base pair. The distance between two base pairs is 3.5 Å. The lysine amide at the C-terminal end was introduced for solubility reasons.

nucleobases connected at the β-position of the side chain can be oligomerized to form a regular peptide strand. These oligomers, which have nucleo amino acids of alternating configuration are repetitive with the backbone in β-sheet conformation and able to form linear double strands based on nucleobase recognition. In the series of alanyl PNA oligomers presented here the pairing of guanine and cytosine shows remarkably high stability and selectivity, as was predicted from model studies. We also found an unexpected sequence-dependent formation of a bandlike, higher order structure.

The oligomers described herein were prepared by solid-phase peptide synthesis (SPPS),[8] purified by HPLC (RP-C18), and characterized by electrospray ionization mass spectrometry (ESI-MS),[9] circular dichroism (CD), and in a few cases by ^{1}H NMR spectroscopy. A C-terminal lysine amide was introduced for solubility reasons. The pairing stabilities were investigated by UV melting curves. The temperature-dependent sigmoidal increase of the absorption corresponds to the destacking of the nucleobases. In order to study the G–C pairing we first examined oligomer **1** (AlaG = β-(guanin-9-yl)alanine, AlaC = β-(cytosin-1-yl)alanine, D-configurated amino acids are underlined), because this sequence usually provides an antiparallel double strand based on six Watson–Crick G–C base pairs (Scheme 2). Neither pairing with parallel strands nor double

H-(AlaG-AlaG-AlaC-AlaG-AlaC-AlaC)-Lys-NH_2 **1**

H-(AlaG-AlaG-AlaC-AlaG-AlaC-AlaC)-Lys-NH_2 *ent*-**1**

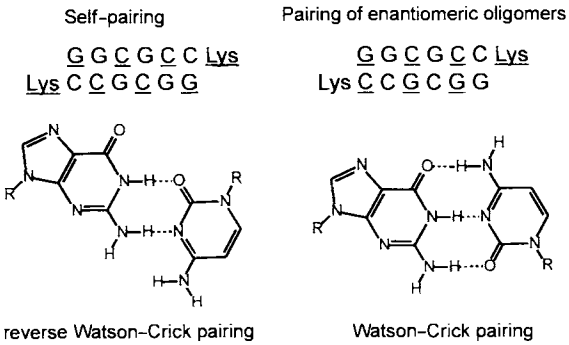

Pairing mode	Possible geometries	
Watson-Crick	antiparallel, homochiral	parallel, heterochiral
reverse Watson-Crick or Hoogsteen	antiparallel, heterochiral	parallel, homochiral

Scheme 2. Dependence of the G–C pairing mode on strand orientation and configuration. In addition, the Hoogsteen mode is possible at pH 4.5 (G = β-(guanin-9-yl)alanine, C = β-(cytosin-1-yl)alanine).

strand formation with G–G, C–C base pairs is likely.[10] In analogy to the A–T pairing discussed earlier[6] formation of antiparallel double strands of alanyl PNA based on the G–C Watson–Crick pairing mode requires that the nucleo amino acids forming the base pair have the same configuration (homochiral). Changing the pairing mode from Watson–Crick to Hoogsteen[11] or to reverse Watson–Crick provides a suitable geometry for antiparallel self-pairing. Therefore, the complex formed from oligomer **1** and its enantiomer *ent*-**1** (Watson–Crick pairing) is expected to be more stable than the self-pairing strands (reverse Watson–Crick pairing).

The pairing stabilities determined by UV spectroscopy (Figure 1) are in agreement with our model: for the self-paired complex of oligomer **1** a melting temperature of $T_m = 40\,^\circ C$ was observed, whereas the complex from a 1:1 mixture of the enantiomeric oligomers **1** and *ent*-**1** showed denaturation at $T_m = 58\,^\circ C$. The Watson–Crick mode is stabilized by three hydrogen bonds, the reverse Watson–Crick mode only by two. The double-strand stability as observed is remarkably high for the pairing of hexamers.

We expected similar UV melting curves when the GGCGCC hexamer sequence was replaced by the G/C alternating oligomers **2** and *ent*-**2**. The self-pairing complex of the G/C

H-(AlaG-AlaC)$_3$-Lys-NH_2 **2**

H-(AlaG-AlaC)$_3$-Lys-NH_2 *ent*-**2**

 © WILEY-VCH Verlag GmbH, D-69451 Weinheim, 1997 0570-0833/97/3617-1887 $ 17.50+.50/0

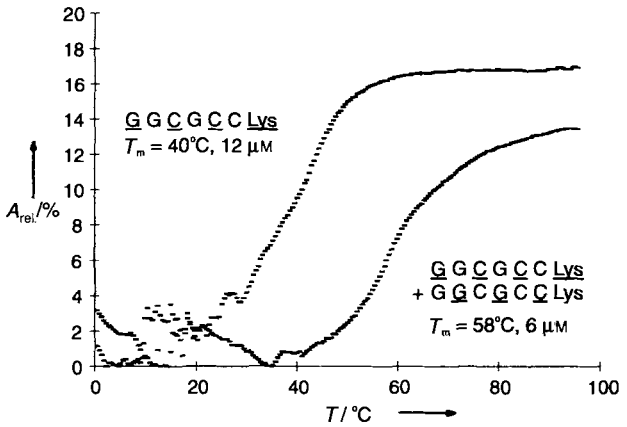

Figure 1. Melting curves of **1** and an equimolar mixture of **1** and *ent*-**1** (260 nm, 0.1 M NaCl, 0.01 M Na_2HPO_4/H_3PO_4, pH 7).

alternating hexamer **2** did indeed have the stability of T_m = 37 °C at 6 μM as expected (Figure 2). Increasing the concentration to 12 and 22 μM resulted in slightly higher stability (at least a bimolecular process) and a strong shift of the hyperchromicity from 15% to 40 and 90%, respectively.

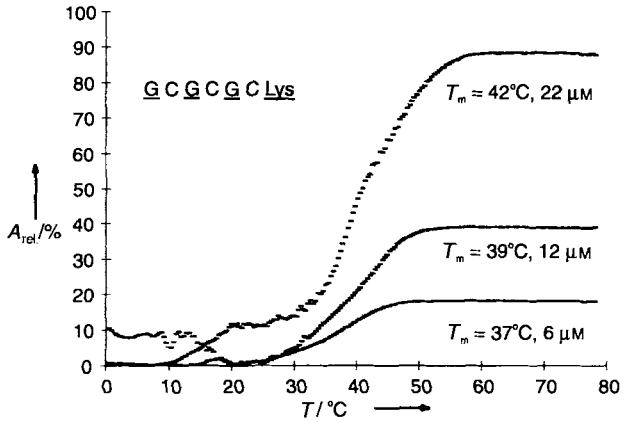

Figure 2. Melting curves of **2** at different concentrations (260 nm, 0.1 M NaCl, 0.01 M Na_2HPO_4/H_3PO_4, pH 7).

The pairing of an equimolar mixture of the enantiomeric hexamers **2** and *ent*-**2** had a stability exceeding that of the corresponding oligomers **1** and *ent*-**1** by 17 °C (Figure 3) and also showed concentration-dependent melting temperatures and hyperchromicities (6 μM: T_m = 75 °C, 50% hyperchromicity; 11 μM: T_m = 79 °C, 150% hyperchromicity).

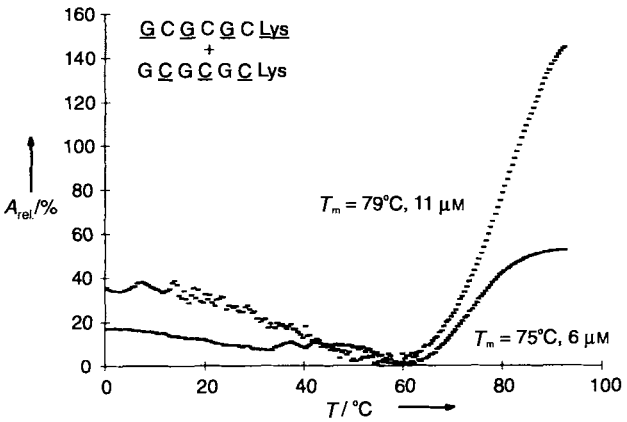

Figure 3. Melting curves of an equimolar mixture of **2** and *ent*-**2** at different concentrations (260 nm, 0.1 M NaCl, 0.01 M Na_2HPO_4/H_3PO_4, pH 7).

Oligomers **1** and **2** differ only in their sequence; they should be identical with respect to number of base pairs and pairing mode. The enormous increase of hyperchromicity of oligomers with alternating G/C sequence indicates the formation of higher order structures. In fact, only G/C alternating oligomers have the potential to form overlapping band structures (Scheme 3).

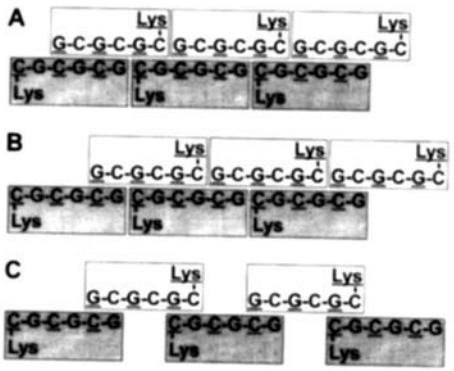

Scheme 3. Possible organization of G/C alternating hexamers in linear, bandlike higher order structures. Overlap as shown in A provides the highest amount of G–C pairs.

Each oligomer can form four Watson–Crick base pairs with an enantiomeric hexamer and in addition two base pairs with a second oligomer. Model studies indicate that by a slight twist of the hexameric strand steric interactions of the C-terminal lysine amide with the neighboring strand can be avoided. This twist favors the formation of four additional hydrogen bonds: two between the ε-amino group of lysine and the guanine (N7, O6) of the neighboring oligomer and two between the NH and the carbonyl groups of the peptide strands overlapping with the lysine amide. This model is feasible for all pairing modes. For self-pairing complexes of G/C alternating oligomers (reverse Watson–Crick mode) the stabilization in higher order structures seems to work only at higher concentrations.

To further prove this model we examined the shorter oligomers **3** and *ent*-**3**, which still should be able to aggregate into bands with a 2+2 overlap. For self-pairing of the tetramers we observed a melting temperature of T_m = 12 °C (10% hyperchromicity), whereas the UV melting curve of the enantiomeric mixture provided T_m = 52 °C (28% hyperchromicity; Figure 4), which again suggests formation of a

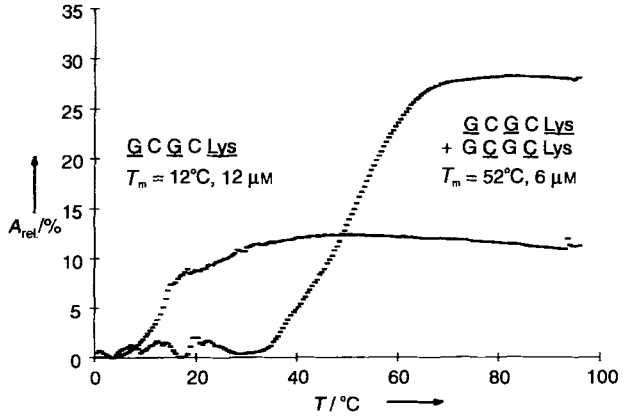

Figure 4. Melting curves of **3** and an equimolar mixture of **3** and *ent*-**3** (260 nm, 0.1 M NaCl, 0.01 M Na_2HPO_4/H_3PO_4, pH 7).

 © WILEY-VCH Verlag GmbH, D-69451 Weinheim, 1997 0570-0833/97/3617-1888 $ 17.50+.50/0

higher order structure. The UV absorptions of equimolar mixtures of the trimers **4** and **5**, and of **4** and *ent*-**5**, are temperature

H-(AlaG-AlaC)$_2$-Lys-NH$_2$ **3**

H-(AlaG-AlaC)$_2$-Lys-NH$_2$ *ent*-**3**

H-(AlaG-AlaC-AlaG)-Lys-NH$_2$ **4**

H-(AlaC-AlaG-AlaC)-Lys-NH$_2$ **5**

H-(AlaC-AlaG-AlaC)-Lys-NH$_2$ *ent*-**5**

independent as is the absorption of the trimers alone (not shown). Formation of a pairing complex by only three G–C base pairs therefore is not feasible.

Three pairing modes can be identified for G/C hexamers: Watson–Crick for the pairing of enantiomeric oligomers (T_m = 58 °C), reverse Watson–Crick in the case of self-pairing (T_m = 40 °C), and the Hoogsteen mode at pH 4.5 (T_m = 23 °C). The observed selectivities as well as comparison of the pairing stabilities of A–A and A–T pairing (T_m = 31 °C and T_m = 25 °C)[6] are in agreement with our model of alanyl PNA pairing in linear double strands. Although the plane of base pairs is oriented orthogonal to the backbone, the experimental results indicate that the strand orientation, configuration of the nucleo amino acids forming a base pair, and pairing mode are dependent on each other. Based on the evidence for organization of G/C alternating oligomers in band structures, we are currently examining the template-directed oligomerization of G/C alanyl PNA oligomers.

Received: February 4, 1997 [Z10074IE]
German version: *Angew. Chem.* **1997**, *109*, 1966–1969

Keywords: band structures · base pairing · peptide nucleic acids · self-organization

[1] W. Saenger, *Principles of Nucleic Acid Structure*, Springer, New York, **1983**.
[2] C. Richert, A. L. Roughton, S. A. Benner, *J. Am. Chem. Soc.* **1996**, *118*, 4518.
[3] a) D. De Prisco Albergo, L. A. Marky, K. J. Breslauer, D. H. Turner, *Biochemistry* **1981**, *20*, 1409; b) F. Seela, H. Driller, *Nucleic Acids Res.* **1989**, *17*, 901.
[4] J. Hunziker, H.-J. Roth, M. Böhringer, A. Giger, U. Diederichsen, M. Göbel, R. Krishnan, B. Jaun, C. Leumann, A. Eschenmoser, *Helv. Chim. Acta* **1993**, *76*, 259.
[5] a) M. Egholm, O. Buchardt, L. Christensen, C. Behrens, S. M. Freier, D. A. Driver, R. H. Berg, S. K. Kim, B. Nordén, P. E. Nielsen, *Nature* **1993**, *365*, 566; b) P. Wittung, P. E. Nielsen, O. Buchardt, M. Egholm, B. Nordén, *ibid.* **1994**, *368*, 561; c) B. Hyrup, P. E. Nielsen, *Bioorg. Med. Chem.* **1996**, *4*, 5.
[6] a) U. Diederichsen, *Angew. Chem.* **1996**, *108*, 458; *Angew. Chem. Int. Ed. Engl.* **1996**, *35*, 445; b) U. Diederichsen, H. W. Schmitt, *Tetrahedron Lett.* **1996**, *37*, 475. For a discussion of a similar model see ref. [7].
[7] V. J. Shah, R. Cepra, J. D. Kuntz, G. L. Kenyon, *Bioorg. Chem.* **1996**, *24*, 201.
[8] The nucleo amino acids Boc-AlaC(Z)-OH and Boc-AlaG-OH (Boc = *tert*-butoxycarbonyl, Z = benzyloxycarbonyl) were prepared by nucleophilic ring opening of Boc-serine lactone with N^6-benzyloxycytosine or 6-chloro-2-aminopurine. The guanine derivative was obtained from the 6-chloro-2-aminopurine nucleo amino acid by reaction with aqueous trifuloroacetic acid (TFA) followed by treatment with Boc_2O. See also: P. Lohse, B. Oberhauser, B. Oberhauser-Hofbauer, G. Baschang, A. Eschenmoser, *Croatica Chim. Acta* **1996**, *69*, 535. The oligomers were synthesized by SPPS on a 4-methylbenzhydrylamine polystyrene support loaded with L- or D-lysine(Z)-OH. Activation with *O*-(7-azabenzotriazol-1-yl)-1,1,3,3-tetramethyluronium hexafluorophosphate (HATU) provided coupling yields of >95%.
[9] MS: **1**: *m/z*: 674.0 $(MH_2)^{2+}$; *ent*-**1**: *m/z*: 674.1 $(MH_2)^{2+}$; **2**: *m/z*: 1368.4 $(MH)^+$, 674.2 $(MH_2)^{2+}$; *ent*-**2**: *m/z*: 674.0 $(MH_2)^{2+}$; **3**: *m/z*: 946.3 $(MH)^+$, 474.0 $(MH_2)^{2+}$; *ent*-**3**: *m/z*: 946.2 $(MH)^+$, 474.0 $(MH_2)^{2+}$; **4**: *m/z*: 766.3 $(MH)^+$; **5**: *m/z*: 726.3 $(MH)^+$; *ent*-**5**: *m/z*: 726.3 $(MH)^+$. The CD spectra of enantiomeric oligomers have the typical plane of symmetry.
[10] U. Diederichsen, unpublished results.
[11] At pH 4.5 cytosine is protonated at N3 and can form a Hoogsteen base pair with guanine. At pH 4.5 both the hexamer **1** and the mixture of the enantiomeric oligomers I and *ent*-I had a melting temperature of T_m = 23 °C (4% hyperchromicity). This indicates that the Hoogsteen mode is irrelevant for G–C pairing in alanyl PNA at pH 7. The higher stability of the self-pairing complex compared to that of the pairing of the enantiomeric oligomers is in agreement with the selectivity requirements (Scheme 2).

Stable Free Dianionic Silicon–Carbon Clusters

Andreas Dreuw, Thomas Sommerfeld, and Lorenz S. Cederbaum*

Many prominent inorganic dianions, such as CO_3^{2-}, SO_4^{2-}, and SO_3^{2-}, known from the solid state are unstable with respect to electron loss in the gas phase.[1, 2] The question as to whether there are small molecules capable of compensating the electrostatic repulsion of two electrons and thereby of forming stable free dianions has been examined theoretically and experimentally. In the meantime several stable free dianions are known,[3, 4] and the smallest of these that have been detected directly in a mass spectrometer are C_7^{2-} [5] and $S_2O_6^{2-}$.[6]

From a theoretical point of view the smallest dianions predicted to be long-lived are the trigonal-planar alkali metal halides MX_3^{2-} (M = alkali metal, X = F, Cl, Br), which can be understood in the framework of an "ionic model".[7, 8] In addition, carbon clusters of the type C_n^{2-} ($n \geq 7$) have been examined at a high level of theory.[9, 10] The results of these studies showed that the smallest stable dianion of this class, C_7^{2-}, has a trigonal-planar structure[11] instead of the expected linear one.

We report herein on dianionic silicon–carbon clusters and focus on the smallest stable cluster from this class. In the following, we first describe the principal differences between the theoretical examination of neutral and dianionic clusters and the theoretical methods used in our calculations. Then we discuss the structures of two stable dianionic silicon–carbon clusters and compare them with structures of typical neutral species.

We begin with the principal differences between the theoretical examination of neutral molecules and dianions. Isolated neutral molecules possess an infinite number of bound states, that is, all electrons can be bound. Thus, a typical goal in their theoretical study is to find the electronic ground state and the lowest minimum on the potential energy surface (PES). In contrast, the theoretical examination of the general stability of a dianion is more difficult, since it is by no means clear whether a dianionic system exists at all. The principal questions pertaining to the examination are whether the given system can bind the two extra electrons, that is whether electronic stability is given, and whether the system is structurally stable, that is whether stability with respect to fragmentation is present. Thus, the theoretical investigation of a given dianion includes the examination of both the electronic stability and the stability with regard to fragmentation.

Let us turn to the quantum chemical methods used to calculate the electron-detachment energy (EDE). The geometries of the examined systems were optimized at the HF-SCF level of theory (HF = Hartree–Fock, SCF = self-consistent field) by using a Gaussian-type double-ζ basis set (dz(sp, d/2d)[12] augmented with additional diffuse and polarization functions, and all presented structures were found to represent local minima, that is their harmonic vibrational frequencies showed real values. A detailed study of the basis sets showed that the additional functions are necessary to account for the diffuse character of the outer valence orbitals of an anion, whereas it is not necessary to apply larger basis sets, such as a triple-ζ basis set because this, has only small effects on the results. For example, the vertical EDE of the dianion **1** is 1.77 eV at the level of Koopmans

[*] Prof. Dr. L. S. Cederbaum, A. Dreuw, Dr. T. Sommerfeld
Theoretische Chemie
Physikalisch-Chemisches Institut der Universität
Im Neuenheimer Feld 253, D-69120 Heidelberg (Germany)
e-mail: q72@ix.urz.uni-heidelberg.de
Fax: Int. code +(6221)545221

 © WILEY-VCH Verlag GmbH, D-69451 Weinheim, 1997 0570-0833/97/3617-1889 $ 17.50+.50/0

Theorem (KT)/dz(sp,d/2d) and 1.81 eV when the enlarged analogous triple-ζ basis set (tz(sp,d/2d)) is used. The adiabatic EDE behaves in the same way and is 0.59 eV at the ΔSCF/dz(sp,d/2d) level compared with 0.61 eV at the ΔSCF/tz(sp,d/2d) level (see Table 1). The effects on the geometries are also minimal; in all cases the observed bond length changes were less than 0.002 Å.

The EDE values can now be obtained in two ways. On the one hand, the EDE can be obtained directly by so-called direct methods. We have employed Koopmans Theorem[13] and the outer valence Green's function (OVGF)[14, 15] approach. The OVGF values represent an improved "orbital energy", which contains orbital relaxation and correlation effects. On the other hand the EDE can be obtained indirectly by calculating the difference in the total energies of the dianion and the monoanion. These indirect methods are also referred to as Δ methods. In our calculations we have used ΔSCF/dz(d,sp/2d) and ΔSDCI (SDCI = singles doubles configuration interaction). We note that the positive EDE indicates that a system is electronically stable.

We present here the results of our calculations on the dianionic silicon–carbon clusters SiC_6^{2-} (**1**) and $Si_2C_6^{2-}$ (**3**). Several smaller dianionic Si–C clusters of general formula SiC_4^{2-} and SiC_5^{2-} were examined but we found no electronically stable isomers. SiC_6^{2-} (**1**) seems to be the smallest dianion of this class capable of binding both excess electrons. We have located several minima on the SiC_6^{2-} PES that have similar total energies, but only **1** represents a stable free dianion. This isomer consists of a central Si atom and three terminal C_2 units. Dianion **1** has the closed-shell $^1A'$ electronic ground state and shows D_{3h} symmetry (Figure 1). At the SCF/dz(d,sp/2d) level the C–C bonds (1.243 Å) show significant triple bond character, whereas the Si–C bonds (1.759 Å) possesses mainly single-bond character.

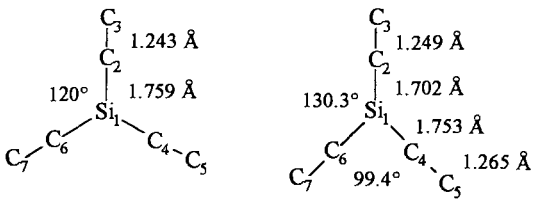

Figure 1. Stable SiC_6^{2-} dianion **1** (D_{3h} symmetry) and its corresponding monoanion **2** (C_{2v} symmetry)

The calculation of possible fragment energies showed that owing to the covalent character of the Si–C bonds and the resulting high binding energy, fragmentations of **1** into two singly negatively charged fragments can be excluded. In contrast, the electronic stability of dianion **1** is not guaranteed. The vertical EDE is 1.77 eV at the level of KT, 1.08 eV at the ΔSCF level, 1.27 eV at the correlated ΔSDCI level, and 1.24 eV according to an OVGF calculation (Table 1). The Overestimation of the EDE by 0.5 to 1.0 eV by Koopmans Theorem is typical. Taking orbital relaxation into account within an ΔSCF calculation leads to a decrease of the EDE, whereas correlation effects within a ΔSDCI or OVGF calculation tend to stabilize the dianion and to increase the EDE.

The adiabatic EDE is obtained by calculating the difference between the total energies of the dianion and the separately optimized monoanion **2** that shows C_{2v} symmetry. At the employed levels of theory the adiabatic EDE is clearly positive (Table 1). Since the dianion **1** is both vertically and adiabatically

Table 1. Vertical and adiabatic electron-detachment energies of the dianions **1** and **3**.

Theoretical method	EAE/eV	
	1	**3**
vertical		
KT	1.77	1.55
ΔSCF	1.08	1.12
ΔSDCI	1.27	1.10
OVGF	1.24	0.98
adiabatic		
ΔSCF	0.59	0.73
ΔSDCI	0.86	0.75

stable with respect to electron loss, and stable with respect to fragmentation, it should be possible to observe it in a mass spectrometer.

Let us now consider the $Si_2C_6^{2-}$ dianion. As for the SiC_6^{2-} system we found only one electronically stable isomer but in contrast to the branched structure of **1** the $Si_2C_6^{2-}$ dianion **3** exhibits a chainlike geometry. Dianion **3** has a ^1A electronic ground state and a C_2 symmetrical structure (Figure 2). The

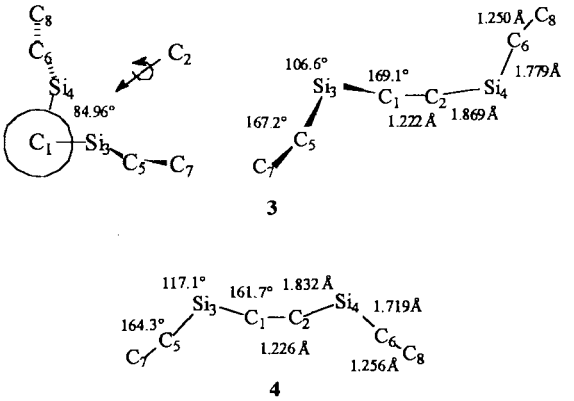

Figure 2. Stable $Si_2C_6^{2-}$ dianion **3** (C_2 symmetry) from two perspectives and its corresponding monoanion **4** (C_{2v} symmetry)

C–C bond C_1–C_2 (1.222 Å) and the bonds C_5–C_7, C_6–C_8 (1.250 Å) can be identified as C–C triple bonds, whereas the Si–C bonds (1.779 and 1.869 Å) have essentially single bond character (Figure 2). As for all chainlike structures we have examined the chain is folded at the silicon atoms. In dianion **3** the angle at the silicon atom is 106°, that is close to the tetrahedral angle. The vertical EDE of dianion **3** is 1.55 eV at the level of KT, and 1.12, 1.10, and 0.98 eV at the ΔSCF, ΔSDCI and OVGF levels respectively (Table 1). The adiabatic EDE has been calculated with respect to a geometrically optimized monoanion with C_{2v} symmetry (**4**); it is clearly positive (Table 1). Based on the sums of possible fragment energies and the arguments presented above, fragmentation can be excluded as a relevant decomposition channel. Thus, we predict that dianion **3** will be long-lived and observable in a mass spectrometer.

Let us now discuss the structures of the stable isomers **1** and **3** from a more general point of view. From the investigation of several classes of free dianions it has been established that stable dianions can roughly be divided into two groups. On the one hand, there are strictly linear or chainlike structures in which the negative charge is mainly localized at the ends of the chain, and the chain itself is essentially neutral. We call this class the "linear neutral group". The most prominent examples are dianions of

 © WILEY-VCH Verlag GmbH, D-69451 Weinheim, 1997 0570-0833/97/3617-1890 $ 17.50+.50/0

aliphatic dicarboxylic acids $^-OOC-(CH_2)_n-COO^-$,[16] and the linear isomers of the carbon clusters C_8^{2-} and C_{10}^{2-}.[10] On the other hand, there are many dianions that form compact structures. These clusters are characterized by a positively charged central atom or group and several electron-withdrawing substructures that enforce the binding of the two extra electrons. We denote this group as the "compact polarized group". The previously mentioned alkali metal halides MX_3^{2-} belong to this group. These dianions have a positively charged central metal atom and three negatively charged halide ligands. The stability of the MX_3^{2-} dianions can be understood in terms of the electrostatic forces present.[7, 8] Another example is the starlike, stable $C(C_2)_3^{2-}$ cluster, which despite its homonuclear, covalent bonding character belongs to the "compact polarized group", since the central carbon atom is clearly positively polarized (+ 0.4) and the negative charge is evenly distributed over the three terminal electron-affinitive C_2 units.

We can now assign the Si–C dianions **1** and **3** to theses groups. The Mulliken charge distribution (Figure 3) shows that the central silicon atom of dianion **1** is positively polarized and

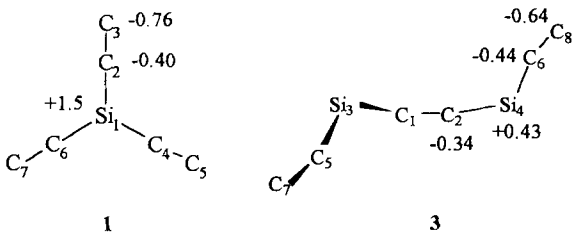

1 3

Figure 3. Mulliken charge distribution of the dianions **1** and **3**.

the three C_2 units carry the negative charge. Thus, the dianion SiC_6^{2-} (**1**) belongs to the group of "compact polarized dianions". The stability of such systems can be explained as follows: The high symmetry (D_{3h}) allows an even distribution of the two negative charges over three electron-affinitive C_2 units. Thus, each "ligand" has to bind effectively less than one electron, the center can be positively polarized, and a favorable electrostatic pattern arises. For dianion **1** the difference of the electronegativities of the elements silicon and carbon additionally favor this charge distribution, such that the positive charge at the central position is increased in comparison with the analogous homonuclear C_7^{2-} cluster. In summary dianion **1** is stabilized, because the polarization of the atoms due to the difference in electronegativities works in the sense of the "ionic model". This is not the case if the silicon atom is not in the central position of the cluster, but in the position of the ligands. In such a case the polarization due to the difference in electronegativities contrasts the favorable charge distribution and indeed all these isomers are not stable with respect to electron autodetachment.

In contrast, the dianion $Si_2C_6^{2-}$ (**3**) belongs to the "linear neutral group". The Si atoms of dianion **3** are likewise positively polarized due to the difference in electronegativities, but there is virtually no difference to the corresponding neutral molecule. In addition, the associated negative charge of the carbon atoms in the center of the molecule (C_1 and C_2) is only slightly smaller in the neutral molecule than in the dianion. Thus, the additional electrons of the dianionic system are mainly bound to the terminal alkyne groups C_5-C_7 and C_6-C_8. Therefore, the picture of dianion **3** resembles that of a neutral chain with the negative charges localized at the ends. Clearly, the stability of dianion **3** originates from the sufficiently large distance between the two extra electrons and not from a stabilization in the sense of the "ionic model".

Finally, let us compare the structures of dianionic Si–C clusters with those of typical neutral Si–C clusters. In neutral carbon-rich systems the Si atoms are placed mainly at the outer positions such that the number of strong C–C bonds is maximized.[17] In contrast, in dianionic species the Si atom is in the central position. This phenomenon is directly related to the criteria of stability of dianions. In contrast to neutral species, electronic stability is the most important requirement for the existence of a given dianion. For example, there are several energetically more favorable isomers of dianion **1**, such as a linear chain with the silicon at the outer position. These structures are stable with respect to fragmentation, but they are not stable with respect to electron autodetachment. Thus, the position of the Si atoms, and thereby the whole geometrical structure, is not controlled by a total energy criterion, but by the necessity to bind both extra electrons.

Received: February 13, 1997 [Z 10108 IE]
German version: *Angew. Chem.* **1997**, *109*, 1849–1951

Keywords: ab initio calculations · carbon · clusters · silicon

[1] A. I. Boldyrev, J. Simons, *J. Phys. Chem.* **1994**, *98*, 2298.
[2] R. Janoschek, *Z. Anorg. Allg. Chem.* **1992**, *616*, 101.
[3] J. Kalcher, A. F. Sax, *Chem. Rev.* **1994**, *94*, 2291.
[4] M. K. Scheller, R. N. Compton, L. S. Cederbaum, *Science* **1995**, *270*, 1160.
[5] S. N. Schauer, P. Williams, R. N. Compton, *Phys. Rev. Lett.* **1990**, *65*, 625.
[6] A. T. Blades, P. Kebarle, *J. Am. Chem. Soc.* **1994**, *116*, 10761.
[7] M. K. Scheller, L. S. Cederbaum, *J. Phys. B* **1992**, *25*, 2257.
[8] M. K. Scheller, L. S. Cederbaum, *J. Chem. Phys.* **1993**, *99*, 441.
[9] T. Sommerfeld, M. K. Scheller, L. S. Cederbaum, *J. Phys. Chem.* **1994**, *98*, 8914.
[10] J. D. Walts, R. J. Bartlett, *J. Chem. Phys.* **1992**, *97*, 3445.
[11] T. Sommerfeld, M. K. Scheller, L. S. Cederbaum, *Phys. Chem. Lett.* **1993**, *209*, 216.
[12] T. H. Dunning, Jr., *J. Chem. Phys.* **1970**, *53*, 2823.
[13] T. Koopmans, *Physika* **1933**, *1*, 1.
[14] L. S. Cederbaum, *J. Phys. B* **1975**, *8*, 290.
[15] W. von Niessen, J. Schirmer, L. S. Cederbaum, *Comput. Phys. Rep.* **1984**, *1*, 57.
[16] W. P. M. Maas, N. M. M. Nibbering, *Int. J. Mass Spectrom. Ion Proc.* **1989**, *88*, 257.
[17] G. Froudakis, A. Zdetsis, M. Mühlhäuser, B. Engels, S. Peyerimhoff, *J. Chem. Phys.* **1994**, *101*, 6790.

 © WILEY-VCH Verlag GmbH, D-69451 Weinheim, 1997 0570-0833/97/3617-1891 $ 17.50+.50/0

Multidentate, Cyclic Phosphorus Ligands with a Silicon–Phosphorus Backbone: Template Synthesis of a 1,4,7-Triphospha-2,3,5,6,8,9-hexasilacyclononane and a 1,3,5,7,9,11-Hexaphospha-2,4,6,8,10,12-hexasilacyclododecane**

Matthias Driess,* Markus Faulhaber, and Hans Pritzkow

Dedicated to Professor Malcolm Chisholm

Multidentate, cyclic ligands containing nitrogen, oxygen, sulfur, or phosphorus donor atoms play an important role in the coordination chemistry of transition metals. They are more suitable than acyclic chelating ligands for the synthesis of complexes with a rigid stereochemistry and with defined redox and magnetic properties. In such complexes the metal is often completely shielded from one side, while the "free" coordination space on the other side can be forged into almost any shape in order to attain a high selectivity. This has already been substantiated by numerous investigations of macrocycles with nitrogen[1] and sulfur atoms as hard and soft donor centers,[2] respectively; however, only a few phosphorus macrocyclic ("phosphacrown") ligands[3] are known to date. The need for such ligands is great, since they are "sterochemically superior" to the analogous acyclic phosphane ligands. However, preparative access to cyclic phosphanes is still very limited. For example, the synthesis of analogues of 1,5,9-triazacyclododecane (tacdo) and 1,4,7-triazacyclononane (tacn) is either difficult or has not been achieved to date. Recently, a template synthesis of a 1,5,9-triphosphacyclodecane[4] was reported. An alternative way to cyclic triphosphorus ligands is the facile synthesis of 1,3,5-triphospha-2,4,6-trisilacyclohexanes, which can also serve as efficient crown ligands, as we have already demonstrated with the synthesis of tricarbonyl metal complexes.[5] 1,4-Diphospha-2,3,5,6-tetrasilacyclohexanes were synthesized by using a metal center as the template.[6] However, larger Si_nP_m skeletons with $n+m>6$ were not known previously. Here we report the template synthesis of the first homologue of tacn, the 1,4,7-triphospha-2,3,5,6,8,9-hexasilacyclononane derivative in complex **1**, and on the unusual "fusion" of two 1,3,5-triphospha-2,4,6-trisilacyclohexane derivatives **2** (Cy = cyclohexyl) in the coordination sphere of Cu^I and Ag^I ions to form the 1,3,5,7,9,11-hexaphospha-2,4,6,8,10,12-hexasilacyclododecane ligand in the complexes **3a** and **3b**.

The starting material, the tris(phosphane) complex *fac*-[Mo(CO)$_3$(PH$_2$R)$_3$] (**4**, R = C_6H_{11}), which is readily obtained from the treatment of [Mo(CO)$_3$(NCMe)$_3$] with three equivalents of RPH$_2$, was lithiated in a surprisingly uniform one-pot reaction with *n*BuLi in THF at $-70\,^\circ C$; subsequent silylation with 1,2-dichlorotetramethyldisilane followed by cyclo-condensation with *t*BuLi produced the desired complex **1** in 48% yield as

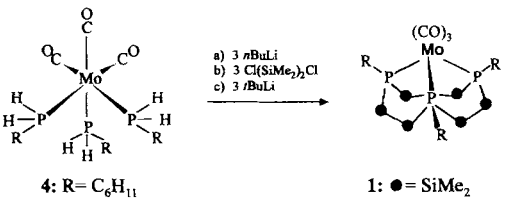

4: R = C_6H_{11} **1**: ● = $SiMe_2$

ocher crystals. The chemical composition was confirmed by mass spectrometry and satisfactory C,H analyses. Surprisingly, the ^{1}H NMR spectrum reveals that the novel Si_6P_3 ligand on the metal is *not* coordinated in a highly symmetrical fashion (C_{3v}): four types of methyl protons at $\delta = 0.4$, 0.5, 0.7, and 1.0 are observed for the Si_2Me_4 bridges. The assignment of these resonance signals to CH, CH_2 (cyclohexyl groups), and CH_3 substituents was verified by a gradient 1D-HMQC NMR experiment (HMQC = Heteronuclear Multiple Quantum Correlation). If **1** had C_{3v} symmetry, only two signals would be observed for the Si_2Me_4 protons. In this case the methyl groups orientated *syn* and *anti* to the Mo center would be arranged in an ecliptical conformation. Apparently, a *gauche*-type conformation of the Me groups in the Si_2Me_4 bridges in **1** is more favorable; this results in different environments for all four Me groups. A singlet at $\delta = -100.2$ is observed in the ^{31}P NMR spectrum. The IR spectrum contains two bands for the CO stretching vibrations at $\tilde{\nu}$ 1837 (s) and 1927 (br) cm^{-1}, which is in agreement with a local C_{3v} symmetry of the [Mo(CO)$_3$] fragment. Though the Si_6P_3 ligand can be released in low yields by the treatment of **1** with multidentate nitrogen and other phosphorus ligands (detected by ^{31}P NMR spectroscopy), it has not yet been isolated.

A new method of constructing cyclic P_6 ligands is offered by the reaction of the P_3 ligand **2**,[7] which can be readily obtained in high yields, with the strongly Lewis-acidic Cu and Ag triflates [M(OSO$_2$CF$_3$)] (M = Cu, Ag). These reactions, which were carried out at $-30\,^\circ C$ in toluene, produce a clear solution. Evaporation of the solvent, subsequent extraction with toluene, and crystallization affords the complexes **3a,b** as colorless, extreme-

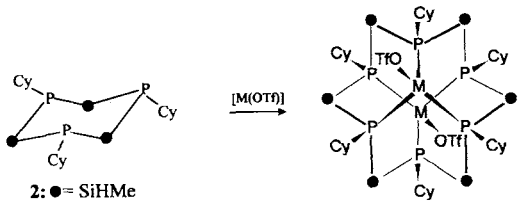

2: ● = SiHMe

3a: M = Cu, OTf = OSO_2CF_3
3b: M = Ag

ly air-sensitive solids. The formation of these complexes is surprising, because silylphosphanes with Cu^I or Ag^I salts usually react to form metal-rich Cu/P or Ag/P clusters.[8] Complexes **3a,b** are diamagnetic, are hardly soluble in aromatic, aliphatic, or ethereal solvents, and gradually decompose to form [(CyH$_2$P)$_3$M(OTf)] (M = Cu: $\delta(^{31}P) = -85$, M = Ag: $\delta(^{31}P) = -100$), which strongly limits their characterization by NMR spectroscopy. In the ^{31}P NMR spectrum of **3b** there was at least a very broad resonance signal at $\delta \approx -140$ with $^{31}P,^{107/109}Ag$ couplings ($J \approx 2600$ Hz), whereas none was observed for **3a** because of the quadrupole broadening by the $^{63/65}$Cu nuclei ($I = 3/2$). The structures of the complexes were determined unambiguously by single-crystal X-ray diffraction analyses[9] (Figure 1), and their compositions were confirmed by correct C,H analyses. The isotypic compounds crystallize in

[*] Prof. Dr. M. Driess, Dipl.-Chem. M. Faulhaber
Lehrstuhl für Anorganische Chemie I der Universität
Fakultät für Chemie
Universitätsstrasse 150, D-44801 Bochum (Germany)
Fax: Int. + (234) 709-4378
e-mail: driess@ibm.anch.ruhr-uni-bochum.de
Dr. H. Pritzkow
Anorganisch-chemisches Institut der Universität
Im Neuenheimer Feld 270, D-69120 Heidelberg (Germany)

[**] This work was supported by the Deutsche Forschungsgemeinschaft (Graduiertenkolleg "Selektivität in der Organischen und Metallorganischen Synthese und Katalyse") and the Fonds der Chemischen Industrie.

 © WILEY-VCH Verlag GmbH, D-69451 Weinheim, 1997 0570-0833/97/3617-1892 $ 17.50+.50/0

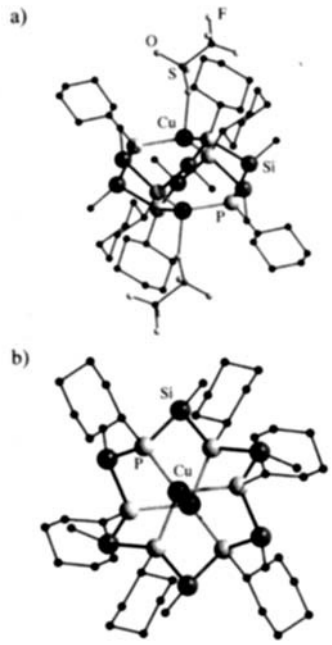

Figure 1. a) Molecular structure of **3a** in the crystal. Compounds **3b** and **3a** are isotypical. Selected distances [Å] for **3a**: Cu–O 2.192(4), Cu–P 2.345(2), 2.348(2), 2.349(2), P–Si (averaged) 2.253(2), P–C (averaged) 1.880(4), Si–C (averaged) 1.851(5). Selected distances [Å] for **3b**: Ag–O 2.507(10), Ag–P 2.510(2), 2.517(2), 2.519(2), P–Si (averaged) 2.257(2), P–C (averaged) 1.874(5), Si–C (averaged) 1.826(6). b) Side view of **3a** along the Cu–Cu axis. The triflate ligands on Cu are not depicted for reasons of clarity.

the triclinic space group $P\bar{1}$. The crownlike Si_6P_6 ligand binds two metal centers, and the M–M distance is 3.521 Å (**3a**) and 3.455 Å (**3b**), which indicates no M–M bond. The M–P distances lie in a narrow range (**3a**: 2.345, 2.349(2) Å; **3b**: 2.510, 2.519(2) Å) and are only slightly longer than those values found in other tris(phosphane)-substituted copper(I)[10] or silver(I)[11] complexes. The unremarkable and only slightly different Si–P distances in **3a** and **3b**, as well as the M–P distance, implies an almost ideal tetrahedral coordination of the Si and P atoms, with somewhat smaller bonding angles on the phosphorus than on the silicon centers as expected. The metal centers, each coordinatively saturated, display a severely flattened tetrahedral environment (sum of the P-M-P angles: **3a** 348.7; **3b** 349.8°).

The high symmetry of the complexes is apparently conserved in solution, since only one type of SiH proton for the potentially stereogenic SiHMe bridge is observed in the ^{1}H NMR spectrum of **3b**. The mechanism of formation of **3a,b** is not yet known. We assume that the metal-template-controlled, multistep fusion of **2** is mainly initiated by two factors: firstly by the thermodynamically favorable tridentate coordination of the Cu^I or Ag^I ion with phosphorus, and secondly, by the ring strain in **2**, which favors a ring extension. On the other hand, the oxidative addition to a reactive intermediate with a d^8-M^{III} center, which, for example, could be formed by the insertion of an M^I ion into a Si–P bond, is very unlikely. NMR spectroscopy gives no hint of any intermediates. Since the electrophilic metal centers in **3a,b** lie embedded in an element–organic pocket, and the triflate group is an excellent nucleofugal leaving group, **3a,b** should be particularly suitable for selective reactions and for mechanistic investigations, such as the isolation of intermediates during the insertion of unsaturated organic substrates into copper(I)–element or silver(I)–element bonds. The relevant investigations and experiments on the liberation of the Si_6P_6 ligand in **3a,b** by decomplexation with other chelate ligands is currently in progress.

Experimental Section

1: A solution of **4** (1.3 g, 2.5 mmol) in THF (80 mL) was treated at −70 °C with a solution of 2.5 M *n*BuLi (3 mL, 7.5 mmol) in hexane. The mixture was warmed to −30 °C. Subsequently, 1,2-dichlorotetramethyldisilane (1.6 g, 7.5 mmol) in THF (20 mL) was added dropwise at −70 °C. The solution was warmed to room temperature, then re-cooled to −70 °C and a solution of 2.0 M *t*BuLi (3.75 mL, 7.5 mmol) in pentane was added to complete the reaction. After partial evaporation of the solvent at room temperature under vacuum (10^{-2} Torr), the residue was extracted with toluene (20 mL). Concentration of the solution to 3 mL gave **1** as ocher crystals. Yield: 48% (1.0 g, 1.2 mmol). M.p. 211 °C (decomp.); ^{1}H NMR (200 MHz, $CDCl_3$): δ = 0.4 (s, SiMe), 0.5 (s, SiMe), 0.7 (s, SiMe), 1.0 (s, SiMe), 1.1 (d, CH-Cy, ^2J(H,P) = 6 Hz), 1,15 (m, CH_2-Cy), 1.35 (m, CH_2-Cy) 1.65 (m, CH_2-Cy); ^{31}P NMR (36 MHz, $CDCl_3$): δ = −100.2 (s); IR (toluene): $\tilde{\nu}$ (CO) = 1837 (s), 1927 (br.) cm^{-1}; MS (EI, 70 eV): m/z(%) = 872 (M^+, 19), 844 ($(M-CO)^+$, 54), 816 ($(M-2CO)^+$, 20), 761 ($(M-CO-C_6H_{11})^+$, 8), 733 ($(M-2CO-C_6H_{11})^+$, 100).

3a: Ligand **2** (455 mg, 0.9 mmol) was treated at −30 °C in toluene (30 mL) with CuOTf·0.5 C_6H_6 (Aldrich; 180 mg, 0.4 mmol). The volume was reduced to ca. 5 mL, and colorless, very air-sensitive crystals were obtained after several days. Yield: 74% (395 mg, 0.3 mmol). M.p. 148 °C (decomp.).

3b: In an analogous synthesis to **3a**, ligand **2** (1.0 g, 2.2 mmol) was treated with AgOTf (Aldrich, 0.51 g, 2.00 mmol) to afford **3b** as colorless crystals. Yield: 85% (1.2 g, 0.83 mmol). M.p. 134 °C (decomp.); ^{1}H NMR (200 MHz, $CDCl_3$): δ = 0.7–2.3 (m, Me and C_6H_{11}), 5.4 (s, Si-H); ^{31}P NMR (36 MHz, $CDCl_3$): $\delta \approx -143$ (br., $J(^{31}P,^{105/107}Ag) \approx 2600$ Hz).

Received: February 10, 1997 [Z10094]
German version: *Angew. Chem.* **1997**, *109*, 1980–1982

Keywords: copper · macrocyclic ligands · P ligands · Si ligands · silver

[1] Reviews: *Coordination Chemistry of Macrocyclic Compounds* (Ed.: G. A. Melson), Plenum, New York, **1979**; L. F. Lindoy, *The Chemistry of Macrocyclic Ligand Complexes*, Cambridge Univ. Press, **1992**; R. I. Haines, A. McAuley, *Coord. Chem. Rev.* **1981**, *39*, 77; G. Haselhorst, S. Stoetzel, A. Strassburger, W. Walz, K. Wieghardt, B. Nuber, *J. Chem. Soc. Dalton Trans.* **1993**, 83, zit. Lit.

[2] Reviews: P. G. Blower, J. R. Dilworth, *Coord. Chem. Rev.* **1987**, *76*, 121; L. Sacconi, F. Mani, A. Bencini, *Comprehensive Coordination Chemistry* (Eds.: G. Wilkinson, R. D. Gillard, J. A. McCleverty), Pergamon, Oxford, **1987**, Vol. 5, Chap. 5, p. 166; J. S. Bradshaw, J. Y. K. Hui, *J. Heterocycl. Chem.* **1974**, *11*, 649; C. McDaniel, J. S. Bradshaw, R. M. Izatt, *Heterocycles* **1990**, *30*, 665, and references therein.

[3] Reviews: F. Vögtle, *Supramolekulare Chemie*, Teubner, Stuttgart, **1991**, p. 45; A.-M. Caminade, J. P. Majoral, *Chem. Rev.* **1994**, *94*, 1183; T. A. DelDonno, W. Rosen, *J. Am. Chem. Soc.* **1977**, *99*, 8051; *Inorg. Chem.* **1978**, *17*, 3714; E. P. Kyba, C. W. Hudson, M. J. McPhaul, A. M. John, *J. Am. Chem. Soc.* **1977**, *99*, 8053; R. Bartsch, S. Hietkamp, S. Morton, O. Stelzer, *Angew. Chem.* **1982**, *94*, 367; *Angew. Chem. Int. Ed. Engl.* **1982**, *21*, 375; D. J. Brauer, T. Lebbe, O. Stelzer, *ibid.* **1988**, *100*, 432 and **1988**, *27*, 438; D. J. Brauer, F. Dörenbach, T. Lebbe, O. Stelzer, *Chem. Ber.* **1992**, *125*, 1785; T. Mizuta, A. Okano, T. Sasaki, H. Nakazawa, K. Niyoshi, *Inorg. Chem.* **1997**, *36*, 200.

[4] S. J. Coles, P. G. Edwards, J. S. Fleming, M. B. Hursthouse, *J. Chem. Soc. Dalton Trans.* **1995**, 1139; *ibid.* **1995**, 4091; S. J. Coles, P. G. Edwards, J. S. Fleming, M. B. Hursthouse, S. S. Liyanage, *Chem. Commun.* **1996**, 293; *J. Chem. Soc. Dalton Trans.* **1996**, 1801.

[5] M. Driess, M. Reisgys, H. Pritzkow, *Angew. Chem.* **1992**, *104*, 1514; *Angew. Chem. Int. Ed. Engl.* **1992**, *31*, 1510; *Chem. Ber.* **1996**, *129*, 247.

[6] G. Johannsen, O. Stelzer, *Chem. Ber.* **1977**, *110*, 3438, and references therein.

[7] M. Driess, M. Faulhaber, H. Pritzkow, M. Reisgys, unpublished results.

[8] Review: D. Fenske in *Clusters and Colloids-From Theory to Applications* (Ed.: G. Schmid), VCH, Weinheim, **1994**, p. 219, and references therein; M. Driess, S. Martin, K. Merz, H. Pritzkow, V. Pinchouk, H. Grützmacher, M. Kaupp, *Angew. Chem.* **1997**, *109*, 1982; *Angew. Chem. Int. Ed. Engl.* **1997**, *36*, 1894.

[9] Crystallographic data: **3a**: triclinic $P\bar{1}$, a = 13.318(7), b = 13.435(7), c = 14.227(7) Å, α = 117.76(2), β = 98.03(3), γ = 103.57(3)°, V = 2103(2) Å^3, Z = 1, θ_{max} = 25°, 7308 independent reflections, of which 5366 observed ($I > 2\sigma(I)$), $R1$ = 0.052, $wR2$ = 0.142, 420 parameters. **3b**: triclinic $P\bar{1}$, a = 13.244(10), b = 13.602(11), c = 14.421(12) Å, α = 117.82(6), β = 96.71(6), γ = 104.77(6)°, V = 2136(3) Å^3, Z = 1, θ_{max} = 25°, 7528 independent reflections, of which 6111 observed ($I > 2\sigma(I)$), $R1$ = 0.046, $wR2$ = 0.126, 548 parameter. The measurements were performed on a Siemens-Stoe AED2 diffractometer ($Mo_{K\alpha}$ radiation, λ = 0.7107 Å, ω scan); empirical correction for absorption. Solution of the structures with direct methods (SHELXS86), refinement with all measured reflections against F^2, non-hydrogen atoms (except solvent hydrogen atoms) anisotropically [12]. For **3a** the H atoms were placed in calculated positions, only common isotropic temperature factors were refined; for **3b** the H atoms were refined isotropically in observed positions. Both compounds contain four toluene molecules in each unit cell; all show disorder. Only the C atoms of the rings were refined isotropically (partly as rigid rings). Further details of the crystal structure investigation data (without structure

 © WILEY-VCH Verlag GmbH, D-69451 Weinheim, 1997 0570-0833/97/3617-1893 $ 17.50+.50/0

factors) are available on request from the Director of the Cambridge Crystallographic Data Centre, 12 Union Road, GB-Cambridge CB2 1EZ (UK) (fax: int. code + (1223) 336-033; e-mail: deposit@chemcrys.cam.ac.uk) on quoting the full journal citation.

[10] C. A. Ghilardi, S. Midollini, A. Orlandini, *Inorg. Chem.* **1982**, *21*, 4096, and references therein.

[11] P. G. Jones, H. W. Roesky, H. Grützmacher, G. M. Sheldrick, *Z. Naturforsch. B* **1985**, *40*, 590; V. Saboonchian, G. Wilkinson, B. Hussain-Bates, M. B. Hursthouse, *Polyhedron* **1991**, *10*, 737.

[12] a) G. M. Sheldrick, SHELXS86, Universität Göttingen, **1986**; b) G. M. Sheldrick, SHELXL93, Universität Göttingen, **1993**.

$[Sn_6(PR)_6]$, $[Sn_3(PR)_2Cl_2]$, and $[Cu_{24}(PR)_{12}]$ (R = Triorganosilyl): New Tin and Copper Phosphanediyl Clusters**

Matthias Driess,* Stefan Martin, Klaus Merz, Vassili Pintchouk, Hans Pritzkow, Hansjörg Grützmacher, and Martin Kaupp

Dedicated to Professor Gottfried Huttner on the occasion of his 60th birthday.

Although monometallic diorganophosphanes MPR_2 containing s-, p-, and d-group metals have been widely investigated, very little is known about the structure of phosphanes with two metal atoms attached to the phosphorus (phosphanediides or phosphanediyl complexes) M_2PR (R = alkyl, aryl, silyl). These complexes show a much greater tendency to oligomerize than the metal diorganophosphanides.[1, 2] We recently reported the structure of the first ionic phosphanediyl heteroaggregates **A**[3] and **B**,[4] whose Li, P frameworks can be described as a close packing of Li cations and RP dianions.

$[(RP)_8Li_{18}O]$ $[(RP)_2Li_4(RF)_2]$

A : R = iPr$_2$(2,4,6-Me$_3$C$_6$H$_2$)Si **B** : R = iPr$_2$(2,4,6-iPr$_3$C$_6$H$_2$)Si

Here we describe the molecular tin(II)-phosphanediyl clusters **1** and **2** as well as the first neutral phosphanediyl-bridged copper cluster **3**, which has no additional terminal donor ligands attached to the Cu(I) center. Compounds **1**–**3** represent new structural motifs for M_2PR aggregates (phosphanediides), with stronger covalent M–P bonds than the Li–P bonds in **A** and **B**. Attractive M–M dispersion forces also contribute to the bonding in **3**.

[*] Prof. Dr. M. Driess, Dipl.-Chem. S. Martin, Dr. K. Merz, Dr. V. Pintchouk
Lehrstuhl für Anorganische Chemie I der Universität
Fakultät für Chemie
Universitätsstrasse 150, D-44801 Bochum (Germany)
Fax: Int. code + (234) 7094378
e-mail: driess@ibm.anch.ruhr-uni-bochum.de

Dr. H. Pritzkow
Anorganisch-chemisches Institut der Universität
Im Neuenheimer Feld 270, D-69120 Heidelberg (Germany)

Prof. Dr. H. Grützmacher
Laboratorium für Anorganische Chemie der ETH Zürich
Universitätsstrasse 6, CH-8092 Zürich (Switzerland)

Dr. M. Kaupp
Max-Planck-Institut für Festkörperforschung
Heisenbergstrasse 1, D-70569 Stuttgart (Germany)

[**] This work was supported by the Deutschen Forschungsgemeinschaft (Schwerpunktprogramm "Polyedermoleküle") and the Fonds der Chemischen Industrie. We thank the Messer Griesheim GmbH for the donation of chemicals. M. K. thanks the Deutschen Forschungsgemeinschaft for a habilitation stipendium and Dr. V. G. Malkin, O. L. Malkina (Bratislava), and Prof. P. Pyykkö (Helsinki) for helpful discussions.

The Sn_6P_6 cluster **1** can be synthesized by two different Brønsted acid–base reaction pathways. The reaction of the primary silylphosphane **4a** with diaminostannanediyl **5a** in a molar ratio of 1:1 in hexane results in an 89% yield of black-red crystals of **1**. Bis[2,4,6-tris(trifluoromethyl)phenyl)]stannanediyl **5b** can also be used as the Sn^{II} source, whereby **1** and 1,3,5-tris(trifluoromethyl)benzene (^{19}F NMR spectroscopy) are obtained in practically quantitative amounts.

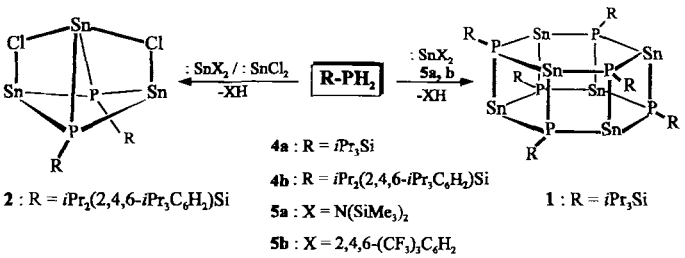

Single-crystal X-ray structure analysis[5] revealed that **1** crystallizes with triclinic symmetry and with two independent half molecules in the unit cell. Since the two molecules differ only very slightly, we will discuss only one form. The molecule has $\bar{1}$ symmetry and forms a distorted hexagonal Sn_6P_6 prism with σ^3,λ^2-coordinated tin and σ^4,λ^3-coordinated phosphorus centers (Figure 1). The atoms P1, P2, P3 and Sn1, Sn2, Sn3 are located just 0.09 Å above (phosphorus) and below (tin) the best hexagonal plane. The average Sn–P bond lengths of 2.626 (3) Å in the Sn_3P_3 plane are only slightly longer than the corresponding Sn–P bond lengths between the two Sn_3P_3 planes (2.665(3) Å). The endocyclic angles at the three symmetry-independent Sn centers are practically identical. For example, the sum of the angles around the Sn1 atom is 276.29(9)° with P1-Sn1-P2a 86.99(9), P3-Sn1-P1 100.76(10) and P3-Sn1-P2a 88.54(9)°. The larger endocyclic angles at the phosphorus atoms are a result of the bulky silyl group attached to the phosphorus. The angles are approximately the same for all three phosphorus centers: for P1 90.19(9) (Sn3a-P1-Sn1), 90.77(10) (Sn3a-P1-Sn2), and 139.13(11)° (Sn1-P1-Sn2).

The Sn–P bond lengths and the endocyclic angle at the tin are virtually the same as the values observed for dimeric[6] and hypercoordinated diphosphinostannanediyl.[7] Monomeric V-shaped $Sn(PR_2)_2$ derivatives (P-Sn-P approximately 97°) have, however, shorter Sn–P bond lengths (average distance 2.567(1) Å).[8] Of particular interest is the unusual highfield position of the ^{31}P NMR singlet signal with Sn satellites at $\delta = -475.2$, with a comparatively low value of $^1J(^{31}P, ^{117/119}Sn) = 708$ Hz. The low solubility of **1** made it impossible to obtain a ^{119}Sn NMR spectrum. DFT-IGLO calculations (density functional theory with individual gauges for localized orbitals)[9] on the parent compound $H_6Sn_6P_6$ (**1***), taking spin–orbital corrections explicitly into account, show that spin–orbital splitting of the 5p orbital of the tin plays a significant role in the unusual high field shift of the ^{31}P resonance. Although calculations without the spin–orbital correction yield a value ($\delta(^{31}P) = -274$) at relatively high field; including the spin–orbital contribution (−80) leads to a further high-field shift to $\delta(^{31}P) = -354$. Because of the amount of computer time required, only a medium-sized basis set was used;[9] experience has shown that the spin–orbital correction is then clearly underestimated. It is therefore probable that the remaining discrepancy between the calculated and experimental values for the high field position of **1** is also due to spin–orbital effects. Calculations at the same level carried out on Sn-

 © WILEY-VCH Verlag GmbH, D-69451 Weinheim, 1997 0570-0833/97/3617-1894 $ 17.50+.50/0

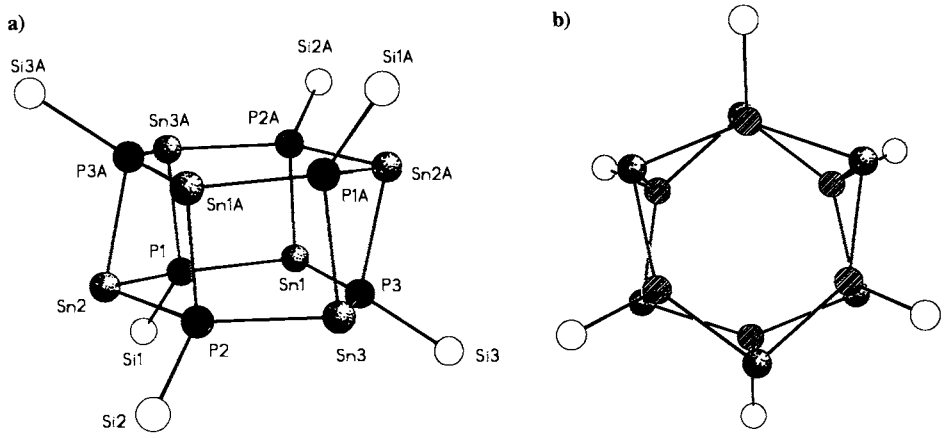

Figure 1. a) Molecular structure of **1** in the crystal. Only one of the two independent molecules in the unit cell is shown, as they can hardly be distinguished. For clarity, the alkyl groups have been omitted. Selected bond lengths [Å] and angles [°]: Sn1–P1 2.611(3), Sn1–P3 2.642(3), Sn1–P2a 2.654(3), Sn2–P1 2.613(3), Sn2–P2 2.628(3), Sn2–P3a 2.669(3), Sn3–P3 2.631(3), Sn3–P1a 2.671(3), Sn3–P2 2.634(3), P1–Si1 2.262(4), P2–Si2 2.269(4), P3–Si3 2.271(4); P1-Sn1-P3 100.76(10), P1-Sn1-P2a 86.99(9), P3-Sn1-P2a 88.54(9), Si1-P1-Sn1 106. 03(13), Si1-P1-Sn2 105.93(13), Sn1-P1-Sn2 139.13(11), Si1-P1-Sn3a 126.59(14), Sn1-P1-Sn3a 90.19(9), Sn2-P1-Sn3a 90.77(10). b) Projection of the Sn_6P_6 cluster in **1** along the Sn_3P_3 rings.

$(PH_2)_2$ gave a value of $\delta(^{31}P) = -105$, with a much lower spin–orbital contribution of -26. This is in good agreement with experimental values obtained for derivatives ($\delta(^{31}P) = -102$ to -121)[8]. The strong influence of the spin–orbital coupling on the ^{31}P chemical shift of **1** (**1***) is a result of the relatively large Sn-P-Sn angles within the Sn_3P_3 ring. This means that the phosphorus 3s orbitals contribute particularly strongly to the Sn–P bonds in the Sn_3P_3 ring and permit a very efficient transfer of the spin–orbital effect from the two neighboring Sn centers.[10a] The mechanism of formation of **1** is unknown. The Sn_6P_6 framework is possibly built up by a stepwise association of three dimeric $(RPSn)_2$ intermediate molecules (Scheme 1).

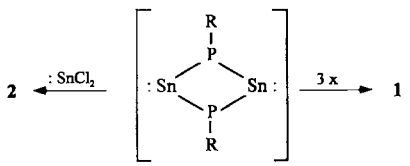

C

Scheme 1. Formation of **1** and **2** from the hypothetical intermediate C.

The formation of a $(RPSn)_2$ molecule as an intermediate is very probable when the following reaction is considered: the diaminostannanediyl **5a** reacts with the bulky silylphosphane **4b** in the presence of $SnCl_2$ to form the unusual cluster $Sn_3P_2Cl_2$ (**2**), which is isolated as yellow crystals in 44% yield. The crystal structure of **2** has been determined and can be described[5] as a complex of the Sn_2P_2 intermediate **C** and $SnCl_2$ (Scheme 1), where the Cl atoms and the phosphanediyl groups act as μ_2- and μ_3-bridging ligands (Figure 2). This description is in agreement with the observation that $SnCl_2$ cleaves off from **2** under mass spectrometry conditions (electron impact ionization (EI), 70 eV). The Sn–P bond lengths in **2** show only slight variations from one another (average 2.622(3) Å) and are virtually identical with those in **1**. The Cl3-Sn2-Cl4 angle is 159.6(1)° and the (somewhat different) Sn2–Cl distances in the $SnCl_2$ dumbbell are approximately 0.3 Å longer than the Sn1–Cl3 (2.583(3) Å) and Sn3–Cl4 bond lengths 2.565(3) Å), which can be explained by higher coordination of the Sn2 atom.

Veith et al. obtained similar complexes (though polymeric in the crystalline state) from the reaction of the four-membered cyclodiazastannanediyl with SnX_2 (X = Cl, Br).[11] The ^{31}P NMR spectrum of **2** shows a singlet with Sn satellites at $\delta = -122.4$ ($^1J(^{31}P, ^{117/119}Sn) = 1037$ Hz). The calculation of the ^{31}P chemical shift[9] of the parent compound $H_2P_2Sn_3Cl_2$ (**2***) gave a value of $\delta = -52$, with a spin–orbital contribution of only -22. The low spin–orbital contribution for **2*** relative to **1*** is due to the large difference in Sn-P-Sn angle, which implies differing amounts of s character of the phosphorus center in the P–Sn bond[10b]. When the reaction is carried out without $SnCl_2$, a deep red solution is formed that has only one singlet signal with Sn satellites ($^1J(P,Sn) = 793$ Hz) at $\delta = -440.5$ in the ^{31}P NMR spectrum, which can be interpreted without doubt as the corresponding Sn_6P_6 cluster. **1** and other derivatives do not react with $SnCl_2$.

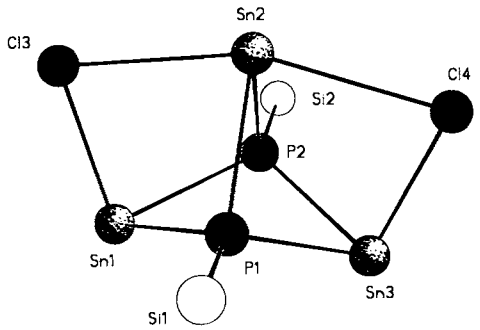

Figure 2. Structure of **2** in the crystal. Selected bond lengths [Å] and angles [°]: Sn1–Cl3 2.583(3), Sn3–Cl4 2.565(3), Sn2–Cl3 2.889(3), Sn2–Cl4 2.947(3), Sn1–P1 2.630(3), Sn1–P2 2.620(3), Sn2–P1 2.636(3), Sn2–P2 2.619(3), Sn3–P1 2.617(3), Sn3–P2 2.614(3), P1–Si1 2.304(4), P2–Si2 2.303(4); Cl3-Sn2-Cl4 159.60(9), P1-Sn2-P2 72.65(9), Cl3-Sn1-P2 88.45(9), Cl3-Sn1-P1 88.59(9), P1-Sn1-P2 72.73(9), P2-Sn2-P1 88.59(8), Si1-P1-Sn2 122.27(11), Si1-P1-Sn1 129.51(12), Si1-P1-Sn3 126.65(12).

A neutral copper phosphanediyl cluster with no additional terminal donor ligands on the copper was prepared for the first time in the synthesis of **3**. Its structure as $(Cu_2PR)_{12}$ (R = Me_2-(*i*PrMe_2C)Si) is very different from that of the dialkali metal phosphanediides, even though it also has a monvalent metal center.[3,4] Cluster **3** forms when **4c** is heated with $[\{CuO tBu\}_4]$ (**6**) in toluene at 60 °C and was isolated in 81% yield, as dark red crystals that are only sparingly soluble.

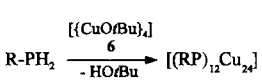

Figure 3 shows the structure of **3**[5] as a cluster of 24 Cu atoms surrounded by 12 triorganosilylphosphanediyl groups. The 24-atom cluster consists of three planar Cu_6 rings and two peripheral Cu_3 rings that all lie parallel to one another. The twelve RP fragments cap alternately the Cu_4 faces of the Cu_{24} polyhedron resulting in five-fold coordinated P centers. The Cu–P and Si–P bond lengths lie within the expected range. The structure of the

 © WILEY-VCH Verlag GmbH, D-69451 Weinheim, 1997 0570-0833/97/3617-1895 $ 17.50+.50/0

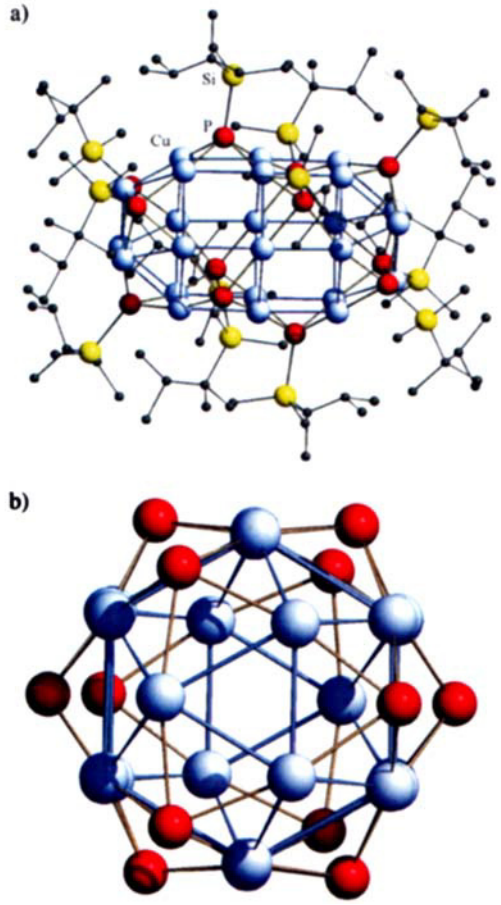

Figure 3. a) Structure of **3** in the crystal. Selected average bond lengths [Å] and angles [°]: Cu–P 2.226(3), Cu–Cu 2.733(2), P–Si 2.239(3); P-Cu-P 164.67(10). b) Projection of the $Cu_{24}P_{12}$ cluster of **3** along the parallel Cu_3 and Cu_6 rings. Cu: blue, P: red.

Cu_{24} polyhedron agrees with that of the recently described $[Cu_{24}(NPh)_{14}]^{4-}$ anionic cluster and can be discussed in an analogous fashion.[12] The construction principle of parallel stacks of hexagonal and trigonal Cu layers to form a polyhedron has also been observed for other Cu clusters.[13]

Experimental Section

1: Silylphosphane **4a** (1.32 g, 7.3 mmol) was added to a solution of **5a** (3.2 g, 7.3 mmol) in 20 mL hexane at 0 °C and then stirred at room temperature for about 2 h. The volatile components were removed under vacuum (10^{-2} Torr) at 25 °C, and the residue was dissolved in about 5 mL hot toluene. Black-red crystals of **1** precipitated upon cooling. Yield: 2.0 g (1.08 mmol, 89%). M.p. = 297 °C (decomp.). ^{1}H NMR (C_6D_6, 200 MHz): δ = 0.98 (d, 108 H, Me, J(H,H) = 5.9 Hz), 1.16 (sept, 18 H, C*H*Me$_2$, J(H,H) = 5.9 Hz); ^{31}P NMR (81 MHz): δ = −475.2 (s, ^1J(P,Sn) = 708 Hz). Correct C,H analysis. Compound **1** was also obtained in quantitative yield by heating **4a** (1.32 g, 7.3 mmol) with an equimolar amount of **5b** in toluene at 90 °C (5 h).

2: Aminostannanediyl **5a** (2.1 g, 4.78 mmol) was added to a suspension of dried $SnCl_2$ (1.0 g, 5.27 mmol) in 50 mL benzene and then treated with **4b** (dissolved in 5 mL benzene). The mixture was heated for 8 h at 60 °C. After cooling, the product crystallized in the form of a yellow solid. Yield: 1.17 g (1.04 mmol, 44%). M.p. = 181 °C (decomp.). ^{1}H NMR (C_6D_6, 200 MHz): δ = 0.91 (pseudo t, 36 H, Me), 1.12 (br. sept, 3 H, C*H*Me$_2$), 1.16 (sept., 3 H, CHMe$_2$, J(H,H) = 5.9 Hz); ^{31}P NMR (81 MHz): δ = −122.4 (s, ^1J(P,Sn) = 1037 Hz); MS (EI, 70 eV): m/z(%) = 1124 (M+, 12), 934 ($(M - SnCl_2)^+$, 6), 774 ($(M - i\mathrm{Pr}_2(i\mathrm{Pr}_3C_6H_2)\mathrm{SiP})^+$, 28), 317 ($(i\mathrm{Pr}_2(i\mathrm{Pr}_3C_6H_2)\mathrm{Si})^+$, 100). Correct C,H analysis.

3: A stirred solution of **6** (0.45 g, 0.82 mmol) in 20 mL toluene was allowed to react with **4c** (0.58 g, 3.29 mmol) and then heated for 5 h at 60 °C. The product crystallized from the deep red solution after cooling to room temperature. Yield: 0.4 g (0.14 mmol, 81%). M.p. = 214 °C (decomp.). Correct C,H analysis.

Received: February 18, 1997 [Z10133IE]
German version: *Angew. Chem.* **1997**, *109*, 1982–1985

Keywords: clusters · copper · phosphorus · tin

[1] Overview: *Clusters and Colloids—From Theory to Applications* (Ed.: G. Schmid), VCH, Weinheim, 1994.
[2] D. Fenske, F. Simon, *Angew. Chem.* **1997**, *109*, 240; *Angew. Chem. Int. Ed. Engl.* **1997**, *36*, 230; R. Ahlrichs, M. von Arnim, J. Eisenmann, D. Fenske, *ibid.*, **1997**, *109*, 243, and **1997**, *36*, 233.
[3] M. Driess, H. Pritzkow, S. Martin, S. Rell, D. Fenske, G. Baum, *Angew. Chem.* **1996**, *108*, 1064; *Angew. Chem. Int. Ed. Engl.* **1996**, *35*, 986.
[4] M. Driess, S. Rell, H. Pritzkow, R. Janoschek, *Chem. Commun.* **1996**, 305.
[5] **1**: triclinic $P\bar{1}$, a = 13.975(7), b = 15.646(8), c = 19.396(10) Å, α = 79.90(4), β = 80.40(4), γ = 74.51(4)°, V = 3991(4) Å^3, Z = 2, θ_{max} = 23°, 11091 unique reflections, 7322 observed ($I > 2\sigma(I)$, $R1$ = 0.052, $wR2$ = 0.111, 687 parameters). **2**: monoclinic $P2_1/c$, a = 15.798(11), b = 19.281(13), c = 17.604(13) Å, β = 107.16(6)°, V = 5124(6) Å^3, Z = 4, θ_{max} = 23°, 7138 unique reflections, 5046 observed ($I > 2\sigma(I)$, $R1$ = 0.049, $wR2$ = 0.135, 487 parameters). **3**: rhombohedral $R3$, a = 26.320(6), c = 19.084(3) Å, V = 11450(4) Å^3, Z = 3, θ_{max} = 25°, 3504 unique reflections, 2145 observed ($I > 2\sigma(I)$, $R1$ = 0.038, $wR2$ = 0.128, 217 parameters). The intensities were measured with a Siemens Stoe AED2 (**1** and **2**) or with a Siemens P4 diffractometer (**3**) ($Mo_{K\alpha}$ radiation, λ = 0.71707 Å, ω scan, T = 203 K), with absorption correction. Structure solution with direct methods [14a], refinement using all measured reflections against F^2 [14b]. Non-hydrogen atoms anisotropic, hydrogen atoms placed in calculated positions and refined with a group isotropic temperature factor only. The crystallographic data (without the structure factors) for the structures described in this publication have been deposited as "supplementary publication no. CCDC-100190" with the Cambridge Crystallographic Data Centre. Copies of the data can be obtained, free of charge, from the following address in Great Britain: The Director, CCDC, 12 Union Road, Cambridge CB21EZ (fax: int. code + (1223) 336033; e-mail: deposit@chemcrys.cam.ac.uk).
[6] A. H. Cowley, D. M. Giolando, R. A. Jones, C. M. Nunn, J. M. Power, *Polyhedron* **1988**, *7*, 1909; M. A. Matchett, M. Y. Chang, W. E. Buhro, *Inorg. Chem.* **1994**, *33*, 1109.
[7] H. H. Karsch, A. Appelt, G. Müller, *Angew. Chem.* **1985**, *97*, 404; *Angew. Chem. Int. Ed. Engl.* **1985**, *24*, 402; *Organometallics* **1986**, *5*, 1664; A. L. Balch, D. E. Oram, *ibid.* **1986**, *5*, 2159.
[8] M. Driess, R. Janoschek, H. Pritzkow, S. Rell, U. Winkler, *Angew. Chem.* **1995**, *107*, 1746; *Angew. Chem. Int. Ed. Engl.* **1995**, *34*, 1614.
[9] For details of the SOS–DFPT method used see: V. G. Malkin, O. L. Malkina, M. E. Casida, D. R. Salahub, *J. Am. Chem. Soc.* **1994**, *116*, 5898. For details of the IGLO method see: W. Kutzelnigg, U. Fleischer, M. Schindler in *NMR Principles and Prog.*, *23*, **1990**, 165. For details of the DFT calculation of spin–orbital corrections of chemical shifts see: V. G. Malkin, O. L. Malkina, D. R. Salahub, *Chem. Phys. Lett.* **1996**, *261*, 335; M. Kaupp, O. L. Malkina, V. G. Malkin, *ibid.* **1996**, *265*, 55. Experimental structure data of the derivatives (**1**, $Sn(PH_2)_2$ derivatives in [8], **2**) were used as the starting values for the calculation of **1***, $Sn(PH_2)_2$, and **2***, and d(P–H) = 1.43 Å was used. IGLO-II basis sets were used for Sn, P, Cl, and H. For **1***, a pseudopotential with a TZ2P valence basis set was introduced for the Sn atoms located further away from the nucleus under consideration: A. Bergner, M. Dolg, W. Küchle, H. Stoll, H. Preuss, *Mol. Phys.* **1993**, *80*, 1431.
[10] a) This can be explained by a Fermi contact mechanism for the interaction of the spin–orbital-induced spin polarization with the magnetic nuclear moment of the phosphorus. A detailed explanation of the underlying concepts will be published elsewhere: M. Kaupp, V. G. Malkin, O. L. Malkina, P. Pyykkö, unpublished. b) A hybridization analysis (NBO/NLMO analysis) for the phosphorus in **2*** yields approximately $sp^{2.6}$ (P–Sn bonds) and $sp^{2.1}$ hybridization (P–H bond); the phosphorus in **1*** has approx. $sp^{2.0}$ (P-Sn bonds in the Sn_3P_3 increment), $sp^{5.2}$ (P-Sn bond from the Sn_2P_2 increment), and $sp^{2.9}$ hybridization (P-H bond).
[11] M. Veith, V. Huch, R. Lisowsky, P. Hobein, *Z. Anorg. Allg. Chem.* **1989**, *569*, 43.
[12] A. Decker, D. Fenske, K. Maczek, *Angew. Chem.* **1996**, *108*, 3025; *Angew. Chem. Int. Ed. Engl.* **1996**, *35*, 2863.
[13] D. Fenske, J. Ohmer, J. Hachgenei, K. Merzweiler, *Angew. Chem.* **1988**, *100*, 1300; *Angew. Chem. Int. Ed. Engl.* **1988**, *27*, 1277 and refs. therein.
[14] a) G. M. Sheldrick, SHELXS86, Universität Göttingen, 1986; b) G. M. Sheldrick, SHELXL93, Universität Göttingen, 1993.

 © WILEY-VCH Verlag GmbH, D-69451 Weinheim, 1997 0570-0833/97/3617-1896 $ 17.50+.50/0

Eight-Coordinate [Bis(oxyiminodiacetate)-titanium(IV)]$^{2-}$ and Nine-Coordinate [Bis(oxyiminodiacetate)aquazirconium(IV)]$^{2-}$; Variation in Coordination Mode in Amavadin-Like Complexes**

Spencer M. Harben, Paul D. Smith, Roy L. Beddoes, David Collison, and C. David Garner*

The synthesis and single-crystal X-ray characterization of $[NH_4][NMe_4][V(hida)_2]$, $(hida)^{3-}$ = oxyiminodiacetate,[1] was important in the development of our understanding of the structure of amavadin ($H_2[V(S,S\text{-hidpa})_2]$, $(hidpa)^{3-}$ = oxyimino-2,2′-dipropionate),[2] the form in which vanadium is accumulated in *Amanita muscaria*. We have confirmed the nature of isolated amavadin,[3] which possesses a novel, eight-coordinate structure. Each $(hidpa)^{3-}$ ligand binds to vanadium through two unidentate carboxylate groups and an η^2-N,O moiety; the two η^2-N,O groups are mutually *trans* and oriented at about 90° to one another. The relative orientations of the two η^2-N,O groups define the Δ and Λ isomers at the stereogenic metal center; amavadin as isolated contains an equal mixture of the two diastereoisomers, $[\Delta,\Lambda\text{-V}(S,S\text{-hidpa})_2]^{2-}$.[3] We have extended this chemistry to other early transition metals, including Mo,[4] Nb, and Ta.[5] Herein we report the synthesis and characterization of $(hida)^{3-}$ complexes of the Group 4 metals Ti and Zr, which further develops the coordination chemistry of the oxyiminodicarboxylate ligands.

The complexes **1** and **2** have been prepared in situ in H_2O, isolated as colorless crystals, and characterized by X-ray crystallography (Figures 1 and 2).[6] Each compound contains Δ and

$[Ca(H_2O)_4][Ti(hida)_2]\cdot 2H_2O$ **1**

$[Ca(H_2O)_5][Zr(hida)_2(H_2O)]$ **2**

Λ isomers of the anions within the crystal lattice. The anion of **1** possesses the same structure as that reported for the complexes of $(hida)^{3-}$ and $(hidpa)^{3-}$ with V^{IV}, V^{V},[1,3] Mo^{V},[4] Nb^{V}, and Ta^{V}.[5] Most of the Ti–O and Ti–N bonds (Figure 1; av. Ti–O_C 2.083, Ti–N 2.075) are similar in length to the equivalent bonds of the V^{IV} complex (av. V–O_C 2.067, V–N 2.003) and longer than those observed for the V^{V} complex (av. V–O_C 1.951, V–N 2.022), but the Ti–O_N bond length of 1.943(4) Å is shorter than that in either of these comparable complexes (V^{IV} av. 1.975 Å, V^{V} av. 1.970 Å; the other Ti–O bond length is 1.975(5) Å). The Zr^{IV} coordinates to two $(hida)^{3-}$ ligands in a manner similar to that of Ti^{IV} but with significantly longer bonds (Figure 2, av. Zr–O_C 2.239, Zr–N 2.227, Zr–O_N 2.125 Å). A water molecule (O16) is also coordinated to the zirconium center and located in a plane between O5 and O6 (Figure 2); consequently, the Zr^{IV} center is nine-coordinate, a unique structural feature for this class of bis-ligand complexes with $(hida)^{3-}$ and $(hidpa)^{3-}$.

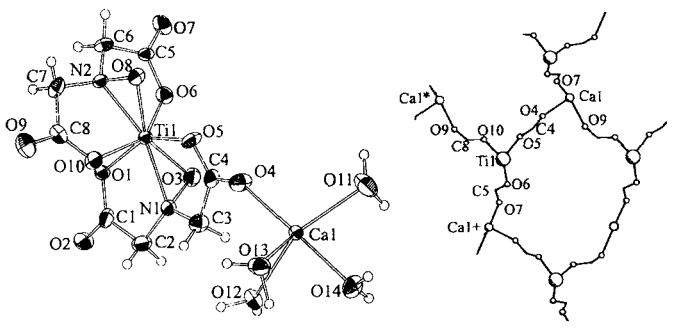

Figure 1. Left: ORTEP view of the asymmetric unit $[Ca(H_2O)_4][\Delta\text{-Ti(hida)}_2]$ in the crystal. Selected bond lengths [Å] and angles [°]: Ti1–O1 2.079(5), Ti1–O5 2.087(5), Ti1–O6 2.077(5), Ti1–O10 2.089(5), Ti1–O3 1.975(5), Ti1–O8 1.943(4), Ti1–N1 2.071(5), Ti1–N2 2.078(5); N1-Ti1-O3 40.6(2), N2-Ti1-O8 41.0(2). Right: schematic representation of the metallacycle in the crystal lattice.

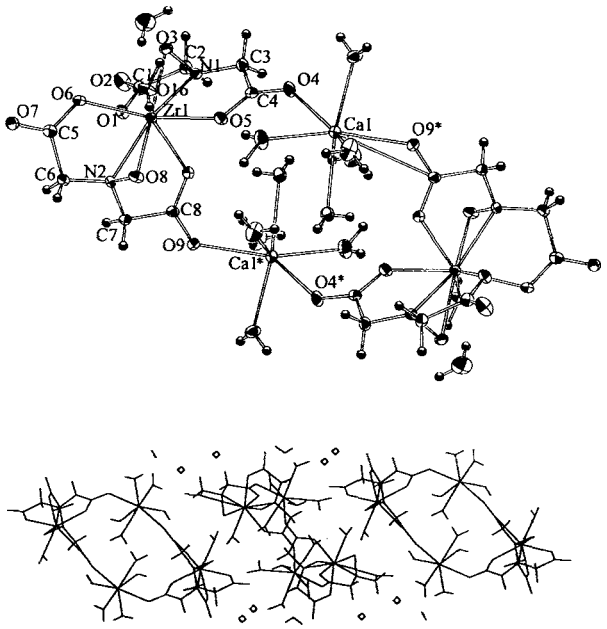

Figure 2. Top: ORTEP view of the metallacycle of $[Ca(H_2O)_5][Zr(hida)_2(H_2O)]$ in the crystal. Selected bond lengths [Å] and angles [°]: Zr1–O1 2.224(4), Zr1–O5 2.240(4), Zr1–O6 2.243(3), Zr1–O10 2.247(4), Zr1–O3 2.126(4), Zr1–O8 2.124(4), Zr1–N1 2.229(4), Zr1–N2 2.225(4), Zr1–O16 2.262(4); N1-Zr1-O3 38.1(1), N2-Zr1-O8 38.2(1). Bottom: packing of the metallacycles in the crystal lattice; water molecules are represented as ◇ and ∧; the plot was obtained with the program PLUTON [11].

If the amavadin-like coordination geometry is considered to be an octahedron in which a pair of *trans* vertices are occupied by the η^2-N,O groups, the extent of distortion from a regular geometry is related to the size of the metal. Thus, the dihedral angle between the two (η^2-N,O)M groups increases, the *trans* angle O1-M-O5 (for the carboxylate oxygen atoms of the same ligand) decreases, and the *cis* angle O5-M-O6 (involving the carboxylate oxygen atoms of different ligands) increases as the size of the metal increases (see Table 1 and Figure 3). This increase in distortion ultimately leads to the ligation of an H_2O molecule in the case of the Zr^{IV} ion. Figure 4 shows a space-filling diagram for $[Ti(hida)_2]^{2-}$ and $[Zr(hida)_2(H_2O)]^{2-}$, illustrating the ligation of the H_2O molecule between the two bonding carboxylate oxygen atoms. Nine-coordination is novel for Zr^{IV} in coordination chemistry, but coordination numbers higher than eight are known for organometallic Zr^{IV} complexes.[8]

The crystal structure of the Ti complex **1** contains 24-membered rings formed from three $[Ti(hida)_2]^{2-}$ anions and three $[Ca(H_2O)_4]^{2+}$ cations (Figure 1); each $[Ti(hida)_2]^{2-}$ binds to three $[Ca(H_2O)_4]^{2+}$ units through the carbonyl oxygen atoms

[*] Prof. Dr. C. D. Garner, Dr. S. M. Harben, Dr. P. D. Smith, R. L. Beddoes, Dr. D. Collison
Department of Chemistry
University of Manchester, M139PL (UK)
Fax: Int. code +(61)275-4616

[**] We gratefully acknowledge the support of this work by British Nuclear Fuels including a studentship (S. M. H.) and a postdoctoral appointment (P. D. S.) and The Royal Society (D. C.) for financial support.

 © WILEY-VCH Verlag GmbH, D-69451 Weinheim, 1997 0570-0833/97/3617-1897 $ 17.50+.50/0

Table 1. Dihedral angle (α) between the two {MNO} groups, and the O1-M-O5 (β) and O5-M-O6 (γ) angles for the $[M(hida)_2]^{n-}$ complexes.

M/ionic radius [pm][10]	α [°][a]	β [°] [b]	γ [°]
V^V/54 [3]	86.6	159	107
V^{IV}/58 [1]	87.7	157.3(1)	103.9(2)
Ti^{IV}/60.5	92.7	149.8(2)	115.8(2)
Nb^V/64 [5]	98.3	148.6(2)	119.8(2)
	95.1	148.8(2)	119.4(2)
Ta^V/64 [5]	98.4	149.4(5)	118.4(4)
	96.9	148.7(4)	119.3(4)
Zr^{IV}/72*	101.3	135.2(1)	146.1(1)

[a] The angle between the N atom of one η^2-N,O group and the O atom of the second η^2-N,O group. [b] In $[Zr(hida)_2(H_2O)]^{2-}$ the *trans* O6-M-O10 angle and the *trans* O1-M-O5 angle are equivalent within the estimated standard deviations.

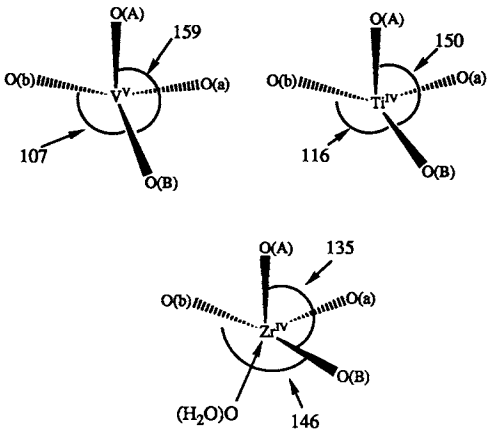

Figure 3. Schematic representation of the four ligating carboxylate oxygen atoms in the $[M(hida)_2]^{n-}$ complexes, viewed perpendicular to the N–O bond axis (not shown), illustrating that as the size of the metal ion increases ($V^V < Ti^{IV} < Zr^{IV}$) the *trans* angle O(A)-M-O(B) (O(A) and O(B) belong to the same ligand) decreases and the *cis* angle O(B)-M-O(b) between the two ligands increases on one side of the molecule ultimately leading to the ligation of an H_2O molecule in the Zr complex.

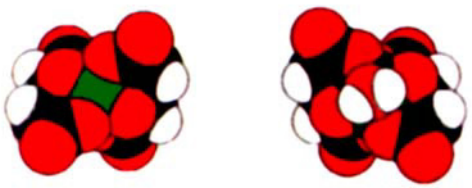

Figure 4. Space-filling model of $[Ti(hida)_2]^{2-}$ (left) and $[Zr(hida)_2(H_2O)]^{2-}$ (right). Red = oxygen, black = carbon, blue = nitrogen, and green = metal; the plot was obtained with the program PLUTON [11].

(Ca–O4 2.375(5), Ca–O7 2.402(5), Ca–O9 2.419(5) Å) and is part of three separate metallacycles. Each Ca^{2+} is seven-coordinate, binding to four H_2O molecules and a single carboxylate oxygen atom from each of three $[Ti(hida)_2]^{2-}$ anions. The crystal lattice is built up from these rings containing common segments as a distorted honeycomb configuration, in which each metal atom is a node of the irregular hexagons (see Figure 1). In Zr complex **2**, two anions are linked by two cations to form 16-membered metallacycles (Figure 2). As in the Ti^{IV} system, each $[Zr(hida)_2(H_2O)]^{2-}$ binds to the $[Ca(H_2O)_5]^{2+}$ cations through the carbonyl oxygens (Ca–O4: 2.400(4), Ca–O9: 2.374(4) Å). However, unlike the Ti^{IV} compound **1** in which the macrocycles are connected through the Ti and Ca units, the rings containing Zr and Ca are discrete. Hydrogen bonding is observed within the rings, and further hydrogen bonding links these metallacycles to form an extended structure (Figure 2, bottom). The rigidity of these extended structures is manifest in the low thermal parameters and R values obtained in the crystal structure determinations at room temperature.

Experimental Section

1: $[TiO(acac)_2]$ (0.131 g, 0.5 mmol) was added to a solution of H_3hida [9] (0.148 g, 1 mmol) in H_2O (10 mL). The resultant mixture was stirred at 22 °C for 16 h. $CaCl_2$ (0.055 g, 0.5 mmol) was added, and the solution stirred for a further 10 min. The solution was concentrated under reduced pressure (to about 3 mL), filtered into a Schlenk tube, a layer of *i*PrOH (15 mL) carefully added, and the Schlenk tube was left to stand at 22 °C. After several days, colorless bipyramidal crystals formed (yield 0.159g, 65%). Elemental analysis calcd for $C_8H_{20}N_2O_{16}CaTi$: C 19.68, H 4.13, N 5.74; found (%): C 19.90, H 4.09, N 5.54.

The Zr compound was prepared analogously from $[Zr(acac)_4]$ (0.244 g, 0.5 mmol), H_3hida [9] (0.148 g, 1 mmol), and $CaCl_2$ (0.055 g, 0.5 mmol). A layer of THF (15 mL) above the reaction solution (3 mL) produced, after several days at 22 °C, colorless tabular crystals (yield 0.127 g, 48%). Elemental analysis calcd for $C_8H_{20}N_2O_{16}CaZr$: C 18.07, H 3.67, N 5.33; found (%): C 18.07, H 3.79, N 5.27.

Received: February 3, 1997 [Z10069IE]
German version: *Angew. Chem.* **1997**, *109*, 1985–1987

Keywords: amavadin · N ligands · O ligands · titanium · zirconium

[1] M. A. A. F. de C. T. Carrondo, M. T. L. S. Duarte, J. C. Pessoa, J. A. L. Silva, J. J. R. Fraústo da Silva, M. C. T. A. Vaz, . F. Vilas-Boas, *J. Chem. Soc. Chem. Commun.* **1988**, 1158–1159.
[2] E. Bayer, H. Kneifel, *Z. Naturforsch. B* **1972**, *27*, 207; H. Kneifel, E. Bayer, *Angew. Chem.* **1973**, *85*, 542; *Angew. Chem. Int. Ed. Engl.* **1973**, *12*, 508; H. Kneifel, E. Bayer, *J. Am. Chem. Soc.* **1986**, *108*, 3075–3077.
[3] E. M. Armstrong, R. L. Beddoes, L. J. Calviou, J. M. Charnock, D. Collison, N. Ertok, J. H. Naismith, C. D. Garner, *J. Am. Chem. Soc.* **1993**, *115*, 807–808.
[4] H. S. Yadav, E. M. Armstrong, R. L. Beddoes, D. Collison, C. D. Garner, *J. Chem. Soc. Chem. Commun.* **1994**, 605–606.
[5] P. D. Smith, S. M. Harben, R. L. Beddoes, M. Helliwell, D. Collison, C. D. Garner, *J. Chem. Soc. Dalton Trans.* **1997**, 685–691.
[6] Crystal data for **1**: dimensions $0.40 \times 0.40 \times 0.50$ mm, orthorhombic, space group $Pca2_1$, $a = 12.036(8)$, $b = 9.169(4)$, $c = 16.76(1)$ Å, $V = 1856(4)$ Å^3, $Z = 4$, $\rho_{calcd} = 1.747$ g cm^{-3}, $2\theta_{max} = 50.0°$, $Mo_{K\alpha}$ radiation ($\lambda = 0.71069$ Å), scan type $\omega/2\theta$, scan rate 4.0° min^{-1} (in ω), scan width $(1.10 + 0.30 \tan\theta)°$, $T = 293$ K, 1894 reflections measured, 1349 data observed with $I > 2.00\sigma(I)$, 252 variables, $\mu = 8.05$ cm^{-1}, corrections: Lorentz-polarization: decay −0.90%; hydrogen atom treatment: included in difference map or in calculated positions ($d_{C-H} = 0.95$ Å); $R = 0.035$, $R_w = 0.027$. Crystal data for **2**: dimensions $0.02 \times 0.15 \times 0.43$ mm, monoclinic, space group $P2_1/c$, $a = 12.305(4)$, $b = 8.622(3)$, $c = 20.164(5)$ Å, $\beta = 106.00(2)°$, $V = 2057(1)$ Å^3, $Z = 4$, $\rho_{calcd} = 1.891$ g cm^{-3}, $2\theta_{max} = 50.0°$, $Mo_{K\alpha}$ radiation ($\lambda = 0.71069$ Å), $\omega/2\theta$ scan, scan rate 2.0° min^{-1} (in ω), scan width $(1.15 + 0.30 \tan\theta)°$, $T = 295$ K, 4085 reflections measured, 2378 data observed with $I > 2.00\sigma(I)$, 280 variables, $\mu = 8.60$ cm^{-1}; corrections: Lorentz-polarization: absorption (transmission factors: 0.89–1.00), decay −0.23%, hydrogen atom treatment: included in difference map or in calculated positions ($d_{C-H} = 0.95$ Å); $R = 0.036$, $R_w = 0.027$. The structures were solved by direct methods with SHELXS-86 [7a]. The non-hydrogen atoms were refined anisotropically. Hydrogen atoms were included in the structure factor calculations. A final cycle of full-matrix least-squares refinement was carried out minimizing the function $\sum\omega(|F_o| - |F_c|)^2$. Neutral atom scattering factors and anomalous dispersion effects [7b] were included in F_{calcd} [7c]. All calculations were performed with the TEXSAN [7d] crystallographic software package. Crystallographic data (excluding structure factors) for the structures reported in this paper have been deposited with the Cambridge Crystallographic Data Centre as supplementary publication no. CCDC-100409. Copies of the data can be obtained free of charge on application to The Director, CCDC, 12 Union Road, Cambridge CB21EZ, UK (fax: int. code +(1223)336-033; e-mail: deposit@chemcrys.cam.ac.uk)
[7] a) G. M.Sheldrick (SHELXS-86) in *Crystallographic Computing 3* (Eds.: G. M. Sheldrick, C. Krueger, R. Goddard), Oxford Univ. Press, **1986**, 175; b) D. T. Cromer, J. T. Waber, *International Tables for X-ray Crystallography*, Vol.4, The Kynoch Press, Birmingham, England, **1974**, Tables 2.2A and 2.3.1; c) J. A. Ibers, W. C. Hamilton, *Acta Crystallogr.* **1964**, *17*, 781–782; d) TEXSAN = *TEXRAY Structure Analysis Package*, Molecular Structure Corporation, USA, **1985** and **1992**.
[8] L. Giannini, E. Solari, C. Floriani, A. Chiesi-Villa, C.Rizzoli, *Angew. Chem.* **1994**, *106*, 2279; *Angew. Chem. Int. Ed. Engl.* **1994**, *33*, 2204–2206.
[9] G. Anderegg, E. Koch, E. Bayer, *Inorg.Chim.Acta*, **1987**, *127*, 183.
[10] R. D. Shannon, *Acta Crystallogr. Sect. A* **1976**, *32*, 751–767.
[11] A. L.Spek, *Acta Crystallogr. Sect. A* **1990**, *46*, C34.

 © WILEY-VCH Verlag GmbH, D-69451 Weinheim, 1997 0570-0833/97/3617-1898 $ 17.50+.50/0

Synthesis, Structure, and Conformational Features of α-Cycloaltrin: A Cyclooligosaccharide with Alternating $^4C_1/^1C_4$ Pyranoid Chairs**

Yasuyoshi Nogami, Kyoko Nasu, Toshitaka Koga, Kazuko Ohta, Kahee Fujita,* Stefan Immel, Hans J. Lindner, Guido E. Schmitt, and Frieder W. Lichtenthaler*

The wealth of knowledge that has accumulated on the starch-derived cyclodextrins and their unique ability to form inclusion complexes[1] is contrasted by a peculiar paucity of data on cyclooligosaccharides composed of sugars other than glucose.[2] Except for certain cyclofructins, obtainable by bacterial action on the polysaccharide inulin,[3] all of the non-glucose cyclooligosaccharides presently known have been acquired synthetically and require laborious multistep procedures to assemble the linear oligosaccharide from its monosaccharide units in a form suitable for cycloglycosylation. In this way, α(1 → 4)-linked cyclooligosaccharides composed of D-mannose[4] (α-, β-, and γ-cyclomannin), of L-rhamnose[5] (α-cyclorhamnin), and of alternating D-mannose/L-rhamnose units[6] have been prepared, yet in such minute amounts as to preclude investigations into their inclusion complex behavior. Molecular modeling studies on α-cyclomannin[7] and its 6-deoxy L-analogue α-cyclorhamnin[2] showed that their axially disposed 2-OH points away from the cavity; thus they fairly closely resemble α-cyclodextrin in backbone structure, cavity dimensions, and lipophilicity patterns. The same, in fact, is to be expected for the cyclohexasaccharide with alternating D-mannose and L-rhamnose units. For a cyclogalactin composed of six β(1 → 4)-linked galactopyranose residues, molecular modeling revealed an α-CD-like geometry, yet a distinctly different lipophilicity distribution such that hydrophobic surface regions at the primary hydroxyl face are substantially enlarged.[7]

More profound changes in shape, cavity dimensions, and guest binding properties are to be anticipated for cyclooligosaccharides with axially disposed 3-OH groups in the pyranoid rings—α-cycloallin for example—as these would be directed towards the interior of the cavity, resulting in considerable steric congestion, which is likely to be released by deformation of the $^4C_1$ chairs. Topologically even more interesting appears to be α-cycloaltrin, as the $^4C_1$ and $^1C_4$ conformations of α-altropyranoid chairs are very similar in stability[8] and, hence, in a macrocyclic array several conformations could be formed, such as the all-$^4C_1$ (**1a**) or all-$^1C_4$ forms (**1b**), or even more likely in solution, an equilibrium between the two, that passes through the skew $^0S_2$ geometries (**1c**) of the pyranoid rings (Scheme 1).

In context with our studies on non-glucose cyclooligosaccharides,[2] we report on a straightforward synthesis of α-cycloaltrin

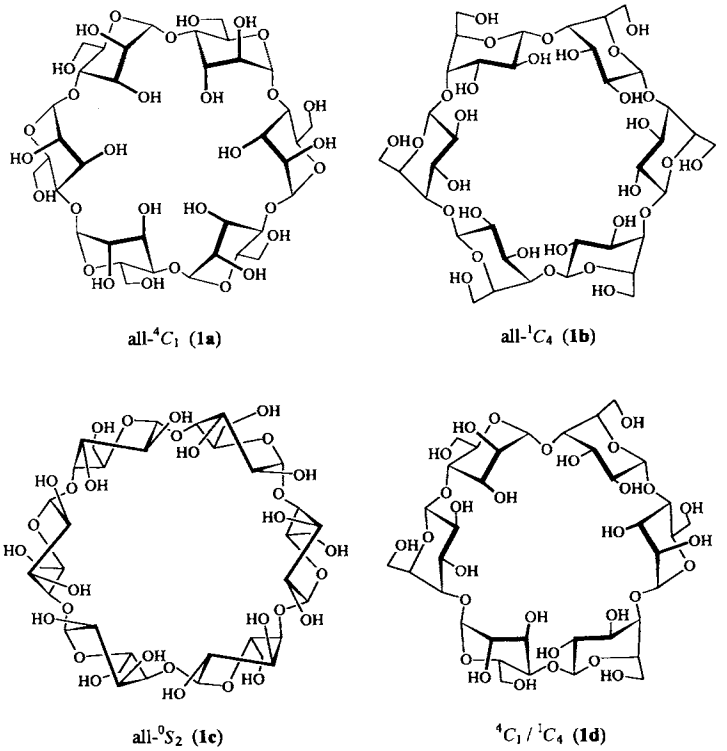

Scheme 1. Molecular geometries for α-cycloaltrin (**1**), a cyclooligosaccharide composed of six α(1 → 4)-linked D-altropyranose residues. In aqueous solution, a dynamic equilibrium prevails between forms **1a**–**1c**, and various other intermediate conformations; in the solid state, the structure is that of **1d**, comprising a unique alternating sequence of $^4C_1$ and $^1C_4$ altropyranoid chair forms.

(**1**) from α-cyclodextrin its molecular geometries in the solid state, revealing a unique alternating sequence of $^4C_1$ and $^1C_4$ chairs (**1d**), and in solution, in which a dynamic equilibrium of the type **1a** ⇌ **1c** ⇌ **1d** prevails.

The conversion of α-cyclodextrin into **1** started with protection of the six primary hydroxyl groups by the *tert*-butyldimethylsilyl moiety (→ **2**[9]). Ensuing deprotonation of the secondary hydroxyls in **2** by treatment with NaH in DMF was followed by the addition of benzenesulfonyl chloride, which not only effected selective 2-*O*-sulfonylation but, concomitantly, displacement of the 2-sulfonyloxy group by the vicinal 3-OH to elaborate the key intermediate, the 6-*O*-protected 2,3-anhydro-α-cyclomannin (**3**, 64%). Deblocking with TBAF/THF yielded

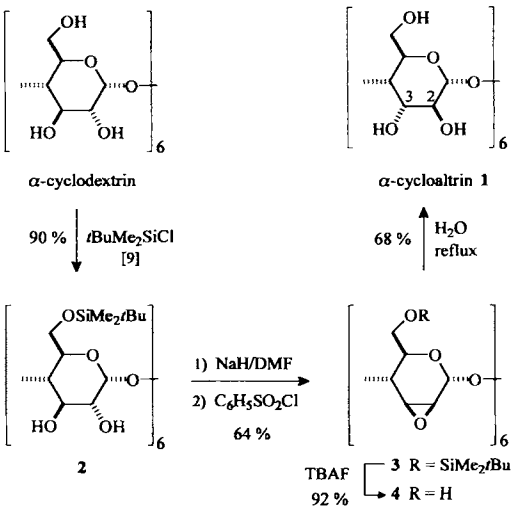

Scheme 2. Synthesis of **1** from α-cyclodextrin.

[*] Prof. K. Fujita, K. Ohta
Faculty of Pharmaceutical Sciences
Nagasaki University
Nagasaki 852 (Japan)
Fax: Int. code +(958)46-5736
Prof. Dr. F. W. Lichtenthaler, Dr. S. Immel, Prof. Dr. H. J. Lindner, Dipl.-Ing. G. E. Schmitt
Institut für Organische Chemie der Technischen Hochschule
D-64287 Darmstadt (Germany)
Fax: Int. code +(6151)16-6674
Prof. Y. Nogami, K. Nasu, Prof. T. Koga
Daiichi College of Pharmaceutical Sciences, Fukuoka 815 (Japan)
Fax: Int. code + (925)53-5698

[**] Molecular Modeling of Saccharides, Part 15. This work was supported by the Fonds der Chemischen Industrie and the Nihon Shokuhin Kako (Japan Maize Products Co.). Part 14: Ref. [2]

 © WILEY-VCH Verlag GmbH, D-69451 Weinheim, 1997 0570-0833/97/3617-1899 $ 17.50+.50/0

4 (92%), which simply by refluxing in water was converted into **1** and isolated by reversed-phase chromatography (68%). The overall yield for the four-step sequence is a satisfactory 36%, but is lower than the conversion of β-cyclodextrin into its all-*altro* analogue (52%[10]), obviously reflecting the lesser steric strain, and hence cleaner reactions, in the cycloheptamer.

Cycloaltrin **1** crystallized with 21 water molecules and is thus embedded in a water matrix in the solid state. Its X-ray structural analysis[11] not only gave evidence of the water molecules built into the crystal lattice (Figure 1), but revealed the unique

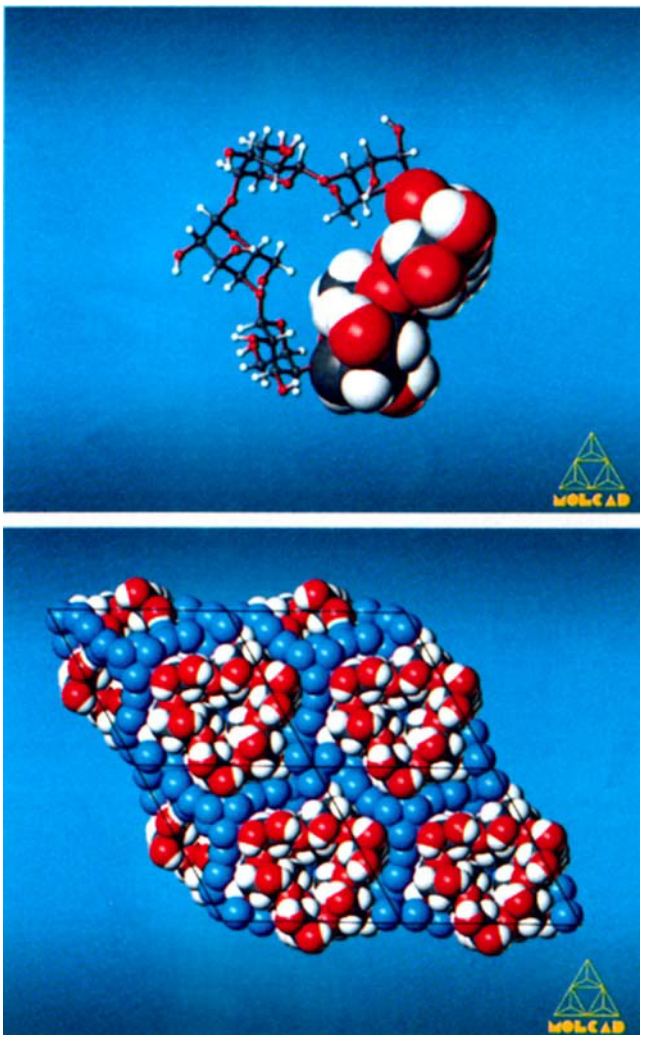

Figure 1. Structure of cyclo-α(1 → 4)-D-altrohexaoside (α-cycloaltrin, **1**) [12]. Top: Ball-and-stick model of the alternating sequence of $^4C_1$ and $^1C_4$ chair conformations of altropyranoid rings; in this way the macrocycle is constructed from three banana-shaped disaccharide units, one of which is depicted in a space-filling representation. Bottom: The macrocycle has a compact, disklike topology, devoid of a cavity and is embedded in a water matrix (**1**·21 H_2O); the disks are stacked in offset layers.

conformational features of the altropyranoid rings: neither the all-$^4C_1$ form **1a** or the all-$^1C_4$ form **1b** is adopted, nor one of the various nonchair conformations conceivable (for instance, **1c**); instead, the altrose units display alternate $^4C_1$ and $^1C_4$ altropyranoid chair conformations (Figure 1, top), entailing the macrocycle to be made up of three banana-shaped disaccharide portions. The molecules are disk-shaped, devoid of a cavity, and stacked in transposed layers (Figure 1, bottom), the space in between being occupied by water molecules.

The closeness of the chair conformations to the ideal is remarkable: nearly perfect geometry in the $^1C_4$-portions with O_4 and C_6 in a fairly antiparallel disposition (167.5°) and with the six pyranoid ring torsion angles in the 52–58° range. The $^4C_1$ chairs, by contrast, are less ideal, as the C_1-C_2-C_3-C_4 torsion angle (−45.7°) reveals some flattening at C-2 and C-3, whilst O_1, O_2, and O_3 are still in a fairly antiparallel disposition (O_1-C_1-C_2-O_2 166.2°, O_2-C_2-C_3-O_3 166.5°). Another salient feature of the structure is the different orientations of the 6-OH groups relative to the pyranoid rings: *gauche–trans* disposition ($\omega = 55.7°$[13]) in the three $^1C_4$ forms in which the CH_2OH groups are directed towards the outside of the macrocycle versus a *gauche–gauche* arrangement ($\omega = -66.8°$[13]) in the three $^4C_1$ forms in which their equatorially disposed CH_2OH groups point towards the center of the macrocycle, thereby closing it (Figure 2). Accordingly, the disk-shaped molecule has a shallow

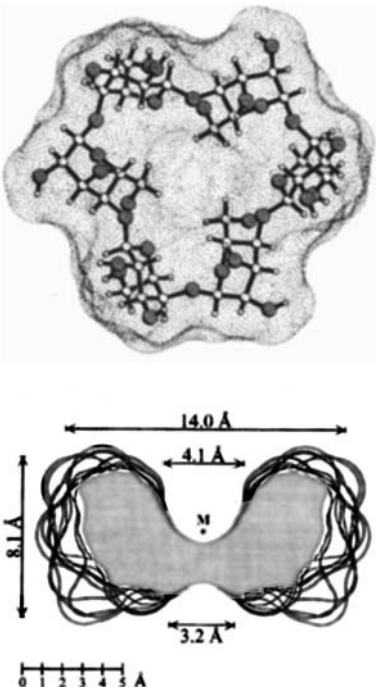

Figure 2. Top: Calculated [12] contact surface (in dotted form) of the solid-state structure of **1** with inserted ball-and-stick-model. The three equatorial hydroxymethyl groups of the $^4C_1$ altropyranoses are directed towards the macrocycle's interior, thereby closing it. Bottom: Cross-sections through the contact surface of **1** (2-OH/3-OH side up) and approximate molecular dimensions; surface contours were obtained for a plane perpendicular to the macrocycle's mean plane through successive 10° rotation steps around the geometrical center *M* and subsequently superimposed.

indentation on one side, and a pronounced hole-like depression on the other. Provided that this disk-shaped, solid-state structure of **1**, already embedded in a water matrix, is retained in aqueous solution, not only separate sets of NMR signals should be observed for the $^4C_1$ and the $^1C_4$ portions, but also distinctly different coupling patterns for the respective pyranoid ring protons as revealed by the calculated *J* values (Table 1).

The high resolution ^1H and ^{13}C NMR spectra of **1** in D_2O,[14] however, unambiguously provide only one set of signals for both the altropyranoid hydrogen atoms and the carbon atoms, and the ^1H coupling constants are an average of those calculated for the $^4C_1$ and $^1C_4$ conformations (Table 1); moreover, the observed *J*-values correlate surprisingly well with those calculated for the all-skew (twist-boat) $^0S_2$ geometry of **1c**, which, in

 © WILEY-VCH Verlag GmbH, D-69451 Weinheim, 1997 0570-0833/97/3617-1900 $ 17.50+.50/0

Table 1. Dihedral angles as well as the $^1H-^1H$ coupling constants measured in D_2O (800 MHz[14], 30 °C) and those calculated for the altropyranoid ring in $^4C_1$, $^1C_4$, and all-$^0S_2$(skew) forms of **1**.

	$^4C_1$[a]	$^1C_4$[a]	$^0S_2$[b]	found
Dihedral angle[°]				
H1-C1-C2-H3	−69.4	−178.0	−138.3	
H2-C2-C3-H3	70.4	−176.0	−176.2	
H3-C3-C4-H4	−61.5	51.8	−44.7	
H4-C4-C5-H5	−71.3	179.8	−141.9	
Coupling constant[Hz][c]				
J(1,2)	2.2	8.0	4.0	4.73
J(2,3)	2.7	10.2	10.2	8.19
J(3,4)	3.4	2.4	4.5	3.71
J(4,5)	9.7	1.4	6.4	5.32

[a] Angles from the solid-state structure of **1**. [b] Data calculated for the global energy minimum (all-skew form) from HTA simulations. [c] Calculation based on the Karplus-type dependence of H-C-C-H torsion angles on coupling constants, including the electronegativity effect of the substitution pattern by use of the generalized Haasnoot equation [15].

fact, emerges from extensive HTA calculations[16] as the global energy minimum structure. Favored over the $^4C_1/^1C_4$ solid-state geometry by as much as 36 kJ mol^{-1}—a major portion of this energy gain undoubtedly stems from hydrogen bonding between the 2-OH of one altrose moiety to the O-3 of the next—this all-skew form features a cavity that pierces the disk (Figure 3) and a pyranose tilt inverse to that of the cyclodextrins.

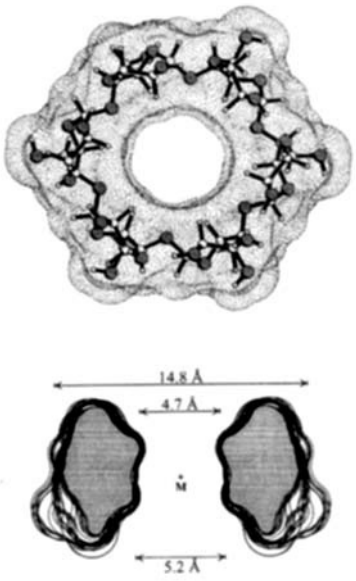

Figure 3. The all-skew (twist-boat) $^0S_2$-geometry of α-cycloaltrin (**1**) emerging from HTA simulations [16] as the global energy minimum structure. Top: Contact surface. Bottom: The contour plots reveal a cavity whose conicity is inverse to that of the cyclodextrins.

Whether, however, the all-skew form **1c** is adopted in aqueous solution—in HTA simulations molecules are in vacuum rather than surrounded by a solvation shell—remains open. If prevalent in aqueous solution, its cavity is conceivably filled with water. Thus not only the six primary, but also the 12 secondary hydroxyl groups are likely to satisfy their hydrogen bonding requirements towards the solvent rather than intramolecularly. This results in a tightly associated first water shell around **1**, which will have to follow any geometry changes within the macrocycle. This hydration sphere could readily be characterized by molecular dynamics (MD) simulations in water, but contributed little to unraveling the nature of the $^4C_1 \rightleftharpoons {}^1C_4$ scrambling observed in the NMR spectra, since on subjection to a 600 ps MD simulation in a box of water,[17] not only the geometry of the hydrated all-skew $^0S_2$ form (**1c**), but also that of the solid-state $^4C_1/^1C_4$ structure **1d**, remained in their respective geometries (Figure 4). Accordingly, no appreciable flexing

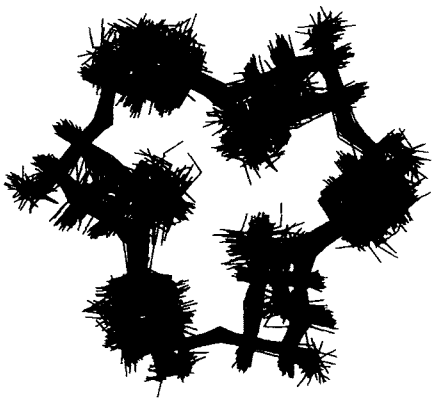

Figure 4. Superimposition of 60 α-cycloaltrin snapshot-geometries taken in 10 ps intervals from a 600 ps molecular dynamic simulation [17] on an assembly comprising α-cycloaltrin in a box of 606 water molecules.

or flip over of the pyranoid chairs or skew forms to alternate topologies takes place within a 600 ps time frame; that is, profound conformational changes like the flipping from $^4C_1$ to $^1C_4$ within the macrocycle are comparatively slow, and require the 10^6 times longer, millisec time frame of NMR spectroscopy to become observable.

The temperature-dependent ^1H and ^{13}C NMR studies proved to be more meaningful in determining the nature of the conformational changes occurring in aqueous solutions of **1**:[14] the coupling constant $J_{2,3}$ of 8.2 Hz at 30 °C in D_2O decreases to 7.6 and 7.1 Hz at 20 and 4 °C, respectively, thereby narrowing the well-separated signal for 3-H; more profound effects are observed for the C-4 and C-5 signals, which, like all other carbon atoms, give rise to sharp singlets at 30 °C but show substantial broadening at 4 °C, which indicates the onset of "freezing out" certain conformations the $^4C_1 \rightleftharpoons {}^1C_4$ equilibrium. Consequently, in water, α-cycloaltrin does not adopt a fixed geometry, such as the all-$^0S_2$-form; rather, the D-altropyranoid rings, tied up in a macrocyclic "straitjacket", adopt a variety of conformations within the $^4C_1 \rightleftharpoons {}^0S_2 \rightleftharpoons {}^1C_4$ pseudorotational "turntable" (Scheme 3), and this necessarily in a coordinated way: flexure of one altropyranoid chair into the intermediate skew $^0S_2$-form via half-chair transition states forces the two adjoining altrose chairs to follow suit, thereby eliciting a consecutive "rolling around" in the probably elliptically distorted macrocycle. NMR data provide an averaged picture thereof and give evidence through the comparatively large $J_{1,2}$ and, particularly, $J_{2,3}$ couplings that the position of the equilibrium in water at 30 °C lies pronouncedly on the $^1C_4 \rightleftharpoons {}^0S_2$ side.

Experimental Section

3: To a solution of NaH (0.40 g, 10.8 mmol) in anhydrous DMF (40 mL) was added **2** (1.0 g, 0.6 mmol) [9], and the mixture was kept under N_2 at 60 °C for 2 h. After cooling, benzenesulfonyl chloride (568 μL, 4.32 mmol) in anhydrous DMF (10 mL) was injected followed by stirring at room temperature for 30 min. Filtration and flash chromatography on a silica gel column (4 × 15 cm) with benzene/EtOAc (4/1, 250 mL) afforded 600 mg (64%) of **3**; m.p. 203 °C (decomp.); $[\alpha]_D^{16} = +70.1$ ($c = 0.36$ in THF). ^1H NMR (500 MHz, $CDCl_3$, relevant data): $\delta = 3.11$ (d, 1H, 2-H), 3.32 (d, 1H, 3-H), 3.56 and 4.24 (two d, 1H, 6-H_2), 3.64 (d, 1H, 4-H), 3.93

 © WILEY-VCH Verlag GmbH, D-69451 Weinheim, 1997 0570-0833/97/3617-1901 $ 17.50+.50/0

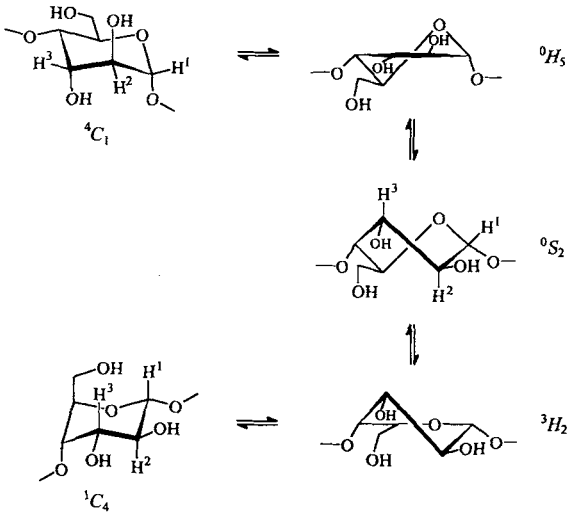

Scheme 3. The chair/half-chair/skew pseudorotational "turntable" between D-altropyranoid rings in $^4C_1$ and $^1C_4$ conformation [18]. Due to the comparatively large $J_{1,2}$ and $J_{2,3}$ values found for **1** (4.7 and 8.2 Hz, respectively, in D_2O), the conformational equilibrium in aqueous solution lies on the $^1C_4 \rightleftharpoons {}^3H_2 \rightleftharpoons {}^0S_2$ side.

(m, 1H, 5-H), 5.16 (s, 1H, 1-H), $J_{1,2}$ and $J_{3,4} = 0$, $J_{2,3} = 3.7$, $J_{4,5} = 11.5$ Hz. MS: $[M^+]$ not detectable. Elemental analysis calculated for $C_{72}H_{132}O_{24}Si_6$: C 55.78, H 8.58; found: C 55.55, H 8.68.

4: A 1 M solution of Bu_4NF in THF (4.6 mL) was added to a solution of silyl epoxide **3** (1.0 g, 0.65 mmol) in anhydrous THF (90 mL) under N_2, and the mixture was stirred at 40 °C for 4 h. Concentration in vacuo, addition of methanol (10 mL), and cooling in a refrigerator overnight resulted in a precipitate: 511 mg (92%) of **4**; m.p. 166 °C (decomp.); $[\alpha]_D^{18} = +83.6$ ($c = 0.34$ in DMSO). ^1H NMR (500 MHz, [D_5] pyridine): $\delta = 3.40$ (d, 1H, 2-H), 3.67 (d, 1H, 3-H), 4.10 (m, 1H, 5-H), 4.30 (m, 2H, 6-H_2), 4.47 (d, 1H, 4-H), 5.57 (s, 1H, 1-H), $J(1,2)$ and $J(3,4) = 0$, $J(2,3) = 3.5$, $J(4,5) = 11.6$ Hz; FAB-MS: m/z: 865 $[M^+]$.

1: A solution of epoxide **4** (1.0 g, 1.14 mmol) in distilled water (250 mL) was heated at reflux for 5 days. Concentration of the mixture in vacuo and chromatography on a reversed-phase column (Merck Lobar, size C) with water yielded **1** (765 mg (68%); m.p. 215 °C (decomp.); $[\alpha]_D^{20} = +70.5$ ($c = 0.3$ in H_2O). ^1H NMR (800 MHz [14], D_2O, 30 °C): $\delta = 3.91$ (dd, 1H, 6-H_a), 4.00 (m, 2H, 2-H, 6-H_b), 4.03 (dd, 1H, 3-H), 4.14 (dd, 1H, 4-H), 4.44 (sext, 1H, 5-H), 4.95 (d, 1H, 1-H), $J_{1,2} = 4.73$, $J_{2,3} = 8.19$, $J_{3,4} = 3.71$, $J_{4,5} = 5.32$, $J_{5,6a} = 3.60$, $J_{5,6b} = 3.46$, $J_{6,6} = 12.42$ Hz. ^{13}C NMR (200 MHz [14], D_2O, 30 °C): $\delta = 63.05$ (C-6), 71.98 (C-3), 73.26 (C-2), 76.07 (C-5), 79.65 (C-4), 105.53 (C-1). FAB-MS: m/z: = 973 $[M + H^+]$), 995 $[M + Na^+]$.

Received: February 19, 1997 [Z10139IE]
German version: *Angew. Chem.* **1997**, *109*, 1987–1991

Keywords: α-cycloaltrin · cyclodextrins · macrocycles · molecular modeling

[1] a) J. Szejtli, *Cyclodextrins and Their Inclusion Complexes*, Académiai Kiadó, Budapest, **1982**; b) *Trends in Cyclodextrins and Derivatives*, (Ed.: D. Duchêne), Edition de la Santé, Paris, **1991**; c) G. Wenz, *Angew. Chem.* **1994**, *106*, 851–870; *Angew. Chem. Int. Ed. Engl.* **1994**, *33*, 803–822; d) *Proceedings of the 8th International Symposium on Cyclodextrins*, (Eds.: J. Szejtli, L. Szente), Kluwer, Dordrecht, **1996**, p. 600 ff.

[2] Recent review: F. W. Lichtenthaler, S. Immel, *J. Inclusion Phenom. Mol. Recognit. Chem.* **1996**, *25*, 3–16.

[3] a) M. Kawamura, T. Uchiyama, T. Kuramoto, Y. Tamura, K. Mizutani, *Carbohydr. Res.* **1989**, *192*, 83–90; b) M. Sawada, T. Tanaka, Y. Takai, T. Hanafusa, T. Taniguchi, M. Kawamura, T. Uchiyama, *ibid.* **1991**, *217*, 7–17; c) The inulin-derived cyclofructins, composed of six to eight β(1 → 2)-linked fructofuranose units, are disk-shaped molecules that are not pierced by the cavity [3d], and are hence unable to accommodate guests as the cyclodextrins can; due to their crown ether constitution, however, they exhibit cation binding properties [3b]; d) S. Immel, F. W. Lichtenthaler, *Liebigs Ann.* **1996**, 39–44.

[4] M. Mori, Y. Ito, T. Ogawa, *Carbohydr. Res.* **1989**, *192*, 131–146; M. Mori, Y. Ito, J. Izawa, T. Ogawa, *Tetrahedron Lett.* **1990**, *31*, 3191-3194.

[5] M. Nishizawa, H. Imagawa, Y. Kan, H. Yamada, *Tetrahedron Lett.* **1991**, *32*, 5551–5554; *Chem. Pharm. Bull.* **1994**, *42*, 1356–1365.

[6] P. R. Ashton, C. L. Brown, S. Menzer, S. A. Nepogodiev, J. F. Stoddart, D. J. Williams, *Chem. Eur. J.* **1996**, *2*, 580–591.

[7] F. W. Lichtenthaler, S. Immel, *Tetrahedron: Asymmetry* **1994**, *5*, 2045–2060.

[8] a) S. J. Angyal, *Aust. J. Chem.* **1968**, *21*, 2737–2746, b) S. J. Angyal, V. A. Pickles, *ibid.* **1972**, *25*, 1695–1710.

[9] K. Takeo, K. Uemura, H. Mitoh, *J. Carbohydr. Chem.* **1988**, *7*, 293–303.

[10] K. Fujita, H. Shimada, K. Ohta, Y. Nogami, K. Nasu, T. Koga, *Angew. Chem.* **1995**, *107*, 1783–1784; *Angew. Chem. Int. Ed. Engl.* **1995**, *34*, 1621–1622.

[11] Crystal structure analysis of **1**: $C_{36}H_{60}O_{30} \cdot 21\,H_2O$, $M_r = 1351.18$, hexagonal, space group $P6_3$, $a = b = 17.241(3)$, $c = 13.323(2)$ Å, $V = 3430(1)$ Å^3, $Z = 2$, $\rho = 1.268$ g cm^{-1}, $\mu(Mo_{K\alpha}) = 0.115$ mm^{-1}, crystal dimensions $0.5 \times 0.15 \times 0.125$ mm, $T = 293$ K. Of 12711 reflections collected on a STOE IPDS diffractometer, graphite-monochromated $Mo_{K\alpha}$ ($\lambda = 0.71069$ Å) radiation, 2253 are independent ($R_{int} = 0.0284$). The structure was solved by direct methods (SHELXS-86) and successive Fourier difference synthesis. Refinement (on F^2) performed by full-matrix least squares method with SHELXL-93. $R(F)$ 0.0568 for 2036 reflections with $I \geq 2\sigma I$, $wR(F^2) = 0.1604$ for all 2253 reflections ($w = 1/(\sigma^2(F_o^2) + (0.1189P)^2 + 0.57P)$; $P = (F_o^2 - 2F_c^2)/3$. All non-hydrogen atoms (except one oxygen atom of the solvent water molecule) were refined anisotropically. Hydrogen atoms on the cycloaltrin were considered in calculated positions with the 1.2 U_{eq} value of the corresponding bound atom. Crystallographic data (excluding structure factors) for the structure reported in this paper have been deposited with the Cambridge Crystallographic Data Centre as supplementary publication no. CCDC-100196. Copies of the data can be obtained free of charge on application to The Director, CCDC, 12 Union Road, Cambridge CB2 1EZ, UK (fax: int. code +(1223) 336-033; e-mail: deposit@chemcrys.cam.ac.uk).

[12] a) The color graphics (Figure 1) and the molecular contact surfaces (Figures 2 and 3) were generated with the MOLCAD molecular modeling program and its texture mapping option: J. Brickmann, *MOLCAD—MOLecular Computer Aided Design*, Technische Hochschule Darmstadt, **1992**. The major part of the MOLCAD program is included in the SYBYL package (TRIPOS Associates, St. Louis, USA); for details, see J. Brickmann, *J. Chim. Phys.* **1992**, *89*, 1709–1721; b) "Interactive Visualization of Molecular Scenarios with MOLCAD/SYBYL": J. Brickmann, T. Goetze, W. Heiden, G. Moeckel, S. Reiling, H. Vollhardt, C.-D. Zachmann, in *Insight and Innovation in Data Visualization* (Ed.: J. E. Bowie), Manning, Greenwich, **1994**, p. 83–97.

[13] The orientation of the 6-OH groups relative to the pyranoid ring is defined by the exocyclic torsion angles O_5-C_5-C_6-O_6 (ω) and C_4-C_5-C_6-O_6; generally preferred are the *gg* and the *gt* forms where the first letter denotes the *gauche* orientation of O_6 towards the pyranoid ring oxygen and the other that of O_6 to C_4.

[14] The ^1H (800 MHz) and ^{13}C (200 MHz) NMR spectra were recorded at the "Large Scale Facility for Biomolecular NMR" in Frankfurt. We are grateful to Prof. Dr. C. Griesinger and Dr. H. Schwalbe, Institut für Organische Chemie, Universität Frankfurt am Main, for support.

[15] C. A. G. Haasnoot, F. A. A. M. De Leeuw, C. Altona, *Tetrahedron* **1980**, *36*, 2783–2792.

[16] High-temperature annealing (HTA) calculations were performed with a force field program specially adapted to carbohydrates, comprising application of the verlet integrator in the MD simulation program CHARMM with a time step of 1 fs at constant temperature and dielectric constant $\varepsilon = 1$. Every 1000 fs the respective conformation from the MD trajectories at 1200 K (4059 ps) was allowed to cool down to 300 K with a rate of 10 K fs^{-1}, was held there for an additional 1100 fs, and was subsequently fully energy-minimized by an adapted Newton–Raphson algorithm of the CHARMM22 program package with a convergence criterion of 10^{-7} kcal mol^{-1}. For **1**, a total of 2736 (67%) different conformers (corresponding to 16416 altrose units) underwent geometry analysis.

[17] The CHARMM force field with **1** in the center of a truncated octahedron ($V \approx 16400$ Å^3) was used for the MD simulations, and the remaining empty space was filled with water molecules.

[18] For conformational notations see IUPAC–IUB Recommendations, *Pure Appl. Chem.* **1981**, *53*, 190–195; *Carbohydr. Res.* **1997**, *297*, 20–21.

 © WILEY-VCH Verlag GmbH, D-69451 Weinheim, 1997 0570-0833/97/3617-1902 $ 17.50+.50/0

Selenoboratoborates $[B_{12}(BSe_3)_6]^{8-}$: A New Class of Chalcogen-Substituted Icosahedral Boron Clusters

Jörn Küper, Olaf Conrad, and Bernt Krebs*

Dedicated to Professor Hans Georg von Schnering

Binary and ternary boron–sulfur and boron–selenium compounds are accessible through high-temperature solid-state syntheses starting from the elements or binary components. This novel class of compounds, which has been established over the past two decades, shows some remarkable structural principles and interesting physical properties. For instance, there are compounds with trigonal-planar coordinated boron atoms such as isolated BS_3^{3-} ions,[1,2] dinuclear strained B_2S_2 four-membered ring systems $B_2S_4^{2-}$,[3] trinuclear $B_3S_6^{3-}$ ions,[2,4-6] dinuclear $B_2S_5^{2-}$ ions with trithiadiborolane rings,[7] octanuclear porphin-analogous B_8S_{16} molecules, and planar two-dimensional polymers formed by interconnected B_2S_2 and B_3S_3 rings.[4,8,9] Thioborates with tetrahedral coordination of the boron atoms show a structural diversity that ranges from chains of corner-sharing tetrahedra over layers of corner- and edge-sharing tetrahedra[10,11] to three-dimensional macrotetrahedra.[4,12-17] Lithium and silver thioborates such as $Ag_6B_{10}S_{18}$, $Li_5B_7S_{13}$, and $Li_9B_{19}S_{33}$ are particularly interesting for use as fast ionic conductors. The only known example of a compound with an isolated BSe_3^{3-} ion is Tl_3BSe_3.[1] In all other reported selenoborates a tetrahedrally coordinated boron atom is present. They form polymeric chain structures with spirocyclically fused B_2Se_3 and B_2Se_4 rings.[11]

The novel chalcogenoborate $Cs_8[B_{12}(BSe_3)_6]$ was obtained from cesium selenide, boron, and selenium by means of high-temperature synthesis. It contains the first B_{12} icosahedron completely saturated with chalcogen ligands (Figure 1). Thus, unlike in all previous chalcogenoborate syntheses, the B_{12} icosahedron is preserved rather than being fragmented by nucleophilic attack. The linkage of trigonal-planar BSe_3 units to an intact B_{12} fragment may be interpreted as an intermediate of the stepwise formation of the "conventional" selenoborates. Evidently, this was not recognized because of the long reaction times in earlier experiments.

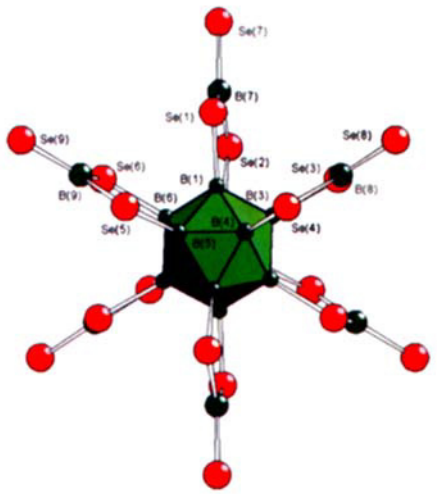

Figure 1. Crystal structure of the $[B_{12}(BSe_3)_6]^{8-}$ ion in cesium hexaselenoborato-*closo*-dodecaborate. Average bond lengths [Å]: B–B 1.783 (range: 1.753(12)–1.803(12)), B(cluster)–Se_{endo} 1.996 (range: 1.981(8)–2.011(8)), B(trig.)–Se_{endo} 1.979 (range: 1.952(8)–1.999(8)), B–Se_{exo} 1.902 (range: 1.886(8)–1.913(8)). Average antipodal B–B distance 3.39 Å.

The unusual cluster $Cs_8[B_{12}(BSe_3)_6]$ contains centrosymmetric, molecular $[B_{12}(BSe_3)_6]^{8-}$ units. Trigonal-planar selenoborate entities functioning as bidentate ligands complete the B_{12} icosahedron to form a persubstituted *closo*-dodecaborate ion. The complex $[B_{12}(BSe_3)_6]^{8-}$ ions are linked through Cs^+ ions (Figure 2), which are eight- and ninefold coordinated by selenium atoms.[22] Thus, the cesium hexaselenoborato-*closo*-dodecaborate is the first representative of a new type of boron cluster compounds.

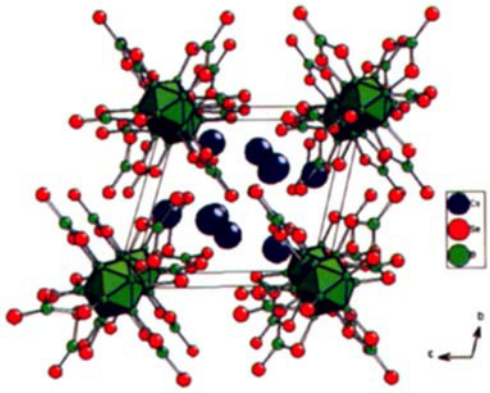

Figure 2. Unit cell of $Cs_8[B_{12}(BSe_3)_6]$. Average Cs–Se distance [Å] in eightfold coordination (Cs(1), Cs(2), Cs(3)) 3.737 (range: 3.533(2)–3.953(2)), and in ninefold coordination (Cs(4)) of the metal atoms 3.941 Å (range: 3.675(2)–4.405(2)).

The electronic counts of the selenium-substituted dodecaborate unit and the hydro-*closo*-dodecaborate are identical. The *closo* cluster contains $2n + 2$ binding electrons for the B_{12} unit and therefore obeys Wade's rules for cluster compounds. Six negative charges are located on the terminal selenium atoms, leaving two negative charges on the central cluster. The comparison between six pairs of hydride ligands in the *closo*-$[B_{12}H_{12}]^{2-}$ ion and the six B–Se_{exo} units present here reveals that each of the latter formally contributes an additional electron, resulting in an overall charge of -8. The antipodal boron–boron distances differ very little due to the symmetrical arrangement of the BSe_3 units (Figure 1). The two types of boron–selenium bonds in the chelate-type B_3Se_2 rings are almost the same length (B(cluster)–Se 1.996 Å and B(trig.)–Se 1.979 Å), whereas the B–Se bonds to the exocyclic selenium atoms, which carry a large portion of the negative charge of the $[B_{12}(BSe_3)]^{8-}$ ion, are significantly shorter (1.902 Å) (Figure 1).

The $[B_{12}(BSe_3)_6]^{8-}$ ion is of additional general interest because of the complete substitution of the *closo*-borate by non-hydrogen atoms. To date this is only known for a few perhalogenated and perhydroxide-substituted *closo*-dodecaborates.[23-26] Replacement of the hydride ligand atoms by selenium-containing substituents has been shown to yield $[B_6(SeCN)_6)]^{2-}$, a per-substituted *closo*-hexaborate.[27] Monosubstituted selenocyanatoborates provided the first indications of the ability of selenium to coordinate to a B_{12} icosahedron.[28]

These results open the way to a series of investigations, which, on the one hand should contribute to the understanding of the steps involved in the reaction of boron with chalcogens, and on the other should provide access to a new field of interesting materials, for example, by replacement of selenium by its homologue sulfur. The size of the selenoboratoborate ion is particu-

[*] Prof. Dr. B. Krebs, Dr. J. Küper, Dipl.-Chem. O. Conrad
Anorganisch-chemisches Institut der Universität
Wilhelm-Klemm-Strasse 8, D-48149 Münster (Germany)
Fax: Int. code + (251)8338366
e-mail: krebs@uni-muenster.de

 © WILEY-VCH Verlag GmbH, D-69451 Weinheim, 1997 0570-0833/97/3617-1903 $ 17.50+.50/0

larly interesting with regard to its use with small cations like Li^+, Ag^+, or Cu^+ to synthesize new ionic conductors. Another strategy for synthesizing polyhedric chalcogenoborates is conceivably available by starting from metal borides with preformed B_{12}, B_6, or other clusters rather than from elemental boron.

Experimental Section

All experiments were carried out in a dry nitrogen atmosphere in a glove box.

$Cs_8[B_{12}(BSe_3)_6]$ was prepared by reacting stoichiometric amounts of dicesium monoselenide (from elemental Cs and HgSe), boron (powdered, amorphous, purity 95%, Alfa-Ventron), and selenium (powdered, purity 99%, Merck) in a molar ratio of 2:9:7. In a quartz glass ampoule coated with glassy carbon the reaction mixture was heated up to 700 °C for 2 h and subsequently annealed (10 h at 600 °C, 24 h at 400 °C, 120 h at 200 °C). Powder diffraction of the resulting pale gray crystalline product showed only traces of impurities. A colorless crystal was chosen for single-crystal X-ray structure determination.

Received: April 1, 1997 [Z10290IE]
German version: *Angew. Chem.* **1997**, *109*, 1995–1996

Keywords: boron · clusters · selenium · solid-phase synthesis · solid-state structures

[1] a) F. Hiltmann, C. Jansen, B. Krebs, *Z. Anorg. Allg. Chem.* **1996**, *622*, 1508; b) P. Vinatier, P. Gravereau, M. Ménétrier, L. Trut, A. Levasseur, *Acta Crystallogr. Sect. C* **1994**, *50*, 1180; c) B. Krebs, W. Hamann, *J. Less-Common Met.* **1988**, *137*, 143.
[2] F. Hiltmann, B. Krebs, *Z. Anorg. Allg. Chem.* **1995**, *621*, 424.
[3] A. Hammerschmidt, C. Jansen, J. Küper, C. Püttmann, B. Krebs, *Z. Anorg. Allg. Chem.* **1995**, *621*, 1330.
[4] B. Krebs, *Angew. Chem.* **1983**, *95*, 113; *Angew. Chem. Int. Ed. Engl.* **1983**, *22*, 113.
[5] C. Püttmann, H. Diercks, B. Krebs, *Phosphorus, Sulfur, Silicon* **1992**, *65*, 179.
[6] a) F. Chopin, G. Turrell, *J. Mol. Struct.* **1969**, *3*, 57; b) F. Chopin, A. Hardy, *C. R. Hebd. Séances Acad. Sci.* **1965**, *261*, 142.
[7] C. Jansen, J. Küper, B. Krebs, *Z. Anorg. Allg. Chem.* **1995**, *621*, 1322.
[8] B. Krebs, H.-U. Hürter, *Angew. Chem.* **1980**, *92*, 479; *Angew. Chem. Int. Ed. Engl.* **1980**, *19*, 481.
[9] P. zum Hebel, H. Diercks, B. Krebs, *Z. Kristallogr.* **1988**, *185*, 401.
[10] a) C. Püttmann, F. Hiltmann, W. Hamann, C. Brendel, B. Krebs, *Z. Anorg. Allg. Chem.* **1993**, *619*, 109; b) B. Krebs, W. Hamann, *Z. Kristallogr.* **1983**, *162*, 149; c) C. Püttmann, W. Hamann, B. Krebs, *Eur. J. Solid State Inorg. Chem.* **1992**, *29*, 857.
[11] A. Hammerschmidt, J. Küper, L. Stork, B. Krebs, *Z. Anorg. Allg. Chem.* **1994**, *620*, 1898.
[12] A. Hardy, *Bull. Soc. Fr. Minéral. Cristallogr.* **1968**, *91*, 111.
[13] P. Hagenmuller, F. Chopin, B. Castagna, *C. R. Séances Acad. Sci. Ser. C* **1966**, *262*, 418.
[14] A. Hammerschmidt, P. zum Hebel, F. Hiltmann, B. Krebs, *Z. Anorg. Allg. Chem.* **1996**, *622*, 76.
[15] B. Krebs, H. Diercks, *Z. Anorg. Allg. Chem.* **1984**, *518*, 101.
[16] C. Püttmann, P. zum Hebel, A. Hammerschmidt, B. Krebs, *Acta Crystallogr. Sect. A* **1990**, *46*, C279.
[17] F. Hiltmann, P. zum Hebel, A. Hammerschmidt, B. Krebs, *Z. Anorg. Allg. Chem.* **1993**, *619*, 293.
[18] a) M. Ménétrier, A. Hojjaji, C. Estournès, A. Levasseur, *Solid State Ionics* **1991**, *48*, 325; b) M. Ménétrier, A. Levasseur, P. Hagenmuller, *J. Electrochem. Soc.* **1984**, *131*, 1971; c) M. Ménétrier, C. Estournès, A. Levasseur, K. J. Rao, *Solid State Ionics* **1992**, *53–56*, 1208, and references therein.
[19] P. zum Hebel, B. Krebs, M. Grüne, W. Müller-Warmuth, *Solid State Ionics* **1990**, *43*, 133.
[20] M. Grüne, H. Meierkord, W. Müller-Warmuth, P. zum Hebel, B. Krebs, M. Wulff, *Ber. Bunsenges. Phys. Chem.* **1989**, *93*, 1313.
[21] M. Grüne, W. Müller-Warmuth, P. zum Hebel, B. Krebs, *Solid State Ionics* **1995**, *78*, 305.
[22] $Cs_8[B_{12}(BSe_3)_6]$: triclinic; space group $P\bar{1}$; $a = 10.711(4)$, $b = 10.747(4)$, $c = 11.144(5)$ Å, $\alpha = 103.59(1)$, $\beta = 91.61(1)$, $\gamma = 109.59(1)°$; $V = 1166.7(8)$ Å^3; $\mu = 20.23$ mm^{-1}; $Z = 1$; $R = 0.0374$ for 3734 independent reflections ($I > 2\sigma(I)$, $2\theta_{max} = 54°$); Siemens P3 diffractometer; $Mo_{K\alpha}$ radiation; graphite monochromator; direct methods (SHELXS), refinement SHELXL-93 (G. M. Sheldrick, Göttingen). Further details of the crystal structure investigation may be obtained from the Fachinformationszentrum Karlsruhe, D-76344 Eggenstein-Leopoldshafen (Germany), on quoting the depository number CSD-406703.
[23] a) K. A. Solntsev, A. M. Mebel, N. A. Votinova, N. T. Kuznetsov, O. P. Charkin, *Koord. Khim.* **1992**, *18*, 340; b) N. T. Kuznetsov, L. A. Zemskova, E. G. Ippolitov, *Zh. Neorgan. Khim.* **1981**, *26*, 1862; *Russ. J. Inorg. Chem.* **1981**, *26*, 1003; c) N. T. Kuznetsov, L. A. Zemskova, Z. M. Alikhanova, E. G. Ippolitov, *ibid.* **1981**, *26*, 1331 and **1981**, *26*, 715.
[24] H.-G. Srebny, W. Preetz, H. C. Marsmann, *Z. Naturforsch. B* **1984**, *39*, 189.
[25] W. H. Knoth, H. C. Miller, J. C. Sauer, J. H. Balthis, Y. T. Chia, E. L. Muetterties, *Inorg. Chem.* **1964**, *3*, 159.
[26] H. C. Miller, E. L. Muetterties, US-A 3551120, **1970** [*Chem. Abstr.* **1971**, *74*, 55815c].
[27] W. Preetz, M. G. Hake, *Z. Naturforsch. B* **1992**, *47*, 1119.
[28] C. Nachtigal, B. Steuer, W. Preetz, *Chem. Ber.* **1996**, *129*, 1531.

The Self-Assembly of a Switchable [2]Rotaxane**

M.-Victoria Martínez-Díaz, Neil Spencer, and J. Fraser Stoddart*

Catenanes and rotaxanes are molecular compounds[1] that hold considerable promise for use in molecular devices as a consequence of the relative movements of their ring and dumbbell-shaped components. Initially researchers learned how to make simple rotaxanes,[2] followed by degenerate rotaxanes with molecular shuttling characteristics,[3] and eventually nondegenerate rotaxanes whose dynamic properties could be addressed selectively with external stimuli of a chemical, electrochemical, or photochemical nature to induce them to behave as molecular switches.[4] However, to our knowledge, no constitutionally asymmetric, two-site [2]rotaxane that exhibits 100% selectivity for one of the binding sites between ring and dumbbell-shaped components has yet been reported. Here, we describe the self-assembly of a [2]rotaxane that possesses two very dissimilar cationic binding sites within its dumbbell-shaped component—specifically, a secondary dialkylammonium center and a bipyridinium unit—each of which shows different affinities[5] toward dibenzo[24]crown-8 (DB24C8), the ring component of the [2]rotaxane. We also report the pH-controlled shuttling of the DB24C8 ring between the two very different recognition sites, or "stations", in this simple molecular shuttle.

The [2]rotaxane **2**-H·3PF_6 was self-assembled (Scheme 1) by using a template-directed threading approach.[6] A pseudorotaxane[7, 8] [DB24C8·**1**-H][PF_6]$_2$ was formed initially in solution between the DB24C8 and **1**-H·2PF_6,[9] which already contains the ammonium center and a stopper (3,5-di-*tert*-butylbenzyl) to prevent unthreading of the ring. Subsequently a single stoppering reaction with 3,5-di-*tert*-butylbenzyl bromide led to the formation of the bipyridinium dicationic unit and the dumbbell-shaped component.[10]

The ^{1}H NMR spectrum of **2**-H·3PF_6 recorded in CD_3COCD_3 at 20 °C shows signals corresponding to the formation of a [2]rotaxane. The spectrum (Figure 1b) demonstrates that the DB24C8 ring binds selectively with the secondary dialkylammonium center, since the characteristic resonance at $\delta = 4.87–4.85$ for the four CH_2 protons adjacent to the NH_2^+ group is observed. These protons experience a downfield shift of about $\Delta\delta = 0.2$ upon association with DB24C8: compare the

[*] Prof. J. F. Stoddart, Dr. M.-V. Martínez-Díaz, Dr. N. Spencer
School of Chemistry, University of Birmingham
Edgbaston, Birmingham B15 2TT (UK)
Fax: Int. code + (121)414-3531

[**] This research was supported by the Ministerio de Educación y Ciencia in Spain in the form of a Postdoctoral Fellowship (to M.-V. M.-D.) and by the Engineering and Physical Sciences Research Council in the United Kingdom. We thank Peter R. Ashton for carrying out the mass spectrometric measurements.

 © WILEY-VCH Verlag GmbH, D-69451 Weinheim, 1997 0570-0833/97/3617-1904 $ 17.50+.50/0

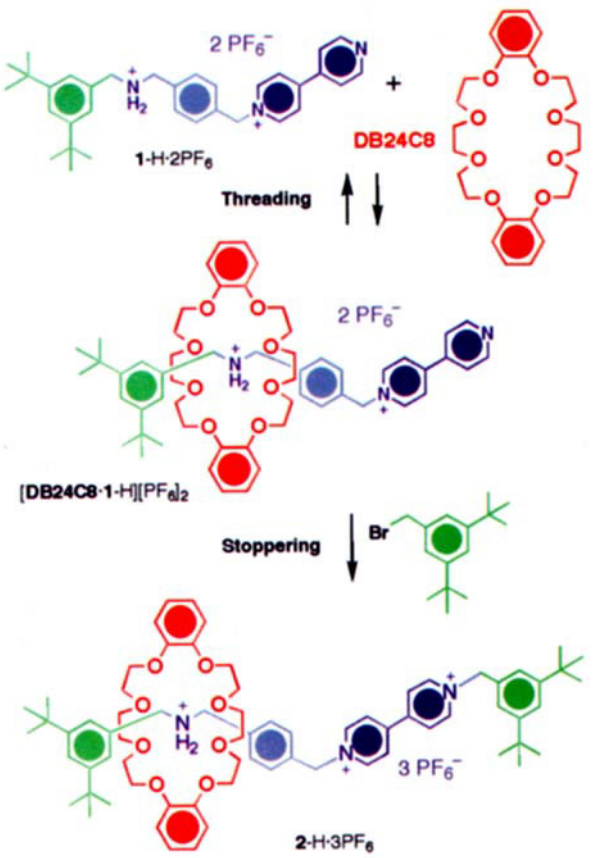

Scheme 1. The self-assembly approach to the [2]rotaxane **2**-H·3 PF_6: threading followed by stoppering.

^{1}H NMR spectrum (Figure 1a) of the dumbbell-shaped compound **3**-H·3 PF_6 with that of the [2]rotaxane **2**-H·3 PF_6 (Figure 1b). This selective binding was confirmed by one-dimensional ^{1}H NMR NOE doubled-pulsed field-gradient spin-echo experiments[11]—GOESY (gradient enhanced nuclear Overhauser effect spectroscopy)—carried out at 400 MHz at room temperature. Selective irradiation of the protons (C) on the *para*-xylyl spacer closest to the NH_2^+ center showed that, in addition to the expected intramolecular NOEs, intercomponent NOEs with some of the OCH_2 protons in the DB24C8 were observed. Since the two faces of the crown ether are diastereotopic, NOEs are observed with protons on only one of its faces. The same effect was noted when the protons in *ortho* positions (A) in the stopper closest to the NH_2^+ center were irradiated selectively. Moreover, since association and dissociation between the NH_2^+ center and DB24C8 is expected to be slow on the ^{1}H NMR time scale,[8] we should observe another set of signals for a second translational isomer if the DB24C8 ring resides anywhere else along the dumbbell-shaped component other than on the NH_2^+ center. In order to establish that the [2]rotaxane **2**-H·3 PF_6 exists as a single translational isomer, a solution of **2**-H·3 PF_6 in CD_3COCD_3 was cooled down to −80 °C. Since no additional set of resonances could be detected, it may be concluded that the DB24C8 ring is bound to the NH_2^+ center with a selectivity of at least 98% in the temperature range between −80 °C and +31 °C.

One reason for the synthesis of interlocked molecules, such as the [2]rotaxane **2**-H·3 PF_6 incorporating an NH_2^+ center and a bipyridinium unit, is to develop them as pH-sensitive or electrochemically driven molecular switches. Since we have established that the potentially mobile component of **2**-H^{3+}—that is the

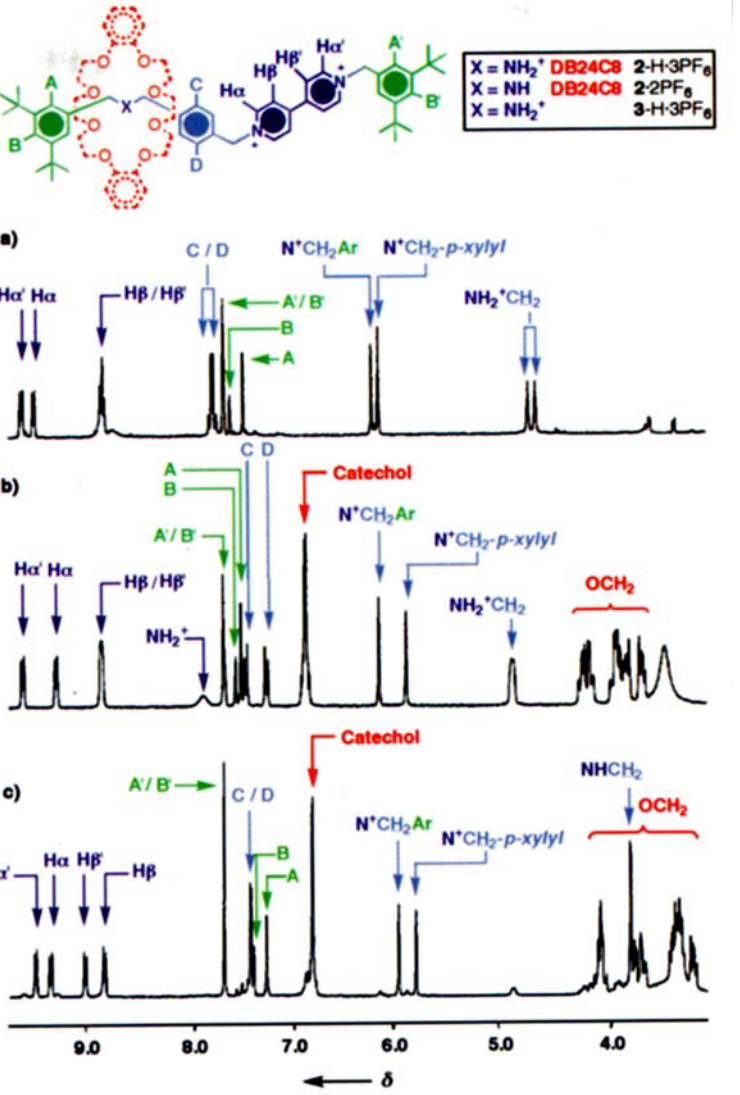

Figure 1. Partial ^{1}H NMR spectra (300 MHz, CD_3COCD_3, room temperature): a) the dumbbell-shaped compound **3**-H·3 PF_6 (ca. 7 mM); b) the [2]rotaxane **2**-H·3 PF_6 (ca. 4.7 mM); c) the deprotonated [2]rotaxane **2**·2 PF_6, after addition of 1.5 μL (2.4 mol equiv) of iPr_2NEt to the solution.

DB24C8 ring—resides initially on the NH_2^+ station, it should be possible (Scheme 2) to deprotonate the NH_2^+ center with base and "drive" the ring to the bipyridinium station. The choice of

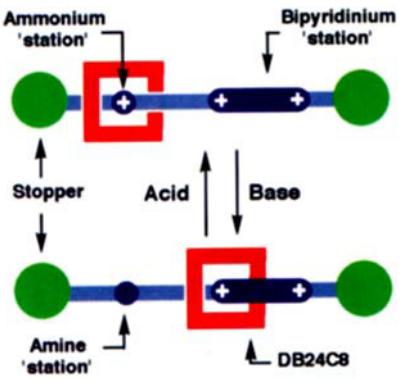

Scheme 2. A cartoon of the switchable [2]rotaxane **2**-H·3 PF_6 showing how the motion of the ring component (red) is driven by deprotonation or reprotonation of the ammonium/amine station in the dumbbell-shaped component (blue and green). The fact that the DB24C8 component interacts asymmetrically with the bipyridinium station is conveyed by the off-center location of the ring with respect to the station.

 © WILEY-VCH Verlag GmbH, D-69451 Weinheim, 1997 0570-0833/97/3617-1905 $ 17.50+.50/0

the base for deprotonation of the NH_2^+ center was not straightforward, since the bipyridinium unit is very sensitive to nucleophilic bases. Addition of a slight excess of a number of bases (e.g. 2,6-lutidine, dibenzylamine, 1,8-diazabicyclo[5.4.0]undec-7-ene (DBU), quinuclidine, hexamethyldisilazane, diisopropylethylamine) to a CD_3COCD_3 solution containing equimolar amounts of DB24C8 and benzyl viologen and dibenzylammonium hexafluorophosphate allowed us to identify an appropriate base for triggering this molecular switching action of **2**-H^{3+}. The deprotonation can be followed by ^1H NMR spectroscopy by noting the disappearance of the multiplet assigned to the CH_2 protons adjacent to the NH_2^+ center. The stability of the bipyridinium dication was monitored by checking the signals for the α-CH and β-CH bipyridinium protons. In the presence of weak bases, such as 2,6-lutidine or dibenzylamine, although the benzyl viologen is stable, the NH_2^+ center is not deprotonated. Upon addition of a much stronger base, such as DBU, or a nucleophilic one such as quinuclidine, deprotonation does occur but the solution turns dark green, indicating the decomposition of the benzyl viologen. Eventually we found that diisopropylethylamine is the ideal base. The ^1H NMR spectrum (Figure 2b) shows that total deprotonation of the NH_2^+ center occurs, while the benzyl viologen is left intact—its resonances only being broadened in the presence of iPr_2NEt. Addition of trifluoroacetic acid (TFA) to this solution results in the reprotonation of the dibenzylamine (Figure 2c) and the recovery of the 1:1 complex between the dibenzylammonium cation and DB24C8. Despite the success of this association–dissociation experiment, no remarkable changes in the ^1H NMR spectrum that might indicate complex formation between the benzyl viologen and DB24C8 were observed. Moreover, the solution remained pale yellow all the time. Since the complex between dibenzylammonium hexafluorophosphate and DB24C8 is colorless, the pale yellow color of the 1:1:1 mixture may be a consequence of charge transfer interactions between the catechol rings of the DB24C8 and the viologen dication.[12] Clearly, once the NH_2^+ center is deprotonated, the affinity of the DB24C8 ring for the viologen is so low that most of the crown ether remains uncomplexed in solution.

This observation poses several questions: can the lack of binding be overcome in a rotaxane in which the DB24C8 ring cannot be expelled from the molecule once the NH_2^+ center is deprotonated? Would it be possible to oblige the DB24C8 ring to associate[12] with the bipyridinium unit in a cliplike manner? In order to test this hypothesis, an excess of iPr_2NEt was added to a solution of **2**-H·3PF_6 in CD_3COCD_3. Immediately, a change in the color of the solution from colorless to yellow was observed, indicative of charge transfer interactions between the catechol rings of the DB24C8 ring and the bipyridinium dication.[12] Moreover, the ^1H NMR spectrum (Figure 1c) of **2**·2PF_6 shows dramatic changes in chemical shifts relative to those for **2**-H·3PF_6 (Figure 1b)—especially in the resonances for the bipyridinium and *para*-xylyl protons—indicating that the DB24C8 ring interacts in an asymmetric fashion with the bipyridinium station. ^1H NMR spectra of the deprotonated [2]rotaxane **2**·2PF_6 from −80 °C to +31 °C in CD_3COCD_3 at 400 MHz revealed that the DB24C8 ring resides *exclusively* on the bipyridinium station. Although the spectrum broadens below −40 °C, no additional set of resonances for another translational isomer are observed. On subsequent addition of TFA to the CD_3COCD_3 solution of the [2]rotaxane **2**·2PF_6, we demonstrated that the system is reversible, since the recorded ^1H NMR spectrum once again shows signals for the translational isomer in which the macrocycle resides on the NH_2^+ station.

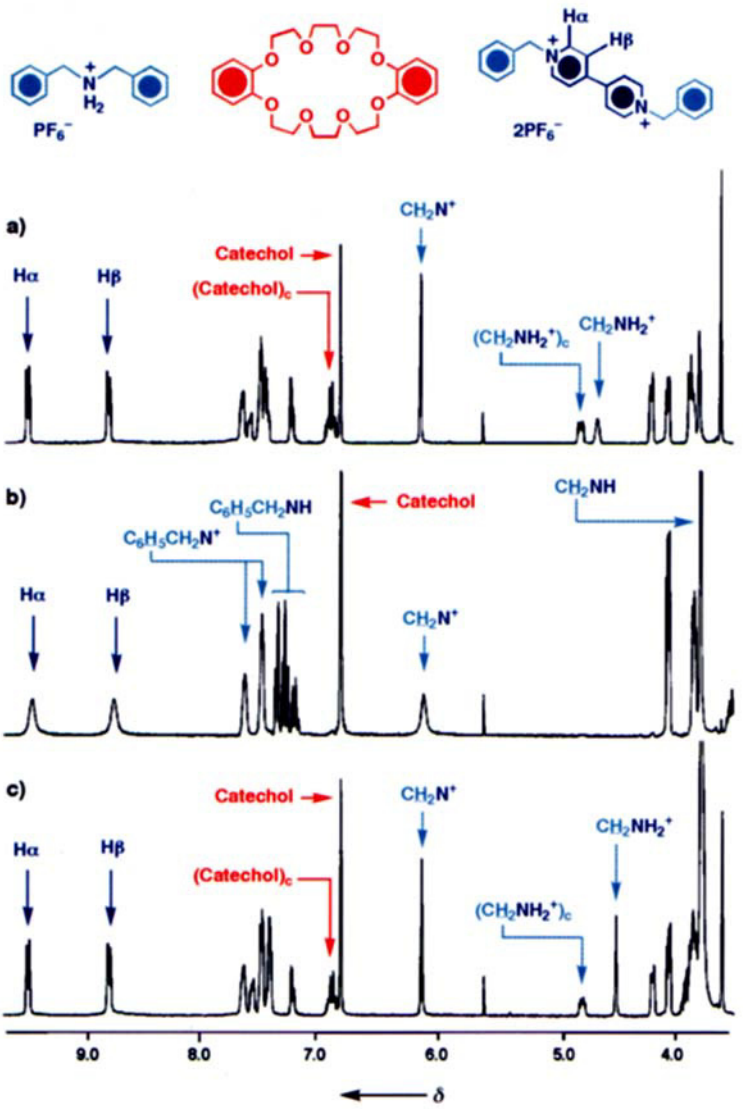

Figure 2. Partial ^1H NMR spectra (300 MHz, CD_3COCD_3, room temperature): a) an equimolar mixture of dibenzylammonium hexafluorophosphate, DB24C8, and benzyl viologen bis(hexafluorophoshate) (ca. 10 mM); b) after addition of 2 μL (1.4 mol equiv) of iPr_2NEt to the CD_3COCD_3 solution, and c) after subsequent addition of 2 μL (3.2 mol equiv) of TFA to the basic solution. The subscript *c* is used in the annotation to indicate signals corresponding to the 1:1 complex formed between the NH_2^+ cation and DB24C8.

In conclusion, we have shown that the dethreading and rethreading of the [2]pseudorotaxane[8] formed between the dibenzylammonium cation and DB24C8 can be controlled chemically by the addition of iPr_2NEt or TFA. However, after the dibenzylammonium cation is deprotonated, complexation of the crown ether with the benzyl viologen also present in the solution is not observed. In order to obtain an efficient switching process in which the bipyridinium dication is bound by the DB24C8 ring upon the transformation of the NH_2^+ center into a neutral amino group, a new [2]rotaxane **2**-H^{3+} was synthesized; in this compound the DB24C8 ring is bound mechanically to a dumbbell-shaped component incorporating both a secondary dialkylammonium center and a bipyridinium dicationic unit. The [2]rotaxane **2**-H·3PF_6 constitutes the most selective switchable molecular shuttle reported to date. When the NH_2^+ center is protonated, the DB24C8 ring resides *exclusively* on this station. The affinity of the crown ether for this NH_2^+ center is decreased dramatically upon the addition of a nonnucleophilic base such as iPr_2NEt—which deprotonates the NH_2^+ center—

 © WILEY-VCH Verlag GmbH, D-69451 Weinheim, 1997 0570-0833/97/3617-1906 $ 17.50+.50/0

and the DB24C8 ring moves to the bipyridinium station. The process is reversible upon addition of TFA, which reprotonates the NH_2^+ center.

Experimental Section

2-H·3PF_6: A solution of 3,5-di-*tert*-butylbenzyl bromide (300 mg, 1.06 mmol) in $CHCl_3$ (5 mL) was added to a stirred suspension of **1**-H·2PF_6 (150 mg, 0.195 mmol) and DB24C8 (200 mg, 0.446 mmol) in $CHCl_3$ (15 mL). The suspension was heated under reflux for 4 days until it became a clear solution. Upon cooling, the reaction mixture was concentrated in vacuo to give a solid residue, which was purified by column chromatography (SiO_2; gradient elution with CH_2Cl_2/MeOH in the proportions 1/0, then 9/1 and then 7/1) to afford a pale yellow solid and characterized as the hydrochloride salt **2**-H·2Cl (97 mg, 40%). After counterion exchange (NH_4PF_6/H_2O/Me_2CO), **2**-H·3PF_6 was isolated as a beige solid (116 mg, 95%); m.p. 169–173 °C; ^{1}H NMR (300 MHz, CD_3COCD_3, 20 °C): δ = 9.55 (d, 2H), 9.23 (d, 2H), 8.80 (d, 2H), 8.79 (d, 2H), 7.62 (s, 3H), 7.51 (s, 1H), 7.46 (s, 2H), 7.41, 7.21 (AA'XX' system, 4H), 6.86–6.83 (m, 8H), 6.14 (s, 2H), 5.88 (s, 2H), 4.87–4.85 (m, 4H), 4.22–3.58 (m, 24H), 1.30 (s, 18H), 1.23 (s, 18H); FABMS (*m*-NBA): *m/z* 1420 [M – PF_6]$^+$, 1275 [M – 2PF_6]$^+$, 1129 [M – 2PF_6 – HPF_6]$^+$.

Received: December 18, 1996 [Z9903IE]
German version: *Angew. Chem.* **1997**, *109*, 1991–1994

Keywords: molecular devices · NMR spectroscopy · rotaxanes · supramolecular chemistry · template synthesis

[1] a) G. Schill, *Catenanes, Rotaxanes and Knots*, Academic Press, New York, **1971**; b) J.-C. Chambron, C. O. Dietrich-Buchecker, J.-P. Sauvage, *Top. Curr. Chem.* **1993**, *165*, 131–162; c) D. B. Amabilino, J. F. Stoddart, *Chem. Rev.* **1995**, *95*, 2725–2828; d) D. Philp, J. F. Stoddart, *Angew. Chem.* **1996**, *108*, 1242–1286; *Angew. Chem. Int. Ed. Engl.* **1996**, *35*, 1155–1196; e) F. Vögtle, R. Jäger, M. Händel, S. Ottens-Hildebrandt, *Pure Appl. Chem.* **1996**, *68*, 225–232.

[2] Examples of simple rotaxanes: a) P. R. Ashton, M. Grognuz, A. M. Z. Slawin, J. F. Stoddart, D. J. Williams, *Tetrahedron Lett.* **1991**, *32*, 6235–6238; b) P. L. Anelli, P. R. Ashton, R. Ballardini, V. Balzani, M. Delgado, M. T. Gandolfi, T. T. Goodnow, A. E. Kaifer, D. Philp, M. Pietraszkiewicz, L. Prodi, M. V. Reddington, A. M. Z. Slawin, N. Spencer, J. F. Stoddart, C. Vicent, D. J. Williams, *J. Am. Chem. Soc.* **1992**, *114*, 193–218; c) A. G. Kolchinski, D. H. Busch, N. W. Alcock, *J. Chem. Soc. Chem. Commun.* **1995**, 1289–1291; d) P. R. Ashton, P. T. Glink, J. F. Stoddart, P. A. Tasker, A. J. P. White, D. J. Williams, *Chem. Eur. J.* **1996**, *2*, 729–736; e) P. R. Ashton, P. T. Glink, J. F. Stoddart, S. Menzer, P. A. Tasker, A. J. P. White, D. J. Williams, *Tetrahedron Lett.* **1996**, *37*, 6217–6220; f) C. Wu, P. R. Lecavalier, Y. X. Shen, H. W. Gibson, *Chem. Mater.* **1991**, *3*, 569–572; g) J.-C. Chambron, V. Heitz, J.-P. Sauvage, *J. Am. Chem. Soc.* **1993**, *115*, 12378–12384; h) F. Vögtle, T. Dunnwald, M. Händel, R. Jäger, S. Meier, G. Harder, *Chem. Eur. J.* **1996**, *2*, 640–643; i) A. G. Johnston, D. A. Leigh, A. Murphy, J. P. Smart, M. D. Deegan, *J. Am. Chem. Soc.* **1996**, *118*, 10662–10663; j) S. Anderson, H. L. Anderson, *Angew. Chem.* **1996**, *108*, 2075–2078; *Angew. Chem. Int. Ed. Engl.* **1996**, *35*, 1956–1959.

[3] Examples of degenerate molecular shuttles: a) P. R. Anelli, N. Spencer, J. F. Stoddart, *J. Am. Chem. Soc.* **1991**, *113*, 5131–5133; b) P. R. Ashton, D. Philp, N. Spencer, J. F. Stoddart, *J. Chem. Soc. Chem. Commun.* **1992**, 1124–1128; c) D. B. Amabilino, P. R. Ashton, V. Balzani, C. L. Brown, A. Credi, J. M. J. Fréchet, J. W. Leon, F. M. Raymo, N. Spencer, J. F. Stoddart, *J. Am. Chem. Soc.* **1996**, *118*, 12012–12020.

[4] Examples of potentially switchable rotaxanes: a) P. R. Ashton, R. A. Bissell, N. Spencer, J. F. Stoddart, M. S. Tolley, *Synlett* **1992**, 914–918; b) P. R. Ashton, R. A. Bissell, R. Górski, D. Philp, N. Spencer, J. F. Stoddart, M. S. Tolley, *ibid.* **1992**, 919–922; c) P. R. Ashton, R. A. Bissell, N. Spencer, J. F. Stoddart, M. S. Tolley, *ibid.* **1992**, 923–926; d) R. A. Bissell, E. Córdova, A. E. Kaifer, J. F. Stoddart, *Nature* **1994**, *369*, 133–137; e) D. B. Amabilino, P. R. Ashton, S. E. Boyd, M. Gómez-López, W. Hayes, J. F. Stoddart, *J. Org. Chem.* **1997**, *62*, 3062–3075; f) P. L. Anelli, M. Asakawa, P. R. Ashton, R. A. Bissell, G. Clavier, R. Górski, A. E. Kaifer, S. J. Langford, G. Mattersteig, S. Menzer, D. Philp, A. M. Z. Slawin, N. Spencer, J. F. Stoddart, M. S. Tolley, D. J. Williams, *Chem. Eur. J.* **1997**, *3*, 1113–1135.

[5] P. R. Ashton, P. T. Glink, M.-V. Martínez-Díaz, J. F. Stoddart, A. J. P. White, D. J. Williams, *Angew. Chem.* **1996**, *108*, 2058–2061; *Angew. Chem. Int. Ed. Engl.* **1996**, *35*, 1930–1933.

[6] a) D. Philp, J. F. Stoddart, *Synlett* **1991**, 445–458; b) J. F. Stoddart, *Chem. Br.* **1991**, 714–718.

[7] For an explanation of the term pseudorotaxane, see a) P. R. Ashton, D. Philp, N. Spencer, J. F. Stoddart, *J. Chem. Soc. Chem. Commun.* **1991**, 1677–1679; b) P. R. Ashton, D. Philp, M. V. Reddington, A. M. Z. Slawin, N. Spencer, J. F. Stoddart, D. J. Williams, *ibid.* **1991**, 1680–1683.

[8] a) P. R. Ashton, P. J. Campbell, E. J. T. Chrystal, P. T. Glink, S. Menzer, D. Philp, N. Spencer, J. F. Stoddart, P. A. Tasker, D. J. Williams, *Angew. Chem.* **1995**, *107*, 1997–2001; *Angew. Chem. Int. Ed. Engl.* **1995**, *34*, 1865–1869; b) P. R. Ashton, E. J. T. Chrystal, P. T. Glink, S. Menzer, C. Schiavo, N. Spencer, J. F. Stoddart, P. A. Tasker, A. J. P. White, D. J. Williams, *Chem. Eur. J.* **1996**, *2*, 709–728.

[9] Compound **1**-H·2PF_6 was prepared in good overall yield (49%) as follows: 3,5-di-*tert*-butylbenzaldehyde was condensed with methyl 4-aminomethylbenzoate, and the resulting imine was reduced in situ with $NaBH_4$ to give the secondary amine. After reduction of the ester function with $LiAlH_4$ and subsequent reaction of the alcohol derivative as hydrochloride salt with an excess of $SOCl_2$, the benzylic chloride in the form of the hydrochloride salt was obtained. Reaction of this compound with a fourfold excess of 4,4'-bipyridine and subsequent counterion exchange (NH_4PF_6/H_2O/Me_2CO) gave **1**-H·2PF_6.

[10] The dumbbell-shaped component of the [2]rotaxane **2**-H·3PF_6 was prepared as compound **3**-H·3PF_6 (Figure 1) in its own right by treating **1**-H·2PF_6 (50 mg, 0.065 mmol) with 3,5-di-*tert*-butylbenzyl bromide (100 mg, 0.35 mmol) in MeCN (10 mL). The reaction mixture was transferred to a Teflon ultrahigh pressure reaction vessel and subjected to a pressure of 12 kbar at 50 °C for 5 days. After removal of the solvent, the crude product was purified by column chromatography (SiO_2: gradient elution with CH_2Cl_2/MeOH 9/1 and then MeOH/2 M NH_4Cl/$MeNO_2$ 7/2/1). After counterion exchange (NH_4PF_6/H_2O/Me_2CO), the dumbbell-shaped compound **3**-H·3PF_6 was isolated as a beige solid (48 mg, 66%). M.p. 187–193 °C (decomp.); ^{1}H NMR (300 MHz, CD_3COCD_3, 20 °C): δ = 9.53 (d, 2H), 9.42 (d, 2H), 8.78 (d, 2H), 8.76 (d, 2H), 7.74, 7.70 (AA'XX' system, 4H), 7.61 (s, 3H), 7.56 (s, 1H), 7.43 (s, 2H), 6.20 (s, 2H), 6.14 (s, 2H), 4.70 (s, 2H), 4.63 (s, 2H), 1.30 (s, 18H), 1.28 (s, 18H); FABMS (*m*-NBA): *m/z* 972 [M – PF_6]$^+$, 827 [M – 2PF_6]$^+$, 681 [M – 2PF_6 – HPF_6]$^+$.

[11] a) J. Stonehouse, P. Adell, J. Keeler, A. J. Shaka, *J. Am. Chem. Soc.* **1994**, *116*, 6037–6038; b) K. Stott, J. Stonehouse, J. Keeler, T. L. Hwang, J. Keeler, *ibid.* **1995**, *117*, 4199–4200.

[12] Complexes between catechol-containing crown ethers—such as DB24C8 and DB30C10—and bipyridinium dications—diquat, paraquat and 2,7-diazapyrenium—show an absorption band at 400 nm, indicative of the charge transfer interaction between the catechol ring of the crown ether and these bipyridinium dications. The crystal structures of some of these complexes show the π–π-stacking of the three aromatic rings leading to a stabilization of a supramolecular entity in which the macrocycle adopts a concave (or cliplike) conformation. Examples: a) H. M. Colquhoun, E. P. Goodings, J. M. Maud, J. F. Stoddart, J. B. Wolstenholme, D. J. Williams, *J. Chem. Soc. Perkin Trans. 2* **1985**, 607–624; b) P. R. Ashton, S. J. Langford, N. Spencer, J. F. Stoddart, A. J. P. White, D. J. Williams, *Chem. Commun.* **1996**, 1387–1388.

 © WILEY-VCH Verlag GmbH, D-69451 Weinheim, 1997 0570-0833/97/3617-1907 $ 17.50+.50/0

Isocyanates Yesterday's News? Think Again!

Chemistry and Technology of Isocyanates. By *H. Ulrich*. Wiley, New York, 1996. 489 pp., hardcover £ 80.00.—ISBN 0-471-96371-2

It is now nearly 150 years since the first synthesis of an isocyanate by Wurtz in 1848. In this book *Chemistry and Technology of Isocyanates,* Henri Ulrich deals with a subject that forms the basis for the 6 Mt/year production of polyurethanes. These are among the most important of polymeric materials, not only in terms of the quantities produced but also because of the enormous variety of polyurethane products and the ability to tailor their properties for different uses.

For this work of almost 500 pages the author has chosen a straightforward and effective structure, dividing it into two main parts: monoisocyanates and diisocyanates. These are subdivided according to the other functional groups present, the synthesis of the compounds, and their reactions. In both parts of the book the chemistry of the isocyanates is described in detail, but in a very effective and concise form, illustrated by over 1100 reaction schemes, mostly with several stages. There are also 80 tables listing reaction parameters. The enormous amount of factual information, taken from almost 2500 publications, is skillfully presented in a form that makes for easy reading, with particular attention to the latest developments in the chemistry of isocyanates. The following is a brief outline of the chapters, mentioning a few highlights.

The treatment of monoisocyanates occupies two-thirds of the book. It ranges over all the areas in which isocyanates are used in agricultural and pharmaceutical chemistry, by dealing with compounds that have aryl, alkenyl, halogen, carbonyl, thiocarbonyl, sulfur, or phosphorus functionalities in addition to the isocyanato group. Thus, for example, the phosphorus-containing compounds offer an elegant route to phosphaheterocycles. Also [2+2]-, [2+3]-, and [2 + 4]-cycloaddition reactions of isocyanates are important for the synthesis of N-heterocycles and alkaloids.

Although phenolic monoisocyanates are of some importance in polymer chemistry, diisocyanates play the dominant role in the polymer area. The two market leaders, MDI and TDI, currently have a combined annual production of about 2.5 Mt, with a strong upward trend. These two, together with other aromatic and nonaromatic diisocyanates, form the basis for the many different polyurethane plastics. The author adds interest to the chapter by including, on page 428, some fascinating highlights from the history of polyurethanes.

Ulrich also treats the synthesis of isocyanates in great detail. With regard to the phosgene-based processes, diphosgene and triphosgene have become important as alternatives to phosgene, whereas nitrene intermediates have become established in the area of non-phosgene processes. The proposed route whereby nitroarenes are allowed to react with carbon monoxide may have the potential to become a low-cost alternative. Processes based on the reactions of isocyanates have special advantages for large-scale industrial production, since addition reactions do not generate waste emissions. This subject of environmental considerations is treated in a short additional section following the two main ones. Here the author discusses on the one hand accident risks and the toxicity and safety aspects of isocyanate chemistry, and on the other hand the use of feedstocks from renewable sources, such as furfural.

Even in such an excellent work as this, there are a few minor details that could be improved. The summary tables 10, 12, 13, and 40–42 in Part 1 and 19–22 in Part 2 should include the relevant literature references, which would allow the reader to extract the required information more quickly. Perhaps this improvement could be incorporated into a second edition of the book, which one hopes will appear in due course.

The author has benefited from discussions with many experts throughout the world and with relevant manufacturers, and this has contributed significantly to the great value of the work. The book is written in such a way that it can be understood by any chemist, but by virtue of the wealth of detailed information provided it will be most useful to specialists working in the area of isocyanate chemistry. It is emphatically recommended for the latter readers, and also for those who intend to become professionally involved in this field, or who wish to gain a more detailed knowledge of it.

Heiner Eckert
Institut für Organische Chemie und Biochemie
der Technischen Universität München
Garching (Germany)

Dictionary of Renewable Resources. Edited by *H. Zoebelein*. WILEY-VCH, Weinheim, 1997. 320 pp., hardcover DM 198.00.—ISBN 3-527-30075-9

In recent years there has been increasing interest in renewable raw materials as feedstocks for the chemical industry. The use of such materials could save fossil resources, improve the CO_2 balance in the atmosphere, help to reduce agricultural surpluses, and lead to new products with biocompatible properties. Although there has been some progress in using renewable resources, no real breakthrough has yet occurred. Hans Zoebelein, the editor of this book, writes in his introduction: "Today renewable resources are in an active stand-by situation". For many years he played a prominent and active role in this field in the chemical industry, and worked on several committees set up to study the subject. His introduction to the book, which discusses in detail the present situation regarding the use of renewable feedstocks and examines the prospects for future developments, is well worth reading. The advantages and disadvantages of

This section contains book reviews and a list of new books received by the editor. Book reviews are written by invitation from the editor. Suggestions for books to be reviewed and for book reviewers are welcome. Publishers should send brochures or (better) books to the editorial office: Redaktion Angewandte Chemie, Postfach 101161, D-69451 Weinheim, Germany. The editor reserves the right of selecting which books will be reviewed. Uninvited books not chosen for review will not be returned.

 © WILEY-VCH Verlag GmbH, D-69451 Weinheim, 1997 0570-0833/97/3617-1909 $ 17.50+.50/0

fossil and renewable raw materials are carefully weighed in the balance.

The main part of this *Dictionary of Renewable Resources* lists and explains a large number of concepts and terms connected with the (sometimes confusing and diverse) subject. The book is intended to be of interest to a broad readership. This includes not only chemists, bioscientists, and process technologists in industry and universities, but also others with backgrounds as varied as agriculture, administration, and policy making, who have an interest in the subject and can benefit from reading the book.

Under the appropriate headings the *Dictionary* explains and discusses renewable resources of both plant and animal origins, and intermediates made from these. For the named chemical compounds the book gives information about their origin and occurrence, extraction, use, chemical structure, and physical properties. Chemical reactions are given under the headings of the individual compounds obtained from the raw materials, sometimes with equations, and the uses of the derivatives are explained.

Economic aspects are also covered in detail, as is evident from the inclusion of entries such as "Starch, EC market" or "Starch industry, world". Data on tonnages produced are also included in many cases. Each article includes carefully chosen cross-references to related entries, and in addition there is usually a short list of literature references. Another nice feature is that each subject heading is also accompanied by a German and a French translation. However, one needs to know the English term in order to find a particular topic.

The editor has recruited appropriate experts from industry and universities to write the contributions on the various specialist areas, thus ensuring competence throughout. This has resulted in a well-balanced coverage of the different aspects.

It is unfortunate that, in contrast to the otherwise high standard of the book and the excellent quality of production, insufficient care has been taken with the structural formulas. The figures are very inconsistent in style, and are even unclear in a few cases. The large number of errors in the formula diagrams is especially annoying. In this first edition of the work it would have been desirable to make the reader aware of the errors in the formulas, for example by including an erratum page. These errors need to be corrected in a future edition and the formulas should be redrawn in a uniform style.

Nevertheless, on the whole we can thoroughly recommend the book. It will undoubtedly be a very useful work of reference for many people in industry and universities who are involved in the area of renewable raw materials. It will serve as a rapid source of information on many different aspects of the subject, which is not available anywhere else in such a clear and concise form.

Stefan Kubik, Günter Wulff
Institut für Organische
und Makromolekulare Chemie
der Universität Düsseldorf (Germany)

Exercises in Synthetic Organic Chemistry. By *C. Ghiron and R. J. Thomas.* Oxford University Press, Oxford, 1997. 139 pp., hardcover £ 40.00.—ISBN 0-19-855944-5

In this book the authors have collected together a selection of 82 total and partial syntheses. These are presented in the form of reaction schemes which are incomplete, so that they serve as exercise problems. In some cases the reader's task is to propose suitable reagents and reaction conditions whereby a desired product can be synthesized, starting from familiar compounds as educts. In others the situation is reversed, by specifying the reagents and inviting the reader to name the end-product. With each synthesis the authors also include suggestions for points that could be discussed, and they refer the reader to recent review articles relating to the key steps. However, there is an inconsistency in one respect: whereas in their preface the authors mention retrosynthetic analysis as being an extremely useful tool for planning a synthesis, they simply leave it at that, providing no examples. In a book of exercises such as this, it would certainly have been appropriate to give a retrosynthetic analysis before the exercise itself, thus affording the reader a preliminary overview of the task.

Unfortunately there is no subject index, which would have made it easier to find material on a particular topic. An index would also allow one to make better use of the well-chosen literature references, so as to get a quick overview of the latest synthetic methods.

The exercises chosen by the authors are of a high and demanding standard, and the syntheses often include a particularly clever key step, or have some other elegant feature. The synthetic targets chosen are mainly natural products of widely different kinds, such as steroids, macrolides, alkaloids, and even taxol. Thus the book tests and extends the reader's knowledge of the areas of heterocyclic chemistry, rearrangement reactions, organometallic chemistry, arenes, and even to some extent carbohydrate chemistry.

But the reader will not achieve very much by merely using this book on its own, because for didactic reasons the answers to the interesting synthetic exercises are not included! Instead, as the authors explain, the reader is referred to the original publications to arrive at a solution, so that there can be no temptation to cut short the exercise by simply looking up the answer. Consequently one must be prepared to make trips to the library, or alternatively to refer to textbooks to find solutions to the simpler problems.

The choice of material and the manner of presentation are undoubtedly suitable for use by a wide readership, from advanced students to experienced chemists. The book could provide exercise material for use in the weekly synthetic seminars that are obligatory in many research groups, or for some other form of group work.

The book is not intended for private study. There would be little motivation to use it in that way, as it does not lend itself to adaptation from the exercise concept on which it is based. To benefit fully from the book one needs a tutor or moderator who can lead the discussion of the exercises on the basis of a knowledge of the original publications.

Jan-Arne Gewert
Institut für Organische Chemie
der Universität Göttingen (Germany)

Grundlagen der Elektrochemie. By *W. Schmickler.* Vieweg, Braunschweig/Wiesbaden, 1996. 214 pp., paperback DM 58.00.—ISBN 3-528-06755-1

The chemical discipline of electrochemistry is of growing importance in many areas of the fundamental and applied sciences. Energy production and conversion, sensor technology, materials science, and many other branches of science and technology make use of electrochemical processes and industrial techniques. As in other analogous situations, the introduction of electrochemistry into these fields has been accompanied by a diversification of the discipline itself. With regard to mechanistic studies, much effort is currently being devoted to investigating the process of electron transfer at an electrode and the great variety of associated chemical reactions, including synthetic applications. Another topical area of study is the role of the electrode–electrolyte interface in electrochemical processes.

 © WILEY-VCH Verlag GmbH, D-69451 Weinheim, 1997 0570-0833/97/3617-1910 $ 17.50+.50/0

The author of this book is mainly concerned with the latter aspect of electrochemistry, the role of surfaces, including the microscopic characterization of the phase boundary. According to his view, as explained in the preface, kinetic studies have not advanced significantly since the 1970s. One might well disagree with that, but nevertheless the appearance of a textbook on electrochemistry in German, incorporating modern developments in this interdisciplinary science, is an event of great interest.

Schmickler takes as his starting point the central concept of the thermodynamic potential and the structure of electrolyte solutions. He then goes on to discuss the phase boundary between a metal and the electrolyte, adsorption (involving a specific interaction between the electrode and constituents of the electrolyte), and electron transfer (treated phenomenologically using the Butler–Volmer kinetic model and its variants, and "theoretically" on the basis of the Marcus–Hush kinetic model). The discussion is then widened to include semiconductor electrodes, and the models are tested against a number of experimental systems. This is followed by three chapters dealing with electrode surface reactions of increasing complexity: gas evolution, the deposition or dissolution of metals, multistage reactions, corrosion. The treatment then moves on to the liquid–liquid interface and liquid electrodes. By far the most familiar example of the latter is the mercury drop electrode, which was the subject of the only Nobel Prize awarded to an electrochemist (Heyrovský in 1959). The book ends with a discussion of mass transport at an electrode and the analytical techniques based on such processes.

From a superficial standpoint it is pleasing to find here detailed figures that are clear, informative, and not over-elaborate. The text contains some printing errors (not many, and mostly confined to the later chapters), but unfortunately there are also some vague or inaccurate statements [examples: "... die Reaktion ist sehr unsymmetrisch" (p. 67); "... so dass der Strom durch ein Maximum fliesst" (p. 193); the word "langsam" (slow) to describe a current (p. 188)]. More seriously, there are occasional errors in symbols, formulas, and equations which alter the meaning, a shortcoming that is especially regrettable in a basic textbook. Sometimes different symbols are used for the same quantity, for example the concentration in the bulk solution is variously denoted by c^0 or c^b.

Schmickler's approach, which is certainly to be welcomed, is to present even complex relationships by deriving them from simple considerations and models. This enables the reader to understand the significance of the essential mathematical "equipment" of electrochemistry, which older textbooks often treat in a way that discourages the student. Usually the technique works well (e.g., in Chapter 11 on the deposition and dissolution of metals), but occasionally the author takes the process too far. For example, the explanation of the nonstationary method of cyclic-voltammetry by relating it to the limiting stationary case would have been better avoided (and, moreover, the formation of the peak is *not* due to the disappearance of the surface concentration but to a depletion in the diffusion layer and an increase of this layer's thickness).

In a basic textbook it is, of course, appropriate to cite only a few key publications, which can then provide a way into the extensive primary literature. However, in a book which frequently emphasizes recent developments in electrochemistry, it is surprising that the references given for some areas of research that have been most active in recent years are limited to very old publications. For example, those for Chapters 7 (theory of electron transfer reactions) and 12 (complex reactions) are all from the 1950s and 1960s, apart from a 1974 review on normal coordinate analysis.

As explained in the preface, this book is a considerably revised translation (from English into German) of the author's *Interfacial Electrochemistry*. It turns out that in the course of this revision certain chapters, including some on surface methods, have been omitted, while new sections on mass transport have been added. Since the author repeatedly emphasizes the surface aspects of electrochemistry, which in my view is exactly where the book's main strength lies, the reason for this choice is not altogether clear. It would have been better to retain the reference to interfaces in the title of the German version, so as to make it clear that this treatment of the "Grundlagen der Elektrochemie" does not include, for example, the (also important) subject of electrochemically induced homogeneous reactions. The title as it stands could lead one to expect more from the book than it actually contains.

Apart from the shortcomings mentioned above (which should certainly be corrected by the author and the publishers), this is a moderately priced volume which offers an overview of the important subject of electrochemistry at interfaces, and it is suitable not only as an introduction but also for advanced students. In this respect, I am shure that there is a demand for such a text book.

Bernd Speiser
Institut für Organische Chemie
der Universität Tübingen (Germany)

 © WILEY-VCH Verlag GmbH, D-69451 Weinheim, 1997 0570-0833/97/3617-1911 $ 17.50+.50/0

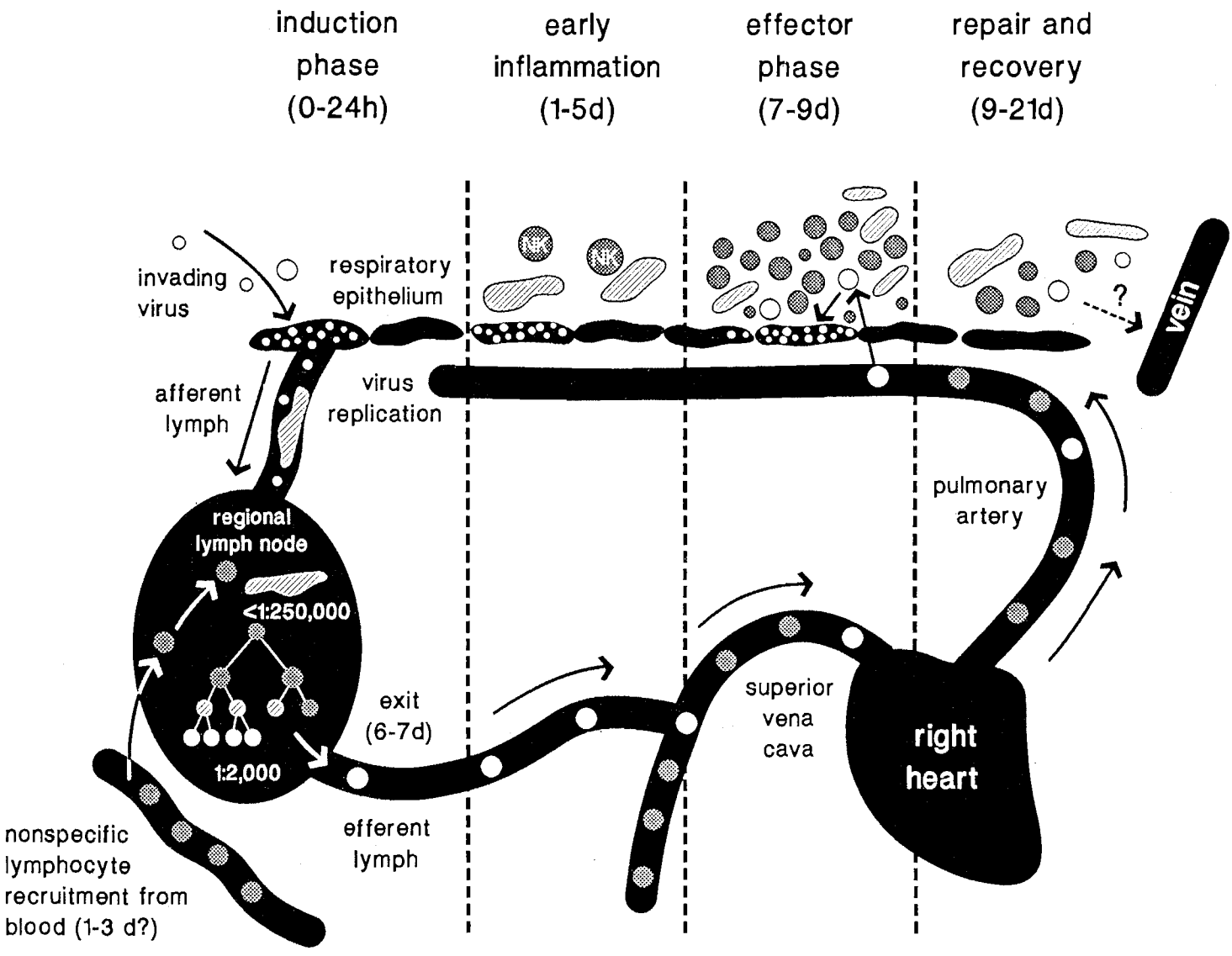

primary CD8$^+$ T cell response upon infection of the respiratory tract

ANGEWANDTE CHEMIE ©WILEY-VCH

Cell-Mediated Immunity in Virus Infections (Nobel Lecture)**

Peter C. Doherty*

Introduction

Many key concepts concerning the nature of immunity have originated from the very practical need to control virus infections. This year, 1996, has been designated the "Year of the Vaccine" commemorating the 200th anniversary of Edward Jenner's vaccination of James Phipps with cowpox virus, and the subsequent challenge with smallpox virus. Insight into the nature of viruses, and how viruses interact with mammalian cells, has evolved since the turn of the century. Our concepts of immunity developed concurrently, beginning with Pasteur's treatment of Joseph Meissner with "aged" rabies virus. Antibody-mediated protection conferred by attenuated, live yellow-fever virus won the Nobel Prize for Max Theiler in 1951. Perhaps the most exciting area of immunology when I graduated from the University of Queensland Veterinary School in 1962 was the nature of virus neutralization,[1] a topic that is still being resolved with the monoclonal antibody (mAb) technology originated by Georges Köhler and César Milstein (Nobel Prize 1985). Crystallographic analysis of influenza virus neuraminidase-mAb complexes and variants of neuraminidase selected by mAbs led to the clear demonstration that Ig molecules normally bind to tertiary structure on proteins.[2]

The present award is for our discovery[3–6] from experiments with lymphocytic choriomeningitis virus (LCMV) that the nature of T cell mediated immunity (CMI) is essentially different, focusing on the recognition of cell-surface major histocompatibility complex (MHC) glycoproteins that have been modified as a consequence of infection (see Figure 1). My intention here is to place these findings in historical context and to develop some aspects to the present day in the context of viral immunity and pathology.

The Australian School of Viral Pathogenesis and Immunity

The strengths in both virology and immunology at the John Curtin School of Medical Research (JCSMR), where we did the LCMV experiments, were a direct consequence of themes developed in Australia by F. M. (Sir Mac) Burnet. Over a period of more than twenty years, Sir Mac built the Walter and Eliza Hall Institute (WEHI) in Melbourne into a major international center for virus (particularly influenza) research. In the late 1940s the only person working there on another virus disease was Frank Fenner, who at Burnet's suggestion studied the epidemiology and pathogenesis of ectromelia (mousepox). Following Burnet's demonstration that ectromelia could be titrated by pock assay on chick chorioallantoic membrane, Fenner did careful quantitative studies of virus distribution in a range of tissues.[7] His conclusion was that the virus replicated initially at the site of inoculation in the dermis, then the regional lymph nodes, then generalized via the liver and spleen, and again to the skin, where it produced a smallpox-like rash. He also noted that delayed-type "allergy" appeared earlier than the serum antibody. In 1949 Fenner became Head of the Department of Microbiology in the JCSMR at the Australian National University, which had just been formed largely as a consequence of initiatives taken by Sir Howard (later Lord) Florey (Nobel Prize 1945). Fenner built a very strong center for virology research.

In 1957, having just enunciated the clonal selection theory,[8] Burnet abandoned virology and redirected the work of the WEHI to basic immunology, a focus continued with great distinction by his protégée G. J. V. Nossal. Nossal recruited J. F. A. P. Miller, who established a strong program in T cell immunology that was to have a major influence both locally and on the international scene. Many of the leading WEHI virologists joined Fenner's department in Canberra. One of the few remaining in Melbourne was G. L. Ada, who switched to immunology. Gordon Ada then moved to Canberra in 1968, replacing Fenner who had become Director of the JCSMR. By the time that I arrived the microbiology department in Canberra had a strong research effort in immunology, interfacing with the virologists remaining from the Fenner era.

Fenner's ectromelia model was subsequently pursued at the JCSMR in two ways that were to influence our discovery. The first was that C. A. Mims made extensive use of fluorescence microscopy to define patterns of virus growth in different organ sites,[9] helping to keep the general area of whole-animal viral pathogenesis alive through the 1960s when most virologists (following Ender, Weller, and Robbins, Noble Prize 1954) turned their attention to in vitro tissue culture systems. Fenner's final contribution to experimental viral immunology was to recruit R. V. Blanden back to Australia from the Trudeau Institute, where he had been working with George Mackaness (a Florey

[*] Prof. P. C. Doherty
Department of Immunology
St. Jude Children's Research Hospital
332 North Lauderdale
Memphis, TN 38104 (USA)
Fax: Int. code +(901)495-3107

[**] Copyright © The Nobel Foundation 1997. We thank the Nobel Foundation, Stockholm, for permission to print this lecture.

trainee and former JCSMR scientist) on CMI in bacterial infections.[10] Bob Blanden applied the approaches that he had developed with Mackaness to the ectromelia model, using both adoptive transfer experiments and depletion with anti-thymocyte serum to show the crucial role of T lymphocytes in controlling the infection.[11-13]

I had followed Mim's papers for many years and returned to Australia from Edinburgh at the end of 1971 to work with him. He had warned me that he might be moving to a Chair in Microbiology in London, and left before the end of 1972. I inherited his laboratory, his technician (Gail Essery), and the LCMV model that had been brought to Canberra some years before by Fritz Lehmann-Grube. Rolf Zinkernagel arrived in 1973 to work with Blanden on CMI in Salmonellosis. Due to space requirements Gordon Ada moved Rolf into the laboratory with me, which is how our collaboration started. Rolf was later to use our experimental data for his Ph.D. thesis but, though I helped him with the writing, the relationship was always as equal colleagues rather than supervisor and student.

Early Experiments with LCMV and the Discovery of MHC Restriction

My initial focus with the LCMV model was to combine contemporary T cell immunology approaches with the capacity to quantitate inflammatory pathology[14] by counting cells in mouse cerebrospinal fluid (CSF), using a CSF tap technique that I had learned from R. I. Carp.[15] This proved to be a very powerful approach (Figure 2), providing strong support for the theme developed initially by W. P. Rowe and J. E. Hotchin (and later by D. H. Gilden, G. A. Cole, and N. Nathanson) that clinical LCM is an immunopathological disease.[16-18] The most visually satisfying experiment done at this time was to use Evan's blue injection to show that the virus-immune T cells were causing a total breakdown of the blood-brain barrier to protein, an experiment that reaches back to the dye studies of Paul Ehrlich (Nobel Prize 1908). Much of this work never appeared in the primary literature and was only published[3] in an article that G. Möller requested for *Transplantation Reviews*. This also carried the first, tentative description of the MHC-restriction finding.

The formal collaboration with Rolf Zinkernagel started when I suggested that we might look to see if the CSF cells that I was obtaining (Figure 2) from clinically affected mice could be shown to have cytotoxic T lymphocyte (CTL) activity. Having worked in Lausanne he was very familiar with the ^{51}Cr-release assay that was being used so effectively by J.-C. Cerottini and K. T. Brunner[19] to study alloreactivity, and had tried (unsuccessfully) to apply the approach to the Salmonella model. The CTL assay had already been used with spleen cells from LCMV-infected mice by M. B. A. Oldstone, O. Marker, M. Volkert, and colleagues.[20, 21] Fortuitously, we were using H-2^k-compatible CBA/H mice and L929 fibroblasts (L cells) as a source of T lymphocytes and virus-infected targets, respectively. The first experiment worked beautifully, and we were able to show that the lytic activity was mediated by Thy-1 positive cells.[22]

At about this time, the very active group of cellular immunologists that made up Gordon Ada's weekly "bible class" had been discussing recent publications on immune response (Ir) gene effects from B. Benacerraf (Nobel Prize 1980) and D. H. Katz at Harvard, which used a very complex in vivo mouse model of T cell/B cell collaboration.[23] We later read of the experiments of E. Shevach and A. Rosenthal at NIH, Bethesda, Maryland, USA, who were looking at the Ir gene question using in vitro stimulation of guinea-pig T cells.[24] The paradigm[25] in this East Coast USA immunology axis was that the Ir genes, which had been mapped to the I-region (now MHC class II) between the loci for the "strong" transplantation antigens (H-2K and H-2D, now MHC class I), encoded all (or part of) the "enigmatic" T cell receptor (TCR). This interpretation would probably have quickly been revised when it became apparent that the Ir gene product (Ia antigen) was expressed on macrophages.[26]

We then saw a report by H. McDevitt, G. R. Mitchell, and M. B. A. Oldstone that there was an "Ir gene" effect in the LCM immunopathology model.[27] This stimulated us to accumulate all the mouse strains that were available in Canberra (CBA/H, BALB/c, and C57BL/6J) to see if we could correlate the level of CTL activity with the H-2 type. The big surprise was that only the H-2^k T cells were lytic for the MHC-compatible, LCMV-infected L cells.[3, 4] We had no appropriate H-2^b or H-2^k cell lines available, so we used primary peritoneal macrophages[28] to

Peter C. Doherty was born in 1940 in Australia. He studied veterinary medicine at the University of Queensland, Australia. From 1963 to 1967 he was at the Animal Research Institute in Brisbane, Australia, and from 1967 to 1971 at the Department of Experimental Pathology of the Moredun Research Institute in Edinburgh, Scotland, where he finished his Ph.D. in 1970. After a position as a Research Fellow in the Department of Microbiology at the John Curtin School of Medical Research at the Australian National University in Canberra, he became a Professor at the Wistar Institute in Philadelphia, PA, USA. In 1982 he went back to Canberra, this time as Professor and Head of the Department of Experimental Pathology. He has been the Chairman of the Department of Immunology at the St. Jude Children's Research Hospital in Memphis, TN, USA since 1988, and, in addition, Adjunct Professor of the Departments of Pathology and Pediatrics of the College of Medicine at the University of Tennessee in Memphis since 1992. He has been awarded numerous scientific fellowships and awards including the Paul-Ehrlich-Preis in Germany, the Gairdner Foundation International Award in Canada, The Albert Lasker Medical Research Award in the USA, and the 1996 Nobel Prize for Medicine and Physiology.

provide a source of LCMV-infected targets to demonstrate reciprocal exclusion of T cell recognition. The next important experiment was with the H-K^kD^d A/J mouse strain,[29] establishing that CTL recognition mapped to H-$2D^d$ and (perhaps) to H-$2K^k$. Later studies on immunodominance hierarchies[30, 31] were to show us how lucky we had been to have a system available where both the H-2K and H-2D alleles were associated with a potent LCMV-specific CTL response. The basic findings with LCMV were rapidly replicated for ectromelia by Bob Blanden's student Ian Gardner.[32] Bob also used his contacts as a more established immunologist to bring in a range of H-2 recombinant and mutant mouse strains over the next 12–18 months that were used (with both the LCMV and ectromelia models) to map virus-specific CTL effector function to the MHC class I alleles.[33, 34] The more detailed description of the actual experiments, the preceding history of the MHC, and the way that the TCR repertoire develops during ontogeny are covered in the accompanying article by Rolf Zinkernagel.[35]

The "Single TCR Altered Self" Hypothesis

Right from the time that we made the discovery[3–6] we considered that there might be two possible explanations for our findings (Figure 1). The first was based on the "TCR"-type

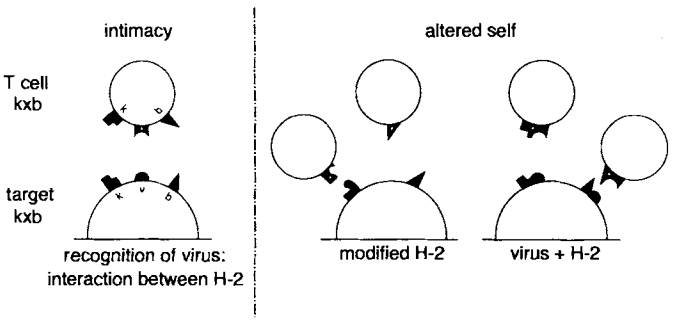

Figure 1. Formulation of the "single T cell receptor altered self" hypothesis. It was published in the second article that appeared in *Nature* [4] about a year after the initial experiment showing MHC restriction of CTL activity. In this paper we discredited the "intimacy" model, which argued that there might be some form of "like–like" interaction between H-2 glycoproteins expressed on the T lymphocyte and the target cell. The experiments and the intellectual context are dealt with in much greater detail in the accompanying article by Rolf Zinkernagel [35].

hypothesis of Katz and Benacerraf, which was formulated as the various dual-recognition models proposed through the 1970s and early 1980s. The second was that the virus was in some way modifying the MHC molecule,[4–6] either by complexing with it on the cell surface or by inducing some other (perhaps allosteric) change. This idea of an "altered-self" molecule recognized by a single TCR seemed reasonable for virus-infected cells, though we were a bit perturbed when the recognition of "minor" histocompatibility antigens was later shown to obey the same rules.[36, 37] Evidence against the dual-recognition model as originally stated (like–like interaction) came from adoptive transfer studies, where we showed that LCMV-primed T cells from H-2 heterozygous mice ("AxB" F1) that would kill virus-infected A and B target cells partitioned into "clonotypes" lytic for A + v (v = virus) alone or B + v alone following further stimulation in irradiated, virus-infected mice of type A or B, respectively.[5] Later variants of "two-receptor" models got around this problem by arguing that the postulated recognition molecules seeing A or B molecules were themselves clonally excluded.

The single TCR altered self hypothesis allowed us to assign a biological role to the strong transplantation antigens, and to explain alloreactivity, Ir gene hierarchies, and the extreme polymorphism of the MHC. We believed from the outset that we had found the mechanistic basis of immunological surveillance of self, though we used the term in a somewhat different context[5, 6, 38, 39] from that employed by Lewis Thomas and Burnet in their discussion of susceptibility to cancer.[40] Many people did not accept the altered-self idea, including some of our colleagues in the JCSMR group.[34] It was to remain controversial and regarded as heretical by most T cell immunologists for the next ten years or so (discussed in ref. [41·42]). The two-receptor models that were generally favored continued, however, to have the problem that they offered no satisfactory generalization that would accommodate alloreactivity and the Ir gene mechanism.

The resolution of the dilemma came with the finding of A. R. Townsend, A. J. McMichael, and colleagues that the class I MHC molecules present viral peptides processed by the "endogenous" pathway.[43] This, together with the publication of the three-dimensional structure of a class I MHC molecule by P. Bjorkman, J. L. Strominger, D. C. Wiley et al[44] and the definition of the two-chain TCR by M. M. Davis, S. Hedrick, T. Mak, J. Allison, P. Marrack, J. Kappler, S. Tonegawa, and others,[45] put the final nail in the coffin of the various "dual-receptor" TCR models. The recent characterization of the tertiary structure of the TCR provides a very satisfactory conclusion to the debate that started with the altered-self hypothesis.[46, 47]

The LCMV Model and T Cell Targeting In Vivo

The MHC restriction of CTL effector function indicated from the outset that the virus-immune T cell must interact directly with the virus-infected target cell. This had already been obvious for alloreactivity, but no one had suggested that the strong transplantation antigens were in any way involved in the immune response to pathogens. Thinking about CMI in infectious diseases had been very much constrained by experiments with *Listeria monocytogenes*, which emphasized the need for T cells in macrophage recruitment and activation.[10] The numbers and the status (in terms of heat shock–protein mRNA expression) of monocyte/macrophages that localize to the lungs of mice infected with an influenza A virus are, for example, clearly a function of the concurrent $CD4^+$ and/or $CD8^+$ T cell response.[48] Macrophages activated during the T cell mediated elimination of LCMV or ectromelia virus can rapidly destroy *L. monocytogenes*.[49]

The MHC-restriction findings with in vitro CTL assays were quickly translated into the in vivo situation. One of the reasons that the LCMV model was so powerful was that we had a very clean in vivo system for analyzing an inflammatory process. Unlike many viruses, LCMV causes little damage and the levels of "background" cellular infiltration independent of the T cell response[3, 50] are low (Figure 2). Combining this with the ca-

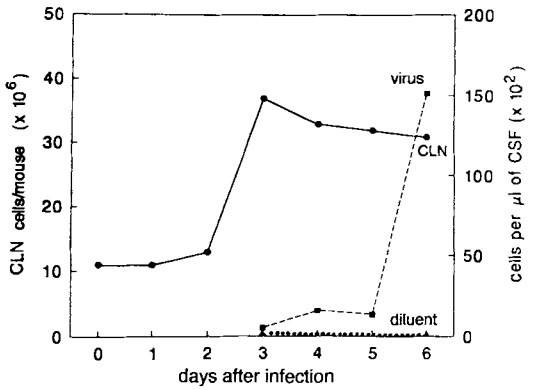

Figure 2. The finding that led to the discovery of MHC restriction was the demonstration that the inflammatory population recovered from the CSF of mice with clinical LCM contains potent CTL effectors [22]. The data shown is from a much later experiment [50], which illustrates the massive influx of cells (dashed line) into the CSF accompanying the onset of CTL activity between days 5 and 6 after infection of the central nervous system. Also shown (solid line) is the preceding increase in cellularity (fourfold) of the cervical lymph nodes (CLN).

pacity to quantitate very accurately by counting cells in the CSF allowed us to determine rapidly by adoptive transfer experiments that the same rules apply for T cell recognition in vitro and in vivo. This was shown for differences in MHC haplotype, particular MHC class I alleles and for H-2 mutant mice.[34, 51, 52]

The interpretation that the T cell must bind directly in vivo to the virus-infected target rather than just to an appropriate antigen-presenting stimulator cell has, however, continued to be subject to challenge. The alternative idea is that cytokines released as a consequence of such interactions are the key effector molecules, an idea that seems to work for the control of a hepatitis virus transgene by interferon-mediated mechanisms.[53] So far this hepatitis model seems to be unique. Adoptively transferred LCMV-immune T cells only caused severe meningitis in virus-infected, chimeric mice when the appropriate MHC restriction element was present on virus-infected epithelial cells in the brain. Neither secondary stimulation of the virus-specific CTL populations in lymphoid tissue nor interaction with inflammatory monocyte/macrophages in the site of pathology were alone sufficient to cause the massive cellular extravasation characteristic of LCM.[54–56]

Perhaps the final indication that the LCMV-immune effector CTL must interact directly with virus-infected CNS epithelia in vivo has come from experiments with perforin −/− mice, which failed to develop the classical symptoms of T cell mediated immunopathology.[57] Cytokine-mediated mechanisms may, however, be responsible for the chronic wasting disease[58–60] that develops in LCMV-infected CD8 "knockout" (−/−) mice and $CD8^+$ T cell deficient mice[61] that are −/− for β2-microglobulin (β2-m), the light chain of the MHC class I glycoproteins. Both these genetically manipulated mouse strains mice are unable to clear LCMV, leading to a persistent confrontation between virus-infected stimulators and the immune $CD4^+$ population. The studies with LCMV and other experiments with respiratory viruses (see below) indicate that the effector mechanisms used by $CD4^+$ and $CD8^+$ T cells to deal with viruses are fundamentally different.

The Non-Self Component: Analysis with Respiratory Viruses

The division of labor in the LCMV experiments at the JCSMR was that Rolf Zinkernagel did the in vitro CTL analysis, while I was responsible for the in vivo immunopathology experiments and for writing the manuscripts with, of course, the benefit of his immediate and constant critique. I thus used respiratory infection with the parainfluenza type 1 virus, Sendai virus, to develop a facility with the CTL assay,[62] and to confirm that MHC restriction was true for more than LCMV and the pox viruses.[27, 32, 63] I returned to the Sendai model[64, 65] years later at St Jude Children's Research Hospital, principally because of the molecular virology expertise available in the laboratory of A. Portner.

When I moved to the Wistar Institute (Philadelphia, USA) in mid 1975, it quickly became apparent that the animal facility was not sufficiently secure to allow extensive experimentation with LCMV, which can easily induce clinically "silent" infections in mouse colonies. The CTL response to Sendai virus was being studied by others at the Wistar, so I took the opportunity to collaborate with W. E. Gerhard on the analysis of T cell mediated immunity to the influenza A viruses (Figure 3).

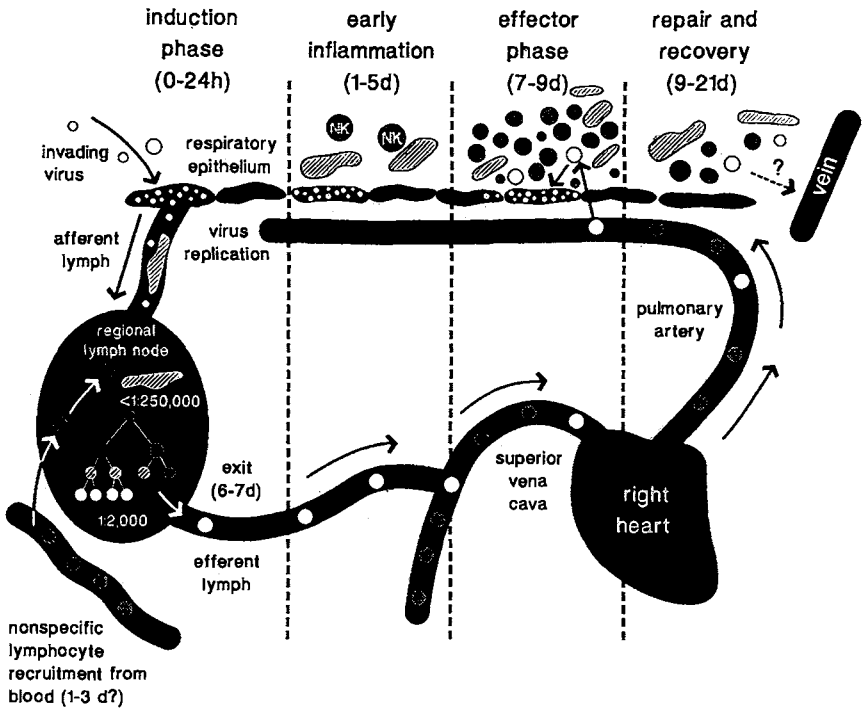

Figure 3. The various events occurring in the respiratory tract and regional lymph nodes are illustrated for mice infected with an influenza A virus or with Sendai virus [64, 98, 83]. Infectious virus cannot generally be recovered from the lung subsequent to day 9 after infection. The $CD8^+$ and $CD4^+$ T cells are responsible for most of the monocyte/macrophage recruitment [48]. The $CD8^+$ set predominates in the inflammatory exudate, but most of these lymphocytes are memory T cells specific for other antigens. Probably less than 1:100 are reactive to the inducing pathogen [99]. Potent CTL effectors and large numbers of cytokine-producing cells are found mainly in the virus-infected lung.

Walter Gerhard had learned his influenza virology at the Institut für Immunologie in Basel from Stephen Fazekas de St. Groth,[1] who had formerly been a leading figure in Fenner's virology department at the JCSMR.

The aim was to exploit "recombinant" influenza A viruses to dissect the other half of the T cell specificity equation, for viral components rather than for MHC glycoproteins. The so-called recombinants result from growing two different influenza A viruses concurrently in the one cell.[66] The eight segments of the influenza genome repackage to give novel variants, the mechanism responsible for the phenomenon of "antigenic shift". The principal focus of immunology-related influenza research, which tends to focus on vaccine studies, was on the viral hemagglutinin (H) and neuraminidase (N) glycoproteins. These virion surface proteins are subject to the antibody-mediated selection pressure that results in "antigenic drift", a further mechanism that can give rise to novel pandemic strains.

We thought that by using serologically distinct variants such as the H1N1 and H3N2 viruses, which do not cross-neutralize, we would be able to map CTL activity to H or N, both of which are expressed on the plasma membrane of the virus-infected cell. The aim then was to use "drifted" variants to map fine specificity. The initial experiments were done by my first graduate student, R. B. Effros, and were later pursued by my second student, J. R. Bennink. Much to our surprise, Rita found that the CTL response for these two viruses was almost totally cross-reactive.[67, 68] Though we were unaware of it at the time, similar findings were being recorded in B. A. (Ita) Askonas's laboratory at the National Institute for Medical Research in London.[69] Our findings with LCMV had induced Ita to drop her long-term studies of the B cell responses to concentrate on virus-specific T cell mediated immunity. Her laboratory was to make an enormous contribution over the next ten years.

Though we failed at this stage to define the nature of the antigenic entity recognized by the influenza specific CTL, these early experiments further supported the conclusion from the MHC restriction analysis that the specificity profiles of T and B lymphocytes are fundamentally different.[34, 70] In addition, we quickly established that exposure to any one influenza A virus will prime T cell memory for a secondary response (Figure 4) to any other influenza A virus.[68, 71] This meant that infection with a "drifted" or "shifted" influenza A virus in an adult person is likely to proceed in the context of a secondary CTL response and a primary humoral response. The albeit imperfect protection conferred by influenza-specific memory T cells[72–74] probably explains why young to middle-aged adults are generally much less likely to die from influenza than are small children or elderly people. These results were quickly confirmed for other viruses that had, after the influenza experiments, also been found to induce CTL specificity profiles that were not predicted by serological analysis.[75]

Other significant experiments that were done with the influenza model at about this time were the extension of MHC restriction to the rat model[76] and, most importantly, the clear demonstration by A. J. McMichael in Askonas's laboratory that this is also true for humans.[77] Further pursuit of this unpredicted cross-reactivity for the influenza viruses led to A. Townsend's (again from the Askonas's laboratory) seminal finding[43, 78] that MHC class I restricted T cells are responding to a peptide derived from the influenza nucleoprotein (NP), which finally explained the molecular mechanism underlying our altered-self hypothesis (Figure 1) and started the whole field of antigen processing in the "endogenous" compartment. Analysis at the Wistar Institute by Jack Bennink and J. R. Yewdell with recombinant vaccinia viruses also showed that much of the CTL recognition in the influenza model is directed at internal components of the virus.[79]

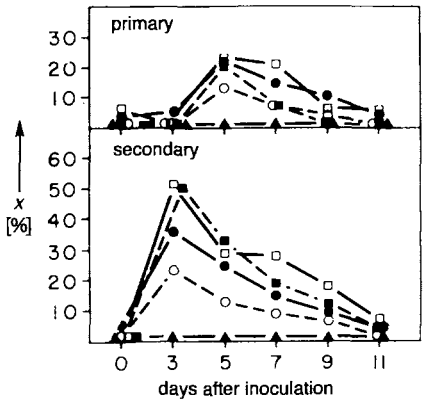

Figure 4. Immunologically naive (primary) CBA/J (H-2^k) mice, or mice that had been infected with the PR8 (H1N1) influenza A virus 52 days previously (secondary), were challenged with the HK × 31 (H3N2) influenza A virus [68]. Spleen cells were assayed (100:1) at the intervals shown on H-2 compatible targets infected with a range of influenza A viruses or with an influenza B virus (triangles). Both the enhanced kinetics and potency of the recall response are very apparent. Later experiments with HK × 31 infection of C57BL/6J (H-2^b) mice have shown very little CTL activity in lymphoid tissue following primary exposure [98]; x = specific ^{51}Cr release.

Latterly, the nonlethal respiratory infections have emerged as the experimental system of choice for analyzing localized, transient viral infections.[80–83] These models have the advantage that it is easy to obtain both the regional lymphoid tissue and the inflammatory cells from the pneumonic lung by bronchoalveolar lavage (BAL). There is also no obvious way that either the virus or the viral genome can persist after infection with such negative strand RNA viruses,[84] which is important when we are considering the difficult area of T cell memory [85].

Some recent experiments addressed again the question of T cell targeting in vivo that we had analyzed earlier with the LCMV model (Figure 2). Using adoptive transfer protocols and bone marrow radiation chimeras made between β2-m $-/-$ and $+/+$ mice, we showed that the clearance of Sendai virus depends on the $CD8^+$ effector T cells interacting directly with virus-infected, MHC class I^+ respiratory epithelium.[86] The opposite conclusion was reached concerning the capacity of $CD4^+$ T cells[87–89] to control influenza virus infection in the absence of the $CD8^+$ subset: Expression of the MHC class II glycoproteins that target the $CD4^+$ T cells is not essential in the respiratory tract.[90] More recent experiments performed by David Topham are confirming the theme developed by Walter Gerhard[91] that complete clearance of the virus by $CD4^+$ T cells requires the concurrent presence of antibody-forming cells.

Quantitating Inflammation and T Cell Mediated Immunity

The essence of the virology-based approach to pathogenesis has always been quantitation, a theme that was started by Mac Burnet with his various plaque assays and continued by Cedric Mims for the fluorescence microscopic localization of virus-infected cells in different organ sites.[9] Measuring the inflammatory process that is the consequence of CMI has, however, traditionally been (at best) semiquantitative. The classical delayed-type hypersensitivity foot-pad swelling assay is a very blunt instrument.

Analyzing Inflammation

My early experience in ultrastructural pathology and immunocytochemistry[92, 93] resulted in an intense curiosity concerning the nature of the lymphocyte populations that invade into tissue sites of virus growth (Figure 5). The experiments that

Figure 5. My interest in the nature of virus-specific CMI was stimulated by the experimental studies of louping-ill encephalomyelitis that Hugh Reid and I did with sheep at the Moredun Research Institute, Edinburgh [92–94]. The electron micrograph shows cells of undetermined identity extravasating from a capillary into the brain parenchyma. Lymphocyte invasion into tissue sites of virus growth is the central feature of CMI.

H. W. Reid and I did with the sheep louping-ill (tick-borne flavivirus) model at the Moredun Research Institute in Edinburgh led to the conclusion that antibody-forming cells were extravasating into the CNS and were responsible for a substantial, in situ virus-specific Ig response.[92, 94] Much later studies by D. E. Griffin have shown that such locally produced antibody controls Sindbis virus infection of mouse brain.[95]

The dual frustrations with morphological approaches are the lack of functional analysis and the difficulty of quantitation, though my current perception is that there is a great need to focus more attention on the anatomical localization of events in immunity that is only possible with microscopy-based protocols. My early attempts at quantitating inflammatory pathology caused me to seize on the CSF tap technique that Richard Carp[15] had developed to look for enzymatic activity in CSF from scrapie-infected mouse brain and apply it to the study of viral meningitis (Figure 2). Experiments with this simple model induced us to develop the LCMV-specific CTL assay, and allowed the later in vivo dissection of MHC-restricted T cell effector function. The capacity to measure statistically significant differences for quite small effects enabled us to operate with unique sensitivity in the in vivo situation.[3, 34] However, because the approach was technically demanding and only really useful with the LCMV model, nobody else adopted this analytical system. The other, great advantage of being able to obtain inflammatory cells directly from the CSF (or from the lung by the BAL) is that the lymphocytes do not need to be freed from tissue by enzymatic techniques. This has been of great benefit for later experiments concentrating on flow cytometric analysis and FACS separation to define functional T cell subsets,[56, 96, 97] experiments that were first started for LCMV (with R. Ceredig in Canberra) and have been a major focus of the respiratory infection studies[98, 99] in Memphis (Figure 3).

Measuring the T Cell Response

Though the in vitro ^{51}Cr-release CTL assay provides numbers, the precursor (p) frequencies that give comparable levels of lytic activity (both during the course of in vivo infection or as a consequence of in vitro culture) can vary enormously.[100, 101] The potency of the $CD8^+$ CTL set in the BAL population from mice with influenza pneumonia is, for example, apparently equivalent by day 10 after infection for $CD4^+$ T cell deficient MHC class II $-/-$ mice and for MHC class II $+/+$ controls.[101, 102] However, the CTLp numbers in both the BAL and regional lymph nodes are much lower for the MHC class II $-/-$ mice, and virus clearance may be slightly delayed. The much smaller CTLp pool in the MHC class II $-/-$ mice is almost totally consumed to provide the level of CTL effector function needed to deal with the infection. A conclusion based on the CTL data alone that the absence of the $CD4^+$ set does not greatly modify the magnitude of the $CD8^+$ T cell response would thus be misleading. Careful kinetic analysis is essential in these in vivo pathogenesis studies.

We first realized this when we tried to quantitate the Ir gene hierarchy that we discovered for the MHC class I alleles H-2K^k, H-2K^b, and H-2D^b with the influenza A viruses.[30, 31] The situation here is that the CTL response associated with H-2D^b + NP peptide is dominant in mice that express H-2K^b, but apparently absent when H-2K^k is present. The same thing happens with vaccinia virus. Jack Bennink and I tried hard to work out the underlying mechanism, using thoracic duct cannulation and negative selection in vivo to remove the alloreactive T cells,[103] a very tedious protocol that we learned from J. A. Sprent. The lack of any useful resolution is a good example of the fact that (though important insights can be generated) molecular mechanisms cannot ultimately be worked out by biological experiments. My current guess is that H-2K^k must greatly out-compete H-2D^b for binding some constant molecule involved in the MHC class I antigen processing pathway,[104] though not to the extent that H-2D^b + NP peptide is no longer present at sufficient levels to be recognized by the appropriate effector CTL on an H-K^{k}D^b target cell.

When J. A. Owen joined the laboratory in Philadelphia she took on the task of developing a quantitative limiting dilution analysis (LDA) for determining influenza virus specific CTLp frequencies,[105] an approach that has been central to my research program over the subsequent years. Judy Owen and Michelle Allouche then applied this technique to the H-2K^{k}D^b hierarchy problem and found that, for mice that had been primed a month or more previously, the CTLp numbers specific for influenza virus components expressed in the context of H-2K^k and H-2D^b may be fairly comparable.[106] Recent experiments with this experimental system by R. A. Tripp in Memphis indicate that the reason that the H-2K^k-restricted CTL effectors are preferentially generated is that this component of the response emerges more quickly.

The Rate Problem in Immunology

The preceding is a good example of one of the major difficulties that we face in developing a detailed understanding of immunity. How do we measure the true kinetics of responses in terms of lymphocyte generation and loss, and in the context of transit times through the various tissue sites that are sampled? A major insight developed from studies with superantigens was that the majority of the T cells that proliferate following such stimulation die as a consequence.[107, 108] We initially thought that this was not the case for "conventional" antigens, such as influenza virus or Sendai virus epitopes, largely because sequential LDA studies indicated a remarkable constancy (Figure 6) in CTLp frequencies (1:2–3000 cells in a lymph node) from about day 7 after infection through to long-term memory.[85, 99, 109] This was somewhat different from the situation that was concurrently being described for LDA studies with LCMV by Rafi Ahmed,[110] but we agreed that the difference was probably due to the fact that systemic LCMV infection undoubtedly gives a much greater antigenic stimulus.

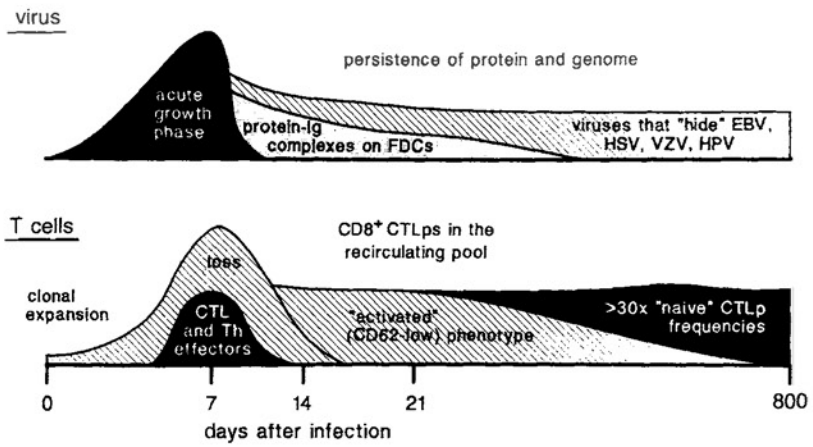

Figure 6. Virus: Replication of the negative strand RNA viruses is generally terminated by the immune response within 7–10 days [84, 118], with the only trace of the infectious agent generally being the long-term maintenance of protein–Ig complexes on the surface of follicular dendritic cells [110]. These do not seem to be necessary for the maintenance of influenza-specific CD4$^+$ T cell memory [119], but are probably essential for B cell memory. Other pathogens, such as the herpes viruses, may persist in a latent form in neurons or B lymphocytes, and periodically reactivate into lytic phase [120]. T cells: Clonal expansion of the CD4$^+$ THp and CD8$^+$ CTLp during the acute phase of the response is greatly in excess of the numbers required to generate the cytokine-producing TH or effector CTL populations that deal with the infection. Many of the CTLp, in particular, either die or are excreted, and CTLp frequencies may remain remarkably stable thereafter for the life of a laboratory mouse. However, the activation phenotype of these T cells may (as first shown by Sam Hou [121]) change with time.

The thymidine analogue bromodeoxyuridine (BrDU) incorporates into the DNA of multiplying cells and causes the formation of toxic thymidine dimers following exposure to bright light, a protocol that was used many years ago to "suicide" in vitro stimulated T cells.[111] Ralph Tripp found that loading proliferating T cells with BrDU in vivo led to the same effect when the lymphocytes were exposed to the laser beam of the flow cytometer.[112] Use of this protocol indicates that the CTLp numbers generated during the acute phase of the response to an influenza A virus are more than tenfold in excess of what would be expected from estimates of CTLp frequencies (Figure 6). Some of these T cells will give rise to the CTL effectors that are found in the virus-infected respiratory tract, but it seems that many others are lost. Measuring a virus specific CD8$^+$ T cell response by effector CTL assays takes no account of the CTLp numbers that are generated. However, the more extensive quantitation of CTLp frequencies shows only the balance between CTLp generation and loss, and does not give a true estimate of the real magnitude of an acute host response. This is less a problem with T cell memory, where the cell populations are turning over at a much slower rate.[113]

Homeostasis: On the Edge of Chaos?

The above experience, together with trying to understand the nature of T cell memory, has left me with the conviction that the major challenge for cellular immunology is to develop a much clearer understanding of lymphocyte homeostasis.[114] In the past many of us would have followed Burnet's insight that the balance between responsiveness and tolerance is the key question, but recent studies (particularly with transgenic mice) have clarified the issues, blurred the distinction, and made the tolerance–response mantra less compelling.[115] It could be argued that tolerance–response is simply a more refined statement of the homeostasis problem, but language conditions perceptions, and defining the area in this way focuses attention solely towards antigen and away from the more physiological mechanisms and quantitative considerations that are also likely to be enormously important.

An obsession with homeostasis is dangerous territory, as it has led in the past to some of the least useful and expensive efforts in immunology. Even so, it may be time for our experimentally based discipline to take greater cognizance of the contribution that can be made by theoreticians, particularly those who are more mathematically inclined. A good example of the way that quantitative analysis can contribute to the development of better predictive models has been provided by recent determinations of the numbers of virus-infected cells[116] in people infected with the human immunodeficiency virus (HIV). Influenza virus specific memory CD8$^+$ T cells seem to show a remarkable constancy in frequency over a very long period (Figure 6). Is this an example[117] of a

chaotic system? Now that we are starting to generate useful numbers, we need the help of people whose business is numbers.

Conclusions

The need to deal with pathogens has driven the evolution of the vertebrate immune system, so it should not be surprising that experiments with infectious agents have often illuminated key elements of the underlying mechanisms. The discovery of MHC restriction and the development of the single TCR altered self hypothesis is a classical example of how interfacing different scientific disciplines and ways of thinking, an inevitable consequence of studying viral pathogenesis, can lead to a major paradigm shift. The progress that was made over the subsequent ten years, and the intellectual directions that were followed as a consequence of this simple, operational hypothesis tell us a great deal about the power of ideas. This is not to decry the importance of technology. Our success depended totally on the availability of the ^{51}Cr-release CTL assay and inbred mouse strains, both of which had been developed to study alloreactivity. The experiments were done in the context of an experimental framework that was being used to dissect T cell responsiveness, the immunopathology of LCMV infection, and the nature of CMI to *L. monocytogenes* and ectromelia virus. The local intellectual environment was strong, and heavily focused on the then current forefront of immunology research. Being isolated in those pre-fax and e-mail days in Australia was a great advantage, as it allowed time to discuss and to think things through. We had outspoken and informed local critics, the freedom and resources to pursue our own ideas, and were given full credit for our efforts. Those of us who have senior roles in science need to do everything possible to ensure that comparable opportunities and environments remain available to young scientists.

My research career has been supported by the taxpayers of Australia, the United Kingdom, and the United States, the National Multiple Sclerosis Societies of the USA and Australia, and by the American Lebanese Syrian Associated Charities who provide much of the funding for St. Jude Children's Research Hospital. I would have achieved nothing without the devotion and encouragement of my wife, Penny, who is my best friend and critic. I owe a very great deal to my students, fellows, colleagues, and collaborators over the years.

Received: April 7, 1997 [A 221 IE]
German version: *Angew. Chem.* **1997**, *109*, 2014–2025

Keywords: antigens · immunology · MHC · Nobel lecture · T cells

[1] "The neutralization of viruses": S. Fazekas de St. Groth, *Adv. Virus Res.* **1962**, *9*, 1.
[2] "Three-dimensional structure of a complex of antibody with influenza virus neuraminidase": P. M. Colman, W. G. Laver, J. N. Varghese, A. T. Baker, P. A. Tulloch, G. M. Air, R. G. Webster, *Nature* **1987**, *326*, 358.
[3] "T-cell-mediated immunopathology in viral infections": P. C. Doherty, R. M. Zinkernagel, *Transplant. Rev.* **1974**, *19*, 89.
[4] "Restriction of in vitro T cell-mediated cytotoxicity in lymphocytic choriomeningitis within a syngeneic or semiallogeneic system": R. M. Zinkernagel, P. C. Doherty, *Nature*, **1974**, *248*, 701.
[5] "Immunological surveillance against altered self components by sensitised T lymphocytes in lymphocytic choriomeningitis": R. M. Zinkernagel, P. C. Doherty, *Nature* **1974**, *251*, 547.
[6] "A biological role for the major histocompatibility antigens": P. C. Doherty, R. M. Zinkernagel, *Lancet* **1975**, *1*, 1406.
[7] "The clinical features and pathogenesis of mouse-pox (infectious ectromelia of mice)" F. Fenner, *J. Pathol. Bacteriol.* **1948**, *4*, 529.
[8] "A modification of Jerne's theory of antibody production using the concept of clonal selection": F. M. Burnet, *Aust. J. Sci.* **1957**, *20*: 67.
[9] "Pathogenesis of rashes in virus diseases": C. A. Mims, *Bacteriol. Rev.* **1966**, *30*, 739.
[10] "Cellular immunity": G. B. Mackaness, R. V. Blanden, *Prog. Allergy*. **1967**, *11*, 89.
[11] "Mechanisms of recovery from a generalized viral infection: mousepox. I. The effects of anti-thymocyte serum": R. V. Blanden, *J. Exp. Med.* **1970**, *132*, 1035.
[12] "Mechanisms of recovery from a generalized viral infection: mousepox. II. Passive transfer of recovery mechanisms with immune lymphoid cells": R. V. Blanden, *J. Exp. Med.* **1971**, *133*, 1074.
[13] "Mechanisms of recovery from a generalized viral infection: mousepox. 3. Regression of infectious foci": R. V. Blanden, *J. Exp. Med.* **1971**, *133*, 1090.
[14] "Quantitative studies of the inflammatory process in fatal viral meningoencephalitis": P. C. Doherty, *Am. J. Pathol.* **1973**, *73*, 607.
[15] "Higher frequency of a protein band in the cerebrospinal fluid from scrapie mice": P. A. Merz, G. S. Merz, R. I. Carp, *Res. Vet. Sci.* **1973**, *14*, 392.
[16] "Protective effect of neonatal thymectomy on mouse LCM infection": W. P. Rowe, P. H. Black, R. H. Levey, *Proc. Soc. Exp. Biol. Med.* **1963**, *14*, 248.
[17] "Protection against the lethal effects of lymphocytic choriomeningitis virus in mice by neonatal thymectomy": J. Hotchin, E. Sikora, *Nature*, **1964**, *202*, 214.
[18] "Immunopathogenesis of acute central nervous system disease produced by lymphocytic choriomeningitis virus. II. Adoptive immunization of virus carriers": D. H. Gilden, G. A. Cole, N. Nathanson, *J. Exp. Med.* **1972**, *135*, 874.
[19] "Cell-mediated cytotoxicity, allograft rejection, and tumor Immunity": J. C. Cerottini, K. T. Brunner, *Adv. Immunol.* **1974**, *18*, 67.
[20] "Tissue injury in lymphocytic choriomeningitis viral infection: virus-induced immunologically specific release of a cytotoxic factor from immune lymphoid cells": M. B. A. Oldstone, F. J. Dixon, *Virology* **1970**, *42*, 805.
[21] "Studies on cell-mediated immunity to lymphocytic choriomeningitis virus in mice": O. Marker, M. Volkert, *J. Exp. Med.* **1973**, *137*, 1511.
[22] "Cytotoxic thymus-derived lymphocytes in cerebrospinal fluid of mice with lymphocytic choriomeningitis": R. M. Zinkernagel, P. C. Doherty, *J. Exp. Med.* **1973**, *138*, 1266.
[23] "Cell interactions between histoincompatible T and B lymphocytes. The H-2 gene complex determines successful physiologic lymphocyte interactions": D. H. Katz, T. Hamaoka, M. E. Dorf, B. Benacerraf, *Proc. Natl. Acad. Sci. USA* **1973**, *70*, 2624.
[24] "Function of macrophages in antigen recognition by guinea pig T lymphocytes. I. Requirement for histocompatible macrophages and lymphocytes": A. S. Rosenthal, E. M. Shevach, *J. Exp. Med.* **1973**, *138*, 1194.
[25] "The histocompatibility-linked immune response genes": B. Benacerraf, D. H. Katz, *Adv. Cancer Res.* **1975**, *21*, 121.
[26] "Biology of the Mouse Histocompatibility-2 Complex": J. Klein, *Springer, Berlin*, **1975**.
[27] "Histocompatibility-linked genetic control of disease susceptibility. Murine lymphocytic choriomeningitis virus infection": M. B. Oldstone, F. J. Dixon, G. F. Mitchell, H. O. McDevitt, *J. Exp. Med.* **1973**, *137*, 1201.
[28] "Peritoneal macrophages as target cells for measuring virus-specific T cell mediated cytotoxicity in vitro": R. M. Zinkernagel, P. C. Doherty, *J. Immunol. Methods* **1975**, *8*, 263.
[29] "H-2 compatibility is required for T-cell-mediated lysis of target cells infected with lymphocytic choriomeningitis virus": P. C. Doherty, R. M. Zinkernagel, *J. Exp. Med.* **1975**, *141*, 502.
[30] "Cytotoxic T-cell responses in mice infected with influenza and vaccinia viruses vary in magnitude with H-2 genotype": P. C. Doherty, W. E. Biddison, J. R. Bennink, B. B. Knowles, *J. Exp. Med.* **1978**, *148*, 534.
[31] "Ir-genes in H-2 regulate generation of anti-viral cytotoxic T cells. Mapping to K or D and dominance of unresponsiveness": R. M. Zinkernagel, A. Althage, S. Cooper, G. Kreeb, P. A. Klein, B. Sefton, L. Flaherty, J. Stimpfling, D. Shreffler, J. Klein, *J. Exp. Med.* **1978**, *148*, 592.
[32] "Cell-mediated cytotoxicity against ectromelia virus-infected target cells. III. Role of the H-2 gene complex": I. D. Gardner, N. A. Bowern, R. V. Blanden, *Eur. J. Immunol.* **1975**, *5*, 122.
[33] "Genes required for cytotoxicity against virus-infected target cells in K and D regions of H-2 complex": R. V. Blanden, P. C. Doherty, M. B. Dunlop, I. D. Gardner, R. M. Zinkernagel, C. S. David, *Nature* **1975**, *254*, 269.
[34] "Specificity of virus-immune effector T cells for H-2K or H-2D compatible interactions: implications for H-antigen diversity": P. C. Doherty, R. V. Blanden, R. M. Zinkernagel, *Transplant. Rev.* **1976**, *29*, 89.
[35] "Cellular immune recognition and the biological role of Major transplantation antigens (Nobel Lecture)": R. M. Zinkernagel, **1996**, *Angew. Chem.* **1997**, *109*, 2026; *Angew. Chem. Int. Ed. Engl.* **1997**, *36*, 1938.
[36] "The major histocompatibility complex determines susceptibility to cytotoxic T cells directed against minor histocompatibility antigens": M. J. Bevan, *J. Exp. Med.* **1975**, *142*, 1349.

[38] "Enhanced immunological surveillance in mice heterozygous at the H-2 gene complex": P. C. Doherty, R. M. Zinkernagel, *Nature* **1975**, *256*, 50.
[39] "Immunological surveillance of tumors in the context of major histocompatibility complex restriction of T cell function": P. C. Doherty, B. B. Knowles, P. J. Wettstein, *Adv. Cancer Res.* **1984**, *42*, 1.
[40] "Immunological surveillance in neoplasia": F. M. Burnet, *Transplant. Rev.* **1971**, *7*, 3.
[41] "The response to H-2-different virus-infected cells is mediated by long-lived T lymphocytes and is diminished by prior virus priming in a syngeneic environment": J. R. Bennink, P. C. Doherty, *Cell. Immunol.* **1981**, *61*, 220.
[42] "Historical developments in understanding the function of class I MHC genes": P. C. Doherty in *H-2 Antigens, Genes Molecules and Functions* (Ed.: C. S. David), NATO ASI series, Plenum Press, New York, **1987**, p. 341.
[43] "The epitopes of influenza nucleoprotein recognized by cytotoxic T lymphocytes can be defined with short synthetic peptides": A. R. Townsend, J. Rothbard, F. M. Gotch, G. Bahadur, D. Wraith, A. J. McMichael, *Cell*, **1986**, *44*, 959.
[44] "The foreign antigen binding site and T cell recognition regions of class I histocompatibility antigens": P. J. Bjorkman, M. A. Saper, B. Samraoui, W. S. Bennett, J. L. Strominger, D. C. Wiley, *Nature* **1987**, *329*, 512.
[45] "T cell receptor gene diversity and selection": M. M. Davis, *Annu. Rev. Biochem.* **1990**, *59*, 475.
[46] "An $\alpha\beta$ T cell receptor structure at 2.5 Å and its orientation in the TCR-MHC complex": K. C. Garcia, M. Degano, R. L. Stanfield, A. Brunmark, M. R. Jackson, P. A. Peterson, L. Teyton, I. A. Wilson, *Science* **1996**, *274*, 209.
[47] "Structure of the complex between human T cell receptor, viral peptide and HLA-A2": D. N. Garboczi, P. Ghosh, Q. R. Fan, W. E. Biddison, D. C. Wiley, *Nature* **1996**, *384*, 134.
[48] "hsp65 mRNA$^+$ macrophages and $\gamma\delta$ T cells in influenza virus-infected mice depleted of the CD4$^+$ and CD8$^+$ lymphocyte subsets": W. Allan, S. R. Carding, M. Eichelberger, P. C. Doherty, *Microb. Pathog.* **1993**, *14*, 75.
[49] "Macrophage activation in mice infected with ectromelia or lymphocytic choriomeningitis viruses": R. V. Blanden, C. A. Mims, *Aust. J. Exp. Biol. Med. Sci.* **1973**, *51*, 393.
[50] "Phenotypic and functional analysis of the cellular response in regional lymphoid tissue during an acute virus infection": F. Lynch, P. C. Doherty, R. Ceredig, *J. Immunol.* **1989**, *142*, 3592.
[51] "Capacity of sensitized thymus-derived lymphocytes to induce fatal lymphocytic choriomeningitis is restricted by the H-2 gene complex": P. C. Doherty, R. M. Zinkernagel, *J. Immunol.* **1975**, *114*, 30.
[52] "Inflammatory process in murine lymphocytic choriomeningitis is maximal in H-2K or H-2D compatible interactions": P. C. Doherty, M. B. Dunlop, C. R. Parish, R. M. Zinkernagel, *J. Immunol.* **1976**, *117*, 187.
[53] "Viral cross talk: Intracellular inactivation of the hepatitis B virus during an unrelated viral infection of the liver": L. G. Guidotti, P. Borrow, M. V. Hobbs, B. Matzke, I. Gresser, M. B. A. Oldstone, F. V. Chisari, *Proc. Natl. Acad. Sci. USA* **1996**, *93*, 4589.
[54] "Role of the major histocompatibility complex in targeting effector T cells into a site of virus infection": P. C. Doherty, J. E. Allan, *Eur. J. Immunol.* **1986**, *16*, 1237, 1646.
[55] "Immunogenetic analysis of cellular interactions governing the recruitment of T lymphocytes and monocytes in lymphocytic choriomeningitis virus-induced immunopathology": P. C. Doherty, R. Ceredig, J. E. Allan, *Clin. Immunol. Immunopathol.* **1988**, *47*, 19.
[56] "Dissection of an inflammatory process induced by CD8+ T cells": P. C. Doherty, J. E. Allan, F. Lynch, R. Ceredig, *Immunol. Today* **1990**, *11*, 55.
[57] "Cytotoxicity mediated by T cells and natural killer cells is greatly impaired in perforin-deficient mice": D. Kagi, B. Ledermann, K. Burki, P. Seiler, B. Odermatt, K. J. Olsen, E. R. Podack, R. M. Zinkernagel, H. Hengartner,
[58] "Immune response against lymphocytic choriomeningitis virus infection in mice without CD8 expression": W. P. Fung-Leung, T. M. Kundig, R. M. Zinkernagel, T. W. Mak, *J. Exp. Med.* **1991**, *174*, 1425.
[59] "Lymphocytic choriomeningitis virus induces a chronic wasting disease in mice lacking class I major histocompatibility complex glycoproteins": P. C. Doherty, S. Hou, P. J. Southern, *J. Neuroimmunol.* **1993**, *46*, 11.
[60] "Antiviral immune responses of lymphocytic choriomeningitis virus-infected mice lacking CD8$^+$ T lymphocytes because of disruption of the beta 2-microglobulin gene": F. Lehmann-Grube, J. Lohler, O. Utermohlen, C. Gegin, *J. Virol.* **1993**, *67*, 332.
[61] "Beta 2-microglobulin deficient mice lack CD4−8$^+$ cytolytic T cells": M. Zijlstra, M. Bix, N. E. Simister, J. M. Loring, D. H. Raulet, R. Jaenisch, *Nature*, **1990**, *344*, 742.
[62] "Specific immune lysis of paramyxovirus-infected cells by H-2-compatible thymus-derived lymphocytes": P. C. Doherty, R. M. Zinkernagel, *Immunology* **1976**, *31*, 27.
[63] "Lysis mediated by T cells and restricted by H-2 antigen of target cells infected with vaccinia virus": U. Koszinowski, H. Ertl, *Nature* **1975**, *255*, 552.
[64] "Delayed clearance of Sendai virus in mice lacking class I MHC-restricted CD8$^+$ T cells": S. Hou, P. C. Doherty, M. Zijlstra, R. Zaenisch, J. M. Katz, *J. Immunol.* **1992**, *149*, 1319.
[65] "Host response to Sendai virus in mice lacking class II major histocompatibility complex glycoproteins": S. Hou, X. Y. Mo, L. Hyland, P. C. Doherty, *J. Virol.* **1995**, *69*, 1429.
[66] "Evolution and ecology of influenza A viruses": R. G. Webster, W. J. Bean, O. T. Gorman, T. M. Chambers, Y. Kawaoka, *Microbiol. Rev.* **1992**, *56*, 152.
[67] "Generation of both cross-reactive and virus-specific T-cell populations after immunization with serologically distinct influenza A viruses": R. B. Effros, P. C. Doherty, W. Gerhard, J. Bennink, *J. Exp. Med.* **1977**, *145*, 557.
[68] "Heterogeneity of the cytotoxic response of thymus-derived lymphocytes after immunization with influenza viruses": P. C. Doherty, R. B. Effros, J. Bennink, *Proc. Natl. Acad. Sci. USA* **1977**, *74*, 1209.
[69] "Cytotoxic T cells kill influenza virus infected cells but do not distinguish between serologically distinct type A viruses": H. J. Zweerink, S. A. Courtneidge, J. J. Skehel, M. J. Crumpton, B. A. Askonas, *Nature* **1977**, *267*, 354.
[70] "MHC-restricted cytotoxic T cells: studies on the biological role of polymorphic major transplantation antigens determining T-cell restriction-specificity, function, and responsiveness": R. M. Zinkernagel, P. C. Doherty, *Adv. Immunol.* **1979**, *27*, 51.
[71] "Characteristics of secondary cytotoxic T-cell responses in mice infected with influenza A viruses": R. B. Effros, J. Bennink, P. C. Doherty, *Cell. Immunol.* **1978**, *36*, 345.
[72] "The roles of influenza virus haemagglutinin and nucleoprotein in protection: analysis using vaccinia virus recombinants": M. E. Andrew, B. E. Coupar, D. B. Boyle, G. L. Ada, *Scand. J. Immunol.* **1987**, *25*, 21.
[73] "Recombinant vaccinia viruses and the development of immunization strategies using influenza virus": P. C. Doherty, W. Allan, D. B. Boyle, B. E. Coupar, M. E. Andrew, *J. Infect. Dis.* **1989**, *159*, 1119.
[74] "Primary pulmonary cytotoxic T lymphocytes induced by immunization with a vaccinia virus recombinant expressing influenza A virus nucleoprotein peptide do not protect mice against challenge": C. M. Lawson, J. R. Bennink, N. P. Restifo, J. W. Yewdell, B. R. Murphy, *J. Virol.* **1994**, *68*, 3505.
[75] "Experiments and speculation on antiviral specificity of T and B cells": R. M. Zinkernagel, K. L. Rosenthal, *Immunol. Rev.* **1981**, *58*, 131.
[76] "The control of specificity of cytotoxic T lymphocytes by the major histocompatibility complex (AG-B) in rats and identification of a new alloantigen system showing no AG-B restriction": A. Marshak, P. C. Doherty, D. B. Wilson, *J. Exp. Med.* **1977**, *146*, 1773.
[77] "HLA restriction of cell-mediated lysis of influenza virus-infected human cells": A. J. McMichael, A. Tig, H. J. Zweerink, B. A. Askonas, *Nature* **1977**, *270*, 524.
[78] "Cytotoxic T cell recognition of the influenza nucleoprotein and hemagglutinin expressed in transfected mouse L cells": A. R. Townsend, A. J. McMichael, N. P. Carter, J. A. Huddleston, G. G. Brownlee, *Cell* **1984**, *39*, 13.
[79] "Recombinant vaccinia viruses as vectors for studying T lymphocyte specificity and function": J. R. Bennink, J. W. Yewdell, *Curr. Top. Microbiol. Immunol.* **1990**, *163*, 153.
[80] "In vivo effector function of influenza virus-specific cytotoxic T lymphocyte clones is highly specific": A. E. Lukacher, V. L. Braciale, T. J. Braciale, *J. Exp. Med.* **1984**, *160*, 814.
[81] "Flow cytometric analysis of pulmonary lymphocytes from mice infected with respiratory syncytial virus": P. J. Openshaw, *Clin. Exp. Immunol.* **1989**, *75*, 324.
[82] "Roles of alpha beta and gamma delta T cell subsets in viral immunity": P. C. Doherty, W. Allan, M. Eichelberger, S. R. Carding, *Annu. Rev. Immunol.* **1992**, *10*, 123.
[83] "Immune response to viruses": P. C. Doherty in *Clinical Immunology. Principles and Practice*, (Eds.: R. R. Rich, T. A. Fleischer, B. D. Schwartz, W. T. Shearer, W. Strober), Mosby, St. Louis, **1996**, p. 535.
[84] "Influenza virus RNA in the lung and lymphoid tissue of immunologically intact and CD4-depleted mice": M. C. Eichelberger, M. Wang, W. Allan, R. G. Webster, P. C. Doherty, *J. Gen. Virol.* **1991**, *72*, 1695.
[85] "Establishment and persistence of virus-specific CD4$^-$ and CD8$^+$ T cell memory": P. C. Doherty, D. J. Topham, R. A. Tripp, *Immunol. Rev.* **1996**, *150*, 23.
[86] "Clearance of Sendai virus by CD8$^+$ T cells requires direct targeting to virus-infected epithelium": S. Hou, P. C. Doherty, *Eur. J. Immunol.* **1995**, *25*, 111.
[87] "Clearance of influenza virus respiratory infection in mice lacking class I major histocompatibility complex-restricted CD8$^+$ T cells": M. Eichelberger, W. Allan, M. Zijlstra, R. Jaenisch, P. C. Doherty, *J. Exp. Med.* **1991**, *174*, 875.
[88] "Transgenic mice lacking class I major histocompatibility complex-restricted T cells have delayed viral clearance and increased mortality after influenza virus challenge": B. S. Bender, T. Croghan, L. Zhang, P. A. Small, Jr. *J. Exp.*
[89] "β2-microglobulin-deficient mice can be protected against influenza A infection by vaccination with vaccinia-influenza recombinants expressing hemagglutinin and neuraminidase": S. L. Epstein, J. A. Misplon, C. M. Lawson, E. K. Subbarao, M. Connors, B. R. Murphy, *J. Immunol.* **1993**, *150*, 5484.

[90] "Immune CD4$^+$ T cells promote the clearance of influenza virus from major histocompatibility complex class II-/-respiratory epithelium": D. J. Topham, R. A. Tripp, S. R. Sarawar, M. Y. Sangster, P. C. Doherty, *J. Virol.* **1996**, *70*, 1288.
[91] "Virus-neutralizing antibodies of immunoglobulin G (IgG) but not of IgM or IgA isotypes can cure influenza virus pneumonia in SCID mice": G. Palladino, K. Mozdzanowska, G. Washko, W. Gerhard, *J. Virol.* **1995**, *69*, 2075.
[92] "Louping-ill encephalomyelitis in the sheep. IV. Nature of the perivascular inflammatory reaction": P. C. Doherty, H. W. Reid, W. Smith, *J. Comp. Pathol.* **1971**, *81*, 545.
[93] "Louping-ill encephalomyelitis in the sheep": P. C. Doherty, H. W. Reid, *J. Comp. Pathol.* **1971**, *81*, 531.
[94] "Louping-ill encephalomyelitis in the sheep. 3. Immunoglobulins in cerebrospinal fluid": H. W. Reid, P. C. Doherty, A. M. Dawson, *J. Comp. Pathol.* **1971**, *81*, 537.
[95] "Virus specificity and isotype expression of intraparenchymal antibody-secreting cells during Sindbis virus encephalitis in mice": W. R. Tyor, D. E. Griffin, *J. Neuroimmunol.* **1993**, *48*, 37.
[96] "Phenotypic analysis of the inflammatory exudate in murine lymphocytic choriomeningitis": R. Ceredig, J. E. Allan, Z. Tabi, F. Lynch, P. C. Doherty, *J. Exp. Med.* **1987**, *165*, 1539.
[97] "Contributions of host and donor T cells to the inflammatory process in murine lymphocytic choriomeningitis": P. C. Doherty, J. E. Allan, R. Ceredig, *Cell. Immunol.* **1988**, *116*, 475.
[98] "Cellular events in the lymph node and lung of mice with influenza. Consequences of depleting CD4$^+$ T cells": W. Allan, Z. Tabi, A. Cleary, P. C. Doherty, *J. Immunol.* **1990**, *144*, 3980.
[99] "Recruitment and proliferation of CD8$^+$ T cells in respiratory virus infections": R. A. Tripp, S. Hou, A. McMickle, J. Houston, P. C. Doherty, *J. Immunol.* **1995**, *154*, 6013.
[100] "Virus-specific CD8$^+$ T-cell memory determined by clonal burst size": S. Hou, L. Hyland, K. W. Ryan, A. Portner, P. C. Doherty, *Nature* **1994**, *369*, 652.
[101] "Characteristics of the influenza virus-specific CD8$^+$ T cell response in mice homozygous for disruption of the H-21A^b gene": R. A. Tripp, S. R. Sarawar, P. C. Doherty, *J. Immunol.* **1995**, *155*, 2955.
[102] "Environmental modulation of the autonomy of cytotoxic T lymphocytes": H. Bodmer, G. Obert, S. Chan, C. Benoist, D. Mathis, *Eur. J. Immunol.* **1993**, *23*, 1649.
[103] "Reciprocal stimulation of negatively selected high-responder and low-responder T cells in virus-infected recipients": J. R. Bennink, P. C. Doherty, *Proc. Nat. Acad. Sci. USA* **1979**, *76*, 3482.
[104] "How selective is the transporter associated with antigen processing?": M. J. Androwlewicz, P. Creswell, *Immunity* **1996**, *5*, 1.
[105] "Limiting dilution analysis of the specificit of influenza-immune cytotoxic T cells": J. A. Owen, M. Allouche, P. C. Doherty, *Cell. Immunol.* **1982**, *67*, 49.
[106] "Limit-dilution analysis of weak influenza-immune T cell responses associated with H-2K^b and H-2D^b": M. Allouche, J. A. Owen, P. C. Doherty, *J. Immunol.* **1982**, *129*, 689.
[107] "Extrathymic tolerance of mature T cells: clonal elimination as a consequence of immunity": S. Webb, C. Morris, J. Sprent, *Cell* **1990**, *63*, 1249.
[108] "Profound deletion of mature T cells in vivo by chronic exposure to exogenous superantigen": J. E. McCormack, J. E. Callahan, J. Kappler, P. C. Marrack, *J. Immunol.* **1993**, *150*, 3785.
[109] "Temporal loss of the activated L-selectin-low phenotype for virus-specific CD8$^+$ memory T cells": R. A. Tripp, S. Hou, P. C. Doherty, *J. Immunol.* **1995**, *154*, 5870.
[110] "Immunological memory and protective immunity: Understanding their relation": R. Ahmed, D. Gray, *Science* **1996**, *272*, 54.
[111] "Independent populations of primed F1 guinea pig T lymphocytes respond to antigen-pulsed parental peritoneal exudate cells": W. E. Paul, E. M. Shevach, S. Pickeral, D. W. Thomas, A. S. Rosenthal, *J. Exp. Med.* **1977**, *145*, 618.
[112] "Laser light suicide of proliferating virus-specific CD8$^+$ T cells in an in vivo response": R. A. Tripp, J. M. Lahti, P. C. Doherty, *J. Immunol.* **1995**, *155*, 3719.
[113] "Turnover of naive- and memory-phenotype T cells": D. F. Tough, J. Sprent, *J. Exp. Med.* **1994**, *179*, 1127.
[114] "Lymphocyte lifespans: homeostasis, selection and competition": A. A. Freitas, B. B. Rocha, *Immunol. Today* **1993**, *14*, 25.
[115] "Tolerance, danger, and the extended family": P. Matzinger, *Annu. Rev. Immunol.* **1994**, *12*, 991.
[116] "HIV-1 dynamics in vivo: virion clearance rate, infected cell life-span and viral generation time": A. S. Perelson, A. U. Neumann, M. Markowit, J. M. Leonard, D. D. Ho, *Science* **1996**, *271*, 1582.
[117] *Complexity: the emerging science at the edge of chaos*, M. W. Waldrop, Simon and Schuster, New York, **1992**.
[118] "Immunity to viruses": P. C. Doherty, *The Immunologist* **1995**, *3*, 231.
[119] "Quantitative analysis of influenza virus-specific CD4$^+$ T cell memory in the absence of B cells and Ig": D. J. Topham, R. A. Tripp, A.-M. Hamilton-Easton, S. R. Sarawar, P. C. Doherty, *J. Immunol* **1996**, *157*, 2947.
[120] "Progressive loss of CD8$^+$ T cell-mediated control of a γ-herpesvirus in the absence of CD4$^+$ T cells": R. D. Cardin, J. W. Brooks, S. R. Sarawar, P. C. Doherty, *J. Exp. Med.* **1996**, *184*, 863.
[121] "Partitioning of responder CD8$^+$ T cells in lymph node and lung of mice with Sendai virus pneumonia by LECAM-1 and CD45RB phenotype": S. Hou, P. C. Doherty, *J. Immunol.* **1993**, *150*, 5494.

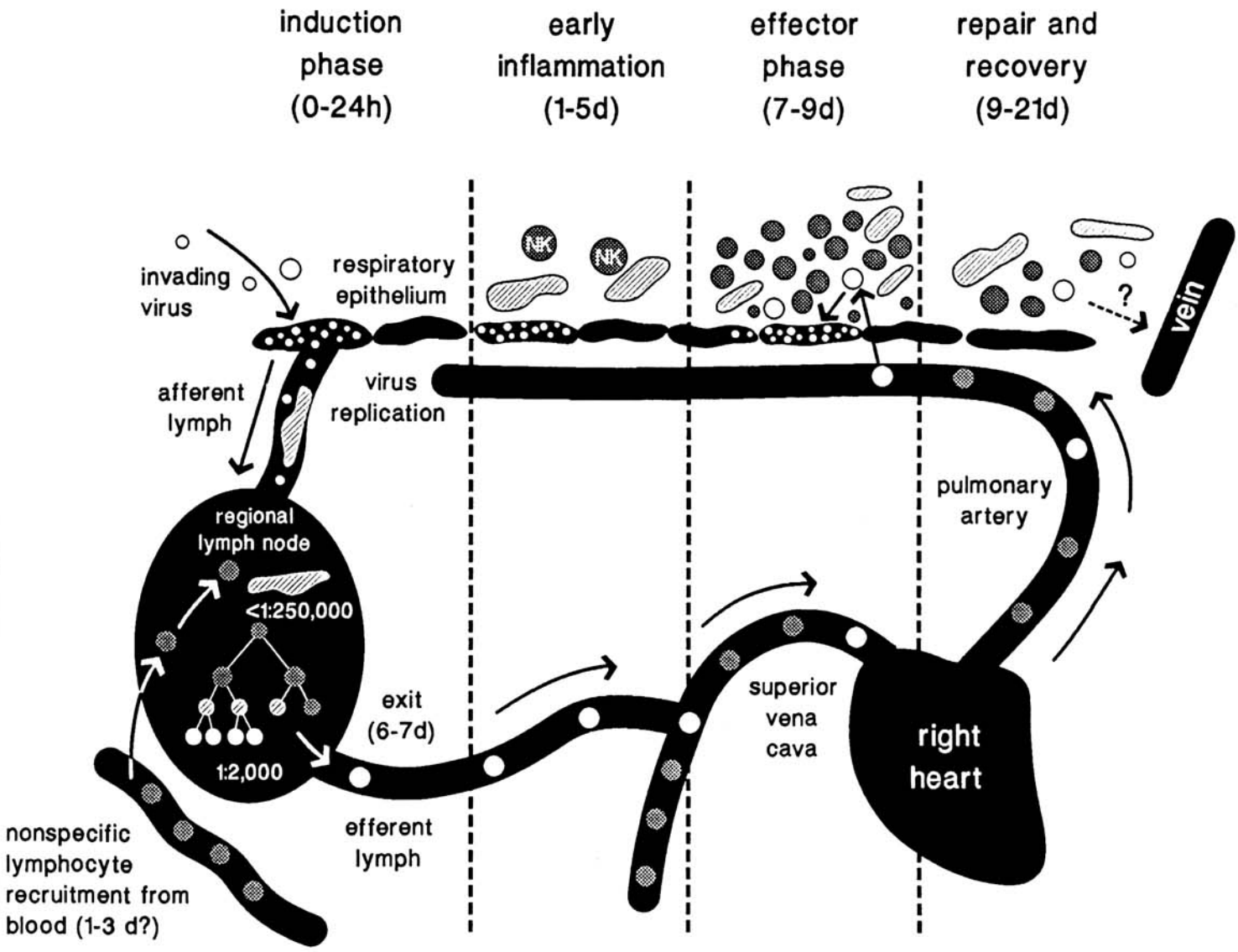

primary CD8$^+$ T cell response upon infection of the respiratory tract

ANGEWANDTE CHEMIE ©WILEY-VCH

Cellular Immune Recognition and the Biological Role of Major Transplantation Antigens (Nobel Lecture)**

Rolf M. Zinkernagel*

The Original Experiment on T cell Specificity

While Immunology began as an attempt to understand immunity against infectious disease, in the 1960s and early 1970s it was largely preoccupied with antibody and T cell responses against easily available foreign protein antigens or chemically defined small molecules (haptens).[1] The mechanisms of graft rejection of foreign organs were also intensively studied, although the biological function of the highly polymorphic, major transplantation molecules coded by the major histocompatibility complex (MHC and HLA in humans, H-2 in mice)[2, 3] was largely unclear. Only a few people studied immunity against infectious agents. The Department of Microbiology at the Australian National University in The John Curtin School of Medical Research in Canberra, headed by G. Ada, was one place where virologists and immunologists worked together on antibacterial and antiviral T cell mediated immunity, particularly on the capacity of immunized cytotoxic $CD8^+$ T cells to destroy either virus-infected or allogeneic target cells in vitro. Peter C. Doherty from Brisbane, who had returned to Australia from Edinburgh at the end of 1971, was working in this Department. He was interested in inflammatory cell responses in the brain against virus infections. When I arrived in Canberra in early 1973 I started working on *Listeria* bacteria with R. V. Blanden and joined forces with Peter to work on cell-mediated immunity to the lymphocytic choriomeningitis virus (LCMV).[4–6] I had come from an institute that was involved in establishing the ^{51}Cr release assays by T. Brunner and J. C. Cerottini in Lausanne, Switzerland,[7, 8] and I therefore attempted to establish the cytotoxicity assay against LCMV in the same way as R. V. Blanden, N. A. Bowern, and I. Gardner were using it to monitor cellular immune responses against ectromelia virus (mouse pox) in mice.[9] Because many papers on cytotoxic T cell responses against LCMV had already been published by various groups[10, 11] and since studies had already been carried out on mouse pox in Canberra by R. V. Blanden's group, members of the Department were sceptical that we should and could run with the strong competition. Although we had some initial problems because of our limited experience with LCMV we successfully established the test with some help from I. D. Gardner. We then used this test to find out whether inflammatory cells in the cerebrospinal fluid of mice infected intracerebrally with LCMV were cytolytic in vitro and whether there was a correlation between cytotoxic T cell activity and severity of choriomeningitis. P. C. Doherty was very good at collecting a few microliters of cerebral spinal fluid from the cisterna magna of a mouse. I miniaturized the ^{51}Cr release assay to be able to measure the activity of such small numbers of cells in microwell plates. These experiments revealed that cytotoxic T cells specifically destroying LCMV-infected target cells could be found in the cerebral spinal fluid of normal mice, but not in that of nude mice lacking a thymus and T cells; this implied that T cells probably also destroyed infected meningial and ependymal cells in vivo and that this was the essential pathogenic mechanism causing lethal choriomeningitis. These findings were published in the *Journal of Experimental Medicine* in March 1973.[12] In this journal a paper by M. B. A. Oldstone, H. O. McDevitt, and collaborators had just appeared, showing that mice with different major histocompatibility gene complexes (H-2) differed with respect to their susceptibility to LCM disease after intracerebral infection.[13] We therefore checked whether a correlation existed between the virus-specific cytotoxic T cell activity in mice and their susceptibility to disease. Six to eight mice of each inbred and cross-bred strain available at the School were infected intracerebrally with LCMV. Two of each were sacrificed when the first mice became sick on day 7 after infection, to test antiviral cytotoxic T cell activities in spleens (Table 1). The remaining mice were monitored for the development of lethal disease during the next ten days. While all the mice died of choriomeningitis by day 10, surprisingly only some strains of mice generated virus-specific cytotoxic T cell activity that was measurable in our in vitro assay (Table 1). This result either signaled that cytotoxic T cells had nothing to do with lethal choriomeningitis, or, alternatively, that our test was in some way inadequate. The latter interpretation proved to be correct: We had used mouse L-929 cells infected with LCMV as target cells to assess cytotoxic T cell activities. This was a fibroblast cell line used by virologists at the John Curtin School of Medical Research to quantifiy viruses by a plaque assay (determination of plaque-forming units (pfu)).[14] Since this was the

[*] Dr. R. M. Zinkernagel
Institut für Experimentelle Immunologie
Departement of Pathologie
UniversitätsSpital Zürich
Schmelzbergstrasse 12, CH-8091 Zürich (Switzerland)

[**] Copyright © The Nobel Foundation 1997. We thank the Nobel Foundation, Stockholm, for permission to print this lecture. A glossary of terms and abbreviations is provided on p. 1947.

Table 1. Experiments demonstrating MHC-restriction specificity and positive selection in the thymus for antiviral cytotoxic T cells [a].

No.	Stem cells (MHC, H-2)	Thymus (MHC, H-2)	Other host cells (MHC, H-2)	Virus-specific $CD8^+$-T-cells, specific for (MHC, H-2) k	d	Lethal $CD8^+$ T Cell mediated choriomeningitis after intracerebral infection [%]
I: Original experiments with normal mice						
1	k	k	k	+	–	100
2	b	b	b	–	–	100
3	d	d	d	–	+	100
4	k/d	k/d	k/d	+	+	100
II: Thymus transplantation to thymus-deficient recipient mice						
1	k/d	–	k/d	–	–	0
2	k/d	k	k/d	+	–	100
3	k/d	d	k/d	–	+	100
4	d	k	d	–	+	100

[a] Normal mice (**I**) as well as mice lacking a thymus that therefore have no T cells and were given a thymus graft under the kidney capsule (**II**) were infected with LCMV intracerebrally. All mice died, except those that had no T cells (**II**, no. 1), because of the lethal $CD8^+$ T cell mediated LCMV-specific immune reaction. The fact that mice without functional T cells survived shows that the noncytopathic LCMV does not cause disease directly. The LCMV-specific cytotoxic T cells lysed infected target cells that have the same MHC molecules (**I** no. 1; immune T cells from infected CBA mice) ($H\text{-}2^k$) lysed infected L929 fibroblast cells ($H\text{-}2^k$) [15]. The MHC of the thymus determines which MHC is recognized by mature T cells. The experimental group **II**, no. 2, shows that ($H\text{-}2^k \times H\text{-}2^d$) mice with a thymus $H\text{-}2^k$ generated virus-specific T cells that lysed virus-infected $H\text{-}2^k$ target cells, but not infected $H\text{-}2^d$ cells [75]. There are, however, experimental exceptions to this rule (**II** no. 4). Thymus-deficient nude mice ($H\text{-}2^d$) reconstituted with an $H\text{-}2^k$ thymus generated $H\text{-}2^d$-restricted T cells [76].

only mouse-cell line usually used in the Department, along with a Vero-cell line derived from monkeys or the BHK-cell line derived from hamsters, we chose it to provide target cells in the virus-specific, cytotoxic T cell assays. By chance, and fortunately, the mice that were most commonly used in the Department were of the CBA strain, while the L cells had been derived from a closely related mouse strain C3H some 50 years earlier. Also by chance, both mice possessed the same MHC molecules ($H\text{-}2^k$). Our critical test now revealed that LCMV-immune spleen cells from all mice that possessed the $H\text{-}2^k$ haplotype (as do, for example, CBA mice), including cross-breeds with $H\text{-}2^k$ mice, lysed L929 ($H\text{-}2^k$) cells infected with the virus, but did not lyse uninfected targets, or those infected with a third-party virus; all spleen cells derived from immunized mice that were not of the $H\text{-}2^k$ type failed to do so.[15]

Two additional experiments carried out within the next few weeks promptly confirmed these findings. It was important to show that LCMV-immune lymphocytes from non-$H\text{-}2^k$ strains of mice were able to lyse LCMV-infected target cells of the corresponding MHC type. This did not prove to be easy, because the other available mouse-cell lines in the Department, such as the $H\text{-}2^d$ mastocytoma P815 or the $H\text{-}2^b$ thymoma EL4, could not be infected with LCMV. Because of my work with R. V. Blanden on *Listeria*—which infects macrophages and is essentially controlled by cell-mediated activation of macrophages as shown by G. B. Mackaness[16]—we tried to use macrophages directly isolated from peritoneal washings of mice as target cells for these tests. Macrophages adhered well to plastic and could be readily infected and labeled with ^{51}Cr. Proper criss-cross experiments showed that LCMV-immune T cells from $H\text{-}2^b$ mice lyse LCMV-infected macrophages of $H\text{-}2^b$ origin but not those of other H-2 types, and vice versa. The report on these findings was sent off via J. Humphrey as a letter to *Nature* in early December;[15] it was accepted in January 1974 and published in April 1974. The first public presentation of our data outside Australia was at a Keystone meeting, in Squaw Valley (California), attended by A. Cunningham in February and a Brook Lodge meeting (Kalamazoo, Michigan) attended by G. Ada in March 1974. A letter sent back to Canberra by A. Cunningham summarized data from G. M. Shearer showing that TNP-specific (TNP = trinitrophenyl), cytotoxic T cells lysed syngeneic TNP-lated targets more efficiently than allogeneic TNP-lated targets; these data were submitted to the *European Journal of Immunology*[17] at about the time our report appeared in *Nature*. Obviously, the two findings had emerged independently.

Rolf M. Zinkernagel was born in 1944 in Basel. After studying medicine (1962–1968) in his home town, he was postdoctorate fellow there (1969–1970) and at the institute for Biochemistry at the University of Lausanne (1971–1973). His doctoral studies as Visiting Fellow (1973–1975) at the Australian National University in Canberra were followed by a position as Assistant Associate and Full Professor at the Department of Immunopathology, Scripps Clinic, in La Jolla, California (1976–1979), and simultaneously (1977–1979) as Adjunct Professor in the Department of Pathology at the University of California, San Diego. Since 1979 he has occupied the chair of Experimental Pathology at the UniversitätsSpital, University of Zürich, and became Director of the Institute of Experimental Immunology in 1992. He has received many awards, such as the Paul-Ehrlich Prize in Germany (1983), the Gairdner Award in Canada (1987), the Albert-Lasker Medical Research Award in the USA (1995), before he won the Nobel Prize for Medicine and Physiology last year.

Interpretations of the Data

The biological function of MHC and of transplantation antigens was largely unknown in the early 1970s. Their function was obviously not simply to frustrate transplantation surgeons. Transplantation antigens have been defined by P. A. Gorer,[18] and by G. D. Snell,[19] based on the work of C. Little, L. Strong, and others, who had developed many inbred strains of mice in order to be able to define the rules of transplantation and rejection of tissue and cell grafts (reviewed by J. Klein[2]). Hematologists, particularly J. Dausset[3] and J. J. van Rood et al.,[20] defined lymphocyte surface antigens in humans as being similar to red blood cell antigens and called them human lymphocyte antigens (HLAs). Once many patients had been typed for their transplantation antigens it became apparent that several disease susceptibilities were somehow linked to the transplantation antigen types. It was revealed in studies by B. Benacerraf et al.,[21] and later in great and critical detail by H. O. McDevitt and coworkers[22,23] and by F. Lilly et al.,[24] that inbred strains of guinea pigs and mice differed in their responses to some of the model antigens or tumors studied. Because of the availability of well-defined inbred strains of mice, this was readily mapped to the MHC and even to subregions of the MHC in mice by H. O. McDevitt et al.[25] In the early 1970s, transplantation antigens were widely discussed because of these findings. MHC polymorphism was thought either to prevent mutual parasitism or transmission of tumor cells,[26] or to prevent viruses or other pathogens from mimicking transplantation antigens and, therefore, from eliminating the species;[27-29] alternatively, it was proposed that transplantation antigens functioned as enzymes or as generators of antibody diversity.[30] A most fascinating proposal had been formulated by H. S. Lawrence in 1959.[31] He proposed that infectious agents complexed with transplantation antigens and formed a (self + x) complex—a fantastically prophetic view of what was to be found later!

There is no doubt that the experiments that were to reveal the essential role of MHC and T cell recognition in all depended upon the foundation built by tumor and transplantation immunologists. Without inbred and MHC (H-2) - congenic or H-2 mutant mouse strains, as developed by G. D. Snell[19] and D. W. Bailey[32] and coworkers, respectively, this problem would not at the time have been accessible to analysis. There is also no doubt that MHC-restricted T cell recognition would have been discovered by others, with a different approach, a few years later. This would certainly have happened once cloned effector T cells were developed by M. H. Schreier, H. Hengartner, H. von Boehmer, and C. G. Fathman,[33,34] when T cell hybridomas were developed by J. W. Kappler, P. Marrack et al., or when T cell receptors were first successfully analyzed by J. W. Kappler, P. Marrack et al., and J. P. Allison et al.[35-37] and then were molecularly defined by M. M. Davis et al. and T. W. Mak et al.[38,39]

From our very first experiments showing the double specificity of cytotoxic T cells for MHC and virus, we immediately knew that we had discovered something important. Our results were not the only ones that hinted at the biological role of major transplantation antigens, and they fitted several observations made during 1972/1973. In addition to the suggestions from cytotoxic T cell studies with leukemia, ectromelia, and LCM viruses,[9,40,41] there were the experiments by B. Kindred and D. C. Shreffler,[42] who had reported that H-2-incompatible T-helper cells transfused to T cell deficient nude mice were not able to help nude B cells make antibodies. Also, P. J. McCullagh and D. H. Katz, T. Hamaoka, and B. Benacerraf had shown that histoincompatible B cells and T cells did not interact successfully to produce a good IgM-to-IgG switch.[43,44] In parallel experiments with inbred strains of guinea pigs, A. S. Rosenthal and E. M. Shevach analyzed antigen-specific, proliferative T cell responses and found them only when primed T cells and antigen-presenting cells were from guinea pigs with the same MHC type.[45] Most of these experiments were, however, complicated and difficult to interpret, because the mixing of T cells and B cells or antigen-presenting cells (APCs) of different MHC type initiated allogeneic mixed lymphocyte reactions, resulting in nonspecific signals. These findings were, therefore, only accepted with hesitation by immunologists; this changed when our data appeared. The simplicity of the in vitro viral assays, the parallel observation by G. M. Shearer with TNP,[17] and its easy reproducibility by R. V. Blanden, I. D. Gardner et al. with ectromelia virus,[46] by U. Koszinowski and H. Ertl with vaccinia virus,[47] by E. Simpson, R. D. Gordon, and L. E. Samelson, and H. von Boehmer et al. with the male H-Y-antigen,[48,49] and by M. J. Bevan with various minor histocompabibility antigens[50] all helped to convince immunologists of the general character of MHC-restricted T cell recognition. Also MHC-restriction of T cell recognition was soon confirmed in vivo to be also important for antiviral protection transmissible from immune to naive recipients by immune T cells. By 1977 A. J. McMichael and coworkers in B. A. Askonas's laboratory showed that cytotoxic T cells specific to human influenza virus were HLA-restricted,[51] as did E. Goulmy et al. for male antigen H-Y-specific cytotoxic T cells.[52]

Our results triggered heated discussions in the Department. We thought that the virus somehow altered the normal cells' MHC molecules and that this virus-specific alteration was recognized by cytotoxic T cells in a similar way to that of foreign transplantation antigens. Everyone's imagination and intellect was stimulated to come up with a more general, simpler, and more convincing explanation for the findings. Discussions were particularly lively because at the same time K. J. Lafferty and A. J. Cunningham developed their ideas on second signals necessary to induce responses against foreign transplantation antigens,[53] G. Ada and R. V. Blanden were studying other virus-specific T cell responses, L. Pilarski and P. Bretscher were thinking about B cell responses and signal requirements along the two-signal theories of P. Bretscher, M. Cohn, and R. E. Langman,[54,55] and C. Parish, I. D. Gardner, I. Ramshaw, A. Happle, S. Kirov, W. Davidson, M. Dunlop, and Y. Rosenberg, working on B cell and T cell response in various virus infections, were discussing the role of enzymes modifying carbohydrates or other self-surface structures to explain the experiments.

Further analysis

According to our interpretation, our findings signified that virus infection somehow caused alterations of transplantation

antigens on the cell surface by forming a complex between the viral antigen and MHC molecules, by undefined structural alterations, or by complexing both, and that these alterations were recognized by T cell receptors (Figure 1).[56] Foreign transplantation antigens (so-called alloantigens) could thus be viewed as a genetically altered form of self-transplantation antigens. This view differed from the then-favored possibility that lymphocytes and target cells interacted mutually through transplantation antigens (see Figure 1A), that is, H-2^k interacted best with H-2^k, H-2^b best with H-2^b molecules in a symmetrical like–like complementarity. This intimacy model was soon excluded by the "F_1-experiment" showing that virus-specific, cytotoxic T lymphocytes from heterozygote (H-2^k × H-2^b) F_1 mice consisted of at least two subpopulations, one of each being specific for infected H-2^k, and the other for infected H-2^b targets. Since both MHC types were codominantly expressed on the lymphocyte surfaces of all host cells, this indicated that some T cell receptors of one T cell subpopulation were probably specific for H-2^k-plus-virus and the other subpopulation was specific for H-2^b-plus-virus (Figure 1B).

Further experiments together with R. V. Blanden carried out with the help of mouse geneticists (including C. S. David and H. O. McDevitt in the U. S. A.) showed that the H-2D and H-2K regions coding for class I MHC molecules were involved in virus-specific, cytotoxic T cell recognition.[46] These findings separated the MHC-restricted recognition by virus-specific, cytotoxic T cells from the MHC class II (Ia) antigen-linked immune response phenomena regulating interactions between T cell and B cell, or T cell and macrophage. Analysis of cytotoxic T cell interactions in vivo causing lethal immunopathology,[57] antiviral protection,[58] and protection against *Listeria monocytogenes*[59] all confirmed that MHC restriction was also valid in vivo.

In our second letter to *Nature*, we therefore concluded that T cells might function essentially by surveying the integrity of transplantation antigens. Recognition of cell surface alteration due to virus infection, chemical modification, or genetic differences (that is, alloantigens) may then be accommodated within the same model. A general hypothesis was formulated in *Lancet* in 1975,[60] which stated explicitly that the function of the major histocompatibility molecules is to signal modifications of self-MHC to the immune system.

What we had discovered and tried to explain for cytotoxic T cells, we also extended to helper T cells, proposing that they might recognize antigen-induced modifications of Ia (as the MHC class II molecules were called at the time) on macrophages and B cells. Importantly, the results offered an explanation of the reasons for the extensive polymorphism of MHC molecules; it minimized both the possibility that some cell-destroying pathogens failed to cause immunogenic modification and the risk of there being general unresponsiveness in a population. Obviously, what was unknown at the time was that MHC molecules or transplantation antigens are the antigen-presenting molecules that are recognized as a complex with the antigenic peptide. This became known in the subsequent ten years, mostly thanks to the work of E. R. Unanue et al.[61] and H. M. Grey and co-workers[62] for class II antigens, as well as to the particularly revealing and eye-opening work of A. R. M. Townsend.[63] He showed that class I molecules of virus-infect-

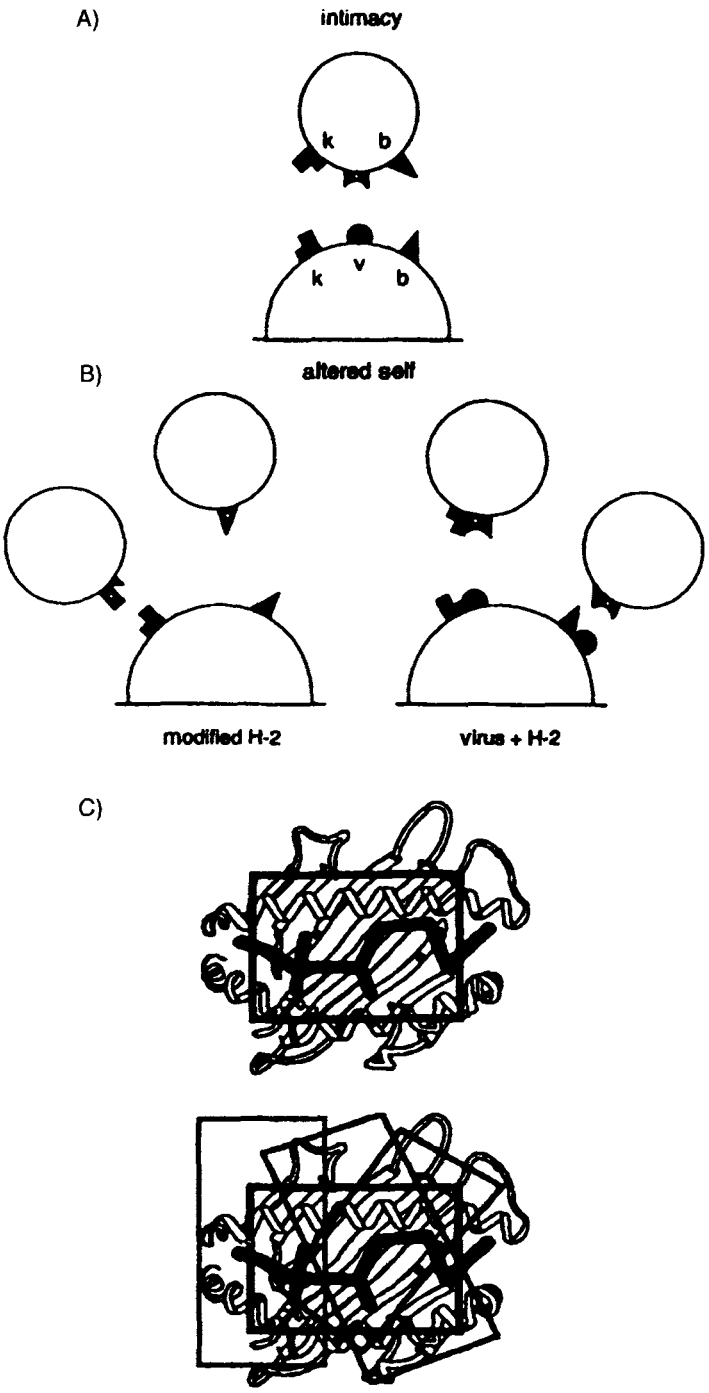

Figure 1. Models originally proposed to explain MHC-restricted T cell recognition. The idea that T cell and target cell come close enough through interactions with MHC molecules (A) was disproven by the demonstration that in H-2^k × H-2^b mice, an F1 cross between H-2^k and H-2^b mice, only two specific T cell populations were present, one specific for virus plus H-2^k and a second for virus plus H-2^b. Therefore T cell receptors were either specific or the virally modified MHC molecule where neither details of either virus antigen nor MHC molecules were recognized in original form (B), or T cells were specific for a complex formed between MHC molecule and viral antigen, and the T cell receptor recognized parts of the viral antigen and parts of the MHC molecule (C). It is now clear (in 1996) [69, 70] that the T cell receptor is composed to two chains Vα and Vβ that recognize a viral peptide presented by the MHC molecule [63]. What is still unclear (C) is whether the T cell receptor, here drawn as a square, interacts with the peptide plus MHC complex always in the same directed fashion, so that certain hypervariable regions of the receptor always interact with corresponding parts of the peptide or of the two MHC domains forming the groove, or whether alternatively the receptor interacts with the complex formed by MHC plus peptide in many possible random ways. (Reproduced with permission of Macmillan Magazines Ltd. from *Nature* **1974**, *251*, 547, and *JAMA* **1995**, *274*, 1070.

ed cells present peptides, 9–10 amino acids in length, to virus-specific cytotoxic T cells. Similar results were obtained by J. Maryanski and coworkers.[64] These peptides became very real when they were first eluted from target cells by the group of H. G. Rammensee.[65] Peptides were also soon shown to be involved in antitumor CTL responses by T. Boon's group.[66] All became convincingly clear in the classical studies of P. J. Bjorkman, J. L. Strominger, D. C. Wiley et al. in 1987, when the X-ray cristallography of class I HLA molecule revealed the peptide binding cleft.[67, 68] It is probably not only by chance that within a few weeks of the news of the Nobel Prize 1996 for specificity of the cell-mediated immune response, the first studies appeared in *Science* and *Nature*, revealing the X-ray structure of the complete complex of the T cell receptor, MHC class I molecule, and bound peptide by I. A. Wilson and by D. C. Wiley and their co-workers.[69, 70] What is still unclear (in 1996) is, which part of the T cell receptor (TCR), and whether always corresponding parts of the TCR, recognized the peptide and the MHC molecule in the same general position (Figure 1).[71, 72]

Implications

The Role of the Thymus in MHC-Restricted T Cell Repertoire Selection

Experiments first published by M. J. Bevan at MIT[73] and conducted in parallel in my laboratory at Scripps with the help of G. N. Callahan, G. Dennert and J. Klein signaled a role of thymic MHC in selection of the MHC-restricted T cell specificity.[74, 75] Reconstitution of lethally radiated H-2^b recipient mice with bone-marrow stem cells of (H-2^k × H-2^b) F_1 origin resulted in bone-marrow chimeras that were tolerant of H-2^k and H-2^b; when immunized, these chimeras reacted against H-2^b plus minor histocompatibility antigens, or, in our experiments, against H-2^b plus virus only (Table 1). This indicated that MHC-restricted T cells were specifically selected during T cell maturation according to the MHC expressed in the thymus. This was formally shown when MHC-restricted T cell specificity was studied in mice that lacked a thymus and therefore did not have mature T cells. When these mice of (H-2^k × H-2^b) F_1 type were given a thymus of fetal H-2^k origin, they eventually generated effector T cells that recognized virus-infected H-2^k, but not infected H-2^b target cells. Surprisingly, thymus-deficient nude mice given a histoincompatible thymus generated T cells that were specific for the nude mice's MHC,[76] but in general the MHC (apparently of the radio-resistant part of the thymus) selected the restriction specificity of virus-specific cytotoxic T cells.

These thymus and bone-marrow-grafting experiments had an immediate impact on clinical medicine by providing rational rules for the reconstitution of immunodeficiency disease. Accordingly, it is not only necessary to deplete T cells in order to avoid lethal graft-versus-host disease, but in addition, the host and the transplanted bone-marrow cells and the host's own or the transplanted thymus grafts must share MHC molecules. Otherwise, T cells capable of recognizing antigen-plus-MHC molecules on infected epithelial, mesenchymal cells, macrophages, or the corresponding B cells would not develop and function appropriately in such reconstituted hosts. These rules for positive selection of T cells according to the MHC of the thymus were subsequently elegantly—and even more convincingly—confirmed with T cell receptor transgenic mice, by H. von Boehmer and collaborators.[77] Subsequently, several other groups also analyzed transgenic TCR-expressing mice—D. Y. Loh et al. with an alloreactive T cell receptor[78] and H. P. Pircher, H. Hengartner, T. W. Mak, and K. Bürki et al. with an LCMV-specific receptor;[79] others used a variety of additional specificities.

New Vaccines

The recognition that peptides derived from viruses, bacteria, or classical parasites are presented to T cells via MHC class I or class II molecules immediately suggested that instead of live, and therefore potentially harmful, infectious agents, peptides could possibly be used as vaccines to induce T cell responses.[80] This was first formally shown for virus-specific peptides in studies by M. Schultz, P. Aichele, and H. Hengartner,[81] (Table 2, Figure 2) and then by C. J. Melief, W. M. Kast, and co-workers.[82] The main problem that slowed things down after the discovery of the key role of peptides by A. R. M. Townsend[63] was the fact that the half-life of such peptides is usually short, and protective T cells could therefore only be induced with the help of adjuvants that guaranteed the relatively slow, long-term release of peptides, triggering T cells over a prolonged period.[83] Peptide treatments were first shown to prevent experimental allergic encephalitis (EAE) under various conditions.[84, 85] More recently, the capacity of peptides to induce cytotoxic T cells so exhaustively and completely that they are deleted has been shown by D. Kyburz, P. Aichele, H. P. Pircher,

Table 2. The role of antigen localization, dose, and time on positive and negative vaccination [a].

vaccination	Infection with				
	cytopathic viruses		noncytopathic viruses		
	localized	generalized	localized		generalized
			choriomeningitis	subcutaneous	
none	survival	death	death	disease	disease but survive (virus eliminated)
positive	protection	protection	protection (virus eliminated)	disease (shorter)	death or protection (virus eliminated)
negative by "exhaustion"	disease and death dependent upon critical role of cytotoxic T cells		treated mice do not develop disease and survive but do not eliminate virus (develop carrier status)		

[a] Data from refs. [81, 87, 88].

H. Hengartner et al. and D. Moskophidis et al.[86–89] T cells were either induced or exhausted, depending on the relative amount and kinetics of the available antigen within a recipient mouse (Figure 2). Thus, with too much peptide, specific T cells

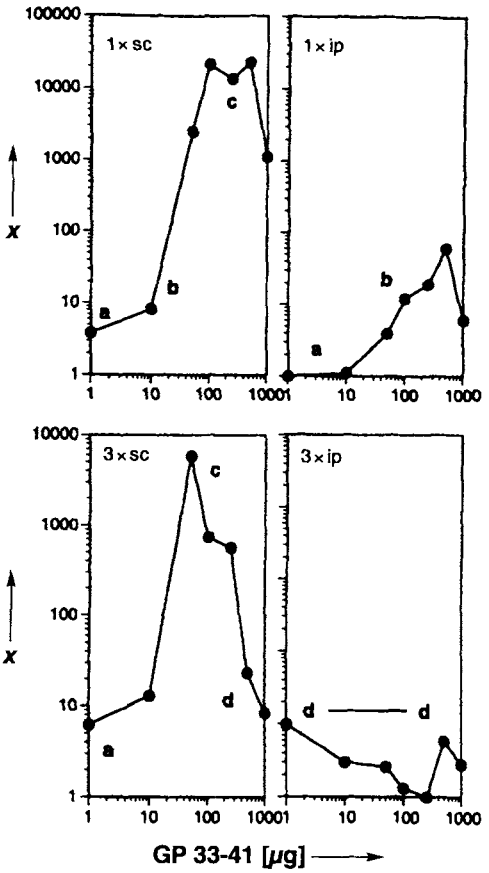

Figure 2. The role of antigen localization and of dose and time on T cell responses: The LCMV glycoprotein peptide GP33–41 presented by MHC class I D^b in C57BL/6-H-2^b mice was used as vaccine. Its half-life in vivo is $\ll$ 12 hours; protection was compared with controls in this experiment to assess T cytotoxic specific, LCMV specific cytotoxic T cell immunity; the x-fold protection relative to the untreated control (x) was titrated against amount of peptide given with adjuvans either once or 3 times subcutaneously (s.c.) or once or 3 times in intraperitoneally (i.p.). No induction was seen if the antigen is available in too small amounts (a), or for too short a period of time (b). Induction of a protective immune T cell response occurs if sufficient antigen is available for long enough (c). If, however, too much antigens spread throughout the organism for a long time causing excessive induction of all inducible T cells, exhaustion/deletion of all specific T-cells results (d). Adapted from ref. [88 b].

could be deleted for aslong as the peptide persisted—even permanently in the case of a thymectomized host. This signaled the possibility of a "negative" vaccination strategy (Figure 2, Table 2): Instead of increasing T cell precursor frequencies to enhance protection (positive vaccination), one could also reduce or delete T cells by means of excess peptides (negative vaccination).[90] The latter possibility may allow the immunopathological T cells that cause disease to be exhausted and deleted. Although one such example has been documented in an MHC class I specific, immunopathological, T cell mediated, transgenic diabetes model,[87] attempts to achieve the same in already primed hosts, before or after initiation of disease, have only met with partial success.

T Cell Epitope Escape Mutant Viruses

It could be expected that noncytopathic viruses would mutate the 9–10 amino acid peptides recognized by T cells in the context of the crucial MHC class I antigen. Mutation of this peptide, so that either its presentation by MHC molecules or its recognition by T cells is no longer possible, could help viruses to escape immune surveillance. A first example of this possibility was found by chance when H. P. Pircher, D. Moskophidis, H. Hengartner, et al. analyzed T cell receptor transgenic mice that expressed a T cell receptor specific for the LCMV glycoprotein peptide 33–41 presented by the MHC class I (D^b) molecule (Figure 3).[91, 92] When we infected such mice in the footpad we found a very early swelling reaction caused by immunopathological cytotoxic T cell response by day 2 to 4, which, however, waned, and a second CTL-mediated response was measurable after day 8 (Figure 3). When this unexpected

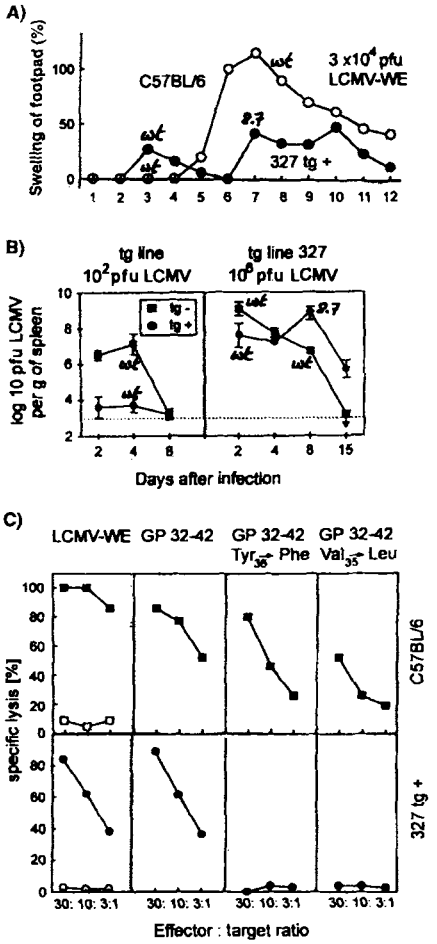

Figure 3. Selection of cytotoxic T cell epitope escape mutants in T cell receptors of transgenic (TCR-tg327) mice. LCMV-WE wildtype (wt) was injected into the footpad (A). The control C57BL/6 developed the expected $CD8^+$ T cell dependent footpad swelling by day 6 or 7; the TCR-tg327 mice exhibited an early swelling caused by the tg-TCR specific for LCMV-GP 33–41 plus D^b. This early response selected a mutant virus 8.7 by about day 7–8, that induced a swelling reaction by the endogenous non-tg T cells specific for other peptides. The virus titers found in the spleen of mice is infected with a low (10^2 plaque-forming units (pfu)) or a high (10^6 pfu) dose of LCMV-WE (B). The cytotoxic T-cell activity found in control C57BL/6 or TCR-tg327 mice on day 8 is shown in C. The peptides of the T cell epitope escape variant virus are not recognized by the tg-TCR, but are still partially (Tyr → Phe) or not (Val → Leu) recognized by effector T cells from control C57BL/6 mice. (Summarized from ref. [91].)

double peak of the T cell mediated footpad swelling reaction was analyzed further, it became clear that the virus had mutated by day 6 of infection; it no longer expressed the original gp 33–41, but exhibited various mutations within this epitope, presented by the MHC class I (D^b) molecule.[91] Apparently the vehement, virtually monoclonal, antiviral $CD8^+$ T cell response in the TCR-transgenic mouse had quickly selected the T cell epitope mutant virus that had escaped the transgenic T cells. A similar mutant virus that escaped the T cell response has subsequently also been found in patients infected with HIV by R. E. Phillips, A. J. McMichael, and co-workers[93] and in HBV-infected patients by A. Bertoletti et al.[94]

Associations between MHC and Disease

The link between some disease susceptibilities and certain HLA types was one of the first findings signaling the important role of MHC molecules in immunity.[95, 96] These diseases are often of autoimmune or immunopathological nature and are often linked to HLA class I, rather than class II, molecules.[97] The critical role of modified MHC molecules in T cell recognition explained why different allelic forms of MHC are randomly distributed in the population and made it likely that infectious agents and their peptides are presented by at least one of the four to ten MHC molecules expressed by an individual; this minimizes the possibility that a virus escapes immune surveillance, endangering survival of the entire population. The fact that some differences with respect to antigenicity and immunogenicity are linked to the MHC and correlate directly with different strengths of the T cell responses shows that different MHC molecules directly determine and regulate resistance to diseases.

Obviously, cytopathic viruses must be controlled efficiently by the immune system, otherwise the host species dies. Therefore, hosts with non-responder or non-presenting MHC molecules have probably been eliminated long ago by natural selection, leaving only high responders to survive. In contrast, for noncytopathic viruses, diseases are not caused by the infectious agent itself, but rather by the damaging effect of protective T cell responses. Because such agents do not directly cause disease, they do not exert a direct selective pressure on survival. But since these viruses may induce immunopathological cytotoxic T cell responses, differences in MHC may influence the severity of the disease. In fact, many of the diseases exhibiting some association with MHC have an aura of being autoimmune or immunopathologically mediated. This has been directly shown for known noncytopathic viruses (Table 3).[97, 98]

As pointed out above, one of the motivations for testing various mouse strains for cytotoxic T cell activity, resulting in the discovery of MHC-restricted T cell recognition was the variable and weak evidence of susceptibility differences of mice to lethal choriomeningitis that somehow correlated with MHC (Table 4). The comparison of a slowly replicating neurotropic strain of LCMV (UBC-A) with a rapidly replicating viscerotropic isolate UBC-B characterized by C. J. Pfau et al.[99] revealed a dramatic and strict correlation with MHC. After intracerebral infection of mice, UBC-A virus caused death in all recipients, irrespective

Table 3. Association between MHC and disease, reflecting $CD8^+$ T cell mediated immunopathological reaction against host cells infected with noncytopathic LCMV [a].

Mouse strain	A. Maximal increase of serum transaminases after intravenous infection with LCMV (pfu): T cell mediated hepatitis				B. Mortality after intracerebral infection with LCMV	
	WE_{UBC} A		WE_{UBC} D		WE_{UBC} A	WE_{UBC} D
	10^2	10^6	10^2	10^6		
BI0.G H-2D^{q}L^q	–	–	–	++	100%	100%
BI0.BR H-2D^k	–	–	++	±	100%	0%

Mice were infected intravenously with the indicated doses of LCMV WE_{UBC} A or D. Maximal increases of serum transaminases were indicated as follows: - less than threefold, +10–20-fold, ++ greater than 100-fold. Damage of liver cells or of choriomeningeal or ependymal cells caused by LCMV-specific $CD8^+$ T cells. In absence of $CD8^+$ T cells, no immunopathology is seen.

C. Role of virus characteristics increasing likelihood to establish persistent LCMV-infection in mice	
Virus parameters	Increased replication rate, increased resistence to interferons, loss of T cell epitopes by mutation, increased tropism for lymphohemopoietic cells.
Host parameters	Decrease in relative interferon levels, loss of presenting MHC class I molecules (e.g., BALB/c-dm2 mice), partial loss of $CD8^+$ T cells (e.g., DBA/2 mice), loss of T-help cells, lack of IL-2.

[a] Data from refs. [98, 100, 101].

Table 4. Transmission of protective immunity from mother to offspring [a,b].

	preexistent antibodies	"activated" T cells
placenta	maternal antibodies transmissible except with chorioepithelial double layered placenta (bovine)[b]	nontransmissible, danger of host-versus-graft disease and rejection
milk	transmissible through gut of offspring (temporarily) passive protection in gut[b]	evidence poorly analyzed
function	altruistic: protection of offspring against infectious diseases during the period of T cell immunodeficiency and protection of mothers during pregnancy	egoistic: protection of original host against spread of noncytopathic infectious agents (control of immunopathology and tumor cells within host)

[a] Because of MHC-restriction of T cell recognition, T cell maturation in offspring is slow and starts after birth to prevent graft-versus-host disease. During this period of physiological immunoincompetence, transfer of maternal antibody-memory is essential for protection of offspring against many infections. [b] Data from refs. [106a].

of MHC. UBC-B caused immunopathological disease in all those possessing the MHC class I H-2D^{q}L^q allele but not in the others.[98, 100] Furthermore, the susceptibility of mice to becoming persistently infected virus-carriers could be linked by D. Moskophidis et al. to the absence of class I MHC molecules that were able to present the critically important dominant immunogenic viral peptide.[101, 102] These studies, in addition, demonstrated that virus dose and virus strain (including T cell epitope variants) also played an important role in the overall virus–host balance and in MHC–disease association.

Thus association between MHC (in humans HLA) and disease may not be found readily for acute cytopathic viral or bacterial infections, because natural selection has favored good combinations between virus and MHC–presenter.[90] In contrast, for noncytopathic viruses, the selection pressures are much weaker and various virus–host immune response balances resulting in more or less immunopathological disease are acceptable for species survival. Because cytotoxic and protective T cell responses directly depend upon class I MHC presentation of peptides, susceptibility to consequential disease may correlate directly with the MHC class I allele, depending upon the localization of infection (choriomeningitis vs. establishment of a virus-carrier status).[98, 101]

One may therefore extrapolate that at least some autoimmune diseases may eventually turn out to be caused by immunopathological T cell responses against viruses that are poorly cytopathic or noncytopathic[95, 96] (Figure 3, 4). Hepatitis B, C, or D virus infections or possibly immunodeficiency virus (HIV) infections in man may represent this type of chronic infection leading to a protective but immunopathological T cell response, causing MHC-regulated immunopathologic disease. Alternatively, infectious agents that are either unknown or not yet recognized may be involved initially in triggering the disease by immunopathological or autoimmune mechanisms. For example, it is suspected that also common cytopathic viruses may be involved in the pathogenesis of some autoimmunity diseases (Figure 4 and 5). Infections of MHC class-I-positive epithelial or

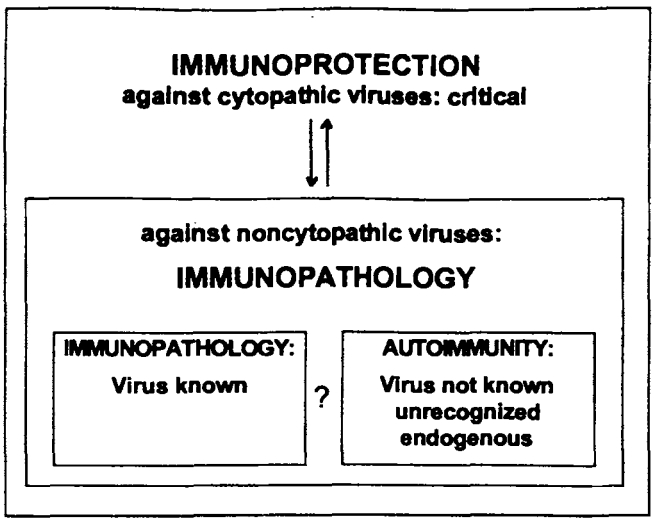

Figure 4. Immunoprotection and immunopathology: Efficient immunoprotection is mandatory for survival of the host infected with a cytophatic virus. Since noncytophatic viruses do not cause cell damage directly, pathology is caused by immune mechanisms. If the virus is not recognized or is unknown, the disease may be mistaken as an autoimmune disease.

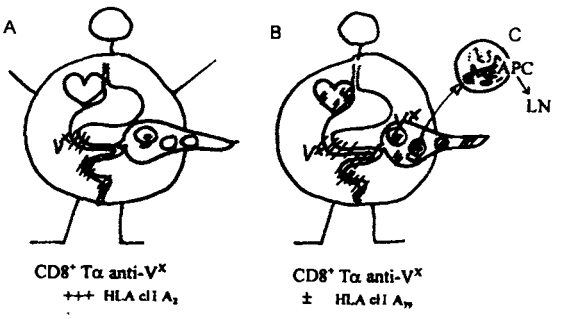

Figure 5. Autoimmunity induced by viruses: If a cytopathic or noncytopathic virus is stopped early enough by MHC class I-(HLA-cl I A_2)-restricted effector T cells (A), sensitive target cells are not destroyed. If the protective HLA-cl I A_{39}-restricted T-cell response is slow (B), virus may reach sensitive target organs and cells that may be destroyed directly or induce disease by T cell mediated immunopathology, that is, T cells cause release of self antigen (S). The self-antigen may then be picked up and presented by APC (C) and in the local lymph node or in the spleen induce autoimmune CTL T cells or autoantibodies. Autoantibody production needs T-help that may be provided by newly induced CD4$^+$ T cells specific either for viral antigens that are linked to self-antigens or for so far segregrated immunologically ignored self-antigens.

neuroendocrine cells should be controlled primarily through CD8$^+$ T cells; their efficiency will, therefore, not only determine the extent and kinetics of destruction of infected host cells, but also whether an autoimmune T cell and B cell response against such sequestered self-antigens is induced.

The reason for MHC class I linkage of autoimmune diseases is, therefore, probably in some diseases that the autoimmune effector T cells are class I restricted (Figure 4), and in other situations that modulations of common or unrecognized infections by the efficiency of class-I-restricted effector T cells may indirectly regulate autoantibody responses (Figure 5).

Consequences for Immunological Memory

The discovery that T cell specificity monitored MHC molecules, that it was positively selected in the thymus, and that this explained the transplantation reaction offered a basis for understanding the role of protective immunological memory. Immunological memory by B and T cells is an important hallmark of immunity and has been exploited successfully by vaccinations.[103–106] However, before vaccinations were used, the idea of immunological memory had no raison d'être. One could argue that if a host dies during the primary infection, he does not need an immunological memory. Also, if he survives the primary infection, he does not need memory, because the system has proven itself efficient. What then is the function of immunological memory? The first and most critical one is transfer of immune antibodies of the mother to protect offspring during the phase of maturation of the immune system after birth, the second is to protect mothers from infections during pregnancy.[106] I will only discuss the first aspect further here.

Calves are born without antibodies because, as for all vertebrates, the immune system is not yet mature enough to produce its own antibody response (Table 4).[106a] In addition, in calves maternal antibodies cannot be transmitted because of the complete doubly layered placenta. All protective antibodies are transmitted in colostral milk from the mother within 24 hours of

birth. If this does not happen, the calf dies within a few weeks as a result of common bacterial infections.

Why then are newborn vertebrates immunoincompetent (Table 4)? My explanation is that because of MHC-restricted T cell recognition, T cells of the fetus should not mature, so as not to endanger pregnancy or cause graft-versus-host disease against maternal MHC molecules.[90, 106] The passively acquired antibodies provide protection during the critical period after birth, during which T cell and B cell maturation slowly takes place over 3–6 months in humans, or four weeks in mice. Since maternal antibodies must cover a wide spectrum of relevant infectious agents that may not be encountered during pregnancy, immunological memory carried by antibodies is mandatory for at least two reasons. Firstly, pregnancy is relatively short compared to the time taken for the host to reach sexual maturity, and therefore antibody memory must be developed over a long period. Secondly, the relevant infections must not occur during pregnancy, because many infections cause damage to and abortion of the foetus.

Evidence has been found in various models and infections that antigens persist both in antibody–antigen complexes and exposed on follicular dendritic cells to maintain antibody responses for many years (Table 5), so that levels of transmissible protection are guaranteed.[107–109]

Table 5. Memory B cells are not protective, whereas preexistent neutralizing levels protect naive recipients against cytopathic infectious agents [a].

Adoptive transfer to naive mice	Booster immunization 2 days before challenge infections	Result of challenge infection
B-cells, naive or normal	no	disease
	yes	disease
"primed" or memory B cells	no	disease
	yes	disease
immune serum with neutralizing antibodies	no	protection
	yes	protection

[a] Data from results of experiments performed in mice with vesicular stomatitis virus (VSV) of refs. [108, 115].

What then is the role of T cell memory? Memory T cells are probably necessary to maintain memory B cells but this is not yet certain. Although increased precursor frequencies of T cells provide some protection, which should suffice to protect mothers during pregnancy, there is a second very important aspect of T cell memory. T cells are critical for controlling persisting noncytopathic viruses that hide in peripheral epithelial or mesenchymal cells and prevent them from reemerging to trigger T cell mediated, immunopathological disease (Tables 4). There is good evidence available now that these protective T cells are also maintained by antigens,[106, 110, 111] although this simple notion is very controversial at the present time.[102, 112, 113] Thus, low levels of ongoing T cell responses reflect antigen-driven, activated effector T cells and not special memory T cells. These serve to protect the host itself and not progeny; these egoistic protective memory T cells cannot be transmitted, due to MHC differences between mother and offspring (Table 4).

Taken together, the summarized evidence suggests that because of MHC-restricted T cell recognition, which causes the transplantation reaction, prolonged physiological immunodeficiency of the offspring is necessary; protection during the period of maturation of the immune system is provided by passively transferred, altruistic antibodies, which necessitate a mandatory antigen-driven elevated antibody level in mothers (Table 4).

Conclusions

In the complex balance between viruses and hosts, T cells play an important role that varies with different host and viral characteristics. The unexpected finding—by chance and also as a matter of course on collaboration between immunologists, geneticists, and virologists—of MHC-restricted T cell recognition has triggered a great number of important subsequent studies by many other groups, resulting in an excellent molecular understanding of T cell recognition of viral-infected target cells. These combined findings have helped to improve the understanding of both immunological specificity and immunological memory. They have furthered our understanding of disease pathogenesis and made possible applications of the acquired knowledge for improving protective immunity and for diminishing immunopathological T cell responses.

Small Glossary

allogen	a substance that stems from another individual of the same species
CTL	cytotoxic T lymphocytes
cytopathic effect	degenerative change in infected cells due to the replication of viruses (formation of giant cells, lysis of cells, etc.)
APC	antigen-presenting cells
EAE	experimental allergic encephalitis
HLA	human lymphocyte antigens (coded by the major histocompatibility complex (MHC)); the MHC controls the transplantation or histocompatibility antigens
H-2	histocompatibility-2, coded by the H-2 gene region (= stronger histocompatibility complex, MHC of the mouse); H-2 controls the transplantation or histocompatibility antigens; the Class 1 antigens are gene products of the K and D region
LCM	lymphocytic choriomeningitis
Listeria monocytogenes	gram-positive, rodlike bacteria without spores that cause the infectious disease Listeriose, which can be tranmitted between animals and humans; the disease can be acute or chronic, with sepsis, meningitis, or often also only as an influenza-like infection or even unnoticed
MHC	major histocompatibility complex
LCMV	the lymphocyte–choriomeningitis virus infects rhodents and occasionally humans; it can attack cells of the meninges and the nervous system without damaging them
TCR	T cell receptor (specific on a T cell)

Looking back over the past 28 years of my professional life since graduating from medical school and marrying my wife, Kathrin, I must admit that life has been very good to me. I was given the chance to work and spend time with many excellent scientists and good friends as well as many eager young students and postdocs. I am part of a caring family, I have the luck to discover new things every once in a while; furthermore, I am paid a salary for enjoying re-searching (in the true sense of the word) the secrets of nature. I thank my families, my mentors, and my

collaborators for all these years. I would also like to thank the Universities of Basel, Zürich, and Lausanne, and especially the John Curtin School of Medical Research, Professor G. Ada, and R. V. Blanden. I am also greatly indebted to the Australian National University in Canberra, the SCRIPPS Clinic and Research Foundation in La Jolla (California), the U. S. National Institutes of Health, the Canton of Zürich, the Swiss Federal Government, the Swiss National Science Foundation, the University of Zürich, and the Fondation Jeantet for their generous financial support.

Received: March 4, 1997 [A 214 IE]
German version: *Angew. Chem.* **1997**, *109*, 2026–2038

Keywords: antigens · immunology · MHC · Nobel lecture · T cells

[1] K. Landsteiner, *The Specificity of Serological Reactions*, Harvard University Press, Boston, **1945**.
[2] J. Klein, *Biology of the Mouse Histocompatibility-2 Complex*, Springer, Berlin, **1975**.
[3] J. Dausset, *Acta Haematol. Basel* **1958**, *20*, 156–166.
[4] J. Hotchin, *Cold Spring Harbor Symp. Quant. Biol.* **1962**, *27*, 479–499.
[5] F. Lehmann-Grube, *Virol. Monogr.* **1971**, *10*, 1–173.
[6] M. J. Buchmeier, R. M. Welsh, F. J. Dutko, M. B. A. Oldstone, *Adv. Immunol.* **1980**, *30*, 275–331.
[7] K. T. Brunner, J. Mauel, J. C. Cerottini, B. Chapuis, *Immunology* **1968**, *14*, 181–196.
[8] J. C. Cerottini, A. A. Nordin, K. T. Brunner, *Nature* **1970**, *228*, 1308–1309.
[9] I. D. Gardner, N. A. Bowern, R. V. Blanden, *Eur. J. Immunol.* **1974**, *4*, 63–67.
[10] O. Marker, M. Volkert, *J. Exp. Med.* **1973**, *137*, 1511–1525.
[11] G. A. Cole, R. A. Prendergast, C. S. Henney, *Nature* **1972**, *238*, 335–337.
[12] R. M. Zinkernagel, P. C. Doherty, *J. Exp. Med.* **1973**, *138*, 1266–1269.
[13] M. B A. Oldstone, F. J. Dixon, G. F. Mitchell, H. O. McDevitt, *J. Exp. Med.* **1973**, *137*, 1201–1212.
[14] R. V. Blanden, *J. Exp. Med.* **1971**, *133*, 1074–1089.
[15] R. M. Zinkernagel, P. C. Doherty, *Nature* **1974**, *248*, 701–702.
[16] G. B. Mackaness, *J. Exp. Med.* **1962**, *116*, 381–406.
[17] G. M. Shearer, *Eur. J. Immunol.* **1974**, *4*, 527–533.
[18] P. A. Gorer, *Br. J. Exp. Pathol.* **1936**, *17*, 42–50.
[19] G. D. Snell, *J. Genet.* **1948**, *49*, 87–108.
[20] J. J. van Rood, A. J. van Leeuwen, *Clin. Invest.* **1963**, *42*, 1382–1390.
[21] B. B. Levine, A. P. Ojeda, B. Benacerraf, *J. Exp. Med.* **1963**, *118*, 953–957.
[22] H. O. McDevitt, M. Sela, *J. Exp. Med.* **1965**, *122*, 517–531.
[23] H. O. McDevitt, A. Chinitz, *Science* **1969**, *163*, 1207–1210.
[24] F. Lilly, E. A. Boyse, L. J. Old, *Lancet* **1964**, *2*, 1207–1209.
[25] H. O. McDevitt, B. D. Deak, D. C. Shreffler, J. Klein, J. H. Stimpfling, G. D. Snell, *J. Exp. Med.* **1972**, *135*, 1259–1278.
[26] F. M. Burnet, *Nature* **1972**, *245*, 359–361.
[27] W. F. Bodmer, *Nature* **1972**, *237*, 139–145.
[28] B. Benacerraf, H. O. McDevitt, *Science* **1972**, *175*, 273–279.
[29] D. B. Amos, W. F. Bodmer, R. Ceppellini, P. G. Condliffe, J. Dausset, J. L. Fahey, *Fed. Proc.* **1972**, *31*, 1087–1104.
[30] N. K. Jerne, *Eur. J. Immunol.* **1971**, *1*, 1–9.
[31] H. S. Lawrence, *Physiol. Rev.* **1959**, *39*, 811–859.
[32] D. W. Bailey, G. D. Snell, M. Cherry, *Proceedings of the Symposium on Immunogenetics of the H-2 System*. Karger, Basel, Schweiz, **1971**, *55*.
[33] C. G. Fathman, H. Hengartner, *Nature* **1978**, *272*, 617–618.
[34] H. von Boehmer, H. Hengartner, M. Nabholz, W. Lernhardt, M. H. Schreier, W. Haas, *Eur. J. Immunol.* **1979**, *9*, 592–597.
[35] J. W. Kappler, B. Skidmore, J. White, P. Marrack, *J. Exp. Med.* **1981**, *153*, 1198–1214.
[36] J. W. Kappler, R. Kubo, K. Haskins, J. White, P. Marrack, *Cell* **1983**, *35*, 295–302.
[37] B. W. McIntyre, J. P. Allison, *Cell* **1983**, *34*, 739–746.
[38] S. M. Hedrick, D. I. Cohen, E. A. Nielsen, M. M. Davis, *Nature* **1984**, *308*, 149–153.
[39] Y. Yanagi, Y. Yoshikai, K. Leggett, S. P. Clark, I. Aleksander, T. W. Mak, *Nature* **1984**, *308*, 145–149.
[40] J. C. Leclerc, E. Gomard, F. Plata, J. P. Levy, *Int. J. Cancer* **1973**, *11*, 426–432.
[41] a) D. H. Lavrin, R. B. Herbermann, M. Nunn, N. Soares, *J. Natl. Cancer Inst.* **1973**, *51*, 1497–1508; b) G. A. Cole, R. A. Prendergast, C. S. Henney, *Fed. Proc.* **1973**, *32*, 964.
[42] B. Kindred, D. C. Shreffler, *J. Immunol.* **1972**, *109*, 940–943.
[43] P. J. McCullagh, *J. Exp. Med.* **1970**, *132*, 916–925.
[44] D. H. Katz, T. Hamaoka, B. Benacerraf, *J. Exp. Med.* **1973**, *137*, 1405–1418.
[45] A. S. Rosenthal, E. M. Shevach, *J. Exp. Med.* **1973**, *138*, 1194–1212.
[46] R. V. Blanden, P. C. Doherty, M. B. Dunlop, I. D. Gardner, R. M. Zinkernagel, C. S. David, *Nature* **1975**, *254*, 269–270.
[47] U. Koszinowski, H. Ertl, *Nature* **1975**, *255*, 552–554.
[48] R. D. Gordon, E. Simpson, L. E. Samelson, *J. Exp. Med.* **1975**, *142*, 1108–1120.
[49] H. von Boehmer, W. Haas, N. K. Jerne, *Proc. Natl. Acad. Sci. USA* **1978**, *75*, 2439–2442.
[50] M. J. Bevan, *Nature* **1975**, *256*, 419–421.
[51] A. J. McMichael, A. Ting, H. J. Zweerink, B. A. Askonas, *Nature* **1977**, *270*, 524–526.
[52] E. Goulmy, A. Termijtelen, B. A. Bradley, J. J. van Rood, *Nature* **1977**, *266*, 544–545.
[53] K. J. Lafferty, A. J. Cunningham, *Aust. J. Exp. Biol. Med. Sci.* **1975**, *53*, 27–42.
[54] P. Bretscher, M. Cohn, *Science* **1970**, *169*, 1042–1049.
[55] M. Cohn, R. E. Langman, *Immunol. Rev.* **1990**, *115*, 11–147.
[56] R. M. Zinkernagel, P. C. Doherty, *Nature* **1974**, *251*, 547–548.
[57] P. C. Doherty, R. M. Zinkernagel, *J. Immunol.* **1975**, *114*, 30–33.
[58] I. D. Gardner, N. A. Bowern, R. V. Blanden, *Eur. J. Immunol.* **1975**, *5*, 122–127.
[59] R. M. Zinkernagel, *Nature* **1974**, *251*, 230–233.
[60] P. C. Doherty, R. M. Zinkernagel, *Lancet* **1975**, *1*, 1406–1409.
[61] B. P. Babbitt, P. M. Allen, G. Matsueda, E. Haber, E. R. Unanue, *Nature* **1985**, *317*, 359–360.
[62] S. Buus, S. Colon, C. Smith, J. H. Freed, C. Miles, H. M. Grey, *Proc. Natl. Acad. Sci. USA* **1986**, *83*, 3968–3971.
[63] A. R. M. Townsend, J. Rothbard, F. M. Gotch, G. Bahadur, D. Wraith, A. J. McMichael, *Cell* **1986**, *44*, 959–968.
[64] J. L. Maryanski, P. Pala, G. Corradin, B. R. Jordan, J. C. Cerottini, *Nature* **1986**, *324*, 578–579.
[65] O. Rötzschke, K. Falk, K. Deres, H. Schild, M. Norda, J. Metzger, G. Jung, H.-G. Rammensee, *Nature* **1990**, *348*, 252–254.
[66] C. Lurquin, A. van Pel, B. Mariame, E. dePlaen, J. P. Szikora, C. Janssens, M. J. Reddchase, J. Lejuene, T. Boon, *Cell* **1989**, *58*, 293–303.
[67] P. J. Bjorkman, M. A. Saper, B. Samraoui, W. S. Bennett, J. L. Strominger, D. C. Wiley, *Nature* **1987**, *329*, 506–511.
[68] P. J. Bjorkman, M. A. Saper, B. Samraoui, W. S. Bennet, J. L. Strominger, D. C. Wiley, *Nature* **1987**, *329*, 512–518.
[69] K. C. Garcia, M. Degano, R. L. Stanfield, A. Brunmark, M. R. Jackson, P. A. Peterson, L. Teyton, I. A. Wilson, *Science* **1996**, *274*, 209–219.
[70] D. N. Garboczi, P. Ghosh, U. Utz, Q. R. Fan, W. E. Biddison, D. C. Wiley, *Nature* **1996**, *384*, 134–141.
[71] J. L. Jorgensen, U. Esser, B. F. de St. Groth, P. A. Reay, M. M. Davis, *Nature* **1992**, *355*, 224–230.
[72] D. B. Sant'Angelo, G. Waterbury, P. Preston-Hurlburt, S. T. Yoon, R. Medzhitov, S. Hong, C. A. Janeway, *Immunity* **1996**, *4*, 367–376.
[73] M. J. Bevan, *Nature* **1977**, *269*, 417–418.
[74] R. M. Zinkernagel, G. N. Callahan, J. Klein, G. Dennert, *Nature* **1978**, *271*, 251–253.
[75] R. M. Zinkernagel, G. N. Callahan, A. Althage, S. Cooper, P. A. Klein, J. Klein, *J. Exp. Med.* **1978**, *147*, 882–896.
[76] R. M. Zinkernagel, A. Althage, E. Waterfield, B. Kindred, R. M. Welsh, G. Callahan, P. Pincetl, *J. Exp. Med.* **1980**, *151*, 376–399.
[77] P. Kisielow, H. S. Teh, H. Bluthmann, H. von Boehmer, *Nature* **1988**, *335*, 730–733.
[78] W. C. Sha, C. A. Nelson, R. D. Newberry, D. M. Kranz, J. H. Russell, D. Y. Loh, *Nature* **1988**, *336*, 73–76.
[79] H. Pircher, T. W. Mak, R. Lang, W. Ballhausen, E. Ruedi, H. Hengartner, R. M. Zinkernagel, K. Bürki, *EMBO J.* **1989**, *8*, 719–727.
[80] K. Deres, H. Schild, K.-H. Wiesmüller, G. Jung, H.-G. Rammensee, *Nature* **1989**, *342*, 561–564.
[81] M. Schultz, R. M. Zinkernagel, H. Hengartner, *Proc. Natl. Acad. Sci. USA* **1991**, *88*, 991–993.
[82] W. M. Kast, L. Roux, J. Curren, H. J. Blom, A. C. Voordow, R. H. Meloen, D. Kolakofsky, C. J. Melief, *Proc. Natl. Acad. Sci. USA* **1991**, *88*, 2283–2287.
[83] C. Widmann, J. L. Maryanski, P. Romero, G. Corradin, *J. Immunol.* **1991**, *147*, 3745–3751.
[84] J. P. Clayton, G. M. Gammon, D. G. Ando, D. H. Kono, L. Hood, E. E. Sercarz, *J. Exp. Med.* **1989**, *169*, 1681–1691.
[85] A. Gaur, B. Wiers, A. Liu, J. Rothbard, C. G. Fathman, *Science* **1992**, *258*, 1491–1494.
[86] D. Kyburz, P. Aichele, D. E. Speiser, H. Hengartner, R. M. Zinkernagel, H. Pircher, *Eur. J. Immunol.* **1993**, *23*, 1956–1962.
[87] P. Aichele, D. Kyburz, P. S. Ohashi, B. Odermatt, R. M. Zinkernagel, H. Hengartner, H. P. Pircher, *Proc. Natl. Acad. Sci. USA* **1994**, *91*, 444–448.
[88] a) S. Oehen, H. Hengartner, R. M. Zinkernagel, *Science*, **1991**, *251*, 195–198; b) P. Aichele, K. Brduscha Riem, R. M. Zinkernagel, H. Hengartner, H. P. Pircher, *J. Exp. Med.* **1995**, *182*, 261–266.
[89] D. Moskophidis, F. Lechner, H. Pircher, R. M. Zinkernagel, *Nature* **1993**, *362*, 758–761.
[90] R. M. Zinkernagel, *Science* **1996**, *271*, 173–178.

[91] H. Pircher, D. Moskophidis, U. Rohrer, K. Bürki, H. Hengartner, R. M. Zinkernagel, *Nature* **1990**, *346*, 629–633.
[92] T. Aebischer, D. Moskophidis, U. Rohrer, R. M. Zinkernagel, H. Hengartner, *Proc. Natl. Acad. Sci. USA* **1991**, *88*, 11047–11051.
[93] R. E. Phillips, S. Rowland-Jones, D. F. Nixon, F. M. Gotch, J. P. Edwards, A. O. Ogunlesi, A. J. McMichael, *Nature* **1991**, *354*, 453–459.
[94] A. Bertoletti, A. Sette, F. V. Chisari, A. Penna, M. Levrero, M. De Carli, *Nature* **1994**, *369*, 407–410.
[95] Review: J. Dausset, A. Svejgaard, *HLA and Disease*, Munksgaard, Kopenhagen, **1977**.
[96] Review: E. Möller, J. Böhme, M. A. Valugerdi, A. Ridderstad, O. Olerup, *Immunol. Rev.* **1990**, *118*, 5–19.
[97] R. M. Zinkernagel, P. C. Doherty, *Adv. Immunol.* **1979**, *27*, 51–177.
[98] R. M. Zinkernagel, C. J. Pfau, H. Hengartner, A. Althage, *Nature* **1985**, *316*, 814–817.
[99] C. J. Pfau, J. K. Valenti, D. C. Pevear, K. D. Hunt, *J. Exp. Med.* **1982**, *156*, 79–89.
[100] T. P. Leist, A. Althage, E. Haenseler, H. Hengartner, R. M. Zinkernagel, *J. Exp. Med.* **1989**, *170*, 269–277.
[101] D. Moskophidis, F. Lechner, H. Hengartner, R. M. Zinkernagel, *J. Immunol.* **1994**, *152*, 4976–4983.
[102] D. Moskophidis, M. Battegay, M. F. van den Broek, E. Laine, U. Hoffmann-Rohrer, R. M. Zinkernagel, *J. Gen. Virol.* **1995**, *76*, 381–391.
[103] Review: D. Gray, T. Leanderson, *Curr. Top. Microbiol. Immunol.* **1990**, *159*, 1–17.
[104] Review: B. D. Jamieson, R. Ahmed, *J. Exp. Med.* **1989**, *169*, 1993–2005.
[105] Review: P. C. Beverley, *Immunol. Today* **1990**, *11*, 203–205.
[106] Reviews: a) R. M. Zinkernagel, M. F. Bachmann, T. M. Kündig, S. Oehen, H. Pircher, H. Hengartner, *Annu. Rev. Immunol.* **1996**, *14*, 333–367; b) R. W. R. Brambell, *The Transmission of Immunity from Mother to Young*, Amsterdam, North Holland. **1970**; c) "Immunology of Feto-Maternal Relationship": G. Möller, *Immunol. Rev.* **1983**, *75*, 5–230.
[107] M. F. Bachmann, B. Odermatt, H. Hengartner, R. M. Zinkernagel, *J. Exp. Med.* **1996**, *183*, 2259–2269.
[108] U. Steinhoff, U. Müller, A. Schertler, H. Hengartner, M. Aguet, R. M. Zinkernagel, *J. Virol.* **1995**, *69*, 2153–2158.
[109] D. Gray, H. Skarvall, *Nature* **1988**, *336*, 70–73.
[110] M. F. Bachmann, T. M. Kündig, H. Hengartner, R. M. Zinkernagel, *Proc. Natl. Acad. Sci. USA* **1997**, *94*, 640–645.
[111] T. M. Kündig, M. F. Bachmann, P. S. Ohashi, H. Pircher, H. Hengartner, R. M. Zinkernagel, *Immunol. Rev.* **1996**, *150*, 63–90.
[112] S. Hou, L. Hyland, K. W. Ryan, A. Portner, P. C. Doherty, *Nature* **1994**, *369*, 652–654.
[113] L. L. Lau, B. D. Jamieson, T. Somasundaram, R. Ahmed, *Nature* **1994**, *369*, 648–652.
[114] P. Aichele, H. Hengartner, R. M. Zinkernagel, M. Schultz, *J. Exp. Med.* **1990**, *171*, 1815–3397.
[115] M. F. Bachmann, T. M. Kündig, B. Odermatt, H. Hengartner, R. M. Zinkernagel, *J. Immunol.* **1994**, *153*, 3386–3397.

Time is money...

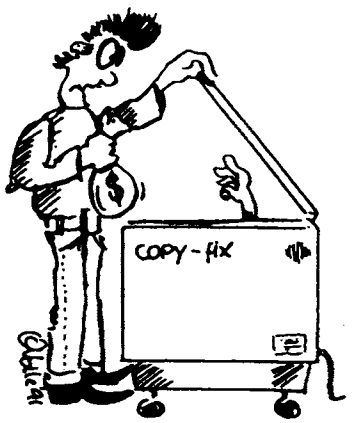

Save both by starting a personal subscription to *Angewandte Chemie*
At 9¢ per page you can't go wrong.
With your own private copy you can read the "hot" articles before they cool, and waste less time in front of the copier.

Order now!
An order form can be found on the last page of this issue.

Inorganic Cauliflower: Functional Main Group Element Dendrimers Constructed from Phosphorus- and Silicon-Based Building Blocks

Dietrich Gudat*

Increased interest in synthetic mesoscopic systems and nanostructures has triggered the rapid development of the chemistry of dendrimers and cascade molecules.[1] Dendrimers are oligo- or polymeric molecules with a treelike, branched backbone, which are constructed in discrete generations by repetitive synthetic cycles. They exhibit interesting properties such as monodispersity, frequently spherical molecular shape, a high degree of internal order, and an accumulation of peripheral functional groups. Although at first mainly dendrimers with organic skeletons were studied, later, dendritic complexes and organometallic compounds and, more recently, main group cascade molecules from silicon- and phosphorus-based building blocks have come to the fore. The incorporation of these elements was stimulated by the availability of a large number of highly reactive monomers suitable for both the assembly of the molecular frame and the attachment of peripheral functional groups. A further advantage of phosphorus-containing dendrimers is that ^{31}P NMR spectroscopy can be applied to directly monitor the construction process.

The known silicon-containing dendrimers may be classified according to three principal categories: silicones and carbosilanes with skeletons of (SiO) and (SiC_n) fragments, respectively, and oligosilanes with pure Si backbones. Silicone dendrimers were obtained as the earliest examples of Si-containing cascade molecules in the late 1980s by the groups led by Zhdanov and Masamune. Starting from $MeSiCl_3$, Zhdanov et al.[2] constructed a dendrimer with 24 $Si(OEt)_2$ end groups by iterative reaction with **1** and subsequent $SOCl_2$-promoted exchange of terminal EtO groups by Cl substituents. Masamune et al.[3] chose the oligosiloxane **2** as the initiator core. The terminal SiH groups were oxidized to SiOH moieties, which were then coupled to the extension unit **3**. Two reiterations of this sequence yielded a third-generation dendrimer ($M \approx 15$ kDa) with 24 SiH end groups, which should be suitable for further functionalization.

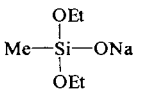

1

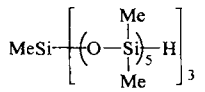

2

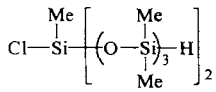

3

[*] Dr. D. Gudat
Institut für Anorganische Chemie der Universität
Gerhard-Domagk-Strasse 1, D-53121 Bonn (Germany)
Fax: Int. code +(228)735327
e-mail: dgudat@uni-bonn.de

An efficient procedure for the generation of carbosilane dendrimers was reported shortly afterwards by van der Made and van Leeuwen[4] and later extended by other groups.[5] Starting from polyfunctional ω-alkenylsilanes as cores, new generations are assembled in two steps by hydrosilylation and subsequent ω-alkenylation (Scheme 1). By deliberate variation of the

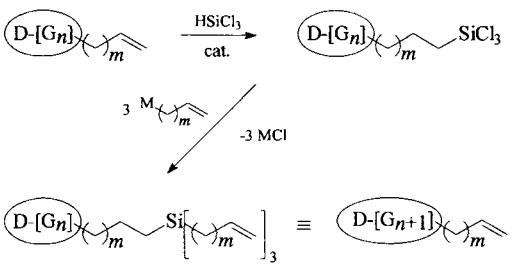

Scheme 1. Construction of carbosilane dendrimers by successive hydrosilylation/alkenylation. D-[G_n]–X denotes a dendrimer of generation n with end groups X.

branch cell multiplicities (e.g. by replacement of $HSiCl_3$ by $HSi(Me)Cl_2$) and segment lengths of each generation (by using alkenyl chains of different lengths) dendrimers can be designed with specific dimensionality and compactness.[4b] Mazerolles et al. recently showed[6] that this procedure can also be used to construct germanium dendrimers up to the second generation; the controlled assembly of still larger molecules has been prevented so far by partial decomposition and side reactions of reactants under the reaction conditions.

Approaches to dendritic polysilanes were elaborated independently by the research groups of Lambert and Sekiguchi. Lambert et al.[7] prepared **4** by chlorinating demethylation of $MeSi(SiMe_3)_3$ and treatment of the resulting product with $LiSi(SiMe_3)_3$. Sekiguchi et al.[8] obtained **7** from the tetrasilanes **5** by repeated cleavage of terminal Si–C bonds with CF_3SO_3H and coupling of the resulting silyl triflates with the lithiosilanes **6** (Scheme 2). Crystal structure determinations revealed that **7** has a rather open, starfishlike molecular structure, whereas **4** is more compact owing to its higher degree of branching. In polysilane **4** the coordination spheres of the inner Si atoms are also distorted due to steric overcrowding.[7] According to UV/Vis studies, the optical properties of both compounds are similar to those of linear oligosilanes.

A growing interest in the functionality of silicon dendrimers is documented by first reports dealing with the linkage

 © WILEY-VCH Verlag GmbH, D-69451 Weinheim, 1997 0570-0833/97/3618-1951 $ 17.50+.50/0

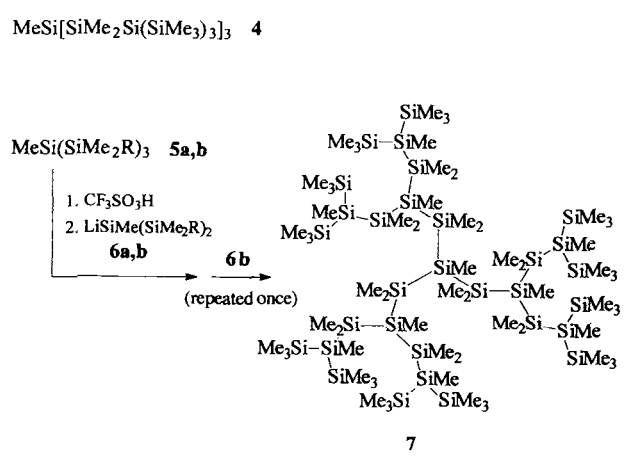

Scheme 2. Polysilane dendrimers. R = Ph (**5a**, **6a**), Me (**5b**, **6b**).

of reactive transition metal fragments to the surface of small dendritic carbosilanes. With the exception of a single report describing the attachment of $Cr(CO)_3$ moieties to terminal phenyl groups,[9] the metal fragments have been anchored by coupling to Si–Cl bonds, either directly or through an additional linker. Examples of this synthetic strategy are the preparation of redox-active ferrocene derivatives and nickel complexes such as **8a**, **b**[10] and **9**,[11] respectively. Complex **9**

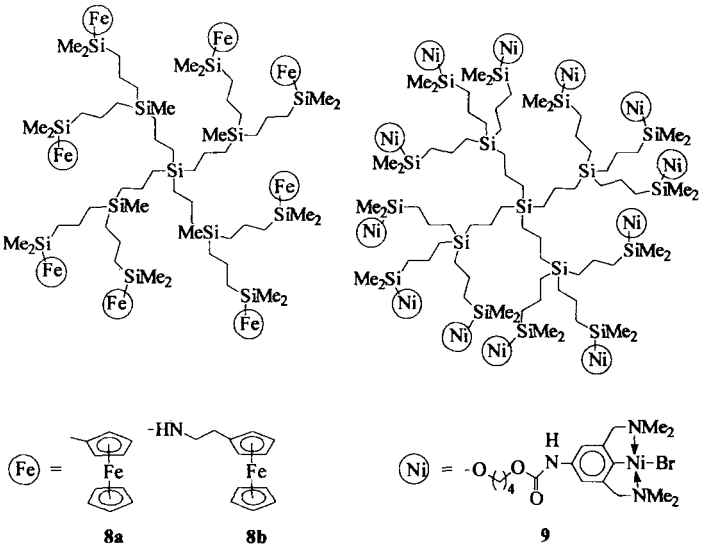

8a **8b** **9**

was successfully employed as a catalyst in Kharasch additions; although its activity was somewhat reduced, its behavior was similar to that of analogous monomeric catalysts. The potential use of SiH_3-terminated carbosilane dendrimers as SiC precursors rather than the explicit exploitation of their terminal functionalities stimulated the synthesis of these compounds by means of hydrogenation of $SiCl_3$-substituted derivatives.[5b] Pyrolysis studies revealed that even if larger dendrimers of this type are in principle suitable as preceramic materials, their use does not lead to any significant improvements that would justify the expensive synthesis.

The structural and functional diversity of dendrimers constructed from phosphorus-based building blocks owes largely to the existence of both neutral and charged framework structures. Rengan and Engel obtained the first charged cascade molecules, polyphosphonium salts in which the three to five dendrons are composed of $[P^+(C_6H_4CH_2)_3]$ repeat units and carry up to 40 positive charges.[12] Reduction of the P=O moiety in the core of such a phosphonium cascade molecule afforded a dendritic phosphane, which is capable of coordinating a metal fragment in the center rather than on the surface, as was demonstrated by the formation of a AuCl complex.[12c]

Neutral phosphorus dendrimers were first reported by the research group headed by Majoral[13] and, shortly afterwards, by the groups led by DuBois and Labarre. DuBois et al.[14] prepared dendritic oligophosphanes by repetitive addition of vinyl phosphonates to primary phosphanes and subsequent reduction of the ester groups to regenerate PH_2 termini; saturation of the outermost PH_2 groups was finally achieved by addition of monovinylphosphanes. The largest molecules of this kind (15 phosphane groups) was treated with $[Pd(MeCN)_4]^{2+}$ to give as the main product the complex **10**, which was found to

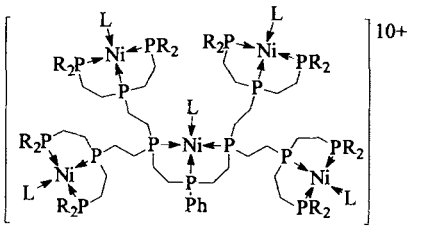

10

catalyze the electrochemical reduction of CO_2 to CO with a rate and selectivity comparable to that attained with analogous monomeric Pd complexes. Similar reactivities were also observed for a mixed Si/P dendrimer accessible from fourfold addition of $HP(CH_2CH_2PPh_2)_2$ to tetravinylsilane and subsequent reaction with $[Pd(MeCN)_4]^{2+}$.

Labarre et al.[15] exploited the functionality of cyclophosphazenes for the generation of highly branched, spherical dendrimers with $N_i = 6$ and $N_b = 5$.[16] Their synthesis started with the exhaustive substitution of hexachlorocyclotriphosphazene by long-chain α,ω-diamines to give a hexamine ("sexapus"), whose terminal amino groups were then capped with new phosphazene "flagstones". This two-step reaction sequence could be reiterated to construct cascade molecules up to the fifth generation, although with increasing molecular size an increasing portion of incompletely substituted side products was noted. Even though these impurities could be removed by chromatography, the analytical data reported for the products give no unequivocal information about possible structure defects (e.g. the growing together of different dendrons, or cyclization reactions), which may lead to polydisperity and molecular weights lower than the theoretically predicted value of approximately 1830 kDa. The authors suggested that the risk of impurities resulting from incomplete reactions might be minimized by a modified reaction sequence in which an existing flagstone is first capped with a sexapus and then with a cyclotriphosphazene to give two new dendrimer generations in two steps.

The largest push so far in the development of phosphorus dendrimers was initiated by the preparation of dendritic polythiophosphoryl amides, whose construction was described by Majoral et al. based on two different reaction sequences starting from aldehyde-based building blocks (Scheme 3). In the first

 © WILEY-VCH Verlag GmbH, D-69451 Weinheim, 1997 0570-0833/97/3618-1952 $ 17.50+.50/0

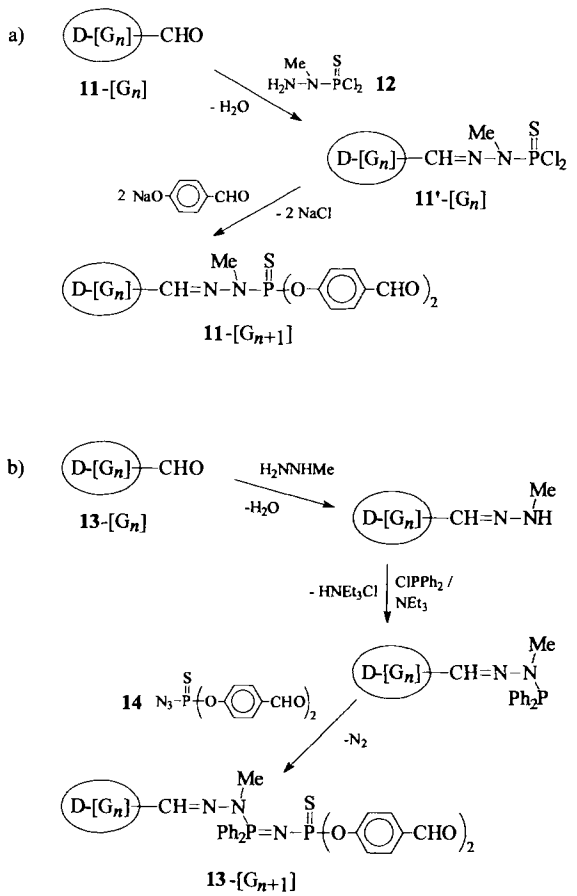

Scheme 3. a),b) Two reaction sequences for the synthesis of thiophosphoryl dendrimers.

addition of phosphonates[21] is possible almost regardless of the size (generation) of the dendrimer. Some examples demonstrating the power of these reactions for the introduction of new functional groups are collected in Scheme 4a. At present investigations of analogous transformations of $P(S)Cl_2$ end groups

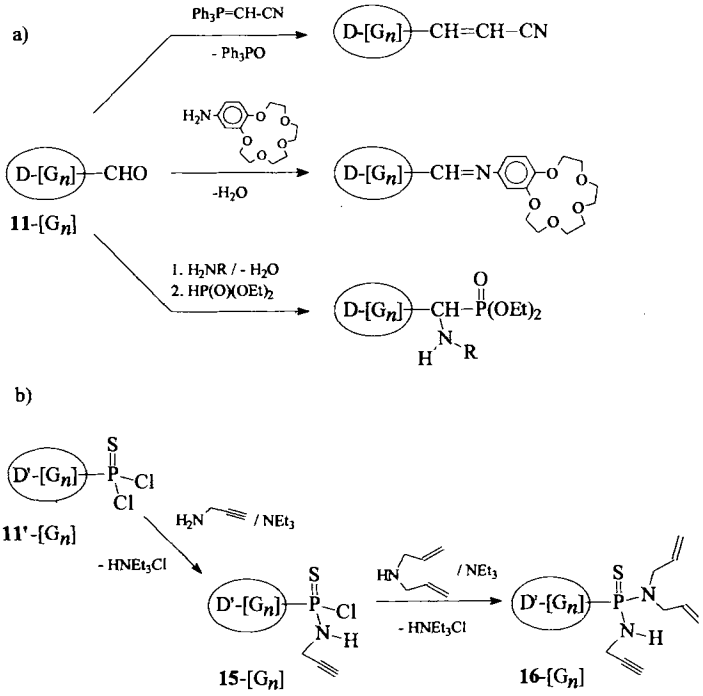

Scheme 4. Functionalization of dendrimers containing a) aldehyde end groups and b) thiophosphoryl end groups.

case a new generation is assembled in two steps by Schiff condensation with the hydrazinothiophosphoryl dichloride **12**, followed by substitution of the Cl groups by the sodium salt of 4-hydroxybenzaldehyde.[13] In the second procedure[17] new generations are formed in three steps by reaction with methylhydrazine, conversion of the formed hydrazone into an aminophosphane (or alternatively[18] Mannich reaction with Ph_2PCH_2OH), and final Staudinger reaction with the thiophosphoryl azide **14**. Since both sequences begin and end with compounds having CHO end groups, their combination affords an easy access to layered block codendrimers with generations of different chemical constitution.[18] Owing to the low degree of branching ($N_b = 2$), large segment lengths, and the ready separation of coproducts, thiophosphoryl dendrimers with three, four, or six dendrons, good solubilities, and large theoretical molecular masses (> 3000 kDa for **11**-[G_{12}]) were easily accessible.[13, 17–19] Confirmation of the calculated molecular masses by mass spectrometry was feasible for first- and second-generation dendrimers,[19] but failed for larger derivatives; however, ^1H and ^{31}P NMR spectroscopic studies indicated that even for the largest molecules any deviations from monodispersity are too small for the observation of structural defects due to incomplete reactions.[13, 17, 19–23]

The highly reactive end groups prove not only useful for backbone construction, but also for the modification of surface groups. Thus, Majoral et al. demonstrated that conversion of peripheral CHO groups in Schiff or Wittig reactions[19, 20] or by are mostly confined to aminolysis and alcoholysis reactions.[20a, 22] A noteworthy finding here is that by appropriate adjustment of reaction conditions the two chlorine atoms of each phosphoryl unit may be replaced successively by two different functional groups.[22] This reaction permits the first directed synthesis of polyfunctional dendrimers such as **15** and **16**, which carry up to four different end groups at the tip of each branch and may, for instance, allow the simultaneous binding of several different chemically active substrates in close proximity (Scheme 4b).

Special attention has been paid to dendrimers with phosphane end groups, which are accessible by the Mannich condensation of hydrazones having NH or NH_2 groups with Ph_2PCH_2OH (Scheme 5a). The potential of these dendrimers to act as mono- or bidentate ligands was confirmed by the syntheses of a number of transition metal complexes.[23] The successful methylation of the Pd complex **18a** with Cp_2ZrMe_2 or MeMgBr to give **18b**, and its further conversion into **18c** and **18d** by sucessive insertion of CO and norbornene into the M–C bonds are impressive examples of synthetically relevant organometallic reactions conducted on the surface of an inorganic dendrimer (Scheme 5b).[23b] Further applications of these and similar reactions in synthetic and catalytic transformations are interesting prospects. After the phosphane surfaces of dendrimers of type **17b** had been covered with between 48 (**17b**-[G_3]) and ca. 3000 AuCl moieties (**17b**-[G_{10}]) the resulting complexes could be visualized directly by electron microscopy. Single dendrimer mol-

 © WILEY-VCH Verlag GmbH, D-69451 Weinheim, 1997 0570-0833/97/3618-1953 $ 17.50+.50/0

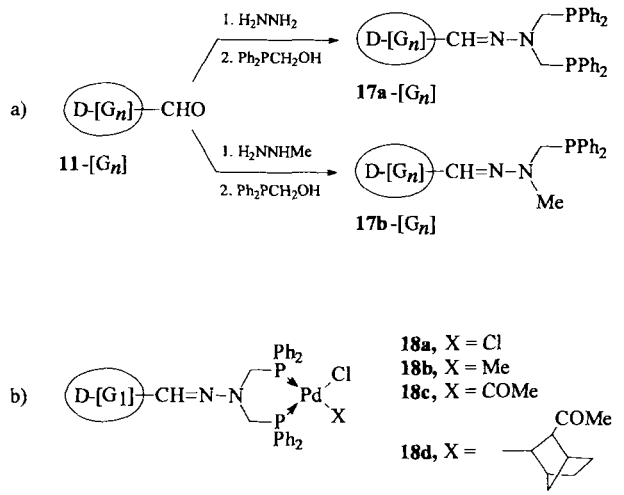

Scheme 5. a) Syntheses of phosphane-functionalized dendrimers and b) dendrimer palladium complexes **18**.

ecules were found with spherical shapes and sizes between 6 [**18b**-[G_3]) and 15 nm [**18b**-[G_{10}]); up to the fifth-generation dendrimer the size increased regularly by 1.5 nm per layer.[23a, c]

^{1}H and ^{31}P NMR spectroscopic studies indicate that for all the surface reactions of thiophosphoryl dendrimers studied a quantitative displacement of end groups within the spectroscopic detection limit can be reached.[19–23] In only a few reactions was a decrease of reaction rates with increasing dendrimer size noted;[20] no generation-dependent variations of the chemical reactivities were detected for the rest. In addition, Majoral et al.[18] were recently able to demonstrate that the inner structures of large thiophosphoryl dendrimers are sufficiently open to allow functionalization even in inner layers. They found that tiered block dendrimers such as **19** react with methyl trifluoromethanesulfonate under regioselective S-alkylation of (Ph_2)-P=NP(S) moieties to give polycations **20**, in which the charges are arranged in well-defined layers at the surface, in the core, in inner cells, or a combination thereof (Scheme 6). Alkylation of the core unit was proven unequivocally by ^{31}P NMR spectroscopy for dendrimers up to the sixth generation. In contrast, for **19**-[G_7] only alkylation of the fourth and seventh layer was ascertained, while the signals of the core evaded spectroscopic detection. The most noteworthy feature of this reaction is not only that the initiator core of an inorganic dendrimer of sixth generation is accessible for defined chemical reactions,[18] but the high chemoselectivity which results in unambigous discrimination between the two types of P=S moieties present. This result suggests that the differences in the reactivity of individual functional groups on the surface and in the interior are comparatively small and paves the way for the further development of organometallic chemistry not only on the surface, but also in interior of dendrimers.

In the study of inorganic dendrimers the focus has also shifted from pure skeleton construction to the preparation of functional molecules.[1c] Earlier studies of functionalities were mostly centered on the consequences of cooperative effects resulting from the accumulation of many functional groups on the surface (e.g. multielectron transfer processes). In the future aspects like the immobilization or fixation of reagents and catalysts on polymers with the aim of facilitating separation from reaction

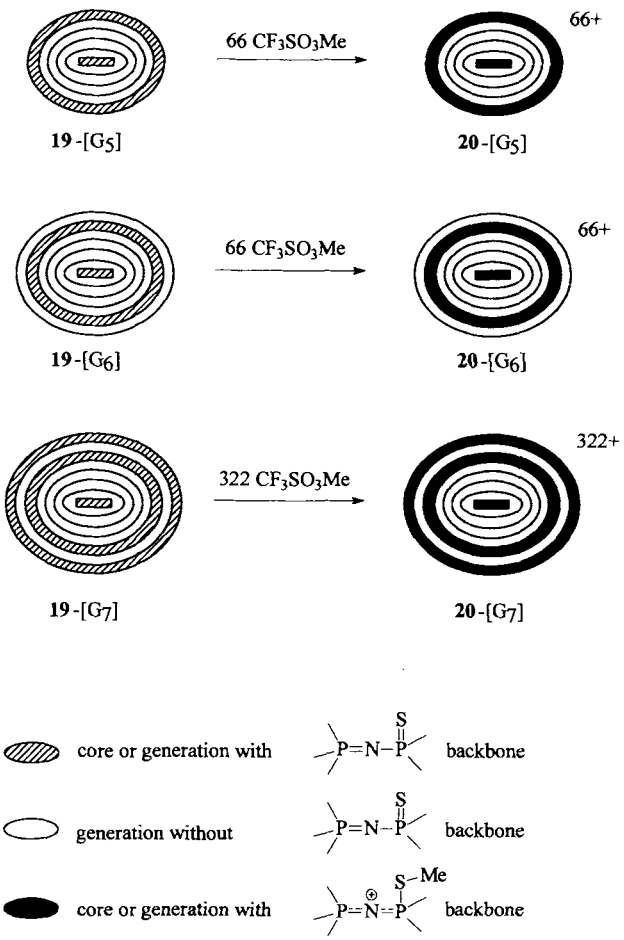

Scheme 6. Polyalkylation reactions of thiophosphoryl dendrimers.

mixtures (for instance, in two-phase or membrane reactors[11]), or the exploitation of "multiply" functionalized dendrimers having several different types of surface groups may gain importance. Another promising area is the application of specific host–guest interactions for the chemoselective control of reactions at interior functionalities, which may lead to the development of novel synthetic reagents or catalysts.

German version: *Angew. Chem.* **1997**, *109*, 2039–2043

Keywords: cascade reactions · dendrimers · phosphorus · silicon

[1] Reviews: a) D. A. Tomalia, A. M. Naylor, W. A. Goddard III, *Angew. Chem.* **1990**, *102*, 119; *Angew. Chem. Int. Ed. Engl.* **1990**, *29*, 138; b) H. B. Mekelburger, W. Jaworek, F. Vögtle, *ibid.* **1992**, *104*, 1609 and **1992**, *31*, 1571; c) J. Issberner, R. Moors, F. Vögtle, *ibid.* **1994**, *106*, 2507 and **1994**, *33*, 2413; d) G. R. Newkome, C. N. Moorefield, F. Vögtle, *Dendritic Molecules, Concepts, Syntheses, Perspectives*, VCH, Weinheim, **1996**.

[2] E. A. Rebrov, A. M. Muzafarov, V. S. Papkov, A. A. Zhdanov, *Dokl. Akad. Nauk SSSR* **1989**, *309*, 376.

[3] H. Uchida, Y. Kabe, K. Yoshino, A. Kawamata, T. Tsumuraya, S. Masamune, *J. Am. Chem. Soc.* **1990**, *112*, 7077.

[4] a) A. W. van der Made, P. W. N. M. van Leeuwen, *J. Chem. Soc. Chem. Commun.* **1992**, 1400; b) A. W. van der Made, P. W. N. M. van Leeuwen, J. C. de Wilde, R. A. C. Brandes, *Adv. Mater.* **1993**, *5*, 466.

[5] a) L. L. Zhou, J. Roovers, *Macromolecules* **1993**, *26*, 963; b) D. Seyferth, D. Y. Son, *Organometallics* **1994**, *13*, 2682.

[6] V. Huc, P. Boussaguet, P. Mazerolles, *J. Organomet. Chem.* **1996**, *521*, 253.

[7] J. B. Lambert, J. L. Pflug, C. L. Stern, *Angew. Chem.* **1995**, *107*, 106; *Angew. Chem. Int. Ed. Engl.* **1995**, *34*, 98.

[8] A. Sekiguchi, M. Nanjo, C. Kabuto, H. Sakurai, *J. Am. Chem. Soc.* **1995**, *117*, 4195.

 © WILEY-VCH Verlag GmbH, D-69451 Weinheim, 1997 0570-0833/97/3618-1954 $ 17.50+.50/0

[9] F. Lobete, I. Cuadrado, C. M. Casado, B. Alonso, M. Morán, J. Losada, *J. Organomet. Chem.* **1996**, *509*, 109.
[10] B. Alonso, I. Cuadrado, M. Morán, J. Losada, *J. Chem. Soc. Chem. Commun.* **1994**, 2575.
[11] J. W. J. Knapen, A. W. van der Made, J. C. de Wilde, P. W. N. M van Leeuwen, P. Wijkens, D. M. Grove, G. van Koten, *Nature* **1994**, *372*, 659.
[12] a) K. Rengan, R. Engel, *J. Chem. Soc. Chem. Commun.* **1990**, 1084; b) *J. Chem. Soc. Dalton Trans.* **1991**, 987; c) R. Engel, K. Rengan, C.-S. Chang, *Heteroat. Chem.* **1993**, *4*, 181.
[13] N. Launay, A.-M. Caminade, R. Lahana, J.-P. Majoral, *Angew. Chem.* **1994**, *106*, 1682; *Angew. Chem. Int. Ed. Engl.* **1994**, *33*, 1589.
[14] A. Miedaner, C. J. Curtis, R. M. Barkley, D. L. DuBois, *Inorg. Chem.* **1994**, *33*, 5482.
[15] F. Sournies, F. Crasnier, M. Graffeuil, J.-P. Faucher, R. Lahana, M.-C. Labarre, J.-F. Labarre, *Angew. Chem.* **1995**, *107*, 610; *Angew. Chem. Int. Ed. Engl.* **1995**, *34*, 578.
[16] N_i and N_b denote the number of branches originating from the core and the individual branch points, respectively.
[17] C. Gaillot, D. Prévoté, A.-M. Caminade, J.-P. Majoral, *J. Am. Chem. Soc.* **1995**, *117*, 5470.
[18] C. Larré, A.-M. Caminade, J.-P. Majoral, *Angew. Chem.* **1997**, *109*, 614; *Angew. Chem. Int. Ed. Engl.* **1997**, *36*, 596.
[19] A.-M. Caminade, M. Slany, N. Launay, M.-L. Lartigue, J.-P. Majoral, *Phosphorus Sulfur Silicon Relat. Elem.* **1996**, *109/110*, 517.
[20] a) N. Launay, A.-M. Caminade, J.-P. Majoral, *J. Am. Chem. Soc.* **1995**, *117*, 3282; b) N. Launay, M. Slany, A.-M. Caminade, J.-P. Majoral, *J. Org. Chem.* **1996**, *61*, 3799.
[21] D. Prévoté, A.-M. Caminade, J.-P. Majoral, personal communication.
[22] a) M. Slany, A.-M. Caminade, J.-P. Majoral, *Tetrahedron Lett.* **1996**, *37*, 9053; b) M.-L. Lartigue, M. Slany, A.-M. Caminade, J.-P. Majoral, *Chem. Eur. J.* **1996**, *2*, 1417.
[23] a) M. Slany, M. Bardaji, M.-J. Casanove, A.-M. Caminade, J.-P. Majoral, B. Chaudret, *J. Am. Chem. Soc.* **1995**, *117*, 9764; b) M. Bardaji, M. Kustos, A.-M. Caminade, J.-P. Majoral, B. Chaudret, *Organometallics* **1997**, *16*, 403; c) M. Slany, M. Bardaji, A.-M. Caminade, B. Chaudret, J.-P. Majoral, *Inorg. Chem.* **1997**, *36*, 1939.

A Chemical Concept for the Treatment of Tay–Sachs Disease

Thomas Kolter*

Tay–Sachs disease belongs to a group of hereditary human diseases in which lipids accumulate in the lysosomes of the cells due to a degradation disorder. With one exception, a causal treatment of these often fatal sphingolipid storage diseases is not possible. Recently, lipid storage was retarded in the central nervous system of an animal model of Tay–Sachs disease with the aid of a low molecular weight inhibitor of glycosphingolipid biosynthesis, *N*-butyldeoxynojirimycin (**1**) (Scheme 1).[1]

Sphingolipidoses

Sphingolipid storage diseases (Scheme 2) are relatively rare hereditary disorders in which at least one step in sphingolipid degradation is deficient.[2, 3] Sphingolipids, components of cell membranes, fulfill functions on the surface of eukaryotic cells that to date have been only partially clarified.[4] They consist of a membrane anchor of ceramide (*N*-acyl-D-*erythro*-sphingosine) and a hydrophilic headgroup, which can be a saccharide or a phosphorylcholine. Sphingolipid biosynthesis[5] starts with the amino acid L-serine and palmitoyl coenzyme A at intracellular membranes. From there the sphingolipids are transported to the plasma membrane to be internalized by endocytosis after a certain time and to be degraded in the digestive system of the cells, the lysosomes.[6] In contrast to phospholipids, for example, sphingolipids are degraded in a strictly sequential manner. Nearly of every of these degradation steps is associated with an inherited defect that gives rise to a human disease. As a consequence of the impaired degradation, undegraded sphingolipids accumulate in the lysosomes and lead to the destruction of certain cells. Since the degradation proceeds at membrane surfaces, activator proteins are needed in addition to hydrolytic enzymes to mediate the interaction between membrane-bound lipid substrates and water-soluble hydrolases. The clinical pictures of sphingolipidoses are rather heterogeneous. Often they are man-

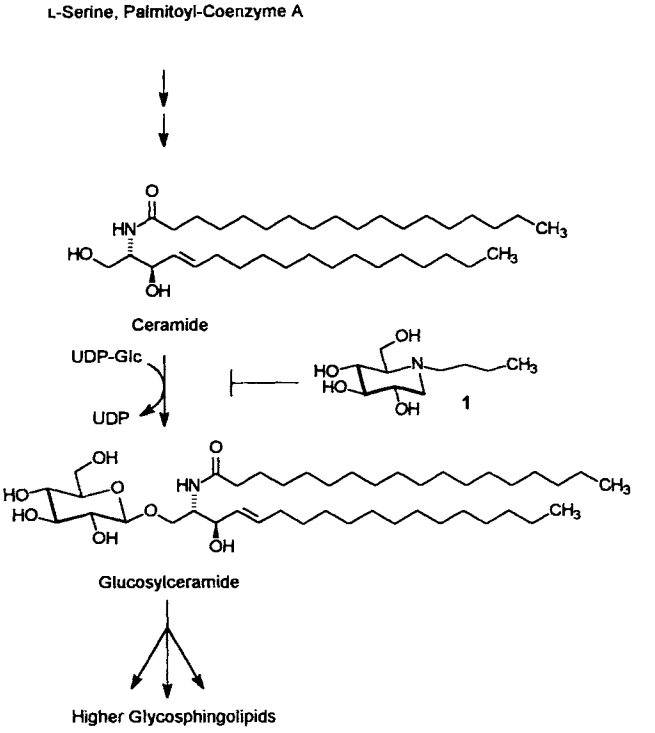

Scheme 1. Part of sphingolipid biosynthesis and site of action of **1**.

[*] Dr. T. Kolter
Institut für Organische Chemie und Biochemie der Universität
Gerhard-Domagk-Strasse 1, D-53121 Bonn (Germany)
Fax: Int. code +(228)737778
e-mail: kolter@snchemie1.chemie.uni-bonn.de

 © WILEY-VCH Verlag GmbH, D-69451 Weinheim, 1997 0570-0833/97/3618-1955 $ 17.50+.50/0

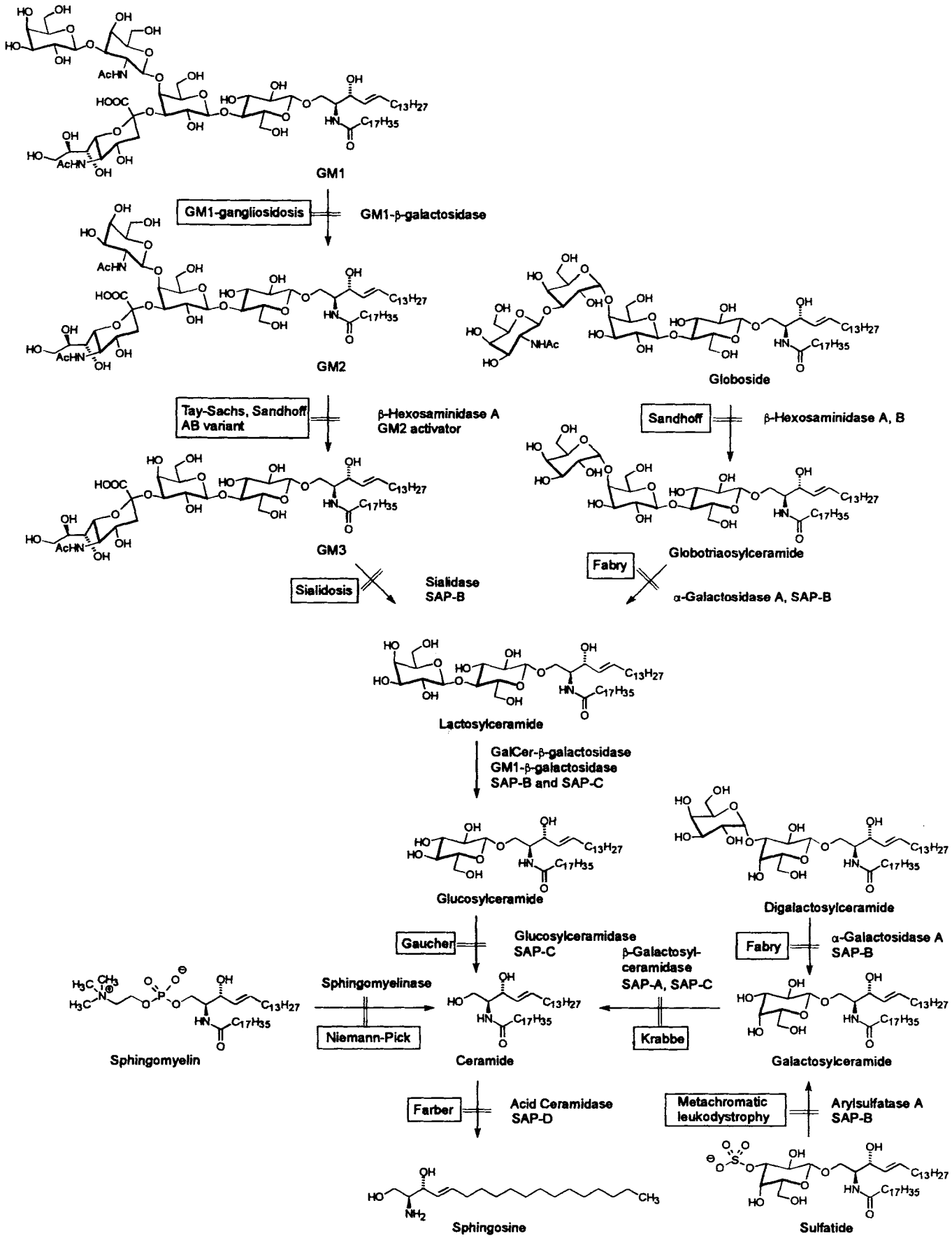

Scheme 2. Degradation of selected sphingolipids in the lysosomes of the cells[2]. The names of individual hereditary diseases (in boxes) are given. The individual compounds show in part considerable heterogeneity within the lipid portion, which is not indicated. Variant AB: AB variant of GM2 gangliosidosis (deficiency of GM2 activator protein); SAP: sphingolipid activator protein.

 © WILEY-VCH Verlag GmbH, D-69451 Weinheim, 1997 0570-0833/97/3618-1956 $ 17.50+.50/0

ifested as mental illnesses that start in early childhood and lead to death of the patients within a few years. However, mild forms of diseases are also known, which do not involve the nervous system, and the patients have a normal life span.

The pathogenesis of these diseases depends essentially on two factors.[2] The expression of glycosphingolipids is cell-type-specific. The gangliosides, for example, glycosphingolipids containing sialic acid, are predominantly found on neuronal cells, so that their accumulation leads to the loss of these cells and impairment of the function of the central nervous system. The other factor is that the course and the severity of the disease depend on the residual enzymatic activity of the gene product in the lysosomes.[7] In general, a complete deficiency leads to an early onset and a severe course of the disease. Many mutations, however, only lead to a partial loss of enzymatic activity. A residual activity of only a few percent can be sufficient to delay the onset of the disease and cause a mild course of the disease.[7]

Tay–Sachs Disease

Human Tay–Sachs disease is characterized by the onset of neurological symptoms in early childhood, rapid progression of the disease, and the death of the patients usually by the age of four years.[8] The earliest symptoms begin within the first three to five months of life. Motoric weakness is evident; patients are extremely startled by sudden sounds since inhibitoric neurons die faster than excitatoric neurons. By the age of six to ten months attention decreases and vision diminishes. Neurological disorders continue until the death of the patients. In Tay–Sachs disease the α-subunit of the enzyme β-hexosaminidase A is defective. β-Hexosaminidase A, which is a heterodimer containing an α- and a β-subunit, cleaves off terminal β-glycosidically linked *N*-acetylglucosamine and *N*-acetylgalactosamine residues from charged and uncharged glycoconjugates. The natural substrate of β-hexosaminidase A is the ganglioside GM2, which is negatively charged under physiological conditions. For GM2 degradation in vivo, the additional presence of a cofactor, the GM2 activator protein, is necessary. Uncharged substrates like the glycolipid GA2 can also be cleaved by β-hexosaminidase B with the subunit composition β_2. Mutations in the β-chain of the hexosaminidases can lead to the loss of both isoenzymes, hexosaminidases A and B, which in humans results in Sandhoff's disease.

The Concept

The new approach is based on the idea that the severity and onset of these diseases are governed by the ratio of residual lysosomal activity and substrate influx into the lysosome.[7] As long as the biosynthesis of substrates continues, the pathological accumulation of substrates in the lysosomes proceeds. Since substrate influx into the lysosomes should be reduced by inhibition of sphingolipid biosynthesis, it should be possible to positively influence the severity as well as the onset of these diseases with the aid of synthetic inhibitors. This approach assumes that a definite residual activity of the enzyme is present in the lysosomes, which is especially the case in juvenile and adult patients.

The Animal Model

The animal model of Tay–Sachs disease was obtained by targeted disruption of the gene of the α-chain of β-hexosaminidase A in murine embryonic stem cells.[9, 10] The animal model of Sandhoff's disease, in which the β-chain of the hexosaminidases A and B are inactivated, has also been described.[11] While both variants of GM2 gangliosidoses mentioned above are only slightly different in the human phenotype, the animal models show drastic differences in severity and course of the disease. Mice with deficient β-hexosaminidase A (the Tay–Sachs mice) are phenotypically normal. They show a mild accumulation of GM2 in the central nervous system, but do not express the neurological symptoms characteristic for Tay–Sachs disease in humans. In contrast, mice with deficient β-hexosaminidase B (Sandhoff mice) develop severe neurological disorders, and the life span of the animals is greatly reduced. The reason for this is the difference in the specificity of sialidase in mice and humans.[11] Mouse sialidase accepts GM2 as a substrate and converts it to GA2. For humans this metabolic pathway is of no significance. GA2 can be degraded by the still-intact β-hexosaminidase B, so that despite the complete loss of β-hexosaminidase A the metabolic barrier is in part circumvented (Scheme 3). Only the loss of both isoenzymes, hexosaminidases A and B, leads to the symptoms corresponding to Sandhoff's disease in humans. Although the mouse sialidase can still convert GM2 to GA2, GA2 cannot be further degraded, since the responsible enzyme, β-hexosaminidase B, is also deficient. For a biosynthetic inhibitor to be useful in the treatment of sphingolipidoses, the degrading system within the lysosomes of the cells should have a certain residual activity. In the animal model of Tay–Sachs disease such a residual activity is present for the degradation of the storage substances through the mouse sialidase, although no intact β-hexosaminidase A can be formed. In this respect the animal model used for the evaluation of the compound is not suitable for studying the effect of the treatment on the symptoms of the disease. But it is particularly well-suited for studying the alteration of morphological parameters of the disease.

The Effect

Through oral application of the inhibitor, serum concentrations of 50 μM are maintained; the same level is also measured in humans who received compound **1** during antiviral therapy.[12] This concentration is sufficient to reduce GM2 storage by 50% (compared to that in untreated mice) after twelve weeks of treatment. In contrast to the findings in untreated mice, cytoplasmic membrane structures due to deposited lipid were hardly detected in the neurons of mice treated for sixteen weeks. The work shows that the compound is well-tolerated, passes the blood–brain barrier,[13] and reaches sufficiently high concentrations in the nervous system to inhibit glucosylceramide formation to the desired extent.

 © WILEY-VCH Verlag GmbH, D-69451 Weinheim, 1997 0570-0833/97/3618-1957 $ 17.50+.50/0

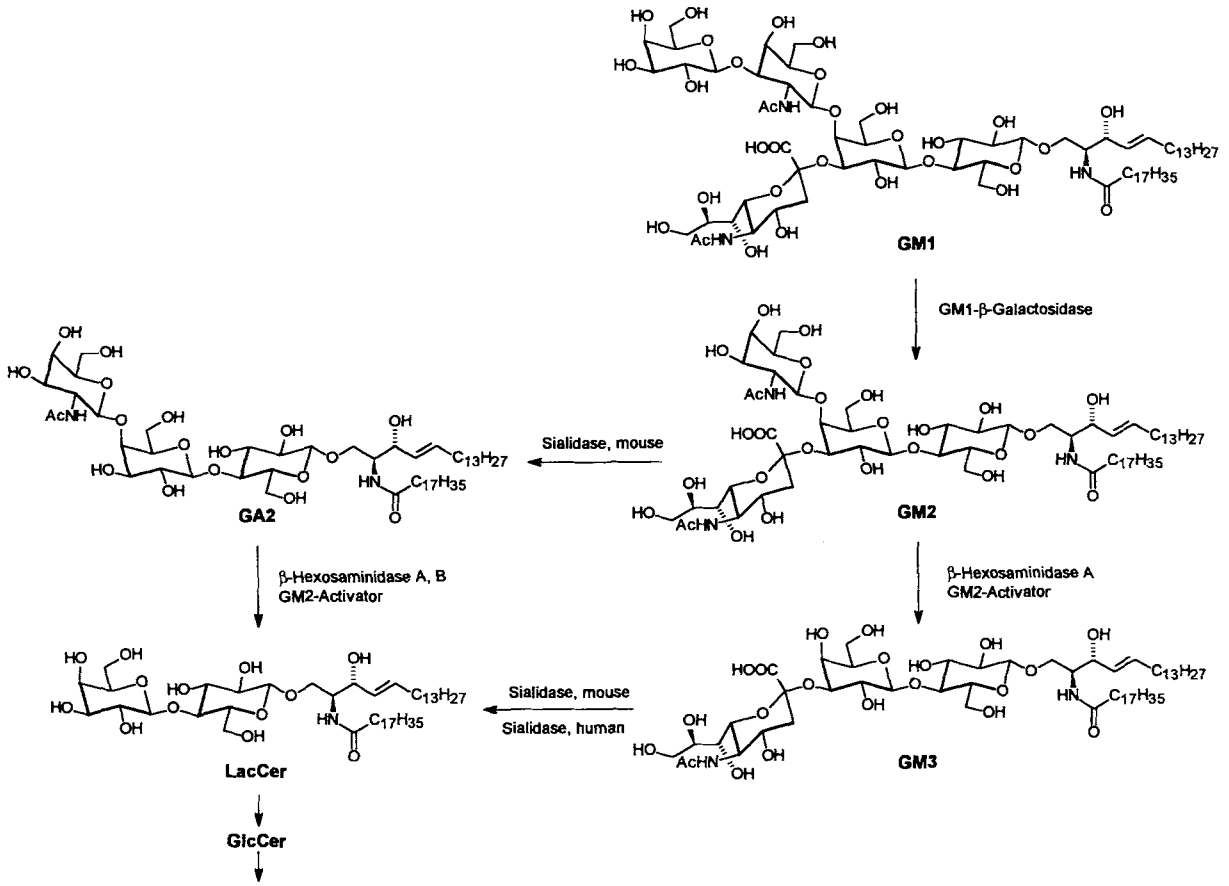

Scheme 3. Degradation pathways for ganglioside GM1 in humans and mice[11].

The Inhibitor

Compound **1** inhibits the glycosyltransferase[14] that transfers glucose from uridine diphosphate-glucose to ceramide (Scheme 1) with an IC_{50} value of 20 μM.[15] The mechanism of the inhibition of the glycosyltransferase by alkylated iminosugars like **1** is not known.[16] However, it is reasonable to assume that the nitrogen atom, which is positively charged under physiological conditions, imitates the carboxonium ion in the transition state of the glycosyltransferase reaction. It can be expected that the mechanism of glycosyltransferases corresponds to the mechanism of glycosidases with the difference that the carbohydrate residue is not transferred to water but to the nucleophilic center of another glycosyl acceptor.[17] In both cases, the enzyme-stabilized intermediate is a carboxonium ion generated by departure of the substituent at the anomeric center. Therefore, **1** should serve as a transition state analog of both the transferase and the glycosidase reaction. Indeed, **1** has been known for some time to be a potent inhibitor of α-glucosidase I and II (IC_{50} = 0.36 μM).[16] Compound **1** is also an inhibitor of HIV replication in vitro; apparently it interferes with the posttranslational processing of viral glycoprotein N-glycosidically linked glycans. Therefore, the compound is neither a particularly potent nor selective inhibitor of glucosylceramide formation, which apparently does not affect its utility.

Structure–activity relationships revealed that the minimum length of the alkyl chain necessary for inhibition of the transferase is three C atoms, and that a chain length of C_4 to C_6 is optimal. Compounds with longer chains led to improved inhibition in vitro, but also had cytotoxic properties in vivo.

Several low molecular weight inhibitors of sphingolipid biosynthesis are known.[18] Inhibition of biosynthesis upstream from glucosylceramide formation can be accompanied by immune suppression or the formation of toxic metabolites.[18] Ceramide-based inhibitors of glucosylceramide formation may interfere with sphingomyelin formation or with ceramide-dependent signal transduction. A compound with improved selectivity compared to that of **1** is the derivative with D-galacto configuration (IC_{50} = 40 μM),[19] which results in little to no inhibition of glycosidases like β-gluco- and β-galactocerebrosidase and α-glucosidase I and II. This compound, however, has not been investigated in the animal model. The results obtained with the alkylated iminosugars are also of importance because attempts at developing potent and selective inhibitors of glycosyltransferases have as yet been of limited success.

Outlook

To date, a causal therapy of sphingolipidoses has been successful only for patients having the adult form (type I) of Gaucher's disease. Here, the central nervous system is not involved due to the high residual activity of the deficient enzyme, the glucosylceramidase. In this very expensive enzyme replacement therapy the patients receive infusions of chemically modified glucocerebrosidase. Gene therapy based approaches and

 © WILEY-VCH Verlag GmbH D-69451 Weinheim. 1997 0570-0833/97/3618-1958 $ 17.50+.50/0

bone marrow transplantations did not lead to the desired success. This underlines the importance of this new approach, in which an orally available and well-tolerated compound has potential for the treatment of an entire group of diseases. Inhibition of glucosylceramide formation should be suitable for the treatment of other sphingolipidoses in which glycosphingolipids are stored that are biosynthetically derived from glucosylceramide and in which residual enzymatic activity is found in the lysosome. Of particularly importance is the ability of the title compound **1** to pass the blood–brain barrier. Owing to its oral availability and low toxicity, the development of **1** constitutes considerable progress towards the treatment of this group of severe diseases.

German version: *Angew. Chem.* **1997**, *109*, 2044–2048

Keywords: bioorganic chemistry · enzymes · glycolipids · inhibitors · sphingolipids

[1] F. M. Platt, G. R. Neises, G. Reinkensmeier, M. J. Townsend, V. H. Perry, R. L. Proia, B. Winchester, R. A. Dwek, T. D. Butters, *Science* **1997**, 276, 428–431.
[2] K. Sandhoff, T. Kolter, *Naturwissenschaften* **1995**, *82*, 403–413.
[3] V. Gieselmann, *Biochim. Biophys. Acta* **1995**, *1270*, 103–136.
[4] S. Hakomori, Y. Igarashi, *J. Biochem.* **1995**, *118*, 1091–1103.
[5] G. van Echten, K. Sandhoff, *J. Biol. Chem.* **1993**, *268*, 5341–5344.
[6] K. Sandhoff, T. Kolter, *Trends Cell Biol.* **1996**, *6*, 98–103.
[7] P. Leinekugel, S. Michel, E. Conzelmann, K. Sandhoff, *Hum. Genet.* **1992**, *88*, 513–523.
[8] K. Sandhoff, E. Conzelmann, E. Neufeld, M. M. Kaback, K. Suzuki in *The Metabolic Basis of Inherited Disease* (Eds.: C. Scriver, A. L. Beaudet, W. S. Sly, D. Valle) McGraw–Hill, New York, **1989**, pp. 1807–1839.
[9] S. Yamanaka, M. D. Johnson, A. Grinberg, H. Westphal, J. N. Crawley, M. Taniike, K. Suzuki, R. L. Proia, *Proc. Natl. Acad. Sci. USA* **1994**, *91*, 9975–9979.
[10] M. Taniike, S. Yamanaka, R. L. Proia, C. Langaman, T. Bonc-Turentine, K. Suzuki, *Acta Neuropathol.* **1995**, *89*, 296–304.
[11] K. Sango, S. Yamanaka, A. Hoffmann, Y. Okuda, A. Grinberg, H. Westphal, M. P. McDonald, J. N. Crawley, K. Sandhoff, K. Suzuki, R. L. Proia, *Nature Genet.* **1995**, *11*, 170–176.
[12] M. A. Fischl, L. Resnick, R. Coombs, A. B. Kremer, J. C. Pottage, R. J. Fass, K. H. Fife, W. G. Powderly, A. C. Collier, R. L. Aspinall, S. L. Smith, K. G. Kowalski, C.-B. Wallemark, *J. Acquir. Immun. Defic. Syndr.* **1994**, *7*, 139–147.
[13] A. Aigner, S. Wolf, H. G. Gassen, *Angew. Chem.* **1997**, *109*, 24–42; *Angew. Chem. Int. Ed. Engl.* **1997**, *36*, 24–41.
[14] Isolation: P. Paul, Y. Kamisaka, D. L. Marks, R. E. Pagano, *J. Biol. Chem.* **1996**, *271*, 2287–2293; Cloning: S. Ichikawa, H. Sakiyama, G. Suzuki, K. Hidari, Y. Hirabayashi, *Proc. Natl. Acad. Sci. USA* **1996**, 93, 4638–4643.
[15] F. M. Platt, G. R. Neises, R. A. Dwek, T. D. Butters, *J. Biol. Chem.* **1994**, *269*, 8362–8365.
[16] F. M. Platt, T. D. Butters, *Trends Glycosci. Glycotechnol.* **1995**, *7*, 495–511.
[17] M. L. Sinnot, *Chem. Rev.* **1990**, *90*, 1171–1202.
[18] T. Kolter, K. Sandhoff, *Chem. Soc. Rev.* **1996**, *25*, 371–381.
[19] F. M. Platt, G. R. Neises, G. B. Karlsson, R. A. Dwek, T. D. Butters, *J. Biol. Chem.* **1994**, *269*, 27108–27114.

 © WILEY-VCH Verlag GmbH, D-69451 Weinheim, 1997 0570-0833/97/3618-1959 $ 17.50+.50/0

Molecular imprinted cavity with a phosphonate ester as template. This template is analogous to the intermediate in basic ester hydrolysis (blue atom either phosphorus or carbon).

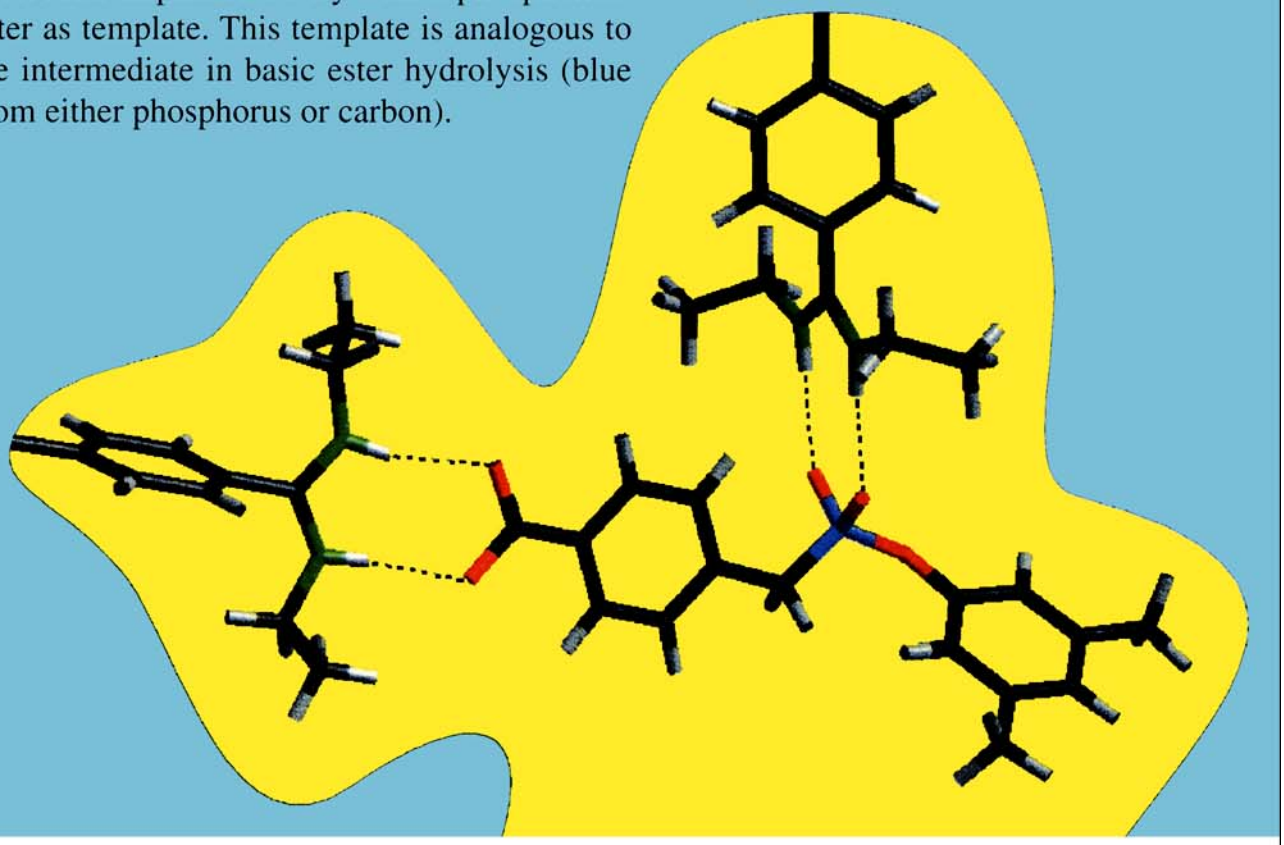

Molecular imprinted cavity with the actual transition state of the basic ester hydrolysis. The amidine activates the carbonyl group and the attacking water molecule. For further details, see the following pages.

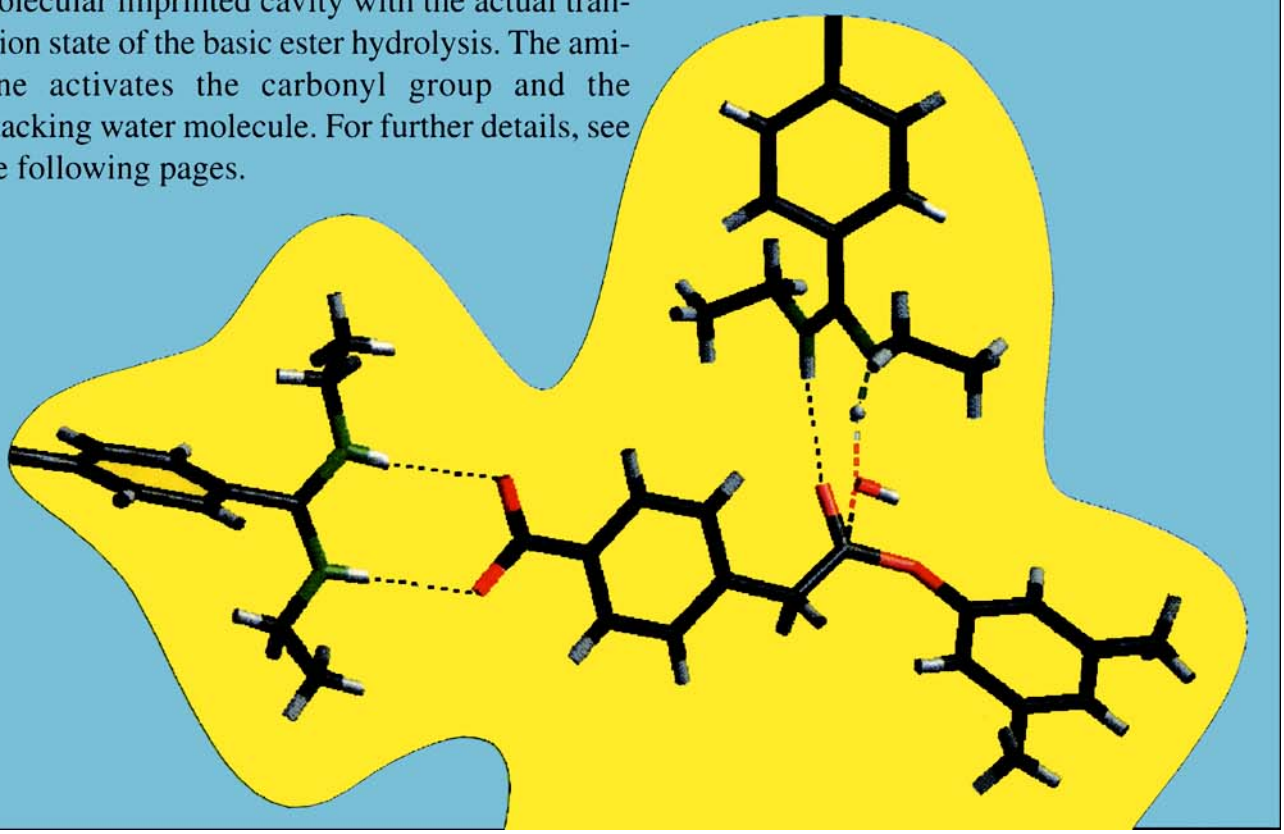

 © WILEY-VCH Verlag GmbH, D-69451 Weinheim, 1997 0570-0833/97/3618-1961 $ 17.50 + .50/0

Enzyme Models Based on Molecularly Imprinted Polymers with Strong Esterase Activity**

Günter Wulff,* Thomas Gross, and Rainer Schönfeld

Enzyme models have roused great general interest[1] since they could be used as efficient synthetic catalysts, and also serve to test theories and hypotheses of enzyme research. Thus, the thesis that the catalytic activity of enzymes relies on the preferred binding of the transition state of the reaction, which was first postulated by L. Pauling[2a] and later justified by W. P. Jencks,[2b] was confirmed by experiments with enzyme models based on transition state imprinted antibodies.[3] For example, a phosphonic ester, as a transition state analogue of the alkaline ester hydrolysis, was used as hapten to generate antibodies that catalytically accelerate the hydrolysis of carboxylic esters by a factor of 10^3–10^4.

We have described a method for obtaining specific microcavities in cross-linked polymers by molecular imprinting.[4, 5] Cross-linking polymerization takes place around a molecule that is used as a template; this is similar to the previously assumed mechanism for the generation of antibodies. The template is then split off, leaving behind an imprint of defined shape and bearing functional groups in specific positions, which are accessible for interaction. This method should be suitable for creating transition state imprinted enzyme models. So far, attempts to design enzyme models with esterase activity by imprinting, for example with phosphonic esters, were disappointing.[6] The attainable acceleration factors of 1.6–2, in one case 6.7, are not satisfying, especially since in most cases neither Michaelis–Menten kinetics nor competitive inhibition or turnover were observed.

The results of others[7] and numerous experiments performed in our laboratory indicate that the transition state analogous shape of a cavity does not alone cause a strong catalytic effect; additional effective groups are necessary. Furthermore, in catalytically active antibodies the correctly positioned functional groups also play an important role in the catalytic mechanism. S. J. Benkovic et al.[8] established that the guanidine group of the amino acid arginine is decisive for the positioning and fixation of the phosphonic monoester during the formation of an antibody, and is also important for the catalysis of the alkaline ester hydrolysis. We have now developed polymerizable amidines[9, 10] and used them as anchor or catalyst groups. Detailed investigations on the interaction of amidines with carboxylic acids and phosphonic acid monoesters showed that, for example, *N*,*N*′-diethyl(4-vinylphenyl)amidine forms readily soluble complexes with very high association constants with both classes of substances. In contrast to the monomer and its hydrochloride, in which the ethyl groups can be (*E*) or (*Z*) configurated, the ethyl groups of the complex are exclusively (*E*) configurated.[11]

Phosphonic acid monoester **1**, which can be prepared in four steps from methyl 4-chloromethylbenzoate in good yields, was used as a transition state analogue of the alkaline ester hydrolysis of **2** [Eq. (a)]. In nonpolar solvents **1a** reacts with two equivalents of amidine **3a** to form the bis(amidinium) complex nearly quantitatively (NMR spectroscopy; see Scheme 1, top). This

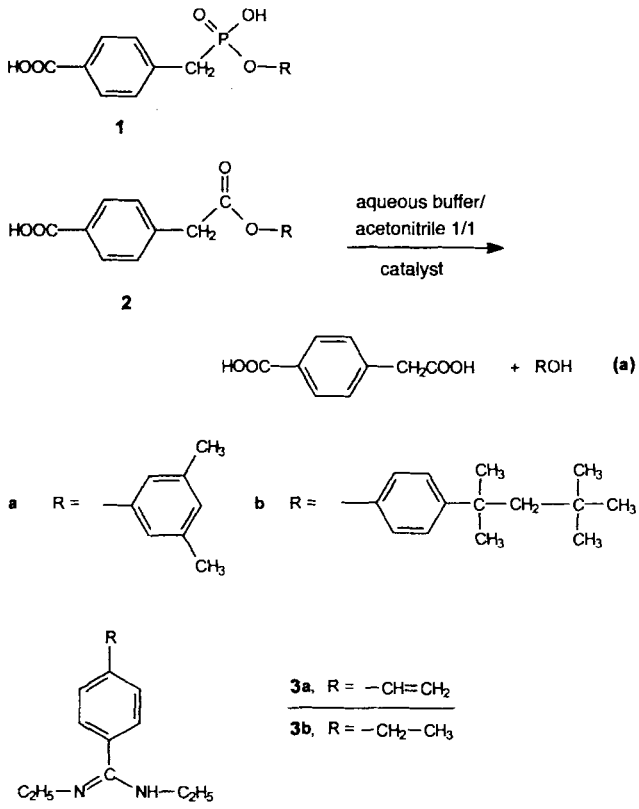

salt is copolymerized in the presence of an inert solvent (THF) with a large excess of ethylene dimethacrylate as cross-linker. About 90% of the template can be split off, leaving cavities containing two amidine groups (Scheme 1, middle). Owing to the high binding constants stoichiometric amounts of the anchor groups can be used, so that all the amidine groups are within the cavities. A larger excess of the anchor group is almost always required for other noncovalent interactions.

The hydrolysis of ester **2a** according to Equation (a) was performed in a 1:1 solution of buffer (pH 7.0, 7.6, and 9.0) and acetonitrile in the presence of the polymer prepared with **1a** (see Table 1). For comparison hydrolysis was performed at each pH

Table 1. Relative reaction rates for hydrolysis of **2a** and **2b** in the presence of different catalysts.

Substrate	pH	k[min^{-1}][a]	Relative reaction rate: Neat solution	Solution + **3b**	Polymer imprinted with **3a**·benzoate	Polymer imprinted with **1a** or **1b**
2a	7.0	$8.9 \cdot 10^{-7}$	1.0	1.5	10.9	49.0
2a	7.6	$9.2 \cdot 10^{-7}$	1.0	2.4	20.5	102.2
2a	9.0	$4.2 \cdot 10^{-6}$	1.0	1.9	4.7	17.6
2b	7.6	$3.1 \cdot 10^{-6}$	1.0	n.b.	n.b.	81.4
2b	9.0	$2.3 \cdot 10^{-6}$	1.0	2.0	14.9	52.4

[a] Reaction rate k refers to the reaction in buffer/acetonitrile (1/1) without addition of amidine or polymer. This value is defined as 1.0.

in a neat solution, in solution with addition of amidine **3b** (equivalent to the amount of amidine groups within the polymer), and with a polymer that was imprinted with the benzoate of **3a** (a polymer containing statistically distributed amidines without microcavities behaves similarly to the solution of the amidine). The reaction at 21 °C was followed with HPLC on a RP8 column with UV detection at 238 nm. All compounds in Equation (a) and the added internal standard propiophenone

[*] Prof. Dr. G. Wulff, Dr. T. Gross, Dipl.-Chem. R. Schönfeld
Institüt für Organische Chemie und Makromolekulare Chemie der Universität
Universitätsstrasse 1, D-40225 Düsseldorf (Germany)
Fax: Int. code +(211)811-4788
e-mail: wulffg@iris-oc2.oc2.uni-duesseldorf.de

[**] These investigations were supported by the Deutsche Forschungsgemeinschaft and the Fonds der Chemischen Industrie.

 © WILEY-VCH Verlag GmbH, D-69451 Weinheim, 1997 0570-0833/97/3618-1962 $ 17.50+.50/0

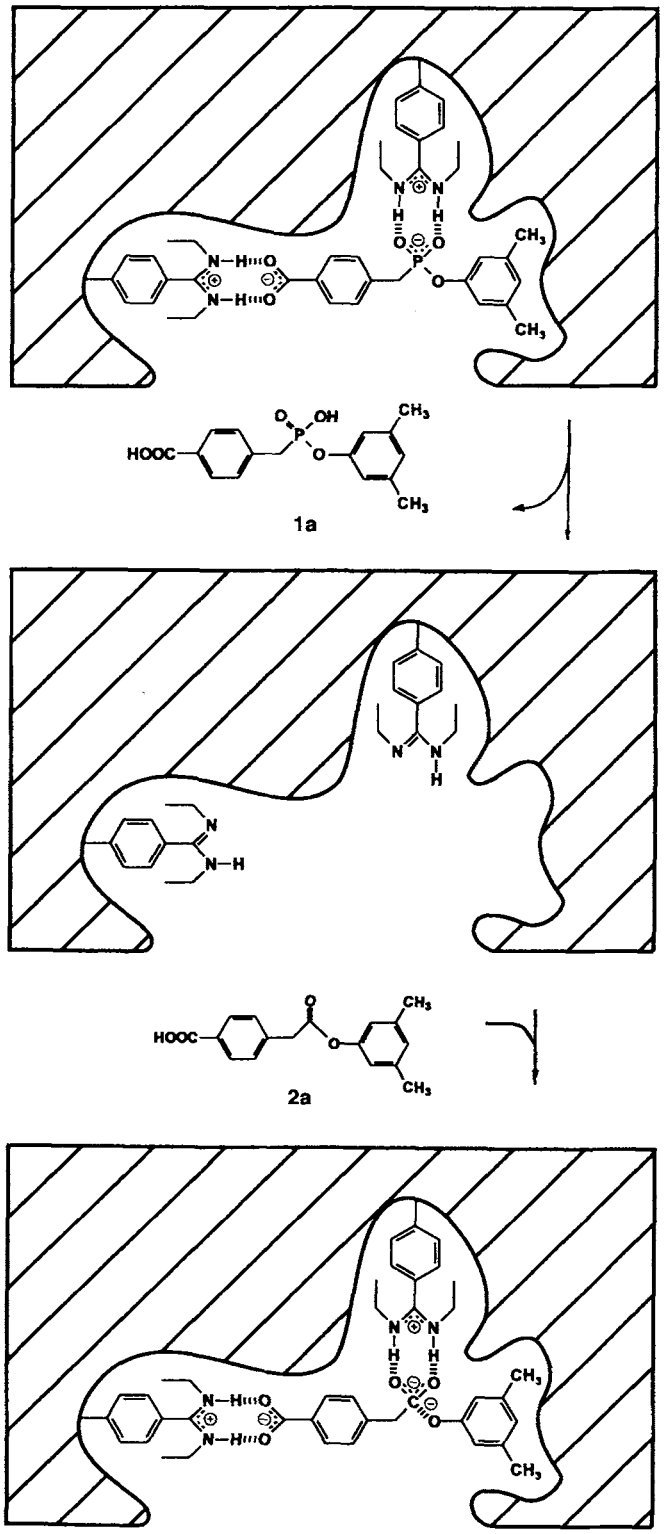

Scheme 1. Schematic representation of a microcavity that was imprinted by the polymerization of bis(amidinium) salt of **3a** with the transition state analogous template **1a** (top). A cavity bearing two *N,N'*-diethylamidine groups remains after removal of the template **1a** (middle). The alkaline hydrolysis of ester **2a** is catalyzed by the polymer that stabilizes the transition state of the reaction (bottom). See also frontispiece of the communications section.

could be completely separated ("baseline-separated"). For the kinetics the formation of homoterephthalic acid was monitored, and the specific reaction rates were calculated from the initial reaction rates.

As in the case of investigations with the catalytic antibodies, the reaction rates given are relative. The rate for hydrolysis in solution at the same pH without addition of a catalyst is defined as 1.0. The amidine **3b** in solution shows a relatively small effect, whereas the acceleration by the polymer imprinted with **1a** is unusually strong, and the reaction rate at pH 7.6 increases by more than 100-fold. Even the polymer imprinted with **3a**·benzoate causes a distinct acceleration by a factor of 20. The polymer imprinted with structurally related template **1b** also shows a strong acceleration (80-fold) of the hydrolysis of the corresponding ester **2b**.

These are by far the strongest catalytic effects for ester hydrolysis achieved with this approach up to now. The activity is only one to two orders of magnitudes lower than that of catalytic antibodies, which is not a big difference considering the fact that we used insoluble polymers with rigid structure and "polyclonal" cavities. It should also be pointed out that in our case only nonactivated phenol esters were employed, in contrast to the strongly activated 4-nitrophenyl esters used in nearly all other investigations.

It is of great interest to assay if this model also shows other typical enzyme characteristics. Therefore, the kinetics of systems with strongly varying substrate:catalyst ratios were measured. Hydrolysis with the polymer imprinted with **1a** reveals typical Michaelis–Menten kinetics with saturation kinetics, while hydrolysis with the neat solution and the solution with **3b** both show a linear relationship between reaction rate and concentration (Figure 1). Surprisingly, even the polymer imprinted with **3b**·benzoate shows a certain substrate saturation.

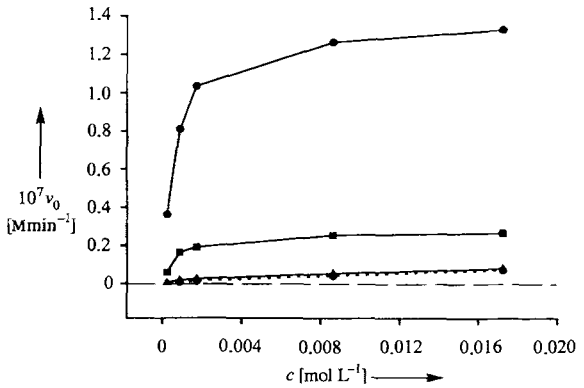

Figure 1. Michaelis–Menten plot for the hydrolysis of ester **2a** in a 1:1 mixture of aqueous buffer (pH 7.6) and acetonitrile at 21 °C in the presence of different catalysts (plot of initial reaction rate v_0 versus substrate concentration c): —●— polymer imprinted with **1a**, —■— polymer imprinted with benzoate, —▲— amidine **3b**, - - ● - - no catalyst.

The double-reciprocal Lineweaver–Burk plot in Figure 2 indicates strong substrate bonding with a Michaelis constant of $K_m = 0.60$ mM. The turnover number is relatively small ($k_{cat} = 0.8 \times 10^{-4}$ min^{-1}), but a turnover unequivocably takes place. Figure 2 also shows that the transition-state analogue **1a** is a very effective competitive inhibitor; its affinity for the imprinted polymer ($K_i = 0.025$ mM) is clearly higher than that of the substrate. Unfortunately the product, homoterephthalic acid, is also a competitive inhibitor, and probably responsible for the small turnover number observed.

The selectivity of our enzyme models is also remarkable. The cross-selectivity of the polymers imprinted with **1a** and **1b** at pH 9.0 is shown in Table 2. The determination of the rates of alkaline hydrolysis of **2a** and **2b** with both polymers proves that

 © WILEY-VCH Verlag GmbH, D-69451 Weinheim, 1997 0570-0833/97/3618-1963 $ 17.50+.50/0

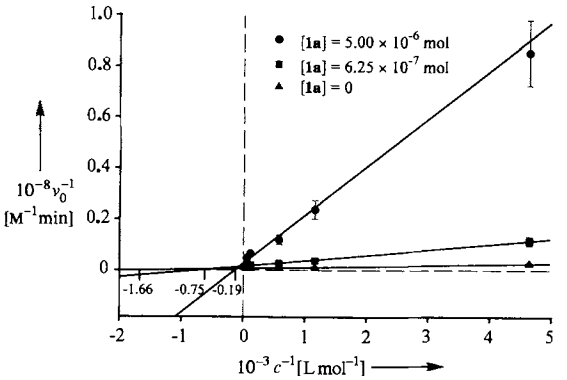

Figure 2. Double-reciprocal Lineweaver–Burk plot of initial reaction rate v_0^{-1} versus substrate concentration c^{-1}. Different concentrations of the competitive inhibitor **1a** were added in two cases. Intersections at $1/v_0 = 0$ provide the $-1/\alpha K_m$ values shown, from which K_i can be determined.

Table 2. Relative reaction rates for the hydrolysis of **2a** and **2b** catalyzed by polymers imprinted with **1a** and **1b** (pH 9) (cross-equilibration).

Substrate	Solution	Imprinted with **1a**	Imprinted with **1b**	Factor
2a	1.0	17.6	11.8	1.5
2b	1.0	40.6	52.4	1.3

each polymer hydrolyzes its "own" substrate significantly better (factor of 1.3–1.5), although both are phenol esters, and the cavities have only a slightly different shape caused by the small structural differences on the aromatic rings.

Experimental Section

General procedure for synthesizing the imprinted polymers: Template **1a** (0.5 equiv), **1b** (0.5 equiv), or benzoic acid (1 equiv) is added with azobis(isobutyronitrile) (1%) to a mixture of ethylene dimethacrylate (87.6 wt%), methyl methacrylate (4.1%), and **3a** (8.3%, 1 equiv). The solution is diluted with the same volume of tetrahydrofuran as the porogen. Polymerization proceeds at 60 °C for 70 h in a fused ampoule. After the polymer is ground, it is washed with methanol in a Soxhlet apparatus for 24 h. The template molecules are then split off by two equilibrations with 0.1 N aqueous NaOH/acetonitrile (1/1). Split-off percentages (typically 90%) are determined by HPLC. The hydrolysis is investigated after adding a solution of **2a** or **2b** (500 μL, 0.01 M) along with benzophenone or propiophenone as internal standard to buffer/acetonitrile (1/1, 5 mL ; phosphate buffer pH 7.0 and 7.6, glycine/NaOH buffer pH 9.0]. The amount of the polymer is based on the number of free cavities. The hydrolysis is monitored at 21 °C by HPLC (RP8 column, UV detection at 238 nm) and referenced to the amount of originating homoterephthalic acid.

Received: April 1, 1997 [Z10293IE]
German version: *Angew. Chem.* **1997**, *109*, 2049–2052

Keywords: enzyme mimetics · heterogeneous catalysis · hydrolyses · imprinting · polymers

[1] Review: A. J. Kirby, *Angew. Chem.* **1996**, *108*, 770–790; *Angew. Chem. Int. Ed. Engl.* **1996**, *35*, 705–724.
[2] L. Pauling, *Chem. Eng. News* **1946**, *24*, 1375–1377; W. P. Jencks, *Catalysis in Chemistry and Enzymology*, McGraw-Hill, New York, **1969**.
[3] Reviews: P. G. Schultz, *Angew. Chem.* **1989**, *101*, 1336–1348; *Angew. Chem. Int. Ed. Engl.* **1989**, *28*, 1283–1295; R. A. Lerner, S. J. Benkovic, P. G. Schultz, *Science* **1991**, *252*, 659–667.
[4] G. Wulff, A. Sarhan, *Angew. Chem.* **1972**, *84*, 364; *Angew. Chem. Int. Ed. Engl.* **1972**, *11*, 341; G. Wulff, A. Sarhan, K. Zabrocki, *Tetrahedron Lett.* **1973**, *44*, 4329–4332; G. Wulff, A. Sarhan, DE-A 2242796, **1974** [*Chem. Abstr.* **1975**, *83*, P 60300w].
[5] Reviews: G. Wulff, *Angew. Chem.* **1995**, *107*, 1958–1979; *Angew. Chem. Int. Ed. Engl.* **1995**, *34*, 1812–1832; K. J. Shea, *Trends Polym. Sci.* **1994**, *2*, 166–173; K. Mosbach, *Trends Biochem. Sci.* **1994**, *19*, 9–14.
[6] D. K. Robinson, K. Mosbach, *J. Chem. Soc. Chem. Commun.* **1989**, 969–970; B. Sellergren, K. J. Shea, *Tetrahedron Asymmetry* **1994**, *5*, 1403–1406; K. Ohkubo, Y. Funakoshi, T. Sagawa, *Polymer* **1996**, *37*, 3993–3995, and references therein.
[7] J. V. Beach, K. J. Shea, *J. Am. Chem. Soc.* **1994**, *116*, 379–380; J. Matsui, I. A. Nicholls, I. Karube, K. Mosbach, *J. Org. Chem.* **1996**, *61*, 5414–5417.
[8] J. D. Stewart, L. J. Liotta, S. J. Benkovic, *Acc. Chem. Res.* **1993**, *26*, 396-404.
[9] G. Wulff, R. Schönfeld, M. Grün, R. Baumstark, G. Wildburg, L. Häußling (BASF AG), German patent registered, **1996**.
[10] The inverse interaction with acrylic acid as the anchor monomer for bis(amidine)s was already used for imprinting: B. Sellergren, *J. Chromatogr. A* **1994**, *673*, 133–141.
[11] G. Wulff, R. Schönfeld, unpublished results.

A Polyoxo–Polyolato Complex of Tantalum(v) with a Double Adamantane-Like $[Ta_7O_{12}]^{11+}$ Core**

Kaspar Hegetschweiler,* Thomas Raber, Guido J. Reiss, Walter Frank, Michael Wörle, Antonio Currao, Reinhard Nesper, and Thomas Kradolfer

In their highest oxidation state, some of the early transition metals, such as V, Nb, Ta, Mo and W, have a pronounced tendency to form polynuclear, oxo-bridged aggregates in aqueous solution.[1] Polyoxometallate anions like $[V_{10}O_{28}]^{6-}$, $[M_6O_{19}]^{8-}$ (M = Nb, Ta), $[Mo_7O_{24}]^{6-}$, $[Mo_8O_{26}]^{4-}$ and $[H_2W_{12}O_{40}]^{6-}$ are well known representatives of this type. The formation of polynuclear complexes is currently being intensively investigated, since such species can be regarded as discrete intermediates in the process of hydrolytic polymerization, which starts from a mononuclear species and leads to the solid oxide.[2] The question arises whether the structural principles of the resulting solid can already be recognized in such intermediate species. A novel molecular architecture of a polynuclear oxo complex would thus be of special interest, since it could open routes to new materials. We have recently demonstrated that polyalcohols with a tripodal arrangement of the hydroxy groups are particularly suitable for stabilizing such polynuclear oxo complexes in solution,[3] since the coordinated polyalcohols shield the periphery of the complex and thus prevent further aggregation. Starting with $[Ta(tdci)_2]^{5+}$ (**1**, tdci = 1,3,5-trideoxy-1,3,5-tris(dimethylamino)-*cis*-inositol) as the mononuclear precursor, this strategy has now been used to prepare a heptanuclear complex having a unique, purely "inorganic" Ta_7O_{12} core with a double adamantane-like structure.

The cation **1** is readily formed by the reaction of $TaCl_5$ with tdci in methanol. It can be isolated in solid state as a hydrated pentachloride.[4] In aqueous medium, the mononuclear species is stable for a few days, thus affording a convenient means of investigating the solution properties. Potentiometric titrations

[*] Prof. Dr. K. Hegetschweiler, Dr. T. Raber
Universität des Saarlandes
Fachrichtung Anorganische Chemie
Postfach 15 11 50, D-66041 Saarbrücken (Germany)
Fax: Int. code + (681) 302-2663
e-mail: hegetsch@rz.uni-sb.de
Dr. G. J. Reiss, Prof. Dr. W. Frank
Fachbereich Chemie der Universität Kaiserslautern (Germany)
Dr. M. Wörle, Dr. A. Currao, Prof. Dr. R. Nesper, Dr. T. Kradolfer
Laboratorium für Anorganische Chemie der Eidgenössischen Technischen Hochschule Zürich (Switzerland)

[**] Metal Binding of Polyalcohols, Part 5. This work was supported by the ETH Zürich (Kredite für Unterricht und Forschung). Part 4: ref. [3].

 © WILEY-VCH Verlag GmbH, D-69451 Weinheim, 1997 0570-0833/97/3618-1964 $ 17.50+.50/0

and NMR measurements established that a total of six protons can be abstracted upon addition of base.[5] Around pH 6, the doubly deprotonated complex is formed. It can be isolated as a crystalline material. The X-ray structure analysis[6] confirmed the presence of a mononuclear complex (Figure 1). The hydroxy

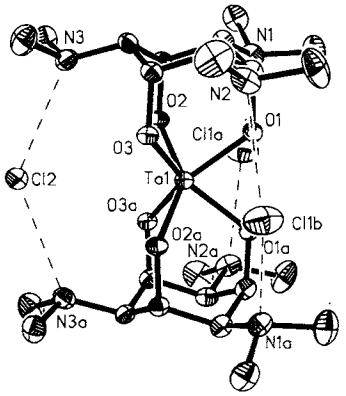

Figure 1. Structure of $[H_{-2}Ta(tdci)_2]^{3+}\cdot 3Cl^-$ (displacement ellipsoids at 50% probability level). The Ta atom is placed on a twofold axis. Main interatomic distances [pm]: Ta–O1 199.2(4), Ta–O2 197.1(3), Ta–O3 198.3(3).

groups of tdci are all deprotonated on coordination to Ta^V, but this does not determine the overall charge of the complex, since internal proton transfer to the peripheral amino groups can occur, leading to a zwitterionic form of the ligand (Scheme 1).[7]

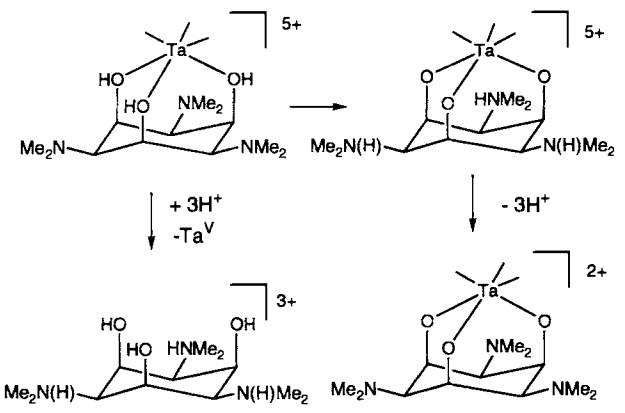

Scheme 1.

The coordination geometry of Ta^V, which is trigonal prismatic rather than octahedral, is somewhat unexpected,[8] and obviously arises from the interactions of the protonated amino groups with the three Cl^- counterions.

Under neutral conditions, **1** reacts slowly to give the heptanuclear hydrolysis product according to Equation (a). All 24

$$7\,[H_{-2}Ta(tdci)_2]^{3+} + 12\,H_2O \longrightarrow [H_{-11}Ta_7O_{12}(tdci)_6] + 5\,H_3tdci^{3+} + 3\,H_2tdci^{2+} \quad (a)$$

protons released upon deprotonation of the 12 water molecules are taken up by the liberated tdci. Additionally, by analogy with the mononuclear species **1**, the dimethylammonium groups of the coordinated tdci ligands are weakly acidic, which allows further deprotonation of the complex and thus a change of the overall charge in the range +11 to −7. At pH 7, upon addition of ethanol, the neutral complex $[H_{-11}Ta_7O_{12}(tdci)_6]$ (**2**) crystallizes as a hydrate. The crystal structure is shown in Figure 2.[9]

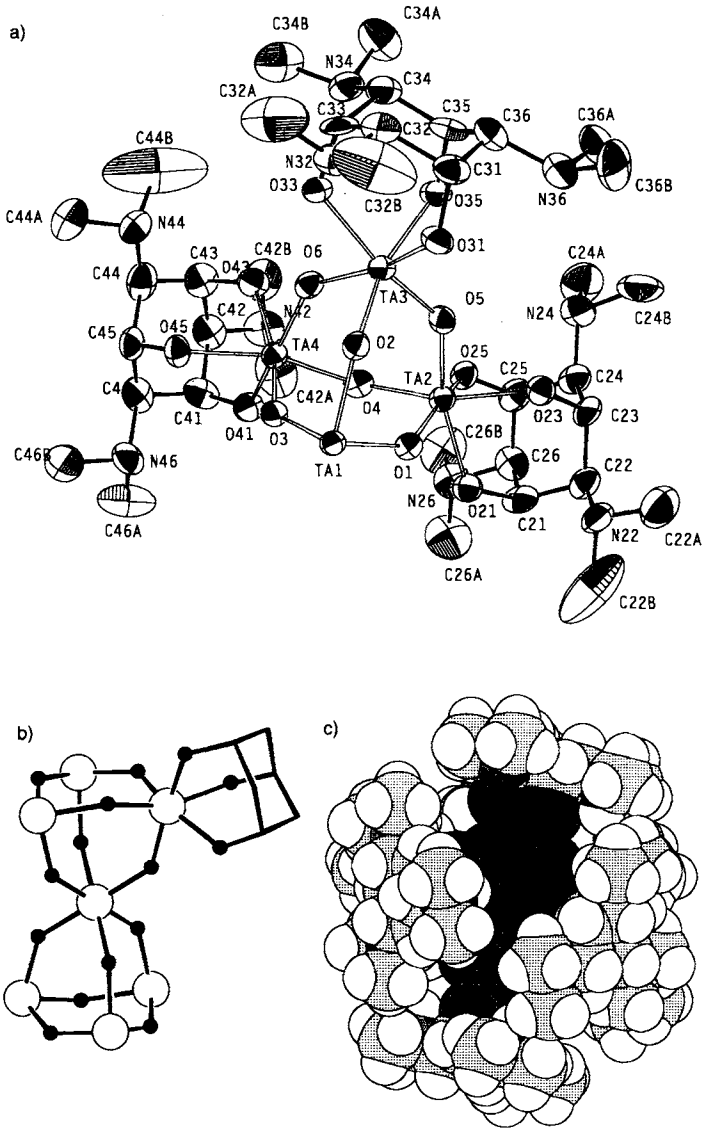

Figure 2. Structure of $[H_{-11}Ta_7O_{12}(tdci)_6]$ (**2**). a) ORTEP view with numbering scheme (ellipsoids at 50% probability). Only the asymmetric unit of the complex is shown for clarity. The second, symmetry-equivalent part of the molecule is generated by inversion on Ta1. b) Representation of the Ta_7O_{12} core with double adamantane structure (oxygen: small, black spheres, Ta: large open spheres). The coordination of the peripheral tdci ligands is indicated for one Ta atom, but the three dimethylamino groups have been omitted for clarity. c) Space filling model: Ta, O, N, C, and H are represented by spheres with decreasing darkness in this order. The Ta–O distances [pm] fall in the range of 198.1(9)–198.3(10) for Ta1, 190.3(10)–195.1(10) for the other $Ta-O_{oxo}$ bonds, and 203.2(10)–205.9(10) for the $Ta-O_{alkoxo}$ bonds [8].

The central Ta1 is connected to six additional Ta atoms by six μ_2-oxo bridges. These peripheral Ta atoms are themselves linked by six additional oxide ions. The structure of the entire Ta_7O_{12} core is exclusively made up of fused six membered Ta_3O_3 rings in chair conformation, and this gives rise to the Ta_7O_{12} double adamantane skeleton, in which Ta1 occupies the common vertex of two Ta_4O_6 cages. Each of the six peripheral Ta atoms is coordinated to another tdci ligand, which significantly distorts the octahedral TaO_6 geometry.[8]

The Ta_7O_{12} core and the eighteen oxygen atoms of the coordinated tdci ligands form a Ta_7O_{30} structure, which can be regarded as an aggregate of seven TaO_6 octahedra. It is noteworthy that these octahedra are all connected by common vertices. This is in contrast to most of the previously described

 © WILEY-VCH Verlag GmbH, D-69451 Weinheim, 1997 0570-0833/97/3618-1965 $ 17.50+.50/0

polyoxo metalates in which the linking of the coordination octahedra occurred mostly through common edges. In the above mentioned $[Ta_6O_{19}]^{8-}$ ion the central oxygen atom has a coordination number of 6, which leads to a much more compact structure. However, in **2** all twelve oxygen atoms have a coordination number of 2, which obviously results in a much more open structure. The higher porosity of this structure is clearly reflected by the cavities formed by the Ta_4O_6 cages (Figure 3).[10]

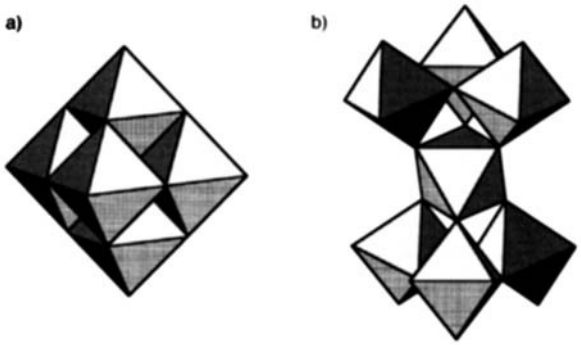

Figure 3. Representation of the coordination polyhedra for $[Ta_6O_{19}]^{8-}$ (a) and the Ta_7O_{30} structure observed in $[H_{-11}Ta_7O_{12}(tdci)_6]$ (**2**) (b). The figures are drawn for maximal symmetry (O_h and D_{3d}), as expected for the two complexes in solution.

The formation of a single tetranuclear M_4O_6 adamantane core is well known [11] and has been established for a variety of metal centers, including Ta^V as $[Ta_4F_{12}O_6]^{4-}$.[12] However, to our knowledge, the M_7O_{12} double-adamantane structure has not previously been described. With a view to controllable construction of new structures, it would be of particular interest to understand the factors that determine the structural motifs in such a continuing polymerization reaction. The peripheral ligands are obviously of crucial significance due to both steric and electrostatic effects. The rigid tdci ligand is restricted to facial coordination, and the bulky dimethylamino groups demand a comparatively large molecular surface leading to the rather open structure observed in the complex core. Moreover, the ability of the 18 dimethylamino groups to serve as a reservoir of protons is also important, as it allows a facile adjustment of the overall charge by simple protonation–deprotonation reactions and thus avoids an unfavorable, highly charged molecular surface.

Received: February 28, 1997
Revised version: May 21, 1997 [Z10182IE]
German version: *Angew. Chem.* **1997**, *109*, 2052–2054

Keywords: cage compounds · multinuclear complexes · O ligands · polyoxometalates · tantalum

[1] Q. Chen, J. Zubieta, *Coord. Chem. Rev.* **1992**, *114*, 107.
[2] A. Müller, W. Plass, E. Krickemeyer, S. Dillinger, H. Bögge, A. Armatage, A. Proust, C. Beugholt, U. Bergmann, *Angew. Chem.* **1994**, *106*, 897; *Angew. Chem. Int. Ed. Engl.* **1994**, *33*, 849.
[3] A. Cornia, D. Gatteschi, K. Hegetschweiler, L. Hausherr-Primo, V. Gramlich, *Inorg. Chem.* **1996**, *35*, 4414.
[4] The C,H,N,Cl analysis is consistent with the formula $[Ta(tdci)_2]Cl_5 \cdot 5.5H_2O$. FAB$^+$-MS: $[Ta(tdci)_2 - 4H]^+$ (100%), $[Ta(tdci)_2Cl_2 - 2H]^+$ (30%).
[5] pK_a values (25.0 °C, 0.1 M KCl): 4.5, 5.7, 7.2, 9.3, 10.5, 11. 2. In the ^{1}H NMR spectrum (D_2O) a closely linear dependence of the chemical shifts on pD is observed in the range $3.8 < pD < 12.9$. Below pD 3.5 the shifts remain constant; δ for pD 3.0 and pD 13.0: 5.77 and 5.18 (6H), 3.79 and 2.11 (6H), 3.17 and 2.37 (36H).
[6] Crystals of $[1 - 2H]Cl_3 \cdot 9H_2O$ (the composition $C_{24}H_{70}Cl_3N_6O_{15}Ta$ was confirmed by C,H,N-analysis) disintegrate upon exposure to air. A crystal of approximate dimensions $0.22 \times 0.12 \times 0.12$ mm was therefore sealed in a glass capillary. Space group $C2/c$, $a = 2319.6(4)$, $b = 1448.8(3)$, $c = 1211.8(2)$ pm, $\beta = 91.62(1)°$, $V = 4070(1) \times 10^6$ pm^3, $Z = 4$, $\rho_{calcd} = 1.583$ Mg m^{-3}. Data were collected on a Siemens-P4 four-circle diffractometer at 293(2) K, $Mo_{K\alpha}$ radiation ($\lambda = 71.073$ pm), $\mu = 2.964$ mm^{-1}, graphite monochromator, numerical absorption correction (min./max. transmission = 0.072/0.461); $2\theta_{max}$: 50.00°. Of 4234 measured reflections 3448 independent reflections were used for the refinement of 284 parameters, structure solution by direct methods (SHELXS-86). All non-hydrogen atoms were refined in the anisotropic mode (full-matrix, least-squares calculations based on F^2). All H-atoms were located and included in the final refinement (SHELXL-93) with either appropriate constraints or on fixed positions as found in the difference Fourier map (H_2O molecules). $R = 0.0382$ ($F_o^2 > 2\sigma(F_o^2)$), $wR_2 = 0.0683$ (all data). Residual electron density $+0.78/-0.50$ e Å^{-3} [13].
[7] The deprotonation of the hydroxy groups is indicated by the short Ta–O bonds. Moreover, the difference Fourier synthesis did not show any electron density in proximity to these oxygen positions. There was, however, additional electron density in proximity to the nitrogen atoms, which could be interpreted as hydrogen atomic positions. In agreement with the elemental analysis, the crystal structure analysis did not give any indication of the presence of additional chloride ions, even if partial occupancy was considered. To achieve the correct charge balance, a 2:1 disorder of protonated and deprotonated amino groups had therefore to be considered. This conclusion was further supported by refined occupancy factors of the hydrogen atoms, which gave a mean value of 2/3, and the rather large displacement parameters of the Cl^- ions, which can be interpreted as a consequence of disorder in the three N–H···Cl···H–N bridges. The rather high pK_a values and the NMR data indicate that the zwitterionic form is also present in solution.
[8] The sum of the Ta–O bond valences of 5.06 for $[1 - 2H]Cl_3 \cdot 9H_2O$ and 5.07–5.23 for the Ta^V centres of $2 \cdot 38.67H_2O$, all fall in the expected range: I. D. Brown, D. Altermatt, *Acta Crystallogr. Sect. B*, **1985**, *41*, 244.
[9] Crystals of the composition $2 \cdot 38.67H_2O$ disintegrate rapidly upon exposure to air. A crystal of approximate dimensions $0.4 \times 0.4 \times 0.25$ mm was therefore sealed in a glass capillary together with its mother liquor: space group $P\bar{1}$, $a = 1759.0(6)$, $b = 1885.7(6)$, $c = 1889.6(7)$ pm, $\alpha = 96.95(3)$, $\beta = 114.32(3)$, $\gamma = 113.91(3)°$, $Z = 1$ (for $Ta_7C_{72}H_{228.33}N_{18}O_{68.67}$), $V = 4900(3) \times 10^6$ pm^3, $\rho_{calcd} = 1.258$ Mg m^{-3}. Data were collected on a STOE IPDS image plate system at 293(2) K, $Mo_{K\alpha}$ radiation ($\lambda = 71.073$ pm), $\mu = 3.957$ mm^{-1}, graphite monochromator; $2\theta_{max}$: 52.1°. Of 34522 measured reflections 17668 independent reflections were used for the refinement of 752 parameters, structure solution by direct methods (SHELXS-86), no absorption correction. All non-hydrogen atoms except some disordered solvent molecules were refined in the anisotropic mode (SHELXL-93, full-matrix least-squares calculations based on F^2). H(–C) atoms were placed at calculated positions. $R = 0.0652$ ($F_o^2 > 2\sigma(F_o^2)$), $wR_2 = 0.0220$ (all data). Residual electron density $+2.18/-1.98$ e/Å^{-3} [13].
[10] The cavity formed by the six oxygen atoms and four tantalum atoms of the adamantane cage of **2** is not large enough to accommodate an additional atom. The mean distance from the center of the cage to the oxygen atoms is 196 pm and to the tantalum atoms is 222 pm. However, some minor displacements of the oxygen positions are sufficient to enlarge the cavity in such away that there is space for an additional oxide ion. A corresponding structure of an $In_4(OH)_6$ adamantane cage with an oxide ion in the center has been described: S. S. Al-Juaid, N. H. Buttrus, C. Eaborn, P. B. Hitchcock, A. T. L. Roberts, J. D. Smith, A. C. Sullivan, *J. Chem. Soc. Chem. Commun.* **1986**, 908.
[11] A comprehensive review is found in J. J. Vittal, *Polyhedron* **1996**, *15*, 1585. See also S. Drüeke, K. Wieghardt, B. Nuber, J. Weiss, E. L. Bominaar, A. Sawaryn, H. Winkler, A. X. Trautwein, *Inorg. Chem.* **1989**, *28*, 4477. G. Bonavia, R. C. Haushalter, C. J. O'Connor, J. Zubieta, *ibid.* **1996**, *35*, 5603.
[12] J. Sala-Pala, J.-E. Guerchais, A. J. Edwards, *Angew. Chem.* **1982**, *94*, 876; *Angew. Chem. Int. Ed. Engl.* **1982**, *21*, 870.
[13] Crystallographic data (excluding structure factors) for the structures reported in this paper have been deposited with the Cambridge Crystallographic Data Centre as supplementary publication no. CCDC-100192 (**1**) and CCDC-100188 (**2**). Copies of the data can be obtained free of charge on application to The Director, CCDC, 12 Union Road, Cambridge CB21EZ, UK (fax: int. code +(1223) 336-033; e-mail: deposit@chemcrys.cam.ac.uk).

 © WILEY-VCH Verlag GmbH, D-69451 Weinheim, 1997 0570-0833/97/3618-1966 $ 17.50+.50/0

Clusters from Vertex- and Face-Sharing Adamantane-Like Units: A New Topology for Multinuclear Complexes**

Euan K. Brechin, Steven G. Harris, Simon Parsons, and Richard E. P. Winpenny*

The discovery of novel metal polyhedra remains one of the chief goals in the synthesis of multinuclear complexes, as new structures may lead to novel properties. The adamantane-like structure featuring a central M_4O_6 core has been reported for the 3d-metals from Ti to Fe;[1-9] however, it remains comparatively rare, and only a dozen or so examples are known. Compounds containing this core have never been reported for later 3d-metals, and only one example exists where adamantane units are linked into higher nuclearity clusters; this is a hexairon complex reported by Nair and Hagen[10] in which two adamantanes share a common edge. Here we report the first nickel and cobalt complexes that contain M_4O_6 units, which are also the first examples of vertex- and face-sharing adamantanes.

Reaction of "$Ni(OH)_2$" with 2.1 equivalents of 6-chloro-2-hydroxypyridine (Hchp) at 130 °C under N_2 gives a green paste, which, after drying in vacuo, can be crystallized from MeCN/MeOH to give green crystals. Structural determination[11] reveals a heptanuclear nickel complex $[Ni_7(chp)_{12}Cl_2(MeOH)_6]$ (**1**, Figure 1). The central Ni site (Ni1) lies on a crystallographic inversion center and is the shared vertex of two Ni_4O_6 adamantanes; the O atoms are provided by the chp ligands. The central Ni atom is bound to six oxygen atoms derived from chp ligands that form chelates with the "basal" Ni sites in the structure. Each basal Ni atom is chelated to one further chp and bound to a bridging O-donor from the chp chelating to a neighboring basal nickel atom. These three chelating chp ligands lie virtually coplanar with the Ni_3 base. Thus chp donors occupy five coordination sites on each basal nickel; the sixth site is occupied by a molecule of MeOH in each case. These three terminal MeOH ligands form strong H-bonds to chloride ions [$\bar{d}$(O···Cl) = 3.11(4) Å] stemming from the nickel chloride used to prepare "$Ni(OH)_2$".

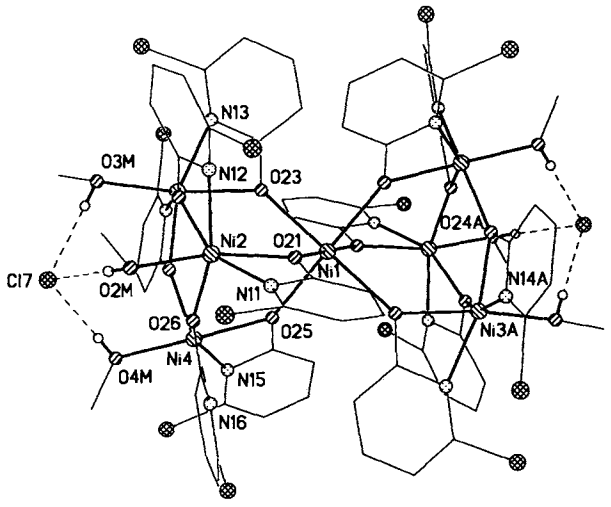

Figure 1. The structure of **1** in the crystal. The structure of **2** is extremely similar in the crystal. Bond length ranges [Å] (in square brackets data for **2**): Ni1–O 2.337–2.369, other Ni–O 2.002–2.145 [1.976–2.165], Ni–N 2.066–2.105 [2.050–2.116], (av. estimated standard deviation (esd): 0.007 [0.010]). Bond angle ranges [°]: *cis* at Ni1 89.4–90.6, *cis* at other Ni 63.2–108.5 [85.8–94.2], *trans* at other Ni 152.6–169.3 [157.0–171.0] (av. esd 0.3 [0.4]).

If the same procedure is utilized, but the nickel chloride is treated with sodium methoxide prior to reaction to produce "$Ni(OMe)_2$", another heptanuclear complex, $[Ni_7(OH)_2(chp)_{12}(MeOH)_6]$ (**2**), can be crystallized. Structure determination[11] shows that a very similar cluster has formed. Again a central Ni atom, disposed on an inversion center and bound to six O donors derived from chp ligands, is the shared vertex of two Ni_4 cages; however, in **2** the ideal adamantane cages are distorted by the presence of a μ_3-hydroxo ligand (O1H) linking the three Ni sites in the basal plane. These three Ni sites are now dissimilar. Ni2 is bound to two chelating chp ligands, the μ_3-OH, and a chp oxygen atom that is μ_2-bridging to Ni3; the pyridine-N donor of this chp ligand forms a hydrogen bond to a MeOH ligand. Ni3 is bound to one chelating chp, the μ_3-OH, μ_2-oxygen atoms from two chp ligands, and a terminal MeOH ligand. Ni4 is bound to one chelating chp, the μ_3-OH, one μ_2-O(chp), and two terminal MeOH ligands.

To remove the influence of MeOH from this chemistry, a similar product was crystallized from MeCN only (see *Experimental Section*). Structure determination[11] revealed a nonanuclear cage $[Ni_9(OH)_2(chp)_{16}(MeCN)_2]$ (**3**, Figure 2), in which a central six-coordinate nickel atom (Ni1) again lay on a symmetry element—in this case a twofold axis. A very similar heptanuclear cage to that in **2** is present, in which a μ_3-OH ligand bridges the three Ni sites, Ni2, Ni3, and Ni4, within the basal plane. However, the absence of MeOH ligands has led to a slightly larger cage, and an additional $[Ni(chp)_3]^-$ unit containing Ni5 is attached to one edge of the triangular base.

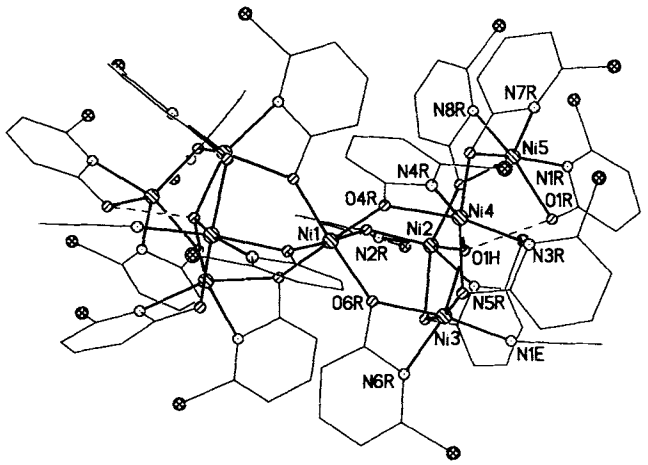

Figure 2. The structure of **3** in the crystal. Bond length ranges [Å]: Ni–O 2.011–2.198, Ni–N 2.053–2.109 (esd 0.005). Bond angle ranges: *cis* at Ni1 85.1–95.3, *trans* at Ni1 175.8–177.7, *cis* at other Ni 62.7–109.4, *trans* at other Ni 148.8–169.6 (esd 0.2).

The three Ni sites in the base are again distinct. Ni2 and Ni4 are identical, bound to two chelating chp ligands, the μ_3-OH ligand, and the μ_2-O-atom that attaches the $[Ni(chp)_3]^-$ unit to the cage. Ni3 is unique, bound to one chelating chp, the μ_3-OH ligand, two μ_2-O-donors from chp ligands chelating to Ni2 and Ni4, and a terminal MeCN ligand.

[*] Dr R. E. P. Winpenny, E. K. Brechin, S. G. Harris, Dr. S Parsons
Department of Chemistry
The University of Edinburgh
West Mains Road, Edinburgh, EH9 3JJ (UK)
Fax: Int. code +(131)667-4743
E-mail: repw01@tattoo.ed.ac.uk

[**] This work was supported by the EPSRC (UK).

 © WILEY-VCH Verlag GmbH, D-69451 Weinheim, 1997 0570-0833/97/3618-1967 $ 17.50+.50/0

The reaction that produced **3** was repeated with cobalt in place of nickel. The nonanuclear cage compound $[Co_9(chp)_{18}]$ (**4**) crystallized from EtOAc in a form suitable for structure determination[11] (Figure 3). The cage has crystallographic D_{3d}

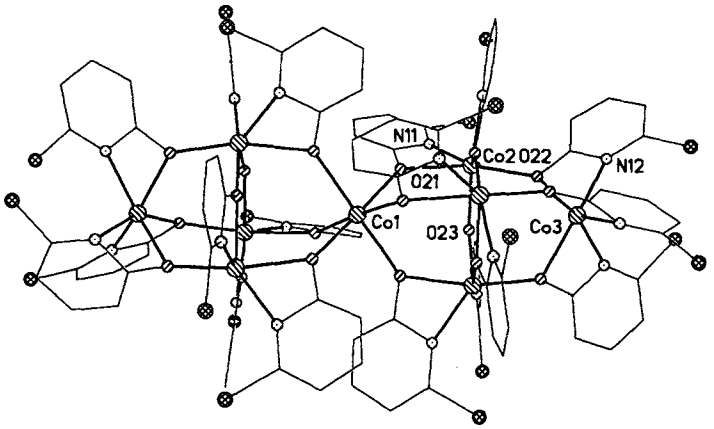

Figure 3. The structure of **4** in the crystal. Bond length ranges [Å]: Co1–O 2.316, Co2–O 2.026–2.211, Co2–N 2.122–2.126, Co3–O 2.185, Co3–N 2.126 (esd 0.007). Bond angles: *trans* at Co1 175.6, *cis* at Co1 85.3 and 91.6, *trans* at Co2 165.3 and 167.2, *cis* at Co2 61.4–132.3, *trans* at Co3 151.9, *cis* at Co3 62.1–104.3 (esd 0.3).

symmetry, and the central cobalt, Co1, lies on both a threefold axis (which also passes through Co3) and a twofold axis. The cage containing four adamantane units is clearly related to the three nickel cages. Two of the adamantane units share Co1 as a common vertex; two additional units share the basal planes (Co2 and symmetry equivalent atoms) with Co3 (and symmetry equivalent) as vertex. The three crystallographically unique Co sites are chemically distinct. Co1 is bound to six O-donors in an identical manner to the central metal sites in **1**–**3**. Co2 is bound to two chelating chp ligands, one μ_2-O atom from a further chp ligand within the basal plane, and one μ_2-O donor that attaches the Co3 vertex to the cage. Co3 is chelated to three chp ligands in *fac* geometry; each O-donor bridges to the Co atoms of the basal plane. A comparison of **4** with **1** shows that the three terminal MeOH ligands and the H-bonded chloride ion have been replaced by a $[Co(chp)_3]^-$ moiety, leaving the connectivity of the heptanuclear metal core unchanged.

Metal coordination geometries in **1**–**4** can be related to an octahedron, with one exception. In each cage the central metal site has a regular geometry (range for *trans* angles 175.8–180.0°; for *cis* angles 85.1–95.3°), whereas the other metal sites are distorted by the narrow bite angle of the chelating chp ligands (range for Ni cages: *trans* angles 148.8–171.0°; for *cis* angles 62.5 to 109.7°). For **4** the distortion at Co2 is so large (only two angles approaching a typical *trans* value at about 166°) that an octahedral description becomes difficult to maintain and the geometry is best described as irregular.

The metal-to-metal distances within the adamantane units vary from 3.808 to 4.143 Å for the nickel cages and 3.742 to 4.116 Å for **4**. The metal-to-ligand bond lengths vary greatly depending on the metal site. The M–O lengths to the central metal in structures **1** and **4** are long, varying from 2.316 to 2.369 Å. The length of these bonds led us to examine the possibility that this site was occupied by Na rather than Ni or Co; however, refinement of the structure with a Na atom in place of Ni1 or Co1 produced physically meaningless results. Analytical data strongly support the formulae given, as does mass spectrometry. Fragments of the three Ni cages are observed in fast atom bombardment mass spectrometry (FAB-MS) which are very close to the molecular ion in mass, and for **4** peaks are seen for fragments containing five Co centers, which would not be feasible if the central metal site were not a cobalt atom. There is no straightforward explanation for the observed bond lengths at this site; steric crowding can be ruled out as the equivalent sites in **2** and **3** have normal bond lengths, as do all other metal sites in the four structures (range for Ni–N 2.050–2.116; for Ni–O 1.976–2.198; for Co–O 2.026–2.211; for Co–N 2.122–2.245 Å).

We have previously stated that the coordinative flexibility of pyridonates and the presence of heteroleptic ligand sets are important factors in the formation of high nuclearity arrays of these ligands;[12] however, **4** is a fascinating exception to this rule in that it is homoleptic, and each pyridonate ligand in the cluster has an identical coordination mode. The homoleptic chp complex of the heavier Group 9 metal rhodium has been reported by Cotton et al.,[13] and the dimer $[Rh_2(chp)_4]$ contains a Rh–Rh single bond. Compound **4** is a beautiful example of the complicated arrays that 3d-metals must adopt to avoid forming metal–metal bonds, and certainly this is a further factor contributing to the novel cages formed by 3d-metals with simple bridging ligands.

Experimental Section

1: Hydrated nickel chloride (1 g, 4.2 mmol) was treated with NaOH (2 equiv) in water (20 mL) to give a green precipitate of nickel hydroxide, which was dried in vacuum. Hchp (1.088 g, 8.4 mmol) was added, and the mixture heated to 130 °C under N_2 for 2 h to produce a paste. This paste was dried in vacuum for 1 h before being dissolved in 1:1 MeCN/MeOH. Green crystals grew over 2 days. Yield: 30%. Elemental analysis calcd (found) for $C_{66}H_{60}Cl_{14}N_{12}Ni_7O_{18}$: C 35.7 (35.6), H 2.71 (2.50), N 7.58 (7.40), Ni 18.5 (17.8)%. FAB-MS: *m/z*: 2181 $[Ni_7(chp)_{12}Cl(MeOH)_6]^+$, 1921 $[Ni_7(chp)_{11}(MeOH)_3]^+$, 1862 $[Ni_6(chp)_{11}(MeOH)_3]$, 1830 $[Ni_6(chp)_{10}(MeOH)_6]^+$, 1734 $[Ni_6(chp)_8(MeOH)_4]^+$, 1605 $[Ni_6(chp)_9(MeOH)_3]^+$, 1509 $[Ni_6(chp)_8(MeOH)_4]^+$, 1477 $[Ni_6(chp)_8(MeOH)_3]^+$, 1413 $[Ni_6(chp)_8(MeOH)]^+$, 1348 $[Ni_6(chp)_7(MeOH)_3]^+$, 1284 $[Ni_6(chp)_7(MeOH)]$, 1205 $[Ni_3(chp)_8]^+$, 889 $[Ni_2(chp)_6]^+$, 573 $[Ni(chp)_4]^+$, 503 $[Ni_2(chp)_3]^+$, 375 $[Ni_2(chp)_2]^+$.

2: Synthesis as for 1, using NaOMe in place of NaOH and MeOH in place of H_2O. Crystals grew after 2 days. Yield: 25%. Elemental analysis calcd (found) for $C_{66}H_{62}Cl_{12}N_{12}Ni_7O_{20}$: C 36.3 (36.0), H 2.84 (2.71), N 7.71 (7.63)%. FAB-MS: as for **1** except peak at *m/z* 2180 assigned as $[Ni_7(chp)_{12}(OH)_2(MeOH)_6]^+$.

3: Synthesis as for **1**, except MeCN alone was used for crystallization. Crystals grew after 1 day. Yield: 80%. Elemental analysis calcd (found) for $C_{84}H_{56}Cl_{16}N_{18}Ni_9O_{18}$: C 37.3 (37.3), H 2.07 (2.00), N 9.33 (9.30)%. FAB-MS: *m/z*: 2490 $[Ni_9(chp)_{13}(OH)_2]^+$, 2174 $[Ni_8(chp)_{13}(OH)_2]^+$, 1602 $[Ni_7(chp)_9(OH)_2]^+$, 1526 $[Ni_6(chp)_9(OH)]^+$, 1288 $[Ni_4(chp)_8(OH)]^+$, 1205 $[Ni_3(chp)_8]^+$, 889 $[Ni_2(chp)_6]^+$, 572 $[Ni(chp)_4]^+$.

4: Synthesis as for **1**, except that cobalt was used in place of nickel, and crystallization was from EtOAc and gave pink crystals after 1 week. Yield: 9%. Elemental analysis calcd (found) for $C_{90}H_{54}Cl_{18}Co_9N_{18}O_{18}$: C 38.0 (37.7), H 1.90 (1.89), N 8.86 (8.80), Co 18.7 (17.8)%. FAB-MS: *m/z*: 1522 $[Co_4(chp)_{10}]^+$, 1323 $[Co_5(chp)_8]^+$, 1264 $[Co_4(chp)_8]^+$, 1195 $[Co_5(chp)_7]^+$, 1136 $[Co_4(chp)_7]^+$, 820 $[Co_3(chp)_5]^+$, 632 $[Co_2(chp)_4]^+$, 573 $[Co(chp)_4]^+$, 504 $[Co_2(chp)_3]^+$, 445 $[Co(chp)_3]^+$, 316 $[Co(chp)_2]^+$.

Received: March 3, 1997 [Z10189IE]
German version: *Angew. Chem.* **1997**, *109*, 2055–2057

Keywords: clusters · cobalt · multinuclear complexes · nickel

[1] K. Wieghardt, D. Ventur, Y. H. Tsai, C. Krüger, *Inorg. Chim. Acta* **1985**, *99*, L25.
[2] L. M. Babcock, V. W. Day, W. G. Klemperer, *J. Chem. Soc, Chem. Commun.* **1987**, 858.
[3] F. Bottomley, C. P. Magill, B. Zhao, *Organometallics* **1990**, *9*, 1700.
[4] D. Wormsbacher, K. M. Nicholas, A. L. Rheingold, *J. Chem. Soc, Chem. Commun.* **1985**, 721.
[5] J. Glerup, H. Weihe, P. A. Goodson, D. J. Hodgson, *Inorg. Chim. Acta* **1993**, *212*, 281.
[6] K. Wieghardt, U. Bossek, B. Nuber, J. Weiss, J. Bonvoisin, M. Corbella, S. E. Vitols, J. J. Girerd, *J. Am. Chem. Soc.* **1988**, *110*, 7398.

 © WILEY-VCH Verlag GmbH, D-69451 Weinheim, 1997 0570-0833/97/3618-1968 $ 17.50+.50/0

[7] K. S. Hagen, T. D. Westmoreland, W. J. Scott, W. H. Armstrong, *J. Am. Chem. Soc.* **1989**, *111*, 1907.
[8] B. P. Murch, F. C. Bradley, P. D. Boyle, V. Papefthymiou, L. Que, Jr., *J. Am. Chem. Soc.* **1987**, *109*, 7993.
[9] S. Drüeke, K. Wieghardt, B. Nuber, J. Weiss, E. L. Bominaar, A. Sawaryn, H. Winkler, A. X. Trautwein, *Inorg. Chem.* **1989**, *28*, 4477.
[10] V. S. Nair, K. S. Hagen, *Inorg. Chem.* **1992**, *31*, 4048.
[11] Crystal data for **1**·1.7 MeCN: $C_{71.4}H_{65.1}Cl_{14}N_{13.7}Ni_7O_{18}$, $M_r = 2310$, triclinic, $P\bar{1}$, $a = 13.706(7)$, $b = 15.216(9)$, $c = 15.431(8)$ Å, $\alpha = 60.68(5)$, $\beta = 67.15(4)$, $\chi = 69.33(4)°$, $V = 2532$ Å^3, $Z = 1$ (the molecule lies on an inversion center), $\rho_{calcd} = 1.515$ g cm^{-3}, $T = 220.0(2)$ K, crystal size $0.51 \times 0.19 \times 0.16$ mm, $\mu(Cu_{K\alpha}) = 5.33$ mm^{-1}. Crystal data for **2**: $C_{66}H_{62}Cl_{12}N_{12}Ni_7O_{20}$, $M_r = 2180$, monoclinic, $P2_1/n$, $a = 12.502(4)$, $b = 19.917(6)$, $c = 17.601(4)$ Å, $\beta = 106.23(2)°$, $V = 4208$ Å^3, $Z = 2$ (the molecule lies on an inversion center), $\rho_{calcd} = 1.720$ g cm^{-3}, $T = 220.0(2)$ K, crystal size $0.31 \times 0.27 \times 0.19$ mm, $\mu(Mo_{K\alpha}) = 1.99$ mm^{-1}. Crystal data for **3**: $C_{84}H_{56}Cl_{16}N_{18}Ni_9O_{18}$, $M_r = 2701$, monoclinic, $C2/c$, $a = 31.570(3)$, $b = 12.784(2)$, $c = 25.371(3)$ Å, $\beta = 101.160(10)°$, $V = 10046$ Å^3, $Z = 4$ (the molecule lies on a twofold axis), $\rho_{calcd} = 1.786$ g cm^{-3}, $T = 220.0(2)$ K, crystal size $0.23 \times 0.16 \times 0.16$ mm, $\mu(Cu_{K\alpha}) = 6.33$ mm^{-1}. Crystal data for **4**·3 EtOAc: $C_{102}H_{78}Cl_{18}Co_9N_{18}O_{24}$, $M_r = 3108$, rhombohedral, $R\bar{3}c$, $a = 18.298(2)$, $c = 67.570(8)$ Å, $V = 19593$ Å^3, $Z = 6$ (the molecule lies on 32 site), $\rho_{calcd} = 1.581$ g cm^{-3}, $T = 220.0(2)$ K, crystal size $0.16 \times 0.16 \times 0.04$ mm, $\mu(Cu_{K\alpha}) = 12.695$ mm^{-1}. Diffraction was very weak, and $Cu_{K\alpha}$ radiation was used for higher intensity. Data were collected with a Stoë Stadi-4 diffractometer equipped with an Oxford Cryosystems low-temperature device. Absorption corrections were applied with Ψ-scan data for **2** and **3** (min./max. transmission: for **2** 0.413/0.594; for 3 0.193/0.343), with SHELXA for **1** (min./max. transmission: 0.165/0.637), and with DIFABS (N. Walker, D. Stuart, *Acta Crystallogr. Sect. A* **1983**, *39*, 158) for **4** (min./max. transmission: 0.176/0.604). All structures were solved by direct methods (SHELXTL, G. M. Sheldrick, Universität Göttingen, **1993**) and completed by iterative cycles of ΔF syntheses and full-matrix, least-squares refinement against F^2 (SHELXTL). Hydrogen atoms were included in all structures in calculated positions, riding on parent C atoms, with $U(H) = 1.2\,U_{eq}(C)$ for chp H atoms and $U(H) = 1.5\,U_{eq}(C)$ for methyl-H atoms. For **1** there were partially occupied, diffuse solvent regions, which were modeled in the manner described by van der Sluis and Spek (*Acta Crystallogr. Sect. A* **1990**, *46*, 194). All non-H atoms were refined with anisotropic displacement parameters: for **1**, 529 parameters, $wR2 = 0.2729$ for 7366 unique data ($2\theta \le 120°$), $R1 = 0.0890$ for 4284 observed reflections, $F_o > 4\sigma(F)$, largest residual difference peak and hole were, respectively, 0.984 and -1.437 e Å^{-3}; for **2** 535 parameters, $wR2 = 0.2220$ for 5474 unique data ($2\theta \le 45°$), $R1 = 0.0827$ for 2899 observed reflections, $F_o > 4\sigma(F)$, largest residual difference peak and hole were, respectively, 0.612 and -0.899 e Å^{-3}; for **3** 655 parameters, $wR2 = 0.1524$ for 7213 unique data ($2\theta \le 120°$), $R1 = 0.0602$ for 4810 observed reflections, $F_o > 4\sigma(F)$, largest residual difference peak and hole were, respectively, 0.496 and -0.504 e Å^{-3}; for **4** 285 parameters, $wR2 = 0.2496$ for 2729 unique data ($2\theta \le 120°$) and 305 restraints, $R1 = 0.0771$ for 1404 observed reflections, $F_o > 4\sigma(F)$, largest residual difference peak and hole were respectively, 0.700 and -1.317 e Å^{-3}. Crystallographic data (excluding structure factors) have been deposited with the Cambridge Crystallographic Data Centre as supplementary publication no. CCDC 100219. Copies of this data can be obtained free of charge on application to The Director, CCDC, 12 Union Road, GB-Cambridge CB21EZ, UK (fax: int. code +(1223)336-033; e-mail: deposit@chemcrys.cam.ac.uk.
[12] S. Parsons, R. E. P. Winpenny, *Acc. Chem. Res.* **1997**, *30*, 89.
[13] F. A. Cotton, T. R. Felthouse, *Inorg. Chem.* **1981**, *20*, 584.

Synthesis, Structure, and Oxidation of Donor-Stabilized Gallium(I) Iodide: $Ga_8I_8 \cdot 6PEt_3$**

Clemens U. Doriat, Markus Friesen, Elke Baum, Achim Ecker, and Hansgeorg Schnöckel*

Dedicated to Professor Wolfgang Beck on the occasion of his 65th birthday

Gallium halides with low-valent gallium have been the subject of intensive study in the fields of solid-state chemistry and molecular compounds.[1] The readily available gallium(II) halides—which are present as gallium(I/III) halides as solids[2] and in donor-free solvents[3] but as genuine gallium(II) species[4] with Ga–Ga bonds ($Ga_2X_4 \cdot 2D$) in donor-containing solvents D—occupy a special position among the gallium halides because they can be used, for example, as starting materials in the synthesis of organic gallium(I) compounds.[5] The mixed-valent $Ga_5Cl_7 \cdot 5OEt_2$ is a peculiarity in which the Ga centers are formally present in the oxidation state 1.5.[6]

A binary Ga^I halide, that is, a compound that contains no Ga^{III} ions, has not yet been structurally characterized. Although solid GaI could be prepared some years ago and its stoichiometric composition substantiated with subsequent reactions,[7] a structure determination of a solid GaX compound remained elusive. As we have been studying donor-stabilized AlX species[8] prepared by cocondensation methods for some time, and were successful in confirming the presence of both AlBr[9] and AlI[10] with planar Al_4 rings ($Al_4X_4 \cdot 4NEt_3$), it was reasonable to consider experiments with analogous GaX systems. We report here the synthesis and structure determination of the first donor-stabilized GaI compound.

Condensing gaseous GaI (31 mmol, prepared from Ga and HI at about 900 °C)[11] with PEt_3 (48 mmol) and toluene (1.05 mol) at −196 °C and then thawing the matrix results in an orange-red solution, from which an orange solid precipitates at −50 °C. The ^{31}P NMR spectrum of the solution (300 MHz, external standard 85% H_3PO_4) shows a downfield-shifted signal at $\delta = -7.2$ in addition to that for free PEt_3 ($\delta = -19.7$).[12] Analysis of the solid (yield about 65%), which decomposes above 133 °C under disproportionation to metallic gallium and $GaI_3 \cdot PEt_3$,[13] gives a Ga:I:PEt_3 ratio of approximately 1:1:0.75. Recrystallization from benzene provides yellow, hexagonal crystals that are suitable for a crystal structure analysis (Figure 1).[14]

The compound, $Ga_8I_8 \cdot 6PEt_3$ (**1**), has a planar eight-membered ring of Ga atoms that is bridged by two I atoms to form a doubly transannular Ga_2I_2 ring. Thus, two of the eight Ga atoms reach the coordination number 4; the remaining six Ga atoms reach this coordination number by binding to one I atom and one PEt_3 donor ligand. The eight Ga–Ga distances (2.47 Å) are of almost equal length. This value seems reasonable when compared to known Ga–Ga distances in compounds of the type $Ga_2X_4 \cdot 2D$ (2.39–2.42 Å for X = Cl, Br),[4] because the radius of the Ga^I ion should be larger than that of the Ga^{II}

[*] Prof. Dr. H. Schnöckel, Dipl.-Chem. C. U. Doriat, Dipl.-Chem. M. Friesen, Dr. E. Baum, Dr. A. Ecker
Institut für Anorganische Chemie der Universität
Engesserstrasse, Geb.-Nr. 30.45, D-76131 Karlsruhe (Germany)
Fax: Int. code +(721)608-4854
e-mail: hg@achpc9.chemie.uni-karlsruhe.de

[**] This work was supported by the Deutsche Forschungsgemeinschaft and the Fonds der Chemischen Industrie. We especially thank Mrs. E. Möllhausen for performing the X-ray diffraction experiments.

 © WILEY-VCH Verlag GmbH, D-69451 Weinheim, 1997 0570-0833/97/3618-1969 $ 17.50+.50/0

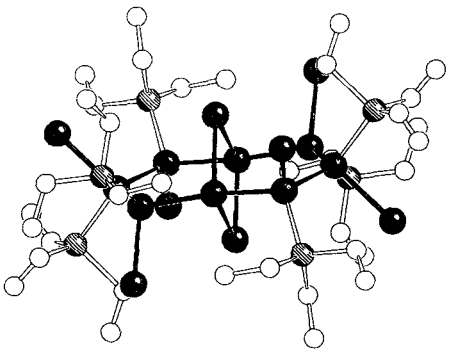

Figure 1. Molecular structure of **1** in the crystal (H atoms omitted). Selected bond lengths [Å] ($d_{min}/d_{max}/\bar{d}$): Ga–Ga 2.4584(11)/2.4726(11)/2.4656), Ga–I_{term} 2.6483(9)/2.6757(10)/2.6648), Ga–I_{br} 2.8522(9)/2.8922(9)/2.8722), Ga–P 2.412(3)/2.428(2)/2.422.

ion. The Ga–I distances are long, as expected for a Ga^I compound: 2.65 Å and 2.87 Å for terminal and bridging I atoms, respectively. The Ga–P distances of 2.42 Å also lie within the expected range; however, they are slightly longer than the Al–P distances in $Al_4I_4 \cdot 4PEt_3$ (2.40 Å).[15] The I-Ga-I angle in the four-membered ring is 98°. The environment of the Ga atoms in the four-membered ring is approximately linear with respect to their neighbors in the Ga_8 framework (168°), whereas the remaining Ga-Ga-Ga angles are about 115°. Thus, the eight-membered metallacycle formally consists of two expanded five-membered rings that are connected to one another. The iodine bridges give the illusion of a shared Ga–Ga "bond";[16] however, the distance of 3.76 Å between these two Ga atoms indicates a nonbonding interaction.

The question of why an eight-membered ring is formed instead of the four-membered rings observed in AlX species is currently being studied by quantum chemical methods.[17] Preliminary results indicate that, in addition to electronic effects, the steric influences of the ligands are of particular importance to the stabilization of the four-membered rings. Therefore, instead of a hypothetical compound $Ga_4I_4 \cdot 4PEt_3$, the sterically less strained $Ga_8I_8 \cdot 6PEt_3$ (**1**) is formed. The isolation of an amine-stabilized $(GaI)_n(NEt_3)_m$ species has been unsuccessful. This system can avoid the electronic and steric forces (stronger Ga-donor interactions weaken the Ga–Ga bonds) in two ways: disproportionation, which begins at low temperature and for $Ga_2I_4 \cdot 2NEt_3$ (**2**) leads to a new donor-stabilized Ga_2I_4 species,[18, 19] or partial oxidation, which would result in relaxation of ring strain in the case of the undetected $Ga_8I_8 \cdot 6NEt_3$.

The latter reaction took place as we attempted to crystallize $Ga_8I_8 \cdot 6NEt_3$ at low temperature to avoid disproportionation. Upon storage at −78 °C traces of oxygen inadvertently came into contact with the solution of GaI. This led to partial oxidation to $Ga_8I_8O_2 \cdot 6NEt_3$ (**3**), a compound with Ga ions in the average oxidation state 1.5. Unfortunately the crystals of **3** thus obtained were only of moderate quality for a crystal structure analysis. The synthesis could not yet be repeated; apparently a very small, defined amount of O_2 must be dosed over a long period of crystal growth. The geometry of the $Ga_8I_8O_2$ species as determined from the X-ray data is shown in Figure 2.[20] Despite the moderate *R* value the geometry of **3** can be regarded as being confirmed.[21]

As expected the Ga–Ga distances in **3** (248–252 pm) are longer than those in the nonoxidized PEt_3-stabilized species, as the relatively strong Ga–N interactions ($d_{Ga-P} = 242$ pm, $d_{Ga-N} = 212$ pm) destabilize the Ga_x system. The $Ga_8I_8O_2$ framework can be described as two near-planar Ga_4O rings

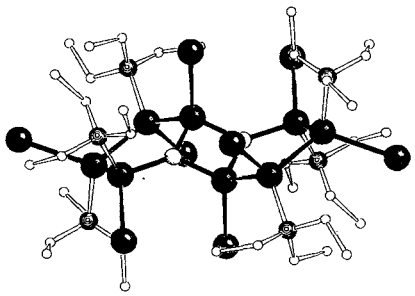

Figure 2. Molecular structure of **3** in the crystal (H atoms omitted). Selected bond lengths [Å] (d_{min}/d_{max}): Ga–Ga 2.478(3)/2.518(3), Ga–O 1.874(11)/1.959(10), Ga–I 2.606(2)/2.670(2), Ga–N 2.12(2)/2.16(2).

connected by a four-membered Ga_2O_2 ring ($d_{Ga-Ga} = 286$ pm); the three Ga atoms bound to a single O atom almost lie in a plane (sum of angles 355°).

The cyclic GaI oligomer **1** is the first structurally characterized gallium(I) halide. The confirmation of a primary product in the oxidation of $Ga_8I_8 \cdot 6D$ with O_2 gives an indication of the strain in this unusual ring system. In addition to its importance for the systematics of structural chemistry, the synthesis of **1** may be of interest for further reactions in Ga^I chemistry.

Received: March 19, 1997 [Z10262IE]
German version: *Angew. Chem.* **1997**, *109*, 2057–2059

Keywords: gallium · low-valent compounds · metallacycles · P ligands

[1] a) G. Gerlach, W. Hönle, A. Simon, *Z. Anorg. Allg. Chem.* **1982**, *486*, 7–21; b) W. Hönle, G. Gerlach, W. Weppner, A. Simon, *J. Solid State Chem.* **1986**, *61*, 171–180; c) W. Frank, W. Hönle, A. Simon, *Z. Naturforsch. B* **1990**, *45*, 1–7; d) W. Uhl, *Angew. Chem.* **1993**, *105*, 1449–1461; *Angew. Chem. Int. Ed. Engl.* **1993**, *32*, 1386–1397; e) C. Dohmeier, D. Loos, H. Schnöckel, *ibid.* **1996**, *108*, 141–161 and **1996**, *35*, 129–149.

[2] a) G. Garton, H. M. Powell, *J. Inorg. Nucl. Chem.* **1957**, *4*, 84–89; b) W. Hönle, A. Simon, G. Gerlach, *Z. Naturforsch. B* **1987**, *42*, 546–552; c) H. Schmidbaur, R. Nowak, W. Bublak, P. Burkert, B. Huber, G. Müller, *ibid.* **1987**, *42*, 553–556.

[3] H. Schmidbaur, *Angew. Chem.* **1985**, *97*, 893–904; *Angew. Chem. Int. Ed. Engl.* **1985**, *24*, 893–904.

[4] a) R. W. H. Small, I. J. Worrall, *Acta Crystallogr. Sect. B* **1982**, *38*, 86–87; b) *ibid.* **1982**, *38*, 250–251; c) J. C. Beamish, R. W. H. Small, I. J. Worrall, *Inorg. Chem.* **1979**, *18*, 220–223; d) J. C. Beamish, A. Boardman, R. W. H. Small, I. J. Worrall, *Polyhedron* **1985**, *4*, 983–987.

[5] a) W. Uhl, W. Hiller, M. Layh, W. Schwarz, *Angew. Chem.* **1992**, *104*, 1378–1380; *Angew. Chem. Int. Ed. Engl.* **1992**, *31*, 1364–1366; b) G. Linti, *J. Organomet. Chem.* **1996**, *520*, 107–113.

[6] According to the crystal structure analysis there are three different types of gallium atoms: one Ga^0, one Ga^I, and three Ga^{II} atoms. Therefore, there is an intermediate on the way to disproportionation from Ga^I to Ga^{III} chloride: D. Loos, H. Schnöckel, D. Fenske, *Angew. Chem.* **1993**, *105*, 1124–1125; *Angew. Chem. Int. Ed. Engl.* **1993**, *32*, 1059–1060.

[7] a) M. L. H. Green, P. Mountford, G. J. Smout, S. R. Speel, *Polyhedron* **1990**, *9*, 2763–2765; b) M. C. Kuchta, J. B. Bonanno, G. Parkin, *J. Am. Chem. Soc.* **1996**, *118*, 10914–10915.

[8] M. Tacke, H. Schnöckel, *Inorg. Chem.* **1989**, *28*, 2895–2896.

[9] M. Mocker, C. Robl, H. Schnöckel, *Angew. Chem.* **1994**, *106*, 1860–1861; *Angew. Chem. Int. Ed. Engl.* **1994**, *33*, 1754–1755.

[10] A. Ecker, H. Schnöckel, *Z. Anorg. Allg. Chem.* **1996**, *622*, 149–152.

[11] The analogous method for GaCl has been described: M. Tacke, H. Kreienkamp, L. Plaggenborg, H. Schnöckel, *Z. Anorg. Allg. Chem.* **1991**, *604*, 35–38.

[12] E. Fluck, J. Lorenz, *Z. Naturforsch. B* **1967**, *22*, 1095–1100.

[13] $GaI_3 \cdot PEt_3$ and $GaI_2 \cdot PEt_3$ were identified as the fragments with the highest intensities upon heating in a mass spectrometer (EI, 70 eV).

[14] a) Crystal structure analysis of **1**: $C_{36}H_{90}Ga_8I_8P_6$ ($M_r = 2281.86$); crystal dimensions $0.7 \times 0.5 \times 0.5$ mm; $T = 200$ K; monoclinic space group $P2_1/n$ (no. 14), $a = 15.125(2)$, $b = 12.7919(7)$, $c = 19.1057(14)$ Å, $\alpha = \gamma = 90$, $\beta = 108.765(7)°$, $V = 3500.0(5)$ Å^3, $Z = 2$, $\rho_{calcd} = 2.165$ g cm^{-3}, $\mu(Mo_{K\alpha}) = 6.718$ mm^{-1}, numerical absorption correction, ω-scan mode ($\Delta\omega = 1.4°$), $5 \le 2\theta \le 55°$; of 7967 reflections measured on a four-circle diffractometer

 © WILEY-VCH Verlag GmbH, D-69451 Weinheim, 1997 0570-0833/97/3618-1970 $ 17.50+.50/0

(STOE STADI4; $Mo_{K\alpha}$, $\lambda = 0.71073$ Å, graphite monochromator) 7886 were independent ($R_{int} = 0.0677$), and 6562 with $F > 4\sigma(F)$; the structure was solved by direct methods (SHELXS-86) [22]; full-matrix refinement of 271 parameters according to the least-squares method against $|F^2|$ (SHELXL-93) [23]; the positions of hydrogen atoms were calculated with the rider model with fixed isotropic U. The molecule has an inversion center. Weighting scheme: $w^{-1} = \sigma^2 F_o^2 + (0.0362\,P)^2 + 28.4990\,P$, with $P = (F_o^2 + 2F_c^2)/3$; $R1 = 0.0489$ ($F > 4\sigma(F)$), weighted R value (all data): $wR2 = 0.1199$, max/min residual electron density: 2.312/ −1.523 e Å^{-3}. b) Crystallographic data (excluding structure factors) for the structures reported in this paper have been deposited with the Cambridge Crystallographic Data Centre as supplementary publication no. CCDC-100292. Copies of the data can be obtained free of charge on application to The Director, CCDC, 12 Union Road, Cambridge CB2 1EZ, UK (fax: int. code +(1223)336-033; e-mail: deposit@chemcrys.cam.ac.uk).

[15] A. Ecker, Dissertation, Universität Karlsruhe (Germany), **1996**.

[16] Attempts to open the iodine bridge by addition of excess PEt_3 gave no evidence for the existence of species of the formula $(GaI \cdot PEt_3)_n$. Instead, **1**·2 toluene was isolated in crystalline form. The molecular structures of **1** and **1**·2 toluene in the crystal do not differ significantly. **1**·2 C_7H_8: monoclinic space group $P2_1/n$, $a = 17.370(10)$, $b = 11.888(6)$, $c = 20.172(9)$ Å, $\alpha = \gamma = 90$, $\beta = 91.06(6)°$, $V = 4164.7(37)$ Å^3, $Z = 2$.

[17] The results obtained so far for the energy values (TURBOMOLE; DFT-RI/SVP; BP 86 parametrization: K. Eichkorn, O. Treutler, H. Öhm, M. Häser, R. Ahlrichs, *Chem. Phys. Lett.* **1995**, *240*, 283–290) confirm the experimental findings. Formation of an eight-membered ring system analogous to **1** from two four-membered Ga or Al rings according to Equation (a) is exothermic for $GaI \cdot PH_3$ (about 200 kJ mol^{-1}). For the corresponding $AlI \cdot NH_3$ oligomer the energy balance is almost zero.

$$2\,M_4I_4 \cdot 4D \rightleftharpoons M_8I_8 \cdot 6D + 2D \qquad (a)$$

Despite the considerable effort involved in the calculation, the results are purely preliminary, as only the simple PH_3 and NH_3 groups were used as donors. Sterically demanding substituents could have a decisive influence on the energy balance, especially in the case of the "forced" Ga_8 system ($d_{Ga-Ga} = 247$ pm; $d_{Al-Al} = 266$ pm in $Al_4I_4 \cdot 4D$).

[18] $Ga_2I_4 \cdot 2AsEt_3$ was the first structurally characterized compound of this type: B. Beagley, S. M. Godfrey, K. J. Kelly, S. Kungwankunakorn, C. A. McAuliffe, R. G. Pritchard, *Chem. Commun.* **1996**, 2179–2180. The Ga–Ga bond of 242.8 pm in this compound is considerably shorter than that in **2** (249 pm). This is in agreement with strengthening of the Ga-donor interaction and resulting weakening of the Ga–Ga bond in **2**.

[19] Crystal structure analysis of **2**: $C_{12}H_{30}Ga_2I_4N_2$ ($M_r = 849.42$); monoclinic space group $P2_1/c$, $a = 7.888(2)$, $b = 14.906(3)$, $c = 19.554(4)$ Å, $\alpha = \gamma = 90$, $\beta = 95.57(3)°$, $V = 2288.3(8)$ Å^3, $Z = 4$, $R1 = 0.0579$ ($F > 4\sigma(F)$), weighted R value (all data): $wR2 = 0.1150$ [14b].

[20] Due to the poor quality of the crystal the caliber of the experimental data and, thus, also of the structural analysis was only moderate. (One of the solvent molecules in the crystal could not be localized.) Crystal structure analysis of **3**: $C_{36}H_{90}Ga_8I_8N_6O_2$ ($M_r = 2212.13$); crystal dimensions $0.4 \times 0.3 \times 0.2$ mm; $T = 200$ K; monoclinic space group $C2/c$, $a = 19.411(4)$, $b = 13.979(3)$, $c = 27.340(6)$ Å, $\alpha = \gamma = 90$, $\beta = 103.45(3)°$, $V = 7215(3)$ Å^3, $Z = 4$, $\rho_{calcd} = 2.066$ g cm^{-3}, $\mu(Mo_{K\alpha}) = 6.393$ mm^{-1}, empirical absorption correction, ω-scan mode ($\Delta\omega = 1.5°$), $3 \le 2\theta \le 50°$; 6279 independent reflections (4783 with $F > 4\sigma(F)$) were measured on a four-circle diffractometer (STOE STADI4; $Mo_{K\alpha}$ $\lambda = 0.71073$ Å, graphite monochromator); the structure was solved by direct methods (SHELXS-86) [22]; full-matrix refinement of 302 parameters according to the least-squares method against $|F^2|$ (SHELXL-93) [23]; the positions of hydrogen atoms were calculated. The molecule has an inversion center. Weighting scheme: $w^{-1} = \sigma^2 F_o^2 + (0.0561\,P)^2 + 411.140\,P$, with $P = (F_o^2 + 2F_c^2)/3$; $R1 = 0.0890$ ($F > 4\sigma(F)$):, weighted R value (all data): $wR2 = 0.2047$, max/min residual electron density: 2.185/ −1.045 e Å^{-3} [14b].

[21] The molecular geometry of **3** described here was also determined for $Ga_8I_8O_2 \cdot 6PEt_3$ (**4**). Crystals of **4** were obtained by treating a solution of GaI in PEt_3 and toluene with a N_2/O_2 mixture at 0 °C. Due to the poor quality of the crystals a precise structural analysis was not possible in this case either. However, the framework structure of **3** was unequivocally confirmed. **4**: triclinic space group $P\bar{1}$, $a = 12.065(5)$, $b = 12.736(4)$, $c = 13.981(4)$ Å, $\alpha = 89.49(3)$, $\beta = 68.54(3)$, $\gamma = 70.32(3)°$, $V = 1866.5(8)$ Å^3, $Z = 1$. The molecule has an inversion center.

[22] G. M. Sheldrick, *Acta Crystallogr. Sect. A* **1990**, *46*, 467–473.

[23] G. M. Sheldrick, Program for Crystal Structure Refinement, Universität Göttingen (Germany), **1993**.

Bi_7RhBr_8: A Subbromide with Molecular $[\{RhBi_7\}Br_8]$ Clusters**

Michael Ruck*

Dedicated to Professor Hans Georg von Schnering

The recently discovered ternary subhalides of bismuth are not only chemically, but also structurally remarkable compounds.[1] One example is $Bi_{5.6}Ni_5I$, the unusual structure of which consists of decagonal tubes of Bi and Ni atoms, and the I atoms intercalated between the tubes.[2] Another compound that belongs to this ternary system is $Bi_{12}Ni_4I_3$. It is composed of ribbons of face-sharing, trigonal $\{NiBiBi_{6/3}\}$ prisms, similar to those found in the intermetallic compound Bi_3Ni.[3] Both $Bi_{13}Pt_3I_7$ and Bi_4RuI_2 are based on different building principles: $Bi_{13}Pt_3I_7$ is composed of Kagomé networks of $\{PtBi_{8/2}\}$ cubes alternating with layers of I atoms and tetraiodobismuthate(III) chains,[4] while Bi_4RuI_2 has a columnar structure with face-sharing, square $\{RuBi_{8/2}\}$ antiprisms.[5]

In contrast to these metal-rich subiodides, which contain one- or two-dimensional intermetallic substructures, the distinctly halogen-richer subbromide Bi_7RhBr_8 reported here consists of discrete molecular clusters of the same composition (Figure 1).[6] These clusters are ordered within the monoclinic crystal structure into an almost perfect hexagonal close packing ($c/a = 1.739 \approx \sqrt{3}$ and $b/a = 1.613 \approx \sqrt{8/3}$) (Figure 2).

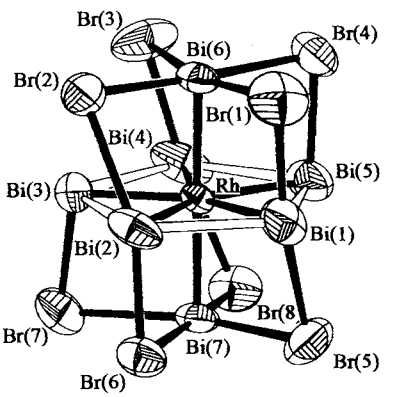

Figure 1. Molecular structure of a $[\{RhBi_7\}Br_8]$ cluster in the crystal (the ellipsoids represent 90% probability). Selected distances [pm] and angles [°]: Rh–Bi(1) 273.2(2), Rh–Bi(2) 273.8(2), Rh–Bi(3) 274.9(2), Rh–Bi(4) 274.2(2), Rh–Bi(5) 271.9(2), Rh–Bi(6) 273.5(2), Rh–Bi(7) 271.9(2) Bi(1)–Bi(2) 326.6(2), Bi(2)–Bi(3) 322.8(2), Bi(3)–Bi(4) 319.1(2), Bi(4)–Bi(5) 320.3(2), Bi(5)–Bi(1) 319.4(2), Bi(1)–Bi(6) 381.3(2), Bi(1)–Bi(7) 388.2(2) Bi(6)–Br(1) 289.7(3), Bi(6)–Br(2) 287.6(3), Bi(6)–Br(3) 296.2(3), Bi(6)–Br(4) 301.0(3); Bi(1)-Rh-Bi(2) 73.32(6), Bi(2)-Rh-Bi(3) 71.08(7), Bi(3)-Rh-Bi(4) 71.05(5), Bi(4)-Rh-Bi(5) 71.81(5), Bi(5)-Rh-Bi(1) 71.73(6), Bi(6)-Rh-Bi(7) 178.91(7).

In this novel $[\{RhBi_7\}Br_8]$ cluster seven Bi atoms are arranged as a pentagonal bipyramid with a Rh atom in the center. The apical Bi atoms are surrounded by four Br atoms in a square-planar environment. Each of these Br atoms is also coordinated to one Bi atom of the central five-membered ring, and two of the five equatorial Bi atoms are coordinated to only one Br atom. The squares are staggered, so that the $\{RhBi_7\}$ bipyramid is enclosed by a distorted, square Br_8 antiprism. The whole mole-

[*] Dr. M. Ruck
Institut für Anorganische Chemie der Universität
Engesserstrasse, Geb.-Nr. 30.45, D-76128 Karlsruhe (Germany)
Fax: Int. code +(721)661-921
e-mail: ruck@achpc1.chemie.uni-karlsruhe.de

[**] This work was supported by the Fonds der Chemischen Industrie, the Karlsruher Hochschulvereinigung, and DEGUSSA AG, Hanau.

 © WILEY-VCH Verlag GmbH, D-69451 Weinheim, 1997 0570-0833/97/3618-1971 $ 17.50+.50/0

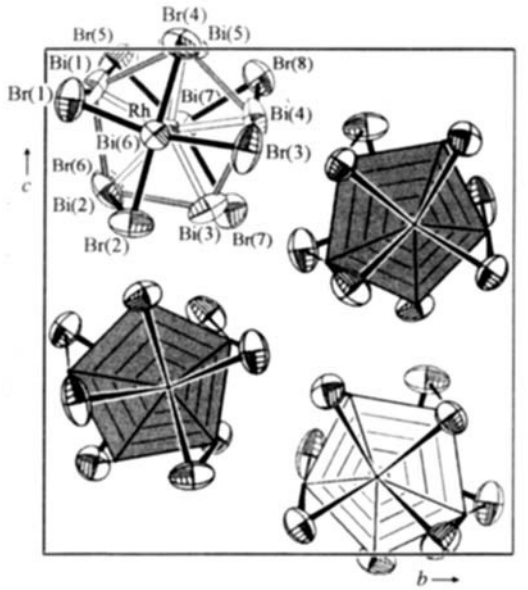

Figure 2. Projection of a part of the crystal structure of Bi_7RhBr_8 onto the b,c plane. The cluster units given in a darker shade are closer to the observer by $\Delta x = 0.5$. (The ellipsoids represent 90% probability).

cule does not display any symmetry dictated by the space group; however, the inner $\{RhBi_7\}$ polyhedron has almost D_{5h} symmetry. The equatorial Bi atoms and the central Rh atom only deviate by a maximum of 1 pm from the average plane defined by these six atoms. If the Br atoms are now taken into consideration, only a two-fold rotational axis through the Rh and the Bi(4) atoms remains from the elements of pseudo-symmetry.

The Br atoms of neighboring molecules are as far apart (d[Br(1)–Br(5′)] = 366.0(3) pm) as those in Bi_6Br_7 (d[Br–Br] ≥ 347.1 pm)[7] and in $BiBr_3$ (d[Br–Br] ≥ 356.8 pm).[8] Together they form gently undulating nets parallel to the (100) plane (Figure 3), which are described by the $3^2434 + 3^34^2 + 3^44 + 3^54$ (1:1:1:1) representation of Schläfli.[9]

The distances between the apical and the equatorial Bi atoms in the $[\{RhBi_7\}Br_8]$ cluster lie in the range 381.3(2) to 391.1(2) pm, so direct interaction can hardly be expected. The smallest distances between the apical Bi atoms of neighboring molecules are of a similar size. In spite of the differing types of coordination of the Br atoms, the distances between the Bi

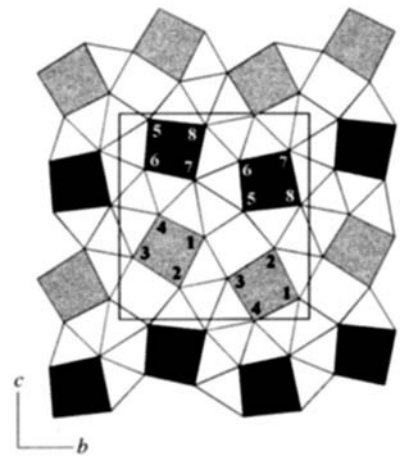

Figure 3. Projection of one of the gently undulating networks of Br atoms in the structure of Bi_7RhBr_8 onto the b,c plane. The numerals represent the number of the Br atom at the junction. The squares formed by the Br atoms of one molecule are shaded, differing in the gray tone according to the set of the atoms involved.

atoms in the five-membered ring only differ slightly (319.1(2)–326.6(2) pm). Consequently, the corresponding Bi-Rh-Bi angles also lie in a very narrow range about the ideal value of 72°. The distances between the Rh atom and all seven surrounding Bi atoms lie between 271.9(2) and 274.9(2) pm. From a comparison with the binary Bi–Rh phases (α-Bi_2Rh: coordination number (CN) = 6, $\bar{d}$[Bi–Rh] = 272 pm;[10] β-Bi_2Rh: CN = 7, $\bar{d}$[Bi–Rh] = 281 pm;[11] α-Bi_4Rh: CN = 8, $\bar{d}$[Bi–Rh] = 280 pm[12]) it is evident that the "disintegration" of the intermetallic structure gives rise to stronger bonds between the transition metal atom and the Bi atoms in the subhalide.

An analysis of the boundary conditions for a regular pentagonal-bipyramidal arrangement highlights a further aspect of the atomic arrangement in the $[\{RhBi_7\}Br_8]$ molecule: in an ideal pentagonal bipyramid with equally sized ligands (radius r_L) at a distance d from the central atom (radius r_Z), the ten apical edges have a length of $\sqrt{2}d = 1.4142\,d$ and the five equatorial edges are $2 \sin 36°\, d = 1.1756\,d$. The ratio of the two edge lengths is 1.2030. For the ligands to be in contact a radius of $r_L = \sin 36°\, d = 0.5878\,d$ is necessary. The maximum radius of the central atom then is $r_Z = (1 - \sin 36°)\,d = 0.4122\,d = 0.7013\,r_L$. In the $[\{RhBi_7\}Br_8]$ molecule, the quotient of the average apical and equatorial edge lengths is 1.201, which is in agreement with an almost ideal pentagonal bipyramid. From the average distance between the Bi atoms and the central Rh atom of 273.3 pm, a radius of the Bi atoms of $r_L = 160.6$ pm and a maximum radius of the Rh atom of $r_Z = 112.7$ pm can be calculated. Since the sum of the covalent radii of the Bi atom (146 pm) and of the Rh atom (125 pm) is 271 pm, which only differs slightly from the observed average Bi–Rh distance, a division of the distance into the respective covalent radii is possible. However, the Bi atoms are then no longer in contact on the basis of the hard sphere model.

The interactions between the Br atoms and the atoms Bi(3) and Bi(5) are only apparently weaker than those between the Br atoms and the other Bi atoms in the five-membered ring. The sums of the bond orders calculated according to the method of Brese and O'Keeffe[13] differ only slightly, even when only an isolated $[\{RhBi_7\}Br_8]$ molecule is considered. However, the interactions between the molecules contributes up to an additional 20% (Table 1). The shortest intermolecular Bi–Br distances of 350.8(3) pm resemble the intramolecular distances. The spatial linkage of the almost spherical molecules that results from this similarity is probably of great importance for the ordered, crystalline structure of the compound.

The sum of the bond orders of the apical Bi atoms also clearly differs from that of the Bi atoms of the five-membered ring: although the Bi–Br bond lengths are similar, the greater number of contacts here leads to an approximate doubling of the sum of the bond orders. If the contributions for the single Bi

Table 1. Sum of the bond orders $\sum_{Br} v_{Bi-Br}$ for the Bi–Br interactions in Bi_7RhBr_8. The total sum is split up into the intra- and intermolecular contributions. Only distances smaller than 400 pm were considered. Bond valence parameter $R_{Bi-Br} = 262$ pm.

Atom	$\sum v_{intra}$	$\sum v_{inter}$	$\sum v_{total}$
Bi(1)	0.844	0.040	0.884
Bi(2)	0.811	0.160	0.971
Bi(3)	0.761	0.134	0.895
Bi(4)	0.740	0.147	0.887
Bi(5)	0.732	0.131	0.863
Bi(6)	1.717	0.032	1.749
Bi(7)	1.673	0.027	1.700
Bi(1) to Bi(5)			4.500
Bi(1) to Bi(7)			7.949

 © WILEY-VCH Verlag GmbH, D-69451 Weinheim, 1997 0570-0833/97/3618-1972 $ 17.50+.50/0

atoms are added, then for the Bi_5 ring the sum of the bond orders is $V_{Bi(1-5)} = \sum_{Bi(1-5)}\sum_{Br} v_{Bi-Br} = 4.50$, and for all seven Bi atoms $V_{Bi(1-7)} = 7.95$. As a result, the sum of the valences of the eight Br atoms and consequently the compensation of the electrostatic charges is almost perfect.

Since the electronegativities of Bi and Rh only differ slightly, covalent bonds between these atoms can be regarded as almost nonpolar. Thus, the central Rh atom should be essentially neutral. If it is assumed that there are seven Bi–Rh single bonds, then the Rh atom has $9 + 7 = 16$ valence electrons. However, in such a calculation the Bi atoms have not been assigned integral oxidation states, but rather values of 8/9 for the equatorial and 16/9 for the apical atoms. In order to avoid fractional oxidation states, Bi_7RhBr_8 can be alternatively formulated as $(Bi^{I})_5(Bi^{II})_2Rh^{-I}(Br^{-I})_8$; note that the Rh atom has been assigned a formal negative charge.

The results of band structure calculations at the extended Hückel level[14] also point to a low negative partial charge on the Rh atom. According to these calculations, the highest occupied and the lowest unoccupied state are distinctly separated in energy (Figure 4), although the band gap is smaller than ≈ 1.7 eV, which is in agreement with the black color of the compound.

The interactions between the central Rh atom and the surrounding Bi atoms are almost exclusively bonding below the band edge, while above it they are strongly antibonding. Again, the equatorial atoms Bi(1) to Bi(5) must be differentiated from the apical atoms Bi(6) and Bi(7): as a result of antibonding contributions, the integration of the overlap population (COOP) curves up to the Fermi level gives a lower positive overlap population of the Rh atom with the equatorial Bi atoms than with the apical atoms. The weaker bond to the central atom, however, is compensated for by an additional, homoatomic bond in the five-membered ring: the Bi–Bi interactions between the atoms in the five-membered ring (distances < 330 pm) are all bonding and those between the equatorial and the apical Bi atoms (distances > 330 pm) are all nonbonding.

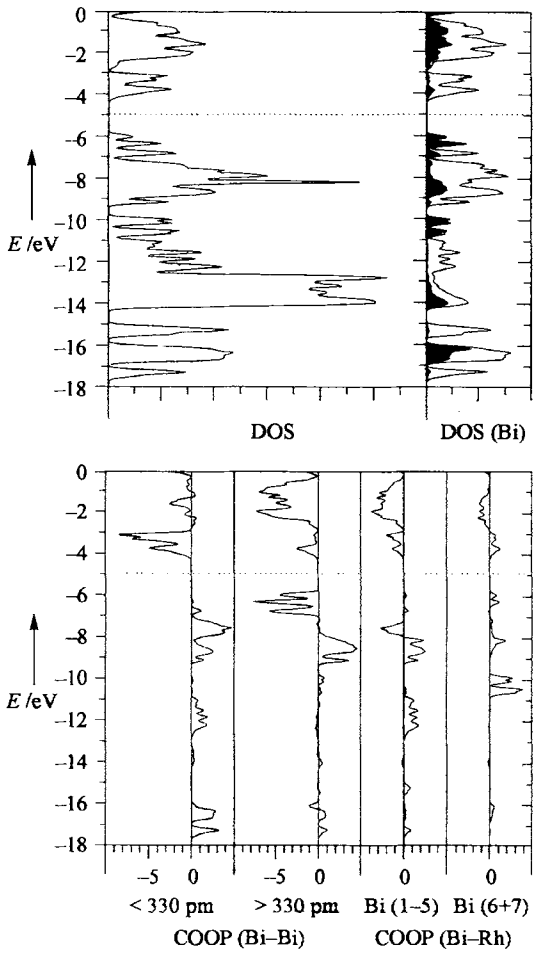

Figure 4. Density of states (DOS) and the projected DOS of the Bi atoms as well as selected overlap populations (COOP) for Bi_7RhBr_8. The dotted line represents the Fermi level. The shaded areas of DOS(Bi) represent the contributions of the apical atoms Bi(6) and Bi(7). The energetically low-lying Bi–Br bonding states at about −22.5 eV have been omitted.

Experimental Procedure

Synthesis of Bi_7RhBr_8: in an evacuated quartz glass ampoule a mixture of the elements (molar ratio Bi:Rh:Br = 7:1:8; $BiBr_3$ can be used instead of Br_2) was heated to 1270 K over a period of 1 h, and subsequently, without a longer tempering phase, cooled to RT over a period of 8 h. Attached to the walls of the ampoule were platelike crystals with a metallic luster, which were contaminated with $BiBr_3$. The impurity was sublimed out of the crystals by storage of the ampoule in a temperature gradient of 520 K to 350 K for 1 d. The black, lustrous platelets of Bi_7RhBr_8 can be left in the air for several weeks without any visible decomposition.

Received: March 4, 1997
Revised version: May 26, 1997 [Z10193IE]
German version: *Angew. Chem.* **1997**, *109*, 2059–2062

Keywords: bismuth · bromine · clusters · subvalent compounds · rhodium

[1] M. Ruck, Habilitation Dissertation, Universität Karlsruhe, **1997**.
[2] M. Ruck, *Z. Anorg. Allg. Chem.* **1995**, *621*, 2034–2042.
[3] M. Ruck, *Z. Anorg. Allg. Chem.* **1997**, *623*, 243–249.
[4] M. Ruck, *Z. Anorg. Allg. Chem.*, in press.
[5] M. Ruck, *Z. Anorg. Allg. Chem.*, in press.
[6] Crystal structure determination of Bi_7RhBr_8: Four-circle diffractometer AED2 (Siemens, Stoe), $Mo_{K\alpha}$ radiation, $\lambda = 71.073$ pm, transmission-optimized ω/θ scan (MESSOPT), $2\theta_{max} = 45°$, crystal dimensions $0.12 \times 0.07 \times 0.03$ mm^3, monoclinic, space group $P2_1/n$ (No. 14), $T = 293$ K, $a = 913.1(2)$, $b = 1472.6(8)$, $c = 1587.6(9)$ pm, $\beta = 91.77(2)°$, $V = 2133.7 \times 10^6$ pm^3, $Z = 4$, $\rho_{calcd} = 6.864$ g cm^{-1}, $\mu(MoK\alpha) = 732$ cm^{-1}, analytical absorption correction (ABSPSI), description of the crystal optimized by 12 ψ-scanned reflections (HABITUS), transmission factors 0.18 to 0.03, extinction correction $x = 0.79(4) \times 10^{-4}$ (SHELXL-93), solution of structure by direct methods (SHELXS-86), least-squares refinement with F_o^2 values, complete matrix (SHELXL-93), 10772 reflections, of which 2762 were independent of symmetry, 146 parameters, $R1$ (1706 $F_o > 4\sigma(F_o)$) = 0.040, $wR2 = 0.042$, residual electron density +1.51 to −1.51 e $10^{-6} \times$ pm^{-3}. Graphical representation: DIAMOND, CORELDRAW. Further details of the crystal structure investigation may be obtained from the Fachinformationszentrum Karlsruhe, D-76344 Eggenstein-Leopoldshafen (FRG) on quoting the depository number CSD-406636, the names of the authors, and the journal citation.
[7] H. von Benda, A. Simon, W. Bauhofer, *Z. Anorg. Allg. Chem.* **1978**, *438*, 53–67.
[8] H. von Benda, *Z. Kristallogr.* **1980**, *151*, 271–285.
[9] W. B. Pearson, *The Crystal Chemistry and Physics of Metals and Alloys*, Wiley, New York, **1972**.
[10] a) R. N. Kuz'min, N. N. Zhuravlev, *Sov. Phys. Crystallogr. (Engl. Transl.)* **1961**, *6*, 209–210; b) A. Kjekshus, T. Rakke, *Acta Chem. Scand. Ser. A* **1977**, *31*, 517–529.
[11] M. Ruck, *Acta Crystallogr. Sect. B* **1996**, *52*, 605–609.
[12] a) Y. Grin, U. Wedig, H. G. von Schnering, *Angew. Chem.* **1995**, *107*, 1318–1320; *Angew. Chem. Int. Ed. Engl.* **1995**, *34*, 1204–1206; b) V. P. Glagoleva, G. S. Zhdanov, *Zh. Eksp. Teor. Fiz.* **1956**, *30*, 248; *Sov. Phys. JETP (Engl. Transl.)* **1956**, *3*, 155.
[13] N. E. Brese, M. O'Keeffe, *Acta Crystallogr. Sect. B* **1991**, *47*, 192–197.
[14] Extended Hückel calculations of Bi_7RhBr_8: calculations of the band structure for the solid were performed with a modified version of the program EHMACC. The STO functions were taken from ref. [15]; for Rh the values of the orbital energy were first subjected to a charge iteration. The calculation of the DOS and COOP curves used 30 k points [16].
[15] a) L. L. Lohr, P. Pykkö, *Chem. Phys. Lett.* **1979**, *62*, 333–338; b) R. H. Summerville, R. Hoffmann, *J. Am. Chem. Soc.* **1976**, *98*, 7240–7254; c) J. Hinze, H. H. Jaffé, *J. Phys. Chem.* **1963**, *67*, 1501–1506.
[16] a) R. Ramirez, M. C. Böhm, *Int. J. Quantum Chem.* **1986**, *30*, 391–411; b) *ibid.* **1988**, *34*, 571–594.

 © WILEY-VCH Verlag GmbH, D-69451 Weinheim, 1997 0570-0833/97/3618-1973 $ 17.50+.50/0

Sc_2Te: A Novel Example of Condensed Metal Polyhedra in a Metal-Rich but Relatively Electron-Poor Compound**

Paul A. Maggard and John D. Corbett*

Dedicated to Professor Hans Georg von Schnering

The earlier transition-metal chalcogenides have both extended the boundaries of solid-state chemistry and challenged our understanding of stability, structure, and bonding. Some recent examples of metal-rich chalcogenides of Group 4 and 5 metals are Ti_9Se_2,[1] Zr_3Te,[2] Hf_3Te_2,[3] Ta_3S_2,[4] and Ta_2Se.[5] Highly reduced binary compounds of the earliest transition metals Sc, Y, La have been limited to a few halides and to the monochalcogenides (NaCl-type), which may be significantly substoichiometric.[6] Only a few truly binary halides are known (Sc_7Cl_{10}, Y_2X_3, and LaI).[7] No phase diagrams exist for any of the scandium or yttrium chalcogenides, and the only binary Sc–Te phases reported are Sc_2Te_3 and ScTe.[8] This situation clearly results from a lack of investigation of these quite refractory compounds. This article describes the first example, Sc_2Te, an exceptional chalcogenide with respect to the nature of its metal–metal bonding.

A [010] projection of the Sc_2Te structure down the short (3.919 Å) axis is given in Figure 1. Both a large complex chain unit and a simple zigzag chain of scandium are evident. The Sc–Sc distances vary from 3.05 Å upward with no distinctive breaks, but the justification of the 3.5 Å limit for "bonds" marked in Figure 1 will be given later. Considerably closer contacts and tighter bonding are found within the larger Sc chain, which is detailed in Figure 2 with atomic numbering and independent distances (the Sc6–Sc6 and Sc4–Sc4 bonds lie on centers of symmetry). The central building block emphasized by the darker bonds is the same as can be visualized in Sc_7Cl_{10}[7] as well as in several interstitial derivatives such as Pr_3I_3Ru,[9] namely, the familiar pairs of quasi infinite chains of distorted *trans*-edge-sharing metal octahedra (for example, (1,1)-5-(6,6)-6) that are further cocondensed through sharing of Sc6–Sc6 side edges. (The choice of Sc1–Sc6 (3.49 Å) as the shared edges and Sc5, Sc6 (d = 3.52 Å) for the apices of the compressed octahedra is fairly arbitrary (see below). The y coordinates around the periphery of the double chain alternate between $^1/_4$ and $^3/_4$.)

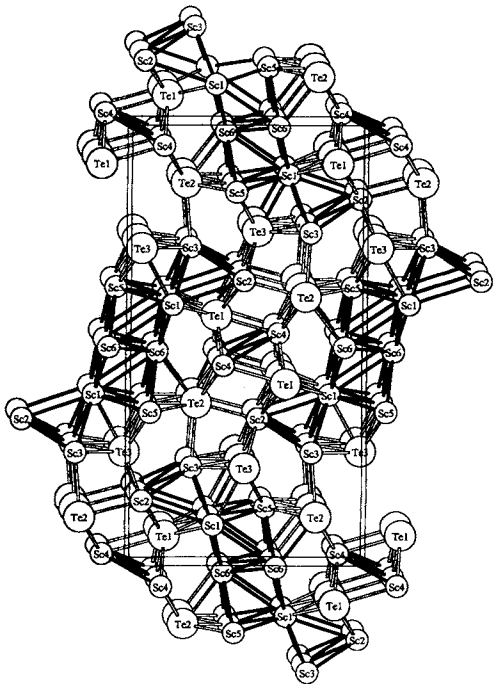

Figure 1. A view of the unit cell of Sc_2Te along [010] (Sc: small circles, Te: large circles). Bonds are drawn for d(Sc–Sc) < 3.50 Å and d(Sc–Te) < 3.15 Å. All atoms lie on mirror planes at $y = {}^1/_4, {}^3/_4$.

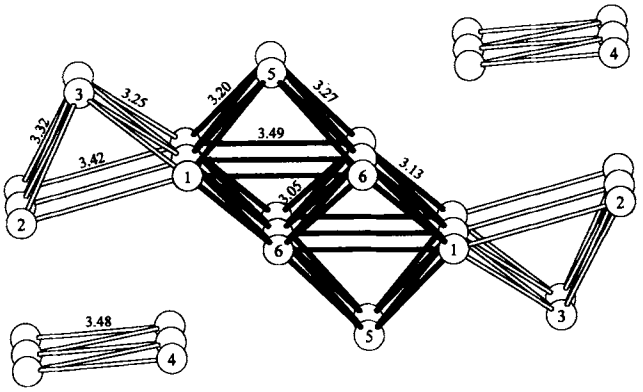

Figure 2. The highly condensed scandium chain and two zigzag chains with atomic labeling and independent distances ($\sigma \leq 0.005$ Å). Inversion centers lie on the Sc6–Sc6 and Sc4–Sc4 bonds.

The shortest Sc–Sc distances in the structure lie within the double chain (3.05–3.27 Å). Surprisingly, these values range from the same length to about 0.1 Å shorter than those in Sc_7Cl_{10}, while both the shared *trans*-edge Sc1–Sc6 and the repeating unit of the chain are about 0.4 Å longer. The first difference may reflect the presence of the Sc2, Sc3 appendages or the bonding within the chain (see below), whereas the increased chain repeat of 3.92 Å logically derives from the larger diameter of closed-shell Te. (An alternate description in terms of metal tetrahedra 1-5-6-6 that are more loosely coupled along the chains is more consistent with observed distances but less useful for comparison with other structures.) There are no short Te–Te separations, so their problematic bonding is not a concern. The metal environments of all tellurium atoms are monocapped trigonal prisms, and Sc–Te distances range between 2.86 and 3.14 Å, less than nearly all Sc–Sc distances.

Generally, the nonmetal-to-metal ratios in metal-rich compounds seem to be the major factor in determining structure, more overtly than electron counts. Although the similar double metal chains in Sc_7Cl_{10} [$= Sc^{3+}(Sc_6Cl_{10})^{3-}$] are easy to assess in terms of average oxidation state (+1.17), a similar partitioning in the more complex Sc_2Te is not very clear. The double-chain framework described above is further augmented by edge-sharing square pyramids (Sc1, Sc2, Sc3; open bonds in Figure 2) that also share Sc1–Sc1 edges along the double chains. The Sc–Sc distances within these appendages are the same or longer (3.25, 3.32, 3.42 Å) than in the double-chain core, befitting the greater amount of tellurium bound to these atoms. The anion-poorer nature of Sc_2Te also allows closer approaches of the metal building blocks. Finally, the 3.48 Å repeat in the Sc4–Sc4 zigzag chain is somewhat larger than within the augmented

[*] Professor J. D. Corbett, P. A. Maggard
Department of Chemistry
Iowa State University
Ames, IA 50011 (USA)
Fax: Int. code +(515)294-5718

[**] This research was supported by the National Science Foundation (Solid State Chemistry grant DMR-9510278) and was carried out in the facilities of Ames Laboratory, U. S. Department of Energy.

 © WILEY-VCH Verlag GmbH, D-69451 Weinheim, 1997 0570-0833/97/3618-1974 $ 17.50+.50/0

double chain and closer to what we assign as interchain separations (3.53(× 2) Å for Sc4–Sc6, 3.67 Å for Sc4–Sc1, 3.68 Å for Sc4–Sc2, and beyond). However, all of these are well segregated by crystal orbital overlap populations (COOP, see below). The larger Sc–Sc separations appear to be attributable to matrix effects and the shortage of bonding electrons.

A novel way to view the Sc_2Te result is as a dissociation product of the metal frameworks in electron-richer chalcogenides of later transition metals with comparable stoichiometries. For example, the metal network in Ta_2Se contains layers of an interpenetrating body-centered cubic (bcc) structure for Ta, as in the element,[5] and similar but more condensed frameworks appear in Ti_8S_3[10] and Ti_9Se_2.[1] Related building blocks can also be perceived in Ti_2S, Zr_2S, Zr_2Se (all the Ta_2P-type),[11] and Hf_3Te_2.[3] A similar feature can be generated from Sc_2Te if each Sc4 is moved toward Sc6 in the closer chain: extended pairs of condensed Sc4-5-6-1 cubes centered by Sc6. The Sc2, Sc3 portions may be further fragments of what was once a sheet.

Extended Hückel calculations have been carried out for the full structure at 48 k points.[12] The total density of states (DOS) shows a Te p-orbital-based valence band (with some Sc mixing through covalency) between about −14.0 and −10.8 eV. A large conduction band (Figure 3) is generated almost entirely

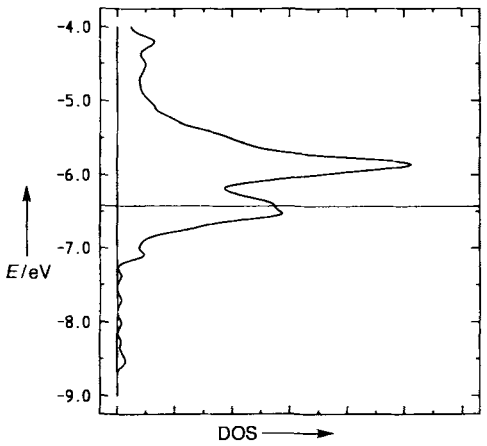

Figure 3. The total densities of states (DOS) for the conduction band in Sc_2Te.

from Sc 3d orbitals, with only traces of Te p orbitals in the upper reaches. Six small DOS features between −7.0 and −8.5 eV all originate with the Sc1–Sc5, Sc1–Sc6, Sc5–Sc6, and Sc6–Sc6 intracluster bonding interactions. The Fermi energy for such an electron-poor compound falls low in the band near −6.4 eV, while the Sc–Sc COOP functions show that the states remain bonding up to about −6.0 eV. (In contrast, all bonding states are occupied in Hf_3Te_2.[3]) The compound appropriately exhibits a Pauli-like paramagnetism ($\chi_{M(298)} = 3.4 \times 10^{-4}$ emu mol^{-1}) and is logically presumed to be a metal.

Interesting features of the bonding are revealed by differences in pairwise Sc–Sc Mulliken overlap populations (MOP) as a function of distance. These emphasize the strength and delocalization of the metal bonding in the double chain region, especially among Sc1, Sc5, and Sc6, and the contrasting weakness of all bonding about Sc4. In fact, directly following the 0.306–0.172 MOP for the three shortest Sc–Sc separations (Figure 2) are those for the longish Sc1–Sc6 separation across the octahedral waist (3.49 Å, MOP 0.166) and for Sc5–Sc6 between its vertices (3.52 Å, 0.170; not interconnected in Figure 2 for clarity). Next is that for the shorter Sc5–Sc6 bond (3.27 Å, 0.146) on the periphery of the chain. These contrasts presumably reflect an enhanced electron concentration and delocalization *within* the chains and suggest a reason for the marked compression of the octahedra across Sc5–Sc6. Still lower populations order fairly well with increasing distances, including those within the Sc1, Sc2, Sc3 appendages (0.119–0.069). Another irregularity appears for the Sc6–Sc6 and Sc3–Sc3 interactions along the chain (0.050–0.040), even at 3.92 Å! Finally, the longish 3.48 Å Sc4–Sc4 separations in the zigzag chains have an MOP of only 0.026, followed by still lower populations for all interchain Sc4–ScX contacts. Thus bonding of Sc4 to all other scandium atoms appears to be weak and not an important part of the stability of this compound. Naturally, Sc4 and Sc2 have, in contrast, the largest Sc–Te overlap populations. A charge flow among the rather different types of scandium atoms from Sc–Sc and Sc–Te bonding is reflected in the relative MOP: largest for Sc6 and Sc1, least for Sc4 and Sc2.

Other highly reduced Group 3 chalcogenides of this type are under study, for example, the result of condensation of four chains of edge-sharing octahedra into four-blocks in Sc_9Te_2.[13] A rich and novel chemistry of these chalcogenides is expected by virtue of the conflicts between the electron-poor but metal-rich characteristics.

Experimental Section

Sc_2Te_3 [8] was prepared by reaction of Sc and Te (2:3) in fused SiO_2 at 900 °C for 72 h. A pressed pellet of Sc_2Te_3 and Sc foil with a Sc_2Te stoichiometry was arc-melted for 20 s per side, sealed into a tantalum tube, allowed to react in a vacuum furnace at 1125 °C for 72 h, and cooled at 5 °C h^{-1} to 850 °C. The structure was determined from crystals in the product, which was later shown to be single phase Sc_2Te according to its Guinier pattern [14].

Received: February 24, 1997 [Z10153IE]
German version: *Angew. Chem.* **1997**, *109*, 2062–2064

Keywords: clusters · lanthanides · scandium · solid-state structures · tellurium

[1] T. E. Weirich, A. Simon, R. Pöttgen, *Z. Anorg. Allg. Chem.* **1996**, *622*, 630.
[2] B. Harbrecht, R. Leersch. *J. Alloys Compd.* **1996**, *238*, 13.
[3] R. L. Abdon, T. Hughbanks, *Angew. Chem.* **1994**, *106*, 2414; *Angew. Chem. Int. Ed. Engl.* **1994**, *33*, 2328.
[4] S.-J. Kim, K. S. Nanjundaswamy, T. Hughbanks, *Inorg. Chem.* **1991**, *30*, 159.
[5] B. Harbrecht, *Angew. Chem.* **1989**, *101* 1696; *Angew. Chem. Int.* Ed. Engl. **1989**, *28*, 1660.
[6] H. F. Franzen, *Eur. J. Solid State Inorg. Chem.* **1996**, *33*, 197.
[7] a) K. R. Poeppelmeier, J. D. Corbett, *Inorg. Chem.* **1977**, *16*, 1107; b) H. Mattausch, J. B. Hendricks, R. Eger, J. D. Corbett, A. Simon, *ibid.* **1980**, *19*, 2128; c) J. D. Martin, J. D. Corbett, *Angew. Chem.* **1995**, *107*, 234; *Angew. Chem. Int. Ed. Engl.* **1995**, *34*, 233.
[8] a) A. A. Men'kov, L. N. Komissarova, Ju. P. Simanov, *Dokl. Akad. Nauk. SSSR.* **1961**, *141*, 364; b) J. G. White, J. P. Dismukes, *Inorg. Chem.* **1965**, *4*, 1760.
[9] J. D. Corbett, *J. Alloys Compd.* **1995**, *229*,10.
[10] J. P. Owens, H. F. Franzen. *Acta Crystallogr. Sect. B.* **1974**, *30*, 427.
[11] H. F. Franzen, L. J. Norrby, *Acta Crystallogr. Sect B*, **1968**, *24*, 601.
[12] R. Hoffmann, *J. Chem. Phys.* **1963**, *39*, 1397; M. Whangbo, R. Hoffman, *J. Am. Chem. Soc.* **1978**, *100*, 6093. Energy parameters for scandium (3d, −6.12; 4s, −6.74; 4p, −3.38 eV) were obtained from charge iterative calculations on the smaller Sc_9Te_2 cell [13], and tellurium parameters were taken from ref. [4]. Orbital size parameters were all program default values.
[13] P. A. Maggard, J. D. Corbett, unpublished.
[14] Structure analysis of Sc_2Te: orthorhombic, space group, *Pnma* (no. 62), $Z = 12$, $a = 20.178(5)$, $b = 3.9186(7)$, $c = 10.675(2)$ Å, $V = 844.1(5)$ Å^3 refined from the Guinier powder pattern ($\lambda = 1.540562$ Å, 23 °C); 2229 reflections ($h,k,\pm l$; $2\theta < 54°$) collected on CAD4 diffractometer ($Mo_{K\alpha}$, $\omega - 2\theta$, $\mu = 146.8$ cm^{-1}) from a crystal 0.4 × 0.1 × 0.1 mm. The structure was solved by direct methods (SHELXS [15]) and refined with the package TEXSAN [16]. Anisotropic refinement gave $R(F)/R_w = 0.043/0.055$ with 839 unique reflections ($I_o > 3\sigma I$) and 56 variables; empirical absorption corrections with the aid

 © WILEY-VCH Verlag GmbH, D-69451 Weinheim, 1997 0570-0833/97/3618-1975 $ 17.50+.50/0

of two Ψ-scans and later, after isotropic refinement, DIFABS [17] gave relative transmission coefficients of 0.470–1.00 (R_{av} = 0.042). The largest residual electron density was 2.5 e Å^{-3}, 0.79 Å from Te3. Further details of the structural investigation and results may be obtained from J. D. C. or from Fachinformationszentrum Karlsruhe, D-76344, Eggenstein-Leopoldshafen (Germany) on quoting the depository number CSD-406579.

[15] M. Sheldrick, SHELXS-86, Universität Göttingen, Germany, **1986**.

[16] TEXSAN, version 6.0, Molecular Structure Corp., The Woodlands, Texas, **1990**.

[17] N. Walker, D. Stuart, *Acta Crystallogr. Sect.* A, **1983**, *39*, 158.

Direct Solid-Phase Glycosylations of Peptide Templates on a Novel PEG-Based Resin**

Axel Schleyer, Morten Meldal,* Renil Manat, Hans Paulsen, and Klaus Bock

Currently the most efficient method to synthesize glycopeptides is by solid-phase synthesis with glycosylated amino acid building blocks.[1–5] However, this method requires the preparation of a new glycosyl amino acid building block for each sugar incorporated. For the generation of a multitude of glycopeptides with variation of both sugar and peptide, it might be more efficient to couple the sugar directly and stereoselectively to the free hydroxyl groups of amino acid side chains on the resin-bound peptides. Thus, libraries of libraries could be produced by glycosylation of a preformed peptide library.

It has been demonstrated that solid-phase bound glycopeptides and oligosaccharides with free hydroxyl groups on the oligosaccharide moiety could be glycosylated with different glycosyl trichloroacetimidates.[6, 8] In contrast, attempts to glycosylate free hydroxyl groups of Thr or Ser in peptides bound to a PEGA resin, Tenta Gel, Polyhipe, and Macrosorb with a Rink linker, as well as polystyrene with a Wang linker, have not been successful.[6] However, a recent report described the glycosylation of N-terminal Thr in a tripeptide on solid-phase, albeit in very low yield.[7]

Systematic studies have demonstrated that the properties of the polymer support can have a large influence on the outcome of solid-phase reactions,[9] so such supports cannot be considered a rigid and inert material in the reaction.[10] The support interacts with reactive intermediates and has a significant role in the solid-phase reaction. With the desire to develop polymeric supports with an optimally balanced hydrophilic–hydrophobic character, a new class of cross-linked polymers, the polyethylene glycol polyacrylamide (PEGA) resins, have been introduced for peptide[11] and glycopeptide[1–5] synthesis. Even though these supports were found to be excellent for glycopeptide synthesis with glycosyl amino acid building blocks,[12] it would be preferrable to eliminate the amide backbone from the polymer matrix to facilitate a larger range of organic reactions. This has led to the development of inert PEG cross-linked resin, namely polyoxyethylene–polyoxypropylene (POEPOP), where all the amide linkages present in PEGA are replaced by fairly stable ether linkages, while the optimized balance of hydrophilic–hydrophobic character is retained.[13] PEG-OH was converted into a mixture of mono- and diepoxylated PEG with epichlorohydrin and polymerized by bulk anion-catalyzed polymerization in the presence of *t*BuOK to yield the POEPOP resin. The product was granulated by passing the wet, swollen polymer through a 1 mm sieve. Gel phase ^{13}C NMR showed a high degree of incorporation of PEG into this type of resin. After acid wash and rinsing the polymer support was dried under high vacuum for 24 h and used in the solid-phase synthesis.

A simple pentapeptide was synthesized as a solid-phase glycosyl acceptor on the POEPOP resin with three different linkers that were attached to the resin through a glycine residue to the resins hydroxy groups: **1a** was prepared with Rink linker,[14] **1b** with hydroxymethyl benzoic acid, and **1c** with a UV-labile linker[15] (Scheme 1). The dried acceptors **1a–c** were glycosylated with perbenzoylated galactopyranosyl trichloroacetimidate (**2**, 8 equiv)[16] in dichloromethane over a few pellets of molecular sieves with slow agitation at room temperature to afford the resin bound glycopeptides **3a–c**. These standard reaction conditions were also used for all the reactions described below. Cleavage of small resin aliquots and TLC analysis of the

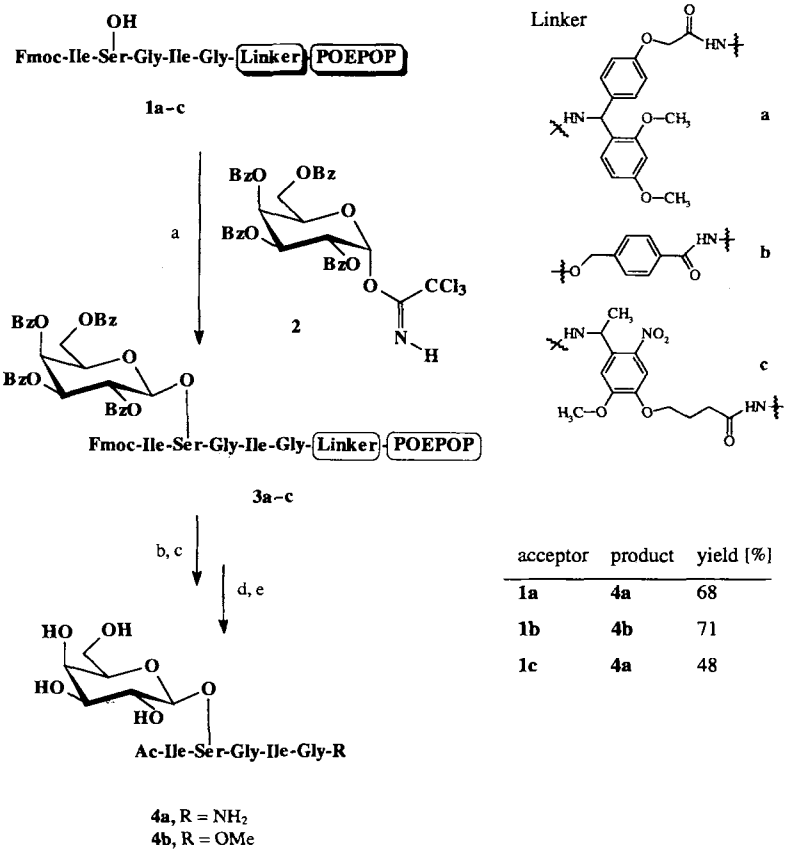

acceptor	product	yield [%]
1a	**4a**	68
1b	**4b**	71
1c	**4a**	48

Scheme 1. Three different linkers were used in the glycosylation of peptides on POEPOP resin. a) Bz_4-α-D-Gal-TCA, TMS-OTf, CH_2Cl_2; b) piperidine; c) Ac_2O; d) 1. 95% TFA, 2. NaOMe/MeOH, 3. *hν* (250–350 nm); e) NaOMe/MeOH. TCA = trichloroacetimidate.

[*] Prof. Dr. M. Meldal, Dr. A. Schleyer, Dr. M. Renil, Prof. Dr. K. Bock
Department of Chemistry, Carlsberg Laboratory
Gamle Carlsberg Vej 10, DK-2500 Valby, Copenhagen (Denmark)
Fax: Int. code +3327-4708
Prof. Dr. H. Paulsen
Institut für Organische Chemie
Universität Hamburg (Germany)

[**] This work was supported by the EU-Science program (grant SCI*-CT92-0765).

 © WILEY-VCH Verlag GmbH, D-69451 Weinheim, 1997 0570-0833/97/3618-1976 $ 17.50+.50/0

product showed the glycosylation to be complete within 24 h. After completion of assembly, N-terminal acetylation, cleavage from the resin, and deprotection, the corresponding glycopeptides **4a** and **4b** were obtained in 48–71% yield (based on the acceptor peptide). A ROESY connectivity between Gal^{H1} and $Ser^{H\beta}$ confirmed the glycosidic linkage (Figure 1). In all three cases quantitative glycosylation could be achieved. The lower yield (48%) of the glycopeptide synthesized on the UV-labile-linker was due to side reactions during the UV-cleavage.

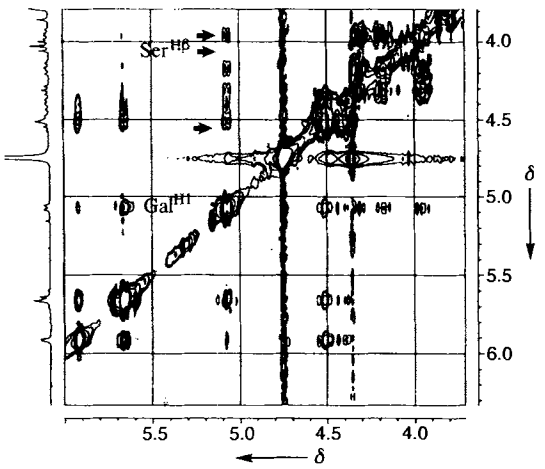

Figure 1. ^{1}H NMR ROESY spectrum of Ac-IS(Bz_4Gal-β)GIG-NH_2. The cross-peaks of the anomeric proton (δ = 5.1) and the $Ser^{H\beta}$ (δ = 3.95 and 4.2) indicates the connectivity between Gal^{H1} and $Ser^{H\beta}$. Fmoc = 9-fluorenylmethoxycarbonyl.

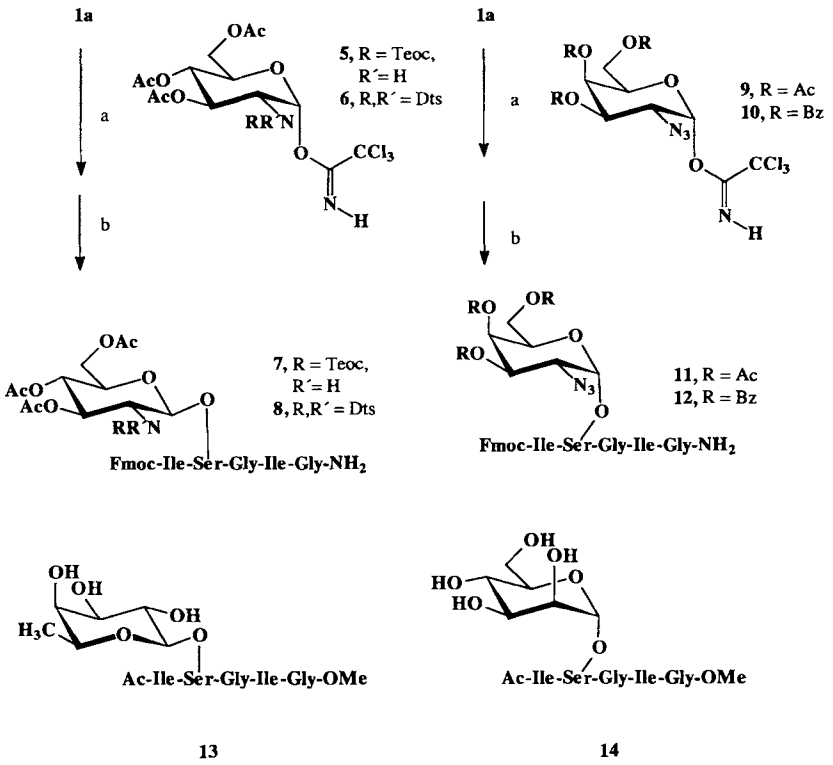

Scheme 2. Stereoselective β- and α-glycosylations of peptides with amino sugars on solid phase with TCAs and TMS-OTf. a) 0.1 equiv TMSOTf in CH_2Cl_2, b) TFA/H_2O, HPLC. β-L-Fucopyranoside (**13**) and α-L-mannopyranoside (**14**) were prepared analogously.

The protection of the 2-amino group of the 2-aminoglucopyranosyl donors is important, since the stereoselectivity of the β-glycosylation and deprotection under mild conditions has to be controlled. The trichloroethoxycarbonyl (Teoc) and the *N*-dithiasuccinyl groups (Dts) are best suited for this 2-amino protection. The acceptor peptide **1a** was glycosylated for 1.5 h (monitored by thin-layer chromatography (TLC)) with the protected 2-amino-2-deoxyglucopyranosyl trichloroacetimidates **5**[17,18] and **6**[19,20] (5 equiv, Scheme 2), and the products were cleaved with 95% trifluoroacetic acid (TFA). The corresponding protected *N*-acetyl-2-amino-2-deoxy-β-D-glucopyranosyl peptides **7** and **8** were obtained in a yield of 53% and 74%, respectively.

The perbenzoylated and peracetylated 2-azido-2-deoxy-α-D-galactopyranosyl trichloroacetimidates **9** and **10** were selected as glycosyl donors to form an α-linkage between the 2-acetamido-2-deoxy-α-D-galactopyranose and acceptor peptide **1a**. The 2-azido-2-deoxyglycosyl donors did not undergo neighboring group participation in the 2-position and led to the corresponding α-glycosylated products. After glycosylation for 2.5 h (monitored by TLC), cleavage with 95% TFA afforded the corresponding protected glycopeptides **11** and **12** in yields of 41% and 78%, respectively (based on the acceptor).

Glycosylation of acceptor **1b** was performed with 8 equivalents of the peracetylated trichloroacetimidates of D-mannose (1 h) and L-fucose (30 min) with trimethylsilyltrifluoromethanesulfonate (TMSOTf, 0.1 equiv) in CH_2Cl_2 at room temperature. Cleavage of the Fmoc group with piperidine in DMF, followed by N-acetylation and treatment with MeOH/NaOMe at pH 9–10, gave cleavage from the resin, and the corresponding glycopeptides **13** and **14** were isolated in 68% and 62% yields, respectively (based on the acceptor).

This method of synthesizing glycopeptides would be more versatile and useful for the synthesis of glycopeptide libraries if more than one free hydroxyl group on the peptide backbone could be glycosylated simultaneously. Therefore, four different acceptor peptides **15a–d** were synthesized in a combinatorial approach. After cleavage of the Fmoc group the obtained free amine was benzoylated with benzoic acid, *O*-(1*H*-benzotriazol-1-yl)-1,1,3,3-tetramethyluronium tetrafluoroborate (TBTU) and *N*-ethyl morpholine (NEM) in THF (Scheme 3). Each of the compounds were first glycosylated in two cycles with perbenzoylated D-galactosyl trichloroacetimidate (**2**, 4 equiv, 24 h) under the standard conditions determined above. The resin was washed carefully with dichloromethane and treated with TFA (95%) for 90 min to remove any remaining *tert*-butyl ether groups. After washing with dichloromethane and drying, the acceptor resin was subjected to a second glycosylation with two cycles of peracetylated L-fucosyl trichloroacetimidate (4 equiv, 30 min). Cleavage from the resin with NaOMe yielded the four different glycopeptides **16a–d**. The products were separated by preparative reversed phase HPLC and were analyzed by one- and two-dimensional ^{1}H NMR spectroscopy and matrix-assisted laser-desorption time-of-flight mass spectrometry (MALDI-TOF-MS). The products contained the expected β-galacto- and β-fucosylated glycopeptides (Table 1).[21]

The method of solid-phase glycoslation on POEPOP resin is a powerful tool for synthesizing a variety of glycopeptides and a valuable alternative in many respects for the introduction of one or several monosaccharides into a peptide template. On Rink-linker-bound glycosyl acceptor peptides, stereoselective β-glycosidation with perbenzoylated or peracetylated trichloroacetimidates of galactose, 2-deoxy-2-dithiosuccimidoglucopyranose and 2-deoxy-2-trichloroethoxycarbamido-D-glucopyra-

 © WILEY-VCH Verlag GmbH, D-69451 Weinheim, 1997 0570-0833/97/3618-1977 $ 17.50+.50/0

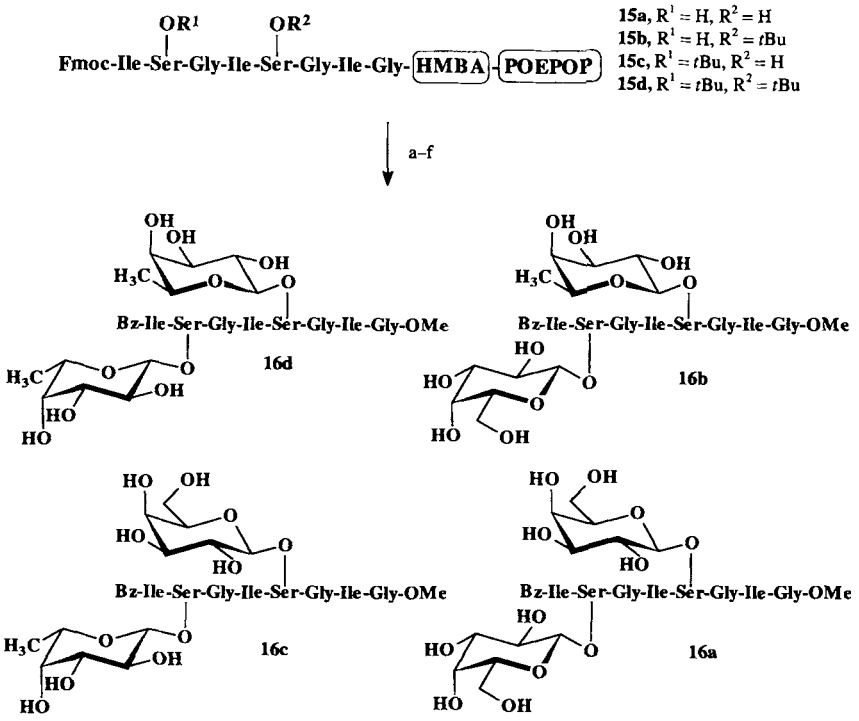

Scheme 3. Synthesis of a small library of glycopeptides by two consecutive, direct glycosylations of a mixture of solid phase-bound peptides. a) Piperidine/DMF; b) BzOH, TBTU, NEM; c) Bz_4Gal-TCA, TMS-OTf; d) TFA/H_2O; e) Ac_3Fuc-TCA, TMS-OTf; f) NaOMe/MeOH.

Table 1. Masses (m/z) of purified compounds determined by MALDI-TOF-MS.

Compound	m/z [M + Na^+]	Compound	m/z [M + Na^+]
4a	670.8	**14**	686.9
4b	689.2	**16a**	1169.7
7	1152.4	**16b**	1154.2
8	1095.1	**16c**	1154.2
11	1002.5	**16d**	1136.7
13	671.8		

nose gave the corresponding glycopeptides in high yields after cleavage. The protected β-galactopyranosyl peptide was deprotected in solution to yield the unprotected D-galactopyranosyl peptide. With perbenzoylated or peracetylated 2-azido-2-deoxy-α-D-galactopyranosyl trichloroacetimidate, the corresponding α-glycosylated products were formed in good yields.

On peptides attached through a HMBA-linker, glycosylation reactions with peracetylated trichloroacetimidates of L-fucopyranose, D-mannopyranose, and D-galactopyranose afforded the corresponding unprotected glycopeptides upon cleavage with NaOMe. *tert*-Butyl ether protecting groups were sufficiently stable when short glycosylation times could be employed. Longer reaction times resulted in some cleavage of *t*Bu, particularly from *tert*-butyl esters (data not presented). Use of temporary *t*Bu-protection of some serine hydroxy groups led to quantitative glycosylation of a model library consisting of four different octapeptide templates with two different glycosyl acceptor sites. The peracetylated trichloroacetimidates of L-fucose and D-galactopyranose were used in two sequential glycosylation steps to produce the four different unprotected glycopeptides obtained after cleavage from the resin.

Received: March 5, 1997 [Z10204IE]
German version: *Angew. Chem.* **1997**, *109*, 2064–2067

Keywords: compound libraries · glycopeptides · glycosylations · solid-phase synthesis

[1] S. Lavielle, N. C. Ling, R. C. Guillemin, *Carbohydr. Res.* **1981**, *89*, 221–228; H. Paulsen, G. Merz, U. Weichert, *Angew. Chem.* **1988**, *100*, 1425–1427; *Angew. Chem. Int. Ed. Engl.* **1988**, *27*, 1365–1367; H. Kunz, B. Dombo, *ibid.* **1988**, *100*, 732–734 bzw. **1988**, *27*, 711–713; M. Meldal, K. J. Jensen, *J. Chem. Soc. Chem. Commun.* **1990**, 483–485;
[2] S. Peters, T. Bielfeld, M. Meldal, K. Bock, H. Paulsen, *J. Chem. Soc. Perkin Trans 1* **1992**, 1163–1171.
[3] M. Meldal, *Curr. Opin. Struct. Biol.* **1994**, *4*, 710–718.
[4] M. Meldal in *Neoglyconjugate: Preperation and Applications* (Eds.: Y. C. Lee, R. T. Lee), Academic Press, San Diego, **1994**, pp. 145–198.
[5] H. Paulsen, S. Peters, T. Bielfeld in *Glycoproteins: Chemical Synthesis of Glycopeptides* (Eds.: J. Montreuil, J. F. G. Vliegenthart, H. Schachter), Elsevier, Amsterdam, **1995**, pp. 87–121.
[6] H. Paulsen, A. Schleyer, N. Mathieux, M. Meldal, K. Bock, *J. Chem. Soc. Perkin Trans. 1* **1997**, 281–293.
[7] O. Seitz, H. Kunz, *J. Org. Chem.* **1997**, *62*, 813–826.
[8] L. Yan, L. C. M. Taylor, R. Goodnow, Jr., D. Kahne, *J. Am. Chem. Soc.* **1994**, *116*, 6953–6954.
[9] M. Meldal in *Methods of Enzymology: Solid-Phase Peptide Synthesis* (Ed.: G. Fields), Academic Press, San Diego, **1997**, in press.
[10] R. C. Sheppard, *Science Tools* **1986**, *33*, 9–16.
[11] M. Meldal, *Tetrahedron Lett.* **1992**, *33*, 3077–3080.
[12] M. Meldal, K. Bock, *Glycoconjugate J.* **1994**, *11*, 59–63.
[13] M. Renil, M. Meldal, *Tetrahedron Lett.* **1996**, *37*, 6185–6188.
[14] H. Rink, *Tetrahedron Lett.* **1987**, *28*, 3787–3790.
[15] C. P. Holmes, D. Jones, *J. Org. Chem.* **1995**, *60*, 2318–2319.
[16] R. R. Schmidt, W. Kinzy, *Adv. Carbhydr. Chem. Biochem.* **1994**, 21–123; S. Rio, J.-M. Beau, J.-C. Jacquinet, *Carbohydr. Res.* **1991**, *219*, 71–90.
[17] T. M. Windholz, B. R. Jonston, *Tetrahedron Lett.* **1967**, 2555–2558.
[18] H. Paulsen, B. Helpap, *Carbohydr. Res.* **1991**, *216*, 289–313.
[19] E. Meinjohans, M. Meldal, H. Paulsen, K. Bock, *J. Chem. Soc. Perkin Trans 1* **1995**, 405–415.
[20] G. Barany, R. B. Merrifield, *J. Am. Chem. Soc.* **1977**, *99*, 7363–7365.
[21] The ^{1}H NMR spectrum indicated the equal formation of Bz-IS(Fuc)GIS-(Gal)GIG-OMe and Bz-IS(Gal)GIS(Fuc)GIG-OMe (eluted from HPLC as a single peak). The combination of the corresponding COSY and NOESY spectra showed the NOE cross-peaks of the Fuc^{H1}/Gal^{H1} and the Ser-H^b at δ = 4.0, 3.9, 3.8, and 3.7 indicate the linkage of the sugar units to the Ser-hydroxy groups.

Multicomponent Self-Assembly: Preferential Generation of a Rectangular [2 × 3]G Grid by Mixed-Ligand Recognition**

Paul N. W. Baxter, Jean-Marie Lehn,* Boris O. Kneisel, and Dieter Fenske

Self-assembly processes offer a particularly attractive method for preparing nanosized supramolecular devices in that the required structural complexity of such entities can be accessed in

[*] Prof. Dr. J.-M. Lehn, Dr. P. N. W. Baxter
Laboratoire de Chimie Supramoléculaire, Institut Le Bel
Université Louis Pasteur, CNRS URA 422
4, rue Blaise Pascal, F-67000 Strasbourg (France)
Fax number: Int. code + 3 884-110
e-mail: lehn@chimie.u-strasbg.fr
B. O. Kneisel, Prof. Dr. D. Fenske
Institut für Anorganische Chemie der Universität Karlsruhe (Germany)

[**] We thank Patrick Maltèse for the ROESY and ^{109}Ag NMR measurements.

 © WILEY-VCH Verlag GmbH, D-69451 Weinheim, 1997 0570-0833/97/3618-1978 $ 17.50+.50/0

a single step from a mixture of suitably tailored molecular components.[1-4] The generation of multimetallic arrays by metal ion directed self-assembly is especially interesting in this respect, as the presence of metal ions may endow the resulting inorganic architecture with novel redox, optical, magnetic, and other properties. Recent examples from this class of compounds include helicates,[3, 5] cages,[6] rotaxanes,[7] and grids.[8, 9] The formation of a [3 × 3]G silver grid[8] demonstrated the feasibility of self-assembling two-dimensional square [$n \times n$] arrays of metal ions ($n = 3$), which may be considered as ion dots. Following the generation of [$n \times n$]G symmetrical grids, their rectangular [$m \times n$]G counterparts are especially attractive synthetic targets, as they constitute a potentially much larger class of compounds, and may therefore present a greater diversity of properties and possible applications.

We herein report the formation of the first example of the rectangular grid **1**, which spontaneously and preferentially self-assembles upon combination of tri- and ditopic ligands **2** and **3** with $AgCF_3SO_3$ in a 2:3:6 stoichiometric ratio in nitromethane (Scheme 1); minor amounts of the corresponding square grids

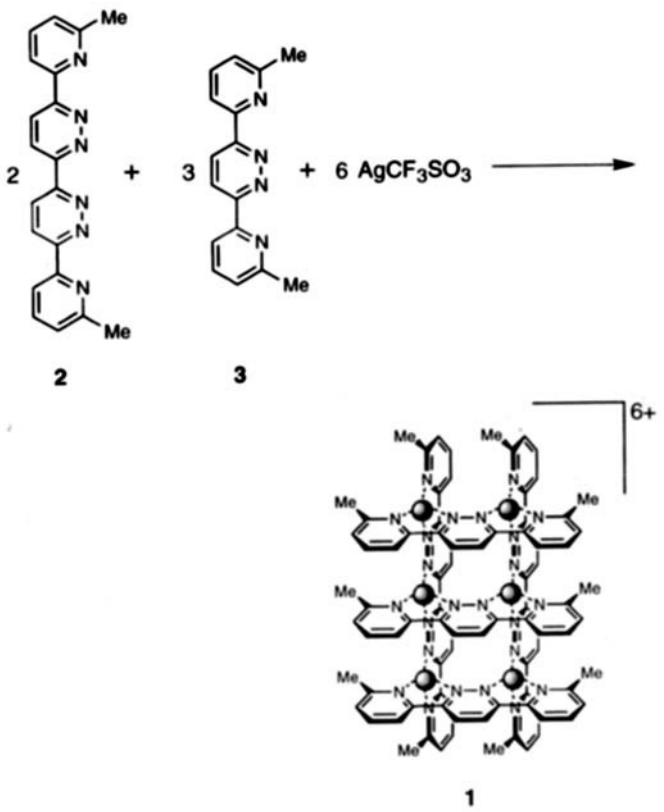

Scheme 1. Self-assembly of the rectangular [2 × 3]G grid complex **1**; the spheres represent Ag^I ions.

are also found (see Scheme 2). The structural formulation of the product as **1**·$(CF_3SO_3)_6$ is based on elemental analysis, X-ray crystallography, and ^1H, ^{13}C, and ^{109}Ag NMR spectroscopy. The product incorporates a two dimensional [2 × 3]G rectangular array of six silver(I) ions, and therefore represents the first member of a homologous series of [$m \times n$]G rectangular grids ($m \neq n$).

The ^1H NMR spectrum[10] of the solution obtained by dissolving **2**, **3**, and $AgCF_3SO_3$ in a 2:3:6 ratio in CD_3NO_2 gave the first indication of structure **1**. The spectrum is clean and free from overlapping bands. Ligand **2** is situated in a single chemical and magnetic environment, as indicated by five aromatic signals in a 2:2:2:2:2 ratio, which correspond to the H3, H4, and H5 protons of the outer pyridine rings and the H4′ and H5′ protons of the inner pyridazine rings. Ligand **3** appears as two sets of signals in a 2:1 ratio, each set comprising four bands due to the H3, H4, and H5 protons of the pyridine rings and the equivalent H4′/H5′ protons on the pyridazine ring. This pattern is consistent with two outer and one inner ligands **3** in **1**. The CH_3 protons give three peaks in a 6:6:3 ratio, which is also indicative of **2** in a single and **3** in two different environments in a ratio of 2(**2**):2(**3**):1(**3**). In addition, the pyridazine H4′/H5′ singlet of the inner **3** ligand is shifted upfield relative to that of the outer two **3** ligands. This shielding effect is what would be expected for protons on a ring situated within structure **1**. The ^{109}Ag NMR spectrum shows two signals in a 2:1 ratio corresponding to four outer and two inner Ag^+ ions, respectively.

An X-ray crystal structural determination[11] of the reaction product confirmed the structure as **1**·$(CF_3SO_3)_6$ (Figure 1). The

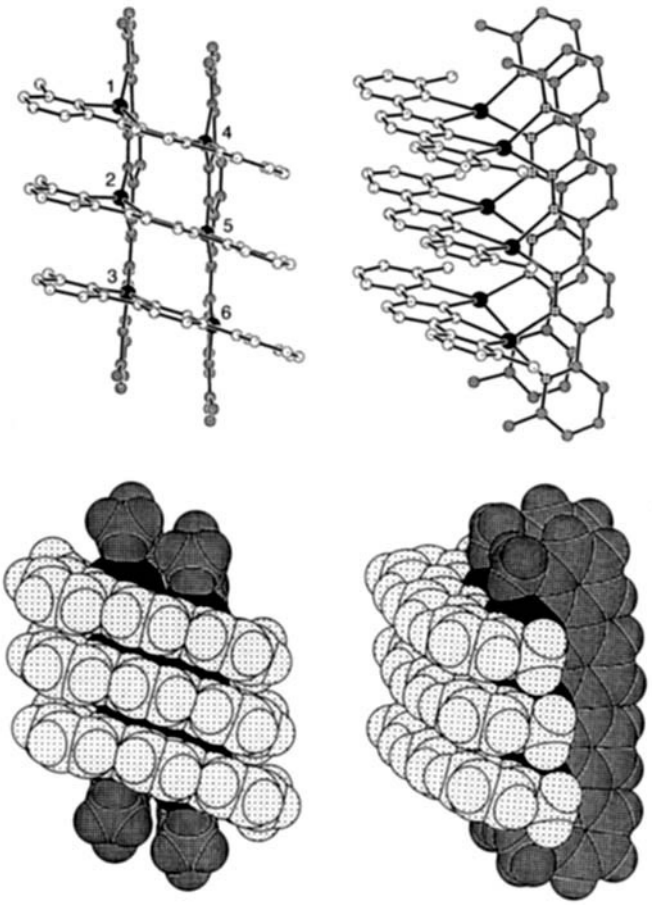

Figure 1. Two views of the crystal structure of the self-assembled [2 × 3]G rectangular grid $[Ag_6(\mathbf{2})_2(\mathbf{3})_3]^{6+}$ (**1**): ball-and-stick (top) and space-filling representations (bottom).

crystals consist of $[Ag_6(\mathbf{2})_2(\mathbf{3})_3]^{6+}$ ions, uncoordinated triflate anions, as well as nitromethane and water molecules. The six silver ions in **1** are arranged in the form of a 2 × 3 rhombohedrally distorted rectangular matrix. The dihedral angle described by the rhombus (between the mean planes of ligands **2** and **3**) is about 66°, and the average Ag–Ag separation is 3.75 Å. The vertex silver ions Ag1, Ag3, Ag4, and Ag6 lie almost in a plane with distances Ag1–Ag4 3.79, Ag1–Ag3 7.63, Ag3–Ag6 3.72, and Ag4–Ag6 7.45 Å, and inner angles Ag4-Ag1-Ag3 65 and

 © WILEY-VCH Verlag GmbH, D-69451 Weinheim, 1997 0570-0833/97/3618-1979 $ 17.50+.50/0

Ag1-Ag4-Ag6 115°. The six silver ions define a slightly U-shaped surface along the longer axis of **1**, in which Ag2 and Ag5 lie 0.19 and 0.25 Å, respectively, above the mean plane through Ag1, Ag3, Ag4, and Ag6. All the silver ions possess a distorted tetrahedral coordination polyhedron with an average dihedral angle of 71° between the N-Ag-N planes of ligands **2** and **1**. The four vertex silver ions are each coordinated to two pyridine and two pyridazine nitrogen atoms (mean Ag–N 2.30 Å), and the two central Ag ions to one pyridine and three pyridazine nitrogen atoms (mean Ag–N 2.35 Å). This situation is reflected in the ^{109}Ag NMR spectrum of **1**, in which the signal due to the vertex Ag ions is shifted downfield by $\Delta\delta = 59$ ppm from that of the central Ag ions. This is in agreement with the chemical shifts observed for a [3 × 3]G nonasilver grid.[8]

The five ligands in **1** are divided into two sets comprising two units of **2** and three units of **3** lying above and below the mean plane through the six Ag^I ions. Each ligand forms a slightly twisted blade conformation due, in part, to the summed effects of intra-ligand steric repulsions (maximum dihedral inter-ring twist angle 12°). The average distance between the ligand mean planes is 3.36 Å and therefore slightly larger than the van der Waals contact distance of about 3.4 Å. The overall dimensions of **1** are 15.19 × 11.07 Å, which places the grid just within the nanostructural domain. The shortest distance between the grid cations within the crystal lattice is 3.4 Å.

The spectroscopic and crystallographic evidence unambiguously supports the identity of the product from the reaction of **2**, **3**, and $AgCF_3SO_3$ in a 1:1.5:3 ratio as that of hexanuclear rectangular [2 × 3]G grid **1** both in solution and in the solid state. Complex **1** forms spontaneously by the self-assembly of eleven particles, that is, five ligand components of two types and six silver ions. On the basis of the instructions contained in the ligands and the coordination algorithm of the metal-ion connectors, the mixed-component process by which a rectangular grid is generated represents a step further in complexity in terms of information content with respect to the formation of symmetric [$n \times n$]G grids, which involves only a single ligand species.

The preferential formation of a mixed-ligand entity is especially noteworthy, as the system made up of **2**, **3**, and Ag^+ in a 1:1.5:3 ratio has the potential to give three different product distributions (Scheme 2): 1) statistical distribution, 2) homo ligand recognition in which ligands only recognize individuals of their own identity to yield [2 × 2]G and [3 × 3]G symmetrical grids, and 3) hetero ligand assembly, that is, selective association between ligands of different type resulting in the generation of **1**. Upon completion of the reaction, **1**·$(CF_3SO_3)_6$ coexists in CD_3NO_2 with a mixture of 8% $[Ag_4(\mathbf{3})_4](CF_3SO_3)_4$ and 2% $[Ag_9(\mathbf{2})_6](CF_3SO_3)_9$, as indicated by the ^{1}H NMR spectrum of the solution. This ratio appears to be independent of concentration. Helicate mixtures exhibit either partial or exclusive homo ligand recognition.[14, 15] The preference for hetero over homo ligand recognition in the case of **1** may derive in part from an avoidance to form the [3 × 3]G complex, which possesses the least stable metal–ligand coordination site, that is, the central $Ag(pyridazine)_4$ unit. Solvation and thermodynamic considerations also play a role. An understanding of the factors which result in a preference for hetero over homo ligand assembly will be of great importance for the future design of disymmetric metal-ion arrays.

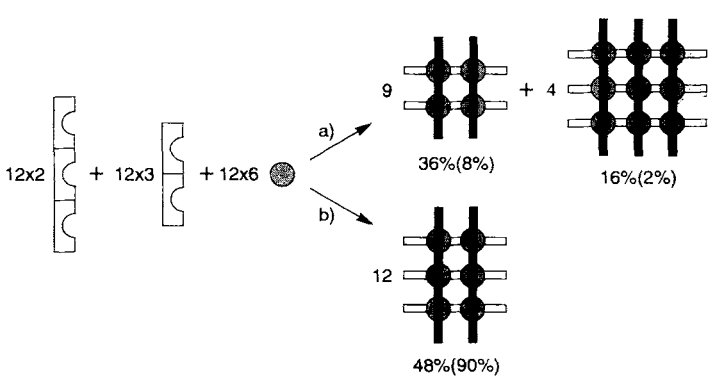

Scheme 2. Possible self-assembly pathways for **2**, **3**, and Ag^+ in a 2:3:6 ratio: a) homo and b) hetero ligand selection; statistically expected values and actual yields (in parentheses) are given for both cases.

The successful preparation of **1** opens the way to metal ion mediated self-assembly of nonsymmetric [$m \times n$]G ion grids ($m \geq 2$, $n \geq 3$, and $m \neq n$ for m and n binding sites). Because such disymmetric grids must, by definition, be mixed-ligand species, they present a larger variety of possible combinations of the ligands involved than their symmetric [$n \times n$]G congeners. Therefore, they could find a greater number of applications, for example as components within a futuristic information storage and processing nanotechnology. To uncover and exploit the novel physicochemical properties that such systems may possess, detailed investigations into electronic, magnetic, surface chemical, and interfacial behavior will be necessary. Furthermore, methods for the fabrication of polynuclear architectures of higher dimensionality and techniques for their incorporation into larger organized superstructures may also be envisioned.

Experimental Section

Nitromethane (3 mL) was added to **2** (0.026 g, 7.64×10^{-5} mol), **3** (0.030 g, 1.14×10^{-4} mol), and $AgCF_3SO_3$ (0.059 g, 2.30×10^{-4} mol), and the mixture subjected to brief ultrasonication. All suspended solids rapidly dissolved to give a yellow solution, which was stirred at room temperature for 36 h and then filtered. The solvent was removed under reduced pressure. The remaining solid was suspended in benzene (8 mL), homogenized by brief ultrasonication, isolated by filtration under vacuum, washed with excess benzene, and dried in the air and then under vacuum at 2×10^{-6} mm Hg and 70 °C. The yellow powder obtained (yield 0.114 g, 99%) could be either pure **1**·$(CF_3SO_3)_6$ or a mixture with the square grids; it was recrystallized quantitatively from nitromethane/benzene [10, 11].

1·$(CF_3SO_3)_6$: ^{1}H NMR (CD_3NO_2, 500 MHz, 25 °C): $\delta = 9.146$ (d, $J(5',4') = 9.4$ Hz, H5′ (**2**)), 9.081 (d, $J(4',5') = 9.4$ Hz, H4′ (**2**)), 8.774 (s, H4′ (outer **3**)), 8.575 (s, H4′ (inner **3**)), 8.264 (d, $J(3,4) = 8.2$ Hz, H3 (**2**)), 8.171 (d, $J(3,4) = 8.0$ Hz, H3 (outer **3**)), 7.977 (t, $J(3,4,5) = 7.9$ Hz, H4 (**2**)), 7.914 (t, $J(3,4,5) = 7.9$ Hz, H4 (outer **3**)), 7.816 (d, $J(3,4) = 8.0$ Hz, H3 (inner **3**)), 7.691 (t, $J(3,4,5) = 7.9$ Hz, H4 (inner **3**)), 7.438 (d, $J(5,4) = 7.7$ Hz, H5 (**2**)), 7.353 (d, $J(5,4) = 7.7$ Hz, H5 (outer **3**)), 7.211 (d, $J(5,4) = 7.7$ Hz, H5 (inner **3**)), 2.373 (s, CH_3 (inner **3**)), 2.258 (s, CH_3 (**2**)), 2.244 (s, CH_3 (outer **3**)). All of the protons assigned represent a symmetric pair of protons on each ligand. ^{13}C NMR (CD_3NO_2, 75 MHz, 25 °C): $\delta = 161.20$, 161.01, 160.83, 158.11, 156.38, 155.28, 153.70, 147.26, 147.05, 145.82, 142.91, 142.20, 142.16, 132.37, 132.31, 131.23, 131.08, 129.98, 129.90, 129.50, 123.81, 123.30, 123.17; 28.40, 27.53, 27.38 (CH_3); 124.59, 120.34 ($CF_3SO_3^-$); ^{109}Ag NMR (CD_3NO_2, 18.625 MHz, 25 °C): $\delta = 572.63$ (Ag, vertex), 513.12 (Ag, central); elemental analysis calcd for $C_{94}H_{74}Ag_6F_{18}N_{24}O_{18}S_6$: C 37.52, H 2.48, N 11.17; found: C 37.35, H 2.61, N 11.32.

Received: March 10, 1997 [Z10219IE]
German version: *Angew. Chem.* **1997**, *109*, 2067–2070

Keywords: coordination modes · multinuclear complexes · N ligands · self-assembly · silver

[1] J. S. Lindsey, *New J. Chem.* **1991**, *15*, 153.
[2] D. S. Lawrence, T. Jiang, M. Levett, *Chem. Rev.* **1995**, *95*, 2229.
[3] J.-M. Lehn, *Supramolecular Chemistry: Concepts and Perspectives*, VCH, Weinheim, **1995**, chap. 9.
[4] D. Philp, J. F. Stoddart, *Angew. Chem.* **1996**, *108*, 1242; *Angew. Chem. Int. Ed. Engl.* **1996**, *35*, 1154.
[5] E. C. Constable, *Tetrahedron* **1992**, *48*, 10013; K. T. Potts, M. Keshavarz-K, F. S. Tham, H. D. Abruña, C. Arana, *Inorg. Chem.* **1993**, *32*, 4436, and references therein.
[6] a) P. N. W. Baxter, J.-M. Lehn, A. De Cian, J. Fischer, *Angew. Chem.* **1993**, *105*, 92; *Angew. Chem. Int. Ed. Engl.* **1993**, *32*, 69; b) M. Fujita, S. Nagao, K. Ogura, *J. Am. Chem. Soc.* **1995**, *117*, 1649.
[7] H. Sleiman, P. N. W. Baxter, J.-M. Lehn, K. Rissanen, *J. Chem. Soc. Chem. Commun.* **1995**, 715.

 © WILEY-VCH Verlag GmbH, D-69451 Weinheim, 1997 0570-0833/97/3618-1980 $ 17.50+.50/0

[8] P. N. W. Baxter, J.-M. Lehn, J. Fischer, M.-T. Youinou, *Angew. Chem.* **1994**, *106*, 2432; *Angew. Chem. Int. Ed. Engl.* **1994**, *33*, 2284.
[9] M.-T. Youinou, N. Rahmouni, J. Fischer, J. A. Osborn, *Angew. Chem.* **1992**, *104*, 771; *Angew. Chem. Int. Ed. Engl.* **1992**, *31*, 733.
[10] ^{1}H NMR spectral assignments were made on the basis of ^{1}H–^{1}H ROESY and COSY measurements. The spectra of the crude and recrystallized materials were identical, indicating that the different grid species present equilibrate. In addition, mixing preformed [2 × 2] and [3 × 3] square grids in the correct ratios generates an equilibrium solution giving the same NMR spectrum. The fact that the species has higher symmetry in solution (NMR spectroscopy) than in the solid state (crystal structure analysis) may be attributed to fast exchange between the two rhombohedral enantiomers, as noted previously [8].
[11] Yellow crystals were grown by slow diffusion of benzene into a solution of **1**·$(CF_3SO_3)_6$ in nitromethane at 20 °C. Crystal data for $\{2[Ag_6(\mathbf{2})_2(\mathbf{3})_3]\cdot 12(O_3SCF_3)\cdot 2C_6H_6\cdot 7H_3CNO_2\cdot 1C_6H_{14}\}$: crystal size 0.1 × 0.1 × 0.2 mm; STOE-IPDS diffractometer with graphite monochromater, $T = -80$ °C, $Mo_{K\alpha}$ radiation ($\lambda = 0.71073$ Å); monoclinic, space group $P2/n$, $a = 29.961(6)$, $b = 21.534(4)$, $c = 38.827(8)$ Å, $V = 25032(9)$ Å^3, $Z = 4$, $\mu = 1.128$ mm^{-1}, $F(000) = 13092$, $\rho_{calcd} = 1.753$ Mg m^{-3}, $M_r = 6604.99$, $2\theta_{max} = 48°$. The primary structure was solved and refined by direct methods (SHELXS-92) [12]. All non-hydrogen atoms except those of some heavily disordered solvent molecules were refined anisotropically (SHELXL-93) [13]. A riding model starting from calculated positions was employed for the hydrogen atoms; due to disorder no hydrogen positions were calculated for solvent molecules. Of 107065 reflections measured 38400 were independent (R(int) = 0.0659), of which 38368 were employed in the refinement of 3795 parameters. Triflate ions and solvent molecules partially show heavy disorder, which could be successfully modeled by use of geometry restraints (planarity, chemically equivalent 1,2-/1,3-distances, and "anti-bumping" principles) and ADP restraints (rigid-bond, similarity, and isotropy). $O_3SCF_3^-$ ions: restraints on S-O (1.42 Å), S-C (1.82 Å), and C-F (1.32 Å) bond lengths. For disordered triflate ions displacement parameters of fluorine and oxygen positions were equated for each split position by means of constraint. N-C and N-O distances in nitromethane were fitted to target values of 1.55 and 1.20 Å, respectively; benzene molecules were refined as variable metric groups; C-C bonds in *n*-hexane were fitted to target values of 1.54 Å. The structure was refined against F^2 (full-matrix-block least squares). Weighting scheme: $w^{-1} = \sigma 2(F_o^2) + (0.0939P)^2 + 172.5727P$, with $P = (F_o^2 + 2F_c^2)/3$, $R1 = 0.0732$ ($F > 4\sigma F$) and $wR2 = 0.2146$ (all data), GOF ($F^2 = S$) = 1.106, max/min residual density +2.34/−1.25 e Å^{-3}, $(R1 = \sum||F_o| - |F_c||/\sum|F_o|$, $wR2 = [\sum w(F_o^2 - F_c^2)^2/\sum wF_o^4]^{1/2}$, GOF = $S = \{\sum[w(F_o^2 - F_c^2)^2]/(n-p)\}^{1/2}$, where n = no. of reflections, and p = no. of parameters). Crystallographic data (excluding structure factors) for the structures reported in this paper have been deposited with the Cambridge Crystallographic Data Centre as supplementary publication no. CCDC-100391. Copies of the data can be obtained free of charge on application to The Director, CCDC, 12 Union Road, Cambridge CB21EZ, UK (fax: int. code +(1223) 336-033; e-mail: deposit@chemcrys.cam.ac.uk).
[12] G. M. Sheldrick, *Acta Crystallogr. Sect. A*, **1990**, *46*, 467.
[13] G. M. Sheldrick, SHELXL-93, program for crystal structure refinement, University of Göttingen, **1993**.
[14] R. Krämer, J.-M. Lehn, A. Marquis-Rigault, *Proc. Natl. Acad. Sci. USA* **1993**, *90*, 5394; D. P. Funeriu, Y.-B. He, H.-J. Bister, J.-M. Lehn, *Bull. Soc. Chim. Fr.* **1996**, *133*, 673.
[15] Heterostrand helicates were obtained with pentacoordinate Cu^{II} ions: B. Hasenknopf, J.-M. Lehn, G. Baum, D. Fenske, *Proc. Natl. Acad. Sci. USA* **1996**, *93*, 1397.

New Copper Telluride Clusters by Light-Induced Tellurolate–Telluride Conversions**

John F. Corrigan and Dieter Fenske*

There is currently considerable interest in the chemistry of metal selenolate and tellurolate complexes,[1] driven in part by their potential utility as single-source precursors for semiconducting binary- and ternary-phase materials.[2] Homoleptic $[M(ER)_2]$ (M = metal, E = chalcogen) complexes decompose with elimination of ER_2 and formation of the corresponding binary solid materials "ME".[3a] Studies in this area have included chalcogenolate complexes of Group 12 elements,[3] and recent efforts have focused on related lanthanide,[4] early transition metal,[5] and main group complexes.[6]

Despite the abundance of research activity in this area, structural reports detailing the manner in which the molecule → bulk transformation occurs are scarce. Arnold et al. described the Lewis base induced conversion of early transition metal selenolate and tellurolate complexes into selenide- and telluride-containing molecules as the first step towards extended solids from molecular precursors.[5] Piers and co-workers also detailed the reversible elimination of dialkyl tellurium from permethyl scandocene tellurolates to yield the dimeric telluride complex $[(Cp^*_2Sc)_2(\mu\text{-Te})]$ ($Cp^* = C_5Me_5$).[7] We set out to exploit this reactivity to access high nuclearity metal telluride clusters. Here we report on the elimination of $TePh_2$ from the phosphane-stabilized copper(I) tellurolate **1**, and its concomitant condensation to yield the mixed telluride/tellurolate cluster **2**.

$[Cu_6(\mu\text{-TePh})(\mu_3\text{-TePh})_5(PEtPh_2)_5]$ **1**

$[Cu_{50}(\mu_3\text{-TePh})_{20}Te_{17}(PEtPh_2)_8][PEtPh_3]_4$ **2**

CuCl readily dissolves in ethers with excess phosphane. When a solution of CuCl and PPh_2Et (1:2) in THF/Et_2O is allowed to react with the silylated tellurium reagent $Te(Ph)SiMe_3$, a yellow, homogenous solution forms, from which yellow crystals of **1** grow in high yield (80–88%) after layering with *n*-heptane [Eq. 1].[8] The molecular structure of **1**[9] (Figure 1) consists of

$$CuCl + 2\,PEtPh_2 + Te(Ph)SiMe_3 \xrightarrow[-Me_3SiCl]{THF/Et_2O} \underset{\mathbf{1}}{[Cu_4(TePh)_6(PEtPh_2)_5]} \quad (a)$$

a nonbonded octahedral array of tellurolate ligands (Te···Te 4.035(1)–4.576(1) Å) that each bridge three Cu sites with the exception of Te3, which forms only two Cu–Te bonds. The μ-TePh–Cu distances (av 2.560(1) Å) are noticeably shorter than their μ_3 counterparts (2.577(1)–2.700(1), av 2.652(4) Å).

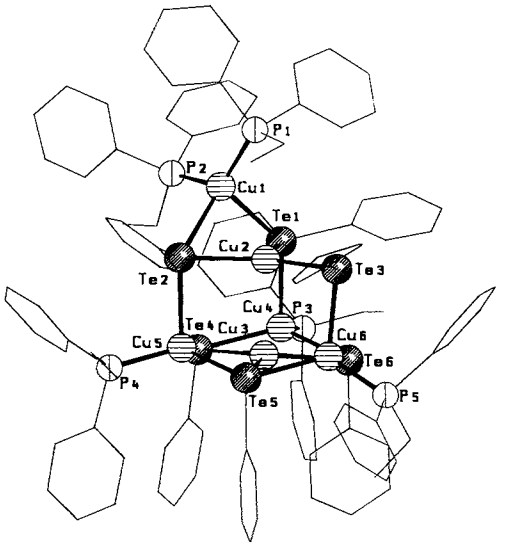

Figure 1. Molecular structure of **1** in the crystal. Important bond lengths and angles are discussed in the text. Te atoms are illustrated as dark spheres, and Cu atoms as spheres with horizontal hashing.

[*] Prof. Dr. D. Fenske, Dr. J. F. Corrigan
Institut für Anorganische Chemie der Universität
Engesserstrasse, Geb. Nr. 30.45, D-76128 Karlsruhe (Germany)
Fax: Int. code (721) 661-921
e-mail john@achibm6.chemie.uni-karlsruhe.de

[**] This work was supported by the the Deutsche Forschungsgemeinschaft (SFB 195), the Fonds der Chemischen Industrie, and the European Union (HCM program). J. F. C. thanks the Natural Sciences and Engineering Research Council (Canada) for a postdoctoral fellowship.

 © WILEY-VCH Verlag GmbH, D-69451 Weinheim, 1997 0570-0833/97/3618-1981 $ 17.50+.50/0

Four of the copper atoms adopt tetrahedral geometries, either with one phosphorus and three tellurium atoms (Cu4–C6) or two Cu–Te and two Cu–P bonds (Cu1). Atoms Cu2 and Cu3 lie in opposite deltahedral faces of the Te_6 octahedron (maximum deviation 0.22 Å, sum of angles 357.8–360.0°). The oxidation state I (d^{10}) can be assigned to the metal centers, and a cluster valence electron count of either 98 or 88, depending on whether the μ_3-TePh ligands are described as five- or three-electron donors, respectively, can be derived. Cluster **1** is related to the recently published homoleptic hexanuclear copper selenolate complex $[Cu_6\{Se(2,4,6\text{-}iPr_3C_6H_2)\}_6]$, in which the Cu^I atoms lie on the faces of a Se_6 antiprism.[10]

We were unable to observe any signals in the ^{125}Te NMR spectrum of **1**; room-temperature $^{31}P\{^1H\}$ NMR spectra display a broad singlet at $\delta = -10.3$. Solutions of **1** are bright yellow and exhibit an intense, broad absorbance band at $\lambda_{max} = 287$ nm ($\varepsilon = 72000$) and a weaker one at $\lambda_{max} = 397$ nm ($\varepsilon = 13500$). The d^{10} electronic configuration at Cu and the high extinction coefficients of these transitions suggest a charge transfer type process. However, intraligand transitions cannot be ruled out for the higher energy band. Upon exposure to light these solutions gradually darken to a brown color, and after four days the bands at 287 and 397 nm are no longer observed. When **1** is dissolved in benzene, brown platelets of the mixed telluride/tellurolate cluster $[Cu_{50}(\mu_3\text{-TePh})_{20}Te_{17}(PEtPh_2)_8]^{4-}$ crystallize over the course of several days as the $[PEtPh_3]^+$ salt (yield 50%); the cation arises from the originally coordinated phosphane ligands.[8] In contrast, solutions of **1** in benzene that are protected from light show no evidence of darkening even after several weeks at room temperature.

A projection of the cluster core determined by X-ray analysis is shown in Figure 2.[9] Although the plate-like crystals scattered

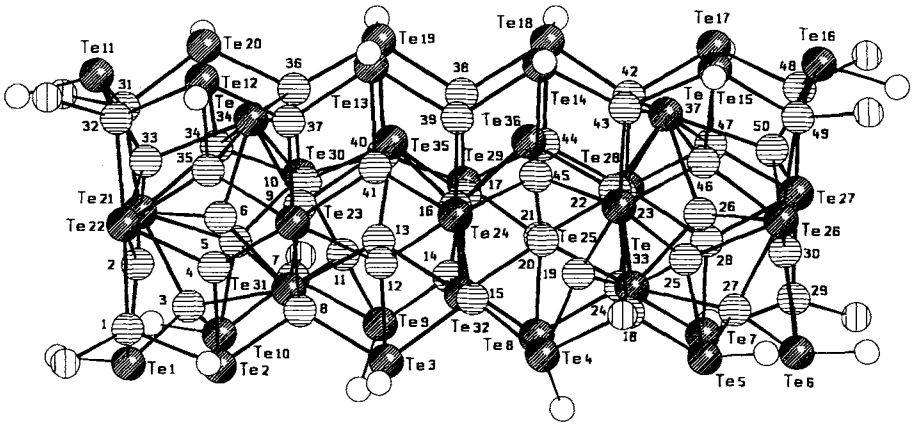

Figure 2. Molecular structure of **2** in the crystal. Important bond lengths and angles are discussed in the text. For clarity all C atoms, with the exception of the *ipso*-C atoms bonded to the tellurolate ligands, have been omitted.

only weakly—which adversely affected the intensity and quality of the data—all carbon atoms, with the exception of those bonded to the disordered $[PEtPh_3]^+$ counterions P11 and P12, could be localized in the difference Fourier maps.[9] The striking feature of the cluster core is the manner in which the tellurium ligands are arranged: the molecule consists of "top" and "bottom" μ_3-TePh layers (Te1–Te10 and Te11–Te20, respectively) with a central telluride layer (Te21–Te30). Sandwiched between these are the 50 copper atoms along with the remaining 7 telluride ligands. The combination of 20 $Te(Ph)^-$ and 17 Te^{2-} ligands accounts for the presence of the four phosphonium ions in the asymmetric unit when an oxidation state of I is assigned to the copper centers. Cluster **2** is diamagnetic, which is in agreement with the above description. The stoichiometric ratio of Cu:Te in **2** is in contrast to the nonstoichiometry observed in more spherical, closely packed Cu/Te clusters[11] but parallels observations on related high-nuclearity Ag/Te/TeR clusters.[12]

The 20 phenyltellurolate ligands are each bonded to three copper atoms (Te–Cu 2.525(4)–2.969(4) Å) and, in conjunction with the eight coordinated $PEtPh_2$ ligands, serve to stabilize effectively the inner CuTe core. The telluride ligands that form the middle Te_{10} layer act as μ_6 and μ_7 bridges between the copper sites to which they are bound with distances between 2.521(4) and 2.983(4) Å. The seven remaining Te^{2-} ligands (Te–Cu 2.561(3)–3.142(4) Å) function as μ_6, μ_7, and μ_8 bridges. Evidence for the presence of $TePh_2$ in reaction solutions, which accounts for the presence of telluride ligands in **2**, was confirmed with $^{125}Te\{^1H\}$ NMR spectroscopy; a signal at $\delta = 688$ was observed.[13] Arnold et al. recently reported the isolation and structural characterization of the mixed telluride/tellurolate clusters $[Ln_5Te_3\{TeSi(SiMe_3)_3\}_9]$ (Ln = La, Ce) by the decomposition of homoleptic metal tellurolate precursors and concomitant generation of $Te[Si(SiMe_3)_3]_2$.[4d]

The Cu···Cu distances in **2** (2.463(5)–3.022(5) Å) are consistent with the oxidation state I assigned to these centers,[14] and their coordination geometries vary from (distorted) trigonal planar to tetrahedral. Despite the layered nature of both **2** and the binary material Cu_2Te,[15] the arrangement in the latter consists of ditelluride (Te_2^{2-}) units and formal Cu–Cu bonds. Therefore, it bears little resemblance to the arrangement observed in **2**.

Although we have yet to isolate any intermediates in the reaction of **1** to **2**, $^{31}P\{^1H\}$ NMR spectra of solutions from which **2** crystallize display broad signals in the range of $\delta = +2$ to -12, suggesting the presence of additional cluster species. Clues into the reaction pathway may be gleaned from the isolation and structural characterization[9] of the dodecanuclear mixed telluride/tellurolate complex **3**,[8] which is the only crystalline

$[Cu_{12}(\mu_6\text{-Te})_3(\mu_3\text{-TePh})_6(PPh_3)_6]$ **3**

product obtained (yield 40%) from reactions analogous to that for **1** but with the ligand PPh_3 under normal daylight conditions (Figure 3). The cluster, not unlike **2**, consists of two tellurolate and a central telluride layers with the 12 Cu atoms lying either slightly above (Cu11, Cu41) or within (Cu21, Cu31) the deltahedral faces of the nonbonded tellurium framework. There are two crystallographically independent but chemically equivalent molecules per asymmetric unit which lie on crystallographic threefold axes.[9] The Te_9 polyhedron consists of two Te_6 octahedra sharing a common face composed of the three telluride ligands. It is thus easily viewed as the product of condensation of two $(PhTe)_6$ units in **1**.

We are currently exploring the general applicability of photolytic methods for the generation of high nuclearity metal/chalcogenide/chalcogenolate clusters and nanoparticle complexes.

Received: February 5, 1997 [Z10077IE]
German version: *Angew. Chem.* **1997**, *109*, 2070–2072

Keywords: clusters · copper · photolysis · tellurium

 © WILEY-VCH Verlag GmbH, D-69451 Weinheim, 1997 0570-0833/97/3618-1982 $ 17.50+.50/0

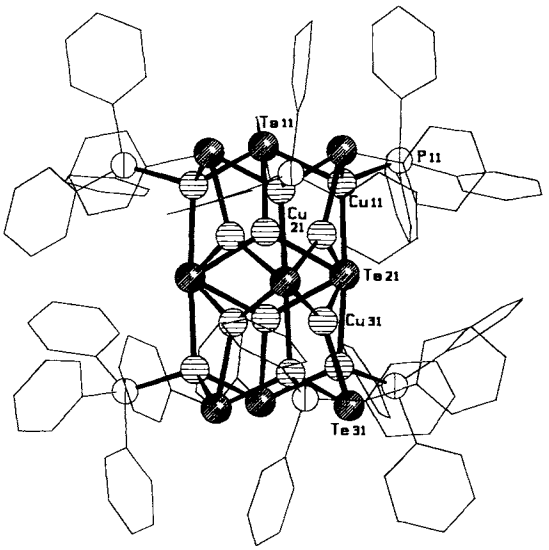

Figure 3. Molecular structure of **3** in the crystal (molecule 1). Selected distances [Å]: TePh–Cu 2.603(2)–2.645(2), μ_6-Te–Cu 2.610(2)–2.731(2), Cu···Cu 2.557(2)–2.675(2).

[1] J. Arnold, *Prog. Inorg. Chem.* **1995**, *43*, 353.

[2] a) W. Hirpo, S. Dhingra, A. C. Sutorik, M. G. Kanatzidis, *J. Am. Chem. Soc.* **1993**, 115, 1597; b) A. R. Strzelecki, P. A. Timinski, B. A. Helsel, P. A.; Bianconi, *ibid.* **1992**, *114*, 3159; c) H. B. Singh, N. Sudha, *Polyhedron* **1996**, *15*, 745, and references therein.

[3] a) D. S. Margolis, R. W. Pitman, *J. Chem. Soc.* **1957**, 799; b) M. L. Steigerwald, C. R. Sprinkle, *J. Am. Chem. Soc.* **1987**, *109*, 7200; c) M. Bochmann, K. Webb, M. Harman, M. B. Hursthouse, *Angew. Chem.* **1990**, *102*, 703; *Angew. Chem. Int. Ed. Engl.* **1990**, *29*, 638.

[4] a) D. R. Cary, J. Arnold, *Inorg. Chem.* **1994**, *33*, 1791; b) D. R. Cary, J. Arnold, *J. Am. Chem. Soc.* **1993**, *115*, 84501; c) M. Berardini, J. Emge, J. G. Brennan, *ibid.* **1993**, *115*, 8501; d) D. R. Cary, G. E. Ball, J. Arnold, *ibid.* **1995**, *117*, 3492.

[5] a) C. P. Gerlach, V. Christou, J. Arnold, *Inorg. Chem.* **1996**, *35*, 2758; b) V. Christou, J. Arnold, *J. Am. Chem. Soc.* **1992**, *114*, 6240.

[6] A. L. Seligson, J. Arnold, *J. Am. Chem. Soc.* **1993**, *115*, 8214.

[7] a) W. E. Piers, D. J. Parks, L. R. MacGillivray, M. J. Zaworotko, *Organometallics* **1994**, *13*, 4547; b) W. E. Piers, L. R. MacGillivray, M. J. Zaworotko, *ibid.* **1993**, *12*, 4723.

[8] Elemental analyses: calcd values (found): $[Cu_6(TePh)_6(PEtPh_2)_5]$ (**1**), $C_{106}H_{105}P_5Cu_6Te_6$: C 47.50 (47.44), H 3.95 (3.83); $[Cu_{50}(TePh)_{20}Te_{17}(PEtPh_2)_8][PEtPh_3]_4$ (**2**), $C_{312}H_{300}P_{12}Cu_{50}Te_{37}$: C 30.42 (30.45), H 2.45 (2.42), P 3.02 (2.80); $[Cu_{12}(Te)_3(TePh)_6(PPh_3)_6]\cdot 1.5C_6H_6$ ($\mathbf{3}\cdot 1.5C_6H_6$), $C_{153}H_{129}P_6Cu_{12}Te_9$: C 45.21 (44.61), H 3.20 (3.15).

[9] Data for the crystal structure analyses were collected with a Stoe IPDS imaging plate diffractometer ($Mo_{K\alpha}$, $\lambda = 0.71073$ Å). $C_{106}H_{105}P_5Cu_6Te_6$ (**1**) at 193 K: yellow polyhedron, $0.40\times0.30\times0.23$ mm, $M = 2680.6$, monoclinic, space group $P2_1/n$, $a = 17.891(4)$, $b = 23.891(5)$, $c = 23.735(5)$ Å, $\beta = 90.39(3)°$, $V = 10145(4)$ Å^3, $Z = 4$, $\rho_{calcd} = 1.755$ g cm^{-3}, $\mu = 3.051$ mm^{-1}, $2\theta_{max} = 52°$; of 41727 reflections collected 18291 were independent ($R_{int} = 0.0433$) and 15469 observed with $F_o > 4\sigma(F_o)$. The structure was solved by direct methods and refined on F^2 using SHELXTL software. Data were corrected for Lorentzian and polarization effects. No absorption corrections were performed. All atoms were refined anisotropically, and hydrogen atoms were included as riding on their respective carbon atoms (1108 parameters). Final $R = 0.0461$ ($wR_2 = 0.1124$) and GOF = 1.111; max/min residual electron density = 2.37/ −1.23 e Å^{-3}. $[C_{232}H_{220}P_8Cu_{50}Te_{37}][C_{20}H_{20}P_4]\cdot 2C_6H_6$ ($\mathbf{2}\cdot 2C_6H_6$) at 200 K: brown platelet, $0.22\times0.22\times0.02$ mm, $M = 12475.6$, monoclinic, space group $P2/c$, $a = 35.986(4)$, $b = 19.955(2)$, $c = 57.004(8)$ Å, $\beta = 106.83(1)°$, $V = 39181(8)$ Å^3, $Z = 4$, $\rho_{calcd} = 2.115$ g cm^{-3}, $\mu = 5.439$ mm^{-1}, $2\theta_{max} = 40°$; of 101160 reflections collected 35173 were independent ($R_{int} = 0.1083$) and 23318 observed with $F_o > 4\sigma(F_o)$. The structure was solved and refined as for **1**; however, only Cu, Te, and P atoms were anisotropically refined (1562 parameters). All phenyl rings were refined as rigid groups, and hydrogen atoms were not included. $[PEtPh_3]$ cations P(10)–P(12) were disordered over inversion centers. P–C and C–C distances about these cations were refined with common values. Not all C atoms about these counterions could be localized. Final $R = 0.0777$ ($wR_2 = 0.2102$) and GOF = 1.11; max/min residual electron density = 1.97/ −1.14 e Å^{-3}. $C_{144}H_{120}P_6Cu_{12}Te_9\cdot 1.5C_6H_6$ ($\mathbf{3}\cdot 1.5C_6H_6$) at 200 K: green hexagonal plate fragment, $0.27\times0.19\times0.04$ mm, $M = 4064.3$, trigonal, space group $R\bar{3}$, $a = 28.049(1)$, $c = 71.959(4)$ Å, $V = 49029(4)$ Å^3, $Z = 12$, $\rho_{calcd} = 1.652$ g cm^{-3}, $\mu = 3.204$ mm^{-1}, $2\theta_{max} = 45°$; of 28704 reflections collected 12849 were independent ($R_{int} = 0.0674$) and 9119 observed with $F_o > 4\sigma(F_o)$. The structure was solved and refined as for **1**; however, solvent atoms C(1S)–C(6S) were isotropically refined (1034 parameters). Final $R = 0.0598$ ($wR_2 = 0.1667$), GOF = 1.036; max/min residual electron density = 1.70/ −0.91 e Å^{-3}. Crystallographic data (excluding structure factors) for the structures reported in this paper have been deposited with the Cambridge Crystallographic Data Centre as supplementary publication no. CCDC-100373. Copies of the data can be obtained free of charge on application to The Director, CCDC, 12 Union Road, Cambridge CB21EZ, UK (fax: int. code +(1223)336-033; e-mail: deposit@chemcrys.cam.ac.uk).

[10] D. Ohlmann, H. Pritzkow, H. Grützmacher, M. Anthamatten, P. Glaser, *J. Chem. Soc. Chem. Commun.* **1995**, 1011.

[11] a) J.-C. Steck, D. Fenske, *Angew. Chem.* **1993**, *105*, 254; *Angew. Chem. Int. Ed. Engl.* **1993**, *32*, 238; b) J. F. Corrigan, S. Balter, D. Fenske, *J. Chem. Soc. Dalton Trans.* **1996**, 729.

[12] J. F. Corrigan, D. Fenske, *J. Chem. Soc. Chem. Commun.* **1996**, 943.

[13] H. C. E. McFarlane, W. McFarlane, *J. Chem. Soc. Dalton Trans.* **1973**, 943.

[14] A. Schäfer, R. Ahlrichs, *J. Am. Chem. Soc.* **1994**, *116*, 10686.

[15] H. Nowotny, *Metallforschung* **1946**, *1*, 40.

Difluorovinylidene, $F_2C{=}C{:}$**

Jürgen Breidung, Hans Bürger,* Carsten Kötting, Rodion Kopitzky, Wolfram Sander,* Michael Senzlober, Walter Thiel,* and Helge Willner*

Vinylidenes $R^1R^2C{=}C{:}$ rearrange so rapidly to alkynes $R^1C{\equiv}CR^2$, which are more stable by 35–45 kcal mol^{-1}, that they could be detected directly only in few cases. The singlet carbenes $H_2CC{:}$ and $FHCC{:}$ were characterized in the gas phase by means of the vibrational progression in the photoelectron (PE) spectra of the anions H_2CC^- [1, 2] and $FHCC^-$.[3] The immediate rearrangement of 1-H-vinylidenes into alkynes by 1,2-H shift is rendered possible by a very low activation barrier[2] calculated to be 2–4 kcal mol^{-1}.[4, 5]

In contrast, the isomerization of $F_2C{=}C{:}$ (difluorovinylidene, **1**) to $FC{\equiv}CF$ (**2**) is impeded by a considerably higher barrier of 35–40 kcal mol^{-1}. The planar, antiaromatic species **A** is the transition state for the corresponding 1,2-F shift.[6] Surprisingly, in spite of this kinetic stabilization there is no direct evidence yet for **1** beyond that based on the vibrational frequencies (see Table 1)[3] measured in the 351.1 nm PE spectrum

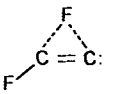

A

[*] Prof. Dr. H. Bürger, Dipl.-Chem. M. Senzlober
Anorganische Chemie, FB 9, Universität-GH
D-42097 Wuppertal (Germany)
Fax: Int. code +(202)439-2901
e-mail: buerger1@wrcs3.urz.uni-wuppertal.de

Prof. Dr. W. Sander, Dipl.-Chem. C. Kötting
Lehrstuhl für Organische Chemie II der Universität
D-44780 Bochum (Germany)
Fax: Int. code +(234)709-4353
e-mail: sander@neon.orch.ruhr-uni-bochum.de

Prof. Dr. W. Thiel, Dr. J. Breidung
Organisch-chemisches Institut der Universität
CH-8057 Zürich (Switzerland)
Fax: Int. code +(1)365-6812
e-mail: thiel@oci.unizh.ch

Prof. Dr. H. Willner, Dr. R. Kopitzky
Institut für Anorganische Chemie der Universität
D-30167 Hannover (Germany)
Fax: Int. code +(511)762-3006
e-mail: willner@mbox.acc.uni-hannover.de

[**] We thank the Deutsche Forschungsgemeinschaft, the Fonds der Chemischen Industrie, and the Schweizerischer Nationalfonds zur Förderung der wissenschaftlichen Forschung for financial support.

 © WILEY-VCH Verlag GmbH, D-69451 Weinheim, 1997 0570-0833/97/3618-1983 $ 17.50+.50/0

of F_2CC^- and assigned with the assistance of ab initio calculations.[7] Experiments to generate **1**, by IR excitation of $F_2C{=}CHF$[8] and $F_2C{=}CHCl$[9] in the gas phase with a CO_2 laser or Hg $6(^3P_1)$ photosensitized decomposition of $F_2C{=}CHF$,[10] yield the geminal elimination products HF and HCl. However, singlet **1**,[10] the presumed intermediate, either adds across the C=C bond of the parent olefin,[7, 10] or by H abstraction[9] immediately forms stable products whose constitution proves the intermediacy of **1**.

This conclusion is further supported by the formation of a mixture of $F_2CC^{12}CO$, $F_2CC^{13}CO$ and ^{13}CO when difluoropropadienone (**3**) with [1-^{13}C] isotopic enrichment is photolyzed in an Ar matrix doped with natural CO ($\lambda > 185$ nm). UV irradiation ($\lambda = 240$ nm) of **3** in an N_2 matrix yields small amounts of difluorodiazoethene F_2CCNN (**4**).[11] Upon flash pyrolysis of difluoromaleic anhydride at 825–975 °C both **2** and **3** are formed, whereas **1** is not obtained.[12] These previous studies suggest that it might be possible to detect and characterize **1**, for example in a matrix in the absence of possible reactive partners, but hardly as a product of photochemical elimination processes.

Our efforts to convert **2**[13] into **1** thermally either by heating to 1100 °C, or by passing over hot Pt wool, failed; only undecomposed **2** was trapped in an Ar matrix at 15 K. We therefore attempted to generate **1** by photochemical isomerization of **2**. A noble gas matrix at low temperature seemed to be more favorable for this purpose than the gas phase, since in the matrix bimolecular trapping reactions and surface-catalyzed back reactions are suppressed. Infrared spectroscopy is apparently particularly suited for the detection of **1**, since the matrix IR spectrum of **2** is well known.[14]

The location of the IR absorptions of **1** has been estimated from ab initio CCSD/DZP calculations[7, 15] by scaling the harmonic wavenumbers with a factor of 0.95. To obtain more reliable ab initio predictions without empirical corrections we recalculated the harmonic wavenumbers at the higher correlated CCSD(T) level using the significantly larger cc-pVQZ basis and determined the anharmonicity corrections to the wavenumbers from the anharmonic MP2/TZ2Pf force field.[15–20] The ab initio predictions are collated in Table 1, columns 1 and 2.

We have recorded the UV/Vis spectrum of gaseous and matrix-isolated **2** in order to determine the wavelength best suited for photochemical conversion of **2** into **1**. Figure 1 illustrates that **2** has an absorption maximum ($\lambda < 200$ nm) with a flank at longer wavelengths. In the UV gas spectrum this flank extends

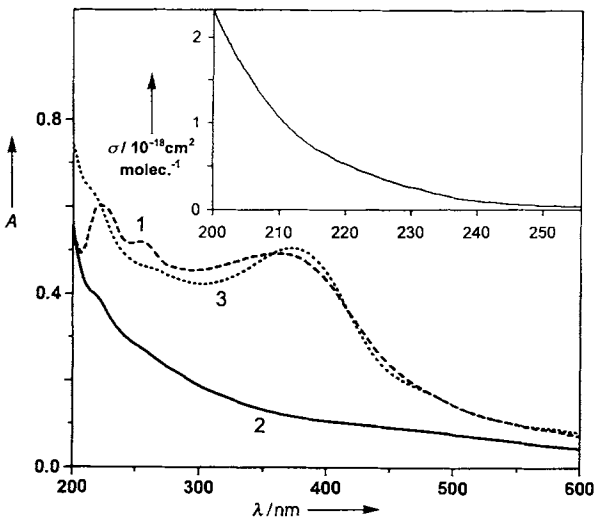

Figure 1. Matrix UV/Vis spectra (A = Absorbance): 1: After 193 nm irraditation of **2**. 2: Compound **2** before irradiation. 3: After irradiation of the carrier of spectrum 1 with $\lambda > 230$ nm. Insert: gas phase spectrum of **2**.

to approximately 250 nm (Figure 1, insert). Irradiation of matrix-isolated **2** with a high-pressure mercury lamp (Heraeus TQ 150, $\lambda > 230$ nm) produced a slow decay of **2** with formation of numerous IR absorption bands, whose number increased with prolongated irradiation. Among the absorptions those typical of **1** at 1672, 1267, and 918 cm^{-1} were discernible, but they only reached low stationary intensity.

Irradiation of matrix-isolated **2** at 10 K with a pulsed ArF laser (Lambda Physik, model COMPex 100; $\lambda = 193$ nm, repetition rate 1 Hz, about 80 mJ per pulse) yielded a photolysis product, which, according to the difference IR spectrum (Figure 2a), revealed absorption bands almost exclusively of the single species ①. These absorptions whose relative intensities did not change grew at the expense of the disappearing **2**. After optimization of the photolysis (5000 pulses) the transformation of **2** into a quasi-stationary equilibrium was completed to more than 90% (Figure 2b).

Altogether six new absorptions were observed, the wavenumbers and relative intensities of which are listed in Table 1,

Table 1. Wavenumbers $\tilde{\nu}$ [cm^{-1}] of the infrared spectra of $F_2C{=}C$: and F_2CS.

		1 Theory		1 Experiment		SCF_2
		1 [a]	2 [b]	3 [c]	4 [d]	5 [e]
a_1	ν_1, ν (CC)	1640	1693 [67]	1670 (25)	1672 [20]	1365
	ν_2, ν_s (CF_2)	893	927 [67]	905 (25)	918 [22]	789
	ν_3, δ (CF_2)	486	512 [5]	510 (25)	511 [3]	526
b_1	ν_4, ν_{as} (CF_2)	1260	1287 [277]		1267 [100]	1190
	$\nu_2 + \nu_5$		1247 [f]		1245 [46]	1219
	ν_5, ρ (CF_2)	322	323 [31]		(334)	420
b_2	ν_6, γ (CF_2)	513	560 [4]		551 [3]	623

[a] Ref. [7], CCSD/DZP, scaling factor 0.95. [b] This work. Harmonic wavenumbers ω_i: CCSD(T)/cc-pVQZ; anharmonicity corrections $\omega_i - \nu_i$ from anharmonicity constants x_{ij} calculated perturbationally, MP2/TZ2Pf. In brackets: intensities [km mol^{-1}] in double harmonic approximation, CCSD(T)/TZ2Pf. [c] Ref. [3]. From vibrational fine structure in the photoelectron spectrum of F_2CC^-. Uncertainty in parentheses. [d] This work, Ar matrix, 10 K. Integrated relative intensity ($\int \ln(I_0/I)d\nu$) in square brackets. Fundamental wavenumber of ν_5 (in parentheses, see text) calculated from deperturbed combination level $\nu_2+\nu_5$. [e] Ref. [21], gas phase. [f] In harmonic approximation the intensity of $\nu_2+\nu_5$ is zero. Due to "Fermi" resonance the intensity of ν_4 is shared by both partners of the resonance.

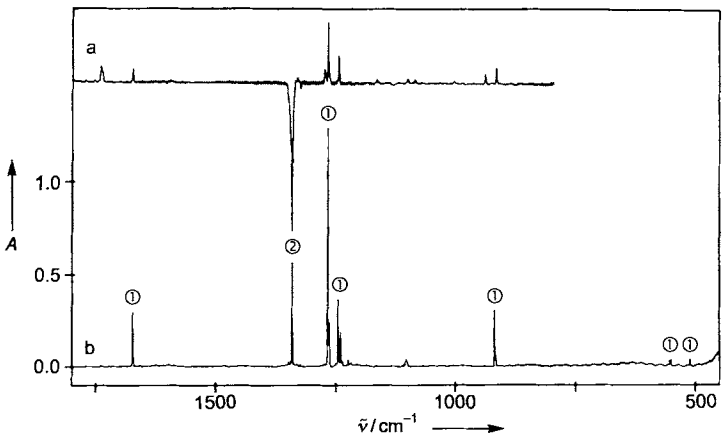

Figure 2. Matrix IR spectra (Ar, 10 K; A = Absorbance). a: Difference spectrum of an irradiated matrix of **2** doped with 1% N_2 and the matrix spectrum of precursor. Absorptions of products formed in the course of the photolysis point upwards, absorptions of depleted starting material point downwards. b: Spectrum of the quasi-stationary equilibrium of the transformation **2** → **1** after 5000 ArF laser pulses (about 80 mJ per pulse, 1 Hz). ①: difluorovinylidene **1**; ②: difluoroethyne **2**. The splitting of the absorption at 1245 cm^{-1} is matrix-dependent (cf. (a) and (b)) and disappears upon annealing.

 © WILEY-VCH Verlag GmbH, D-69451 Weinheim, 1997 0570-0833/97/3618-1984 $ 17.50+.50/0

column 4. The assignment of five of these bands to the fundamentals $\nu_1-\nu_4$ and ν_6 of planar difluorovinylidene **1** with C_{2v} symmetry follows unambiguously from a comparison with ab initio predictions of vibrational frequencies and intensities (Table 1, column 2). The excellent agreement of observed and predicted vibrational spectra and the trapping reactions described below ascertain that difluorovinylidene **1** is the exclusive product of the 193 nm photolysis of **2**.

The IR absorption at 1245 cm^{-1}, which is the second most intense, is assigned to the combination $\nu_2+\nu_5$ belonging to the same species b_1 as ν_4 at $\tilde{\nu}_{eff}=1267\ cm^{-1}$, with which it interacts by anharmonic ("Fermi") resonance. Exactly the same situation is met in the closely related SCF_2 molecule (Table 1, column 5).[21] Here a pair of absorptions assigned to $\nu_4/\nu_2+\nu_5$ at 1190 and 1219 cm^{-1} (gas phase)[21] is observed; the intensity ratio is about 3:2 and compared to the spectrum of **1** the relative position of ν_4 and $\nu_2+\nu_5$ is inverted.

Assuming that the transition moment of ν_4 is very large relative to that of $\nu_2+\nu_5$ (cf. Table 1, footnote [f]), the anharmonic resonance of ν_4 with $\nu_2+\nu_5$ can be deperturbed by means of the observed relative intensities (100:46). The coupling term W_{245} is determined to be 10.25 cm^{-1} (analogous value of 13 cm^{-1} for SCF_2), which is in excellent agreement with the ab initio prediction (10.81 cm^{-1} from the corresponding cubic force constant, MP2/TZ2Pf). The deperturbed vibrational frequencies $\tilde{\nu}^*$ are $\tilde{\nu}_4{}^*=1260$ and $(\tilde{\nu}_2+\tilde{\nu}_5)^*=1252\ cm^{-1}$ (ab initio: 1284 and 1249 cm^{-1}). The vibrational fundamental, which could not be observed for experimental reasons, is calculated from $\tilde{\nu}_2=918\ cm^{-1}$ and an estimated anharmonicity constant χ_{25} of 0 (ab initio: $-0.34\ cm^{-1}$) to be $\tilde{\nu}_5=(1252-918)\ cm^{-1}=334\ cm^{-1}$.

The photochemical transformation **2** → **1** may also be monitored by the UV/Vis spectrum (Figure 1). Upon irradiation of **2** with an ArF laser (193 nm) in an Ar matrix whose concentration was higher than that employed for the IR experiment, the UV absorption of **2** changed, and new maxima at $\lambda=228$ and 254 nm emerged, which were assigned to **1** (Figure 1 (1)). Under the given experimental conditions additional products absorbing at $\lambda=380$ nm were formed, which were retained when **1** was converted back into **2** by irradiation with $\lambda>230$ nm (Figure 1 (3)). Quantitative reconversion was achieved by irradiation with a high-pressure mercury lamp (Osram HBO, 500 W, $\lambda>230$ nm) for merely 15 minutes. This behavior explains why irradiation of **2** with $\lambda>230$ nm produces **1** in a photostationary equilibrium only in very low concentration.

The previous experiments of Brahms and Dailey[11] suggest that **1** would react in a matrix with CO to yield **3** and with N_2 to form **4**. To prove this we have photochemically generated **1** from **2** in an Ar matrix doped with 1% CO or 1% N_2 at 10 K. Under these conditions **1** is sufficiently separated from CO or N_2 that they coexist in the matrix. On annealing the matrix at 35–42 K a synchronous depletion of the IR absorptions of **1**, and growth of those of **3** and **4** is observed.[22]

While **3**, as reported,[11] is "pseudo" inert towards irradiation with $\lambda=254$ nm, **4** decomposes to **2** and N_2 under these conditions. The transformation of **2** isolated in a matrix in contact with N_2 into **1** by irradiation at $\lambda=193$ nm could not be repeated, because N_2 and **1** rapidly react to form **4**, which then immediately decomposes to N_2 and **2** (Scheme 1).

As the essential result of the present investigation we stress that matrix-isolated difluorovinylidene **1** can be made by 193 nm excimer laser photolysis of difluoroethyne **2**. It is protected against isomerization to **2**, which is more stable by about 30 kcal mol^{-1}, by a substantial barrier (calculated to be ca. 35 kcal mol^{-1}). Nevertheless **1** is so reactive that addition of CO

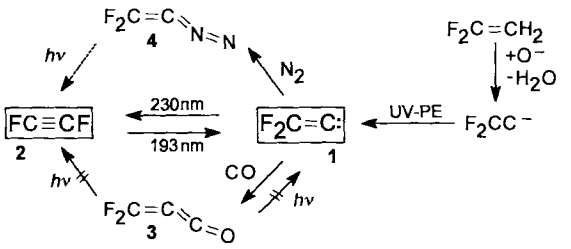

Scheme 1.

and N_2 occurs at temperatures as low as 10 K. Previous attempts to generate **1** by photofragmentation of other precursors failed, because **1** reacted immediately, even in a matrix, with other concomitantly formed photofragments or precursors. All vibrational fundamentals of **1** have been determined experimentally, ν_5 by an indirect method. Their frequencies are in excellent agreement with those from high-level ab initio calculations.

Received: February 19, 1997 [Z10137IE]
German version: *Angew. Chem.* **1997**, *109*, 2072–2075

Keywords: alkynes · carbenes · fluorine · matrix isolation · photochemistry

[1] S. M. Burnett, A. E. Stevens, F. S. Feigerle, W. C. Lineberger, *Chem. Phys. Lett.* **1983**, *100*, 124–128.
[2] K. M. Ervin, J. Ho, W. C. Lineberger, *J. Chem. Phys.* **1989**, *91*, 5974–5992.
[3] M. K. Gilles, W. C. Lineberger, K. M. Ervin, *J. Am. Chem. Soc.* **1993**, *115*, 1031–1038.
[4] T. Carrington Jr., L. M. Hubbard, H. F. Schaefer III, W. H. Miller, *J. Chem. Phys.* **1984**, *80*, 4347–4354.
[5] M. M. Gallo, T. P. Hamilton, H. F. Schaefer III, *J. Am. Chem. Soc.* **1990**, *112*, 8714–8719.
[6] M. J. Frisch, R. Krishnan, J. A. Pople, P. von R. Schleyer, *Chem. Phys. Lett.* **1981**, *81*, 421–423.
[7] M. M. Gallo, H. F. Schaefer III, *J. Chem. Phys.* **1990**, *93*, 865–866.
[8] R. A. Stachnik, G. C. Pimentel, *J. Phys. Chem.* **1984**, *88*, 2205–2210.
[9] a) C. Reiser, J. I. Steinfeld, *J. Phys. Chem.* **1980**, *84*, 680–681; b) M. W. Thomsen, B. F. Kimmich, *Macromolecules* **1991**, *24*, 6343–6345.
[10] R. J. Norstrom, H. E. Gunning, O. P. Strausz, *J. Am. Chem. Soc.* **1976**, *98*, 1454–1461.
[11] J. C. Brahms, W. P. Dailey, *J. Am. Chem. Soc.* **1990**, *112*, 4046–4047.
[12] J. C. Brahms, W. P. Dailey, *J. Am. Chem. Soc.* **1989**, *111*, 8940–8941.
[13] H. Bürger, S. Sommer, *J. Chem. Soc. Chem. Commun.* **1991**, 456–458.
[14] H. Bürger, W. Schneider, S. Sommer, W. Thiel, H. Willner, *J. Chem. Phys.* **1991**, *95*, 5660–5669.
[15] Abbreviations: CCSD = coupled cluster method with single and double excitations [16], CCSD(T) = CCSD with perturbational treatment of triple excitations [17], MP2 = Møller-Plesset second-order perturbation theory [18], DZP = polarized double zeta basis [7], TZ2Pf = triple zeta basis [19] with cc-pVTZ polarization functions [20], cc-pVQZ = multiply polarized quadruple zeta basis [20].
[16] G. D. Purvis III, R. J. Bartlett, *J. Chem. Phys.* **1982**, *76*, 1910–1918.
[17] K. Raghavachari, G. W. Trucks, J. A. Pople, M. Head-Gordon, *Chem. Phys. Lett.* **1989**, *157*, 479–483.
[18] C. Møller, M. S. Plesset, *Phys. Rev.* **1934**, *46*, 618–622.
[19] T. H. Dunning, Jr., *J. Chem. Phys.* **1971**, *55*, 716–723.
[20] T. H. Dunning,Jr., *J. Chem. Phys.* **1989**, *90*, 1007–1023.
[21] A. J. Downs, *Spectrochim. Acta* **1963**, *19*, 1165–1171; W. Jerzembeck, Diplom thesis, University of Wuppertal, **1994**.
[22] **3**: obs. $\tilde{\nu}$ in cm^{-1} [relative intensity] 2160 [100], 1763 [31], 1251 [23]/1233 [23], 1189 [14]. Data in ref. [23] (gas phase) in cm^{-1} [relative intensity] 2169.1 [54.5], 1763.6 [19.3], 1248.4 [16.2], 1194.4 [6.2]. **4**: obs. $\tilde{\nu}$ in cm^{-1} [relative intensity] 2105 [21], 2085 [26], 1674 [22], 1646 [100], 1268 [16], 1143 [5], 837 [18]. Data in ref. [11] (N_2 matrix) in cm^{-1} 2104.7, 2085.2, 1672.7, 1650.7, 1262.8, 1143.9, 834.9.
[23] J. C. Brahms, W. P. Dailey, *J. Am. Chem. Soc.* **1989**, *111*, 3071–3073.

 © WILEY-VCH Verlag GmbH, D-69451 Weinheim, 1997 0570-0833/97/3618-1985 $ 17.50+.50/0

Self-Assembly of Thirty-Six Atom Clusters ($Li_{12}S_6O_6N_{12}$) Containing Diazasulfite Anions**

Justin K. Brask, Tristram Chivers,* Masood Parvez, and Gabriele Schatte

Recently there has been considerable interest in alkali metal derivatives of polyimido anions of p-block elements, for example $[Sb(NR)_3^{3-}]$ ($R = PhCH_2CH_2$),[1a] $[Sb_2(NCy)_4^{2-}]$,[1b] and $[E(NR)_3^{2-}]$ (**1**, R = *t*Bu; E = S,[2] Se,[3] Te[4]). In addition to the novelty of their cluster structures, the anions themselves are potentially important reagents for the incorporation of main group elements into chalcogen–nitrogen rings [4b] and the development of the coordination chemistry of anionic polyimido ligands.[5] The dimeric dilithium derivatives of the dianions $[E(NtBu)_3^{2-}]$ (E = S, Se, Te) all adopt distorted hexagonal prismatic structures.[2–4] The replacement of one (or more) of the bulky NR groups in the anions of these clusters by the isoelectronic oxo ligand may have significant structural consequences, but the diazasulfite anions $[OS(NR)(NR')]^{2-}$ (**2**) are unknown. We describe here the syntheses of dilithium derivatives of the bis(*tert*-butylimido)sulfite dianion, $[OS(NtBu)_2]^{2-}$ (**2a**), and the (*tert*-butylimido)(trimethylsilylimido)sulfite dianion, $[OS(NtBu)(NSiMe_3)]^{2-}$ (**2b**), which adopt unique cluster structures derived from the aggregation of hexagonal prisms and eighteen atom cages, respectively.

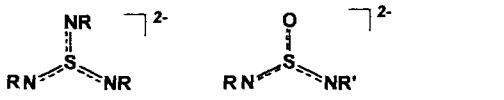

The reactions of the chalcogen diimides, *t*BuN=E=N*t*Bu, with two equivalents of LiNH*t*Bu produce the dianions $[E(NtBu)_3]^{2-}$ (E = S, Se, Te) in excellent yields.[2–4] By analogy, the treatment of *tert*-butylsulfinylimine, *t*BuNSO, or trimethylsilylsulfinylimine, Me_3SiNSO, with two equivalents of lithium *tert*-butylamide leads to hexameric dilithium bis(*tert*-butylimido)sulfite **3** and hexameric dilithium (*tert*-butylimido)-(trimethylsilylimido)sulfite **4**, respectively [Eq. (a), cf. reac-

$$6\,RNSO + 12\,LiNHtBu \xrightarrow{C_7H_8} [\{Li_2[OS(NtBu)(NR)]\}_6] + 6\,H_2NtBu \quad (a)$$

3, R = *t*Bu

4, R = $SiMe_3$

tions of RNSO with other bases, e.g. $Li[N(SiMe_3)R']$, which lead to mixed sulfurdiimides, RNSNR'].[6]

A crystal structure determination of **3** revealed a remarkable arrangement of thirty-six atoms of main group elements in a $Li_{12}N_{12}O_6S_6$ cluster with a central Li_6O_6 core, which comprises two parallel, six-membered Li_3O_3 rings in their chair conformations (Figure 1).[7, 8] The cage structure consists of six pyramidal $[OS(NtBu)_2]^{2-}$ ions (mean bond angles: NSN 104.2(5)°, OSN 101.6(4)°); the oxygen atom of each of these ions participates in the formation of the central Li_6O_6 core with Li–O distances in the range 1.86(2)–2.20(2) Å. In addition, one nitrogen atom of each $[OS(NtBu)_2]^{2-}$ ion is attached to one Li atom of the Li_6O_6 core with Li–N distances in the range 1.91(2)–2.15(2) Å. The mean S–O and S–N distances of 1.587(7) and 1.625(9) Å imply bond orders of 1.44 and 1.46,[9] respectively, in reasonable agreement with the values of 1.33 expected for these bonds in the resonance hybrid **2**. The six sulfur atoms are all three-coordinate, as expected for the pyramidal $[OS(NtBu)_2]^{2-}$ ion, and all oxygen atoms are four-coordinate. However, this novel structural arrangement results in different coordination environments for the N*t*Bu ligands as well as the Li atoms. All the N atoms are four-coordinate with the exception of N6 and N11, which are three-coordinate. The atoms Li3, Li4, Li5, and Li7 of the Li_6O_6 core are four-coordinate, whereas the remaining Li atoms of the Li_6O_6 core and the other six Li atoms are three-coordinate.

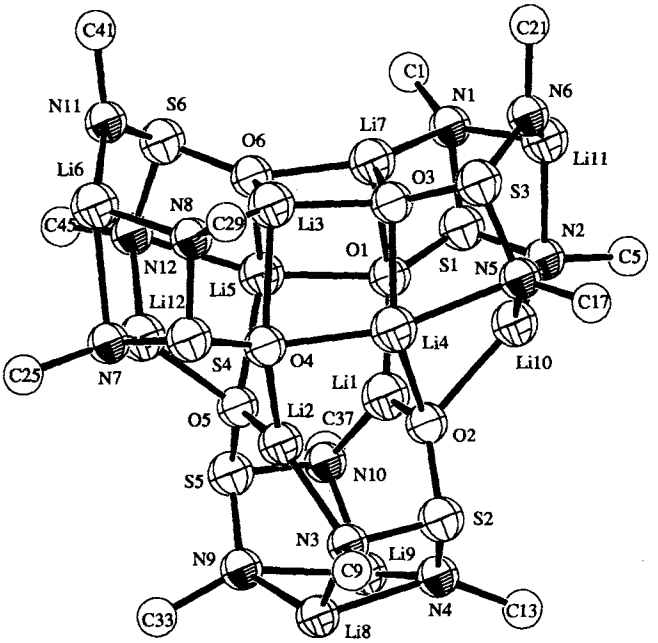

Figure 1. Crystal structure of $[\{Li_2[OS(NtBu)_2]\}_6]$ (**3**) with the atomic numbering scheme. For clarity only the α-carbon atoms of the *t*Bu groups are shown. The range and mean values of selected bond lengths and bond angles are given in the text.

Hexagonal prismatic arrangements based on A_6X_6 clusters are well known,[10–16] and the dimers $[\{Li_2[E(NtBu)_3]\}_2]$ are examples of such structures involving $A_4B_2X_6$ cores.[2–4] The thirty-six atom cluster **3** can be visualized to result from the trimerization of three $Li_4S_2N_4O_2$ ($A_4B_2X_4Y_2$) hexagonal prisms through their Li_2O_2 faces (Figure 2). To our knowledge **3** is the first cluster derived from the aggregation of hexagonal prisms. The $[\{Li_2[OS(NtBu)_2]\}_6]$ cluster **3** has C_2 symmetry; the C_2 axis passes through the center of the [Li3-O3-Li7-O6] square. As a result, there are six inequivalent environments for both the Li atoms and the *tert*-butyl groups. Therefore, six resonances of equal intensity are expected in both the ^1H and the ^7Li NMR spectra. However, very complex sets of both ^1H and ^7Li resonances are observed in C_7D_8 solution throughout the temperature range 183–298 K (see Experimental Section for details) suggesting a dissociative equilibrium, for example according to Equation (b) (cf. $[\{Li_2Sb_2(NCy)_4\}_2]$).[17]

$$[\{Li_2[OS(NtBu)_2]\}_6] \rightleftharpoons [\{Li_2[OS(NtBu)_2]\}_4] + [\{Li_2[OS(NtBu)_2]\}_2] \quad (b)$$

[*] Prof. Dr. T. Chivers, J. K. Brask, Dr. M. Parvez, Dr. G. Schatte
Department of Chemistry
The University of Calgary
Calgary, Alberta T2N 1N4 (Canada)
Fax: Int. code +(403) 289-9488

[**] We gratefully acknowledge the Natural Sciences and Engineering Research Council (Canada) and the Province of Alberta Graduate Fellowships program (J. K. B.) for financial support.

 © WILEY-VCH Verlag GmbH, D-69451 Weinheim, 1997 0570-0833/97/3618-1986 $ 17.50+.50/0

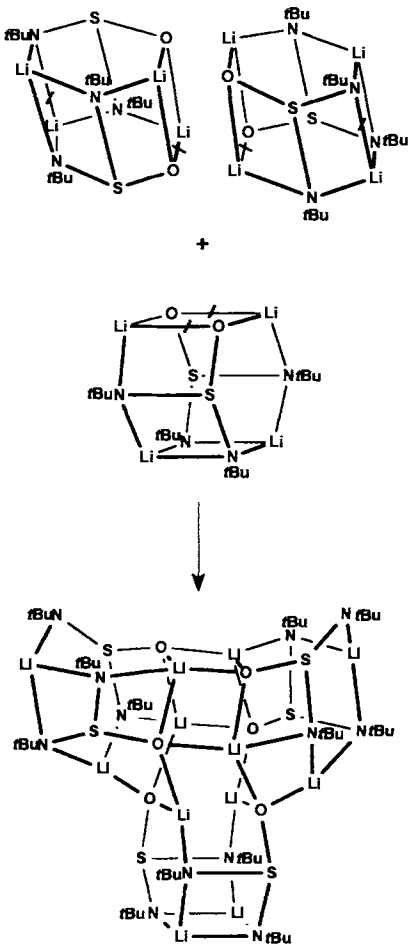

Figure 2. Schematic representation of the formation of the hexameric cluster **3** by the trimerization of $Li_4S_2N_4O_2$ hexagonal prisms (only the α-carbon atoms of the *t*Bu groups are shown for clarity). The designation + indicates the bonds broken in this process.

A comparison of the ^1H and ^7Li NMR data for **3** in C_7D_8 solution with the corresponding data for **4** suggest a different structure for **4**. Indeed, a crystal structure determination of **4** revealed a second unique arrangement for the thirty-six atom cluster in which two $Li_6N_6O_3S_3$ cages are joined by their Li_3O_3 faces (Figure 3).[8, 18] The dimerization of two $Li_6N_6O_3S_3$ cages is depicted schematically in Figure 4. Structurally similar eighteen-atom (A_9X_9) cages are known for the nonamers $[(t\text{Bu-MO})_9]$ (M = Al, Ga)[15, 19] and $[Na(OtBu)_9]$.[20] In **4** each $Li_6N_6O_3S_3$ cage contains three pyramidal $[OS(NtBu)(NSiMe_3)]^{2-}$ ions arranged to form two six-membered rings (Li_3N_3 and Li_3O_3) linked by three SN(R) units. A channel resulting from the parallel arrangement of these six-membered rings passes through the center of the molecule (viewed down the S_6 axis). The lithium atoms in the Li_3N_3 ring are three-coordinate, whereas those in the Li_3O_3 ring are four-coordinate. The crystal structure exhibited disorder in which the N-bonded silicon and carbon atoms were scrambled over all positions, and no distinctions could therefore be made about their positions (see ref. [18]). The solvent toluene molecules were also highly disordered, and the structure analysis thus had high *R* values. The mean values and ranges for important bond lengths and bond angles for **4** are summarized in the caption to Figure 3.

Although it is not possible to define the positions of the silicon and α-carbon atoms from the structure determination due to the disorder, they can be assigned by using the ^1H and ^7Li NMR data for **4**. The ^7Li NMR spectrum of **4** in C_7D_8 at 23 °C shows four well-resolved resonances of approximately equal intensity, and the ^1H NMR spectrum shows two equally intense resonances for the *t*Bu as well as for the $SiMe_3$ groups. In view of the S_6 symmetry of the $Li_{12}S_6N_{12}O_6$ cluster in **4** the ^1H NMR spectrum should exhibit two resonances, one singlet for the *t*Bu groups and one singlet for the $SiMe_3$ groups. The analysis of the NMR results is consistent with the presence of the two clusters **4a** and **4b** in which the nitrogen atoms of the Li_3N_3 rings are attached to either $SiMe_3$ or *t*Bu groups (Figure 4). Apparently **4a** and **4b** are present in equal amounts in solution. Each of these two molecules should exhibit two ^7Li NMR resonances of equal intensity consistent with the finding of four resonances of approximately equal intensity in the ^7Li NMR spectrum of **4**.

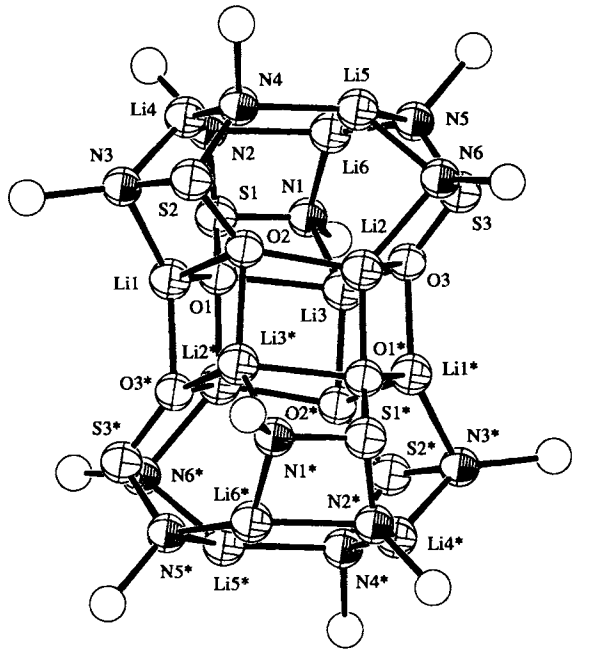

Figure 3. Crystal structure of $[\{Li_2[OS(NtBu)(NSiMe_3)]\}_6]$ (**4**). For clarity only the α-carbon atoms of the *t*Bu groups and the Si atoms of the $SiMe_3$ groups are shown. Mean bond lengths [Å] and bond angles [°]: S–O 1.546(13), S–N 1.62(2); N-S-N 102.4(9), O-S-N 101.1(1). The Li–O and Li–N bond lengths are in the ranges 1.87(4)–2.17(4) Å and 1.89(4)–2.14(4) Å, respectively.

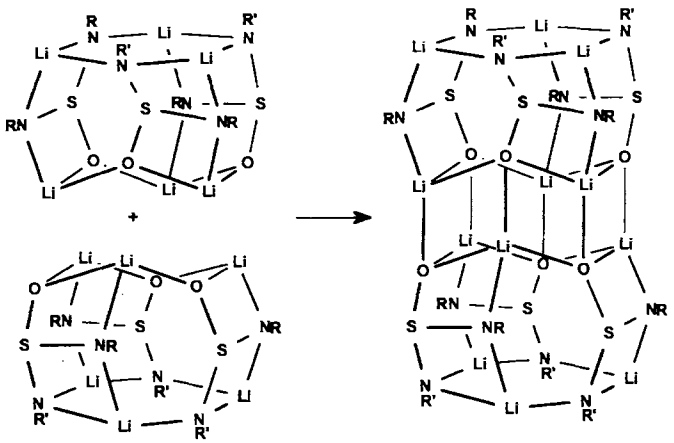

4a, R = $C(CH_3)_3$, R' = $Si(CH_3)_3$
4b, R = $Si(CH_3)_3$, R' = $C(CH_3)_3$

Figure 4. Schematic representation of the formation of the hexameric cluster **4** by the dimerization of $Li_6S_3N_6O_3$ cages.

 © WILEY-VCH Verlag GmbH, D-69451 Weinheim, 1997 0570-0833/97/3618-1987 $ 17.50+.50/0

In summary, we have prepared two examples of the novel diazasulfite ion $[OS(NtBu)(NR)]^{2-}$. Their dilithium derivatives are hexameric and represent the first examples of main group element clusters formed by the aggregation of either hexagonal prisms or eighteen atom cages. The self-assembly of these thirty-six atom clusters is envisaged to occur by oligomerization of smaller clusters through their Li_xO_x faces ($x = 2$ or 3). Consequently, the replacement of two NR groups in $[S(NR)_3]^{2-}$ by two oxygen atoms is likely to produce more highly associated clusters. This possibility and the effects of subtle changes to the size of the R/R′ groups on the aggregation of $\{Li_2[OS(NR)(NR')]\}$ units are under investigation.

Experimental Section

3: A slurry of LiHN*t*Bu (7.21 g, 91.2 mmol) in toluene (15 mL) was added dropwise to a stirred, yellow solution of *t*BuNSO [21] (5.43 g, 45.6 mmol) in toluene (75 mL) at −78 °C. The reaction mixture turned orange. After 1 h at −78 °C, it was allowed to warm slowly to 23 °C to give a transparent, pale yellow solution. All volatiles were removed under dynamic vacuum, and the off-white precipitate was washed with *n*-hexane (10 mL). The yield of **3** was 7.93 g (6.47 mmol, 85%); m.p. 210 °C (decomp.). IR (KBr, Nujol): $\nu\sim$ [cm^{-1}]: above 1000 (N*t*Bu groups), 960–977 (S–N stretching vibrations), 814–837 (S–O stretching vibrations) [22]; ^{1}H NMR (400 MHz, C_7D_8/C_7H_8, TMS in $CDCl_3$): δ(25 °C) = 1.37–1.11 (12 signals), δ(−90 °C) = 1.59 (very broad); ^{7}Li NMR (400 MHz, C_7D_8/C_7H_8; standard: 4 M LiCl in D_2O)]: δ(25 °C) = 0.68– −2.03 (7 signals), δ(−90 °C) = 0.14– −2.86 (6 signals). Satisfactory C,H, N analysis.

4: A yellow solution of Me_3SiNSO [23] (0.536 g, 3.96 mmol) in toluene (10 mL) was added dropwise to a stirred slurry of LiHN*t*Bu (0.626 g, 7.92 mmol) in toluene (20 mL) at 0 °C. After 0.5 h at 0 °C, the mixture was allowed to warm to 23 °C to give a transparent, bright yellow solution, which was stirred for a further 3.5 h. All volatiles were removed under dynamic vacuum, and the oily yellow residue was washed with *n*-pentane (10 mL) to give a white solid. The yield of $[Li_2S(O)(NtBu)(NSiMe_3)]_4$ was 0.707 g (3.21 mmol, 81%); m.p. 207 °C (decomp.). IR (KBr, Nujol): $\nu\sim$ [cm^{-1}]: above 1000 (Me_3Si and N*t*Bu groups), 951–894 (S–N stretching vibrations), 856–831 (S–O stretching vibrations); ^{1}H NMR (200 MHz, 23 °C, C_7D_8, TMS in $CDCl_3$): δ = 1.41 (18 H, s, *t*Bu), 1.32 (18 H, s, *t*Bu), 0.37 (18 H, s, Me_3Si), 0.28 (18 H, s, Me_3Si); ^{7}Li NMR (200 MHz, 23 °C, C_7D_8; standard: 4 M LiCl in D_2O): δ = 2.79, 2.15, 1.64, 1.39. Satisfactory C,H, N analysis.

Received: December 2, 1996
Revised version: April 21, 1997 [Z9844IE]
German version: *Angew. Chem.* **1997**, *109*, 2075–2078

Keywords: clusters · lithium · self-organisation · structure elucidation · sulfur

[1] a) A. J. Edwards, M. A. Paver, P. R. Raithby, M.-A. Rennie, C. A. Russell, D. S. Wright, *Angew. Chem.* **1994**, *106*, 1334–1336; *Angew. Chem. Int. Ed. Engl.* **1994**, *33*, 1277–1278; b) R. A. Alton, D. Barr, A. J. Edwards, M. A. Paver, P. R. Raithby, M.-A. Rennie, C. A. Russell, D. S. Wright, *J. Chem. Soc. Chem. Commun.* **1994**, 1481–1482.

[2] R. Fleischer, S. Freitag, F. Pauer, D. Stalke, *Angew. Chem.* **1996**, *108*, 208–211; *Angew. Chem. Int. Ed. Engl.* **1996**, *35*, 204–206.

[3] T. Chivers, M. Parvez, G. Schatte, *Inorg. Chem.* **1996**, *35*, 4094–4095.

[4] a) T. Chivers, M. Parvez, X. Gao, *Inorg. Chem.* **1996**, *35*, 4336–4341; b) *Angew. Chem.* **1995**, *107*, 2756–2758; *Angew. Chem. Int. Ed. Engl.* **1995**, *34*, 2549–2551.

[5] D. Barr, A. J. Edwards, M. A. Paver, P. R. Raithby, M.-A. Rennie, C. A. Russell, D. S. Wright, *Angew. Chem.* **1994**, *106*, 1960–1962; *Angew. Chem. Int. Ed. Engl.* **1994**, *33*, 1875–1876.

[6] M. Herberhold, B. Distler, H. Maisel, W. Millius, B. Wrackmeyer, P. Zanello, *Z. Anorg. Allg. Chem.* **1996**, *622*, 1515–1523.

[7] Colorless, square-pyramidal crystals of **3** were obtained by recrystallization from toluene at −8 °C (6 weeks). Crystal data for **3**: $(C_8H_{18}N_2OSLi_2)_6 \cdot 2.5\ C_7H_8$, M_r = 1455.44, monoclinic, space group $P\ 2_1/n$ (No. 14), a = 14.416(8), b = 24.718(9), c = 24.676(11) Å, b = 95.15(5)°, V = 8757(7) Å^3, Z = 4, ρ_{calcd} = 1.104 g cm^{-3}, $\mu(Mo_{K\alpha})$ = 0.205 mm^{-1}, $\lambda(Mo_{K\alpha})$ = 0.71069 Å, T = −123(1) °C, $F(000)$ = 3140. Data were collected on a Rigaku AFC6S diffractometer on a colorless prism (0.7 × 0.5 × 0.5 mm^3) mounted directly from the solution (toluene solvation was maintained) into a glass capillary tube (i.d. 1.0 mm) by the $\omega - 2\theta$/scan method ($2° < \theta < 25°$). Of a total of 15896 collected reflections, 15465 were independent (R_{int} = 0.057), 3553 were observed [$I > 2\sigma(I)$], and 15384 reflections were used to refine 897 parameters. Maximum and minimum of the final difference Fourier synthesis: 0.325 and −0.401 e Å^{-3}. The structure was solved by direct methods (SAPI91, Fan Hai-Fu, Rigaku Corp., Tokyo, **1991**). The data were corrected for absorption, Lorentz, and polarization effects. The non-hydrogen atoms were allowed anisotropic temperature factors. The H-atoms were included at geometrically idealized positions with CH distances of 0.95 Å. For each asymmetric unit, which contains 12 Li atoms and six $(NtBu)_2SO$ groups, there are 2.5 molecules of toluene; one of the toluene molecules lies on a special position and is disordered. The C atoms of the toluene were constrained to be regular hexagons and the hydrogen atoms of the disordered solvate ignored. Refinement by full-matrix, least-squares calculations on F^2 converged at R = 0.079 (for the observed reflections) and R_w = 0.217 (all data) with $R = \sum||F_o| - |F_c||/\sum|F_o|$ and $R_w = [\sum w(|F_o|^2 - |F_c|^2)/\sum w(F_o^2)]^{\frac{1}{2}}$, $w = [\sigma^2(F_o^2) + (0.131P)^2 + 16.3897P]^{-1}$ and $P = (F_o^2 + 2F_c^2)/3$ (SHELXL-92) [24].

[8] Crystallographic data (excluding structure factors) for the structures **3** and **4** reported in this paper have been deposited with the Cambridge Crystallographic Data Centre as supplementary publication no. CCDC-406170 (**3**) and CCDC-100287 (**4**). Copies of the data can be obtained free of charge on application to The Director, CCDC, 12 Union Road, Cambridge CB21EZ, UK (fax: int. code +(1223)336-033; e-mail: deposit@chemcrys.cam.ac.uk).

[9] a) The order b of a bond X–Y, length $D(n)$, is given by $b = 10^{[D(1)-D(n)]/0.71}$, where $D(1)$ = sum of the the covalent radii of X and Y (S 1.04, O 0.66 Å). See L. Pauling, *The Nature of the Chemical Bond*, Cornell University Press, Ithaca NY, **1960**, p. 239. b) The S–N bond order is calculated by Nyburg's equation: $b(SN) = 0.429 + 6.85\,D_b - 3.825\,D_b^2$. See S. C. Nyburg, *J. Cryst. Mol. Struct.* **1973**, *3*, 331–336.

[10] T. Hascall, K. Ruhlandt-Senge, P. P. Power, *Angew. Chem.* **1994**, *106*, 350; *Angew. Chem. Int. Ed. Engl.* **1994**, *33*, 356–357.

[11] M. Cesari, S. Cucinella in *The Chemistry of Inorganic Homo- and Heterocycles, Vol. 1* (Eds.: I. Haiduc, D. B. Sowerby), Academic Press Inc. London, **1987**, p. 167.

[12] P. G. Willard, G. B. Carpenter, *J. Am. Chem. Soc.* **1986**, *108*, 462–468.

[13] D. Barr, W. Clegg, R. E. Mulvey, R. Snaith, K. Wade, *J. Chem. Soc. Chem. Commun.* **1986**, 295–297.

[14] C. E. Housecroft, *Cluster Molecules of the p-Block Elements*, Oxford University Press, Oxford, **1994**, p. 31.

[15] a) J. E. Davies, J. Kopf, E. Weiss, *Acta Crystallogr. Sect. B* **1982**, *38*, 2251–2253; b) E. Weiss, *Angew. Chem.* **1993**, *105*, 1565–1587; *Angew. Chem. Int. Ed. Engl.* **1993**, *32*, 1501–1523.

[16] M. R. Mason, J. M. Smith, S. G. Bott, A. R. Barron, *J. Am. Chem. Soc.* **1993**, *115*, 4971–4984.

[17] Unpublished results quoted in M. A. Paver, C. A. Russell, D. S. Wright, *Angew. Chem.* **1995**, *107*, 1679–1688; *Angew. Chem. Int. Ed. Engl.* **1995**, *34*, 1545–1554.

[18] Crystals of $\mathbf{4} \cdot 2C_6H_5CH_3$ were obtained by recrystallization from toluene at −17 °C (3 weeks). Crystal data for **4**: $(C_7H_{18}N_2OSSiLi_2)_6 \cdot 2C_7H_8$, M_r = 1505.84, monoclinic, space group $P\ 2_1/n$ (No. 14), a = 15.560(4), b = 19.728(6), c = 15.629(8) Å, β = 104.24(3)°, V = 4650(3) Å^3, Z = 2, ρ_{calcd} = 1.075 g cm^{-3}, $\mu(Mo_{K\alpha})$ = 0.268 mm^{-1}, $\lambda(Mo_{K\alpha})$ = 0.71069 Å, T = −103(1) °C, $F(000)$ = 1616. Data were collected on a Rigaku AFC6S diffractometer on a colorless prism (0.50 × 0.40 × 0.15 mm^3) mounted directly from the solution on a glass fiber coated with epoxy resin. Of a total of 8822 reflections, 8494 were unique (R_{int} = 0.085), 2188 were observed [$I > 3.00\sigma(I)$] and used to refine 283 parameters. The structure was solved by direct methods and expanded using Fourier techniques [25]. The S, O, N, and Si/C positions were refined anisotropically, while the remaining carbon and hydrogen atoms were refined isotropically. The silicon atoms of the Me_3Si groups and the carbon atoms of the *t*Bu groups were scrambled over all positions. Therefore, these positions were refined as Si with partial occupancy factors leading to electron populations corresponding to three Si and three C atoms over six sites. No distinctions could be made about the positions of C and Si atoms, and hence C–C and Si–C distances are not typical. The solvent molecules were highly disordered; therefore the C atoms with partial occupancy factors were included at fixed positions. Hydrogen atoms were included but not refined. Refinement converged at R = 0.125 and R_w = 0.084.

[19] M. B. Power, J. W. Ziller, A. R. Barron, *Organometallics* **1992**, *11*, 2783–2790.

[20] T. Greiser, E. Weiss, *Chem. Ber.* **1977**, *110*, 3388–3396.

[21] G. Kresze, A. Maschke, R. Albrecht, K. Bederke, H. P. Patzschke, H. Smalla, A. Trede, *Angew. Chem.* **1962**, *74*, 135–144; *Angew. Chem. Int. Ed. Engl.* **1962**, *1*, 89–98.

[22] $\lambda(S-N) = 0.1941\,d(S-N) - 20.66$ and $\lambda(S-O) = 0.2364\,d(S-N) - 25.84$, where $\lambda(S-N)$ and $\lambda(S-O)$ are the stretching vibrations in 10^{-4}cm, and $d(S-N)$ and $d(S-O)$ the bond lengths in pm. See A. J. Banister, J. A. Durrant, I. B. Gorrell, *J. Chem. Soc. Faraday Trans.* **1985**, *81*, 1771–1782.

[23] E. Parkes, J. D. Woollins, *Inorg. Synth.* **1989**, *25*, 48–49.

[24] G. M. Sheldrick, *SHELXL-92, Program for crystal structure refinement*, Universität Göttingen (Germany) **1993**.

[25] *DIRDIF94*: P. T. Beurskens, G. Admiraal, G. Beurskens, W. P. Bosman, R. de Gelder, R. Israel, J. M. M. Smith, *The DIRFIX-94 Program System*, Technical Report of the Crystallography Laboratory, University of Nijmegen, The Netherlands, **1994**.

 © WILEY-VCH Verlag GmbH, D-69451 Weinheim, 1997 0570-0833/97/3618-1988 $ 17.50+.50/0

A Modular System for the Synthesis of Complex *N*-Glycans**

Carlo Unverzagt*

The aparagine-bound oligosaccharides found in glycoproteins (*N*-glycans) vary in their degree of branching, the terminal sugars, and the substitution of the core pentasaccharide.[1] A divergent combination of the possible linkages leads to thousands of related oligosaccharide structures. This phenomenon is also known as microheterogeneity.[2] Therefore, glycoproteins can be viewed as natural libraries, whose elements are very similar but show a high degree of diversity in the detailed structures. Complex *N*-glycans are classified by the number of branches, ranging from two to five, and by characteristic substitutions of the core pentasaccharide (Scheme 1). In the case of the pharmaceutically important glycoprotein hormone erythropoietin (EPO), the in vivo biological activity[3] of the glycoform with tetraantennary *N*-glycans was significanty greater that that of biantennary structures.

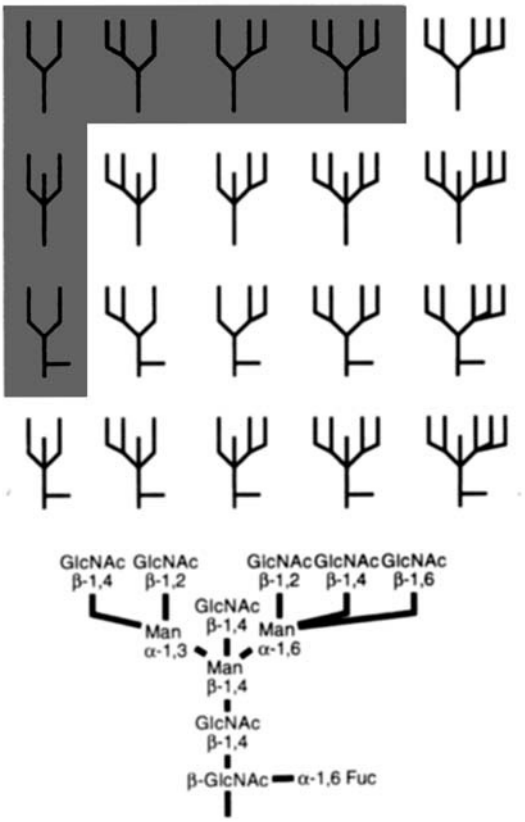

Scheme 1. Twenty individual basic structues can be distinguished for complex *N*-glycans. They result from a combination of five different degrees of branching (first row) with core substitutions by "bisecting" GlcNAc residues (second row) or core fucosylation (third row), or both modifications (fourth row). Seven examples of this class of compounds (in the grey box) were synthesized by a flexible system of oligosaccharide building blocks.

[*] Dr. C. Unverzagt[+]
Institut für Organische Chemie und Biochemie
der Technische Universität München
Lichtenbergstrasse 4, D-85748-Garching (Germany)
[+]Current address:
Institut für Organische Chemie der Universität
Karlstrasse 23, D-80333 München (Germany)
Fax: Int. code +(89)5902-483
e-mail: unv@org.chemie.uni-muenchen.de

[**] This work was supported by the Deutsche Forschungsgemeinschaft and the Leonhard-Lorenz-Stiftung. I would like to thank the Hoechst AG and Boehringer Mannheim for funding, and Prof. Dr. H. Kessler for his generous support.

Up to now the synthesis[4] of biantennary sialylated *N*-glycans[5] was only demonstrated in a few examples. Partial structures of complex tri- and tetraantennary *N*-glyans were chemically synthesized.[6] Entire multiantennary *N*-glycans are only accessible in small amounts by tedious isolation procedures[7] from natural sources or by semisynthesis.[8] The biosynthesis of *N*-glycans is carried out stepwise by a number of glycosyltransferases, however, only a few of the *N*-acetylglucosaminyltransferases[2c] responsible for branching have been cloned and overexpressed. In the course of this work a series of modular building blocks which provide access to synthetic tri- and tetraantennary *N*-glycans was devised (Scheme 2).

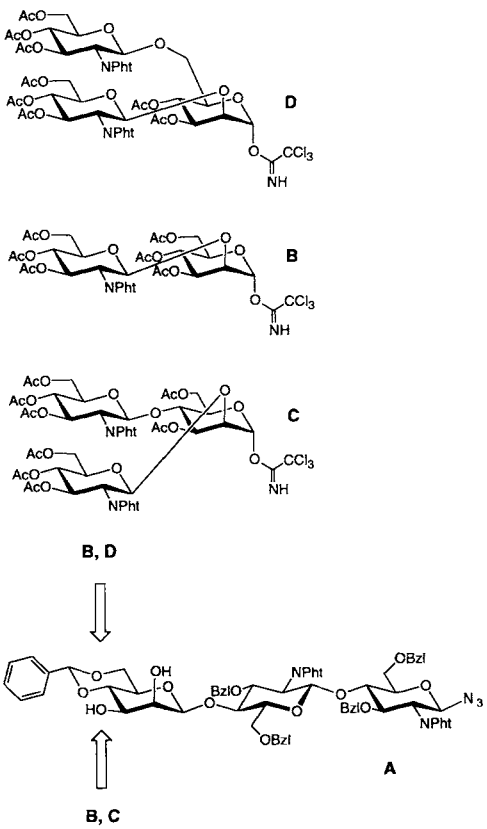

Scheme 2. The building blocks **A**–**D**; Pht = phthaloyl.

A new strategy was developed recently to obtain biantennary *N*-glycans by chemical synthesis.[9] Starting from core trisaccharide **A** (Scheme 2), positions 3 and 6 of the central β-mannosyl residue were glycosylated regio- and stereoselectively[5c] using donor **B**. Subsequent elongation of the carbohydrate chains by enzymatic synthesis gave sialylated biantennary *N*-glycans.[5c] The concept of double regioselective glycosylation of **A** could be extended and applied to the synthesis of the tri- and tetraantennary *N*-glycans **2**, **5**, and **6**. The products shown in Schemes 3 and 4 represent the most frequently found branching patterns for *N*-glycans. Together with **A** and **B** the newly synthesized trisaccharide building blocks **C** and **D** form a modular system. This allowed the multiple use of valuable intermediates to obtain various basic structures of *N*-glycans. A crucial requisite for the success of this concept was the optimized protecting-group pattern of the building blocks, and the high reactivity at the connection points provided by the vicinal diol structure of the acceptors.

 © WILEY-VCH Verlag GmbH, D-69451 Weinheim, 1997 0570-0833/97/3618-1989 $ 17.50+.50/0

The temporary allyl and benzyl groups required for the synthesis of **C**[10] und **D**[13] were replaced by acetate groups. Benzyl functionalitites in the mannosyl part of the donors may lead to β-configured side products during glycosylation.[6c] The three α-configured imidates **B**–**D** follow the same protecting-group pattern which was expected to facilitate deprotection of these parts of the molecule.

Pentasaccharide **1** was obtained as an intermediate[5c] during the synthesis of biantennary *N*-glycans starting from core trisaccharide **A** and donor **B** (Scheme 3). Elongation of pentasaccharide **1** with the imidate **B** gave the heptasaccharide in 73% yield. To achieve selective reaction at the primary hydroxyl group, the glycosylation was performed under dilute conditions. Otherwise overreaction at the second OH functionality occurred. As an initial test of the glycosylating properties of the branched and thus sterically more demanding trisaccharide imidate **D**, the coupling with pentasaccharide **1** was examined. Activation of the imidate **D** under dilute conditions with $BF_3 \cdot OEt_2$ gave the triantennary octasaccharide **2**[16] in 76% yield (Table 1). The α-1,6-linked product was formed selectively. This was confirmed by the characteristic downfield shift of the ^{13}C NMR signal for C-6^3 (60.4 → 66.3) and a C-1,H-1 coupling constant[17] of 176.2 Hz for C-$1^{4'}$, which is typical for α-mannosides.

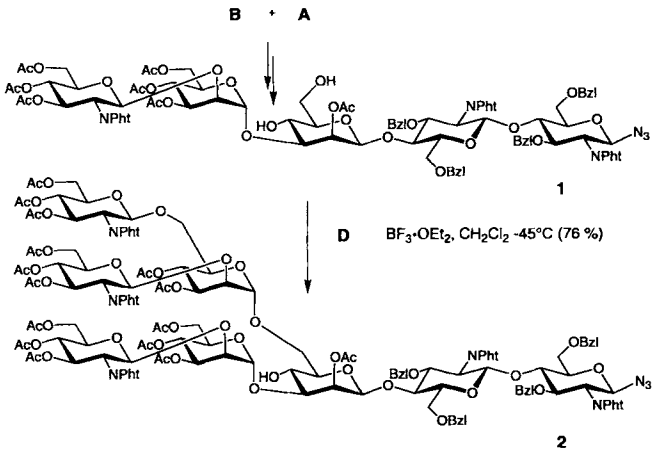

Scheme 3. Synthesis of **1** and **2**.

A steric hindrance during the regioselective glycosylation at OH-3^3 of the core trisaccharide **A** with the branched donor **C** was not observed. The coupling to hexasaccharide **3** proceeded with an unexpectedly high yield of 93%(Scheme 4). The newly formed α-1,3-linkage was verified by NMR spectroscopy: the signal for C-3^3 of **3** is shifted from $\delta = 69.9$ to 78.0, and J(C-1,H-1) is 172.7 Hz for C-1^4. Acetylation of the free hydroxyl group in **3** followed by debenzylidenation with *p*-toluenesulfonic acid gave the hexasaccharide diol **4**. These conditions permitted acidic acetal cleavage without affecting the numerous acetyl groups. Subsequently, the linear donor **B** was coupled with the acceptor **4** to the triantennary octasaccharide **5**[16] in 70% yield (Table 1). The presence of the branched mannoside in the 1,3-arm of **4** did not affect the reaction at the primary OH group.

The sterically most demanding glycosylation of the hexasaccharide acceptor **4** also proceeded regio- and stereoselectively with the trisaccharide building block **D** (Scheme 4). Nonasaccharide **6**,[16] a partial structure of tetraantennary *N*-glycans, was obtained in 78% yield (Table 1). Others have reported difficulties in the formation of glycosidic linkages using branched donors.[18]

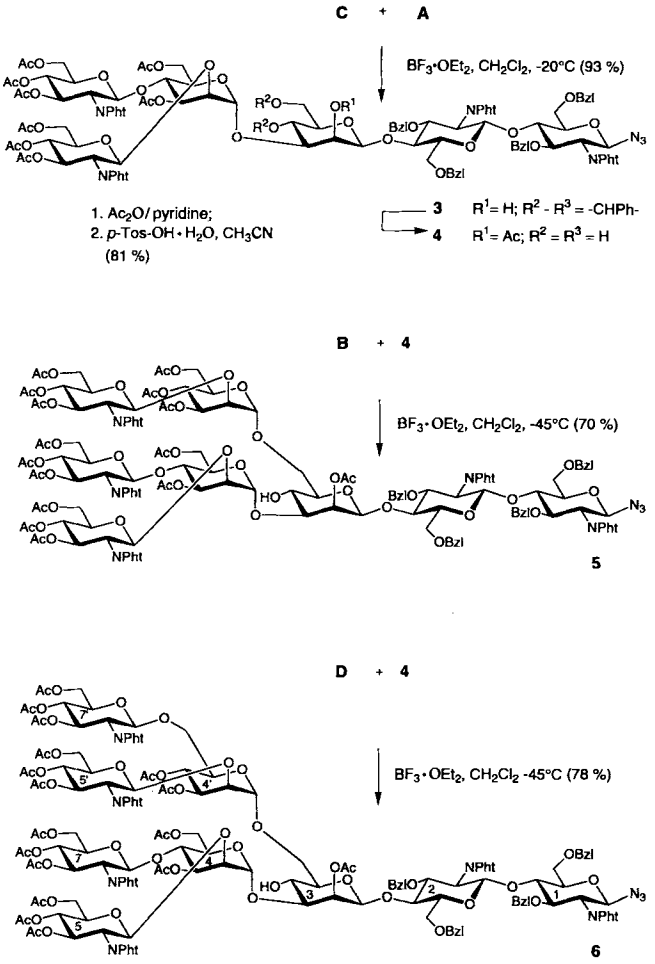

Scheme 4. Synthesis of **3**–**6**.

Surprisingly, a comparison of the glycosylation yields showed that under identical conditions the branched trisaccharide imidates **C** and **D** gave even higher yields than the linear disaccharide **B**. It may be assumed that the reactivity of the trisaccharides **C** and **D** is lower than that of **B**, and, because of the slower rearrangement to the unreactive trichloroacetamides,[19] higher yields are obtained. However, higher yields should only be observed when steric hindrance is not increased. Therefore, combining donors **C** and **D** with the complex acceptors carrying two adjacent OH groups is favored from a steric point of view. The protected compounds **1**–**6** were purified by flash chromatography and characterized by NMR spectroscopy with HMQC, HMQC-COSY, HMQC-DEPT, HMQC-TOCSY, TOCSY, and NOESY experiments.[20]

The often problematic removal of phthalimido groups was examined for compound **6**, which was converted into the water-soluble nonasaccharide **7** in three steps (Scheme 5). A one-pot reaction with ethylenediamine in *n*-butyl alcohol[21] followed by an acetylation–deacetylation sequence proceeded smoothly, as seen previously for the deprotection of the biantennary parent compound.[5c] Solid-phase extraction furnished the deprotected nonasaccharide **7**[16] in high yield. The remaining protecting groups in the chitobiosyl part are strategically valuable. They allow the construction of glycoconjugates through an *N*-glycosidic bond at the anomeric center, and facilitate purification by reversed-phase HPLC.[5c]

An additional extension of this flexible synthesis concept was demonstrated recently by incorporation of a modified building block **A**, which led to core-fucosylated *N*-glycans.[22] Further-

 © WILEY-VCH Verlag GmbH. D-69451 Weinheim. 1997 0570-0833/97/3618-1990 $ 17.50+.50/0

Table 1. Physical and spectroscopic data for **2**, **5**, **6**, and **7** [16]. Only representative NMR data are given for compounds **2** and **5** [a].

2: $[\alpha]_D^{23} = -13.3°$ ($c = 0.5$ in dichloromethane); $C_{146}H_{150}N_8O_{60}$ (2976.81); FAB-MS (NBA): $M_{calcd} = 2974.9$, $M_{found} = 2976$ ($M+H^+$); ^{13}C NMR (125 MHz, [D$_6$]DMSO): $\delta = 97.7$ (C-1$^4\alpha$, J(C-1,H-1) = 176.2 Hz in a coupled HMQC spectrum), 97.6 (C-1$^{7'}$), 96.9 (C-1^3), 96.64 (C-1$^{4'}\alpha$, J(C-1,H-1) = 176.2 Hz), 96.62 (C-1^2), 96.0 (C-1^5), 95.9 (C-1$^{5'}$), 84.7 (C-1^1).

5: $[\alpha]_D^{23} = +4.0°$ ($c = 0.5$ in dichloromethane); $C_{146}H_{150}N_8O_{60}$ (2976.81); FAB-MS (NBA): $M_{calcd} = 2974.9$, $M_{found} = 2099.1$ ($M+Na^+$); ^{13}C NMR (125 MHz, [D$_6$]DMSO): $\delta = 97.7$ (C-1$^4\alpha$, J(C-1,H-1) = 177.6 Hz), 97.1 (C-1$^{4'}\alpha$, J(C-1,H-1) = 177.6 Hz), 96.8 (C-1^2), 96.7 (C-1^3), 96.4 (C-1$^{5'}$), 96.2 (C-1^5), 95.3 (C-1^7), 84.8 (C-1^1).

6: $[\alpha]_D^{23} = -2.1°$ ($c = 0.5$ in dichloromethane); $C_{164}H_{167}N_9O_{68}$ (3352.14); FAB-MS (NBA): $M_{calcd} = 3350.0$, $M_{found} = 3377.5$ ($M+Na^+$); ^1H NMR (500 MHz, [D$_6$]DMSO): $\delta = 8.04-7.60$ (m, 24H, Pht), 7.30–6.70 (m, 20H, Ar), 5.64 (m, 1H, H-3^5), 5.62 (m, 1H, H-3^7), 5.48–5.39 (m, 3H, H-1^7, H-3$^{5'}$, H-3$^{7'}$), 5.31 (d, J(1,2) = 8.5 Hz, 1H, H-1^5), 5.29 (d, J(OH-4,4) = 5.2 Hz, 1H, OH-4^3), 5.25 (d, J(1,2) = 9.5 Hz, 1H, H-1^1), 5.18–5.12 (m, 2H, H-1^2, H-1$^{5'}$), 5.04–4.97 (m, 3H, H-2^3, H-4^5, H-4^7), 4.94 (d, J(1,2) = 8.2 Hz, 1H, H-1^7), 4.89 (dd, J(3,4) = J(4,5) = 9.5 Hz, 1H, H-4$^{5'}$), 4.85–4.80 (m, 3H, H-4$^{7'}$, H-3$^{4'}$, CH$_2$O), 4.76–4.70 (m, 3H, H-1^4, H-3^4, H-4$^{4'}$), 4.50–4.42 (m, 3H, H-1^3, CH$_2$O), 4.39 (d, J_{gem} = 12.2 Hz, 1H, CH$_2$O), 4.37–3.82 (m, 25H), 3.80–3.62 (m, 6H, H-2^1, H-2$^{7'}$, H-4^4, H-5^4, H-5$^{4'}$, H-6b$^{5'}$), 3.59 (m, 1H, H-6a^2), 3.57–3.50 (m, 2H, H-5^1, H-5^7), 3.48–3.36 (m, 4H, H-6a^1, H-6b^2, H-6b^4, H-6a$^{4'}$), 3.30–3.17 (m, 6H, H-3^3, H-4^3, H-5^2, H-5$^{5'}$, H-6b^1, H-6a^3), 3.04–2.94 (m, 2H, H-6b^3, H-6b$^{4'}$), 2.90 (m, 1H, H-5^3), 2.02, 2.015, 2.01, 2.0, 1.98, 1.96, 1.92, 1.78, 1.77, 1.76, 1.75, 1.74, 1.73, 1.68, 1.63 (15s, 51H, OAc); ^{13}C NMR (125 MHz, [D$_6$]DMSO): $\delta = 170.1-167.2$ (C=O), 138.3, 138.1, 138.0 (*ipso*-C, Ar), 135.1, 134.9, 134.6 (C-4/5, Pht), 130.9, 130.7, 130.6, 130.5 (C-1/2, Pht), 128.2–127.0 (C-Ar), 123.8, 123.7, 123.4 (C-3/6, Pht), 97.9 (C-1$^4\alpha$, J(C-1,H-1) = 180.0 Hz), 97.7 (C-1$^{7'}$), 96.70 (C-1^2, C-1$^3\beta$, J(C-1,H-1) = 162.7 Hz), 96.65 (C-1$^{4'}\alpha$, J(C-1,H-1) = 172.6 Hz), 96.2 (C-1^5), 96.0 (C-1$^{5'}$), 95.3 (C-1^7), 84.7 (C-1^1), 77.0 (C-4^2), 76.8 (C-3^1), 76.6 (C-3^3), 75.7 (C-5^1), 75.5 (C-3^2), 75.3 (C-4^1), 74.3 (C-5^3), 74.2 (C-5^2), 73.9 (CH$_2$O), 73.4 (C-2^4), 73.3 (C-2$^{4'}$), 73.2, 72.3 (CH$_2$O), 71.6 (CH$_2$O, C-4^4), 71.0 (C-5^5), 70.8 (C-5$^{7'}$), 70.7 (C-5$^{5'}$), 70.5 (C-5^7), 70.3 (C-2^3), 70.1 (C-3$^{7'}$), 69.9 (C-3$^{5'}$, C-3^7), 69.8 (C-3^5), 69.6 (C-3$^{4'}$), 68.8 (C-3^4), 68.6 (C-4^5), 68.5 (C-5$^{4'}$), 68.4 (C-4$^{7'}$), 68.3 (C-4$^{5'}$), 68.2 (C-4^7), 67.9 (C-5^4, C-6$^{4'}$), 67.4 (C-6^1, C-6^2), 66.5 (C-6^3), 66.2 (C-4^3), 64.8 (C-4$^{4'}$), 61.9 (C-6^4, C-6^5), 61.5 (C-6$^{7'}$), 61.4 (C-6$^{5'}$, C-6^7), 55.8 (C-2^2), 54.6 (C-2^1), 54.5 (C-2^7), 53.9 (C-2$^{7'}$), 53.8 (C-2^5, C-2$^{5'}$), 20.4, 20.2, 20.1, 20.0, 19.8 (OAc).

7: $[\alpha]_D^{23} = -27.9°$ ($c = 0.5$ in water); $C_{94}H_{133}N_9O_{45}$ (2109.12); ESI-MS (water/methanol, 1/1): $M_{calcd} = 2107.8$, $M_{found} = 1055.4$ [$(M+2H)^+$]; ^1H NMR (500 MHz, D_2O, [D$_6$]acetone as internal standard): $\delta = 7.36-7.12$ (m, 20H, Ar), 4.98 (d, 1H, J(1,2) < 1.0 Hz, H-1^4), 4.78 (d, J_{gem} = 12.2 Hz, 1H, CH$_2$O), 4.68 (d, J_{gem} = 12.0 Hz, 1H, CH$_2$O), 4.61 (d, 1H, J(1,2) < 1.0 Hz, H-1$^{4'}$), 4.53–4.50 (m, 2H), 4.47–4.31 (m, 6H, H-1^3, H-1^5, H-1^7, H-1$^{7'}$, CH$_2$O), 4.25 (m, 3H, H-1^2, CH$_2$O), 4.10 (m, 2H, H-1$^{5'}$, H-2^4), 3.97–3.92 (m, 3H, H-2^3, H-3^4, H-6a$^{4'}$), 3.22–3.18 (m, 2H, H-5^2, H-5^3), 2.86 (m, 1H, H-5$^{5'}$), 1.91, 1.90, 1.89, 1.88, 1.66, 1.62 (6s, 18H, NAc); ^{13}C NMR (125 MHz, D_2O, [D$_6$]acetone as internal standard): $\delta = 174.9-174.0$ (C=O), 138.6, 138.4, 137.7, 137.6 (*ipso*-C, Ar), 129.1–128.2 (C-Ar, C-1$^{7'}$), 101.8 (C-1$^{7'}$), 100.7 (C-1^2), 100.5 (C-1^3), 100.2 (C-1^5), 99.8 (C-1$^{5'}$), 99.5 (C-1^4), 96.9 (C-1$^{4'}$), 88.8 (C-1^1), 81.0 (C-3^3), 80.4 (C-3^1), 80.3 (C-3^2), 78.4 (C-4^4), 77.6 (C-4^2), 76.9 (C-2$^{4'}$), 76.5 (C-2^4), 76.3 (C-5^1), 76.24 (C-5^7), 76.16 (C-5^5), 76.14 (C-5$^{7'}$), 75.8 (C-5$^{5'}$), 75.4 (C-4^1), 74.6 (C-5^3), 74.2, 74.10 (CH$_2$O), 74.07 (C-5^2, C-3$^{7'}$), 73.9, 73.6 (C-3^5, C-3^7), 73.3 (C-3$^{5'}$, CH$_2$O), 72.1 (C-5^4), 71.8 (C-5$^{4'}$), 70.7 (C-2^3), 70.3, 70.1 (C-4^5, C-4^7, C-4$^{7'}$, C-6$^{4'}$), 69.9 (C-3$^{4'}$, C-4$^{5'}$), 68.4 (C-3^4), 68.3 (C-6^2), 68.0 (C-6^1), 67.8 (C-4$^{4'}$), 65.8 (C-4^3), 65.6 (C-6^3), 61.4 (C-6^4), 61.1, 61.0 (C-6^5, C-6^7, C-6$^{7'}$), 60.5 (C-6$^{5'}$), 55.9 (C-2$^{5'}$, C-2^7, C-2$^{7'}$), 55.7 (C-2^5), 55.3 (C-2^2), 54.0 (C-2^1), 22.8, 22.7, 22.5, 22.3 (NAc).

[a] NBA = *m*-Nitrobenzyl alcohol, Pht = phthaloyl.

more, the glycosylation of the free OH-4^3 functionality of the heptasaccharide[5c] obtained from compounds **A** and **B** gave access to the class of "bisecting" *N*-glycans.[23]

For the first time the most frequently found basic structures of *N*-glycans could be assembled by a single synthetic scheme. The versatile building blocks **A**–**D** provide an efficient chemical equivalent for the modular structure of these natural oligosaccharides. In the future this will facilitate the synthesis of those *N*-glycans that display biological functions and are difficult to isolate. The final compounds were obtained in high yields throughout. After removal of the majority of the protecting groups, the synthetic *N*-glycans are accessible for functionalization at the anomeric center and enzymatic elongation of the oligosaccharide portion.

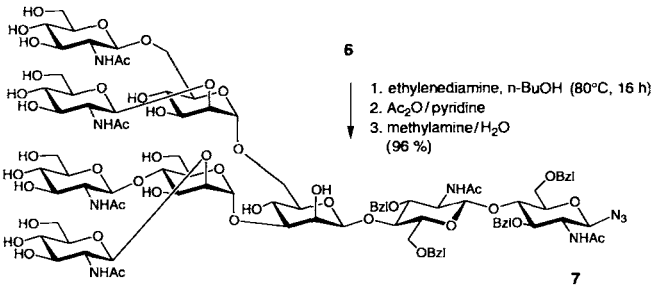

Scheme 5. Selective cleavage of the protecting groups: synthesis of **7**.

Received: January 27, 1997 [Z10037IE]
German version: *Angew. Chem.* **197**, *109*, 2078–2081

Keywords: carbohydrates · glycans · glycosides · glycosylations · polysaccharides

[1] Review: E. G. Berger, E. Buddecke, J. P. Kamerling, A. Kobata, J. C. Paulson, J. F. G. Vliegenthart, *Experientia* **1982**, *38*, 1129–1162.

[2] Reviews: a) R. A. Dwek, *Chem. Rev.* **1996**, 96, 683–720; b) A. Varki, *Glycobiology* **1993**, *3*, 97–130; c) H. Schachter, *Biochem. Cell. Biol.* **1984**, *64*, 163–181.

[3] M. Takeuchi, N. Inoue, T. W. Strickland, M. Kobuta, M. Wada, R. Shimizu, S. Hoshi, H. Kozutsumi, S. Takasaki, A. Kobata, *Proc. Natl. Acad. Sci. USA* **1989**, *86*, 7819–7822.

[4] Review: H. Paulsen, *Angew. Chem.* **1990**, *102*, 851–857; *Angew. Chem. Int. Ed. Engl.* **1990**, *29*, 823–839.

[5] a) T. Ogawa, M. Sugimoto, T. Kitajma, K. K. Sadozai, T. Nukada, *Tetrahedron Lett.* **1986**, *27*, 5739–5742; b) Y. Nakahara, S. Shibayama, Y. Nakahara, T. Ogawa, *Carbohydr. Res.* **1996**, *280*, 67–84; c) C. Unverzagt, *Angew. Chem.* **1996**, *108*, 2507–2510; *Angew. Chem. Int. Ed. Engl.* **1996**, *35*, 2350–2353.

[6] a) H. Paulsen, B. Helpap, *Carbohydr. Res.* **1991**, *216*, 289–313; b) J. Kerekgyarto, J. P. Kamerling, J. B. Bouwstra, J. F. G. Vliegenthart, A. Liptak, *ibid.* **1989**, *186*, 51–62; c) K. K. Sadozai, Y. Ito, T. Nukada, T. Ogawa, A. Kobata, *ibid.* **1986**, *150*, 91–101; d) K. K. Sadozai, T. Nukada, Y. Ito, Y. Nakahara, T. Ogawa, A. Kobata, *ibid.* **1986**, *157*, 101–123; e) J. Arnarp, M. Haraldsson, J. Lönngren, *J. Chem. Soc. Perkin Trans. 1* **1982**, 1841–1844; f) *Carbohydr. Res.* **1981**, *97*, 307–313; g) J. Arnarp, J. Lönngren, *J. Chem. Soc. Perkin Trans. 1* **1981**, 2070–2074.

[7] a) S. W. Homanns, R. A. Dwek, D. L. Fernandes, T. W. Rademacher, *Proc. Natl. Acad. Sci. USA* **1984**, *81*, 6286–6289; b) T. Endo, *J. Chromatogr. A* **1996**, *720*, 251–261; c) K. G. Rice, M. L. Corradi Da Silva, *ibid.* **1996**, *720*, 235–249.

[8] a) M. H. Chiu, T. Tamura, M. S. Wadhwa, K. G. Rice, *J. Biol. Chem.* **1994**, *269*, 16195–16202; b) M. H. Chiu, V. H. Thomas, H. J. Stubbs, K. G. Rice, *ibid.* **1995**, *270*, 24024–24031; c) C.-H. Lin, M. Shimazaki, C.-H. Wong, M. Koketsu, R. R. Juneja, M. Kim, *Bioorg. Med. Chem.* **1995**, *3*, 1625–1630; d) J. Helin, H. Maaheimo, A. Seppo, A. Keane, O. Renkonen, *Carbohydr. Res.* **1995**, *266*, 191–209.

[9] C. Unverzagt, *Angew. Chem.* **1994**, *106*, 1170–1173; *Angew. Chem. Int. Ed. Engl.* **1994**, *33*, 1102–1104.

[10] Donor **C** was obtained by the following reaction sequence: a) benzyl 3,6-di-*O*-allyl-α-D-mannopyranoside [11] and 3,4,6-tri-*O*-acetyl-2-deoxy-2-phthalimido-α,β-D-glucopyranosylfluoride [12], CH_2Cl_2, molecular sieves (4 Å), $BF_3 \cdot Et_2O$ (81%); b) 1. $PdCl_2$, NaOAc, AcOH; 2. Ac_2O/pyridine, 4-dimethylaminopyridine (DMAP) (77%); c) 1. Pd/H_2, MeOH; 2. CCl_3CN, 1,8-diazabicyclo[5.4.0]undec-7-ene (DBU), CH_2Cl_2 (80%).

[11] J. Arnarp, J. Lönngren, *Acta Chem. Scand. B* **1978**, *32*, 696–697.

[12] C. Unverzagt, H. Kunz, *J. Prakt. Chem.* **1992**, *334*, 570–578.

[13] Donor **D** was obtained by the following reaction sequence: a) benzyl 3,4-di-*O*-benzyl-α-D-mannopyranoside [14] and 3,4,6-tri-*O*-acetyl-2-deoxy-2-phthalimido-β-D-glucopyranosyl-trichloroacetimidate [15], CH_2Cl_2, molecular sieves (4 Å), $BF_3 \cdot Et_2O$ (53%); b) 1. Pd/H_2, MeOH; 2. Ac_2O/pyridine (70%); c) 1. hydrazine acetate, DMF; 2. CCl_3CN, DBU, CH_2Cl_2 (68%).

[14] J. Arnarp, M. Haraldsson, J. Lönngren, *Carbohydr. Res.* **1981**, *97*, 307–313.

[15] R. R. Schmidt, W. Kinzy in *Adv. Carbohydr. Chem. Biochem. Vol. 50* (Ed.: D. Horton), Academic Press, New York, **1994**, pp. 21–123.

[16] The individual residues are assigned according to **6**.

[17] a) K. Bock, C. Pedersen, *J. Chem. Soc. Perkin Trans. 2* **1974**, 293–297; b) S. Wolfe, B. M. Pinto, V. Varma, R. Y. N. Leung, *Can. J. Chem.* **1990**, *68*, 1051–1062.

[18] a) Y.-M. Zhang, A. Brodzky, P. Sinai, G. Saint-Marcoux, B. Perly, *Tetrahedron: Asymmetry* **1995**, *6*, 1195–1216; b) P. Grice, S. V. Ley, J. Pietruszka, H. W. M. Priepke, *Angew. Chem.* **1996**, *108*, 206–208; *Angew. Chem. Int. Ed. Engl.* **1996**, *35*, 197–200.

 © WILEY-VCH Verlag GmbH, D-69451 Weinheim, 1997 0570-0833/97/3618-1991 $ 17.50+.50/0

[19] F. Cramer, N. Hennrich, *Chem. Ber.* **1961**, *94*, 976–989.
[20] a) H. Kessler, M. Gehrke, C. Griesinger, *Angew. Chem.* **1988**, *100*, 507–554; *Angew. Chem. Int. Ed. Engl.* **1988**, *27*, 490–536; b) H. Kessler, P. Schmieder, M. Kurz, *J. Magn. Reson.* **1989**, *65*, 400–405.
[21] O. Kanie, S. C. Crawley, M. M. Palcic, O. Hindsgaul, *Carbohydr. Res.* **1993**, *243*, 139–164.
[22] J. Seifert, C. Unverzagt, *Tetrahedron Lett.* **1996**, *37*, 6527–6530.
[23] a) C. Unverzagt, *Abstr. Pap. 17th Int. Carbohydr. Symp.* (Ottawa, Canada), **1994**, B1.66; b) C. Unverzagt, J. Seifert, unpublished results.

Phosphorus(v) Nitride Imide HP_4N_7: Synthesis from a Molecular Precursor and Structure Determination with Synchrotron Powder Diffraction**

Stefan Horstmann, Elisabeth Irran, and Wolfgang Schnick*

The ammonolysis of phosphorus(v) chloride (PCl_5) leads to chlorine-rich compounds such as $[NPClNH_2]_x$ or to totally substituted compounds such as $[NP(NH_2)_2]_x$, depending on the reaction temperature and the distribution ratio NH_3:PCl_5.[1] Already in the last century a polymeric compound HPN_2 was postulated to be the final product of substitution and condensation.[2–4] However, the ammonolysis of PCl_5 leads to countless oligomeric and polymeric phosphazenes; no single-phase and well-defined product HPN_2 was obtained. Pure and crystalline HPN_2 was synthesized recently by heterogeneous pressure ammonolysis of phosphorus(v) nitride [Eq. (a)].[5] Phosphorus(v)

$$P_3N_5 + NH_3 \xrightarrow{580\,^\circ C} 3\,HPN_2 \qquad (a)$$

nitride imide (HPN_2) has the framework structure $^3_\infty[(PN_{4/2})^-]$ built up of PN_4 tetrahedra linked by corner-sharing through all four vertices. This structure, which is also found in $LiPN_2$,[6] is derived from the isosteric β-cristobalite type.[5] The hydrogen atoms are bound in an ordered manner to half of the nitrogen atoms.[7]

We recently obtained the novel phosphorus(v) nitride imide HP_4N_7[8] by the reaction of P_3N_5 with ammonium chloride in closed, thick-walled quartz ampoules [Eq. (b)]. However, X-ray

$$4\,P_3N_5 + NH_4Cl \xrightarrow{820\,^\circ C} 3\,HP_4N_7 + HCl \qquad (b)$$

powder diffraction measurements indicate that HP_4N_7 is not formed as a single-phase product by this reaction. Furthermore, since it was not possible to obtain single crystals of HP_4N_7, the crystal structure could not yet be elucidated. This structure is nevertheless of particular interest, because HP_4N_7, in addition to P_3N_5, is one of a few highly condensed phosphorus(v) nitrides (molar ratio P:N > 1:2). Therefore, the structure of HP_4N_7 should not be analogous to that of silicates.

[*] Prof. Dr. W. Schnick, Dr. S. Horstmann, Mag. E. Irran
Laboratorium für Anorganische Chemie der Universität
D-95440 Bayreuth (Germany)
Fax: Int. code +(921)55-2788
e-mail: wolfgang.schnick@uni-bayreuth.de

[**] This work was supported by the Fonds der Chemischen Industrie, the Deutsche Forschungsgemeinschaft (project SCHN 377/2-2 and Gottfried-Wilhelm-Leibniz-Programm), and the Bundesministerium für Bildung, Wissenschaft, Forschung und Technologie as part of the project "Erforschung kondensierter Materie" (project 03-SC4 BAY). We thank Dr. D. E. Cox and Dr. Q. Zhu (NSLS, Brookhaven) for their help during the synchrotron experiment, and Dr. R. Dinnebier (Lehrstuhl Kristallographie, Universität Bayreuth) for discussions during the structure refinement.

While systematically investigating the development of molecular precursors for the synthesis of well-defined, crystalline nonmetal nitrides (molecular preorganization[9, 10]), we obtained $(NH_2)_2P(S)NP(NH_2)_3$ (**1**).[11] According to thermoanalytical investigations diphosphazene **1** loses H_2S already at 145 °C with formation of amorphous poly(aminoiminophosphazene)s. In contrast, the pyrolysis of **1** in closed pressure ampoules at 750 °C (see Experimental Section) leads to pure and crystalline HP_4N_7 [**2**; Eq. (c)]. During this procedure phosphorus(v) nitride imide

$$\underset{\mathbf{1}}{2\,(NH_2)_2P(S)NP(NH_2)_3} \xrightarrow{750\,^\circ C} \underset{\mathbf{2}}{HP_4N_7} + 2\,H_2S + 5\,NH_3 \qquad (c)$$

(**2**) is formed as a microcrystalline, colorless powder. It is stable in a nonoxidizing atmosphere up to 800 °C; further increase of temperature leads to loss of NH_3 and formation of P_3N_5. HP_4N_7 is insoluble in common solvents as well as in hot acids and alkaline solutions.

The determination and refinement of the crystal structure of HP_4N_7 were based on powder X-ray diffraction data. The measurements were made with synchrotron radiation at the National Synchrotron Light Source in Brookhaven, USA (Beamline X7A). The powder pattern obtained (Figure 1) could be indexed unambiguously, and the structure determination by direct methods as well as the subsequent Rietveld refinement were successful (see Experimental Section).

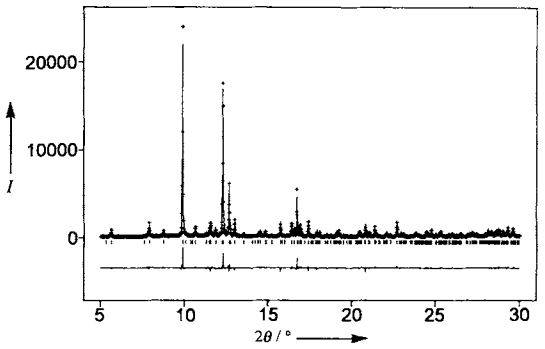

Figure 1. The observed (crosses) and calculated X-ray powder diffraction pattern (line) as well as the difference profile of the Rietveld refinement of HP_4N_7 (only the section until $2\theta = 30°$ is shown). The possible positions of the peaks are marked by vertical lines. The powder pattern was obtained at the National Synchrotron Light Source (NSLS) at Brookhaven, USA, on the Beamline X7A ($\lambda = 69.906$ pm). I = intensity in counts.

Solid HP_4N_7 is made up of a three-dimensional network structure of connected PN_4 tetrahedra, according to $^3_\infty[(P^{[4]}_4N^{[2]}_5N^{[3]}_2)^-]$ (Figure 2). Whereas in β-cristobalite-analogous HPN_2[5] the nitrogen atoms are only bound to two phosphorus atoms ($N^{[2]}$), in HP_4N_7 there are also nitrogen atoms connected to three phosphorus atoms ($N^{[3]}$).[*] The situation resembles that in phosphorus(v) nitride $^3_\infty[(P^{[4]}_3N^{[2]}_3N^{[3]}_2)]$.[12] In HP_4N_7 there exist pairs of edge-sharing PN_4 tetrahedra. This structural motive has so far only been found in P_3N_5[12] and P_4N_6O.[13] In the nitridosilicates $Ba_5Si_2N_6$[14] and $BaSi_7N_{10}$[15] analogous edge-sharing pairs of tetrahedra are found, while in oxosilicates a comparable edge linkage has not yet been confirmed.

The three-dimensional network structure of HP_4N_7 may be separated into two different open-branched zweier single chains (Figure 3). The main cords of both arrangements are built up of corner-sharing PN_4 tetrahedra; in one case the branch results by

[*] The superscripted numbers in square brackets define the coordination number of the element.

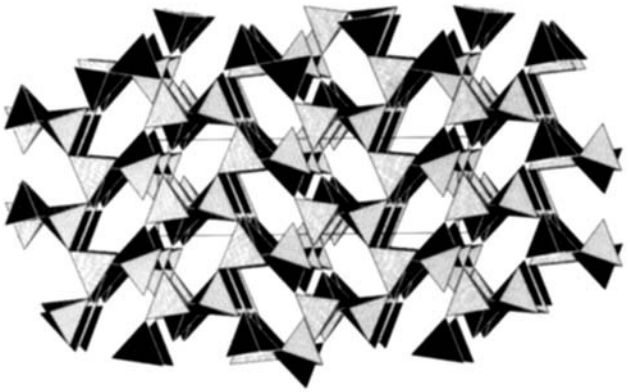

Figure 2. Crystal structure of HP_4N_7 as viewed along [001]. Open-branched zweier single chains, in which the PN_4 tetrahedra are linked alternately through common corners and edges, are connected by further PN_4 tetrahedra. The pairs of tetrahedra resulting from edge-sharing are shown in black.

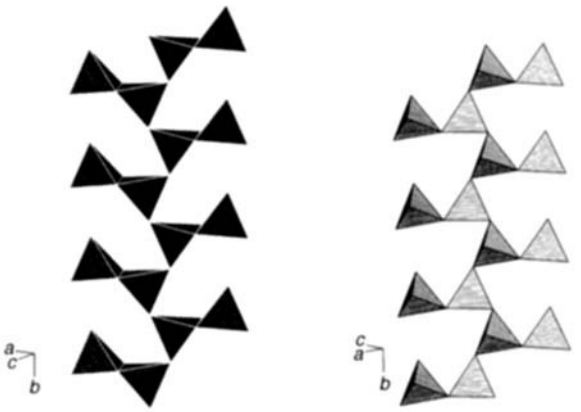

Figure 3. Two different open-branched zweier single chains of PN_4 tetrahedra are found in HP_4N_7. Branching results from edge-sharing (left) and corner-sharing (right).

edge-sharing, and in the other by corner-sharing. The whole network is formed from the alternating arrangement and vertex-sharing of these cords. As in α-P_3N_5[12] all ring sizes P_nN_n with the exception of $n = 3$ are found in the P–N network of HP_4N_7. In contrast, analogously condensed Si_3N_3 rings often occur in highly condensed nitridosilicates (Si:N > 1:2).[16]

Though P_4N_6O and HP_4N_7 are isoelectronic, different three-dimensional network structures exist in the solid-state topologically.[17] However, in the case of silicon, Si_2N_2O[18] and Si_2N_2NH[19] are homeostructural.

Although we used synchrotron radiation for the X-ray structure analysis based on powder data, we could not localize the hydrogen-atom positions. However, based on structure-chemical estimations[20] conclusions of the probable hydrogen-atom positions are possible. On average the bond lengths $P-N^{[2]}$ (152.6(7)–166.9(6) pm) are shorter than the corresponding values for $P-N^{[3]}$ (164.7(8)–172.2(7) pm). This effect occurs similarly in P_3N_5[12] and nitridosilicates.[16] The angular sum of the nitrogen atoms bonded to three phosphorus atoms is nearly 360°; therefore, these $N^{[3]}$ atoms must be considered as sp^2-hybridized. These circumstances as well as the analysis of the valence sums and effective coordination numbers[20] point to no further demand of coordination for the $N^{[3]}$ atoms. Two of the four crystallographically independent $N^{[2]}$ atoms possess largely saturated bond valences; only the remaining nitrogen atoms are suitable for bonding to hydrogen atoms. These nitrogen atoms are similar, and emerge into channels along [001] built up of P_6N_6 rings. It is possible that all hydrogen atoms are bound intrinsically disordered to these nitrogen atoms.

We are currently synthesizing DP_4N_7 to prove the postulated hydrogen-atom positions as well as their order and dynamic behavior by neutron diffraction. In the case of DPN_2, the corresponding order in the hydrogen-atom positions has recently been described.[7] The proposed arrangement of the hydrogen atoms in channels of HP_4N_7 leads to the supposition that phosphorus(v) nitride imide is suitable as a proton conductor. In the case of HPN_2, orientating measurements[21] have already shown remarkable thermal proton conductivity. The advantage of phosphorus(v) nitride imides over traditional proton conductors might be their chemical and thermal stability.

Experimental Section

HP_4N_7: $(NH_2)_2P(S)NP(NH_2)_3$ (100 mg, 53.2 mmol) was transferred under an argon atmosphere to a quartz ampoule ($d = 15$ mm, wall thickness 2 mm). The ampoule was sealed off to a length of 12 cm, and heated for 3 d in an electrical tube furnace at 750 °C. The colorless solid product remained at the bottom of the ampoule (45.7 mg, 20.3 mmol, 76.3%). Elemental analysis by Mikroanalytisches Labor Pascher, Remagen, Germany (calcd): P 55.1% (55.6%), N 40.6% (43.9%). IR (1 mg substance per 500 mg KBr): $\tilde{\nu}$ = 3089 (NH), 1338, 1262, 938 (PN), 778, 691, 651, 549, 473 cm^{-1} (framework).

The diffraction investigations with synchrotron radiation were carried out in Debye–Scherrer geometry. The sample was enclosed in a glass capillary ($d = 1.0$ mm). A wavelength of 69.906 pm was maintained by a Ge(111) double-crystal monochromator, and a Ge(220) crystal used as analyzer. A scintillation counter was used, and the measured diffraction intensities were normalized for storage ring decay by an ionization chamber monitor. The diffraction pattern was indexed unambiguously with the programs ITO [22] and TREOR-90 [23] (de Wolff figure of merit $M_{20} = 45.9$). The space group $P2_1/a$ (no. 14) resulted from the systematic extinctions. With the program EXTRA [24] 1574 integrated intensity data were extracted, and used as input for the program SIRPOW.92 [25] for structure determination by direct methods. As a result, all P and N could be localized immediately. The atomic coordinates were refined with the program system GSAS [26]. HP_4N_7: $P2_1/a$, (no. 14), $a = 1507.95(2)$, $b = 480.304(6)$, $c = 710.722(8)$ pm, $\beta = 92.191(1)°$, $Z = 4$, $F(000) = 440$, $\mu = 1.333$ mm^{-1}, measured range $4 \le 2\theta \le 60°$, 5500 data points, 1689 observed reflections, $wR_p = 0.082$, $R_p = 0.063$, $R_F = 0.038$. At the beginning of the calculation the scale factor, lattice constants, zero point, and background were refined. The profile was fitted by a pseudo Voigt function [27], and its asymmetry corrected according to ref. [28]. A total of 33 atomic parameters were refined; the thermal ellipsoids of all P atoms were refined independently, and those of N atoms as dependent on each other. Further details of the crystal structure investigation may be obtained from the Fachinformationszentrum Karlsruhe, D-76344 Eggenstein-Leopoldshafen, Germany on quoting the depository number CSD-406655.

Received: March 7, 1997 [Z10210IE]
German version: *Angew. Chem.* **1997**, *109*, 2085–2087

Keywords: nitrides · phosphorus · solid-state chemistry · structure elucidation

[1] a) A. Schmidpeter, C. Weingand, E. Hafner-Roll, *Z. Naturforsch. B* **1969**, *24*, 799; b) H. Moureu, P. Rocquet, *Bull. Soc. Chim. Fr.* **1935**, *3*, 821.
[2] H. Schiff, *Justus Liebigs Ann. Chem.* **1857**, *101*, 299.
[3] W. Couldridge, *J. Chem. Soc.* **1888**, *53*, 398.
[4] C. Gerhardt, *Ann. Chim. Phys.* **1846**, *18*, 188.
[5] W. Schnick, J. Lücke, *Z. Anorg. Allg. Chem.* **1992**, *610*, 121.
[6] W. Schnick, J. Lücke, *Z. Anorg. Allg. Chem.* **1990**, *588*, 19.
[7] H. Jacobs, R. Nymwegen, S. Doyle, T. Wroblewski, W. Kockelmann, *Z. Anorg. Allg. Chem.* **1997**, in press.
[8] W. Schnick, *Angew. Chem.* **1993**, *105*, 846; *Angew. Chem. Int. Ed. Engl.* **1993**, *32*, 806.
[9] H. P. Baldus, W. Schnick, J. Lücke, U. Wannagat, G. Bogedain, *Chem. Mater.* **1993**, *5*, 845.
[10] W. Schnick, *Comments Inorg. Chem.* **1995**, *17*, 189.
[11] S. Horstmann, W. Schnick, *Z. Naturforsch. B* **1997**, *52*, 490.
[12] S. Horstmann, E. Irran, W. Schnick, *Angew. Chem.* **1997**, *109*, 1938; *Angew. Chem. Int. Ed. Engl.* **1997**, *36*, 1873.
[13] J. Ronis, B. Bondars, A. Vitola, T. Millers, J. Schneider, F. Frey, *J. Solid State Chem.* **1995**, *115*, 265.
[14] H. Yamane, F. J. DiSalvo, *J. Alloys Compounds* **1996**, *240*, 33.
[15] H. Huppertz, W. Schnick, *Chem. Eur. J.* **1997**, *3*, 249.
[16] W. Schnick, H. Huppertz, *Chem. Eur. J.* **1997**, *3*, 679.
[17] Network structures of linked TX_4 tetrahedra (T = Si, P; X = O, N) can be characterized topologically by the "cycle class sequences", which give the rela-

 © WILEY-VCH Verlag GmbH, D-69451 Weinheim, 1997 0570-0833/97/3618-1993 $ 17.50+.50/0

tive frequency of the T_nX_n ring sizes (for $n = 1, 2, 3, \ldots$) which occur in the unit cell. Cycle class sequence of HP_4N_7: $\{-, 4, 0, 4, 16, 60, 72, 252, \ldots\}$, P_4N_6O: $\{-, 2, 0, 2, 8, 16, 40, 132, \ldots\}$; see also A. Beukemann, W. E. Klee, *Z. Kristallogr.* **1994**, *209*, 709.
[18] I. Idrestedt, C. Brosset, *Acta Chem. Scand.* **1964**, *18*, 1879.
[19] D. Peters, H. Jacobs, *J. Less-Common Met.* **1989**, *146*, 241.
[20] Effective coordination numbers according to R. Hoppe, S. Voigt, H. Glaum, J. Kissel, H. P. Müller, K. Bernet, *J. Less-Common Met.* **1989**, *156*, 105; bond length–bond strength correlation according to N. E. Brese, M. O'Keeffe, *Acta Crystallogr. Sect. B* **1991**, *47*, 192.
[21] J. Lücke, W. Schnick, unpublished results.
[22] J. W. Visser, *J. Appl. Crystallogr.* **1969**, *2*, 89.
[23] P.-E. Werner; *TREOR 90—Trial and Error Program for Indexing of Unknown Powder Patterns*, University of Stockholm, **1990**; P.-E. Werner, L. Eriksson, M. Westdahl, *J. Appl. Crystallogr.* **1985**, *18*, 367.
[24] A. Altomare, M. C. Burla, G. Cascarano, C. Giacovazzo, A. Guagliardi, A. G. G. Moliterni, G. Polidori, *J. Appl. Crystallogr.* **1995**, *28*, 842.
[25] A. Altomare, G. Cascarano, C. Giacovazzo, A. Guagliardi, M. C. Burla, G. Polidori, M. Camalli, *J. Appl. Crystallogr.* **1994**, *27*, 435.
[26] R. B. von Dreele, A. C. Larson, *General Structure Analysis System*, Los Alamos National Laboratory Report LAUR 86-748, **1990**.
[27] P. Thompson, D. E. Cox, J. B. Hastings, *J. Appl. Crystallogr.* **1987**, *20*, 79.
[28] L. W. Finger, D. E. Cox, A. P. Jephcoat, *J. Appl. Crystallogr.* **1994**, *27*, 892.

Trimethylplatinum Triflate: A Versatile Building Block in Coordination Chemistry**

Sabine Schlecht, Jörg Magull, Dieter Fenske, and Kurt Dehnicke*

The well-known trimethylplatinum compounds $[\{Me_3PtX\}_4]$ (**1**; for example, X = Cl, Br, I, N_3, OH)[1] form very stable, relatively inert heterocubane structures, in which Pt and X atoms occupy alternate corners of slightly distorted cubes. In contrast to **1**, we have found the previously reported[2] but structurally uncharacterized trimethylplatinum triflate **2** to be a versatile reagent in coordination chemistry. Its tetrameric structure (Figure 1)[3] can be "deaggregated" successively into trimeric, dimeric, and momomeric complexes by bases of various strengths (Scheme 1).

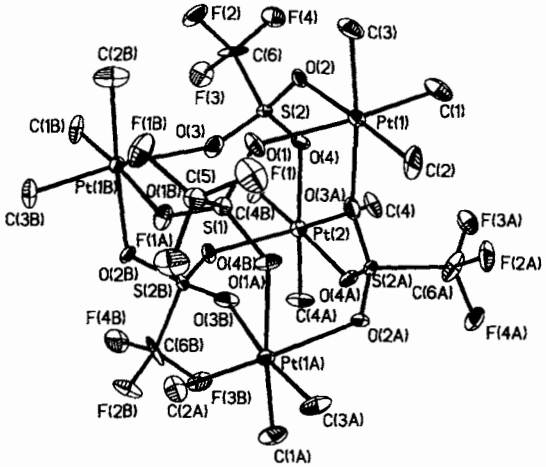

Figure 1. Crystal structure of **2**. Selected average bond lengths [pm] and angles [°]: Pt–C 200(3), Pt–O 227(2), S–O 144(2); C-Pt-C 91.2(12), O-Pt-O 87.4(7), Pt-O-S 138.8(12), O-S-O 113.9(10).

[*] Prof. Dr. K. Dehnicke, Dipl.-Chem. S. Schlecht
Fachbereich Chemie der Universität
Hans-Meerwein-Strasse, D-35032 Marburg (Germany)
Fax: Int. code +(6421)288917
Priv.-Doz. Dr. J. Magull, Prof. Dr. D. Fenske
Institut für Anorganische Chemie der Universität Karlsruhe (Germany)

[**] This work was supported by the Deutsche Forschungsgemeinschaft and the Fonds der Chemischen Industrie.

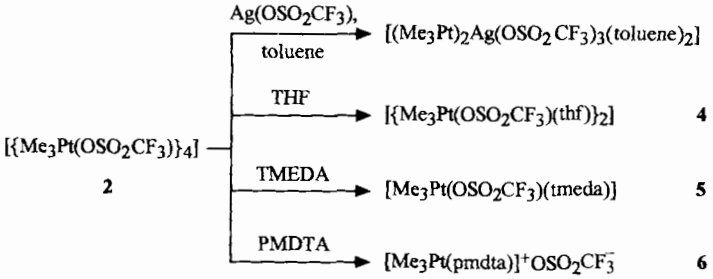

Scheme 1. Deaggregation of **2**. TMEDA = *N,N,N',N'*-tetramethylethylenediamine; PMDTA = *N,N,N',N'',N''*-pentamethyldiethylenetriamine.

This is associated with a change in the donor function of the triflate ions from μ_3 to μ_2 to nonbridging O coordination. Known examples of these types of coordination are **7**, with μ_3 and μ_2 coordination, which leads to chain formation,[4] **8**, which exhibits μ_2-coordination of a bicapped heterocubane,[5] and **9**, which contains monodentate triflate ion.[6]

$[Cu(O_3SCF_3)(\text{cyclohexene})]_\infty$ **7**

$[Cu_4(OH)_4(O_3SCF_3)_2\{N(py)_3\}_4]^{2+}$ **8**

$[Me_2Au(H_2O)(O_3SCF_3)]$ **9**

The structure of **2** is stretched relative to the heterocubane structure of **1**, and the platinum atoms of **2** are bridged by oxygen atoms of the triflate ion in a μ_3 fashion. Due to the weak donor strength of the triflate ions[7] the resulting Pt–O bonds of average length 228 pm are significantly longer than those in $[Me_3PtOH]_4$[8] (222 pm). The associated weakening of the Pt–O bonds is reflected in the relatively low-field position of the ^{1}H NMR resonance[9] for the methyl groups in the *trans* position ($\delta = 1.36$) and the large coupling constant $^2J(^1H, ^{195}Pt) = 81.6$ Hz.[1] This also explains the deaggregation of **2** by the very weak Lewis base silver triflate to give the trinuclear complex **3**, in which three triflate ions each bridge the platinum atoms of two Me_3Pt fragments through two μ_2-O atoms (Figure 2). One oxygen atom of each of two triflate ions, O(6) and O(9), is bonded to a silver ion, the coordination sphere of which is completed by two η^2-coordinated toluene molecules. This bonding mode, which has often been observed in arene complexes of silver,[10] is the reason for the relatively long Ag–O bonds of 250.7 and 245.5 pm in **3**. The ^{1}H NMR spectrum indicates a slightly increased electron density at the Me_3Pt

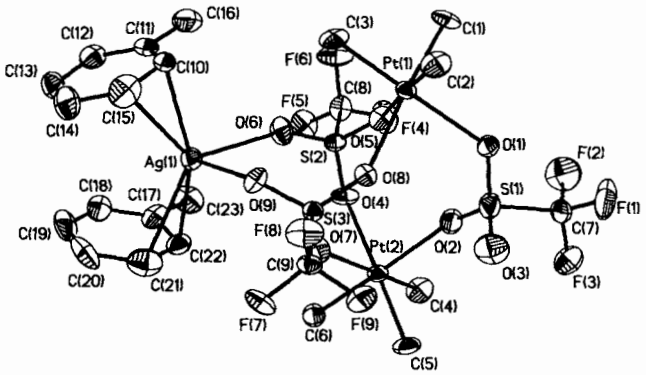

Figure 2. Crystal structure of **3**. Selected (sometimes averaged) bond lengths [pm] and angles [°]: Ag1–C10 239.2(11), Ag1–C15 257(2), Ag1–C21 268(2), Ag1–C22 238.5(12), Ag1–O6 250.7(8), Ag1–O9 245.5(8), Pt–C 200.3(12), Pt–O 226.9(7), S1–O3 147.1(10), other S–O 143.1(8); O6-Ag1-O9 84.4(3), Ag1-O6-S2 150.1(6), Ag1-O9-S3 128.3(5), Pt-O-S 138.1(5) C-Pt-C 89.1(6).

 © WILEY-VCH Verlag GmbH, D-69451 Weinheim, 1997 0570-0833/97/3618-1994 $ 17.50+.50/0

unit ($\delta = 1.28$) and correspondingly weaker coupling to the platinum atom [$^2J(^1H,^{195}Pt) = 79.4$ Hz].

With the somewhat stronger Lewis base tetrahydrofuran, **2** can be deaggregated to the dimeric complex **4**, which according to the crystal structure analysis[3] (Figure 3) contains a centrosymmetric, corrugated $Pt_2O_4S_2$ eight-membered ring, in which the platinum atoms are additionally coordinated by the O atom of a THF molecule. The Pt–O(THF) bond (222.9 pm) is slightly shorter than the Pt–O bonds to the triflate ions (227.2 pm on average), which are very similar to those in **2** and **3**. In **4** only two of the three O atoms of each triflate ion capable of coordinating are actually used for coordination. However, the corresponding S–O bonds of the bridge, with lengths of 144.6 and 145.6 pm, are only marginally longer than the nonbridging S–O bond (143.0 pm), and this indirectly reflects the weak donor strength of the triflate ion. In spite of the different donor strengths of triflate and THF, the ^{1}H NMR data of the Me_3Pt unit in **4** differ only slightly from those of **3** and show one set of signals for the methyl groups at 293 K ($\delta = 1.29$, $^2J = 80.7$ Hz). At 193 K (CD_2Cl_2, 500 MHz) two sets of signals are observed at $\delta = 1.09$ (3H, $^2J = 81.0$ Hz) and 1.21 (6H, $^2J = 76.7$ Hz), as required by the molecular symmetry.

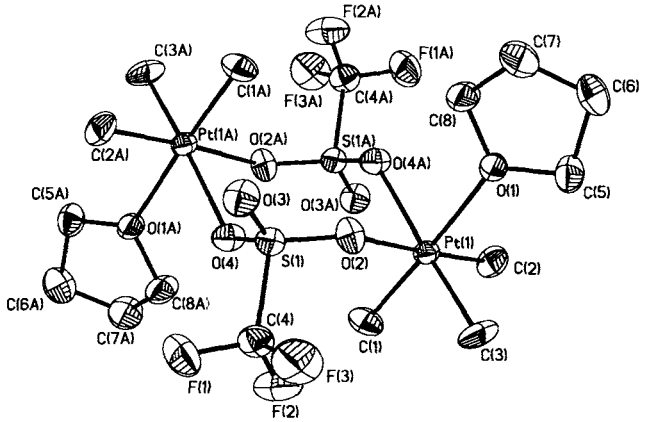

Figure 3. Crystal structure of **4**. Selected (sometimes averaged) bond lengths [pm] and angles [°]: Pt–C 201.9(6), Pt–O1 222.9(4), Pt–O2/4 227.2(4), S1–O3 143.0(4), S1–O2/4 145.1(4); C-Pt-C 89.3(3), O1-Pt1-O2 82.9(2), O1-Pt-O4A 82.4(2), O2-Pt1-O4A 87.6(2), Pt-O-S 134.7(1), O-S-O 114.7(3).

The reaction of **2** with the strong chelating base TMEDA leads to the monomeric complex **5**, in which the triflate ion is monodentate (Figure 4). Surprisingly, the Pt–O bond (232.1 pm) is now significantly longer than those of complexes **2**–**4**, which contain bridging triflate ions. Because of this very weak coordination of the triflate ion, the ^{1}H NMR signals of the Me_3Pt group are broadened by intramolecular dynamic processes at room temperature.[11] On cooling to 253 K they split into two sets of signals at $\delta = 0.79$ (3H, $^2J = 82.9$ Hz) and 1.01 (6H, $^2J = 67.2$ Hz), which are shifted upfield relative to those of **4**. The triflate ion is therefore readily substituted on reaction of **2** with the trifunctional base PMDTA to give the complex cation **6**, in which the Me_3Pt group gives rise to two sets of resonances in the ^{1}H NMR spectrum at $\delta = 0.66$ (3H, $^2J = 65.1$ Hz) and 0.80 (6H, $^2J = 68.7$ Hz). Their significant high-field shift is in good agreement with the strong donor capacity of PMDTA.

Received: April 3, 1997 [Z10305IE]
German version: *Angew. Chem.* **1997**, *109*, 2087–2089

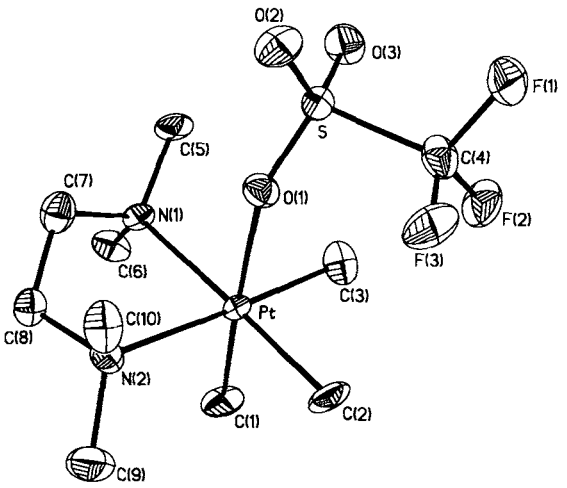

Figure 4. Crystal structure of **5**. Selected (sometimes averaged) bond lengths [pm] and angles [°]: Pt–C 203.9(7), Pt–O1 232.1(6), Pt–N 224.3(6), S–O1 145.3(6), S–O2/3 143.8(6); C-Pt-C 87.8(4), N1-Pt-N2 82.6(3) O1-Pt-N 87.2(2).

Keywords: arene complexes · bridging ligands · platinum · silver

[1] Review: V. K. Jain, G. S. Rao, L. Jain, *Adv. Organomet. Chem.* **1987**, *27*, 113.
[2] J. C. Baldwin, W. C. Kaska, *Inorg. Chem.* **1979**, *18*, 686.
[3] Crystal structure determinations: four-circle diffractometer STOE *STADI IV*, graphite monochromated $Mo_{K\alpha}$ radiation, $\omega-2\theta$ scans, Patterson techniques, refined against F^2, semiempirical absorption correction, H atoms in calculated positions; the calculations were performed with the programs SHELXS-86, SHELXL-93. **2**: $C_{16}H_{36}F_{12}O_{12}Pt_4S_4$, trigonal, space group $R\bar{3}$, $a = b = 1151.8(6)$, $c = 484.7(2)$ pm, $V = 5568(5)$ Å^3, $Z = 6$, $\rho_{calcd} = 2.786$ g cm^{-3}, 203(2) K, $\mu(Mo_{K\alpha}) = 153.59$ cm^{-1}, 2452 measured reflections, of which 2207 were unique with $I > 2\sigma(I)$, 150 parameters, $R_1 = 0.102$, wR_2 (all data) = 0.2932. **3**: $C_{23}H_{34}AgF_9O_9Pt_2S_3$, monoclinic, space group $P2_1/n$, $a = 1147.6(4)$, $b = 1976.1(5)$, $c = 1583.1(4)$ pm, $\beta = 93.84(4)°$, $V = 3582(2)$ Å^3, $Z = 4$, $\rho_{calcd} = 2.262$ g cm^{-3}, 203(2) K, $\mu(Mo_{K\alpha}) = 85.98$ cm^{-1}, 6259 measured reflections, 5619 unique reflections ($R_{int} = 0.0765$), 4575 of which with $I > 2\sigma(I)$, 432 parameters, $R_1 = 0.047$, wR_2 (all data) = 0.1284. **4**: $C_{16}H_{34}F_6O_8Pt_2S_2$, triclinic, space group $P\bar{1}$, $a = 852.7(2)$, $b = 917.5(2)$, $c = 958.3(2)$ pm, $\alpha = 85.82(2)$, $\beta = 70.62(2)$, $\gamma = 67.592(14)°$, $V = 652.6(2)$ Å^3, $Z = 2$, $\rho_{calcd} = 2.348$ g cm^{-3}, 203(2) K, $\mu(Mo_{K\alpha}) = 109.47$ cm^{-1}, 3144 measured reflections, 3047 of which with $I > 2\sigma(I)$, 157 parameters, $R_1 = 0.030$, wR_2 (all data) = 0.0795. **5**: $C_{10}H_{25}F_3N_2O_3PtS$, orthorhombic, space group $P2_12_12_1$, $a = 787.58(7)$, $b = 1373.63(13)$, $c = 1466.94(13)$ pm, $V = 1587.0(2)$ Å^3, $Z = 4$, $\rho_{calcd.} = 2.116$ g cm^{-3}, 203(2) K, $\mu(Mo_{K\alpha}) = 90.12$ cm^{-1}, 4153 measured reflections, 2773 unique reflections ($R_{int} = 0.0278$), 2734 reflections with $I > 2\sigma(I)$, 188 parameters, Flack's parameter −0.010(13), $R_1 = 0.030$, wR_2 (all data) = 0.0785. Further details of the crystal structure investigations may be obtained from the Fachinformationszentrum Karlsruhe, 76344 Eggenstein-Leopoldshafen (Germany), on quoting the depository numbers CSD-406 778 (**2**), -406 779 (**3**), -406 780 (**4**), and -406 781 (**5**).
[4] P. J. J. A. Timmermans, A. Mackor, A. L. Spek, B. Kojić-Prodić, *J. Organomet. Chem.* **1984**, *276*, 287.
[5] P. L. Dedert, T. Sorrell, T. J. Marks, J. A. Ibers, *Inorg. Chem.* **1982**, *21*, 3506.
[6] S. Komiya, J. C. Huffman, J. K. Kochi, *Inorg. Chem.* **1977**, *16*, 2138.
[7] G. A. Lawrence, *Chem. Rev.* **1986**, *86*, 17.
[8] T. G. Spiro, D. H. Templeton, A. Zalkin, *Inorg. Chem.* **1968**, *7*, 2165.
[9] ^{1}H NMR: 300 MHz, $CDCl_3$, Bruker AM 300, 20 °C.
[10] H. G. Smith, R. E. Rundle, *J. Am. Chem. Soc.* **1958**, *80*, 5075; S. H. Strauss, M. D. Noirot, O. P. Anderson, *Inorg. Chem.* **1985**, *24*, 4307; M. J. Begley, D. B. Sowerby, R. D. Verma, A. Vig, *J. Organomet. Chem.* **1994**, *481*, 243.
[11] T. G. Appleton, J. R. Hall, T. G. Jones, *Inorg. Chim. Acta* **1979**, *32*, 127.

 © WILEY-VCH Verlag GmbH, D-69451 Weinheim, 1997 0570-0833/97/3618-1995 $ 17.50+.50/0

Polycyclic Aromatic Hydrocarbons in the Nanometer Range**

Benedikt Schlicke,
A.-Dieter Schlüter,*
Petra Hauser, and Jürgen Heinze

Both the discovery of fullerenes with all their exciting aspects[1] and the improved understanding of optoelectronic properties of polycyclic aromatic hydrocarbons (PAHs) as well as other unsaturated molecules[2] have considerably stimulated research on unsaturated compounds of all sorts. A few years ago, a two-step methodology for the synthesis of fully unsaturated, double-stranded polymers was established, which uses Diels–Alder (DA) polyaddition of unsaturated, bifunctional monomers followed by dehydration or dehydrogenation of the initially resulting prepolymer.[3,4] This chemistry has now been used to push the size of extended, yet monodisperse and structurally well-defined PAHs to its (present) limits. We report here on the synthesis of the novel PAHs **6** and **7**, which contain 19 and 29 condensed five- and six-membered rings, respectively, as well as their chemical, electrochemical, and optical characterization.

The synthetic strategy involves the bifunctional central building block **3** and its linear extension by DA end-capping reactions with cyclopentadienones **4b**[5] and **5**. Compound **3** was synthesized from **1**[3d] and bisaryne precursor **2**.[6] The more extended analogue of the cyclopentadienone derivative **4**, compound **5**, was synthesized by cycloaddition between diene **4a** and the dienophilic group of compound **1**. This cycloaddition proceeds at a significantly higher rate than the self-addition[3c,d] of the DA monomer **1**. This may be explained in terms of a reduced DA reactivity of the cyclopentadienone moiety in **1** as compared with that in **4a** presumably due to the substitution of the latter with electron-withdrawing ester groups in this inverse DA reaction. The very minor amounts of oligomers of **1** formed during synthesis of **5** (<2%) were removed in the workup, which gave the isolated target compound in a yield of 91%. In the final step, two equivalents of **4b** and **5** were treated with the central building block **3** to afford the PAHs **6** and **7**, respectively. They were easily purified by column chromatography and obtained in yields of 85 and 92%, respectively. Due to the substitution with dodecyl chains, these quite extended, flat (tabular) molecules show an exceptionally high solubility in common organic sol-

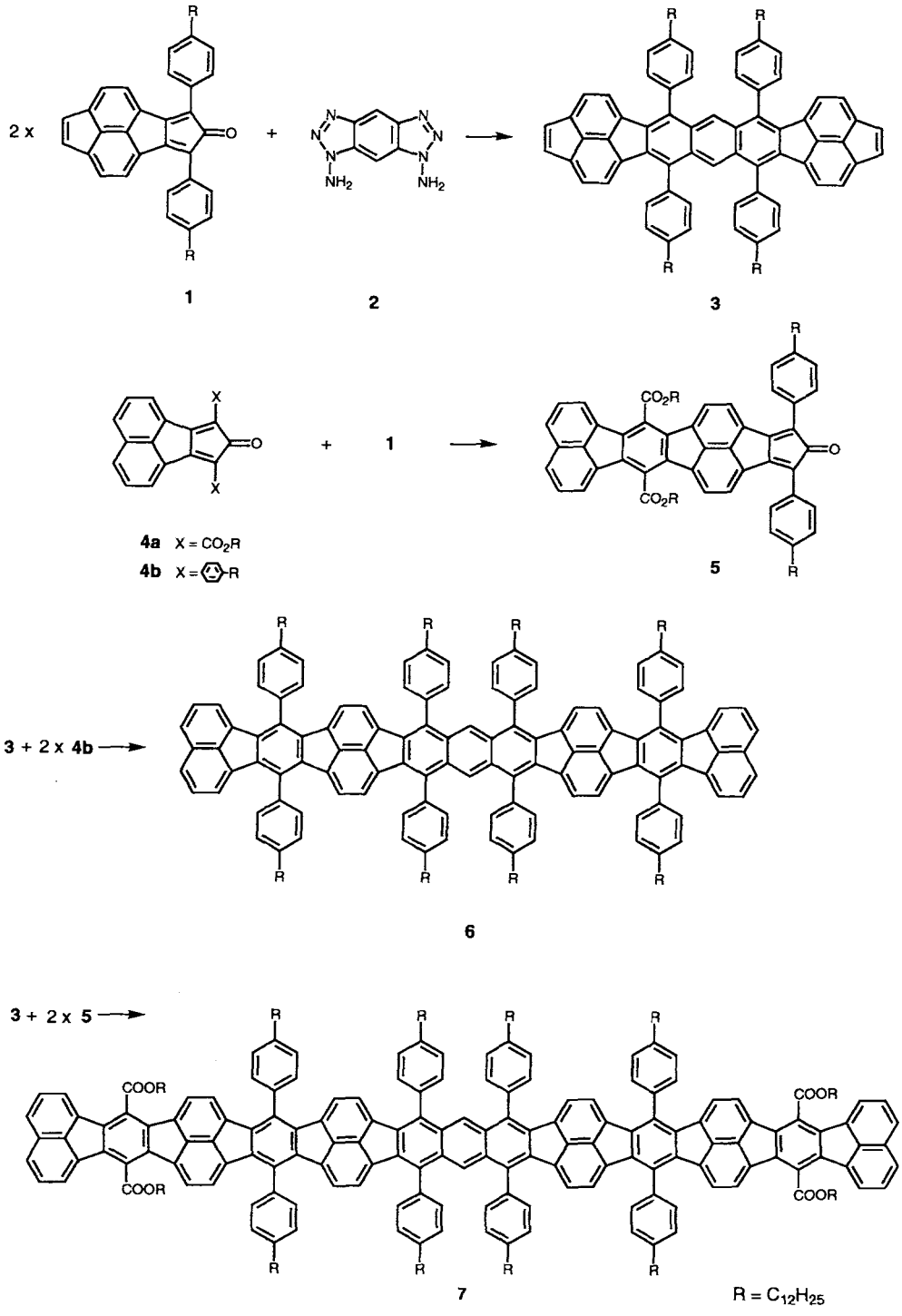

[*] Prof. Dr. A.-D. Schlüter, Dr. B. Schlicke
Freie Universität Berlin
Institut für Organische Chemie
Takustrasse 3, D-14195 Berlin (Germany)
Fax: Int. code +(30)838-3357
e-mail: adschlue@chemie.fu-berlin.de
Dipl.-Chem. P. Hauser, Prof. Dr. J. Heinze
Institut für Physikalische Chemie der Universität Freiburg (Germany)

[**] This work was supported by the Deutsche Forschungsgemeinschaft and the Fonds der Chemischen Industrie. Dr. Roelofs (Fachbereich Physik, FU Berlin) is thanked for the τ measurements for **6** and **7**, Prof. Röder (Fachbereich Physik, HU Berlin) for the determination of the quantum yields, Dr. Francke (FU Berlin), Dr. Just (BAM Berlin), and Dr. Räder (MPI-P, Mainz) for recording the LDI-TOF mass spectra and for help with their interpretation. J. Full is thanked for his help with some of the experiments.

 © WILEY-VCH Verlag GmbH, D-69451 Weinheim, 1997 0570-0833/97/3618-1996 $ 17.50+.50/0

vents like chloroform, toluene, and THF at room temperature. For example, at room temperature CH_2Cl_2 dissolves 5.0 gL^{-1} of **6** (1.8 $mmol L^{-1}$) and 4.5 gL^{-1} of **7** (1.1 $mmol L^{-1}$). The NMR spectra are in agreement with the proposed structures, including the integrals, which show correct proportions. The laser-desorption time-of-flight (LDI-TOF) mass spectra show the molecular ions at 2778 (**6**) and 4024 kDa (**7**) and no higher signals.[7] Compound **7** gives a correct elemental analysis.[8] Gel permeation chromatography (GPC) elution curves referenced to polystyrene standard are monomodal and give $M_n(\mathbf{6}) = 3380$ ($M_w/M_n = 1.02$) and $M_n(\mathbf{7}) = 4280$ ($M_w/M_n = 1.03$).

Compounds **6** and **7** were studied by cyclic voltammetry (Table 1).[9] Experiments were carried out in tetrahydrofuran

Table 1. Redox potentials ([V] vs. Ag/AgCl) of compounds **6** and **7** [a].

	Reduction						Oxidation			
	$E^6_{1/2}$	$E^5_{1/2}$	$E^4_{1/2}$	$E^3_{1/2}$	$E^2_{1/2}$	$E^1_{1/2}$	$E^1_{1/2}$	$E^2_{1/2}$	$E^3_{1/2}$	$E^4_{1/2}$
6	−3.10	−2.92 [b]	−2.00	−1.82	−1.50	−1.40	+0.89	+1.28	+1.54	
7	−2.55	−2.42	−2.16	−2.04	−1.41 [b]	−1.13 [b]	+0.85	+1.21	+1.34	+1.52

[a] The cyclic voltammograms were recorded in THF/$TBAPF_6$ (reductions) and CH_2Cl_2/$TBAPF_6$ (oxidations) at −40 °C (scan rate: 200 mVs^{-1}; TBA = Tetrabutylammonium). [b] Two-electron transfer steps.

(reductions) and dichloromethane (oxidations) under superdry conditions. With **7** the onset of reduction and oxidation shifts to lower energies than that with **6**. Compound **6** can be reduced to the heptaanion and **7** to the octaanion within a relatively small potential range (Figure 1). Fullerenes cannot be reduced further

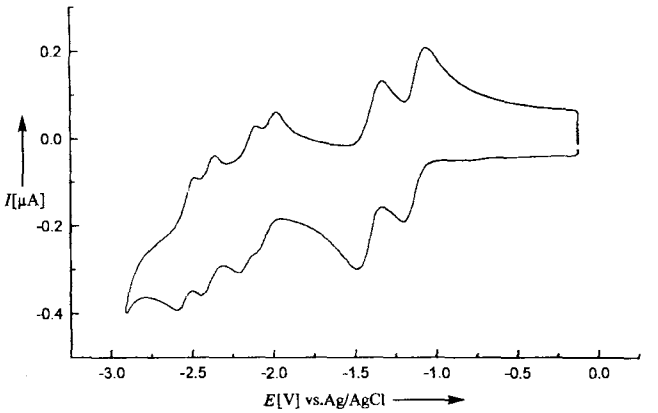

Figure 1. Reduction part of the cyclic voltammogram of compound **7** in THF/$TBAPF_6$ at −40 °C (scan rate: 200 mVs^{-1}).

than the hexaanions.[1, 10] Persistent trications and tetracations can be generated for species **6** and **7**, respectively. The redox states are stable. Their lifetimes are at least in the range of seconds. During reduction two-electron transfer steps take place up to the tetraanion, whereas for the oxidation well-separated one-electron transfer steps are observed. This is surprising because typically the energetical order of reduction and oxidation is symmetrical.

Some optical properties of **6** and **7** are summarized in Table 2. The absorption bands at longest wavelength (^1L_a) have a typical vibronic pattern (Figure 2). The fluorescence spectra show small Stokes shifts, indicating a high rigidity of the molecules.[11] The fluorescence quantum yield is high for the shorter and surprisingly weak for the longer arene.[12] The apparent lifetime of the excited states (τ) lies in the range of ns as for anthracene and perylene.[13]

Table 2. Absorption and emission maxima, fluorescence quantum yields (Φ_F), Stokes shifts, and lifetimes of the excited state (τ) of compounds **6** and **7**.

	Color	Absorption λ_{max} [nm]	lg ε	Emission λ_{max} [nm]	Φ_F	Stokes shift [nm]	τ [ns]
6	red	582	5.28	597	0.81	17	2.76
7	green	611	5.21	641	0.01	30	0.74

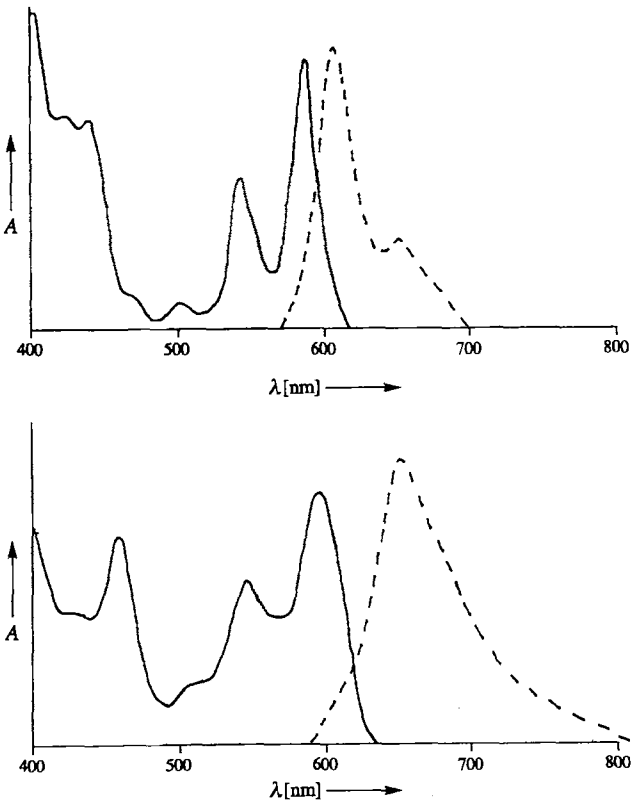

Figure 2. Absorption and emission spectra of compounds **6** (top) and **7** (bottom) in dichloromethane at room temperature. A = absorption in arbitrary units.

Table 3. Physical and spectroscopic data of compounds **6** and **7** [a].

6: ^1H NMR (270 MHz, $CDCl_3$): $\delta = 7.6$ (d, $J = 8.2$ Hz, 4 H, 3,4,18,19-H), 7.6 (s, 2 H, 11,26-H), 7,4 (d, $J = 8$ Hz, 8 H, phenyl-H), 7.4 (d, $J = 8$ Hz, 8 H phenyl-H), 7.3 (dd, $J = 8.1$, 7.1 Hz, 4 H, 2,5,17,20-H), 7.2 (d, $J = 8$ Hz, 8 H, phenyl-H), 7.2 (d, $J = 8$ Hz, 8 H, phenyl-H), 6.7 (d, $J = 7.1$ Hz, 4 H, 1,6,16,21-H), 6.3 (dd, 8 H, 8,9,13,14,23,24,28,29-H), 2.8 (t, $J = 7.1$ Hz 8 H, α-CH), 2.6 (t, $J = 7.5$ Hz, 8 H, α-CH), 1.8 (m, 8 H, β-CH), 1.7 (m, 8 H, β-CH), 1.4 (m, 144 H, alkyl-H), 0.9 (m, 24 H, CH_3); ^{13}C NMR (67.9 MHz, $CDCl_3$): $\delta = 142.6$ and 142.0 (7,10,12,15,22,25,27,30-C, phenyl-C), 139.3, 137.3, 136.6, 135.6, 134.9, 134.6, 133.1, 132.2, 129.5, 129.2, 128.7, 128.4, 128.2, 126.3, 122.9 (1,2,3,4,5,6,16,17,18,19,20,21-C), 122.8 (11,26-C), 35.9 (α-C), 32.0, 31.6, 29.7, 29.5, 22.7, 14.1 (alkyl-C); UV/Vis (CH_2Cl_2): λ_{max} (lg ε) = 582.2 (5.276), 537.8 (5.073), 499.8 (4.644), 434.9 (5.103), 415.4 (5.068), 393.3 (5.231), 317.4 (5.053) nm.

7: ^1H NMR (270 MHz, $CDCl_3$): $\delta = 7.9$ (2d, $J = 8.2$, 7.2 Hz, 8 H, 1,3,4,6,22,24,25,27-H), 7.6 (m, 6 H, 2,5,14,23,26,35-H), 7.4 (2d, $J = 7.9$, 16 H, terminal phenyl), 7.2 (m, 16 H, internal phenyl), 6.3 (m, 12 H, 9,11,12,16,17,19,30,32, 33,37,38,40-H), 4.6 (t, $J = 6$ Hz, 8 H, α-CH (ester)), 2.8 (t, $J = 6.8$ Hz, 8 H, α-CH (phenyl)), 1.8 (m, 24 H, β-CH), 1.2 (m, 216 H, alkyl-H), 0.9 (m, 36 H, CH_3); ^{13}C NMR (67.9 MHz, $CDCl_3$): $\delta = 142.7$, 142.0, 140.0, 139.9, 138.3. 138.2, 136.9, 136.4, 136.1, 135.6, 135.2, 134.9, 134.7, 134.1, 133.9, 133.3, 133.0, 132.7, 129.3, 129.1, 128.5, 128.4, 127.7, 126.4, 125.4, 124.9, 124.3, 122.7 (arom. C), 66.2 (α-C, ester), 37.6, 35.9, 32.0, 31.9, 31.6, 31.4, 29.8, 29.6, 29.5, 29.4, 29.3, 28.5, 26.9, 26.1, 24.9, 22.7, 22.6, 14.1 (alkyl-C); UV/Vis (CH_2Cl_2): λ_{max} (lg ε) = 611.2 (5.206), 563.2 (4.979), 474.3 (4.962), 399.9 (5.208) nm; C,H analysis (%) calcd for $C_{294}H_{362}O_8$ (4024.09): C 87.75, H 9.02; found: C 87.62, H 9.12.

 © WILEY-VCH Verlag GmbH, D-69451 Weinheim, 1997 0570-0833/97/3618-1997 $ 17.50+.50/0

We have devised a facile route to monodisperse PAHs of 3.0 (**6**) and 4.5 nm (**7**) length,[14] which, regardless of their considerable size, can be handled and characterized (Table 3) like any low molecular weight compound. To our knowledge PAH **7** is the most extended, fully characterized aromatic compound known today.

Received: March 7, 1997 [Z10209IE]
German version: *Angew. Chem.* **1997**, *109*, 2091–2093

Keywords: arenes · cyclic voltammetry · Diels–Alder reactions · fluorescence · polycycles

[1] See, for example, A. Hirsch, *The Chemistry of Fullerenes*, Thieme, Stuttgart, **1994**.
[2] See, for example, *Conjugated Polymers* (Eds.: J.-L. Brédas, R. Silbey), Kluwer, Dordrecht, **1991**.
[3] a) A.-D. Schlüter, *Adv. Mater.* **1991**, *3*, 282; b) M. Löffler, A.-D. Schlüter, K. Gessler, W. Saenger, J.-M. Toussaint, J.-L. Brédas, *Angew. Chem.* **1994**, *106*, 2281; *Angew. Chem. Int. Ed. Engl.* **1994**, *33*, 2209; c) B. Schlicke, H. Schirmer, A.-D. Schlüter, *Adv. Mater.* **1995**, *7*, 544; d) B.Schlicke, J. Frahn, A.-D. Schlüter, *Synth. Met.* **1996**, *83*, 173–176.
[4] For an alternative approach to double-stranded, unsaturated polymers, see U. Scherf, K. Müllen, *Synthesis* **1992**, 23.
[5] Compound **4** was prepared according to the method of C. F. Allen, *Chem. Rev.* **1962**, *62*, 653. See also B. Schlicke, A.-D. Schlüter, *Synlett* **1996**, 425.
[6] H. Hart, D. Ok, *J. Org. Chem.* **1986**, *51*, 979. See also M. Löffler, A.-D. Schlüter, *Synlett* **1994**, 75.
[7] The LDI-TOF spectra of **6**, **7**, and other related compounds show, besides the molecular ion peak (low intensity), patterns of signals with a Gaussian type distribution at somewhat lower masses (relatively high intensity). The peaks of these patterns are separated by a constant $m/e = 28$ Da. The reason for this finding is not yet understood. A possible systematic distribution of molecular weights caused by an inadvertent employment of reagents with an even distribution of methylene groups in the alkyl chains is unlikely. The alkyl chains are introduced into the whole sequence as bromides and alcohols (see Refs. [3d, 5]), the purity of which was greater than 98% (checked by (GC)).
[8] Despite several attempts we were not able to get correct analytical data from compound **6**; the values for H were always slightly too small.
[9] J. Heinze, *Angew. Chem.* **1984**, *96*, 823; *Angew. Chem. Int. Ed. Engl.* **1984**, *23*, 831.
[10] Q. Xie, E. Pérez-Cordero, L. Echegoyen, *J. Am. Chem. Soc.* **1992**, 114, 3978; Y. Ohsawa, T. Saji, *J. Chem. Soc. Chem. Commun.* **1992**, 781; K. Meerholz, P.Tschunky, J. Heinze, *J. Electroanal.* **1993**, *347*, 425.
[11] For comparison, see A. Bohnen, K.-H. Koch, W. Lüttke, K. Müllen, *Angew. Chem.* **1990**, *102*, 548; *Angew. Chem. Int. Ed. Engl.* **1990**, *29*, 525.
[12] The reason for the weak fluorescence of **7** is presently under investigation.
[13] See, for example, W. Schmidt, *Optische Spektroskopie*, VCH, Weinheim, **1994**.
[14] The lengths were calculated with the program Spartan Silicon Graphics, Version 4.1.1., on the assumption that conformations are planar. Hydrogen atoms were disregarded.

Efficient Synthesis of Ganglioside GM2 for Use in Cancer Vaccines**

Julio C. Castro-Palomino, Gerd Ritter,*
Sheila R. Fortunato, Stefan Reinhardt, Lloyd J. Old,
and Richard R. Schmidt*

A number of carbohydrate antigens that are expressed on human cancer cells on glycolipids and glycoproteins are considered attractive targets for immunotherapy with monoclonal antibodies and vaccines.[1] Examples include the gangliosides GM2, GD2, GD3, *O*-acetyl-GD3, and fucosyl-GM1, the neutral glycosphingolipid globo-H, the T, Tn, and sTn epitopes expressed on glycoproteins, and the Le^Y epitope expressed on both glycolipids and glycoproteins. Of these potential targets, ganglioside GM2 is of particular interest, because a) GM2 is expressed on the cell surface of a number of human cancers, including melanoma, sarcoma, and renal cancer;[2] b) GM2-reactive antibodies (mouse and human polyclonal and monoclonal antibodies) are cytotoxic in vitro against $GM2^+$ human cancer cells;[3,4] c) GM2 is immunogenic in humans due to the presence of naturally occurring low-titer IgM serum antibodies against GM2,[4] to the relative ease of isolating GM2 monoclonal antibodies from humans,[5] and to the induction of GM2 antibodies in melanoma patients following immunization with GM2-containing vaccines;[3,4,6–8] d) the presence of GM2 antibodies in melanoma patients appears to be associated with an improved survival rate and a longer disease-free interval;[4] and e) no deleterious side effects associated with an immune response to GM2 have been observed.[4]

Various approaches for inducing an immune response against $GM2^+$ cancer cells in melanoma patients have been pursued, including immunization with GM2-expressing tumor cells,[7] with purified GM2 mixed with various immunological adjuvants,[3,4] and more recently, with vaccines consisting of purified GM2 chemically conjugated to an immunogenic carrier protein.[6] Antibodies induced by whole cell vaccines or GM2 adherent to bacillus Calmette Guerin (BCG) were generally of the IgM isotype (low-titer, short-lived, and nonboostable), consistent with a T-cell-independent immune response.[3,4] In more recent studies vaccination with GM2 chemically conjugated to keyhole hemocyanin (KLH) and mixed with QS21, an adjuvant of the saponin family, resulted in more strongly cytotoxic IgM antibodies and the frequent induction of IgG antibodies against GM2 in ELISA (enzyme-linked immunosorbent assay).[6,8] However, the majority of the IgG antibodies against GM2 failed to react with GM2-expressing human cancer cells.[8] This could be due, among other explanations, to the induction of IgG antibodies against GM2 epitopes that are hidden or buried on the cell surface, possibly as a consequence of the particular vaccine formulation.

The GM2 used in these studies was derived from mammalian tissues (e.g., bovine brain, cat Tay–Sachs brain, or human melanoma). However, extraction and purification of GM2 from tissue bears the risk of biological contamination. In addition, mammalian tissue-derived GM2 comprises a mixture of different molecular species, mostly varying in the ceramide moiety. For systematic clinical vaccine development, a consistent source of a single, well-defined, synthetic GM2 species would be desirable, particularly for vaccines to be used in large groups of patients. We have therefore developed a practical method for the chemical synthesis of ample quantities of GM2 oligosaccharide building blocks and GM2 ganglioside for use in GM2 cancer vaccines.

The strategies pursued in previous GM2 syntheses[9–11] follow the GA2 or the GM3 route,[12] which is also employed here (Scheme 1). The most important synthetic problems in this endeavor are a) convenient generation of a suitable lactose building block, b) α-selective attachment of a sialyl donor to the 3b-hydroxyl group of this lactose constituent, c) high-yield β-selective attachment of an N-protected galactosamine residue to the low-reactive 4b-hydroxyl group of the GM3 trisaccharide intermediate, and d) convenient transformation of the N-protected galactosamine residue into the *N*-acetyl-galactosamine constituent. Problems (a)–(d) can be solved by means of build-

[*] Dr. G. Ritter, S. R. Fortunato, Dr. L. J. Old
Ludwig Institute for Cancer Research
New York Branch at Memorial Sloan Kettering Cancer Center
1275 York Avenue, New York, NY 10021 (USA)
Prof. Dr. R. R. Schmidt, J. C. Castro-Palomino, S. Reinhardt
Fakultät für Chemie der Universität
D-78457 Konstanz (Germany)
Fax: Int. code +(7531)88-3135

[**] This work was supported by the Deutsche Forschunggemeinschaft and the Fonds der Chemischen Industrie.

 © WILEY-VCH Verlag GmbH, D-69451 Weinheim, 1997 0570-0833/97/3618-1998 $ 17.50+.50/0

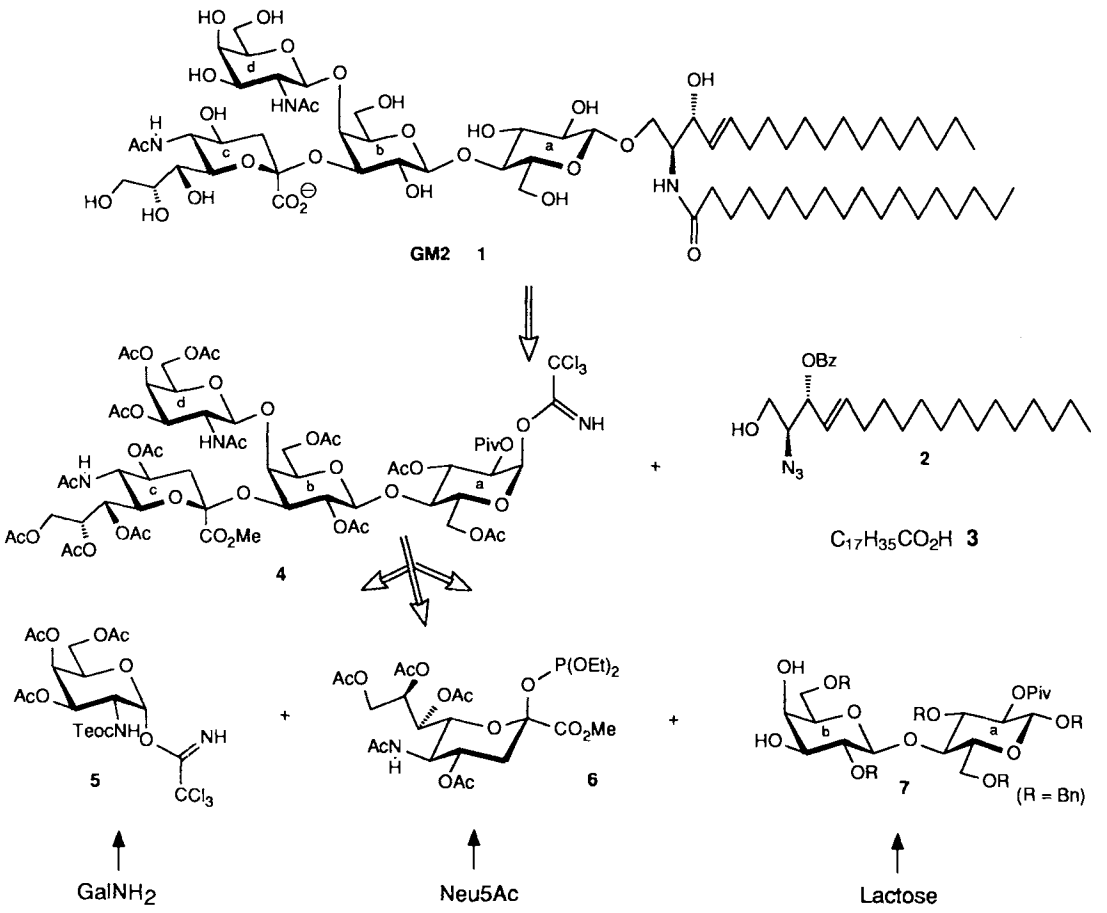

Scheme 1. Retrosynthesis of GM2 (**1**).

ing blocks **2**,[13] **3**, and **5**–**7**, which constitute tetrasaccharide intermediate **4**.

After investigating various galactosamine donors, we selected *N*-trichloroethoxycarbonyl(Teoc)-protected trichloroacetimidate **5**,[14] which was obtained from galactosamine in three convenient steps via the 1-O unprotected intermediate **8** in high yield (Scheme 2). This procedure avoided the tedious azidogalactose production[11,12] and the difficult removal of *N*-phthaloyl protecting groups in the presence of Neu5Ac residues, required in previous GM2 syntheses.[9,10] Simple treatment of *N*-Teoc-containing compounds with Zn/acetic anhydride leads to direct replacement of *N*-Teoc by an acetyl group.[15] The known diethyl phosphite derivative **6**[16] was employed as Neu5Ac donor.

The 3b,4b-O-unprotected 2a-*O*-pivaloyllactose residue **7**[17] facilitates the desired consecutive regioselective attack at the 3b- and then at the 4b-hydroxyl group, because of the very different

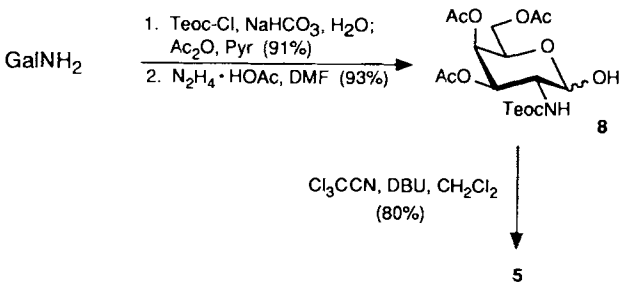

Scheme 2. Synthesis of the trichloroacetimidate **5** (Pyr = pyridine).

reactivities of these groups. The number of steps required for the reported synthesis of **7**[17] was greatly reduced by employing 1a,2a-*O*-silyl-group migration[18] for the regioselective introduction of the 2a-*O*-pivaloyl group. Isopropylidenation of lactose[19] and then silylation with thexyldimethylsilyl chloride (TDS-Cl) in the presence of base led to 1-*O*-silylated 3b,4b-*O*-isopropylidenelactose **9** (Scheme 3), which can be conveniently obtained also via the per-O-acetyl derivative of 3b,4b-*O*-isopropylidenelactose.[20] Benzylation of **9** with benzyl bromide and NaH as base in DMF leads to reversible silyl-group migration between the 1a and 2a oxygen atoms. Owing to the high nucleophilicity of the oxide oxygen atom of the β anomer, **10** is directly obtained from these intermediates in good yield by an irreversible anomeric *O*-alkylation process[18,21]. Removal of the 2a-*O*-silyl group with tetra-*n*-butylammonium fluoride (TBAF) in THF, pivaloylation, and acid-catalyzed cleavage of the isopropylidene group furnished target molecule **7** in high yield.

Reaction of sialyl donors with 2,3,4-*O*-unprotected galactosyl residues provides generally good α-glycosylation results. This is usually not found for 3,4-*O*-unprotected galactose derivatives.[16,22] Investigations with donor **6** and acceptor **7** and various catalysts showed that tin(II) triflate in acetonitrile at $-40\,^{\circ}C$ leads to high α selectivity ($\alpha:\beta = 9:1$) and good yields of GM3 intermediate **11** (Scheme 4); at room temperature sialoside yields of up to 80% were obtained with a slightly higher content of the β anomer ($\alpha:\beta = 4:1$); the α product **11** can be separated by flash chromatography in high purity. Subsequent glycosylation with donor **5** gave the desired tetrasaccharide in almost quantitative yield. Replacement of the Teoc group

 © WILEY-VCH Verlag GmbH, D-69451 Weinheim, 1997 0570-0833/97/3618-1999 $ 17.50+.50/0

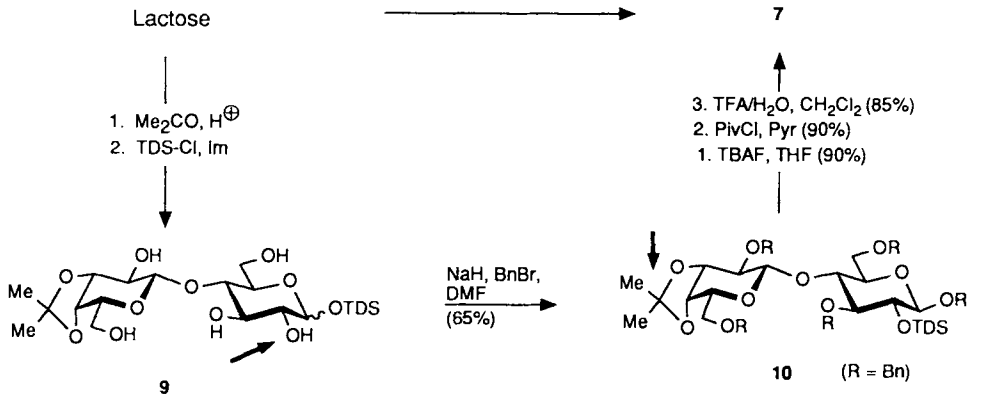

Scheme 3. Synthesis of the pivaloyllactose **7**. Im = imidazole, Piv = pivaloyl, TFA = trifluoroacetic acid. For synthesis of **7** from lactose, see also ref. [17].

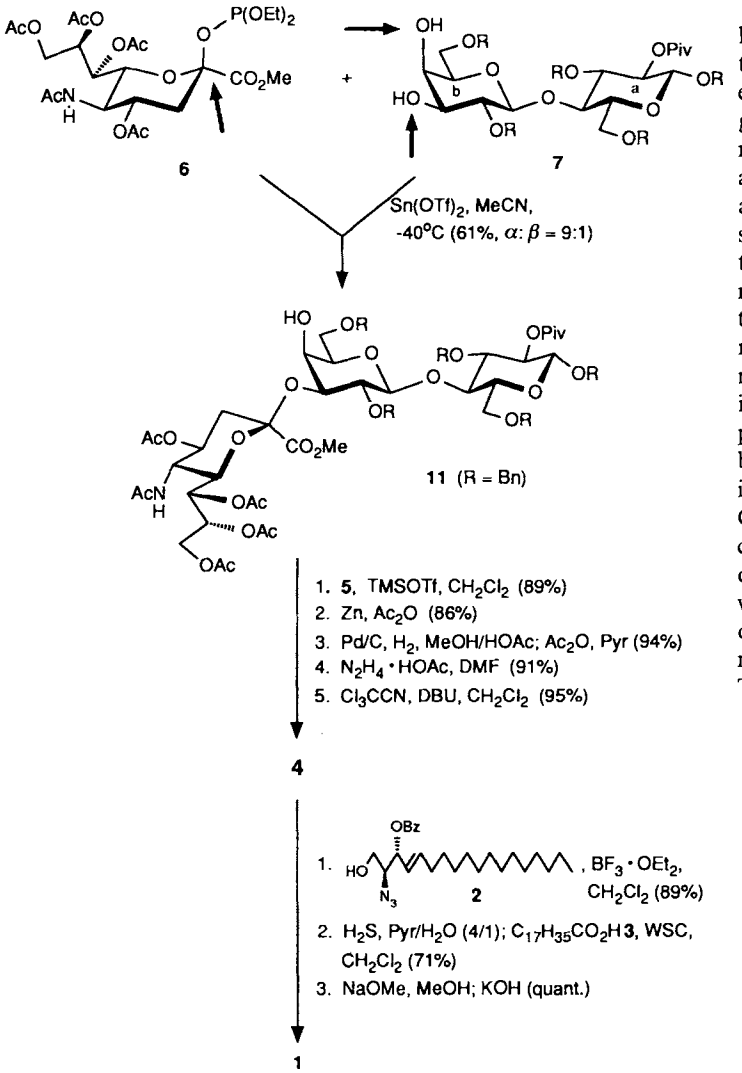

Scheme 4. Synthesis of GM2 (**1**) from the building blocks **6**, **7**, **5**, and **2**. Tf = F_3CSO_2, TMS = trimethylsilyl, WSC = water-soluble carbodiimide [*N*-(3-dimethylaminopropyl)-*N'*-ethylcarbodiimide hydrochloride].

by an acetyl group with Zn/Ac_2O proceeded smoothly. Hydrogenolysis with Pd/C in MeOH/HOAc, followed by treatment with Ac_2O in pyridine led to replacement of all *O*-benzyl groups by *O*-acetyl groups. All subsequent procedures followed our previously introduced standard methods:[12] regioselective removal of the anomeric *O*-acetyl group with $N_2H_4 \cdot$HOAc and then treatment with CCl_3CN in the presence of 1,8-diazabicyclo[5.4.0]undec-7-ene (DBU) as base afforded tetrasaccharide donor **4**. Application of the "azidosphingosine glycosylation procedure"[13] to azidosphingosine derivative **2**,[13] transformation of the azido into the amino group, attachment of the stearoyl residue (or other acyl group; see below), and then removal of all protective groups under basic conditions furnished target molecule **1** that was identical to previously synthesized material.[8, 9]

The availability of a GM2 oligosaccharide building block in large quantities by chemical synthesis facilitates the construction of GM2 gangliosides with different defined ceramide moieties and novel GM2 neoglycoconjugates for use as immunogens in GM2 vaccines. For instance, we have synthesized by this methodology GM2 having fatty acids of various lengths (capric acid, stearic acid, and lignoceric acid) in the ceramide moiety, and we have linked GM2 oligosaccharide to a short lipophilic spacer molecule (azidohexanol) to facilitate further conjugation to carrier molecules. To identify potential serological differences resulting from the composition of the lipid moiety, we tested these compounds and GM2 derived from bovine brain for their reactivity with a number of serological reagents (including mouse and human monoclonal antibodies against GM2, rabbit immune serum with GM2 reactivity, and sera from melanoma patients who had been immunized with vaccines containing bovine-brain GM2) by ELISA, dot blot immune stains, and immune thin-layer chromatography. We found that synthetic GM2 with stearic acid or lignoceric acid and sphingosine in the ceramide moiety was serologically indistinguishable from GM2 derived from bovine brain (Figures 1 and 2). However, GM2 with a ceramide containing a shorter fatty acid (e.g., capric acid) or GM2 oligosaccharide linked to azidohexanol showed dramatically reduced reactivity towards GM2-reactive antibodies. This suggests that ceramide containing a fatty acid longer than

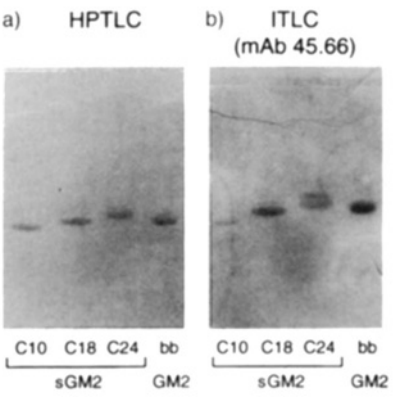

Figure 1. Reaction of a human monoclonal GM2 antibody (mAb 45.66) from a patient with malignant melanoma with synthetic GM2 containing capric acid (C10sGM2), stearic acid (C18sGM2), lignoceric acid (C24sGM2), or GM2 derived from bovine brain (bbGM2). The amount of ganglioside spotted per lane was 1 mg. The TLC was developed in chloroform/methanol/$CaCl_2$ (0.2%) in H_2O (55/45/10 v/v/v) and treated with hybridoma supernatant 45.66 diluted 1:10 with phosphate-buffered saline. Specific reactivity was made visible by using an anti-human IgM antibody conjugated to horseradish peroxidase and diaminobenzidine (b). Gangliosides were stained with orcinol/H_2SO_4 after immunostaining (a).

 © WILEY-VCH Verlag GmbH, D-69451 Weinheim, 1997 0570-0833/97/3618-2000 $ 17.50+.50/0

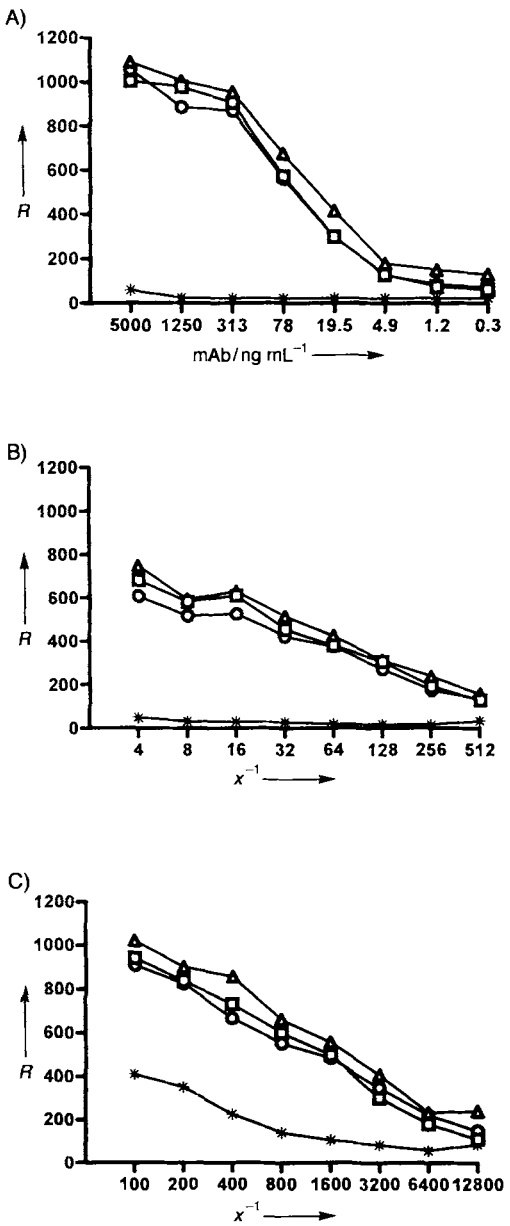

Figure 2. ELISA reactivity of GM2 antibodies with synthetic GM2 containing C10:0 (•), C18:0 (○), or C24:0 (△) fatty acid or with bovine brain-derived GM2 (□). A) Mouse monoclonal antibody 10.11 (purified IgM). B) Human monoclonal antibody 45.66 (tissue culture supernatant, IgM). C) Serum of a melanoma patient immunized with bovine brain-derived GM2-KLH/QS21 vaccine (IgG). No reactivity was observed with control antibodies or other gangliosides. Method: 200 pmol GM2 were incubated with varying amounts of GM2 antibody, and reactivity was quantitated by using Fitc-conjugated species, isotype specific secondary antibodies, and a microplate fluorospectrometer.

ten carbon atoms is required for full and specific immune recognition of GM2. Based on this observation, we have now prepared GM2–KLH conjugate vaccines by using synthetic GM2 containing stearic acid. Clinical trials with these vaccines will be initiated in the near future in patients with advanced malignant melanoma. By utilizing fully synthetic GM2, which is structurally well defined and free of biological contaminants, we hope to come a step closer towards our goal of developing a safe and efficient vaccine able to induce consistently a high-titered and long-lived cytotoxic antibody response in cancer patients.

Received: December 16, 1996
Revised version: May 15, 1997 [Z9886IE]
German version: *Angew. Chem.* **1997**, *109*, 2081–2085

Keywords: antigens · antitumor agents · gangliosides · glycoside synthesis · tumor therapy

[1] H. F. Oettgen, L. J. Old in *Biologic Therapy of Cancer* (Eds.: V. DeVita, S. Hellmann, S. A. Rosenberg), J. B. Lippincott Company, Philadelphia, PA, **1991**; G. Ritter, P. O. Livingston, *Seminars Cancer Biol.* **1991**, *2*, 401–409.
[2] W. B. Hamilton, F. Helling, K. O. Lloyd, P. O. Livingston, *Int. J. Cancer* **1993**, *53*, 566–573.
[3] P. O. Livingston, E. J. Natoli, M. Jones Calves, E. Stockert, H. F. Oettgen, L. J. Old, *Proc. Nat. Acad. Sci. USA* **1987**, *84*, 2911–2915.
[4] P. O. Livingston, G. Y. C Wong, S. Adluri, Y. Tao, M. Padavan, R. Parente, C. Hanlon, M. Calves, F. Helling, G. Ritter, H. F. Oettgen, L. J. Old, *J. Clin. Oncol.* **1994**, *12*, 1036–1044.
[5] H. Yamaguchi, K. Furukawa, S. R. Fortunato, P. O. Livingston, K. O. Lloyd, H. F. Oettgen, L. J. Old, *Proc. Nat. Acad. Sci. USA* **1990**, *87*, 3333–3337; Y. Nishinaka, M. H. Ravindranath, R. F. Irie, *Cancer Res.* **1996**, *56*, 5666–5671.
[6] F. Helling, S. Zhang, A. Shang, S. Adluri, M. Calves, R. Koganty, B. M. Longenecker, T.-H. Tao, H. F. Oettgen, P. O. Livingston, *Cancer Res.* **1995**, *55*, 2783–2788.
[7] T. Tai, L. D. Cahan, T. Tsuchida, R. E. Saxton, R. F. Irie, D. L. Morton, *Int. J. Cancer* **1985**, *35*, 607–612.
[8] K. Kitamura, P. O. Livingston, S. R. Fortunato, E. Stockert, F. Helling, G. Ritter, H. F. Oettgen, L. J. Old, *Proc. Nat. Acad. Sci. USA* **1995**, *92*, 2805–2809.
[9] M. Sugimoto, M. Numata, K. Koike, Y. Nakahara, T. Ogawa, *Carbohydr. Res.* **1986**, *156*, C1–C5.
[10] A. Hasegawa, T. Nagahama, H. Ohki, M. Kiso, *J. Carbohydr. Chem.* **1992**, *11*, 699–714.
[11] T. Stauch, Dissertation, Universität Konstanz, **1995**; R. R. Schmidt in *Synthetic Oligosaccharides—Indispensible Probes for Life Sciences* (Ed.: P. Kovac), Washington DC, **1994**, pp. 276–296 (*ACS Symp. Ser.* **1994**, *560*).
[12] T. Stauch, U. Greilich, R. R. Schmidt, *Liebigs Ann.* **1995**, 2101–2111; U. Greilich, R. Brescello, K.-H. Jung, R. R. Schmidt, *ibid.* **1996**, 663–672, and references therein.
[13] R. R. Schmidt, P. Zimmermann, *Tetrahedron Lett.* **1986**, *27*, 481–484; *Angew. Chem.* **1986**, *98*, 722–723; *Angew. Chem. Int. Ed. Engl.* **1986**, *25*, 725–726.
[14] Corresponding glucosamine derivatives have already been employed in glycosylation reactions: H. Paulsen, B. Helpap, *Carbohydr. Res.* 1991, **216**, 289–313; and ref. [15].
[15] W. Dullenkopf, J. C. Castro-Palomino, L. Manzoni, R. R. Schmidt, *Carbohydr. Res.* **1996**, *296*, 135–147.
[16] T. J. Martin, R. R. Schmidt, *Tetrahedron Lett.* **1992**, *33*, 6123–6126; T. J. Martin, R. Brescello, A. Toepfer, R. R. Schmidt, *Glycoconj. J.* **1993**, *10*, 16–25, and references therein.
[17] Y. Ito, M. Numata, M. Sugimoto, T. Ogawa, *J. Am. Chem. Soc.* **1989**, *111*, 8508–8510; N. Numata, M. Sugimoto, Y. Ito, T. Ogawa, *Carbohydr. Res.* **1990**, *203*, 205–217.
[18] J. M. Lassaletta, R. R. Schmidt, *Synlett* **1995**, 925–927; J. M. Lassaletta, M. Meichle, S. Weiler, R. R. Schmidt, *J. Carbohydr. Chem.* **1996**, *15*, 241–254.
[19] H. H. Baer, S. A. Abbas, *Carbohydr. Res.* **1980**, *84*, 53–60.
[20] L. Lay, R. Windmüller, S. Reinhardt, R. R. Schmidt, *Carbohydr. Res.*, in press.
[21] R. R. Schmidt, *Angew. Chem.* **1986**, *98*, 213–236; *Angew. Chem. Int. Ed. Engl.* **1986**, *25*, 212–235.
[22] T. Murase, H. Ishida, M. Kiso, A. Hasegawa, *Carbohydr. Res.* **1988**, *184*, C1–C4.

 © WILEY-VCH Verlag GmbH, D-69451 Weinheim, 1997 0570-0833/97/3618-2001 $ 17.50+.50/0

Effects of Environment on Intramolecular Electron Transfer in Mixed-Valence 1′,1‴-Dinaphthylmethyl(biferrocenium) Triiodide: Structural and ^{57}Fe Mössbauer Characteristics**

Teng-Yuan Dong,* Xiao-Qian Lai, Zhi-Wei Lin, and Kuan-Jiuh Lin

Electron transfer in chemical[1] and biological[2] systems has received considerable attention in the last few years. Recent studies of electron transfer in mixed-valence biferrocenium complexes **1**–**6** revealed that the environment surrounding a cation is perhaps the most important factor in determining the rate of intramolecular electron transfer.[1c, 3] Complexes **1**–**6** give unusual temperature-dependent Mössbauer spectra.[4] At temperatures below 77 K they each show two doublets, one for the Fe^{II} and one for the Fe^{III} site (electron-transfer rate $< 10^7\ s^{-1}$). In each case the two doublets move together upon increasing temperature and eventually become a single "average-valence" doublet. Hendrickson et al. suggested that the temperature dependence of the Mössbauer spectrum is due to the onset of lattice dynamics associated with the triiodide counterions and alkyl substituents.[4] At low temperatures (< 100 K) all parts of the crystal lattice of the complex are static. As the temperature is increased, the thermal energy formed could be sufficient to trigger a cooperative phase transition in the crystal lattice.[3a] A crystallographic phase change was not observed in **1**–**6**; we believe that the transition may be described in terms of a gradual (second-order) change with temperature.

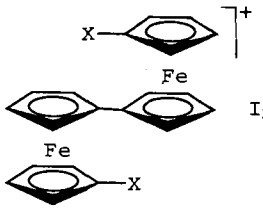

1 X = H
2 X = CH_3
3 X = C_2H_5
4 X = n-C_3H_7
5 X = n-C_4H_9
6 X = benzyl
7 X = 1-naphthylmethyl

The mixed-valence complex **6** has two distinct crystallographic phases that show that the electron-transfer rates are extremely sensitive to changes in the crystal lattice.[3a] Two different crystalline morphologies (needle and platelike crystals) of **6** were found. The needle crystal in the triclinic space group $P\bar{1}$ shows a Mössbauer spectrum characteristic of a valence-detrapped electronic structure down to 25 K. The platelike crystal in the space group $P2_1/n$ shows a valence-trapped Mössbauer spectrum up to 300 K. However, because of the poor quality of the diffraction data and disorder in the triiodide anion, a satisfactory refinement of the structure was not obtained. Here we report on **7**, the first mixed-valence complex in two crystallographic phases with satisfactory structural refinements. Compound **7** was formed from **8** via **9** and **10** (see Experimental Section).

[*] Prof. T.-Y. Dong, X.-Q. Lai, Z.-W. Lin
Department of Chemistry
National Sun Yat-Sen University
Kaohsuing (Taiwan)
Fax: Int. code +(7)525-3908

Dr. K. J. Lin
The Institute of Chemistry, Academia Sinica
Nankang, Taipei (Taiwan)

[**] This work was supported by the National Science Council (NSC86-2113-M-110-003) and National Sun Yat-Sen University.

Dark crystals in the triclinic space group $P\bar{1}$ were formed when a solution of **7** in CH_2Cl_2 was slowly concentrated.[5] An ORTEP plot of the molecular structure is given in Figure 1a. The refinement of the structure imposed inversion centers on both the cation and the triiodide anion. Thus, the two ferrocenyl moieties are crystallographically equivalent. The average Fe–C distance of 2.059(5) Å is intermediate to values for ferrocene (2.045(1) Å)[6] and the ferrocenium ion (2.075(1) Å).[7] The distances from the iron atom to the planes of the Cp ligands (1.668(2) and 1.676(2) Å) are also between the corresponding values for ferrocene (1.65 Å)[6] and the ferrocenium ion (1.70 Å).[7] The plane of the Cp ring forms a dihedral angle of 4.4° with the fulvalenide plane, and the two Cp rings in each ferrocenyl moiety are not perfectly eclipsed but rotated relative to one another by 7.0°.

Dark crystals in the monoclinic space group $P2_1/n$ were obtained when a layer of hexane was allowed to diffuse slowly into a solution of **7** in CH_2Cl_2.[5] The molecular structure is shown in Figure 1b. The two metallocene moieties in the cation are not equivalent. The average Fe1–C distance (2.052(4) Å) and the Fe1–Cp distance (1.660(4) Å) indicate that the iron in this metallocene is in the oxidation state II. In contrast, the average Fe2–C (2.086(5) Å) and Fe2–Cp distances (1.693(4) Å) indi-

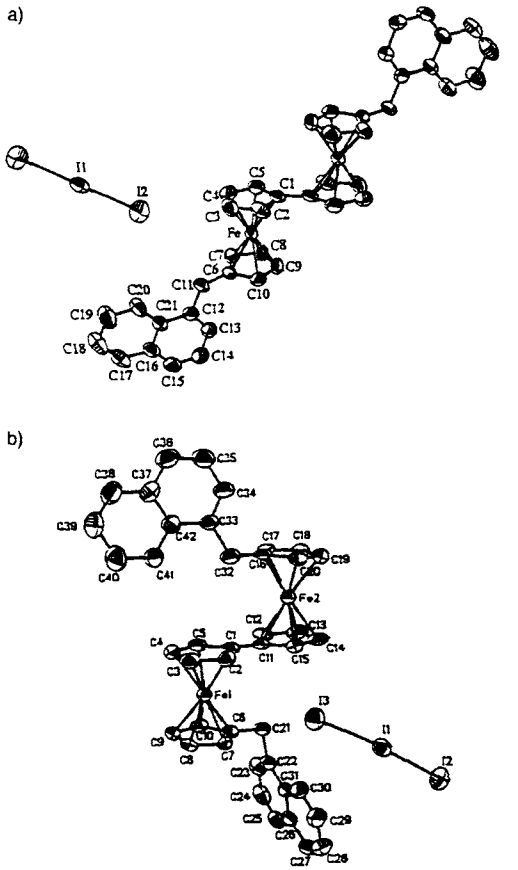

Figure 1. a) ORTEP plot of the crystal structure of **7**, space group $P\bar{1}$. Selected distances [Å] and angles [°] (standard deviations are given in parentheses): Fe–C1 2.090(5), Fe–C2 2.055(6), Fe–C3 2.039(6), Fe–C4 2.046(6), Fe–C5 2.050(6), Fe–C6 2.074(5), Fe–C7 2.043(5), Fe–C8 2.053(6), Fe–C9 2.064(6), Fe–C10 2.073(6), I1–I2 2.8936(8); I2-I1-I2 180. b) ORTEP plot of the crystal structure of **7**, space group $P2_1/n$. Selected distances [Å] and angles [°]: Fe1–C1 2.053(6), Fe1–C2 2.054(7), Fe1–C3 2.067(7), Fe1–C4 2.056(7), Fe1–C5 2.028(7), Fe1–C6 2.065(6), Fe1–C7 2.046(6), Fe1–C8 2.043(6), Fe1–C9 2.055(6), Fe1–C10 2.043(6), Fe2–C11 2.129(6), Fe2–C12 2.095(7), Fe2–C13 2.047(7), Fe2–C14 2.050(7), Fe2–C15 2.079(7), Fe2–C16 2.126(7), Fe2–C17 2.091(7), Fe2–C18 2.067(7), Fe2–C19 2.069(7), Fe2–C20 2.1107, I1–I2 2.89(1), I1–I3 2.932(1); I2-I1-I3 176.31.

 © WILEY-VCH Verlag GmbH, D-69451 Weinheim, 1997 0570-0833/97/3618-2002 $ 17.50+.50/0

cate that the iron in this metallocene is in the oxidation state III. The two Cp rings associated with Fe1 and Fe2 are not quite parallel; the dihedral angles are 2.1 and 5.5°. Furthermore, the two Cp rings associated with Fe1 and Fe2 are nearly eclipsed with average staggering angles of 3.0 and 2.3°.

A comparison of the structural features of the two different crystallographic phases of **7** is interesting. The naphthylmethyl substituents on the Cp rings are situated differently. The two nonequivalent naphthylmethyl groups in the cation of the $P2_1/n$ phase show a cisoid conformation relative to the fulvalenide ligand; this is similar to other dialkyl mixed-valence biferrocenium triiodide salts.[4, 8, 9] In the case of the cation of the $P\bar{1}$ phase the two equivalent naphthylmethyl groups show a transoid conformation relative to the fulvalenide ligand. Consequently, the packing arrangement of the cations and anions of **7** in the $P2_1/n$ phase is different from that in the $P\bar{1}$ phase. In the case of the latter the packing arrangement can be described as columns of cations and anions developing approximately along the *a* axis. In $P2_1/n$ phase the packing arrangement has a layer structure. Furthermore, it appears that the naphthylmethyl substituents lead to further slippage of the cations from the steplike stacks seen in dialkyl biferrocenium cations.

In the $P\bar{1}$ phase the I_3^- anion is at the inversion center and shows a symmetric structure. The I–I bond length is 2.8936(8) Å. In the case of the $P2_1/n$ phase the I_3^- anion is asymmetric (I1–I2 2.895(1), I1–I3 2.932(1) Å). In other words, the I3 atom carries more negative charge and shows I2–I1···I3$^-$ character. Furthermore, the I_3^- anion is not quite linear. In the $P\bar{1}$ phase an intermolecular phenyl–phenyl (π–π) interaction is observed between adjacent cations.

These structural characteristics are consistent with the results of the Mössbauer studies. The variable-temperature ^{57}Fe Mössbauer spectra of the two different crystallographic phases are shown in Figures 2 and 3. The ^{57}Fe Mössbauer spectrum of the $P\bar{1}$ phase at 80 K shows two doublets (Fe^{II}, ΔE_Q = 1.610 mms^{-1}; Fe^{III}, ΔE_Q = 0.818 mms^{-1}), which is characteristic of a valence-trapped cation in which the rate of intramolecular electron transfer is less than 10^7 s^{-1}.[10] The two doublets move together as the temperature is increased, and finally become a single average doublet (valence-detrapped) at about 130 K. On the other hand, the sample of the $P2_1/n$ phase exhibits a Mössbauer spectrum that is characteristic of a valence-trapped cation which remains trapped even at 300 K (Fe^{II}, ΔE_Q = 2.085 mms^{-1}; Fe^{III}, ΔE_Q = 0.407 mms^{-1}; Figure 3). The differences in the ^{57}Fe Mössbauer spectral properties of the two phases of **7** are attributable to differences in the molecular conformation around the mixed-valence cation. The crystal structure analysis of the $P\bar{1}$ phase shows that the environment of the cation is symmetric with respect to the two iron ions; rapid electron transfer is therefore possible. The asymmetric environment of the cations in the $P2_1/n$ phase energetically favors one valence state over the other, and, as a consequence, slow electron transfer results.[11]

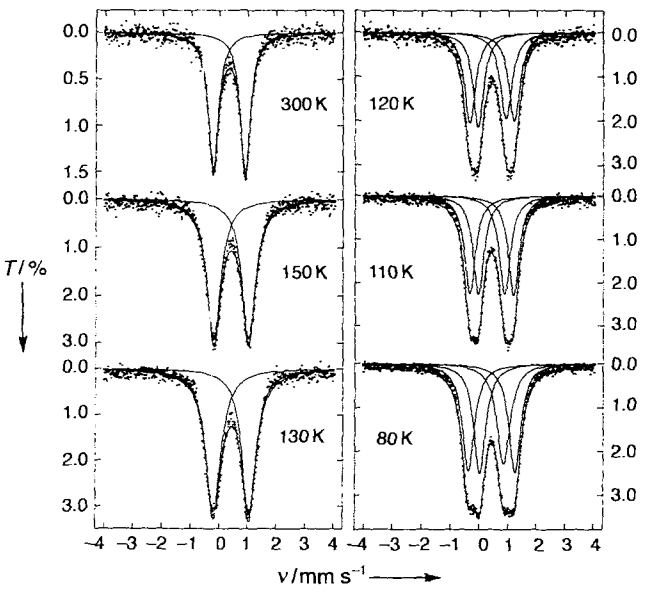

Figure 2. Variable-temperature ^{57}Fe Mössbauer spectra of **7** in the $P\bar{1}$ phase; T = transmission, v = velocity.

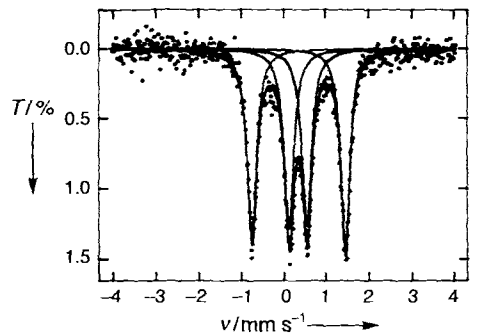

Figure 3. ^{57}Fe Mössbauer spectra of **7** in the $P2_1/n$ phase at 300 K.

The observations for the mixed-valence cation **7** definitively show that the crystallographic properties of the lattice play an important role in controlling the rate of electron transfer. There are several cases known in chemical and biological systems in which sluggish solvent–molecule motion and lattice dynamics can dramatically affect the rate of electron transfer.[1a, 12] In biological systems conformational changes of protein and the motion of amino acid groups have been suggested as providing control and specificity in electron transfer between proteins.[2] Our observation is an interesting result, which shows that the crystallographic properties can turn the electron transfer on or off.

Experimental Section

1′-Naphthoyl-1-bromoferrocene (**8**): Dibromoferrocene [13] (1.72 g, 5 mmol) was placed in a freshly dried flask (250 mL), and dried under vacuum at 2 Torr and 30 °C for 4 h. Dry THF (20 mL) and then butyllithium (3.15 mL, 1.6 M in hexane) were added under N_2. The solution was stirred at −25 °C for 30 min, during which 1-lithio-1′-bromoferrocene gradually precipitated. 1-Naphthylnitrile (5 mmol) was then added, and the solution stirred at −25 °C for another 25 min. Water (20 mL) was added, and the mixture extracted with CH_2Cl_2 (50 mL × 2). The combined extracts were dried over sodium sulfate and concentrated under reduced pressure. The residue was purified by chromatography on a column of neutral alumina (activity grade II). Elution with hexane gave fractions containing dibromoferrocene and bromoferrocene. Further elution with ethylacetate/hexane (1/25) provided the desired **8** in 20 % yield. ^{1}H NMR (300 MHz, $CDCl_3$, TMS): δ = 8.25 (t, 1H), 7.94 (m, 2H), 7.77 (d, 1H), 7.53 (m, 3H), 4.87 (s, 2H), 4.60 (s, 2H), 4.45 (s, 2H), 4.19 (s, 2H); MS (40 eV): m/z (%) = 418, 420 (100) [M^+].

Reduction of **8** to 1′-naphthylmethyl-1-bromoferrocene (**9**): Small portions of $AlCl_3$ were carefully added with stirring to a mixture of **8** and $LiAlH_4$ in dry ether. After 1 h the solution became yellow. An excess of H_2O was added, and the ether layer isolated, washed with H_2O, and dried over $MgSO_4$. After removal of the solvent the crude product was purified by chromatography on neutral Al_2O_3 with hexane as eluant. The first fraction contained the desired **9** in 71 % yield. ^{1}H NMR (300 MHz, $CDCl_3$, TMS): δ = 8.10 (d, 1H), 7.85 (t, 1H), 7.72 (d, 1H), 7.44 (m, 4H), 4.38 (t, 2H), 4.19 (s, 2H), 4.16 (s, 2H), 4.08 (t, 2H); MS (40 eV): m/z (%) = 404, 406 (100) [M^+]; m.p. 113.5–114.5 °C.

1′,1‴-Dinaphthylmethylbiferrocene (**10**): A mixture of **9** (1 g) and activated copper (5 g) was heated under N_2 at 120 °C for 24 h. After the mixture was cooled to room temperature, it was repeatedly extracted with CH_2Cl_2 until the extracts were colorless. The extracts were concentrated and purified by chromatography. The first fraction eluted with hexane yielded starting material. Further elution with CH_2Cl_2 afforded the desired **10** in 78% yield, which was recrystallized from hexane/

 © WILEY-VCH Verlag GmbH, D-69451 Weinheim, 1997 0570-0833/97/3618-2003 $ 17.50+.50/0

benzene. ^{1}H NMR (300 MHz, $CDCl_3$, TMS): $\delta = 7.94$ (d, 2H), 7.81 (t, 2H), 7.66 (d, 2H), 7.48 (m, 4H), 7.31 (m, 2H), 7.08 (d, 2H), 4.42 (s, 4H), 4.30 (s, 4H), 4.01 (s, 8H), 3.79 (s, 4H); MS (40 eV): m/z (%) = 650 (100) [M^+]; m.p. 170.0 °C (decomp).

7: A stoichiometric amount of I_2 in benzene/hexane (1/1) was added to a solution of **10** in benzene at 0 °C. The resulting dark green crystals were isolated by filtration and washed with cold hexane. A better crystalline sample was prepared by slowly concentrating a solution of **7** in CH_2Cl_2 (method 1) or by slowly diffusing hexane into a solution of **7** in CH_2Cl_2 (method 2). Microanalyses of the two different preparations were identical within experimental error. Elemental analysis calcd for **7** ($C_{42}H_{34}Fe_2I_3$): C 50.91, H 3.14; found: C 51.02, H 3.53 (method 1); found: C 50.99, H 3.55 (method 2).

Received: December 30, 1996
Revised version: May 23, 1997 [Z9941IE]
German version: *Angew. Chem.* **1997**, *109*, 2093–2096

Keywords: electron transfer · iron · mixed-valent compounds · Moessbauer spectroscopy

[1] a) R. D. Cannon, *Electron Transfer Reactions*, Butterworths, London, **1980**; b) A. Haim, *Comments Inorg. Chem.* **1985**, *4*, 113; c) D. N. Hendrickson, S. M. Oh, T.-Y. Dong, M. F. Moore, *ibid.* **1985**, *4*, 329; d) J. Jortner, M. Bixon, *J. Chem. Phys.* **1988**, *88*, 167.

[2] a) G. McLendon, *Acc. Chem. Res.* **1988**, *21*, 160; b) G. Williams, G. R. Moore, R. J. P. Williams, *Comments Inorg. Chem.* **1985**, *4*, 55.

[3] a) R. J. Webb, T.-Y. Dong, C. G. Pierpont, S. R. Boone, R. K. Chadha, D. N. Hendrickson, *J. Am. Chem. Soc.* **1991**, *113*, 4806; b) T.-Y. Dong, C. C. Shei, M. Y. Hwang, T. Y. Lee, S. K. Yeh, Y. S. Wen, *Organometallics* **1992**, *11*, 574; c) R. J. Webb, A. L. Rheingold, S. J. Geib, D. L. Staley, D. N. Hendrickson, *Angew. Chem.* **1989**, *101*, 1422; *Angew. Chem. Int. Ed. Eng.* **1989**, *28*, 1388.

[4] a) T.-Y. Dong, M. J. Cohn, D. N. Hendrickson, C. G. Pierpont, *J. Am. Chem. Soc.* **1985**, *107*, 4777; b) T.-Y. Dong, D. N. Hendrickson, K. Iwai, M. J. Cohn, A. L. Rheingold, H. Sano, I. Motoyama, S. Nakashima, *ibid.* **1985**, *107*, 7996; c) M. J. Cohn, T.-Y. Dong, D. N. Hendrickson, S. J. Geib, A. L. Rheingold, *J. Chem. Soc. Chem. Commun.* **1985**, 1095; d) S. Iijima, R. Saida, I. Motoyama, H. Sano, *Bull. Chem. Soc. Jpn.* **1981**, *54*, 1375.

[5] The X-ray structures of **7** ($C_{42}H_{34}Fe_2I_3$, $M = 1031.14$) were determined at 298 K. a) Crystals were obtained by slowly concentrating a solution of **7** in CH_2Cl_2: triclinic, space group $P\bar{1}$, $a = 9.836(2)$, $b = 10.418(2)$, $c = 10.638(3)$ Å, $\alpha = 62.83(1)$, $\beta = 86.06(1)$, $\gamma = 69.74(1)°$, $V = 904.5(4)$ Å^3, $F(000) = 497$, $\lambda(Mo_{K\alpha}) = 0.71073$ Å, $\mu = 3.391$ mm^{-1}, $Z = 1$, $\rho_{calcd} = 1.893$ g cm^{-3}. Data were collected on an Enraf Nonius CAD4 diffractometer in the range $2.16 < \theta < 22.42°$ (of 2356 reflections collected 1973 were independent). The structure was solved by heavy-atom methods, and refined, based on F^2, by full-matrix least-squares techniques. All non-hydrogen atoms were refined anisotropically, and hydrogen atoms were included in calculated positions and allowed to ride on the relevant carbon atom. Final residuals were $R1 = 0.0354$ and $wR(f^2) = 0.0875$ for 2356 unique data with $I > 2\sigma(I)$. Absorption corrections were made with empirical ψ rotation. b) Crystals were obtained by slowly diffusing hexane into a solution of **7** in CH_2Cl_2: monoclinic, space group $P2_1/n$, $a = 17.286(5)$, $b = 9.188(7)$, $c = 23.069(4)$ Å, $\beta = 93.44(2)°$, $V = 3658(3)$ Å^3, $F(000) = 1988$, $\lambda(Mo_{K\alpha}) = 0.71073$ Å, $\mu = 3.355$ mm^{-1}, $Z = 4$, $\rho_{calcd} = 1.873$ g cm^{-3}. Data were collected in the range $1.43 < \theta < 22.43°$ (of 4764 reflections collected 4764 were independent). The structure was refined as described above. Final residuals were $R1 = 0.0348$ and $wR(f^2) = 0.0980$ for 3289 unique data with $I > 2\sigma(I)$. Crystallographic data (excluding structure factors) for the structures reported in this paper have been deposited with the Cambridge Crystallographic Data Centre as supplementary publication no. CCDC-100423. Copies of the data can be obtained free of charge on application to The Director, CCDC, 12 Union Road, Cambridge CB21EZ, UK (fax: int. code +(1223)336-033; e-mail: deposit@chemcrys.cam.ac.uk).

[6] P. Seiler, J. D. Dunitz, *Acta Crystallogr. Sect. B* **1979**, *35*, 1068.

[7] N. J. Mammano, A. Zalkin, A. L. Rheingold, *Inorg. Chem.* **1977**, *16*, 297.

[8] K. Michiko, H. Sano, *Bull. Chem. Soc. Jpn.* **1988**, *61*, 1455.

[9] K. Michiko, H. Sano, *Bull. Chem. Soc. Jpn.* **1982**, *55*, 2327.

[10] W. H. Morrison Jr., D. N. Hendrickson, *Inorg. Chem.* **1975**, *14*, 2331.

[11] K. Y. Wong, P. N. Schatz, *Prog. Inorg. Chem.* **1981**, *28*, 369.

[12] a) H. G. Jang, S. J. Geib, Y. Kaneko, M. Nakano, M. Sorai, A. L. Rheingold, B. Montez, D. N. Hendrickson, *J. Am. Chem. Soc.* **1989**, *111*, 173; b) S. M. Oh, S. R. Wilson, D. N. Hendrickson, S. E. Woehler, R. J. Wittebort, D. Inniss, C. E. Strouse, *ibid.* **1987**, *109*, 1073; c) S. E. Woehler, R. J. Wittebort, S. M. Oh, T. Kambara, D. N. Hendrickson, D. Inniss, C. E. Strouse, *ibid.* **1987**, *109*, 1063; d) Y. Kaneko, M. Nakano, M. Sorai, H. G. Jang, D. N. Hendrickson, *Inorg. Chem.* **1989**, *28*, 1067; e) R. D. Cannon, R. P. White, *Prog. Inorg. Chem.* **1988**, *36*, 195.

[13] T.-Y. Dong, L. L. Lai, *J. Organomet. Chem.* **1996**, *509*, 131.

$[Ru(Ph)(CO)(PtBu_2Me)_2]^+$: A Unique 14-Electron Ru^{II} Complex with Two Agostic Interactions**

Dejian Huang, William E. Streib, Odile Eisenstein,* and Kenneth G. Caulton*

In a number of molecular settings the ligand $PtBu_2Me$ (L) is very bulky, even in comparison to $PiPr_3$ and PCy_3 (Cy = cyclohexyl). Thus, this ligand significantly diminishes the enthalpy of addition of PhCCPh and even compact MeNC to $[Ru(CO)_2L_2]$, and this phosphane spontaneously and completely dissociates from $[Ru(CO)_2L_3]$.[1] The two *t*Bu groups have a similarly large influence, for example, on promoting *ortho* metalation of $[Ir(H)_2X(PtBu_2Ph)_2]$ to form $[IrHX(PtBu_2Ph)\{\eta^2\text{-}P(C_6H_4)tBu_2\}]$, and in causing even this 16-electron complex to eliminate $PtBu_2Ph$.[2] Indeed, phenyl metalation is accompanied by metalation of the *t*Bu carbon atoms. We reported that $[RuH(CH_3)(CO)(PtBu_2Me)_2]$ loses methane already at −40 °C with metallation of a *t*Bu group.[1] We report here that $PtBu_2Me$ is the phosphane which leads to a remarkable example of two agostic aliphatic interactions with a single metal center.

Essential to this observation is the production of a metal center with two empty valence orbitals. This is tantamount to the synthesis of a 14-valence-electron complex. Our approach to this goal is halide removal from a 16-electron complex. For optimum electrophilicity in a 14-electron complex, it is desirable to exclude π-donor ligands from the coordination sphere. This also diminishes the possibility of loss ("quenching") of unsaturation by dimerization through halide bridges (e.g., $[L_nM(\mu\text{-}Cl)_2ML_n]$). Unlike in the case of $[Ru(CO)(NO)L_2][BAr'_4]$ (L = $PtBu_2Me$, Ar' = 3,5-$(CF_3)_2C_6H_3$),[3] which can be made by salt metathesis of $[RuCl(CO)(NO)L_2]$ with $Na[BAr'_4]$, $Na[BAr'_4]$ does not remove Cl^- from $[Ru(Ph)Cl(CO)L_2]$. Replacement of Cl^- in $[Ru(Ph)Cl(CO)L_2]$ by OTf^- with AgOTf ($OTf^- = CF_3SO_3^-$) also fails. However, $[Ru(Ph)Cl(CO)L_2]$ can be transformed into $[Ru(Ph)F(CO)L_2]$ quantitatively by salt metathesis with CsF in acetone. Reaction of $[Ru(Ph)F(CO)L_2]$ with one equivalent of Me_3SiOTf affords $[Ru(Ph)(OTf)(CO)L_2]$ in quantitative yield. Subsequent reaction with $Na[BAr'_4]$ in dichloromethane at 20 °C (5 min) gives $[Ru(Ph)(CO)L_2][BAr'_4]$ in quantitative yield [Eq. (1)].

$$[Ru(Ph)F(CO)L_2] \xrightarrow{Me_3SiOTf} [Ru(Ph)(OTf)(CO)L_2] \xrightarrow[-NaOTf]{Na[BAr'_4]} [Ru(Ph)(CO)L_2][BAr'_4] \quad (1)$$

The ^{1}H NMR spectrum (CD_2Cl_2, 20 °C) of $[Ru(Ph)(CO)L_2][BAr'_4]$ shows only three broad signals for the phenyl-ring

[*] Prof. O. Eisenstein
Laboratoire de Structure et Dynamique des Systèmes Moléculaire et Solides, UMR5636
Université de Montpellier 2
F-34095 Montpellier Cedex 5 (France)
Fax: Int. code +(4)6714-4798
e-mail: eisenst@lsd.univ-montp2.fr
Prof. K. G. Caulton, D. Huang, W. E. Streib
Department of Chemistry and Molecular Structure Center
Indiana University
Bloomington, IN 47405-4001 (USA)
Fax: Int. code +(812)855-8300
e-mail: caulton@indiana.edu

[**] We thank the National Science Foundation (NSF) and the Centre National de la Recherche Scientifique (CNRS) for support of the US–France collaboration through an international NSF/PICS grant. O. E. thanks E. R. Davidson for a generous donation of computational time.

 © WILEY-VCH Verlag GmbH, D-69451 Weinheim, 1997 0570-0833/97/3618-2004 $ 17.50+.50/0

protons. In contrast, five phenyl-proton signals appear for the five-coordinate $[Ru(Ph)X(CO)L_2]$ species reported here, indicating that phenyl-ring rotation is slow on the ^1H NMR time scale.[4] Two *t*Bu virtual triplets reveal that the molecule has a rigid, nonplanar geometry with two mutually *trans* phosphanes. The CO stretching frequencies (1958 cm^{-1}) of this complex in CD_2Cl_2 or fluorobenzene are identical, indicating the lack of solvent coordination to Ru. This very high ν(CO) value is consistent with a very electron-poor metal center. The other species in Equation (1) have ν(CO) values from 1890 to 1921 cm^{-1}. Additionally, two bands at 2722 and 2672 cm^{-1} are observed in the two solvents.[5] These two bands, which are in the stretching-frequency range of agostic C–H bonds, suggest that there are agostic interactions in this complex. However, attempts to observe the agostic protons by ^1H NMR spectroscopy in CD_2Cl_2 failed, even at −60 °C.[6]

To have conclusive evidence of an agostic interaction and the structure of this complex, a single crystal grown from a solution of fluorobenzene layered with pentane at room temperature was selected for an X-ray diffraction study. The crystal structure[7] of $[RuPh(CO)L_2][BAr'_4]$ confirms that the $[BAr'_4]^-$ anion does not bind directly to Ru, and shows a nonplanar geometry for the $Ru(C_{ipso})(CO)P_2$ moiety; this resembles an octahedron in which two *cis* ligands are missing (Figure 1). The phosphanes are transoid (∢ P-Ru-P 167.9°), and the CO and phenyl C_{ipso} atom *cis* (∢ C-Ru-C 93.5°). There is no evidence for agostic *ortho* phenyl interactions with Ru ($Ru\text{-}C_{ipso}\text{-}C_{ortho}$ 121 ± 4°); this phenyl ligand is therefore monohapto bound. However, the complex cation shows two agostic C-H-Ru interactions, one from one *t*Bu group of each phosphane. The shortest $Ru\text{–}C_{phosphane}$ distances are 2.87 Å (to C13) and 2.88 Å (to C28), which are within the range for strong agostic interactions.[8] Consequently, Ru-P-C angles are smaller when agostic interactions are involved: ∢ Ru1-P10-C11 (98.1(3)°) is 28° smaller than ∢ Ru1-P10-C15 (126.1(4)°), and ∢ Ru1-P20-C25 (96.6(3)°) is 25° smaller than ∢ Ru1-P20-C21 (121.7(6)°). In contrast, normal ∢ Ru-P-CMe_3 angles are typically around 115°. It is also true that the P-C-CH_3 angles for the which the CH_3 group is involved in an agostic interaction (C13 and C28: 103.3(11) and 104.2(12)°, respectively) are among the smallest in this molecule. While the C–C bonds in which the agostic methyl groups participate are not significantly longer than other C–C bonds, P–C bonds involving agostic *t*Bu groups are 3–4 σ (0.06 Å) longer than those to non-agostic *t*Bu groups. Thus, agostic interactions form primarily by angular deformation at P and C, but there is some evidence that P–C bonds may be "soft" enough to be lengthened.

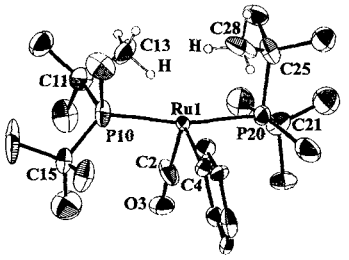

Figure 1. ORTEP diagram of the crystal structure of $[Ru(Ph)(CO)L_2]^+$. Hydrogen-atom positions are modeled. Only the hydrogen atoms of agostic methyl groups are shown, and these are idealized (C–H 1.05 Å, staggered conformation); Ru–C2 1.799(14), Ru–C4 2.058(12) Å.

The two agostic interactions formally provide four electrons to two vacant Ru orbitals. The occurrence of two (not one) agostic interactions in this cation reveals the reluctance of retaining even a 16-electron count in the absence of a π-donor ligand. Finally, since an intramolecular agostic interaction is evidently preferred to interaction with F, H or the π system of $[BAr'_4]$, this anion is quite effective at being "inert". The preference for *t*Bu over methyl C–H as donor must be attributed to the better steric approach of the former (giving a five-membered ring) than the latter (giving a four-membered ring). In summary, the existence of two agostic interactions in this complex reveals that this Ru^{II} complex is a strong Lewis acid but a weak π base.

The structure of the model complex $[Ru(Ph)(CO)(PH_3)_2]^+$ was optimized by density functional theory (DFT) calculations (B3LYP) with no symmetry constraint using the Gaussian 94 package (Figure 2).[9] The objective was to determine the inherent structural preferences of Ru and of the phenyl group (*ortho* agostic or not) in the absence of the influence of bulky phosphane substituents. The minimum-energy geometry is that of an octahedron with two empty *cis* sites. The calculated P-Ru-P and $OC\text{-}Ru\text{-}C_{ipso}$ angles are 176.6 and 97.4°, and the experimental values 167.9 and 93.5°, respectively. This shows that the (nonintuitive)[10] nonplanar structure of Ru and the four attached atoms is not caused by the two agostic interactions observed in $[Ru(Ph)(CO)(PtBu_2Me)_2]^+$. Instead, a d^6 configuration prefers a bent ML_4 structure with one angle close to 90°. This permits the three occupied metal d orbitals to be nonbonding (versus antibonding). The ligands with the strongest *trans* influence, CO and phenyl, prefer a position *trans* to an empty site. This structure keeps the (two) LUMOs, directed *trans* to CO and to phenyl, at a relatively high energy and, thus, makes the species persistent. The CO ligand (π* orbital) stabilizes two of the occupied d orbitals, but it (and the cationic charge) prevents oxidative addition of any C–H bond onto the metal. The slight twist (18°) of the phenyl ring out of the $OC\text{-}Ru\text{-}C_{ipso}$ plane observed in the crystal structure of $[Ru(Ph)(CO)(PtBu_2Me)_2]^+$ is not reproduced by the calculation involving PH_3, and is attributed to the *t*Bu and methyl substituents of the experimental species. The optimized structure shows no agostic interaction involving the *ortho*-phenyl hydrogen atom adjacent to the empty coordination site (Ru–H 2.84 Å). A phenyl ring is apparently too rigid to be a good *ortho* agostic donor to the metal to which it is σ bonded.

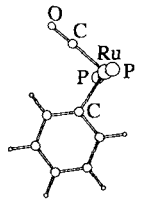

Figure 2. Calculated structure of $[Ru(Ph)(CO)(PH_3)_2]^+$; selected structural parameters: Ru–C(O) 1.83, Ru–C(Ph) 2.03, Ru–P 2.42 Å, ∢ Ru-C-O 178.9°.

$[Ru(Ph)(CO)L_2][BAr'_4]$ is highly air-sensitive. However, it is thermally stable up to 100 °C (eight hours in $[D_8]$toluene). It reacts with H_2 (CD_2Cl_2, 20 °C) within the time of mixing to form benzene, HL^+, and several other phosphane-containing products. The reaction with Me_3SiCCH occurs within the time of mixing at 25 °C (in CH_2Cl_2) to produce exclusively $PhCCSiMe_3$ and $[Ru\{\eta^3\text{-}(Me_3Si)CH{=}CHC{=}CH(SiMe_3)\}(CO)L_2][BAr'_4]$[11] in quantitative yield (Scheme 1). Since $[Ru(Ph)(CO)L_2^+]$ is a weak π base, it is unlikely to undergo oxidative addition. We therefore propose that this reaction undergoes a sigma bond metathesis mechanism in a highly selective way. This shows that agostic interactions in no way suppress the reactivity of this operational equivalent of a 14-electron species.

 © WILEY-VCH Verlag GmbH, D-69451 Weinheim, 1997 0570-0833/97/3618-2005 $ 17.50+.50/0

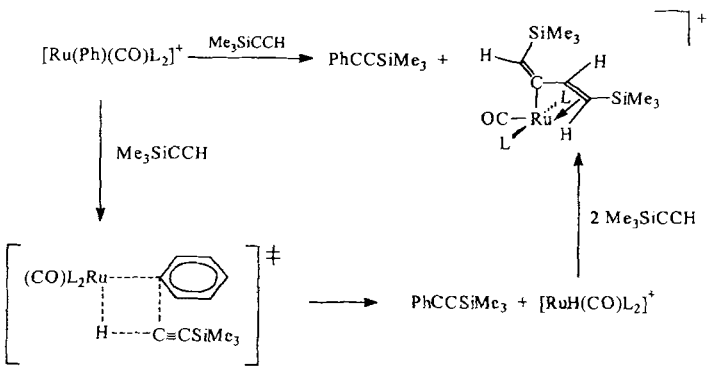

Scheme 1.

Experimental Section

[Ru(Ph)Cl(CO)L_2]: A solution of [RuHCl(CO)L_2] [12] (2.0 g, 4.1 mmol) and $HgPh_2$ (2.9 g, 8.0 mmol) in toluene (40 mL) was heated at reflux for 12 h and freed of volatile components [13]. The residue was extracted with pentane ($\approx$120 mL), and the extract evaporated to dryness to afford a crude product. Recrystallization from methanol gave dark orange crystals. Yield 1.92 g (83%). ^{1}H NMR (C_7D_8, 20 °C): δ = 8.32 (d, J = 7.2 Hz, 1H, *ortho*-H), 7.31 (d, J = 7.2 Hz, 1H, *ortho*-H), 6.78 (m, 1H, *para*-H), 6.69 (m, 2H, *meta*-H), 1.44 (virt. t, N = 5.4 Hz, 6H, PMe), 1.04 (virt. t, N = 12 Hz, 18H, P*t*Bu), 1.02 (virt. t, N = 12 Hz, 18H, P*t*Bu); N = ^3J(P,H) + ^5J(P,H); ^{31}P{^{1}H} NMR (C_7D_8, 20 °C): δ = 34.0 (s); IR (C_6D_6): $\tilde{\nu}$(CO) = 1902 cm^{-1}.

[Ru(Ph)F(CO)L_2]: [Ru(Ph)Cl(CO)L_2] (200 mg, 0.36 mmol) and CsF (100 mg, 0.66 mmol) were mixed with acetone (5 mL) and stirred for 12 h. The mixture was filtered, and the residue washed with pentane. The combined filtrate was evaporated to dryness in vacuo. The crude product was recrystallized from pentane (− 40 °C). Yield 150 mg (77%). ^{1}H NMR (C_6D_6, 20 °C): δ = 8.44 (d, J(H,H) = 6.6 Hz, 1H, *ortho*-H), 7.50 (d, J(H,H) = 8.1 Hz, 1H, *ortho*-H), 6.92 (m, 1H, *para*-H), 6.90 (m, *meta*-H), 6.83 (m, *meta* H), 1.31 (virt. t, N = 5.7 Hz, 6H, PCH_3), 1.08 (virt. t, N = 13.2 Hz, 18H, P*t*Bu), 0.99 (virt. t, N = 12.6 Hz, 18H, P*t*Bu); ^{31}P{^{1}H} NMR (C_6D_6, 20 °C): δ = 42.0 (d, J(P,F) = 24 Hz); ^{19}F NMR (C_6D_6, 20 °C): δ = −124.5 (t, J(P,F) = 24 Hz, Ru−F); IR (C_6D_6): $\tilde{\nu}$(CO) = 1890 cm^{-1}.

[Ru(Ph)(OTf)(CO)L_2]: [Ru(Ph)F(CO)L_2] (150 mg, 0.28 mmol) was dissolved in cyclohexane (10 mL), and Me_3SiOTf (54 µL, 0.28 mmol) added. The mixture was stirred for 10 min and then freed of volatile components. Recrystallization from a solution in toluene layered with pentane gave orange crystals. Yield 110 mg (58%). ^{1}H NMR (C_6D_6, 20 °C): δ = 8.0 (d, J(H,H) = 7.8 Hz, 1H, *ortho*-H), 7.31 (d, J(H,H) = 7.8 Hz, 1H, *ortho*-H), 6.90 (t, J(H,H) = 7.4, 1H, *para*-H), 6.73 (m, 1H, *meta*-H), 6.72 (m, 1H, *meta*-H), 1.50 (br s, 6H, PCH_3), 1.04 (virt. t, N = 13.2 Hz, 18H, P*t*Bu), 0.76 (virt. t, N = 13.2 Hz, 18H, P*t*Bu); ^{31}P{^{1}H} NMR (C_6D_6, 20 °C): δ = 40.5 (s); ^{19}F NMR (CD_2Cl_2, 20 °C): δ = −77.7 (s, O_3SCF_3); IR (C_6D_6): $\tilde{\nu}$(CO) = 1921 cm^{-1}.

[Ru(Ph)(CO)L_2][BAr$'_4$]: [Ru(Ph)(OTf)(CO)L_2] (150 mg, 0.22 mmol) and NaBAr$'_4$ (201 mg, 0.23 mmol) were mixed in fluorobenzene (5 mL) in a Schlenk tube under argon. The mixture was shaken for 10 min and then centrifuged. The liquid was transferred to a Schlenk flask in a glovebox under argon and layered with pentane. After 2 d red crystals were obtained. Yield 160 mg (52%). ^{1}H NMR (CD_2Cl_2, 20 °C): δ = 7.73 (s, 8H, BAr$'_4$), 7.57 (s, 4H, BAr$'_4$), 7.15 (br s, 2H, Ph), 7.01 (br s, 2H, Ph), 6.88 (m, 1H, *para*-H), 1.22 (virt. t, N = 4.8 Hz, 6H, PCH_3), 1.18 (virt. t, N = 13.2 Hz, 18H, P*t*Bu), 1.12 (virt. t, N = 14.4, 18H, P*t*Bu); ^{19}F NMR (CD_2Cl_2, 20 °C): δ = − 65.2 (s, BAr$'_4$); ^{31}P{^{1}H} NMR (CD_2Cl_2, 20 °C): δ = 41.4 (s); IR (CD_2Cl_2 or fluorobenzene): $\tilde{\nu}$(CO) = 1958, $\tilde{\nu}$(C−H(agostic)) = 2722, 2672 cm^{-1}; elemental analysis calcd for $C_{57}H_{59}BF_{24}OP_2Ru$: C 48.59, H 4.22; found: C 48.61, H 4.10.

Received: February 10, 1997 [Z10098IE]
German version: *Angew. Chem.* **1997**, *109*, 2096–2098

Keywords: agostic interactions · alkyl complexes · density functional calculations · ruthenium

[1] M. Ogasawara, S. A. Macgregor, W. E. Streib, K. Folting, O. Eisenstein, K. G. Caulton, *J. Am. Chem. Soc.* **1996**, *118*, 10189; C. Li, M. Ogasawara, S. P. Nolan, K. G. Caulton, *Organometallics* **1996**, *16*, 4900.
[2] A. C. Cooper, K. G. Caulton, *Inorg. Chim. Acta* **1996**, *251*, 41.
[3] M. Ogasawara, D. Huang, W. E. Streib, J. C. Huffman, O. Eisenstein, K. G. Caulton, *J. Am. Chem. Soc.* **1997**, in press.
[4] For the hindered rotation in [RuXY(CO)L_2], see J. U. Notheis, R. H. Heyn, K. G. Caulton, *Inorg. Chim. Acta* **1995**, *229*, 187.
[5] M. Brookhart, M. L. H. Green, L. K. Wong, *Prog. Inorg. Chem.* **1988**, *36*, 1.
[6] The ^{31}P{^{1}H} NMR spectrum of this complex in CD_2Cl_2 at −64 °C shows a slightly broader singlet than that at room temperature. However, in the ^{1}H NMR spectrum at −64 °C five phenyl-proton chemical shifts are recorded, indicating the slower rotation of the phenyl ring at this temperature.
[7] Crystal data for $C_{57}H_{59}BF_{24}OP_2Ru$ (−170 °C): a = 18.716(3), b = 18.495(3), c = 18.090(3) Å, Z = 4, space group $P2_12_12_1$; $R(F)$ = 0.0618 for 3443 reflections with $F > 3\sigma(F)$. Crystallographic data (excluding structure factors) for the structure reported in this paper have been doposited with the Cambridge Crystallographic Data Centre as supplementary publication no. CCDC-100415. Copies of the data can be obtained free of charge on application to The Director, CCDC, 12 Union Road, Cambridge CB2 1EZ, UK (fax: int. code + (1223) 336-033; e-mail: deposit@chemcrys.cam.ac.uk).
[8] D. Braga, F. Grepioni, K. Biradha, G. R. Desiraju, *J. Chem. Soc. Dalton Trans.* **1996**, 3925.
[9] The calculations were performed with the Gaussian 94 package. The pseudopotential and basis sets of Ru, P, C, and O are those of LANL2DZ. Polarization functions were added to P, C, and O. A STO-3G basis set was used for the H of PH_3. Optimization of the geometry was carried out at the B3LYP level. Gaussian 94, Revision D. I.: M. J. Frisch, G. W. Trucks, H. B. Schlegel, P. M. W. Gill, B. G. Johnson, M. A. Robb, J. R. Cheeseman, T. Keith, G. A. Petersson, J. A. Montgomery, K. Raghavachari, M. A. Al-Laham, V. G. Zakrzewski, J. W. Ortiz, J. B. Foresman, J. Cioslowski, B. B. Stefanov, A. Nanayakkara, M. Challacombe, C. Y. Peng, P. Y. Ayala, W. Chen, M. W. Wong, J. L. Andres, E. S. Reploge, R. Gomperts, R. L. Martin, D. J. Fox, J. S. Binkley, D. J. Dfrees, J. Baker, J. P. Stewart, M. Head-Gordon, C. Gonzalez, J. A. Pople, Gaussian, Inc., Pittsburgh, PA, USA **1995**.
[10] For four ligands a planar and not an SF_4 structure might be expected; see, however, M. Elian, R. Hoffmann, *Inorg. Chem.* **1975**, *14*, 1058.
[11] This complex is synthesized independently from [RuH(CO)L_2] with two equivalents of Me_3SiCCH: D. Huang, K. G. Caulton, unpublished results.
[12] D. F. Gill, B. L. Shaw, *Inorg. Chim. Acta* **1979**, *32*, 19.
[13] C. E. F. Rickard, W. R. Roper, G. E. Taylor, J. M. Waters, L. J. Wright, *J. Organomet. Chem.* **1990**, *389*, 375.

Solution Structures of a Pair of Stable Hexaaminecobalt(III/II) Conformers**

Peter Comba* and Achim F. Sickmüller

Dedicated to Professor Gottfried Huttner on the occasion of his 60th birthday

Hexaaminecobalt(III) complexes generally are yellow, and their redox potentials clustered around (− 0.2 ± 0.25) V (aqueous solutions, versus standard hydrogen electrode (SHE)). Some highly strained species were reported with "extremely" low ligand fields, in which the first d–d transition ($^1A_1 \rightarrow {}^1T_1$) is shifted from about 480 nm (20800 cm^{-1}) to about 510 nm (19600 cm^{-1}), and the redox potentials up to about + 0.3 V. The recent report[1] of an exciting blue hexaaminecobalt(III) cage compound with a $^1A_1 \rightarrow {}^1T_1$ transition at 600 nm (16700 cm^{-1}) and a redox potential of + 0.84 V (versus SHE) beats all records, and indeed opens an entirely new area of hexaaminecobalt(III) chemistry and ways of changing electronic and structural properties of metal complexes profoundly. Also of interest is the fact that this challenging new compound occurs in two forms which appear to be conformers of similar stability. The second species is a "normal" yellow hexaaminecobalt(III) complex with a $^1A_1 \rightarrow {}^1T_1$ transition at 480 nm (20800 cm^{-1}) and a redox potential not far from 0 V versus SHE. The X-ray structure of the yellow form was determined, but not that of the blue species.[1] There are two important questions addressed here: a) What are the structural differences between the yellow

[*] Prof. Dr. P. Comba, Dr. A. F. Sickmüller
Anorganisch-chemisches Institut der Universität
Im Neuenheimer Feld 270, D-69120 Heidelberg (Germany)
Fax: Int. code + (6221) 54-6617
e-mail: comba@akcomba.oci.uni-heidelberg.de

[**] We are grateful to Professor Alan M. Sargeson for interesting and helpful discussions. Generous financial support by the Volkswagen Stiftung, the Deutsche Forschungsgemeinschaft, and the Fonds der Chemischen Industrie is gratefully acknowledged.

and blue conformers? b) What causes the unprecedented shift of over 4000 cm^{-1} in the ligand-field band and of about 800 mV in the redox potential?

The structure of the yellow conformer is shown in Figure 1b. The calculated structure is in excellent agreement with the experimental data (see below). The three pairs of methyl substituents on the annular six-membered chelating rings are oriented towards the periphery of the complex, leading to a twist (skew-boat) conformation of these rings. The orientation of each of these rings is such that they are quasi perpendicular (oblique) to the C_3 axis through the metal center and the two trigonal planes defined by the "caps" of the cage ligand (*ob* conformations). The configuration of the coordination polyhedron of the computed molecule is Δ, and that of each of the six nitrogen donors (S); the two caps have the same orientation. As a result, the symmetry of the complex is D_3, and the overall geometry of the conformer may be described as $twist_3$-D_3ob_3. Simple geometric considerations suggest that the corresponding lel_3 conformer would have a cavity that is elongated along the C_3 axis. Structural studies on smaller cage complexes, which are based on ethane-1,2-diamine and have five-membered chelating rings, support this idea.[2] Therefore, an lel_3 conformer would have a larger cavity, leading to longer Co–N bonds and, thus, a weaker ligand field and a preference for the larger cobalt(II) ion, that is, to a more positive redox potential. Qualitatively, these are the properties of the blue conformer.

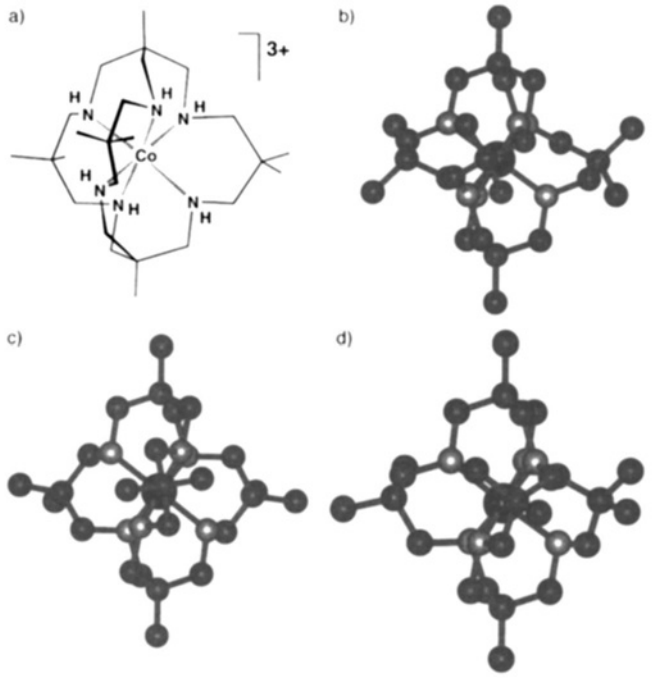

Figure 1. a) Lewis structure and computed structures of the most stable isomers: b) $twist_3$-D_3ob_3, c) $twist_3$-D_3lel_3, and d) $chair_3$-C_3.

These ideas were tested by computing various possible conformers of the hexaaminecobalt(III) cage compound. The calculations were restricted to the most important geometries. Conformers containing six-membered chelating rings in different geometries and structures including mixed chiralities at the nitrogen donors (R and S) were neglected, because they are distorted and high in energy. The strain energy minimized structures were obtained with the MOMEC program[3] and the corresponding force field.[4] Since the expected long cobalt(III)–amine bonds are outside the allowed interpolation limit of force-field calculations,[5] a Morse potential was used to model these stretching interactions.[6–8] The strain energies and the computed Co–N distances are assembled in Table 1, together with those for the reduced cobalt(II) species. It emerges that the $twist_3$-D_3ob_3, $twist_3$-D_3lel_3, and $chair_3$-C_3 cobalt(III) conformers are the most stable. The first two conformers have skew-boat conformations for all three six-membered chelating rings, and the third one has the three six-membered chelating rings in chair conformations.

Table 1. Calculated metal–ligand distances and strain energies of the most stable conformers.

Conformer	Co^{III}–N (Co^{II}–N) [Å]	Strain energy $H_{Co^{III}}$ ($H_{Co^{II}}$) [kJ mol^{-1}]
$twist_3$-D_3ob_3	1.985[a]	279.01
	(2.124)	(238.40)
$twist_3$-D_3lel_3	2.046	281.8
	(2.224)[b]	(177.11)
$chair_3$-C_3	2.031	268.77
	(2.189)	(190.37)
$twist_3$-C_2lel_2ob	2.008	312.1
	(2.204)	(194.42)
$twist_3$-C_2lelob_2	2.001	313.27
	(2.219)	(201.47)

[a] Observed [1]: 1.990 Å. [b] Observed [1]: 2.235 Å.

The electronic transitions and redox potentials of all conformers listed in Table 1 were also computed based on the strain energy minimized structures using MM-AOM[5, 9–11] and MM-Redox[5, 7, 13] calculations. These are given in Table 2. The calculated redox potentials and electronic transitions of the $twist_3$-D_3lel_3 and $twist_3$-D_3ob_3 conformers are in excellent agreement with the experimental data of both the yellow and blue species, which are also listed in Table 2.

Table 2. Calculated [a] and observed redox potentials [1] as well as ligand-field transitions of the three most stable and the two isolated conformers.

Conformer	Co^{III}–N [Å]	Redox potential [V]	Absorption maxima [nm]
$twist_3$-D_3ob_3	1.985	−0.10	481
			344
$twist_3$-D_3lel_3	2.046	+0.89	612
			416
$chair_3$-C_3	2.031	+0.49	583
			402
orange	1.990	~0	480
			350
blue	–	+0.84	600
			370

[a] $E^\circ = \{[(H_{Co^{III}} - H_{Co^{II}})/64.818] - 0.724\}$ V [7].

The good agreement between the computed and the observed structural data for the yellow isomer and for the reduced form of the blue isomer as well as the agreement between observed and computed spectroscopic and electrochemical properties are a strong basis for the structural assignment of the blue cobalt(III) hexaamine compound. This supports our view that the combination of force-field calculations with the simulation of d–d absorption spectra and/or redox potentials, based on the computed structures, is a reliable tool for the determination of structures of cobalt(III) hexaamines in general.

Received: March 14, 1997 [Z 102437 IE]
German version: *Angew. Chem.* **1997**, *109*, 2089–2090

 © WILEY-VCH Verlag GmbH, D-69451 Weinheim, 1997 0570-0833/97/3618-2007 $ 17.50+.50/0

Keywords: cobalt · conformation analysis · electrochemistry · molecular modeling · N ligands

[1] R. J. Geue, J. Hanna, A. Höhn, C. J. Qin, S. F. Ralph, A. M. Sargeson, A. C. Willis in *Electron Transfer Reactions* (Ed.: S. Isied), *ACS Symp. Ser.* **1997**, chap. 8.
[2] P. Comba, *Inorg. Chem.* **1989**, *28*, 426.
[3] P. Comba, T. W. Hambley, N. Okon, *MOMEC, A Strain Energy Minimization Package*, Lauer & Okon, Heidelberg, Germany, **1995**, e-mail: CVS-HD@T-Online.de
[4] P. Comba, T. W. Hambley, M. Ströhle, *Helv. Chim. Acta* **1995**, *78*, 2042.
[5] P. Comba, T. W. Hambley, *Molecular Modeling of Inorganic Compounds*, VCH, Weinheim, **1995**.
[6] P. M. Morse, *Phys. Rev.* **1929**, *34*, 57.
[7] P. Comba, A. F. Sickmüller, *Inorg. Chem.* **1997**, *36*, in press.
[8] Due to the strongly elongated bonds the compounds modeled here are the first examples of cobalt(III) hexaamines for which an anharmonic potential is required, and for which this may be accurately parameterized. The quality of the parameters is based on structural data, including that of the yellow isomer and a set of cobalt(III) amines with moderately long bonds, and on the computed ligand field and redox properties (see below and ref. [7]).
[9] a) P. V. Bernhardt, P. Comba, *Inorg. Chem.* **1993**, *32*, 2798; b) P. Comba, *ibid.* **1994**, *33*, 4755; c) P. Comba, T. W. Hambley, M. A. Hitchman, H. Stratemeier, *ibid.* **1995**, *34*, 3903; d) P. Comba, P. Hilfenhaus, *Helv. Chim. Acta*, in press.
[10] a) P. Comba, *Coord. Chem. Rev.* **1993**, *123*, 1; b) P. Comba, *Comments Inorg. Chem.* **1994**, *16*, 133; c) P. Comba in *Fundamental Principles of Molecular Modeling* (Eds.: W. Gans, A. Amann, J. C. A. Boeyens), Plenum Press, New York, **1996**, p. 167.
[11] CAMMAG [12] was used for the AOM calculations.
[12] a) M. Gerloch, M. *CAMMAG, a Fortran Program for AOM Calculations*, University of Cambridge, U. K.; b) H. Stratemeier, M. A. Hitchman, P. Comba, P. V. Bernhardt, M. J. Riley, *Inorg. Chem.* **1991**, *30*, 4088; the parameterization is described in ref. [9].
[13] Ligand-induced steric strain is not the only contribution to the redox potential of coodination compounds, and other effects have been discussed in detail [5, 7]. The admittedly simplistic approach used here was shown to lead to valuable results for hexaaminecobalt(III/II) couples [7].

$Ln_3Au_2Al_9$ (Ln = Dy, Tb): Heteronuclear versus Homonuclear Bonding in Intermetallic Phases**

Karen J. Nordell and Gordon J. Miller*

Dedicated to Professor Hans Georg von Schnering

Main-group intermetallic phases can be classified into three groups based on the valence electron concentration (VEC) per atom: Hume–Rothery phases with VEC < 2, Zintl phases with VEC > 4, and compounds with 2 < VEC < 4 whose structures cannot be rationalized by any simple electron-counting rules. Compounds of these three classes display a rich variety of structures and compositions ranging from close-packed structures with wide phase widths to valence compounds containing covalent two-center, two-electron bonds.[1] Many of these intermetallic phases offer chemists the challenge of complex structural features such as fractional and mixed site occupancies, site preferences, vacancy ordering, and structural phase transitions.

[*] Prof. Dr. G. J. Miller, K. J. Nordell
Department of Chemistry
Iowa State University
Ames, IA 50011-3111 (USA)
Fax: Int. code +(515)294-0105
e-mail: gmiller@iastate.edu

[**] This work was supported by the U. S. National Science Foundation (DMR-96-27161). We thank Dr. R. Jacobson for use of a diffractometer, and Dr. J. Ostenson for magnetic susceptibility measurements.

In addition to careful crystallography, calculations of electronic structure are essential for understanding the structures of these compounds. To explore the connection between VEC and structure type for the compounds between the Hume–Rothery phases and the Zintl phases, we focused on the synthesis, characterization, and determination of electronic structure of new ternary aluminum-rich intermetallic phases with 2 < VEC < 4.

The electronic structures of several binary aluminides—for example $BaAl_4$,[2a] $CaAl_4$,[2b] and $LaAl_3$[2c]—were investigated recently. These studies suggest phase stability within narrow ranges of VEC, and optimization of Al–Al bonding according to their calculated overlap populations. The ternary compound $BaCu_xAl_{13-x}$ ($5 < x < 6$) has the $NaZn_{13}$ structure, in which Ba atoms are surrounded by a $^3_\infty[Cu(Cu_y\text{-}Al_{12-y})]$ ($4 < y < 5$) cubic framework of Cu-stuffed icosahedra with randomly arranged Cu (ca. 33%) and Al atoms (ca. 67%). This is an example of a ternary aluminide whose VEC maximizes the bonding within the $^3_\infty[Cu_5Al_8]$ network, as observed in its overlap populations. These theoretical results provide justification for attractive Al–Al, Cu–Al, and Cu–Cu interactions in these intermetallic phases. When the more electronegative Au is used instead of Cu, we also observe a different structure that is related to the $BaAl_4$ structure.

While $BaAl_4$ represents one of the most prolific structural types,[3] isostructural compounds involving main-group metals are restricted to VEC ≤ 3.5.[4] The rare-earth elements (except Eu) do not form binary aluminides of composition $LnAl_4$ in this structural type (VEC = 3.75); rather, they form Ln_3Al_{11}.[5] Low-temperature $\alpha\text{-}Ln_3Al_{11}$ (Ln = La, Ce, Pr, Nd) has a body-centered orthorhombic structure which undergoes a phase transition (above 976 °C for La_3Al_{11}) to $\beta\text{-}Ln_3Al_{11}$ ($Ln\square_{0.33}Al_{3.67}$), a tetragonal $BaAl_4$ structural type with ordered vacancies. The structure of $\alpha\text{-}Ln_3Al_{11}$ is also closely related to that of $BaAl_4$ (Figure 1). The reason that these rare-earth elements form

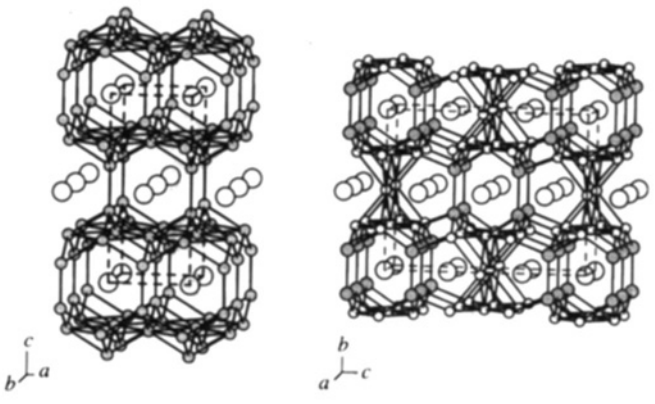

Figure 1. Left: structure of $BaAl_4$; large open circles Ba and small gray circles Al. Right: structure of $Dy_3Au_2Al_9$ ($\alpha\text{-}La_3Al_{11}$); large open circles Dy, small open circles nearly exclusively Al, and large gray circles 48% Au and 52% Al.

Ln_3Al_{11} rather than $LnAl_4$ is probably a combination of several factors including cation size and electron count. In the ternary rare-earth/Au/Al systems $LnAu_xAl_{4-x}$ ($x = 1\text{–}1.5$, Ln = La–Tb) with VEC = 3.0–3.25 form the $BaAl_4$ structure if Au and Al are disordered, but form the $BaNiSn_3$ structural type if the Al atoms are ordered.[6a] $LnAu_xAl_{4-x}$ ($x = 1.5\text{–}2$, Ln = La–Tb) with VEC = 2.75–3.0 are reported to form the $CaBe_2Ge_2$ structural type.[6b] We observed several rare-earth gold aluminides (e.g., $EuAu_{0.75}Al_{3.25}$, VEC = 3.125) that form the $BaAl_4$ structural type with no ordering of the Au and Al atoms.[6c]

 © WILEY-VCH Verlag GmbH, D-69451 Weinheim, 1997 0570-0833/97/3618-2008 $ 17.50+.50/0

We prepared the new compounds $Ln_3Au_2Al_9$ (Ln = Dy, Tb)[7] from their elements in an arc welding furnace. Both crystallize in a ternary derivative of the α-La_3Al_{11} type. According to single crystal X-ray diffraction studies, $Dy_3Au_2Al_9$ crystallizes in the space group *Immm* with $a = 4.265(1)$, $b = 9.952(2)$, and $c = 12.563(4)$ Å (see Table 1).[8] Several crystallites of

Table 1. Important structural parameters for $Dy_3Au_2Al_9$.

Refined composition				$Dy_3Au_{2.08}Al_{8.92}$		
Space group				*Immm* (no. 71)		
Unit-cell dimensions [7]				$a = 4.265(1)$ Å $b = 9.952(2)$ Å $c = 12.563(4)$ Å		
Atom	Wyckoff position	x	y	z	Occupation	U_{eq}
Dy1	2*a*	0	0	0	1.0	0.0080(4)
Dy2	4*i*	0	0	0.3155(1)	1.0	0.0081(3)
Au1	8*n*	0	0.3608(1)	0.3401(1)	0.484(3)	0.0092(5)
Al1	8*n*	0	0.3927(2)	0.3462(8)	0.516(3)	0.0092(5)
Au2	4*h*	0	0.2137(4)	0.5	0.068(4)	0.0097(14)
Al2	4*h*	0	0.2137(4)	0.5	0.932(4)	0.0097(14)
Al3	8*l*	0	0.2716(4)	0.1477(3)	1.0	0.0099(9)
Al4	2*d*	0	0.5	0	1.0	0.013(2)

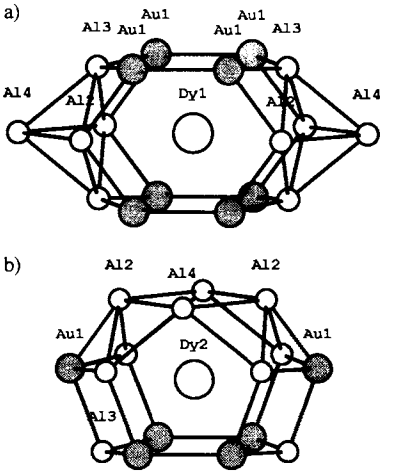

Figure 2. a) Structure of the 18-vertex elongated rhombic dodecahedron around Dy1. Au1 atoms are shown, but Al1 are not. Distances [Å] between Dy1 and framework atoms: Dy1–Au1 3.238(1), Dy1–Al2 3.555(2), Dy1–Al3 3.275(2), Dy1–Al4 4.971(3). Bond lengths [Å] within the framework: Au1–Au1 2.767(2), Al1–Al1 2.13(2), Au1–Al1 2.452(1), Au1–Al3 2.509(2), Au1–Al2 2.484(2), Al1–Al2 2.625(1), Al4–Al3 2.931(4), Al4–Al2 3.009(3). Bond length Dy1–Al1 3.067(7) Å (not shown). b) Structure of the 16-vertex polyhedron around Dy2. Au1 atoms are shown, but Al1 are not. Selected distances [Å]: Dy2–Al1 3.130(9), Dy2–Au1 3.204(1), Dy2–Au2/Al2 3.143(3), Dy2–Al3 3.148(3), Dy2–Al4 3.1474(9).

$Dy_3Au_2Al_9$ were analyzed with energy-dispersive spectroscopy in a Jeol 6100 scanning electron microscope, which indicated that Dy, Au, and Al were the only elements present in the sample. Magnetic-susceptibility measurements of $Dy_3Au_2Al_9$ showed Curie–Weiss paramagnetism with an effective moment of 18.54(4) μ_B per formula unit (for $T > 100$ K), which corresponds to three noninteracting Dy^{3+} centers (f^9) or 10.70 μ_B per Dy atom.[9]

$Dy_3Au_2Al_9$ forms the α-La_3Al_{11} structural type whose body-centered orthorhombic unit cell contains two formula units, or 28 atoms, and is related to $BaAl_4$ (see Figure 1). In $BaAl_4$, sheets of square pyramids are linked together along the *c* axis by direct connections between apex atoms, which results in 18-vertex polyhedra surrounding the Ba atoms. Calculations suggest that these linkages are two-center, two-electron bonds.[2a] In α-Ln_3Al_{11} the unit cell is three times larger, and two of the apex–apex connections have been condensed to single atoms (Al4), which have square-prismatic coordination and account for the deficiency in Al (the composition is $Dy_3Au_2Al_9$ and not "$Dy_3Au_2Al_{10}$"). This difference from $BaAl_4$ also leads to the disruption of the square network of Al atoms (the bases of the square pyramids) into ribbons along the *a* axis. There are two types of polyhedra surrounding the Dy atoms: 1) an elongated rhombic dodecahedron composed of 18 Al and Au atoms surrounding the Dy1 atoms on the corners and body center of the cell (Figure 2a) and 2) an irregular polyhedron composed of 16 Al and Au atoms encapsulating each Dy2 atom (Figure 2b). The large gray atoms in Figure 2 (labeled Au1), which represent averaged positions of the Au1 and Al1 atoms (see Table 1), form a cube around the Dy1 atom and are occupied by 48.4(3)% Au and 51.6(3)% Al.

Extended Hückel calculations[10] were performed on $Ln_3Au_2Al_9$ to examine the electronic structure of this compound and to help understand the mixing of Au and Al within the structure. Valence atomic orbitals of Y were selected to mimic Dy without its localized 4f orbitals, since the ionic radius of Y^{3+} (0.93 Å) is similar to that of Dy^{3+} (0.99 Å). Usually we can treat these elements as classical cations (Ln^{3+}); we included them in the calculation with the shortest Dy–Al and Dy–Au distances of 3.067(7) and 3.204(1) Å, respectively. To initially investigate the electronic structure of the aluminum-rich framework, we considered the homonuclear $^3_\infty[Al_{11}]^{n-}$ framework from α-La_3Al_{11} with an electron count of 38, which is appropriate for $Ln_3Au_2Al_9$. Mulliken populations were calculated for each atomic position: 3.676 (8*n*), 3.374 (4*h*), 3.266 (8*l*), and 3.512 (2*d*). For 42 electrons per formula unit, the electron count appropriate for La_3Al_{11}, the Mulliken populations are 3.900 (8*n*), 3.653 (4*h*), 3.810 (8*l*), and 3.853 (2*d*). The position with the largest population for both electron counts is 8*n*. Using Mulliken populations for the $^3_\infty[Al_{11}]^{n-}$ framework as a guide for the atomic ordering in the ternary compound, the positions with the largest Mulliken populations would be those most likely occupied by the atoms with the largest electronegativity.[11] The Pauling electronegativity of Au is 2.4, and that of Al 1.5. In the ternary compound $Dy_3Au_2Al_9$ this 8*n* position is occupied by 48.4(3)% Au and 51.6(3)% Al.

Since the X-ray diffraction experiment indicated no special ordering of Au and Al atoms on the 8*n* position, calculations were performed on model structures in which the Au and Al atoms were arranged with either homoatomic (Au–Au and Al–Al) or only heteroatomic (Au–Al) contacts. The partial density of states (DOS) curve for the $^3_\infty[Au_2Al_9]^{9-}$ framework in $Ln_3Au_2Al_9$ and the crystal orbital overlap population (COOP) curve for the Au1–Al1 contacts are shown in Figure 3. The Fermi energy lies in an area of nonzero DOS, and falls in the region of the crossover from bonding to antibonding levels in the Au1–Al1 COOP curve, which indicates near optimization of the bonding at this VEC. The total energy of the structure with only heteroatomic contacts is 0.5 eV per formula unit lower than that of the structure with homoatomic contacts.[12] Having two such bonding contacts per formula unit with only heteroatomic Au-Al contacts places an upper limit of two gold atoms per formula unit. These results indicate that there may be a range in composition of $x = 0$–2 for $Ln_3Au_xAl_{11-x}$; we are currently investigating this point. The stability of heteroatomic contacts may also be a factor in the ordered $LnAu_xAl_{4-x}$ ($x = 1.5$–2, Ln = La–Tb),[6b] which form the $CaBe_2Ge_2$ structure type in which there are only heteroatomic contacts for $x = 2$, or Au-Al and Al-Al contacts for $x < 2$. Given the large

 © WILEY-VCH Verlag GmbH, D-69451 Weinheim, 1997 0570-0833/97/3618-2009 $ 17.50+.50/0

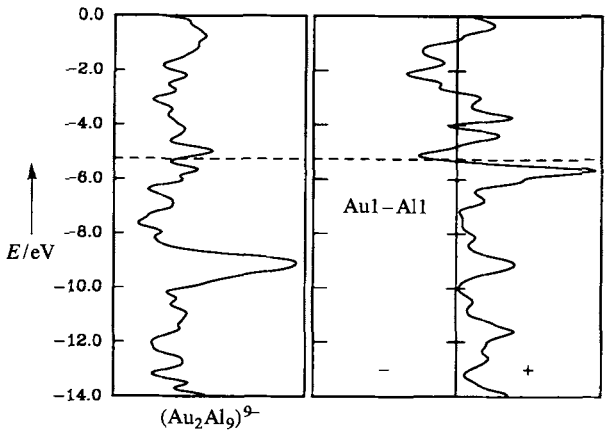

Figure 3. Left: Partial DOS curve for the $^3_\infty[Au_2Al_9]^{9-}$ framework of $Y_3Au_2Al_9$. Right: The COOP curve for the Au1–Al1 interaction, which shows the nearly optimal filling of bonding orbitals (+) and leaves the antibonding orbitals unfilled (−). The Fermi energy (dotted line) is at −5.21 eV.

DOS at the Fermi energy, we are also exploring electronic instabilities in these phases, in particular "$Y_3Au_2Al_9$", for a possible superconducting or structural phase transition.

Experimental Section

$Dy_3Au_2Al_9$ and $Tb_3Au_2Al_9$ were synthesized by allowing the elements to react in an argon-filled arc welding furnace with a zirconium getter for further atmosphere purification. Dysprosium and terbium (Materials Preparation Center, Ames Lab, 99.0%) as well as aluminum wire (Aesar 99.95%) and foil were cut into stoichiometric amounts in an argon-filled glovebox. The aluminum foil was used to wrap the metals into a small ball for transfer to the arc welding chamber. In the X-ray powder pattern no lines except those of the $Dy_3Au_2Al_9$ pattern and the silicon standard were observed. Samples that were annealed in niobium foil and evacuated fused silica at 800 °C for several weeks showed no structural change.

Received: February 27, 1997
Supplemented version: May 23, 1997 [Z10169IE]
German version: *Angew. Chem.* **1997**, *109*, 2098–2101

Keywords: aluminum · electronic structure · gold · intermetallic phases · solid-state chemistry

[1] W. B. Pearson, *The Crystal Chemistry and Physics of Metals and Alloys*, Wiley, New York, **1972**.

[2] a) J. K. Burdett, G. J. Miller, *Chem. Mater.* **1989**, *2*, 12; C. Zheng, R. Hoffmann, *Z. Naturforsch. B* **1986**, *41*, 292; b) G. J. Miller, F. Li, H. F. Franzen, *J. Am. Chem. Soc.* **1993**, *115*, 3739; c) G. J. Miller in *Chemistry, Structure, and Bonding of Zintl Phases and Ions* (Ed.: S. M. Kauzlarich), VCH, New York, **1996**, pp. 1–59.

[3] P. Villars, L. D. Calvert, *Pearson's Handbook of Crystallographic Data for Intermetallic Phases, 2nd ed.*, ASM International, Metals Park, OH, USA, **1991**.

[4] The VEC is calculated per Al atom in $BaAl_4$.

[5] A. H. Gomes de Mesquita, K. H. J. Buschow, *Acta Crystallogr.* **1967**, *22*, 497; K. A. Gschneidner, Jr., F. W. Calderwood, *Bull. Alloy Phase Diagrams* **1988**, *9*, 686.

[6] a) F. Hulliger, *J. Alloys Compds*, **1995**, *218*, 255; b) F. Hulliger, H. U. Nissen, R. Wessicken, *J. Alloys Compds*, **1994**, *206*, 263; c) K. J. Nordell, G. J. Miller, unpublished results.

[7] Lattice parameters obtained with an Enraf–Nonius Guinier camera ($Cu_{K\alpha 1}$ with Si standard): for $Dy_3Au_2Al_9$: $a = 4.265(1)$, $b = 9.952(2)$, $c = 12.563(4)$ Å; for $Tb_3Au_2Al_9$: $a = 4.276(3)$, $b = 9.970(5)$, $c = 12.583(8)$ Å.

[8] a) Crystal data for $Dy_3Au_2Al_9$ (23 °C, $Mo_{K\alpha}$ radiation, $\lambda = 0.7107$ Å): space group *Immm* (no. 71), $a = 4.262(1)$, $b = 9.941(2)$, $c = 12.552(3)$ Å, $V = 531.8(2)$ Å^3, $Z = 2$; $2\theta_{max} = 50°$; of 588 reflections collected 295 were unique; 33 variables; final $R = 0.025$, $R_w = 0.059$, GOF = 1.008 ($\rho_{calcd} = 7.106$ Mg m^{-3}). Lorentzian and polarization corrections were applied to the data set, and a semiempirical absorption correction was applied based on a series of azimuthal reflections. The structure was solved by using direct methods with calculations performed on a Digital Equipment Micro VAX 3100 computer using SHELXS-86 and SHELXTL-93 [8b] programs. Further details of the crystallographic investigation are available upon request from the authors, or from the Fachinformationszentrum Karlsruhe, D-76344 Eggenstein-Leopoldshafen (Germany) under the depository number CSD-406656. b) G. M. Sheldrick, in *Crystallographic Computing 3* (Eds.: G. M. Sheldrick, C. Kruger, R. Goddard), Oxford University Press, Oxford, **1985**, p. 175; SHELXTL-93, Siemens Industrial Automation, Inc., Madison, WI, USA.

[9] A small piece from the button (0.0392 g) was glued inside a straw for a magnetic susceptibility measurement from 6–300 K at a field strength of 3 T.

[10] a) The electronic structure of "$Y_3Au_2Al_9$" was evaluated with the tight-binding approximation in the extended Hückel calculations [10b]. The atomic orbital parameters of Y, Au, and Al [10c] are as follows: Y: 5s = −8.13 eV ($\zeta_1 = 1.74$), 5p = −5.13 eV ($\zeta_1 = 1.70$), 4d = −8.32 eV ($\zeta_1 = 1.56$, 0.8316, $\zeta_2 = 3.55$, 0.3014); Al: 3s = −12.30 eV ($\zeta_1 = 1.37$), 3p = −6.50 eV ($\zeta_1 = 1.36$); Au: 6s = −10.92 eV ($\zeta_1 = 2.60$), 6p = −5.55 eV ($\zeta_1 = 2.58$), 5d = −15.07 eV ($\zeta_1 = 6.16$, 0.6851, $\zeta_2 = 2.79$, 0.5696). Densities of states and crystal orbital overlap population curves were determined by summing over a set of k points (usually 30–50 special k points in the irreducible wedge of the first Brillouin zone); b) R. Hoffmann, W. N. Lipscomb, *J. Chem. Phys.* **1962**, *36*, *2179*, 3489; R. Hoffmann, *ibid.* **1963**, *39*, 1397; J. H. Ammeter, H. B. Bürgi, J. C. Thibeault, R. Hoffmann, *J. Am. Chem. Soc.* **1978**, *100*, 3686; M.-H. Whangbo, R. Hoffmann, R. B. Woodward, *Prog. R. Soc. London A* **1979**, *366*, 23; c) E. Clementi, C. Roetti, *At. Data Nucl. Data Tables* **1974**, *14*, 177.

[11] B. M. Gimarc, *J. Am. Chem. Soc.* **1983**, *105*, 1979.

[12] This result was confirmed by LMTO calculations on identical models [6c].

$[NH_4]_3[Ir(S_4)(S_6)_2]$: A Reevaluation of Hofmann and Höchtlen's Report of $[NH_4]_3[Ir(S_5)_3]$ from 1904**

Thomas E. Albrecht-Schmitt and James A. Ibers*

Dedicated to Professor Hans Georg von Schnering

Hofmann and Höchtlen were among the first to synthesize polysulfidometalates. In seminal work they reported on a number of novel compounds including $[NH_4]_2[PtS_{15}]\cdot 2H_2O$[1,2] and $[NH_4]_3[IrS_{15}]$.[2] Sixty-six years later $[NH_4]_2[PtS_{15}]\cdot 2H_2O$ was shown by single-crystal X-ray diffraction to be $[NH_4]_2[Pt(S_5)_3]\cdot 2H_2O$.[3] When a reaction mixture containing $[NH_4]_2[Pt(S_5)_3]$ is acidified to about pH 9.4, a second complex forms; from analytical data the complex was formulated as $[NH_4]_2[PtS_{17}]\cdot 2H_2O$.[4] Presumably the anion in this complex is either $[Pt(S_5)(S_6)_2]^{2-}$ or $[Pt(S_5)_2(S_7)]^{2-}$.[4]

Whereas the chemistry of $[PtS_{15}]^{2-}$, initiated by Hofmann and Höchtlen, was subsequently pursued and clarified, the chemistry of their $[IrS_{15}]^{3-}$ anion was not investigated until our recent studies of reactions between Ir^I and Ir^{III} complexes and polychalcogenides. We isolated the α-$[Ir(Se_4)_3]^{3-}$,[5,6] β-$[Ir(Se_4)_3]^{3-}$,[6] $[Ir(S_6)_3]^{3-}$,[6] and $[Ir(NCCH_3)_2(Se_4)_2]^{1-}$ anions;[6] with the exception of the latter, all have Pt^{IV} analogues.[7–9] We found that under certain conditions a polysulfidoiridate other than $[NH_4]_3[Ir(S_6)_3]$ could be isolated. We now report the synthesis and X-ray crystal structure of this product, $[NH_4]_3[Ir(S_4)(S_6)_2]$. We demonstrate that this is the material Hofmann and Höchtlen characterized as $[NH_4]_3[IrS_{15}]$ in 1904.

When $IrCl_3\cdot n H_2O$ is allowed to react with 25 wt% $[NH_4]_2S_n$ in water at 30–50 °C, the major product is $[NH_4]_3[Ir(S_6)_3]\cdot H_2O\cdot 0.5CH_3CH_2OH$.[6] However, after isolation of

[*] Prof. J. A. Ibers, T. E. Albrecht-Schmitt
Department of Chemistry
Northwestern University
2145 Sheridan Road, Evanston, IL 60208-3113 (USA)
Fax: Int. code +(847)491-2976
e-mail: ibers@chem.nwu.edu

[**] This research was supported by the U. S. National Science Foundation (grant CHE-9531232). We thank Dr. H. S. Genin for helpful discussions, and D. M. Smith for assistance with semiquantitative EDX.

this product, the mother liquor can be cooled to yield small amounts of $[NH_4]_3[Ir(S_4)(S_6)_2]$ in the form of brown, polycrystalline hemispheres. If 20 wt% $[NH_4]_2S_n$ is employed the product is predominantly $[NH_4]_3[Ir(S_4)(S_6)_2]$ as small red plates. When $RhCl_3 \cdot nH_2O$ is allowed to react under identical conditions $[NH_4]_3[Rh(S_5)_3] \cdot 3H_2O$ is the only product isolated.[10, 11]

The $[Ir(S_4)(S_6)_2]^{3-}$ anion (Figure 1), which has crystallographically imposed twofold symmetry, has the $\Lambda\lambda\lambda\delta$ conformation. This and its enantiomer $\Lambda\delta\delta\lambda$ are the expected conformations.[6, 9] The geometry about the Ir atom is a distorted octahedron with S-Ir-S bond angles ranging from 85.5(2) to 98.8(2)°, comparable to those of other octahedral polychalcogenometalates.[6, 8] The Ir–S and S–S bond lengths are within expected[6] ranges of 2.347(5) to 2.367(4) and 2.042(9) to 2.079(9) Å, respectively.

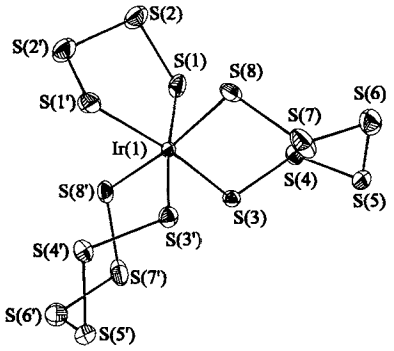

Figure 1. Structure of the $[Ir(S_4)(S_6)_2]^{3-}$ anion; ellipsoids for 50% displacement are shown.

Hofmann and Höchtlen's formulation of their product as $[NH_4]_3[IrS_{15}]$ was based upon the assumption that $[NH_4]_2S_n$ contained polysulfide exclusively in five-atom chains,[1] and upon accurate and reproducible elemental analyses.[1, 2] Although their work from 1904 was carried out a decade before the discovery of X-ray diffraction, they did report sufficient crystallographic data to enable us to establish beyond doubt that their product was $[NH_4]_3[Ir(S_4)(S_6)_2]$, that is $[NH_4]_3[IrS_{16}]$. They reported that their product crystallized in the tetragonal system as octahedra with interplanar angles of 52.30° for (001):(111) and 68.40° for (111):($\bar{1}$11).[2] The assignment of {111} to octahedral faces is arbitrary though standard in mineralogy in the absence of information about the space group. In fact, if we assign the octahedral faces as {101}, then from our unit-cell measurements the interplanar angles are calculated to be 51.60° for (001):(101) and 67.31° for (10$\bar{1}$):(011). There is thus excellent agreement between the interplanar angles reported by Hofmann and Höchtlen from room-temperature measurements and those calculated from our unit cell obtained at 113 K. There is no doubt that $[NH_4]_3[IrS_{15}]$ is $[NH_4]_3[Ir(S_4)(S_6)_2]$, and that all references to the former compound are in error.

Individual crystals of $[NH_4]_3[Ir(S_4)(S_6)_2]$ are enantiomerically pure, but, since batches of single crystals fail to rotate polarized light and since Ir^{III} complexes are kinetically inert,[12, 13] other crystals contain anions in the $\Lambda\delta\delta\lambda$ conformation. Thus, $[NH_4]_3[Ir(S_4)(S_6)_2]$ is an example of a material that undergoes spontaneous resolution. It is interesting that such crystals were available a decade before Werner's classic paper from 1914,[14] in which he resolved the first completely inorganic chiral compound.

Remarkably, Hofmann and Höchtlen briefly described the existence of small, orange plates as a second product from their reaction. $[NH_4]_3[Ir(S_6)_3]$, which we characterized,[6] crystallizes as orange plates.

Hofmann and Höchtlen's seminal work in this field was characterized by superb elemental analyses, reproducible reaction conditions, and thorough descriptive analysis of isolated products. The incorrect formulation of $[NH_4]_3[IrS_{16}]$ as $[NH_4]_3[IrS_{15}]$ simply resulted from a low S analysis, a problem also noted for $[NH_4]_3[Rh(S_5)_3] \cdot 3H_2O$.[11] By analogy to Rh^{III} and Pt^{IV} chemistry,[4, 10, 11] the existence of $[NH_4]_3[Ir(S_5)_3]$ is entirely plausible. But neither the remarkable chemistry of Hofmann and Höchtlen from 1904 nor the present chemistry provides evidence for its existence.

Experimental Section

$[NH_4]_3[Ir(S_4)(S_6)_2]$ was prepared by allowing $IrCl_3 \cdot nH_2O$ (1.000 g), dissolved in water (10 mL), to react with $[NH_4]_2S_n$ (30 mL), which was prepared by dissolving sulfur (5 g) in 20 wt% $(NH_4)_2S$ (30 mL) at 50 °C. The resultant deep red solution was stirred at 50 °C for 1 h, and then filtered through a plug of celite. The filtrate was divided into two portions, each of which was layered with ethanol/2-propanol (1/1, 40 mL). Crystals were usually observed after 24 h. The mother liquor was decanted, and the crystals were washed with CS_2 and 2-propanol. By appearance, three different products were formed: orange octagonal plates, small red crystals, and brown polycrystalline masses. The orange plates were previously shown to be $[NH_4]_3[Ir(S_6)_3] \cdot H_2O \cdot 0.5\,CH_3CH_2OH$ [6]. The other two products were both identified as $[NH_4]_3[Ir(S_4)(S_6)_2]$ by means of Raman spectroscopy and energy-dispersive X-ray spectroscopy (EDX). The ratio of $[NH_4]_3[Ir(S_6)_3] \cdot H_2O \cdot 0.5\,CH_3CH_2OH$ to $[NH_4]_3[Ir(S_4)(S_6)_2]$ was approximately 1:4, as determined by manual separation of the crystals. The total yield was 1.430 g ($\approx$ 57%). Semiquantitative EDX ratios of Ir:S for $[NH_4]_3[Ir(S_6)_3] \cdot H_2O \cdot 0.5\,CH_3CH_2OH$ and $[NH_4]_3[Ir(S_4)(S_6)_2]$ were recorded on a Hitachi S-4500 SEM, since standard elemental analyses can be misleading and inaccurate for polysulfidometalates [4, 11].

X-ray structure analysis of $[NH_4]_3[Ir(S_4)(S_6)_2]$: red, irregular blocks, crystal dimensions $0.16 \times 0.17 \times 0.13$ mm, tetragonal, D_4^8-$P4_32_12$, $Z = 4$, $a = 12.009(2)$, $c = 15.154(3)$ Å, $V = 2186(1)$ Å^3 ($T = 113$ K), Enraf-Nonius CAD4 diffractometer: $\theta_{max} = 49.94°$, $Cu_{K\alpha}$, $\lambda = 1.54056$ Å, ω-scan mode; of 2487 reflections measured 1121 were independent and included in the refinement. The data were corrected for Lorentz–polarization and absorption effects (empirical method), $\mu = 261$ cm^{-1}. The structure was solved by the Patterson method [15], and refined anisotropically on F^2 by full-matrix least squares [16]; 101 parameters, $R_w(F^2) = 0.120$, $R_1 = 0.054$ for 929 reflections with $F_o^2 > 2\sigma(F_o^2)$, absolute structure parameter $-0.07(5)$, residual electron density 1.12 e Å^{-3}. Further details of the crystal structure investigation may be obtained from the Fachinformationszentrum Karlsruhe, D-76344 Eggenstein-Leopoldshafen (Germany) on quoting the depository number CSD-406601.

Received: February 24, 1997 [Z10156IE]
German version: *Angew. Chem.* **1997**, *109*, 2101–2102

Keywords: chirality · iridium · S ligands · structure elucidation

[1] K. A. Hofmann, F. Höchtlen, *Ber. Dtsch. Chem. Ges.* **1903**, *36*, 3090–3093.
[2] K. A. Hofmann, F. Höchtlen, *Ber. Dtsch. Chem. Ges.* **1904**, *37*, 245–249.
[3] P. E. Jones, L. Katz, *Acta Crystallogr. Sect. B* **1969**, *25*, 745–753.
[4] R. D. Gillard, F. L. Wimmer, J. P. G. Richards, *J. Chem. Soc. Dalton Trans.* **1985**, 253–258.
[5] T. E. Albrecht-Schmitt, J. A. Cody, J. T. Hupp, J. A. Ibers, *Inorg. Chem.* **1995**, *34*, 5101–5102.
[6] T. E. Albrecht-Schmitt, J. A. Ibers, *Inorg. Chem.* **1996**, *35*, 7273–7278.
[7] M. A. Ansari, J. A. Ibers, *Inorg. Chem.* **1989**, *28*, 4068–4069.
[8] J. M. McConnachie, M. A. Ansari, J. A. Ibers, *Inorg. Chem.* **1993**, *32*, 3250–3255.
[9] R. Sillanpaa, P. S. Cartwright, R. D. Gillard, J. Valkonen, *Polyhedron* **1988**, *7*, 1801–1806.
[10] R. A. Krause, *Inorg. Nucl. Chem. Lett.* **1971**, *7*, 973–975.
[11] P. Cartwright, R. D. Gillard, R. Sillanpaa, J. Valkonen, *Polyhedron* **1987**, *6*, 1775–1779.
[12] R. A. Bauer, F. Basolo, *Inorg. Chem.* **1969**, *8*, 2231–2236.
[13] F. Basolo, R. G. Pearson, *Mechanisms of Inorganic Reactions. A Study of Metal Complexes in Solution, 2nd ed.*, Wiley, New York, **1967**.
[14] A. Werner, *Ber. Dtsch. Chem. Ges.* **1914**, *47*, 3087–3094.
[15] G. M. Sheldrick in *Crystallographic Computing 3* (Eds.: G. M. Sheldrick, C. Krüger, R. Goddard), Oxford University Press, London, **1985**, pp. 175–189.
[16] A. L. Spek, *Acta Crystallogr. Sect. A* **1990**, *46*, C34.

 © WILEY-VCH Verlag GmbH, D-69451 Weinheim, 1997 0570-0833/97/3618-2011 $ 17.50+.50/0

NADH-Dependent Halogenases Are More Likely To Be Involved in Halometabolite Biosynthesis Than Haloperoxidases**

Kathrin Hohaus, Annett Altmann, Wassily Burd, Ilona Fischer, Philip E. Hammer, Dwight S. Hill, James M. Ligon, and Karl-Heinz van Pée*

The detection of chloroperoxidase from the fungus *Caldariomyces fumago*[1] and the development of a simple spectrophotometric assay[2] for the detection of halogenating enzymes based on the synthetic compound monochlorodimedone (**1**) as organic substrate resulted in the subsequent isolation of a number of haloperoxidases from different organisms. All these enzymes produce hypohalogenic acid, which is the actual halogenating agent. Thus, halogenation catalyzed by haloperoxidases lacks substrate and regiospecificity.[3-4] However, investigations of the biosynthetic pathways of different halometabolites have shown that biological halogenation must be specific.[3, 5] Furthermore, the formation of fluorinated metabolites by haloperoxidases is difficult to explain, as fluoride cannot be oxidized in the haloperoxidase reaction.[6]

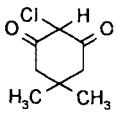

1

Recently, genetic investigations showed that haloperoxidase-type enzymes are definitely not involved in the biosynthesis of chlorotetracycline and pyrrolnitrin.[7-8] These results raise some interesting questions. What other type of halogenating enzymes could exist, and how can they be detected? It had always been assumed that the enzyme oxidizes the halide ion and that the oxidized halide reacts with the organic substrate. However, why couldn't the enzyme first react with the organic substrate in a way that would make it suitable for nucleophilic attack by the halide ion itself?

Apparently all groups working on enzymatic halogenation have ignored the fact that, if they were looking for specific enzymes, they should use the natural substrates for these enzymes and not a substrate like **1**. One reason that this approach was ignored is the lack of knowledge about the structure of these substrates. Thus, prior to the use of a "natural" substrate it had to be established that this compound actually is halogenated in vivo.

Tryptophan (**2**) would be such a substrate, if the chlorination of **2** to 7-chlorotryptophan (**3**) is the first step in the biosynthesis of the antifungal antibiotic pyrrolnitrin (**6**, Scheme 1).[9] To check this hypothesis, the growth medium of a mutant of *Pseudomonas fluorescens* blocked in the second step of pyrrolnitrin biosynthesis was analyzed. The isolated **3** was identified as the L-isomer by employing D- and L-amino acid oxidases. Thus, chlorination of the L-isomer of **2** was identified as the first step

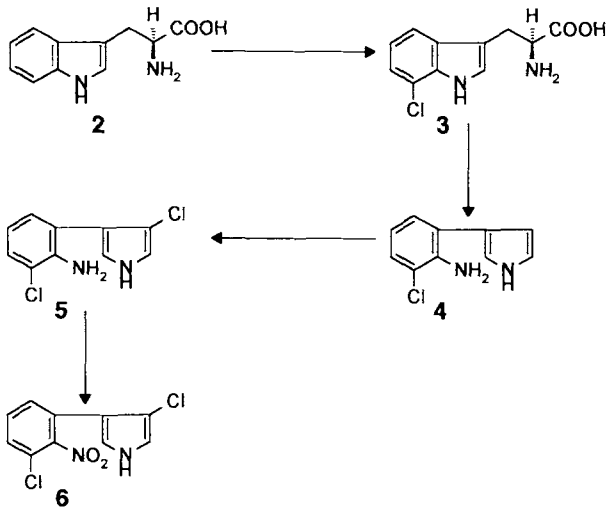

Scheme 1. Pathway for pyrrolnitrin (**6**) biosynthesis based on the isolation of metabolites and cloning of the biosynthetic genes [9,11].

in pyrrolnitrin biosynthesis by *P. fluorescens*, and this strain therefore must contain an enzyme that catalyzes the specific chlorination of the L-isomer of **2** to the L-isomer of **3**. A second chlorination occurs later, where monodechloroaminopyrrolnitrin (**4**) is chlorinated to aminopyrrolnitrin (**5**, Scheme 1).[9]

Using the L-isomer of **2** as the substrate and a *Pseudomonas fluorescens* mutant that lacked all chromosomal pyrrolnitrin-biosynthesis genes but harbored the gene for the first step on a plasmid, we searched for tryptophan halogenase activity by means of an HPLC assay. As we did not know what kind of cofactor, if any, would be needed, a number of different cofactors were tested. The chlorinated **3** could only be detected when NADH was added to the cell-free extract (Scheme 2a).

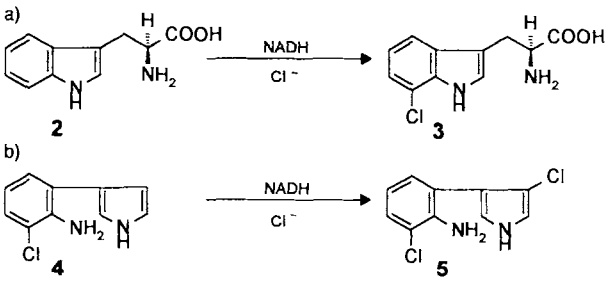

Scheme 2. NADH-dependent chlorination of a) L-tryptophan (**2**) to 7-chloro-L-tryptophan (**3**) catalyzed by tryptophan halogenase and b) monodechloroaminopyrrolnitrin (**4**) to aminopyrrolnitrin (**5**) by monodechloraminopyrrolnitrin halogenase.

Attempts to chlorinate **2** with haloperoxidases only resulted in the formation of the oxindole derivative of tryptophan and not in a halogenated product.[10] Chemical chlorination of **2** in the 7-position is also not possible. The enzymatic chlorination of **2** can therefore be regarded as a specific and unusual reaction, although there are a number of naturally produced antibiotics that are derived from **3**.[5]

The addition of NADH to cell-free extracts of a *P. fluorescens* pyrrolnitrin-deletion mutant containing the gene coding for the enzyme that catalyzed the second chlorination step on a plasmid was also necessary for activity. Thus the halogenase chlorinating **4** to **5** is also NADH-dependent (Scheme 2b). As the oxidation of halide ions in an NADH-dependent reaction can be ruled

[*] Prof. Dr. K.-H. van Pée, Dipl.-Chem. K. Hohaus, Dipl.-Chem. A. Altmann, Dr. W. Burd, Dipl.-Ing. (FH) I. Fischer
Institut für Biochemie der Technischen Universität
Mommenstrasse 13, D-01062 Dresden (Germany)
Fax: Int. code +(351)463-5506
e-mail: Karl-Heinz.vanPee@chemie.tu-dresden.de
Dr. P. E. Hammer, Dr. D. S. Hill, Dr. J. M. Ligon
Novartis, Research Triangle Park (USA)

[**] This work was supported by the Sächsische Staatsministerium für Umwelt und Landesentwicklung (SMU), the Deutsche Forschungsgemeinschaft (DFG), the Environment and Climate Research and Technology Development Programme of the European Union, and the Fonds der Chemischen Industrie. We are grateful to Dr. Kronbach and Dr. Hempel, Arzneimittelwerk Dresden, for HPLC-MS analysis of isolated and enzymatically produced **2** and to Dr. Kroschwitz, Institut für Organische Chemie, TU Dresden, for GC-MS analysis of enzymatically produced **4**.

 © WILEY-VCH Verlag GmbH, D-69451 Weinheim, 1997 0570-0833/97/3618-2012 $ 17.50+.50/0

out, the NADH-dependence could be explained by the involvement of oxygen leading to the intermediate formation of an epoxide (**7**). From this enzyme-bound epoxide a halohydrin (**8**) could be formed by the incorporation of halide ion with subsequent specific removal of water (Scheme 3). Thus the organic substrate can not only be chlorinated, brominated, and iodated, but also fluorinated, depending on the specificity of the enzyme for the halide ion. No substantially different halogenating enzyme would be needed for the introduction of fluoride ions.

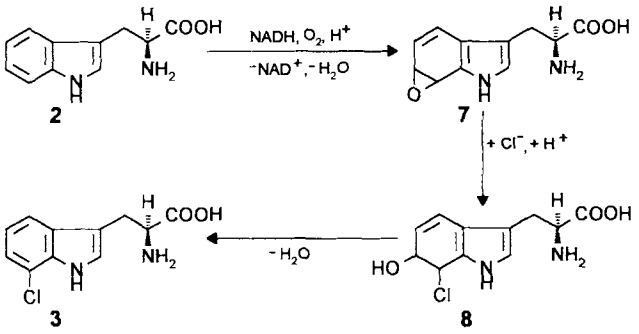

Scheme 3. Hypothetical mechanism for the NADH-dependent halogenation. Compounds **7** and **8** would probably not be released by the enzyme.

No enzymatically formed products other than **3** or **5** could be detected in the enzyme assays. The enzymes are specific, and tryptophan halogenase does not catalyze the chlorination of **4** or vice versa. Comparison of the amino acid sequences of the two halogenases showed no sequence homology. However, monodechloroaminopyrrolnitrin halogenase was found to be homologous to the halogenase that catalyzes the chlorination in 7-chlorotetracycline biosynthesis.[7, 11]

The newly detected NADH-dependent halogenases, in contrast to haloperoxidases, have at least some of the properties expected of specifically halogenating enzymes. It was always difficult to understand why halogenation by haloperoxidases in vitro produces halocompounds that could not be found in the organisms from which these haloperoxidases had been isolated. It is very likely that haloperoxidases are not the halogenating enzymes involved in the specific biosynthesis of halometabolites. For these reactions NADH-dependent halogenases are much better candidates. Thus, in organisms where discrepancies arise between the halometabolites produced in vivo and the products formed in vitro, the involvement of haloperoxidases should be reinvestigated and NADH-dependent halogenases sought.

Experimental Section

For the isolation of **3**, bacteria were grown in 2 L of glycerol minimal medium [9] in the presence of 8.5×10^{-5} M kanamycin and 6.2×10^{-5} M tetracycline at 30 °C for two days. As **3**, like **2**, is metabolized by a number of different pathways, it was not expected to accumulate in large amounts. Therefore the growth medium was adjusted to pH 5.3 with 1 N HCl and loaded onto an Amberlite CG-120I cation exchange column with a column volume of 25 mL, equilibrated with 0.35 M citrate buffer (pH 5.3). After elution with 1% aqueous ammonia the fractions (2.4 mL) were neutralized with 1 M acetic acid and analyzed by HPLC [12]. Fractions containing **3** were pooled, concentrated under vacuum, and desalted over a Sephadex G-10 column (column volume 5 mL). The fractions (1 mL) were analyzed by HPLC and those containing **3** were pooled and concentrated. The isolated compound was identified by comparison of its retention time, UV spectra, and mass spectra with those of authentic, synthesized **3** [13].

Oxidation of isolated **3** to 3-(3-indolyl)-pyruvic acid by amino acid oxidases was performed in a total volume of 75 µL in 0.2 M Tris/HCl buffer (pH 8.3) in the presence of 9×10^{-4} units of catalase. The reactions were started by addition of 5×10^{-1} units of D-amino acid oxidase or 5×10^{-2} units of L-amino acid oxidase. The assays were incubated at 30 °C with continuous shaking. Samples (20 µL) were analyzed at the start of the reaction, after 60, and after 90 min.

For detection of the halogenase activities, a *Pseudomonas fluorescens* mutant that lacked all pyrrolnitrin-biosynthesis genes but contained the genes for tryptophan or monodechloroaminopyrrolnitrin halogenase on a plasmid was grown for three days as described for the isolation of **3**. Cells were harvested by centrifugation, resuspended in 2 mL g^{-1} cells volume of 100 mM ammonium acetate buffer (pH 6.8) and disrupted by sonication at 2 °C for 6 min. The cell debris was removed by centifugation, and the crude extracts were used for analysis of the halogenase activities. The assays used contained the following components: 200 µL of crude extract, 20 mM NaCl, 0.2 mM **2** or **4** as the organic substrate, 2 mM cofactor, and 0.1 mM ammonium acetate buffer (pH 6.8) in a total volume of 1 mL. After incubation for 16 h at room temperature the reaction was stopped by boiling in water for 5 min in the case of tryptophan halogenase. After removal of precipitated protein by centrifugation, the assay mixture (20 µL) was analyzed by HPLC [12]. With **4** as the substrate, the assay mixture was extracted with 2 × 0.5 mL ethyl acetate. After evaporation of the organic solvent, the extracted compounds were redissolved in methanol (50 µL), and a 20 µL sample of the solution was analyzed by HPLC [14]. The products were identified by comparison of their retention times, HPLC-UV spectra, HPLC-MS spectrum in the case of **3**, and GC-MS spectrum in the case of **5** with those of authentic samples [13,15].

Received: March 11, 1997 [Z10223IE]
German version: *Angew. Chem.* **1997**, *109*, 2102–2104

Keywords: antibiotics · biosynthesis · chlorinations · enzyme catalysis · halogenases

[1] P. D. Shaw, L. P. Hager, *J. Am. Chem. Soc.* **1959**, *81*, 6527–6528.
[2] L. P. Hager, D. R. Morris, F. S. Brown, H. Eberwein, *J. Biol. Chem.* **1966**, *241*, 1769–1777.
[3] K.-H. van Pée, *Annu. Rev. Microbiol.* **1996**, *50*, 375–399.
[4] M. C. R. Franssen, *Biocatalysis* **1994**, *10*, 87–111.
[5] G. W. Gribble, *Prog. Chem. Org. Nat. Prod.* **1996**, *68*, 119–166.
[6] S. L. Neidleman, J. Geigert, *Biohalogenation: Principles, Basic Roles and Applications*, Ellis Horwood, Chichester, **1986**.
[7] T. Dairi, T. Nakano, K. Aisaka, R. Katsumata, M. Hasegawa, *Biosci. Biotechnol. Biochem.* **1995**, *59*, 1099–1106.
[8] S. Kirner, S. Krauss, G. Sury, S. T. Lam, J. M. Ligon, K.-H. van Pée, *Microbiology* **1996**, *142*, 2129–2135.
[9] K.-H. van Pée, O. Salcher, F. Lingens, *Angew. Chem.* **1980**, *92*, 855-856; *Angew. Chem. Int. Ed. Engl.* **1980**, *19*, 828–829.
[10] M. Morrison, G. R. Schonbaum, *Annu. Rev. Biochem.* **1976**, *45*, 861–888.
[11] P. E. Hammer, D. S. Hill, S. T. Lam, K.-H. van Pée, J. M. Ligon, *Appl. Environ. Microbiol.*, **1997**, *63*, 2147–2154.
[12] HPLC analysis of **3**: LiChrospher 100, RP-18, 5 µm, 250 mm × 4.6 mm, MeOH/H_2O/trifluoroacetic acid 40/60/0.1, 1 mL min^{-1}. UV detection at 280 nm; retention time of the isolated compound, the enzymatically produced product, and authentic **3** is 13.7 min.
[13] K.-H. van Pée, O. Salcher, F. Lingens, *Liebigs Ann. Chem.* **1981**, 233–239.
[14] HPLC for the analysis of **4**: LiChrospher 100, RP-18, 5 µm, 250 × 4.6 mm, MeOH/H_2O 60/40, 0.8 mL min^{-1}, UV detection at 280 nm; retention time of the enzymatically produced product and of **4** is 10.0 min.
[15] K.-H. van Pée, O. Salcher, P. Fischer, M. Bokel, F. Lingens, *J. Antibiotics* **1983**, *36*, 1735–1742.

 © WILEY-VCH Verlag GmbH, D-69451 Weinheim, 1997 0570-0833/97/3618-2013 $ 17.50+.50/0

Boratabenzene Zirconium(II) Complexes: An Unusual Annulation with Ethynes**

Arthur J. Ashe III,* Saleem Al-Ahmad, Jeff W. Kampf, and Victor G. Young, Jr.

Dedicated to Professor Gerhard E. Herberich on the occasion of his 60th birthday

1-Substituted boratabenzenes can serve as six-electron, π-bound, anionic ligands towards a variety of metals.[1] The well-investigated late transition metal complexes, for example **1**[2] and **2**,[3] are closely analogous to the corresponding cyclopentadienyl metal compounds. Early transition metal complexes have been more sparingly studied. We recently reported the first zirconium(IV) boratabenzene complex **3a**, which on activation by methylaluminoxane polymerizes ethene with an activity similar to that of $[Cp_2ZrCl_2]$.[4] Since Cp_2Zr^{II} compounds are particularly useful in organic synthesis,[5] an investigation of the corresponding boratabenzene Zr^{II} complexes is appropriate. We have prepared boratabenzene Zr^{II} complex **4b** and find that the PMe_3 ligands are displaced under very mild conditions. The reaction of **4b** with ethyne involves an unprecedented ring annulation to afford complex **5**, which contains the novel ligand 4a-phenyl-8a *H*-4a-boratanaphthalene.

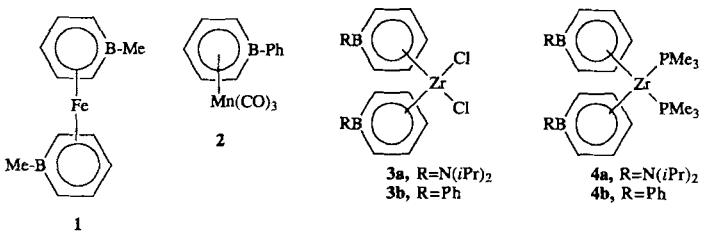

The reaction of **3a** and **3b**[4b] with butyllithium in ether in the presence of an excess of PMe_3 affords the zirconium(II) derivatives **4a** and **4b** in 70% and 75% yields, respectively.[5, 6] In contrast to the corresponding reactions of $[Cp_2ZrCl_2]$, neither the presumed intermediate, an (η^2-1-butene)Zr complex,[6b] nor Zr^{III}-bridged products are detected.[7] The structure of **4a** was confirmed by an X-ray diffraction study (Figure 1).[8]

Comparison of the structures **4a** and **3a**[4] illustrates the differences between Zr^{II}- and Zr^{IV}-coordinated boratabenzenes. Both molecules possess pseudo tetrahedral coordination spheres about the metal centers, which are typical of Group 4 bent metallocenes. However, the B–Zr distances (2.980(7) Å for **3a**, 2.830(3) Å for **4a**) are longer, and the B–N distances (1.396(6) Å for **3a**, 1.438(3) Å for **4a**) are shorter for the Zr^{IV} derivatives. Apparently, the more electron-withdrawing Zr^{IV} slip-distorts away from the boron atom, which is stabilized by B–N π-bonding.[4, 9] Consequently the boratabenzene ligands are η^5-bonded to the central metal in **3a** and η^6-bonded in **4a**.

At ambient temperature the ^1H NMR spectrum (Table 1) of a solution of equivalent amounts of **4b** and PMe_3 in toluene

[*] Prof. Dr. A. J. Ashe III, Dr. S. Al-Ahmad, Dr. J. W. Kampf
Department of Chemistry
The University of Michigan
Ann Arbor, MI 48109-1055 (USA)
Fax: Int. code +(313)747-4865
e-mail: ajashe@umich.edu
Dr. V. G. Young, Jr.
University of Minnesota, Minneapolis (USA)

[**] This work was supported by the National Science Foundation and the Petroleum Research Fund administered by the American Chemical Society.

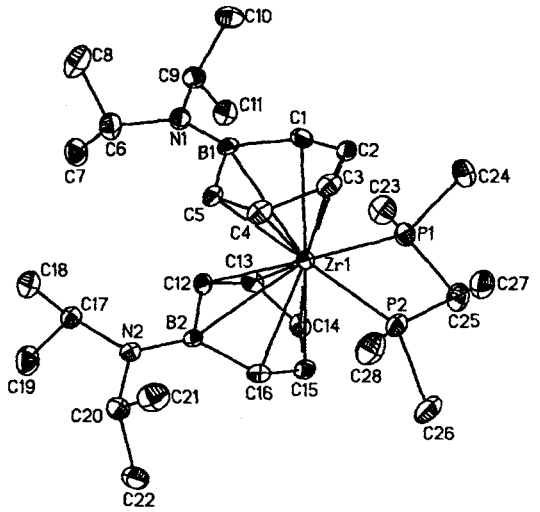

Figure 1. Molecular structure of **4a** in the crystal. Selected average bond lengths [Å]: Zr–C 2.506(21), Zr–B 2.830(3), Zr–P 2.742(9), B–C 1.544(4), B–N 1.438(3), C–C (ring), 1.419(14).

Table 1. NMR spectroscopic data for **4–9** [a, b].

4a: ^1H NMR (360 MHz, C_6D_6): $\delta = 0.72$ (br., PMe), 1.18 (br., CMe), 3.80 (br. d, $J = 10$; H_α), 4.95 (br., H_γ), 5.95 (br., H_β). Other peaks very broad. ^{13}C NMR (90.6 MHz, C_6D_6): $\delta = 21.3$ (CMe), 24.1 (br., PMe), 101.2 (C_β), C_α, C_γ, *CH* not observed). ^{11}B NMR (115.5 MHz, C_6D_6): $\delta = 24.5$. ^{31}P NMR (145.8 MHz, C_6D_6): $\delta = -10.2$.

4b: ^1H NMR (360 MHz, C_6D_6): $\delta = 0.67$ (d, $J = 5.2$; PMe), 4.85 (br. t, H_γ), 5.15 (br., H_β), 5.04 (br. d, $J = 10.5$; H_α), 7.26 (t, $J = 7.2$; *p*-H), 7.43 (t, $J = 7.2$; *m*-H), 7.72 (d, $J = 7.2$; *o*-H). ^{13}C NMR (90.6 MHz, C_6D_6): $\delta = 22.1$ (d, $J = 16.4$; PMe_3), 100.2 (br., C_α), 103.9 (C_β), 107.0 (C_γ), 128.8, 132.6, 133.6 (Ph), C_{ipso} not observed. ^{11}B NMR (115.5 MHz, C_6D_6): $\delta = 27.5$. ^{31}P NMR (145.8 MHz, C_6D_6): $\delta = -5.8$.

5: ^1H NMR(500 MHz, C_6D_6): $\delta = 1.05$(br. m, H17), 3.60 (dd, $J = 7.0$, 5.4; H16,27), 4.35 (d, $J = 10.4$; H13,24), 4.57 (t, $J = 7.0$; H15,26), 4.76 (tt, $J = 6.6$; 1.6, H10), 5.34 (dd, $J = 10.4$; 7.0; H14,25), 5.41 (d, $J = 9.4$; H8,12), 5.73 (dd, $J = 9.6$, 7.0; H9,11), 7.02 (br. d, $J = 7.1$; H19,23), 7.08 (tt, $J = 7.3$, 3.6; H21), 7.15 (t, $J = 7.3$; H20,22), 7.32 (tt, $J = 7.3$, 2.6; H4), 7.40 (t, $J = 7.3$; H3,5), 7.75 (d, $J = 7.3$; H2,6). ^{13}C NMR (90.6 MHz, C_6D_6): $\delta = 16.1$ (C17), 69.8 (C16,27), 92.3 (C15,26), 100.3 (C10), 104.1 (C14,25), 106.9 (C13,C24), 115.7 (C9,11), 125.7 (C20,22), 129.1 (C3,5), 131.6 (C19,23), 132.5 (C2,6). C1, C4, C18, and C21 not observed. ^{11}B NMR (115.5 MHz C_6D_6): $\delta = 28.7$ (B1), -23.8 (B2).

6: ^1H NMR (360 MHz, C_6D_6): $\delta = 0.62$ (d, $J = 2.8$; PMe), 1.26 (br., PCH_2), 4.50 (d, $J = 10.5$; H_α), 4.61 (t, $J = 6.5$; H_γ), 5.56 (dd, $J = 10.5$, 6.5; H_β), 7.25 (t, $J = 7.2$; *p*-H), 7.32 (t, $J = 7.2$; *m*-H), 7.87 (d, $J = 7.2$; *o*-H). ^{13}C NMR (90.6 MHz, C_6D_6): $\delta = 18.2$ (d, $J = 7$; PMe), 31.6 (br., PCH_2), 93.9 (br., C_α), 100.0 (C_γ), 106.8 (C_β), 108.3 (*p*-C), 128.0 (*m*-C), 132.9 (*o*-C). C_{ipso} not observed. ^{11}B NMR (115.5 MHz, C_6D_6): $\delta = 28.3$. ^{31}P NMR (145.8 MHz, C_6D_6): $\delta = 18.4$.

7: ^1H NMR (360 MHz, C_6D_6): $\delta = -0.08$ (ZrMe), 6.33 (t, $J = 6.3$, H_γ), 6.39 (m, H_α) 6.52 (m, H'_α), 7.05 (m, $2H_\beta$), 7.28 (t, $J = 7.2$; *p*-H), 7.37 (t, $J = 7.2$; *m*-H), 7.87 (d, $J = 7.2$; *o*-H). ^{13}C NMR (90.6 MHz, C_6D_6): $\delta = 112$ (C_γ), 128.9 (*m*-C), 130.3 (*p*-C), 133.5 (*o*-C), 139.8 (H_β), 142.5 (H'_β). Cα, C_{ipso} not observed. ^{11}B NMR (115.5 MHz, C_6D_6): $\delta = 35.8$.

8: ^1H NMR (360 MHz, C_6D_6): $\delta = 6.26$ (t, $J = 6.8$; H_γ), 6.40 (d, $J = 11.0$; H_α), 6.91 (dd, $J = 11.0$, 7.0; H_β), 6.85 (t, $J = 7.2$; SPh), 6.89 (t, $J = 7.2$; SPh), 7.07 (t, $J = 7.2$; BPh), 7.32 (t, $J = 7.2$; BPh), 7.70 (d, $J = 7.2$; SPh), 7.89 (d, $J = 7.2$; BPh). ^{13}C NMR (90.6 MHz, C_6D_6): $\delta = 117.7$ (C_γ), 125.1 (br., C_α), 128.8 (BPh), 129.1 (BPh), 129.7 (SPh), 130.3 (SPh), 132.8 (SPh), 133.8 (BPh), 137.8 (*ipso* SPh), 139.0 (C_β). BPh-C_{ipso} not observed. ^{11}B NMR (115.5 MHz, C_6D_6): $\delta = 36.8$.

9: ^1H NMR (300 MHz, C_6D_6): $\delta = 1.35$ (br., H17), 1.57(s, Me), 1.71(s, Me), 1.79(s, Me), 2.07 (s, Me) 3.71 (dd, $J = 7.2$, 6.0; H16), 4.23 (d, $J = 10.4$; H13) 4.57 (t, $J = 7.3$; H15), 4.87 (tt, $J = 7.0$, 1.7; H10), 5.31 (m, H14), 5.36, 5.45 (ddd, $J = 10.3$, 3.5, 1.7; H8,12) 5.63, 5.69 (m, H9,11), 7.01 (br. d, $J = 7.2$; H19,23), 7.09 (t, $J = 7.2$; H21), 7.17 (t, $J = 7.2$; H20,22), 7.28 (t, $J = 7.2$; H4), 7.37 (t, $J = 7.2$; H3,5), 7.70 (t, $J = 7.2$; H2,6). ^{13}C NMR (90.5 MHz, C_6D_6): $\delta = 16.8$, 17.6, 20.4, 21.5 (Me), 26.0 (C17), 59.0 (C27), 78.0 (C16), 93.1 (C10), 98.4 (C15), 102.1 (C25), 106.0 (C26), 106.6 (C24), 105.8 (C14), 109.0 (C8), 109.2 (C12), 114.5 (C13), 118.6 (C11), 119.0 (C9), 125.6 (C20,22), 128.8 (C3,5), 132.1 (C19,23), 132.7 (C2,6). C(1), C(4), C(18), and C(21) not observed. ^{11}B NMR (115.5 MHz, C_6D_6): $\delta = 30.2$ (B1), -19.6 (B2).

[a] The spectral assignments for **5** and **9** use the crystallographic numbering scheme illustrated in Figure 2. [b] *J* values are in Hz.

 © WILEY-VCH Verlag GmbH, D-69451 Weinheim, 1997 0570-0833/97/3618-2014 $ 17.50+.50/0

shows two separate PMe_3 signals ($\delta = 0.58$, 0.78), which reversibly coalesce ($\delta = 0.70$) on heating to 57 °C. Thus **4b** shows rapid PMe_3 exchange.[7, 10] Both PMe_3 groups are readily displaced from **4b** by the addition of the chelating ligand 1,2-bis(dimethylphosphino)ethane to form **6** in 75% yield.[7, 10, 11] Treating **4b** with methyl iodide affords the oxidative addition product **7**,[7, 10, 11] which shows a characteristic ^{1}H NMR spectrum indicating five nonequivalent ring protons.[4a] Similarly the reaction of **4b** with diphenyl disulfide results in cleavage of the S–S bond to afford **8** in 72% yield.[12, 13] These reactions of **4b** are completely analogous to those of $[Cp_2Zr(PMe_3)_2]$ and $[Cp_2Ti(PMe_3)_2]$.

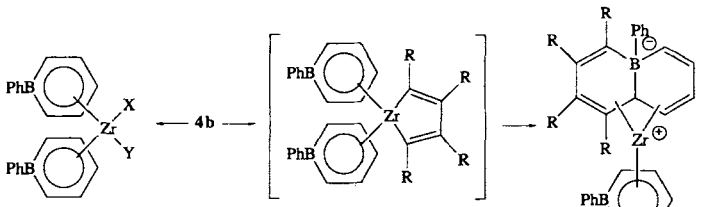

6, X = Y = $Me_2PCH_2CH_2PMe_2$
7, X = I, Y = Me
8, X = Y = SPh

5, R=H
9, R=Me

The reaction of **4b** with ethyne proceeds rapidly to produce adduct **5** as a crystalline solid in 78% yield as well as some polyacetylene. 2-Butyne reacts with **4b** in a similar manner to produce **9**, but no polyacetylenes are observed. Since the ^{1}H, ^{11}B, and ^{13}C NMR spectra of **5** are inconsistent with its formulation as the expected metallacyclopentadiene **10**,[5–7, 14] we have obtained an X-ray structure.

The crystal structural analysis of **5** reveals that two ethyne molecules have added to one of the 1-phenylboratabenzene rings to produce a novel 4a-phenyl-8a-*H*-4a-boratanaphthalene ligand (Figure 2). The zirconium atom is π-coordinated to the butadiene units C13–C16 and C24–C27 of the boratanaphthalene and η^6-coordinated to the phenylboratabenzene. Complex **5** exists as a zwitterion with a formal positive charge on zirconium center, which balances the negative charge on B2.[15] The borate structure is independently indicated by the characteristic high-field signal[16] ($\delta = -23.8$) in the ^{11}B NMR spectrum of **5**. It is particularly significant that C17 and B2 at the ring fusion are well within bonding distance to the metal (C17–Zr 2.390(7) Å, B2–Zr 2.508(7) Å). It seems likely that the electron deficiency at zirconium is partially compensated by bonding to these atoms, which is also suggested by the long B2–C17 bond (1.706(9) Å). Several electrophilic Cp_2Zr^{IV} derivatives feature similar pentacoordinated carbon atoms with C–Zr bonds in the range 2.39–2.58 Å,[17, 18] although **5** is to our knowledge the first example with a zirconium(II) center.

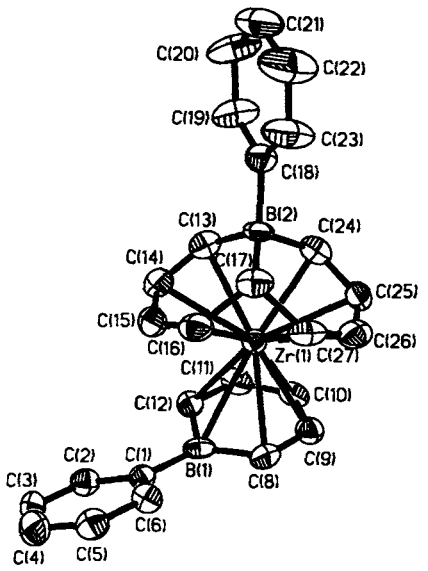

Figure 2. Molecular structure of **5** in the crystal. Selected interatomic distances [Å]: Zr–B1 2.683(7), Zr–C (boratabenzene) 2.498(7)–2.553(7), Zr–B2 2.508(7), Zr–C17 2.390(7), Zr–C(dienes) 2.401(7)–2.495(7), C–C(dienes) 1.356(9)–1.463(10), C16–C17 1.517(9), C17–C27 1.502(9), B2–C13 1.620(10), B2–C17 1.706(9), B2–C18 1.624(10), B2–C24 1.645(10).

Formation of **5** by the addition of two ethyne molecules to a boratabenzene ring is unprecedented. We speculate that the reaction proceeds "normally" to afford metallacycle **10**,[5–7, 10] which is diverted to **5** by transfer of an alkenyl unit to the electrophilic boron followed by carbometalation at the α-C atom by the pendant Zr–dienyl group. Work on this rearrangement continues in our laboratory.[19]

Experimental Section

4a: A solution of **3a** (100 mg, 0.19 mmol) and PMe_3 (150 mg, 1.9 mmol) in 20 mL of ether was treated with BuLi (0.38 mmol) in 150 μL of hexane at −78 °C. The reaction mixture was stirred for 1 h at −78 °C and then allowed to warm to 25 °C for 1 h. The solvent was removed in vacuo, and the residue extracted with pentane. On cooling to −20 °C dark green crystals of **4a** (81 mg, 70%; m.p. 195 °C) were obtained. Correct C,H,N analysis.

4b: In the same manner **3b** was converted into **4b** (84%; brown powder, m.p. 91 °C). High resolution EI-MS calcd. for $C_{28}H_{38}{}^{11}B_2P_2{}^{90}Zr$: 548.1682; found 548.1626.

6: An excess (100 μL) of 1,2-bis(dimethylphosphino)ethane was added to a solution of **4b** (100 mg, 0.18 mmol) in 8 mL of toluene. After stirring for 2 h at 25 °C the solvent was removed in vacuo. The residue was taken up in pentane, which when cooled to −78 °C afforded **6** as a brown red solid (75 mg, 75%). High resolution EI-MS calcd. for $C_{28}H_{36}{}^{11}B_2P_2{}^{90}Zr$: 546.1525; found: 546.1526.

7: A solution of **4b** (100 mg, 0.18 mmol) in 5 mL of toluene was treated with iodomethane (130 mg, 0.91 mmol) at 25 °C. After 2 h the solvent was removed, and the residue was extracted with hexane. Cooling to −20 °C afforded **8** (76 mg, 77%; m.p. 105 °C (decomp.)). High resolution EI-MS calcd. for $C_{22}H_{20}{}^{11}B_2I^{90}Zr$ ($M^+ - CH_3$): 522.9843; found: 522.9827.

8: A solution of **4b** (60 mg, 0.11 mmol) in toluene (5 mL) was treated with diphenyl disulfide (30 mg, 0.13 mmol). The reaction mixture was stirred for 2 h at 25 °C. After removal of the solvent the residue was extracted with pentane. On cooling to −78 °C **7** (50 mg, 72%) was obtained as a solid with m.p. 147 °C. High resolution EI-MS calcd. for $C_{34}H_{30}{}^{11}B_2S_2{}^{90}Zr$: 614.1022; found 614.1041.

5: A solution of **4b** (200 mg, 0.36 mmol) in toluene (10 mL) was stirred for 2 h at 25 °C under ethyne at 1 atm pressure. The solvent was removed under reduced pressure, and the residue was extracted with pentane. Cooling the extracts to −20 °C afforded **5** (100 mg, 62%) as dark red crystals with m.p. 207 °C. High resolution EI-MS calcd. for $C_{26}H_{22}{}^{11}B_2{}^{90}Zr$ ($M^+ - 2H$): 446.0955; found: 446.0961.

9: Analogously **4b** was treated with 2-butyne to give **9** (68%, m.p. 138 °C). High resolution MS calcd. for $C_{30}H_{32}{}^{11}B_2{}^{90}Zr$: 504.1737; found: 504.1747.

Received: March 25, 1997 [Z102791E]
German version: *Angew. Chem.* **1997**, *109*, 2104–2106

Keywords: agostic interactions · boron · heterocycles · zirconium

[1] a) G. E. Herberich, G. Greiss, H. F. Heil, *Angew. Chem.* **1970**, *82*, 838; *Angew. Chem. Int. Ed. Engl.* **1970**, *9*, 805; b) G. E. Herberich in *Comprehensive Organometallic Chemistry*, Vol. 1 (Eds: G. Wilkinson, F. G. A Stone, E. W. Abel), Pergamon, Oxford, **1982**, p. 381; c) G. E. Herberich, H. Ohst, *Adv. Organomet. Chem.* **1986**, *25*, 199; d) G. E. Herberich in *Comprehensive Organometallic Chemistry II, Vol. 1*, (Volume Ed.: C. E. Housecroft), Pergamon, Oxford, **1995**, p 197.

[2] A. J. Ashe III, E. Meyers, P. Shu, T. Von Lehmann, J. Bastide, *J. Am. Chem. Soc.* **1975**, *97*, 6865.

[3] G. E. Herberich, H. J. Becker, *Angew. Chem.* **1973**, *85*, 817; *Angew. Chem. Int. Ed. Engl.* **1973**, *12*, 764.

[4] a) G. C. Bazan, G. Rodriguez, A. J. Ashe III, S. Al-Ahmad, C. Müller, *J. Am. Chem. Soc.* **1996**, *118*, 2291; b) G. C. Bazan, G. Rodriguez, A. J. Ashe III, S. Al-Ahmad, J. W. Kampf, *Organometallics*, **1997**, *16*, 2492.

 © WILEY-VCH Verlag GmbH, D-69451 Weinheim, 1997 0570-0833/97/3618-2015 $ 17.50+.50/0

[5] a) R. D. Broene, S. L. Buchwald, *Science* **1993**, *261*, 1696; S. L. Buchwald, R. B. Nielsen, *Chem. Rev.* **1988**, *88*, 1047; J. H. Tidwell, S. L. Buchwald, *J. Am. Chem. Soc.* **1994**, *116*, 11797; b) E. Negishi, *Acc. Chem. Res.* **1987**, *20*, 65; E. Negishi, D. Choueiry, T. B. Nguyen, D. R. Swanson, *J. Am. Chem. Soc.* **1994**, *116*, 9751; c) P. J. Fagan, W. A. Nugent, J. C. Calabrese, *ibid.* **1994**, *116*, 1880; d) G. Erker, *Acc. Chem. Res.* **1984**, *17*, 103.

[6] a) E. Negishi, F. E. Cederbaum, T. Takahashi, *Tetrahedron Lett.* **1986**, *27*, 2829; b) E. Negishi, D. R. Swanson, F. E. Cederbaum, T. Takahashi, *ibid.* **1987**, *28*, 917; c) P. Binger, P. Müller, R. Benn, A. Rufinska, B. Gabor, C. Krüger, P. Betz, *Chem. Ber.* **1989**, *122*, 1035.

[7] L. B. Kool, M. D. Rausch, H. G. Alt, M. Herberhold, B. Honold, U. Thewalt, *J. Organomet. Chem.* **1987**, *320*, 37.

[8] Crystal structure analysis of **4a**: Triclinic, space group $P\bar{1}$, $a = 10.8156(10)$, $b = 11.3629(10)$, $c = 15.019(2)$ Å, $\alpha = 74.236(7)$, $\beta = 77.967$ (8), $\gamma = 66.813(6)°$, $V = 1622.1(3)$ Å^3, $Z = 2$ ($\rho_{calcd} = 1.219$ g cm^{-3}), $T = 178(2)$ K ($Mo_{K\alpha}$, $\lambda = 0.71073$ Å, $\mu = 16.22$ cm^{-1}); 6330 unique reflections were used in refinement (SHELXTL-93); $R(I > 2\sigma(I))$: $R_1 = 0.0360$, $wR_2 = 0.0987$; GOF = 1.179; (all data): $R_1 = 0.0411$, $wR_2 = 0.1032$. **5**: Monoclinic, space group $P2_1/c$, $a = 25.0086(9)$, $b = 8.1319(3)$, $c = 20.9628(8)$ Å, $\beta = 104.0970(10)°$, $V = 4134.8(3)$ Å^3, $Z = 8$ ($\rho_{calcd} = 1.444$ g cm^{-3}), $T = 173(2)$ K ($Mo_{K\alpha}$, $\lambda = 0.71073$ Å, $\mu = 16.22$ cm^{-1}), 7171 unique reflections were used in refinement (SHELXTL-V 5.0); R ($I > 2\sigma(I)$): $R_1 = 0.0801$, $wR_2 = 0.1103$, GOF = 1.083; (all data): $R_1 = 0.1506$, $wR_2 = 0.1369$. Crystallographic data (excluding structure factors) for the structures reported in this paper have been deposited with the Cambridge Crystallographic Data Centre as supplementary publication no. CCDC-100254 for **4a** and no. CCDC-100279 for **5**. Copies of the data can be obtained free of charge on application to the Director, Cambridge Crystallographic Data Centre, 12 Union Road, GB-Cambridge CB21EZ, UK (fax: int. code +(1223)336-033; e-mail: deposit@chemcrys.cam.ac.uk).

[9] A. J. Ashe III, J. W. Kampf, C. Müller, M. Schneider, *Organometallics* **1996**, *15*, 387.

[10] K. I. Gell, J. Schwartz, *J. Am. Chem. Soc.* **1981**, *103*, 2687.

[11] G. S. Girolami, G. Wilkinson, M. Thornton-Pett, M. B. Hursthouse, *J. Chem. Soc. Dalton Trans* **1984**, 2347.

[12] G. Fochi, G. Guidi, C. Floriani, *J. Chem. Soc. Dalton Trans* **1984**, 1253.

[13] W. A. Howard, T. M. Trnka, G. Parkin, *Inorg. Chem.* **1995**, *34*, 5900.

[14] H. G. Alt, C. E. Denner, *J. Organomet. Chem.* **1990**, *390*, 53.

[15] A number of related zironocene–borane zwitterions have been reported: G. Erker, W. Ahlers, R. Fröhlich, *J. Am. Chem. Soc.* **1995**, *117*, 5853; J. Ruwwe, G. Erker, R. Fröhlich, *Angew. Chem.* **1996**, *108*, 108; *Angew. Chem. Int. Ed. Engl.* **1996**, *35*, 80.

[16] B. Wrackmeyer, *Ann. Rep. NMR Spectrosc.* **1988**, *20*, 1.

[17] Y. Sun, W. E. Piers, S. J. Rettig, *Organometallics* **1996**, *15*, 4110; R. E. von H. Spence, D. J. Parks, W. E. Piers, M.-A. MacDonald, M. J. Zaworotko, S. J. Rettig, *Angew. Chem.* **1995**, *107*, 1337; *Angew. Chem. Int. Ed. Engl.* **1995**, *34*, 1230; R. F. Jordan, *Adv. Organomet. Chem.* **1991**, *32*, 325.

[18] U. Radius, S. J. Silverio, R. Hoffmann, R. Gleiter, *Organometallics* **1996**, *15*, 3737.

[19] The reaction of 2-butyne with **4a** forms an analogous but more labile product, which has been detected by NMR spectroscopy.

Chemistry at the crossroads

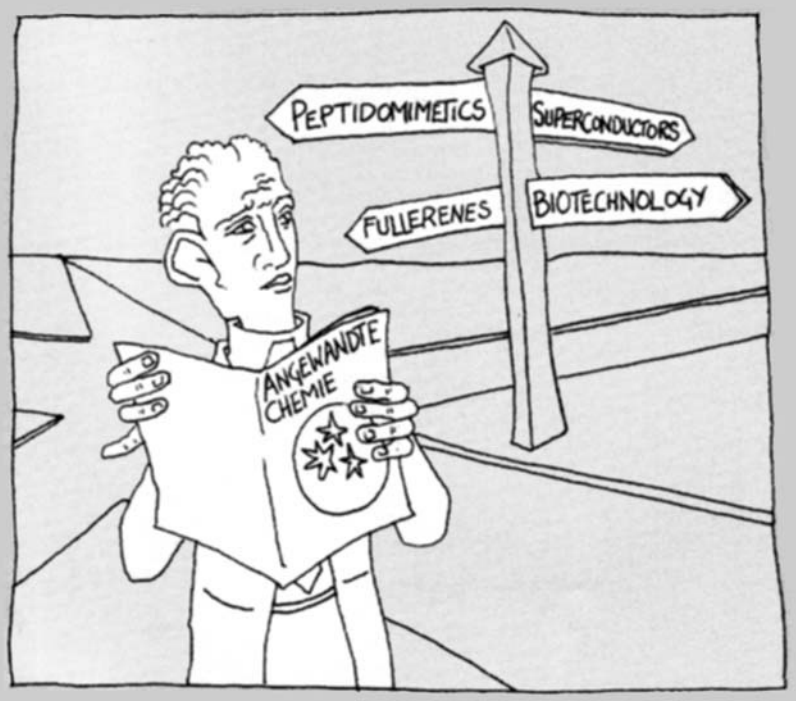

Pioneering scientists guide your way through newly charted territory with their topical reviews and discriminating highlights in **Angewandte Chemie.**

To start your own personal subscription, just fax.

An order form is provided on the last page for your convenience.

WILEY-VCH

 © WILEY-VCH Verlag GmbH, D-69451 Weinheim, 1997 0570-0833/97/3618-2016 $ 17.50+.50/0

Practical Approaches to Analysis, Liquid Crystals, and Alkenes

Trace Analysis: A Structured Approach to Obtaining Reliable Results. Edited by *E. Pritchard, G. MacKay and U. Points*. Royal Society of Chemistry, London, 1996. XIV, 404 pp., hardcover £ 69.50.—ISBN 0-85404-417-5

Within its approximately 400 pages this book contains a lot of useful practical advice. However, it is essential that the reader should already have a certain amount of knowledge about the secrets of trace analysis.

When I started to read this book for the first time, I was struck by the abundance of information on what "trace analysis" really means. The editors have their power-play in the first three chapters. In Chapter 1 the author explains the requirements for a valid and proper trace analysis, including an outline of the possible and necessary methodologies and their characteristics. Here I do not agree with the classification of ICP-MS as a semiquantitative technique for field screening (p. 27). Also the claim that the journals *Analytical Chemistry* and *The Analyst* are all that one needs as a direct route to useful methodology and review articles in analytical chemistry is not justified. Other mothers (publishing houses) also have beautiful daughters (journals) ...

Chapter 2 is probably the most useful one in the whole monograph. All the hints and comments are extremely valuable. Unfortunately the warning at the bottom of page 44 about the use of strong acids is incomplete! Possible artifacts include, for example, effects of filtration on the concentration of PAHs in water. Likely sources of contamination during sample pretreatment are also identified.

Chapter 3 overlaps to some extent with Chapter 2, since sample preparation is again the topic. All the various digestion techniques are discussed in great detail.

Unfortunately, the following chapters provide only a superficial treatment of the subject. Chapter 4 deals with the determination of inorganic analytes, after the sample has undergone the necessary preparation steps. The most popular techniques are presented in a very general way. Here some concrete examples would have been useful. Some modern techniques such as laser-excited spectroscopy or the very successful method of total reflection X-ray fluorescence analysis are not covered. In contrast, a separate section (4.3) is entirely devoted to elemental mass spectrometry with all the known variants. On the other hand, Section 4.4, on ion chromatography, is again at a trivial level. The references given for this topic do not reflect the state of the art.

Chapter 5 ("Organic Analytes: Sample Preparation") covers more or less all the important treatment techniques, but is again not very up-to-date. Emerging methods such as solid phase extraction techniques (SPME) or immunoaffinity columns are not discussed. Here it becomes apparent that the authors' view of organic trace analysis is limited to the more conventional and well-established methods.

This is also seen in Chapter 6 ("Organic Analytes: Determination"). Recently developed techniques such as GC-AED or HPTLC-AMD are not treated. The resolution of MS techniques is given in "plates" (see Table 6.5.3)—why? A typical example, such as dioxin analysis, would have given a much better insight into the use of the various methods, especially for congener analysis (a subject that does not exist in this book!). On the other hand some practical matters, such as the safety aspects of MS, are discussed in more detail than is necessary.

The very important topic "Analysis of Speciated Elements" is treated briefly in Chapter 7, unfortunately without relating it to what has been discussed in the previous chapters. Some very general remarks are offered, for example that HPLC and GC are relatively inexpensive (Table 7.3.1). Here, a great chance to discuss exciting developments in trace analysis is wasted.

Chapter 8 is intended to bridge the gap between organic and inorganic trace analysis (if indeed there is one). Spectrophotometry is introduced at a student level. Colorimetric procedures are certainly not state-of-the-art. Luminescence is treated without introducing the advantages of time resolution. Electrochemical detection is briefly mentioned.

Chapter 8.3 treats a more modern subject, bioanalytical techniques. Enzymatic reactions, immunoassays, and PCR techniques as tools for trace analysis are discussed, and some relatively recent literature is cited.

Chapter 9 ("From Signal Processing to Reporting") is completely unnecessary. Here the reader is introduced to the formula for the standard deviation ...

The strengths of this monograph lie in the discussions of sample treatment and possible artifacts, but there are serious weaknesses in the description of the separation and detection techniques. Modern times have touched this book only slightly. It's a pity.

Reinhard Niessner
Institut für Wasserchemie
und Chemische Balneologie
der Technischen Universität München
(Germany)

Introduction to Liquid Crystals. Chemistry and Physics. By *P. J. Collings* and *M. Hird*. Taylor & Francis, London, 1997. 298 pp., paperback £ 15.95.—ISBN 0-7484-0483-X

Over a century has passed since the discovery of liquid crystals in 1988. During that time liquid crystals have developed from just a scientific curiosity to become a very active interdisciplinary field of research with many technological applications. However, although there are a large number of specialized, mainly physics-oriented, monographs on the subject, there are few introductory textbooks. The interdisciplinary nature of the field is an obstacle here, as its study requires some

This section contains book reviews and a list of new books received by the editor. Book reviews are written by invitation from the editor. Suggestions for books to be reviewed and for book reviewers are welcome. Publishers should send brochures or (better) books to the editorial office: Redaktion Angewandte Chemie, Postfach 101161, D-69451 Weinheim, Germany. The editor reserves the right of selecting which books will be reviewed. Uninvited books not chosen for review will not be returned.

knowledge of both chemistry and physics. This book is the first in a series of monographs on liquid crystals that is planned. It is intended to serve as a general introduction suitable for both physicists and chemists. Thus the authors needed to construct a bridge between tensor algebra on the one hand and synthetic methods (transition metal catalyzed and enantioselective) on the other hand. The book's 13 chapters strike a good balance, with six that are chemistry-oriented and six physics-oriented, together with a general introduction.

The work begins with an introduction to the main classes of liquid crystals and their phase types, accompanied by a brief outline of the history. Regrettably, the latter includes no mention of the pioneering work of D. Vorländers in the period 1900–1935. Vorländers synthesized over 1100 liquid-crystalline substances (which up to 1960 still comprised 90 % of all the then known liquid crystals!), and discovered some important relationships between molecular structure and liquid-crystalline properties.

Chapter 2 deals briefly with some important physical aspects, such as order parameters, X-ray methods, and defects in liquid crystals. This is followed by five chapters which discuss in detail the most important types of mesophases and the molecular structures of the units that form them.

Structure–property relationships in calamitic liquid crystals are discussed in great detail. With the help of well-chosen examples, the authors explain very clearly how the different types of structural units, such as aromatic and alicyclic ring systems, bridging groups, and terminal and lateral substituent groups, determine the stability of the liquid crystalline phases, their types, and their special properties (dielectric properties, elastic constants, viscosity, etc.).

The chapters on discotic liquid crystals, polymeric liquid crystals, and lyotropic systems are less detailed, but they provide a good overview of typical structures and important types of phases.

The chapter on chiral liquid crystals describes not only the cholesteric and ferroelectric mesophases but also some more recent developments, including antiferroelectric, ferrielectric, TGB phases, and chiral discotic phases.

Chapter 8 reviews important methods for synthesizing a wide variety of classes of liquid crystalline materials, and this is an innovative feature of the book. The main emphasis is on modern synthetic methods such as orthometalation reactions and Suzuki cross-coupling reactions, which are illustrated by numerous examples.

The chapter entitled "Identification of Liquid-Crystalline Phases" briefly describes the use of polarization microscopy (including measurements on self-supporting films) and calorimetric methods, and explains some important distinguishing characteristics of nematic phases and different types of smectic phases. However, the choice of texture types shown as examples is disappointing and seems rather arbitrary. Also there is no mention here of the standard works by Demus and Richter and by Gray and Goodby. Furthermore, it would have been useful to include here some representative textures of the new chiral phases and of the columnar and lyotropic phases for comparison. One would also have expected to find X-ray diffraction methods included in this chapter; although the relevant theory has already been covered in Chapter 2, a brief description of typical X-ray diffraction patterns and their interpretation would have been useful.

The chapters that follow deal with dielectric and magnetic properties, instabilities, optical properties, some important theoretical approaches (the Landau–De Gennes theory, the Maier–Saupe theory, and the McMillan model), and the principles of construction of liquid crystal displays (LCDs) and a few other application devices. Thus, the book provides a survey of the many different aspects of liquid crystals, ranging from methods of synthesis to theoretical models.

An appendix contains a list of books for further reading and some selected review articles. However, there are no references to the extensive collections of data on liquid crystals that exist.

The features of this book that especially distinguish it from other introductory monographs on liquid crystals are: a) a detailed discussion of structure–property relationships for calamitic liquid crystals, b) descriptions of antiferroelectric and TGB phases, and c) the description of methods for synthesizing liquid crystals. On the other hand, many topical aspects are not covered. Some examples of those omitted are: polycatenated compounds, liquid-crystalline carbohydrate derivatives, the concept of amphotropic liquid crystals, the induction of columnar phases by charge transfer interactions, thermotropic cubic mesophases, and reentrant phases. Also, apart from one phthalocyanine derivative there is no mention of the metallomesogens, a class of liquid crystalline compounds that has grown at a remarkable rate. Moreover, the appendix contains no references to important review articles on these topics.

The formula schemes and the figures are mainly very clear and easy to understand. Exceptions are the diagrams showing columnar phases on page 12 and discotic nematic phases on page 81, both of which would be difficult for a beginner to understand. Also Figure 3.2 fails to give a clearly recognizable impression of the structure of smectic low-temperature phases, and the phase diagram for a lyotropic system on page 141 is somewhat oversimplified. It would also have been useful to include cubic phases at this point.

To summarize, this book can be strongly recommended as an excellent introduction to the interdisciplinary subject of liquid crystals. All the concepts and terms are introduced in a way that can be widely understood, and therefore one can confidently recommend the book for all readers with scientific interests. In particular, it will be valuable to both undergraduate and postgraduate students wishing to specialize in the field of liquid crystals, by giving them an initial overview of the subject and serving as an important companion to their studies. The book will also be useful to scientists who wish to gain a general overview of liquid crystals.

Carsten Tschierske
Institut für Organische Chemie
der Universität Halle (Germany)

Preparation of Alkenes. A Practical Approach. (Series: The Practical Approach in Chemistry.) Edited by *J. M. J. Williams*. Oxford University Press, Oxford, 1996. 253 pp., ring-binding £ 29.95.—ISBN 0-19-855794-9

Alkenes are among the most important compounds in organic chemistry, since they not only function as almost universally applicable precursors and intermediates in syntheses, but are often present as structural elements in molecules that one wishes to synthesize. Every chemist who engages in synthetic work is certain to become involved with alkene groups more than once in the laboratory.

In accordance with the aims of the series *The Practical Approach in Chemistry*, of which this is the third volume, *Preparation of Alkanes* is a very useful, clear, and well produced laboratory handbook. It consists of nine chapters by various authors, together with two appendices, covering modern methods for the synthesis of alkenes.

 © WILEY-VCH Verlag GmbH, D-69451 Weinheim, 1997 0570-0833/97/3618-2018 $ 17.50+.50/0

Each of the first eight chapters has as its central core a very detailed description of experimental procedures, broken down into individual steps. Chapter 1 lays the foundation for the chapters that follow, and consists mainly of detailed descriptions of general methods, including especially techniques for working in inert atmospheres. It covers aspects such as setting up the apparatus, transferring materials, and determining the activity of organometallic reagents.

Chapters 2–4 deal with alkene syntheses in which the olefinic double bond is formed by bringing together two components. These methods include the highly successful Wittig reaction and its offshoots (the Horner–Wadsworth–Emmons and Horner–Wittig olefination reactions, the Schlosser and Still–Gennari variants, and the Corey–Fuchs homologization of aldehydes). These are followed in Chapter 3 by olefinations of carbonyl compounds, which are formally derived from the Wittig reaction, the role of phosphorus being fulfilled instead by another heteroatom such as silicon (Peterson), sulfur (Johnson, Julia), or boron. The treatment of olefination methods is completed by Chapter 4, which describes chromium- and titanium-mediated olefinations of carbonyl compounds, including the McMurry, Oshima–Lombardo, and Tebbe reactions, and the use of *gem*-dichromium reagents.

Chapter 5 describes strategies based on elimination and addition–elimination reactions. This is followed in Chapter 6 by methods for preparing alkenes from alkynes. As well as practical advice on performing catalytic hydrogenations of alkynes, this also includes examples of the use of metal hydrides and dissolved metals, and a description of the reduction of alkynes using diimides. To complete the treatment of approaches based on alkynes, Chapter 7 deals with reactions involving the addition of organometallic reagents, including detailed descriptions of hydro- and carbometallations using organoboron, organoaluminum, organozirconium, and organocopper reagents. The preparative part of the book ends with Chapter 8, which is devoted to the increasingly important catalytic coupling reactions, especially those involving palladium catalysts; examples described include the Stille, Suzuki, and Heck reactions.

Finally, Chapter 9 consists of a detailed summary (almost 40 pages) of synthetic methods, classified according to the types of alkenes rather than the strategies employed. The nine sections describe, for example, methods for preparing derivatives with a specified number of substituents (1–4), methods for cyclic olefins, and methods for dienes. This compilation, which does not give detailed laboratory procedures, also introduces some methods, such as the Baylis–Hillman reaction, that were not mentioned in the preceding chapters.

Each of the eight chapters dealing with preparative methods also includes a short theoretical treatment, which is mainly concerned with the configuration of the olefinic double bond created, and with the stereoselectivity of the reaction. Unfortunately, however, as in many other monographs and reviews on preparative methods, hardly any information is given about the chemoselectivity and tolerance with regard to other functions present in the molecules, including protecting groups, an aspect that is especially important in reactions of complex compounds. Another shortcoming is the absence of laboratory recipes for some important types of olefins, such as enol ethers, or for vinyltriflates and *trans*-vinylboronic acids prepared with Matteson's reagent.

To summarize, this practically oriented handbook is recommended for use by advanced students and synthetic chemists, as a resource to help with the more demanding areas of organic synthesis. It should be available in every departmental library, and especially in advanced teaching laboratories and in research groups involved in synthetic work.

Andreas Kirschning
Institut für Organische Chemie
der Technischen Universität
Clausthal-Zellerfeld (Germany)

Color Atlas of Biochemistry. By *J. Koolman* and *K.-H. Röhm*. Thieme, Stuttgart, 1996. 435 pp., softcover DM 49.80.—ISBN 3-13-100371-5

The *Color Atlas of Biochemistry* is an illustrated text, aimed at students of medicine and the biological sciences. It not only provides an introduction to biochemistry but also gives the reader the basic supporting knowledge of organic, inorganic, and physical chemistry necessary to gain the most from this unique book. Before discussing the contents in detail, here are a few general comments. First, the quality of the diagrams and figures, all in color, is first class. The color plates produced by Jürgen Wirth are well presented, with complex molecular graphics where necessary, and finely detailed chemical structures. Graphical representations of biochemical metabolic pathways are necessarily complex, but by a combination of color coding with astute use of figure legends the biochemical charts at the back of the book serve as an excellent reference source for any student wishing to rapidly glean the most important information from a number of key biosynthetic pathways. Secondly, the figures are all strategically placed on the page facing the relevant text, which is especially important when complex principles are being explained.

The atlas begins with a section termed *basics* and includes areas of chemistry and physical chemistry essential for a rudimentary grasp of biochemistry. These include orbital hybridization and chemical bonding, molecular structure, with explanatory paragraphs on bond polarity, hydrogen bonding, and effective atomic radii, and an excellent section on energetics and reaction kinetics.

The second section, *biomolecules*, discusses carbohydrates, lipids, amino acids and proteins, and nucleic acids. The carbohydrates subsection details the nomenclature of each of the saccharide families and discusses stereochemical aspects, amply supported by Fischer and Haworth projections. The chemistry of sugars is also outlined: redox processes, hydrolysis, acylation, and glycosylation. The lipids subsection offers an initial overview of their classification and biological roles, followed by an in-depth analysis of the biochemistry of fats, phospholipids, glycolipids, isoprenoids, and steroids. Excellent color plates help to simplify the otherwise complex area of plant and animal steroid and isoprenoid biosynthesis. The amino acids subsection comprises an overview dealing with the stereochemistry of the L and D series and a clear explanation of the pK_a values of amino-acids and proteins. The major content then outlines the importance of the peptide bond, subsequent secondary and tertiary protein structure development, and finally the function of structural and globular proteins, such as collagen, α-keratin, and insulin. The subsection discussing nucleosides and nucleotides starts with an outline of the nucleobase structures and progresses to their function. The interplay throughout the cell between the nucleic acids, DNA, mRNA, rRNA, and tRNA during transcription and translation is well illustrated.

The third section, *metabolism*, deals with the reactions involved in the interconversion of the biomolecules discussed in the previous section. The section begins with an explanation of the key role of enzymes in biosystems and includes a useful explanation of enzyme classification, something of a black art to most chemists

 © WILEY-VCH Verlag GmbH, D-69451 Weinheim, 1997 0570-0833/97/3618-2019 $ 17.50+.50/0

such as ourselves. There then follows a brief outline of enzyme catalysis, with necessarily simplified views of mechanisms by which enzymes are known to effect catalysis, including transition-state stabilization, covalent catalysis, and acid–base catalysis. The discussion of mathematical modeling of enzyme kinetics and inhibition introduces the fundamentals such as the Michaelis–Menten model and the important inhibition mechanisms that a student needs to understand. The following subsection focusses on the mechanisms of metabolic regulation and includes transcriptional control with a specific example of the *lac* operon, hormonal regulation of glycogen biosynthesis, and allosteric regulation of aspartate transcarbamoylase. The biochemistry of so-called 'energy metabolism' processes is then discussed. This includes a thermodynamic profile of the phosphoric acid anhydride bond in ATP, photosynthesis, the citric acid cycle, glycolysis, the respiratory chain, ATP biosynthesis, and studies of the key enzymes as components and regulatory elements in these processes. This is followed by catabolic and anabolic metabolic processes in which carbohydrates, fats, proteins, and nucleic acids are the key components. Specific examples to note are the β-degradation of fatty acids, transamination and deamination of amino acids, purine, pyrimidine, and porphyrin biosynthesis.

Section 4, *organelles*, gives a preliminary introduction to cell structure and methods for cell fractionation, before describing in detail the functions of some of the component organelles, including the mitochondria, the cell membrane, the endoplasmic reticulum, and lysosomes. This section contains a much more detailed study of genomic function than given earlier (Section 2), with particular reference to gene technology, DNA sequencing and cloning, PCR, and RFLP.

Section 5, *tissues and organs*, forms a major part of the book and reinforces the utility of this atlas to the medical biochemistry student. The authors discuss the biochemistry and, where necessary for clarification, the relevant physiology of most of the major organ classes in the human body, including the blood, liver, kidneys, muscle, connective tissue, and brain.

Section 6, *nutrition*, presents a biochemical perspective of this area and outlines the natural sources and functions of vitamins, minerals, and trace elements in the human body.

Section 7, *hormones*, describes some examples of the different hormone classes and their mechanisms of action. Specific examples include lipophilic hormones such as the steroids involved in reproduction and metabolic control, and their biosynthesis and inactivation are described. Secondary messengers are also described in this section and clear diagrams help to delineate the mechanisms of adenylate cyclase activation and signal transduction by G proteins.

The book ends with a number of clear and very well constructed metabolic charts as mentioned earlier. For students these charts may serve to make the process of learning and memorizing these key complex biochemical transformations much less soul-destroying than from a standard text.

On the whole the book serves as an excellent visual portrayal of the key biochemical processes occurring in humans and mammals. In conjunction with other larger and more detailed works on biochemistry, this atlas supplies the necessary information for the student of biochemistry.

Paul Wentworth Jr., Kim D. Janda
Department of Chemistry
Scripps Research Institute and
Skaggs Institute for Chemical Biology
La Jolla, CA (USA)

Molecular Modeling. Basic Principles and Applications. By *H.-D. Höltje* and *G. Folkers*. VCH Verlagsgesellschaft, Weinheim, 1996. 194 pp., hardcover DM 198.00.—ISBN 3-527-29384-1

Molecular Modelling. Principles and Applications. By *A. R. Leach*. Longman, Singapore, 1996. 595 pp., paperback £ 35.00.—ISBN 0-582-23933-8

Molecular modeling, more accurately described as computer-aided simulation of molecular properties, is now a widely used method in many areas of chemistry. When used correctly by someone with the necessary know-how, the techniques grouped together under this heading can lead to a better understanding of molecular processes, and can provide knowledge for planning experiments and for developing chemical compounds with novel properties. However, the attitudes of many scientists towards these methods are far from realistic. At one extreme there is the view that any chemist can easily use modeling methods, whereas at the other they are regarded as merely games for computer freaks, and are thought to need much further development before they can become a useful tool of chemical research. From my own observations, anyone believing the first statement usually changes sooner or later to the second. Modeling methods are of great value for the purposes mentioned above, but only in the hands of those who know how to use them effectively. On the other hand, anyone (and not only chemists) can produce meaningless colorful images on the computer screen. The two books reviewed here aim to provide their readers with the background knowledge needed to use molecular modeling techniques effectively.

Molecular Modeling. In the first book Höltje and Folkers have set out to provide a broadly-based practical introduction to molecular modeling methods. Appropriately, a distinction is made between the treatment of "small molecules" and that of proteins, and one example of each type is discussed.

The topics treated in the chapter on small molecules are: methods for generating three-dimensional atomic coordinates, methods of geometrical optimization, conformational analysis, methods for calculating molecular interaction potentials, the identification of pharmacophores, and the use of data banks. For each of these topics the authors discuss in detail the different approaches and the critical steps. The main emphasis is not on the scientific background (e.g., details of force-field calculations), but on practical aspects such as different minimization techniques, the calculation of atomic charges and of their effects, hydrophobic interactions, or the overlapping of molecules.

The introduction to the modeling of proteins describes in detail methods for predicting the structures of homologous proteins. Each of the individual steps in sequence alignment from predictions of side-chain and main-chain structures, and in the refinement of models using force field and molecular dynamics models, is briefly described. Methods for taking into account solvent effects are also described, and the authors discuss possible ways of validating a structural model that has been developed. This part of the book ends with a discussion of protein properties and of protein–ligand complexes. The only section that seems rather out of place here is the brief description of the principles of three-dimensional protein structures, which can be found in any textbook of biochemistry.

Each of the above two subject areas is illustrated by discussing an instructive example. For the small molecule case the example chosen is the simulation of a receptor binding pocket, leading to the identification of a pharmacophore. For proteins the example described in detail is the modeling of a protein–ligand com-

 © WILEY-VCH Verlag GmbH, D-69451 Weinheim, 1997 0570-0833/97/3618-2020 $ 17.50+.50/0

plex involved in antigen presentation by a protein belonging to MHC Class I.

This book is ideally suitable for scientists or advanced students who need a quick up-to-date overview of the methods and capabilities of molecular modeling, and who wish to be able to evaluate alternative methods in cases where there are several possible approaches. In most cases the authors have deliberately limited their treatment to brief descriptions of the various methods, leaving the reader to obtain background information and further details from the literature references attached to each chapter. This is the only aspect of the book that I would criticize, since here it would have been a great advantage to also include the titles of the papers cited. However, despite this minor complaint I hope that the book will reach a wide readership. It will be of great value in helping the reader to realistically evaluate the capabilities of these methods.

Molecular Modelling. Although the title of Leach's book is almost identical to that of the one reviewed above, the concept on which it is based is quite different. Whereas the book from the VCH publishing house has a strong practical bias with only a brief sketch of the theory, Leach has set out to present the theoretical background of molecular modeling methods.

A short introductory chapter with definitions of some important concepts is followed by one of about 100 pages containing a well written and informative, but very theoretical, treatment of quantum-mechanical models. Chapter 3 then gives a detailed account of empirical force-field models for the simulation of larger molecules. Although this subject is covered in many books on quantum-mechanical aspects, this is one of the best treatments that I have yet seen.

Chapter 4 discusses the various energy minimization techniques that are used in conjunction with both quantum-mechanical and force-field methods. The author also considers practical questions about the applicability of the techniques. Applications of modeling methods to the simulation of molecular properties are discussed in Chapter 5. The next two chapters are concerned with molecular dynamics simulation methods and Monte Carlo methods, both of which can be used to generate large numbers of states for describing the dynamics and statistics of molecular systems. The author discusses the differences between the methods, and considers the best choice for a given situation.

Chapter 8 deals with conformational analysis, including studies involving the molecular conformation space, molecular fitting methods, the use of structural data banks, and the problem of predicting conformational structures of proteins. There are many points in this chapter where one would have preferred to see the topics treated in greater depth. The last two chapters are concerned with some of the more sophisticated applications of molecular modeling methods, such as calculations of free enthalpy, the simulation of solvation processes and of chemical reactions, and the discovery or design of new molecules; aspects covered include drug design, ligand design, docking, QSAR, and lead structures.

The book is heavily biased towards theory (480 pp.) as compared with applications (about 100 pp.). Nevertheless, it clearly brings out the variety of uses of the methods. Each chapter ends with suggestions for further reading and a comprehensive list of references (including titles of publications). It is a carefully written work which is satisfying to read, and can be recommended for everyone who wishes to understand modeling methods. It should also serve as a reference source to provide essential background information when one is using modeling software packages in practical situations. It is not a suitable book for gaining a quick overview of the subject.

These two books have been written with different aims, and both fill real gaps. In many respects they are, in fact, complementary. Anyone with a serious intention to work in the field of molecular modeling should ideally use the two books in combination. On the other hand, the reader who expects to make only occasional use of these methods should rely on the book by Höltje and Folkers, while reserving the option to refer to Leach's book or to the original literature in doubtful cases. Both books have the potential to become standard works.

Dietmar Schomburg
Institut für Biochemie
der Universität Köln (Germany)

 © WILEY-VCH Verlag GmbH, D-69451 Weinheim, 1997 0570-0833/97/3618-2021 $ 17.50+.50/0

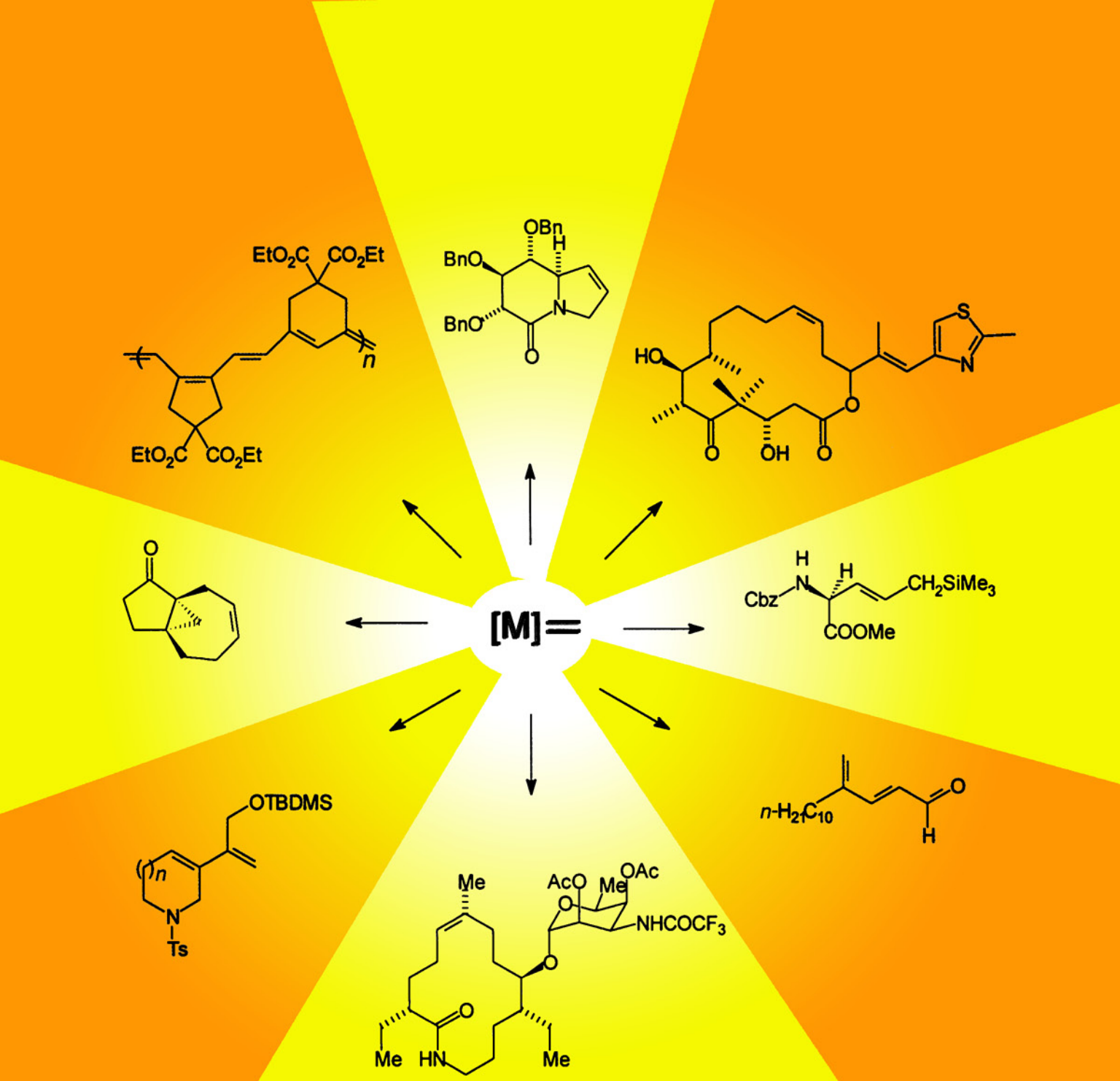

The development of stable alkylidene–ruthenium and alkylidene–molybdenum complexes has resulted in a significant broadening of the application potential of olefin metathesis in organic chemistry.

ANGEWANDTE CHEMIE ©WILEY-VCH

Olefin Metathesis in Organic Chemistry

Matthias Schuster and Siegfried Blechert*

Transition metal catalyzed C–C bond formations belong to the most important reactions in organic synthesis. One particularly interesting reaction is olefin metathesis, a metal-catalyzed exchange of alkylidene moieties between alkenes. Olefin metathesis can induce both cleavage and formation of C–C double bonds. Special functional groups are not necessary. Although this reaction—which can be catalyzed by numerous transition metals—is used in industry, its potential in organic synthesis was not recognized for many years. The recent abrupt end to this Sleeping-Beauty slumber has several reasons. Novel catalysts can effect the conversion of highly functionalized and sterically demanding olefins under mild reaction conditions and in high yields. Improved understanding of substrate–catalyst interactions has greatly contributed to the recent establishment of olefin metathesis as a synthetic method. In addition to the preparation of polymers with fine-tuned characteristics, the metathesis today also provides new routes to compounds of low molecular weight. The highly developed ring-closing metathesis has been proven to be a key step in the synthesis of a growing number of natural products. At the same time interesting applications can be envisioned for newly developed variants of bimolecular metathesis. Improvements in the selective cross-metathesis of acyclic olefins as well as promising attempts to include alkynes as viable substrates provide for a vivid development of the metathesis chemistry.

Keywords: carbene complexes · heterocycles · homogeneous catalysis · metathesis · olefins

1. Introduction

Olefin metathesis is a transition metal catalyzed reaction in which formally a mutual exchange of alkylidene groups between two substituted alkenes occurs (Scheme 1). In other words, the

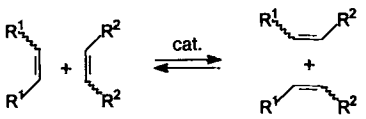

Scheme 1. General principle of olefin metathesis of symmetrically substituted olefins.

metathesis constitutes a catalytic method for both cleaving and forming C–C double bonds. The new developments reported here point out the large potential of this reaction type in organic synthesis. Although catalyzed C–C bond formations play an important role in synthetic chemistry, and the reaction principle has been known in polymer chemistry for a long time, thanks to the emergence of novel catalysts, olefin metathesis has recently advanced to a widely applicable synthetic method.

[*] Prof. Dr. S. Blechert, Dr. M. Schuster
Institut für Organische Chemie
der Technische Universität, Sekr. C3
Strasse des 17. Juni 135, D-10623 Berlin (Germany)
Fax: Int. code +(30)3142-3619
e-mail: sibl@wap0105.chem.tu-berlin.de

In 1955 Anderson and Merckling described the catalytic polymerization of norbornene by Ti^{II} compounds formed in situ.[1] In 1964 Banks and Bailey observed disproportionation of olefins at elevated temperatures in the presence of heterogeneous catalysts.[2] At about the same time Natta and co-workers reported the ring-opening polymerization of cyclic olefins by homogeneous catalysis.[3–5] Fundamental studies towards the understanding of this reaction were performed by Calderon et al.[6–8] and Mol et al.[9] By investigating the conversion of labeled olefins, it was demonstrated that an exchange of alkylidene groups occurs during metathesis. At first it was assumed that the alkylidene rearrangement proceeds through a bis(alkylidene)metal intermediate in which both olefin ligands are coordinated to the metal atom.[10–12] Chauvin et al. were the first to postulate that the reaction proceeds via a metallacyclobutane (Scheme 2).[13] According to these ideas,[14–17, 36]

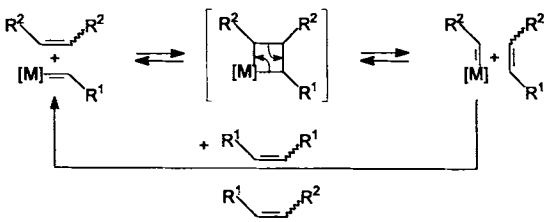

Scheme 2. Mechanism of olefin metathesis according to the Chauvin model.

 © WILEY-VCH Verlag GmbH, D-69451 Weinheim, 1997 0570-0833/97/3619-2037 $ 17.50+.50/0

which are still valid today, olefin metathesis proceeds by a [2+2]cycloaddition between a C–C double bond and a metal–carbene complex followed by cycloreversion. The double-bond formation generally does not proceed under stereocontrol—that is, with the exclusion of numerous intramolecular reactions—and *E*/*Z* mixtures result as metathesis products. The use of 1,2-disubstituted olefins results in the formation of regioisomeric metallacyclobutane intermediates, which lead to mixtures of differently substituted products.

2. Industrial Applications

Olefin metathesis was used early on in technical processes.[18] One classical example is the Phillips triolefin process[19] (Scheme 3), in which propene is converted into a mixture of ethane and 2-butene. The reverse reaction can also be used as needed; the required butene is obtained by dimerization of ethane. Technically the most important current application of the metathesis is a partial step within the Shell Higher Olefin Process (SHOP),[20, 21] a combination process starting with ethane to produce C_{10}–C_{18} olefins. The metathesis is applied in this process to make use of the early and late distillation fractions of the nickel-catalyzed ethane oligomerization. By double-bond isomerization and subsequent metathesis, it is possible to obtain additional olefins with the desired number of carbon atoms in a cyclic controlled process (Scheme 3). Since the establishment of the SHOP in 1979 plants with a capacity of several 100000 metric tons annually have been erected.[22]

Another area of application for metathesis chemistry is the polymerization of olefins. Representative for a series of established processes, we list here only the Norsorex process[23] of the CDF-Chimie company and the Hüls–Vestenamer process (Scheme 3).[24, 25] These processes are based on the ring-opening polymerization of norbornene (Norsorex, 45000 annual tons)[22] and cyclooctene (Vestenamer), respectively. Current developments in the area of metathesis polymerization are the subject of Section 4.

A) Phillips triolefin process

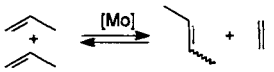

B) Shell higher olefin process (excerpt)

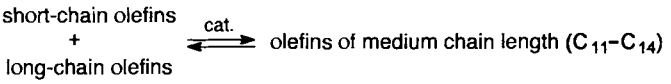

C) Norsorex process

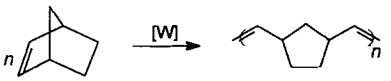

D) Hüls–Vestenamer process

Scheme 3. Important technical metathesis processes.

Additional applications include preparation of neohexene (3,3-dimethyl-1-butene)[26] by reaction of 2,4,4-trimethylpentene with ethane, ring opening of cyclic olefins to α,ω-diolefins[27] as crosslinkers for the olefin polymerization, and ring expansion of cyclic olefins to cyclic diolefins containing twice the number of carbon atoms. Interesting perspectives could arise from other intensively studied reactions, including those for use in replenishing raw materials. Therefore, with metathesis reactions it is possible to convert unsaturated fatty esters[18, 28] into chain-shortened fatty acids,[29, 30] long-chain dicarboxylic acids,[31] and synthetic triglycerides.[32]

Siegfried Blechert, born 1946 in Aalborg (Denmark), studied chemistry at the Universität Hannover (Germany), and received his Ph.D. in 1974 from Prof. E. Winterfeld. After holding a research position in Gif-sur-Yvette (France) with Prof. P. Potier, he finished his habilitation at the Universität Hannover. In 1986 he held positions at the Universität Bonn and Universität Münster. After a four-year appointment as a C3 professor in Bonn, he succeeded Prof. F. Bohlmann at the Technische Universität Berlin in 1990. His research interests include the development of synthetic methods and strategies as well as the chemistry of natural and biologically active compounds.

S. Blechert

M. Schuster

Matthias Schuster, born 1963 in Bad Muskau (Germany), studied biochemistry in Leipzig (Germany) and received his Ph.D. in 1991 from Prof. H.-D. Jakubke. He received a research stipend from the Deutsche Forschungsgemeinschaft and joined Prof. C.-H. Wong's group at the Scripps Research Institute, La Jolla, CA (USA), where he investigated enzyme-catalyzed accesses to unnatural peptides and glycoconjugates. After holding a research position with Prof. S. Dieckmann at the Institut für Moleculare Biotechnologie in Jena (Germany), he is now a research fellow at the Institut für Organische Chemie der Technischen Universität Berlin.

3. Catalysts

In recent decades a large number of homogeneous, microheterogeneous, and heterogeneous metathesis catalysts have been reported.[22, 33–36] Catalyst activities and reaction conditions are determined by both the catalyst type and the transition metal. The catalysis proceeds by the formation of salts or complexes of the early and late transition metals; however, abnormal reaction systems such as catalysis with irradiated silica gel surfaces have also been reported.[37]

Heterogeneous catalysts that have long been used as contacts in petrochemical metathesis include $MoO_3/CoO/Al_2O_3$, $WO_3/SiO_2/Al_2O_3$, and Re_2O_7/Al_2O_3. The reaction temperature necessary for heterogeneous catalysis is strongly dependent on the catalyst metal. Whereas the Co/Mo catalyst is active at temperatures as low as 150 °C, other systems require temperatures over 300 °C.

The "classical" complex catalysts are obtained by combining transition metal salts (WCl_6, $MoCl_5$, $ReCl_5$, etc.) and their complexes with main group organometallic compounds (for example $RAlCl_2$, SnR_4). Therefore, they can be included in the group of Ziegler–Natta type catalysts. Typical homogeneous classical catalyst systems include $WCl_6/EtOH/EtAlCl_2$, $WCl_6/Et_2O/SnR_4$, $MoCl_2(NO)_2(PR_3)_2/RAlCl_2$, and $ReCl_5/Al_2O_3$. The use of small amounts of oxygen-containing compounds (ROH, ROR, O_2) leads to an increase in activity. These catalysts are generally active at room temperature. Catalysts based on late transition metals such as ruthenium and osmium (for example $[Ru(H_2O)_6](tos)_2$; tos = $MeC_6H_4SO_3^-$) are less active than the salts of early transition metals.[38] In comparison to other systems, however, they tolerate polar functional groups including protic compounds such as water.[39] Although the classical catalysts based on transition metal salts are easily obtained, they are poorly defined with respect to the actual active catalytic component, since only a part of the metal is directly involved in the catalytic process. Their activity is therefore controllable only to a certain extent, which complicates their specific application in organic synthesis.

Important advancements in this area have been the identification of methyltrioxorhenium (MTO) as the actual catalyst precursor of the $Re_2O_7/SnMe_4$ system, and its synthesis by Herrmann and co-workers.[40, 41] Immobilized MTO on acidic metal oxide supports (for example $MTO/Al_2O_3–SiO_2$) catalyzes reactions such as the self-metathesis of allyl halides, ethers, and silanes, unsaturated carboxylates and nitriles, as well as ethenolyses and ring closing metathesis polymerization already at room temperature.[42] Herrmann recently presented another molecularly defined, surface-bound carbene precursor based on tris(neopentyl)nitridomolybdenum(VI).[43] The application spectrum of olefin metathesis to organic synthesis has been significantly expanded mainly by the introduction of stable alkylidene–metal complexes (Scheme 4).

The first catalysts of this type were obtained by Osborn[44–48] (for example **1**) and Schrock[49–53] (for example **2**) by thermal H_α abstraction. The majority of the applications described below are based on the fourfold-coordinated neopentylidene and neophylidene complexes of molybdenum (**3** in Scheme 4) introduced by Schrock and co-workers,[54] as well as the ruthenium–alkylidene compounds (**4** in Scheme 4) developed by Grubbs et al.[55–58] The stabilized alkylidene–transition metal complexes used as catalysts are correctly referred to as initiators, as they must first be converted into the actual catalytically active metal–carbene complex by alkylidene exchange with a double bond. This initiation rate is very high in the case of **3**, and strongly dependent on the substituent R′ in the case of **4**. A significant advantage of the new ruthenium catalysts such as **4c** is their high rate of initiation. The dependence of catalyst activity on the ligand is shown for **4**; **4b** shows significantly higher metathesis activity than **4a**. Both **3b** and **4c** are commercially available. In contrast to **3**, Grubbs's ruthenium–alkylidene complexes tolerate a large number of polar functional groups and are less sensitive towards humidity and oxygen. Thus, they meet a crucial criterion for application in organic synthesis. Moreover, they are more easily available by ring opening of cyclopropanes[55, 56] (**4a** and **4b**) and by carbene transfer in the presence of diazoalkanes[57, 58] (for example **4c**). The lower tolerance of the Schrock molybdenum complexes towards functional groups is often compensated by significantly higher metathesis activity, which also allows the conversion of sterically demanding double bonds. In addition to Grubbs's ruthenium(II) complexes, allyl ruthenium(IV) complexes which constitute highly active metathesis catalysts in the presence of aliphatic diazo compounds were recently introduced.[59]

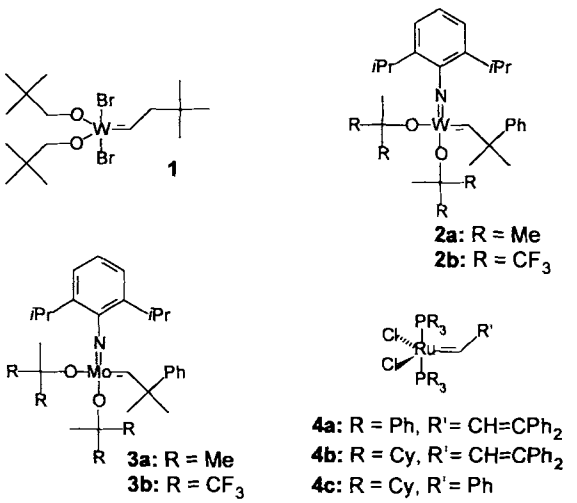

Scheme 4. Selected stable metal–carbene initiators.

In light of the repeated application of these expensive alkylidene–metal complexes, and to avoid contamination of the synthesized products with the used metal, immobilization of the catalysts on polymeric supports is an interesting concept. First studies in this area were reported by Grubbs et al.[60] based on ruthenium–carbene complexes of type **4**. The catalysts bound to polystyrene (2% divinylbenzene (DVB)) show lower metathesis rates than the corresponding soluble systems; they are, however, significantly more durable. Recently developed photoactivatable metathesis catalysts[61, 111, 112] are of great interest for application in polymerization.

4. Current Developments in Polymer Synthesis

The long established *r*ing-*o*pening *m*etathesis *p*olymerization[1] (ROMP) has been described in many re-

views.[34, 35, 61–66] The application potential of this method was greatly expanded by the development of highly active and defined alkylidene–metal complexes. In contrast to the classical catalysts, the modern alkylidene–metal initiators allow for the realization of "living" polymerizations due to their high metathesis activity and initiation rates; the metal–carbene intermediate formed during ring opening is stable on the time scale of the polymerization reaction.[35] As shown in Scheme 5,

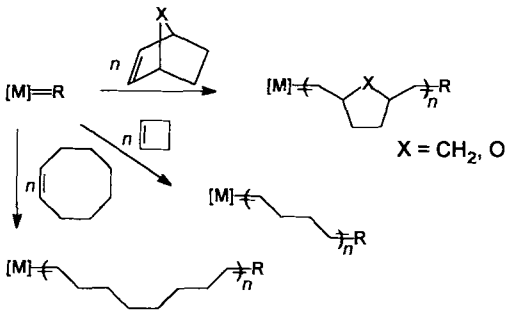

Scheme 5. "Living" ROMP of various strained cycloolefins.

the catalytic metal complex remains attached to the growing polymer chain during living ROMP. Strained cyclic olefins are used as monomers, since, due to the ring strain, the double bonds react highly selectively with the catalyst and enhance product formation.

Since the polymerization can be terminated selectively by addition of an aldehyde (for example benzaldehyde), which causes oxygen transfer to the catalyst, polymers of defined chain lengths are easily available. By alternating the addition of two or more monomers to the living chain, it is possible to synthesize defined block copolymers.[67–69]

A relatively new polymerization variant is the *a*cyclic *d*iene *met*athesis[70] (ADMET) in which terminal dienes (such as 1,9-decadiene or 1,5-hexadiene) are used as starting materials. Furthermore, polymerization of functionalized[71–75] and conjugated[76] olefins was also investigated. The polymerization proceeds as a stepwise cross-metathesis of the terminal double bonds (Scheme 6A). As opposed to the ROMP, which proceeds

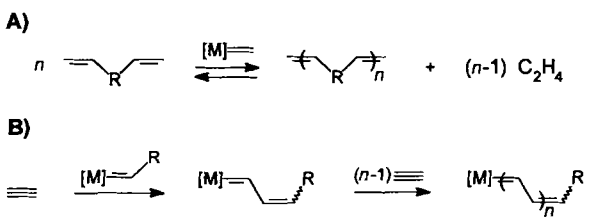

Scheme 6. Acyclic metathesis polymerization (ADMET) of A) dienes and B) acetylenes.

atom economically, the formation of the stoichiometric by-product ethene leads to an irreversible reaction for ADMET.[74–78] This nonliving polymerization yields products of high dispersity with (*E*) and (*Z*) double bonds.

Although metathesis of acetylenes has long been known,[79, 80] the development of the new alkylidene–metal initiators has only recently permitted living polymerizations.[81] The mechanism correlates to that proposed by Chauvin, in which conjugated metal–carbene complexes are formed.[13] When asymmetrically substituted acetylenes are used, two isomeric carbene complexes are obtained that exhibit different reactivities. An interesting variant of the acetylene polymerization is the cyclopolymerization of derivatives of 1,6-heptadiyne.[82–88] Starting from diethyl dipropargyl malonate (**5**) and **3b**, Schrock and co-workers synthesized cyclopolymer **6** with very low dispersity by living polymerization (Scheme 7).[35]

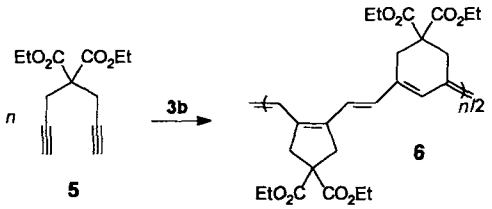

Scheme 7. Molybdenum-catalyzed cyclopolymerization of diethyl dipropargyl malonate.

Modern catalysts allow controlled construction of metal and semiconductor clusters[89–94] as well as redox-active polymers.[95, 96] The redox-active polymer **9** in Scheme 8 was

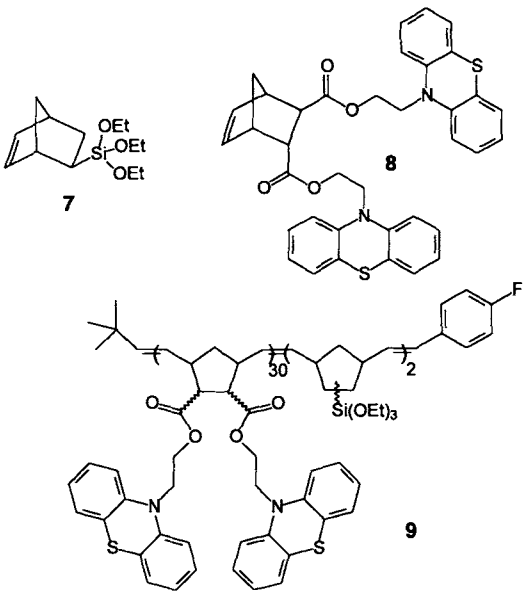

Scheme 8. Redoxactive copolymer **9**, synthesized by ROMP from **7** and **8**, that is suitable for the direct coating of electrode surfaces.

obtained by molybdenum-catalyzed copolymerization of monomers **7** and **8**.[97] While the redox-active properties of **9** can be traced back to the side chain of **8**, the triethoxysilyl functionality allows efficient and direct fixation of the polymer to the various electrode types.

Liquid-crystal polymers are also readily available by polymerization of suitable monomers.[83, 98–104] While polymers with mesogenic side chains can be prepared by ring-opening polymerization, ADMET opens the way to main-chain liquid

crystals. One interesting application in this area is the ruthenium-catalyzed polymerization of mesogenic "α,ω-dienes" to yield oligomeric ferroelectric liquid crystals such as **11** (Scheme 9).[105]

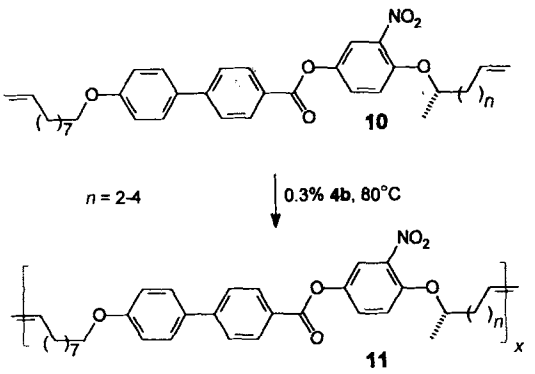

Scheme 9. Synthesis of a main-chain liquid-crystalline polymer **11** by ADMET.

The pronounced tolerance of Grubbs's ruthenium catalyst **4b** enabled the ROMP of the unprotected, sugar-substituted norbornene **12** (Scheme 10) in an aqueous-organic two-phase system.[106] Living polymerizations with **4c** were recently reported in predominantly aqueous solutions.[107]

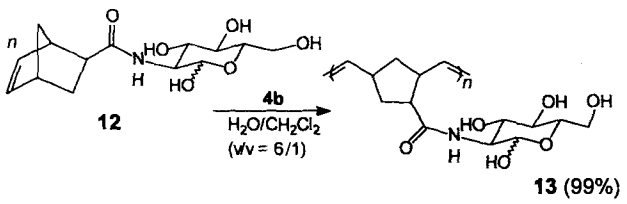

Scheme 10. Ruthenium-catalyzed ROMP of an unprotected sugar-substituted norbornene (**12**).

A fundamental problem of polymerizations is their stereochemical control. In addition to undergoing *cis*/*trans* isomerism, polymers with chiral centers adjacent to the formed double bonds can have various tacticities. By choosing specific ligands one can obtain all-*cis* and all-*trans* polymers with partly uniform tacticites. Using 2,3-bis(trifluoromethyl)norbornadiene with the hexafluoro-*tert*-butoxide catalyst **3b** led to exclusive formation of the *cis*-polymer[108] (75% tactical), while the use of the *tert*-butoxide catalyst **3a** resulted in the corresponding all-*trans* polymer ($\approx$100% tactical).[109] Furthermore, the stereochemistry can be controlled by the use of chiral catalysts. Therefore, use of the racemic form of [Mo(CHCMe$_2$Ph)(N-2,6-Me$_2$C$_6$H$_3$){BINO(SiMe$_2$Ph)$_2$}] (BINO = 1,1'-binaphthyl-2,2'-dioxy) yielded completely tactical all-*cis* poly-(dicarbomethoxynorbornadiene) and poly-[2,3-(bis)trifluoromethylnorbornadiene).[110]

Olefin metatheses can also be initiated photochemically. It was only recently discovered that sandwich complexes of the type [(η^6-arene)Ru(η^6-arene)]$^{2+}$ as well as nitrile complexes of the type [(NC–R)$_6$Ru]$^{2+}$ can be activated by UV radiation,[61, 111] and thus allow *p*hotoinduced *r*ing *o*pening *m*etathesis *p*olymerization (PROMP). Activation of the catalytically inactive sandwich complex occurs by photoinduced solvation of the metal. Since [Ru(solvent)$_6$]$^{2+}$ functions as the catalytically active complex, PROMP with ruthenium–sandwich complexes corresponds to ROMP with [Ru(H$_2$O)$_6$](tos)$_2$. To date the latter is the most active ruthenium complex for the polymerization of strained cyclic olefins in aqueous solution.[39] Activation of the nitrile complex occurs by photoinduced labilization of the extremely stable Ru–CN bond and corresponding ligand exchange. Complexes of the type [Ru(NCR)$_{6-x}$(H$_2$O)$_x$]$^{2+}$ are being discussed as catalytically active species. For both catalyst systems a nonlinear dependence of the molecular weight of the polymeric products on the monomer:catalyst ratio is observed, which is typical for nonliving polymerizations. The first PROMP based on photochemically formed catalysts of the Schrock type was also recently introduced.[112]

5. Ring-Closing Metathesis (RCM)

The intramolecular olefin metathesis of α,ω-diolefins leads to cyclic products (Scheme 11). The driving force for this transformation is the release of highly volatile ethylene. Although *r*ing-*c*losing *m*etathesis (RCM) was used relatively early for synthetic purposes, for example by Tsuji[113] and Villemin,[114] it has not become established as a method.

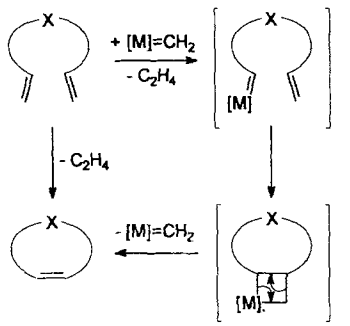

Scheme 11. Mechanism of RCM.

In recent years significant activity has been observed in this area. The versatility of the molybdenum catalysts **3b** and the ruthenium complexes **4b,c** in carbo- and heterocyclizations of very different ring sizes was demonstrated for many examples, even in the presence of diverse functional groups. Ring-closing metatheses have proven to be key steps in various total syntheses.

5.1. Synthesis of Five- to Seven-Membered Rings

Acyclic dienes can be used as substrates for metathesis polymerizations (ADMET) or ring-closing reactions (RCM). Which reaction path applies depends primarily on ring size, dilution, substrate, and catalyst. Four-membered rings cannot be obtained in this way, while five- to seven-membered rings should form readily due to their relatively low ring strain.

Catalyst dependency can be demonstrated with the conversion of **14** into **15** (Scheme 12). Even at high dilution the heterogeneous rhenium system affords primarily oligomers with the

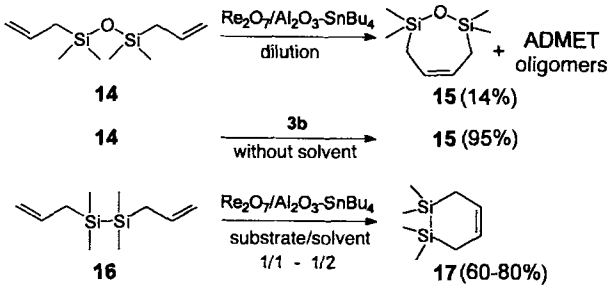

Scheme 12. RCM at different dilutions.

seven-membered ring as a by-product.[115] In contrast, the homogeneous Schrock molybdenum complex cyclizes the same substrate in high yield, even without solvent.[116] The rhenium catalyst does not always fail during RCM. In fact, disilacyclohexene **17** was obtained in useful yields even at increased concentrations.[115] Instead of the corresponding five-membered ring, oligomers are again primarily formed with the same catalyst.

Intermolecular olefin metatheses of acyclic dienes can generally be prevented by applying the dilution principle. However, RCM at higher concentration is advantageous due to the more rapid conversion. The required dilution for a specific ring size is often strongly dependent on the substituents. Forbes et al. reported systems in which ring closure with **3b** was favored by the Thorpe–Ingold effect, and thus also possible without solvent (Scheme 13).[116] Due to the geminal dimethyl substituents, **18a**

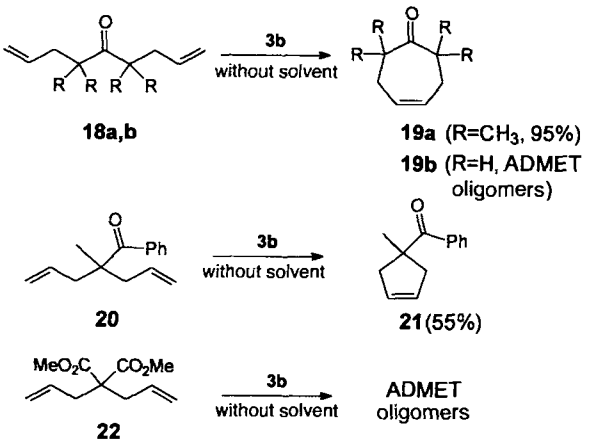

Scheme 13. Olefin metathesis without solvent.

reacts to form the seven-membered ring **19a** in high yield, whereas **18b** reacted exclusively intermolecularly under the same conditions. The reaction paths are in agreement with results of MM2 calculations. The different reactivities of the diallyl derivatives **20** and **22**, however, are not easily predictable. Compound **20** cyclizes even in its pure form, whereas the ring closure of **22** occurs only in solution.[117]

Ring-closing metatheses in which five- to seven-membered carbocycles are formed often proceed without complications; they do, however, require selection of the proper catalyst depending on functional groups as well as steric demands. A valuable resource is Grubbs's ruthenium complex **4c**. Due to its high tolerance towards substituents, it can cyclize allyl alcohol **23**, obtained by aldol addition, cleanly to the almost enantiomerically pure cyclopentenol derivative **24** (Scheme 14), which is a precursor for a carbocyclic nucleoside.[118] The optically active

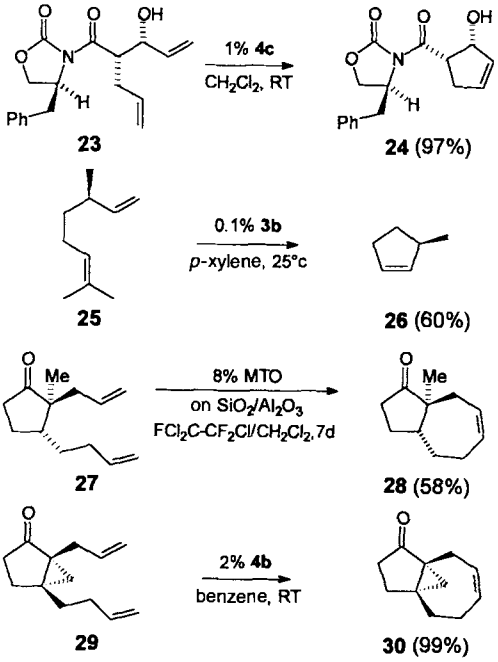

Scheme 14. Carbocyclic ring closures; RT = room temperature.

methylcyclopentene **26**, which is interesting for the synthesis of chiral polymers, was obtained by Sita with only 0.1% of the molybdenum catalyst **3b** from β-citronellene.[119] The relatively low amount of catalyst required for this reaction is presumably based on the lack of heteroatoms and the tendency of **3b** to induce the metathesis of higher-substituted olefins. Although **25** can be cyclized with **4c**, it requires higher amounts of catalyst.[117] The perhydroazulenes we prepared demonstrate the suitability of metathesis for constructing condensed ring systems.[120] In contrast to **28**, the more strained tricycle **30** cannot be obtained using MTO; with **4b**, however, it is formed nearly quantitatively.[121]

Olefin metatheses with derivatives of allyl alcohols are not unproblematic, since many catalysts are consumed by β-elimination of the generated carbene complex. The new generation of ruthenium complexes **4b** and **4c** as well as the molybdenum catalyst **3b** tolerate allyl ethers and acetals without problem, and are therefore suitable for the synthesis of cyclic ethers. The rate of RCM correlates well with the degree of substitution of the olefin substrates and with the ring size. Seven-membered rings and especially higher-substituted alkenes generally require longer reaction times. Examples for the synthesis of cyclic ethers are given in Scheme 15. Both types of catalyst are suitable for cyclization to seven-membered rings such as **32**; however, the more readily accessible and less sensitive ruthenium catalyst is generally preferred.[122] Ring-closing metatheses with di- or even trisubstituted double bonds generally require the more reactive Schrock complex **3b**.[123] The RCM to form **34** demonstrates the principle suitability of the metathesis for constructing tetrasubstituted double bonds.

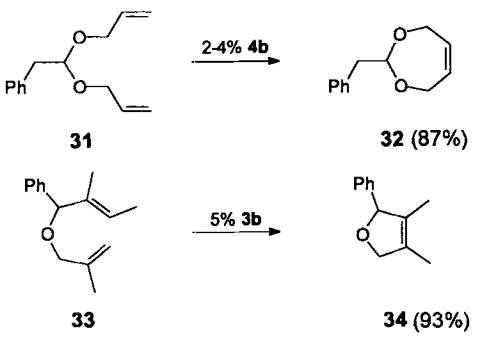

Scheme 15. Synthesis of cyclic ethers.

As Grubbs et al. have shown, **3b** also reacts with enol ethers. This opens versatile possibilities for the synthesis of O-heterocycles such as dihydropyran **36** or benzofuran **38** (Scheme 16).[124]

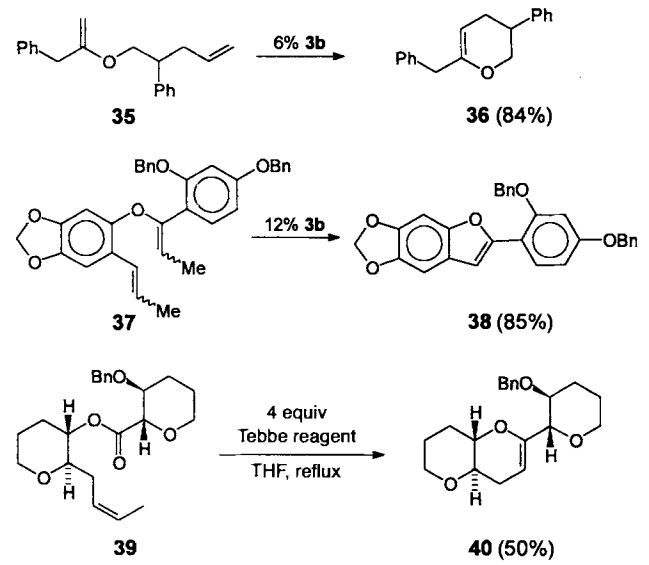

Scheme 16. Synthesis of cyclic enol ethers.

Depending on the position of the enol ether double bond, RCM can also be used for synthesizing enolizable cyclic ketones. The used enol ethers can be obtained by carbonyl olefination of the ester by the Utimoto–Takai method or with the Tebbe reagent.[125, 126] Under extreme conditions metatheses can even be catalyzed by the Tebbe reagent. Thus, one can combine olefination of an ester with RCM. Such cyclizations were recently used by Nicolaou for synthesizing ring systems of type **40**, which are interesting as they represent a subunit of naturally occurring neurotoxic polyethers.[174, 128] However, this two-step reaction in which the olefination occurs first requires an excess of the organometallic reagent. Catalytic cyclizations with **3b** to form brevetoxin subunits have been described by Clark and Kettle.[129] In contrast, **4c** is not suitable for such ring-closing reactions.

Various studies in recent years have demonstrated the usefulness of RCM for constructing N-heterocycles. Due to the importance of nitrogen-containing compounds, for instance in the synthesis of alkaloids and other biologically active substances, the method is an enrichment of synthetic chemistry. In some cases the ring-closing reactions are not unproblematic, because the catalysts may be inhibited by the complex-forming properties of amines and amides. RCM reactions with basic amines present a substantial problem, even with the use of Grubbs's ruthenium catalyst, which is relatively inert towards various functional groups. Benzyldiallylamine, for instance, could be cyclized only after conversion into the hydrochloride **41** (Scheme 17).[122] In contrast, tertiary amines are converted

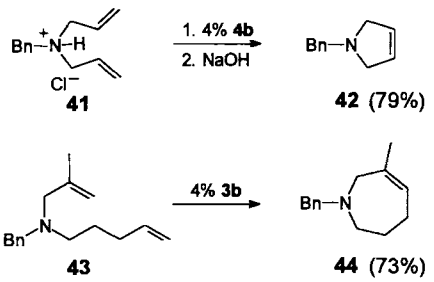

Scheme 17. RCM of tertiary amines.

cleanly to N-heterocycles such as **44** with the use of the generally more sensitive Schrock complex **3b**.[130] We discovered that the catalyst-inhibiting complexation with basic nitrogen can often be suppressed by steric hindrance.

Although **3b** is very suitable for RCM of basic tertiary amines, it causes problems for the conversion of certain amides. In reactions with α,β- or β,γ-unsaturated compounds, the catalysts may become inhibited by intramolecular interaction with the carbonyl group (**45** and **46**, Scheme 18). Grubbs was able to

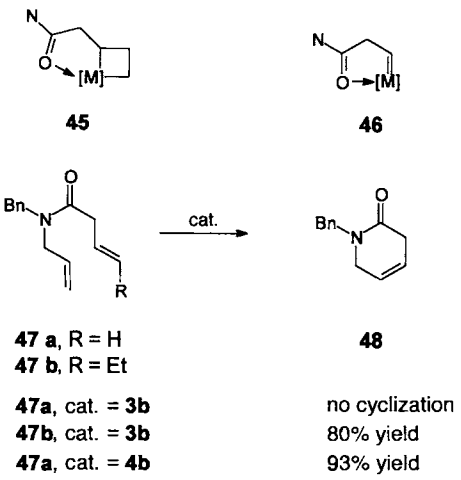

Scheme 18. Effects of complexating structural elements.

solve this problem by using higher-substituted double bonds.[130] The ring closing initiating first metathesis reaction can be directed by steric effects. Primary attack at the *N*-allyl group of **47b** prevents formation of an inhibiting chelating structure. However, **47a** cannot be converted with **3b**. Fortunately, the two above-mentioned catalyst types complement each other even in this case. Complexes **4b** or **4c** have considerably less problems with α,β- or β,γ-unsaturated monosubstituted amides such as **47a**, and provide **48** in good yields (Scheme 18).

In many cases Grubbs's ruthenium catalysts are active even in the presence of free NH-amides. This leads to interesting application possibilities for the conversion of amino acids and peptides.[131] However, the tolerance of these functional groups cannot be generalized. Starting with optically active vinyl and allyl glycine, we prepared various pyrrolidine and piperidine derivatives by RCM (Scheme 19),[132] and thereby discovered

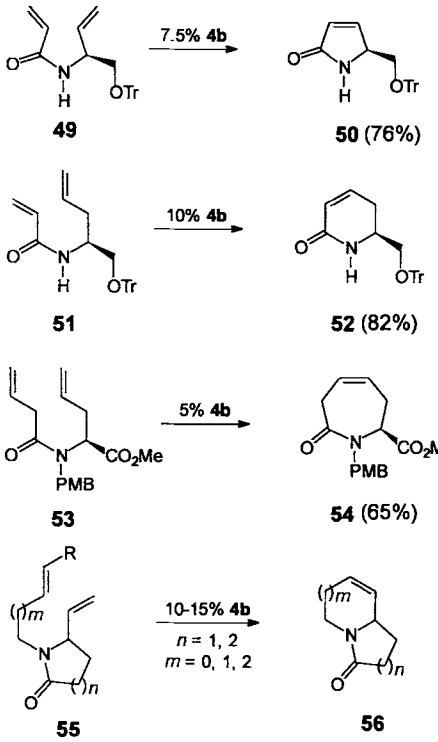

Scheme 19. Synthesis of substituted N-heterocycles; Tr = Ph_3C, PMB = *p*-$MeOC_6H_4CH_2$.

that the NH-amides **49** and **51** could be cleanly cyclized. Ring closure of such structural units is apparently favored due to steric blocking of the NH group by the neighboring trityl group. Sterically less demanding protecting groups provide significantly lower yields for RCM. Comparable effects were observed by Rutjes et al. for amino acid synthesis.[133] For cyclization of amide derivatives of allyl glycine, additional blocking of the nitrogen proved to be advantageous. For example, when the corresponding free NH compound was used instead of the *p*-methoxybenzyl-protected amide **53**, the yield of the cyclization decreased to 20%. Recently Guibé et al. also used a protected amide for synthesizing an unsaturated lactam with a six-membered ring.[134] Numerous biologically interesting alkaloids contain pyrrolizidine, indolizidine, or chinolizidine ring systems. Such structural units are also accessible by RCM. Martin et al. synthesized amides of type **55**, which provided the molybdenum-catalyzed bicyclic compounds of type **56**, from succinimide or glutarimide.[135] We were able to prepare similar bicycles with the use of **4b**; unfortunately cyclizations to yield the more strained pyrrolizidinone derivative were unsuccessful with this method.[136]

Ring-closing metatheses have also been used for synthesizing phosphorus and sulfur heterocycles.[137, 138] These functional substituents are apparently tolerated by only few catalysts. Diallylsulfide, for example, was not converted with **4c** at all. However, RCM to 2,5-dihydrothiophene proceeded smoothly with **3b**; this transformation was also described with an aryloxo(chloro)neopentylidene–tungsten complex.[138, 139]

Triple bonds are also suitable probes for metathesis reactions, even though ring-closing metatheses with triple bonds are seldom. Fundamental studies were performed by Katz,[140] who was able to cyclize the rigid enyne system **57** in moderate yields using the tungsten–carbene complex **58** as the initiator (Scheme 20). A methylidene–tungsten complex presumably

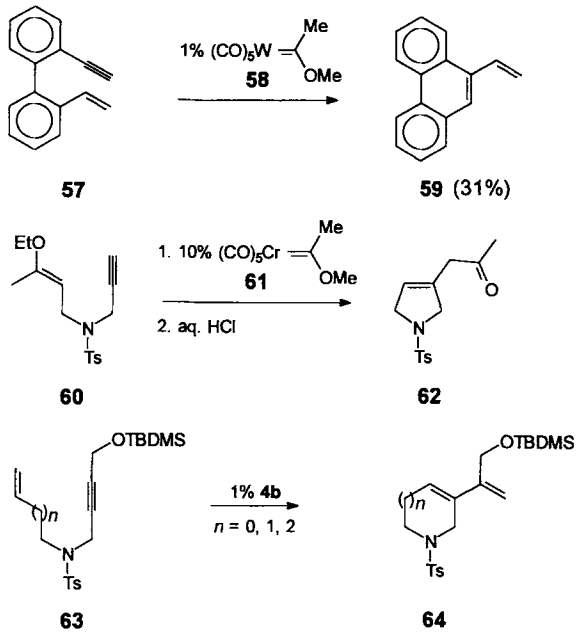

Scheme 20. RCM with enynes; Ts = *p*-$MeC_6H_4SO_2$, TBDMS = *tert*-butyldimethylsilyl.

functions as the catalytically active species. Mori reported heterocyclizations with the Fischer chromium–carbene complex **61**.[141, 142] Cyclization between enol ethers and triple bonds to form five-membered rings allows regeneration of the Fischer complex. Depending on the substituents at the double bond, various enol ethers can be obtained in addition to their hydrolytic products. One positive example is the two-step transformation of **60** to **62**. More attractive is RCM of enynes of type **63**, which proceed with relatively low amounts of the catalyst and in good yields, since the required substrates are readily accessible.[143] Carbocyclizations of monosubstituted acetylene derivatives were described by Murai et al. with $[RuCl_2(CO)_3]_2$ and CO.[144]

Ring-closing metatheses are also possible between an olefin and a carbonyl group (Scheme 21). Oxygen transfer to the metal during these reactions leads to inactivation of the catalyst. Therefore, the reaction is not catalytic. In contrast to the previously described olefination and metathesis sequence using the Tebbe reagent (see **39** → **40**, Scheme 16), in the case of **3b** primary attack occurs at the C–C double bond.[145] Cyclization of esters requires the more reactive analogous tungsten complex **2b**.[146]

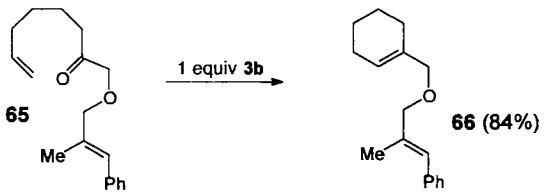

Scheme 21. RCM with a ketone.

5.2. Synthesis of Medium-Sized and Large Rings

The efficiency of a cyclization reaction often becomes apparent in the preparation of medium-sized rings. Here also, the metathesis appears to be quite a powerful tool. A particular challenge is the synthesis of eight-membered rings, since the olefins required are often suitable monomers for competing ROMP. The balance between RCM and ROMP is certainly affected by ring strain. In the cyclization of diallylethers to eight-membered rings, Grubbs observed relatively smooth ring closure of **67** (Scheme 22), whereas the analogous *cis* compound provided the more strained eight-membered ring in only 20% yield.[147]

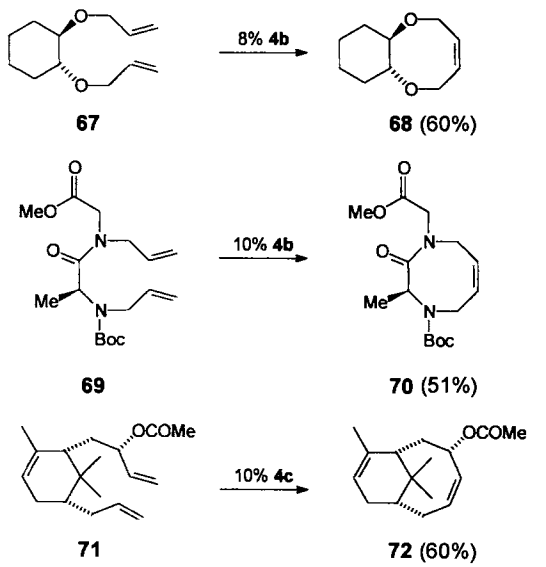

Scheme 22. Synthesis of eight-membered rings; Boc = *tert*-butoxycarbonyl.

In cyclizations which can compete with bimolecular C–C bond formations, it is absolutely crucial to maintain a high degree of dilution. A conformationally favored cyclization to an eight-membered ring, which was performed at a concentration of 0.005 M, yielded the diazocine derivative **70** in 51% yield from a dipeptide (Scheme 22). Upon replacement of the allyl amide substituent with an allyl ester under the same reaction conditions, the conformation of the substrate changed and prohibited cyclization. Grubbs et al., Martin et al., and Winkler et al. reported the use of RCM to access acozine ring systems, which are contained in many natural products.[147–150] The metathesis was also used for synthesizing various carbocycles.[147] Recently, we were able to use the ruthenium-catalyzed ring closure of **71** for synthesizing an AB-taxane system (**72**), which has a relatively strained structure due to the geminal dimethyl group and the annelation of the six-membered ring.[151]

Cyclization to an eight-membered ring does not present the biggest challenge. More problematic are ring-closing metathesis reactions to yield nine-membered rings. Barrett, Giles et al. used RCM with β-lactams in reaction with **3b** to obtain the eight-membered ring in 53% yield; the homologous nine-membered ring was obtained in only 12% yield.[152] Comparable observations were recently made by Clark and Kettle for cyclizations to form brevetoxin subunits.[153] Little is known about the synthesis of other medium-sized rings.

Larger ring systems are generally more readily accessible. Due to the ring size, *cis* and/or *trans* double bonds can be formed. The yields are not only dependent on the ring size, but also on the position of the resulting double bond. Ring-closing metathesis has been successfully used in the synthesis of various substance classes (Scheme 23). Despite the low yield the construction of the highly functionalized pentacycle **73**, which contains the ABCD system of the alkaloid manzamine A, is noteworthy.[154] However, the **4b**-catalyzed cyclization to the 13-membered ring required a reaction time of five days. Significantly more rapid was the ring closure to the 14-membered tetrapeptide **74** when using the same catalyst.[131] For the synthesis of the acyclic peptide, Grubbs used racemic allyl glycine. From the mixture of the four resulting diastereomers, only one cyclized. In the reaction of the pure compound with 20% **4b** at a dilution of 0.002 M, **74** was obtained in 60% yield. Beyond these conformationally favored cyclizations, Fürstner et al. described ring closure to large and very large rings starting from other substrates.[155] With small amounts of catalyst, König and Horn successfully synthesized crown ethers in good yields with only 1% **4c** at a relatively high concentration of 0.1 M.[156] Besides the 17-membered ring **75**, larger benzannelated compounds were also prepared.

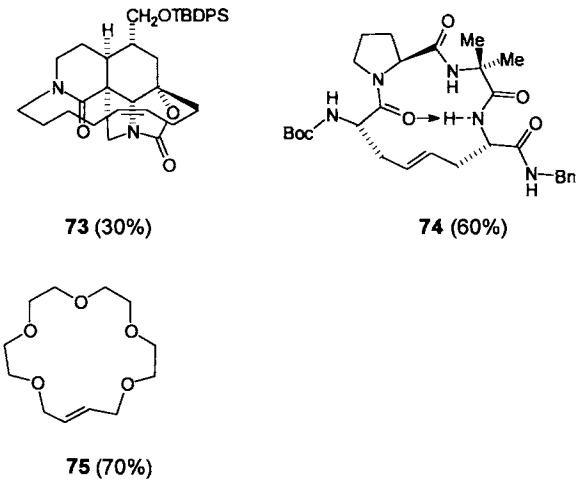

Scheme 23. Macrocylic compounds prepared by RCM; TBDPS = *tert*-butylphenylsilyl.

Ring-closing metathesis was also used successfully in the area of supramolecular chemistry. Wasserman et al.[157] reported the formation of catenanes in the process of RCM to form large rings. In contrast to earlier assumptions, these reactions proceed by a statistical threading process.[158] McKervey and Pitarch

used the metathesis for synthesizing cage compounds.[159] Calix[4]arenes were converted into diethers with pentenyl bromide, and bridged by RCM. One of the largest cyclic compounds constructed by metathesis is the 38-membered ring **77**.[160] Supramolecular interactions between cyclopeptides **76** were used in the synthesis of this ring. In nonpolar solvents, these molecules arrange themselves to cylindrical arrangements by intermolecular hydrogen bonding. Based on the C_2 symmetry of the peptide unit, two diasteromeric dimer structures can be formed. In one of the diastereomers the homoallyl glycine units are in adjacent positons, which allows the noncovalent interactions to be used for the synthesis of the tricyclic cylindrical peptide **77**. The two-step reaction with **4b**, in which the last step is an RCM occured with an impressive yield of 65% (Scheme 24). Three double-bond isomers were isolated. As expected in polar solvents, no cyclizations occured due to the missing H bonds.

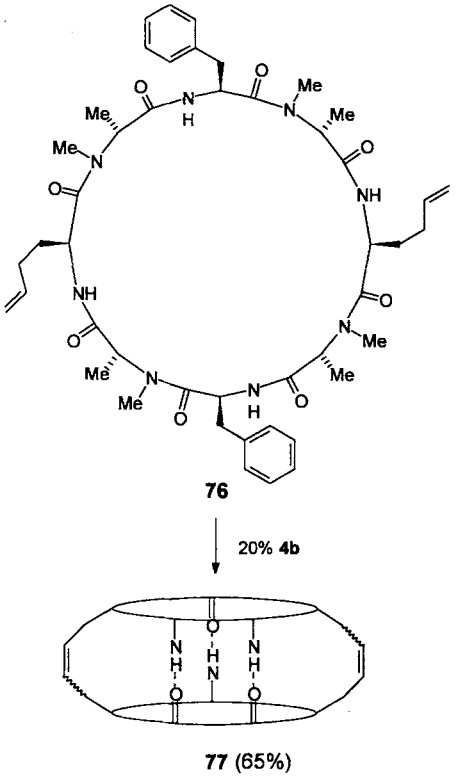

Scheme 24. Use of the template effect for the synthesis of peptide suprastructures.

5.3 Asymmetric RCM

Due to the large synthetic potential of ring-closing metathesis, asymmetric variants are particularly important. In this area there is still a great need for development. Although chiral catalysts have been used for polymerizations, as illustrated in Section 4, the first example of an asymmetric RCM with a chiral catalyst was only recently reported.[161] This case followed the concept of converting racemates of chiral diolefins of type **78** with the chiral catalyst **81**, a modification of **3b**, into diastereomeric metal–carbene complexes (Scheme 25). Due to the different energies of the transition states resulting from the diastereomers, it was possible to achieve a kinetic racemic separation based on the different cyclization rates of **79** and **80**. The degree of substitution of the olefin controls the primary attack. In light of the *ee* values obtained to date, synthetic applications of this process are currently not envisioned.

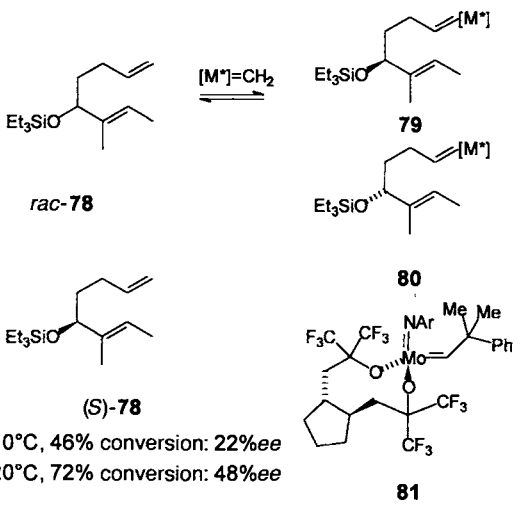

Scheme 25. Kinetic racemic separation by olefin metathesis with **81**.

As numerous natural products and biologically active substrates contain α,α′-disubstituted heterocyclic units, we investigated the stereocontrolled construction of such systems with asymmetric RCM. In principle, an existing chiral center should control the cyclization with a prochiral diene unit. The required control of the primary attack was also achieved by using differently substituted double bonds. Surprisingly, the ring closure of **82** with **3b** afforded the product with *syn* orientation of the two substituents, while the *anti*-isomer of **83** was obtained with high diastereoselectivities when using **4b** (Scheme 26).[162] Although the catalysts lead to different ligand orientations during the metatheses, a clear explanation and predictability of the observed selectivities are not yet possible. Polyhydroxylated pyrrolidine derivatives are of interest as enzyme inhibitors. This prompted us to use this process for synthesizing the homoazasugar (−)-**84** from enantiomerically pure vinyl glycinol.[163]

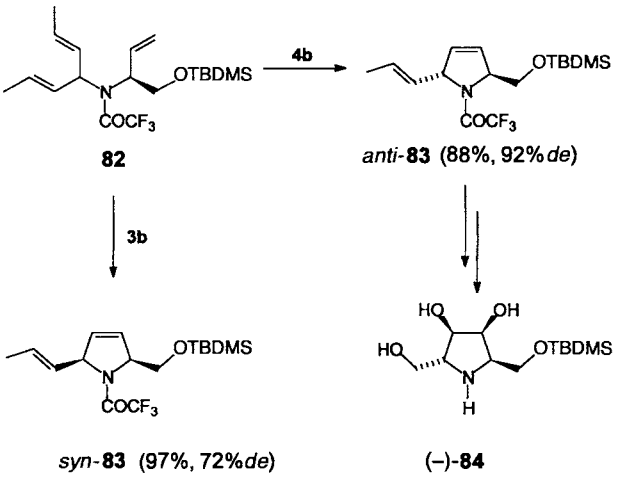

Scheme 26. Catalyst-specific asymmetric RCM.

5.4 Synthesis of Natural Products

In recent years the ring-closing metathesis developed into an efficient, widely applicable method for forming C–C bonds. As a result of the pronounced tolerance to many different functional groups, the method has increasingly been used in the area of natural-product synthesis. We used RCM for synthesizing naturally occurring prolinol derivatives.[163] (+)-Castanospermin (**87**) belongs to the same family of polyhydroxylated alkaloids, which are interesting as aza analogues of saccharides. Overkleeft and Pandit synthesized lactam **85** from tetrabenzylglucopyranose.[164] This RCM, in which an acrylic ester resulting from a Wittig olefination is cleaved instead of a volatile alkene, requires relatively drastic reaction conditions (Scheme 27). The corresponding substrates with two terminal

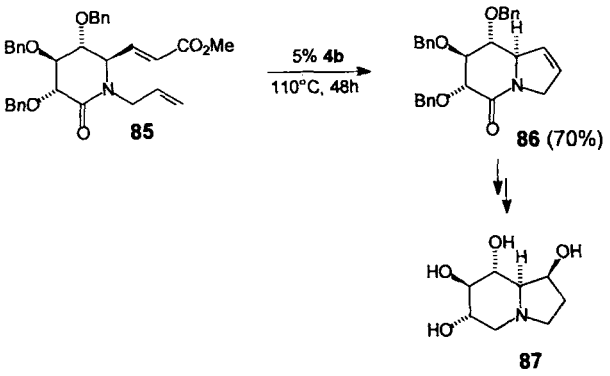

Scheme 27. Synthesis of castanospermin (**87**).

olefins or a phenyl-substituted double bond cyclize much more readily, but are more difficult to obtain because of the competing elimination of benzyl alcohol during the Wittig reaction. The multistep introduction of the fourth OH group was accomplished by oxidation with osmium tetroxide, since epoxidations gave only unsatisfactory results.

Coronatin (**90b**) is a strong phytotoxic fungus metabolite which has found new interest due to its analogy to some phytohormones. We prepared coronafacinic acid (**90a**) by metathetic ring closure of diene **88**,[165] in which the double bond is not further functionalized, but instead isomerized (Scheme 28). Due to steric hinderance, only one diastereomer of the 1:1 dia-

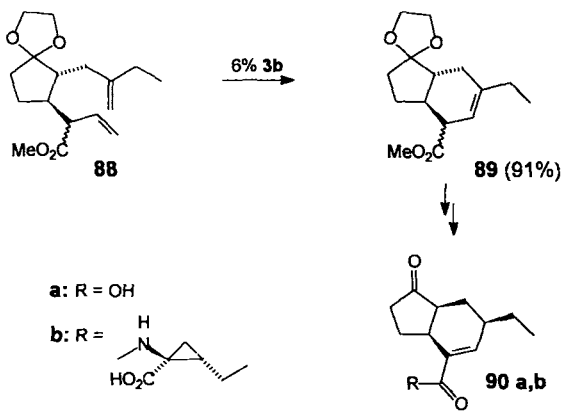

Scheme 28. Synthesis of coronafacinic acid (**90a**).

stereomeric mixture which resulted from a Michael addition could be cyclized with the ruthenium catalyst **4b**. On the other hand, with **3b** complete conversion into the bicyclic substrate **89** was achieved. During RCM with the unprotected ketone within the five-membered ring, partial carbonyl olefination was observed with simultaneous consumption of the catalyst. Deprotection, ester hydrolysis, and acid-catalyzed isomerization lead from **89** to **90a**.

Enyne metathesis to a seven-membered ring is the key step in a total synthesis of (−)-stemoamide **93**, according to Kinoshita and Mori.[166] The synthesis of the insectizidal tricyclic alkaloid starts from the acetylene ester **91**, which is obtained enantiomerically pure from pyroglutamate. Enyne metatheses with these functional groups provided poor yields in earlier studies, which was attributed to the instability of the resulting ester-substituted conjugated butadiene unit.[143] In the present case a disruption of the conjugation by steric effects was desired, and ruthenium-catalyzed RCM did in fact provide bicycle **92** in good yield, the ester group of which was used for acidic lactone annellation with $CuBr_2$ on Al_2O_3 (Scheme 29).

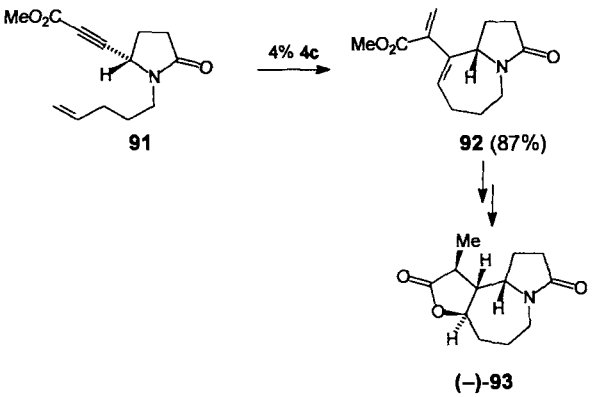

Scheme 29. Synthesis of stemoamide (**93**).

Eight-membered rings can also be prepared by olefin metathesis. Fürstner and Langemann recently reported a short synthesis of dactylol (**95**; Scheme 30), an isoprene isolated from

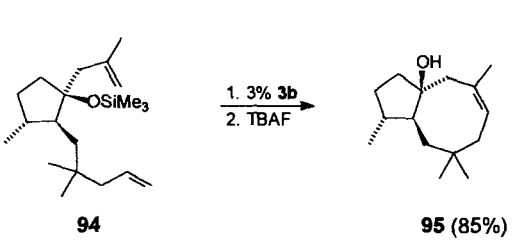

Scheme 30. Synthesis of dactylol (**95**); TBAF = tetrabutylammonium fluoride.

maritime organisms.[167] The precursor **94** was prepared in five steps from cyclopentenone. The synthesis of the tertiary carbinol by addition of a methallyl–cerium compound afforded an approximately 1:1 diastereomeric mixture, which was used for synthesizing 3-α-*epi*-dactylol. Protection of the OH group proved to be crucial, since the free carbinol was recovered after treatment with **3b**. It apparently deactivated the catalyst by complexation.

Ring-closing metathesis is very suitable for synthesizing large rings. Although many macrolactonization methods are known, it is attractive to prepare such compounds by olefin metathesis. The synthetic route chosen by Fürstner and Kindler to obtain (+)-lasiodiplodine (**97**) starts from enantiomerically pure propene oxide (Scheme 31).[168] The outstanding yield of 94% for the cyclization step underlines the efficiency of this ring-closing method. The resulting mixture of *E*/*Z* isomers in a ratio of approximately 2.3:1 can be combined by hydrogenation, making the 12-membered lactone **97** easily accessible. The synthesis of the 14-membered lactam fluvirucin (**99**) by Hoveyda et al. (Scheme 31) is a nice example for the highly developed status of metal-catalyzed reactions.[169, 170] This natural-product synthesis includes no less than nine transition metal catalyzed reactions. The key step, the molybdenum-catalyzed RCM of the highly functionalized diene **98**, proceeds with very good yields and affords the desired (*E*)-configurated cycloolefin almost exclusively. Subsequent hydrogenation of the relatively rigid macrocycle provides the desired stereochemical orientation of the methyl group.

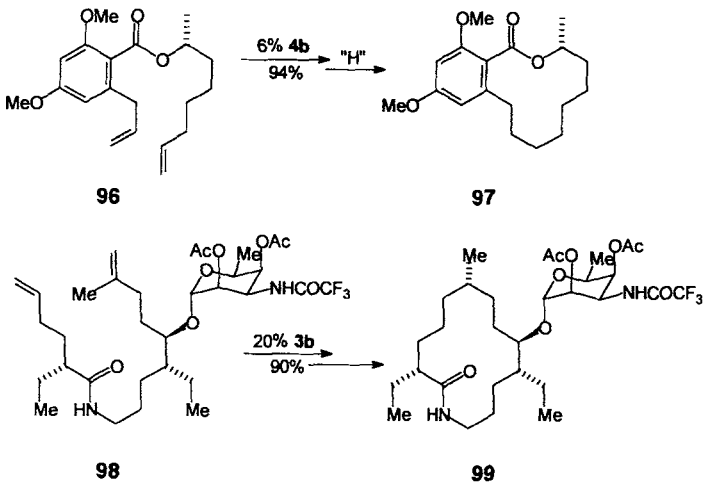

Scheme 31. Synthesis of lasiodiplodin (**97**) and fluvirucin (**99**).

Epothilon A (**101**) is a promising new 16-membered macrolactone which was isolated from myxo bacteria.[171] It exhibits selective cytotoxic activity with an activation mechanism similar to that of taxol, and has therefore awakened high expectations. Soon after the publication of the complete structure, total syntheses were reported. Nicolaou et al. used an RCM as the key step.[172] The metathesis of **100** proceeds under mild conditions in 85% yield (Scheme 32), demonstrating once more the potential of the ring-closing metathesis for the construction of complex molecules. Less satisfactory is the poor *E*/*Z* selectivity, since the (*Z*) isomer necessary for the epoxidation is obtained in only 50% yield. A comparable synthetic strategy using RCM as the key step was recently reported by Schinzer et al.[173] The *E*/*Z* selectivity of the cyclization could possibly be improved by substituent effects.[174]

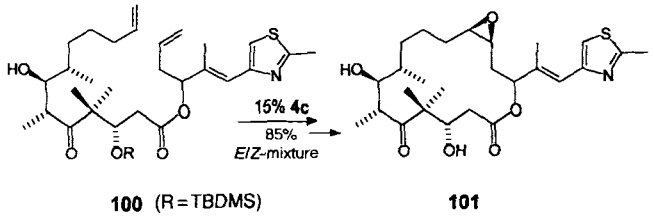

Scheme 32. Synthesis of epothilon A.

6. Cross-Metathesis

Cross-metatheses between two acyclic olefins offer interesting possibilities for synthesizing higher-substituted alkenes. The use of highly substituted asymmetric olefins is not practical because of the expected complex spectrum of products. Use of terminal olefins results in the formation of volatile ethylene as a by-product, which provides the driving force for the reaction. Therefore, almost all relevant studies to develop cross-metathesis as a synthetic method employ reactions between terminal olefins. The reaction is generally not very stereoselective.

The self-metathesis of terminal olefins is a reaction which has been known for a long time for synthesizing symmetrically substituted olefins.[175–177] Every cross-metathesis of two terminal olefins **102** and **103** faces the danger that not only the desired product **104** but also the homodimers **105** and **106** form (Scheme 33). For this reason, investigations of the factors responsible for the selectivity are extremely important.

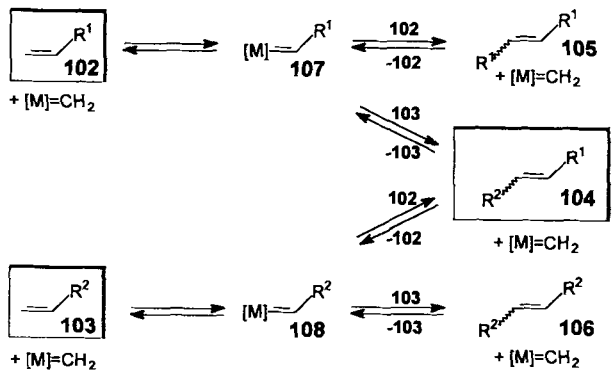

Scheme 33. General reaction scheme of the cross-metathesis of terminal olefins.

In 1988 Marciniec and co-workers published the first cross-metatheses of vinyl silanes,[178] and later of vinylalkoxy- and alkenyl-substituted silanes[179–181] with terminal alkenes, using classic ruthenium and rhodium complexes. However, these catalysts require reaction temperatures over 100 °C. Moreover, with equimolar amounts of the substrates, the dimeric silane was formed in significant yields along with the cross-product. In the case of the cross-metathesis of alkenyl-substituted vinyl silanes, self-metathesis could be suppresed only by the use of a tenfold excess of the respective coupling partner.[181]

Crowe et al. performed first reactions with defined catalysts of type **3**. They described selective molybdenum-catalyzed conversions of styrene[182] and acrylonitrile[183] with a series of nonconjugated terminal olefins (Scheme 34). While cross-metathesis reactions with styrene afford the (*E*) olefin almost exclusively, the respective (*Z*) isomer predominates in the reactions with acrylonitrile. The pronounced selectivity with which these conjugated, terminal olefins react with nonconjugated

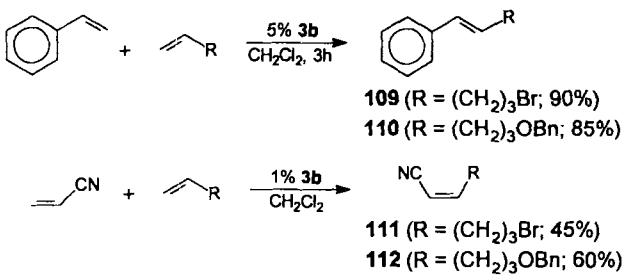

Scheme 34. Selected cross-metatheses of conjugated olefins.

olefins was first explained by the formation of a conjugated, and thus stabilized, alkylidene–metal donor from styrene or acrylonitrile (see **107** and **108**, respectively, in Scheme 33), followed by selective [2+2]cycloaddition with a "nucleophilic" isolated double bond.[183] The high selectivity of cross-metatheses of allyltrimethylsilane,[184] especially with π-substituted reaction partners, recently reported by Crowe et al. could thus be traced back to the pronounced nucleophilic character of the silane (β effect of silicon). A drawback of this model is that the results obtained with acrylonitrile and styrene are so far not transferable to other π-substituted olefins. Furthermore, we have results which suggest that not only electronic factors, but also others can control the selectivity of the reaction. For instance, we observed that 4,4-dimethylpentene, a carbon analogue of allyltrimethylsilane, shows comparable reactivities and selectivities in cross-metatheses although it lacks a β effect.[185] In addition, with the use of **3** and **4** selective cross-metatheses could be carried out between reaction partners with double bonds of comparable electron densities.

Our studies on cross-metatheses of allyltrimethylsilanes show that high yields of cross products are typically observed when the double bonds of the reaction partners are different either with regard to their steric requirements or the polarity of their substituents (Scheme 35).[185] Of practical value is the synthesis of **117**, which proceeds with high stereoselectivity. The nearly isomerization-free conversion of the strongly C,H-acidic vinylglycine derivative **116** is achievable only under the mild conditions of olefin metathesis. The preparation of **119** demonstrates the possibility of differentiating between various terminal double bonds on the basis of their steric effects. The most

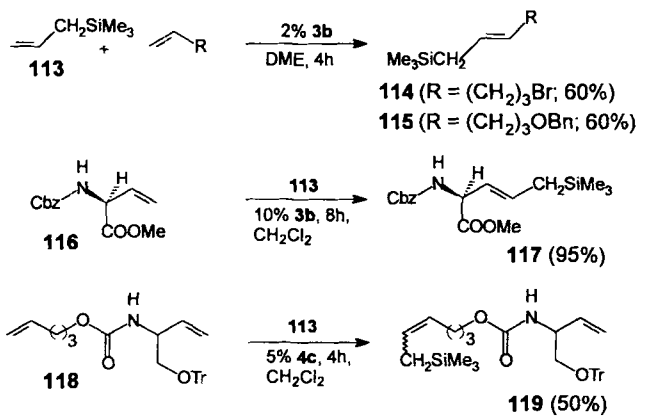

Scheme 35. Cross-methatheses with allyltrimethylsilane; Cbz = benzyloxycarbonyl.

efficient catalyst in this case is the ruthenium catalyst **4c**, whereas for the conversion of the sterically demanding vinyl group in **116** the more active **3b** is necessary. In both reactions 1.5 equivalents of the silane were used. The allylsilanes that are readily available in large variety by cross-metathesis react with a large number of electrophiles either inter- or intramolecularly.[186, 187]

With a twofold excess of allyltriphenylstannane we were able to prepare, among others, the allylstannanes **121** and **123** shown in Scheme 36.[188] These examples demonstrate that biologically

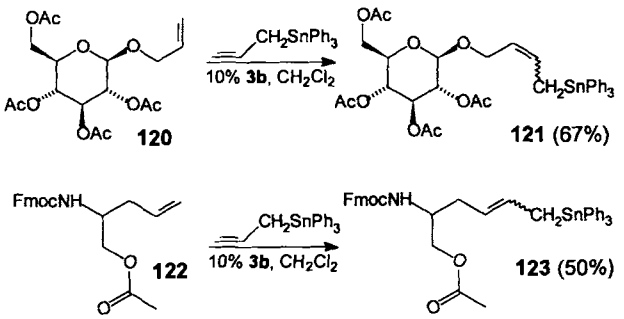

Scheme 36. Cross-methatheses with allyltriphenylstannane; Fmoc = 9-fluorenylmethoxycarbonyl.

relevant polyfunctional structures can also be selectively converted in molybdenum-catalyzed reactions. Allylstannanes as well as allylsilanes are valuable substrates, for example in Sakurai [189, 190] and radical reactions.[191]

We have also used selective cross-metatheses to prepare various substituted derivatives of jasmonic acid, a highly potent plant hormone. The ruthenium-catalyzed reactions with **124** shown in Scheme 37 point towards a large synthetic potential of the cross-metathesis.

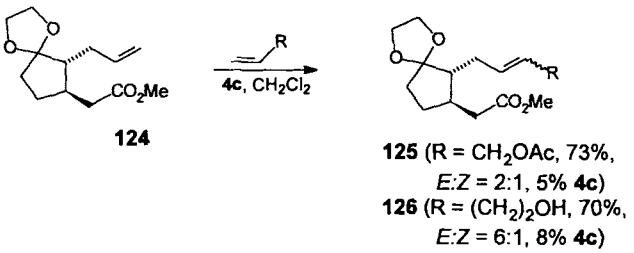

Scheme 37. Synthesis of selected jasmonic acid derivatives by ruthenium-catalyzed cross-methathesis.

To date there is no general model for the selectivity of the cross-metathesis. The reduced tendency of sterically hindered and conjugated olefins to undergo self-metathesis,[58] along with the possible precomplexation of the metal complex by heteropolar substituents, offers a viable starting point for increasing the understanding of the observed selectivities. Since the cross product can be formed by various reaction pathways, the suppression of the self-metathesis of one reaction partner alone does not allow for the proposal of a selective mode of action. On the other hand, selective cross-metatheses are often observed between olefins which completely dimerize in the absence of a partner component. The current knowledge is still insufficient for the directed use of the cross-metathesis.

Recently, we found that cross-metatheses between monosubstituted acetylenes and terminal olefins are also possible with **4c** (Scheme 38).[192] The use of **3b** under identical reaction conditions led to the exclusive polymerization of the acetylene component (see Scheme 6B). The selectivities of the bimolecular yne–ene metatheses are surprisingly high. Disubstituted triple bonds could not be coupled. Based on the current results, we favor a reaction path in which the catalytic carbene complex attacks the triple bond in the first step (Scheme 38). The resulting conjugated metal–carbene complex **127** subsequently reacts with a double bond to form the cross product **128**. The products were isolated as *E*/*Z* mixtures. The isomerization to the thermodynamically more stable (*E*) compounds is currently under investigation. To synthesize the natural antifungal α-triticen[193] (**129**), we coupled dodecyne with allyl alcohol protected with a *tert*-butyldimethylsilyl group. The metathesis product was deprotected and directly oxidized with MnO_2 in a one-pot reaction. The desired (*E*) product was obtained exclusively in a total yield of 58%.[192]

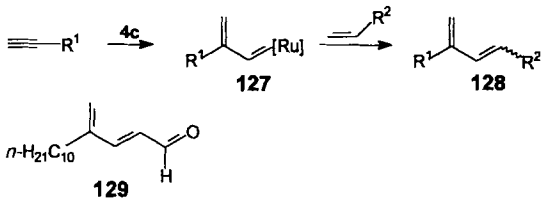

Scheme 38. Ruthenium-catalyzed yne–ene cross-metathesis.

7. Ring-opening Metathesis (ROM)

The metathetic opening of strained cyclic olefins to give open-chain metal–carbene complexes provides the basis for ring-opening metathesis polymerization (ROMP). The polymerization is induced by the conversion of an intermediate metal–carbene species with another molecule of the cycloolefin (Scheme 39). In the presence of a second open-chain olefin, the same intermediate has the opportunity to react to a monomeric ring-opening product by a cross-metathesis. The benefit of this *r*ing-*o*pening *m*etathesis (ROM) is, for example, the conversion of bicycles of defined configuration into monocyclic compounds of defined configuration. In contrast to cross-metathesis, ROM proceeds atom economically.

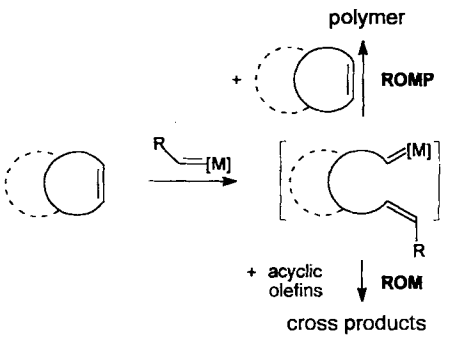

Scheme 39. Comparison between ROMP and ROM.

Since the driving force of ROM is presumed to be the ring strain of the cyclic starting materials, the first systematic investigations were performed on norbornene derivatives.[194, 195] The examples shown in Scheme 40 prove that both norbornene as well as 7-oxanorbornene derivatives **130** and **132** can be opened in high yield to the expected bicycles **131** and **133**, respectively. To suppress the polymerization of norbornene, however, it was necessary to use up to a tenfold excess of the respective acyclic component.

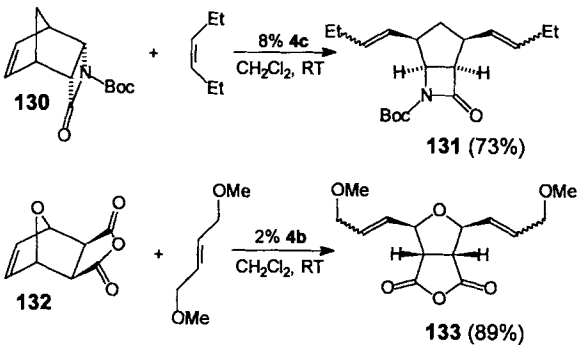

Scheme 40. ROM of norbornene derivatives with symmetrically substituted olefins.

Recent studies showed that the use of terminal olefins as the acyclic component alleviate the use of a large excess.[196] The molybdenum- and ruthenium-catalyzed reactions (Scheme 41) proceeded with surprising selectivity, although only equimolar amounts or up to 1.5-fold excesses of the respective terminal olefins were used. Noteworthy is also the exclusive formation of the monosubstituted diene. On the other hand, the investigated reactions generally proceeded with low stereoselectivities, that is, the *E*:*Z* ratios ranged between 5:1 and 1:6. These products represent interesting synthetic building blocks as they are highly substituted cyclopentane and furan derivatives. The selection of the catalyst is decided by the functionalities of the starting materials. While the highly reactive molybdenum initiator **3b** is required for ring opening of **134** with acrylonitrile to form **135**, it is not suitable for the conversion of **138** into **139**. In this case the ruthenium initiator **4c**, which remains active even in the presence of unprotected hydroxyl groups, was used. However, the use of silyl-protected derivatives of **138** resulted in higher

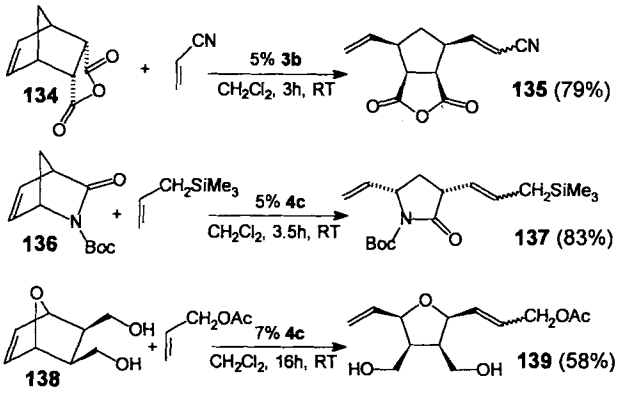

Scheme 41. ROM of norbornene derivatives with terminal olefins.

yields. The conversion of lactam **136** proceeded with surprisingly high regioselectivity. The regioisomer of the 3,5-pyrrolidinone **137** could not be detected. The application potential of the ROM is greatly increased by the possibility of performing regioselective reactions.

The high yields and the fact that no products with two disubstituted double bonds were isolated (Scheme 40) indicates that the self-metathesis of acyclic compounds can be suppressed successfully in the presence of cyclic compounds. We assume that the highly reactive methylidene–metal complex originally formed by the reaction of the alkylidene–metal initiator with the terminal olefin preferentially attacks the strained double bond of the cyclic olefin. Due to steric reasons, the resulting intermediate (Scheme 39, R = H) reacts preferentially with the acyclic component to form the observed products. Thus, the regioselectivity is caused by either steric effects during the attack of the catalytic metal–carbene complex at the double bond of the cycloolefin or a precomplexation by electron-rich heteroatoms.

In addition to norbornenes, other strained cycloolefins were employed in ring-opening reactions.[196, 197] Snapper et al. investigated the ruthenium-catalyzed ring-opening of cyclobutene-containing bicycles to form monocyclic products (Scheme 42).[197] Here too, only small excesses of the acyclic

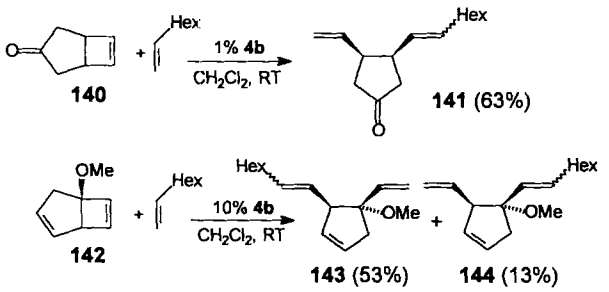

Scheme 42. ROM of functionalized bicyclic cyclobutene derivatives with terminal olefins.

components were used. Remarkable is the reaction of the unprotected ketone **140** to give **141**. The sterically demanding cyclobutene double bond in **142** is selectively opened by **4b** in the presence of the more accessible double bond of the cyclopentane ring to form a mixture of **143** and **144**.

We have described the formation of open-chain 1,5-dienes starting from the cyclobutene diester **145**.[196] Both allyltrimethylsilane as well as the carbon analogue 4,4-dimethylpentene react with high yields to form **146** and **147**, respectively. Similar to cyclobutene, cyclooctene represents a suitable starting material for ROM due to its ring strain. Bespalova et al. used the WCl_6/1,1,3,3-tetramethyl-1,3-disilacyclobutane cocatalyst system (**148**) for ring opening of cyclooctene to afford 1,9-dienes **149** and **150** (Scheme 43).[195] Since cyclooctene can also be opened by Grubbs's ruthenium initiators,[196] polar functionalized 1,9-dienes are also accessible by ROM. Bespalova et al. also presented the ring opening of cyclopentene by allylnitrile to yield the open-chain 1,6-diene **151**.[195] Due to the high tendency to form five-membered rings in RCM, the yield is surprisingly high. It may be possible that the disadvantage of the lower ring strain relative to the other

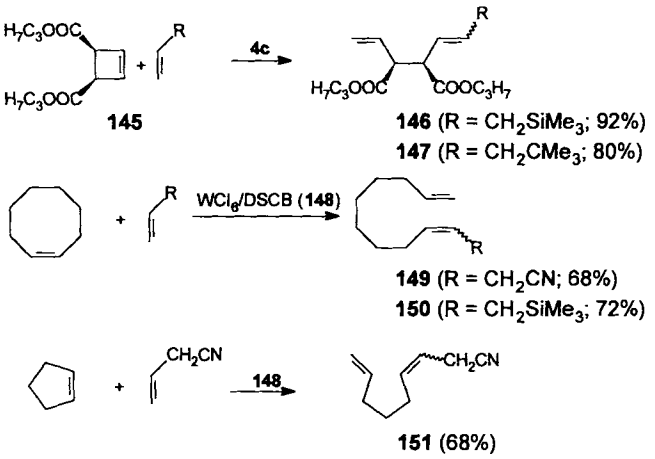

Scheme 43. ROM of monocyclic olefins with terminal olefins; DSCB = disilacyclobutane.

examined cycloolefins is compensated by the simultaneously reduced tendency towards polymerization. The catalytic ring-opening of cycloolefins, especially by terminal olefins, opens an interesting access to asymmetrically substituted acylic olefins, and therefore possesses a high synthetic potential.

8. Tandem Metathesis

Tandem or domino reactions can shorten synthetic routes significantly and are very interesting for synthetic strategies and methods.[198] Sequences of multiple subsequent olefin metathesis reactions are also known. Grubbs reported double ring closing metatheses using dienes which lead to various bicyclic [*m*,*n*,0] systems.[199, 200] An example is the conversion of **152**, in which an enyne RCM occurs in the first step, to form the vinyl carbene complex **153**, which in the second step yields the perhydroazulene skeleton **154** by loss of propene (Scheme 44). As the reaction sequence obviously starts with the monosubstituted olefin, asymmetric dienes require differentiation between the two double bonds with different degrees of substitution. If one removes the olefinic methyl group in **152**, the tandem metathesis yields a 1:1 mixture of a [4.4.0] bicyclic and the [3.5.0] system

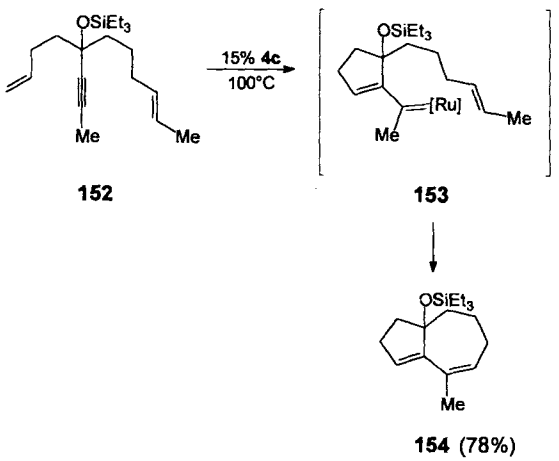

Scheme 44. Tandem metathesis with a dienyne.

154. Ring-closing metatheses of two olefins to form monocyclic products were found only in the case of a seven-membered ring in trace amounts. Substituent variation at the triple bond showed that bulky substituents drastically slow down the reaction, and for some functional substituents, such as $SiMe_3$ or halogens, no reaction occurs.

The RCM can also be combined with a ROM. Grubbs used various *syn*-configurated bis(allyl) or bis(homoallyl) ethers such as **155** in the reaction with **4c** to obtain oxygen-containing heterocyclic compounds such as **156** (Scheme 45).[201] Remarkable

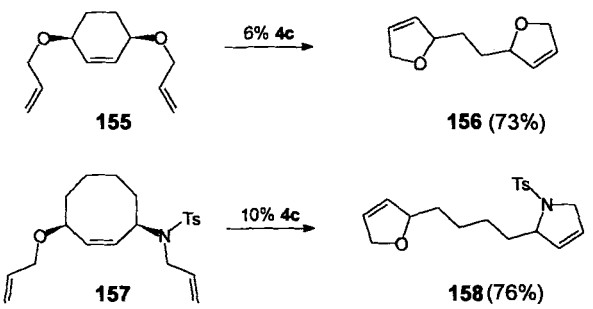

Scheme 45. Tandem ring-opening/ring-closing metathesis.

in this case is the rarely observed opening of a relatively unstrained six-membered ring. This reaction, however, was carried out at high dilution to prevent bimolecular bond formation. Considering the ring system and the corresponding ring strain, various mechanisms are possible which all involve primary attack at the ring or the terminal olefin. We have used similar ring-opening/ring-closing sequences with cyclooctene derivatives for synthesizing mixed chain linked hetero- and carbocycles such as **158**.[202]

After we demonstrated that norbornene derivatives can be opened very selectively by terminal olefins,[196] we investigated the combination of this method with a RCM.[203] Norbornenes with *endo* olefinic side chains as in **159** or **161** can easily be obtained by Diels–Alder reactions with acrolein and subsequent addition to the carbonyl group. Tandem metathesis in the presence of approximately a threefold excess of another alkene affords stereocontrolled access to various bicyclic compounds such as **160** and **162** in one step (Scheme 46). Compound **159** was used as a diasteromeric mixture. In the reaction of the separated, stereochemically homogeneous compounds, however, we obtained different conversion rates and different yields. Without the use of a second olefin, only the oligomerization of the bicyclic is observed. The combination of ring opening, ring closing, and cross-metathesis provides interesting possibilities for converting readily available bridged bicyclic compounds of definite configuration into substituted [*m*,*n*,0] bicycles of defined configurations.

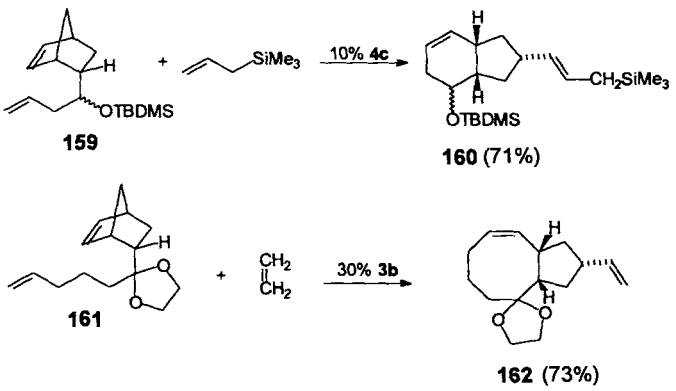

Scheme 46. Combined ring-opening/ring-closing cross-metathesis.

9. Reactions of Olefins on Solid Supports

In light of the increasing importance of combinatorial synthesis[204] for the development of biologically active substances, there is great interest in new synthetic methods on the surface of polymeric supports. The potential, especially of Grubbs's ruthenium catalysts, for the synthesis of highly functionalized heterocyclic structures by metathetic ring closures suggests applications that combine combinatorial construction of such structures with simultaneously variable modifications thereof.

Initial studies of ruthenium-catalyzed solid-phase synthesis of heterocyclic compounds demonstrate that such a concept may be feasible.[205] We prepared functionalized precursors, such as **165**, for the RCM by sequential coupling of a polymer-bound amino alcohol, an aldehyde, and a carbon nucleophile (Scheme 47). The ruthenium-catalyzed cyclization can be carried out successfully on the polymer with high yields (>90%). By varying the individual components, it is possible to obtain differently substituted rings of various sizes.

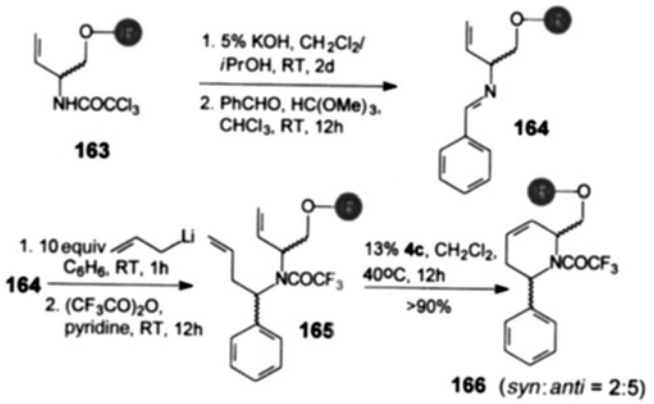

Scheme 47. Synthesis of α,α'-disubstituted tetrahydropyridine **166** by ruthenium-catalyzed RCM (R = trityl polystyrene, 1% DVB).

Grubbs and co-workers used a tentacle polymer bound hexapeptide with two olefinic side chains as the substrate for ruthenium-catalyzed ring-closing reactions.[206] As previously observed in solution,[131] a macrocyclic structure was obtained which represents the redox-stable analogue of a loop of glutaredoxin stabilized by a disulfide bond. The avoidance of solubility problems represents a significant advantage of the cyclization of peptide systems on polymers.

A cyclizing cleavage from the support was presented by van Maarseveen et al (Scheme 48).[207] The double bond, which functions as the linker between the resin and the component to be cleaved, is also involved in the ruthenium-catalyzed cyclization of polymer-bound **167**. This cleavage method provides the

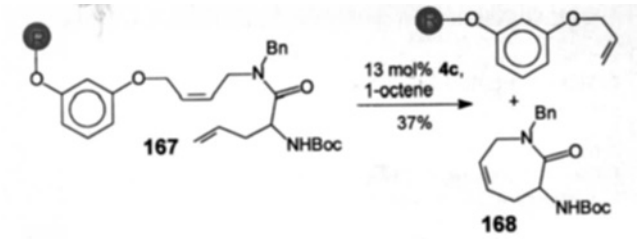

Scheme 48. Cyclizing cleavage of polymer-bound diolefin **167** by ruthenium-catalyzed RCM (R = methylene polystyrene, 1% DVB).

concept of a "traceless" linker,[208, 209] that is, no additional polar functionalities are needed to create the link to the support. Furthermore, the cyclizing cleavage provides very pure products if the terminal double bond necessary for RCM is introduced in the last reaction step.

The catalytic performance of the cyclizing cleavage requires the use of olefinic cofactors such as ethylene or 1-octene, which can guarantee in an exchange reaction the renewed mobility of the metal that remains on the resin after cleavage. In contrast to cyclizing cleavage, when using the diolefinic linker shown in Scheme 49, the resulting cyclic compounds remain attached to

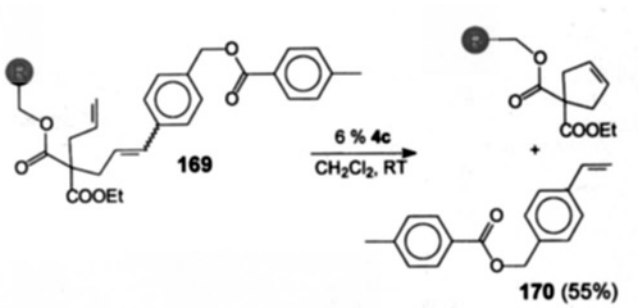

Scheme 49. Cleavage of the styrene derivative **170** by ruthenium-catalyzed cyclization of a diolefinic linker (R = polystyrene, 1% DVB).

the support.[210] Under the very mild metathesis conditions, the linker is catalytically cleaved by C–C bond breakage. The driving force of this reaction is the high tendency of formation of the resulting five-membered ring.

The interest of our group focuses not only on the ring-closing reaction but also especially on cross-metathesis with inclusion of olefinic supports. First experiments have shown that cross-metathesis between a soluble olefin and an immobilized olefin can be carried out with good yields.[205] The prerequisite for such reactions is the careful optimization of the reaction system to suppress the macrocyclic ring-closing reaction on the polymer surface. The allylsilyl polymer **171** shown in Scheme 50 can be attacked by electrophiles in solution under C–Si bond breakage (Sakurai conditions) after a terminal olefin has been catalytically attached. Since the electrophilic attack can occur either inter- or intramolecularly, a large number of open-chain as well as cyclic products of type **173** are easily accessible.[211]

The studies performed to date have shown that olefin metathesis reactions can also be carried out on polymeric supports with high yields. The potential application spectrum of metathesis ranges from binding of olefins over their further modification on the support to cleavage of the products.

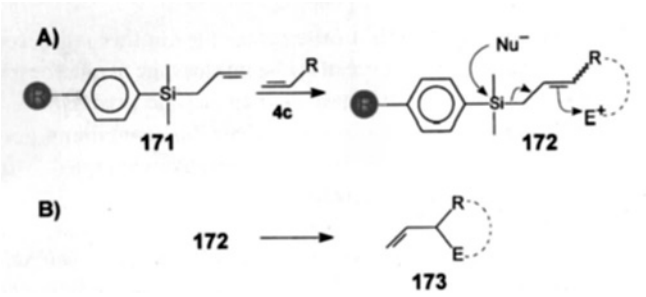

Scheme 50. General scheme of A) ruthenium-catalyzed coupling of terminal olefins onto allylsilylpolystyrene (**171**) and B) inter- and intramolecular electrophilic cleavage of polymer-bound allyl silane (**172**, R = polystyrene, 1% DVB).

10. Summary and Outlook

The results discussed herein show that olefin metathesis has proven to be an efficient synthetic method, especially for the preparation of rings. Initial investigations in other areas such as the selective cross-coupling or asymmetric synthesis show promising results for future developments. For the establishment of this reaction as a broadly applicable method, however, much work remains to be done. Fundamentals have been established for the mechanistic understanding of these reactions; these, however, are still insufficient for predicting and directing chemo- and stereoselectivities. A lucrative goal is to establish metathesis as a widely applicable method for the wasteless and atom economical stereoselective synthesis of olefins. Enhanced activities can be expected in the area of olefin metathesis in the near future. The recently seen developmental rush caused by the new generation of catalysts will most likely continue. Application opportunities in organic synthesis will continue to grow, as we can count on the future development of even more active and tolerant metal complexes.

Addendum

Since submission of this review, several new publications regarding mechanistic and applied aspects of olefin metathesis have appeared. In the following, important contributions are supplemented without claiming completeness (state as of August 1997).

Investigations performed by Grubbs and co-workers[212] on the reaction mechanism justify the conclusion that catalysis by **4** is accompanied by dissociation of one phosphane ligand from the metal center. This is strongly supported by the recent isolation and characterization of a ruthenium–carbene intermediate by Snapper et al., in which one phosphane ligand is replaced by a double bond.[213] Several authors described the application of ring-closing metathesis for preparing small, polar molecules (e. g. from amino acids or β-lactams).[214–218] Fürstner et al. achieved ring closure to the ten-membered jasmine ketolactone.[219] Exploitation of templating effects has enabled the synthesis of unsaturated crown ethers as well as [*n*]catenanes[220] and topologically related systems.[221] Besides novel cross-metatheses,[222] ring-opening[223,224] and tandem reactions[225] have been reported. Noteworthy is a combinatorial approach for preparing epothilone derivatives devised by Nicolaou et al., in which the key step is cyclizing cleavage of a highly function-

alized precursor assembled on a resin.[226] Another study concentrates on the dependence of cyclizing cleavage of macrocyclic peptides on the conformation of their acyclic precursors.[227] The preparations of thymine- and penicilline-containing polymers[228, 229] are mentioned as representative examples in the area of metathesis polymerization.

We thank the co-workers listed in the references for their valuable contributions and efforts, and the Fonds der Chemischen Industrie for financial support.

Received: March 10, 1997 [A 218 IE]
German version: *Angew. Chem.* **1997**, *109*, 2124–2145
Translated by Dr. Detlef Klingberg, Toledo, OH (USA)

[1] A. W. Anderson, M. G. Merckling (du Pont de Nemours & Co.), US-A 2721189, **1955** [*Chem. Abstr.* **1955**, *50*, 3008i].
[2] R. L. Banks, G. C. Bailey, *Ind. Eng. Chem. Process Des. Dev.* **1964**, *3*, 170.
[3] G. Natta, G. Dall'Asta, G. Mazzanti, G. Mortoni, *Makromol. Chem.* **1963**, *69*, 163.
[4] G. Natta, G. Dall'Asta, G. Mazzanti, *Angew Chem.* **1964**, *76*, 765; *Angew. Chem. Int. Ed. Engl.* **1964**, *3*, 723.
[5] G. Natta, G. Dall'Asta, I. W. Bassi, G. Carella, *Makromol. Chem.* **1966**, *91*, 87.
[6] N. Calderon, *Acc. Chem. Res.* **1972**, *5*, 127.
[7] N. Calderon, H. Y. Chen, K. W. Scott, *Tetrahedron Lett.* **1967**, 3327.
[8] N. Calderon, E. A. Ofstead, J. P. Ward, W. A. Judy, K. W. Scott, *J. Am. Chem. Soc.* **1968**, *90*, 4133.
[9] J. C. Mol, J. A. Moulijn, C. Boelhouwer, *Chem. Commun.* **1968**, 633.
[10] C. P. C. Bradshaw, E. J. Howman, L. Turner, *J. Catal.* **1967**, *7*, 269.
[11] G. S. Lewandos, R. Pettit, *Tetrahedron Lett.* **1971**, 789.
[12] R. H. Grubbs, T. K. Brunck, *J. Am. Chem. Soc.* **1972**, *94*, 2538.
[13] J. L. Herisson, Y. Chauvin, *Makromol. Chem.* **1970**, *141*, 161.
[14] N. Calderon, E. A. Ofstead, W. A. Judy, *Angew. Chem.* **1976**, *88*, 433; *Angew. Chem. Int. Ed. Engl.* **1976**, *15*, 401.
[15] R. H. Grubbs, *J. Organomet. Chem. Libr.* **1976**, *1*, 423.
[16] T. J. Katz, *Adv. Organomet. Chem.* **1978**, *16*, 283.
[17] R. H. Grubbs, W. Thomas *Science* **1989**, *243*, 907.
[18] S. Warwel, *Nachr. Chem. Tech. Lab.* **1992**, *40*, 314.
[19] Phillips Petroleum Company, *Hydrocarbon Process* **1967**, *46*, 232.
[20] E. R. Freitas, C. R. Gum, *Chem. Eng. Prog.* **1979**, *75*, 73.
[21] Shell International Chemical Company, *SHOP-Linear Alpha Olefins* (company publication), **1982**.
[22] W. A. Herrmann, *Kontakte (Darmstadt)* **1991**, *3*, 29.
[23] R. F. Ohm, *Chemtech* **1980**, 198.
[24] A. Dräxler, *Lichtbogen* **1980**, *29*, 4.
[25] A. Dräxler, A. Konietzny, *Lichtbogen* **1986**, *35*, 24.
[26] R. L. Banks, D. S. Banasiak, P. S. Hudson, J. R. Norell, *J. Mol. Catal.* **1982**, *15*, 21.
[27] R. L. Banks in *Applied Industrial Catalysis, Vol. 2* (Ed.: B. E. Leach), Academic Press, New York, **1984**, p. 215.
[28] J. C. Mol, *J. Mol. Catal.* **1994**, *90*, 185.
[29] R. H. A. Bosma, F. van den Aardweg, J. C. Mol, *J. Chem. Soc. Chem. Commun.* **1981**, 1132.
[30] S. Warwel, A. Deckers, *Tenside Surfactants Deterg.* **1989**, *26*, 252.
[31] S. Warwel, H.-G. Jägers, S. Thomas, *Fett Wiss. Technol.* **1992**, *94*, 323.
[32] E. Sh. Finkel'shtein, V. I. Bykov, E. B. Portnykh, *J. Mol. Catal.* **1992**, *76*, 33.
[33] M. Biermann, *Methoden Org. Chem. (Houben-Weyl) 4th ed. 1952–* Bd. 1 E18/2, **1986**, p. 1163.
[34] R. H. Grubbs, *J. Macromol. Sci. Chem.* **1994**, *A31*(11), 1829.
[35] R. R. Schrock, *Pure Appl. Chem.* **1994**, *66*, 1447
[36] K. J. Ivin, J. C. Mol, *Olefin Metathesis and Metathesis Polymerisation*, Academic Press, New York, **1997**.
[37] H. Yoshida, T. Tanaka, S. Matsuo, T. Funabiki, S. Yoshida, *J. Chem. Soc. Chem. Commun.* **1995**, 761.
[38] A. Mühlebach, P. Bernhard, N. Bühler, T. Karlen, A. Ludi, *J. Mol. Catal.* **1994**, *90*, 143.
[39] B. M. Novak, R. H. Grubbs, *J. Am. Chem. Soc.* **1988**, *110*, 960.
[40] W. A. Herrmann, J. G. Kuchler, J. K. Felixberger, E. Herdtweck, W. Wagner, *Angew. Chem.* **1988**, *100*, 420; *Angew. Chem. Int. Ed. Engl.* **1988**, *27*, 394.
[41] W. A. Herrmann, F. E. Kühn, E. W. Fischer, W. R. Thiel, C. C. Romao, *Inorg. Chem.* **1992**, *31*, 4431.
[42] W. A. Herrmann, W. Wagner, U. N. Flessner, U. Volkhardt, H. Komber, *Angew. Chem.* **1991**, *103*, 1704; *Angew. Chem. Int. Ed. Engl.* **1991**, *30*, 1636.
[43] W. A. Herrmann, A. W. Stumpf, T. Priermeier, S. Bogdanovic, V. Dufaud, J.-M. Basset, *Angew. Chem.* **1996**, *108*, 2978; *Angew. Chem. Int. Ed. Engl.* **1996**, *35*, 2803.
[44] J. Kress, J. A. Osborn, V. Amir-Ebrahimi, K. J. Ivin, J. J. Rooney, *J. Chem. Soc. Chem. Commun.* **1988**, 1164.
[45] K. J. Ivin, J. Kress, J. A. Osborn, *J. Mol. Catal.* **1988**, *46*, 351.
[46] R. M. E. Greene, K. J. Ivin, J. J. Rooney, J. Kress, J. A. Osborn, *Makromol. Chem.* **1988**, *189*, 2797.
[47] R. M. E. Greene, , K. J. Ivin, J. Kress, J. A. Osborn, J. J. Rooney, *Br. Polym. J.* **1989**, *21*, 237.
[48] J. Kress, J. A. Osborn, K. J. Ivin, *J. Chem. Soc. Chem. Commun.* **1989**, 1234.
[49] C. J. Schaverien, J. C. Dewan, R. R. Schrock, *J. Am. Chem. Soc.* **1986**, *108*, 2771.
[50] R. R. Schrock, J. Feldman, L. F. Cannitzo, R. H. Grubbs, *Macromolecules* **1987**, *20*, 1172.
[51] R. R. Schrock, S. A. Krouse, K. Knoll, J. Feldman, J. S. Murdzek, D. C. Yang, *J. Mol. Catal.* **1988**, *46*, 243.
[52] R. R. Schrock, R. T. DePue, J. Feldman, C. J. Schaverien, J. C. Dewan, A. H. Liu, *J. Am. Chem. Soc.* **1988**, *110*, 1423.
[53] R. R. Schrock, *Acc. Chem. Res.* **1990**, *23*, 158.
[54] R. R. Schrock, J. S. Murdzek, G. C. Bazan, J. Robbins, M. DiMare, M. O'Regan, *J. Am. Chem. Soc.* **1990**, *112*, 3875.
[55] S. T. Nguyen, L. K. Johnson, R. H. Grubbs, *J. Am. Chem. Soc.* **1992**, *114*, 3974.
[56] S. T. Nguen, R. H. Grubbs, J. W. Ziller, *J. Am. Chem. Soc.* **1993**, *115*, 9858.
[57] P. Schwab, M. B. France, J. W. Ziller, R. H. Grubbs, *Angew. Chem.* **1995**, *107*, 2179; *Angew. Chem. Int. Ed. Engl.* **1995**, *34*, 2039.
[58] P. Schwab, R. H. Grubbs, J. W. Ziller, *J. Am. Chem. Soc.* **1996**, *118*, 100.
[59] W. A. Herrmann, W. C. Schattenmann, O. Nuyken, S. C. Glander, *Angew. Chem.* **1996**, *108*, 1169; *Angew. Chem. Int. Ed. Engl.* **1996**, *36*, 1087.
[60] S. T. Nguyen, R. H. Grubbs, *J. Organomet. Chem.* **1995**, *497*, 195.
[61] A. Hafner, P. A. van der Schaaf, A. Mühlebach, *Chimia* **1996**, *50*, 131.
[62] F. Stelzer, *J. Macromol. Sci. Chem.* **1996**, *A33*(7), 941.
[63] W. J. Feast, E. Khosravi in *New Methods Polym. Synth.* (Eds.: J. R. Ebdon, G. C. Eastmond), Blackie, Glasgow, **1995**, p. 69.
[64] W. J. Feast, V. C. Gibson, E. Khosravi, E. L. Marshall, B. Wilson, *Ziegler Catal.* **1995**, 469.
[65] V. C. Gibson, C. Verno, *Adv. Mater.* **1994**, *6*, 37.
[66] R. R. Schrock in *Ring-Opening Polym.* (Ed.: D. J. Brunelle), Hanser, München, **1993**, p. 129.
[67] "Olefin Metathesis and Polymerisation Catalysts": Y. Imamoglu, B. Zümreoglu-Karan, A. J. Amass, *NATO ASI Ser. Ser. C* **1990**, *326*, 571.
[68] W. A. Nugent, J. M. Mayer, *Metal-Ligand Multiple Bonds*, Wiley, New York, **1988**.
[69] G. Bazan, R. R. Schrock, *Macromolecules* **1991**, *24*, 817.
[70] M. Lindmark-Hamberg, K. B. Wagener, *Macromolecules* **1987**, *20*, 2951.
[71] K. B. Wagener, D. W. Smith, Jr. *Macromolecules* **1991**, *24*, 6073.
[72] K. B. Wagener, K. Brzwzinska, *Macromolecules* **1991**, *24*, 5273.
[73] J. T. Patton, J. M. Boncella, K. B. Wagener, *Macromolecules* **1992**, *25*, 3862.
[74] K. B. Wagener, J. T. Patton, *Macromolecules* **1993**, *26*, 249.
[75] D. W. Smith, Jr, K. B. Wagener, *Macromolecules* **1993**, *26*, 1633.
[76] D. Tao, K. B. Wagener, *Macromolecules* **1994**, *27*, 1281.
[77] K. B. Wagener, J. G. Nel, J. Konzelman, J. M. Boncella, *Macromolecules* **1990**, *23*, 5155.
[78] K. B. Wagener, J. M. Boncella, J. G. Nel, *Macromolecules* **1991**, *24*, 2649.
[79] T. Masuda, T. Higashimura, *Acc. Chem. Res.* **1984**, *17*, 51.
[80] T. Masuda, T. Higashimura, *Adv. Polym. Sci.* **1987**, *81*, 121.
[81] R. Schlund, R. R. Schrock, W. E. Crowe, *J. Am. Chem. Soc.* **1989**, *111*, 8004.
[82] S. H. Jin, S. H. Kim, H. N. Cho, S. K. Choi, *Macromolecules* **1991**, *24*, 6050.
[83] S. H. Jin, S. W. Kang, J. G. Park, J. C. Lee, K. S. Choi, *J. Macromol. Sci. Chem.* **1995**, *A32*(3), 455.
[84] H. K. Ahn, Y.-H. Kim, S. H. Jin, S. K. Choi, *Polym. Bull.* **1992**, *29*, 625.
[85] Y. S. Gal, S. K. Choi, *J. Polym. Sci. Part A Polym. Chem.* **1993**, *31*, 345.
[86] S. H. Jin, H. N. Cho, S. K. Choi, *J. Polym. Sci. Part A Polym. Chem.* **1993**, *31*, 69.
[87] J. W. Park, J. H. Lee, H. N. Cho, S. K. Choi, *Macromolecules* **1993**, *26*, 1191.
[88] K. M. Koo, S. H. Han, Y. S. Kang, U. Y. Kim, S. K. Choi, *Macromolecules* **1993**, *26*, 2485.
[89] R. Tassoni, R. R. Schrock, *Chem. Mater.* **1994**, *6*, 744.
[90] J. N. C. Chan, R. R. Schrock, R. E. Cohen, *Chem. Mater.* **1993**, *5*, 566.
[91] V. Sankaran, J. Yue, R. E. Cohen, R. R. Schrock, R. J. Silbey, *Chem. Mater.* **1993**, *5*, 1133.
[92] J. Yue, V. Sankaran, R. E. Cohen, R. R. Schrock, *J. Am. Chem. Soc.* **1993**, *115*, 4409.
[93] J. N. C. Chan, G. S. W. Craig, R. R. Schrock, R. E. Cohen, *Chem. Mater.* **1992**, *4*, 885.
[94] J. N. C. Chan, R. R. Schrock, R. E. Cohen, *Chem. Mater.* **1992**, *4*, 24.
[95] M. M. Rock, T. H. Jozefiak, R. H. Grubbs, *Polym. Prepr.* **1993**, *34*, 358.
[96] G. C. Bazan, M. S. Wrighton, R. R. Schrock, *J. Am. Chem. Soc.* **1992**, *114*, 4150.
[97] D. Albagli, G. C. Bazan, R. R. Schrock, M. S. Wrighton, *J. Am. Chem. Soc.* **1993**, *115*, 7328.
[98] Z. Komiya, R. R. Schrock, *Macromolecules* **1993**, *26*, 1387.
[99] Z. Komiya, R. R. Schrock, *Macromolecules* **1993**, *26*, 1393.

[100] M. Weck, B. R. Maughon, B. Mohr, R. H. Grubbs, *Polym Prepr.* **1996**, *37*, 587.
[101] G. Widawski, W. J. Feast, P. Dounis, *J. Mater. Chem.* **1995**, *5*, 1847.
[102] M. Ungerank, B. Winkler, E. Eder, F. Stelzer, *Macromol. Chem. Phys.* **1995**, *196*, 3623.
[103] C. Pugh, *Macromol. Symp.* **1994**, *77*, 325.
[104] C. Pugh, R. R. Schrock, *Polym. Prepr.* **1993**, *34*, 18.
[105] D. M. Walba, P. Keller, R. Shao, N. A. Clark, M. Hillmyer, R. H. Grubbs, *J. Am. Chem. Soc.* **1996**, *118*, 2740.
[106] C. Fraser, R. H. Grubbs, *Macromolecules* **1995**, *28*, 7248.
[107] D. M. Lynn, S. Kanaoka, R. H. Grubbs, *J. Am. Chem. Soc.* **1996**, *118*, 784.
[108] W. J. Feast, V. C. Gibson, E. L. Marshal, *J. Chem. Soc. Chem. Commun.* **1992**, 1157.
[109] G. C. Bazan, E. Khosravi, R. R. Schrock, W. J. Feast, V. C. Gibson, M. B. O'Regan, J. K. Thomas, W. M. Davies, *J. Am. Chem. Soc.* **1990**, *112*, 8378.
[110] D. H. McConville, J. R. Wolf, R. R. Schrock, *J. Am. Chem. Soc.* **1993**, *115*, 4413.
[111] T. Karlen, A. Ludi, A. Mühlebach, P. Bernhard, C. Pharisa, *J. Polym. Sci. Part A Polym. Chem.* **1995**, *33*, 1665.
[112] P. A. van der Schaaf, A. Hafner, A. Mühlebach, *Angew. Chem.* **1996**, *108*, 1974; *Angew. Chem. Int. Ed. Engl.* **1996**, *35*, 1845.
[113] J. Tsuji, S. Hashiguchi, *Tetrahedron Lett.* **1980**, *21*, 2955.
[114] D. Villemin, *Tetrahedron Lett.* **1980**, *21*, 1715.
[115] E. Sh. Finkel'shtein, N. V. Ushakov, E. B. Portnykh, *J. Mol. Catal.* **1992**, *76*, 133.
[116] M. D. E. Forbes, J. T. Patton, T. L. Myers, H. D. Maynard, D. W. Smith, Jr., G. R. Schulz, K. B. Wagener, *J. Am. Chem. Soc.* **1992**, *114*, 10978.
[117] S. Blechert, unpublished results.
[118] M. T. Crimmins, B. W. King, *J. Org. Chem.* **1996**, *61*, 4192.
[119] L. R. Sita, *Macromolecules* **1995**, *28*, 656.
[120] H. Junga, S. Blechert, *Tetrahedron Lett.* **1993**, *34*, 3731.
[121] M. F. Schneider, H. Junga, S. Blechert, *Tetrahedron* **1995**, *51*, 13003.
[122] G. C. Fu, S. T. Nguyen, R. H. Grubbs, *J. Am. Chem. Soc.* **1993**, *115*, 9856.
[123] G. C. Fu, R. H. Grubbs, *J. Am. Chem. Soc.* **1992**, *114*, 5426.
[124] O. Fujimura, G. C. Fu, R. H. Grubbs, *J. Org. Chem.* **1994**, *59*, 4029.
[125] T. Okazoe, K. Takai, K. Oshima, K. Utimoto, *J. Org. Chem.* **1987**, *52*, 4410.
[126] S. H. Pine, R. Zahler, D. A. Evans, R. H. Grubbs, *J. Am. Chem. Soc.* **1980**, *102*, 3270.
[127] K. C. Nicolaou, M. H. D. Postema, C. Claiborne, *J. Am. Chem. Soc.* **1996**, *118*, 1565.
[128] K. C. Nicolaou, M. H. D. Postema, E. W. Yue, A. Nadin, *J. Am. Chem. Soc.* **1996**, *118*, 10335.
[129] J. S. Clark, J. G. Kettle, *Tetrahedron Lett.* **1997**, *38*, 123.
[130] G. C. Fu, R. H. Grubbs, *J. Am. Chem. Soc.* **1992**, *114*, 7324.
[131] S. J. Miller, R. H. Grubbs, *J. Am. Chem. Soc.* **1995**, *117*, 5855.
[132] C. M. Huwe, O. C. Kiehl, S. Blechert, *Synlett* **1996**, *1*, 65.
[133] F. P. J. T. Rutjes, H. E. Schoemaker, *Tetrahedron Lett.* **1997**, *38*, 677.
[134] F. Garro-Hélion, F. Guibé, *Chem. Commun.* **1996**, 641.
[135] S. F. Martin, H.-J. Chen, A. K. Courtney, Y. Liao, M. Pätzel, M. N. Ramser, A. S. Wagman, *Tetrahedron* **1996**, *52*, 7251.
[136] C. M. Huwe, S. Blechert, *Tetrahedron Lett.* **1995**, *36*, 1621.
[137] M. Leconte, I. Jourdan, S. Pagano, F. Lefebvre, J.-M. Basset, *J. Chem. Soc. Chem. Commun.* **1995**, 857.
[138] J.-L. Couturier, K. Tanaka, M. Leconte, J.-M. Basset, J. Ollivier, *Angew. Chem.* **1993**, *105*, 99; *Angew. Chem. Int. Ed. Engl.* **1993**, *32*, 112.
[139] S. K. Armstrong, B. A. Christie, *Tetrahedron Lett.* **1996**, *37*, 9373.
[140] T. J. Katz, T. M. Sivavec, *J. Am. Chem. Soc.* **1985**, *107*, 737.
[141] S. Watanuki, N. Ochifuji, M. Mori, *Organometallics* **1995**, *14*, 5062.
[142] S. Watanuki, N. Ochifuji, M. Mori, *Organometallics* **1994**, *13*, 4129.
[143] A. Kinoshita, M. Mori, *Synlett* **1994**, 1020.
[144] N. Chatani, T. Morimoto, T. Muto, S. Murai, *J. Am. Chem. Soc.* **1994**, *116*, 6049.
[145] G. C. Fu, R. H. Grubbs, *J. Am. Chem. Soc.* **1993**, *115*, 3800.
[146] R. R. Schrock, R. T. DePue, J. Feldman, C. J. Schaverien, J. C. Dewan, A. H. Liu, *J. Am. Chem. Soc.* **1988**, *110*, 1423.
[147] S. J. Miller, S.-H. Kim, Z.-R. Chen, R. H. Grubbs, *J. Am. Chem. Soc.* **1995**, *117*, 2108.
[148] S. F. Martin, Y. Liao, Y. Wong, T. Rein, *Tetrahedron Lett.* **1994**, *35*, 691.
[149] S. F. Martin, A. S. Wagman, *Tetrahedron Lett.* **1995**, *36*, 1169.
[150] J. D. Winkler, J. E. Stelmach, J. Axten, *Tetrahedron Lett.* **1996**, *37*, 4317.
[151] S. Blechert, M. Wenz, unpublished results.
[152] A. G. M. Barrett, S. P. D. Baugh, V. C. Gibson, M. R. Giles, E. L. Marshall, P. A. Procopiou, *Chem. Commun.* **1996**, 2231.
[153] J. S. Clark, J. G. Kettle, *Tetrahedron Lett.* **1997**, *38*, 127.
[154] B. C. Borer, S. Deerenberg, H. Bieräugel, U. K. Pandit, *Tetrahedron Lett.* **1994**, *35*, 3191.
[155] A. Fürstner, K. Langemann, *J. Org. Chem.* **1996**, *61*, 3942.
[156] B. König, C. Horn, *Synlett* **1996**, 1013.
[157] E. Wassermann, D. A. Ben-Efraim, R. Wolovski, *J. Am. Chem. Soc.* **1968**, *90*, 3286.
[158] G.-J. M. Gruter, O. S. Akkerman, F. Bickelhaupt, *Tetrahedron* **1996**, *52*, 2565.
[159] M. A. McKervey, M. Pitarch, *Chem. Commun.* **1996**, 1689.
[160] T. D. Clark, M. R. Ghadiri, *J. Am. Chem. Soc.* **1995**, *117*, 12364.
[161] O. Fujimura, R. H. Grubbs, *J. Am. Chem. Soc.* **1996**, *118*, 2499.
[162] C. M. Huwe, J. Velder, S. Blechert *Angew. Chem.* **1996**, *108*, 2542; *Angew. Chem. Int. Ed. Engl.* **1996**, *35*, 2376.
[163] C. M. Huwe, S. Blechert, *Synthesis* **1997**, 61.
[164] H. S. Overkleeft, U. K. Pandit, *Tetrahedron Lett.* **1996**, *37*, 547.
[165] S. Hölder, S. Blechert, *Synlett* **1996**, 505.
[166] A. Kinoshita, M. Mori, *J. Org. Chem.* **1996**, *61*, 8356.
[167] A. Fürstner, K. Langemann, *J. Org. Chem.* **1996**, *61*, 8746.
[168] A. Fürstner, N. Kindler, *Tetrahedron Lett.* **1996**, *37*, 7005.
[169] A. F. Houri, Z. Xu, D. A. Kogan, A. H. Hoveyda, *J. Am. Chem. Soc.* **1995**, *117*, 2943.
[170] Z. Xu, C. W. Johannes, S. S. Salman, A. H. Hoveyda, *J. Am. Chem. Soc.* **1996**, *118*, 10926.
[171] K. Gerth, N. Bedorf, G. Höfle, H. Irschik, H. Reichenbach, *J. Antibiot.* **1996**, *49*, 560.
[172] Z. Yang, Y. He, D. Vourloumis, H. Vallberg, K. C. Nicolaou, *Angew. Chem.* **1997**, *109*, 170; *Angew. Chem. Int. Ed. Engl.* **1997**, *36*, 166.
[173] D. Schinzer, A. Limberg, A. Bauer, O. M. Böhm, M. Cordes, *Angew. Chem.* **1997**, *109*, 543; *Angew. Chem. Int. Ed. Engl.* **1997**, *36*, 523.
[174] D. Meng, D.-S. Su, A. Balog, P. Bertinato, E. J. Sorensen, S. J. Danishefsky, H.-H. Zheng, T.-C. Chou, L. He, S. B. Horwitz, *J. Am. Chem. Soc.* **1997**, *119*, 2733.
[175] B. Marciniec, J. Gulinski, *J. Organomet. Chem.* **1984**, *266*, C19.
[176] B. Marciniec, Maciejewski, J. Gulinski, Z. Rzejak, *J. Organomet. Chem.* **1989**, *362*, 273.
[177] B. Marciniec, C. Pietraszuk, Z. Foltynowicz, *J. Organomet. Chem.* **1994**, *474*, 83.
[178] B. Marciniec, L. Rzejak, J. Gulinski, Z. Foltynowicz, W. Urbaniak, *J. Mol. Catal.* **1988**, *46*, 329.
[179] Z. Foltyniwics, B. Marciniec, *J. Organomet. Chem.* **1989**, *376*, 15.
[180] Z. Foltynowics, B. Marciniec, C. Pietraszuk, *J. Mol. Catal.* **1991**, *65*, 113.
[181] B. Marciniec, C. Pietraszuk, *J. Organomet. Chem.* **1993**, *447*, 163.
[182] W. E. Crowe, Z. J. Zhang, *J. Am. Chem. Soc.* **1993**, *115*, 10998.
[183] W. E. Crowe, D. R. Goldberg, *J. Am. Chem. Soc.* **1995**, *117*, 5162.
[184] W. E. Crowe, D. R. Goldberg, Z. J. Zhang, *Tetrahedron Lett.* **1996**, *37*, 2117.
[185] O. Brümmer, A. Rückert, S. Blechert, *Chem. Eur. J.* **1997**, *3*, 441.
[186] I. Fleming, J. Dunogues, R. Smithers, *Org. React.* **1989**, *37*, 57.
[187] D. Schinzer, *Synthesis* **1988**, 263.
[188] J. Feng, M. Schuster, S. Blechert, *Synlett* **1997**, 129.
[189] H. Yatagi, Y. Yamamoto, K. Maruyama, *J. Am. Chem. Soc.* **1980**, *102*, 4548.
[190] Y. Yamamoto, *Acc. Chem. Res.* **1987**, *20*, 243.
[191] G. E. Keck, J. B. Yates, *J. Am. Chem. Soc.* **1982**, *104*, 5829.
[192] M. Schuster, R. Stragies, S. Blechert, unpublished results.
[193] P. J. Spendley, P. M. Bird, J. P. Ride, D. P. Leworthy, *Phytochemistry* **1982**, *21*, 2403.
[194] M. F. Schneider, S. Blechert, *Angew. Chem.* **1996**, *108*, 479; *Angew. Chem. Int. Ed. Engl.* **1996**, *35*, 411.
[195] N. B. Bespalova, M. A. Bovina, M. B. Sergeeva, V. D. Oppengeim, V. G. Zaikin, *J. Mol. Catal.* **1994**, *90*, 21.
[196] M. F. Schneider, N. Lucas, J. Velder, S. Blechert, *Angew. Chem. Int. Ed. Engl.* **1997**, *109*, 257; *Angew. Chem. Int. Ed. Engl.* **1997**, *36*, 257.
[197] M. L. Randall, J. A. Tallarico, M. L. Snapper, *J. Am. Chem. Soc.* **1995**, *117*, 9610.
[198] L. F. Tietze, U. Beifuss, *Angew. Chem.* **1993**, *105*, 137; *Angew. Chem. Int. Ed. Engl.* **1993**, *32*, 131.
[199] S.-H. Kim, N. Bowden, R. H. Grubbs, *J. Am. Chem. Soc.* **1994**, *116*, 10801.
[200] S.-H. Kim, W. J. Zuercher, N. B. Bowden, R. H. Grubbs, *J. Org. Chem.* **1996**, *61*, 1073.
[201] W. J. Zuercher, M. Hashimoto, R. H. Grubbs, *J. Am. Chem. Soc.* **1996**, *118*, 6634.
[202] S. Kannenberg, Diplomarbeit, Technische Universität Berlin, **1997**.
[203] R. Stragies, Diplomarbeit, Technische Universität Berlin, **1997**.
[204] F. Balkenhohl, C. von dem Bussche-Hühnefeld, A. Lansky, Z. Zechel, *Angew. Chem.* **1996**, *108*, 2436; *Angew. Chem. Int. Ed. Engl.* **1996**, *35*, 2288.
[205] M. Schuster, J. Pernerstorfer, S. Blechert, *Angew. Chem.* **1996**, *108*, 2111; *Angew. Chem. Int. Ed. Engl.* **1996**, *35*, 1979.
[206] S. Miller, H. E. Blackwell, R. H. Grubbs, *J. Am. Chem. Soc.* **1996**, *118*, 9606.
[207] J. H. van Maarseveen, J. A. J. den Hartog, V. Engelen, G. Visser, C. G. Kruse, E. Finner, *Tetrahedron Lett.* **1996**, *37*, 8249.
[208] M. J. Plunkett, J. A. Ellman, *J. Org. Chem.* **1995**, *60*, 6006.
[209] B. Chenera, J. A. Finkelstein, D. F. Veber, *J. Am. Chem. Soc.* **1995**, *117*, 11999.
[210] J. Peters, S. Blechert, *Synlett* **1997**, 348.
[211] M. Schuster, N. Lucas, S. Blechert, *Chem. Commun.* **1997**, 823.
[212] E. L. Dias, S. T. Nguyen, R. H. Grubbs, *J. Am. Chem. Soc.* **1997**, *119*, 3887.
[213] J. A. Tallarico, P. J. Bonitatebus, Jr., M. L. Snapper, *J. Am. Chem. Soc.* **1997**, *119*, 7157.

[214] K. Hammer, K. Undheim, *Tetrahedron* **1997**, *53*, 2309.
[215] K. Hammer, K. Undheim, *Tetrahedron* **1997**, *53*, 10603.
[216] A. G. M. Barrett, S. P. D. Baugh, D. C. Braddock, K. Flack, V. C. Gibson, P. A. Procopiou, *Chem. Commun.* **1997**, 1375.
[217] A. B. Dyatkin, *Tetrahedron Lett.* **1997**, *38*, 2065.
[218] S. Chang, R. H. Grubbs, *Tetrahedron Lett.* **1997**, *38*, 4757.
[219] A. Fürstner, T. Müller, *Synlett* **1997**, 1010.
[220] M. J. Marsella, H. D. Maynard, R. H. Grubbs, *Angew. Chem.* **1997**, *109*, 1147; *Angew. Chem. Int. Ed. Engl.* **1997**, *36*, 1101.
[221] B. Mohr, M. Weck, J.-P. Sauvage, R. H. Grubbs, *Angew. Chem.* **1997**, *109*, 1365; *Angew. Chem. Int. Ed. Engl.* **1997**, *36*, 1308.
[222] S. E. Gibson, V. C. Gibson, S. K. Keen, *Chem. Commun.* **1997**, 1107.
[223] M. L. Snapper, J. A. Tallarico, M. L. Randall, *J. Am. Chem. Soc.* **1997**, *119*, 1478.
[224] G. D. Cuny, J. Cao, J. R. Hauske, *Tetrahedron Lett.* **1997**, *38*, 5237.
[225] J. P. A. Harrity, M. S. Visser, J. D. Gleason, A. H. Hoveyda, *J. Am. Chem. Soc.* **1997**, *119*, 1488.
[226] K. C. Nicolaou, N. Winssinger, J. Pastor, S. Nincovic, F. Sarabia, Y. He, D. Vourloumis, Z. Yang, T. Li, P. Giannakakou, E. Hamel, *Nature* **1997**, *387*, 268.
[227] J. Pernerstorfer, M. Schuster, S. Blechert, *Chem. Commun.* **1997**, in press.
[228] V. C. Gibson, E. L. Marshall, M. North, D. A. Robson, P. J. Williams, *Chem. Commun.* **1997**, 1095.
[229] S. C. G. Biagini, V. C. Gibson, M. R. Giles, E. L. Marshall, M. North, *Chem. Commun.* **1997**, 1097.

Chemistry at the crossroads

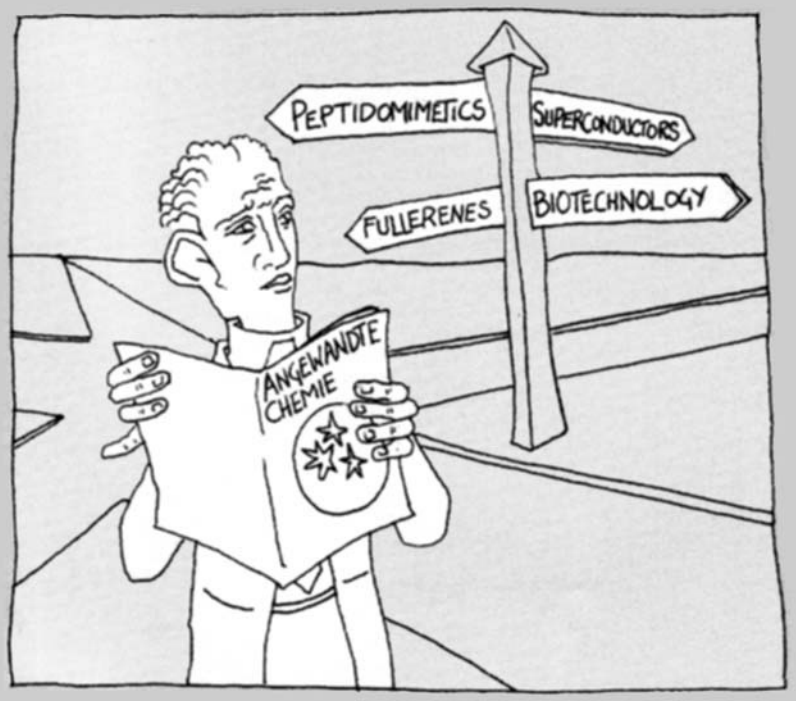

Pioneering scientists guide your way through newly charted territory with their topical reviews and discriminating highlights in **Angewandte Chemie.**

To start your own personal subscription, just fax.

An order form is provided on the last page for your convenience.

WILEY-VCH

Fluorous Biphase Systems—The New Phase-Separation and Immobilization Technique

Boy Cornils*

Something new is afoot in chemistry: FBS (fluorous biphase systems) is a new phase-separation and immobilization technique which makes use of the restricted and thermally controllable solubility and miscibility of perfluorinated hydrocarbons (or derivatives such as ethers or tertiary amines) and organic liquids. The method was first used in reactions with FBS-compatible, homogeneous catalysts,[1, 2] and goes back to the unpublished thesis of M. Vogt,[1] who in 1991 attempted to utilize the solvophobic properties of perfluorinated ethers of the Hostinert 216 type (structure **1**) and homogeneous catalysts dissolved therein for phase separation after successful homogeneous catalysis.

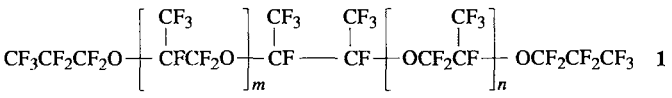

1

The actual "inventive" idea was to utilize "... the high chemical inertness of such perfluorinated compounds ..."[1] to create a medium for a variety of homogeneously catalyzed reactions, and to modify the homogeneous catalysts needed by introducing perfluorinated groups into their ligand sphere in order to make them soluble in the perfluorinated ethers. At elevated temperatures the biphase system, which contains the corresponding modified complex catalysts and the organic reactants, forms a single phase and thus provides the best conditions for the desired reaction. Since the reaction system is again biphasic upon subsequent cooling, organic reaction products and the catalysts dissolved in the FBS can be readily separated ("thermal regulation", see Figure 2). As with the oxo process of Ruhrchemie/Rhône-Poulenc[3] or the SHOP process of Shell,[4] this would have made it possible to convert the homogeneous catalyst into a "heterogenized" form and to immobilize it in an extremely effective and elegant way by means of simple phase separation without having to anchor the catalyst on solid supports (as has also been described for perfluoroalkyl-substituted supports[5]).

Following the old alchemist's rule "similia similibus solvuntur", which he cites, Vogt synthesized ligands based on hexafluoropropene oxide oligomers that gave transition metal complexes of Co, Ni, or Mn (structure **2**), which were active as

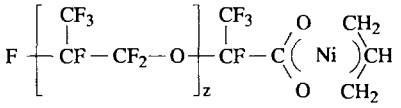

2

homogeneous catalysts and could be employed in the oxidation of cyclohexene, the polymerization and telomerization of butadiene, and the oligomerization of ethylene.

German theses which, as in the case of Vogt, do not lead to publications do not become internationally known. As a result, the phase properties of amphiphilic, perfluorinated species for solvophobic perfluorinated head groups and solvophilic hydrocarbon tail groups ("bilayer assemblies")[6] and the separation behavior of high-boiling, reactant-immiscible Fluorinert solvents[7] for etherifications, alkylations, and other reactions were described later, but clearly independent of Vogt. The same applies to work by Horváth et al. since 1994,[2, 8-10] which has the following focal points:

- Using perfluorinated solvents in FBS or FMS (fluorous multiphase systems)
- Solubilizing catalysts for homogeneously catalyzed reactions by replacing customary ligands with partially fluorinated or perfluorinated ligands
- Carrying out selected reactions, for instance hydroformylation or hydroboration,[11] as biphasic reactions catalyzed by immobilized homogeneous catalysts.[3]

Quite obviously independent of Vogt, Horváth and Rábai as well as Gladysz et al. described the genesis of the FBS methodology very logically and with virtually the same words for the hydroformylation of *n*-decene to give undecanals [Eq. (1)].

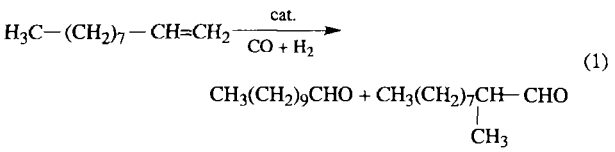

(1)

Their search for two-phase systems other than water/organic liquids—which provides the foundation for the industrially important aqueous, two-phase oxo process[8]—began with studies of solubility diagrams and the influence of intermolecular dissolution forces, as shown in Figure 1.[12]

[*] Prof. Dr. B. Cornils
Hoechst AG
D-65926 Frankfurt am Main (Germany)
Fax: Int. code + (69) 305-83128

 © WILEY-VCH Verlag GmbH, D-69451 Weinheim, 1997 0570-0833/97/3619-2057 $ 17.50+.50/0

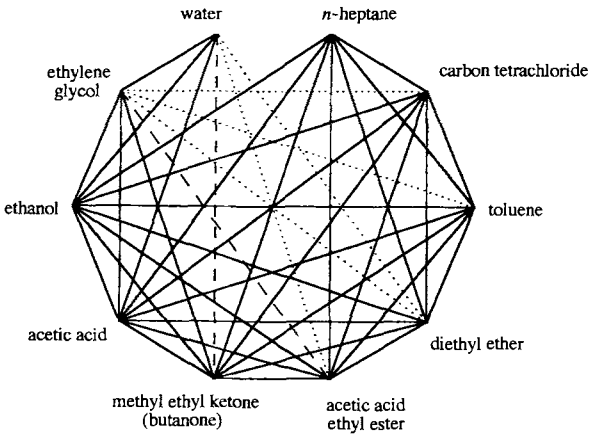

Figure 1. Miscibility diagram [12a]. Solvents not connected by a binding line are immiscible; solvents of unlimited miscibility are connected by a solid line, those of limited miscibility by a dashed line, and those of low miscibility with a dotted line.

As in the case of Vogt, the substances chosen were perfluorinated hydrocarbons which are largely immiscible with organic liquids at room temperature (and thus also with the preferably oxygen-containing reaction products of customary organic syntheses). In addition, as already emphasized by Zhu,[7] they are stable to hydrolysis but nevertheless have a measurable solubilizing capability for nonpolar reactants (for example the feed olefins of hydroformylations), especially at elevated temperatures.

Taking the two-phase hydroformylation[3] as a model, the auxiliary solvent in the reaction (in this case water) should be able to dissolve the complex catalyst completely in order to retain it after phase separation and removal of the reaction products (aldehydes), and to make them immediately available for a further catalysis cycle. Therefore, as in the case of Vogt, the ligand-modified rhodium carbonyl hydrides as oxo catalysts had to be made FBS-compatible by introducing alkylene perfluoroalkyl phosphanes. Here the tailor-made "ponytail" ligands[9] are ascribed particular electronic properties which, as a result of the thermal and leaching stability of the central atom Rh, make them more suitable than Vogt's ligands. In the hydroformylation reaction, complex catalysts of type **3** modified with these ligands display satisfactory activities in the two-phase system perfluoromethylcyclohexane/toluene and an *n*:*i* ratio of about 3, which is astonishing for the use of higher olefins.[8, 10]

$[HRh(CO)\{P[CH_2CH_2(CF_2)_5CF_3]_3\}_3]$ **3**

The FBS complex catalysts have the general formula $[M_x\{L(R)_n(R_f)_m\}_y]$; they contain not only a hydrocarbon group R but also a fluorine-containing part R_f, which is similar to the requirements of Kunitake et al.[6] for particular two-phase structures. Incorporation of CH_2 groups between the P atom of the phosphanes and the perfluorinated R_f groups (the ponytails)[8, 9] is, according to the authors, necessary for matching reactivity and compatibility for electronic reasons.[8] The corresponding patent[10] claims catalyzed and stoichiometric reactions in addition to hydroformylations; however, the only other reactions described are oxidations of cyclohexene (to give traces of the epoxide) and of sulfur compounds (for example, diphenyl sulfide to sulfone) as well as extractions.

The FBS method of immobilizing homogeneous catalysts is also used for Rh-catalyzed hydroboration[11] (in yields of up to 95%) and for oxidation reactions. The good solubility of oxygen in the FBS auxiliary liquids, which was earlier an argument for proposing that they be used as synthetic blood substitutes,[13] indicates that they may be particularly suitable for oxidation reactions.[10] Pozzi et al.[14] used Co complexes of perfluorohydrocarbon-soluble tetraalkylporphyrins in substrate:catalyst ratios of up to 1000:1 for the epoxidation of alkenes (albeit in the presence of considerable amounts of aldehydes, preferably isobutyraldehyde, as reducing agents). For cycloolefins yields of up to 100% are reported; for 1-dodecene the yield is still 60%. As desired, the cobalt–porphyrin complex is present in the FBS phase after the reaction and can be recycled. Knochel et al.[15] described the oxidation of aldehydes to carboxylic acids and of sulfides to sulfoxides and sulfones using the Ni complexes as well as the epoxidation of carbocyclic olefins (likewise in the presence of aliphatic aldehydes) using the Ru complexes of perfluorinated diketones of structure **4**.

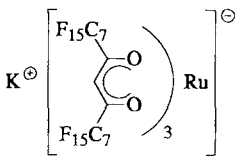

4

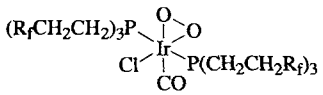

5

Also in these reactions, use is made of perfluorinated hydrocarbons as the FBS solvent; above 60 °C the reaction solution is a single phase in which the desired reaction proceeds without mass-transfer limitation. Upon cooling, the solution reverts to a two-phase system with the catalysts remaining in the FBS phase (Figure 2). According to Knochel et al.[15] the catalyst undergoes no leaching and displays only little ageing. The extent to which transition metal/oxygen complexes, as first described by Horváth and Gladysz et al.[16] for the partially fluorinated Vaska complex **5**, play a role in the oxidation is still unknown.

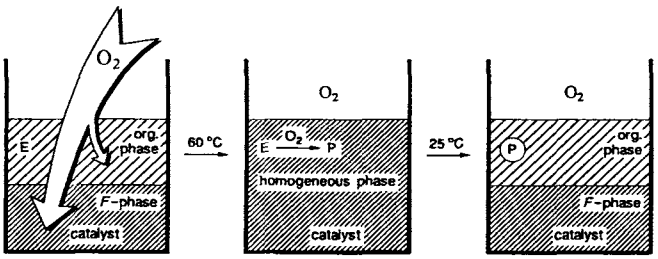

Figure 2. Principle of the FBS oxidation; E = starting material, P = product.

The importance of FBS for the quick separation of homogeneous catalyst and reaction product is so evident that a number of other studies have attempted to utilize the phase-separation effect even for reaction systems which do not contain transition metal catalysts. For example, Schultz et al.[17] proposed carry-

 © WILEY-VCH Verlag GmbH, D-69451 Weinheim, 1997 0570-0833/97/3619-2058 $ 17.50+.50/0

ing out the photoinduced singlet oxidation of cyclohexenes in this way [Eq. (2)].

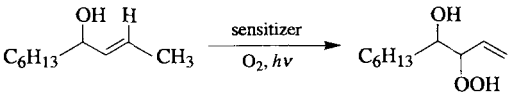

(2)

Exchanging the sensitizer tetraphenylporphyrin for 5,10,15,20-tetrakis(heptafluoropropyl)porphyrin in an FBS medium produced the desired effects: increase in the chemical stability of the sensitizer towards oxidative degradation and separation of the reaction solution from the sensitizer solution, which prevents further decomposition. The increase in yield and the reduction in decomposition of the sensitizer are considerable. Curran et al.[18] used FBS systems to recover and purify liquids (typical FBS applications) in specific reactions of organic chemistry, for example, nitrile oxidations/cycloadditions, Grignard and Ugi reactions, and the Bignelli condensation.

In the wider sense catalysis in supercritical CO_2 ($scCO_2$) is also a FBS reaction, although the ability to adjust the dissolution and phase-separation behavior of $scCO_2$ by changing the pressure and temperature provides the actual impetus for their use in two-phase processes. The FBS aspect becomes involved because, as Leitner et al.[19] showed, the customary arylphosphane ligands which are important for homogeneous catalysis can only be sufficiently dissolved in $scCO_2$ if alkenylperfluoroalkyl chains are incorporated in their periphery. The catalytic properties of the parent phosphanes, and also those of their chiral derivatives, are retained (see Noyori et al.,[20] who proposed the external addition of perfluoroalkyl alcohols). In the method of Leitner et al. (see **3** and Figure 3) the solubilizers are, as in the case of Horváth et al., fixed directly to the aryl radical and thus part of the ligand. The hydroformylation of 1-octene demonstrates the effectiveness of this technique: Comparatively high conversions and *n*:*i* ratios are obtained in the homogeneous phase in $scCO_2$.

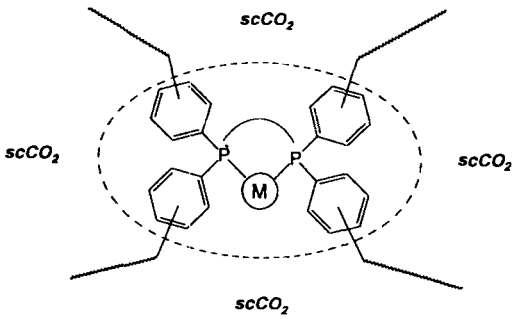

Figure 3. Catalysts with fluorine-containing ligands for use in $scCO_2$ according to Leitner et al. [19]. The "tails" on the phenyl rings represent m-$(CH_2)_2(CF_2)_6F$.

The FBS method will be secured a place in preparative organic chemistry and homogeneous catalysis in the future because its thermoselective phase behavior offers an opportunity to carry out reactions in one phase and thus homogeneously (and without serious mass transfer problems). Furthermore after cooling the mixture to separate the reaction products and by-products (and also decomposition products), the catalyst can be recycled by simple decantation. The question of the industrial importance of the FBS method is more difficult to answer. Some things do stand in the way of its wider use in industrial homogeneous catalysis: The complex catalysts are tailor-made and, like Savile Row suits, expensive; it is not so much the price of the catalytically active noble metals but rather the cost of the ligands and their recovery which becomes important. Furthermore, since they are inert fluorinated materials, ligands and FBS solvents can very easily raise questions about their presence in the atmosphere (ozone-depletion or greenhouse-warming potential of fluorine compounds) and the fate of even traces during any further processing steps (for example the hydrogenation of aldehydes to alcohols). Nevertheless, the properties of this particular type of two-phase catalysis leave no doubt that this is a spectacular but also important new development.

German version: *Angew. Chem.* **1997**, *109*, 2147–2149

Keywords: fluorocarbons · homogeneous catalysis · immobilization · supercritical fluids

[1] M. Vogt, Dissertation, Technische Hochschule Aachen, August 26, 1991.
[2] I. T. Horváth, oral presentation on August 31, 1994 at the NATO Advanced Research Workshop on *Aqueous Organometallic Chemistry and Catalysis* in Debrecen, Hungary; see *Aqueous Organometallic Chemistry and Catalysis* (Eds.: I. T. Horváth, F. Joó), Kluwer, Dordecht, **1995**.
[3] B. Cornils, E. Wiebus, *CHEMTECH* **1995**, *25*, 33.
[4] W. Keim, *Chem. Ing. Tech.* **1984**, *56*, 850.
[5] T. Umemoto, *Tetrahedron Lett.* **1984**, *25*, 81.
[6] H. Kuwahara, M. Hamada, Y. Ishikawa, T. Kunitake, *J. Am. Chem. Soc.* **1993**, *115*, 3002.
[7] D.-W. Zhu, *Synthesis* **1993**, 953
[8] I. T. Horváth, J. Rábai, *Science* **1994**, *266*, 72.
[9] J. A. Gladysz, *Science* **1994**, *266*, 55.
[10] Exxon Research and Engineering Comp. (I. T. Horváth, J. Rábai), US 5.463.082 (**1995**).
[11] J. J. J. Juliette, I. T. Horváth, J. A. Gladysz, *Angew. Chem.* **1997**, *109*, 1682; *Angew. Chem. Int. Ed. Engl.* **1997**, *36*, 1610.
[12] a) G. Duve, O. Fuchs, H. Overbeck, *Lösemittel Hoechst*, 6th ed., p. 49, Hoechst AG, Frankfurt am Main, **1976**; b) J. H. Hildebrand, D. R. F. Cochran, *J. Am. Chem. Soc.* **1949**, *71*, 22.
[13] See ref. [1] in [15].
[14] G. Pozzi, F. Montanari, S. Quici, *Chem. Commun.* **1997**, 69.
[15] I. Klement, H. Lütjens, P. Knochel, *Angew. Chem.* **1997**, *109*, 1605; *Angew. Chem. Int. Ed. Engl.* **1997**, *36*, 1454.
[16] M.-A. Guillevec, A. M. Arif, I. T. Horváth, J. A. Gladysz, *Angew. Chem.* **1997**, *109*, 1685; *Angew. Chem. Int. Ed. Engl.* **1997**, *36*, 1612.
[17] S. G. DiMagno, P. H. Dussault, J. A. Schultz, *J. Am. Chem. Soc.* **1996**, *118*, 5312.
[18] A. Studer, S. Hadida, R. Ferritto, S.-Y. Kim, P. Jeger, P. Wipf, D. P. Curran, *Science* **1997**, *275*, 823.
[19] W. Baumann, S. Kainz, D. Koch, W. Leitner, *Angew. Chem.* **1997**, *109*, 1699; *Angew. Chem. Int. Ed. Engl.* **1997**, *36*, 1628.
[20] J. Xiao, S. C. A. Nefkens, P. G. Jessop, T. Ikariya, R. Noyori, *Tetrahedron Lett.* **1996**, *37*, 2813.

 © WILEY-VCH Verlag GmbH, D-69451 Weinheim, 1997 0570-0833/97/3619-2059 $ 17.50+.50/0

The Jacobsen–Katsuki Epoxidation and Its Controversial Mechanism

Torsten Linker*

Epoxidation reactions have been established as an important method for the formation of carbon–oxygen bonds. In 1980 Sharpless and Katsuki developed an enantioselective variant for allylic alcohols which is still one of the most elegant methods in asymmetric synthesis.[1] Over the last few years unfunctionalized olefins have also become the focal point of interest as substrates, yielding epoxides in high enantiomeric excess when the optically active (salen)manganese(III) complexes **1** designed by

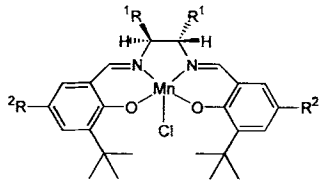

1a: R^1, R^1 = -$(CH_2)_4$-, R^2 = *t*Bu
1b: R^1, R^1 = -$(CH_2)_4$-, R^2 = OMe
1c: R^1, R^1 = -$(CH_2)_4$-, R^2 = OSi*i*Pr$_3$
1d: R^1 = Ph, R^2 = Br

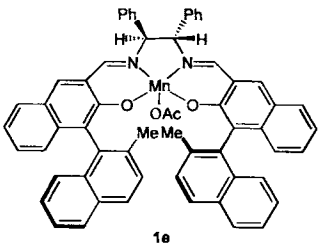

1e

Jacobsen and Katsuki are used.[2] The best selectivities are achieved with *cis*-alkenes; however, recently the epoxidation of olefins having tri- and tetrasubstituted double bonds has also been successful with enantiomeric excesses of over 90%.[3] The oxidants of choice are iodosobenzene and sodium hypochlorite at room temperature as well as *meta*-chloroperbenzoic acid at −78 °C. The proposed mechanism of the Jacobsen–Katsuki epoxidation is based on investigations by Kochi et al. with achiral salen ligands, where the Mn^V–oxo complexes **2** are postulated to be the catalytically active species (Scheme 1).[4]

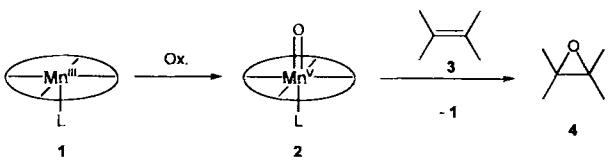

1 **2** **4**

Scheme 1. Formation of Mn^V–oxo complexes **2** in the Jacobsen–Katsuki epoxidation. Ox = oxidant, L = counterion or amine *N*-oxide ligand.

While the existence of analogous Cr^V–oxo complexes has been established by X-ray crystallographic analysis, the more reactive Mn^V complexes could only be speculated on. Recently, however, Plattner et al. made an important contribution to the mechanistic understanding by proving such intermediates with electrospray tandem mass spectrometry.[5]

[*] Priv.-Doz. Dr. T. Linker
Institut für Organische Chemie der Universität
Am Hubland, D-97074 Würzburg (Germany)
Fax: Int. code +(931)888-4606
e-mail: linker@chemie.uni-wuerzburg.de

Soon after the discovery of the Jacobsen–Katsuki epoxidation, the first models were developed (which were later refined) to explain the high enantioselectivities in the transformation of *cis*-alkenes (Figure 1).[2] A side-on approach of the double bond

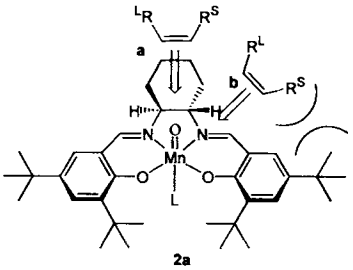

2a

Figure 1. Preferred directions of attack of alkenes **3** on complex **2**: **a** according to Jacobsen, **b** according to Katsuki.

parallel to the salen ligand is generally accepted; the sterically demanding *tert*-butyl groups shield the aryl rings. Jacobsen proposes attack from the direction of the diimine bridge (path **a**) such that the smaller substituent (R^S) is on the same side as the axial hydrogen atom of the chiral center.[2c] Katsuki favors path **b** due to π–π interactions;[2d] however, the two models differ only marginally and both explain the observed facial selectivities. Besides steric influences, the electronic character of the salen ligand also plays a decisive role. In an interesting study Jacobsen et al. found that the enantioselectivities can be increased significantly by donor substituents R^2 (in **1**), thus leading to the development of the efficient catalysts **1b** and **1c**.[6] An explanation is that the reactive manganese(v)–oxo species **2** is stabilized, and the rate of oxygen transfer is decreased. According to the Hammond postulate, this would imply a late transition state, in which the interaction between the olefin and the chiral salen ligand is more important.

The influence of additives on the reaction rate, yield, and enantioselectivity of the Jacobsen–Katsuki epoxidation was recognized early on.[7] Amine *N*-oxides proved to be the best axial coligands, because they also stabilize the manganese(v)–oxo complex **2** (Scheme 1). Recently, Jacobsen was able to impressively substantiate the importance of additives by synthesizing the (salen)manganese(III) complex **1f**.[8] While the yield and

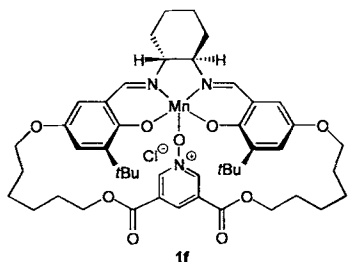

1f

 © WILEY-VCH Verlag GmbH, D-69451 Weinheim, 1997 0570-0833/97/3619-2060 $ 17.50+.50/0

enantiomeric excess of epoxide obtained with the catalyst **1b** can be drastically increased when 4-phenylpyridine *N*-oxide (PPNO) is added, the concentration of PPNO has no influence on the reactivity of complex **1f**.

Although the factors controlling the reactivity and enantioselectivity of (salen)manganese(III) complexes **1** are now well understood, a controversy has recently erupted over the mechanism of oxygen transfer to the double bond. The concerted path **A** and pathways proceeding via radical intermediates (path **B**) and manganaoxetanes (path **C**) are under discussion (Scheme 2).

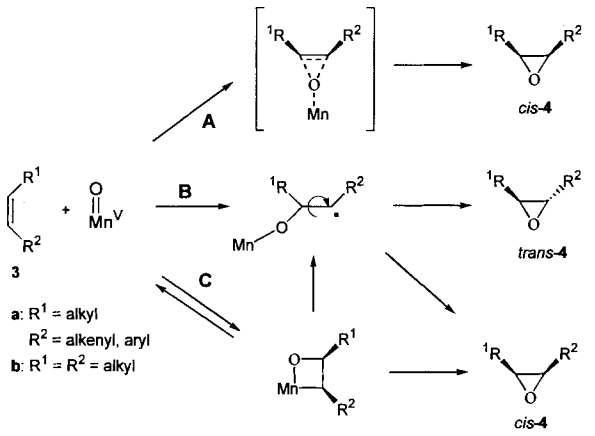

Scheme 2. Three mechanisms for oxygen transfer: **A** concerted, **B** via radicals, **C** via manganaoxetane intermediates.

Even in the first examples of the Jacobsen–Katsuki epoxidation, conjugated olefins **3a** were reported to give mixtures of *cis*- and *trans*-epoxides **4**, while the alkyl-substituted derivatives **3b** stereoselectively gave only the *cis* products. These findings were explained by evoking the concerted pathway **A** for alkyl-substituted alkenes and a radical mechanism (path **B**) for conjugated alkenes, in which rotation about the C–C single bond leads to both epoxides **4**. However, if one compares experiments with the prime example *cis*-β-methylstyrene (**3c**) under various reaction conditions, then it becomes clear that contrary to the enantiomeric excesses the diastereoselectivities are strongly dependent on the oxidant, the catalyst, and the additives (Table 1).

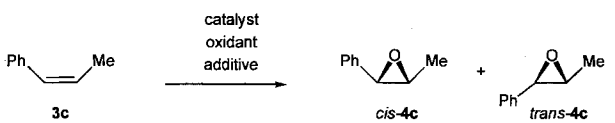

Table 1. Epoxidation of *cis*-β-methylstyrene (**3c**) with 0.04 equiv catalyst.

Entry [ref.]	Cat.	Oxidant[a]	Additive	Yield [%]	*cis*:*trans*	ee_{tot} [%][e]
1[8]	**1d**	NaOCl	4-PPNO [b]	98	95:5	81
2[8]	**1d**	MCPBA	NMO[c]	91	94:6	82
3[9]	**1a**	NaOCl	–	86	92:8	81
4[2d]	**1e**	PhIO	4-PPNO[b]	48	77:23	88
5[8]	**1d**	PhIO	4-PPNO[b]	76	75:25	72
6[9]	**1c**	NaOCl	–	86	71:29	81
7[9]	**1c**	NaOCl	CAS[d]	86	5:95	81

[a] NaOCl: in phosphate buffer/chlorobenzene; *m*-chloroperbenzoic acid (MCPBA): in dichloromethane; iodosobenzene (PhIO): in acetonitrile. [b] 0.2–0.4 equiv 4-phenylpyridine *N*-oxide (4-PPNO). [c] 10.0 equiv *N*-methylmorpholine *N*-oxide (NMO). [d] 0.2 equiv of a quaternary quinine ammonium salt (QAS). [e] $ee_{tot} = \%\,cis \times ee_{cis} + \%\,trans \times ee_{trans}$.

What is especially surprising is the high *trans* selectivity when quaternary quinine ammonium salts are added (Table 1, entry 7),[9] as it is difficult to bring this into line with radical intermediates. To date, only scant attention has been paid to the electronic interactions in the Jacobsen–Katsuki epoxidation; however, recent studies on the kinetic resolution of chiral dihydronaphthalenes have shown that polar substituents on the substrate have a strong influence on the diastereoselectivity of the reactions.[10]

The discussion on the mechanism of the Jacobsen–Katsuki epoxidation was revived by theoretical investigations conducted by Norrby, Linde, and Åkermark.[11] The diastereomeric manganaoxetanes (path **C**) were calculated with MacroModel/MM3*, and the energy differences well reflected the observed enantioselectivities. According to Scharf et al., no linear Eyring correlation should be found if these intermediates are formed reversibly.[12] Indeed, experiments by Katsuki et al. support the formation of metallaoxetanes, since inversion temperatures are found in the epoxidation of various olefins.[13] However, Jacobsen et al. question these results in a recent study and obtain a linear Eyring correlation with their salen ligands.[8] Unfortunately, the two investigations were conducted with different catalysts and under different reaction conditions, which have a significant influence on the reaction mechanism (Table 1) and thereby make comparisons rather difficult.

The epoxidation of the vinylcyclopropanes **3d–g** should provide a good indication for radical intermediates, as these "radical clocks" undergo ring-opening at a rate of approximately $10^{11}\ s^{-1}$. Jacobsen et al. published investigations with the unsubstituted vinylcyclopropane **3d** already in 1991;[14] however, an interesting paper on the phenyl-substituted derivatives **3e–g** (Scheme 3) appeared only recently.[15] Although the exclusive formation of the epoxides *cis*-**4d** according to a concerted mechanism (path **A** or **C**) was expected, the highly selective formation of the epoxides **4e** and **4f** with sodium hypochlorite without epimerization and cyclopropane ring-opening is surprising. This speaks against radical intermediates in this case and was interpreted by the authors as proof for manganaoxetanes (path **C**).[15] However, the argumentation is again based on a nonlinear Eyring correlation, which is contested by Jacobsen et al.[8] What is more striking are the different product distributions with sodium hypochlorite and iodosobenzene, something also observed in the epoxidation of *cis*-β-methylstyrene (Table 1, entries 1 and 5). The reaction conditions ap-

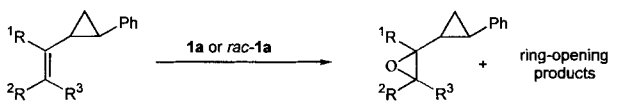

3	oxidant	*cis*-4 : ring-opening
d: $R^1 = R^2 = R^3 = H$	NaOCl	100 : 0
e: $R^1 = Ph$, $R^2 = R^3 = H$	NaOCl	100 : 0
e: $R^1 = Ph$, $R^2 = R^3 = H$	PhIO	57 : 43
f: $R^1 = Ph$, $R^2 = H$, $R^3 = Me$	NaOCl	100 : 0
f: $R^1 = Ph$, $R^2 = H$, $R^3 = Me$	PhIO	83 : 17
g: $R^1 = Ph$, $R^2 = Me$, $R^3 = H$	NaOCl	56 : 44
g: $R^1 = Ph$, $R^2 = Me$, $R^3 = H$	PhIO	54 : 46

Scheme 3. Epoxidation of vinylcyclopropanes **3d–g** as "radical clocks".

 © WILEY-VCH Verlag GmbH, D-69451 Weinheim, 1997 0570-0833/97/3619-2061 $ 17.50+.50/0

parently play a fundamental role in the Jacobsen–Katsuki epoxidation, so that a general mechanistic interpretation is not possible to date.

In summary, Mn^V–oxo complexes could be detected as catalytically active species in the Jacobsen–Katsuki epoxidation by electrospray tandem mass spectrometry. The synthesis of catalyst **1f** impressively demonstrates the importance of amine *N*-oxide ligands. The excellent enantioselectivities can be explained by the preferred side-on approach of the olefin. Finally, the epoxidation of phenyl-substituted vinylcyclopropanes provided evidence for radical intermediates in the *cis–trans* isomerization; however, the influence of different reaction conditions has to be taken into account. To what extent the manganaoxetanes or possibly polar intermediates play a part in the mechanism cannot be conclusively decided due to the contradictory results; further work on this point is necessary. Nonetheless, the great synthetic use of the Jacobsen–Katsuki epoxidation remains indisputable and makes this reaction one of the most important methods of asymmetric catalysis.

German version: *Angew. Chem.* **1997**, *109*, 2150–2152

Keywords: asymmetric syntheses · catalysis · epoxidations · oxidations · reaction mechanisms

[1] a) T. Katsuki, K. B. Sharpless, *J. Am. Chem. Soc.* **1980**, *102*, 5974–5976; b) R. A. Johnson, K. B. Sharpless in *Comprehensive Organic Sythesis, Vol. 7* (Eds.: B. M. Trost, I. Fleming), Pergamon, New York, **1991**, pp. 389–436; c) R. A. Johnson, K. B. Sharpless in *Catalytic Asymmetric Synthesis* (Ed.: I. Ojima), VCH, Weinheim, **1993**, pp. 103–158; d) T. Katsuki, V. S. Martin, *Org. React.* **1996**, *48*, 1–299.

[2] a) W. Zhang, J. L. Loebach, S. R. Wilson, E. N. Jacobsen, *J. Am. Chem. Soc.* **1990**, *112*, 2801–2803; b) R. Irie, K. Noda, Y. Ito, N. Matsumoto, T. Katsuki, *Tetrahedron Lett.* **1990**, *31*, 7345–7348; c) E. N. Jacobsen in *Catalytic Asymmetric Synthesis* (Ed.: I. Ojima), VCH, Weinheim, **1993**, pp. 159–202; d) T. Katsuki, *J. Mol. Catal.* **1996**, 87–107.

[3] a) B. D. Brandes, E. N. Jacobsen, *J. Org. Chem.* **1994**, *59*, 4378–4380; b) T. Fukuda, R. Irie, T. Katsuki, *Synlett* **1995**, 197–198; c) B. D. Brandes, E. N. Jacobsen, *Tetrahedron Lett.* **1995**, *36*, 5123–5126.

[4] a) T. S. Siddall, N. Miyaura, J. C. Huffman, J. K. Kochi, *J. Chem. Soc. Chem. Commun.* **1983**, 1185–1186; b) E. G. Samsel, K. Srinivasan, J. K. Kochi, *J. Am. Chem. Soc.* **1985**, *107*, 7606–7617; c) K. Srinivasan, P. Michaud, J. K. Kochi, *ibid.* **1986**, *108*, 2309–2320.

[5] D. Feichtinger, D. A. Plattner, *Angew. Chem.* **1997**, *109*, 1796–1798; *Angew. Chem. Int. Ed. Engl.* **1997**, *36*, 1718–1719.

[6] a) E. N. Jacobsen, W. Zhang, M. L. Güler, *J. Am. Chem. Soc.* **1991**, *113*, 6703–6704; b) S. Chang, R. M. Heid, E. N. Jacobsen, *Tetrahedron Lett.* **1994**, *35*, 669–672; c) S. L. Vander Velde, E. N. Jacobsen, *J. Org. Chem.* **1995**, *60*, 5380–5381.

[7] a) R. Irie, Y. Ito, T. Katsuki, *Synlett* **1991**, 265–266; b) R. Irie, K. Noda, Y. Ito, N. Matsumoto, T. Katsuki, *Tetrahedron: Asymmetry* **1991**, *2*, 481–494; c) M. Palucki, P. J. Pospisil, W. Zhang, E. N. Jacobsen, *J. Am. Chem. Soc.* **1994**, *116*, 9333–9334.

[8] N. S. Finney, P. J. Pospisil, S. Chang, M. Palucki, R. G. Konsler, K. B. Hansen, E. N. Jacobsen, *Angew. Chem.* **1997**, *109*, 1798–1801; *Angew. Chem. Int. Ed. Engl.* **1997**, *36*, 1720–1723.

[9] S. Chang, J. M. Galvin, E. N. Jacobsen, *J. Am. Chem. Soc.* **1994**, *116*, 6937–6938.

[10] T. Linker, F. Rebien, *Angew. Chem.*, submitted.

[11] P.-O. Norrby, C. Linde, B. Åkermark, *J. Am. Chem. Soc.* **1995**, *117*, 11035–11036.

[12] H. Buschmann, H.-D. Scharf, N. Hoffmann, P. Esser, *Angew. Chem.* **1991**, *103*, 480–518; *Angew. Chem. Int. Ed. Engl.* **1991**, *30*, 477–515.

[13] T. Hamada, T. Fukuda, H. Imanishi, T. Katsuki, *Tetrahedron* **1996**, *52*, 515–530.

[14] H. Fu, G. C. Look, W. Zhang, E. N. Jacobsen, C.-H. Wong, *J. Org. Chem.* **1991**, *56*, 6497–6500.

[15] C. Linde, M. Arnold, P.-O. Norrby, B. Åkermark, *Angew. Chem.* **1997**, *109*, 1802–1803; *Angew. Chem. Int. Ed. Engl.* **1997**, *36*, 1723–1725.

 © WILEY-VCH Verlag GmbH, D-69451 Weinheim, 1997 0570-0833/97/3619-2062 $ 17.50+.50/0

Oxidation of ethene–rhodium (I) complexes with H_2O_2 selectively leads to stable 2-rhodaoxetanes.

Such species have frequently been invoked as intermediates in the metal-catalyzed oxidation of olefins.

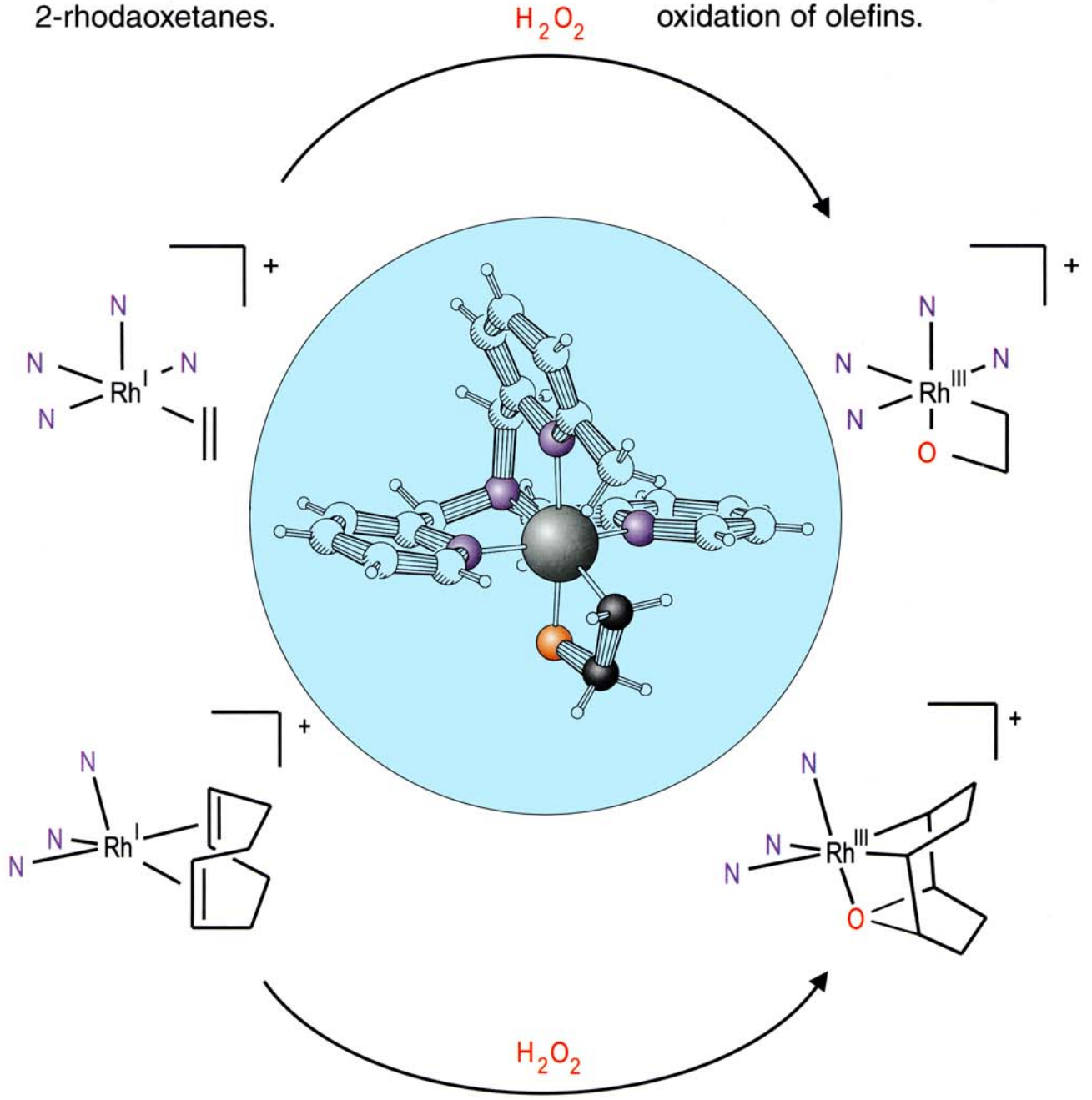

Analogous cyclooctadiene complexes react under the same conditions to form unprecedented Rh^{III} complexes of THF derivatives.

More about these interesting rhodium complexes is reported by Gal et al. on the following pages.

 © WILEY-VCH Verlag GmbH, D-69451 Weinheim, 1997 0570-0833/97/3619-2063 $ 17.50 + .50/0

Oxidation of Rh^{I}(olefin) Fragments to 2-Rhoda(III)oxetanes**

Bas de Bruin, Mark J. Boerakker, Jack J. J. M. Donners, Boukje E. C. Christiaans, Paul P. J. Schlebos, René de Gelder, Jan M. M. Smits, Anthony L. Spek, and Anton W. Gal*

The intermediacy of 2-metallaoxetanes (1,2-oxametallacyclobutanes) has been proposed in important conversions, such as the hydroxylation of olefins by $KMnO_4$, CrO_2Cl_2, or OsO_4,[1] the catalytic epoxidation of olefins,[2] and the catalytic rearrangement of epoxides to ketones.[3] Most recently, 2-metallaoxetanes have also been invoked in the Rh^{I}-catalyzed, asymmetric hydrogenolysis of epoxides.[4] Few isolated 2-metallaoxetanes are known, and those reported are stabilized by various substituents. Previous results suggest that substituents at the β-position of 2-rhodaoxetanes are required to prevent β-hydrogen elimination.[5] Substituted[6] 2-metallaoxetanes have been prepared by oxidative addition of an epoxide to a low valent metalcomplex,[4, 5b, 7] or, in the case of 2-rhoda- and 2-iridaoxetanes, by deprotonation of a β-hydroxyethyl metal halide.[5, 8] To our knowledge, the reaction of $[Ir^{I}(P_3O_9)(cod)]^{2-}$ (cod = (*Z*,*Z*)-1,5-cyclooctadiene) with dioxygen is the only example of a reaction in which a 2-metallaoxetane is obtained upon oxygenation of a coordinated olefin.[9] In this paper we describe some new $[Rh^{I}(cod)'N_3']^{+}$ ('N_3' = cn*, dpbn) and $[Rh^{I}(ethene)'N_4']^{+}$ ('N_4' = tpa, Me-tpa) complexes and their selective oxidation by H_2O_2. The $[Rh^{I}(cod)'N_3']^{+}$ complexes are oxidized to oxarhoda(III)tetracyclodecanes, possibly via 2-rhodaoxetane intermediates. Oxidation of the $[Rh^{I}(ethene)'N_4']^{+}$ complexes results in unsubstituted 2-rhodaoxetanes as isolable compounds.

The cationic five-coordinate cod complexes **1** and **2** were prepared as their PF_6^- salts (Scheme 1).[10] Compound **1** contains the rigid *fac* coordinating cn* ligand, whereas **2** contains the flexible dpbn ligand in its *fac* coordination mode.

In methanol at room temperature **1**-PF_6 and **2**-PF_6 are air-stable. Upon reaction of **1**-PF_6 with an excess of aqueous H_2O_2 (95%) in methanol, the color of the solution immediately changed from bright yellow to pale yellow. The ^1H NMR spectrum of the pale yellow powder, obtained by evaporation of the solvent, indicated quantitative conversion of **1**-PF_6 to **3**-PF_6 (Scheme 1).

Upon treatment of **2**-PF_6 with an excess of aqueous H_2O_2 (35%) in [D_6]acetone at room temperature, a reaction similar to that for **1**-PF_6 occurred. Comparison of the ^1H NMR spectrum of the resulting solution with the ^1H NMR spectrum of **3**-PF_6 in [D_6]acetone indicated the presence of two isomeric oxidation products, **4a**-PF_6 (symmetric) and **4b**-PF_6 (asymmetric) (Scheme 1), in a ratio 1:5.[11] Selective formation of the asymmetric isomer **4b** was observed when the reaction was carried out at $-10\,^{\circ}C$. We observed no isomerization of **4b** to **4a** at room temperature in [D_6]acetone.[12]

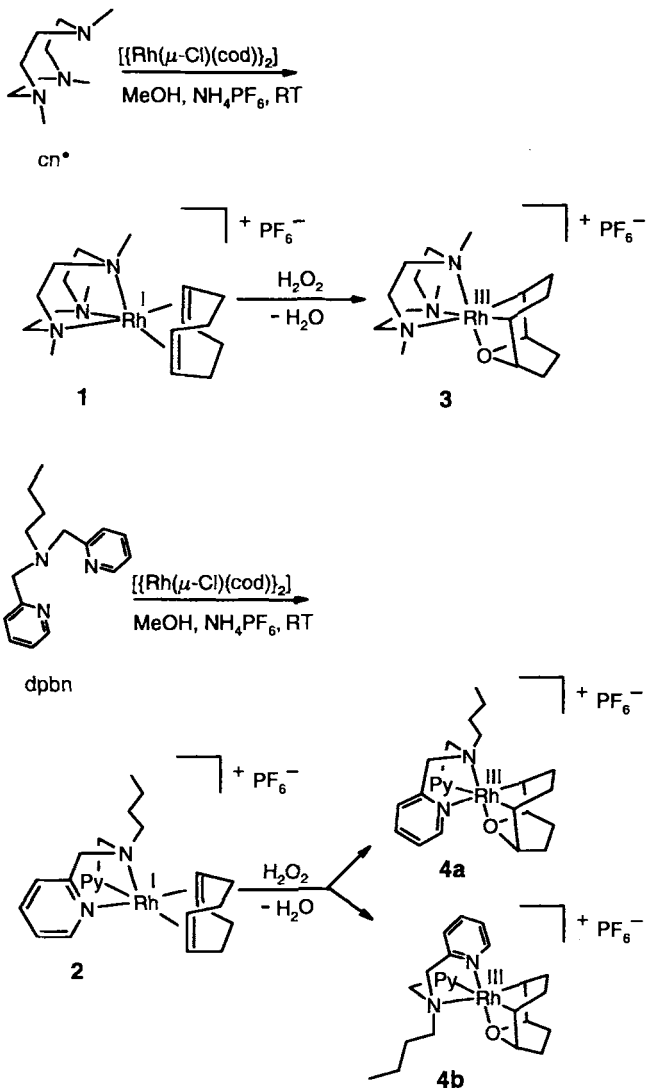

Scheme 1. Synthesis of the $[Rh^{I}(cod)'N_3']^{+}$ complexes **1**-PF_6 and **2**-PF_6, and their oxidation by H_2O_2 to **3**-PF_6 and **4a**-PF_6/**4b**-PF_6 (cn* = 1,4,7-trimethyl-1,4,7-triazacyclononane, dpbn = *n*-butylbis(pyridine-2-ylmethyl)amine).

The crystal structure of cation **3** was determined by X-ray diffraction (Figure 1).[13] The Rh^{I}(cod) fragment in **1** has been oxidized to a 6,7-oxarhoda(III)tetracyclodecane fragment that contains two Rh–C bonds and one $Rh-O_{ether}$ bond. Omission of the coordinative $Rh-O_{ether}$ bond from the nomenclature makes the fragment a 9,10-oxarhoda(III)tricyclodecane. Thus, oxidation of both double bonds of cod in the five-coordinate Rh^{I}(cod) complex **1** has resulted in a six-coordinate (9-oxabicyclo[4.2.1]nonane-2,5-diyl)rhodium(III) complex. The oxabicyclononanediyl ligand can formally be considered a tetrahydrofuran derivative. The observed oxidation reaction bears some resemblance to the stoichiometric permanganate oxidation of 1,5-hexadienes to tetrahydrofurans.[14] Though the structure of oxidation product **3** is unprecedented, it has some structural similarity to the 1,4-cycloaddition product of $[\{Rh(\mu\text{-}Cl)(cod)\}_2]$ with hexafluorobut-2-yne.[15] The coordination geometry of the rhodium atom is pseudooctahedral. The Rh–C distances (2.052 and 2.069 Å) are normal for Rh^{III}, as are the Rh–N distances. The Rh–N3 distance (2.098 Å) is shorter than the Rh–N11 and Rh–N21 distances (2.228 and 2.219 Å), reflecting

[*] Prof. Dr. A. W. Gal, Dipl.-Chem. B. de Bruin, M. J. Boerakker, J. J. J. M. Donners, B. E. C. Christiaans, P. P. J. Schlebos, Dr. R. de Gelder, J. M. M. Smits
Department of Inorganic Chemistry
University of Nijmegen
Toernooiveld 1, NL-6525 ED Nijmegen (The Netherlands)
Fax: Int. code +(24)355-3450
e-mail: gal@sci.kun.nl.

Dr. A. L. Spek
Laboratory of Crystal and Structural Chemistry
Bijvoet Centre for Biomolecular Research
University of Utrecht (The Netherlands)

[**] We thank Unilever Research Laboratory, Vlaardingen, for a generous gift of 1,4,7-trimethyl-1,4,7-triazacyclononane.

 © WILEY-VCH Verlag GmbH, D-69451 Weinheim, 1997 0570-0833/97/3619-2064 $ 17.50+.50/0

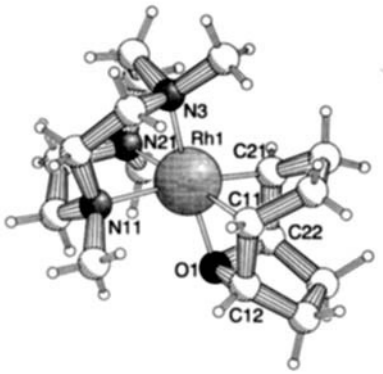

Figure 1. X-ray crystal structure of cation **3**. Selected bond lengths [Å] and angles [°]: Rh1–C11 2.069(4), Rh1–C21 2.052(4), Rh1–O1 2.077(3), Rh1–N11 2.228(3), Rh1–N21 2.219(4), Rh1–N3 2.098(3), O1–C12 1.515(5), O1–C22 1.503(5); C11-Rh1-C21 77.2(2), N11-Rh1-N3 81.87(13), N21-Rh1-N3 82.14(13), N11-Rh1-N21 80.37(13), C12-O1-C22 102.0(3), Rh1-O1-C12 92.2(2), Rh1-O1-C22 92.0(2), O1-Rh1-C11 69.81(14), O1-Rh1-C22 92.0(2), C11-Rh1-N21 173.4(2), C21-Rh1-N11 171.4(2), C11-Rh1-N3 104.2(2), C21-Rh1-N3 106.6(2), O1-Rh1-N3 173.62(13).

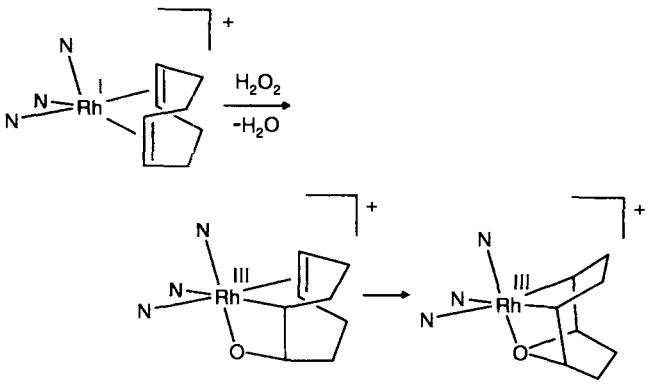

Scheme 2. Formation of oxarhoda(III)tretracyclodecanes via proposed 2-rhoda(III)oxetane intermediates.

In view of the proposed intermediacy of 2-rhodaoxetanes in the above selective oxidation of $[Rh^{I}(cod)'N_3']^+$ complexes, we argued that unsubstituted 2-rhodaoxetanes might form upon similar oxidation of $[Rh^{I}(ethene)'N_4']^+$ complexes. We therefore prepared the five-coordinate ethene complex **5a**, containing the 'N_4' ligand tpa, and studied its reaction with H_2O_2 (Scheme 3).

The color changed from yellow to pale yellow upon addition of an excess of aqueous H_2O_2 (35%) to a methanolic solution of **5a**-PF_6 at $-10\,^{\circ}C$ (Scheme 3).[17] A single compound was obtained as an off-white solid by precipitation with diethyl ether. Its ^1H NMR spectrum shows a triplet at $\delta = 4.97$ ($^3J_{H,H} = 7.5$ Hz) and a triplet with rhodium coupling at $\delta = 2.35$

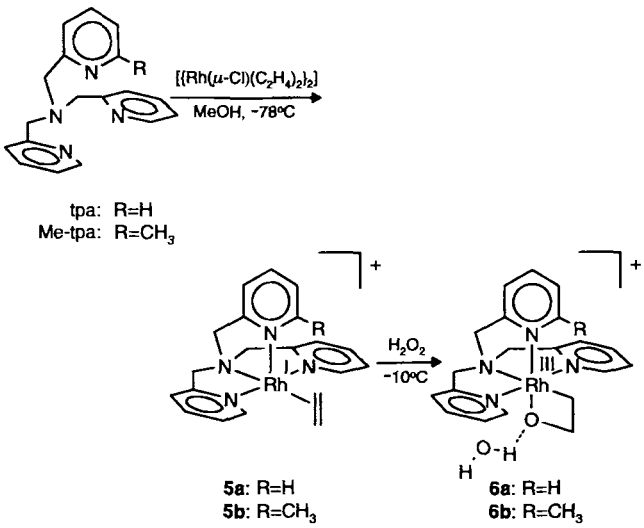

Scheme 3. Synthesis of the $[Rh^{I}(ethene)'N_4']^+$ complexes **5a** and **5b**, and their oxidation by H_2O_2 to **6a** and **6b**. (tpa = tris(pyridin-2-ylmethyl)amine).

($^3J_{H,H} = 7.5$ Hz, $^2J_{H,Rh} = 2.5$ Hz), indicating the presence of a $RhCH_2CH_2O$ fragment. Further spectroscopic and analytical data led us to propose the 2-rhodaoxetane structure **6a**-PF_6 for this compound. Repeated CHN analysis and ^1H NMR spectra of samples from various experiments indicated that the product coprecipitates with water.

As we were not able to grow X-ray quality crystals of **6a**-PF_6, we also investigated the oxidation of a Rh^{I}(ethene) fragment stabilized by the monomethyl substituted 'N_4' ligand Me-tpa.[18] Stirring $[\{Rh(\mu\text{-Cl})\}_2(ethene)_2]$[19] with Me-tpa in methanol afforded **5b**-Cl, which was quantitatively oxidized in situ to **6b**-Cl by adding an excess of 35% aqueous H_2O_2. Both **6b** and **5b** could be isolated as their BPh_4 salt by precipitation with one equivalent of $NaBPh_4$.

Spectroscopic and analytical data indicated the composition **6b**-$BPh_4 \cdot 1.5H_2O$. The crystal structure of **6b**-$BPh_4 \cdot 1.5H_2O$ was determined by X-ray diffraction. It proved to be a pseudo-centrosymmetric arrangement of two cations (**6b**^{A} and **6b**^{B}), two anions, and three water molecules per unit cell. The molecular structure of cation **6b**^{A} is shown in Figure 2[13].

Two-thirds of the water molecules in the crystal are found as independent water dimers. Interestingly, one-third of the water

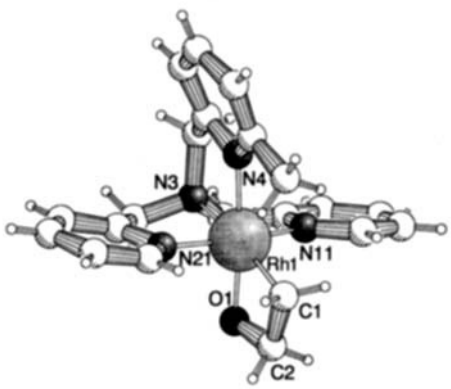

Figure 2. X-ray crystal structure of cation **6b**^{A}. Selected bond lengths [Å] and angles [°] for both cations **6b**^{A} and **6b**^{B}: Rh1–O1 2.000(5), 2.013(6); Rh1–N21 2.021(6), 2.019(8); Rh1–N11 2.045(10), 2.033(9); Rh1–C1 2.070(7), 2.075(8); Rh1–N3 2.140(8), 2.124(8); Rh1–N4 2.132(10), 2.079(13); O1–C2 1.446(10), 1.435(14); C1–C2 1.514(11), 1.49(2); O1-Rh1-C1 70.3(3), 70.0(4); C2-O1-Rh1 94.8(4), 93.5(6); C2-C1-Rh1 90.0(5), 89.4(6); O1-C2-C1 104.6(6), 106.4(7)

 © WILEY-VCH Verlag GmbH, D-69451 Weinheim, 1997 0570-0833/97/3619-2065 $ 17.50+.50/0

molecules connect the cations **6b**^{A} and **6b**^{B} through two O_{water}-H$\cdots$$O_{oxetane}$ hydrogen bonds. The O_{water} atoms are also involved in a bifurcated hydrogen bond with the hydrogen atoms on the C^4 and C^5 pyridyl groups of a neighboring **6b**^{A} cation (Figure 3). The observed hydrogen bonding of H_2O to the 2-rhodaoxetane fragment parallels the frequently observed hydrogen bonds between alcohols and late transition metal alkoxides.[20]

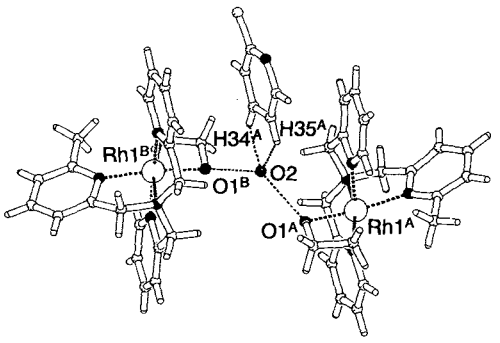

Figure 3. Hydrogen bonding interactions of the bridging water molecule as found in the X-ray structure of **6b**-$BPh_4\cdot1.5H_2O$. O1^{A} and O1^{B}: oxygen atoms of cationic 2-rhodaoxetanes **6b**^{A} and **6b**^{B}; O2: oxygen atom of bridging H_2O. Selected interatomic distances [Å]: O2–O1^{A} 2.645(6), O2–O1^{B} 2.713(7), O2–H34^{A} 1.900(15), O2–H35^{A} 2.037(11).

Rhodium–alkoxy compounds are rare. The Rh–O distances in 2-rhodaoxetane **6b** (**6b**^{A}: 2.00 Å, **6b**^{B}: 2.01 Å) are shorter than those of all the known Rh–O_{alkoxy} distances (2.01–2.11 Å),[20a, 21] including the Rh–O_{alkoxy} distance (2.10 Å) in the β,β-disubstituted 2-rhodaoxetane [RhBr{$CH_2C(Me)_2O$}-$(PMe_3)_3$] (**7**), the only 2-rhodaoxetane reported thus far.[5] The difference between the cationic **6b** and the neutral **7** seems to be the result of a weaker *trans* influence of the hard N ligand in **6b** than of the soft P ligand in **7**. A M–O distance of 1.96 Å, similar to that in **6b**, is observed for the dianionic 2-iridaoxetane $[Ir(P_3O_9)(O\text{-}cod)]^{2-}$ (**8**).[9] The C–O distances found for **6b** (**6b**^{A}: 1.45 Å, **6b**^{B}: 1.44 Å) are much shorter than the rather long C–O distance in the strained 2-iridaoxetane **8** (1.86 Å), but compare well with those in the 2-rhodaoxetane **7** (1.42 Å). The Rh–C and C–C distances in 2-rhodaoxetane **6b** compare well with the corresponding distances of **7** and **8**.[5, 9]

To our best knowledge **6a** and **6b** are the first isolated examples of unsubstituted 2-metallaoxetanes. Their formation upon oxidation of a Rh^{I}(ethene) fragment could well be relevant to a better understanding of late transition metal mediated oxidation of olefins.

Experimental Section

All procedures were performed under N_2 with standard schlenk techniques.

1-PF_6: cn* (92 mg, 0.54 mmol) and [{Rh(μ-Cl)}$_2$(cod)] [22] (134 mg, 0.27 mmol) were stirred in 25 mL MeOH for 1 h. Subsequently, NH_4PF_6 (354 mg, 2.16 mmol) was added. Partial evaporation of the solvent caused the precipitation of **1**-PF_6 as a yellow powder, which was filtered and vacuum-dried. Yield 202 mg (71%). ^{1}H NMR (200.13 MHz, [D$_6$]acetone, 298 K): δ = 3.56 (m, 4H; CH=CH), 3.1–2.85 (m, 12H; NCH_2), 3.00 (s, 9H; NCH_3), 2.46 (m, 4H; C=CCH_2-*exo*), 1.67 (m, 4H; C=CCH_2-*endo*); ^{13}C{^{1}H} NMR (50.33 MHz, [D$_6$]acetone, 298 K): δ = 74.2 (d, J(Rh,C) = 13.8 Hz; CH=CH), 58.4 (NCH_2), 51.2 (NCH_3), 30.7 (C=CCH_2). FAB-MS (*m*-nitrobenzyl alcohol (*m*-Noba)/CH_3CN): 382 $[M]^+$, 909 $[2M+PF_6]^+$. Elemental analysis calcd for $C_{17}H_{33}N_3RhPF_6$: C 38.72, H 6.31, N 7.97; found: C 38.47, H 6.22, 7.85.

2-PF_6: Prepared by a procedure similar to that of **1**-PF_6 but with the ligand dpbn [23]. ^{1}H NMR (200.13 MHz, [D$_6$]acetone, 298 K): δ = 9.20 (d, ^3J(H,H) = 5.4 Hz, 2H; Py-H6), 7.74 (m, 2H; Py-H4), 7.37–7.27 (m, 4H; Py-H5, and Py-H3), 4.62 (d[AB], ^2J(H,H) = 16.3 Hz, 2H; N-CH_2-Py), 4.25 (d[AB], ^2J(H,H) = 16.3 Hz, 2H; NCH_2Py), 4.06 (m, 2H; N$CH_2CH_2CH_2CH_3$), 3.83 (m, 4H; CH=CH), 2.65 (m, 4H; C=CCH_2-*exo*), 2.12 (m, 2H; $NCH_2CH_2CH_2CH_3$), 1.86 (m, 4H; C=CCH_2-*endo*), 1.59 (m, 2H; $NCH_2CH_2CH_2CH_3$), 1.09 (t, ^3J(H,H) = 7.4 Hz, 3H; $NCH_2CH_2CH_2CH_3$); ^{13}C{^{1}H} NMR (50.33 MHz, [D$_6$]acetone, 298 K): δ = 160.4 (Py-C2), 151.5 (Py-C6), 139.0 (Py-C4), 124.9 (Py-C3), 123.7 (Py-C5), 75.9 (d, J(Rh,C) = 13.8 Hz; CH=CH), 64.1 ($NCH_2CH_2CH_2CH_3$), 63.4 (NCH_2Py), 31.4 (C=CCH_2), 27.2 ($NCH_2CH_2CH_2CH_3$), 21.0 ($NCH_2CH_2CH_2CH_3$), 14.0 ($NCH_2CH_2CH_2CH_3$). FAB-MS (*m*-Noba/CH_3CN): 466 $[M]^+$, 1077 $[2M+PF_6]^+$. Elemental analysis calcd for $C_{24}H_{33}N_3RhPF_6$: C 47.15, H 5.44, N 6.87; found: C 46.43, H 5.33, 6.84.

3-PF_6: **1**-PF_6 (37 mg) was dissolved in MeOH (5 mL), and 35% aqueous H_2O_2 solution (0.1 mL) was added. The solution was stirred at room temperature for 1 h. Addition of Et_2O caused the precipitation of **3**-PF_6 as a light yellow powder, which was filtered, washed with Et_2O, and vacuum-dried. Yield 38 mg (100%). ^{1}H NMR (200.13 MHz, [D$_6$]acetone, 298 K): δ = 5.95 (m, 2H; OCH), 3.35–3.15 (m, 4H; NCH_2), 3.18 (s, 6H; NCH_3), 3.15–3.05 (m, 4H; NCH_2), 2.952.73 (m, 4H; NCH_2), 2.68 (m, 2H; RhCH), 2.63 (d, ^3J(Rh,H) = 1.7 Hz, 3H; NCH_3), 2.29–1.96 (m, 4H; RhCHCH_2-*exo*/OCHCH_2-*exo*), 1.53 (m, 2H; OCHCH_2-*endo*), 1.41 (m, 2H; RhCHCH_2-*endo*); ^{13}C{^{1}H} NMR (50.33 MHz, [D$_6$]acetone, 298 K): δ = 107.3 (d, ^2J(Rh,C) = 4.6 Hz; OCH), 62.3, 58.3, and 56.1 (NCH_2), 54.5 and 49.6 (NCH_3), 28.1 and 27.0 (RhCHCH_2/OCHCH_2), 21.7 (d, ^1J(Rh,C) = 23.0 Hz; RhCH). FAB-MS (*m*-Noba/CH_3CN): 398 $[M]^+$, 941 $[2M+PF_6]^+$. Elemental analysis calcd for $C_{17}H_{33}N_3ORhPF_6$: C 37.58, H 6.12, N 7.73; found: C 37.26, H 5.93, 7.65.

4b-PF_6: Prepared by a method similar to that of **3**-PF_6 except that the reaction was carried out at -10 °C. ^{1}H NMR (200.13 MHz, [D$_6$]acetone, 298 K): δ = 9.23 (d, ^3J(H,H) = 5.4 Hz, 1H; Py-H6), 8.50 (d, ^3J(H,H) = 5.6 Hz, 1H; Py-H6), 7.10–8.10 (m, 6H; Py-H4, Py-H5, and Py-H3), 6.08 (m, 1H; OCH), 6.04 (m, 1H; OCH), 4.85 (d[AB], ^2J(H,H) = 15.6 Hz, 1H; NCH_2Py), 4.67 (d[AB], ^2J(H,H) = 17.2 Hz, 1H; NCH_2-Py), 4.53 (d[AB], ^2J(H,H) = 15.6 Hz, 1H; NCH_2Py), 4.16 (d[AB], ^2J(H,H) = 17.2 Hz, 1H; NCH_2-Py), 3.90–3.45 (m, 2H; N$CH_2CH_2CH_2CH_3$), 3.42 (m, 1H; RhCH), 2.91 (m, 1H; RhCH), 2.3–2.0 (m, 4H; RhCHCH_2-*exo*/OCHCH_2-*exo*), 1.85–1.05 (m, 8H; OCHCH_2-*endo*/RhCHCH_2-*endo*/$NCH_2CH_2CH_2CH_3$/$NCH_2CH_2CH_2CH_3$), 0.91 (t, ^3J(H,H) = 7.4 Hz, 3H; $NCH_2CH_2CH_2CH_3$). ^{13}C{^{1}H} NMR (50.33 MHz, [D$_6$]acetone, 298 K): δ = 162.5 (Py_a-C2), 161.5 (Py_b-C2), 153.8 (Py_a-C6), 150.8 (Py_b-C6), 139.0 (Py_a-C4), 137.6 (Py_b-C4), 125.2 (Py_a-C3), 125.0 (Py_b-C3), 123.6 (Py_a-C5), 122.2 (Py_b-C5), 106.6 (d, ^2J(Rh,C) = 4.0 Hz; OCH_a), 105.7 (d, ^2J(Rh,C) = 4.0 Hz; OCH_b-), 66.4 ($NCH_2CH_2CH_2CH_3$), 63.3 (NCH_2-Py_a), 63.2 (NCH_2-Py_b), 28.8 ($NCH_2CH_2CH_2CH_3$), 28.2, 27.7, 26.7, and 26.6 (RhCHCH_2/OCHCH_2), 25.2 (d, ^1J(Rh,C) = 19.4 Hz; $RhCH_a$), 23.5 (d, ^1J(Rh,C) = 19.4 Hz; $RhCH_b$), 20.9 ($NCH_2CH_2CH_2CH_3$), 13.9 ($NCH_2CH_2CH_2CH_3$). FAB-MS (*m*-Noba/CH_3CN): 482 $[M]^+$. Elemental analysis calcd for $C_{24}H_{33}N_3ORhPF_6$: C 45.95, H 5.36, N 6.76; found: C 44.29, H 5.07, N 6.45.

5a-PF_6: [{Rh(μ-Cl)(ethene)$_2$}$_2$] (100 mg, 0.30 mmol) and tpa (150 mg, 0.54 mmol) were stirred in MeOH (25 mL) at -78 °C for 1 h. Subsequently KPF_6 (441 mg, 2.4 mmol) was added. Partial evaporation of the solvent caused the precipitation of **5a**-PF_6 as a yellow powder, which was filtered and vacuum-dried. Yield 200 mg (59%). In both the ^{1}H and ^{13}C NMR spectra of **5a** at 298 K, the ethene fragment is observed as two broad singlets. At 263 K the ethene fragment is observed as two double triplets in the ^{1}H NMR spectrum and two doublets in the ^{13}C NMR spectrum. ^{1}H NMR (500.14 MHz, [D$_6$]acetone, 263 K): δ = 9.43 (d, ^3J(H,H) = 4.7 Hz, 1H; Py_a-H6), 8.16 (d, 2H, ^3J(H,H) = 5.8 Hz, 2H; Py_b-H6), 7.90–7.10 (m, 9H; Py-H4, Py-H5, and Py-H3), 5.69 (d[AB], ^2J(H,H) = 15.6 Hz, 2H; NCH_2-Py_b), 5.02 (d[AB], ^2J(H,H) = 15.6 Hz, 2H; NCH_2-Py_b), 4.76 (s, 2H; NCH_2-Py_a), 2.11 (dt, ^3J(H,H) = 9.5 Hz, J(H,Rh) = 1.7 Hz, 2H; C_2H_4), 1.82 (dt, 2H, ^3J(H,H) = 9.5 Hz, J(Rh,H) = 1.7 Hz, 2H; C_2H_4); ^{13}C{^{1}H} NMR (125.77 MHz, [D$_6$]acetone, 263 K): δ = 163.9 (Py_b-C2), 159.6 (Py_a-C2), 151.9 (Py_a-C6), 151.4 (Py_b-C6), 138.1 (Py_a-C4), 137.3 (Py_b-C4), 125.2 (Py_b-C3), 124.4 (Py_a-C3), 123.1 (Py_b-C5), 122.2 (Py_a-C5), 69.6 (NCH_2-Py_b), 64.3 (NCH_2-Py_a), 27.2 (d, J(C,Rh) = 18.0 Hz; C=C), 25.0 (d, J(C,Rh) = 19.7 Hz; C=C). FAB-MS (*m*-Noba/CH_3CN): 421 $[M]^+$, 589 $([M + Na + PF_6]^+$, 393 $[M - C_2H_4]^+$. Elemental analysis calcd for $C_{20}H_{22}N_4RhPF_6$: C 42.42, H 3.93, N 9.98; found: C 40.54, H 3.60, N 9.70. The same procedure with $NaBF_4$ gave **5a**-BF_4. Calculated for $C_{20}H_{22}N_4RhBF_4$: C 47.28, H 4.36, N 11.03; found: C 47.25, H 4.46, N 10.80.

5b-BPh_4: Prepared by a procedure similar to that of **5a**-PF_6, with Me-tpa and 1 equiv $NaBPh_4$. ^{1}H NMR (200.13 MHz, CD_2Cl_2, 298 K): δ = 7.86 (d, ^3J(H,H) = 5.3 Hz, 2H; Py_a-H6), 7.55–6.65 (m, 9H; Py-H4, Py-H5, and Py-H3), 7.37 (m, 8H; BAr-H2), 7.02 (t, ^3J(H,H) = 7.4 Hz, 8H; BAr-H3), 6.87 (t, ^3J(H,H) = 7.4 Hz, 4H; BAr-H4), 5.07 (d[AB], ^2J(H,H) = 15.3 Hz, 2H; NCH_2-Py_b), 4.23 (d[AB], ^2J(H,H) = 15.3 Hz, 2H; NCH_2-Py_b), 4.11 (s, 2H; NCH_2-Py_a), 3.33 (s, 3H; Py_a-CH_3), 2.07 (br. s, 2H; C_2H_4), 1.94 (br. s, 2H; C_2H_4). FAB-MS (*m*-Noba/CH_2Cl_2): 435 $[M]^+$, 407 $[M - C_2H_4]^+$. Elemental analysis calcd for $C_{45}H_{44}BN_4Rh$: C 71.63, H 5.88, N 7.42; found: C 71.15, H 5.93, N 7.42.

6a-PF_6: **5a**-PF_6 (50 mg) was dissolved in MeOH (5 mL) and 35% aqueous H_2O_2 solution (0.1 mL) was added. The solution was stirred at -10 °C for 1 h. Addition of Et_2O caused the precipitation of **6a**-PF_6 as a pale yellow powder, which was filtered, washed with Et_2O, and vacuum-dried. Yield 51 mg (100%). ^{1}H NMR (200.13 MHz, [D$_6$]acetone, 298 K): δ = 9.03 (d, ^3J(H,H) = 5.7 Hz, 1H; Py_b-H6), 8.70 (d, ^3J(H,H) = 5.5 Hz, 2H; Py_a-H6), 8.10–7.20 (m, 9H; Py-H4, Py-H5, and Py-H3), 5.32 (d[AB], ^2J(H,H) = 15.4 Hz, 2H; NCH_2-Py_b), 5.13 (d[AB], ^2J(H,H) = 15.4 Hz, 2H; NCH_2-Py_b), 5.04 (s, 2H; NCH_2-Py_a), 4.97 (t,

 © WILEY-VCH Verlag GmbH, D-69451 Weinheim, 1997 0570-0833/97/3619-2066 $ 17.50+.50/0

^3J(H,H) = 7.5 Hz, 2H; RhCH$_2$CH$_2$O), 2.90 (s, approx. 3H; H$_2$O), 2.35 (dt, ^3J(H,H) = 7.5 Hz, ^2J(H,Rh) = 2.5 Hz, 2H; RhCH$_2$CH$_2$O); ^{13}C{^{1}H} NMR (50.33 MHz, [D$_6$]acetone, 298 K): δ = 165.4 (Py$_b$-C2), 162.6 (Py$_a$-C2), 151.9 (Py$_b$-C6), 150.9 (Py$_a$-C6), 139.4 (Py$_b$-C4), 138.4 (Py$_a$-C4), 125.9 (Py$_b$-C3), 125.1 (Py$_a$-C3), 124.6 (Py$_b$-C5), 122.2 (Py$_a$-C5), 78.8 (d, ^2J(Rh,C) = 4.0 Hz; RhCH$_2$CH$_2$O), 66.8 (NCH$_2$-Py$_b$), 64.7 (NCH$_2$-Py$_a$), 1.3 (d, ^1J(C,Rh) = 18.4 Hz; RhCH$_2$CH$_2$O). FAB-MS (*m*-Noba/CH$_3$CN): 437 [*M*]$^+$, 393 [*M* − CH$_2$CH$_2$O]$^+$. Compound **6a** appears to coprecipitate with H$_2$O: elemental analysis calcd for **6a**-PF$_6$·1.5H$_2$O (C$_{20}$H$_{25}$N$_4$O$_{2.5}$RhPF$_6$): C 39.42, H 4.14, N 9.20; found: C 38.60, H 3.62, N 9.41. The same procedure with NaBPh$_4$ gave [**6a**](BPh$_4$). Calcd for [**6a**]-BPh$_4$·1.5H$_2$O (C$_{44}$H$_{45}$N$_4$O$_{2.5}$RhB): C 57.44, H 5.79, N 7.15; found: C 67.15, H 5.43, N 7.04.

6b-[BPh$_4$]: [{(C$_2$H$_4$)$_2$Rh(μ-Cl)}$_2$] (200 mg, 0.51 mmol) and Me-tpa (320 mg, 1.05 mmol) were added to MeOH (25 mL) at −78 °C, and stirred for 1 h. A 35% aqueous solution of H$_2$O$_2$ (0.2 mL) was added, and the solution was allowed to slowly warm up to room temperature. Any undissolved material was removed by filtration. NaBPh$_4$ (0.36 mg, 1.06 mmol) in MeOH (7 mL) was added to the solution, causing the precipitation of a light yellow solid, which was collected by filtration. After recrystalization from dichloromethane/hexane, pure **6b**-BPh$_4$·1.5H$_2$O was obtained as bright yellow crystals, suitable for X-ray diffraction. Yield 654 mg (64%). ^{1}H NMR (200.13 MHz, CD$_2$Cl$_2$, 298 K): δ = 8.77 (d, ^3J(H,H) = 5.6 Hz, 2H; Py$_a$-H6), 7.80–6.50 (m, 9H; Py-H4, Py-H5, and Py-H3), 7.36 (m, 8H; BAr-H2, 7.01 (t, ^3J(H,H) = 7.4 Hz, 8H; BAr-H3), 6.86 (t, ^3J(H,H) = 7.4 Hz, 4H; BAr-H4), 4.81 (d[AB], ^2J(H,H) = 15.3 Hz, 2H; NCH_2-Py$_b$), 4.80 (t, ^3J(H,H) = 7.6 Hz, 2H; RhCH$_2$CH_2O), 4.29 (d[AB], ^2J(H,H) = 15.3 Hz, 2H; NCH_2-Py$_b$), 4.10 (s, 2H; NCH$_2$-Py$_a$), 2.90 (s, 3H; H$_2$O), 2.83 (s, 3H; Py$_a$-CH$_3$), 2.35 (dt, ^3J(H,H) = 7.6 Hz, ^2J(H,Rh) = 2.6 Hz. 2H, RhCH_2CH$_2$O); ^{13}C{^{1}H} NMR (75.47 MHz, CD$_2$Cl$_2$, 298 K): δ = 164.7 (q, ^1J(C,B) = 48.6 Hz; BAr-C1), 164.5 (Py$_b$-C2), 164.2 (Py$_a$-C2), 161.6 (Py$_a$-C6), 152.5 (Py$_b$-C6), 139.5 (Py$_b$-C4), 138.5(Py$_a$-C4), 136.8 (BAr-C2), 125.8 (q, ^3J(C,B) = 2.8 Hz; BAr-C3), 126.2 (Py$_b$-C3), 125.8 (Py$_a$-C3), 124.6 (Py$_b$-C5), 122.8 (BAr-C4), 119.6 (Py$_a$-C5), 80.6 (d, ^2J(Rh,C) = 4.2 Hz; RhCH$_2$CH$_2$O), 66.6 (NCH$_2$-Py$_b$), 65.5 (NCH$_2$-Py$_a$), 26.7 (Py$_a$-CH$_3$), 2.5 (d, ^1J(C,Rh) = 18.0 Hz; RhCH$_2$CH$_2$O). FAB-MS (*m*-Noba/CH$_2$Cl$_2$): 451 [*M*]$^+$, 407 [*M* − CH$_2$CH$_2$O]$^+$. Elemental analysis calcd for **6b**-BPh$_4$·1.5H$_2$O (C$_{45}$H$_{47}$BN$_4$O$_{2.5}$Rh): C 67.76, H 5.94, N 7.02; found: C 66.96, H 5.81, N 6.94.

Received: April 8, 1997 [Z10346IE]
German version: *Angew. Chem.* **1997**, *109*, 2153–2157

Keywords: alkene complexes · N ligands · oxidations · peroxides · rhodium

[1] See, for example, a) F. Freeman, C. O. Fuselier, C. R. Armstead, C. E. Dalton, P. A. Davidson, E. M. Karchesfski, D. E. Krochman, M. N. Johnson, N. K. Jones, *J. Am. Chem. Soc.* **1981**, *103*, 1154; b) D. G. Lee, N. A. Noureldin, *ibid.* **1983**, *105*, 3188; c) A. K. Rappé, W. A. Goddard, *ibid.* **1982**, *104*, 3287; d) M. Schröder, E. C. Constable, *J. Chem. Soc. Chem. Commun.* **1982**, 734.

[2] Excellent overviews: a) K. A. Jørgensen, *Chem. Rev.* **1989**, *89*, 431; b) K. A. Jørgensen, B. Schiøtt, *ibid.* **1990**, *90*, 1483.

[3] J. Blum, B. Zinger, D. Milstein, O. Buchman, *J. Org. Chem.* **1978**, *43*, 2961

[4] J. Bakos, Á. Orosz, S. Cserépi, I. Tóth, D. Sinou, *J. Mol. Catal. A* **1997**, *116*, 85

[5] a) A. A. Zlota, F. Frolow, D. Milstein, *J. Am. Chem. Soc.* **1990**, *112*, 6411; b) M. J. Calhorda, A. M. Galvão, C. Ünaleroglu, A. A. Zlota, F. Frolow, D. Milstein, *Organometallics* **1993**, *12*, 3316

[6] 2-metallaoxetanes stabilized by exocyclic double bonds have been synthesized by the reaction of a peroxo–metal complex with a ketene: a) S. Baba, T. Ogura, S. Kawaguchi, H. Tokunan, Y. Kai, N. Kashi, *J. Chem. Soc. Chem. Commun.* **1972**, 910; b) L. Pandolfo, G. Paiaro, G. Valle, P. Ganis, *Gazz. Chim. Ital.* **1985**, *115*, 65; c) W. A. Herrmann, U. Küsthardt, A. Schäfer, E. Herdtweck, *Angew. Chem.* **1986**, *98*, 818; *Angew. Chem. Int. Ed. Engl.* **1986**, *25*, 817.

[7] a) R. Schlodder, J. A. Ibers, M. Lenarda, M. Graziani, *J. Am. Chem. Soc.* **1974**, *96*, 6893; b) M. Lenarda, N. B. Pahor, M. Calligaris, M. Graziani, L. Randaccio, *J. Chem. Soc. Dalton Trans.* **1978**, 279.

[8] D. P. Klein, J. C. Hayes, R. G. Bergman, *J. Am. Chem. Soc.* **1988**, *110*, 3704.

[9] In [Ir^{III}(P$_3$O$_9$)(O-cod)]$^{2-}$ the C atoms of one double bond of the cod ligand are connected by an Fr and on O atom to form a 2-iridaoxetane ring. V. W. Day, W. G. Klemperer, S P. Lockledge, D. J. Main, *J. Am. Chem. Soc.* **1990**, *112*, 2031

[10] The structures of compound **1** and a dinuclear analogue of **2** have been determined by X-ray diffraction (as yet unpublished).

[11] Most of the ^{1}H NMR signals of **4a** are obscured by those of **4b**, yet some characteristic signals indicate its formation: ^{1}H NMR (200.13 MHz, [D$_6$]acetone, 298 K): δ = 8.95 (d, ^3J(H,H) = 5.4 Hz, 2H, Py-H6), 5.92 (m, 2H, OC*H*), 2.77 (m, 2H, RhC*H*).

[12] In solution, the η^4-cod fragment of **2** appears to be rotating fast on the NMR timescale from T = 298 K to at least 183 K. This (pseudo)rotation is interpreted as a rapid interchange of the trigonal-bipyramidal and square-pyramidal coordination geometry of **2**. The formation of the two isomers **4a** and **4b** at room temperature upon oxidation of **2** possibly results from H$_2$O$_2$ attack at both geometrical structures and the distribution results from a kinetic preference for one of them.

[13] Pale yellow crystals of **3**-PF$_6$ were obtained by slow crystallization from a saturated methanolic solution. The X-ray diffraction data were collected at 150 K on an Enraf-Nonius CAD4T diffractometer with graphite monochromatized Mo$_{K\alpha}$ (λ = 0.710730 Å). The structure was solved by the program system DIRDIF [24a], and the program PATTY [24b] was used to locate the heavy atoms. Crystal data for **3**-PF$_6$: C$_{17}$H$_{33}$F$_6$N$_3$OPRh, M_r = 543.34, monoclinic, space group $P2_1/c$ (no. 14, a = 10.2472(10), b = 13.0331(8), c = 15.5345(8) Å, β = 90.012(6)°, V = 2074.7(3) Å^3, Z = 4, ρ_{calcd} = 1.740 g cm^{-3}. All hydrogen atoms were placed at calculated positions and were subsequently freely refined. Final R indices: R_1 = 0.0441 (for 3399 reflections considered observed ($I > 2\sigma(I)$), wR_2 = 0.0929 (all data) for all 394 parameters. Crystal data for **6b**-BPh$_4$·1.5H$_2$O: C$_{45}$H$_{47}$BN$_4$O$_{2.5}$Rh, M_r = 794.56, triclinic, space group $P\bar{1}$, a = 9.3022(3), b = 11.8120(2), c = 18.3852(4) Å, α = 78.781(5), β = 88.275(3), γ = 85.428(3)°, V = 1974.99(8) Å^3, Z = 2, ρ_{calcd} = 1.336 g cm^{-3}. The X-ray diffraction data were collected at 173 K on an Enraf-Nonius CAD4 diffractometer with graphite monochromatized Cu$_{K\alpha}$ (λ = 1.541838 Å). The structure was solved by the program system DIRDIF [24a], and the program PATTY [24b] was used to locate the heavy atoms. The initial results showed severe disorder. The structure then proved to be a pseudocentrosymmetric arrangement of two cations, two anions, and three water molecules per unit cell (in spacegroup $P1$), which could be adequately refined with an inversion-disorder model in space group $P\bar{1}$. The non-rhodium atoms were subjected to restrained refinement procedures (SHELXL-93) [c]. Final R indices: R_1 = 0.0566 (for 6908 reflections considered observed ($I > 2\sigma(I)$), wR_2 = 0.1786 (all data) for all 727 parameters. Crystallographic data (excluding structure factors) for the structures reported in this paper have been deposited with the Cambridge Chrystallographic Data Centre as supplementary publication no. CCDC-100377. Copies of the data can be obtained free of charge on application to The Director, CCDC, 12 Union Road, Cambridge CB21EZ, UK (fax: int. code +(1223)336-033; e-mail: deposit@chemcrys.cam.ac.uk)

[14] a) D. M. Walba, M. D. Wand, M. C. Wilkes, *J. Am. Chem. Soc.* **1979**, *101*, 4396; b) J. E. Baldwin, M. J. Crossley, E. M. M. Lehtonen, *J. Chem. Soc. Chem. Commun.* **1979**, 918.

[15] D. R. Russell, P. A. Tucker, *J. Chem. Soc. Dalton.* **1976**, 841.

[16] a) M. Alvarez, N. Lugan, R. Mathieu, *J. Organomet. Chem.* **1994**, *468*, 249; b) R. Graziani, G. Bombieri, L. Volponi, C. Panattoni, R. J. H. Clark, *J. Chem. Soc. A* **1969**, 1236; c) S. C. Haefner, K. R. Dunbar, C. Bender, *J. Am. Chem. Soc.* **1991**, *113*, 9540; d) G. E. Efe, E. O. Schlemper, *Polyhedron* **1991**, *10*, 1611; e) E. Lindner, Q. Wang, H. A. Meyer, R. Fawzi, M. Steimann, *J. Organomet. Chem.* **1993**, *453*, 289; f) S. J. Chadwell, S. J. Coles, P. G. Edwards, M. B. Hursthouse, *J. Chem. Soc.Dalton Trans.* **1995**, 3551.

[17] Reaction at room temperature results in a mixture of **6a** and at least one other compound, possibly a geometrical isomer of **6a**.

[18] H. Nagao, N. Komeda, M. Mukaida, M. Suzuki, K. Tanaka, *Inorg. Chem.* **1996**, *35*, 6809

[19] R. Cramer, J. A. McCleverty, J. Bray, *Inorg. Synth.* **1990**, *28*, 86.

[20] a) S. E. Kegley, C. J. Schaverien, J. H. Freudenberger, R. G. Bergman, S. P. Nolan, C. D. Hoff, *J. Am. Chem. Soc.* **1987**, *109*, 6563; b) Y. J. Kim, K. Osakada, A. Takenaka, A, Yamamoto, *ibid.* **1990**, *112*, 1096; c) G. M. Kapteijn, A. Dervisi, D. M. Grove, H. Kooijman, M. T. Lakin, A. L. Spek, G. van Koten, *ibid.* **1995**, *117*, 10939; d) C. D. Bugno, M. Pasquali, P. leoni, P. Sabatino, D. Braga, *Inorg. Chem.* **1989**, *28*, 1390.

[21] a) M. P. Doyle, W. R. Winchester, S. H. Simonsen, R. Ghosh, *Inorg. Chim. Acta* **1994**, *220*, 193; b) P. Caddy, M. Green, J. A. K. Howard, J. M. Squire, N. J. White, *J. Chem. Soc. Dalton Trans.* **1981**, 400; c) M. A. Calvo, A. M. M. Lanfredi, L. A. Oro, M. R. Pinillos, C. Tejel, A. Tiripicchio, F. Ugozzoli, *Inorg. Chem.* **1993**, *32*, 1147.

[22] G. Giordano, R. H. Crabtree, *Inorg. Synth.* **1990**, *28*, 88.

[23] The ligand dpbn has been prepared by a method similar to that reported for tpen: H. Toftlund, S. Yde-Andersen, *Acta Chem. Scand. Ser. A* **1981**, *35*, 575.

[24] a) DIRDIF-96 (a computer program system for crystal structure determination by Patterson methods and direct methods applied to difference structure factors): P. T. Beurskens, G. Beurskens, W. P. Bosman, R. de Gelder, S. Garcia-Granda, R. O. Gould, R. Israel, J. M. M. Smits, Laboratory of Crystallography, Department of Inorganic Chemistry, University of Nijmegen, The Netherlands, **1996**; b) P. T. Beurskens, G. Beurskens, M. Strumpel, C. E. Nordman in *Patterson and Pattersons* (Eds.: J. P. Glusker, B. K. Patterson, M. Rossi), Clarendon, Oxford, **1987**, p. 356; c) SHELXL-93 (program for the refinement of crystal structures), G. M. Sheldrick, University of Göttingen (Germany), **1993**.

 © WILEY-VCH Verlag GmbH, D-69451 Weinheim, 1997 0570-0833/97/3619-2067 $ 17.50+.50/0

Anion-Assisted Self-Assembly**

Matthew C. T. Fyfe, Peter T. Glink, Stephan Menzer, J. Fraser Stoddart,* Andrew J. P. White, and David J. Williams*

Dedicated to Professor Dieter Seebach on the occasion of his 60th birthday

On account of its pivotal role in several essential chemical and biological processes, anion binding and recognition[1] is currently arousing considerable attention within the domain of supramolecular chemistry.[2] Traditionally, supramolecular chemists have positioned anion recognition sites within covalent macro(poly)cyclic frameworks[3] in a preorganized[4] manner, so as to achieve strong anion binding. However, the discovery of self-assembled[5] supermolecules that are capable of binding anions has been accomplished,[6] as supramolecular science has developed. Nevertheless, to the best of our knowledge, there has been no report to date of a self-assembled anion receptor whose components are held together *entirely* by hydrogen bonds. We describe here the discovery of two novel supermolecules—self-assembled utilizing only hydrogen bonds—which display either partial or complete envelopment of PF_6^- ions in the solid state.

Recently, we reported[7] that macrocyclic polyethers form inclusion complexes, termed pseudorotaxanes,[8] of varying stoichiometries with secondary dibenzylammonium ions. In these pseudorotaxanes the ammonium ions are threaded through the macrorings and are held in place by a combination of $[N^+-H\cdots O]$ and $[C-H\cdots O]$ hydrogen bonds, with occasional assistance from $\pi-\pi$ stacking interactions. For instance, the ditopic crown ether bis-*p*-phenylene[34]crown-10 (BPP34C10) has been shown[7] to form complexes with the dibenzylammonium ion (**1**-H^+), in which two of these threadlike cations interpenetrate the macroring's void simultaneously to form (Figure 1) a double-stranded [3]pseudorotaxane. While researching these systems, we became intrigued by the possibility that higher homologues[9] of BPP34C10—specifically, the crown ethers tris-*p*-phenylene[51]crown-15 (TPP51C15) and tetrakis-*p*-phenylene[68]crown-20 (TPP68C20)—could incorporate three and four **1**-H^+ cations within their respective cavities. Moreover, on account of the increased dimensions of the circumferences of their crown ether precursors, the resultant [4]- and [5]pseudorotaxanes should possess ammonium centers ideally predisposed to associate with anions by means of hydrogen bonding and anion–dipole interactions, that is, where the macrocyclic polyethers effect supramolecular preorganization[10] of the anion binding sites. Indeed, we have found (vide infra) that the $[TPP51C15\cdot(\mathbf{1}\text{-}H)_3]^{3+}$ and $[TPP68C20\cdot(\mathbf{1}\text{-}H)_4]^{4+}$

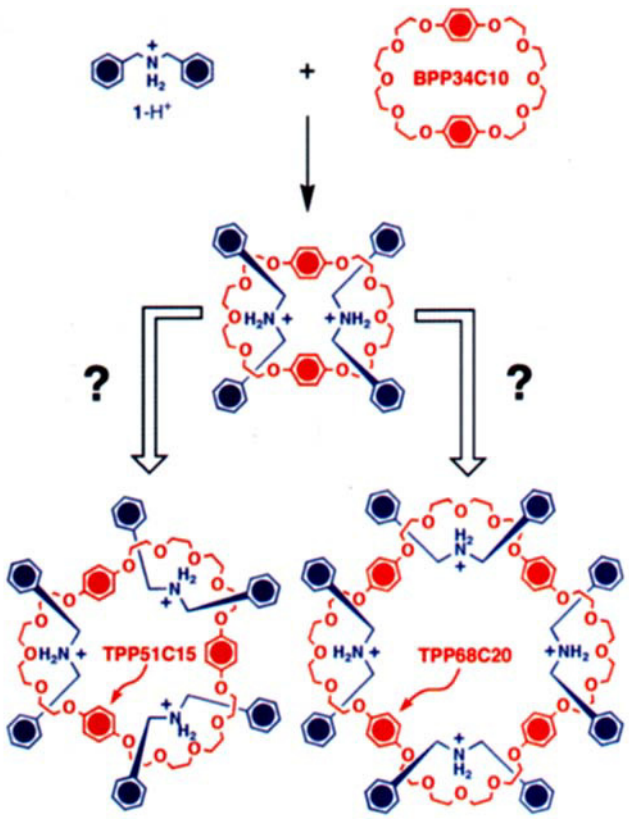

Figure 1. Complexation of the dibenzylammonium ion (**1**-H^+) with the crown ether BPP34C10 yields a double-stranded [3]pseudorotaxane. The question is: would larger macrocycles such as TPP51C15 and TPP68C20 allow the concurrent threading of three and four **1**-H^+ ions through their respective cavities?

pseudorotaxanes interact with PF_6^- ions in the solid state. Furthermore, it appears that the bound anions can dictate the overall three-dimensional topology of the pseudorotaxane complexes, thus assisting the overall self-assembly processes.[11]

TPP51C15 is capable of extracting three molar equivalents of [**1**-H]PF_6 from a suspension of a large excess of the salt in CD_2Cl_2. Since [**1**-H]PF_6 is practically insoluble in this solvent in the absence of the crown ether, this observation provides a semiquantitative guide to the likely stoichiometry of the complex. Analysis of the resulting CD_2Cl_2 solution by ^1H NMR spectroscopy reveals[12] significant chemical shift changes for the proton resonances associated with both species, indicative of host–guest complex formation. An analysis of a single crystal (obtained by liquid diffusion of *n*-hexane into a 1:3 molar mixture of TPP51C15 and [**1**-H]PF_6 in CH_2Cl_2) by X-ray crystallography[13] revealed the solid-state structure depicted in Figure 2. The complex's supramolecular architecture corresponds

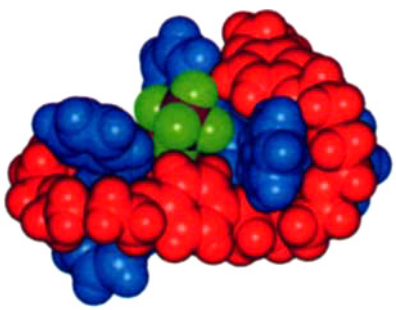

Figure 2. Space-filling representation of the $[TPP51C15\cdot(\mathbf{1}\text{-}H)_3\cdot PF_6]^{2+}$ superstructure formed in the solid state, depicting both the threading of the three **1**-H^+ cations (blue) through the cavity of the macrocyclic polyether TPP51C15 (red), and the coordination of a PF_6^- ion (phosphorus in purple, fluorines in green) within the cleft formed by the $[TPP51C15\cdot(\mathbf{1}\text{-}H)_3]^{3+}$ complex.

[*] Prof. J. F. Stoddart,[+] M. C. T. Fyfe, Dr. P. T. Glink
School of Chemistry, University of Birmingham
Edgbaston, Birmingham B15 2TT (UK)
Prof. D. J. Williams, Dr. S. Menzer, Dr. A. J. P. White
Chemical Crystallography Laboratory
Department of Chemistry, Imperial College
South Kensington, London SW7 2AY (UK)
Fax: Int. code +(171) 594-5804

[+] Current address:
Department of Chemistry and Biochemistry
University of California at Los Angeles
405 Hilgard Avenue, Los Angeles, CA 90095 (USA)
Fax: Int. code +(310) 206-1843
e-mail: stoddart@chem.ucla. edu

[**] This research was funded in the UK primarily by the ZENECA Strategic Research Fund, and was supported additionally by the Biotechnology and Biological Sciences Research Council and the Engineering and Physical Sciences Research Council.

 © WILEY-VCH Verlag GmbH, D-69451 Weinheim, 1997 0570-0833/97/3619-2068 $ 17.50+.50/0

to a triple-stranded [4]pseudorotaxane, in which each of the enthreaded **1**-H^+ ions is independently involved in stabilizing $[N^+-H\cdots O]$ and $[C-H\cdots O]$ hydrogen bonding interactions with TPP51C15's separate polyether loops. The macroring adopts a folded conformation with approximate C_s symmetry. A closer investigation of the location of the three PF_6^- ions reveals that one of the three anions is located almost centrally within a cleft generated by the saddlelike co-conformation[14] of the 1:3 complex (Figure 2). Complexation of this anion is achieved by a series of $[C-H\cdots F]$ hydrogen bonds to hydrogen atoms on the hydroquinone rings of the crown ether and the benzylic methylene groups of the bound **1**-H^+ ions. Hence, the crown ether participates simultaneously in both of the anion's first and second coordination spheres.[15] A noticeable feature of this binding is the order bestowed upon the bound PF_6^- ion.

This discovery of partial anion envelopment by the $[TPP51C15\cdot(\mathbf{1}\text{-}H)_3]^{3+}$ supermolecule led us to believe that the total encapsulation of anions by self-assembled pseudorotaxane superstructures of this type could be achieved with suitably expanded crown ethers. Four molar equivalents of the [**1**-H]PF_6 salt are solubilized in a CD_2Cl_2 solution containing one molar equivalent of TPP68C20. Significant changes in the chemical shifts of probe protons in both the salt and the crown ether are observed[16] in the ^1H NMR spectrum of this solution, suggesting that cation complexation is occurring in this solvent. Single crystals were obtained when a 1:4 molar solution of TPP68C20 and [**1**-H]PF_6 in CH_2Cl_2 was layered with *n*-hexane. The X-ray analysis[13] of one of these crystals reveals that, when the macrocyclic polyether is extended by an additional hydroquinone-spaced polyether loop, a crystalline aggregate results which contains two independent quadruple-stranded [5]pseudorotaxane complexes (Figure 3). The asymmetric unit also

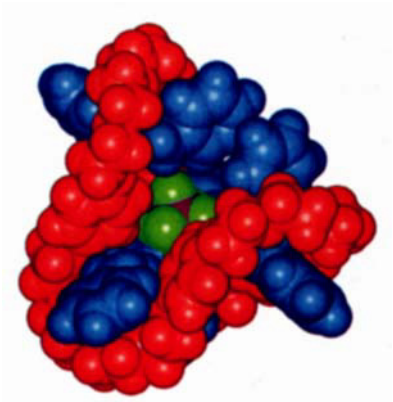

Figure 3. Space-filling view of one of the $[TPP68C20\cdot(\mathbf{1}\text{-}H)_4\cdot PF_6]^{3+}$ supermolecules formed in the solid state, illustrating both the threading of the four **1**-H^+ ions (blue) through the cavity of the macrocyclic polyether TPP68C20 (red), and the encapsulation of a PF_6^- ion (phosphorus in purple, fluorines in green) within the cavity formed by the $[TPP68C20\cdot(\mathbf{1}\text{-}H)_4]^{4+}$ complex. The $[H\cdots F]$ distances range between 2.41 and 2.73 Å; the associated $[C\cdots F]$ contacts are between 3.16 and 3.52 Å.

accommodates a pair of unassociated C_s-symmetric dibenzylammonium ions with their allied PF_6^- counterions. The two [5]pseudorotaxane complexes have essentially identical co-conformations[14]; the TPP68C20 macrocycle adopts a conformation that possesses local S_4 symmetry and resembles the seam of a tennis ball. The four dibenzylammonium ions are clipped over each of the macrocycle's four polyether loops. The tetracationic complex is stabilized by a combination of $[N^+-H\cdots O]$ and $[C-H\cdots O]$ hydrogen bonds between both the ammonium centers' hydrogen atoms and their adjacent CH_2 groups and the polyether's oxygen atoms. On the other hand, the remaining cations, which lie on the crystallographic C_s plane, are not involved in any hydrogen bonding interactions. The most striking feature of both independent [5]pseudorotaxane complexes is the siting of a single PF_6^- ion at each of their cores in ordered arrangements (Figure 3). In this case, the anion is totally encapsulated[17] by both the four hydroquinone rings, which are oriented with their planes intersecting on the phosphorus center, and the four tetrahedrally disposed, positively charged $CH_2-NH_2^+-CH_2$ regions of the four **1**-H^+ cations. The phosphorus atoms lie only about 0.3 Å from the complexes' centroids. In view of the "spherical" shape of PF_6^- ions, they tend to assume random orientations in crystal lattices. However, in this example, the anion is fully ordered—an ordering which is undoubtedly a consequence of a series of $[C-H\cdots F]$ hydrogen bonds, involving the cooperative action of hydroquinone methine and benzylic methylene hydrogen atoms which, in addition to coulombic forces, direct the physical envelopment of the anion. Thus, the self-assembled [5]pseudorotaxanes provide elegant concentric spheres of cationic and neutral ligands for the total encapsulation of the anions (Figure 4).

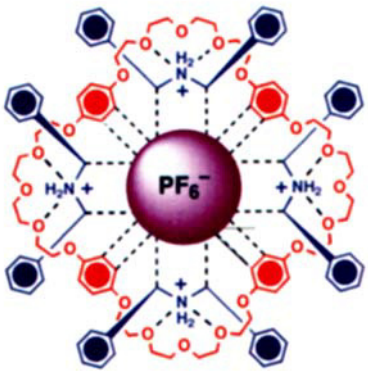

Figure 4. Cartoon representation of the $[TPP68C20\cdot(\mathbf{1}\text{-}H)_4\cdot PF_6]^{3+}$ superstructure.

It is not unreasonable to conclude that the enfolded geometries of the 1:4:1 complexes—and, indeed, the 1:3:1 complex as well—have been programmed by the negatively charged PF_6^- ions; that is, the supramolecular system could be equally well viewed as receiving its instructions from the anionic core, which are then relayed through a four-component, tetracationic, first sphere to the neutral, second-sphere ligand.

Received: March 12, 1997 [Z10232IE]
German version: *Angew. Chem.* **1997**, *109*, 2158–2160

Keywords: anion complexation · host–guest chemistry · noncovalent interactions · self-assembly · supramolecular chemistry

[1] Recent reviews: a) P. D. Beer, *Chem. Commun.* **1996**, 689–696; b) J. L. Atwood, K. T. Holman, J. W. Steed, *ibid.* **1996**, 1401–1407; c) J. Scheerder, J. F. J. Engbersen, D. N. Reinhoudt, *Recl. Trav. Chim. Pays-Bas* **1996**, *115*, 307–320.

[2] J.-M. Lehn, *Supramolecular Chemistry—Concepts and Perspectives*, VCH, Weinheim, **1995**.

[3] For instance, see: a) B. Dietrich, J. Guilhem, J.-M. Lehn, C. Pascard, E. Sonveaux, *Helv. Chim. Acta* **1984**, *67*, 91–104; b) K. Worm, F. P. Schmidtchen, A. Schier, A. Schäfer, M. Hesse, *Angew. Chem.* **1994**, *106*, 360–362; *Angew. Chem. Int. Ed. Engl.* **1994**, *33*, 327–329; c) K. Ichikawa, M. A. Hossain, *Chem. Commun.* **1996**, 1721–1722.

[4] a) D. J. Cram, *Angew. Chem.* **1986**, *98*, 1041–1060; *Angew. Chem. Int. Ed. Engl.* **1986**, *25*, 1039–1057; b) D. J. Cram, *ibid.* **1988**, *100*, 1041–1052 and **1988**, *27*, 1009–1020.

 © WILEY-VCH Verlag GmbH, D-69451 Weinheim, 1997 0570-0833/97/3619-2069 $ 17.50+.50/0

[5] a) D. S. Lawrence, T. Jiang, M. Levett, *Chem. Rev.* **1995**, *95*, 2229–2260; b) D. Philp, J. F. Stoddart, *Angew. Chem.* **1996**, *108*, 1242–1286; *Angew. Chem. Int. Ed. Engl.* **1996**, *35*, 1154–1196.

[6] a) D. M. Rudkevich, W. Verboom, Z. Brzozka, M. J. Palys, W. P. R. V. Stauthamer, G. J. van Hummel, S. M. Franken, S. Harkema, J. F. J. Engbersen, D. N. Reinhoudt, *J. Am. Chem. Soc.* **1994**, *116*, 4341–4351; b) B. Hasenknopf, J.-M. Lehn, B. O. Kneisel, G. Baum, D. Fenske, *Angew. Chem.* **1996**, *108*, 1987–1990; *Angew. Chem. Int. Ed. Engl.* **1996**, *35*, 1838–1840; c) R. W. Saalfrank, S. Trummer, H. Krautscheid, V. Schünemann, A. X. Trautwein, S. Hien, C. Stadler, J. Daub, *ibid.* **1996**, *108*, 2350–2352 and **1996**, *35*, 2206–2208; d) S. Mann, G. Huttner, L. Zsolnai, K. Heinze, *ibid.* **1996**, *108*, 2983–2984 and **1996**, *35*, 2808–2809.

[7] a) P. R. Ashton, E. J. T. Chrystal, P. T. Glink, S. Menzer, C. Schiavo, N. Spencer, J. F. Stoddart, P. A. Tasker, A. J. P. White, D. J. Williams, *Chem. Eur. J.* **1996**, *2*, 709–728; b) P. T. Glink, C. Schiavo, J. F. Stoddart, D. J. Williams, *Chem. Commun.* **1996**, 1483–1490; c) P. R. Ashton, P. T. Glink, M.-V. Martinez-Diaz, J. F. Stoddart, A. J. P. White, D. J. Williams, *Angew. Chem.* **1996**, *108*, 2058–2061; *Angew. Chem. Int. Ed. Engl.* **1996**, *35*, 1930–1933.

[8] Pseudorotaxanes have been defined as inclusion complexes in which one or more threadlike molecules (or ions) are encircled by one or more macrocyclic molecules (or ions) in the absence of an intercomponent mechanical or covalent bond. Consequently, pseudorotaxanes are free to dissociate into their separate components. The prefix [*n*] implies that an [*n*]pseudorotaxane is comprised of *n* components. For instance, the 1:2 complex $[BPP34C10\cdot(\mathbf{1}\text{-}H)_2]^{2+}$ depicted in Figure 1 is a double-stranded [3]pseudorotaxane.

[9] D. B. Amabilino, P. R. Ashton, C. L. Brown, E. Córdova, L. A. Godínez, T. T. Goodnow, A. E. Kaifer, S. P. Newton, M. Pietraszkiewicz, D. Philp, F. M. Raymo, A. S. Reder, M. T. Rutland, A. M. Z. Slawin, N. Spencer, J. F. Stoddart, C. Vicent, D. J. Williams, *J. Am. Chem. Soc.* **1995**, *117*, 1271–1293.

[10] P. R. Ashton, A. N. Collins, M. C. T. Fyfe, S. Menzer, J. F. Stoddart, D. J. Williams, *Angew. Chem.* **1997**, *109*, 760–763; *Angew. Chem. Int. Ed. Engl.* **1997**, *36*, 735–739.

[11] For other examples of anion-controlled self-assembly, see: J. L. Sessler, A. Andrievsky, P. A. Gale, V. Lynch, *Angew. Chem.* **1996**, *108*, 2954–2957; *Angew. Chem. Int. Ed. Engl.* **1996**, *35*, 2782–2785, and references therein.

[12] $\Delta\delta$ values for the resonances associated with the polyether's α-, β-, γ-, δ-OCH_2 and hydroquinone methine protons [solution of TPP51C15 (approximately 5×10^{-3} M) and [**1**-H]PF_6 (approximately 1.5×10^{-2} M) in CD_2Cl_2 at 20 °C]: $\delta = 0.00, -0.17, -0.29, -0.36, +0.13$.

[13] Crystal data for $[TPP51C15\cdot(\mathbf{1}\text{-}H)_3][PF_6]_3\cdot2CH_2Cl_2$, $M_r = 2004.5$, orthorhombic, $a = 19.592(1)$, $b = 25.240(1)$, $c = 20.117(3)$ Å, $V = 9948(2)$ Å^3, space group $Pca2_1$, $Z = 4$, $\rho_{calcd} = 1.338$ g cm^{-3}, $\mu(Cu_{K\alpha}) = 23.5$ cm^{-1}, $\lambda = 1.54178$ Å, $F(000) = 4176$, $T = 293$ K, 6518 unique reflections ($\theta \le 60°$), of which 3846 were observed [$I_o > 2\sigma(I_o)$]. Final *R*-factors: $R_1 = 0.103$, $wR_2 = 0.269$ for 670 parameters. Crystal data for $[TPP68C20\cdot(\mathbf{1}\text{-}H)_4][PF_6]_4\cdot0.5(C_6H_5CH_2)_2NH_2\cdot0.5PF_6\cdot1.75CH_2Cl_2$, $M_r = 2766.4$, monoclinic, $a = 19.179(3)$, $b = 70.669(7)$, $c = 19.993(2)$ Å, $\beta = 90.55(1)°$, $V = 27096$ Å^3, space group $P2_1/m$, $Z = 8$ (two independent supermolecules), $\rho_{calcd} = 1.356$ g cm^{-3}, $\mu(Cu_{K\alpha}) = 20.8$ cm^{-1}, $\lambda = 1.54178$ Å, $F(000) = 11532$, $T = 293$ K, 34335 unique reflections ($\theta \le 55°$), of which 20274 were observed ($I_o > 2\sigma(I_o)$). Final *R*-factors: $R_1 = 0.100$, $wR_2 = 0.269$ for 3282 parameters. Data for both structures were collected on a Siemens P4/RA diffractometer with $Cu_{K\alpha}$ radiation (graphite monochromated) using ω scans. The data were corrected for Lorentz and polarization factors, but not for absorption. The structures were solved by direct methods and refined by least-squares based on F^2. The N–H hydrogen atoms were located from ΔF maps, the C–H hydrogen atoms were placed in calculated positions. Both were allowed to ride on their parent atoms. The polarity of the $[TPP51C15\cdot(\mathbf{1}\text{-}H)_3][PF_6]_3$ superstructure was determined using the Flack parameter, which refined to 0.2(2). All computations were carried out using the SHELXTL 5.03 package. Crystallographic data (excluding structure factors) for the structures reported in this paper have been deposited with the Cambridge Crystallographic Data Centre as supplementary publication no. CCDC-100264. Copies of the data can be obtained free of charge on application to The Director, CCDC, 12 Union Road, Cambridge CB21EZ, UK (Fax: Int. code +(1223)336-033; e-mail: deposit@chemcrys.cam.ac.uk).

[14] Strictly speaking, the term "conformation" refers only to discrete molecular species. Consequently, we have used "co-conformation" to designate the different three-dimensional spatial arrangement of a) the constituent parts (e.g., host and guest) in supramolecular systems and of b) the components of interlocked molecular systems.

[15] Simultaneous first- and second-sphere coordination by macrocyclic polyethers has been noted previously in our laboratories. See: H. M. Colquhoun, S. M. Doughty, A. M. Z. Slawin, J. F. Stoddart, D. J. Williams, *Angew. Chem.* **1985**, *97*, 124–125; *Angew. Chem. Int. Ed. Engl.* **1985**, *24*, 135–136.

[16] $\Delta\delta$ values for the resonances associated with the polyether's α-, β-, γ-, δ-OCH_2 and hydroquinone protons [solution of TPP68C20 (approximately 5×10^{-3} M) and [1-H]PF_6 (approximately 2.0×10^{-2} M) in CD_2Cl_2 at 20 °C]: $\delta = -0.03, -0.15, -0.23, -0.38, +0.16$.

[17] For the encapsulation of neutral species by self-assembled hosts, see: J. Rebek, Jr., *Chem. Soc. Rev.* **1996**, *25*, 255–264, and references therein.

The Five-Stage Self-Assembly of a Branched Heptacatenane**

David B. Amabilino, Peter R. Ashton, Sue E. Boyd, Ju Young Lee, Stephan Menzer, J. Fraser Stoddart,* and David J. Williams*

The controlled creation of macromolecular chain compounds—that is, oligo- and polycatenanes—comprising mechanically linked macrocycles, which recognize each other link by link as a result of noncovalent bonding interactions is one of the most intellectually appealing goals in synthetic polymer chemistry today. Self-assembly processes[1] provide versatile means of achieving this objective, operating in the first instance by thermodynamically controlled recognition between the appropriate acyclic and cyclic intermediates, followed by kinetically controlled[2] ring closures in which both covalent and mechanical bonds are formed. Clearly, the ease of construction of the higher order catenanes becomes a function of just how efficiently additional rings can be clipped around existing ones.[3]

Previously we have reported[3] the self-assembly (Scheme 1) of a tricatenane $\mathbf{3}\cdot4PF_6$ incorporating two tris-1,5-naphtho[57]crown-15 macrocycles linked by the large tetracationic cyclophane, cyclobis(paraquat-4,4'-biphenylene). We have also shown[4] that $\mathbf{3}\cdot4PF_6$ can be employed as a template to clip on, in a stepwise manner, smaller tetracationic cyclophanes like cyclobis(paraquat-*p*-phenylene) tetracations. This approach to the construction of oligo- and polycatenanes has already yielded[4, 5] the pentacatenane $\mathbf{5}\cdot12PF_6$, dubbed olympiadane.[6] Here we report how subsequent repetitive self-assembly steps have been rendered more efficient by the use of ultrahigh pressure, leading to the isolation of a branched heptacatenene ($\mathbf{7}\cdot20PF_6$), and describe its solid-state molecular structure as determined by X-ray diffraction analysis.

When $\mathbf{3}\cdot4PF_6$[4] was treated (Scheme 1) with $\mathbf{2}\cdot2PF_6$ and **1** in *N*,*N*-dimethylformamide at 12 kbar for 6 days, the [7]catenane $\mathbf{7}\cdot20PF_6$ was isolated after chromatography in 26% yield, together with $\mathbf{5}\cdot12PF_6$ (30%) and $\mathbf{6}\cdot16PF_6$ (28%). No $\mathbf{4}\cdot8PF_6$ was obtained and only traces of $\mathbf{5}'\cdot12PF_6$ were detected.[7] The [7]catenane was characterized initially from its mass spectrum (LSI-MS) and ^{1}H NMR spectrum (see *Experimental Section*). Subsequently, single crystals of $\mathbf{7}\cdot20PF_6$, suitable for X-ray crystallography, were obtained by vapor diffusion of diisopropyl ether into an acetonitrile solution of the [7]catenane.

The X-ray analysis[8] of $\mathbf{7}\cdot20PF_6$ (Figure 1) reveals a molecular structure that fulfills every one of the anticipated design features of the interlocked molecule: all the recognition sites are

[*] Prof. J. F. Stoddart,[+] Dr. D. B. Amabilino, P. R. Ashton, Dr. S. E. Boyd, Dr. J. Y. Lee
School of Chemistry, University of Birmingham
Edgbaston, Birmingham B15 2TT (UK)
Prof. D. J. Williams, Dr. S. Menzer
Chemical Crystallography Laboratory
Department of Chemistry, Imperial College
South Kensington, London SW7 2AY (UK)
Fax: Int. code +(171)594-5804

[+] Current address:
Department of Chemistry and Biochemistry
University of California at Los Angeles
405 Hilgard Avenue, Los Angeles, CA90095 (USA)
Fax: Int. code +(310)206-1843
e-mail: stoddart@chem.ucla.edu

[**] This research was sponsored in the UK by the British Council and the Engineering and Physical Sciences Research Council, and the Biotechnology and Biological Sciences Research Council. We would like to thank Dr. E. R. Hovestreydt and Siemens, Karlsruhe, for making available their charge-coupled device (CCD) detector system and for assistance.

 © WILEY-VCH Verlag GmbH, D-69451 Weinheim, 1997 0570-0833/97/3619-2070 $ 17.50+.50/0

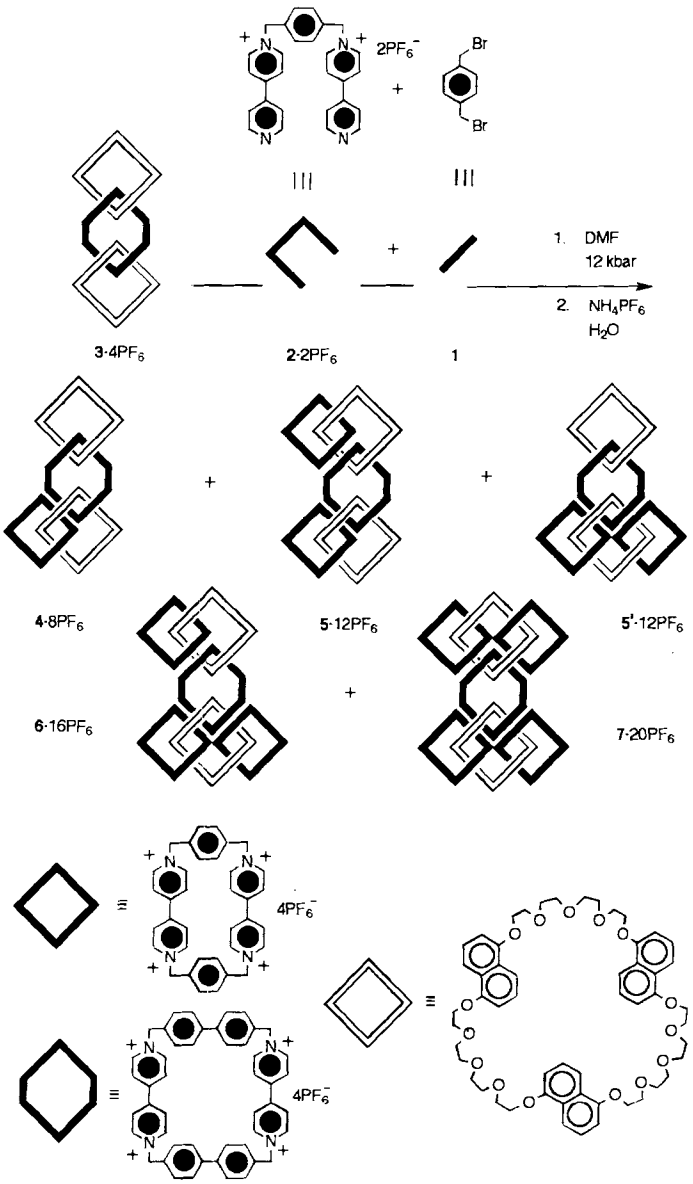

Scheme 1. The multistep template-directed syntheses of the [4]catenane $4\cdot 8\,PF_6$, two [5]catenanes $5\cdot 12\,PF_6$ (olympiadane) and $5'\cdot 12\,PF_6$, the [6]catenane $6\cdot 16\,PF_6$, and finally, the [7]catenane $7\cdot 20\,PF_6$.

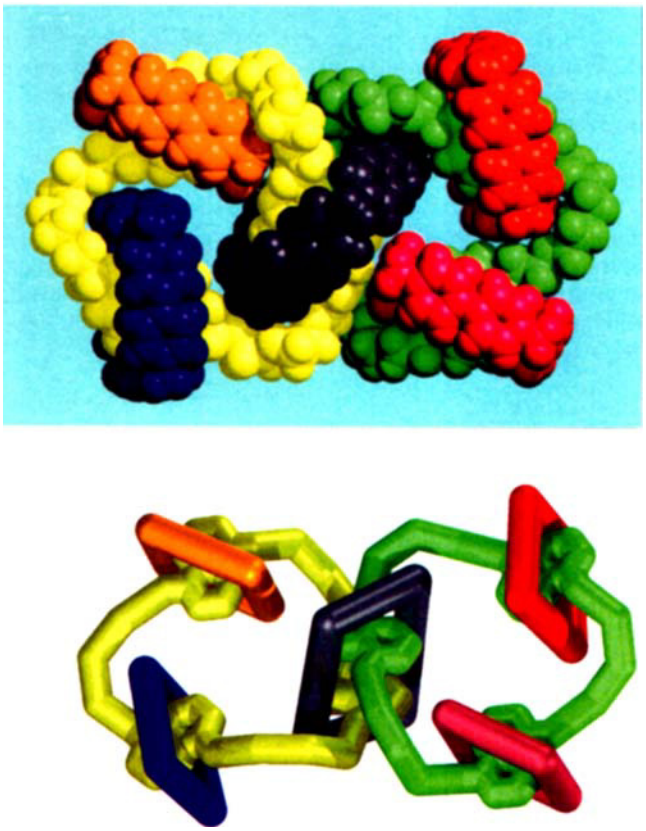

Figure 1. Top: A space-filling representation of the solid state structure of the branched [7]catenane 7^{20+}. Green and yellow: tris-1,5-dinaphtho[57]crown-15 rings; black: cyclobis(paraquat-4,4'-biphenylene) tetracation; other contrasting colors: cyclobis(paraquat-*p*-phenylene) tetracations. Bottom: A tubular representation of 7^{20+}. The pipe sections within the crown ethers define the 1,5-dioxynaphthalene rings and link the oxygen atoms of the polyether chains. Within the tetracationic cyclophanes they link the corner methylene carbon atoms. The pipe diameters are approximately 2.5 Å. This representation was generated with the Persistence of Vision (POV) package, version 3.0, on an SGI workstation.

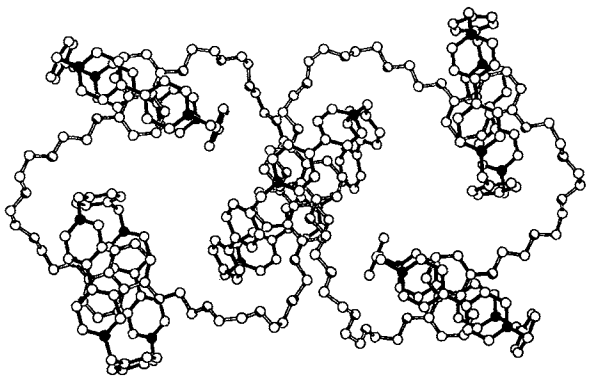

Figure 2. A ball-and-stick representation of the branched [7]catenane 7^{20+}.

utilized in a mutually compatible manner; that is, all six π-electron-rich 1,5-dioxynaphthalene units (belonging to the two discrete but identical macrocyclic polyethers) enter into π-π-stacking interactions with the π-electron-deficient bipyridinium units of all five tetracationic cyclophanes—one cyclobis(paraquat-4,4'-biphenylene) tetracation centrally located between the two macrocyclic polyethers and the other four, all cyclobis(paraquat-*p*-phenylene) tetracations, divided equally between the two macrocyclic polyethers on the periphery of the molecule (Figure 2). Although this branched [7]catenane can adopt a C_i-symmetrical arrangement, this particular symmetry is not realized in the deep violet crystals. However, despite the absence of crystallographic symmetry, the overall molecular structure deviates only marginally from this potential, centrosymmetric arrangement of the ring components. Indeed, molecular pseudosymmetry appears to dominate: the centers of the three 1,5-dioxynaphthalene rings within each of the macrocyclic polyether components define approximate equilateral triangles with sides of about 12 Å. Additionally, the inclinations of the $-OC_{10}H_6O-$ vectors of all six 1,5-dioxynaphthalene rings with respect to the average N···N axes of the bipyridinium units in their associated tetracationic cyclophanes are in a narrow range (51–54°). Furthermore, the interplanar separation between the π-π-stacked donors and acceptors throughout the molecule are bunched together between 3.37 and 3.47 Å: the sandwiched pair of 1,5-dioxynaphthalene rings within the central tetracationic cyclophane lie 3.50 Å apart. The only other arene–arene interactions[9] present within the molecule are between this sandwiched pair of rings and the orthogonally aligned, proximal

 © WILEY-VCH Verlag GmbH, D-69451 Weinheim, 1997 0570-0833/97/3619-2071 $ 17.50+.50/0

p-xylyl spacers in the tetracationic cyclophanes in the 4 and 10 o'clock positions in Figures 1 and 2: the associated ring centroid/ring centroid distances are 4.94 and 5.02 Å. The surface of the molecule has a capsular shape with nanometer dimensions of about 1.5 × 2.0 × 4.0 nm. The only extended intermolecular interaction is an off-set π-π-stacking between the peripheral *p*-xylyl rings of the pair of tetracationic cyclophanes at 4 and 10 o'clock in lattice-translated molecules.

The solid-state crystal structure of this branched heptacatenane serves as a significant marker and symbolic reminder to us of the effectiveness and efficiency of the relatively new methods of template-directed synthesis[10] where interlocked molecular compounds[5, 11] are the result of self-assembly processes[1] that are kinetically controlled.[2]

Experimental Section

7·20PF_6: 1,4-Bis(bromomethyl)benzene (**1**, 43 mg, 0.165 mmol), the dicationic salt **2**·2PF_6 (106 mg, 0.150 mmol), and the [3]catenane **3**·4PF_6 (60 mg, 0.019 mmol) were allowed to react at 12 kbar in DMF (12 mL) in an ultrahigh pressure reaction vessel for two days at 20 °C. Additional quantities of **1** (43 mg, 0.165 mmol) and **2**·2PF_6 (106 mg, 0.150 mmol) were added to the solution, and the reaction vessel was repressurized (12 kbar for four more days). The solvent was removed under vacuum, and the residue subjected to column chromatography (SiO_2; gradient elution: MeOH/2 M NH_4Cl(aq)/$MeNO_2$/DMF from 4/2/2/2 to 4/6/2/5) to afford, after counterion exchange (NH_4PF_6/H_2O), **5**·12PF_6 (30 mg, 30%), a trace of **5'**·12PF_6, **6**·16PF_6 (34 mg, 28%), and the [7]catenane **7**·20PF_6 (37 mg, 26%) as a purple solid, m.p. > 300 °C, LSI-MS: m/z = 7275, 7130, 6985, 6840, 6694, and 6549 for $[M-2PF_6]^+$, $[M-3PF_6]^+$, $[M-4PF_6]^+$, $[M-5PF_6]^+$, $[M-6PF_6]^+$, and $[M-7PF_6]^+$, respectively; ^{1}H NMR (CD_3CN, 400 MHz, 12 °C) δ = 2.28 (d, J = 7.5 Hz, 8H), 3.40–4.06 (m, 68H), 4.10–4.19 (m, 16H), 4.20–4.29 (m, 16H), 5.33–5.41 (m, 8H), 5.43 (s, 8H), 5.52–5.66 (m, 32H), 5.88 (t, J = 7.5 Hz, 8H), 6.17 (d, J = 7.5 Hz, 8H), 6.89 (d, J = 6.5 Hz, 8H), 7.08 (d, J = 6.5 Hz, 16H), 7.26 (d, J = 6.5 Hz, 16H), 7.74 (d, J_{AB} = 8.0 Hz, 8H), 7.85 (s, 16H), 7.98 (s, 16H), 8.03 (d, J_{AB} = 8.0 Hz, 8H), 8.53 (d, J = 6.5 Hz, 16H), 8.60 (d, J = 6.5 Hz, 8H), 8.87 (d, J = 6.5 Hz, 16H).

Received: April 7, 1997 [Z 10319 IE]
German version: *Angew. Chem.* **1997**, *109*, 2160–2162

Keywords: catenanes · donor–acceptor systems · self-assembly · supramolecular chemistry · template synthesis

[1] a) J. S. Lindsey, *New J. Chem.* **1991**, *15*, 153–180; b) G. M. Whitesides, J. P. Mathias, C. T. Seto, *Science* **1991**, *254*, 1312–1319; c) D. Philp, J. F. Stoddart, *Synlett* **1991**, 445–458; d) D. S. Lawrence, T. Jiang, M. Levett, *Chem. Rev.* **1995**, *95*, 2229–2260; e) D. Philp, J. F. Stoddart, *Angew. Chem.* **1996**, *108*, 1242–1286; *Angew. Chem. Int. Ed. Engl.* **1996**, *35*, 1154–1196.

[2] D. B. Amabilino, P. R. Ashton, L. Pérez-García, J. F. Stoddart, *Angew. Chem.* **1995**, *107*, 2569–2572; *Angew. Chem. Int. Ed. Engl.* **1995**, *34*, 2378–2380.

[3] A multistep self-assembly procedure has been used to construct [4]- and [5]catenanes: D. B. Amabilino, P. R. Ashton, A. S. Reder, N. Spencer, J. F. Stoddart, *Angew. Chem.* **1994**, *106*, 450–453; *Angew. Chem. Int. Ed. Engl.* **1994**, *33*, 433–437.

[4] D. B. Amabilino, P. R. Ashton, A. S. Reder, N. Spencer, J. F. Stoddart, *Angew. Chem.* **1994**, *106*, 1316–1319; *Angew. Chem. Int. Ed. Engl.* **1994**, *33*, 1286–1290.

[5] D. B. Amabilino, J. F. Stoddart, *Chem. Rev.* **1995**, *95*, 2725–2828.

[6] X-ray crystal structure of olympiadane: R. Dagani, *Chem. Eng. News* **1996**, Sept. 2, 31. This trivial name for a pentacatenane was proposed, because it resembles the emblem of the International Olympics: N. van Gulick, *New J. Chem.* **1993**, *17*, 619–625.

[7] When the reaction was performed during 3 days at 10 kbar, some **4**·8PF_6 was isolated, along with the higher order catenanes in yields somewhat lower than those achieved for the longer and higher pressure reactions—in agreement with the kinetic regime that characterizes this self-assembly process. It is clear that the [4]-, [5]-, and [6]catenanes are intermediates on the way to the [7]catenane from the [3]catenane. There is no reason why these intermediate catenanes cannot be used for the preparation of 7·20PF_6—or indeed, other higher order catenanes.

[8] Crystal data for 7·20PF_6: $C_{300}H_{300}N_{20}O_{30}$·20$PF_6$·10$CH_3CN$·$CH_3OH$·18$H_2O$, M_r = 8327.84, triclinic, a = 24.179(1), b = 28.066(1), c = 31.108(1) Å, α = 90.04(1), β = 98.44(1), γ = 100.96(1)°, V = 20491(1) Å^3, space group $P\bar{1}$, Z = 2, ρ_{calcd} = 1.350 g cm^{-3}, μ = 0.200 mm^{-1}, T = 173 K, $F(000)$ = 8556. Data were collected with a Siemens SMART diffractometer (graphite monochromated $Mo_{K\alpha}$ radiation). The unit cell was determined by least-squares refinement of all the observed data. A total of 84390 reflections were collected up to 2θ = 52°, merged to give 55802 unique data, and of these, 18937 (2θ < 40°) reflections with $|F_o| > 4\sigma|F_o|$ were considered observed. The data were corrected for Lorentz and polarization effects but not for absorption. The structure was solved with some difficulty by direct methods with the XS module of SHELXTL 5.03. To complete the first model, solvent molecules and anions were located from electron density maps with XtalView 3.1. The ring systems and polyether linkages were then subjected to geometric restraints, and the structure refined by blocked least-squares refinement on F^2 with the observed data (2θ < 40°). All full weight anions, solvent molecules, and polyether linkages were refined anisotropically, while the remainder of the structure was left isotropic. Hydrogen atoms in the macrocyclic polyether and tetracationic cyclophane components were located in idealized positions with U(H) = 1.2 U_{eq}(C) and allowed to ride on their parent atoms. Hydrogen atoms for solvent molecules were not located. The refinement converged to give R_1 = 0.1968 and wR_2 = 0.4498 for 3748 refined parameters. The high value for R_1 is a consequence of the extensive solvation, the large number of very weak reflections, and serious and unresolved inconsistencies in the high-angle data (very asymmetric intensity distributions and negative overall U values from Wilson plots), discrepancies that necessitated weighting of the data before a solution could even be obtained and the abandoning of the data in the range 40° < θ < 52° for the refinements. Crystallographic data (excluding structure factors) for the structure reported in this paper have been deposited with the Cambridge Crystallographic Data Centre as supplementary publication no. CCDC-100468. Copies of the data can be obtained free of charge on application to The Director, CCDC, 12 Union Road, Cambridge CB2 1EZ, UK (fax: int. code +(1223) 336-033; e-mail: deposit@chemcrys.cam.ac.uk).

[9] In view of the limited accuracy of the data and the presence of disorder within parts of the polyether linkages, we have not carried out a detailed analysis of the possible intercomponent [CH···O] hydrogen bonding, although undoubtedly these interactions will have additional stabilizing effects on the overall molecular geometry.

[10] a) S. Anderson, H. L. Anderson, J. K. M. Sanders, *Acc. Chem. Res.* **1993**, *26*, 469–475; b) R. Hoss, F. Vögtle, *Angew. Chem.* **1994**, *106*, 389–398; *Angew. Chem. Int. Ed. Engl.* **1994**, *33*, 375–384; c) D. H. Busch, A. L. Vance, A. G. Kolchinski in *Comprehensive Supramolecular Chemistry*, Volume 9 (Eds. J. L. Atwood, J. E. D. Davis, D. D. MacNicol, F. Vögtle), Pergamon, **1996**, pp. 1–42.

[11] The self-assembly of [3]catenates directed by a copper(I) ion template led subsequently to the production of catenates containing up to seven interlocked rings—comprising one very large macrocycle with up to six smaller macrocycles threaded around its circumference—from a one-pot reaction: a) F. Bitsch, C. O. Dietrich-Buchecker, C. Hemmert, A.-K. Khémiss, J.-P. Sauvage, *J. Am. Chem. Soc.* **1991**, *113*, 4023–4025; b) F. Bitsch, G. Hegy, C. O. Dietrich-Buchecker, E. Leize, J.-P. Sauvage, A. van Dorsselaer, *New J. Chem.* **1994**, *18*, 801–807.

Halozeotypes: a New Generation of Zeolite-Type Materials**

James D. Martin* and Kevin B. Greenwood

Solid-state chemists have followed nature's geological examples by transforming common silicate, aluminate, and phosphate building blocks into zeolitic materials with elaborate microporous frameworks.[1] These microporous materials are used as molecular sieves and catalysts that are vital to countless applications in industry as diverse as petrochemicals, personal-care products, and environmental decontamination. In spite of extensive substitution of the framework cations to fine tune the properties of such materials, zeolite-type structures with frame-

[*] Prof. J. D. Martin, Dr. K. B. Greenwood
Department of Chemistry
North Carolina State University
Raleigh, NC 27695 (USA)
Fax: Int. code +(919) 515-5079
e-mail: jdmartin@ncsu.edu

[**] This work was supported by the U. S. National Science Foundation (DMR-9501370 and CHE-9509532) and the North Carolina State University, Department of Chemistry.

 © WILEY-VCH Verlag GmbH, D-69451 Weinheim, 1997 0570-0833/97/3619-2072 $ 17.50+.50/0

work anions other than oxide are rare.[2] The refractory nature of the metal oxides provides remarkable stability to the microporous frameworks, albeit at the expense of reactivity and tractability. For this reason there is considerable interest in the synthesis of microporous solids whose micropores incorporate reactive species that enhance reactivity,[3] and in the synthesis of microporous solids from organic[4] and inorganic/organic[5] building blocks to obtain greater control of framework design.

Here we report the development of a new generation of zeotype materials constructed from the reactive metal halide building blocks CuCl and $ZnCl_2$. These halozeotype materials represent novel non-oxide analogues of microporous aluminosilicates, and provide the foundation for new developments in host–guest chemistry for crystal engineering of chemically reactive framework building units. The halozeotypes have the general formula T_mX_{2m} (T = tetrahedraly coordinated atom, X = halide) and are constructed by linking tetrahedral cations through two-coordinate halide anions. A divalent metal halide such as $ZnCl_2$, in which the metal cation exhibits tetrahedral coordination, acts as a silicate analogue in this family of framework materials. Compounds $[A_n][Cu_nZn_{m-n}X_{2m}]$ (A = cationic template), analogues of the aluminosilicates $[A_n][Al_nSi_{m-n}O_{2m}]$, can be prepared by substituting certain Zn^{II} sites with Cu^{I} cations; an interstitial cation A^+ is required with each Cu^{I} ion to balance the charge in the framework. Although there is no evidence for binary Cu/Zn halides in the $CuCl/ZnCl_2$ phase diagram,[6] a novel family of framework materials can be prepared from the ternary system alkylammonium/copper halide/zinc halide. The materials CZX-1, CZX-2, and CZX-3 (CZX = copper zinc halide) are the first examples of halozeotypes.

$[HNMe_3][CuZn_5Cl_{12}]$ CZX-1

$[H_2NEt_2][CuZn_5Cl_{12}]$ CZX-2

$[H_2NMe_2]_n[Cu_nZn_{6-n}Cl_{12}]$ ($n = 1, 2$) CZX-3

Single crystals of CZX-1, CZX-2, and CZX-3 were grown from solutions in superheated benzene (160 °C, autogeneous pressure) with a 5:1:1 ratio (2:1:1 for CZX-3) of $ZnCl_2$, CuCl, and $HNMe_3Cl$, H_2NEt_2Cl, or H_2NMe_2Cl, respectively. The resulting materials are colorless and diamagnetic with melting points between 160 and 180 °C. The framework structures are dictated by the size and shape of the ammonium cation template. The CZX-1 framework, formed with the more symmetrical $HNMe_3^+$ template, adopts the well-known sodalite structure.[1, 7–11] The less symmetrical dialkylammonium cations $H_2NEt_2^+$ and $H_2NMe_2^+$ afford the isostructural compounds CZX-2 and CZX-3, whose frameworks exhibit novel three-dimensional channel structures.

Halozeotype CZX-1 crystallizes in the cubic space group $I\bar{4}3m$ with $a = 10.5887(3)$ Å. Refinement of the single crystal X-ray diffraction data revealed a sodalite structure (Figure 1), in which truncated octahedral metal halide cages are packed in a body-centered cubic arrangement.[12] Since the trimethylammonium cation is too small to completely fill the space inside the metal halide cage (the distance from the centroid of the cage to Cl is 4.41 Å), it is disordered over four orientations with hydrogen bonding of the N–H group to the three chloride atoms of the six-ring faces (N–Cl 3.49 Å). Halozeotype CZX-1 exhibits the smallest T-X-T angle (110.04(3)°) of all known sodalite structures;[7–11] this results in an unprecedented contraction of the cage. The T-O-T angle in oxidic sodalites ranges from 124 to 160° (145° is preferred), and in the only other nonoxide sodalite, $[P_{12}N_{24}]^{12-}$, the P-N-P angle is 125.8(4)°.[13]

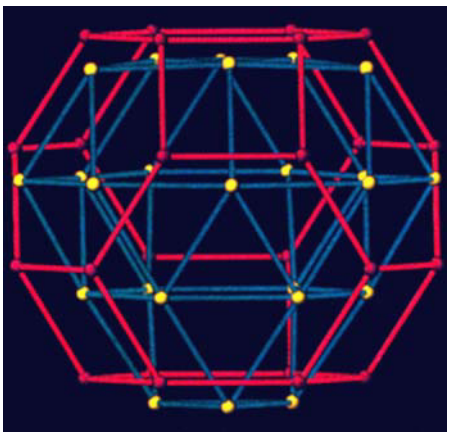

Figure 1. View of the sodalite cage of CZX-1 perpendicular to the 111 axis; T–T contacts are shown in red, and X–X contacts in blue.

To our knowledge the question of the maximal contraction of the sodalite cage has not yet been addressed, although the flexibility of the sodalite framework by T-atom substitution or thermal expansion is well documented. The angular constraints of the sodalite framework have been described by Depmeier[10] and Taylor,[11] who showed that the flexibility of the sodalite cage is a function of bond length l between the T atom and the anion, the X-T-X angle (α), the T-X-T angle (γ), and the angle by which the tetrahedra are twisted cooperatively about the $\bar{4}$ axis (φ). Thus, given the tetrahedral angle α of 109.5°, the maximum value of γ is 160.5°. This maximum expansion of the cage is obtained for $\varphi = 0°$. Structures close to this limit have been observed in several oxide-based sodalites.[7–11] However, when $\varphi = 45°$, then $\alpha = \gamma = 109.5°$. In this contracted limit, the anions form a cubic closest packed sublattice (. .ABCA. .) in which 4/16 of the anion positions are vacant. These anion vacancies provide the host cavity for the template cation(s). The sodalite cage of CZX-1 adopts just such a closest-packed structure with $\gamma = 110.04(3)°$, $\alpha = 112.82(3)°$, and $\varphi = 43.38°$. (The most highly contracted sodalite previously reported is $Zn_3As_3O_{12}^{3-}$, in which $\gamma = 123.8°$.[7])

The limits to the contraction of a sodalite cage are determined by the T–T distances u and the X–X distances m, which can be expressed as functions of l, α, and γ or φ.[14] It follows that m and u are related by the geometric limits of the sodalite cage according to Equation (a).

$$m = 2u - 2\sqrt{2}l\cos\alpha/2 \qquad \text{(a)}$$

A consequence of closest packing is that m and u must be equal. Thus, a closest-packed sodalite structure can only be obtained when $2\sqrt{2}l\cos\alpha/2$ [Eq. (a)] is greater than the radius of the X and T atoms, since the minimum value of m or u is twice the radius of the X or T atom, respectively. The radius of Si (1.55 Å) exceeds this limit. The short (Si,Al)–O distances, which range from $l = 1.58$ to 1.78 Å, define a radius limit of less than 1.29 to 1.45 Å; the oxidic sodalites are thus restricted to structures in which the T-O-T angle γ is limited to about 120°. In contrast, the longer (Zn,Cu)–Cl bond length of 2.285(1) Å defines a radius limit of 1.87 Å for a "closest-packed" sodalite with $\alpha \approx 109.5$. Chloride anions fit comfortably within this radius limit, and the van der Waals radii of copper and zinc (1.40 Å) are well below it. Whereas the most contracted structure for oxide-based sodalites is limited by T–T repulsions, the novel metal halide sodalite CZX-1 exhibits the maximum frame-

 © WILEY-VCH Verlag GmbH, D-69451 Weinheim, 1997 0570-0833/97/3619-2073 $ 17.50+.50/0

work contraction limited by anion–anion contacts. A similar conclusion was presented by O'Keeffe and Hyde for the structural limitations of cristobalite-like structures.[15]

Compounds CZX-2[16] and CZX-3[17] crystallize in the orthorhombic space group $I2_12_12_1$ with $a = 9.6848(5)$, $b = 9.5473(4)$, and $c = 14.0003(9)$ Å and $a = 9.5677(16)$, $b = 9.4554(12)$, and $c = 13.6435(16)$ Å, respectively. Refinement of the single crystal X-ray diffraction data revealed a novel open-framework structure (Figure 2). The dialkylammonium

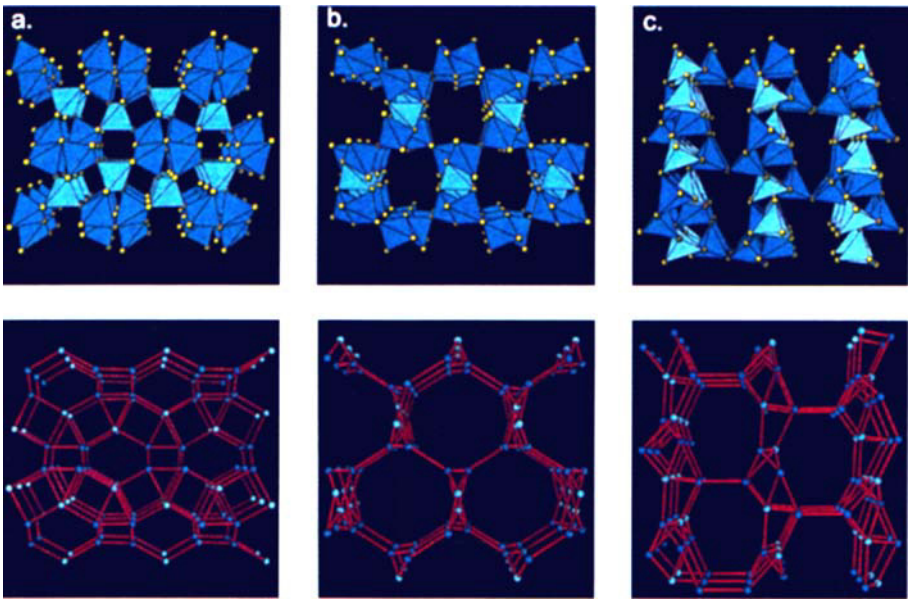

Figure 2. Polyhedral and ball-and-stick views of the open-framework structure of CZX-2 and CZX-3 a) along the *a* axis, b) along the *b* axis (the unit cell boundaries are also shown), and c) along the body diagonal. The two types of metal sites are royal blue (eightfold site) and light blue (fourfold site).

cations form hydrogen bonds with the chloride anions that form the interior of the channels (N–Cl(4) 3.25 Å × 2 and N–Cl(6) 3.21 Å in CZX-2; N–Cl(5) 3.64 Å × 2 and N–Cl(4) 3.66 Å × 2 in CZX-3) and act as templates for the formation of the open framework. In CZX-2 the ammonium cations refine to a crystallographically imposed occupancy of 50% (the methyl carbon atom is common to two diethylammonium cations), which is consistent with the ammonium:copper:zinc ratio of 1:2:5 observed by energy-dispersive X-ray spectroscopy (EDS) and elemental analysis. In contrast, the smaller dimethylammonium cation is fully occupied in CZX-3, giving an ammonium:copper:zinc ratio of 1:1:2. There are two crystallographically distinct metal sites in this framework with multiplicities of four and eight. However, it is not possible to assign uniquely the Cu or Zn cations to either site on the basis of X-ray diffraction data.

Consistent with our zeolitic analogy, frameworks CZX-2 and CZX-3 are constructed from corner-sharing tetrahedral primary building blocks. This framework structure can also be described as being constructed from three-ring secondary building units that consist of one type-one and two type-two metal sites. To our knowledge, this framework structural type has not been observed for any other zeolite-type materials. The projection of the metal framework along the *a* axis (Figure 2a) is reminiscent of a projection of the faujasite framework structure. However, the apparent six-rings and one-third of the apparent four-rings are actually projections of helical connectivity. The most open dimension of this novel framework consists of chiral channels running along the 2_1 axes parallel to the *b* axis (Figure 2b). The smallest ring that circumscribes this channel consists of eleven tetrahedra (Figure 3a). The shortest cross-channel contacts between Cl(4) and Cl(4′) are 6.34 Å for CZX-2, and 6.22 Å for CZX-3. This corresponds to free diameters of 2.9 Å and 2.8 Å, respectively, if the radius of Cl (1.7 Å) is taken into account. The Cl(6)–Cl(6′) distance is 7.87 Å for CZX-2 and 7.51 Å for CZX-3. Four eight-ring windows (Figure 3b) provide access to this primary eleven-ring channel and themselves form smaller channels along the body diagonal (Figure 2c). The smallest cross-channel contacts of this eight-ring channel between Cl(3) and Cl(3′) are 4.32 Å in CZX-2 and 4.11 Å in CZX-3. The largest remaining void in the fully occupied CZX-3 structure lies directly in the eight-ring window and also corresponds to the channel parallel to the *c* axis; the shortest void centroid to halide distance is 2.69 Å.

On investigating the microporosity of these novel frameworks we discovered that addition of methanol or water in quantities insufficient for complete solvation results in the formation of a colloidal suspension of CZX-1, CZX-2 and CZX-3. This is in contrast to $ZnCl_2$, which forms a liquid methanol solvate similar to the zinc chloride hydrates. Neither CuCl nor the known $[A]_2ZnCl_4$ phases ($A^+ = HNMe_3$, H_2NEt_2, and H_2NMe_2) absorb methanol under similar conditions. Thermogravimetric analysis (TGA) and NMR measurements indicate that up to about three equivalents of methanol can be absorbed into the framework of these halozeotypes. The frameworks with the lowest template content absorb the most methanol. Additional methanol, up to about 12–15 equivalents per framework unit ($M_6Cl_{12}^n$) are absorbed to stabilize the colloid. The size and extent of flocculation of the colloids can be controlled by the ratio of framework to solvent. Adding 40 equivalents of methanol to one equivalent of the metal halide framework gives a suspension of 100-nm particles (measured by optical microscopy), which remain suspended for days. Concentrating this suspension by removal of solvent in a

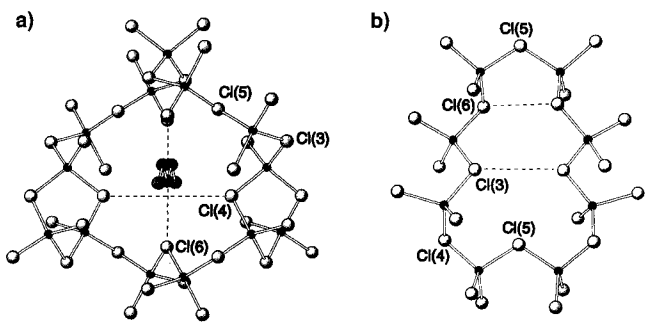

Figure 3. Ball-and-stick drawings of a) the eleven-ring that circumscribes the channels running along the *b* axis, and b) the eight-ring that circumscribes the channels running along the body diagonals in CZX-2. The location of the template cation is also shown in a).

 © WILEY-VCH Verlag GmbH, D-69451 Weinheim, 1997 0570-0833/97/3619-2074 $ 17.50+.50/0

nitrogen-filled dry-box yields a homogenous paste with the appearance and consistency of Elmer's glue. After being allowed to stand open to the dry-box atmosphere for two or three days, microcrystalline CZX-1, CZX-2, or CZX-3 was observed by Guinier X-ray powder diffraction. While the CZX frameworks are not nearly as robust as silicate frameworks, this remarkable formation of colloidal particles requires some degree of integrity of the anionic framework to yield negatively charged particles, likely $\{[A]_x[Cu_nZn_{m-n}Cl_{2m}]\}^{(n-x)-}$. (A small amount of CuCl is also observed by X-ray powder diffraction; free $ZnCl_2$ remains in the solution in methanol.) In addition, since the parent crystalline CZX materials can be grown by evaporation of methanolic colloidal suspensions, these colloidal particles are implicated as intermediates in the formation of the open-framework solids. This novel metal halide system, in which colloidal intermediates are involved in the formation of open frameworks, may also provide a useful model for understanding the growth of zeolite frameworks from sol–gel processing of colloidal suspensions.[18]

Experimental Section

All manipulations were performed under an atmosphere of dry nitrogen; CuCl and $ZnCl_2$ were freshly sublimed; benzene was distilled from sodium benzophenone and stored over 4-Å molecular sieves; and methanol was freshly distilled from magnesium methoxide. Crystalline CZX-1, CZX-2, and CZX-3 were synthesized from superheated solutions of the respective alkylammonium chloride, CuCl, $ZnCl_2$, and benzene in a 1:1:5:45 molar ratio. For example CuCl (25 mg), $ZnCl_2$ (170 mg) and $HNMe_3Cl$ (24 mg) were added to a thick-walled fused silica tube. Benzene (1.0 mL) was added to the reaction vessel with standard Schlenk techniques. The reaction mixture was frozen in liquid nitrogen and sealed with a torch, such that the reaction tube was filled to 25%. Hardened solids from which colorless single crystals could be cleaved were prepared by cooling the solutions in benzene from 160 to 60 °C at 0.01° min^{-1}. Bulk materials could also be prepared from a melt of CuCl, $ZnCl_2$, and the respective alkylammonium chloride.

Elemental analyses: CZX-1: calcd for $C_3H_{10}Cl_{12}CuNZn_5$: C 4.1, H 1.2, N 1.6; found: C 4.3, H 1.3, N 1.6; CZX-2: calcd for $C_4H_{12}Cl_{12}CuNZn_5$: C 5.4, H 1.4, N 1.6; found: C 5.3, H 1.5, N 1.4; CZX-3: calcd for $C_4H_{16}Cl_{12}Cu_2N_2Zn_4$: C 5.3, H 1.8, N 3.1; found: C 5.3, H 2.0, N 3.0.

Received: February 24, 1997 [Z 10151 IE]
German version: *Angew. Chem.* **1997**, *109*, 2162–2166

Keywords: copper · microporosity · solid-state structures · zeolite analogues · zinc

[1] W. M. Meier, D. H. Olson, *Atlas of Zeolite Structure Types*, Butterworth-Heinemann, London, **1992**; R. Szostak, *Handbook of Molecular Sieves*, Van Nostrand Reinhold, New York, **1992**.

[2] C. L. Bowes, G. A. Ozin, *Adv. Mater.* **1996**, *8*, 13; W. Schnick, *Stud. Surf. Sci. Catal.* **1994**, *84c*, 2221.

[3] a) *Inclusion Chemistry with Zeolites: Nanoscale Materials by Design* (Eds.: N. Herron, D. R. Corbin), Kluwer, Dordrecht, **1995**; b) D. E. DeVos, J. L. Meinershagen, T. Bein, *Angew. Chem.* **1996**, *108*, 2355; *Angew. Chem. Int. Eng. Ed.* **1996**, *35*, 2211.

[4] Z. Wu, S. Lee, J. S. Moore, *J. Am. Chem. Soc.* **1992**, *114*, 8730.

[5] a) O. M. Yaghi, G. Li, H. Li, *Nature* (London) **1995**, *378*, 703; b) G. B. Gardner, D. Venkataraman, J. S. Moore, S. Lee, *ibid.* **1995**, *374*, 792; c) D. Venkataraman, G. B. Gardner, S. Lee, J. S. Moore, *J. Am. Chem. Soc.* **1995**, *117*, 11600; d) B. F. Abrahams, B. F. Hoskins, D. M. Michail, R. Robson, *Nature (London)* **1994**, *369*, 727.

[6] A. P. Palkin, G. P. Chepurko, *J. Inorg. Chem.* **1956**, *1*, 144.

[7] T. M. Nenoff, W. T. A. Harrison, T. E. Gier, N. L. Keder, C. M. Zaremba, V. I. Srdanov, J. M. Nicol, G. D. Stucky, *Inorg. Chem.* **1994**, *33*, 2472.

[8] M. T. Weller, M. E. Brenchley, D. C. Apperley, N. A. Davies, *Solid State Nucl. Magn. Res.* **1994**, *3*, 103.

[9] M. A. Camblor, S. B. Hong, M. E. Davis, *Chem. Commun.* **1996**, 425.

[10] W. Depmeier, *Acta Crystallogr. Sect. B* **1984**, *40*, 185. The geometric constraints of the sodalite cage were shown to be functions of α, γ, and φ according to Equations (1) and (2).

$$-\cos\gamma = \cos\varphi \sin\alpha - \sin^2\varphi \sin^2\alpha/2 \quad (1)$$

$$\cos\varphi = \sqrt{2}\frac{\sin\gamma/2}{\sin\alpha/2} - \cot\alpha/2 \quad (2)$$

[11] D. Taylor, *Mineral. Mag.* **1972**, *38*, 593.

[12] Crystal data for CZX-1: $C_3H_{10}Cl_{12}CuNZn_5$, $M_r = 876.0\ g\,mol^{-1}$, cubic, $I\bar{4}3m$ (no. 217), $a = 10.5887(3)$ Å, $V = 1187.21(3)$ Å^3, $Z = 2$, $\rho_{calcd} = 2.451\ g\,cm^{-3}$, $\mu(Mo_{K\alpha}) = 7.34\ mm^{-1}$, $Mo_{K\alpha}$ radiation ($\lambda = 0.71073$ Å). Data were collected at 293 K on a crystal with dimensions $0.25 \times 0.20 \times 0.14$ mm. Final cell constants were determined from a set of 24 reflections with $38 < 2\theta < 41°$. Intensity data were collected over an octant with an Enraf-Nonius CAD4 diffractometer by the $\theta-2\theta$ scan method to the limit of $\theta < 30°$. Of 986 reflections collected, 201 were unique. An absorption correction was made from empirical psi-scan data. The X-ray powder pattern indicated a sodalite structure, which was used as a starting model for the structure solution. The final refinement of 14 parameters was carried out by a full-matrix least-squares method on 191 independent reflections [$I > 1.0\sigma(I)$]. All non-hydrogen atoms were refined anisotropically. The structure refined to $R = 0.0194$ and $R_w = 0.0232$. The maximum and minimum residual electron density was 0.28 and $-0.43\ e\,Å^{-3}$.

[13] a) W. Schnick, J. Lücke, *Angew. Chem.* **1992**, *104*, 208; *Angew. Chem. Int. Ed. Engl.* **1992**, *31*, 213; b) J. Weitkamp, S. Ernst, F. Cubero, F. Wester, W. Schnick, *Adv. Mater.* **1997**, 9, 247; c) F. Wester, W. Schnick, *Z. Anorg. Allg. Chem.* **1996**, 622, 1281.

[14] $u = 2l\sin\gamma/2 = \sqrt{2}l(\sin\alpha/2\cos\varphi + \cos\alpha/2)$ and $m = 2l(2\sin\gamma/2 - \sqrt{2}\cos\alpha/2) = 2\sqrt{2}l\sin\alpha/2\cos\varphi$

[15] M. O'Keeffe, B. G. Hyde, *Acta Crystallogr. Sect. B* **1976**, *32*, 2923.

[16] Crystal data for CZX-2: $C_4H_{12}Cl_{12}CuNZn_5$, $M_r = 890.1\ g\,mol^{-1}$, orthorhombic, $I2_12_12_1$ (no. 24), $a = 9.6848(5)$, $b = 9.5473(4)$, $c = 14.0003(9)$ Å, $V = 1294.52(12)$ Å^3, $Z = 2$, $\rho_{calcd} = 2.284\ g\,cm^{-3}$, $\mu(Mo_{K\alpha}) = 6.73\ mm^{-1}$, $Mo_{K\alpha}$ radiation ($\lambda = 0.71073$ Å). Data were collected at 293 K on a crystal with dimensions $0.32 \times 0.20 \times 0.10$ mm crystal. Final cell constants were determined from a set of 24 reflections with $40 < 2\theta < 46°$. An Enraf-Nonius CAD4 diffractometer data was used to collect intensity data for 3962 reflections (1887 unique) over a hemisphere by the $\theta-2\theta$scan method out to $\theta < 30°$. An absorption correction was made from empirical psi-scan data. The structure was solved by SIR92 and conventional Fourier techniques. A full-matrix least-squares calculation on 1696 independent reflections [$I > 1.0\sigma(I)$] was used in the final refinement of 44 parameters. The Cu, Zn, and Cl atoms were refined anisotropically; H atoms were not included in the refinement. The structure refined to $R = 0.0330$ and $R_w = 0.0516$. The maximum and minimum residual electron density was 1.16 and $-1.06\ e\,Å^{-3}$.

[17] Crystal data for CZX-3: $C_2H_8Cl_{12}Cu_2N_2Zn_4$, $M_r = 906.3\ g\,mol^{-1}$, orthorhombic, $I2_12_12_1$ (no. 24), $a = 9.5677(16)$, $b = 9.4554(12)$, $c = 13.6435(16)$ Å, $V = 1234.3(3)$ Å^3, $Z = 2$, $\rho_{calcd} = 2.439\ g\,cm^{-3}$, $\mu(Mo_{K\alpha}) = 6.73\ mm^{-1}$, $Mo_{K\alpha}$ radiation ($\lambda = 0.71073$ Å). Data were collected at 293 K on a crystal of dimensions $0.26 \times 0.14 \times 0.07$ mm. Final cell constants were determined from a set of 24 reflections with $23 < 2\theta < 28°$. An Enraf-Nonius CAD4 diffractometer was used to collect intensity data for 1231 reflections (1095 unique) over an octant by the $\theta-2\theta$ scan method out to $\theta < 25°$. The structure was solved by using the CZX-2 structure as a model and conventional Fourier techniques. A full-matrix least-squares calculation on 814 independent reflections [$I > 1.5\sigma(I)$] was used in the final refinement of 58 parameters. All non-hydrogen atoms were refined anisotropically. $R = 0.0418$, $R_w = 0.0343$. The maximum and minimum residual electron density was 0.54 and $-0.58\ e\,Å^{-3}$. Crystallographic data (excluding structure factors) for the structures reported in this paper have been deposited with the Cambridge Crystallographic Data Centre as supplementary publication no CCD-100302 Copies of the data can be obtained free of charge on application to The Director, CCDC, 12 Union Road, Cambridge CB2 1EZ, UK (fax: int. code +(1223) 336-033; e-mail: deposit@chemcrys.cam.ac.uk).

[18] M. Tsapatsis, M. Lovallo, T. Okubo, M. E. Davis, M. Sadakata, *Chem. Mater.* **1995**, *7*, 734.

 © WILEY-VCH Verlag GmbH, D-69451 Weinheim, 1997 0570-0833/97/3619-2075 $ 17.50+.50/0

Binuclear Vanadium(III) Squarates with Layered and Framework Structures: Hydrothermal Synthesis and Structures of $[\{V(OH)(C_4O_4)(H_2O)\}_2]$ and $[\{V(OH)(C_4O_4)\}_2]\cdot 4H_2O$**

Kuan-Jiuh Lin* and Kwang-Hwa Lii

Studies of self-assembly of inorganic structures have blossomed during the 1990s. Supermolecules or coordination polymers with infinite two- or three-dimensional frameworks are of intense current interest[1] because of their unique physical and chemical properties, such as magnetism,[2] host–guest chemistry,[3] and catalysis.[4] Crystal engineering of supramolecular architectures based on a transition metal macrocyclic motif with rigid organic ligands has become a rapidly expanding field.[4–6] In our approach we chose as bridging ligand the squarate anion, $C_4O_4^{2-}$, together with vanadium oxide to synthesize V/O/squarate polymeric compounds with hydrothermal methods. The anion with its fourfold C=O functionality is not only a potential multiple acceptor of hydrogen bonds,[7, 8] but also can be engaged in polydentate coordination modes such as μ_2, μ_3, and μ_4 coordination.[9–11] Here we present two novel polymeric structures, **1** and **2**, where open frameworks are achieved by a combination of such interactions.

$[\{V(OH)(C_4O_4)(H_2O)\}_2]$ **1**

$[\{V(OH)(C_4O_4)\}_2]\cdot 4H_2O$ **2**

Hydrothermal reactions of NH_4Cl, V_2O_5, and squaric acid in the molar ratios 0.3:1:1 at 180 °C and 0.6:1:2 at 200 °C in water produced compounds **1** and **2**, respectively. Both were structurally characterized by single-crystal X-ray diffraction analyses.[12] The structure of **1** (Figure 1) consists of layers stacked on each other along the *a* axis with an interplanar separation of $1/a^* = 7.576$ Å. Each layer is constructed from dimers of edge-sharing $V^{III}O_6$ octahedra, which are linked by squarate anions in μ_3 mode. Within the layer, rectangular windows (3.0×6.5 Å) are surrounded by four vanadium dimers and four squarates. Adjacent layers are displaced with respect to each other such that the windows are aligned to form straight tunnels along the [101] direction. The geometry at the vanadium site is defined by two bridging OH groups, one H_2O ligand, and one oxygen donor from each of three squarates. The squarate retains a pendant group which has a somewhat shorter C=O distance than the other three substituents and an O atom that is involved in both an intra- and intermolecular hydrogen bond to the water molecule.

The structure of **2** reveals a neutral, three-dimensional framework again containing dimers of edge-sharing $V^{III}O_6$ octahedra besides the squarate anions (Figure 2). The vanadium atoms are coordinated by two bridging hydroxides and four squarates, two of which coordinate in a true μ_4 mode (to four dimers) and the other two in a μ_2/μ_2 mode (to two dimers). The binuclear cores are connected to four μ_4 squarates to form a

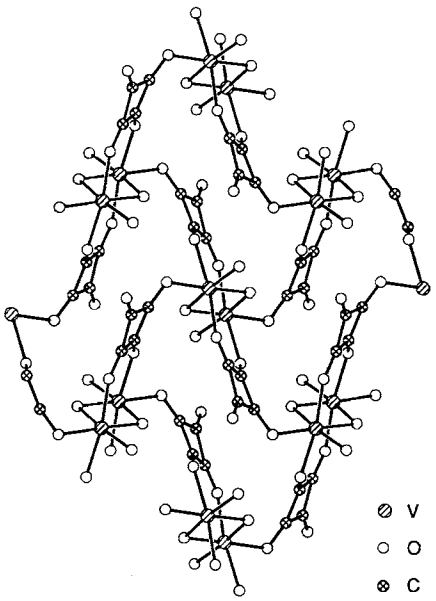

Figure 1. An inclined view onto the layer of **1**.

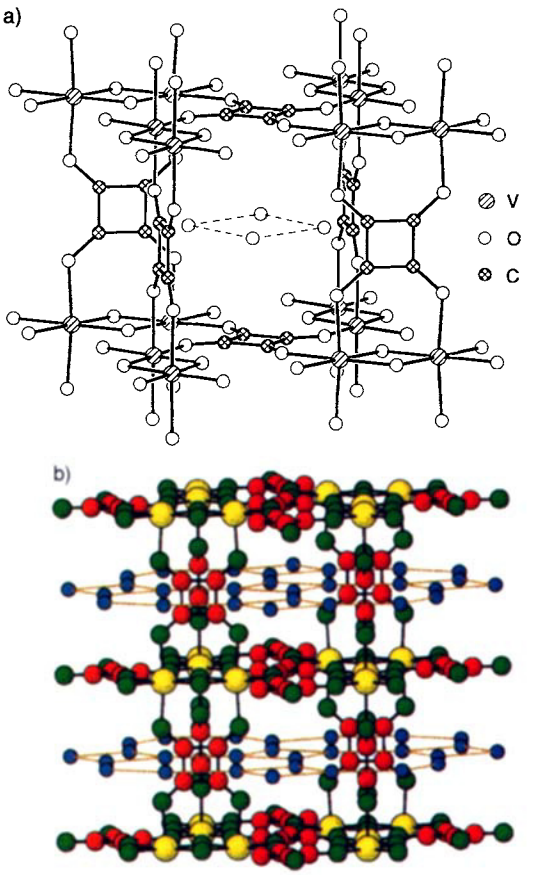

Figure 2. Structure of **2**. a) The water tetramer is depicted at the intersection of two channels, one of which is nearly horizontal and the other in viewing direction; b) projection of a large part of the layered framework showing how the water tetramers also form layers by further hydrogen bonding. Yellow V, red C, green O, blue O (from water).

$_\infty[V_2(OH)_2(C_4O_4)^{2+}]$ layer parallel to the *ab* plane. Adjacent layers with a separation of $c = 7.113$ Å are covalently linked by the μ_2/μ_2 squarates, with resulting square channels along the [110] and [1$\bar{1}$0] directions. Rare cyclic tetrameric clusters of

[*] Dr. K.-J. Lin, Dr. K.-H. Lii
Institute of Chemistry
Academia Sinica
Nankang, Taipei (Taiwan)
Fax: Int. code +(2)783-1237
e-mail: kjlin@chem.sinica.edu.tw.

[**] We thank Professor Y. Wang (National Taiwan University) for her many stimulating discussions, a referee for valuable comments, and the Institute of Chemistry, Academia Sinica, for support.

 © WILEY-VCH Verlag GmbH, D-69451 Weinheim, 1997 0570-0833/97/3619-2076 $ 17.50+.50/0

hydrogen-bonded water molecules are located at the intersections of the channels. The μ_4 squarate has C_{4h} crystallographic symmetry, whereas the μ_2/μ_2 squarate and vanadium dimer have D_{2h} symmetry. The window of the square channels has dimensions $\sqrt{2}a/2 \times c = 7.04 \times 7.11$ Å, which is comparable to the pore size of SAPO-40 zeolite (6.7×6.9 Å).[13] The water cluster in the *ab* plane is further hydrogen-bonded into a layer, resulting in additional eight-membered rings condensed with themselves and the four-membered rings. It is interesting to note that the O···O separation of 2.88 Å in the water tetramer compares well with the results of vibration-rotation tunneling spectroscopy[14] and of ab initio calculations.[15]

In summary, the two polymeric structures are composed of similar macrocyclic units constructed from cationic octahedral vanadium dimers and squarate anions, a new building principle for supramolecular architectures and microporous structures. The pore sizes are determined by the coordination modes of the bridging squarates: **2** provides large square channels where cyclic water tetramers are located, whereas **1** has a layer structure with rectangular windows within the layer. These first examples show that there is a great potential for the preparation of topologically unique zeolitic materials in the metal squarate system by hydrothermal methods.

Experimental Section

1: A mixture of NH_4Cl (0.60 mL, 0.5 M), V_2O_5 (0.0929 g), $H_2C_4O_4$ (0.2276 g) ($V:H_2C_4O_4$ molar ratio = 1:2), and H_2O (10 mL) was sealed in a Teflon-lined stainless autoclave (volume 23 mL), heated at 180 °C for three days, and cooled to 90 °C at 5 °C h^{-1}. The product (yellow green crystals of **1**; yield: 0.1740 g, 88% based on V), was filtered off and washed with deionized water. This compound is stable in air and insoluble in water. Monophasic crystalline material was confirmed by X-ray powder diffraction. Thermogravimetric analysis in air showed one-step weight loss of 54.41% over the temperature range 150–400 °C, which agrees well with the theoretical values of 54.1% assuming that the final decomposition product is V_2O_5. IR(KBr): $\tilde{\nu}$ = 3483 (s, OH), 3145 (br, w, H_2O), 1621 (s, pendant C=O), 1518 and 1456 (s, C=O and C=C), 1086(m), 1145(m), 861 and 843 cm^{-1} (m, V-(OH)-V).

2: A mixture of NH_4Cl (0.60 mL, 0.5 M), V_2O_5 (0.0904 g), $H_2C_4O_4$ (0.1143 g) ($V:H_2C_4O_4$ molar ratio = 1), and H_2O (10 mL) was sealed in a Teflon-lined stainless autoclave (23 mL), heated at 200 °C for three days, cooled to 150 °C at 5 °C h^{-1}, and quenched to room temperature. The product (0.1877 g), which is a mixture of dark purple crystals of **2** and an about equal amount of **1**, was filtered off and washed with deionized water. This compound is stable in air and insoluble in water. The compound retains its structure at 200 °C in air with partial loss of water molecules, and decomposes at 250 °C, as indicated from powder X-ray diffraction and thermogravimetric analysis. IR(KBr): $\tilde{\nu}$ = 3463 (m, OH), 2900 (br, w), 1500 (s, C=C and C=O), 870 cm^{-1} (m, V-(OH)-V).

Received: December 23, 1996
Revised version: May 9, 1997 [Z9928IE]
German version: *Angew. Chem.* **1997**, *109*, 2166–2167

Keywords: channel structures · hydrothermal syntheses · squarates · supramolecular chemistry · vanadium

[1] a) C. L. Bowes, G. A. Ozin, *Adv. Mater.* **1996**, *8*, 13–28, and references therein; b) A. Müller, H. Reuter, S. Dillinger, *Angew. Chem.* **1995**, *107*, 2505–2539; *Angew. Chem. Int. Ed. Engl.* **1995**, *34*, 2328–2361, and references therein.

[2] a) S. Turner, O. Kahn, L. Rabardel, *J. Am. Chem. Soc.* **1996**, *118*, 6428–6432; b) H. O. Stumpf, L. Ouahab, Y. Pei, D. Grandjean, O. Kahn, *Science* **1993**, *261*, 447–449; c) S. Decurtins, H. W. Schmalle, R. Pellaux, R. Huber, P. Fischer, B. Ouladdiaf, *Adv. Mater.* **1996**, *8*, 647–652; d) G. De Munno, M. Julve, G. Viau, F. Lloret, J. Faus, D. Viterbo, *Angew. Chem.* **1996**, *108*, 1931–1934; *Angew. Chem. Int. Ed. Engl.* **1996**, *35*, 1807–1810.

[3] a) B. F. Hoskins, R. Robson, *J. Am. Chem. Soc.* **1990**, *112*, 1546–1554; b) B. F. Abrahams, B. F. Hoskins, D. M. Michail, R. Robson, *Nature* **1994**, *369*, 727–729.

[4] M. Fujita, Y. J. Kwon, S. Washizu, K. Ogura, *J. Am. Chem. Soc.* **1994**, *116*, 1151–1152.

[5] a) P. Losier, M. J. Zaworotko, *Angew. Chem.* **1996**, *108*, 2857–2960; *Angew. Chem. Int. Ed. Engl.* **1996**, *35*, 2779–2781; b) S. Subramanian, M. J. Zaworotko, *ibid.* **1995**, *107*, 2295–2297 and **1995**, *34*, 2127–2128.

[6] P. J. Stang, D. H. Cao, S. Saito, A. M. Arif, *J. Am. Chem. Soc.* **1995**, *117*, 6273–6283.

[7] a) Y. Wang, G. D. Stucky, *J. Chem. Soc. Perkin Trans 2* **1974**, 925–928; b) K. J. Lin, M. C. Cheng, Y. Wang, *J. Phys. Chem.* **1994**, *98*, 11685–11693.

[8] I. L. Karle, D. Ranganathan, V. Haridas, *J. Am. Chem. Soc.* **1996**, *118*, 7128–7133.

[9] Two-dimensional squarate coordination polymers: C. R. Lii, C. C. Wang, Y. Wang, *Acta Crystallogr. Sect. B* **1996**, *52*, 966–975, and references therein.

[10] Few examples of discrete bimetal squarates have been reported: a) M. I. Khan, Y. D. Chang, Q. Chen, J. Salta, Y. S. Lee, C. J. O'Connor, J. Zubieta, *Inorg. Chem.* **1994**, 33, 6340–6350, b) A. Müller, R. Rohlfing, E. Krickemeyer, H. Bögge, *Angew. Chem.* **1993**, *105*, 916–918; *Angew. Chem. Int. Ed. Engl.* **1993**, *32*, 909–911.

[11] Q. Chen, S. Liu, J. Zubieta, *Angew. Chem.* **1990**, *102*, 100–101; *Angew. Chem. Int. Ed. Engl.* **1990**, *29*, 70–72.

[12] Diffractometer Enraf-Nonius CAD4, $Mo_{K\alpha}$ radiation, graphite monochromator, $\omega/2\theta$ scan, direct methods with NRCVAX [16], refinement on F^2 with SHELXL-93 [17]. Structure of **1**: $C_8H_6O_{12}V_2$, monoclinic, space group $P2_1/c$ (no. 14); $a = 7.637(3)$, $b = 8.410(3)$, $c = 9.082(3)$ Å, $\beta = 97.25(4)°$; $V = 578.7(4)$ Å^3, $Z = 2$, $2\theta_{max} = 55°$, $R_1 = 0.035$, $wR_2(F^2) = 0.077$, $GOF = 0.900$, residual electron density between -0.51 and 0.47 e Å^{-3}. Structure for **2**: $C_8H_{10}O_{14}V_2$, tetragonal, space group $P4/mbm$ (no. 127); $a = 9.959(1)$, $c = 7.113(2)$ Å; $V = 705.5(2)$ Å^3, $Z = 2$, $2\theta_{max} = 50°$, $R_1 = 0.032$, $wR_2(F^2) = 0.074$, $GOF = 0.983$, residual electron density between -0.45 and 0.32 e Å^{-3}. Further details of the crystal structure investigations may be obtained from the Fachinformationszentrum Karlsruhe, D-76344 Eggenstein-Leopoldshafen (Germany), on quoting the depository numbers CSD-406215 (**1**) and 406216 (**2**).

[13] W. M. Meier, D. H. Olson, *Atlas of Zeolite Structure Types*, 3rd ed., Butterworth-Heinemann, Boston, **1992**.

[14] J. D. Cruzan, L. B. Braly, K. Liu, M. G. Brown, J. G. Loeser, R. J. Saykally, *Science* **1996**, *271*, 59–62.

[15] S. S. Xantheas, T. H. Dunning, Jr., *J. Chem. Phys.* **1993**, *99*, 8774–8792.

[16] E. J. Gabe, Y. Le Page, J. -P. Charland, F. L. Lee, P. S. White, *J. Appl. Cryst.* **1989**, *22*, 384–387.

[17] G. M. Sheldrick, SHELXL-93, Program for Crystal Structure Refinement, Universität Göttingen, Germany, **1993**.

Topological Bifurcation Analysis: Electronic Structure of CH_5^+ **

Dominik Marx* and Andreas Savin

CH_5^+, the product of the formal addition of a proton to methane, a stable and rigid molecule, is highly fluxional and elusive. The reason is that the electronic energy penalty to switch from one of the many degenerate eclipsed *e*-C_s global minima to another one is tiny,[1–5] the most recent best estimate being as small as 0.8 kcal mol^{-1} to the C_{2v} transition state.[5] This led to speculations that the hydrogen atoms in CH_5^+ may easily scramble in the rotational-vibrational ground state as a result of pseudorotational rearrangements.[3, 6] This picture was recently confirmed by ab initio quantum simulations in which all the nuclei of CH_5^+ were treated as quantum particles.[7] More importantly, it was demonstrated that a H_2 unit attached to the apex of a CH_3 tripod is a characteristic geometric feature of the *quantum* ground state of CH_5^+.

A fundamental question which arises is what type of chemical bonding ultimately holds such a highly fluxional molecule together. The *e*-C_s structure is commonly described as consisting

[*] Dr. D. Marx
Max-Planck-Institut für Festkörperforschung
Heisenbergstrasse 1, D-70569 Stuttgart (Germany)
Fax: Int. code + (711)689-1701
e-mail: marx@prr.mpi-stuttgart.mpg.de

Dr. A. Savin
Laboratoire de Chimie Théorique (CNRS)
Université Pierre et Marie Curie
place Jussieu, F-75252 Paris (France)
Fax: Int. code +(1)44274117
e-mail: savin@lct.jussieu.fr.

[**] We thank Bernard Silvi and Jürg Hutter for useful discussions.

 © WILEY-VCH Verlag GmbH, D-69451 Weinheim, 1997 0570-0833/97/3619-2077 $ 17.50+.50/0

of three standard two-center, two-electron CH bonds, and one electron-deficient three-center, two-electron bond involving the carbon nucleus and the two hydrogen nuclei that form the H_2 unit.[8, 9] To what extend is this picture valid taking into account the floppiness that is present even in the ground state? We will answer this question by a topological analysis of the electron localization function ELF[10] of representative configurations sampled from ab initio quantum simulations.[7]

Let us now concisely describe some important features of the electron localization function. It can be viewed as a local measure of the Pauli repulsion between electrons in three-dimensional space due to the exclusion principle. It thus allows us to define regions of space that are associated with different electron pairs in a molecule or solid. The definition of ELF $\eta(\mathbf{r})$ is given by Equations (a)–(d), where the sum in (b) and (d) is over

$$\eta(\mathbf{r}) = \frac{1}{1 + (D/D_h)^2} \quad \text{(a)}$$

$$D = \frac{1}{2}\sum_{i=1}^{N} |\nabla\psi_i|^2 - \frac{1}{8}\frac{|\nabla\rho|^2}{\rho} \quad \text{(b)}$$

$$D_h = \frac{3}{10}(3\pi^2)^{2/3}\rho^{5/3} \quad \text{(c)}$$

$$\rho = \sum_{i=1}^{N} |\psi_i|^2 \quad \text{(d)}$$

all singly occupied one-electron (spin-) orbitals $\psi_i(\mathbf{r})$ in an N-electron system. This function is normalized to the interval between 0 and 1, and is large where the Pauli repulsion is small, that is, where two electrons with antiparallel spin are paired in space. Conversely, it is small in the regions between electron pairs. By locating the electron pairs, ELF makes a direct connection with the chemist's view of the chemical bond, often drawn as a line connecting atoms; this property of ELF is not restricted to the equilibrium structure of a molecule and can even be followed during a chemical reaction. We refer to previous work[10–13] for an in depth discussion of the properties of ELF, and in particular to Ref.[14] for an interpretation within the framework of density functional theory.

The position where ELF attains a maximum value, the attractor, can be used as an electron pair's signature. To identify a region around a maximum, one can consider all the points in space with $\eta(\mathbf{r}) \geq f$, which defines the f-localization domain; f is a positive constant smaller than the value of the maximum. This region in space can be visualized by showing the isosurface $\eta(\mathbf{r}) = f$. The isosurface surrounds only one attractor when f is close to the value of the corresponding ELF maximum. For a given value of f, several closed isosurfaces surrounding different attractors can appear. As the value of f is lowered, different spatially separated f-localization domains merge, and closed isosurfaces that contain more than one attractor appear. In other words: there is at least one path which joins different attractors as f is lowered. Of course, the isosurface encompasses all attractors, that is, all electron pairs, in the $\eta \to 0$ limit, whereas all attractors are separated in the opposite limit ($\eta \to 1$).[15]

This behavior can be visualized by a bifurcation diagram, which includes only the maxima of ELF and the saddle points where merging occurs.[16] The connectivity of these characteristic points represents the hierarchical merging pattern of the isosurfaces. By focussing on that part of the bifurcation diagram with $\eta(\mathbf{r}) > f$ one can identify the number of attractors within a particular f-localization domain, as all maxima within this domain will appear connected. This suggests that a covalent bond is the better defined the larger the difference between the ELF-maximum and the saddle point where the first merging occurs.

The usefulness of these ideas is illustrated by depicting two f-localization domains with $\eta(\mathbf{r}) \geq 0.98$ and 0.6 (Figure 1a–c) for the textbook example, methane; only the chemically relevant valence electrons are included explicitly in the calculations, and the inert core electrons are represented by pseudopotentials. There are clearly four well-separated maxima for $\eta > 0.71$ (Figure 1a), which can be assigned to the four CH bonds, whereas all four localization domains coalesce below this bifurcation value $\eta^* \approx 0.71$ (Figure 1b, c). This leads to the particularly simple bifurcation diagram displayed in Figure 1d.

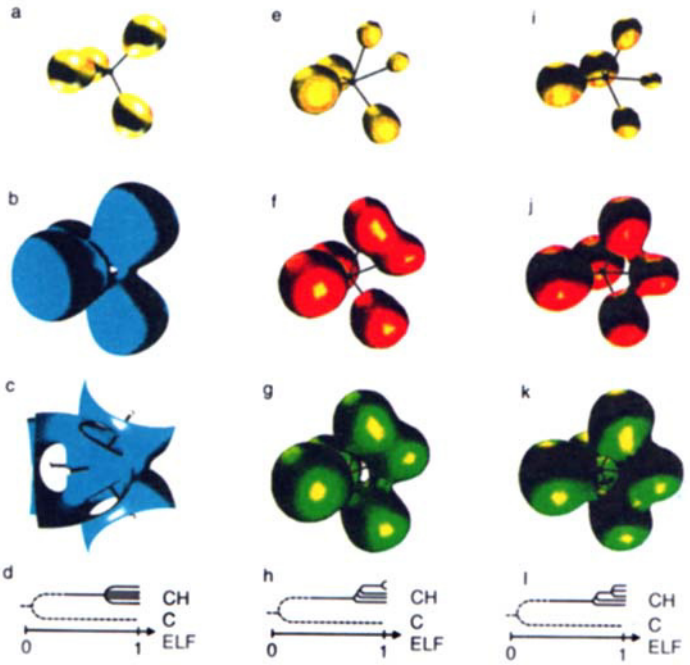

Figure 1. ELF isosurfaces ($\eta(\mathbf{r}) = f$) depicting the f-localization domains for the global minimum of methane CH_4 with $f = 0.98$ (yellow, a), $f = 0.60$ (blue, b), and $f = 0.60$ with isosurface cut open (blue, c); for protonated methane e-C_s-CH_5^+ with $f = 0.98$ (yellow, e), $f = 0.88$ (red, f), and $f = 0.70$ (green, g); for C_{2v}-CH_5^+ with $f = 0.98$ (yellow, i), $f = 0.88$ (red, j), and $f = 0.70$ (green, k). Resulting valence bifurcation diagrams for methane CH_4 (d), protonated methane e-C_s-CH_5^+ (h), and C_{2v}-CH_5^+ (l). Dotted lines (only schematic): the electrons forming the $1s^2$ shell of the carbon core are inluded in the calculations.

Moreover, the attractor structure of ELF allows disjoint spatial regions to be defined from the gradients of ELF.[12, 17, 18] From any point in space the gradient is followed to an attractor in that region, and this point is then attributed to this attractor. The collection of all the points in space that were assigned to a given attractor is called its basin. In the example of the valence shell of CH_4, space is divided into four equivalent basins corresponding to the four CH bonds. Integrating the electron density separately in these valence basins yields 1.98 electrons per basin, very close to two as expected in the idealized Lewis picture of a covalent bond; the last reported digit is assumed to be inaccurate due to the numerical integration on a finite grid. The chemically inert core basin would appear in an all-electron calculation.

The nontrivial case of the quantum-fluxional CH_5^+ can now be approached analogously. First, we have to find the characteristic ELF values at the relevant bifurcation points η^* for the two most important stationary points on the potential energy surface, namely, the e-C_s global minimum (Figure 1e–g) and the lowest energy C_{2v} transition state (Figure 1i–k). For the global minimum we find five separated maxima for $\eta \to 1$, but two localization domains around them merge already at a surpris-

 © WILEY-VCH Verlag GmbH, D-69451 Weinheim, 1997 0570-0833/97/3619-2078 $ 17.50+.50/0

ingly high value of $\eta^* \approx 0.97$. The resulting basin can clearly be associated with the bonding electron pair of the H_2 unit to the carbon nucleus, whereas the other three separated basins stem from the three standard two-center CH bonds in the CH_3 tripod. Integration of the electron density (from the eight valence electrons) over the basins yields values of about two electrons per basin in all four cases (1.72, 1.97, 1.98 for the CH basins, and 2.27 for the CH_2 basin with corresponding CH bonds lengths of about 1.10 Å, 1.08 Å, 1.08 Å, and 1.17 Å, respectively), so one can clearly denote the particular bond that involves two hydrogen nuclei and the carbon nucleus to be a three-center, two-electron bond.[8, 9] However, these numerical values seem furthermore to suggest that the three-center bond „needs more electrons than just two" to bind three nuclei, and that the necessary electron density is mainly „borrowed" from one particular two-center CH bond, which becomes weakened and thus is the longest of the three two-center bonds. This topological pattern is stable over a wide range on the ELF scale down to about $\eta^* \approx 0.78$, where the merging of all the valence localization domains starts. The full valence shell is finally established at $\eta^* \approx 0.7$; see Figure 1h for the resulting bifurcation diagram. Thus, we find two distinct bifurcation points η^*: the first where the two isosurfaces surrounding the two hydrogen nuclei of the H_2 unit coalesce and the second where the resulting isosurface now encompassing the H_2 unit merges with the other three isosurfaces stemming from the normal CH bonds.

The bifurcation hierarchy for the C_{2v} transition state derived from its ELF landscape (Fig. 1i–k) is topologically different (Figure 1l). At $\eta^* \approx 0.89$ three of the five localization domains merge, and the resulting basin contains four electrons (4.01) that are distributed over four centers (see ref. [5] for such a conjecture), whereas the remaining two basins with about two electrons each (1.97 and 1.96) stem from the two standard two-center, two-electron CH bonds. The full valence shell, that is, the merging of all previously separated basins, occurs at $\eta^* \approx 0.74$.

After having determined the characteristic points in the bifurcation hierarchy for the two limiting structures, we can analyze the quantum mechanical ground state of CH_5^+ including tunneling and zero-point motion effects.[7] The bifurcation analysis as outlined for the stationary points corresponding to the *e*-C_s and C_{2v} structures is applied to a statistical sample of 64 configurations obtained from previous ab initio quantum simulations.[7] We obtain for each of these configurations the ELF from electronic structure calculations based on first principles.[19] This gives access to the associated bifurcation diagrams and thus to the ELF values η^* where the two major bifurcations in the valence shell occur in each configuration. The resulting quantity of interest is a histogram or probability distribution $P(\eta^*)$ of these bifurcation points, and its broadness is entirely due to quantum mechanical tunneling and rotational-vibrational zero-point fluctuations; simulations where the nuclei are approximated as classical particles show that thermal fluctuations are negligible at low temperatures, whereas they are of similar magnitude at room temperature.[20]

The two branches of the distribution function depicted separately in Figure 2 show two prominent peaks at the bifurcation points $\eta^* \approx 0.78$ and 0.97, signaling a major contribution of C_s-like configurations to the quantum ground state of CH_5^+. Furthermore, the distribution function actually has minima at $\eta^* \approx 0.74$ and 0.89, the values that were found to characterize the bifurcation hierarchy of the ideal C_{2v} structure of CH_5^+. Thus, the electronic structure analysis based on the bifurcations of ELF clearly supports the concept of a three-center, two-electron bond that holds CH_5^+ together.

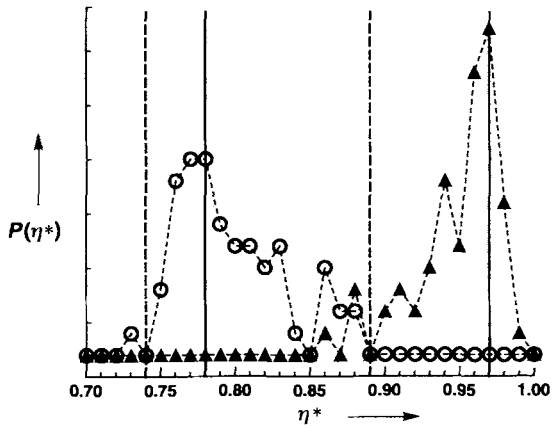

Figure 2. Distribution function $P(\eta^*)$ of the ELF bifurcation points η^* in the quantum ground state of CH_5^+; P and η^* are dimensionless quantities. The two partial distribution functions obtained from separate histograms of the bifurcation points with the largest (filled triangles) and second largest (open circles) ELF values are shown. The sum of these two contributions constitutes the full distribution function (not shown) and the connecting dotted lines are only visual guides. For the two relevant individual stationary point structures (discussed in the text and presented in Figures 1e–g and i–k) the same analysis yields necessarily very sharp peaks at two ELF values in each case: the vertical solid lines mark these four characteristic peak positions for the *e*-C_s global minimum ($\eta^* \approx 0.78, 0.97$), the dashed lines those for the C_{2v} transition state ($\eta^* \approx 0.74, 0.89$).

In conclusion, we have presented a powerful addition to the arsenal of topological analysis methods of the electronic structure of molecules that is tailored to cope with highly fluxional molecules. In particular, we have demonstrated that a three-center, two-electron bond emerges naturally from this analysis, even for the quantum ground state of such a floppy molecule as protonated methane CH_5^+. Furthermore, we believe that our method will find widespread applications in the emerging realm of ab initio simulations of molecules at finite temperatures, where one does not deal with a few high-symmetry stationary points, but with an ensemble encompassing many configurations that all deviate from ideal symmetries.

Received: March 3, 1997 [Z 10184 IE]
German version: *Angew. Chem.* **1997**, *109*, 2168–2170

Keywords: ab initio calculations · electron localization · electronic structure · hypervalent compounds

[1] W. Klopper, W. Kutzelnigg, *J. Phys. Chem.* **1990**, *94*, 5625–5630.
[2] P. von R. Schleyer, J. W. d. H. Carneiro, *J. Comput. Chem.* **1992**, *13*, 997–1003.
[3] P. R. Schreiner, S.-J. Kim, H. F. Schaefer III, P. von R. Schleyer, *J. Chem. Phys.* **1993**, *99*, 3716–3720.
[4] M. Kolbuszewski, P. R. Bunker, *J. Chem. Phys.* **1996**, *105*, 3649–3653.
[5] H. Müller, W. Kutzelnigg, J. Noga, W. Klopper, *J. Chem. Phys.* **1997**, *106*, 1863–1869.
[6] G. A. Scuseria, *Nature (London)* **1993**, *366*, 512–513.
[7] D. Marx, M. Parrinello, *Nature (London)* **1995**, *375*, 216–218.
[8] G. A. Olah, *Angew. Chem.* **1995**, *107*, 1519–1532; *Angew. Chem. Int. Ed. Engl.* **1995**, *34*, 1393–1405.
[9] a) G. A. Olah, *Carbocations and Electrophilic Reactions*, VCH, Weinheim, **1974** (see in particular Chapters 3 and 4); b) G. A. Olah, G. K. S. Prakash, J. Sommer, *Superacids*, Wiley, New York, **1985** (see in particular Chapters 3 und 5); c) G. A. Olah, G. K. S. Prakash, R. E. Williams, L. D. Field, K. Wade, *Hypercarbon Chemistry*, Wiley, New York, **1987** (see in particular Chapters 1, 5, and 7).
[10] A. D. Becke, K. E. Edgecombe, *J. Chem. Phys.* **1990**, *92*, 5397–5403.
[11] A. Savin, A. D. Becke, J. Flad, R. Nesper, H. Preuß, H. G. von Schnering, *Angew. Chem.* **1991**, *103*, 421–424; *Angew. Chem. Int. Ed. Engl.* **1991**, *30*, 409–412.
[12] B. Silvi, A. Savin, *Nature (London)* **1994**, *371*, 683–686.
[13] R. F. W. Bader, S. Johnson, T.-H. Tang, P. L. A. Popelier, *J. Phys. Chem.* **1996**, *100*, 15398–15415.

 © WILEY-VCH Verlag GmbH, D-69451 Weinheim, 1997 0570-0833/97/3619-2079 $ 17.50+.50/0

[14] A. Savin, O. Jepsen, J. Flad, O. K. Andersen, H. Preuß, H. G. von Schnering, *Angew. Chem.* **1992**, *104*, 186–188; *Angew. Chem. Int. Ed. Engl.* **1992**, *31*, 187–188.
[15] P. Mezey in *Reviews in Computational Chemistry, Vol. 1* (Eds.: K. B. Lipkowitz, D. B. Boyd), VCH, Weinheim, **1990**, pp. 265–294.
[16] A. Savin, B. Silvi, F. Colonna, *Can. J. Chem.* **1996**, *74*, 1088–1096.
[17] R. Thom, *Stabilité structurelle et morphogénèse*, Intereditions, Paris, **1972**.
[18] R. W. F. Bader, *Atoms in Molecules: A Quantum Theory*, Oxford University Press, Oxford, **1990**.
[19] The Hohenberg–Kohn–Sham density functional formalism in a plane-wave pseudopotential representation is used: R. O. Jones, O. Gunnarsson, *Rev. Mod. Phys.* **1989**, *61*, 689–746. In particular we use the local density approximation supplemented by Becke's exchange gradient correction: J. P. Perdew, A. Zunger, *Phys. Rev. B* **1981**, *23*, 5048–5079 and A. Becke, *Phys. Rev. A* **1988**, *38*, 3098–3100. This method was shown to yield excellent results [7] in particular for the crucial energy difference between the $e\text{-}C_s$ and C_{2v} stationary points of CH_5^+ as judged by comparison with correlated high-level calculations [1–5]. Our ELF module is based on the program CPMD version 2.5, written by Jürg Hutter, Max-Planck-Institut für Festkörperforschung, Stuttgart, **1995**, with the help of the group for Numerical Intensive Computations of IBM Research Laboratory Zürich and the Abteilung Parrinello at the Max-Planck-Institut für Festkörperforschung, Stuttgart. Graphics program: E. Pepke, J. Murray, J. Lyons, T.-Z. Hwu, *SciAn*, SCRI, Florida State University, Tallahassee, FL (USA), **1993**.
[20] D. Marx, M. Parrinello, *Z. Phys. D*, in press.

Nonclassical Shapes of Noble-Metal Colloids by Synthesis in Microgel Nanoreactors**

Markus Antonietti,* Franziska Gröhn, Jürgen Hartmann, and Lyudmila Bronstein

The controlled synthesis of colloids on a nanometer scale is important for bridging the gap between microlithography and micromechanics, which deal with structures down to 250 nm, and supramolecular chemistry, in which molecules of increasing size are built up by means of sophisticated classical chemistry. Structural design on the intermediate scale of several nanometers requires special techniques; nanomechanics would be inefficient, and classical chemical methods too complex and tedious.

Nature teaches us that effective control of structure is possible. In biomineralization, for instance, functional biomolecules (such as proteins or polysaccharides) act as templates for growing nanocrystals, platelets, and needles.[1–6] The specific interaction of these molecules with distinct crystallographic planes or sites of the growing nuclei allows control of the size, shape, and crystal structure of the inorganic product.

This approach for the nanostructuration of materials has been transferred to synthetic chemistry by utilizing Langmuir films of sparingly water soluble organic compounds to direct the growth of calcium carbonate and to tailor its crystal structure and morphology.[7] A three-dimensional biomimetic extension was described by Walsh et al., who synthesized highly defined, spongelike inorganic structures by precipitating calcium and magnesium carbonates from the microemulsion phases of nonionic surfactants.[8]

[*] Prof. Dr. M. Antonietti, F. Gröhn, Dr. J. Hartmann
Max Planck Institut für Kolloid- und Grenzflächenforschung
Kantstrasse 55, D-14513 Teltow-Seehof (Germany)
Fax: Int. code +(3328)46204
e-mail: pape@mpikg-teltow.mpg.de
Dr. L. Bronstein
Nesmeyanov Institute of Organoelement Compounds, Moscow (Russia)

[**] Financial support by the Max Planck Society is gratefully ackowledged. L. B. thanks the Volkswagen Foundation for a Russian–German exchange grant. We thank M. Giersig of the Hahn Meitner Institute (Berlin, Germany) for help with high-resolution electron microscopy.

Another route to matter organized on the nanometer scale consists of controlling the intermolecular arrangement of colloids. Fendler and co-workers obtained periodic arrays of noble-metal colloids beneath or in monolayers.[9] Möller et al. generated spherical gold particles in block copolymer micelles and examined the surface patterns of drying films.[10] Andres et al.[11] and Whetten et al.[12,13] crystallized gold and silver clusters to give two-dimensional superlattices. All these alignment techniques are restricted to producing crystallike, ordered two-dimensional or three-dimensional arrays of preformed particles, but do not address the original growth process. Nevertheless, these approaches indicate what the further structural layout of nanomaterials may look like.

Currently two general strategies for particle-growth control can be distinguished.[14] In host–guest nanoscale synthesis, a cage or structure-directing molecular container is formed by supramolecular or colloidal preorganization in which the nanostructure is fabricated (exo-template approach). In the interfacial molecular recognition route, crystallization is nucleated in the proximity of a structure-directing molecule or assembly. Growth is controlled by the presence of these molecules at some of the crystal surfaces, but no imprinting of an outer shape occurs (endo-template approach).

For a broader application of these principles, simpler, nonbiogenic templates are required, and modern polymer chemistry provides some promising candidates. We here describe the use of "microgels",[15,16] spherical polymer gel particles with a well-defined diameter in the nanometer range and an adjustable chemical functionality, as exo-templates and the generation of colloid particles by chemical reactions within the microgels. The tuning parameters of the local chemical environment (cross-linking density, abundance and type of functional groups) and the related physical properties of the microgel (swellability, elasticity) were systematically varied, and the resulting structures of the colloids produced within the nanoreactors investigated.

Using the reduction of gold salts to gold colloids (the classical Faraday experiment) as a model reaction allows a simple evaluation of the experiment by the naked eye. This is because the color of metallic gold colloids is caused by collective oscillations (plasmons) of the electrons relative to the atomic cores, the energy distribution of which is sensitive to the size and shape of the colloidal particles.[17]

Figure 1 shows a selection of gold colloids in polystyrene sulfonate microgels. Variation of cross-linking density, reducing agent, and reducing conditions resulted in a variety of stable colloidal solutions with very different colors. In addition to the classical Faraday colors, Barolo red and purple, shades from bengal rose to apricot and black were obtained.

These colloids were characterized by transmission electron microscopy (TEM). Three typical morphologies obtained by varying the reduction conditions are shown in Figure 2. Fast reduction with $NaBH_4$ in water resulted in the limiting case of small spherical gold colloids located as swarms inside the microgels (Figure 2a). Decreasing the reduction rate by changing the pH ($NaBH_4$ in 0.1 N NaOH), but maintaining all other parameters, led to a second morphology: long and winding gold threads (Figure 2b). With hydrazine as a reducing agent, gold "nanonuggets" that resemble algae were formed (Figure 2c).

The estimated amount of gold in a thread or a nugget is one order of magnitude too large to have originated from the gold load of a single microgel. Dynamic light scattering before and after reduction indicated that the reaction occurred only in some of the dispersed particles, which led to a bimodal particle size distribution. That is, the colloids were nucleated in some of the microgels, while the others served as a source of gold salt which

 © WILEY-VCH Verlag GmbH, D-69451 Weinheim, 1997 0570-0833/97/3619-2080 $ 17.50+.50/0

Figure 1. A selection of gold colloids prepared in polystyrene sulfonate microgels under different reaction conditions. The different colors of the solutions indicate the adjustable range of colloid sizes and morphologies. The colors yellow, red, and blue can be assigned to spherical gold particles of increasing size. All other colors are generated by the overlap of more than one plasmon resonance; this requires the presence of nonspherical particles with more than one "resonator" length.

migrated towards the growing colloids. This was confirmed by analytical ultracentrifugation, since the inclusion of a gold colloid increases the average density of the microgels. Scanning the optical density simultaneously at the wavelength of the plasmon band and at the absorption of the polymer, we found that only 15 (for the nuggets) to 20% (for the threads) of the microgels produce a colloid; the others were "empty" at the end of the reaction.

Formation of larger, more complex colloids implies that the rate of nucleation is sufficiently lower than the rate of mass transfer and growth to allow effective templating by the microgel. In the case of the nugget morphology, the microgel indeed acts as an exo-template, and the stretched polymer shell around the particles is clearly visible (Figure 2c). In the case of the nanothreads, the gold structures are significantly larger than the original microgels. Thus, the gold must have been extruded from the reaction core. The final threads are clustered and adhere to more than one microgel. It is noteworthy that, for some unknown reason, the ends of the threads usually occur in groups.

The switching between threads and nuggets upon using different reducing agents is not easy to explain. We assume that this morphology change reflects the fact that the colloid can grow at one site (thread) or many sites (nugget) as a result of the different surface binding of sodium borates and hydrazine.

The colloid morphology not only depends on the type of reduction, but also on the cross-linking density of the microgel. Higher cross-linking densities led to thinner structures as well as the formation of spherical colloids under a wider range of reac-

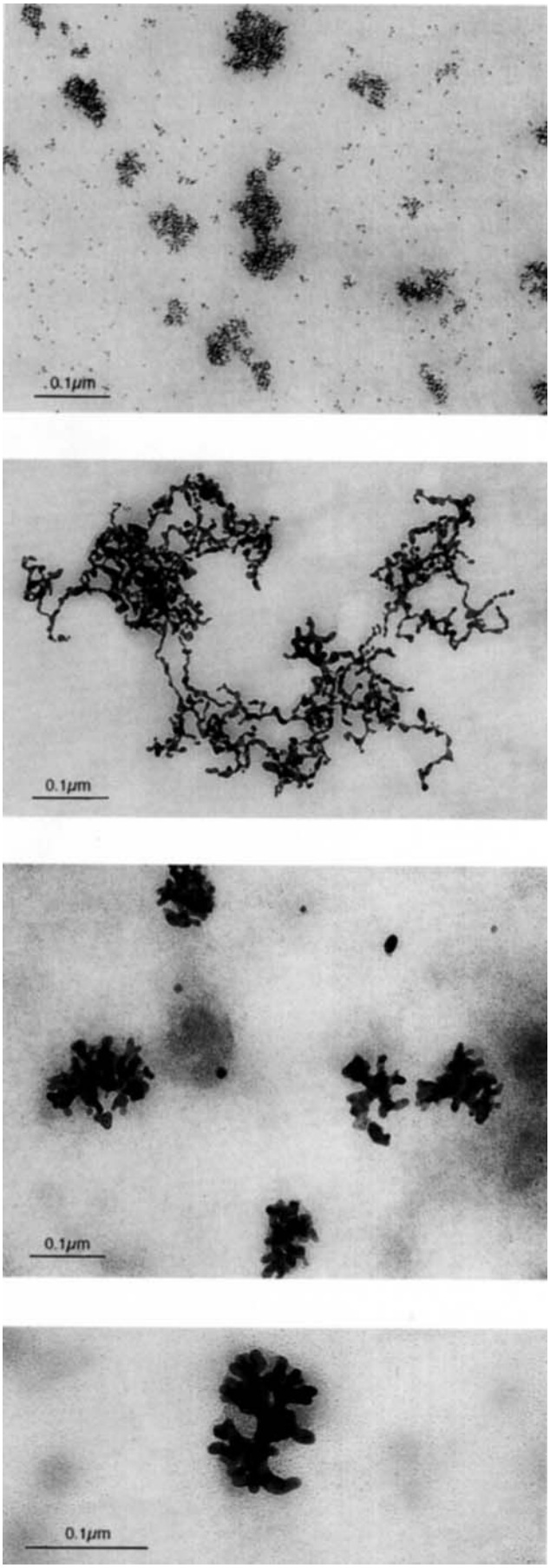

Figure 2. Transmission electron micrographs of colloids synthesized with different gels and reducing agents: a) uncontrolled particle morphology arising from fast reduction with multiple nucleation; b) threadlike morphology after slow reduction with sodium borohydride; c) nuggetlike morphology after reduction with hydrazine.

 © WILEY-VCH Verlag GmbH, D-69451 Weinheim, 1997 0570-0833/97/3619-2081 $ 17.50+.50/0

tion conditions, whereas the structures become thicker and less structured at lower cross-linking densities. This is due to the limitation of growth by the elastic forces of the surrounding gel matrix; that is, the particles stop growing in one direction as soon as the surrounding polymer chains are fully stretched.

Additional information was obtained from the determination of the crystallite size d_{cr} by linewidth analysis of the X-ray peaks. From the width of the Au(111) peak for the three samples shown in Figure 2, sizes of $d_{cr} = 4.5$ nm (small spheres in the microgel), $d_{cr} = 7$ nm (threads), and $d_{cr} = 25$ nm (nuggets) were calculated, which correlate well with the sizes of the colloids or the diameter of the threads observed by electron microscopy.

Further details of the inner structure of the colloids were obtained by high-resolution TEM (Figure 3). A remarkable

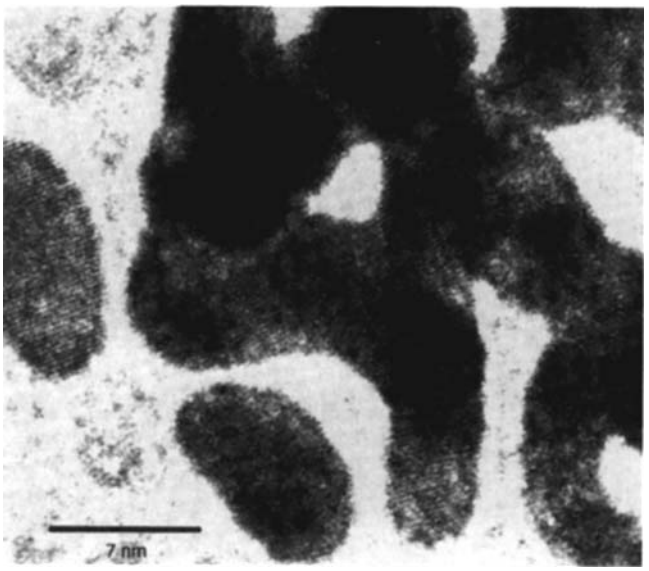

Figure 3. High-resolution electron micrographs of an end zone of the threads. The (111) crystallographic planes of the gold colloids can be seen. The correlation proves that the particles undergo directed growth rather than statistical agglomeration.

correlation of the crystallographic Au(111) planes was observed, which is apparently only weakly disturbed by the outer particle curvature. This proves that the particles grew from one nucleus, whereas the outer shape has to follow the chemical and physical structure of the microgel environment. This structure is not defect-free; grain boundaries are visible between slightly tilted regions.

We also investigated whether the use of microgel templates can be extended to control the structure of other chemically different colloids, such as oxidic colloids obtained by the precipitation of metal salts with hydroxide ions. To this end, we precipitated iron oxide under similar conditions inside the same microgels. The iron oxide does not precipitate macroscopically and is colloidally stable at pH 12, which would not be the case in the absence of the microgel. TEM revealed that again colloids with nonclassical shape, similar to the nugget morphology, are produced (Figure 4). This shows that the exo-template approach is not restricted to a particular chemistry or polymer/salt combination.

Biomineralization of iron oxides, with size and shape control, is performed by a number of living organisms, such as magnetotactic bacteria[14, 18]—this is source of inspiration. However, production of such structures is not a peculiarity of living matter, but seems to lie also within the capabilities of synthetic colloidal chemical systems.

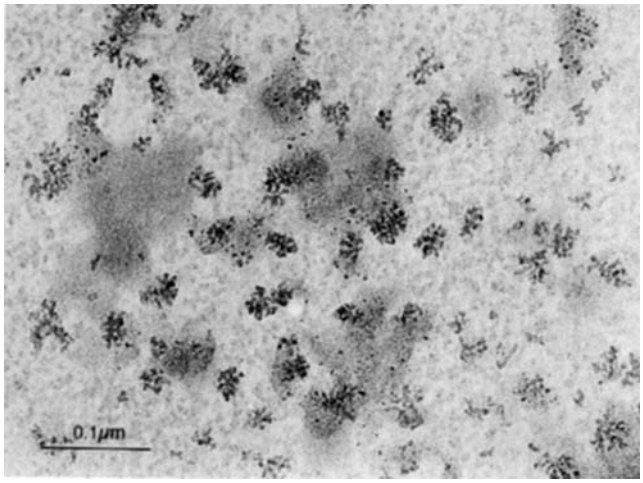

Figure 4. Transmission electron micrograph of iron oxide colloids synthesized by alkaline precipitation of iron salts in microgels. Templated, nonspherical objects are obtained.

The polymeric templates described here could potentially control properties other than size and shape. In the case of possible crystal polymorphism, the crystal structure can also depend on the microenvironment, and for binary systems, a composition control must also be considered. An extension of this set of "molecular tools" for the organized formation of matter on the nanometer scale is a topic of future experiments.

Experimental Section

The synthesis of polystyrene sulfonate microgels with defined size and cross-linking density and the characterization of their molecular properties are described elsewhere [19]. In the course of the synthesis, cross-linking density and degree of sulfonation were varied independently. For the experiments presented here, different microgels with a radius between 20 and 60 nm and cross-linking densities with one cross-link per 20 to 80 monomer units were selected.

The microgels were loaded with metal salt by mixing the aqueous solutions of microgel with the appropriate amounts of metal salts ($AuCl_3$ and $FeCl_3$; Aldrich Co.). To obtain stable systems a slight excess of negative charges is preferable; hence, ratios of Au:sulfonate slightly lower than 1:3 were employed. The colloidal stability is presumably due to enrichment of the gold salts inside the microgels, driven by osmotic forces and counterion condensation. This enrichment was required to produce the gold colloids within the microgels. No influence of the microgel template on the colloid structure is expected for nucleation in the continuous phase. The gold salt was reduced with an excess of $N_2H_4 \cdot H_2O$ or with $NaBH_4$ in aqueous solution at various pH values. Metal colloids formed immediately, as indicated by the color change. Iron oxide colloids were prepared by adding 0.1 N NaOH to solutions of $FeCl_3$ and microgel.

The colloidal solutions were characterized by static and dynamic light scattering, analytical ultracentrifugation, wide-angle scattering with linewidth analyis, and TEM. Experimental details of these techniques can be found elsewhere [20]. Samples for electron microscopy were prepared by suspension preparation. The dilute colloidal solutions were applied to a 400-mesh carbon-coated copper grid and left to dry. Electron microscopy was performed with a Zeiss 912 Omega electron microscope operating at 100 kV. High-resolution electron microscopy was performed with a Philips CM 120 equipped with Super Twin lenses at 120 kV.

Received: March 12, 1997 [Z10231IE]
German version: *Angew. Chem.* **1997**, *109*, 2170–2173

Keywords: colloids · crystal engineering · microgels · nanoreactors · nanostructures

[1] S. Mann, D. D. Archibald, J. M. Didymus, T. Douglas, B. R. Heywood, F. C. Meldrum, N. J. Reeves, *Science* **1993**, *261*, 1286.
[2] B. R. Heywood, S. Mann, *Adv. Mater.* **1994**, *6*, 9.
[3] G. Falini, S. Albeck, S. Weiner, L. Addadi, *Science* **1996**, *271*, 67.
[4] A. Berman, L. Addadi, S. Weiner, *Nature* **1988**, *331*, 546.
[5] J. Aizenberg, S. Albeck, S. Weiner, L. Addadi, *J. Cryst. Growth* **1994**, *142*, 156.
[6] C. S. Sikes, A. Wierzbicki, V. J. Fabry, *Bulletin de l'Institut oceanographique*, Monaco, **1994**.
[7] B. R. Heywood in ref. [14], pp. 143.

 © WILEY-VCH Verlag GmbH, D-69451 Weinheim, 1997 0570-0833/97/3619-2082 $ 17.50+.50/0

[8] D. Walsh, S. Mann, *Nature (London)* **1995**, *377*, 320.
[9] K. C. Yi, V. S. Mendieta, R. L. Castanarez, F. C. Meldrum C. Wu, J. H. Fendler, *J. Phys. Chem.* **1995**, *99*, 9869.
[10] J. P. Spatz, A. Roescher, M. Möller, *Adv. Mater.* **1996**, *8*, 337.
[11] R. P. Andres, J. D. Bielefeld, J. I. Henderson, D. B. Janes, V. R. Kolagunta, C. P. Kubiak, W. J. Mahoney, R. G. Osifchin, *Science* **1996**, *273*, 1690.
[12] R. L. Whetten, J. T Khoury, M. M. Alvarez, S. Murthy, I. Vezmar, Z. L. Wang, P. W. Stephens, C. L. Cleveland, W. D. Luedtke, U. Landman, *Adv. Mater.* **1996**, *8*, 428.
[13] S. A. Harfenist, Z. L. Wang, M. M. Alvarez, I. Vezmar, R. L. Whetten, *J. Phys. Chem.* **1996**, *100*, 13904.
[14] *Biomimetic Material Chemistry* (Ed.: S. Mann), VCH, Weinheim, **1996**.
[15] M. Antonietti, *Angew. Chem.* **1988**, *100*, 1813; *Angew. Chem. Int. Ed. Engl.* **1988**, 27, 1743.
[16] M. Antonietti, W. Bremser, M. Schmidt, *Macromolecules* **1990**, *23*, 3796.
[17] M. Vollmer, U. Kreibig, *Springer Ser. Mater. Sci.*, Springer, New York, **1995**.
[18] *Iron Biominerals* (Eds.: R. B. Frankel, R. P. Blakemore), Plenum Press, New York, **1989**.
[19] M. Antonietti, A. Briel, S. Förster, *J. Chem. Phys.* **1996**, *105*, 7795.
[20] M. Antonietti, A. Thünemann, E. Wenz, *Colloid. Polym. Sci.* **1996**, *274*, 795.

Addition of Nitriles to Metal Sulfides: Possible Insight into the Metal Sulfide Catalyzed Hydrogenation of Nitriles and Dinitrogen**

Jonathan T. Goodman and Thomas B. Rauchfuss*

The study of soluble metal sulfides provides insight into the function of biological and industrial catalysts as well as the design of new materials.[1] One remarkable aspect is the high reactivity of certain metal sulfides towards small substrates. While the binding of alkynes to metal sulfides is widely observed,[2] the corresponding addition of alkenes is relatively rare.[3] Hence, we were interested in the finding that the simple inorganic anion $[ReS_4]^-$ binds a variety of alkenes, for example ethylene [Eq. (1)].[4]

$$[ReS_4]^- + 2\,C_2H_4 + R_3NO \xrightarrow[-\,R_3N]{} \quad (1)$$

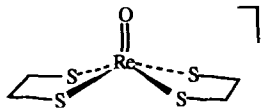

We examined the reaction of $PPh_4[ReS_4]$ with the relatively inert olefin *trans*-stilbene in the presence of sulfur in benzonitrile at reflux. Analysis of the crude reaction products by negative-ion FAB mass spectrometry revealed the presence of alkanedithiolates $[ReS(Ph(CHS)(CHS)Ph)]^-$ and $[ReS_5(Ph(CHS)(CHS)Ph)]^-$. Unexpectedly, we also observed comparable amounts of nitrile adducts $[ReS_5(NCPh)_2]^-$ and $[ReS_7(NCPh)]^-$ as well as the mixed complex $[ReS_3(Ph(CHS)(CHS)Ph)(NCPh)]^-$. We report here on this novel reaction.

Activation of nitriles by metal sulfides has been examined. Certain metal sulfides, notably WS_2 and MoS_2, catalyze the hydrogenation of nitriles.[5] The enzyme nitrogenase is also known to catalyze hydrogenation and hydrogenolysis of certain nitriles.[6] Furthermore, $[Cp_2Mo_2(S)(SH)(SCH_2S)]^+$ and MeCN react in the presence of acid to give imidothiolate $[Cp_2Mo_2(SC(=NH_2)Me)(S)(SCH_2S)]^+$,[7] a process related to the addition of H_2S to RCN.[8]

We initially focused on the reaction of $PPh_4[ReS_4]$ with S_8 and ArCN. Electrophilic substituents enhanced the rate of reaction. Thus, 4-substituted benzonitriles (X = CF_3, CO_2Me, NO_2) proved to be effective substrates, as judged by mass spectrometric and ^1H NMR spectroscopic analysis of the products. We optimized the reaction of methyl-4-cyanobenzoate with $PPh_4[ReS_4]$ in the presence of 0.5 equivalents of S_8 (see *Experimental Section*). Analysis showed the product to be $PPh_4[ReS_7NCC_6H_4CO_2Me]$. Alkene adducts of comparable stoichiometry consist of a thiorhenium(v) center bound to tetrasulfido and 1,2-dithiolato ligands.[4] The ^1H NMR spectrum of this material confirmed the 1:1 ratio of PPh_4^+ to nitrile. The IR spectrum revealed a medium-intensity band at 1602 cm^{-1}, assigned to $\nu_{C\equiv N}$, but no bands in the region normally associated with nitriles. On the basis of these results we propose that the reaction proceeds as shown in Equation (2).

We examined the connection between the nitrile adducts and the structurally related bis(tetrasulfido) complex ion $[ReS_9]^-$.[9] Under conditions employed for the formation of **1** [Eq. (2)],

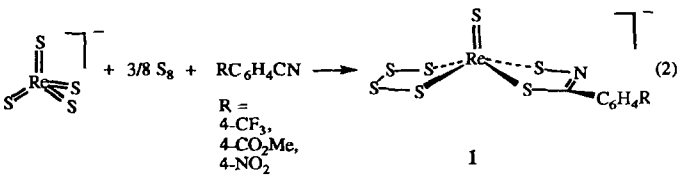

$CF_3C_6H_4CN$ is unreactive towards $[ReS_9]^-$ (= $[ReS(S_4)_2]^-$). Thus, we propose that Re^{VII} is required for adduct formation; that is, a redox process takes place. In addition, solutions of PPh_4-**1** (R = CO_2Me) do not react with sulfur to give $[ReS_9]^-$.

We were unable to obtain well-formed single crystals of the aryl nitrile adducts for an X-ray structure analysis. Studies with CF_3CN[10] proved more fruitful in this regard. The interaction of this reactive nitrile with metal sulfides had not yet been studied, but the related alkyne hexafluoro-2-butyne is known to bind sulfido ligands.[11] The violet color characteristic of solutions of $[ReS_4]^-$ is rapidly discharged in the presence of CF_3CN, even at low temperatures. We conducted reactions at −47 °C with MeCN as solvent and one equivalent of *N*-methylmorpholine-*N*-oxide (NMO) as an O-atom donor. The synthesis was completed by warming the mixture to room temperature. Recrystallization of the product from ethanol/hexane afforded straw-colored crystals of $PPh_4[ReO(S_2NCCF_3)_2]$ [PPh_4-**2**, Eq. (3)].

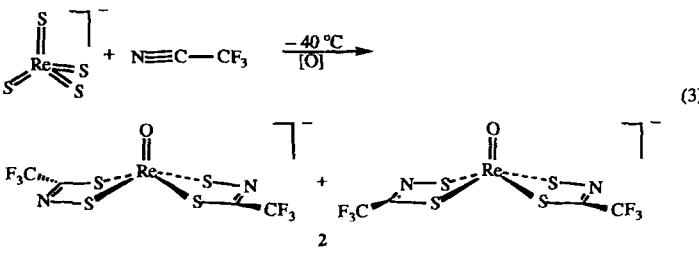

The ^{19}F NMR spectrum of this species showed two equally intense signals at $\delta = 13.80$ and 13.95, which we attribute to *cis* and *trans* isomers. Reaction of $[ReS_4]^-$ with CF_3CN in the presence of sulfur yielded a compound that is assigned as

[*] Prof. T. B. Rauchfuss, J. T. Goodman
School of Chemical Sciences
University of Illinois
Urbana, IL 61801 (USA)
Fax: Int. code (217)333-2685
e-mail: rauchfuz@uiuc.edu

[**] This research was supported by the U. S. National Science Foundation. We thank Dr. S. Inomata for preliminary results.

 © WILEY-VCH Verlag GmbH, D-69451 Weinheim, 1997 0570-0833/97/3619-2083 $ 17.50+.50/0

$PPh_4[ReS(S_2NCCF_3)_2]$ based on ^{19}F NMR and IR spectroscopy. The reaction of $[ReS_4]^-$ and CF_3CN also proceeded readily in the absence of an oxidant, but produced a complex mixture.

Single crystal X-ray diffraction analysis[12] of PPh_4-**2** confirmed the presence of ReSC=NS rings (Figure 1). The structure of the azadithiolene moieties compare well with that in

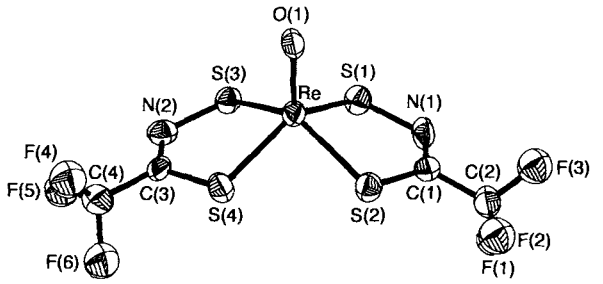

Figure 1. Structure of the anion in PPh_4-**2**. Selected distances [Å]: Re–S(2) 2.323(2), S(2)–C(1) 1.757(10), C(1)–N(1) 1.266(13), N(1)–S(1) 1.720(9), S(1)–Re 2.286(3).

$(C_5H_5)CoS_2NCPh$, which Sugimori et al. synthesized by oxidative addition of $CpCo^I$- containing compounds on preformed RCNS heterocycles.[13] Within the ReSCNS rings the Re–S distance to the nitrogen-bound sulfur atom is slightly shorter than that to the carbon-bound sulfur atom. The remaining Re–S bond lengths are similar to those seen in related Re^V–S compounds.[14]

We obtained evidence that even conventional nitriles add to $[ReS_4]^-$ in the presence of S_8. This surprising aspect was established by careful analysis of the products obtained from solutions of $PPh_4[ReS_4]$ and elemental sulfur (three equivalents) in acetonitrile, which were heated at reflux for 24 h. After removal of $[ReS_9]^-$ (≈80% yield) and a small amount of starting $[ReS_4]^-$ by fractional crystallization,[15] we obtained a crude sample in less than 5% yield that we assign as $PPh_4[ReS_7NCMe]$. The following data support this assignment: a band for $\nu_{C=N}$ at 1477 cm^{-1} in the IR spectrum, a signal at $\delta = 3.13$ (s) for the methyl group in the ^1H NMR spectrum, and negative-ion ESI MS peaks corresponding to $[ReS_7NCMe]^-$ ($m/z = 451.8$) and $[ReS_5(NCMe)_2]^-$ ($m/z = 387.9$). The aryl nitrile adducts and $[ReS_7NCMe]^-$ display very similar fragmentation patterns.

Metal sulfides are active catalysts for the reduction of nitriles.[5] We have confirmed that solutions of $[ReS_4]^-$ give very active catalysts for the hydrogenation of benzonitrile to NH_3 and dibenzylamine (typical reaction conditions: neat nitrile, 175 °C, H_2 (1000 psi), 16 h to give 75% conversion with a turnover number of about 3400). This suggests that mechanistic models for metal sulfide catalyzed hydrogenation of nitriles should consider the possibility of substrate binding at a sulfur atom. A speculative but logical extension of these findings is that similar pathways may apply to biological nitrogen fixation, which is catalyzed by clusters[16, 17] featuring highly exposed sulfido ligands.

Experimental Section

$NEt_4[ReS_4]$ was synthesized by the modification from Exxon of the procedure by Müller et al, and converted to the PPh_4^+ salt by metathesis in MeCN [18]. CF_3CN was purchased from PCR (Gainesville, FL, USA).

PPh_4-**1**, R = CO_2Me: A mixture of $PPh_4[ReS_4]$ (0.36 g, 0.55 mmol), sulfur (0.054 g, 0.21 mmol), and 4-$NCC_6H_4CO_2Me$ (2.0 g, 12.41 mmol) was held at 85 °C for 1.5 h, during which time its color changed from violet to dark brown. The product was extracted with THF (5 mL) and precipitated by cooling (yield 0.36 g, 72%). Analytically pure samples were obtained by recrystallization from THF/hexane. Elemental analysis calcd (found) for $C_{33}H_{27}NO_2PReS_7$: C 43.50 (43.47), H 2.99 (3.24), N 1.54 (1.24), S 24.63 (24.62), P 3.40 (3.14); ^1H NMR (500 MHz, CD_3CN): $\delta = 3.90$ (Me, 3H), 7.83 (m, 16H), 7.98 (m, 4H), 8.06 (Ar, 2H, $J = 0.75$ Hz), 8.36 (Ar, 2H, $J = 0.75$ Hz); ^{13}C NMR (125 MHz, [D$_6$]acetone): $\delta = 52.41$ (OMe), 118.94 (PPh, $J = 88.8$ Hz), 129.87, 130.40, 131.37 (PPh, $J = 12.9$ Hz), 131.58, 135.65 (PPh, $J = 10$ Hz), 136.34 (PPh, $J = 2.75$ Hz), 139.3, 166.85 (C = O), 181.5 (SCN); IR (KBr): $\tilde{\nu} = 1714$ (C=O), 1603 (C=N), 1278 cm^{-1} (C=O); MS (negative-ion ESI): $m/z = 571.8$ ($C_9H_7NO_2ReS_7^-$).

The above procedure applies to syntheses with 4-$CF_3C_6H_4CN$ and 4-$O_2NC_6H_4CN$: Et_4N-**1**, R = CF_3: ^1H NMR (400 MHz, CD_3CN): $\delta = 1.17$ (tt, 12H), 3.11 (q, 8H), 7.77 (d, 2H, $J = 10$ Hz), 8.42 (d, 2H, $J = 10$ Hz); MS (negative-ion ESI): $m/z = 581.7$ ($C_8H_4NF_3ReS_7^-$). Et_4N-**1**, R = NO_2: ^1H NMR (500 MHz, CD_3CN) $\delta = 1.09$ (tt, 12H), 2.98 (q, 8H), 8.28 (d, 2H, $J = 9$ Hz), 8.46 (d, 2H, $J = 9$ Hz); MS (negative-ion ESI): $m/z = 558.9$ ($C_7H_4N_2O_2ReS_7^-$).

PPh_4-**2**: A solution of $PPh_4[ReS_4]$ (0.25 g, 0.38 mmol) and NMO (0.051 g, 0.43 mmol) in CH_3CN (20 mL) was cooled to −47 °C, and treated with gaseous CF_3CN. The solution immediately assumed a brown color. The solution was allowed to warm to room temperature. After 1 h solvent was removed under vacuum from the pale yellow solution leaving yellow microcrystals, which were washed with hexane (50 mL; yield 0.28 g, 86%). Analytically pure single crystals were obtained by slow diffusion of hexane into a solution of PPh_4-**2** in ethanol. Elemental analysis calcd (found) for $C_{28}H_{20}N_2F_6OPReS_4$: C 39.11 (39.38), H 2.34 (2.28), N 3.26 (3.48), S 14.92 (14.75), F 13.26 (12.84), P 3.60 (3.47); ^{19}F NMR (CD_3CN, 376 MHz; as ext. ref. CF_3CO_2H): $\delta = 13.80$, 13.95; IR (KBr): $\tilde{\nu} = 1560$ (C=N), 1278 (CF), 1194 (CF), 1182 (CF), 1125 (CF), 960 (Re=O), 630 (CS). MS (negative-ion ESI): $m/z = 520.8$ ($C_4N_2F_6OReS_4^-$).

Received: March 17, 1997 [Z10250IE]
German version: *Angew. Chem.* **1997**, *109*, 2173–2175

Keywords: nitrogen fixation · oxidoreductases · redox chemistry · rhenium · sulfur

[1] *Transition Metal Sulfur Chemistry* (Eds.: E. I. Stiefel, K. Matsumoto), American Chemical Society, Washington, DC, **1996**.
[2] H. Kawaguchi, K. Tatsumi, *J. Am. Chem. Soc.* **1995**, *117*, 3885; A. A. Eagle, S. M. Harben, E. R. T. Tiekink, C. G. Young, *ibid.* **1994**, *116*, 9749; T. Shibahara, G. Sakane, S. Mochida, *ibid.* **1993**, *115*, 10408.
[3] M. Rakowski DuBois, B. R. Jagirdar, S. Dietz, B. C. Noll, *Organometallics* **1997**, *16*, 294, and references therein.
[4] J. T. Goodman, S. Inomata, T. B. Rauchfuss, *J. Am. Chem. Soc.* **1996**, *118*, 11674.
[5] O. Weisser, S. Landa, *Sulphide Catalysts, Their Properties and Applications*, Pergamon, New York, **1973**, p. 248.
[6] B. K. Burgess, D. J. Lowe, *Chem. Rev.* **1996**, *96*, 2983.
[7] P. Bernatis, J. C. V. Laurie, M. Rakowski DuBois, *Organometallics* **1990**, 9, 1607; D. E. Coons, J. C. V. Laurie, R. C. Haltiwanger, M. Rakowski DuBois, *J. Am. Chem. Soc.* **1987**, *109*, 283.
[8] A. Fatidi, *Chemistry of Triple-Bonded Functional Groups, Part 2* (Eds.: S. Patai, Z. Rappoport), Wiley, Chichester, **1983**.
[9] A. Müller, M. Lemke, E. Krickemeyer, H. Bögge, M. Penk, *Monatsh. Chem.* **1993**, *124*, 857.
[10] H. Gilman, R. G. Jones, *J. Am. Chem. Soc.* **1943**, *65*, 1458.
[11] C. M. Bolinger, T. B. Rauchfuss, A. L. Rheingold, *J. Am. Chem. Soc.* **1983**, *105*, 6321.
[12] Crystal data for $C_{28}H_{20}F_6N_2OPReS_4$: monoclinic, space group $P2_1/n$, $a = 11.0735(5)$, $b = 12.5437(6)$, $c = 22.2448(10)$ Å, $\beta = 94.065(2)°$, $V = 3082.1(2)$ Å^3, $Z = 4$, $\rho_{calcd} = 1.922$ g cm^{-3}, $Mo_{K\alpha}$ radiation ($\lambda = 0.71073$ Å), crystal dimentions $0.08 \times 0.14 \times 0.36$ mm. The structure was solved by direct methods; Re, S, C, and N atoms were refined anisotropically (SHELXS-86 and SHELXL-93). Some disorder is evident in the fluorine-atom positions. For 5415 unique observed reflections with $I > 2\sigma(I)$ collected at $T = 198(2)$ K on a Siemens 3-circle platform in the range $3.68 < 2\vartheta < 56.60$, the final R value is 0.0663 ($wR_2 = 0.1574$). Crystallographic data (excluding structure factors) for the structures reported in this paper have been deposited with the Cambridge Crystallographic Data Centre as supplementary publication no. CCDC-100280. Copies of the data can be obtained free of charge on application to The Director, CCDC, 12 Union Road, Cambridge CB21EZ, UK (fax: int. code +(1223) 336-033; e-mail: deposit@chemcrys.cam.ac.uk).
[13] A. Kato, M. Tono, N. Hisamatsu, S. Nozawa, K. Ninomiya, T. Sugiyama, M. Kajitani, T. Akiyama, A. Sugimori, *J. Organomet. Chem.* **1994**, *473*, 313; A. Kato, M. Tono, N. Hisamatsu, S. Nozawa, T. Sugiyama, M. Kajitani, T. Akiyama, A. Sugimori, *Chem. Lett.* **1992**, 243.
[14] M. Herberhold, G.-X. Jin, A. L. Rheingold, *J. Chem. Soc. Chem. Commun.* **1996**, 2645; M. Herberhold, G.-X. Jin, W. Milius, *J. Organomet. Chem.* **1996**, 512, 111, and references therein.

 © WILEY-VCH Verlag GmbH, D-69451 Weinheim, 1997 0570-0833/97/3619-2084 $ 17.50+.50/0

[15] Control experiments: In the absence of S_8, solutions of $[ReS_4]^-$ in MeCN are stable for extended periods at 80 °C. Nitriles per se do not accelerate the conversion of $[ReS_4]^-$ into $[ReS_9]^-$; this conversion also proceeds readily for solutions in pyridine.
[16] J. B. Howard, D. C. Rees, *Chem. Rev.* **1996**, *96*, 2965; D. C. Rees, M. K. Chen, J. Kim, *Adv. Inorg. Chem.* **1994**, *40*, 89.
[17] Recent work on catalytically active metal sulfide clusters: T. Wakabayashi, Y. Ishii, K. Ishikawa, M. Hidai, *Angew. Chem.* **1996**, *108*, 2268; *Angew. Chem. Int. Ed.* **1996**, *35*, 2123; K. D. Demadis, S. M. Malinak, D. Coucouvanis, *Inorg. Chem.* **1996**, *35*, 4038; M. D. Curtis, S. H. Drucker, *J. Am. Chem. Soc.* **1997**, *119*, 1027.
[18] Jp. Patent 02 08 8428 (Exxon), **1990**; *Chem. Abstr.* **1990**, *113*, 214804; A. Müller, E. Krickemeyer, H. Bögge, *Z. Anorg. Allg. Chem.* **1987**, *554*, 61.

Site-Specific Photocleavage of Proteins**

Challa V. Kumar* and Apinya Buranaprapuk

Dedicated to Professor Nicholas J. Turro on the occasion of his 59th birthday

Reagents that cleave proteins with high specificity under thermal or photochemical conditions could be useful for structure–activity studies of proteins, investigation of protein structural domains, design of new therapeutic agents, and conversion of large proteins into smaller fragments that are more amenable for sequencing.[1] The proliferation of chemical nucleases in DNA-cleavage studies is an example of how reagents based on small molecules can be of use in molecular biology.[2, 3] Analogously, chemical proteases are useful for the manipulation of proteins.[1, 4, 5] Two approaches for the design of chemical proteases can be distinguished: 1) use of affinity-based reagents, and 2) covalent linking of redox-active metal complexes to specific residues of the protein with subsequent activation of the metal to achieve protein cleavage. We describe here a new reagent for the photocleavage of proteins that has a) high affinity for hydrophobic sites of proteins, b) strong absorption bands in the near-visible region, c) a long-lived singlet excited state (which is convenient for photoreactions), and d) a chromophore that has been extensively used to probe microenvironments. Use of light as a reagent in protein-cleavage reactions provides strict control of the initiation and termination of the reaction. Vanadate was used as a photoprobe for phosphate-binding sites of proteins.[6] Vanadate has a low extinction coefficient (>320 nm),[6] and high concentrations of vanadate are needed to capture a significant fraction of the incident light. The presence of several vanadium species in vanadate solutions makes it difficult to identify the photochemically active species,[6c] and vanadate induces photocleavage at many sites other than serine residues.[6d] We now observed that Py-Phe (Scheme 1) complements vanadate photochemistry and that Py-Phe induces site-specific photocleavage of bovine serum albumin (BSA) and chicken-egg lysozyme under mild conditions.[7]

The design of Py-Phe was prompted by earlier studies in our laboratory with bifunctional probes consisting of hydrophobic and hydrophilic groups separated by a linker.[8–10] Bifunctional

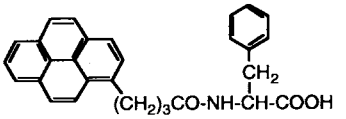

Py-Phe

Scheme 1. Structure of the bifunctional probe Py-Phe, which is obtained by linking 4-(1-pyrenyl)butyric acid with L-phenylalanine.

probes seek out binding sites on proteins that have an arrangement of hydrophobic and hydrophilic microenvironments with complementary interactions. Covalent linking of 4-(1-pyrenyl)-butyric acid with L-phenylalanine resulted in fluorescent Py-Phe (Scheme 1).[11] The hydrophilic carboxy functionality of Py-Phe and the amide linkage improve the aqueous solubility of the hydrophobic pyrene moiety of Py-Phe. The hydrophilic functionalities may also participate in electrostatic and hydrogen-bonding interactions. The size of the separation between the hydrophobic and hydrophilic moieties (the length of the linker) plays an important role in probe binding to proteins. Probe affinity for proteins, for example, increases with increasing linker length as well as with the size of the hydrophobic moiety.[8] The long-lived singlet excited state of the pyrenyl chromophore ($t_{1/2}$ > 100 ns), when coupled with the redox activity of amminecobalt(III) complexes, results in site-specific protein cleavage.

Studies show that Py-Phe binds to proteins. For example, the electronic absorption spectrum of Py-Phe (3 μM) is red-shifted upon binding to BSA (Figure 1). The intensities of Py-Phe absorption bands decrease with increased protein concentration;

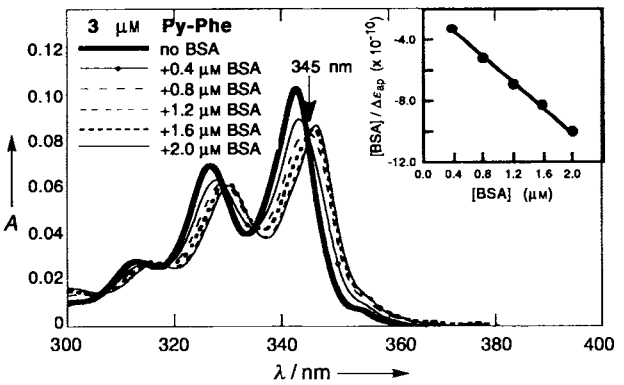

Figure 1. Absorption spectra of Py-Phe (3 μM) with and without BSA. The spectra are red-shifted by 4 nm with an isosbestic point at 345 nm. A plot of the quotient of the BSA concentration and $\Delta\varepsilon_{ap}$ versus the BSA concentration is shown at the top right corner; the estimated binding constant for the binding of Py-Phe to BSA is $(2.8\pm0.5)\times10^6\ M^{-1}$. The binding constant for the binding of Py-Phe to lysozyme is $(7\pm0.5)\times10^5\ M^{-1}$. A = absorbance.

the isosbestic point is at 345 nm. The red shift and hypochromicity indicate a hydrophobic environment around the pyrenyl chromophore.[8] The binding plot[12] derived from the absorption titration data (inset of Figure 1) provided a binding constant of $(2.8\pm0.5)\times10^6\ M^{-1}$. Binding of Py-Phe to BSA was also confirmed by circular dichroism (CD) and fluorescence spectra. New positive CD bands appeared at 330 and 345 nm when BSA (50 μM) was added to Py-Phe (50 μM), whereas the free probe had negative CD bands at 336, 351, and 360 nm. Binding of Py-Phe to BSA increases the fluorescence lifetime of Py-Phe from 106 ns (free probe, air-saturated buffer) to 125 ns (1:1 ratio of Py-Phe to BSA). Fluorescence-quenching studies indicate that Py-Phe bound to BSA is well protected from the

[*] Prof. C. V. Kumar, A. Buranaprapuk
Department of Chemistry
University of Connecticut
Storrs, CT 06269-3060 (USA)
Fax: Int. code +(860)486-2981
e-mail: cvkumar@nucleus.chem.uconn.edu

[**] Financial support from the University of Connecticut Research Foundation is gratefully acknowledged.

 © WILEY-VCH Verlag GmbH, D-69451 Weinheim, 1997 0570-0833/97/3619-2085 $ 17.50+.50/0

aqueous medium. The Stern–Volmer quenching constants obtained with CoHA (= $[Co(NH_3)_6]^{3+}$) as the quencher decrease from 1.9 mM^{-1} (free probe) to 0.25 mM^{-1} (bound to BSA). Taken together, these spectroscopic studies indicate that the probe binds to the protein through its pyrenyl moiety, which is protected from the aqueous medium by the surrounding protein matrix.

Photocleavage of BSA was achieved by irradiating into the absorption bands of the pyrenyl chromophore at 344 nm in the presence of CoHA (1, 2, and 10 mM) as an electron acceptor. Progress of the protein photocleavage was monitored by sodium dodecyl sulfate polyacrylamide gel electrophoresis (SDS PAGE; 6% acrylamide, 0.4% bis(acrylamide), 13% glycerol, pH 8.4).[13] Two new bands for BSA fragments with molecular weights of 41 and 28 kDa appear in the gel (Figure 2), illustrating the high degree of specificity in cleavage. If the photocleavage were random, one would observe a smear in these lanes. No photocleavage is observed in the absence of either of the two reagents or light (Figure 2, bottom, lanes 3 and 8–10). Irradiation of BSA and CoHA without Py-Phe does not yield any fragmentation (lane 10). Similarly, irradiation of BSA in the presence or absence of Py-Phe without CoHA does not result in fragmentation (lanes 9 and 8, respectively). Py-Phe, CoHA, and light are essential for the observed photocleavage. Photocleavage with Py-Phe is also observed for lysozyme (two fragments of lower molecular weight (11 kDa, 3.5 kDa) appear), myoglobin, and carboxypeptidase, demonstrating the general nature of the methodology.

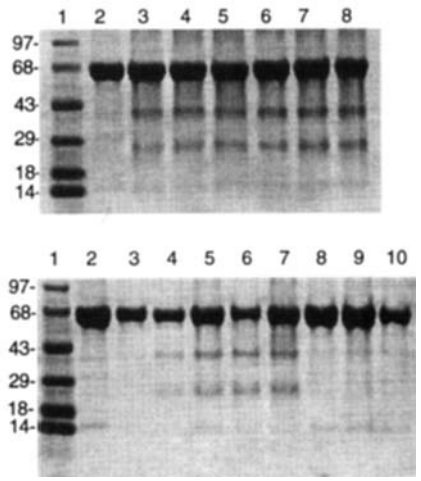

Figure 2A. Top: the gel-electrophoresis pattern of BSA under various conditions: lane 1, molecular weight standard for the mass values given on the left; lanes 2–8 contained BSA (15 μM) and Py-Phe (15 μM); lanes 3–5 also contained CoHA (1 mM); lanes 6–8 also contained CoHA (2 mM). Samples in lanes 3–5 were irradiated at 344 nm for 20, 40, and 60 min, respectively. Samples in lanes 6–8 were irradiated for 20, 40, and 60 min, respectively. The samples were run from top to bottom. Bottom: the gel-electrophoresis pattern of BSA under various conditions: lane 1, molecular weight standard for the mass values given on the left; lane 2 contained BSA (15 μM); lanes 3–7 contained BSA (15 μM), CoHA (10 mM), and Py-Phe (15 μM), and the sample was irradiated for 0, 10, 20, 30, and 60 min, respectively; lane 8 contained only BSA (15 μM), and the sample was irradiated for 30 min; lane 9 contained BSA (15 μM) and Py-Phe (15 μM), and the sample was irradiated for 30 min; lane 10 contained BSA (15 μM) and CoHA (10 mM), and the sample was irradiated for 30 min.

Use of Co^{III} complexes other than CoHA—such as chloropentamminecobalt(III) chloride, $[Co(bpy)]_3^{3+}$, or sepulchratecobalt(III) chloride—also results in the same fragments for the cleavage of BSA with Py-Phe. The cleavage most likely occurs at the pyrenyl-binding site rather than at the metal-binding site. Singlet oxygen is not involved in these reactions, as degassing of the reaction mixture does not alter or reduce photoproduct formation. Addition of sodium azide, a known singlet-oxygen quencher, does not inhibit the photoreaction. Irradiation for longer than 20 min enhances the formation of photoproducts only marginally (maximum conversion of 21% for BSA and 44% for lysozyme). The pyrenyl radical cation, generated by electron transfer from the Py-Phe singlet excited state by CoHA, may be responsible for the photocleavage. The following support this view: Py-Phe fluorescence is quenched by CoHA at a diffusion-controlled rate (4.6×10^9 $dm^3 mol^{-1} s^{-1}$), amminecobalt(III) complexes are necessary for cleavage, Py-Phe is gradually consumed in the photoreaction, and $[Co^{II}(H_2O)]_6^{2+}$ is detected at the end of the photocleavage reaction. Fluorescence from protein-bound Py-Phe is quenched by CoHA at a slower rate than that with the free probe (K_{SV} is reduced by a factor of about 8 upon binding to BSA). When Py-Phe is omitted from the reaction mixture, irradiation does not lead to protein cleavage. The pyrenyl chromophore is important in the light-absorption process and in the subsequent photoreaction. The N-terminal sequencing of the photoproducts to identify the cleavage site was not successful, which suggests possible N-terminal blockage similar to those observed with other protein-cleavage protocols.[1a–c, 6] Experiments are in progress to identify the cleavage site and the mechanistic pathways responsible for photocleavage. The appearance of two sharp bands in the gels demonstrates a single cut in the peptide backbone with a high degree of specificity. The low diffusional mobility of the pyrenyl radical cation (compared to that of the hydroxy radical)[14] and the high affinity of Py-Phe for hydrophobic and hydrophilic microenvironments in proteins may be responsible for the observed high specificity.

Received: December 30, 1996
Revised version: April 14, 1997 [Z9946IE]
German version: *Angew. Chem.* **1997**, *109*, 2175–2177

Keywords: cleavage reactions · gel electrophoresis · photochemistry · proteins · pyrene

[1] a) A. Schepartz, B. Cuenoud, *J. Am. Chem. Soc.* **1990**, *112*, 3247; b) B. Cuenoud, T. M. Tarasow, A. Schepartz, *Tetraheron Lett.* **1992**, *33*, 895; c) D. Hoyer, H. Cho, P. G. Schultz, *J. Am. Chem. Soc.* **1990**, *112*, 3249; d) M. R. Ermacora, J. M. Delfino, B. Cuenoud, A. Schepartz, R. O. Fox, *Proc. Natl. Acad. Sci.* USA **1992**, *89*, 6383; e) T. M. Rana, C. F. Meares, *J. Am. Chem. Soc.* **1991**, *113*, 1859; f) *Proc. Nat. Acad. Sci.* USA **1991**, *88*, 10578; g) *J. Am. Chem. Soc.* **1990**, *112*, 2457.

[2] A. H. Krotz, L. Y. Kuo, T. P. Shields, J. K. Barton, *J. Am. Chem. Soc.* **1993**, *115*, 3877; C. C. Cheng, S. E. Rokita, C. Burrows, *Angew. Chem.* **1993**, *105*, 290; *Angew. Chem. Int. Ed. Engl.* **1993**, *32*, 277; N. Gupta, N. Grover, G. A. Neyhart, P. Singh, H. H. Thorpe, *Inorg. Chem.* **1993**, *32*, 310; A. Sitlani, E. C. Long, A. M. Pyle, J. K. Barton, *J. Am. Chem. Soc.* **1992**, *114*, 2303.

[3] S. A. Strobel, P. B. Dervan, *Methods Enzymol.* **1992**, *216*, 309; D. P. Mack, P. B. Dervan, *Biochemistry* **1992**, *31*, 9399; S. F. Singleton, P. B. Dervan, *J. Am. Chem. Soc.* **1992**, *114*, 6957; P. B. Dervan, *Nature* **1992**, *359*, 87.

[4] N. Ettner, G. A. Ellestad, W. Hillen, *J. Am. Chem. Soc.* **1993**, *115*, 2546; N. Ettner, J. W. Metzger, T. Lederer, J. D. Hulmes, C. Kisker, W. Hinrichs, G. Ellestad, W. Hillen, *Biochemistry* **1995**, *34*, 22.

[5] S. A. Strobel, P. B. Dervan, *Science* **1991**, *254*, 1639; K. S. Graham, P. B. Dervan, *J. Biol. Chem.* **1990**, *265*, 6534; K. Nagai, S. M. Hecht, *ibid.* **1991**, *266*, 3994.

[6] a) J. J. Correia, L. D. Lipscomb, J. C. Dabrowiak, N. Isern, J. Zubieta, *Arch. Biochem. Biophys.* **1994**, *309*, 94; b) D. C. Crans, K. Sudhakar, T. Zamborelli, *Biochemistry* **1992**, *31*, 6812; c) D. Rehder, *Angew. Chem.* **1991**, *103*, 152; *Angew. Chem. Int. Ed. Engl.* **1991**, *30*, 148; d) C. R. Cremo, J. A. Loo, C. G. Edmonds, K. M. Hatlelid, *Biochemistry* **1992**, *31*, 491.

[7] C. V. Kumar, A. Buranaprapuk, poster presentation at the 213th ACS National Meeting, August 1996, Orlando, FL, USA.

[8] a) C. V. Kumar, L. M. Tolosa, *J. Phys. Chem.* **1993**, *97*, 13913; b) *FASEB J.* **1993**, *7*, A1131.

[9] C. V. Kumar, E. H. Asuncion, *J. Chem. Soc. Chem. Commun.* **1992**, 470; *J. Am. Chem. Soc.* **1993**, *115*, 8547.

[10] C. V. Kumar, W. B. Tan, *J. Inorg. Biochem.*, in press.

 © WILEY-VCH Verlag GmbH, D-69451 Weinheim, 1997 0570-0833/97/3619-2086 $ 17.50+.50/0

[11] L-Phenylalanine ethyl ester (0.4 g) and dicyclohexylcarbodiimide (0.4 g) were added 4-(1-pyrenyl)butyric acid (0.5 g) in acetonitrile (50 mL). The mixture was stirred at room temperature (4 h), and excess DCC deomposed. The solvent was removed under reduced pressure, and the reaction mixture subjected to acid hydrolysis (1 N HCl, 12 h, room temperature). Pure product was isolated after chromatography on silica gel. ^{1}H NMR (270 MHz, DMSO): $\delta = 8.06-8.34$ (m, 9H), 7.2 (m, 5H), 4.5 (exchangeable NH, 1H), 2.0 (m, 1H), 2.1–2.5 (m, 6 aliphatic H); IR (KBr): $\tilde{\nu} = 3300$ (OH), 1703 (acid C=O), 1640 cm^{-1} (amide C=O); the absorption maxiama at 313, 326, and 343 nm as well as the fluorescence maxima at 376, 396, and 417 nm (340 nm excitation) correspond to those of the pyrenyl chromophore. The circular-dichroism maxima are at 336, 351, and 360 nm.

[12] A. Wolfe, G. H. Shimer, Jr., T. Mechan, *Biochemistry* **1987**, *26*, 6392; A. M. Pyle, R. M. Rehman, C. V. Kumar, N. J. Turro, J. K. Barton, *J. Am. Chem. Soc.* **1989**, *111*, 3051. The equation used is $([BSA]/\Delta\varepsilon_{ap}) = ([BSA]/\Delta\varepsilon) + (1/\Delta\varepsilon K)$ where $\Delta\varepsilon_{ap} = [\varepsilon_a - \varepsilon_f]$, $\Delta\varepsilon = [\varepsilon_b - \varepsilon_f]$, K is the binding constant, $\varepsilon_a =$ (absorbance at 343 nm)/[Py-Phe], ε_b = extinction coefficient of the bound form (2.211×10^4 M^{-1} cm^{-1}), and ε_f is the extinction coefficient of free Py-Phe.

[13] The reaction mixture (0.1 mL) was irradiated at 344 nm for various lengths of time with a xenon lamp source and a monochromator (3.0×10^{-8} einsteins min^{-1} at 340 nm). Filters were used to remove stray UV light, and the band pass on the monochromator was adjusted to 10 nm. Irradiated solutions of the protein and probe were dried under reduced pressure, and the residue was redissolved in the sample buffer (0.024 mL) made of glycerol (1 mL), sodium dodecyl sulfate (3 mL, 10% aqueous solution), tris(hydroxymethyl)aminomethane hydrochloride (1.25 mL, 0.5 M), bromophenol blue (0.6 mL, 0.1% solution), and deionized distilled water (4.5 mL). The gels were run by applying a voltage of 60 V until the dye (Coomassie blue) passed through the stacking gel. The voltage was then increased to 110 V, and the gels were run for a total of 2 h; see H. Schagger, G. V. Jagow, *Anal. Biochem.* **1987**, *166*, 368.

[14] P. A. King, E. Jamison, D. Strahs, V. E. Anderson, M. Brenowitz, *Biophys. J.* **1993**, *64*, A179; *Nucleic Acids Res.* **1993**, *21*, 2473; P. A. King, V. E. Anderson, J. O. Edwards, G. Gustafson, R. C. Plumb, J. W. Suggs, *J. Am. Chem. Soc.* **1992**, *114*, 5430.

Design of Thermotropic Liquid Crystals with Micellar Cubic Mesophases: Amphiphilic *N*-(2,3-Dihydroxypropyl)benzamides**

Konstanze Borisch, Siegmar Diele, Petra Göring, Horst Kresse, and Carsten Tschierske*

Cubic mesophases are common in surfactant/solvent and lipid/solvent systems and are ordered supermolecular arrangements with isotropic physical properties. They have attracted considerable interest because of their potential use in drug release systems, as templates for the preparation of mesoporous silicates, and as models for cell fusion processes.[1] Several different cubic mesophases are observed in these systems depending on the concentration of the surfactant.[2] They can occur as intermediate phases either between lamellar and hexagonal columnar phases (bicontinuous cubic phases, V-phases) or between the hexagonal columnar phases and the micellar solutions (discontinuous cubic phases, I-phases). The first type can be regarded as interwoven networks of branched columns, the second one consists of closed micelles arranged in a cubic lattice. The interface curvature between hydrophilic regions and lipophilic regions was recognized as the key factor determining the phase type. Depending on the sign of the interface curvature either normal phases (type 1; the interface curvature is directed away from the regions with stronger cohesive interactions) or inverted phases (type 2; the interface is curved toward the regions with stronger cohesive forces) can occur.

In contrast to the large number of lyotropic systems with cubic mesophases, relatively few thermotropic compounds with cubic phases are known.[3, 4] In most cases, bicontinuous structures with body-centered cubic lattices (*Ia3d*, *Im3m*), which represent intermediate phases between columnar and smectic phases, have been proposed for these thermotropic cubic phases.[4] More recently different types of thermotropic cubic phases have been observed for amphiphilic carbohydrate derivatives.[5, 6] For some of these compounds inverted micellar cubic phases with primitive cubic lattices (*Pm3n* or *P43n*) have been found.[6] Because this type of primitive cubic phase has never been observed in thermotropic systems, their more detailed investigation should be of special interest;[7] however, the transition temperatures of these carbohydrate derivatives are rather high such that their study is hampered by decomposition. In an effort to overcome these difficulties, we decided to decrease the number of attractive hydrogen bonds in the head group regions.

Here we describe the first stable model compounds for these carbohydrate derivatives. These are amphiphiles in which one, two, or even three lipophilic alkyl chains were grafted to a hydrophilic N-(2,3-dihydroxypropyl)benzamide group (**1**–**3**). As

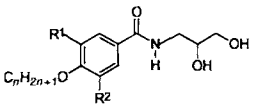

1, $R^1 = R^2 = H$
2, $R^1 = C_nH_{2n+1}O$, $R^2 = H$
3, $R^1 = R^2 = C_nH_{2n+1}O$

in the case of related D-glucamides,[6] three different types of mesophases were found depending on the number of alkyl chains: compound **1** with only one dodecyloxy chain, $n = 12$, forms a smectic A_d phase, a hexagonal columnar phase (Col_{H2}) is found for the double chain compound **2**, and a cubic phase was detected for compound **3** with three dodecyloxy chains (Table 1). The X-ray diffraction pattern of this cubic phase can be indexed on the basis of a primitive cubic lattice (*Pm3n* or *P43n*; $a_{cub} = 7.45$ nm at $T = 90$ °C; Table 2). Thus, simply by changing the number of lipophilic chains grafted to the aromatic linking units the supermolecular organization of these molecules can be changed from layerlike through columnar to cubic. In this respect the thermotropic mesomorphism of these compounds, which depends on the number of lipophilic chains, is analogous to the lyotropic mesomorphism of surfactant/solvent

Table 1. Transition temperatures T of the compounds **1**–**3**, $n = 12$, and lattice parameter a of their mesophases [a].

Compd.	R^1	R^2	T[°C][a]	a[nm] (T[°C])
1, $n = 12$	H	H	cr 89 S_A 132 is	4.03 (85)
2, $n = 12$	$C_{12}H_{25}O$	H	cr 98 Col_{H2} 148 is	4.18 (105)
3, $n = 12$	$C_{12}H_{25}O$	$C_{12}H_{25}O$	cr 69 Cub_{12} 126 is	7.45 (90)

[a] Abbreviations: cr = crystalline solid, S_A = smectic A-phase, Col_{H2} = hexagonal columnar mesophase, Cub_{12} = inverted micellar cubic mesophase (space group *Pm3n* or *P43n*), is = isotropic liquid. The designation of the Col and Cub phases is given as subscripts using descriptors of lyotropic phases as proposed by Tiddy [2c]. The polar/lipophilic interfaces are curved in the direction of the polar regions (negative curvature) and thus represent type 2 phases (inverted phases).

[*] Prof. Dr. C. Tschierske, K. Borisch
Institut für Organische Chemie der Universität
Kurt-Mothes-Strasse 2, D-06120 Halle (Germany)
Fax: Int. code +(345)5527030
e-mail: coqfx@rmlucom.urz.uni-halle.de
Dr. S. Diele, P. Göring, Prof. Dr. H. Kresse
Institut für Physikalische Chemie der Universität Halle (Germany)

[**] This work was supported by the Deutsche Forschungsgemeinschaft and the Fonds der Chemischen Industrie.

 © WILEY-VCH Verlag GmbH, D-69451 Weinheim, 1997 0570-0833/97/3619-2087 $ 17.50+.50/0

Table 2. Bragg reflections of the cubic mesophase of compound **3**, $n = 12$, at $T = 70\,^{\circ}C$.

$\theta_{exp.}$[°]	$\theta_{calcd.}$[°]	*hkl*
1.19	–	200
1.32	1.32	210
1.47	1.45	211
1.68	1.68	220
1.88	1.88	310
2.13	2.13	320
2.22	2.22	321
2.36	2.37	400
2.64	2.65	420
2.72	2.71	421

systems. In analogy to lyotropic systems it can be expected that by increasing the number of chains the interface curvature between the segregated regions of the lipophilic chains and the polar *N*-(2,3-dihydroxypropyl)amide groups increases and gives rise to the transition from a smectic phase (S_A) through an inverted hexagonal columnar phase (Col_{H2}) to a cubic phase consisting of closed inverted micelles (Cub_{I2}).

The comparison of several homologous compounds **3** with alkyl chains of different length (Figure 1) indicates that the

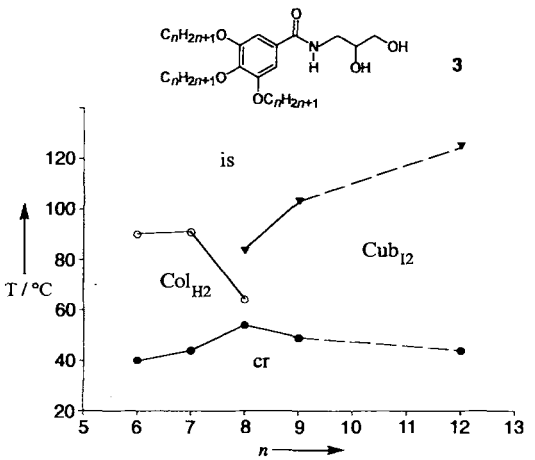

Figure 1. Dependence of the thermotropic transition temperatures T of the aminopropanediol derivatives **3** on the chain length n (● = cr/Col_{H2}, cr/Cub_{I2}; ○ = Col_{H2}/is, Col_{H2}/Cub_{I2}; ▼ = Cub_{I2}/is). Abbreviations: see Table 1.

cubic phase is destabilized on decreasing the chain length and a hexagonal columnar phase is found for the short-chain derivatives. This is in accordance with the proposed inverted micellar structure of the cubic phase. Compound **3**, $n = 8$, exhibits a cubic–columnar dimorphism. This provided the opportunity to investigate the structural changes that occur at the transition from the thermotropic columnar to the thermotropic cubic phase.[8] The hexagonal lattice parameter of the Col_{H2} phase is $a_{hex} = 3.3$ nm at $T = 60\,^{\circ}C$. The cubic phase has a primitive cubic lattice (*Pm3n* or *P43n*) with a lattice parameter a_{cub} of 6.9 nm at $T = 75\,^{\circ}C$.

In order to confirm the inverted micellar structure of the cubic phase of **3**, $n = 8$, proton conductivity investigations were carried out. If the cubic mesophase is built up by closed inverted micelles, the hydrogen bonding networks between the head groups should be located inside the micelles and therefore they should be isolated from each other by the lipophilic regions of the alkyl chains. In a bicontinuous cubic phase and in columnar phases however, the hydrogen bonding network should be extended over large distances. Since these hydrogen bonding networks can act as proton conductors, the conductivity is expected to decrease at the transition from the hexagonal columnar to the inverted micellar cubic mesophase, whereas it should remain approximately constant at the transition in a bicontinuous cubic phase. Indeed, a strong decrease in the specific conductivity is found at the transition from the hexagonal columnar phase to the cubic phase (Figure 2), which strongly supports the inverted micellar structure of this cubic phase.

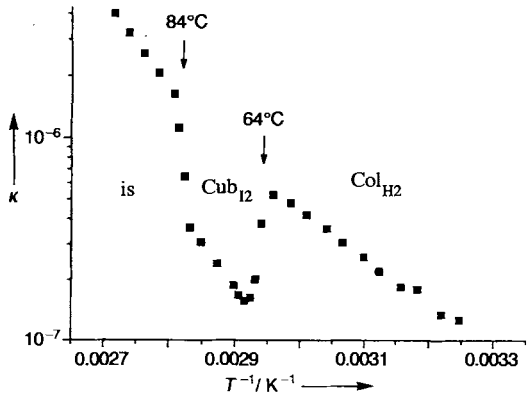

Figure 2. Dependence of the specific conductivity κ (in $AV^{-1}m^{-1}$) of compound **3**, $n = 8$, on the temperature. Measurements were carried out in a microcapacitor ($A = 2\,cm^2$, $d = 0.02$ cm) without orientation ($f = 1$ K Hz).

What shape are these closed micelles in the cubic phases? If one assumes that spherical micelles exist and that these are arranged in a primitive cubic cell, their diameter should be equal to the lattice parameter ($a_{cub} = 6.9$ nm). The length of a single molecule of **3**, $n = 8$, as estimated from CPK models under the assumption of an all-*trans* conformation of the chains is, however, only 2.2 nm and is thus significantly smaller than the radius of the spherical micelles. This contradiction between molecular size and cell dimensions is often observed in cubic phases. Therefore, Fontell et al.[9] suggested an alternative structure for lyotropic micellar cubic phases (Cub_{I1}) located between the micellar solution and the normal hexagonal phase in surfactant/solvent systems. They proposed that the cubic unit cell is built up by eight short rodlike aggregates with an axial ratio of approximately 2:1. One of these rod-shaped micelles is placed in each corner of the unit cell, one in the center, and two on each face of the cell.[10] The micelles centered at the corners and in the center should be statistically disordered or freely rotating, whereas those on the faces of the cell are only rotationally disordered.[9]

We propose that the thermotropic cubic phases of the compounds **3**, $n = 8$–12, have the same structure (Figure 3). How-

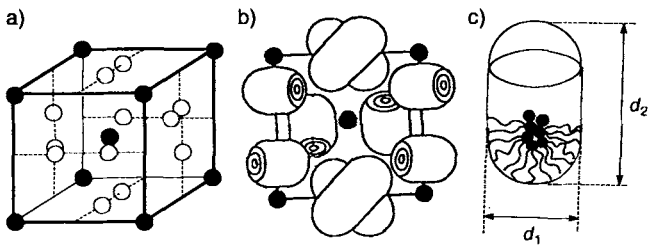

Figure 3. a) Structure of the thermotropic cubic phase Cub_{I2} of the compounds **3**, $n = 8$–12, based upon the proposal by Fontell et al. [9]. a) Arrangement of the micelles in the primitive cubic lattice. The rodlike micelles are indicated as open circles, the statistically disordered micelles at the corners and in the center are indicated by filled circles. b) View upon a face of the cubic lattice. c) Schematic representation of a rodlike micelle.

 © WILEY-VCH Verlag GmbH, D-69451 Weinheim, 1997 0570-0833/97/3619-2088 $ 17.50+.50/0

ever, they are built up by *inverted micelles* and appear in the *absence of any solvent*. Thus, the cubic lattice of the compound **3**, $n = 8$, should be built up by short rodlike micelles, each consisting of approximately 44 individual molecules.[11] The proposed model (Figure 3) requires that two micelles are arranged side by side at each cell face of the cubic lattice (edge length 6.9 nm). Therefore the short diameter d_1 of these rods ($d_1 = a_{cub}/2$) should not exceed 3.45 nm. In order to organize 44 molecules in each of these closed cylindrical micelles (see Figure 3) with a diameter of about 3.4 nm, these micelles should be about 5 nm long (d_2). Thus, an axial ratio $d_2:d_1$ of the order of about 1.5:1 results.[12]

Remarkably the short diameter (d_1) of the rodlike micelles in the cubic mesophase is nearly identical with the diameter of the columns in the hexagonal columnar mesophase of **3**, $n = 8$, formed at lower temperature ($a_{hex} = 3.3$ nm at 60 °C). Thus, we conclude that the short rodlike micelles of the cubic mesophase result from the collapse of the extended columns of the hexagonal columnar phase into small segments. Probably the arrangement of eight rodlike micelles in such a cubic lattice represents an energetic minimum that could be stabilized by quadrupole interactions[9] and allows an efficient packing of the molecules. If spherical micelles are formed, their packing coefficient in this arrangement would amount to only 0.52. Therefore, it is expected that spherical micelles preferably arrange in a body-centered (0.68) or in a face-centered lattice (0.74), which allow more efficient packing.

A related model was recently proposed for thermotropic cubic phases of some dendrimers.[7] A nearly spherical shape was assumed for the micelles of these cubic phases.[13] However, since both compounds differ in their chemical structure, they could not be compared directly. Further detailed investigations are necessary to elucidate the general principles for the directed design of thermotropic cubic mesophases.

Received: January 13, 1997
Revised version: May 30, 1997 [Z9988IE]
German version: *Angew. Chem.* **1997**, *109*, 2188–2190

Keywords: amphiphiles · cubic mesophases · hydrogen bonds · liquid crystals · micelles

[1] G. Lindblom, L. Rilfors, *Biochim. Biophys. Acta* **1989**, *988*, 221.
[2] a) V. Luzzati, A. P. Spengt, *Nature (London)* **1967**, *215*, 701; b) J. M. Seddon, R. H. Templer, *Philos. Trans. R. Soc. London A* **1993**, *344*, 377; c) G. J. T. Tiddy, *Phys. Rep.* **1980**, *57*, 1.
[3] a) D. Demus, G. Kunicke, J. Neelsenand, H. Sackmann, *Z. Naturforsch. A* **1968**, *23*, 84; b) G. Etherington, A. J. Leadbetter, X. J. Wang, T. Tajbakhsh, *Liq. Cryst.* **1986**, *1*, 209; c) G. Lattermannn, G. Staufer, *Mol. Cryst. Liq. Cryst.* **1990**, *191*, 199; d) U. Stebani, G. Lattermann, R. Festag, M. Wittenberg, J. H. Wendorff, *J. Mater Chem.* **1995**, *5*, 2247; e) W. Weissflog, G. Pelzl, I. Letko, S. Diele, *Mol. Cryst. Liq. Cryst.* **1995**, *260*, 157.
[4] a) Y. Fang, A. M. Levelut, C. Destrade, *Liq. Cryst.* **1990**, *7*, 265; b) A. M. Levelut, Y. Fang, *Colloq. Phys.* **1990**, 299; c) D. W. Bruce, B. Donnino, S. A. Hudson, A. M. Levelut, S. Megtert, D. Petermann, M. Veber, *J. Phys. II* **1995**, *5*, 289, and references therein.
[5] a) K. Praefcke, B. Kohne, A. Eckert, J. Hempel, *Z. Naturforsch. B* **1990**, *45*, 1084; b) S. Fischer, H. Fischer, S. Diele, G. Pelzl, K. Jankowski, R. R. Schmidt, V. Vill, *Liq. Cryst.* **1994**, *17*, 855.
[6] a) K. Borisch, S. Diele, P. Göring, C. Tschierske, *J. Chem. Soc. Chem. Commun.* **1996**, 237; b) *Liq. Cryst.* **1997**, *22*, 427.
[7] After submission of this work a *Pm3n* phase was proposed for dendrimers: V. S. K. Balagurusamy, G. Ungar, V. Percec, G. Johansson, *J. Am. Chem. Soc.* **1997**, *119*, 1539.
[8] The hexagonal–cubic transition in normal lyotropic systems was recently studied: Y. Rancon, J. Charvolin, *J. Phys. Chem.* **1988**, *92*, 2646; P. Mariana, L. Q. Amaral, L. Saturni, H. Delacroix, *J. Phys. II* **1994**, *4*, 1393.
[9] K. Fontell, K. K. Fox, E. Hansson, *Mol. Cryst. Liq. Cryst. Lett. Sect.* **1985**, *1*, 9; K. Fontell, *Colloid Polym. Sci.* **1990**, *268*, 264.
[10] The micelle in the center contributes as a whole micelle, each of the 8 micelles in the corners contribute 1/8, and each of the 12 micelles at the faces contribute 1/2 to the unit cell.
[11] By using the equation $n = V_{cell}N_A/M\rho$ and by assuming a density of $\rho = 1$ g cm^{-3} it can be calculated that each cubic unit cell contains about 350 molecules.
[12] A value of 1.35:1 was obtained by fluorescence quenching experiments of normal cubic mesophases of lyotropic systems (type 1): L. B.-A. Johansson, O. Söderman, *J. Phys. Chem.* **1987**, *91*, 5275.
[13] Two different kinds of micelles were found: spherical and tetrahedral distorted.

Absolute Sense of Twist of the C12–C13 Bond of the Retinal Chromophore in Bovine Rhodopsin Based on Exciton-Coupled CD Spectra of 11,12-Dihydroretinal Analogues**

Qiang Tan, Jihong Lou, Babak Borhan, Elena Karnaukhova, Nina Berova, and Koji Nakanishi*

Rhodopsin, the photoreceptor responsible for dim-light vision in vertebrate species, is located in the outer segment of rod cells. This membrane protein is composed of seven transmembrane α-helices and contains the 11-*cis*-retinal chromophore **1** (Figure 1), which is attached to the ε-amino group of Lys(K)296 on helix G through a protonated Schiff base (PSB).[1, 2] Glu 113 serves as a counterion to stabilize the positive charge of the PSB.[3] The 11-*cis* → *trans* isomerization triggered by light initiates changes in the protein conformation leading to a cascade of events referred to as the visual transduction process.[4] The structure of the protonated Schiff base (PSB) of 11-*cis*-retinal, with the long conjugated polyene side chain, five methyl groups, the cyclohexene ring, and the C11–C12 double bond, together with the nonplanar 6-s-*cis* and 12-s-*trans* arrangements, is ideally suited for the very subtle regulation of the pigment absorption maximum.[5] Depending on the fit of the pigment within the rhodopsin binding site, this single chromophore can cover the entire range from the UV region up to wavelengths of around 640 nm, a range most suited for the environment surrounding the organism.[5]

The UV/Vis and circular dichroism (CD) spectra of bovine rhodopsin in octyl glucoside are shown in Figure 1. Native rhodopsin ($\lambda_{max} = 500$ nm) exhibits two positive Cotton effects in its CD spectrum at 480 nm ($\Delta\varepsilon = +2.8$, α-band) and 337 nm ($\Delta\varepsilon = +9.8$, β-band). A rhodopsin incorporating a retinal analogue in which planes B and C are coplanar due to a five-membered ring (linkage of C10 and 13-methyl group) exhibit CD spectra with a negligible α-band. Similarly, the pigment formed from a retinal with coplanar A and B planes as a result of a bridged five-membered ring between the 5-methyl group and C8 showed weak β-band. Based on these findings, Ito and co-workers[6] have assigned the origin of the α- and β-bands to distortions around 12-s-*trans* and 6-s-*cis* bonds, respectively. Although the two positive Cotton effects reflect the interaction between the twisted chromophore and its environment, at this stage it is not possible to gain further information regarding the sense of twist around the 6-s-*cis* and 12-s-*trans* bonds, that is, the arrangement of planes A, B, and C in Figure 1. We have

[*] Prof. K. Nakanishi, Q. Tan, J. Lou, Dr. B. Borhan, Dr. E. Karnaukhova, Prof. N. Berova
Department of Chemistry, Columbia University
New York, NY 10027 (USA)
Fax: Int. code +(212)932-8273
e-mail: kn5@columbia.edu

[**] This study was supported by grants from the U. S. National Institutes of Health (GM 36564 and 34509).

 © WILEY-VCH Verlag GmbH, D-69451 Weinheim, 1997 0570-0833/97/3619-2089 $ 17.50+.50/0

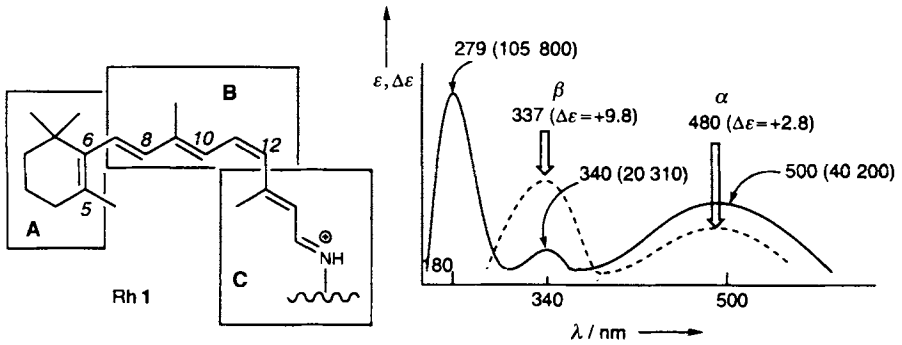

Figure 1. The 11-*cis*-retinal chromophore **1** in native rhodopsin attached in PSB form, and the UV/Vis (——, ε) and CD spectrum (– – – –, $\Delta\varepsilon$) of bovine rhodopsin in octyl glucoside.

therefore disrupted the conjugated polyene system by a single bond so that the two polyene moieties flanking the single bond would couple. The sign of the resulting bisignate couplet would reflect the twist in a nonempirical manner. Here we present data that determine the absolute sense of twist of planes B and C planes.

Previous photoaffinity labeling experiments have shown that the C3 and C4 atoms of the ionone ring lie very close to the transmembrane helix F of rhodopsin (Figure 2).[7, 8] The next essential structural feature to be clarified is the absolute sense of twist of the retinal chromophore, that is, the twists between planes A and B and planes B and C. The polyene side chain comprising C7 to C12 (plane B) is perpendicular to the axis of the transmembrane helices of rhodopsin (Figure 2). By establishing the absolute twist around the C12–C13 bond one can determine whether plane C is tilted up or down with respect to plane B. We have now established the helicity between planes B and C by incorporating 11,12-dihydroretinals into opsin and measuring their CD spectra. To our knowledge this is the first time that exciton-coupled CD spectroscopy has been applied to elucidate subtle conformational details of protein-bound substrates.

Exciton-coupled circular dichroism is observed when two or more chromophoric systems with no or only negligible molecular orbital overlap in a chiral fashion and interact through space. Hence, a twist of the polyene chain along the C12–C13 single bond in retinal bound to rhodopsin does not lead to an exciton-coupled CD band because the polyene chain is in conjugation with the rest of the molecule. However, saturation of the C11–C12 double bond in retinal breaks the chromophore into two independent conjugated systems: the triene and the protonated Schiff base (PSB) moieties. If the through-space interaction between these two chromophores in the pigment results in a couplet, then the "sign" of the split CD band should reflect the absolute twist of 11,12-dihydroretinal within the pigment binding site (Figure 3). Provided 11,12-dihydroretinal

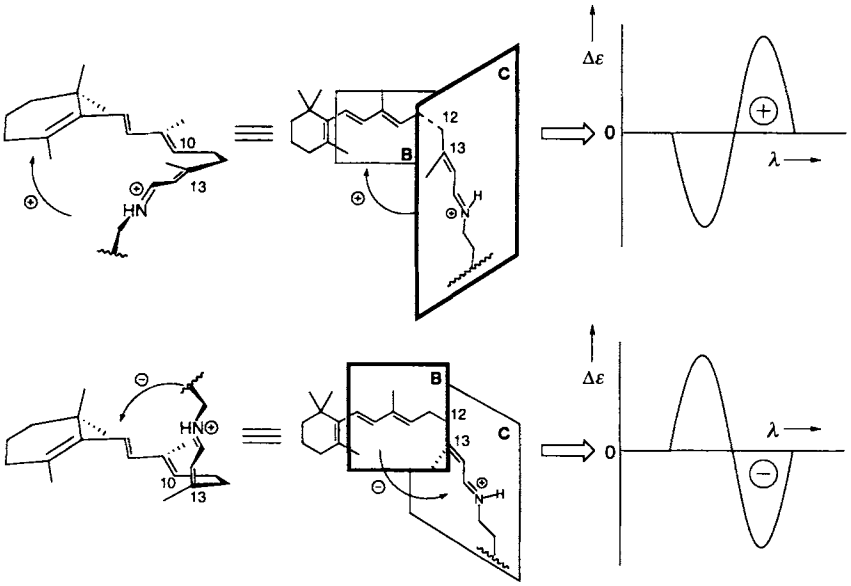

Figure 3. Absolute sense of twist between planes B and C and the predicted CD exciton couplets. The exciton-coupled CD curve is defined as positive if the sign of the first Cotton effect of the couplet at longer wavelength is positive, and vice versa.

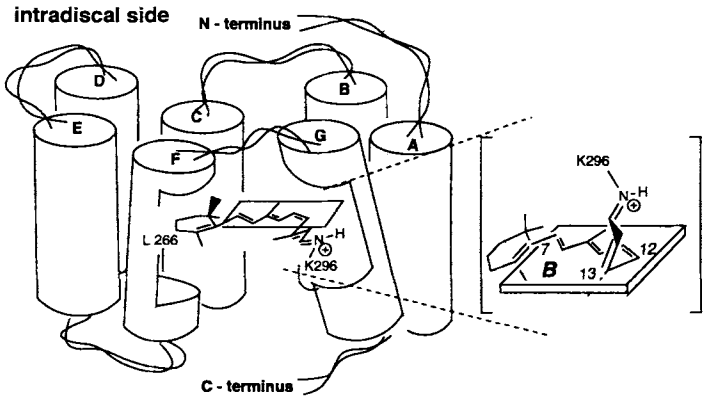

Figure 2. Schematic drawing of rhodopsin showing the location and twist of the chromophore. The residue cross-linked in the photoaffinity labeling study[7], L 266 on helix F, is indicated. The triene moiety C7 to C12 is in plane B, which is parallel to the lipid bilayer membrane. The PSB moiety is twisted around the C12–C13 bond so that it is directed toward the intradiscal side of the membrane.

adopts a conformation similar to that of 11-*cis*-retinal in rhodopsin, the exciton coupling between the triene and PSB should appear as either a "positive" or "negative" CD couplet depending on whether planes B and C assume a positive or negative twist (Figure 3).[9, 10]

The triene and enal moieties of 11,12-dihydroretinal (2H-ret, **2**)[11] absorb at 255 nm (shoulder) and 236 nm, respectively. The triene absorption of the corresponding Schiff base (2H-PSB, **3**) at 255 nm overlaps with the red-shifted PSB absorption at 270 nm (Figure 4). The UV spectrum of 11,12-dihydrorhodopsin (2H-Rh, **4**) in octyl glucoside has one broad maximum centered around 279 nm;[12] the accompanying CD spectrum shows negative and positive Cotton effects at 295 nm ($\Delta\varepsilon = -1.2$) and 275 nm ($\Delta\varepsilon = +2.5$), respectively; the difference between the extrema or *A* value is −3.7. In contrast the CD spectrum of native rhodopsin shows two positive Cotton effects (Figure 1). Thus the CD spectrum of **4** with negative and positive Cotton effects can be ascribed to the expected exciton coupling between the triene and PSB moieties, which absorb around

 © WILEY-VCH Verlag GmbH, D-69451 Weinheim, 1997 0570-0833/97/3619-2090 $ 17.50+.50/0

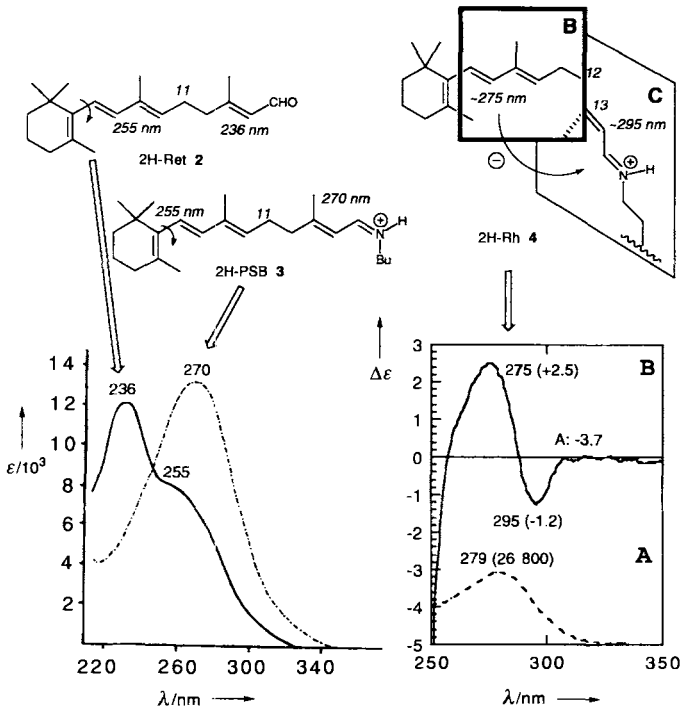

Figure 4. Left: 11,12-Dihydroretinal (**2**), its protonated Schiff base **3** obtained with *n*-butylamine, and their UV spectra in methanol. Right: Dihydrorhodopsin **4** and its UV (A) and CD spectra (B) in octyl glucoside. The chromophore analogue was bound by incubating 3.5 molequiv of analogue with a suspension of bovine opsin in 67 mM phosphate buffer (pH 7.0) at 25 °C for 5 h. All spectra were recorded in 23 mM octyl glucoside solution at pH 7.0 with opsin as a control.

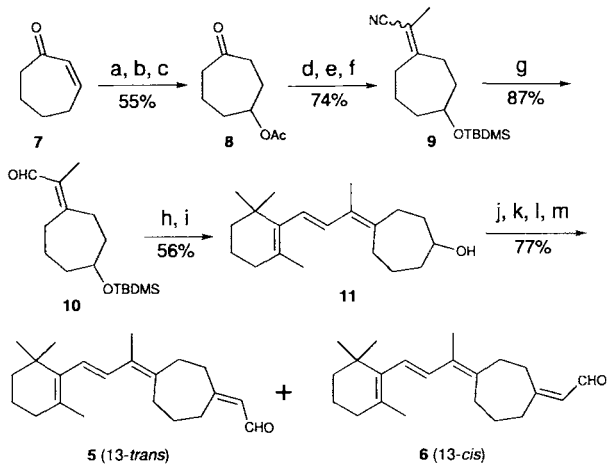

Scheme 1. Synthesis of retinal analogues **5** and **6**. a) *N*-bromosuccinimide (NBS), benzoyl peroxide, CCl_4; b) potassium acetate, 3-methyltrioctylammonium chloride (Aliquat 336), H_2O; c) H_2, Pd/C, acetic acid, CH_2Cl_2; d) diethyl 1-cyanoethyl phosphonate, NaH, THF; e) potassium carbonate, methanol, H_2O; f) *tert*-butyldimethylsilyl chloride (TBDMSCl), imidazole, DMF; g) diisobutylaluminum hydride (DIBAL-H), CH_2Cl_2, 1:1 mixture of isomers separated by column chromatography; h) *β*-cyclocitryl triphenylphosphonium bromide, potassium *tert*-butoxide, THF; i) $Bu_4N^+F^-$, THF; j) tetra-*N*-propylammonium perruthenate (TPAP), 4-methylmorpholine *N*-oxide (NMO), finely powered 4 Å molecular sieves, CH_2Cl_2; k) diethyl cyanomethyl phosphonate, NaH, THF; l) DIBAL-H, CH_2Cl_2; m) HPLC separation of 1:1 mixture of isomers[15].

275 and 295 nm, respectively. The red shift of the PSB band from 270 nm in **3** to roughly 295 nm in **4** is due to the effect of the electrostatic charges operating within the binding site[13] and is not unexpected. The extremum at 275 nm represents the positive Cotton effect of the negative couplet; the contribution from the opsin should be negligible since the CD spectrum depicted in Figure 4 is a difference spectrum between that of the pigment and that of the opsin. Thus it appears that the triene band in pigment **4** is red-shifted by 20 nm relative to the band in **3** (255 nm in methanol). This implies that the twist around the 6-s-*cis* bond in pigment **4** is smaller than in **3** in solution; in other words, planes A and B (Figure 1) adopt a more planar arrangement in the protein due to constraints within the binding site. The conclusion arising from the negative couplet of **4** is that planes B and C are twisted as depicted in Figure 4.

It is conceivable that the 11,12-dihydrochromophore is flexible and subject to many degrees of freedom, which ultimately lead to the weak amplitudes observed in the exciton-coupled CD spectra. To check the validity of the conclusion reached from studies with the dihydropigment **4**, the same set of experiments were performed with the 13-*trans*- and 13-*cis*-11,12-dihydrocycloheptatrienylidene retinal (13-*trans*-2H-ret7 **5** and 13-*cis*-2H-ret7 **6**). The synthesis of the retinal analogues is outlined in Scheme 1. After HPLC separation, **5** and **6** were characterized by their NMR and mass spectra.[14] The rationale to pursue a dihydro analogue of pigment **4** in which the conformation is locked with a seven-membered ring lies in earlier data obtained with cycloheptatrienylidene retinal (ret7 **12**). The UV and CD spectra of the pigment obtained from **12** and opsin closely resemble the UV and CD spectra of native rhodopsin.[15] It was therefore concluded that the geometry of **12** within the binding site and the corresponding protein–substrate interactions are very similar to those of 11-*cis*-retinal in the native rhodopsin. Based on these observations we felt that 13-*trans*-2H-ret7 **5** would be a more appropriate choice for a dihydro-11-*cis* locked retinal analogue of 11,12-dihydroretinal (Figure 5).

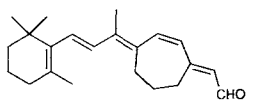

12

The enal moiety in **5** absorbs at 244 nm in methanol. The absorption of the nonplanar triene moiety was assigned to be around 266 nm (the synthetic intermediate **11** with the same triene system exhibits an absorption maximum at 266 nm) and appears as a shoulder around 270 nm (Figure 5; the UV and CD spectra of **6** are very similar). In the protonated Schiff base **13**

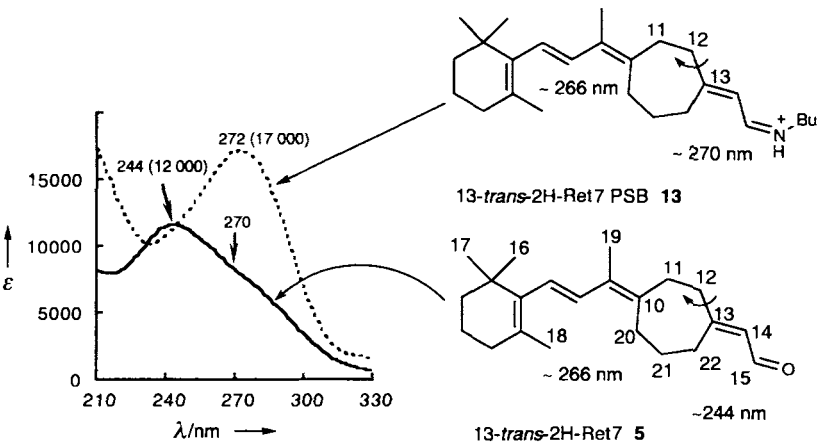

Figure 5. 13-*trans*-2H-ret7 **5**, its PSB derivative **13**, and their UV spectra in methanol. The UV spectra of 13-*cis*-2H-ret7 **6** and its PSB derivative are very similar to those of the *trans* isomer.

 © WILEY-VCH Verlag GmbH, D-69451 Weinheim, 1997 0570-0833/97/3619-2091 $ 17.50+.50/0

obtained with *n*-butylamine, the absorption maximum of the enal unit is shifted to around 270 nm (Figure 5) and overlaps with the triene absorption.

Rhodopsin analogues **14** and **15**, which incorporate **5** and **6**, respectively, have absorption maxima at 283 nm ($\varepsilon = 28000$) and 284 nm ($\varepsilon = 29000$), respectively (Figure 6).[16] Repeated addition of 11-*cis*-retinal to incubation mixtures of each failed to generate the native rhodopsin as determined by the absorption at 500 nm. Therefore, it was concluded that no opsin was left and the analogues bound to opsin could not be replaced by 11-*cis*-retinal.

13-*trans*-2H-Rh7 **14** exhibits a negative split CD band at 297 nm ($\Delta\varepsilon = -6.5$) and 273 nm ($\Delta\varepsilon = +5.2$; $A = -11.7$). Rhodopsin analogue **15** also shows a negative couplet with a slightly larger A value of -14.1 at similar wavelengths, 298 nm ($\Delta\varepsilon = -7.5$) and 272 nm ($\Delta\varepsilon = +6.6$; Figure 6). The bisignate CD spectra can again be ascribed to the coupling between the triene and protonated Schiff base (PSB) moieties, thus confirming the conclusion resulting from experiments with analogue **4**. To secure further support for the origin of the couplet, the amplitudes of the split CD bands of 13-*trans* and 13-*cis* isomers **14** and **15** were compared. It is known that the A value of bisignate exciton-coupled split CD curves increases as the projection angle of the two interacting chromophores approaches 70°.[9, 10] The estimated angle between the triene and protonated Schiff base moieties is roughly 60° for the 13-*cis* isomer and 20° for the 13-*trans* isomer based on molecular modeling calculations (MM2 force field).[17] This is in agreement with the observed larger A value for the 13-*cis* isomer (-14.1) relative to that for the 13-*trans* isomer (-11.7), and supports the conclusion that the observed split CD band is due to exciton coupling between the two chromophores within the binding site.

The smaller A value of the pigment incorporating 11,12-dihydroretinal (**2**), in which the 11-s-*cis* conformation is not fixed, is most probably due to the flexibility of the side chain leading to conformations in which the angles between the two interacting chromophores are smaller and/or the chromophores are more distal. Nevertheless, the fact that the CD spectrum of 11,12-dihydrorhodopsin (**4**) displays a negative bisignate curve is in agreement with the results obtained with 13-*trans*-2H-Rh7 **14** and 13-*cis*-2H-Rh7 **15**.

The experimental results indicate that the negative helicity between planes B and C is as depicted in Figure 3; they also suggest that the twist between planes A and B of chromophores bound to opsin is smaller than in the same chromophore in solution. The handedness of the arrangement of the planes B and C agrees with the theoretical prediction of Kakitani and co-workers,[18] according to which the C12–C13 bond in rhodopsin is twisted by -130 to $-150°$ when the torsion angle is measured clockwise from the planar *cis* conformation. (Han and Smith have also arrived at the same conclusion by theoretical considerations.[19]) It is remarkable that the conformation of the chromophore in the binding pocket of a large protein can be determined from the sign of the bisignate exciton-coupled split CD spectra. As mentioned above, the twist of the chromophore is reflected in the CD spectrum of the original rhodopsin by the presence of the α- and β-bands. The characteristics shape and sign of these bands are dictated by the interaction between the chromophore and the opsin binding site. Therefore, in other visual pigments that exhibit similar positive α- and β-bands, it can be postulated that the chromophoric twist along their polyene chain will be similar to that in bovine rhodopsin.

These results further demonstrate the versatility of the exciton-coupled split CD method in probing subtle conformational aspects of ligand–receptor interactions. Further studies directed toward determining the absolute sense of twist between planes A and B and clarifying the mechanism of the visual transduction process on a molecular structural basis are in progress.

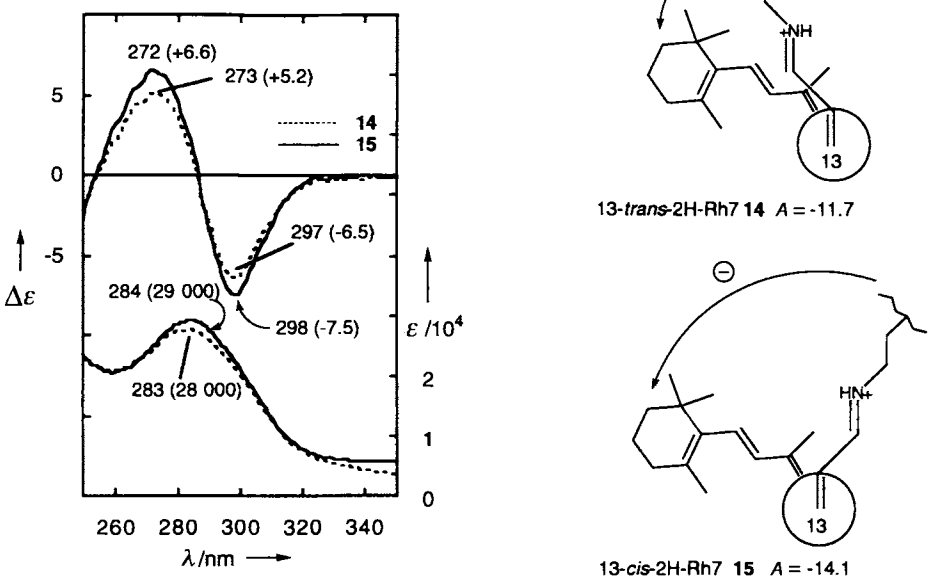

Figure 6. UV and CD spectra of 13-*trans*-2H-Rh7 **14** and 13-*cis*-2H-Rh7 **15**. The projected structures of the chromophores show that the angle between the coupled chromophores is larger for the 13-*cis* pigment, and this is reflected in the slightly larger amplitude in its CD spectrum. The chromophore analogues were bound by incubating 1.5 mol equiv of analogue with a suspension of bovine opsin in 67 mM phosphate buffer (pH 7.0) at 25 °C for 5 h. All spectra were recorded in 23 mM octyl glucoside solution at pH 7.0 with opsin as a control.

Received: March 17, 1997 [Z102551E]
German version: *Angew. Chem.* **1997**, *109*, 2190–2194

Keywords: chirality · circular dichroism · exciton coupling · retinal analogues · rhodopsin

[1] a) T. Yoshizawa, G. Wald, *Nature* **1963**, *197*, 1279; b) D. Bownds, *ibid* **1967**, *216*, 1178; c) G. Wald, *ibid* **1968**, *219*, 800; e) G. F. X. Schertler, C. Villa, R. Henderson, *ibid* **1993**, *362*, 770.

[2] a) "Photophysics and Photochemistry of Retinal Proteins": *Israel J. Chem.* **1995**, *35* (special issue); b) K. Nakanishi, R. Crouch, *ibid.* **1995**, *35*, 253.

[3] a) T. Sakmar, R. R. Franke, H. G. Khorana, *Proc. Natl. Acad. Sci. USA* **1989**, *86*, 8309; b) E. A. Zhukovsky, D. D. Oprian, *Science* **1989**, *246*, 928.

[4] a) B. König, A. Arendt, J. H. McDowell, M. Kohlert, P. A. Hargrave, K. P. Hofmann, *Proc. Natl. Acad. Sci. USA* **1989**, *86*, 6878; b) L. Stryer, *J. Biol. Chem.* **1991**, *266*, 1071; c) P. A. Hargrave, J. H. McDowell, *FASEB J.* **1992**, *6*, 2323; d) H. G. Khorana, *J. Biol. Chem.* **1992**, *26*, 1; e) J. Nathans, *Biochemistry* **1992**, *31*, 4923.

 © WILEY-VCH Verlag GmbH, D-69451 Weinheim, 1997 0570-0833/97/3619-2092 $ 17.50+.50/0

[5] a) K. Nakanishi, *Am. Zool.* **1991**, *31*, 479; b) *Pure Appl. Chem.* **1991**, *63*, 161; c) R. R. Rando, *Chem. Biol.* **1996**, *3*, 255.
[6] a) M. Ito, A. Kodama, K. Tsukida, Y. Fudaka, Y. Shichida, T. Yoshizawa, *Chem. Pharm. Bull.* **1982**, *30*, 1913; b) see also G. G. Kochendoerfer, P. E. Verdegem, I. van der Hoef, J. Lugtenburg, R. A. Mathies, *Biochemistry* **1996**, *35*, 16230.
[7] a) H. Zhang, K. A. Lerro, T. Yamamoto, T. H. Lien, L. Sastry, M. A. Gawinowicz, K. Nakanishi, *J. Am. Chem. Soc.* **1994**, *16*, 10165; b) K. Nakanishi, H. Zhang, K. Lerro, S. Takekuma, T. Yamamoto, T. Lien, L. Sastry, D. Baek, C. Moquin-Pattey, F. Derguini, M. Gawinowicz, *Biophys. Chem.* **1995**, *56*, 13.
[8] a) T. A. Nakayama, H. G. Khorana, *J. Biol. Chem.* **1990**, *265*, 15762; b) see also D. L. Farrens, C. Altenbach, K. Yang, W. H. Hubbell, H. G. Khorana, *Science*, **1996**, *274*, 768.
[9] N. Harada, K. Nakanishi, *Circular Dichroic Spectroscopy—Exciton Coupling in Organic Stereochemistry*, University Science Books, Mill Valley, **1983**, p. 73.
[10] K. Nakanishi, N. Berova in *Circular Dichroism: Principles and Applications* (Eds.: K. Nakanishi, N. Berova, R. W. Woody), VCH, Weinheim, **1994**, pp. 361–398.
[11] a) M. A. Gawinowicz, Doctoral Thesis, Columbia University, **1978**; b) M. A. Gawinowicz, N. V. Balog-Nair, J. S. Sabol, K. Nakanishi, *J. Am. Chem. Soc.* **1977**, *99*, 7720.
[12] a) M. Arnaboldi, M. G. Motto, K. Tsujimoto, V. Balogh-Nair, K. Nakanishi, *J. Am. Chem. Soc.* **1979**, *101*, 7082; b) Y. Koutalos, T. G. Ebrey, M. Tsuda, K. Odashima, T. Lien, M. H. Park, N. Shimizu, F. Derguini, K. Nakanishi, H. R. Gilson, B. Honig, *Biochemistry* **1989**, *28*, 2732.
[13] B. Honig, U. Dinur, K. Nakanishi, V. Balogh-Nair, M. A. Gawinowicz, M. Arnaboldi, M. G. Motto, *J. Am. Chem. Soc.* **1979**, *101*, 7084.
[14] Compounds **5** and **6** were separated by HPLC on a YMC-Pack SIL column (250 × 10 mm i.d.). The chromophores were eluted with ethyl acetate/hexane (5/95, v/v) at a flow rate of 2.0 mL min^{-1}. The retention times for **5** and **6** were 22.6 and 21.0 min, respectively. ^{1}H NMR ($CDCl_3$, TMS): **5**: δ = 1.00 (s, 6H, 1-CH_3), 1.46 (m, 2H, 2-H), 1.61 (m, 2H, 3-H), 2.00 (t, J = 6.4 Hz, 2H, 4-H), 1.68 (s, 3H, 5-CH_3), 1.83 (s, 3H, 9-CH_3), 6.06 (d, J = 15.8 Hz, 1H, 7-H), 6.38 (d, J = 15.8 Hz, 1h, 8-H), 5.85 (d, J = 8.2 Hz, 1H, 14-H), 9.95 (d, J = 8.2 Hz, 1H, 15-H), 2.52 (t, J = 5.8 Hz, 2H, 11-H), 2.48 (t, J = 5.8 Hz, 2H, 12-H), 2.45 (t, J = 6.5 Hz, 2H, 20-H), 1.75 (m, 2H, 21-H), 2.72 (t, J = 6.4 Hz, 2H, 22-H); **6**: δ = 1.00 (s, 6H, 1-CH_3), 1.46 (m, 2H, 2-H), 1.60 (m, 2H, 3-H), 2.00 (t, J = 6.4 Hz, 2H, 4-H), 1.68 (s, 3H, 5-CH_3), 1.82 (s, 3H, 9-CH_3), 6.06 (d, J = 16.3 Hz, 1H, 7-H), 6.39 (d, J = 16.3 Hz, 1H, 8-H), 5.85 (d, J = 8.1 Hz, 1H, 14-H), 9.96 (d, J = 8.1 Hz, 1H, 15-H), 2.57 (t, J = 6.6 Hz, 2H, 11-H), 2.91 (t, J = 6.6 Hz, 2H, 12-H), 2.45 (t, J = 6.3 Hz, 2H, 20-H), 1.71 (m, 2H, 21-H), 2.37 (t, J = 6.3 Hz, 2H, 22-H); positive-ion CI-MS (NH_3): m/z: 313 $[M + H]^+$, 331 $[M + NH_4]^+$.
[15] H. Akita, S. P. Tanis, M. Adams, V. Balogh-Nair, K. Nakanishi, *J. Am. Chem. Soc.* **1980**, *102*, 6370.
[16] Bovine rod outer segments (ROS) were isolated and bleached according to published procedures[20]. The artificial pigments **4**, **14**, and **15** were prepared at 25 °C in the dark. Screw-capped vials equipped with magnetic stirrer bars were charged with 1 OD of opsin suspended in 67 mM sodium phosphate buffer (pH 7.0, 500 μL) per vial. Retinal analogue **2** (3.5 molequiv for making pigment **4**), or retinal analogue **5** or **6** (1.5 molequiv for making pigment **14** or **15**) in EtOH (5 μL) was added to each vial containing opsin. The control sample was prepared by adding EtOH (5 μL) to 1 OD of opsin. All samples were stirred for 5 h then centrifuged at 50000 *g* for 15 min. The pellets were dissolved in 23 mM octyl glucoside in phosphate buffer (67 mM, pH 7.0, 1 mL) and centrifuged at 50000 *g* for 10 min. The supernatants were used to obtain UV and CD spectra. All UV and CD spectra of the rhodopsin pigments were corrected by subtraction of the UV and CD spectra of the control sample.
[17] F. Mohamadi, N. Richards, W. C. Guida, R. Liskamp, M. Lipton, C. Caufield, G. Chang, T. Hendrickson, W. C. Still, *J. Comput. Chem.* **1990**, *4*, 440.
[18] H. Kakitani, T. Kakitani, S. Yomosa, *J. Phys. Soc. Japan* **1977**, *42*, 996.
[19] M. Han, S. O. Smith, *Biochemistry*, **1997**, *36*, 7280.
[20] D. S. Papermaster, *Methods Enzymol.* **1982**, *81*, 49–52.

Structure–Activity Relationships of the Epothilones and the First In Vivo Comparison with Paclitaxel**

Dai-Shi Su, Aaron Balog, Dongfang Meng, Peter Bertinato, Samuel J. Danishefsky,* Yu-Huang Zheng, Ting-Chao Chou, Lifeng He, and Susan B. Horwitz

The discovery and characterization of the bacterial natural products epothilones A (**1**) and B (**2**) have evoked a great deal of interest.[1] Their high levels of cytotoxicity and their potent stabilization of microtubules are reminiscent of the biological activity of paclitaxel (**3**), a clinically valuable resource in cancer

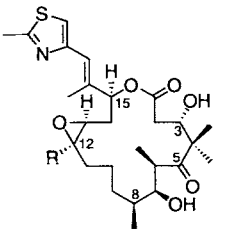

1, R = H: epothilone A
2, R = Me: epothilone B

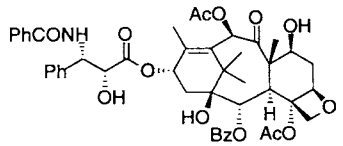

3: paclitaxel

chemotherapy.[2] Paclitaxel (**3**), which has been in use for the treatment of ovarian and breast carcinomas, is also being evaluated against a variety of other tumors. Nonetheless, its application is hampered by difficulties in formulation and susceptibility to multiple drug resistance (MDR). Though a massive amount of analog synthesis based on the paclitaxel structure has been accomplished, the framework appears to be intolerant to major simplification with maintenance of biological activity. To the best of our knowledge, no compound which is of a significantly lower level of structural complexity than paclitaxel has been of clinical interest as a replacement for the parent drug.

Since the epothilones are more water-soluble than paclitaxel and, in preliminary in vitro studies, seemed to perform better against several MDR cell lines, this series warranted evaluation. Our laboratory and several others have attacked the problem of the total synthesis of **1** and **2**.[3–9] This goal, in the case of **1**, was first accomplished in a stereocontrolled fashion by using a boron-alkyl Suzuki coupling strategy to establish the C11–C12

[*] Prof. S. J. Danishefsky,[+] Dr. D.-S. Su, Dr. A. Balog, D. Meng,[+]
Dr. P. Bertinato
Laboratory for Bioorganic Chemistry
Sloan-Kettering Institute for Cancer Research
1275 York Avenue, New York, NY 10021 (USA)
Fax: Int. code +(212)772-8691
Dr. Y.-H. Zheng, Dr. T.-C. Chou
Laboratory for Preclinical Pharmacology
Sloan-Kettering Institute, New York, NY (USA)
L. He, Dr. S. B. Horwitz
Department of Molecular Pharmacology
Albert Einstein College of Medicine, Bronx, NY (USA)
[+]Additional address:
Columbia University, Department of Chemistry
Havemeyer Hall, New York, NY 10021 (USA)

[**] This research was supported by the National Institutes of Health (grants to S. J. D. (CA-28824) and S. B. H. (CA-39821) and postdoctoral fellowships to A. B. (CA-GM 72231) and P. B. (CA-62948)). We gratefully acknowledge Dr. George Sukenick (NMR Core Facility, Sloan-Kettering Institute) for NMR and mass spectrometric analyses. Professor Dr. G. Höfle, of the Gesellschaft für Biotechnologische Forschung, Braunschweig (Germany), is gratefully acknowledged for providing natural epothilone A and B for comparative analysis. We also thank Professor Gunda Georg of the University of Kansas, Lawrence, KS (USA), for bringing the epothilone problem to our attention.

 © WILEY-VCH Verlag GmbH, D-69451 Weinheim, 1997 0570-0833/97/3619-2093 $ 17.50+.50/0

bond.[3c, e] Our total synthesis was followed by three reports of total syntheses involving nonstereoselective ring-forming olefin metathesis reactions to establish the C12–C13 bond.[3d, 4, 5] More recently, a stereoselective Wittig reaction to establish the C12–C13 bond en route to **1** has also been described.[4c]

The first synthesis of epothilone B (**2**) was accomplished in our laboratory, again, through the use of a highly stereoselective boron-alkyl Suzuki coupling reaction to form the trisubstituted olefin.[3e] A Wittig-based route, generating a mixture of olefin isomers leading to **2**, was recently reported.[4d] An important advance in the field was the stereocontrolled epoxidation of the C12–C13 double bond in desoxyepothilones A (**4**) and B (**5**) through the agency of 3,3-dimethyldioxirane.[3c–e]

While none of our syntheses described thus far are practical for the full-scale pharmaceutical development of an epothilone, they have provided more than ample quantities for biological evaluations of the natural products both in vitro and in vivo, and for early evaluations of a range of fully synthetic analogs. Presently, we are examining compounds obtained by obvious explorations of key intermediates in the total syntheses of **1** and **2**. At this writing, we have not yet generated analogs derived from extended operations on the completed natural products themselves. We have focused on structure–activity relationships (SAR) to determine zones of the molecule that are tolerant or intolerant of structural change. Such insights would be valuable in focusing studies on molecular modeling. Furthermore, it was hoped to gather in vivo data for a direct comparison of epothilone B and paclitaxel.

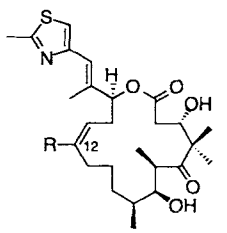

4, R = H
5, R = methyl
8, R = ethyl
10, R = propyl
11, R =

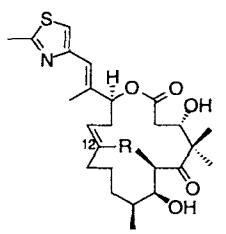

6, R = H
7, R = methyl
9, R = propyl

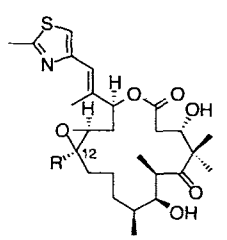

12, R = ethyl
13, R = propyl
14, R = hexyl

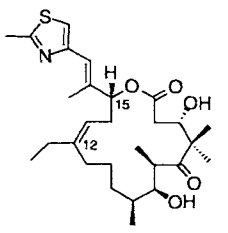

15, C15-epimer

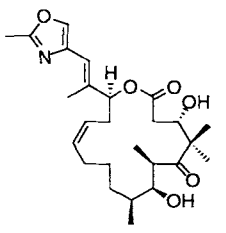

16

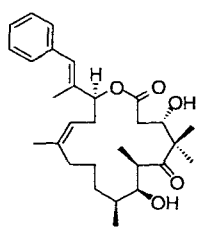

17

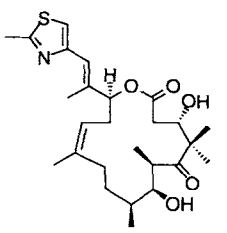

18

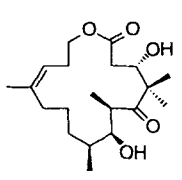

19

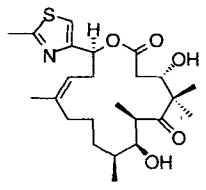

20

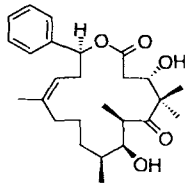

21

For the definition of the SAR of the epothilones, it is convenient to divide the structure of the drug into an acyl sector (shown arbitrarily as C1–C8), an O-alkyl sector (C9–C15), and a pendant aryl sector projecting from C15. In our preliminary SAR studies on epothilones we found that the acyl sector is rather intolerant of modification. For instance, inversion of stereochemistry at C3 ($S \rightarrow R$), or reduction at C5 results in serious abrogation of activity. Wholesale deletion of functionality at C3, C5, C6, C7, and C8 results in a loss of cytoxicity and of activity in the tubulin/microtubule system.[10] Indeed, as we recently demonstrated, a single permutation—deletion of the 8-methyl group—has a highly deleterious effect on biological function.[11] We now report that deletion of the "C9" methylene group (see the 15-membered macrolide **18**) also results in a major loss of activity in the tubulin polymerization/depolymerization assays, which have correlated rather closely with other indicators of biological function.[12]

Turning to the O-alkyl sector, we have expanded on the original[13] and subsequent findings to the effect that epothilone B (**2**) is more potent than epothilone A (**1**) with regards to tubulin polymerization/depolymerization and cytotoxicity (Figure 1 and Table 1). It was also found that the (*Z*)-desoxy compounds **4** and **5** retain a function closely comparable to their natural counterparts, **1** and **2**, respectively. Once again, the "B" precursor, compound **5**, is more active than the "A" precursor, compound **4**. Even the (*E*)-desoxy compounds **6** and **7** maintain significant biological activity, although less than that of the (*Z*) analogs, **4** and **5**, respectively.[3d, e, 4d] We now report that epothilone B is approximately 3400 times more active than paclitaxel against the resistant human leukemic cell line CCRF-CEM/VBL in cell-culture cytotoxicity studies.

The alkyl sector has been studied in greater detail.[14] Thus, substitution of an ethyl group at C12 in epothilone B is well tolerated (see compounds **8** and **12**, the ethyl versions of **5** and **2**, respectively) as are the higher homologues **10**, **13** and **14**.[15] Interestingly, biological activity is not lost in compound **11** bearing the polar acetal functionality on C12, nor in the *E*-desoxy compound **9**.[16] Further, activity is still retained, though in attenuated form, upon inversion of stereochemistry at C15 (see compound **15**). In summary, the O-alkyl sector is remarkably tolerant of modification with basic maintenance of in vitro function.

We also investigated the aryl sector.[14] Our studies indicate that this sector is also quite tolerant to permutation. For instance, the substitution of oxygen for sulfur was well tolerated. Thus, compound **16** (an oxazole rather than a thiazole) is equipotent with **4** in the tubulin polymerization assay (Figure 1)[17] as well as in cytotoxicity assays (Table 1).[18] We then studied a more drastic variant of the aryl domain with phenyl in place of the thiazolyl unit, and found that compound **17** retains 60% of the activity of **2** in the tubulin polymerization assay. Though there is a loss of one order of magnitude in the cytotoxicity assay, compound **17** is still highly cytotoxic.

 © WILEY-VCH Verlag GmbH, D-69451 Weinheim, 1997 0570-0833/97/3619-2094 $ 17.50+.50/0

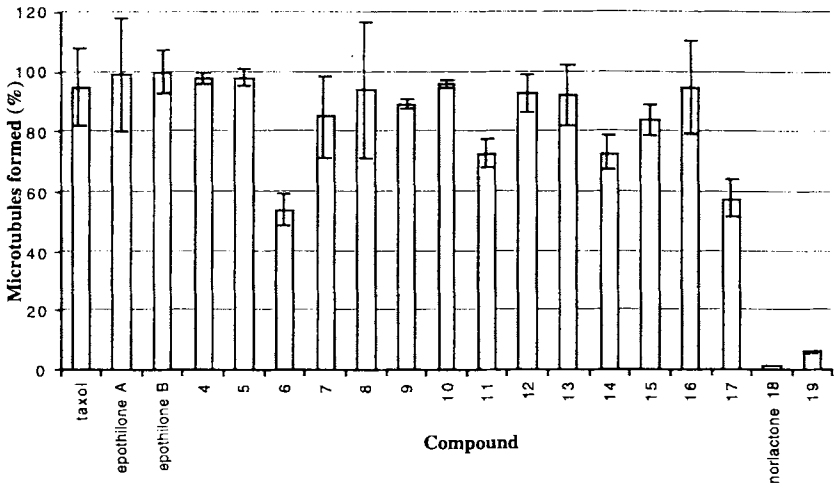

Figure 1. Formation of microtubules in the presence of 10 μM of the tested compounds. (Microtubules formed in the presence of 10 μM epothilone B defined as 100%.)

Table 1. Relative efficacy of epothilone compounds against drug-sensitive and -resistant CCRF-CEM cell lines[18].

Compound	CCRF-CEM IC_{50} [μM]	CCRF-CEM/VBL IC_{50} [μM]
paclitaxel (**3**)	0.002	4.140
epothilone A (**1**)	0.003	0.020
epothilone B (**2**)	0.0002	0.001
4	0.022	0.012
5	0.009	0.017
6	0.052	0.035
7	0.090	0.262
8	0.021	0.077
9	0.090	0.254
10	0.039	0.067
11	0.003	0.009
12	0.001	0.007
13	0.004	0.006
14	0.027	0.049
15	0.055	0.197
16	0.030	0.049
17	0.098	0.146
18	>10.0	8.95
19	>10.0	>10.0
20	3.52	1.20
21	1.80	>5.00

Given these data, we wondered whether the aryl sector is even necessary. Could it be replaced by a single hydrogen at C15? Toward this end, we prepared compound **19**. However, it has very low cytotoxicity (IC_{50} > 10.0 μM) and shows almost no activity in tubulin polymerization/depolymerization assays. We then asked whether the olefinic spacer element connecting the aromatic rings with C15 is needed. Therefore, we prepared compounds **20** and **21**. These substances showed a major loss of cytotoxicity. Accordingly, the aryl sector can now be defined with greater precision: it requires an olefinic spacer linking the lactone at C15 to an aromatic subsection which is substantially tolerant to modification.

Of course, it will be necessary to prepare and evaluate many more compounds to provide a definitive mapping of the SAR profile of this series with single carbon atom resolution. However, it is already clear that the acyl sector constitutes a "hot spot" with great sensitivity to structural change (Scheme 1). By contrast, the O-alkyl and aryl sectors exhibit significant tolerance, both in the tubulin assays and in cytotoxicity screens.

We have also initiated in vivo evaluations of the epothilones. As a first line of inquiry, we conducted a direct comparison of fully synthetic epothilone B (**2**) with paclitaxel (**3**). Since the susceptibility to drug resistance is one of the vulnerabilities of paclitaxel, we scrutinized the in vivo efficacy of the two drugs against resistant tumor tissues.[19] In the initial studies, CCRF-CEM/VBL tumor tissue was implanted subcutaneously in SCID mice. The tumor-bearing mice were treated periodically, according to a set protocol, with epothilone B (**2**, 0.7 mg kg^{-1}) and paclitaxel (**3**, 2 mg kg^{-1}). Although the concentration of paclitaxel used was higher than that of epothilone B (ca. 1.7:1 molar ratio), the reduction in tumor size was substantially greater with epothilone B at each interval of measurement (Table 2).

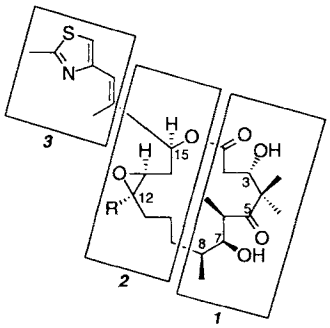

Scheme 1. The three arbitrarily defined sectors of the epothilones: aryl (1), alkyl (2), and acyl (3) sectors. Sector 1 is very sensitive to modifications; sectors 2 and 3 are more tolerant.

Table 2. Chemotherapeutic effect of daily treatments with epothilone B and paclitaxel in CB-17 SCID mice bearing drug-resistant human CCRF-CEM/VBL xenografts[a].

Drug	Dose [mg kg^{-1}][c]	Average tumor volume (T/C)[b] day 7	day 12	day 17	day 22
control	0	1.0	1.0	1.0	1.0
epothilone B	0.7	1.0	0.32	0.40	0.33
paclitaxel	2.0	1.0	0.60	0.58	0.70

[a] Multidrug resistant CCRF-CEM/VBL tumor tissue, 50 μL per mouse, was implanted subcutaneously on day 0. Solutions of the drugs in DMSO were injected intraperitoneally on days 7, 8, 9, 10, 14, and 15. There were seven CB-17 SCID mice in each treated group and in the control group. [b] The tumor volumes for each group on day 7 were about 1 mm^3. The average tumor volumes of the control group on days 12, 17, and 22 were 35, 107 and 278 mm^3, respectively. [c] On day 12, the average decreases in body weight due to treatment with epothilone B and paclitaxel were 2.7 and 3.4%, respectively.

In a subsequent experiment, epothilone B and paclitaxel were administered weekly (Table 3).[22] In these experiments both the sensitive (CCRF-CEM) and resistant (CCRF-CEM/VBL) tumor tissues were implanted in SCID mice. Epothilone B was given both intraperitoneally (H_2O) and intravenously (DMSO) for comparison. Epothilone B and paclitaxel show similar reduction of tumor size in treatment of the sensitive tumor (CCRF-CEM). Against the resistant tumor (CCRF-CEM/VBL), epothilone B shows a significant advantage over paclitaxel. It is also interesting to note that epothilone B is more

 © WILEY-VCH Verlag GmbH, D-69451 Weinheim, 1997 0570-0833/97/3619-2095 $ 17.50+.50/0

Table 3. Chemotherapeutic effect of weekly treatments with epothilone B and paclitaxel in CB-17 SCID mice bearing human CCRF-CEM and CCRF-CEM/VBL xenografts[a].

Tumor	Drug	Route	Dose [mg kg^{-1}][b]	Average tumor volume (T/C) [c] day 10	day 15	day 20	day 25
CCRF-CEM	control	i.p.	0	1.0	1.0	1.0	1.0
	epothilone B	i.p.	1.5	0.40	0.40	0.37	0.34
		(H_2O)	3.0[d]	0.41	0.35	0.38	0.50
	epothilone B	i.v.	1.5	0.38	0.34	0.42	0.37
		(DMSO)	3.0[e]	0.28	0.38	0.29	0.24
	paclitaxel	i.p.	20.0[f]	0.33	0.28	0.31	0.34
		(DMSO)	30.0[g]	0.43	0.25	0.23	0.25
CCRF-CEM/ VBL	control	i.p.	0	1.0	1.0	1.0	1.0
	epothilone B	i.p.	1.5[h]	0.23	0.34	0.27	0.26
		(H_2O)	3.0[i]	0.26	0.25	0.20	0.22
	epothilone B	i.v.	1.5	0.21	0.19	0.27	0.26
		(DMSO)	3.0	0.24	0.27	0.14	0.20
	paclitaxel	i.p.	20.0[j]	0.77	0.51	0.60	0.59
		(DMSO)	30.0[k]	0.58	0.46	0.42	0.61

[a] CCRF-CEM and CCRF-CEM/VBL tumor tissue, 50 µL per mouse, implanted subcutaneously on day 0. The drugs were administered on day 5, 12, 19 (i.p. = intraperitoneally, i.v. = intravenously). There were five CB-17 SCID mice in each group. [b] On day 20 the average decrease in body weight due to epothilone B doses of 1.5 and 3.0 mg kg^{-1} was 5.0 and 6.6%, respectively. [c] The tumor volumes for each group on day 5 was about 8 mm^3. The average tumor volumes in the CCRF-CEM control group on days 10, 15 and 20 were 57, 145, 335 mm^3; those of the CCRF-CEM/VBL control group were 62, 173, and 386 mm^3, respectively. [d]–[k] A number of mice died of drug toxicity: two on day 23 (d), two on day 19 (e), three on days 13, 21, and 21 (f), three on days 6, 6, and 21 (g), one on day 24 (h), two on day 24 (i), two on day 13 (j), and four on day 6 (k).

effective against the resistant tumor tissues than sensitive tissues in these experiments.

At present, none of our analogs are more potent in vitro than the naturally occurring epothilone B (**2**), although the ethyl compound **12** is fully competitive in all comparisons thus far available. However, we have established zones of the molecule that are most likely to be responsive to molecular modification (see Scheme 1). Also, early in vivo data suggest a potentially valuable margin of advantage of epothilone B (**2**) relative to paclitaxel (**3**) against a highly resistant MDR tumor implant. In all in vivo experiments conducted so far, epothilone B and paclitaxel were equally effective in reducing the size of sensitive (CCRF-CEM) tumor tissues. While it is far too early to argue that we have demonstrated a superior alternative to paclitaxel, the data already in hand mark the epothilones as worthy of continuing interest. Our present focus is on selecting the most promising compounds for further development, and on a major restructuring of our synthesis for the preparation of any desirable compound in the series in an eminently practical fashion.

Received: July 8, 1997 [Z 10647 IE]
German version: *Angew. Chem.* **1997**, *109*, 2178–2181

Keywords: antitumor agents · epothilones · in vivo testing · natural products · structure–activity relationships

[1] G. Höfle, N. Bedorf, H. Steinmetz, D. Schomberg, K. Gerth, H. Reichenbach, *Angew. Chem.* **1996**, *108*, 1671; *Angew. Chem. Int. Ed. Engl.* **1996**, *35*, 1567.

[2] a) "Taxane Anticancer Agents, Basic Science and Current Status": *ACS Symp. Ser.* **1995**, 583; b) "The Chemistry and Pharmacology of Taxol® and its Derivatives": *Pharmacochem. Libr.* **1995**, *22*; c) K. C. Nicolaou, W.-M. Dai, K. Guy, *Angew. Chem.* **1994**, *106*, 38; *Angew. Chem. Int. Ed. Engl.* **1994**, *33*, 15.

[3] Model reactions: a) D. Meng, E. J. Sorensen, P. Bertinato, S. J. Danishefsky, *J. Org. Chem.* **1996**, *61*, 7998; b) P. Bertinato, E. J. Sorensen, D. Meng, S. J. Danishefsky, *ibid.* **1996**, *61*, 8000; Total syntheses: c) A. Balog, D. Meng, T. Kamenecka, P. Bertinato, D.-S. Su, E. J. Sorensen, S. J. Danishefsky, *Angew. Chem.* **1996**, *108*, 2976; *Angew. Chem. Int. Ed. Engl.* **1996**, *35*, 2801; d) D. Meng, D.-S. Su, A. Balog, P. Bertinato, E. J. Sorensen, S. J. Danishefsky, Y.-H. Zheng, T.-C. Chou, L. He, S. B. Horwitz, *J. Am. Chem. Soc.* **1997**, *119*, 2733; e) D.-S. Su, D. Meng, P. Bertinato, A. Balog, E. J. Sorensen, S. J. Danishefsky, Y.-H. Zheng, T. -C. Chou, L. He, S. B. Horwitz, *Angew. Chem.* **1997**, *109*, 775; *Angew. Chem. Int. Ed. Engl.* **1997**, *36*, 757.

[4] Model reactions: a) K. C. Nicolaou, Y. He, D. Vourloumis, H. Vallberg, Z. Yang, *Angew. Chem.* **1996**, *108*, 2554; *Angew. Chem. Int. Ed. Engl.* **1996**, *35*, 2399; Total syntheses: b) Z. Yang, Y. He, D. Vourloumis, H. Vallberg, K. C. Nicolaou, *ibid.* **1997**, *109*, 170 and **1997**, *36*, 166; c) K. C. Nicolaou, F. Sarabia, S. Ninkovic, Z. Yang, *ibid.* **1997**, *109*, 539 and **1997**, *36*, 525; d) K. C. Nicolaou, N. Winssinger, J. Pasto, S. Ninkovic, F. Sarabia, Y. He, D. Vourloumis, Z. Yang, T. Li, P. Giannakakout, E. Hamel, *Nature (London)* **1997**, *387*, 268.

[5] Model reactions: a) D. Schinzer, A. Limberg, O. M. Böhm, *Chem. Eur. J.* **1996**, *2*, 1477; Total synthesis: b) D. Schinzer, A. Limberg, A. Bauer, O. M. Böhm, M. Cordes, *Angew. Chem.* **1994**, *106*, 543; *Angew. Chem. Int. Ed. Engl.* **1997**, *36*, 523.

[6] T. Gabriel, L. Wessjohann, *Tetrahedron Lett.* **1997**, *38*, 1363.

[7] E. Claus, A. Pahl, P. G. Jones, H. M. Meyer, M. Kalesse, *Tetrahedron Lett.* **1997**, *38*, 1359.

[8] J. Mulzer, A. Mantoulidis, *Tetrahedron Lett.* **1996**, *37*, 9179.

[9] R. E. Taylor, J. D. Haley, *Tetrahedron Lett.* **1997**, *38*, 2061.

[10] Unpublished results using compounds described in refs. [3a,b].

[11] A. Balog, P. Bertinato, D.-S. Su, D. Meng, E. Sorensen, S. J. Danishefsky, Y.-H. Zheng, T.-C. Chou, L. He, S. B. Horwitz, *Tetrahedron Lett.* **1997**, *38*, 4529.

[12] Identification of the deleted carbon in compound **18** as C9 is arbitrary; it could also be looked upon as deletion of C10 or C11. For the purpose of this discussion, we look upon this compound as a "C9 deletion" corresponding to an alteration of the substituents at C8.

[13] a) D. M. Bollag, P. A. McQueney, J. Zhu, O. Hensens, L. Koupal, J. Liesch, M. Goetz, E. Lazarides, C. M. Woods, *Cancer Res.* **1995**, *55*, 2325; b) R. J. Kowalski, P. Giannakakou, E. Hamel, *J. Biol. Chem.* **1997**, *272*, 2534.

[14] All new analogs described here were prepared by extensions of our previously published methodology: D. Meng, P. Bertinato, A. Balog, D.-S. Su, T. Kamenecka, E. Sorensen, S. J. Danishefsky, *J. Am. Chem. Soc.* **1997**, in press.

[15] The (*Z*)-desoxy compound with *n*-hexyl at C12 was also found to have significant biological activity; however, the solubility of this compound in DMSO is very low. Therefore, the results are not included in Figure 1.

[16] Compound **9** was treated with 3,3-dimethyldioxirane to create the *trans*-epoxide, which was found to have significant biological activity. However, the absolute configuration of the *trans*-epoxide has not been determined.

[17] Microtubule protein (MTP) was purified from calf brains by two cycles of temperature-dependent assembly and disassembly[20]. The concentration of tubulin in the preparation was approximately 85%. Assembly experiments were done in the presence or absence of 10 µM drug plus MTP (1 mg mL^{-1} diluted in assembly buffer containing 0.1 M 2-(*N*-morpholino)ethanesulfonic acid (MES), 1 mM 1,2-di(2-aminoethoxy)ethane-*N*,*N*,*N*′,*N*′-tetracetic acid (EGTA), 0.5 mM $MgCl_2$, and 3 M glycerol, pH 6.6). This concentration of drug gives an approximate 1:1 ratio to tubulin dimer. Assembly was followed spectrophotometrically at 350 nm, 37 °C for 40 min, by monitoring changes in turbidity as a measure of polymer mass[21]. Aliquots (200 µL) were taken from each assembly reaction and centrifuged at 28000 rpm, 27 °C for 30 min. The amount of protein remaining in the supernatant was determined, allowing the protein concentration in the microtubule pellet to be calculated. Controls with assembly buffer or DMSO were included. The value obtained for microtubules formed with 10 µM epothilone B was defined as 100%.

[18] The cytotoxicities of test compounds were determined by the growth of human lymphoblastic leukemic cells CCRF-CEM or their sublines resistant to vinblastine and taxol (CCRF-CEM/VBL). XTT-microculture tetrazolium/fromazan assays were used. The IC_{50} values were calculated based on five or six assays at various concentrations; a median-effect plot was generated using computer software[23].

[19] The multidrug resistant CCRF-CEM/VBL tumor tissue was implanted subcutaneously to CB-17 SCID mice, and the tumor-bearing mice were treated on days 7, 8, 9, 10, 14, and 15 with 0.7 mg kg^{-1} epothilone B intraperitoneally. The average tumor sizes were reduced by 68, 60, and 67% on days 12, 17, and 22, respectively. In the parallel experiments, 2 mg kg^{-1} taxol reduced tumor size by 40, 42, and 30%, respectively.

[20] R. C. Weisenberg, *Science* **1972**, *177*, 1104.

[21] F. Gaskin, C. R. Cantor, M. L. Shelanski, *J. Mol. Biol.* **1974**, *89*, 737.

[22] Experiments were also conducted with daily (0.7 and 1.0 mg kg^{-1}) and twice daily (0.15 and 0.25 mg kg^{-1}) treatments of epothilone B. The efficacy of once and twice daily treatments with epothilone B was similar to the weekly treatments, but the drug toxicity was slightly higher.

[23] J. Chou, T. C. Chou, IBM-PC Software "Dose-Effect Analysis with Microcomputers", Biosoft, Cambridge, **1987**.

 © WILEY-VCH Verlag GmbH, D-69451 Weinheim, 1997 0570-0833/97/3619-2096 $ 17.50+.50/0

Designed Epothilones: Combinatorial Synthesis, Tubulin Assembly Properties, and Cytotoxic Action against Taxol-Resistant Tumor Cells**

K. C. Nicolaou,* Dionisios Vourloumis, Tianhu Li, Joaquin Pastor, Nicolas Winssinger, Yun He, Sacha Ninkovic, Francisco Sarabia, Hans Vallberg, Frank Roschangar, N. Paul King, M. Ray V. Finlay, Pareskevi Giannakakou, Pascal Verdier-Pinard, and Ernest Hamel

The isolation of epothilones A (**1**) and B (**2**) from the myxobacterium *Sorangium cellulosum* strain 90 by Höfle et al.[1] and the recognition of their cytotoxic action against tumor cells prompted intense research activities in chemistry and biology. In 1995 Bollag et al.[2] reported the Taxol (paclitaxel)-like mechanism of action of these compounds through induction of tubulin assembly and microtubule stabilization.[3] The recognition of their unique action against Taxol-resistant tumor cell lines[4] added to their novelty and potential importance in cancer chemotherapy. In 1996 Höfle et al. published the complete elucidation of the stereochemistry as determined by spectroscopic and X-ray crystallographic techniques.[5] Soon thereafter, a flurry of reports announced several approaches[6] to, and total syntheses of, epothilones A (**1**)[7-11,13] and B (**2**).[10,12,13] In addition to the natural products themselves, several precursors and analogues have been synthesized[7-17] and biologically investigated.[7,10,12,14,17] Notable amongst these are the 12,13-desoxy analogues (lacking the epoxide oxygen) first reported by Danishefsky et al.[7,12] and independently by ourselves,[8,10,11,13] Schinzer et al.,[9] and Höfle et al.[14] Herein we report on a) the solid-phase synthesis of several epothilone A analogues based on a combinatorial approach, b) the tubulin assembly properties of an extensive library of compounds, and c) the cytotoxic actions against breast and ovarian carcinoma cells (including a number of Taxol-resistant tumor cell lines) of a selected number of these designed epothilones. The results provide comprehensive information on structure–activity relationships of epothilones and set the foundation for their further development.

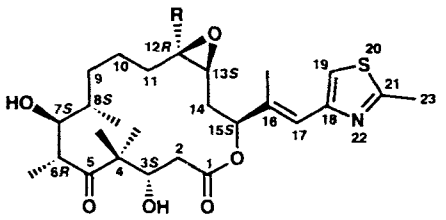

1: R = H : epothilone A
2: R = Me: epothilone B

The structures of epothilones are amenable to modification by changing the configuration of certain stereocenters, the geometry of the double bonds, the size of the rings, and the nature of their substituents. Our synthetic strategies towards these molecules were, therefore, designed on the premise of modifying these elements so as to reach optimum molecular diversity and obtain a maximum number of library members. Table 1 includes the structures of an epothilone library obtained by solution[6a,8,10,11,13,15,16,28] and solid-phase[10,28] combinatorial methods. Biological screening of these compounds was expected to lead to the establishment of sufficient structure–activity relationships to allow the next phase of the program, the design, synthesis, and identification of potential drug candidates, to proceed along a narrower track.

The strategy for the construction of a library of epothilone A analogues was based on our previously reported solid-phase synthesis[10] of epothilone A and Radiofrequency Encoded Combinatorial (REC) chemistry.[18] Scheme 1 summarizes the synthesis of a library of 12,13-desoxyepothilones A from the three key fragments generically denoted as **A**, **B**, and **C**.[19] Thus, SMART Microreactors[20] (SMART = single or multiple addressable radiofrequency tag) containing Merrifield resin were smoothly converted to Microreactors **I** by chain extension and phosphonium salt formation. Phosphonium salt resin **I** was then sorted according to the radiofrequency tag and treated with sodium hexamethyldisilazide (NaHMDS) to generate the corresponding ylides which were treated with the aldehydes **A**. The SMART Microreactors **II** were pooled for washing and subsequent deprotection and oxidation to obtain the polymer-bound aldehydes **III**. Further sorting and treatment with the dianion of the ketoacids **B** provided the polymer-bound carboxylic acids **IV** as a mixture of diastereoisomers. Resorting and esterification with alcohols **C** afforded dienes **V**. The SMART Microreactors were separately treated with $[RuCl_2(=CHPh)(PCy_3)_2]$ catalyst to simultaneously effect cyclization by olefin metathesis[6a,7a,8a,9-11,15,21,22] and cleavage of the products, leading to products as mixtures of four 12,13-desoxyepothilones A (**VII**, **VIII**, **IX**, **X**). Each mixture was identified and subjected to preparative thin-layer chromatography to provide pure compounds, which were individually deprotected by treatment with TFA in dichloromethane and then epoxidized accordingly.[6a,7b,8-11,13,15-17]

The epothilone library (Table 1) was screened for induction of tubulin assembly with 5 μM compound at 37 °C.[2] Previously tested compounds (see references in Table 1) were reevaluated for comparative purposes. Most analogues were subjected to more detailed investigation in cytotoxicity assays with human ovarian and breast cancer cells, including Taxol-resistant lines,[23] and a quantitative tubulin assembly assay that differentiates between potent taxoid compounds (Table 2).[24] It soon became apparent that compounds with assembly values below 40% in the screen yielded high EC_{50} values in the quantitative

[*] Prof. Dr. K. C. Nicolaou, Dr. D. Vourloumis, Dr. T. Li, Dr. J. Pastor
N. Winssinger, Y. He, Dr. S. Ninkovic, Dr. F. Sarabia, Dr. H. Vallberg
Dr. F. Roschangar, Dr. N. P. King, Dr. M. R. V. Finlay
Department of Chemistry and The Skaggs Institute for Chemical Biology
The Scripps Research Institute
10550 North Torrey Pines Road, La Jolla, CA 92037 (USA)
Fax: Int. code +(619)784-2469
e-mail: kcn@scripps.edu
and
Department of Chemistry and Biochemistry
University of California, San Diego
9500 Gilman Drive, La Jolla, CA 92093 (USA)
Dr. P. Giannakakou
Medicine Branch, Division of Clinical Sciences
National Cancer Institute, National Institutes of Health
Bethesda, MD 20892 (USA)
Dr. P. Verdier-Pinard, Dr. E. Hamel
Laboratory of Drug Discovery Research and Development
Developmental Therapeutics Program, Division of Cancer Treatment
Diagnosis and Centers National Cancer Institute
Frederick Cancer Research and Development Center
Frederick, MD 21702 (USA)

[**] We thank Drs. D. H. Huang and G. Siuzdak for assistance with the NMR spectroscopic and mass spectrometric measurements, respectively. This work was supported by the National Institutes of Health USA, The Skaggs Institute for Chemical Biology, the CaP CURE Foundation, and fellowships from the George E. Hewitt Foundation (N. P. K.), the Deutsche Forschungsgemeinschaft (DFG) (F. R), Novartis (D. V), the Fundación Ramón Areces (Spain) (F. S.) and a Fulbright Scholarship (M. R. V. F), and grants from Merck, DuPont–Merck, Schering Plough, Hoffmann La Roche, and Amgen.

 © WILEY-VCH Verlag GmbH, D-69451 Weinheim, 1997 0570-0833/97/3619-2097 $ 17.50+.50/0

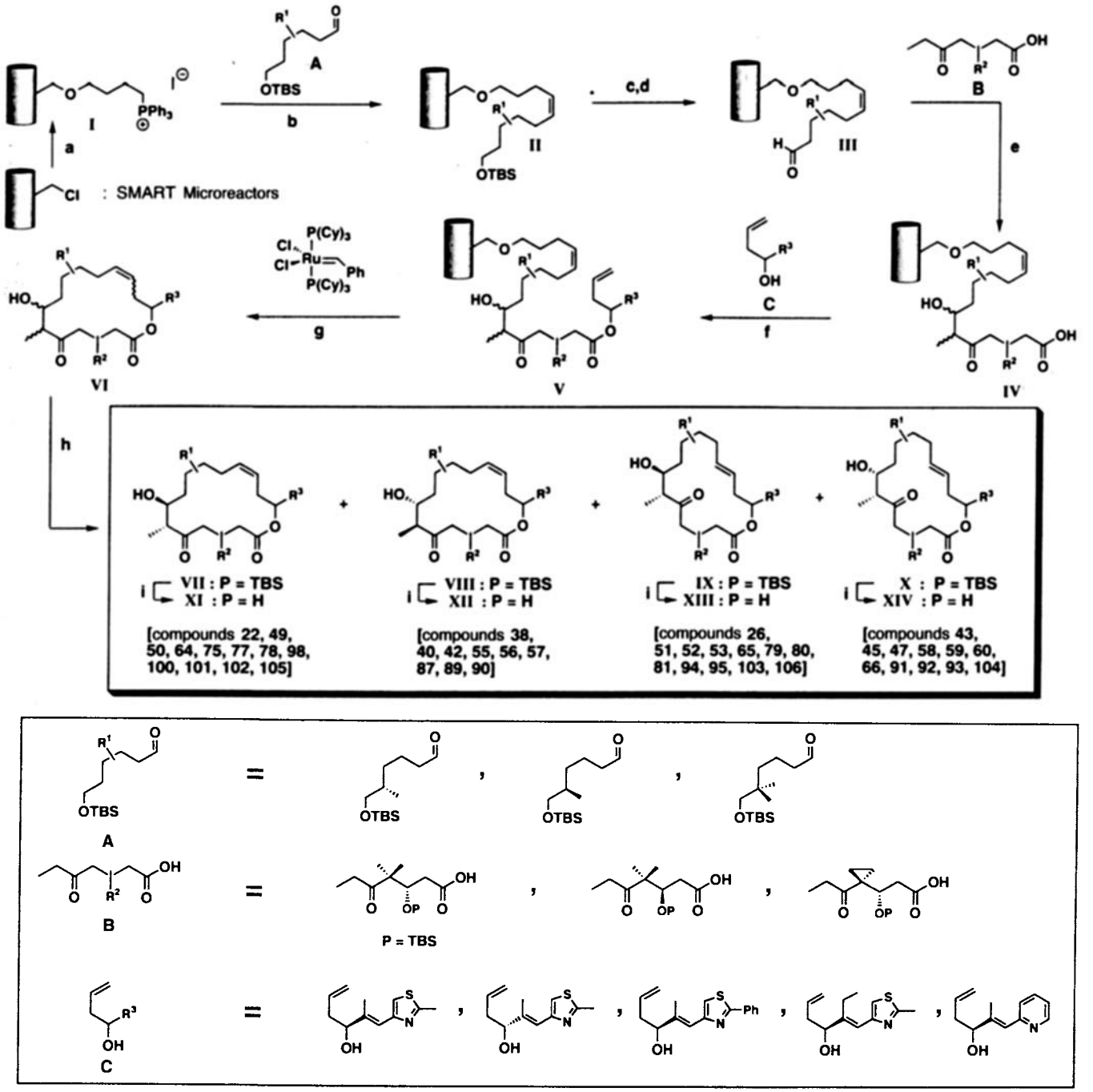

Scheme 1. Solid-phase synthesis of epothilone A analogues by a combinatorial approach. a) 1. 1,4-butanediol (5.0 equiv), NaH (5.0 equiv), nBu$_4$NI (0.1 equiv), DMF, 25 °C, 12 h; 2. Ph_3P (4.0 equiv), I_2 (4.0 equiv), imidazole (4.0 equiv), CH_2Cl_2, 25 °C, 3 h; 3. Ph_3P (10 equiv), 90 °C, 12 h; b) 1. sort SMART Microreactors (with an Accutag-100 apparatus); 2. NaHMDS (3.0 equiv), THF:DMSO (1:1), 25 °C, 12 h; 3. **A** (2.0 equiv), THF, 0 °C, 3 h (≈75% from chloromethyl polystyrene loading based on recovered aldehyde upon ozonolysis); 4. pool; c) 0.2 M HCl in THF, 25 °C, 12 h; d) $(COCl)_2$ (4.0 equiv), DMSO (8.0 equiv), Et_3N (12.5 equiv), −78 → 25 °C (≥95% for two steps, the reactions were monitored by IR analysis of polymer-bound material and by TLC analysis of the products obtained by ozonolysis); e) 1. sort; 2. **B** (2.0 equiv), LDA (2.2 equiv), THF, −78 → −40 °C, 1 h; then add resulting enolate to the resin suspended in a $ZnCl_2$ (2.0 equiv) solution in THF, −78 → −40 °C, 2.0 h (≥90%, based on recovered aldehyde upon ozonolysis); 3. pool; f) 1. sort; 2. **C** (5.0 equiv), DCC (5.0 equiv), 4-DMAP (5.0 equiv), 25 °C, 15 h (≥85% yield as determined by recovered heterocycle fragments obtained upon treatment with NaOMe); g) 1. separation of individual SMART Microreactors; 2. $[RuCl_2(=CHPh)(PCy_3)_2]$ (0.20 equiv), CH_2Cl_2, 25 °C, 48 h; h) automated HPLC (SiO_2, EtOAc/hexane, or C_{18}, H_2O/THF), or preparative thin-layer chromatography, EtOAc/hexanes. The stereochemisty at C-6 and C-7 as well as the geometry of the olefin was tentatively assigned by ^{1}H NMR spectroscopy; i) 20% TFA in CH_2Cl_2 (v/v), 25 °C, 2–12 h. The purity of individual compounds was established by ^{1}H NMR spectroscopy and HPLC. P = protecting group; TBS = *tert*-butyldimethylsilyl; DMSO = dimethyl sulfoxide; TFA = trifluoroacetic acid; LDA = lithium diisopropylamide; DCC = *N*,*N*′-dicyclohexylcarbodiimide; 4-DMAP = 4-dimethylaminopyridine.

assay and had little inhibitory effect on cell growth (only positive results shown in Table 2).

The glutamate assay was devised to test the hypothesis that taxoids more active than Taxol in tubulin assembly would also be more cytotoxic,[24] and this was validated with over fifty analogues (Hamel et al., unpublished results).[33] With the epothilones, however, the quantitative assay was less successful. A low glutamate concentration resulted in a high false negative rate in predicting cytotoxicity (data not shown), while higher glutamate concentrations (e.g. 0.7 M, Table 2) were comparable

 © WILEY-VCH Verlag GmbH, D-69451 Weinheim, 1997 0570-0833/97/3619-2098 $ 17.50+.50/0

Table 1. Structures and tubulin polymerization properties of epothilone analogues. Footnotes [a]–[i] are on page 2101.

Ref.	Structure	Tubulin polymerization [%][a]	Ref.	Structure	Tubulin polymerization [%][a]	Ref.	Structure	Tubulin polymerization [%][a]
[7-13] [10, 12, 13] [15] [16]	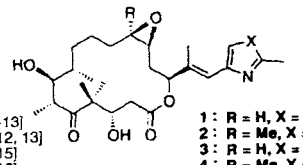	1: R = H, X = S 76 [b] 2: R = Me, X = S 98 [b] 3: R = H, X = O 58 4: R = Me, X = O 93 Taxol 50	[11]	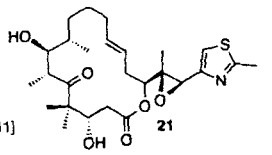	21 12	[11] [15] [28] [28] [28]	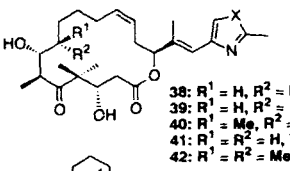	38: R¹ = H, R² = Me, X = S 13 39: R¹ = H, R² = Me, X = O 18 40: R¹ = Me, R² = H, X = S 5 41: R¹ = R² = H, X = S 23 42: R¹ = R² = Me, X = S 5
[11, 13] [16] [15]	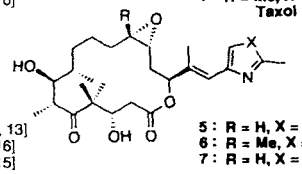	5: R = H, X = S 17 6: R = Me, X = O 71 7: R = H, X = O 24	[7-13] [10, 12, 13] [15] [16]	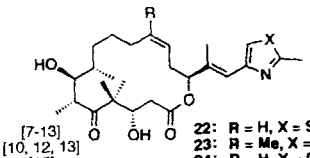	22: R = H, X = S 72 [d] 23: R = Me, X = S 94 [d] 24: R = H, X = O 75 25: R = Me, X = O 93	[11] [15] [28] [28]	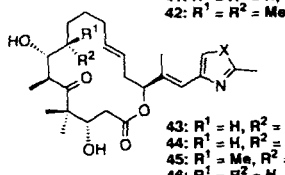	43: R¹ = H, R² = Me, X = S 13 44: R¹ = H, R² = Me, X = O 20 45: R¹ = Me, R² = H, X = S 11 46: R¹ = R² = H, X = S 21 47: R¹ = R² = Me, X = S 4
[11]	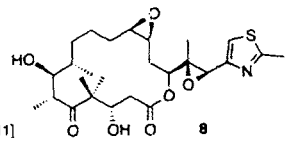	8 16	[7, 10-13] [10, 12, 13] [15] [16]	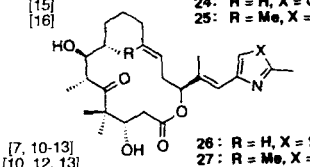	26: R = H, X = S 76 [e] 27: R = Me, X = S 84 [d] 28: R = H, X = O 43 29: R = Me, X = O 54	[28]	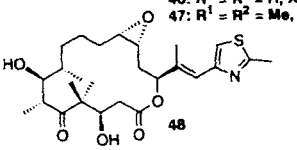	48 25
[11]	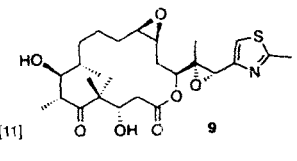	9 14	[11] [11]	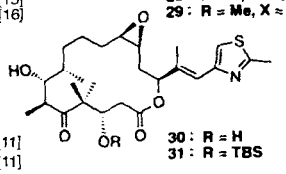	30: R = H 25 31: R = TBS 6	[7] [28]	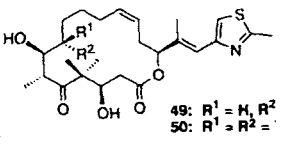	49: R¹ = H, R² = Me 16 [f] 50: R¹ = R² = [illegible] 3
[11]	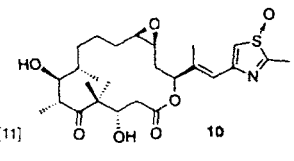	10 26	[11]	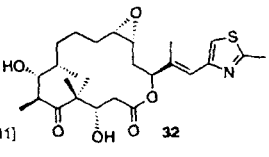	32 20	[28] [28] [28]	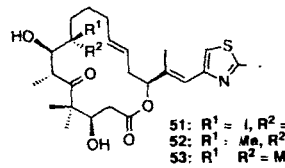	51: R¹ = [illegible], R² = Me 21 52: R¹ = Me, R² = H 3 53: R¹ = R² = Me 4
[8, 11]	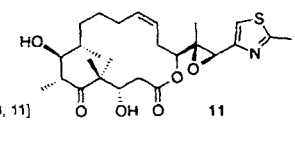	11 20	[11]	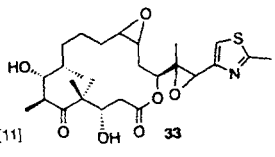	33 7	[28]	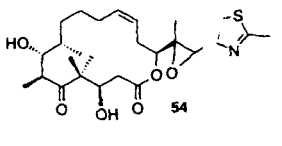	54 7
[8, 11]	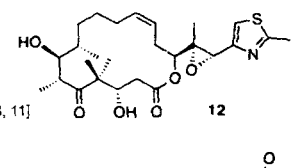	12 9	[11]	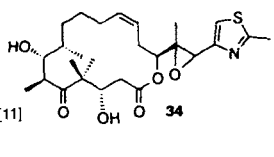	34 23	[28] [28] [28]	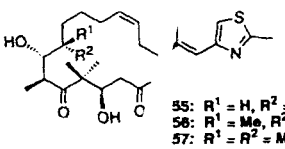	55: R¹ = H, R² = Me 23 56: R¹ = Me, R² = H 5 57: R¹ = R² = Me 1
[11]	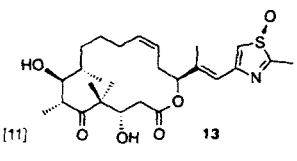	13 22	[11]	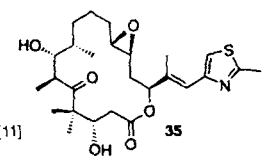	35 19	[28] [28] [28]	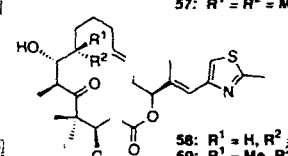	58: R¹ = H, R² = Me 24 59: R¹ = Me, R² = H 7 60: R¹ = R² = Me 5
[10, 11, 13] [10, 13] [15] [16]	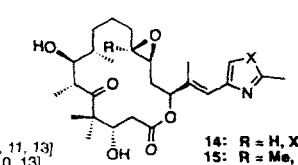	14: R = H, X = S 92 15: R = Me, X = S 84 [c] 16: R = H, X = O 64 17: R = Me, X = O 95	[11]	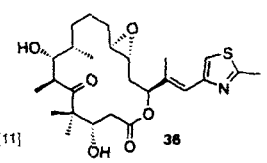	36 16	[28]	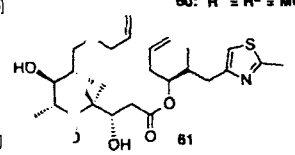	61 18
[11, 13] [10, 13] [15]	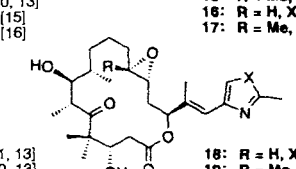	18: R = H, X = S 17 19: R = Me, X = S 63 20: R = H, X = O 46	[11]	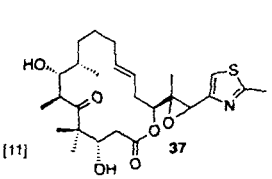	37 22	[28]	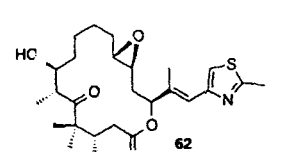	62 21

 © WILEY-VCH Verlag GmbH, D-69451 Weinheim, 1997 0570-0833/97/3619-2099 $ 17.50+.50/0

Table 1 (cont.)

Ref.	Structure	Tubulin polymerization [%] [a]
[28]	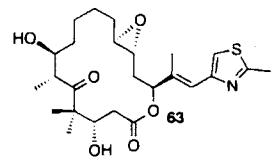 **63**	27
[28]	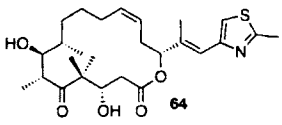 **64**	10
[28]	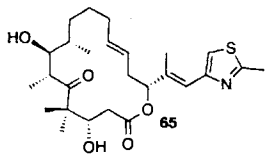 **65**	10
[28]	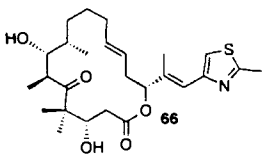 **66**	15
[28] [h]	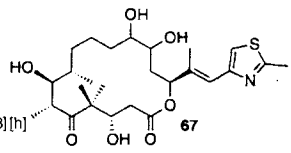 **67**	12
[28] [h]	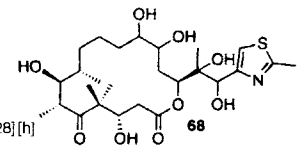 **68**	13
[15] [16]	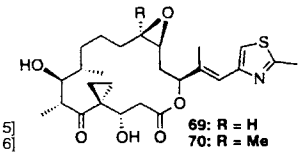 **69: R = H** **70: R = Me**	20 19
[15] [16]	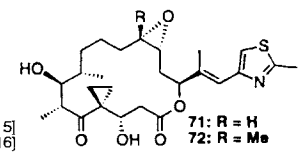 **71: R = H** **72: R = Me**	5 6
[16]	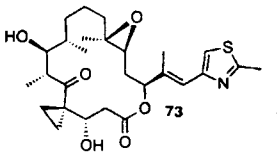 **73**	31
[16]	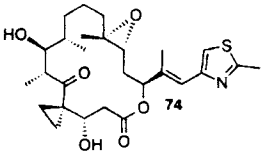 **74**	18

Ref.	Structure	Tubulin polymerization [%] [a]
[15] [16] [28] [28]	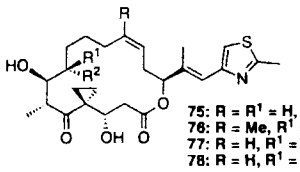 **75: R = R¹ = H, R² = Me** **76: R = Me, R¹ = H, R² = Me** **77: R = H, R¹ = Me, R² = H** **78: R = H, R¹ = R² = Me**	17 22 5 4
[15] [28] [28]	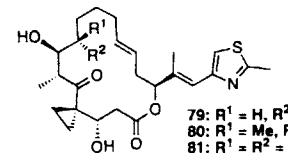 **79: R¹ = H, R² = Me** **80: R¹ = Me, R² = H** **81: R¹ = R² = Me**	25 9 5
[15] [16]	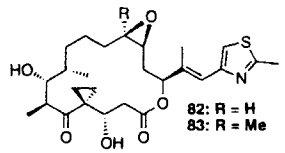 **82: R = H** **83: R = Me**	10 27
[15] [16]	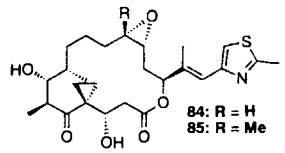 **84: R = H** **85: R = Me**	9 18
[15]	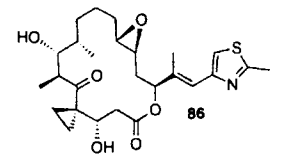 **86**	3
[15] [16] [28] [28]	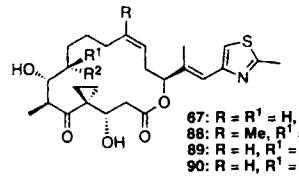 **87: R = R¹ = H, R² = Me** **88: R = Me, R¹ = H, R² = Me** **89: R = H, R¹ = Me, R² = H** **90: R = H, R¹ = R² = Me**	13 6 1 5
[15] [16] [28]	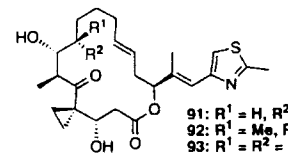 **91: R¹ = H, R² = Me** **92: R¹ = Me, R² = H** **93: R¹ = R² = Me**	18 5 4
[28] [28] [28] [28]	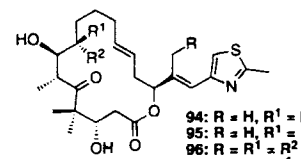 **94: R = H, R¹ = Me, R² = H** **95: R = H, R¹ = R² = Me** **96: R = R¹ = R² = H** **97: R = Me, R¹ = H, R² = Me**	11 3 24 48
[28] [17, 28] [28] [28]	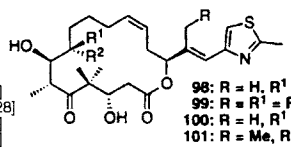 **98: R = H, R¹ = Me, R² = H** **99: R = R¹ = R² = H** **100: R = H, R¹ = R² = Me** **101: R = Me, R¹ = H, R² = Me**	11 23 5 [g] 34
[28]	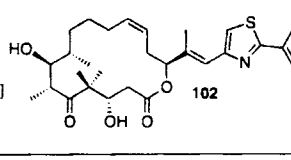 **102**	25

Ref.	Structure	Tubulin polymerization [%] [a]
[28]	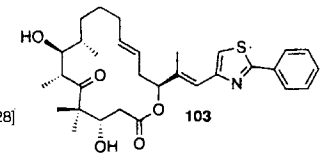 **103**	16
[28]	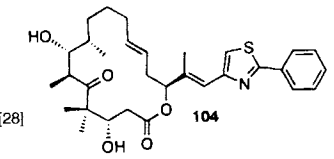 **104**	12
[28]	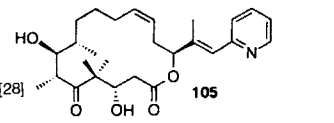 **105**	51
[28]	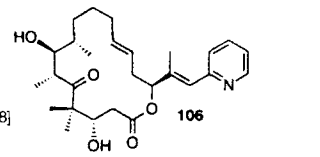 **106**	61
[11]	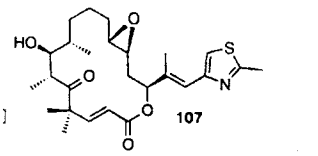 **107**	46
[11]	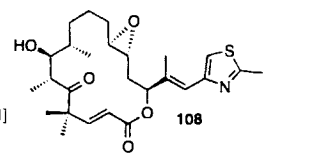 **108**	28
[11]	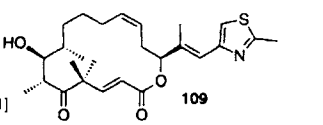 **109**	27
[11]	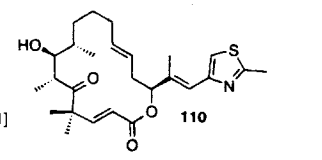 **110**	58
[11]	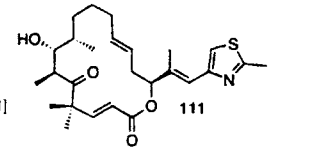 **111**	20
[28] [i]	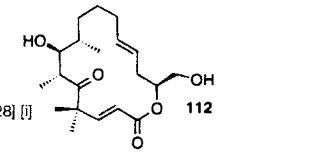 **112**	17

 © WILEY-VCH Verlag GmbH, D-69451 Weinheim, 1997 0570-0833/97/3619-2100 $ 17.50+.50/0

Table 2. Biological properties of selected epothilone analogues.

Cmpd.	Induction of tubulin polymerization: Screening-assay [a] polymer formation [%]	quantitative glutamate assay [b] EC_{50} [μM]	Inhibition of carcinoma cell growth: Ovarian [d] parental 1A9	Ovarian [d] β-tubulin mutations 1A9PTX10 IC_{50} [nM] [relative resistance] [f]	Ovarian [d] β-tubulin mutations 1A9PTX22 IC_{50} [nM] [relative resistance] [f]	Breast [e] MCF7
Taxol	50	4.7	1.4	32 [23]	38 [27]	4.2
1	76	4.6	2.2	20 [9.1]	5.9 [2.7]	5.1
2	98	3.4	0.13	1.0 [7.7]	0.31 [2.4]	1.0
3	58	5.3	3.0	25 [8.3]	8.0 [2.7]	6.1
4	93	–	0.2	1.1 [5.5]	0.9 [4.5]	–
6	71	6.1	1.5	11 [7.3]	3.0 [2.0]	6.2
14	92	6.2	2.0	18 [9.0]	3.0 [1.5]	5.4
15	84	5.6	1.0	8.5 [8.5]	1.0 [1.0]	1.8
16	64	7.8	3.5	32 [9.1]	9.5 [2.7]	>100
19	63	13	6.0	30 [5.0]	6.5 [1.1]	14
20	46	8.1	4.8	34 [7.1]	9.0 [1.9]	5.7
22	72	8.3	32	>100	100	38
23	94	3.9	6.5	23 [3.5]	9.0 [1.4]	9.3
24	75	6.1	68	>100	90	74
25	93	3.3	8.0	30 [3.8]	12 [1.5]	>100
26	76	9.8	60	>100	100	>100
27	84	7.5	61	>100	85	75
28	43	13	>100	–	–	>100
29	54	6.0	32	>100	>100	68
101	34	17	>100	–	–	>100
105	51	7.6	32	>100	70	57
106	61	11	82	>100	>100	78
107	46	–	28	>100	50	–

[a] From Table 1. [b] Assay performed as described in ref. [24]; reaction mixtures contained 10 μM purified tubulin [29], 0.7 M monosodium glutamate, 5% DMSO and drug; incubation was for 20 min at room temperature and reaction mixtures were centrifuged at 14000 rpm; supernatant protein concentration was measured and the EC_{50} value is defined as the drug concentration resulting in a 50% reduction in supernatant protein relative to control values; each EC_{50} value shown is an average (standard deviations ≤20%) obtained in two to four independent assays. [c] Cell growth was evaluated by measurement of increase in cellular protein [30]. [d] The parental ovarian cell line, derived as a clone of line A2780 [31], was used to generate Taxol-resistant cell lines by incubating the cells with increasing concentrations of Taxol with verapamil [23]; the cells were grown in the presence of drug for 96 h; values shown in the table were single determinations, except for those of Taxol, **1** and **2** (average of six determinations each); the values for **1** and **2** are averages of data obtained with both synthetic and natural samples (generously provided to E. H. by Merck Research Laboratories), which did not differ significantly. [e] The MCF7 cells were obtained from the National Cancer Institute drug screening program [32]; cells were grown in the presence of drug for 48 h; each value represents an average of two determinations. [f] Relative resistance is defined as the IC_{50} value obtained for the β-tubulin mutant line divided by that obtained for the parental cell line.

to the screening assay in identifying cytotoxic analogues. If "significant" cytotoxicity is defined as an IC_{50} value below 10 nM, we identified nine analogues with activity against the breast and ovarian lines (**3**, **6**, **14**–**16**, **19**, **20**, **23**, and **25**). With the screening assay, there were no false negatives, but there were seven false positives (agents with limited cytotoxicity yielding >40% polymerization) among examined compounds. With the glutamate assay, the same results were obtained. The nine cytotoxic analogues had EC_{50} values of 3.3–13 μM, but an additional nine agents had EC_{50} values of 6.0–17 μM.

Two Taxol-resistant lines were generated from the 1A9 ovarian cells, and resistance resulted from mutations in the M40 gene, which codes for a highly expressed β_1 isotype in the parental and resistant cell lines.[23] The altered amino acids were residue 270 in the 1A9PTX10 line (Phe → Val) and 364 in 1A9PTX22 (Ala → Thr). This agreed with other observations that the Taxol binding site is on β-tubulin.[25–27] In preliminary results[10] we had reported with **1** and several analogues that 1A9PTX22 cells retained nearly complete sensitivity to epothilones, while 1A9PTX10 cells remained partially resistant to the drugs. These findings have been confirmed (Table 2). The relative resistance observed with 1A9PTX22 cells was 27-fold with Taxol and 1.0–2.7-fold with the eleven cytotoxic epothilones. With 1A9PTX10 cells, relative resistance was 23-fold with Taxol and 3.5–9.1-fold with the epothilones. The Taxol and epothilone binding sites could overlap, since **1** and **2** are competitive inhibitors of Taxol binding to tubulin polymer.[4] If one assumes that Phe270 and Ala364 interact directly with Taxol, the results with the resistant cells suggest that Phe270 is more important than Ala364 in the interaction of epothilones at the Taxol binding site.

The data in Tables 1 and 2, together with previously reported results,[1, 2, 7, 10, 12, 17] revealed important information regarding structure–activity relationships for in vitro tubulin polymerization and in vitro cytotoxicity, and lead to several conclusions. The importance of the macrocycle was confirmed by the lack of significant tubulin polymerization activity of the open-chain olefin metathesis precursor **61**. This conclusion was also reached by Höfle et al.[14] with a degradation product of epothilone A. Inversion of the configuration at C3 resulted in reduced tubulin polymerization potency. Interestingly, however, α,β-unsaturated lactones (e.g. **107** and **110**) retained significant tubulin assembly properties (Table 1) suggesting a conformational, rather than a direct binding effect for this hydroxyl group. Neither **107** nor **110**, however, exhibited significant cytotoxicity indicating an additional role for the 3-OH group. Substitution of the 4-*gem*-dimethyl with a 4,4-ethano moiety (e.g. **69** and **70**) resulted in loss of tubulin polymerization activity in all cases, pointing to the crucial importance of a proper conformation of epothilones for biological activity. Apparently the partial sp^2 character and the accompanied widening of the C3-C4-C5 angle introduced intolerable conformational changes within the macrocycle for effective interaction with tubulin. Another clear requirement for tubulin polymerization activity was the (6*R*,7*S*) configuration as revealed by the failure of all (6*S*,7*R*) stereoisomers to induce tubulin polymerization at significant concentrations (e.g. **30**, **47**, **54**–**60**, **66**, **82**–**93**, **104**, **111**, Table 1). Interestingly, there was a notable decrease in interaction with tubulin upon inversion of

Footnote to Table 1:

[a] Tubulin polymerization was determined by the filtration-colorimetric assay following the procedure of Bollag et al.[2]; purified tubulin [29] (1 mg/mL) was incubated at 37 °C for 30 min in the presence of each compound (5 μM) in MEM buffer [(100 mM 2-(*N*-morpholino)ethanesulfonic acid, pH 6.75, 1 mM ethylene glycol bis(β-aminoethyl ether). *N,N,N',N'*-tetraacetic acid, and 1 mM $MgCl_2$]; the mixture was then filtered to remove unpolymerized tubulin by using a 96-well Millipore Multiscreen Durapore hydrophilic 0.22 μm pore size filtration plate; the collected polymerized tubulin was stained with amido black solution and quantified by measuring absorbance of the dyed solution on a Molecular Devices Microplate Reader; the [%] polymerization was calculated relative to the absorbance produced by incubation with 0.5 M GTP + 10% glycerol in MEM buffer (presumed to cause 100% tubulin polymerization); these values represent the average of three experiments. [b] Refs. [1, 2, 10, 12, 17]. [c] Ref. [10]. [d] Refs. [10, 12, 17]. [e] Refs. [7, 12]. [f] Ref. [7]. [g] Ref. [17]. [h] Compounds **67** and **68** were obtained by reaction of compound **22** with OsO_4-NMO. [i] Compound **112** was prepared by desilylation of the corresponding primary *tert*-butyldiphenylsilyl ether (Ref. [11]).

 © WILEY-VCH Verlag GmbH, D-69451 Weinheim, 1997 0570-0833/97/3619-2101 $ 17.50+.50/0

the C8 methyl group (e.g. **98** vs **22**), introduction of a *gem*-dimethyl group at C8 (**100** vs **22** and **95** vs **26**), and removal of the C8 methyl group (e.g. **99** vs **22** and **96** vs **26** and **62** vs **14**). The latter observation was also made independently by Danishefsky et al.[17]

The importance of the natural (12*R*,13*S*) configuration for the epoxide was demonstrated by the general trend of the unnatural (12*S*,13*R*) epoxides to exhibit lower activities in inducing tubulin assembly (e.g. **5** vs **1**, **6** vs **4**, **7** vs **3**; although compound **6** had activities similar to those of epothilone A (**1**), but not B (**2**)). Most interestingly, both the *cis* and *trans* olefins corresponding to epothilones A and B were active in the tubulin assembly assays, and the activities of the *cis* olefins were comparable to those of the natural substances. Similar observations were independently made by Danishefsky et al.[7b, 12, 17] and Höfle et al.[14] However, we found that the *cis* and especially the *trans* olefins were significantly less cytotoxic than the naturally occurring epoxides (**22** and **26** vs **1**, **23** and **27** vs **2**). Moreover, both the α- and β-epoxides derived from the 12,13*E*-olefinic precursors exhibited considerable ability to induce tubulin assembly and inhibit cell growth (**14**, **16**, and **20** vs **1**, **15**, and **19** vs **2**; in fact, compound **15** appears to be one of the most cytotoxic analogues from those shown in Table 2).

The C12 methyl group consistently bestowed higher potency to all epothilones studied as compared to the C12 *des*-methyl counterparts (e.g. **2** vs **1** and **4** vs **3**), with the exception of compounds **14** and **15** where comparable results were obtained. Inversion of configuration at C15 led to loss of ability to induce tubulin polymerization (**64** vs **22**, **65** vs **26**). Replacement of the C16 methyl group with an ethyl group also reduced activity in the tubulin assay (**101** vs **22**, **97** vs **26**) suggesting that the methyl group may play a role in maintaining the planar conformation[5] of the side chain. The inactivity of the C16,C17 epoxides (**8**, **9**, **11**, and **12**) further supports this conclusion. The epothilone pharmacophore tolerated some heterocycle modifications. Thus, a number of oxazole derivatives exhibited activity comparable to the corresponding thiazoles (e.g. **3** vs **1**, **4** vs **2**, **16** vs **14**, **24** vs **22**, **25** vs **23**, **20** vs **18**). Furthermore, replacement of the thiazole with a 2-pyridyl moiety led only to a slight decrease in activity (e.g. **105** vs **22**, **106** vs **26**) in the tubulin assays, whereas substitution of the C23-methyl with a phenyl group yielded inactive compounds (**102**, **103**). Scheme 2 summarizes graphically the structure–activity relationships within the epothilone family of compounds as derived from these and previous studies.[1, 2, 7, 10, 12, 17]

The reported work demonstrates the power of interfacing combinatorial chemistry with chemical biology as facilitated by solid-phase synthesis, REC chemistry, and modern biological assays. Furthermore, this research should facilitate the process of drug discovery and development in the area of cancer chemotherapy.

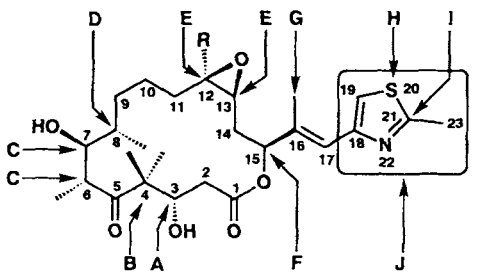

Scheme 2. Epothilone structure–activity relationships (tubulin binding assay): A) (3*S*) configuration important; B) 4,4-ethano group not tolerated; C) (6*R*,7*S*) configuration crucial; D) (8*S*) configuration important, 8,8-dimethyl group not tolerated; E) epoxide not essential for tubulin polymerization activity, but may be important for cytotoxicity; epoxide configuration may be important; R group important; both olefin geometries tolerated; F) (15*S*) configuration important; G) bulkier group reduces activity; H) oxygen substitution tolerated; I) substitution important; J) heterocycle important.

Received: July 9, 1997 [Z10666IE]
German version: *Angew. Chem.* **1997**, *109*, 2181–2187

Keywords: antitumor agents · combinatorial chemistry epothilones · microreactors · structure–activity relationships

[1] a) G. Höfle, N. Bedorf, K. Gerth, H. Reichenbach (GBF), DE-B 4138042, **1993** [*Chem. Abstr.* **1993**, *120*, 52841]; b) K. Gerth, N. Bedorf, G. Höfle, H. Irschik, H. Reichenbach, *J. Antibiot.* **1996**, *49*, 560–563.

[2] D. M. Bollag, P. A. McQueney, J. Zhu, O. Hensens, L. Koupal, J. Liesch, M. Goetz, E. Lazarides, C. M. Woods, *Cancer Res.* **1995**, *55*, 2325–2333.

[3] S. B. Horwitz, J. Fant, P. B. Schiff, *Nature* **1979**, *277*, 665–667.

[4] R. J. Kowalski, P. Giannakakou, E. Hamel, *J. Biol. Chem.* **1997**, *272*, 2534–2541.

[5] G. Höfle, N. Bedorf, H. Steinmetz, D. Schomburg, K. Gerth, H. Reichenbach, *Angew. Chem.* **1996**, *108*, 1671–1673; *Angew. Chem. Int. Ed. Engl.* **1996**, *35*, 1567–1569.

[6] a) K. C. Nicolaou, Y. He, D. Vourloumis, H. Vallberg, Z. Yang, *Angew. Chem.* **1996**, *108*, 2554–2556; *Angew. Chem. Int. Ed. Engl.* **1996**, *35*, 2399–2401; b) D. Meng, E. J. Sorensen, P. Bertinato, S. J. Danishefsky, *J. Org. Chem.* **1996**, *61*, 7998–7999; c) P. Bertinato, E. J. Sorensen, D. Meng, S. J. Danishefsky, *J. Org. Chem.* **1996**, *61*, 8000–8001; d) D. Schinzer, A. Limberg, O. M. Böhm, *Chem. Eur. J.* **1996**, *2*, 1477–1482; e) J. Mulzer, A. Mantoulidis, *Tetrahedron Lett.* **1996**, *37*, 9179–9182; f) E. Claus, A. Pahl, P. G. Jones, H. M. Meyer, M. Kalesse, *ibid.* **1997**, *38*, 1359–1362; g) T. Gabriel, L. Wessjohann, *ibid.* **1997**, *38*, 1363–1366; R. E. Taylor, J. D. Haley, *ibid.* **1997**, *38*, 2061–2064.

[7] a) A. Balog, D. Meng, T. Kamenecka, P. Bertinato, D.-S. Su, E. J. Sorensen, S. J. Danishefsky, *Angew. Chem.* **1996**, *108*, 2976–2978; *Angew. Chem. Int. Ed. Engl.* **1996**, *35*, 2801–2803; b) D. Meng, D.-S. Su, A. Balog, P. Bertinato, E. J. Sorensen, S. J. Danishefsky, Y.-H. Zheng, T.-C. Chou, L. He, S. B. Horwitz, *J. Am. Chem. Soc.* **1997**, *119*, 2733–2734.

[8] a) Z. Yang, Y. He, D. Vourloumis, H. Vallberg, K. C. Nicolaou, *Angew. Chem.* **1997**, *109*, 170–172; *Angew. Chem. Int. Ed. Engl.* **1997**, *36*, 166–168; b) K. C. Nicolaou, F. Sarabia, S. Ninkovic, Z. Yang, *ibid.* **1997**, *109*, 539–540 and **1997**, *36*, 525–526.

[9] D. Schinzer, A. Limberg, A. Bauer, O. M. Böhm, M. Cordes, *Angew. Chem.* **1997**, *109*, 543–544; *Angew. Chem. Int. Ed. Engl.* **1997**, *36*, 523–524.

[10] K. C. Nicolaou, N. Winssinger, J. A. Pastor, S. Ninkovic, F. Sarabia, Y. He, D. Vourloumis, Z. Yang, T. Li, P. Giannakakou, E. Hamel, *Nature* **1997**, *387*, 268–272.

[11] K. C. Nicolaou, Y. He, D. Vourloumis, H. Vallberg, F. Roschangar, F. Sarabia, S. Ninkovic, Z. Yang, J. I. Trujillo, *J. Am. Chem. Soc.* **1997**, *119*, 7960–7973.

[12] D.-S. Su, D. Meng, P. Bertinato, A. Balog, E. J. Sorensen, S. J. Danishefsky, Y.-H. Zheng, T.-C. Chou, L. He, S. B. Horwitz, *Angew. Chem.* **1997**, *109*, 775–777; *Angew. Chem. Int. Ed. Engl.* **1997**, *36*, 757–759.

[13] K. C. Nicolaou, S. Ninkovic, F. Sarabia, D. Vourloumis, Y. He, H. Vallberg, M. R. V. Finlay, Z. Yang, *J. Am. Chem. Soc.* **1997**, *119*, 7974–7991.

[14] G. Höfle, personal communication.

[15] K. C. Nicolaou, H. Vallberg, N. P. King, F. Roschangar, Y. He, D. Vourloumis, C. G. Nicolaou, *Chem. Eur. J.* **1997**, *3*, no. 12.

[16] K. C. Nicolaou, F. Sarabia, M. R. V. Finlay, S. Ninkovic, N. P. King, D. Vourloumis, Y. He, *Chem. Eur. J.* **1997**, *3*, no. 12.

[17] A. Balog, P. Bertinato, D.-S. Su, D. Meng, E. J. Sorensen, S. J. Danishefsky, Y.-H. Zheng, T.-C. Chou, L. He, S. B. Horwitz, *Tetrahedron Lett.* **1997**, *38*, 4529–4532.

[18] a) K. C. Nicolaou, X.-Y. Xiao, Z. Parandoosh, A. Senyei, M. P. Nova, *Angew. Chem.* **1995**, *107*, 2476–2479; *Angew. Chem. Int. Ed. Engl.* **1995**, *34*, 2289–2291; b) E. J. Moran, S. Sarshar, J. F. Cargill, M. M. Shahbaz, A. Lio, A. M. M. Mjalli, R. W. Armstrong, *J. Am. Chem. Soc.* **1995**, *117*, 10787–10788.

[19] These fragments were synthesized by standard synthetic operations and according to similar known sequences [11·13·15·16].

[20] We thank Dr. M. P. Nova of IRORI Quantum Microchemistry, San Diego, CA, for a gift of an AccuTag-100 instrument and SMART Microreactors (MicroKans and MicroTubes). The reported combinatorial chemistry was performed by using MicroKans, while a single MicroTube was utilized to synthesize a set of four epothilones A (i.e. **42**, **47**, **95**, and **100**, Table 1). K. C. N. is an advisor of IRORI Quantum Microchemistry.

[21] For the development of the olefin metathesis as a ring forming reaction, see: a) W. J. Zuercher, M. Hashimoto, R. H. Grubbs, *J. Am. Chem. Soc.* **1996**, *118*, 6634–6640; b) P. R. Schwab, H. Grubbs, J. W. Ziller, *ibid.* **1996**, *118*, 100–110; c) R. H. Grubbs, S. J. Miller, G. C. Fu, *Acc. Chem. Res.* **1995**, *28*, 446–452 and references therein; d) J. Tsuji, S. Hashiguchi, *Tetrahedron Lett.* **1980**, *21*, 2955–2959; for some earlier pioneering studies on this reaction, see: e) T. J. Katz, S. J. Lee, N. Acton, *ibid.* **1976**, 4247–4250; f) T. J. Katz, N. Acton, *ibid.* **1976**,

 © WILEY-VCH Verlag GmbH, D-69451 Weinheim, 1997 0570-0833/97/3619-2102 $ 17.50+.50/0

4241–4254; g) T. J. Katz, J. McGinnis, C. Altus, *J. Am. Chem. Soc.* **1976**, *98*, 606–608; h) T. J. Katz, *Adv. in Organomet. Chem.* **1977**, *16*, 283–317.
[22] For a number of applications of the olefin metathesis reaction in medium- and large-ring synthesis, see: a) B. C. Borer, S. Deerenberg, H. Bieräugel, U. K. Pandit, *Tetrahedron Lett.* **1994**, *35*, 3191–3194; b) T. D. Clark, M. R. Ghadiri, *J. Am. Chem. Soc.* **1995**, *117*, 12364–12365; c) A. F. Houri, Z. Xu, D. A. Cogan, A. H. Hoveyda, *ibid.* **1995**, *117*, 2943–2944; d) A. Fürstner, K. Langemann, *J. Org. Chem.* **1996**, *61*, 3942–3943; e) S. F. Martin, H.-J. Chen, A. K. Courtney, Y. Liao, M. Pätzel, M. N. Ramser, A. S. Wagman, *Tetrahedron* **1996**, *52*, 7251–7264; f) Z. Xu, C. W. Johannes, S. S. Salman, A. H. Hoveyda, *J. Am. Chem. Soc.* **1996**, *118*, 10926–10927.
[23] P. Giannakakou, D. L. Sackett, Y.-K. Kang, Z. Zhan, J. T. M. Buters, T. Fojo, M. S. Poruchynsky, *J. Biol. Chem.* **1995**, *272*, 17118–17125.
[24] C. M. Lin, Y. Q. Jiang, A. G. Chaudhary, J. M. Rimoldi, D. G. I. Kingston, E. Hamel, *Cancer Chemother. Pharmacol.* **1996**, *38*, 136–140.
[25] S. Rao, N. E. Krauss, J. M. Heerding, C. S. Swindell, I. Ringel, G. A. Orr, S. B. Horwitz, *J. Biol. Chem.* **1994**, *269*, 3132–3134.
[26] S. Rao, G. A. Orr, A. G. Chaudhary, D. G. I. Kingston, S. B. Horwitz, *J. Biol. Chem.* **1995**, *270*, 20235–20238.
[27] E. Nogales, S. G. Wolf, I. A. Khan, R. F. Luduena, K. H. Downing, *Nature* **1995**, *375*, 424–427.
[28] This work.
[29] E. Hamel, C. M. Lin, *Biochemistry* **1984**, *23*, 4173–4184.
[30] P. Skehan, R. Storeng, D. Scudiero, A. Monks, J. McMahon, D. Vistica, J. T. Warren, H. Bokesh, S. Kenney, M. R. Boyd, *J. Natl. Cancer Inst.* **1990**, *82*, 1107–1112.
[31] B. C. Behrens, T. C. Hamilton, H. Masuda, K. R. Grotzinger, J. Whang-Peng, K. G. Louie, T. Knutsen, W. M. McKoy, R. C. Young, R. F. Ozols, *Cancer Res.* **1987**, *47*, 414–418.
[32] A. Monks, D. Scudiero, P. Skehan, R. Shoemaker, K. Paull, D. Vistica, C. Hose, J. Langley, P. Cronise, A. Vaigro-Wolff, M. Gray-Goodrich, H. Campbell, J. Mayo, M. Boyd, *J. Natl. Cancer Inst.* **1991**, *83*, 757–766.
[33] E. Hamel, P. Giannakakou, D. G. I. Kingston, unpublished results.

5,6,11,12,17,18-Hexadehydro-1,4,7,10,13,16-hexaethynyltribenzo[*a*,*e*,*i*]cyclododecene: Synthesis and CpCo-Catalyzed Cycloisomerization to the First Superdelocalized Oligophenylenes**

Christian Eickmeier, Heiko Junga, Adam J. Matzger, Frank Scherhag, Moonsub Shim, and K. Peter C. Vollhardt*

The title molecule ("hexaethynyltribenzocyclyne") **1a** is of great interest as a subunit of graphyne **2**,[1] a partially carbomeric[2] graphitic carbon allotrope,[3] as an extended π framework for ligating transition metals with unusual properties,[4] and as a precursor to antikekulene **3** by means of threefold CpCo-catalyzed cycloisomerization.[5] Compound **3** constitutes a much theoretically scrutinized[6] member of the as yet unknown circular phenylenes.[7]

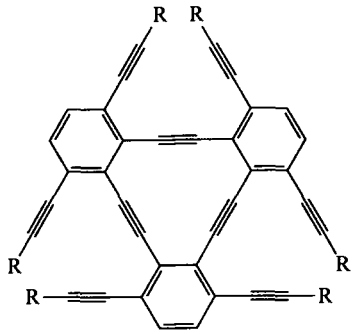

1a, R = H
1b, R = $Si(CH_3)_2[C(CH_3)_2CH(CH_3)_2]$
1c, R = Pr
1d, R = $CH_2C_6H_{11}$

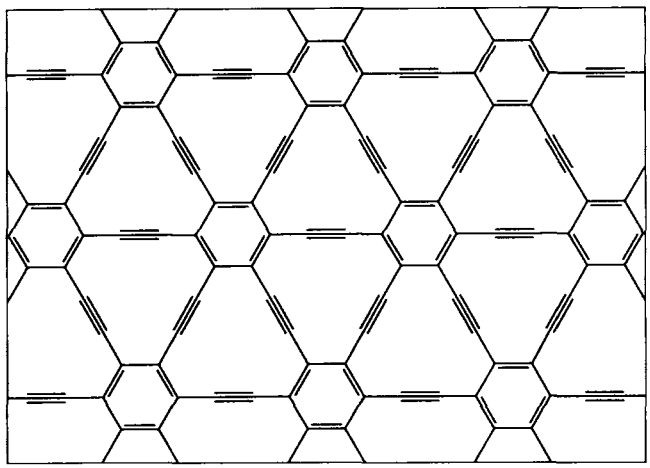

2

Compound **3** is intriguing in its juxtaposition to kekulene **4**,[8] which has the same number of rings but inner and outer π perimeters with a $4n+2$ electron count, whereas in **3**, the corresponding circuits are of the $4n$ type. However, in **4**, the annulenoid resonance forms suffer from the disruption of all benzenoid circuits and appear to be negligible contributors, as borne out by theory[6c, e, f, 9] and experiment.[8] In contrast, the nonannulenoid resonance alternatives to that depicted in **3** are all expected to be considerably destabilized by cyclobutadienoid antiaromaticity, an underlying feature of all phenylenes.[7] Thus, **3** might be a better candidate than **4** for probing the phenomenon of superdelocalization, although the notion of the

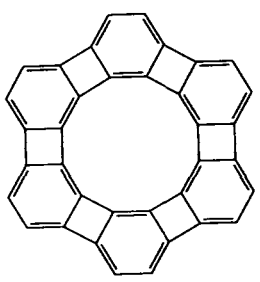

3

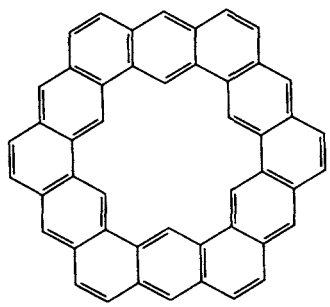

4

[*] Prof. Dr. K. P. C. Vollhardt, Dr. C. Eickmeier, Dr. H. Junga, A. J. Matzger, Dr. F. Scherhag, M. Shim
Department of Chemistry, University of California at Berkeley
and
The Chemical Sciences Division, Lawrence Berkeley National Laboratory
Berkeley, CA 94720 (USA)
Fax: Int. code +(510)643-5208
e-mail: vollhard@cchem.berkeley.edu

[**] This work was supported by the National Science Foundation (CHE-9202152). C. E. and F. S. thank the Deutsche Forschungsgemeinschaft for postdoctoral fellowships. A. J. M. received a predoctoral fellowship from Syntex (1994–1995) and from the ACS Division of Organic Chemistry (1995–1996; sponsored by Rohm and Haas Co). We are indebted to Professors M. M. Haley (University of Oregon) and W. J. Youngs (University of Akron) for preprints of their work and Dr. K. Oertle (Ciba-Geigy AG) for a gift of chlorodimethyl(1,1,2-trimethylpropyl)silane.

 © WILEY-VCH Verlag GmbH, D-69451 Weinheim, 1997 0570-0833/97/3619-2103 $ 17.50+.50/0

latter has been met with skepticism by some theoreticians.[6] We report here the total synthesis of **1a–d** and their reactivity in the presence of $[CpCo(CO)_2]$, which has led to the first superdelocalized oligophenylenes **9a,b** and **10a,b**.

Scheme 1 details the synthetic strategy toward **1**, which has as its cornerstone the discovery that 1,2,3,4-tetrabromobenzene

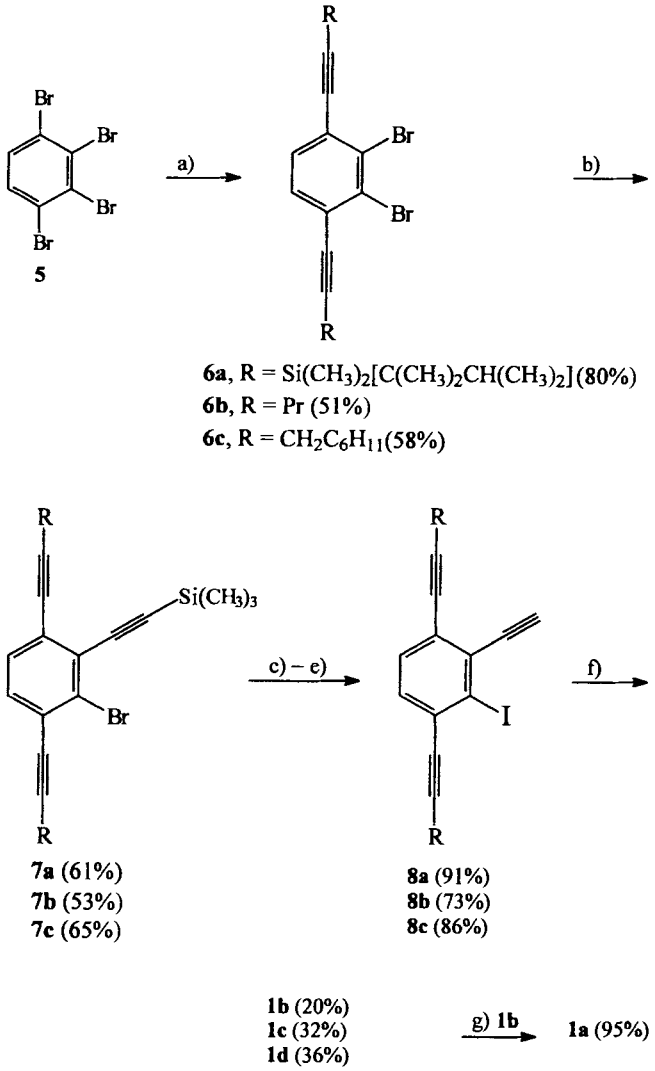

Scheme 1. a) RC≡CH, 1–2% CuI, 1–2% $[PdCl_2(PPh_3)_2]$, Et_3N, 23–60 °C, 3 d; b) $(CH_3)_3SiC_2H$, 1–2% CuI, 1–2% $[PdCl_2(PPh_3)_2]$, Et_3N, 100 °C, 4 h–2.5 d; c) BuLi, $(CH_3CH_2)_2O$, −78 °C, 30 min; d) I_2, $(CH_3CH_2)_2O$, −78 → 23 °C; e) K_2CO_3, CH_3OH or NaOH, CH_3OH or $Bu_4N^+F^-$, THF, 1 h; f) CuCl, NH_4OH, EtOH (DMSO for **8c**), pyridine, Δ, 6 h; g) $Bu_4N^+F^-$, THF, CH_3CN, 5 h.

(**5**)[10] can be regioselectively alkynylated at C1 and C4 to furnish **6**, then at C3 to give **7**, using Pd catalysis.[11] The regiochemistry of **6** was confirmed by debromination to the *p*-dialkynylbenzenes (1. *t*BuLi, 2. H_2O) and further transformations (vide infra). The bromine substituent in **7** is unsuitable for the protocol that constructs the tribenzocyclyne frame of **1**[12] and therefore was replaced by iodine. The C2-ethynyl group was selectively deprotected and cyclization of **8a–c** yielded **1b–d**.

The parent nonayne **1a** was readily accessible by desilylation of **1b**. It is relatively stable even in the solid state, and it can be conveniently handled in solution, which bodes well for its continuing elaboration into larger networks. Models show that the R groups in **1** are severely congested and indeed the X-ray structural analysis of **1d** (Figure 1)[13] reveals a severely distorted cyclyne frame with local C_2 symmetry, dihedral angles between the mean planes of the three benzene rings of 25.4, 30.8, and 31.4°, and deviations from linearity of the triple bonds within (average 174.3°, range 169.6–178.1°) and without (average 175.5°, range 171.7–179.9°) the cyclyne ring. All cyclohexyl groups adopt chair conformations. Apart from these features, the molecular structure is remarkably similar to that of the unsubstituted core system.[14b] The most noteworthy aspect of the spectral data of **1** (Table 1) is the much lower intensity of the longest wavelength UV band (π–π* transition) observed for the parent tribenzocyclyne at 290 nm ($\lg\varepsilon = 5.57$), which was associated with the rigid planarity of the latter,[14] a characteristic that is absent in **1**.

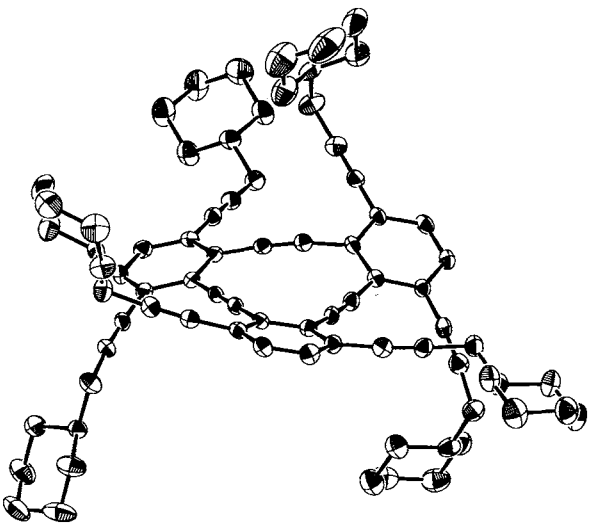

Figure 1. Molecular structure of **1d** in the crystal.

With **1a** in hand, our first concern was its potential to isomerize to **3** in the presence of $[CpCo(CO)_2]$. Calculations were encouraging in this respect, suggesting each of the three individual [2+2+2]cycloadditions to be exothermic (−14.5, −13.4, and −10.0 kcal mol^{-1} (PM3);[15a] for the last step: −31.0 kcal mol^{-1} (HF/6-31G*),[15b] −45.50 kcal mol^{-1} (B3LYP/6-31G*);[15b] comparable to the values calculated for the cyclization to angular [3]phenylene). Unfortunately, in practice, **1a** gave only insoluble dark brown powders. Suspecting lack of solubility of the target (or intermediates en route) as a potential problem in these experiments, we turned to the substituted nonaynes **1b–d**, with better, albeit not complete, success. Thus, while **1b** gave intractable mixtures, **1c** and **1d** provided **9a,b** and **10a,b**, respectively, either directly as mixtures or by a stepwise sequence (Scheme 2, Table 1).[11] The isolation of **9a,b** was possible because they cyclize noticeably slower than **1c,d**. This trend continues for **10a,b** which, despite extensive experimentation with conditions (solvent, temperature, addition rates, light sources), could not be induced to furnish the antikekulene core, but rather gave either recovered starting material or decomposition (>170 °C, sulfolane or 1-methylnaphthalene).

Because of the novelty of the "circularly" conjugated phenylenes **9** and **10**, X-ray structural determinations of **9b** and **10b** were carried out (Figures 2 and 3, respectively).[13] Similar to **1d** (Figure 1), the twelve-membered ring in **9b** is significantly (although less) distorted from planarity; the plane of the nonphenylene benzene forms an angle of 18.4° with the mean plane of the dehydro[12]annulene cycle. Unlike the parent angular

 © WILEY-VCH Verlag GmbH, D-69451 Weinheim, 1997 0570-0833/97/3619-2104 $ 17.50+.50/0

Table 1. Selected physical data for **1a**, **1b**, **1d**, **9b**, **10a,b**, and **11** [11].

1a: yellow solid ($CHCl_3$), m.p. > 100 °C (decomp); MS (70 eV): *m/z* (%): 444 (M^+, 10), 149 (100); ^{1}H NMR (400 MHz, $CDCl_3$): δ = 7.33 (s, 6H), 3.32 (s, 6H); $^{13}C\{^1H\}$ NMR (100 MHz, [D$_{10}$]1,2-dimethoxyethane): δ = 133.4, 128.9, 126.0, 106.5, 99.2, 94.9; IR (KBr): $\tilde{\nu}$ = 3292, 2957, 2924, 2854, 2108, 1461, 830, 660, 621 cm^{-1}; UV/Vis (isooctane): λ_{max} (lgε) = 222 (3.20), 243 (3.31), 261 (3.34), 288 (3.30), 306 (3.37), 316 (3.29), 329 (3.66) nm

1b: yellow crystals (*i*PrOH), m.p. 197–198 °C; MS (70 eV): *m/z* (%): 1298 (M^+, 20), 1213 (22), 1129 (100), 1044 (50); ^{1}H NMR (400 MHz, $CDCl_3$): δ = 7.31 (s, 6H), 1.73 (sept, *J* = 6.9 Hz, 6H), 0.93 (s, 36H), 0.90 (d, *J* = 6.9 Hz, 36H), 0.28 (s, 36H); $^{13}C\{^1H\}$ NMR (100 MHz, $CDCl_3$): δ = 132.2, 129.4, 126.2, 104.0, 102.3, 96.8, 34.5, 23.8, 20.8, 18.7, −2.40; IR (KBr): $\tilde{\nu}$ = 2958, 2866, 2153, 1462, 1250, 838, 822, 776, 674 cm^{-1}; UV/Vis (isooctane): λ_{max} (lgε) = 253 (4.71), 285 (4.93), 308 (4.97), 340 (4.81), 385 sh (3.8) nm. High-resolution FAB-MS calcd for $C_{84}H_{121}Si_6$: 1297.8084; found: 1297.8075

1d: yellow crystals (*i*PrOH/CH_2Cl_2), m.p. 144–145 °C; FAB-MS: *m/z* (%) : 1021 (M^+,100); ^{1}H NMR (400 MHz, $CDCl_3$): δ = 7.18 (s, 6H), 2.31 (d, *J* = 6.8 Hz, 12H), 1.91–1.79 (m, 12H), 1.72—1.52 (m, 24H), 1.28–0.93 (m, 30H); $^{13}C\{^1H\}$ NMR and DEPT 135 (100 MHz, $CDCl_3$): δ = 132.0 (CH), 129.0, 126.2, 96.0, 95.8, 80.1, 37.6 (CH), 32.9 (CH_2), 28.0 (CH_2), 26.3 (CH_2), 26.1 (CH_2); IR (KBr): $\tilde{\nu}$ = 2923, 2851, 2226, 1465, 1448, 1118, 827 cm^{-1}; UV/Vis (isooctane): λ_{max} (lgε) = 232 (4.73), 243 sh (4.77), 248 (4.83), 275 (4.97), 301 (4.90), 313 (4.89), 319 sh (4.82), 336 (5.02), 382 (3.87), 402 (3.84) nm. High-resolution MS calcd for $C_{78}H_{84}$: 1020.6573; found: 1020.6564

9b: orange crystals (*i*PrOH/CH_2Cl_2), m.p. 210–211 °C; FAB-MS: *m/z* (%): 1021 (M^+, 100); ^{1}H NMR (500 MHz, CD_2Cl_2): δ = 7.16 (s, 2H), 7.00 (d, *J* = 7.4 Hz, 2H), 6.61 (d, *J* = 7.3 Hz, 2H), 2.34 (d, *J* = 6.9 Hz, 4H), 2.30 (d, *J* 6.9 Hz, 4H), 2.15 (d, *J* = 7.0 Hz, 4H), 1.91–1.82 (m, 8H), 1.81–1.48 (m, 24H), 1.48–1.38 (m, 2H), 1.33–0.86 (m, 32H); $^{13}C\{^1H\}$ NMR and DEPT 135 (100 MHz, CD_2Cl_2): δ = 151.5, 150.2, 146.6, 134.5 (CH), 133.6, 132.8 (CH), 131.6, 128.8, 126.6, 125.1, 118.0 (CH), 116.4, 96.7, 94.3, 94.0, 93.4, 81.2, 80.4, 39.4, (CH), 38.2 (CH), 38.1 (CH), 37.2 (CH_2), 34.0 (CH_2), 33.3 (CH_2, 2C), 28.3 (CH_2), 26.9 (CH_2), 26.8 (CH_2), 26.73 (CH_2), 26.71 (CH_2), 26.59 (CH_2, 2C); IR (KBr): $\tilde{\nu}$ = 2923, 2850, 2224, 1448, 1068, 824 cm^{-1}; UV/Vis (THF): λ_{max} (lgε) = 250 (4.94), 261 (4.81), 269 (4.81), 306 (5.05), 327 (4.67), 335 sh (4.59), 372 (4.18), 389 (4.34), 399 sh (4.23), 415 (4.08), 444 (3.94), 484 (3.78), 516 (3.11) nm. High-resolution MS calcd for $C_{78}H_{84}$: 1020.6573; found: 1020.6584

10a: red solid (CH_2Cl_2), m.p. > 250 °C (decomp); MS (70 eV): *m/z* (%): 696 (M^+, 100), 207 (6), 97 (6), 83 (8), 69 (13), 57 (22); ^{1}H NMR (400 MHz, CD_2Cl_2): δ = 6.93 (d, *J* = 7.2 Hz, 2H), 6.54 (d, *J* = 7.2 Hz, 2H), 6.30 (s, 2H), 2.39 (t, *J* = 7.8 Hz, 4H), 2.33–2.25 (m, 8H), 1.68–1.46 (m, 12H), 1.02 (t, *J* = 7.8 Hz, 6H), 0.97 (br t, *J* = 7.8 Hz, 12H); $^{13}C\{^1H\}$ NMR (100 MHz, CS_2): δ = 151.6, 150.4, 149.3, 148.5, 146.0, 135.0, 134.4, 134.3, 133.0, 132.8, 132.0, 125.4, 117.8, 116.8, 116.7, 94.8, 91.9, 81.1, 31.7, 31.6, 30.4, 23.52, 23.49, 23.2, 22.7, 14.8, 14.3; IR (KBr): $\tilde{\nu}$ = 2959, 2928, 2226, 1457, 1384, 818 cm^{-1}; UV/Vis (CH_2Cl_2): λ_{max} = 263, 294, 326, 343, 379, 480, 554 nm. High-resolution MS calcd for $C_{54}H_{48}$: 696.3756; found: 696.3760

10b: dark red crystals (CCl_4), m.p. 290–295 °C; MS (70 eV): *m/z* (%): 1021 (M^+, 7), 285 (7), 263 (24), 207 (47), 169 (56), 146 (62), 103 (72), 69 (100); ^{1}H NMR (500 MHz, CD_2Cl_2): δ = 6.93 (d, *J* = 7.4 Hz, 2H), 6.54 (d, *J* = 7.3 Hz, 2H), 6.30 (s, 2H), 2.40–0.70 (m, 78H); ^{1}H NMR (500 MHz, C_6D_6): δ = 7.03 (d, *J* = 7.3 Hz, 2H), 6.27 (s, 2H), 6.25 (d, *J* = 7.3 Hz, 2H), 2.44 (d, *J* = 6.8 Hz, 4H), 2.20 (d, *J* = 6.9 Hz, 4H), 2.11 (d, *J* = 6.8 Hz, 4H), 1.94 (dm, *J* = 11.6 Hz, 4H), 1.87 (dm, *J* = 11.3 Hz, 4H), 1.80 (dm, *J* = 12.5 Hz, 4H), 1.75–0.85 (m, 54H); IR (KBr): $\tilde{\nu}$ = 2922, 2850, 2222, 1449, 1262, 1176, 1096, 1032, 818 cm^{-1}; UV/Vis (CH_2Cl_2): λ_{max} (lgε) = 255 sh (4.96), 264 (5.03), 295 (4.93), 326 (4.61), 342 (4.54), 380 (4.46), 399 sh (4.12), 432 (3.82), 456 (3.74), 484 (3.68), 520 (3.00), 554 (3.13) nm

11: red crystals (CH_2Cl_2), m.p. 230–232 °C; MS (70 eV): *m/z* (%): 458 (M^+, 100), 398 (13), 229 (10), 200 (9); ^{1}H NMR (400 MHz, CD_2Cl_2): δ = 6.97 (m, 4H), 6.90 (m, 2H), 6.83 (m, 2H), 6.47 (s, 2H), 6.17 (s, 2H), 2.36 (t, *J* = 7.3 Hz, 4H), 1.62 (sex, *J* = 7.4 Hz, 4H), 0.98 (t, *J* = 7.4 Hz, 6H); $^{13}C\{^1H\}$ NMR (100 MHz, CD_2Cl_2): δ = 151.8, 149.9, 149.5, 148.9, 143.4, 137.8, 136.4, 132.9, 131.5, 129.5, 128.2, 119.1, 118.6, 117.7, 116.2, 34.9, 23.0, 14.0; IR (KBr): $\tilde{\nu}$ = 2959, 2925, 2854, 1262, 1098, 1023, 802, 737 cm^{-1}; UV/Vis (CH_2Cl_2): λ_{max} (lgε) = 262 (4.82), 273 (4.86), 330 (4.69), 352 (4.71), 4.02 (3.81), 4.30 (3.93), 454 (3.93) nm

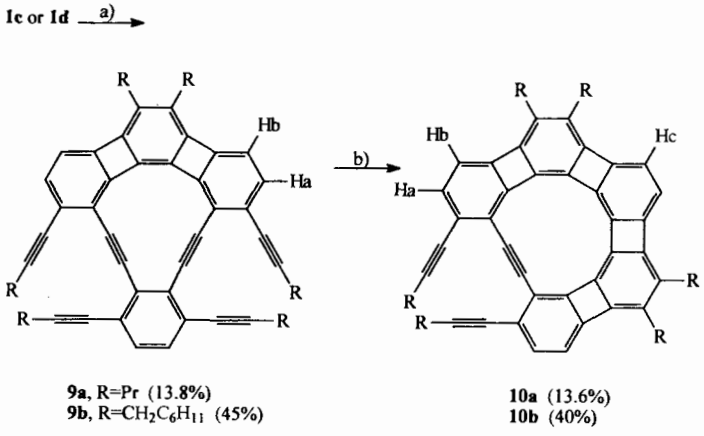

Scheme 2. a) [CpCo(CO)$_2$] (0.3–1 equiv), *m*-xylene, △, *hv*, 20 min; b) as in a) but with 1,2,4-trichlorobenzene as solvent, 160 °C, 3 h.

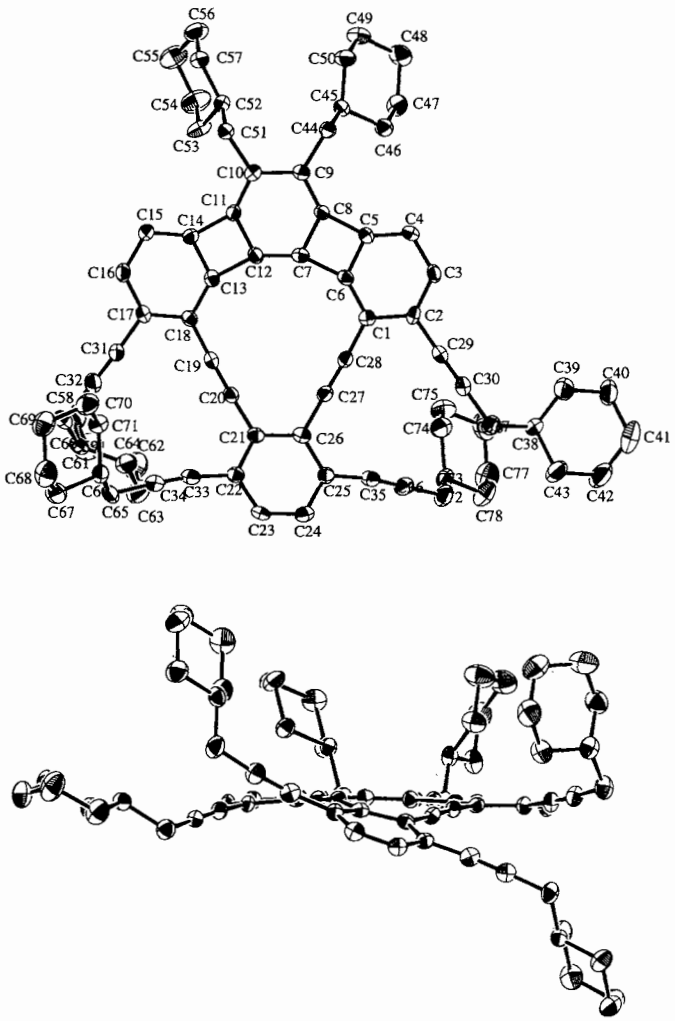

Figure 2. Structure of **9b** in the crystal: views from above (top) and the side (bottom). Selected distances [Å] and angles [°], averaged for idealized symmetry: C1–C2 1.430(4), C2–C3 1.400(4), C3–C4 1.400(4), C4–C5 1.371(4), C5–C6 1.418(4), C6–C1 1.381(4), C6–C7 1.499(4), C7–C8 1.459(4), C8–C5 1.505(4), C8–C9 1.357(4), C9–C10 1.465(4), C7–C12 1.353(4), C1–C28 1.429(4), C21–C22 1.410(4), C22–C23 1.399(4), C23–C24 1.375(4), C24–C25 1.399(4), C25–C26 1.410(4), C26–C27 1.432(4), C27–C28 1.204(4); C1-C2-C3 121.0(3), C2-C3-C4 122.9(3), C3-C4-C5 116.2(3), C4-C5-C6 121.1(3), C5-C6-C1 123.5(3), C5-C6-C7 90.5(3), C6-C7-C8 89.8(2), C7-C8-C5 88.7(2), C8-C5-C6 91.1(2), C7-C8-C9 126.7(3), C8-C9-C10 116.5(3), C12-C7-C8 116.9(3).

[3]phenylene,[5] the phenylene subunit in **9b** is slightly curved (dihedral angles between the mean planes of adjacent benzene and cyclobutadiene rings between 0.44 and 3.14°), a phenomenon that appears to be general.[16] In other respects, the structure of this unit, especially the pronounced bond alternation of its central benzene ring, is remarkably similar to that of the parent system; small deviations are due to the presence of the additional substituents, especially the alkyne groups which generally cause slight elongations in attached benzene ring

 © WILEY-VCH Verlag GmbH, D-69451 Weinheim, 1997 0570-0833/97/3619-2105 $ 17.50+.50/0

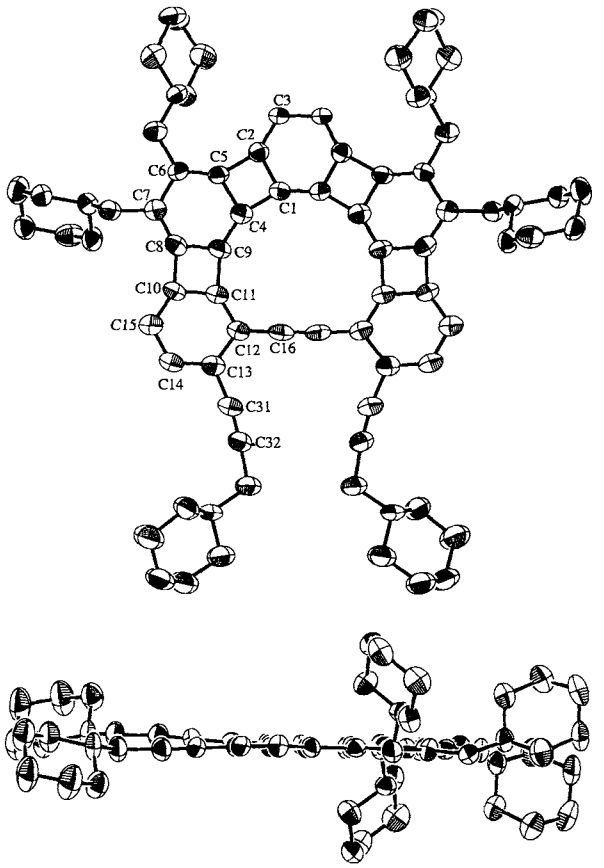

Figure 3. Structure of **10b** in the crystal: views from above (top) and the side (bottom). Selected distances [Å] and angles [°]: C1–C1′ 1.34(1), C1–C2 1.449(8), C2–C3 1.367(8), C3–C3′ 1.41(1), C1–C4 1.479(8), C4–C5 1.473(8), C2–C5 1.527(8), C5–C6 1.351(8), C6–C7 1.472(8), C7–C8 1.352(9), C8–C9 1.461(9), C9–C4 1.351(8), C8–C10 1.507(8), C10–C11 1.433(9), C9–C11 1.496(8), C11–C12 1.387(8), C12–C13 1.440(8), C13–C14 1.398(9), C14–C15 1.399(9), C10–C15 1.357(8), C12–C16 1.423(8), C16–C16′ 1.21(1), C13–C31 1.446(9), C31–C32 1.190(8); C1′-C1-C2 118.9(4), C1-C2-C3 122.1(6), C2-C3-C3′ 119.0(4), C1-C2-C5 89.8(5), C2-C5-C4 88.3(5), C1-C4-C5 90.9(5), C2-C1-C4 91.0(5), C4-C5-C6 125.2(6), C5-C6-C7 116.9(6), C6-C7-C8 117.1(7), C7-C8-C9 125.9(6), C4-C8-C9 117.1(6), C5-C4-C9 117.8(6), C8-C9-C11 90.9(6), C9-C11-C10 89.5(5), C8-C10-C11 91.5(5), C9-C8-C10 88.1(6), C10-C11-C12 124.8(6), C11-C12-C13 112.8(7), C12-C13-C14 121.9(7), C13-C14-C15 123.0(7), C10-C15-C14 116.5(7), C11-C12-C16 123.3(6), C12-C16-C16′ 177.5(5).

bonds.[1c, 3e, 14b] While the overall rigidity of the carbon frame increases noticeably when going from **1d** to **9b**, this effect is much more pronounced when continuing from **9b** to **10b** (Figure 3). The latter lies on a C_2 axis and exhibits a slightly helical angular [5]phenylene frame (dihedral angles between the mean planes of adjacent rings between 0.53 and 2.31°). The distances between the three alkyne units that would be called on in cyclotrimerization increase along the series **1**, **9**, **10**. That, along with the increasing rigidity of the structures, provides a rationale for their decreasing reactivity in the presence of [CpCo].

Because the parent angular [5]phenylene[17] could not be obtained in the form of crystals suitable for X-ray analysis and hence comparison with **10b**, the appropriately crystalline dipropyl derivative **11** (Table 1)[11] was prepared by a new, much shorter route (five steps) starting from **6a** (Scheme 3) in a variation of Scheme 1. The crystal structure of **11** is shown in Figure 4. The molecule is more pronouncedly helical than **10b** (dihedral angles between adjacent ring planes between 0.94 and 4.91°), and there is no significant contact between 5-H and 26-H (distance 2.59 Å, assuming a C–H bond length of 1.08 Å). Otherwise, the two structures are quite similar; minor deviations can be ascribed to the presence of the adjacent cyclohexylmethyl substituents and the added alkyne functions (vide supra) in **10b**. As indicated by the ^{1}H NMR data (Table 1),[17] the internal benzene rings have significant cyclohexatriene character. The bridging triple bond (C16–C16′) flattens **10b** relative to **11** and decreases the distance between the terminal benzene rings some-

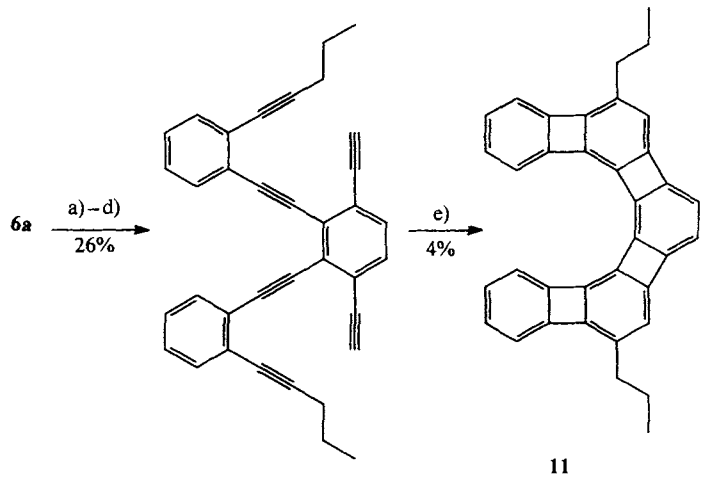

Scheme 3. a) $(CH_3)_3SiC_2H$ (excess), 15% CuI, 15% $[PdCl_2(PPh_3)_2]$, piperidine, 110 °C, 7 d; b) K_2CO_3, CH_3OH, THF, 1 h; c) 1-iodo-2-(1-pentynyl)benzene (4 equiv), 10% CuI, 10% $[PdCl_2(PPh_3)_2]$, Et_3N, 100 °C, 7 d; d) $Bu_4N^+F^-$, THF, 1 h; e) $[CpCo(CO)_2]$ (2 equiv), xylenes, △, *hv*, 1 h.

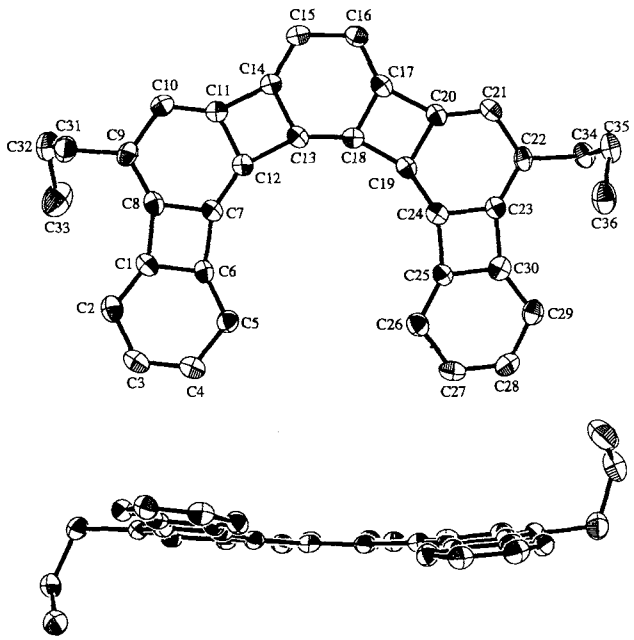

Figure 4. Structure of **11** in the crystal: views from above (top) and the side (bottom). Selected distances [Å] and angles [°], averaged for idealized symmetry: C1–C2 1.371(3), C2–C3 1.405(3), C3–C4 1.378(3), C4–C5 1.407(3), C5–C6 1.362(3), C1–C6 1.415(2), C6–C7 1.504(2), C7–C8 1.448(2), C1–C8 1.508(2), C8–C9 1.364(3), C9–C10 1.443(3), C10–C11 1.354(3), C11–C12 1.449(2), C7–C12 1.352(3), C12–C13 1.496(2), C13–C14 1.443(2), C11–C14 1.506(2), C14–C15 1.366(3), C15–C16 1.423(3), C13–C18 1.352(3); C1-C2-C3 116.1(3), C2-C3-C4 121.9(3), C3-C4-C5 122.0(3), C4-C5-C6 115.8(3), C1-C6-C5 122.7(3), C2-C1-C6 121.5(3), C1-C6-C7 90.2(2), C6-C7-C8 90.0(2), C1-C8-C7 88.8(2), C6-C1-C8 91.1(2), C7-C8-C9 125.8(3), C8-C9-C10 115.9(3), C9-C10-C11 118.8(3), C10-C11-C12 124.5(3), C7-C12-C11 117.7(3), C8-C7-C12 117.4(3), C11-C12-C13 90.3(2), C12-C13-C14 90.1(2), C11-C14-C13 90.2(2), C12-C11-C14 89.5(2), C13-C14-C15 124.0(3), C14-C15-C16 118.0(3), C18-C13-C14 118.0(3).

 © WILEY-VCH Verlag GmbH, D-69451 Weinheim, 1997 0570-0833/97/3619-2106 $ 17.50+.50/0

what (e.g. C5–C26 in **11**: 4.69 Å; calculated for its planar conformer: 4.55 Å; C12–C12′ in **10b**: 4.06 Å). This change does not appear to greatly alter bond angles and lengths.[18] Thus, as perhaps expected, the X-ray data for **9b** and **10b** do not reveal any structural evidence for superdelocalization imparted by the bridging alkyne units.

Much more sensitive probes for such a phenomenon are UV and, especially, ^{1}H NMR measurements. Indeed, the longest wavelength maxima in the electronic spectra of **9a,b** (λ_{max} = 514 and 516 nm, respectively) and **10a,b** (554 nm) are drastically bathochromically shifted relative to those of angular [3]- (394 nm)[19] and [5]phenylene (470 nm),[17] considerably more than expected by simple substituent contributions,[7, 20] and consistent with increased antiaromaticity[21] due to superdelocalization. The latter would be expected to increase the cyclobutadienoid character of the four-membered rings, causing increased shielding of close-lying benzenoid hydrogens. Indeed, H_b in **9a,b** is shielded ($\Delta\delta$ = 0.28; all measurements in CD_2Cl_2), relative to the corresponding nuclei in angular [3]phenylene.[17] More convincingly, in **10a,b**, not only is H_b shielded ($\Delta\delta$ = 0.33) relative to the parent angular [5]phenylene (and **11**), but also the remote H_c ($\Delta\delta$ = 0.21). While H_a in **9** and **10**, respectively, appear unchanged in these comparisons, we believe that they experience the same shielding effect as H_b and H_c, since the added *ortho*-alkynyl substitution causes deshielding by $\Delta\delta \approx 0.2$ (and negligible *meta* and *para* effects).[7, 22] The operation of aromatic π-stacking effects[23] on the observed chemical shifts was ruled out by measurements at varying concentrations (5–170 mM). Moreover, the slight increase in σ-strain introduced by the alkyne bridge is unlikely to be the cause of these shieldings, since the δ(H) values of highly strained biphenylene derivatives are normal.[24]

We conclude that superdelocalization effects are operational in annelated oligophenylenes[25] of the type **9** and **10** and anticipate that they will be accentuated in **3**. The successful execution of the final cyclization step from **10** may have to rely on derivatives in which the [5]phenylene grid is rendered more flexible by chemical alteration.

Experimental Section

Cycloisomerization of **1d**: To degassed, boiling *m*-xylene (100 mL) was added within 10 s a degassed solution of **1d** (110 mg, 1.08 mmol) and $[CpCo(CO)_2]$ (41 μL, 0.324 mmol) in *m*-xylene (20 mL). The reaction mixture was irradiated with a 300 W projector lamp (60 V). After 20 min, the solvent was evaporated, and the crude product was dissolved in CH_2Cl_2, absorbed on silica gel, and chromatographed on silica gel (35 × 3 cm, 18–32 μm) eluting with hexanes/CH_2Cl_2 (20:1–10:1) to provide **9b** as an orange solid (49 mg, 45%), followed by **10b** as a red solid (5 mg, 5%).

Cycloisomerization of **9b**: A solution of compound **9b** (20 mg, 0.02 mmol) in degassed, boiling 1,2,4-trichlorobenzene (100 mL) was irradiated with a 300 W projector lamp (60 V) while a solution of $[CpCo(CO)_2]$ (7 μL, 0.055 mmol) in 1,2,4-trichlorobenzene (12 mL) was added with a syringe pump over 3 h. The solvent was evaporated and the crude product was chromatographed on a silica gel preparative TLC plate (1 mm), eluting with hexanes/CH_2Cl_2 (4:1) to provide **10b** (8.1 mg, 40%).

Received: April 14, 1997 [Z 10348 IE]
German version: *Angew. Chem.* **1997**, *109*, 2194–2199

Keywords: aromaticity · carbon allotropes · cyclotrimerizations · phenylenes · superdelocalization

[1] a) R. H. Baughman, H. Eckhardt, M. Kertesz, *J. Chem. Phys.* **1987**, *87*, 6687; b) R. H. Baughman, D. S. Galvão, C. Cui, Y. Wang, D. Tománek, *Chem. Phys. Lett.* **1993**, *204*, 8; graphdiyne: c) M. M. Haley, S. C. Brand, J. J. Pak, *Angew. Chem.* **1997**, *109*, 864; *Angew. Chem. Int. Ed. Engl.* **1997**, *36*, 836.

[2] R. Chauvin, *Tetrahedron Lett.* **1995**, *36*, 397.

[3] a) F. Diederich, Y. Rubin, *Angew. Chem.* **1992**, *104*, 1123; *Angew. Chem. Int. Ed. Engl.* **1992**, *31*, 1101; b) F. Diederich, *Nature (London)* **1994**, *369*, 199; c) F. Diederich in *Modern Acetylene Chemistry* (Eds.: P. J. Stang, F. Diederich), VCH, Weinheim, **1995**, p. 443; d) U. H. F. Bunz, *Angew. Chem.* **1994**, *106*, 1127; *Angew. Chem. Int. Ed. Engl.* **1994**, *33*, 1073; e) R. Boese, A. J. Matzger, K. P. C. Vollhardt, *J. Am. Chem. Soc.* **1997**, *119*, 2052.

[4] See, inter alia: a) D. Zhang, D. B. McConville, C. A. Tessier, W. J. Youngs, *Organometallics* **1997**, *16*, 824; b) J. D. Bradshaw, L. Guo, C. A. Tessier, W. J. Youngs, *ibid.* **1996**, *15*, 2582; c) L. Guo, J. D. Bradshaw, C. A. Tessier, W. J. Youngs, *ibid.* **1995**, *14*, 586; d) D. Solooki, J. D. Bradshaw, C. A. Tessier, W. J. Youngs, *ibid.* **1994**, *13*, 451, and references therein.

[5] R. Diercks, K. P. C. Vollhardt, *Angew. Chem.* **1986**, *98*, 268; *Angew. Chem. Int. Ed. Engl.* **1986**, *25*, 266.

[6] a) J. M. Schulman, R. L. Disch, *J. Am. Chem. Soc.* **1996**, *118*, 8470; b) I. Gutman, *Rev. Roum. Chim.* **1994**, *39*, 943; c) J. Aihara, *Bull. Chem. Soc. Jpn.* **1993**, *66*, 57; d) I. Gutman, S. J. Cyvin, *J. Mol. Struct.* **1993**, *288*, 85; e) D. Plavšić, S. Nikolić, N. Trinajstić, *ibid.* **1992**, *277*, 213; f) N. Trinajstić, T. G. Schmalz, T. P. Živković, S. Nikolić, G. E. Hite, D. J. Klein, W. A. Seitz, *New J. Chem.* **1991**, *15*, 27.

[7] a) D. L. Mohler, K. P. C. Vollhardt in *Advances in Strain in Organic Chemistry, Vol. 5* (Ed.: B. Halton), JAI, London, **1996**, p. 121; b) K. P. C. Vollhardt, *Pure Appl. Chem.* **1993**, *65*, 153.

[8] a) H. A. Staab, F. Diederich, *Chem. Ber.* **1983**, *116*, 3487; b) H. A. Staab, F. Diederich, C. Krieger, D. Schweitzer, *ibid.* **1983**, *116*, 3504.

[9] See: H. Jiao, P. von R. Schleyer, *Angew. Chem.* **1996**, *108*, 2548; *Angew. Chem. Int. Ed. Engl.* **1996**, *35*, 2383, and references therein.

[10] I. Collins, H. Suschitzky, *J. Chem. Soc. C* **1969**, 2337.

[11] All new compounds gave satisfactory analytical and/or spectroscopic data (see Table 1).

[12] J. D. Kinder, C. A. Tessier, W. J. Youngs, *Synlett* **1993**, 149.

[13] X-ray structural analyses: **1d**: Crystal size 0.30 × 0.15 × 0.10 mm^3, space group $P\bar{1}$ (no. 2), scan range $3 \le 2\theta \le 52°$, a = 13.8004(8), b = 15.0002(8), c = 15.9651(9) Å, α = 74.522(1), β = 75.560(1), γ = 89.755(1)°, V = 3077.56(50) Å^3, Z = 2, ρ_{calcd} = 1.102 g cm^{-3}, μ = 0.62 cm^{-1}. 10 140 unique reflections at −90 °C, of which 6060 were taken as observed [$F_o \ge 4\sigma(F)$], R = 0.060, R_w = 0.074. **9b**: Crystal size 0.22 × 0.13 × 0.11 mm^3, space group $P\bar{1}$ (no. 2), scan range $3 \le 2\theta \le 45°$, a = 13.8868(3), b = 14.1342(3), c = 17.3725(1) Å, α = 76.678(1), β = 67.149(1), γ = 75.552(1)°, V = 3008.59(11) Å^3, Z = 2, ρ_{calcd} = 1.128 g cm^{-3}, μ = 0.63 cm^{-1}, 8326 unique reflections at −90 °C, of which 5570 were taken as observed [$F_o \ge 3\sigma(F)$], R = 0.058, R_w = 0.064. **10b**: Crystal size 0.20 × 0.20 × 0.12 mm^3, space group $C2/c$ (no. 15), scan range $3 \le 2\theta \le 45°$, a = 20.393(1), b = 27.399(1), c = 10.7872(5) Å, β = 109.760(1)°, V = 5672.38(77) Å^3, Z = 4, ρ_{calcd} = 1.196 g cm^{-3}, μ = 0.67 cm^{-1}, 4160 unique reflections at −151 °C, of which 1905 were taken as observed [$F_o \ge 2\sigma(F)$], R = 0.080, R_w = 0.076. **11**: Crystal size 0.44 × 0.18 × 0.04 mm^3, space group $P2_1/n$ (no. 14), scan range $3 \le 2\theta \le 45°$, a = 17.8936(4), b = 5.0829(1), c = 27.4744(8) Å, β = 104.106(1)°, V = 2423.49 (9) Å^3, Z = 4, ρ_{calcd} = 1.257 g cm^{-3}, μ = 0.71 cm^{-1}, 3889 unique reflections at −102 °C, of which 1980 were taken as observed [$F_o \ge 3\sigma(F)$], R = 0.040, R_w = 0.044. Crystallographic data (excluding structure factors) for the structures reported in this paper have been deposited with the Cambridge Crystallographic Data Centre as supplementary publication no. CCDC-100238. Copies of the data can be obtained free of charge on application to The Director, CCDC, 12 Union Road, Cambridge CB2 1EZ, UK (fax: Int. code +(1223)336-033; e-mail: deposit@chemcrys.cam.ac.uk).

[14] a) H. A. Staab, F. Graf, *Chem. Ber.* **1970**, *103*, 1107; b) H. Irngartinger, L. Leiserowitz, G. M. J. Schmidt, *ibid.* **1970**, *103*, 1119; c) I. D. Campbell, G. Eglinton, W. Henderson, R. A. Raphael, *J. Chem. Soc. Chem. Commun.* **1966**, 87.

[15] a) Using the program MOPAC, Version 6.11; b) Calculations performed with Gaussian 94, Revision B.1, M. J. Frisch, G. W. Trucks, H. B. Schlegel, P. M. W. Gill, B. G. Johnson, M. A. Robb, J. R. Cheeseman, T. Keith, G. A. Peterson, J. A. Montgomery, K. Raghavachari, M. A. Al-Laham, V. G. Zakrzewski, J. V. Ortiz, J. B. Foresman, J. Cioslowski, B. B. Stefanov, A. Nanayakkara, M. Challacombe, C. Y. Peng, P. Y. Ayala, W. Chen, M. W. Wong, J. L. Andres, E. S. Replogle, R. Gomperts, R. L. Martin, D. J. Fox, J. S. Binkley, D. J. Defrees, J. Baker, J. P. Stewart, M. Head-Gordon, C. Gonzalez, J. A. Pople, Gaussian, Inc., Pittsburgh, PA, **1995**.

[16] R. Boese, A. J. Matzger, D. L. Mohler, K. P. C. Vollhardt, *Angew. Chem.* **1995**, *107*, 1630; *Angew. Chem. Int. Ed. Engl.* **1995**, *34*, 1478.

[17] R. H. Schmidt-Radde, K. P. C. Vollhardt, *J. Am. Chem. Soc.* **1992**, *114*, 9713. In this paper the assignments for H1–H4 in Table II were inadvertently inverted (see ref. [7]).

[18] All phenylene topologies synthesized in our laboratory have been scrutinized by theory at the HF/6-31G* and B3-LYP/6-31G* level: A. J. Matzger, K. P. C. Vollhardt, first reported at the 6th Annual Symposium on Frontiers in Chemistry, Scripps Research Institute, La Jolla, CA, **1995**. See also: Z. B. Maksić, D. Kovaček, M. Eckert-Maksić, M. Böckmann, M. Klessinger, *J. Phys. Chem.* **1995**, *99*, 6410; ref. [6a].

[19] J. W. Barton, R. B. Walker, *Tetrahedron Lett.* **1978**, 1005.

 © WILEY-VCH Verlag GmbH, D-69451 Weinheim, 1997 0570-0833/97/3619-2107 $ 17.50+.50/0

[20] See, inter alia: a) R. Diercks, J. C. Armstrong, R. Boese, K. P. C. Vollhardt, *Angew. Chem.* **1986**, *98*, 270; *Angew. Chem. Int. Ed. Engl.* **1986**, *25*, 268; b) C. F. Wilcox, Jr., K. A. Weber, *J. Org. Chem.* **1986**, *51*, 1088.
[21] See, inter alia: J. Anthony, C. B. Knobler, F. Diederich, *Angew. Chem.* **1993**, *105*, 437; *Angew. Chem. Int. Ed. Engl.* **1993**, *32*, 406.
[22] H. Vogler, *J. Am. Chem. Soc.* **1978**, *100*, 7464.
[23] See, inter alia: a) A. S. Shetty, J. Zhang, J. S. Moore, *J. Am. Chem. Soc.* **1996**, *118*, 1019; b) C. Nuckols, T. J. Katz, L. Castellanos, *ibid.* **1996**, *118*, 3767.
[24] a) F. Vögtle, J. E. Schulz, K. Rissanen, *Chem. Commun.* **1992**, 120; b) K. Saitmacher, J. E. Schulz, M. Nieger, F. Vögtle, *ibid.* **1992**, 175; c) C. F. Wilcox, Jr., K. R. Lassila, G. Van Duyne, H. Lu, J. Clardy, *J. Org. Chem.* **1989**, *54*, 2190.
[25] For the effects of conjugative 1,8-annelation on biphenylene, see: a) A. Rajca, A. Safronov, S. Rajca, C. R. Ross, II, J. J. Stezowski, *J. Am. Chem. Soc.* **1996**, *118*, 7272; b) C. F. Wilcox, Jr., K. A. Weber, *J. Org. Chem.* **1986**, *51*, 1088; c) C. F. Wilcox, Jr., D. A. Blain, *Tetrahedron* **1986**, *42*, 6389; d) C. F. Wilcox, Jr., D. A. Blain, J. Clardy, G. Van Duyne, R. Gleiter, M. Eckert-Maksić, *J. Am. Chem. Soc.* **1986**, *108*, 7693; e) C. F. Wilcox, Jr., E. N. Farley, *J. Org. Chem.* **1985**, *50*, 351, and references therein.

Palladium-Catalyzed Allylic Alkylation with Phosphinoaryldihydrooxazole Ligands: First Evidence and NMR Spectroscopic Structure Determination of a Primary Olefin–Pd^0 Complex**

Henning Steinhagen, Michael Reggelin,* and Günter Helmchen*

Palladium-catalyzed allylic substitution reactions are well established in organic synthesis.[1] We and others showed that an enantioselective reaction can be realized with ligands containing electronically different donor centers;[2] of these, chiral phosphinoaryldihydrooxazole (phosphinooxazoline) ligands were found to be particularly useful.[3] With the prototype **1** of this ligand class it was possible to obtain substitution products with enantiomeric purity of $\geq 98\%$ from acyclic substrates.

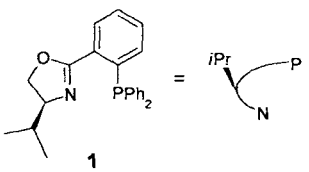

1

The postulated catalytic cycle for the examined system is shown in Scheme 1. The cycle contains the essential intermediates **2**–**5**, of which only the easily preparable allylic complexes **4** could be characterized so far. In the case of an unsymmetrical ligand such as **1**, an *exo*- (**4x**) and an *endo*-π-complex (**4n**) are fundamentally possible; these are in equilibrium through π-σ-π rearrangement.[4] As a consequence, there are in principle four reaction pathways, of which two lead to the preferred product (*S*)-**6**. Attack of the nucleophile can occur at C-3 of **4x** or at C-1 of **4n**. In spite of contrary assumptions (early[4, 5b] and late transition state[5a]), mechanistic interpretations up to now were all based on the postulate that the first reaction pathway is the faster one. We were now able to detect a primarily formed η^2-olefin–Pd^0 complex in the catalytic cycle and unambiguously determine its conformation. Therefore, it is now possible to make a well-founded statement about a late transition state.

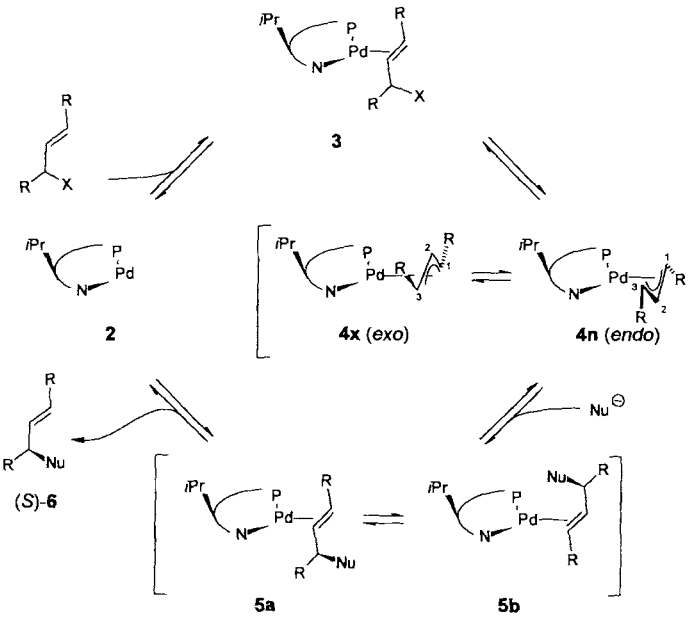

Scheme 1. Catalytic cycle of the Pd-catalyzed allylic substitution; R = Ph, X = OAc, Nu = $CH(COOCH_3)_2$.

Initially the stoichiometric reaction between the π-allyl complexes **4**[6] (10:1 mixture of **4x** and **4n**) and sodium dimethylmalonate (NaDMM) as a nucleophile was examined. A solution of the complexes in [D_8]THF (0.5 mL, 88 mM), prepared at room temperature, was cooled to −78 °C, and a precooled solution of NaDMM (20.3 mg, 0.132 mmol) in [D_8]THF (0.5 mL) added. The sample was allowed to warm to room temperature inside the NMR probehead, and the progress of the reaction was monitored by ^{31}P NMR spectroscopy (Figure 1).

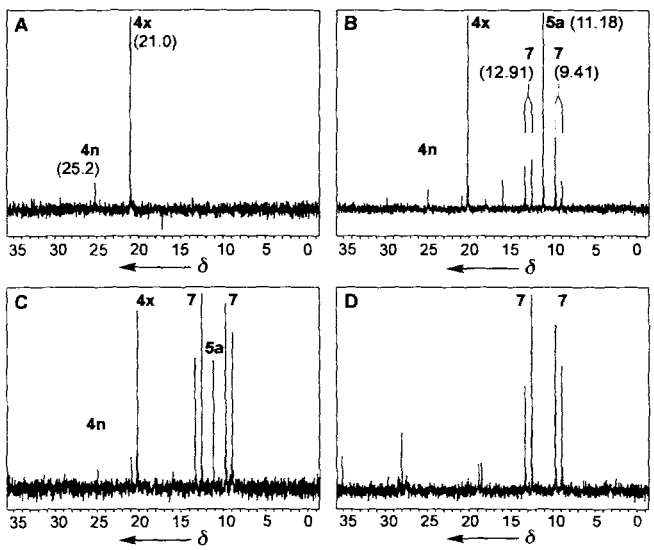

Figure 1. $^{31}P\{^1H\}$ NMR spectra recorded at various times during the reaction (161.98 MHz, −60 °C): A) equilibrating π-allyl complexes **4x** and **4n**; B–D) reaction mixtures at 370 s, 500 s, and 1 h, respectively, after addition of NaDMM.

[*] Priv.-Doz. Dr. M. Reggelin
Institut für Organische Chemie der Universität
Marie-Curie-Strasse 11, D-60439 Frankfurt am Main (Germany)
Fax: Int. code +(69) 7982-9128
e-mail: re@krypton.org.chemie.uni-frankfurt.de
Prof. Dr. G. Helmchen, Dipl.-Chem. H. Steinhagen
Organisch-chemisches Institut der Universität
Im Neuenheimer Feld 270, D-69120 Heidelberg (Germany)
Fax: Int. code +(6221) 54-4205
e-mail: en4@ix.urz.uni-heidelberg.de

[**] This work was supported by the Deutsche Forschungsgemeinschaft (SFB 247) and the Fonds der Chemischen Industrie. We thank Prof. Dr. C. Griesinger for his generous support.

 © WILEY-VCH Verlag GmbH, D-69451 Weinheim, 1997 0570-0833/97/3619-2108 $ 17.50+.50/0

During the course of the reaction **4x** and **4n** were always in rapid equilibrium.[4] As the first new species, a compound with a singlet at $\delta = 11.18$ appeared, whose concentration reached a maximum already after 90 s before it was consumed within a few minutes. This compound is the olefin–Pd^0 complex **5a**, whose structure determination is described below. Consumption of **5a** was accompanied by the appearance of a new species with a characteristic AB spin system ($\delta_A^{corr} = 9.41$, $\delta_B^{corr} = 12.91$, $^2J_{P,P} = 128$ Hz), which was the main component after a reaction time of about one hour. We propose structure **7** for this long-lived intermediate; the precise geometry could not yet be determined.[7]

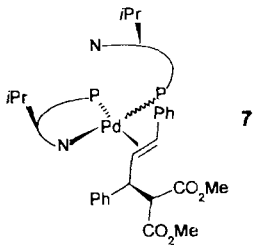

7

Only traces of the metal-free product (*S*)-**6**, which is formed from **7**, were detected in the reaction mixture when the reaction was stopped after conversion of approximately 50% of **4**. The concentration of (*S*)-**6** only increased when conversion exceeded 50%. Therefore, complex **7** is a stable by-product of the stoichiometric reaction.[8]

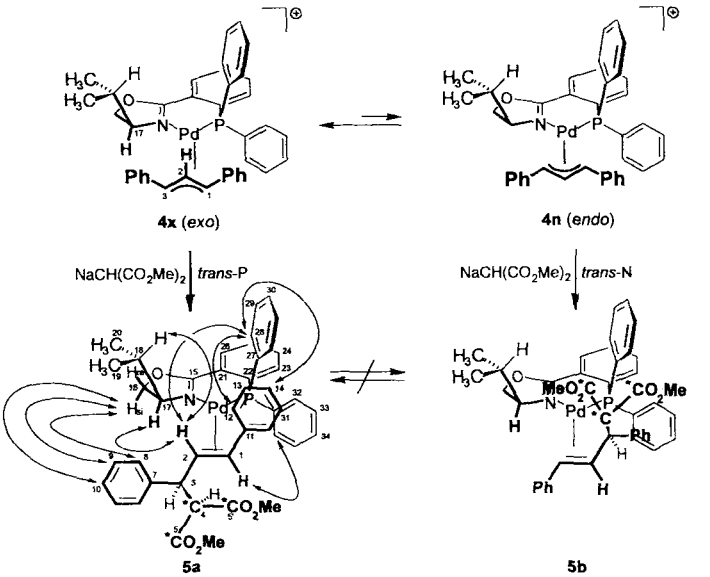

Scheme 2. Possible reaction pathways leading to (*S*)-**6**. The arrows mark NOE contacts between protons that were used for determining the conformation of **5a** [16]; C-4, C-5 and C-5′ are ^{13}C-labeled (99.5%).

To determine the constitution of the mechanistically meaningful transient species **5a**, the reaction was carried out with $^{13}C_3$-labeled NaDMM at -20 to $-30\,^\circ C$ and stopped after two minutes by cooling to $-78\,^\circ C$. A sample thus prepared contained about 75% of the phosphorus in the form of the olefin–Pd^0 complex **5a**,[9] and was stable for several weeks at $-78\,^\circ C$ under an inert atmosphere. This sample contained less than one percent of **7**, which is only formed at temperatures above about $-20\,^\circ C$.

Assignment of the resonances of all NMR-active nuclei was possible by use of $^{13}C_3$-labeled NaDMM and a large set of two-dimensional (2D) NMR experiments, of which only a few are described here. The starting point was a $^{31}P-^1H$ HMBC experiment[10] with a sample at $-60\,^\circ C$, which, in addition to ^{31}P correlations to aromatic protons (Scheme 2), showed correlations to protons with chemical shifts in the range of $\delta = 3-4.5$. By further analysis these could be unambiguously identified as belonging to the allyl system of the olefin–Pd^0 complex **5a** (Figure 2A: $\delta = 4.24$ (1-H), 3.23 (2-H), 3.43 (3-H)).

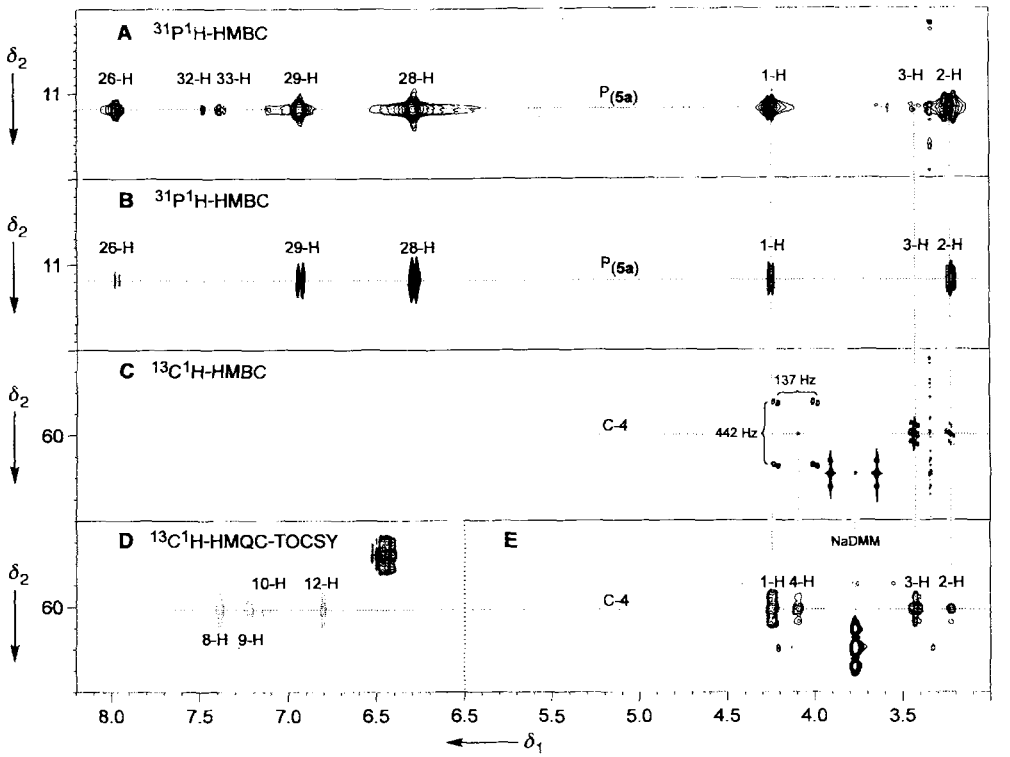

Figure 2. Sections of heteronuclear NMR spectra of **5a** ([D_8]THF, $-60\,^\circ C$): A) 400-MHz $^{31}P-^1H$ HMBC, stoichiometric reaction; B) 400-MHz $^{31}P-^1H$ HMBC, catalysis [19]; C) 600-MHz $^{13}C-^1H$ HMBC, stoichiometric reaction; D) 400-MHz $^{13}C-^1H$ HMQC TOCSY, stoichiometric reaction; the dotted crosspeaks are TOCSY-derived ROE signals between the protons of the allyl spin system and the marked aromatic protons; E) high-field region of spectrum D with a tenfold-increased contour level.

The $^{13}C-^1H$ HMBC spectrum of **5a** (Figure 2C) showed the expected $^2J_{C,H}$ and $^3J_{C,H}$ correlations between the central carbon C-4 of the malonic ester moiety and 3-H ($\delta = 3.43$) and 2-H ($\delta = 3.23$), respectively; the crosspeaks were split in the $\omega 1$ dimension due to $^1J_{C,C}$ coupling (57.3 Hz), which became apparent with ^{13}C labeling. An unusual crosspeak pattern at the position of the direct correlation ($^1J_{C,H}$) between 4-H and C-4 was of particular diagnostic value. As a consequence of ^{13}C labeling of C-4, C-5 and C-5′, marked in Scheme 2, the $^{13}C-^1H$ HMBC spectrum showed, among others, coherences that gave rise to signals at the positions $\Omega_{C-4} \pm (\Omega_{C-5} - \Omega_{C-5'})$;[11] this explained the separation of signals by 442 Hz in the $\omega 1$ dimension (Figure 2C). In addition, this provided definite proof for the assignment, because no such arrangement of nuclei could ap-

 © WILEY-VCH Verlag GmbH, D-69451 Weinheim, 1997 0570-0833/97/3619-2109 $ 17.50+.50/0

pear elsewhere in the molecule. By further projecting the proton spin system onto the C-4 with a HMQC-TOCSY experiment[12] (Figure 2D and E) the missing 1-H of the allylic system could be found at $\delta = 4.24$, in addition to 2-H and 3-H, which were formerly identified in the $^{13}C-^{1}H$ HMBC spectrum. The constitution of the η^2-olefin–Pd^0 complex **5a** (Scheme 2) was unambiguously determined by this analysis.[13]

The olefin–Pd^0 complex **5a** was not only found in the stoichiometric reaction but also under catalytic reaction conditions. A reaction catalyzed with 10 mol% Pd in [D_8]THF was carried out under standard conditions.[14] After a reaction time of three minutes at room temperature the mixture was cooled to $-60\,^{\circ}C$, and the $^{31}P-^{1}H$ HMBC spectrum shown in Figure 2B recorded. The characteristic P–H correlation of **5a** is apparent on comparison with Figure 2A. This proof of the presence of **5a** under catalytic reaction conditions stresses the relevance of structure determination for interpretating the mechanism.

It was also important to determine the conformation of the olefin fragment relative to the coordination plane N-Pd-P. This was achieved with the help of 2D NOESY (τ_{mix} = 200, 300, 400 ms) and 2D JS-ROESY experiments[15] (τ_{mix} = 260 ms). By quantitative analysis of NOE and ROE data, information on distances was gained[16] that is only in accordance with conformer **5a** and not **5b** (Scheme 2). For example, the NOE contact between 2-H and 17-H that appeared during the transformation of **4x** to **5a** is characteristic. The value of this NOE contact corresponds to a reduction in the distance between 2-H and 17-H by 1.4 Å[4, 17] compared to that in **4x**, which was determined by X-ray diffraction analysis.

Statements concerning the mechanism of the allylic substitution require the following plausible assumptions: a) Attack of the nucleophile NaDMM on **4x** under formation of **5a** proceeds by a "least-motion" reaction path, that is, a rotation of the allyl fragment by 30° from **4x** to **5a** is the main process. b) Rotation of the olefin fragment relative to the N-Pd-P-plane in complex **5a** is sufficiently slow, so that equilibration between **5a** and **5b** does not occur during the reaction time.[18] The second assumption is supported by experiments in which the reaction was carried out in a temperature gradient ($-78\,^{\circ}C$ to room temperature) and monitored by ^{1}H NMR spectroscopy.[19] In this experiment broadening of the resonances of **5a**, which would be expected for a dynamic exchange process, was not observed.

Under assumption b), the configuration of the more reactive allyl complex **4x** is conserved in the olefin–Pd^0 complex **5a**. Considering the known absolute configuration of the product, attack of the nucleophile *trans* to the phosphorus center at the *exo*-π-allyl complex **4x** can be derived. This result is in accordance with earlier interpretations,[4, 5] but is here based on a precisely characterized olefin–Pd^0 product complex in the Pd-catalyzed allylic substitution.

Received: May 6, 1997 [Z10413IE]
German version: *Angew. Chem.* **1997**, *109*, 2199–2202

Keywords: allyl complexes · asymmetric catalysis · NMR spectroscopy · palladium · reaction mechanisms

[1] a) R. F. Heck, *Palladium Reagents in Organic Synthesis*, Academic Press, London, **1985**; review: b) C. G. Frost, J. Howarth, J. M. J. Williams, *Tetrahedron: Asymmetry* **1992**, *3*, 1089–1122; c) T. Hayashi in *Catalytic Asymmetric Synthesis, Vol. 1* (Ed.: I. Ojima), VCH, New York, **1993**, pp. 325–365; d) B. M. Trost, D. L. van Vranken, *Chem. Rev.* **1996**, *96*, 395–422.

[2] R. D. Adams, D. F. Chodosh, J. W. Faller, A. M. Rosan, *J. Am. Chem. Soc.* **1979**, *101*, 2570–2578.

[3] a) J. Sprinz, G. Helmchen, *Tetrahedron Lett.* **1993**, *34*, 1769–1772; b) P. von Matt, A. Pfaltz, *Angew. Chem.* **1993**, *105*, 614–615; *Angew. Chem. Int. Ed. Engl.* **1993**, *32*, 566–567; c) G. J. Dawson, C. G. Frost, J. M. J. Williams, S. J. Coote, *Tetrahedron Lett.* **1993**, *34*, 3149–3150.

[4] a) J. Sprinz, M. Kiefer, G. Helmchen, M. Reggelin, G. Huttner, O. Walter, L. Zsolnai, *Tetrahedron Lett.* **1994**, *35*, 1523–1526; b) P. S. Pregosin, R. Salzmann, A. Togni, *Organometallics* **1995**, *14*, 842–847.

[5] a) J. M. Brown, D. I. Hulmes, P. J. Guiry, *Tetrahedron* **1994**, *50*, 4493–4506; b) P. B. Mackanzie, J. Whelan, B. Bosnich, *J. Am. Chem. Soc.* **1985**, *107*, 2046–2054.

[6] The salt [Pd^{II}(**1**){η^3-(1,3-diphenylallyl)}]$^+$[SbF_6]$^-$ was used [4a].

[7] The structure determination and dynamic aspects of intermediate **7**, which are irrelevant for our interpretation, will be described elsewhere.

[8] Complex **7** could not be detected under catalytic reaction conditions.

[9] Of the remaining 25% approximately 15% belong to **4x**, and 10% to unknown species with resonances at $\delta = 16.01$ and 18.08.

[10] HMBC = Heteronuclear Multiple Bond Correlation: A. Bax, M. F. Summers, *J. Am. Chem. Soc.* **1986**, *108*, 2093–2094.

[11] The symbol Ω_C marks the chemical shift of the corresponding carbon atom. In a 2D NMR spectrum the indirectly sampled dimension is usually the $\omega 1$ dimension.

[12] HMQC-TOCSY = Heteronuclear Multiple Quantum Coherence Total Correlation Spectroscopy: A. M. Gronenborn, A. Bax, P. T. Wingfield, G. M. Clore, *FEBS Lett.* **1988**, *243*, 93.

[13] Selected NMR data for **5a**: ^{31}P NMR (161.98 MHz, [D_8]THF, 213 K, H_3PO_4): $\delta = 11.18$; ^{1}H NMR (400.13 MHz, [D_8]THF, 213 K, TMS): $\delta = -0.11/0.51$ (19-H/20-H), 1.77 (18-H), 1.86 (17-H), 3.20 (CH_3O), 3.23 (2-H), 3.36 (CH_3O), 3.43 (3-H), 3.71 (16-H_{Si}), 3.83 (16-H_{Re}), 4.11 (4-H), 4.25 (1-H), 6.29 (28-H), 6.71 (14-H), 6.79 (12-H), 6.82 (13-H), 6.93 (23-H), 6.96 (29-H), 7.12 (30-H), 7.13 (10-H), 7.23 (9-H), 7.38 (8-H), 7.39 (33-H), 7.44 (24-H), 7.45 (34-H), 7.47 (32-H), 7.50 (25-H), 7.98 (26-H); ^{13}C NMR (100.61 MHz, [D_8]THF, 213 K, TMS): $\delta = 14.35/18.60$ (C-19/C-20), 32.40 (C-18), 52.06 (CH_3O), 52.22 (C-3), 52.40 (CH_3O), 58.76 (C-2), 60.0 (C-4), 60.71 (C-1), 67.08 (C-16), 74.43 (C-17), 122.12 (C-14), 124.45 (C-12), 126.45 (C-8), 127.90 (C-31), 128.35 (C-13), 128.85 (C-29), 128.90 (C-9), 129.30 (C-34), 129.58 (C-30), 130.10 (C-10), 130.20 (C-33), 130.28 (C-25), 130.98 (C-21), 132.39 (C-26), 132.43 (C-24), 133.79 (C-28), 135.10 (C-23), 136.0 (C-27), 136.12 (C-22), 137.50 (C-32), 147.50 (C-7), 148.25 (C-11), 162.0 (C-15), 168.6/170.0 (C-5/C-5').

[14] A solution of NaDMM, prepared from malonic acid dimethylester (132 μmol) and NaH (123 μmol) in [D_8]THF (0.5 mL), was added at room temperature to a solution of [{(η^3-C_3H_5)PdCl}$_2$] (4.4 μmol), **1** (9.7 μmol), and 1,3-diphenylpropenyl acetate (88 μmol) in [D_8]THF (0.5 mL). The reaction was stopped at various intervals by cooling to $-60\,^{\circ}C$, and the reaction mixture analyzed by NMR spectroscopy.

[15] J. Schleucher, J. Quant, S. Glaser, C. Griesinger, *J. Magn. Reson.* **1995**, *A112*, 144–151.

[16] Selected distances [Å]: 1-H–32-H 3.84, 2-H–17-H 3.20, 2-H–18-H 3.01, 2-H–28-H 4.09, 8-H–16$_{Si}$-H 4.34, 9-H–16$_{Si}$-H 3.20, 10-H–16$_{Si}$-H 3.24, 12-H–28-H 2.46, 14-H–28-H 3.09. The distances based on the correlated crosspeak volumina were calculated according to the isolated spin pair approximation (ISPA; B. A. Borgias, M. Gochin, D. J. Kerwood, T. L. James, *Progr. NMR Spectrosc.* **1990**, *22*, 83–100), for which the conformation-independent distance of the geminal pair of protons at C-16 ($r = 1.78$ Å) was used as the reference. As a result of the r^{-6} dependence of the crosspeak volumina, the distances given here are nonlinear standardized values.

[17] A trigonal-planar conformation is in accordance with the results of numerous X-ray analyses of olefin–Pd^0 complexes: a) R. Goddard, G. Hopp, P. W. Jolly, C. Krüger, R. Mynott, C. Wirtz, *J. Organomet. Chem.* **1995**, *486*, 163–170; b) R. van Asselt, C. J. Elsevier, W. J. J. Smeets, A. L. Spek, *Inorg. Chem.* **1994**, *33*, 1521–1531; c) M. Hodgson, D. Parker, R. J. Taylor, G. Ferguson, *Organometallics* **1988**, *7*, 1761–1766.

[18] Values for the rotational barriers of olefin–Pd^0 complexes of 15 to 25 kcal mol^{-1} were derived from calculations and experiments: a) T. A. Albright, R. Hoffmann, J. C. Thibeault, D. L. Thorn, *J. Am. Chem. Soc.* **1979**, *101*, 3801–3812; b) J. Krause, W. Bonrath, K. R. Pörschke, *Organometallics* **1992**, *11*, 1158–1167; c) ref. [17b].

[19] For this purpose a sample prepared at $-78\,^{\circ}C$ was placed in the NMR probehead of a NMR spectrometer at room temperature. The reaction that started upon warming could be monitored by recording 512 proton FIDs every 2.69 s. The sample temperature was determined with a methanol sample within a capillary.

 © WILEY-VCH Verlag GmbH, D-69451 Weinheim, 1997 0570-0833/97/3619-2110 $ 17.50+.50/0

Phase Transformations and Phase Stability in Epitaxial β-GaN Films**

Achim Trampert,* Oliver Brandt, and Klaus H. Ploog

Dedicated to Professor Hans Georg von Schnering

Internal interfaces and phase boundaries determine the physical and chemical properties of low-dimensional heterostructures and nanosized composite materials. The nature of the interfaces, that is, their atomic configuration, is of fundamental importance for understanding the various material properties. In the case of GaN and its related compounds, which are of great interest because of their potential for optoelectronic devices, internal interfaces such as domain boundaries frequently occur and are believed to degrade the material's suitability for applications. Thus, the atomic structure of these interfaces is of great current interest.[1]

In general, nitrides of elements from the third main group crystallize in the thermodynamically stable hexagonal wurtzite structure (α) as well as in the metastable cubic zinc blende modification (β). First-principle calculations predict that the energy difference between these structure modifications is smallest for GaN.[2] In fact, during epitaxial growth of GaN the phenomenon of phase mixing frequently occurs and may be overcome only by choosing the appropriate growth conditions and suitable substrate materials. However, even hexagonal and cubic GaN made by state-of-the-art procedures still contain fractions of their polytypic counterparts.

Assuming that the lattice parameter ratio in the hexagonal lattice is ideal ($c/a \approx 1.633$), the wurtzite and zinc blende structures differ only in the sequence of their closed packed planes: ...γAαBβCγAαBβCγA... for the {111} planes in zinc blende and ...AαBβAαBβAαBβA... for the {00.2} basal planes in wurtzite crystals. Consequently, a structural phase transformation, introduced by a single stacking fault, would be expected to appear along the direction of closed packed planes[3] by simultaneously creating a coherent phase boundary of low energy.[4, 5] In fact, this orientation relationship has been found in GaN layers grown on (111)A- and (111)B-oriented GaAs substrates,[6] in predominantly hexagonal GaN layers on Al_2O_3,[7] and in predominantly cubic GaN epilayers on GaAs(001).[8] However, this type of phase boundary is rather unlikely in the latter case because a fault in the stacking sequence does not exist in growth direction unless the growth front is faceted. Herein we report the dominant orientation relationship between the cubic and hexagonal phases in epitaxially grown β-GaN by high-resolution transmission electron microscopy (HRTEM) and demonstrate the importance of the interface character for the cubic–hexagonal phase transformation.

The β-GaN films investigated were grown by molecular beam epitaxy on (001) GaAs substrates.[8] The nucleation and growth of these films as well as their structural quality has already been discussed in detail.[9] Figure 1 shows a typical ⟨110⟩ cross-sectional bright field TEM image and the corresponding electron diffraction pattern of the β-GaN/GaAs(001) heterostructure under consideration. The TEM experiments demonstrate the comparatively high crystalline quality of the β-GaN layer and its perfect epitaxial orientation with respect to the GaAs substrate. Stacking faults and nanotwins are the prevalent crystal defects, as is evidenced by the dark lines along the {111} planes in the bright field image (Figure 1a) and by the streaks and the weak twin spots along the ⟨111⟩ directions in the diffraction pattern (Figure 1b). These structural defects are an indirect result of the strain relief caused by the large lattice mismatch between GaN and GaAs, as discussed in more detail in reference [9].

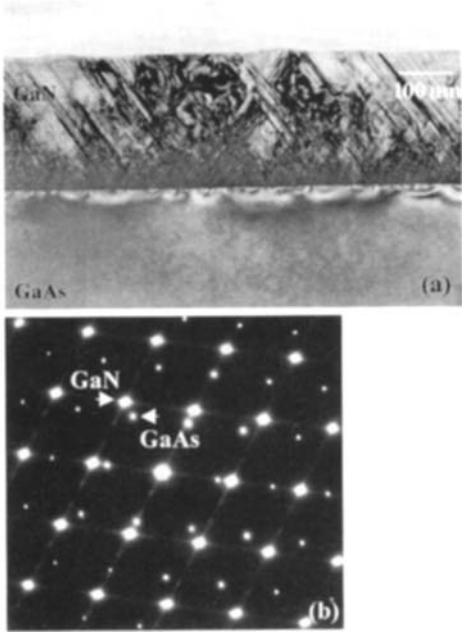

Figure 1. a) ⟨110⟩ cross-sectional bright field TEM image and b) corresponding electron diffraction pattern of the β-GaN/GaAs(001) heterostructure.

In these β-GaN layers two different kinds of hexagonal inclusions are detected. The first, which is typically of nanometer size, is located in direct vicinity of the β-GaN/GaAs heterointerface, meaning that these hexagonal inclusions are formed during nucleation. They show a random orientation with respect to the substrate, and thus, in general, their interface energy is significantly higher than that of the critical nuclei in the (epitaxial) "cube-on-cube" orientation. In fact, these hexagonal nuclei are rapidly overgrown during the subsequent coalescence process (an example is given in Figure 2). The rare occurrence of these

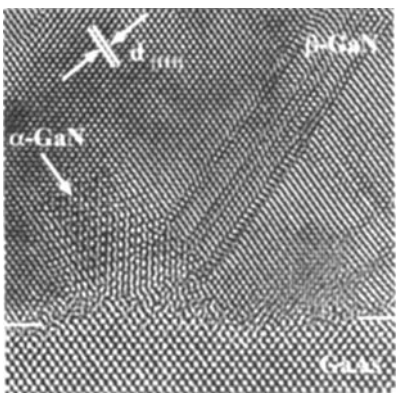

Figure 2. HRTEM image of the GaN/GaAs heterointerface showing a buried hexagonal nucleus at the boundary.

[*] Dr. A. Trampert, Dr. O. Brandt, Prof. Dr. K. H. Ploog
Paul-Drude-Institut für Festkörperelektronik
Hausvogteiplatz 5-7, D-10117 Berlin (Germany)
Fax: Int. code +(30)20377-425
e-mail: trampert@pdi.wias-berlin.de

[**] We thank the Institut für Mikrostrukturforschung at the Forschungszentrum Jülich for the use of their TEM facilities. This work was supported by the German Bundesministerium für Bildung und Forschung (BMBF).

 © WILEY-VCH Verlag GmbH, D-69451 Weinheim, 1997 0570-0833/97/3619-2111 $ 17.50+.50/0

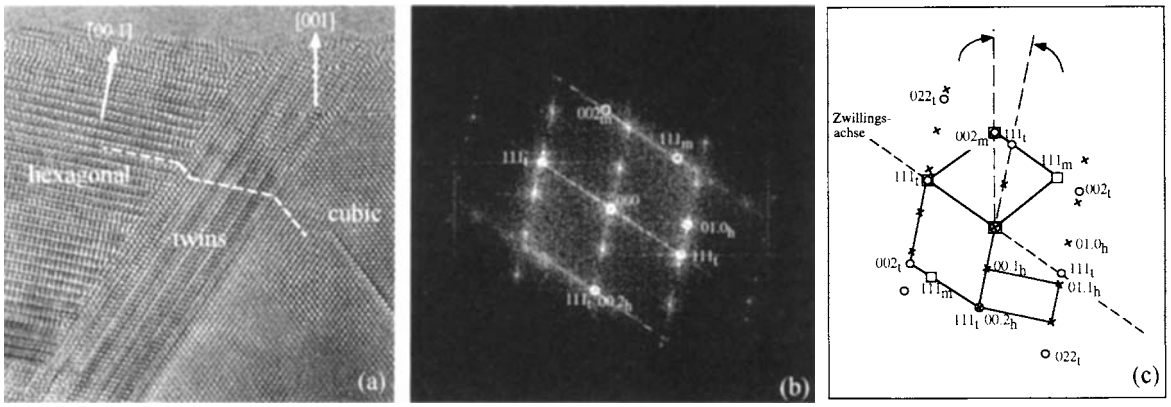

Figure 3. a) HRTEM image of a hexagonal inclusion with the specific orientation relationship to the matrix (see text). b) The corresponding Fourier spectrum: The [11.0] zone axis of the hexagonal phase and the [110] zone axis of the cubic twin are emphasized in the scheme given in (c). t = twin, m = matrix, h = hexagonal.

hexagonal inclusions implies that their influence on the layer's properties is negligible.

The second kind of hexagonal inclusions is detected within the layer and is more important than the first kind discussed above because of its apparently higher stability within the cubic matrix. Furthermore, this kind of hexagonal inclusion exhibits a specific orientation relationship to the cubic matrix: $[110]_\beta \parallel [11.0]_\alpha \measuredangle ([001]_\beta, [00.1]_\alpha) \approx 15°$.

At the first glance, this orientation seems to be arbitrary and purely accidental. However, a closer analysis reveals this orientation to be actually quite favorable. Figure 3 shows a magnified part of a HRTEM image of the interface between the hexagonal precipitate and the cubic matrix along the [11.0] and [110] zone axes respectively. The hexagonal basal plane runs parallel to closed packed planes belonging to a twinned region in the cubic layer [along the white line in Figure 3a]. The Fourier spectrum in Figure 3b directly shows the coincidence of the {111} twin and the {00.2} hexagonal reflections and also the tilt between the cubic matrix and the hexagonal inclusion. The closed packed planes of the twin can now act as seeds for the phase transformation by generating a coherent phase boundary (indicated as I in Figure 4) by simultaneously aligning the fast growing basal plane nearly parallel to the growth front and thus making the precipitate stable in the course of subsequent growth (see Figure 4). In addition, the phase boundary to the cubic matrix (indicated as II in Figure 4) is also coherent, since the {111} planes of the matrix match the {00.2} basal planes of the inclusion. Thus, this specific orientation relationship results in a phase boundary that is analogous to a cubic twin boundary except that one part of the twin is formed by the wurtzite structure.

To summarize, phase transformations from cubic to hexagonal GaN may occur due to the favorable orientation of the basal plane to the growth front. This condition is met by twinning within the cubic matrix, which aligns the closed packed planes closer to the growth front and subsequently creates a coherent phase boundary. The stability of the secondary phase is then a result of the coherent character of the phase boundaries having minimal interfacial energies.

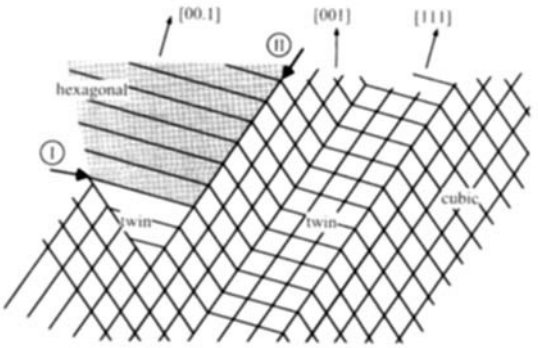

Figure 4. Schematic representation of the specific orientation between the hexagonal inclusion and the cubic matrix, which demonstrates the role of nanotwins.

Received: March 25, 1997 [Z10278IE]
German version: *Angew. Chem.* **1997**, *109*, 2202–2204

Keywords: gallium · interfaces · metastable compounds · nitrogen · phase transformations

[1] J. E. Northrup, J. Neugebauer, L. T. Romano, *Phys. Rev. Lett.* **1996**, *77*, 103.
[2] C. Y. Yeh, Z. W. Lu, S. Froyen, A. Zunger, *Phys. Rev. B* **1992**, *46*, 10086.
[3] a) S. C. Strite in *Properties of Group III Nitrides* (Ed.: J. H. Edgar) INSPEC, London, **1994**, pp. 262–267; b) P. Pirouz, J. W. Yang, *Ultramicroscopy* **1993**, *51*, 189.
[4] The energy of a crystalline interface (γ_i) can generally be subdivided into two parts (see for example ref. [5]). The first part takes into account the interaction between the atoms at both sides of the interface and is often interpreted as the coherent (chemical) interface energy (γ_i^{chem}), whereas the second portion considers the strain energy caused by the lattice mismatch (γ_i^{struc}): $\gamma_i = \gamma_i^{chem} + \gamma_i^{struc}$. In the case of a coherent GaN interface there is $\gamma_i^{struc} \approx 0$ and γ_i^{chem} should also be small because the bonding relations scarcely differ between the α- and the β-phase.[2]
[5] D. A. Porter, C. E. Easterling, *Phase Transformation in Metals and Alloys*, Van Nostrand, Wokingham, **1981**, p. 142.
[6] J. W. Yang, J. N. Kuzina, M. Asif Khan, T. George, M. De Graef, S. Mahajan, *Appl. Phys. Lett.* **1995**, *67*, 3759.
[7] M. S. H. Leung, R. Klockenbrink, C. Kisielowski, H. Fujii, J. Krüger, G. S. Sudhir, A. Anders, Z. Liliental-Weber, M. Rubin, E. R. Weber, *Mater. Res. Soc. Symp.* **1997**, in press.
[8] O. Brandt, H. Yang, B. Jenichen, Y. Suzuki, L. Däweritz, K. H. Ploog, *Phys. Rev. B* **1995**, *52*, R2253.
[9] A. Trampert, O. Brandt, H. Yang, K. H. Ploog, *Appl. Phys. Lett.* **1997**, *70*, 583.

 © WILEY-VCH Verlag GmbH, D-69451 Weinheim, 1997 0570-0833/97/3619-2112 $ 17.50+.50/0

Oscillation of NO_x Concentration in the Selective Catalytic Reduction of Nitrogen Oxides on Platinum-Containing Zeolite Catalysts**

Yvonne Traa, Marcus Breuninger, Beate Burger, and Jens Weitkamp*

The emission of nitrogen oxides, carbon monoxide, and hydrocarbons from spark-ignition engines can nowadays be effectively reduced with the three-way catalyst. Since diesel and lean-burn engines operate with an excess of oxygen, conventional three-way catalysts cannot be used for purifying exhaust gases from these engines. While oxidation catalysts, which are already being used in diesel engines, do reduce the amount of carbon monoxide and hydrocarbons in the exhaust gas, they do not bring about a reduction in the amount of nitrogen oxides. Since the discovery by Iwamoto et al.[1] and Held et al.[2] that the selective catalytic reduction of nitrogen oxides with hydrocarbons can be achieved in an oxidizing atmosphere (*h*ydrocarbon *s*elective *c*atalytic *r*eduction, HC-SCR), the potential of HC-SCR in the purification of exhaust gases from diesel and lean-burn engines has been intensively scrutinized. In addition to copper-containing zeolite catalysts favored earlier, platinum-containing catalysts are employed in modern research, because they are insensitive to water in the exhaust gas.[3] However, the reaction also takes place on transition metal free catalysts (for example, on γ-Al_2O_3—see below).

In 1992 Obuchi et al. observed oscillations in the concentrations of NO_x, CO_2, and CO in the product gas of the selective catalytic reduction of NO with propene on γ-Al_2O_3 in an oxidizing atmosphere.[4] Oscillations are not uncommon in heterogeneous catalysis, and the phenomenon is well-known for CO oxidation, oxidation of other substrates with O_2, and reduction of NO with CO, H_2, or NH_3.[5] In contrast, there are very few reports on oscillations for HC-SCR in a strongly oxidizing atmosphere. In addition to Obuchi et al.[4] two other groups found oscillations in such systems, namely, Halasz et al. on zeolite H-ZSM-5[6] and Cho et al. on Pt/ZSM-5.[7] Interestingly, Cho et al. were only able to observe oscillations when ^{15}NO was employed; no oscillations occurred with ^{14}NO.

In the present study, oscillations of NO_x concentration in the HC-SCR with propene on different Pt–V/H zeolites were fortuitously found. As an example, the conversion of NO_x as a function of time is depicted in Figure 1 for 2.6Pt-1.0V/H-ZSM-35 zeolite as catalyst.[8] The oscillations could only be observed at high NO_x conversion and within a temperature range of about 20 K. The temperature of the catalyst was constant within ± 1 K. C_3H_6 and CO were completely oxidized to CO_2. It can be seen from Figure 1 that the amplitude of the oscillations decreases with increasing temperature, whereas their frequency increases. The oscillations are fully reproducible, that is, they also occur on other freshly prepared Pt-V/H-ZSM-35 batches and under slightly different experimental conditions. However, on zeolite Pt/H-ZSM-35, only irregular fluctuations in NO_x conversion were noticed. Therefore, the presence of vanadium

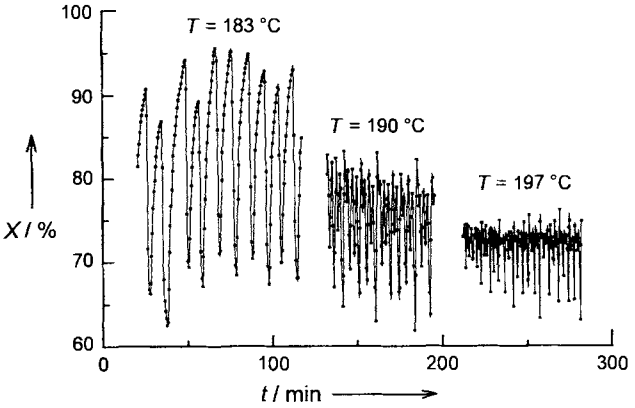

Figure 1. NO_x conversion X for HC-SCR on 2.6Pt-1.0V/H-ZSM-35 zeolite ($n_{Si}/n_{Al} = 8$) as a function of time t for different catalyst temperatures T.

seems to be important for the occurrence of regular oscillations in this system. Moreover, the oscillations are not limited to zeolite ZSM-35. They can also be observed on zeolites with other pore systems, for example on Pt-V/H-Beta and Pt-V/H-ZK-5. Figure 2 shows the dependency of the oscillation on water content for the example of 2.0Pt-1.1V/H-ZK-5 as catalyst:

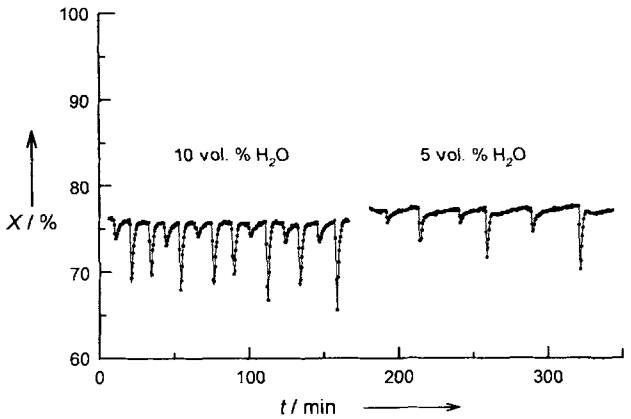

Figure 2. NO_x conversion X for HC-SCR on 2.0Pt-1.1V/H-ZK-5 zeolite ($n_{Si}/n_{Al} = 4$) for different partial pressures of water; $T_{cat.} = 189$ °C.

The amplitude and frequency of the oscillation decrease with decreasing water concentration. Without water in the feed no oscillations were observed at all. In contrast to the systems employed by Obuchi et al., Halasz et al., and Cho et al.,[4, 6, 7] who used dry model exhaust gases, the presence of relatively large amounts of water seems to be essential for the occurrence of oscillations on the catalysts described here. As Figure 3 shows, only minor changes occur in the amplitude and the frequency of the oscillation, even over a time period of 17 h.

In the literature there are different models to account for the occurrence of oscillations in HC-SCR. One possibility is the formation of carbon-containing deposits which react periodically with NO.[4] Another possibility is the slow formation of nitroxy compounds and the fast decomposition of the radicals that form from them.[6] Cho et al. interpreted the oscillations in terms of a periodic change of the catalyst between states of different catalytic activity.[7] This can be caused either by phase transitions at the platinum sites of the Pt/ZSM-5 catalyst, which are induced by NO adsorption, or by blocking of the surface by NO, which inhibits the reaction.

[*] Prof. Dr.-Ing. J. Weitkamp, Dipl.-Chem. Y. Traa, Dipl.-Chem. M. Breuninger, Dr. B. Burger
Institut für Technische Chemie I der Universität
D-70550 Stuttgart (Germany)
Fax: Int. code +(711)685-4065
e-mail: yvonne.traa@po.uni-stuttgart.de

[**] Most valuable discussions with G. Wenninger and Dr. B. Krutzsch (Department of Fuels and Reaction Kinetics, Daimler-Benz AG, Stuttgart) are gratefully acknowledged. This work was supported by the Fonds der Chemischen Industrie and the Max-Buchner-Forschungsstiftung. B. B. is indebted to the Dr.-Leni-Schöninger-Stiftung for financial support.

 © WILEY-VCH Verlag GmbH, D-69451 Weinheim, 1997 0570-0833/97/3619-2113 $ 17.50+.50/0

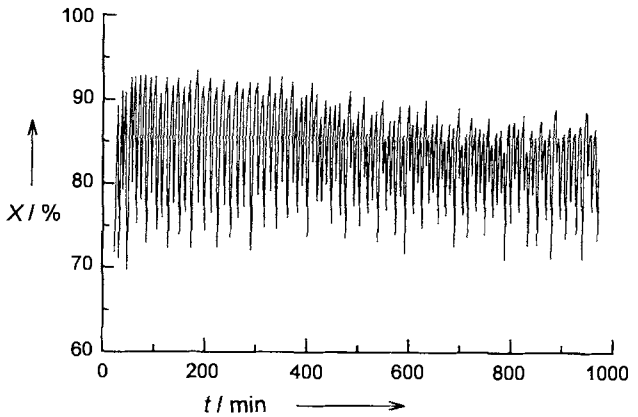

Figure 3. Long-duration experiment on 2.6Pt-1.0V/H-ZSM-35 zeolite ($n_{Si}/n_{Al} = 8$); $T_{cat.} = 187\,^{\circ}C$.

In an attempt to determine the reasons for the occurrence of the oscillations, the H-ZSM-35 samples loaded with Pt and/or V were investigated by means of temperature-programmed oxidation/reduction (Figure 4). On samples loaded with Pt or V only,

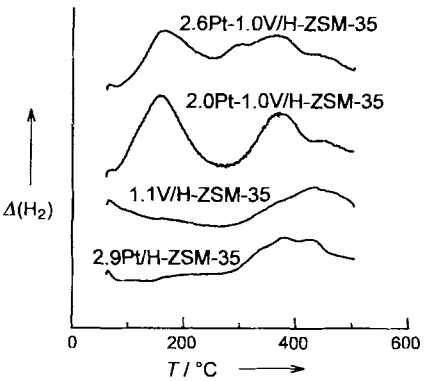

Figure 4. Results of the temperature-programmed reduction on different metal-containing H-ZSM-35 zeolites. $\Delta(H_2) = H_2$ consumption.

no significant hydrogen consumption occurred at temperatures below 300 °C. In contrast, on Pt-V/H-ZSM-35 large amounts of hydrogen were consumed already at 150 to 200 °C, that is, exactly in the temperature range in which the oscillations occur. Furthermore, the total hydrogen consumption on these bimetallic zeolites was considerably larger. From this we conclude that the reducible portion of metals in the catalyst is enhanced through synergistic effects between platinum and vanadium. Hence, it is straightforward to assume that the observed oscillations have their origin in redox reactions; this hypothesis is further supported by the simultaneous presence of oxygen and propene in the feed.

Experimental

The zeolites (ZSM-35, Beta, and ZK-5) were first transformed into their ammonium forms by ion exchange. The resulting samples were treated with aqueous solutions of $[Pt(NH_3)_4]Cl_2$ and VCl_3; the water was removed by heating after every step. Normally, the dry catalysts contained about 3 wt% Pt and 1 wt% V. The catalytic experiments were performed in a flow-type apparatus with a fixed-bed reactor at atmospheric pressure. The hydrated zeolite (200 mg) was activated in a flow of synthetic air for 1 h at 500 °C and then overnight at 450 °C. The gaseous components of the model exhaust gas were premixed in a pressure vessel, and then saturated with water vapor at 45 °C. The feed typically contained NO_x (0.02 vol%), C_3H_6 (0.06 vol%), CO (0.03 vol%), CO_2 (4 vol%), O_2 (9 vol%), and H_2O (10 vol%) in He at a flow rate of 150 $cm^3\,min^{-1}$. The product stream was analyzed for nitrogen oxides with a chemiluminescence detector; all other components were analyzed by capillary gas chromatography. Prior to the temperature-programmed reduction with H_2 (10 vol%) in Ar, the catalyst samples were oxidized in a gas stream containing O_2 (10 vol%) in He.

Received: April 10, 1997 [Z10332IE]
German version: *Angew. Chem.* **1997**, *109*, 2207–2208

Keywords: heterogeneous catalysis · nitrogen oxides · oscillations · platinum · vanadium

[1] M. Iwamoto in *Proceedings of the Meeting on Catalytic Techniques for Removal of Nitrogen Monoxide* (Ed.: M. Misono), University of Tokyo, **1990**, pp. 17–22.
[2] W. Held, A. König, T. Richter, L. Puppe, *SAE Trans. Sect. 4* **1990**, *99*, 209–216.
[3] H. Hirabayashi, H. Yahiro, N. Mizuno, M. Iwamoto, *Chem. Lett.* **1992**, 2235–2236.
[4] A. Obuchi, M. Nakamura, A. Ogata, K. Mizuno, A. Ohi, H. Ohuchi, *J. Chem. Soc. Chem. Commun.* **1992**, 1150–1152.
[5] a) R. Imbihl, G. Ertl, *Chem. Rev.* **1995**, *95*, 697–733; b) F. Schüth, B. E. Henry, L. D. Schmidt in *Advances in Catalysis, Vol. 39* (Eds.: D. D. Eley, H. Pines, P. B. Weisz), Academic Press, San Diego, **1993**, pp. 51–127.
[6] I. Halasz, A. Brenner, M. Shelef, K. Y. S. Ng, *J. Phys. Chem.* **1995**, *99*, 17186–17191.
[7] B. K. Cho, J. E. Yie, K. M. Rahmoeller, *J. Catal.* **1995**, *157*, 14–24.
[8] a) The numbers before the metals indicate the content of the metal [wt%] in the dry catalyst. b) The structures of the zeolites ZSM-35, Beta, and ZK-5, which were used in this work, have been described in, for example, W. M. Meier, D. H. Olson, C. Baerlocher, *Zeolites* **1996**, *17*, A1–A6, 1–230.

Multilayer Dendrimer–Polyanhydride Composite Films on Glass, Silicon, and Gold Wafers**

Yuelong Liu, Merlin L. Bruening, David E. Bergbreiter,* and Richard M. Crooks*

Organic thin films are of current interest because of their use in adhesion, corrosion passivation, sensor chemistry, photonics, electronics, and membrane chemistry.[1] Here we describe a new way to prepare thin films using functional dendrimers and a reactive copolymer that is covalently attached to a surface as a solvent-swollen, brush-like polymer. The synthesis proceeds by an alternating deposition and reaction process leading to a covalent assembly of multilayers of dendrimers contained within layers of Gantrez (poly(maleic anhydride)-*c*-poly(methyl vinyl ether) lightly cross-linked with 1% ethylenediamine). The product films are densely functionalized, semi-organized, and easily modified. The chemistry used is general, and can be extended to include the synthesis of composite interfaces using other nano- or mesoscopic surface-functionalized objects or polyfunctional molecular assemblies.

Prior syntheses of organic thin films on inorganic solids include deposition of monolayers and multilayers by self-assembly or Langmuir–Blodgett techniques,[1] deposition of polymers by adsorptive binding,[2] sequential deposition of cationic and anionic polymers, organic polymers, and inorganic sheets or mutually reactive layers,[3–9] and graft polymeriza-

[*] Prof. D. E. Bergbreiter, Prof. R. M. Crooks, Dr. Y. Liu, Dr. M. L. Bruening
Department of Chemistry
Texas A & M University
College Station, TX 77845-3255 (USA)
Fax: Int. code +(409)845-4719
e-mail: bergbreiter@chemvx.tamu.edu
crooks@chemvx.tamu.edu

[**] Support of this work by the U. S. National Science Foundation (grant nos. DMR-96341196 for D. E. B. and CHE-9313441 for R. M. C.) and the Texas Advanced Technology Program is acknowledged. We thank Mingqi Zhao, Dr. Yuefen Zhou, and Dr. Laurel Knott for suggestions and advice, and the Michigan Molecular Institute (MMI) and Dendritech Inc. (Midland, MI, USA) for samples of the Starburst PAMAM dendrimer. M. L.B acknowledges a postdoctoral fellowship from the U. S. National Institutes of Health.

 © WILEY-VCH Verlag GmbH, D-69451 Weinheim, 1997 0570-0833/97/3619-2114 $ 17.50+.50/0

tions.[8-10] The chemistry presented here combines features of these approaches for preparing thin-film composites containing highly functionalized nanomolecules in a polymeric network.

Silicon- or glass-wafer modification begins with aminosilylation.[11] The resulting aminated surface is then modified with a monolayer of Gantrez (Figure 1). Ellipsometry shows that this

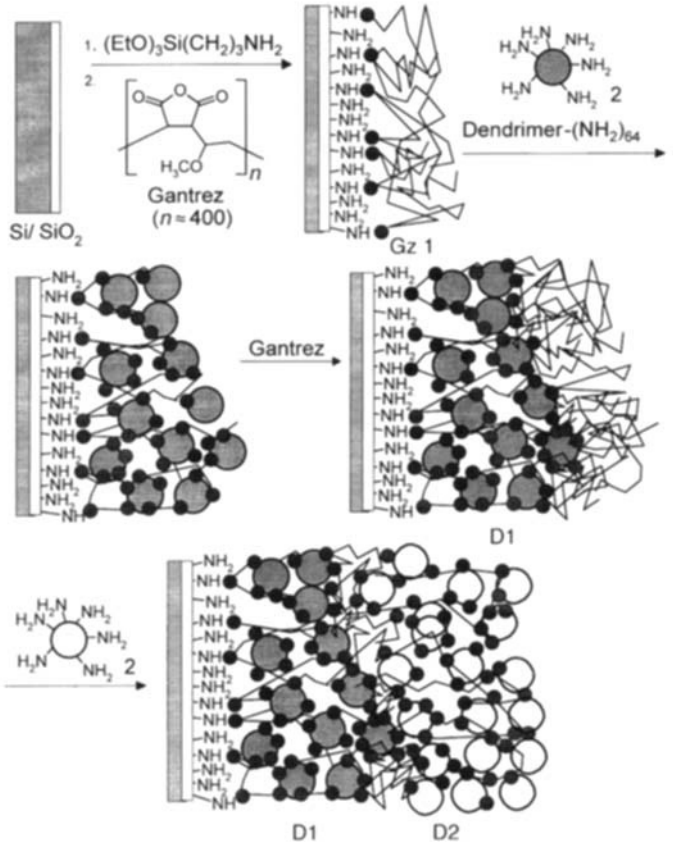

Figure 1. Schematic drawing showing the growth of multilayers of Gantrez and a PAMAM dendrimer beginning with an amino-functionalized silica/silicon-wafer surface (PAMAM = Starburst polyamidoamine). The amic acid binding sites of Gantrez are shown as smalled filled circles, and the fourth-generation PAMAM dendrimer as large filled circles (D1) or large open circles (D2).

layer (Gz1) is 2.6 ± 0.4 nm thick. The silicon atoms of the underlying layer are detectable by X-ray photoelectron spectroscopy (XPS) at this stage, though the intensity of the Si_{2p} signal is attenuated from 28 to 3 atom% with silicon or from 19 to 2 atom% with glass as substrate. The Gz1 surface presumably consists of polymer chains covalently attached to the amino surface through amic acid groups at multiple sites distributed throughout the adsorbent. As Equation (1) and Figure 1 show,

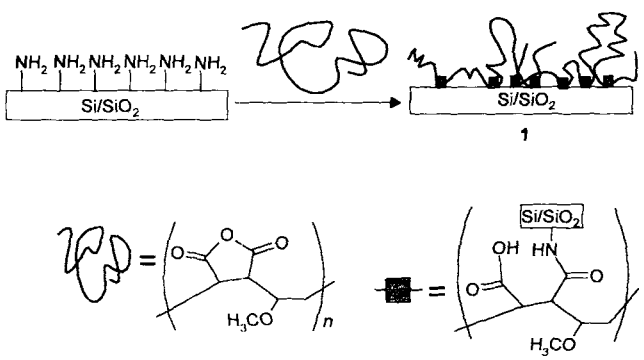

(1)

this results in a polydisperse mixture (1) of random-sized loops containing unchanged anhydrides. This surface is presumably like those produced by chemisorptive binding of "sticky" polymers containing thiols or carboxylic acids to metal or metal oxide surfaces.[2, 7]

The key to this chemistry is the use of unchanged anhydride groups of these sticky surfaces for additional reactions.[7, 10] Since most of the anhydride groups of the film **1** have not reacted, the loopy brush-like polymer layer should react further, as suggested by the synthesis of cross-linked multilayer surfaces with another Gantrez derivative and 2-aminoethanol.[7] Exposure of this solvent-swollen reactive brush to a dendrimer that has terminal amino groups results in covalent attachment of multilayers of the dendrimer to the loopy brush surface through amic acids (Figure 1). Specifically, reaction of an amine-functionalized Starburst PAMAM dendrimer (**2**) with the initial Gz1 Gantrez layer yields a first-generation, dendrimer-modified surface (D1), whose ellipsometric thickness is 14.6 ± 0.4 nm (an increase of 7.9 nm). Since the fourth-generation dendrimer **2** has a diameter of 4.5 nm[12] and previous depositions of a single layer of dendrimers yields a thickness of about 4 nm,[6] a change of 7.9 nm implies that more than a single layer of dendrimer is attached in each step.

Elaboration of these surfaces by sequential deposition of Gantrez and dendrimer leads to increasingly thick films (Figure 2). Subsequent Gantrez-deposition steps (Gz2, Gz3, and

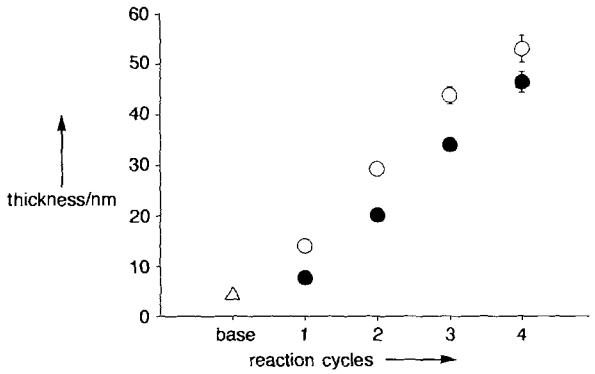

Figure 2. Ellipsometric thickness of Gantrez–dendrimer composite grafts on a silicon wafer. The thickness of the initial layer (△) includes the SiO_2 and the grafted aminopropylsilyl layer. The other data are for films after deposition of Gantrez (Gz1–Gz4, ●) and after the addition of the multilayers of dendrimer (D1–D4, ○).

Gz4) lead to larger increases in film thickness (6 nm versus 2.6 nm for Gz1). Likewise, further dendrimer additions (D2, D3, and D4) lead to larger increases in thickness (10–11 nm versus the initial increase of 7.9 nm). These increases too are in accord with addition of more than a single layer of dendrimer at the D2, D3, and D4 stages. Control experiments in which a surface without amine groups was treated first with Gantrez and then with dendrimer **2** did not lead to film growth.

XPS and IR spectroscopy as well as contact-angle analysis provide further evidence for the structure of these composite dendrimer grafts. XPS data show the disappearance of the peak due to the underlying Si atoms at the D1 stage, and changes in atom percentage that are consistent with the alternating layered structure shown in Figure 1. The anhydride-rich Gz1 and Gz2 films contain an enhanced amount of oxygen (29 atom%) and a reduced amount of nitrogen (1 atom%), while the amine-rich D1, D2, and D3 films have 19 atom% oxygen and 15 atom% nitrogen. Contact-angle measurements also cycle as film growth

 © WILEY-VCH Verlag GmbH, D-69451 Weinheim, 1997 0570-0833/97/3619-2115 $ 17.50+.50/0

proceeds; the dendrimer-rich surface is more hydrophilic than the Gantrez-rich surface (Figure 3). The IR spectra also change with film growth. Bands for anhydride groups are observed at 1860 and 1790 cm^{-1} (Figure 4) for sticky films (Gz1–Gz3).

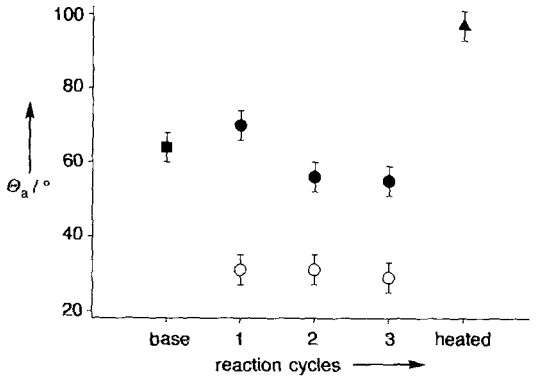

Figure 3. Contact-angle data (θ_a, water) for silicon surfaces modified with Gantrez (base, ■; Gz1–Gz3, ●) and dendrimer multilayers (D1–D3, ○) showing the cyclic changes in hydrophilicity with layer deposition and the change in hydrophilicity of layer D3 on heating (▲).

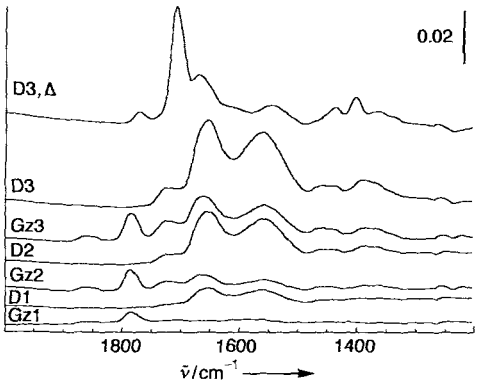

Figure 4. IR spectra (extinction) of films grafted onto silicon wafers that were polished on both sides. Spectra are shown for films after deposition of Gantrez (Gz1–Gz3) and after deposition of **2** (D1–D3) as well as for the final D3 layer after heating (D3, Δ); see text for details.

These bands disappear after addition of dendrimer **2**, and new bands for amides at 1660 and 1560 cm^{-1} appear. Moreover, the latter gradually increase in intensity as the film thickness grows. We cannot distinguish between bands for amides within **2** and bands for amides of amic acids resulting from reaction of **2** with Gantrez.

Thermal treatment of a D3 film (2 h, 120 °C) leads to a decrease of 15% in thickness and the appearance of bands for imide carbonyl groups at 1772 and 1710 cm^{-1} in the IR spectrum (Figure 4, top). We believe that imide groups form from the amic acid groups that are produced by reaction of Gantrez with the initial amine surface and with the amine-functionalized dendrimer. The IR spectrum shows that other changes occur in this film upon heating. Preliminary work with films on gold (see below) suggests that the "imidized" film is highly impermeable.

Use of a smaller second-generation Starburst PAMAM dendrimer (diameter 2.9 nm)[12] in place of the larger dendrimer **2** shows that dendrimer size may modestly affect the thickness of these multilayer films. Changes in ellipsometric thickness upon addition of the Gz1, D1, Gz2, D2, Gz3, D3, Gz4, and D4 layers were 2.3, 7.5, 4.5, 7.0, 4.6, 7.9, 5.5, and 8.5 nm, respectively.

Composite layers of **2** and Gantrez form on gold substrates upon use of an aminated base layer, which is formed by reaction of ethylenediamine with a self-assembled monolayer of 11-mercaptoundecanoic acid. In this case the D3 layer is 42.3 nm thick, as determined by ellipsometry. The D3 layer has modest blocking ability in electrochemistry experiments.[13] Heating this layer leads to an imidized film of 36.2 nm thickness that is electrochemically passivating.[13]

The chemistry described here is a new approach for the formation of thin-film composites. The coupling of a reactive surface to a polyfunctional polymer leads to a covalently attached reactive brush, that in turn allows us to incorporate multilayers of a large reactive structure (the dendrimer here) in a polyfunctional film of 40–50 nm thickness.

Experimental Section

Typical procedure for preparing a film with alternating layers of Gantrez and a polyamine dendrimer: A base layer of Gantrez on an aminopropylated glass slide was prepared by dipping the slide in a clear, pre-formed solution of Gantrez (200 mg, $M_n = 6.2 \times 10^4$, $M_w/M_n = 3.4$) and 1,2-diaminoethane (0.8 mg) in THF (4 mL). The slides were then heated in an oven at 120 °C under vacuum for 5 min. Sonication in DMF (5 min) followed by washing in THF removed any physically absorbed polymer. A dendrimer multilayer was then added to the base layer by immersing the slide in a solution of **2** in CH_3OH (10% by weight). After maintaining the slides at 25 °C for 20 min they were placed in hot THF for 5 min, washed thoroughly with CH_3OH, and dried under N_2 before being characterized by ellipsometry, XPS, and/or FT-IR spectroscopy. The next Gantrez layer was attached to the dendrimer-modified surface by allowing the dendrimer-grafted slides to react with Gantrez in THF (50 mg mL^{-1}) for 20 min with occasional heating of the reaction solution. The slides were then washed with THF and dried with N_2.

Received: March 11, 1997 [Z102251E]
German version: *Angew. Chem.* **1997**, *109*, 2204–2207

Keywords: dendrimers · materials science · nanostructures · polymers · surface chemistry

[1] A. Ulman, *Chem. Rev.* **1996**, *96*, 1533–1554; *An Introduction to Ultra Thin Films*, Academic Press, New York, **1991**.
[2] a) J. M. Stouffer, T. J. McCarthy, *Macromolecules* **1988**, *21*, 1204–1208; b) F. Sun, D. G. Castner, G. Mao, W. Wang, P. Mckeown, D. W. Grainger, *J. Am. Chem. Soc.* **1996**, *118*, 1856–1866; c) J. Rühe, G. Blackman, V. J. Novotny, T. Clarke, G. B. Street, S. J. Kuan, *Appl. Polym. Sci.* **1994**, *53*, 825–836.
[3] Y. Lvov, H. Haas, G. Decher, H. Möhwald, A. Mikhailov, B. Mtchedlishvily, E. Morgunova, B. Vainshtein, *Langmuir* **1994**, *10*, 4332–4336.
[4] V. V. Tsukruk, F. Rinderspacher, V. N. Bliznyuk, *Langmuir* **1997**, *13*, 2171–2176.
[5] E. R. Kleinfeld, G. S. Ferguson, *Science* **1994**, *265*, 370–373.
[6] S. Watanabe, S. L. Regen, *J. Am. Chem. Soc.* **1994**, *116*, 8855–8856.
[7] D. Beyer, T. M. Bohanon, W. Knoll, H. Ringsdorf, G. Elender, E. Sackmann, *Langmuir* **1996**, *12*, 2514–2518.
[8] G. Decher, J. Schmitt, L. Heiliger, H.-U. Siegmund, DE 4333107, **1995** [*Chem. Abstr.* **1995**, *123*, P202227y].
[9] T. Corner, *Adv. Polym. Sci.* **1984**, *62*, 95–142.
[10] a) Y. Zhou, M. L. Bruening, D. E. Bergbreiter, R. M. Crooks, M. Wells, *J. Am. Chem. Soc.* **1996**, *118*, 3773–3774; b) Y. Zhou, M. L. Bruening, Y. Liu, R. M. Crooks, D. E. Bergbreiter, *Langmuir* **1996**, *12*, 5519–5521; c) M. L. Bruening, Y. Zhou, G. Aguilar, R. Agee, D. E. Bergbreiter, R. M. Crooks, *ibid.* **1997**, *13*, 770–778.
[11] R. H. Wieringa, A. J. Schouten, *Macromolecules* **1996**, *29*, 3032–3034.
[12] The dendrimer diameters are based on estimates of molecular size based on size-exclusion chromatography (SEC) as determined by Dendritech, Midland, MI, USA (private communication to R. M. Crooks).
[13] M. Zhao, Y. Zhou, M. L. Bruening, D. E. Bergbreiter, R. M. Crooks, *Langmuir* **1997**, *13*, 1388–1391; M. Zhao, Y. Liu, D. E. Bergbreiter, R. M. Crooks, unpublished results.

 © WILEY-VCH Verlag GmbH, D-69451 Weinheim, 1997 0570-0833/97/3619-2116 $ 17.50+.50/0

Tetra-*tert*-butyltetraborane(6) $B_4H_2tBu_4$: A Derivative in the Series B_nH_{n+2}

Andreas Neu, Theo Mennekes, Ulli Englert, Peter Paetzold,* Matthias Hofmann, and Paul von Ragué Schleyer

Dedicated to Professor Gottfried Huttner on the occasion of his 60th birthday

In the series of tetraboranes B_4H_4, B_4H_6, B_4H_8, and B_4H_{10}, *arachno*-B_4H_{10} has been known for 85 years;[1] many *arachno* derivatives of the type B_4H_8L (L = Lewis base) represent well-characterized substances.[2] B_4Cl_4[3] and B_4R_4 (R = *t*Bu),[4] derivatives of the unknown B_4H_4, have also been known for years. All four tetraboranes were investigated by theoretical methods.[5]

We report here on the synthesis of $B_4H_2R_4$, a derivative of B_4H_6. When $RBBr_2$ is reduced with Na/K alloy in toluene, $B_4H_2R_4$ is obtained in 13% yield [Scheme 1, Eq. (a)]. The two boron-bound H atoms in the product do not originate from the solvent but apparently from *t*Bu groups, since $B_4H_2R_4$ does not contain deuterium when [D_8]toluene is used. The same product is formed in 74% yield when B_4R_4[4] in THF is reduced by Na/K alloy in the presence of [18]crown-6, and the anionic intermediate subsequently protonated by HCl [Scheme 1, Eq. (b)].

The NMR spectra of $B_4H_2R_4$ reveal the presence of one type of B atom and *t*Bu group, even at −80 °C. The signals of the two framework H atoms can be observed in the $^1H\{^{11}B\}$ NMR spectrum at −80 °C, but not at ambient temperature; a corresponding cross-peak is detected in the ^1H–^{11}B HMQC NMR spectrum. The molecule gives the highest peak in the mass spectrum (2%). Although a structural model could not be refined on the basis of X-ray diffraction data[6] of crystalline $B_4H_2R_4$, the tetrahedral structure could be deduced. All experimental findings support a structure that can be derived from a tetrahedral structure by adding two bridging H atoms across the opposite edges (D_{2d} symmetry).

To confirm this structural proposal, we performed ab initio calculations at the MP2(fc)/6-31G* level[7] for B_4H_6 and $B_4H_2Me_4$ as model compounds. Three minima could be localized on the potential hyperface (Figure 1). The lowest-energy

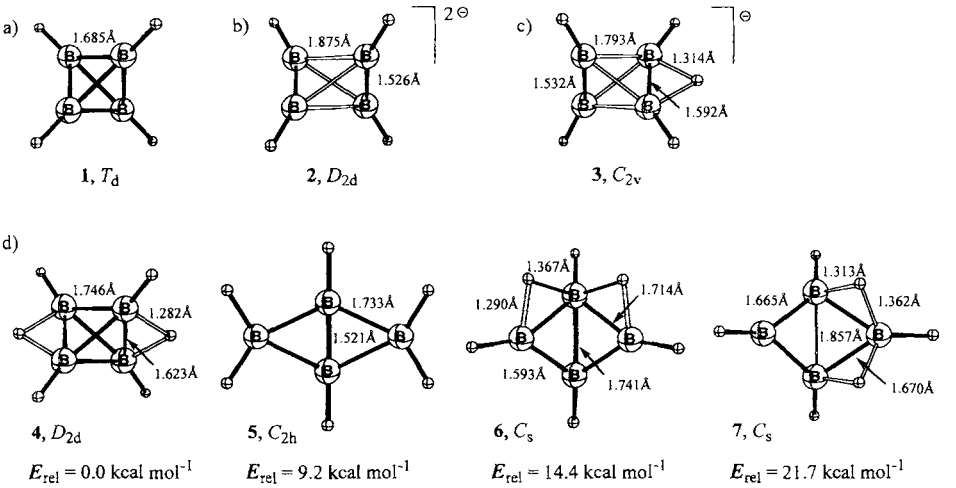

Figure 1. Geometries optimized at the MP2(fc)/6-31G* level: a) B_4H_4, b) $[B_4H_4]^{2-}$, c) $[B_4H_5]^-$, d) B_4H_6.

species corresponds to a stretched tetrahedron with two opposite hydrogen bridges (**4**, D_{2d} symmetry); the same structure is postulated for $B_4H_2R_4$. The two bridged edges (1.623 Å) are shortened and the four non-bridged edges (1.746 Å) are elongated with respect to those in B_4H_4 (1.685 Å).

Both the electron-deficient B_4H_4 and the electron-precise C_4H_4 exhibit T_d symmetry. The two *e* orbitals are unoccupied in B_4H_4 and completely occupied in C_4H_4. In the case of $B_4H_4^{2-}$, occupation of these orbitals by one electron pair causes a Jahn–Teller distortion from T_d to D_{2d} symmetry. The large difference in the B–B distances (1.526 versus 1.875 Å) is diminished by H bridges in $B_4H_5^-$ (1.592 versus 1.793 Å) and B_4H_6 (1.632 versus 1.746 Å). A similar situation is found for the tetramethyl derivatives (see Figure 2). The observed ^{11}B NMR shift of $\delta = 14.8$ is in very good agreement with that calculated for the D_{2d} structure of $B_4H_2Me_4$ with IGLO/DZ[8] ($\delta = 13.9$), leaving no doubt about the structure of $B_4H_2R_4$. The extreme change of $\Delta\delta = 120$ in the ^{11}B NMR signal by going from B_4R_4 ($\delta = 135.4$) to $B_4H_2R_4$ ($\delta = 14.6$) is worth mentioning.

Upon treating $B_4H_2R_4$ in tetrahydropyrane (L) with lithium, a bridging H atom is replaced by Li. Two solvent molecules are bound to the bridging Li atom in the crystalline product [Eq. (c)]. Only one type of BR fragment, Li cation, and cluster

$$B_4H_2R_4 + Li + 2L \longrightarrow (L_2Li)B_4HR_4 + 1/2H_2 \qquad (c)$$

H atom is recognized in the NMR spectra (^1H, ^7Li, ^{11}B, ^{13}C) of the product in [D_{10}]Et_2O. Upon cooling, the NMR signals split, and another set of signals for an isomeric product appears, which makes up one fifth of the total product at −80 °C. Two types of BR fragment as well as one type of Li cation and cluster H atom are observed for the major product at low temperature, pointing to a distorted tetrahedron of C_{2v} symmetry. The structure in which the opposite edges are bridged by an H and a Li atom is also present in the crystalline state. The coordination of

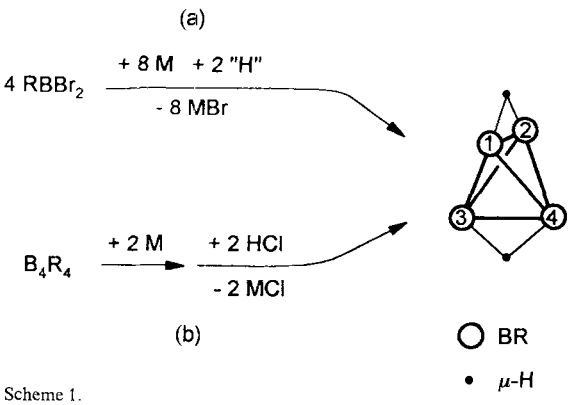

Scheme 1.

[*] Prof. Dr. P. Paetzold, A. Neu, Dr. T. Mennekes, Dr. U. Englert
Institut für Anorganische Chemie der Technischen Hochschule
D-52056 Aachen (Germany)
Fax: Int. code +(241)888-8288
e-mail: peter.paetzold@ac.rwth-aachen.de
Dr. M. Hofmann, Prof. Dr. P. von R. Schleyer
Institut für Organische Chemie der Universität Erlangen-Nürnberg (Germany)

 © WILEY-VCH Verlag GmbH, D-69451 Weinheim, 1997 0570-0833/97/3619-2117 $ 17.50+.50/0

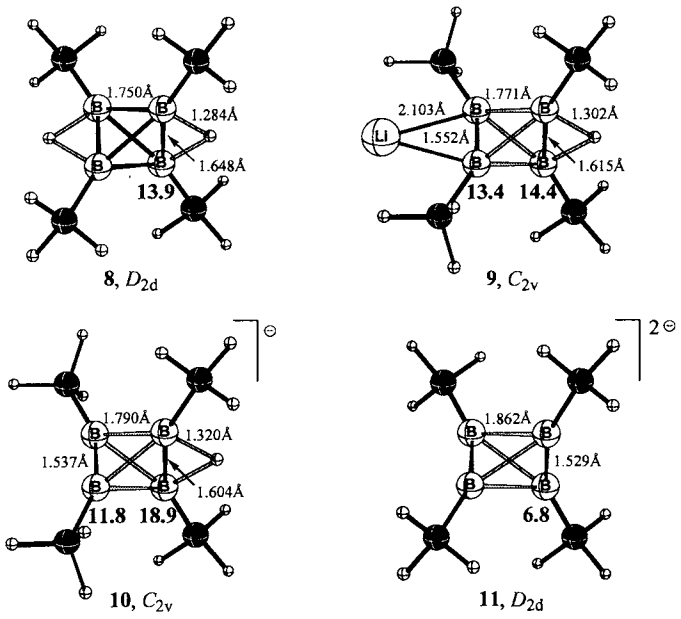

Figure 2. Geometries optimized at the MP2(fc)/6-31G* level and ^{11}B NMR shifts (boldface) calculated by IGLO/DZ for $B_4H_2Me_4$, LiB_4HMe_4, $[B_4HMe_4]^-$, and $[B_4Me_4]^{2-}$.

the Li cation by the solvent or by tetrahydropyrane remains obscure. The minor isomer observed at low temperature may represent a product that is dissociated into a solvated Li cation and the anion $[B_4HR_4]^-$; the fluctuation of the H atom between the six bridging positions, rapid even at $-80\,^{\circ}C$, results in simulated T_d symmetry in the NMR spectra. Rapid movement of the H atom and the more or less solvated Li cation apparently describes the predominating situation of LiB_4HR_4 in Et_2O at room temperature. In [D$_8$]THF as solvent, NMR signals are observed that are not principally altered upon cooling to $-80\,^{\circ}C$. These signals correspond to the minor isomer in Et_2O at low temperature. We suppose that the product dissociates into ions already at room temperature in the slightly more polar THF.

Molecules $(L_2Li)B_4HR_4$ of C_2 symmetry are found in the crystal (Figure 3). Again, the bridged edges (1.63 and 1.57 Å)

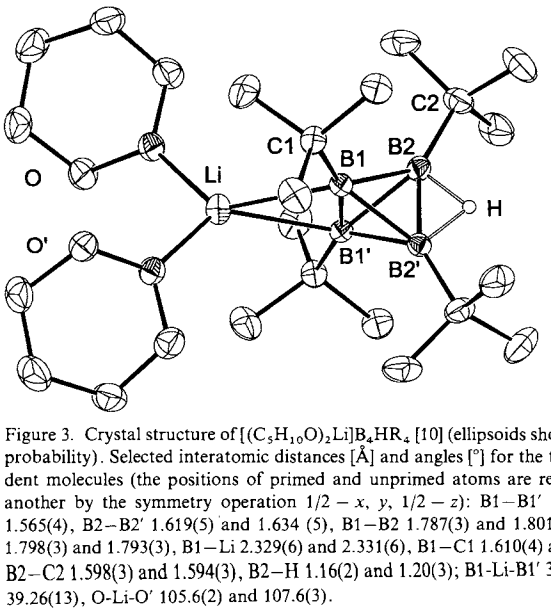

Figure 3. Crystal structure of $[(C_5H_{10}O)_2Li]B_4HR_4$ [10] (ellipsoids shown for 30% probability). Selected interatomic distances [Å] and angles [°] for the two independent molecules (the positions of primed and unprimed atoms are related to one another by the symmetry operation $1/2-x$, y, $1/2-z$): B1–B1′ 1.582(4) and 1.565(4), B2–B2′ 1.619(5) and 1.634 (5), B1–B2 1.787(3) and 1.801(3), B1–B2′ 1.798(3) and 1.793(3), B1–Li 2.329(6) and 2.331(6), B1–C1 1.610(4) and 1.620(3), B2–C2 1.598(3) and 1.594(3), B2–H 1.16(2) and 1.20(3); B1-Li-B1′ 39.79(14) and 39.26(13), O-Li-O′ 105.6(2) and 107.6(3).

are considerably shorter than the four nonbridged edges (1.79 and 1.80 Å). The calculated geometric parameters for LiB_4HM_4 (**9**, C_{2v} symmetry, Figure 2) are in accordance with the experimental values for $(L_2Li)B_4HR_4$. Only the distances between the B atoms and the Li atom are too short, as expected, since the Li atom is unsolvated in the model compound. As it is bound to the cluster by ionic forces, the influence of lithium on the cluster geometry is smaller than that of covalently bound hydrogen bridges. The ^{11}B NMR signals calculated for LiB_4HMe_4 and measured for LiB_4HR_4 at $-80\,^{\circ}C$ in ether are in excellent agreement (see Figure 2).

Closed polyhedral boranes of the type B_nH_{n+2} are in general not available. This is in contrast to the corresponding anions $[B_nH_n]^{2-}$ ($n = 6-12$), which are more or less well-known as stable salts $M[B_nH_n]$. In the larger anions $[B_nH_n]^{2-}$ ($n = 10-12$) the negative charge is distributed over a large polyhedral skeleton. The anions are therefore very weak Brønsted bases, whereas the corresponding hypothetical acids B_nH_{n+2} must be very strong acids. The basicity of the smaller anion $[B_6H_6]^{2-}$ ($pK_B = 7$) is in the range of weak but not very weak bases.[11] The basicity of a hypothetical anion $[B_4R_4]^{2-}$, in which the negative charge can only be distributed over a tetrahedral skeleton, must be very strong, since even our single-charged lithium tetraborate LiB_4HR_4 is completely protonated by the weak acid $(Me_3Si)_2NH$ to give the borane $B_4H_2R_4$. In contrast $B_4H_2R_4$ cannot be deprotonated by strong bases such as LiMe, LiBu, or K[BHEt$_3$]. We shall report on experimental and theoretical results concerning the *nido*-tetraborane $B_4H_4R_4$ and the corresponding anion $[B_4H_3R_4]^-$ in the near future.

Experimental Section

Tetra-*tert*-butyltetraborane(6): Na/K alloy (20 g) was added to dibromo-*tert*-butylborane [12] (51.30 g, 0.225 mmol) in toluene (120 mL). The mixture boiled at reflux for 15 min without additional heating, and cooled to room temperature within 3 h. The solids were then removed by filtration over a G4 frit. The volatile components were transfered from the filtrate finally at 80 °C/0.001 Torr into a condenser that was cooled to $-196\,^{\circ}C$. The volatile material was treated with butyllithium in hexane (20 mL, 1.6 M) at 0 °C. The solvent was then removed in vacuo at room temperature. After condensation of the crude product at 70 °C/0.001 Torr, colorless $B_4H_2R_4$ (2.00 g, 13%) was crystallized from acetonitrile; m.p. 112 °C. The same product was obtained by dropwise addition of tetra-*tert*-butyltetraborane [4] (100 mg, 0.37 mmol) in THF (2 mL) to a mixture of Na/K alloy (0.10 g) and [18]crown-6 (190 mg, 0,72 mmol) at 0 °C. After the insoluble components were removed by filtration, a solution of HCl in Et_2O (1 mL, 2 M) was added, the solvent removed in vacuo, and the product again dissolved in hexane. After renewed filtration, removal of hexane in vacuo, and condensation of the crude product, pure $B_4H_2R_4$ was crystallized from acetonitrile (75 mg, 74%). ^{1}H NMR (500 MHz, [D$_8$]toluene, $-80\,^{\circ}C$): $\delta = 0.85$ (br, μ-H), 1.05 (s, *t*Bu); ^{11}B NMR (160.4 MHz, [D$_8$]toluene): $\delta = 14.8$; ^{13}C NMR (125.7 MHz, [D$_8$]toluene, $-80\,^{\circ}C$): $\delta = 31.3$ (q, Me), 21.3 (br, BC).

Bis(tetrahydropyrane)lithium tetra-*tert*-butylhydrotetraborate: A mixture of lithium (40 mg, 5.8 mmol) and $B_4H_2R_4$ (200 mg, 0.73 mmol) in tetrahydropyrane (4 mL) was treated with ultrasound for 10 h. The volatile components were removed at 11 mbar, and the product dissolved in warm hexane. The hot solution was filtered over diatomaceous earth. All reaction vessels and the kieselguhr had to be dried carefully with $HN(SiMe_3)_2$. Pure product crystallized upon cooling the solution (140 mg, 42%). ^{1}H{^{11}B} NMR (500 MHz, [D$_{10}$]Et$_2$O, 22 °C): $\delta = 0.29$ (μ-H), 1.00 (s, *t*Bu), 1.53, 1.62, 3.60 (3mc, 2:1:2, CH$_2$); ^{7}Li NMR (194.2 MHz, [D$_{10}$]Et$_2$O, 22 °C): $\delta = 1.24$; ^{11}B NMR (160.4 MHz, [D$_{10}$]Et$_2$O, 22 °C): $\delta = 14,9$; ^{13}C NMR (125.6 MHz, [D$_{10}$]Et$_2$O, 22 °C): $\delta = 24.3, 27.4, 69.3$ (3t, 1:2:2, CH$_2$), 20.1 (br, BC), 34.1 (q, Me); measurements at $-80\,^{\circ}C$: ^{1}H{^{11}B} NMR: $\delta = -0.08$ (μ-H), 0.92, 1.03, 1.08 (3s, ≈5:5:2, *t*Bu), 1.57, 1.64, 1.86, 3.50, 4.11 (5mc, 1:4:1:2:2, CH$_2$); ^{7}Li NMR: $\delta = -1.21, 1.27$ (1:5); ^{11}B NMR: $\delta = 13.3, 15.5, 20.6$ (≈5:5:2); ^{13}C NMR: $\delta = 23.6, 26.7, 69.1$ (3t, 1:2:2, CH$_2$), 34.1, 33.3, 34.5 (3q); MS (Finnigan MAT 95; 70 eV): $M_{found} = 280.343$, $M_{calcd} = 280.343$ ($LiB_4HR_4^+$, 100%); elemental analysis calcd for $C_{26}H_{57}B_4LiO_2$: C 69.10, H 12.71, B 9.57, Li 1.55; found: C 68.67, H 12.75, B 9.57, Li 1.55.

Received: April 24, 1997 [Z 10380 IE]
German version: *Angew. Chem.* **1997**, *109*, 2211–2213

Keywords: ab initio calculations · boron · clusters · electron deficiency · tetraborane

 © WILEY-VCH Verlag GmbH, D-69451 Weinheim, 1997 0570-0833/97/3619-2118 $ 17.50+.50/0

[1] A. Stock, C. Massenez, *Ber. Dtsch. Chem. Ges.* **1912**, *45*, 3539–3568.

[2] *Gmelin Handbook of Inorganic Chemistry*, 8th ed. *Boron Compounds 3rd Suppl. Vol. 1*, Springer, Berlin, **1987**, pp. 100–103.

[3] G. Urry, T. Wartik, H. I. Schlesinger, *J. Am. Chem. Soc.* **1952**, *74*, 5809.

[4] T. Daran, J. A. Morrison, *J. Chem. Soc. Chem. Commun.* **1981**, 250–251; T. Mennekes, P. Paetzold, R. Boese, D. Bläser, *Angew. Chem.* **1991**, *103*, 199–200; *Angew. Chem. Int. Ed. Engl.* **1991**, *30*, 173–175.

[5] M. Bühl, J. Gauss, M. Hofmann, P. von R. Schleyer, *J. Am. Chem. Soc.*, **1993**, *115*, 12385–12390.

[6] Crystals of $B_4H_2R_4$ exhibited measurable intensities of the reflections only at small diffraction angles. Crystal data at 243 K gave the orthorhombic space group *Pba*2 (no. 32); $a = 33.56(1)$, $b = 28.74(1)$, $c = 9.066(5)$ Å, $V = 8743(9)$ Å^3, $Z = 16$, $\rho_{calcd} = 0.832$ g cm^{-3}, $\mu(Cu_{K\alpha}) = 2.79$ cm^{-1}, $F(000) = 2464$. Efforts to solve the structure by direct methods gave three symmetry-independent molecular fragments (substituted tetrahedra) in a general position and two fragments with crystallographic C_2 symmetry; unconstrained refinement was not possible, and refinement with rigid idealized *t*Bu groups yielded unweighted factors R of about 0.25 and large displacement parameters of the peripheral atoms. More demanding disorder models did not work because of the small number of significant intensity data. Low-temperature data could not be recorded because of a phase transition.

[7] Optimizations of energy and calculations of frequency were performed at the MP2(fc)/6-31G* level with the Gaussian 94 program: M. J. Frisch, G. W. Trucks, H. B. Schlegel, P. M. W. Gill, B. G. Johnson, M. A. Robb, J. R. Cheeseman, T. Keith, J. A. Petersson, J. A. Montgomery, K. Raghavachari, M. A. Al-Laham, V. G. Zakrzewski, J. Y. Ortiz, J. B. Foresman, J. Cioslowski, B. B. Stefanov, A. Nanayakkara, M. Challcombe, C. Y. Peng, P. Y. Ayala, W. Chen, M. W. Wong, J. L. Andres, E. S. Replogle, R. Gomperts, R. L. Martin, D. J. Fox, J. S. Blinkley, D. J. DeFrees, J. Baker, J. J. P. Stewart, M. Head-Gordon, C. Gonzalez, J. A. Pople, Gaussian Inc., Pittsburgh, PA, USA **1995**. Relative energies correspond to the MP2(fc)/6-31G* level, and include corrections by the scaling factor 0.93 with respect to the zero-point vibrational energy.

[8] a) W. Kutzelnigg, *Israel J. Chem.* **1980**, *19*, 193–200; b) M. Schindler, W. Kutzelnigg, *J. Chem. Phys.* **1982**, *76*, 1919–1933; c) W. Kutzelnigg, U. Fleischer, M. Schindler, *NMR: Basic Princ. Prog.* **1990**, *23*, 165. DZ designates Huzinga's "double-zeta" basis set in the recommended contraction: S. Huzinaga, Approximate Atomic Wave Functions, University of Alberta, Edmonton, **1971**.

[9] Crystal structure analysis: ENRAF-Nonius CAD4; $Mo_{K\alpha}$ radiation, graphite monochromator; intensity data were collected at 203 K in the $\omega - 2\theta$ scan mode. $[(C_5H_{10}O)_2Li]B_4HR_4$: colorless, transparent parallelepiped, 0.80 × 0.72 × 0.48 mm, monoclinic space group $P2/n$ (no. 13); $a = 14.463(3)$, $b = 12.634(3)$, $c = 18.395(6)$ Å, $\beta = 112.05(2)°$, $V = 3115(1)$ Å^3, $Z = 4$, $\rho_{calcd} = 0.963$ g cm^{-3}, $\mu(Mo_{K\alpha}) = 0.51$ cm^{-1}, $F(000) = 1008$; of 9521 reflections with $3 < \theta < 28°$, 3752 were independent ($I > \sigma(I)$) and used for the structure solution [13]; refinement with 528 parameters [14]; the H atoms were refined with isotropic displacement parameters; $R = 0.063$, $R_w = 0.056$, $w^{-1} = \sigma^2(F_o)$; the asymmetric unit contains two independent molecules of crystallographic C_2 symmetry. Crystallographic data (excluding structure factors) for the structures reported in this paper have been deposited with the Cambridge Crystallographic Data Centre as supplementary publication no. CCDC-100346. Copies of the data can be obtained free of charge on application to The Director, CCDC, 12 Union Road, Cambridge CB21EZ, UK (fax: int. code +(1223)336-033; e-mail: deposit@chemcrys.cam.ac.uk).

[10] A. L. Spek, PLATON 94, Utrecht, **1994**.

[11] W. Preetz, A. Heinrich, J. Thesing, *Z. Naturforsch. B* **1988**, *43*, 1319–1326.

[12] P. A. McCusker, E. C. Ashby, H. S. Makowski, *J. Am. Chem. Soc.* **1957**, *79*, 5182–5188.

[13] G. M. Sheldrick, SHELXS-86, Göttingen, **1986**.

[14] B. A. Frenz and ENRAF-Nonius, SDP, version 5.0, **1989**.

A New Strategy for Extending *N*-Acyl Imides as Chiral Auxiliaries for Aldol and Diels–Alder Reactions: Application to an Enantioselective Synthesis of α-Himachalene**

David A. Evans,* David H. Brown Ripin, Jeffrey S. Johnson, and Eileen A. Shaughnessy

The development of enantioselective transformations involving the ketone functional group continues to be a problem of general interest in asymmetric synthesis due to the ubiquity of this functionality. While chiral Lewis acids have been employed to promote enantioselective aldol and Diels–Alder reactions of carboxylic acid derivatives and aldehydes, stereocontrol is generally low in reactions of ketones due to the lack of differentiation in Lewis acid coordination to the two nonbonding electron pairs of the carbonyl group.[1] One strategy for creating a stereochemical bias in ketone-derived enolate–electrophile reactions [Eq. (1)] or in the transformations of α,β-unsaturated ketones such as the Diels–Alder reaction [Eq. (2)] has been developed. In

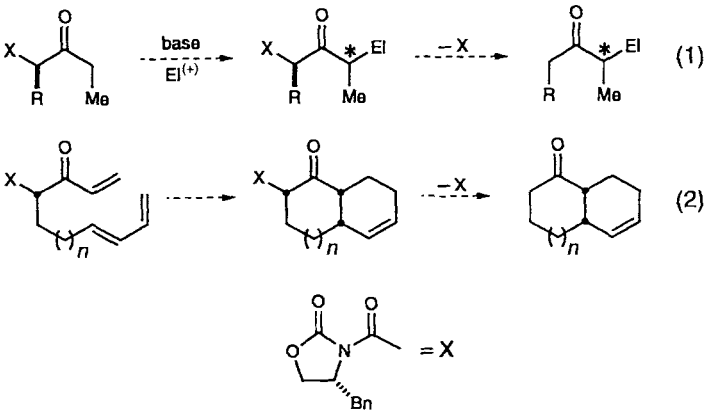

these processes, a stereogenic center, created by the incorporation of the removable substituent X, is positioned proximal to the trigonal carbon centers undergoing reaction, thus establishing a diastereofacial bias for the transformation. The implementation of this strategy for enolates and enolsilanes of α-trialkylsilyl ketones [Eq. (1), X = SiR_3] has been reported by Enders and Lohray,[2, 3] while Heathcock and Masamune have demonstrated that the aldol and Diels–Alder reactions of α-alkoxyketones [Eqs. (1) and (2), X = OR] are highly diastereoselective.[4]

Here we define the removable auxiliary X = COX_c (X_c = 4-benzyl-2-oxazolidinon-3-yl), which can be used in the previously described enolate bond constructions and combined with a mild hydrolysis/decarboxylation procedure to extend the utility of β-ketoimides[5] to the production of enantiopure ketones [Eq. (1)]. We also demonstrate that this strategy is applicable to the implementation of enantioselective Diels–Alder reactions [Eq. (2), X = COX_c].

We have previously demonstrated that the β-ketoimide **1**[6] undergoes metal ion dependent stereoselective *syn*-[7] and *anti*-aldol[6] reactions. In addition, the titanium enolate[8] derived

[*] Prof. D. A. Evans, D. H. B. Ripin, J. S. Johnson, E. A. Shaughnessy
Department of Chemistry and Chemical Biology, Harvard University
Cambridge, MA 02138 (USA)
Fax: Int. code +(617)495-1460
e-mail: evans@chemistry.harvard.edu

[**] Financial support was provided by the U. S. National Science Foundation and the National Institutes of Health.

 © WILEY-VCH Verlag GmbH, D-69451 Weinheim, 1997 0570-0833/97/3619-2119 $ 17.50+.50/0

from **1** has also been shown to undergo diastereoselective orthoester acylation.[9]

The focus of the current investigation has been the development of a mild decarboxylation process that might be applied to the enolate-derived reaction products that are prone to epimerization and/or elimination.[10] A successful solution to this transformation is transesterification with ethanethiolate[11] followed by silver(I)-promoted hydrolysis/decarboxylation[12] of the resulting thioester (Scheme 1).

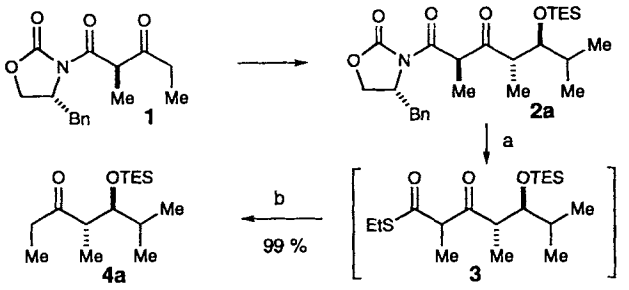

Scheme 1. Thiolate displacement, hydrolysis, and decarboxylation of β-oxoimide **2a**[6]: a) EtSH, KH, THF, 25 °C; b) $AgNO_3$, 2,6-lutidine, THF/H_2O (5/1), 25 °C. TES = triethylsilyl.

Treatment of **2a** with potassium ethanethiolate afforded a mixture of C_α-diastereomeric β-ketothioesters **3**.[13] Subjecting thioesters **3** to silver(I)-promoted hydrolysis and subsequent decarboxylation at ambient temperature provided ethyl ketone **4a** over the course of 48 hours. In most instances the reaction time may be reduced without compromising yield by mild heating during the hydrolysis step (70 °C, 3 h). The two steps may be merged into a single-flask operation (see Experimental Section). The decarboxylation of β-ketoimide-derived aldol and orthoester acylation adducts **2a–2f** was investigated using this procedure (Table 1). The mild reaction conditions accommodate the presence of ketal, silyl ether, alkene, and acetate functionalities.

Table 1. One-flask decarboxylation of representative β-ketoimide adducts[a].

Imide	Product	Yield [%][b]	*t* [h][c]
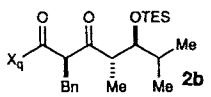 **2b**	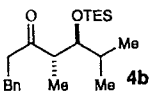 **4b**	98	24
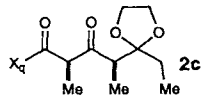 **2c**	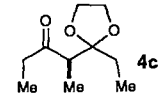 **4c**	79 74	24 3[d]
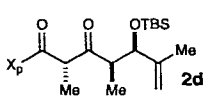 **2d**	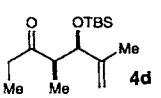 **4d**	88	48
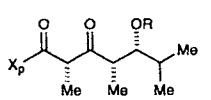 **2e**, R = TBS	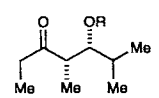 **4e**	93 92	48 3[d]
2f, R = Ac	**4f**	83	48

[a] X_p = (*S*)-4-benzyl-2-oxazolidinon-3-yl, X_q = (*R*)-4-benzyl-2-oxazolidinon-3-yl, TBS = *tert*-butyldimethylsilyl. [b] Yield after purification. [c] Reaction time for the hydrolysis step. [d] Hydrolysis run at reflux.

These ketone decarboxylation products are useful building blocks for the rapid synthesis of extended polypropionate chains.[14] In the example shown in Scheme 2, polypropionate **5**, containing six stereocenters, was synthesized in four steps (63 % yield) from β-ketoimide **1**; all stereocenters were formed with a combined diastereoselectivity exceeding 95 %.[14e]

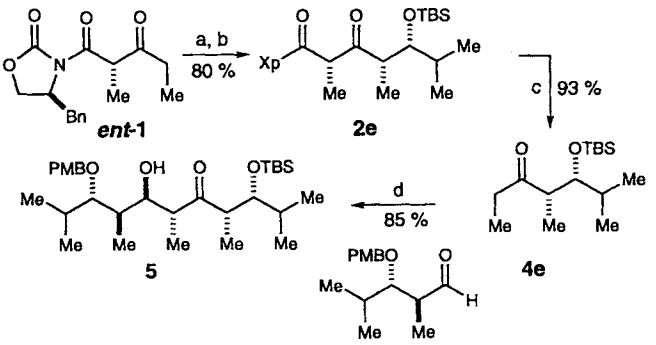

Scheme 2. Strategy for the rapid assembly of polypropionate chains. a) 1. $TiCl_4$, Et_3N, 0 °C, 2. *i*PrCHO, −78 °C; b) TBSOTf, 2,6-lutidine, −78 °C; c) 1. EtSH, KH, 2. $AgNO_3$, 2,6-lutidine, H_2O; d) *c*hex$_2$BCl, Et_3N, −78 °C. OTf = trifluoromethanesulfonate, PMP = 4-methoxybenzyl.

This auxiliary-based methodology can be applied to achieve control of the absolute stereochemistry in the Diels–Alder process [Eq. (2)]. In this context, we investigated an intramolecular Diels–Alder reaction that comprises the pivotal bond construction in an enantioselective synthesis of the sesquiterpene α-himachalene (**11**).[15] Dienimide **6**, prepared in five steps from 3,3-dimethyl-4-propenal, underwent a highly diastereoselective boron-mediated aldol reaction with acrolein to afford the allylic alcohol **7** as the sole isomer (Scheme 3).[16] Compound **7** was subjected to Parikh–Doering oxidation[17] and the resulting trienone **8** was treated with $ZnBr_2$ (0 °C, CH_2Cl_2, 1.5 h) to effect cycloaddition (78 % yield, two steps) to the desired crystalline *endo* adduct **9** (97:3 diastereoselectivity), which was isolated as

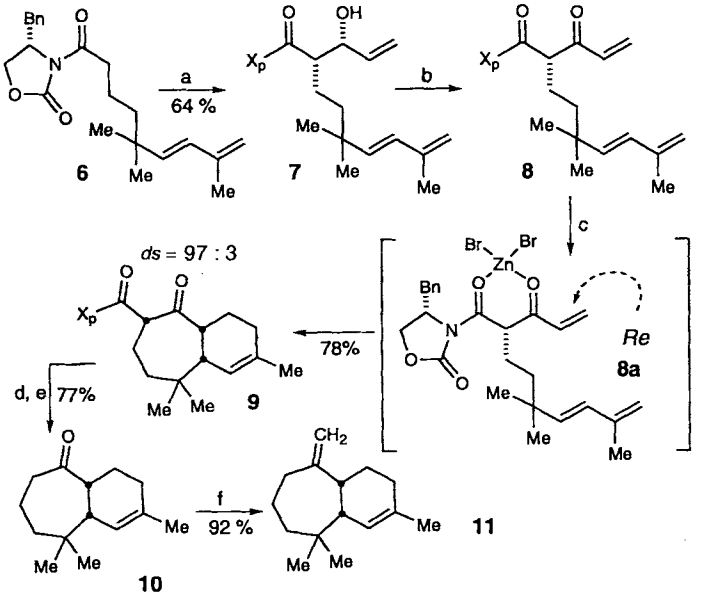

Scheme 3. Enantioselective synthesis of α-himachalene (**11**). a) 1. Bu_2BOTf, *i*Pr_2NEt, isoprene, 0 °C, 2. acrolein, −78 °C; b) SO_3·pyridine, DMSO/CH_2Cl_2, *i*Pr_2NEt, −10 °C; c) $ZnBr_2$, 0 °C; d) LiSEt; e) $AgNO_3$, 2,6-lutidine, THF/H_2O, 70 °C; f) $[Cp_2Ti(\mu\text{-Cl})(\mu\text{-CH}_2)AlMe_2]$, −40 °C.

 © WILEY-VCH Verlag GmbH, D-69451 Weinheim, 1997 0570-0833/97/3619-2120 $ 17.50+.50/0

a single diastereomer by chromatography. The sense of asymmetric induction in this cycloaddition is consistent with a Lewis acid catalyzed Diels–Alder reaction on the *s-cis* $ZnBr_2$ complex **8a**.

In analogy to previous experiments, Diels–Alder adduct **9** was transformed to the corresponding β-ketothioester in 90% yield and smoothly decarboxylated (70 °C, 24 h) to afford ketone **10** in 86% yield without epimerization at the ring fusion. The synthesis was completed by treatment of **10** with Tebbe reagent[18] to afford synthetic α-himachalene (**11**) (92% yield), whose spectroscopic and analytical data are identical in all respects to literature values (^{1}H NMR, IR, TLC, $[\alpha]_D$).[15]

The removable auxiliary X = COX_c described here should prove useful in enantioselective ketone-based bond constructions. Although the methodology has been highlighted with aldol and Diels–Alder reactions, absolute stereochemical control of other transformations such as the Michael reaction should also be possible. Studies extending the scope of these concepts are currently underway.

Experimental Section

General one-flask procedure for the decarboxylation of β-ketoimides: A stirred suspension of KH (1.2 mmol) in THF (10 mL) under argon was charged with EtSH (1.3 mmol) and gas evolved. The white suspension was stirred for 1 h before a solution of β-oxoimide (1 mmol) in THF (10 mL) was added by cannula. The reaction mixture was stirred until the starting material had been consumed. To the reaction mixture was added water (4 mL) and 2,6-lutidine (10 mmol), followed by $AgNO_3$ (2.5 mmol). The reaction mixture was protected from light and stirred for two days. The pale yellow suspension was filtered through Celite with ether, and the organic solution was extracted between ether (50 mL) and aqueous $CuSO_4$ solution (50 mL). The ether layer was separated, dried over $MgSO_4$, and concentrated in vacuo. Chromatography on silica gel using an appropriate solvent mixture provided pure ketone.

Received: April 7, 1997 [Z10313IE]
German version: *Angew. Chem.* **1997**, *109*, 2208–2210

Keywords: aldol reactions · chiral auxiliaries · decarboxylations · Diels–Alder reactions · himachalene

[1] S. Shambayati, S. L. Schreiber in *Comprehensive Organic Synthesis, Vol. 1* (Eds.: B. M. Trost, I. Fleming), Pergamon, New York, **1991**, pp. 283–324.
[2] a) D. Enders, B. B. Lohray, *Angew. Chem.* **1988**, *100*, 594–596; *Angew. Chem. Int. Ed. Engl.* **1988**, *27*, 581–582; b) B. B. Lohray, D. Enders, *Helv. Chim. Acta* **1989**, *72*, 980–984; c) B. B. Lohray, R. Zimbiniski, *Tetrahedron Lett.* **1990**, *31*, 7273–7276.
[3] Another important approach to the construction of ketone-derived chiral auxiliaries has been through the use of chiral metalloenamines: a) S. F. Martin in *Comprehensive Organic Synthesis, Vol. 2* (Eds.: B. M. Trost, I. Fleming), Pergamon, New York, **1991**, pp. 475–502.
[4] a) C. H. Heathcock, M. C. Pirrung, C. T. Buse, J. P. Hagen, S. D. Young, J. E. Sohn, *J. Am. Chem. Soc.* **1979**, *101*, 7077–7079; b) S. Masamune, W. Choy, F. A. Kerdesky, B. Imperiali, *J. Am. Chem. Soc.* **1981**, *103*, 1566–1568; c) S. Masamune, L. A. Reed III, J. T. Davis, W. Choy, *J. Org. Chem.* **1983**, *48*, 1154–1156.
[5] D. A. Evans, M. D. Ennis, T. Le, N. Mandel, G. Mandel, *J. Am. Chem. Soc.* **1984**, *106*, 1154–1156.
[6] The experimental details for the synthesis of **1** have been reported: D. A. Evans, H. P. Ng, J. S. Clark, D. L. Rieger, *Tetrahedron* **1992**, *48*, 2127–2142.
[7] D. A. Evans, J. S. Clark, R. Metternich, V. J. Novack, G. S. Sheppard, *J. Am. Chem. Soc.* **1990**, *112*, 866–868.
[8] D. A. Evans, F. Urpi, T. C. Somers, J. S. Clark, M. T. Bilodeau, *J. Am. Chem. Soc.* **1990**, *112*, 8215–8216.
[9] a) D. A. Evans, H. P. Ng, D. L. Rieger, *J. Am. Chem. Soc.* **1993**, *115*, 11446–11459 (see the transformation **7** → **18** in Scheme VIII); b) D. A. Evans, A. M. Ratz, B. E. Huff, G. S. Sheppard, *J. Am. Chem. Soc.* **1995**, *117*, 3448–3467 (see the transformation **4** → **17** in Scheme VII).
[10] Initial studies utilizing the Krapcho decarboxylation conditions (DMSO, H_2O, 140 °C) on β-oxoimide aldol adducts afforded only moderate yields of the desired ketone products accompanied by significant amounts of β-elimination: a) A. P. Krapcho, *Synthesis* **1982**, 805–822, b) 893-914.
[11] R. E. Damon, G. M. Coppola, *Tetrahedron Lett.* **1990**, *31*, 2849–2852.
[12] a) E. J. Corey, M. C. Bock, *Tetrahedron Lett.* **1975**, 3269–3270; b) R. Schwyzer, C. Hurlimann, *Helv. Chim. Acta* **1954**, *18*, 155–166.
[13] Thiophenolate and 2-methyl-2-propanethiolate both failed to react, while benzylthiolate provides results comparable to those of ethanethiolate.
[14] a) J. L. Duffy, T. P. Yoon, D. A. Evans, *Tetrahedron Lett.* **1995**, *36*, 9245–9248; b) D. A. Evans, M. G. Yang, M. J. Dart, J. L. Duffy, *ibid.* **1996**, *37*, 1957–1960; c) D. A. Evans, M. G. Yang, M. J. Dart, J. L. Duffy, A. S. Kim, *J. Am. Chem. Soc.* **1995**, *117*, 9598–9599; d) D. A. Evans, D. L. Rieger, M. T. Bilodeau, F. Urpi, *J. Am. Chem. Soc.* **1991**, *113*, 1047–1049; e) D. A. Evans, M. J. Dart, J. L. Duffy, D. L. Rieger, *ibid.* **1995**, *117*, 9073–9074.
[15] a) T. C. Joseph, S. Dev, *Tetrahedron Lett.* **1961**, 216–222; b) *Tetrahedron* **1968**, *24*, 3841–3852, 3853–3859; c) W. Oppolzer, R. L. Snowden, *Helv. Chim. Acta* **1981**, *64*, 2592–2597; d) E. Wenkert, K. Naemura, *Synth. Comm.* **1973**, *3*, 45–48.
[16] D. A. Evans, J. Bartroli, T. L. Shih, *J. Am. Chem. Soc.* **1981**, *103*, 2127–2129.
[17] J. R. Parikh, W. von E. Doering, *J. Am. Chem. Soc.* **1967**, *89*, 5505–5507.
[18] S. H. Pine, R. Zahler, D. A. Evans, R. H. Grubbs, *J. Am. Chem. Soc.* **1980**, *102*, 3270–3272.

One-Component Catalysts for Thermal and Photoinduced Ring Opening Metathesis Polymerization

Andreas Hafner,* Andreas Mühlebach, and Paul A. van der Schaaf

New generations of stereospecific olefin polymerization catalysts have catapulted the polymer industry into a new area. A large variety of thermoplastic materials, based on α-olefins, of well-defined tacticity and block length are expected to be commercialized in the near future.[1] A similar development can be foreseen for thermoset materials. In this respect ring opening metathesis polymerization (ROMP)[2] offers new types of polymers with attractive mechanical and electrical properties. Currently applied industrial catalysts for ROMP are multicomponent systems based on early transition metal complexes and water-sensitive alkylaluminum cocatalysts. In the mid 1980s the first well-defined, one-component catalysts for ROMP were developed by Osborn (e. g., $[WCl_2(=CHCMe_3)(OR)_2]$)[3] and Schrock (e. g., $[Mo(=CHCMe_3)(=NAr)(OR)_2]$).[4] However, these catalysts are air- and moisture-sensitive as well, and sparsely tolerate monomers bearing protic substituents, fillers, or other additives.

In contrast to early transition metal catalysts, ruthenium- and osmium-based complexes are water-stable and possess remarkable tolerance towards most functional groups.[5] Therefore, the use of these catalysts goes far beyond the classical scope of olefin-metathesis reactions.

When we started our work in the field of ROMP by studying the reactivity of $[Ru(H_2O)_6]^{2+}$, we were able to prepare polymers and copolymers from cyclic olefins containing a large variety of functional groups.[6] Using the concept of photoinduced arene displacement, we developed the first photocatalysts for ROMP (PROMP) by generating $[Ru(H_2O)_6]^{2+}$ from $[Ru(\eta^6\text{-arene})_2]^{2+}$.[7, 8] A disadvantage of these catalysts is their cationic character, which restricts their applicability to polar environments, and their moderate reactivities. Therefore, we focused our attention on more soluble and more active arene complexes of ruthenium and osmium.

In 1992 Grubbs et al. reported the synthesis of the first well-defined, metathesis-active ruthenium–carbene complex by ring opening of a substituted cyclopropene with $[RuCl_2(PPh_3)_3]$.[9]

[*] Dr. A. Hafner, Dr. A. Mühlebach, Dr. P. A. van der Schaaf
Ciba Specialty Chemicals Inc.
Additives Research
CH-1723 Marly 1 (Switzerland)
Fax: Int. code +(26)435-6219
e-mail: andreas.hafner@chma.mhs.ciba.com

 © WILEY-VCH Verlag GmbH, D-69451 Weinheim, 1997 0570-0833/97/3619-2121 $ 17.50+.50/0

In 1995 Noels et al. reported the in situ formation of carbene complexes from arene ruthenium phosphane complexes and (trimethylsilyl)diazomethane.[10] These studies showed that the cone angle θ of the coordinating phosphane determines the activity of the catalyst. We also investigated the photoactivity of a series of arene ruthenium phosphane and arene osmium phosphane complexes.[11]

Osmium complexes of the type $[Os(p\text{-cymene})Cl_2(PR_3)]$ (R = cyclohexyl (Cy; **1**), *i*Pr (**2**), *n*Bu (**3**), Ph (**4**), Me (**5**), $C_6H_4CH_3$-3 (*m*-Tol; **6**)) do not initiate the thermal polymerization of norbornene (NBE). However, when they were activated by UV irradiation (200-W Hg lamp, 5 min), active ROMP catalysts were obtained. The results of the photoinduced polymerization of NBE in toluene initiated by **1**–**6** are depicted in Figure 1a. Figure 1b shows the comparison of ROMP and PROMP activity for **1**.

Active photocatalysts were obtained with the sterically demanding phosphane ligands PCy_3 and $P\textit{i}Pr_3$ ($\theta = 170$ and 160°, respectively), whereas very slow or no polymerization was observed for complexes with less bulky phosphanes (PPh_3, $P\textit{n}Bu_3$, or Pme_3; $\theta = 145$, 130, and 120°, respectively). Surprisingly, **6** ($\theta = 165°$) was inactive as well.

The corresponding ruthenium complexes $[Ru(p\text{-cymene})Cl_2(PR_3)]$ (R = Cy (**7**), *n*Bu (**8**), *m*-Tol (**9**)) showed much higher reactivity for NBE polymerization;[12] none of these complexes was thermally latent towards NBE. Complex **7** was already known to initiate NBE polymerization without activation of diazomethane derivatives as cocatalyst (80% poly(NBE) after 15 min at 50 °C).[13] Both **8** and **9** yield traces of poly(NBE) after 1 h at 80 °C. However, under similar conditions **8** yields 80% poly(NBE) when irradiated for 5 min at room temperature.

The low reactivity of **6** and **9** can be explained by the work of von Philipsborn et al.[11i] The ^{187}Os NMR chemical shift for arene osmium phosphane complexes, including **1**–**6**, correlates extremely well with Toleman's steric parameters.[14] The reported θ for P*m*-Tol_3 is 165°, assuming C_{3v} symmetry, whereas a value of 150° was measured with the chemical-shift method. This can be explained by a nonsymmetrical orientation of the phenyl rings of the phosphane ligand in **9**.[15] To have direct proof for the proposed importance of the steric parameters (for example the asymmetry of the P*m*-Tol_3 ligand), X-ray structure determinations of **7** and **9** were carried out (Figure 2).[16]

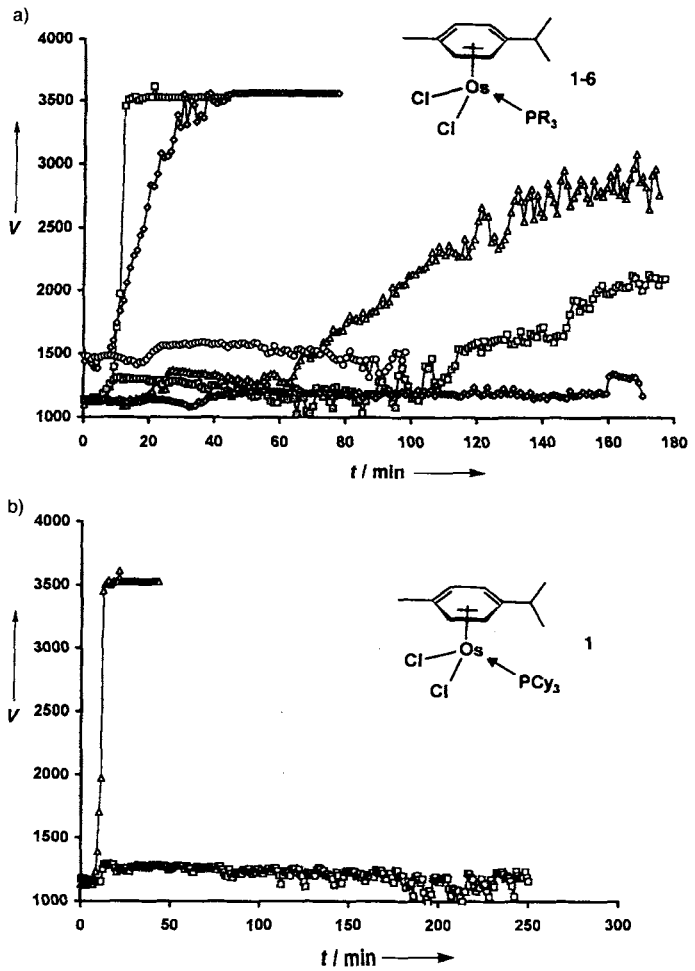

Figure 1. a) Real-time viscosimetric measurements of the photopolymerization of norbornene in toluene (10 wt%) with **1**–**6** (2 mol% each; □: R = Cy (**1**); ◇: R = *i*Pr (**2**); △: R = *n*Bu (**3**); ○: R = Ph (**4**); □: R = Me (**5**); ◇: R = *m*-Tol (**6**)). b) Thermal latency versus the photoactvity of **1** in the polymerization of norbornene (△: 30 °C, UV irradiation; □: 80 °C, without irradiation). *V* = viscosity (arbitrary units).

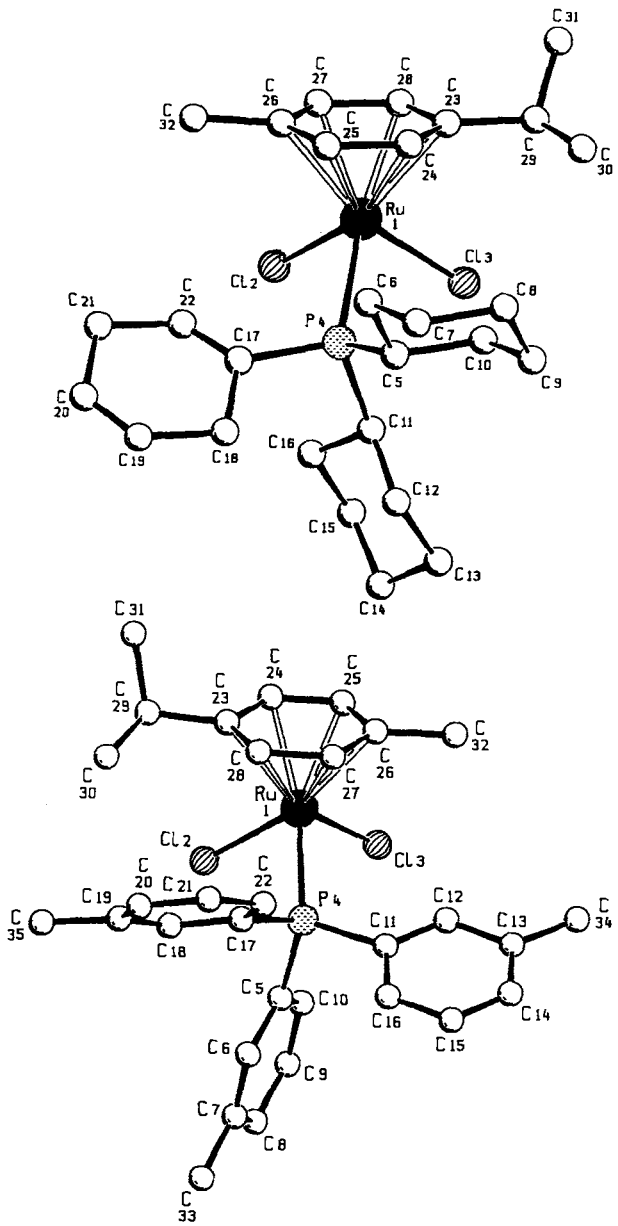

Figure 2. Molecular structures of **7** (top) and **9** (bottom); hydrogen atoms are ommited for clarity. In both cases only one of two molecules from the asymmetric unit cell is depicted.

 © WILEY-VCH Verlag GmbH, D-69451 Weinheim, 1997 0570-0833/97/3619-2122 $ 17.50+.50/0

The assumed asymmetry of the P*m*-Tol_3 ligand was confirmed with the molecular structure of **9**: C33 points into the ligand sphere of the phosphane, whereas C34 and C35 point outwards. The larger tilting of the *p*-cymene ring relative to the Cl-Cl-P plane in **7** (6°) than in **9** (1.5°) can be explained by the steric interaction with the more bulky PCy_3 ligand. This is also reflected by the fact that *p*-cymene is liberated at lower temperatures from **7** (150 °C) than from **8** and **9** (180 and 200 °C, respectively), as measured by differential scanning calorimetry (DSC).

By allowing **7** to react with less reactive monomers we coincidentally found that it is a very efficient catalyst for the thermal, solvent-free polymerization of dicyclopentadiene (DCPD) at temperatures above 80 °C. This was completely unexpected, since, to our knowledge, no ruthenium catalysts were known for the polymerization of DCPD. In fact, it was reported that DCPD is a poison for ruthenium-initiated ROMP.[17] Surprisingly, "solutions" of **7** in DCPD are stable for weeks at room temperature with no increase in viscosity. We think that the active species is an arene-free ruthenium phosphane complex, as described by Noels et al., formed by thermal arene displacement. Furthermore, the arene-free complexes $[Ru(PCy_3)_2(MeOH)_2Tos_2]$ (**10**) and $[RuCl_2(PCy_3)_3]$ (**11**) are also active with DCPD.[18]

Figure 3 shows a dynamic and isothermic DSC scan of the DCPD polymerization initiated with **7** (0.3 wt%). The exothermic curing reaction starts around 100 °C, and the curing heat reaches a maximum of $\Delta H = 364\ J\,g^{-1}$. This ΔH value corresponds well to the theoretical value, calculated from the ring strains of NBE and cyclopentene, for about 95% conversion and a cross-link density of 10–20% for the polymer. This cross-link density is supported by swelling experiments of poly(DCPD) in toluene (weight increase of about 100%). Another fascinating aspect of the DSC experiment is the flatness of the curve up to 100 °C, which demonstrates the excellent latency of the system at room temperature. Gel times of more than three weeks at 20 °C, 270 min at 60 °C, 102 min at 70 °C, and 38 min at 80 °C were determined with vicosimetric measurements under the conditions described above. The isothermal DSC scan at 100 °C shows a fast polymerization reaction with a peak maximum after 6 min. At this temperature the polymerization is completed after about 40 min.

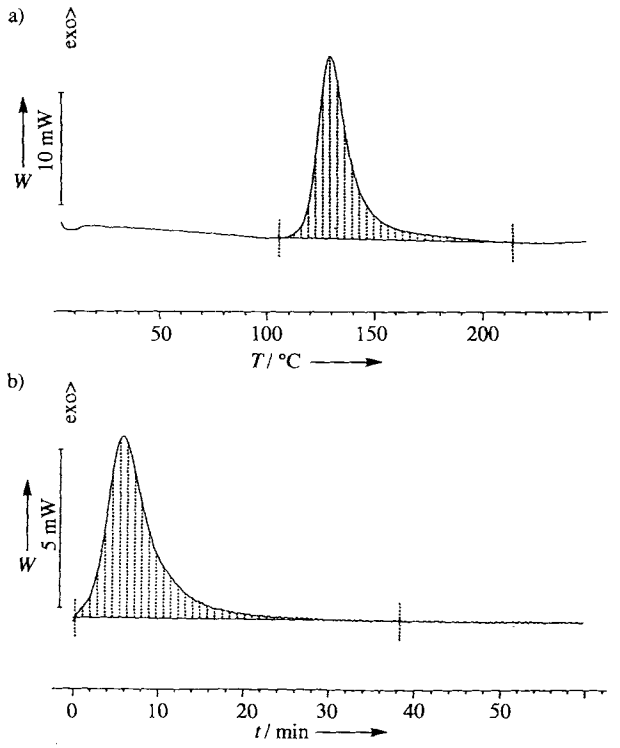

Figure 3. Dynamic (top) and isothermal DSC scan (bottom) of the polymerization of DCPD initiated by **7** (0.3 wt%). *W* = heat flow.

Due to the amazing tolerance of **7** towards impurities and water, we were able to incorporate almost any type of filler (for example SiO_2, $Al(OH)_3$, Al powder, or $CaCO_3$) in amounts of up to 70 wt%; the good electrical and mechanical properties of poly(DCPD) were thus preserved. These properties makes this system extremely interesting for new types of thermosets. For example, the dielectric constant for poly(DCPD) with quartz powder (60 wt%) is still as low as 3.3 with an E modulus of 6200 MPa. Poly(DCPD) loaded with Al powder (60 wt%) is a perfect insulator with a surface resistivity of greater than $10^{11}\ \Omega$ up to 1000 V.[19] Catalyst **7** even allows aqueous dispersion polymerization of NBE and DCPD.[20]

The good mechanical properties of this material are partially due to additional cross-linking of the cyclopentene ring. A second ring opening metathesis reaction is the accepted mechanism for the cross-linking in poly(DCPD) polymerized with early transition metal catalysts.[21] However, Wagener et al. recently reported a model study from which they concluded that cross-linking occurs by a vinyl-addition reaction.[22] To elucidate the structure of cross-linked poly(DCPD) obtained by solvent-free polymerization of DCPD with **7** (0.3 wt%), ^{13}C CP-MAS NMR spectra of the material were measured (Figure 4). Integration of the olefinic and aliphatic ^{13}C signals provided a ratio of exactly 2:3. This strongly suggests that in this case ring opening of the cyclopentene ring is the predominant cross-linking mechanismpoly(DCPD).

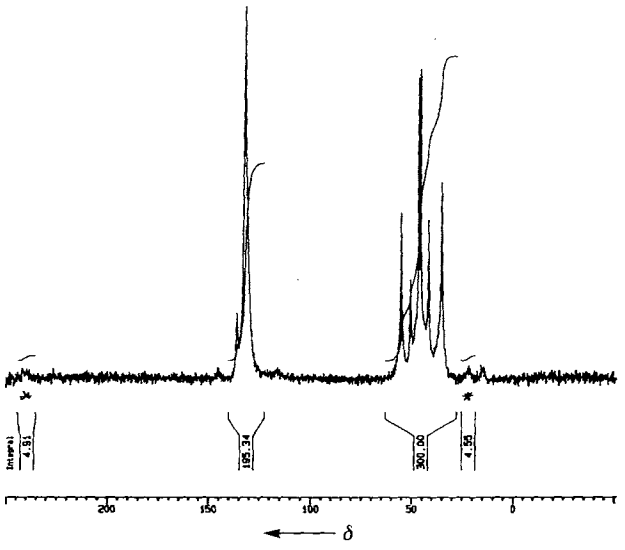

Figure 4. ^{13}CP-MAS NMR spectrum of poly(DCPD); the asterisk indicates spinning side bands.

Polymers with two double bonds per repeat unit are supposed to be oxidatively very unstable. However, almost no weight loss (<1%) was measured for 4-mm plates of unstabilized poly(DCPD) heated in air at 180 °C for 100 days. We suppose that the oxidized surface forms a dense layer which hinders O_2 penetration and therefore protects the deeper material from further oxidation. The thickness of this hard and dense oxide layer was estimated to be about 4 μm from surface-roughness and micro-hardness measurements.

 © WILEY-VCH Verlag GmbH, D-69451 Weinheim, 1997 0570-0833/97/3619-2123 $ 17.50+.50/0

Due to the tolerance of catalyst **7** in combination with the interesting properties of poly(DCPD), new filled or unfilled thermosets could be prepared, which should find novel applications in the field of electro casting, insulation, and tooling (among others) in the near future. Work to improve catalysts and polymer systems are ongoing.

Experimental Section

The ruthenium and osmium complexes were prepared according to literature procedures [11]. NBE was purchased from Fluka, and DCPD (technical quality, 94%) from Shell and used as received. Viscosimetric measurements were performed on a home-built, real-time viscosimeter. Gel times were recorded on a Brookfield viscosimeter, DSCs on a Mettler DSC30 with a Mettler TC11 controller, TGAs on a Mettler TG50 with a Mettler TC10A controller, and surface roughness on a Form Talysurf S3C-50. Micro hardness was determined on a Fischerscope H100. ^{13}C CP-MAS NMR spectra of a piece of poly(DCPD) that was tightly fitted into the spinner were recorded on a Bruker 400-MHz instrument with a MAS rate of 11 kHz and a pulse delay of 5 s (a pulse delay of 60 s gave an identical result).

Received: March 17, 1997 [Z102521E]
German version: *Angew. Chem.* **1997**, *109*, 2213–2216

Keywords: metathesis · osmium · polymers · ring-opening polymerization · ruthenium

[1] a) J. Boor, *Ziegler-Natta Catalysts and Polymerization*, Academic Press, New York, **1979**; b) H. H. Brintzinger, D. Fischer, R. Mülhlhaupt, B. Rieger, R. Waymouth, *Angew. Chem.* **1995**, *107*, 1255; *Angew. Chem. Int. Ed. Engl.* **1995**, *34*, 1143, and references therein.

[2] K. J. Ivin, J. C. Mol, *Olefin Metathesis and Metathesis Polmerization*, Academic Press, London, **1996**.

[3] a) J. Kress, J. A. Osborn, V. Amir-Ebrahimi, K. J. Ivin, J. J. Rooney, *J. Chem. Soc. Chem. Commun.* **1988**, 1164; b) J. Kress, J. A. Osborn, K. J. Ivin, *ibid.* **1989**, 1234; c) K. J. Ivin, J. Kress, J. A. Osborn, *J. Mol. Catal.* **1988**, *46*, 351; d) R. M. E. Greene, K. J. Ivin, J. J. Rooney, J. Kress, J. A. Osborn, *Makromol. Chem.* **1988**, *189*, 2797; e) R. M. E. Greene, K. J. Ivin, J. Kress, J. A. Osborn, J. J. Rooney, *British Polymer J.* **1989**, *21*, 237.

[4] a) R. R. Schrock, *Acc. Chem. Res.* **1990**, *23*, 158; b) C. J. Schaverien, J. C. Dewan, R. R. Schrock, *J. Am. Chem. Soc.* **1986**, *108*, 2771; c) R. R. Schrock, R. T. DePue, J. Feldman, C. J. Schaverien, J. C. Dewan, A. H. Liu, *ibid.* **1988**, *110*, 1423; d) R. R. Schrock, J. Feldman, L. F. Cannizzo, R. H. Grubbs, *Macromolecules* **1987**, *20*, 1172; e) R. R. Schrock, S. A. Krouse, K. Knoll, J. Feldman, J. S. Murdzek, D. C. Yang, *J. Mol. Catal.* **1988**, *46*, 243.

[5] a) B. M. Novak, R. H. Grubbs, *J. Am. Chem. Soc.* **1988**, *110*, 960; b) B. M. Novak, R. H. Grubbs, *ibid.* **1988**, *110*, 7542; b) W. J. Feast, D. B. Harrison, *J. Mol. Catal.* **1991**, *65*, 63.

[6] a) A. Mühlebach, P. Bernhard, N. Bühler, T. Karlen, A. Ludi, *J. Mol. Catal.* **1994**, *90*, 143; b) A. Mühlebach, U. Schädeli, *Irradiation of Polymers* (Eds.: R. L. Clough, S. W. Shalaby), *ACS Symp. Ser.* **1996**, *620*, 364.

[7] a) A. Mühlebach, P. Bernhard, A. Hafner, T. Karlen, A. Ludi, (Ciba-Geigy AG), *WO Pat. 95 07,310* **1995** [*Chem. Abstr.* **1993**, *123*, 314873]; b) T. Karlen, A. Ludi, A. Mühlebach, P. Bernhard, C. Pharisa, *J. Polym. Sci. Polym. Chem. Ed.* **1995**, *33*, 1665.

[8] Our second-generation PROMP catalysts are based on high-valent alkyl tungsten complexes: P. A. van der Schaaf, A. Hafner, A. Mühlebach, *Angew. Chem.* **1996**, *108*, 1974; *Angew. Chem., Int. Ed. Engl.* **1996**, *35*, 1845.

[9] a) S. T. Nguyen, L. K. Johnson, R. H. Grubbs, J. W. Ziller, *J. Am. Chem. Soc.* **1992**, *114*, 3974; b) S. T. Nguyen, R. H. Grubbs, J. W. Ziller, *ibid.* **1993**, *115*, 9858.

[10] A. W. Stumpf, E. Saive, A. Demonceau, A. F. Noels, *J. Chem. Soc. Chem. Commun.* **1995**, 1127.

[11] a) A. J. Lindsay, G. Wilkinson, M. Motevalli, M. B. Hursthouse, *J. Chem. Soc. Dalton Trans.* **1985**, 2321; b) A. J. Lindsay, G. Wilkinson, M. Motevalli, M. B. Hursthouse, *ibid.* **1987**, 2723; c) F. A. Cotton, V. M. Miskowski, B. Zhong, *J. Am. Chem. Soc.* **1989**, *111*, 6177; d) R. A. Zelonka, M. C. Baird, *Can. J. Chem.* **1972**, *50*, 3063; e) J. A. Cabeza, P. M. Maitlis, *J. Chem. Soc. Dalton Trans.* **1985**, 573; f) H. Werner, K. Zenkert, *J. Organomet. Chem.* **1988**, *345*, 151; g) W. A. Kiel, R. G. Ball, W. A. Graham, *ibid.* **1990**, *383*, 481; h) T. Arthur, T. A. Stephenson, *ibid.* **1981**, *208*, 396; i) A. Bell, W. Kozminski, A. Linden, W. von Philipsborn, *Organometallics* **1996**, *15*, 3124.

[12] Reaction of NBE (0.5 g) and catalyst (0.6 wt%) in $CHCl_3$ (3 mL).

[13] A. Demonceau, A. F. Noels, E. Saive, A. J. Hubert, *J. Mol. Catal.* **1992**, *76*, 123.

[14] C. A. Tolman, *Chem. Rev.* **1977**, *77*, 313.

[15] On the basis of a nonsymmetrical arrangement of the phenyl rings, $\theta = 148°$ was calculated: D. White, N. J. Coville, *J. Organomet. Chem.* **1992**, *440*, 15.

[16] Crystals of $7 \cdot CH_3OH$ were grown by cooling a saturated solution in methanol to $-30\,°C$; crystal size $0.90 \times 0.36 \times 0.12$ mm; triclinic, space group $P\bar{1}$; $Z = 4$; $a = 20.148$, $b = 15.333$, $c = 10.337$ Å, $\alpha = 89.41$, $\beta = 102.34$, $\gamma = 107.26°$; $V = 3046.2$ Å^3, $\rho_{calcd} = 1.336\ g\,cm^{-3}$; $6 \le 2\theta \le 44°$ ($Mo_{K\alpha}$, $\lambda = 0.70926$ Å, graphite monochromator, 2θ-θ scan, $T = 298$ K); of 8003 reflections measured, 5879 were observed with $F > 3\sigma(F)$. Crystals of **9** were grown by cooling a saturated solution in methanol to $-30\,°C$; crystal size $0.8 \times 0.3 \times 0.1$ mm; monoclinic, space group $P2_1/n$; $Z = 8$; $a = 17.632$, $b = 18.450$, $c = 17.872$ Å, $\beta = 96.60°$; $V = 5775.4$ Å^3, $\rho_{calcd} = 1.402\ g\,cm^{-3}$; $6 \le 2\theta \le 46°$ ($Mo_{K\alpha}$, $\lambda = 0.70926$ Å, graphite monochromator, 2θ-θ scan, $T = 298$ K); of 8677 reflections measured, 6158 were observed with $F > 3\sigma(F)$. Crystallographic data (excluding structure factors) for the structures reported in this paper have been deposited with the Cambridge Crystallographic Data Centre as supplementary publication no. CCDC-100452. Copies of the data can be obtained free of charge on application to The Director, CCDC, 12 Union Road, Cambridge CB21EZ, UK (fax: int. code +(1223)336-033; e-mail: deposit@chemcrys.cam.ac.uk).

[17] C. Tanielian, A. Kiennemann, T. Osparpucu, *Can. J. Chem.* **1979**, *57*, 2022.

[18] NBE (0.5 g) with **10** (5 ppm!) gave poly(NBE) quantitatively after 48 hr at 50 °C.

[19] Physical properties of poly(DCPD) filled with 60% quarz powder and unfilled poly(DCPD) (values for the latter are given in parentheses): density: 1.64 (1.04) $g\,cm^{-3}$; glass-transition temperature, 120 (120) °C; e-modulus: 6200 (2020) MPa; elongation at break: 2.6 (14.5)%; double-torsion test: K_{1C}: 3.0 (3.7) $MPa\,m^{-1/2}$, G_{1C}: 1300 (5800) Jm^{-2}; coefficient of linear thermal expansion: 56–59 (109–115) ppm K; water absorption (10 d at 23 °C): 0.06 (0.13)%; dielectric constant (ε, 50 Hz, RT): 3.3 (2.4).

[20] A. Mühlebach, P. A. van der Schaaf, A. Hafner, unpublished results.

[21] a) A. Bell, *The Role of Catalysts in Polymer Synthesis* (Eds.: E. J. Vandenberg, J. C. Salamone), *ACS Symp. Ser.* **1992**, *469*, 21; b) R. A. Fischer, R. H. Grubbs, *Makromol. Chem. Macromol. Symp.* **1992**, *63*, 271.

[22] T. A. Davidson, K. B. Wagener, D. B. Priddy, *Macromolecules* **1996**, *29*, 786.

The Amidinium–Carboxylate Salt Bridge as a Proton-Coupled Interface to Electron Transfer Pathways**

Yongqi Deng, James A. Roberts, Shie-Ming Peng, C. K. Chang, and Daniel G. Nocera*

Proton motion coupled to electron transfer is a basic energy conversion mechanism. Many proteins and enzymes function by utilizing the energy gathered along a charge-separating network to drive a proton pump, which in turn is manifested in a transmembrane chemical potential that provides the energy for the synthesis of complex biomolecules.[1] Yet some thirty years after Mitchell's initial proposal of proton translocation driven by electron transfer,[2] the mechanistic details of how the electron couples to the proton remain undefined.[1a, 3] To unravel the relationship between the proton and the electron, we have developed the following approach: electron transfer is photoinduced within photoexcitable electron donor–acceptor supramolecule complexes formed from the association of a proton transfer interface.[4] We have concentrated on asymmetric inter-

[*] Prof. D. G. Nocera
Department of Chemistry
Massachusetts Institute of Technology
77 Massachusetts Avenue, Cambridge, MA 02139-4307 (USA)
Fax: Int. code +(617)253-7670
e-mail: nocera@mit.edu
Y. Deng, J. A. Roberts, Prof. C. K. Chang
Department of Chemistry
Michigan State University
East Lansing, MI 48824 (USA)
Prof. S. M. Peng
Department of Chemistry
National Taiwan University
Taipei (Taiwan)

[**] This work was supported financially by the National Institutes of Health (GM 47274). J. A. R. acknowledges support from the Carl H. Brubaker Jr. Fellowship in Chemical Sciences.

faces such as salt bridges, because they provide an important model for proton-coupled electron transfer (PCET) in biology, where reaction dynamics are modulated by coupling the charge redistribution accompanying both proton *and* electron motion to the surrounding environment.[5] Such is the case for the donor–(salt bridge)–acceptor supramolecule systems. Changes in polarity, charge, and energetics resulting from the transfer of an electron from the donor to the acceptor are augmented by the charge shift accompanying proton displacement within the salt bridge interface.

One attractive salt bridge for PCET studies is the amidinium–carboxylate interface, which models the arginine–aspartate salt bridges important to many biological structures.[6] But unlike the guanidinium–carboxylate interaction of Arg–Asp, amidinium group shows only one specific binding mode for carboxylate, thereby simplifying PCET studies. Though high association constants are characteristic of salt bridge supramolecules, an electron donor–acceptor complex assembled by such noncovalent interactions at the interface has yet to be structurally characterized. We now report the X-ray crystal structure of **1**·benzoate and show that the salt bridge is preserved in solutions of high dielectric constant. The salt bridge is maintained upon replacement of the phenyl ring by the electron-withdrawing 3,5-dinitro phenyl moiety, but with an attenuated association constant. When the porphyrin is made photoexcitable by Zn^{II} substitution of Ni^{II}, we observe an unusually slow rate of electron transfer for the porphyrinatozinc(II)–(amidinium carboxylate)–3,5-dinitrobenzene complex. Electronic spectroscopy indicates that the salt-bridge is strongly coupled to the electron transfer pathway and that it significantly influences the rate of electron transfer.

The syntheses of compounds **1** and **2** are outlined in Scheme 1. Dipyrrylmethane **5**, obtained from acid-catalyzed condensation of bromomethylpyrrole **3** and α-unsubstituted pyrrole **4**, was reduced by diborane (generated in situ by addition of BF_3 to $NaBH_4$) to give dipyrrylmethane **6**, which was then hydrolyzed and decarboxylated by heating with sodium hydroxide in ethylene glycol to give compound **7**. A modified MacDonald condensation[7] between **7** and **8** produced **9** in about 45% yield. Alcohol-derivatized porphyrin **9** was converted into vinyl porphyrin **11** by chlorination and elimination from **10** following standard procedures.[8] The vinyl group was oxidized to aldehyde **12** with osmium tetraoxide followed by sodium periodate. The aldehyde was converted into the nitrile ($\tilde{\nu}_{CN}$ at 2250 cm^{-1}) by heating at reflux with hydroxyamine hydrochloride in formic acid. After nickel complexation, **14** was converted into **1**[9] with Weinreb's reagent ($AlCl(CH_3)(NH_2)$) to deliver the amide.[10] The conversion of the Ni complex into the Zn complex can be accomplished by published procedures.[10]

The formation of the salt bridge is confirmed by X-ray crystallography of **1**·benzoate (Figure 1).[11] The relatively short N to O distances of 2.757(11) and 2.812(11) Å of the salt bridge indicates substantial stability and relatively strong hydrogen bonding ($d_{calcd}(O\cdots H) = 1.800$ and 1.874 Å). These bond lengths are usual for this type of salt bridge; according to a crystal structure analysis of the doubly hydrogen-bonded salt bridge formed between a bicyclic guanidinium unit and a carboxylate group, the N–O length is 2.85(4) and the attendant O···H bond length 1.97(4) Å.[12] An S_4 ruffling of the porphyrin ring is common for Ni^{II} porphyrin complexes and results from the contraction of the metal coordination site owing to the small size and high electrophilicity of the Ni^{II} atom.[13] The amidinium group is rotated by 42° with respect to the plane of the porphyrin ring, defined by the four pyrrole nitrogens (0.016 Å mean deviation from plane).[14] This canting of the

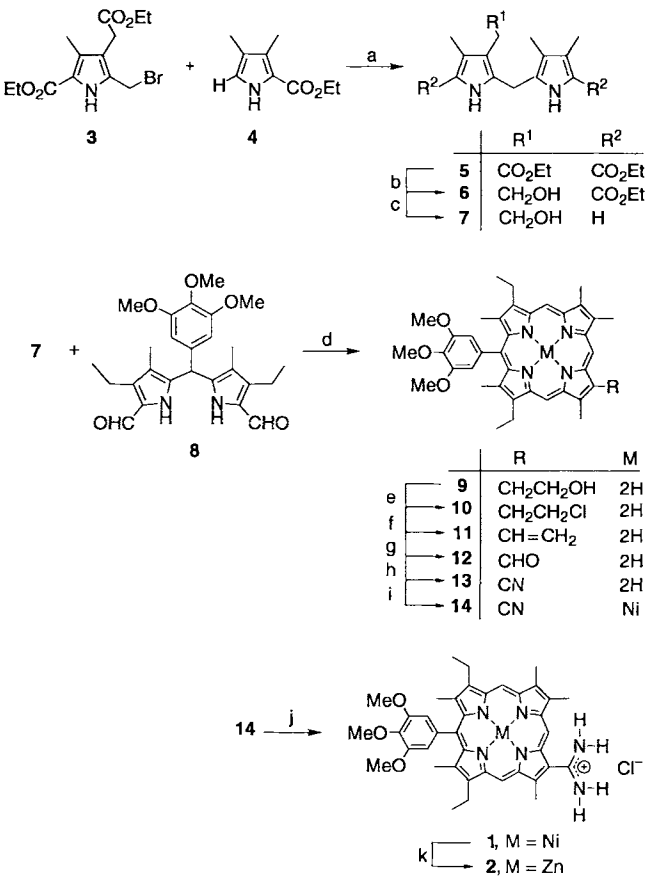

Scheme 1. a) HCl, ethanol, 80%; b) $NaBH_4$, BF_3, THF, 81%; c) NaOH, ethylene glycol, reflux, 95%; d) 1. $HClO_4$, methanol/THF; 2. chloranil, 48%; e) 1. $POCl_3$, DMF; 2. Na_2CO_3, 88%; f) DBU, pyridine, reflux, 95%; g) 1. OsO_4, CH_2Cl_2; 2. H_2S; 3. $NaIO_4$ in pyridine, 78%; h) $NH_2OH\cdot HCl$, formic acid, reflux, 95%; i) $Ni(OAc)_2$, DMF; j) $AlCl(CH_3)(NH_2)$, toluene, 93%; k) 1. concd H_2SO_4; 2. NaOH; 3. $Zn(OAc)_2$ in CH_2Cl_2, 90%.

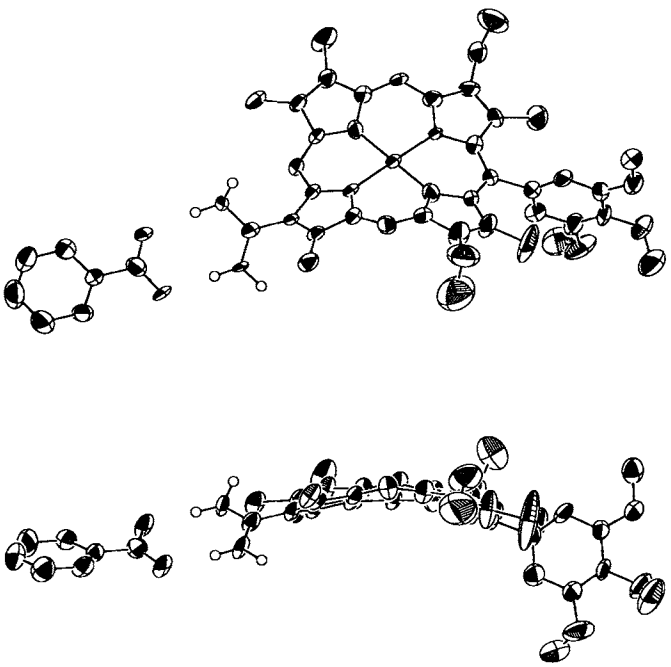

Figure 1. Top and side views of the ORTEP diagrams of the salt-bridged supramolecular assembly **1**·benzoate.

 © WILEY-VCH Verlag GmbH, D-69451 Weinheim, 1997 0570-0833/97/3619-2125 $ 17.50+.50/0

amidinium is not fully compensated by a counter rotation of the carboxylate, and a slight twist of 5.4° is observed within the salt bridge interface (dihedral angle defined by the planes of the CN_2 and CO_2 atoms of the salt bridge).

The amidinium–carboxylate salt bridge is very stable, and it persists in solutions, even when the dielectric constant of the solvent is high. Figure 2 shows the ^{1}H NMR spectral changes

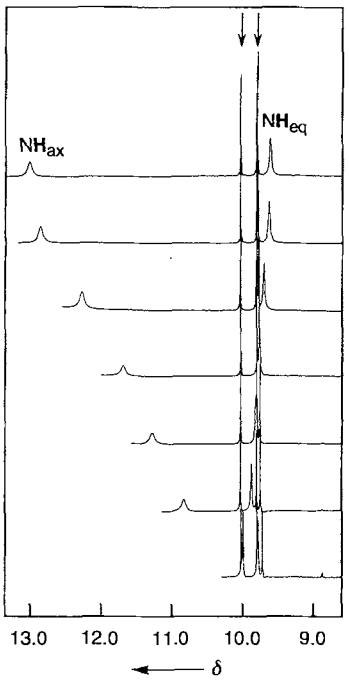

Figure 2. Selected ^{1}H NMR spectra of **1** (3.63 mM) in the presence of 0.00, 1.39, 2.08, 2.77, 4.16, 7.62, and 13.9 mM (bottom to top) tetrabutylammonium benzoate in [D_6]DMSO. The spectral range captures the signals of the amidinium protons internal (NH_{ax}) and external (NH_{eq}) to the salt bridge interface and the three *meso* protons of the porphyrin ring (indicated by arrows).

resulting from the association of the Ni^{II} porphyrin to benzoate ions in [D_6]DMSO. The chemical shift of the *meso* proton adjacent to the amidinium group at $\delta = 10.0$, and the nearly coincident singlets of two distal *meso* protons (indicated by the arrows) at $\delta = 9.8$, do not vary with addition of benzoate, indicating that π-stacking is not an important association mechanism (the *meso* protons are a sensitive measure of π-stacking in porphyrin systems[15]). As observed previously for the bicyclic guanidinium–carboxylate salt bridge,[12] a signature of salt bridge formation is the concentration-dependent downfield shift of amidinium protons involved in hydrogen bonding (NH_{ax} varies by more than 4 ppm) to carboxylate and the insensitivity of the chemical shift ($\delta < 0.5$) for the amidinium protons external to the salt bridge (NH_{eq}). A linear least-squares fit of chemical shift of the hydrogen-bonded amidinium protons vs. the carboxylate concentration, as described by Wilcox,[16] yields an association constant (K_a) of 1550(9) M^{-1} for **1**·benzoate in DMSO. A 1:1 stoichiometry of the complex is established by a Job's plot[17] of the ^{1}H NMR titration data, which shows that the optimal formation of **1**·benzoate occurs at equimolar concentrations of the amidinium and carboxylate (that is, 0.5 mole fraction). The exceptionally high association of the salt bridge accords well with Jorgensen's classification for two favorable secondary interactions that compose the hydrogen bonded interface,[18] bolstered by the stabilization imparted by the molecular recognition of the negatively charged carboxylate by the positively charged amidinium groups. When the benzoate ion is replaced by the well-known electron acceptor 3,5-dinitrobenzoate (3,5-DNBCOO$^-$), similar behavior is observed. The chemical shifts of the *meso* protons ($\delta = 9.72$) and NH_{eq} ($\delta = 9.96$) exhibit an insignificant shift upon 3,5-DNBCOO$^-$ addition ($\Delta\delta < 0.1$ over 12 mM), while NH_{ax} varies by 2 ppm over the same concentration range. However, we observe a smaller K_a of 267 M^{-1}, which is consistent with a decreased basicity of the carboxylate group conferred by the electron-withdrawing nitro groups, which results in a weaker hydrogen bonding interaction.

In less polar solvents the association constant greatly increases. Indeed the binding in CH_2Cl_2 is so high that the association can conveniently be followed by absorption spectroscopy. The Soret and Q-bands of the porphyrin undergo a blue shift immediately upon association of **1** to the carboxylate ion (λ_{max}(**1**) = 406, 530, 574 nm; λ_{max} (**1**·benzoate) = 403, 525, 570 nm; λ_{max} (**1**·3,5-DNBCOO$^-$) = 404, 526, 571 nm). Benesi–Hildebrand fits of these shifts in the absorption maxima with added carboxylate yields K_a of $5.7(11) \times 10^6$ M^{-1} and $7.7(11) \times 10^5$ M^{-1}. As above, the electron-withdrawing nitro groups engender a smaller association constant.

The perturbation of the absorption profile upon salt-bridge formation suggests that the interface is strongly coupled to the porphyrinic chromophore and correspondingly to the electron transfer pathway. When Ni^{II} is replaced by Zn^{II}, the amidinium porphyrin exhibits luminescence, which decays monoexponentially with a lifetime of 1.5 ns (λ_{exc} = 588 nm, λ_{det} = 620 nm) for **2**·benzoate in CH_2Cl_2 at 25 °C. Replacement of the benzoate ion by the 3,5-DNBCOO$^-$ ion results in luminescence quenching, and a unimolecular rate constant of 6.4×10^7 s^{-1} is calculated from the decay kinetics. This observation is consistent with electron transfer from the singlet excited state of **2** to 3,5-DNBCOO$^-$ mediated by the amidinium–carboxylate salt bridge. The electron transfer rate constant for **2** is considerably smaller than that of covalently linked Zn^{II} porphyrin donor–acceptor systems. For instance, an electron transfer rate constant of $k = 3 \times 10^{10}$ s^{-1} is interpolated from Wasielewski's data on Zn^{II}porphyrin-L-quinone (L = rigid polycyclic spacer) systems at driving forces equivalent to **2** ($\Delta G = -0.30$ eV).[19] This considerably faster rate of the covalently tethered donor–acceptor system is further augmented by its longer electron transfer distance (edge-to-edge distance: Zn^{II}porphyrin-L-quinone = 10.5 Å; **2** 7.0 Å) and hence weaker electronic coupling.

The dramatic attenuation in the electron transfer rate constant through the salt bridge may have several origins. First, the electron transfer is in the direction of the permanent dipole of the salt bridge. The presence of an internal electric field contained within the electron transfer pathway will alter the driving force of reaction relative to the isolated constituents.[20] Second, the charge shift of the electron will be stabilized by an accompanying proton shift within the salt bridge. PCET through a salt bridge therefore includes Franck–Condon factors arising from the charge shift of the electron *and* the proton coupling to the polarization of the surrounding environment.[21] Finally, differences in H-bonding strengths of the asymmetric interfaces are manifested in differences in electronic coupling efficiencies.[22] The studies reported herein thus show that salt bridges can be used to form electron transfer networks by self-assembly, and as a constituent of the electron transfer pathway, the salt bridge can profoundly affect the rate of electron transport.

Received: January 17, 1997
Revised version: May 9, 1997 [Z 10003 IE]
German version: *Angew. Chem.* **1997**, *109*, 2216–2219

 © WILEY-VCH Verlag GmbH, D-69451 Weinheim, 1997 0570-0833/97/3619-2126 $ 17.50+.50/0

Keywords: electron transfer · hydrogen bonding · porphyrinoids · proton transfer

[1] a) M. Y. Okamura, G. Feher, *Annu. Rev. Biochem.* **1992**, *61*, 861; b) *Electron and Proton Transfer in Chemistry and Biology*; (Eds.: A. Müller, H. Ratajczaks, W. Junge, E. Diemann), Elsevier, Amsterdam, **1992**; c) S. Ferguson-Miller, G. T. Babcock, *Chem. Rev.* **1996**, *96*, 2889.

[2] P. Mitchell *Nature* **1961**, *191*, 144.

[3] a) M. S. Graige, M. L. Paddock, J. M. Bruce, G. Feher, M. Y. Okamura, *J. Am. Chem. Soc.* **1996**, *118*, 9005; b) B. G. Malmström, *Acc. Chem. Res.* **1993**, *26*, 332; c) G. T. Babcock, C. Varotsis, *Proc. SPIE Int. Soc. Opt. Eng.* **1993**, *1890*, 104.

[4] a) C. Turró, C. K. Chang, G. E. Leroi, R. I. Cukier, D. G. Nocera, *J. Am. Chem. Soc.* **1992**, *114*, 4013; b) J. A. Roberts, J. P. Kirby, D. G. Nocera, *ibid.* **1995**, *117*, 8051; c) J. P. Kirby, J. A. Roberts, D. G. Nocera, *ibid.*, in press.

[5] B. Honig, A. Nicholls, *Science* **1995**, *268*, 1144.

[6] a) J. M. Berg, *Acc. Chem. Res.* **1995**, *28*, 14; b) B. R. Crane, L. M. Siegel, E. D. Getzoff, *Science* **1995**, *270*, 59; c) J. D. Puglisi, L. Chen, A. D. Frankel, J. R. Williamson, *Proc. Natl. Acad. Sci. USA* **1993**, *90*, 3680; d) N. P. Pavletich, C. O. Pabo *Science* **1991**, *252*, 809; e) E. H. Howell, J. E. Villafranca, M. S. Warren, S. J. Oatley, J. Kraut, *ibid.* **1986**, *231*, 1125.

[7] a) C. K. Chang, *J. Org. Chem.* **1985**, *50*, 411; b) J. L. Sessler, B. Wang, A. Harriman, *J. Am. Chem. Soc.* **1993**, *115*, 10418.

[8] C. K. Chang, H. H. Marcos, A. J. Tulinsky, *J. Chem. Soc. Perkin Trans. 2* **1983**, 371.

[9] Analytical data for **1**: ^{1}H NMR (300 MHz, [D$_6$]DMSO, TMS): $\delta = 1.58$ (t, $J = 7.5$ Hz, 3H; CH_2CH_3), 1.59 (t, $J = 7.4$ Hz, 3H; CH_2CH_3), 2.45 (s, 3H; CH_3), 3.38 (s, 6H; CH_3), 3.41 (s, 3H; CH_3), 3.65 (s, 3H; CH_3), 3.80 (s, 6H; *m*-OCH_3), 3.86 (q, $J = 7.5$ Hz, 2H; CH_2CH_3), 3.87 (q, $J = 7.4$ Hz, 2H; CH_2CH_3), 3.94 (s, 3H; *p*-OCH_3), 7.18 (s, 2H; arom. CH), 9.71 (s, 1H; *meso*-CH), 9.77 (br.s, 2H; NH_{ax}), 9.79 (s, 1H; *meso*-CH), 9.98 (br.s, 2H; NH_{eq}), 10.01 (s, 1H; *meso*-CH). FABMS: calcd for $C_{39}H_{43}N_6NiO_3^+$: $m/z = 701.26$; found, 701.5.

[10] J. P. Kirby, N. A. van Dantzig, C. K. Chang, D. G. Nocera, *Tetrahedron Lett.* **1995**, *36*, 3477.

[11] Crystallographic data: $C_{39}H_{43}N_6NiO_3 \cdot C_7H_5O_2^-$ from CH_3CN, $M_r = 882.11$, triclinic, space group P, $a = 15.497(3)$, $b = 16.268(3)$, $c = 19.483(7)$ Å, $\alpha = 113.598(23)$, $\beta = 109.687(22)$, $\gamma = 93.435(14)°$, $V = 4128.8(18)$ Å^3, $Z = 4$, $\rho_{calc} = 1.323$ g cm^{-3}, $F(000) = 1732$, $\lambda(Mo_{K\alpha}) = 0.7107$ Å, $\mu = 5.219$ cm^{-1}, crystal dimensions $0.05 \times 0.50 \times 1.50$ mm. A total of 10761 unique reflections and 5300 reflections ($I > 2\sigma(I)$) were collected at 25 °C on a Nonius diffractometer ($\theta/2\theta$) to $2\theta < 45°$. The crystal structure was solved by direct methods with the NRCVAX program package, and 1045 parameters were refined to $R = 0.065$ ($Rw = 0.058$). All non-hydrogen atoms were refined anisotropically. The hydrogen atoms were placed at calculated positions with fixed isotropic thermal parameters. Crystallographic data (excluding structure factors) for the structure(s) reported in this paper have been deposited with the Cambridge Crystallographic Data Centre as supplementary publication no. CCDC-100 179. Copies of the data can be obtained free of charge on application to The Director, CCDC, 12 Union Road, Cambridge CB2 1EZ, UK (fax: int. code +(1223) 336-033; e-mail: deposit@chemcrys.cam.ac.uk).[12] G. Müller, J. Riede, P. Schmidtchen, *Angew. Chem. Int. Ed. Engl.* **1988**, *27*, 1516.

[13] C. Kratky, A. Fässler, A. Pfaltz, B. Kräutler, B. Juan, A. Eschenmoser, *J. Chem. Soc. Chem. Commun.* **1984**, 1368.

[14] The structure consists of the packing of two crystallographically independent molecular complexes, one of which is shown in Figure 1. While the overall features of the two are similar (for example, hydrogen bond lengths in the second complex: 1.854(6) and 1.838(6) Å), the amidinium group of the second complex rotates 61.8° out of the porphyrin plane, and the salt bridge interface is more twisted (25.9° between the CN_2 and the carboxylate planes). Such variabilities in the solid state accentuate the high degree of rotational freedom of the salt bridge that is surely present in the solution phase.

[15] a) R. J. Abraham, F. Eivazi, H. Pearson, K. M. Smith, *J. Chem. Soc. Chem. Commun.* **1976**, 698; b) C. K. Chang, *J. Heterocycl. Chem.* **1977**, *14*, 1285.

[16] C. S. Wilcox, *Frontiers in Supramolecular Organic Chemistry and Photochemistry* (Eds.: H.-J. Schneider, H. Durr), VCH, Weinheim, **1991**, p. 123.

[17] J. S. Albert, M. S. Goodman, A. D. Hamilton, *J. Am. Chem. Soc.* **1995**, *117*, 1143.

[18] a) J. Pranata, S. G. Wierschke, W. L. Jorgensen, *J. Am. Chem. Soc.* **1991**, *113*, 2810; b) W. L. Jorgensen, J. Pranata, *ibid.* **1990**, *112*, 2008.

[19] a) M. R. Wasielewski, *Chem. Rev.* **1992**, *92*, 435; b) M. R. Wasielewski, M. P. Niemczyk, W. A. Svec, E. B. Pewitt, *J. Am. Chem. Soc.* **1985**, *107*, 1080.

[20] a) T. Scherer, I. M. H. van Stokkum, A. M. Brouwer, J. W. Verhoeven, *J. Phys. Chem.* **1994**, *98*, 10539; b) E. Galoppini, M. A. Fox, *J. Am. Chem. Soc.* **1996**, *118*, 2299.

[21] a) R. I. Cukier, *J. Phys. Chem.* **1995**, *99*, 16101; b) R. I. Cukier, *J. Phys. Chem.* **1996**, *100*, 15428.

[22] H. B. Gray, J. R. Winkler, *Annu. Rev. Biochem.* **1996**, *65*, 537.

Corrigendum

In the communication "Synthesis and Structure of the Nanoclusters $[Hg_{32}Se_{14}(SePh)_{36}]$, $[Cd_{32}Se_{14}(SePh)_{36}(PPh_3)_4]$, $[P(Et)_2(Ph)C_4H_8OSiMe_3]_5[Cd_{18}I_{17}(PSiMe_3)_{12}]$, and $[N(Et)_3C_4H_8OSiMe_3]_5[Cd_{18}I_{17}(PSiMe_3)_{12}]$" by S. Behrens, M. Bettenhausen, A. C. Deveson, A. Eichhöfer, D. Fenske, A. Lohde, and U. Woggon (*Angew. Chem. Int. Ed. Engl.* **1996**, *35*, 2215–2218), Equation (c) was inadvertently omitted at a late stage of production. Equation (c) should read:

$$[CdCl_2(PPh_3)_2] \xrightarrow[\text{acetone}]{PhSeSiMe_3} [Cd_{32}Se_{14}(SePh)_{36}(PPh_3)_4]$$

 © WILEY-VCH Verlag GmbH, D-69451 Weinheim, 1997 0570-0833/97/3619-2127 $ 17.50+.50/0

Medicine, Membranes, and Mechanisms

Medicinal Chemistry: Today and Tomorrow. Proceedings of the AFMC Int. Medicinal Chemistry Symposium. Edited by *M. Yamakazi*. Blackwell Science, Oxford, 1996. 278 pp., hardcover £ 49.50.—ISBN 0-632-04272-9

This book contains the texts of 41 papers by industrial and academic scientists that were presented at the AFMC International Medicinal Chemistry Symposium (AIMECS 95) in Tokyo in September 1995, under the auspices of the Pharmaceutical Society of Japan. These short papers (typically 4–6 pages) touch on practically all general aspects of modern research in medicinal chemistry with relevant examples, although unfortunately they are not grouped under subject areas.

Several contributions are concerned with the isolation and characterization of biologically active natural products from various sources such as marine organisms or tropical plants, and of microbial metabolites and biologically active constituents of traditional Chinese medicines. Some of these articles also describe syntheses of natural products and their analogs. This leads into a further group of papers dealing specifically with the synthesis of biologically active natural products (e.g., inositol phosphates, brevetoxin, oligosaccharides) and with more general methods such as those that are being developed for achieving enantioselective reactions. The prospects for developing these into industrial processes based on conventional chemistry or biocatalytic reactions are discussed in relation to specific medical indications or targets. These include AIDS, diabetes, receptors for glutamates, for opiates, for angiotensin II, for prostanoids, for endothelin, and for kainates, as well as renin and DNA-gyrase inhibitors. These articles also contain sections on combinatorial synthesis and molecular diversity, on drug design and drug metabolism, polymer-bound pharmaceutical agents, drug delivery systems, and new strategies for increasing the membrane permeability of peptides.

Another group of articles is concerned with biological processes and proteins that could serve as starting points for developing new or improved therapies. These include, for example, cytokin and integrin receptors, apoptosis, the regulation of gene expression, the role of sphingoglycolipids in signal transduction, and the modulation of carbohydrates in the expression of recombinant glycoprotein therapeutic agents.

The symposium also served as a forum for official bodies: the European Commission, the United States FDA, and the Japanese Health Ministry each provided a representative to offer guidelines for the development of "orphan drugs", that is, drugs for the treatment of comparatively rare conditions, the development of which tends to be neglected on economic grounds.

This symposium report contains papers on a wide range of topics, giving it considerable variety and interest. The excellent choice of topics and presenters demonstrates the organizers' keen awareness of the latest research trends in this field. Many aspects of modern medicinal chemistry are included, but I regret that some important ones are absent, for example tumor suppressors, kinase inhibitors, and SH2 and SH3 domains. However, that is not a serious criticism. A symposium such as this one, dealing with a rapidly developing field of research, can only offer a snapshot of the current state of knowledge and development. Future snapshots will, by their very nature, emphasize different topics of special interest at the time. In accordance with its character as a symposium report, this book is mainly suitable for specialists in the field, rather than for nonspecialists who may have an interest in the subject but no close familiarity with it. It will be read with particular interest by pharmaceutical chemists seeking the latest information about developments in their area of work, and will also provide useful reading for natural products chemists and synthetic chemists, and for biologists who wish to learn whether their research is of possible relevance for medicinal chemistry, or to enrich their lectures or publications by including interdisciplinary aspects.

Herbert Waldmann
Institut für Organische Chemie
der Universität Karlsruhe (Germany)

Basic Principles of Membrane Technology. (Second edition). By *M. Mulder*. Kluwer, Dordrecht, 1996. 564 pp., hardcover £ 174.00.—ISBN 0-7923-4247-X

"If you are tired of membranes, you are tired of life". This remark by Richard Bowen, cited in the preface of the book by M. Mulder, highlights the importance of membranes and their functions for the living cell. The ability of membranes to function as highly selective barriers is also used in industrial processes. Examples are simple particle filtration, ultrafiltration for the retention of macromolecules, or the recovery of solvents from the gas phase. This book, now available in its second edition, gives an exhaustive overview of existing membrane processes and describes the necessary fundamentals. The book is well structured and easy to understand. The figures are clear and informative. Compared to the first edition the number of pages has been increased by 200. There are three reasons for this: i) to cover recent developments new chapters have been added, for example, those on nanofiltration and membrane reactors; ii) the line spacing has been increased, resulting in better readability and clarity; iii) 80 pages with problems and solutions have been added, which is the most appealing aspect of the second edition. These exercise problems relate to the principles covered in the text. Examples are simple calculations for the design of membrane modules, considerations for the selection of suitable membranes, and more com-

This section contains book reviews and a list of new books received by the editor. Book reviews are written by invitation from the editor. Suggestions for books to be reviewed and for book reviewers are welcome. Publishers should send brochures or (better) books to the editorial office: Redaktion Angewandte Chemie, Postfach 101161, D-69451 Weinheim, Germany. The editor reserves the right of selecting which books will be reviewed. Uninvited books not chosen for review will not be returned.

plex calculations of the transport through a membrane using different models. Examples based on everyday problems are also included: "How long will it take before a bicycle tire is flat?", or "What is the principle behind the function of Gore-tex® or Sympatex® membranes?"

The book is divided into eight chapters, varying in length between 20 and 130 pages. Each chapter has its own literature references and problems. Only a few references are from 1995, most of them are older. Here some more recent data would have been useful, including selected examples of applications of membrane processes. Some interesting examples can be found in the problems, but these are not covered by the index.

The first chapter describes the historical development and provides the basic definitions. Chapter 2 summarizes membrane materials, and Chapter 3 gives an introduction to membrane production. In Chapter 4 methods for the characterization of membranes are described. Chapter 5 summarizes different models used to describe transport through membranes. These five chapters form the first part of the book.

The second part begins with Chapter 6 which is the longest in the book (130 pages). Here various membrane processes are described, such as particle filtration, ultrafiltration, pervaporation, membrane contactors or electrodialysis, classified according to their driving forces. There is also a short section dealing with membrane reactors. Chapter 7 discusses the problem of membrane fouling. Finally, Chapter 8 describes different types of membrane modules including guidelines for their design.

To summarize, this is an excellent textbook and reference source for everyone working with membrane processes. It also gives valuable advice for the reader who has a separation problem and is looking for new approaches to solving it. But it requires careful reading—there is no 'quick solution'. Here the limited number of applications described restricts the book's usefulness. The index contains some errors: bipolar membranes can be found on page 390, not on page 277. There is no index of membrane suppliers. But a search in the Internet using the keyword 'membrane' reveals enough helpful information.

It is to be hoped that this book will be read by scientists from a range of disciplines, not solely by process engineers. However, the high price may be an obstacle to its wide distribution. Difficulties in the filtration of precipitates or the desalting of samples are typical of everyday problems that might be solved easily using appropriate membrane processes.

By the way: a bicycle tire is entirely flat after 169 days.

Udo Kragl
Institut für Biotechnologie
der Forschungszentrum Jülich GmbH
Jülich (Germany)

An Introduction to Enzyme and Coenzyme Chemistry. By *T. Bugg*. Blackwell Science, Oxford, 1997. 247 pp., softcover, £ 19.95.—ISBN 0-86542-793-3

In this book the author, Tim Bugg, has succeeded well in his aim of writing an introduction to the modes of action of enzymes and coenzymes from the standpoint of organic chemistry, and of explaining the underlying mechanisms. Concisely and in clearly understandable language, the book also provides the reader with much valuable background knowledge, which is not available elsewhere in so compact a form.

The structure of the book is well suited for such an introduction. First, in a general overview, the reader learns a little about enzyme kinetics and enzymatic reactions in general. The different types of reactions are then introduced in turn, plentifully illustrated with the help of many two-color formula schemes: hydrolytic and group transfer reactions, redox enzyme reactions, carbon–carbon bond-forming reactions, addition and elimination reactions, transformations of amino acids, and isomerase reactions. Lastly there is a chapter on nonenzymatic catalysis. A short appendix contains answers to the questions and exercises that are given at the end of each chapter.

We consider this book to be very suitable for use by students as an introduction to the various aspects of enzymatic reactions and the role of coenzymes. However, our very favorable impression on first glancing through it was modified to some extent on closer examination, as there are a number of errors that suggest a lack of care in proofreading (see the examples below). The reader already familiar with the subject would perhaps not be troubled by these, but it is especially important that the student using the book as a first introduction should be able to rely on consistent accuracy in both text and figures.

The fact that 21 proteinogenic amino acids are now known, together with their corresponding codons, should nowadays be part of every student's basic knowledge. However, it seems quite unnecessary to repeat at several places the explanation of the three-letter symbols for amino acids in the text and in the figures. The role of chaperones as "helpers" in the folding of many proteins should at least have been briefly mentioned, to avoid giving the impression that folding always occurs spontaneously (p. 12). The formula schemes do not always accurately identify all the compounds involved; it is essential to check in each case to ensure that all the reactants are shown, as the reader is likely to be confused if there are omissions. The definitions of specificity and selectivity on pages 26 and 27 do not agree with those usually found in textbooks of biochemistry and in original publications; for example, substrate specificity is normally taken to mean the selectivity of an enzyme with regard to the substrate that is converted.

A few printing errors need to be corrected in a subsequent edition of the book. In addition, however, there are numerous other mistakes and points that invite criticism, as shown by the following list:

page 4: "Many of the vitamins are in fact coenzymes ...";

page 8: the stereochemistry of the side-chain in threonine is shown wrongly (*S* instead of *R*);

pages 9 ff: the names for nucleobases, nucleosides, and nucleotides are not always used correctly;

page 16: hemoglobin is said to consist of identical subunits;

the determination of the structure of lysozyme by X-ray crystallography was the first achieved for an enzyme, not for a protein;

the statement that the active center is usually in a hydrophilic environment is over-simplified; the situation is described correctly two pages later;

page 17: the definitions of H-donors and H-acceptors given here are not the usual ones;

page 46: in giving the specific activity the protein concentration is referred to, whereas this should instead be the protein mass;

page 51: in the legend to Figure 4.5 the symbol *V* should instead be *v*;

page 66: in the first paragraph C-2 should be C-4;

page 69: the appendix does not give a solution to Problem 3;

page 87: transesterification is incorrectly printed as "*trans*-esterification", which is likely to confuse (one wonders what *cis*-esterification might mean!);

page 114: in mentioning cytochromes reference is made to Table 6.1, but the word

 © WILEY-VCH Verlag GmbH, D-69451 Weinheim, 1997 0570-0833/97/3619-2130 $ 17.50+.50/0

cytochrome does not appear in the table as such, nor does it in the index;
page 229: in the statement "... the C-1 centre is designated as *S*", *R* should appear instead.

Wolf-Peter Kuhl and *Karl-Heinz van Pée*
Institut für Biochemie
der Technische Universität Dresden
(Germany)

NMR of Polymers. By *F. A. Bovey* and *P. A. Mireau*. Academic Press, San Diego, 1996. 459 pp., hardcover $ 85.00.—ISBN 0-12-119765-4

The declared aim of this book is to provide an overview of the applications of NMR spectroscopy to polymer characterization. Frank A. Bovey and Peter A. Mireau have succeeded well in their objective. Naturally, in view of the enormous growth in the scope of this field, such an overview cannot cover every aspect of the current situation, and the authors make this clear in their preface. Rather than attempting an exhaustive treatment, they have set out to illustrate the range of problems in the polymer sciences that can be solved using NMR spectroscopy. The particular strength of the book lies in the adoption of this approach.

Chapter 1 explains the basic principles of nuclear magnetic resonance at a level understandable by the nonspecialist. The authors provide a good introduction to the subject, with a very broad choice of material forming a grounding in the subject that is suitable for an interdisciplinary readership. Thus we find, for example, a drawing of a cross-section through a superconducting magnet, a description of the frequency spectrum responsible for magnetic relaxation, and detailed tables of chemical shifts. A possible criticism is that some of the figures are very basic and lacking in detail, and contribute little to the reader's understanding. This applies, for example, to Figure 1.5 showing the separation of the alternating magnetic field into two counterrotating components, and Figure 1.15 illustrating the origin of the quadrupolar interaction. A necessarily brief introduction such as this cannot, of course, be expected to give the newcomer a real working knowledge. Accordingly, the later discussions of specific technique areas such as solid-state NMR spectroscopy or two-dimensional NMR methods are similarly limited to describing the most important pulse sequences and the interpretation of the resulting spectra.

Chapter 2 begins with a brief and lucid explanation of the different types of constitutional and configurational isomerism of polymers. The authors then deal with the various statistical models used to derive the sequence frequencies of the polymer chains resulting from different growth mechanisms.

In Chapter 3 the reader learns how one can determine the constitution and configuration of a polymer using high-resolution liquid-state NMR spectroscopy. This chapter achieves its purpose very well by using a large number of examples to illustrate how NMR spectroscopy can be used. These begin with regioisomerism in polythiophenes, and progress to problems such as solvent association in solutions of polymethylmethacrylate and polyvinylchloride. The reader's understanding is greatly helped by the frequent explanations of how one goes about predicting the characteristic chemical shift for a given structural element, using aids such as incremental rules, synthesizing model compounds, or recording multidimensional spectra. The authors offer many helpful hints on experimental aspects; for example, they point out that the chemical shifts of methyl groups are especially sensitive to solvent effects.

Chapters 4 and 5 contain a very wide-ranging description of the capabilities of solid-state NMR spectroscopy applied to polymers. For example, the authors explain how the chain conformations of the most important technical polymers can be deduced from features in their ^{13}C NMR spectra, how one can study long-range structures using a great variety of NMR techniques, how the molecular mobilities of the individual constituents in polymer blends can be investigated, etc., etc. The treatment is very up-to-date, as shown, for example, by the fact that a large proportion of the book is devoted to multidimensional methods. The work is rounded off by a very informative chapter on applications of NMR imaging.

The authors have been astute in their choice of topics for inclusion in these chapters. I noticed one error that has crept in: in Figure 5.1 showing the spectral density for relaxation processes, the extreme cases of very slow and very fast relaxation have been interchanged, and are opposite to those in Figure 1.8.

Which readers are most likely to benefit from this book? It does not give enough background on NMR fundamentals to enable a newcomer to the field to make effective use of the methods described. On the other hand, experienced NMR users will find nothing new here about techniques, although it may be useful in filling gaps in their knowledge of the literature. Probably those most likely to find the book useful are postgraduate students and research scientists who have a special interest in polymer science and are already familiar with NMR methods. It will make them aware of the wide variety of problems that can be investigated using NMR spectroscopy, and will bridge the gaps in their knowledge to enable them to use the techniques effectively. For these readers the outlay of $ 85.00 should prove both worthwhile and profitable.

Bernhard Blümich
Lehrstuhl für Makromolekulare Chemie
der Technischen Hochschule
Aachen (Germany)

Introduction to Medicinal Chemistry. How Drugs Act and Why. By *A. Gringauz*. WILEY-VCH, Weinheim, 1997. 721 pp., hardcover, DM 109.00.—ISBN 0-471-18545-0

Compared to the situation in other countries, the facilities for teaching medicinal chemistry in German universities, as an optional extra subject for students of organic or pharmaceutical chemistry, are somewhat rudimentary, despite the fact that many graduates hope to find work in pharmaceutical research. It is not surprising, therefore, that whereas the classical disciplines of chemistry are served by a few good quality works for each level of study, which have become established as standard textbooks, it is difficult to identify corresponding books in the area of medicinal chemistry. Alex Gringauz, the author of the book reviewed here, explains that it is intended for students of pharmaceutical and medicinal chemistry, and aims to provide an introductory overview of this specialized area of biomedical research, which is of steadily growing importance. It contains 15 self-contained chapters, the first three of which introduce the reader to the most important concepts of the molecular mechanisms involved in the activity of pharmaceutical agents. These chapters, occupying about 90 pages, explain the principles of the molecular interactions between low molecular weight compounds and macromolecular target systems, and discuss the various types of metabolic breakdown reactions undergone by medicinal compounds in the biochemical context. Unfortunately, however, the stereochemical aspects which are of such importance for pharmaceutical research are only touched on briefly.

 © WILEY-VCH Verlag GmbH, D-69451 Weinheim, 1997 0570-0833/97/3619-2131 $ 17.50+.50/0

After these introductory chapters the monograph becomes an encyclopedia-like collection of data, arranged according to the clinical conditions that the therapeutic substances are designed to treat. However, this arrangement of the subject matter is contrary to what one might expect in a modern textbook, as it does not correspond to current practice in pharmaceutical research. Instead we find a rather antiquated juxtaposition of often unrelated types of compounds under the following headings: agents for cancer therapy, analgesics, anti-inflammatory agents, antibiotics (two chapters consisting of 140 pages), cholinergic and adrenergic agents, cardiovascular drugs (two chapters), psychotherapeutic drugs, antihistamines, and steroids. The final chapter, entitled "New Developments and New Problems", occupies a mere twelve pages. Consequently it contains only very brief treatments of gene therapy, drug resistance, antisense technology, cytokins, and the applications of computers in pharmaceutical research.

Unfortunately, this attempt to convey the essence of pharmaceutical research fails so badly that it belongs to that generation of textbooks which cannot meet the standard of a modern works capable of motivating students. Some important aspects of this field of research are not covered at all, such as the concept of searching for lead structures and subsequent optimization, the study of structure–activity relationships in the context of the targeted receptor or enzyme, the importance of combinatorial chemistry in conjunction with high-throughput screening, and the topic of peptide mimetics, which has undergone a renaissance in the last few years. These are just a few of the topics that currently occupy organic chemists engaged in pharmaceutical research, and in relation to which this book can offer no help at all.

On a more positive note, the book deals with each of the above listed types of clinical conditions against the background of the physiological processes involved, with a wealth of detailed medical information. However, the standard of production, especially with regard to graphical layout, is much inferior to that normally found in the chemical literature. For example, the structural formulas are not numbered consecutively, and are generally of such poor quality that it is often difficult to distinguish between single and multiple bonds. Moreover, stereogenic centers are simply ignored, the orientations of substituents (e.g., in perspective representations of cyclohexane rings) are shown in ways that are very confusing and contrary to all the usual conventions, and the mechanisms of organic reactions are misrepresented to such an extent that even the experienced synthetic chemist will have difficulty in deciphering the relationship between educts and products. Here one begins to doubt whether the manuscript was ever subjected to copy-editing. It is not unusual in this book to come across hypervalent atomic centers in the structural formulas; pentavalent carbon atoms or tetravalent (neutral) nitrogen atoms are by no means rare. In the list of contents one occasionally finds a question mark instead of a page number. The overall appearance of the book in its chemical parts is more like a hastily prepared lecture manuscript than a modern textbook, and the reader will be amazed that it has been put onto the market at all in this state. When compared with other textbooks on medicinal chemistry that are currently available, such as those by R. B. Silverman or by H.-J. Böhm, G. Klebe, and H. Kubinyi, the book reviewed here cannot be recommended, either to students or to working chemists. In any case, it does not really convey the impression of a textbook intended for students; it is at best only suitable as a reference source for use by the scientist who occasionally needs information about some aspect of medicinal chemistry. Perhaps it would be fair to say, in conclusion, that Alex Gringauz's *Introduction to Medicinal Chemistry* will find few friends in the books market in view of the competition from genuine modern textbooks.

Gerhard Müller
Bayer AG, Leverkusen (Germany)

Spectra Interpretation of Organic Compounds. (Series: Spectroscopic Techniques. An Interactive Course.) By *E. Pretsch* and *J. T. Clerc*. WILEY-VCH, Weinheim, 1997. xiii, 175 pp., hardcover DM 128.00.—ISBN 3-527-28826-0

Spectroscopy is often seen by synthetic chemists as having a rather low status. It is only a slight exaggeration to say that spectroscopy is sometimes regarded as a necessary evil that one has to accept in order to meet the minimum requirements for characterizing a reaction product. Therefore it is hardly surprising that in many university chemistry departments the teaching of spectroscopy is undertaken by a lecturer for whom it is only a peripheral subject, and the students undergo an obligatory course of a minimal standard, from which they gain only a rudimentary knowledge. As a result of the low priority afforded to it, spectroscopy comes to be treated as a rather insignificant little wallflower bordering the main garden of preparative chemistry. Consequently the chemistry graduate who then moves into an industrial environment regards analysis as an overhead cost that should be minimized, so that there is a tendency, on the grounds of economy, to turn a blind eye to poor standards of analysis. Synthetic work that is not backed up by high quality analysis is worthless, and this fact is likely to be understood by the student who has learned to evaluate the capabilities of the various analytical methods. Any learning tool with the potential for helping to achieve that must be welcomed. This book by Pretsch and Clerc is the first volume in a new series from Wiley-VCH with the general title *Spectroscopic Techniques: An Interactive Course*.

The book is intended to be used as a self-study course. Its main part consists of 15 chapters, each of which is devoted to a particular compound whose structure is to be determined. These are moderately difficult exercises, with a gentle trend towards increasing difficulty in the later chapters.

Each chapter begins by showing a mass spectrum (produced by electron impact ionization), an IR spectrum (always of a solution in chloroform), a proton NMR spectrum (usually at 400 MHz, with expansions of the multiplets), and ^{13}C NMR spectra under different conditions (a normal spectrum together with DEPT-135 and DEPT-90 spectra for determining the degree of substitution). UV/vis spectral data are also given in three of the exercises, and in three other cases NMR spectra obtained in different solvents are shown.

In each case the above listed spectra are followed by a section explaining how the empirical formula can be determined from the spectroscopic data (without access to an elemental analysis or to a high-resolution mass spectrum), and how one can identify the characteristic structural groups of the unknown compound. Next it is shown how the partial structures thus obtained may be fitted together to give the required molecular structure, and how one can distinguish between possible isomeric structures. Here, however, the authors must be criticized for failing to mention the existence of two-dimensional and multidimensional NMR spectra. Surely nowadays there can hardly remain any laboratories where the structural analysis of organic compounds is carried out without the help of 2D NMR spectra! Would

 © WILEY-VCH Verlag GmbH, D-69451 Weinheim, 1997 0570-0833/97/3619-2132 $ 17.50+.50/0

anyone now contemplate managing without these very informative techniques? Pretsch and Clerc do not mention 2D NMR anywhere in their book, nor do they show any H,H-COSY, H,C-HMQC, or related types of spectra.

Each chapter ends with a section headed "Comments", usually quite long, in which the authors draw attention to special points that are illustrated by the compound concerned in relation to the various spectroscopic methods. Thus, for example, they explain why a molecule containing no nitrogen can sometimes give a mass spectrum that is dominated by fragments of even-numbered mass, or why a ^{13}C spectrum recorded under the DEPT-90 conditions may contain residual signals from carbon nuclei other than those of CH fragments. Although these points only emerge at the stage where the solution to the structural problem is being discussed, the reader cannot afford to ignore them, as they include a wealth of useful information, and are in my opinion the most valuable part of the text.

The 15 exercises are followed by three short chapters headed "Additional Remarks", dealing in turn with mass spectrometry (6 pp.), infrared spectroscopy (4 pp.), and NMR spectroscopy (14 pp.). These chapters give details of the conditions under which the spectra were recorded, and some general advice about using each of the spectroscopic methods. The advice offered is certainly useful, but the notes are too brief to be really adequate, and they are not a substitute for consulting more detailed textbooks. The book ends with two further chapters, one on the SpecTool computer program (see below) and the other introducing the reader to the formula generating program ChemWindow, which allows the user to input structures to SpecTool.

The most noteworthy feature of the book, which distinguishes it from other works with a similar purpose, is the combination with a CD-ROM containing a demo version ("teaching version") of the SpecTool program together with all the spectra belonging to Chapters 1–15. The software allows one to display the spectra on the PC monitor screen and expand them at will, so that chemical shifts or wavenumbers can be read off easily and precisely. Installing the program was simple and straightforward, and it performed satisfactorily with both Windows 3.11 and Windows 95. SpecTool in its full version is a good program, and is worthy of a separate review in its own right. It contains reference data, auxiliary programms ("tools"), and examples of actual spectra for each of the above spectroscopic methods. A feature deserving special mention is the suite of methods developed by Pretsch and colleagues, which identify the key partial structures within any structural formula that is fed in, and then apply appropriate incremental relationships to estimate the ^{1}H and ^{13}C chemical shifts.

In the text of the book, whenever a problem occurs for which SpecTool contains a useful function that should help in arriving at a solution, the reader is advised of this and of how to use it. Thus, in working through the exercises, one also becomes familiar with the use of the program. However, the user may be rather disappointed with the demo version of SpecTool supplied here, as it only contains a limited selection of spectral data, namely those that are relevant to the compounds mentioned in the book (and not always all of those: for example it does not give ^{13}C NMR data for lactones, which are needed for Chapter 1). Also the chemical shift estimation works only for the examples treated in the book.

When first trying out the system I initially thought that there must be a programming error, because data or spectra displayed on the monitor screen remained for only a few tenths of a second before they were hidden by a window carrying an advertisement ("Other books in this series: ..."). However, I felt cheated on realizing that there is method in this device, which ensures that for this price one receives only a limited version. Such a sales ploy is perhaps understandable, but could it not have been handled in a more acceptable way? For example, the publishers might have offered a deal whereby one could buy the book and a full version of the program together at a special reduced price. In any case, the extravagant promise of "powerful software tools and data" on the book's cover led me to expect more than this.

The standard of production of the book is excellent, with a sturdy binding and clear type and figures. However, the CD-ROM which is supplied in a plastic sleeve attached within the book is not easy to remove without destroying the sleeve or risking scratching the disk itself. Also, the practice here of listing the chemical shifts in ^{13}C NMR spectra with four digits after the decimal point is not sensible, as the implied precision is illusory.

To sum up, the concept underlying this combined book and CD-ROM is an excellent one, and apart from the failure to cover 2D NMR spectroscopy the result is very good. The package should serve effectively to familiarize the user with the spectroscopic methods that are important in the structural analysis of organic compounds. However, the prospective buyer needs to be warned about the limitations of the facilities provided by the software, lest there should be any suggestion of deception.

Ludger Ernst
NMR-Laboratorium
der Chemischen Institute
der Technischen Universität
Braunschweig (Germany)

 © WILEY-VCH Verlag GmbH, D-69451 Weinheim, 1997 0570-0833/97/3619-2133 $ 17.50+.50/0

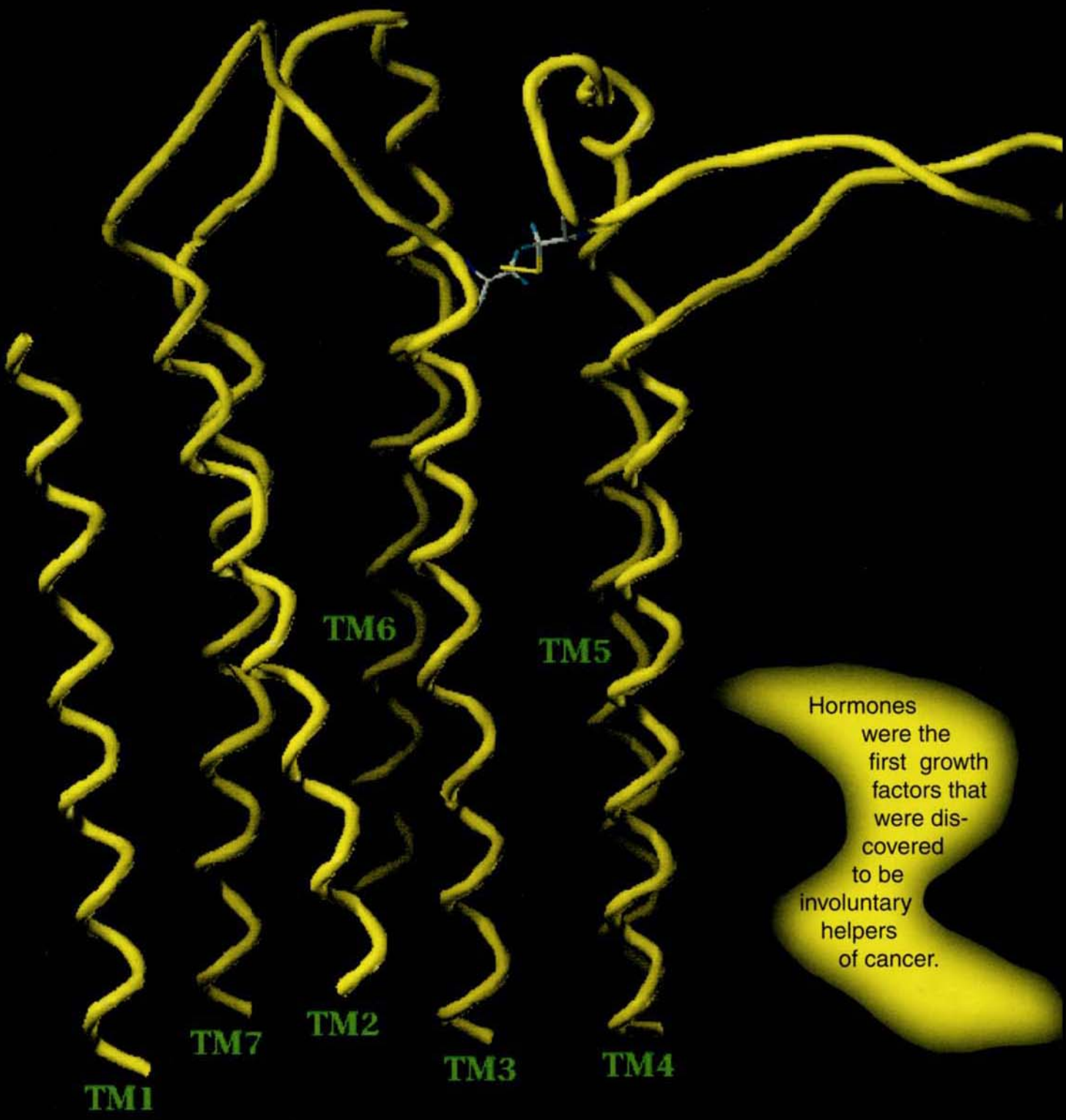

Hormones were the first growth factors that were discovered to be involuntary helpers of cancer.

Both the peptidic derivatives that are already employed clinically and new peptidomimetics, as well as the growing understanding of the three-dimensional structure of the receptor, fuel the expectation of a new generation of clinically active LHRH antagonists.

ANGEWANDTE CHEMIE ©WILEY-VCH

Chemistry and Molecular Biology in the Search for New LHRH Antagonists

Bernhard Kutscher,* Michael Bernd, Thomas Beckers, Emmanuel E. Polymeropoulos, and Jürgen Engel

Dedicated to Professor Heribert Offermanns on the occasion of his 60th birthday

Hormones—and in particular, the sex hormones—were the first growth factors discovered to be involuntary helpers of cancer. Female breast cancer and male prostate cancer are the best known examples of tumors acknowledged to be hormone-dependent. A look at cancer statistics shows that breast cancer is still the most frequent cancer in women; in men, prostate cancer plays a similarly dominant role with increasing age. Shutting down the main production site of the sex hormones estrogen and testosterone either by removing the ovaries or by castration is a well-known and often effective therapy; however, these procedures can be problematic due to the concomittant psychological stress. Modern hormone therapy for advanced breast cancer and prostate cancer attempts to spare the patient such irreversible operative procedures for as long as possible, by using hormone antagonists, such as the LHRH antagonists, which hinder deployment of the hormone itself and thus its growth-promoting activity.

Keywords: conformation analysis · LHRH antagonists · peptidomimetics · receptors · tumor therapy

1. Introduction

The releasing hormone, gonadorelin (GnRH, synonymous with LHRH, luteinizing hormone-releasing hormone or gonadoliberin), together with its specific receptor, plays a central role in neuroendocrinology.[1] The decapeptide LHRH, discovered by A. V. Schally et al. and R. Guillemin et al.,[2] is formed in the cell bodies of hypothalamic neurons and is secreted in pulses into the blood stream. Ultimately it stimulates secretion of the sex-specific hormones in the testes and ovaries. Intensive research has revealed that specific receptors for LHRH and synthetic analogues are also present in the pituitary gland and other tissues (for example, tumor cells)[3] and organs.

Three concepts for therapeutic application have emerged. The first is the restoration of normal physiology by administration of LHRH by infusion pump to promote fertility in men and women who are infertile due to defective endogenous LHRH secretion. Second, long-lasting LHRH agonists are used in a depot form, which bring about desensitization of the pituitary receptors and thus interrupt the signal cascade. This results in a biochemical "castration", which opens up new therapeutic possibilities for hormone-dependent diseases such as prostate cancer, breast cancer, and endometriosis. Although superagonists are generally well tolerated, they have the disadvantage that hormone secretion (estrogen, testosterone) is initially stimulated before the depletion of receptors or "down" regulation can take place, and thus the illness temporarily worsens.[4] This has led to the development of the third concept: use of LHRH antagonists.[5] At present, about 5000 LHRH analogues have been synthesized worldwide and tested in vitro or in vivo.[6a–c] Whilst LHRH agonists have been on the market for about ten years (see Section 2), the LHRH antagonists that have been developed furthest are still in clinical testing (Figure 1).[7]

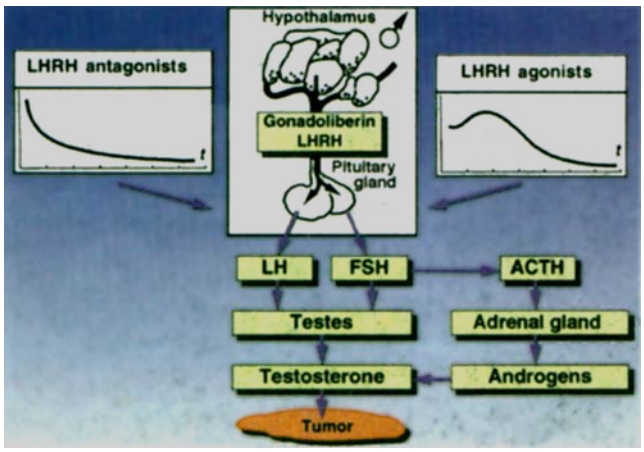

Figure 1. Antitumor activity of LHRH agonists and antagonists in man. FSH = follicle-stimulating hormone, ACTH = adrenocorticotropic hormone.

[*] Prof. B. Kutscher, Dr. M. Bernd, Dr. T. Beckers, Dr. E. E. Polymeropoulos, Prof. J. Engel
ASTA Medica AG, Konzernforschung
Weismüllerstrasse 45, D-60315 Frankfurt (Germany)
Fax. Int. code +(69)4001-2628
e-mail: Dr_Bernhard.Kutscher@astamedica.de

 © WILEY-VCH Verlag GmbH, D-69451 Weinheim, 1997 0570-0833/97/3620-2149 $ 17.50+.50/0

Complemetary to the reviews on LHRH agonists and antagonists which are already available,[8-10] this contribution covers not only the current developments in synthesis, but in addition, the establishment of the human receptor for specific characterization of substances, and presents methods and progress in the search for, and development of, peptidomimetics.

2. LHRH Peptides as Therapeutic Agents

2.1. Agonists

The first years after the discovery of the gondarelins were marked by the search for more active agonists, since their therapeutic potential as, for example, antitumor agents or in gynecology, was apparent.[5, 11] Such "superagonists" bring about a very effective reversible inhibition of the release of steriodal sex hormones. The exchange of glycine[6] of the native LHRH for other, always D-configured, amino acids, is common to all modern superagonists; some have a C-terminal ethylamide (buserelin, leuprorelin) or azaglycinamide (goserelin) residue instead of glycinamide. Eight to ten amino acids of the LHRH sequence are conserved in all clinically relevant superagonists; by exchange at a maximum of two positions, the biological activity, or hormone suppression in tumor patients, can be increased by a factor of up to 100 on subcutaneous application.[5, 11, 12] Table 1 summarizes the most important derivatives currently on the market.

Buserelin^{INN} (Profact, Suprecur), leuprorelin^{INN} (Carcinil, Enatone), triporelin^{INN} (Decapeptyl) and goserelin^{INN} (Zoladex) (trade names in Germany) are the products on the market with the highest turnover; worldwide, a turnover of about two billion

M. Bernd B. Kutscher J. Engel T. Beckers E. E. Polymeropoulos

Bernhard Kutscher, born in 1957, completed his chemistry studies in 1984 at the Universität Frankfurt (Germany) with a doctorate under the supervision of Prof. H. Kessler in the field of peptide synthesis. He then joined Degussa as laboratory manager (Laborleiter) in the research department "Pharmazeutische Chemie". Since 1987 he has headed the Department "Chemische Forschung Wirkstoffe" of ASTA Medica. Today he is responsible for the Department "Chemische Forschung". In 1992 he was appointed lecturer at the Technische Universität München and became Honorary Professor there in 1996. His fields of research include the synthesis of peptides, phospholipids and heterocycles, automation of synthesis, and combinatorial chemistry.

Michael Bernd, born in 1954, completed his doctorate in Chemistry with Professor H. Kessler at the Universität Frankfurt in 1983. In 1984 he became Laborleiter in the Department "Organische Forschung" of Degussa and in 1989 moved to ASTA Medica where he is responsible for peptide synthesis in the Department "Chemische Forschung Tumor".

Thomas Beckers, born in 1961, studied Biology specializing in Biochemistry at the Universität Frankfurt. His diploma was completed at the Max-Planck-Institut für Biophysik in Frankfurt. After graduating with a doctorate under Prof. J. Engels, Institut für Organische Chemie, Universität Frankfurt, in the field of Molecular Biology and a postdoctorate at the Massachusetts General Hospital/Harvard Medical School in the research group of Dr. B. Seed, Boston (USA), he joined the department for cancer research at ASTA Medica in the field of tumor research.

Emmanuel E. Polymeropoulos, born in Athens in 1943, obtained his doctorate in Physical Chemistry from Rutgers University, New Jersey (USA). From 1974 to 1980 he was scientific assistant in the research group of Prof. H. Kuhn at the Max-Planck-Institut für biophysikalische Chemie Göttingen (Germany) and thereafter as scientific assistant in the research group of Prof. J. Brickmann at the Institut für Physikalische Chemie der Technischen Hochschule Darmstadt (Germany) till 1984. After one and a half years at the Department of Physics of the research institute "Demokritos" in Athens he joined ASTA Medica in 1986, where he is responsible for computer applications in the Department "Chemische Forschung".

Jürgen Engel, born in 1945, completed his engineering studies at the Naturwissenschaftlich-technische Akademie in Isny (Germany) and began his studies in Chemistry at the Technische Hochschule Braunschweig (Germany) in 1969. He ended these studies in 1979 with a doctorate at the Institut für Organische Chemie der Universität Braunschweig with Prof. H. H. Inhoffen. From 1976 to 1981 he was Laborleiter in the Department "Chemische Forschung Wirkstoffe" at ASTA Medica, in 1981 head of research coordination, and in addition was promoted to head of the "Chemische Forschung Wirkstoffe" in 1982. Since 1981 he has given a series of lectures at the Universität Regensburg, where he completed his habilitation in 1985, and became Professor in 1990. In May 1993 he was appointed Honorary Professor at the Universität Dresden. Since 1996 he has been chairman of the Fachgruppe Medizinische Chemie of the Gesellschaft Deutscher Chemiker.

Table 1. Structure of LHRH, and the LHRH agonists on the market (given are only those amino acid residues that are different in LHRH).

Name (Co.)	Structure									
	1	2	3	4	5	6	7	8	9	10
LHRH	Glp[a]	His	Trp	Ser	Tyr	Gly	Leu	Arg	Pro	Gly-NH_2
Buserelin (Hoechst)						D-Ser(*t*Bu)				Gly-NHEt
Nafarelin (Syntex)						D-(2)Nal				
Leuprorelin (Abbott, Takeda)						D-Leu				Gly-NHEt
Goserelin (Zeneca)						D-Ser(*t*Bu)				Azagly-NH_2
Histrelin (Ortho)						D-His(Bzl)				Gly-NHEt
Triptorelin (Ferring)						D-Trp				

[a] Glp = pyroglutamic acid.

German marks with active compound formulations corresponding to these peptides was achieved in 1994; of this, over half belonged to the firms Abbott and Takeda with leuprorelin. A total market volume of about 2.4 billion German marks across all indications is expected at the end of the century.[12b]

Annual production of peptide pharmaceuticals is of the magnitude of less than 100 kg for buserelin and significantly over 100 kg for the market leader, leuprorelin. At this order of magnitude, these substances are only made by classical organic preparative synthesis (fragment condensation in solution). The firm Hoechst, for example, synthesizes the nonapeptide buserelin from the units Glp-His, Trp-Ser-Tyr, and D-Ser(*t*Bu)-Leu-Arg-Pro-NHEt; the tri- and tetrapeptide units are coupled to form the corresponding C-terminal heptapeptide, and then the N-terminal dipeptide is condensed with this to form the complete sequence. Control of the physicochemical process parameters, such as concentrations, precipitations, separations, reaction temperature profiles, and purification techniques, is important for successful peptide synthesis on a technical scale, since there is naturally a significant difference to those required for laboratory scale synthesis.[13a]

2.2. Antagonists

Common to the intrinsic activity of all superagonists is the initial temporary stimulation of gonadotrophin release. Soon after the use of highly active agonists became an established therapy, a search began for corresponding antagonists, which do not bring about an initial hormone release, to avoid this therapeutically counterproductive effect. A final big hurdle for clinical use of highly active anatagonists was the inherent anaphylactic potential of these peptides.

Starting from the sequence of native LHRH, the individual positions of the peptide chain were examined in rapid succession for their contribution to biological activity. Particular attention was paid to side effects. The most effective early improvements in antagonistic activity were achieved by using D-Phe^2 instead of histidine, by D-amino acids at position 6 instead of Gly^6, and the exchange of C-terminal glycine for D-Ala^{10}. Further stepwise optimization led to the sequence scheme now usual for all modern antagonists of D-Nal^1-D-Cpa^2-D-Pal^3 (Nal = 2-naphthylalanine, Cpa = Phe(4-Cl), Pal = 3-pyridylalanine) as hydrophobic cluster, plus a D-configured aromatic or aliphatic, yet hydrophilic, aminocarboxylic acid^6, and the C-terminal hydrophilic sequence Xxx^8-Pro^9-D-Ala^{10}, where Xxx is either arginine or isopropyllysine. Excellent documentation of the stepwise optimization can be found in many classical review articles.[14, 15]

Antagonists of the second generation caused formation of temporary edemas of the face and extremities in animal experiments, due in part to massive histamine release by mast cell degranulation. Cyanosis and respiratory impairment were also observed.[16] The cause of these intolerable side effects is thought to be the combination of D-arginine at position 6 with the three aromatic amino acids at the N-terminus of the sequence.[17] For the desired biological antagonist potency, an R-configured basic amino acid is necessary at position 6; A. V. Schally et al. achieved the breakthrough to highly active antagonists free of side effects with the derivatives SB-75 (INN: cetrorelix) and SB-88, by incorporating hydrophilic, nonbasic amino acids with side-chain carbamoyl functions (D-citrulline^6 (D-Cit^6), D-homocitrulline^6).[17]

The biological activity of such sequences that are free of significant anaphylactic potential is limited exclusively to R-configured amino acids at position 6; peptides with L-citrulline^6 are practically inactive in vivo due to rapid enzymatic degradation (Figure 2).[18]

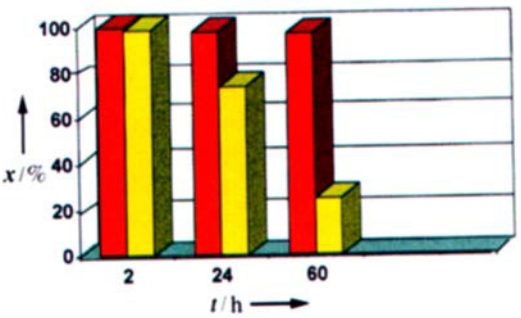

Figure 2. Stability of [D-Cit^6]SB-75 (cetrorelix; red) and [L-Cit^6]SB-75 (yellow) under the influence of human serum (HPLC peptide content x[%] over 60 h).

Today, cetrorelix is manufactured exclusively by classical fragment condensation, on a kilogram scale. Two synthesis strategies, worked out in detail and optimized over several years, proceed via either the N-terminal tripeptide (D-Nal^1-D-Cpa^2-D-Pal^3) or the C-terminal tripeptide (Arg^8-Pro^9-D-Ala^{10}) and the complementary heptapeptide (Ser^4–D-Ala^{10}) or (Nal^1–Leu^7) to the protected decapeptide with *tert*-butyl side-chain protection; the hydrochloric acid deprotection is followed by final purification by preparative HPLC. The C- and N-terminal functionalization of the acetylated decapeptide amide, nec-

essary for biological activity and to avoid rapid enzymatic degradation, is introduced at the level of the terminal tripeptide, by acetylation of the free α-amino group of naphthylalanine[1] with acetylhydroxysuccinimide, or saponification of the resulting alanine methyl ester in alcoholic ammonia.[13b,c]

Folkers et al. were able to improve active antagonists successively by consistent and systematic modifications both at the relevant sequence positions and the side-chain substituents; the most successful were complex substitutions at the positions 5, 6 and, in part, 8. Starting from antide, a highly potent but poorly water-soluble decapeptide with nicotinoyl-substituted lysine[5], or with D-lysine[6] (Scheme 1), the analogues [PicLys[5],D-(6ANic)Lys[6]]antide (= nictide where pic = picolinyl, 6ANic = 6-aminonicotinoyl), [D-3-Qal[1],c-PzACAla[5],D-PicLys[6],Arg[8]]-antide (= argtide where Qal = 3-(3-quinolyl)alanine, c-PzAC = *cis*-3(4-pyrazinylcarbonyl-aminocyclohexyl), and [PicLys[5],D-(PicSar)Lys[6]]antide (= sartide where Sar = sarcosine (*N*-methylglycine)) were synthesized and their biological activity characterized.[19-23]

Flouret et al. have reported over 104 analogues of antide, the clinical use of which is impaired by unfavorable solubility characteristics. They describe the exchange of the antide-typical nicotinoyl group for a variety of other acyl substituents, and exchange of lysine for other short-chained amino acids such as 2,3-diaminopropionic acid or 2,4-diaminobutyric acid, and the biological activity in relation to these modifications.[9] Xiao et al. have synthesized a number of active antagonists (Tx series) with unnatural amino acids at positions 5 and 6; the most active sequence Tx-44 contains the amino acid 4-(morpholinomethyl)-phenylalanine (Mop) derived from phenylalanine instead of tyrosine[5].[24-26]

An important contribution was made by Rivier et al., whose optimization led to the decapeptide "azaline" with novel modifications at positions 5 and 6, where aminotriazole-subsituted p-aminophenylalanine or lysine are positioned.[27,28] Azaline B is probably one of the most active antagonists presently available worldwide. The current status of work on the "Azaline B family" is documented in a review by Rivier.[29]

An interesting strategy for discovery of antagonists with good water solubility was published by Roeske et al.[30] Decapeptide sequences with side chain modifications of D-Glu[6] or D-Lys[6] derivatives were synthesized with strongly polar and hydrophilic groups such as taurine. The strongest antiovulatory activity (AOA) was found on substitution of D-Lys[6] with gulonic acid or D-Glu[6] substitution with tris(hydroxymethyl)aminomethane (Tris; 75 and 50% AOA, respectively, 1 μg, rat model).

Deghenghi published a highly active decapeptide sequence with minimal histamine release and good water solubility. This structure, known as antarelix, differs from SB-75 (cetrorelix) in that it has homocitrulline[6] instead of citrulline[6] and isopropyllysine[8] instead of arginine[8].[31,32] By using Lys(*i*Pr)[8], residual potential for histamine release can be further reduced.

The firm Organon is developing the antagonist ganirelix (RS-26306) under licence from the firm Syntex; this is a decapeptide with novel alkyl-modified D- and L-homoarginine units at positions 6 and 8.[33] The development of a similar forerunner derivative called detirelix (Arg[8]-ganirelix) was suspended by Syntex. With ramorelix (HOE 013), the firm Hoechst (HMR) has a peptide antagonist with a sugar–amino acid unit D-α-L-rhamnosyl-D-serine[6], that has improved water solubility; however, its biological activity is possibly insufficient for clinical use as an antitumor agent.[34,35] The firm Schering is also developing peptide antagonists, using nonproteinogenic amino acids, such as ε-dialkylated lysine or benzodiazepine aminocarboxylic acids.[36,37] ZK-157348 contains *N*-6-morpholinolysine at the positions 6 (D-Morlys) and 8 (L-Morlys); biological data have not been published.

An interesting method for the manufacture of orally administered LHRH antagonists is being pursued by the Australian firm Biotech, who are concerned with the synthesis of conjugates of antide and vitamin B_{12}. The derivatives have similar in vitro and in vivo activity to antide; however, they have much better aqueous solubility and can thus be administered parenterally.[38,39] Scheme 1 shows the relevant derivatives and known candidates for development.

The search for peptide and peptidomimetic structures of the next (that is, the fourth) generation with improved pharmacologic activity continues undiminished worldwide. In addition to the classical indication of hormone-dependent tumor treatment, the LHRH antagonists can also be used to treat nonmalignant tissue abnormalities, for example, uterine myoma or benign prostate hyperplasia (BPH), with good prospects of success. In modern reproductive medicine, LHRH antagonists have significant advantages over the agonists used exclusively until now.

Today, the highly active decapeptides SB-88 and SB-75 (INN: cetrorelix)[40] are used in various laboratories as lead structures for the discovery of stable derivatives with good aqueous solubility and long-lasting in vivo activity. For peptide antagonists, one looks for cetrorelix analogues with modifications particularly at positions 5, 6, and 7. Nonproteinogenic amino acids, D-alkyl derivatives and amino acids with specifically altered side chains are introduced at these positions. Characteristic substitution patterns of such modifications of cetrorelix analogues are explained in Figure 3, with D-lysine[6] as an example.

The best derivatives with the highest receptor affinities have so far been obtained by suitable modifications of the ε-amino function of D-lysine[6] with polar, hydrophilic carboxylic acids. With T-148, Schally et al. found a sequence that has bisacetyl-2,3-diaminopropionic acid bound through an amide linkage to the ε-amino function of D-lysine[6]-SB-75 and that is highly active in vitro. Sugar units of the D-glucopyranuronic acid type as D-lysine[6] side chain also give highly active antagonists with long-lasting hormone suppression in vivo.[42,43] Insertion of α-amino carboxylic acids at positions of the peptide scaffold other than position 6 also brings about stronger receptor affinity in certain cases, but has not yet achieved increased activity in vivo.[24]

D-24308, an L-Cpa[2] analogue of antarelix is a spectacular example of how reversal of chirality at a sensitive position on the molecular scaffold, which has a characteristic sequence of optically active centers, can bring about a dramatic loss of activity (Scheme 1). With exchange of D-Cpa[2] for L-Cpa[2], the biological activity is completely lost.

The work of Haviv et al. with restrictions, cyclizations and sequence truncations[44-50] is a good example of intensive research on effective antagonists. Abbott's A-76154 is an octapeptide antagonist with LHRH receptor affinity of a similar order of magnitude to that of active decapeptides such as A-75998 or "Nal-Glu".[51]

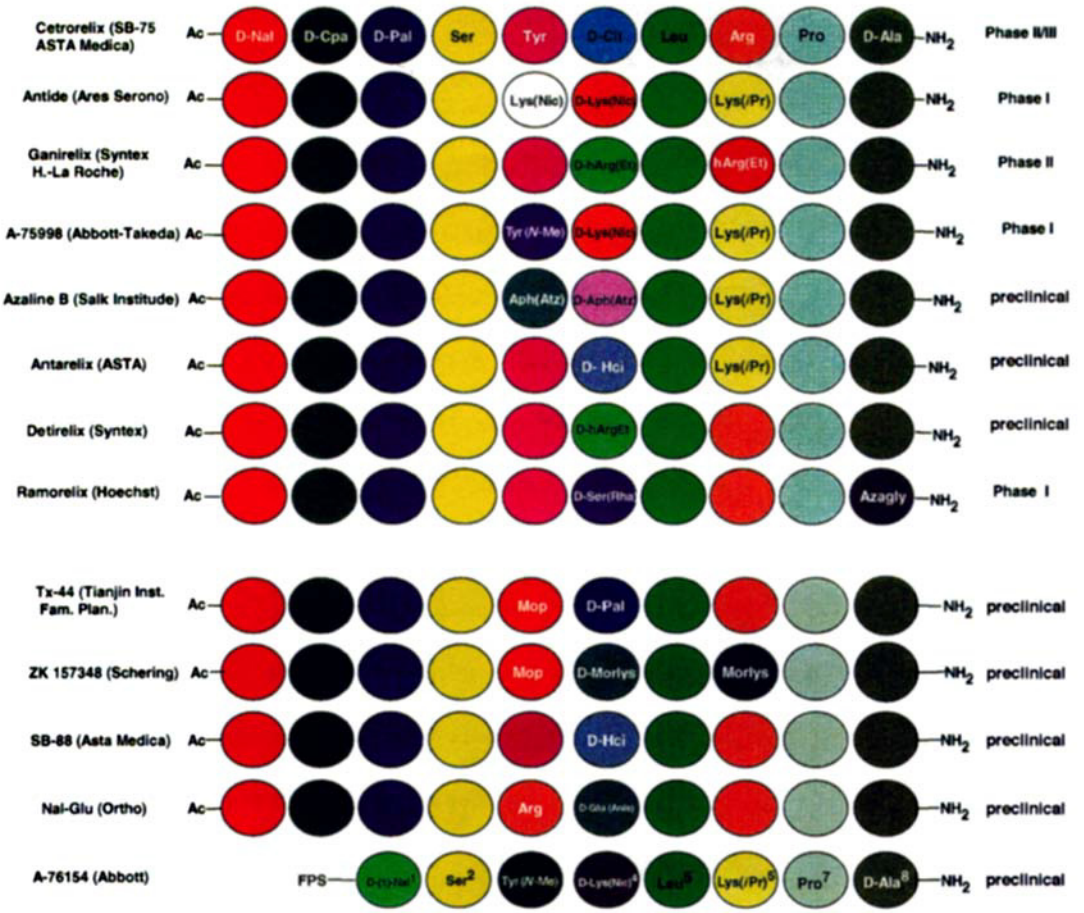

Scheme 1. Structures of LHRH antagonists (cetrorelix, the compound furthest along in clinical tests, serves as basis). $hArg(Et_2)$ = homoarginine(N^G,N^G-diethyl), Anis = anisol, Aph = *p*-aminophenylalanine, FPS = 4-fluorophenylpropionic acid, Hci = homocitrulline, Mop = morpholinomethylphenylamine, Morlys = *N*-morpholinolysine, Rha = rhamnosyl.

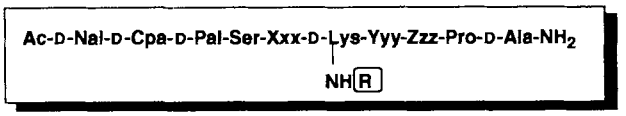

Xxx = Tyr or other amino acids
Yyy = Leu or other amino acids
Zzz = Arg or Lys(*i*Pr)
R = carboxylic acids

Example : T-148

Ac-D-Nal-D-Cpa-D-Pal-Ser-Tyr-D-Lys(Ac_2Dap)-Leu-Arg-Pro-D-Ala-NH2

Figure 3. Side chain variation in (D-Lys^6)-cetrorelix analogues. Ac_2Dap = N^2,N^3-diacetyl-2,3-diaminopropionic acid.

Molecular restrictions, such as head-to-tail cyclization, can be accompanied by improved stability and duration of activity in peptides and also in heterocyclic lead structures, if the restriction includes the bioactive conformation (matched core).[52] The same applies to dimerization and partial dimerization through binding of suitable (partial) sequences, for example on the Lys^6 side chain, and also for cyclization from the C-terminus to the middle of the molecule. A multitude of cyclopeptides with LHRH sequences have been synthesized which confirm this (see Schemes 3 and 4). Their conformational properties are discussed in Section 3.

3. Structure and Conformation

Modeling of peptide systems such as LHRH as a means to explain the biologically active conformation began in the 1970s with the development of potential functions to examine energetic and entropic terms that contribute to the stabilization of the conformation of a peptide chain in solution.[53, 54] The first NMR investigations of LHRH indicated that there was no preferred conformation in solution.[55, 59, 60] Monahan et al. explained the significant difference in both in vitro and in vivo activity between [Ala^6]LHRH and [D-Ala^6]LHRH by the formation of a β-turn in the Ser^4-Tyr^5-Gly^6-Leu^7 segment of LHRH.[56] This assumption was supported by empirical conformational analyses of LHRH and analogous compounds by Momany (Figure 4).[57, 58] Substitution of the segment Tyr^5-Gly^6-Leu^7-Arg^8 by a sterically hindered β-lactam[61] as a model of a βII'-turn resulted in an LHRH-analogous compound that was more potent than LHRH both in vitro and in vivo.

Molecular dynamics (MD) simulation calculations performed by Struthers et al.[62a, b] supported the presence of a βII turn and indicated spatial separation of the hydrophobic side chains (Trp^3, Tyr^5, Leu^7), which possibly interact with a hydrophobic region of the receptor.[56] These calculations led to the synthesis of the cyclic LHRH antagonist cyclo[$\Delta^{3,4}$-Pro^1-D-Cpa^2-D-Trp^3-Ser^4-Tyr^5-Trp^6-N-Me-Leu^7-Arg^8-Pro^9-β-Ala^{10}-] (I, Scheme 2), which, however, binds more weakly to the recep-

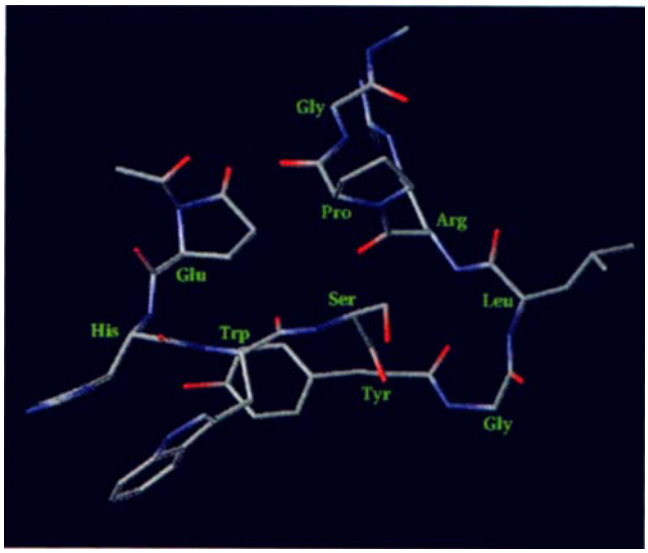

Figure 4. Conformation of LHRH, reproduced according to data in Refs. [57,58].

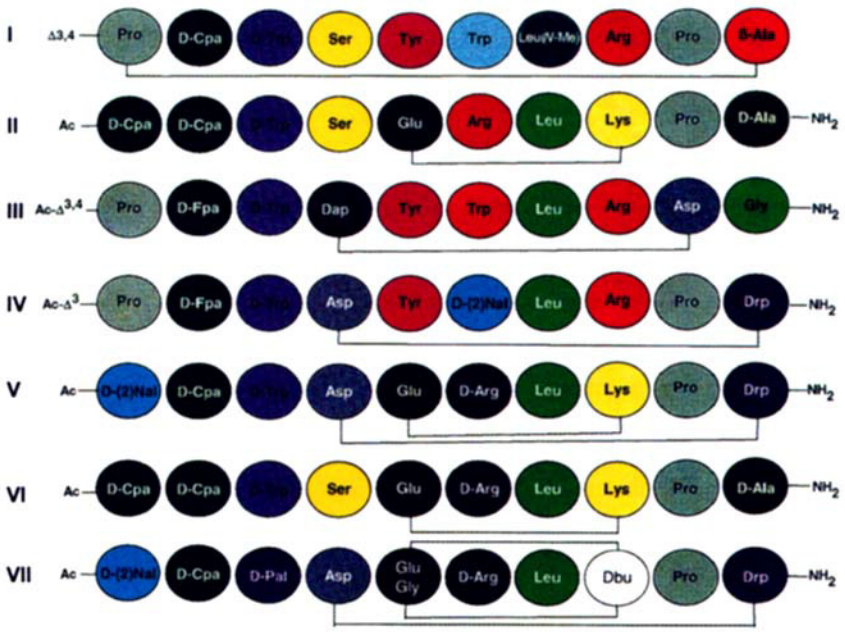

Scheme 2. Structures of cyclized LHRH analogues, whose conformations have been elucidated.

tor than LHRH itself. This compound has two βII′-turns,[63] which are formed with the help of an internal network of hydrogen bonds. This stabilizing effect was also examined by the isosteric substitution of -CH_2NH- instead of -CONH- at all amino acid positions of the antagonist [N-Ac-D-Nal[1], D-Phe[2,3], D-Arg[6], Phe[7], D-Ala[10]]-LHRH, except for position 9.[64a] These substitutions brought about a reduction or even absence of antiovulatory activity in biological tests. Such an interpretation assumes that these modifications do not lead to changed binding to the receptor. However, it is known that amide bonds of a substrate are also involved in receptor binding.[64b]

To gain a better understanding of the interaction between LHRH antagonists and the human receptor, a head-to-tail cyclization of cetrorelix to cyclic cetrorelix ("cyclorelix"), of antrarelix to cycloantrarelix, and of SB-88 to cyclo-SB-88 was carried out (Scheme 3).[65] All three cyclopeptides have significantly weaker binding than the linear derivatives (see Section 5b). NMR investigations in methanol and DMSO did not give any indication of preferred conformations for these cyclized compounds; thus no further insight into receptor-binding conformations was gained.[66] By 2D-NMR investigations of LHRH in various solvents[67] and NMR investigations of cetrorelix in DMSO, trifluoroethanol (TFE), H_2O, and H_2O/SDS (SDS = sodium dodecylsulfate),[68] preferred extended conformations were found for LHRH, and evidence was found for a possible fold in the Tyr[5]-Arg[8] segment of cetrorelix that, however, bears no resemblance to a βII′-turn.

The search for active, conformationally restricted LHRH antagonists was continued by Dutta et al.[69,70] By targeted cyclization of linear peptides, a range of cyclic derivatives was obtained, in which the side chains of the amino acids at positions 5 and 8 formed part of the ring system. The most potent compound of this group was Ac-D-Cpa[1]-D-Cpa[2]-D-Trp[3]-Ser[4]-cyclo(Glu[5]-D-Arg[6]-Leu[7]-Lys[8])-Pro[9]-D-Ala[10]-NH_2 (**II**), which showed threefold stronger ovulatory inhibition than the corresponding linear compound. As a result of conformational analysis of this antagonist and its linear analogue, bicyclic LHRH antagonists were obtained in which the amino acids 5 and 8, and also both termini, were bridged.[71] The examination of this compound led to structures in which a β-turn was present between positions 3 and 6 (Figure 5). Since the in vivo results were generally less favorable for the bicyclic peptides than for monocyclic 5–8 bridged derivatives, this was an indication that the free end groups play an important role in binding to the receptor.

Use of a novel starting point for design of LHRH antagonists was attempted by Struthers et al.;[72] based on analysis of MD simulations on **I**,[73] they suggested a receptor–binding conformation (supported by NMR investigations) for LHRH antagonists. However, in vitro results gave a K_D value greater than 100 nM for binding to the LHRH receptor, which was much higher than the K_D value of the corresponding linear compound (K_D = 0.21 nM). These findings suggest that 1) the free N- or C-terminus of the linear derivative plays an important role in receptor binding, and 2) fitting of the cyclic antagonist to the receptor binding pocket was suboptimal.

By optimization, the antagonist Ac-$\Delta^{3,4}$Pro[1]-D-Fpa[2]-D-Trp[3]-cyclo(Dap[4]-Tyr[5]-D-Trp[6]-Leu[7]-Arg[8]-Asp[9])-Gly[10]-NH_2 (**III**, Fpa = 4-fluorophenylalanine) was obtained, in which the side chains of Dap[4] and Asp[9] are bridged. The substance has a binding constant of K_D = 55 nM. The compound Ac-$\Delta^{3,4}$-Pro[1]-D-Fpa[2]-D-Trp[3]-cyclo(Asp[4]-Tyr[5]-D-(2)Nal[6]-Leu[7]-Arg[8]-Pro[9]-Dpr[10])-NH_2 (Dpr = 2,3-diaminopropionic acid, **IV**)[74,75] was synthesized by bridging amino acids 4 and 10, whereby a βII′-turn in segment 5-6-7-8 is stabilized by two hydrogen bridges. The influence of incorporation of L-Tic (Tic = tetrahydroisoquinoylalanine) at various positions of the linear antagonist Ac-D-Nal[1]-D-Cpa[2]-D-Pal[3]-Ser[4]-Tyr[5]-D-Pal[6]-Leu[7]-Arg[8]-Pro[9]-D-Ala[10]-NH_2 was also examined, with molecular mechanics cal-

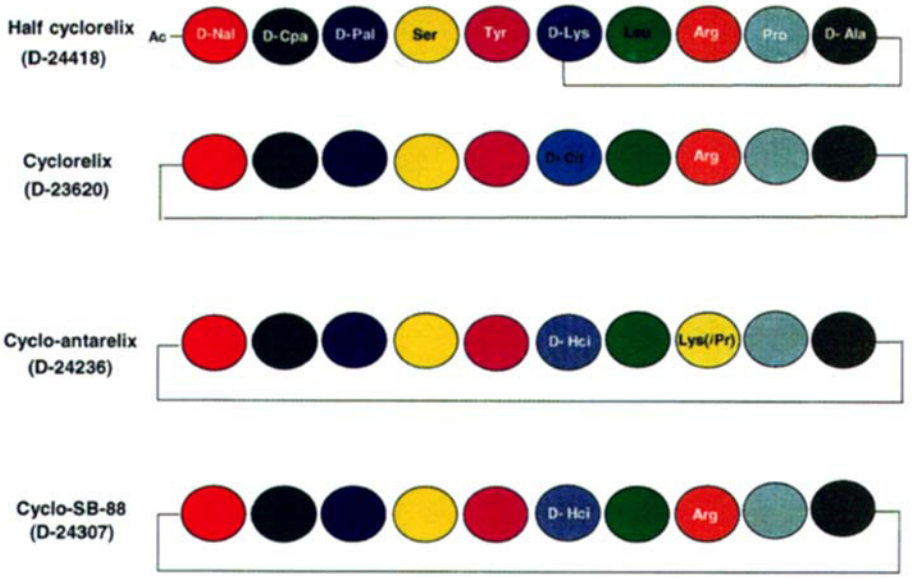

Scheme 3. Cyclized analogues of cetrorelix and structurally related compounds (code numbers).

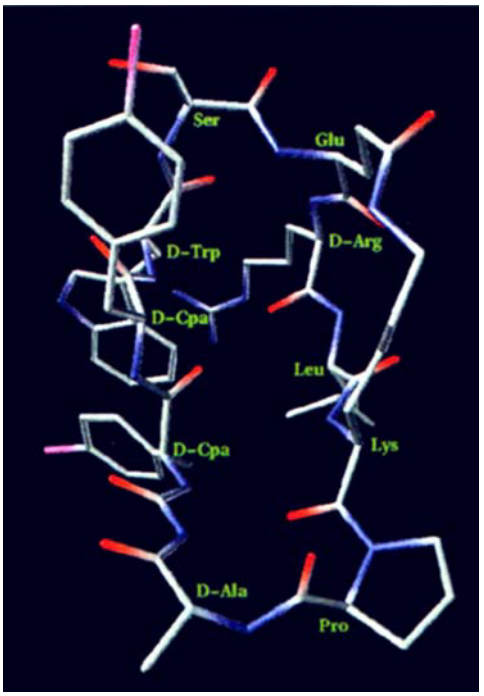

Figure 5. Conformation of the antagonist bicyclo(1-10/5-8)(-D-Cpa^1-D-Cpa^2-D-Trp^3-Ser^4-cyclo(Glu^5-D-Arg^6-Leu^7-Lys^8)-Pro^9-D-Ala^{10}-), reproduced according to the data in Ref. [71].

culations.[76] Substitution of D-Tic at position 6 seems to contribute to the maintenance of a βII′-turn. It is known that a D-amino acid flanked by L-amino acids is a strong βII′-turn inducer. The D-amino acid then occupies the $i+1$ position. D-Pro, which is the natural counterpart of D-Tic, exerts a particularly strong effect.[76b] Further mimetic models for βII-turns were discussed by Rizo and Gierasch in a review article on theoretical considerations of conformationally restricted peptides.[77]

N-methylation of α-amide bonds in LHRH agonists[78] and antagonists[45] has the surprising effect of converting some agonists into antagonists. In the majority of cases, the N-methylated agonists were less active than the corresponding nonmethylated compounds. All Tyr^5(*N*-Me) derivatives of antagonists had surprisingly good aqueous solubility. In particular, for the sequence Ac-D-(2)Nal^1-D-Cpa^2-D-(3)Pal^3 - Ser^4 - Tyr^5(*N* - Me) - D - Lys-(Nic)^6-Leu^7-Lys(*i*Pr)^8-Pro^9-D-Ala^{10}-NH_2 (A-75998), the conformational change was crucial for both solubility and binding affinity to the receptor. On N-methylation, the ratio of *cis*/*trans* isomers is changed and hydrogen-bridge formation is not possible, which leads to poorer association or aggregation. In addition, a hydrogen bridge, which normally contributes to stabilization of the βII-turn, is broken by the methylation. A further development was attempted by Liff et al., who tried to bring about targeted changes in the conformation of LHRH-analogous compounds by methylation of C_α atom centers.[79] However, such substitutions have not resulted in any significant conformational changes.

Comprehensive conformational analyses of native LHRH and of LHRH agonists and antagonists were performed by Nikiforovich and Marshall.[80, 81] A high flexibility was established for LHRH, in agreement with previous NMR investigations on linear peptides of corresponding chain length. Due to the function of Gly as a D-amino acid, the fragment Tyr^5-Gly^6-Leu^7-Arg^8 has a preferred conformation, yet without forming a marked βII-turn. Calculations indicate different conformations for agonists and antagonists in segment 5–8. However, the geometry of the N-terminal tripeptide was similar for agonists and antagonists.

A further attempt to determine the "biologically active conformation" of LHRH and analogues was made with NMR and MD investigations on the conformationally restricted bicyclic antagonist bicyclo(4-10/5-8)[Ac-(2)Nal^1-D-Cpa^2-D-Trp^3-Asp^4-Glu^5-D-Arg^6-Leu^7-Lys^8-Pro^9-Dpr^{10}]-NH_2 (**V**).[82] The existence of a βII′-turn in segment 5–8 (D-Arg at $i+1$ position) could be shown here. The additional 5–8 ring closure changed the conformation of the 4–10 bridge in the original monocyclic compound only slightly.

NMR investigations on a series of cyclized LHRH antagonists and their linear analogues (best cyclic antagonist: Ac-D-Cpa^1-D-Cpa^2-D-Trp^3-Ser^4-cyclo(Glu^5-D-Arg^6-Leu^7-Lys^8)-Pro^9-D-Ala^{10}-NH_2, **VI**) resulted in a structure with a β-turn present in segment 3–6, as in Refs. [71, 83]. In addition, the side chains 1 and 10 were now in direct proximity to one another, due to the existence of a network of hydrogen bridges. These cyclic compounds showed higher potency in the antiovulation assay (AOA) than the corresponding linear peptides.

Recent results on putative binding conformations of LHRH antagonists were obtained by Rizo et al. in a study of the bicyclic antagonist bicyclo(4-10/5,5′-8)(Ac-D-(2)Nal^1-D-Cpa^2-D-Pal^3-Asp^4-Glu^5(Gly)-D-Arg^6-Leu^7-Dbu^8-Pro^9-Dpr^{10}-NH_2) (**VII**, Dbu = 2,4-diaminobutyric acid).[84] This antagonist has a βII-turn at amino acids 5–6, a βI′-turn at 6–7 and a βII-like

turn between Pro^9 and the side chain of Dpr^{10}. Comparison with the results in Ref. [82] clearly shows that 4-10/5-8 bicyclic structures—despite double restriction—can adopt many conformations.

Until now, cyclized LHRH agonists and antagonists have not shown any significantly better biological activity than linear derivatives. It is clear that the termini must be free to take part in binding to the receptor. Although NMR investigations and MD simulations indicate the existence of a β-turn in segment 5–8 or 3–6, the high flexibility of oligopeptides remains the main problem in the search for the biologically active conformation and in optimization of structure–activity relationships. It is becoming more and more obvious that new methods are needed to solve this problem.

4. Receptor Assays

4.1. The Pituitary LHRH Receptor—A Representative of the Rhodopsin-Like G-Protein-Coupled Family of Serpentine Receptors

Although the hypothalamic peptide luteinizing hormone-releasing hormone was isolated and its sequence determined in 1971 by A. V. Schally and coworkers,[2, 85] the corresponding cDNA was not successfully cloned until 1984. This coded for the precursor protein of 92 amino acids, from which the decapeptide is formed by proteolytic processing.[86] Almost another ten years of intensive research passed until in 1992, various research groups managed to clone the high affinity receptor for LHRH from the murine gonadotrophic αT3-1 cell line.[87, 88] This immortalized murine pituitary cell line shows relatively high LHRH receptor expression, which enabled isolation of the cDNA by expression cloning in oocytes of *Xenopus laevis*.[87, 89–91] Based on the murine LHRH receptor cDNA sequence, the homologous cDNA genes of human, rat, cow, and sheep receptors were subsequently cloned.[92–97] The homology of the murine receptor to that of the rat is 97% and to the human receptor 89%. The pituitary high-affinity receptor for LHRH belongs to the rhodopsin-like family of G-protein-coupled 7-helix receptors, which are also described as serpentine receptors (a review is given in Iismaa et al.[98]). Further representatives of this family are the receptors for the peptides somatostatin, thyrotropin-releasing hormone (TRH), cholecystokinin (CCK), neurokinins A and B, and Substance P.[99] The cDNA of the human LHRH receptor codes for a protein of 328 amino acids. It is striking that the receptor has practically no C-terminal cytoplasmic domain (only two amino acid residues) and that the "signature sequence" typical for many G-protein-coupled receptors is changed from DRY^{140} to DRS^{140}.[100] Complementary to the LHRH cDNA, the chromosomal gene of the human receptor, composed of three exons and two introns, was recently cloned.[101] LHRH induces dose-dependent synthesis of the "second messenger" D-*myo*-inositol-1,4,5-triphosphate ($InsP_3$) and a biphasic rise in the intracellular calcium [Ca_i^{2+}] both in cultivated gonadotrophic pituitary cells and in the αT3-1 cell line (Figure 6).[102] Since these signals could not be inhibited by pertussis toxin, participation of the G_i and G_o subfamily of trimeric G-proteins could be excluded.[103] Recent work on the gonadotrophic αT3-1 cell line shows, however, that signal transmission following activation of the receptor takes place through a G protein of the subtype G_q/G_{11} and is thus coupled by phospholipase C subtype β (PLCβ) to the inositol phospholipid signal pathway.[104] The heterologously expressed LHRH receptor is also functional in recombinant cell systems, that is, stimulation with agonists leads, after G-protein coupling, to synthesis of $InsP_3$.[105, 93]

4.2. The Human LHRH Receptor—Cloning, Heterologous Expression and Recombinant Systems for Testing LHRH Antagonists

Cloning of the human receptor is of great importance for discovery and characterization of potent LHRH antagonists for clinical application, and this has become possible with the development of relevant, simple test systems. In the past, an initial in vitro characterization of peptide LHRH antagonists was done with classical receptor-ligand binding tests with iodinated LHRH derivatives, which mostly use crudely purified membrane fractions from the rat pituitary.[106, 107] Since a species-dependent binding of LHRH derivatives has been reported by various authors, this was a pragmatic method although not without problems.[97, 108–109] In particular, species-specific binding might be the case for nonpeptide receptor ligands, since these probably

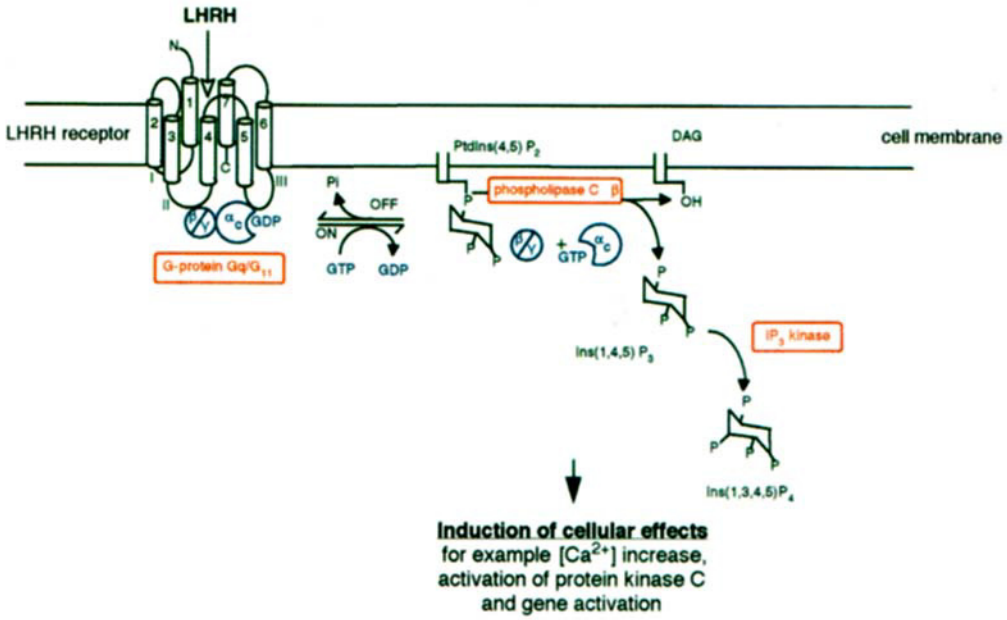

Figure 6. Simplified representation of the signal transduction pathway of the LHRH receptor. DAG = diacylglycerol.

interact with nonconserved amino acids outside the peptide-binding pocket of the receptor protein. This was shown for the neurokinin-1 receptor, for example, with Substance P as endogenous ligand and chemically very diverse, antagonistic, non-peptide compounds.[110] Taking this into consideration, the human LHRH receptor was thus stably expressed in different mammalian cell lines such as murine L cells. The individual cell clones overexpressing the receptor were isolated, and a pharmacological characterization/validation of the test system was performed with receptor–ligand binding tests on intact cells under physiological conditions, with the authentic hormone and relevant LHRH superagonists and antagonists.[105] A multitude of further structurally diverse peptide LHRH antagonists were tested with this system in displacement binding experiments with [^{125}I]-cetrorelix. The results for both clinically relevant and cyclized peptides are discussed in Section 5 (see also Figure 8).

In addition to the determination of binding affinity, expressed as the dissociation constant K_D [nM], the functional characterization of a ligand is also of importance. In early work, cultivated primary cell cultures from, for example, chicken pituitary, were used for this purpose, and agonist-stimulated or antagonist-inhibited release of luteinizing hormone (LH) was measured in a radioimmunoassay (RIA).[109] This reliable but complicated method has been simplified by determination of intracellular messenger substances such as $InsP_3$ in permanent cell lines or, alternatively, in suitable reporter gene test systems. In Figure 7a, detection of $InsP_3$ following stimulation with LHRH and with the superagonist [D-Trp^6]LHRH is shown as an example of the use of recombinant cell lines overexpressing the human LHRH receptor. The agonist-stimulated signal is dose-dependently reduced to the level in unstimulated cells, using an antagonist such as cetrorelix (Figure 7b).[105]

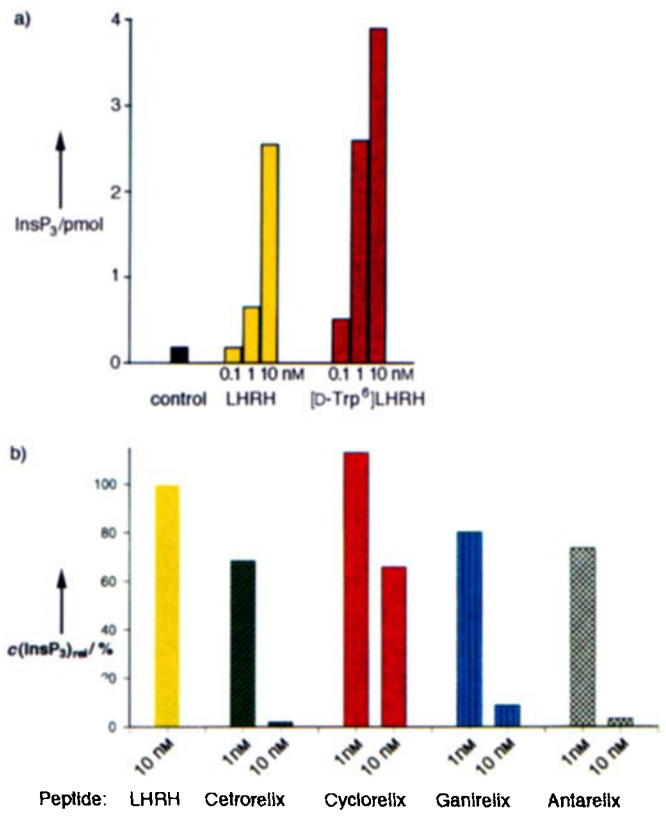

Figure 7. Functional characterization of peptide LHRH antagonists. a) Stimulation of $InsP_3$ synthesis by LHRH or by the superagonists [D-Trp^6]LHRH (triporelin/decapeptyl) in murine L cells, which overexpress the human LHRH receptor. The $InsP_3$ concentration is given for 4×10^6 cells; cells not stimulated with peptide are shown as control. b) Inhibition of stimulation by 10 nM LHRH by various antagonists (1 nM and 10 nM). The cellular $InsP_3$ concentration $c(InsP_3)_{rel}$ [%] is given relative to the maximum $InsP_3$ concentration specifically induced by 10 nM LHRH (100% corresponds to 7.63 pmol and 11.68 pmol $InsP_3$, respectively, per 4×10^6 cells).

At present, selected peptides are being tested in vivo by measuring the testosterone concentration in male rat serum. Here, a single subcutaneous application of a potent LHRH antagonist leads to persistent testosterone suppression. According to our current knowledge, the activity in animals generally correlates well with the binding affinity determined in vitro on human receptors. In cases where no in vivo activity was observed despite high binding affinity, the peptide probably had pharmacokinetic characteristics that played a decisive role. In the future, transgenic animals will also be very important for in vivo testing.

5. Comparative Studies

5.1. Comparison of Clinically Relevant Antagonists

The binding affinity and also the functional characteristics of certain, in part clinically relevant, peptide LHRH antagonists have been tested on the human LHRH receptor. The antagonists tested were cetrorelix (SB-75, D-20761), SB-88 (D-20455), antide (Serono), antarelix (D-23234), ganirelix (Organon/D-24598), and a truncated-sequence antagonist from Abbott, (ProNHEt)-A-76154 (D-24710). The binding affinity was determined as the dissociation constant K_D [nM] with suitable displacement binding tests with [^{125}I]-cetrorelix as labeled ligand and various concentrations of the peptide to be tested (Figure 8 and Table 2). Cetrorelix showed the highest affinity for the human receptor, followed by its analogue SB-88.

Selected peptide antagonists were tested with a functional assay in the cell line used for the radioligand binding tests (see Figure 7b). Here, inhibition of $InsP_3$ synthesis induced by 10 nM

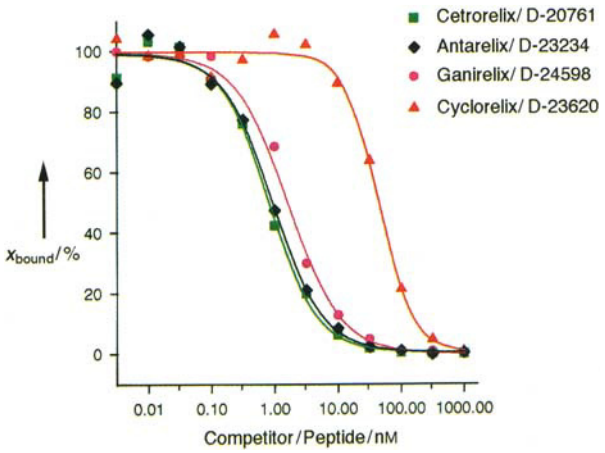

Figure 8. Binding affinity of selected peptide LHRH antagonists. Dose–response curves of competitive binding tests with [^{125}I]-cetrorelix as labeled ligand are given for cetrorelix (K_D = 0.18 nM), antarelix (K_D = 0.26 nM), ganirelix (K_D = 0.45 nM), and cyclorelix (K_D = 9.81 nM). Evaluation of many experiments and a comparison of the binding affinities are shown in Tables 2 and 3.

Table 2. Binding affinity of clinically relevant peptide LHRH receptor antagonists[a].

Peptide	Binding affinity K_D[nM]
LHRH	3.610±0.89 (4)
Cetrorelix (D-20761)	0.202±0.03 (10)
SB88 (D-20455)	0.209±0.002 (2)
Antarelix (D-23234)	0.233±0.04 (3)
Antide (Bachem)	0.360±0.13 (3)
Ganirelix (D-24598)	0.405±0.04 (2)
[Pro^8-NHEt]A-76154 (D-24710)	2.371±0.69 (2)

[a] The binding affinity of the peptide LHRH antagonists was determined in a displacement binding test with [^{125}I]cetrorelix as labeled ligand. The dose–response curves and the dissociation constants $K_D \pm \sigma_n$ (n = number of experiments, in parentheses) were calculated with the program EBDA/Ligand 3.0[133]. The binding affinity of the authentic LHRH ligand is shown for comparison.

LHRH was measured at antagonist concentrations of 1 nM and 10 nM. In this test, cetrorelix is also the most effective inhibitor of secondary messenger formation.

5.2. Comparison of Cyclized Antagonistic LHRH Derivatives

Several cyclized peptide LHRH antagonists were tested for binding affinity to the human LHRH receptor: cyclized cetrorelix ("cyclorelix", D-23620), cycloantarelix (D-24236), cyclo-SB-88 (D-24307) and partially cyclized cetrorelix ("half-cyclorelix", D-24418). The binding affinities, calculated as dissociation constants K_D [nM], are summarized in Table 3. All cyclopeptide analogues of the potent antagonists show significantly weaker binding than the linear precursors.

Table 3. Binding affinity of cyclized peptide LHRH receptor antagonists[a].

Peptide	Binding affinity K_D[nM]
Cyclorelix (D-23620)	12.87±3.1
Cyclo-Antarelix (D-24236)	13.64±1.69
Cyclo-SB88 (D-24307)	24.74±10.57
Halbcyclorelix (D-24418)	10.41±0.27

[a] The binding affinity of the cyclized LHRH antagonists was determined in a displacement binding test with [^{125}I]cetrorelix as labeled ligand. In each case two experiments were performed. The dose–response curves and the dissociation constants $K_D \pm \sigma_n$ (n = number of experiments, here $n = 2$) were calculated with the program EBDA/Ligand 3.0[133].

6. LHRH-Receptor Modeling

It has not yet been possible to determine the structure of a receptor coupled to a G-protein. Knowledge of the molecular structure and the functionality of the receptor has only been obtained by targeted mutagenesis experiments.[111–113] Molecular modeling offers the opportunity to obtain an approximate, three-dimensional structure of a receptor. Hoflack et al. have suggested a model for binding and activation of the gonadothyrotrophin hormone at the receptor.[114] A model of the LHRH receptor was outlined by Kühne et al.,[115] which is based on the well-known crystal structure of bacteriorhodopsin[116] and on material published on bovine rhodopsin.[117–118] The amino acids of the human LHRH receptor were positioned on the seven transmembrane helices of bacteriorhodopsin by means of homology modeling. The extracellular turns were modeled in the same way with data from the Brookhaven Protein Bank.[119] The orientation of the helices was fixed by hydropathy studies. Following energy minimization of the entire model with the AMBER force field, an MD simulation was performed over 100 ps. The model structure was stable under the conditions of this simulation; the relative orientation of the seven helices to each other changed little. In addition, the proline-containing helices formed the bend typical for such structures (Figure 9). This model could give information about the biologically active conformation of LHRH agonists and antagonists and thus facilitate the way to optimization of structure–activity relationships.

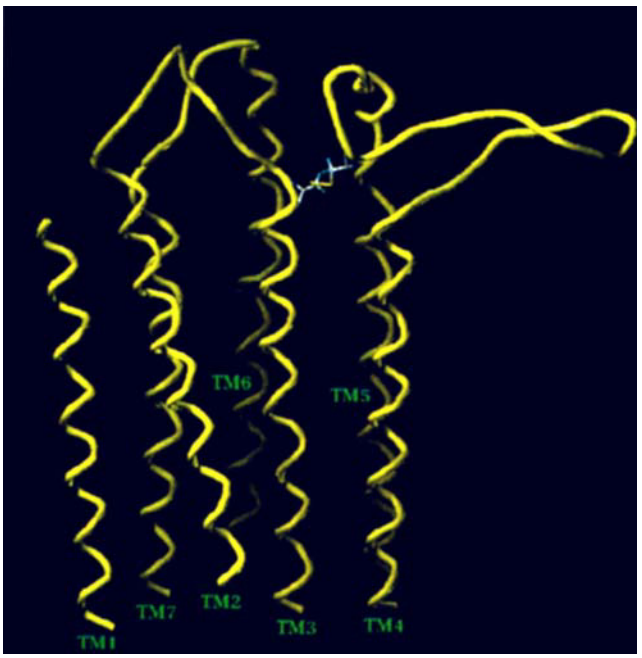

Figure 9. Energy-minimized structure of the human LHRH receptor model.

7. The Search for Peptidomimetics for the LHRH Receptor

The search for peptidomimetic substances to replace peptides as active substances is being undertaken worldwide; prominent examples are angiotensin II antagonists such as Losartan, and (substituted) benzodiazepinones as high affinity ligands for the somatostatin receptor. Literature on the endothelin receptor antagonists (Ro 46-2005, L-744453), growth hormone analogues (MK-0677), CCK antagonists (MK-329), bradykinin B_2 receptor antagonists (Win-64338), and Substance P antagonists (CP-99994) is rapidly expanding.[120–124] Intensive efforts are being made particularly in the area of fibrinogen receptor antagonists, to replace the native Arg-Gly-Asp sequence ("RGD") and to obtain active substances that can be administered orally.[125]

For some years, increased efforts have also been made to find substances with affinity to the LHRH receptor that do not have

the characteristic substance-specific properties and also disadvantages of peptides (short half-life, lack of bioavailability), yet have a high binding affinity. Ideally, such substances should be able to be administered orally, be sufficiently stable in the organism, and possess favorable pharmacological parameters comparable to peptide antagonists. Clinical investigations of the influence of the antimycotic ketoconazole on prostate cancer and testosterone suppression indicate that it may have a LHRH-mimetic effect.[126, 127] Further investigations by the firm Abbott showed weak antagonistic activity both in vitro and in vivo for ketoconazole and modified analogues (Scheme 4); however, the biological activity of such derivatives is most probably not mediated mainly by LHRH antagonism.[128, 129]

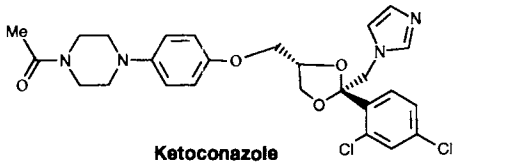

Ketoconazole

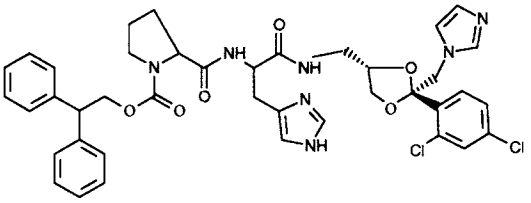

Ketoconazole partial skeleton with dipeptide unit

Scheme 4. LHRH mimetics based on the ketoconazole partial structure [128,129].

A multitude of publications on stabilization and modification of peptide sequences (pseudo-peptides) with the help of mimetic structures, for example, the use of *N*-alkyl amino acids, cyclization and sequence truncation without loss of activity, originate from Abbott.[51, 45, 78, 130]

Complex, highly substituted nitrogen heterocycles such as those published by the firm McNeillab (Scheme 5) seem to have LHRH antagonistic potential.[135] In patent literature, Takeda describe benzodiazepines, benzodiazepinones, heterocyclic benzo-substituted alkylamines, and recently, thienopyridine carboxylic acid derivatives as LHRH receptor antagonists with receptor-binding inhibition at submicromolar concentrations, suitable amongst other uses as antitumor agents for hormone-dependent tumors.[131, 133] A lead structure from the latter substance class is currently in extensive pharmacological trials.

ASTA Medica is also developing substances with potential as antagonistic LHRH mimetics. Based on our work with sequence-truncated and cyclized peptides, both short-chain cyclopeptides and low molecular weight mimetics based on condensed heterocyclenes are being synthesized and evaluated. This strategy is confirmed by recent publications from the firm Takeda, who report cyclopentapeptides with affinity to the human LHRH receptor of the order of $IC_{50} = 0.07\ \mu M$.[134] The search for lead structures is facilitated and further accelerated by the use of compound libraries and high-throughput screening systems.[136, 137]

8. Conclusions and Outlook

LHRH agonists are well-established, high-turnover pharmaceuticals with the main area of application in tumor therapy and gynecology. Despite an early start to the search and intensive worldwide research activity, no LHRH antagonists are on the market today; cetrorelix, with its improved selectivity, high stability, and long-lasting action, is in an advanced stage of development and thus has the best chance of being the first LHRH antagonist to be launched.

With the help of molecular biology, human receptor assays have been established and functional tests developed, so that targeted optimization and characterization of clinically relevant antagonists can follow. Intensive conformational analyses on both linear and cyclized antagonists have not yet delivered any strategy for enhancing the activity or bioavailability. Despite advanced formulation technologies, the goal of a simple, economical, easily administrable form has not yet been adequately achieved in this research area. Assuming similar activity characteristics, peptidomimetics are, in general, superior with respect to cost of manufacture and method of application to the peptide derivatives on which they are based; with the available methods and lead structures, the search for these pharmacologically important substances will certainly be intensified in the future, so that the fourth generation of LHRH derivatives will meet the challenges of modern pharmaceutical research.

We would like to thank H. Kessler, Technische Universität München, for many NMR spectroscopic investigations and for suggestions during drafting of the manuscript, and A. V. Schally, Tulane University, New Orleans, for the introduction to the topic of endocrinology and his constant support. The cooperation with H. Michel and M. Reiländer, MPI Frankfurt, and with G. Krause and R. Kühne, Forschungsinstitut für molekulare Pharmakologie Berlin, in the field of the human LHRH receptor was supported by a project of the Bundesministerium für Bildung und Forschung (BMBF No. 0310697).

Received: November 4, 1997 [A 196 IE]
German version: *Angew. Chem.* **1997**, *109*, 2240–2254
Translated by Dr. J. Cooper, Frankfurt (Germany)

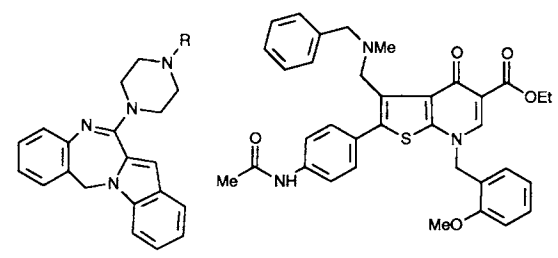

McNeil, US-A 4678784

Takeda, WO 95/28405

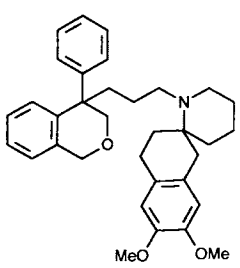

Takeda, EP 679642 A1

Scheme 5. Peptidomimetic LHRH antagonists [131,132].

[1] "The Privileges of a Nobel Laureate": A. V. Schally, S. M. McCann, *Fertil. Steril.* **1995**, *64*, 452–453.

[2] a) A. V. Schally, A. Arimura, A. J. Kastin, *Science* **1971**, *173*, 1036–1038; b) H. Matsuo, Y. Baba, R. M. Nair, A. Arimura, A. V. Schally, *Biochem. Biophys. Res. Commun.* **1971**, *43*, 1334–1339; c) K. Amoss, R. Burgus, R. Blackwell, W. Vale, R. Fellows, R. Guillemin, *ibid.* **1971**, *44*, 205–210; d) Y. Baba, H. Matsuo, A. V. Schally, *ibid.* **1971**, *44*, 459–463.

[3] G. Emons, A. V. Schally, *Hum. Reprod.* **1994**, *9*, 1364–1370.

[4] P. M. Conn, W. Crowley, *New Engl. J. Med.* **1991**, *324*, 93–103.

[5] G. F. Weinbauer, E. Nieschlag in *Peptides in Oncology I* (Ed.: K. Höffgen), Springer, Heidelberg, **1992**, pp. 113–136.

[6] a) A. S. Dutta, *Drugs of the Future* **1988**, *13*, 43–57; b) M. Filicori, C. Flamingi, *Drugs* **1988**, *35*, 63–82; c) J. J.Nestor, B. H. Vickery, *Annu. Rep. Med. Chem.* **1988**, *23*, 211–220.

[7] a) M. T.Goulet, *Annu. Rep. Med. Chem.* **1995**, *30*, 169–178; b) T. Reissmann, R. Felberbaum, K. Diedrich, J. Engel, A. M. Comaru-Schally, A. V. Schally, *Hum. Reprod.* **1995**, *20*, 1974–1981.

[8] M. J. Karten in *Modes of Action of GnRH and GnRH Analogs* (Eds.: W. F. Crowley, P. M. Conn), Springer, Heidelberg, **1992**, pp. 277–297.

[9] G. Flouret, Z. S. Arnold, T. Majewski, N. H. Petousis, K. Mahan, F. Farooqui, K. A. Blum, D. Konopinska, S. Natarajan, D. Crich, *Pept. Sci.* **1995**, *1*, 89–105.

[10] P. M. Conn, W. F. Crowley, *Annu. Rev. Med.* **1994**, *45*, 391.

[11] A. V. Schally in *Cancer Medicine*, 3rd ed. (Eds.: J. F. Holland, E. Frei, R. C. Bast, D. W. Kufe, D. L. Morton, R. R. Weichselbaum), Lee & Febiger, Philadelphia, PA (USA), pp. 827–840.

[12] a) A. V. Schally in *Advances in Gynecology and Obstetrics, Vol. 6* (Eds.: P. Belfort, J. Pinotti, T. K. Eskes), Parthenon, Cornforth, **1989**, 3–22; b) *Scrip* **1995**, *2066*, 22.

[13] a) A. Friedrich, G. Jaeger, K. Radscheit, R. Uhmann, *Pept. Proc. Eur. Pept. Symp. 22nd 1992* **1993**, 47–49; b) A. Kleemann, K. Drauz, J. Engel, B. Kutscher, E. Wünsch, *Proc. Akabori Conf. Ger. Jpn. Symp. Pept. Chem. 4th* **1991**, 96–101; c) F. R. Kunz, T. Müller, K. Drauz, *Proc. Akabori Conf. Ger. Jpn. Symp. Pept. Chem. 5th*, **1994**, 15–16

[14] M. J.Karten, J. E. Rivier, *Endocrine Rev.* **1986**, *7*, 44–66.

[15] R. L. Barbieri, *Trends Endocrinol. Metab.* **1992**, *3*, 30–34.

[16] R. Schmidt, K. Sundaram, R. B. Thau, C. W. Badrin, *Contraception* **1984**, *29*, 283–289.

[17] S. Bajusz, V. J. Csernus, T. Janaky, L. Bokser, M. Fekete, A. V. Schally, *Int. J. Pept. Protein Res.* **1988**, *32*, 425–435.

[18] J. Pinski, A. V. Schally, T. Yano, K. Groot, G. Srkalovic, P. Serfozo, T. Reissmann, M. Bernd, W. Deger, B. Kutscher, J. Engel, *Int. J. Pept. Protein Res.* **1995**, *45*, 410–417.

[19] A. Ljungqvist, D. M. Feng, W. Hook, Z. X. Shen, C. Bowers, K. Folkers, *Proc. Natl. Acad. Sci. USA* **1988**, *85*, 8236–8240.

[20] J. Leal, K. Gordon, D. R. Danforth, R. F. Williams,G. D. Hodgen, *Drugs of the Future* **1991**, *16*, 529–537.

[21] A. Janecka,T. Janecki, S. M. Shan, C. Bowers, K. Folkers, *J. Med. Chem.* **1994**, *37*, 2238–2241.

[22] A. Janecka, A. Ljungqvist, M. Suzuki, J. C. Xu, C. Bowers, K. Folkers, *Med. Chem. Res.* **1991**, *1*, 306–311.

[23] A. Janecka, T. Janecki, C. Bowers, K. Folkers, *Int. J. Pept. Protein Res.* **1994**, *44*, 19–23.

[24] K. Liu, B. He, S. Xiao, Q. Xia, X. Fang, Z. Wang, *Int. J. Pept. Protein Res.* **1990**, *35*, 157–160.

[25] K. Liu, B. He, S. Xiao, Q. Xia, X. Fang, Z. Wang, *Sci. China Ser. B* **1991**, *34*, 201–208.

[26] Y. Ge, S. Xiao, *Contraception* **1992**, *46*, 131–133.

[27] P. Theobald, J. Porter, C. Rivier, A. Corrigan, M. Perrin, W. Vale, J. Rivier, *J. Med. Chem.* **1991**, *34*, 2395–2402.

[28] J. Rivier, J. Porter, C. Hoeger, P. Theobald, A. G. Craig, J. Dykert, A. Corrigan, M. Perrin, W. A. Hook, R. P. Siraganian, W. Vale, C. Rivier, *J. Med. Chem.* **1992**, *35*, 4270–4278.

[29] J. E. Rivier, G. Jiang, J. Porter, C. A. Hoeger, A. G. Craig, A. Corrigan, W. Vale, C. L. Rivier, *J. Med. Chem.* **1995**, *38*, 2649–2662.

[30] Z. P. Tian, Y. L. Zhang, P. J. Edwards, R. W. Roeske, *Pept. Proc. Am. Pept. Symp. 13th*, **1994**, 562–564.

[31] R. Deghenghi, F. Boutignon, P. Wüthrich, V. Lenaerts, *Biomed. Pharmacother.* **1993**, *47*, 107–110.

[32] R. Deghenghi (Europeptides), WO 92/19651-A1, **1992**.

[33] J. Nestor, Jr., R. Tahilramani, T. L. Ho, J. C. Goodpasture, B. H. Vickery, P. Ferrandon, *J. Med. Chem.* **1992**, *35*, 3942–3948.

[34] K. Stoeckemann, J. Sandow, *J. Cancer Res. Clin. Oncol.* **1993**, *119*, 457–462.

[35] J. Knolle, W. König, G. Breipohl, *Pept. Proc. Eur. Pept. Symp. 21st 1990* **1991**, 414–415.

[36] J. Mulzer in *Stereoselective Synthesis* (Eds.: E. Ottow, U. Schöllkopf, B. G. Schulz), Springer, Heidelberg, **1994**, pp. 37–61.

[37] J. Mulzer, F. Schröder, A. Lobbia, J. Buschmann, P. Luger, *Angew. Chem.* **1994**, *106*, 1813–1815; *Angew. Chem. Int. Ed. Engl.* **1994**, *33*, 1737–1739.

[38] G. J. Russell-Jones, S. W. Westwood, P. G. Farnworth, J. K. Findlay, H. G. Burger, *Bioconj. Chem.* **1995**, *6*(1), 34–42.

[39] G. J. Russell-Jones (Biotech Australia Pty.), WO 94/28015, **1994**.

[40] T. Reissmann, J. Engel, B. Kutscher, M. Bernd, P. Hilgard, M. Peukert, I. Szelenyi, S.Reichert, D. Gonzalez-Barcena, E. Nieschlag, A. M. Comaru-Schally, A. V. Schally, *Drugs of the Future* **1994**, *19*, 228–237.

[41] J. Pinski, T. Yano, T. Janaky, A. Nagy, A. Juhasz, L. Bokser, K. Groot, A. V. Schally, *Int. J. Pept. Protein Res.* **1993**, *41*, 66–70.

[42] E. Graf von Roedern, Dissertation, Technische Universität München, **1994**; E. von Roedern, H. Kessler, B. Kutscher, M. Bernd, T. Klenner (ASTA Medica), DE 4338015, US-A 5,556,836, **1995/1996**.

[43] H. Kessler, E. Graf von Roedern, *Angew. Chem.* **1994**, *106*, 684–686; *Angew. Chem. Int. Ed. Engl.* **1994**, *33*, 687–689.

[44] F. Haviv, C. A. Palabrica, E. N. Bush, G. Diaz, E. S. Johnson, S. Love, J. Greer, *J. Med. Chem.* **1989**, *32*, 2340–2344.

[45] F. Haviv, T. D. Fitzpatrick, C. J. Nichols, R. E. Swenson, N. A. Mort, E. N. Bush, G. Diaz, A. T. Nguyen, M. R. Holst, V. A. Cybulski, J. A. Leal, G. Bammert, N. S. Rhutasel, P. W. Dod, E. S. Johnson, J. B. Cannon, J. Knittle, J. Greer, *J. Med. Chem.* **1993**, *36*, 928–933.

[46] F. Haviv (Abbott Laboratories), PCT/US 95/02410, **1995**.

[47] F. Haviv (Abbott Laboratories), WO 95/04540, **1995**.

[48] F. Haviv (Abbott Laboratories), WO 94/14841, **1994**.

[49] J. Greer (Abbott Laboratories), WO 94/13313, **1994**.

[50] F. Haviv (Tap Pharmaceuticals), US-A 5300492, **1994**.

[51] F. Haviv, T. D. Fitzpatrick, C. J. Nichols, E. N. Bush, G. Diaz, G. Bammert, A. T. Nguyen, E. S. Johnson, J. Knittle, J. Greer, *J. Med. Chem.* **1994**, *37*, 701–705.

[52] H. Kessler, *Angew. Chem.* **1982**, *94*, 509–520; *Angew. Chem. Int. Ed. Engl.* **1982**, *21*, 512–523.

[53] H. A. Scheraga, *Chem. Rev.* **1971**, *71*, 195–217.

[54] 5. P. N. Lewis, F. A. Momany, H. A. Scheraga, *Israel J. Chem.* **1973**, *11*, 121–152.

[55] R. Deslauriers, R. Walter, I. C. P. Smith, *Biochem. Biophys. Res. Commun.* **1973**, *53*, 244–250.

[56] M. W. Monahan, M. S. Amos, H. A. Anderson, W. Vale, *Biochemistry* **1973**, *12*, 4616–4620.

[57] F. A. Momany, *J. Am. Chem. Soc.* **1976**, *98*, 2990–2996.

[58] F. A. Momany, *J. Am. Chem. Soc.* **1976**, *98*, 2996–3000.

[59] P. L. Wessels, J. Feeney, H. Gregory, J. J. Gormley, *J. Chem. Soc. Perkin Trans. 2* **1973**, 1691–1698.

[60] R. Deslauriers, G. C. Levy, W. H. McGregor, D. Sarantakis, I. C. P. Smith, *Biochemistry* **1975**, *14*, 4335–4343.

[61] R. M. Freidinger, D. F. Veber, D. Schwenk Perlow, J. R. Brooks, R. Saperstein, *Science* **1980**, *210*, 656–658.

[62] a) R. S. Struthers, J. Rivier, A. T. Hagler, *Ann. NY Acad. Sci.* **1984**, *439*, 81–96; b) "Design of Peptide Analogs": R. S. Struthers, A. T. Hagler, J. Rivier in *Conformationally Directed Drug-Design—Peptides and Nucleic Acids as Templates or Targets* (Eds.: J. A. Vida, M. Gordon), American Chemical Society, Washington DC, **1984**, pp. 239–261.

[63] E. L. Baniak, J. E. Rivier, R. S. Struthers, A. T. Hagler, L. M. Gierasch, *Biochemistry* **1987**, *26*, 2642–2656.

[64] a) S. J. Hocart, M. V. Nekola, D. H. Coy, *J. Med. Chem.* **1988**, *31*, 1820–1824; b) J. Wermuth, S. L. Goldmann, A. Jonczyk, H. Kessler, *J. Am. Chem. Soc.* **1997**, *119*, 1328–1335

[65] B. Kutscher, M. Bernd, T. Beckers, T. Klenner, E. E. Polymeropoulos, M. Bachelin, T. Dierks, H. Kessler, *Proc. Akabori Conf. Ger. Jpn. Symp. Pept. Chem.* 6th, **1996**, 127–132.

[66] H. Kessler, personal communication.

[67] K. V. R. Chary, S. Srivastava, R. V. Hosur, K. B. Roy, G. Govil, *Eur. J. Biochem.* **1986**, *158*, 323–332.

[68] A. Müller, E. Busker, J. Engel, B. Kutscher, M. Bernd, A. V. Schally, *Int. J. Pept. Protein Res.* **1994**, *43*, 264–270.

[69] A. S. Dutta, J. J. Gormley, P. F. McLachlan, J. R. Woodburn, *Biochem. Biophys. Res. Commun.* **1989**, *159*, 1114–1120.

[70] P. K. C. Paul, P. Dauber-Osguthorpe, M. M. Campbell, D. J. Osguthorpe, *Biochem. Biophys. Res. Commun.* **1989**, *165*, 1051–1058.

[71] A. S. Dutta, J. J. Gormley, J. R. Woodburn, P. K. C. Paul, D. J. Osguthorpe, M. M. Campbell, *Bioorg. Med. Chem. Lett.* **1993**, *3*, 943–948.

[72] R. S. Struthers, G. Tanaka, S. C. Koerber, T. Solmajer, E. L. Baniak, L. M. Gierasch, W. Vale, J. Rivier, A. T. Hagler, *Proteins* **1990**, *8*, 295–304.

[73] "GnRH analogs: Structure–activity relationships": J. Rivier, C. Rivier, M. Perrin, J. Porter, W. Vale in *LHRH Peptides as Male & Female Contraceptives* (Eds.: G. I. Zatuchni, J. D. Shelton, J. J. Sciarra), Harper & Row, Philadelphia, **1991**, pp. 13–23.

[74] J. Rizo, S. C. Koerber, R. J. Bienstock, J. Rivier, A. T. Hagler, L. M. Gierasch, *J. Am. Chem. Soc.* **1992**, *114*, 2852–2859.

[75] J. Rizo, S. C. Koerber, R. J. Bienstock, J. Rivier, L. M. Gierasch, A. T. Hagler, *J. Am. Chem. Soc.* **1992**, *114*, 2860–2871.

[76] a) S. C. Koerber, M. Ibea, A. T. Hagler, C. L. Rivier, J. E. Rivier, *Biochem. Biophys. Res. Commun.* **1992**, *187*, 1035–1041; b) H. Matter, H. Kessler, *J. Am. Chem. Soc.* **1995**, *117*, 3347–3359.

[77] J. Rizo, L. M. Gierasch, *Annu. Rev. Biochem.* **1992**, *61*, 387–418.

[78] F. Haviv, T. D. Fitzpatrick, R. E. Swenson, C. J. Nichols, N. A. Mort, E. N. Bush, G. Diaz, G. Bammert, A. Nguyen, N. S. Rhutasel, H. N. Nellans, D. J. Hoffman, *J. Med. Chem.* **1993**, *36*, 363–369.
[79] M. I. Liff, K. D. Kopple, Z. Tian, R. W. Roeske, *Int. J. Pept. Protein Res.* **1994**, *43*, 471–476.
[80] G. V. Nikiforovich, G. R. Marshall, *Int. J. Pept. Protein Res.* **1993**, *42*, 171–180.
[81] G. V. Nikiforovich, G. R. Marshall, *Int. J. Pept. Protein Res.* **1993**, *42*, 181–193.
[82] R. J. Bienstock, J. Rizo, S. C. Koerber, J. E. Rivier, A. T. Hagler, L. M. Gierasch, *J. Med. Chem.* **1993**, *36*, 3265–3273.
[83] D. V. Reddy, B. Jagannadh, A. S. Dutta, A. C. Kunwar, *Int. J. Pept. Protein Res.* **1995**, *46*, 9–17.
[84] J. Rizo, R. B. Sutton, J. Breslau, S. C. Koerber, J. Porter, A. T. Hagler, J. E. Rivier, L. M. Gierasch, *J. Am. Chem. Soc.* **1996**, *118*, 970–976.
[85] H. Matsuo, Y. Baba, R. M. Nair, A. Arimura, A. V. Schally, *Biochem. Biophys. Res. Commun.* **1971**, *43*, 1334–1339.
[86] P. H. Seeburg, J. P. Adelman, *Nature* **1984**, *311*, 666–668.
[87] M. Tsutsumi, W. Zhou, R. P. Millar, P. L. Mellon, J. L. Roberts, C. A. Flanagan, K. Dong, B. Gillo, S. C. Sealfon, *Mol. Endocrinol.* **1992**, *6*, 1163–1169.
[88] J. Reinhart, L. M. Mertz, K. J. Catt, *J. Biol. Chem.* **1992**, *267*, 21281–21284.
[89] J. J. Windle, R. I. Weiner, P. L. Mellon, *Mol. Endocrinol.* **1990**, *4*, 597–603.
[90] F. Horn, L. M. Bilezikjian, M. H. Perrin, M. M. Bosma, J. J. Windle, K. S. Huber, A. L. Blount, B. Hille, W. Vale, P. L. Mellon, *Mol. Endocrinol.* **1991**, *5*, 347–355.
[91] S. C. Sealfon, B. Gillo, S. Mundamattom, P. L. Mellon, J. J. Windle, E. Landau, J. L. Roberts, *Mol. Endocrinol.* **1990**, *4*, 119–124.
[92] S. S. Kakar, L. C. Musgrove, D. C. Devor, J. C. Sellers, J. D. Neill, *Biophys. Biochem. Res. Commun.* **1992**, *189*, 289–295.
[93] L. Chi, W. Zhou, A. Prikhozhan, C. Flanagan, J. S. Davidson, M. Golembo, N. Illing, R. P. Millar, S. C. Sealfon, *Mol. Cell. Endocrinol.* **1993**, *91*, R1–R6.
[94] K. A. Eidne, R. E. Sellar, G. Couper, L. Anderson, P. L. Taylor, *Mol. Cell. Endocrinol.* **1992**, *90*, R5–R9.
[95] U. B. Kaiser, D. Zhao, G. R. Cardona, W. W. Chin, *Biochem. Biophys. Res. Commun.* **1992**, *189*, 1645–1652.
[96] S. S. Kakar, C. H. Rahe, J. D. Neill, *Domest. Anim. Endocrinol.* **1993**, *10*, 335–342.
[97] N. Illing, G. F. Jacobs, I. I. Becker, C. A. Flanagan, J. S. Davidson, A. Eales, W. Zhou, S. C. Sealfon, R. P. Millar, *Biochem. Biophys. Res. Commun.* **1993**, *196*, 745–751.
[98] T. P. Iismaa, T. J. Biden, J. Shine, *Molecular Biology Intelligence Unit: G-protein coupled receptors*, Springer, Heidelberg, **1995**.
[99] W. C. Probst, L. A. Snyder, D. L. Schuster, J. Brosius, S. C. Sealfon, *DNA Cell Biol.* **1992**, *11*, 1–20.
[100] A. Bairoch, *Nucleic Acids Res.* **1991**, *19*, 2241–2245.
[101] N. C. Fan, C. Peng, J. Krisinger, P. C. K. Leung, *Mol. Cell. Endocrinol.* **1995**, *107*, R1–R8.
[102] S. S. Stojilkovic, K. J. Catt, *Recent Prog. Horm. Res.* **1995**, *50*, 161–205.
[103] S. G. Rhee, K. D. Choi, *J. Biol. Chem.* **1992**, *267*, 12393–12396.
[104] K. P. Hsieh, T. F. Martin, *J. Mol. Endocrinol.* **1992**, *6*, 1673–1681.
[105] T. Beckers, K. Marheineke, H. Reiländer, P. Hilgard, *Eur. J. Biochem.* **1995**, *231*, 535–543.
[106] R. N. Clayton, R. A. Shakespear, J. A. Duncan, J. C. Marshall, P. J. Munson, D. Rodbard, *Endocrinology* **1979**, *105*, 1369–1381.
[107] E. Loumaye, P. C. Wynn, D. Coy, K. J. Catt, *J. Biol. Chem.* **1984**, *259*, 12663–12671.
[108] P. J. Wormald, K. A. Eidne, R. P. Millar, *J. Clin. Endocrinol. Metab.* **1985**, *61*, 1190–1194.
[109] R. P. Millar, C. A. Flanagan, R. C. Milton, J. A. King, *J. Biol. Chem.* **1989**, *264*, 21007–21013.
[110] U. Gether, X. Emonds-Alt, J.-C. Breliére, T. Fujii, D. Hagiwara, C. Garret, T. E. Johansen, T. W.Schwartz, *Mol. Pharm.* **1994**, *45*, 500–508
[111] J. S. Davidson, C. A. Flanagan, I. I. Becker, N. Illing, S. C. Sealfon, R. P. Millar, *Mol. Cell. Endocrinol.* **1994**, *100*, 9–14.
[112] W. Zhou, C. Flanagan, J. A. Ballesteros, K. Konvicka, J. S. Davidson, H. Weinstein, R. P. Millar, S. C. Sealfon, *Mol. Pharmacol.* **1994**, *45*, 1991–1995.
[113] W. Zhou, V. Rodic, S. Kitanovic, C. A. Flanagan, L. Chi, H. Weinstein, S. Maayani, R. P. Millar, S. C. Sealfon, *J. Biol. Chem.* **1995**, *270*, 18853–18857.
[114] J. Hoflack, M. F. Hibert, S. Trumpp-Kallmeyer, J. M. Bidart, *Drug Des. Discovery* **1993**, *10*, 157–171.
[115] R. Kühne, G. Krause, E. E. Polymeropoulos, B. Kutscher, unpublished.
[116] R. Henderson, J. M. Baldwin, T. A. Ceska, F. Zemlin, E. Beckmann, K. H. Downing, *J. Mol. Biol.* **1990**, *213*, 899–929.
[117] J. Baldwin, *EMBO J.* **1993**, *12*, 1693–1703.
[118] J. Baldwin, *J. Curr. Opin. Cell Biol.* **1994**, *6*, 180–190.
[119] Protein Data Bank (Version January 1996), Chemistry Department, Brookhaven National Laboratory, Upton, NY (USA).
[120] J. Gante, *Angew. Chem.* **1994**, *106*, 1780–1802; *Angew. Chem. Int. Ed. Engl.* **1994**, *33*, 1699–1720.
[121] D. C. Rees, *Curr. Med. Chem.* **1994**, *1*, 145–158.
[122] A. Giannis, T. Kolter, *Angew. Chem.* **1993**, *105*, 1303–1326; *Angew. Chem. Int. Ed. Engl.* **1993**, *32*, 1244–1267.
[123] D. Fairlie, G. Abbenante, D. March, *Curr. Med. Chem.* **1995**, *2*, 654–686.
[124] R. M. Freidinger, *Prog. Drug Res.* **1993**, *40*, 33–89.
[125] V. Austel, F. Himmelsbach, T. Müller, *Drugs of the Future* **1994**, *19*, 757–764.
[126] J. Trachtenberg, A. Pont, *Lancet* **1984**, *2*, 433–435.
[127] S. Bhasin, S. Sikka, T. Fielder, U. Sod-Moriah, H. Levine, R. Swerdloff, J. Rajfer, *Endocrinology* **1986**, *118*, 1229–1232.
[128] B. De, J. Plattner, E. Bush, H. S. Jae, G. Diaz, E. Johnson, T. Perun, *J. Med. Chem.* **1989**, *32*, 2036–2038.
[129] B. De (Abbott Laboratories), US-A 4992421, **1991**.
[130] F. Haviv, C. A. Palabrica, E. N. Bush, G. Diaz, E. S. Johnson, S. Love, J. Greer, *J. Med. Chem.* **1989**, *32*, 2340–2344.
[131] S. Furuya (Takeda Chemical Industries), WO 95/28405, **1995**.
[132] K. Kato (Takeda Chemical Industries), EP 679642 A1, **1995**.
[133] G. A. McPherson, *J. Pharmacol. Methods* **1985**, *14*, 213–228.
[134] C. Kitada (Takeda Chemical Industries), WO 96/34012 A1, **1996**.
[135] C. Y. Ho (McNeillab Inc.), US-A 4678784, **1987**.
[136] M. Goulet (Merck) WO 97/21435, **1997**.
[137] S. Furuya (Takeda Chemical Industries) WO 97/14697, **1997**.

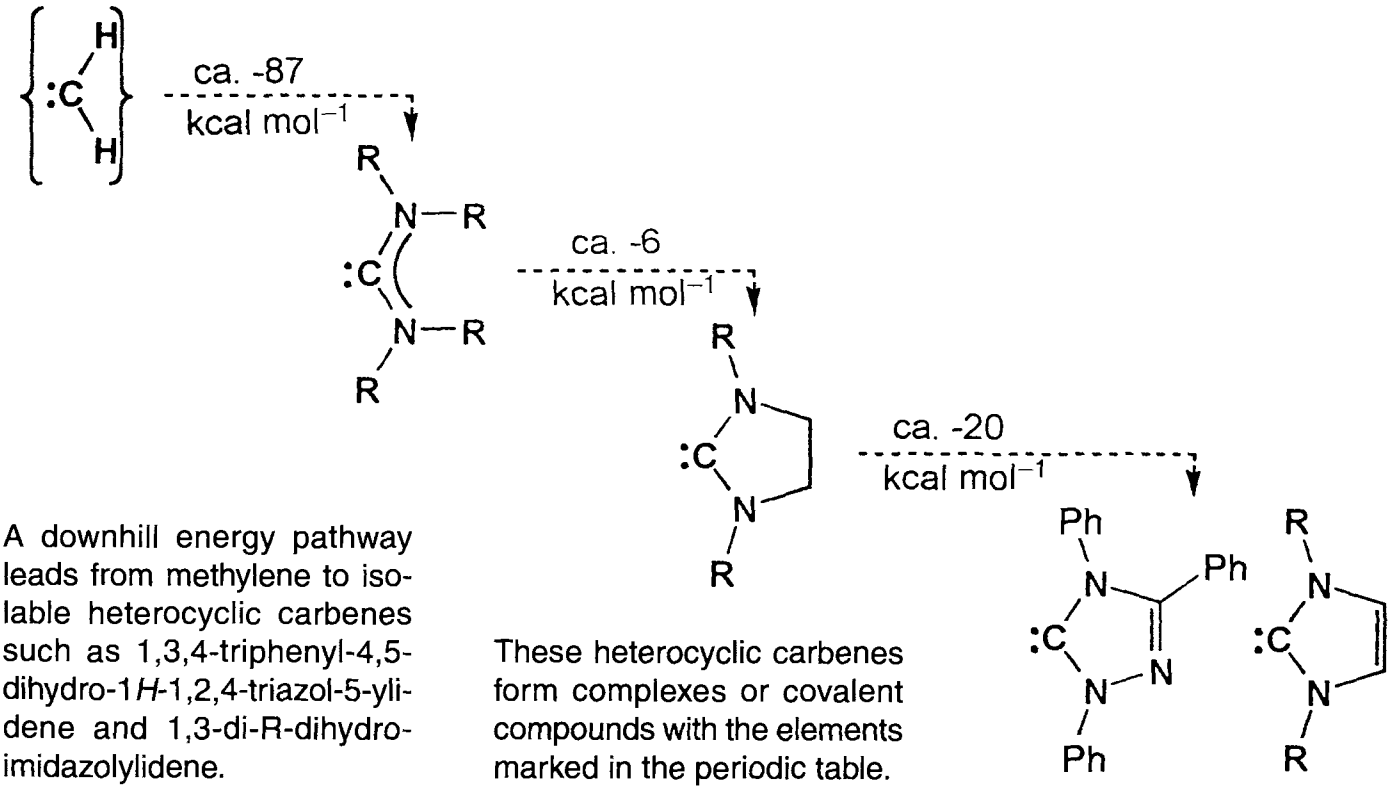

A downhill energy pathway leads from methylene to isolable heterocyclic carbenes such as 1,3,4-triphenyl-4,5-dihydro-1*H*-1,2,4-triazol-5-ylidene and 1,3-di-R-dihydroimidazolylidene.

These heterocyclic carbenes form complexes or covalent compounds with the elements marked in the periodic table.

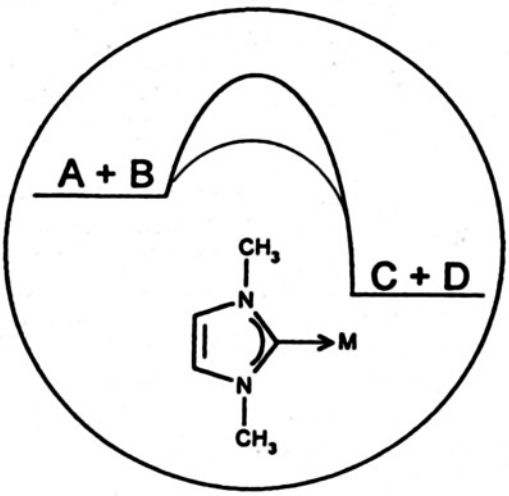

Several of the metal complexes can be successfully used as homogeneous catalysts, as indicated by the schematic representation of the energy profile.

H																	He
Li	Be											B	C	N	O	F	Ne
Na	Mg											Al	Si	P	S	Cl	Ar
K	Ca	Sc	Ti	V	Cr	Mn	Fe	Co	Ni	Cu	Zn	Ga	Ge	As	Se	Br	Kr
Rb	Sr	Y	Zr	Nb	Mo	Tc	Ru	Rh	Pd	Ag	Cd	In	Sn	Sb	Te	I	Xe
Cs	Ba	La	Hf	Ta	W	Re	Os	Ir	Pt	Au	Hg	Tl	Pb	Bi	Po	At	Rn
Fr	Ra	Ac	Rf	Ha	Sg	Ns	Hs	Mt	Unn	Unu							

Ce	Pr	Nd	Pm	Sm	Eu	Gd	Tb	Dy	Ho	Er	Tm	Yb	Lu
Th	Pa	U	Np	Pu	Am	Cm	Bk	Cf	Es	Fm	Md	No	Lr

ANGEWANDTE CHEMIE
© WILEY-VCH

N-Heterocyclic Carbenes**

Wolfgang A. Herrmann* and Christian Köcher

Dedicated to Professor Heribert Offermanns on the occasion of his 60th birthday

The chemistry of N-heterocyclic carbenes has long been limited to metal coordination compounds derived from azolium precursors, a development that was started by Öfele and Wanzlick in 1968. Since free carbenes are now available through the work of Arduengo (1991), a renaissance in this little-recognized area of chemistry has occurred. A leading motive is the advantage of N-heterocyclic carbenes as ligands in organometallic catalysts, where they extend the scope of application reached by phosphanes (functionalized, chiral, water-soluble, and immobilized derivatives). The present review summarizes the state of the art with regard to synthesis, structure, bonding theory, metal coordination chemistry, and catalysis. Chelating, functionalized, chiral, and immobilized ligands can be generated and attached to metal centers in straightforward procedures under mild conditions. A wealth of new chemistry is thus opened. It is also shown how carbenes derived from imidazoles and triazoles behave as ligands in catalysis. It is reasonable to assume that N-heterocyclic carbenes surpass the ubiquitous phosphanes as ligands in a number of organometallic catalytic reactions.

Keywords: carbenes · heterocycles · homogeneous catalysis · metal complexes

1. Introduction

Carbenes have played an important role in organic chemistry ever since the first firm evidence of their existence. While much of the early chemistry of these laboratory curiosities was established in the 1950s by Skell,[1] it was Fischer and his students who introduced carbenes into inorganic and organometallic chemistry in 1964.[2] Suffice it to say that metal carbenes have become quite significant, particularly in organic synthesis, catalysis, and macromolecular chemistry.[3–6] Shortly after the discovery of the first authentic metal–carbene complexes of type **1**, two little-recognized reports by Öfele (Technische Universität München)[7] and Wanzlick et al. (Technische Universität Berlin)[8] appeared that described complexes **2** and **3** with N-heterocyclic carbenes as ligands. These complexes, which at that time were highly unusual compounds, were both obtained from imidazolium salts and metal-containing precursors of sufficient basicity to deprotonate the organic substrate. In the first case a carbonylmetalate was used, while the mercury complex resulted simply from the metal acetate [Eqs. (1), (2)].

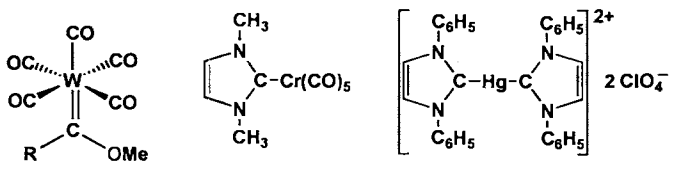

1 **2** **3**

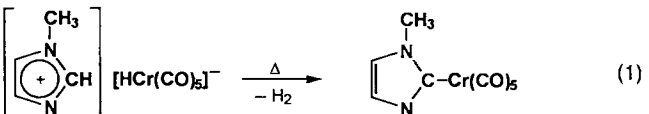

(1)

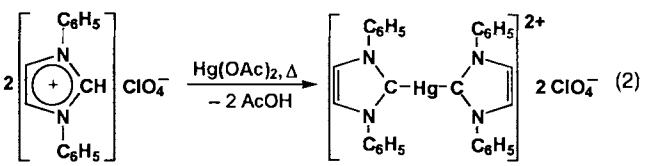

(2)

Öfele and his students established several basic features of this chemistry before Arduengo opened the access to free, isolable N-heterocyclic carbenes in 1991.[33] According to Equation (3),

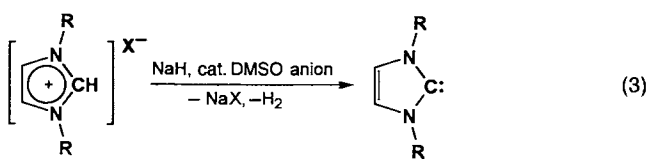

(3)

[*] Prof. Dr. W. A. Herrmann, Dr. C. Köcher
Anorganisch-chemisches Institut der Technischen Universität München
Lichtenbergstrasse 4, D-85748 Garching (Germany)
Fax: Int. code +(89)2891-3473
e-mail: herrmann@zaphod.anorg.chemie.tu-muenchen.de

[**] Essays on Organometallic Chemistry, Part 9. Part 8: W. A. Herrmann, B. Cornils, *Angew. Chem.* **1997**, *109*, 1074; *Angew. Chem. Int. Ed. Engl.* **1997**, *36*, 1047.

 © WILEY-VCH Verlag GmbH, D-69451 Weinheim, 1997 0570-0833/97/3620-2163 $ 17.50+.50/0

deprotonation of the imidazolium ion is effected by NaH and catalytic amounts of KO*t*Bu or the DMSO anion. Although this methodology has its limitations with regard to substituent R, Arduengo's work proved that a carbene of type **4** is in principle thermodynamically stable. At roughly the same time we synthesized the crystalline divalent germanium(II) congener **5** from diimine *t*BuN=CH–CH=N*t*Bu, lithium, and germanium(II) chloride.[10] As a result of this discovery Denk et al. and Lappert et al. successfully synthesized the stable silylenes **6** by reduction of the corresponding silicon(IV) cyclodiamides with potassium.[11] Compound **5** proved to be a successful precursor for chemical vapor deposition (CVD) of amorphic germanium.[134–137]

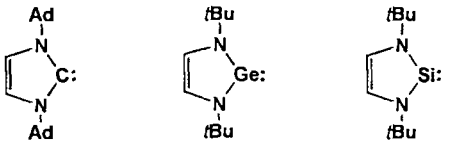

4 **5** **6**

Based on earlier work in the Munich laboratory,[12a–e] we suggested that N-heterocyclic carbenes **4** would exhibit ligand properties similar to those known from electron-rich phosphanes. This led to the conclusion that an equally rich coordination and catalysis chemistry should arise from these pronouncedly C-nucleophilic compounds.[13] Experimental evidence has increasingly been keeping track with our predictions.

1.1. The Way to Isolable Carbenes

There has been continued and growing interest in persistent intermediates since the days of Gomberg.[14, 15] However, almost no efforts were made to isolate carbenes, and stable "ylidene carbenes" were only recently isolated. Carbene intermediates such as dihalocarbenes are now well established in synthetic chemistry.[1, 16, 17] Carbenes are uncharged compounds with a divalent carbon atom and two unshared electrons, which can be assigned to two nonbonding orbitals in different ways. For this reason, the chemistry of carbenes, nitrenes, and arynes is similar in many respects.

1.1.1. Hybridization and Structure

Depending on spin multiplicity and ground state, the (electronic) structure of a given carbene varies as follows: If the carbene has a nonlinear structure with an sp^2-hybridized carbon atom, the structures of the singlet ground state and the triplet state compare to that of carbenium ions $(CR_3)^+$ and free radicals $^{\bullet}CR_3$, respectively. For the triplet state and excited singlet states linear structures with sp-hybridized carbon atoms also need to be considered.[18] A nonlinear triplet ground state is experimentally established for the majority of carbenes; singlet-state dihalocarbenes and carbenes with oxygen, sulfur, or nitrogen substituents are exceptions.

1.1.2. Triplet Carbenes

Electrophilic carbenes $:CR^1R^2$ with substituents R^1 and R^2 that are not electron donors were originally regarded as being too reactive to be isolated. As these triplet carbenes cannot be stabilized through thermodynamic effects, they have to be rendered unreactive by steric protection. Considerable progress was made by Tomioka et al., who stabilized diphenylcarbenes with methyl or chloro substituents in *ortho* positions. Whereas laser flash photolysis (LFP) of phenyl(2,4,6-tris-*tert*-butylphenyl)diazomethane yielded a nascent singlet carbene which intramolecularly inserted into a *tert*-butyl C–H bond before undergoing intersystem crossing, LFP in the presence of the triplet sensitizer benzophenone produced a transient triplet carbene.[19] In 1995 they synthesized 2,2′,4,4′,6,6′-hexabromodiphenylcarbene (**7**),

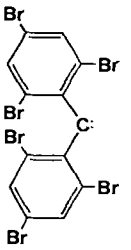

7

Wolfgang A. Herrmann, born in 1948, recieved his organometallic academic education with E. O. Fischer (Munich, Germany), H. Brunner (Regensburg, Germany), and P. S. Skell (Pennsylvania, USA) before becoming a professor at Regensburg (1979) and Frankfurt (1982). In 1985 he was appointed the chair professor of inorganic chemistry at the Technische Universität München as the successor to E. O. Fischer. His research focuses on homogeneous catalysis with a strong emphasis on synthesis, spectroscopy, and structures. He has authored about 450 scientific publications, 38 patents, and a number of review articles. He holds honorary doctoral degrees and has received numerous scientific awards. In 1996 he became president of the Technische Universität München.

W. A. Herrmann

C. Köcher

Christian Köcher, born in 1968 in Munich, studied chemistry at the Technische Universität München. For his Diplomarbeit in the group of W. A. Herrmann he investigated functionalized derivatives of C_{60}. This year he finished his dissertation "New Ways to N-Heterocyclic Carbenes and their Transition Metal Complexes—Applications in Homogeneous Catalysis". He is coauthor of eight publications and five international patents.

triplet carbene (ESR spectroscopy), again by photolysis of the parent diazo compound. In glassy (77 K) and completely fluid (120 K) 2-methyltetrahydrofuran, **7** is stable without significant decomposition. The crystalline compound can be kept at room temperature.[20]

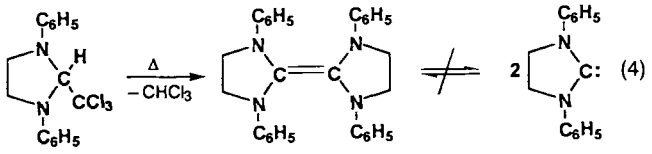

8 **8a** **9** (4)

1.1.3. Singlet Carbenes: Heteroatoms at the Divalent Carbon

Heteroatom donor groups on a carbene center render the originally degenerate orbitals on carbon unequal in energy, thus enhancing the nucleophilicity of the carbon atom and the thermodynamic stability. The singlet–triplet splitting correlates with increasing electronegativity of the π-donor substituents X and Y in carbenes of the type :CXY. Although several combinations of heteroatoms (O, S, N) are conceivable, only singlet carbenes with two nitrogen atoms (amino groups) were isolated as crystalline compounds so far ("carbon diamides"). These singlet carbenes have a pronounced low-energy HOMO and a high-energy LUMO.[21] Because of the lower electronegativity of carbon, they are stronger electron-pair donors than amines. The electron-accepting capability is more significant than that of boranes (electronegativity!). Since the amino groups are π-donating (mesomeric) and σ-withdrawing (inductive), 2,3-dihydro-1*H*-imidazol-2-ylidenes benefit from a "push–pull" effect.[22, 23] Although the methoxy and trifluoromethyl groups also display push–pull stabilization, methoxy(trifluoromethyl)carbene, $CH_3O(CF_3)C$:, is unstable at room temperature and electronically indiscriminant upon reaction with different alkenes.[24] Dialkoxycarbenes could be generated in situ by thermolysis of, for example, 2,2-dialkoxy-Δ^3-1,3,4-oxadiazolines,[25] and amino(chloro)carbenes by deprotonation of Vilsmeier reagents such as chloromethylene iminium salts;[26] however, attempts at their isolation resulted in dimeric or oligomeric products.

Therefore, the extent of "stability" and "aromaticity" (for 6π-electron systems) of free carbenes and their homologues depends on the point of view. For preparative chemistry kinetic stability is crucial. Stable N-heterocyclic carbenes are being studied for several reasons. Structure, reactivity, and theoretical understanding of these highly Lewis basic (one of the strongest known neutral bases) and nucleophilic molecules are of interest per se. Moreover, stable ylidene carbenes are used to prepare main group and transition metal complexes, although there are several in situ methods for synthesizing metal ylidene complexes without having to isolate free carbenes or their equivalents.

1.1.4. N-Heterocyclic Singlet Carbenes

In the early 1960s Wanzlick et al. investigated saturated and unsaturated heterocyclic carbenes.[27] The focus was first put on C–C-saturated molecules of type **9**. Imidazoline **8**, one possible precursor of **9**, was obtained from the reaction of 1,2-dianilinoethane with chloral; it underwent thermal α-elimination of chloroform. The resulting product dimerized, however, to yield the electron-rich olefin **8a** as a colorless crystalline compound [Eq. (4)]. Reactions with oxygen, water, nitromethane, and cyclopentanone confirmed the nucleophilic properties of what was incorrectly described as a "monomeric carbene". Cross-coupling experiments with differently substituted "dimers" showed that they are not in equilibrium with their monomers. Most notably, Lappert et al. developed a general synthesis of metal–carbene complexes by treatment of electron-rich (Wanzlick) olefins with transition metal complexes such as chlorotris(triphenylphosphane)rhodium(I). It is interesting that this particular rhodium complex catalyzes the metathetical cleavage of electron-rich olefins.

Numerous five- and six-membered heterocyclic cations display CH-acidic properties and base-catalyzed H–D exchange. The *N*-methylbenzthiazolium cation was most easily deprotonated by triethylamine in *N*,*N*-dimethylformamide or acetone, as shown by Wanzlick, Vorsanger, and Hünig. Once again, only the electron-rich olefin could be isolated in place of the free carbene,[28] but numerous transition metal complexes have become known since.

Wanzlick et al. recognized that aromatic resonance structures in unsaturated N-heterocyclic five-membered rings contribute to carbene stability. Free carbenes, such as 1,3,4,5-tetraphenyl-2,3-dihydro-1*H*-imidazol-2-ylidene (**10**), were generated by deprotonation of imidazolium salts with KO*t*Bu [Eq. (5)] and then allowed to react with isothiocyanates or

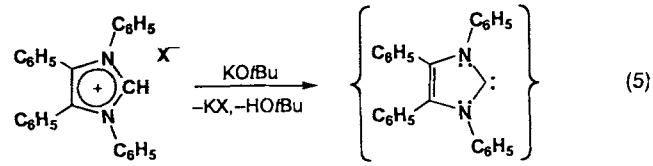

10 (5)

metal-containing precursors.[29, 30] Although Wanzlick et al. were so close to carbenes, they lacked the luck needed to isolate them.[31] Gleiter and Hoffmann pointed out that the ground state of a carbene will be a singlet state if the energy difference between the σ and π orbitals is greater than 2 eV, and that this splitting may be achieved by interaction of the unoccupied carbene p orbital with an aromatic system of $(4n+2)$ π electrons.

1.1.4.1. Synthesis and NMR Spectroscopy

In 1895 Nef announced that the isolation of methylene would be his next challenge.[32] After he and many others failed, however, no one believed any longer that carbenes would ever be isolated. Only the careful investigations by Arduengo et al. yielded the surprise of stable, crystalline (ylidic) carbenes almost one hundred years later.[33] For example, 1,3-diadamantyl-2,3-dihydro-1*H*-imidazol-2-ylidene (**11**; Figure 1) was obtained as

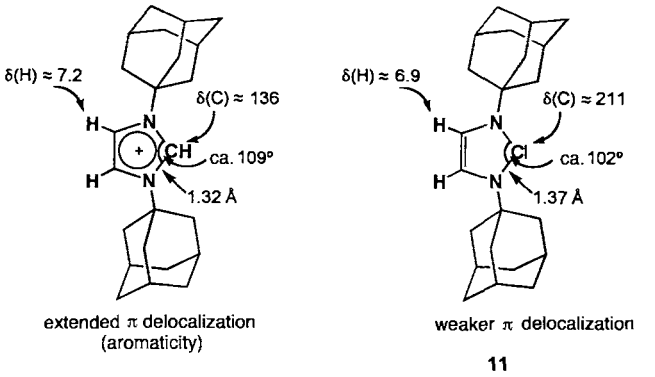

11

Figure 1. Geometric and spectroscopic parameters of the first isolated free carbene **11** and the corresponding imidazolium ion.

a colorless, crystalline solid by deprotonation of 1,3-diadamantylimidazolium iodide with NaH in the presence of catalytic amounts of DMSO anion [see Eq. (3)].

The thermal stability of solid **11** is surprising (melting point 240–241 °C without decomposition). In contrast, decomposition occurs rather quickly at room temperature in solution. To obtain reasonable rates for the deprotonation, catalytic amounts of either KO*t*Bu or the DMSO anion have to be applied, since sodium hydride and potassium hydride (and in most cases also the imidazolium salt) are insoluble in THF. Alternatively, stoichiometric amounts of KO*t*Bu may be used, but the less volatile *tert*-butyl alcohol is generated in place of hydrogen. Major progress in the synthesis was achieved with liquid ammonia as solvent: Deprotonation with sodium hydride or potassium amide occurred quickly and quantitatively in a homogeneous phase, and provided carbenes that were not previously accessible, such as oxygen-, nitrogen-, and diarylalkylphosphino-functionalized or chiral carbenes.[34]

Kuhn et al. reported a versatile two-step approach to thermally stable, alkyl-substituted N-heterocyclic carbenes.[35] To give an example, reducing 1,3,4,5-tetramethylimidazol-2(3*H*)-thion with potassium in boiling THF yielded analytically pure 1,3,4,5-tetramethyl-2,3-dihydro-1*H*-imidazol-2-ylidene [**12**, Eq. (6)] after filtration and removal of the solvent under vacuum.

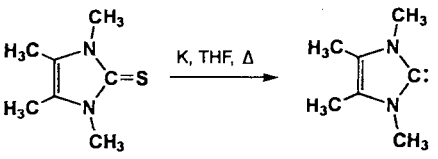

(6)

12

The thiones were accessible through condensation of *N*,*N*′-dialkylthioureas with 3-hydroxy-2-butanone. 1,3,4,5-Tetramethylimidazol-2(3*H*)-thione was obtained in a stoichiometric mixture with the pentamethylimidazolium ion when 1,3,4,5-tetramethyl-2-(methylthio)imidazolium iodide was reduced with potassium. The only drawback to this technique is the thermal lability of 2,3-dihydro-1*H*-imidazol-2-ylidenes in solution, which is dependant on the nature of the substituents R on nitrogen. The same problems are encountered upon generation of free carbenes under "Arduengo conditions".

1,3-Disubstituted ylidenes with aryl residues (*p*-tolyl, *p*-chlorophenyl, and 2,4,6-trimethylphenyl; m.p. 157 (decomp), 154 (decomp), and 153 °C (decomp), respectively) or higher alkyl groups (*tert*-butyl, cyclohexyl, adamantyl) and 1,3,4,5-tetramethyl-2,3-dihydro-1*H*-imidazol-2-ylidene (m.p. 109 °C) are colorless crystalline solids; 1,3-dimethyl-2,3-dihydro-1*H*-imidazol-2-ylidene is an oily liquid.[36] Under an inert-gas atmosphere they can be kept in the solid state for months at −30 °C. 1,3-Dicyclohexyl-2,3-dihydro-1*H*-imidazol-2-ylidene does not fully decompose upon heating at 160 °C for 24 h. In solution they are stable to approximately 50 °C for several hours; this is even valid for 1,1′-(1,2-ethylene)-3,3′-dimethylbis(2,3-dihydro-1*H*-imidazol)-2-ylidene.[37] As long as the solid carbenes or their solutions are colorless, they are very pure and contain no decomposition products. (Slightly colored solutions, from yellow to orange, are in most cases NMR spectroscopically pure.)

It was clear from the constitution of the stable, sterically unencumbered ylidenes named above that not kinetic (steric hindrance) but rather thermodynamic stabilization (electronic structure) is the essential feature. Two electronic effects deserve consideration. Firstly, the difference in electronegativity of nitrogen and carbon accounts for the (−I) inductive σ effect, which stabilizes the pair of unshared electrons in the in-plane carbene orbital. Secondly, the unoccupied p orbital yields a π-resonance interaction; in the ylidic resonance structures the nitrogen atoms donate their lone pairs to carbon (+M effect). Steric hindrance quite certainly contributes to stability, but the electronic situation in the N-C-N moiety seems to be crucial.

Imidazolium salts, which are promising solvents for two-phase catalysis,[38–40] are electron-rich heteroaromatic compounds. Hence, the ^{13}C NMR shift of the N-C-N sp^2 carbon (which later becomes the carbene center) appears at $\delta \approx 137$. The $H^4(H^5)$ ring protons and the CH-acidic H^2 proton resonate at $\delta = 7.9-7.3$ and 8–10, respectively (Figure 1).

Free 2,3-dihydro-1*H*-imidazol-2-ylidenes are also diamagnetic. The divalent carbon atoms resonates at rather low field ($\delta = 210-220$ in $[D_8]$THF). The substituents on nitrogen exert only little influence (!) on the chemical shift. The $H^4(H^5)$ ring protons typically resonate at $\delta = 6.9-7.0$. However, in 2,3-dihydro-1*H*-imidazol-2-ylidenes with aryl residues adopting a roughly coplanar arrangement (no *ortho* substituents!), anisotropic effects of the aryl substituents account for chemical shifts at $\delta = 7.6-7.8$.[36] Deprotonation of the imidazolium salts to the corresponding 2,3-dihydro-1*H*-imidazol-2-ylidenes entails a significant high-field shift of the $H^4(H^5)$ proton resonances in the case of N-alkyl substitution. This indicates a different magnetic anisotropy of the ring system, which is consistent with a decrease in 6π-electron delocalization.[41]

1.1.4.2. Isoelectronic Congeners

π Backdonation also contributes to the stability of isoelectronic stable nitrenium and phosphenium ions LN^+ and LP^+ (L = *N*,*N*-di-*tert*-butyl-1,4-diaza-2-butene or -butane).[42, 43] Isoelectronic Group 13 congeners, for example N-heterocyclic gallium and aluminum complexes containing the fragments

$NR_2Ga(R)NR_2$ and $NR_2Al(R)NR_2$, were experimentally verified with 1,4-diazabutadiene (DAB) ligands.[44,45] They are either stabilized by intramolecular coordination of a hemilabile dimethylamino side group or by dimerization. Alkyl- and aryl-substituted diyls $:E[CH(SiMe_3)_2]_2$ and $:E(2,4,6\text{-}t\text{Bu}_3C_6H_2)_2$ (E = Ge and Sn), which are monomeric in solution, were studied earlier;[46,47] in the meantime numerous compounds are known.[141] Stability and resistance to dimerization or insertion reactions once again reach a maximum for N-heterocyclic ring systems containing the DAB fragment and a Group 13–15 element.[10,11]

1.1.4.3. Solid-State Structures

The solid-state structures of 2,3-dihydro-1*H*-imidazol-2-ylidenes and representatives of C–C-saturated and acyclic carbenes were extensively studied by X-ray and neutron diffraction techniques. In the case of 2,3-dihydro-1*H*-imidazol-2-ylidenes, the N-C-N angles at the divalent carbon atom are all within a narrow range (±1°). For ylidenes with methyl, *p*-tolyl, or adamantyl substituents $R^1(R^3)$ on nitrogen, the carbenic angles are 101.5(1), 101.2(1), and 102.2(2)°, respectively.[33,35,142] These data are in excellent agreement with predictions for prototypical singlet ($^1A'$) carbenes bearing π-donor substituents (CF_2: F-C-F 102°).[48] These angles are significantly smaller than the typical range known for imidazolium salts (108.5–109.7°).[49] It was established for 1,3-diadamantyl-2,3-dihydro-1*H*-imidazol-2-ylidene that the $C^2-N^1(N^3)$ bonds (1.37 Å) are longer than in the imidazolium cation (1.33 Å). Considering this together with a slight elongation of the $N^1(N^3)-C^4(C^5)$ bonds, it was concluded that π delocalization is less pronounced in 2,3-dihydro-1*H*-imidazol-2-ylidenes than in imidazolium cations.

1.1.5. Acyclic carbenes

The success story of stable carbenes culminated in 1996 when Alder et al. synthesized bis(diisopropylamino)carbene (**13**), the first stable acylic carbene, by C-deprotonation of *N*,*N*,*N*′,*N*′-tetraisopropylformamidinium chloride with lithium diisopropylamide (LDA) in THF [Eq. (7)].[50] It is more sensitive to oxygen

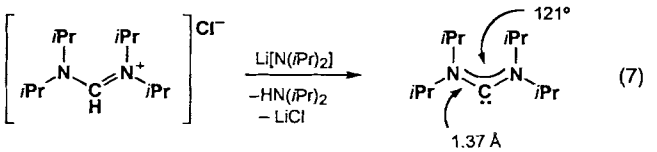

(7)

13

and moisture than the cyclic congeners. The N-C-N (121.0°) angle is significantly larger than in 1,3-dimesityl-1*H*-imidazolidin-2-ylidene (104.7°) and ylidene **11** (102.2°). The barrier to N–C rotation gives proof of substantial double-bond character.[50] The ^{13}C NMR chemical shift of the divalent carbon atom in **13** is shifted downfield by about 40 ppm relative to that for the divalant carbon atom in 2,3-dihydro-1*H*-imidazol-2-ylidenes and downfield by 10 ppm relative to that for **15** (see below).

1.2. Monomer or Dimer? The Singlet–Triplet Gap

1.2.1. C–C-Unsaturated Carbenes

After carbon monoxide and isocyanides, unsaturated N-heterocyclic carbenes have the largest singlet–triplet gap (about 85 kcal mol^{-1} according to ab initio calculations) of any divalent carbon compounds.[51] They show no tendency to dimerize, which is in contrast to their C–C-saturated analogues. Despite the predicted (thermodynamic) lability for tetraazafulvalene, the formal dimer **14** of 2,3-dihydro-1*H*-imidazol-2-ylidenes with a genuine double bond was isolated by Chen et al. by deprotonation of a doubly trimethylene-bridged diimidazolium salt [Eq. (8)] and structurally characterized.[52] The bond energy was

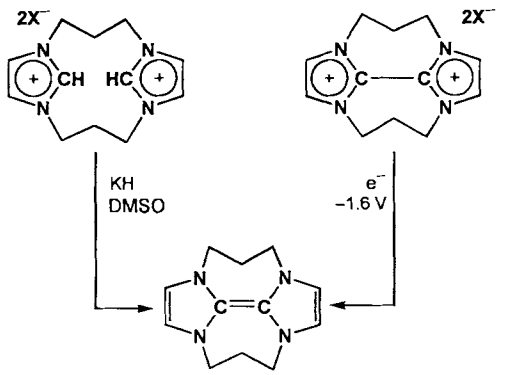

(8)

14

estimated to be 4±3 kcal mol^{-1}. The tetramethylene-bridged analogue, however, readily converts into the corresponding dicarbene. Monobridged and untethered imidazolium salts exist in the monomeric ylidene form after deprotonation and show no tendency to dimerize. Thummel et al. independently reported that **14** is accessible by bulk electrolysis (−1.6 V) of the corresponding doubly tethered diimidazolium salt in acetonitrile.[55] Doubly tethered benzo- and naphtho-2,3-dihydro-1*H*-imidazol-2-ylidene dimers which are reluctant to undergo C–C bond cleavage were also obtained through bulk electrolyis. It has long been recognized that enetetramines are strong reducing agents. For example, 2,2′-dibenzo-2,3-dihydro-1*H*-imidazolylidene shows the first ionization potential at about 6 eV and is easily oxidized to the corresponding dication.[54]

1.2.2. C–C-Saturated Carbenes

The singlet–triplet gap becomes smaller upon saturation of the C–C bond, since five-center six-electron (5c-6e) π delocalization as a stabilizing factor is no longer possible. As dimers of saturated carbenes, electron-rich olefins **8a** were used by Lappert et al. to prepare imidazolidine–carbene metal complexes. In 1995 Arduengo et al. succeeded in synthesizing imidazolidine-2-ylidene **15**, a stable and crystalline monomer of the electron-rich olefins [Eq. (9)].[55]

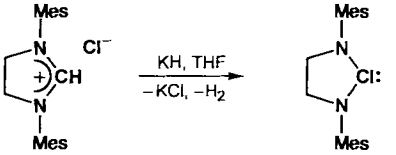

(9)

15

2,3-Dihydro-1*H*-imidazol-2-ylidenes, ylidene **15**, and the acyclic diaminocarbene **13** were synthesized by deprotonation of amidinium salts. This showed that the different degree of aromaticity in the precursor has no first-order effect on deprotonation in this special case. Semiempirical calculations (AM 1 method) suggest that the proton affinities of similarly substituted representatives of all three systems vary by less than 1% of the absolute values.[50]

1.2.3. Triazole-Derived Carbenes

The first crystalline triazole-derived carbene, 1,3,4-triphenyl-4,5-dihydro-1*H*-1,2,4-triazol-5-ylidene, was not prepared by deprotonation of the highly protic triazolium salt, because the latter forms—in contrast to imidazolium salts—(isolable) 5-methoxytriazoles upon treatment with NaOMe.[56] 4,5-Dihydro-1*H*-1,2,4-triazol-5-ylidene **16** was obtained at 80 °C and 0.1 mbar by endothermic elimination of methanol from the corresponding 5-methoxytriazole in the solid state [Eq. (10)].

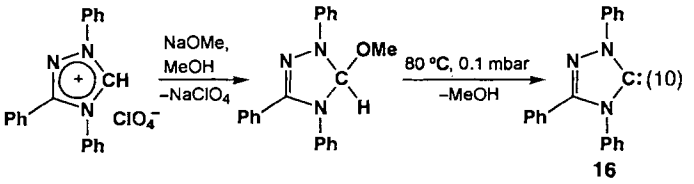

16

The bond lengths N^1–C and N^3–C (1.351(3) and 1.373(4) Å) are much shorter than expected for a single bond. This result and ab initio calculations indicate strong interaction of the filled nitrogen 2p orbitals with the unoccupied carbon 2p orbital. As in the case of imidazole-derived carbenes, no dimers are formed in solution. Ylidene **16** decomposes unspecifically above 150 °C (differential scanning calorimetry/thermogravimetry (DSC/TG) studies). 1,3,4-Triphenyl-4,5-dihydro-1*H*-1,2,4-triazol-5-ylidene is the first carbene to be commercially available (ACROS). Cyclic voltammetry and ESR measurements demonstrated that **16** can be reversibly reduced to the corresponding radical anion.[57] Density functional theory (DFT) calculations on the spin density in the most stable structure of the radical anion suggested that the single electron is delocalized between the N^2–C^3 double bond and the adjacent phenyl substituent.

1.2.4. Thiazole-Derived Carbenes

Substituted 2,3-dihydrothiazol-2-ylidenes as well as the unsubstituted parent compound as a thiazole tautomer were investigated experimentally and by quantum chemical calculations only very recently. These compounds are close analogues of the intermediate involved in enzymatic C–C bond forming and breaking transformations catalyzed by thiamin (vitamin B_1). The parent species were characterized by matrix-isolation techniques as well as in the gas phase: Prolonged irradiation (254 nm) of thiazol-2-caboxylic acid in an argon matrix (12 K) yielded unsubstituted 2,3-dihydrothiazol-2-ylidene (**17**) with loss of CO_2 [Maier et al.; Eq. (11)].[58] The analysis of calculated and measured IR spectra together with ^{13}C labeling experiments confirmed the formation of **17**·CO_2. Ylidene **17** isomerized, probably by an intermolecular pathway, to thiazole under further irradiation or upon heating to 60 K. Dissociative electron ionization (EI) of acetyl-2-thiazole yielded the 2,3-dihydrothiazol-2-ylidene radical cation, from which neutral ylidene **17** was generated by neutralization-reionization mass spectroscopy [Eq. (12); Schwarz and Terlouw et al.].[59]

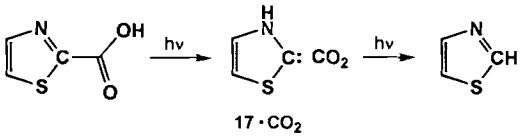

17·CO_2

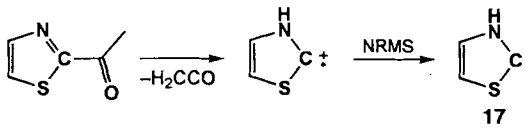

17

The geometric parameters and energies of neutral thiazole, 2,3-dihydrothiazol-2-ylidene, and the corresponding radical cations were calculated using the hybrid DFT option. Ylidene **17** is 31.5 kcal mol^{-1} less stable than thiazole; the energy barrier is 72.4 kcal mol^{-1}. The calculated geometry of planar **17** (1*A'*)[59] is in perfect agreement with the X-ray diffraction data of 3-(2,6-diisopropylphenyl)-2,3-dihydrothiazol-2-ylidene (**18**), the first stable crystalline 2,3-dihydrothiazol-2-ylidene synthesized by Arduengo et al. through deprotonation of the corresponding thiazolium chloride with potassium hydride in THF [Eq. (13)].[60] With 104.2° the angle at the carbene carbon

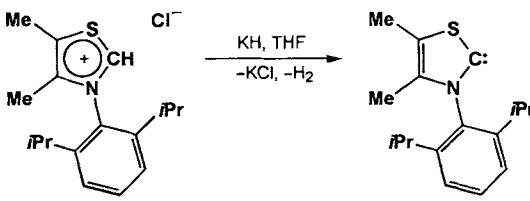

18

atom (S-$C_{carbene}$-N) is again smaller than in the azolium ion (112.0°). As for other singlet carbenes, the bond lengths between C2 and the heteroatoms are greater than those in azolium salts. Monomeric 2,3-dihydrothiazol-2-ylidenes with sterically less demanding groups on nitrogen can be observed in solution at low temperature but are prone to fast dimerization. With **18** an equilibrium between a stable carbene and its dimer was observed for the first time in the presence of a protic acid catalyst.

1.2.5. Functionalized Chiral and Multidentate Carbenes

N-Heterocyclic carbenes form a plethora of metal complexes, either over carbenes, which are formed by deprotonation of CH-acidic imidazolium salts, or by in situ deprotonation by metal-bound basic ligands (e. g. amides, alkoxides, or acetate; see Section 5). Free carbenes with oxygen, nitrogen, and diarylalkylphosphino donors in the side chain(s) or with chiral residues were synthesized in our group using the particularly beneficial liquid-ammonia route (Figure 2).[34, 61, 62] When the

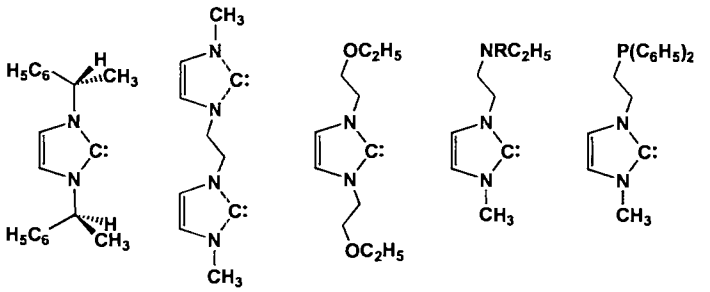

Figure 2. Side chain functionalized, chiral, and multidentate 2,3-dihydro-1*H*-imidazol-2-ylidenes.

imidazolium salts were deprotonated in a mixture of liquid ammonia and aprotic polar solvents such as THF, the desired carbene was obtained in exellent yield and purity; in most cases the reaction went to completion within about 30 min at −40 °C. Many otherwise inaccessible carbenes have thus been prepared.

As two-electron ligands, carbenes are related to ethers, amines, isonitriles, and phosphanes with regard to their coordination chemistry. Chelating derivatives are of special interest. Asymmetric precursors are accessible from commercially available starting materials in four-step syntheses with yields of up to 90%.[63] Because of the rigid geometry of the planar five-membered rings, the optimum number of atoms forming an appropriate chelate ligand does not match that found with diphosphanes or diamines. Methylene-bridged 2,3-dihydro-1*H*-imidazol-2-ylidenes and 1,2,4-1*H*-triazol-5-ylidenes form six-membered rings upon metal complexation. However, the natural bite angle of 78–79° found in transition metal complexes (W, Pd) of these ligands is exactly that of 1,1′-bis(diphenylphosphino)methane (four-membered ring).[63, 64] At rhodium centers this dicarbene exhibits a bridging coordination mode.[65] In ethylene-bridged 2,3-dihydro-1*H*-imidazol-2-ylidenes an unfavorable eclipsed conformation of the hydrogen atoms in the ethylene bridge also favors dinuclear structures.[37] With an *o*-xylylene backbone (C_4), however, bidentate ligands well suited for chelating metal coordination on Rh were obtained.[66] In addition to phenyl- and naphthylethyl-substituted carbenes, other chiral 1,3-di-R-2,3-dihydroimidazol-2-ylidenes and complexes thereof were prepared in our group. Enantiomerically pure acetylated 1,1′-bis(1-hydroxyethyl)ferrocene reacted with imidazole under retention of configuration at the pseudobenzylic positions. Chiral diimidazolium salts were obtained after alkylation. Differrocenyl-substituted imidazolium salts were synthesized from enantiomerically pure 1-ferrocenylamine by a ring-closure synthesis.[67] Complexes of chelating oxazoline/carbene donors are available by a simple general route from 2-amino alcohols.[119]

A tripodal carbene ligand of the Trofimenko type, tris(2,3-dihydro-1*H*-imidazol-2-ylidene)borate, resulted from deprotonation of the corresponding precursor salt with *n*BuLi/*n*-hexane in THF. The homoleptic hexacarbene–iron complex **19** resulted from subsequent treatment with $FeCl_2$ (Figure 3).[68] Another tridentate carbene ligand, [1,3,5-{tris(3-*tert*-butyl-2,3-dihydro-1*H*-imidazol-2-ylidene)methy}-2,4,6-trimethyl benzene] (**20**), was isolated as a solid. Inter- or intramolecular interactions of the carbene groups with each other were not found.[69]

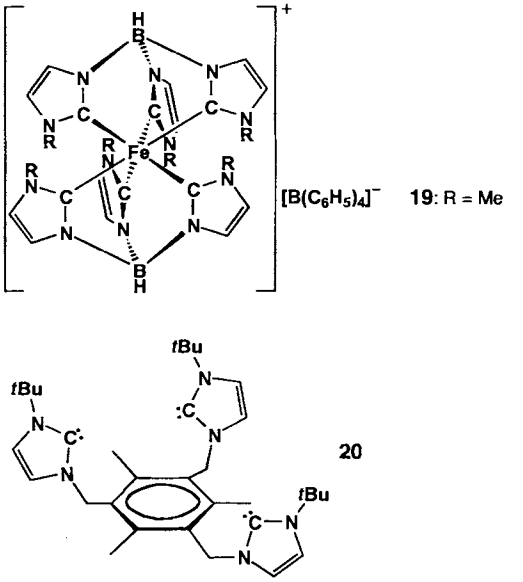

Figure 3. Tridentate carbenes as ligands in the hexacarbene complex **19** and as free carbene **20**.

1.3. Nomenclature of Ylidenes

The suffixes of the systematical names of heterocyclic compounds are determined by the kind of heteroatoms in the ring. The first differentiation is made between a ring system containing at least one nitrogen atom and all other heterocyclic rings. Five-membered rings containing at least one nitrogen atom have the suffixes -olidine (saturated ring systems), -oline (ring containing one double bond), and -ole (ring containing the maximum number of double bonds).

The N-heterocyclic ylidenes first isolated by Arduengo are formal tautomers of 1*H*-imidazole **a**. Protonation of 1*H*-imidazole at the basic N3 position and subsequent deprotonation of the resulting 1,3-dihydroimidazolium ion **b** at the C^2 center yields the 1,3-dihydrosubstituted ylidene **c**. The number of π electrons (six) remains unchanged. The addendum -ylidene refers to compounds in which two hydrogen substituents are replaced by two electrons or one pair of electrons. The parent compound of **c** (**d**) is unequivocally described as 2,3-dihydro-1*H*-imidazole. Thus, **c** is called 2,3-dihydro-1*H*-imidazol-2-ylidene. As **d** represents a ring system with only one double bond, it may also by called an imidazoline (see above). Although the

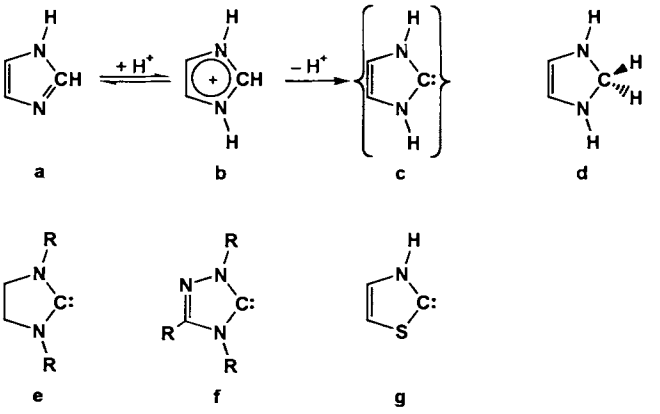

name imidazoline by itself comprises other tautomers, 1,3-di-R-imidazoline-2-ylidene is unequivocal for compounds of type **c**. The names 1,3-di-R-2,3-dihydro-1*H*-imidazol-2-ylidene and 1,3-di-R-imidazoline-*2*-ylidene are synonymous here because of the substitution pattern of imidazole-derived carbenes with (organic) substituents in positions 1 and 3, and the carbenic center at the C^2 atom. Definitely not correct, however, is the name "1,3-di-R-imidazol-2-ylidene". N-heterocyclic ylidenes of type **e** with a saturated C–C bond are correctly called 1,3-di-R-2,3,4,5-tetrahydro-1*H*-imidazol-2-ylidenes or 1,3-di-R-imidazolidine-2-ylidenes. Triazole-derived carbenes of type **f** are 1,3,4-tri-(R)-4,5-dihydro-1*H*-triazol-5-ylidenes, and thiazole-derived **g** 2,3-dihydro-thiazol-2-ylidenes.

2. Electronic Structure of N-Heterocyclic Carbenes, Silylenes, and Germylenes

2.1. Singlet–Triplet Gap in Methylene

Due to a small HOMO–LUMO gap, the energy difference between the singlet and triplet states can be very small or even negative because of the energy gain from increased exchange interaction in the triplet state. It was experimentally verified that the parent carbene $:CH_2$ has a triplet ground state. This fact has served as a reference for various ab initio methods, since the contribution of electron correlation in singlet and triplet states is significantly different, and an accurate value for the singlet–triplet gap can be calculated only by using large basis sets and extensive configuration interaction (CI).[70]

2.2. π Delocalization in N-Heterocyclic Carbenes

In their first theoretical work Dixon and Arduengo calculated singlet–triplet splitting and proton affinity of unsubstituted 2,3-dihydro-1*H*-imidazol-2-ylidene by ab initio methods (singlet: TCSCF, triplet: ROHF).[71] With 79.4 kcal mol^{-1} the energy gap is nearly twice as large as that of $:CF_2$ (calcd: 45, found: $\approx$57 kcal mol^{-1}). On the other hand, the proton affinity is estimated to be about 250 kcal mol^{-1}, making 2,3-dihydro-1*H*-imidazol-2-ylidenes one of the strongest organic Brønsted bases known. Interestingly, this value is larger then that for $:CH_2$ (205 kcal mol^{-1}), whereas $:CF_2$ has a lower proton affinity (172 kcal mol^{-1}). It was concluded that a) **A** is similar to $:CF_2$ and b) ylidic resonance structures do not dominate. An analysis of the MP2 wavefunction using the localized orbital approach provided a similar conclusion:[72] The stability of **A** is due to σ donation of charge to the nitrogen atoms, whereas π backdonation plays only a minor role.

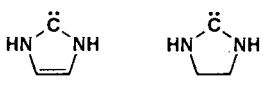

A **B**

This point of view was reconfirmed.[73] The electron distribution of perdeuterated tetramethyl-2,3-dihydro-1*H*-imidazol-2-ylidene was determined experimentally by neutron and X-ray diffraction. In addition, the electron density was calculated by DFT methods using a gradient-corrected function. Experimental and theoretical electron distributions matched each other very well. Based on contour line diagrams of the electron density, the authors reestablished their picture of similarity between $:CF_2$ and **A**. The "egg-shaped" density at the carbenic carbon resembles that of $:CF_2$ and was interpreted as significant electron deficiency above and below the molecular plane. Accordingly, contour plots 70 pm above the molecular plane showed separate maxima for the two nitrogen atoms and one for the C–C double bond, which was interpreted as a lack of π delocalization in the N-C-N fragment and a separated double bond. The authors concluded that the stability of 2,3-dihydro-1*H*-imidazol-2-ylidenes must be due to kinetic hindrance because of electrostatic repulsion between the localized π electrons and an attacking nucleophile.

The above-mentioned theoretical studies judged N-C-N π delocalization to be of minor importance. However, it is a necessary prerequisite for an aromatic type of delocalization in the 6π-electron system in **A**. The appartent difference in the stability of isolated **A** and **B** provoked skepticism of this point of view.

Avoiding the question of aromaticity, Thiel et al. attributed the difference between **A** and **B** to the larger singlet–triplet separation in **A** entailing a higher barrier to dimerization.[74] However, the reason for the higher singlet–triplet gap in the unsaturated system **A** remains unexplained.

2.3. Aromaticity

On the basis of (hypothetical) isostructural and isodesmic reactions, the relative thermodynamic stability of a given set of species can be estimated. Sauers therefore verified the influence of heteroatoms in heterocyclic 6π-electron carbenes.[75] The aromatic stabilization energy (ASE) is the negative of the isodesmic reaction energy in Equation (14) (including the zero point energy correction).

$$AH_2 + B \longrightarrow A + BH_2 \qquad (14)$$

Significant stabilization for the 6π-electron system can be achieved with two nitrogen atoms. In contrast, two oxygen atoms, with higher electronegativity than N and S, afford the lowest stabilization. This rules out stabilization merely by σ effects, as proposed by Cioslowski.[72] Consequently, as long as 6π-electron delocalization plays a role, N-C-N π delocalization must also be present.

Two profound theoretical studies by Heinemann et al.[76] as well as Frenking and Böhme[77] came to essentially the same conclusion. It was demonstrated that, even in systems such as pyridine or pyrrole, the analysis of electron-density contour plots 70 pm above the molecular plane exhibit the same features of "separated" π electron density above the individual nuclei.[77] Therefore, the method of density mapping employed by Arduengo et al. is not very reliable for analyzing the presence of electron delocalization.

The isodesmic reaction energies in Equation (15) are very interesting.[76] For R = NH_2 (the plane of the NH_2 frag-

$$R_2C: + CH_4 \longrightarrow R_2CH_2 + H_2C: \qquad (15)$$

ments is perpendicular to the carbene plane) the reaction energy of about 20 kcal mol^{-1} demonstrates the stabilization with respect to singlet methylene due to the higher electronegativity of the nitrogen atoms. However, in a completely planar conformation, where π delocalization from the nitrogen lone pairs into the "empty" carbene p-type orbital is possible, this stabilization energy is increased by 70 kcal mol^{-1}. Thus, π backdonation dominates carbene stabilization. Addition of a CH_2-CH_2 bridge increases the stabilization by only 6 kcal mol^{-1}, whereas the unsaturated CH=CH linkage effects an additional stabilization of 26 kcal mol^{-1} with respect to the planar aminocarbene. This demonstrates a significant stabilization effect of the double bond and indicates the presence of a certain degree of cyclic electron delocalization. On the other hand, this stabilization is small compared to that originating from N-C-N π delocalization.

Thermodynamic calculations led to two main conclusions: a) The major contribution to carbene stabilization is due to $p\pi-p\pi$ electron donation from the two nitrogen atoms to the carbene carbon atom, and b) the unsaturated cyclic carbene **A** is about 20 kcal mol^{-1} more stable than the saturated analogue **B**.

2.4. Heterocyclic Silylenes and Germylenes

Because of their similarity, silylenes and germylenes were studied in parallel to the carbene by a number of methods mentioned above.[11, 21, 73, 76–79] Arduengo et al. concluded that the electron-density distribution of silylenes and germylenes differs significantly from that of carbenes, and resembles chelation of a Group-14 element by a DAB ligand.[73] However, numerous thermodynamic calculations performed in various studies led directly to the conclusion that also silylenes and germylenes are stabilized by $p\pi-p\pi$ delocalization.[76, 77] On the other hand, 6π-electron delocalization was judged to be present but less pronounced than in carbene **A**. As an example, an isodesmic reaction energy affords an increased thermodynamic stability of about 9 kcal mol^{-1} for the unsaturated silylene with respect to the cyclic saturated analogue (about 20 kcal mol^{-1} for the carbene).[76]

2.5. Magnetic Properties

The thermodynamic calculations clearly demonstrated the increased stability of the 6π-electron system. However, this was only an indication for aromaticity but no proof. A large anisotropy between in-plane and out-of-plane magnetic susceptibility is known to be a good indicator for ring currents, and therefore a good measure for what is meant by "aromaticity". It should be noted here that there are at least two noncompatible scales of aromaticity.[80]

Heinemann et al. as well as Frenking and Böhme calculated magnetic susceptibilities. They pointed out that the absolute values of susceptibility are not very accurate, but the relative parallel and perpendicular components should be reliable.[77] A reference value of $\Delta\chi = 50$ was given for pyridine. As expected the 6π-electron carbene **A** is "less aromatic" than pyridine with an anisotropy $\Delta\chi$ of only 28, which is nevertheless much larger than the value of $\Delta\chi = 9$ for **B**. The protonated imidazolium cation has a slightly higher anisotropy of $\Delta\chi = 31$. It is reasonable to conclude that cyclic electron delocalization in **A** is less developed as in, for example, benzene or pyridine, as expected for five-membered heteroaromatic rings.[80] However, there is a distinct difference between **A** and **B**, which suggests a relation between cyclic electron delocalization and increased thermodynamic stability.

2.6. Chemical Shielding Tensor

In addition to these studies that focus on the electronic structure of 2,3-dihydro-1*H*-imidazol-2-ylidene, a number of theoretical investigations concerning experimental properties were performed. The chemical shielding tensor of carbenes was calculated based on the local density functional and Hartree–Fock (HF) theories,[41] and compared with the experimental CP-MAS solid-state NMR spectra of 1,3,4,5-tetramethyl-2,3-dihydro-1*H*-imidazol-2-ylidene. The large chemical shielding anisotropy at the carbene carbon atom could be reproduced by all theoretical methods. Because of a large deshielding component of the tensor in the molecular plane orthogonal to the lone pair, the resonance for the carbene carbon atom appears at very low field. This tensor element is dominated by a paramagnetic (deshielding) contribution arising from a low-lying $n \rightarrow \pi^*$ transition. This large deshielding paramagnetic contribution is missing in the shielding tensors of the doubly bonded carbon atoms C^4 and C^5 of **A** and also for the protonated carbene carbon C^2 in the imidazolium cation AH^+, which indicates the absence of π delocalization in the N-C-N fragment (carbenic structure). However, this reasoning is somewhat misleading, since the presence of such a large paramagnetic contribution is not necessarily due to different π^* energy levels. The most significant difference between the carbenic carbon atom C^2 in **A** and the carbon atoms C^4 and C^5 as well as the C^2 center in the imidazolium cation is the fact that the lone pair is replaced by a significantly stabilized electron pair forming the C–H bond. The extent of paramagnetic contribution is proportional to the inverse of the energy difference of the related transition. Therefore, this contribution will be much larger for carbene carbon atoms, for which the $n \rightarrow \pi^*$ transition has a low energy gap, than for other cases for which the equivalent $\sigma \rightarrow \pi^*$ transition out of the C-H bond will have a much larger energy gap and therefore a much smaller paramagnetic contribution. Exactly this kind of simplified picture was established to explain the difference between the ^{13}C NMR chemical shielding tensors of benzene and the *ipso* carbon atom of phenyllithium.[81]

2.7. Photoelectron Spectroscopy

Since photoelectron spectra can shed light on the electronic structure of molecules, the whole series of isolated, cyclic 6π-electron carbenes, silylenes, and germylenes was investigated.[21] Density functional calculations were employed to explain the experimental data. Based on Koopman's theorem on the Kohn–Sham orbitals and using first-order time-dependent per-

turbation theory, the spectra could be simulated very well. The most important feature is the fact that, in contrast to the Si and Ge homologues, the lowest-energy ionization process is the removal of an electron from the in-plane lone-pair orbital which appears as the HOMO in the DFT calculation. The next two bands correspond to π-type orbitals of the five-membered ring.

The HF orbital energies for all carbenes, silylenes, and germylenes show a π-type HOMO, and that the second highest molecular orbital (HOMO − 1) is that for the in-plane lone pair.[76] The question of why the classical Koopman's theorem is violated only in the case of the 6π-electron carbene then appears. In fact, it implies that the errors in neglecting electron correlation in the HF wavefunction and electronic relaxation upon ionization cancel out. This apparently does not apply to carbenes. These deficiencies can be overcome by using correlated ab initio methods to calculate also the energy of the radical cation: Ionization energies of **A** were reproduced very well with respect to both order and absolute value at the PUMP4/6-31G(d) or CCSD(T)/6-31G(d) level of theory. The analysis revealed that significant relaxation of the wavefunction occurs upon removing an electron from the in-plane lone pair, which results in increased electron delocalization. This is in line with the increased aromaticity of the cationic imidazolium, for which charge density of the former lone pair is diminished by "adduct formation" with a proton. The authors concluded that the in-plane electron density acts as a barrier that reduces the extent of cyclic electron delocalization. Because of the energy gained upon removing an electron from the lone pair, this ionization appears to be the lowest-energy ionization process. This fact was confirmed by the Kohn–Sham orbital energies.

3. Reactivity

Whereas triplet carbenes exhibit radical-like reactivity, singlet carbenes are expected to show nuleophilic and electrophilic reactivity due to the σ-type lone pair and the vacant p orbital. As a result of small HOMO–LUMO gaps, carbenes are very reactive. One of the most intriguing and controversial questions regarding the reactivity and stability of 2,3-dihydro-1*H*-imidazol-2-ylidenes, imidazolidine-2-ylidene, and bis(diisopropylamino)ylidene focuses on their electronic structure. The theoretical investigations discussed above, however, concluded that unsaturated as well as saturated N-heterocyclic carbenes of the imidazole type benefit very well from π donation from the adjacent amino groups; this is equivalent to a contribution of the two ylidic mesomeric structures to the electronic structure of diaminocarbenes.

It is doubtful whether much can be learned about the behavior of transient, highly reactive singlet carbenes by studying the stable ones. Transient carbenes generally react with unsaturated nucleophiles such as allenes, acetylenes, arenes, or olefins. Following Skell's theory the spin multiplicity of the carbene correlates with the stereochemistry of cyclopropanes resulting from [1 + 2] cycloadditions to olefins.[82, 83] However, it has long been known that nucleophilic carbenes in which the singlet state is stabilized by interaction of the vacant π orbital with a delocalized π system do not react with nucleophilic olefins (e. g. hexene) but with electrophilic olefins such as fumaric esters. This rule is confirmed by 2,3-dihydro-1*H*-imidazol-2-ylidenes, which do not undergo electrophilic reactions like insertions or cycloadditions; furthermore, they can be handled in typical donor solvents including THF, liquid ammonia, or acetonitrile. 2,3-Dihydro-1*H*-imidazol-2-ylidene adducts are also reluctant to add to nucleophiles. This shows that the pπ LUMO lies rather high in energy as a result of nitrogen lone pair conjugation, thus decreasing the electrophilic character of the carbene carbon atom. The stability of 2,3-dihydro-1*H*-imidazol-2-ylidenes with respect to dimerization (nucleophilic perpendicular attack of one singlet carbene at the vacant out-of-plane orbital of another singlet carbene) suggests that the term "carbene" is misleading.[30]

3.1. Bertrand's Carbene

Ab initio calculations indicate that Bertrand's phosphanylsilylcarbenes $[(R_2N)_2P](SiMe_3)C{:}$ (R = *i*Pr (**21**), *c*-C_6H_{11}) and the more temperature-sensitive phosphanylphosphoniumcarbenes $[\{(iPr_2N)_2P\}\{P(iPr_2N)_2H\}C{:}]X$ are best regarded as λ^5-phosphaacetylenes with polar P^+-C^- multiple bonds [Eq. (16)]; reactivity typical for λ^3-phosphanylcarbenes results.[51, 84, 85] The P-C-P angle in $[(iPr_2N)_2PCP\{(iPr_2N)_2H\}]^+$ (165°) is significantly larger than that expected for singlet carbenes. A singlet–triplet energy seperation of only 3 kcal mol^{-1} was computed. However, reactivity typical for carbene is known, for example, for intramolecular insertion into C–H bonds, stereospecific cyclopropanation with electron-poor olefins (dimethyl fumarate), addition to aldehydes to yield oxiranes, [1 + 1] addition to isocyanides to yield ketene imines, and concerted or stepwise (cyclo)additions to nitriles to give 2*H*-azirins and 1,2-λ^5-azaphosphetes, respectively.[86]

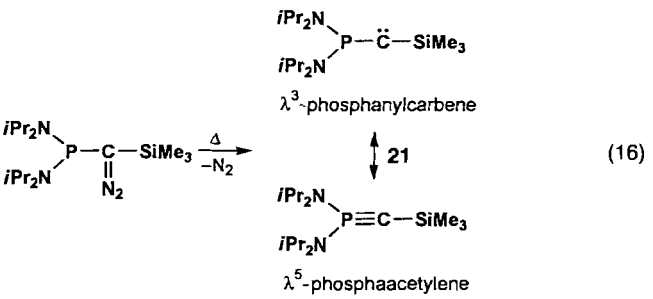

(16)

3.2. Basicity and Nucleophilicity

The basicity following the concept of Brønsted–Lowry and the nucleophilicity of 2,3-dihydro-1*H*-imidazol-2-ylidenes were examined by Alder et al. With $pK_a = 24$ in $[D_6]$DMSO (fluorene: $pK_a = 22.9$; 2,3-benzofluorene: $pK_a = 23.5$) 1,3-diisopropyl-4,5-dimethyl-2,3-dihydro-1*H*-imidazol-2-ylidene is a stronger base than 1,5-diazabicyclo[4.3.0]non-5-ene (DBN), 1,8-diazabicyclo[5.4.0]undec-7-ene (DBU), and proton sponges but weaker than phosphazene bases.[87] The rate of proton transfer between a free carbene and its conjugate acid is close to the exchange limit at room temperature, but the carbene is too

nucleophilic for synthetic applications as a strong base due to a sterically unhindered conformer which is only slightly higher in energy than the preferred congested conformer. The ratio of elimination to substitution in the reaction with 2-bromopropane (20:80) is similar to that for DBN and DBU. Proton exchange between the acyclic bis(diisopropylamino)carbene and its conjugate acid is much slower due to steric hindrance; this may also explain the stability of the acyclic carbene, for example, towards dimerization.

3.3. N-Heterocyclic Carbenes as Nucleophilic Catalysts

N-Heterocyclic carbenes acting as nucleophiles have manifold catalytic applications in synthetic chemistry as well as in nature: Breslow showed in the context of ylidene-catalyzed benzoin condensations[88] that the vitamin B_1 enzyme cofactor thiamin (**22**), a naturally occurring thiazolium salt, plays a key role in biochemistry (Figure 4).[89] As thiamin diphosphate (the

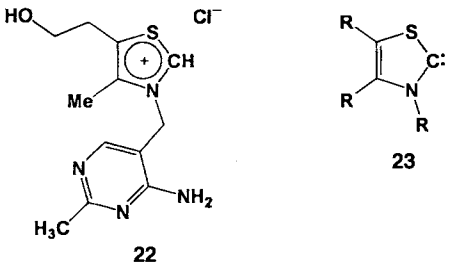

Figure 4. Structure of thiamin (**22**) as well as the framework of the corresponding catalytically active 1,3-dihydrothiazol-2-ylidene **23**.

coenzyme of pyruvate decarboxylase), it catalyzes the decarboxylation of pyruvic acid to active acetaldehyde as well as the benzoin condensation of benzaldehyde. In basic aqueous buffers the active catalyst of this reaction is a 2,3-dihydrothiazol-2-ylidene of the form **23**. Stetter recognized that aliphatic aldehydes that undergo aldol condensation in the presence of cyanides are activated for a benzoin-type condensation upon addition of ylidene catalysts.[90-92]

2,3-Dihydro-1*H*-imidazol-2-ylidenes and 4,5-diyhdro-1*H*-1,2,4-triazol-5-ylidenes also found catalytic applications in organic synthesis, for example in the benzoin condensation of higher aldehydes to α-hydroxyketones, the oxidative benzoin condensation of aldehydes, alkohols, and aromatic nitro compounds to yield esters, and selective formoin reactions of formaldehyde to give C_2 to C_6 building blocks.[93] The catalytic activity and selectivity of a given system composed of a 1,3-heteroazolium salt and a base correlated nicely with the kinetic acidity of the 1,3-heteroazolium salt. The transient formation of dimers was ruled out. Nucleophilic ylidenes also served as catalysts in the Michael–Stetter reaction (Scheme 1). In this "umpolung" reaction yielding 1,4-dicarbonyl compounds, a nucleophilic heterocyclic ylidene attacks an aldehyde; the generated acyl carbanion equivalent then adds to α,β-unsaturated ketones in a 1,4 manner. Intramolecular variants of this reaction provided furanones, pyranones, and chromanones. Asymmetric variants of ylidene-catalyzed benzoin condensations and

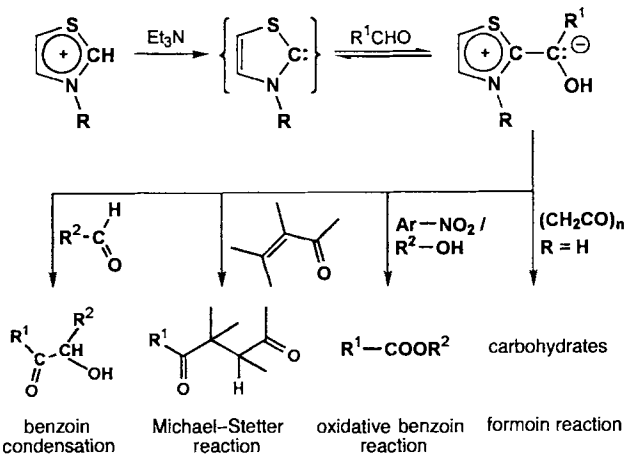

Scheme 1. Organic transformations of aldehydes catalyzed by N-heterocyclic ylidenes.

Michael–Stetter reactions were achieved using chiral triazolium salts as catalyst presursors.[94]

3.4. N-Heterocyclic Carbenes as Lewis Bases

The transition metal coordination chemistry of 2,3-dihydro-1*H*-imidazol-2-ylidenes is discussed in detail in Section 5. 2,3-Dihydro-1*H*-imidazol-2-ylidenes form stable adducts with soft and weak Lewis acids, such as iodine, in which the carbenes,[9,95] just like tertiary phosphanes, act as pronouncedly basic σ donors. The nearly linear arrangement together with other structural and spectroscopic data of the imidazole moiety suggest a hypervalent (10e-I-2c) central iodine atom (I^-) with an expanded I···I bond and a positively charged imidazole moiety of slightly augmented π delocalization. 2-Iodo-1,3-dimesitylimidazolium iodide further reacted with 1,3-dimesityl-2,3-dihydro-1*H*-imidazol-2-ylidene to give almost linear cationic bis(carbene) adducts of hypervalent iodine with only slightly different C–I bond distances [Eq. (17)].[96]

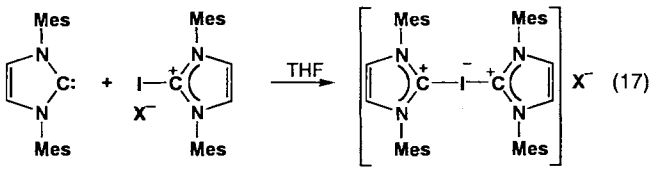

X = I, $[B(C_6H_5)_4]$

Adducts (1:1) of 2,3-dihydro-1*H*-imidazol-2-ylidenes with iodopentafluorobenzene[9] also display a characteristic linear arrangement [Eq. (18); R = adamantyl]. Increased π delocaliza-

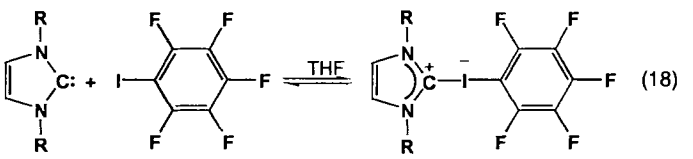

tion in the imidazole ring indicates a formal charge assignment opposite to that in halonium methylides. These halonium methylides ($RX^+ \leftarrow {}^-CR_2$) with a small C-X-C angle are typically formed from reactions of electrophilic carbenes with halogen centers.

Upon complexation to a Lewis acid, electron density at C^2 decreases, and ylidic mesomeric structures become more important. In this sense a (hetero)aromatic imidazolium salt is an adduct of free carbene with the strongest Lewis acid, a proton. By allowing 1,3-dimesityl-2,3-dihydro-1*H*-imidazol-2-ylidene to react with the corresponding imidazolium salt, a linear 3c–4e C-H-C hydrogen bridge is formed [172.5°; Eq. (19)].[97] This

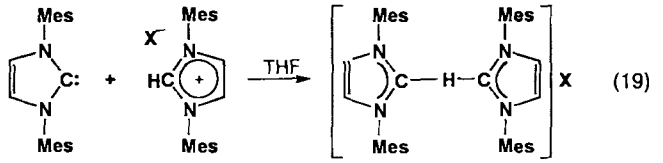

X = PF_6, CF_3SO_3

"proton complex" has two significantly different C–H bond lengths (202.6(45) versus 115.9(45) pm, X-ray diffraction). It was suggested that mesityl substituents favor the formation of homoleptic bis(carbene) adducts because of the "cavity" seen in the structure of the 2,3-dihydro-1*H*-imidazol-2-ylidene.

There is only one example of backbone functionalization of N-heterocyclic carbenes. A new type of bimetallic complex was obtained by *cis*-osmylation of the isolated double bond of 1,3-dimethyl-2,3-dihydro-1*H*-imidazol-2-ylidene in $[M(CO)_5$(carbene)] (M = Cr, Mo, W) with osmium tetraoxide [Eq. (20)]. Upon oxidation the ylidene ligand becomes slightly more nucleophilic. There is no interaction between Os^{IV} and Cr^0, as seen from cyclic voltammetry.[98]

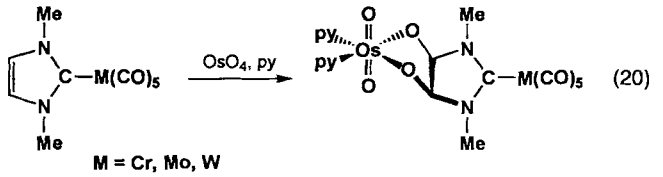

M = Cr, Mo, W

3.5. Electronic Properties of N-Heterocyclic Carbene Ligands

It has been standard textbook knowledge for several decades that divalent carbon species $:CR^1R^2$ exhibit σ-donor and π-acceptor properties upon binding to transition metals. In principle, a "double bond" situation represented in formula **1** results, depending somewhat on the nature of R^1 and R^2. In all cases, however, metal–carbon bonds shorter than single bonds in metal–alkyl complexes are present. Unfortunately, there is only little thermodynamic data on metal–carbene bonds. With regard to the reactivity of the metal-bonded carbon fragment, the literature discriminates between electrophilic (Fischer) and nucleophilic (Schrock) carbenes.[2] In many cases the carbene (alkylidene) ligand can be transferred to other substrates; cyclopropanation and metathesis of olefins are probably the most prominent examples.[3] A general reaction scheme is not easy to produce since particularly the nature of the metal influences the reactivity of the carbene. However, metal–carbene complexes often react with cleavage of the metal–carbon bond. For this reason the common carbenes $:CR^1R^2$ (R^1, R^2 = H, alkyl, aryl, alkoxy, amino) are not considered as ligands that would survive the standard reaction conditions of organometallic catalysis.

The quite distinctive role of diamino-substituted carbenes (singlet ground state) was anticipated in coordination chemistry, and the classification into "Fischer-" and "Schrock-type" complexes ($[Cr(CO)_5\{C(OMe)Ph\}]$ and $[(\eta^5\text{-}C_5H_5)_2Ta(CH_3)(CH_2)]$, respectively) does not hold for N-heterocyclic carbenes of the imidazole and imidazolidine series. At first glance these may be classified as Fischer-type compounds which are formally derived from rather "soft" nucleophilic carbenes and are susceptible to nuleophilic attack at the carbene carbon.

Conventional carbenes are rather weak σ donors. Their bonding to metals depends on pronounced π backbonding; metals in low formal oxidation states therefore prevail in this domain of coordination chemistry. The CO stretching frequencies in metal–carbonyl complexes are a sensitive probe for electronic ligand properties. The differences between single-faced two-electron ligands in a series of isoelectronic compounds $[M(CO)_nL]$ can be derived from the IR spectra. The ratio of σ donors to π acceptors (that is, the electron density induced at the metal center) of $Fe(CO)_4$-bonded heteroatom-substituted carbenes increases in the order $:C(OR)R < :C(NR)R < :C(NR)_2$ ≙ imidazolidine-2-ylidene ≙ 2,3-dihydro-1*H*-imidazol-2-ylidene (see Table 2).

The stretching frequencies of the *trans*-CO ligands in carbene complexes $[M(CO)_nL]$ are identical within the limit of error with those of imidazolidine-2-ylidene and 2,3-dihydro-1*H*-imidazol-2-ylidene complexes (Table 1 and 2). The latter induces a remarkably higher electron density at the metal center than the basic trimethylphosphane.[12a, 65]

Table 1. The ν(CO) absorptions [cm^{-1}] in carbene complexes $[Cr(CO)_5L]$ [139].

L	$A_1^{(1)}$	$A_1^{(2)}$	E
$:C(OCH_3)C_6H_5$	1963	2062	1952
$:C(CH_3)(NHC_6H_5)$	1937	2057	1937
$:C(NH_2)C_6H_5$	1921	2058	1944
imidazolidine-2-ylidene	covered by E	2061	1928
2,3-dihydro-1*H*-imidazol-2-ylidene	1897	2056	1925

Table 2. The ν(CO) absorptions [cm^{-1}] in carbene complexes $[Fe(CO)_4L]$ [139].

L	A_1	A_1	E
$:C(NHCH_3)_2$	1967	2046	1931, 1925
imidazolidine-2-ylidene	1963	2044	1929
2,3-dihydro-1*H*-imidazol-2-ylidene	1959	2040	1938

The π-acceptor ability of N-heterocyclic carbenes is negligible, and lies between that of nitriles and pyridine, as shown for the examples in Table 3. The π-acceptor character decreases

in the order NO > CO > RNC > PF_3 > $P(OR)_3$ > $P(aryl)_3$ > $P(alkyl)_3$ > RCN > N-heterocyclic carbenes > py. Tables 4 and 5 compare further IR characteristics of the complexes discussed here.

Table 3. The ν(CO) absorptions [cm^{-1}] in carbene complexes *fac*-[$MoL_3(CO)_3$] [139, 140].

[$Mo(PPh_3)_3(CO)_3$]	1835	1934
[$Mo(CH_3CN)_3(CO)_3$]	1783	1915
[$Mo(CH_3CN)(L-L)(CO)_3$][a]	1780	1896
[Mo(py)(L–L)$(CO)_3$][a]	1772	1891
[$MoL_3(CO)_3$][a]	1764	1881
[$Mo(py)_3(CO)_3$]	1746	1888

[a] L and L–L are heterocyclic mono- and dicarbene ligands, respectively.

Table 4. The ν(CO) absorptions in *trans*-[$RhL^1L^2(CO)X$] complexes [65].

L^1, L^2[a]	X	$\tilde{\nu}$ [cm^{-1}] (medium)
L^{Me}, L^{Me}	Cl	1924 (KBr)
L^{Cy}, L^{Cy}	Cl	1929 (KBr)
PCy_3, PCy_3	Cl	1939 (benzene)
PMe_3, PMe_3	Cl, Br, I	1957, 1958, 1960 (benzene)
L^{CHPh_2}, PPh_3	Br	1968 (KBr)
PPh_3, PPh_3	Cl	1983 (benzene)
$L^{CHPh_2}, P(OPh)_3$	Br	1994 (KBr)
$P(C_6F_5)_3, P(C_6F_5)_3$	Cl	2003 (benzene)
$P(OPh)_3, P(OPh)_3$	Cl, Br	2018, 2020 (benzene)

[a] L^{Me} = 1,3-Dimethyl-2,3-dihydro-1*H*-imidazol-2-ylidene, L^{Cy} = 1,3-bis(cyclohexyl)-2,3-dihydro-1*H*-imidazol-2-ylidene, L^{CHPh_2} = 1,3-bis(diphenylmethyl)-2,3-dihydro-1*H*-imidazol-2-ylidene.

Table 5. Average CO force constants *f* [N cm^{-1}] in [$M(CO)_nL_m$] complexes [12].

	L: CO	PMe_3	[a]
[$Ni(CO)_3L$]	16.73	15.65	15.45
[$Fe(CO)_4L$]	16.72	15.76	15.62
[$Cr(CO)_5L$]	16.98	15.77	15.25
[$Mo(CO)_5L$]	16.65	15.66	15.31
[$W(CO)_5L$]	16.52	15.75	15.38
cis-[$W(CO)_4L_2$]	16.52	15.16	14.61

[a] 1,3-Dimethyl-2,3-dihydro-1*H*-imidazol-2-ylidene.

"Conventional" carbene ligands such as alkoxy(alkyl)-carbenes are similar in their bonding properties (with respect to low-valent metals) to carbon monoxide, and N,O-heterocyclic carbenes may also act as π acceptors.[12c–e] N-heterocyclic carbenes, however, very much resemble electron-rich alkylphosphanes and N donors such as nitriles and pyridine.[12a, b]

4. Main Group Element and Rare Earth Metal Complexes

With this background it was not surprising that metals incapable of π backbonding also coordinate these N-heterocyclic carbenes as nucleophilic two-electron ligands, which are in this sense similar to the distant relatives amines and ethers. Both the genesis of these complexes and their structural data suggest that they could be viewed as donor adducts, just like ammonia and ether complexes.

4.1. Alkaline Earth Metals and Zinc

The chemistry of beryllium shows unique aspects among the alkaline earth metals, since Be^{2+} is one of the hardest Lewis acids known. Tetrahedral adducts of the formula $BeCl_2 \cdot L_2$ formed upon treatment of $BeCl_2$, a polymer in the solid state, with donors. Use of the sterically unencumbered 1,3-dimethyl-2,3-dihydro-1*H*-imidazol-2-ylidene (L^{Me}) resulted in the formation of complexes $BeCl_2(L^{Me})_2$ and [$BeCl(L^{Me})_3$]Cl (Figure 5).[99] An X-ray diffraction analysis of the latter showed

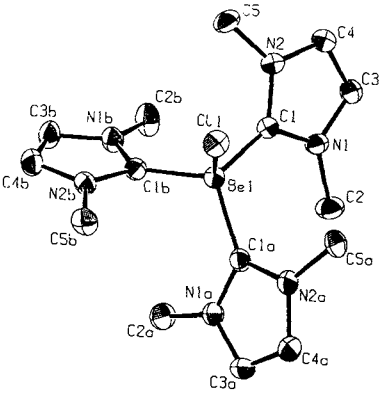

Figure 5. Structure of the cation $[BeCl(L^{Me})_3]^+$ in the chloride salt.

distorted tetrahedral coordination at the beryllium atom. With 1.822(3) (1.807(3) Å) the $Be-C_{carbene}$ distances are in the range of Be–alkyl or Be–aryl single bonds (1.708(6)–1.85(3) Å), and under consideration of the different ionic radii they can be compared to Be–O and Be–N bonds. The Be–Cl bond (2.083 Å) is significantly longer than in other tetravalent complexes and in $BeCl_2$. An excess of free carbene did not displace the second chloride ion. Complete solvation to yield dicationic complexes was only observed for $[Be(H_2O)_4]^{2+}$ and $[Be(NH_3)_4]^{2+}$.

Monomeric and dimeric 1:1 adducts of Mg^{2+} and Zn^{2+} were obtained from the reaction of diethyl zinc and diethyl magnesium with 1,3-diadamantyl- and 1,3-dimesityl-2,3-dihydro-1*H*-imidazol-2-ylidene (L^{Mes}, L^{Ad}) [Eq. (21)].[100] The solid-state

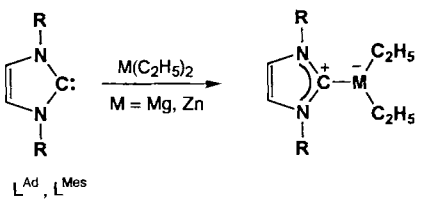

L^{Ad}, L^{Mes} (21)

structure of $(C_2H_5)_2Zn \cdot L^{Ad}$ shows trigonal-planar coordination at zinc. The angle between the coordination sphere of zinc and the imidazole plane is 81.6°. Mesityl groups do not provide as much steric protection as adamantyl groups, as seen in the dimeric magnesium adduct $(C_2H_5)_2Mg \cdot L^{Mes}$ with bridging ethyl groups. The ^{13}C NMR resonances of the imidazole C^2 nuclei are shifted upfield by 25–30 ppm. There is evidence that in THF the trivalent adducts are coordinatively saturated by THF.

The metal–donor bonds are predominately ionic and more labile in complexes of the heavier analogues of beryllium and

magnesium. 2,3-Dihydro-1*H*-imidazol-2-ylidene complexes of calcium, strontium, and barium were nevertheless obtained for bis(trimethylsilyl)amides $[M\{N(SiMe_3)_2\}_2(thf)_2]$ (M = Ca, Sr, Ba) upon displacement of the two THF molecules by two equivalents of 1,3-dimethyl-2,3-dihydro-1*H*-imidazol-2-ylidene [Eq. (22)]. The solubility and stability of the adducts decrease

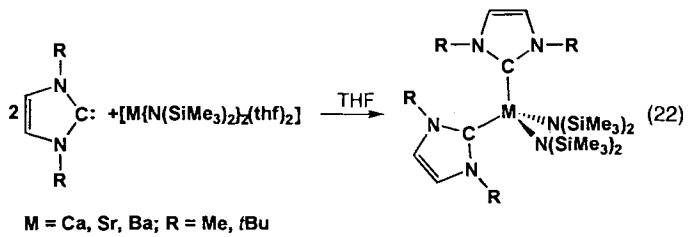

(22)

M = Ca, Sr, Ba; R = Me, *t*Bu

from calcium to barium. Whereas the calcium and strontium adducts can be isolated in the solid state at −36 °C, the barium adduct is stable only in solution. For the barium adduct a dissociation equilibrium is observed. Upon complexation to strontium and barium the resonances of the carbene centers are only slightly shifted to higher field (δ = 198 and 203, respectively).[101]

4.2. Boron, Aluminum, and Gallium

Borane adducts with (formally) neutral carbon donors such as carbon monoxide, isonitriles, or phosphane ylides are well established. Since conventional carbene complexes show pronounced metal-to-ligand π backdonation, electron-poor (coordination) fragments are not well suited for stabilizing carbene ligands. However, N-heterocyclic carbenes do not depend on backdonation due to delocalization of the nitrogen lone pair; 1:1 adducts with BH_3 or BF_3 (Scheme 2) are thermally stable

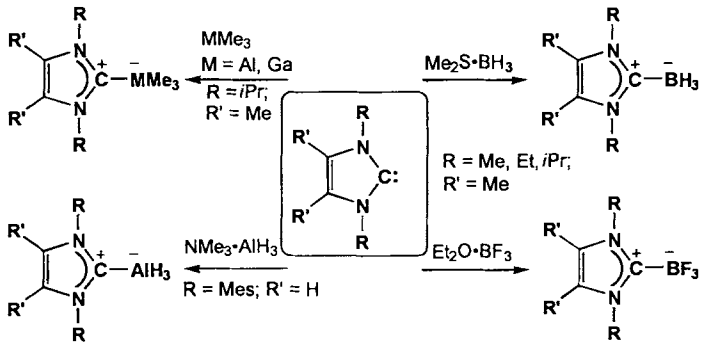

Scheme 2. Adducts of 2,3-dihydro-1*H*-imidazol-2-ylidenes and Lewis acids MR_3 (M = Al, Ga; R = H, Me), BH_3, and BF_3.

and can even be sublimed without decomposition. The ^{11}B NMR chemical shift of 1,2,3,4-tetramethyl-2,3-dihydro-1*H*-imidazol-2-ylidene → BH_3 at δ = −35 is typical for ylide–borane adducts, and between that of amine– and phosphane–borane adducts. The $^1J(^1H,^{11}B)$ coupling constant, however, is very similar to that of the anionic analogue $[(C_6H_5)BH_3]^-$. Both X-ray analysis and ab initio calculations on these borane adducts imply alternating bond lengths and only weak π interactions between the N-C-N moiety and the C–C π systems within the five-membered rings.[102] When 1,3-dialkyl-2,3-dihydro-1*H*-imidazol-2-ylidenes were allowed to react with 2-bromo-2,3-dihydro-1*H*-1,3,2-diazaboroles, borolylimidazolium salts formed under displacement of the halide.[143] Borane adducts are also known for N,O-heterocyclic carbenes.[144] A silylene–borane adduct was reported recently.[145]

When 1,3-bis(2,4,6-trimethylphenyl)-2,3-dihydro-1*H*-imidazol-2-ylidene was allowed to react with $H_3Al\cdot NMe_3$, a 1:1 adduct with AlH_3 formed.[103] The upfield shift of the ^{13}C NMR signal for the carbenoid carbon center is, agreement with π delocalization, even more pronounced (δ = 175.3; parent carbene: δ = 219.7; imidazolium salt: $\delta \approx 136$). 1,3-Diisopropyl-4,5-dimethyl-2,3-dihydro-1*H*-imidazol-2-ylidene adducts with Me_3Al or Me_3Ga are also stable. The metal–$C_{carbene}$ bonds in the monomeric, tetrahedrally coordinated adducts are significantly longer than the metal–C_{methyl} bonds (Al–$C_{carbene}$ 2.124(6) Å; Al–C_{methyl} 1.940(5) and 2.062(7) Å). In the trimethylaluminum dimer, Al_2Me_6, the Al–C_{bridge} bond length is 2.14(1) Å (3c–2e alkyl bridge), and a distance of 1.97(1) Å is found for the Al–$C_{terminal}$ bonds.[104]

4.3. Carbon and Higher Homologues

The pronounced ability of the N-heterocyclic fragment to take on a formal positive charge is demonstrated by ylidic olefins (exocyclic C_{ylide}–C bond), which form upon deprotonation of pentamethylimidazolium salts [Eq. (23)]. The chemical

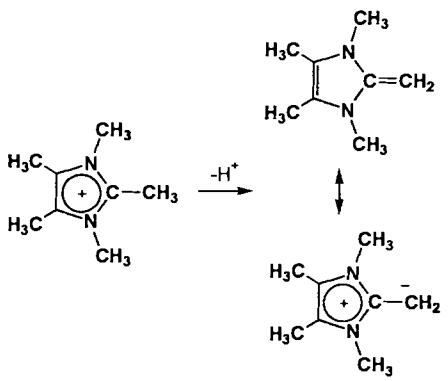

(23)

reactivity of the methylene carbon atom in $C_8H_{14}N_2$ and the strong shielding in the ^{13}C NMR signal (δ = 40.2) reveal high electron density on the methylene carbon atom and extended charge separation.[105a] The exocyclic double bond is extremely polarized due to a combination of the enamine structure and π delocalization; it acts as a strong ylidic donor towards boranes and metal–carbonyl complexes.[105b,c] In these complexes the exocyclic double bond is clearly bound to the metal in the otherwise unusual end-on mode. This ylidic olefin also allowed the preparation of mono adducts with 4f elements such as La^{III}, Nd^{III}, and Y^{III} from $Ln[N(Me_3Si)_2]_3$ (Ln = La, Nd) and $[(C_8H_8)Y(C_5Me_5)]$, respectively. Whereas coordination to low-valent metal–carbonyl complexes ($[M(CO)_5(C_8H_{14}N_2)]$, M = Mo, W) entails a significant high-field shift of the

methylene carbon resonance ($\Delta\delta \approx 45$), there is almost no change in the exocyclic ylidic bond upon coordination to lanthanide ions.[105d] Like these ylidic olefins, the 2-iminoimidazolines[146a] with exocyclic C_{ylide}–NH bonds display interesting chemistry.[147b,c]

Similar to organophosphanes, N-heterocyclic carbenes form stable adducts with carbon disulfide. In the crystal structure the plane of the CS_2 fragment is perpendicular to the five-membered ring (decoupled π systems).[105e,f] Strongly polarized structures are most clearly observed in the mono adducts $GeI_2 \cdot L$ (**24**, L = 1,3-dimesityl-2,3-dihydro-1*H*-imidazol-2-ylidene) and $SnR_2 \cdot L$ (**25**, L = 1,3-diisopropyl-4,5-dimethyl-2,3-dihydro-1*H*-

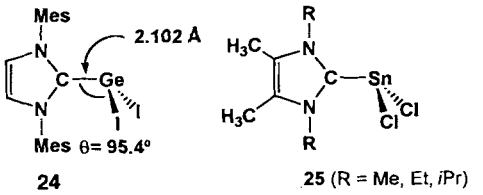

imidazol-2-ylidene; R = Cl, 2,4,6-iPr$_3$C$_6$H$_6$), which were used as models for the dimerization of singlet carbenes along a non-least-motion pathway.[106,107] The heavier main group elements show pronounced pyramidalization of the coordination sphere (sum of angles at Ge 290°, at Sn 282°, C-Ge-I 95.4 and 100.1°) and the two halves of the adducts are twisted with respect to one another. The ^{13}C NMR resonance of the carbene carbon atom in the GeI_2 adduct is shifted upfield by 61 ppm, and the N-C-N angle opened from 101.4 to 107.0°. Long C–Ge and C–Sn distances (2.102 and 2.290(5) Å, respectively) suggest that the adducts be described as Lewis acid–base adducts. Tetravalent dicarbene adducts of the less Lewis acidic $SnCl_2$ with sterically unencumbered carbenes are very insoluble.

The chemistry of hypervalent silicon compounds is dominated by complex anions with sixfold coordination. Substituents are in most cases negatively charged organic alkyl or aryl residues or fluoro, alkoxy, or hydrido ligands. A new way of forming element–carbon bonds was opened with the isolation of nucleophilic carbenes. The reaction of carbenes with main group element halides may yield several possible products (Scheme 3): a) neutral or ionic compounds resulting from simple adduct formation or displacement of a halide ion, or b) reduction of the central element with formation of 2-haloimidazolium ions. Lewis acidic silanes such as tetrachlorosilane as well as diaryl- or dialkyldichlorosilanes form monomeric and neutral pentavalent 1:1 adducts with 2,3-dihydro-1*H*-imidazol-2-ylidenes. The $SiCl_4$ adducts are rather labile. The less Lewis acidic trimethylsilanes Me_3SiCX are inert or, such as Me_3SiI, form ionic 2-(trimethylsilyl)imidazolium salts.[107]

The tendency to form complexes is more pronounced for tetravalent tin than for silicon. Pentavalent tin adducts are prepared from diphenyldichlorostannane. The solid-state structure of $Sn(C_6H_5)_2Cl_2 \cdot L$ (L = 1,3-diisopropyl-4,5-dimethyl-2,3-dihydro-1*H*-imidazol-2-ylidene) shows that the three organic substituents adopt the equatorial positions of a distorted trigonal bipyramid. With 2.179(3) Å the Sn–$C_{carbene}$ bond is longer than the Sn–Ph bonds (2.122(5) and 2.139(3) Å). The ^{119}Sn NMR resonance is shifted to higher field by about 30 ppm relative to that of the phosphane adducts.[107] Allowing 1,3-dimesityl-2,3-dihydro-1*H*-imidazol-2-ylidene to react with suitable phosphorous precursors yielded adducts with two- and six-coordinate phoshorus centers ($L^{Mes} \cdot PF_4Ph/L^{Mes} \cdot PPh$) which were also structurally characterized.[147]

4.4. Sulfur, Selenium, and Tellurium

Ylidic structures with a positively charged imidazolium group have spotlighted a new perspective in organotellurium chemistry. In general the existence of tellurocarbonyl compounds such as telluroaldehydes or telluroketones can only be proven by stabilization with metals. In contrast, 2,3-dihydro-1*H*-imidazol-2-ylidenes readily react with elemental sulfur, selenium, and tellurium to form stable adducts [Eq. (24)].[108] According to

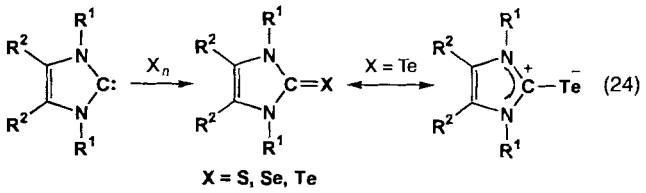

(24)

the crystal structure analysis the formal C_{ylide}–Te double bond is almost as long as a single bond (2.087(4) Å). The stability of this compound, in contrast to the analogous selenium compound, results from the decrease in double-bond character. The signals in the ^{125}Te and ^{77}Se NMR spectra of the telluro- and selenoimidazolines, respectively, resonate upfield with respect to that of other chalcocarbonyl compounds. This shielding is explained by π delocalization. Oxidation of the sulfur imidazoline with iodine yields a charge-transfer complex; in the cases of the seleno and telluroimidazolines, however, structures with covalent bonds are formed; the latter exists as a dimer. Chalcogenoimidazolines also serve as ligands in transition metal complexes.[148]

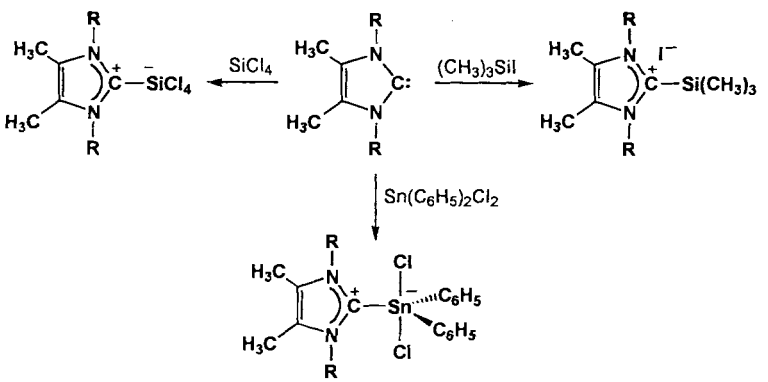

Scheme 3. Possible reactions of 4,5-dimethyl-2,3-dihydro-1*H*-imidazol-2-ylidene with main group elements. R = Me, Et, *i*Pr.

1,3,4-Triphenyl-4,5-dihydro-1*H*-1,2,4-triazol-5-ylidene similarly reacts with chalcogenes such as oxygen, sulfur and selenium to give the respective triazolinone, triazothion, and triazoselenone. The free triazolylidene also inserts into the O–H, N–H, and S–H bonds of alcohols, amines, and thiols, but no case of insertion into C–H bonds has been reported yet.[109] Reaction with protonation or alkylation occurs with acids and trialkyoxonium salts, respectively. The products formed from reaction with activated double bonds such as those in fumaric and maleic esters, amides, and nitriles suggest [2+1] cycloaddition with subsequent 1,2-hydrogen shift. Nonactivated double bonds are not attacked. Heterocumulenes (e. g. CS_2, $C_6H_5N{=}C{=}O$, and $C_6H_5N{=}C{=}S$) are also susceptible to nucleophilic attack by the triazol-derived carbene.

4.5 Rare Earth Metals

Until a few years ago isonitriles were the only neutral ligands in organolanthanide chemistry that coordinate through just one carbon atom. In view of the isolation of stable alkaline earth metal complexes of nucleophilic carbenes, it was not surprising that rare earth metals, which are nearly incapable of π backbonding, also coordinate N-heterocyclic carbenes (Scheme 4). 2,3-Dihydro-1*H*-imdidazol-2-ylidenes are not reduced by cyclopentadienyl precursors of Yb^{II} or Sm^{II}: 1,3,4,5-Tetraalkyl-2,3-dihydro-1*H*-imidazol-2-ylidenes readily replace the THF molecule in $[(\eta^5\text{-}C_5R_5)_2M^{II}(thf)]$ (M = Yb, Sm). The mono- and bis(carbene) adducts obtained $[(\eta^5\text{-}C_5R_5)_2Yb^{II}(L)]$ and $[(\eta^5\text{-}C_5R_5)_2Sm^{II}(L)_n]$ ($n = 1$ or 2) are more stable to air and moisture than the THF adducts.[110–113]

In the solid-state ^{13}C NMR spectra of the diamagnetic and thermally very stable ytterbium complexes, the resonances for the ligating carbon atom are shifted to higher field by only 10 ppm with respect to that of the free carbenes. Solid-state structures were determined in two cases. With 2.552(4) and 2.598(3) Å the $Yb{-}C_{carbene}$ bond lengths in the pseudotrigonal complexes are in the range of "elongated single bonds".[111, 112] The analogous monocarbene samarium(II) complexes are also high-melting stable solids. Addition of a second equivalent of 1,3,4,5-tetraalkyl-2,3-dihydro-1*H*-imidazol-2-ylidene to $[(\eta^5\text{-}C_5Me_5)_2Sm^{II}(L)]$ yielded the bis(carbene) adduct $[(\eta^5\text{-}C_5Me_5)_2Sm^{II}(L)_2]$. The X-ray structure analysis of this complex shows pseudotetrahedral coordination and rather long metal–$C_{carbene}$ bonds (2.837(7) and 2.845(7) Å). With 101.1(6) and 101.9(6)° the internal valence angles $N\text{-}C_{carb}\text{-}N$ are very close to that for free carbenes.[110]

Seven-coordinate monocarbene adducts of Eu^{III} and Y^{III} were prepared from the dionato precursors $[Eu(thd)_3]$ and $[Y(thd)_3]$ (thd = 2,2,6,6-tetramethylheptane-3,5-dionate).[110] In the ^{13}C NMR spectrum the former $C_{carbene}$ in $[Y(thd)_3L]$ resonates at $\delta = 199.4$ with a $^1J(Y,C)$ coupling constant of 33 Hz. Although the metal–carbene bond lengths are longer for lanthanides than for s-, p-, and d-block metals, the carbene does not dissociate on the NMR time-scale. With 2.663(4) Å the $Eu{-}C_{carbene}$ bond length in $[Eu(thd)_3L]$ is similar to Pr^{III}–C and Sm^{III}–C distances in isonitrile complexes.

Lanthanide amides (with or without additional donors such as THF) are also versatile starting compounds for carbene complexes. Addition of one or two equivalents of 1,3-dimethyl-2,3-dihydro-1*H*-imidazol-2-ylidene to $[Y\{N(SiHMe_2)_2\}_3(thf)_2]$ yielded $[Y\{N(SiHMe_2)_2\}_3(L^{Me})]$ and $[Y\{N(SiHMe_2)_2\}_3(L^{Me})_2]$, which were both structurally characterized. The $Y{-}C_{carbene}$ distances are 2.55(1) and 2.648(8)/2.671(9) Å, and in the range of elongated Y–C single bonds. The bond lengths compare well to other lanthanide–carbene distances. Monocarbene adducts of lanthanum $[La\{N(SiMe_3)_2\}_3(L^{Me})]$ are available from $[La\{N(SiMe_3)_2\}_3]$.[114, 115]

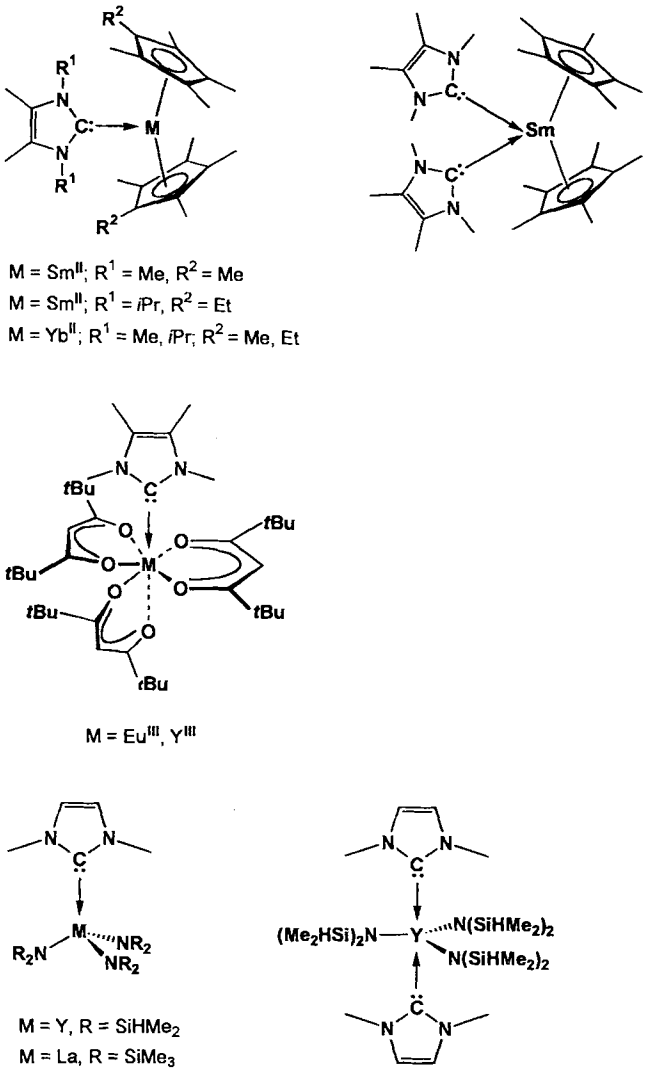

Scheme 4. Complexes of 2,3-dihydro-1*H*-imidazol-2-ylidenes and rare earth metals.

5. Transition Metal Complexes

Transition metal complexes of heterocyclic carbenes are accessible by three different routes (Scheme 5). Most common is the treatment of simple metal salts or coordination compounds (neutral, cationic, or anionic) with azolium precursors (route A). The coordination properties of the anion X^- determine whether it enters the inner coordination sphere of the resulting carbene complex; the most commonly employed azolium iodides normally yield iodo complexes in which the iodide

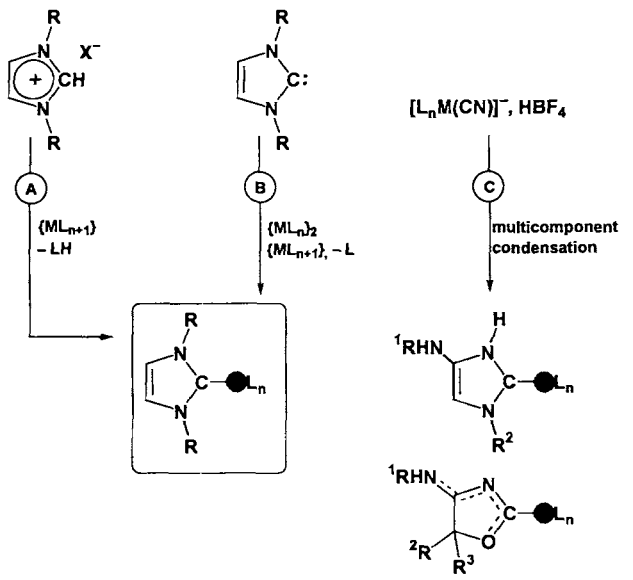

Scheme 5. Synthesis of transition metal carbene complexes by A) in situ deprotonation of azolium salts, B) reaction with free N-heterocyclic carbenes, or C) reaction with anionic metal–cyano complexes

has replaced other ligands (e. g. chloride, bromide, acetate, carbon monoxide).

This is certainly not the case when non- or weakly coordinating anions are employed, for example tetraphenylborate or hexafluorophosphate. In some cases the metal complexes act as a reducing agent for imidazolium salts (evolution of hydrogen). The scope of heterocyclic carbenes which can be directly generated at metal centers is more varied following route A because of the broad variety of CH-acidic, cationic heteroaromatic compounds (Scheme 6).

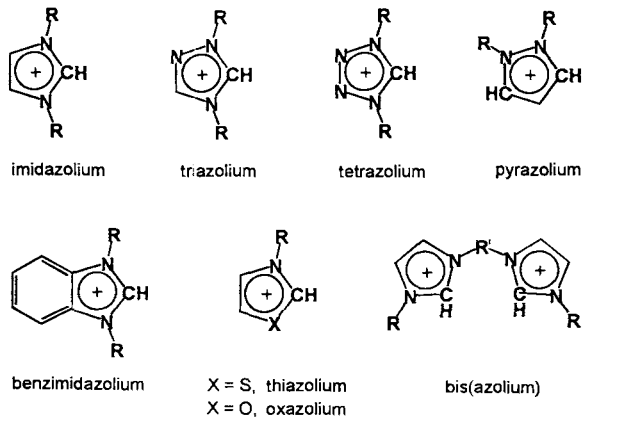

Scheme 6. Heteroaromatic azolium salts which can be deprotonated in situ to give coordinated N-heterocyclic carbenes.

It is useful to have a basic ligand in the precursor that effects deprotonation of the azolium salt. C-Deprotonation of azolium salts is also feasible with (anionic) carbonylmetalates, which are normally generated through typical Hieber base reactions. Both variants were reported in 1968 for the first time: Wanzlick's homoleptic mercury(II) carbene complex and Öfele's chromium(0) complex were already mentioned [see Eqs. (2) and (1)]. Palladium(II) complexes were prepared similarly from the metal acetate [Eqs. (25) and (26)].[13, 116]

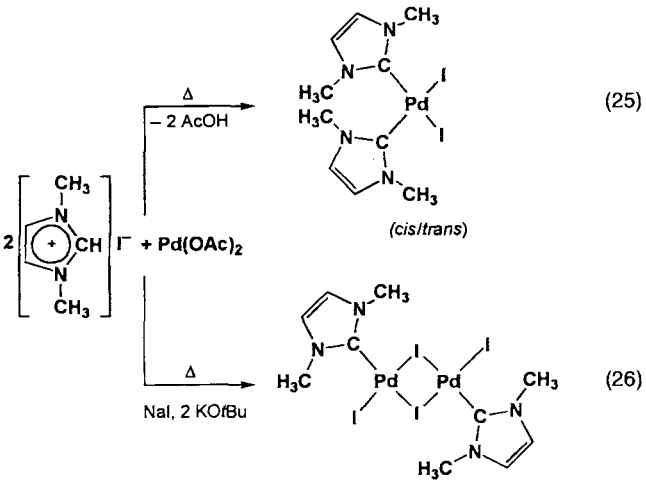

(25)

(26)

Öfele pointed out that this procedure is not limited to imidazolium salts. Also triazolium, tetrazolium, benzimidazolium, and even the less acidic pyrazolium salts yield complexes of the respective N-heterocyclic carbene ligands. Other metal bases from elements of Groups 6–8 were identified as suitable precursors, for example metalates of chromium, molybdenum, and tungsten, some of which contain μ-hydroxo or μ-alkoxo bridges (Table 6). In the case of the di- and tetranuclear complexes, the acidic azolium protons are not transferred to the hydroxy or methoxy ligands but reduced to hydrogen [Eq. (27)].[63]

Table 6. Multinuclear Group-6 metalates capable of reducing azolium salts with formation of carbene ligands.

		Metal M	Product [a]
dinuclear	$[M_2(CO)_{2n}]^{2-}$	Cr, Mo, W	$[M(CO)_5L]$
	$[M_2(CO)_6(\mu\text{-}OH)_3]^{2-}$	Cr	$[M(CO)_4L_2]$
	$[M_2(CO)_6(\mu\text{-}OH)_3]^{3-}$	Mo, W	$[M(CO)_4L_2]$
tetranuclear	$[M_4(CO)_{12}(\mu\text{-}OMe)_4]^{4-}$	Cr, Mo, W	$[M(CO)_4L_2]$

[a] L = carbene ligands derived from imidazole, triazole, tetrazole, benzimidazole, or pyrazole.

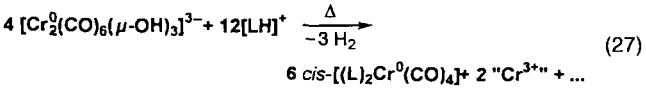

(27)

$K[Re_2(CO)_6(\mu^2\text{-}OR)_3]$ was successfully applied to synthesize dicarbene complexes *fac*-$[Re(CO)_3(L)_2I]$, and $Na_2[Fe_2(CO)_8]$ was a suitable precursor for carbene complexes of the type *trans*-$[Fe(CO)_3L_2]$ and *cis*-$[Fe(CO)_3(L-L)]$. Again the metal precursor was partially oxidized during the synthesis.[63]

A variety of rhodium and iridium complexes were synthesized from easily available μ-alkoxy complexes and azolium salts. Carbene-complex formation is exclusively effected by proton transfer to the metal-bound ethoxy group (Scheme 7). The reactions seem to be thermodynamically controlled, as further acidic protons in the azolium unit did not inhibit carbene-complex formation. Even when an excess of base and azolium salt was employed, neutral monocarbene complexes of the type [M(η^4-1,5-cod)LX] (M = Rh, Ir; cod = cyclooctadiene) are formed selectively in almost quantitative yield.[65] On the other hand, free carbenes displaced the halide ligands to yield cationic complexes of the type $[Rh(\eta^4\text{-}1,5\text{-cod})L_2]^+X^-$ (Scheme 7). The acidic protons are therefore transferred to metal-bound ethoxide groups exclusively. However, cationic dicarbene complexes are also accessible when the imidazolium halides are first transferred to imidazolium ethoxides salts with potassium ethoxide in ethanol (2-ethoxyimidazoles are not observed).[62]

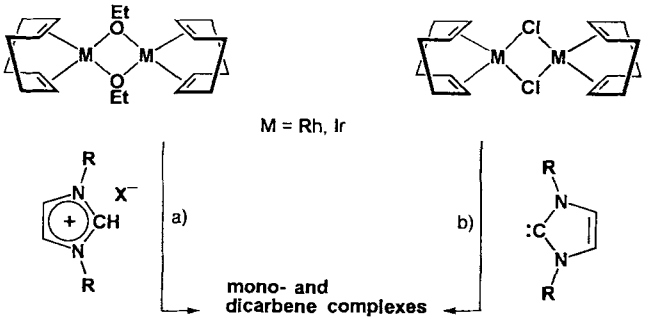

Scheme 7. Mono- and diylidene complexes of Rh and Ir are accessible a) directly from metal alkoxides and azolium salts or b) from free N-heterocyclic ylidenes and dinuclear μ-chloro complexes.

According to route B in Scheme 5, nucleophilic N-heterocyclic carbenes may replace other ligands, for example a two-electron ligand (such as halide, carbon monoxide, or acetonitrile) in the complex. From carbonyl complexes such as $[M(CO)_6]$ (M = Cr, Mo, W), $[Fe(CO)_5]$, or $[Ni(CO)_4]$, one or two molecules of carbon monoxide are displaced. Further substitution requires photolytic conditions.[12a, b]

Two-electron donors are displaced by 2,3-dihydro-1*H*-imidazol-2-ylidenes in smooth reactions from the adducts $[(Me_2S)MCl]$ (M = Cu, Ag, Au), $[MCl_4(thf)_2]$ (M = Ti, Zr, Hf), $[MCl_4(py)_2]$ (M = Nb, Ta), and $[VCl_2(tmeda)_2]$.[150] Free N-heterocyclic carbenes thus act as conventional two-electron donors, and react with a broad variety of precursors. Bridging moieties of dinuclear precursor complexes are split by the carbene. Dinuclear halo- or acetato-bridged complexes of Ru, Os, Rh, Ir, and Pd yield mononuclear carbene complexes in excellent yields.[13, 34, 37, 61]

Acyclic carbenes with heteroatoms can be generated at the metal centers by transforming other C-bound ligands, for example isonitriles [Eqs. (28), (29)]. Nucleophilic attack of an alcohol or an amine at the electrophilic carbon atom starts the reaction sequence.[117] The four-component condensation (4CC) following route C, established by Fehlhammer et al., yielded the ligand framework of 2,3-dihydro-1*H*-imidazol-2-ylidene. Metal complexes of hydrogen cyanide (normally generated from anionic metal–cyano precursors) were treated successively with an aldehyde, an isocyanide and an amine to form (ring-substituted) N-heterocyclic carbene complexes. Because of the isolobal analogy between an oxygen atom and a ML_5 d^6 transition metal complex fragment, this route represents the organometallic analogue of Ugi's 4CC reaction to hydantoins.[118] The same principle can be employed to generate oxazolidine-derived carbenes bound to transition metals by a 3CC [2+1+2] cycloaddition of hydrogen isocyanide metal complexes, isocyanides, and carbonyl compounds [see Eq. (28)].[119, 120]

$$[M(CN)(CO)_5]^- + HBF_4 + CNR^1 + R^2R^3C{=}O \xrightarrow[-BF_4]{3\,CC} \quad (28)$$

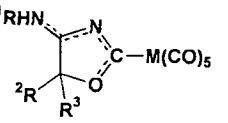

$$[Cp(CN)_2(CO)Fe]^- + CNtBu + PhCHO + PhNH_3Cl \xrightarrow{4\,CC} \quad (29)$$

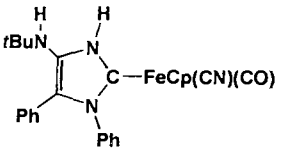

Less general routes were mentioned in the recent literature. For example, Matsumara reported that palladium und rhodium complexes of six-membered 2,6-diazocarbenes result in a most peculiar manner from 10-S-3-tetraazapentalene derivatives [Eq. (30)].[121] Sellmann et al. obtained nickel and platinum complexes with tridentate dibenzenethiolate-imidazolidine-2-ylidene ligands according to Equation (31).[122] Furthermore, Ghosh discussed the analogy between the "N-disordered porphyrines" [Eq. (32), Ar = p-Tolyl] and Arduengo carbenes.[123]

6. Structural Chemistry

The structure of bis(1,3-dimethyl-2,3-dihydro-1*H*-imidazol-2-ylidene)mercury(II) perchlorate was determined[151] three years after its synthesis by Wanzlick in 1968.[8] In the twenty years since 1971 only a few solid-state structures of this type were reported in the literature. On the other hand, there are many examples of structurally characterized complexes with C–C-saturated carbene ligands not considered in this review.

The data rather suggest a bonding order near, or even below, one. In comparison to Schrock- and Fischer-type carbene complexes, imidazole-derived ylidenes show long metal–carbon bonds. This is expected from the contribution of the ylidic resonance structures to the free 2,3-dihydro-1*H*-imidazol-2-ylidenes. Significant metal-to-carbon backdonation can only be observed in linear homoleptic bis(1,3-dimesityl-2,3-dihydro-1*H*-imidazol-2-ylidene) complexes $[M(L^{Mes})_2]$ of of zero-valent nickel and platinum. The $Ni-C_{carbene}$ distances are 0.15 Å shorter than in $[Ni(CO)_2(L^{Mes})_2]$, which cannot be

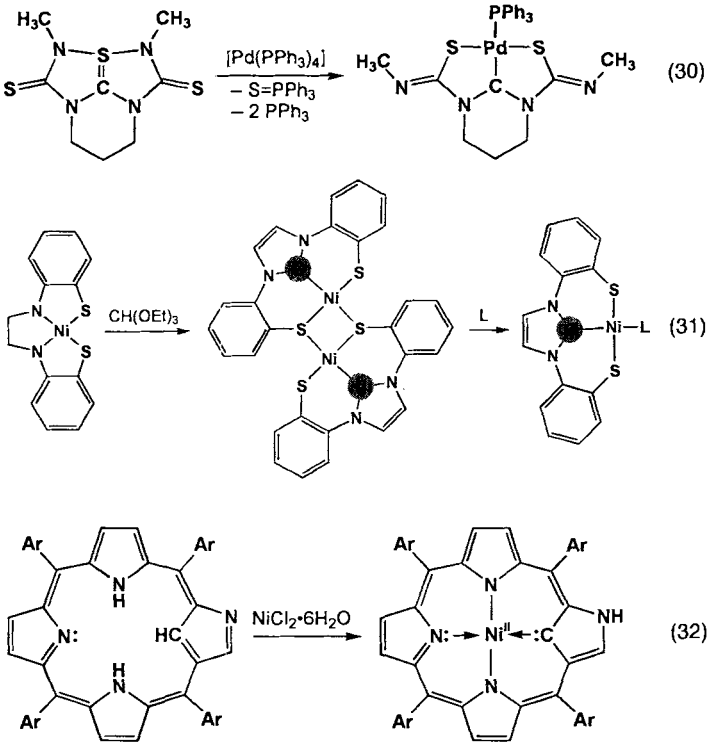

explained with the decrease in coordination number from four to two. A barrier to rotation has not been observed for the metal–carbene bond, which is in agreement with single-bond character. The position of the carbene ligands relative to the remaining complex fragment is strongly influenced by packing effects: For $[W(CO)_5L]$ three different rotamers with an eclipsed, a staggered, and an intermediate arrangement are structurally characterized for nearly identical carbene ligands.[61]

The structures of free 2,3-dihydro-1*H*-imidazol-2-ylidenes, as determined by X-ray and neutron diffraction, all show nearly identical geometries (Table 7). Considering a 3σ limit of error for X-ray and neutron diffraction data, the only difference worth discussing is an increase of about 2° in the ring angle N-$C_{carbene}$-N upon metal coordination. Whereas the geometric details of free and metal-bound carbenes hardly differ from each other, the structures of azolium cations are very different. In accordance with an increase in π delocalization in the five-membered ring upon protonation, the N–C bond lengths decrease and the C=C bond lengths increase. The angles in the ring become more similar. Apart from the C–C double bond all structural parameters of the carbene ligands are between those of the two extreme structures.

A dependence of the ring parameters on the metal is seen when the average bond lengths are considered (Figure 6).

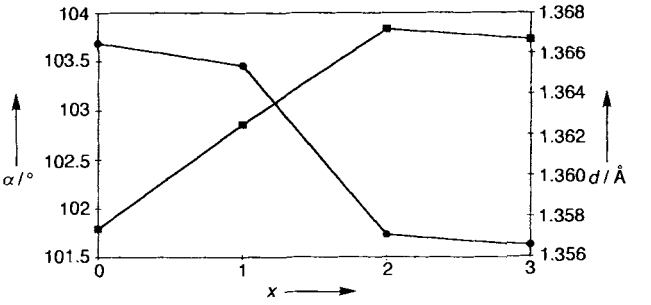

Figure 6. Averaged values of the $C_{carbene}$–N bond lengths d (circles) and the N-$C_{carbene}$-N angles α (squares) as a function of the metal from the transition metal series x. The first column ($x = 0$) lists the values for free carbenes [115].

Whereas isolated data are not meaningful, the trend in Figure 6 is more elucidating: Angle N-$C_{carbene}$-N increases for the heavier metals, while the $C_{carbene}$-N bond length decreases. This supports the general rule that metal–carbon bonds become stronger when going from 3d to 4d and 5d transition metals.

7. Catalysis

Applications of C–C-unsaturated N-heterocyclic carbenes as ligands in metal-containing catalysts were disclosed in a series of patents (1994). Previous investigations on catalytic properties were limited to C–C-saturated derivatives, but no advantage over the standard metal–phosphane catalysts was achieved.[124, 125] A recent publication on the Heck olefination sparked renewed interest in the catalysis-related aspect of carbenes.[13] Reactions such as hydroformylation, hydrogenation, isomerization, furan synthesis,[126] and olefin metathesis were investigated. The synthesis of chiral 2,3-dihydro-1*H*-imidazol-2-ylidene complexes and their application in asymmetric catalysis was another important development.

7.1. Hydrosilylation of Alkenes and Alkynes

The hydrosilylation of terminal alkenes catalyzed by rhodium–carbene complexes such as $[RhCl(\eta^4\text{-}1,5\text{-cod})L]$, $[RhCl(PPh_3)_2L]$, and $[RhCl(CO)(PPh_3)L]$ led to selective anti-Markovnikov addition of the silane [Eq. (33)].[124, 125] The

$$C_6H_{13}CH{=}CH_2 + HSiX_3 \xrightarrow{cat.} C_6H_{13}CH_2{-}CH_2SiX_3 \quad (33)$$

$X = OC_2H_5, C_2H_5, \ldots$

hydrosilylation products were obtained in yields of up to 98%, depending on the silane and the rhodium–carbene catalyst.

Table 7. Average bonding parameters of the 2,3-dihydro-1*H*-imidazol-2-ylidene system (see text; distances in Å, angles in °) [115].

	$C_{carbene}$–N	N–C	C–C	N-$C_{carbene}$-N	$C_{carbene}$-N-C	N-C-C
free carbene	1.367	1.390	1.335	101.8	112.8	106.3
carbene ligand [a]	1.360	1.384	1.329	103.5	111.4	106.9
imidazolium ion	1.322	1.374	1.345	109.2	108.2	107.2

Other rhodium(I) catalysts, for example $[RhCl(PPh_3)_3]$, gave lower yields. Conjugated dienes with rhodium–carbene catalysts yielded mixtures of 1,4- and 1,2-addition products, while $[RhCl(PPh_3)_3]$ led to pure 1,4-isomers.

In the hydrosilylation of alkynes[127] [Eq. (34)] the product distribution depended on the reaction conditions and the catalyst. With the rhodium(I) carbene complexes $[RhCl(\eta^4\text{-}1,5\text{-cod})L]$ and $[RhCl(PPh_3)_2L]$, silane addition gave mixtures of *cis* and *trans* adducts. Upon further heating in the presence of both the catalyst and the silane, complete *cis* → *trans* isomerization occurred.

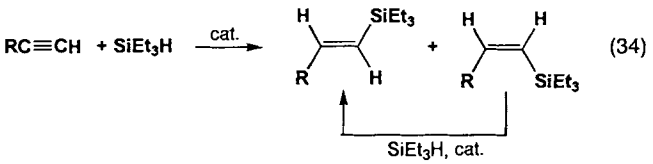

(34)

The rates of the hydrosilylation of alkynes increased in the presence of air and/or ultraviolet light. For example, irradiation of a mixture of phenylacetylene, triethylsilane, and catalyst $[RhCl(\eta^4\text{-}1,5\text{-cod})L]$ effected quantitative conversion within one hour, whereas in the absence of ultraviolet irradiation or the catalyst no reaction was observed. No such effects were seen for $[RhCl(PPh_3)_3]$.

7.2. Hydrosilylation of Ketones

The hydrosilylation of ketones according to Equation (35) is of synthetic interest, since this reaction followed by hydrolysis

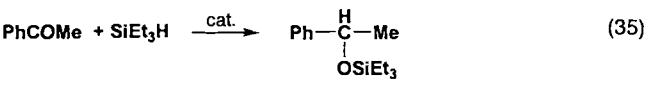

(35)

of the resulting silylether is a mild route for reducing ketones to secondary alcohols. The use of triethylsilane requires relatively high temperatures. $[RhCl(\eta^4\text{-}1,5\text{-cod})L]$, $[RhCl(PPh_3)_2L]$, $[RhCl(CO)L_2]$, and several ruthenium–carbene complexes were tested as catalysts.[124, 125] The rhodium complexes proved to be efficient catalysts. Only the dicarbene complex $[RhCl(CO)L_2]$ was rather unreactive; the mixed phosphane–carbene derivative $[RhCl(PPh_3)_2L]$ showed the best performance (98% conversion, 4 h, 100 °C). The nature of the N substituent on the carbene ligand also effected the catalytic activity, indicating that the carbene ligand is indeed involved in the catalysis. Ruthenium(II) complexes are less active.

The reaction temperatures could be significantly lowered if diphenylsilane was used as the silylating agent [Eq. (36)]. However, with some catalysts considerable amounts of the silyl enol ether side product formed.[125] The best results were obtained with the monocarbene complex $[RhCl(\eta^4\text{-}1,5\text{-cod})L]$ (*N*-phenyl derivative, 98% conversion, 24 h, 25 °C). Increasing number of carbene ligands lowered the yields.

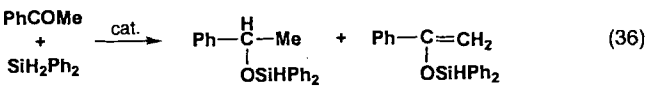

(36)

Treating silanes with a rhodium(I) carbene complex in the absence of another substrate resulted in coupling to disilanes. This reaction was exploited for the synthesis of disilanes.[125] The asymmetric version of the catalytic hydrosilylation is particularly interesting. For example, prochiral ketones are converted into optically active secondary alcohols. Although chiral carbene complexes were synthesized by Lappert et al. in a multistep approach, they failed to generate significant enantiomeric excesses. Therefore, our recently published asymmetric hydrosilylation of acetophenone [Eq. (37)] represents the first successful asymmetric catalysis using chiral metal–carbene complexes.[128, 129]

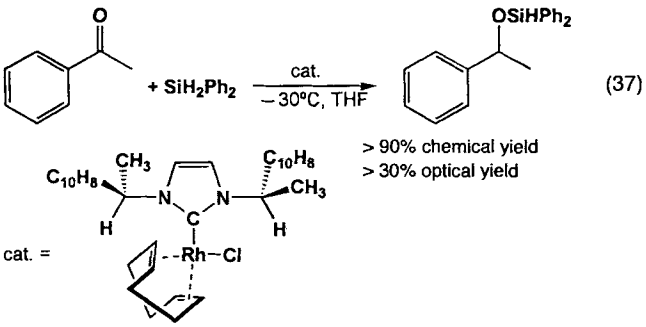

(37)

The synthesis of the chiral carbene complex is straightforward: the C_2-symmetrical imidazolium salt is synthesized in one step from enantiomerically pure α-naphthylethylamine and directly converted into the catalytically active rhodium–carbene complex (alkoxo route). With this chiral rhodium complex as catalyst, the hydrosilylation of ketones proceeds smoothly, even at low temperatures (–30 °C); asymmetric inductions over 30% (not optimized) are obtained.[128]

Although the enantiomeric excesses are subject to improvement, they are not influenced by the amount of catalyst or the degree of conversion. It should be mentioned that a free carbene ligand reacts with a hydrosilane with insertion into the Si–H bond. If there were free ligands present in the reaction mixture, they would be irreversibly destroyed and the enantiomeric excess would then decrease in the course of the reaction. It can therefore be taken for granted that the metal–carbene bond is kinetically inert under the reaction conditions.

7.3. Hydrogenation of Olefins

Mixed carbene–phosphane complexes, for example $[RhCl(PPh_3)_2L]$ and $[Ru(Cl)L(PPh_3)_2]$, are so far the most active of the carbene-containing catalysts for the hydrogenation of olefins. Hydrogenation of C–C double bonds proceeds smoothly under atmospheric pressure [Eq. (38)].[125]

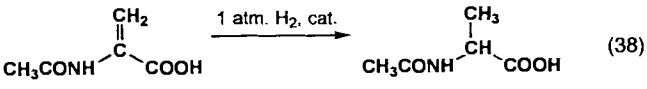

(38)

The hydrogenation of olefins catalyzed by rhodium(I) carbene complexes is being investigated further in our group.[130] Preliminary results suggest that carbenes are best combined with other ligands that lower the electron density at the metal center and dissociate in solution to generate coordination sites for the respective substrate ("hemilabile coordination"). This is plausible, since the activation of H_2 proceeds more readily when rather strong p-accepting phosphanes, for example pyrollyl phosphane, are employed.[131] Combined phosphane–carbene complexes, however, exhibit pronounced stability under the conditions of catalysis.

7.4. Heck Olefination

The application of palladium complexes $[PdL_2I_2]$ as catalysts for the Heck olefination of aryl halides according to Equation (39) has been subject to intense research.[13] The new catalysts are extraordinarily stable with respect to heat, moisture, and oxygen. Kinetic studies show that they become very active after a short induction period: Treatment with reducing agents yielded Pd(0) derivatives which are the true active spiecies (Figure 7) and have remarkable long-term stability in the Heck

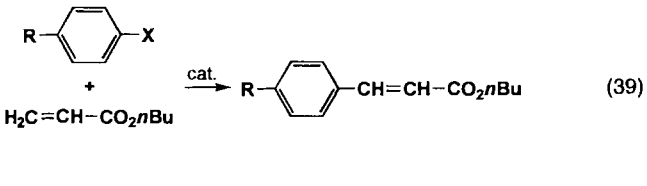

(39)

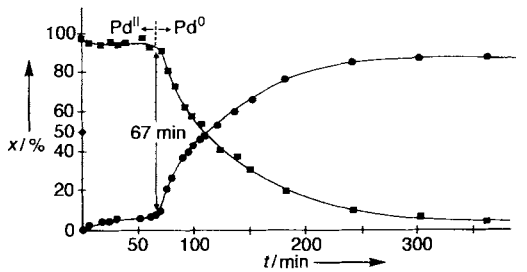

Figure 7. Palladium(0) carbene complexes as active species in the Heck olefination with the example of the reaction of 4-bromoacetophenone (squares) with *n*-butyl acrylate to form *n*-butyl-(*E*)-4-acetylcinnamate (circles). Hydrazine hydrate was added after 67 min; x = concentration.

olefination. No colloidal palladium was observed. These properties make carbene complexes of this type suitable for the activation of chloroarenes.

Enders et al. reported the synthesis of chiral palladium–carbene complexes and their application in asymmetric Heck reactions. However, they have not yet obtained significant optical inductions.[116]

7.5. Hydroformylation

Rhodium(I) phosphane complexes are commonly used as catalysts in the hydroformylation of olefins. To avoid decomposition of the complex and to obtain a good ratio of linear to branched products, a large excess of phosphanes (up to 1000-fold) is required. Stoichiometric rhodium triphenylphosphane complexes slowly decompose under the conditions of a catalytic hydroformylation.

In contrast, since the long-term stability of rhodium(I) carbene complexes—for example $[RhCl(\eta^4\text{-}1,5\text{-cod})L]$, $[RhCl(PPh_3)_2L]$, or $[RhCl(CO)L_2]$—is much higher , they can be used without ligand excess; this is quite an advantage over conventional catalysts. However, the higher electron density at the metal entails reduced activities in comparison with triphenylphosphane complexes (e. g. $[RhH(CO)(PPh_3)_3]$). Higher activities in combination with long-term stability were observed in the case of mixed rhodium carbene phosphane complexes.[132] All experimental observations lead to the conclusion that the carbene ligands remain at the metal center during the catalytic cycle.

7.6. Furan Synthesis

In 1996 Dixneuf et al. reported an interesting application of ruthenium(II) carbene complexes of the general type [Ru(*p*-cymene)Cl_2L].[126] In a catalytic reaction (*Z*)-3-methylpent-2-en-4-yn-1-ol was converted into 2,3-dimethylfuran [Eq. (40)].

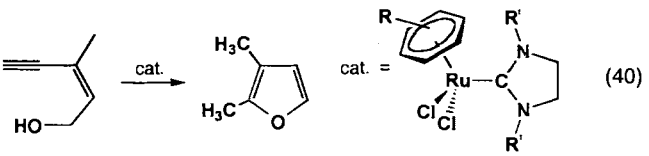

(40)

The reactivity of the catalyst is strongly dependent on the nature of the carbene ligand. Best results were obtained with a benz-2,3-dihydro-1*H*-imidazol-2-ylidene derivative.

7.7. Olefin Metathesis

Ruthenium(II) carbene complexes were successfully employed as catalysts in olefin metathesis. The bond between ruthenium and the N-heterocyclic carbene carbon atom does not react with strained cyclic olefins; norbornene is not polymerized with [Ru(*p*-cymene)Cl_2L]. This suggests that the carbene acts as a stabilizing "spectator ligand". The ruthenium catalyst has a high activity in the metathesis of norbornene (turnover number (TON) at room temperature >8000) only when an alkylidene moiety is generated with trimethylsilyldiazomethane. Functional groups as in *exo*/*endo*-bicyclo-[2.2.1]hept-5-en-2-acetate are tolerated (TON >100).[62] Ruthenium(II) complexes with N-heterocyclic carbenes are similar to analogous complexes with basic phosphanes, for example [Ru(*p*-cymene)$Cl_2(PCy_3)_3$], in their catalytical performance. Further work in our laboratories is in progress.[133]

7.8. Conclusions

N-Heterocyclic carbene complexes exhibit promising properties for a number of catalytic reactions in organic chemistry. The

cheap synthesis of imidazolium salts makes them attractive for industrial applications. Since the strong σ-donating abilities of the carbene ligands lead to increased electron density at the metal centers, heterocyclic carbenes can generally be seen as alternatives and extensions to more basic phosphanes.

Since this new class of catalysts feature strong metal–carbene bonds, immobilization techniques have a realistic chance for catalytic applications; the first results are now available. A number of methods to immobilize either the imidazolium salt or a preformed catalyst have been tested. For example, the coupling of a functionalized rhodium(I) carbene complex with a Merrifield resin works well [Eq. (41)]. Many different functionalized

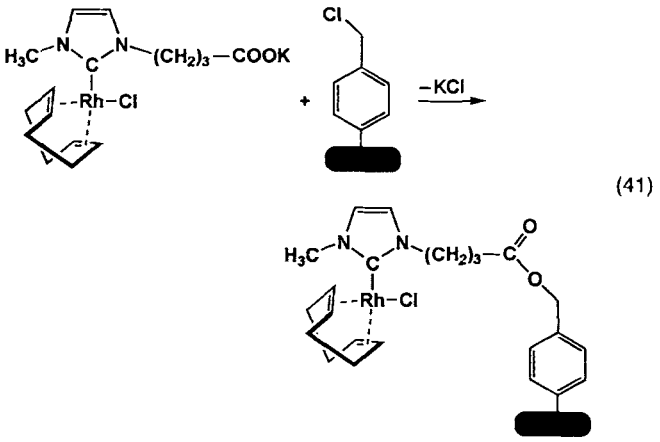

(41)

metal–carbene complexes with amino, ester, ether, hydroxy, and keto groups were synthesized for the purpose of subsequent attachment to organic and inorganic polymers.[135]

8. Chemical Vapor Deposition (CVD) of Germanium

Photoelectron spectroscopy (PES) and thermolytic studies opened an interesting application of the C–C-saturated cyclogermylene (**B**, Scheme 8) in materials science.[10, 134] The compound yielded [Ge/GeH] layers, isobutylene, HCN, and (possibly) isobutane but no hydrogen upon heating to 900 K, and [Ge/GeH] layers, **A**, and *N*,*N*′-bis-*tert*-butylethylenediamine upon heating to 470 K (Scheme 8).

A comprehensive CVD study by Veprek et al. established that these cyclogermylenes are suitable precursors for generating thin films of amorphic α-germanium by MOCVD (sublimation at about 40 °C/0.25 mbar).[135–137] Depending somewhat on the nature of the support meterial, germanium coatings began growing around 245 °C. At lower temperatures selective deposition of germanium on silicon patterned with SiO_2 was possible. To demonstrate the selectivity, silicon wafers covered with 1.8 μ thick patterned SiO_2 were used. The contact holes were filled at a substrate temperature of 230 °C with germanium without any deposition onto the SiO_2 surface. X-ray diffraction analysis showed that all films were amorphous without detectable crystallite (sensitivity about 1 vol%). The dark conductivity of the germanium film on SiO_2 ("ball-like film") reached values of 6.6×10^{-3} S cm^{-1}. This relatively high value and low activation

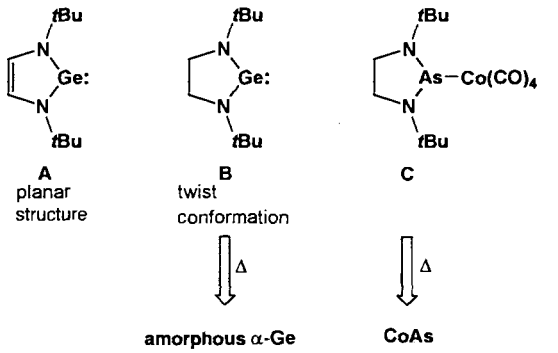

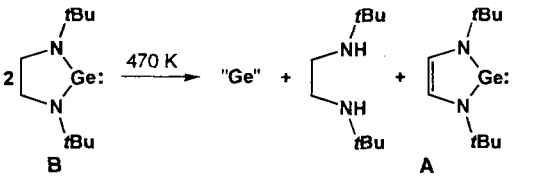

Scheme 8. Germylenes as a source for depositing α-Ge films by CVD.

energy of 0.20 eV are due to the dendritic-like nature of these films. The compact films deposited on clean SiO_2 surfaces had a relatively high dark conductivity (7.2×10^{-4} S cm^{-1}, 25 °C) and activation energy (0.25 eV). Hydrogen contents were around 0.2 atom%.

The decomposition of cyclogermylene **B** follows a bimolecular mechanism: One germanium atom is deposited, while an equivalent amount of the C–C-unsaturated derivative **A** is formed together with the diamine. The precision of this decomposition seems to arise from a predissociative bond lengthening along with the occupation of antibonding orbitals residing at germanium approaching the surface. This corresponds to a weakening of the Ge–N bonds and consequently promotes decomposition. The same feature was recognized in the case of the arsenic–cobalt heterobimetallic compound **C** (Scheme 8), which formed thin films of cobalt arsenide under CVD conditions at temperatures as low as 210 °C.[138] Electron micrographs showed uniform films, energy dispersive X-ray spectroscopy and electron spectroscopy confirmed their bulk composition, and powder diffraction patterns and conductivity measurements proved the crystallinity and electrical properties. As in the case of germanium above, impurities due to carbon, oxygen, and nitrogen were below 1%.

9. N-Heterocyclic carbenes—Quo vadis?

Heterocyclic carbenes of the imidazole, triazole, and thiazole families are no longer laboratory curiosities, since general avenues for synthesis have been opened following Arduengo's discovery of stable, isolable carbenes. A specific strength of these compounds is their universal capability to coordinate to metal centers, ranging from electron-rich transition metals (e. g. Pd^0, Rh^I) to electron-poor main group metal cations (e. g. Be^{2+}) and high oxidation state metals such as Ti^{IV}, Nb^V, and Re^{VII}.

Considering this versatility, N-heterocyclic carbenes surpass even phosphanes in that pure σ donation suffices to form stable "adducts" with certain metals and nonmetals—just as for amines and ethers. In addition, unexpectedly stable bonds are formed with catalytically relevant metals, as exemplified by the palladium(0) carbene complexes that easily survive temperatures as high as 140 °C under the harsh conditions of catalytic Heck coupling reactions.

These specific ligand properties make N-heterocyclic carbenes ideally suited for redox-dependent catalytic cycles because they tolerate rather different electronic situations. The future is thus seen in homogeneous catalysis. Effects to be expected from ligand functionalization are far from being explored. Side chains containing hemilabile phosphorus, nitrogen, and oxygen functionalities should trigger the chemistry at the metal center and, at the same time, enhance the catalyst's stability.

Chelating dicarbenes have already been verified in the free state and attached to metal centers. Water-soluble and immobilized derivatives may bridge the gap between homogeneous and heterogeneous catalysis. Finally, chiral derivatives will exploit the advantageous flexibility of composition, not least because simple ring syntheses are available. Chiral carbenes synthesized from α-phenylethylamine, glyoxal, and formaldehyde work reasonably well as part of a rhodium(I) complex in asymmetric hydrosilylation, but can certainly be improved by generating a fixed geometry (no rotation around the N–C bonds). We do not think that the planar core geometry of this class of ligands, as compared to the conical geometry of phosphanes, will reduce the efficiency of chirality transfer, not least because of the chance to synthesize bulky, chelating derivatives. It is reasonable to assume that N-heterocyclic carbenes will extend the well-established phosphanes as catalyst ligands, both alone and in combination with the latter.

What have we learned from the foregoing discussion? There are three major reasons why N-heterocyclic carbenes enter a new era in chemistry thirty years after the landmark publications of Wanzlick[8] and Öfele:[7] a) They are available as free compounds from an efficient general route (deprotonation of azolium salts in liquid ammonia), thus making a plethora of substituted, functionalized, chiral, or immobilized derivatives important in catalytic applications accessible. b) They are compatible with literally any type of main group and transition metal element of the periodic table, both in low and high formal oxidation states. However, the syntheses of catalytically relevant metal complexes does not depend on the availability of the free carbenes, but rather rests on several indirect ways to convert an azolium precursor into the metal-bound carbene. c) They form highly efficient catalysts with certain metals; palladium(II) complexes of the type $[PdL_2X_2]$ were first used successfully in the Heck-type C–C coupling,[13] and another example is the enantioselective hydrosilylation.[128]

We conclude that N-heterocyclic carbenes have long been an overlooked class of catalytically relevant ligands in coordination chemistry. Although Wanzlick pointed out in his very first publication (1968) that nucleophilic carbenes are "close relatives of isonitriles" (!), they have always been viewed as curiosities. Their renaissance in the past several years, however, justifies the assessment that they will play a major role in tomorrow's organometallic chemistry.

The authors are grateful to Dr. K. Öfele (Technische Universität München) for his continuous participation in our research related to N-heterocyclic carbenes. We acknowledge generous support by the Deutsche Forschungsgemeinschaft and the Fonds der Chemischen Industrie. The (former) students Dr. M. Elison, Dr. J. Fischer, Dr. G. R. J. Artus, Dr. D. Mihalios, C.-P. Reisinger, G. M. Lobmaier, Dr. O. Runte, M. Steinbeck, T. Weskamp, R. Eckl, M. Prinz, and G. Gerstberger deserve our gratitude for their experimentally skillful contributions to our work on the coordination chemistry of N-heterocyclic carbenes and their applications in catalysis. We thank Dr. R. Schmidt and Dr. L. J. Goosen for contributions to the manuscript.

Received: May 12, 1997 [A230IE]
German version: *Angew. Chem.* **1997**, *109*, 2256–2282

[1] P. S. Skell, S. R. Sandler, *J. Am. Chem. Soc.* **1958**, *80*, 2024.
[2] a) E. O. Fischer, A. Maasböl, *Angew. Chem.* **1964**, *76*, 645; *Angew. Chem. Int. Ed. Engl.* **1964**, 580; b) E. O. Fischer, *ibid.* **1974**, *86*. 651 (Nobel lecture).
[3] *Applied Homogeneous Catalysis with Organometallic Complexes* (Eds.: B. Cornils, W. A. Herrmann), VCH, Weinheim, **1996**.
[4] R. H. Grubbs in *Comprehensive Organometallic Chemistry, Vol. 8* (Eds.: G. Wilkinson, F. G. A. Stone, E. W. Abel), Pergamon, Oxford, **1982**, p. 499.
[5] M. Brookhart, W. B. Studabaker, *Chem. Rev.* **1987**, *87*, 411.
[6] K. H. Dötz in *Organometallics in Organic Synthesis* (Eds.: A. de Meijere, H. tom Dieck), Springer, Berlin, **1988**.
[7] K. Öfele, *J. Organomet. Chem.* **1968**, *12*, P42.
[8] H.-W. Wanzlick, H.-J. Schönherr, *Angew. Chem.* **1968**, *80*, 154; *Angew. Chem. Int. Ed. Engl.* **1968**, *7*, 141.
[9] A. J. Arduengo III, M. Kline, J. C. Calabrese, F. Davidson, *J. Am. Chem. Soc.* **1991**, *113*, 9704.
[10] W. A. Herrmann, M. Denk, J. Behm, W. Scherer, F. R. Klingan, H. Bock, B. Solouki, M. Wagner, *Angew. Chem.* **1992**, *104*, 1489; *Angew. Chem. Int. Ed. Engl.* **1992**, *31*, 485.
[11] a) M. Denk, R. Lennon, R. Hayashi, R. West, A. V. Belyakov, H. P. Verne, A. Haaland, M. Wagner, N. Metzler, *J. Am. Chem. Soc.* **1994**, *116*, 2691; b) B. Gehrhus, M. F. Lappert, J. Heinicke, R. Boese, D. Bläser, *J. Chem. Soc. Chem. Commun.* **1995**, 1931; c) B. Gehrhus, P. B. Hitchcock, M. F. Lappert, J. Heinicke, R. Boese, D. Bläser, *J. Organomet. Chem.* **1996**, *521*, 211.
[12] a) K. Öfele, C. G. Kreiter, *Chem. Ber.* **1972**, 105, 529; b) K. Öfele, M. Herberhold, *Z. Naturforsch.* **1973**, *28b*, 306; c) C. G. Kreiter, K. Öfele, G. W. Wieser, *Chem. Ber.* **1976**, *109*, 1749; d) K. Öfele, M. Herberhold, *Angew. Chem.* **1970**, *82*, 775; *Angew. Chem. Int. Ed. Engl.* **1970**, *9*, 739; e) K. Öfele, E. Roos, M. Herberhold, *Z. Naturforsch.* **1976**, *31b*, 1070; f) K. Öfele, W. A. Herrmann, D. Mihalios, M. Elison, E. Herdtweck, W. Scherer, J. Mink, *J. Organomet. Chem.* **1993**, *459*, 177; g) N. Kuhn, T. Kratz, R. Boese, D. Bläser, *ibid.* **1994**, *470*, C8; h) *ibid.* **1994**, *479*, C32; i) F. E. Hahn, L. Imhof, *Organometallics* **1997**, *16*, 763; j) F. E. Hahn, M. Tamm, *J. Organomet. Chem.* **1993**, *456*, C11; k) *J. Chem. Soc. Chem. Commun.* **1993**, 42.
[13] W. A. Herrmann, M. Elison, J. Fischer, C. Köcher, G. R. J. Artus, *Angew. Chem.* **1995**, *107*, 2602; *Angew. Chem. Int. Ed. Engl.* **1995**, *34*, 2371.
[14] a) M. Gomberg, *Chem. Ber.* **1900**, *33*, 3150; b) A. R. Forrester, J. M. Hay, R. H. Thomso, *Organic Chemistry of Stable Radicals*, Academic Press, London, **1968**.
[15] D. Griller, K. U. Ingold, *Acc. Chem. Res.* **1976**, *9*, 13.
[16] D. Seyferth, *Acc. Chem. Res.* **1971**, *5*, 65.
[17] W. E. Parham, E. E. Schweizer, *Organic Reactions, Vol. 13*, Wiley, New York, **1963**.
[18] W. Kirmse, *Carbene Chemistry*, Academic Press, New York, **1971**.
[19] K. Hirai, K. Komatsu, H. Tomioka, *Chem. Lett.* **1994**, 503.
[20] H. Tomioka, T. Watanabe, K. Hirai, K. Furukawa, T. Takui, K. Itoh, *J. Am. Chem. Soc.* **1995**, *117*, 6376.
[21] A. J. Arduengo III, H. Bock, H. Chen, M. Denk, D. A. Dixon, J. C. Green, W. A. Herrmann, N. L. Jones, M. Wagner, R. West, *J. Am. Chem. Soc.* **1994**, *116*, 6641.
[22] E. A. Carter, W. A. Goddard, *J. Phys. Chem.* **1986**, *90*, 998.
[23] S. S. Krishnamurthy, *Curr. Sci.* **1991**, *60*, 619.
[24] R. A. Moss, T. Zdrojewski, G. J. Ho, *J. Chem. Soc. Chem. Commun.* **1991**, 946.
[25] M. Elsaidi, K. Kassam, D. L. Pole, T. Tadey, J. Warkentin, *J. Am. Chem. Soc.* **1992**, *114*, 8751.
[26] Y. Cheng, S. Goon, O. Methcohn, *Chem. Commun.* **1996**, 1395.
[27] a) H. W. Wanzlick, E. Schikora, *Angew. Chem.* **1960**, *72*, 494; b) M. F. Lappert, R. W. McCabe, J. J. MacQuitty, P. L. Pye, P. I. Riley, *J. Chem. Soc. Dalton Trans.* **1980**, 90; c) M. F. Lappert, P. L. Pye, *J. Chem. Soc. Dalton Trans.* **1978**, 837, and references therein.

[28] H. Quast, S. Hünig, *Angew. Chem.* **1964**, *76*, 989; *Angew. Chem. Int. Ed. Engl.* **1964**, *3*, 800.
[29] H.-W. Wanzlick, H.-J. Schönherr, *Justus Liebigs Ann. Chem.* **1970**, *731*, 176.
[30] M. Regitz, *Angew. Chem.* **1991**, *103*, 691; *Angew. Chem. Int. Ed. Engl.* **1991**, *30*, 674.
[31] R. Gleiter, R. Hoffmann, *J. Am. Chem. Soc.* **1968**, *90*, 5457.
[32] J. V. Nef, *Justus Liebigs Ann. Chem.* **1895**, *287*, 359.
[33] A. J. Arduengo III, R. L. Harlow, M. Kline, *J. Am. Chem. Soc.* **1991**, *113*, 361.
[34] W. A. Herrmann, C. Köcher, L. Goossen, G. R. J. Artus, *Chem. Eur. J.* **1996**, *2*, 1627.
[35] N. Kuhn, T. Kratz, *Synthesis* **1993**, 561.
[36] A. J. Arduengo III, H. V. R. Dias, R. L. Harlow, M. Kline, *J. Am. Chem. Soc.* **1992**, *114*, 5530.
[37] W. A. Herrmann, M. Elison, J. Fischer, C. Köcher, *Chem. Eur. J.* **1996**, *2*, 772.
[38] J. Fuller, R. T. Carlin, H. C. DeLong, D. Haworth, *J. Chem. Soc. Chem. Commun.* **1994**, 299.
[39] Y. Chauvin, L. Mussmann, H. Olivier, *Angew. Chem.* **1995**, *107*, 2941; *Angew. Chem. Int. Ed. Engl.* **1995**, *34*, 2698.
[40] Y. Chauvin, H. Olivier-Bourbigou, *Chemtech* **1995**, 26.
[41] A. J. Arduengo III, D. A. Dixon, K. K. Kumashiro, C. Lee, W. P. Power, K. W. Zilm, *J. Am. Chem. Soc.* **1994**, *116*, 6361.
[42] N. Burford, P. Losier, C. Macdonald, V. Kyrimis, P. K. Bakshi, T. S. Cameron, *Inorg. Chem.* **1994**, *33*, 1434.
[43] M. K. Denk, S. Gupta, R. Ramachandran, *Tetrahedron Lett.* **1996**, *37*, 9025.
[44] D. S. Brown, A. Decken, A. H. Cowley, *J. Am. Chem. Soc.* **1995**, *117*, 5421.
[45] D. S. Brown, A. Decken, C. A. Schnee, A. H. Cowley, *Inorg. Chem.* **1995**, *34*, 6415.
[46] D. E. Goldberg, P. B. Hitchcock, M. L. Lappert, K. M. Thomas, A. J. Thorne, T. Fjeldberg, A. Haaland, B. E. R. Schilling, *J. Chem. Soc. Dalton Trans.* **1986**, 2387.
[47] P. J. Davidson, D. H. Harris, M. F. Lappert, *J. Chem. Soc. Dalton Trans.* **1976**, 2268.
[48] C. W. Bauschlicher, Jr., H. F. Schaefer III, P. S. Bagus, *J. Am. Chem. Soc.* **1977**, *99*, 7106.
[49] V. Langer, K. Huml, G. Reck, *Acta Crystallogr. Sect. B* **1982**, *38*, 298.
[50] R. W. Alder, P. R. Allen, M. Murray, A. G. Orpen, *Angew. Chem.* **1996**, *108*, 1211; *Angew. Chem. Int. Ed. Engl.* **1996**, *35*, 1121.
[51] D. A. Dixon, K. D. Dobbs, A. J. Arduengo III, G. Bertrand, *J. Am. Chem. Soc.* **1991**, *113*, 8782.
[52] T. A. Taton, P. Chen, *Angew. Chem.* **1996**, *108*, 1098; *Angew. Chem. Int. Ed. Engl.* **1996**, *35*, 1011.
[53] Z. Q. Shi, V. Goulle, R. P. Thummel, *Tetrahedron Lett.* **1996**, *37*, 2357.
[54] E. Çetinkaya, P. B. Hitchcock, H. Kücükbay, M. F. Lappert, S. Al-Juaid, *J. Organomet. Chem.* **1994**, *481*, 89.
[55] A. J. Arduengo III, J. R. Goerlich, W. J. Marshall, *J. Am. Chem. Soc.* **1995**, *117*, 11027.
[56] D. Enders, K. Breuer, G. Raabe, J. Runsink, J. H. Teles, J. P. Melder, K. Ebel, S. Brode, *Angew. Chem.* **1995**, *107*, 1119; *Angew. Chem. Int. Ed. Engl.* **1995**, *34*, 1021.
[57] D. Enders, K. Breuer, G. Raabe, J. Simonet, A. Ghanimi, H. B. Stegmann, J. H. Teles, personal communication, **1996**.
[58] G. Maier, J. Endres, H. P. Reisenauer, *Angew. Chem.* **1997**, *109*, 1788; *Angew. Chem. Int. Ed. Engl.* **1997**. *36*, 1709.
[59] G. A. McGibbon, J. Hrusák, D. J. Lavorato, H. Schwarz, J. K. Terlouw, *Chem. Eur. J.* **1997**, *3*, 232.
[60] A. J. Arduengo III, J. R. Goerlich, W. J. Marshall, *Liebigs Ann.* **1997**, 365.
[61] W. A. Herrmann, L. J. Goossen, G. R. J. Artus, C. Köcher, *Organometallics* **1997**, *16*, 2472.
[62] C. Köcher, Dissertation, Technische Universität München, **1997**.
[63] D. Michalios, Dissertation, Technische Universität München, **1992**.
[64] W. A. Herrmann, C. P. Reisinger, unpublished results, **1997**.
[65] C. Köcher, W. A. Herrmann, *J. Organomet. Chem.* **1997**, *532*, 261.
[66] W. A. Herrmann, T. Weskamp, unpublished results, **1997**.
[67] W. A. Herrmann, T. Weskamp, R. Eckl, unpublished results, **1996**.
[68] U. Kernbach, M. Ramm, P. Luger, W. P. Fehlhammer, *Angew. Chem.* **1996**, *108*, 333; *Angew. Chem. Int. Ed. Engl.* **1996**, *35*, 310.
[69] H. V. R. Dias, W. Jin, *Tetrahedron Lett.* **1994**, *35*, 1365.
[70] a) K. K. Irikura, W. A. Goddard III, J. L. Beauchamp, *J. Am. Chem. Soc.* **1992**, *114*, 48; b) C. W. Bauschlicher, Jr., S. R. Langhoff, P. R. Taylor, *J. Chem. Phys.* **1987**, *87*, 387; c) S. K. Shin, W. A. Goddard III, J. L. Beauchamp, *ibid.* **1990**, *93*, 4986; d) *ibid.* **1990**, *94*, 6963.
[71] D. A. Dixon, A. J. Arduengo III, *J. Phys. Chem.* **1991**, *95*, 4180.
[72] J. Cioslowski, *Int. J. Quantum Chem.* **1993**, *27*, 309.
[73] A. J. Arduengo III, H. V. R. Dias, D. A. Dixon, R. L. Harlow, W. T. Klooster, T. F. Koetzle, *J. Am. Chem. Soc.* **1994**, *116*, 6812.
[74] C. Heinemann, W. Thiel, *Chem. Phys. Lett.* **1994**, *217*, 11.
[75] R. R. Sauers, *Tetrahedron Lett.* **1996**, *37*, 149.
[76] C. Heinemann, T. Müller, Y. Apeloig, H. Schwarz, *J. Am. Chem. Soc.* **1996**, *118*, 2023.
[77] C. Boehme, G. Frenking, *J. Am. Chem. Soc.* **1996**, *118*, 2039.
[78] C. Heinemann, W. A. Herrmann, W. Thiel, *J. Organomet. Chem.* **1994**, *475*, 73.
[79] M. Denk, J. C. Green, N. Metzler, M. Wagner, *J. Chem. Soc. Dalton Trans.* **1994**, 2405.
[80] A. R. Katritzky, M. Karelson, N. Malhotra, *Heterocycles* **1991**, *32*, 127.
[81] S. Berger, U. Fleischer, C. Geletneky, J. C. W. Lohrenz, *Chem. Ber.* **1995**, *128*, 1183.
[82] R. Hoffmann, *J. Am. Chem. Soc.* **1968**, *90*, 1475.
[83] R. Hoffmann, R. B. Woodward, *Acc. Chem. Res.* **1968**, *1*, 17.
[84] G. Bertrand, R. Reed, *Coord. Chem. Rev.* **1994**, *137*, 323.
[85] G. Alcaraz, U. Wecker, A. Baceiredo, F. Dahan, G. Bertrand, *Angew. Chem.* **1995**, *107*, 1358; *Angew. Chem. Int. Ed. Engl.* **1995**, *34*, 1246.
[86] P. Dyer, A. Baceiredo, G. Bertrand, *Inorg. Chem.* **1996**, *35*, 46.
[87] R. W. Alder, P. R. Allen, S. J. Williams, *J. Chem. Soc. Chem. Commun.* **1995**, 1267.
[88] R. Breslow, *J. Am. Chem. Soc.* **1958**, *80*, 3719.
[89] R. Kluger, *Chem. Rev.* **1987**, *87*, 863.
[90] W. Kreiser, *Nachr. Chem. Tech. Lab.* **1981**, *29*, 172.
[91] H. Stetter, *Angew. Chem.* **1976**, *88*, 695; *Angew. Chem. Int. Ed. Engl.* **1976**, *15*, 639.
[92] H. Stetter, H. Kuhlmann, *Org. React. (NY)* **1991**, *40*, 407.
[93] J. H. Teles, J.-P. Melder, K. Ebel, R. Schneider, E. Gehrer, W. Harder, S. Brode, D. Enders, K. Breuer, G. Raabe, *Helv. Chim. Acta* **1996**, *79*, 61.
[94] a) D. Enders, K. Breuer, J. H. Teles, *Helv. Chim. Acta* **1996**, *79*, 1217; b) D. Enders, K. Breuer, J. Runsink, J. H. Teles, *ibid.* **1996**, *79*, 1899.
[95] N. Kuhn, T. Kratz, G. Henkel, *J. Chem. Soc. Chem. Commun.* **1993**, 1778.
[96] A. J. Arduengo III, M. Tamm, J. C. Calabrese, *J. Am. Chem. Soc.* **1994**, *116*, 3625.
[97] A. J. Arduengo III, S. F. Gamper, M. Tamm, J. C. Calabrese, F. Davidson, H. A. Craig, *J. Am. Chem. Soc.* **1995**, *117*, 572.
[98] W. A. Herrmann, P. W. Roesky, M. Elison, G. R. J. Artus, K. Öfele, *Organometallics* **1995**, *14*, 1085.
[99] W. A. Herrmann, O. Runte, G. R. J. Artus, *J. Organomet. Chem.* **1995**, *501*, C1.
[100] A. J. Arduengo III, H. V. R. Dias, F. Davidson, R. L. Harlow, *J. Organomet. Chem.* **1993**, *462*, 13.
[101] O. Runte, Dissertation, Technische Universität München, **1997**.
[102] N. Kuhn, G. Henkel, T. Kratz, J. Kreutzberg, R. Boese, A. H. Maulitz, *Chem. Ber.* **1993**, *126*, 2041.
[103] A. J. Arduengo III, H. V. R. Dias, J. C. Calabrese, F. Davidson, *J. Am. Chem. Soc.* **1992**, *114*, 9724.
[104] X.-W. Li, J. Su, G. H. Robinson, *Chem. Commun.* **1996**, 2683.
[105] a) N. Kuhn, H. Bohnen, J. Kreutzberg, D. Blaser, R. Boese, *J. Chem. Soc. Chem. Commun.* **1993**, 1136; b) N. Kuhn, H. Bohnen, D. Bläser, R. Boese, *Chem. Ber.* **1994**, *127*, 1405; c) N. Kuhn, H. Bohnen, G. Henkel, J. Kreutzberg, *Z. Naturforsch. B* **1996**, *51*, 1267; d) H. Schumann, M. Glanz, J. Winterfeld, H. Hemling, N. Kuhn, H. Bohnen, D. Bläser, R. Boese, *J. Organomet. Chem.* **1995**, *493*, C14; e) N. Kuhn, H. Bohnen, G. Henkel, *Z. Naturforsch. B* **1994**, *49*, 1473; f) N. Kuhn, G. Weyers, G. Henkel, *Chem. Commun.* **1997**, 627.
[106] A. J. Arduengo III, H. V. R. Dias, J. C. Calabrese, F. Davidson, *Inorg. Chem.* **1993**, *32*, 1541.
[107] a) N. Kuhn, T. Kratz, D. Bläser, R. Boese, *Chem. Ber.* **1995**, *128*, 245; b) A. Schäfer, M. Weidenbruch, W. Saak, S. Pohl, *J. Chem. Soc. Chem. Commun.* **1995**, 1157.
[108] Se: a) N. Kuhn, G. Henkel, T. Kratz, *Z. Naturforsch. B* **1993**, *48*, 973; b) D. J. Williams, M. R. Fawcett-Brown, R. R. Raye, D. VanDerveer, Y. T. Pang, R. L. Jones, K. L. Bergbauer, *Heteroat. Chem.* **1993**, *4*, 409; Te: c) N. Kuhn, G. Henkel, T. Kratz, *Chem. Ber.* **1993**, *126*, 2047.
[109] D. Enders, K. Breuer, J. H. Teles, K. Ebel, *Org. Synth.* **1997**, submitted.
[110] A. J. Arduengo III, M. Tamm, S. J. McLain, C. J. Calabrese, F. Davidson, W. J. Marshall, *J. Am. Chem. Soc.* **1994**, *116*, 7927.
[111] H. Schumann, M. Glanz, J. Winterfeld, H. Hemling, N. Kuhn, T. Kratz, *Angew. Chem.* **1994**, *106*, 1829; *Angew. Chem. Int. Ed. Engl.* **1994**, *33*, 1733.
[112] H. Schumann, M. Glanz, J. Winterfeld, H. Hemling, N. Kuhn, T. Kratz, *Chem. Ber.* **1994**, *127*, 2369.
[113] R. D. Fischer, *Angew. Chem.* **1994**, *106*, 2253; *Angew. Chem. Int. Ed. Engl.* **1994**, *33*, 2165.
[114] F. Munck, Dissertation, Technische Universität München, **1996**.
[115] G. R. J. Artus, Dissertation, Technische Universität München, **1996**.
[116] D. Enders, H. Gielen, G. Raabe, J. Runsink, J. H. Teles, *Chem. Ber.* **1996**, *129*, 1483.
[117] W. P. Fehlhammer, K. Bartel, A. Völkl, D. Achatz, *Z. Naturforsch. B* **1982**, *37*, 1044.
[118] I. Ugi, K. Offermann, *Isonitrile Chemistry, Vol. 20*, Academic Press, London, **1971**.
[119] D. Rieger, S. D. Lotz, U. Kernbach, C. André, J. Bertran-Nadal, W. P. Fehlhammer, *J. Organomet. Chem.* **1995**, *491*, 135.
[120] W. P. Fehlhammer, M. Fritz, *Chem. Rev.* **1993**, *93*, 1243.
[121] N. Matsumura, J.-I. Kawano, N. Fukunishi, H. Inoue, *J. Am. Chem. Soc.* **1995**, *117*, 3623.
[122] D. Sellmann, W. Prechtel, F. Knoch, M. Moll, *Inorg. Chem.* **1993**, *32*, 538.

[123] A. Ghosh, *Angew. Chem.* **1995**, *107*, 1117; *Angew. Chem. Int. Ed. Engl.* **1995**, *34*, 1028.
[124] J. E. Hill, T. A. Nile, *J. Organomet. Chem.* **1977**, *137*, 293.
[125] M. F. Lappert in *Transition Metal Chemistry* (Eds.: A. Müller, E. Diemann), Verlag Chemie, Weinheim, **1981**.
[126] B. Çetinkaya, I. Özdemir, C. Bruneau, P. H. Dixneuf, *J. Mol. Catal. A* **1997**, *118*, L1.
[127] M. F. Lappert, R. K. Maskell, *J. Organomet. Chem.* **1984**, *264*, 217.
[128] W. A. Herrmann, L. J. Goossen, C. Köcher, G. R. J. Artus, *Angew. Chem.* **1996**, *108*, 2980; *Angew. Chem. Int. Ed. Engl.* **1996**, *35*, 2805.
[129] L. Goossen, Dissertation, Technische Universität München, **1997**.
[130] W. A. Herrmann, M. Steinbeck, unpublished results, **1997**.
[131] A. M. Trzeciak, J. J. Ziolkowski, *Abstr. Pap. XX. Colloquy on Organometallic Chemistry, Germany–Poland* (Halle-Wittenberg), **1996**, p. 11.
[132] C. Köcher, Dissertation, Technische Universität München, **1997**.
[133] W. A. Herrmann, unpublished results.
[134] F.-R. Klingan, Dissertation, Technische Universität München, **1995**.
[135] J. Procop, R. Merica, F. Glatz, S. Veprek, F.-R. Klingan, W. A. Herrmann, *J. Non-Cryst. Solids* **1996**, 2638.
[136] S. Veprek, J. Procop, R. Merica, F. Glatz, F.-R. Klingan, W. A. Herrmann, *Mat. Res. Soc. Symp. Proc.* **1994**, *336*, 541.
[137] S. Veprek, J. Procop, R. Merica, F. Glatz, F.-R. Klingan, W. A. Herrmann, *Abstr. Pap. CVD-13 American Chemical Society Spring Meeting*, (Los Angeles, CA) **1996**.
[138] F.-R. Klingan, A. Miehr, R. A. Fischer, W. A. Herrmann, *Appl. Phys. Lett.* **1995**, *67*, 822.
[139] M. Elison, Dissertation, Technische Universität München, **1995**.
[140] C. Elschenbroich, A. Salzer, *Organometallchemie*, 3. Aufl., Teubner, Stuttgart, **1990**, p. 279.
[141] M. Driess, H. Grützmacher, *Angew. Chem.* **1996**, *108*, 900; *Angew. Chem. Int. Ed. Engl.* **1996**, *35*, 828.
[142] R. Boese, unpublished results.
[143] L. Weber, E. Dobbert, H.-G. Stammler, B. Neumann, R. Boese, D. Bläser, *Chem. Ber.* **1997**, *130*, 705.
[144] M. Tamm, T. Lügger, F. E. Hahn, *Organometallics* **1996**, *15*, 1251.
[145] N. Metzler, M. Denk, *Chem. Commun.* **1996**, 2657.
[146] a) N. Kuhn, R. Fawzi, M. Steimann, J. Wiethoff, D. Bläser, R. Boese, *Z. Naturforsch. B* **1995**, *50*, 1779; b) N. Kuhn, R. Fawzi, M. Steimann, J. Wiethoff, *Z. Anorg. Allg. Chem.* **1997**, *623*, 769; c) N. Kuhn, R. Fawzi, M. Steimann, J. Wiethoff, *Chem. Ber.* **1996**, *129*, 479.
[147] A. J. Arduengo III, R. Krafczyk, W. J. Marshall, R. Schmutzler, *J. Am. Chem. Soc.* **1997**, *119*, 3381.
[148] a) N. Kuhn, T. Kratz, G. Henkel, *Chem. Ber.* **1994**, *127*, 849; b) N. Kuhn, T. Kratz, G. Henkel, *Z. Naturforsch. B* **1996**, *51*, 295.
[149] N. Kuhn, R. Fawzi, T. Kratz, M. Steimann, *Phosphorus Sulfur Silicon Relat. Elem.* **1996**, *108*, 107.
[150] a) W. A. Herrmann, K. Öfele, M. Elison, F. E. Kühn, P. W. Roesky, *J. Organomet. Chem.* **1994**, *480*, C7; b) N. Kuhn, T. Kratz, D. Bläser, R. Boese, *Inorg. Chim. Acta* **1995**, *238*, 179.
[151] P. Luger, G. Ruban, *Acta Crystallogr. Sect. B* **1971**, *27*, 2276.

Deposition of Data from X-Ray Structure Analyses

In order to make life easier for authors and referees the Cambridge Crystallographic Data Centre (CCDC) and the Fachinformationszentrum Karlsruhe (FIZ) have unified their procedures for the deposition of data from single-crystal X-ray structure analyses.

Prior to submitting your manuscripts please deposit the data for your compound(s) **electronically** at the appropriate data base, that is, at the CCDC for organic and organometallic compounds and at the FIZ for inorganic compounds. Both data bases will be pleased to provide help (see our *Notice to Authors* in the first issue of this year). In general, you will receive a depository number from the data base within two working days after electronic deposition; please include this number with the appropriate standard text (see our *Notice to Authors*) in your manuscript. This will enable the referees to retrieve the structure data quickly and efficiently if they need this information to reach their decision.

This is now the uniform procedure for manuscripts submitted to the journals *Advanced Materials, Angewandte Chemie, Chemische Berichte/Recueil, Chemistry—A European Journal,* and *Liebigs Annalen/Recueil.*

The Direct Synthesis of a *closo*-Borate from Elemental Boron

Lars Wesemann*

The significance of the icosahedron in the chemistry of boron is certainly unique. Whereas Platonic forms such as tetrahedra, octahedra, and cubes are known as structures of a diverse range of very different compounds, the icosahedron is a characteristic structural motif for boron and its compounds. The known element modifications[1] of boron all contain B_{12} icosahedra, which in α-rhombohedral boron are linked together through three-center bonds and through usual two center bonds in such a way that a near cubic face-centered packing of B_{12} icosahedra is formed. β-Rhombohedral boron has a considerably more complicated structure with 105 boron atoms per unit cell; the central icosahedron in this case is surrounded by twelve additional icosahedra. The modification of boron that was earlier designated as α-tetragonal boron should be described as boron carbide or boron nitride, in which four B_{12} icosahedra and two heteroatoms are present per unit cell.

In the boron-deficient borides the boron atoms are either isolated or linked one- or two-dimensionally, whereas the boron-rich borides all have a three-dimensional covalent linkage of the boron atoms. Icosahedra occur as a structural motif for the linkage of the boron atoms in several of these borides (B_4C, B_6P, B_6O, SiB_6, α-AlB_{12}, γ-AlB_{12}).[2]

In the chemistry of the boranes, which began with the pioneering investigations by Stock,[3] a regular icosahedron is found for the *closo*-borate $[B_{12}H_{12}]^{2-}$ (**1**).

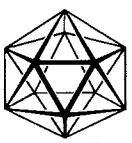

$[B_{12}H_{12}]^{2-}$

1

Of the structures of the *closo*-borates the regular, closed deltahedra $[B_nH_n]^{2-}$ with $n = 6-12$ are known; the icosahedron is the upper limit ($n = 12$). The relationship between the structure of the boranes and the number of electrons in their frameworks shows that the *closo*-borates with n framework atoms have $2n + 2$ electrons.[4] For closed, dodecagonal heteroboranes, which can be derived formally by the exchange of a BH unit of the $[B_{12}H_{12}]^{2-}$ ion (**1**) for a heteroatom or a substituted heteroatom, the descriptive term icosahedron is now used despite their lower symmetry. The best known compound of this class of substances is *o*-carborane ($C_2B_{10}H_{12}$); however, syntheses are also known for other disubstituted as well as a large number of monosubstituted icosahedra.[5] An icosahedron of the higher homologue $[Al_{12}iBu_{12}]^{2-}$ was prepared in a surprising reaction by the reduction of diisobutylaluminum chloride.[6]

Although there is a close structural relationship between elemental boron and the icosahedral dodecaborate dianion $[B_{12}H_{12}]^{2-}$ (**1**), no synthesis of such a *closo* cluster directly from the element was known. As starting materials for the synthesis of the icosahedral polyborate dianion $[B_{12}H_{12}]^{2-}$ (**1**), which was isolated for the first time by Hawthorne et al. in 1960,[7] either smaller borane clusters and sodium boranate[8] or sodium borates or boron oxide are used in the presence of sodium and hydrogen.[9] The chemistry of **1** and other polyhedral boranate ions has become more significant because these compounds show potential for application in cancer therapy. The large effective nuclear cross section of the ^{10}B isotope for capture of thermal neutrons is used to achieve a localized destruction of the cell by the products of the nuclear reaction. Boron-rich soluble compounds such as the polyhedral borates are particularly promising for such medical applications.[10]

Many examples are known for the substitution of the hydrogen atoms in the *closo*-borate ion; the derivatization to give a halogen compound has been described for monosubstitution up to persubstitution.[11] The isolation and characterization of a B_{12} icosahedron that is completely substituted by selenium atoms and has the composition $[B_{12}(BSe_3)_6]^{8-}$ (**2**) (Figure 1) was recently described by Krebs et al.[12]

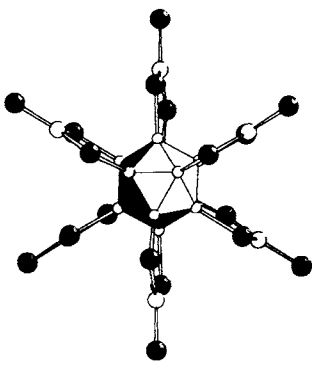

Figure 1. Structure of the anion of $Cs_8[B_{12}(BSe_3)_6]$ (o = B, • = Se).

It is not the complete substitution but rather the synthesis from elemental boron that is surprising. Hitherto, the reactions typical for solid-state chemistry have described the dissolution of boron network structures to give boron compounds completely substituted by chalcogen atoms. These products highlight the novel remarkable structural principles; the boron

[*] Priv.-Doz. Dr. L. Wesemann
Institut für Anorganische Chemie der Technischen Hochschule
Professor-Pirlet-Strasse 1, D-52056 Aachen (Germany)
Fax: Int. code +(241)8888288
e-mail: lars.wesemann@ac.rwth-aachen.de

 © WILEY-VCH Verlag GmbH, D-69451 Weinheim, 1997 0570-0833/97/3620-2189 $ 17.50+.50/0

atoms reside in trigonal-planar and tetrahedral environments, coordinated by chalcogen atoms. The short reaction times are considered as a possible explanation for the formation of the unusual cluster **2**, which obeys Wade's rules. Future experiments will surely determine whether this substance is an intermediate on the way to selenium borates. The bridging substituents in **2**, which in this form are not known for boron clusters, lower the icosahedral symmetry to D_{3d}. In the solid state the anion only shows crystallographic inversion symmetry. A substituent that bridges two neighboring atoms of the icosahedron framework, as in the cluster anion described here, was reported for an annelated six-membered ring at the azadodecaborane by Paetzold et al. and at the *o*-carborane by Wade et al.[13] The bridging of two neighboring boron atoms by a triazenium ligand has been confirmed for two open derivatives.[14]

The fascination of compound **2** originates on the one hand from its aesthetically pleasing structure and on the other from its synthesis, which reveals a direct link between the element boron and a substituted borane cluster.

German version: *Angew. Chem.* **1997**, *109*, 2283–2284

Keywords: boron · clusters · selenium

[1] N. N. Greenwood, A. Earnshaw, *Chemistry of the Elements*, Pergamon Press, Oxford, **1984**.
[2] T. Lundström in *Encyclopedia of Inorganic Chemistry* (Ed.: R. B. King), Wiley, New York, **1994**.
[3] A. Stock, *Hydrides of Boron and Silicon. The George Fisher Baker Non-Resident Lectureship in Chemistry at Cornell University*, Cornell University Press, Ithaca, New York, **1933**.
[4] K. Wade, *Adv. Inorg. Chem. Radiochem.* **1976**, *18*, 1–66.
[5] a) T. L. Heying, J. W. Ager, Jr., S. L. Clark, D. J. Mangold, H. L. Goldstein, M. Hillman, R. J. Polak, J. W. Szymanski, *Inorg. Chem.* **1963**, *2*, 1089–1092; b) L. I. Zakharkin, V. I. Stanko, V. A. Brattsev, Y. A. Chapovskii, Y. T. Struchkov, *Izv. Akad. Nauk. SSSR Ser. Khim.* **1963**, 2069; c) W. H. Knoth, *J. Am. Chem. Soc.* **1967**, *89*, 1274–1275; d) J. L. Little, S. S. Pao, K. K. Sugathan, *Inorg. Chem.* **1974**, *13*, 1752–1756; e) J. Plešek, S. Heřmánek, *J. Chem. Soc. Chem. Commun.* **1975**, 127–128; f) G. D. Friesen, L. J. Todd, *ibid.* **1978**, 349–350; g) J. L. Little, *Inorg. Chem.* **1979**, *18*, 1598–1600; h) T. D. Getman, S. G. Shore, *ibid.* **1988**, 27, 3439–3440; i) N. S. Hosmane, J. A. Maguire, *Adv. Organomet. Chem.* **1989**, *30*, 99–150; j) T. D. Getman, H.-B. Deng, L.-Y. Hsu, S. G. Shore, *Inorg. Chem.* **1989**, *28*, 3612–3616; k) D. Seyferth, K. Büchner, W. S. Rees, Jr., W. M. Davis *Angew. Chem.* **1990**, *102*, 911–913; *Angew. Chem. Int. Ed. Engl.* **1990**, *29*, 918–920; l) J. Müller, J. Runsink, P. Paetzold, *ibid.* **1991**, *103*, 201 and **1991**, *30*, 175; m) R. W. Chapman, J. G. Kester, K. Folting, W. E. Streib, L. J. Todd, *Inorg. Chem.* **1992**, *31*, 979–983; n) L. Wesemann, U. Englert, *Angew. Chem.* **1996**, *108*, 586–587; *Angew. Chem. Int. Ed. Engl.* **1996**, *35*, 527.
[6] W. Hiller, K.-W. Klinkhammer, W. Uhl, J. Wagner, *Angew. Chem.* **1991**, *103*, 182-183; *Angew. Chem. Int. Ed. Engl.* **1991**, *30*, 179–180.
[7] A. R. Pitochelli, M. F. Hawthorne, *J. Am. Chem. Soc.* **1960**, *82*, 3228–3229.
[8] a) Gmelin, *Handbuch der Anorganischen Chemie*, supplement to the 8th ed., *vol. 54*, Boron Compounds, Part 20, Boron-Hydrogen Compounds, Springer, Heidelberg, **1979**; b) see ref. [8a], pp. 216–222, and references therein.
[9] C. Harzdorf, H. Niderprüm, H. Odenbach, *Z. Naturforsch. B* **1970**, *25*, 6–10.
[10] M. F. Hawthorne, *Angew. Chem.* **1993**, *105*, 997–1033; *Angew. Chem. Int. Ed. Engl.* **1993**, *32*, 950–986.
[11] Ref. [8a] pp. 231–239, and references therein.
[12] J. Küper, O. Conrad, B. Krebs, *Angew. Chem.* **1997**, *109*, 1995–1996; *Angew. Chem. Int. Ed. Engl.* **1997**, *36*, 1903–1904, and references therein.
[13] a) L. Schneider, U. Englert, P. Paetzold, *Chem. Ber.* **1994**, *127*, 87–90; b) R. C. B. Copley, M. A. Fox, W. R. Gill, J. A. K. Howard, J. A. H. MacBride, R. J. Peace, G. P. Rivers, K. Wade, *Chem. Commun.* **1996**, 2033–2034.
[14] a) S. Küpper, P. J. Carroll, L. G. Sneddon, *J. Am. Chem. Soc.* **1992**, *114*, 4914–4915; b) F. Meyer, P. Paetzold, U. Englert, *Chem. Ber.* **1992**, *125*, 2025–2026.

Biosynthesis of Taxol

Jürgen Rohr*

Yew trees contain a broad spectrum of biologically active compounds.[1] Indeed "slips of yew" were already esteemed as important ingredients of certain recipies by well-known "chemists" in Elizabeathen literature (Shakespeare: Macbeth IV, I).[1b,c] Today, interest in yews is concentrated mostly upon taxol (**1**, paclitaxel),[2a] a novel cytostatic occurring in the bark of the Pacific yew *Taxus brevifolia*. Taxol, related taxoids, and the semisynthetically prepared taxotère (**2**, docetaxel)[2a] are antimitotic agents. They presumably[2b] stop the growth of cancer cells by stabilizing the mitotic spindles through inhibition of the depolymerization of their major component, tubulin. The hollow spindle fibers play an essential role in mitosis (cell division), since they pull the two chromosomes to opposite poles of the cell. Epothilone[3] is another natural product with this mode of action.[2b,3] Taxol and taxotère are successfully used for the treatment of a variety of solid tumors, in particular ovarian and breast cancer, even in advanced stages.

[*] Prof. Dr. J. Rohr
Institut für Organische Chemie der Universität
Tammannstrasse 2, D-37077 Göttingen (Germany)
Fax: Int. code +(551)39-9660
e-mail: jrohr@gwdg.de

The problem hindering wider application of this promising drug has been its limited supply from its original source. Only 100–170 mg of taxol can be isolated from one kilogram of bark, and the slow-growing yews (a tree needs about 200 years to reach its full size) have to be cut down (ca. 1000 trees for 1 kg of taxol). The treatment of only one cancer patient requires at least 3 g, and approximately 50000 patients die each year of ovarian and breast cancer in the USA alone.[1,4]

An alternative source that preserves natural resources and is currently used for both taxol and taxotère is semisynthesis. 10-Deacetylbaccatin III (**3**) and baccatin III (**4**) are extracted from regenerable twigs of various yew species and then converted to taxotère (**2**) and taxol (**1**), respectively, through the linkage of the synthetically prepared side chains.[4,5] Taxol has also been prepared by a number of total syntheses,[4,6] but none of these are realistic for commercial production. In the most recent, and conceptually most attractive approach, which was devised by P. A. Wender et al. (the so-called pinene route),[6d] the overall yield is ten times that of the first taxol syntheses.

Further sources for taxol production are (endophytic) fungi such as *Taxomyces andreanae*,[7a] *Fusarium*, *Penicillium*, and *Phoma*, and *Alternaria alternata* ssp. *Taxus hicksii*, which have

 © WILEY-VCH Verlag GmbH, D-69451 Weinheim, 1997 0570-0833/97/3620-2190 $ 17.50+.50/0

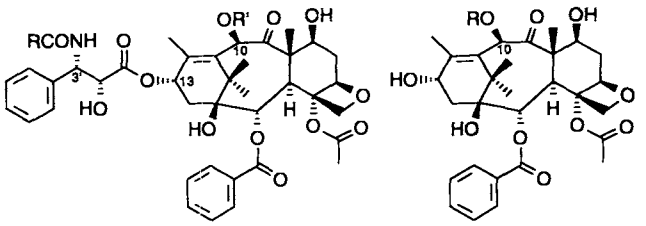

1: R = , R' = CH_3CO

2: R = , R' = H

3: R = H

4: R = CH_3CO

been isolated from the Pacific yew and *Taxus hicksii*, respectively.[7a,b] These organisms probably "learned" to biosynthesize taxol from the tree by horizontal gene transfer.[7c] The fermentation of *Alternaria alternata* yields about 116 mg of taxol per liter.[7b] Further sources being developed include plant tissue cultures (production rates of roughly 55 mg of taxol per liter per week are already reached[7d]) and cell-free biosynthesis.[8] For the optimization of such complex biochemical systems exact information on taxol biosynthesis and its enzyme apparatus is essential, and recently tremendous advances in this area have been achieved.[9–18]

Initial information on the biogenetic origin of the taxol molecular frame was gained through radiolabeling studies by Zamir et al. using *Taxus baccata* and *Taxus canadensis*.[9b] The expected precursors were found: phenylalanine (for the side chain), acetate (for the acetyl residues), and mevalonate (**7**, for the taxane frame). However, the incorporation rates of mevalonate turned out to be very low, and no further degradation studies were undertaken to pinpoint the exact sites of incorporation (see below). Further biosynthetic hypotheses were suggested based on molecular modeling studies and on the structures of isolated side products.[9c]

More exact biosynthetic studies have been reported only recently, and virtually nothing was known about early stages in taxol biosynthesis up until 1995. These studies were led by R. Croteau et al. partially in collaboration with H. G. Floss and R. M. Williams[10,12–15]. The Munich-based teams headed by M. H. Zenk et al. and A. Bacher et al. also contributed interesting results.[10] The first step in the biosynthesis of the taxane diterpenoid frame is the formation of the common building block geranylgeranyl diphosphate (**10**). In this context it was surprising that the taxane frame is not of mevalonoid origin.[10] In incorporation experiments using cell cultures of *Taxus chinensis* with [U-$^{13}C_6$]glucose, [1-^{13}C]glucose, and [1,2$^{13}C_2$]acetate the labeled acetate reached only the acetyl residues (NMR analysis), but not the tricyclic taxane ring frame. The labeled glucose, in contrast, was incorporated in the acetyl groups as well as in the frame of taxol-related compound taxuyunnanine C (**11**, Scheme 1). Especially interesting was the analysis of long-range $^{13}C,^{13}C$ couplings in **11** after the incorpo-

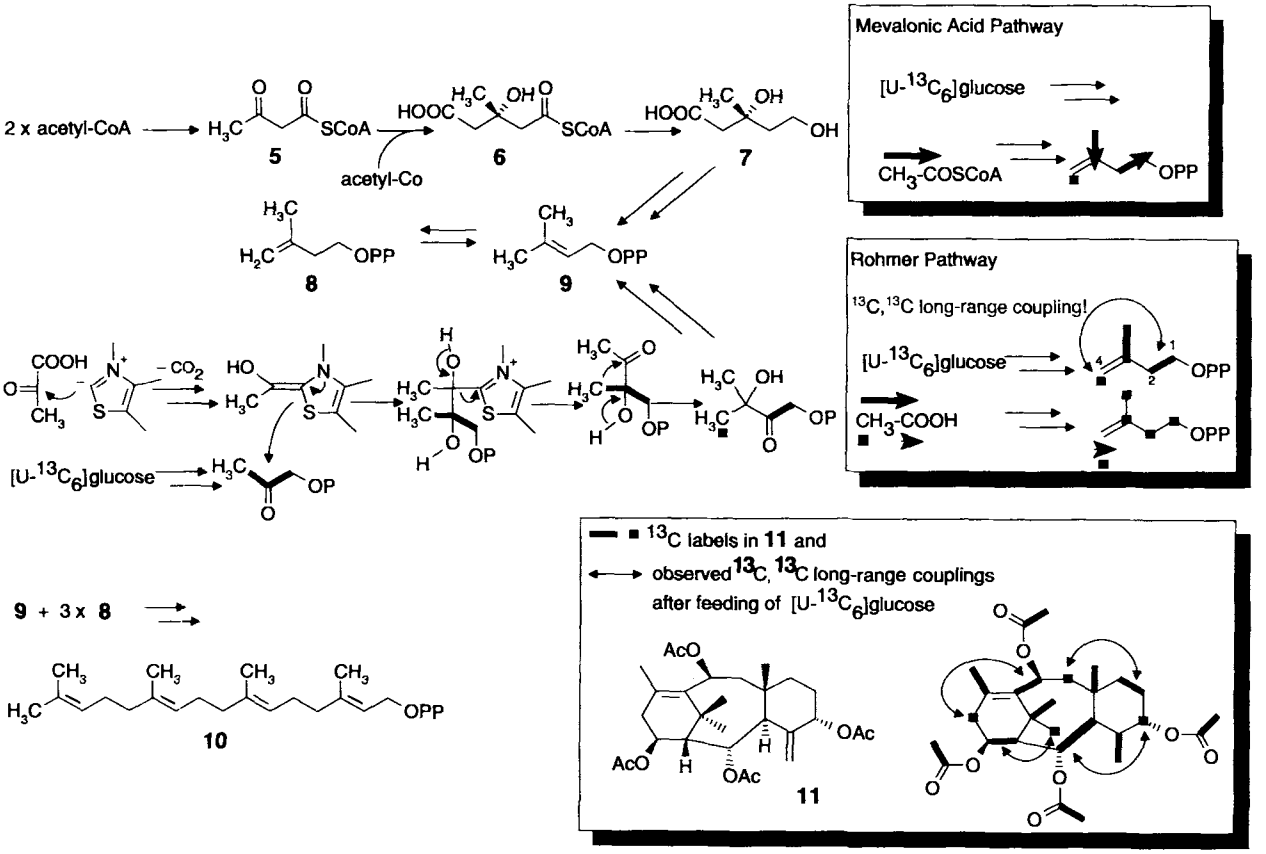

Scheme 1. The classical mevalonic acid and Rohmer's "non-mevalonoid" biosynthetic pathway to isopentenyl pyrophosphate (**8**) and dimethylallyl pyrophosphate (**9**). The labeling pattern in taxoid **11** after the incorporation of [U-$^{13}C_6$]glucose and especially the observed $^{13}C,^{13}C$ long-range couplings within each isoprenoid unit indicate that the taxane skeleton is biosynthesized by a "non-mevalonoid" pathway.

 © WILEY-VCH Verlag GmbH, D-69451 Weinheim, 1997 0570-0833/97/3620-2191 $ 17.50+.50/0

ration of [U-$^{13}C_6$]glucose, since this proved that a C_3 precursor rearranges intramolecularly during the formation of each isoprene unit. This is not consistent with the classical mevalonate pathway,[11a] but remarkably resembles the alternative biosynthetic pathway for isoprenoids recently recognized by M. Rohmer et al. as predominant for the biosynthesis of hopane triterpenoids and ubiquinones in eubacteria (Scheme 1).[11b]

The fundamental building blocks of all isoprenoids, including terpenes such as geranylgeranyl diphosphate (**10**), are isopentenyl pyrophosphate (IPP, **8**) and dimethylallyl pyrophosphate (DMAPP, **9**). These are biosynthesized via acetoacetyl-CoA (**5**), 3-hydroxy-3-methylglutaryl-CoA (HMG-CoA, **6**) and mevalonic acid (MVA, **7**). IPP **8** and DMAPP **9** are in an isomerase-mediated equilibrium. This leads to a labeling pattern showing the same incorporation rates everywhere when [1,2-$^{13}C_2$]acetate or [U-$^{13}C_6$]glucose is used (Scheme 1). In the alternative pathway discovered by Rohmer et al.[11b] IPP and DMAPP are constructed presumably via thiamine-activated acetic aldehyde (which is generated in the course of pyruvate decarboxylation) and dihydroxyacetone phosphate. Cleavage of the thiamine residue is followed by a rearrangement (CH_3 shift) and further reductions, and dehydration and phosphorylation steps (Scheme 1). The characteristic labeling pattern of IPP **8** and DMAPP **9** biosynthesized in this way is principally similar to that arising from the classical pathway when [U-$^{13}C_6$]glucose serves as the source of the isotopic label. But typically one finds different incorporation rates for the carbons of the C_2 and C_3 precursors and characteristic $^{13}C,^{13}C$ long-range couplings between the carbons of the former C_3 precursor within each isoprenoid unit which are separated due to the rearrangement. In contrast to their classically assembled counterparts, alternatively biosynthesized IPP **8** and DMAPP **9** cannot be labeled directly by acetate (one finds either no clear label at all or "scrambling", i.e. indirect incorporation after further metabolism, Scheme 1). This pathway may be in effect in many other organisms,[11c] possibly also in humans, since cholesterol inhibitors such as the HMG-CoA reductase inhibitors compactin and mevinolin (lovastatin) do not disturb the biosynthesis of ubiquinone which is essential for mitochondrial respiration.

The first committed biosynthetic step towards the construction of the tricyclic taxane skeleton is catalyzed by taxadiene synthase, an enzyme responsible for the formation of three C–C bonds.[12] Its final product is taxa-4(5),11(12)-diene **13** and not the isomeric 4(20),11(12)-diene **12** (Scheme 2), which had been favored due to the common occurrence of such taxanes (e.g. **11**). Feeding experiments with [1-^{3}H]geranylgeranyl diphosphate proved that **13** is the first cyclization product. The radiolabeled taxa-4(5),11(12)-diene was converted further into baccatin III (**4**), taxol (**1**), and other taxanes, which proved its role as a biosynthetic intermediate. A cell-free enzyme system was used in these experiments which was prepared from four-year-old *Taxus brevifolia* saplings.[12] After this success the responsible taxadiene synthase was sought. To find the genes encoding this enzyme, DNA primers were constructed based on known conserved gene fragments of putative related terpene cyclases. Amplification of two of these primers by polymerase chain reaction (PCR) yielded a DNA fragment 83 base pairs (bp) in length, whose sequence was homologous to that of a cyclase. A cDNA library of *Taxus brevifolia* DNA was then screened, and one of the hybridizing cDNA fragments was expressed in *E. coli*. The resulting protein (862 amino acids, 98303 g mol^{-1}) proved to be the desired taxadiene synthase and catalyzed the cyclization of geranylgeranyl diphosphate (**10**) to give taxa-4(5),11(12)-diene **13**. This work paved the way for more detailed studies of the mechanisms of this important key enzyme in the taxol biosynthesis.[13]

A taxa-4(20),11(12)-diene intermediate and its rearrangement into the thermodynamically more stable **13** could be ruled out

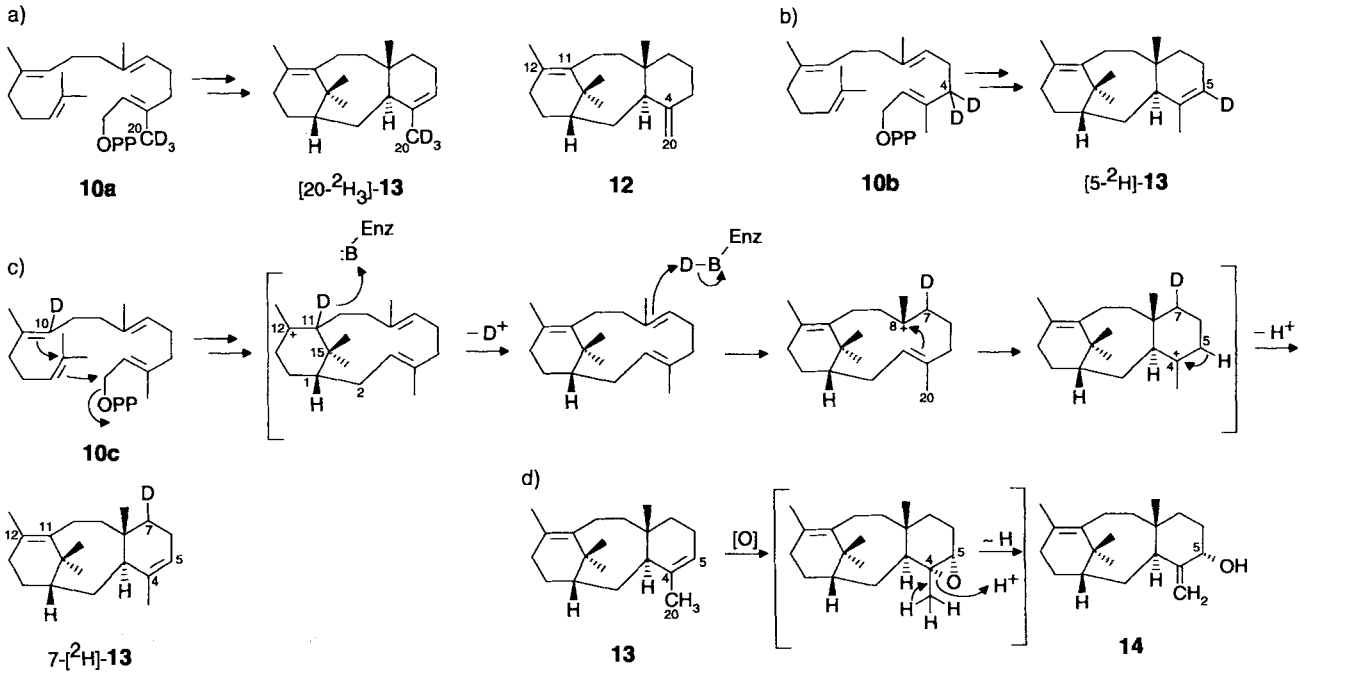

Scheme 2. Experiments with taxadiene synthase (see text for details). The taxa-4(5),11(12)-diene **13** oxygenase reaction: 4,5-α-epoxidation and subsequent rearrangement to give taxa-4(20),11(12)-dienol **14**.

 © WILEY-VCH Verlag GmbH, D-69451 Weinheim, 1997 0570-0833/97/3620-2192 $ 17.50+.50/0

conclusively, since all three deuterium atoms of [20-$^2H_3$]-geranylgeranyl diphosphate (**10a**) were retained during the taxadiene synthase reaction (Scheme 2a). In other work one deuterium atom disappeared when taxadiene synthase was fed [4-$^2H_2$]geranylgeranyl diphosphate (**10b**). This is a clear indication of a direct H^+ abstraction at C-5, and thus direct formation of **13** (Scheme 2b). Particularly interesting was the conversion of [10-^{2}H]geranylgeranyl diphosphate (**10c**), which yielded **13** labeled in the 7-position. This result proves that the C-11/C-15 and the C-1/C-2 connections are made prior to the formation of the C-3/C-8 bond, since the abstraction of one of the protons from C-11 (this was 10-H in **10**) leading to the formation of the C-11/C-12 double bond must occur prior to its reconnection at C-7. This last step generates the cation that enables formation of the last C–C bond in the biosynthesis of the tricyclic taxane skeleton, namely the one between C-3 and C-8. The resulting cation (at the 4-position) undergoes H^+ abstraction from C-5 and the C-4/C-5 double bond of taxa-4(5),11(12)-diene **13** is formed (Scheme 2c).[14]

The biosynthetic conversion of taxa-4(5),11(12)-diene **13** into taxol (**1**) requires extensive oxidative modification of the taxane skeleton, all in all eight oxygenation steps, including the formation of the important oxetane ring. Recently, the first and perhaps most important of these oxygenation steps has been elucidated,[15] namely the 5α-hydroxylation catalyzed by taxadiene-5-hydroxylase. This occurs with the simultaneous shift of the double bond from the 4,5- to the 4,20-position. The enzyme responsible, taxa-4(5),11(12)-diene-5α-hydroxylase could be characterized as a membrane-bound, NADPH-dependent, P450 oxygenase that uses molecular oxygen. Cell-free preparations from *Taxus brevifolia* saplings and cell cultures from *Taxus cupsidata* containing this oxygenase catalyze the reaction of radiolabeled [^{3}H]- and [20-$^2H_3$]taxa-4(5),11(12)-diene. The latter experiment showed a loss of one deuterium in agreement with the shift of the double bond into the 4,20-position. The former experiment allowed access to radiolabeled taxa-4(20),11(12)-dien-5α-ol **14**, which was shown to be a true biosynthetic intermediate by conversion into 10-deacetylbaccatin III (**3**) and taxol (**1**). The absolute configuration of alcohol **14** at the 5-position (5α and not 5β) was proven by TLC comparison with the diastereomers prepared by total synthesis.[15]

The proof that **14** is a biosynthetic intermediate of taxol (**1**) immediately following **13** and that the 5α-hydroxylation is the first oxygenation step and accompanied by the shift of the double bond gave rise to interesting mechanistic consequences, especially regarding the formation of the oxetane ring in **1** and related taxanes. The formation of the oxetane ring always was postulated to be initiated by epoxidation of the 4,20-double bond.[16] This is also the reason why taxa-4(20),11(12)-diene **12** was favored for such a long time as a biosynthetic intermediate (see above). There is evidence[15a] that the rearranged dienol **14** is formed by 4,5-epoxidation of **13** and subsequent opening of this epoxide along with H-migration (Scheme 2d). The observed formation of a 4,20-olefin along with the 5-hydroxylation confirms all the hypotheses favoring 4,20-epoxidation as the first step in the formation of the oxetane ring. The configuration in **14** (5α-OH) and in the oxetane moiety of **1**, however, exclude a direct intramolecular attack of the 4,20-epoxide by the 5-OH group (Scheme 3a). Instead, a more complicated acetate

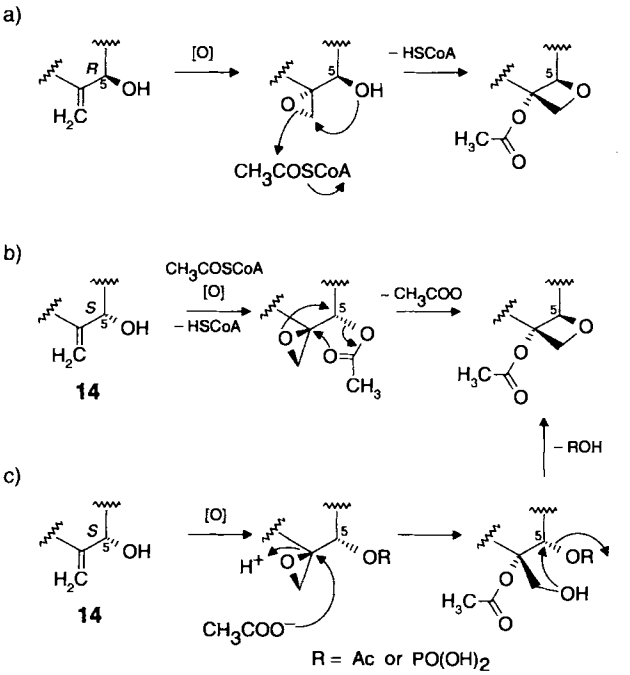

Scheme 3. Alternative mechanisms for the formation of the oxetane ring in **1**. The stereochemistry in taxadienol **14** and the oxetane ring in **1** exclude direct intramolecular opening of the epoxide (as shown in a)). The alternatives shown in b) and c) are still open.

rearrangement with concomitant opening of the epoxide and an S_N2 reaction at C-5 must be considered (Scheme 3b). It is still unclear whether this is an intramolecular acetate migration (Scheme 3b) or an intermolecular acetate opening (Scheme 3c).

The route from taxa-4(20),11(12)-dien-5α-ol **14** to taxol (**1**) is still quite long and for the most part unexplored. Late steps in the biosynthesis in which the taxol side chain is assembled were examined intensively by H. G. Floss et al. The side chain derives entirely from the biogenetic building block phenylalanine (**15**).[9, 17] Debenzoyltaxol **18** is an intermediate, the last one in the long biosynthetic cascade leading to **1**. One reaction that has been never detected before in biosyntheses in plants, a phenylalanine aminomutase reaction, plays a key role in the formation of the side chain from phenylisoserine (**17**), which is essential for the antitumor activity of taxol. In this reaction phenylalanine (**15**) is turned into the corresponding β-amino acid **16** through the 1,2-shift of the amino group (Scheme 4). Another plausible alternative via cinnamic acid (**19**), its isomerization (to the (*Z*) isomer **20**), epoxidation (to **21**), and final ring opening with concurrent amination could be ruled out because of negative incorporation experiments with [$^2H_5$]-**19** and analogously labeled (*Z*)-epoxide **21**. The reaction of the interesting enzyme phenylalanine aminomutase has since been examined closely with cell-free extracts from *Taxus brevifolia* cambial tissue cultures by using selected isotopically labeled precursors and analyzing the products by mass spectrometry. An experiment with [$^2H_5$,^{15}N]phenylalanine (**15a**) showed that the migration of the amino group from the α- to the β-position is strictly intramolecular, since addition of unlabeled **15** yielded only **16**, which gives rise to the molecular ion M^+ and $M+6$, but never $M+5$.[17b] Also the steric course of the reaction could

 © WILEY-VCH Verlag GmbH, D-69451 Weinheim, 1997 0570-0833/97/3620-2193 $ 17.50+.50/0

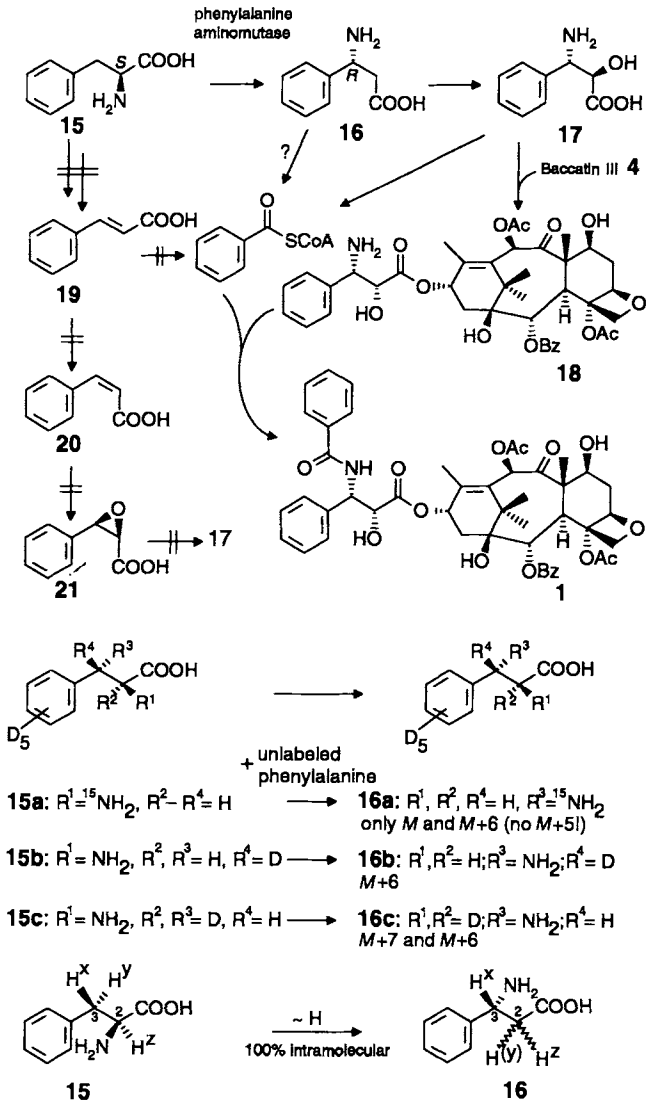

Scheme 4. Late steps in the biosynthesis of taxol (**1**). Both arene rings of the side chain derive from phenylalanine (**15**), which is first rearranged into the corresponding β-phenylalanine (**16**). The alternative path via cinnamic acid (**19**) was ruled out (see text for details). Designed experiments to examine the mechanisms of the phenylalanine aminomutase reaction lead to the stereochemical course shown and a strict intramolecular course of reaction.

be determined. Conversion reactions of [3*R*-^{2}H]- and [2*S*,3*R*-$^2H_2$]-labeled phenylalanine (**15b** and **15c**, respectively) showed that the reaction proceeds with retention of the pro-*R* hydrogen at the 3-position and (partial) migration of the pro-*S* hydrogen from C-3 (in **15**) to C-2 of **16** (Scheme 4).[17b] The biosynthesis of the benzoate residue of the side chain is also performed differently in *Taxus brevifolia* than in other plants, in which a route via cinnamic acid (**19**) is preferred. Incorporation experiments with [$^2H_5$]-β-phenylalanine gave in part double incorporation, as indicated by the $M+10$ peak in the mass spectrum. Thus, the benzoyl group must also be constructed via β-phenylalanine (**16**) (or phenylisoserine (**17**)).

Although many questions regarding the biosynthesis of taxol (**1**) are still unanswered, recent results have pinpointed "bottlenecks" in the pathway. The primary time-consuming, rate-limiting key reactions are the taxadiene synthase and the subsequent oxygenase reaction. Now it is necessary to accelerate these reactions, taking advantage of well-established gene technological methods. A functioning transformation system to amplify the necessary genes coding the biosynthesis of the rate-limiting enzymes and to transform the enhancer genes that regulate certain biosynthetic steps has been already established.[18] It is based on the mutagenic bacterium *Agrobacterium tumefaciens*, a common tool for the targeted mutation of plants. With such methods, the chances are good that the rate of taxol production in plant tissue cultures can be stimulated further. Alternatives include targeted mutations of taxol-producing fungi for further increase of the taxol biosynthesis, and the development of an organism-independent, cell-free enzyme system,[8] a strategy currently under investigation.[8c]

German version: *Angew. Chem.* **1997**, *109*, 2284–2289

Keywords: antitumor agents · biosynthesis · enzymes · isotopic labeling · taxol

[1] a) B. Schneider, *Dtsch. Apoth. Ztg.* **1994**, *134*, 3389–3400, and references therein; b) W. Shakespeare, in *The Complete Works of William Shakespeare*, Avenel Books, New York, **1975**, p. 1060; c) J. Mann, in *Murder, Magic and Medicine*, Oxford University Press, Oxford, **1992**, pp. 1–2.

[2] a) Taxol is now a registered trademark of Bristol-Myers-Squibb; the generic name is paclitaxel; taxotère is a registered trademark of Rhône-Poulenc Rorer; its generic name is docetaxel. Because of the greater familiarity of the words taxol and taxotère, only these are used in the text in lieu of the corresponding generic names; b) There are other microtubuli-stabilizing compounds which, however, are not cytostatics. Therefore the simple equation depolymerization inhibitor = cytotoxic compound is questionable.

[3] a) G. Höfle, N. Bedorf, H. Steinmetz, D. Schomburg, K. Gerth, H. Reichenbach, *Angew. Chem.* **1996**, *108*, 1671–1673; *Angew. Chem. Int. Ed. Engl.* **1996**, *35*, 1567–1569; b) K. Gerth, N. Bedorf, G. Höfle, H. Irschik, H. Reichenbach, *J. Antibiot.* **1996**, *49*, 560–563; c) L. Wessjohann, *Angew. Chem.* **1997**, *109*, 739–742; *Angew. Chem. Int. Ed. Engl.* **1997**, *36*, 738–742.

[4] a) P. Poitier, S. Irseer Naturstofftage, Kloster Irsee, **1993**, see also: J. Rohr, *Nachr. Chem. Tech. Lab.* **1993**, 41, 559–564; b) K. C. Nicolaou, W.-M. Dai, R. K. Guy, *Angew. Chem.* **1994**, *106*, 38–69; *Angew. Chem. Int. Ed. Engl.* **1994**, *33*, 45–76.

[5] a) J.-N. Denis, A. Correa, A. E. Greene, *J. Org. Chem.* **1990**, *55*, 1957–1959; b) G. Li, H.-T. Chang, K. B. Sharpless, *Angew. Chem.* **1996**, *108*, 449–452; *Angew. Chem. Int. Ed. Engl.* **1996**, *35*, 448–451; c) C. Gennari, A. Vulpetti, M. Donghi, N. Mongelli, E. Vanotti, *ibid.* **1996**, *108*, 1809–1812 and **1996**, *35*, 1723–1725, and references therein.

[6] a) R. A. Holton, C. Somoza, H.-B. Kim, F. Liang, R. J. Biediger, P. D. Boatman, M. Shindo, C. C. Smith, S. Kim, H. Nadizadeh, Y. Suzuki, C. Tao, P. Vu, S. Tang, P. Zhang, K. K. Murthi, L. N. Gentile, J. H. Liu, *J. Am. Chem. Soc.* **1994**, *116*, 1597–1600; b) K. C. Nicolaou, Z. Yang, J. J. Liu, H. Ueno, P. G. Nantermet, R. K. Guy, C. F. Claiborne, J. Renaud, E. A. Couladouros, K. Paulvannan, E. J. Sorensen, *Nature* **1994**, *367*, 630–634; c) S. J. Danishefsky, J. J. Masters, W. B. Young, J. T. Link, L. B. Snyder, T. V. Magee, D. K. Jung, R. C. A. Isaacs, W. G. Bornmann, C. A. Alaimo, C. A. Coburn, M. J. Di-Grandi, *J. Am. Chem. Soc.* **1996**, *118*, 2843–2859; d) P. A. Wender, N. F. Badham, S. P. Conway, P. E. Floreancig, T. E. Glass, J. B. Houze, N. E. Krauss, D. Lae, D. G. Marquess, P. L. McGrane, W. Meng, M. G. Natchus, A. J. Shuker, J. C. Sutton, R. E. Taylor, *ibid.* **1997**, *119*, 2757–2758; e) L. Wessjohann, *Angew. Chem.* **1994**, *106*, 1011–1013; *Angew. Chem. Int. Ed. Engl.* **1994**, *33*, 959–961.

[7] a) A. Stierle, G. Strobel, D. Stierle, *Science* **1993**, *260*, 214–216; b) J. S. Dahiya (Novopharm Ltd.), WO 9632490 A1, **1996** [*Chem. Abstr.* **1996**, *125*, 326547]; c) Horizontal gene transfer may also have been performed the other way around, or could have even developed co-evolutively. However, since taxoids are typical plant products, the direction favored here seems to be most likely; d) Y. Yukimune, *Nat. Biotech.* **1996**, *14*, 1129.

[8] a) C. A. Roessner, A. I. Scott, *Chem. Biol.* **1996**, *3*, 325–330; b) A. I. Scott, *Tetrahedron* **1992**, *48*, 2559–2578; c) personal communication, **1996**.

[9] a) S. Borman, *Chem. Eng. News* **1996**, *74(27)*, 27–29; b) L. O. Zamir, M. E. Nedea, F. X. Garneau, *Tetrahedron Lett.* **1992**, *33*, 5235–5236; c) Y. Boulanger, A. Khiat, Z.-H. Zhou, G. Caron, L. O. Zamir, *Tetrahedron* **1996**, *52*, 8957–8968.

[10] W. Eisenreich, B. Menhard, P. J. Hylands, M. H. Zenk, A. Bacher, *Proc. Natl. Acad. Sci. USA* **1996**, *93*, 6431–6436.

 © WILEY-VCH Verlag GmbH, D-69451 Weinheim, 1997 0570-0833/97/3620-2194 $ 17.50+.50/0

[11] a) D. Voet, J. G. Voet, *Biochemie*, **1994**, VCH, Weinheim, p. 639–659; b) M. Rohmer, M. Knani, P. Simonin, B. Sutter, H. Sahm, *Biochem. J.* **1993**, *295*, 517–524; c) H. Seto, H. Watanabe, K. Furihata, *Tetrahedron Lett.* **1996**, *37*, 7979–7982.
[12] A. E. Koepp, M. Hezari, J. Zajicek, B. Stofer Vogel, R. E. LaFever, G. N. Lewis, R. Croteau, *J. Biol. Chem.* **1995**, *270*, 8686–8690.
[13] M. R. Wildung, R. Croteau, *J. Biol. Chem.* **1996**, *271*, 9201–9204.
[14] X. Lin, M. Hezari, A. E. Koepp, H. G. Floss, R. Croteau, *Biochemistry* **1996**, *35*, 2968–2977.
[15] a) J. Hefner, S. M. Rubenstein, R. E. B. Ketchum, D. M. Gibson, R. M. Williams, R. Croteau, *Chem. Biol.* **1996**, *3*, 479–489; b) S. M. Rubenstein, R. M. Williams, *J. Org. Chem.* **1995**, *60*, 7215–7223.
[16] a) F. Guéritte-Voegelein, D. Guénard, P. Poitier, *J. Nat. Prod.* **1987**, *50*, 9–18; b) H. G. Floss, U. Mocek, in *Taxol: Science and Applications* (Ed.: M. Suffness), **1995**, CRC Press, Boca Raton, FL, USA, pp. 191–208.
[17] a) P. E. Fleming, U. Mocek, H. G. Floss, *J. Am. Chem. Soc.* **1993**, *115*, 805–807; b) H. G. Floss, personal communication, **1997**.
[18] K.-H. Han, P. Fleming, K. Walker, M. Loper, W. S. Chilton, U. Mocek, M. P. Gordon, H. G. Floss, *Plant Sci.* **1994**, *95*, 187.

EVENTS

Announcing the

XXIII International Symposium on Macrocyclic Chemistry

Macrocycles in Academe and Industry

June 7th–12th, 1998
Turtle Bay, Hawai

Imaging, Chelation, Catalysis, Molecular Recognition, Sensing.
Poster Presentations Currently Being Accepted.

Site of symposium is the Turtel Bay Hilton on the North Shore of the Island of Oahu. Activities of interest include golf, surfing, and tennis. An excursion to the Polynesian Center is planned. Organized by Jonathan Sessler, Eric Anslyn, and Eiichi Kimura.

To acquire registration and poster contribution forms please write: Eric V. Anslyn, Department of Chemistry and Biochemistry, The University of Texas at Austin, Austin TX 78712, or e-mail anslyn@ccwf.cc.utexas.edu.

 © WILEY-VCH Verlag GmbH. D-69451 Weinheim, 1997 0570-0833/97/3620-2195 $ 17.50+.50/0

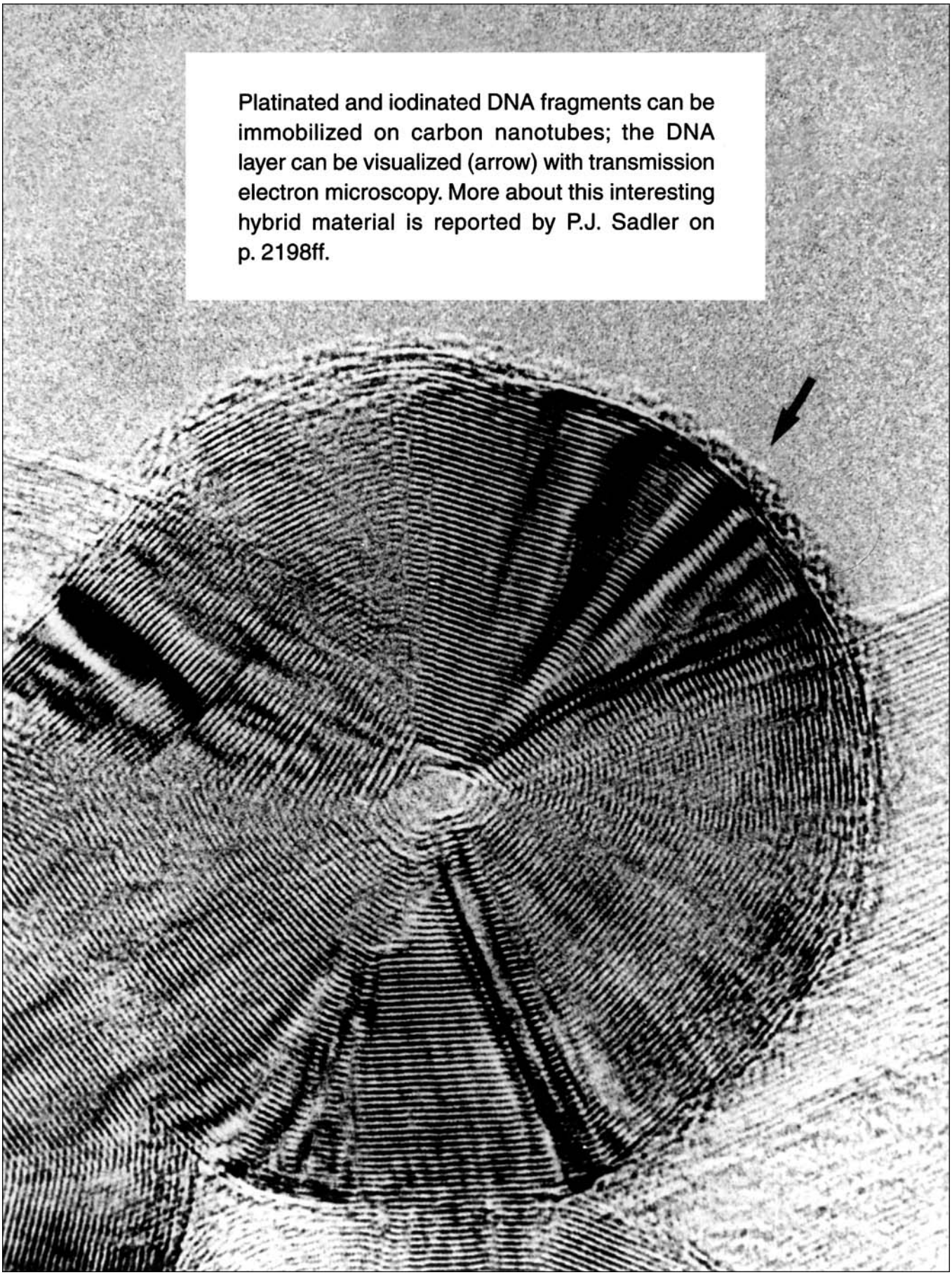

 © WILEY-VCH Verlag GmbH, D-69451 Weinheim, 1997 0570-0833/97/3620-2197 $ 17.50+.50/0

Immobilization of Platinated and Iodinated Oligonucleotides on Carbon Nanotubes**

Shik Chi Tsang, Zijian Guo, Yao Kuan Chen, Malcolm L. H. Green, H. Allen O. Hill, Trevor W. Hambley, and Peter J. Sadler*

Rapid advances in biotechnology are making major contributions to our understanding of health and disease, stimulating much current interest in designing novel systems for detecting abnormalities and for delivering (bio)chemicals to target diseases with limited side effects. In this context, the development of techniques for the study of molecular recognition is particularly important in the area of biochemical sensing, drug delivery, and gene therapy. For example, there has been recent interest in anchoring DNA onto a solid surface so that it may function as a chemical recognition agent for complementary DNA or for specific proteins.[1]

Carbon is the most common support material for the immobilization of biomolecules because of its strength, stability, and electrical conductivity.[2] However, only a limited amount of work on the structure and morphology of biomolecules adsorbed onto carbon materials has been reported. Recently discovered nanotubes have fullerene-type structures of concentric tubular carbon layers and a prominent central cavity 30–60 Å in diameter. This novel form of carbon has a higher electrical conductivity than graphite[3] and can be prepared on a gram-scale by high-temperature arc vaporization of graphite electrodes.[4, 5] We report here the synthesis and immobilization of small, platinated and iodated DNA oligomers and their immobilization on carbon nanotubes. These heavy-atom-labeled oligomers readily scatter electrons, which allows indirect visualization by high-resolution transmission electron microscopy (TEM).

Carbon nanotubes were prepared as previously reported.[6] TEM examination of the nanotube-rich distillate showed it to consist of fiberlike nanotubes (about 30%) and graphitic particles (about 70%). The TEM images of the tip region showed that the carbon tubes invariably had closed ends. In order to investigate whether DNA could be trapped inside nanotubes, opened nanotubes were prepared by treatment with HNO_3, and most of the surface acidic groups were removed by heat treatment.[7] TEM examination of the sample showed that more than 80% of the tubes were selectively opened in the cap region[8] and that the internal cavities were clean and empty.

The nanotubes were then treated with a DNA duplex labeled with a heavy atom, which could be clearly seen by the TEM technique. For this purpose a self-complementary 14-mer (**I**)

d(5'A-T-**G**-**G**-T-A-G-^{I}**C**-T-A-^{I}**C**-^{I}**C**-A-T3') **I**

containing 5-iodocytosine (^{I}C) and a GG pair, which could be labeled with chelated *cis*-$[Pt(NH_3)_2]^{2+}$ was chosen. The ^{1}H NMR spectrum of this oligonucleotide over the pH range of 4.4 to 7 (H_2O/D_2O (9/1), 0.1 M $NaClO_4$) showed 5 to 11 peaks in the region $\delta = 11.5-13.5$, typical of imino NH protons in Watson–Crick base pairs.[9] The duplex (**II**) was platinated specifically at G(3)·G(4) by treatment with 0.9 equivalents (i.e., ca. one Pt per duplex) of a solution containing equimolar amounts of *cis*-$[Pt(H_2O)_2(^{15}NH_3)_2]^{2+}$ and *cis*-$[PtCl(H_2O)(^{15}NH_3)_2]^{+}$, the reactive hydrolysis products of the anticancer drug cisplatin.[10] The reaction was monitored by [^{1}H,^{15}N] HSQC 2D NMR spectroscopy.[11, 12] The diaqua complex reacted very rapidly to give the GG chelate, and no monofunctional aqua intermediates were seen, whereas the monoaquamonochloro complex gave rise to two monofunctional intermediates *cis*-$[PtCl(NH_3)_2$(G3-N7)] and *cis*-$[PtCl(NH_3)_2$(G4-N7)] (Figure 1). One of the monofunctional adducts predominated,

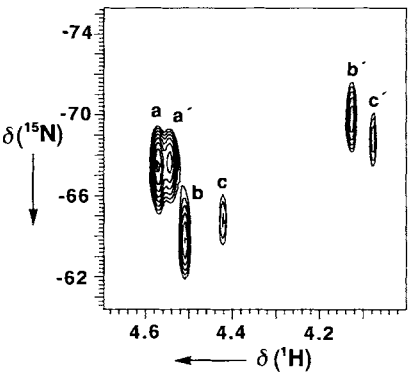

Figure 1. Two-dimensional [^{1}H,^{15}N] NMR spectrum recorded 12 h after mixing duplex **II** with 0.9 equiv of a solution of *cis*-$[Pt(H_2O)_2(^{15}NH_3)_2]^{2+}$ and *cis*-$[PtCl(H_2O)(^{15}NH_3)_2]^{+}$. At the end of the reaction (about 72 h) only peaks **a** and **a'** were present, which are assignable to the nonequivalent Pt-NH_3 ligands in the GG chelate Pt-**II**. Peaks **b**, **b'**, and **c**, **c'** are assignable to the monofunctional intermediates platinated at G(3) or G(4) (two peaks in each case: NH_3 *trans* to N7 and Cl).

an effect which has been observed recently for a 14-mer DNA oligonucleotide duplex.[12] After three days the GG chelate was the only final product detected by [^{1}H,^{15}N] NMR spectroscopy. The presence of about ten resonances in the imino region of the ^{1}H NMR spectrum suggested that the duplex structure of **II** was retained after platination, as is usual for such adducts.[10] The model of Pt-**II** shown in Figure 2 serves to indicate the position of the heavy atoms in this duplex.

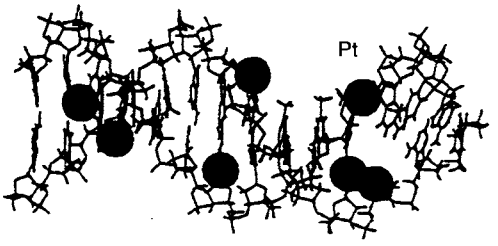

Figure 2. B-DNA model of Pt-**II** showing the positions of the heavy atoms (artificially enlarged; unlabeled heavy atoms are iodine atoms).

[*] Prof. Dr. P. J. Sadler, Dr. Z. Guo, Dr. T. W. Hambley[+]
Department of Chemistry
University of Edinburgh
West Mains Road, Edinburgh EH9 3JJ (UK).
Fax: Int. code +(131)650-6452
e-mail: p.j.sadler@ed.ac.uk

[+] Permanent address: School of Chemistry, University of Sydney (Australia)

Dr. S. C. Tsang
The Catalysis Research Centre, Department of Chemistry
University of Reading (UK).

Y. K. Chen, Prof. Dr. M. L. H. Green, Prof. Dr. H. A. O. Hill
Inorganic Chemistry Laboratory, University of Oxford (UK)

[**] This work was supported by the Association for International Cancer Research and BBSRC. PJS thanks the EC and EPSRC for support of HCM and COST programs, and SCT The Royal Society for a University Fellowship. We thank the MRC NMR Centre, Mill Hill, for provision of NMR facilities, and Dr. J. L. Hutchinson, Department of Materials, University of Oxford, for use of the JEOL 4000 EX microscope and for helpful discussions, and Dr R. Henderson (MRC Laboratory of Molecular Biology, Cambridge) for critical comments on the script.

 © WILEY-VCH Verlag GmbH, D-69451 Weinheim, 1997 0570-0833/97/3620-2198 $ 17.50+.50/0

Both closed and opened nanotubes were treated with Pt-**II**. Figure 3 shows closed nanotubes (with graphitic layers) entirely embedded beneath a layer of amorphous material. A small amount of the amorphous material could be due to contamination of the sample during preparation and transfer, and local electrical charges induced by the electron beam could lead to the attraction of amorphous material inside the microscope chamber. However, contamination by such a large quantity of amorphous material on nanotube surfaces such as those shown in Figure 3 has never been observed. Nanotubes treated similarly

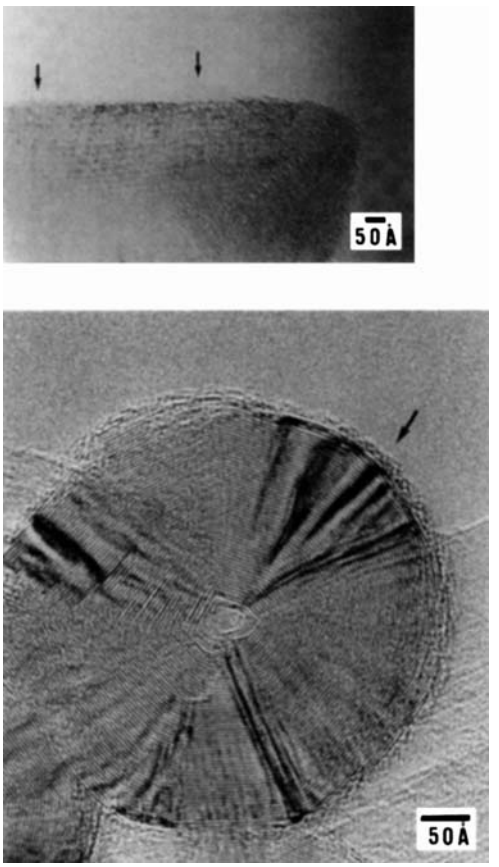

Figure 3. TEM images of closed nanotubes after treatment with Pt-**II**. Top: side view; bottom: an end. The arrows indicate adsorbed layers of amorphous material (DNA) on the surface.

but without the presence of Pt-**II** showed clear surfaces free of contamination. X-ray dispersive analysis (EDX) indicated that adsorbed material contained Pt, P, I, Cl, Na, and some Ca. We therefore infer that the amorphous surface layer is due to Pt-**II** (and $NaClO_4$). The immobilized material gave IR absorption peaks at 1630 cm^{-1} (NH_2 bending mode), 1097 cm^{-1} (phosphate backbone), 1000–1400 cm^{-1} (nucleobases), and 800 cm^{-1} (deoxyribose), typical of DNA.[13]

Good contrast from the amorphous material was obtained in some TEM images. This may arise from the heavy elements Pt and I, which scatter electrons more readily than the background. The amorphous material tended to cover the nanotube surface very evenly with an average thickness of 7–13 Å, although some larger aggregation patches were also observed (Figure 3, top). This indicates that the material interacts strongly with the carbon surface and has good surface-wetting properties. The strong binding was illustrated by the fact that material was still observable on open nanotubes (2 mg) after treatment with Pt-**II** (1 mL of a 3 μM solution) for 24 h and followed by incubation in water for 24 h. The adsorption of duplex **II** was studied by UV spectroscopy (see Experimental Section). Even after washing, about 25 μg of **II** (46% of added DNA) was adsorbed onto 2 mg of closed tubes and 12 μg of **II** (22% of added DNA) onto open tubes. The material washed off the tubes was shown to be double helical DNA by melting experiments. The greater adsorption of DNA onto closed nanotubes is consistent with the introduction of negative charges on the surface after oxidation of the tubes.

No clear image of the surface adsorbed DNA was obtainable, perhaps because of radiation damage. Blurring of images due to beam-induced specimen movement and charging has been reported previously.[14] Nevertheless the fairly uniform thickness of adsorbed molecules (7–13 Å) indicates excellent surface recognition properties. The large major groove of B-DNA results in it having a regular cross-section and is consistent with the observed two-dimensional width variation of 7–13 Å, being dependent on the projection angle and position relative to the electron beam. Thus, the surface layer coating the nanotubes is likely to be double-stranded helical DNA. DNA on some inert surfaces (for example, glass) can have a similar morphology as in bulk aqueous solution.[15] Some TEM pictures appeared to show the presence of highly coiled Pt-**II** trapped inside open nanotubes with filling along the entire length of the tube but in a discontinuous manner. Presumably when the tubes were dried and water was removed, the DNA anchored to the internal surface in a regular fashion. The included materials appeared to form long aggregates inside the nanotubes.

We have previously reported[6] immobilization of proteins and enzymes in and on the nanotubes and now anticipate that carbon nanotubes with their well-defined structures, defect-free surfaces and tubular morphology may be of general utility in the study of molecular recognition processes including biomolecule–carbon interactions of importance to the design of biosensors.

Experimental Section

Chemicals: The iodinated oligonucleotide I was supplied by OSWEL DNA Service (University of Southampton). *cis*-$[PtCl_2(^{15}NH_3)_2]$ was synthesized by a standard method [16], and the solution of *cis*-$[Pt(H_2O)_2(^{15}NH_3)_2]^{2+}$ and *cis*-$[PtCl(H_2O)(^{15}NH_3)_2]^{+}$ was prepared by treating *cis*-$[PtCl_2(^{15}NH_3)_2]$ with 1.5 equiv of $AgNO_3$ for 24 h followed by removal of AgCl. Carbon nanotubes were prepared by the arc vaporization method [6]. Open tubes were obtained by suspending closed tubes in HNO_3 and heating at reflux for 4 h [8]. The open tubes were washed thoroughly with H_2O, dried in air at 100 °C, and heated at 700 °C for 4 h to remove most of the surface acidic groups [7]. Immobilization was carried out by mixing 0.5 mL of a 0.5 mM solution of Pt-**II** (as used for NMR) with 2 mg of closed or opened tubes. To avoid DNA damage, no sonication was used. Typically the sample was preconcentrated under vacuum, and a droplet of the suspension was placed on a copper grid (400 mesh) covered with perforated carbon film. Tubes for the control experiments were treated in the same way except for the absence of added Pt-**II**.

Instruments: DNA samples were characterized by UV, IR, NMR, and HRTEM. UV spectra were recorded on a Perkin Elmer Lambda 16 spectrometer in 1 cm cells and a PTP-1 Peltier temperature programmer. The NMR spectra were recorded on Varian UNITY plus-500 and UNITY-600 spectrometers fitted with pulsed-field-gradient modules. ^1H chemical shifts were internally referenced to TSP ($Me_3Si(CD_2)_2CO_2Na$), and the ^{15}N shifts to 1.5 M NH_4Cl in 1 M HCl. The 2D [^1H, ^{15}N] HSQC spectra (optimized for $J(N,H) = 72$ Hz) were recorded as previously reported [11,12,17] with the sequence of Stonehouse et al. [18]. The electron micrographs were recorded on JEOL 4000EX and 2000FX high resolution microscopes. The accelerating voltages were adjusted to 200 kV in all cases. The microscopes were operated at their optimum defocusing conditions. In order to reduce contamination, short illumination times (less than one minute), low beam intensity, and improved vacuum by use of liquid nitrogen traps were employed. Energy X-ray analysis (EDX) was used to confirm the presence of Pt and I on nanotubes treated with Pt-**II**.

UV studies of DNA adsorption: Open or closed nanotubes (2 mg) were incubated with 1 mL of a 7 μM solution of duplex II in 0.1 M $NaClO_4$ for 24 h at ambient

 © WILEY-VCH Verlag GmbH, D-69451 Weinheim, 1997 0570-0833/97/3620-2199 $ 17.50+.50/0

temperature with occasional agitation. The supernatant was separated by ultrafiltration (Centricon, Amicon, cut-off 30 kDa, 6 h at 15 °C). The nanotubes were then washed with water (0.6 mL), and the separation was repeated. In a control experiment (to check for adsorption of DNA onto the membrane filter), DNA solution was added to the ultrafiltration tube in the absence of nanotubes, and the separation and washing steps carried out as before. DNA concentrations were determined from the absorption at 260 nm. The recovery of DNA in the control experiment was >87%. A second set of experiments was carried out with 0.1 M $NaClO_4$ to wash the tubes, and then melting curves for the desorbed DNA were determined by UV.

Molecular modeling: A bifunctional Pt adduct was constructed on one strand of a B-DNA model with the HyperChem program [19] and restrained energy minimization, followed by docking of the ammine ligands in an appropriate geometry. This produced a model of the bifunctional adduct similar to those obtained with Newton–Raphson energy minimization and a force field developed for Pt/DNA interactions [20]. Iodine atoms were then added to the 5-positions of each cytidine base.

Received: December 3, 1996
Revised version: May 23, 1997 [Z9850IE]
German version: *Angew. Chem.* **1997**, *109*, 2291–2294

Keywords: electron microscopy · immobilization · molecular recognition · nanotubes · oligonucleotides

[1] K. M. Millan, A. J. Spurmanis, S. R. Mikkelsen, *Electroanalysis* **1992**, *4*, 929–932.
[2] P. Pantano, W. G. Kuhr, *Electroanalysis* **1995**, *7*, 405–416.
[3] H. J. Dai, E. W. Wong, C. M. Lieber, *Science* **1996**, *272*, 523–526.
[4] S. Iijima, *Nature* **1991**, *354*, 56–58.
[5] T. W. Ebbesen, P. M. Ajayan, *Nature* **1992**, *358*, 220–222.
[6] S. C. Tsang, J. J. Davis, M. L. H. Green, H. A. O. Hill, Y. C. Leung, P. J. Sadler *J. Chem. Soc. Chem. Commun.* **1995**, 1803–1804.
[7] R. M. Lago, S. C. Tsang, K. L. Lu, Y. K. Chen, M. L. H. Green, *J. Chem. Soc. Chem. Comm.* **1995**, 1355–1356.
[8] S. C. Tsang, Y. K. Chen, P. J. F. Harris, M. L. H. Green, *Nature* **1994**, *372*, 159–162.
[9] G. C. K. Roberts, *NMR of Macromolecules, a Practical Approach*, Oxford University Press, Oxford, **1993**.
[10] J. Reedijk, *Chem. Commun.* **1996**, 801–806.
[11] K. J. Barnham, S. J. Berners-Price, T. A. Frenkiel, U. Frey, P. J. Sadler, *Angew. Chem.* **1995**, *107*, 2040–2043; *Angew. Chem. Int. Ed. Engl.* **1995**, *34*, 1874–1877.
[12] S. J. Berners-Price, K. J. Barnham, U. Frey, P. J. Sadler, *Chem. Eur. J.* **1996**, *2*, 1283–1291.
[13] R. J. H. Clark, E. E. Hester, *Spectroscopy of Biological Systems*, Wiley, Chichester, **1986**.
[14] R. Henderson, *Q. Rev. Biophys.* **1995**, *28*, 171–193.
[15] Y. S. Melnikova, N. Kumazawa, K. Yoshikawa, *Biochem. Biophys. Res. Commun.* **1995**, *214*, 1040–1044.
[16] S. J. S. Kerrison, P. J. Sadler, *J. Chem. Soc. Chem Commun.* **1977**, 861–863.
[17] S. J. Berners-Price, U. Frey, J. D. Ranford, P. J. Sadler, *J. Am. Chem. Soc.* **1993**, *115*, 8649–8659.
[18] J. Stonehouse, G. L. Shaw, J. Keeler, E. D. Laue, *J. Magn. Reson. Ser. A* **1994**, 174–184.
[19] HyperChem, Release 2 for Windows, Autodesk, Sausalito, California, USA.
[20] T. W. Hambley, *Inorg. Chem.* **1991**, *30*, 937–942.

Beltlike Aromatic Hydrocarbons by Metathesis Reaction with Tetradehydrodianthracene**

Stefan Kammermeier, Peter G. Jones, and Rainer Herges*

One of the main motivations for the synthesis of cyclophanes is the preparation and investigation of compounds in which the π-electron system is spherically deformed by the introduction of bridging ligands (Scheme 1, left).[1] Fully conjugated belt- and

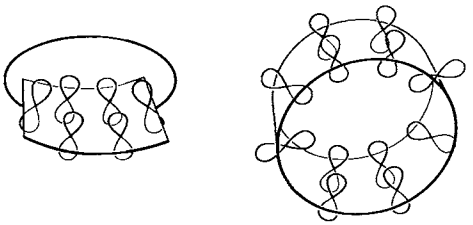

Scheme 1. Spherically deformed π systems in a cyclophane (left) and in a beltlike conjugated system (right).

tubelike structures can be viewed as an extreme example of such a deformation (Scheme 1, right).[2] The p orbitals in these structures are perpendicular to the surface of a cylinder and their inner lobes point towards the axis of the cylinder. To date, three such systems have been prepared by conventional synthesis and isolated as stable compounds.[3–5] Formally, the nanotubes generated by vaporization of carbon[6] and chemical vapor deposition (CVD)[7] also belong to this class of compounds.

Our approach to the synthesis of molecular belts and tubes is based on the ring enlargement metathesis[8] of tetradehydrodianthracene **1** (TDDA).[9] Scheme 2 illustrates the molecular unit construction system employed. a) Bianthraquinodimethanes are obtained starting from TDDA **1** and noncyclic alkenes;[3] b) cyclophanelike, bridged bianthraquinodimethanes are available from TDDA and cyclic alkenes;[3] c) tubelike anthracene-9,10-bisylidenes, which are connected by quinoid double bonds, can be constructed by dimerizing metathesis;[4] and d) bianthraquinodimethanes bridged by conjugated chains are formed from [*n*]annulenes.[3] The double bonds in the bridge of these beltlike conjugated systems should again be able to undergo metathesis with TDDA. This should provide access to larger conjugated systems composed of anthracenylidene units connected by quinoid double bonds and diene units in an alternating sequence. We now report on the synthesis of the smallest of these beltlike, fully conjugated systems which has 20 carbon atoms in its perimeter ($n = 0$, Scheme 2d).

In principle, cyclobutadiene, the smallest [*n*]annulene, would be suitable for the synthesis of the conjugated, bridged bianthraquinodimethane. Cyclobutadiene can be generated in situ[10] and also undergoes [2+2]cycloadditions;[11] however,

[*] Prof. Dr. R. Herges, Dr. S. Kammermeier
Institut für Organische Chemie der Technischen Universität
Hagenring 30, D-38106 Braunschweig (Germany)
Fax: Int. code +(531)391-5266
e-mail: r.herges@tu-bs.de
Prof. Dr. P. G. Jones
Institut für Anorganische und Analytische Chemie der Technischen Universität Braunschweig

[**] This work was supported by the Deutsche Forschungsgemeinschaft and by the Fonds der Chemischen Industrie (scholarship for S. K.).

 © WILEY-VCH Verlag GmbH, D-69451 Weinheim, 1997 0570-0833/97/3620-2200 $ 17.50+.50/0

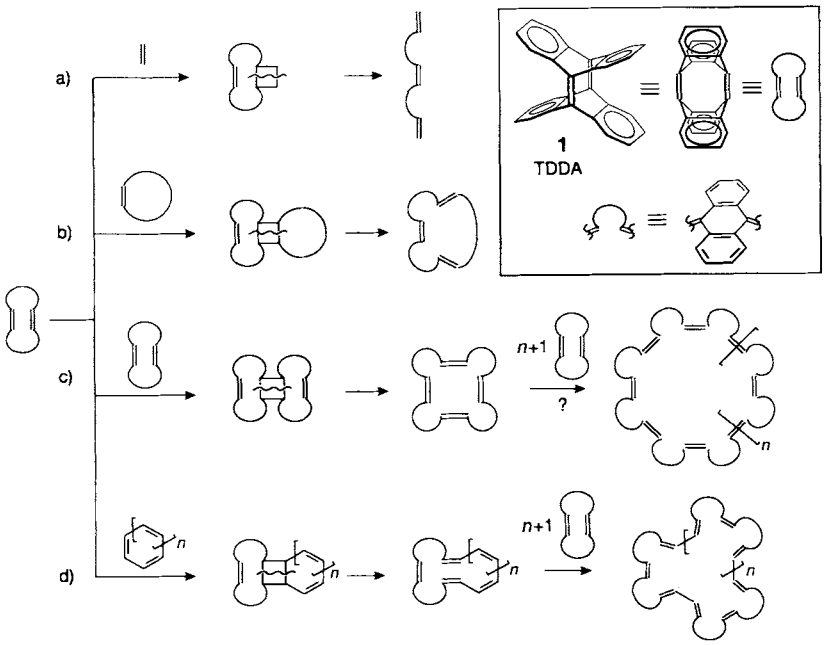

Scheme 2. Molecular unit construction system for the synthesis of molecular belts and tubes.

we chose the more comfortable detour via α-pyrone and 1,2-diazine. Both dienes react with TDDA **1** in boiling toluene yielding the Diels–Alder adducts **2**[12] and **3**, which eliminate CO_2 and N_2, respectively (Scheme 3). Electrocyclic ring opening results in the desired product **5** ("Kammermeierphane 1"[13]). In contrast to **3**, adduct **2** can be isolated and characterized.

According to the X-ray analysis (Figure 1),[14] the bridging ethene unit in **5** is *syn* with respect to the two quinoid double bonds. The C_s-symmetrical structure is also in agreement with a thermochemically allowed electrocyclic ring opening of **4**.

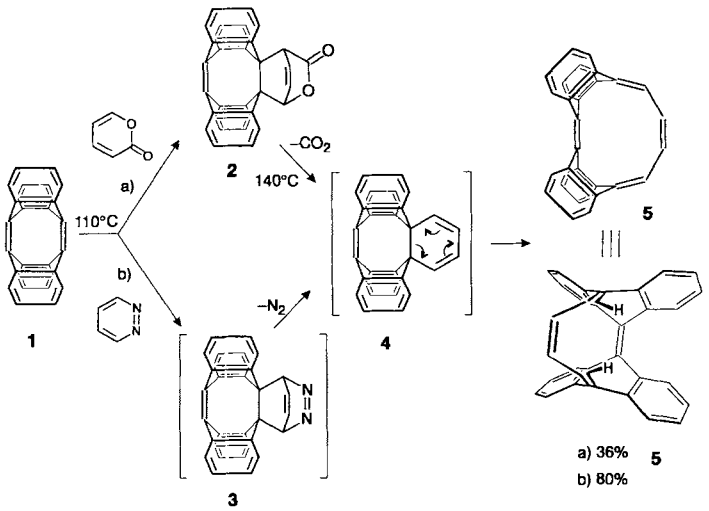

Scheme 3. Synthesis of "Kammermeierphane 1" **5** by reaction of **1** with a) α-pyrone and b) 1,2-diazine.

The sterically easily accessible double bond in the bridging part of **5** can serve as the reaction partner in a second metathesis reaction with TDDA **1**. Photochemically induced metathesis of **1** with **5** (benzene, 150W high-pressure mercury lamp, quartz filter,[15] room temperature, 1 h) directly leads to cyclophane **6** ("Kammermeierphane 2"[13]), which has the molecular formula $C_{60}H_{36}$ (Scheme 4).

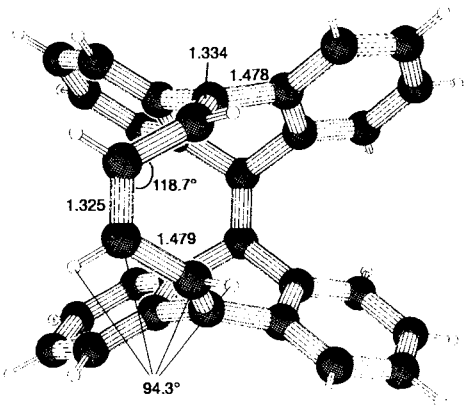

Figure 1. X-ray crystal structure of **5**.

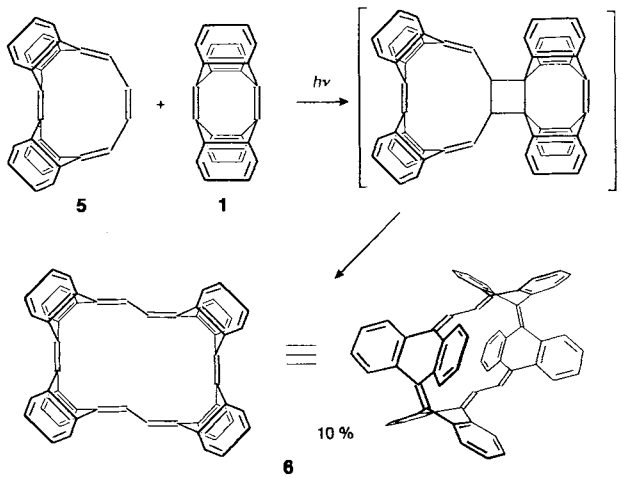

Scheme 4. Synthesis of **6** by metathesis of **1** with **5**.

Compound **6** is composed of two bianthraquinodimethane units, which are connected by C–C bonds such that a fully conjugated beltlike system is formed. The structure of **6** can be viewed as a subunit of a (5,5)-armchair nanotube.[16] According to AM1 calculations[17] and simple considerations based on space-filling models, the 1,3-butadiene units in the bridge must have s-*trans* configuration (C_{2h}). The s-*cis*/s-*trans* (C_1) and s-*cis*/s-*cis* (C_{2v}) configurations are not possible for steric reasons and would be highly strained. The NMR spectra confirm the C_{2h}-symmetrical structure. Because the structure itself prevents rotation about the single bonds, **6** has a rigid conformation. According to AM1 calculations the cavity of the approximately rectangular tube has dimensions of 7.9 × 4.8 Å. Figure 2 shows the calculated van der Waals surface of **6**. Based on the strategy illustrated in Scheme 2, it should be possible to synthesize larger belt- and tubelike π systems.

Experimental Section

2: A solution of **1** (100 mg, 0.284 mmol) and α-pyrone (82 mg, 0.852 mmol) in toluene (60 mL) was heated at reflux for 30 h. During the reaction two portions of α-pyrone were added (82 mg each). The solvent was removed in vacuo and the residue was purified by chromatography with hexane/ethyl acetate 2/1 on silica gel

 © WILEY-VCH Verlag GmbH, D-69451 Weinheim, 1997 0570-0833/97/3620-2201 $ 17.50+.50/0

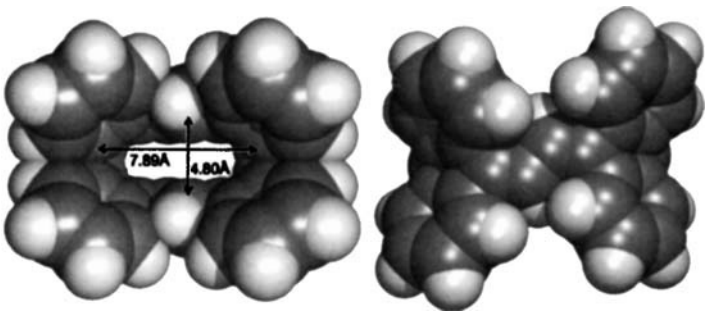

Figure 2. AM1-calculated van der Waals surface of "Kammermeierphane 2" **6** ($C_{60}H_{36}$).

(R_f = 0.37). Compound **2** was obtained as a colorless solid. Yield: 90 mg (71%). M.p. 229 °C (decomp); ^{1}H NMR (400 MHz, $CDCl_3$): δ = 7.72 (m, 1H; CH, arom.), 7.58 (m, 1H; CH, arom.), 7.17 (m, 6H; CH, arom. and CH=CH), 6.90 (m, 10H; CH, arom.), 5.95 (dd, J = 4.3 Hz, J = 2.9 Hz, 1H; CH, saturated), 4.39 (dd, J = 5.1 Hz, J = 2.7 Hz, 1H; CH, saturated); ^{13}C NMR (100.6 MHz, $CDCl_3$): δ = 174.16 (C=O), 150.76 (C_q), 150.76 (C_q), 147.95 (C_q), 147.29 (C_q), 147.26 (C_q), 146.95 (C_q), 144.38 (C_q), 143.56 (C_q), 143.09 (C_q), 142.87 (C_q), 133.43 (CH=CH), 132.23 (CH=CH), 126.79 (CH, arom.), 126.51 (CH, arom.), 126.38 (CH, arom.), 126.38 (CH, arom.), 126.38 (CH, arom.), 126.12 (CH, arom.), 125.98 (CH, arom.), 125.21 (CH, arom.), 125.21 (CH, arom.), 125.07 (CH, arom.), 124.78 (CH, arom.), 124.71 (CH, arom.), 124.10 (CH, arom.), 123.93 (CH, arom.), 123.56 (CH, arom.), 123.56 (CH, arom.), 79.04 (CH, saturated), 66.12 (C_q, saturated), 61.78 (C_q), 49.46 (CH, saturated); IR (KBr): $\tilde{\nu}$ = 3061, 3037 cm^{-1} (m, C–H, arom.), 1754 (s, C=O), 1634 (w, C=C, olef.),1451 (s, C=C, arom.), 1361 (m), 1181 (m), 1019 (m), 768 (s, C–H, arom.); UV/Vis (CH_2Cl_2): λ_{max} (ε) = 230 (20100), 272 (1700, sh), 280 nm (1200, sh); MS (70 eV): m/z (%): 448 (47) [M^+], 404 (100) [$M^+ - CO_2$]; C,H analysis ($C_{33}H_{20}O_2$): calcd C 88.36, H 4.50; found C 88.06, H 4.90.

5 (Kammermeierphane 1): Method a from Scheme 3: Thermolysis of **2**: A solution of **2** (106 mg, 0.237 mmol) in xylene (50 mL) was heated at reflux for 16 h. After removal of the solvent in vacuo the residue was purified by chromatography on silica gel with hexane/dichloromethane 2/1. **5** was obtained as a colorless solid. Yield: 54 mg (51%). M.p. 242 °C; ^{1}H NMR (400 MHz, $CDCl_3$): δ = 7.58 (m, 2H; CH, arom.), 7.47 (m, 2H; CH, arom.), 7.19 (m, 2H; CH, arom), 7.07 (m, 6H; CH, arom.), 6.96 (m, 4H; CH, arom.), 6.45 (m, 2H; HC=C), 5.86 (m, 2H; HC=C); ^{13}C NMR (100.6 MHz, $CDCl_3$): δ = 142.20 (C_q), 140.56 (C_q), 140.12 (C_q), 139.96 (C_q), 136.59 (C_q), 136.00 (C_q), 130.00 (CH, arom.), 126.84 (CH, arom.), 126.71 (CH, arom.), 126.53 (CH, arom.), 126.42 (CH, arom.), 125.75 (CH, arom.), 125.19 (CH, arom.), 125.19 (CH, arom.), 124.56 (CH, arom.), 121.44 (CH, arom.); IR (KBr): $\tilde{\nu}$ = 3061, 3035, 3013 cm^{-1} (m, C–H, arom, olef.), 1633 (m, C=C, olef.), 1450 (s, C=C, arom.), 768 (s, C–H, arom.); UV/Vis (CH_2Cl_2): λ_{max} (ε) = 230 (41000), 272 nm (20400, sh); MS (70 eV): m/z (%): 404 (100) [M^+], 200 (10); C,H analysis ($C_{32}H_{20}$): calcd C 95.02, H 4.98; found C 94.81, H 5.04.

Method b from Scheme 3: Diels–Alder reaction of **1** with 1,2-diazine: A solution of **1** (100 mg,0.284 mmol) and 1,2-diazine (350 mg, 4.38 mmol) in toluene (70 mL) was heated at reflux for 20 h. After removal of the solvent in vacuo the residue was purified by chromatography on silica gel with hexane/dichlormethane 2/1 (R_f = 0.26). **5** was obtained as a colorless solid. Yield: 92 mg (80%).

6 (Kammermeierphane 2): A solution of **5** (40 mg, 0.010 mmol) and **1** (53 mg, 0.015 mmol) in benzene (120 mL) was irradiated in a quartz reactor for 3 h. The solvent was removed in vacuo and the residue was purified by chromatography on silica gel with hexane/dichloromethane 2/1 (R_f = 0.08). After further purification by HPLC (PSS-SDV gel 100 Å, 10 mm, $CHCl_3$) the product was recrystallized from toluene. **6** was obtained as a lemon-yellow solid. Yield: 7 mg (10%). M.p. 380 °C (decomp); ^{1}H NMR (400 MHz, $CDCl_3$): δ = 7.79 (m, 8H; CH, arom.), 7.54 (m, 4H; CH, arom.), 7.27 (m, 4H; CH, arom.), 7.16 (m, 16H; CH, arom.), 6.82 (s, 4H; CH, olef.); ^{13}C NMR (100.6 MHz, CS_2/C_6D_6 10/1): δ = 140.55 (C_q), 139.96 (C_q), 139.45 (C_q), 138.56 (C_q), 136.17 (C_q), 135.70 (C_q), 128.72 ($CHR=CR_2$), 128.67 (CH, arom.), 127.55 (CH, arom.), 127.16 (CH, arom.), 126.20 (CH, arom.), 125.57 (CH, arom.), 124.91 (CH, arom.), 123.39 (CH, arom.), 122.98 (CH, arom.); IR (KBr): $\tilde{\nu}$ = 3090, 3060, 3028 cm^{-1} (m, C–H, arom, olef.), 1644 (m, C=C, olef.), 1451 (s, C=C, arom.), 769 (s, C–H, arom.); UV/Vis (CH_2Cl_2): λ_{max} (ε) = 230 (56000), 246 (58000), 316 (27000), 358 nm (60000); MS (70 eV): m/z (%): 756 (100) [M^+]; HRMS: calcd for $C_{60}H_{36}$: 756.2817, found: 756.2815.

Received: April 14, 1997 [Z10338IE]
German version: *Angew. Chem.* **1997**, *109*, 2317–2319

Keywords: cycloadditions · cyclophanes · metatheses · photochemistry

[1] a) F. Vögtle, *Cyclophane Chemistry*, Wiley, Chichester, **1993**; b) F. Diederich, *Cyclophanes*, The Royal Society of Chemistry, London, **1991**; c) G. J. Bodwell, *Angew. Chem.* **1996**, *108*, 2221–2224, *Angew. Chem. Int. Ed. Engl.* **1996**, *35*, 2085–2088.

[2] For a review of beltlike but not fully conjugated molecules see a) A. Schröder, H.-B. Mekelburger, F. Vögtle, *Top. Curr. Chem.*, **1994**, *172*, 178–201; for more recent work see b) H. Meier, K. Müller, *Angew. Chem.* **1995**, *107*, 1598–1600; *Angew. Chem. Int. Ed. Engl.* **1995**, *34*, 1437–1438; c) M. G. Banwell, D. C. R. Hockless, J. M. Walter, *Chem. Commun.* **1996**, 1469–1470; d) S. Breidenbach, S. Ohren, F. Vögtle, *Chem. Eur. J.* **1996**, *2*, 832–837.

[3] S. Kammermeier, R. Herges, *Angew. Chem.* **1996**, *108*, 470–472; *Angew. Chem. Int. Ed. Engl.* **1996**, *35*, 417–419.

[4] S. Kammermeier, P. G. Jones, R. Herges, *Angew. Chem.* **1996**, *108*, 2834–2836; *Angew. Chem. Int. Ed. Engl.* **1996**, *35*, 2669–2671.

[5] T. Kawase, H. R. Darabi, M. Oda, *Angew. Chem.* **1996**, *108*, 2803–2805; *Angew. Chem. Int. Ed. Engl.* **1996**, *35*, 2664–2666.

[6] a) S. Iijima, *Nature* **1991**, *354*, 56–58; b) S. Iijima, T. Ichihashi, Y. Ando, *ibid.* **1992**, *356*, 776–778; c) for a review see: R. S. Ruoff, *ibid.* **1994**, *372*, 731–732.

[7] K. Hernadi, A. Fonseca, J. B. Nagy, D. Bernaerts, J. Riga, A. Lucas, *Synth. Met.* **1996**, *77*, 31–43.

[8] a) G. Schröder, J. F. M. Oth, *Tetrahedron Lett.* **1966**, 4083–4088; Reviews: b) G. Mehta, *J. Chem. Educ.* **1982**, *59*, 313–316; c) G. Kaupp, *Methoden Org. Chem (Houben Weyl) 4th ed. 1952–, Vol. IV*/5a, pp. 298–299; d) H. Quast, P. Eckert, *Angew. Chem.* **1976**, *88*, 150–151, *Angew. Chem. Int. Ed. Engl.* **1976**, *15*, 168–169; e) B. A. R. C. Bulusu, P. R. Spur, R. Pinkos, C. Grund, W.-D. Fessner, D. Hunkler, H. Fritz, W. R. Roth, H. Prinzbach, *Chimia* **1987**, *41*, 32–36.

[9] a) R. L. Viavattene, F. D. Greene, L. D. Cheung, R. Majeste, L. M. Trefonas, *J. Am. Chem. Soc.* **1974**, *96*, 4342–4343; b) R. Herges, H. Neumann, *Liebigs Ann.* **1995**, 1283–1289; c) R. Herges, H. Neumann, F. Hampel, *Angew. Chem.* **1994**, *106*, 1024–1026; *Angew. Chem. Int. Ed. Engl.* **1994**, *33*, 993–995; d) S. Kammermeier, H. Neumann, F. Hampel, R. Herges, *Liebigs Ann.* **1996**, 1795–1800.

[10] a) G. F. Emerson, L. Watts, R. Pettit, *J. Am. Chem. Soc.* **1965**, *87*, 131–133; b) R. P. Dodge, V. Schomacher, *Nature* **1960**, *186*, 798–799.

[11] a) L. Watts, J. D. Fitzpatrick, R. Pettit, *J. Am Chem. Soc.* **1966**, *88*, 623–624; b) J. C. Barborak, L. Watts, R. Pettit, *ibid.* **1966**, *88*, 1328–1329.

[12] This proves the high reactivity of TDDA **1** in [4+2]cycloadditions. Under these conditions reactions of α-pyrone with even very reactive dienophiles like maleic anhydride do not proceed with more than 50% yield: E. Pfaff, H. Plieninger, *Chem. Ber.* **1982**, *115*, 1967–1981, and references therein.

[13] Named after one of the authors, Stefan Kammermeier.

[14] Crystal structure analysis of **5**: **5**·$CHCl_3$, $C_{33}H_{21}Cl_3$, M_r = 523.85, monoclinic, space group $P2_1/n$, a = 799.2(1), b = 2137.7(3), c = 1477.4(2) pm, β = 90.06(1)°, V = 2.5242 nm^3, Z = 4, ρ_{calcd} = 1.378 Mg m^{-3}, $F(000)$ = 1080, $\mu(Mo_{K\alpha})$ = 0.39 mm^{-1}, T = −100 °C. A colorless plate 0.5 × 0.5 × 0.3 mm was mounted in inert oil and brought into a stream of cold gas in the diffractometer (Siemens, P4). 4772 Reflections were registered up to 2θ = 50° by ω-scans, of which 4438 were independent (R_{int} = 0.023). The structure was solved with direct methods and refined anisotropically versus F^2 (program SHELXL-93, G. M. Sheldrick, Universität Göttingen). Hydrogen atoms were considered using a riding model. The final $wR(F^2)$ value was 0.129 for all reflections, with conventional $R(F)$ = 0.050; S = 0.95, max. $\Delta\rho$ = 592 e nm^{-3}. Crystallographic data (excluding structure factors) for the structures reported in this paper have been deposited with the Cambridge Crystallographic Data Centre as supplementary publication no. CCDC-100360. Copies of the data can be obtained free of charge on application to The Director, CCDC, 12 Union Road, Cambridge CB21EZ, UK (fax: Int. code +(1223)336-033; e-mail: deposit@chemcrys.cam.ac.uk).

[15] The π–π* transition of TDDA lies at 280 nm. With a Pyrex filter the irradation time is much longer due to absorption of light with wavelengths <300 nm.

[16] Two other compounds that have been synthesized in our laboratory following the same construction principle correspond to sections of (4,4)nanotubes, see refs.[3,4]. For a review on the nomenclature, properties, and synthesis of nanotubes see: M. S. Dresselhaus, G. Dresselhaus, P. C. Eklund, *Science of Fullerenes and Carbon Nanotubes*, Academic Press, San Diego, **1996**.

[17] M. J. S. Dewar, E. G. Zoebisch, E. F. Healy, J. J. P. Stewart, *J. Am. Chem. Soc.* **1985**, *107*, 3902–3909.

 © WILEY-VCH Verlag GmbH, D-69451 Weinheim, 1997 0570-0833/97/3620-2202 $ 17.50+.50/0

Organic-Soluble Neutral and Ionic Indium Siloxane Cages: Potential Precursors for Indium-Containing Silicates**

Andreas Voigt, Mrinalini G. Walawalkar, Ramaswamy Murugavel, Herbert W. Roesky,* Emilio Parisini, and Paolo Lubini

Dedicated to Professor Achim Müller on the occasion of his 60th birthday

Zeolites and metal-doped zeolites have attracted increasing attention from chemists and material scientists because of their excellent catalytic and ion exchange properties, which also find wide applications in the chemical industry. While aluminum-containing silicates have been well known and studied over the decades, there has been a recent upsurge in the study of Ga-doped molecular sieves and phosphate compounds in the light of their usefulness in catalytic conversions.[1-3] In spite of the widespread applications of Al and Ga zeolites, there are only a very few reports on the synthesis or on the catalytic activity of In-containing zeolites.[4] Studies on In-based zeolites warrant attention in the light of their recently reported utility in the catalytic reduction of nitrogen oxides (NO_x),[4] a process that has implications in cleaning up exhaust gases of combustion engines.

Studies on metallasiloxanes are also important because of their ability to act as model compounds for complex zeolite systems.[5] Starting from a series of stable silanetriols we have synthesized a range of metallasiloxanes incorporating metals such as Al, Ga, Sn, Ti, Zr, Ta, and Re that exhibit novel structural features.[6, 7] In particular, silanetriols are excellent starting materials for three-dimensional Al- and Ga-containing siloxanes, which could function as models for zeolites.[8] Continuing our efforts in the utilization of stable and discrete silanetriols for the preparation of useful metallasiloxanes, we report here on the first successful synthesis of new polyhedral indium siloxanes **2**–**5** (Scheme 1) that are soluble in common organic solvents such as pentane, diethyl ether, THF, and toluene. While the reaction between **1** and $InMe_3$ in the ratio 1:2 results in the partial elimination of methyl groups on indium leading to the drum-shaped In–siloxane **2**, a 1:1 reaction between the same reactants under similar conditions leads to the complete elimination of all the methyl groups on indium and the isolation of the cube-shaped In–siloxane **3**. The reactions between **1** and the ionic alkylindium compounds $Li[InMe_4]$ and $Na[InMe_4]$ lead to the ionic In–siloxanes **4** and **5**, respectively (Scheme 1).

The reaction leading to the Na–In–siloxane **5** is particularly interesting. The formation of this product should have proceeded by a self-condensation of the silanetriol **1** resulting in the tetrahydroxydisiloxane $[(OH)_2RSi]_2O$ and water.[9] This process is presumably catalyzed by highly ionic reactants such as $Na[InMe_4]$ in the reaction medium.[10] Evidently, the reactive $N-SiMe_3$ bonds in the initially formed In–siloxane are partially hydrolyzed over the period of crystallization (ca. three months) to yield the siloxane **5**, which contains NHAr groups.

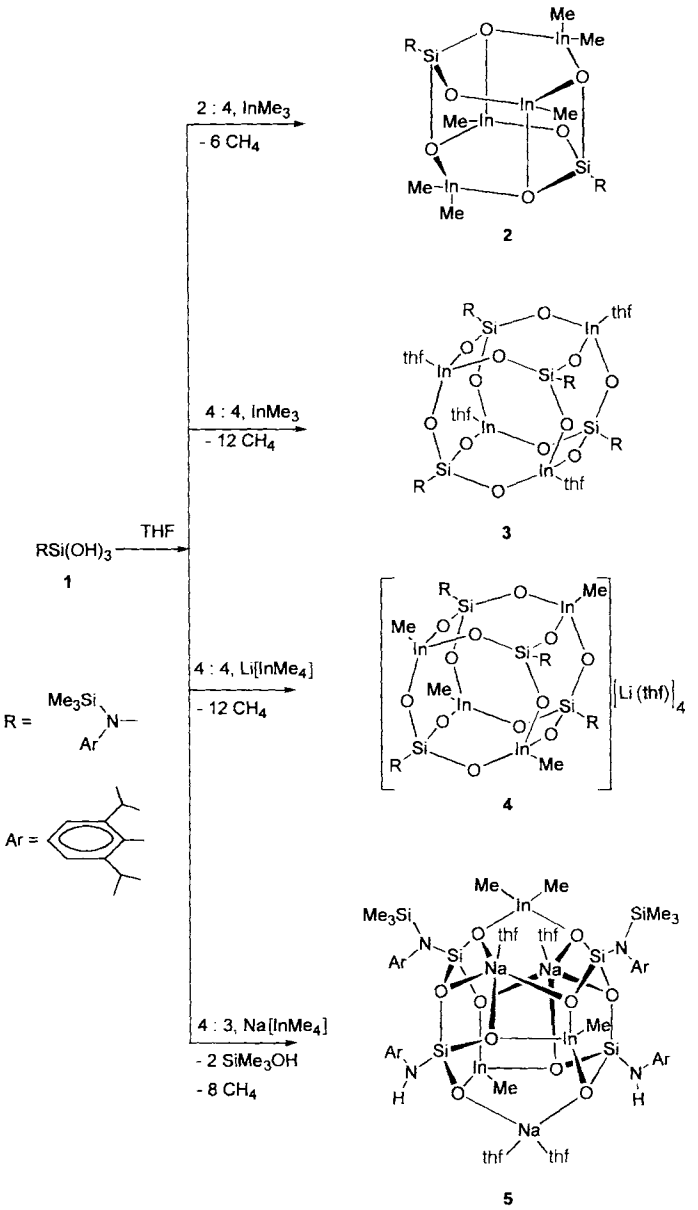

Scheme 1. Synthesis of indium siloxanes **2**–**5**.

All the new In–siloxanes have been characterized based on their analytical, spectroscopic (IR, ^1H and ^{29}Si NMR), and mass spectrometric (EI MS) data. In addition the solid-state structures of **2**, **4**, and **5** have been unambiguously established by single-crystal X-ray diffraction studies.[11] In the case of **3**, it has so far not been possible to obtain suitable single crystals. The spectroscopic data are consistent with the structural formulation of all the compounds. The EI mass spectra of all compounds yield molecular ion peaks or the peaks due to loss of solvent molecules or methyl groups. Three ^{29}Si NMR signals are observed for the three different types of silicon centers in **5** ($\delta = -73.9$, -72.8, and 2.3); the spectra of all the other compounds show only two ^{29}Si NMR signals corresponding to the $SiMe_3$ and SiO_3 moieties.

The molecular structure of the heterosiloxane **2** (Figure 1) can best be described as a cylindrical-drum whose top and bottom faces are made up of six-membered In_2O_3Si rings. The side faces

[*] Prof. Dr. H. W. Roesky, Dr. A. Voigt, M. G. Walawalkar, Dr. R. Murugavel, Dr. E. Parisini, Dr. P. Lubini
Institut für Anorganische Chemie der Universität
Tammannstrasse 4, D-37077 Göttingen (Germany)
Fax: Int. code +(551) 39 33 73
e-mail: hroesky@gwdg.de

[**] This work was supported by the Deutsche Forschungsgemeinschaft and the Witco GmbH, Bergkamen. R. M. thanks the Alexander-von-Humboldt foundation, Bonn, for a research fellowship. E. P. and P. L. are grateful to the European Union for post-doctoral grants (ERB CHBG CT 940731 and BBW 94.0162 CHBG CT 940731).

 © WILEY-VCH Verlag GmbH, D-69451 Weinheim, 1997 0570-0833/97/3620-2203 $ 17.50+.50/0

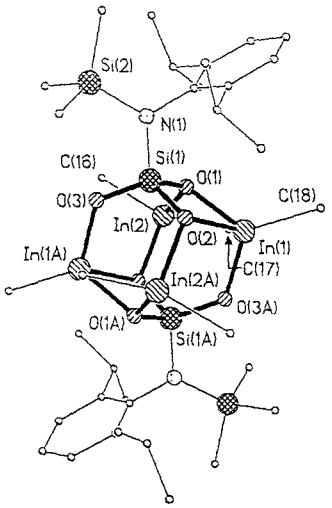

Figure 1. Molecular structure of **2** in the crystal. Selected bond lengths [Å] and angles [°]: In(1)–O(1) 2.148(6), In(1)–O(2) 2.150(6), In(1)–C(18) 2.100(9), In(1)–O(3A) 2.033(6), Si(1)–O(1) 1.654(6), Si(1)–O(2) 1.666(6), Si(1)–O(3) 1.590(6), Si(1)–N(1) 1.722(7), In(2)–C(16) 2.136(6), In(2)–C(17) 2.132(10); O(1)-In(1)-O(2) 71.0(2), O(1)-In(1)-O(3A) 97.8(2), O(2)-In(1)-O(3A) 100.1(2), C(16)-In(2)-C(17) 136.9(4).

are composed of two such six-membered rings (existing in a boat conformation) in addition to two planar four-membered InO_2Si rings. The shape of the $In_4O_6Si_2$ framework in compound **2** is similar to that observed for the previously characterized Al and Ga analogues.[8] Given the differences in the covalent radii of the metal atoms, the In–O distances (2.11 Å) are longer than the Ga–O (1.91 Å) and Al–O (1.83 Å) distances in the corresponding compounds. As a consequence, the internal O-M-O angles of the drum also decrease on going from Al to In. The In–O distances in **2** are comparable with the values reported for $[\{InC(Me_3Si)_3\}_4O(OH)_6]$ (2.12 Å)[12a] and $[\{In(OH)(O_2PPh_2)Me(py)\}_4]$ (2.23 Å) (py = pyridine).[12b]

Both **3** and **4** are made up of a central $In_4O_{12}Si_4$ cubic core (Scheme 1). In the ionic compound **4** (Figure 2), four of the six faces of the $In_4O_{12}Si_4$ cube are further surrounded by Li^+ ions. Although the overall shape of the cage appears to be comparable to that of the Al analogue,[8b] the substitution of Al by In seems to provide a greater flexibility to the cubic core. In particular, the chair conformation for the four eight-membered $In_2O_4Si_2$ rings facing the coordinated Li^+ ions is absent in the other two faces of the cage. Also there is a pronounced deviation from regular tetrahedral coordination of the four-coordinate In atoms. The Li^+ ions adopt a nearly ideal square-pyramidal coordination geometry. As a consequence of the *side-on* coordination of the oxygen atoms to the Li^+ ions, the cubic cage is slightly squeezed along the axis perpendicular to the plane defined by these four lithium ions. The conformation adopted by the N-bonded ligands in **2** and **4** is almost identical; owing to the bulkiness of the isopropyl groups, the aromatic ring is forced to lie perpendicular to the Si-N-Si plane.

The molecular structure of In–siloxane **5** is made up of a central $In_3Na_3O_{10}Si_4$ core that resembles the shape of a bird-cage (Figure 3). Two formal $[\{N(Ar)(SiMe_3)\}O_2(\mu\text{-}O)O_2Si(NHAr)]^{4-}$ ligands coordinate to two $[InMe]^{2+}$, one $[InMe_2]^+$, and three Na^+ moieties. There are two InO_3Si_2 six-membered

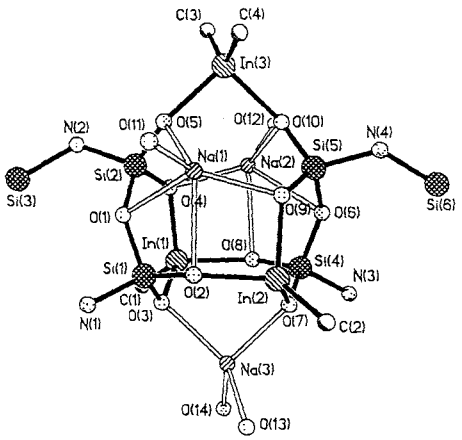

Figure 3. Structure of the central core in **5** in the crystal. Selected bond lengths [Å] and angles [°]: In(1)–O(3) 2.078(5), In(1)–O(4) 2.069(5), In(1)–O(8) 2.080(5), In(1)–C(1) 2.144(8), Si(1)–O(1) 1.640(5), Si(1)–O(2) 1.606(5), Si(1)–O(3) 1.619(5), Na(1)–O(1) 2.647(5), Na(1)–O(2) 2.512(6), Na(1)–O(5) 2.313(6), Na(1)–O(9) 2.310(6), Na(1)–O(11) 2.295(6); Si(1)-O(1)-Si(2) 141.4(3), Si(1)-O(2)-In(2) 137.4(3), Si(1)-O(3)-In(1) 123.2(3).

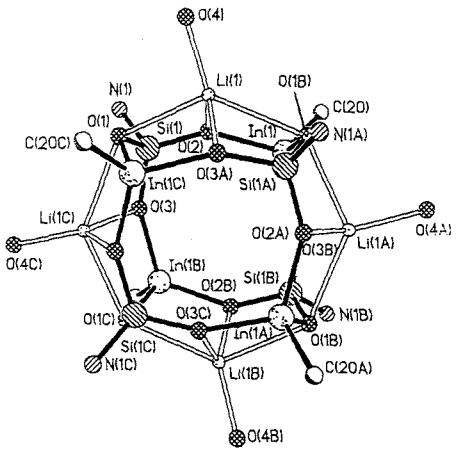

Figure 2. Structure of the central core in **4** in the crystal. Selected bond lengths [Å] and angles [°]: In(1)–O(2) 2.036(3), In(1)–O(1B) 2.068(3), In(1)–O(2A) 2.056(3), In(1A)–C(20A) 2.131(4), Si(1)–O(1) 1.609(3), Si(1)–O(2) 1.618(3), Si(1)–O(3) 1.615(3), Li(1)–O(4) 1.953(8), Li(1)–O(1B) 2.561(10), Li(1)–O(2) 1.933(8), Li(1)–O(3A) 1.974(8); O(2)-In(1)-O(2A) 115.65(11), O(2)-In(1)-O(1B) 92.19(12), O(2A)-In(1)-O(1B) 95.21(12).

rings in the molecule that are linked by two In-O-Si bridges. All the oxygen atoms in the molecule are triply bridging (μ_3) the In, Na, and Si centers. All In atoms have a tetrahedral coordination sphere.

While the two pentacoordinate Na^+ ions (bonded to four cage oxygen atoms and one THF molecule) have an approximate square-pyramidal geometry, the third Na^+ ion is tetrahedrally coordianted by two cage oxygen atoms and two THF molecules. There are two distinct types of Si–O distances in the molecule: the Si–O(Si) bonds are considerably longer (av 1.65 Å) than the Si–O(In) bonds (av 1.60 Å). All the In–O distances are nearly equal; the average value is 2.08 Å. The Na–O distances in the molecule vary from 2.28 to 2.66 Å.

In summary, small variations in the reaction conditions and the choice of starting materials has allowed us to prepare indium siloxanes with different polyhedral structures, which would potentially model the In–silicate frameworks. Furthermore, the hydrolyzable functionalities make compounds **2**–**5** promising starting materials for the synthesis of new synthetic In-containing zeolites under mild conditions or by sol–gel processes.

 © WILEY-VCH Verlag GmbH, D-69451 Weinheim, 1997 0570-0833/97/3620-2204 $ 17.50+.50/0

Experimental Section

2: A solution of $InMe_3$ (1.60 g, 10 mmol) in *n*-hexane/THF (10 mL/5 mL) was added to a suspension of **1** (1.64 g, 5 mmol) in *n*-hexane (40 mL) at room temperature. The resulting clear solution was heated under reflux for 2 h and then slowly allowed to cool to room temperature to yield colorless crystals of **2** after two days. Yield 2.45 g (82%); MS (EI, 70 eV): *m/z* (%): 1198 (20) [M^+], 1183 (100) [M^+ − Me]; ^{1}H NMR ($CDCl_3$): δ = − 0.10 (s, 6H; In*Me*), 0.04 (s, 12H; InMe_2), 0.30 (s, 18H, SiMe_3), 1.32 (m, 24H; CHMe_2), 3.57 (m, 4H; C*H*Me$_2$), 7.05 (s, 6H; aromat.); ^{29}Si NMR ($CDCl_3$): δ = −70.9 (SiO_3), 6.3 ($SiMe_3$); IR (Nujol): $\tilde{\nu}$ = 1500, 1317, 1260, 1249, 1180, 1106, 1043, 1014, 969, 955, 905, 875, 838, 802, 752, 688, 613, 542 cm^{-1}; elemental analysis (%) calcd for $C_{36}H_{70}In_4N_2O_6Si_4$: C 36.1, H 5.8, N 2.4; found: C 35.1, H 5.2, N 2.1.

3: A solution of $InMe_3$ (0.80 g, 5 mmol) in *n*-hexane/THF (10 mL/5 mL) was added to a suspension of **1** (1.64 g, 5 mmol) in *n*-hexane (40 mL) at 60 °C. After the evolution of methane gas ceased, the heating was continued for an additional 1.5 h. The solvent was removed in vacuo to afford **3** as a white solid which was purified by crystallization from hot *n*-hexane. Yield 2.43 g (95%); MS (EI, 70 eV): *m/z* (%): 2045 (10) [M^+], 1756 (100) [M^+ − 4THF]; ^{1}H NMR ($CDCl_3$): δ = 0.15 (s, 36H; SiMe_3), 1.26 (m, 48H; CHMe_2), 1.28 (m, 16H; OCH_2CH_2), 3.46 (m, 16H; OCH_2), 3.74 (m, 8H; C*H*Me$_2$), 7.10 (m, 12H; aromat.); ^{29}Si NMR ($CDCl_3$): δ = −72.4 (SiO_3), 6.4 ($SiMe_3$); IR (Nujol): $\tilde{\nu}$ = 1499, 1321, 1258, 1180, 1109, 1046, 1012, 968, 954, 908, 879, 836, 801, 755, 656, 617, 551, 474, 443, 397 cm^{-1}; elemental analysis (%) calcd for $C_{72}H_{136}In_4N_4O_{16}Si_8$: C 51.9, H 7.7, N 3.2; found: C 50.1, H 7.1, N 2.9.

4: A solution of LiInMe$_4$ [13] (0.91 g, 5 mmol) in *n*-hexane/THF (10 mL/5 mL) was slowly added to a suspension of **1** (1.64 g, 5 mmol) in *n*-hexane (40 mL). The reaction mixture was heated under reflux for 1.5 h and then allowed to cool to room temperature. From this solution, colorless crystals of **4** were obtained after two days. Yield 2.27 g (85%), MS (EI, 70 eV): *m/z* (%): 1844 (5) [M^+ − 4THF], 1770 (100) [M^+ − 4THF − $SiMe_3$]; ^{1}H NMR (C_6D_6): δ = − 0.15 (s, 12H; In*Me*), 0.15 (s, 36H: SiMe_3), 1.23 (m, 16H; OCH_2CH_2), 1.37 (m, 48H; CHMe_2), 3.54 (m, 16H; OCH_2), 3.82 (m, 8H; C*H*Me$_2$), 7.12 (m, 12H; aromat.); ^{29}Si NMR ($CDCl_3$): δ = −75.9 (SiO_3), 5.8 ($SiMe_3$); elemental analysis (%) calcd for $C_{80}H_{148}In_4Li_4N_4O_{16}Si_8$: C 45.0, H 6.9, N 2.6; found: C 44.3, H 6.4, N 2.4.

5: A solution of Na[InMe$_4$] [13] (0.59 g, 3 mmol) in *n*-hexane/THF (10 mL/5 mL) was slowly added to a suspension of **1** (1.31 g, 4 mmol) in *n*-hexane (40 mL). The reaction mixture was heated under reflux for 1.5 h and and then allowed to cool to room temperature and left to crystallize. The colorless solution turned brown over three months with the formation of large colorless single crystals of **5**. Yield: 0.94 g (40% based on 1); m.p. 200 °C (decomp), MS (EI, 70 eV): *m/z* (%): 1839 (2) [M^+ − 3Me], 1695 (3) [M − 3Me − 2THF], 162 (100) [iPr$_2$C$_6$H$_3$NH$_2$ − Me]; ^{1}H NMR (C_6D_6): δ = − 0.77 (s, 12H; In*Me*), 0.41 (s, 18H; SiMe_3), 1.23 (d, ^3J(H,H) = 6.8 Hz, 24H; CHMe_2), 1.29 (d, ^3J(H,H) = 6.8 Hz, 24H; CHMe_2), 1.40 (t, ^3J(H,H) = 6.4 Hz, 16H; OCH_2CH_2), 3.45 (t, ^3J(H,H) = 6.4 Hz, 16 H; OCH_2), 4.04 (sept., 4H; C*H*Me$_2$), 4.14 (sept., 4H; C*H*Me$_2$), 6.82–7.20 (m, 12H; aromat.); ^{29}Si NMR (C_6D_6): δ = −73.86 (SiO_3), −72.76 (SiO_3), 2.30 ($SiMe_3$); IR (Nujol): $\tilde{\nu}$ = 1319, 1256, 1245, 1185, 1099, 1049, 1019, 941, 919, 834, 801, 720, 592, 546, 515, 462 cm^{-1}; elemental analysis: calcd for $C_{74}H_{132}In_3N_4Na_3O_{14}Si_6$: C 47.2, H 7.1, N 3.0; found: C 46.8, H 7.3, N 2.6. The observed low values of carbon analysis for **2**–**5** are due to the formation of silicon carbide during the combustion process.

Received: April 10, 1997 [Z10331IE]
German version: *Angew. Chem.* **1997**, *109*, 2313–2315

Keywords: alkali metals · cage compounds · indium · silicon

[1] G. Giannetto, R. Monque, R. Galiasso, *Catal. Rev. Sci. Eng.* **1994**, *36*, 271.
[2] M. Estermann, L. B. McCusker, C. Baerlocher, A. Merrouche, H. Kessler, *Nature* **1991**, *352*, 320.
[3] a) M. Guisnet, N. S. Gnep, F. Alario, *Appl. Catal. A* **1992**, *89*, 1; b) Y. Ono, *Catal. Rev. Sci. Eng.* **1992**, *34*, 179; c) L. S. Marchenko, D. Z. Levin, V. A. Plakhotnik, E. S. Mortikov, *Bull. Acad. Sci. USSR Div. Chem. Sci. Engl. Transl.* **1986**, *35*, 81.
[4] a) E. Kikuchi, M. Ogura, I. Terasaki, Y. Goto, *J. Catal.* **1996**, *161*, 465; b) E. Kikuchi, K. Yogo, *Catal. Today* **1994**, *22*, 73.
[5] a) R. Murugavel, A. Voigt, M. G. Walawalkar, H. W. Roesky, *Chem. Rev.* **1996**, *96*, 2205; b) M. G. Voronkov, E. A. Maletina, V. K. Roman, *Heterosiloxanes*, (*Soviet Scientific Review Supplement, Series Chemistry, Vol. 1*), Academic Press, London, **1988**; c) F. J. Feher, T. A. Budzichowski, *Polyhedron* **1995**, *14*, 3239.
[6] R. Murugavel, V. Chandrasekhar, H. W. Roesky, *Acc. Chem. Res.* **1996**, *29*, 183.
[7] A. Voigt, R. Murugavel, M. Montero, H. Wessel, F.-Q. Liu, H. W. Roesky, I. Usón, T. Albers, E. Parisini, *Angew. Chem.* 1997, 109, 1020–1022; *Angew. Chem. Int. Ed. Engl.* **1997**, *36*, 1001–1003, and references therein.
[8] a) M. Montero, I. Usón, H. W. Roesky, *Angew. Chem.* **1994**, *106*, 2198; *Angew. Chem. Int. Ed. Engl.* **1994**, *33*, 2103; b) M. Montero, A. Voigt, M. Teichert, I. Usón, H. W. Roesky, *ibid.* **1995**, *107*, 2761 and **1995**, *34*, 2504; c) A. Voigt, R. Murugavel, E. Parisini, H. W. Roesky, *ibid.* **1996**, *108*, 823 and **1996**, *35*, 748; d) V. Chandrasekhar, R. Murugavel, A. Voigt, H. W. Roesky, H.-G. Schmidt, M. Noltemeyer, *Organometallics* **1996**, *15*, 918.
[9] R. Murugavel, P. Böttcher, A. Voigt, M. G. Walawalkar, H. W. Roesky, E. Parisini, M. Teichert, M. Noltemeyer, *Chem. Commun.* **1996**, 2417.
[10] Self-condensation of silanols in the presence of ionic acidic or basic impurities is well known, see ref. [9].
[11] Crystal structure analysis for **2**: $C_{36}H_{70}In_4N_2O_6Si_4$, M_r = 1198.55, triclinic, $P\bar{1}$, a = 10.086(2), b = 10.462(2), c = 13.151(3) Å, α = 98.01(3), β = 96.16(3), γ = 113.80(3)°, V = 1237(1) Å^3, Z = 1, ρ_{calcd} = 1.609 g cm^{-3}, 3679 independent reflections, $R1$ = 0.0518 for $I > 2\sigma(I)$, $wR2$ = 0.1215 for all data. Crystal data for **4**: $C_{64}H_{116}In_4Li_4N_4O_{12}Si_8 \cdot (OC_4H_8)_4$, M_r = 2133.8, tetragonal, $I4_1/a$, $a = b$ = 29.200(4), c = 12.870(3) Å, V = 10974(3) Å^3, Z = 4, ρ_{calcd} = 1.344 g cm^{-3}, 4061 independent refelctions, $R1$ = 0.0424 for $I > 2\sigma(I)$, $wR2$ = 0.1172 for all data. Crystal structure analysis for **5**: $C_{74}H_{132}In_3N_4Na_3O_{14}Si_6$, M_r = 1883.81, triclinic, $P\bar{1}$, a = 14.799(3), b = 15.520(3), c = 23.361(5) Å, α = 91.03(3), β = 106.18(3), γ = 97.49(3)°, V = 5101(2) Å^3, Z = 2, ρ_{calcd} = 1.227 g cm^{-3}, 13329 independent reflections, $R1$ = 0.0530 for $I > 2\sigma(I)$, $wR2$ = 0.1376 for all data. The data were collected on a Stoe-Siemens-AED2 four-circle diffractometer equipped with a graphite monochromator, Mo$_{K\alpha}$ radiation (λ = 0.71073 Å). The measurements were made with a cooled crystal coated with an oil drop by using the Learnt Profile Method [14]. The structures were solved by direct methods (SHELXS-90) [15] and refined on all data by full-matrix least-squares on F^2 [16]. All non-hydrogen atoms were refined anisotropically. Hydrogen atoms were added in idealized positions and included in the refinement. Crystallographic data (excluding structure factors) for the structures reported in this paper have been deposited with the Cambridge Crystallographic Data Centre as supplementary publication no. CCDC-100353. Copies of the data can be obtained free of charge on application to The Director, CCDC, 12 Union Road, Cambridge, CB2 1EZ, UK (fax: int. code +(1223)336-033; e-mail: deposit@chemcrys.cam.ac.uk).
[12] a) S. S. Al-Juaid, N. H. Buttrus, C. Eaborn, P. B. Hitchcock, A. T. L. Roberts, J. D. Smith, A. C. Sullivan, *J. Chem. Soc. Chem. Commun.* **1986**, 908; b) A. M. Arif, A. R. Barron, *Polyhedron* **1988**, *7*, 2091.
[13] K. Hoffmann, E. Weiss, *J. Organomet. Chem.* **1972**, *37*, 1.
[14] W. Clegg, *Acta Crystallogr. Sect. A* **1981**, *37*, 22.
[15] G. M. Sheldrick, SHELXS-90/96, Program for Structure Solution: *Acta Crystallogr. Sect. A* **1990**, *46*, 467.
[16] G. M. Sheldrick, SHELXL-93/96, Program for Crystal Structure Refinement, Universität Göttingen, **1993**.

The Distortive Tendency of Benzene π Electrons: How Is It Related to Structural Observables?**

Avital Shurki and Sason Shaik*

Many computational experiments have demonstrated that benzene π electrons tend to distort to a localized D_{3h} structure, while the final D_{6h} symmetry is determined by the σ framework.[1a] However, the notion of π distortive tendency would have remained elusive without experimental probes. Although the exalted b_{2u} frequency of the $^1B_{2u}$ excited state was recently pointed out as such an observable,[1b, 2] there is still a need for a more "chemical" observable which can be associated with π distortive tendency. Structure is an essential chemical observable, and the recent exciting syntheses of cyclohexatriene motifs[3, 4] (for example **1**, in which there is strong bond alternation)[3b] pose an excellent opportunity for drawing a link between π distortive tendency and structure as well as predicting novel structures.

Our approach for establishing the requisite link between π distortive tendency and structural probes relies on the struc-

[*] Prof. S. Shaik, A. Shurki
Department of Organic Chemistry and
The Lise Meitner-Minerva Center for Computational Quantum Chemistry
The Hebrew University
91904 Jerusalem (Israel)
Fax: Int. code +(2)658-5345
e-mail: sason@shiva02.ch.huji.ac.il

[**] This work was supported by the Israel Science Foundation, which was founded by the Israel Academy of Sciences and Humanities.

 © WILEY-VCH Verlag GmbH, D-69451 Weinheim, 1997 0570-0833/97/3620-2205 $ 17.50+.50/0

tural patterns of the ground state and the $^1B_{2u}$-like excited state. These two states for benzene derivatives are described as the bonding and antibonding combinations of the Kekulé structures (Scheme 1).[1b, 5]. Thus, they arise from avoided crossing,

Scheme 1. Description of the ground state and the $^1B_{2u}$-like excited state of benzene as the linear combinations of Kekulé structures.

that is, resonance mixing along the bond alternation distortion mode (b_{2u} for benzene[1b]), and are two twin states which are expected to exhibit mirror-image behavior along the bond-alternating mode. We therefore decided to compute[6] the properties of these two states for the target molecules **1**[3b] and **2**.[8] The

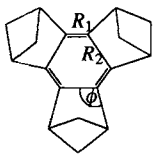

1

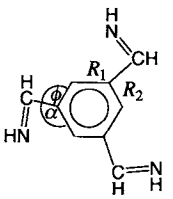

2

$R_1 = 1.349$Å
$R_2 = 1.438$Å
$\phi = 102.3°$

ground states ($^1A'_1$ and $^1A'$, respectively) were calculated at the restricted Hartree–Fock (RHF) level, the Møller–Plesset (MP2) level, and the hybrid density functional theory (DFT) level B3LYP. Calculations with the latter two methods were used to ascertain that the localization of the bonds is not due to the deficiency of the RHF method.[9] The $^1B_{2u}$-like excited states ($^1A'_1$ and $^1A'$, respectively) were calculated at the *c*onfiguration *i*nteraction with single excitations (CIS) level, which proved useful for these states.[10] The results are collected in Table 1.

In agreement with experiment (entry 1) and previous computations,[3b, c] our results (entries 2–7) show that the ground state of **1** exhibits significant bond alternation. In contrast, the calculations of the $^1A'_1$ excited state (entries 8–11) reveal a very small bond alternation, which is one order of magnitude smaller than in the ground state. Therefore, unlike the cyclohexatriene structure of the ground state of **1**, the $^1B_{2u}$-like excited state, which arises from $\pi \rightarrow \pi^*$ promotion is almost symmetrical. What are the origins of this structural switch?

Table 1. Experimental and calculated angles ϕ [°], bond lengths R_1 and R_2 [Å], and bond length alternations ΔR for **1** in the ground and exited states [a].

Entry	Method	ϕ	R_1	R_2	ΔR
ground state ($^1A'_1$)					
1	X-ray diffraction [3b]	102.3	1.349	1.438	0.089
2	HF/STO-3G	101.6	1.339	1.448	0.109
3	HF/6-31G	102.0	1.346	1.443	0.097
4	HF/6-31G(d) [3b]	101.8	1.344	1.440	0.096
5	HF/6-31G(dp)	101.8	1.342	1.441	0.099
6	MP2/6-311G(dp) [b]	102.2	1.377	1.431	0.054
7	B3LYP/6-311G(dp) [b]	102.0	1.361	1.440	0.079
excited state ($^1A'_1$) [c]					
8	CIS/STO-3G	102.1	1.411	1.428	0.017
9	CIS/6-31G	102.4	1.406	1.426	0.020
10	CIS/6-31G(d)	102.3	1.407	1.419	0.012
11	CIS/6-31G(dp)	102.3	1.407	1.419	0.012

[a] See the formula of **1** for definitions of R_1, R_2, and ϕ; $\Delta R = R_2 - R_1$. [b] Virtually identical to the results from MP2 and DFT calculations in ref. [3b]. [c] This state is the $^1B_{2u}$-like state of benzene (Scheme 1).

Scheme 2 provides a model for this behavior of the two states. Scheme 2a shows the behavior of the Kekulé structures contain-

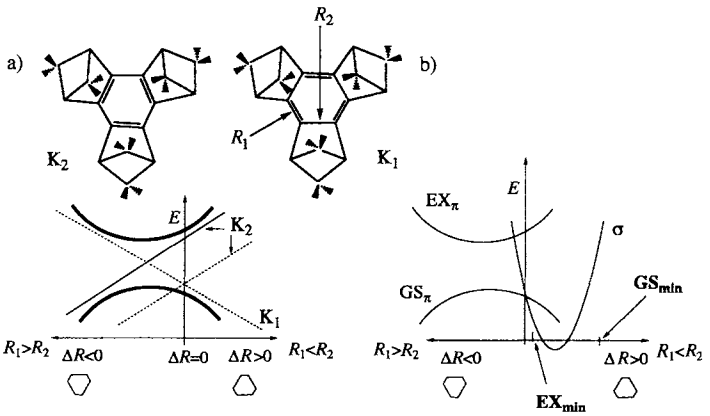

Scheme 2. Behavior of the π and σ energy curves of **1** along the bond-alternation coordinate; see text for details.

ing only π electrons, K_1 and K_2, along the bond-alternation coordinate.[1b] The dashed lines describe the situation for benzene, for which the Kekulé structures cross at $R_1 = R_2$ ($\Delta R = 0$). In **1** the C–H bonds and the C–C Walsh orbitals of the bicyclic moieties lie above and below the benzene unit, and therefore have a repulsive interaction with the π orbitals. This effect is stronger in K_2, and, hence, K_2 rises in energy relative to K_1, as shown by the solid thin line in Scheme 2a. This displacement of K_2 shifts the crossing point of the two Kekulé curves to a geometry were $R_1 > R_2$ ($\Delta R < 0$). By resonance mixing the Kekulé structures avoid the crossing and form the delocalized ground and excited states represented by the solid thick lines in Scheme 2a. The lower π curve, which is the bonding combination of the two Kekulé structures (that is, the ground state), has a maximum at $R_1 > R_2$ ($\Delta R < 0$). The upper π curve describes the excited state, which is the antibonding combination of the two Kekulé structures and possesses a minimum at $R_1 > R_2$ ($\Delta R < 0$) above the ground-state maximum.

Scheme 2b shows the two π curves (GS_π and EX_π) along with the σ curve. As discussed previously,[1a, 11–13] due to angular strain the σ minimum is located at $R_1 < R_2$ ($\Delta R > 0$), and ΔR increases as the endocyclic angle ϕ decreases from the ideal value of 120° in benzene. Furthermore, as we demonstrated,[1a] since the distortion caused by the σ electrons is small, the σ minimum lies very close to the D_{6h} geometry ($\Delta R = 0$). Thus, were it only a σ effect, the ground state of **1** would exhibit marginal bond alternation. The total energy of the ground state is determined by the sum of the σ curve, which has a minimum, and the π curve, which has a maximum. This sum will shift the ground-state minimum (GS_{min}) relative to the σ minimum to a higher degree of bond alternation in the sense $R_1 < R_2$ ($\Delta R > 0$). In contrast, the total energy of the excited states is the sum of σ and π curves with minima. As a consequence, the minimum of the excited state (EX_{min}) will be an average of the σ and π minima and possess a much lower degree of bond alternation relative to the ground-state minimum, if at all. Therefore, the opposite behavior of the ground state and its twin covalent excited state derive from the avoided crossing of the π curves and is associated with the tendency of π electrons in the ground state to distort, which is enhanced by the repulsive interaction with the bicyclic bridge. If the GS_π curve had a minimum like the

 © WILEY-VCH Verlag GmbH, D-69451 Weinheim, 1997 0570-0833/97/3620-2206 $ 17.50+.50/0

ES_π curve, the bond alternation would have also been marginal in the ground state.

The model can now be applied to **2**. Here, σ repulsion between the NH moieties and the *ortho* hydrogen atoms of the benzene ring will increase angle α and decrease angle ϕ. According to previous studies,[1a, 11, 12] the σ minimum will be shifted very slightly[1a] in the direction of $R_1 < R_2$ ($\Delta R > 0$; Scheme 3).

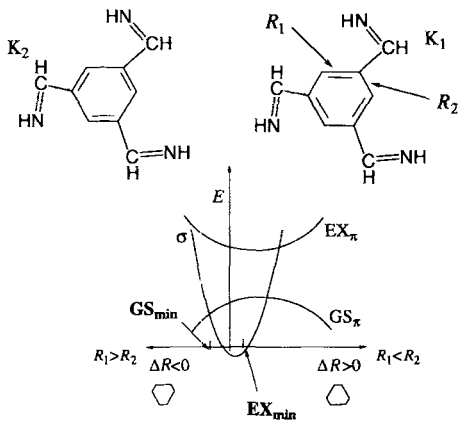

Scheme 3. Behavior of the π and σ energy curves of **2** along the bond-alternation coordinate; see text for details.

The π interaction of the C=NH groups with the benzene moiety will now raise K_1 relative to K_2. Following the same argument as for Scheme 2a, this π effect will shift the avoided crossing of the π curves to $R_1 < R_2$ ($\Delta R > 0$), which is precisely opposite to the situation with molecule **1**. The ground state, which is the sum of a σ curve with a minimum and a π curve with a maximum, will attain a minimum (GS_{min}) to the left of the σ minimum where $R_1 > R_2$ ($\Delta R < 0$). In contrast, the excited state, which is a sum of two curves with minima, will have a minimum (EX_{min}) between the two minima ($\Delta R > 0$).

This prediction is supported by the computational data presented in Table 2. The ground state has a small (negatively signed) bond alternation, that is, $\Delta R < 0$, while the twin excited state alternates in the opposite direction. Thus, as predicted by the qualitative model, this small but opposite alternation of the ground state and its twin excited states is a result of the π electronic behavior along the bond-alternating mode.

Table 2. Calculated angles ϕ [°], bond lengths R_1 and R_2 [Å], and bond length alternations ΔR for **2** in the ground and exited states [a].

Entry	Method	ϕ	R_1	R_2	ΔR
ground state ($^1A'$)					
1	HF/6-31G	119.6	1.398	1.382	−0.016
2	HF/6-31G(d)	119.5	1.399	1.378	−0.021
3	B3LYP/6-311G(dp)	119.6	1.405	1.390	−0.015
excited state ($^1A'$)[b]					
4	CIS/6-31G	119.7	1.412	1.417	0.005
5	CIS/6-31G(d)	119.6	1.410	1.416	0.006

[a] See the formula of **2** for definitions of R_1, R_2, and ϕ; $\Delta R = R_2 - R_1$. [b] This state is the $^1B_{2u}$-like state of benzene (Scheme 1).

This link between distortion and structure can be quantified. Assuming that the total energy is the sum of π and σ energies which have a parabolic behavior in the bond-alternation coordinate ΔR, one obtains Equation (1), in which k represents the corresponding force constants. The quantities δR are shifts relative to the minimum of the σ curve on the ΔR coordinate[14]. Since $k_\sigma > k_\pi$, the denominator is always positive irrespective of the sign of k_π. The numerator depends on the sign of k_π. Due to the avoided-crossing mechanism, which generates the π curves, k_π is negative for the ground state and positive for the excited state. Consequently, the structural distortion $\delta R_{(\sigma+\pi)min}$ will be opposite for the two states. Moreover, since the denominator is small for the ground state ($k_\pi < 0$) and large for the excited state ($k_\pi > 0$), Equation (1) predicts that the ground state will undergo significant bond alternation upon appropriate constraints (for example, as with **1**), whereas the corresponding twin excited state will hardly alternate and virtually conserve local D_{6h} symmetry. These predictions, which are supported by the quantitative calculations, are amenable to experimental scrutiny.

$$\delta R_{(\sigma+\pi)min} = k_\pi \delta R_\pi / (k_\pi - k_\sigma) \quad (1)$$

At the onset we stated the importance of linking the distortive tendency of the π electrons to a chemical observable. The work reported here steps toward this goal by drawing a simple and predictive relationship between π distortion and bond-alternation patterns in the ground and covalent excited states (Scheme 1) of constrained and perturbed benzene derivatives. This, together with the vibrational characteristics of the bond-alternating mode in the two states of benzene,[1, 15] provide well-defined observables for probing the balance between the σ and π electrons in benzene and its derivatives.

Received: March 10, 1997
Supplemented version: May 28, 1997 [Z 10217 IE]
German version: *Angew. Chem.* **1997**, *109*, 2322–2324

Keywords: arenes · bond-length alternation · cyclohexatriene · strained molecules

[1] a) P. C. Hiberty, D. Danovich, A. Shurki, S. Shaik, *J. Am. Chem. Soc.* **1995**, *117*, 7760; b) S. Shaik, A. Shurki, D. Danovich, P. C. Hiberty, *ibid.* **1996**, *118*, 666; see also c) K. Jug, A. Köster, *ibid.* **1990**, *112*, 6772; d) A. Gobbi, Y. Yamaguchi, G. Frenking, H. F. Schaefer III, *Chem. Phys. Lett.* **1995**, *244*, 27.
[2] Y. Haas, S. Zilberg, *J. Am. Chem. Soc.* **1995**, *117*, 5387.
[3] a) K. K. Baldridge, J. S. Siegel, *J. Am. Chem. Soc.* **1992**, *114*, 9583; b) H. B. Bürgi, K. K. Baldridge, K. Hardcastle, N. L. Frank, P. Gantzel, J. S. Siegel, J. Ziller, *Angew. Chem.* **1995**, *107*, 1575; *Angew. Chem. Int. Ed. Engl.* **1995**, *34*, 1454; c) N. L. Frank, K. K. Baldridge, J. S. Siegel, *J. Am. Chem. Soc.* **1995**, *117*, 2102.
[4] a) R. Diercks, K. P. C. Vollhardt, *J. Am. Chem. Soc.* **1986**, *108*, 3150; b) R. Boese, A. J. Matzger, D. L. Mohler, K. P. C. Vollhardt, *Angew. Chem.* **1995**, *107*, 1630; *Angew. Chem. Int. Ed. Engl.* **1995**, *34*, 1478; c) F. Cardullo, D. Giuffrida, F. H. Kohnke, F. M. Raymo, J. F. Stoddart, D. J. Williams, *ibid.* **1996**, *108*, 347 bzw. **1996**, *35*, 339.
[5] E. C. da Silva, J. Gerratt, D. L. Cooper, M. Raimondi, *J. Chem. Phys.* **1994**, *101*, 3866.
[6] Various levels and basis sets were used for the calculations to show self-consistency. All calculations were performed with the Gaussian 94 package of programs [7]. The geometry of **1** was optimized, and the frequency calculated. The geometry of **2** was optimized under C_{3h} constraint to prevent rotation of the substituents. The $^1A'$ excited state ($^1B_{2u}$-like) of **2** is always the first excited state but for **1** it is the second excited state according to all levels of calculation except STO-3G, in which it is predicted to be the first excited state.
[7] Gaussian 94, Revision D.4: M. J. Frisch, G. W. Trucks, H. B. Schlegel, P. M. W. Gill, B. G. Johnson, M. A. Robb, J. R. Cheeseman, T. Keith, G. A. Petersson, J. A. Montgomery, K. Raghavachari, M. A. Al-Laham, V. G. Zakrzewski, J. V. Ortiz, J. B. Foresman, J. Cioslowski, B. B. Stefanov, A. Nanayakkara, M. Challacombe, C. Y. Peng, P. Y. Ayala, W. Chen, M. W. Wong, J. L. Andres, E. S. Replogle, R. Gomperts, R. L. Martin, D. J. Fox, J. S. Binkley, D. J. Defrees, J. Baker, J. P. Stewart, M. Head-Gordon, C. Gonzalez, J. A. Pople, Gaussian, Inc., Pittsburgh, PA, **1995**.
[8] A molecule that is closely related to **2** was recently discussed by T. M. Krigowski, R. Anulewicz, P. C. Hiberty, *J. Org. Chem.* **1996**, *61*, 8533.
[9] a) M. Merchán, E. Ortí, B. O. Roos, *Chem. Phys. Lett.* **1994**, *221*, 136; b) J. Almlöf, T. H. Ficher, P. G. Gassman, A. Ghosh, M. Häser, *J. Phys. Chem.* **1993**, *97*, 10964.
[10] a) S. Zilberg, Y. Haas, *J. Chem. Phys.* **1995**, *103*, 20; b) S. Zilberg, S. Kendler, Y. Haas, *J. Phys. Chem.* **1996**, *100*, 10869.
[11] A. Stanger, *J. Am. Chem. Soc.* **1991**, *113*, 8277.

 © WILEY-VCH Verlag GmbH, D-69451 Weinheim, 1997 0570-0833/97/3620-2207 $ 17.50+.50/0

[12] E. D. Jemmis, B. Kiran, *J. Org. Chem.* **1996**, *61*, 9006.
[13] For such a distorted σ framework see L. D. Mohler, K. P. Vollhardt, S. Wolff, *Angew. Chem.* **1990**, *102*, 1200; *Angew. Chem. Int. Ed. Engl.* **1990**, *29*, 1151.
[14] The variable δR is defined as $\Delta R - \Delta R_{\sigma\,min}$. Using this definition and parabolic equations for the energy curves, one obtains $E_\sigma = 0.5k_\sigma(\delta R)^2$ for the σ curve, and $E_\pi = 0.5k_\pi(\delta R - \delta R_\pi)^2 + \text{const}$ for the π curve; δR_π is the deviation of the maximum or minimum of the π curve from the σ minimum at $\delta R = 0$. The curve of the total energy E_{tot} (the sum of σ and π energies) is then given by $0.5k_\sigma(\delta R)^2 + 0.5k_\pi(\delta R - \delta R_\pi)^2 + \text{const}$, and its minimum by Equation (1).
[15] a) A. G. Ozkabak, L. Goodman, J. M. Berman, *Chem. Phys. Lett.* **1990**, *168*, 253; b) for a summary, see S. Shaik, S. Zilberg, Y. Haas, *Acc. Chem. Res.* **1996**, *29*, 211.

Anaerobic Copper-Catalyzed Oxidation of Alcohols to Aldehydes and Ketones**

István E. Markó,* Masao Tsukazaki, Paul R. Giles, Stephen M. Brown, and Christopher J. Urch

We recently reported on an efficient, copper-catalyzed oxidation of alcohols to carbonyl compounds that uses oxygen or air as the ultimate, stoichiometric oxidant.[1] In light of the extensive research on copper chemistry[2] and some of our own mechanistic studies,[3] we proposed the catalytic cycle depicted in Figure 1.

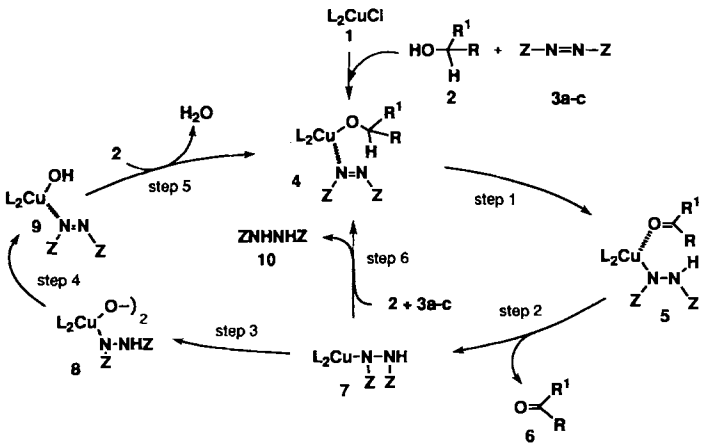

R, R¹ = alkyl, aryl, H; **3a**: Z = COOEt, **3b**: Z = COO*i*Pr, **3c**: Z = COO*t*Bu; L_2 = phen

Figure 1. Proposed mechanism for the copper-catalyzed oxidation of alcohols.

In this catalytic process, we assumed that the reaction of CuCl·phen (phen = 1,10-phenanthroline) with the alcohol **2** and azodicarboxylate **3** forms the ternary complex **4**. This copper(I) derivative **4** then undergoes an intramolecular hydride transfer reaction leading to complex **5** and the formation of a carbon–oxygen double bond.[4] Release of the bound carbonyl compound **6** generates the hydrazidocopper(I) system **7** which, in the presence of oxygen, is subsequently oxidized to the binuclear copper(II) complex **8**.[5] Homolytic cleavage of the peroxo linkage, enables the second intramolecular hydrogen-atom transfer of the catalytic cycle, which affords the hydroxycopper(I) derivative **9** and leads to the regeneration of the key diazo functionality. Addition of alcohol **2** with concomitant loss of water leads to reformation of the loaded catalyst **4** and a new catalytic cycle ensues.

As this mechanism suggests, in the absence of the azo derivatives **3**, little if any turnover was observed.[6] The key role played by the azodicarboxylates **3** (DEAD: Z = COOEt, DIAD: Z = COO*i*Pr and DBAD; Z = COO*t*Bu) is apparent from the catalytic cycle. They act both as hydride acceptors in step 1 and also as ligands for the metal in the various complexes involved in the oxidation process. The continuous regeneration of **3** in the presence of oxygen ensures efficient turnover.

In order to gain more information on the hydride transfer (step 1) and thereby to substantiate our proposed mechanism, we decided to perform some experiments in the absence of oxygen. Under these anaerobic conditions, the conversion of alcohol **2** into carbonyl compound **6** should stop once the azo derivative **3** has been reduced. Reoxidation of the intermediate copper–hydrazine complex **7** to the active species **4** cannot occur and the reaction should cease after **3** is consumed.[7] An equimolar quantity of hydrazine **10** should also be produced in this process. For catalysis to still take place under these anaerobic conditions, a ligand exchange between the hydrazidocopper(I) complex **7**, alcohol **2** and azo compounds **3** should operate with simultaneous generation of hydrazine **10** (step 6).[8]

To test these hypotheses, we performed some initial experiments on *p*-chlorobenzyl alcohol **11**. The most important results are displayed in Table 1.

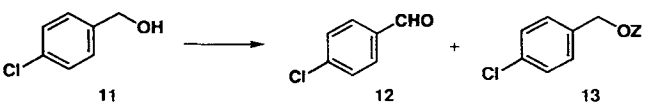

Table 1. Influence of the azo derivative **3** on the copper-catalyzed, anaerobic oxidation of alcohols [a].

Entry	Z	**3** [mol%]	Conversion [%] [b]	Ratio **12**/**13** [c]
1	COO*t*Bu	10	11	>99/<1
2	COO*t*Bu	50	42	>99/<1
3	COO*t*Bu	120	>99 [d]	>99/<1
4	COO*i*Pr	120	81	36/64
5	COOEt	130	73	26/74

[a] 20 °C; other conditions see Experimental Section. [b] Determined by ^{1}H NMR spectroscopy. [c] Determined by ^{1}H NMR spectroscopy and by capillary gas chromatography. [d] Aldehyde **12** was isolated in 82% yield.

Addition of one equivalent of alcohol **11** to a suspension containing 5 mol% CuCl·phen, 10 mol% DBAD **3c**, and 10 mol% K_2CO_3 in toluene, in the absence of oxygen, led to the partial transformation of **11** into aldehyde **12** (11% conversion, Table 1, entry 1). Raising the quantity of DBAD **3c** (50 mol%) used resulted in an increase in the yield of the aldehyde (entry 2). Finally, when DBAD **3c** (1.2 equiv) was used, a quantitative conversion was observed and high yields of *p*-chlorobenzalde-

[*] Prof. I. E Markó, Dr. M. Tsukazaki, Dr. P. R Giles
Département de Chimie
Université Catholique de Louvain
Place Louis Pasteur 1, B-1348 Louvain-la-Neuve (Belgium)
Fax: Int. code +(10)47 27 88
e-mail: marko@chor.ucl.ac.be
Dr. S. M. Brown
Zeneca Process Technology Department, Huddersfield Works, Huddersfield (UK)
Dr. C. J. Urch
Zeneca Agrochemicals, Berkshire (UK)

[**] This work was supported by Zeneca Limited, through the Zeneca Strategic Research Fund. I. E. M. is grateful to Zeneca for a Zeneca Fellowship (1994–1997).

hyde **12** were obtained (Table 1, entry 3). One equivalent of $DBADH_2$ was also produced in this last reaction. Whilst the use of one equivalent of DIAD **3b** also resulted in complete consumption of **11**, the mixed carbonate **13** was now the major product (Table 1, entry 4). The amount of **13** increased even further when DEAD **3a** was employed instead of DIAD **3b** (Table 1, entry 5). Thus, to avoid the undesired formation of carbonate **13**, a bulky carboalkoxy residue is required on the azo derivatives **3**. DBAD **3c** therefore appears to be the best adjuvant and all subsequent oxidations were performed with this diazo compound.[9]

In addition to substantiating our proposed mechanism, the anaerobic, copper-catalyzed oxidation system proved to be particularly useful for the laboratory-scale oxidation of a wide variety of alcohols into the corresponding carbonyl derivatives (Table 2).

As can be seen from Table 2, primary, secondary, allylic, and benzylic alcohols can all be smoothly oxidized to the corresponding aldehydes and ketones in excellent yields. Sensitive products, such as geranial and neral are not isomerized under the reaction conditions (Table 2, entries 3 and 4, respectively). Remarkably, benzoin is oxidized to benzil with virtually no competitive C–C bond cleavage (Table 2, entry 9).[10] Importantly, optically active β-amino alcohols are oxidized to the corresponding β-amino aldehydes without any detectable racemization (Table 2, entry 10), which demonstrates the mildness of the reaction conditions.[11] In contrast to the aerobic oxidation system[1] in which two equivalents of K_2CO_3 were required for optimum catalytic activity, only a small amount of K_2CO_3 (10 mol%) is necessary in our anaerobic version. Remarkably, in all cases studied so far, complete conversion of the alcohol to the carbonyl derivative took place. This situation is different in the aerobic process in which the presence of oxygen hampers complete transformation of primary alcohols to aldehydes.[12]

In summary, we have established a new, efficient copper-catalyzed anaerobic protocol for the oxidation of a wide range of alcohols into carbonyl compounds under mild conditions. In addition, these studies support our proposals for the mechanism of such Cu-catalyzed oxidations and form the foundations for the development of this interesting oxidation system.

Table 2. Anaerobic, copper-catalyzed oxidation of alcohols [a].

Entry	Substrate **2**	Product **6**	Yield [%][b]	*t* [min]
1	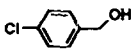	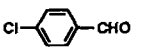	82	240 [c]
2	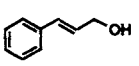	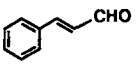	93	60
3	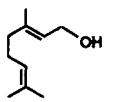	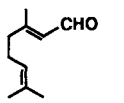	89	60 [d]
4	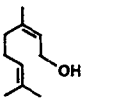	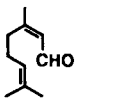	87	60 [e]
5	$C_9H_{19}CH_2OH$	$C_9H_{19}CHO$	79	180 [f]
6	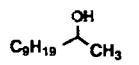	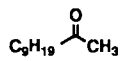	84	180
7	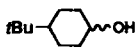	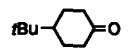	88	180
8	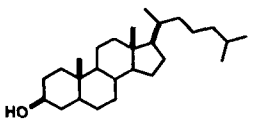	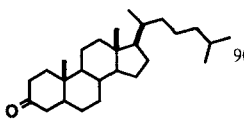	90	180
9	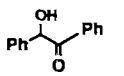	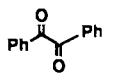	93	120 [f]
1	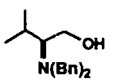	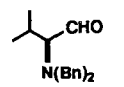	91	120 [g]

[a] 70 °C; other conditions see Experimental Section. [b] All yields are for pure, isolated products. [c] Reaction performed at 20 °C. [d] >95% (*E*). [e] >95% (*Z*). [f] Reaction conducted under degassed conditions. [g] >95% *ee*.

Experimental Section

Typical procedure for the oxidation of 2-undecanol to 2-undecanone: CuCl (5 mg, 0.05 mmol) and 1,10-phenanthroline (9 mg, 0.05 mmol) were mixed in dry toluene (5 mL) and the mixture was stirred for 10 min at room temperature. K_2CO_3 (14 mg, 0.10 mmol), DBAD **3c** (230 mg, 1.00 mmol), and 2-undecanol (172 mg, 1.00 mmol) were added successively and the mixture was heated at 70 °C for 3 h. After cooling to room temperature, the mixture was diluted by adding Et_2O (5 mL) and filtered through a pad of celite. Evaporation of the solvent under vacuum afforded a crude product that was further purified by column chromatography (EtOAc/hexane 1/20) to give pure 2-undecanone (142 mg, 84%).

Received: March 20. 1997 [Z10265IE]
German version: *Angew. Chem.* **1997**, *109*, 2297–2299

Keywords: alcohols · carbonyl compounds · copper · homogeneous catalysis · oxidations

[1] I. E. Markó, P. R. Giles, M. Tsukazaki, S. M. Brown, C. J. Urch, *Science* **1996**, *274*, 2044–2046.

[2] a) C. Jallabert, H. Rivière, *Tetrahedron Lett.* **1977**, 1215–1218; b) C. Jallabert, C. Lapinte, H. Rivière, *J. Mol. Catal.* **1980**, *7* 127–136; c) C. Jallabert, H. Rivière, *Tetrahedron* **1980**, *36*, 1191–1194; d) C. Jallabert, C. Lapinte, H. Rivière, *J. Mol. Catal.* **1982**, *14*, 75–86; e) P. Capdevielle, D. Sparfel, J. Baranne-Lafont, N. K. Cuong, M. Maumy, *J. Chem. Res. Synop.* **1993**, 10–11, and references therein; f) M. Munakata, S. Nishibayashi, H. Sakamoto, *J. Chem. Soc. Chem. Commun.* **1980**, 219–220; g) S. Bhaduri, N. Y. Sapre, *J. Chem. Soc. Dalton Trans.* **1981**, 2585–2586; h) M. F. Semmelhack, C. R. Schmid, D. A. Cortes, C. S. Chou, *J. Am. Chem. Soc.* **1984**, *106*, 3374–3376.

[3] I. E. Markó, P. R. Giles, M. Tsukazaki, S. M. Brown, C. J. Urch, unpublished results.

[4] For general reviews on Oppenauer-type oxidations, see a) C. F. de Graauw, J. A. Peters, H. Vandekkum, J. Huskens, *Synthesis* **1994**, 1007–1017; b) C. Djerassi, *Org. React. N. Y.* **1951**, *6*, 207–212; c) K. Krohn, B. Knauer, J. Kupke, D. Seebach, A. K. Beck, M. Hayakawa, *Synthesis* **1996**, 1341–1344. The use of stoichiometric amounts of dipiperidinyl azodicarboxamide to oxidize magnesium alkoxides to the corresponding carbonyl compounds has been described: K. Narasaka, A. Morikawa, K. Saigo, T. Mukaiyama, *Bull. Chem. Soc. Jpn.* **1977**, *50*, 2773–2776. No reaction is observed under our catalytic anaerobic conditions if DBAD is replaced by the azodicarboxamide derivative. The stoichiometric oxidation of copper(I) alkoxides to aldehydes and ketones by O_2, though in very low yields, has been reported previously: P. Capdevielle, P. Audebert, M. Maumy, *Tetrahedron Lett.* **1984**, *25*, 4397–4400.

[5] For reviews on the formation, isolation and reactions of dinuclear copper(II) peroxides, see a) K. D. Karlin, Y. Gultneh, *Prog. Inorg. Chem.* **1987**, *35*, 219–327; b) A. D. Zuberbühler in *Copper Coordination Chemistry: Biochemical and Inorganic Perspectives* (Eds.: K. D. Karlin, J. Zubieta), Adenine Press, Guilderland, NY, **1983**; c) A. M. Sakharov, I. P. Skibida, *Kinet. Catal. Engl. Transl.* **1988**, *29*, 96–102; d) Z. Tyleklar, R. R. Jacobson, N. Wei, N. N. Murthy, J. Zubieta, K. D. Karlin, *J. Am. Chem. Soc.* **1993**, *115*, 2677–2689; e) N. Kitajima, K. Fujisawa, C. Fujimoto, Y. Morooka, S. Hashimoto, T. Kitagawa, K. Toriumi, K. Tatsumi, A. Nakamura, *ibid.* **1992**, *114*, 1277–1291; f) S. Fox, A. Nanthakumar,

 © WILEY-VCH Verlag GmbH, D-69451 Weinheim, 1997 0570-0833/97/3620-2209 $ 17.50+.50/0

M. Wikstrom, K. D. Karlin, N. J. Blackburn, *ibid.* **1996**, *118*, 24–34; g) E. I. Solomon, U. M. Sundaram, T. E. Machonkin, *Chem. Rev.* **1996**, *96*, 2563–2605.

[6] In the absence of azo derivatives **3** highly active benzylic alcohols undergo some aerobic oxidation to the corresponding aldehydes. For example, using 5 mol% CuCl·phen, 200 mol% K_2CO_3, benzene, 80 °C, and bubbling O_2 through the reaction mixture, a 60% conversion of *p*-chlorobenzylalcohol into *p*-chlorobenzaldehyde can be achieved. Allylic substrates gave much lower conversions (<30%) and aliphatic alcohols are virtually inert under these conditions. No reaction is observed with any of these substrates under anaerobic conditions, in the absence of the azo derivatives **3**.

[7] The intermediacy of complex **7** in the aerobic oxidations was supported by the following observations: 1) independently generated hydrazido complex **7** (CuCl·phen/DBADH$_2$/NaH) proved to be unreactive under anaerobic conditions; 2) passing O_2 through the reaction mixture containing **7** and alcohol **2** restored the catalytic activity, and good yields of aldehyde **6** were again obtained.

[8] This new catalytic cycle, involving steps 2 and 6, is in some ways reminiscent of analogous oxidation shunts that take place in aerobic bacteria placed under anaerobic conditions.

[9] The oxidation of alcohols with azodicarboxylates has been previously reported: F. Yoneda, K. Suzuki, Y. Nitta, *J. Org. Chem.* **1967**, *32*, 727–729. Control experiments were therefore performed to establish the need for copper salts in our anaerobic oxidation procedure. Thus, under our reaction conditions, no aldehyde or ketone could be detected in the absence of the CuCl·phen catalyst, even when phenanthroline was added as an activating base. Moreover, certain reactive alcohols were oxidized partially by CuCl·phen in the absence of the azo derivative **3**, though only in moderate yields.

[10] With most oxidants, α-hydroxyketones are oxidized with concomitant cleavage of the C–C bond: a) R. C. Larock, *Comprehensive Organic Transformations*, VCH, New York, **1989**, pp. 604–615; b) R. A. Sheldon, J. K. Kochi, *Metal-Catalyzed Oxidations of Organic Compounds*, Academic Press, New York, **1981**; c) G. Procter in *Comprehensive Organic Synthesis*, *Vol. 7* (Eds.: B. M. Trost, I. Flemming, S. V. Ley), Pergamon, Oxford, **1991**; d) W. S. Trahanovsky, *Oxidation in Organic Chemistry*, *Part A–D*, Academic Press, New York.

[11] See for example M. T. Reetz, M. W. Drewes, A. Schmitz, *Angew. Chem.* **1987**, *99*, 1186–1188; *Angew. Chem. Int. Ed. Engl.* **1987**, *26*, 1141–1143.

[12] This difference appears to be due to competitive autooxidation of the aldehyde to the corresponding carboxylic acid by oxygen at high conversions of the alcohol. See also ref. [9b].

Electron-Density Relaxation and Oppositely Signed Reaction Constants in Dual Substituent Parameter Relationships in Dediazoniation Reactions**

Rainer Glaser,* Christopher J. Horan, and Heinrich Zollinger*

Dedicated to Professor Dieter Seebach on the occasion of his 60th birthday

The reasons why relationship between σ and ρ in the Hammett equation [Eq. (1)][1] has been fairly well applicable since 1935 to several thousand heterolytic reactions of substituted benzene derivatives are by no means obvious. In the Hammett equation, the constants σ and ρ represent a combination of field (inductive) and resonance effects (mesomeric). One can therefore conclude that in all of these reactions both effects influence the reactivity in the same direction and to the same relative extent. This is indeed the case if one evaluates the same kinetic data with a dual substituent parameter (DSP) treatment, as, for example, developed by Taft and co-workers [Eq. (2); subscripts F and R indicate field and resonance effect contributions, respectively, to reaction rate constants k_X of X-substituted benzene derivatives relative to that of the unsubstituted compounds (k_0)].[2] Effects of electronic substituent can be classified[3a] into those that are associated with the substituent's polarity (I_σ, F, π_s, π_F) and those that are assigned to the substituent's ability to transfer charge (R, σ_π).[3b] This classification relates the substituent constants σ_F and σ_R in Equation (2) to polarity and charge-transfer factors, as indicated in Equation (3).

$$\lg(k_X/k_0) = \sigma\rho \quad (1)$$

$$\lg(k_X/k_0) = \sigma_F\rho_F + \sigma_R\rho_R \quad (2)$$

$$\lg(k_X/k_0) = (\text{polarity})\rho_F + (\text{charge transfer})\rho_R \quad (3)$$

The substituent constants in the Hammett equation are assumed to be independent of the reaction.[4] Dual substituent parameter treatments can thus be regarded as a necessary consequence of the two classes of intrinsic substituent effects. Experience shows that in the large majority of cases the ratio $\rho_R/\rho_F = \lambda \approx 1$. We estimate that values of λ larger than 1.1 or smaller than 0.9 (but still positive) are present in fewer than 10% of all equilibria and rates for which a Hammett relationship was tested. This result seems surprising, as the field and resonance effects are, in principle, considered to be independent of each other. There are, however, sixteen reactions with opposite signs for ρ_F and ρ_R, that is, λ is negative.[5] Examples are dediazoniations of benzenediazonium ions in water, 1,2-dichloromethane, and trifluoroethanol; these reactions all show $\rho_F < -3.5$, $\rho_R > +2.2$, and $|\rho_F| > |\rho_R|$.

Due to our interest in the structure of benzenediazonium ions,[6] the nature of C–N dative bonding,[7] and its dediazoniations,[5–8] we investigated the theoretical basis for the opposing influences of the field and resonance effects on dediazoniation of *para*-substituted benzenediazonium ions *para*-X-C_6H_4-N_2^+ (**1a**, X = H; **1b**, X = NH_2; **1c**, X = NO_2) to the respective *para*-substituted phenyl cations **2a–c** (see Figure 1). Zollinger interpreted the opposite signs of the reaction constants ρ_F and ρ_R by proposing that the cleavage of the σ bond between the N_2 lone pair and the sp^2 LUMO of **2** is slowed by inductively withdrawing substituents and should give rise to a substantial negative field reaction constant ρ_F. If N–C σ bonding is reinforced by C → N π backbonding, a positive reaction constant ρ_R is plausible, since dissociation leads to an increase in π density on the phenyl fragment and brings π-electron density closer to the substituent. While this interpretation cannot be demonstrated experimentally, it is possible to examine it with electronic structure methods. We carried out electron-density analyses of the unimolecular dissociations **1**→**2** + N_2 (X = H, NH_2, NO_2).

Our objectives here are to show that the reaction constants of the dediazoniation reactions are consistent with the hypothesis of combined C←N σ dative and C→N π backdative bonding. Furthermore, we want to learn about the mechanisms by which two important substituents affect electronic structure. The electron-density analysis is based on the topological features of total electron densities, which are observable in the quantum me-

[*] Prof. Dr. R. Glaser, Dr. C. J. Horan
Department of Chemistry
University of Missouri-Columbia
Columbia, Missouri 65211 (USA)
Fax: Int. code +(573)882-2754
e-mail: chemrg@showme.missouri.edu
Prof. Dr. H. Zollinger
Technisch-chemisches Laboratorium der Eidgenössische Technische Hochschule
Universitätstrasse 16, CH-8092 Zürich (Switzerland)
Fax: Int. code +(1)632-1072

[**] Presented in part at the Gordon Conference on Electron Distribution and Chemical Bonding, Plymouth State College, Plymouth, NH, USA, July 2–7, 1995, and at the 30th Midwest Theoretical Chemistry Conference, University of Illinois, Urbana-Champaign, IL, USA, May 22–24, 1997.

 © WILEY-VCH Verlag GmbH, D-69451 Weinheim, 1997 0570-0833/97/3620-2210 $ 17.50+.50/0

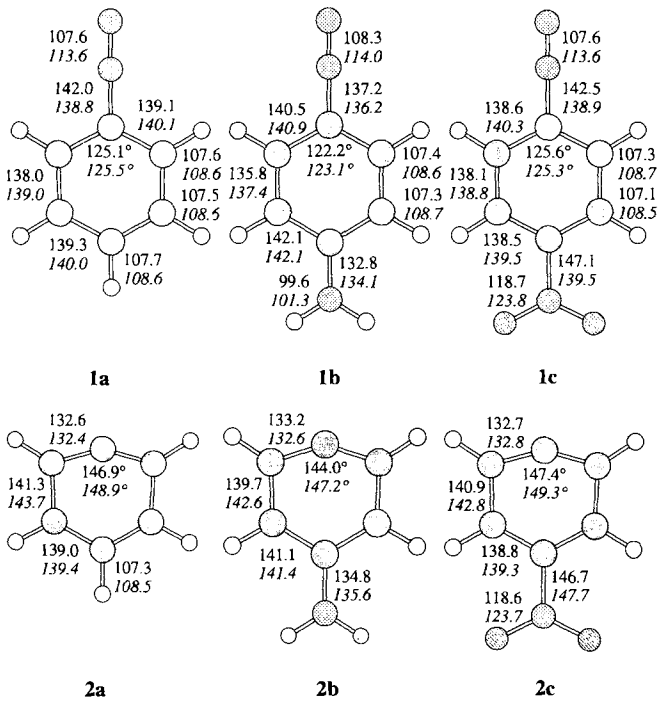

Figure 1. Structural parameters for **1a–c** and **2a–c** calculated at the levels RHF/6-31G* and MP2(full)/6-31G* (in italics). The *para* subsituent is H, NH_2, and NO_2, respectively. The bond lengths are given in pm.

chanical sense. We also determined the σ and π components of the atom populations. Although these components are not observable, the concept of σ/π separation is successful and central to all models invoking dative and backdative bonding. In essence, our analysis links shifts in electron density in the σ and π systems with the reaction constants ρ_F and ρ_R. This approach differs slightly from Topsom's formulation,[3] in which we would weigh π_σ and π_F with ρ_R. Ideally, an analysis of this relatively clear and qualitatively explainable case[5] of a reaction with opposing field and resonance effects may lead to an understanding of why thousands of equilibria and reactions can be explained with the simple Hammett equation and show an almost constant ratio of the two effects ($1.1 > \lambda > 0.9$).

Structures along the dissociation pathways of **1a–c** were optimized at the RHF/6-31G* level,[9, 10] and vibrational analyses were carried out for stationary structures. These dissociations proceed without an activation barrier, as in other diazonium ions.[6, 7] Zero point energy corrections to binding energies were scaled by a factor of 0.9135.[11] Geometries of stationary structures were refined at the MP2(full)/6-31G* level; the molecular models are shown in Figure 1. More reliable binding energies were computed at the levels up to QCISD(T,fc)/6-31G*//MP2(full)/6-31G* (Table 1).

Table 1. Binding energies and corrections of the vibrational zero point energy (VZPE) of **1** [a, b].

X	Reaction	RHF //RHF	Δ(VZPE)	MP2 //MP2	MP3(fc) //MP2	MP4(fc) //MP2	QCISD(T) //MP2
H	**1a** → **2a** + N_2	107.22	−19.72	161.78	139.96	143.52	134.81
NH_2	**1b** → **2b′** + N_2	141.18	−19.05	199.75	178.02	177.86	165.67
NO_2	**1c** → **2c** + N_2	118.82	−19.30	180.12	154.87	160.73	150.93

[a] All values were calculated with the 6-31G* basis set. All energies are given in kJ mol^{-1}. [b] The Δ(VZPE) values need to be added to the reaction energies to obtain approximate reaction enthalpies: $\Delta H = \Delta E + \Delta(\mathrm{VZPE})$.

The C_{2v} structures **1a–c** are minima on the potential energy hypersurface, and **2a** and **2c** also prefer C_{2v} symmetry. However, a C_{2v} structure is not a minimum for **2b**. The most stable structure, labeled **2b′**, is nonplanar and chiral (C_1 symmetrical), and it appears advantageous for reducing ring strain at C_{ipso}. Structures **2b′** and **2b** are nearly isoenergetic, and the distortions do not play a role until late stages in the dissociation. Although we report binding energies for **2b′** in Table 1, we consider **2b** for the remaining discussion. The structural differences between **1a** and **1c** are minor (within 1 pm and 1°; Figure 1), while the effects of push–pull interaction are clearly manifest in **1b**. The structural relaxation upon N_2 dissociation is steady for all substituents X, and the major structural consequences are common. The main event concerns the rehybridization of C_{ipso} upon heterolysis: The $C_{ipso}-C_{ortho}$ bond lengths shorten dramatically (by 0.06–0.08 pm), and the angle at C_{ipso} increases. Systematic studies of X/N_2^{+2} systems showed that binding energies computed at the MP3 level or higher that include vibrational zero point energies reproduce experimental gas-phase binding energies nearly quantitatively.[12] The good agreement between the data measured in the gas phase and in solution[13, 14] suggests that primarily intrinsic properties of **1** are important in the solution chemistry. The binding energies of **1b** and **1c** are higher than for **1a**. The NH_2 and NO_2 groups are overall both electron-withdrawing groups, and are expected to destabilize the phenyl cation more than the diazonium ion. But why is the dissociation of **1b** more endothermic than that of **1c**? One might expect the opposite, since the nitro group is more electron-withdrawing, and because the π donor might better compensate for the electron deficiency in the σ framework. Therefore, qualitative considerations of **2** require significant differences in the electronic structures of **1b** and **1c** that provide an extra stabilization to **1b**. This realization leads to the idea of push–pull stabilization of spacer-connected π-donor–acceptor systems.

Topological electron density analyses[15, 16] at the RHF/6-31G* level were carried out for stationary structures **1a–c** and **2a–c** and the associated reaction pathways; important results are shown in Figures 2 and 3. In general, aliphatic and aromatic diazonium ions are best thought of as carbenium ions closely associated with an N_2 molecule that is internally polarized in the fashion $N_\alpha^{\delta-}-N_\beta^{\delta+}$. This bonding model implies C–N dative bonding instead of covalent C–N bond formation with charge transfer, as suggested by the formal Lewis notation. With a combination of theory and experiment, we have shown that the idea of a carbenium ion within the diazonium ion is fully warranted.[17, 18] The integrated phenyl charge of **1a** is +0.974, and the N_2 group is nearly neutral and polarized ($q(N_\alpha) = -0.540$, $q(N_\beta) = +0.558$). The charge distributions in the CN_2 regions of **1a** and **1c** are similar (Figure 2, top), and, as expected, **1c** exhibits a slightly higher positive N_2 charge.

In **1b** the charge $q(H_2N-Ph)$ exceeds +1, and a negatively charged N_2 group occurs as the result of strong C→N π backdonation of 0.338 electrons. This backdonation is about half as much in **1a** (0.211) and **1c** (0.185). For all ions **1**, the N → C σ donation is the same, and the σ charge hardly varies from 0.231. The charge transfer associated with C–N bonding in **1** can thus be described by a bonding model that involves N→C σ donation and C→N π backdonation of about equal magnitudes (Scheme 1). The H_{para} atom in **1a** acts like the other aromatic H atoms to delocalize positive charge to the periphery of the molecule, while the X groups are negatively charged in **1b** and **1c**. The NH_2 group is a π donor (0.156 electrons), but overall it withdraws 0.475 electrons! The NO_2 group withdraws in total 0.531 electrons, of which 0.063 is due to π withdrawal.

 © WILEY-VCH Verlag GmbH, D-69451 Weinheim, 1997 0570-0833/97/3620-2211 $ 17.50+.50/0

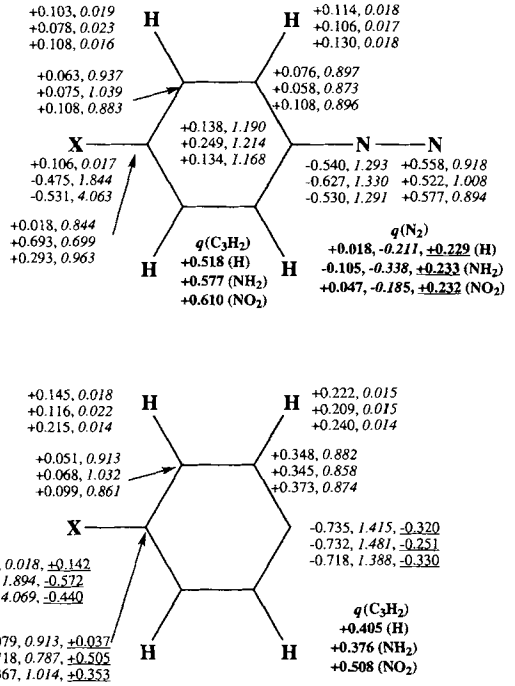

Figure 2. Integrated atom and fragment charges as well as populations (RHF/6-31G*) for **1a–c** and **2a–c**. The π populations are given in italics, and σ charges are underlined.

σ dative interaction between the N_2 lone pair and the vacant σ orbital of the phenyl cation

π backdative bonding between a π orbital of the phenyl cation and the π* orbital of the N_2 group

Scheme 1. Schematic representation of the primary MO interactions associated with N→C σ dative and C→N π backdative bonding in diazonium ions.

The density shifts show enhance C→N π backdative bonding in **1b**, but the electronic mechanism is more complex than the simplistic π-pushing picture and leaves the amino group very negative. The σ density of the N_2 group is changed slightly, but that of C_{ipso} is depleted; these events should strengthen N → C σ dative bonding in **1b**. Therefore, both components of the C–N interaction are enhanced in **1b**. Compared to **1a**, the total changes in the charge of the N_2 group in **1c** are very similar to the changes in the π system. The NO_2 group leads to depletion of π density at C_{meta}, C_{ipso}, and N_β. These density shifts suggest that the NO_2 group hardly affects N→C σ dative bonding but weakens C→N π backdative bonding. The electron-density analysis suggests that C–N bonding is enhanced in **1b** and weakened in **1c**; the C–N bond lengths in **1a–c** are perfectly consistent with this trend.

Our analysis of the phenyl cations **2** focused on the C_3H_2 fragment and showed that its overall positive charge is greatly diminished during dediazoniation: by 0.113 for X = H, by 0.102 for X = NO_2, and by as much as 0.201 for X = NH_2. The σ-hole formation causes such extreme polarizations in the σ system that the majority of the positive charge is located on the other half of the molecule! Interestingly, the population analysis of **2** assigns a negative charge to C_{ipso} and large positive charges to the *ortho*-CH groups. These atom populations reflect C_{ipso}–C_{ortho} bond polarization toward C_{ipso} and, with the zero-flux surfaces at a greater distance from C_{ipso}, an expanding C_{ipso} basin.[7a, b] The topological analysis of the electronic relaxation along the dissociation path shows that the associated population changes at C_{ipso} reflect primarily inductomeric effects on the location of the C_{ipso}–C_{ortho} partitioning surface.[16]

The plots in Figure 3 depict the changes in C–N bonding during heterolysis of **1a**; similar plots were obtained for the

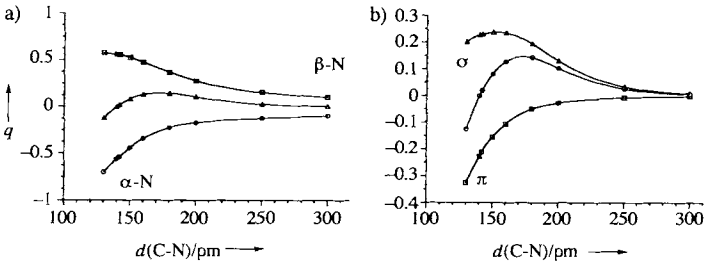

Figure 3. Variation of the charge q of a) the N atoms and b) the N_2 group as well as the σ and π components of the charge for **1a** along the unimolecular dissociation pathway as a function of the C–N bond length. The top and bottom curves describe the different components, and the middle curve describes the corresponding combination.

substituted systems. The dissociation is essentially complete when the bond length d(C–N) is about 300 pm. The charges of N_α and N_β change steadily, and the negative charge at N_α drops faster than the positive charge at N_β. Consequently, the charge of the N_2 group goes through a maximum around d(C–N) = 175 pm. Cleavage of the C–N bond may increase (X = H, NO_2) or decrease (X = NH_2) the overall positive charge on the phenyl fragment. Irrespective of their charge in the equilibrium structures **1a–c**, the N_2 groups become more positive in the early phase of the dissociation, reach a maximum charge of 0.1–0.2 at d(C–N) ≈ 175 pm, and then smoothly become neutral in the later stages. The value $q_{max}(N_2)$ for the NO_2-substituted system exceeds that of the parent system; $q_{max}(N_2)$ of the NH_2-substituted ion is the lowest. Our analysis illustrates in a compelling way that the C→N π backdative bond breaks earlier than the N→C σ dative bond.

These results are consistent with and provide additional support for the electron density based model that describes C–N bonding in diazonium ions by synergistic C←N σ dative and C→N π backdative bonding. The analysis provides a straightforward theoretical basis for interpretating the oppositely signed DSP relationship and, in addition, furnishes details about the electronic structure that cannot be deduced from physical-organic studies alone. For example, the kinetic analysis does not answer the question as to whether the negative reaction constant ρ_F is due to positive charge being transferred from the diazo function onto the phenyl fragment (e. g. Lewis notation) or whether it is merely the result of charge shifts within the phenyl fragment (as we show). Only the theoretical analysis reveals how C–N bonding is achieved. The kinetic analysis quantifies substituent effects on the overall energy difference between reagents and products, which form the basis for deducing stabilization mechanisms. Theory allows one to pinpoint

 © WILEY-VCH Verlag GmbH, D-69451 Weinheim, 1997 0570-0833/97/3620-2212 $ 17.50+.50/0

these mechanisms by providing independent information on both. While the overall charge of the phenyl fragments in **1** and **2** differ relatively little, the extreme polarizations in the σ systems of the phenyl cations cause a pronounced shift of positive charge from the C_3H_2 fragment into the other half of the molecule. We consider this electron density shift responsible for the negative reaction constant ρ_F. The phenyl ring gains π density upon dediazoniation, which is consistent with the positive reaction constant ρ_R.

Received: February 12, 1997
Supplemented version: May 2, 1997 [Z10106IE]
German version: *Angew. Chem.* **1997**, *109*, 2324–2328

Keywords: bond theory · dediazoniation · diazonium ions · electronic structure · linear free energy relation

[1] L. P. Hammett, *Chem. Rev.* **1935**, *17*, 125.
[2] a) R. W. Taft, *J. Am. Chem. Soc.* **1957**, *79*, 1045; b) S. Ehrenson, R. T. C. Brownlee, R. W. Taft, *Prog. Phys. Org. Chem.* **1973**, *10*, 1.
[3] a) R. D. Topsom, *Prog. Phys. Org. Chem.* **1976**, *12*, 1; b) *ibid.* **1987**, *16*, 125.
[4] a) E. R. Vorpagel, A. Streitwieser, S. D. Alexandratos, *J. Am. Chem. Soc.* **1981**, *103*, 3777; b) J. Niwa, *Bull. Chem. Soc. Jpn.* **1989**, *62*, 226.
[5] H. Zollinger, *J. Org. Chem.* **1990**, *55*, 3856.
[6] a) R. Glaser, C. J. Horan, *J. Org. Chem.* **1995**, *60*, 7518, zit. Lit.; b) R. Glaser, M.-S. Son, *J. Am. Chem. Soc.* **1996**, *118*, 10942.
[7] a) R. Glaser, G. S.-C. Choy, M. K. Hall, *J. Am. Chem. Soc.* **1991**, *113*, 1109; b) R. Glaser, G. S.-C. Choy, *ibid.* **1993**, *115*, 2340; c) R. Glaser, D. Farmer, *Chem. Eur. J.* **1997**, *3*, 1244.
[8] H. Zollinger, *Diazo Chemistry I*, VCH, Weinheim, **1994**, chapters 8–10.
[9] Gaussian94, revision C.3: M. J. Frisch, G. W. Trucks, H. B. Schlegel, P. M. W. Gill, B. G. Johnson, M. A. Robb, J. R. Cheeseman, T. Keith, G. A. Petersson, J. A. Montgomery, K. Raghavachari, M. A. Al-Laham, V. G. Zakrzewski, J. V. Ortiz, J. B. Foresman, J. Cioslowski, B. B. Stefanov, A. Nanayakkara, M. Challacombe, C. Y. Peng, P. Y. Ayala, W. Chen, M. W. Wong, J. L. Andres, E. S. Replogle, R. Gomperts, R. L. Martin, D. J. Fox, J. S. Binkley, D. J. Defrees, J. Baker, J. J. P. Stewart, M. Head-Gordon, C. Gonzalez, J. A. Pople, Gaussian, Inc., Pittsburgh, PA, **1995**.
[10] W. J. Hehre, L. Radom, P. von R. Schleyer, J. A. Pople, *Ab Initio Molecular Orbital Theory*, Wiley, New York, **1986**.
[11] J. A. Pople, A. P. Scott, M. W. Wong, L. Radom, *Isr. J. Chem.* **1993**, *33*, 345.
[12] C. J. Horan, R. Glaser, *J. Phys. Chem.* **1994**, *98*, 3989.
[13] a) T. Kuokkanen, P. O. I. Virtanen, *Acta Chem. Scand. Ser. B* **1979**, *33*, 725; b) T. Kuokkanen, *ibid.* **1990**, *44*, 394.
[14] P. Burri, G. H. Wahl, H. Zollinger, *Helv. Chim. Acta* **1974**, *57*, 2099.
[15] a) R. F. W. Bader, *Atoms in Molecules, A Quantum Theory*, Oxford University Press, New York, **1990**; b) F. W. Biegler-König, R. F. W. Bader, T.-H. Tang, *J. Comput. Chem.* **1982**, *3*, 317; c) R. F. W. Bader, P. L. A. Popelier, T. A. Keith, *Angew. Chem.* **1994**, *106*, 647; *Angew. Chem. Int. Ed. Engl.* **1994**, *33*, 620.
[16] Electron-density analyses were also carried out for **1a** and **2a** at the correlated levels MP2(full)/6-31G* (including dissociation pathways) and CISD(full)/6-31G*//RHF/6-31G*; similar results were obtained: R. Glaser et al., unpublished results.
[17] a) R. Glaser, G. S. Chen, C. L. Barnes, *Angew. Chem.* **1992**, *104*, 749; *Angew. Chem. Int. Ed. Engl.* **1992**, *31*, 740; b) G. S. Chen, R. Glaser, C. L. Barnes, *J. Chem. Soc. Chem. Commun.* **1993**, 1530.
[18] R. Glaser, C. J. Horan, *Can. J. Chem.* **1996**, *74*, 1200, and references therein.

Hexavinylogous Porphyrins with Aromatic 30 π-Electron Systems**

Christian Eickmeier and Burchard Franck*

The seminal work of Sondheimer et al. on the synthesis of cyclic conjugated compounds, including the aromatic [18]annulene (**1a**), culminated with the preparation of [30]annulene (**1b**).[1] Although **1b** follows the $(4n+2)$ rule[2] for aromatic systems, it is unstable. Perfect conformational stabilization of a C_{30} perimeter is achieved in kekulene **2** synthesized by Staab and Diederich.[3] However, the π-electron sextets of its annelated benzene rings do not allow the formation of a conjugated 30 π perimeter. Recently it has been shown with numerous examples that planar cyclopolyenes can be stabilized by insertion of pyrrole units,[4–7] but no aromatic compound corresponding to [30]annulene (**1b**) has been synthesized so far.

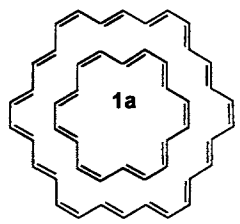

1b

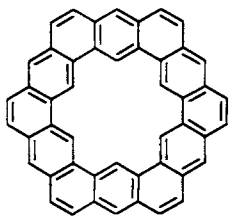

2

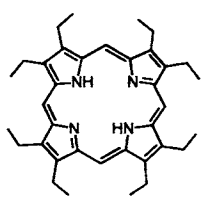

3

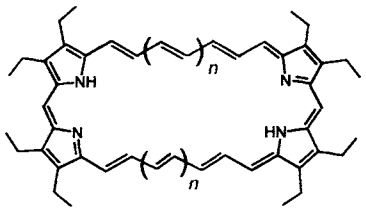

4: $n = 0$
5: $n = 1$

After we had found that the *tetravinylogous* porphyrin **4** has a stable aromatic 26 π-electron system,[8] the question arose whether the stabilizing effect of the pyrrole units would be sufficient for a *hexavinylogous* porphyrin **5**, which has a conjugated perimeter corresponding to the [30]annulene (**1b**) of Sondheimer et al.[1] One serious impedement was that the synthesis of **5** would have to proceed via the highly reactive pyrrylpolyene **11** (Scheme 1).

We report here on the first synthesis of a hexavinylogous porphyrin **5** with an aromatic 30 π-electron system. In addition to its importance for the understanding of aromaticity, this octaethyl[30]porphyrin is also of practical interest, as its parent compound, octaethyl[18]porphyrin **3**,[9] is the most extensively used porphyrin in chemistry and medicine.

[*] Prof. Dr. B. Franck
Organisch-chemisches Institut der Universität
Corrensstrasse 40, D-48149 Münster (Germany)
Fax: Int. code +(251)83-39972
e-mail: franck@uni-muenster.de.

Dr. C. Eickmeier
Boehringer Ingelheim KG
D-55216 Ingelheim am Rhein (Germany)

[**] Novel Porphyrinoids, Part 16. This work was supported by the Deutsche Forschungsgemeinschaft, the Fonds der Chemischen Industrie, and the BASF AG (Ludwigshafen). Part 15: [7].

 © WILEY-VCH Verlag GmbH, D-69451 Weinheim, 1997 0570-0833/97/3620-2213 $ 17.50+.50/0

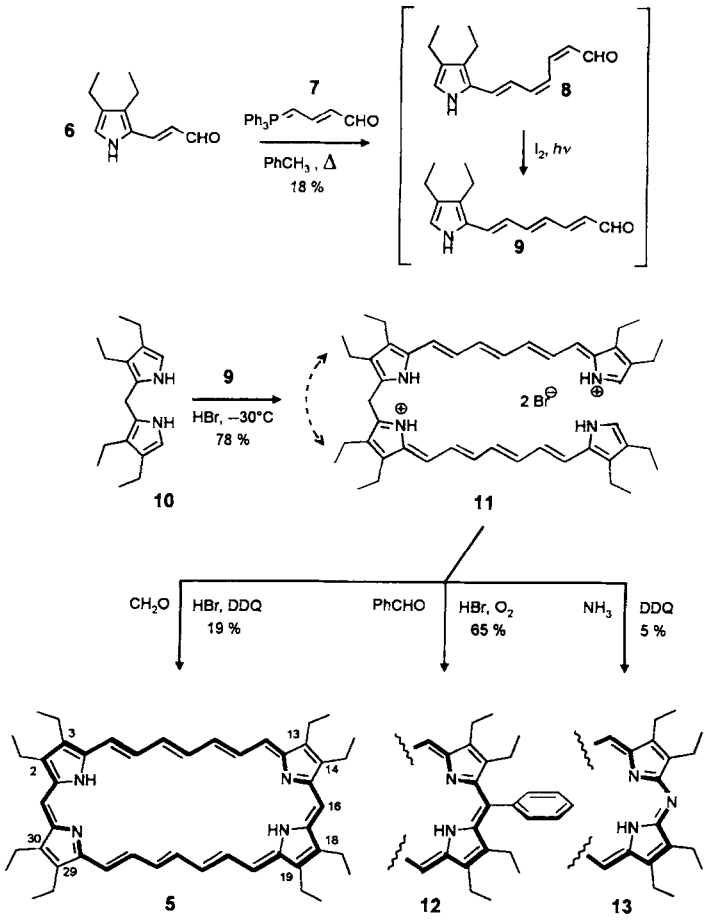

Scheme 1. Synthesis of the hexavinylogous biladiene **11** and its cyclocondensation to give the octaethyl[30]porphyrins **5**, **12**, and **13**[13].

The key building block for the synthesis of the octaethyl[30]porphyrin **5** was the hexavinylogous biladiene bishydrobromide or bilaoctaene **11** (Scheme 1). The deep green bishydrobromide **11** was prepared starting from pyrrylacrolein **6**[4c, 10] by chain extension through Wittig reaction with phosphorane **7**[11] and acid-catalyzed condensation with dipyrrylmethane **10**.[12] 7-(3,4-Diethylpyrrol-2-yl)hepta-2,4,6-trienal **8**/**9** was obtained as a mixture of the (4*E*) and (4*Z*) isomers, from which the (all-*E*) product **9** was separated as rust-colored reddish crystals by column chromatography (silica gel, ether/cyclohexane 2:1) and recrystallization (ether/*n*-hexane). The oily (4*Z*) isomer **8** yielded a further amount of **9** by isomerization with iodine/*hv* (24 h, daylight).

The bilaoctaene salt **11**, which contains two heptavinylogous amidine structures, is stable to air but decomposed in solution. Its cyclocondensation with formaldehyde was achieved in methanol/HBr. After subsequent in situ dehydrogenation with 2,3-dichloro-5,6-dicyano-1,4-benzoquinone (DDQ), 2,3,13,14, 18,19,29,30-octaethyl[30]porphyrin(7.1.7.1) (**5**)[14] was isolated and purified by twofold flash chromatography[15] (silica gel, CH_2Cl_2/MeOH 10:1). Compound **5** is deep violet in solution, and despite its limited stability as a solid and in solution, it could be completely characterized.[13] The considerably more stable 16-phenyl[30]porphyrin **12** was obtained by acid-catalyzed condensation of biladiene **11** with excess benzaldehyde.[13] In this case air oxidation sufficed for the dehydrogenation of the initially formed cyclic intermediate. After column chromatography (silica gel, CH_2Cl_2/MeOH 20:1) **12** was obtained as thin green needles. As in earlier investigations[4g, 7] the high yield of 65% can be explained by the favored hairpin-type conformation of **11**, which results from steric repulsion of the ethyl groups in the dipyrrylmethane unit (indicated with an arrow in Scheme 1; "helical effect"[4g]). Of the new [30]porphyrins, the 16-aza-[30]porphyrin **13**[13] is the least stable. Its synthesis required careful optimization of the conditions for the condensation of the biladiene salt **11**: NH_3/MeOH at room temperature in the presence of a stoichiometric amount of DDQ.

Although the [30]porphyrins **5** and **12** have limited solubility, their ^{1}H NMR spectra could be recorded in [D_6]dimethylsulfoxide/[D_1]trifluoroacetic acid ([D_6]DMSO/[D_1]TFA); the observed diatropic ring current effects provide proof of aromacity (Figure 1). For **5** the maximum difference $\Delta\delta$ in the chemical shifts of the inner (H_c) and outer (H_a) protons is 23.7. This value is slightly lower than that of the [26]porphyrin **4** ($\Delta\delta = 24.1$),[8] and indicates that extending the conjugated perimeter from **4** to **5** does not result in a further increase of aromaticity, as expressed by the diatropic ring current effect. Thus we conclude that the planar stabilization of annulenes through four pyrrole units ends with the 30π perimeter **5** because of its two long C_7 bridges.

Further evidence for the interdependence of the ring current effect and planarity of the ring system can be gained from the δ values of 16-phenyl-[30]porphyrin **12** (Figure 1). The maximum

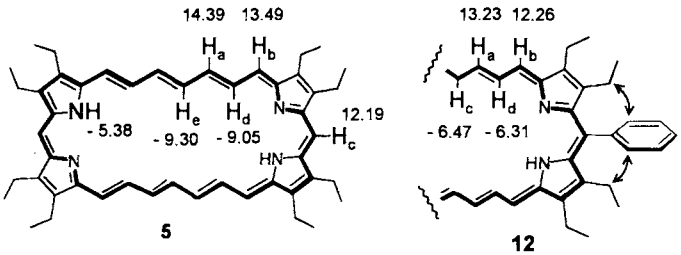

Figure 1. ^{1}H NMR chemical shifts of [30]porphyrin **5** and 16-phenyl-[30]porphyrin **12**[13].

difference $\Delta\delta$ in the chemical shifts of the inner (H_c) and outer protons (H_a) amounts to 19.7, which is four units less than for **5**. In agreement with earlier results[16] this may be explained by distortion of the 30π perimeter due to interactions of the phenyl group with adjacent ethyl groups.

It can be concluded that even [30]annulene systems are aromatic and follow E. Hückel's $(4n+2)$ rule[2] when they are stabilized and held planar. The stabilization of the [30]π systems in **5**, **12**, and **13** by insertion of four pyrrolic units follows the porphyrin model in nature.

Received: March 24, 1997 [Z10275IE]
German version: *Angew. Chem.* **1997**, *109*, 2302–2304

Keywords: annulenes · aromaticity · porphyrinoids · Wittig reactions

[1] a) F. Sondheimer, R. Wolovsky, Y. Amiel, *J. Am. Chem. Soc.* **1962**, *84*, 274–284; b) F. Sondheimer, *Acc. Chem. Res.* **1972**, *5*, 81–91.
[2] a) E. Hückel, *Z. Phys.* **1931**, *70*, 204–286; b) S. Kikuchi, *J. Chem. Educ.* **1997**, *74*, 194–201.
[3] H. A. Staab, F. Diederich, *Chem. Ber.* **1983**, *116*, 3487–3503.
[4] Vinylogous porphyrins: a) R. A. Berger, E. LeGoff, *Tetrahedron Lett.* **1978**, 4225–4228; b) E. LeGoff, O. G. Weaver, *J. Org. Chem.* **1987**, *52*, 710–711; c) M. Gosmann, B. Franck, *Angew. Chem.* **1986**, *98*, 1107–1108; *Angew. Chem. Int. Ed. Engl.* **1986**, *25*, 1100–1101; d) B. Franck, M. Gosmann, DOS DE 3635820, 28. April 1988, BASF AG [*Chem. Abstr.* **1988**, *109*, 94748u]; e) B. Franck, H. König, C. Eickmeier, DOS DE 4029768, 26. March 1992, BASF AG [*Chem. Abstr.* **1992**, *117*, 26197d]; f) B. Franck, H. König, C. Eickmeier, M. Völker, T. Wessel, DE 4029768, Eur. Pat. Appl. EP 477,611, 1. April 1992, BASF AG [*Chem. Abstr.* **1992**, *117*, 7740j]; g) B. Franck, A. Nonn, K. Fuchs, M. Gosmann, *Liebigs Ann. Chem.* **1994**, 503–510.

 © WILEY-VCH Verlag GmbH, D-69451 Weinheim, 1997 0570-0833/97/3620-2214 $ 17.50+.50/0

[5] Vinylogous porphycenes: a) N. Jux, P. Koch, H. Schmickler, J. Lex, E. Vogel, *Angew. Chem.* **1990**, *102*, 1429–1431; *Angew. Chem. Int. Ed. Engl.* **1990**, *29*, 1385–1387; b) E. Vogel, *Pure Appl. Chem.* **1993**, *65*, 143–152.
[6] Expanded porphyrins: a) J. L. Sessler, S. J. Weghorn, V. Lynch, M. R. Johnson, *Angew. Chem.* **1994**, *106*, 1572–1575; *Angew. Chem. Int. Ed. Engl.* **1994**, *33*, 1509–1512; b) J. L. Sessler, A. K. Burrel, *Top. Curr. Chem.* **1991**, *161*, 177–273.
[7] B. Franck, A. Nonn, *Angew. Chem.* **1995**, *107*, 1941–1957; *Angew. Chem. Int. Ed. Engl.* **1995**, *34*, 1795–1811.
[8] T. Wessel, B. Franck, M. Möller, U. Rodewald, M. Läge, *Angew. Chem.* **1993**, *105*, 1201–1203; *Angew. Chem. Int. Ed. Engl.* **1993**, *32*, 1148–1151.
[9] a) H. Fischer, R. Bäumler, *Justus Liebigs Ann. Chem.* **1929**, *468*, 58–98; b) H. H. Inhoffen, J.-H. Fuhrhop, H. Voigt, H. Brockmann, *Justus Liebigs Ann. Chem.* **1966**, *695*, 133–143.
[10] M. Gosmann, A. Vogt, B. Franck, *Liebigs Ann. Chem.* **1990**, 163–168.
[11] M. J. Berenguer, J. Castells, R. M. Galard, M. Moreno-Manas, *Tetrahedron Lett.* **1971**, 495–496.
[12] J. B. Paine, R. B. Woodward, *J. Org. Chem.* **1976**, *41*, 2826–2835.
[13] Selected spectroscopic and analytical data. **5**: ^{1}H NMR (300 MHz, [D$_6$]DMSO/[D$_1$]TFA, TMS): $\delta = -9.30$ (t, $J = 12.8$ Hz, 2H, $(CH)_3CH(CH)_3$), −9.05 (m, 4H, $CHCH(CH)_3CHCH$), −5.38 (s, NH), 12.19 (s, 2H, monomethine bridge-CH), 13.49 (d, $J = 13.9$ Hz, 4H, $CH(CH)_5CH$), 14.39 (t, $J = 12.8$ Hz, 4H, $(CH_2)CHCHCH(CH_2)_2$); IR (KBr): $\tilde{\nu} = 2960$, 2920, 2860 (CH), 1440 cm^{-1} (conj. C=C); UV/Vis (CH_2Cl_2): λ_{max} (lg ε) = 545 (5.62), 7.17 nm (4.55); UV/Vis (CH_2Cl_2/TFA): λ_{max} (lg ε) = 562 (5.77), 588 (5.36), 761 nm (4.56); MS (70 eV): *m/z* (%) = 690 (34) [M^+], 661 (8) [$M^+ - C_2H_5$], 345 (8) [M^{++}]; HRMS: $C_{48}H_{58}N_4$: calcd 690.4662, found 690.4679. **12**: ^{1}H NMR (300 MHz, [D$_6$]DMSO/[D$_1$]TFA, TMS): $\delta = -6.72$, −6.47, −6.31 (3t, $J = 13.3$ Hz, 2H each, $CHCHCHCHCHCHCH$), −3.09, −1.72 (2s, NH), 8.15–8.21 (m, 3H, *m*- and *p*-phenyl-H), 8.86 (d, $J = 6.5$ Hz, 2H, *o*-phenyl-H), 10.95 (s, 1H, monomethine bridge-CH), 12.26 (br. d, 2H, $(CH)_6CH$), 12.42 (d, $J = 13.3$ Hz, 2H, $CH(CH)_6$), 13.23 (t, $J = 12.9$ Hz, $(CH)_2CHCHCH(CH)_2$); IR (KBr): $\tilde{\nu} = 3400$ (NH), 2960, 2920, 2860 (CH), 1590 cm^{-1} (conj. C=C); UV/Vis (CH_2Cl_2): λ_{max} (lg ε) = 553 (5.67), 599 (5.00), 726 nm (4.66); UV/Vis (CH_2Cl_2/TFA): λ_{max} (lg ε) = 574 (5.74), 778 nm (4.64); MS (70 eV): *m/z* (%) = 766 (100) [M^+], 736 (32) [$M^+ - C_2H_5$], 689 (20) [$M^+ - C_2H_5$], 383 (100) [M^{++}]; HRMS: $C_{54}H_{62}N_4$: calcd 766.4975, found 766.4989; correct C,H,N analyses. **13**: UV/Vis (CH_2Cl_2): $\lambda_{max} = 519$ nm; UV/Vis (CH_2Cl_2 + 1% TFA): $\lambda_{max} = 550$, 567 nm; MS (70 eV): *m/z* (%) = 691 (38) [M^+], 662 (4) [$M^+ - C_2H_5$]; HRMS: $C_{47}H_{57}N_5$: calcd 691.4614, found 691.4600.
[14] For the nomenclature of vinylogous porphyrins see refs.[4c,g]. Following the designation of the annulenes, the number of π-electrons in the aromatic perimeter precedes in brackets. The name finishes with the C-atom numbers of the *meso* bridges between the pyrrole units, starting in the upper left, in parentheses. Thus the porphyrin system of **5** is [30]porphyrin(7.1.7.1).
[15] Flash column chromatography according to W. C. Still, M. Kahn, A. Mitra, *J. Org. Chem.* **1978**, *43*, 2923–2925; silica gel (Merck), particle size < 0.063 mm, N_2 pressure 1.3 bar.
[16] B. Franck, G. Krautstrunk, *Liebigs Ann. Chem.* **1993**, 1069–1073.

The Crystal Structure of Aziridine**

Norbert W. Mitzel,* Jürgen Riede, and Christoph Kiener

Dedicated to Dr. C. Arnold Beevers on the occasion of his 89th birthday

The structure of the aziridine molecule in the gas phase is well established by microwave spectroscopy[1] and electron diffraction[2] studies. Ab initio calculations on aziridine confirm most of the experimental results.[3] The structures of crystalline, substituted aziridines, elucidated by X-ray diffraction, deviate from these results in some cases.[4] We report here on the crystal structure determination of this simplest nitrogen heterocycle at low temperature.

The toxic, extremely carcinogenic, and teratogenic free aziridine, which tends to polymerize spontaneously (potentially explosively), was prepared following a known synthetic procedure[6] starting with β-aminoethylsulfate. It was purified by repeated distillation and condensed into a thin-walled glass capillary. A single crystal was grown by carefully cooling the melt after generation of a suitable seed crystal. X-ray diffraction intensities were collected at 145 K and analyzed following established procedures.[7]

Aziridine crystallizes with three independent molecules in the asymmetric unit, which show very similar geometries. As in crystalline oxirane studied by Luger et al.,[8] aziridine is an equilateral triangle (Figure 1), although the bond lengths are significantly longer in aziridine [average values aziridine/oxirane: C–C 1.462(2)/1.438(4) Å, C–N and C–O 1.467(2)/1.431(4) Å, respectively]. Cyclopropane, also isoelectronic, shows even longer C–C distances of 1.500 Å on average,[9] which suggests that the ring bond lengths are primarily dependent on the electronegativity of the heteroatom.

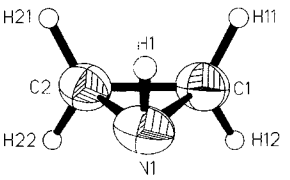

Figure 1. Molecular structure of aziridine in the crystal at 145 K. Selected bond lengths and angles for the three independent molecules: C–C 1.459(1), 1.465(2), 1.463(2) Å; C–N 1.463(2), 1.464(2); 1.469(2), 1.470(2); 1.465(2), 1.468(2) Å; C-N-C 59.8(1), 59.8(1), 59.8(1)°; N-C-C 60.1(1), 60.1(1); 60.1(1), 60.2(1); 60.0(1), 60.2(1)°.

Using all available lone pairs of electrons and hydrogen atoms, aziridine forms a hydrogen-bonded chain aggregate (Figure 2). In contrast to crystal structures of other very small secondary amines like F_2NH, which shows a zig-zag arrangement of molecules ABAB, the chains of aziridine follow an ABCABC motif with three molecules per repeat unit, although an ideal N–H···N angle of 180° cannot be attained (the N–H···N angles are 157, 179, and 161°). Two molecules are oriented toward one side of the chain axis, while the third one points in the other direction. The cavity generated on the side of the latter molecule is filled by a symmetry-equivalent molecule from the neighboring chain.

A comparison of the structure of aziridine in the crystal and in the gas phase (Table 1) shows that the molecule suffers no

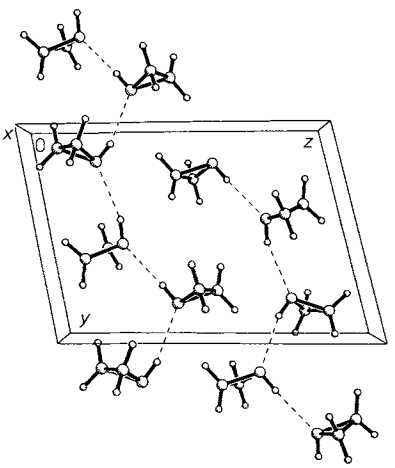

Figure 2. View of the hydrogen-bonded molecules in the crystal showing the ABCABC arrangement in the chains. The intermolecular N–N distances are 3.085(2), 3.069(2), and 3.082(2) Å.

[*] Dr. N. W. Mitzel, J. Riede, C. Kiener
Anorganisch-chemisches Institut der Technischen Universität München
Lichtenbergstrasse 4, D-85747 Garching (Germany)
Fax: Int. code +(89)289-13125
e-mail: N.Mitzel@lrz.tu-muenchen.de

[**] This work was supported by the Bayerisches Staatsministerium für Unterricht, Kultus, Wissenschaft und Kunst (Bayerischer Habilitationsförderpreis 1996 to N. W. M.). We thank Professor H. Schmidbaur for his generous support.

 © WILEY-VCH Verlag GmbH, D-69451 Weinheim, 1997 0570-0833/97/3620-2215 $ 17.50+.50/0

Table 1. Comparison of the structures of aziridine determined by different methods (XRD = X-ray diffraction, MW microwave spectroscopy, GED = gas-phase electron diffraction; distances in Ångströms, angles in degrees).

		XRD[a]	MW[1]	GED[2]	Calculations SCF/ 6-31G*[3]	QCISD/ 6-311 + G**
C–C		1.462(2)	1.481(1)	1.48(1)	1.471	1.487
C–N		1.467(2)	1.475(1)	1.49(1)	1.449	1.477
C–H		0.96(2)	1.084(1)	1.08(3)	1.077	1.087
N–H		0.89(2)	1.016(1)	1.05(7)	1.001	1.017
C-C-N	60.1(1)	59.86(1)	60.2		59.5	59.8
C-N-C	59.8(1)	60.25(1)	59.6		61.0	60.5
H-C-H	116.8(20)	115.72(1)	117		114.4	115.2
C-N-H	109.3(10)	109.31(1)	–		111.7	109.3

[a] Average values from three independent molecules in the asymmetric unit.

significant structural distortions on incorporation into the crystal lattice. Even the electron density maxima, which roughly represent the positions of the hydrogen atoms bound to nitrogen, are described by C-N-H angles that are only marginally different from the gas-phase values (Table 1).

To our knowledge, the best ab initio calculations of the structure of aziridine were performed at the SCF/6-31G(d) level of theory in 1989.[3] The predicted C–C and C–N bond lengths differ significantly from the experimental values (Table 1). Consequently, we conducted calculations at much more sophisticated levels of theory. As expected, the deviations decrease when the effects of electron correlation are taken into consideration. Already at the MP2/6-31G* level of theory good results are obtained, which deviate only slightly from those calculated at QCISD/6-311 + G**, the highest level applied (Table 1). In particular the calculated C–N distance and C-N-H angle are much more realistic.

A rigid-body correction[11] of the results of the crystal structure analysis with all the anisotropic displacement parameters of one molecule yields average C–N and C–C bond lengths of 1.474 and 1.469 Å, respectively. These values are very close to those calculated and determined by microwave spectroscopy. However, even after application of these corrections, the aziridine C–C bond in the crystal is shorter than the C–N bond, whereas microwave spectroscopy and theory both indicate the C–C distance to be the longer one. The remaining deviations can be explained at least in part by the fact that X-ray diffraction analysis measures the maxima of electron density rather than the average nuclear positions, which may be significantly different, in particular in the presence of light atoms and in extreme bonding situations. Nevertheless, the descriptions of the molecular structure of the simplest nitrogen heterocycle are now consistent in the solid state and gas phase, and according to theory.

Received: May 5, 1997 [Z102821E]
German version: *Angew. Chem.* **1997**, *109*, 2299–2300

Keywords: ab initio calculations · aziridine · heterocycles · structure elucidation

[1] B. Bak, S. Skaarup, *J. Mol. Struct.* **1971**, *10*, 385–391.
[2] M. Igarashi, *Bull. Soc. Chim. Jpn.* **1961**, *34*, 369–373.
[3] J. A. Boatz, M. S. Gordon, *J. Phys. Chem.* **1989**, *93*, 3025–3029.
[4] Examples: a) J. A. Deyrup (*"Aziridines"*) in *Small Ring Heterocycles* (Ed.: A. Hassner), Part I, Chapter 1, p. 4ff., Wiley, New York, **1983**; b) E. S. Gould, R. A. Pasternak, *J. Am. Chem. Soc.* **1961**, *83*, 2658; c) T. Skarzynski, T. Olszak, R. Bvartnik, G. Mloston, *Acta Crystallogr. Sect. C* **1988**, *44*, 205; d) J. Portas, P. Courtot, A. El Gadi, *ibid.* **1989**, *44*, 205.
[5] *Dictionary of Organic Compounds*, 6th ed., Chapman & Hall, London, **1996**.
[6] C. F. H. Allen, F. W. Spangler, E. R. Webster, *Org. Synth. Coll. Vol. 4*, **1963**, 433–435.
[7] Crystal system triclinic, space group $P\bar{1}$, $Z = 6$, $a = 4.795(1)$, $b = 8.042(1)$, $c = 11.210(2)$ Å, $\alpha = 76.85(1)$, $\beta = 85.77(1)$, $\gamma = 76.98(1)°$, $V = 410.0(1)$ Å^3 at 145 K. Diffractometer: Enraf-Nonius Turbo-CAD4, $Mo_{K\alpha}$ radiation, graphite monochromator, $2\theta_{max} = 54.08°$, ω/θ-scan, 1734 independent reflections, 1732 of which have $F_0 > 4\sigma(F_0)$. Solution by direct methods (SHELXTL-PC[12]), refinement using SHELXL-93[13], 142 parameters, $R(F)$ (obsd) = 0.048, $wR(F^2) = 0.130$, maximum residual electron density 0.27 and −0.15 e Å^{-1}. All non-hydrogen atoms were refined by applying anisotropic thermal displacement parameters, all hydrogen atoms were located in difference Fourier maps and refined by applying isotropic thermal displacement parmeters. Crystallographic data (excluding structure factors) for the structure reported in this paper have been deposited with the Cambridge Crystallographic Data Centre as supplementary publication no. CCDC-100303. Copies of the data can be obtained free of charge on application to The Director, CCDC, 12 Union Road, Cambridge CB2 1EZ, UK (Fax: Int. code +(1223)336–033; e-mail: deposit@chemcrys.cam.ac.uk).
[8] P. Luger, C. Zaki, R. Rudert, *Angew. Chem.* **1986**, *98*, 254–255.
[9] D. Nijveldt, A. Vos, *Acta Crystallogr. Sect. B* **1988**, *44*, 289–296.
[10] M. F. Klapdor, H. Willner, W. Poll, D. Mootz, *Angew. Chem.* **1996**, *108*, 336; *Angew. Chem. Int. Ed. Engl.* **1996**, *35*, 320.
[11] V. Schomaker, K. N. Trueblood, *Acta Crystallogr. Sect. B*, **1968**, *24*, 63–76.
[12] *SHELXTL PLUS, Structure Determination System—Revision 4.21/V*, Siemens Analytical X-Ray Instruments, Madison, WI, USA, **1990**.
[13] G. M. Sheldrick, *Program for the Refinement of Crystal Structures*, Universität Göttingen, **1993**.

The Chiral S–N Axis in Sulfenamides: Enantiomeric Resolution, Direct Demonstration of Optical Activity, and Kinetics of Interconversion**

Merav Ben-David Blanca, Eric Maimon, and Daniel Kost*

Sulfenamides **1** have a chiral ground-state geometry (when $R'' \neq R'$), since the R-S-N and the average R′-N-R″ planes are mutually perpendicular.[1] Interconversion of the enantiomers (**1**⇌*ent*-**1**) takes place by rotation about the S–N bond [Eq. (1)], which constitutes a stereolabile chiral axis. The factors

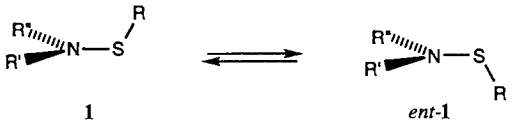

1 *ent*-**1** (1)

affecting the magnitude of the rotational barrier have been known for some time:[2] a) electron-withdrawing groups in the substituent R attached to the sulfur atom, and b) steric hindrance in the rotational transition state. Barriers ranging from 10 to 22 kcal mol^{-1} have been reported.[1] Sulfenamides with barriers that are high enough to permit potential isolation of stereoisomers at ambient temperature were described, however no resolution was attempted.[3, 4]

Here we describe the preparation of the *stereostable* sulfenamide **6**, and the direct demonstration of its chirality by enan-

[*] Prof. Dr. D. Kost, M. Ben-David Blanca, E. Maimon
Department of Chemistry
Ben Gurion University of the Negev
Beer-Sheva 84105 (Israel)
Fax: Int. code +(7)647-2943
e-mail: kostd@bgumail.bgu.ac.il

[**] We thank Dr. Shulamit Levin for assisting with the HPLC separation, Ms. Marina Sterin for measuring the CD spectra, and Ms. Hadar Kost for solving the differential equations.

 © WILEY-VCH Verlag GmbH, D-69451 Weinheim, 1997 0570-0833/97/3620-2216 $ 17.50+.50/0

tiomeric resolution and measurement of circular dichroism (CD) spectra.[5] Furthermore, the determination of the rate constants for enantiomer interconversion over a wide range of temperatures is described. Sulfenamide **6** was prepared according to Equation (2). The ^1H and ^{13}C NMR spectra of **6** at ambient

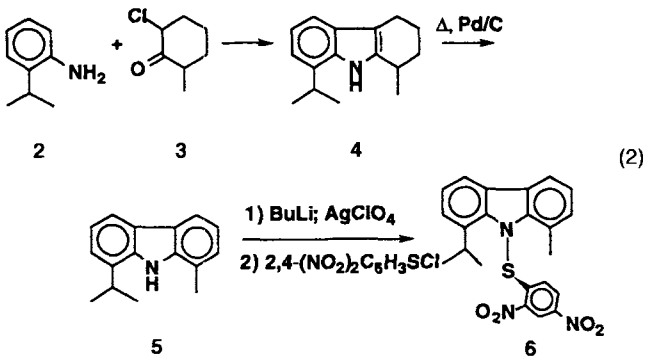

temperature feature separate signals for each of the diastereotopic isopropyl methyl groups, which confirms the chiral ground-state geometry of **6**.

The Gibbs energy of activation for rotation about the S–N bond was determined by the coalescence of the methyl signals in the ^1H NMR spectrum ([D_5]nitrobenzene) to be $\Delta G^{\neq} = 21.0\ kcal\,mol^{-1}$ at 417 K;[6] this is insufficient for isolation of the rotamers at room temperature. However, the enantiomers were resolved at 0° by HPLC on a chiral column, and immediately cooled and stored in liquid nitrogen. The CD spectra of the enantiomers of **6** in the HPLC eluents are shown in Figure 1 (bottom) along with the corresponding UV spectrum of the racemate (top), which is identical to the UV spectrum of the

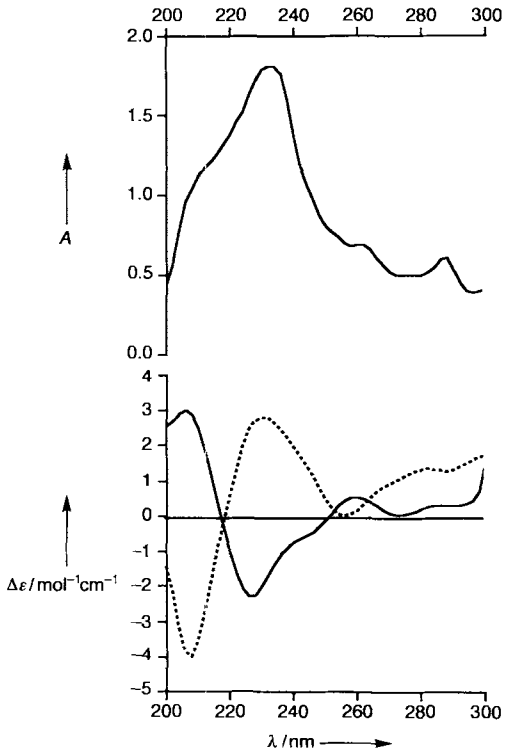

Figure 1. CD spectra for the enantiomers of **6** at 0° (bottom), and the corresponding UV spectrum of the racemic mixture (top).

enantiomers. The approximate mirror-image shapes of the superimposed CD spectra confirm the enantiomeric nature of the components. This constitutes the first direct observation of optical activity due to restricted rotation about a S–N single bond, and renders this bond a stereogenic axis.[7]

Relatively rapid racemization took place during the CD measurements, as manifested by the variation in the CD spectra with time (Figure 2). A first-order rate constant of $k = 0.0028\ s^{-1}$

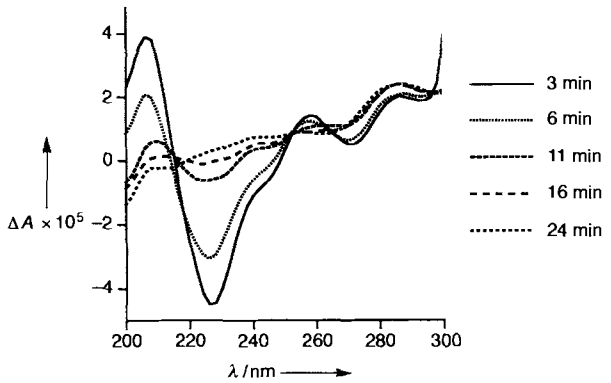

Figure 2. Decay of CD spectrum of **6** at 0° as a function of time; concentration of the initial sample: 8.91×10^{-5} M.

was obtained from the linear correlation of $\ln(\Delta A)$ versus time, and extrapolation to $t = 0$ s afforded the differential absorbances ($\Delta A = A_L - A_R$) of the pure enantiomer. The total concentrations of the solutions, determined from their UV spectra after racemization, were used to calculate the molar differential absorbances at maximum and minimum points on the CD spectrum (Table 1). Several Cotton effects were found that correspond to the UV maxima of **6**.

Table 1. Bands in the CD spectrum of **6** at 0 °C [a]: differences in the molar absorption coefficients of left- and right-handed circularly polarized light.

Wavelength [nm]	$\Delta\varepsilon$ [$cm^{-1}M^{-1}$] [b]
206	+3.79
226	−4.33
258	+0.58
270	−0.62
286	+0.39
310	+1.38

[a] Obtained by extrapolation of ΔA values to $t = 0$; concentration: 8.91×10^{-5} M in 2-propanol/hexane (3/7), pathlength: 0.2 cm. [b] CD Cotton effects are sometimes reported in terms of molar ellipticity [θ], which may be obtained from $\Delta\varepsilon$ values by multiplying by 3298.2 and is expressed in $10^3\,cm^2\,mol^{-1}$ (ref. [7b], p. 1005).

To obtain accurate values for the activation enthalpy and entropy, rate constants at four additional temperatures were measured by NMR magnetization transfer using the selective inversion recovery technique.[8] Selective inversion was applied to one of the isopropyl methyl signals (at temperatures below the coalescence temperature), and variations of the inverted and the unperturbed signals back to their equilibrium intensities were followed as a function of the delay time τ between the inversion and the observation pulses. The unperturbed signal first decreased in intensity as a result of kinetic magnetization transfer from the inverted methyl signal, and then returned exponentially to its steady-state intensity (Figure 3). This behav-

 © WILEY-VCH Verlag GmbH, D-69451 Weinheim, 1997 0570-0833/97/3620-2217 $ 17.50+.50/0

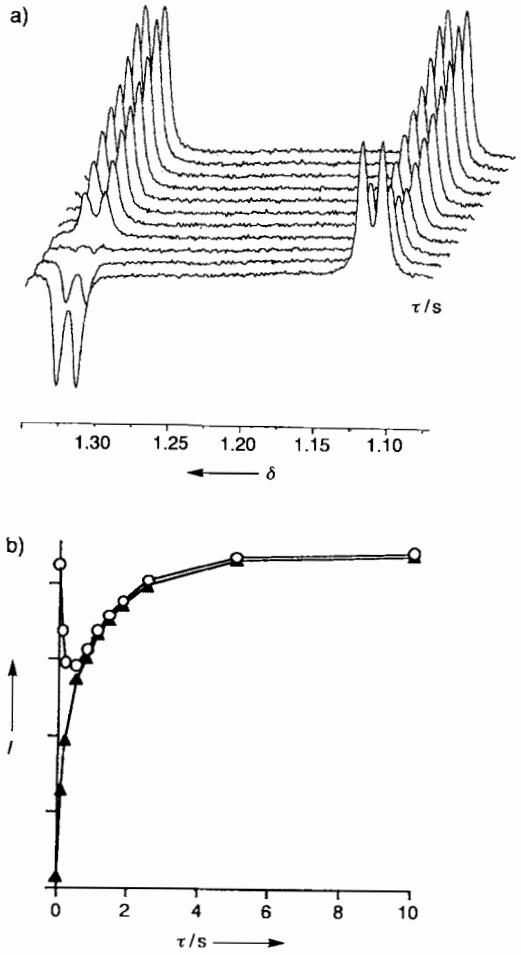

Figure 3. Selective inversion recovery ^{1}H NMR spectra (500 MHz, [D$_5$]nitrobenzene) of the isopropyl methyl region of **6** at various delay times τ between 0.01 and 10 s at 360 K; a) time-dependent presentation of the measured spectra; b) plot of signal intensities versus delay time τ; I = intensity in arbitrary units.

ior is described by Equations (3) and (4) and their linear solutions [Eq. (5), (6)]. (k = first-order rate constant; T_1 = spin-lattice relaxation time, I_A, I_B = signal intensities.)

$$\frac{dI_A}{dt} = \frac{1}{T_1}(I_A^\infty - I_A) + k(I_B - I_A) \quad (3)$$

$$\frac{dI_B}{dt} = \frac{1}{T_1}(I_B^\infty - I_B) - k(I_B - I_A) \quad (4)$$

$$\ln\left(1 - \frac{I_A + I_B}{I_A^\infty + I_B^\infty}\right) = -\frac{t}{T_1} \quad (5)$$

$$\ln\frac{I_B - I_A}{I_B^0 - I_A^0} = -\left(2k + \frac{1}{T_1}\right)t \quad (6)$$

The graphic solutions of Equations (5) and (6) at four temperatures are presented in Figures 4a and 4b, respectively. The excellent linear relationships indicate the precision of the method for kinetic measurements. The first-order rate constants for rotation about the S–N bond (k) and the spin-lattice relaxation times T_1 were obtained from the slopes of the lines (Table 2). The relaxation times compare well with T_1 values obtained at the corresponding temperatures by the conventional (nonselective) inversion recovery method.

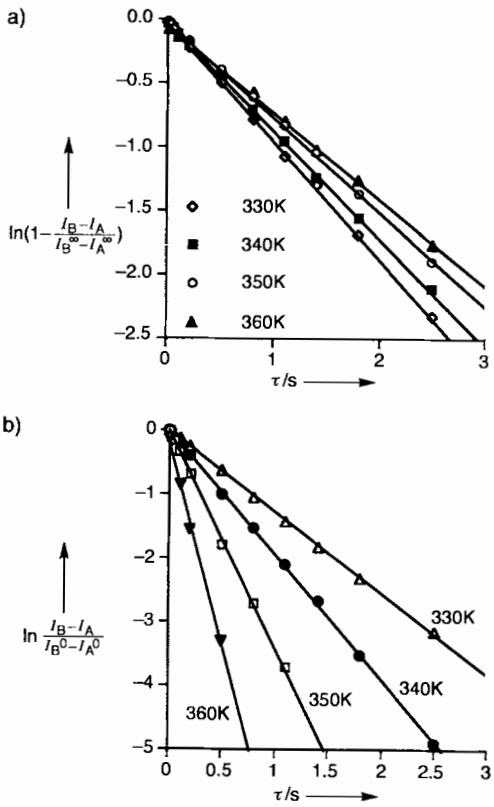

Figure 4. Graphic solution of Equations (5) (a) and (6) (b) from the inversion recovery experiments at four temperatures (see text).

Table 2. Rate constants for rotation about the S–N bond and spin-lattice relaxation times for **6** obtained by selective inversion recovery experiments.

T [K]	k [s^{-1}]	T_1 [s] (selective)	T_1 [s] (nonselective)
330	0.17	1.09	1.00
340	0.55	1.18	1.17
350	1.34	1.40	1.39
360	3.47	1.49	1.50

The rate constants determined by the coalescence and magnetization transfer methods over a wide temperature range were correlated in an Eyring plot as $\ln(k/T)$ versus $1/T$. A perfect linear correlation was obtained (correlation coefficient 1.000), from which the enthalpy and entropy of activation were calculated: (21.7 ± 0.4) kcal mol^{-1} and (3.7 ± 1.0) cal mol^{-1} K^{-1}, respectively.

The rate constant obtained at 0° from the decay of the CD spectrum was left out of the correlation because it was much too high. This was evident earlier from the observation that, although HPLC resolution was achieved at 0° without significant racemization over 22 min, the optical activity decayed almost completely over the same period of time. Since the CD measurement was carried out under adequate temperature control, it seems that the rate of enantiomer interconversion is increased by the influence of the light beam.[9]

Experimental Section

1-Isopropyl-8-methylcarbazole (**5**) was synthesized from **3** [10] (0.07 mol) and 2-isopropylaniline (**2**, 0.14 mol) according to a literature procedure [11] via **4** followed by Pd/charcoal dehydrogenation [12]. Compounds **4** and **5** were purified by chromatography over silica gel and obtained in 55 and 60% yields, respectively (m.p. 57–58 and 79–81 °C, respectively (petroleum ether (40–60)). To a solution of **5**

 © WILEY-VCH Verlag GmbH, D-69451 Weinheim, 1997 0570-0833/97/3620-2218 $ 17.50+.50/0

(0.8 g, 36 mmol) in THF at -20° under nitrogen was added *n*BuLi in hexane (2.5 M, 1.5 mL, 36 mmol) with stirring. The reaction mixture was cooled to -78°, and $AgClO_4$ (0.74 g, 36 mmol) in THF added. After 30 min a solution of 2,4-dinitrobenzenesulfenyl chloride (0.84 g, 36 mmol) in THF was added dropwise. The temperature was allowed to rise to room temperature, and stirring maintained for 20 h. The solid residue was removed by filtration, and the filtrate purified by chromatography on silica gel with petroleum ether (40–60)/CH_2Cl_2 (3/1) as eluent. Compound **6** was obtained in 46% yield (0.7 g); m.p. 145–146° (methanol); HRMS (CI) calcd for $C_{22}H_{20}N_3O_4S$ ($M+1$): 422.117; found: 422.119.

Resolution of **6**: $T = 0^{\circ}$, Chiralpak-AD column (25 × 0.46 cm) packed with dimethylphenylcarbamoylamylose from DAICEL Chemical, hexane/2-propanol (7/3), Waters 996 HPLC instrument. Retention times of the enantiomers: 8.5 and 21.5 min.

Selective inversion was applied by the sequence of hard pulses: $\pi/2 \rightarrow 1/2\Delta\nu \rightarrow \pi/2$ on resonance with one of the methyl signals.

Received: April 11, 1997 [Z10334IE]
German version: *Angew. Chem.* **1997**, *109*, 2294–2297

Keywords: chirality · enantiomeric resolution · NMR spectroscopy · restricted rotation · sulfenamides

[1] Reviews on sulfenamide chemistry: a) D. Kost, M. Raban in *The Chemistry of Sulphenic Acids and their Derivatives* (Ed.: S. Patai), Wiley, Chichester, **1990**, pp. 23–82; b) M. Raban, D. Kost in *Acyclic Organonitrogen Stereodynamics* (Eds.: J. B. Lambert, Y. Takeuchi), VCH, New York, **1992**, pp. 57–88; c) *Tetrahedron* **1984**, *40*, 3345–3381; d) L. Craine, M. Raban, *Chem. Rev.* **1989**, *89*, 689–712.

[2] a) M. Raban, F. B. Jones, Jr., *J. Am. Chem. Soc.* **1971**, *93*, 2692–2699; b) M. Raban, H. Chang, L. Craine, E. Hortelano, *J. Org. Chem.* **1985**, *50*, 2205–2210.

[3] M. Raban, V. A. Martin, L. Craine, *J. Org. Chem.* **1990**, *55*, 4311–4316.

[4] Atkinson et al. isolated diastereomers with one asymmetric carbon center and a sulfenamide bond. However, it was argued that the second stereogenic unit responsible for the observation of diastereomers was the N–N bond, which was also present: R. S. Atkinson, B. D. Judkins, B. H. Patwardhan, *Tetrahedron Lett.* **1978**, 3137–3140.

[5] Chiroptical measurements of diastereomeric stereolabile sulfenamides also containing an asymmetric carbon center were reported: M. Raban, S. K. Lauderback, *J. Am. Chem. Soc.* **1971**, *93*, 2781–2783. However, optical activity could not be assigned directly to one or the other stereogenic unit.

[6] The validity of coalescence measurements for estimating intramolecular exchange barriers was studied: D. Kost, E. H. Carlson, M. Raban, *J. Chem. Soc. Chem. Commun.* **1971**, 656–657.

[7] a) K. Mislow, J. Siegel, *J. Am. Chem. Soc.* **1984**, *106*, 3319–3328; b) E. L. Eliel, S. H. Wilen, L. N. Mander, *Stereochemistry of Organic Compounds*, Wiley, New York, **1994**, p. 53; c) for the definition of absolute configuration in a chiral axis see V. Prelog, G. Helmchen, *Angew. Chem.* **1982**, *94*, 614–631; *Angew. Chem. Int. Ed. Engl.* **1982**, *21*, 567–583.

[8] K. G. Orrell, V. Sik, *Annu. Rep. NMR Spectrosc.* **1993**, *27*, 103–171.

[9] The possible effect of UV and polarized light on the rate of rotation about the S–N bond is being studied further.

[10] G. A. Olah, L. Ohannesian, M. Arvanaghi, G. K. Surya Prakash, *J. Org. Chem.* **1984**, *49*, 2032–2034.

[11] N. Campbell, E. B. McCall, *J. Chem. Soc.* **1950**, 2870–2874.

[12] M. Kuroki, Y. Tsunashima, *J. Heterocycl. Chem.* **1981**, *18*, 709–714.

Synthesis of a Triiodide-Like Pentamesityltritellurium Cation by Addition of Dimesityltelluride to the Remarkably Electrophilic Trimesityltelluronium Ion**

Jörg Jeske, Wolf-Walther du Mont,* and Peter G. Jones

Dedicated to Professor Manfred Weidenbruch on the occasion of his 60th birthday

It has been observed that linear Te_3 building units in some nonclassical polytellurides and polytelluride-chelate complexes[1–5] are analogous to the I_3^- ion. This raises questions such as whether matrix effects or metal coordination are essential[3] for the existence of such Te_3 units and whether the hypervalent Te_3 units and the I_3^- ion also show similar reactivities. Answers to such questions could be provided by a model reaction in which linear Te_3 units would be formed from Te_1 and Te_2 units with "normal" valencies. Calculations of a hypothetical Te_3^{n-} ion, under the assumption of a Te–Te bond length of 307.7 pm (Te coordinated in a linear manner in the $[CsTe_6]^{2-}$ layer of Cs_3Te_{22}),[6] predict linear structures for $n = 3-5$.[7] The Te_3^{4-} ion, which is isoelectronic with I_3^-,[3, 7] can be formally obtained by the addition of Te^{2-} to Te_3^{2-}, but has not yet been detected either in the solid state or in solution. In contrast, the first cationic pentaaryl derivative of the hypothetical Te_3^{4-} ion has proved to be remarkably stable. The synthesis of $[Mes_5Te_3]^+$ described herein exploits the pronounced electrophilic character of the ditelluronium ion $[Mes_3Te_2]^+$; it readily undergoes addition to Mes_2Te (**1**) (Mes = 2,4,6-trimethylphenyl). Normally telluronium cations interact only very weakly with tellurium nucleophiles,[8] but the Lewis acidity of the divalent tellurium atom in the triaryldittelluronium ion $[Mes_3Te_2]^+$ is strongly increased by the proximity of the neighboring telluronium center. Although corresponding trialkyldisulfonium ions $[R_2SSR]^+$[9] can be used as reagents for the transfer of RS^+ units,[10] they avoid violating the octet rule by cation–anion interaction[11] or by the addition of further dialkyl sulfide. The stable ditelluronium salt $[Mes_3Te_2][SbF_6]$ (**2**) was synthesized by coordinating **1** with the $[MesTe]^+$ ion, which was produced in situ from dimesityldittelluride, silver hexafluoroantimonate, and bromine [Eq. (a)].

$$2\,\underset{\mathbf{1}}{Mes_2Te} + Mes_2Te_2 + Br_2 \xrightarrow[-2\,AgBr]{+2\,AgSbF_6} 2\,\underset{\mathbf{2}}{[Mes_2TeTeMes][SbF_6]} \qquad (a)$$

The description of the ditelluronium ion in **2** as a mesitylenetellurenyl cation $MesTe^+$ donor-stabilized by the Lewis base **1** is supported by the interaction of the cation in **2** with the SbF_6^- counterion in the solid state (see crystal structure).[12] The structure of the cation in **2** is fundamentally different from the structures of the original ditelluride[13] and from those of known disulfonium ions.[11] In **2**, two cations and two anions form ring-shaped units through secondary Te···F interactions (Figure 1). The coordination geometries of the two tellurium atoms in **2** can be described as pseudo trigonal-bipyrami-

[*] Prof. Dr. W.-W. du Mont, Dipl.-Chem. J. Jeske, Prof. Dr. P. G. Jones
Institut für Anorganische und Analytische Chemie der Technischen Universität
Postfach 3329, D-38023 Braunschweig (Germany)
Fax: Int. code +(531)3915387
e-mail: dumont@mac1.anchem.nat.tu-bs.de

[**] Properties of Chalcogen–Chalcogen Bonds, Part 22. This work was supported by the Deutsche Forschungsgemeinschaft and the Fonds der Chemischen Industrie. Part 21.: Ref. [8].

 © WILEY-VCH Verlag GmbH, D-69451 Weinheim, 1997 0570-0833/97/3620-2219 $ 17.50+.50/0

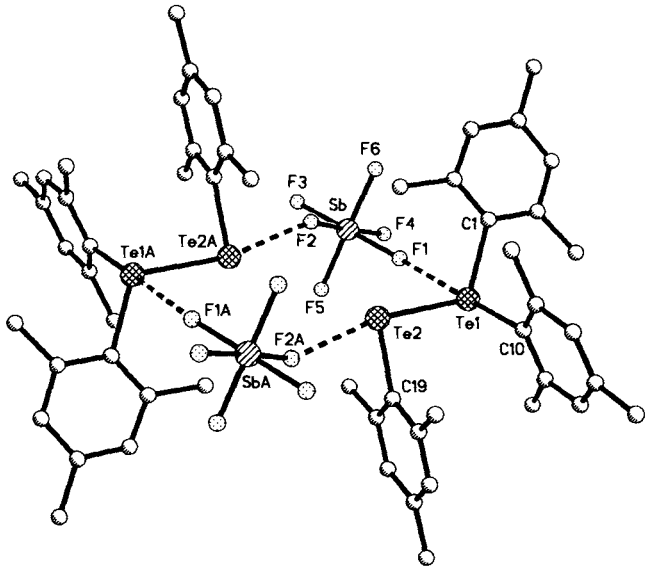

Figure 1. Crystal structure of **2**. Symmetry operators for the equivalent A: $1-x$, $2-y$, $1-z$; Te1–Te2 276.45(5), Te1–F1 308.9(3), Te2–F2A 276.8(3) pm; C1-Te1-Te2 112.76(12), C10-Te1-F1 175.65(12), Te2-Te1-C10 95.34(11), Te2-Te1-F1 88.94(6), C19-Te2-Te1 86.18(12), Te1-Te2-F2A 168.27(9), C19-Te2-F2A 83.01(14)°.

dal when the Te–F contacts are taken into consideration. Relative to Te1 (*one* lone pair of electrons, 10-Te-4[14]), the neighboring F atom is in an apical position (C10-Te1-F1 175.6°) and the neighboring divalent Te2 atom is in an equatorial position. The T-shaped geometry is clearly apparent from the coordination sphere of Te2 (Te1-Te2-F2A 168.3°, Te1-Te2-C19 86.2°, C19-Te2-F2A 83°). This is because the divalent tellurium atom in the α position in **2** has an appreciably stronger contact with the counterion than the telluronium center, which formally carries the charge (Te2–F2A 276.8 pm, Te1–F1 308.9 pm). This surprising phenomenon distinguishes the cation in **2** clearly from disulfonium ions and permits a comparison with the known acceptor behavior of iodophosphonium ions. For example, in solid [tBu$_3$PI][BF$_4$], donor–acceptor interactions exist between the F atoms of ordered tetrafluoroborate ions and the iodine atom of the onium center, whereas P···F contacts do not occur.[15] The F2A···Te2-Te1 (n $\rightarrow \sigma^*$) interaction is accompanied by a Te–Te bond length that is approximately 6 pm longer than that in Mes$_2$Te$_2$.[13] As a consequence, the d(Te1–Te2) and d(Te2–F2A) bonds are almost the same length. The strong cation–anion interaction in **2** indicates the pronounced electrophilic character of the Te atom in the α position to the telluronium center. Red-black **2** reacts smoothly with excess **1** by addition to Te2 to form the brown-red **3** [Eq. (b)], which contains the new pentaaryltritellurium cation. Compound **2** can therefore be described as a salt of a tellurenyl cation that is, despite coordination with a diaryltelluride nucleophile, still not saturated.[16, 17]

$$\underset{\mathbf{1}}{\text{Mes}_2\text{Te}} + \underset{\mathbf{2}}{[\text{Mes}_2\text{TeTeMes}][\text{SbF}_6]} \longrightarrow \underset{\mathbf{3}}{[(\text{Mes}_2\text{Te})_2\text{TeMes}][\text{SbF}_6]} \qquad \text{(b)}$$

The compound **3** is much more soluble in dichloromethane than **2**, which enabled the ^{125}Te NMR spectrum in solution to be measured. The two Mes$_2$Te groups in the cation in **3** are magnetically equivalent. The varying degrees of broadening of the two ^{125}Te NMR signals from **3** and the absence of Te–Te coupling indicate dynamic exchange equilibria in solution. When a further equivalent of **1** is added, no separate signals for **1** and the terminal Te atoms in **3** are observed. This means that fast exchange of coordinated **1** with free **1** occurs at room temperature. Crystals of **3** contain [Mes$_5$Te$_3$]$^+$ and SbF$_6^-$ ions and CH$_2$Cl$_2$ (Figure 2). The cation of **3** contains an almost linear Te$_3$ unit. The Te–Te bond lengths differ by about 7 pm but they are both clearly longer than the single bond in **2**. The one

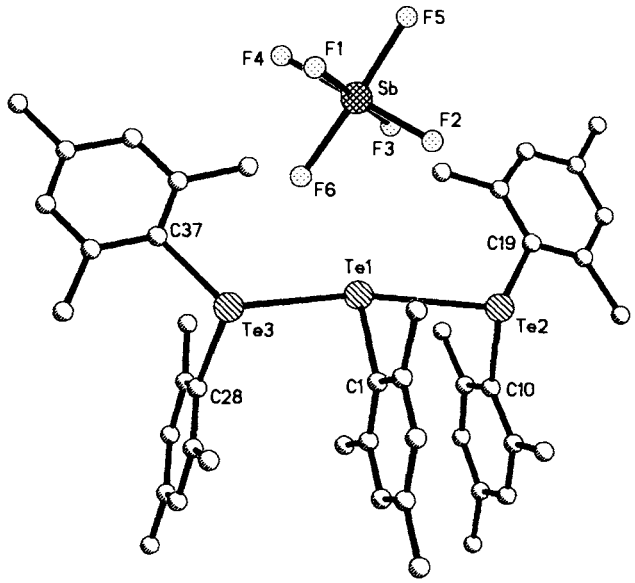

Figure 2. Crystal structure of **3** (without dichloromethane). Te1–Te2 304.91(10), Te1–Te3 297.91(10) pm; Te2-Te1-Te3 159.51(3)°; shortest distance to the fluorine atoms; Te1–F3 390.9(11), Te3–F6 358.3(15) pm.

Te···F contact in **3** (Te3–F6 358.3 pm) is much longer than those in **2** and is accompanied by a shortening of the neighboring Te–Te bond (Te3–Te1 297.9 pm); the other Te–Te bond is correspondingly longer (Te1–Te2 304.9 pm). The average Te–Te bond length in **3** (301.5 pm) is one of the shortest Te–Te distances known for linear Te-Te-Te units (for example the I_5^+-analogous Te_5^{4-} ion of NaTe: linear: d(Te–Te) 308 pm, terminal: d(Te–Te) 282 pm.[1, 18] Therefore the cation in **3** is undoubtedly a slightly asymetric cation similar to triiodide, in which the valence shell of the central tellurium atom is expanded to contain 10 electrons. Compound **3** is the first organotellurium compound with a "hypervalent" Te$_3$ unit.

The addition of **1** to **2** to form **3** represents the first well-defined combination of two eight-electron tellurium species to form a linear ten-electron Te$_3$ species. The smooth access to **2** and **3** and the remarkable acceptor properties of the cation in **2** raise expectations that ditelluronium ions could be of significance for the synthesis of new cationic organotellurium compounds and for doping experiments. The formation of **3** is analogous to the known reaction of iodine with iodide. Similar bonding characteristics (homonuclear n $\rightarrow \sigma^*$ donor–acceptor interaction or 3-center-4-electron bonding) and the kinetic lability of the stable Te$_3$ unit in **3** show how closely related the unusual properties of many polytellurides, the significance of which has only become clear within the past ten years, are to the known phenomena of iodine chemistry.

Experimental Section

2: Mes$_2$Te (**1**) (0.55 g, 1.5 mmol) and Mes$_2$Te$_2$ (0.49 g, 0.75 mmol) in dichloromethane (30 mL) were oxidized with bromine (0.12 g, 0.75 mmol) and then allowed to react with AgSbF$_6$ (0.5 g, 1.5 mmol) in dichloromethane (5 mL). The initially brown solution turned blood-red immediately and silver bromide slowly precipitated. The reaction was allowed to proceed to completion in the dark for 1 h at room

 © WILEY-VCH Verlag GmbH, D-69451 Weinheim, 1997 0570-0833/97/3620-2220 $ 17.50+.50/0

temperature with stirring, then the precipitate was removed by filtration. Hexane (50 mL) was added to the now brown solution and the product was obtained as a violet-brown powder. Crystals suitable for X-ray structure analysis were obtained by using the diffusion method (dichloromethane solution/hexane). Yield: 0.94 g (74%); m.p.: 189 °C (decomp), $C_{27}H_{33}F_6SbTe_2$; $M = 848.50\ g\,mol^{-1}$, calcd.: C 38.22, H 3.92; found: C 38.37, H 4.03; ^1H NMR (CD_2Cl_2): $\delta = 7.05$ (2H), 2.34 (6H), 2.32 (3H); ^{125}Te NMR: no signal was observed because of low solubility; positive-ion FAB-MS (NBA): *m/z* (%): 741 (5, $[Mes_3Te_3]^+$), 613 (40, $[Mes_3Te_2]^+$), 494 (22, $[Mes_2Te_2]^+$), 368 (100, $[Mes_2Te]^+$), 248 (24, $[MesTe^+ - H]^+$), 119 (70, Mes^+); negative-ion FAB-MS: *m/z* (%): 494 (7, $[Mes_2Te_2]^-$), 472 (2.5, $[Sb_2F_{12}]^-$), 235 (100, $[SbF_6]^-$), 216 (2, $[SbF_5]^-$), 197 (2, $[SbF_4]^-$).

3: **2** (0.43 g, 0.5 mmol) and **1** (0.25 g, 0.7 mmol) were taken up in dichloromethane (2 mL) by warming and subsequently crystallized at -18 °C to give crystals suitable for X-ray structure analysis. The transparent red-brown needlelike crystals obtained by filtration crumbled to a brown powder after drying in vacuum (yield, melting point, and elemental analysis refer to the solvent-free substance). Yield: 0.45 g (74%); m.p.: 169 °C (decomp), $C_{45}H_{55}F_6SbTe_3$; $M = 1214.47\ g\,mol^{-1}$; calcd.: C 44.50, H 4.56; found C 44.64, H 4.48; ^1H NMR (CD_2Cl_2): $\delta = 7.04$ (2H), 2.32 (6H), 2.30 (3H); ^{125}Te NMR (CH_2Cl_2/C_6D_6): $\delta = 854$, 388, (20% excess of 1: 842, 385); positive-ion FAB-MS (NBA): *m/z* (%): 741 (2, $[Mes_3Te_3]^+$), 613 (40, $[Mes_3Te_2]^+$), 494 (14, $[Mes_2Te_2]^+$), 368 (100, $[Mes_2Te]^+$), 248 (20, $[MesTe^+ - H]^+$), 119 (55, Mes^+); negative-ion FAB-MS: *m/z* (%): 494 (7, $[Mes_2Te_2]^-$), 472 (3, $[Sb_2F_{12}]^-$), 235 (100, $[SbF_6]^-$), 216 (2, $[SbF_5]^-$), 197 (2, $[SbF_4]^-$).

Received: February 11, 1997
Revised version: May 16, 1997 [Z 10101 IE]
German version: *Angew. Chem.* **1997**, 2304–2306

Keywords: cations · chalcogens · hypervalent compounds · tellurium

[1] P. Böttcher, *Angew. Chem.* **1988**, *100*, 781–794; *Angew. Chem Int. Ed. Engl.* **1988**, *27*, 759–772.
[2] D. Y. Valentine, O. B. Cavin, H. L. Yakel, *Acta Crystallogr. Sect. B.* **1977**, *33*, 1389–1396.
[3] M. G. Kanatzidis, *Angew. Chem.* **1995**, *107*, 2281–2283, *Angew. Chem. Int. Ed. Engl.* **1995**, *34*, 2109–2111.
[4] a) U. Müller, C. Grebe, B. Neumüller, B. Schreiner, K. Dehnicke, *Z. Anorg. Allg. Chem.* **1993**, *619*, 500–506; b) B. Schreiner, K. Dehnicke, K. Maczek, D. Fenske, *ibid.* **1993**, *619*, 1414–1418.
[5] a) M. A. Ansari, J. C. Bollinger, J. A. Ibers, *Inorg. Chem.* **1993**, *32*, 231–232; b) D. M. Smith, L. C. Roof, M. A. Ansari, J. M. McConnachie, J. C. Bollinger, M. A. Pell, R. J. Salm, J. A. Ibers, *ibid.* **1996**, *35*, 4999–5006.
[6] W. S. Sheldrick, M. Wachold, *Angew. Chem.* **1995**, *107*, 490–492; *Angew. Chem. Int. Ed. Engl.* **1995**, *34*, 450–451.
[7] Q. Liu, N. Goldberg, R. Hoffmann, *Chem. Eur. J.* **1996**, *2*, 390–397.
[8] W.-W. du Mont, J. Jeske, P. G. Jones, *Angew. Chem.* **1996**, *108*, 2822–2824; *Angew. Chem. Int. Ed. Engl.* **1996**, *35*, 2653–2655.
[9] T. P. Hilditch, S. Smiles, *J. Chem. Soc.* **1907**, *91*, 1394–1399; D. J. Pettit, G. K. Helmkamp, *J. Org. Chem.* **1963**, *28*, 2932–2933.
[10] a) G. Capozzi, O. De Lucchi, V. Lucchini, G. Modena, *Synthesis* **1976**, 677–678; b) B. M. Trost, T. Shibata, *J. Am. Chem. Soc.* **1982**, *104*, 3225–3228 and references therein.
[11] R. Laitinen, R. Steudel, R. Weiss, *J. Chem Soc. Dalton Trans.* **1986**, 1095–1100; R. Minkwitz, H. Prenzel, H. Pritzkow, *Z. Naturforsch. B* **1987**, *42*, 750–755.
[12] X-ray structure analysis: **2**: $C_{27}H_{33}F_6SbTe_2$, $M_r = 848.48$; monoclinic, space group $P2_1/c$: $a = 843.52(10)$, $b = 1424.2(2)$, $c = 2459.7(3)$ pm, $\beta = 90.977(5)°$, $V = 2.9544(6)\ nm^3$; $Z = 4$; $\sigma_{calcd.} = 1.908\ Mg\,m^{-3}$, $\lambda = 0.71073$ pm, $T = 173$ K; crystal dimensions $0.52 \times 0.40 \times 0.40$ mm; Siemens R3 diffractometer, 2θ range 6–50°, 5931 reflections, 5189 unique ($R_{int} = 0.0156$). Absorption correction after Psi-scans. Solution with direct methods (SHELXS90); refinement against F^2 (SHELXL93). Hydrogen atoms refined by using the riding model or with freely rotating methyl groups. Final *wR2* value = 0.0713 for all data, conventional *R(F)* value *R1* = 0.0290, 334 parameters and 234 restraints; max. Δ_ρ 701 e nm^{-3}. **3**: $C_{48}H_{61}Cl_6F_6SbTe_3$, $M_r = 1469.22$; monoclinic, space group $P2_1/c$: $a = 818.1(2)$, $b = 2184.3(4)$, $c = 3158.4(6)$ pm; $V = 5.604(2)\ nm^3$; $Z = 4$; $\sigma_{calcd.} = 1.741\ Mg\,m^{-3}$, $\lambda = 0.71073$ pm, $T = 173$ K; crystal dimensions $0.66 \times 0.50 \times 0.45$ mm, 2θ range 6–50°, Psi-scans, 12315 reflections, 9747 unique ($R_{int} = 0.0362$); structure solution and refinement as above, *wR2* = 0.1855, *R1* = 0.0645, 574 parameters and 429 restraints; max. Δ_ρ 1701 e nm^{-3}. The relatively high residual value results from the disordered dichloromethane molecules. Crystallographic data (excluding structure factors) for the structures reported in this paper have been deposited with the Cambridge Crystallographic Data Centre as supplementary publication no. CCDC-100-165. Copies of the data can be obtained free of charge on application to The Director, CCDC, 12 Union Road, Cambridge CB2 1EZ, UK (fax: int. code +(1223) 336-033; e-mail: deposit@chemcrys.cam.ac.uk).
[13] A. Edelmann, S. Brooker, N. Bertel, M. Noltemeyer, H. W. Roesky, G. M. Sheldrick, F. T. Edelmann, *Z. Naturforsch. B* **1992**, *47*, 305–309.
[14] "10-Te-4" denotes 10 valence electrons around the central Te atom, to which four substituents are attached: C. W. Perkins, J. C. Martin, A. J. Arduengo III., W. Lau, A. Alegria, J. K. Kochi, *J. Amer. Chem. Soc.* **1980**, *102*, 7753–7759.
[15] M. Bätcher, W.-W. du Mont, S. Pohl, W. Saak, *Phosphorus, Sulfur Silicon Relat. Elem.* **1990**, *49/50*, 147–150.
[16] S. Hauge, O. Vikane, *Acta Chem. Scand. Ser A* **1983**, *37*, 723–729.
[17] W.-W. du Mont, H.-H. Meyer, S. Kubiniok, S. Pohl, W. Saak, *Chem. Ber.* **1992**, *125*, 761–766.
[18] P. Böttcher, R. Keller, *J. Less-Common Met.* **1985**, *109*, 311–321.

The First Di-μ_3-hydroxo-Bridged Tetramanganese(II) Complex**

Lutz Stelzig, Bruno Donnadieu, and Jean-Pierre Tuchagues*

Tetranuclear manganese complexes are currently of interest as models for the manganese cluster in the oxygen-evolving center (OEC) of photosystem 2 (PS2) for which four manganese centers per active site have been proposed.[1] In terms of the synthesis of model complexes for the various states of the OEC, the coordination of water or its derivatives (OH^- or O^{2-}) to a tetranuclear manganese cluster is of great significance. Many manganese complexes containing hydroxo, oxo, and peroxo bridges have been synthesized.[2] However, only two hydroxo-bridged tetranuclear manganese complexes that include $Mn^{I}(\mu_3\text{-}OH)$[3a] and $Mn^{IV}(\mu_2\text{-}OH)$[3b] bonds are known. This communication describes **1**, the first tetranuclear manganese(II) complex including bridging μ_3-hydroxo ligands.

$[Mn_2(L)(OH)(thf)]_2 \cdot 2THF$ **1**

LH_3 = 1,5-bis(3,5-dinitrosalicylideneamino)pentan-3-ol)

LH_3 has proven a suitable ligand for the synthesis of di- and tetranuclear metal complexes; in particular, a tetranuclear μ_3-oxo-bridged manganese(III) complex based on the unsubstituted analogue, 1,5-bis(salicylideneamino)pentan-3-ol ($L'H_3$), has been previously reported by Mikuriya et al.[4] Under strictly anaerobic conditions, reaction of twice the molar amount of $Mn(OAc)_2 \cdot 2H_2O$ with LH_3 in a methanolic sodium hydroxide solution leads to a very air-sensitive orange compound. Subsequent crystallization of this orange powder from THF/pentane yielded **1** as well-shaped, orange-red crystals.

The molecular structure[5] of the tetranuclear complex **1** (Figure 1) shows that the trianionic pentadentate ligand L bridges two Mn^{II} ions through its alkoxo oxygen atom. Each Mn^{II} is additionally bonded to one azomethine nitrogen and one phenolate oxygen atom of L. A hydroxo bridge further stabilizes the two Mn^{II} centers of each dinuclear unit. The structure of complex **1** is best viewed as two layers of dinuclear subunits linked by two bridging phenolate-O atoms of L and two μ_3-OH^- ions. The bis-dinuclear molecule is located at a crystallographic inversion center. Different coordination spheres for the two man-

[*] Prof. J.-P. Tuchagues, Dr. L. Stelzig, B. Donnadieu,
Laboratoire de Chimie de Coordination du CNRS
UP 8241 liée par conventions à l'Université Paul Sabatier et à l'Institut National Polytechnique
205 route de Narbonne, 31077 Toulouse Cedex (France)
Fax: Int. code +561-553003
e-mail: tuchague@lcc-toulouse.fr

[**] This work was supported by a grant from the European community to L. S. (Human Capital and Mobility Programme, ERBCHBGCT 93-0417).

 © WILEY-VCH Verlag GmbH, D-69451 Weinheim, 1997 0570-0833/97/3620-2221 $ 17.50+.50/0

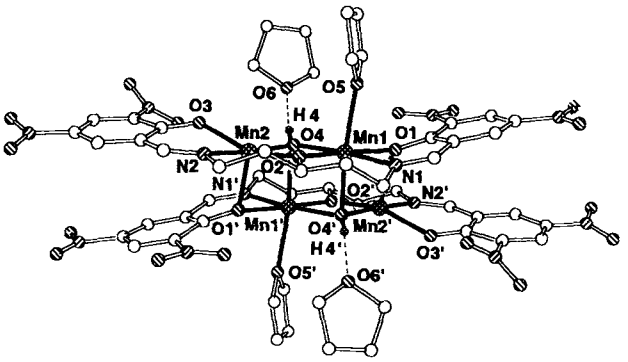

Figure 1 ORTEP view of complex **1** (hydrogen atoms are omited for clarity). Selected distances [Å] and angles [°]: Mn1–O1 2.199(3), Mn1–O2 2.089(3), Mn1–O4 2.136(3), Mn1–N1 2.206(3), Mn1–O5 2.259(3), Mn1–O4′ 2.203(3), Mn2–O2 2.045(3), Mn2–O3 2.105(3), Mn2–O4 2.106(3), Mn2–N2 2.223(3), Mn2–O1′ 2.196(3); O1-Mn1-O2 173.7(1), O1-Mn1-O4 105.5(1), O2-Mn1-O4 80.8(1), O1-Mn1-N1 82.0(1), O2-Mn1-N1 91.7(1), O4- Mn1-N1 171.9(1), O1-Mn1-O5 84.2(1), O2-Mn1-O5 95.8(1), O4- Mn1-O5 94.7(1), N1-Mn1-O5 89.0(1), O2-Mn2-O3 157.8(1), O2- Mn2-O4 82.6(1), O3-Mn2-O4 101.4(1), O2-Mn2-N2 90.8(1), O3-Mn2-N2 83.4(1), O4-Mn2-N2 172.3(1), Mn1-O2-Mn2 100.0(1), MN1-O4-Mn2 96.6(1), Mn1-O1-Mn2′ 96.45(3), Mn1-O4′-Mn2′ 99.45(4), Mn1-O4-Mn1′ 98.24(3), O4-Mn1-O4′ 81.76(3).

ganese atoms in the same subunit result from the weak binding of a THF molecule at the remaining apex of the Mn1 coordination octahedron. Consequently, Mn2 is in a square-pyramidal environment of one N and four O atoms, whereas Mn1 has donor set of one N and five O atoms.

The Mn1 $\cdots$ Mn2 distance of 3.166(3) Å is mainly dominated by the ligand bite angle. The Mn1 $\cdots$ Mn1′ distance involving bis-hydroxo-bridged metal centers (3.281(3) Å) is very close to those involving hydroxo-phenoxo-bridged metal centers (Mn1 $\cdots$ Mn2′ = Mn2 $\cdots$ Mn1′ = 3.278(3) Å). The Mn2 $\cdots$ Mn2′ distance (5.547(7) Å) is the largest Mn $\cdots$ Mn separation inside the Mn_4 unit.

The bond lengths between Mn and μ_3-OH oxygen atoms range from 2.106(3) Å (within a dinuclear layer) to 2.203(3) Å (between dinuclear layers). These values are in agreement with those previously reported for $Mn^{II}(\mu_2\text{-OH})_2Mn^{II}$ bonds[2b] and for the $Mn^{II}\mu_2$-OH bond of a $Mn^{II}(\mu_2\text{-OH})(\mu_2\text{-OAc})_2Mn^{III}$ complex,[2h] and longer than that reported for a $Mn^{II}(\mu_2\text{-OH})Mn^{II}$ bond.[2f] On the other hand, these $Mn^{II}(\mu_3\text{-OH})Mn^{II}$ bonds are significantly longer than the $Mn^{III}(\mu_3\text{-O})Mn^{III}$ bonds (1.89–1.94 Å) in the related $[Mn_4(L')_2(\mu\text{-O})_2(CH_3COO)_2]$ complex.[4] The oxidation state of the manganese ions and the presence of the hydroxo bridges are deduced from stoichiometric considerations and the good correspondence with established Mn–O bond lengths; furthermore, the hydroxide proton is easily located in difference Fourier maps as a result of the hydrogen bond between the oxygen atom of uncoordinated THF molecules and the bridging hydroxo anions. A broad and weak band at 3400–3500 cm^{-1} in the IR spectra of **1** is unambiguously attributable to a $\tilde{\nu}_{O-H}$ stretch. This observation is in agreement with the presence of a hydrogen bond between the hydroxide anion and the oxygen of the uncoordinated THF molecule, which should broaden and exert a downfield shift on the hydroxide $\tilde{\nu}_{O-H}$ stretch, usually a relatively sharp absorption in the 3520–3688 cm^{-1} range.[2a–c, g, 3a] However, due to the possible presence of water, unambiguous assignment of this $\tilde{\nu}_{O-H}$ stretch requires labeling experiments. The band at 558 cm^{-1} may be attributed to the $\tilde{\nu}_{Mn-OH}$ stretch.

The X-band powder spectra of complex **1** exhibit a temperature-independent (from 300 to 80 K) and featureless broad resonance with a g value of about 2. The broadness of this isotropic EPR absorption is consistent with the presence of magnetically interacting manganese(II) ions in the solid state.[6] The X-band EPR spectra of the compound in DMF/toluene glasses at 100 K exhibit a resonance without fine or hyperfine features centered at $g \approx 2$, indicating that the tetranuclear structure is retained in solution.

The magnetic susceptibility of complex **1** has been measured betweem 300 and 2 K. The μ_{eff} value per Mn center is lower than the spin only value at 300 K and decreases from 5.56 to 2.31 μB at 2 K, indicating overall antiferromagnetic coupling of the $S = 5/2$ spin systems of the Mn^{II} ions in complex **1**.

The vacant coordination site at the Mn2 center may be of interest in oxidation reactions. Air oxidation, for example, proceeds rapidly with formation of a not yet structurally characterized solid. Oxidation reactions of related compounds containing acetate anions yield tetranuclear, mixed-valence, methoxo-bridged Mn^{II}_2/Mn^{III}_2[7] or oxo-bridged Mn^{III}_4[4] compounds. As the nature of the oxidized complex is considerably influenced by the salicylaldimine ring substituents of L, it is expected that **1**, which bears strongly electron-withdrawing nitro groups, may be oxidized to a mixed-valent tetramanganese(II)/(III) complex.

Experimental Section

A solution of NaOH (0.06 g) in MeOH (20 mL) was added to a suspension of the ligand[4] (0.252 g, 5×10^{-4} mol) in MeOH (20 mL). The reaction mixture was stirred until dissolution was complete. The resulting solution was added dropwise to a methanolic solution of $Mn(OAc)_2 \cdot 2H_2O$ (0.244 g, 10^{-3} mol in 10 mL) and stirred for 24 h. The orange precipitate was suction filtered, washed with MeOH and Et_2O, and dried under vacuum. Yield: 260 mg (65%) of a complex which analyzed well for $Mn_2(L)(OH)(MeOH)_2$. Orange-red crystals of **1** suitable for X-ray diffraction where grown by vapor diffusion of pentane into a THF solution of **1**. IR, EPR, and magnetic measurements were carried out on ground crystals of **1**.

Received: March 18, 1997 [Z 10259 IE]
German version: *Angew. Chem.* **1997**, *109*, 2315–2317

Keywords: manganese · multinuclear complexes · N ligands · O ligands · photosynthesis

[1] See, for example, *Manganese Redox Enzymes* (Ed.: V. L. Pecoraro), VCH, New York, **1992**; R. J. Debus, *Biochim. Biophys. Acta* **1992**, *1102*, 269; A. W. Rutherford, J.-L. Zimmerman, A. Boussac, in *The Photosystems: Structure, Function and Molecular Biology* (Ed.: J. Barber), Elsevier, New York, **1992**, Chap. 5.

[2] See, for example, a) K. Wieghardt, U. Bossek, B. Nuber, J. Weiss, J. Bonvoisin, M. Corbella, S. E. Vitols, J.-J. Girerd, *J. Am. Chem. Soc.* **1988**, *110*, 7398; b) N. Kitajima, U. P. Singh, H. Amagai, M. Osawa, Y. Moro-oka, *ibid.* **1991**, *113*, 7757; c) M. J. Baldwin, T. L. Stemmler, P. J. Riggs-Gelasco, M. L. Kirk, J. E. Penner-Hahn, V. L. Pecoraro, *ibid.* **1994**, *116*, 11349; d) B. C. Dave, R. S. Czernuszewicz, *New J. Chem.* **1994**, *18*, 149; e) R. Manchanda, G. W. Brudvig, R. H. Crabtree, *Coord. Chem. Rev.* **1995**, *144*, 1; f) D. Tetard, A. Rabion, J.-B. Verlhac, J. Guilhem, *Chem. Commun.* **1995**, 531; g) N. Kitajima, M. Osawa, S. Imai, K. Fujisawa, Y. Moro-oka, K. Heerwegh, C. A. Reed, P. D. W. Boyd, *Inorg. Chem.* **1994**, *33*, 4613; h) A. Darovsky, V. Kezerashvili, P. Coppens, T. Weyhermüller, H. Hummel, K. Wieghardt, *ibid.* **1996**, *35*, 6916.

[3] a) M. D. Clerk, M. J. Zaworotko, *Chem. Commun.* **1991**, 1607; b) K. S. Hagen, T. D. Westmoreland, M. J. Scott, W. H. Armstrong, *J. Am. Chem. Soc.* **1989**, *111*, 1907.

[4] M. Mikuriya, Y. Yamato, T. Tokii, *Bull. Chem. Soc. Jpn.* **1992**, *65*, 2624.

[5] **1**: $[C_{23}N_6O_{13}H_{24}Mn_2] \cdot THF$, $M_r = 806.46$, orange-red crystal ($0.55 \times 0.25 \times 0.13$ mm), triclinic, space group $P\bar{1}$, $a = 12.227(2)$, $b = 12.891(4)$, $c = 13.009(3)$ Å, $\alpha = 69.73(3)$, $\beta = 69.57(2)$, $\gamma = 67.53(2)°$, $V = 1721.0(3)$ Å^3, $Z = 2$, $\rho_{calcd} = 1.56$ g cm^{-3}, $\mu(Mo_{K\alpha}) = 7.82$ cm^{-1}, 13436 measured reflections (4741 independent), 462 parameters, $R = 0.038$, and $R_w = 0.042$. Crystallographic data (excluding structure factors) have been deposited with the Cambridge Crystallographic Data Centre as supplementary publication no. CCDC 100270. Copies of the data can be obtained free of charge on application to The Director, CCDC, 12 Union Road, Cambridge CB21EZ (UK) (fax: int. code +(1223)336-033; e-mail: deposit@chemcrys.cam.ac.uk).

[6] a) R. D. Dowsing, J. F. Gibson, D. M. Goodgame, M. Goodgame, P. J. Hayward, *Nature (London)* **1968**, *219*, 1037; b) *J. Chem. Soc. (A)* **1969**, 1242; c) R. D. Dowsing, J. F. Gibson, M. Goodgame, P. J. Hayward, *J. Chem. Soc. (A)* **1969**, 187; d) B. A. Goodman, J. B. Raynor, *Adv. Inorg. Chem. Radiochem.* **1970**, *13*, 205; e) B. Mabad, P. Cassoux, J.-P. Tuchagues, D. N. Hendrickson, *Inorg. Chem.* **1986**, *25*, 1420.

[7] Z.-Y. Zhang, C. Brouca-Cabarrecq, F. Dahan, J.-P. Tuchagues, unpublished results.

 © WILEY-VCH Verlag GmbH, D-69451 Weinheim, 1997 0570-0833/97/3620-2222 $ 17.50+.50/0

Isolation and X-ray Crystallographic Analysis of a Stable Selenenic Acid**

Toshiyuki Saiki, Kei Goto, and Renji Okazaki*

Selenenic acids (RSeOH) play a central role in the oxidation and reduction processes of organoselenium compounds, for example, in the *syn* elimination of selenoxides, the reduction of seleninic acids, and the oxidation of selenols and diselenides.[1] They are also of great interest from a biological point of view as illustrated by a number of reports that postulate the intermediacy of a selenenic acid in the catalytic cycle of glutathione peroxidase[2] and its synthetic model compounds.[3] However, despite the importance of selenenic acids, much of our knowledge on their chemistry has been derived in quite an indirect and speculative fashion because of their extremely high instability; they are known to undergo a rapid disproportionation to form the corresponding diselenides and seleninic acids. Several areneselenenic acids stabilized by coordination to *ortho*-nitro,[4] -carbonyl,[5] or -amino groups[3c] have been reported to be observable, but only in solution.[6] Even the employment of the 2,4,6-tri-*tert*-butylphenyl group, one of the most effective steric protection groups, cannot prevent the disproportionation of a selenenic acid.[7] Thus, to date, no selenenic acid has been isolated in pure form,[8] and the development of a new methodology to stabilize this important but elusive species has long been awaited.

Herein we report the synthesis and structure of the first isolable selenenic acid. In this work we have applied the recently developed 1,4-bridged calix[6]arene **1**[9,10] as a reaction environment; we had previously verified the usefulness of **1** as a stabilizing environment for a reactive species by incorporating a sulfenic acid functionality (X = SOH) into the calixarene **1** as a probe.[9b]

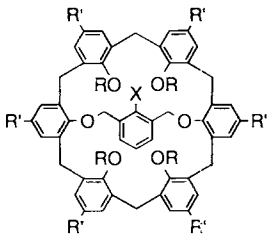

1

The reaction of *p-tert*-butylcalix[6]arene with selenide **2** under basic conditions afforded a bridged calix[6]arene **3** bearing a butylselanyl group on the bridge (Scheme 1). Treatment of **3** with benzyl bromide in the presence of NaH gave the tetrabenzyl ether **4** as the main product. Oxidation of **4** by *m*-chloroperoxybenzoic acid (*m*CPBA) followed by thermolysis in toluene (80 °C, 2 h) afforded the selenenic acid **5**, which was isolated by silica gel chromatography as colorless crystals (74%).

Compound **5** was fully characterized by NMR and IR spectroscopy, as well as FAB mass spectrometry, and elemental analysis. The ^{77}Se NMR spectrum ($CDCl_3$) revealed a signal at $\delta = 1134$ and the ^{1}H NMR spectrum showed the signal of the hydroxyl proton at $\delta = -0.05$ (readily exchangeable with D_2O), suggesting that it is highly shielded by the calix[6]arene macrocycle. The ^{1}H NMR spectrum of **5** is consistent with the *cone* conformation and hardly changes up to 130 °C: it shows essentially the same features as those in the spectrum of the *cone*

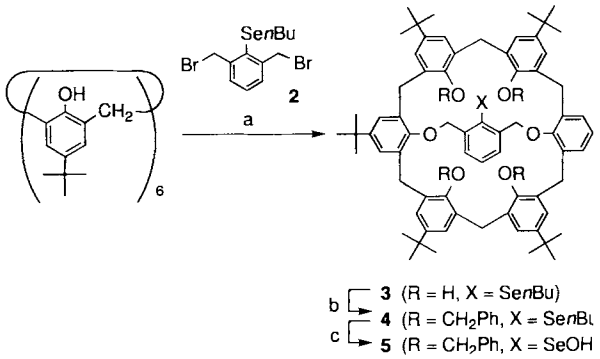

Scheme 1. Synthesis of selenenic acid **5**. a) KOH, THF/DMF (80%); b) NaH, $PhCH_2Br$, THF/DMF (59%); c) *m*CPBA, CH_2Cl_2, then toluene, 80 °C, 2 h (74%).

conformer of its bromide analogue (X = Br instead of SeOH).[9d] The OH absorption in the IR spectrum (CH_2Cl_2) was observed at 3523 cm^{-1}, indicating the absence of significant intramolecular hydrogen bonding.

The structure of **5** was established by X-ray crystallographic analysis (Figure 1).[11] This is the first X-ray structure analysis

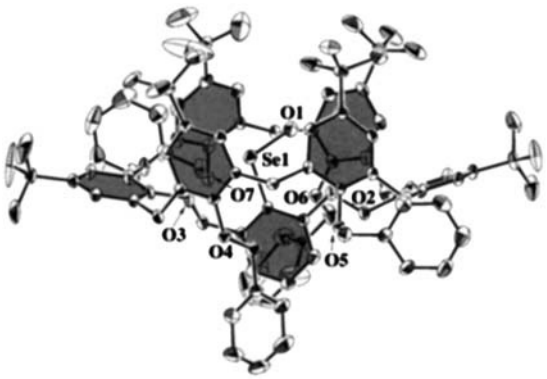

Figure 1. Crystal structure of **5** (ORTEP drawing; thermal ellipsoids at 20% probability level). The aromatic rings of the calix[6]arene macrocycle and that of the bridging unit are shaded.

of a selenenic acid. The SeOH functionality is deeply buried in the cavity of the *p-tert*-butylcalix[6]arene macrocycle with a *cone* conformation; evidently this situation is unfavorable for the intermolecular processes that normally lead to its decomposition. The distance between the selenium atoms on the neighboring molecules is more than 10 Å, indicating that there is no intermolecular interaction between the SeOH functionalities. The Se1–O1 bond length is 1.763(7) Å, which is almost the same as that of the Se–O single bond in benzeneseleninic acid.[12] The distances between O1 and O2–O7 lie between 3.88 and 6.21 Å, and are thus much longer than the average distance of hydrogen-bonded HO···O (2.72 Å),[13] clearly showing the lack of hydrogen bonding between the OH group and the atoms O2–O7 also in the solid state. The Se1–O3 distance is 2.64 Å, which is significantly shorter than the sum of the corresponding van der Waals radii (3.42 Å).[14] The atoms O3, Se1, and O1 adopt a nearly linear arrangement (bond angle 168°). These structural parameters indicate the existence of the nonbonding interaction between the Se1 and O3 atoms of **5** in the solid state.[15]

Selenenic acid **5** is remarkably stable both in the crystalline state and in solution. Even after **5** had been heated at 120 °C for 5 h in $CDCl_2CDCl_2$, no decomposition was observed. Considering that 2,4,6-*tert*-butylbenzeneselenenic acid disproportion-

[*] Prof. Dr. R. Okazaki, Dr. T. Saiki, Dr. K. Goto
Department of Chemistry, Graduate School of Science
The University of Tokyo
7-3-1 Hongo, Bunkyo-ku, Tokyo 113 (Japan)
Fax: Int. code +(3)5800-6899.
e-mail: okazaki@chem.s.u-tokyo.ac.jp

[**] This work was partly supported by Grants-in-Aid for Scientific Research (No. 08454197 and 08740487) from the Ministry of Education, Science and Culture, Japan. We also thank Tosoh Akzo Co., Ltd. for the generous gift of alkyllithium compounds.

 © WILEY-VCH Verlag GmbH, D-69451 Weinheim, 1997 0570-0833/97/3620-2223 $ 17.50+.50/0

ates completely within 2 h in 4% D_2O/CD_3CN at 25 °C,[7] this stability of **5** is remarkable. In order to clarify its origin, a control experiment was carried out using selenoxide **6**, which does not have the macrocyclic structure (Scheme 2). Upon heating at 80 °C for 5 min in [D_8]toluene, **6** decomposed to afford diselenide **7** and seleninic acid **8**; the intermediary selenenic acid Ar'SeOH was not detected. After separation, **7** and **8** were isolated in 59 and 28% yields, respectively. These results clearly indicate that the high stability of **5** is caused by the steric protection, and not the coordination by the *ortho* substituent.

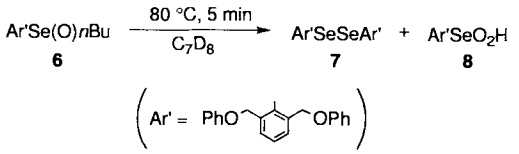

Scheme 2. Control experiment with the selenoxide **6**.

The reaction of **5** with *m*CPBA (1.2 equiv) or 1-butanethiol (10 equiv) afforded the corresponding seleninic acid **9** (88%) or selanyl sulfide **10** (78%), respectively (Scheme 3), indicating that **5** retains its reactivity as a selenenic acid although it has the unprecedented stability.

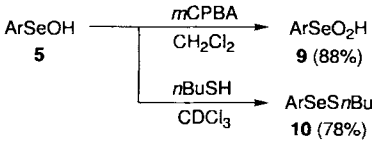

Scheme 3. Reactions of selenenic acid **5**.

In summary, an isolable selenenic acid was synthesized for the first time by taking advantage of the bridged calix[6]arene framework, and its structure was determined by X-ray crystallographic analysis. This stable compound should enable us to elucidate the chemistry of selenenic acids directly.

Experimental Section

To a solution of **4** (282 mg, 0.18 mmol) in CH_2Cl_2 (5 mL) was added a solution of *m*CPBA (80%, 47 mg, 0.22 mmol) in CH_2Cl_2 (4 mL) at 0 °C. After the mixture had been stirred at the same temperature for 2 h, it was washed with 5% aqueous $NaHCO_3$ and dried over anhydrous $MgSO_4$. After removal of the solvent, the residue was heated in toluene (9 mL) at 80 °C for 2 h. After removal of the solvent, the residue was separated by chromatography ($SiO_2/CHCl_3$:hexane = 1:1) to give **5** (204 mg, 74%) in the form of colorless crystals. M.p. 168 °C (decomp); ^{1}H NMR (500 MHz, $CDCl_3$): $\delta = -0.05$ (s, 1H; SeOH), 1.04 (s, 36H; *t*Bu), 1.44 (s, 18H; *t*Bu), 3.24 (d, $^2J = 14.3$ Hz, 2H; $ArCH_2Ar$), 3.34 (d, $^2J = 15.3$ Hz, 4H; $ArCH_2Ar$), 4.21 (s, 4H; $ArCH_2OAr$), 4.47 (d, $^2J = 11.9$ Hz, 4H; $PhCH_2O$), 4.500 (d, $^2J = 14.3$ Hz, 2H; $ArCH_2Ar$), 4.501 (d, $^2J = 15.3$ Hz, 4H; $ArCH_2Ar$), 4.58 (d, $^2J = 11.9$ Hz, 4H; $PhCH_2O$), 6.44 (t, $^3J = 7.3$ Hz, 1H), 6.81 (d, $^4J = 2.3$ Hz, 4H), 6.99–7.007 (m, 8H), 7.012 (d, $^3J = 7.3$ Hz, 2H), 7.08–7.11 (m, 8H), 7.13–7.17 (m, 4H), 7.20 (d, $^4J = 2.3$ Hz, 4H), 7.29 (s, 4H); ^{13}C NMR (125 MHz, $CDCl_3$): $\delta = 26.9$ (t), 31.3 (t), 31.5 (q), 31.7 (q), 34.17 (s), 34.19 (s), 72.7 (t), 74.7 (t), 124.2 (d), 124.7 (d), 125.9 (d), 126.0 (d), 127.0 (d), 127.5 (d), 127.9 (d), 128.5 (d), 131.9 (s), 132.1 (s), 133.8 (s), 135.1 (s), 137.7 (s), 137.9 (s), 144.4 (s), 145.6 (s), 152.2 (s), 152.6 (s); ^{77}Se NMR (95 MHz, $CDCl_3$): $\delta = 1134$; IR (CH_2Cl_2): $\tilde{\nu} = 3523$ cm^{-1} (OH); HR-MS (FAB): calcd. for $C_{102}H_{114}O_7{}^{80}Se$ 1530.7730; found: 1530.7737; elemental analysis (%): calcd for $C_{102}H_{114}O_7Se \cdot H_2O$: C 79.09, H 7.55, Se 5.10; found: C 79.31, H 7.53, Se 4.72. The NMR signals were assigned by HH-COSY, CH-COSY, and differential NOE experiments.

Received: May 5, 1997 [Z10412IE]
German version: *Angew. Chem.* **1997**, *109*, 2320–2322

Keywords: calixarenes · selenium · steric hindrance · structure elucidation

[1] For reviews, see: a) *The Chemistry of Organic Selenium and Tellurium Compounds, Vol. 1 and 2* (Eds.: S. Patai, Z. Rappoport), Wiley, New York, **1986**, and **1987**, respectively; b) *Organoselenium Chemistry* (Ed.: D. Liotta), Wiley, New York, **1987**; c) P. D. Magnus in *Comprehensive Organic Chemistry, Vol. 3* (Ed.: D. N. Jones), Pergamon, Oxford, **1979**, pp. 491–538.

[2] a) L. Flohé in *Free Radicals in Biology, Vol. V.* (Ed.: W. A. Pryor), Academic Press, New York, **1982**, pp. 223–254; b) H. E. Ganter, R. J. Kraus in *Methods Enzymol.* **1984**, *107*, 593–602.

[3] For recent examples, see: a) T. G. Back, B. P. Dyck, *J. Am. Chem. Soc.* **1997**, *119*, 2079–2083; b) L. Engman, C. Andersson, R. Morgenstern, I. A. Cotgreave, C. M. Andersson, A. Hallberg, *Tetrahedron* **1994**, *50*, 2929–2938; c) M. Iwaoka, S. Tomoda, *J. Am. Chem. Soc.* **1994**, *116*, 2557–2561, and references therein.

[4] a) O. Behaghel, W. Müller, *Ber. Dtsch. Chem. Ges.* **1935**, *68*, 1540–1549; b) H. Rheinboldt, E. Giesbrecht, *Chem. Ber.* **1955**, *88*, 666–678; c) *ibid.* **1955**, *88*, 1037–1042; d) *ibid.* **1955**, *88*, 1974–1978.

[5] a) O. Behaghel, W. Müller, *Ber. Dtsch. Chem. Ges.* **1934**, *67*, 105–108; b) W. Jenny, *Helv. Chim. Acta.* **1958**, *41*, 317–326; c) H. Rheinboldt, E. Giesbrecht, *Chem. Ber.* **1956**, *89*, 631–636; d) H. J. Reich, C. A. Hoeger, W. W. Willis, Jr., *J. Am. Chem. Soc.* **1982**, *104*, 2936–2937.

[6] Although some of those relatively stable selenenic acids were claimed to be isolable [4,5c], reinvestigations of the structures of the isolated products revealed that they are not selenenic acids but the corresponding selenenic anhydrides: a) H. J. Reich, W. W. Willis, Jr., S. Wollowitz, *Tetrahedron Lett.* **1982**, *23*, 3319–3322; b) J. L. Kice, F. McAfee, H. Slebocka-Tilk, *ibid.* **1982**, *23*, 3323–3326.

[7] H. J. Reich, C. P. Jasperse, *J. Org. Chem.* **1988**, *53*, 2389–2390.

[8] Possible exceptions are anthraquinoneselenenic acids [5a,b], whose structural determination was based only on elemental analysis and UV/Vis spectra.

[9] a) N. Tokitoh, T. Saiki, R. Okazaki, *J. Chem. Soc. Chem. Commun.* **1995**, 1899–1900; b) T. Saiki, K. Goto, N. Tokitoh, R. Okazaki, *J. Org. Chem.* **1996**, *61*, 2924–2925; c) T. Saiki, K. Goto, N. Tokitoh, M. Goto, R. Okazaki, *Tetrahedron Lett.* **1996**, 37, 4039–4042; d) T. Saiki, K. Goto, R. Okazaki, *Chem. Lett.* **1996**, 993–994. For related compounds, see: e) K. Goto, N. Tokitoh, R. Okazaki, *Angew. Chem.* **1995**, *107*, 1202–1203; *Angew. Chem. Int. Ed. Engl.* **1995**, *34*, 1124–1126; f) K. Goto, M. Holler, R. Okazaki, *J. Am. Chem. Soc.* **1997**, *119*, 1460–1461.

[10] Recently, the bridged calix[6]arenes containing a functional group on the bridge were also described by Lüning et al. a) H. Ross, U. Lüning, *Angew. Chem.* **1995**, *107*, 2723–2725; *Angew. Chem., Int. Ed. Engl.* **1995**, *34*, 2555–2557; b) *Liebigs Ann.* **1996**, 1367–1373; c) *Tetrahedron* **1996**, *52*, 10879–10882.

[11] Crystal data for **5**: $C_{102}H_{114}O_7Se$, $M_r = 1530.98$, crystal dimensions $0.80 \times 0.30 \times 0.20$ mm, crystal system triclinic, space group $P\bar{1}$, unit cell dimensions $a = 12.949(4)$, $b = 28.743(8)$, $c = 12.230(2)$ Å, $\alpha = 96.90(2)$, $\beta = 101.55(2)$, $\gamma = 78.70(2)°$, $V = 4357(1)$ Å^3, $Z = 2$, $\rho_{calcd} = 1.167$ g cm^{-3}, $2\theta_{max} = 55.2°$. The intensity data were collected at 296 K on a Rigaku AFC5R diffractometer with $Mo_{K\alpha}$ radiation ($\lambda = 0.71069$ Å), the scan mode being ω. Of the 20951 reflections which were collected, 20064 were independent. The linear absorption coefficient μ for $Mo_{K\alpha}$ radiation is 4.9 cm^{-1}. An empirical absorption correction using the program DIFABS [16] was applied that resulted in transmission factors ranging from 0.81 to 1.00. The data were corrected for Lorenz and polarization effects. The structure was solved by heavy-atom Patterson methods (PATTY [17]) and expanded by using Fourier techniques (DIRDIF94 [18]). The non-hydrogen atoms were refined anisotropically. Hydrogen atoms except that of the SeOH group were included but not refined. Full-matrix least-squares refinement based on F weighted with $1/\sigma^2(F_o)$ gave final values $R = 0.063$ and $wR = 0.066$ for 5001 observed reflections [$I > 3.00\sigma(I)$] and 991 variable parameters. Maximum/minimum residual electron density: 0.81/ −0.55 e Å^{-3}. Crystallographic data (excluding structure factors) for the structure reported in this paper have been deposited with the Cambridge Crystallographic Data Centre as supplementary publication no. CCDC-100401. Copies of the data can be obtained free of charge on application to The Director, CCDC, 12 Union Road, Cambridge CB2 1EZ, UK (fax: int. code +(1223) 336-033; e-mail: deposit@chemcrys.cam.ac.uk).

[12] J. H. Bryden, J. D. McCullough, *Acta Crystallogr.* **1954**, *7*, 833–838.

[13] L. N. Kuleshova, P. M. Zorkii, *Acta Crystallogr. Sect. B* **1981**, *37*, 1363–1366.

[14] A. Bondi, *J. Phys. Chem.* **1964**, *68*, 441–451.

[15] The intramolecular interaction between a divalent selenium and an amino group has been studied in detail: a) M. Iwaoka, S. Tomoda, *Phosphorus Sulfur Silicon Relat. Elem.* **1992**, *67*, 125–130; b) *J. Am. Chem. Soc.* **1996**, *118*, 8077–8084. Also see ref. [3c].

[16] N. Walker, D. Stuart, *Acta Crystallogr. Sect. A* **1983**, *39*, 158–166.

[17] P. T. Beurskens, G. Admiraal, G. Beurskens, W. P. Bosman, S. Garcia-Granda, R. O. Gould, J. M. M. Smits, C. Smykalla, The DIRDIF program system, Technical Report of the Crystallography Laboratory, University of Nijmegen, The Netherlands, **1992**.

[18] P. T. Beurskens, G. Admiraal, G. Beurskens, W. P. Bosman, R. de Gelder, R. Israel, J. M. M. Smits, The DIRDIF-94 program system, Technical Report of the Crystallography Laboratory, University of Nijmegen, The Netherlands, **1994**.

 © WILEY-VCH Verlag GmbH, D-69451 Weinheim, 1997 0570-0833/97/3620-2224 $ 17.50+.50/0

Anti-Markovnikov Functionalization of Olefins: Rhodium-Catalyzed Oxidative Aminations of Styrenes**

Matthias Beller,* Martin Eichberger, and Harald Trauthwein

Amines and their derivatives are of great importance for organic chemistry as natural products, pharmacological agents, fine chemicals, and dyes. Despite the many uses for amines, the direct addition of ammonia as well as primary and secondary amines to olefins has not been investigated in detail.[1] The advantage of direct aminations of olefins over classical methods[2] is that in principle no coupled products are formed, that is every atom from the starting material is still present in the product molecules (100% atom economy).

Aminations of olefins catalyzed by transition metals can follow two different paths (Scheme 1):[3] a) coordinative binding

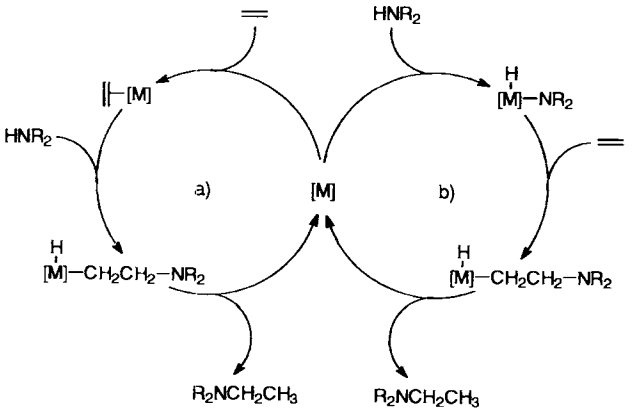

Scheme 1. Transition metal catalyzed amination of olefins as exemplified by ethene. a) The first step is the coordinative binding of the olefin to the metal center. b) The first step is the insertion of a metal complex into the N–H bond.

of an olefin, for example ethene, to the central atom of an electron-poor metal complex activates the olefin for a direct attack of the amine; b) oxidative insertion of an electron-rich metal complex into the N–H bond of an amine leads to the corresponding amidohydrido complex with subsequent insertion of an olefin into the metal–nitrogen bond.

Both paths present several problems, and to date, there is no broadly applicable method for the catalytic amination of olefins. Rhodium-catalyzed aminations of ethene and norbornene are well-known,[4–6] as are palladium-catalyzed intramolecular aminations of amines and amides[7] as well as recently developed hydroaminations in the presence of lanthanoid complexes.[8] The metal complexes previously employed for transition metal catalyzed aminations are not very active, and some of the aminations only progress intramolecularly. In addition the Markovnikov products are always favored when unsymmetrical olefins are used. An exception is the intramolecular oxidative amination of *o*-aminostyrene, in which for reasons of ring strain in the product only attack at a terminal position is possible.[9]

Here we report on a catalytic system which for the first time enables regioselective intermolecular oxidative anti-Markovnikov aminations of different olefins with secondary amines. Because of the significance of the pharmacologically important structural unit $ArylCH_2CH_2NR_2$[10] we examined the reaction of styrene with amines. During the course of a catalyst screening we discovered that rhodium complexes with the general formula $[RhL_4]X$ (L = olefin, phosphane, $X = BF_4^-$) surprisingly catalyze the selective formation of the enamines **3**, that is of the anti-Markovnikov products (Scheme 2)!

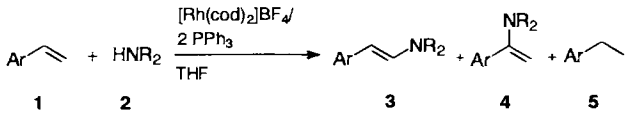

Scheme 2. Rhodium-catalyzed regioselective oxidative amination of styrenes. Ar = aryl; R = alkyl, aryl; cod = (*Z*,*Z*)-1,5-cyclooctadiene.

Formally this is an oxidation of the olefin, similar to the Wacker process.[11] Hydrolysis of the enamines leads to phenylacetaldehydes that are regioisomeric to the products of a Wacker oxidation. The reaction conditions were optimized for the model reaction between styrene and piperidine. In the presence of 2.5 mol% $[Rh(cod)_2]BF_4$ and two equivalents of triphenylphosphane in THF, the desired product *N*-styrylpiperidine **3** (Ar = Ph, R_2 = pentane-1,5-diyl) is obtained after 20 h in 55% yield. According to the ^1H NMR spectrum the *E* isomer is formed exclusively ($^3J = 14$ Hz). Hydrogenation of styrene leads to ethylbenzene **5** as a further main product. The other possible amination product, the Markovnikov regioisomer **4**, was not detected. Brunet et al. obtained the Markovnikov product of oxidative amination as main product besides the product of the hydroamination reaction when styrene and aniline were converted in the presence of $[\{RhCl(PEt_3)_2\}_2]$/lithium anilide.[12]

The reaction of piperidine with styrene is catalyzed not only by $[Rh(cod)_2]BF_4$, but also by the corresponding norbornadiene (nbd) complex $[Rh(nbd)_2]BF_4$. More strongly coordinating anions such as halide ions suppress enamine formation. Likewise no reaction takes place when $[\{RhCl(cod)\}_2]$/2 PPh_3 is used as a catalyst. The addition of phosphane to the cationic olefin–rhodium complex is essential, as only traces of the product are obtained without PPh_3. The optimal phosphane–rhodium ratio is 2:1. Besides triphenylphosphane, electron-rich, sterically less demanding phosphanes such as tri-*n*-butylphosphane or tri-*p*-tolylphosphane are highly suitable catalyst ligands. On the other hand, chelating phosphorus and amine ligands completely inhibit the reaction. The choice of solvent is also crucial to the productivity of the catalytic system. The best results are obtained in THF. As expected, the use of polar and coordinating solvents such as dimethyl sulfoxide or dimethylacetamide significantly reduces the activity.

To examine the range of applications for this method, different amines and olefins were transformed under optimized conditions. Table 1 shows that a series of secondary amines can be used for oxidative aminations. The highest reactivity is displayed by cyclic and acyclic aliphatic amines, but *N*-methylani-

[*] Prof. Dr. M. Beller, Dipl.-Chem. M. Eichberger, Dipl.-Chem. H. Trauthwein
Anorganisch-chemisches Institut der Technischen Universität München
Lichtenbergstrasse 4, D-85747 Garching (Germany)
Fax: Int. code +(89)289-13473
e-mail: mbeller@arthur.anorg.chemie.tu-muenchen.de

[**] Anti-Markovnikov Fuctionalization of Unsaturated Compounds, Part 1. We thank Degussa AG, Heraeus AG, and Hoechst AG for gifts of chemicals. We also thank Dr. J. Herwig, Dr. H. Geissler, Dr. R. Fischer, and Prof. Dr. K. Kühlein (all from the Hoechst AG, Frankfurt) for suggestions and discussions. Harald Trauthwein thanks the Fonds der Chemischen Industrie for a doctoral scholarship.

 © WILEY-VCH Verlag GmbH, D-69451 Weinheim, 1997 0570-0833/97/3620-2225 $ 17.50+.50/0

Table 1. Oxidative aminations of styrene [a].

Amine	Yield [%] enamine	ethyl benzene
diethylamine	40	54
di-*n*-butylamine	48	44
piperidine	55	57
hexahydroazepine	45	80
N-methylaniline	9	9

[a] Ratio of styrene:amine 4:1, 2.5 mol% $[Rh(cod)_2]BF_4$/2 PPh_3 relative to amine, 20 h reflux in THF.

line, whose nucleophilicity is strongly reduced because of the phenyl ring, can also be made to react.

Surprisingly, electronically different substituents at the aryl ring can significantly influence the efficiency of the reaction (Table 2). Thus a methyl group clearly increases the yield,

Table 2. Variation of olefins in the reaction with piperidine [a].

Olefin	Yield [%] Enamine [b]	Ethyl benzene [c]	Amine after hydrogenation [c]
styrene	55	57	55
4-methylstyrene	75	65	69
3-methylstyrene	75	94	42
4-methoxystyrene	55	49	45(33)
3,4-dimethoxystyrene	44	64	44(35)
2-vinylnaphthalene	99	99	99
4-vinylbiphenyl	24	8	16
4-fluorostyrene	18	13	18(10)
4-trifluoromethylstyrene	14	6	14
acrylamide	18	- [d]	-

[a] Ratio of styrene:amine 4:1, 2.5 mol% $[Rh(cod)_2]BF_4$/2 PPh_3 relative to amine, 20 h reflux in THF. [b] The yield was determined by gas chromatography by percentage area. [c] The yield was determined by gas chromatography using an internal standard. The values in parentheses correspond to yields of isolated product. [d] The yield of the hydrogenated product could not be determined by gas chromatographic methods as the retention time coincides with that of acrylamide.

whereas a methoxy group in the 4-position decreases it. A further methoxy group in 3-position only has a negligible influence on the yield. Distinctly lower yields of enamine are obtained with electron-poor styrenes. Therefore electronic reasons also seem to be responsible for the low reactivity of 4-vinylbiphenyl.

Preliminary experiments aimed at broadening the spectrum of suitable olefins showed that functionalized olefins also undergo the reaction. For example, acrylamide, which without catalyst selectively reacts in a Michael reaction resulting in the hydroamination product, can be transformed into the enamine in 18% yield; however, the hydroamination product is also detected. In principle, further functionalized aliphatic olefins should be convertible into enamines.

The oxidative amination and the simultaneous hydrogenation of a further olefin molecule make a mechanism similar to that of the oxidative silylation seem plausible (Scheme 3).[13] We postulate that the catalytically active species **6** reacts with the olefin, leading to the formation of the η^2 complex **7**. Nucleophilic attack of the amine on the thus activated olefin affords the Rh–alkylamine compound **8**; β-H elimination then leads to the Rh–H species **9** and the enamine **3**. The active species **6** is then reformed from **9** and a further olefin molecule. Interestingly, only the styrene is hydrogenated, which can be explained by its easy hydrogenability.[14] Unlike in the palladium-catalyzed oxidative amination with benzoquinone as an oxidant, the

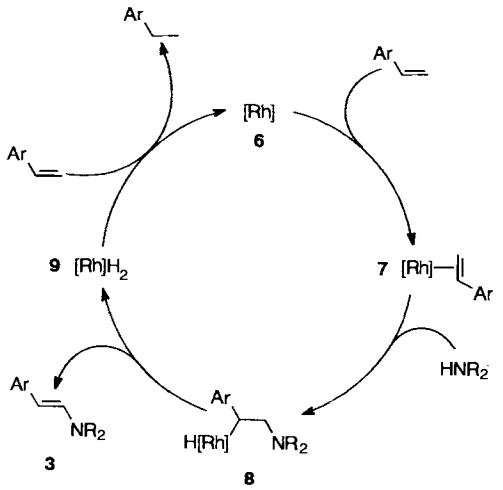

Scheme 3. Postulated mechanism of the oxidative amination. Ar = aryl; R = alkyl, aryl.

olefin added in excess serves as an oxidizing agent. The yield of enamine falls with decreasing styrene–amine ratio.

We have thus developed a method that for the first time allows oxidative aminations of simple olefins. The resulting enamines are reactive intermediates that can be further transformed;[15] thus, in future new cascade processes should become possible. The excellent regioselectivity of the reaction is of particular importance, as it provides evidence that transition metal catalyzed reactions of simple olefins with nucleophiles in the anti-Markovnikov sense are possible.

Experimental Section

All experiments were carried out under exclusion of air and moisture. The chemicals were dried according to standard procedures and stored under N_2 or argon. $[Rh(cod)_2]BF_4$ was prepared according to reference[16].

Procedure for the catalysis experiments: $[Rh(cod)_2]BF_4$ (45.0 mg, 0.11 mmol) and PPh_3 (58.0 mg, 0.22 mmol) were suspended in THF (10.0 mL) under argon. Addition of the amine (4.40 mmol) afforded a yellow solution to which the olefin was added. Subsequently the mixture was heated to reflux for 20 h. The reaction mixtures were then either distilled or hydrogenated to the corresponding alkylamines (48 h, 1 bar H_2, 0.5 g 5% Pd/C). After the hydrogenation catalyst had been removed by filtration, the solvent was removed in vacuo and the residue was taken up in dichloromethane (20.0 mL). After extraction with 5% HCl (3 × 20.0 mL) the combined aqueous phases were carefully brought to pH 9 by using NaOH pellets and then extracted with dichloromethane (3 × 20.0 mL). The combined organic phases were dried over magnesium sulfate. After the solvent had been removed in vacuo, the product was purified by column chromatography and dried in high vacuum. The products were characterized by ^1H NMR and (DEPT)^{13}C NMR spectroscopy as well as by GC-MS. The yields with respect to the amine were determined after gas chromatography with hexadecane as internal standard.

Received: March 17, 1997 [Z10246IE]
German version: *Angew. Chem.* **1997**, *109*, 2306–2308

Keywords: aminations · enamines · homogeneous catalysis · oxidations · rhodium

[1] D. M. Roundhill, *Chem. Rev.* **1992**, *92*, 1.
[2] G. Heiler, H. J. Mercker, D. Frank, R. A. Reck, R. Jäckh in *Ullmann's Encyclopedia of Industrial Chemistry, Vol. A2* (Ed.: W. Gerhartz), 5th ed., VCH, Weinheim, **1985**, p. 1.
[3] R. Taube in *Applied Homogeneous Catalysis with Organometallic Compounds* (Ed.: B. Cornils, W. A. Herrmann), VCH, Weinheim, **1996**, p. 507.
[4] D. R. Coulson (Du Pont), US 3.758.586, **1973**; [*Chem. Abstr.* **1973**, *79*, P125808g]; *Tetrahedron Lett.* **1971**, 429.
[5] D. Steinborn, B. Thies, I. Wagner, R. Taube, *Z. Chem.* **1989**, *29*, 333.
[6] A. L. Casalnuovo, J. L. Calabrese, D. Milstein, *J. Am. Chem. Soc.* **1988**, *110*, 6738.
[7] L. S. Hegedus, *Angew. Chem.* **1988**, *100*, 1147; *Angew. Chem. Int. Ed. Engl.* **1988**, *27*, 1113.

 © WILEY-VCH Verlag GmbH, D-69451 Weinheim, 1997 0570-0833/97/3620-2226 $ 17.50+.50/0

[8] M. R. Gagné, C. L. Stern, T. J. Marks, *J. Am. Chem. Soc.* **1992**, *114*, 275.
[9] R. C. Larock, T. R. Hightower, L. A. Hasvold, K. P. Peterson, *J. Org. Chem.* **1996**, *61*, 3584.
[10] E. Mutschler, *Arzneimittelwirkungen*, 6th ed., Wiss. Verlagsges., Stuttgart, **1991**; W. Forth, D. Henschler, W. Rummel, K. Starke, *Pharmakologie und Toxikologie*, 6th ed., Bibliographisches Institut, Mannheim, **1992**.
[11] J. Tsuji in *Comprehensive Organic Synthesis*, *Vol. 7* (Ed.: B. M. Trost), Pergamon Press, Oxford, **1991**, p. 449.
[12] J.-J. Brunet, D. Neibecker, K. Philippot, *Tetrahedron Lett.* **1993**, *34*, 3877.
[13] R. Takeuchi, H. Yasue, *Organometallics* **1996**, *15*, 2098.
[14] H. Takaya, R. Noyori in *Comprehensive Organic Synthesis*, *Vol. 8* (Ed.: B. M. Trost), Pergamon Press, Oxford, **1991**, p. 443.
[15] P. W. Hickmott, *Tetrahedron* **1982**, *38*, 1975.
[16] R. R. Schrock, J. A. Osborn, *J. Am. Chem. Soc.* **1971**, *93*, 3089.

$[Ru_{20}H_4Cu_6Cl_2(CO)_{48}]^{4-}$: A New High Nuclearity Copper–Ruthenium Cluster**

Michael A. Beswick, Jack Lewis, Paul R. Raithby,* and M. Carmen Ramirez de Arellano

Mixed-copper alloys are of interest as catalysts, particularly in the selective reforming of petroleum naptha fractions to aromatic hydrocarbons.[1] We have recently embarked on the study of high nuclearity mixed-metal ruthenium–copper carbonyl clusters, and the three cluster anions characterized so far, $[Ru_8H_2Cu_7Cl_3(CO)_{24}]^{2-}$, $[Ru_{12}H_2Cu_6Cl_2(CO)_{34}]^{2-}$, and $[Ru_{12}Cu_4Cl_2C_2(CO)_{32}]^{2-}$ all have different Ru:Cu ratios, 8:7, 2:1, and 3:1, respectively.[2] These mixed-metal clusters illustrate the use of copper cations as linking agents in the formation of high nuclearity mixed-metal clusters. We now report the synthesis and structure of the highest nuclearity ruthenium–copper carbonyl hydrido cluster $[Ru_{20}H_4Cu_6Cl_2(CO)_{48}]^{4-}$, so far characterized crystallographically.

The reaction of the dianion $[Ru_{10}H_2(CO)_{25}]^{2-}$ with excess $[Cu(MeCN)_4]^+$ in CH_2Cl_2 in the presence of $[Bu_4N]OH/H_2O$ and $[(Ph_3P)_2N]Cl$, with stirring at room temperature, leads after purification by thin-layer chromatography to the isolation of **1** in 60–70% yield. Complex **1** was initially

$[Bu_4N]_4[Ru_{20}H_4Cu_6Cl_2(CO)_{48}]$ **1**

characterized by spectroscopy,[3] but in order to establish the structure of the complex a crystal structure analysis was undertaken. Crystals suitable for X-ray analysis were grown from the layered diffusion of ethanol into a solution of **1** in CH_2Cl_2.[4]

The structure of the tetraanion of **1** (Figure 1) may be viewed as two decaruthenium clusters sandwiching the hexacopper cluster metal core. The geometry of the decaruthenium units in cluster **1** is different from that observed in the precursor dianion $[Ru_{10}H_2(CO)_{25}]^{2-}$.[5, 6] This geometry can be viewed as the condensation of two octahedra through the triangular face Ru2-Ru3-Ru4, generating three butterflies, one of which is capped. This is very similar to the metal core geometry found in $[Ru_{11}H(CO)_{27}]^{3-}$[6, 7] but in this case two of the butterflies are capped. In the cluster precursor $[Ru_{10}H_2(CO)_{25}]^{2-}$ the geometry is that of two trigonal bipyramids fused to an octahedron. The ruthenium metal core arrangement in the anion of **1** has not been observed previously for decanuclear clusters, although the use of Group 11 metals has been shown to introduce a polarity into ruthenium metal frameworks, generating metal geometries not observed in homometal clusters.[8] The Cu_6 metal core may be described as two tetrahedra fused through a common edge (Cu(1)–Cu(1a)) the center of which is the crystallographic center of symmetry.

The central section of the metal core is reminiscent of that in $[Ru_{12}H_2Cu_6Cl_2(CO)_{34}]^{2-}$, which consists of four fused octahredra; in the case of **1** a further four Ru atoms have condensed on each end. Two chloride ligands each symmetrically bridge two of the copper atoms in the Cu_6 core. The distance between the Cu centers bridged by the two chloride ligands is 2.840(5) Å, and the shortest Cu–Cu distance is between the two central copper atoms Cu(1) and Cu(1a) (2.440(6) Å). The structure of the tetraanion of **1** has 12 asymmetrically bridging carbonyl ligands, each Ru_{10} unit containing six.

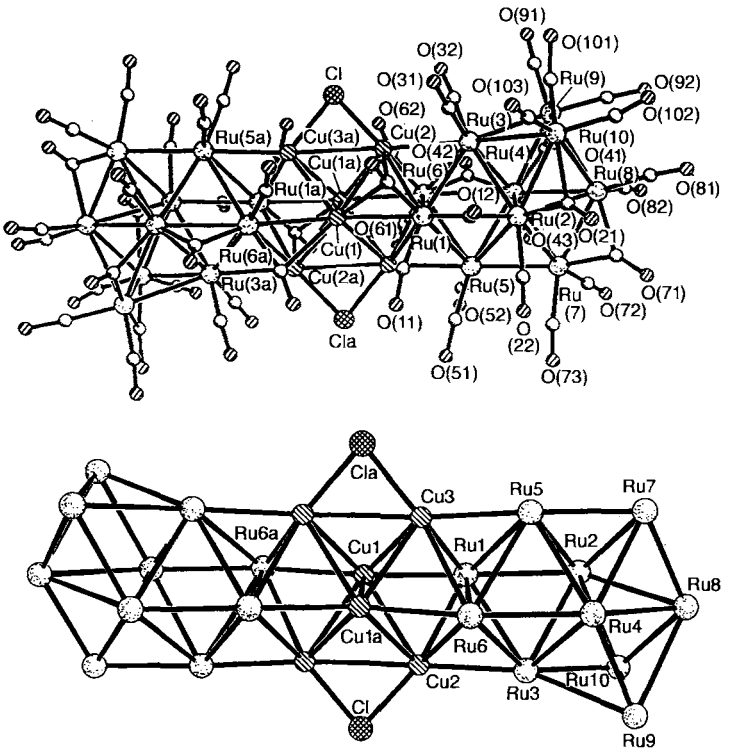

Figure 1. Top: Structure of the anion of **1** showing the atom numbering scheme. Selected bond lengths [Å] and angles [°]: Ru(1)–Cu(1) 2.595(4), Ru(1)–Cu(2) 2.667(5), Ru(1)–Cu(3) 2.720(4), Ru(1)–Ru(2) 2.835(3), Ru(1)–Ru(3) 2.882(3), Ru(1)–Ru(5) 2.994(3), Ru(1)–Ru(6) 3.073(3), Ru(2)–Ru(3) 2.852(4), Ru(2)–Ru(4) 2.855(3), Ru(2)–Ru(5) 2.806(3), Ru(2)–Ru(7) 2.836(4), Ru(2)–Ru(8) 2.837, Ru(2)–Ru(10) 2.807(4), Ru(3)–Cu(2) 2.657(4), Ru(3)–Ru(4) 2.851(3), Ru(3)–Ru(6) 2.924(3), Ru(3)–Ru(9) 2.916(3), Ru(3)–Ru(10) 2.960(3), Ru(4)–Ru(5) 2.842(4), Ru(4)–Ru(6) 2.860(3), Ru(4)–Ru(7) 2.823(4), Ru(4)–Ru(8) 2.885(3), Ru(5)–Cu(3) 2.608(4), Ru(5)–Ru(6) 2.937(4), Ru(5)–Ru(7) 2.697(4), Ru(6)–Cu(2) 2.678(4), Ru(6)–Cu(3) 2.715(4), Ru(6)–Cu(1a) 2.615(4), Ru(7)–Ru(8) 2.685(4), Ru(8)–Ru(9) 2.925(4), Ru(8)–Ru(10) 2.924(4), Ru(9)–Ru(10) 2.798(4), Cu(1)–Cu(2) 2.668(5), Cu(1)–Cu(3) 2.674(5), Cu(1)–Cu(1a) 2.440(6), Cu(1)–Cu(2a) 2.647(5), Cu(1)–Cu(3a) 2.631(5), Cu(2)–Cu(3a) 2.840(5). Cu(2)–Cl 2.229(7), Cu(3)–Cl 2.244(7); Cu(3)-Cl(a)-Cu(2a) 78.8(2). The atoms denoted "a" are related to the atoms with the same number through the center of symmetry. Bottom: The metal core geometry of **1** showing the position of the chlorine ligands.

[*] Dr. P. R. Raithby, Dr. M. A. Beswick, Prof. The Lord Lewis, Dr. M. C. Ramirez de Arellano.
Department of Chemistry, University of Cambridge
Lensfield Road, Cambridge CB2 1EW (UK)
Fax: Int. code +(1223) 336 362
e-mail: mab16@cam.ac.uk

[**] We thank the Engineering and Physical Sciences Research Council and Johnson Matthey plc for support (for M. A. B.) and the European Union for a Human Capital and Mobility grant (to M. C. R. de A).

 © WILEY-VCH Verlag GmbH, D-69451 Weinheim, 1997 0570-0833/97/3620-2227 $ 17.50+.50/0

If the decaruthenium units are each considered to have a formal 4 − charge, that is $[Ru_{10}H_2(CO)_{24}]^{4-}$, the two chloride ions contribute a 2 − charge, and each of the six copper atoms is in a formal +I oxidation state, then the overall charge on the cluster is 4 − , consistent with the presence of the four $[Bu_4N]^+$ ions. As in the precursor $[Ru_{10}H_2(CO)_{25}]^{2-}$ and the related anion $[Ru_{11}H(CO)_{27}]^{3-}$ the four hydrides in the anion of **1** could not be located from the structural analyses[6] or from potential energy calculations.[9] However, the presence of a strong, but broad, ^{1}H NMR signal at $\delta = -5.00$, in a similar position to that observed in the anion $[Ru_{11}H(CO)_{27}]^{3-}$,[7] is consistent with the presence of hydrides that are undergoing a dynamic process. Attempts to carry out low-temperature NMR studies were unsuccessful because of the poor solubility of **1** at lower temperatures. The assignment of four hydrides to the anion of **1** is consistent with the ^{1}H NMR data, the charge assignment to the cluster and the precursor complexes, and follows the trends observed in the synthesis of other high nuclearity, mixed-metal clusters in this series.[2]

Experimental Section

1: $[(Ph_3P)_2N]_2[Ru_{10}H_2(CO)_{25}]$ (100 mg) in CH_2Cl_2 (50 mL) with $[Et_4N][OH]/H_2O$ (100 mg), excess $[Cu(MeCN)_4][BF_4]$ (250 mg), and $[(Ph_3P)_2N]_2Cl$ (100 mg) was stirred for 10 min. The mixture was filtered hot and the volume reduced to 10 mL under vacuum. The mixture was separated by thin-layer chromatography with CH_2Cl_2 as eluent.

Received: September 27, 1996
Supplemented version: May 20, 1997 [Z 9599 IE]
German version: *Angew. Chem.* **1997**, *109*, 2311–2312

Keywords: carbonyl complexes · clusters · copper · ruthenium · structure elucidation

[1] K. Christmann, G. Ertl, H. Shimizu, *J. Catal.* **1980**, *61*, 397; H. Shimizu, K. Christmann, G. Ertl, *J. Catal.* **1980**, *61*, 412; R. D. Adams, W. A. Hermann, *Polyhedron*, **1988**, *7*, 2255.

[2] M. A. Beswick, P. R. Raithby, J. Lewis, M. C. Ramirez de Arellano, *Angew. Chem.* **1997**, *109*, 303; *Angew. Chem. Int. Ed. Engl.* **1997**, *36*, 291; *J. Chem. Soc. Dalton Trans.* **1996**, 4033.

[3] Spectroscopic data for **1**: IR (CH_2Cl_2) υ(CO)/cm^{-1}: 2055 (m, br), 2020 (s, br), 1805 (w, br). ^{1}H NMR (CD_2Cl_2): $\delta = -5.00$ (s, 2H), and signals corresponding to the $[Bu_4N]^+$ ion. Elemental analysis calcd: C 28.06, H 3.11, N 1.17; found: C 23.84, H 3.05, N 1.01.

[4] Crystal data for **1**: $C_{112}H_{148}Cl_2Cu_6N_4O_{48}Ru_{20}$, $M_r = 4791.88$, monoclinic, space group $P2_1/n$, $a = 18.997(5)$, $b = 17.117(6)$, $c = 24.940(7)$ Å, $\beta = 112.14(2)°$, $V = 7512(4)$ Å^3, $Z = 2$, $\rho_{calcd} = 2.119$ Mg m^3, $F(000) = 4640$, $\lambda(Mo_{K\alpha}) = 0.71073$ Å, $\mu(Mo_{K\alpha})$ 2.882 mm^{-1}, $T = 298$ K. 10550 intensity data were recorded on a Siemens R3 mV diffractometer in the range $2.04 < \theta < 22.55°$, and the structure solution and refinement carried out on F^2 using SHELXS86 and SHELXL93 (G. M. Sheldrick, University of Göttingen) with all 10550 reflections, $R_1 = 0.0894$, $wR_2 = 0.1109$ (all non-H atoms anisotropic; butyl H atoms in idealised positions; hydrides not located). Crystallographic data (excluding structure factors) for the structure reported in this paper have been deposited with the Cambridge Crystallographic Data Centre as supplementary publication number CCDC-100 548. Copies of the data can be obtained free of charge on application to the Director of the Cambridge Crystallographic Data Centre, 12 Union Road, GB-Cambridge CB2 1EZ (UK) (fax: int. code + (1223) 336033; e-mail: deposit@chemerys.cam.ac.uk).

[5] P. J. Bailey, E. Charalambous, J. Hoyle. B. F. G. Johnson, J. Lewis, M. McPartlin, *J. Chem. Soc. Chem. Commun.* **1990**, 1444.

[6] P. J. Bailey, M. A. Beswick, B. F. G. Johnson, J. Lewis, M. McPartlin, P. R. Raithby, M. C. Ramirez de Arellano, *J. Chem. Soc. Dalton Trans.* **1996**, 3515.

[7] P. J. Bailey, M. A. Beswick, B. F. G. Johnson, J. Lewis, P. R. Raithby, M. C. Ramirez de Arellano, *J. Chem. Soc. Dalton Trans.* **1992**, 3159.

[8] I. D. Salter, *Adv. Organomet. Chem.* **1989**, *93*, 249; P. J. Bailey, M. A. Beswick, J. Lewis, P. R. Raithby, M. C. Ramirez de Arellano, *J. Organomet. Chem.* **1993**, *459*, 293.

[9] A. G. Orpen, *J. Chem. Soc. Dalton Trans.* **1980**, 2509.

Cationic Metallatricarbadecaboranyl Analogues of Metallocene Antitumor Agents: Synthesis, Structure, and Antineoplastic Activity of $[1\text{-}(\eta^5\text{-}C_5H_5)Fe\text{-}2\text{-}Me\text{-}2,3,4\text{-}C_3B_7H_9]^+[X]^-$ Salts ($X^- = AsF_6^-$, SbF_6^-)**

Michael D. Wasczcak, Christian C. Lee, Iris H. Hall,* Patrick J. Carroll, and Larry G. Sneddon*

The success of the antitumor reagent cisplatin[1] has stimulated the search for new metal complexes having cytotoxic properties. Studies of metallocenes of the general formulae $[(\eta^5\text{-}C_5H_5)_2MX_2]$ and $[(\eta^5\text{-}C_5H_5)_2M]^+[X]^-$[2] continue to show promise. We report here the synthesis, structure, and bioactivity of new types of hybrid cationic ferratricarbadecaboranyl analogues of ferrocenium complexes that demonstrated significant cytotoxicity and inhibition of topoisomerase II activity.

The synthesis[3] of the ferrocene analogue **1** [Eq. (a)] illustrates that the *nido*-[6-Me-5,6,9-$C_3B_7H_9$] tricarbadecaboranyl

$$[(\eta^5\text{-}C_5H_5)Fe(CO)_2I] + Na[6\text{-}Me\text{-}5,6,9\text{-}C_3B_7H_9] \xrightarrow{-2CO,\ -NaI} closo\text{-}[(\eta^5\text{-}C_5H_5)Fe\text{-}2\text{-}Me\text{-}2,3,4\text{-}C_3B_7H_9] \quad \mathbf{1} \qquad (a)$$

cage can, like the cyclopentadienyl ligand, coordinate to transition metals as a monoanionic six-electron donor. However, tricarbadecaboranyl complexes have higher chemical, oxidative, and thermal stabilities than their cyclopentadienyl analogues.[3] They are also less prone to hydrolytic metal–ligand cleavage, which can deactivate metallocenes under biological conditions. These observations suggested that cationic ferratricarbadecaboranyl complexes might, like the ferrocenium cation,[4, 5] exhibit significant bioactivity.

Oxidation of **1** with silver ion gave quantitative formation of the paramagnetic ferratricarbadecaboranyl cation [Eq. (b)].

$$\mathbf{1} + AgX \longrightarrow [1\text{-}(\eta^5\text{-}C_5H_5)Fe\text{-}2\text{-}Me\text{-}2,3,4\text{-}C_3B_7H_9][X] + Ag^0 \qquad (b)$$

$$X = AsF_6^- \ (\mathbf{1}^+\cdot AsF_6^-)$$
$$X = SbF_6^- \ (\mathbf{1}^+\cdot SbF_6^-)$$

As shown in Figure 1 for $\mathbf{1}^+\cdot AsF_6^-$,[6] crystallographic determination of both salts established that the complexes are hybrid ferratricarbadecaboranyl analogues of the ferrocenium cation, in which the iron atom is sandwiched between the planar cyclopentadienyl ring and the puckered six-membered face of the tricarbadecaboranyl ligand. The cage structure of $\mathbf{1}^+$ is remarkably similar to that of **1**,[3] with only a shortening of the Fe–C3 (by 0.02 Å), Fe–C4 (by 0.04 Å), and Fe–B7 bond lengths (by 0.05 Å). The lengthening of Fe–C_5H_5(centroid) from 1.69 Å in **1** to 1.75 Å in $\mathbf{1}^+$ suggests removal of an electron from an Fe–C_5H_5 bonding molecular orbital.[7]

[*] Prof. L. G. Sneddon, M. D. Wasczcak, Dr. P. J. Carroll
Department of Chemistry
University of Pennsylvania
Philadelphia, PA 19104-6323 (USA)
Fax: Int. code + (215) 573-2112
e-mail: sneddon@a.chem.upenn.edu
Prof. I. H. Hall, C. C. Lee
Division of Medicinal Chemistry and Natural Products
School of Pharmacy
University of North Carolina
Chapel Hill, NC 27559-7360 (USA)
Fax: Int. code + (919) 966-6919

[**] At the University of Pennsylvania, we thank the National Science Foundation for support of this research. At the University of North Carolina the research was done with the assistance of a North Carolina Biotechnology grant.

 © WILEY-VCH Verlag GmbH, D-69451 Weinheim, 1997 0570-0833/97/3620-2228 $ 17.50+.50/0

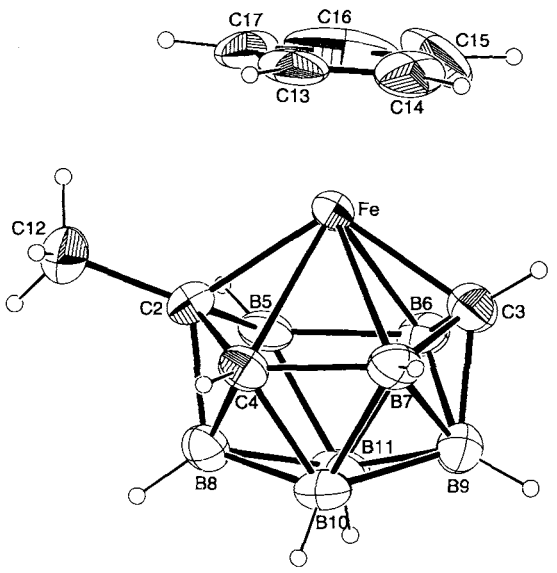

Figure 1. ORTEP view of the crystal structure of the cation in $1^+ \cdot AsF_6^-$.

Both $1^+ \cdot AsF_6^-$ and $1^+ \cdot SbF_6^-$ demonstrated selective cytotoxicity in certain cultured tumor cell lines, and produced more effective ED_{50} values than 5-fluorouracil (5-FU), 6-mercaptopurine (6-MP), β-cytosine arabinoside (Ara-C), etoposide (VP-16), and hydroxyurea standards.[8] The best ED_{50} values for $1^+ \cdot AsF_6^-$ were obtained for human HeLa uterine carcinoma (0.90 $\mu g mL^{-1}$), human lung bronchogenic MB-9812 (1.83 $\mu g mL^{-1}$), and A431 skin cells (1.32 $\mu g mL^{-1}$), while $1^+ \cdot SbF_6^-$ gave best activities for murine L-1210 leukemia (0.75 mg mL^{-1}) and P388 lymphocytic leukemia cells (1.49 $\mu g mL^{-1}$). The two salts also demonstrated excellent activity in the $Tmolt_3$ leukemia cell line, (2.39 and 2.59 $\mu g mL^{-1}$, respectively). The neutral compound **1** also showed significant activity for P388 (1.80 $\mu g mL^{-1}$), HL-60 lymphoma (2.41 $\mu g mL^{-1}$), $Tmolt_3$ (2.41 $\mu g mL^{-1}$), HeLaS^3 (1.50 $\mu g mL^{-1}$), and A431 skin cells (2.73 $\mu g mL^{-1}$). It is significant that the complexes had different activity than the corresponding $[(\eta^5\text{-}C_5H_5)_2Fe]^+[X]^-$ ($X^- = AsF_6^-$ or SbF_6^-) salts or ferrocene.[9]

Complexes $1^+ \cdot SbF_6^-$ and $1^+ \cdot AsF_6^-$ were examined for their effects on DNA, RNA, and protein synthesis in L-1210 cells. Use of $1^+ \cdot SbF_6^-$ (100 μM, 1 h) resulted in reductions of 92% for ^{3}H-thymidine incorporation into DNA, 59% for ^{3}H-uridine incorporation into RNA, and 32% for ^{3}H-leucine incorporation into the protein. Use of $1^+ \cdot AsF_6^-$ (100 μM, 1 h) caused 22% reduction in RNA synthesis, but no reduction in DNA and protein synthesis.[9]

Most significantly, the complexes inhibited L-1210 DNA topoisomerase activity. Salt $1^+ \cdot SbF_6^-$ afforded an IC_{50} value of 68.7 μM, and $1^+ \cdot AsF_6^-$ a value of 78.17 μM with inhibition of DNA synthesis. These values are in the range provided by the standard VP-16 (22.5 μM), but the complexes exhibited a different mode of action, since L-1210 DNA protein linked breaks were not produced by the metal compounds themselves at 100 μM. Yet, when incubated with VP-16 at 40 μM there was a 25% increase in breaks over those observed for VP-16 alone. The metal complexes inhibited topoisomerase II phosphorylation by protein kinase C from 59 to 64% at 30 min. The suppression of topoisomerase II phosphorylation is positively linked with increased DNA fragmentation and apoptosis. These metal salts thus offer a different mode of action for regulating topoisomerase II activity.

The initial bioactivity results strongly suggest that the tricarbadecaboranyl analogues of other more potent metallocene antitumor agents, such as the early transition metal compounds $[(\eta^5\text{-}C_5H_5)_2MX_2]$,[2] *should exhibit significant and selective anticancer activities. The syntheses and bioactivities of corresponding metallatricarbaboranes, including* $[(RC_3B_7H_9)_2MX_2]$ *and* $[(\eta^5\text{-}C_5H_5)(RC_3B_7H_9)MX_2]$ *are currently being investigated.*

Experimental Section

$1^+ \cdot AsF_6^-$ and $1^+ \cdot SbF_6^-$: Under a nitrogen atmosphere, of $AgAsF_6$ (0.122 g, 0.41 mmol) or $AgSbF_6$ (0.221 g, 0.61 mmol) suspended in dry Et_2O (10 mL) was added dropwise to solutions of **1** (0.016 g, 0.06 mmol and 0.024 g, 0.09 mmol, respectively) in Et_2O (10 mL). The precipitates were isolated by filtration, and washed with Et_2O and CH_2Cl_2. Recrystallization from CH_2Cl_2 gave air-stable, purple-pink crystals of $1^+ \cdot AsF_6^-$ (0.026 g, 0.06 mmol) and $1^+ \cdot SbF_6^-$ (0.043 g, 0.09 mmol) in quantitative yields. $1^+ \cdot AsF_6^-$: elemental analysis: calcd: C 24.26, H 3.84; found: C 23.98, H 3.50; IR (KBr, cm^{-1}): $\tilde{\nu}$ = 3122s, 2579s, 2554s, 1450m, 1428s, 1391m, 1273m, 1196w, 1164w, 1122m, 1105m, 1096m, 1061w, 1015w, 967m, 954w, 932w, 904w, 875m, 860m, 830m, 706vs; UV/Vis (CH_2Cl_2): λ_{max} [nm] (ε [$M^{-1}cm^{-1}$]) = 538 (1060), 360 (2894), 242 (25265). $1^+ \cdot SbF_6^-$: elemental analysis: calcd: C 21.95, H 3.48; found: C 21.89, H 3.35; IR (KBr, cm^{-1}): $\tilde{\nu}$ = 3120s, 3036m, 2579vs, 1452m, 1429s, 1390m, 1272m, 1164w, 1123m, 1094m, 1059m, 1021m, 952m, 874s, 860m, 827m, 789w, 752w, 723m, 677s, 650vs, 521w; UV/Vis (CH_2Cl_2): λ_{max} [nm] (ε [$M^{-1}cm^{-1}$]) = 538 (356), 358 (1450), 244 (11535).

Cytotoxicity assay: The four salts ($1^+ \cdot AsF_6^-$, $1^+ \cdot SbF_6^-$, $[Cp_2Fe]^+AsF_6^-$, $[Cp_2Fe]^+Sb_6^-$), controls, standards, and **1** were tested for cytotoxic activity by homogenizing the drugs (1 mM) in 0.05% Tween 80/H_2O. Solutions were sterilized through an acrodisc filter (0.45 μM). The cell lines were maintained by standard techniques. The National Cancer Institute (NCI) protocol was used to assess the cytotoxicity [10]. Values for cytotoxicity are expressed as ED_{50} in $\mu g mL^{-1}$, that is, the concentration of the compound inhibiting 50% of the cell growth after 3 d. Growth of solid tumor cell lines was determined with crystal violet/methanol and assessed at 580 nm in a plate reader [11].

Incorporation studies: ^{3}H-labeled precursors (2 μCi) were incorporated into 10^6 L-1210 lymphoid leukemia cells over 60 min. The reaction was stopped with cold acids and filtered [12]. Incorporation into DNA, RNA, or protein was expressed in dpm per 10^6 cells. Drugs were incubated at concentrations of 25, 50 and 100 μM.

Topoisomerase inhibition studies: P4 phage knotted DNA was isolated by the method of Liu et al [13]. L-1210 topoisomerase II was isolated and the enzyme activity determined according to Miller et al. [14]. The drugs were measured at concentrations of 0–100 μM over 1 h with VP-16 as a standard. IC_{50} values (50% inhibition of protein content) were determined by densitometry.

Received: January 23, 1997
Supplemented version: April 22, 1997 [Z 10029 IE]
German version: *Angew. Chem.* **1997**, *109*, 2300–2302

Keywords: antitumor agents · boron · iron · metallocenes · topoisomerase

[1] S. E. Sherman, S. J. Lippard, *Chem. Rev.* **1987**, *87*, 1153–1181, and references therein.

[2] a) K. E. Dombrowski, W. Baldwin, J. E. Sheats, *J. Organomet. Chem.* **1986**, *302*, 281–306; b) P. Köpf-Maier, H. Köpf, *Structure Bonding* **1988**, *70*, 103–185.

[3] a) C. A. Plumb, P. J. Carroll, L. G. Sneddon, *Organometallics* **1992**, *11*, 1665–1671; b) *ibid.* **1992**, *11*, 1672–1680.

[4] a) P. Köpf-Maier, H. Köpf, E. W. Neuse, *Angew. Chem.* **1984**, *96*, 446–447; *Angew. Chem. Int. Ed. Engl.* **1984**, *23*, 456–457; b) E. W. Neuse, B. S. Mojapelo, J. Ensling, *Transition Met. Chem.* **1985**, *10*, 135–141; c) N. Motohashi, R. Meyer, S. R. Gollapudi, K. R. Bhattiprolu, *J. Organomet. Chem.* **1990**, *398*, 205–217; d) C.-W. Ong, J.-Y. Jeng, S.-S. Juang, C.-F. Chen, *Bioorg. Med. Chem. Let.* **1992**, *2*, 929–932; e) L. V. Popova, V. N. Babin, Y. A. Belousov, Y. S. Nekrasov, A. E. Snegireva, N. P. Borodina, G. M. Shaposhnikova, O. B. Bychenko, P. M. Raevskii, N. B. Morozova, A. I. Iiyina, K. G. Shitkov, *Appl. Organomet. Chem.* **1993**, *7*, 85–94; f) V. J. Fiorina, R. J. Dubois, S. Brynes, *J. Med. Chem.* **1978**, *21*, 393–395.

[5] A. Houlton, R. M. G. Roberts, J. Silver, *J. Organomet. Chem.* **1991**, *418*, 107–112.

[6] Structural data for $1^+ \cdot AsF_6^-$: M_r = 445.66, 0.40 × 0.12 × 0.03 mm; monoclinic, $P2_1/n$, a = 8.4551(4), b = 27.945(2), c = 7.0102(3) Å, β = 92.405(5)°, V = 1654.9(1) Å^3, Z = 4, ρ_{calcd} = 1.789 g cm^{-3}, $\mu(Mo_{K\alpha})$ = 29.44 cm^{-1}, $2\theta_{max}$ = 49.7°, T = 295 K; of 11105 refection measured 2836 were independent ($1868 > 3.0\sigma$); 254 parameters, residual electron density +0.77/−0.77. X-ray intensity data were collected on an MSC/RAXIS IIc area detector employing

 © WILEY-VCH Verlag GmbH, D-69451 Weinheim, 1997 0570-0833/97/3620-2229 $ 17.50+.50/0

graphite-monochromated $Mo_{K\alpha}$ radiation ($\lambda = 0.7107$ Å). The structure was solved by direct methods (SIR92). The full-matrix least-squares refinement (teXsan package, Molecular Structure Corp.) was based on F to minimize the quantity $\sum w(|F_o| - |F_c|)^2$ with $w = 1/\sigma^2(F)$. Non-hydrogen atoms were refined anisotropically; hydrogen atoms were included as constant contributions to the structure factors and were not refined. The refinement converged at $R_1 = 0.0612$ and $R_2 = 0.0650$. Crystallographic data (excluding structure factors) for the structures reported in this paper have been deposited with the Cambridge Crystallographic Data Centre as supplementary publication no. CCDC-100113. Copies of the data can be obtained free of charge on application to The Director, CCDC, 12 Union Road, Cambridge CB21EZ, UK (fax: int. code +(1223)336-033; e-mail: deposit@chemcrys.cam.ac.uk).

[7] Y.-K. Yan, D. M. P. Mingos, T. E. Müller, D. J. Williams, M. Kurmoo, *J. Chem. Soc. Dalton Trans.* **1994**, 1735–1741.

[8] Compounds with ED_{50} values of less than 4 $\mu g\,mL^{-1}$ after 3 d are considered to be significantly active in reducing tumor cell growth.

[9] At anion molar concentrations equivalent to those of $1^+ \cdot AsF_6^-$ and $1^+ \cdot SbF_6^-$, Na^+ and K^+ salts of AsF_6^- and SbF_6^- were inactive as cytotoxic agents in L-1210 cells. They also did not suppress DNA or RNA syntheses over 60 min at 100 mM. See also: I. H. Hall, A. E. Warren, C. C. Lee, M. D. Wasczcak, L. G. Sneddon, *Anticancer Res.* submitted.

[10] R. I. Geran, N. H. Greenberg, M. M. Macdonald, A. M. Schumacher, B. J. Abbott, *Cancer Chemother. Rep. Part 3* **1972**, *3*, 7–24.

[11] A. Leibovitz, J. C. Stinson, W. B. McCombs III, C. E. McCoy, K. C. Mazur, N. D. Mabry, *Cancer Res.* **1976**, *36*, 4562–4569.

[12] L.-L. Liao, S. M. Kupchan, S. B. Horwitz, *Mol. Pharmacol.* **1976**, *12*, 167–176.

[13] L. F. Liu, J. L. Davis, R. Calendar, *Nuclei Acids Res.* **1981**, *9*, 3979–3989.

[14] K. G. Miller, L. F. Liu, P. T. Englund, *J. Biol. Chem.* **1981**, *256*, 9334–9339.

Enhanced α-CH Acidity and Reactivity of Lewis Acid–Base Complexes in the Gas Phase**

Jianhua Ren, Derek B. Workman, and Robert R. Squires*

Lewis acid catalysis provides a powerful means for accelerating many different types organic and organometallic reactions, and recent work with chiral Lewis acids has demonstrated the tremendous potential of this approach for catalytic asymmetric induction.[1] A key component of the general mechanism for Lewis acid catalysis is the coordination of the substrate and the resulting activation of its reactive site(s).[2] This activation may take the form of, inter alia, enhanced electrophilicity of a carbonyl group, increased Brønsted acidity of α-C–H bonds or amplified dienophilicity of an alkenyl moiety in the substrate. We are interested in developing quantitative models for the activation of Lewis acids, and in the use of gas-phase ion chemistry techniques for determining the changes in fundamental physical properties such as acidity, basicity, and bond energy that accompany coordination of a molecule by a Lewis acid. Herein we examine the gas-phase negative-ion chemistry of a series of prototype Lewis acid–base complexes: Me_2SBH_3, Me_3NBH_3, Me_3PBH_3 and Et_3NBH_3. We show that the α-CH acidities in the complexes are up to 20 kcal mol^{-1} higher than in the uncomplexed molecules, and that deprotonation of such α-CH groups produces stable, dipole-stabilized carbanions.[3] Coordination by BH_3 is also shown to switch-on substitution and elimination reactions involving the alkyl groups of the Lewis bases that are either kinetically or thermodynamically inaccessible to the uncomplexed molecules.

The experiments were carried out at room temperature in a flowing afterglow-triple quadrupole apparatus.[4] The gas-phase reaction between OH^- and the head vapors sampled from a 10 M solution of Me_2SBH_3 in Me_2S produces an ion with the formula $C_2H_8BS^-$ [Eq. (1)], in addition to a series of $B_nH_m^-$

$$Me_2SBH_3 + OH^- \rightarrow C_2H_8BS^- + H_2O \quad (1)$$

($n = 1-3$; $m = 4-10$) ions derived from the diborane present in the sample mixture. Likely structures for this ion are either the carbanion **1**, formed by simple deprotonation of Me_2SBH_3, or the alkylborate ion **2**, which could result from rearrangement.

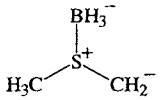

1

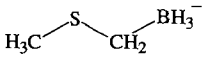

2

Ab initio calculations carried out at the G2(MP2) level of theory[5] predict that **2** is lower in energy than **1** by 28 kcal mol^{-1}, but unimolecular rearrangement of **1** to **2** by a 1,2-borane shift has an energy barrier of 30 kcal mol^{-1}.

We have carried out collision-induced dissociation (CID) and ion–molecule reaction experiments with the product of reaction (1) in order to identify its structure. Authentic isomer **2** was synthesized independently from the reaction between B_2H_6 and $CH_3SCH_2^-$ (formed by deprotonating Me_2S with NH_2^-). Low-energy CID of both $C_2H_8BS^-$ and the authentic $MeSCH_2BH_3^-$ ion under identical conditions in the triple quadrupole analyzer yields two different fragment ion spectra (Figure 1). Three product ions are common to both spectra, but the relative intensities are quite different. For example, loss of methyl radical is the dominant fragmentation for $C_2H_8BS^-$ (Figure 1a), while it

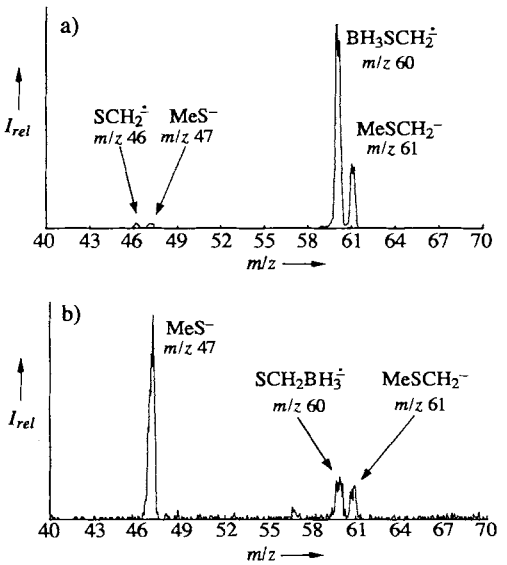

Figure 1. CID spectra of a) $MeS(BH_3)CH_2^-$, the product of reaction (1), and b) $MeSCH_2BH_3^-$, which is produced by reaction of $MeSCH_2^-$ with B_2H_6. The argon target pressure was 7×10^{-5} Torr and the center-of-mass collision energy was 3.5 eV.

[*] Prof. R. R. Squires, J. Ren
Department of Chemistry, Purdue University
West Lafayette, IN 47907 (USA)
Fax : Int. code +(765)494-0239
e-mail: squires@vm.cc.purdue.edu
Dr. D. B. Workman
Delco Electronics, Kokomo, IN 46902 (USA)

[**] This work was supported by the National Science Foundation.

 © WILEY-VCH Verlag GmbH, D-69451 Weinheim, 1997 0570-0833/97/3620-2230 $ 17.50+.50/0

is only a minor channel for ion **2**, which fragments mainly by heterolytic cleavage to give MeS^- (Figure 1b). The qualitative differences between these two CID spectra clearly indicate that the $C_2H_8BS^-$ ion formed in reaction (1) is not the alkylborate isomer **2**.

The most compelling evidence in support of structure **1** comes from the results of H/D exchange experiments.[6] Reaction of $C_2H_8BS^-$ with either D_2O or CH_3OD in the flow tube results in a maximum of five sequential H/D exchanges (Figure 2). This is clearly indicative of the structure **1**, which has five exchangeable hydrogen atoms. In contrast, the authentic $MeSCH_2BH_3^-$ ion does not undergo any H/D exchange because it has no hydrogen-bearing carbanionic sites.

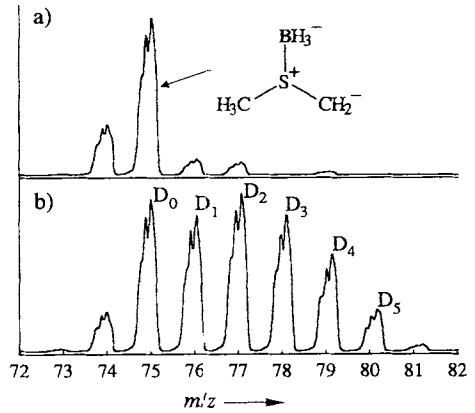

Figure 2. Mass spectra that illustrate the H/D exchange reaction between $MeS(BH_3)CH_2^-$ and D_2O. a) Spectrum without D_2O, b) spectrum after addition of D_2O; D_0, D_1 etc. denote how many H atoms were replaced by D atoms.

Structure **1** is further confirmed by the occurrence of "electrophile switching" reactions of $MeS(BH_3)CH_2^-$ with other Lewis acids such as CO_2, BEt_3, and CS_2 (Scheme 1). For instance, the $MeS(BH_3)CH_2^-$ ion reacts with CO_2 and BEt_3 to

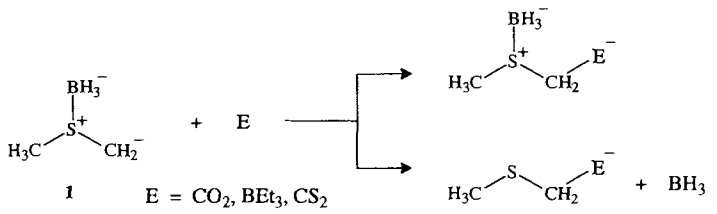

Scheme 1. Reactivity of the product of reaction (1) with electrophiles.

produce adducts and electrophilic substitution products, whereas only substitution occurs with the stronger Lewis acid CS_2. In contrast, isomer **2** is completely unreactive with these reagents. Thus, the CID results and the observed reactivity indicate that deprotonation of Me_2SBH_3 in the gas phase produces a stable carbanion, $MeS(BH_3)CH_2^-$.

The original motivation for this study derives, in part, from our earlier observation[7] that Me_2SBH_3 was readily deprotonated by anionic bases that are too weak to deprotonate uncomplexed Me_2S (ΔH_{acid} = 393.2 kcal mol^{-1}).[8] This means that the α-CH acidity of Me_2S increases upon borane coordination at the sulfur atom. To quantify the extent of the acidity enhancement, we determined the gas-phase acidity of Me_2SBH_3 by the bracketing method.[9] Reactions of Me_2SBH_3 with a series of anionic bases having known basicities,[8] and reactions of $MeS(BH_3)CH_2^-$ with a series of acids having known gas-phase acidities gave consistent behavior with respect to the preferred direction for proton transfer [Eq. (2)].

$$Me_2SBH_3 + A^- \rightleftharpoons MeS(BH_3)CH_2^- + HA \quad (2)$$

The bracketing results indicate $\Delta G_{acid} = 364.3 \pm 2.0$ kcal mol^{-1} for the gas-phase acidity of Me_2SBH_3, which corresponds to $\Delta H_{acid} = 372.5 \pm 2.0$ kcal mol^{-1} at 298 K.[10] The predicted acidity obtained from G2(MP2) calculations, ΔH_{acid} = 373.4 kcal mol^{-1}, is in good agreement with the experimental results.

Thus, Me_2SBH_3 is a stronger acid than uncomplexed Me_2S by 20 kcal mol^{-1}, which corresponds to a difference in acid dissociation equilibrium constants of about 10^{15}. The gas-phase acidity of Me_2SBH_3 is virtually identical to that of the isoelectronic molecule dimethyl sulfoxide (DMSO, ΔH_{acid} = 373.5 kcal mol^{-1}),[8] and the enhancement relative to Me_2S probably originates from the same dipolar effects as with DMSO.[11] G2(MP2) calculations give C–H bond energies for Me_2S and Me_2SBH_3 of 94.5 and 98.7 kcal mol^{-1}, respectively, whereas the electron affinities for the radicals $MeSCH_2^{\bullet}$ and $MeS(BH_3)CH_2^{\bullet}$ are computed to be 13.8 and 38.6 kcal mol^{-1}, respectively. Therefore, most of the acidity enhancement is due to the increase in electron affinity of $MeSCH_2$ that accompanies complexation by BH_3.

Analogous results are obtained for the volatile amine and phosphane complexes, Me_3NBH_3 and Me_3PBH_3, respectively. Both species can be deprotonated by anionic bases to yield product ions that display reactivity consistent with the dipole-stabilized carbanions **3** and **4**, respectively. For example, car-

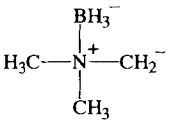

3

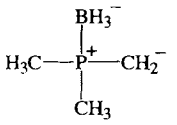

4

banions **3** and **4** both undergo up to eight H/D exchanges upon reaction with added D_2O, and both ions undergo electrophilic addition and/or switching reactions like those shown in Scheme 1. The observation of carbanion **3** is significant since the uncomplexed α-aminocarbanion $Me_2NCH_2^-$ is unknown, and is believed to be thermodynamically unstable with respect to electron detachment.[12] Organolithium reagents analogous to the ion **4** have found use as organic synthons for the asymmetric synthesis of C_2-symmetric *P*-chiral diphosphanes.[13]

Acid–base bracketing measurements give gas-phase acidities (ΔH_{acid}) for Me_3NBH_3 and Me_3PBH_3 of 393 ± 2 and 374 ± 2 kcal mol^{-1}, respectively. Therefore, borane coordination leads to acidity increases of more than 11 kcal mol^{-1} for Me_3N ($\Delta H_{acid}(Me_3N) > 404$ kcal mol^{-1}),[14] and 17 kcal mol^{-1} for Me_3P ($\Delta H_{acid}(Me_3P)$ = 391.1 ± 2.1 kcal mol^{-1}).[15] The acidity enhancements in these complexes are similar to that found for Me_2SBH_3, and their absolute acidities are essentially the same as those calculated (B3LYP/cc-pVTZ) for the isoelectronic amine and phosphane oxides: $\Delta H_{acid}(Me_3NO)$ = 389 kcal mol^{-1} and $\Delta H_{acid}(Me_3PO)$ = 375 kcal mol^{-1}.

Borane coordination at the heteroatom also enhances the reactivity of the pendant alkyl groups. This is shown, for example, by the occurrence of a novel S_N2 reaction between F^- and Me_2SBH_3 [Eq. (3)], and by a Hoffmann-like elimination reaction that occurs when Et_3NBH_3 reacts with OH^- [Eq. (4)].

 © WILEY-VCH Verlag GmbH, D-69451 Weinheim, 1997 0570-0833/97/3620-2231 $ 17.50+.50/0

$$Me_2SBH_3 + F^- \rightarrow MeSBH_3^- + CH_3F \quad (3)$$

$$Et_3NBH_3 + OH^- \rightarrow Et_2NBH_3^- + H_2C{=}CH_2 + H_2O \quad (4)$$

For comparison, F^- is completely unreactive in the gas-phase with uncomplexed Me_2S, and OH^--induced ethylene elimination from uncomplexed Et_3N is actually endothermic by 14 kcal mol^{-1}[8] and does not occur at room temperature. The absence of $Me_2NBH_3^-$ as a product from the reaction between OH^- and Me_3NBH_3 indicates that $Et_2NBH_3^-$ must be formed by elimination rather than substitution. In neither of the above reactions is the proton abstraction product observed.

In conclusion, complexation of methyl sulfides, methylamines, and methylphosphanes with BH_3 causes a dramatic increase in the gas-phase acidity of the α-C–H bonds, amounting to 11–20 kcal mol^{-1}. Deprotonation of borane Lewis base complexes in the gas phase produces stable carbanions that do not rearrange to the more stable "borate" forms. Borane coordination at a heteroatom is also found to enable new reactions of the attached alkyl groups, such as α-substitution and β-elimination.

Received: April 16, 1997 [Z10356IE]
German version: *Angew. Chem.* **1997**, *109*, 2330–2332

Keywords: acidity · carbanions · gas-phase chemistry · ion–molecule reactions · Lewis acids

[1] a) D. A. Evans, D. M. Barnes, *Tetrahedron Lett.* **1997**, *38*, 57; b) Y. Hayashi, J. J. Rohde, E. J. Corey, *J. Am. Chem. Soc.* **1996**, *118*, 5502; c) D. A. Evans, J. A. Murry, M. C. Kozlowski, *ibid.* **1996**, *118*, 5814; d) K. Ishihara, H. Kurihara, H. Yamamoto, *ibid.* **1996**, *118*, 3049; e) E. J. Corey, K. A. Cimprich, *ibid.* **1994**, *116*, 3151.

[2] a) S. V. Kessar, P. Singh, *Chem. Rev.* **1997**, *97*, 721; b) Y. Nishigaichi, A. Takuwa, Y. Naruta, K. Maruyama, *Tetrahedron* **1993**, *49*, 7395; c) L. Deloux, M. Srebnik, *Chem. Rev.* **1993**, *93*, 763; d) H. B. Kagan, O. Riant, *ibid.* **1992**, *92*, 1007; e) H. Yamamoto, K. Maruoka, K. Furuta in *Selectivities in Lewis Acid Promoted Reactions* (Ed.: D. Schinzer), Kluwer, Dordrecht, **1988**, p. 281.

[3] P. Beak, D. B. Reitz, *Chem. Rev.* **1978**, *78*, 275.

[4] a) S. T. Graul, R. R. Squires, *Mass Spectrom. Rev.* **1988**, *7*, 263; b) P. J. Marinelli, J. A. Paulino, L. S. Sunderlin, P. G. Wenthold, J. C. Poutsma, R. R. Squires, *Int. J. Mass Spectrom. Ion Processes* **1994**, *130*, 89.

[5] L. A. Curtiss, K. Raghavachari, J. A. Pople, *J. Chem. Phys.* **1993**, *98*, 1293.

[6] a) J. H. Stewart, R. H. Shapiro, C. H. DePuy, V. M. Bierbaum, *J. Am. Chem. Soc.* **1977**, *99*, 7650; b) C. H. DePuy, V. M. Bierbaum, G. K. King, R. H. Shapiro, *ibid.* **1978**, *100*, 2921.

[7] D. B. Workman, Ph.D Thesis, Purdue University, **1990**.

[8] S. G. Lias, J. E. Bartmess, J. F. Liebman, J. L. Holmes, R. D. Levin, W. G. Mallard, *J. Phys. Chem. Ref. Data* **1988**, *17*, Suppl. 1; updated: J. E. Bartmess, NIST Std. Ref. Database 19B (Negative Ion energetics Database Ber. 3.00), **1993**.

[9] J. E. Bartmess, R. T. McIver, Jr. in *Gas Phase Ion Chemistry, Vol. 2* (Ed.: M. T. Bowers), Academic Press, London, **1979**, p. 87.

[10] $\Delta H_{acid} = \Delta G_{acid} + T\Delta S_{acid}$ For a concise description of the calculation of ΔS_{acid} by statistical mechanics, see: G. E. Davico, V. M. Bierbaum, C. H. DePuy, G. B. Ellison, R. R. Squires, *J. Am. Chem. Soc.* **1995**, *117*, 2590. Note that the first term of Equation A2 in this paper contains a minor typographical error, it should read 5/2R ln(T).

[11] a) P. Speers, K. E. Laidig, A. Streitwieser, *J. Am. Chem. Soc.* **1994**, *116*, 9257; b) K. B. Wiberg, H. Castejon, *ibid.* **1994**, *116*, 10489.

[12] K. M. Downard, J. C. Sheldon, J. H. Bowie, D. E. Lewis, R. N. Hayes, *J. Am. Chem. Soc.* **1989**, *111*, 8112.

[13] A. R. Muci, K. R. Campos, D. A. Evans, *J. Am. Chem. Soc.* **1995**, *117*, 9075.

[14] G. I. Mackay, R. S. Hemsworth, D. K. Bohme, *Can. J. Chem.* **1976**, *54*, 1624.

[15] S Ingemann, N. M. M. Nibbering, *J. Chem. Soc. Perkin Trans. 2*, **1985**, 837. Grabowski, et al. report a value of 384.2 ± 3.2 kcal mol^{-1} based on bracketing experiments (J. J. Grabowski, P. D. Roy, R. Leone, *ibid.* **1988**, 1627). However, B3LYP/cc-PVTZ and CBS-4 calculations using an isodesmic reaction approach predict $\Delta H_{acid}(PMe_3)$ = 390 kcal mol^{-1}, in support of the higher value.

Cyclopropenylidene Adducts of Divalent Germanium, Tin, and Lead**

Herbert Schumann,* Mario Glanz, Frank Girgsdies, F. Ekkehardt Hahn, Matthias Tamm,* and Alexander Grzegorzewski

Dedicated to Professor Wolfgang Beck on the occasion of his 65th birthday

Adducts of nucleophilic carbenes[1] (especially imidazol-2-ylidenes[2]) with main group Lewis acids have been studied intensively in recent years.[3] In the course of our work on ligands containing cycloheptatrienylium[4] and cyclopropenylium[5] rings we became interested in the coordination chemistry of bis(dialkylamino)cyclopropenylidenes, which according to calculations[6, 7] have a stability comparable to imidazol-2-ylidenes. Whereas cyclopropenylidene transition metal complexes[8] have been known for many years,[8] analogous derivatives with main group elements have not yet been described.

The bis(dialkylamino)cyclopropenylidene (**2**) can be obtained from cyclopropenylium salts like **1** by treatment with *n*-butyllithium. At low temperature **2** forms a stable lithium adduct that

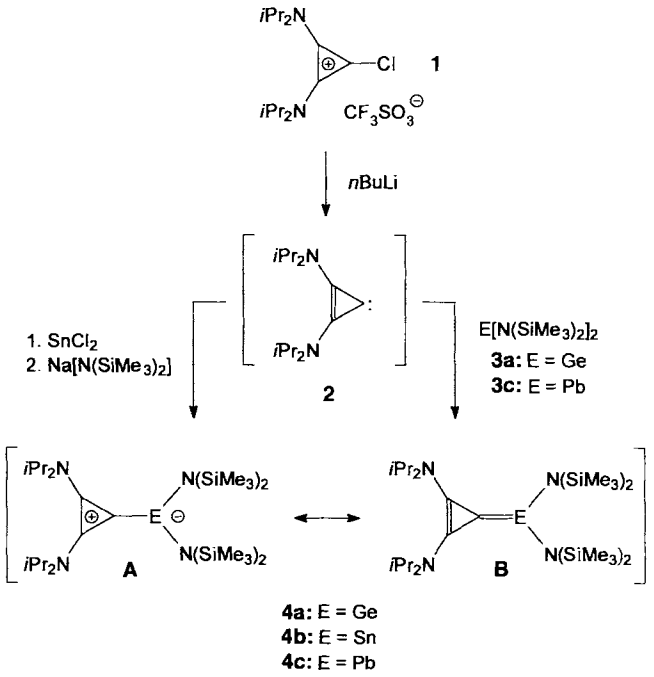

can be used directly for the synthesis of carbene complexes.[5, 7, 8b] Thus, the reaction of **2** with the bisamides **3a** and **3c** affords the cyclopropenylidene complexes **4a** and **4c**, respectively. The analogous tin compound **4b** is synthesized by reaction of **2** with $SnCl_2$ followed by amidation of the intermediate

[*] Prof. Dr. H. Schumann, Dr. M. Glanz, Dipl.-Chem. F. Girgsdies
Institut für Anorganische und Analytische Chemie der Technischen Universität
Strasse des 17. Juni 135, D-10623 Berlin (Germany)
Fax: Int. code +(30)314-22168
e-mail: schumann@mailszrz.zrz.tu-berlin.de
Dr. M. Tamm, Prof. Dr. F. E. Hahn, Dipl.-Chem. A. Grzegorzewski
Institut für Anorganische und Analytische Chemie der Freien Universität
Fabeckstrasse 34–36, D-14195 Berlin (Germany)

[**] This work was supported by the Deutsche Forschungsgemeinschaft and the Fonds der Chemischen Industrie.

carbene adduct. Compounds **4a–c** are isolated as thermally stable yellow crystals, which are soluble in aprotic solvents such as tetrahydrofuran and diethyl ether and in aromatic and aliphatic hydrocarbons. In the crystalline state the monomeric complexes **4** have a trigonal-pyramidal structure (Figure 1, top) with the E atom (E = Ge, Sn, Pb) on top and the two silylamine-N atoms and the carbene-C atom forming the basal plane of the pyramid (Figure 1, bottom). The plane defined by the three-membered carbene ring approximately includes the nitrogen

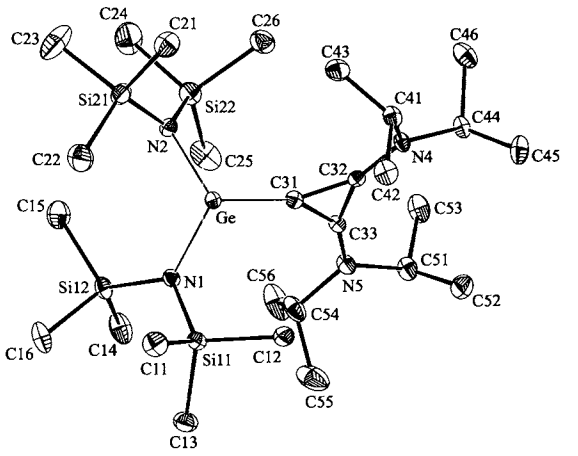

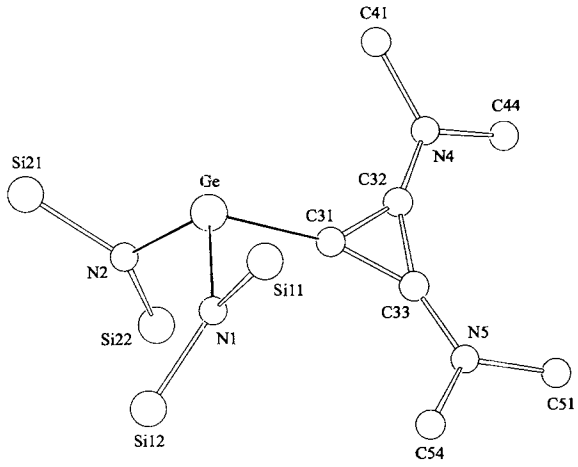

Figure 1. Top: ORTEP drawing [11] of **4a** (thermal ellipsoids at the 30% probability level); compounds **4b** and **4c** have analogous structures. Bottom: Schematic ORTEP drawing [11] of **4a** (all methyl groups have been omitted for clarity). Selected bond lengths [pm] and angles [°] [12]: Ge–C31 208.5(3), Ge–N1 199.1(3), Ge–N2 196.5(3); N1-Ge-C31 98.67(12), N2-Ge-C31 98.65(12), N1-Ge-N2 105.67(11). **4b**: Sn–C31 230.3(9), Sn–N1 221.2(7), Sn–N2 215.7(7); N1-Sn-C31 95.1(3), N2-Sn-C31 94.3(3), N1-Sn-N2 110.5(3). **4c**: Pb–C31 242.3(8), Pb–N1 230.1(7), Pb–N2 230.8(7); N1-Pb-C31 95.0(2), N2-Pb-C31 91.9(2), N1-Pb-N2 110.2(2).

and secondary carbon atoms of the *iso*-propyl groups. The distances between the E atom and the carbene-C atom are appreciably longer than those in "true" germaethenes (180/183 pm)[9] and stannaethenes (202 pm)[10] and fall in the range expected for single bonds. This indicates a bond type best described by the ylidic resonance structure **A**, which corresponds to that in imidazol-2-ylidene adducts,[3a–c] rather than the metallaethene structure **B**.

Comparison of the molecular structures of the adducts **4** with the compound **3**[16] reveals only slight changes in the N-E-N angles upon coordination of the carbene ligand, whereas the E–N distances show the expected lengthening. Resonance stabilization of the carbene ligand is clearly indicated by the equivalence (3σ) of the C–C bonds (137–139 pm). The exocyclic C–N distances (133–134 pm) are significantly shorter than typical C–N single bonds.

The ^{1}H NMR spectra of complexes **4** below $-60\,^\circ$C exhibit four multiplets for the methine protons and four doublets for the methyl protons of the *iso*-propyl groups, which are all magnetically inequivalent due to hindered rotation around the N–C(ring) and E–C bond axes. As the temperature increases the signals broaden, and at room temperature only two very broad resonances are observed for the CH_3 groups. As the exchange processes are concurrent, it is not possible to determine the coalescence temperatures. The ^{13}C NMR signals for the ring carbon atoms in **4a–c** are observed at $\delta \approx 145-150$ and fall in the range typical for cyclopropenylium compounds.[5, 7] In imidazol-2-ylidenes the carbene-C resonance is shifted significantly to higher field upon coordination.[3a–c] Here, an analogous trend is purely speculative, as a free cyclopropenylidene **2** has not yet been isolated and characterized by NMR spectroscopy. Comparison of the ^{119}Sn NMR resonance signals in **3b** ($\delta = 766$)[17] and in **4b** ($\delta = -45$) indicates strong shielding of the tin nucleus by interaction with the carbene ligand.[3b, c] The new compounds presented here illustrate that nucleophilic bis(dialkylamino)cyclopropenylidenes could be interesting alternatives to the intensively studied imidazol-2-ylidenes.

Experimental Section

1 [18], **3a**, and **3c** [19] were prepared according to published procedures. NMR spectra were recorded on Bruker AMX-200 and AMX-400 instruments. Microanalyses were performed on a Perkin-Elmer Series II CHNS/O 2400 analyzer.

4a: A solution of *n*BuLi (3.5 mL of a 1.6 M solution in hexane, 5.6 mmol) was added dropwise to a stirred suspension of **1** (2.35 g, 5.6 mmol) in THF (70 mL) at $-78\,^\circ$C. After the mixture had been stirred for about 15 min, solid **3a** (2.20 g, 5.6 mmol) was added in small portions to the clear solution. The reaction mixture was allowed to warm up to 25 °C and was subsequently stirred for 12 h. After removal of the solvent the residue was suspended in hexane (70 mL) and filtered. The solution was concentrated to about 35 mL, and yellow crystals of **4a** were obtained at $-78\,^\circ$C. Yield 2.15 g (61%). M.p. (0.1 mbar) 125 °C (decomp); ^{1}H NMR (400 MHz, C_6D_6, 25 °C): $\delta = 1.23$ (br. s, 120 Hz, 12H; $CHCH_3$), 0.86 (br. s, 120 Hz, 12H; $CHCH_3$), 0.47 (s, 36H; $SiCH_3$); ^{1}H NMR (400 MHz, C_7D_8, $-73\,^\circ$C): $\delta = 4.95$ (m, 1H; $CHCH_3$), 3.92 (m, 1H; $CHCH_3$), 2.88 (m, 1H; $CHCH_3$), 2.74 (m, 1H; $CHCH_3$), 1.39 (d, ^3J(H,H) = 5.7 Hz, 6H; $CHCH_3$), 1.09 (d, ^3J(H,H) = 5.8 Hz, 6H; $CHCH_3$), 0.77 (d, ^3J(H,H) = 6.1 Hz, 6H; $CHCH_3$), 0.67 (d, ^3J(H,H) = 6.0 Hz, 6H; $CHCH_3$), 0.57 (s, 36H; $SiCH_3$); ^{13}C NMR (100.64 MHz, C_6D_6, 25 °C): $\delta = 145.45$ (CC_2), 144.62 (CC_2), 52.50 (250 Hz; $CHCH_3$), 49.26 (250 Hz; $CHCH_3$), 22.51 (120 Hz; $CHCH_3$), 21.70 (120 Hz; $CHCH_3$), 6.74 ($SiCH_3$); elemental analysis calcd (%) for $C_{27}H_{64}GeN_4Si_4$ (629.76): C 51.50, H 10.24, N 8.90; found: C 51.84, H 10.01, N 8.47.

4b: A solution of *n*BuLi (3.9 mL of a 1.6 M solution in hexane. 6.22 mmol) was added dropwise to a stirred suspension of **1** (2.61 g, 6.2 mmol) in THF (70 mL) at $-78\,^\circ$C. After the mixture had been stirred for about 15 min, solid $SnCl_2$ (1.18 g, 6.2 mmol) was added in small portions to the clear solution. The reaction mixture was allowed to warm up to 25 °C and was subsequently stirred for 12 h. $Na[N(SiMe_3)_2]$ (2.27 g, 12.3 mmol) was added and the mixture was stirred for another 12 h. Compound **4b** was isolated as described for **4a**. Yellow crystals of **4b** are obtained from hexane at $-78\,^\circ$C. Yield 2.30 g (55%). m.p. (0.1 mbar) 137 °C (decomp); ^{1}H NMR (400 MHz, C_6D_6, 25 °C): $\delta = 1.26$ (br. s, 75 Hz, 12H; $CHCH_3$), 0.85 (br. s, 75 Hz, 12H; $CHCH_3$), 0.49 (s, 36H; $SiCH_3$); ^{1}H NMR (400 MHz, C_7D_8, $-61\,^\circ$C): $\delta = 4.87$ (m, 1H; $CHCH_3$), 3.91 (m, 1H; $CHCH_3$), 2.80 (m, 2H; $CHCH_3$), 1.38 (d, ^3J(H,H) = 6.3 Hz, 6H; $CHCH_3$), 1.09 (d, ^3J(H,H) = 6.1 Hz, 6H; $CHCH_3$), 0.78 (d, ^3J(H,H) = 6.8 Hz, 6H; $CHCH_3$), 0.68 (d, ^3J(H,H) = 6.2 Hz, 6H; $CHCH_3$), 0.57 (s, 36H; $SiCH_3$); ^{13}C NMR (50.32 MHz, C_6D_6, 25 °C): $\delta = 150.17$ (CC_2), 146.66 (CC_2), 51.13 (120 Hz; $CHCH_3$), 49.73 (120 Hz; $CHCH_3$), 21.89 (100 Hz; $CHCH_3$), 7.09 ($SiCH_3$); ^{14}N NMR (28.91 MHz, C_6D_6, 25 °C): $\delta = -316.7$, -353.1; ^{29}Si NMR (79.49 MHz, C_6D_6, 25 °C): $\delta = -3.03$; ^{119}Sn NMR (149.21 MHz, C_6D_6, 25 °C): $\delta \approx -44.69$; elemental analysis calcd (%) for $C_{27}H_{64}N_4Si_4Sn$ (675.86): C 47.98, H 9.54, N 8.29; found: C 46.76, H 8.85, N 7.90.

4c: **4c** was prepared from **1** (1.16 g, 2.8 mmol), *n*BuLi (1.8 mL of a 1.6 M solution in hexane, 2.8 mmol) and **3c** (1.45 g, 2.8 mmol) by a procedure similar to that for **4a**. Yield 1.66 g (79%) of yellow crystals. M.p. (0.1 mbar) 135 °C (decomp); ^{1}H NMR (400 MHz, C_6D_6, 25 °C): $\delta = 1.20$ (br. s, 120 Hz, 12H; $CHCH_3$), 0.81 (br.

s, 120 Hz, 12H; $CHCH_3$), 0.47 (s, 36H; $SiCH_3$); ^1H NMR (400 MHz, C_7D_8, $-61\,^\circ C$): $\delta = 4.92$ (m, 1H; $CHCH_3$), 3.95 (m, 1H; $CHCH_3$), 2.84 (m, 1H; $CHCH_3$), 2.78 (m, 1H; $CHCH_3$), 1.32 (br. s, 15 Hz, 6H; $CHCH_3$), 1.16 (br. s, 15 Hz, 6H; $CHCH_3$), 0.84 (br. s, 15 Hz, 6H; $CHCH_3$), 0.75 (br. s, 15 Hz, 6H; $CHCH_3$), 0.60 (s, 36H; $SiCH_3$); ^{13}C NMR (100.64 MHz, C_6D_6, 25 °C): $\delta = 148.53$ (C_3), 50.71 (400 Hz; $CHCH_3$), 21.46 (175 Hz; $CHCH_3$), 6.89 ($SiCH_3$); elemental analysis calcd (%) for $C_{27}H_{64}N_4Si_4Pb$ (764.37): C 42.43, H 8.44, N 7.33; found: C 42.54, H 8.45, N 6.66.

Received: April 4, 1997 [Z 10311 IE]
German version: *Angew. Chem.* **1997**, *109*, 2328–2330

Keywords: carbene complexes · germanium · lead · tin

[1] M. Regitz, *Angew. Chem.* **1996**, *108*, 791–794; *Angew. Chem. Int. Ed. Engl.* **1996**, *35*, 725–728.

[2] H.-W. Wanzlick, H.-J. Schönherr, *Angew. Chem.* **1968**, *80*, 154; *Angew. Chem. Int. Ed. Engl.* **1968**, *7*, 141–142; A. J. Arduengo III, R. L. Harlow, M. Kline, *J. Am. Chem. Soc.* **1991**, *113*, 361–363; A. J. Arduengo III, H. V. R. Diaz, R. L. Harlow, M. Kline, *ibid.* **1992**, *114*, 5530–5534; N. Kuhn, T. Kratz, *Synthesis* **1993**, 561–562; W. A. Herrmann, M. Elison, J. Fischer, C. Köcher, G. R. J. Artus, *Chem. Eur. J.* **1996**, *2*, 772–780.

[3] a) A. J. Arduengo III, H. V. R. Diaz, J. C. Calabrese, F. Davidson, *Inorg. Chem.* **1993**, *32*, 1541–1542; b) N. Kuhn, T. Kratz, D. Bläser, R. Boese, *Chem. Ber.* **1995**, *128*, 245–250; c) A. Schäfer, M. Weidenbruch, W. Saak, S. Pohl, *J. Chem. Soc. Chem. Commun.* **1995**, 1157–1158; d) A. J. Arduengo III, H. V. R. Diaz, J. C. Calabrese, F. Davidson, *J. Am. Chem. Soc.* **1992**, *114*, 9724–9725; e) N. Kuhn, G. Henkel, T. Kratz, J. Kreutzberg, R. Boese, A. H. Maulitz, *Chem. Ber.* **1993**, *126*, 2041–2045; f) X.-W. Li, J. Su, G. H. Robinson, *Chem. Commun.* **1996**, 2683–2684.

[4] M. Tamm, A. Grzegorzewski, I. Brüdgam, *J. Organomet. Chem.* **1996**, *519*, 217–220; M. Tamm, A. Grzegorzewski, T. Steiner, W. Werncke, T. Jentzsch, *Organometallics* **1996**, *15*, 4984–4990; M. Tamm, W. Werncke, T. Jentzsch, *ibid.* **1997**, *16*, 1418–1424.

[5] M. Tamm, A. Grzegorzewski, F. E. Hahn, *J. Organomet. Chem.* **1995**, *501*, 309–313.

[6] M. Driess, H. Grützmacher, *Angew. Chem.* **1996**, *108*, 900–929; *Angew. Chem. Int. Ed. Engl.* **1996**, *35*, 828–856, and references therein.

[7] Z. Yoshida, *Pure Appl. Chem.* **1982**, *54*, 1059–1074.

[8] a) K. Öfele, *Angew. Chem.* **1968**, *80*, 1032–1033; *Angew. Chem. Int. Ed. Engl.* **1968**, *7*, 950–951; b) R. Gompper, E. Bartmann, *ibid.* **1978**, *90*, 490–491 and **1978**, *17*, 456–457; c) R. Weiss, C. Priesner, *ibid.* **1978**, *90*, 491–492 and **1978**, *17*, 457–458; d) R. D. Wilson, Y. Kamitori, H. Ogoshi, Z. Yoshida, J. A. Ibers, *J. Organomet. Chem.* **1979**, *173*, 199–209; e) U. Kirchgässner, H. Piana, U. Schubert, *J. Am. Chem. Soc.* **1991**, *113*, 2228–2232; f) J. Schubert, S. Mock, U. Schubert, *Chem. Ber.* **1993**, *126*, 657–664; g) M. S. Morton, J. P. Selegue, A. Carillo, *Organometallics* **1996**, *15*, 4664–4666.

[9] a) H. Meyer, G. Baum, W. Massa, A. Berndt, *Angew. Chem.* **1987**, *99*, 790–791; *Angew. Chem. Int. Ed. Engl.* **1987**, *26*, 798–799; b) M. Lazraq, J. Escudié, C. Couret, J. Satgé, M. Dräger, R. Dammel, *ibid.* **1988**, *100*, 885–887 and **1988**, *27*, 828–830.

[10] H. Meyer, G. Baum, W. Massa, S. Berger, A. Berndt, *Angew. Chem.* **1987**, *99*, 559–560; *Angew. Chem. Int. Ed. Engl.* **1987**, *26*, 546–547.

[11] L. Zsolnai, H. Prizkow, ORTEP—Program for Personal Computer, Universität Heidelberg, **1994**.

[12] General X-ray structure data: Enraf-Nonius CAD 4 diffractometer, $Mo_{K\alpha}$ radiation ($\lambda = 71.069$ pm), graphite-monochromator, $T = 163(2)$ K, correction for Lorentz and polarization effects, structure solution with direct methods (SHELXS 86 [13]), refinement against F^2 (SHELXL 93 [14]) with anisotropic thermal parameters for all non-hydrogen atoms, hydrogen positions with fixed isotropical thermal parameters ($U_{iso} = 0.08 \times 10^4$ pm^2) on calculated positions, $R_1 = \sum||F_o| - |F_c||/\sum|F_o|$, $wR_2 = [\sum w(F_o^2 - F_c^2)^2/\sum w(F_o^2)^2]^{1/2}$. Crystallographic data (excluding structure factors) for the structures reported in this paper have been deposited as supplementary publication no. CCDC-100297 with the Cambridge Crystallographic Data Centre. Copies of the data can be obtained free of charge on application to the following address: The Director, CCDC, 12 Union Road, Cambridge CB2 1EZ (fax: int. code +(1223)336-033, e-mail: deposit@chemchrys.cam.ac.uk). **4a**: crystal dimensions $0.48 \times 0.36 \times 0.24$ mm, monoclinic, $P2_1/c$, $a = 1629.8(4)$, $b = 1283.6(5)$, $c = 1796.2(8)$ pm, $\beta = 101.70(3)^\circ$, $V = 3680(3) \times 10^6$ pm^3, $Z = 4$, $\rho_{calcd} = 1.137 \times 10^3$ kg m^{-3}, $\mu = 0.984$ mm^{-1}, $F(000) = 1368$, $2.56^\circ \le 2\theta \le 54.92^\circ$, $0 \le h \le 15$, $0 \le k \le 16$, $-23 \le l \le 23$, 5500 data collected, 5207 unique data, ($R_{int} = 0.0316$), 5197 data with $I > 2\sigma(I)$, 345 refined parameters, GOF (F^2) = 1.053, $R_1 = 0.0360$, $wR_2 = 0.0874$, max./min. residual electron density $0.497/-0.313 \times 10^{-6}$ e pm^{-3}. **4b**: crystal dimensions $0.45 \times 0.36 \times 0.24$ mm, monoclinic, Cc, $a = 1140.6(2)$, $b = 1948.3(8)$, $c = 1802.5(6)$ pm, $\beta = 104.08(2)^\circ$, $V = 3885(2) \times 10^6$ pm^3, $Z = 4$, $\rho_{calcd} = 1.156 \times 10^3$ kg m^{-3}, $\mu = 0.801$ mm^{-1}, $F(000) = 1440$, $4.18^\circ \le 2\theta \le 54.88^\circ$, $0 \le h \le 14$, $0 \le k \le 25$, $-23 \le l \le 22$, 4661 data collected, 4659 unique data ($R_{int} = 0.0142$), 4651 data with $I > 2\sigma(I)$, 345 refined parameters, GOF(F^2) = 1.061, $R_1 = 0.0529$, $wR_2 = 0.1238$, max./min. residual electron density $1.349/-2.409 \times 10^{-6}$ e pm^{-3}; **4c**: crystal dimensions $0.48 \times 0.24 \times 0.18$ mm, monoclinic, $P2_1/n$, $a = 1239.8(3)$, $b = 1873.4(4)$, $c = 1693.4(5)$ pm, $\beta = 103.54(2)^\circ$, $V = 3824(2) \times 10^6$ pm^3, $Z = 4$, $\rho_{calcd} = 1.328 \times 10^3$ kg m^{-3}, $\mu = 4.558$ mm^{-1}, $F(000) = 1568$, $4.02^\circ \le 2\theta \le 54.90^\circ$, $0 \le h \le 16$, $0 \le k \le 18$, $-16 \le l \le 16$, 7590 data collected, 7298 unique data ($R_{int} = 0.0763$), 5476 data with $I > 2\sigma(I)$, empirical absorption correction DIFABS [15] (min. 0.786, max. 1.423 ∅ 1.011), 345 refined parameters, GOF (F^2) = 1.170, $R_1 = 0.0436$, $wR_2 = 0.1097$, max./min. residual electron density $3.420/-2.672 \times 10^{-6}$ e pm^{-3}.

[13] G. M. Sheldrick, SHELX-86, Program for Crystal Structure Solution, Universität Göttingen, **1986**.

[14] G. M. Sheldrick, SHELX-93, Program for Crystal Structure Determination, Universität Göttingen, **1993**.

[15] N. Walker, D. Stuart, *Acta Crystallogr. Sect. A* **1983**, *39*, 158–166.

[16] T. Fjeldberg, H. Hope, M. F. Lappert, P. P. Power, A. J. Thorne, *J. Chem. Soc. Chem. Commun.* **1983**, 639–641; R. W. Chorley, P. B. Hitchcock, M. F. Lappert, W.-P. Leung, P. P. Power, M. M. Olmstead, *Inorg. Chim. Acta* **1992**, *198–200*, 203–209.

[17] H. Braunschweig, R. W. Chorley, P. B. Hitchcock, M. F. Lappert, *J. Chem. Soc. Chem. Commun.* **1992**, 1311–1312.

[18] Z. Yoshida, Y. Tawara, *J. Am. Chem. Soc.* **1971**, *93*, 2573–2574.

[19] M. J. S. Gynane, D. H. Harris, M. F. Lappert, P. P. Power, P. Rivière, M. Rivière-Baudet, *J. Chem. Soc. Dalton Trans.* **1977**, 2004–2009.

On the Mechanism of the McMurry Reaction**

Martin Stahl, Ulrich Pidun, and Gernot Frenking*

The use of low-valent titanium reagents for the reductive coupling of carbonyl compounds is an important synthetic technique in organic chemistry. Although an impressively broad range of alkenes is accessible by this method, for a long time only a few mechanistic details were known and only in the last few years have experiments shed new light on the mechanism. The current status of research in this field has recently been described in a review article.[1]

Typically the reaction is conducted with $TiCl_3$ as the source of titanium and a reducing agent such as $LiAlH_4$, Zn/Cu, or Mg. It was long believed that highly dispersed Ti^0 particles are initially formed and that the carbonyl coupling proceeds heterogeneously on their surface via ketyl radical intermediates.[2–4] New experiments by Fürstner et al. and Bogdanović et al., however, indicate that when the coupling is performed with Zn/Cu in dimethoxyethane (DME), a different reaction path is followed.[5, 6] They propose a nucleophilic rather than a radical mechanism, as depicted in Scheme 1.[1]

Because the postulated intermediates **1**–**4** have not been characterized experimentally and the energetics of the reaction course suggested by Fürstner and Bogdanović are not known, we have carried out quantum mechanical calculations of the proposed reaction profile by means of density functional theory (DFT)[7] using formaldehyde as a model carbonyl compound. All intermediates and transition states have been located on the singlet potential energy surface and confirmed by frequency calculations. The transition states have been further characterized by calculating the intrinsic reaction coordinates (IRC).[16]

[*] Prof. Dr. G. Frenking, Dr. M. Stahl, Dr. U. Pidun
Fachbereich Chemie der Universität
Hans-Meerwein-Strasse, D-35032 Marburg (Germany)
Fax: Int. code +(6421)282189
e-mail: frenking@ps1515.chemie.uni-marburg.de

[**] Theoretical Studies of Organometallic Compounds, Part XXVII. This work was supported by the Deutsche Forschungsgemeinschaft (SFB 260, Graduiertenkolleg Metallorganische Chemie) and the Fonds der Chemischen Industrie. Part XXVI: R. K. Szilagyi, G. Frenking, *Organometallics*, **1997**, in press.

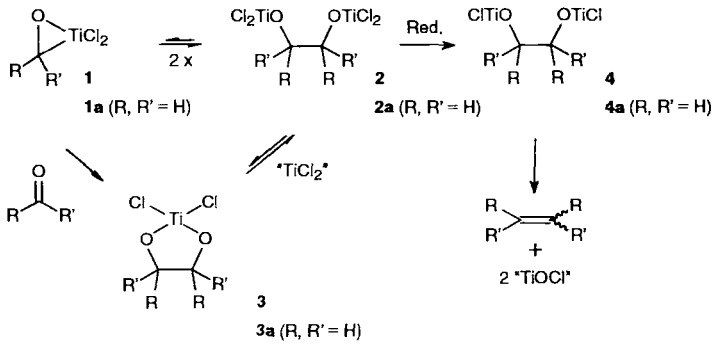

Scheme 1. Nucleophilic reaction mechanism for the McMurry reaction proposed by Fürstner and Bogdanović [1].

Three key experimental observations led to the formulation of the Ti^{II} complex **1** as the starting point for the proposed nucleophilic mechanism: a) Pure $TiCl_3$ in DME is not reduced by Zn/Cu. b) Reduction takes place only after addition of the carbonyl compound. A complex between $TiCl_3$ and the carbonyl compound has been observed by IR spectroscopy, and it has been shown that only one reduction equivalent is consumed per equivalent of titanium.[6] c) The resulting complex **1** has been formulated as a side-on coordinated carbonyl complex, since at low temperatures reaction mixtures can be quenched with D_2O to yield the corresponding secondary alcohol deuterated in the α-position.[6] Side-on coordinated formaldehyde complexes of early transition metals are known[17] and have frequently been observed to undergo C–C coupling reactions.[17, 18] In our calculations the only minimum found for the complex of CH_2O with $TiCl_2$ is indeed the side-on coordinated structure **1a** (Figure 1), which has pseudotetrahedral coordination at titanium. The C–O bond length of 1.399 Å is considerably closer to the length of a typical C–O single bond (1.43 Å[19]) than to the length of the C–O bond in free formaldehyde (1.21 Å[20]). The term titanaoxacyclopropane is thus justified and the formal oxidation state IV can be assigned to the titanium atom.

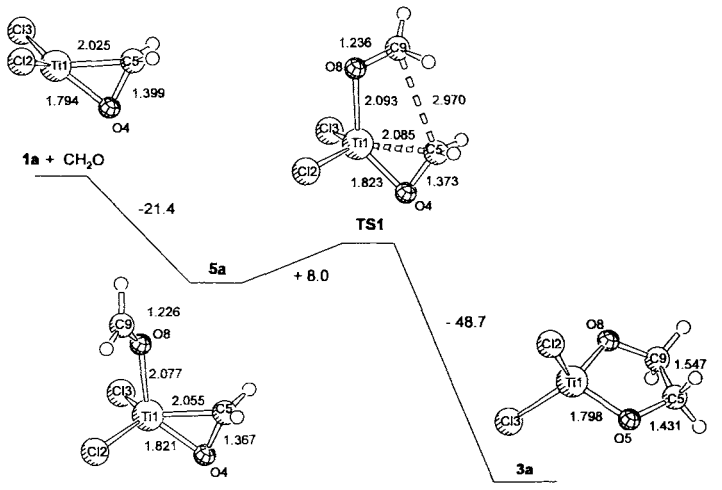

Figure 1. Energy profile and structures of stationary points in the pathway for intramolecular C–C coupling; bond lengths [Å] and reaction energies [kcal mol^{-1}] corrected for zero-point vibrational energies at the B3LYP/II level.

At room temperature the reaction can be quenched with water to yield the pinacol.[6] This has been rationalized by the formation of the pinacolate complex **2**, in which the Ti centers must have the formal oxidation state III, since only one reduction equivalent per equivalent of titanium is consumed up to this stage. A reversible disproportionation reaction to give a Ti^{IV} pinacolate complex **3** and a Ti^{II} compound of low solubility is observed.[6] While Fürstner and Bogdanović consider the pathway **1** → **2** to be the C–C bond forming process, we have found that the reaction **1** → **3** is energetically accessible as well. Figure 1 shows the structures and the energy profile for the reaction **1a** + CH_2O → **3a**. The complex **1a** acts as a Lewis acid towards another molecule of formaldehyde to yield structure **5a**. This complex is the only energy minimum in which two CH_2O molecules are coordinated to a $TiCl_2$ fragment. Structures with two side-on or two end-on coordinated molecules of formaldehyde could not be located. The formation of the adduct **5a** is exothermic by 21.4 kcal mol^{-1}. A series of linear synchronous transit (LST) optimizations showed that the addition of formaldehyde to **1a** takes place without an activation barrier. The end-on coordinated formaldehyde can rotate with a barrier of only 2.9 kcal mol^{-1} about the Ti–O bond, describing a semicircle above the $TiCl_2$ moiety. The transition state structure of this rotation (not shown in Figure 1) is C_s-symmetric with an antiperiplanar arrangement of the two carbon atoms. At the same time rotation of the end-on coordinated formaldehyde about the O–Ti axis towards the other carbon atom, combined with rotation around the C–O bond, leads to the transition state **TS1** for the formation of the pinacolate complex **3a**. This step has an activation barrier of only 8.0 kcal mol^{-1}. The long C–C bond (2.97 Å) in **TS1** and the only slight elongation of the Ti1–C5 and O8–C9 distances indicate an early transition state, which is in agreement with the Hammond postulate. Reaction **5a** → **3a** is exothermic by 40.7 kcal mol^{-1}. The product pinacolate complex **3a** has a nonplanar five-membered ring with an O-C-C-O dihedral angle of 31.1° and a C–C distance of 1.547 Å, typical of a C–C single bond.[19]

The results of the calculations for the intermolecular C–C coupling by means of the dimerization reaction 2 × **1a** → **2a** (Scheme 1) are shown in Figure 2. The highly unsymmetric transition state **TS2** was located for the C–C coupling step leading to the dimetalated pinacolate **2a**. One of the two titanaoxacyclopropanes **1a** almost retains its ground state geometry, while the other has a widened Ti-O-C bond angle to allow for the bond formation between the two carbon atoms. At the same time the coordinative unsaturation of the titanium atom is compensated by one of the chlorine ligands (Cl3) of the first reaction partner, which now forms a bridge between the two titanium atoms. The C–C distance of 2.171 Å and the significant pyramidalization at C10 show that this is a rather late transition state compared to **TS1**. IRC calculations prove that complex **6a** must be formed before the dimerization can occur. Intermediate **6a** is 15.9 kcal mol^{-1} more stable than two molecules of **1a**. The activation barrier for the C–C coupling step **6a** → **2a** is 27.1 kcal mol^{-1}, which means that the overall reaction has an activation barrier of 11.2 kcal mol^{-1}. The pinacolate complex **2a** is 24.0 kcal mol^{-1} lower in energy than **6a**. The most striking feature of the pinacolate **2a** is the long Ti–Ti distance of 2.813 Å. The weak Ti–Ti bond[21] leads to a closed-shell electron configuration for **2a**, while the postulated intermediate **2** (Scheme 1) was originally formulated without a Ti–Ti bond.[6] Despite careful searching, no other energy minimum structure of **2** was found. In particular, we could not locate a diradical structure on the potential energy surface.[22] This is in agreement with the fact that in ESR studies of the reaction course signals for paramagnetic species could not be observed.[23]

 © WILEY-VCH Verlag GmbH, D-69451 Weinheim, 1997 0570-0833/97/3620-2235 $ 17.50+.50/0

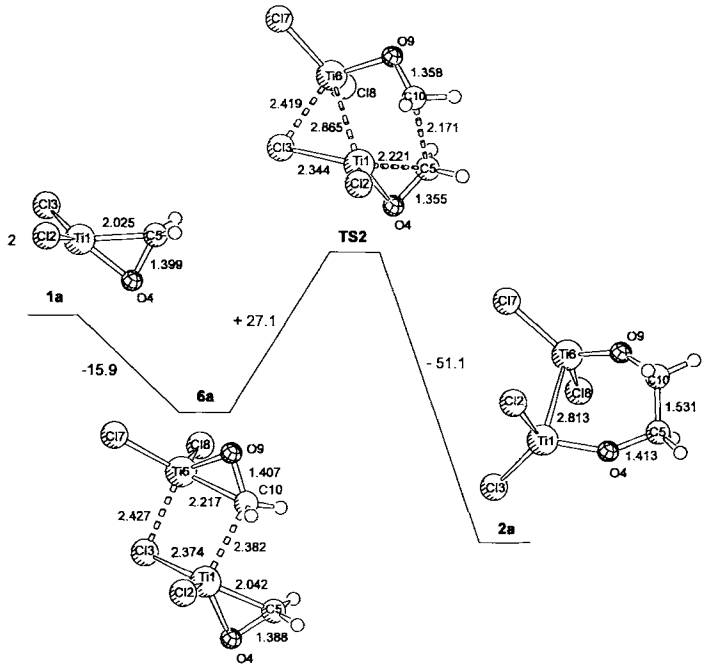

Figure 2. Energy profile and structures of stationary points in the pathway for intermolecular C–C coupling; bond lengths [Å] and reaction energies [kcal mol^{-1}] corrected for zero-point vibrational energies at the B3LYP/II level.

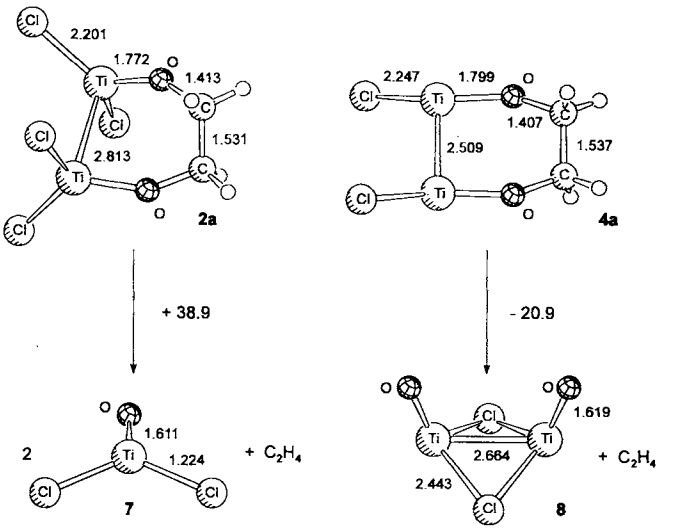

Figure 3. Comparison of the ethylene elimination reactions of the pinacolate complexes **2a** and **4a**; bond lengths [Å] and reaction energies [kcal mol^{-1}] corrected for zero-point vibrational energies at the B3LYP/II level.

The theoretical reaction profiles for the intramolecular (Figure 1) and intermolecular (Figure 2) closed-shell C–C coupling reactions indicate that both pathways should be possible. The calculated energies favor the intramolecular mechanism. It may depend on the reaction conditions whether there is a sufficient proportion of uncomplexed carbonyl compound available which can then react easily via **5a** to **3a**. The energetics of the reaction will also be influenced by solvent molecules stabilizing the ground and transition state structures to different extents.

The final reaction step of the proposed mechanism is the reduction of the pinacolate complex to the alkene. A very recent experimental study of a related C–C coupling reaction with UCl_4 and Li/Hg as the reducing agent showed that the alkene is formed directly from the mononuclear pinacolate complex of UCl_4 corresponding to **3** (Scheme 1).[24] However, experimental evidence proved unequivocally that in the case of titanium the direct formation of the alkene from **3** can be excluded.[25] Therefore, the dinuclear complex **2** must be an intermediate in the alkene-forming process. Furthermore, it is known that when Zn/Cu is used as a reducing agent, the formation of the alkene takes place only if a further reduction equivalent is consumed per equivalent of titanium and that the titanium finally precipitates as $TiClO(ZnCl_2)_{0.93}$.[6] It was suggested that further reduction, **2** → **4** (Scheme 1), takes place prior to dissocation of the alkene.[6] To test this hypothesis we calculated the energetics of the elimination of ethylene from the Ti^{III} compound **2a** and from the Ti^{II} species **4a** (Figure 3). Compound **4a** has a significantly shorter Ti–Ti bond (2.509 Å) than **2a**, indicative of a Ti–Ti double bond. The calculations predict that the reaction **2a** → ethylene + $2TiOCl_2$ (**7**) is strongly endothermic by 38.9 kcal mol^{-1}, while the reaction **4a** → ethylene + $Ti_2O_2Cl_2$ (**8**) is exothermic by 20.9 kcal mol^{-1}. No energy minimum structure corresponding to a $TiOCl_2$ dimer could be located. Even though the calculated energies are not exact reaction energies, because they may be significantly influenced by solvent effects and the solubility of the inorganic products, the calculations indicate that formation of ethylene from a Ti^{II} pinacolate is energetically clearly favored over the Ti^{III} pinacolate pathway.

Although our results do not rule out that the McMurry reaction may follows a radical pathway under different reaction conditions, the calculations presented here support the interpretation of the experimental results of Fürstner and Bogdanović[1, 5, 6] in terms of a nucleophilic mechanism. The calculations show that a closed-shell nucleophilic pathway for the C–C coupling step is a reasonable mechanistic hypothesis. In particular, intermediates **1**–**4** which have hitherto been postulated only, were characterized as energy minima **1a**–**4a** on the potential energy surface, and the energy profile of the postulated reaction course was found to be favorable.

Received: February 14, 1997
Revised version: April 24, 1997 [Z10125IE]
German version: *Angew. Chem.* **1997**, *109*, 2308–2311

Keywords: ab initio calculations · carbonyl compounds · C–C coupling · reaction mechanisms · titanium

[1] A. Fürstner, B. Bogdanović, *Angew. Chem.* **1996**, *108*, 2582; *Angew. Chem., Int. Ed. Engl.* **1996**, *35*, 2442.
[2] J. E. McMurry, *Chem. Rev.* **1989**, *89*, 1513.
[3] R. Dams, M. Malinowski, I. Westdorp, H. Y. Geise, *J. Org. Chem.* **1982**, *47*, 248.
[4] N. Balu, S. K. Nayak, A. Banerji, *J. Am. Chem. Soc.* **1996**, *118*, 5932.
[5] a) A. Fürstner, D. N. Jumbam, *Tetrahedron* **1992**, *48*, 5991; b) A. Fürstner, A. Hupperts, A. Ptock, E. Janssen, *J. Org. Chem.* **1994**, *59*, 5215.
[6] B. Bogdanović, A. Bolte, *J. Organomet. Chem.* **1995**, *502*, 109.
[7] All calculations were performed with the program package Gaussian 94[8]. The geometries were optimized at the DFT[9] level by means of the Becke three parameter hybrid method (B3LYP)[10]. The accuracy of the B3LYP method is well known[11]. Calculations at the MP2 level of theory gave similar geometries and relative energies as the B3LYP calculations. For titanium, we used a (small core) nonrelativistic effective core potential (ECP) with a (441/2111/41) basis set for the twelve valence and outer-core electrons[12]. For chlorine, we also used an ECP in combination with a (31/31/1) basis set for the seven valence electrons[13]. For carbon, oxygen, and hydrogen a 6-31G(d) basis set was employed. This is our standard basis set II[14]. Frequency calculations were performed at the same level of theory. Zero-point energies were used unscaled[15]. The calculated total energies [Hartree] and zero-point vibrational energies [kcal mol^{-1}] of all stationary points are: **1a**: −202.79952, 20.6; CH_2O: 114.49822, 16.8; **5a**: −317.33510, 39.4; **TS1**: −317.32200, 39.2; **3a**: −317.40519, 42.7; **6a**: −405.62620, 42.3; **TS2**: −405.58359, 42.7; **2a**: −405.66890, 45.1; **7**: −163.50559, 3.4; **4a**: −375.43133, 42.7; **8**: −296.87155, 6.0; $TiCl_2$: −88.16417, 1.4; $H_2C{=}CH_2$: −78.58582, 32.1.

 © WILEY-VCH Verlag GmbH, D-69451 Weinheim, 1997 0570-0833/97/3620-2236 $ 17.50+.50/0

[8] Gaussian 94 (Revision A.1): M. J. Frisch, G. W. Trucks, H. B. Schlegel, P. M. W. Gill, B. G. Johnson, M. A. Robb, J. R. Cheeseman, T. A. Keith, G. A. Petersson, J. A. Montgomery, K. Raghavachari, M. A. Al-Laham, V. G. Zakrzewski, J. V. Ortiz, J. B. Foresman, J. Cioslowski, B. B. Stefanov, A. Nanayakkara, M. Challacombe, C. Y. Peng, P. Y. Ayala, W. Chen, M. W. Wong, J. L. Andres, E. S. Replogle, R. Gomperts, R. L. Martin, D. J. Fox, J. S. Binkley, D. J. Defrees, J. Baker, J. J. P. Stewart, M. Head-Gordon, C. Gonzalez, J. A. Pople, Gaussian, Inc., Pittsburgh PA, USA, **1995**.
[9] *Density Functional Methods in Chemistry* (Eds.: J. Labanowski, J. Andzelm), Springer, Heidelberg, **1991**.
[10] a) A. D. Becke, *J. Chem. Phys.* **1993**, *98*, 5648; b) P. J. Stevens, F. J. Devlin, C. F. Chablowski, M. J. Frisch, *J. Phys. Chem.* **1994**, *98*, 11623.
[11] a) A. Ricca, C. W. Bauschlicher, Jr., *Theor. Chim. Acta* **1995**, *92*, 123; b) O. Wiest, K. A. Black, K. N. Houk, *J. Am. Chem. Soc.* **1994**, *116*, 10336.
[12] P. J. Hay, W. R. Wadt, *J. Chem. Phys.* **1985**, *82*, 299.
[13] a) A. Bergner, M. Dolg, W. Küchle, H. Stoll, H. Preuss, *Mol. Phys.* **1993**, *80*, 1431; b) M. Kaupp, P. von R. Schleyer, H. Stoll, H. Preuss, *J. Am. Chem. Soc.* **1991**, *113*, 6012. From the basis set in this reference the diffuse s- and p-functions were discarded.
[14] G. Frenking, I. Antes, M. Böhme, S. Dapprich, A. W. Ehlers, V. Jonas, A. Neuhaus, M. Otto, R. Stegmann, A. Veldkamp, S. F. Vyboishchikov in *Reviews in Computational Chemistry, Vol. 8* (Eds.: K. B. Lipkowitz, D. B. Boyd), VCH, New York, **1996**, p. 63.
[15] A. P. Scott, L. Radom, *J. Phys. Chem.* **1996**, *100*, 16502.
[16] a) K. Fukui, *Acc. Chem. Res.* **1981**, *14*, 363; b) C. Gonzalez, H. B. Schlegel, *J. Chem. Phys.* **1991**, *95*, 5853.
[17] G. Erker, U. Dorf, P. Czisch, J. L. Petersen, *Organometallics* **1986**, *5*, 668, and references therein.
[18] a) P. Hofmann, P. Stauffert, M. Frede, K. Tatsumi, *Chem. Ber.* **1989**, *122*, 1559; b) D. M. Roddick, J. E. Bercaw, *ibid.* **1989**, *122*, 1579.
[19] *Handbook of Chemistry and Physics* (Ed.: D. R. Lide), 75th ed., CRC Press, Boca Raton, FL, USA, **1994**.
[20] C. Sato, S. Konaka, T. Iijima, M. Kimura, *Bull. Chem. Soc. Jpn.* **1969**, *42*, 2148.
[21] The analysis of the related Ti–Ti bond in Cl_3Ti–$TiCl_3$ shows that both Ti centers are sd^3-hybridized. The bond energy at the CCSD(T)/II level is approximately 17 kcal mol^{-1}: a) M. Diedenhofen, G. Frenking, unpublished results; b) M. Diedenhofen, Diploma Thesis, Marburg, Germany, **1997**.
[22] Structures not having a Ti–Ti interaction (singlet diradicals) are 60–80 Kcal mol^{-1} higher in energy **2a** and are higher order saddle points.
[23] A. Fürstner, personal communication.
[24] O. Maury, C. Villiers, M. Ephritikhine, *Angew. Chem.* **1996**, *108*, 1215; *Angew. Chem., Int. Ed. Engl.* **1996**, *35*, 1129.
[25] J. E. McMurry, M. P. Fleming, K. L. Kees, L. R. Krepski, *J. Org. Chem.* **1978**, *43*, 3255.

Sb_8R_4, R = $(Me_3Si)_2CH$—A Polycyclic Organostibane**

Hans Joachim Breunig,* Roland Rösler, and Enno Lork

Dedicated to Professor Gottfried Huttner on the occasion of his 60th birthday

Whereas several examples of monocyclic organostibanes are known,[1] polycycles of the type Sb_nR_m ($n > m$, R = monovalent substituent) have not yet been described. Polycyclic structures have been observed, however, for polyantimonides and their derivatives.[2]

Since monocyclic stibanes can be stabilized kinetically by bulky substituents, it seemed appropriate to try to protect polycyclic stibanes in a similar way. Attempts to produce polycycles by methods analogous to those applied for organophosphorus polycycles[3] by reactions of magnesium and mixtures of $RSbCl_2$ [R = *t*Bu, $(Me_3Si)_2CH$)] and $SbCl_3$ in the molar ratios 3:1, 1:1, or 1:3 were, however, unsuccessful. When a 3:1 mixture was used the known Sb_4 monocycles were formed.[1a,c,d] In the other cases no ring formation was observed; only insoluble black solids were obtained.

Yellow crystals of the polycycle Sb_8R_4 (**1**) (R = $(Me_3Si)_2CH$) have now been obtained as a product of the previously described[1c] reaction of $RSbCl_2$ with magnesium filings in tetrahydrofuran, in which a variation of the work-up conditions was crucial. When the main product, Sb_4R_4, is separated by chromatography before crystallization, the novel polycycle is obtained from a fraction that also contains Sb_3R_3, SbR_3, and Sb_7R_5 (**2**). The yield of **1** and **2** is small, but the synthesis is very reproducible. The pathway of the reaction is not yet known. A thermal decomposition of Sb_3R_3 to give **1** or **2** and SbR_3 may be assumed, which corresponds to reaction patterns known in phosphorus chemistry.[3]

According to an X-ray structure analysis of **1**[4] (Figure 1), the eight Sb atoms form a tricyclic cage consisting of Sb_5 monocycles sharing common edges. The alkyl substituents occupy

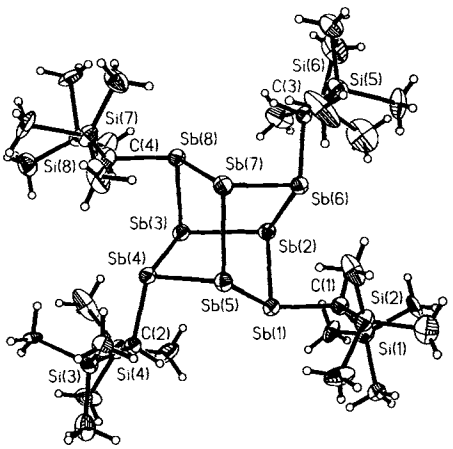

Figure 1. Structure of **1** in the crystal. Selected bond lengths [pm] and angles [°]: Sb(1)–Sb(2) 281.0(4), Sb(2)–Sb(3) 281.4(3), Sb(3)–Sb(4) 285.2(4), Sb(4)–Sb(5) 278.4(4), Sb(5)–Sb(1) 284.3(3), Sb(5)–Sb(7) 281.9(3), Sb–C (mean) 220; C(1)-Sb(1)-Sb(2) 96.2(8), C(1)-Sb(1)-Sb(5) 110.2(7), Sb(2)-Sb(1)-Sb(5) 99.65(10), Sb(3)-Sb(2)-Sb(6) 109.66(10), Sb(3)-Sb(2)-Sb(1) 91.22(10), Sb(1)-Sb(2)-Sb(6) 87.32(10).

1,3-positions in a *trans* orientation to each other in the five-membered rings, which each adopt an approximate envelope conformation. The structure of **1** can be derived from a Sb_4 tetrahedron that is bridged on four edges with SbR groups. Therefore a close relationship exists between **1** and realgar, As_4S_4, whose structure is explained by insertion of sulfur atoms into four As–As bonds of a tetrahedral As_4 molecule. The structure of **1** cannot be derived from a known modification of antimony; however, it corresponds to the P_8 cage in Hittorf's phosphorus. Thus, **1** supplements the structural patterns of organophosphorus polycycles since the analogous octaphosphanes P_8R_4[5] have not yet been investigated crystallographically.

The distances and angles in the structure of **1** display wider variations than those in monocyclic organostibanes. The Sb–Sb bond lengths are approximately equal only between antimony atoms bearing no alkyl substituents (av 281.7 pm). In the [Sb–Sb(R)-]$_4$ skeleton there is a systematic variation of shorter [278.4(4)–281.0(4) pm] and longer distances [284.3(3)–286.1(4) pm]. In the four-membered ring $(SbR)_4$ (R =

[*] Prof. Dr. H. J. Breunig, R. Rösler, Dr. E. Lork
Institut für Anorganische und Physikalische Chemie (FB 02) der Universität
Postfach 330 440, D-28334 Bremen (Germany)
Fax: Int. code +(421) 218 4042
e-mail: breunig@chemie.uni-bremen.de

[**] This work was supported by Deutsche Forschungsgemeinschaft (Br 630/16, Antimonpolycyclen).

 © WILEY-VCH Verlag GmbH, D-69451 Weinheim, 1997 0570-0833/97/3620-2237 $ 17.50+.50/0

$(Me_3Si)_2CH$) the differences between the Sb–Sb bond lengths (282.2–286.6 pm) are considerably smaller. The bond angles at the antimony atoms of **1** range between 84.66(9)° and 113.2(7)°. A similar wide range of Sb–Sb bond lengths and bond angles has also been observed in other antimony clusters, such as the anions Sb_7^{3-} [2d] or $[Sb_7M(CO)_3]^{3-}$ (M = Cr[2b], Mo[2a]). The differences in the distances and angles of **1** cause some deviations from the geometry of the realgar structure. This is apparent for the antimony atoms Sb(1), Sb(4), Sb(8), and Sb(6) bearing alkyl substiuents. They are not exactly situated in a plane; the deviations from the best plane are between −39.1 and 38.6 pm. The nonbonding distances between the antimony atoms without alkyl substituents [Sb(2)–Sb(5), Sb(2)–Sb(7), Sb(3)–Sb(5), Sb(3)–Sb(7)] vary only little between 429.0 and 432.3 pm. This corresponds quite well to the idealized geometry of the realgar type. A detailed examination of the structure of the five-membered rings reveals some deviations from an ideal envelope conformation. The atoms Sb(2), Sb(3), Sb(4), and Sb(5), for example, are not exactly in a plane either; the deviations from the best plane vary from −21.4 to 20.9 pm.

Apart from crystallographic analysis, mass spectrometry is also suitable for detecting the novel polycycles. In the chemical ionization mass spectrum, in addition to **1**, Sb_7R_5 (**2**, $R = (Me_3Si)_2CH$) was also detected through the intensive group of signals of the molecular ion. Attempts to determine the structure of **2** by X-ray structure analysis or NMR spectroscopy have not yet been successful. Analogous phosphorus compounds of the type P_7R_5 have the bicyclic norbornane structure.[3]

Experimental Section

All operations were carried out with strict exclusion of air in an argon atmosphere. Al_2O_3 was heated under reduced pressure and loaded under argon.

A solution of $RSbCl_2$ [R = $(Me_3Si)_2CH$] [6] (1.58 g, 4.5 mmol) in THF (20 mL) was added dropwise within 30 min with stirring to magnesium filings (0.15 g, 6 mmol) in THF (5 mL) activated with $BrCH_2CH_2Br$. The dark brown mixture was stirred for 1 h, the solvent was removed at reduced pressure, and the residue was washed three times with portions of petroleum ether (100 mL). The extracts were combined, concentrated to a volume of 10 mL, and separated by chromatography with petroleum ether on Al_2O_3 (Al_2O_3 neutral according to Brockmann, activity Super I, particle size 0.063–0.200 mm; column 8 × 1.5 cm). The first, intensely orange fraction contained $(SbR)_4$ (yield 0.76 g, 60%). The second, less intensely colored fraction was concentrated to a volume of 10 mL under reduced pressure. It contained $(SbR)_3$ as main component as well as SbR_3 and the polycycles **1** and **2**. Small yellow crystals of **1** were obtained when the concentrated solution was stored at −27 °C for two months (MS (CI, positive-ion mode, NH_3): **1**: *m/z* :1608–1612 [M^+]; **2**: *m/z*: 1643–1658 [M^+H]).

Received: February 10, 1997
Revised version: April 29, 1997 [Z10091IE]
German version: *Angew. Chem.* **1997**, *109*, 2333–2334

Keywords: antimony · main group elements · polycycles · structure elucidation

[1] a) K. Issleib, B. Hamann, L. Schmidt, *Z. Anorg. Allg. Chem.* **1965**, *339*, 298–303; b) J. Ellermann, A. Veit, *Angew. Chem.* **1982**, *94*, 377; *Angew. Chem. Int. Ed. Engl.* **1982**, *21*, 375; c) H. J. Breunig, A. Soltani-Neshan, *J. Organomet. Chem.* **1984**, *262*, C 27–C 29; d) M. Ates, H. J. Breunig, K. Ebert, S. Gülec, R. Kaller, M. Dräger, *Organometallics* **1992**, *11*, 145–150; e) T. F. Berlitz, H. Sinning, L. Lorberth, U. Müller, *Z. Naturforsch. B* **1988**, *43*, 744–748; f) O. M. Kekia, R. L. Jones, Jr., A. L. Rheingold, *Organometallics* **1996**, *15*, 4104–4106; g) review: H. J. Breunig in *The Chemistry of Organic Arsenic, Antimony and Bismuth Compounds* (Ed.: S. Patai), Wiley, Chichester, **1994**, p. 563.

[2] a) U. Bolle, W. Tremel, *J. Chem. Soc. Chem. Commun.* **1992**, 91–93; b) S. Charles, B. W. Eichhorn, A. L. Rheingold, S. G. Bott, *J. Am. Chem. Soc.* **1994**, *116*, 8077–8086; c) C. J.Warren, D. M. Ho, R. C. Haushalter, A. B. Bocarsely, *Angew. Chem.* **1993**, 1684–1687; *Angew. Chem. Int. Ed. Engl.* **1993**, *32*, 1646–1649; d) S. C. Critchlow, D.Corbett, *Inorg. Chem.* **1984**, *23*, 770–774.

[3] Review: M. Baudler, K. Glinka in *The Chemistry of Inorganic Homo- and Heterocycles, Vol.2* (Eds.: I. Haiduc, D. B. Sowerby), Academic Press, London, **1987**, p. 423.

[4] Crystal dimensions 0.5 × 0.4 × 0.15 mm, crystal system triclinic, space group $P\bar{1}$, cell parameters $a = 915.6(7)$, $b = 1781.5(7)$, $c = 1794.7(10)$ pm, $\alpha = 93.54(3)$, $\beta = 92.82(7)$, $\gamma = 104.56(6)°$, $V = 2.822(3)$ nm^3, $Z = 2$, $\rho_{calcd} = 1.897$ Mg m^{-3}, $2\theta_{max.} = 45.4°$, Siemens-P4 four-circle diffractometer, $Mo_{K\alpha}$ radiation, $\lambda = 71.073$ pm, scan mode 2θ-ω, $T = 173(2)$ K, 9170 measured reflections, 7365 independent reflections ($R_{int} = 0.090$) 3630 independent reflections with $(I > 2\sigma I)$, absorption coefficient 3.956 mm^{-1}, absorption correction Difabs, method of structure solutions: direct methods, program used for structure solution SHELXS-86, method of refinement full-matrix least squares at F^2, refinement program SHELXL-93, 424 free parameters, hydrogen atoms geometrically positioned and refined with a riding model, final $R(I > 2\sigma(I))$, $R1 = 0.0957$, $wR2 = 0.2507$. Crystallographic data (excluding structure factors) for the structure reported in this paper have been deposited with the Cambridge Crystallographic Data Centre as supplementary publication no. CCDC-100169. Copies of the data can be obtained free of charge on application to The Director, CCDC, 12 Union Road, Cambridge CB2 1EZ, UK (fax: int. code +(1223) 336-033; e-mail deposit@chemcrys.cam.ac.uk).

[5] M. Baudler, V. Arndt, *Z. Naturforsch. B* **1984**, *39*, 275–283.

[6] H. J. Breunig, W. Kanig, A. Soltani-Neshan, *Polyhedron*, **1983**, *2*, 291–292.

Chemoenzymatic Synthesis of Fluorescent N-Ras Lipopeptides and Their Use in Membrane Localization Studies In Vivo**

Herbert Waldmann,* Michael Schelhaas, Edgar Nägele, Jürgen Kuhlmann, Alfred Wittinghofer,* Hans Schroeder, and John R. Silvius*

Dedicated to Professor Heribert Offermanns on the occasion of his 60th birthday

The lipidation of proteins, specifically the covalent attachment of a myristoyl group to an N-terminal glycine, and the S-palmitoylation and S-alkylation of cysteines by farnesyl or geranylgeranyl moieties, is among the most important modifications of proteins in nature.[1] Lipoproteins play decisive roles in numerous biological processes; in particular they are critically involved in the transduction of hormonal and mitogenic signals across the plasma membrane and from there towards the nucleus. For instance, the transmembrane G-protein-coupled receptors are S-palmitoylated, the heterotrimeric G-proteins are N-myristoylated, S-palmitoylated, and S-farnesylated, nonreceptor protein tyrosine kinases are N-myristoylated and S-palmitoylated, and the Ras proteins carry S-palmitoyl- and S-farnesyl groups. In addition, numerous further membrane-associated proteins are lipidated, for example the enzyme NO_x-synthetase,[2] and various viral envelope proteins[3] are S-palmitoylated.

Due to the important biological roles of lipid-modified proteins, the study of protein lipidation and its biological significance is at the forefront of biological research.[1] Correct lipidation of G-protein-coupled receptors[4] and the Ras proteins (vide infra) is known to be important for the proper execution

[*] Prof. Dr. H. Waldmann, Dr. M. Schelhaas, Dr. E. Nägele
Institut für Organische Chemie der Universität
Richard-Willstätter-Allee 2, D-76128 Karlsruhe (Germany)
Fax: Int. code +(721)608-4825
e-mail: waldmann@ochhades.chemie.uni-karlsruhe.de
Prof. Dr. F. Wittinghofer, Dr. J. Kuhlmann
Max-Planck-Institut für Molekulare Physiologie
Rheinlanddamm 201, D-44026 Dortmund (Germany)
Prof. J. R. Silvius, H. Schroeder
Department of Biochemistry, McGill University
Montréal, Quebec H3G1Y6 (Canada)

[**] This research was supported by the Deutsche Forschungsgemeinschaft, the Fonds der Chemischen Industrie, and the Medical Research Council of Canada.

of their biological functions. However, the general biological significance of different lipid groups, in particular their possible roles in biological signal transduction processes, is largely unclear and the subject of numerous hypotheses.[1] Furthermore, the detailed knowledge of the requirements for either transient or stable insertion of lipopeptides into biological bilayers may help in the design of drugs that influence pathological signal transduction processes such as those employing oncogenic Ras.

For the study of such phenomena by a combination of biophysical[5] and cell-biological[6] methods[7] useful reagents are lipidated peptides that contain the lipid groups and amino acid sequences of their parent lipoproteins, and also carry labels by which they can be traced in biological systems (i.e. fluorescent labels that can be detected by fluorescence microscopy).

We report here on an efficient method for the synthesis of fluorescent-labeled lipopeptides and on their application in the study of the specific membrane localization of lipopeptides and lipoproteins by means of membrane fusion/fluorescence microscopy and microinjection/confocal laser fluorescence microscopy.

For the development of a new synthetic, flexible method for the construction of differently lipidated peptides we have drawn from our previous experience in the construction of acid- and base-labile S-palmitoylated and S-farnesylated Ras lipopeptides.[8] The Ras proteins, a class of membrane-bound lipidated proteins that convey signals sent by growth factors further towards the nucleus, are often involved in malignant transformation.[9] They can fulfill their biological roles in the normal and the transformed state only if they are lipidated.[9]

The differently labeled N-Ras heptapeptides **14**–**16**, **17**, and **18** were chosen as target compounds. In retrosynthetic analysis they were divided into differently labeled N-terminal dipeptides and a constant C-terminal pentapeptide **13**, which carries an acid-labile farnesyl sulfanyl group (Scheme 1). Peptide **13** can be constructed in high yield by enzymatic removal of the N-terminal *p*-acetoxybenzyloxycarbonyl (AcOZ) group[8a] or base-mediated cleavage of the fluorenylmethoxycarbonyl (Fmoc) group[8c] as key steps. The synthesis of the selectively deprotected, S-palmitoylated peptides **14**–**16** is complicated by the pronounced base-lability of the sulfanylcarbonyl group. Thus, we found that in S-palmitoylated peptides these groups hydrolyze spontaneously even at pH 7 in aqueous solution.[8b] We now report that S-palmitoylated peptides can be synthesized efficiently by the combination of Pd^0-mediated cleavage of an allyl ester[10] for deprotection of the peptide chain at the C-terminus and enzymatic removal of an AcOZ group[8a] for unmasking at the N-terminus.

Thus, cystine (bis)allyl ester **1** was condensed with AcOZ-glycine **2** to give the corresponding peptide in high yield. After reductive cleavage of the disulfide bond by means of dithiothreitol (DTT), the sulfanyl groups were palmitoylated and then the N-terminal AcOZ residue was cleaved by means of the enzyme acetyl esterase from oranges to deliver the selectively unmasked, S-palmitoylated dipeptide allyl ester **3** in a straightforward manner. Dipeptide **3** was then condensed with different labels. The fluorescent 7-nitrobenz-2-oxa-1,3-diazolyl (NBD) and bimanyl groups were introduced with reagents **4** and **5**, respectively, and **3** was also coupled to the biotin derivative **6**. The fully masked peptides **7**–**9** were then treated with $[Pd(PPh_3)_4]$ in the presence of morpholine as an allyl-accepting nucleophile to give the selectively deprotected, fluorescent-labeled dipeptides **10**–**12** in high yields. In the N- and the C-terminal deprotections no undesired side reactions occurred. Thus, the conditions for the enzymatic cleavage of the AcOZ residue and the allyl ester are so mild that neither an attack on the base-sensitive thioester group nor a base-induced β-elimination[8] occurs. Finally, **10**–**12** were condensed with the N-terminally deprotected pentapeptide **13** to give the desired, differently labeled, S-farnesylated and S-palmitoylated N-Ras heptapeptides **14**–**16**. Similarly, the NBD-tagged heptapeptides **17** and **18** were prepared. In addition, the farnesylated pentapeptide **13** was coupled with NBD-aminocaproic acid **4** to give the labeled peptide **19** (Scheme 2).

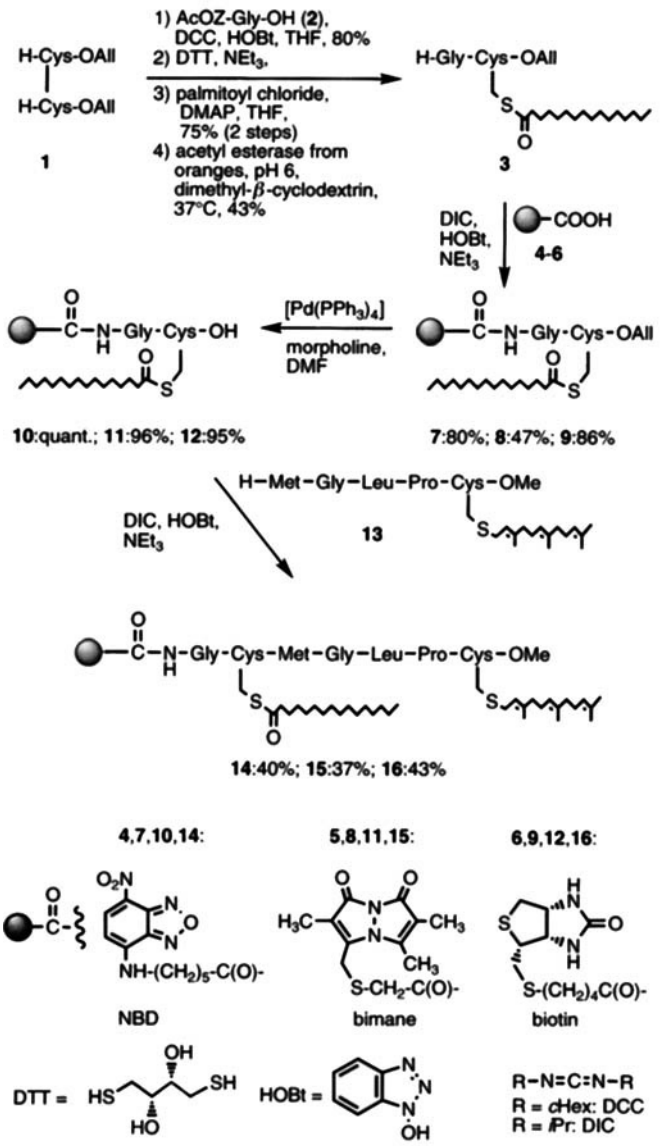

Scheme 1. Chemoenzymatic synthesis of the labeled, farnesylated and palmitoylated N-Ras lipopeptides **14**–**16**.

The NBD- and the bimanyl-labeled peptides can be detected directly in biological systems and in vitro model systems by fluorescence microscopy and fluorescence spectroscopy. The biotin label can be traced with the protein streptavidin, which is also available in a fluorescent-labeled form or can be modified with colloidal gold, thus facilitating the study of model lipoproteins by fluorescence microscopy and electron microscopy.[11]

One of the prevailing questions in the study of the biological roles of the lipidation of proteins is whether particular lipidation motifs target lipoproteins to specific membranes.[5–8] Thus, the observation that several proteins in the plasma membrane carry farnesyl residues, whereas proteins in intracellular membranes

 © WILEY-VCH Verlag GmbH, D-69451 Weinheim, 1997 0570-0833/97/3620-2239 $ 17.50+.50/0

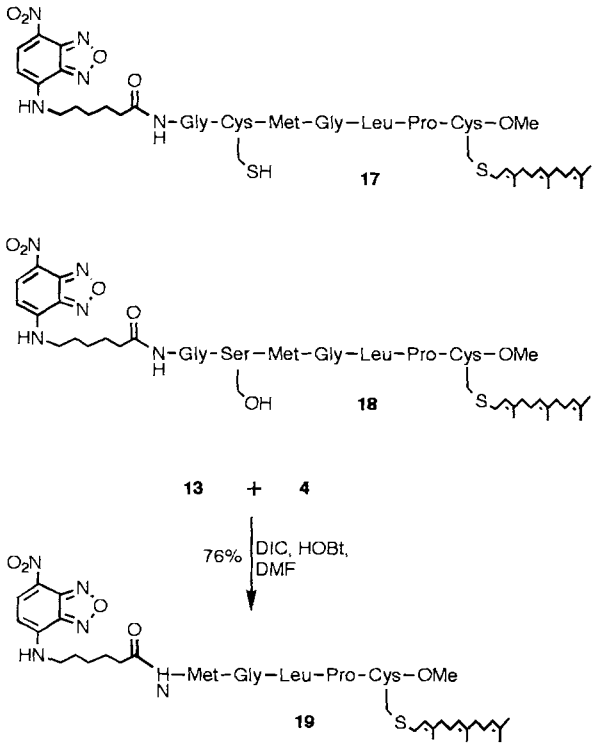

Scheme 2. Synthesis of the labeled farnesylated N-Ras peptides **17**–**19**.

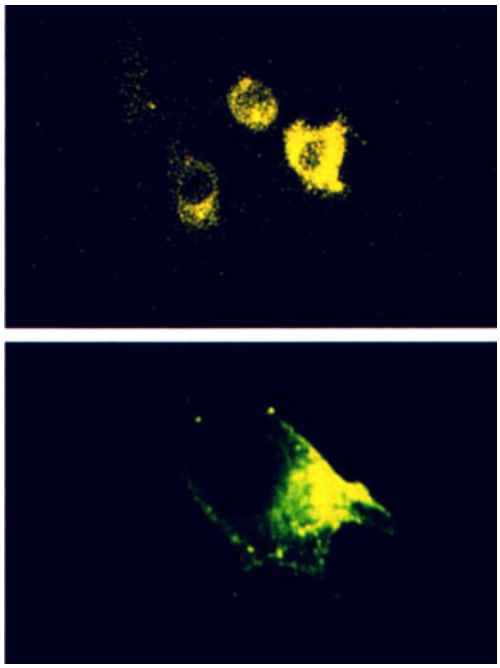

Figure 1. Fluorescence micrographs of NIH-3T3 fibroblast cells. Top: After microinjection of pentapeptide **19**; bottom: after microinjection of heptapeptide **14**. The top micrograph shows that **19** is not localized to the plasma membrane; the bottom micrograph indicates that **14** is localized in the plasma membrane.

are often geranylgeranylated (e.g. the Rab proteins[12]) has raised the notion that S-farnesylation might serve to target lipidated proteins specifically to the plasma membrane, for example by interactions with respective receptors.[1, 13]

To address this question and to determine whether the different lipidation motifs and amino acid sequences present in the Ras model peptides **14**, **17**, **18** and **19** determine a specific localization of the probes in a particular subcellular membrane, in particular the plasma membrane, the labeled peptides were subjected to in vivo studies. In one set of experiments the exclusively farnesylated and non-palmitoylable NBD-labeled pentapeptide **19** and the palmitoylated and farnesylated NBD-labeled lipoheptapeptide **14** were microinjected into NIH-3T3 fibroblast cells. After 30 min the distribution of the peptides in the cells was investigated by means of confocal laser fluorescence microscopy. The image obtained for **19**, shown at the top of Figure 1, demonstrates that the peptide is not localized in the plasma membrane. At the bottom of Figure 1 the corresponding result for **14** indicates clearly that the doubly modified peptide is specifically located in the plasma membrane. In the micrograph the fluorescence intensity is highest in the membrane around the site of injection (large yellow spot) and extends from there into the membrane of the dendrites of the cell. Several notable "hot spots" seem to represent compartments of the plasma membrane that are particularly enriched with the lipidated peptide.

In a second set of experiments the palmitoylation of the lipopeptides **17** and **18** was studied, and the subcellular locus at which this reaction occurs was determined. To this end, cultured CV-1 fibroblasts were incubated with [^{3}H]palmitic acid and sonicated vesicles (composed of phosphatidyl choline extracted from egg yolk and 1-palmitoyl-2-oleoyl phosphatidylethanolamine in a ratio of 90:10) loaded with lipopeptides.[6] The palmitoylation of the fluorescent peptides after fusion of the vesicles with the cell membrane was determined by extraction of the fibroblast cells and analysis by two-dimensional thin-layer chromatography and scintillation counting.[6] Visualization of the S-acylated peptide spot by fluorescence employing peptide **14** as reference compound revealed that the N-Ras peptide **17**, which contains a farnesylated and an unacylated cysteine, was readily S-acylated in the fibroblasts and thereby converted into the palmitoylated and farnesylated lipopeptide **14**. In contrast, the serinyl lipopeptide **18** was not acylated under these conditions at all.

The subcellular locus of S-acylation of **17** was examined by fluorescence microscopy.[6] After incubation of CV-1 fibroblasts with lipid-loaded vesicles and selective extraction of unacylated peptide, inspection of the cells revealed a preferential accumulation of fluorescence, that is, the S-acylated lipopeptide **14**, in the plasma membrane. To determine whether the peptide might have been acylated at an intracellular membrane, for example in a compartment of the endoplasmatic reticulum or of the Golgi apparatus, and then rapidly transferred in the S-acylated form to the plasma membrane, presumably by vesicular membrane transport,[14] the experiments were carried out at different temperatures. However, neither at 37 °C (at which vesicular transport is regular) nor at 15 °C (at which vesicular transport of materials from the Golgi to the plasma membrane is strongly suppressed[15]) was fluorescence detected in the Golgi apparatus or trans Golgi compartments. At both temperatures fluorescence accumulated in the plasma membrane. Given the additional fact that doubly lipid-modified peptides like **14** exhibit negligible rates of spontaneous transfer between distinct membranes[5, 6] (as opposed to lipopeptides like **19** carrying only a farnesyl group, which rapidly exchange between different membranes), these observations suggest that the plasma membrane is itself a major site of cellular S-acylation. In contrast, cells incubated with the serinyl-peptide **18** showed little residual fluorescence.

These in vivo experiments with the labeled N-Ras peptides support the mechanism for the selective subcellular localization

 © WILEY-VCH Verlag GmbH, D-69451 Weinheim, 1997 0570-0833/97/3620-2240 $ 17.50+.50/0

of lipoproteins recently proposed by Silvius et al.[5] (Scheme 3). According to this mechanism, the farnesylated but unacylated N-Ras C-terminal heptapeptide **17** (as well as the analogous pentapeptide **19**) can diffuse freely between different membranes. Upon S-acylation of **17** (which is not possible for **19**) in

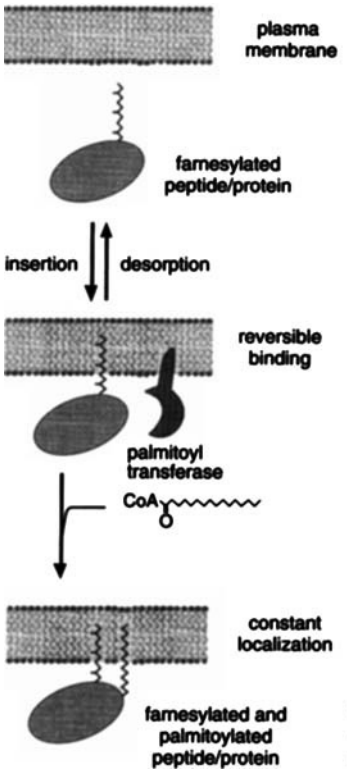

Scheme 3. Proposed model for the targeting of lipoproteins to the plasma membrane by S-palmitoylation.

a given cellular membrane compartment the now doubly lipidated peptide can no longer be transferred between different membranes. It is thus localized to the membrane where the S-acylation reaction takes place, which in the case of the N-Ras peptide is the plasma membrane. The injected, doubly modified conjugate **14** might be rapidly incorporated into the plasma membrane near the injection site and remain there due to the anchoring influence of two lipid groups. In addition, it could undergo enzymatic[16] or nonenzymatic (vide supra) deacylation on sulfur and subsequent repalmitoylation at the plasma membrane during the time of assay.

This model should also be valid for the co- and posttranslational modification of membrane-bound lipid-modified proteins by S-farnesylation and S-palmitoylation, in particular of the Ras proteins themselves. According to this model the specific localization of lipoproteins in particular membranes would not only be determined by the first lipid group introduced in the course of their biosynthesis, but even more by the attachment of the second lipid residue at the site at which the protein remains localized. The recent identification of a plasma membrane bound protein S-acyltransferase,[17] which acylates the free cysteine in the farnesylated C-terminal hexadecapeptide of N-Ras, and similarly positioned cysteine residues in full length H-Ras strongly supports this notion.

This model of "kinetic targeting" does not address the participation of transport proteins that might be involved in the membrane targeting of lipoproteins. However, it explains how very small regions of proteins such as Lck, Fyn, and H- and N-Ras containing S-acylation sites are both necessary and sufficient for targeting to the plasma membrane when they are introduced artificially into chimeric or mutated proteins.[18] Also, a recent study has concluded that the protein Fyn is targeted to the plasma membrane by a kinetic-targeting mechanism based on acylation at that membrane[19] just as was observed for simple lipopeptides that are S-acylation substrates and that resemble the termini of proteins such as Fyn and Lck.[6]

Received: April 14, 1997 [Z10283IE]
German version: *Angew. Chem.* **1997**, *109*, 2334–2337

Keywords: fluorescence spectroscopy · lipoproteins · membranes · Ras proteins · signal transduction

[1] Reviews: a) P. J. Casey, *Science* **1995**, *268*, 221; b) G. Milligan, M. Parenti, A. I. Magee, *TIBS* **1995**, 181.
[2] L. J. Robinson, T. Michel, *Proc. Natl. Acad. Sci. USA* **1995**, *92*, 11776.
[3] a) E. Ponimaskin, M. F. G. Schmidt, *Biochem. Soc. Trans.* **1995**, *23*, 565; b) C. Yang, C. P. Spies, R. W. Compans, *Proc. Natl. Acad. Sci. USA* **1995**, *92*, 9871; c) J. Hensel, M. Hintz, M. Kargs, D. Linder, B. Stahl, R. Geyer, *Eur. J. Biochem.* **1995**, *232*, 373.
[4] For the G protein coupled β_2-adrenoceptor (S. Moffet, B. Mouillac, H. Bonin, M. Bouvier, *EMBO J.* **1993**, *12*, 349) and rhodopsin (E. R. Weiss, S. Osawa, W. Shi, C. D. Dickerson, *Biochemistry* **1994**, *33*, 7587) it has been demonstrated that S-palmitoylation plays a central role in regulating the respective effector systems.
[5] S. Shahinian, J. R. Silvius, *Biochemistry* **1995**, *34*, 3813 and references therein.
[6] H. Schroeder, R. Leventis, S. Shahinian, P. A. Walton, J. R. Silvius, *J. Cell Biol.* **1996**, *134*, 647.
[7] Review: R. S. Bhatnagar, J. I. Gordon, *Trends Cell Biol.* **1997**, 14.
[8] a) H. Waldmann, E. Nägele, *Angew. Chem.* **1995**, *107*, 2425; *Angew. Chem. Int. Ed. Engl.* **1995**, *34*, 2259; b) M. Schelhaas, S. Glomsda, M. Hänsler, H.-D. Jakubke, H. Waldmann, *ibid.* **1996**, *108*, 82 and **1996**, *35*, 106; c) P. Stöber, M. Schelhaas, E. Nägele, P. Hagenbuch, J. Rétey, H. Waldmann, *Bioorg. Med. Chem.* **1997**, *5*, 75. For reviews on the enzymatic synthesis of lipo-, glyco-, phospho-, and nucleopeptides see: M. Schelhaas, H. Waldmann, *Angew. Chem.* **1996**, *108*, 2192; *Angew. Chem. Int. Ed. Engl.* **1996**, *35*, 2056; T. Kappes, H. Waldmann, *Liebigs Ann.* **1997**, 803; K. Hinterding, D. Alonso-Diaz, H. Waldmann, *Angew. Chem.* in press; *Angew. Chem. Int. Ed. Engl.* in press.
[9] Reviews: a) S. E. Egan, R. A. Weinberg, *Nature* **1993**, *365*, 781; b) M. S. Boguski, F. McCormick, *ibid.* **1993**, *366*, 643.
[10] S. Friedrich-Bochnitschek, H. Waldmann, H. Kunz, *J. Org. Chem.* **1989**, *54*, 751.
[11] G. T. Hermanson, *Bioconjugate Techniques*, Academic Press, San Diego, **1996**.
[12] A. Valencia, P, Chardin, A. Wittinghofer, C. Sander, *Biochemistry* **1991**, *30*, 4637.
[13] a) A. I. Magee, *J. Cell Science* **1990**, *97*, 581; b) W. A. Maltese, *FASEB J.* **1990**, *4*, 3319; c) K. A. Cadwallader, H. Paterson, S. G. Macdonald, J. T. Hancock, *Mol. Cell. Biol.* **1994**, *14*, 4722; d) O. G. Kisselev, M. V. Ermolaeva, N. Gautam, *J. Biol. Chem.* **1994**, *269*, 21399; e) A. Scheer, P. Gierschik, *Biochemistry* **1995**, *34*, 4952
[14] L. Guttierez, A. I. Magee, *Biochim. Biophys. Acta* **1991**, *1978*, 147.
[15] a) K. S. Matlin, K. Simons, *Cell* **1983**, *34*, 233; b) J. Saraste, E. Cuismanen, *ibid.* **1984**, *35*, 535; c) M. R. Kaplan, R. D. Simoni, *J. Cell Biol.* **1985**, *101*, 446; d) R. E. Pagano, O. C. Martin, H. C. Kang, R. P. Haugland, *ibid.* **1991**, *113*, 1267; e) Y.-J. Shiao, J. E. Vance, *J. Biol. Chem.* **1993**, *268*, 26085; f) C. N. Connolly, C. E. Futter, A. Gobson, C. R. Hopkins, D. F. Cutler, *J. Cell Biol.* **1994**, *127*, 641.
[16] For the identification of a palmitoylthioesterase that H-Ras depalmitoylates see: J.-Y. Lu, S. Hofmann, *J. Biol. Chem.* **1995**, *270*, 7251.
[17] L. Liu, T. Dudler, M. H. Gelb, *J. Biol. Chem.* **1996**, *271*, 23269.
[18] a) L. Alland, S. M. Peseckis, R. E. Atherton, L. Berthiaume, M. Resh, *J. Biol. Chem.* **1994**, *269*, 16701; b) L. Berthiaume, M. D. Resh, *ibid.* **1995**, *270*, 22399; c) J. F. Hancock, K. Cadwallader, H. Patterson, C. J. Marshall, *EMBO J.* **1991**, *10*, 4033; d) A. M. Shenoy-Scaria, L. K. Timson Gauen, J. Kwong, A. S. Shaw, D. M. Lublin, *Mol. Cell. Biol.* **1991**, *13*, 6385; e) A. M. Shenoy-Scaria, D. J. Dietzen, J. Kwong, D. C. Link, D. M. Lublin, *J. Cell Biol.* **1994**, *126*, 353.
[19] W. van't Hof, M. D. Resh, *J. Cell Biol.* **1997**, *136*, 1023.
[20] NIH-3T3 cells were grown in Dulbecco's Modified Eagle Medium (DMEM) supplemented with 10% fetal bovine serum (Gibco) in a humidified CO_2 (7.5%) incubator at 37 °C. Microinjections were performed in culture medium buffered with 20 mM Na-HEPES, pH 7.4. For injections a Zeiss Microinjection Workstation (AIS) was used along with thin borosilicate glass capillaries with filaments (Hilgenberg) having a diameter of ≤ 0.5 µm at the tip. Distribution of the fluorophore was observed 30 min after injection with a confocal laser scanning microscope (CLSM) based on the MRC 500 system (BioRad) with an excitation wavelength at 488 nm.

 © WILEY-VCH Verlag GmbH, D-69451 Weinheim, 1997 0570-0833/97/3620-2241 $ 17.50+.50/0

Bimetallic Nanoparticle Catalysts Anchored Inside Mesoporous Silica**

Douglas S. Shephard, Thomas Maschmeyer, Brian F. G. Johnson,* John Meurig Thomas,* Gopinathan Sankar, Dogan Ozkaya, Wuzong Zhou, Richard D. Oldroyd, and Robert G. Bell

There has been considerable interest in the formation, structure and further exploitation of the catalytic activity of bimetallic particles ever since Sinfelt et al.[1] demonstrated the powerful, catalytic, reforming properties of alumina-supported Ru–Cu, Pt–Ir, and Pt–Re ensembles. With the advent[2, 3] of readily preparable mesoporous solids possessing pore diameters in the range 25 to 100 Å and the feasibility[4–6] of inserting "single-site" centers that are catalytically active (such as Ti^{IV} ions anchored through Si–O bonds) in atomically well-defined locations inside such mesopores, the incentive for extending such strategies to the insertion of bimetallic nanoparticles is high. One of the key aims in this work has been the design and production of discrete, supported bimetallic particles of well-defined and tuneable atomic composition; another is to secure the clusters to the support in such a way that they are prevented from sintering.

In this communication we report: a) the synthesis and characterization of a novel Ag_3Ru_{10} complex anion $[Ag_3Ru_{10}C_2(CO)_{28}Cl]^{2-}$ (**2**) from Ag^+ ions and $[Ru_5C(CO)_{14}]^{2-}$ (**1**); b) the adsorption of **2** onto the inner walls of the mesoporous silica (MCM-41), with a pore diameter of about 30 Å,[7] together with spectroscopic proof that it retains its integrity; c) the subsequent thermolytic conversion of the bound complex $[Ag_3Ru_{10}C_2(CO)_{28}Cl][AsPh_4]_2$ (**2**) into discrete nanoparticles that have been shown (by bright-field and annular dark-field high-resolution electron microscopy and extended X-ray absorption fine structure (EXAFS)) to be firmly anchored inside the siliceous mesopores; and finally d) the performance of the nanoparticles as a catalyst for the hydrogenation of hex-1-ene.

Several important criteria influence the choice of bimetallic cluster precursor for the production of supported nanoparticles. First, the protective sheath surrounding the organometallic precursor must be readily removable (for **2** mild thermolysis is sufficient to activate and secure the bimetallic particles). Second, to ensure an even distribution of the precursor over the surface of the support the sheath must undergo favorable interactions with the functional groups on the surface, the solvent, and the counterion. The interaction with the surface must be stronger than that involved both in solvation and between the precursor species, so that aggregation into small molecular crystallites on the surface is suppressed, as these may sinter on removal of the CO sheath. Anionic carbonyl clusters[8] fulfill these criteria; their interaction with the MCM-41 surface is between the Si-OH group of the surface and the OC-M group,[9] and the intermolecular coulombic repulsion prevents aggregation prior to thermolysis. A loading corresponding to about 0.2 occupancy of the internal volume (127 mg PPN-**2** per 427 mg MCM-41) was used for both the microscopy and catalysis experiments (PPN = $^+N(PPh_3)_2$).

The selected anionic bimetallic cluster **2** was fully characterized before deposition inside the mesoporous silica. According to a single crystal X-ray analysis of $[Ph_4As]_2$-**2** (Figure 1) the dianion is composed of two $Ru_5C(CO)_{14}$ units linked by three

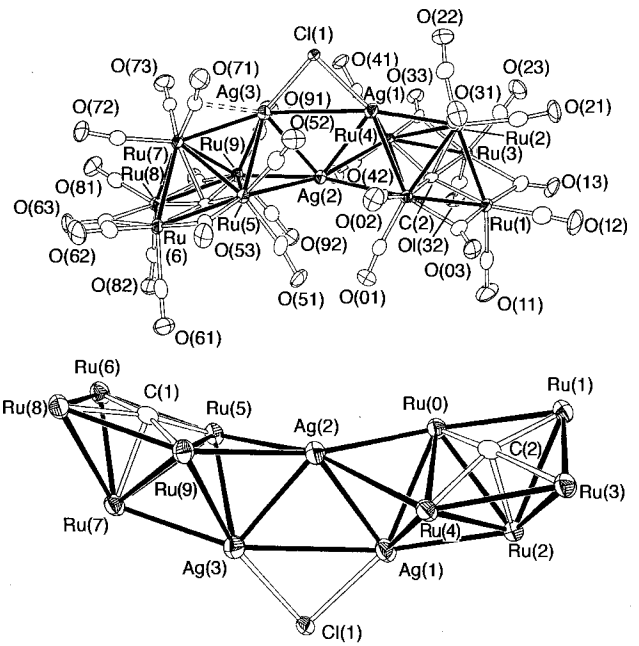

Figure 1. The molecular structure of **2** in the crystal. Top: the full dianion; bottom: $Ag_3Ru_{10}C_2$ core. Selected bond lengths [Å] and standard deviations (in parentheses): Ru0–Ru1 2.7753(10), Ru0–Ru2 2.8580(10), Ru0–Ag2 2.8587(10), Ru0–Ag1 2.9645(10), Ru0–Ru4 3.1078(10), Ru1–Ru3 2.7877(11), Ru1–Ru2 2.8296(10), Ru2–Ru3 2.8173(11), Ru2–Ag1 2.8411(10), Ru2–Ru4 2.8922(11), Ru3–Ru4 2.7708(10), Ru4–Ag1 2.8366(10), Ru4–Ag2 3.0507(10), Ru5–Ru6 2.7795(11), Ru5–Ru7 2.8669(10), Ru5–Ag3 2.9646(10), Ru5–Ag2 3.0613(10), Ru5–Ru9 3.0756(11), Ru6–Ru8 2.7633(11), Ru6–Ru7 2.8534(10), Ru7–Ru8 2.8173(12), Ru7–Ag3 2.8419(10), Ru7–Ru9 2.8852(10), Ru8–Ru9 2.8061(10), Ru9–Ag3 2.8279(11), Ru9–Ag2 2.9181(10), Ag1–Cl(1 2.501(2), Ag1–Ag2 2.8199(11), Ag1–Ag3 3.3498(10), Ag2–Ag3 2.7949(10), Ag3–Cl1 2.486(2).

silver atoms in a triangular arrangement, which is in turn bridged by a chlorine atom. The Ru–Ru contacts in the bimetallic core lie in the unusually broad range between 2.7633(10) and 3.1078(10) Å (cf. $Ru_5C(CO)_{15}$),[10] the two longest distances arising between two basal ruthenium atoms bridged by silver atoms [Ru0–Ru4 3.1078(10) Å, Ru5–Ru9 3.0756(10) Å]. Consequently the geometries of the two pentaruthenium moieties of the anion are distorted from those of regular square pyramids. The silver atoms occupy two distinct environments (see Figure 1) and form an isosceles triangle with two short sides and one long side, which is bridged by the chlorine atom [Ag1–Ag2 2.8199(11) Å, Ag2–Ag3 2.7949(10) Å, Ag1–Ag3 3.3498(10) Å].

The chemical integrity of the cluster accommodated inside the MCM-41 was established by IR (Nujol mull) and EXAFS spectroscopies (Table 1). The major bands in the infrared spectrum were somewhat broader and shifted to lower energy (by about 3 cm^{-1}), which may be due to interactions with the pore wall. The structural parameters extracted from the EXAFS analysis (Ru and Ag K-edges) correspond well to those established from the single crystal X-ray structure.

Activation and anchoring of adsorbed **2** on the MCM-41 support was achieved by heating the sample under dynamic

[*] Prof. B. F. G. Johnson, Dr. D. S. Shephard, Dr. W. Zhou
The University Chemical Laboratories
Lensfield Road, Cambridge CB2 1EW (UK)
Prof. Sir J. M. Thomas, Dr. T. Maschmeyer, Dr. G. Sankar,
Dr. R. D. Oldroyd, R. G. Bell
Davy-Faraday Research Laboratories, The Royal Institution of Great Britain
21 Albemarle Street,
London, W1X 4BS (UK)
Dr. D. Ozkaya
Deptartment of Materials Science, University of Cambridge

[**] This work was supported by a ROPA award and rolling grant from the EPSRC (UK) to J. M. T., a EPSRC post-doctoral research award to B. F. G. J. and a EU Fellowship (T. M.).

 © WILEY-VCH Verlag GmbH, D-69451 Weinheim, 1997 0570-0833/97/3620-2242 $ 17.50+.50/0

Table 1. Local structural parameters from Ag and Ru K-edge EXAFS for MCM-41-supported **2**.

Absorber	Scatterer	N	R [Å]	σ^2 [Å^2]
Before thermolysis				
Ag	Cl	0.66	2.43	0.002
	Ag	1.33	2.69	0.004
	Ru	2.87	2.83	0.004
	Ag	0.66	3.36	0.010
Ru	C	2.4	1.91	0.002
	C	1.3	1.89	0.002
	C	1.0	2.06	0.002
	Ru	3.2	2.81	0.004
	Ag	1.0	2.89	0.002
	O	3.6	3.07	0.003
After thermolysis				
Ag	Ru	2.0	2.81	0.006
	Ag	2.2	2.92	0.010
	O	1.0	2.29	0.003
Ru	Ru*	5.2	2.65	0.007
	O	2.0	2.48	0.002
Two-edge refinement				
Ru	O	1.8	2.53	0.002
	Ru	4.6	2.66	0.002
	Ag	1.0	2.80	0.002
Ag	O	1.1	2.30	0.002
	Ru	1.0	2.80	0.002
	Ag	1.5	2.93	0.002

[*] Averaged environment; the Ru–Ag shell is statistically not significant due to the dominant Ru–Ru environment.

vacuum [10^{-4} Torr] for 1 hr at 473 K, during which the sample turned from pink to grey. Upon thermolysis, the CO-stretching region in the IR spectrum became featureless, and the interatomic distances as well as the coordination numbers changed dramatically as determined by EXAFS measurements obtained in situ in a custom made cell.[11] The K-edge EXAFS data, corresponding Fourier transformations, and calculated fits for Ru and Ag are given in Figure 2. The data were modeled bearing in mind the propensity of the bimetallic particle to contract and rearrange on losing its CO sheath. The structural parameters extracted from the analysis of the EXAFS spectra are summarized in Table 1. The Ag K-edge EXAFS data establish the bimetallic nature of the cluster, since, in addition to Ag–Ag interactions at 2.92 Å, the metal–metal distance of 2.81 Å, in between the bulk metal–metal distances for Ru-Ru (2.65 Å) and Ag-Ag (2.92 Å) is consistent with a Ag–Ru contact. Ru–Ru scattering is the dominant feature in the Ru K-edge data and the inclusion of a Ag–Ru shell does not result in a statistically meaningful improvement. However, we have been able to refine one combined model to both Ru and Ag K-edge data sets simultaneously using the XFIT (for Windows 95) suite of programs.[17] This procedure clearly confirms the presence of Ag–Ru contacts and establishes beyond doubt the bimetallic nature of the particles. This result highlights the importance and need of EXAFS measurements of both metals in bimetallic systems, as concentration on the Ru data only would not have been able to establish the bimetallic nature of the particles. In addition, the simultaneous two edge data refinement represent a major step forward in the structural elucidation of particles for which one scatterer dominates.

In addition to the metal–metal contacts, there is clear evidence of the light scatterer oxygen, in the case of Ag at a distance of 2.30 Å (close to a covalent Ag-O bond) and in the case of Ru at a distance of 2.53 Å (most likely associated with a surface oxygen, as such anchoring metal–O distances have been observed in other supported catalysts and zeolitic materials[12]). These structural features are consistent with the model of the carrier-bound bimetallic cluster shown in Figure 3, which is about 12 Å across. It should be noted that the interatomic dis-

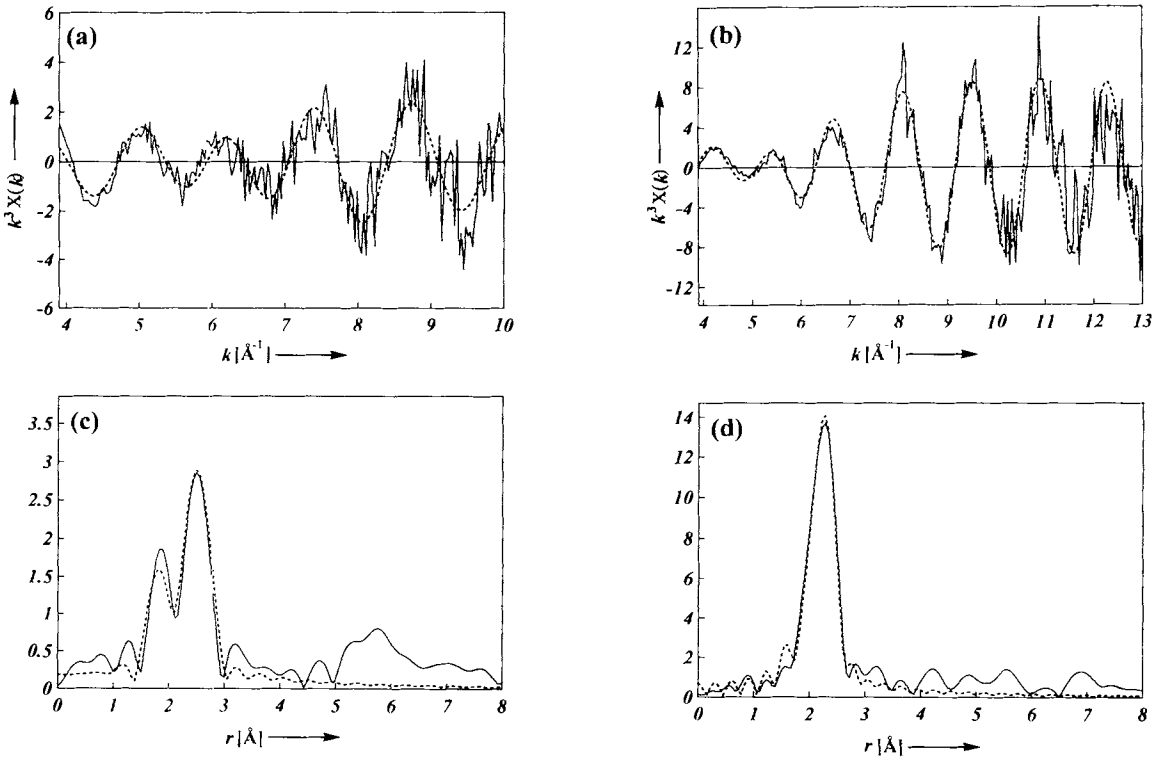

Figure 2. EXAFS data for **2** after thermolysis (Ag K-edge (a) and Ru K-edge (b)), and their Fourier transforms (Ag K-edge (c) and Ru K-edge (d)). Solid lines represent observed data, and dashed lines the fitted curves. The fits shown are obtained from simultaneous two-edge refinement.

 © WILEY-VCH Verlag GmbH, D-69451 Weinheim, 1997 0570-0833/97/3620-2243 $ 17.50+.50/0

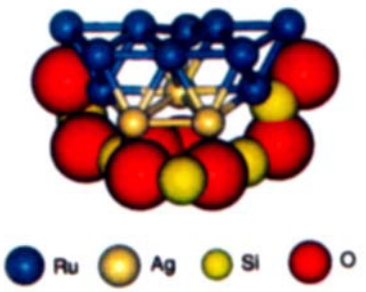

Figure 3. A possible structure of nanoparticles of the bimetallic catalyst anchored inside MCM-41 generated from **2** by thermolysis (see text).

tances of the metal atoms are larger than expected for small metal particles and approach those of the bulk metals. This may be due to the surface interaction with the particle and their bimetallic nature. Different starting clusters can yield contractions,[13] possibly pointing to different particle shapes (for example, spherical versus flat, yielding contraction and expansion, respectively).

Conventional high-resolution electron microscopy (*JEOL* 200CX TEM microscope) of the heat-treated material yielded the bright-field image shown in Figure 4, viewed perpendicular

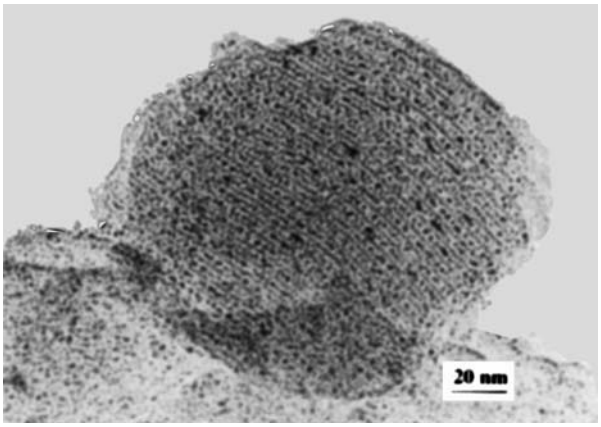

Figure 4. A bright-field HRTEM micrograph of **2** after heat-treatment showing alignment of particles (about 15 Å inddiameter) inside the channels.

to the pore axis. The uniform distribution of the bimetallic nanoparticles, aligned along the channels, is clearly discerned.[14] A scanning transmission electron microscope (STEM, *Vacuum Generators HB501* equipped with a field-emission gun) yielded the high-resolution, annular-dark-field (so-called *Z* contrast) image (Figure 5, top left) and the bright field image (Figure 5, top right). Electron-induced X-ray emission maps (Figure 5, bottom) further confirm the spatial uniformity of the distribution of the nanoparticles.[15]

The catalytic performance of the activated, supported bimetallic particles was tested for hydrogenation of hex-1-ene to hexane. Initial experiments show a high selectivity (in excess of 99%) and a turnover frequency of at least 6300 mol hexane per mol $[Ag_3Ru_{10}]$ per hour.[16]

Experimental Section

Synthesis of **2**: Reaction of $[Ru_6C(CO)_{15}]^-$ [18] with $AgBF_4$ (3 equiv) and $(Ph_3)_2NCl$ (PPN-Cl, 1 equiv) or $(Ph_3)_4AsCl$ (TPACl) in dichloromethane gave a ruby red solution within 10 min. The reaction was monitored by infrared spectroscopy in the $\tilde{\nu}$(CO) region, which showed the growth of a new set of bands at 2053 (s), 2024 (vs), 2001 (vs), and 1830 (br s) cm^{-1}. Addition of a small amount of hexane/ether gave a deep red precipitate showing the same profile in the $\tilde{\nu}$(CO) region. In a similar synthesis in which no Cl^- was added, a similar red solution was

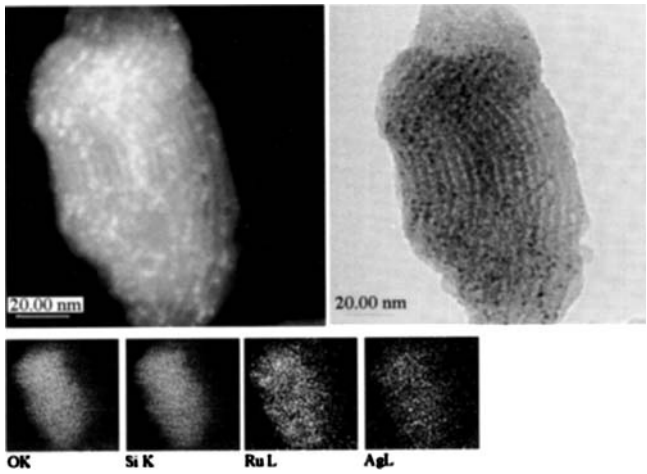

Figure 5. High-resolution annular dark-field (*Z* contrast) and bright-field scanning transmission electron micrographs (top left and right, respectively) of adsorbed PPN-**2** in MCM-41 after heat treatment at 150 °C for 1 h. Bottom: Electron-induced X-ray emission maps of the same sample.

produced; however, the resulting compound has proved difficult to isolate and characterize. Positive fast atom bombardment (FAB) mass spectrometry also showed only peaks assignable to the presence of PPN^+ or TPA^+, whilst negative FAB mass spectrometry of the PPN salt gave broad peaks at *m/z* 2718, 2550, 2178, and 2011. The highest peak was tentatively assigned to $\{[Ru_5C(CO)_{14}]_2Ag_3Cl \cdot PPN\}^-$ (calcd 2717), whilst the peak at 2178 corresponds to $\{[Ru_5C(CO)_{14}]_2Ag_3Cl\}^-$ (calcd 2178). Elemental analysis gave 31.18% C, 1.20% H, 0.00% N (calcd for $C_{78}H_{40}Ag_3As_2Cl_1O_{28}Ru_{10}$ gives 31.81% C, 1.37% H).

Crystals of the TPA salt of **2** suitable for a single crystal X-ray diffraction study were grown from a solution mixture of dichloromethane/ethylacetate into which pentane was allowed to diffuse at about 253 K. Crystal data for $[Ag_3Ru_{10}C_2(CO)_{28}Cl][Ph_4As]_2$: $C_{79}H_{42}Ag_3As_2Cl_3O_{28}Ru_{10}$, $M = 3039.63$, triclinic, space group $P\bar{1}$, $a = 14.6991(5)$, $b = 26.1473(8)$, $c = 12.7729(4)$ Å, $\alpha = 102.146(2)$, $\beta = 112.439(3)$, $\gamma = 82.522(2)°$, $U = 4429.1(2)$ $Å^3$, $\rho_{calcd} = 2.272$ $g\,cm^{-3}$, $Z = 2$, $Mo_{K\alpha}$ radiation, $\lambda = 0.71069$ Å, $\mu = 3.206$ mm^{-1}, $T = 153(2)$ K. Data were collected on a Rigaku AFC7 image plate diffractometer for an RS 3000 coated, rapidly cooled crystal of dimensions $0.40 \times 0.30 \times 0.10$ mm, mounted directly from solution (T. Kottke, D. Stalke, *J. Appl. Crystallogr.* **1993**, *26*, 615) by the θ/ω method ($3° < 2\theta < 50°$). Of a total of 23085 reflections collected, 13750 were independent ($R_{int} = 0.0642$). The structure was solved by direct methods (SHELXTL PLUS, SHELXL-93, Göttingen Univeristy, **1993**) and refined by full-matrix least-squares analysis on F^2 with $R_1(F > 4\sigma(F)) = 0.0603$ and wR_2(all data) = 0.1724. H atoms were placed in calculated positions and allowed to refine riding on their C atoms. Largest peak/hole in final difference map: 3.677/ − 2.085 e $Å^{-3}$. Crystallographic data (excluding structure factors) for the structure(s) reported in this paper have been deposited with the Cambridge Crystallographic Data Centre as supplementary publication no. CCDC-100617. Copies of the data can be obtained free of charge on application to The Director, CCDC, 12 Union Road, Cambridge CB2 1EZ, UK (fax: int. code +(1223)336-033; e-mail: deposit@chemcrys.cam.ac.uk).

Adsorption of PPN-**2** into MCM-41: PPN-(**2**) was slurried in ether with MCM-41 (3:10 *m/m*) for 48 h in which time the white mesoporous silica became pink in color. The ether was removed by filtration and the solid dried under high vacuum [0.01 mmHg] at ambient temperature.

HRTEM of activated **2**: The dry sample ground in air was deposited on a copper grid with a carbon film, transferred to a Jeol TEM-200CX electron microscope operating at 200 kV, and kept in the microscope vacuum overnight. The images were recorded at 49000-fold magnification.

The EXAFS data were analyzed with the XFIT (for Windows 95) [17] and EXCURVE suites of programs. The simultaneous refinement of two edges was performed with XFIT (WIN95). The S_0^2 parameters were taken from the single-edge refinements and held constant. The σ^2 parameters were constrained to be equal for the silver and ruthenium atoms. Two E_0 parameters were included in the model, one for silver and one for ruthenium. All parameters (coordination numbers, distances, E_0, and σ^2 values) were refined simultaneously. The precise fitting protocol and theoretical underpinning will be published elsewhere.

Hydrogenation of hex-1-ene: A 200 mL teflon-lined autoclave equipped with a magnetic follower was charged with catalyst (20 mg), hex-1-ene (3.0 mL), and H_2 (65 atm). The ensemble was heated to 393 K for 4 h, after which the vessel was cooled to ambient temperature, and the contents were analyzed by ^1H NMR to reveal greater than 99% conversion to *n*-hexane.

Received: March 12, 1997 [Z10233IE]
German version: *Angew. Chem.* **1997**, *109*, 2337–2341

 © WILEY-VCH Verlag GmbH, D-69451 Weinheim, 1997 0570-0833/97/3620-2244 $ 17.50+.50/0

Keywords: clusters · electron microscopy · EXAFS spectroscopy · heterogeneous catalysis · mesoporosity

[1] J. H. Sinfelt, *Bimetallic Catalysts*, Wiley, New York, **1983**, and references therein; J. H. Sinfelt, *Int. Rev. Phys. Chem.* **1988**, *7*, 281.
[2] J. S. Beck, J. C. Vartuli, *Curr. Opinion Solid State Mater. Sci.* **1996**, *1*, 76.
[3] D. A. Antonelli, J. Y. Ying, *Curr. Opinion Colloid Sci.*, **1996**, *1*, 523.
[4] T. Maschmeyer, F. Rey, G. Sankar, J. M. Thomas, *Nature*, **1995**, *378*, 159.
[5] R. D. Oldroyd, J. M. Thomas, T. Maschmeyer, P. A. MacFaul, D. W. Snelgrove, K. U. Ingold, D. D. M. Wagner, *Angew. Chem.* **1996**, *108*, 2966; *Angew. Chem. Int. Ed. Engl.* **1996**, *35*, 2787.
[6] J. M. Thomas, *Faraday Discuss.* **1996**, *105*, 1.
[7] D. Ozkaya, J. M. Thomas, W. Zhou, unpublished.
[8] M. A. Beswick, Dissertation, University of Cambridge, **1992**, and references therein; M. A. Beswick, J. Lewis, P. R. Raithby, M. C. Ramirez de Arellano, *Angew. Chem.* **1997**, *108*, 303; *Angew. Chem. Int. Ed. Engl.* **1997**, *36*, 291.
[9] S. J.Taverner, J. H.Clark, G. W.Gray, P. A.Heath, D. J.Macquarrie, *J. Chem. Soc. Chem. Commun.* **1997**, 1073.
[10] C. R. Eady, B. F. G. Johnson, J. Lewis, *J. Organomet. Chem.* **1979**, *57*, C82.
[11] P. A. Barrett, G. Sankar, C. R. A. Catlow, J. M. Thomas, *J. Phys Chem.* **1996**, *100*, 8977.
[12] M. Vaarkamp, J. T. Miller, F. S. Modea, D. C. Koningsberger, *J. Catal.* **1996**, *163*, 294; M. Vaarkamp, B. L. Mojet, M. J. Kappers, J. T. Miller, D. C. Koningsberger, *J. Phys. Chem.* **1995**, *99*, 16067.
[13] Unpublished results.
[14] The sample was unstable under the electron beam, and therefore images were recorded at low magnification. In this case no structural fringes from the particles could be discerned, and the size of the black dots (about 15 Å) do not necessarily correspond to the size of the real particles.
[15] The *Z*-contrast image is formed from electrons scattered through wide angles (50 to 250 mrad). Such an image is formed from electron beams that have undergone Rutherford scattering, in which the intensity of the signal is proportional to Z^2, where Z is the atomic number of the scattering atom. A. V. Crewe, J. Wall, *J. Mol. Biol.* **1970**, *48*, 375.
[16] This compares very favorably with a TOF of 250 h^{-1} given in E. Linder, M. Haustein, R. Fawzi, M. Steinmann, P. Wegner, *Organometallics* **1994**, *13*, 5021 for homogeneous ruthenium hydrogenation catalysts under similar conditions.
[17] XFIT (for Windows95), P. J. Ellis, H. C.Freeman, *J. Synchroton Radiation* **1995**, *2*, 190.
[18] B. F. G. Johnson, J. Lewis, W. J. H. Nelson, J. N. Nicholls, J. Puca, P. R. Raithby, M. J. Rosales, M. Schroder, M. D. Vargas, *J. Chem. Soc. Dalton Trans.* **1983**, 2447.

Chemistry at the crossroads

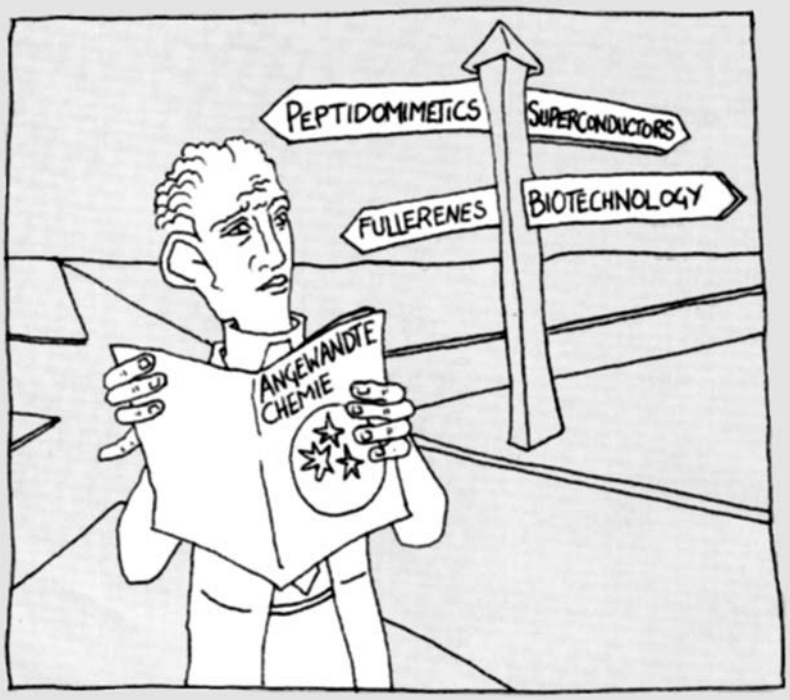

Pioneering scientists guide your way through newly charted territory with their topical reviews and discriminating highlights in **Angewandte Chemie.**

To start your own personal subscription, just fax.

An order form is provided on the last page for your convenience.

WILEY-VCH

 © WILEY-VCH Verlag GmbH, D-69451 Weinheim, 1997 0570-0833/97/3620-2245 $ 17.50+.50/0

Modern Materials

The Chemistry of Ceramics. Edited by *H. Yanagida, K. Kuomoto and M. Miyayama.* John Wiley & Sons, Chichester, 1996. 263 pp., hardcover £ 19.99.—ISBN 0-471-96733

Engineering ceramics or high-performance ceramics are playing an increasingly important role in the development of new technologies, especially in the fields of microelectronics and telecommunications, automotive and turbine engineering, power generation, medical technology, and special materials such as cermets. In this book, which is an English translation of the second edition of a monograph first published in 1993, the editors' main aim was to present the basic chemistry and physics of this new class of constructional materials. The detailed engineering and technical aspects of ceramics, such as processing methods or fracture mechanics, are only touched on at an elementary level.

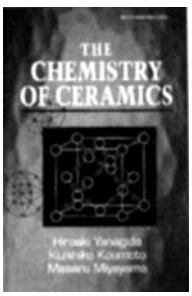

The work consists of just four chapters, resulting in a structure that is clear and easy to grasp. The first chapter is an introduction which explains the special importance of ceramic materials, reviews their history and the present situation, and considers the potential for future developments.

The second chapter describes the characteristic solid state structures of ceramics and glasses. The crystal structures are classified according to the coordination number and the arrangement of the ions. Point defects and dislocations, which are of fundamental importance for understanding the relevant powder processing technology and the properties of polycrystalline materials, are treated in detail. The microstructures of both dense sintered and porous materials in molded components are then described, and are related to their properties. Surface structures are discussed, first in a general way, then with special reference to thin films, fibers, and interfaces.

For a thorough understanding of solid state syntheses and the properties of the resulting materials it is essential to have a detailed knowledge of the different reactions that can occur in ceramics, especially at high temperatures. Therefore the third chapter begins by concentrating on phase equilibria, phase diagrams, and phase transformations. Diffusion and mass transport in solids, and the many different types of reactions that solids can undergo with gases or liquids, are treated in detail. These discussions then provide the basis for a section devoted to the sintering processes that play a key role in the compaction of ceramic powders, and make possible the manufacture of a variety of technologically important refractory materials. The development of suitable sintering methods has made it possible to produce a whole range of new synthetic ceramics with especially valuable properties, such as those based on barium or aluminum titanates, zirconium dioxide, silicon nitride, and silicon carbide. As well as dealing with the purely physical fundamentals of sintering, the chapter also describes the most important technological compaction processes. This part ends with a description of processes for manufacturing ceramic powders, thin films, fibers, porous structures, and composite materials.

The final chapter is devoted to the physical properties of ceramic materials in relation to their technological applications. These are discussed under the headings of thermal properties (melting point, coefficient of expansion, thermal conductivity), electrical and magnetic properties, and optical, mechanical, and chemical properties. The treatment of electrical and magnetic properties is quite detailed, but some of the other properties, such as corrosion behavior, are only covered rather superficially. A more extensive and thorough treatment of these aspects in a future edition would add further to the generally very favorable impression given by this monograph.

In its structure and content *The Chemistry of Ceramics* is an excellent textbook which provides a good treatment of the fundamental relationships between the structure and properties of modern technical ceramics. It can therefore be recommended unreservedly for chemistry students specializing in solid state chemistry, and for students of materials science subjects and applied mineralogy.

Ralf Riedel
Fachbereich Materialwissenschaft
der Technischen Hochschule Darmstadt
(Germany)

CVD of Nonmetals. Edited by *W. S. Rees Jr.* VCH Verlagsgesellschaft, Weinheim, 1996. 424 pp., hardcover DM 238.00.—ISBN 3-527-29295-0

This book is a further addition to those recently published by VCH Verlagsgesellschaft on the topical theme of chemical vapor deposition (T. Kodas, M. Hampden-Smith, *The Chemistry of Metals CVD*, 1994; A. C. Jones, P. O'Brien, *CVD of Compound Semiconductors*, 1996).

Chapter 1 is a short introduction which explains how the book should be used, and briefly summarizes the basic principles of physical and chemical gas phase deposition techniques. The reader wishing to gain a deeper insight should consult the more advanced literature listed in the bibliography. The topics treated in the main text are: superconductors (Ch. 2, D. L. Schulz and T. J. Marks), nonmetallic (transparent) conductors (Ch. 3, T. Gerfin and K.-H. Dahmen), compound semiconductors (Ch. 4, G. S. Tompa), insulators (Ch. 5, A. R. Barron), and structured ceramics and composites (Ch. 6, W. J. Lackey). The book ends with a chapter by G. E. Kräuter and W. S. Rees entitled "Other Materials", in which the authors have carefully gathered together all the topics that would not naturally fit in under any of the other headings.

This section contains book reviews and a list of new books received by the editor. Book reviews are written by invitation from the editor. Suggestions for books to be reviewed and for book reviewers are welcome. Publishers should send brochures or (better) books to the Redaktion Angewandte Chemie, Postfach 101161, D-69451 Weinheim, Federal Republic of Germany. The editor reserves the right of selecting which books will be reviewed. Uninvited books not chosen for review will not be returned.

A focus of considerable interest in this area, as in CVD methods generally, is the chemistry of the starting materials. On this aspect one is helped by the very detailed documentation that the editor has provided, with about 1230 literature references extending up to 1993/94. The book is intended for a heterogeneous readership with backgrounds in different disciplines. Thus the users are likely to include, among others, synthetic organometallic chemists, electrical engineers, and solid state physicists whose common interest is an involvement in the design and manufacture of novel types of microelectronic components.

The chapter on superconductors is especially interesting and well written. The established systems such as Nb_3Ga and Nb_3Sn are compared with the new ceramic high temperature superconductors (Section 2.4, pp. 67–132). The problems of producing these materials from organometallic precursors by CVD or VPE (vapor phase epitaxy) are discussed in detail. For example, Section 2.4.1.2 (pp. 71 ff) considers "Limitations of Alkaline Earth β-Diketonate Complexes for HTS CVD", and describes recent developments (e.g., the use of an alternative precursor for the barium component). The comparison of different methods for introducing the relatively involatile precursors (β-diketonates and β-ketoiminates) is well worth reading. The following section, "Conducting Materials", is mainly concerned with TiN, In_2O_3, SnO_2, and ZnO. There is an interesting and useful description of the recently clarified mechanistic details of the breakdown of the tetrakis-dialkylamidotitanium precursor to give TiN or TiN_xC_y, a reaction which depends critically on the process conditions (thermal CVD with or without NH_3, or plasma methods). This part of the book is highly recommended; it is well structured and carefully written, and is ideally suitable to be adapted for use in undergraduate courses related to materials chemistry. Aspects such as the interaction between the surface and the chemistry of the gas phase, the effects of different process conditions (reactor type, means of energy supply), positionally selective deposition, prenucleation in the gas phase, purity, electrical and morphological properties, mechanisms that incorporate carbon, transamination, labeling studies, and plasma chemistry, are treated concisely but thoroughly. For completeness CVD of compound semiconductors is briefly discussed in Chapter 4. However, this subject is already covered by some other excellent monographs (examples are those mentioned above and: G. B. Stringfellow, *Organometallic Vapor Phase Epitaxy*, Academic Press, 1989). The book does not cover new trends in the chemistry of precursors. Chapter 5 deals with the important topic of the deposition of electrically insulating layers, and also extends the analogy to discuss "chemically insulating" films, such as diffusion barriers and passivating layers. The materials discussed include SiO_2, Al_2O_3, AlN, and Si_3N_4.

Chapter 6 describes methods for deposition from the gas phase onto ceramic fibers and various types of composites, for example porous materials treated by chemical vapor infiltration. Here again the deposited materials are mainly oxides of aluminum, zirconium, and tin, and in some cases SiC. Thus, from the chemical point of view there is little here that is new. Instead the emphasis is on aspects such as reactor design, a very detailed description of the processes involved, and the analysis of the morphology and materials properties of the layers produced.

Chapter 7, which occupies the last 20 pages of the book, presents an interesting collection of research results taken from the widely scattered sources in the literature. These relate to a wide variety of deposited substances, from metal fluorides via metal carbides to metal tellurides.

On the whole the book has been carefully written and produced. However, the quality of the figures is not consistently good, and a few are disappointingly crude in appearance; for example one may contrast Figure 1-3 with Figure 6-1. It is also noticeable that the literature coverage only extends to about 1993/94, and is mainly concentrated within the years 1988 to 1993. There are scarcely any references to more recent developments from 1995 onward. Nevertheless, the work is a useful additional resource, both for molecular chemists with an interest in this field and for users of vapor deposition, and will provide them with quick and convenient access to the literature on CVD of nonmetals.

Roland A. Fischer
Anorganisch-chemisches Institut
der Universität Heidelberg (Germany)

Introduction to glass science and technology. By *J. E. Shelby*. Royal Society of Chemistry, Cambridge, 1997. 244 pp., paperback £ 18.95.—ISBN 0-85404-533-3

This book, written by a well recognized glass scientist, is intended as an introduction for students or beginners. The material is limited to what can be covered in a single semester of course work, and assumes no more than a general knowledge of physical and inorganic chemistry. Depending on the extent of prior knowledge, the reader will therefore find that some chapters can be read more quickly than others. Each of the ten chapters of the book, with one exception, ends with a concise summary. The bibliography is necessarily short, due to the brevity of monography although somewhat one-sided, and the index is sufficiently detailed.

The first two chapters deal with the principles of glass formation and glass melting, including technological aspects such as the formation of bubbles or inhomogeneities. Immiscibility and phase separation is discussed in a separate chapter. The attempt to elaborate the structures of glasses in only 37 pages is obviously only possible in a very limited way. Although the author emphasizes that he wants to restrict himself to general principles (including the trivial statement: "... the author now proposes the Fundamental Law of Structural Models: 'no model can be considered to be valid unless that model can explain *all* of the available data' "), he does not always meet this claim, and sometimes loses himself in details that are out of place in a book of this kind. For example, there are mini-subchapters on rare earth alumino/galliosilicate glasses, fluorogermanate glasses, and $ZnCl_2$ glasses. Instead a little more space could have been allocated to the treatment of organic and metallic glasses, which are given only half a page each. The viscosity of glass-forming melts is treated in a fairly general way in the following chapter, which also includes a section on viscosity measurement techniques. The next chapter discusses the influence of composition, thermal history, phase separation and crystallization, radiation exposure, and pressure on the density and thermal expansion behavior of glasses. Under the heading "Transport Properties", a concise general introduction to the fundamentals of diffusion is followed by discussions of ionic diffusion, ion exchange, ionic conductivity, chemical durability, weathering, gas permeation, and diffusion. In the chapters on mechanical and optical properties a more detailed discussion of how these are related to the structure and composition of glasses would have been desirable. The title of the final chapter, "Glass Technology", is rather misleading, as it deals with forming methods. Its 12 pages are definitely insufficient to give more than a rough overview. For example, the one page on sol–gel processing is hardly enough to give the uninformed reader a clear impression of this method.

 © WILEY-VCH Verlag GmbH, D-69451 Weinheim, 1997 0570-0833/97/3620-2248 $ 17.50+.50/0

In summary, the author has succeeded in writing a comprehensible introduction to glass science. The diagrams are clear, and the use of physical and chemical formulas is restricted to an essential minimum. Of course, one can have different opinions on the weighting of the different topics in such a book. The book cannot be recommended as a *textbook* on glass, but, in accordance with the intentions of the author, as an introductory overview dealing with all important aspects.

Ulrich Schubert
Institut für Anorganische Chemie
der Technischen Universität Wien
Vienna (Austria)

Chemistry of Powder Production. (Series: Powder Technology.) By *Y. Arai.* Chapman & Hall, London, 1996. 281 pp., hardcover £ 69.00.—ISBN 0-412-39540-1

This book is an English translation of the original Japanese version published in 1987. Consequently it does not cover the latest methods for the production and characterization of powders, but describes conventional and well-established methods. The book can therefore best serve as an introduction to powder technology, which now plays an increasingly important role in the manufacture of high-performance materials such as polymers, metals, and ceramics. Materials in powder form are also important in the areas of pharmaceuticals and agricultural products. A large proportion of modern industrial manufacturing involves the production and processing of raw materials in powder form.

The book consists of five chapters covering the basic principles of the production of powders and measurements of powder properties. The main part of the contents is arranged under three subject areas: the physical properties of powders (Chapter 3), the production of powders (Chapter 4), and methods for the measurement and analysis of powder properties (Chapter 5).

Chapter 1 is an excellent introduction, which begins by discussing what is meant by a powder, and goes on to give a definition. According to this, powders can be regarded as a fourth state of matter alongside the three aggregated states: gas, liquid, and solid. The powder state has features in common with all the latter three. The essential differences between a powder and a bulk solid are discussed in terms of their characteristic physical properties. Lastly, the author explains the distinction between powders and granular materials on the basis of their typical particle size ranges.

Chapter 2 discusses powder specifications by considering various examples: ceramic sintering powders, powders for magnetic applications (e.g., sound recording), and pigment powders for use in plastics, paints, and paper. The different combinations of properties needed for each of these three areas of application are described. In each case the author explains how the critical properties of the powder (e.g., sintering behavior, magnetic induction at saturation, coloring power) are affected by the size and/or shape of the particles.

Chapter 3 is concerned with the fundamental physical properties of powders. The main aspects treated are particle size, structure, surface energy, and surface properties such as adsorption behavior, wettability, and catalysis. Mechanochemistry, i.e. the influence of mechanical energy input on the physical and chemical properties of powders, is also included here.

Chapter 4 deals with methods for manufacturing powders. A distinction is drawn between purely physical processes, such as comminution or milling, and the thermal decomposition of inorganic or organic metal salts to yield finely-divided ceramic powders, where the chemical decomposition reactions determine the constitution of the product. Another important topic discussed is the precipitation of solids from liquid phases (especially solutions). The chapter deals with the mechanistic details of nucleation, or of processes where a precipitate is laid down on a substrate, as well as crystal growth, hydrolysis of metal alkoxides, and hydrothermal reactions. Next the author discusses the production of powders by gas phase reactions, with special attention to the thermodynamics of the formation of oxide and non-oxide powder particles from the gas phase. The chapter ends by considering the internal structure of the solid phase, and discusses solid state reactions, a fundamental understanding of which is important in the production of ceramics from powders.

Having thus dealt with the production of powders, the final chapter is devoted to their properties, which are of crucial importance for technological applications. The physicochemical methods used for studying the properties of powders are discussed in detail. The central topics are particle size analysis and the measurement of surface properties (wetting energy, surface energy, heat of adsorption, zeta potential, and surface activity).

Considering the book as a whole, its special virtues are the orderly arrangement of the material and the easily understandable presentation of the main features. At the end of each chapter is a list of references which includes the most important original papers on the subjects covered. However, it is unfortunate that the chapters are not as up-to-date as they should be. If the translation from the Japanese had been combined with a thorough revision and enlargement, the result would have been an up-to-date standard work of great value for both teaching and research. Bearing in mind this limitation, the book can be recommended mainly for advanced or postgraduate students of chemistry, mineralogy, or materials science, who wish to learn about the fundamentals of powder technology, and more particularly about the production, characterization, and properties of inorganic powders.

Ralf Riedel
Fachgebiet Disperse Feststoffe
der Technischen Hochschule
Darmstadt (Germany)

Hydrocarbon Resins. By *R. Mildenberg, M. Zander* and *G. Collin.* WILEY-VCH, Weinheim, 1997. 179 pp., hardcover DM 198.00.—ISBN 3-527-28617-9

Synthetic hydrocarbon resins consist of rather complex oligomers and monomers which are derived from coal tar, cracked petroleum, and turpentine feedstocks. Such resins—frequently consisting of complicated reaction products and blends of numerous compounds—find many applications in formulated multicomponent systems such as adhesives, coatings, printing inks, packaging, sealants, paints, wood protection treatments, surface modification treatments, foundry industry chemicals, mineral oil additives, flooring, etc.

The authors of the book *Hydrocarbon Resins* have compiled information about raw materials, production processes, methods of characterization, and chemical and physical properties of hydrocarbon resins, excluding natural resins. Special emphasis is placed upon applications and opportunities for improving performance of formulated products in specific end uses. The aim of the book is to provide background information on hydrocarbon resins for chemists, engineers, applications technologists, and sales personnel, who are concerned with production and quality control of products involving hydrocarbon resins.

The book is organized in nine chapters: 1. terminology (2 pp.); 2. raw materials

 © WILEY-VCH Verlag GmbH, D-69451 Weinheim, 1997 0570-0833/97/3620-2249 $ 17.50+.50/0

for the manufacture of resins such as indene–cumraone resins, petroleum-based resins, dicyclopentadienes, or polyterpenes (14 pp.); 3. resin manufacture including resin modification (21 pp.); 4. resin structure and properties (34 pp.); 5. applications (80 pp.); 6. chemical composition and resin selection (6 pp.); 7. quality and quality assurance (2 pp.); 8. toxicology and legal aspects (4 pp.); 9. economic aspects (4 pp.). Instead of writing a concise manual, the authors have preferred to summarize their extensive practical experience. The applications section describes some specific formulations, and offers advice on incorporating hydrocarbon resins in formulated products.

In conclusion, this very specialized book represents a valuable asset for everybody who does not have hands-on experience with hydrocarbon resins and is planning to exploit the potential of hydrocarbon resins in formulated systems or to solve quality control problems. Unfortunately, there are only 46 literature references, which is not adequate to give access to more detailed information on specific topics.

Rolf Mülhaupt
Institut für Makromolekulare Chemie
der Universität Freiburg (Germany)

Chemometrics in Environmental Analysis. By *J. W. Einax, H. W. Zwanziger* and *S. Geiss*. WILEY-VCH, Weinheim, 1997. 384 pp., hardcover DM 238.00.—ISBN 3-527-28772-8

Chemometrics is a relatively new discipline that is undergoing great developments, not least in its applications to environmental analysis using automated multielement and multicomponent instrumental methods. Modern analytical techniques generate a vast amount of data, and to digest this and arrive at a description of complex environmental processes requires powerful mathematical and statistical methods. For this reason, chemometrics is important to everyone working in the area of environmental analysis.

From the first chapter the reader learns that chemometrics may be defined as a chemical discipline in which mathematical and statistical methods are used to design measurement procedures and experiments or to choose the best alternatives, and then to analyze the resulting data so as to extract the maximum amount of chemical information. From this definition one can already form a first impression of the potential applications of chemometrics.

The book is divided into two main parts. The first part consists of five chapters that are essentially concerned with methods, dealing with the mathematical fundamentals of chemometrics and illustrating these with examples from environmental analysis. The second part (four chapters) is more problem-orientated, and describes applications of chemometrics, dealing in turn with specific types of problems related to the interpretation of analytical data or with sampling strategies.

About one-half of the first part is devoted to methods for the analysis of multivariate data and of time series. As well as graphical methods such as box–whisker plots, Chernoff diagrams, and time series plots, the authors describe in detail the most important mathematical methods (cluster analysis, principal components analysis, factor analysis, multivariate variance analysis, smoothing and filtering, regression and correlation techniques, ARIMA modeling, etc.). The methods are illustrated and put into a practical context by including examples of applications in environmental analysis, with numerical data (e.g., comparative studies of analytical results from different laboratories, or the variation with time of the nitrate concentration in a drinking water reservoir). This makes the book especially interesting for the analyst who has not yet begun to make serious use of chemometrics.

This first part also familiarizes the reader with all the important aspects of the statistics of experimental data, factorial and sequential design of experiments, and the planning of sampling procedures. Designing a system to give truly representative sampling is a very important aspect of environmental analysis, and accordingly it is considered in more detail, with up-to-date practical examples, in the second part.

The second part of the book, entitled "Case Studies", has separate sections devoted to the three main environmental matrices: atmosphere, hydrosphere, and pedosphere. These are followed by a further section on the applications of chemometrics in food research and in optimizing an analytical method. Each section begins by describing a topical problem in environmental analysis, then explains how various chemometric methods can be used to plan the sampling procedure, analyze the data output, and interpret the results. The chapter on the pedosphere (soil) contains a discussion of the problems that arise in studying the deposition of heavy metals, including the planning of methods for representative sampling, the minimum number of samples needed, and comparing the burden of pollutants at different sites. The chapter describes how these problems are approached using chemometric methods such as principal components anaysis, MANOVA, and discrimination analysis. From this part of the book the reader gains an appreciation of the scope of chemometrics, and is prompted to refer back to the first part to learn more about the methods applied here.

Each chapter includes a list of references, extending up to 1995 in most cases. This should be useful also for readers who already have a good knowledge of chemometrics.

In summary, this is a very clearly written and easily readable book. The typesetting is clear, including the mathematical formulas, and the figures help the reader's understanding, although they are not of a uniformly high quality. It can be thoroughly recommended for all analytical chemists who wish to learn about chemometrics and its applications to environmental analysis, without having to work only through a rigorous mathematical description of the methods.

Christian Zwiener
Engler-Bunte-Institut der Universität
Karlsruhe (Germany)

Inorganic Chemistry. An Industrial and Environmental Perspective. By *T. W. Swaddle*. Academic Press, San Diego, 1997. 428 pp., hardcover $ 65.00.—ISBN 0-12-678550-3

Writing a new book on inorganic chemistry is an ambitious task, as there are already such a large number of comprehensive treatments of the subject. Nevertheless, Thomas W. Swaddle has set out to do just that. He teaches as Professor of Inorganic Chemistry at the University of Calgary (Canada), and this is his second book on the subject. Although it was originally conceived as a textbook for undergraduates, the author intends that in its now completed form it will also enable a broader public to appreciate the role of inorganic chemistry in modern life and its importance for industry and care of the environment, as well as being a convenient reference source for scientists, technologists, and students.

The 19 chapters cover a wide range of topics in general and inorganic chemistry. As well as explaining important concepts of thermodynamics and kinetics, the book contains several rather theoretically oriented chapters discussing the crystal structures of metals and salts, the main types of defects present in non-ideal solids, and some aspects of electrochemistry and complex chemistry. The author

 © WILEY-VCH Verlag GmbH, D-69451 Weinheim, 1997 0570-0833/97/3620-2250 $ 17.50+.50/0

then builds on this basic knowledge by describing the types of inorganic reactions that occur and their practical applications, such as the separation and refining of metals, corrosion and corrosion protection, the principles of batteries and fuel cells, and the manufacture of industrial diamonds. The reader is introduced to topics such as zeolites and their uses in washing powders and as catalysts, and to inorganic fertilizers, building materials, and different types of explosives, to mention just a few examples. Catalytic processes are discussed in detail in the chapters on "Inorganic Solids as Heterogeneous Catalysts" and on "Organometallics". Some examples of other topics covered in the book are water treatment processes, the greenhouse effect, the depletion of the ozone layer caused by the use of CFCs, and technologies for reducing emissions of sulfur and nitrogen oxides in flue gases.

The standard of writing and production is excellent. The principles are clearly explained and are illustrated by interesting examples. Consequently the book makes agreeably easy reading and invites browsing. At the end of each chapter there are some exercise problems and a very comprehensive list of references for further reading, enabling the reader to build on the foregoing material. On the other hand, the discussions are often rather superficial and seldom go much beyond providing a basic knowledge. The choice of topics seems a little haphazard and could not be described as comprehensive. The reader seeking an overview of the most important compounds of a particular element, or of the different processes for manufacturing a given product, will be disappointed in many cases. Moreover, finding such information is made more difficult by the fact that the material is not arranged under elements or compound classes. For example, α-sulfur (S_8), polysulfanes, and polythioacids appear in Chapter 3 ("Catenation: Inorganic Macromolecules"), oxides of sulfur in Chapter 8 ("The Atmosphere and Atmospheric Pollution"), and sulfates in Chapter 9 ("N, P and K in Agriculture"). The manufacture of sulfur and sulfuric acid is described in Chapter 10 ("Sulfur and Sulfur Compounds"), but the main emphasis in this chapter is on paper manufacturing processes based on sulfur compounds. Lastly we find sulfides in Chapter 17 ("Extractive Metallurgy"). Many inorganic substances, including some that are of great technological importance, are not covered at all. Thus, although Chapter 3 treats diamond and the fullerenes in great detail, some other forms of carbon such as graphite and carbon black are mentioned only briefly or not at all.

To summarize, this book can provide the newcomer to inorganic chemistry with a good first insight into a variety of interesting topics, but it cannot be recommended as a comprehensive textbook nor as a work of reference.

Steffen Hasenzahl
Degussa AG, Hanau (Germany)

NMR Data Processing. By *J. C. Hoch* and *A. S. Stern*. John Wiley & Sons, Chichester, 1996. 196 pp., hardcover £ 50.00.—ISBN 0-471-03900-4

Pulsed nuclear magnetic resonance spectroscopy generates time domain signals that have to be transformed to obtain a spectrum. The present book shows in a convincing manner that there are other ways of doing this besides the usual Fourier transformation, and that they can sometimes even yield better results.

The book begins with a flashy introduction about NMR signal processing, featuring Richard Ernst, 26 years before his Nobel Prize award, performing the first pulsed Fourier transform NMR measurement. It is pointed out that the signal processing methods now used in multidimensional NMR spectroscopy have only become possible as a result of the breathtaking development of computer performance during the last 20 years. The time domain signal or free induction decay (FID) is then introduced.

Chapter 2 deals with the fundamentals of digitization in the time and amplitude domains in the context of Fourier transformation, and introduces all the important concepts such as the Nyquist frequency, aliasing and folding, and Parceval's theorem, which are discussed using only a minimum of mathematics. The fact that the FID and the spectrum form a Fourier pair has a number of important consequences that are discussed. These include, for example, the relationship between sampling rate and spectral range, the equivalence between phase correction in the spectrum and a shift of the time coordinate in the FID, and between convolution of the spectrum and multiplication of the FID by a time-dependent function, and the Hilbert transform which, when applied to the real component of the spectrum, allows one to restore the imaginary component (provided that no information has been discarded). This chapter is really great for the reader who wishes to understand how Fourier transformation works, without having to deal with more mathematics than is absolutely necessary.

Chapter 3 gives some examples, with special emphasis on zero-filling and apodization. The different functions that can be used, and their relative merits with regard to resolution versus signal-to-noise enhancement, are discussed. Some topics that have only come into prominence quite recently, such as oversampling, are also covered. Phase correction, quadrature, baseline, and solvent-induced artifacts are treated at length. However, modified pulse sequences for reducing such artifacts are only mentioned briefly, as detailed treatments would be beyond the intended scope of the book. There is also a subchapter dealing with the transformation of multidimensional data.

In Chapter 4 we move on to non-FT methods of signal processing, which have now been in use for over ten years. One such method is linear prediction, which again is introduced with only a minimum of mathematics. The underlying principle is explained and the most important equations are given. The two alternative modes of linear prediction are described. In the first of these, linear prediction of the FID in the forward or backward direction is used to generate a new FID which, after conventional Fourier transformation, yields a spectrum with improved resolution, and possibly also improved signal-to-noise ratio. The second mode is the direct evaluation of the spectrum by linear prediction (parametric approach). The most important recipes are discussed (least squares, Hankel–SVD method, minimum variance estimate, Burg method). The chapter could profit from the inclusion of more figures; for example, the regularization could have been explained more clearly with the help of a figure. Another criticism is that only one example is given to show the result of applying linear prediction to a two-dimensional COSY experiment. The fact that linear prediction is widely used in multidimensional NMR spectroscopy is not obvious from this book.

Chapter 5 is devoted to the maximum entropy reconstruction method (MaxEnt), an area in which the authors are themselves actively involved. The method is introduced using a lot of mathematics in a concise form. The underlying principle, in which a synthesized spectrum is fitted to match the experimentally observed FID, is clearly explained. The many examples will be a valuable aid for the reader who is mainly interested in the application of the MaxEnt method. In contrast to apodization methods and Fourier transformation, the MaxEnt method can achieve an increase in the signal-to-noise ratio at the same time as improving the

 © WILEY-VCH Verlag GmbH, D-69451 Weinheim, 1997 0570-0833/97/3620-2251 $ 17.50+.50/0

resolution. This seemingly paradoxical situation is explained with the help of examples. MaxEnt is able to make use of preknowledge about the spectrum, such as the expectation of a particular line shape or of certain coupling constant values, and provides deconvoluted spectra accordingly. This is also possible in principle with FT methods, but in that case it would amount to division of the FID by the time domain function of the known spectral feature, and in many cases the result would be numerically unstable due to a division by zero. MaxEnt, by contrast, compares the spectrum with the FID, so that the procedure amounts to multiplying the time domain function of the spectrum by that of the known spectral feature, thereby avoiding such numerical instabilities. The chapter also contains many examples illustrating how the MaxEnt treatment can overcome problems of truncated FIDs, poor resolution, and low signal-to-noise ratio. Finally, the potential advantages of nonlinear sampling of the FID are discussed. Nonlinear sampling is not compatible with the FT method, but with MaxEnt reconstruction it becomes possible, since the FID is compared with the time domain function of the spectrum (a feature which also allows one to deal with partially corrupted FIDs). Nonlinear sampling is recommended for acquisition of multidimensional data that achieve good resolution.

Chapter 6 describes some emerging methods that have not yet entered the practice of NMR spectroscopy. Those discussed include "iterated soft thresholding", "smoothing by wavelets", and Bayesian techniques. However, it is not clear why the latter methods should be included under this heading, as they are already in use.

Finally, Chapter 7 reviews procedures for the visualization of the results of data processing, for extracting quantitative data, and for error analysis. This chapter is not well integrated with the main body of the book. However, it contains valuable information about matters such as the pitfalls of integrating peak areas in multiple dimensions, the use of color in plotting results, and suggestions for error analysis as applied to peak integrals, peak positions determined from spectra, etc.

Altogether the book is easy to read, and is valuable for NMR spectroscopists who wish to learn more about the processing of the data. It covers all the modern approaches that are available in commercially available software packages, and will help inexperienced users to apply them. The examples are mainly from solution state NMR, but the spectroscopist using high-resolution solid state techniques will find the book equally beneficial. I can therefore recommend it for all NMR laboratories as an aid to ensuring that the data generated are processed in the most effective way.

Christian Griesinger
Institut für Organische Chemie
der Universität Frankfurt a. M.
(Germany)

Handbook of Palladium-Catalyzed Reactions. By *J.-L. Malleron, J.-C. Fiaud,* and *J.-Y. Lagros.* Academic Press, San Diego, 1997. 304 pp., in ring-binder with demo diskette £ 50.00.—ISBN 0-12-466615-9

Transformations catalyzed by palladium are among the most important of all organometallic reactions. Many highly efficient syntheses based on palladium-catalyzed reactions have been developed during the last 30 years. Some important examples are the allylic alkylations due to Trost and Tsuji, and the palladium-catalyzed cross-coupling reactions developed by Heck, Stille, Negishi, and Suzuki. The versatility of palladium-catalyzed reactions is of interest not only for use in basic research (asymmetric catalysis, etc.) but for enabling the synthetic chemist to prepare classes of compounds that present difficulties due to their complexity or sensitivity. This handbook is intended mainly for those wishing to carry out syntheses using such reactions.

The work is based on a palladium data base covering more than 3000 publications (there is an accompanying demo diskette), which was originally set up by one of the authors, Dr. J.-L. Malleron of Rhone-Poulenc-Rorer. The actual handbook contains over 2500 literature references (extending up to November 1995), which relate to 84 different palladium-catalyzed reactions. For convenience these reactions (numbered RXN1 to RXN84) are not only listed in the table of contents but are shown in a diagrammatic form and cross-referenced to the list, so that the reader can find a desired reaction very quickly. The detailed descriptions of the individual reactions are linked to the latter system. First the reaction mechanism (taken from a recent publication) is shown diagrammatically, and this is followed by data on the reaction itself (substrate, substitution pattern, nucleophile, leaving group, etc.). For the more complex reactions a detailed reaction scheme is usually shown. This allows the reader to pick out the most interesting example from his or her standpoint, and to obtain additional information from the cited literature as necessary.

This handbook can be thoroughly recommended for everyone concerned with palladium-catalyzed reactions.

Uli Kazmaier
Organisch-Chemisches Institut
der Universität Heidelberg (Germany)

Database of Palladium Chemistry. Reactions, Catalytic Cycles and Chemical Parameters on CD-ROM. By *J.-L. Malleron* and *A. Juin.* Academic Press, San Diego, 1997. $ 875.00.—ISBN 0-12-466760-0

The complete version of the *Database of Palladium Chemistry* is a collection of data on the best known catalytic reactions of organopalladium chemistry. It covers the literature up to May 1996 and lists 3481 reactions, classified under 85 reaction types. This review is based on a demo version of the database containing just a representative sample of the reactions that are included in the full version of the data bank, while offering the user the same facilities.

The user can access the data bank in three different ways as described in detail below.

a) In the first mode nothing is specified. One obtains a list of all the available reactions, which can then be worked through in sequence. However, considering the large number of reactions listed, this method is hardly suitable as a way of searching for information on special topics.

b) As a second alternative one can specify a given type of reaction, which produces a list of reactions that one can then search through for information on the aspect of special interest. For each reaction one obtains key information in a clearly set out form. Thus, one sees at a glance the reaction scheme, the solvent used, the catalyst and ligands (but no clear explanation of the abbreviations used for the ligands, at least in the demo version), the reaction conditions, and the yield. There are also comments on the reaction, which contain information about the purpose of the investigation, any other examples that are known, and relevant review articles if these exist. The picture is completed by a reference to the original

 © WILEY-VCH Verlag GmbH, D-69451 Weinheim, 1997 0570-0833/97/3620-2252 $ 17.50+.50/0

publication describing the example of the reaction. In addition it is possible to request information about the catalytic cycle on which the reaction is based and the relevant reaction parameters (substrate, substitution pattern, nucleophile, leaving groups, etc.). The catalytic cycle and the list of reaction parameters can also be found in identical form in the *Handbook of Palladium-Catalyzed Organic Reactions*.

c) Probably the most effective way of using the data bank is by means of the various search facilities that are provided. These allow one to specify keywords relating to the solvent, catalyst, reaction conditions, ligands, yield, and authors. By carrying out a search with two or more simultaneous criteria one can limit the number of matching reactions that it produces and thus arrive more quickly at the required data. One can also perform a search in which these criteria are combined with a chosen reaction scheme described by using the ISIS/Draw facility. In fact, however, it is often advantageous to use such a reaction scheme by itself, either by searching directly for the reaction that the scheme depicts, or by carrying out a search to list all those reactions in which the structures of the educt and product are present as subunits. In another type of situation one's interest might lie not in a particular reaction but in reactions that involve a given substrate. In that case the program allows one to specify the substrate structure together with a reaction arrow and obtain a list of all reactions in which that structure is present, either in its own right or as a subunit. In a similar way one can also carry out a search to find a synthesis giving a particular product.

Thus, the *Database of Palladium Chemistry* provides a toolkit that affords the user rapid access to important information of all kinds. Furthermore, the data bank is to be kept up-to-date by continually adding new reactions, typically at a rate of 500–700 each year. That prospect will be of great interest to everyone concerned with organopalladium chemistry.

Franz Zumpe
Organisch-Chemisches Institut
der Universität Heidelberg (Germany)

Protein and Peptide Analyis by Mass Spectrometry. Edited by *J. R. Chapman*. (Series: Methods in Molecular Biology, Vol. 61.) Humana Press, Totowa, 1996. 350 pp., hardcover $ 69.50.—ISBN 0-896-03345-7

J. R. Chapman has already edited several successful books on mass spectrometry. The present book of 21 chapters is concerned with applications of modern mass spectrometric methods to the analysis of proteins and peptides.

In the first, introductory chapter P. Roepstorff gives a short summary of the past and present development of mass spectrometry. Here also the work of the late Michael Barber, 'father' of FAB ionization, to whom the book is dedicated, is honored. Then follows an introduction to mass spectrometry by Chapman, in which soft ionization methods, mass analyzers, and modern techniques such as MS/MS are explained.

The choice of the topics of the subsequent chapters is well balanced and covers many current analytical problems in protein chemistry. However, special problems of synthetic peptide chemistry, such as the characterization of synthetic peptides or analytical problems of combinatorial chemistry, are not discussed. Some of the topics dealt with in detail are the determination of the primary structure of proteins by tandem mass spectrometry, by low- and high-energy CID, PSD or ladder sequencing, mass spectrometric fingerprinting for the identification and characterization of proteins, determination of post-translational modifications (determination of the disulfide bridges), and the analysis of glycopeptides and protein conjugates. Also quantitative aspects are discussed in one chapter (quantitative analysis of neuropeptides). Further chapters deal with the secondary structural analysis of proteins, the determination of noncovalent (supramolecular) interactions of proteins, the computer-assisted analysis of mass spectra, and the identification of proteins by means of protein databases.

Since the chapters have been written by different authors (all of whom are recognized experts in the field of biochemical mass spectrometry), one might expect some overlapping and repetition. Fortunately, however, this is not the case. The individual chapters are on different and well-demarcated topics, and repetitions are rare (one of the few exceptions: a table containing the masses of the amino acid residues appears both in Chapter 12 and in Appendix III).

In accordance with their increasing importance for protein analysis, the two modern soft ionization techniques of electrospray ionization (ESI) and matrix-assisted laser desorption ionization (MALDI) are treated most thoroughly. Nevertheless, the classical methods such as SIMS und FAB have not been forgotten.

As usual for books of the series *Methods in Molecular Biology*, each chapter is organized in sections entitled 'Introduction', 'Materials', 'Methods', and 'Notes'. These sections contain much advice and many practical tips, so that the scientist with the required analytical equipment at his disposal can put the particular method into practice right away in his own laboratory. At the end of each chapter is a bibliography, which also, commendably, includes very recent literature (up to the year 1996). In addition the appendix contains over 180 further references, most of them from 1995.

The text is well illustrated by numerous figures and tables and contains only a few typing errors (e.g., p. 322, 'Vat' instead of 'Val'; p.327, 'Tryp' instead of 'Trp'). The subject index could be more detailed. Some terms, such as 'FTMS' or 'ion trap', which occur in the text, are not listed here.

The book provides the protein chemist with comprehensive information about the capabilities of modern mass spectrometry for biopolymer analysis. Because it is also helpful for practical applications in the laboratory (for example in explaining which detergents interfere with the analysis of proteins by ESI-MS), it can be recommended unreservedly for all scientists working in the field of protein chemistry. Before one picks up this book, however, one should take seriously the warning that Chapman gives in the preface: 'the use of mass spectrometry might be habit-forming'!

Jörg W. Metzger
Institut für Siedlungswasserbau
der Universität Stuttgart (Germany)

 © WILEY-VCH Verlag GmbH, D-69451 Weinheim, 1997 0570-0833/97/3620-2253 $ 17.50+.50/0

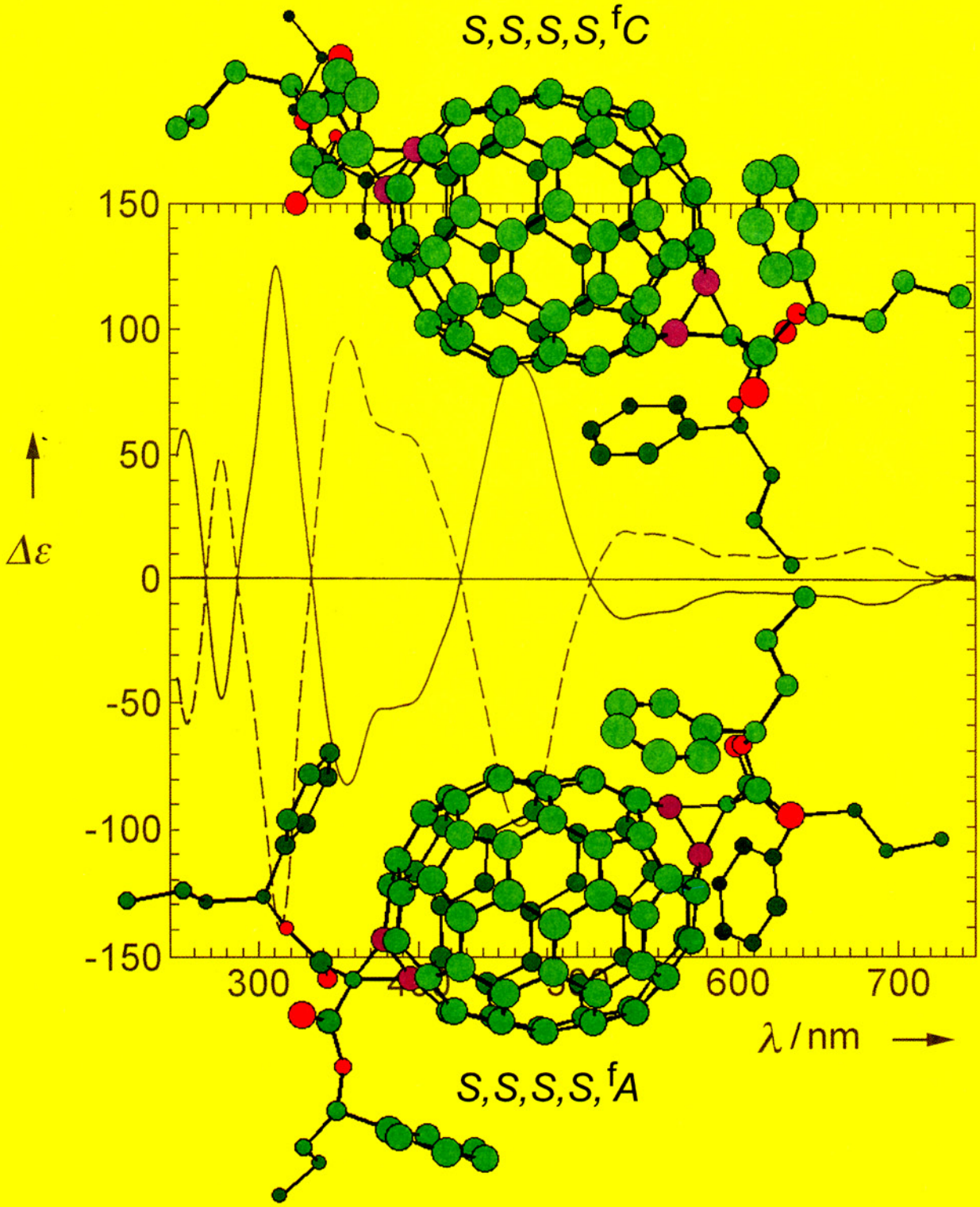

The chiroptical contributions from the chiral addition pattern of higher fullerenes greatly dominate those from the chiral addends, as shown by CD spectra of the diastereoisomeric bis-adducts formed in the reaction of bis[(*S*)-1-phenylbutyl] 2-bromomalonate with C_{70} in the presence of base.

ANGEWANDTE CHEMIE ©WILEY-VCH

The Covalent Chemistry of Higher Fullerenes: C_{70} and Beyond

Carlo Thilgen, Andreas Herrmann, and François Diederich*

Dedicated to Professor Dieter Seebach on the occasion of his 60th birthday

Although higher fullerenes are not yet available in larger amounts, their accessibility, like that of C_{60}, has gradually improved since the early days of fullerene chemistry. Today, many of the soluble larger carbon cages can be purchased either in pure form or as isomeric mixtures. In particular, pure C_{70} is available in preparative amounts from fullerene soot without the need for tedious separation by high-performance liquid chromatography; this has had a major impact on the progress of the chemistry of this higher fullerene. Over the last years C_{70} has been functionalized in many ways, and pure derivatives of even the larger, more complex carbon spheres C_{76}, C_{84}, and recently also C_{78}, have been isolated and characterized. From the collected body of data, first general principles of reactivity and selectivity begin to emerge for these fullerenes, which are all less symmetric than C_{60}. Important information is provided by multiple additions to higher fullerenes, in which certain isomers are formed with a remarkable selectivity that exceedes that observed for C_{60}. A particularly attractive aspect is the chirality of certain allotropes and many derivatives. Although the chirality of fullerene derivatives is not restricted to the larger carbon cages, it was sofar mostly explored through their chemistry and can be related to different structural characteristics. A recently proposed system allows simple specification by a single descriptor of the configuration of chiral fullerenes and fullerene derivatives with a chiral functionalization pattern, including highly branched carbon frameworks with a multitude of possible stereogenic centers.

Keywords: carbon allotropes · chirality · fullerenes · reactivity

1. Introduction

Shortly after the discovery of the bulk fullerene soot production process by Krätschmer, Huffman, and co-workers[1] and the isolation of macroscopic quantities of C_{60} and C_{70}, evidence for soluble carbon molecules with more than 70 carbon atoms was obtained.[2] Together with C_{70}, these homologues of C_{60} are designated as "higher fullerenes". Isolation of single species proved to be difficult due not only to their structural similarity and the occurrence of isomerism, but also to their low abundance in the soot.[3, 4]

Whereas simple protocols are available for isolating pure C_{60}[5, 6] and C_{70},[7] separation of higher fullerenes is based on multistage chromatography.[2–4] Currently, pure species are available in quantities of up to 100 mg by high-performance liquid chromatography (HPLC) of fullerene-soot extract that has been previously depleted of most of the far more abundant C_{60} and C_{70}.[8, 9] The first isolation of D_2-C_{76}[10] and C_{78}[11],

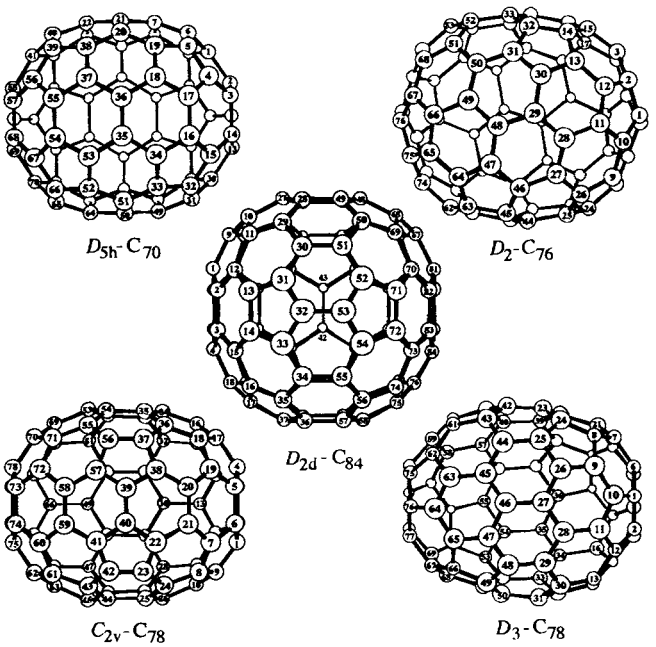

Figure 1. Five higher fullerenes of which pure derivatives have been isolated: D_{5h}-C_{70}, D_2-C_{76}, C_{2v}-C_{78}, D_3-C_{78}, and D_{2d}-C_{84}. The atoms are numbered according to refs. [13, 14].

[*] Prof. Dr. F. Diederich, Dr. C. Thilgen, Dr. A. Herrmann
Laboratorium für Organische Chemie
ETH-Zentrum
Universitätstrasse 16, CH-8092 Zürich (Switzerland)
Fax: Int. code +(1)632-1109
e-mail: diederich@org.chem.ethz.ch

 © WILEY-VCH Verlag GmbH, D-69451 Weinheim, 1997 0570-0833/97/3621-2269 $ 17.50+.50/0

which could be separated into two isomers of C_{2v} and D_3 symmetry (Figure 1), was achieved by HPLC on a polymeric C18 reversed-phase column. Preparative-scale separation was subsequently improved considerably by using π-acidic stationary phases, of which the Buckyclutcher I column developed by Welch and Pirkle merits particular mentioning.[12]

Even though the number of possible isomers increases dramatically with fullerene size,[15] unambiguous structural assignment based on ^{13}C NMR spectroscopy or X-ray crystallography was possible for D_2-C_{76},[10, 16, 17] C_{2v}-C_{78},[11, 16, 18] D_3-C_{78},[11, 16, 18] C'_{2v}-C_{78},[16, 18] and D_{2d}-C_{84} (Figure 1).[19] If rigorous experimental assignment of an isomer is impossible, calculations of heats of formation in conjunction with ^{13}C NMR spectroscopy may provide a structural lead. This was the case for the isolated fullerenes D_2-C_{80},[20] C_2-C_{82},[18] and D_2-C_{84} (obtained as a mixture with D_{2d}-C_{84}).[4, 16, 18]

Due to their hollow cage structure, C_{60} and higher fullerenes can form endohedral inclusion compounds with metal ions[21] or noble-gas atoms.[22] Depending on the size of the cavity, up to three metal ions can be incarcerated. Preparative amounts of the first helium compounds He@C_n (n = 60, 70, 76, 78, 84) were produced by heating fullerene samples at about 600 °C under a high He pressure ($\approx$2700 atm).[23, 24] Based on energetic considerations, different mechanisms have been discussed for the incorporation of He atoms.[25] ^3He NMR spectroscopy revealed strong and specific magnetic shieldings of ^3He atoms inside the cages of different fullerenes and their covalent derivatives; this gave rise to a unique resonance for each compound measured so far.[26, 27]

Although the covalent chemistry of the most abundant fullerene, C_{60}, developed fastest after 1990 and led to a rich variety of tailor-made building blocks for materials and biological applications,[28–31] investigations into the chemical reactivity of the higher fullerenes also made enormous progress in recent years. Of particular interest are the understanding of chemo- and regioselectivity of covalent derivatizations as well as the structural aspects related to chirality.[32, 33]

2. Chirality of Fullerenes and Their Derivatives

Many higher fullerenes are chiral.[3, 4, 16, 18, 20, 32] With increasing cage size, the number of chiral isomers increases rapidly: Of the 5 isomeric C_{78} structures obeying the isolated pentagon rule (IPR), 2 are chiral, whereas there exist 10 chiral representatives among the 24 IPR-satisfying isomers of C_{84}.[15, 32] These compounds are among the rare examples of chiral element modifications, and the enantiomers of D_2-C_{76}, D_3-C_{78}, and D_2-C_{84} could be separated in small amounts.[34, 35]

Functionalized fullerenes can be chiral even if they are derived from achiral parent cages. Depending on the origin of their chirality, four classes of chiral fullerene compounds can be distinguished.[32, 33]

1) All inherently chiral fullerenes and their derivatives.
2) Chiral adducts obtained by functionalizing achiral fullerenes in such a way that stereogenic elements are exclusively located in the addends.
3) Fullerene derivatives with an inherently chiral functionalization pattern, that is, the addends create a chiral addition pattern on an achiral fullerene core irrespective of the addends being identical or different.
4) Fullerene derivatives with a noninherently chiral addition pattern that is chiral due only to differences in the addends.

Carlo Thilgen was born in Luxembourg in 1961. He received his Ph.D. from the Universität Bonn in 1990, and was a postdoctoral fellow of NATO and the Government of Luxembourg at the University of California at Los Angeles (UCLA) with François Diederich. Since 1993 he has been a research associate at the Eidgenössische Technische Hochschule (ETH) Zürich. His current research focuses on the stereochemical aspects of fullerene functionalization.

C. Thilgen

A. Herrmann

F. Diederich

Andreas Herrmann was born in Karlsruhe, Germany in 1969, and studied chemistry at the Universität Karlsruhe and the Ecole Européenne des Hautes Etudes des Industries Chimiques de Strasbourg (EHICS). In 1997 he received his Ph.D. at the ETH Zürich, where he was working on the chemistry and chiroptical properties of higher fullerenes and their derivatives. Since March 1997 he has been employed at Firmenich SA in Geneva, Switzerland.

François Diederich was born in Ettelbrück, Luxembourg, in 1952 and received his Ph.D. in 1979 at the Universität Heidelberg. Following postdoctoral studies at UCLA from 1979 to 1981, he was a research associate at the Max-Planck-Institut für medizinische Forschung in Heidelberg. After his Habilitation in 1985 he joined the faculty of the Department of Chemistry and Biochemistry at UCLA where he advanced to full professor of organic and bioorganic chemistry in 1989. Since April 1992 he has been a professor of organic chemistry at the ETH Zürich.

A compound can belong to several of the above classes when different stereogenic elements are superimposed in the same molecule. From a slightly different viewpoint, adducts of both chiral and achiral parent fullerenes can be usefully classified as outlined in Scheme 1.

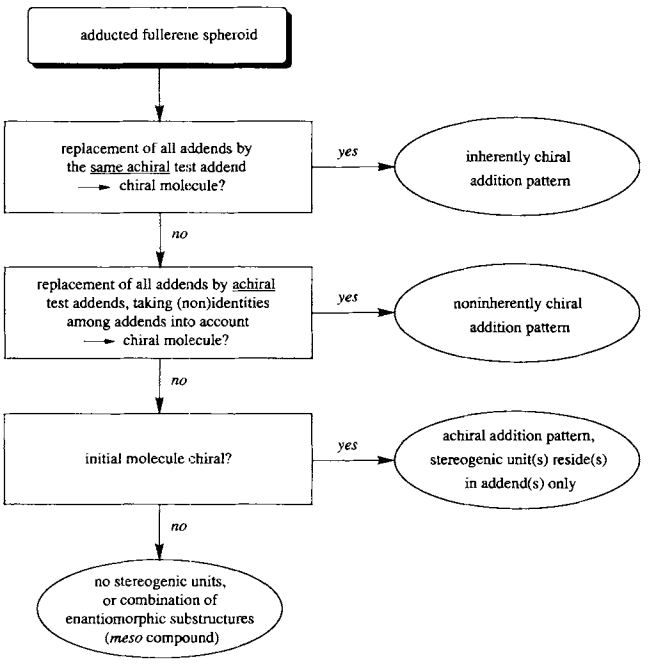

Scheme 1. Flow diagram for classifying different types of fullerene-spheroid chirality by applying a simple, stepwise substitution test. Checking the structure resulting after each step for chirality quickly reveals the type of addition pattern of the starting structure.

The configurational description of compounds in categories 1, 3, and 4 by application of the Cahn, Ingold, and Prelog (CIP) rules[36] can be excessively complicated, especially when there is a multitude of stereogenic centers within the highly branched carbon framework. For this reason, we proposed a new system that allows configurational specification of chiral spheroids by a single descriptor, regardless of the degree of functionalization.[33] It is based on the fact that the numbering schemes proposed for fullerenes, which can be developed with a set of rules from their structure,[37] are themselves chiral (helical) and thus constitute an ideal reference for differentiating between enantiomeric carbon cages. Whereas two isometric, mirror-symmetric numbering schemes can be applied to an achiral parent fullerene, a unique scheme is associated with a specific enantiomer of an inherently chiral carbon spheroid.[37] Similarly, for a chiral derivative resulting from a specific addition pattern of an achiral parent fullerene, there is a unique numbering pattern leading to the lowest set of locants[38] for the addends. Depending on whether the direction of this numbering from C(1) over C(2) to C(3) is clockwise (*C*) or anticlockwise (*A*), the descriptors are ^{f}C or ^{f}A, respectively (f = fullerene; Figure 2).[33]

3. Reactivity and Regioselectivity in the Functionalization of Higher Fullerenes

Fullerene bonds are located either between two six-membered rings (6–6 bonds) or between a six- and a five-membered ring (6–5 bonds). In buckminsterfullerene, C_{60}, primary addition takes place preferentially at 6–6 bonds, which have higher double bond character.[28, 29] Whereas buckminsterfullerene contains only a single type of 6–6 bond, C_{70} contains 4, C_{76} 15, C_{2v}-C_{78} 18, and D_3-C_{78} 10. This leads to a growing number of possible adduct isomers with increasing fullerene size and decreasing symmetry.

In general, the mode of addition to higher fullerenes is similar to that of C_{60}:[28, 29] Whereas nucleophilic and carbene addition, hydrogenation, formation of transition metal complexes, and cycloadditions give rise to 1,2-adducts, most radical reac-

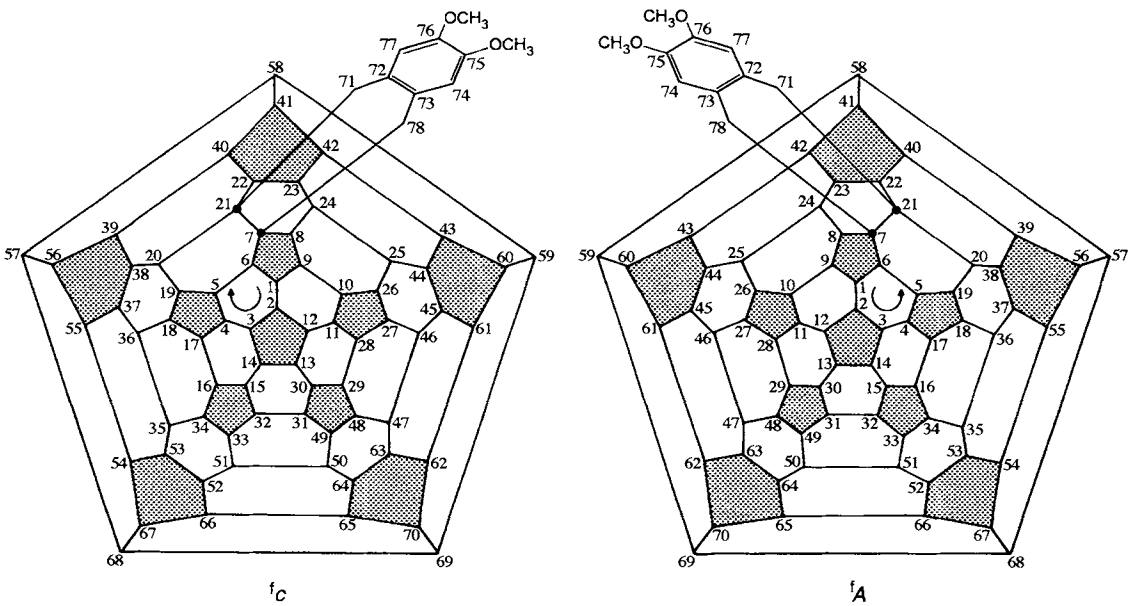

Figure 2. Schlegel diagrams of the enantiomers of 75,76-dimethoxy-7,21-(methano[1,2]benzenomethano)[70]fullerene, a C_{70} adduct with an inherently chiral addition pattern. Interchanging the numbering schemes and, therefore, the descriptors would afford the locant set 8,24 for the addend(s), which, being higher than 7,21, is unacceptable.

tions, for example halogenations, occur as intrahexagonal 1,4-additions, especially if sterically demanding groups are introduced. With C_{60}, 1,4-addition results in at least one double bond within a five-membered ring; this situation is energetically unfavorable in fullerene structures.[39] However, some of these energetic costs may be compensated by a reduction in steric interactions.

Bond reactivities in higher fullerenes can be estimated by considering π bond orders[13,40] or the local spheroid curvature,[34,41] which is expressed as pyramidalization angles of the corresponding carbon atoms.[42] To make simple predictions of the expected isomeric product distributions, we consider a qualitative model for evaluating local curvature.[8] As the latter results from incorporation of pentagons into a network of hexagons, the reactivity of a 6–6 bond should increase with the number of surrounding five-membered rings and a decrease in their distance to the 6–6 bond being considered. According to this description, the most strained bonds in C_{70} and C_{76} are located at the poles (type α, surrounded by type β), whereas the flatter equatorial region contains a number of different, less curved bonds (Figure 3).

Figure 3. Pyracylene substructures (shaded) with the three most curved fullerene bond types α, β, and γ at their center (marked with a cross).[8]

4. Functionalization of C_{70}

4.1. Oxidation Reactions

The first derivative of a higher fullerene described in the literature was the epoxide $C_{70}O$, which formed as a by-product during fullerene-soot production in the presence of traces of oxygen.[2,43] It is conveniently generated by the reaction of C_{70} with oxidizing agents such as dioxygen,[44,45] ozone,[46] or *m*-chloroperbenzoic acid.[47] As evidenced by X-ray crystallography of an iridium complex obtained from the isomeric epoxide mixture **1** and **2**,[48] oxygen addition occurs at the most curved α- and β-type bonds in the polar region of the fullerene (Scheme 2). This characteristic addition pattern was also observed for the osmylation of C_{70} to yield the mono-osmates **3** and **4** in a ratio of approximately 2:1.[41]

4.2. Transition Metal Complexes

Transition metal complexes of fullerenes are characterized by reversible, thermodynamically controlled association and a pronounced tendency to form crystals suitable for X-ray analysis. As illustrated for mono-adducts **5**[49] and **6** (Scheme 2)[50] as well as bis-adduct (±)-**7** (Scheme 3),[51] there is a high selectivity for η^2-complexation by Ir and Pt at the bonds nearest the pole of C_{70}. The addition patterns seen in the chiral bis-adduct (±)-**7** and the C_{2v}-symmetrical tetrakis-adduct **8**[52] were also realized in functionalizations with C-nucleophiles (see Section 4.8).

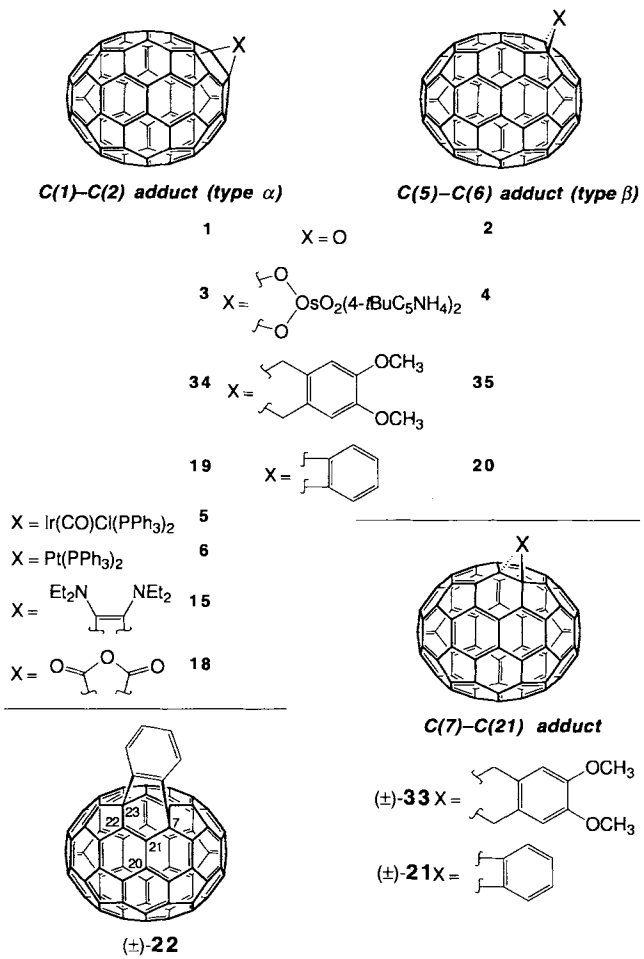

Scheme 2. Mono-adducts of C_{70} with bridging addends, and their isomeric distribution. All chiral adducts are represented by a single enantiomer only.

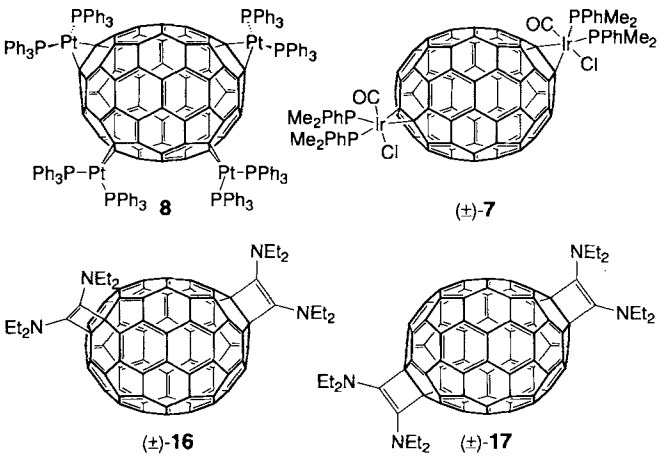

Scheme 3. Bis-adducts of C_{70} with an inherently chiral functionalization pattern resulting from addition to α-type bonds at opposite poles as well as a C_{2v}-symmetrical tetrakis(platinum) complex. Only a single enantiomer is shown in each case.

4.3. Hydrogenation

As in the case of C_{60},[28,53] 1,2-addition is preferred over 1,4-addition for the hydrogenation of C_{70} despite eclipsing interactions between vicinal hydrogen atoms on the carbon spheroid. Two isomeric bis-adducts, **9** (major product) and **10**,

were formed by the reaction of C_{70} with diimide[54] or $BH_3 \cdot THF$[55] (Scheme 4). Conversion of the less stable **10** into a mixture of **9** and **10** by Pt-catalyzed equilibration allowed experimental determination of the corresponding difference in free energy as (1.4 ± 0.2) kcal mol^{-1}.[55] Diimide reduction of

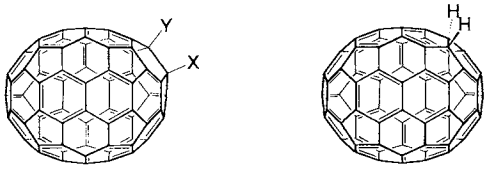

9 X = Y = H
36 X = CH_3, Y = H
37 X = H, Y = CH_3

10

Scheme 4. Isomeric hydrogenation and hydromethylation products of C_{70}.

C_{70} also afforded the tetrahydro[70]fullerenes 1,2,3,4-$C_{70}H_4$ and (±)-1,2,5,6-$C_{70}H_4$, in which all four hydrogen atoms are located at adjacent positions in one of the six-membered rings of the polar corannulene substructure.[54] Although a number of more highly hydrogenated derivatives of C_{70} bearing 8, 10, 12,[16, 56] 30,[57] or 36[58] hydrogen atoms as well as a mixture of hydrogenated higher fullerenes[59] were generated by various methods, in no case was a conclusive structural assignment possible.

4.4. Halogenations

Possibly due to crystal packing effects, solid C_{70} is more reactive towards fluorination than C_{60}.[60, 61] As revealed by mass spectrometry, the reaction with F_2[60–63] or the more selective MnF_3[64] affords $C_{70}F_{38}$,[60, 61, 64] $C_{70}F_{40}$,[62] and $C_{70}F_{52}$[63] as prominent species of high symmetry (^{19}F NMR spectroscopy). Fluorofullerenes are sensitive towards moisture or solvents.[61, 63] An S_N2' mechanism was proposed for nucleophilic attack, for example by OH^- or H_3CO^-, which clearly cannot take place from the back side of the fluorinated carbon atoms of the fullerene shell.[65] The most interesting halide of a higher fullerene is the well-characterized $C_{70}Cl_{10}$, which was obtained by Taylor and co-workers as a single C_s-symmetrical isomer (**11**) in the reaction of C_{70} with ICl (Scheme 5).[14] Presumably

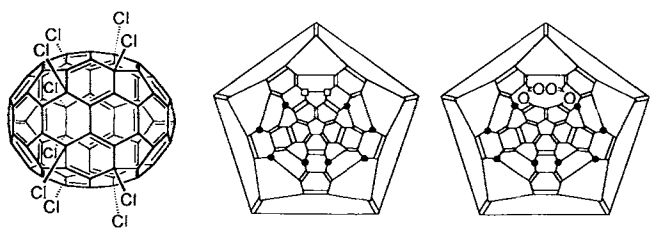

11

11 • = C-Cl, □ = C-Cl
12 • = C-Ph, □ = C-Ph
13 • = C-Ph, □ = C•

14 • = C-Ph

Scheme 5. $C_{70}Cl_{10}$ (**11**), $C_{70}(Ph)_{10}$ (**12**), $C_{70}(Ph)_8$ (**13**), and oxidative cage opening of **13** yielding the C_s-symmetrical bis(lactone) **14** with an eleven-membered ring in the fullerene shell. The two representations on the right are Schlegel diagrams.

taking place by a radical mechanism, 1,4-addition leads to sterically favorable "*para*" relationships of the Cl atoms in a belt of adjacent six-membered rings with only one vicinal ("*ortho*") neighborship.[14, 66] In addition, all double bonds are exocyclic to the five-membered rings.

4.5. Chemistry of $C_{70}Cl_{10}$

$C_{70}Cl_{10}$ is an interesting starting material for further chemical transformations. In analogy to $C_{60}Cl_6$, $C_{70}Cl_{10}$ undergoes Friedel–Crafts alkylation with benzene/$FeCl_3$ to yield $C_{70}Ph_{10}$ (**12**) via the octakis-adduct $C_{70}Ph_8$ (**13**), which contains an intrapentagonal double bond.[67] A by-product of this reaction, fullerenol $C_{70}Ph_9OH$ is formed by nucleophilic substitution of another intermediate, $C_{70}Ph_9Cl$, by water.[68]

When left in CCl_4 under air for several weeks, **13** is spontaneously oxidized to the C_s-symmetrical bis(lactone) $C_{70}Ph_8O_4$ (**14**; Scheme 5) with an eleven-membered hole in the fullerene cage.[69] It presumably results from insertion of two oxygen atoms into σ bonds followed by oxidative cleavage of the adjacent, electron-rich intrapentagonal bis(enol ether) double bond.

4.6. Addition of Radicals

Studies with C_{60} showed that, for reasons of allylic stabilization, the unpaired electron resulting from radical attack is preferentially located at the position α to the addition site.[28] With five different types of carbon atoms in its shell, C_{70}, which seems to have a somewhat lower affinity for radicals than C_{60},[70] can give rise to a maximum of five isomeric mono-adducts. Three were detected with ESR spectroscopy for the addition of alkyl or Cl_3C radicals,[71, 72] up to four for H, aryl, and F_5C_2 radicals,[72–75] and all five for H_3CO[76] and F_3C radicals.[74] Whereas structural assignments are in general difficult, calculations on $HC_{70}^{\bullet}$ regioisomers indicate that attack at the equator is the most unlikely.[72, 74, 75, 77]

4.7. Cycloadditions

Together with the addition of C-nucleophiles, cycloadditions represent the most important reaction for the formation of C–C bonds with the fullerene framework.[28, 29, 78] Ando and coworkers described a [2+1]cycloaddition in which they treated C_{70} with photochemically generated bis(2,6-diisopropylphenyl)silylene.[79] As in most cycloadditions with this fullerene, the reaction occurred selectively at the C(1)—C(2) (α) and C(5)—C(6) (β) bonds in a 2:1 ratio.

Zhang and Foote reported [2+2]cycloaddition of ethynediamines and thioethynamines to C_{70} and, for the former, obtained a single mono-adduct isomer (**15**; see Scheme 2) in addition to a mixture of two chiral bis-adducts ((±)-**16** and (±)-**17**; see Scheme 3). This demonstrated a remarkable selectivity for attack at the most curved bonds of type α nearest the poles.[80] After self-sensitized photooxygenation of the mixture, the authors obtained the tetrakis(carboxamide) corresponding to (±)-**16**. Starting from a thioethynamine α-type mono-adduct,

photooxidative cleavage to a thioester amide followed by acid treatment afforded **18** as the first fullerenedicarboxylic acid anhydride.

Up to ten equivalents of benzyne readily add to C_{70}.[81, 82] ^1H and ^{13}C NMR spectroscopic analysis of the generated monobenzeno[70]fullerene mixture revealed the formation of three out of four possible 6–6 bond cycloadducts (**19**, **20**, and (±)-**21**, see Scheme 2); no reaction occurred at the equatorial biphenyl-type bond C(20)–C(21). A fourth, presumably transequatorial 1,4-adduct in which C(7) and C(23) are bridged ((±)-**22**) is a fullerene analogue of triptycene. In contrast to [2+2]cycloaddition at the equatorial C(20)–C(21) bond, [4+2]cycloaddition leading to (±)-**22** does not generate new double bonds in the five-membered rings. Furthermore, by taking into account the high reactivity of α-type bonds and possible steric interactions, as well as avoidance of intrapentagonal double bonds, a structure was proposed for the decakis(benzeno) adduct.[82] Its π system includes five benzenoid six-membered rings and is a substructure of the $C_{70}Cl_{10}$ chromophore.[14, 66] [2+2]Cycloadditions between carbon spheres seem to be the origin of polymers produced from C_{70} films upon irradiation or application of high temperature and pressure.[83]

Methanofullerenes can be obtained by [3+2]cycloaddition of diazo compounds to 6–6 bonds and subsequent photochemical or thermal extrusion of N_2 from the intermediate pyrazolines.[28, 29, 84] Two regioisomeric pyrazolines, **23** and **24**, arise from addition at the α-type bond C(1)—C(2), and a racemic mixture of a third constitutional isomer ((±)-**25**) with a noninherently chiral addition pattern is obtained from addition to the β-type bond C(5)–C(6) (12:1:2 ratio; Scheme 6).[85] The same isomerism was found by Meier et al.[86] and Irngartinger et al.[87] for the reaction of isonitrile oxides with C_{70}, and by Yamago and Nakamura for the addition of a dipolar trimethylenemethane derivative generated by thermolytic ring opening of a methylenecyclopropane derivative.[88]

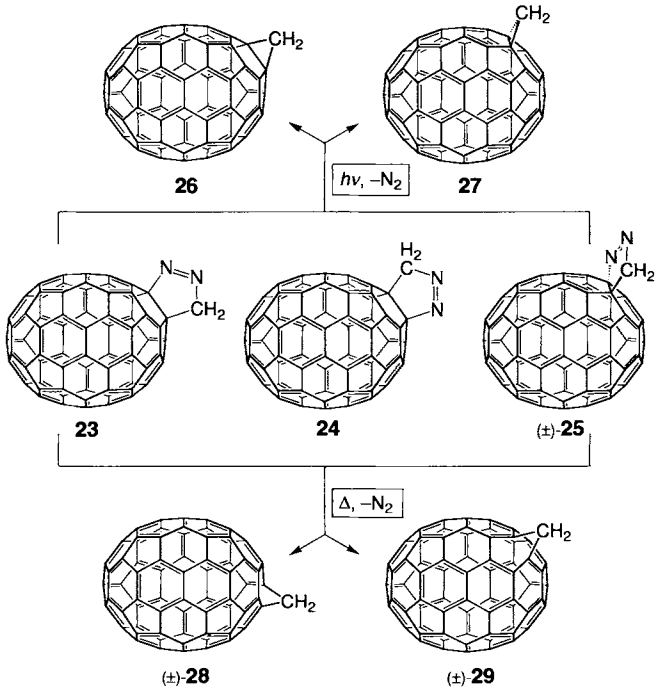

Scheme 6. Photochemical N_2 extrusion from diazomethane adducts of C_{70} **23**, **24**, and (±)-**25** yields 6–6 closed methanofullerenes **26** and **27**, whereas the corresponding thermal process generates the 6–5 open derivatives (±)-**28** and (±)-**29**.

Irradiation of the mixture of pyrazolines **23**, **24**, and (±)-**25** yielded methanofullerenes **26** and **27** (7:1) with a closed transannular 6–6 bond in addition to minor amounts of a third constitutional isomer ((±)-**28**), whereas thermolysis of the same mixture gave (±)-**28** and (±)-**29** (4:1) with an open transannular 6–5 "bond".[85] As to the mechanism of this combination of N_2 extrusion and rearrangement, thermolysis of the corresponding pyrazolo[60]fullerene was proposed to give a 6–5 open methanofullerene by an orbital symmetry controlled [$\pi^2s+\pi^2s+\sigma^2s+\sigma^2a$] reaction, whereas photolysis to a 6–6 closed methanofullerene proceeds by a diradical mechanism.[89]

Similar to the reaction of diazomethane, [3+2]cycloaddition of alkyl azides to C_{70} afforded three constitutionally isomeric triazolines, of which the regioisomer analogue of **23** predominated.[90, 91] Subsequent thermal elimination of N_2 under formation of N-bridged compounds showed a preference for the 6–5 open analogues of (±)-**28** and (±)-**29** over the 6–6 closed isomers corresponding to **26** and **27**.[90]

Twofold addition of azide yielded C_s-symmetrical **30** with two bridged, adjacent 6–5 open "bonds" (Scheme 7).[92, 93] Compound **30** is a suitable starting material for the macroscopic

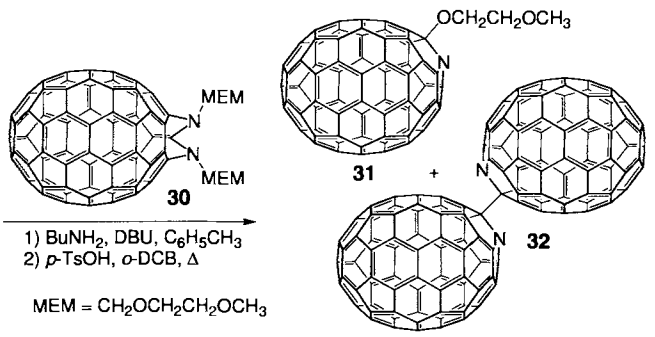

Scheme 7. Generation of aza[70]fullerene derivatives from a geminally N-bridged precursor.

synthesis of aza[70]fullerene derivatives **31** and **32**, provided that facile deprotection of the N-bridges is possible.[93] Whereas **31** could be well characterized, **32** gave no ^1H NMR signal, as expected, and its solubility was too low to obtain sufficient ^{13}C NMR data; it did however provide a UV absorption typical for a 1,2-dihydro[70]fullerene. In analogy to $(C_{59}N)_2$,[93, 94] the mass spectra of **32** showed only a peak for half of the dimeric structure.

Wilson and Lu found that *N*-methylazomethine ylide adds under formation of fused *N*-methylpyrrolidines not only to the reactive α- and β-type bonds of C_{70}, but, to a minor extent, also to the C(7)–C(21) bond.[95] This led to an addition pattern previously seen in Diels–Alder adduct **33** (see Scheme 2).[8] The transequatorial 1,4-addition mode of **22** (see Scheme 2) was also suggested[82] for the product of the photochemically induced addition of 1,1,2,2-tetramesityl-1,2-disilirane to C_{70}.[96]

We investigated the regioselectivity of the Diels–Alder [4+2]cycloaddition of 4,5-dimethoxy-*o*-quinodimethane to C_{70} and C_{76}.[8] In the case of C_{70}, three out of four possible 6–6

adducts ((±)-**33**, **34**, and **35**) were isolated and unambiguously assigned by ^{13}C NMR or variable-temperature ^{1}H NMR spectroscopy. Boat-to-boat interconversion of the newly formed cyclohexene ring is fast on the NMR time scale around 80 °C, and the spectroscopically observed average symmetry of the adducts changes upon crossing the coalescence temperature T_c. A unique symmetry combination at $T<T_c$ and $T>T_c$ allowed structural assignment of all three isolated constitutional isomers. The two most abundant products were **34** and **35** (Scheme 2), and their structures were confirmed by X-ray crystallography.[97] The third, minor constitutional isomer (±)-**33**, formed by addition to the C(7)–C(21) bond, has an inherently chiral addition pattern which is also found in other adducts of C_{70}.[82, 95] Addition at the equatorial C(20)–C(21) bond did not occur.

Cyclopenta-1,3-dienes readily and reversibly add to C_{70}.[98–100] An interesting method for purifying C_{60} and C_{70} was developed by Rotello and Nie; it takes advantage of the differential reactivity of the two fullerenes towards a silica gel supported cyclopentadiene.[101] An [8 + 2]cycloaddition of 8-methoxyheptafulvene to an α-type bond of C_{70} was reported by Daub and co-workers in addition to Diels–Alder reactions with electron-rich Danishefsky dienes.[102]

4.8. Addition of Nucleophiles

Kinetically controlled nucleophilic 1,2-additions to C_{70} followed by quenching with an electrophile display a particularly high selectivity for the polar α-type C(1)–C(2) bond.[103–107] This can be rationalized by the preference of the sp^3-hybridized carbanionic center, which develops in the transition state α to the site of nucleophilic attack,[28] for a region of high curvature. Hirsch and co-workers found that hydroalkylations or hydroarylations, in which the carbanion resulting from nucleophilic attack is quenched by a proton as electrophile, afford two isomers (e. g. **36** and **37**; see Scheme 4) by addition to the C(1)–C(2) bond.[103, 108]

In one of the most practical methanofullerene syntheses, the Bingel reaction,[104] attack of 2-bromomalonate carbanions on the fullerene is followed by intramolecular halide displacement. Starting from phosphonium[109] or sulfonium ylides,[105, 110] a similar addition–elimination mechanism also yields methanofullerenes. The Bingel reaction shows high preference for monofunctionalization of C_{70} at the C(1)–C(2) bond, and we selected it for studying the formation of multiple adducts of higher fullerenes.[9, 106] Our objective was to learn about the changes in chemical reactivity and physical properties which occur when the conjugated fullerene chromophore is reduced as a result of increasing functionalization.[111]

The X-ray crystal structures of C_{70} mono-adducts **34** and **35** revealed that the electronic configuration at the unfunctionalized pole closely resembles that of the parent fullerene.[97] As a consequence, second Bingel[106, 112] or other[51, 80] additions to C_{70} take place at the unfunctionalized pole (see Schemes 3 and 8).[97] If both malonate addends are achiral, three constitutionally isomeric bis(methano)fullerenes are formed: an achiral (C_{2v}-symmetrical **38**) and two chiral compounds (C_2-symmetrical (±)-**39** and (±)-**40**) that are obtained as pairs of enantiomers with an inherently chiral addition pattern.[106] The analogous addition of bis[(*S*)-1-phenylbutyl] 2-bromomalonate leads to a superimposition of the chirality of the addend and, when present, that of the core functionalization pattern. This affords a total of five optically active isomers, two constitutionally isomeric pairs of C_2-symmetrical diastereoisomers (**41a, 42a** and **43a, 44a**) as well as a third constitutional C_2-symmetrical isomer (**45a**).[106] All these and the products **41b**–**45b** resulting from addition of the respective (*R,R*)-configured esters could be separated by HPLC on silica gel.[113] As a consequence, ten pure, optically active compounds were obtained; they include five pairs of enantiomers, four with an inherently chiral fullerene functionalization pattern and chiral side chains (**41a, b, 42a, b, 43a, b, 44a, b**), and one with stereogenic units in the addends only (**45a, b**). Inherently chiral addition patterns lead to very strong Cotton effects in the circular dichroism (CD) spectra,[106, 114–116] which is in contrast to sole perturbation of achiral fullerene chromophores by chiral addends.[32, 106, 117, 118] Furthermore, identical core functionalization patterns lead to

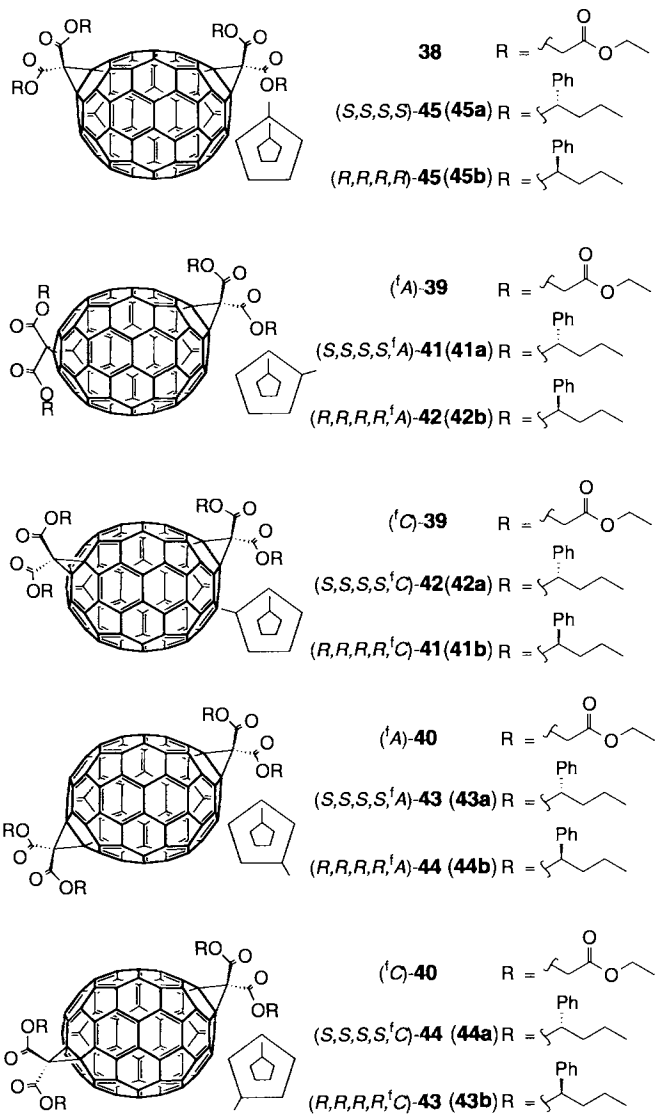

Scheme 8. Different combinations of inherently chiral or achiral [70]fullerene functionalization patterns and chiral or achiral addends. The addition patterns are schematically represented by Newman-type projections along the C_5 axis of the C_{70} framework; the inner pentagon corresponds to that nearest the viewer.

(nearly) the same spectra irrespective of the side chain configuration. This is nicely illustrated by the spectra of diastereoisomeric bis-adducts ($S,S,S,S,^{f}A$)-**43** and ($S,S,S,S,^{f}C$)-**44**, which have enantiomeric addition patterns and display nearly mirror-image shapes since the chiroptical contributions from the chiral addition pattern of the fullerene greatly dominate those from the chiral addends (Figure 4b).[106] A characteristic band around 460 nm was observed in the CD spectra of all C_{70} adducts with an inherently chiral functionalization pattern and may be helpful in assigning absolute configurations.[113]

Further functionalization of the major bis-adducts **38** and (±)-**39** with diethyl bromomalonate yielded tetrakis-adducts **46** and (±)-**47**, respectively, in addition to the intermediate tris-adducts (Scheme 9, top).[106] Once C_{70} bis-adducts are formed, further addition must take place in a hemisphere that is already functionalized. For steric and probably also electronic reasons, this does not occur at another α-type bond. Instead, an addition mode similar to that of a second bromomalonate addition to C_{60}, which preferentially occurs at an equatorial bond, is observed. Given the two alternatives corresponding to this relative arrangement in a C_{70} hemisphere, the next addition takes place at a β-type bond rather than at bond x in the less curved equatorial region (Scheme 9, bottom), thus leading to tris- and tetrakis-adducts.[106] Compared to C_{60},[119,120] C_{70} shows higher selectivity in multiple nucleophilic additions.[106,108]

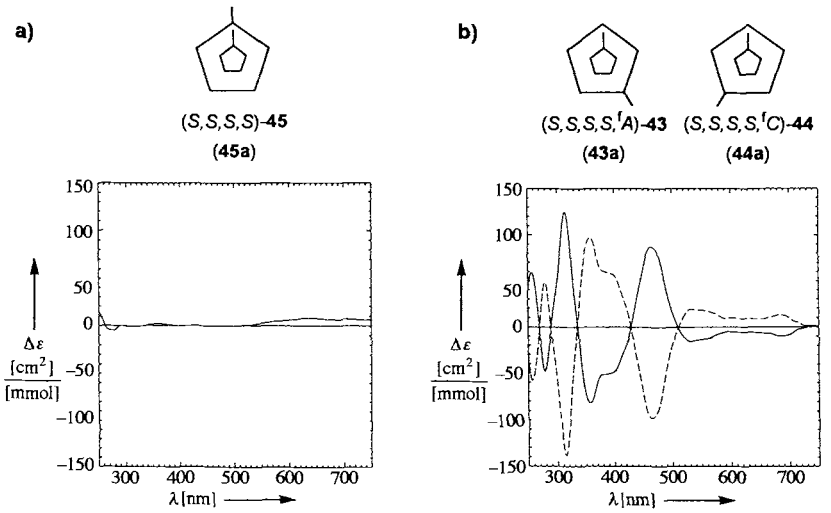

Figure 4. CD spectra of a) **45a** and b) the diastereoisomeric bis-adducts **43a** and **44a**. The Cotton effects shown by **43a** and **44a**, which have an inherently chiral addition pattern, are much larger than those observed for **45a**, in which the achiral fullerene chromophore is only perturbed by the chiral side chains. In addition, the spectra of **43a** and **44a** with their enantiomeric fullerene addition patterns display near mirror-image shapes despite the fact that the molecules are diastereoisomers.

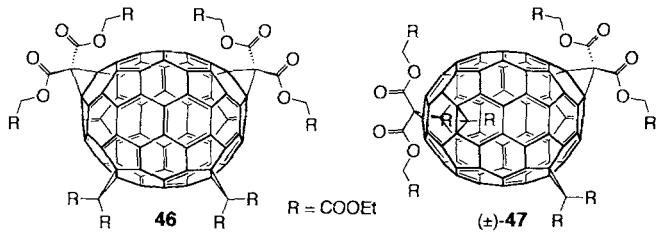

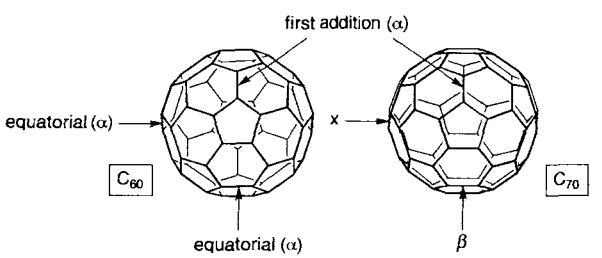

Scheme 9. C_2- and C_{2v}-symmetrical tetrakis-adducts of C_{70} as well as a comparison of the modes of second intrahemispheral addition for C_{60} and C_{70}. In C_{60}, the second addition preferentially takes place at one of the two different equatorial bonds (both of type α). In C_{70}, the same favorable relative addend arrangement can be realized by addition of a second nucleophile either at the marked bond of type β or in the less curved equatorial region (bond x). Of the two possibilities, only the former was observed.

5. Functionalization of the Fullerenes Beyond C_{70}

The chemistry of the fullerenes beyond C_{70} is much less explored, and, other than for the derivatives derscribed in this review, product mixtures from ozonation[46], hydrogenation[59], and methylenation[121] have been reported. Making use of the asymmetric Sharpless osmylation, Hawkins et al. achieved a small-scale kinetic resolution of D_2-C_{76}, D_3-C_{78}, and D_2-C_{84}.[34,35] No racemization of C_{76}, or of D_2-C_{84} by Stone–Wales rearrangements[122] via D_{2d}-C_{84}, occurred below 700 °C and upon UV irradiation.[35]

By selective crystallization of [{η^2-(D_{2d}-C_{84})}Ir(CO)Cl(PPh_3)$_2$] (**48**) from a mixture of D_{2d}-C_{84} and D_2-C_{84}, Balch et al. obtained the first isomerically pure adduct of [84]fullerene (Scheme 10).[19] Fluorination of a higher fullerene mixture yielded $C_{70}F_x$ ($x = 44-56$), $C_{78}F_y$ ($y = 54-60$), and $C_{84}F_z$ ($z = 56-62$).[123] The difluorinated anions $C_{72}F_2^-$, $C_{74}F_2^-$, $C_{76}F_2^-$, and $C_{78}F_2^-$ were produced in Knudsen-cell mass-spectrometric experiments.[124–127]

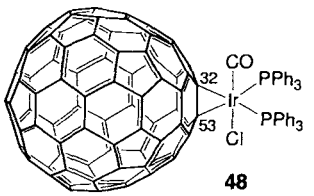

Scheme 10. Formula of the first isomerically pure adduct of [84]fullerene.

Photochemically induced addition of 1,1,2,2-tetramesityl-1,2-disilirane to endohedral metallofullerenes such as La@C_{82}, Gd@C_{82}, La_2@C_{80}, and Sc_2@C_{84} yielded isomeric mixtures of mono-adducts.[128] In contrast to the empty cages, most of the more strongly electron-accepting metallofullerenes also react thermally with this disilirane.

5.1. Diels–Alder Addition and Nucleophilic Addition to C_{76}

At least six isomers were formed by the addition of 4,5-dimethoxy-*o*-quinodimethane to D_2-C_{76}.[8] ^{1}H NMR spectroscopy, together with consideration of bond reactivities modulated by local curvature, led to the tentative assignment of the C_1-symmetrical C(2)–C(3) adduct structure (±)-**49** (Scheme 11) resulting from attack at the polar α-type bond to the major

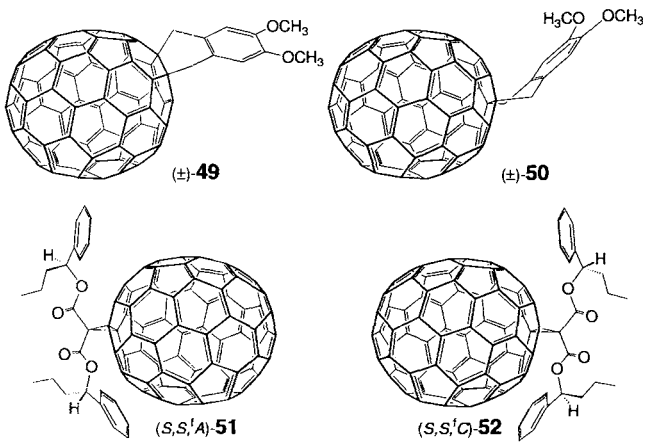

Scheme 11. Isolated mono-adducts of C_{76} for which confident structural assignments were possible.

product, which was isolated in pure form. Based on similar reasoning, the structure of the C(1)–C(6) adduct (±)-**50** formed by attack at another α-type bond, was assigned to a C_2-symmetrical mono-adduct, which was isolated as a mixture with two C_1-symmetrical isomers.[8]

In a Bingel reaction of C_{76} with an (*S,S*)-configured 2-bromomalonate, superimposition of the chirality of the addend and that of the inherently chiral fullerene mainly yielded three constitutionally isomeric pairs of diastereoisomeric mono-adducts, two of C_1, and one (**51**, **52**) of C_2 symmetry (Scheme 11; ratio approximately 8:7:1).[115] All six compounds were isolated by HPLC, and represent the first optically pure adducts of an inherently chiral fullerene. UV/Vis, CD, and ^{13}C NMR spectra showed distinct similarities for isoconstitutional stereoisomers, thus allowing facile identification of the three pairs. The CD spectra of these derivatives of an inherently chiral fullerene display very pronounced Cotton effects with maximum Δε values ($\approx 250\ cm^2\ mmol^{-1}$)[115] that are twice as high as those[106] measured for optically active adducts of achiral fullerenes with a chiral addition pattern.

According to the local curvature model for bond reactivities, the minor C_2-symmetrical diastereoisomeric pair (**51,52**) most probably results from addition to the α-type bond C(1)–C(6) that is intersected by a C_2 axis of D_2-C_{76}. This leaves another α bond (C(2)–C(3)) for malonate addition leading to one of the C_1-symmetrical pairs; the third C_1-symmetrical constitutional isomer must arise from addition to a bond located in a less curved region. The fact that a minor product results from α-bond addition, whereas reaction at a less curved bond leads to a major adduct, indicates that other factors, such as electronic effects, contribute to the regioselectivity in C_{76} and possibly other higher fullerenes.[115]

5.2. Nucleophilic Addition to C_{78}

Cyclopropanation of a 3:1 isomeric mixture of C_{2v}-C_{78} and D_3-C_{78} with about two equivalents of diethyl 2-bromomalonate showed high reactivity of these fullerene isomers, since at least eight tris-adducts, colored from green to brownish yellow in CH_2Cl_2, were formed as main products in addition to two C_1-symmetrical bis-adducts.[9] Most of the adducts were isolated in a pure state by HPLC and characterized by UV/Vis and ^1H and ^{13}C NMR spectroscopy, as well as mass spectrometry. A minor fraction of mono-adducts consisting of at least four isomers could not be analyzed in detail.

In the case of the tris-adducts, three isomers displayed higher symmetry than C_1 and could therefore be unambiguously assigned to the C_{78} isomer from which they arose. By comparing the spectra obtained for a C_2-symmetrical tris-adduct of C_{2v}-C_{78} to those of the bis-adducts, three possible structures ((±)-**53**) were proposed for one of the C_1-symmetrical bis-adducts that is the direct precursor to the corresponding tris-adduct (±)-**54** (Scheme 12). A common addend position in

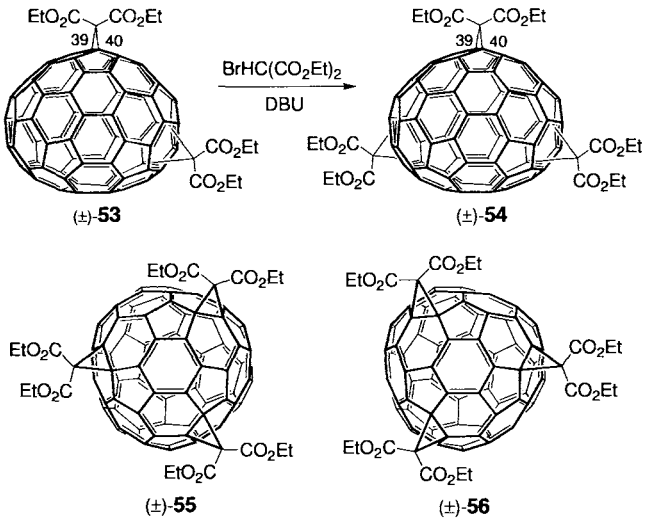

Scheme 12. Proposed structures for a C_2-symmetrical tris-adduct of C_{2v}-C_{78} ((±)-**54**), its bis-adduct precursor ((±)-**53**), and a C_3-symmetrical tris-adduct of D_3-C_{78} ((±)-**55** or (±)-**56** are possible).

(±)-**53** and (±)-**54** can be identified as the γ-type bond C(39)–C(40) at the intersection of the mirror planes of the parent fullerene. For the second addend, one out of three positions within the same six-membered ring containing one bond of type α and two of type β is most likely.[9] Considerations of π bond orders[13] that take into account steric effects predict C(9)–C(10) and C(69)–C(70) to be the most likely positions for the second and third addends in (±)-**54** (see Figure 1).

Two constitutionally isomeric structures, (±)-**55** or (±)-**56** (Scheme 12), were finally proposed for a pure C_3-symmetrical tris-adduct of D_3-C_{78}; both show the same relative pairwise arrangement of addends that is observed within a hemisphere of tris- and tetrakis-adducts of C_{70} (see Scheme 9).[9] This functionalization pattern (equatorial in C_{60}) therefore seems to be commonly realized in multiple adducts of fullerenes. According to considerations of π bond orders,[13] (±)-**56** should be formed preferentially. Even though a mixture of two C_{78} isomers was used as the starting material for the syntheses, most products were chromatographically isolated as (racemic) single isomers and represent the first pure adducts of C_{2v}-C_{78} and D_3-C_{78}. Reversible functionalization may therefore be a useful method for separating isomers of higher fullerenes.[19]

6. Conclusions

The chemical reactivity of C_{70} is becoming increasingly understood. Noteworthy is the general tendency for additions at 6–6 bonds in areas of highest local curvature near the poles, and for bis-additions at 6–6 bonds in opposite hemispheres. Furthermore, the pronounced regioselectivity in multiple additions exceeds that observed for C_{60}.

Although the number of studies concerning the reactivity of higher fullerenes beyond C_{70} is still small, it appears that relatively few mono-adduct isomers are formed despite the large number of potentially reactive 6–6 bonds. Also, the regioselectivity in multiple additions to the C_{78} isomers is quite remarkable. Many of these features cannot be satisfactorily explained by sole differences in bond reactivities resulting from differences in local curvature (C-atom pyramidalization) or steric effects. Rather, electronic effects must additionally be taken into account, and the consideration of π bond orders was proposed as a different way of looking at reactivities of fullerene bonds. Furthermore, the view of fullerenes as having the reactivity of simple alkenes with isolated double bonds might need significant adjustment. From the chemistry of higher fullerenes known today, it emerges that the different "double bonds" cannot be considered as independent. Further elucidation of the interrelationships between bonds in fullerene π systems has to be the object of future investigations, which, however, still await easier availability of the higher fullerenes.

Fullerene chirality is a novel chapter in stereochemistry that has largely been developed in work on higher fullerenes and their covalent derivatives. Hopefully, the remarkable, yet poorly understood chiroptical properties of fullerenes with chiral addition patterns will attract the interest of theoretical chemists in the future.

This work was supported by the Swiss National Science Foundation. We also thank Hoechst AG for samples of pure C_{70} and fullerene-soot extract enriched in higher fullerenes.

Received: April 7, 1997 [A 222IE]
German version: *Angew. Chem.* **1997**, *109*, 2362–2374

[1] W. Krätschmer, L. D. Lamb, K. Fostiropoulos, D. R. Huffman, *Nature (London)* **1990**, *347*, 354–358.
[2] F. Diederich, R. Ettl, Y. Rubin, R. L. Whetten, R. Beck, M. Alvarez, S. Anz, D. Sensharma, F. Wudl, K. C. Khemani, A. Koch, *Science* **1991**, *252*, 548–551.
[3] F. Diederich, R. L. Whetten, *Acc. Chem. Res.* **1992**, *25*, 119–126.
[4] C. Thilgen, F. Diederich, R. L. Whetten in *Buckminsterfullerenes* (Eds.: W. E. Billups, M. A. Ciufolini), VCH, New York, **1993**, pp. 59–81.
[5] W. A. Scrivens, P. V. Bedworth, J. M. Tour, *J. Am. Chem. Soc.* **1992**, *114*, 7917–7919.
[6] L. Isaacs, A. Wehrsig, F. Diederich, *Helv. Chim. Acta* **1993**, *76*, 1231–1250.
[7] W. A. Scrivens, A. M. Cassell, B. L. North, J. M. Tour, *J. Am. Chem. Soc.* **1994**, *116*, 6939–6940.
[8] A. Herrmann, F. Diederich, C. Thilgen, H.-U. ter Meer, W. H. Müller, *Helv. Chim. Acta* **1994**, *77*, 1689–1706.
[9] A. Herrmann, F. Diederich, *J. Chem. Soc. Perkin Trans. 2* **1997**, 1679–1684.
[10] R. Ettl, I. Chao, F. Diederich, R. L. Whetten, *Nature (London)* **1991**, *353*, 149–153.
[11] F. Diederich, R. L. Whetten, C. Thilgen, R. Ettl, I. Chao, M. M. Alvarez, *Science* **1991**, *254*, 1768–1770.
[12] C. J. Welch, W. H. Pirkle, *J. Chromatogr.* **1992**, *609*, 89–101.
[13] R. Taylor, *J. Chem. Soc. Perkin Trans. 2* **1993**, 813–824.
[14] P. R. Birkett, A. G. Avent, A. D. Darwish, H. W. Kroto, R. Taylor, D. R. M. Walton, *J. Chem. Soc. Chem. Commun.* **1995**, 683–684.
[15] P. W. Fowler, D. E. Manolopoulos, *An Atlas of Fullerenes*, Clarendon, Oxford, **1995**.
[16] R. Taylor, G. J. Langley, A. G. Avent, T. J. S. Dennis, H. W. Kroto, D. R. M. Walton, *J. Chem. Soc. Perkin Trans. 2* **1993**, 1029–1036.
[17] R. H. Michel, M. M. Kappes, P. Adelmann, G. Roth, *Angew. Chem.* **1994**, *106*, 1742–1746; *Angew. Chem. Int. Ed. Engl.* **1994**, *33*, 1651–1654.
[18] K. Kikuchi, N. Nakahara, T. Wakabayashi, S. Suzuki, H. Shiromaru, Y. Miyake, K. Saito, I. Ikemoto, M. Kainosho, Y. Achiba, *Nature (London)* **1992**, *357*, 142–145.
[19] A. L. Balch, A. S. Ginwalla, J. W. Lee, B. C. Noll, M. M. Olmstead, *J. Am. Chem. Soc.* **1994**, *116*, 2227–2228.
[20] F. H. Hennrich, R. H. Michel, A. Fischer, S. Richard-Schneider, S. Gilb, M. M. Kappes, D. Fuchs, M. Bürk, K. Kobayashi, S. Nagase, *Angew. Chem.* **1996**, *108*, 1839–1841; *Angew. Chem. Int. Ed. Engl.* **1996**, *35*, 1732–1734.
[21] a) J. R. Heath, S. C. O'Brien, Q. Zhang, Y. Liu, R. F. Curl, H. W. Kroto, F. K. Tittel, R. E. Smalley, *J. Am. Chem. Soc.* **1985**, *107*, 7779–7780; b) Y. Chai, T. Guo, C. Jin, R. E. Haufler, L. P. F. Chibante, J. Fure, L. Wang, J. M. Alford, R. E. Smalley, *J. Phys. Chem.* **1991**, *95*, 7564–7568; c) D. S. Bethune, R. D. Johnson, J. R. Salem, M. S. de Vries, C. S. Yannoni, *Nature (London)* **1993**, *366*, 123–128; d) F. T. Edelmann, *Angew. Chem.* **1995**, *107*, 1071–1075; *Angew. Chem. Int. Ed. Engl.* **1995**, *34*, 981–985; e) S. Nagase, K. Kobayashi, T. Akasaka, *Bull. Chem. Soc. Jpn.* **1996**, *69*, 2131–2142.
[22] a) M. M. Ross, J. H. Callahan, *J. Phys. Chem.* **1991**, *95*, 5720–5723; b) K. A. Caldwell, D. E. Giblin, M. L. Gross, *J. Am. Chem. Soc.* **1992**, *114*, 3743–3756; c) H. Schwarz, T. Weiske, D. K. Böhme, J. Hrusák in *Buckminsterfullerenes* (Eds.: W. E. Billups, M. A. Ciufolini), VCH, New York, **1993**, pp. 257–283.
[23] M. Saunders, H. A. Jiménez-Vázquez, R. J. Cross, R. J. Poreda, *Science* **1993**, *259*, 1428–1430.
[24] M. Saunders, H. A. Jiménez-Vázquez, R. J. Cross, S. Mroczkowski, M. L. Gross, D. E. Giblin, R. J. Poreda, *J. Am. Chem. Soc.* **1994**, *116*, 2193–2194.
[25] a) R. L. Murry, G. E. Scuseria, *Science* **1994**, *263*, 791–793; b) S. Patchkovskii, W. Thiel, *J. Am. Chem. Soc.* **1996**, *118*, 7164–7172.
[26] a) M. Saunders, H. A. Jiménez-Vázquez, R. J. Cross, S. Mroczkowski, D. I. Freedberg, F. A. L. Anet, *Nature (London)* **1994**, *367*, 256–258; b) M. Saunders, R. J. Cross, H. A. Jiménez-Vázquez, R. Shimshi, A. Khong, *Science* **1996**, *271*, 1693–1697; c) M. Saunders, H. A. Jiménez-Vázquez, R. J. Cross, W. E. Billups, C. Gesenberg, A. Gonzalez, W. Luo, R. C. Haddon, F. Diederich, A. Herrmann, *J. Am. Chem. Soc.* **1995**, *117*, 9305–9308.
[27] M. Rüttimann, R. F. Haldimann, L. Isaacs, F. Diederich, A. Khong, H. Jiménez-Vázquez, R. J. Cross, M. Saunders, *Chem. Eur. J.* **1997**, *3*, 1071–1076.
[28] A. Hirsch, *The Chemistry of the Fullerenes*, Thieme, Stuttgart, **1994**.
[29] a) F. Diederich, C. Thilgen, *Science* **1996**, *271*, 317–323; b) F. Diederich, *Pure Appl. Chem.* **1997**, *69*, 395–400.
[30] *Tetrahedron Symposia-In-Print 60, Fullerene Chemistry* (Ed.: A. B. Smith III), Elsevier, Oxford, **1996**.
[31] a) *Proceedings of the Symposium on Fullerenes, Recent Advances in the Chemistry and Physics of Fullerenes and Related Materials, Vol. 1* (Eds.: K. M. Kadish, R. S. Ruoff), The Electrochemical Society, Pennington, New Jersey, **1994**; b) *Proceedings of the Symposium on Fullerenes, Recent Advances in the Chemistry and Physics of Fullerenes and Related Materials, Vol. 2* (Eds.: K. M. Kadish, R. S. Ruoff), The Electrochemical Society, Pennington, New Jersey, **1995**; c) *Proceedings of the Symposium on Fullerenes, Recent Advances in the Chemistry and Physics of Fullerenes and Related Materials, Vol. 3* (Eds.: K. M. Kadish, R. S. Ruoff), The Electrochemical Society, Pennington, New Jersey, **1996**.
[32] F. Diederich, C. Thilgen, A. Herrmann, *Nachr. Chem. Tech. Lab.* **1996**, *44*, 9–16.
[33] C. Thilgen, A. Herrmann, F. Diederich, *Helv. Chim. Acta* **1997**, *80*, 183–199.
[34] J. M. Hawkins, A. Meyer, *Science* **1993**, *260*, 1918–1920.
[35] J. M. Hawkins, M. Nambu, A. Meyer, *J. Am. Chem. Soc.* **1994**, *116*, 7642–7645.
[36] a) R. S. Cahn, S. C. Ingold, V. Prelog, *Angew. Chem.* **1966**, *78*, 413–447; *Angew. Chem. Int. Ed. Engl.* **1966**, *5*, 385–415, 511; b) V. Prelog, G. Helmchen, *Angew. Chem.* **1982**, *94*, 614–631; *Angew. Chem. Int. Ed. Engl.* **1982**, *21*, 567–583.
[37] E. W. Godly, R. Taylor, *Pure Appl. Chem.* **1997**, *69*, 1411–1434.
[38] R. Panico, W. H. Powell in *A Guide to IUPAC Nomenclature of Organic Compounds* (Ed.: J.-C. Richter), Blackwell, Oxford, **1993**.
[39] N. Matsuzawa, D. A. Dixon, T. Fukunaga, *J. Phys. Chem.* **1992**, *96*, 7594–7604.
[40] a) J. Baker, P. W. Fowler, P. Lazzeretti, M. Malagoli, R. Zanasi, *Chem. Phys. Lett.* **1991**, *184*, 182–186; b) A. Rathna, J. Chandrasekhar, *Fullerene Sci. Technol.* **1995**, *3*, 681–705.

[41] J. M. Hawkins, A. Meyer, M. A. Solow, *J. Am. Chem. Soc.* **1993**, *115*, 7499–7500.
[42] R. C. Haddon, *Science* **1993**, *261*, 1545–1550.
[43] a) J. M. Wood, B. Kahr, S. H. Hoke II, L. Dejarme, R. G. Cooks, D. Ben-Amotz, *J. Am. Chem. Soc.* **1991**, *113*, 5907–5908; b) J. B. Howard, A. L. Lafleur, Y. Makarovsky, S. Mitra, C. J. Pope, T. K. Yadav, *Carbon* **1992**, *30*, 1183–1201.
[44] M. Wohlers, H. Werner, D. Herein, T. Schedel-Niedrig, A. Bauer, R. Schlögl, *Synth. Met.* **1996**, *77*, 299–302.
[45] D. Heymann, L. P. F. Chibante, *Chem. Phys. Lett.* **1993**, *207*, 339–342.
[46] D. Heymann, L. P. F. Chibante, *Recl. Trav. Chim. Pays-Bas* **1993**, *112*, 639–642.
[47] A. B. Smith, R. M. Strongin, L. Brard, G. T. Furst, J. H. Atkins, W. J. Romanow, M. Saunders, H. A. Jiménez-Vázquez, K. G. Owens, R. J. Goldschmidt, *J. Org. Chem.* **1996**, *61*, 1904–1905.
[48] A. L. Balch, D. A. Costa, M. M. Olmstead, *Chem. Commun.* **1996**, 2449–2450.
[49] A. L. Balch, V. J. Catalano, J. W. Lee, M. M. Olmstead, S. R. Parkin, *J. Am. Chem. Soc.* **1991**, *113*, 8953–8955.
[50] M. Iyoda, Y. Ogawa, H. Matsuyama, *Fullerene Sci. Technol.* **1995**, *3*, 1–9.
[51] A. L. Balch, J. W. Lee, M. M. Olmstead, *Angew. Chem.* **1992**, *104*, 1400–1402; *Angew. Chem. Int. Ed. Engl.* **1992**, *31*, 1356–1358.
[52] A. L. Balch, L. Hao, M. M. Olmstead, *Angew. Chem.* **1996**, *108*, 211–213; *Angew. Chem. Int. Ed. Engl.* **1996**, *35*, 188–190.
[53] C. C. Henderson, C. M. Rohlfing, P. A. Cahill, *Chem. Phys. Lett.* **1993**, *213*, 383–388.
[54] A. G. Avent, A. D. Darwish, D. K. Heimbach, H. W. Kroto, M. F. Meidine, J. P. Parsons, C. Remars, R. Roers, O. Ohashi, R. Taylor, D. R. M. Walton, *J. Chem. Soc. Perkin Trans. 2* **1994**, 15–22.
[55] C. C. Henderson, C. M. Rohlfing, K. T. Gillen, P. A. Cahill, *Science* **1994**, *264*, 397–399.
[56] M. S. Meier, J. A. Laske Cooke, B. R. Weedon, H. P. Spielmann in ref. [31c], pp. 1193–1199.
[57] A. Govindaraj, A. Rathna, J. Chandrasekhar, C. N. R. Rao, *Proc. Indian Acad. Sci. Chem. Sci.* **1993**, *105*, 303–309.
[58] a) M. Gerst, H.-D. Beckhaus, C. Rüchardt, E. E. B. Campbell, R. Tellgmann, *Tetrahedron Lett.* **1993**, *34*, 7729–7732; b) M. I. Attalla, A. M. Vassallo, B. N. Tattam, J. V. Hanna, *J. Phys. Chem.* **1993**, *97*, 6329–6331; c) K. Shigematsu, K. Abe, *Chem. Express* **1992**, *7*, 905–908; d) K. Shigematsu, K. Abe, M. Mitani, K. Tanaka, *ibid.* **1992**, *7*, 957–960; e) *Fullerene Sci. Technol.* **1993**, *1*, 309–318; f) A. D. Darwish, A. K. Abdul-Sada, G. J. Langley, H. W. Kroto, R. Taylor, D. R. M. Walton, *J. Chem. Soc. Perkin Trans. 2* **1995**, 2359–2365; g) *Synth. Met.* **1996**, *77*, 303–307.
[59] A. D. Darwish, H. W. Kroto, R. Taylor, D. R. M. Walton, *J. Chem. Soc. Perkin Trans. 2* **1996**, 1415–1418.
[60] A. Hamwi, C. Fabre, P. Chaurand, S. Della-Negra, C. Ciot, D. Djurado, J. Dupuis, A. Rassat, *Fullerene Sci. Technol.* **1993**, *1*, 499–535.
[61] R. Taylor, G. J. Langley, J. H. Holloway, E. G. Hope, A. K. Brisdon, H. W. Kroto, D. R. M. Walton, *J. Chem. Soc. Perkin Trans. 2* **1995**, 181–187.
[62] H. Selig, C. Lifshitz, T. Peres, J. E. Fischer, A. R. McGhie, W. J. Romanow, J. P. McCauley, Jr., A. B. Smith III, *J. Am. Chem. Soc.* **1991**, *113*, 5475–5476.
[63] A. A. Tuinman, P. Mukherjee, J. L. Adcock, R. L. Hettich, R. N. Compton, *J. Phys. Chem.* **1992**, *96*, 7584–7589.
[64] O. V. Boltalina, A. Y. Borschevskii, L. N. Sidorov, J. M. Street, R. Taylor, *Chem. Commun.* **1996**, 529–530.
[65] R. Taylor, G. J. Langley, A. K. Brisdon, J. H. Holloway, E. G. Hope, H. W. Kroto, D. R. M. Walton, *J. Chem. Soc. Chem. Commun.* **1993**, 875–878.
[66] S. J. Austin, P. W. Fowler, J. P. B. Sandall, P. R. Birkett, A. G. Avent, A. D. Darwish, H. W. Kroto, R. Taylor, D. R. M. Walton, *J. Chem. Soc. Perkin Trans. 2* **1995**, 1027–1028.
[67] A. G. Avent, P. R. Birkett, A. D. Darwish, H. W. Kroto, R. Taylor, D. R. M. Walton, *Tetrahedron* **1996**, *52*, 5235–5246.
[68] P. R. Birkett, A. G. Avent, A. D. Darwish, H. W. Kroto, R. Taylor, D. R. M. Walton, *Chem. Commun.* **1996**, 1231–1232.
[69] P. R. Birkett, A. G. Avent, A. D. Darwish, H. W. Kroto, R. Taylor, D. R. M. Walton, *J. Chem. Soc. Chem. Commun.* **1995**, 1869–1870.
[70] M. Ohno, S. Shibata, S. Eguchi, *Fullerene Sci. Technol.* **1995**, *3*, 29–35.
[71] P. N. Keizer, J. R. Morton, K. F. Preston, *J. Chem. Soc. Chem. Commun.* **1992**, 1259–1261.
[72] R. Borghi, L. Lunazzi, G. Placucci, P. J. Krusic, D. A. Dixon, L. B. Knight, Jr., *J. Phys. Chem.* **1994**, *98*, 5395–5398.
[73] J. R. Morton, F. Negri, K. F. Preston, *Magn. Reson. Chem.* **1995**, *33*, S20–S27.
[74] R. Borghi, L. Lunazzi, G. Placucci, P. J. Krusic, D. A. Dixon, N. Matsuzawa, M. Ata, *J. Am. Chem. Soc.* **1996**, *118*, 7608–7617.
[75] J. R. Morton, F. Negri, K. F. Preston, *Chem. Phys. Lett.* **1994**, *218*, 467–474.
[76] R. Borghi, B. Guidi, L. Lunazzi, G. Placucci, *J. Org. Chem.* **1996**, *61*, 5667–5669.
[77] I. D. Reid, E. Roduner, *Hyperfine Interact.* **1994**, *86*, 809–815.
[78] a) W. Sliwa, *Fullerene Sci. Technol.* **1995**, *3*, 243–281; b) S. Eguchi, M. Ohno, S. Kojima, N. Koide, A. Yashiro, Y. Shirakawa, H. Ishida, *ibid.* **1996**, *4*, 303–327.
[79] T. Akasaka, E. Mitsuhida, W. Ando, K. Kobayashi, S. Nagase, *J. Chem. Soc. Chem. Commun.* **1995**, 1529–1530.
[80] X. Zhang, C. S. Foote, *J. Am. Chem. Soc.* **1995**, *117*, 4271–4275.
[81] A. D. Darwish, A. K. Abdul-Sada, G. J. Langley, H. W. Kroto, R. Taylor, D. R. M. Walton, *J. Chem. Soc. Chem. Commun.* **1994**, 2133–2134.
[82] A. D. Darwish, A. G. Avent, R. Taylor, D. R. M. Walton, *J. Chem. Soc. Perkin Trans. 2* **1996**, 2079–2084.
[83] a) A. M. Rao, M. Menon, K.-A. Wang, P. C. Eklund, K. R. Subbaswamy, D. S. Cornett, M. A. Duncan, I. J. Amster, *Chem. Phys. Lett.* **1994**, *224*, 106–112; b) Y. P. Sun, B. Ma, C. E. Bunker, B. Liu, *J. Am. Chem. Soc.* **1995**, *117*, 12705–12711.
[84] F. Diederich, L. Isaacs, D. Philp, *Chem. Soc. Rev.* **1994**, *23*, 243–255.
[85] A. B. Smith III, R. M. Strongin, L. Brard, G. T. Furst, W. J. Romanow, K. G. Owens, R. J. Goldschmidt, R. C. King, *J. Am. Chem. Soc.* **1995**, *117*, 5492–5502.
[86] M. S. Meier, M. Poplawska, A. L. Compton, J. P. Shaw, J. P. Selegue, T. F. Guarr, *J. Am. Chem. Soc.* **1994**, *116*, 7044–7048.
[87] H. Irngartinger, C.-M. Kohler, G. Baum, D. Fenske, *Liebigs Ann.* **1996**, 1609–1614.
[88] S. Yamago, E. Nakamura, *Chem. Lett.* **1996**, 395–396.
[89] R. F. Haldimann, F. G. Klärner, F. Diederich, *Chem. Commun.* **1997**, 237–238.
[90] B. Nuber, A. Hirsch, *Fullerene Sci. Technol.* **1996**, *4*, 715–728.
[91] C. Bellavia-Lund, F. Wudl, *J. Am. Chem. Soc.* **1997**, *119*, 943–946.
[92] I. Lamparth, B. Nuber, G. Schick, A. Skiebe, T. Grösser, A. Hirsch, *Angew. Chem.* **1995**, *107*, 2473–2476; *Angew. Chem. Int. Ed. Engl.* **1995**, *34*, 2257–2259.
[93] B. Nuber, A. Hirsch, *Chem. Commun.* **1996**, 1421–1422.
[94] J. C. Hummelen, B. Knight, J. Pavlovich, R. González, F. Wudl, *Science* **1995**, *269*, 1554–1556.
[95] S. R. Wilson, Q. Lu, *J. Org. Chem.* **1995**, *60*, 6496–6498.
[96] T. Akasaka, E. Mitsuhida, W. Ando, K. Kobayashi, S. Nagase, *J. Am. Chem. Soc.* **1994**, *116*, 2627–2628.
[97] P. Seiler, A. Herrmann, F. Diederich, *Helv. Chim. Acta* **1995**, *78*, 344–354.
[98] H. Becker, G. Javahery, S. Petrie, D. K. Bohme, *J. Phys. Chem.* **1994**, *98*, 5591–5592.
[99] L. S. K. Pang, M. A. Wilson, *J. Phys. Chem.* **1993**, *97*, 6761–6763.
[100] M. F. Meidine, A. G. Avent, A. D. Darwish, H. W. Kroto, O. Ohashi, R. Taylor, D. R. M. Walton, *J. Chem. Soc. Perkin Trans. 2* **1994**, 1189–1193.
[101] B. Nie, V. M. Rotello, *J. Org. Chem.* **1996**, *61*, 1870–1871.
[102] T. Gareis, O. Köthe, E. Beer, J. Daub in ref. [31c], pp. 1244–1253.
[103] A. Hirsch, T. Grösser, A. Skiebe, A. Soi, *Chem. Ber.* **1993**, *126*, 1061–1067.
[104] C. Bingel, *Chem. Ber.* **1993**, *126*, 1957–1959.
[105] Y. Wang, D. I. Schuster, S. R. Wilson, C. J. Welch, *J. Org. Chem.* **1996**, *61*, 5198–5199.
[106] A. Herrmann, M. Rüttimann, C. Thilgen, F. Diederich, *Helv. Chim. Acta* **1995**, *78*, 1673–1704.
[107] J.-F. Nierengarten, A. Herrmann, R. R. Tykwinski, M. Rüttimann, F. Diederich, C. Boudon, J.-P. Gisselbrecht, M. Gross, *Helv. Chim. Acta* **1997**, *80*, 293–316.
[108] H. R. Karfunkel, A. Hirsch, *Angew. Chem.* **1992**, *104*, 1529–1531; *Angew. Chem. Int. Ed. Engl.* **1992**, *31*, 1468–1470.
[109] H. J. Bestmann, D. Hadawi, T. Röder, C. Moll, *Tetrahedron Lett.* **1994**, *35*, 9017–9020.
[110] Y. Wang, J. Cao, D. I. Schuster, S. R. Wilson, *Tetrahedron Lett.* **1995**, *36*, 6843–6846.
[111] C. Boudon, J.-P. Gisselbrecht, M. Gross, L. Isaacs, H. L. Anderson, R. Faust, F. Diederich, *Helv. Chim. Acta* **1995**, *78*, 1334–1344.
[112] C. Bingel, H. Schiffer, *Liebigs Ann.* **1995**, 1551–1553.
[113] A. Herrmann, T. Gibtner, F. Diederich, unpublished results.
[114] J. M. Hawkins, A. Meyer, M. Nambu, *J. Am. Chem. Soc.* **1993**, *115*, 9844–9845.
[115] A. Herrmann, F. Diederich, *Helv. Chim. Acta* **1996**, *79*, 1741–1756.
[116] J.-F. Nierengarten, V. Gramlich, F. Cardullo, F. Diederich, *Angew. Chem.* **1996**, *108*, 2242–2244; *Angew. Chem. Int. Ed. Engl.* **1996**, *35*, 2101–2103.
[117] A. Bianco, M. Maggini, G. Scorrano, C. Toniolo, G. Marconi, C. Villani, M. Prato, *J. Am. Chem. Soc.* **1996**, *118*, 4072–4080.
[118] S. R. Wilson, Q. Lu, J. R. Cao, Y. Wu, C. J. Welch, D. I. Schuster, *Tetrahedron* **1996**, *52*, 5131–5142.
[119] F. Djojo, A. Herzog, I. Lamparth, F. Hampel, A. Hirsch, *Chem. Eur. J.* **1996**, *2*, 1537–1547.
[120] A. Hirsch, I. Lamparth, H. R. Karfunkel, *Angew. Chem.* **1994**, *106*, 453–455; *Angew. Chem. Int. Ed. Engl.* **1994**, *33*, 437–438.

[121] P. R. Birkett, A. D. Darwish, H. W. Kroto, G. J. Langley, R. Taylor, D. R. M. Walton, *J. Chem. Soc. Perkin Trans. 2* **1995**, 511–514.
[122] A. J. Stone, D. J. Wales, *Chem. Phys. Lett.* **1986**, *128*, 501–503.
[123] O. V. Boltalina, L. N. Sidorov, V. F. Bagryantsev, V. A. Seredenko, A. S. Zapol'skii, J. M. Street, R. Taylor, *J. Chem. Soc. Perkin Trans. 2* **1996**, 2275–2278.
[124] O. V. Boltalina, L. N. Sidorov, E. V. Sukhanova, I. D. Sorokin, *Chem. Phys. Lett.* **1994**, *230*, 567–570.
[125] O. V. Boltalina, D. B. Ponomarev, A. Y. Borschevskii, I. D. Sorokin, L. N. Sidorov in ref. [31c], pp. 108–120.
[126] A. Y. Borschevskii, O. V. Boltalina, L. N. Sidorov, V. Y. Markov, I. N. Ioffe in ref. [31c], pp. 509–521.
[127] O. V. Boltalina, E. V. Dashkova, L. N. Sidorov, *Chem. Phys. Lett.* **1996**, *256*, 253–260.
[128] a) T. Akasaka, T. Kato, K. Kobayashi, S. Nagase, K. Yamamoto, H. Funasaka, T. Takahashi, *Nature (London)* **1995**, *374*, 600–601; b) T. Akasaka, S. Nagase, K. Kobayashi, T. Suzuki, T. Kato, K. Yamamoto, H. Funasaka, T. Takahashi, *J. Chem. Soc. Chem. Commun.* **1995**, 1343–1344; c) T. Akasaka, S. Nagase, K. Kobayashi, T. Suzuki, T. Kato, K. Kikuchi, Y. Achiba, K. Yamamoto, H. Funasaka, T. Takahashi, *Angew. Chem.* **1995**, *107*, 2303–2304; *Angew. Chem. Int. Ed. Engl.* **1995**, *34*, 2139–2141.

Deposition of Data from X-Ray Structure Analyses

In order to make life easier for authors and referees the Cambridge Crystallographic Data Centre (CCDC) and the Fachinformationszentrum Karlsruhe (FIZ) have unified their procedures for the deposition of data from single-crystal X-ray structure analyses.

Prior to submitting your manuscripts please deposit the data for your compound(s) **electronically** at the appropriate data base, that is, at the CCDC for organic and organometallic compounds and at the FIZ for inorganic compounds. Both data bases will be pleased to provide help (see our *Notice to Authors* in the first issue of this year). In general, you will receive a depository number from the data base within two working days after electronic deposition; please include this number with the appropriate standard text (see our *Notice to Authors*) in your manuscript. This will enable the referees to retrieve the structure data quickly and efficiently if they need this information to reach their decision.

This is now the uniform procedure for manuscripts submitted to the journals *Advanced Materials, Angewandte Chemie, Chemische Berichte/Recueil, Chemistry—A European Journal,* and *Liebigs Annalen/Recueil.*

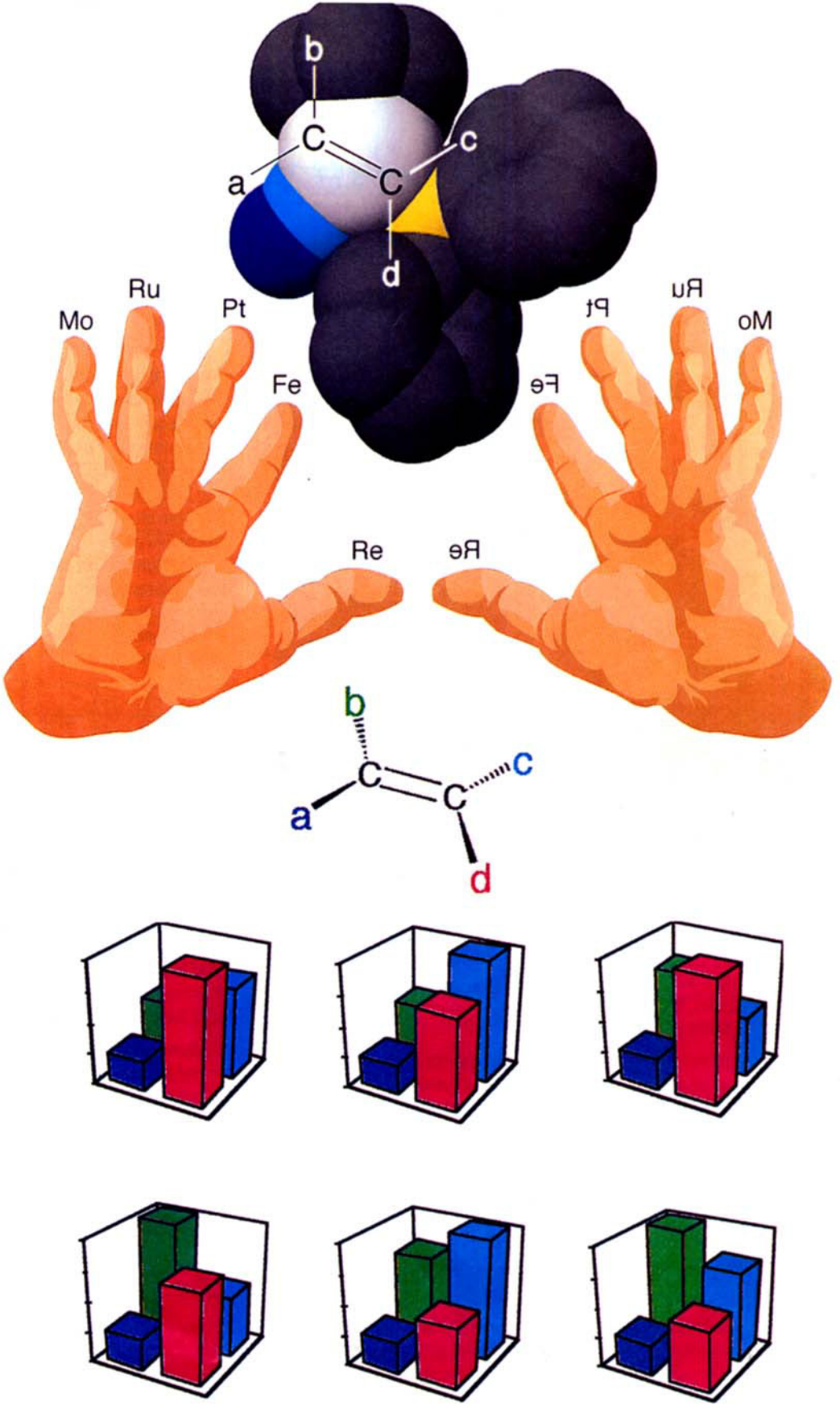

$[(\eta^5\text{-}C_5H_5)Re(NO)(PPh_3)]^+$ and analogons unsaturated chiral complexes (see element symbols along the fingertips) can form two diastereomeric adducts with prochiral alkenes, aldehydes, and ketones. The ratio of these diastereomers is a measure of the chiral recognition, symbolized by the hands, of the reaction partners. The rhenium complex mentioned is depicted above the hands (Re: light gray, P: yellow, N: light blue, O: dark blue, Ph, Cp: dark gray). The selectivity of alkene complexation can be analyzed (and predicted) by considering the sizes of the substituents a–d on the alkene and correlating them with the steric conditions in the chiral complexes, which can be represented with three-dimensional bar graphs.

Enantioselective Synthesis with Lithium/(−)-Sparteine Carbanion Pairs

Dieter Hoppe* and Thomas Hense

Dedicated to Professor Dieter Seebach on the occasion of his 60th birthday

"Chiral carbanions"—that is, enantiomerically enriched lithium–carbanion pairs in which the carbanionic center carries the chiral information—were regarded until recently as "exotic species." In the past ten years it has become clear that they can, in fact, play a meaningful role in enantioselective synthesis, since substitution for lithium occurs here stereospecifically, usually with retention of configuration. They are also more readily and commonly accessible than was originally assumed. The trick lies in the use of lithium cations with chiral ligands, whether in the form of alkyllithium species used as bases in kinetically controlled, enantiotopically discriminating deprotonation, or in thermodynamically controlled equilibration in configurationally labile epimeric ion pairs. The lupine alkaloid (−)-sparteine has shown itself admirably suited as a chiral bidentate ligand, and its efficiency and breadth of application are so far unsurpassed. This contribution constitutes an overview of the preparation of chiral reagents, covering primarily "umpoled" synthons such as homoenolates, 1-oxyalkanides with a broad pattern of substitution, and α-aminobenzyl anions.

Keywords: asymmetric synthesis · chiral building blocks · lithium · (−)-sparteine

1. Introduction and Delineation of the Problem

In a series of reviews that also provide insight into the fundamental contributions of his research group, D. Seebach has since 1969 popularized the concept of "reactivity umpolung."[1] As a consequence, the synthetic chemist has acquired not only a simple tool for the rational planning of syntheses, but has also been stimulated in the search for new synthetic building blocks. A higher standard has been achieved particularly in the case of reagents for carbanionic synthons of the d^1 and d^3 type, which now leaves little to be desired with respect to controlling reactivity and various levels of selectivity. Seebach has repeatedly noted that the reactivity and selectivity of carbanionic reagents is heavily dependent on the nature of the counterion and the structure of the relevant aggregates.[2] It will become clear in what follows that it is precisely the apparent disadvantage of most d^1 and d^3 reagents—a lack or at least a weakening of resonance stabilization, and thus restricted accessibility—that lends new qualities to these species.

The carbanionic center of a lithium–carbanion pair in the vicinity of +M substituents seeks to achieve a pyramidal and therefore potentially chiral configuration; in this way it is able, under appropriate conditions, to act as a carrier of chiral information, thereby opening the way to new strategies for enantioselective synthesis. Chiral ligands attached to the cation—here primarily the alkaloid (−)-sparteine (**1**) (Scheme 1)—have shown themselves to be astonishingly efficient aids.

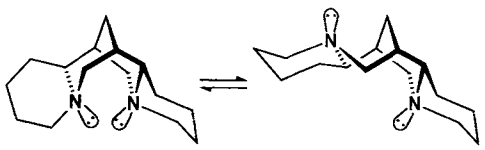

1A **1B**

Scheme 1. Conformations of (−)-sparteine (**1**).

In nonpolar solvents lithium salts of carbanions form tight ion pairs, usually present as dimers, tetramers, and occasionally also higher aggregates.[2, 3] The lithium cation usually prefers an approximately tetrahedral coordination geometry saturated by four donor ligands. It is thus tempting to provide the cation with chiral, enantiomerically pure ligands and to hope that stereoselectivity will be introduced in reactions with achiral, prostereogenic substrates. For purposes of clarity our first "thought experiment" will involve a bidentate, C_2-symmetric ligand[4, 5] and a η_1-bound anion; in addition, we will consider a monomeric ion pair. The ion pair **A** bears an achiral alkanide residue; that means that any chiral induction must be due to the chiral cation (Scheme 2). If both components of the ion pair (the cation as well as the anion) are chiral, the result is the pair of epimers **B** and *epi*-**B**. The consequences will be explored in more detail.

[*] Prof. Dr. D. Hoppe, Dr. T. Hense
Organisch-chemisches Institut der Universität
Corrensstrasse 40, D-48149 Münster (Germany)
Fax: Int. code +(251)833-9772

 © WILEY-VCH Verlag GmbH, D-69451 Weinheim, 1997 0570-0833/97/3621-2283 $ 17.50+.50/0

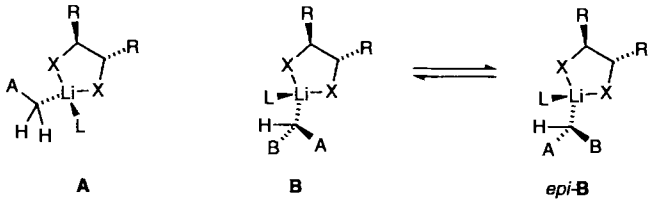

Scheme 2. Types of chiral lithium–carbanion pairs. X is, for example, OR, NR_2; L is, for example, OEt_2, THF; A,B are C- or heterosubstituents.

A is already in a position to "recognize" enantiotopic faces and groups in prochiral[6] reaction partners, since it will proceed through diastereomorphic transition states, which will in principle be energetically nonequivalent (Scheme 3). This is apparent in complex **D**, comprising a combination of **A** and **C**: the previously enantiotopic faces *Re* and *Si* are now diastereotopic in the intermediate **D**, and the alkanide residue ACH_2^- will be transferred at different rates to form the adducts **E** and *epi*-**E**. Hydrolysis leads finally to the enantiomers **F** and *ent*-**F**, one of which will be present in excess.[7] Scheme 4 depicts several examples from the early stages of the development of this technique.

A similar problem is posed when **A** interacts as a chiral base with the prostereogenic substrate $A-CH_2-B$: in this case the enantiotopic groups *pro-S*-H atom H_s and *pro-R*-H atom H_R must display different reactivities. Insofar as the resulting ion pairs **B** and *epi*-**B** are configurationally stable under the reaction conditions and substitution occurs stereospecifically (that is, with either retention or inversion), the enantiomeric relationship **G**:*ent*-**G** reflects directly the result of enantiotopic differentiation between H_S and H_R (Scheme 5). Thus, the newly created stereocenter at the carbanionic C atom determines the stereochemistry of substitution.

However, with few exceptions (which will be discussed later), configurational stability of the carbanionic intermediate cannot be assumed;[15] the ion pairs **B** and *epi*-**B** are subject to equilibration. Scheme 6 summarizes the possible situations, where for simplicity only stereoretentative substitution is illustrated. Under the simplifying assumption that $k_R \approx k_s > k_{epi}$, the ratio **G**:*ent*-**G** corresponds to the position of equilibrium **B**:*epi*-**B**. Especially fortunate circumstances obtain when one of the diastereomers **B** or *epi*-**B** crystallizes, so that in the reaction mixture essentially only one diastereomer arises. This special case of a dynamic kinetic resolution through crystallization is also referred to as "asymmetric transformation of the second order."[16] An additional limiting case—kinetically controlled

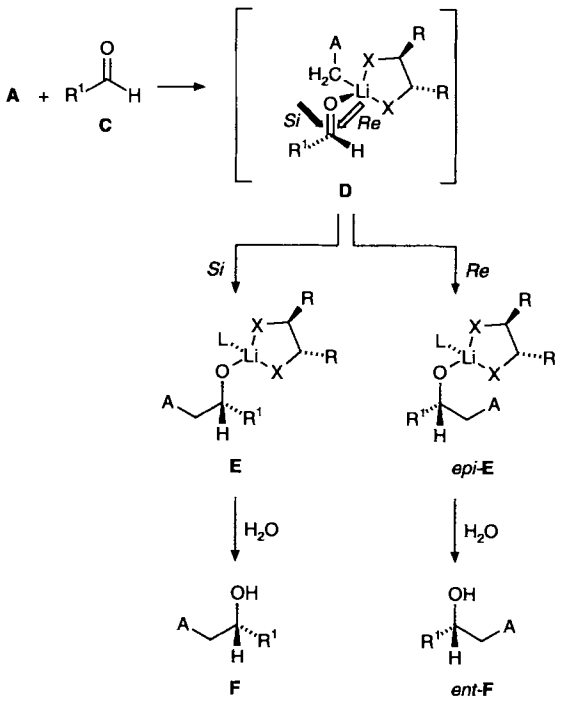

Scheme 3. Enantiofacial selection in a prochiral carbonyl compound on use of an ion pair containing an achiral residue.

Dieter Hoppe, born in Berlin in 1941, worked as a chemical technician in Hannover before beginning his chemistry studies at the University of Göttingen in 1965. He received his doctorate in 1970 with U. Schöllkopf, submitting a dissertation on metalated isonitriles and completed his habilitation there in 1977 with a topic drawn from the realm of β-lactam chemistry. From 1977 to 1978 he was a postdoctoral fellow with R. B. Woodward at Harvard University in Cambridge (Massachusetts). After serving as a Privatdozent at the University of Göttingen he accepted a call to a C-4 professorship at the University of Kiel in 1985. Then followed a call to the University of Münster (1992), after a call he had declined to Hamburg (1991). His work was recognized in 1993 with an Otto-Bayer Award. He is a coeditor of "Synthesis." His areas of research relate to the development of stereoselective and especially enantioselective synthetic methods based on carbanion chemistry.

D. Hoppe

T. Hense

Thomas Hense, born in 1964 in Oldenburg, began his studies in 1987 in Münster, and joined the research group of D. Hoppe in 1992. He completed his dissertation in 1996 on the subject of kinetic resolution of racemates through (−)-sparteine-induced deprotonation. In 1997 he entered upon a postdoctoral appointment with J. Otera in Okayama (Japan) in the field of enantioselective catalysis.

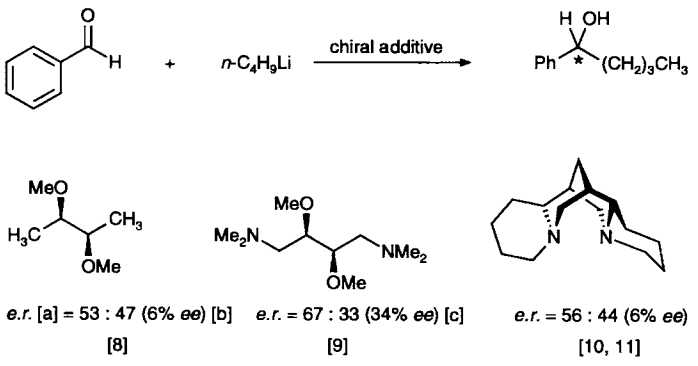

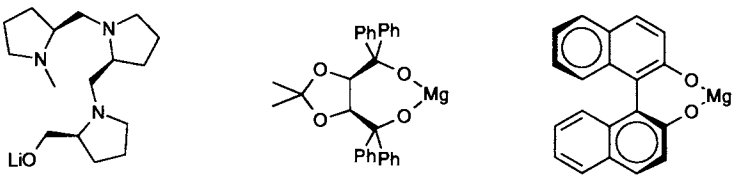

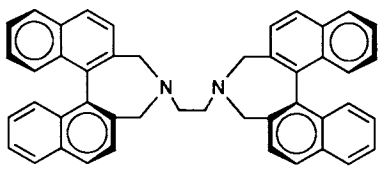

Scheme 4. Addition of complexes of *n*-butyllithium and chiral ligands to benzaldehyde with differentiation between enantiotopic faces. [a] *e.r.* = enantiomeric ratio; [b] 2.0 equivalents of ligand utilized; [c] with 9 equivalents, 86% *ee* was achieved; [d] With butylmagnesium chloride.

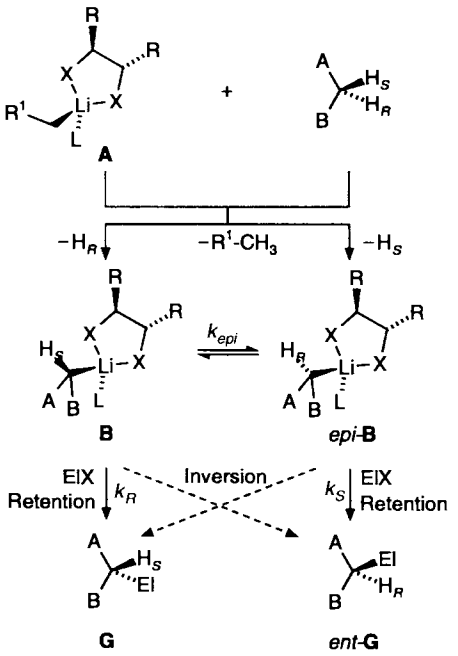

Scheme 5 Deprotonation of a prochiral CH acid ACH_2B by a chiral base and stereoselective substitution of the epimeric ion pairs.

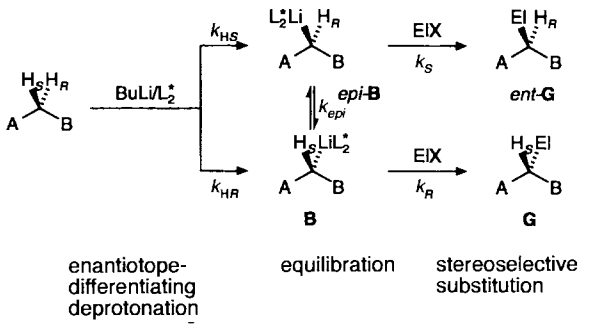

Scheme 6. Limiting cases in the substitution of chiral ion pairs.

stereoselective substitution with dynamic kinetic resolution[16a, c, d]—occurs when the rate constants k_R and k_S differ greatly, and k_{epi} much larger than these. In this limiting case (e.g., $k_R \gg k_S > k_{epi}$), the enantiomeric ratio **G**/*ent*-**G** is determined solely by the quotient k_R/k_S.[17]

It should also be recalled that achiral carbanions, which in the ground state are planar and which bear three different substituents at the carbanionic center, become chiral in the course of interacting with a cation (Scheme 7). Since exchange of the

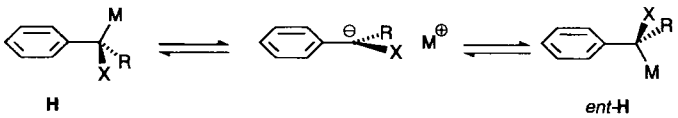

Scheme 7. Chiral tight ion pairs and their racemization via achiral separated ion pairs.

cation between the enantiotopic faces on the "top" and "bottom" of the benzylmetal compounds **H** and *ent*-**H** normally occurs with exceptional ease, enantiomerically enriched ion pairs are subject to rapid racemization, as demonstrated by D. J. Cram.[18] However, if the cation is provided with a configuratively uniform ligand, the result is epimeric, configurationally stable ion pairs, to which the above argument applies.

Thus, the areas of application for chiral lithium carbanions in enantioselective synthesis can be subdivided according to the effective mechanisms:

1. Enantiofacial selection with achiral carbanions bearing a chiral cation.
2. Kinetically determined enantiotopic selection through deprotonation by a chiral base.
3. Thermodynamically controlled selection between epimeric ion pairs.
4. Kinetically controlled selection between diastereomeric ion pairs during a substitution step.

We will also discuss and then utilize the complications that arise out of interaction with other stereocenters that may be present.

2. (—)-Sparteine-Modified Ion Pairs—Early Experiments and Disappointments

The alkaloid (−)-sparteine[19] (**1**) is extremely well-suited to the chiral modification of cations in carbanion pairs,[20] because in the only slightly more energy-rich conformation **1A** (see

Scheme 1)[21] it can function as a bidentate ligand. (−)-Sparteine is available in large quantity and is obtained through the extraction of certain papilionaceous plants such as Scotch broom.[22] In contrast to its diastereomers[23] (−)-α-isosparteine (**2**) and (−)-β-isosparteine (**3**) (Scheme 8) it deviates

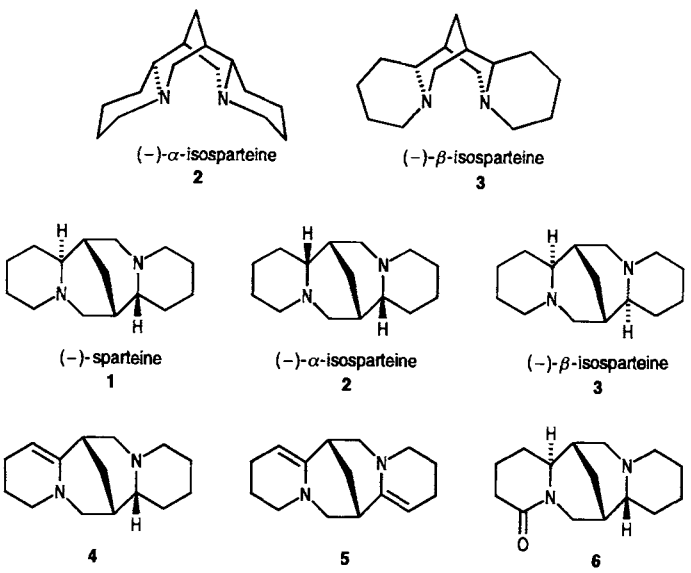

Scheme 8. Various sparteine diastereomers, along with starting material **6** and intermediates **4** and **5** for semisynthetic transformations.

slightly from C_2-symmetry; it is true that **2** and **3** also occur naturally, but they are best obtained by isomerization of (−)-sparteine (**1**) via the dehydro derivatives **4** and **5**.[24] (+)-Sparteine (*ent*-**1**) has been described as a constituent of the shrub *Sophora pachycarpa C. A. Mey*.[25] It is most conveniently obtained in the form of the racemic lactam *rac*-lupanine (**6**) by extraction of seeds of the bitter lupine *Lupinus albus*, followed by racemate resolution through the salt of (−)-camphor-10-sulfonic acid and finally by deoxygenation to give *ent*-**1**.[26] All the sparteine diastereomers can be easily recovered from alkaline suspensions as a result of their low water solubility.

Nozaki, Aratani, Toraya, and Noyori[10, 27] first studied the suitability of (−)-sparteine (**1**) as a chiral additive in carbanion reactions in the years 1968–70 (Scheme 9). The greatest enan-

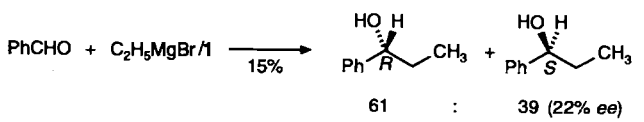

Scheme 9. Early attempts at (−)-sparteine-mediated nucleophilic alkylation of benzaldehyde. [10, 27a]

tiomeric excess (22% *ee*) was achieved by addition of ethylmagnesium bromide/**1** to benzaldehyde.[10, 27a] The procedure they utilized is only of historical significance,[28] since today efficient catalytically asymmetric methods are known for nucleophilic alkyl transfer.[7a, h, o, 29]

Other early applications relate to the asymmetric lithiation of isopropylferrocene[27c, d] and ethylbenzene,[27a] as well as attempts at rearranging cyclopropyl carbenoids;[27a, b] the best results achieved in each case are illustrated without comment in Scheme 10.

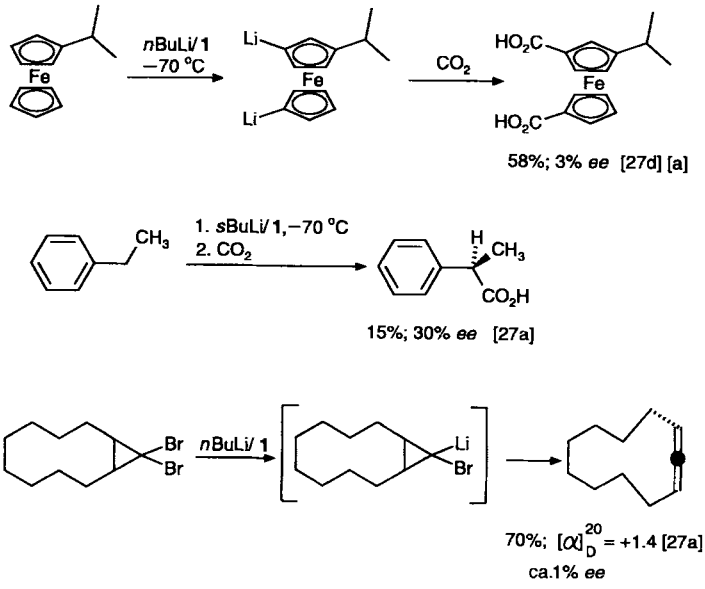

Scheme 10. Early applications of (−)-sparteine-mediated lithiation. [a] The configuration is unknown.

Only very small enantiomeric excesses have been observed in (−)-sparteine-mediated conjugate addition to enones,[30] allylation utilizing palladium catalysis,[31] methyltitanium trichloride addition to alkanals,[32] and the acylation of lithiomethyl *p*-tolyl sulfoxide.[33]

An astonishingly high chiral induction of 98% *ee* was achieved in the case of **7** by M. Guetté, J.-P. Guetté, and J. Capillon in the Reformatzky reaction of ethyl bromoacetate and benzaldehyde in the presence of (−)-sparteine[34] (Scheme 11). However, the authors themselves and others as well[35, 36] established, for unknown reasons, much lower *ee* values with substrates that differ only slightly.

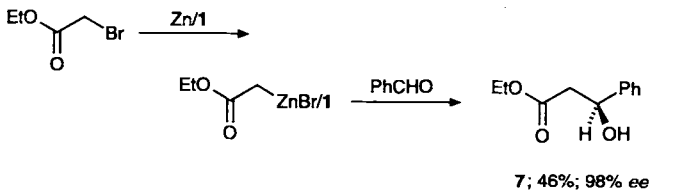

Scheme 11. (−)-Sparteine-catalyzed Reformatzky reaction [34a].

(−)-Sparteine-modified alkyllithium and alkylmagnesium complexes found early application in stereoselective anionic polymerization.[37, 24b] Remarkable in this context is the reaction of racemic 1-phenylethyl methacrylate (*rac*-**8**) with cyclohexylmagnesium bromide/(**1**), as well as with other Grignard complexes (Scheme 12). Under kinetic resolution, (*S*)-**8** is largely transformed into isotactic poly(methacrylate), whereas (*R*)-**8** remains behind.[24b].

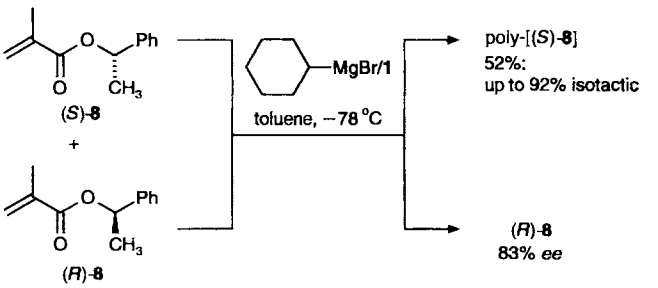

Scheme 12. Anionic polymerization of a methacrylic acid ester with kinetic resolution via (−)-sparteine [24b].

Kinetic ^{1}H NMR studies by Fraenkel et al. document relatively slow ligand exchange in dialkylmagnesium/(−)-sparteine complexes.[38]

The metal complexes of (−)-sparteine and its isomers display a strong tendency toward crystallization. This has permitted corresponding X-ray crystal structure analyses of various Grignard compounds,[39] an allylpalladium complex,[40] and several transition-metal salts.[41]

White, Raston, et al. solved the structure of the (−)-sparteine complex with (methylphenylphosphinyl)methyllithium[42] (**9**), which crystallized as a dimer, and that with 1-pyrid-2-yl-1-(trimethylsilyl)methyllithium[43] (**10**), which can be regarded as an azaallyllithium derivative. The structure of α-isocyanodiphenylmethyllithium/**1**/2THF (**11**) was characterized by Boche et al. (Scheme 13).[44] It is interesting that here lithium

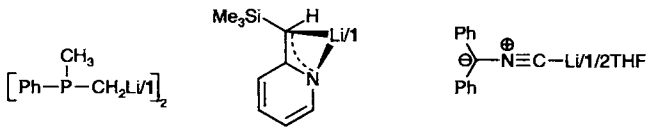

9 [42] **10** [43] **11** [44]

	9 [a]	**10**	**11**
Li-N_2 (*cis*)	221.3 (218.3)	206.0	206.5
Li-N_3 (*trans*)	216.2 (210.2)	202.0	210.3

Scheme 13. Li–N bond lengths [pm] in selected lithium/(−)-sparteine complexes. [a] Two different aggregates are present in the unit cell.

seeks contact with the isonitrile C atom, but not with the carbanionic center. The bond lengths between lithium and the (nonequivalent) N atoms of (−)-sparteine are quite variable: 202–216 pm and 206–221 pm. The structures of additional lithium complexes that possess stereogenic carbanionic centers are discussed in Section 3.

3. Enantioselective Syntheses with Configurationally Labile Lithium/Sparteine-Carbanion Pairs

3.1. Lithiated Allyl Carbamates and Enantioselective Homoaldol Reactions

We established in 1985 that enantiomerically enriched secondary 2-alkenyl diisopropylcarbamates can be deprotonated with retention of configuration using butyllithium.[45] This formed the basis for an enantioselective variant of the homoaldol reaction.[46] Not aware at the time of the previously described sparteine efforts, O. Zschage began in 1988 a diplom a thesis[47] with the task of deprotonating the (*E*)-2-butenyl carbamate **12** in the presence of (−)-sparteine instead of the ordinarily employed achiral complexing agent *N*,*N*,*N*′,*N*′-tetramethylethylenediamine (TMEDA), and subsequently investigating the resulting capture products with respect to possible enantiomeric excesses. We anticipated that the chiral base *sec*-butyllithium/(−)-sparteine would distinguish between the enantiotopic protons *pro*-*R*-H and *pro*-*S*-H in the methylene groups. In that case, one of the epimeric ion pairs (*R*)-**13**·**1** or (*S*)-**13**·**1** should be generated in excess, which would be discernible from a corresponding enantiomeric excess in the capture product **14** (Scheme 14, Table 1).

It quickly became apparent that the deprotonation here is not kinetically controlled, but the process is nevertheless extremely efficient.[52,48] In the very first experiment deprotonation with *sec*-butyllithium/(−)-sparteine (**1**) in isopentane/cyclohexane and addition of tetra(isopropoxy)titanium[53] to the suspension of the organolithium intermediate, followed by 2-methylpropanal, led to the (*Z*)-*anti*-configured homoaldol adduct **17a** [R^1 = $CH(CH_3)_2$] with 83% *ee*. Because of the complete 1,3-chirality transfer[54] during carbonyl addition, the titanated intermediate (*R*)-**14** must have been present here with the same enantiomeric excess, corresponding to the diastereomeric excess in the (−)-sparteine complex **13**·**1**. Nevertheless, the reaction at first proved not to be reproducible; only a nearly racemic product was subsequently isolated. In contrast to the successful experiment, crystallization failed to occur after deprotonation. Our suspicion was confirmed that dynamic kinetic racemate resolution[55] occurred in the course of crystallization; the epimeric (*R*)- and (*S*)-**13**·**1** are in equilibrium in solution, and one diastereomer crystallizes preferentially. A certain amount of cyclohexane is required for the crystallization, however, and this had been introduced in sufficient quantity into the first experiment only due to the use of a *sec*-butyllithium solution in isopentane/cyclopentane with the unusually low concentration of 0.5 M. An optimized procedure, in which a defined quantity of cyclohexane was added to the hexane solution and *n*-butyllithium was employed as the base, resulted unambiguously in substitution products with 90–94% *ee*.[55]

Metal exchange occurs under the refined conditions[55] with complete inversion of configuration, and the titanium intermediate (*R*)-**14** is configurationally stable up to at least −40 °C. Thus the epimeric ratio of (*S*)- and (*R*)-**13**·**1** determines the enantiomeric ratio of the homoaldol adducts **17**/*ent*-**17**. The stereoselectivity is predominantly reagent-controlled; that is, equally good results are achieved for the "mismatched pair"[16c,d,56] with chiral aldehyde components.[57,58]

The crystalline suspension of (*S*)-**13**·**1** can also be trapped with retention of optical activity using trialkyltin chloride (Scheme 15).[55] This results, with low regioselectivity and about 80% *ee*, in a mixture of the α-adduct (*S*)-**20** (inversion) and the γ adduct (*S*)-**19** from an *anti*-S_E' reaction. However, stannylation of the titanium intermediate (*R*)-**14** leads with high efficiency to the (1*Z*,3*R*)-configured stannane **19**, from which the tributylstannyl derivative (*R*)-**19b** is obtained with about 95% *ee*.

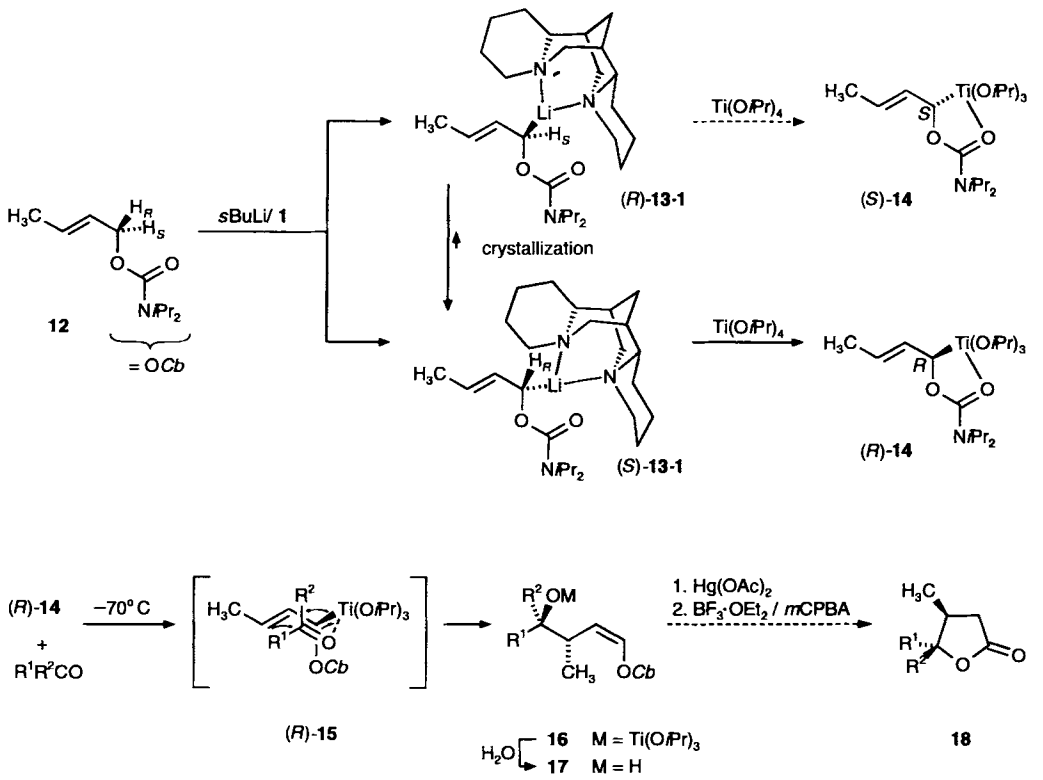

Scheme 14. Dynamic kinetic racemate resolution in the (−)-sparteine-induced deprotonation of **12**; lithium–titanium exchange and enantioselective homoaldol reaction [48, 51, 52, 55].

Table 1. Various optically active homoaldol products that were prepared.

17	R^1	R^2	Yield [%]	*ee* [%]	Yield (**18**) [%]	Ref.
a	$(CH_3)_2CH$	H	90	90[a]	89	[48]
b	CH_3	H	95	80[a]	[b]	[48]
c	$CH_3C(CH_2)_2$	H	93	84[a]	90	[48]
d	CH_3CCH_2	H	90	[b]	-	[49]
e	$(CH_3)_2C{=}CH{-}CH_2$	H	62	92	70[c]	[50]
f	$H_2C{=}CMe$	H	78	86[a]	[b]	[51]
g	$H_2C{=}i$PrC	H	81	90	[b]	[51]
h	CH_3	CH_3	92	82	[b]	[48]

[a] Nonoptimized preparation of **13**·**1**. [b] Not determined. [c] A different oxidation method was utilized; see text.

The stannanes **19** are storable homoenolate reagents that are activated by the addition of titanium tetrachloride (Scheme 16, Table 2).[55, 59, 60] All indications suggest a stereospecific tin–titanium exchange (similar to that shown by Marshall for tin–tin exchange[61]) to give a trichlorotitanate, and pericyclic *syn*-S_E' addition of the latter to the aldehyde. Starting with stannane (*R*)-**19** one obtains the enantiomerically enriched homoaldol adduct **22**, whereas the antipode (*S*)-**19** leads to *ent*-**22**. Thus, both series of enantiomers are accessible via this Lewis acid mediated variant from the same lithium intermediate (*S*)-**13**·**1**. The strength of the variant lies in a smooth reaction with sterically demanding ketones.

The extension of thermodynamically controlled asymmetric lithiation with a subsequent homoaldol reaction to the diisopropylcarbamates of (*E*)-2-hexen-1-ol, 3-methyl-2-butenol, or (*E*)-3-trimethylsilyl-2-butenol provided only modest enantiomeric excesses (41–76% *ee*), because optimized conditions for the crystallization had not yet been established.[48]

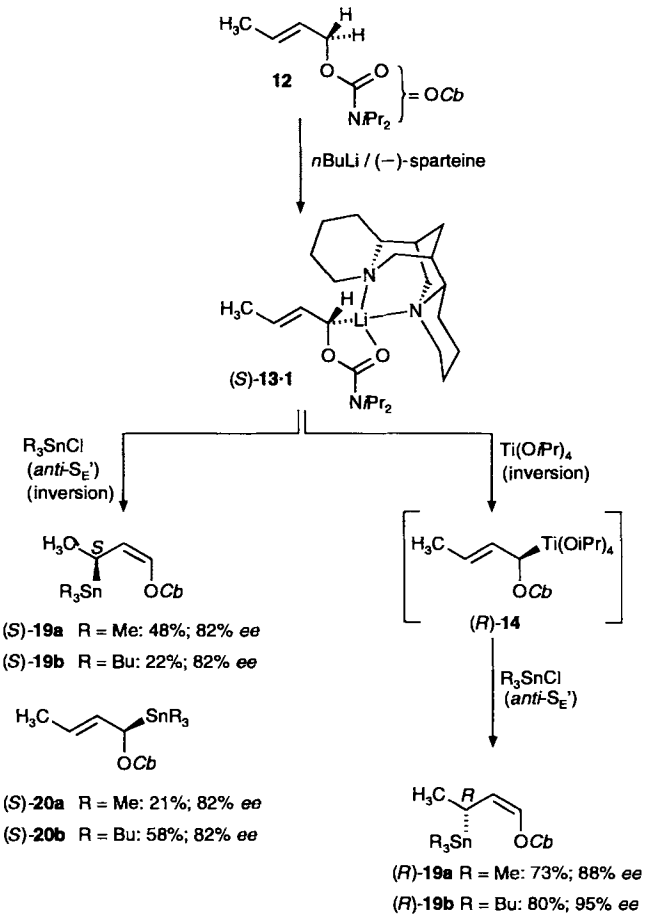

Scheme 15. Synthesis of enantiomerically enriched alkenylstannanes from the lithium complex (*S*)-**13**·**1** [55].

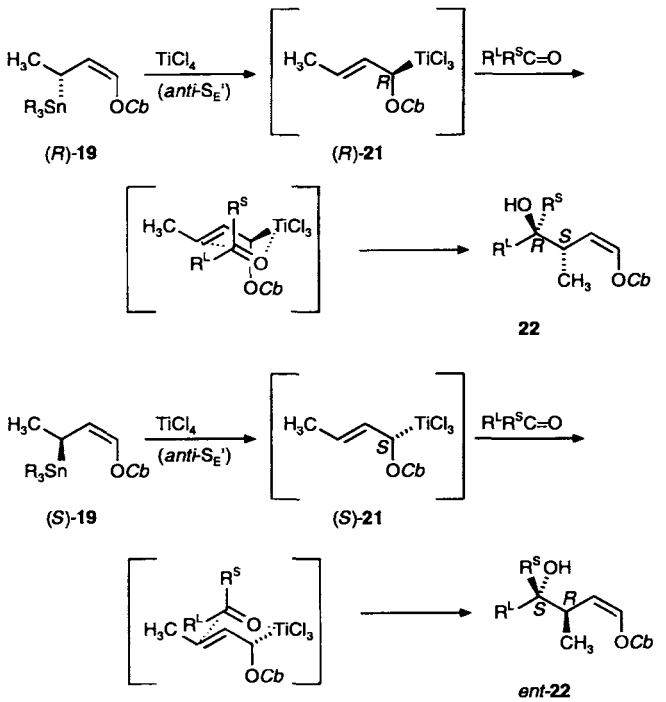

Scheme 16. Lewis acid induced enantioselective homoaldol reaction with 3-stannyl-1-alkenyl carbamates [55]. R^S, R^L: see Table 2; $OCb = O_2CON(iPr)_2$.

Table 2. Enantioselective Lewis acid catalyzed homoaldol reactions [55].

22	Starting material	R^L	R^S	Yield[%]	*ee*[%]	Ref.
22a	(*R*)-**19a**	$(CH_3)_2CH$	H	91	88	[55]
ent-**22a**	(*S*)-**19a**	$(CH_3)_2CH$	H	82	82	[55]
22a	(*R*)-**19b**	$(CH_3)_2CH$	H	96	96	[55]
22b	(*R*)-**19b**	$(CH_3)_3C$	CH_3	80	74	[55]
22c	(*R*)-**19b**	$EtOCO(CH_2)_3$	CH_3	84	94	[55]
22d	(*R*)-**19b**	$EtOCO(CH_2)_2$	CH_3	91[a]	94	[55]
22e	(*R*)-**19b**	C_2H_5	$PhCO(CH_2)_3$	67[a]	94	[62]

[a] See text.

In collaboration with Boche et al. it proved possible to obtain an X-ray crystal structure analysis of sparteine complex **23**·**1** (Figure 1).[63] This revealed the (*1S*)-configuration at the carbanionic center and verified our earlier assumptions regarding the structure of lithioallyl carbamates: they are monomeric even in the crystalline state, because the lithium cation is offered optimal preconditions for four-fold coordination in the α-position. The allylic system is η^1-bonded, and the electron-donating carbamoyl oxo group and the nitrogen atom of the tertiary diamine function as residual ligands. Firm attachment of the cation at the α-position is the key to high γ-selectivity in the course of carbonyl addition. This also causes the observed torsional stability in most cases of the β,γ-double bond[64] and presumably contributes much to increasing the barrier to racemization in chiral lithium derivatives.

The lithiated secondary 2-alkenyl and 2,4-alkadienyl carbamates **24** and **25** (Scheme 17), readily accessible in enantiomerically enriched form, are configurationally stable below $-70\,^{\circ}C$;[45] to our knowledge they represent the first known examples of allyllithium derivatives with configurationally

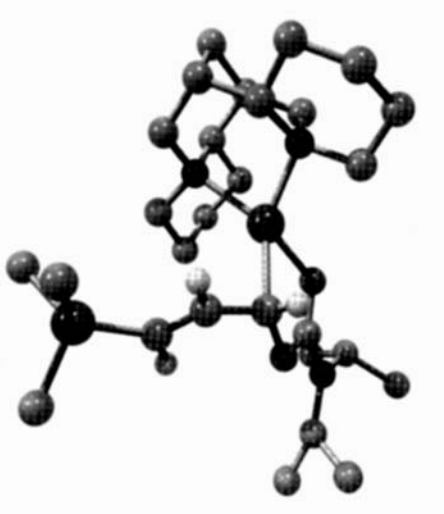

Figure 1. X-Ray crystal structure analysis of η^1-[(1*S*,2*E*)-1-(*N*,*N*-diisopropylcarbamoyloxy)-3-trimethylsilyl-2-propen-1-yl]lithium·(−)-sparteine (**23**·**1**)[63]. All hydrogen atoms have been omitted, with the exception of H-1 and H-2. (C Atoms gray, O atoms dark gray, N atoms black).

24 **25**

Scheme 17. Configurationally stable alkenyl carbamates **24** and **25**. L_2 = TMEDA.

stable stereogenic, metal-bearing C atoms. As we reported in 1990, the enantiomerically enriched lithium derivative **24** can be obtained not only from the optically active carbamate, but also with *sec*-butyllithium/(−)-sparteine under kinetic resolution of the corresponding racemic allyl carbamate **24** (H for Li/L_2 in *rac*-**24**).[59,60] The rich chemistry of the compound[45,60,65] and **25**,[66] as well as their analogues, is governed by their torsional behavior; further discussion of this point would exceed the bounds of this review, however.

The value of the enantiomerically enriched homoaldol adducts in stereoselective synthesis extends far beyond formal hydrolysis to carbonyl compounds; numerous stereoselective transformations of the (*Z*)-vinyl carbamate group have been developed by P. Kocienski as well as by us.[67] Oxidative deblocking[71] of adduct **17c** or **17e** (Table 1) leads to completion of the syntheses of (+)-quercus lactone A[52,48] (**18c**) and (+)-eldanolide (**18e**).[50] This procedure is readily transferable to the synthesis of diverse γ-lactones (Scheme 18).

3.2. Benzyllithium Compounds

Primary and secondary benzyl *N*,*N*-dialkylcarbamates are deprotonated with the same ease as the corresponding allyl esters.[72] Whereas the lithium derivatives of chiral secondary benzyl carbamates are configurationally stable at $-70\,^{\circ}C$, this is not true for lithiated primary benzyl carbamates, although the "Hoffmann test"[57] for the complex **27**·TMEDA demonstrates

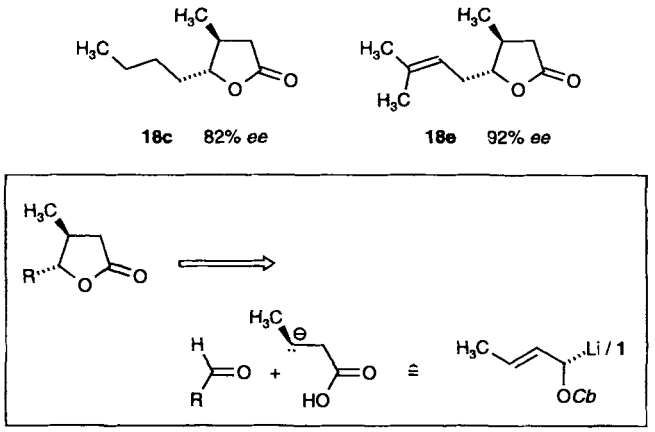

Scheme 18. Synthesis of optically active β-methyl-γ-lactones by enantioselective homoaldol reactions [50].

increased stability at the microscopic level.[73] This can also be concluded from the following series of experiments: Benzyl *N*,*N*-diisopropylcarbamate (**26**) was deprotonated with *sec*-butyllithium/(−)-sparteine in ether at −78 °C, and after 4 h the epimeric mixture of ion pairs **27**·**1** was trapped by introduction of carbon dioxide into the homogeneous reaction mixture (Scheme 19). After esterification with diazomethane one isomer

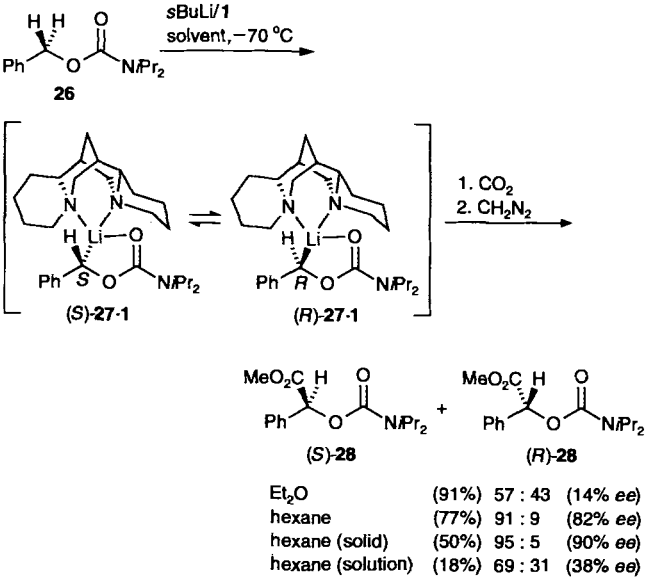

Et_2O	(91%)	57 : 43	(14% *ee*)
hexane	(77%)	91 : 9	(82% *ee*)
hexane (solid)	(50%)	95 : 5	(90% *ee*)
hexane (solution)	(18%)	69 : 31	(38% *ee*)

Scheme 19. Investigations into the configurational stability of lithiated benzyl carbamates.

lates the mandelic acid derivatives (+)-(*S*)-**28** and (−)-(*R*)-**28** with only 14% *ee* in favor of (*S*)-**28**. Under identical experimental conditions but with hexane as the solvent crystallization occurred, and (+)-(*S*)-**28** was formed with 82% *ee*. In a third experiment the solution was separated from the crystalline mass, and the two were treated separately; the enantiomeric excesses amounted to 38% and 90% *ee*, respectively.

It is thus very probable that the lithium complexes equilibrate even at −70 °C, and that here also the crystallization of one epimer leads to a dynamic resolution. The configuration of the favored ion pair has not been established with certainty; since we have found inversion in carboxylation of a similar complex (**29**, CH_3 for 1-H),[74a,b] there are strong arguments for the (*S*) configuration.[75, 76]

P. Beak et al. succeeded in carrying out stereoselective lithiation of a series of benzyl systems; the results are collected along with an extensive discussion of the mechanistic aspects in a recent review.[17]

N-Methyl-3-phenylpropionamide (**30**) reacts with two equivalents of butyllithium/(−)-sparteine to give the dilithium derivative **31**·**1**,[77] which leads with various electrophiles to amides substituted at the benzyl position with 60–94% *ee* (Scheme 20). Similar results were achieved when **30** was prepared first in the absence of (−)-sparteine (**1**) and the latter was added only subsequently. This argues in favor of equilibration between the epimers **31**·**1**, a suspicion that has recently been verified.[78] On the other hand, racemization-free lithiodestannylation/silylation proved successful with the enantiomerically enriched stannane **32f** to give silane **32a**; under these reaction conditions the carbanionic intermediate was configurationally stable. It is noteworthy that reaction in this case can be carried out in THF without displacement of (−)-sparteine.[77b] Equally efficient are transformations of the 2-methoxyphenyl derivative; adducts of the type **32** (2-$MeOC_6H_4$ for C_6H_5) offer the possibility of transformation into enantiomerically enriched coumarins.[77b]

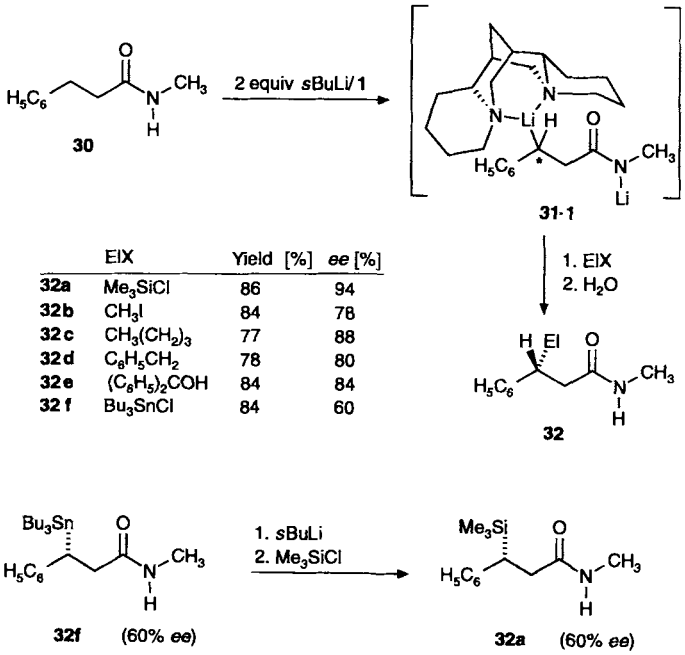

	EIX	Yield [%]	*ee* [%]
32a	Me_3SiCl	86	94
32b	CH_3I	84	78
32c	$CH_3(CH_2)_3$	77	88
32d	$C_6H_5CH_2$	78	80
32e	$(C_6H_5)_2COH$	84	84
32f	Bu_3SnCl	84	60

Scheme 20. Enantioselective substitution of *N*-alkyl-3-phenylpropionic acid amides [77].

As in the case of **31**·**1**, configurational stability at −78 °C was demonstrated for a series of additional benzyllithium–(−)-sparteine complexes. Warming of the reaction mixture is required to cause epimerization. This opens up interesting pathways for controlling stereoselectivity, as will be demonstrated.

M. Schlosser and D. Limat[79] discovered that *N*-Boc-*N*-methylbenzylamine (**33**) is smoothly deprotonated by *sec*-butyllithium/(−)-sparteine (Scheme 21). The resulting enantiomeric excess and the direction of chiral induction depend not only on the solvent and electrophile, but also on the length of time the

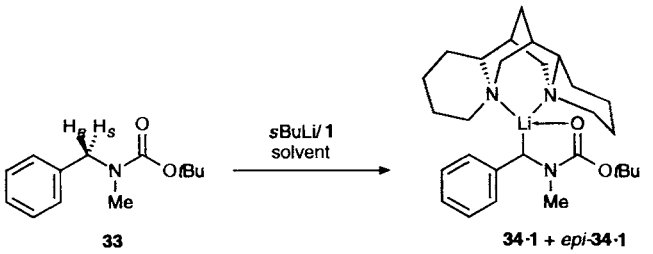

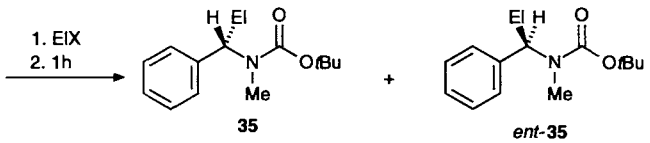

EIX	solvene	35 : *ent*-35	*ee* [%]
DC≡CPh	hexane [a]	95.0 : 5.0	90
	THF	7.5 : 92.5	85
CH_3I	hexane	87.5 : 12.5	75
	THF	10.0 : 90.0	80
CO_2	hexane	91.5 : 9.5	81
	THF	7.5 : 92.5	85

Scheme 21. Enantioselective lithiation and substitution of *N*-Boc-*N*-methylbenzylamine (**33**) [79]. [a] The same excess enantiomer is formed in ether.

reagent was kept before quenching it. Only after about 2 h at −75 °C is maximum enantiomeric excess achieved; exchange of hexane for THF causes the configuration of the product to be reversed, and precipitation of a solid is observed in THF after 1 h.

Through deprotonation and subsequent carboxylation of (*S*)-[1*D*]**33** with *sec*-butyllithium/TMEDA[80] it was established that the ion pair was configurationally labile in all the solvents employed at 75 °C. The ratio of the ion pairs **34·1** and *epi*-**34·1** is therefore thermodynamically determined.[81] Boche et al. conducted an X-ray crystal structure analysis on the *N*-pivaloyl derivative **36·1** and found it to possess the (1*S*)-configuration (Figure 2).[82] What is the cause of the solvent-dependent stereoselectivity of the substitution step? The authors suspect that in both cases an ion pair with the (*S*)-configuration is present, but the stereoselectivity in the substitution step is reversed under the influence of the solvent. However, all the results are also consistent with the following interpretation: The predominant ion pairs in hexane and ether solution possess a reversed configuration relative to the aggregate obtained through THF crystallization, and the substitution step follows the same configurational pathway in each case.

Beak et al. describe a (−)-sparteine-mediated lithiation of *N*-Boc-*N*-(*p*-methoxyphenyl)benzylamine (**37**), followed by enantioselective alkylation or addition to carbonyl compounds and imines (Scheme 22).[83] In a formal sense the *pro-S* H atom

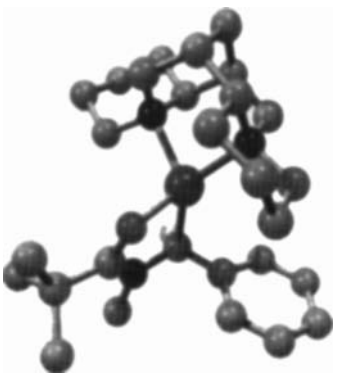

Figure 2. X-Ray crystal structure analysis of α-(*N*-methyl-*N*-pivaloylamino)-benzyllithium·(−)-sparteine (**36·1**)[82]. All hydrogen atoms have been omitted with the exception of the benzylic hydrogen atoms. (C atoms gray, O atoms dark gray, N atoms black).

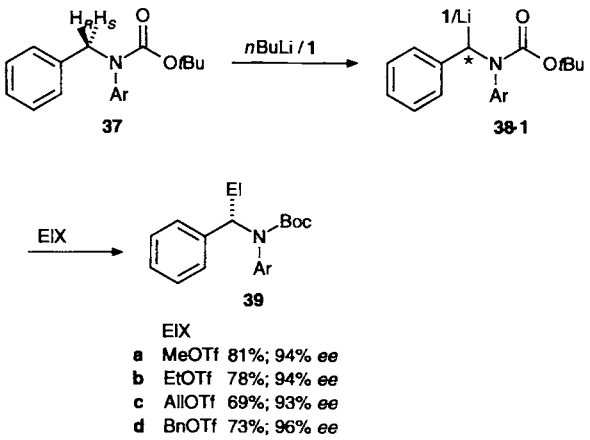

Scheme 22. Enantioselective lithiation and substitution of *N*-Boc-*N*-(*p*-methoxyphenyl)benzylamine (**37**) [83]. Ar = 4-MeO-C_6H_4; Tf = F_3CSO_2; All = CH_2=$CHCH_2$.

in **37** is substituted, and the resulting enantiomeric excesses in most cases range around 95% *ee*.

The configuration of the dominant intermediate **38·1** is unknown.[84] As we have previously demonstrated for a lithiated benzyl carbamate,[74a] it can be reversed by stannylation–delithiostannylation (Scheme 23).[83] It is important to note here that the intermediates complexed with (−)-sparteine are configurationally stable. It follows that one can obtain the oppositely configured tertiary amines (*S*)- and (*R*)-**41** by the same sequence of methylation, deprotonation, and alkylation, with subsequent oxidative deblocking.[83a]

In the case of the *N*-Boc-*N*-(3-chloropropyl)benzylamine **42a** it proved possible to show with the aid of the (*R*)-deuterium derivative **42b** that the (−)-sparteine reagent preferentially abstracts the *pro-S*-proton in **42a** (Scheme 24).[85] Intramolecular cycloalkylation of the (*S*)-configured lithium derivative **42a·1** to pyrrolidine (*S*)-**44a** occurs very rapidly, and therefore virtually free of racemization. Alkylation with stereoretention is an astonishing fact.[75] The reaction is transferable with comparable efficiency to a whole series of arylmethyl- and heteroarylmethylamines of the type **42**.

N,*N*-Diisopropyl-2-ethylbenzamide (**45**) was transformed by P. Beak et al. into the (−)-sparteine–lithium complex **46·1**[86]

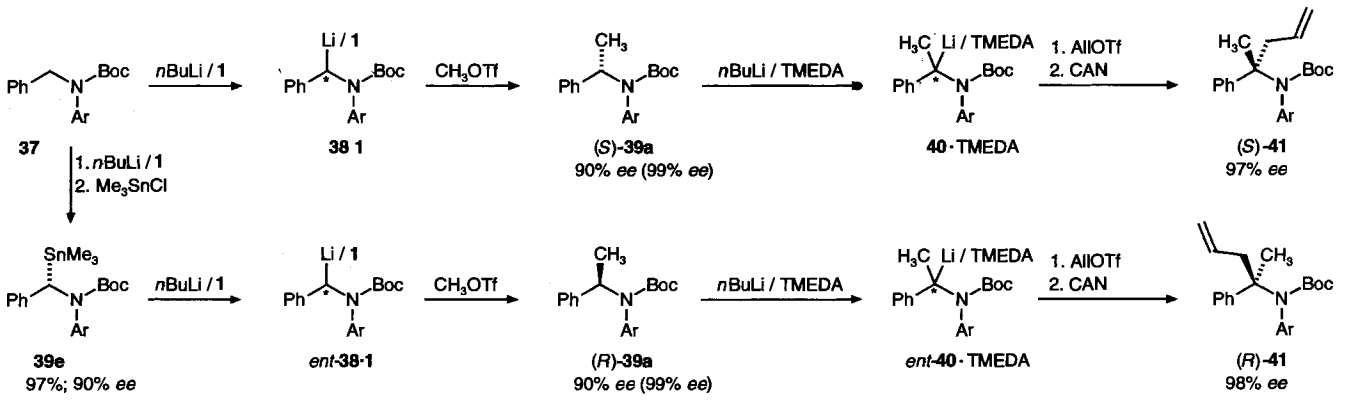

Scheme 23. Enantiodivergent synthesis of tertiary benzylamines [83a]. CAN = $(NH_4)_2Ce(NO_3)_6$; Ar = p-$MeOC_6H_4$.

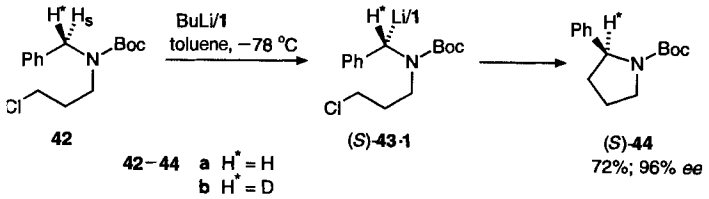

Scheme 24. Synthesis of (*S*)-*N*-Boc-2-phenylpyrrolidine by intramolecular substitution [85].

and then alkylated. All experimental indications are that the rare case of dynamic kinetic resolution (Scheme 6) has been realized.[87] The epimers (*R*)- and (*S*)-**46**·**1** are in equilibrium, and one [presumably (*S*)-**46**·**1**] reacts preferentially. In the process, substitutions with alkyl halides and alkyl tosylates take opposite courses (Scheme 25). No such strong dependence on the leaving group[75] had previously been observed for alkylating agents.

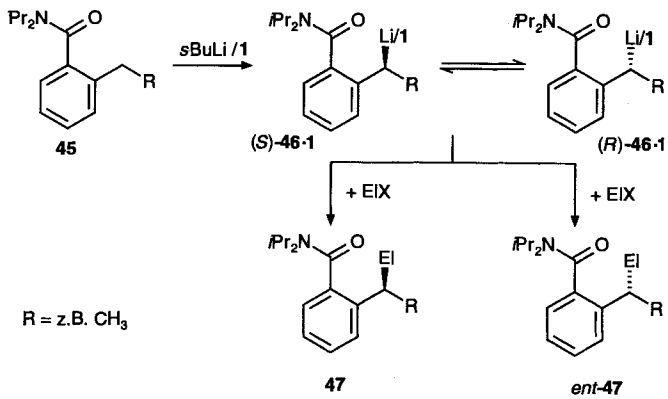

Scheme 25. Enantioselective lithiation and substitution of 2-alkyl-*N*,*N*-diisopropylbenzamides [86·87].

The (−)-sparteine complex of the dilithium salt of 2-ethyl-*N*-pivaloylaniline (**49**·**1**) is configurationally stable at −78 °C. Only after equilibration between the epimers **49**·**1** and *epi*-**49**·**1**, which occurs upon raising the temperature, does electrophilic substitution lead to good enantiomeric excesses[88] (Scheme 26).

The two diastereomeric complexes **49**·**1** and *epi*-**49**·**1** are present before equilibration in roughly equal amounts. Their re-

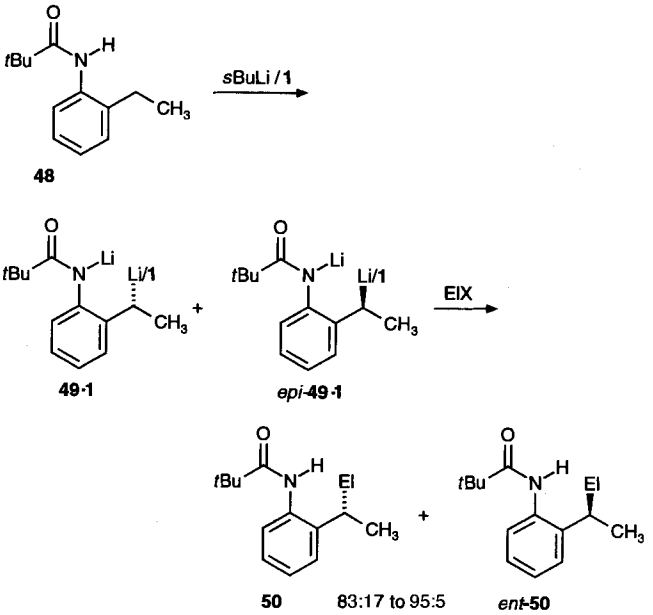

Scheme 26. Enantioselective lithiation and substitution of 2-ethyl-*N*-pivaloylaniline [88]. El = alkyl, Me_3Si, and others.

activities toward electrophiles differ; from subsequent experiments a difference $\Delta G^{\ddagger}_{epi-49\cdot1} - \Delta G^{\ddagger}_{49\cdot1} = 3.4\ kJ\,mol^{-1}$ was established for trimethylsilylation at −78 °C.[88b] This can be exploited as follows (Scheme 27): If one adds to this mixture only half an equivalent of trimethylsilyl chloride, primarily **49**·**1** is trapped, with formation of the (*R*)-configured silane **50a**. Excess allyl bromide transforms the residual *epi*-**49**·**1** into the oppositely configured product *ent*-**50b**.

The configurational lability of lithiated intermediates at higher temperature permits recycling of the less reactive epimer into the other ("diastereomeric recycling"[88b]) through a warming and cooling sequence ("warm and cool protocol"[88b]) as a means of increasing the enantiomeric excess. As a result of warming to −25 °C, a **49**·**1**:*epi*-**49**·**1** ratio of 92:8 is established, which is then frozen by cooling the reaction mixture to −78 °C. A trapping experiment with excess trimethylsilyl chloride produces the enantiomers **50a** and *ent*-**50a** in a ratio of 92:8 (84% *ee*). However, if the electrophile is added in two portions of 0.45 equivalents each, with warming to −25 °C in between, the result is **50a** with a 98% *ee* (*e.r.* = 99:1).

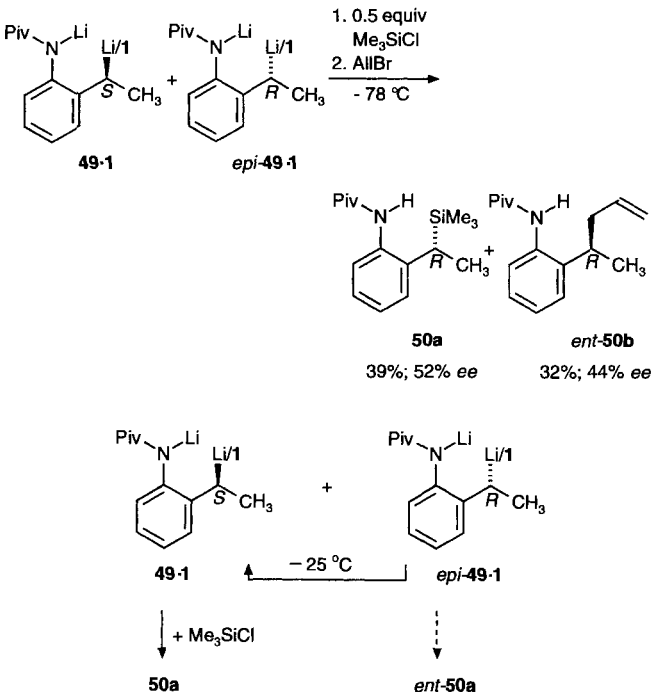

Scheme 27. Differing reactivities of the diastereomeric ion pairs **49·1** and *epi*-**49·1**; "diastereomeric recycling."[88b]

α-Monosubstituted benzyllithium compounds thus assume an intermediate position with respect to their configurational stability, and in favorable cases their behavior can be prearranged by the selected reaction temperature. Configurational lability permits efficient dynamic kinetic resolution at higher temperature, whereas freezing the equilibrium between the epimers opens the possibility of thermodynamically governed reaction control.

V. Snieckus et al. established a high enantiomeric excess by deprotonation of the 2-ethylphenyl carbamate **51** with subsequent silylation (Scheme 28).[90] The configuration of the dominant products **53** and intermediates **52·1**, as well as the extent of the configurational stability, are so far unknown.

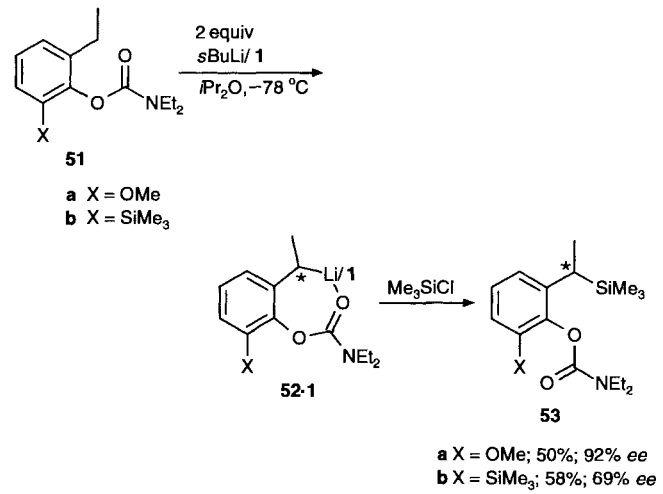

Scheme 28. Enantioselective lithiation and substitution of 2-ethylphenyl *N*,*N*-diethylcarbamates [90].

3.3. Chiral Lithium Indenides

The epimeric (−)-sparteine complexes of 1-lithioindenyl *N*,*N*-diisopropylcarbamate[91] (**55a·1** and *epi*-**55a·1**) rapidly equilibrate at temperatures around 0 °C, and produce upon silylation the optically active silane (+)-**56a**[92] with only 16% *ee* (Scheme 29). In a similar way, one obtains from the 2-methylindenyl derivative **54b** via the corresponding indenides

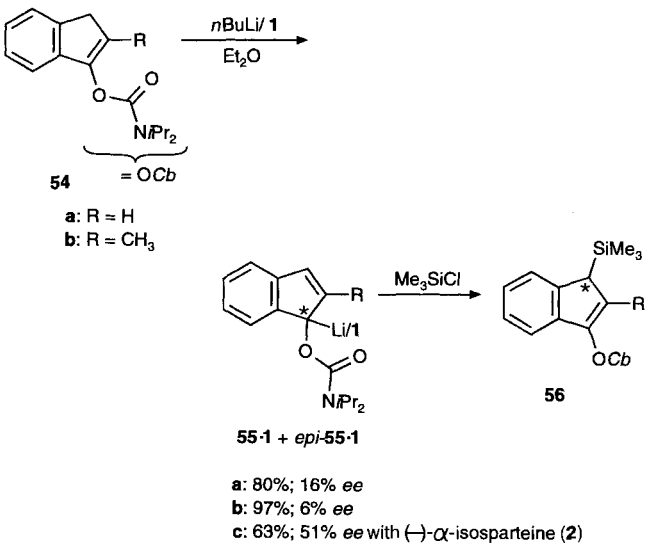

Scheme 29. Lithiation and silylation of indenyl carbamates [91, 96].

55b·1 and *epi*-**55b·1** the silane (+)-**56b**[92] with only 6% *ee*. ^{1}H NMR spectra in [D_8]toluene could be obtained from both of the indenide complexes **55a·1** and **55b·1** (Figures 3 and 4), and

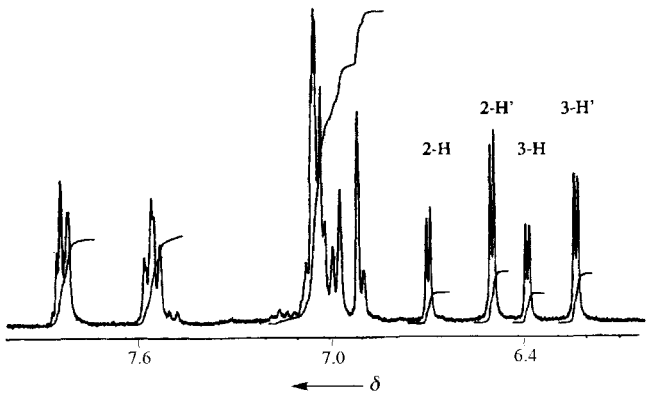

Figure 3. Excerpt from a ^{1}H NMR spectrum (300 MHz) of [1-(*N*,*N*-diisopropylcarbamoyloxy)-1*H*-inden-1-yl)lithium·(−)-sparteine (**55a·1** and *epi*-**55a·1**) in [D_8]toluene at −15 °C [91]. The spectrum indicates the presence of two diastereomers in the ratio 60:40; these interconvert only slowly, if at all.

these verify the presence in each case of two diastereomers in a ratio of roughly 60:40.[91–94] This in turn indicates an energy difference ΔG_{263} of 0.9 kJ mol^{-1}.

Semiempirical calculations (MOPAC, PM3)[95] predict for the ground state energies of the complexes **55b·2** and *epi*-**55b·2**,

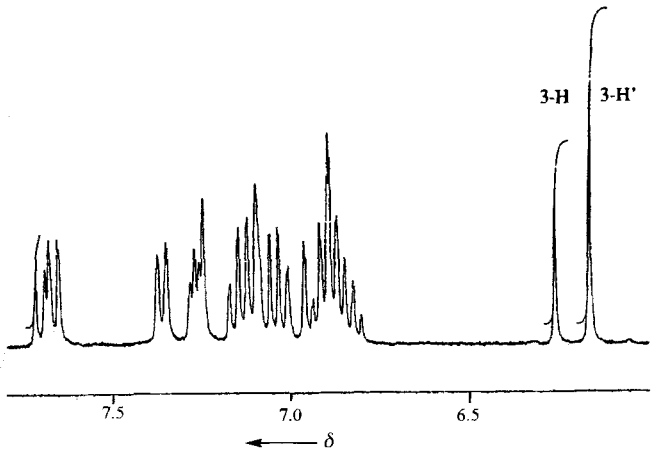

Figure 4. Excerpt from a ^{1}H NMR spectrum (300 MHz) of [1-(*N*,*N*-diisopropylcarbamoyloxy)-2-methyl-1*H*-inden-1-yl]lithium·(−)-sparteine (**55b**·**1** and *epi*-**55b**·**1**) in [D$_8$]toluene at −10 °C [91]. The sharp signals of the "cyclopentadienyl protons" H-3 and H-3′ (in the diastereomers) are $\Delta\delta \approx 0.1$ apart.

which bear the C_2-symmetric (−)-α-isosparteine as ligand, a higher difference of 2.5 kJ mol^{-1}, and the silylation experiment in fact led to (+)-**56b** with 51% *ee*.[96]

To our great surprise, the ion pairs **58**·**1** derived from 1-alkyl-3*H*-indenes **57** proved to be the most efficient representatives (Scheme 30).[97] As I. Hoppe observed as early as 1990, the

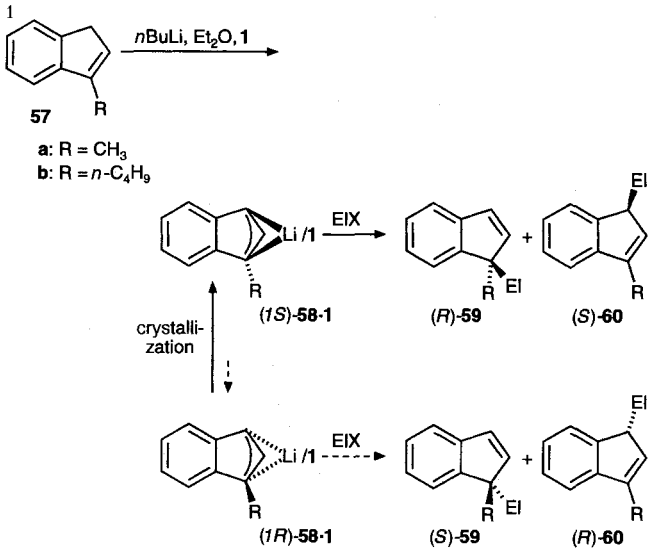

Scheme 30. Lithiation, dynamic kinetic resolution of (1*S*)-**58**·**1** by crystallization and enantioselective substitution of 1-alkyl-3*H*-indenes [97].

1-methyl derivative **57a** is rapidly deprotonated by *n*-butyllithium/(−)-sparteine in ether, and a yellow solid crystallizes upon warming the reaction mixture. After addition of an acid chloride or an aldehyde[98] the 1-substitution product (*R*)-**59** is usually isolated with an enantiomeric purity greater than 95% *ee*. Only with bulky carbonyl compounds such as 2,2-dimethylpropanal or acetone does a 3-substitution product of the type (*S*)-**60** predominate (Table 3). Similar results are provided by the 1-butyl derivative **57b**, although here the regioselectivity is reversed even sooner to the benefit of the γ-adduct (*S*)-**60h**.

Table 3. Lithiation and stereoselective substitution of 1-alkyl-3*H*-indenes [97].

Starting material	EIX	Products[a]	El	**59**:**60**	Yield [%]
57a	MeO_2Cl	(*R*)-**59a**	MeOCO	>97:3	64
57a	MeCOCl	(*R*)-**59b**	MeCO	>97:3	63
57a	PhCOCl	(*R*)-**59c**	PhCO	>97:3	74
57a	PhCHO	(*R*)-**59d**[b]	PhCHOH	>97:3	67
57a	*t*BuCHO	(*R*)-**59e**[b]	*t*BuCHOH	<3:97	55
57a	MeCOMe	(*R*)-**59f** + (*S*)-**60f**	Me_2COH	31:69	36
57b	PhCOCl	(*R*)-**59g**	PhCO	>95:5	79
57b	PhCHO	(*R*)-**59h**[b] + (*S*)-**60h**[b,c]	PhCHOH	35:65	52

[a] Unless indicated otherwise, the enantiomeric excess is greater than 95% *ee*. [b] Epimers with respect to the 1′-stereocenter. [c] The *ee* value could not be determined.

These results are best interpreted with an assumption of equilibrating dissolved ion pairs (1*S*)- and (1*R*)-**58**·**1**, from which one epimer crystallizes and reacts stereoselectively as a solid at low temperature with the carbonyl compound added as electrophile. It was long unknown which configuration applied to the crystallizing ion pair. An X-ray structural analysis[97] was ultimately successful for the dominant complex **58b**·**1** (Figure 5). This established a (1*S*)-configuration along with η^3-coordination for the indenide to the lithium cation. The C1−Li and C3−Li distances of 243.2 and 233.4 pm are unusually long.

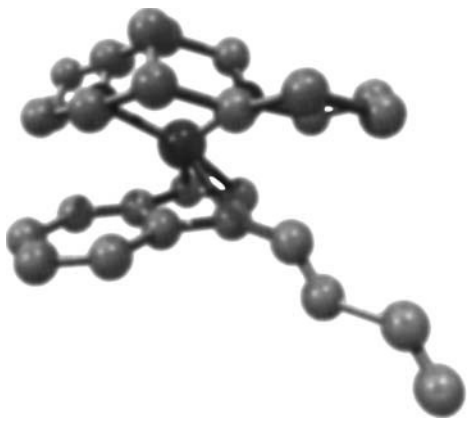

Figure 5. X-Ray crystal structure analysis of η^3-[(1*S*)-1-butylindenyl]lithium·(−)-sparteine **58b**·**1** [47]. All hydrogen atoms have been omitted.

Carbonyl addition thus proceeds with retention. Apparently the attacking carbonyl group reversibly displaces one coordination site of the allyl anion with the formation of intermediates **61** or **62**, which react further by transfer of the carbonyl compound with allylic inversion to give adducts **63** or **64** (Scheme 31).[99] Route A should be favored because of the weaker C1−Li interaction. Only when the C−C bonding step leading to **63** is heavily burdened sterically should route B with formation of the γ-adduct **60** gain the upper hand.

The (−)-sparteine complexes **58**·**1** are quite labile. Addition of THF causes one coordination site of the indenide and also

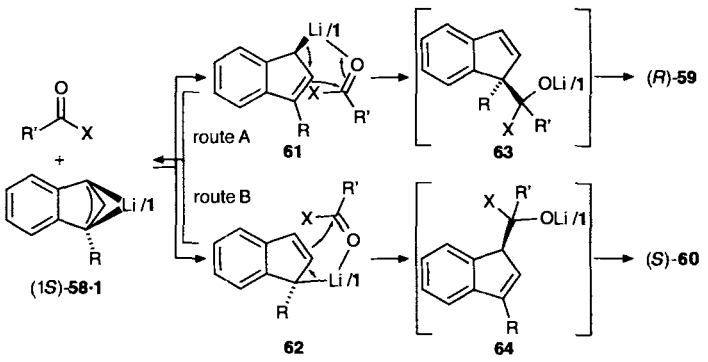

Scheme 31. Formation of the α- and γ-adducts **59** and **60**.

sparteine on lithium to be displaced; (1*S*)-**58a**·**1** is transformed into the η^1-$(THF)_3$ complex *rac*-**65**, which has also been characterized by crystal structure analysis (Scheme 32, Figure 6).[97, 100] Reaction of the latter with benzaldehyde produces the completely racemic γ-adduct *rac*-**60a**. Quite generally, the regioselectivity of substitution is strongly influenced by the ligands on lithium, since in the complex **58**·TMEDA there is a considerable tendency toward γ-substitution.[101]

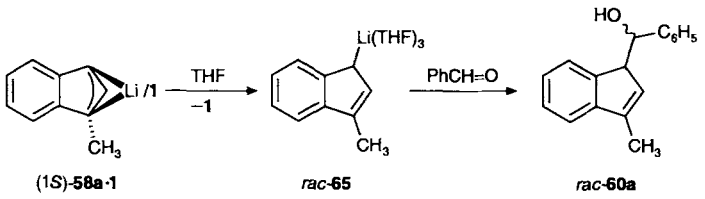

Scheme 32. Formation of the complex *rac*-**65** and its addition to benzaldehyde.

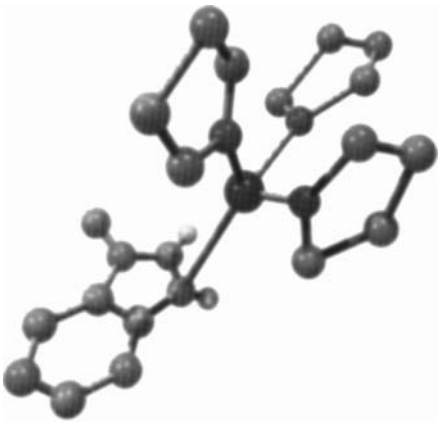

Figure 6. X-Ray crystal structure analysis of *rac*-(3-methylinden-1-yl)lithium·(3THF) (*rac*-**65**) [97]. All hydrogen atoms with the exception of those on C-1 and C-2 have been omitted.

3.4 Lithiated Cinnamylamides

As P. Beak and G. A. Weisenburger recently found,[102] one of the enantiotopic methylene protons in (*E*)-*N*-(*p*-methoxyphenyl)cinnamylamide (**66**) is released with outstanding differentiation by *n*-butyllithium/(−)-sparteine (Scheme 33, Table 4). The η^3-allyllithium compound[103] **67**·**1** has been formulated as an intermediate, which can be trapped with various electrophiles to give products with high enantiomeric enrichments. Conclusive control experiments prove the configurational stability of **67**·**1** under the selected reaction conditions. The configuration of **67**·**1** was derived under the assumption that transformations with alkylating and silylating agents proceed as *anti*-E′ reactions, and hydroxyalkylations with ketones as *syn*-E′ reactions.[104]

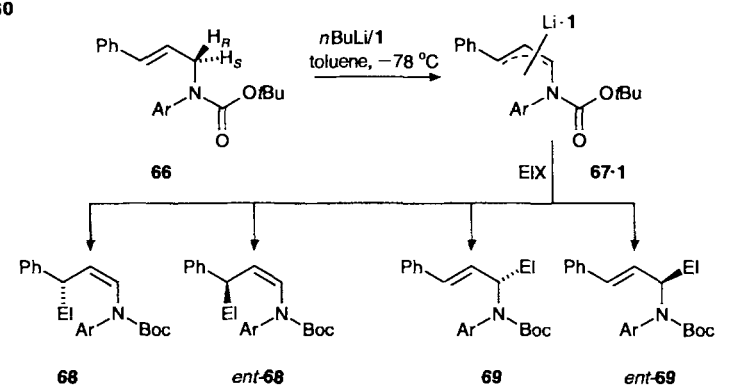

Scheme 33. Enantioselective lithiation and substitution of *N*-Boc-*N*-(*p*-methoxyphenyl)cinnamylamine (**66**) [102]. Ar = 4-$MeOC_6H_4$, Boc = $OCOtBu$.

Table 4. Enantioselective deprotonation and substitution of **66**.

*El*X	Major product	Yield[%]	*ee*[%]
H_3COTf	**68a**	74	92
H_3Cl	**68a**	73	95
$H_2C{=}CHCH_2Br$	**68b**	72	94
$PhCH_2Br$	**68c**	70	96
Me_3SiOTf	**68d**[a]	46	96
Me_3SnCl	*ent*-**68e**[b]	49	90
$(CH_2)_5C{=}O$	*ent*-**68f**[c]	77	98

[a] Together with 24% of the γ-silane **69d** (94% *ee*). [b] Together with 24% of the γ-stannane *ent*-**69e**. [c] El = 1-hydroxycyclohexyl.

In order to gain access to the opposite series of enantiomers, the authors again utilized the sequence of stannylation of **67**·**1** followed by lithium–tin exchange,[105] which led to *ent*-**68** (Scheme 34). This lithiostannylation was carried out in the pres-

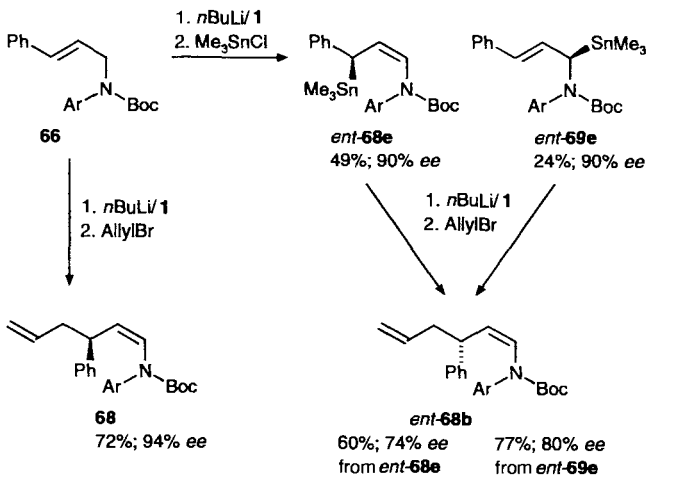

Scheme 34. Configurational inversion through stannylation and lithiodestannylation [102].

ence of (−)-sparteine, because uncomplexed **67** is configurationally labile.

The high γ-selectivity and enantioselectivity of the methylation remains intact in corresponding transformations of the cyclohexylallyl derivative **70** as well, although the result is the oppositely configured products **71** and **72**, with (*Z*)- and (*E*)-double bonds[106] (Scheme 35). Since the enamides of the corresponding aldehydes are subject to hydrolysis, these experiments demonstrate an additional route to enantiomerically enriched homoenolate equivalents.

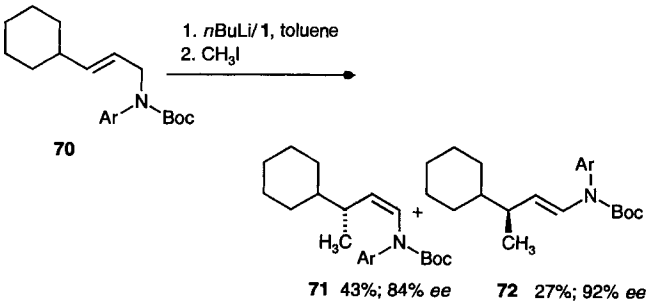

Scheme 35. Lithiation and methylation of the cyclohexyl derivative **70** [102]. Ar = 4-MeOC$_6$H$_4$.

4. Configurationally Stable Chiral Ion Pairs through Deprotonation of Achiral and Racemic Precursors

4.1. Preparations of Non-Resonance-Stabilized 1-Hydroxyalkyllithium Derivatives

Enantiomerically enriched 1-(alkoxymethoxy)alkyllithium derivatives of the type **74** were recognized to be configurationally stable by W. C. Still and C. Streekumar in 1980; the compounds fail to racemize below −40 °C in ethereal solvents.[107, 108] They were prepared by lithium–tin exchange starting from the precursor **73**. Transmetalation is accomplished, as is the subsequent methylation to **75**, with stereoretention (Scheme 36).[107, 109, 110]

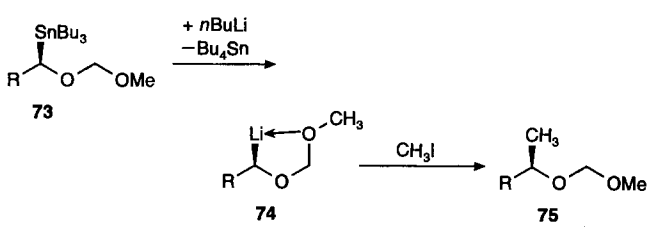

Scheme 36. Preparation of enantiomerically enriched 1-oxyalkyllithium derivatives by lithiodestannylation [107].

The tin derivative **73** was obtained through a laborious racemate resolution by way of diastereomeric esters, although simpler pathways are now known, most of which involve asymmetric reduction of acylstannanes.[111]

In contrast to the above-described lithiodestannylation, reductive cleavage of chiral monothioacetals **76** is not suitable for stereoselective carbanion generation (Scheme 37),[112] because

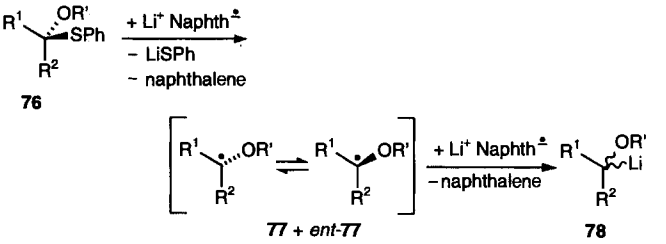

Scheme 37. Preparation of racemic α-oxyalkyllithium derivatives by reductive desulfenylation.

it proceeds via a configurationally labile radical intermediate **77** due to the single-electron transition involved. This reaction thus leads to the racemic products **78**.[113]

Formation via deprotonation is ruled out by the extraordinarily low CH-acidity of dialkyl ethers. The situation is more favorable for esters because of the possibility of efficient complexation of the lithium reagent[114] and the associated increase in kinetic acidity, as well as dipole stabilization of the ion pair, although a competitive nucleophilic attack is a potential threat. Thus, only lithiomethyl derivatives of a *tert*-butyl methyl ether[115] (**79**) and sterically blocked benzoic acid esters (**80**[116] and **81**[117]) could be obtained (Scheme 38); persistent homologues with primary alkyl chains cannot be generated in this way.[118]

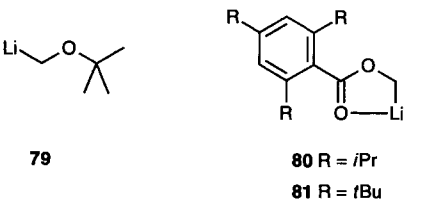

Scheme 38. 1-Oxymethyllithium derivatives accessible by deprotonation [115, 116a, 117].

As expected, the methyl *N*,*N*-diisopropylcarbamate[119] **82** is easily deprotonated by *sec*-butyllithium/TMEDA in diethyl ether or pentane as solvent (Scheme 39); addition of the lithium intermediate **83**·**TMEDA** to aldehydes and ketones to give diol derivatives of type **84** is straightforward.[120]

This reaction is applicable to the ethyl carbamate, although "the faithful servants" that one called upon in the case of the

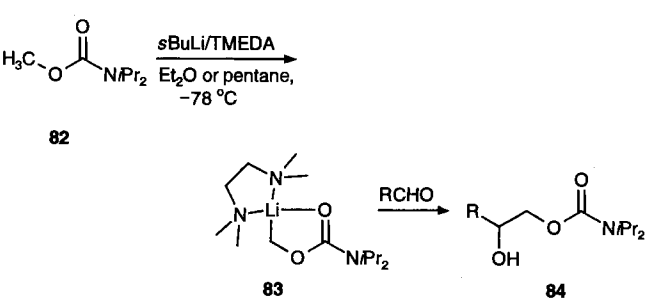

Scheme 39. Preparation and carbonyl addition of 1-(*N*,*N*-diisopropylcarbamoyloxy)methyllithium (**83**) [120b].

bulky carbamoyl group proved hard to dismiss; subsequent hydrolytic cleavage of *N,N*-dialkylcarbamates of saturated alcohols cause considerable difficulties, and only reductive methods with large excesses of diisobutylaluminum hydride[121] under drastic conditions have so far led to success.

A general solution to the problem was achieved with 1,3-oxazolidine-3-carboxylic esters of the types **89**[122] and **90**[123] (Scheme 40).[122] 2,2,4,4-Tetrasubstitution accomplishes extremely efficient shielding of the carbonyl group, but incorporation of an aminoketal group also ensures the presence of an acid-labile potential cleavage site. The acid chlorides **87** and **88** required for introduction of an activating *O*-protective group are obtained by condensation[124] of 2-amino-2-methylpropanol with acetone or cyclohexanone to give the distillable oxazolidines **85** and **86**, followed by chlorocarbonylation with diphosgene.[122, 123] The carbamates **89** and **90**, generally obtained by the acylation of alcohols with acid chlorides **87** and **88**, are present as *E*/*Z* mixtures, which in the time frame of ^{1}H NMR spectroscopy interconvert only slowly. The consequence is a doubling of the signals when ^{1}H NMR spectra are recorded without special precautions.[125] Spectroscopic evaluation is less hampered for *Cby*-esters of the type **89** than for the originally utilized spirocyclic *Cbx*-esters **90**.

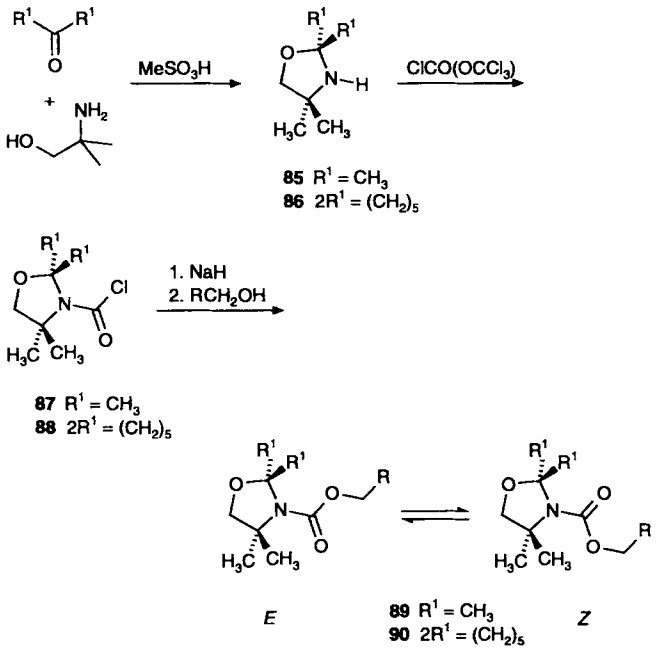

Scheme 40. General synthesis of 1,3-oxazolidine-3-carboxylic acid esters.

The 2,2,4,4-tetramethyl-1,3-oxazolidinyl group corresponds approximately in terms of spatial demand to a di-(*tert*-butylamino) group, so it is hardly surprising that secondary alkyl esters **91** (R and El = alkyl) usually are not attacked even by lithium aluminum hydride[126] in boiling THF. Stirring in methanol containing methanesulfonic acid releases the *N*-(β-hydroxyalkylurethane) **92** from the *N,O*-acetonide **91**. Thereafter, the hydroxy group plays an active role in base- or acid-catalyzed deblocking to alcohol **93** (Scheme 41).

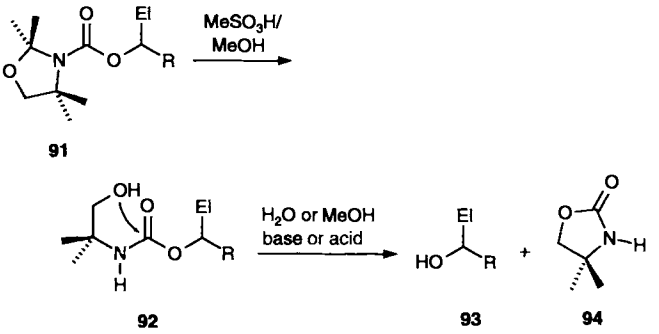

Scheme 41. Stepwise cleavage of the 1,3-oxazolidine-3-carbonyl residue.

4.2. (−)-Sparteine-Induced Deprotonation of Achiral Alkyl Carbamates

The deprotonation of "ordinary" achiral primary alkyl carbamates of types **89** or **90** with *sec*-butyllithium/(−)-sparteine in diethyl ether or hydrocarbons proceeds with a reliable preference for the *pro-S*-proton to give the lithium derivatives **95**·**1** or **96**·**1**, which can be substituted with various electrophiles under stereoretention to give **97** or **98**, respectively (Scheme 42, Table 5). The resulting enantiomeric enrichment is normally

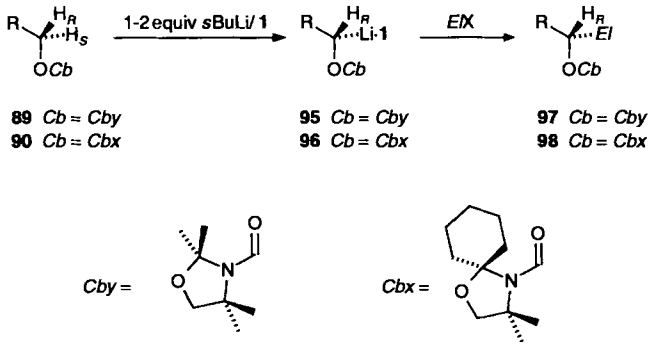

Scheme 42. Enantioselective deprotonation and substitution of "oxazolidine carbamates" **89** and **90**.

Table 5. Selected examples of the (−)-sparteine-mediated lithiation and substitution of alkyl carbamates.

Product	R	El	ElX	Yield[%]	Config.[a]	Ref.
98aa	CH_3	CO_2Me	CO_2[b]	75	*R*	[123, 130]
98ab	CH_3	Me_3Sn	Me_3SnCl	76	*S*	[123, 130]
97ac	CH_3	PhCHOH	PhCHO	76	*R*	[130]
97ad	CH_3	$H_2C{=}CHCH_2$	AllBr	60	*R*(42)	[130]
97aa	CH_3	CO_2Me	MeOCOCl	73	*R*	[130]
97ae	CH_3	PhC=O	PhCOCl	38	*R*	[130]
97af	CH_3	Me_3Si	Me_3SiCl	86	*S*	[130]
97ag	CH_3	Me_3Sn	Me_3SnCl	72	*S*	[130]
97ah	CH_3	Me_3Pb	Me_3PbBr	61	*S*(93)	[130]
97ba	$(CH_3)_2CH$	CO_2Me[b]	CO_2	52	*R*	[123, 130]
97bg	$(CH_3)_2CH$	Me_3Sn	Me_3SnCl	62	*S*	[123, 130]
97ci	$H_3C(CH_2)_6$	CH_3	CH_3I	87	*S*	[123, 130]
97ca	$H_3C(CH_2)_6$	CO_2Me	CO_2	79	*R*	[123, 130]
97da	$PhCH_2CH_2$	CO_2Me	CO_2	88	*R*	[131]
97ek	$FcCH_2$[e]	Ph_2P	Ph_2PCl	70	*S*	[132]
97fi	$H_3C(CH_2)_{11}$	CH_3	CH_3I	60[d]	*S*(98)	[122, 130]
97gi	[f]	CH_3	CH_3I	64	*S*(>92)	[130]

[a] The enantiomeric excess is greater than 95% *ee*. Deviations are indicated in parentheses. [b] Subsequent methylation of the carboxylic acid with diazomethane. [c] Mixture of epimers. [d] Use of 3 equivalents of *sec*-butyllithium/**1**. [e] *Fc* = ferrocenyl. [f] $(H_3C)_2C{=}CH{-}(CH_2)_2$.

more than 95% *ee*. Suitable reaction partners include methyl iodide, CO_2, alkyl chloroformates, aldehydes, ketones, carboxylic acid chlorides and esters, and trialkylsilyl and trialkyltin chlorides. Partial racemization is observed in reactions with benzylic and allylic halides, which speaks for the involvement here of single-electron transfer (SET)[127] in the substitution step, which is favored by resonance stabilization of the benzylic or allylic radical. Primary alkyl iodides can be caused to react[128] by the addition of HMPTA-substitutes such as 1,3-dimethyltetrahydro-2(1*H*)-pyrimidinone (DMPU).[129] It is especially noteworthy that acylation occurs without racemization. This points to weak kinetic basicity of the lithium compounds **95** and **96**, which presumably has its origin in the severe steric burden of the lithium cation, that in turn hinders "docking" at the ketone on the carbonyl group and thus activation of the neighboring CH-bond.

Methylation product **97fi** led, with 98% *ee*[122] after deblocking and acetylation, to (*S*)-(+)-2-tridecylacetate **99**, a pheromone of the fruit fly *Drosophila muelleri*,[133] whereas (*S*)-(−)-sulcatol (**100**),[134a] a pheromone of the beetle *Gnathotricus sulcatus*,[134b] (92% *ee*) was obtained from **97gi** (Scheme 43).[130]

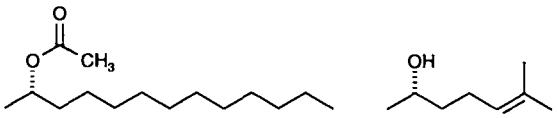

99 **100**

Scheme 43. Synthetic insect pheromones **99**[122] and **100**[130].

Unlike in the case of the lithium ion pairs of resonance-stabilized α-carbamoyloxyalkanides (see Section 3.1), substitution reactions of the saturated analogues **95·1** and **96·1** always occur with retention of configuration. Thus, the synthetic ester **97aa** is identical with a sample prepared from (*R*)-lactic acid.[123] (*R*)-**97aa** was also obtained via the detour of stannylation of **101·1** to (*S*)-**97ag** and destannylation with *n*-butyllithium/TMEDA by way of the sparteine-free complex **101**·TMEDA (Scheme 44).[123]

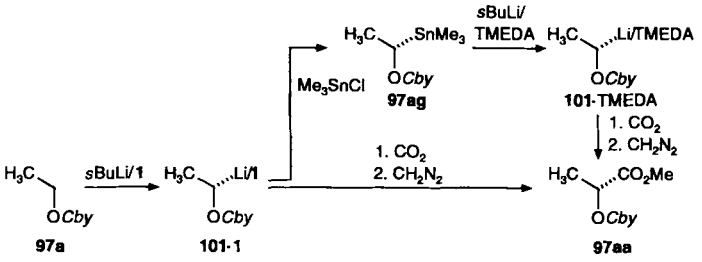

97a **101-1** **97aa**

Scheme 44. Stereochemical correlation of the metal derivatives with (*R*)-lactic acid [123].

Since according to all previous experience[109,135] the lithiodestannylation step is always accompanied by retention, stannylation must also have taken this configurative course.

Thus, the process permits a broad range of electrophilic substitution reactions of *pro-S*-protons in alkanols; the lithiated carbamates **95·1** or **96·1** correspond to the chiral synthon **I** (Scheme 45).

Irregularities can arise if the starting material contains heterosubstituents. The following causes will be discussed in Sections 4.1–4.6: 1,2- and 1,3-elimination of nucleofugic leaving groups;

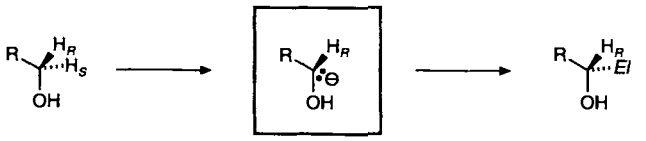

I

Scheme 45. General synthetic strategy.

displacement of (−)-sparteine by Lewis-basic substituents in the substrate; opposite stereochemical preferences in chiral substrates through the formation of "mismatched pairs."[56]

First, however, we discuss insights gained to date into the mechanistic pathway of (−)-sparteine-mediated deprotonation.

4.3. On the Mechanism of Kinetically Controlled Carbamate Deprotonation

A series of simple experiments[136] with the deuterium-labeled substrate [1*D*]**97a** supports the validity of the previously described interpretation (Scheme 46):[137] Through double application of the sequence (−)-sparteine-induced deprotonation

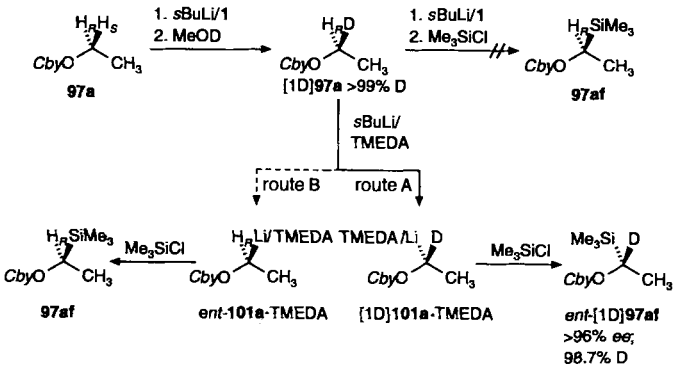

97a [1D]**97a** >99% D **97af**

ent-**101a**-TMEDA [1D]**101a**-TMEDA *ent*-[1D]**97af** >96% *ee*; 98.7% D

Scheme 46. Determination of the kinetic isotope effect k_H/k_D in the deprotonation of an alkyl carbamate [136].

and deuterolysis of the organolithium intermediate it was possible to isolate the α-deuterioethyl carbamate [1*D*]**97a** with a 1-D_1-content higher than 99%. An attempt at renewed deprotonation with *sec*-butyllithium/(−)-sparteine (**1**) and subsequent trapping with chlorotrimethylsilane failed; the anticipated silane **97af** was detectable at most in trace amounts. Deprotonation of [1*D*]**97a** with the achiral base pair *sec*-butyllithium/TMEDA, on the other hand, is not subject to any stereochemical restriction: the ratio of rates according to which reaction pathways A and B proceed is determined exclusively by the kinetic isotope effect k_H/k_D. The reaction produced, after silylation, the silane *ent*-[1*D*]**97af** with greater than 96% *ee* and a ^1H content of less than 1.3%.[138] From this one can calculate a k_H/k_D ratio of >70.[139]

The following conclusions can be drawn from these results: 1) Lithiated alkyl carbamates are completely stable configurationally in the form of TMEDA or (−)-sparteine complexes under the reaction conditions. 2) The deprotonation step is kinetically controlled, and this step determines the stereochemical course. 3) A *pro-S*-proton is abstracted with high selectivity

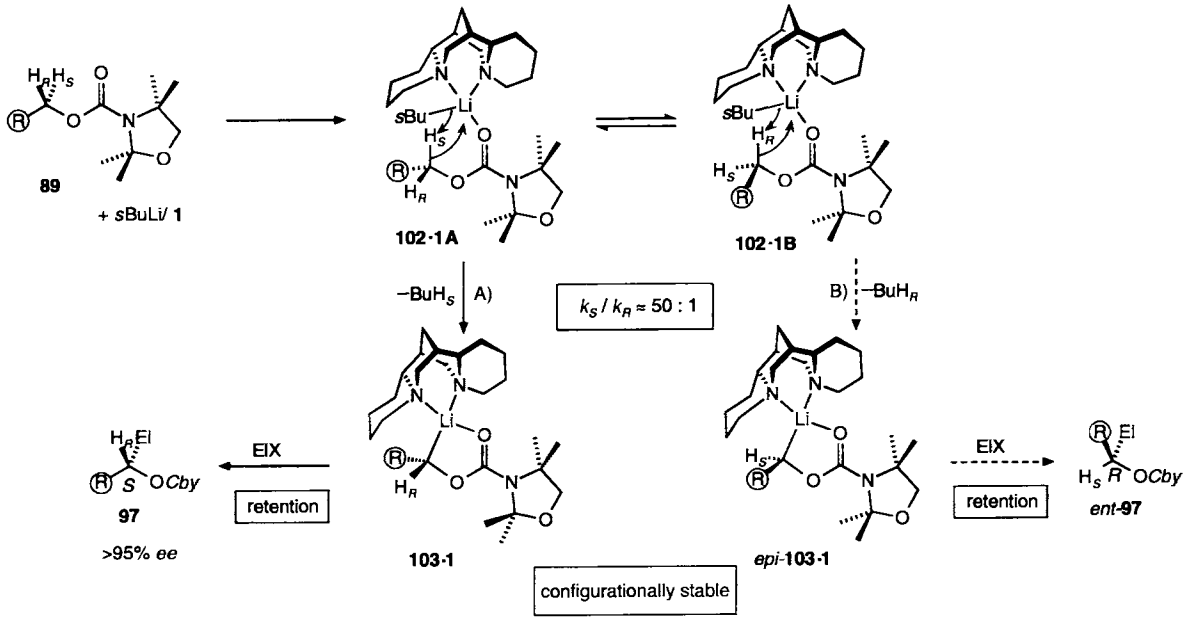

Scheme 47. Diastereomorphic transition states in the (−)-sparteine-mediated deprotonation of ethyl carbamate **97a** with *sec*-butyllithium.

under the influence of (−)-sparteine, and the incoming electrophile occupies its topochemical position. 4) The observed kinetic isotope effect k_H/k_D of at least 70 points to the intervention of a quantum-mechanical tunneling effect.[139, 140] Powerful H/D tunneling effects are observed when the reactants and products are separated by high, very "thin" potential barriers. This applies to proton transfer when the base and the resulting carbanion have similar basicities, and when the reacting centers are heavily shielded sterically. To our knowledge, the largest H/D kinetic isotope effect for a deprotonation reaction ($k_H/k_D = 24.3$) was determined in the deprotonation of 2-nitropropane with 2,4,6-trimethylpyridine.[140b]

Additional experimental facts are also important if one wishes to propose a solid mechanistic model: 1) Without addition of a bidentate ligand such as TMEDA or (−)-sparteine (**1**), deprotonation of "simple" alkyl carbamates is excluded. 2) A reactive alkyl carbamate like **89** or **90** added to an equimolar mixture of *sec*-butyllithium, (−)-sparteine (**1**), and the (not deprotonateable) isopropyl carbamate *i*prO*Cby* at −78 °C is also not attacked.[141] This means that prior to the deprotonation step a complex consisting of alkyllithium, the bidentate ligand, and the carbamate forms virtually irreversibly. Beak et al.[142] verified by NMR spectroscopy the presence in ethereal solution of an unsymmetrical complex of the composition $[(RLi)_2(Et_2O)_2 \cdot \mathbf{1}]$, which is, however, under the conditions applicable here for the kinetics of the deprotonation step of no significance.

Proton transfer in the aggregate **102·1** is turned in this way into an intramolecular process with differentiation between diastereotopic protons (Scheme 47). Abstraction of the *pro-S*-H from conformation **A** occurs roughly 50 times more rapidly than that of the *pro-R*-H from conformation **B**, which leads to the minor diastereomer *epi*-**103·1**. From this result a free energy difference $\Delta G^{\neq}$ of about 6.3 kJ mol^{-1} is calculated.

The limits of the deprotonation of very weak CH acids have nearly been reached; it is apparent here that the combination *sec*-alkyllithium/(−)-sparteine was a fortunate choice, and with respect to the basicity and steric demands of base and ligand an optimum has almost surely been reached: Deprotonation of nonactivated alkyl carbamates does not occur with use of *n*- or *tert*-butyllithium/(−)-sparteine (**1**) or *sec*-butyllithium/(−)-α-isosparteine (**2**).[131]

J. Haller and E.-U. Würthwein simulated the energy minima for transition states along the diastereomorphic reaction pathways **A** and **B** with the aid of semiempirical calculations (MOPAC, PM3).[95] For this process, *sec*-butyllithium was replaced by the achiral isopropyllithium,[143] and lithium parameters from Anders[95b] were utilized. In both transition structures **104·1A** and **104·1B** (Figure 7) the reaction center inserts into a "niche" that is left free by a "wing" of the ligand (−)-sparteine.

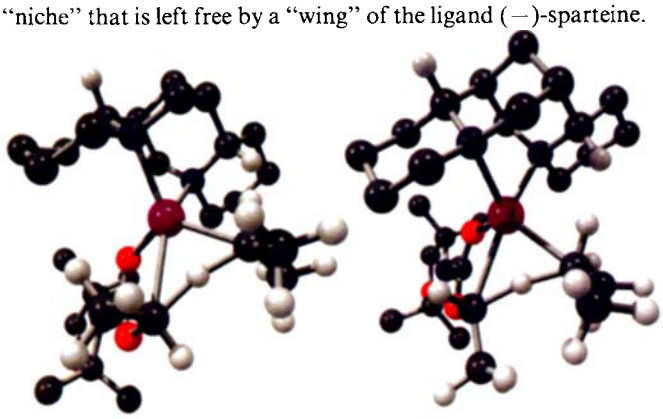

Figure 7. Models of the calculated diastereomorphic transition states (MOPAC, PM3) in the intramolecular removal of the *pro-S*-proton (left) and the *pro-R*-proton (right) in carbamate **97a** by isopropyllithium/(−)-sparteine [141]. In the case of sparteine (top of both illustrations) all hydrogen atoms have been omitted except for those at the bridgeheads; the same applies to the 2,2,4,4-tetramethyloxazolidin-3-carbonyl residue (bottom left). The view into the reaction center [the "triangle" consisting of the lithium cation (violet), C-1 of the substrate (left), the proton to be transferred (white), and C-2 of the base (right)] has been held constant. In both transition states, the bulky base (bottom right) extends into the niche left free by the *cis*-annelated outer six-membered ring of the sparteine. The *pro-S*-transition state (left) corresponds to the experimentally observed stereochemical course; here the methyl group (bottom left) extends forward. In the *pro-R*-transition state (right) it points downward; here the distance to the isopropyl group of the base is smaller, and therefore the steric interaction greater.

The structures differ from each other in that the urethane alkyl group in structure **104·1A** extends into the free space, whereas that in **104·1B** collides with the isopropyl group. The calculated energy difference $\Delta\Delta G^{\ddagger}$ of 0.8 kJ mol^{-1} is much too small in comparison to the experimental value of $\geq$6.3 kJ mol^{-1}; we suspect that the calculation method selected for the exact solution of this complex problem is, like other semiempirical methods, inadequate for the task, which is complicated further by the appearance of tunneling effects.[144]

Better agreement between experimental and calculated results is obtained when diastereotopic differentiation is established through a neighboring stereogenic center in the substrate:[145] (*R*)-2-Phenylpropyl carbamate[146] **105** leads after deprotonation and methoxycarbonylation to the diastereomeric esters **108** and **109** in a ratio of 95:5 (Scheme 48); that is, the *pro-S*-proton is removed roughly 20 times more rapidly than the *pro-R*-proton. However, in (1-tetrahydronaphthyl)methyl carbamate **110**, which has an equivalent configuration,[146] a reverse preference for **113**:**114** is registered with a ratio of 13:87.[147]

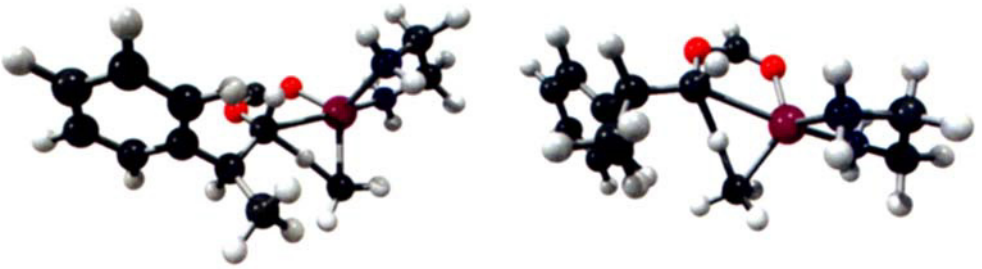

Figure 8. Models of the calculated diastereomorphic transition states (MOPAC, PM3) for removal of the *pro-R*-proton in a complex consisting of methyllithium/ethylenediamine and (*S*)-1-phenylethyl formate (left) or (*R*)-1-phenylethyl formate (right)[145]. In the transition state a triangle is formed consisting of the now pentacoordinated lithium cation (violet), the (also pentacoordinated) carbon atom of the base, and the C–H acid, on the basis of which the attacked proton wanders. The calculated energy difference $\Delta\Delta H^{\ddagger}$ in favor of the *ul*-proton (left) relative to the *lk*-process (right) amounts to 2.9 kJ mol^{-1}. In the most favorable conformations in each case the plane of the phenyl residue is parallel to the C–H bond at the stereogenic center in order to avoid 1,3-allyl strain. In the favorable *ul*-transition state (left) the C1–C2 bond can assume a completely eclipsed conformation at the expense of an interaction between an *ortho*-H atom and the remaining 1-H atom, whereas that conformation in the *lk*-transition state apparently represents a poor compromise. The two experiments are possible only by computer, since in a reaction flask the system would discover that removal of an N–H proton and subsequent attack of lithium amide on the formyl group would be the favored reaction pathway.

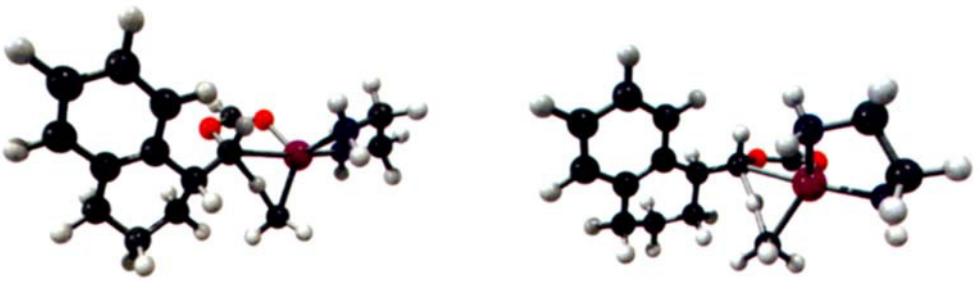

Figure 9. Models of the calculated diastereomorphic transition states (MOPAC, PM3) for removal of the *pro-R*-proton in a complex consisting of methyllithium/ethylenediamine and (*R*)-(left) or (*S*)-(1,2,3,4-tetrahydronaphth-1-yl)methyl formate (right)[145]. In this case calculations ($\Delta\Delta H^{\ddagger}$ = 2.9 kJ mol^{-1}) and experiment ($\Delta G^{\ddagger}_{-78\,^{\circ}C}$ = 2.9 kJ mol^{-1}) show the *lk*-transition state (left) to be the more favorable. Since the phenyl residue and the attached alkyl group are constrained in a plane by the ring, the conformational energies are reversed relative to the α,β-(1,1')-C–C bond. In the *ul*-transition state (right) the interaction of the C-2-methylene group of the tetrahydronaphthyl residue with the reaction center ia apparently stronger than that of the *lk*-transition state (left).

Although the PM3 calculations[95] are carried out with simplified substrates (formyl in place of oxazolidinecarbonyl) and reagents (MeLi for *sec*-BuLi and ethylenediamine for TMEDA), they correctly reflect the observed trend (Figures 8, 9).[148]

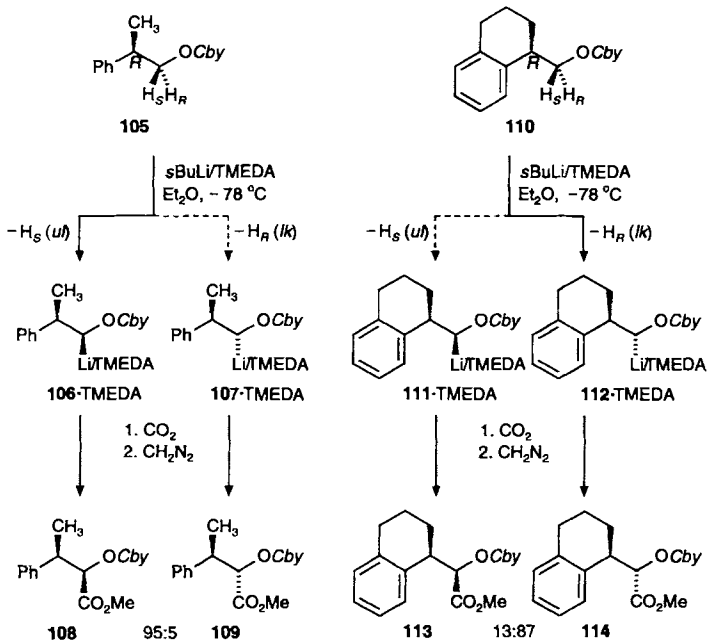

Scheme 48. Diastereotope-differentiating deprotonation of chiral alkyl carbamates [145].

Calculated energy differences $\Delta(\Delta H^{\ddagger}_{lk} - \Delta H^{\ddagger}_{ul})$ correspond well with the experimentally determined values $\Delta(\Delta G^{\ddagger}_{lk} - \Delta G^{\ddagger}_{ul}$ in parentheses): 2.5 (5.0) kJ mol^{-1} for the system **105** and −2.5 (−2.5) kJ mol^{-1} for **110**.

It is apparent that significant differences in the energies of diasteromorphic reaction pathways for a kinetic racemate resolution under the influence of the chiral base pair *sec*-butyllithium/(−)-sparteine are susceptible to exploitation.[145, 149] The enantiomer that reacts most rapidly is the one in which the *pro-S* preference of substrate matches that of the reagent, namely (*R*)-**105** and (*S*)-**110**.[145, 149]

4.4. Deprotonation of Heterosubstituted Alkyl Carbamates

As described in the preceding section, the formation of a complex consisting of alkyl carbamate, *sec*-butyllithium, and (−)-sparteine is essential for achieving highly stereoselective deprotonation. If the alkyl group bears a strong donor substituent, this may displace the sparteine.

Thus, deprotonation of the 3-(*N*,*N*-dimethylamino)propyl carbamate **117a**, followed by reaction with various electrophiles, leads to the nearly racemic product **118a** (Scheme 49).[150, 151] The bulkier *N*,*N*-dibenzylamino group on

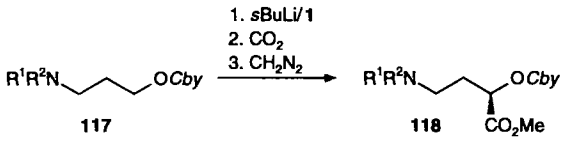

	R^1	R^2	Yield [%]	*ee* [%]
a	CH_3	CH_3	92 [a]	<10
b	CH_3	$PhCH_2$	70	80
c	$PhCH_2$	$PhCH_2$	94	97

Scheme 49. (−)-Sparteine-induced deprotonation of 3-(dialkylamino)alkyl carbamates [152]. [a] CH_3 instead of CO_2Me.

the other hand does not interfere, and the product **118c** of electrophilic substitution is obtained with the customary enantiomeric enrichment of greater than 95% *ee*.[150] In this respect the (*N*-benzyl-*N*-methylamino) group in **117b** (80% *ee*) occupies an intermediate position.[150]

The 3-, 4-, and 5-carbamoyloxy,[153] 4-methoxy or 5-silyloxy,[153a] and 2-dibenzylamino groups[154] do not disrupt the enantioselectivity of deprotonation in the presence of (−)-sparteine (Scheme 50, Table 6).

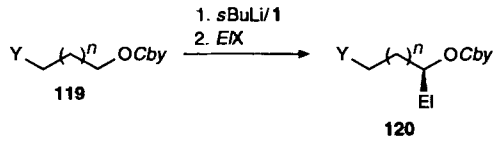

Scheme 50. Enantioselective deprotonation and substitution of ω-heterosubstituted alkyl carbamates.

Table 6. Enantioselective deprotonation and substitution of achiral ω-heterosubstituted alkyl carbamates **119**. TBDMS = *tert*-butyldimethylsilyl, MEM = methoxyethoxymethyl.

Starting material	Product	*n*	Y	*EIX*	Yield[%]	*ee*[%]	Ref.
119a	**120a**	1	O*Cby*	*MeI*	83	>97	[153a]
119b	**120b**	2	O*Cby*	*MeI*	92	97	[153a]
119c	**120c**	2	OMe	Me_3SnCl	70	99	[153a]
119d	**120d**	2	OTBDMS	CO_2[a]	77	>95	[153a]
119e	**120e**	2	OMEM	CO_2[a]	69	62	[155]
119f	**120f**	3	O*Cby*	Me_3SiCl	70	96	[153b]
119g	**120g**	0	NBn_2	CO_2[a]	56	>95	[154]

[a] Isolated as the methyl ester after treatment with diazomethane.

Compound **120g** is a protected derivative of D-isoserine.[154] Carboxylation of lithiated 1,3-dicarbamates leads in two steps to essentially enantiomerically pure γ-lactones, as illustrated in an exemplary way by the synthesis of D-pantolactone (**124**) (Scheme 51).[153a, 156]

1,3-Dicarbamates like **122·1** (Scheme 52) bear potential leaving groups that are activated by Lewis acids. In fact, we observed upon treatment with chlorotrimethylsilane the formation of the cyclopropyl carbamate **125** with 1,3-elimination of the lithium carbamate salt.[136, 153a, 157, 158] In the process the (*S*)-enantiomer **125** results with greater than 95% *ee*, as could be demonstrated by transformation into the carboxylic acid ester **126** and crystalline ketone **127** via the configurationally stable[159] intermediate lithium cyclopropanide. Investigations with the deuterium labeled, enantiomerically enriched starting material (*S*)-[1*D*]**121** proved without question that ring closure

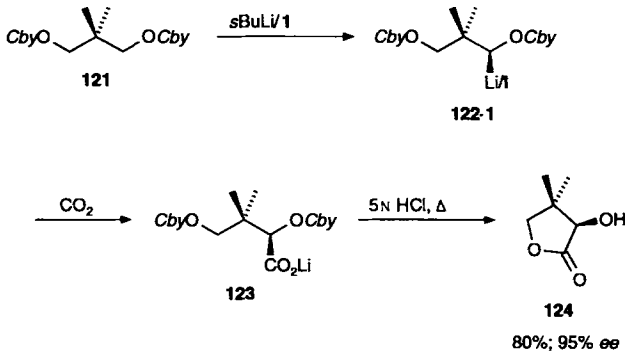

Scheme 51. Synthesis of (*R*)-pantolactone [153a].

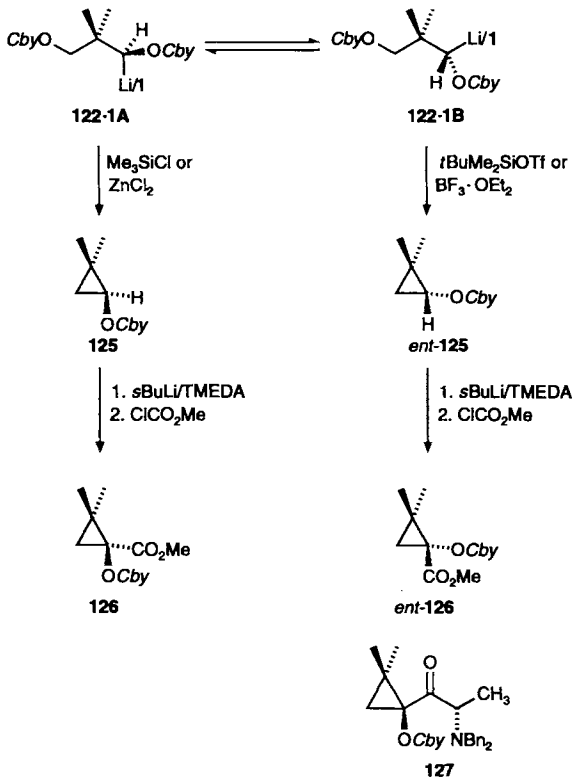

Scheme 52. Stereochemistry of the 1,3-elimination of a 1,3-dicarbamate [157, 160].

here occurs stereospecifically, with retention at C-1 as well as inversion at C-3, hence out of conformation **122·1a**.[136] To our great surprise, stronger Lewis acids like *tert*-butyldimethylsilyl triflate or boron trifluoride caused formation of the opposite enantiomerically enriched cyclopropane, *ent*-**125** (>95% *ee* and 74% *ee*); stereoinversion at both reactive centers was verified.[160–163]

Despite many possible complications, the carbamate group is distinguished by its unsurpassed directing effects. The following "acid test" (Scheme 53) underscores this assertion: Carbamate

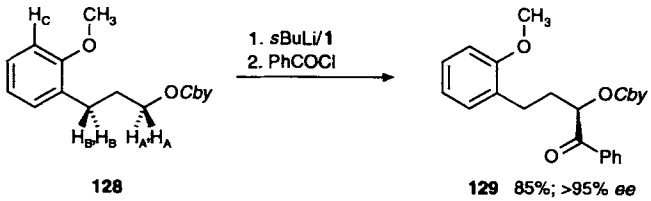

Scheme 53. Competing acidic positions in (−)-sparteine-induced lithiation [165].

128 bears three extraordinarily easily activable protons in H_C, H_B, and $H_{B'}$;[164] nevertheless, under the usual conditions of (−)-sparteine-induced deprotonation, exclusively the *pro-S*-proton H_A is released.[165]

4.4.1. Competition with Stereogenic Centers in the Substrate; Kinetic Resolution

Provided that a good donor substituent is attached to a stereogenic C atom in the γ- or δ-position, it can ensure a significant amount of chiral induction in the deprotonation step. It is useful when this chelate effect is subordinate in the competition with (−)-sparteine (**1**). In favorable cases—as with 1,3-dicarbamate **130a**—lithiation can then be directed preferentially in either of the two directions.[166] Application of the sparteine variant with subsequent methylation led to the (*S,S*)-2,4-pentanediol derivative **132a** with high selectivity, whereas in the presence of TMEDA the *meso*-compound *epi*-**132a** dominated (Scheme 54).[166] We suspect that a bicyclic chelate complex of

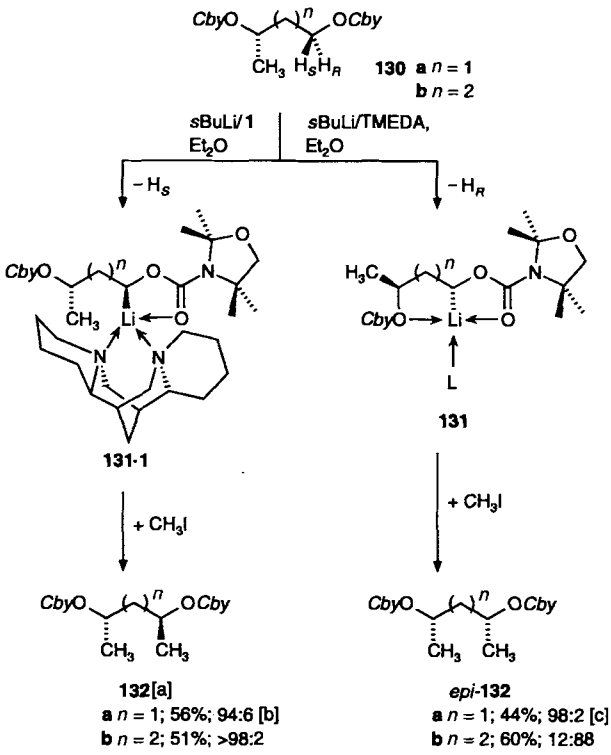

Scheme 54. (−)-Sparteine- vs. substrate-directed diastereoselective lithiation of 1,3- and 1,4-dicarbamates [166]. [a] Conducted with the carbamate residue *Cbx*. [b] Ratio **132**:*epi*-**132** [= (*S,S*):(*S,R*)]. [c] Ratio *epi*-**132**:**132** [= (*S,R*):(*S,S*)].

the type **131**[167] forms, and the more favorable *exo*-position of the stationary methyl group determines the transition state.[168] In the homologous (*S*)-2-methyl-1,4-butanediyl dicarbamate **130b**, reagent- and substrate-controlled deprotonations take the identical stereochemical course, and lead with differing efficiency to the (*S,S*)-diol derivative **132b**.

An effective substrate-inherent chiral induction can also be exploited with the acetonide of the (*S*)-3,4-dihydroxybutyl carbamate **133**.[169] Deprotonation in diethyl ether (without any other additive) and reaction of the resulting ion pairs **134** and *epi*-**134** with trimethyltin chloride produces mainly the (1*S*,3*S*)-diastereomer **135** (Scheme 55, Table 7). From this one can conclude that there is highly selective formation of the *anti*-annelated tricyclic chelate complex **134**.[168,170] In the presence of (−)-sparteine (**1**) the tendency toward release of the *pro-S* pro-

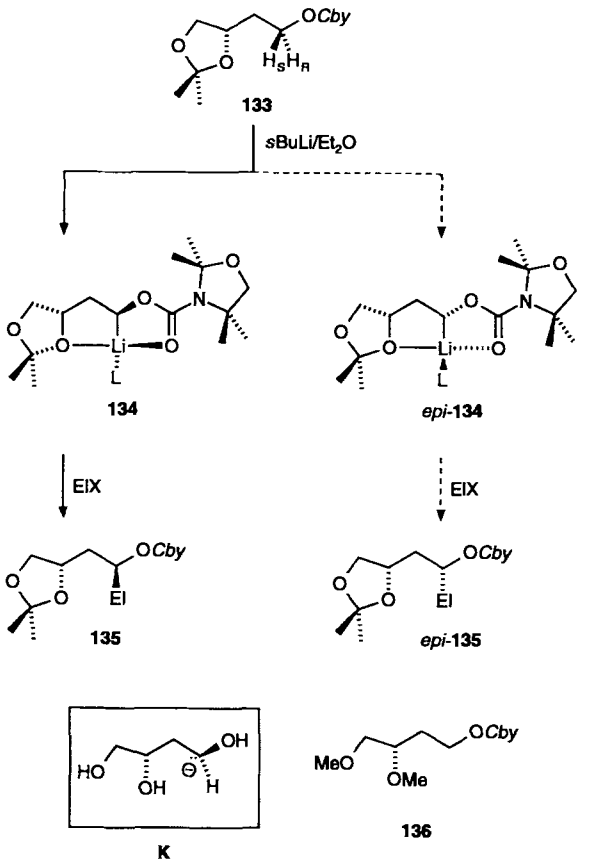

Scheme 55. Diastereoselective lithiation of the chiral acetonide **133** [169].

Table 7. Deprotonation of the acetonide **133** and reaction with various electrophiles [169].

Additive L	Products	*ElX*	Yield[%]	**135**:*epi*-**135**
Et_2O	**135a**	Me_3SnCl	63	98:2
TMEDA	**135a**	Me_3SnCl	71	75:35
1	**135a**	Me_3SnCl	61	>99:1
ent-**1**	**135a**	Me_3SnCl	75	28:72
Et_2O	**135b**	*MeI*	70	>95:5
Et_2O	**135b**	*MeOCO*(OMe)	35	98:2
Et_2O	**135c**	*HCO*OEt	69	96:4
Et_2O	**135e**	*iPrCO*Cl	57	>95:5
Et_2O	**135f**	Ph_2CO	76	>95:5
Et_2O	**135g**	[a]	39	>95:5
Et_2O	**135h**	[b]	51	>95:5
Et_2O	**135i**	[c]	62	>95:5

[a] (*E*)-Crotonyl chloride. [b] (*S*)-2-(*N,N*-Dibenzyl)alanine benzyl ester. [c] δ-Valerolactone.

ton is further increased, because in this case *epi*-**135a** is no longer identifiable in the reaction mixture. The 2,2-dimethyl-substituted 1,3-dioxolane ring is only a weak ligand for lithium, for in the deprotonation step, as with sparteine, it is displaced by TMEDA. As Table 7 indicates, diastereoselectivity decreases

under these conditions and is reversed by means of (+)-sparteine (*ent*-**1**)[171] with its preference for the *pro-R*-proton. In other words, in the presence of a bidentate complexing ligand, intramolecular complexation is not involved, and the normal deprotonation pathway applies. Conformational rigidity in the form of the acetonide is essential for achieving high substrate-controlled stereoselectivity, for the 3,4-dimethoxy derivative **136** reacts unselectively under the above-described conditions.[169]

As Table 7 shows, the ion pair **134** reacts smoothly with a wide variety of electrophiles, and acylation also poses no problems. For this reason the substrate constitutes a valuable synthetic equivalent to the (*S*)-1,3,4-trihydroxybutanide (**K**).[172] The method should be generalizable to the transfer of longer chains and more highly functionalized analogues.

How might one now gain entrance to the epimeric series *epi*-**135** without the need for the awkwardly available (+)-sparteine? This is easy so long as a deuteration of the product can be tolerated (Scheme 56).[65e] Acetonide **133** is lithiated and

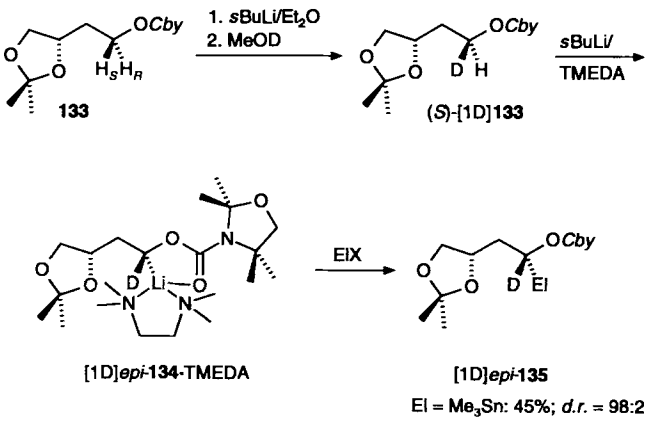

Scheme 56. Reversal of diastereoselectivity through deuteration of **133** [65e].

deuterated under substrate control. Because of the large kinetic H/D isotopic effect (see Section 4.2), TMEDA-assisted lithiation leads from (*S*)-[1*D*]**133** to the diastereomerically pure ion pair [1*D*]*epi*-**134**, which is configurationally stable and can be substituted to give [1*D*]*epi*-**135** under stereoretention.

High substrate-controlled diastereoselectivities are also achievable if the substituent capable of chelating is not itself on a stereogenic center, but rather adjacent to one. Upon deprotonation according to either the TMEDA or the (−)-sparteine variant, followed by reaction with electrophiles, dicarbamate **137** of (*S*)-2-(dibenzylamino)-1,4-butanediol,[173a,c] derived from (*S*)-asparaginic acid, leads to mixtures of regio- and diastereomers.[173b] However, if the transformation is carried out in diethyl ether (without addition of a diamine), the pure 1-substitution product **139** results (Scheme 57, Table 8). The breadth of the applicable electrophiles and the high reactivity are noteworthy. We therefore conclude that formation of the chelate complex **138** is kinetically controlled;[174,176] the cause of the highly stereoselective course of the reaction is thought to be the strong tendency of the 2-dibenzylamino and 4-carbamoyloxy groups to occupy an equatorial position in the developing six-membered ring.

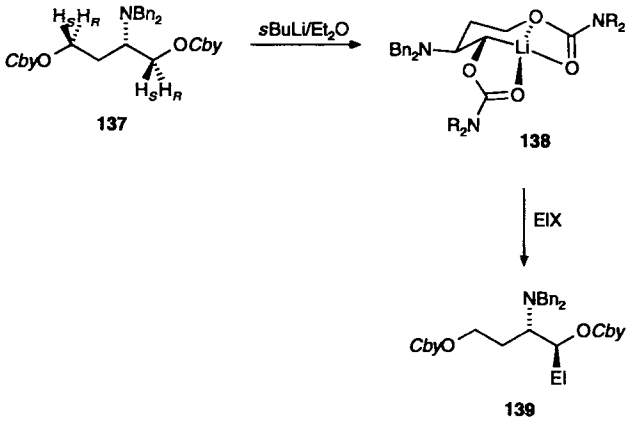

Scheme 57. Substrate-directed regio- and diastereoselective deprotonation of dicarbamate **137** [173b].

Table 8. Substrate-directed deprotonation and substitution of the dicarbamate **137** [173b].

Product[a]	El	*EIX*	Yield[%]
139a	D	*D*OMe	95
139b	Me	*Me*I	93
139c	CO_2Me[b]	*CO*$_2$	92
139d	Me_2COH	*Me*$_2$*C*=*O*	85
139e	iPr_2COH	*i*Pr$_2$*C*=*O*	75
139f	EtC=O	*EtCO*Cl	80
139g	[c]	[d]	71
139h	Me_3Si	*Me*$_3$*Si*Cl	73
139i	Me_3Sn	*Me*$_3$*Sn*Cl	75
139k[e]	PhS	*PhS*SPh	73
1391[e]	PPh_2	*Ph*$_2$*P*Cl	56

[a] In no case could a second diastereomer be verified by ^{1}H NMR, so the diastereomeric ratio was at least 97:3. [b] After esterification with diazomethane. [c] (*E*)-MeCH=CH−C=O. [d] (*E*)-MeCH=CHCOCl. [e] Ref. [175].

The 4-methyl ether **142** shows very similar selectivity,[173b,177] whereas the 4-*O*-TBDMS ether **143** is unreactive,[177] which also supports the important role played by the complexing substituent in the 4-position.

If the 1-*pro-S*-position of substrate **137** is blocked, whether by an alkyl group or deuterium,[178,179] the (−)-sparteine-mediated deprotonation "at the other end" takes its usual course, with the abstraction of *pro-S*-H-4 (Scheme 58). Obviously the 1-posi-

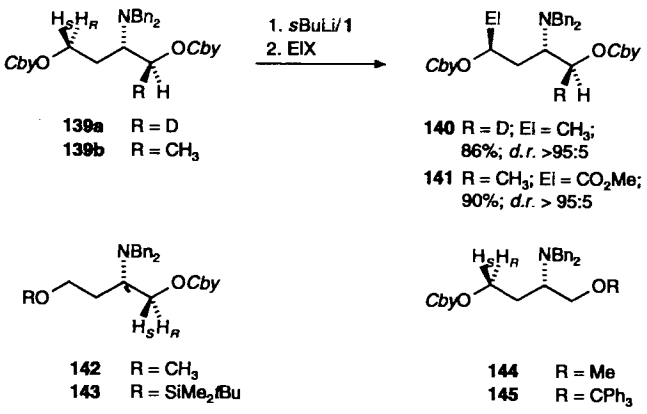

Scheme 58. Lithiation of 2-amino-1,4-butanediol derivatives in the 4-position [173b, 177].

tion can also be blocked in a classical way after introduction of a nonactivating protective group such as methyl or trityl at O-1 (**144** and **145**, Scheme 58), leading to regio- and stereoselective deprotonation at C-4.[177]

In the corresponding 2-amino-1,5-pentanediol derivative **146**, made from (*S*)-glutamic acid, internally assisted deprotonation is apparently retarded due to the unfavorable ring size of the resulting lithium chelate complex (Scheme 59).[173b] Thus, in

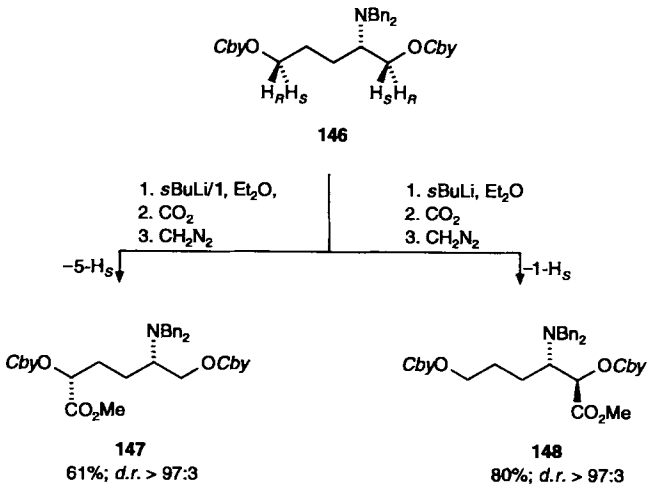

Scheme 59. Regio- and diastereoselective substitution of the 2-amino-1,5-pentanediol derivative **146** [173b].

the presence of (−)-sparteine, proton 5-H_S is abstracted almost exclusively, whereas in the absence of a diamine a slower deprotonation at C-1 is initiated; the intermediate lithium compounds produce, after trapping with carbon dioxide and *O*-methylation, the regioisomeric esters **147** and **148**.

Therefore, the procedures described offer extremely facile access to equivalents for the stereoisomerically pure carbanionic synthons **L** through **O** (Scheme 60).

Scheme 60. Carbanionic synthons accessible from 2-amino-1,ω-alkanediols [173b].

(*S*)-2-(*N*,*N*-Dibenzylamino)alkyl carbamates, accessible in a small number of steps from the natural amino acids,[180] display marked *ul*-induction[6a] in TMEDA-assisted deprotonation[154] (L_2 = TMEDA). Therefore, the *pro-R*-proton is preferentially abstracted, and one obtains after reaction, irrespective of the electrophile, an excess of the diastereomer **152** (Scheme 61, Table 9). The (*S*)-alaninol derivative **149a** constitutes an excep-

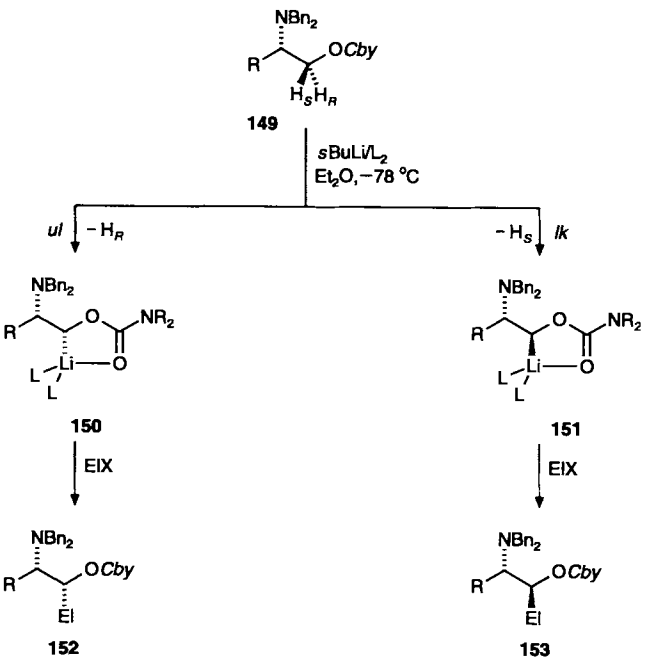

Scheme 61. Deprotonation of (*S*)-2-(*N*,*N*-dibenzylamino)alkyl carbamates. For R, see Table 9.

tion. One presumes that proton abstraction takes place in the antiperiplanar conformation, and in the normal case the *pro-R*-H is more accessible (Figure 10).[181] As described above, we have so far found no indication that the dibenzylamino group interacts as a complexing ligand.[182]

In the presence of (−)-sparteine (L_2 = 1) as complexing partner, the situation of a "mismatched pair" arises due to its preference for the *pro-S*-proton.[56] Strong substrate-directed stereoselection is directed toward the *pro-R*-H, and thus retards

Table 9. Substrate- and reagent-directed deprotonation of 2-(dibenzylamino)alkyl carbamates **149**.

Starting material	R	L_2 = TMEDA *EIX*	Products	L_2 = 1 Yield [%]	**152**:**153**	Yield [%]	**152**:**153**	Ref.
149a	CH_3	*CH*$_3$I	**152aa**, **153aa**	82	37:63	56	<3:97	[183]
149a	CH_3	*Bu*$_3$*Sn*Cl	**152ab**, **153ab**	49	36:64	59	<3:97	[183]
149a	CH_3	*CO*$_2$*Me*[a]	**152ac**, **153ac**	76	31:69	48	<3:97	[183]
149b	H_3CCH_2	*CH*$_3$I	**152ba**, **153ba**	72	88:12	[b]	–	[183]
149b	H_3CCH_2	*Bu*$_3$*Sn*Cl	**152bb**, **153bb**	70	89:11	[b]	–	[183]
149b	H_3CCH_2	*PhCO*Cl	**152bd**, **153bd**	74	88:12	[b]	–	[183]
ent-**149b**	H_3CCH_2	*CO*$_2$*Me*[a]	*ent*-**152bc**, *ent*-**153bc**	–	–	57	>97:3	[183]
149c	$Bn_2N(CH_2)_3$	Cl*CO*$_2$*Me*	**152cc**, **153cc**	78	84:16	[c]	–	[183]
149d	$(CH_3)_2CHCH_2$	*CO*$_2$*Me*[a]	**152dc**, **153dc**	56	>95:5	[b]	–	[154]
149e	$C_6H_5CH_2$	*CO*$_2$*Me*[a]	**152ec**, **153ec**	–	–	43	11:89	[184]
149e	$C_6H_5CH_2$	*PhCO*OMe	**152ed**, **153ed**	74	92:8	65	7:93	[184]
rac-**149f**	*c*-$C_3H_5CH_2$	*CO*$_2$*Me*[a]	*ent*-**152fc**, *ent*-**153fc**	89	83:17	[d]	[d]	[185]

[a] Isolated after esterification with diazomethane; CO_2 was used as electrophile. [b] No deprotonation. [c] Not carried out. [d] See text.

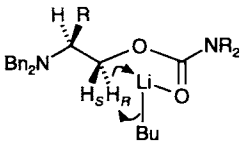

Figure 10. Favored conformation for substrate-directed deprotonation of (*S*)-2-(*N*,*N*-dibenzylamino)alkyl carbamates.

formation of the diastereomeric ion pair **151**, which in the presence of large residues R may be completely excluded.

Also with the (*S*)-prolinol derivative **154** there is a strong preference for abstraction of the *pro-R*-proton, which leads via the ion pair **155** to the diastereomerically pure substitution products **156** (Scheme 62).[154] Quite surprisingly, when deprotonation is carried out in ether solution in the presence of (−)-sparteine[154] or entirely without the addition of a diamine, the very same diastereomer results.[184] This observation permits only one conclusion: Here the less shielded amino function intervenes in the deprotonation step in an intra- or intermolecular way.

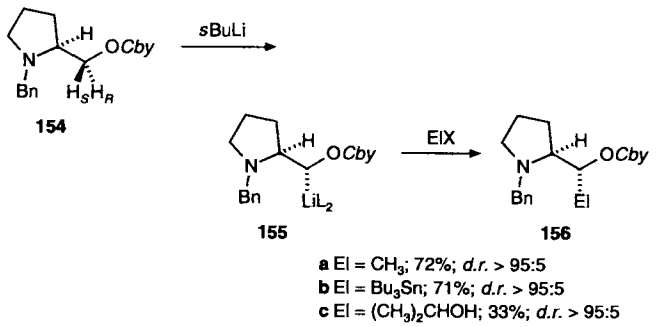

Scheme 62. Diastereoselective deprotonation of the prolinol carbamate **154** [154].

In the (−)-sparteine-induced deprotonation of (*R*)-2-(dibenzylamino)alkyl carbamates *ent*-**149**, both the substrate- and the reagent-controlled preferences point to the *pro-S*-proton. As a consequence, the reaction is rapid and stereoselectivity virtually complete (compare with *ent*-**149b** in Table 9) (Scheme 63).[183, 184] The sharply differing reactivities of the

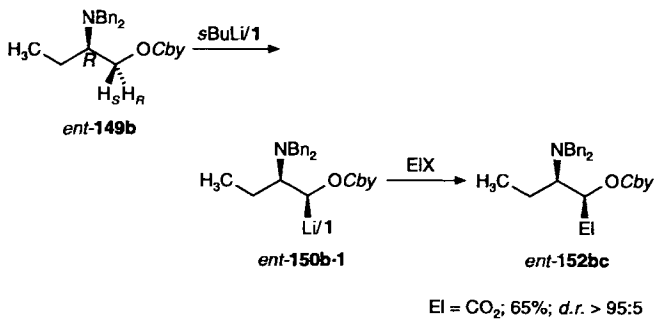

Scheme 63. Highly diastereoselective deprotonation and substitution of the (*R*)-2-(*N*,*N*-dibenzylamino)butyl carbamate *ent*-**149b** [183].

two enantiomers with respect to *sec*-butyllithium/(−)-sparteine can be exploited for efficient kinetic racemate resolution. As with all kinetic racemate resolutions with carbamates, at least one equivalent of alkyllithium is required; apparently this is irreversibly bound in a precomplex even with the less reactive enantiomer. From the racemic β-cyclopropylalaninol derivative *rac*-**149f** it was possible in this way to acquire the ester *ent*-**152fc** (>95% *ee*) and recover (*S*)-carbamate (*S*)-**149f** (Scheme 64).[128, 185] The advantage relative to classical or enzymatic racemate resolution lies in the possibility of accomplishing a highly diastereoselective C–C coupling in addition.

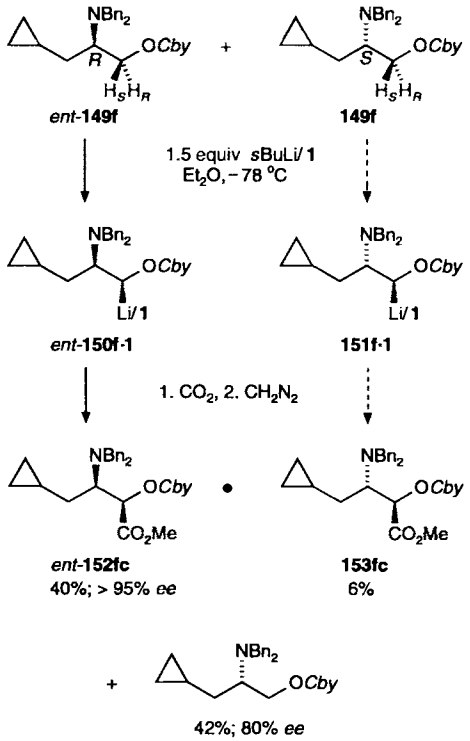

Scheme 64. Kinetic resolution of the carbamate *rac*-**149f** [129, 185].

As was demonstrated with 3-(piperidine-2-yl)ethyl carbamate *rac*-**156**, the method can also prove valuable when differentiation between the enantiomers is less efficient.[186] One obtains after methylation the epimeric (2*S*)-alkyl carbamates **157** (>95% *ee*) and **158** (89% *ee*), which after deblocking lead to the alkaloids (+)-sedridine[187] (**159**) and (+)-allosedridine (**160**) (Scheme 65). The sequence possesses the character of a

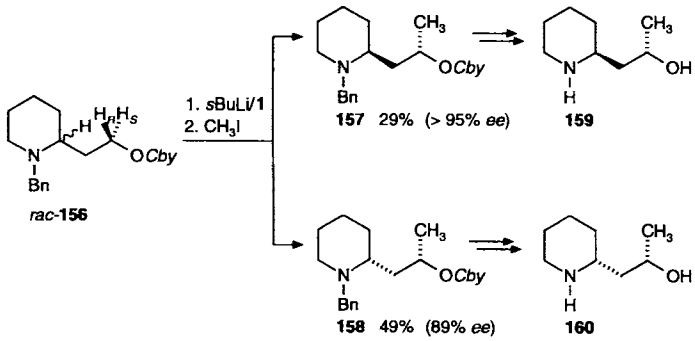

Scheme 65. Synthesis of (+)-sedridine and (+)-allosedridine [186].

highly enantioselective substitution on a racemic starting material, which simplifies racemate resolution of the starting material by turning it into a separation of product diastereomers.

An interesting stereochemical problem is presented by *meso*-dicarbamate **161** (Scheme 66).[153b, 188] The compound bears two enantiotopic side groups, each with two diastereotopic protons. The chiral base *sec*-butyllithium/(−)-sparteine abstracts that *pro-S*-proton whose removal is supported by the substrate-inherent preference, namely *R*-H_S.[189] The [1*R*,1(1*R*),2*S*]-configured lithium intermediate **162**·**1** arises in excess together with the [1*S*,1(1*R*),2*R*]-diastereomer and leads to the substitution products **164** with high stereoselectivity.

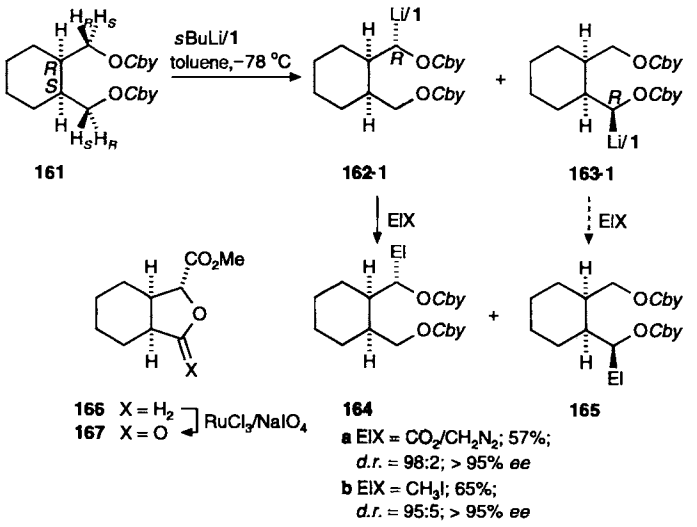

Scheme 66. Desymmetrization of a *meso*-1,4-dicarbamate [153b].

Carboxylic acid ester **164a** was transformed with 5N hydrochloric acid into the tetrahydrofuran derivative **166**, which was oxidized to the lactone acid ester **167**.[190] At this stage the expected configuration was verified by an X-ray crystal structure analysis.[191] All in all, desymmetrization of the *meso*-substrate was associated with highly diastereoselective C−C bond formation.

4.5. Enantioselective Lithiation of *N*-Boc-Pyrrolidines

As Beak et al. were able to show as early as 1984 that *N*-(*tert*-butoxycarbonyl)pyrrolidines and -piperidines are easily deprotonated to the corresponding racemic dipole-stabilized lithium–carbanion pairs.[192] Application of *sec*-butyllithium/(−)-sparteine to *N*-Boc-pyrrolidine leads through enantiotopic differentiation, after removal of the *pro-S*-2-H atom, to the configurationally stable intermediate **169**·**1**, which can be substituted with retention by various electrophiles (Scheme 67).[193]

The (*R*)-diphenylprolinol derivative **170c** can be enriched to 99.3% *ee* by recrystallization and provides a valuable ligand for enantioselective ketone reduction according to Corey–Itsuno.[194] Tin compound **170d** is the starting material for the synthesis of enantiomerically enriched 2-lithio-*N*-methylpyrrolidines developed by R. E. Gawley.[195] Double lithiation/methylation offers easy access to the (*S*,*S*)-2,5-dimethylpyrrolidine derivative **171**; a possibility has also been worked out for separation of the roughly 10% content of *meso*-compound **172**

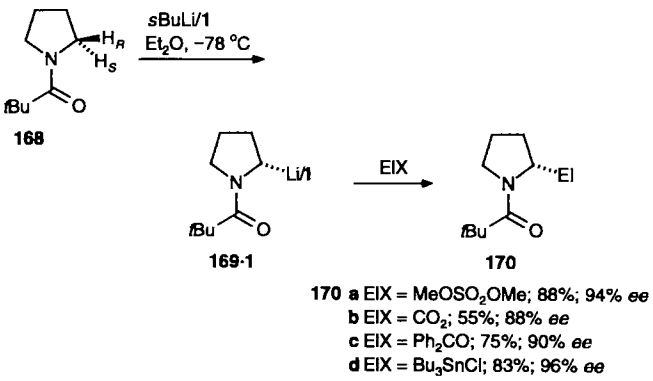

Scheme 67. (−)-Sparteine-controlled deprotonation of *N*-Boc-pyrrolidine [193].

(Scheme 68).[193b] As expected, reagent-induced chiral induction dominates, as has also been shown to be the case with the 2-phenylpyrrolidine derivative **173**.[85]

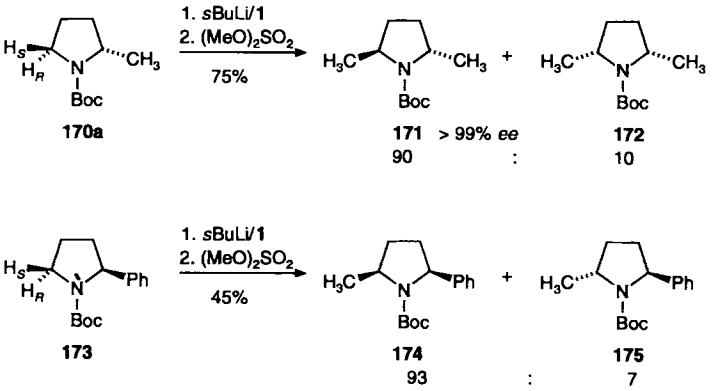

Scheme 68. Reagent-directed deprotonation of chiral 2-substituted *N*-Boc-pyrrolidines [85].

From a mechanistic standpoint there are many parallels to the deprotonation of *O*-alkyl carbamates (Sections 4.1–4.3);[196] kinetic and deuteration studies suggest rapid formation of a precomplex of the reaction partners.[142, 197] M. E. Kopach and A. I. Meyers were able to show with a conformationally biased pyrrolidine that both the deprotonation and substitution steps proceed with retention.[198] In a paper that is well worth reading, about two dozen ligands—mainly chiral diamines—were investigated to see to what extent they could replace (−)-sparteine (**1**), or even lead conveniently into the other series of enantiomers.[199] The most effective among them have been collected in Scheme 69.

Essential, sufficiently high configurational stability of the lithiated intermediates seems to be limited to pyrrolidines like **168**.[200] The greater configurational lability of the corresponding piperidines can be compensated for to some extent through a rapid, intramolecular subsequent reaction. Thus, Y. S. Park and P. Beak obtained the 1-azabicyclo[3.1.0]hexane **182** with 55% *ee* after deprotonation of *N*-Boc-4-tosylpiperidine (**179**) in the presence of (−)-sparteine by the addition of chlorotrimethylsilane; the configuration is still unknown (Scheme 70).[201] In this case, rapid 1,3-substitution of the enantiomerically enriched intermediate **180**·**1** preserves most of the chiral information.

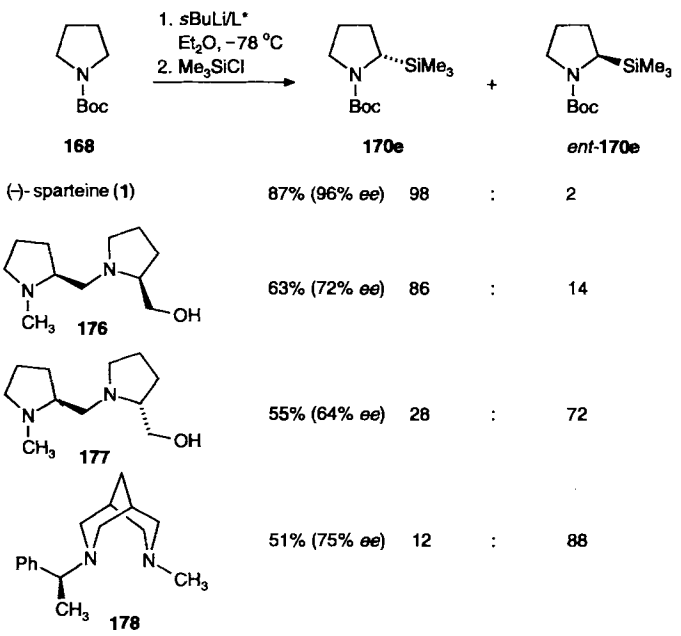

Scheme 69. Testing of various bidentate ligands in reagent-controlled deprotonation of *N*-Boc-pyrrolidine [199].

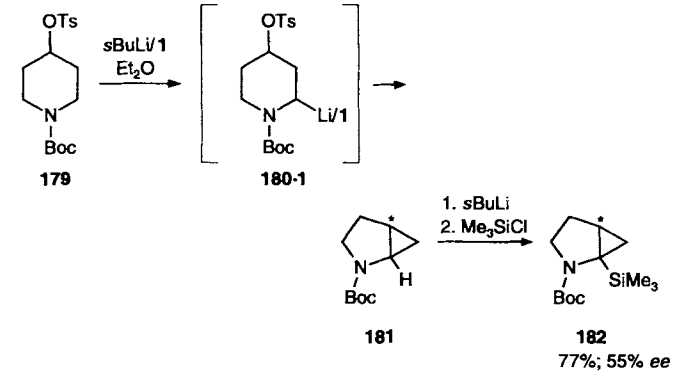

Scheme 70. Enantioselective deprotonation and intramolecular alkylation of an *N*-Boc-piperidine [201]. Ts = 4-$MeC_6H_4SO_2$.

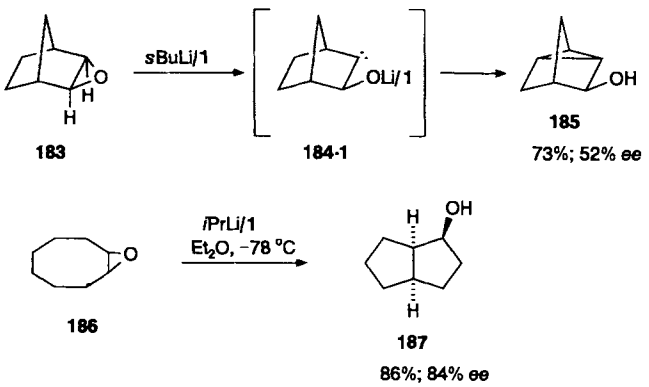

Scheme 71. (−)-Sparteine-induced rearrangement of *meso*-epoxides via **184·1**.

ing of the epoxide ring and insertion into the γ-*endo*-CH bond. *cis*-Epoxides of medium-sized cycloalkanes undergo similar reactions with transannular CH-insertion.[202a]

An interesting vinylogous nucleophilic ring opening of *meso*-oxabicyclic system **188** by *n*-butyllithium/(−)-sparteine was discovered by M. Lautens et al. (Scheme 72).[203] The best results [60% yield of (−)-**189** with 52% *ee*] were obtained with five equivalents of butyllithium and 15 mol% (−)-sparteine at −40 °C in pentane/hexane.

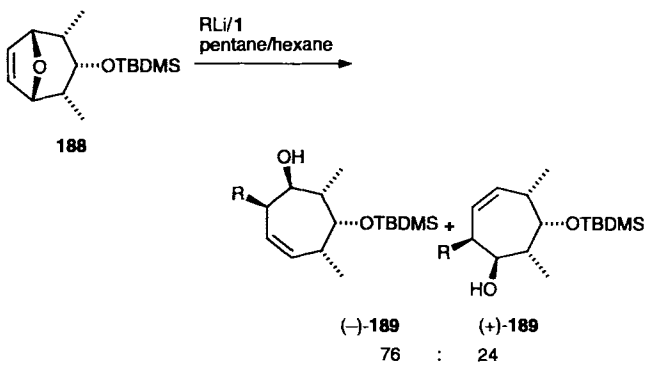

Scheme 72. Nucleophilic ring opening of *meso*-oxabicyclic compound **188**. R = Bu.

4.6. Enantiotopically Differentiating Lithiation at Other Prochiral Groups; Planar- and Axial-Chiral Intermediates

In the preceding sections, chirality was in most cases introduced through differentiation by the chiral base between enantiotopic protons of a methylene group. This means that configurational stability of the lithiated intermediate under the reaction conditions as well as a subsequent stereoselective substitution are necessary prerequisites. A few other cases in which no stereogenic carbanionic C atom is formed will now be discussed.

Hodgson et al. investigated a rearrangement of *meso*-epoxides induced by chiral bases.[202] Treatment of *exo*-norbornene epoxide (**183**) with *sec*-butyllithium/(−)-sparteine in pentane permitted the isolation of (−)-nortricyclanol[185] in 73% yield and 52% *ee* (Scheme 71).[202b] The base differentiates between the (*R*)- and (*S*)-sites on the oxirane unit during proton abstraction, and the carbenoid stabilizes immediately through open-

Both methyl groups in the dimethylphosphane derivatives **190**–**192** (Scheme 73) are enantiotopic, and the attached hydrogen atoms are acidified. During deprotonation to **191·1**–**193·1** the phosphorus atom becomes a stereogenic center. First experiments in deprotonation of dimethylphenylphosphine oxide (**190a**, R = C_6H_5) with *n*-butyllithium/(−)-sparteine were described in very brief form by Raston, White, et al.,[42] with an observed diastereomeric ratio in the range of 60:40.

Better results were obtained by D. A. Evans et al. with aryldimethylphosphine sulfides **190b** and the borane complex **190c**;[204] *ee* values of 74–94% were achieved in the capture products with benzophenone (**194b** and **194c**).

Oxidative coupling of the lithium derivative **193·1** with copper(II) pivalate to give the bis(phosphonium) complexes **195** and **196** is associated with an enhancement of the enantiomeric ratio to 98:2 (96% *ee*) (Scheme 73), because the greatest part of the epimer (P_R)-**193·1** (present to the extent of about 12%) is removed as the *meso*-diastereomer (*R*,*S*)-**196**. Deblocking of the

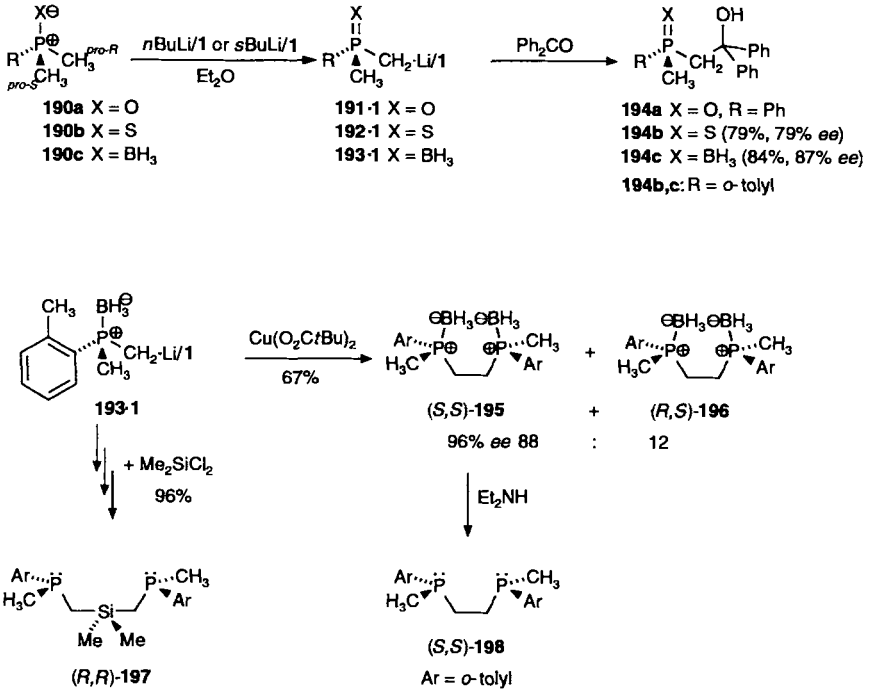

Scheme 73. Enantioselective, (−)-sparteine-induced deprotonation of aryldimethylphosphane derivatives [204].

borane complex (*S*,*S*)-**195** with diethylamine leads to the free diphosphane (*S*,*S*)-**198**. Just as in the case of the bis(phosphinyl)-substituted silane (*R*,*R*)-**197**, C_2-symmetric diphosphanes obtained in this way represent valuable potential ligands for enantioselective catalyst systems.

Based on the seminal work by I. Ugi and H. B. Kagan,[205] ferrocenes are extraordinarily versatile chiral auxiliaries and catalyst ligands. When one succeeds in using an enantiomerically pure base to distinguish between the enantiotopic sites of the achiral monosubstituted ferrocene **199** (Scheme 74), racemization of the enantiomerically enriched planar-chiral intermediates **200** and *ent*-**200** remains possible only through a proton transfer reaction or dissociation–recombination of the ferrocene; that is, configurational stability can be presupposed.[206]

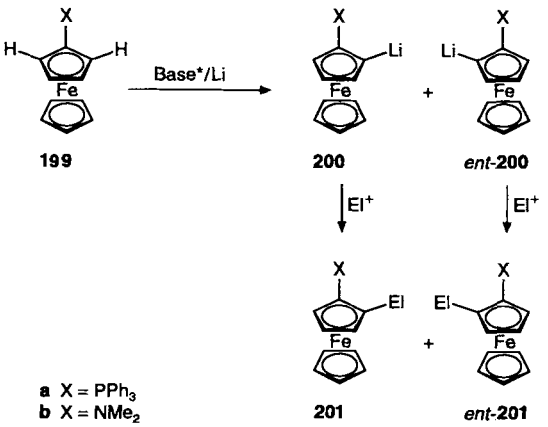

Scheme 74. (−)-Sparteine-induced *ortho*-lithiation of a ferrocene derivative [207].

Good enantiomeric enrichments have also been achieved through enantioselective deprotonation of other ferrocene derivatives: (diphenylphosphanyl)ferrocene (**201a**) with lithium (*R*,*R*)-bis(1-phenylethyl)amide, 55% *ee*,[208] and (dimethylaminomethyl)-ferrocene (**201b**) with (*R*,*R*)-*N*,*N*,*N*′,*N*′-tetramethyl-1,2-cyclohexanediamine/*n*-butyllithium,[209] 80% *ee* (Scheme 74).

A breakthrough was achieved by V. Snieckus et al.,[207] when they subjected *N*,*N*-diisopropylferrocene carboxamide (**202**) to deprotonation with *n*-butyllithium/(−)-sparteine in diethyl ether (Scheme 75). The expected products **203** were isolated with a host of electrophiles in 62–96% yield and 81–99% *ee*.

Related stereochemical problems are posed by monosubstituted arenetricarbonylchromium complexes; in this case chiral bases other than alkyllithium/(−)-sparteine prove to be most useful. Scheme 76 collects examples from the research groups of Kündig,[210] Uemura,[211] Simpkins,[212, 213] and Schmalz.[214]

Axial chirality can also be created through enantiotopically discriminating deprotonation. The first examples, with 2,2′-dimethyl-1,1′-binaphthyl and 2,2′,6,6′-tetramethyl-1,1′-biphenyl

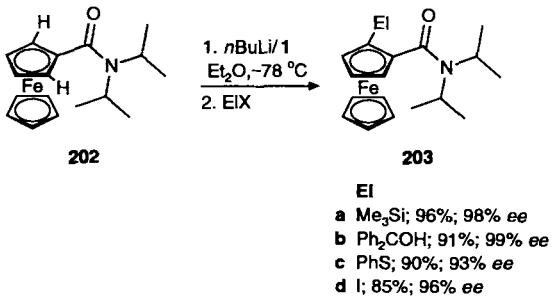

Scheme 75. Lithiation and substitution of monosubstituted ferrocenes with enantiotopic differentiation.

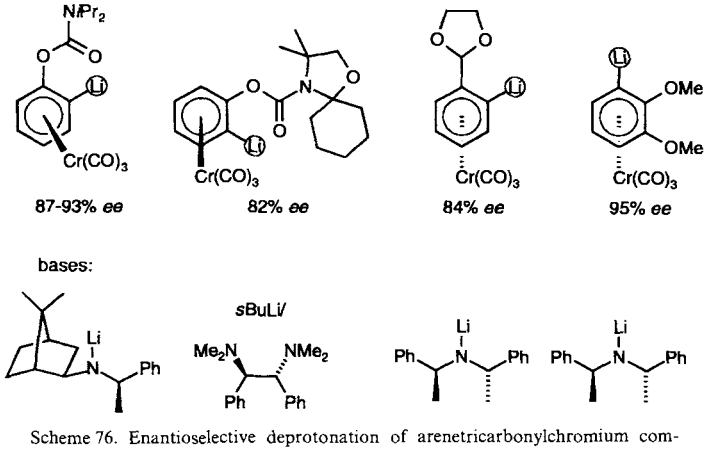

Scheme 76. Enantioselective deprotonation of arenetricarbonylchromium complexes [210–212, 214].

from Raston et al., are unfortunately not well documented with respect to quantitative results and configurational assignment.[215] P. Beak and D. P. Curran recently described a (−)-sparteine-induced deprotonation and methylation of the 1-naphthoic acid amide **204** with 50% *ee* (Scheme 77).[216] The yield at −78 °C amounted to only 53%, and from that one can conclude that the chiral base apparently accomplishes a kinetic racemate resolution between conformers that are interconverted only very slowly at −78 °C.[217]

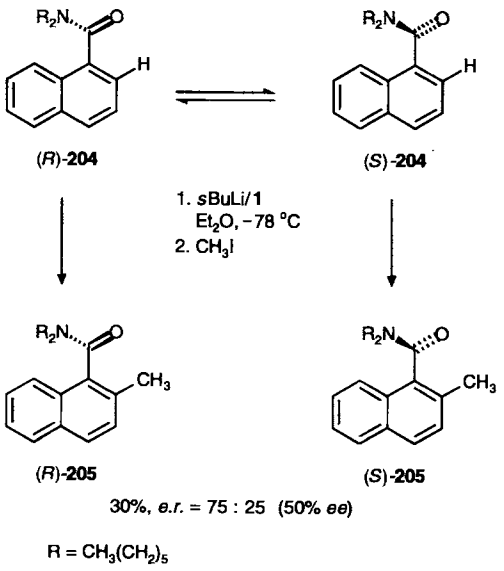

Scheme 77. Induction of axial chirality through (−)-sparteine-induced deprotonation [216].

5. Sparteine-Induced Carbolithiation

So far we have discussed only the most popular route to "carbanion generation", the deprotonation of CH-acidic precursors. The addition of organolithium to C=C double bonds (carbolithiation)[218] is an attractive alternative, because it yields an additional C−C bond "gratis" (Scheme 78). This reaction represents the first step in anionic polymerization;[218] its use in organic synthesis depends upon retarding (relative to the first step) addition of the intermediate **208** to another molecule of alkene **206**. This can be accomplished, for example, by conducting carbolithiation with a 5-alkenyllithium derivative in an intramolecular way according to W. F. Bailey,[219, 220] or in a case where the adduct **208** is specially stabilized.

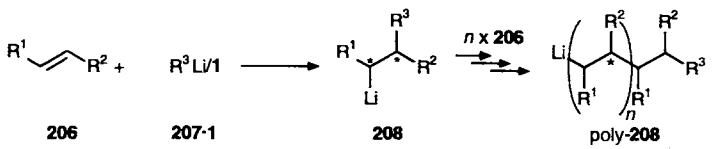

Scheme 78. Sparteine-induced asymmetric polymerization.

As a benefit, control is extended over two or even three (if the residue R^3 is chiral) stereogenic centers in the product. I. Marek, J.-F. Normant, and co-workers succeeded in carrying out an enantioselective (−)-sparteine-controlled addition of alkyllithium to cinnamyl alcoholates and cinnamylamines (Scheme 79).[221] Reaction of the (*E*)-alcoholate (*E*)-**209** with

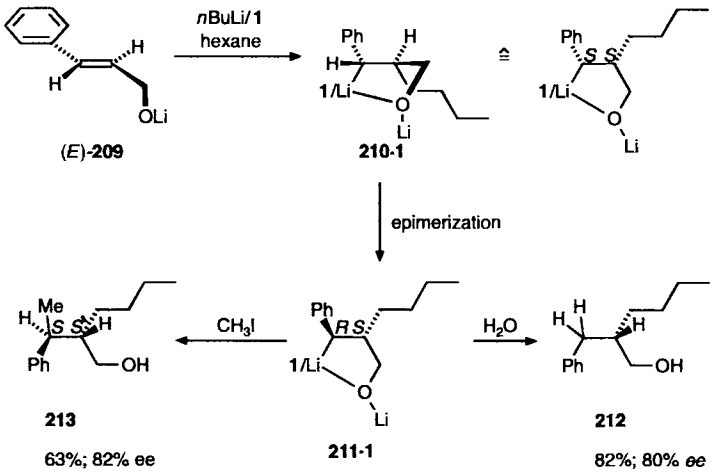

Scheme 79. Enantio- and diastereoselective carbolithiation of lithium (*E*)-3-phenyl-2-propen-1-olate [221].

butyllithium/(−)-sparteine provides good insight into the course of the reaction. In a *syn*-addition, typical for carbometalation,[222] butyllithium/(−)-sparteine [presumably bonded in a precomplex to the alcoholate (*E*)-**209**] attacks the C=C double bond from the *Si*-face. The resulting five-membered ring chelate complex **210·1** bears phenyl and butyl residues in *cis*-orientation, hence the configurationally labile benzyllithium derivative epimerizes with formation of the more stable *trans*-substituted chelate **211·1**. Protonation produces the (*S*)-configured alcohol **212** with 80% *ee*, whereas methylation with inversion[223] leads to the doubly branched (*S,S*)-alkanol **213**. Locking the intermediate into the chelate and the formation of reactive, presumably hexameric[224] lithium alcoholate clusters with diminished reactivity protects adducts **210·1** and **211·1** from polymerization. Quite remarkably, 5 mol% of (−)-sparteine is sufficient to produce enantioselective reaction.[225]

Enantiofacial differentiation on the part of the (−)-sparteine reagent at C-2 of the double bond in the conformationally restricted complex determines the stereochemical course of the reaction, since a configurationally stable stereocenter is created at C-2. Consequently, the (*Z*)-alcoholate (*Z*)-**209** leads to the opposite series of enantiomers.[221a] Similarly successful additions have been realized with (*E*)-cinnamylamines and -acetals.[221b]

Kündig et al. have recently reported on enantioselective carbolithiation of the arenetricarbonylchromium complex **214** from 4,4-dimethyl-2-phenyl-1,3-oxazolidine (Scheme 80).[226] Here the (−)-sparteine reagent attacks one of the enantiotopic sites preferentially from the "upper side," and treatment of the carbanionic intermediate[227] with propargyl bromide leads to a 5,6-*trans*-disubstituted cyclohexadiene **215**. Greater enantiomeric excesses (65–93% *ee*) with somewhat lower yields (51–67%) were achieved on using (*S,S*)-1,2-dimethoxy-1,2-diphenylethane (**216**) in place of (−)-sparteine.[226]

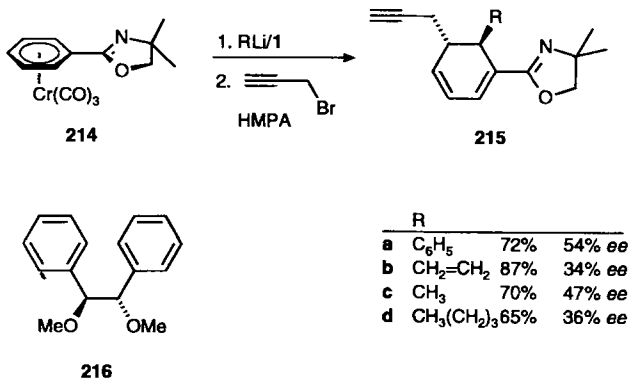

	R		
a	C_6H_5	72%	54% *ee*
b	$CH_2{=}CH_2$	87%	34% *ee*
c	CH_3	70%	47% *ee*
d	$CH_3(CH_2)_3$	65%	36% *ee*

Scheme 80. Diastereo- and enantioselective reaction of the tricarbonylchromium arene complex **214** [226]. HMPA = hexamethylphosphoramide.

Orientational investigations with α-styryl-*N*,*N*-diisopropyl carbamate (**217**) reveal a pathway to enantiomerically enriched secondary benzyl alcohols (Scheme 81).[228] Attack by alkyllithium/(−)-sparteine leads—albeit with reduced enantiofacial selectivity—to the configurationally stable adducts **218**·**1**, which are carboxylated with inversion[74b] and protonated with retention of configuration.[229]

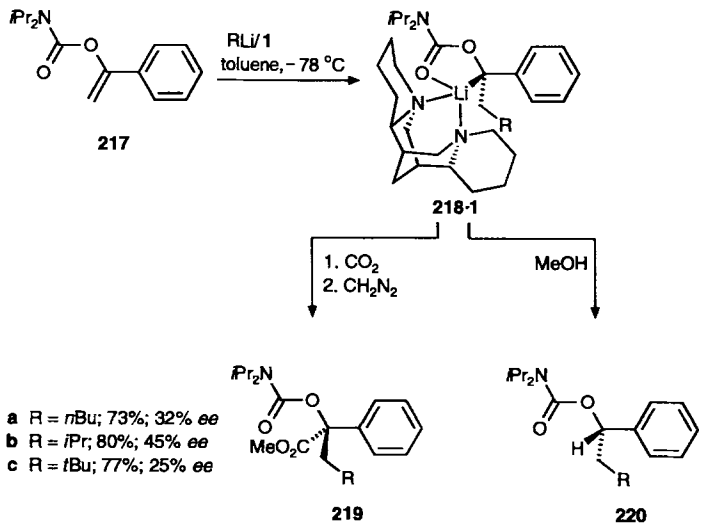

Scheme 81. Enantioselective carbolithiation of α-styryl carbamate **217** [228].

Intramolecular carbolithiations of (*E*)-alkenyllithium compounds proceed rapidly, as documented by numerous studies by Bailey et al., by 5-*exo*-*trig*-ring closure.[219, 230] However, this pathway has so far been used only to synthesize racemic or achiral cyclopentane derivatives. The gap has been closed by a highly stereoselective carbolithiation developed by us, which also assures control over the configuration of the attacking C-nucleophile; it produces in the case of the substituted cyclopentane **222**, for example, three consecutive, uniformly configured stereogenic centers (Scheme 82).[231]

6. Ion Pairs from α-Thiocarbanions

In contrast to α-alkoxyalkyllithium derivatives, α-thio-substituted alkyllithium[232] and benzyllithium compounds[232] **223**·**1**

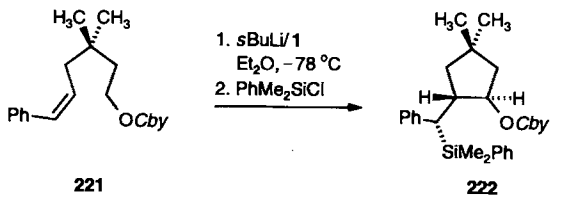

Scheme 82. Stereohomogeneous cyclopentyl carbamates through cyclocarbolithiation [231].

have turned out in all the relevant studies to be especially configurationally labile. Experimental results from Reich et al. point to the fact that the formation of solvent-separated ion pairs tends to increase the barrier to inversion rather than lower it.[232b] Nevertheless, we thought it might be possible that incorporation into a rigid chelate complex might lead to an increase in configurational stability. Alkyl[233] and vinyl *N*,*N*-dimethylmonothiocarbamates[234] are distinguished by high kinetic acidity. B. Kaiser thus investigated the (−)-sparteine-induced deprotonation of *S*-alkyl thiocarbamates of the type **224**;[235, 236] the reactions with *S*-butyl esters (Scheme 83) will be discussed as

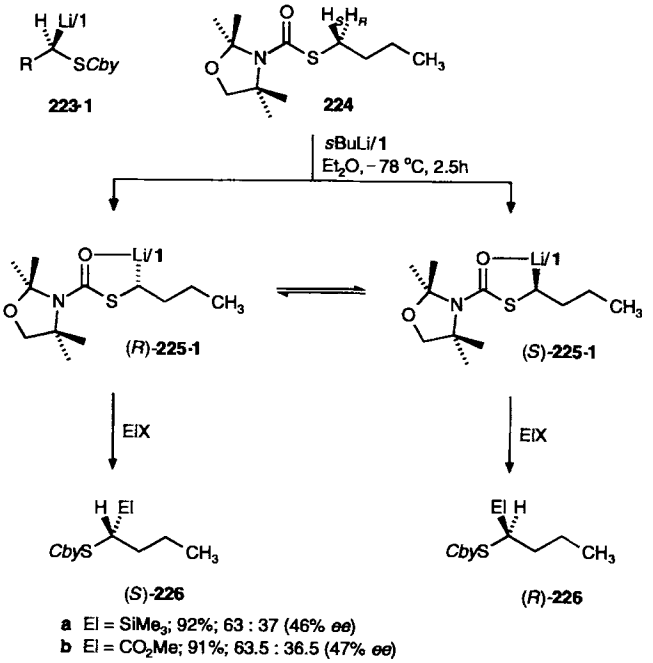

Scheme 83. (−)-Sparteine-mediated deprotonation of *S*-alkyl thiocarbamates [235].

an example of the results of this study. Deprotonation of **224a** with *sec*-butyllithium/(−)-sparteine in diethyl ether and trapping of the carbanionic intermediate with chlorotrimethylsilane led to the silane (+)-(*S*)-**226a** with 46% *ee*. A nearly identical result was recorded in carboxylation and esterification to (−)-(*S*)-**226b**.[236]

Is the cause here insufficient configurational stability of the diastereomeric intermediates (*R*)-**225**·**1** and (*S*)-**225**·**1**, which enter into equilibrium under the reaction conditions, or inadequate enantiotopic differentiation in the deprotonation step? As demonstrated by the following series of experiments with the

deuterated substrate *rac*-[*D*]**224**, in this case both factors are responsible (Scheme 84).[235] During deprotonation with *sec*-butyllithium/TMEDA (a) and capture of the intermediate ion

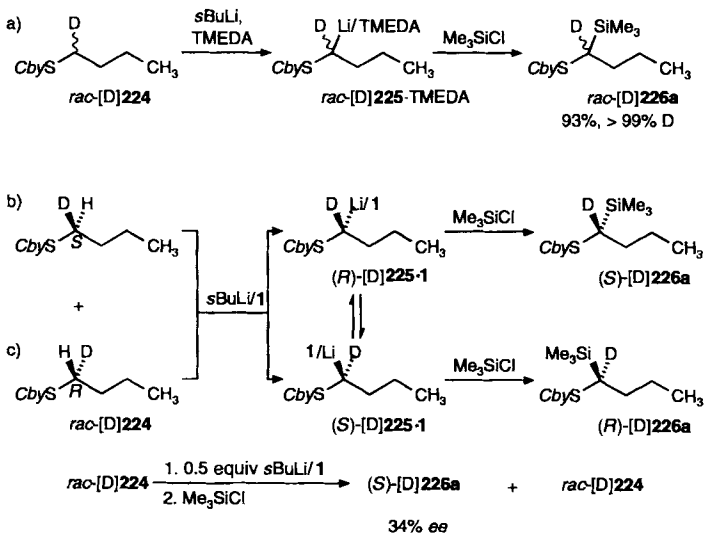

Scheme 84. Reactions with deuterium-labeled thiocarbamates.

pair *rac*-[*D*]**225** to give the silane *rac*-[*D*]**226a**, all the deuterium remains in the molecule; that is, the kinetic H/D isotope effect is on the order of about 100. In the next experiment (b), *rac*-[*D*]**224** was treated with one equivalent of the chiral base system *sec*-butyllithium/(−)-sparteine, and silylation was initiated; the result was a greater than 99% deuterated product (*S*)-[*D*]**226a** in 93% yield and 34% *ee*.[237] If there were a great preference for one of the enantiotopic protons *pro-S*-H or *pro-R*-H, one of the enantiomers would have been preferentially deprotonated, thus introducing a kinetic resolution like that observed with the corresponding *O*-alkyl carbamates (Section 4.2). However, the substrate was nearly completely deprotonated; nevertheless, an overproportional amount of enantiomerically enriched product was isolated. From this it can be concluded that the diastereomeric ion pairs (1*R*)- and (1*S*)-[*D*]**225**·**1** equilibrate under the reaction conditions. Experiment (c) solidifies this conclusion; it differs from experiment (b) only in a reduced amount of base (0.5 equivalents). Again the product was (*S*)-[*D*]**224a** with 34% *ee*, and the recovered unchanged substrate [*D*]**224** took the form of a racemate. There was thus no kinetic resolution, and the product ratio was determined thermodynamically at the stage of the ion pairs.

Also for the (−)-sparteine complex of the dilithium compound derived from *N*-methyl-3-phenylthiopropionamide, which represents a valuable homoenolate reagent, Takei et al. found evidence of configurational lability in THF at −78 °C, as well as similarly low enantiomeric enrichment in the aldehyde adducts.[238]

For an efficient utilization of chiral α-thiocarbanions, conditions and ligands must be found that lead to the largest possible energy difference between the diastereomeric lithium complexes. Corresponding investigations with (similarly configurationally labile) lithium-1-(phenylselenyl)alkanides carried out by R. W. Hoffmann et al. show through an NMR study that this is not a simple venture.[239]

Why do *S*- and *O*-lithioalkyl derivatives behave so differently? Presumably the relatively long C(= O)−S and C−S bonds (about 180 pm compared to 140 pm for C−O) establish a less compact transition state for deprotonation, coupled with diminished enantiotopic differentiation. Moreover, the mechanisms of enantiomer interconversion differ. Evidence is increasing that rotation of the attached C−S bond from the antiperiplanar to the synperiplanar conformation is the rate-determining step in the enantiomer interconversion, whereas for α-hydroxyalkyllithium derivatives inversion at the carbanionic center appears to be the slowest step (Scheme 85).[240]

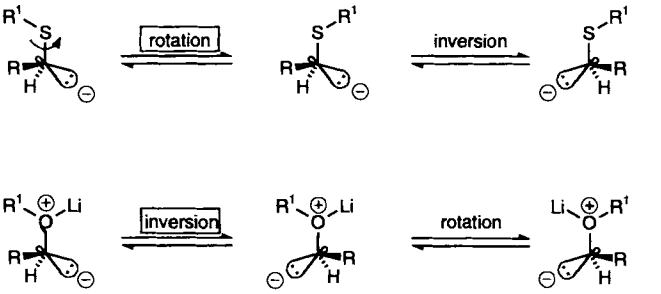

Scheme 85. The rate-determining step in enantiomer interconversion of α-heterosubstituted alkyllithium compounds.

It can be concluded from the work of R. W. Hoffmann et al. on racemic 1-(arylselenyl)alkyllithium derivatives that bulky arylthio residues increase the barrier to enantiomer interconversion.[241] An increased crowding of groups at the carbanionic center should for the same reason lead to increased configurational stability. Indeed, the lithium compound (*S*)-**225a**·TMEDA prepared from (*S*)-**224a** (46% *ee*) with *sec*-butyllithium in diethyl ether proved to be configurationally stable at −78 °C, because after standing for 2.5 h, deuterolysis produces the capture product (*S*)-[*D*]**226a** with 44% *ee* (Scheme 86).[235]

This is, to the best of our knowledge, the first enantiomerically enriched α-thioalkyllithium derivative. The world record with respect to configurational stability is held by benzyllithium derivative (*S*)-**227** (99% *ee*).[242, 243] No racemization could be demonstrated after standing for 24 h at −78 °C, and even 10 min of warming the reaction mixture to 0 °C caused less than 1% racemization.

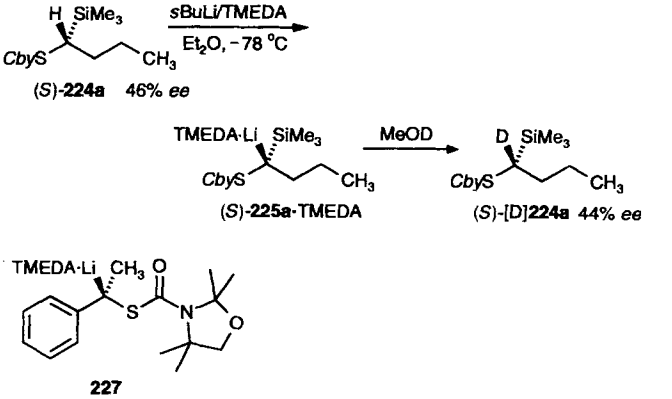

Scheme 86. Configurationally stable α-thioalkyllithium derivatives [235, 241, 242].

7. Summary and Prospects

The interaction between a lithium ion bearing chiral ligands and a developing or previously formed carbanion forces the latter into a specific configuration, whether through a preferred diastereomorphic transition state in the course of deprotonation or because of the establishment of a state of equilibrium. In combination with a stereoselective substitution step, this provides a new and effective strategy for enantioselective synthesis. The synthetic value of the process is increased by the fact that the carbanionic reagents are obtained by simple deprotonation of the corresponding CH acids. The examples discussed above were discovered through intuition, whereby spontaneous crystallization of one of the diastereomers occasionally played a crucial role in increasing efficiency. One goal is to understand the interaction between chiral ligand, cation, and substrate or carbanion better, as well as to quantify it through quantum-mechanical calculations in order ultimately to succeed in predicting favorable ligand–carbanion combinations. We are closer to this goal with respect to estimating the relative energies of diastereomeric ion pairs than for diastereomorphic transition states.

The results described from our own research group have been achieved over the past eight years by capable and enthusiastic co-workers. Their names are included in the bibliography. Special thanks are due to Prof. Dr. E.-U. Würthwein, who convinced me (D. H.) of the value of quantum-mechanical computational methods for the solution of our problems, introduced several co-workers to the application of these methods, and stood at our side with unselfish advice and assistance. A. Deiters and Dipl.-Chem. T. Heinl gave valuable support with the presentation of the manuscript and the graphics. The work was supported for many years by the Deutsche Forschungsgemeinschaft, the Fonds der Chemischen Industrie, the Stiftung Volkswagenwerk, and Bayer AG.

Received: March 5, 1997 [A 215 IE]
German version: *Angew. Chem.* **1997**, *109*, 2376–2410
Translated by Dr. W. E. Russey, Huntingdon, PA (USA)

[1] a) D. Seebach, *Angew. Chem.* **1979**, *91*, 259; *Angew. Chem. Int. Ed. Engl.* **1979**, *18*, 239; b) D. Seebach, *Synthesis* **1969**, 17; c) D. Seebach, *Angew. Chem.* **1969**, *81*, 690; *Angew. Chem. Int. Ed. Engl.* **1969**, *8*, 639; d) D. Seebach, D. Enders, *ibid.* **1975**, *87*, 1; and **1975**, *14*, 15; e) D. Seebach, K.-H. Geiss, *J. Organomet. Chem. Libr.* **1976**, *101*, 1; f) D. Seebach, A. R. Sting, M. Hoffmann, *Angew. Chem.* **1996**, *108*, 2881; *Angew. Chem. Int. Ed. Engl.* **1996**, *35*, 2795.

[2] a) D. Seebach, *Angew. Chem.* **1990**, *102*, 1363; *Angew. Chem. Int. Ed. Engl.* **1990**, *29*, 1320; b) D. Seebach, *ibid.* **1988**, *100*, 1685; and **1988**, *27*, 1624.

[3] Reviews of the structure of organolithium compounds: a) P. von R. Schleyer, *Pure Appl. Chem.* **1984**, *56*, 151; b) G. Boche, F. Haller, K. Harms, D. Hoppe, W. Koch, J. Lorenz, M. Marsch, A. Opel, C. Tümmler, O. Zschage, "Crystal Structure and Reactivity (Selectivity) of Oxygen (Aryloxy; Carbamoyloxy; Silyloxy)-Substituted Lithium Compounds" in *New Aspects of Organic Chemistry II*, Kodansha, Tokyo, **1992**, pp. 159–179; c) E. Weiss, *Angew. Chem.* **1993**, *105*, 1565; *Angew. Chem. Int. Ed. Engl.* **1993**, *32*, 1501; d) C. Lambert, P. von R. Schleyer, *ibid.* **1994**, *106*, 1187 and **1994**, *33*, 1129; e) C. Lambert, P. von R. Schleyer, "Carbanionen - Polare Organometall-Verbindungen," in *Methoden Org. Chem.* 1952– *(Houben–Weyl), Carbanionen*, 4th ed., Vol. E19d, **1993**, pp. 1–106.

[4] Regarding the advantages of C_2-symmetric ligands, see the following reviews: a) J. K. Whitesell, *Chem. Rev.* **1989**, *89*, 1581; b) H. Waldmann, *Nachr. Chem. Tech. Lab.* **1991**, *39*, 1142.

[5] In the preceding example, a nonsymmetric C_2 ligand would have had the consequence that an additional stereogenic center would have been established at the lithium cation, and it would have been necessary for us to consider twice as many diastereomers.

[6] The term "two-dimensional stereogen" has been considered better defined: a) D. Seebach, V. Prelog, *Angew. Chem.* **1982**, *94*, 696; *Angew. Chem. Int. Ed. Engl.* **1982**, *21*, *654*. Although not as well defined, we continue to use the simpler designation "prochiral": b) E. L. Eliel, S. H. Wilen, *Stereochemistry of Organic Compounds*, 1st ed., Wiley, New York, **1994**.

[7] On applying the term "cation" rather generously and even including covalently bonded metal substituents (e.g., magnesium, boron, zinc, and titanium), this simple concept has been shown to be exceptionally successful. Magnesium: a) R. Noyori, M. Kitamura, *Angew. Chem.* **1991**, *103*, 34; *Angew. Chem. Int. Ed. Engl.* **1991**, *31*, 49; b) B. Weber, D. Seebach, *Tetrahedron* **1994**, *50*, 6117; Boron: c) H. C. Brown, P. V. Ramachandran, *J. Organomet. Chem.* **1995**, *500*, 1; d) D. S. Matteson, *Chem. Rev.* **1989**, *89*, 1535; e) W. R. Roush, "Formation of C–C Bonds by Addition of Allyl-Type Organometallic Compounds to Carbonyl Compounds. Allylboron Reagents," in *Methoden Org. Chem* 1952– *(Houben–Weyl), Stereoselective Synthesis*, 4th ed., 1952–, E21b, **1995**, pp. 1410–1486; f) R. W. Hoffmann, *Angew. Chem.* **1987**, *99*, 503; *Angew. Chem. Int. Ed. Engl.* **1987**, *26*, 489; g) R. W. Hoffmann, R. Stürmer, "Synthesis of Natural Products of Polyketide Origin, An Exemplary Case," in *Stereoselective Synthesis* (Eds.: E. Ottow, K. Schöllkopf, B. G. Schulz), Springer, Berlin, **1994**, pp. 91–108; Zinc: h) P. Knochel, *Synlett* **1995**, 393; Titanium: i) R. O. Duthaler, A. Hafner, *Chem. Rev.* **1992**, *92*, 807; k) D. Seebach, A. K. Beck, R. Imwinkelried, S. Roggo, A. Wonnacott, *Helv. Chim. Acta* **1987**, *70*, 954; l) D. Seebach, L. Behrendt, D. Felix, *Angew. Chem.* **1991**, *103*, 991; *Angew. Chem. Int. Ed. Engl.* **1991**, *30*, 1006; m) D. Seebach, D. A. Plattner, A. K. Beck, Y. M. Wang, D. Hunziker, W. Petter, *Helv. Chim. Acta* **1995**, *75*, 2171; n) A. L. Costa, M. G. Piazza, E. Tagliavini, C. Trombini, A. Umani-Ronchi, *J. Am. Chem. Soc.* **1993**, *115*, 7001; o) D. Seebach, A. K. Beck, B. Schmidt, Y. M. Wang, *Tetrahedron* **1994**, *50*, 4363.

[8] H. L. Cohen, G. F. Wright, *J. Org. Chem.* **1953**, *18*, 432.

[9] D. Seebach, G. Grass, E.-M. Wilka, D. Hilvert, E. Brunner, *Helv. Chim. Acta* **1979**, *62*, 2695.

[10] H. Nozaki, T. Aratani, T. Toraya, *Tetrahedron Lett.* **1968**, 4097.

[11] D. Seebach, H. Dörr, B. Bastani, V. Ehrig, *Angew. Chem.* **1969**, *81*, 1002; *Angew. Chem. Int. Ed. Engl.* **1969**, *8*, 982.

[12] T. Mukaiyama, K. Soai, T. Sato, H. Shimuzu, K. Suzuki, *J. Am. Chem. Soc.* **1979**, *101*, 1455.

[13] R. Noyori, S. Suga, K. Kawai, S. Okada, M. Kitamura, *Pure Appl. Chem.* **1988**, *60*, 1597.

[14] J.-P. Mazaleyrat, D. J. Cram, *J. Am. Chem. Soc.* **1981**, *103*, 4585.

[15] For this reason, the first successful examples involving this strategy of enantiotopically differentiated deprotonation relate to the formation of chiral enolates from 4-substituted cyclohexanones; here the stereogenic (C-4) and the carbanionic (C-2) centers are separated from each other; reviews: a) K. Koga, *Pure Appl. Chem.* **1994**, *66*, 1487; b) K. Koga, M. Shindo, *J. Synth. Org. Chem. Jpn.* **1995**, *53*, 1021; c) N. S. Simpkins, *Pure Appl. Chem.* **1996**, *68*, 691; d) P. J. Cox, N. S. Simpkins, *Tetrahedron: Asymmetry* **1991**, *2*, 1.

[16] a) R. Kuhn, *Ber. Dtsch. Chem. Ges.* **1932**, *65*, 49; b) M. M. Harris, *Progr. Stereochem.* **1958**, *2*, 157; overviews of dynamic racemate resolution: c) S. Caddick, K. Jenkins, *Chem. Soc. Rev.* **1996**, 447; d) M. Reggelin, *Nachr. Chem. Tech. Lab.* **1997**, *45*, 789.

[17] A somewhat more penetrating discussion is provided in P. Beak, A. Basu, D. J. Gallagher, Y. S. Park, S. Thayumanavan, *Acc. Chem. Res.* **1996**, *29*, 552.

[18] D. J. Cram, J. L. Mateos, F. Hauck, A. Langemann, K. R. Kopecky, W. D. Nielsen, J. Allinger, *J. Am. Chem. Soc.* **1959**, *81*, 5774; b) D. J. Cram, C. A. Kingsbury, B. Rickborn, *ibid.* **1961**, *83*, 3688.

[19] a) J. Stenhouse, *Ann. Chem. Pharm.* **1851**, *78*, 1; b) E. J. Mills, *ibid.* **1863**, *125*, 71; c) W. Boczon, *Heterocycles* **1992**, *33*, 1101.

[20] "(−)-Sparteine": D. Hoppe in *Encyclopedia of Reagents for Organic Synthesis, Vol. 7* (Ed.: L. A. Paquette), 1st ed., Wiley, Chichester, **1995**, p. 4662.

[21] a) F. Bohlmann, D. Schumann, C. Arndt, *Tetrahedron Lett.* **1965**, 2705; b) M. Wiewiorowowski, O. E. Edwards, M. D. Bratek-Wiewiorowska, *Can. J. Chem.* **1967**, *45*, 1447–1457.

[22] (−)-Sparteine is commercially available as the free amine (SIGMA, about 450 US dollars per mol^{-1}) or as a sulfate pentahydrate (about 280 US dollars per mol^{-1}).

[23] M. Carmack, B. Douglas, E. W. Martin, H. Suss, *J. Am. Chem. Soc.* **1955**, *87*, 4435.

[24] a) F. Bohlmann, *Chem. Ber.* **1959**, *92*, 1798; b) Y. Okamoto, K. Suzuki, T. Kitayama, H. Yuki, H. Kageyama, K. Miki, N. Tanaka, N. Kasai, *J. Am. Chem. Soc.* **1982**, *104*, 4618; c) F. Galinovsky, P. Knoth, W. Fischer, *Monatsh. Chem.* **1955**, *86*, 1014.

[25] A. Orechoff, M. Rabinowitch, R. Kolowanowa, *Ber. Dtsch. Chem. Ges.* **1933**, 66, 621.

[26] a) T. Ebner, M. Eichelbaum, P. Fischer, C. O. Meese, *Arch. Pharm.* **1989**, *322*, 399; b) G. R. Clemo, R. Raper, W. S. Short, *J. Chem. Soc.* **1949**, 663.

[27] a) H. Nozaki, T. Aratani, T. Toraya, R. Noyori, *Tetrahedron* **1971**, *27*, 905; b) H. Nozaki, T. Aratani, R. Noyori, *Tetrahedron Lett.* **1968**, *26*, 2087; c) T. Aratani, T. Gonda, H. Nozaki, *ibid.* **1969**, *27*, 2265; d) T. Aratani, T. Gonda, H. Nozaki, *Tetrahedron* **1970**, *26*, 5453.

[28] In a recent paper by Denmark et al. it was shown, however, that **1** is a very efficient catalyst for the nucleophilic alkylation of imines: S. E. Denmark, N. Nakajima, O. J.-C. Nicaise, *J. Am. Chem. Soc.* **1994**, *116*, 8797.

[29] a) P. Knochel, *Chemtracts: Org. Chem.* **1995**, *8*, 205; b) K. Soai, S. Niwa, *Chem. Rev.* **1992**, *92*, 833.
[30] R. A. Kretchmer, *J. Org. Chem.* **1972**, *37*, 2744.
[31] B. M. Trost, T. J. Dietsche, *J. Am. Chem. Soc.* **1973**, *95*, 8200.
[32] M. T. Reetz, J. Westermann, *Syn. Commun.* **1981**, *11*, 647.
[33] N. Kunieda, M. Kinoshita, *Phosphorous Sulfur Relat. Elem.* **1981**, *10*, 383.
[34] a) M. Guetté, J.-P. Guetté, J. Capillon, *Tetrahedron Lett.* **1971**, 2863; b) M. Guetté, J. Capillon, J.-P. Guetté, *Tetrahedron* **1973**, *29*, 3659.
[35] M. M. Hansen, P. A. Bartlett, C. H. Heathcock, *Organometallics* **1987**, *6*, 2069.
[36] K. Soai, A. Oshio, T. Saito, *J. Chem. Soc. Chem. Commun.* **1993**, 811.
[37] a) Y. Okamoto, K. Ohta, H. Yuki, *Chem. Lett.* **1977**, 617; b) G. Wulff, R. Sczepan, A. Steigel, *Tetrahedron Lett.* **1986**, *27*, 1991; c) Review: Y. Okamoto, T. Nakano, *Chem. Rev.* **1994**, *94*, 349.
[38] a) G. Fraenkel, C. Cottrell, J. Ray, J. Russell, *Chem. Commun.* **1971**, 273; b) G. Fraenkel, B. Appleman, J. G. Ray, *J. Am. Chem. Soc.* **1974**, *96*, 5113.
[39] a) EtMgBr·**1** and EtMgBr·**2**: [24b]; b) EtMgBr·**1**: H. Kageyama, K. Miki, N. Tanaka, N. Kasai, Y. Okamoto, H. Yuki, *Bull. Soc. Chem. Jpn.* **1983**, *56*, 1319; c) EtMgBr·**2**: H. Kageyama, K. Miki, Y. Kai, N. Kasai, Y. Okamoto, H. Yuki, *Acta Crystallogr. B* **1982**, *38*, 2264; d) *t*BuMgCl·**1** and $MgCl_2$·**1**: H. Kageyama, K. Miki, Y. Kai, N. Kasai, Y. Okamoto, H. Yuki, *Bull. Chem. Soc. Jpn.* **1983**, *56*, 2411.
[40] [(η_3-Cyclopentenyl)Pd/**1**]$^+PF_6^-$: A. Togni, G. Rihs, P. S. Pregosin, C. Ammann, *Helv. Chim. Acta* **1990**, *73*, 723.
[41] a) $CoCl_2$·**1**: R. Kuroda, S. F. Mason, *J. Chem. Soc. Dalton Trans.* **1977**, 371; b) $CoCl_2$·**2**: R. Kuroda, S. F. Mason, *ibid.* **1979**, 727; c) $CuCl_2$·**3**: L. S. Childers, K. Folting, L. L. Merritt Jr, W. E. Streib, *Acta Crystallogr. B* **1975**, *31*, 924.
[42] L. T. Byrne, L. M. Engelhardt, G. E. Jacobsen, W.-P. Leung, R. I. Papasergio, C. L. Raston, B. W. Skelton, P. Twiss, A. H. White, *J. Chem. Soc. Dalton Trans.* **1989**, 105.
[43] R. I. Papasergio, B. W. Skelton, P. Twiss, A. H. White, C. L. Raston, *J. Chem. Soc. Dalton Trans.* **1990**, 1161.
[44] B. Ledig, M. Marsch, K. Harms, G. Boche, *Angew. Chem.* **1992**, *104*, 80; *Angew. Chem. Int. Ed. Engl.* **1992**, *31*, 79.
[45] D. Hoppe, T. Krämer, *Angew. Chem.* **1986**, *98*, 171; *Angew. Chem. Int. Ed. Engl.* **1986**, *25*, 160.
[46] Reviews: a) D. Hoppe, *Angew. Chem.* **1984**, *96*, 930; *Angew. Chem. Int. Ed. Engl.* **1984**, *23*, 932; b) D. Hoppe, T. Krämer, J.-R. Schwark, O. Zschage, *Pure Appl. Chem.* **1990**, *62*, 1999; c) D. Hoppe, O. Zschage, "Chiral Metalated Carbamates: Tools for New Strategies in Asymmetric Synthesis" in *Organic Synthesis via Organometallics* (Ed.: K. H. Dötz, R. W. Hoffmann), 1st ed., Vieweg, Braunschweig **1990**, pp. 267; d) H. Kunz, H. Waldmann, *Chemtracts: Org. Chem.* **1990**, *3*, 421; e) "Formation of C–C Bonds by Addition of Allyl-Type Organometallic Compounds to Carbonyl Compounds": D. Hoppe, *Methoden Org. Chem. (Houben-Weyl), 4th ed., 1952–*, E21b, **1995**, p. 1551; f) "Generation and Reactions of Chiral, Mesomerically Stabilized Lithium Carbanions": D. Hoppe in *New Horizons in Organic Synthesis* (Eds.: V. Nair, S. Kumar), New Age, New Delhi, **1996**, p. 130.
[47] O. Zschage, Diplomarbeit, Universität Göttingen, **1989**.
[48] Correction of the configuration for **13**·**1**: O. Zschage, D. Hoppe, *Tetrahedron* **1992**, *48*, 5657.
[49] a) P. Le Ménez, V. Fargeas, J. Poisson, J. Ardisson, J.-Y. Lallemand, A. Pancrazi, *Tetrahedron Lett.* **1994**, *35*, 7767; b) P. Le Ménez, N. Firmo, V. Vargeas, J. Ardisson, A. Pancrazi, *Synlett* **1994**, 995.
[50] H. Paulsen, D. Hoppe, *Tetrahedron* **1992**, *48*, 5667.
[51] B. Peschke, J. Lüßmann, M. Dyrbusch, D. Hoppe, *Chem. Ber.* **1992**, *117*, 1421.
[52] D. Hoppe, O. Zschage, *Angew. Chem.* **1989**, *101*, 67; *Angew. Chem. Int. Ed. Engl.* **1989**, *28*, 67.
[53] Reviews of lithium–titanium exchange: a) "Titanium in Organic Synthesis": M. T. Reetz in *Organometallics in Synthesis* (Ed.: M. Schlosser), Wiley, Chichester, **1994**, p. 1994; b) ref[7i]; c) M. T. Reetz, *Organotitanium Reagents in Organic Synthesis*, Springer, Berlin, **1986**; d) "Titanium and Zirconium Derivatives in Organic Synthesis": D. Seebach, B. Weidmann, L. Widler in *Modern Synthetic Methods 1983* (Ed.: R. Scheffold), Salle und Sauerländer, Frankfurt und Aarau, **1983**, p. 217; e) B. Weidmann, D. Seebach, *Angew. Chem.* **1983**, *95*, 12; *Angew. Chem. Int. Ed. Engl.* **1983**, *22*, 32.
[54] The configurational stability of the titanium intermediate, together with complete 1,3-chirality transfer, must be concluded from the distinctively different diastereomeric ratios achieved on addition of enantiomerically pure and racemic aldehydes [57].
[55] H. Paulsen, C. Graeve, D. Hoppe, *Synthesis* **1996**, 141.
[56] Review: S. Masamune, W. Choy, J. S. Petersen, L. R. Sita, *Angew. Chem.* **1985**, *97*, 1; *Angew. Chem. Int. Ed. Engl.* **1985**, *24*, 1.
[57] R. W. Hoffmann, J. Lanz, R. Metternich, G. Tarara, D. Hoppe, *Angew. Chem.* **1987**, *99*, 1196; *Angew. Chem. Int. Ed. Engl.* **1987**, *26*, 1145.
[58] D. Hoppe, G. Tarara, M. Wilckens, *Synthesis* **1989**, 83.
[59] O. Zschage, J.-R. Schwark, D. Hoppe, *Angew. Chem.* **1990**, *102*, 336; *Angew. Chem. Int. Ed. Engl.* **1990** *29*, 296.
[60] O. Zschage, D. Hoppe, *Tetrahedron* **1992**, *48*, 8389.
[61] Reviewen: a) J. A. Marshall, *Chemtracts: Org. Chem.* **1992**, *5*, 75; b) *Chem. Rev.* **1996**, *96*, 31.
[62] H. Paulsen, C. Graeve, R. Fröhlich, D. Hoppe, *Synthesis* **1996**, 145.
[63] M. Marsch, K. Harms, O. Zschage, D. Hoppe, G. Boche, *Angew. Chem.* **1991**, *103*, 338; *Angew. Chem. Int. Ed. Engl.* **1991**, *30*, 321.
[64] D. Hoppe, R. Hanko, A. Brönneke, F. Lichtenberg, E. van Hülsen, *Chem. Ber.* **1985**, *118*, 2822.
[65] a) D. Hoppe, T. Krämer, J.-R. Schwark, O. Zschage, *Pure Appl. Chem.* **1990**, *62*, 1999; b) T. Krämer, D. Hoppe, *Tetrahedron Lett.* **1987**, *28*, 5149; c) T. Krämer, J.-R. Schwark, D. Hoppe, *ibid.* **1989**, *30*, 7037; d) O. Zschage, J.-R. Schwark, T. Krämer, D. Hoppe, *Tetrahedron* **1992**, *48*, 8377; e) H. Helmke, Dissertation, Universität Münster, **1995**.
[66] J.-R. Schwark, Dissertation, Universität Kiel, **1991**.
[67] For reasons of space, a presentation in context must be deferred to a planned separate review article. A few representative examples are provided in refs. [68, 69, 70] as well as [46].
[68] Metalate rearrangements and related reactions: a) P. Kocienski, N. J. Dixon, *Synlett* **1989**, 52; b) A. Pimm, P. Kocienski, S. D. A. Street, *ibid.* **1992**, 886; c) P. Kocienski, C. Barber, *Pure Appl. Chem.* **1990**, *62*, 1933; d) [49a]; e) D. Madec, S. Pujol, V. Henryon, J. P. Férézou, *Synlett* **1995**, 435.
[69] Epoxidation and furanoside synthesis: a) D. Hoppe, J. Lüßmann, P. G. Jones, D. Schmidt, G. M. Sheldrick, *Tetrahedron Lett.* **1986**, *27*, 3591; b) J. Lüßmann, D. Hoppe, P. G. Jones, C. Fittschen, G. M. Sheldrick, *ibid.* **1986**, *31*, 3595; c) ;[58] d) G. Tarara, D. Hoppe, *Synthesis* **1989**, 89; e) [50]; 3-acyltetrahydrofurans: f) D. Hoppe, T. Krämer, C. Freire Erdbrügger, E. Egert, *Tetrahedron Lett.* **1989**, *30*, 1233; synthesis of dipeptide isosteres: g) R. Hanko, K. Rabe, R. Dally, D. Hoppe, *Angew. Chem.* **1991**, *103*, 1725; *Angew. Chem. Int. Ed. Engl.* **1991**, *30*, 1690; h) F. Rehders, D. Hoppe, *Synthesis* **1992**, 859; i) F. Rehders, D. Hoppe, *ibid.* **1992**, 865.
[70] Applications in the synthesis of complex natural products: Dehydroavermectin $B1_b$: a) J. P. Férézou, M. Julia, R. Khourzom, Y. Li, A. Pancrazi, P. Robert, *Synlett* **1991**, 611; Desepoxy-Rosaramycin: b) ref.[49b]; c) P. Le Ménez, I. Berque, V. Fargeas, J. Ardisson, A. Pancrazi, *Synlett* **1994**, 998; d) Le Ménez, N. Firmo, V. Fargeas, J. Ardisson, A. Pancrazi, *ibid.* **1994**, 995; jaspamide: e) P. Ashworth, B. Broadbelt, P. Jankowski, A. Pimm, P. Kocienski, *Synthesis* **1995**, 199; herboxidiene A: f) N. D. Smith, P. J. Kocienski, S. D. A. Street, *ibid.* **1996**, 652; *rac*-tylosine: g) P. Le Ménez, V. Fargeas, I. Berque, J. Poisson, J. Ardisson, J.-Y. Lallemand, A. Pancrazi, *J. Org. Chem.* **1995**, *60*, 3592.
[71] D. Hoppe, A. Brönneke, *Tetrahedron Lett.* **1983**, *24*, 1687.
[72] D. Hoppe, A. Brönneke, *Synthesis* **1982**, 1045.
[73] R. W. Hoffmann, T. Rühl, J. Harbach, *Liebigs Ann. Chem.* **1992**, 725.
[74] a) A. Carstens, D. Hoppe, *Tetrahedron* **1994**, *50*, 6097; b) C. Derwing, D. Hoppe, *Synthesis* **1996**, 149; c) F. Hammerschmidt, A. Hanninger, *Chem. Ber.* **1995**, *128*, 1069.
[75] Information on the stereochemical course of electrophilic substitution of chiral benzyllithium compounds is still quite fragmentary. Only in the case of (1-lithio-1-phenylethyl)-*N*,*N*-diisopropyl carbamate [74a,b] and 2,4,6-triisopropyl benzoate,[74c] which are accessible in enantiomerically enriched form with known configuration through deprotonation of optically active precursors, do there exist firm correlations between the configurations of starting materials and products. The trend toward stereoinversion in reactions with alkyl and acyl halides, carbon dioxide, carbon disulfide, and silyl and stannyl chlorides is strong. Protonation with alcohols and carboxylic acids, hydroxyalkylation with aliphatic aldehydes, and acylation with esters occur with retention; in these cases one can assume a preassociation of the reagent at the cation. The experimental basis is too small for solid generalization; moreover, a strong dependence on individual factors is to be anticipated.
[76] Zhang and Gawley carried out similar experiments in THF and isolated racemic products. This once again verifies that (–)-sparteine is easily displaced from the lithium cation by THF: P. Zhang, R. E. Gawley, *J. Org. Chem.* **1993**, *58*, 3223.
[77] a) P. Beak, H. Du, *J. Am. Chem. Soc.* **1993**, *115*, 2516; b) G. P. Lutz, H. Du, D. J. Gallagher, P. Beak, *J. Org. Chem.* **1996**, *61*, 4542.
[78] D. J. Gallagher, H. Du, S. A. Long, P. Beak, *J. Am. Chem. Soc.* **1996**, *118*, 11391.
[79] M. Schlosser, D. Limat, *J. Am. Chem. Soc.* **1995**, *117*, 12342.
[80] As we have already established in related cases [136, 235], deprotonation is subject to an unusually large kinetic H/D isotope effect.
[81] Synthesis of (*R*)-phenylsarcosine: N. Voyer, J. Roby, *Tetrahedron Lett.* **1995**, *36*, 6627.
[82] G. Boche, M. Marsch, J. Harbach, K. Harms, B. Ledig, F. Schubert, J. C. W. Lohrenz, H. Ahlbrecht, *Chem. Ber.* **1993**, *126*, 1887.
[83] a) Y. S. Park, M. L. Boys, P. Beak, *J. Am. Chem. Soc.* **1996**, *118*, 3757; other applications and examples: b) Y. S. Park, P. Beak, *J. Org. Chem* **1997**, *62*, 1574.
[84] We refrain here from providing an interpretation in depth. If the individual lithiation and substitution steps are subject to the same stereochemical course as was proven to be the case for the lithium derivatives of secondary benzyl carbamates [75], **38**·**1** must possess the (*R*)-configuration [83b].
[85] S. Wu, S. Lee, P. Beak, *J. Am. Chem. Soc.* **1996**, *118*, 715.

[86] S. Thayumanavan, S. Lee, C. Liao, P. Beak, *J. Am. Chem. Soc.* **1994**, *116*, 9755.
[87] The configuration at the benzylic center is unknown.
[88] a) A. Basu, P. Beak, *J. Am. Chem. Soc.* **1996**, *118*, 1575; b) A. Basu, D. J. Gallagher, P. Beak, *J. Org. Chem.* **1996**, *61*, 5718.
[89] Configurational assignment is based on the assumption of stereoinversion in the course of silylation.
[90] V. Snieckus, lecture on December 16, 1996, in Münster.
[91] S. Retzow, dissertation, Universität Kiel, **1993**.
[92] The absolute configuration of the predominant stereoisomer is unknown.
[93] For **55a**·**1**/*epi*-**55a**·**1**, a free energy of epimerization $\Delta G^{\ddagger}_{epi}$ of about 67 kJ mol^{-1} was estimated from the coalescence temperature, whereas for the pair **55b**·**1**/*epi*-**55b**·**1** a value of >78 kJ mol^{-1} results in the same way.
[94] An additional problem will be touched upon only briefly: Since (−)-sparteine is not C_2-symmetric, a stereogenic center is also created at the tetrahedrally coordinated lithium cation. In this way four diastereomers compete. All experimental indications are consistent with the view that epimerization at lithium is much more rapid than that at the carbanionic C atom.
[95] a) J. J. P. Stewart, *J. Comp. Chem.* **1989**, *10*, 209; b) E. Anders, R. Koch, P. Freunscht, *ibid.* **1993**, *14*, 1301.
[96] T. Heinl, Diplomarbeit, Universität Münster, **1996**.
[97] I. Hoppe, M. Marsch, K. Harms, G. Boche, D. Hoppe, *Angew. Chem.* **1995**, *107*, 2328; *Angew. Chem. Int. Ed. Engl.* **1995**, *34*, 2158.
[98] The addition of tetra(isopropoxy)titanium leads to increases in the yield and product purity of the resulting carbinols, but does not change either the enantio- or the diastereoselectivity. From this we conclude that metal exchange does not arise in the carbanionic intermediate. Rather, we suspect that the lithium alcoholate is bound as a titanate, and hence possible subsequent and retroreactions are prevented.
[99] In a general sense, and with the same consequences with respect to regioselectivity, intermediates can be formulated in which the carbonyl oxygen atom has displaced one coordination site of (−)-sparteine.
[100] A lithium–sparteine contact has also been demonstrated by NMR spectroscopy in diethyl ether solution, whereas in THF solution no such evidence was discovered; S. Gessler, Diplomarbeit, Universität Marburg, **1996**.
[101] I. Hoppe, unpublished.
[102] G. A. Weisenburger, P. Beak, *J. Am. Chem. Soc.* **1996**, *118*, 12218.
[103] The authors suggest a η^3-structure **67**·**1** and not a η^1-α-lithio ion pair [102]. Presumably the marked γ-selectivity of the substitution reaction serves as an argument. We were able to show that related η^1-α-lithioallyl ion pairs (for which the α-chelate structure was established) display a strong tendency toward γ-alkylation [46a, 64, 65d].
[104] Only the (*S*)-configuration of **68d** was rigorously proven [102].
[105] The authors claim that the provisional assignments of absolute configuration for the stannanes *ent*-**68e** and *ent*-**69e** are based on analogies to our results [102]. On this basis we come to the reverse conclusion (**68e** and **69e**), but then encounter contradictions with respect to the configurational assignment of the alkylation products **68b** and *ent*-**68b**.
[106] The high enantioselectivity is only useful in a preparative sense if the (*E*)- and (*Z*)-enamides **71** and **72** are separated and they do not interconvert during workup and separation.
[107] W. C. Still, C. Sreekumar, *J. Am. Chem. Soc.* **1980**, *102*, 1201. See also ref. [108].
[108] J. S. Sawyer, A. Kucerovy, T. L. Macdonald, G. J. McGarvey, *J. Am. Chem. Soc.* **1988**, *110*, 842.
[109] J. S. Carey, T. S. Coulter, D. J. Hallett, R. J. Maguire, A. H. McNeill, S. J. Stanway, A. Teerawutgulrag, E. J. Thomas, *Pure Appl. Chem.* **1996**, *68*, 707.
[110] As demonstrated by many examples, sp^3-hybridized (thus non-resonance-stabilized) alkyllithium derivatives react with retention of configuration, apart from a few very special exceptions.
[111] a) P. C.-M. Chang, J. M. Chong, *J. Org. Chem.* **1988**, *53*, 5584; b) J. A. Marshall, W. Y. Gung, *Tetrahedron* **1989**, *45*, 1043; c) Ref. [135].
[112] a) T. Cohen, M.-T. Lin, *J. Am. Chem. Soc.* **1984**, *106*, 1130; b) C. G. Screttas, M. Micha-Screttas, *J. Org. Chem.* **1978**, *43*, 1064.
[113] For elegant synthetic applications based on diastereoselective "capture" of the lithium cation as well as thermodynamically controlled equilibrations, see a) S. D. Rychnovsky, D. E. Mickus, *Tetrahedron Lett.* **1989**, *30*, 3011; b) S. D. Rychnovsky, *J. Org. Chem.* **1989**, *54*, 4982.
[114] N. G. Rondan, K. N. Houk, P. Beak, W. J. Zajdel, J. Chandrasekhar, P. von R. Schleyer, *J. Org. Chem.* **1981**, *46*, 4108.
[115] E. J. Corey, T. M. Eckrich, *Tetrahedron Lett.* **1983**, *24*, 3165.
[116] a) P. Beak, B. G. McKinnie, *J. Am. Chem. Soc.* **1977**, *99*, 5213; b) P. Beak, L. G. Carter, *J. Org. Chem.* **1981**, *46*, 2363.
[117] R. Schlecker, D. Seebach, W. Lubosch, *Helv. Chim. Acta* **1978**, *61*, 512.
[118] The 2-(dimethylaminoethyl) ester of type **80** constitutes an exception; activation through the chelating dialkylamino group here certainly plays a significant role; cf. [116b].
[119] First application of *N,N*-dialkylcarbamoyl groups in the activation of alcohols: D. Hoppe, R. Hanko, A. Brönneke, *Angew. Chem.* **1980**, *92*, 637; *Angew. Chem. Int. Ed. Engl.* **1980**, *19*, 625.
[120] a) P. Tebben, dissertation, Universität Kiel, **1991**; b) T. Raffel, Diplomarbeit, Universität Kiel, **1990**.
[121] T. Nakai, personal communication, **1996**.
[122] F. Hintze, D. Hoppe, *Synthesis* **1992**, 1216.
[123] D. Hoppe, F. Hintze, P. Tebben, *Angew. Chem.* **1990**, *102*, 1457; *Angew. Chem. Int. Ed. Engl.* **1990**, *29*, 1422.
[124] P. Mickon, A. Rassat, *Bull. Soc Chim. Fr.* **1971**, 3561; see also Ref. [122].
[125] Coalescence is achieved in $CDCl_3$ by warming to about 70°C; J. Haller, Diplomarbeit, Universität Kiel, **1992**.
[126] If there are additional hydroxy groups in the vicinity of the carbamoyloxy group, reductive ester cleavage with lithium aluminum hydride occurs readily. Apparently these bring the metal hydride into place.
[127] a) J. Tanaka, *J. Chem. Soc. Perkin Trans. 2* **1989**, 1009; b) K. S. Rein, *Tetrahedron Lett.* **1991**, *32*, 1941; c) Gawley, *J. Org. Chem.* **1989**, *54*, 175; d) J. J. Eisch, *Res. Chem. Intermed.* **1996**, *22*, 145.
[128] T. Hense, dissertation, Universität Münster, **1996**.
[129] a) D. Seebach, R. Henning, T. Mukhopadhyay, *Chem. Ber.* **1982**, *115*, 1705; b) T. Mukhopadhyay, D. Seebach, *Helv. Chim. Acta* **1982**, *65*, 385.
[129] T. Hense, Dissertation, Universität Münster, **1996**.
[130] F. Hintze, Dissertation, Universität Kiel, **1993**.
[131] K. Behrens, dissertation, Universität Münster, **1997**.
[132] I. Hoppe, unpublished (1991).
[133] R. H. Bartelt, A. M. Schaner, C. L. Jackson, *J. Chem. Ecol.* **1989**, *15*, 399.
[134] a) K. Mori, *Tetrahedron* **1975**, *31*, 3011; b) J. H. Borden, E. Stokkink, *Can. J. Zool.* **1973**, *51*, 469.
[135] Y. Yamamoto, *Chemtracts: Org. Chem.* **1991**, *4*, 255.
[136] D. Hoppe, M. Paetow, F. Hintze, *Angew. Chem.* **1993**, *105*, 430; *Angew. Chem. Int. Ed. Engl.* **1993**, *32*, 394.
[137] We wish to thank Professor D. O. Collum for stimulating us to carry out this investigation through a comment at the Gordon Conference in Newport (1992).
[138] Starting from (*S*)-configured 1-deuterocarbamates of the type **97** one is able to enter the series of enantiomeric products *ent*-**97**. However, these suffer the blemish of being deuterated. We are aware of no precedent in which a kinetic isotope effect has been similarly utilized for the synthesis of highly enantiomerically enriched products.
[139] A high, though not quantified, kinetic H/D isotope effect was observed in the deprotonation of *S*-ethyl thiobenzoates; D. B. Reitz, P. Beak, R. F. Farney, L. S. Helmick, *J. Am. Chem. Soc.* **1978**, *100*, 5428.
[140] a) Review: "Isotope Effects in Hydrogen Atom Transfer Reactions," E. S. Lewis in *Isotopes in Organic Chemistry*, Vol. 2 (Eds. E. Buncel, C. C. Lee), Elsevier, Amsterdam **1976**, p. 127; b) E. S. Lewis, L. H. Funderburg, *J. Am. Chem. Soc.* **1967**, *89*, 2322.
[141] J. Haller, dissertation, Universität Münster, **1995**.
[142] D. J. Gallagher, S. T. Kerrick, P. Beak, *J. Am. Chem. Soc.* **1992**, *114*, 5872.
[143] In this way the useless stereogenic center in the base is avoided. It follows from studies by Beak that this exchange has virtually no influence on the stereoselectivity [142].
[144] We believe that despite the small calculated energy difference the calculated structures portray the decisive distinction. It is very likely that the "true" transition states are more compact than the calculated ones. For the ground state of the lithium–sparteine–methylindenide complex **58a**·**1**: Li–N distances measured in the crystal structure (209.5 pm and 214.1 pm) are noticeably shorter than the calculated distances (225.2 pm und 226.4 pm). T. Heinl, Diplomarbeit, Universität Münster, **1996**.
[145] J. Haller, T. Hense, D. Hoppe, *Liebigs Ann. Chem.* **1996**, 489.
[146] These investigations were carried out with racemic mixtures; for greater clarity, one enantiomer has been singled out.
[147] T. Hense, Diplomarbeit, Universität Münster, **1993**.
[148] Those with little practice in stereochemistry are asked to forgive us for the confusion we may have perpetrated. For reasons of clarity we have held constant the configurational arrangement at the reaction center in the calculations, and instead varied the configuration at the stationary center. This is legitimate, since all such transformations that obey the relative topicity *lk* (*like*) [6a]—irrespective whether *R,Re*, *S,Si* or *R*,Re**—must overcome the same energy barrier. The same applies in principle to the *ul* (*unlike*) series.
[149] J. Haller, T. Hense, D. Hoppe, *Synlett* **1993**, 726.
[150] P. Sommerfeld, D. Hoppe, *Synlett* **1992**, 764.
[151] The great tendency toward complexation for γ-Me_2N groups in organolithium compounds is well known: G. W. Klumpp, M. Vos, F. J. J. de Kanter, C. Slob, H. Krabbendam, A. L. Spek, *J. Am. Chem. Soc.* **1985**, *107*, 8292.
[152] Because of the unfavorable solubility characteristics of the intermediate carboxylic acid, methyl iodide was used as trapping reagent. The observed enantiomeric excesses are independent of the electrophile [150].
[153] a) M. Paetow, H. Ahrens, D. Hoppe, *Tetrahedron Lett.* **1992**, *33*, 5323; b) H. Ahrens, dissertation, Universität Münster, **1994**.
[154] J. Schwerdtfeger, D. Hoppe, *Angew. Chem.* **1992**, *104*, 1547; *Angew. Chem. Int. Ed. Engl.* **1992**, *31*, 1505.
[155] S. Kleinfeld, Diplomarbeit, Universität Münster, **1996**.
[156] D-Pantolactone (**124**) is produced by BASF. The key step here is a sophisticated racemate resolution on a technical scale.

[157] M. Paetow, M. Kotthaus, M. Grehl, R. Fröhlich, D. Hoppe, *Synlett* **1994**, 1034.

[158] It is unclear whether Me_3SiCl or LiCl formed in the process functions as Lewis acid.

[159] Cyclopropyl anions possess a very high barrier to inversion: H. M. Walborsky, C. Hamdouchi, *J. Am. Chem. Soc.* **1993**, *115*, 6406 and earlier papers by these authors.

[160] M. Kotthaus, dissertation, Universität Münster, **1996**.

[161] This represents the only case in which stereoinversion of a lithiated alkyl carbamate was observed during the reaction.

[162] The stereochemistry at the nucleophilic center during 1,3-eliminations was accorded little attention until recently: a) B. Beruben, I. Marek, J.-F. Normant, N. Platzer, *Tetrahedron Lett.* **1993**, *34*, 7575; b) *J. Org. Chem.* **1995**, *60*, 2488; c) J.-F. Normant, *Chemtracts: Org. Chem.* **1994**, *7*, 59; d) A. Krief, M. Hobe, *Tetrahedron Lett.* **1992**, *33*, 6529; e) A. Krief, M. Hobe, W. Dumont, E. Badaoui, E. Guittet, G. Evard, *ibid.* **1992**, *33*, 3381; f) N. Isono, M. Mori, *J. Org. Chem.* **1996**, *61*, 7867.

[163] Similar findings are obtained with 2-monosubstituted 1,3-dicarbamates of the type **121** [160]. Because of the complicated stereochemical relationships (the CH_2OCby groups are enantiotopic, their protons diastereotopic), a presentation will be dispensed with in this context.

[164] Reviews of directed lithiation: a) P. Beak, A. I. Meyers, *Acc. Chem. Res.* **1986**, *19*, 356; b) D. D. Clark, A. Jahangir, *Organic Reactions* **1995**, *47*, 1; c) V. Snieckus, *Chem. Rev.* **1990**, *90*, 879.

[165] a) C. Boie, dissertation, Universität Münster, **1996**; b) C. Boie, D. Hoppe, *Synthesis* **1997**, 176.

[166] H. Ahrens, M. Paetow, D. Hoppe, *Tetrahedron Lett.* **1992**, *33*, 5327.

[167] We do not know the precise structure of bis-chelate complexes like **131**. It is also possible that the more effectively donating carbonyl group of the γ- or δ-carbamoyloxy residue binds, but then a seven- or eight-membered ring would need to form. We can also only speculate about the fourth ligand L; Et_2O or $Me_2NCH_2CH_2NMe_2$ (TMEDA) bound in monodentate fashion are possible candidates.

[168] Irrespective of the fact that the deprotonation step is kinetically directed, the energetically more favorable bicyclic chelate complex is formed in excess.

[169] H. Helmke, D. Hoppe, *Synlett 1995*, 978.

[170] Based on MOPAC calculations [65e], there is an energy difference of 4.6 kJ mol^{-1} between the simplified complexes **134** and *epi*-**134** ($Me_2NC{=}O$ for *Cby*, L = Me_2O).

[171] For the preparation of (+)-sparteine from *rac*-lupinane, which is obtained from the seeds of *Lupinus alba*, see ref. [26a].

[172] Another elegant route for diastereoselective generation of protected 1,3-dihydroxyalkanides was developed by S. E. Rychnovsky: a) [113b]; b) T. I. Richardson, S. D. Rychnovsky, *J. Org. Chem.* **1996**, *61*, 4219; review: c) S. D. Rychnovsky, *Chem. Rev.* **1995**, *95*, 2021.

[173] a) W. Guarnieri, Diplomarbeit, Universität Kiel, **1992**; b) W. Guarnieri, M. Grehl, D. Hoppe, *Angew. Chem.* **1994**, *106*, 1815; *Angew. Chem. Int. Ed. Engl.* **1994**, *33*, 1734; c) P. Gmeiner, A. Kärtner, *Synthesis* **1995**, 83.

[174] The energy difference in the ground state between the complexes (1*S*)-**138** and (1*R*)-**138** is apparently smaller than the relevant free energies of activation, because the addition of lithium bromide initiates an epimerization that leads to a 1:2 mixture [175]. Nevertheless, the possibility that a further LiBr-containing aggregate enters into competition cannot be ruled out [175].

[175] M. Sendzik, Diplomarbeit, Universität Kiel, **1995**.

[176] We do not know the structure of **138**; our suggestion offers one plausible interpretation of the experimental findings. In particular, it remains unclear in what way the 4-O*Cby* group is bound to the lithium cation, and whether an additional ligand L (here Et_2O) is acquired.

[177] M. Sendzik, dissertation, Universität Münster, **1997**.

[178] This experiment proves that there is a kinetically determined deprotonation.

[179] As demonstrated here, the high H/D kinetic isotope effect permits a very general utilization of deuterium as protective group in the deprotonation of alkyl carbamates.

[180] Preparation of 2-(dibenzylamino)alkanols: a) L. Velluz, D. Amiard, R. Heymes, *Bull. Soc. Chim. Fr.* **1954**, 1012; b) M. T. Reetz, M. W. Drewes, A. Schmidt, *Angew. Chem.* **1987**, *99*, 1186; *Angew. Chem. Int. Ed. Engl.* **1987**, *26*, 1141; c) ref. [173c].

[181] The following problem has been avoided in Figure 10: With the exception of two energetically unfavorable conformational arrangements, the pyramidal dibenzylamino group contributes to varying degree to the shielding of the front and rear faces. It is quite conceivable that the influence of the "small" methyl group is overcompensated in this way.

[182] For experiments with *N*-(diphenylmethylene) derivatives see ref. [165]

[183] S. Kolczewski, dissertation, Universität Münster **1995**.

[184] B. Weber, D. Hoppe, unpublished.

[185] T. Hense, D. Hoppe, *Synthesis* **1997**, in press.

[186] P. Sommerfeld, dissertation, Universität Münster, **1995**.

[187] Enantioselective total syntheses of (+)-sedridine: a) S. Murahashi, Y. Imada, M. Kohno, T. Kawakami, *Synlett* **1993**, 395; b) C. Louis, C. Hootelé, *Tetrahedron: Asymmetry* **1995**, *6*, 2149; c) B. J. Littler, T. Gallagher, I. K. Boddy, P. D. Riordan, *Synlett* **1997**, 22.

[188] J. van Bebber, D. Hoppe, unpublished.

[189] No indications of participation by the δ-O*Cby*-group were detected.

[190] P. H. J. Carlsen, T. Katsuki, V. S. Martin, K. B. Sharpless, *J. Org. Chem.* **1981**, *46*, 3936.

[191] R. Fröhlich, M. Grehl, personal communication (1994).

[192] P. Beak, W. J. Zajdel, *J. Am. Chem. Soc.* **1984**, *106*, 1010.

[193] a) S. T. Kerrick, P. Beak, *J. Am. Chem. Soc.* **1991**, *113*, 9708; b) P. Beak, S. T. Kerrick, S. Wu, J. Chu, *ibid.* **1994**, *116*, 3231.

[194] a) E. J. Corey, R. K. Bakshi, S. Shibata, *J. Am. Chem. Soc.* **1987**, *109*, 5551; b) E. J. Corey, R. K. Bakshi, S. Shibata, C. P. Chen, K. K. Singh, *ibid.* **1987**, *109*, 7925; c) review: S. Wallbaum, J. Martens, *Tetrahedron: Asymmetry* **1992**, *3*, 1475.

[195] a) R. E. Gawley, Q. Zhang, *J. Am. Chem. Soc.* **1993**, *115*, 7515; b) T. R. Elworthy, A. I. Meyers, *Tetrahedron* **1994**, *50*, 6089; c) R. E. Gawley, Q. Zhang, *J. Org. Chem.* **1995**, *60*, 5763; d) R. E. Gawley, Q. Zhang, S. Campagna, *J. Am. Chem. Soc.* **1995**, *117*, 11817; e) I. Coldham. R. Hufton, D. J. Snowden, *ibid.* **1996**, *118*, 5322.

[196] For a detailed discussion, see a very recent review by Beak: ref. [17].

[197] D. J. Gallagher, P. Beak, *J. Org. Chem.* **1995**, *60*, 7092.

[198] M. E. Kopach, A. I. Meyers , *J. Org. Chem.* **1996**, *61*, 6764.

[199] D. J. Gallagher, S. Wu, N. A. Nikolic, P. Beak, *J. Org. Chem.* **1995**, *60*, 8148.

[200] In orientational experiments with *N*-Boc-piperidine we obtained nearly racemic products; I. Hoppe, unpublished (1990).

[201] Y. S. Park, P. Beak , *Tetrahedron* **1996**, *52*, 12333.

[202] a) D. M. Hodgson, G. P. Lee, *Chem. Commun.* **1996**, 1015; b) D. M. Hodgson, R. Wisedale, *Tetrahedron: Asymmetry* **1996**, *7*, 1275; c) D. M. Hodgson, G. P. Lee, *ibid.* **1997**, 2303.

[203] M. Lautens, C. Gajda, P. Chiu, *J. Chem. Soc. Chem. Commun.* **1993**, 1193.

[204] R. A. Muci, K. R. Campos, D. A. Evans, *J. Am. Chem. Soc.* **1995**, *117*, 9075.

[205] Brief reviews: a) A. Togni, *Angew. Chem.* **1996**, *108*, 1581; *Angew. Chem. Int. Ed. Engl.* **1996**, *35*, 1475; b) S. Borman, *Chem. Eng. News* **1996**, *74* (30), 38.

[206] With respect to relevant experiments with isopropylferrocene (**199**, X = $CHMe_2$) by Nozaki et al. see Section 2 and refs. [27c,d].

[207] a) M. Tsukazaki, M. Tinkl, A. Roglans, B. J. Chapell, N. J. Taylor, V. Snieckus, *J. Am. Chem. Soc.* **1996**, *116*, 685; b) an application: H. Jendralla, E. Paulus, *Synlett* **1997**, 471.

[208] D. Price, N. S. Simpkins, *Tetrahedron Lett.* **1995**, *36*, 6135.

[209] Y. Nishibayashi, Y. Arikawa, K. Ohe, S. Uemura, *J. Org. Chem.* **1996**, *61*, 1172.

[210] E. P. Kündig, A. Quattropani, *Tetrahedron Lett.* **1994**, *35*, 3497.

[211] M. Uemura, Y. Hayashi, Y. Hayashi, *Tetrahedron: Asymmetry* **1994**, *5*, 1427.

[212] D. A. Price, N. S. Simpkins, A. M. MacLeod, A. P. Watt, *J. Org. Chem.* **1994**, *59*, 1961.

[213] J. Aubé, *Chemtracts: Org. Chem.* **1994**, *7*, 413.

[214] H.-G. Schmalz, K. Schellhaus, *Tetrahedron Lett.* **1995**, *36*, 5515.

[215] L. M. Engelhardt, W.-P. Leung, C. L. Raston, G. Salem, P. Twiss, A. H. White, *J. Chem. Soc. Dalton Trans.* **1988**, 2403.

[216] S. Thayumanavan, P. Beak, D. P. Curran, *Tetrahedron Lett.* **1996**, *37*, 2899.

[217] A very effective approach to (−)-sparteine-assisted synthesis of enantiomerically enriched binaphthyls consists of the oxidative coupling of naphthols: a) M. Smrčina, J. Poláková, S. Vyskočil, P. Kočovský, *J. Org. Chem.* **1993**, *58*, 4534; b) T. Osa, Y. Kasiwagi, Y. Yanagisawa, J. M. Bobbitt, *J. Chem. Soc. Chem. Commun.* **1994**, 2535.

[218] Reviews: a) P. Knochel, *Comprehensive Organic Synthesis, Vol. 4* (Eds.: B. M. Trost, I. Flemming, M. F. Semmelhack), Pergamon, Oxford, **1991**, p. 865; b) R. L. Subramanian, *Methoden Org. Chem. (Houben-Weyl), 4th ed. 1952–*, E19d, **1993**, p. 744.

[219] a) W. F. Bailey, K. V. Gavaskar, *Tetrahedron* **1994**, *50*, 5957; b) V. N. Drozd, Uy. A. Ustynyuk, M. A. Tsel'eva, L. B. J. Dmitriev, *J. Gen. Chem. USSR (Engl. Transl.)* **1968**, *38*, 2144; *Zh. Obsch. Khim.* **1968**, *38*, 2144.

[220] A. Krief, B. Kenda, B. Remacle, *Tetrahedron Lett.* **1995**, *36*, 7917.

[221] a) S. Klein, I. Marek, J.-F. Poisson, J.-F. Normant, *J. Am. Chem. Soc.* **1995**, *117*, 8853; b) S. Norsilian, I. Marek, J.-F. Poisson, J. F. Normant, *J. Org. Chem.* **1997**, *62*, 4898.

[222] Brief review: ref. [162c]

[223] Proof of stereoinversion in the alkylation of benzyllithium derivatives: ref. [74b].

[224] Structure of lithium alcoholates in nondonor solvents: B. Goldfuss, P. von R. Schleyer, F. Hampel, *J. Am. Chem. Soc.* **1996**, *118*, 12183 and references therein.

[225] To our knowledge, this discovery constitutes the first example of a catalytic enantioselective lithiation induced by (−)-sparteine.

[226] D. Amurrio, K. Khan, E. P. Kündig, *J. Org. Chem.* **1996**, *61*, 2258.

[227] Suggestions regarding the structure of the carbanionic intermediate were not published [226]. The propargyl residue enters from the side complexed by chromium; thus a bonding interaction between the metal and the alkynyl residue is very probable.

[228] J. G. Peters, Diplomarbeit, Universität Münster, **1996**.

[229] Stereochemistry of the electrophilic substitution of lithiated secondary benzyl carbamates: ref. [74].

[230] a) J. E. Baldwin, *J. Chem. Soc. Chem. Commun.* **1976**, 738; b) review: C. D. Johnson, *Acc. Chem. Res.* **1993**, *26*, 476.

[231] M. J. Woltering, R. Fröhlich, D. Hoppe, *Angew. Chem.* **1997**, *109*, 1804–1805; *Angew. Chem. Int. Ed. Engl.* **1997**, *36*, 1764–1766.
[232] a) H. J. Reich, M. D. Bowe, *J. Am. Chem. Soc.* **1990**, *112*, 8994; b) H. J. Reich, R. R. Dykstra, *Angew. Chem.* **1993**, *105*, 1489; *Angew. Chem. Int. Ed. Engl.* **1993**, *32*, 1469; c) H. J. Reich, R. R. Dykstra, *J. Am. Chem. Soc.* **1993**, *115*, 7041; d) H. J. Reich, K. J. Kulicke, *ibid.* **1995**, *117*, 6621; e) H. J. Reich, K. J. Kulicke, *ibid.* **1996**, *118*, 273; f) ref. [73]; g) R. W. Hoffmann, M. Julius, F. Chemla, T. Ruhland, G. Frenzen, *Tetrahedron* **1994**, *50*, 6049; h) H. Ahlbrecht, J. Harbach, R. W. Hoffmann, T. Ruhland, *Liebigs Ann. Chem.* **1995**, 211; i) R. W. Hoffmann, W. Klute, *Chem. Eur. J.* **1996**, *2*, 694; k) R. W. Hoffmann, R. K. Dress, T. Ruhland, A. Wenzel, *Chem. Ber.* **1995**, *128*, 861.
[233] P. Beak, P. D. Becker, *J. Org. Chem.* **1982**, *47*, 3855.
[234] D. Hoppe, L. Beckmann, R. Follmann, *Angew. Chem.* **1980**, *92*, 305; *Angew. Chem. Int. Ed. Engl.* **1980**, *19*, 303.
[235] B. Kaiser, D. Hoppe, *Angew. Chem.* **1995**, *107*, 344; *Angew. Chem. Int. Ed. Engl.* **1995**, *34*, 323.
[236] The (*R*)-configuration of the predominant lithiated intermediate **225** was derived from the carboxylic ester (*S*)-**226b** under the assumption of stereoretention during carboxylation (in analogy to the corresponding reactions of oxygen analogues). The configurational assignment is thus not completely secured.
[237] We do not know how to account for the marked deviation of the *ee* value (34%) from that obtained with the undeuterated substrate (46% *ee*). Is it likely that equilibrium between the diastereomers would be upset by a thermodynamic isotope effect on the order of magnitude of $\Delta\Delta G = 0.4\ \mathrm{kJ\,mol^{-1}}$?
[238] T. Shinozuka, Y. Kikori, M. Asaoka, H. Takei, *J. Chem. Soc. Perkin Trans 1*, **1996**, 119.
[239] R. W. Hoffmann, W. Klute, R. K. Dress, A. Wenzel, *J. Chem. Soc. Perkin Trans. 2*, **1995**, 1721.
[240] G. Boche, A. Opel, M. Marsch, K. Harms, F. Haller, J. C. W. Lohrenz, C. Thümmler, W. Koch, *Chem. Ber.* **1992**, *125*, 2265.
[241] T. Ruhland, R. Dress, R. W. Hoffmann, *Angew. Chem.* **1993**, *105*, 1487; *Angew. Chem. Int. Ed. Engl.* **1993**, *32*, 1467.
[242] B. Kaiser, dissertation, Universität Münster, **1995**.
[243] D. Hoppe, B. Kaiser, O. Stratmann, R. Fröhlich, *Angew. Chem.* **1997**, *109*, No. 24; *Angew. Chem. Intl. Ed. Engl.* **1997**, *36*, No. 24.

Time is money...

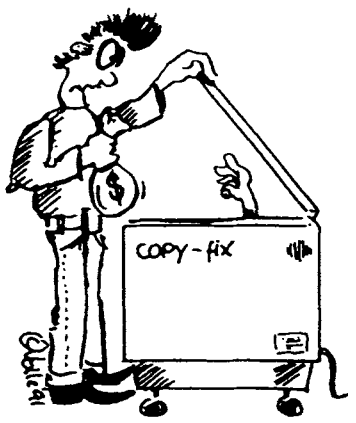

Save both by starting a personal subscription to *Angewandte Chemie*
At 9¢ per page you can't go wrong.
With your own private copy you can read the "hot" articles before they cool, and waste less time in front of the copier.

Order now!
An order form can be found on the last page of this issue.

Charge Transfer in DNA: A Controversy

Ulf Diederichsen*

Interest has increased in the scrutiny of linear molecular structures with regard to their conductivity, and several models that define charge propagation have evolved; one concept describes a molecular wire in which an electron tunnels through a valence-bound, linear, saturated carbon chain.[1] Thus, the probability that the charge remains within the chain is very low. A new model, which was developed for positive charge transfer in small peptides in the gas phase, follows a stepwise charge transport through energetically varied intermediate states.[2] Various amino acids in the peptide backbone function to control the mechanism of charge transfer. However, for large, complex folded proteins electron transfer in solution is described as a tunneling process that proceeds along the peptide backbone and passes through space.[3]

A well-defined linear helix and repetitive structure is found in the DNA double strand. It consists of a stack of purine–pyrimidine base pairs which are topologically stabilized by a ribosyl phosphodiester double strand. The interaction of the π electrons, which are 3.4 Å apart, provides an important contribution to DNA double strand stability. The question of whether DNA has a structurally inherent potential for transport of electrons over greater distances has been discussed for some time.[4] An early experiment that points out electron migration in DNA defines the photoinduced interaction between intercalating ethidium donors with acceptors that are unspecifically bound to the DNA backbone.[5] In recent years experiments by Barton et al., which confirm indications that efficient charge migration within the DNA duplex might be possible over distances up to 40 Å, have raised attention.[6] Initially, a fast hopping mechanism through the stack of base pairs (π way) was suggested.[6] An alternate model is based on quantum mechanical tunneling, which is supported by the valence orbitals of the π stack; however only moderate electron-transport properties can be expected.[7] Another approach based on conductivity measurements suggests electron transport through the outer sphere of the ribosyl phosphodiester backbone with tightly bound water molecules.[8]

Due to original difficulties in the synthesis of DNA strands with covalently linked metal-complex intercalators (1% yield) and the high concentration necessary for determining electron-transport rates, some of the electron-transport studies were carried out with *noncovalently linked intercalators*. (Figure 1a).[9]

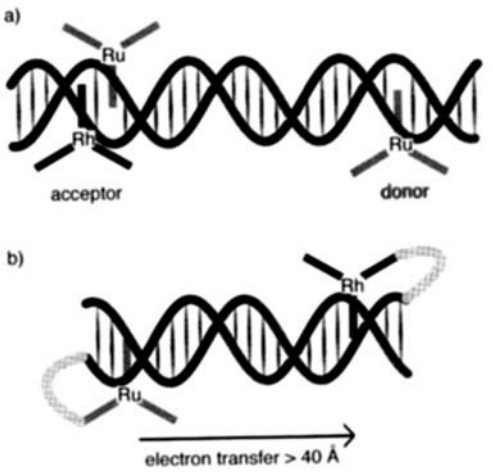

Figure 1. a) Intercalation of nontethered ruthenium and rhodium complexes to DNA takes place without a defined distance between electron donors and acceptors. The high rates observed for electron transport most likely result from clustering of the intercalators. b) DNA double strands with metal intercalators covalently tethered to the 5'-termini ensure electron transfer between separated donor and acceptor complexes.

These experiments provide limited information, primarily because the real distance of electron transport with unspecifically bound intercalators is unknown. In some instances cooperative binding of donor and acceptor intercalators in clusters could explain the rapid exchange of electrons. Circular dichroism (CD) spectra indicate cooperative binding of the intercalators, thus suggesting the influence of the neighboring intercalators.[10] Furthermore, by simulating electron transport as a function of the distance between the metal complex, the experiment with noncovalently linked intercalators is correlated advantageously by the pairing of donor–acceptor complexes.[11]

On the other hand, the stoichiometry of DNA and intercalator has no kinetic effect, and the rate of electron transport is clearly dependent on the sequence, which is in contrast to a direct exchange between donor and acceptor intercalator; electron exchange on poly d(AT) is 30 times faster than on poly d(GC).[6] As long as the distances between the intercalators are not defined, it is difficult to determine which effect

[*] Dr. U. Diederichsen
Institut für Organische Chemie und Biochemie
der Technischen Universität München
Lichtenbergstrasse 4, D-85747 Garching (Germany)
Fax: Int. code +(89)2891-3210
e-mail: ud@linda.org.chemie.tu-muenchen.de

 © WILEY-VCH Verlag GmbH, D-69451 Weinheim, 1997 0570-0833/97/3621-2317 $ 17.50+.50/0

influences electron transport. This requires a system in which the *intercalators are covalenty bound* to the DNA strands.

When a DNA double strand consisting of 15 base pairs is covalently linked through the 5′-terminus to the electron-donating metal intercalator $[Ru(phen)_2(dppz)]^{2+}$ and through the opposite 5′-position to the acceptor $[Rh(phen)(phi)_2]^{3+}$ (phen = 1,10-phenanthroline, dppz = dipyrido[2,3-*a*:2′,3′-*c*]phenazine, phi = 9,10-phenanthrenequinonediimine), intercalation of the metal ligands over a distance of 40 Å is possible (Figure 1b); the luminescence usually present in intercalated ruthenium complexes is not observed.[12] This luminescence quenching is interpreted as electron transfer from the activated ruthenium to the rhodium complex and back at a rate of at least $3 \times 10^9\ s^{-1}$. Control experiments on photochemical DNA cleavage at the intercalation site proved that the positions of intercalation are usually two base pairs away from the ends. Furthermore, at least 85% of the quenching of the ruthenium-complex emission is due to an intramolecular process.[12] The dependence of electron transport on the distance between donor and acceptor remains an important issue. Recently, Lewis et al. described photoinduced electron transport between a stilbene molecule, which functions as a loop for two DNA strands forming a double helix, and a guanine residue of a G–C base pair.[13] Decreasing fluoresence quenching with increasing distance between the G–C base pair and stillbene was established. Also Tanaka et al. observed a distance-dependent electron transfer between an acridine derivative that is covalently anchored into an internucleotide site in DNA and a guanine residue.[14] Furthermore, experiments are expected in the near future from Meade[15] and Barton et al.[6] The latter use covalenty bound ethidium instead of ruthenium donors with donor–acceptor distances of 17–36 Å, and observe a negligible distance dependency for fluorenscence quenching.

Because of the great biological significance of charge transport, the development of artificial electron transfer systems for simulating biologically relevant functions has received much attention. The Barton group investigated DNA mutation by electron transfer for a guanine residue oxidized at C8[16] and the repair of thymine-dimer damage resulting from [2+2]cycloaddition.[17] These experiments support the concept of electron transport through the stack of DNA base pairs. In addition, they indicate a new principle for the formation and possible repair of DNA damage, because, in contrast to the position of electron transfer, the mutation location can be precisely established. Photochemical activation (365 nm) of the electron acceptor $[Rh(bpy')(phi)_2]^{3+}$ (bpy′ = 4-butyric acid 4′-methylbipyridine) that is covalently linked to the DNA duplex at the 5′-terminus (Figure 2) generates an electron hole that might equilibrate in the DNA base pair stack. Positions such as GG or GGG sequences are susceptible to oxidation because of the electron-donor properties of the adjacent guanine residue; therefore, oxidation at C8 of the 5′-terminal guanine residue proceeds with a low quantum yield of 10^{-7}. When several GG sequences are present, the more distant ones are more easily oxidized.[16]

Quantitative repair of the damaged thymine dimer is achieved through photochemical activation of the statistically intercalated metal complex $[Rh(phi)_2(dmb)]^{3+}$ (dmb = 4,4′-dimethyl-2,2′-bipyridine). The reaction is catalytic, since only substoichiometric amounts of intercalator are required.[17] Full

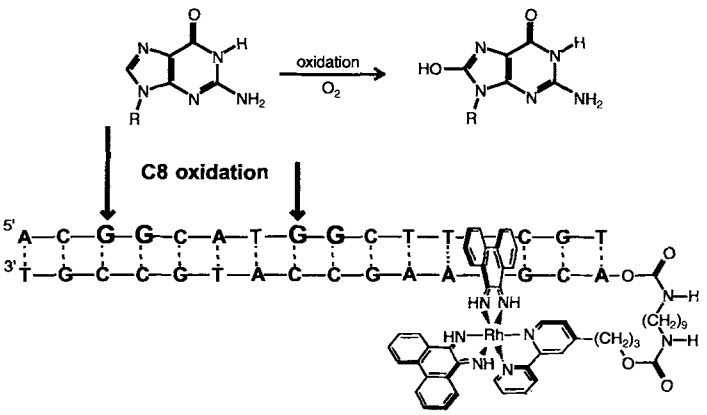

Figure 2. Electron transport initiated by photochemical activation of a covalently tethered rhodium-complex intercalator selectively oxidizes the 5′-guanine residue of a G–G dimer.

repair is observed even when $[Rh(phi)_2(dmb)]^{3+}$ is covalently tethered to the 5′-terminus of the DNA (Figure 3). The yields strongly depend on how the base pairs stack and how closely the intercalator interacts with the nucleobases. In this manner, effective damage repair of a less than ideally stacked thymine dimer is indicated, in which a thymine dimer projects out of the helix; this provides better contact with the nontethered inter-

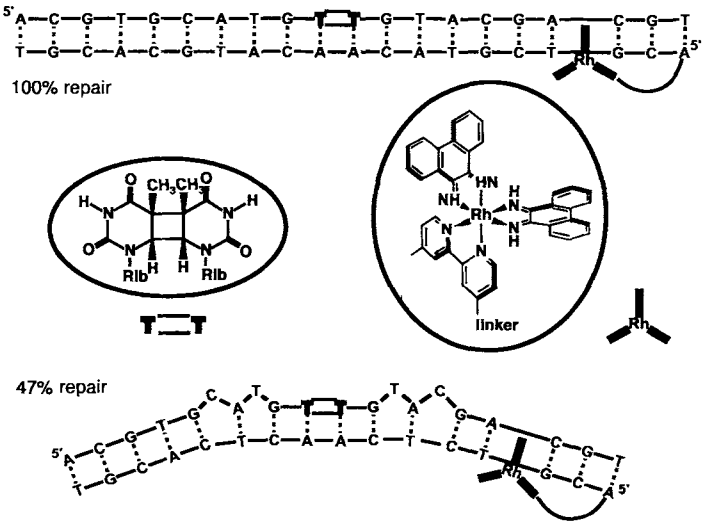

Figure 3. Photochemical activation of a rhodium-complex intercalator covalently tethered to the 5′-position of DNA initiates complete repair of the damage to a thymine dimer. Perfect stacking of the nucleobases is required for most effective repair.

calator. Control experiments show that repair of the T–T dimer with covalently bound metal complex does not result from an intermolecular reaction between DNA double strands. Furthermore, the repair efficiency is independent of the distance or the binding of the intercalator to either end of the double strand.[17]

The investigated DNA electron transfer systems are controversial with respect to the distance dependency of electron transport. In contrast to studies on systems clearly showing distance-dependent electron transport,[13, 14] Barton's results indicate that with ideal DNA geometry the electron transfer is virtually distance independent.[6, 16, 17] Effective stacking of arenes in-

 © WILEY-VCH Verlag GmbH, D-69451 Weinheim, 1997 0570-0833/97/3621-2318 $ 17.50+.50/0

volved in the transport process (intercalator, base pairs, thymine dimers) seems to be neccessary for uninterrupted electron transport. Mismatched base pairs, bulges that disturb the strand geometry, and loosely bound intercalators with weak stacking interaction have negative effects on the transport.[6] Sequence dependency of electron transport also seems reasonable, because nucleobases contribute differently to double-strand stability through stacking. Interference in base stacking could be important for regulating usually unrestricted electron transfer within the DNA stack.

Investigations based on past results are already in progress using DNA electron transport as a sensor. To detect a DNA sequence, one could advantageously use the fact that a single DNA strand has low and a helical double strand high conductivity. The presence of a sought after DNA sequence can be clarified by a great increase in conductivity when bound to a complementary DNA strand which is placed in a conducting matrix.[18] The efficiency of electron transport provides an additional measurement of the structural interference of a DNA double helix through base-pair mismatch, DNA damage, or bulges.

The present interesting experiments concerning electron transport in DNA raise many questions, which call for a mechanistic understanding of the electronic properties of DNA. The development of satisfactory theories and prognosis requires cooperation between bioorganic chemistry for the molecular design of and experiments with appropriate test systems, physical chemistry for diagnostics (transport rates), and theoretical chemistry for mechanistic interpretation.

German version: *Angew. Chem.* **1997**, *109*, 2411–2413

Keywords: DNA oxidation · DNA repair · electron transfer · intercalations

[1] M. A. Ratner, *J. Phys. Chem.* **1990**, *94*, 4877–4883.
[2] a) R. Weinkauf, P. Schanen, D. Yang, S. Soukara, E. W. Schlag, *J. Phys. Chem.* **1995**, *99*, 11255–11265; b) R. Weinkauf, P. Schanen, A. Metsala, E. W. Schlag, M. Bürgle, H. Kessler, *ibid.* **1996**, *100*, 18567–18585; c) R. Weinkauf, E. W. Schlag, R. Levine, *ibid.* submitted.
[3] a) J. N. Onuchic, D. N. Beratan, *J. Chem. Phys.* **1990**, *92*, 722–733; b) D. N. Beratan, J. N. Onuchic, J. R. Winkler, H. B. Gray, *Science* **1992**, *258*, 1740–1741.
[4] a) D. D. Eley, D. I. Spivey, *Trans. Faraday Soc.* **1962**, *58*, 411–415; b) T. A. Hoffmann, J. Ladik, *Adv. Chem. Phys.* **1964**, *7*, 84; c) R. S. Snart, *Biopolymers*, **1968**, *6*, 293–297; d) S. Suhai, *J. Chem. Phys.* **1972**, *57*, 5599–5603; e) D. Dee, M. E. Baur, *ibid.* **1974**, *60*, 541–560; f) P. M. Cullis, J. D. McClymont, M. C. R. Symons, *J. Chem. Soc. Farad. Trans.* **1990**, *86*, 591–592.
[5] P. Fromherz, B. Rieger, *J. Am. Chem. Soc.* **1986**, *108*, 5361–5362.
[6] R. E. Holmlin, P. J. Dandliker, J. K. Barton, unpublished results.
[7] a) A. K. Felts, W. T. Pollard, R. A. Friesner, *J. Phys. Chem.* **1995**, *99*, 2929–2940; b) D. N. Beratan, S. Priyadarshy, S. M. Risser, *Chem. Biol.* **1997**, *4*, 3–8; c) S. Priyadarshy, S. M. Risser, D. N. Beratan, *J. Phys. Chem.* **1996**, *100*, 17678–17682; d) A. M. Brun, A. Harriman, *J. Am. Chem. Soc.* **1992**, *114*, 3656–3660.
[8] J. M. Warman, M. P. de Haas, A. Rupprecht, *Chem. Phys. Lett.* **1996**, *249*, 319–322.
[9] M. R. Arkin, E. D. A. Stemp, R. E. Holmlin, J. K. Barton, A. Hörmann, E. J. C. Olson, P. F. Barbara, *Science* **1996**, *273*, 475–479.
[10] P. Lincoln, E. Tuite, B. Nordén, *J. Am. Chem. Soc.* **1997**, *119*, 1454–1455.
[11] E. J. C. Olson, D. Hu, A. Hörmann, P. F. Barbara, *J. Phys. Chem. B* **1997**, *101*, 299–303.
[12] C. J. Murphy, M. R. Arkin, Y. Jenkins, N. D. Ghatlia, S. H. Bossmann, N. J. Turro, J. K. Barton, *Science* **1993**, *262*, 1025–1029. Metal complexes covalently tethered to the ends of a DNA double strand: T. J. Meade, J. F. Kayyem, *Angew. Chem.* **1995**, *107*, 358–360; *Angew. Chem. Int. Ed. Engl.* **1995**, *34*, 353–354; see also the cover page, *ibid.* **1995**, *107*, no. 3 and **1995**, *34*, no. 3.
[13] F. D. Lewis, T. Wu, Y. Zhang, R. L. Letsinger, S. R. Greenfield, M. R. Wasielewski, *Science* **1997**, *277*, 673–676.
[14] a) K. Fukui, K. Tanaka, *Angew. Chem.* **1997**; *Angew. Chem. Int. Ed. Engl.* **1997**, *in press*; b) K. Fukui, K. Iwane, T. Shimidzu, *Tetrahedron Lett.* **1996**, *37*, 4983–4986.
[15] See ref. [7b]; personal communication from T. J. Meade to D. N. Beratan.
[16] a) D. B. Hall, R. E. Holmlin, J. K. Barton, *Nature* **1996**, *382*, 731–735; b) E. D. A. Stemp, M. R. Arkin, J. K. Barton, *J. Am. Chem. Soc.* **1997**, *119*, 2921–2925; c) M. R. Arkin, E. D. A. Stemp, S. Coates Pulver, J. K. Barton, *Chem. Biol.* **1997**, *4*, 389–400.
[17] a) P. J. Dandliker, R. E. Holmlin, J. K. Barton, *Science* **1997**, *275*, 1465–1468; b) G. Taubes, *ibid.* **1997**, *275*, 1420–1421.
[18] T. J. Meade, American Association for the Advancement of Science Meeting, Atlanta, USA, **1995**.

 © WILEY-VCH Verlag GmbH, D-69451 Weinheim, 1997 0570-0833/97/3621-2319 $ 17.50+.50/0

How Can One Recognize a Triple Bond between Main Group Elements?

Karl Wilhelm Klinkhammer*

The synthesis of compounds containing a double bond between heavy main group elements has challenged chemists since the double-bond rule was established by Goubeau in 1957. According to this rule, no double bond, which is stable towards polymerization, should exist between elements for which the sum of their electronegativities exceeds a certain amount (approximately 5).[1] Thus—with the exception of the combinations P/S, S/S, P/Cl, S/Cl, and Cl/Cl—a double bond is stable only if at least one of the atoms is a second-row element.

The ingenuity of some chemists, however, canceled out this rule with a trick called *kinetic stabilization*.[2] By using very bulky substituents a few dozen compounds containing formal double bonds between heavy electropositive elements were synthesized.[3] Compounds with corresponding triple bonds remained unknown. Some of the synthesized alkene homologues, however, show unexpected differences to "ordinary" double bonds: a) The four substituents no longer lie in a plane with the double-bonded atoms (idealized D_{2h} symmetry), but rather show a typical *trans*-bent orientation (idealized C_{2h} symmetry). b) The double bond is only marginally shorter and, in a few cases, even longer than the corresponding single bond. c) Cleaving the double bond requires less energy than cleaving the corresponding single bond; the compound and its carbene-type fragments are often in thermal equilibrium in solution.

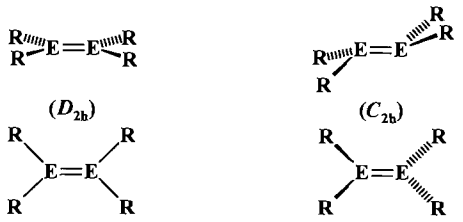

In accordance with Goubeau's rule, these "abnormalities" become more important for elements of low electronegativity. Therefore, no (isolable) molecular compound is known to date containing homonuclear double bonds between the heaviest elements of Group 14, 15, or 16. Molecules showing multiple bonds between the more electropositive heavier elements of Group 13 were unknown until very recently, when the research groups of Uhl, Pörschke, and Power reported the syntheses of radical anions such as $[Al_2R_4]^-$ or $[Ga_2R_4]^-$ (bond order 3/2), and Robinson et al. described the anionic cyclotrigallenes $[R_3Ga_3]^{2-}$ (bond order 4/3).[4] These compounds display the expected shortening of Al–Al and Ga–Ga bond lengths compared to dialanes and digallanes, Al_2H_4 and Ga_2H_4. However, for dimeric cyclopentadienyl derivatives of indium(I) and thallium(I)—which, from a classical point of view, may be double-bonded species (R–E=E–R)—only very long E–E distances (> 350 pm) are observed. Moreover, only monomers are present in solution.[5]

What are then the typical features which unambiguously define a multiple bond? Is a short E–E bond imperative? A recent paper by Robinson et al. allowed us to ask this question again. They reported a compound they call "the first gallyne", that is, the first species showing a triple bond between heavy main group elements.[6] The synthesis was accomplished by using an extremely bulky *m*-terphenyl substituent. During the last years substituents of this type had been frequently used, mainly by the groups of Power and Robinson, to stabilize molecules with atoms of unusually low coordination.[4, 7]

"How short is a –Ga≡Ga– triple bond?" is the question posed at the beginning of the paper on the synthesis and characterization of gallyne **1**, a compound containing two-coordinate

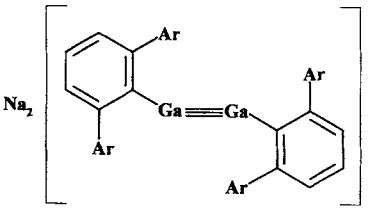

1

Ar = 2,4,6-*i*Pr$_3$C$_6$H$_2$

gallium and an almost planar but nonlinear C-Ga-Ga-C framework.[8] This question possibly reflects a preliminary discussion with Power, who thinks that a Ga–Ga distance of 2.32 Å is too long to be called a triple bond. In his opinion, the observed C-Ga-Ga angles of 129–134° seem to fit better the alternative description of a digallane with one lone pair at each gallium atom (**B**) than a formulation as a triply bonded system (**A**).[9] How can one verify the presence of a multiple bond? Classical criteria are short bond distances, high bond energies, and large force constants as well as a characteristic geometry. Thus, C–C double bonds within alkenes are always shorter than corresponding single bonds within alkanes, much more energy is needed to cleave them, and both carbon atoms exhibit trigonal-planar coordination. On the other hand, the C–C triple bond is shorter and stronger than a double bond, and both carbon atoms are linearly coordinated.

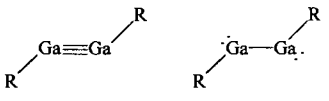

A **B**

Theoretical analyses with ab initio methods show that the elements from the second row of the periodic table have an exceptional position, and the criteria mentioned above are not imperative for multiple bonds between heavy main group elements.[3, 10] This is caused by the different radial extension of

[*] Dr. K. W. Klinkhammer
Institut für Anorganische Chemie der Universität
Pfaffenwaldring 55, D-70569 Stuttgart (Germany)
Fax: Int code +(711)685-4241
e-mail: kw@anorg55.chemie.uni-stuttgart.de

 © WILEY-VCH Verlag GmbH, D-69451 Weinheim, 1997 0570-0833/97/3621-2320 $ 17.50+.50/0

the s and p valence orbitals, which corresponds to a lower inclination to hybridize, and by markedly lower E–E bond energies. Simply said: The amount of energy gained by the hypothetical formation of a double bond from the corresponding carbene homologues is diminished by the energy needed to promote the fragments R_2E from their singlet ground state to their triplet valence state. The same holds for the formation of a triple bond from carbyne- or borylene-homologous fragments.

For most of the carbene fragments R_2C, the sum of the promotion energies is much lower than the C=C bond energy and may even be zero in certain cases. In the case of the analogous silylene, germylene, and stannylene fragments, however, the promotion energy often amounts to more than half of the bond energy of the E–E double bond.[3] In the case of lead, the heaviest Group 14 element, as well as the corresponding EH fragments of Group 13 (E = Al, Ga, In, Tl), promotion energies are even higher, and, at least for this simple model, dimerization is totally inhibited. Lowering the energy of dimerization also results in geometrical changes. The trigonal-planar and linear coordination of the double or triple bonded atoms is distorted. The E–E bond is lengthened, and pyramidalization or tilting of the $E-EH_2$ and E–EH fragments, respectively, occurs.

That means that neither the bond length, nor the bond strength or the topology are reliable criteria for determining the bond order of bonds between heavy main group elements. How can one find a way out of this dilemma? If there are no reliable experimental criteria for a multiple bond, we have to go back to the original definition of a bond and analyze the mode of bonding with quantum mechanics: A *covalent* bond consists of an electron pair which is *localized* on only two atoms, and a *triple* bond is defined by *three* covalent bonds connecting two atoms.

Quantum mechanical calculations are nowadays mainly performed with the widespread LCAO (*l*inear *c*ombination of *a*tomic *o*rbitals) method, which leads to canonical molecular orbitals, that is, delocalized orbitals with coefficients on all atoms. By using the NBO (*n*atural *b*ond *o*rbitals) analysis, however, one may easily transform the canonical orbitals into orbitals which are localized at one or two centers, corresponding to lone pairs or bonds, respectively.[11, 12] The derived model is virtually the same as the simple picture obtained using the octet rule. In the cases of ethylene and acetylene, two and three bonds between the carbon atoms, one σ bond and one or two π bonds, are obtained. Applying this method to gallyne $[Ga_2H_2]^{2-}$, which differs from acetylene by a nonlinear *trans*-bent H-Ga-Ga group, three bonds are also obtained: a) a σ bond, b) an "ordinary" π bond constructed from p orbitals perpendicular to the molecular plane, and c) a "slipped" π bond in which the maxima of electron density is shifted towards the gallium atoms (Figure 1).[13] Closer inspection reveals that this view is equivalent to a model with two donor–acceptor bonds, which was proposed as early as 1976 by Lappert et al. for describing bonding within the distannene $[(Me_3Si)_2CH]_2Sn{=}Sn[CH(SiMe_3)_2]_2$ (Figure 2).[14] In the present gallyne, the donor-acceptor bonds are augmented by an additional π bond to yield a Ga–Ga triple bond.[15]

A pure quantum mechanical definition of a multiple bond which is not further verified by experimental data may or may not be accepted. However, the very existence of compounds such as the gallyne remains exciting, because established, apparently unique conceptions and models lead to ambiguous statements and, therefore, have to be modified. The principle of kinetic stabilization supported by extremely bulky substituents will hopefully yield further thrilling compounds.

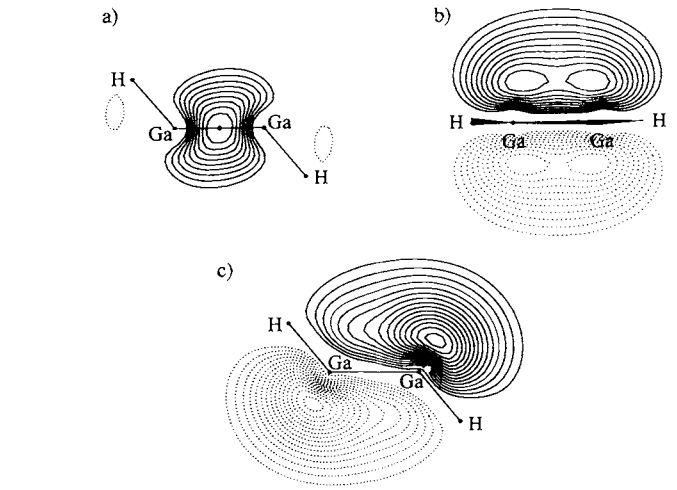

Figure 1. Ga≡Ga bond orbitals derived from NBO analysis. The different signs of the wave functions are represented by solid and dotted contours; a) σ bond, b) π bond, c) "slipped" π bond.

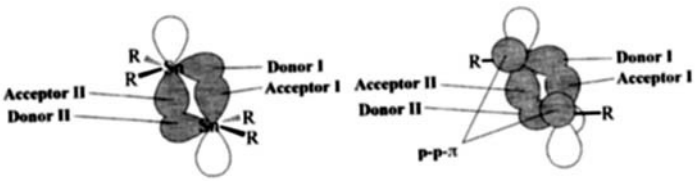

Figure 2. Description of the bonding situation in Sn_2R_4 (left) and $[Ga_2R_2]^{2-}$ (right) according to the model of donor–acceptor bonds [14].

German version: *Angew. Chem.* **1997**, *109*, 2414–2416

Keywords: ab initio calculations · bond theory · main group elements · multiple bonds · subvalent compounds

[1] J. Goubeau, *Angew. Chem.* **1957**, *69*, 3.

[2] From the point of view of physics, the term "kinetic stabilization" should not be used because it intermingles kinetics and thermodynamics. The effects which are described by this term, however, do consist of both a kinetic and a thermodynamic contribution in many cases: On the one hand, the oligomerization reactions are slowed down, and, on the other, the oligomerization products are thermodynamically destabilized.

[3] Review: M. Driess, H. Grützmacher, *Angew. Chem.* **1996**, *108*, 900; *Angew. Chem. Int. Ed. Engl.* **1996**, *35*, 828.

[4] W. Uhl, A. Vester, W. Kaim, J. Poppe, *J. Organomet. Chem.* **1993**, *454*, 9; C. Pluta, K.-R. Pörschke, C. Krüger, K. Hildenbrand, *Angew. Chem.* **1993**, *105*, 451; *Angew. Chem. Int. Ed. Engl.* **1993**, *32*, 388; R. J. Wehmschulte, K. Ruhlandt-Senge, M. M. Olmstead, H. Hope, B. E. Sturgeon, P. P. Power, *Inorg. Chem.* **1993**, *32*, 2983; X. He, R. A. Bartlett, M. M. Olmstead, K. Ruhlandt-Senge, B. E. Sturgeon, P. P. Power, *Angew. Chem.* **1993**, *105*, 761; *Angew. Chem. Int. Ed. Engl.* **1993**, *32*, 717; X.-W. Li, W. T. Pennington, G. H. Robinson, *J. Am. Chem. Soc.* **1995**, *117*, 7578; X.-W. Li, Y. Xie, P. R. Schreiner, K. D. Gripper, R. C. Crittendon, C. F. Campana, G. H. Robinson, H. F. Schaefer III, *Organometallics* **1996**, *15*, 3798.

[5] H. Schumann, C. Janiak, J. Pickardt, U. Börner, *Angew. Chem.* **1987**, *99*, 788; *Angew. Chem. Int. Ed. Engl.* **1987**, *26*, 789; H. Schumann, C. Janiak, F. Görlitz, J. Loebel, *J. Organomet. Chem.* **1989**, *363*, 243.

[6] J. Su, X.-W. Li, R. C. Crittendon, G. H. Robinson, *J. Am. Chem. Soc.* **1997**, *119*, 5471.

[7] R. S. Simons, L. H. Pu, M. M. Olmstead, P. P. Power, *Organometallics* **1997**, *16*, 1920; J. J. Ellison, P. P. Power, *J. Organomet. Chem.* **1996**, *526*, 263; J. J. Ellison, K. Ruhlandt-Senge, H. H. Hope, P. P. Power, *Inorg. Chem.* **1995**, *34*, 49.

 © WILEY-VCH Verlag GmbH, D-69451 Weinheim, 1997 0570-0833/97/3621-2321 $ 17.50+.50/0

[8] There are additional, presumably ionic contacts (Ga··Na 308 pm (mean value)) to both sodium atoms, which are held in place by two chelating arene rings and probably reduce the electrostatic repulsion between the negatively charged Ga atoms.
[9] R. Dagani, *Chem. Eng. News*, June 10, **1997**, 9.
[10] W. Kutzelnigg, *Angew. Chem.* **1984**, *96*, 262; *Angew. Chem. Int. Ed. Engl.* **1984**, *23*, 272.
[11] J. E. Carpenter, F. Weinhold, *J. Mol. Struct.* **1988**, *169*, 41, and references therein.
[12] The ELF (*e*lectron *l*ocalization *f*unction) is a further suitable tool for interpreting results of quantum chemical calculations in terms of such vivid concepts as "lone pair" or "bond": B. Silvi, A. Savin, *Nature* **1994**, *371*, 683; A. D. Becke, E. Edgecombe, *J. Chem. Phys.* **1990**, *92*, 5397; A. Savin, A. D. Becke, J. Flad, R. Nesper, H. G. von Schnering, *Angew. Chem.* **1991**, *103*, 421; *Angew. Chem. Int. Ed. Engl.* **1991**, *30*, 409; A. Savin, R. Nesper, S. Wengert, T. F. Fässler, *ibid.* **1997**, *109*, 1892 and **1997**, *36*, 1808. This function, which measures the probability of finding two electrons of opposite spin in the same space, is in accordance with a triple bond within gallyne $[Ga_2H_2]^{2-}$.
[13] I carried out the NBO analyses employing the NBO module implemented in Gaussian 94: NBO Version 3.1, E. D. Glendening, A. E. Reed, J. E. Carpenter, F. Weinhold implemented in Gaussian 94, Revision D.1: M. J. Frisch, G. W. Trucks, H. B. Schlegel, P. M. W. Gill, B. G. Johnson, M. A. Robb, J. R. Cheeseman, T. Keith, G. A. Petersson, J. A. Montgomery, K. Raghavachari, M. A. Al-Laham, V. G. Zakrzewski, J. V. Ortiz, J. B. Foresman, J. Cioslowski, B. B. Stefanov, A. Nanayakkara, M. Challacombe, C. Y. Peng, P. Y. Ayala, W. Chen, M. W. Wong, J. L. Andres, E. S. Replogle, R. Gomperts, R. L. Martin, D. J. Fox, J. S. Binkley, D. J. Defrees, J. Baker, J. P. Stewart, M. Head-Gordon, C. Gonzalez, J. A. Pople, Gaussian, Pittsburgh (PA), **1995**. The gallium atoms were described by LANL2 pseudopotentials. Basis sets of double-zeta quality were used for hydrogen, carbon, and gallium.
[14] P. J. Davidson, D. H. Harris, M. F. Lappert, *J. Chem. Soc. Dalton Trans.* **1976**, 2268; D. E. Goldberg, P. B. Hitchcock, M. F. Lappert, K. M. Thomas, A. J. Thorne, T. Fjeldberg, A. Haaland, *J. Chem. Soc. Dalton Trans.* **1986**, 2387. Double or triple bond models with equivalent "banana bonds" instead of σ and π bonds are obtained by unitary transformations. An analogous relationship exists between the bonding model for gallyne $[Ga_2H_2]^{2-}$ derived here and the model by Lappert of two donor–acceptor bonds (augmented by a further π bond)
[15] Quantum chemical investigations of the bonding within homologues systems of alkenes and alkines, E_2H_4 and E_2H_2, yield analogous results. A survey is given in ref. [3] as well as in K. Kobayashi, S. Nagase, *Organometallics* **1997**, *16*, 2489, and references therein. The latter demonstrates that the introduction of bulky ligands further stabilizes the *trans*-bent form of disilynes (R_2Si_2), which are isolelectronic to Robinson's gallyne.

EVENTS

Announcing the

XXIII International Symposium on Macrocyclic Chemistry

Macrocycles in Academe and Industry

June 7th–12th, 1998
Turtle Bay, Hawai

Imaging, Chelation, Catalysis, Molecular Recognition, Sensing.
Poster Presentations Currently Being Accepted.

Site of symposium is the Turtel Bay Hilton on the North Shore of the Island of Oahu. Activities of interest include golf, surfing, and tennis. An excursion to the Polynesian Center is planned. Organized by Jonathan Sessler, Eric Anslyn, and Eiichi Kimura.

To acquire registration and poster contribution forms please write: Eric V. Anslyn, Department of Chemistry and Biochemistry, The University of Texas at Austin, Austin TX 78712, or e-mail anslyn@ccwf.cc.utexas.edu.

 © WILEY-VCH Verlag GmbH, D-69451 Weinheim, 1997 0570-0833/97/3621-2322 $ 17.50+.50/0

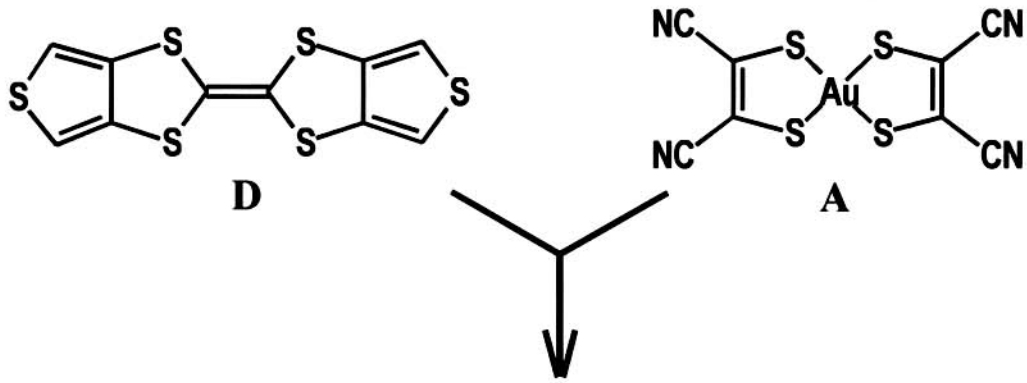

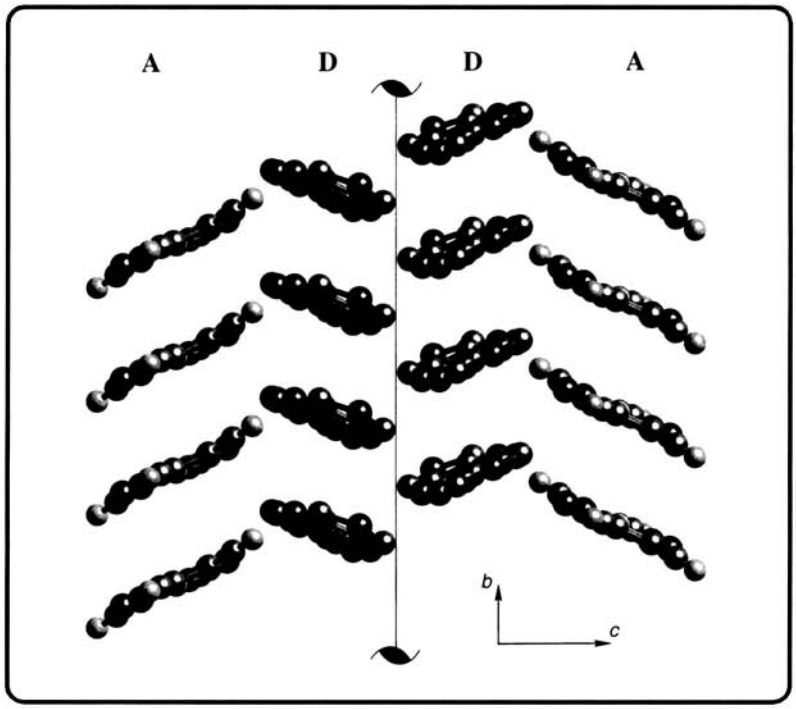

Electrocrystallization of the donor D and the nBu$_4$N salt of the acceptor A gave crystals (structure in the center) whose donor stacks form a two-leg spin ladder

223 K

by localization of unpaired electrons in D_2^{+} units (principles of the construction depicted at the bottom). For further details, see the following pages.

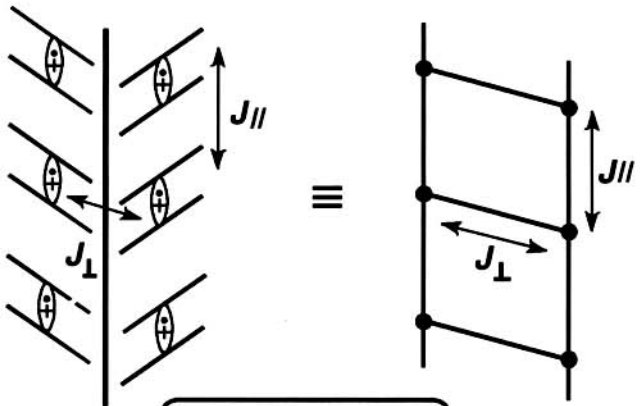

spin ladder

 © WILEY-VCH Verlag GmbH, D-69451 Weinheim, 1997 0570-0833/97/3621-2323 $ 17.50+.50/0

An Organic Spin-Ladder Molecular Material**

Concepció Rovira,* Jaume Veciana, Elisabet Ribera, Judit Tarrés, Enric Canadell, Roger Rousseau, Montserrat Mas, Elies Molins, Manuel Almeida, Rui T. Henriques, Jorge Morgado, Jean-Philippe Schoeffel, and Jean-Paul Pouget

Materials with a ladder type arrangement of the spins ("spin-ladder compounds") have brought a lot of excitement to the quantum magnets community.[1] The initial expectations concerning these materials have been fully confirmed by recent findings of a puzzling dependence of the bulk magnetic properties with the even/odd number of legs in the ladder. Recent results on metal-based compounds (mainly oxides) indicate that while odd-leg ladders are gapless and have magnetic behavior similar to one-dimensional chains, even-leg ladders have only short-range order and a finite spin gap. In addition, holes injected into even-leg ladders are predicted to pair and possibly show superconductivity.[2] Until now only very few two-leg and three-leg ladder compounds formed by connected chains of transition metal atoms have been studied.[2a, 3] Because of their structural flexibility molecular solids offer many possiblities to finely tune interesting physical situations such as those exhibited by spin-ladder materials. Molecular organic solids with this kind of behavior could be obtained by assembling a finite number of molecular chains one next to the other to form "ladder-structures" of increasing width. We have succeeded in preparing and characterizing $[(DT\text{-}TTF)_2][Au(mnt)_2]$ (**1**, DT-TTF = "dithiophentetrathiafulvalene", mnt = maleonitrile dithiolate), one of these wide spin-ladder organic solids.

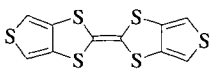

DT-TTF

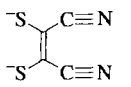

mnt

By analogy with the metallic α phases of the $(Per)_2M(mnt)_2$ family (Per = perylene, M = metal), which crystallize in a structure containing pairs of perylene chains surrounded by $M(mnt)_2$ chains,[4] we sought to construct a ladder molecular organic compound by replacing perylene by an appropriate aromatic donor. As electron donor we chose DT-TTF, [5] which tends to stack to form chainlike structures and which contains sulfur atoms on the periphery that are able to promote close contacts between the chains,[6] to provide the rungs of the spin ladder system. As counterion we chose the closed-shell monoanion $[Au(mnt)_2]^-$,[7] which might magnetically isolate the ladder chains.

The target compound $[(DT\text{-}TTF)_2][Au(mnt)_2]$ (**1**) was obtained as dark needles by electrocrystallization from a dichloromethane solution containing the donor and the tetrabutylammonium salt of $[Au(mnt)_2]^-$. The mixed valence character of this salt was confirmed by the presence in the near infrared (NIR) spectrum of the characteristic "A" band of the mixed valence states centered at 2700 nm.[8] Compound **1** crystallizes in the monoclinic system,[9] and the asymmetric unit comprises one molecule of DT-TTF and 0.5 molecule of $[Au(mnt)_2]$. At room temperature the DT-TTF and $[Au(mnt)_2]$ molecules form segregated regular stacks of donors and acceptors along *b* in a herringbone pattern (Figure 1). Inside each stack, donors **D** (DT-TTF) and acceptors **A** ($[Au(mnt)_2]$) slip parallel to the shortest axis of the molecule and have interplanar distances of 3.555(3) and 3.581(4) Å, respectively. The DT-TTF stacks are arranged in pairs related by a twofold screw axis, and they alternate with single stacks of $[Au(mnt)_2]$ along the $a-c$ direction. Apparently the pairs of organic donor stacks form a structural two-leg ladder, since they are strongly linked by three interstack S···S close contacts (Figure 1b). As shown later, the double donor stacks form a two-leg spin ladder below 225 K due

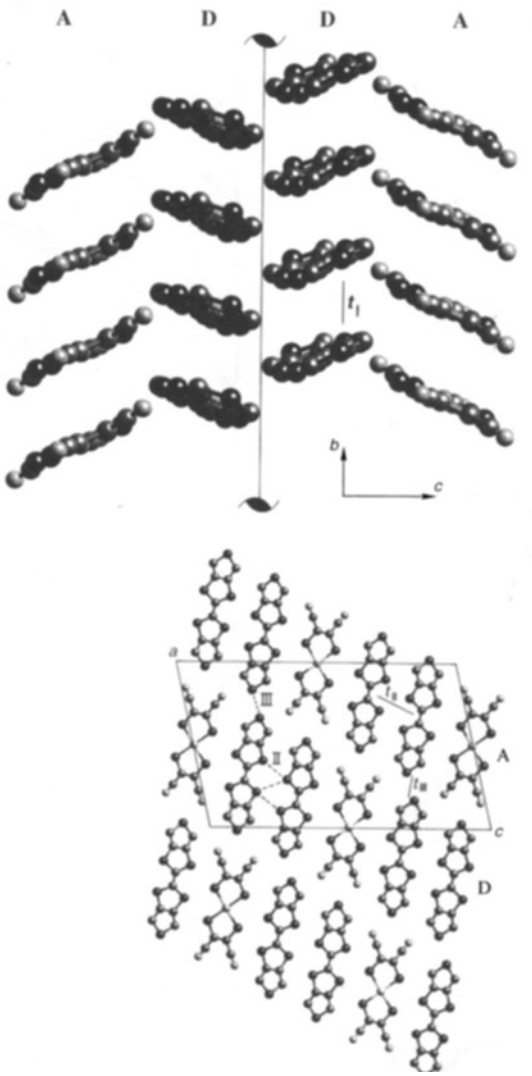

Figure 1. Top: Crystal packing of $[(DT\text{-}TTF)_2][Au(mnt)_2]$ (**1**) at 293 K showing the organic DT-TTF stacks **D** related by a twofold screw axis. Bottom: Projection of the crystal structure along *b*, short S···S contacts (between 3.460 and 3.944 Å) are indicated by dotted lines. This figure represents the average structure. It does not include the local dimerization discussed in the text.

[*] Dr. C. Rovira, Prof. J. Veciana, E. Ribera, J. Tarrés, Prof. E. Canadell, Dr. R. Rousseau, Dr. M. Mas, Dr. E. Molins
Institut de Ciència dels Materials de Barcelona (CSIC)
Campus de la U. A. B., E-08193 Bellaterra (Spain)
Fax: Int. code +(3)580-5729
e-mail: c.rovira@icmab.es

Dr. M. Almeida
Departamento de Química, Instituto Tecnológico e Nuclear
P-2686 Sacavém Codex (Portugal)

Dr. R. T. Henriques, Dr. J. Morgado
Departamento de Engenharia Química, Instituto Superior Técnico
P-1096 Lisboa Codex (Portugal)

Prof. J.-P. Pouget, J.-P Schoeffel
Laboratoire de Physique des Solides (CNRS URA 02), Batiment 510
Université Paris-Sud, F-91405 Orsay (France)

[**] This work was supported by the Programa Nacional de Química Fina (CIRIT-CICyT; grant, QFN93-4510-C01) and by the Generalitat de Catalunya (SGR95-0057) in Barcelona, by PRAXIS 2/2.1/QUI/203/94, in Sacavém and by JNICT-CSIC agreement. E. R. thanks CIRIT for a fellowship.

 © WILEY-VCH Verlag GmbH, D-69451 Weinheim, 1997 0570-0833/97/3621-2324 $ 17.50+.50/0

to the localization of unpaired electrons in $(DT\text{-}TTF)_2^{+}$ dimeric units.

The electrical conductivity along the chain axis b is thermally activated and is about 8 $S\,cm^{-1}$ at room temperature. Its temperature dependence (Figure 2) has an inflexion point at about 220 K, denoting that the gap increases significantly below this temperature. The thermopower $S(T)$ is positive (about 40 $\mu v\,K^{-1}$ at 300 K), indicating a hole transport as expected in a partially oxidized (quarter empty) donor band.

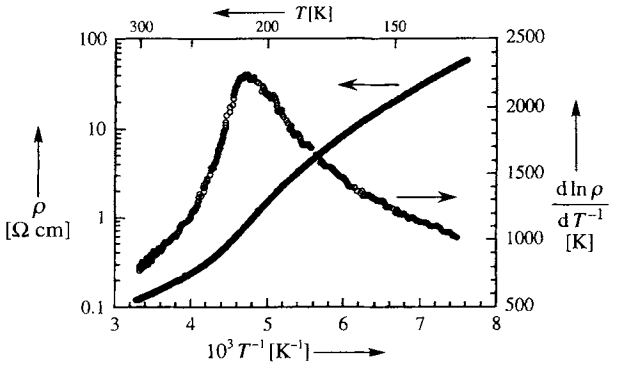

Figure 2. Electrical resistivity ρ of $[(DT\text{-}TTF)_2][Au(mnt)_2]$ as a function of the reciprocal temperature (left) and its first derivative, $d\ln\rho/dT^{-1}$ (right), measured along the needle axis b by the standard four-probe method.

Taken together, the 2:1 stoichiometry, the closed-shell character of $[Au(mnt)_2]^{-}$, and the electrical transport measurements clearly show that below 220 K the unpaired electrons are quite localized in the organic, DT-TTF, interacting double chains. Consequently, depending on the strength of the interactions within and between the double chains, this organic system could well fulfill the requirements for spin-ladder behavior. In order to quantify this point we have calculated the HOMO–HOMO transfer integrals for the different donor $\cdots$ donor interactions of the lattice.[10] There are only three types of DT-TTF interactions (Figure 1): 1) those within the DT-TTF molecular chains (I), 2) those connecting the two molecular chains that form the pair (II), and 3) those between the extremities of the molecules in different paired chains (III). The calculated $t_{HOMO-HOMO}$ transfer integrals are 36 meV for t_I, 21 meV for t_{II}, and 6 meV for t_{III}. Three important implications may be drawn from these values. First, the transfer integral t_{III} between the pairs of chains is quite small relative to those within chains (t_I and t_{II}). Thus, the different pairs of chains of the lattice are probably quite isolated. Second, the transfer integrals up the chain (t_I) and coupling the two paired chains (t_{II}) are nonnegligible. Third, these transfer integrals within chains (t_I and t_{II}), although nonnegligible, are smaller than those of related molecular metals. This agrees with the relatively high but activated conductivity. These three observations suggested a possible spin-ladder behavior for **1** in which the paired chains constitute the ladder. However, before pursuing along this line, we must consider additional structural features that explain more clearly the observed electronic localization.

In order to study this point, X-ray diffuse scattering experiments were performed.[11] X-ray patterns taken at 15 K reveal a weak scattering consisting of single diffuse lines located midway between successive layers of main Bragg reflections perpendicular to the chain direction b. Its reduced wave vector ($0.5b^*$) shows that a dimerization is achieved in the chain direction. These lines are broader than the experimental resolution, which means that the dimerization takes place only on a local scale. At 15 K their half width at half maximum (HWHM) along b is of $\Delta Q = 0.035$ Å^{-1}. The inverse of this quantity, corrected by the (gaussian) resolution, leads to an intrachain correlation length ξ_b of 60(40) Å, if one assumes an intrinsic Lorentzian (gaussian) profile for the diffuse scattering. As shown in Figure 3 (top) these diffuse lines begin to broaden substantially above about 225 K and at 295 K ξ_b amounts to about 20 Å.

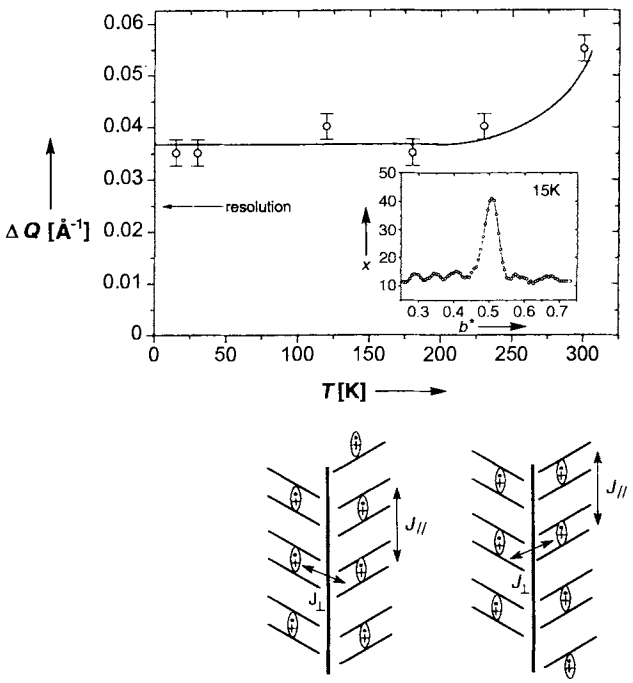

Figure 3. Top: Thermal dependence of the HWHM along the b axis of the $1/2b^*$ diffuse lines of **1**. The inset shows the profile along b^* of such a line (χ is the number of counts in arbitary units). Bottom: Schematic illustration of the two possible two-leg ladders formed by the dimerization of DT-TTF stacks, where $J_{\parallel}$ is the exchange coupling along the chains, and $J_{\perp}$ is the coupling along the rungs.

The weakness of the scattering suggests that the dimerization occurs on the pairs of strongly linked DT-TTF stacks. The observation of diffuse lines means that there is no sizable phase relation between the dimerization of first pairs of adjacent stacks. Their finite width shows that the dimerization locally breaks the twofold screw axis symmetry, which relates the two stacks that form the ladder. As there are two ways to break this symmetry (see Figure 3, bottom), it can be easily understood that their simultaneous realization on a given pair of stacks will limit the intrachain correlation length. From the previous determination of ξ_b, one can estimate an average domain size at low temperature of about $L_b (= \pi\xi_b) = 150$ Å (i.e. $40b$). Therefore, this structural study indicates that at low temperature (15–225 K) this molecular system consists of isolated ladders with a finite number (about 40) of rungs. The decrease of this number above 225 K leads to a better conducting state.

In this picture each dimer has one localized electron (Figure 3, bottom). Since $[Au(mnt)_2]^{-}$ has a closed-shell nature, the magnetic properties of this compound arise only from the spins located in the organic $(DT\text{-}TTF)_2^{+}$ units of the ladders, in agreement with the observed ESR g factor. Thus the ESR g factor of the radical cation $[DT\text{-}TTF]^{\cdot+}$ in solution,[5] is very close to the average g value of the crystals of **1**. As expected, the minimum g value is observed when the magnetic field is applied parallel to the stacking b axis.[12] The relatively large paramagnetism thus associated with these $[(DT\text{-}TTF)_2]^{\cdot+}$ units does not show any significant anomaly around 220 K, where the trans-

 © WILEY-VCH Verlag GmbH, D-69451 Weinheim, 1997 0570-0833/97/3621-2325 $ 17.50+.50/0

port properties displayed anomalies; this fact indicates that, due to electronic correlations, the spin and charge degrees of freedom in the DT-TTF chains are separated. The most important result (Figure 4) is that the static magnetic susceptibility[13] $\chi(T)$

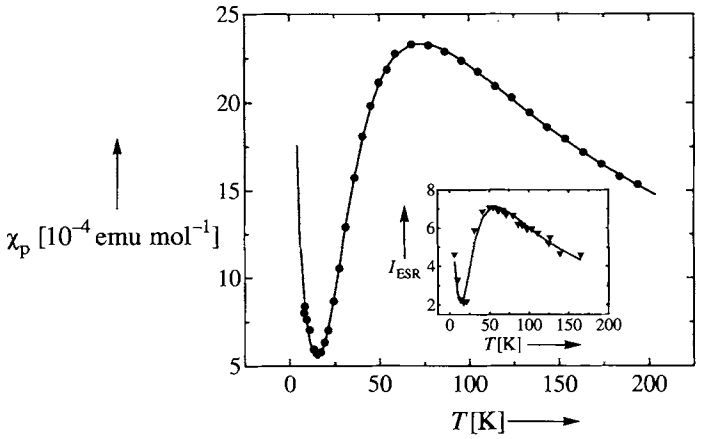

Figure 4. Temperature dependence of the paramagnetic susceptibility. The solid line is the fit to the expression (2) of reference [2c] (see text). Inset shows the temperature dependence of paramagnetic susceptibility measured by ESR on a single crystal.

shows an activated behavior above 70 K together with a Curie–Weiss behavior at higher temperatures. This is characteristic of a system having localized spins with strong antiferromagnetic interactions, which displays a spin gap. In this respect the experimental data from 8 to 45 K can be fitted to the low temperature expression for the susceptibility of a two-leg ladder model found by Troyer et al. [Eq. (1)],[14] where α is a constant corresponding

$$\chi_{ladder} = \alpha T^{-1/2} \exp(-\Delta/kT) \quad (1)$$

to the dispersion of the excitation energy, and Δ is the finite energy gap in the spin-excitation spectrum. For such a fit Equation (2), which takes into account the Curie contribution due

$$\chi = f\chi_{ladder} + (1-f)\chi_{Curie} \quad (2)$$

both to the finite sizes of the ladders and to the magnetic defects present in the crystals, was used. In Equation (2) f is the molar fraction of $[(DT\text{-}TTF)_2]^{\bullet+}$ units forming the regular ladder. The resulting parameters of this fit were $f = 0.98$, $\alpha = 7.22 \times 10^{-4}$ emu $K^{1/2}$ mol^{-1}, and $\Delta/k = 78$ K ($r^2 = 0.9972$). The experimental susceptibility was also fitted with the expression (2) given by Barnes and Riera,[2c] for a two-leg ladder model (solid line in Figure 4), which provides the exchange coupling parameters $J_{\parallel}$ and $J_{\perp}$, of the ladder spin configuration. The resulting parameters of such a fit were $f = 0.980$, $J_{\parallel}/k = -83$ K and $J_{\perp}/k = -142$ K ($r^2 = 0.9989$). The ratio between $J_{\parallel}$ and $J_{\perp}$ is in good agreement with the ratio between the transfer integrals evaluated from the t_I and t_{II} values once the dimeric nature of the elementary building block of the ladder is taken into account. The spin gap has also been calculated from the resulting values of $J_{\parallel}$ and $J_{\perp}$ by using the expression $\Delta = |J_{\perp}| - |J_{\parallel}| + J_{\parallel}^2/2J_{\perp}$,[14] to give $\Delta/k = 83$ K, in good agreement with the previous value. The intensity of the ESR signal, which is proportional to the paramagnetic spin susceptibility, also exhibits the same thermal dependence as the static spin susceptibility (inset of Figure 4), confirming that the spin-ladder behavior occurs on the organic $[(DT\text{-}TTF)_2]^{\bullet+}$ stacks.

The results presented here characterize $[(DT\text{-}TTF)_2][Au(mnt)_2]$ as the first example of a purely organic system with a ladder spin configuration that shows this magnetic behavior below 225 K. This result opens new possibilities to apply supramolecular chemistry for tailoring ladder architectures with different structural characteristics and promising magnetic properties.

Received: April 17, 1997 [Z10360IE]
German version: *Angew. Chem.* **1997**, *109*, 2417–2421

Keywords: conducting materials · crystal engineering · magnetic properties · radical ions · spin-ladder compounds

[1] a) E. Dagotto, T. M. Rice, *Science* **1996**, *271*, 618–623; b) Z. Hiroi, M. Takano, *Nature* **1995**, *377*, 41–43; c) D. J. Scalapino, *ibid.* **1995**, *377*, 12–13.

[2] a) E. Dagotto, J. Riera, D. J. Scalapino, *Phys. Rev. B* **1992**, *45*, 5744–5747; b) S. Gopalan, T. M. Rice, M. Sigrist, *ibid.* **1994**, *49*, 8901–8910; c) T. Barnes, J. Riera, *ibid.* **1994**, *49*, 6817–6822; d) S. R. White, R. M. Noack, D. J. Scalapino, *Phys. Rev. Lett.* **1994**, *73*, 882–886; e) C. A. Hayward, D. Poilblanc, L. P. Lévy, *ibid.* **1995**, *75*, 926–929.

[3] a) H. Imai, T. Inabe, T. Otsuka, T. Okuno, K. Awaga, *Phys. Rev. B* **1996**, *54*, 6838–6840; b) R. S. Eccleston, T. Barnes, J. Brody, J. W. Johnson, *Phys. Rev. Lett.* **1994**, *73*, 2626–2629; c) M. Azuma, Z. Hiroi, M. Takano, K. Ishida, Y. Kitaoka, *ibid.* **1994**, *73*, 3463–3466; d) T. M. Rice, S. Gopalan, M. Sigrist, *Europhys. Lett.* **1993**, *23*, 445–450.

[4] M. Almeida, V. Gama, R. T. Henriques, L. Alcácer in *Inorganic and Organometallic Polymers with Special Properties*; (Ed.: R. M. Laine), Kluwer, Dordrecht, The Netherlands, **1992**, pp. 163–177.

[5] C. Rovira, J. Veciana, N. Santaló, J. Tarrés, J. Cirujeda, E. Molins, J. Llorca, E. Espinosa, *J. Org. Chem.* **1994**, *59*, 3307–3313.

[6] J. J. Novoa, M. C. Rovira, C. Rovira, J. Veciana, J. Tarrés, *Adv. Mater.* **1995**, *7*, 233–237.

[7] A. Davison, N. Edelstein. R. H. Holm, A. H. Maki, *Inorg. Chem.* **1963**, *2*, 1227–1232.

[8] J. B. Torrance, B. A. Scott, B. Welber, F. B. Kaufmann, P. E. Seiden, *Phys. Rev. B* **1979**, *19*, 730–741.

[9] Crystallographic data for $C_{28}H_{16}N_4S_{16}Au$: crystal dimensions $0.37 \times 0.23 \times 0.065$ mm; $M_r = 1110.31$, monoclinic, space group $P2_1/n$, $a = 16.334(1)$, $b = 3.912(1)$, $c = 27.348(2)$ Å, $\beta = 101.787(6)°$; $Z = 2$; $V = 1710.7(2)$ Å^3, $\rho_{calcd} = 2.16$ g cm^{-3}. Data were collected at 293 K on an Enraf-Nonius CAD4 diffractometer equipped with a Mo X-ray tube, and a graphite monochromator selected $Mo_{K\alpha}$ radiation (absorption coefficient $\mu = 5.31$ mm^{-1}. Data collection up to $2\theta = 62°$ and $-23 \le h \le 23$, $0 \le k \le 5$, $-39 \le l \le 0$ affords 7898 reflections measured with $\omega - 2\theta$ scans. Lorentz, polarization, and absorption (DIFABS: max/min absoption factors 1.254/0.793) effects were corrected. The structure was refined using full-matrix least-squares methods (SHELXL-93). The minimized function was $\omega(F_o^2 - F_c^2)^2$ with $\omega = 1/\sigma^2F^2 + (AP)^2 + BP$ and $A = 0.0419$, $B = 0.57$, $P = [\mathrm{Max}(0 \cdot F_o) + 2F_c]/3$ and s, the standard deviation estimated from counting statistics. At convergence the final R indices were $R_1 = 0.068$, $wR_2 = 0.078$ (for all data) and $R_1 = 0.027$, $wR_2 = 0.066$ (for $I > 2\sigma(I)$ reflections). The final max/min residuals were $1.11/-0.91$ e Å^{-3}. Crystallographic data (excluding structure factors) for the structure reported in this paper have been deposited with the Cambridge Crystallographic Data Centre as supplementary publication no. CCDC-100375. Copies of the data can be obtained free of charge on application to The Director, CCDC, 12 Union Road, Cambridge CB21EZ, UK (fax: int. code +(1223)336-033; e-mail: deposit@chemcrys.cam.ac.uk).

[10] As in previous studies of related materials (L. F. Veiros, M. J. Calhorda, E. Canadell, *Inorg. Chem.* **1994**, *33*, 4290–4294), the calculations use an extended Hückel type hamiltonian (R. Hoffmann, *J. Chem. Phys.* **1963**, *39*, 1397-1412) and a modified Wolfsberg–Helmholz formula (J. H. Ammeter, H.-B. Bürgi, J. Thibeault, R. Hoffmann, *J. Am. Chem. Soc.* **1978**, *100*, 3686–3692) to calculate the nondiagonal H_{ij} matrix elements and a single-ζ atomic orbital basis set.

[11] The experiment was performed with the so-called "fixed film-fixed crystal" method with a monochromatized $Cu_{K\alpha}$ ($\lambda = 1.542$ Å) beam.

[12] The ESR spectra consists in a single Lorentzian line in all the orientations of the crystal with respect to the external magnetic field. The room temperature line-widths measured in the three orthogonal orientations of the crystal are $\Delta H_{pp} = 42$, 25, and 26 G, with g factors of 2.0127, 2.0050, and 2.0020, respectively.

[13] Magnetic susceptibility was measured by the Faraday method in the range 4–300 K in a polycrystalline sample with an applied magnetic field of 1 T. A correction for the diamagnetic contribution estimated as 4.6×10^{-4} emu mol^{-1} from tabulated Pascal constants was applied.

[14] M. Troyer, H. Tsunetsugu, D. Würtz, *Phys. Rev. B* **1994**, *50*, 13515–13527.

 © WILEY-VCH Verlag GmbH, D-69451 Weinheim, 1997 0570-0833/97/3621-2326 $ 17.50+.50/0

Anion Control in Bipyridylsilver(I) Networks: A Helical Polymeric Array**

Matthew A. Withersby, Alexander J. Blake, Neil R. Champness, Peter Hubberstey,* Wan-Sheung Li, and Martin Schröder*

The construction of inorganic supramolecular arrays based on covalent interactions[1] or hydrogen bonding[2] is a rapidly developing area of research that has implications for the rational design of functional materials. A variety of architectures have been reported including adamantoid,[3-5] octahedral,[6] ladder,[7] honeycomb,[8] and "brick wall".[9] We have been investigating the effect of ligand functionality in the construction of arrays based on Cu^I and Ag^I,[4] and report here what we believe to be a unique helical structural motif in inorganic supramolecular architectures. Furthermore, the structure of $[Ag(pytz)(X)]_\infty$[10] is both anion-controlled for $X = NO_3^-$—the structure contrasts markedly with that of the corresponding $X = PF_6^-$ and BF_4^- analogues—and dependent upon ligand functionality. This gives a completely different structural motif from that of the corresponding 4,4′-bipyridyl complex, $[Ag(4,4'\text{-bpy})(NO_3)]_\infty$.[11]

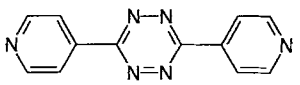

3,6-di(4-pyridyl)-1,2,4,5-tetrazine

pytz

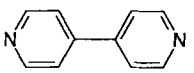

4,4′-bipyridine

4,4′-bpy

$[Ag(pytz)(NO_3)]_\infty$ was prepared as scarlet-red hexagonal crystals by layering a solution of $AgNO_3$ in MeCN over a solution of pytz in CH_2Cl_2. The crystals grew over a period of two days, and could be prepared from the reaction of either one or two equivalents of ligand per equivalent of $AgNO_3$. The single-crystal X-ray structure of the product[12] shows that each Ag^I ion is coordinated to two pytz ligands in a linear arrangement (Ag–N11 2.154(3), Ag–N21 2.151(3) Å, N11-Ag-N21 180°) to give linear chains of alternating Ag^I ions, separated by 15.34 Å, and pytz ligands. As in $[Ag(4,4'\text{-bpy})(NO_3)]_\infty$, the chains align in a parallel fashion to form two-dimensional sheets. In the 4,4′-bpy complex alternate sheets, which are linked by Ag···Ag interactions, are oriented at 90° with respect to each other. In the pytz complex, however, the sheets stack along a 6_1 screw axis to give a helical staircase motif. In fact, each Ag^I center interacts weakly with two NO_3^- ions (d(Ag–O31) = d(Ag–O32) = 2.787(2) Å),[16] which adopt positions perpendicular to the pytz-Ag-pytz axis, to give a pseudo square planar geometry at the Ag^I center (Figure 1). The NO_3^- ions bridge adjacent chains through two of their oxygen atoms; each chain is related to the next by a 60° rotation and by a step of 5.18 Å to generate the helical staircase motif (Figure 2). Thus, despite their weakness, the resultant 3D structure is controlled by $Ag^I \cdots NO_3^-$ interactions. The points at which the chains cross—one may consider these as the center of the helix—correspond to overlapping pyridine units (Figures 2 and 3). We believe this helical motif to be unique in inorganic supramolecular architectures, and, significantly, it contrasts markedly with the structure observed for $[Ag(4,4'\text{-bpy})(NO_3)]_\infty$,[11] which consists of linear Ag^I–bpy chains linked in a T-shape through Ag···Ag interactions (Ag–Ag 2.970(2) Å). This confirms the importance of ligand functionality in determining the structure of these types of inorganic supramolecular arrays.

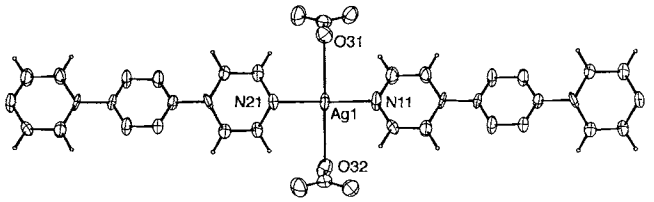

Figure 1. View of the pseudo square planar environment at the Ag centers in $[Ag(pytz)(NO_3)]_\infty$.

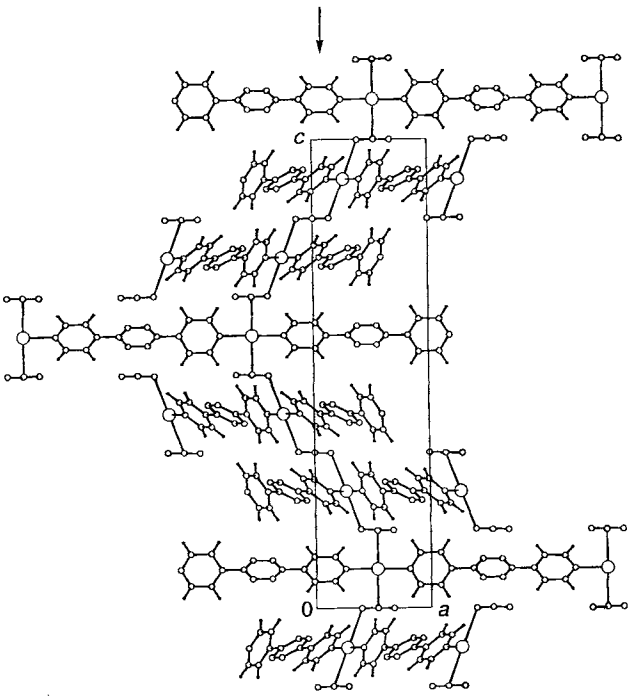

Figure 2. View of the helical structure of $[Ag(pytz)(NO_3)]_\infty$ from the side, which illustrates the pivotal role of the NO_3^- ions. The 6_1 screw axis is marked with an arrow.

The degree of anion control observed in the structure of $[Ag(pytz)(NO_3)]_\infty$ is illustrated by the structure of the isomorphous PF_6^- and BF_4^- complexes, $[Ag(pytz)(PF_6)(MeCN)]_\infty$ and $[Ag(pytz)(BF_4)(MeCN)]_\infty$. Both were prepared analogously to the NO_3^- complex, and deep-red crystals were obtained over similar time periods. The single-crystal X-ray structure of these complexes[17,18] revealed a completely different and comparatively simple structure based on linear chains of alternating Ag^I ions and pytz ligands which align themselves along the [101] direction. However, the 3D structure is different to that of the 4,4′-bpy analogue in that the chains formed pairs which were joined through Ag···Ag interactions (3.230(1) Å (PF_6^- compound) and 3.312(1) Å (BF_4^- compound)) and $\pi-\pi$ interactions between adjacent pytz ligands (Figure 4). In addition, each Ag^I ion in these structures interacts with a MeCN solvent mole-

[*] Dr. P. Hubberstey, Prof. M. Schröder, M. A. Withersby, Dr. A. J. Blake, Dr. N. R. Champness, Dr. W.-S. Li
Department of Chemistry
University of Nottingham
University Park, Nottingham, NG7 2RD (UK)
Fax: Int code +(115)951-3563
e-mail: p.hubberstey@nottingham.ac.uk
m.schröder@nottingham.ac.uk

[**] This work was supported by the Engineering and Physical Sciences Research Council (UK) and by the University of Nottingham.

 © WILEY-VCH Verlag GmbH, D-69451 Weinheim, 1997 0570-0833/97/3621-2327 $ 17.50+.50/0

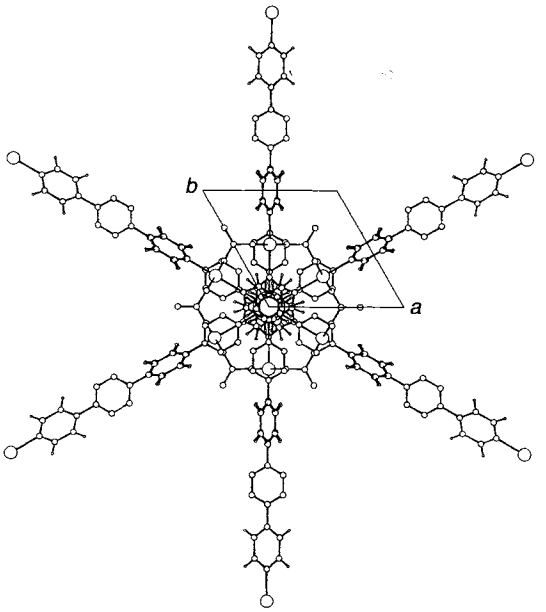

Figure 3. View of $[Ag(pytz)(NO_3)]_\infty$ along the helical axis that illustrates the hexagonal arrangement of the polymeric chains.

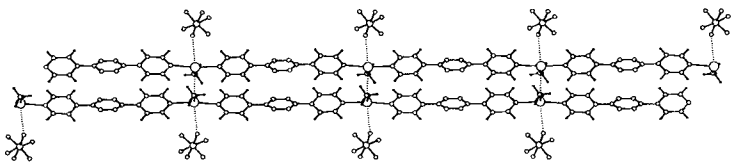

Figure 4. View of the linear chain pairs formed by $[Ag(pytz)(X)(MeCN)]_\infty$ ($X = PF_6^-$, BF_4^-).

cule (Ag–N 2.648(4) Å (PF_6^- compound) and 2.637(2) Å (BF_4^- compound)). However, these pairs of Ag–bpy chains are all parallel to each other, in contrast to the those in NO_3^- complex, and there are no significant interactions between adjacent pairs of chains, most significantly not even through the anion.

These results not only represent the first example of a helical staircase structural motif but also a remarkable case of anion control of supramolecular architecture construction. We are currently investigating whether this control can be transferred to other metal–ligand arrays and indeed to other anions.[20]

Experimental Section

$[Ag(pytz)(NO_3)]_\infty$: A solution of $AgNO_3$ (0.0365 g, 0.2 mmol) in MeCN (3 mL) was layered onto a solution of pytz (0.0505 g , 0.214 mmol) in CH_2Cl_2 (10 mL). The solutions were left for two days at room temperature, and red hexagonal crystals were obtained. Elemental analysis calcd for $C_{12}H_8AgN_7O_3$: C 35.49, H 1.99, N 24.14; found: C 35.42, H 1.81, N 23.98; IR (KBr): $\tilde{\nu}$ = 3048 (w), 2952 (w), 2905 (w), 1616 (m), 1589 (m), 1558 (m), 1411 (m), 1384 (s), 1262 (m), 1111 (m), 1055 (m), 917 (m), 833 (m), 716 (m), 599 (s) cm^{-1}.

$[Ag(pytz)(PF_6)(MeCN)]_\infty$ was prepared analogously to $[Ag(pytz)(NO_3)]_\infty$ but with $AgPF_6$ (0.0522 g, 0.207 mmol) in place of $AgNO_3$. Elemental analysis calcd for $C_{14}H_{11}AgF_6N_7P$: C 31.72, H 2.09, N 18.50; found: C 32.21, H 2.00, N 18.81; IR (KBr): $\tilde{\nu}$ = 3086 (w), 3003 (w), 2952 (w), 1616 (m), 1590 (m), 1560 (m), 1411 (m), 1391 (s), 1262 (m), 1112 (m), 1056 (m), 917 (m), 833 (s), 717 (m), 599 (s), 560 (m) cm^{-1}.

$[Ag(pytz)(BF_4)(MeCN)]_\infty$ was prepared analogously to $[Ag(pytz)(NO_3)]_\infty$ but with $AgBF_4$ (0.0406 g, 0.209 mmol) in place of $AgNO_3$. Elemental analysis calcd for $C_{14}H_{11}AgBF_4N_7$: C 35.63, H 2.35, N 20.77; found: C 35.52, H 2.18, N 20.67; IR (KBr): $\tilde{\nu}$ = 3090 (w), 3009 (w), 2953 (w), 1611 (m), 1589 (m), 1559 (m), 1411 (m), 1391 (s), 1263 (w), 1221 (w), 1055 (s), 919 (m), 834 (m), 717 (m), 599 (s) cm^{-1}.

Received: April 7, 1997
Revised version: June 19, 1997 [Z10317IE]
German version: *Angew. Chem.* **1997**, *109*, 2421–2423

Keywords: helical structures · N ligands · silver · supramolecular chemistry

[1] R. Robson, B. F. Abrahams, S. R. Batten, R. W. Gable, B. F. Hoskins, J. Liu, *Supramolecular Architecture*, American Chemical Society, Washington DC, **1992**, chap. 19; M. Fujita, Y. J. Kwon, S. Washizu, K. Ogura, *J. Am. Chem. Soc.* **1994**, *116*, 1151.

[2] G. R. Desiraju, *Crystal Engineering: The Design of Organic Solids*, Elsevier, Amsterdam, **1989**; *Angew. Chem.* **1995**, *107*, 2541; *Angew. Chem. Int. Ed. Engl.* **1995**, *35*, 2311.

[3] L. R. MacGillvary, S. Subramanian, M. J. Zaworotko, *J. Chem. Soc. Chem. Commun.* **1994**, 1325; M. J. Zaworotko, *Chem. Soc. Rev.* **1994**, 283.

[4] A. J. Blake, N. R. Champness, S. S. M. Chung, W.-S. Li, M. Schröder, *Chem. Commun.* **1997**, 1005, and unpublished results.

[5] L. Carlucci, G. Ciani, D. M. Proserpio, A. Sironi, *J. Chem. Soc. Chem. Commun.* **1994**, 2755.

[6] S. Subramanian, M. J. Zaworotko, *Angew. Chem.* **1995**, *107*, 2295; *Angew. Chem. Int. Ed. Engl.* **1995**, *34*, 2127.

[7] P. Losier, M. J. Zaworotko, *Angew. Chem.* **1996**, *108*, 2957; *Angew. Chem. Int. Ed. Engl.* **1996**, *35*, 2779.

[8] G. B. Gardner, D. Venkataraman, J. S. Moore, S. Lee, *Nature* **1995**, *374*, 792.

[9] M. Fujita, Y. J. Kwon, O. Sasaki, K. Yamaguchi, K. Ogura, *J. Am. Chem. Soc.* **1995**, *117*, 7287.

[10] R. Charonnat, P. Fabiani, *C. R. Hebd. Seances Acad. Sci.* **1955**, *241*, 1783.

[11] F. Robinson, M. Zaworotko, *J. Chem. Soc. Chem. Commun.* **1995**, 2413; O. M. Yaghi, H. Li, *J. Am. Chem. Soc.* **1996**, *118*, 295.

[12] X-ray structure crystal analysis of $[Ag(pytz)(NO_3)]_\infty$: $C_{12}H_8AgN_7O_3$, red hexagonal plates, crystal dimensions $0.61 \times 0.31 \times 0.19$ mm^3, hexagonal, space group $P6_122$ (no. 178), $a = 8.865(4)$, $c = 31.08(2)$ Å, $V = 2115.3(8)$ Å^3, $Z = 6$, $F(000) = 1200$, $\rho_{calcd} = 1.913$ g cm^{-3}, $\mu(Mo_{K\alpha}) = 1.44$ mm^{-1}, $T = 300(2)$ K. Data were collected on a Stoe Stadi-4 four-circle diffractometer with graphite-monochromated $Mo_{K\alpha}$ radiation in the $\omega-\theta$ scan mode with a scan width of $(1.50+0.347\tan\theta)°$ ($5.2 \le 2\theta \le 50.0°$, $-10 \le h \le +10$, $-10 \le k \le +10$, $-36 \le l \le +36$). A numerical absorption correction was applied to the data (T_{min} 0.772, T_{max} 0.842); 1251 unique reflections ($R_{int} = 0.0371$), of which 1050 had $I \ge 2\sigma(I)$, were used in all calculations. The structure was solved by direct methods [13] and refined using full-matrix least squares on F^2 [14]. All non-hydrogen atoms were refined anisotropically, and hydrogen atoms were treated with a riding model (d(C–H) = 1.00 Å, U_{iso} = 0.03 Å^2). A four-term Chebychev weighting scheme was adopted [15]. Final R values: $R = 0.033$, wR_2(all data) = 0.049 [19].

[13] A. Altomare, G. Cascarano, G. Giacovazzo, A. Guagliardi, M. C. Burla, G. Polidori, M. Camalli. (SIR-92), *J. Appl. Crystallogr.* **1994**, *27*, 435.

[14] D. J. Watkin, C. K. Prout, R. J. Carruthers, P. Betteridge, CRYSTALS Issue 10, Chemical Crystallography Laboratory, Oxford, UK, **1996**.

[15] J. R. Carruthers, D. J. Watkin, *Acta Crystallogr. Sect A* **1979**, *35*, 698.

[16] The Ag–O distances of 2.787(2)Å are typical for such interactions between Ag^I centers and NO_3^- ions [11].

[17] X-ray crystal structure analysis of $[Ag(pytz)(PF_6)(MeCN)]_\infty$: $C_{14}H_{11}AgF_6N_7P$, red plates, crystal dimensions $0.62 \times 0.54 \times 0.27$ mm^3, monoclinic, space group $P2_1/n$ (no. 14), $a = 9.242(3)$, $b = 13.695(2)$, $c = 14.010(2)$ Å, $\beta = 99.68(3)°$, $V = 1747.9(8)$ Å^3, $Z = 4$, $F(000) = 1040$, $\rho_{calcd} = 2.014$ g cm^{-3}, $\mu(Mo_{K\alpha}) = 1.31$ mm^{-1}, $T = 220.0(2)$ K. Data were collected on a Stoe Stadi-4 four-circle diffractometer with graphite-monochromated $Mo_{K\alpha}$ radiation in the $\omega-\theta$ scan mode with a scan width of $(4.0+0.347\tan\theta)°$ ($5.7 \le 2\theta \le 50.1°$, $-10 \le h \le +11$, $0 \le k \le +16$, $-5 \le l \le +16$). A ψ-scan absorption correction was applied to the data (T_{min} 0.521, T_{max} 0.628); 2914 unique reflections ($R_{int} = 0.0567$), of which 2385 had $I \ge 2\sigma(I)$, were used in all calculations. The structure was solved by direct methods [13] and refined using full-matrix least squares on F^2 [14]. All non-hydrogen atoms were refined anisotropically, and hydrogen atoms were treated with a riding model (d(C–H) = 1.00 Å, U_{iso} = 0.03 Å^2), except those on methyl groups (d(C–H) = 1.00 Å, U_{iso} = 0.06 Å^2). A three-term Chebychev weighting scheme was adopted [15]. Final R values: $R = 0.0738$, wR_2 (all data) = 0.0414 [19].

[18] X-ray crystal structure analysis of $[Ag(pytz)(BF_4)(MeCN)]_\infty$: $C_{14}H_{11}AgBF_4N_7$, red plates, crystal dimensions $0.55 \times 0.33 \times 0.16$ mm^3, monoclinic, space group $P2_1/n$ (no. 14), $a = 8.754(3)$, $b = 13.565(3)$, $c = 14.049(5)$ Å, $\beta = 98.46(3)°$, $V = 1650.1(7)$ Å^3, $Z = 4$, $F(000) = 928$, $\rho_{calcd} = 1.813$ g cm^{-3}, $\mu(Mo_{K\alpha}) = 1.254$ mm^{-1}, $T = 220.0(2)$ K. Data were collected on a Stoe Stadi-4 four circle diffractometer with graphite-monochromated $Mo_{K\alpha}$ radiation in the $\omega-\theta$ scan mode with scan width of $(1.50+0.347\tan\theta)°$ ($5.2 \le 2\theta \le 50.0°$, $-10 \le h \le +10$, $-16 \le k \le +16$, $-16 \le l \le +16$). A numerical absorption correction was applied to the data (T_{min} 0.653, T_{max} 0.799); 5494 unique reflections ($R_{int} = 0.1252$), of which 4394 had $I \ge 2\sigma(I)$, were used in all calculations. The structure was solved by direct methods [13] and refined using full-matrix least squares on F^2 [14]. The structure was disordered along the direction of the Ag-pytz-Ag chains, and all atoms with the exception of the BF_4^- anion and the MeCN molecule were affected. The relative occupancies were 0.8 and 0.2; the geometry of the lower-occupancy ligand was restrained to the average geometry of the higheroccupancy ligand. All higher occupancy

atoms were refined anisotropically, and all lower-occupancy atoms isotropically. No hydrogen atoms were modelled on atoms of the lower occupancy ligand. Hydrogen atoms were treated with a riding model (d(C–H) = 1.00 Å, U_{iso} = 0.03 Å^2). A two-term Chebychev weighting scheme was adopted [15]. Final R values: R = 0.1065, wR_2(all data) = 0.1095 [19].

[19] Further details of the crystal structure investigations can be obtained from the Fachinformationszentrum Karlsruhe, D-76344 Eggenstein-Leopoldshafen, Germany upon quoting the deposit numbers CSD-407272 ([Ag(pytz)$(NO_3)]_x$), CSD-407273 ([Ag(pytz)(BF_4)(MeCN)]$_x$), and CSD-407274 ([Ag(pytz)-(PF_6)(MeCN)]$_x$).

[20] **Note added in proof** (September 15, 1997): A related helical coordination polymer, also in the space group $P6_122$, recently appeared after submission of this communication: S. R. Batten, B. F. Hoskins, R. Robson, *Angew. Chem.* **1997**, *109*, 652; *Angew. Chem. Int. Ed. Engl.* **1997**, *36*, 636.

Electronic Structure of Manganese(III) Compounds from High-Frequency EPR Spectra

Anne-Laure Barra, Dante Gatteschi,* Roberta Sessoli, Gian Luca Abbati, Andrea Cornia, Antonio C. Fabretti, and Myriam G. Uytterhoeven

EPR spectra of transition metal ions with an even number of unpaired electrons are very difficult to obtain, principally because the ground state spin multiplet is largely split in a zero magnetic field by the low symmetry components of the crystal field. When the zero field splitting is much larger than the microwave quantum used in the spectrometer, transitions can be observed only at extremely high fields, much larger than usually available. This is a very unfortunate situation, because EPR spectroscopy can, in principle, provide a great deal of information on the geometrical and electronic structure of the transition metal ion. This situation is changing rapidly following the introduction of high-frequency–high-field EPR spectrometers (HF-EPR),[1] which allow the detection of spectra of integer spin multiplets with very large zero field splittings.

Manganese(III) is certainly one of the unfavorable metal ions for EPR studies. In an octahedral ligand environment, its four unpaired electrons result in a ^5E_g ground state, which is unstable to Jahn–Teller distortions. The inherent low symmetry of the complexes gives rise to large zero field splitting and to date the reports of EPR spectra of manganese(III) are exceedingly rare[2] and most of them refer to forbidden transitions within the non-Kramers doublets.[3] Far-IR techniques have been used to characterize manganese(III)-doped rutile[4] and some porphyrins;[5] however, no HF-EPR spectrum of simple complexes has to our knowledge been reported so far. Given the large interest in the electronic structure of manganese(III), which is relevant to such diverse topics as photosystem II,[6] colossal magneto-resistance,[7] and single-molecule magnets,[8] we decided to investigate simple manganese(III) complexes by using the high-field EPR spectrometer at Grenoble, which can reach 500 GHz and 30 T. We report here the HF-EPR spectra of [Mn(dbm)$_3$] (Hdbm = 1,3-diphenyl-1,3-propanedione) to illustrate how EPR spectra can be easily detected and reproduced with ligand field models. This work opens exciting perspectives for the investigation of manganese(III) compounds.

A low-quality X-ray crystal structure analysis of [Mn(dbm)$_3$] was previously reported.[9] As the coordination geometry of the manganese ion needs to be determined precisely for a detailed analysis of the HF-EPR results, we collected a new data set[10] and refined the structure. The coordination polyhedron is tetragonally elongated as a result of Jahn–Teller distortion and thus shows significant deviation from idealized D_{4h} symmetry.[11]

Powder EPR spectra of polycrystalline [Mn(dbm)$_3$] were recorded at 245.0 and 349.3 G Hz in the range between 4.2 and 30 K on a laboratory-made spectrometer by using a far-IR laser as radiation source.[12] The spectra recorded at 349.3 GHz at 15 K are shown in Figure 1. The relative intensities changed markedly on varying the temperature because the Zeeman energy is similar to the thermal energy. This allows the determination of the sign of the zero field splitting. At least eleven features are observed in the range 0–12 T; the strongest absorption bands appear at low field. The corresponding spectra recorded at 245.0 GHz (Figure 2) show fewer features (only nine are clearly observed), and also the pattern of intensities of the transitions changes dramatically. The spectra of [Mn(dbm)$_3$] clearly indicate that the amount of energy required for the zero field splitting is similar in size to the radiation used in the experiments (8.17 and 11.65 cm^{-1}, respectively). Therefore, it is very difficult to perform even a qualitative assignment of the transitions, because in this case many "forbidden" transitions may be present. The fit of the spectra was performed with a program written by H. Weihe et al.,[13] which diagonalizes the full Hamiltonian matrix within the basis of five $S = 2$ spin functions [Eq. (a)].

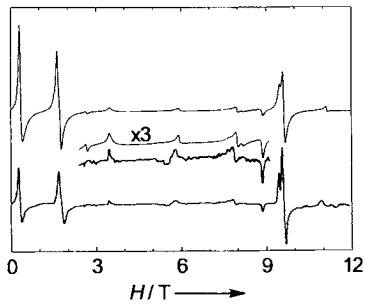

Figure 1. Experimental (bold) and simulated powder HF-EPR spectrum of polycrystalline [Mn(dbm)$_3$] at 349.3 GHz and 15 K. The free electron resonates at about 12.46 T.

$$H = \boldsymbol{B}\cdot\boldsymbol{g}\cdot\boldsymbol{S} + \boldsymbol{S}\cdot\boldsymbol{D}\cdot\boldsymbol{S} \quad \text{(a)}$$

The calculated transitions are very sensitive to the zero field splitting parameters D and E, which are therefore accurately determined, both in terms of their size and sign; however, these transitions are much less sensitive to the g values, which therefore are determined with less accuracy. To avoid over-parameterization we assumed $g_x = g_y$. The best fit calculated spectra are shown in Figures 1 and 2. The agreement is very good both in terms of the position and the intensity of the bands. The best fit parameters are: $g_x = g_y = 1.99$; $g_z = 1.97$; $D = -4.35$ cm^{-1}, $E = 0.26$ cm^{-1}. Attempts were also made at including fourth-order crystal field terms that are symmetry-allowed,[14] but no significant improvement on the fit was found, therefore we neglect these terms here.

[*] Prof. D. Gatteschi, Dr. R. Sessoli
Department of Chemistry, University of Florence
Via Maragliano 75/77, I-50144 Firenze (Italy)
Fax: Int. code +(55) 354845
e-mail gattesch@chim1.unifi.it
G. L. Abbati, Prof. A. C. Fabretti, Dr. A. Cornia
Department of Chemistry, University of Modena (Italy)
Dr. A. L. Barra
Laboratoire Champs Magnetiques Intenses-C. N. R. S. Grenoble (France)
M. G. Uytterhoeven
SIS-Consult, B-3002 Heverlee (Belgium)

 © WILEY-VCH Verlag GmbH, D-69451 Weinheim, 1997 0570-0833/97/3621-2329 $ 17.50+.50/0

The assignment of the features to the transitions can be performed by using pseudo-rotation plots and the high-field labeling of the energy levels. The resonance fields of the transitions are calculated in the three principal planes of the $\boldsymbol{g}$ tensor, which is assumed to be parallel to the $\boldsymbol{D}$ tensor. The intense feature observed at the lowest fields in Figure 1 is associated with the z component of the forbidden $M = +2 \rightarrow M = -1$ transition, which is partially allowed by the mixing of the $M = +1$ and $M = -1$ states, while the feature at about 1.8 T is attributed to the y component of the $1 \rightarrow 0$ transition and the z component of the $2 \rightarrow 1$ transition. The other intense and structured feature at about 9.8 T corresponds to the x and y components of the $0 \rightarrow 1$ transition. In Figure 2 the strongest absorptions at 6.1 T and 6.8 T are attributed to y and x components, respectively, of the allowed $0 \rightarrow 1$ transition.

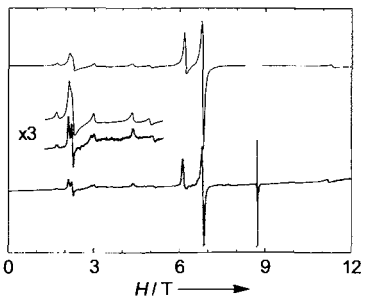

Figure 2. Experimental (bold) and simulated powder HF-EPR spectrum of polycrystalline [Mn(dbm)$_3$] at 245.0 GHz and 15 K. The narrow line at about 8.75 T is attributed to the standard (α,α-diphenyl-β-picrylhydrazyl, dpph).

At the simplest level the parameters for an elongated octahedral complex with rhombic distortion are related to the electronic structure [15] according to Equation (b), in which g_e is the free

$$g_z = g_e - \frac{8\lambda}{\Delta E(xy \rightarrow x^2 - y^2)};\quad g_x = g_e - \frac{2\lambda}{\Delta E(yz \rightarrow x^2 - y^2)};\quad g_y = g_e - \frac{2\lambda}{\Delta E(xz \rightarrow x^2 - y^2)}; \qquad \text{(b)}$$

electron value, and the energy differences ΔE refer to the indicated d orbitals; $\lambda = \zeta/2S$, where ζ, the spin-orbit coupling constant, is about 90 cm^{-1} for the free manganese(III) ion.

The zero field splitting parameters can be evaluated by general relations [Eq. (c)], which are expected to be valid if only the states belonging to the same Russell–Saunders manifold $^{2S+1}$L are included.

$$D = 1/2\,\lambda[g_z - 1/2\,(g_x + g_y)];\ E = 1/4\,\lambda[g_x - g_y] \qquad \text{(c)}$$

The ΔE energy differences of the transitions can be obtained from the electronic spectra. Spectra recorded in toluene solution showed a maximum at 9000 cm^{-1} and shoulders at about 18000 and 21000 cm^{-1}. In analogy to [Mn(acac)$_3$][16] (Hacac = 2,4-pentanedione) we assign the lowest energy band to $^5A_1 \leftarrow {}^5B_1$, that is the transition between the two split levels of the ^5E_g ground state in octahedral symmetry. The other two bands correspond to $^5B_2 \leftarrow {}^5B_1$ and $^5E \leftarrow {}^5B_1$. We assume that the ground state of [Mn(dbm)$_3$] is $^5B_1$ in agreement with the elongated octahedral geometry experimentally observed; thus, $\Delta E(xy \rightarrow x^2 - y^2) = 18000$ cm^{-1} and $\Delta E(xz,yz \rightarrow x^2 - y^2) = 21000$ cm^{-1}. Using these values and the free ion spin orbit coupling constant we calculate $g_{\parallel} = 1.96$ and $g_{\perp} = 1.99$, which are in fair agreement with the experimental data. Using Equation (c) we obtain the zero field splitting parameter $D = -1.4$ cm^{-1}. The agreement is good for the sign, but not acceptable for the value. A similar discrepancy was previously observed for the spectra of manganese(III)-doped rutile.[4] The disagreement between experiment and calculation was attributed to the neglect of the $^3T_{2g}$ excited state, formed by placing the four electrons in the t_{2g} orbitals, which at the simplest level of approximation contributes to the zero field splitting parameter with an additive term [Eq. (d)]. B and C are electron repulsion terms, which in

$$D' = -\frac{\zeta^2}{6B + 5C + \Delta E(xz,\ yz \rightarrow z^2)} \qquad \text{(d)}$$

the free ion take the values $B = 1140$ cm^{-1} and $C = 3675$ cm^{-1}. Using Equations (c) and (d), the calculated zero field splitting parameter becomes $D = -4.9$ cm^{-1}, which is in good agreement with the experiment.

We calculated the parameters of the spin Hamiltonian operator also in a more general way by developing a suitable computer program that uses the angular overlap model (AOM) for the ligand field.[17] The energies of the states appropriate to the d^4 configuration are calculated within the weak field formalism by a full matrix diagonalization. The computed electronic energies and eigenfunctions are therefore correct to all orders in perturbation theory. Details of the computer program and its applications to selected systems will be published elsewhere. The parameters of the spin Hamiltonian operator obtained in this way can be considered as the best improvement to the perturbative approach [Eqs. (a)–(c)].

The fitting strategy was that of finding the AOM parameters from the electronic spectra and then calculating the parameters of the spin Hamiltonian operator. The structure of [Mn(dbm)$_3$] is essentially orthoaxial; the O-Mn-O angles are close to 90° or 180°. Therefore we assumed that the differences in bond lengths are primarily responsible for the electronic structure of the complex. In an orthoaxial complex the energies of the d levels can be described as reported in reference [18]. By using these values the energies of the electronic transitions can be expressed by Equations (e)–(g).

$$E(^5A_1 \leftarrow {}^5B_1) = \nu_1 = e_\sigma^x + e_\sigma^y - 2e_\sigma^z \qquad \text{(e)}$$

$$E(^5B_2 \leftarrow {}^5B_1) = \nu_2 = 3/2\ e_\sigma^x + 3/2\ e_\sigma^y - 2\ e_\pi^x - 2\ e_\pi^y \qquad \text{(f)}$$

$$E(^5E \leftarrow {}^5B_1) = \nu_3 = 3/2\ e_\sigma^x + 3/2\ e_\sigma^y - 2\ e_\pi^x - 2\ e_\pi^z \qquad \text{(g)}$$

Since we have no evidence of symmetry lower than axial from the electronic spectra we first set $e_{\sigma,\pi}^x = e_{\sigma,\pi}^y$. With this approach the three electronic transitions can be fitted with four parameters. By using the appropriate values for the observed transitions, and fixing for instance e_π^z to 1000 cm^{-1}, the other parameters are calculated as $e_\sigma^z = 4833$ cm^{-1}, $e_\sigma^x = 9333$ cm^{-1}, and $e_\pi^x = 2500$ cm^{-1}. Translating the AOM parameters into the usual crystal field parameter Dq, by applying the relation Dq = 3/10 e_σ − 4/10 e_π the calculated Dq value for the axial ligands is 1050 cm^{-1} and for the equatorial ligands 1800 cm^{-1}.

These values were used to calculate the parameters of the spin Hamiltonian operator by using the procedure described above. First the parameters were calculated by neglecting the contribution from the excited Russell–Saunders multiplets with $S < 2$. The calculated D value of -1.35 cm^{-1} corresponds nicely to that obtained with the perturbative formulas in Equations (b) and (c). The same calculations were repeated with the inclusion of all the excited Russell–Saunders terms, and the results are

 © WILEY-VCH Verlag GmbH, D-69451 Weinheim, 1997 0570-0833/97/3621-2330 $ 17.50+.50/0

$g_x = g_y = 1.99$, $g_z = 1.96$, and $D = -4.57\ cm^{-1}$. In this case the agreement between observed and calculated zero field splitting can be considered as very satisfactory. Interestingly, non-zero fourth-order parameters of the order of $10^{-4}\ cm^{-1}$ are calculated. This can have a large significance for the interpretation of the magnetic properties of clusters that show quantum tunneling of the magnetization at low temperature.[19]

Improvements to the fit can be achieved by taking into consideration the difference in the ligand field parameters of the equatorial ligands. The average Mn–O distance on the x axis is 1.913 Å, and that for the ligands on the y axis is 1.933 Å; thus some anisotropy may be anticipated. If we assume that the calculated difference in the Dq values for the axial and equatorial ligands is due to an exponential decrease of the parameter with the metal–ligand distance, the Dq parameters for the ligands on the x and y axes can be calculated as 1850 and $1750\ cm^{-1}$, respectively. By setting $e_\sigma^x = 9595\ cm^{-1}$, $e_\pi^x = 2570\ cm^{-1}$, $e_\sigma^y = 9080\ cm^{-1}$, $e_\pi^y = 2430\ cm^{-1}$, and leaving the parameters of the axial ligand at the previously determined value, we calculate $g_x = 1.99$, $g_y = 1.99$, $g_z = 1.96$, $D = -4.55\ cm^{-1}$, and $E = 0.28\ cm^{-1}$, in good agreement with the experimental data.

$[Mn(dbm)_3]$ is the first molecular manganese(III) complex for which a detailed analysis of the EPR parameters could be performed. The results given here show that HF-EPR can easily provide the g factors and the zero field splitting of manganese(I–II) complexes. The success of the ligand field analysis confirms that structural information can be readily obtained from the spectra. Furthermore, we have shown how reasonable estimates of the $\boldsymbol{g}$ and $\boldsymbol{D}$ tensors in pseudo-octahedral manganese(III) complexes can be made simply by recording the electronic spectra in solution. We have not observed hyperfine splittings in our sample, but, given the success in the interpretation of the other tensors it is reasonable to assume that the ligand field analysis is applicable also for the **A** tensor. This is of great significance for the current efforts in the understanding of the structure of photosystem II.

Experimental Section

$[Mn(dbm)_3]$ was obtained by an alternative procedure to those already reported for the synthesis of manganese(III) tris(β-diketonate) complexes [20]. A solution of Hdbm (4.4 mmol) and triethylamine (12 mmol) in anhydrous, oxygen-free CH_3CN (40 mL) was prepared under dinitrogen. Solid $MnBr_2 \cdot 4H_2O$ (2 mmol) was then added, and the solution was stirred for 1.5 h under dinitrogen. The yellow precipitate was collected by filtration and suspended in CH_3CN with stirring. Upon contact with air, the precipitate progressively dissolved and the mixture turned brown; black lustrous crystals of $[Mn(dbm)_3]$ formed quickly. The purity of the samples was checked by microanalysis: Calcd. for $MnC_{45}H_{33}O_6$ (%): C 74.58, H 4.59; found: C 74.84, H 4.57.

Received: April 29 1997 [Z10397IE]
German version: *Angew. Chem.* **1997**, *109*, 2423–2426

Keywords: electronic structure · EPR spectroscopy · manganese

[1] G. R. Eaton, S. S. Eaton, *Magn. Reson. Rev.* **1993**, *16*, 157; G. R. Eaton, S. S. Eaton in *Handbook of Electron Spin Resonance, Vol. 2*, (Eds.: C. P. Poole Jr., H. Farach), American Institute of Physics, in press.
[2] F. E. Mabbs, D. Collison, *Electron Paramagnetic Resonances of d-Transition Metal Compounds*, Elsevier, Amsterdam, **1992**.
[3] S. L. Dexheimer, J. W. Gohdes, M. K. Chan, K. S. Hagen, W. H. Armstrong, M. P. Klein, *J. Am. Chem. Soc.* **1989**, *111*, 8923; R. A. Serway, K. Berlinger, K. A. Müller. R. W. Collins, *Phys. Rev. B.* **1977**, *16*, 4761.
[4] H. J. Gerritsen, E. B. Sabisky, *Phys. Rev.* **1963**, *132*, 1507.
[5] G. C. Brackett, P. L. Richards, W. S. Caughey, *J. Chem. Phys.* **1971**, *54*, 4383.
[6] K. Wieghardt, *Angew. Chem.* **1989**, *101*, 1179; *Angew. Chem. Int. Ed. Engl.* **1989**, *28*, 1153.
[7] S. Jin, T. H. Tiefel, M. McCormach, R. A. Fastnacht, *Science* **1994**, *264*, 413.
[8] R. Sessoli, D. Gatteschi, A. Caneschi, M. A. Novak, *Nature* **1993**, *365*, 141.
[9] E. G. Zaitseva, I. A. Baidina, P. A. Stabnikov, S. V. Borisov, I. K. Igumenov, *Zh. Strukt. Khim.* **1990**, *31*, 184; *Chem. Abstr.* **1990**, *113*, 88602h.
[10] Crystal data for $MnC_{45}H_{33}O_6$: $M_r = 724.69$, crystal dimensions $0.5 \times 0.6 \times 0.5$ mm, $Mo_{K\alpha}$ radiation, $\lambda = 0.71069$ Å, $T = 298$ K, monoclinic, space group $P2_1/c$, $a = 16.882(1)$, $b = 9.989(1)$, $c = 21.466(2)$ Å, $\beta = 92.730(6)°$, $Z = 4$, $V = 3615.8(5)$ Å^3. Further details of the crystal structure investigation may be obtained from the Fachinformationszentrum Karlsruhe, D-76344 Eggenstein-Leopoldshafen (Germany), on quoting the depository number CSD-406981.
[11] The *trans* M–O bond lengths are: Mn–O1 2.109(2), Mn–O3 2.142(2); Mn–O5 1.935(2), Mn–O4 1.931(2); Mn–O2 1.917(2), Mn–O6 1.908(2) Å. The angles around the Mn atom deviate less than 4.0° from the idealized value of 90°.
[12] F. Muller, M. A. Hopkins, N. Coron, M. Grynberg. L. C. Brunel. G. Martinez, *Rev. Sci. Instrum.* **1989**, *60*, 3681; A. L. Barra, L. C. Brunel, J. B. Robert, *Chem. Phys. Lett.* **1990**, *165*, 107.
[13] C. J. H. Jacobsen, E. Pedersen, J. Villadsen, H. Weihe, *Inorg. Chem.* **1993**, *32*, 1216.
[14] A. Abragam, B. Bleaney, *Electron Paramagnetic Resonance of Transition Metal Ions*, Dover, New York, **1986**.
[15] J. S. Griffith, *The Theory of Transition Metal Ions*, Cambridge University Press, **1961**.
[16] J. P. Fackler, Jr., T. S. Davis, I. D. Chawla, *Inorg. Chem.* **1965**, *4*, 130.
[17] A. Bencini, I. Ciofini, M. G. Uytterhoeven *Inorg. Chim. Acta*, in press.
[18] A. B. P. Lever, *Inorganic Electron Spectroscopy*, Elsevier, Amsterdam, **1984**.
[19] J. R. Friedman, M. P. Sarachilk, J. Tejada, R. Ziolo, *Phys. Rev. Lett.* **1996**, *76*, 3830; L. Thomas, F. Lionti, R. Ballou, D. Gatteschi, R. Sessoli, B. Barbara, *Nature* **1996**, *383*, 145; A. L. Barra, D. Gatteschi, R. Sessoli, *Phys. Rev. B.* **1997**, *56*, 8192.
[20] R. G. Charles, B- E. Bryant, *Inorg. Syn.* **1963**, *7*, 183; J. G. Gordon II, M. J. O'Connor, R. H. Holm, *Inorg. Chim. Acta* **1971**, *5*, 381.

Controlling Microstructure in Polymeric Molecular Shuttles: Solvent-Induced Localization of Macrocycles in Poly(urethane/crown ether) Rotaxanes**

Caiguo Gong and Harry W. Gibson*

Polyrotaxanes, which are formed by threading macrocycles onto polymeric backbones or side chains, have been studied extensively in the last decades.[1–6] Cyclodextrins[2–4] and crown ethers[5, 6] are often used as the cyclic components. In poly(ester rotaxane)s, crown ether can freely translate along the backbone and aggregate into a separate phase, because no significant interaction between the ester linkages and the cycles exists.[5c, 5d] However, the crown ether is influenced by blocking groups (BG) bearing tetraphenylmethyl moieties in the chain.[6] While small molecular shuttles have been widely studied,[1b, 1c] oligomeric[7] and polymeric[8, 9] counterparts based on paraquat charge transfer systems, in which the cycles shuttle between solvent and backbone, have only recently been addressed. We now report the preparation of novel polymeric molecular shuttles with polyurethanes containing BG units as backbones and [30]crown-10 (30C10) as the cyclic unit; the latter only move on the chain. Furthermore, we demonstrate for the first time the ability to control the locus of the macrocycles in these polyrotaxanes with solvent effects.

Copoly(urethane/30C10 rotaxane)s **4a–c** and homopoly(urethane/30C10 rotaxane) **4d** were prepared from diol BG **1**,

[*] Prof. H. W. Gibson, C. Gong
Department of Chemistry
Virginia Polytechnic Institute and State University
Blacksburg, VA 24061 (USA)
Fax: Int. code +(540)231-8517
e-mail: hwgibson@vt.edu

[**] This work was supported by the U. S. National Science Foundation, Division of Materials Research (grant no. DMR-93-20196). We also thank Prof. H. Dorn in our department for suggesting the T_1 measurements.

 © WILEY-VCH Verlag GmbH, D-69451 Weinheim, 1997 0570-0833/97/3621-2331 $ 17.50+.50/0

tetra(ethylene glycol) (**2**) and 4,4′-methylenebis(phenyl isocyanate) (MDI, **3**) by solution polymerization with 30C10 as solvent (Scheme 1 and Table 1). The methodology used was essentially the same as reported for analogous systems without BG.[5c]

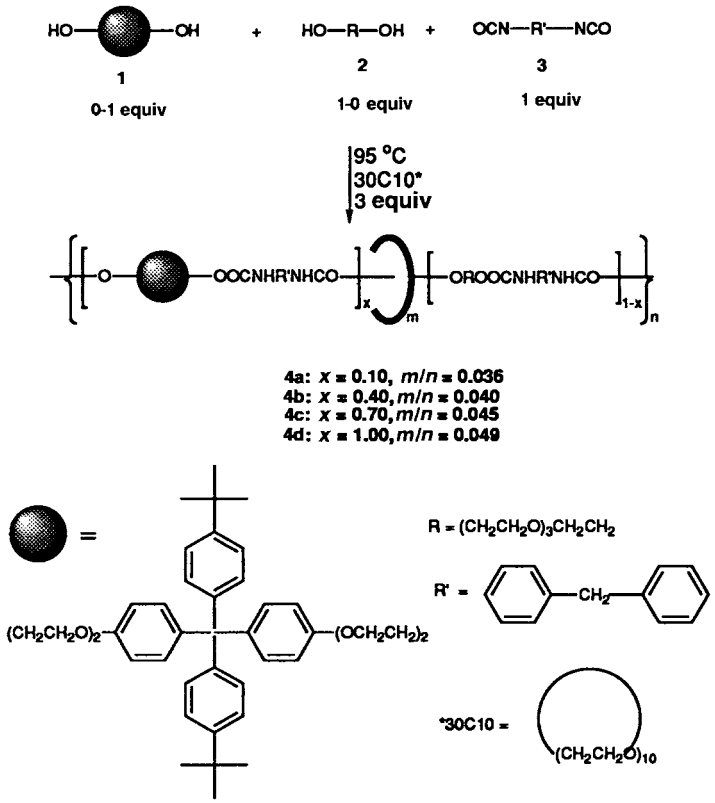

Scheme 1. Synthesis of poly(urethane/30C10 rotaxane)s **4a–d**.

Table 1. The feed compositions for **4a–d**[a].

Products	BG diol **1** [mg/mmol]	Glycol **2** [mg/mmol]	MDI (**3**) [mg/mmol]	30C10 [g/mmol]
4a	63.9/0.100	174.8/0.900	250.3/1.000	1.321/3.000
4b	255.5/0.400	116.5/0.600	250.3/1.000	1.321/3.000
4c	447.2/0.700	58.3/0.300	250.3/1.000	1.321/3.000
4d	638.8/1.000	0/0	250.3/1.000	1.321/3.000

[a] Polymerization at 95 °C for 7 h.

While free 30C10 has a chemical shift of $\delta = 3.67$ in $CDCl_3$,[6a] threaded 30C10 in **4a–d** only displays one signal at $\delta = 3.51$ (Figure 1). However, for copoly(ester rotaxane)s made from **1**, 1,10-decanediol, and sebacoyl chloride, threaded 30C10 showed a range of chemical shifts.[6b] What causes the difference in the ^{1}H NMR spectra of these two polyrotaxanes? In the polyesters, threaded 30C10 is shielded by the phenyl groups of the BG units and shifted upfield. It displays different time-averaged chemical shifts corresponding to the various sequence structures in which it is constrained; in the sequences with longer distances between the BG units, the crown ether is less shielded.[6b] Nuclear Overhauser effect spectroscopy (NOESY) revealed the correlation between 30C10 and the phenyl groups of the BG moieties,[6] and it is believed that 30C10 tends to stay close to these phenyl groups. With polyurethane as the backbone, hydrogen bonding between the in-chain NH groups and the crown ethers takes place,[10] and, therefore, 30C10 is localized at the NH groups. Such hydrogen bonding induces the well-defined polymeric microstructure **5** (Scheme 2), in which

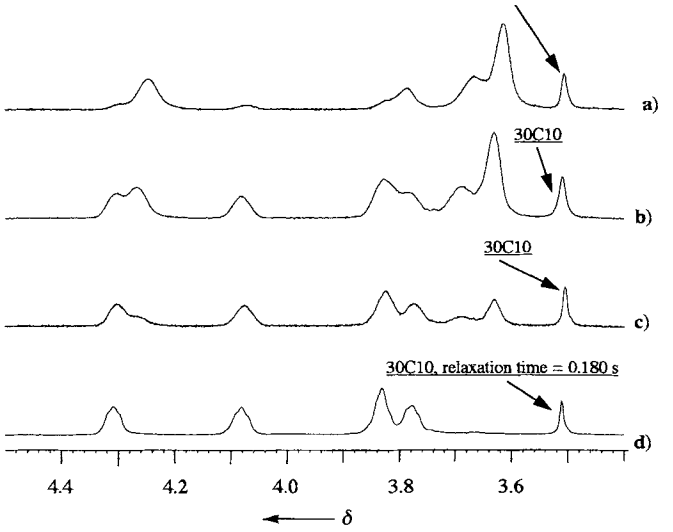

Figure 1. Section from the aliphatic region in the 400-MHz ^{1}H NMR spectra of a) **4a**, b) **4b**, c) **4c**, and d) **4d** in $CDCl_3$ at 30 °C.

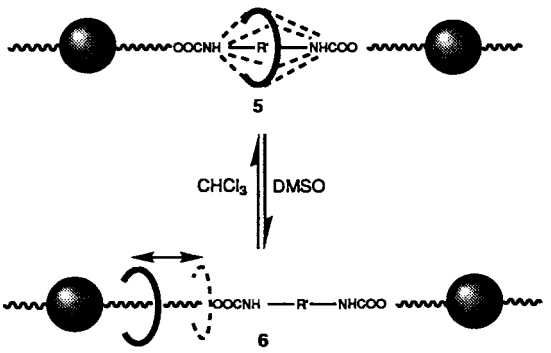

Scheme 2. Polymeric molecular shuttles: solvent-induced localization of 30C10 in **4a–d**.

30C10 is confined near the phenyl groups of the MDI units. The upfield shift for threaded 30C10 in the polyurethanes is caused by these phenyl rings. Therefore, in $CDCl_3$ threaded 30C10 in **4a–d** display the same chemical shift, even in different sequence structures.

To confirm the above hypothesis, ^{1}H NMR studies of poly(urethane rotaxane)s were also performed in [D_6]DMSO. As shown in Figure 2, threaded 30C10 in copolyurethanes **4a–c** indeed displays a range of chemical shifts from $\delta = 3.33$ to 3.38, while free 30C10 has a chemical shift at $\delta = 3.52$. DMSO is a very good solvent for displacing hydrogen bonding between NH groups and crown ethers, and, therefore, the macrocycles in polyurethanes are no longer localized at the NH groups but are instead forced away and move along the rest of the backbone between the BGs (structure **6** in Scheme 2). The signal for 30C10 is shifted upfield because it is shielded in a time-averaged man-

 © WILEY-VCH Verlag GmbH, D-69451 Weinheim, 1997 0570-0833/97/3621-2332 $ 17.50+.50/0

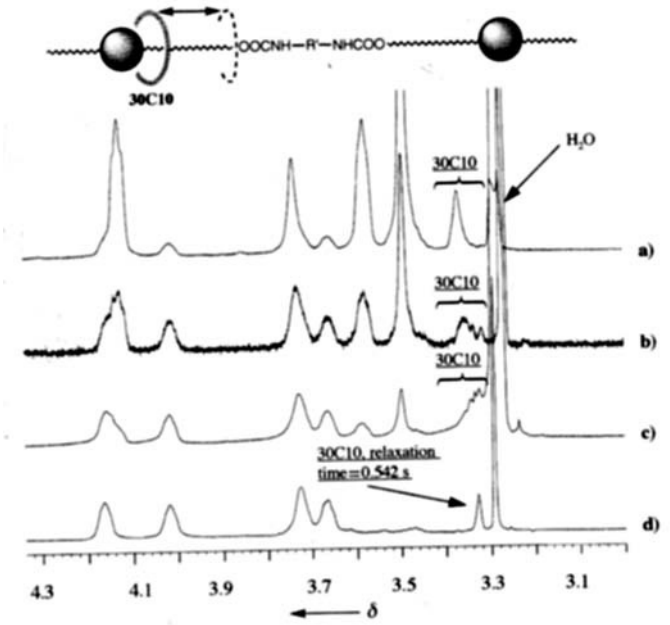

Figure 2. Section from the aliphatic region in the 400-MHz ^{1}H NMR spectra of a) **4a**, b) **b**, c) **4c**, and d) **4d** in [D$_6$]DMSO at 30 °C.

ner by the phenyl groups of the BG units and the MDI units; this is the same reason as for polyesters.[6] Since the copolyurethanes have different sequence structures with different lengths between the BG units, a range of chemical shifts for threaded 30C10 reflecting these sequence structures was observed (Figure 2). Therefore, 30C10 tends to be more mobile in DMSO and spend most of its time away from the NH group which interacts strongly with the solvent.

All these observations are supported by the measurements of spin-lattice relaxation times (T_1). Threaded 30C10 in **4d** has a T_1 of 0.178 and 0.542 s in chloroform and DMSO, respectively.[11] The smaller value in chloroform confirms the restriction of ring movement (both translation and rotation) due to hydrogen bonding (**5** in Scheme 2), while the larger T_1 in DMSO indicates relatively free translational and rotational movement of the macrocycle (**6** in Scheme 2). However, the macrocycle in **4d** is still restricted to a large extent even in DMSO, since its T_1 is smaller than that of unthreaded 30C10 (1.78 s). The large difference in T_1 values between threaded and unthreaded macrocycles provides a novel, easy, and reliable method for characterizing the formation of polyrotaxanes, and augments chemical-shift changes and NOESY.[6]

Polymeric shuttles were successfully prepared with polyurethanes as backbones and the crown ethers as macrocycles, and a novel method for controlling microstructures of the polymeric materials in solution was demonstrated. The crown ethers in **4a**–**d** are localized at the NH groups by hydrogen bonding in $CHCl_3$, in which both rotation and translation are restricted, while they are delocalized (mobile) but removed from the NH groups in DMSO. In principal, this concept can be used for other polymers bearing similar functional groups, for example polyamides.

Experimental Section

The diols (1 equiv **1** and **2**) were dissolved in 30C10 (3 equiv) at 95 °C, and the solution was stirred for 0.5 h. After addition of **3**, polymerization proceeded for 7 h under a nitrogen atmosphere. The product was precipitated from DMF into methanol three times to remove unthreaded 30C10. The specific feed compositions for **4a**–**d** are detailed in Table 1. Their threading efficiencies and molecular weights are summarized in Table 2.

Table 2. Threading efficiencies and results of gel permeation chromatography (GPC) of **4a**–**d**.

Products	x	m/n[a]	M_n[b] [kg mol^{-1}]	M_w[b] [kg mol^{-1}]
4a	0.10	0.036	22.6	39.4
4b	0.40	0.040	12.4	18.0
4c	0.70	0.045	18.7	52.9
4d	1.00	0.049	23.5	37.8

[a] Threading efficiencies (m/n, the average number of cycles per repeat unit) were measured by ^{1}H NMR spectroscopy[6]. [b] Measured by GPC with universal calibration in *N*-methylpyrrolidone (NMP) at 60 °C.

Received: April 7, 1997
Revised version: June 12, 1997 [Z10320IE]
German version: *Angew. Chem.* **1997**, *109*, 2426–2428

Keywords: crown compounds · hydrogen bonds · molecular machines · rotaxanes · supramolecular chemistry

[1] a) H. W. Gibson, M. C. Bheda, P. T. Engen, *Prog. Polym. Sci.* **1994**, *19*, 843–945; b) D. B. Amabilino, J. F. Stoddart, *Chem. Rev.* **1995**, *95*, 2725–2828; c) D. Philp, J. F. Stoddart, *Angew. Chem.* **1996**, *108*, 1242–1286; *Angew. Chem. Ed. Int. Engl.* **1996**, *35*, 1154–1196; d) H. W. Gibson in *Large Ring Molecules* (Ed.: J. A. Semlyen), Wiley, New York, **1996**, pp. 191–262.

[2] a) G. Wenz, B. Keller, *Angew. Chem.* **1992**, *104*, 201–204; *Angew. Chem. Ed. Int. Engl.* **1992**, *31*, 197–199; b) G. Wenz, F. Wolf, M. Wagner, S. Kubik, *New J. Chem.* **1993**, *17*, 729–738; c) G. Wenz, *Macromol. Symp.* **1994**, *87*, 11–16; d) M. Weickenmeier, G. Wenz, *Macromol. Rapid. Commun.* **1996**, *17*, 731–736; e) M. B. Steinbrunn, G. Wenz, *Angew. Chem.* **1996**, *108*, 2274–2277; *Angew. Chem. Int. Engl.* **1996**, *35*, 2139–2142.

[3] a) M. Born, H. Ritter, *Acta Polym.* **1994**, *45*, 68–72; b) *Angew. Chem.* **1995**, *107*, 342–345; *Angew. Chem. Int. Ed. Engl.* **1995**, *34*, 309–311; c) *Adv. Mater.* **1996**, *8*, 149–151; d) *Macromol. Rapid Commun.* **1996**, *17*, 197–202.

[4] a) A. Harada, J. Li, M. Kamachi, *Nature* **1993**, *364*, 516–518; *ibid.* **1994**, *370*, 126–129; b) A. Harada, J. Li, M. Kamachi, *Macromolecules* **1993**, *26*, 5698–5703; *ibid.* **1994**, *27*, 4538–4543; A. Harada, M. Okada, J. Li, M. Kamachi, *ibid.* **1995**, *28*, 8406–8411.

[5] a) H. W. Gibson, H. Marand, *Adv. Mater.* **1993**, *5*, 11–21; b) Y. X. Shen, D. Xie, H. W. Gibson, *J. Am. Chem. Soc.* **1994**, *116*, 537–548; c) H. W. Gibson, S. Liu, P. Lecavalier, C. Wu, Y. X. Shen, *ibid.* **1995**, *117*, 852–874; d) H. W. Gibson, S. Liu, C. Gong, Q. Ji, E. Joseph, *Macromolecules* **1997**, *30*, 3711–3727.

[6] a) C. Gong, H. W. Gibson, *Macromolecules* **1996**, *29*, 7029–7033; b) C. Gong, H. W. Gibson, *Macromol. Chem. Phys.* **1997**, *198*, 2331–2342; c) C. Gong, Q. Ji, T. E. Glass, H. W. Gibson, *Macromolecules* **1997**, *30*, 4807–4813.

[7] P. E. Mason, I. W. Parsons, M. S. Tolley, *Angew. Chem.* **1996**, *108*, 2405–2408; *Angew. Chem. Int. Ed. Engl.* **1996**, *35*, 2238–2241.

[8] H. W. Gibson, S. Liu, Y. X. Shen, M. C. Bheda, S.-H. Lee, F. Wang *NATO ASI Ser. Ser. C* **1995**, *456*, 41–58.

[9] G. J. Owen, P. Hodge *Chem. Commun.* **1997**, 11–12.

[10] E. Marand, Q. Hu, H. W. Gibson, B. Veytsman, *Macromolecules* **1996**, *29*, 2555–2562.

[11] The T_1 values were measured by standard 180-τ-90° acquisition techniques.

 © WILEY-VCH Verlag GmbH, D-69451 Weinheim, 1997 0570-0833/97/3621-2333 $ 17.50+.50/0

The First Lithiated Phosphane Oxide with Li–C Bonds: Synthesis and Structure of $[\{Ph_2P(O)CHLiC(H)MeEt\}_4]$**

John E. Davies, Robert P. Davies, Lorraine Dunbar, Paul R. Raithby, Matthew G. Russell, Ronald Snaith,* Stuart Warren, and Andrew E. H. Wheatley

Lithiated phosphane oxides, Horner–Wittig reagents,[1] are extremely important in synthetic organic chemistry, for example in the stereoselective syntheses of alkenes[2] and the asymmetric synthesis of chiral compounds.[2, 3] Despite such importance, relatively little is known about the detailed structures of these reagents. Six solid-state, THF-complexed structures have been solved; five are dimers obtained by lithiation of *P*-benzylphosphorinane-1-oxide (**1**-H),[4] phosphonamides **2**-H, **3**-H, and **4**-H,[5a–c] and thiophosphonamide **5**-H.[5d] The structures of all

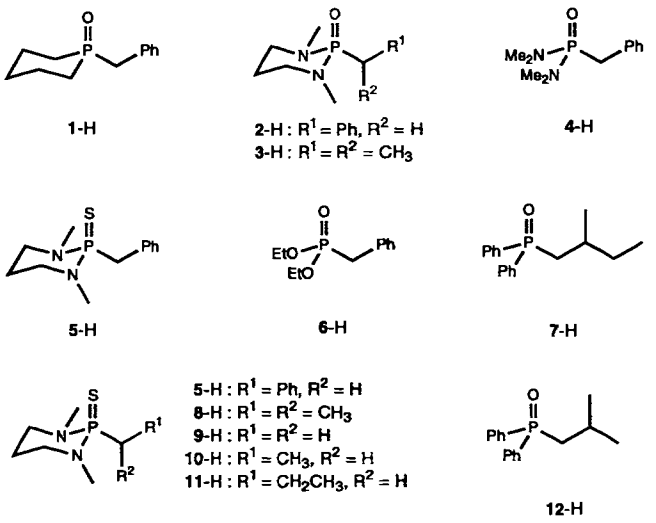

five are similar. They contain planar $(LiX)_2$ rings (X = O, S) with two THF ligands solvating each Li^+ center. There are no Li–C contacts, and, reflecting this coordinative inactivity, the carbanionic carbon centers are nearly planar and formally sp^2-hybridized. Similar features are seen in the DABCO complex (DABCO = $N(CH_2CH_2)_3N$) of the lithiated phosphonate ester **6**-H, except that here the $(LiO)_2$ rings are connected by DABCO ligands to give an infinite layered network.[6] Here we describe the very different structure of a lithiated phosphane oxide, tetrameric $[\{Ph_2P(O)CHLiC(H)MeEt\}_4]$ (**7**-Li). It is the first uncomplexed lithiated phosphane oxide and the first that is not a monomer or a dimer. Each unit of the tetramer contains two stereogenic centers, a feature which, as far as we are aware, has not been seen before in any lithiated organic molecule. Most importantly, each unit has a Li–C bond and, hence, an sp^3-hybridized, pyramidalized carbanionic center.

Our investigation was prompted by solution studies on lithiated thiophosphonamides derived from **5**-H and **8**-H to **11**-H. In THF **5**-Li (a dimer in the solid state, as noted above) and **8**-Li (a tris(THF)-complexed monomer in the solid state)[5e] are monomeric, solvent-separated ion pairs with nearly planar sp^2-hybridized carbanionic centers.[5d] In marked contrast, however, in solutions at low temperatures **9**-Li to **11**-Li have sp^3-carbanionic centers and Li–C contacts, as shown by NMR spectroscopy (^1H, $^{6,7}Li$, ^{13}C, ^{31}P); direct ^6Li–^{13}C coupling was observed.[7] This dramatic structural switch was attributed to two main factors: a) the accessibility of localized charge to metal cation contact and b) the degree of solvation of the attendant cation. We reasoned that a C–Li contact, and thus an sp^3-hybridized carbon center, could best be encouraged by lithiating a phosphane oxide with small and/or flat substituents in, above all, non-Lewis base media. By excluding such solvent molecules, the P-bound carbanionic center should be primed to act, in effect, as a donor to the lithium atom. Our initial efforts concentrated on lithiating $Ph_2P(O)CH_3$[2b] in toluene, but this gave only microcrystalline material.[8] We therefore switched to **7**-H. A suspension of **7**-H in toluene at −78°C gave a yellow solution after treatment with one equivalent of *n*BuLi in hexane. At room temperature a yellow solid precipitated which could best be dissolved for crystallization by heating after addition of one-third of an equivalent of HMPA ($O=P(NMe_2)_3$). Subsequent cooling afforded crystals identified as **7**-Li by elemental analyses as well as ^1H and ^{13}C NMR spectroscopy in THF (see Experimental Section). It was readily apparent that HMPA had not been incorporated; presumably, it merely aids dissolution of the precipitated product by increasing the polarity of the solvent mixture. Furthermore, the position of the ^{13}C NMR resonance due to the P-CH_2 group in **7**-H (δ = 36.92) had barely changed after lithiation to **7**-Li (δ(P-CHLi) = 36.78). This strongly indicates retention of sp^3 hybridization at this carbon center.

The crystal structure of **7**-Li [9] revealed a tetramer (Figure 1). In crystallographic terms the structure is not good. It has a high *R* value (R_1 = 0.1316) as a result of the poor quality of the crystals, which is consistent with the presence of highly disor-

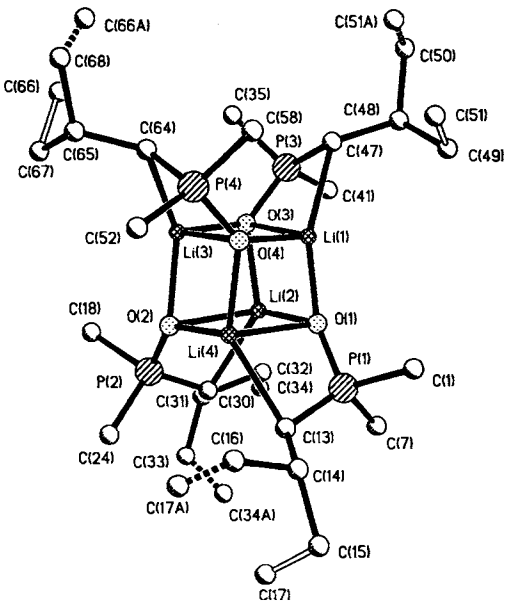

Figure 1. The molecular structure of **7**-Li. The toluene solvent molecules, H atoms, and C atoms of the phenyl group (except for the α-C atoms) have been omitted for clarity. The methyl and ethyl groups were disordered, and two positions are shown for the ethyl β-C atoms.

[*] Dr R. Snaith, Dr J. E. Davies, R. P. Davies, L. Dunbar, Dr P. R. Raithby, M. G. Russell, Dr S. Warren, A. E. H. Wheatley
Department of Chemistry
University of Cambridge
Lensfield Road, Cambridge CB2 1EW (UK)
Fax: Int. code +(1223)336-362
e-mail: cmc1006@cam.ac.uk

[**] This work was supported by the UK Engineering and Physical Sciences Research Council (R. P. D., L. D., M. G. R., A. E. H. W.) and the Royal Society (low-temperature X-ray diffraction apparatus; J. E. D., P. R. R.).

 © WILEY-VCH Verlag GmbH, D-69451 Weinheim, 1997 0570-0833/97/3621-2334 $ 17.50+.50/0

dered toluene solvate molecules (one per tetramer) in the lattice. Inspection of the structure shows that two of the new stereogenic centers of the PCH(R)Li groups are *R* (C(13) and C(30)) and two are *S* (C(47) and C(64)). However, it is impossible to decide which diastereoisomers are present because of the uncertainty of the positions of the PCHLi·CHMe·CH_2*Me* methyl groups (C(17), C(51), C(66), and C(34)). Nonetheless, the key features of **7**-Li in the solid state are clear. The core consists of a $(LiO)_4$ pseudo-cubane formed by stacking two dimeric rings, Li(3)-O(3)-Li(1)-O(4) and Li(2)-O(2)-Li(4)-O(1). Such a $(LiX)_4$ unit is common in complexes of the type $(RLi \cdot L)_n$, where the R^- anion is alkoxide, enolato (X = O), alkyl, aryl (X = C), or imide (X = N) and L is an added monodentate Lewis base such as THF, HMPA, or an internal single-base center (e. g. MeO, Me_2N) within the anion.[10] In **7**-Li the internal Lewis base is the carbanionic center of the $^-$CHC(H)MeEt unit. Within each monomeric unit, this carbanionic center has a contact with a Li^+ center to give an O-P-C-Li ring. The Li–C distances (av 2.23 Å, range 2.21(3)–2.26(3) Å) can be compared with those in lithiated phosphonamides **2**-Li , **3**-Li, and **4**-Li, in which the Li···C distances (3.83(1), 3.778(10), and 3.678(6) Å respectively) exceed the sum of the van der Waals radii, and with those in typical lithium alkyls such as $(EtLi)_4$ (av Li–C 2.25 Å)[11] and $(t$BuLi$)_4$ (av Li–C 2.246 Å).[12] The Li–O distance (av 2.27 Å, range 2.25(2)–2.28(2) Å) within each chelated monomeric unit is similar to the Li–C distance, and rather longer than the Li–O contacts which connect these units together in the cube (av 1.91 Å, range 1.85(3)–1.95(3) Å). The Li–O(P) distances are similar to those in THF complexes **1**-Li to **4**-Li, as are the P–O and P–C(H) distances in **7**-Li (av 1.541 Å, range 1.525(10)–1.555(9) Å, and av 1.682 Å, range 1.669(14)–1.702(13) Å, respectively).

Without question, the above structural features for tetrameric **7**-Li prove that it contains sp^3-hybridized carbanionic centers with contacts to lithium. We also lithiated the related but achiral phosphane oxide **12**-H in toluene. The X-ray analysis of **12**-Li was also plagued with disordered toluene solvent molecules, but the basic structure is akin to that of **7**-Li, that is, a tetrameric cubane with both Li–O and Li–C bonds. Given such disorder, **7**-Li and related systems are being synthesized (starting from enantiomerically pure precursors) in benzene in the hope of obtaining more accurate structures. These should provide good stereochemical information on the effect an extant and adjacent stereogenic center exerts on the new stereogenic center produced by lithiation. Finally, lithiation of **7**-H in toluene gives a solution at −78°C that persists until close to ambient temperature, and the then precipitated **7**-Li can be recrystallized from toluene/HMPA without incorporation of HMPA (an exceptionally good complexant for lithium). In a similar vein, it is clear from ^{13}C NMR spectroscopic data that solid **7**-Li dissolves in [D_8]THF with retention of its Li–C bonds. These results indicate that it will be profitable to examine the reactivity and selectivity of solutions of reagents such as **7**-Li in solvents such as toluene, HMPA, and THF.

Experimental Section

7-Li: *n*BuLi in hexane (5 mmol) was added to a suspension of **7**-H (1.36 g, 5 mmol) in toluene (6 mL) at −78 °C. Warming the yellow solution to room temperature caused precipitation of a yellow powder, which dissolved upon heating after addition of HMPA (0.29 mL, 1.67 mmol). Cooling the ensuing red solution afforded cubic yellow crystals of **7**-Li, $[\{Ph_2P(O)CH(Li)C(H)MeEt\}_4] \cdot C_6H_5CH_3$, $C_{75}H_{88}Li_4O_4P_4$. The yield of the first batch was 18%; m.p. decomp (loss of toluene) from 98 °C; calcd elemental analysis: C 74.7, H 7.4, Li 2.3, P 10.3; found: C 74.0, H 7.4, Li 2.1, P 10.3; ^{1}H NMR ([D_8]THF, 400.136 MHz, 25 °C): δ = 7.91 (m, 4H, Ph), 7.15 (m, 6H. Ph), 1.93 (m, 1H, CH), 1.76 (m, 1H, P-CH), 1.41 (m, 1H, CH_AH_B), 1.25 (m, 1H, CH_AH_B), 0.98 (d, 3H, CH_3), 0.86 (t, 3H, CH_2CH_3); toluene resonances have been excluded; ^{13}C/APT NMR ([D_8]THF, 100.614 MHz, 25 °C): δ = 143.77 (d, *ipso*-C, Ph), 133.35 (d, *meta*-C, Ph), 128.77 (s, *para*-C, Ph), 127.58 (d, *ortho*-C, Ph), 37.24 (d, CH_2, ^3J(C,P) = 11.1 Hz), 36.78 (d, P-CH, J(C,P) = 138.4 Hz), 34.50 (d, CH, ^2J(C,P) = 6.5 Hz), 27.62 (d, CH_3, ^3J(C,P) = 9.3 Hz), 12.68 (s, CH_2CH_3); toluene resonances have been excluded.

Received: April 24, 1997 [Z 10381 IE]
German version: *Angew. Chem.* **1997**, *109*, 2428–2430

Keywords: lithium · phosphorus · structure elucidation · Wittig reactions

[1] L. Horner, H. Hoffmann, H. G. Wippel, G. Klahre, *Chem. Ber.* **1959**, *92*, 2499–2505.
[2] a) B. E. Maryanoff, A. B. Reitz, *Chem. Rev.* **1989**, *89*, 863–927; b) J. Clayden, S. Warren, *Angew. Chem.* **1996**, *108*, 261–291; *Angew. Chem. Int. Ed. Engl.* **1996**, *35*, 241–270.
[3] a) S. E. Denmark, N. Chatani, S. V. Pansare, *Tetrahedron* **1992**, *48*, 2191–2208; b) S. E. Denmark, C.-T. Chen, *J. Am. Chem. Soc.* **1992**, *114*, 10674–10676.
[4] S. E. Denmark, K. A. Swiss, S. R. Wilson, *Angew. Chem.* **1996**, *108*, 2686–2688; *Angew. Chem. Int. Ed. Engl.* **1996**, *35*, 2515–2517.
[5] a) S. E. Denmark, R. L. Dorow, *J. Am. Chem. Soc.* **1990**, *112*, 864–866; b) S. E. Denmark, P. C. Miller, S. R. Wilson, *ibid.* **1991**, *113*, 1468–1470; c) C. J. Cramer, S. E. Denmark, P. C. Miller, R. L. Dorow, K. A. Swiss, S. R. Wilson, *ibid.* **1994**, *116*, 2437–2447; d) S. E. Denmark, K. A. Swiss, S. R. Wilson, *ibid.* **1993**, *115*, 3826–3827; e) M. Kranz, S. E. Denmark, K. A. Swiss, S. R. Wilson, *J. Org. Chem.* **1996**, *61*, 8551–8563.
[6] W. Zarges, M. Marsch, K. Harms, F. Haller, G. Frenking, G. Boche, *Chem. Ber.* **1991**, *124*, 861–866.
[7] S. E. Denmark, K. A. Swiss, *J. Am. Chem. Soc.* **1993**, *115*, 12195–12196.
[8] D. R. Armstrong, D. Barr, M. G. Davidson, G. Hutton, P. O'Brien, R. Snaith, S. Warren, *J. Organomet. Chem.* **1997**, *529*, 29–33.
[9] X-ray crystal data for **7**-Li: $[Ph_2P(O)CHLiC(H)MeEt]_4 \cdot C_6H_5Me$: $C_{75}H_{88}Li_4O_4P_4$, triclinic, $P\bar{1}$ (no. 2), a = 16.851(9), b = 16.921(13), c = 15.516(12) Å, α = 116.26(5), β = 109.49(5), γ = 90.25(6)°, V = 3679(4) Å^3, T = 153(2) K, $F(000)$ = 1284, ρ_{calcd} = 1.088 mg m^{-3}, Z = 2, $\mu(Mo_{K\alpha})$ = 1.47 cm^{-1} (no correction), 0.20 × 0.20 × 0.40 mm, Rigaku AFC7R diffractometer, $Mo_{K\alpha}$ radiation. Of 7358 reflections measured ($2\theta_{max}$ = 45°), 6856 were unique (R_{int} = 0.214). The structure was solved by direct methods (SHELXL PLUS, Version 4.21, Siemens Analytical X-Ray Instruments Inc., Madison, WI, **1990**), and refined by full-matrix least squares based on F^2 (SHELXL 93, G. M. Sheldrick, Universität Göttingen, **1993**); 679 parameters, R_1 = 0.132 (for 3516 data with $F_o > 4\sigma(F_o)$), wR_2 = 0.431 (all data). Methyl and ethyl groups were disordered and refined with partial occupancies over two sites. The toluene solvent molecule was also disordered, and two sites for the methyl group were refined with partial occupancies; phenyl H-atoms were placed in idealized positions and allowed to ride on the relevant carbon atom. Crystallographic data (excluding structure factors) for the structure reported in this paper have been deposited with the Cambridge Crystallographic Data Centre as supplementary publication no. CCDC-100549. Copies of the data can be obtained free of charge on application to The Director, CCDC, 12 Union Road, Cambridge CB21EZ, UK (fax: int. code +(1223)336-033; e-mail: deposit@chemcrys.cam.ac.uk).
[10] Reviews of structures with O–Li, C–Li, and N–Li bonds: a) W. Setzer, P. von R. Schleyer, *Adv. Organomet. Chem.* **1985**, *24*, 353–451; b) D. Seebach, *Angew. Chem.* **1988**, *100*, 1685–1715; *Angew. Chem. Int. Ed. Engl.* **1988**, *27*, 1624–1654; c) G. Boche, *ibid.* **1989**, *101*, 286–306 and **1989**, *28*, 277–297; d) R. E. Mulvey, *Chem. Soc. Rev.* **1991**, *20*, 167–209; e) K. Gregory, P. von R. Schleyer, R. Snaith, *Adv. Inorg. Chem.* **1991**, *37*, 47–142; f) E. Weiss, *Angew. Chem.* **1993**, *105*, 1567–1587; *Angew. Chem. Int. Ed. Engl.* **1993**, *32*, 1501–1523; g) *Lithium Chemistry: A Theoretical and Experimental Overview* (Eds.: A. M. Sapse, P. von R. Schleyer), Wiley, New York, **1995**.
[11] H. Dietrich, *Acta Crystallogr.* **1963**, *16*, 681–689.
[12] T. Kottke, D. Stalke, *Angew. Chem.* **1993**, *105*, 619–621; *Angew. Chem. Int. Ed. Engl.* **1993**, *32*, 580–582.

 © WILEY-VCH Verlag GmbH, D-69451 Weinheim, 1997 0570-0833/97/3621-2335 $ 17.50+.50/0

The Structure of $[Zn(bix)_2(NO_3)_2]\cdot 4.5H_2O$ (bix = 1,4-Bis(imidazol-1-ylmethyl)benzene): A New Type of Two-Dimensional Polyrotaxane**

Bernard F. Hoskins, Richard Robson,* and Damian A. Slizys

Rotaxanes and polyrotaxanes currently attract considerable interest.[1] Polyrotaxanes resembling strings of beads have been reported, in which macrocycles such as cyclodextrins and cyclic polyethers provide the beads and polymers of various sorts act as the string; however, these have generally been structurally irregular. The first three examples of structurally regular polyrotaxanes amenable to single-crystal X-ray diffraction study were reported very recently within a short time by Kim et al[2] and by ourselves.[3] The examples from Kim et al. consist of a one-dimensional Cu^{II} coordination polymer and an analogous 2D Ag^{I} derivative of the same ligand with a macrocyclic cucurbituril bead encircling every repeat unit; in both cases the beads are secured in place by hydrogen bonds between their oxygen atoms and NH_2^+ groups incorporated into the polymer for this purpose. The 2D polyrotaxane that we reported[3] is also a coordination polymer, but it differs fundamentally from that of Kim et al. in that the rings associated with the rotaxane are themselves part of a 1D polymeric chain. It has the composition $[Ag_2(bix)_3(NO_3)_2]$ (bix = 1,4-bis(imidazol-1-ylmethyl)benzene, **I**; Scheme 1) and consists of 1D polymeric chains of the type represented schematically by **II**, in which the threefold connecting nodes are provided by three-coordinate Ag^{I}. The metal centers are connected by two types of bridging bix units: those forming $Ag_2(bix)_2$ rings and those that connect the rings with each other (referred to here as "rods"). Each polymeric chain is entangled through rotaxane interactions with an infinite number of other chains, so that every one of its $Ag_2(bix)_2$ rings encircles an Ag-bix-Ag rod of another chain and every one of its Ag-bix-Ag rods passes through an $Ag_2(bix)_2$ ring of another chain. This generates the 2D polyrotaxane sheet represented by **III**.

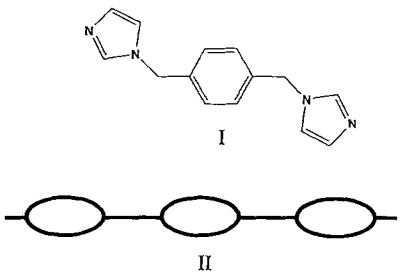

Scheme 1.

We report here the structure of $[Zn(bix)_2(NO_3)_2]\cdot 4.5H_2O$, which, like the silver derivative, has a 2D polyrotaxane structure. Its topology, however, is entirely different. The outstanding structural features are polyrotaxane columns of the type represented schematically by **IV**.

Crystals suitable for single crystal X-ray diffraction studies were obtained directly from reaction mixtures containing zinc nitrate and bix in aqueous methanol. The zinc centers are all equivalent and in a distorted tetrahedral N_4 coordination environment. The N-Zn-N angles vary from 96.2(1) to 125.0(1)°, and the Zn–N bond lengths from 1.994(3) to 2.056(4) Å. There are two independent 2D polymeric sheets of the type represented schematically by **V** (Scheme 2), in which the fourfold connecting nodes are provided by zinc; two such sheets interpenetrate as shown by **VI**. Therefore, three types of bridging bix ligands are present: those that form the macrocyclic $Zn_2(bix)_2$ rings (Zn···Zn 11.902(2) Å), the rods that pass through these rings (Zn···Zn 15.037(2) Å), and those that connect columns of type **IV** (Zn···Zn 14.146(2) Å). The C/N/Zn arrangement within columns of type **IV**, which are oriented parallel to the *a* axis, is shown in Figure 1, and that within an entire interpenetrating double sheet in Figure 2. Water molecules and nitrate ions located largely within the double-sheet structure are highly disordered.

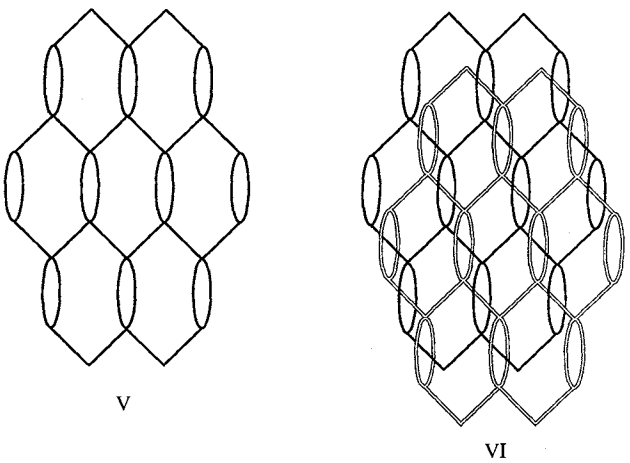

Scheme 2.

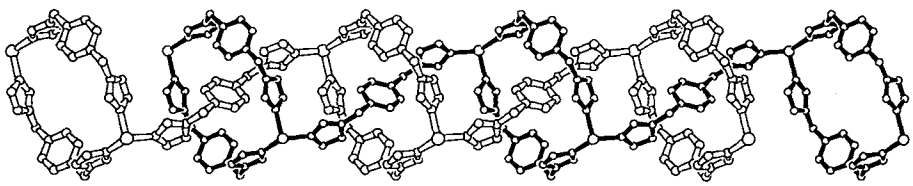

Figure 1. A polyrotaxane column present in the $\{Zn(bix)_2^{2+}\}_n$ framework structure. Small circles represent C and N atoms, and large circles Zn atoms. The components of two independent networks are indicated by filled and open connections.

[*] Dr. R. Robson, Dr. B. F. Hoskins, D. A. Slizys
School of Chemistry
University of Melbourne
Parkville, Victoria 3052 (Australia)
Fax: Int. code +(3)9347-5180
e-mail: r.robson@chemistry.unimelb.edu.au

[**] The authors gratefully acknowledge support from the Australian Research Council and the American Chemical Society Petroleum Research Fund.

 © WILEY-VCH Verlag GmbH, D-69451 Weinheim, 1997 0570-0833/97/3621-2336 $ 17.50+.50/0

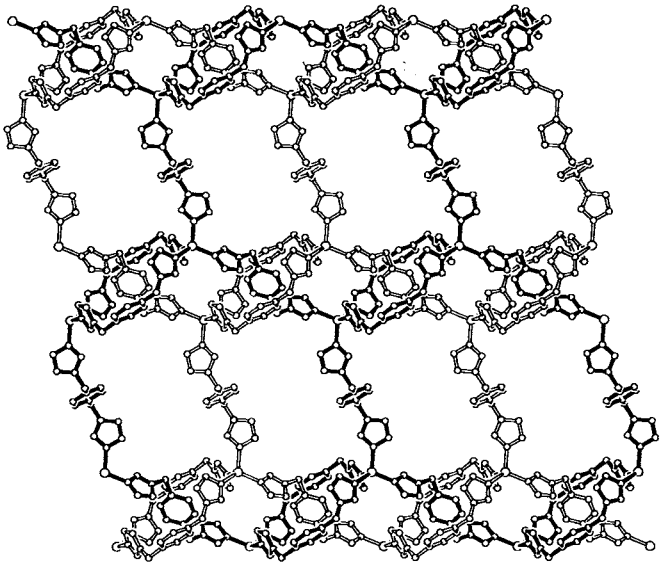

Figure 2. A view of the pair of independent and interpenetrating extended 2D $\{Zn(bix)_2^{2+}\}_n$ networks.

The stereochemical relationships between the $M_2(bix)_2$ ring and the bix rod passing through it are contrasted for the silver and zinc derivatives in Figure 3. In both cases the macrocyclic ring is arranged around a center of symmetry, but the two differ

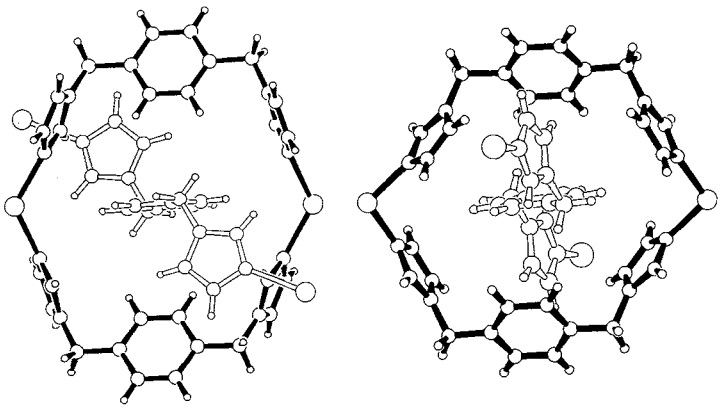

Figure 3. Comparison of the stereochemical relationships between a metal-bix-metal rod and the $metal_2(bix)_2$ ring through which it passes for $[Ag_2(bix)_3(NO_3)_2]$ (left) and $[Zn(bix)_2(NO_3)_2]\cdot 4.5H_2O$ (right).

in conformation. The Ag···Ag separation across the ring (10.503(1) Å) is significantly smaller than the Zn···Zn separation (11.902(2) Å), mainly as a result of the larger N-M-N angle for trigonal silver (127.3(1)° internal to the ring) than for tetrahedral zinc (103.2(1)° internal to the ring). Another conformational difference arises in the direction of inclination for the phenylene units of the macrocycle. In the case of zinc, the C–C edge of the phenylene units that appears on the same side of the macrocycle as the C–C edges of the two adjacent imidazoles is oriented outwards, away from the center of the macrocycle, whereas in the case of silver it is oriented inwards. As is apparent in Figure 3, the central phenylene unit of the rod relative to the surrounding macrocycle is much the same in the two cases. However, the orientation of the rod metal–metal vector relative to the macrocyclic average plane is significantly different: it is inclined away from the perpendicular to the ring much more in the case of silver, as can be clearly seen in Figure 3. In both cases many contacts between H atoms and aromatic C or N atoms in the range of 2.9 to 3.2 Å participate in the rod-to-ring interaction; in the case of silver there are also two shorter interactions (2.684(4) and 2.772(5) Å), both involving coordinated N atoms. The shortest interaction in the case of zinc (2.954(4) Å) also involves a coordinated N atom of the macrocycle, but no particular rod-to-ring interaction appears to be of significance.

Bridging ligands derived from 1,4-xylyl appear to have some propensity for forming catenanes and rotaxanes by penetrating parts of independent components through $M_2(ligand)_2$ rings. Thus, in addition to the two bix-based polyrotaxanes described here, the related 1,4-xylyl-derived ligands, 1,4-bis(4-pyridylmethyl)benzene and *N,N'-p*-phenylenedimethylenebis(pyridin-4-one) were reported to form discrete molecular catenanes[4] and infinite polycatenanes,[5] respectively. Related cyclophanes derived from 1,4-xylyl involving C–C and C–N covalent bonds rather than metal–ligand bonds have also been extensively used by Stoddart et al. to generate a wide range of catenanes and rotaxanes.[6]

Experimental Section

Hydrated $[Zn(bix)_2(NO_3)_2]$ was obtained by adding a solution of bix dihydrate [3] (58.8 mg, 0.214 mmol) in methanol (5 mL) to a solution of zinc nitrate hexahydrate (21.3 mg, 0.072 mmol) in water (5 mL). The crystals that separated after 18 h were collected, washed with aqueous methanol, and dried under air. Elemental analysis calcd for $C_{28}H_{33}N_{10}O_{8.5}Zn$ ($[Zn(bix)_2(NO_3)_2]\cdot 2.5H_2O$): C 47.3, H 4.7, N 19.7, Zn 9.2; found: C 47.4, H 4.5, N 19.8, Zn 9.2. Crystal data: $[Zn(bix)_2(NO_3)_2]\cdot 4.5H_2O$, $M_r = 747.04$, triclinic, space group $P\bar{1}$ (no. 2), $a = 10.489(1)$, $b = 13.539(2)$, $c = 13.659(2)$ Å, $\alpha = 70.53(1)$, $\beta = 83.21(1)$, $\gamma = 77.27(1)°$, $U = 1781(4)$, $Z = 2$, $\rho_{calcd} = 1.39\ g\,cm^{-3}$, $\rho_{found} = 1.44(2)\ g\,cm^{-3}$, $\mu(Mo_{K\alpha}) = 7.6\ cm^{-1}$, $F(000) = 778$. Intensity data for 7145 reflections, yielding 6280 independant reflections ($R_{int} = 0.0124$), were measured at 295(1) K with $Mo_{K\alpha}$ radiation (graphite monochromator) using an Enraf-Nonius CAD-4 MachS diffractometer and employing the $\omega/2\theta$ scan method; absorption corrections were applied [7]. All non-hydrogen atoms of the polymeric cation, together with oxygen atoms attributed to two of the waters of solvation, were located using the Patterson interpretation routine of the SHELXS-86 program [8]. Subsequent cycles of least-squares refinement and difference syntheses (SHELXL-93) [9] indicated that both of the crystallographically independent anions and the remainder of the water structure were extensively disordered; these features were incorporated in the model. The ligand hydrogen atoms, all of which were revealed in the difference syntheses during the last stages of refinement, were included in the refinement at their geometrically constrained positions. Anisotropic displacement parameters were applied to all non-hydrogen atoms of the coordination polymer and the full-weight oxygen atoms of the water structure. Full-matrix least-squares refinement based on F^2 converged with $R_1 = 0.0716$, $wR_2 = 0.2163$, and goodness of fit = 1.041; minimum and maximum residual electron density were -0.733 and $0.881\ e\,Å^{-3}$. Crystallographic data (excluding structure factors) for the structures reported in this paper have been deposited with the Cambridge Crystallographic Data Centre as supplementary publication no. CCDC-100 532. Copies of the data can be obtained free of charge on application to The Director, CCDC, 12 Union Road, Cambridge CB2 1EZ, UK (fax: int. code +(1223) 336-033; e-mail: deposit@chemcrys.cam.ac.uk).

Received: April 17, 1997 [Z10361IE]
German version: *Angew. Chem.* **1997**, *109*, 2430–2432

Keywords: coordination polymers · N ligands · rotaxanes zinc

[1] An indication of the extent of this interest can be obtained from the following reviews and the references therein: D. B. Amabilino, J. F. Stoddart, *Chem. Rev.* **1995**, *95*, 2725; P. T. Glink, C. Schiavo, J. F. Stoddart, D. J. Williams, *Chem. Commun.* **1996**, 1483; F. Vögtle, T. Dunnwald, T. Schmidt, *Acc. Chem. Res.* **1996**, *29*, 451; see also R. Jäger, F. Vögtle, *Angew. Chem.* **1997**, *109*, 966; *Angew. Chem. Int. Ed. Engl.* **1997**, *36*, 930.
[2] D. Whang, Y.-M. Jeon, J. Heo, K. Kim, *J. Am. Chem. Soc.* **1996**, *118*, 11 333; D. Whang, K. Kim, *ibid.* **1997**, *119*, 451.
[3] B. F. Hoskins, R. Robson, D. A. Slizys, *J. Am. Chem. Soc.* **1997**, *119*, 2952.
[4] M. Fujita, F. Ibukuro, K. Yamaguchi, J. Ogura, *Nature* **1994**, *367*, 720.
[5] D. M. L. Goodgame, S. Menzer, A. M. Smith, D. J. Williams, *Angew. Chem.* **1995**, *107*, 605; *Angew. Chem. Int. Ed. Engl.* **1995**, *34*, 574.

 © WILEY-VCH Verlag GmbH, D-69451 Weinheim, 1997 0570-0833/97/3621-2337 $ 17.50+.50/0

[6] D. Philp, J. F. Stoddart, *Angew. Chem.* **1996**, *108*, 1242; *Angew. Chem. Int. Ed. Engl.* **1996**, *35*, 1154.
[7] G. M. Sheldrick, SHELX-76, Program for crystal structure determination, University of Cambridge, UK, **1976**.
[8] G. M. Sheldrick, SHELXS-86, Program for crystal structure determination, in *Crystallographic Computing 3* (Eds.: G. M. Sheldrick, C. Kruger, R. Goddard), Oxford University Press, Oxford, **1985**, 175.
[9] G. M. Sheldrick, SHELXL-93, Program for crystal structure refinement, University of Göttingen, **1993**.

Incorporation of a First Row Element into the Bridge of a Strained Metallocenophane: Synthesis of a Boron-Bridged [1]Ferrocenophane**

Holger Braunschweig,* Regina Dirk, Matthias Müller, Paul Nguyen, Rui Resendes, Derek P. Gates, and Ian Manners*

[1]Ferrocenophanes **1** are unusual, strained organometallic species that have attracted considerable interest with respect to their structures, reactivity, and, more recently, their propensity to undergo ring-opening polymerization (ROP) reactions.[1–5] The latter provide access to novel, high molecular weight poly(ferrocene)s **2**.[3] The first [1]ferrocenophane, the silicon-bridged

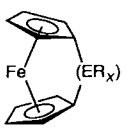

1

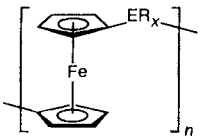

2

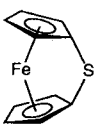

3

species **1** (ER$_x$ = SiPh$_2$), was prepared in 1975 by the reaction of dilithioferrocene·TMEDA (TMEDA = *N*,*N*,*N*′,*N*′-tetramethylethylenediamine) with Ph_2SiCl_2 and was shown to possess a strained structure in which the tilt angle between the planes of the cyclopentadienyl ligands is about 19°.[6] The range of [1]ferrocenophanes has subsequently been extended to include compounds whose bridges contain other main group elements of the second period and below from Group 14 (Ge and Sn; tilt angles 14–19°),[7] Group 15 (P and As; tilt angles 23–27°),[8] and also Group 4 transition metals (Ti, Zr, Hf; tilt angles = ca. 6°).[9] In general, the smaller the covalent radius of the atom in the bridge, the larger the tilt angle, and the higher the ring strain present. With this in mind, one of our groups recently reported the preparation of a sulfur-bridged [1]ferrocenophane **3**, the first ferrocenophane with a Group 16 element in the bridge.[10] This species possessed the highest tilt angle recorded to date for a strained [1]ferrocenophane (31.05(10)°).[11] As the covalent radii of first row elements are even smaller than that of sulfur their incorporation into the bridged structure would be expected to provide access to even more highly strained species. We have investigated the preparation of such compounds because of our interests concerning the use of ROP to access new metal-based polymers,[3] possible interactions between the iron and the bridging element,[12] and the opportunity of accessing novel species with bonds between transition metals and main group elements by insertion reactions.[13, 14] In the case of a bridging boranediyl moiety, insertion processes might provide a new synthetic route to transition metal boryl complexes, which, to date, are mainly restricted to the use of the 1,2-phenylenedioxy group as the boron bound ligand.[15] With this in mind, we report here the first [1]ferrocenophane containing a first row element in the bridge, a boron-bridged [1]ferrocenophane.[16]

Reaction of a suspension of dilithioferrocene·TMEDA with $(Me_3Si)_2NBCl_2$[17] in benzene or toluene at 25 °C, followed by recrystallization from hexanes at −30 °C afforded dark red crystals. NMR spectroscopic data were consistent with the formation of the highly strained [1]boraferrocenophane **4a**. For example, a characteristically large separation ($\Delta\delta = 0.50$ ppm) of the α and β protons of the cyclopentadienyl groups was detected by ^{1}H NMR spectroscopy, and the ^{13}C NMR signal ([D$_8$]toluene, −30 °C) of the *ipso*-C atom was detected at δ = 45.0 and is upfield shifted compared to the signal for unstrained systems (ferrocene, $\delta = 68.0$). Surprisingly though, it is shifted much further downfield with respect to those of compound **3** ($\delta = 14.3$) and other less strained [1]ferrocenophanes.[18] The ^{11}B NMR signal ($\delta = 48.3$) was in the range expected for a planar three-coordinate boron atom. In hexanes, **4a** exhibits a UV/Vis absorbance at 479 nm which is considerably red-shifted with respect to ferrocene (λ_{max} = 440 nm); however, interestingly, it is not as low energy as that of **3** (λ_{max} = 504 nm). The [1]boraferrocenophane **4b** was prepared by a method analogous to that employed for **4a** and was characterized similarly.

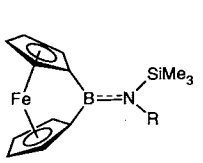

4a, R = SiMe$_3$
4b, R = *t*Bu

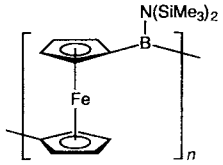

5

In order to completely characterize and probe the strain present in **4a**, a single-crystal X-ray diffraction study was undertaken.[19] This indicated that molecules of **4a** are highly strained with a tilt angle of 32.4(2)°, the largest reported to date for a [*n*]metallocenophane (Figure 1). The large ring tilting in **4a** is accompanied by a Cp$_c$1-Fe-Cp$_c$2 angle (Cp$_c$ = ring centroid) of 155.2(2)° (ferrocene: 180°), which is smaller than that in **3** [156.9(1)°]. The cyclopentadienyl rings are in an eclipsed conformation with a C(10)-Cp$_c$1-Cp$_c$2-C(20) torsion angle of 1.0(2)°. Additional structural distortions include angles of 33.7(2)° and 34.0(2)° between the cyclopentadienyl ring planes and the exo-

[*] Dr. H. Braunschweig, Dr. R. Dirk
Institut für Anorganische Chemie der Technischen Hochschule
Templergraben 55, D-52056 Aachen (Germany)
Fax: Int. code +(241) 8888-288
e-mail: holger.braunschweig@ac.rwth-aachen.de
Prof. I. Manners, Dr. P. Nguyen, R. Resendes, D. P. Gates
Department of Chemistry, University of Toronto
80 St. George Street
Toronto, Ontario, M5S 1A1 (Canada)
Fax: Int. code +(416) 978-8775
e-mail: imanners@alchemy.chem.utoronto.ca
Dr. M. Müller
Chemical Crystallography Laboratory, University of Oxford
Oxford, OX1 3PD (UK)

[**] H. B. thanks the Deutsche Forschungsgemeinschaft (DFG) and the Fonds der Chemischen Industrie for financial support of this work. M. M. gratefully acknowledges a scholarship from the DFG and thanks Prof. K. Prout for his support. I. M. thanks the donors of the Petroleum Research Fund (PRF), administered by the American Chemical Society, for financial support of this work, the Natural Sciences and Engineering Research Council of Canada (NSERC) for a Graduate Student Fellowship for D. P. G. and a Postdoctoral Fellowship for P. N, the Alfred P. Sloan Foundation for a Research Fellowship (1994–1998), NSERC for an E. W. R. Steacie Fellowship (1997–98), and the University of Toronto for a McLean Fellowship (1997).

 © WILEY-VCH Verlag GmbH, D-69451 Weinheim, 1997 0570-0833/97/3621-2338 $ 17.50+.50/0

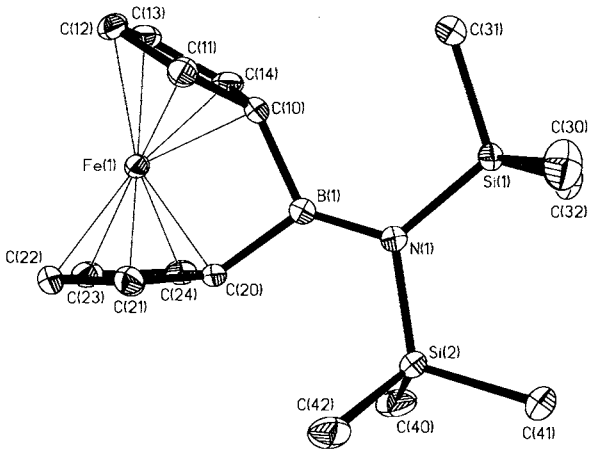

Figure 1. Molecular structure of **4a** in the crystal (ellipsoids drawn at 50% level).

cyclic C–B bonds. The B–N bond length is 1.399(2) Å, which is typical for a B–N double bond (1.41 Å).[20] The Fe(1) and B(1) atoms do not appear to show a substantial interaction; the Fe(1)–B(1) distance is 2.590(2) Å, which is significantly longer than for a single bond (in $[CpFe(BPh_2)(CO)_2]$, d(Fe–B) = 2.034(3) Å[15c]) and longer than the sum of the covalent radii (2.15 Å).[21]

In order to explore the polymerization behavior of **4a** a differential scanning calorimetry (DSC) investigation was undertaken. A DSC thermogram of **4a** (Figure 2) showed a melt

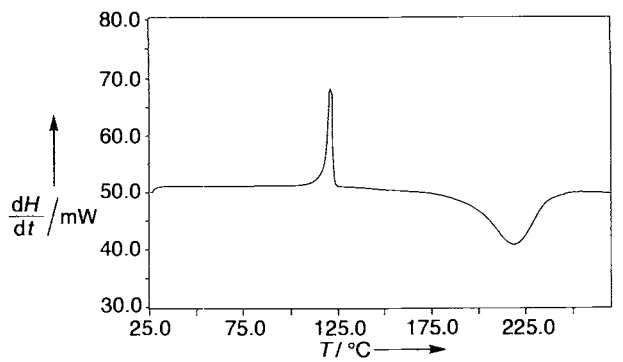

Figure 2. DSC thermogram of **4a**.

endotherm at about 115 °C, followed by a ROP exotherm at about 190 °C. Similar behavior has been detected by DSC for strained silicon-bridged [1]ferrocenophanes. In the case of **4a** the ΔH for the ROP was 95 kJ mol^{-1}, which is significantly greater than for silicon-bridged [1]ferrocenophanes (70–80 kJ mol^{-1}) (tilt angles 16–21°).[22]

The product **5** formed from heating **4a** at 180 °C for 2 h was found to be mainly insoluble in organic solvents. However, ^{1}H NMR analysis of a soluble extract in C_6D_6 showed the presence of oligomers. Pyrolysis mass spectrometry of **5** confirmed the presence of the ferrocenylborane repeat unit, and peaks were observed that could be assigned to cyclic oligomers **5** ($n = 2$) and **5** ($n = 3$).

We are now carrying out detailed studies on the chemical behavior of **4a** and **4b**. As mentioned above, the possibility of the insertion of transition metals into the strained *ipso*-C–B bond is of particular interest. Work aimed at the preparation and characterization of soluble poly(boraferrocene)s is also in progress.

Experimental Section

4a: $[Fe(\eta^5\text{-}C_5H_4Li)_2]\cdot$TMEDA (1.20 g, 2.79 mmol) was suspended in benzene (70 mL) at room temperature and $[(Me_3Si)_2N]BCl_2$ (0.67 g, 2.79 mmol) was added dropwise by a syringe. After the mixture had been stirred for 6 h, all volatile components were removed in high vacuum (25 °C/0.001 Torr) and the residue was taken up in hexane (30 mL). After filtration, **4a** (0.35 g; 35%) was obtained at −30 °C as dark red crystals. NMR spectra in C_6D_6 at 25 °C: ^{1}H NMR (500 MHz, TMS): $\delta = 0.37$ (s, 18H; $SiMe_3$), 3.91, 4.41 (2m, 8H; C_5H_4); ^{11}B NMR (160 MHz, $Et_2O\cdot BF_3$): $\delta = 48.3$; ^{13}C NMR (126 MHz, TMS): $\delta = 5.1$ ($SiMe_3$), 45.0 (*ipso*-C), 72.4, 77.1 (C_5H_4); UV/Vis (hexanes): λ_{max} (ε) = 479 nm (593 L mol^{-1} cm^{-1}); MS (70 eV): m/z (%): 355 (100) [M^+], 340 (80) [$M^+ - CH_3$], 299 (70) [$M^+ - Fe$], 73 (30) [$SiMe_3$] (the calculated isotopic distribution for each ion was in agreement with experimental values); elemental analysis (%): calcd for $C_{16}H_{26}BFeNSi_2$: C 54.10, N 3.94, H 7.38; found C 53.43, N 4.13, H 7.79.

4b: As described for **4a**, $[Fe(\eta^5\text{-}C_5H_4Li)_2]\cdot$TMEDA (1.38 g, 3.21 mmol) suspended in benzene (70 mL) was treated with [*t*Bu(Me_3Si)N]BCl_2 [17] (0.73 g, 3.21 mmol), and **4b** (0.48 g; 44%) was obtained as dark red crystals. NMR spectra (same conditions as for **4a**); ^{1}H NMR: $\delta = 0.43$ (s, 9H; $SiMe_3$), 1.50 (s, 9H, *t*Bu), 3.92, 3.94, 4.40, 4.42 (4m, 8H; C_5H_4); ^{11}B NMR: $\delta = 44.7$; ^{13}C NMR: $\delta = 7.5$ ($SiMe_3$), 34.6 (CMe_3), 44.3, 46.1 (*ipso*-C), 57.9 (CMe_3), 72.0, 72.8, 76.6, 76.7 ($2C_5H_4$); elemental analysis (%): calcd for $C_{17}H_{26}BFeNSi$: C 60.21, N 4.13, H 7.73; found C 58.70, N 4.00, H 7.89.

5: **4a** (80 mg) was heated at 180 °C in a sealed, evacuated Pyrex tube. After about 15 min. the contents of the tube melted and became increasingly viscous, becoming immobile after 2 h. The red glassy material obtained quantitatively was found to be essentially insoluble in common organic solvents. A small amount was extracted with C_6D_6. ^{1}H NMR (400 MHz): $\delta = 0.25$, 0.33, 0.46 (3s, $SiMe_3$), 4.19, 4.26, 4.38, 4.53, 4.66, 4.94 (6t, C_5H_4). Pyrolysis MS of the crude product **5** (70 eV, 450 °C): m/z (%): 1065 (45) [$n = 3$], 710 (100) [$n = 2$], 355 (78) [$n = 1$], 73 (80) [$SiMe_3$] (the calculated isotopic distribution for each ion was in agreement with experimental values).

Received: April 21, 1997 [Z10373IE]
German version: *Angew. Chem.* **1997**, *109*, 2433–2435

Keywords: boron · iron · metallocenophanes · ring-opening polymerization · sandwich complexes

[1] G. Osborne, R. H. Whiteley, R. E. Meads, *J. Organomet. Chem.* **1980**, *193*, 345.
[2] A. B. Fischer, J. B. Kinney, R. H. Staley, M. S. Wrighton, *J. Am. Chem. Soc.* **1979**, *101*, 6501.
[3] D. A. Foucher, B.-Z. Tang, I. Manners, *J. Am. Chem. Soc.* **1992**, *114*, 6246; I. Manners, *Adv. Organomet. Chem.* **1995**, *37*, 131; *Angew. Chem.* **1996**, *108*, 1712; *Angew. Chem. Int. Ed. Engl.* **1996**, *35*, 1602 and references therein.
[4] M. Herberhold, *Angew. Chem.* **1995**, *107*, 1985; *Angew. Chem. Int. Ed. Engl.* **1995**, *34*, 1837.
[5] For recent work on poly(ferrocene)s see: O. Nuyken, T. Pöhlmann, M. Herberhold, *Macromol. Rev.* **1992**, *A29*, 211; R. Bayer, T. Pöhlmann, O. Nuyken, *Makromol. Chem. Rapid Commun.* **1993**, *14*, 359; M. Rosenblum, H. M. Nugent, K.-S. Jang, M. M. Labes, W. Cahalane, P. Klemarczyk, W. M. Reiff, *Macromolecules*, **1995**, *28*, 6330; M. Morán, M. C. Pascual, I. Cuadrado, J. Losada, *Organometallics*, **1993**, *12*, 811; M. T. Nguyen, A. F. Diaz, V. V. Demente'ev, K. H. Pannell, *Chem. Mater.* **1993**, *5*, 1389; C. E. Stanton, T. R. Lee, R. H. Grubbs, N. S. Lewis, J. K. Pudelski, M. R. Callstrom, M. S. Erickson, M. L. McLaughlin, *Macromolecules*, **1995**, *28*, 8713; P. F. Brandt, T. B. Rauchfuss, *J. Am. Chem. Soc.* **1992**, *114*, 1926; D. L. Compton, P. F. Brandt, T. B. Rauchfuss, D. F. Rosenbaum, C. F. Zukoski, *Chem. Mater.* **1995**, *7*, 2342.
[6] A. G. Osborne, R. H. Whiteley, *J. Organomet. Chem.* **1975**, *101*, C27.
[7] H. Stoeckli-Evans, A. G. Osborne, R. H. Whiteley, *J. Organomet. Chem.* **1980**, *194*, 91; R. Rulkens, A. J. Lough, I. Manners, *Angew. Chem.* **1996**, *108*, 1929; *Angew. Chem. Int. Ed. Engl.* **1996**, *35*, 1805.
[8] H. Stoeckli-Evans, A. G. Osborne, R. H. Whiteley, *J. Organomet. Chem.* **1980**, *194*, 91; D. Seyferth, H. P. Withers, *Organometallics* **1982**, *1*, 1275; I. R. Butler, W. R. Cullen, F. W. B. Einstein, S. J. Rettig, A. J. Willis, *ibid.* **1983**, *2*, 128.
[9] R. Broussier, A. Da Rold, B. Gautheron, Y. Dromzee, Y. Jeannin, *Inorg. Chem.* **1990**, *29*, 1817; R. Broussier, A. Da Rold, B. Gautheron, *J. Organomet. Chem.* **1992**, *427*, 231;
[10] J. K. Pudelski, D. P. Gates, R. Rulkens, A. J. Lough, I. Manners *Angew. Chem.* **1995**, *107*, 1633; *Angew. Chem. Int. Ed. Engl.* **1995**, *34*, 1506;
[11] Herberhold and co-workers have reported the synthesis and structure of the [2]ruthenocenophane $[Ru\{(\eta\text{-}C_5H_4)_2C_2Me_4\}]$ (average tilt angle (α) = 31°), see M. Herberhold, T. Bärtl, *Z. Naturforsch. B* **1995**, *50*, 1692.
[12] J. Silver, *J. Chem. Soc. Dalton Trans.* **1990**, 3513.
[13] H. Braunschweig, T. Wagner, *Angew. Chem.* **1995**, *107*, 904; *Angew. Chem. Int. Ed. Engl.* **1995**, *34*, 825; H. Braunschweig, B. Ganter, M. Koster, T. Wagner *Chem. Ber.* **1996**, *129*, 1099; H. Braunschweig, J. Müller, B. Ganter *Inorg. Chem.* **1996**, *35*, 7443.
[14] Oxidative addition at low-valent transition metal centers is known for the bond between the strained Cp *ipso*-carbon atom and the bridging atom present in strained silicon-bridged [1]ferrocenophanes: see, J. B. Sheridan, A. J. Lough, I. Manners, *Organometallics* **1996**, *15*, 2195.

 © WILEY-VCH Verlag GmbH, D-69451 Weinheim, 1997 0570-0833/97/3621-2339 $ 17.50+.50/0

[15] a) J. R. Knorr, J. S. Merola, *Organometallics* **1990**, *9*, 3008; b) P. Nguyen, H. P. Blom, S. A. Westcott, N. J. Taylor, T. B. Marder, *J. Am. Chem. Soc.* **1993**, *115*, 9329; c) J. F. Hartwig, S. Huber, *ibid.* **1993**, *115*, 4908; d) C. N. Iverson, M. R. Smith, *ibid.* **1995**, *117*, 4403.
[16] For the recent report of the first [2]diboraferrocenophane see M. Herberhold, U. Doerfler, B. Wrackmeyer, *J. Organomet. Chem.* **1997**, *530*, 117.
[17] P. Geymayer, E. G. Rochow, U. Wannagat, *Angew. Chem.* **1964**, *76*, 499; *Angew. Chem. Int. Ed. Engl.* **1964**, *3*, 633.
[18] For example, the following ^{13}C NMR shifts were measured for *ipso* cyclopentadienyl carbon atoms of compounds of type **1**: $ER_x = SiPh_2$: 31.0 ($CDCl_3$); $ER_x = GePh_2$: 28.5 ($CDCl_3$); $ER_x = PPh$: 18.7 (C_6D_6); $ER_x = AsPh$: 18.3 (C_6D_6); $ER_x = S$: 14.3 (C_6D_6). a) References [1], [8], and [10]; b) D. Seyferth, H. P. Withers, *J. Organomet. Chem.* **1980**, *185*, C1.
[19] Crystallographic data for **4a** ($C_{16}H_{26}BFeNSi_2$): monoclinic, $P2_1/c$, $a = 11.614(1)$, $b = 11.506(1)$, $c = 13.601(1)$ Å, $\beta = 98.526(2)°$, $V = 1797$ Å^3, $Z = 4$, $\mu = 9.62$ cm^{-1}, $Mo_{K\alpha}$ ($\lambda = 0.71069$ Å), $\rho_{calcd} = 1.31$ g cm^{-3}, 100 K, Enraf-Nonius DIP2020 image plate diffractometer with graphite monochromator, dark red crystal (dimensions $0.21 \times 0.26 \times 0.31$ mm^3). Of 18806 reflections recorded ($1 < \theta < 27°$, $-13 \le h \le 13$, $-14 \le k \le 14$, $-16 \le l \le 16$), 3605 were unique and 3186 were observed with $I > 3\sigma(I)$. The images were processed with the DENZO and SCALEPACK programs [23]. Solution by direct methods and refinement by the full-matrix least-squares method. Subsequent difference Fourier analysis revealed that one of the $Si(CH_3)_3$ groups was disordered over two sites with 80% and 20% fractional occupancy. In the final stages of the structure determination all methyl hydrogen atoms were added geometrically after each refinement cycle and included in the structure factor calculations: 235 refined parameters for 3189 observations. Corrections for Lorentz and polarization effects, secondary extinction and anomalous scattering were applied. Refinement was completed by using Chebyshev weighting scheme with three parameters [24]. Refinement on F, $R = 0.028$, $R_w = 0.035$, GOF = 1.056, $\Delta\rho_{max} = 0.46$ e Å^{-3}, and $\Delta\rho_{min} = 0.46$ e Å^{-3}. All crystallographic calculations were carried out using the CRYSTALS package [25]. Crystallographic data (excluding structure factors) for the structure reported in this paper have been deposited with the Cambridge Crystallographic Data Center as supplementary publication no. CCDC-100378. Copies of the data can be obtained free of charge on application to The Director, CCDC, 12 Union Road, Cambridge CB2 1EZ (fax: Int. code +(1223) 336-033; e-mail: deposit@chemcrys.cam.ac.uk)
[20] P. Paetzold, *Adv. Inorg. Chem.* **1987**, *31*, 123, see p. 137.
[21] J. E. Huheey, E. A. Keiter, R. L. Keiter, *Inorganic Chemistry*, Harper Collins, New York, **1993**.
[22] J. K. Pudelski, D. A. Foucher, C. H. Honeyman, P. M. Macdonald, I. Manners, S. Barlow, D. O'Hare, *Macromolecules*, **1996**, *29*, 1894.
[23] D. Gewirth, Z. Otwinoski, W. Miner, The HKL Manual, Yale University, **1995**.
[24] E. Prince, *Mathematical Techniques in Crystallography and Material Sciences*, Springer, New York, **1982**.
[25] D. J. Watkin, C. K. Prout, J. R. Carruthers, P. W. Belteridge, CRYSTALS, Issue 10, Chemical Crystallography Laboratory, University of Oxford, **1996**.

Recognition of Anions through NH–π Hydrogen Bonds in a Bicyclic Cyclophane—Selectivity for Nitrate**

Adrian P. Bisson, Vincent M. Lynch, Mary-Katherine C. Monahan, and Eric V. Anslyn*

The molecular recognition of anions with synthetic receptors is an expanding field of research. Synthetic anion receptors to date have typically employed various combinations of Lewis acids,[1] protonated polyammonium macrocycles,[2] pyrroles,[3] guanidiniums,[4] and amides.[5] The selectivity these hosts exhibit comes from both size and shape complementarity as well as anion basicity.[6] With anions such as carboxylates and phosphates, hydrogen bonding from these receptors is typically targeted to the guest heteroatom's lone pairs. Herein we introduce a novel C_3-symmetric host capable of hydrogen bonding to the anion's π systems. The combination of geometric and electrostatic complementarity leads to stronger binding of nitrate than might be expected based upon its basicity.

Nature in part uses amide hydrogen bonding for the binding of sulfate and phosphate when they are bound within proteins.[7] With this in mind, we designed an amide-linked C_3-symmetric bicyclic cyclophane (**1**, Scheme 1) capable of

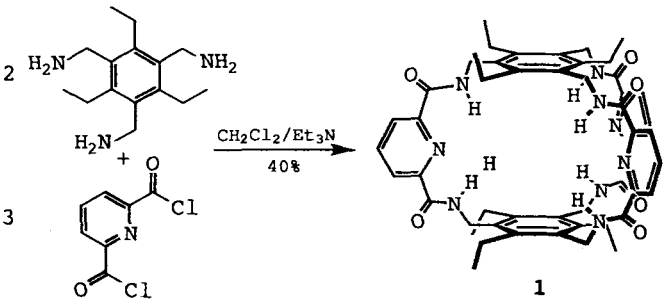

Scheme 1. Synthesis of the bicyclic cyclophane **1**.

recognizing anions exclusively through neutral hydrogen bonding.[8] The C_3 symmetry comes from two rigid building blocks, 2,6-pyridine dicarbonyl dichloride and 1,3,5-triaminomethyl-2,4,6-triethylbenzene.[9] Amides formed by 2,6-pyridine dicarbonyl dichloride are oriented such that the amide NH protons are hydrogen bonded to the pyridine nitrogen, forcing a converged geometry.[10] Also the alternating steric interactions in 1,3,5-triaminomethyl-2,4,6-triethylbenzene ensure that the amine groups are oriented on the same face of the aromatic ring.[11] The bicyclic cyclophane produced converges six amide hydrogens into the center of a binding pocket. Due to the geometry imposed by the cyclophane, a host–guest complex with nitrate or acetate would involve hydrogen bonding to π electrons in preference to lone pair electrons.

The preorganization of both building blocks for **1** greatly facilitated the synthesis (Figure 1). On treatment of two equivalents of 1,3,5-triaminomethyl-2,4,6-triethylbenzene with three equivalents of 2,6-pyridine dicarbonyl dichloride the rigid bicyclic cyclophane is formed in surprisingly high yield (40%).

X-ray quality crystals of the host were grown from a CH_2Cl_2/CH_3CN solution (Figure 1a).[12a] As expected, the cavity is lined by six hydrogens all oriented toward the center. The cavity size measures 78.3 Å^3; the aromatic rings are separated by 7.0 Å. The cavity of the free receptor is occupied by two water molecules and one molecule of CH_3CN. The latter forms hydrogen bonds with the amides of one of the acyl pyridine units and π–π stacks between the faces of the aromatics.

X-ray quality crystals of the chloride complex were also grown from the same solvent mixture in the presence of excess tetrabutylammonium chloride (Figure 1b).[12b] In this case, a 2:1 stoichiometry of guest to host was found; each chloride forms hydrogen bonds with the amides of one acyl pyridine. The remaining space within the cavity is occupied by a water molecule which is hydrogen bonded to each chloride and to the last acyl pyridine unit, forming a cooperative network of eight hydrogen bonds.

[*] Prof. E. V. Anslyn, Dr. A. P. Bisson, Dr. V. M. Lynch, M.-K. C. Monahan
Department of Chemistry and Biochemistry
University of Texas at Austin
Austin, Texas, 78712 (USA)
Fax: Int. code +(512)471-8696
e-mail: anslyn@ccwf.cc.utexas.edu

[**] This work was funded by the National Science Foundation, the Texas Advanced Technology Program, and the Welch Foundation, as well as by monies from Sloan and Dreyfus Teacher Scholar Awards (to E. V. A.). A. P.B thanks Dr. P. A. Gale (Oxford University) for helpful discussions. We gratefully acknowledge Dr. K. A. Abboud of the University of Florida at Gainesville for X-ray analysis of $2Bu_4NCl \cdot 1$.

 © WILEY-VCH Verlag GmbH, D-69451 Weinheim, 1997 0570-0833/97/3621-2340 $ 17.50+.50/0

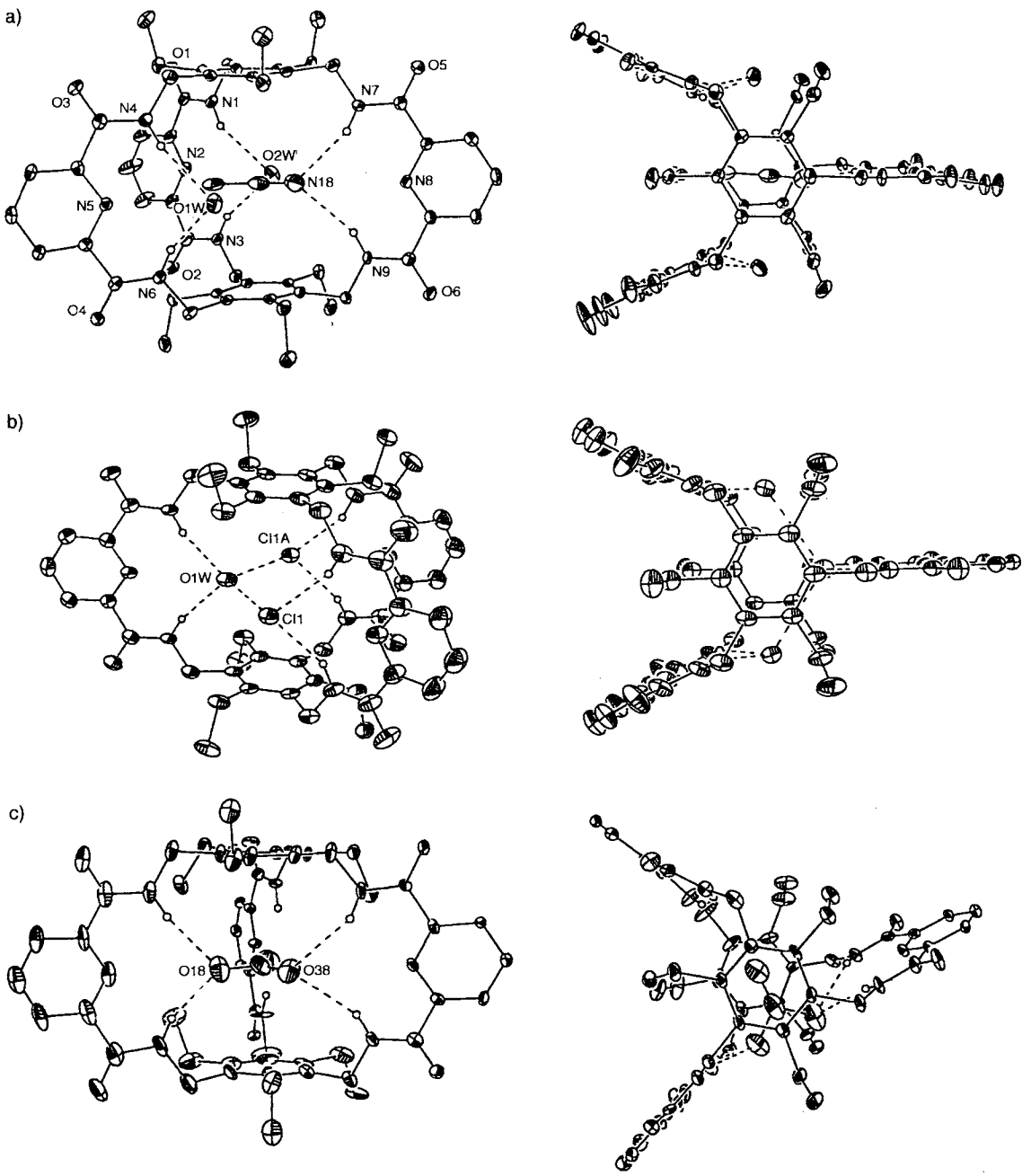

Figure 1. Two views of the crystal structures of a) free host **1** (thermal ellipsoids scaled to 30%), b) $2\,Bu_4NCl\cdot\mathbf{1}$ (thermal ellipsoids scaled to 20%) c) $2\,Bu_4NOAc\cdot\mathbf{1}$ (thermal ellipsoids scaled to 20%).

Crystals of the acetate complex suitable for X-ray analysis were grown from a $H_2O/EtOH/CH_2Cl_2$ solution in the presence of excess ammonium acetate (Figure 1c).[12c] In this case, the acetate is bound within the cavity to form a 1:1 complex. The anion is bound by two hydrogen bonds from the amides of two acyl pyridines.

The solution state anion binding properties of **1** were determined both by Job plots[13] and ^1H NMR titration experiments, the latter being analyzed with EQNMR[14] (Table 1). In all experiments the change in chemical shift of the amide NH resonances was followed. These signals shifted downfield, indicative of hydrogen bonding. Initial studies were carried out in CD_2Cl_2. However, the association constants were too large to determine at NMR concentrations, suggesting values in excess of

Table 1. Association constants K [M^{-1}] determined by ^1H NMR titration experiments[a] in 25% CD_2Cl_2/CD_3CN (1/3 v/v) at 298 K and pK_a values of the acids corresponding to the anion X^-.

Anion X^-	K [M^{-1}]	pK_a of HX
AcO^-	770±120	4.6
NO_3^-	300±30	−1.4
CN^-	115±10	9.2
Cl^-	40±8	−7
$H_2PO_4^-$	25±5	2
Br^-	15±8	−9
HSO_4^-	<5	−9

[a] Titrations were typically run at 10 mM host concentrations with aliquots of a 0.3 M tetrabutylammonium salt solution added. Association constants were determined by EQNMR[14].

 © WILEY-VCH Verlag GmbH, D-69451 Weinheim, 1997 0570-0833/97/3621-2341 $ 17.50+.50/0

$10^4-10^5\,M^{-1}$. Increasing the polarity of the solvent to 25% CD_2Cl_2 in CD_3CN (v/v) allowed association constants to be determined. In all cases the stoichiometry of the solution state complexes was determined to be 1:1.

The host was found to exhibit enhanced binding of acetate and nitrate over cyanide, chloride, dihydrogen phosphate and bromide, while the binding of hydrogen sulfate was negligible. This enhanced binding is most likely due to encapsulation of these geometrically equivalent guests and the formation of several hydrogen bonds from both above and below the plane defined by the anions.

Several pieces of data lead to the conclusion that the host/guest complex with nitrate involves the encapsulation of this anion in the cavity with six hydrogen bonds. First is the comparison of the geometry of acetate and nitrate, and the fact that acetate is encapsulated. Moreover, acetate binds only a factor of 2.6 times better than nitrate, although it is 10^6 times more basic. Further, dihydrogen phosphate is also significantly more basic than nitrate, yet it is precluded from the cavity due to size and therefore has a much lower affinity.

The results presented here demonstrate that amide NH proton donors are effective for hydrogen bonding to planar anions. Although acetate had the largest association constant of all the anions studied, hydrogen bonding between the geometrically matched host and nitrate led to enhanced binding, overcoming the weak coordinative ability of this anion.

Received: April 15, 1997 [Z10351IE]
German version: *Angew. Chem.* **1997**, *109*, 2435–2437

Keywords: anion recognition · cyclophanes · host–guest chemistry · hydrogen bonds

[1] M. T. Reetz, C. M. Miemeyer, K. Harms, *Angew. Chem.* **1991**, *103*, 1515; *Angew. Chem. Int. Ed. Engl.* **1991**, *30*, 1472; M. T. Reetz, C. M. Miemeyer, K. Harms, *ibid.* **1991**, 103, 1517 bzw. **1991**, *30*, 1474; M. T. Blanda, J. H. Horner, M. Newcomb, *J. Org. Chem.* **1989**, *54*, 4626; D. M. Rudkevich, W. P. R. V. Stathamer, W. Verbomm, J. F. J. Engbersen, S. Harkema, D. N. Reinhoudt, *J. Am. Chem. Soc.* **1992**, *114*, 9671; M. E. Jung, H. Xia, *Tetrahedron Lett.* **1988**, *29*, 297.

[2] C. H. Park, H. E. Simmons, *J. Am. Chem. Soc.* **1968**, *90*, 2431; E. Kimura, M. Kodama, T. Yatsunami, *ibid.* **1982**, *104*, 3182; D. Heyer, J.-M. Lehn, *Tetrahedron Lett.* **1986**, *27*, 5869; M. W. Hosseini, J.-M. Lehn, *Helv. Chim. Acta.* **1988**, *71*, 749; J.-M. Lehn, R. Meric, J.-P. Vigneron, B. Waksman, C. Pascard, *J. Chem. Soc. Chem. Commun.* **1991**, 62; B. Hinzen, P. Seiler, F. Diederich, *Helv. Chim. Acta.* **1996**, *79*, 942.

[3] P. A. Gale, J. L. Sessler, V. Král, V. Lynch, *J. Am. Chem. Soc.* **1996**, *118*, 5140; V. Král, J. L. Sessler, *Tetrahedron* **1995**, *51*, 539; V. Král, A. Andrievsky, J. L. Sessler, *J. Am. Chem. Soc.* **1995**, *117*, 2953; J. L. Sessler, S. J. Weghorn, V. Lynch, M. R. Johnson, *Angew. Chem.* **1994**, *106*, 1572; *Angew. Chem. Int. Ed. Engl.* **1994**, *33*, 1509.

[4] F. P. Schmidtchen, *Tetrahedron Lett.* **1989**, *30*, 4493; A. Echavarren, A. Galan, J.-M. Lehn, J. de Mendoza, *J. Am. Chem. Soc.* **1989**, *111*, 4994; E. F. Scott, V. Arman, S. Kincaid, A. D. Hamilton, *ibid.* **1993**, *115*, 369; A. Gleich, F. P. Schmidtchen, P. Miculcik, G. Muller, *J. Chem. Soc. Chem. Commun.* **1990**, 55; P. H. Boyle, M. A. Convery, A. P. Davis, G. D. Hopsken, B. A. Murray, *ibid.* **1992**, 239; D. M. Kneeland, K. Ariga, V. M. Lynch, C.-Y. Huang, E. V. Anslyn, *J. Am. Chem. Soc.* **1993**, *115*, 10042; P. H. Boyle, M. A. Convery, A. P. Davis, G. D. Hosken, B. A. Murray, *J. Chem. Soc. Chem. Commun.* **1992**, 239.

[5] P. D. Beer, D. Hesek, J. Hodacova, S. E. Stokes, *J. Chem. Soc. Chem. Commun.* **1992**, 270; P. D. Beer, C. Hazlewood, D. Hesek, J. Hodacova, S. E. Stokes, *J. Chem. Soc. Dalton Trans.* **1993**, 1327; P. D. Beer, Z. Chen, A. J. Goulden, A. Graydon, S. E. Stokes, T. Wear, *J. Chem. Soc. Chem. Commun.* **1993**, 1834; P. D. Beer, S. E. Stokes, *Polyhedron* **1995**, *14*, 873; P. D. Beer, P. A. Gale, D. Hesek, *Tetrahedron Lett.* **1995**, *36*, 767; P. D. Beer, *J. Chem. Soc. Chem. Commun.* **1996**, 689; C. Seel, F. Vögtle, *Angew. Chem.* **1992**, *104*, 542; *Angew. Chem. Int. Ed. Engl.* **1992**, *31*, 528; S. Valiyaveettil, J. F. J. Engbersen, W. Verboom, D. N. Reinhoudt, *ibid.* **1993**, *105*, 942 and **1993**, *32*, 900; J. Scheerder, J. F. J. Engbersen, A. Casnati, R. Ungaro, D. N. Reinhoudt, *J. Org. Chem.* **1995**, *60*, 6448; J. Scheerder, J. P. M. van Duynhoven, J. F. J. Engbersen, D. N. Reinhoudt, *ibid.* **1996**, *108*, 1172.

[6] D. A. Bell, E. V. Anslyn, *J. Org. Chem.* **1994**, *59*, 512; K. M. Neder, H. W. Whitlock, Jr., *J. Am. Chem. Soc.* **1990**, *112*, 9412; A. M. Kelly-Rowley, V. M. Lynch, E. V. Anslyn, *ibid.* **1995**, *117*, 3438.

[7] H. Luecke, F. A. Quiocho, *Nature* **1990**, *347*, 402; J. J. He, F. A. Quiocho, *Science* **1991**, *251*, 1479; J. W. Pflugrath, F. A. Quiocho, *Nature* **1985**, *314*, 257.

[8] R. J. Pieters, F. Diederich, *J. Chem. Soc. Chem. Commun.* **1996**, 2255.

[9] A. Metzger, V. M. Lynch, E. V. Anslyn, *Angew. Chem.* **1997**, *109*, 911; *Angew. Chem. Int. Ed. Engl.* **1997**, *36*, 862.

[10] For further examples of the use of 2,6-pyridine diamides to control conformation, see: S. J. Geib, S. C. Hirst, C. Vincent, A. D. Hamilton, *J. Chem. Soc. Chem. Commun.* **1991**, 1293; Y. Hamuro, S. J. Geib, A. D. Hamilton, *Angew. Chem.* **1994**, *106*, 465; *Angew. Chem. Int. Ed. Engl.* **1994**, *33*, 446; C. A. Hunter, D. H. Purvis, *ibid.* **1992**, *104*, 779 and **1992**, *31*, 792; C. A. Hunter, L. D. Sarson, *ibid.* **1994**, *106*, 2424 and **1994**, *33*, 2313.

[11] D. Iverson, G. Hunter, J. F. Blount, J. R. Damewood, Jr., K. Mislow, *J. Am. Chem. Soc.* **1981**, *103*, 6073; T. D. P. Stack, Z. Hou, K. N. Raymond, *ibid.* **1993**, *115*, 6466; C. Walsdorff, W. Saak, S. Pohl, *J. Chem. Res. Synop.* **1996**, 282.

[12] a) Crystal structure analysis of **1**: Data were collected on a Siemens P4 diffractometer with a graphite monochromator; $Mo_{K\alpha}$ radiation; $\lambda = 0.71073$ Å; 183 K. Crystal system: monoclinic; space group $P2_1/n$, $Z = 4$; cell dimensions $a = 21.424(1)$, $b = 12.395(2)$, $c = 23.670(2)$ Å; $\beta = 95.87(1)°$; $V = 6251.6(6)$ Å^3; $\rho_{calcd} = 1.18\ g\,cm^{-3}$; $2\theta_{max} = 45°$; reflections (measured/independent) 8331/8150; $R_{int} = 0.040$. The structure was refined on F^2 using SHELXTL-PLUS to an $R_w = 0.181$, with a conventional $R = 0.0792$ (4773 reflections with $F_0 > 4(\sigma(F_0))$ and a goodness of fit = 2.158. b) Crystal structure analysis of $2Bu_4NCl\cdot$**1**: Data were collected on a Siemens Smart CCD Area Detector with a graphite monochromator; $Mo_{K\alpha}$ radiation; $\lambda = 0.71073$ Å; 173 K. Crystal system: orthorhombic; space group *Cmcm*, $Z = 8$; cell dimensions $a = 14.0416(4)$, $b = 46.9852(12)$, $c = 13.4714(4)$ Å; $V = 8887.7(6)$ Å^3; $\rho_{calcd} = 1.157\ g\,cm^{-3}$; $2\theta_{max} = 45°$; reflections (measured/independent) 16623/3077; $R_{int} = 0.053$. The structure was refined on F^2 with SHELXTL-PLUS to $R_w = 0.232$, with conventional $R = 0.104$ (2091 reflections having $F_0 > 4(\sigma(F_0))$ and a goodness of fit = 3.993. c) Crystal structure analysis of $Bu_4NOAc\cdot$**1**: Data were collected on a Siemens P4 diffractometer with a graphite monochromator; $Mo_{K\alpha}$ radiation; $\lambda = 0.71073$ Å; 188 K; crystal system: triclinic; space group $P\bar{1}$, $Z = 4$; cell dimensions: $a = 12.847(2)$, $b = 18.304(4)$, $c = 22.266(3)$ Å; $\alpha = 107.28(1)$, $\beta = 94.46(1)$, $\gamma = 91.42(1)°$; $V = 4978.9(15)$ Å^3; $\rho_{calcd} = 1.315\ g\,cm^{-3}$; $2\theta_{max} = 45°$; reflections (measured/independent) 13330/12758; $R_{int} = 0.085$. The structure was refined on F^2 with SHELXTL-PLUS to $R_w = 0.235$, with conventional $R = 0.116$ (4505 reflections having $F_0 > 4(\sigma(F_0))$ and a goodness of fit = 1.144. Crystallographic data (excluding structure factors) for the structures reported in this paper have been deposited with the Cambridge Crystallographic Data Centre as supplementary publication no. CCDC-100347. Copies of the data can be obtained free of charge on application to The Director, CCDC, 12 Union Road, Cambridge CB2 1EZ, UK (fax: int. code +(1223)336-033; e-mail: deposit@chemcrys.cam.ac.uk).

[13] P. Job, *Ann. Chim. (Paris)* **1928**, *9*, 113; K. A. Connors, *Binding Constants*, 1st ed., Wiley, New York, **1987**.

[14] M. J. Hynes, *J. Chem. Soc. Dalton Trans.* **1993**, 311.

Tetraethylammonium Trichloride: A Versatile Reagent for Chlorinations and Oxidations**

Thierry Schlama, Kiroubagaranne Gabriel, Véronique Gouverneur, and Charles Mioskowski*

Functional-group manipulation is fundamental to synthetic organic chemistry, and the development of new reagents remains of great interest. Organic polyhalide salts have established themselves as useful reagents for halogenations.[1] Solid organic tribromides are a practical source of electrophilic bromine. However, the development of new reagents for chlorination is still unexplored, and only a few organic salts have been studied.[2] Here we demonstrate the efficiency of tetraethylammonium trichloride, a new organic salt that is a practical source of chlorine. This reagent was easily prepared by bubbling

[*] Dr. C. Mioskowski, T. Schlama, K. Gabriel, Dr. V. Gouverneur
Laboratoire de Synthèse Bioorganique associé au CNRS
Faculté de Pharmacie
Université Louis Pasteur
74, route du Rhin-BP 24, F-67401 Illkirch (France)
Fax: Int. code +38867-8891
e-mail: mioskow@aspirine.u-strasbg.fr

[**] This work was supported by Rhône-Poulenc and the Centre National de la Recherche Scientifique.

 © WILEY-VCH Verlag GmbH, D-69451 Weinheim, 1997 0570-0833/97/3621-2342 $ 17.50+.50/0

chlorine through a solution of tetraethylammonium chloride in dichloromethane. The content of active chloride was 3.2 mmol g^{-1}, and no decrease in activity was observed upon storage for several months at room temperature.

Several substrates including alkynes, alkenes, aldehydes, ketones, esters, acetals, and arenes were easily chlorinated under mild conditions (Scheme 1, Table 1). Alkenes and alkynes were converted into vicinal dichloroalkanes and dichloroalkenes, respectively, in good yields (entries 1–13). All reactions of the alkynes afforded the (*E*) stereoisomer exclusively, as determined from ^{1}H NMR spectra of the crude mixtures and confirmed by comparison with authentic samples. The reagent is equally compatible with alkynols (entry 4) or silylated alcohols (entry 5). THP-protected alkynols gave the desired product in low yields (entry 6, THP = tetrahydro-2*H*-pyran-2-yl), since side products probably arose from chlorination of the acetal group (entries 21 and 22).

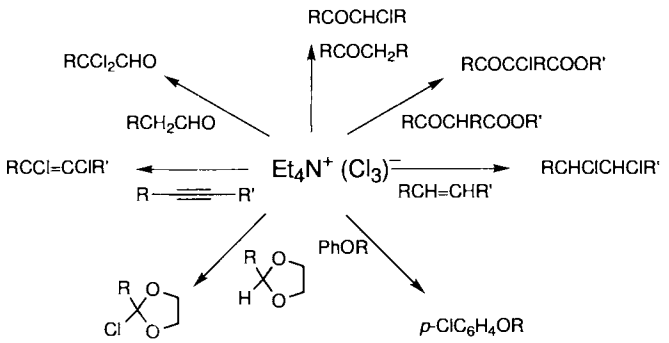

Scheme 1. Reactions with tetraethylammonium trichloride.

Table 1. Chlorinations with tetraethylammonium trichloride.

Entry	Starting material	Product	Yield [%]
1	$CH_3(CH_2)_3$—≡—$(CH_2)_3CH_3$	(*E*)-$CH_3(CH_2)_3CCl{=}CCl(CH_2)_3CH_3$	88
2	$CH_3(CH_2)_8$—≡	(*E*)-$CH_3(CH_2)_8CCl{=}CHCl$	100
3	$CH_3(CH_2)_5$—≡—$CH(OEt)_2$	(*E*)-$CH_3(CH_2)_5CCl{=}CClCH(OEt)_2$	82
4	$CH_3(CH_2)_6$—≡—CH_2OH	(*E*)-$CH_3(CH_2)_6CCl{=}CClCH_2OH$	100
5	$CH_3(CH_2)_6$—≡—$CH_2OSi\,tBuMe_2$	(*E*)-$CH_3(CH_2)_6CCl{=}CClCH_2OSi\,tBuMe_2$	56
6	$THPOCH_2$—≡—$(CH_2)_2OTHP$	(*E*)(*E*)-$THPOCH_2CCl{=}CCl(CH_2)_2OTHP$	29
7	3-hexyne	(*E*)-3,4-dichlorohexene	100
8	≡—COOEt	(*E*)- CHCl=CClCOOEt	76
9	$CH_3(CH_2)_5CH{=}CH_2$	$CH_3(CH_2)_5CHClCH_2Cl$	100
10	(*E*)-$EtOOCCH_2CH{=}CHCH_2COOEt$	$EtOOCCH_2CHClCHClCH_2COOEt$	100
11	$CH_3(CH_2)_2CH{=}CH\text{-}CH_2OH$	$CH_3(CH_2)_2CHClCHClCH_2OH$	100
12	cyclooctene	*trans*-1,2-dichlorocyclooctane	100
13	$PhCH_2CH{=}CH_2$	$PhCH_2CHCl\text{-}CH_2Cl$	100
14	$CH_3(CH_2)_9CH_2CHO$	$CH_3(CH_2)_9CCl_2CHO$	83
15	$PhCOCH_3$	$PhCOCH_2Cl$	100
16	(*E*)-PhCOCH=CHPh	(*Z*)-PhCOCCl=CHPh	100
17	cyclohexenone	2-chlorocyclohexenone	100
18	$CH_3COCHEtCOOEt$	$CH_3COCClEtCOOEt$	100
19	$PhOCH_3$	*p*-$ClC_6H_4OCH_3$	80
20	$PhOCH_2$—≡	*p*-$ClC_6H_4OCH_2$—≡	100
21	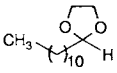	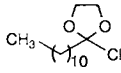	100
22	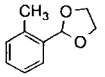	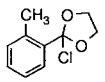	100

Direct dichlorination of saturated aldehydes at the α-position was achieved under mild conditions with two equivalents of tetraethylammonium trichloride (entry 14). Even with one equivalent of reagent, the reaction proceeded beyond the monochlorinated product. Ketones were selectively monochlorinated at the α-position (entry 15), but, unlike in the case of aldehydes, the reactions did not proceed to di- or trichloro derivatives. α,β-Unsaturated ketones (entries 16 and 17) were converted into the corresponding α,β-unsaturated α-chloroketones, probably via vicinal α,β-dichloroketones which underwent spontaneous dehydrohalogenation. Esters, with the exception of activated β-keto esters, failed to react (entry 18). Aromatic compounds activated with an electron-donating group were easily chlorinated at the *para* position (entry 19), and a bifunctional compound with both an activated aromatic ring and an alkyne functionality was preferentially chlorinated at the *para* ring position (entry 20).

Interestingly, the diethylene acetal of *n*-dodecanal was successfully chlorinated; the chlorine atom is on the dioxy carbon atom (entries 21 and 22). Treating this compound with 10% aqueous HCl afforded the corresponding ester in quantitative yield (Scheme 2). This is an unusual transformation, because the product usually isolated from the reaction of acetals with halogens is an α-halogenated acetal.[3] However, it was reported that acetals derived from non-enolizable aldehydes can be oxidized to the corresponding ester with *N*-bromosuccinimide under photolytic conditions[4] or in the presence of a radical initiator such as azobis(isobutyronitrile) (AIBN) or *t*-butyl peroxide.[5] However, in contrast to our chlorinated acetal derivatives, the intermediate brominated acetal could not be isolated.

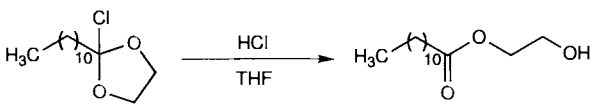

Scheme 2. Hydrolysis of the chlorinated acetal.

In the presence of pyridine/1,4-diazabicyclo[2.2.2]octane (DABCO) in acetonitrile, tetraethylammonium trichloride oxidizes secondary and benzylic alcohols to the corresponding ketones or aldehydes (Table 2). The oxidation failed when dichloromethane was used instead of acetonitrile, or triethylamine in place of pyridine. Secondary alcohols were selectively

Table 2. Oxidations with tetraethylammonium trichloride.

Entry	Starting material	Product	Yield [%]
1	$PhCH_2OH$	PhCHO	100
2	$PhCHOHCH_2CH_3$	$PhCOCH_2CH_3$	71
3	menthol	menthone	100
4	$CH_3(CH_2)_2CH{=}CHCH_2OH$	$CH_3(CH_2)_2CHClCHClCH_2OH$	100
5	cyclohexanol	cyclohexanone	56
6	cyclooctanol	cyclooctanone	70
7	$CH_3(CH_2)_5CHOHCH_2OH$	$CH_3(CH_2)_5COCH_2OH$	100

 © WILEY-VCH Verlag GmbH, D-69451 Weinheim, 1997 0570-0833/97/3621-2343 $ 17.50+.50/0

oxidized over primary alcohols (entry 7). Allyl alcohols were not oxidized, but chlorinated at the double bond (entry 4).

Compared to other reagents,[2] tetraethylammonium trichloride has several advantages as a chlorinating or oxidizing agent. This stable, crystalline solid is more convenient to handle, and—unlike in the case of iodoperchloride salts—the reaction times are greatly reduced, and no iodine is produced that can give rise to by-products. In general, chlorination of alkenes or alkynes proceeded stereoselectively in excellent yields. Interesting results were obtained with acetals, which afforded stable chloroacetals in which the chlorine atom is located on the dioxy carbon atom.

Experimental Section

Synthesis of $Et_4N^+(Cl_3)^-$: A solution of Et_4NCl in CH_2Cl_2 was saturated with Cl_2. The solvent was then removed in vacuo to afford a yellow solid which can be stored for months under an argon atmosphere.

Chlorination: $Et_4N^+(Cl_3)^-$ (1.5–3 equiv) was added in one portion under an argon atmosphere at −78 or 0 °C to a solution of the substrate (1 equiv) in CH_2Cl_2 (0.3 M). After addition of water, the organic phases were dried over $MgSO_4$ and filtered on celite. The solvent was removed in vacuo, and the crude compound purified by column chromatography.

Oxidation: $Et_4N^+(Cl_3)^-$ (1–3 equiv) was added to a solution of the alcohol in CH_3CN (0.3 M) and pyridine (4 equiv) at room temperature. After disappearance of the yellow color, DABCO (1 equiv) was added. After completion of the reaction, the crude mixture was concentrated in vacuo, and the residue was purified by column chromatography.

Received: April 18, 1997 [Z10365IE]
German version: *Angew. Chem.* **1997**, *109*, 2440–2442

Keywords: chlorinations · oxidations · reagents · synthetic methods

[1] S. Kajigashi, M. Mariwashi, T. Tanabe, S. Fujisaki, T. Kakiuami, T. J. Okamoto, *J. Chem. Soc. Perkin Trans. 1* **1990**, 897, and references therein.
[2] a) S. E. Fuller, J. R. L. Smith, R. O. C. Norman, R. Higgins, *J. Chem. Soc. Perkin Tran. 2* **1981**, 545; b) J. R. L. Smith, L. C. McKeer, *Tetrahedron Lett.* **1983**, *24*, 3117; c) A. Debon, S. Masson, A. Thuillier, *Bull. Soc. Chim. Fr.* **1975**, *11*, 2493; d) S. Kajigaeshi, T. Kakinami, H. Yamasaki, S. Fujisaki, M. Kondo, T. J. Okamoto, *Chem. Lett.* **1987**, 2109; e) A. I. Popov, R. E. Buckles, *Inorg. Synth.* **1957**, *5*, 176; f) R. E. Buckles, D. F. Knaack, *J. Org. Chem.* **1960**, *25*, 20; g) F. Manescalchi, A. Bongini, G. Cainelli, M. Contento, *J. Chem. Soc. Chem. Commun.* **1980**, 1278.
[3] A. Bongini, G. Cainelli, M. Contento, F. Manescalchi, *Synthesis* **1980**, 143.
[4] E. N. Marvell, M. J. Joncich, *J. Am. Chem. Soc.* **1951**, *73*, 973.
[5] J. D. Prugh, W. C. McCarthy, *Tetrahedron Lett.* **1966**, 1351.

The First Total Synthesis of Tricolorin A

Shou-Fu Lu, QinQin O'yang, Zhong-Wu Guo, Biao Yu,* and Yong-Zheng Hui*

Tricolorin A, a member of the resin glycoside family, was first isolated by Pereda-Miranda et al. in 1993 from *Ipomoea tricolor cav.* (convolvulaceae), a plant used in traditional Mexican agriculture as a weed controller.[1] Bioassays showed that tricolorin A was not only largely responsible for weed-growth inhibition by the plant, but it also possessed significant cytotoxic activity against cultured P-388 and human breast cancer cells ($ED_{50} = 2.2\ \mu g\,mL^{-1}$).[1a] What attracted us most was the beauty of the structure of tricolorin A, which, bearing a disaccharide containing a 19-membered macrolactone, represents a perfect balance between hydrophobicity and hydrophilicity. We therefore directed our efforts towards the total synthesis of this interesting molecule, during the course of which Schmidt et al. accomplished a first total synthesis of another molecule of the resin glycoside family (calonyctin A).[2] Heathcock recently reported the synthesis of a macrolactone disaccharide subunit (**2**) of tricolorin A.[3] Coincidentally, we employed a similar strategy for assembling **2** in our total synthesis. Here we describe this total synthesis of tricolorin A. Of particular interest is the regioselective macrolactonization of a 1-hydroxycarbonyl-pentadec-10(s)-yl disaccharide to form the macrolactone disaccharide **2**, and a one-pot assembly of two monosaccharide donors (**3** and **4**, Scheme 1).[4]

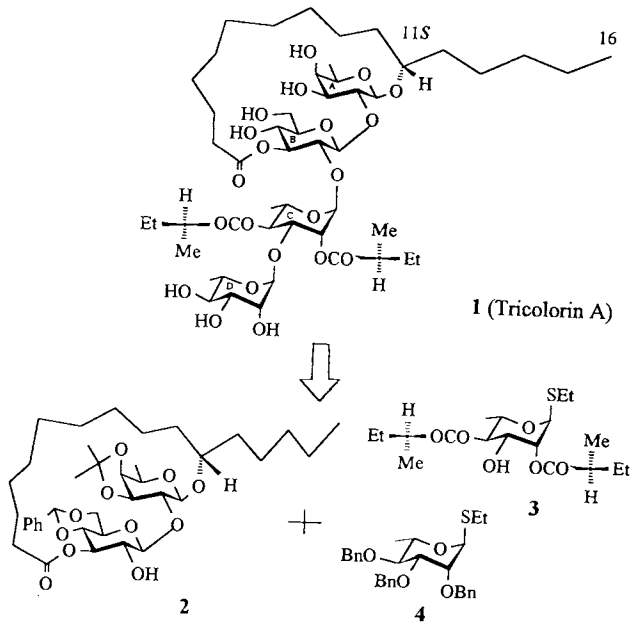

Scheme 1. Retrosynthesis of tricolorin A.

First, four monosaccharide building blocks (**6**,[5] **8**,[6] **3**,[7] and **4**[4c]) were prepared as shown in Schemes 2–4. All are glycosyl donors either with a neighboring participating group (**6**, **8**, **3**) or with a strong anomeric effect (**3**, **4**) that is sufficient to cause highly selective β-glycosidation (for **6**, **8**) or α-glycosidation (for **3**, **4**). Methyl 11(s)-jalapinolate [methyl 11(s)-hydroxyhexadecanoate (**14**)][8] was prepared by employing a chiral-pool approach starting from D-(+)-mannitol (Scheme 5).[9]

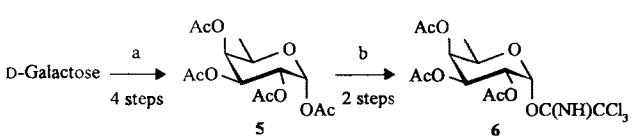

Scheme 2. Preparation of monosaccharide synthon **6**: a) 1. anhydrous Cu_2SO_4, acetone, H_2SO_4 (concd, cat.), RT, 29 h, 62%; 2. *p*-TsCl (Ts = $H_3CC_6H_4SO_2$), pyridine (Py), 55 °C, 4 h, 94%; 3) $NaBH_4$, Me_2SO (DMSO), 120 °C, 5 h, 75%; 4. Ac_2O/HOAc (2/1), H_2SO_4 (concd, cat.), −15 °C, 4 h, 20%; b) 1. NH_3 in MeOH/THF (3:7), 0 °C, 3 h, 50%; 2. $CNCCl_3$, 1,8-diazabicyclo[5.4.0]undec-7-ene (DBU), CH_2Cl_2, RT, 14 h, 79%.

[*] Dr. B. Yu, Prof. Y.-Z. Hui, S.-F. Lu, Z.-W. Guo
State Key Laboratory of Bio-organic and Natural Products Chemistry
Shanghai Institute of Organic Chemistry, Chinese Academy of Sciences
354 Fenglin Road, Shanghai 200032 (China)
Fax: Int. code +(21)641-66128
e-mail: byusioc@fudan.ac.cn
Q. O'yang
Textile University (China)

[**] This work was supported by the state Science and Technology Committee of China. We are also grateful to Prof. Hou-Ming Wu for helping with the 600 MHz NMR experiments, and Prof. R. Pereda-Miranda for kindly providing an authentic sample and NMR spectra of tricolorin A.

 © WILEY-VCH Verlag GmbH, D-69451 Weinheim, 1997 0570-0833/97/3621-2344 $ 17.50+.50/0

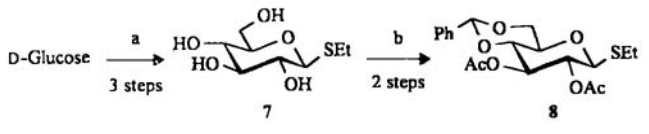

Scheme 3. Preparation of monosaccharide synthon **8**: a) 1. Ac_2O, NaOAc (cat.), reflux, 4 h, 87%; 2. EtSH, $BF_3 \cdot OEt_2$, CH_2Cl_2, RT, 15 min, 71%; 3. NaOMe (cat.), MeOH, 0°C, 2 h, 90%; b) 1. $PhCH(OMe)_2$, *p*-TsOH, 50°C, 4.5 h, 61%; 2) Ac_2O, Py, 14 h, 84%.

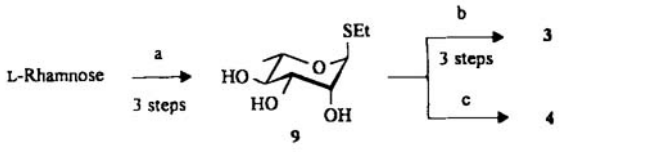

Scheme 4. Preparation of monosaccharide synthons **3** and **4**: a) 1. Ac_2O, Py, 87%; 2. EtSH, $BF_3 OEt_2$, CH_2Cl_2, 74% ($\alpha:\beta = 4:1$); 3. NaOMe, HOMe, 99%; b) 1. Bu_2SnO, toluene, reflux, 1 h, then *p*-$MeOC_6H_4CH_2Cl$ (PMBCl), CsF, Bu_4NI, DMF, RT, 33 h, 79%; 2. 2(*s*)-methylbutyric anhydride (2.0 equiv), 4-(dimethylamino)pyridine (DMAP), Py, RT, 27 h, 70%; 3. ceric ammonium nitrate (CAN, 2.0 equiv), CH_3CN/H_2O (9:1), 25 min, 97%; b) BnBr, NaH, DMSO, 0°C, 11 h, 52%.

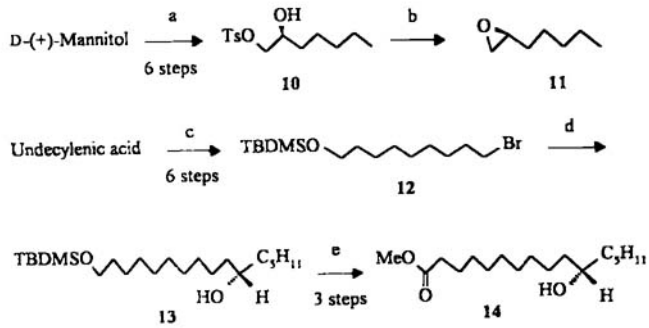

Scheme 5. Synthesis of methyl 11(*s*)-jalapinolate (**14**): a) 1. $ZnCl_2$, acetone, RT, 21 h, 32%; 2. $NaIO_4$, CH_2Cl_2/H_2O (20:1), RT, 1 h, 97%; 3. $Ph_3P^+(CH_2)_3CH_3Br^-$, THF, *n*BuLi/hexane, −78°C → 0°C, 2.5 h, 64%; 4. H_2, 10% Pd/C (cat.), 3 d; 5. 80% HOAc, 40°C, 20 h, 77% (2 steps); 6. *p*-TsCl, CH_2Cl_2, 0°C, 16 h, 44%; b) *t*BuLi/pentane (1.5 mol mL^{-1}), −30°C → RT, 1 h, 70%; c) 1. $LiAlH_4$, THF, reflux, 12 h, 95%; 2. Ac_2O, Py, RT, 2 h, 95%; 3. $KMnO_4$, benzene/H_2O/HOAc (4/4/1), Bu_4NI, RT, 14 h, 91%; 4. Br_2, HgO, CCl_4, reflux, 5 h, 83%; 5. *p*-TsOH (cat.), CH_3OH, reflux, 1.5 h, 92%; 6. *t*$BuMe_2SiCl$ (TBDMSCl), imidazole, RT, 3 h, 97%; d) Mg, THF, reflux, 2 h, then CuI (cat.), **11** (1.0 equiv), −78°C → RT, 2.5 h, 66%; e) 1. Ac_2O, Py, RT, 14 h, 91%; 2. Jones reagent, acetone, RT, 1.5 h, 89%; 3. $BF_3 \cdot OEt_2$ (3.0 equiv), MeOH, 40°C, 4 h, 97%.

With methyl 11(*s*)-jalapinolate (**14**) and monosaccharide donors **6** and **8** at hand, we sought to construct the macrolactone disaccharide **2** (Scheme 6). Alcohol **14** was readily glycosylated by imidate **6** using the procedure of Schmidt et al.[10] to afford **15**, which was sequentially subjected to deacetylation and isopropylidenization to give **16** with only the 2′-OH group free. Treatment of alcohol **16** with thioglycoside donor **8** in the presence of *N*-iodosuccinimide (NIS) and AgOTf (Tf = F_3CSO_2) in CH_2Cl_2 at −15°C led to disaccharide **17** in 76% yield, which was saponified with 3% KOH in MeOH/H_2O (9:1) to provide acid **18** with the 2″- and 3″-OH groups free. Regioselective macrolactonization of **18** by the Corey–Nicolaou protocol[11] gave the desired 3″-OH macrolactonized product **2** in 69% yield, together with the 2″-OH macrolactonized product **19** in 11% yield.[12]

Macrolactone tetrasaccharide **21** was finally assembled in 43% yield (based on consumed **2**) by a facile one-pot, two-step glycosylation of **2** with thioglycoside donors **3** and **4** using NIS/TfOH (cat., Scheme 7).[4] Alternatively, **21** was also constructed stepwise; disaccharide synthon **20**, the intermediate in the above

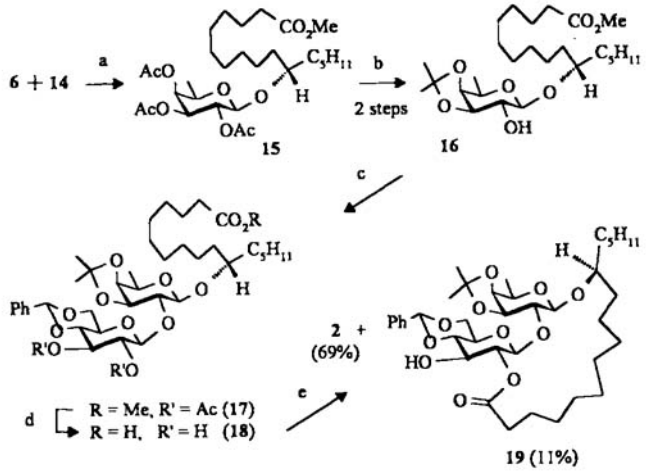

Scheme 6. Synthesis of macrolactone disaccharide **2**: a) **6** (0.9 equiv), $BF_3 \cdot OEt_2$ (1.2 equiv), CH_2Cl_2, −15°C, 1 h, 66%; b) 1. 1% NaOMe in MeOH, −15°C, 25 min; 2. $Me_2C(OMe)_2$, *p*-TsOH, acetone, 14 h, 82% (2 steps); c) **8** (1.6 equiv), NIS (3.0 equiv), AgOTf (1.0 equiv), 4-Å molecular seives, CH_2Cl_2, −15°C, 0.5 h, 76%; d) 3% KOH, MeOH/H_2O (9/1), reflux, 24 h, 91%; e) $(PyS)_2$, Ph_3P, toluene, reflux, 7 d, 69% for **2**, 11% for **19**.

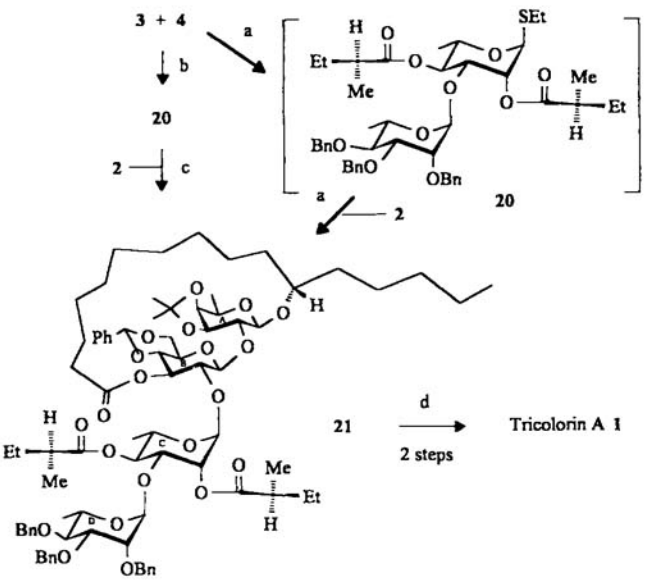

Scheme 7. Synthesis of tricolorin A (**1**): a) **3** (1.2 equiv), **4** (1.0 equiv), NIS (1.4 equiv), TfOH (cat.), 4-Å molecular seives, Et_2O/DCE (1:1; DCE = 1,2-dichloroethane), −15°C, 15 min, then **2** (1.6 equiv), NIS (1.4 equiv), TfOH (cat.), 4-Å molecular seives, RT, 1 h, 43% (based on **2**); b) IDCP (2.3 equiv), 4-Å molecular seives, CH_2Cl_2, RT, 0.5 h, 98%; c) NIS (4.5 equiv), AgOTf (0.5 equiv), 4-Å molecular seive, CH_2Cl_2, RT, 1 h, 86%; d) 1. DDQ (3.0 equiv), CH_3CN/H_2O (9/1), reflux, 4 h, 80%; 2. H_2 (6 MPa), 10% Pd/C, 60°C, 7 h, 88%.

one-pot protocol, was efficiently synthesized by a reaction of thioglycosides **3** and **4** involving the well-known "armed–disarmed" glycosidation approach[13] in the presence of iodium di-*sym*-collidine perchlorate (IDCP).[14] Glycosylation of macrolactone disaccharide **2** by disaccharide donor **20** in the presence of a promoter (NIS/AgOTf)[15] afforded the important precursor (**21**) of tricolorin A in good yield (86%). Final deprotection of the 3′,4′-*O*-isopropylidene and 4″,6″-*O*-benzylidene of **21** by DDQ[16] followed by removal of the benzyl groups by hydrogenation provided tricolorin A in 70.4% yield. The physical data obtained were essentially identical to those reported.[1, 17]

We have achieved the first total synthesis of tricolorin A in a total of 45 steps, where the longest linear sequence consists of

 © WILEY-VCH Verlag GmbH, D-69451 Weinheim, 1997 0570-0833/97/3621-2345 $ 17.50+.50/0

20 steps, and the overall yield is 0.65% starting from D-(+)-mannitol. The synthetic route features regioselective macrolactonization of a disaccharide bearing a 19-membered ring and a one-pot glycosidation for construction of a macrolactone tetrasaccharide.

Received: April 28, 1997 [Z10392IE]
German version: *Angew. Chem.* **1997**, *109*, 2442–2444

Keywords: glycosylations · macrocycles · one-pot reactions · total synthesis · tricolorin A

[1] a) R. Pereda-Miranda, R. Mata, A. L. Anaya, D. B. M. Wickramaratne, J. M. Pezzuto, A. D. Kinghorn, *J. Nat. Prod.* **1993**, *56*, 571–582; b) M. Bah, R. Pereda-Miranda, *Tetrahedron* **1996**, *52*, 13063–13080.

[2] a) Z.-H. Jiang, A. Geyer, R. R. Schmidt, *Angew. Chem.* **1995**, 107, 2730–2734; *Angew. Chem. Int. Ed. Engl.* **1995**, *34*, 2520–2524; b) Z.-H. Jiang, R. R. Schmidt, *Liebigs Ann. Chem.* **1994**, 645–651.

[3] D. P. Larson, C. H. Heathcock, *J. Org. Chem.* **1996**, *61*, 5208–5209.

[4] For previous one-pot glycosylations, see a) P. Grice, S. V. Ley, J. Pietruszka, H. M. I. Osborn, H W. M. Priepke, S. L. Warriner, *Chem. Eur. J.* **1997**, *3*, 431–440; b) M.-K. Cheng, N. L. Douglas, B. Hinzen, S. V. Ley, X. Pannecoucke, *Synlett* **1997**, 257–260; c) S. V. Ley, H. W. M. Priepke, *Angew. Chem.* **1994**, *106*, 2412–2414; *Angew. Chem. Int. Ed. Engl.* **1994**, *33*, 2292–2294; d) P. Grice, S. V. Ley, J. Pietruszka, H. W. M. Prieke, E. P. E. Walther, *Synlett* **1995**, 781–784; e) H. Yamada, T. Harada, T. Takahashi, *J. Am. Chem. Soc.* **1994**, *116*, 7919–7920; f) H. K. Chenault, A. Castro, *Tetrahedron Lett.* **1994**, *35*, 9145–9148; g) H. Yamada, T. Harada, H. Miyazaki, T. Takahashi, *ibid.* **1994**, *35*, 3979–3982; h) S. Raghavan, D. Kahne; J. *Am. Chem. Soc.* **1993**, *115*, 1580–1581.

[5] Compound **5** was prepared according to L. M. Lerner, *Carbohydr. Res.* **1993**, *41*, 291–294.

[6] Compound **7** was prepared according to B. Erbing, B. Lindberg, *Acta Chem. Scand. B* **1976**, *30*, 611–612.

[7] The procedure was based on the preparation of methyl 3-*O*-(4-methoxybenzyl)-1-thio-(L-rhamnopyranoside): P. Kovac, *Carbohydr. Res.* **1993**, *245*, 219–231.

[8] For the synthesis of 11(s)-jalapinoate, see a) N. Nodo, M. Ono, K. Miyahara, T. Kawasaki, M. Okabe, *Tetrahedron* **1987**, *43*, 1889–3902; b) H. Shibaya, I. Kitagawa, *Chem. Pharm. Bull.* **1989**, *37*, 260–262; c) M. Ono, K. Kubo, K. Miyahara, T. Kawasaki, *ibid.* **1989**, *37*, 241–244.

[9] Compound **10** was prepared according to J. Barry, H. B. Kagan, *Synthesis* **1981**, 453.

[10] R. R. Schmidt, J. Michel, *Angew. Chem.* **1980**, *92*, 201–202; *Angew. Chem. Int. Ed. Engl.* **1980**, *19*, 731–732.

[11] E. J. Corey, K. C. Nicolaou, *J. Am. Chem. Soc.* **1974**, *96*, 5614–5616.

[12] Selected spectroscopic data for **2**: white needles; $R_f = 0.47$ (petroleum ether/EtOAc, 7/3); m.p. = 209–211 °C. $[\alpha]_D^{19} = -59.09$ ($c = 0.07$ in $CHCl_3$); IR (KBr): $\tilde{\nu}$ = 3484 (OH), 1742 and 1722 (CO_2), 1458, 1372, 1243, 1184, 1094, 1075, 1038, 1005, 867, 800, 748, 697 cm^{-1}; ^1H NMR (300 MHz, $CDCl_3$, TMS): δ = 7.45–7.35 (m, 5H, Ph), 5.52 (s, 1H, PhC*H*), 5.22 (t, $J(3'',2'') = J(3'',4'') = 8.82$ Hz, 1H, H-3''), 5.06 (d, $J = 7.43$ Hz, 1H, H-1''), 4.30–4.23 (m, 2H, H-$6''_{aq}$, H-1'), 4.16 (t, $J(3',4') = J(3',2') = 6.03$ Hz, 1H, H-3'), 3.97–3.73 (m, 5H), 3.60–3.54 (m, 2H), 3.42 (m, 1H), 2.79 (br s, 1H, 2''-OH), 2.51 and 2.31 (both m, 2H, CH_2-2), 1.67–1.25 (m, 22H, 11CH_2), 1.49 and 1.34 (both s, 6H, Me_2C), 1.38 (d, $J(6',5') = 6.72$ Hz, 3H, H-6'), 0.88 (t, $J = 6.92$ Hz, 3H, H-16); ^{13}C NMR (75.6 MHz, $CDCl_3$): δ = 174.9 (CO_2), 137.2, 129.2, 128.3, 109.9 (Me_2C), 102.5 (PhCH), 101.8 (C-1''), 98.9 (C-1'), 83.2, 79.5, 78.4, 75.2, 74.8, 68.9, 66.3, 36.0, 35.7, 34.8, 32.0, 30.6, 29.8, 29.4, 28.5, 28.4, 27.9, 27.0, 26.6, 25.9, 22.7, 16.8, 14.2; ESI-MS: *m/z*: 713 ($M + Na^+$), 729 ($M + K^+$); C,H analysis calcd for $C_{38}H_{58}O_{11}$: C 66.07, H 8.46; found: C 65.88, H 8.59. **19**: amorphous solid; $R_f = 0.71$ (petroleum ether/EtOAc, 7/3); $[\alpha]_D^{19} = -38.60$ ($c = 0.27$ in $CHCl_3$); IR (KBr): $\tilde{\nu}$ = 3484 (OH), 1751 (CO_2), 1458, 1382, 1182, 1133, 1099, 1076, 869, 699 cm^{-1}; ^1H NMR (300 MHz, $CDCl_3$, TMS): δ = 7.50–7.36 (m, 5H, Ph), 5.55 (s, 1H, PhC*H*), 5.23 (d, $J = 7.43$ Hz, 1H, H-1''), 4.91 (t, $J = 8.05$ Hz, 1H, H-2''), 4.28 (dd, $J = 4.77$, 10.43 Hz, 1H, H-$6''_{aq}$), 4.16 (d, $J = 8.29$ Hz, 1H, H-1'), 4.07 (m, 1H), 4.00 (m, 1H), 3.92–3.67 (m, 5H), 3.50 (m, 2H), 3.07 (br s, 1H, OH-3''), 2.45 (m, 2H), 1.53 and 1.36 (both s, 6H, Me_2C), 1.75–1.26 (m, 25H, 22CH_2, Me-5'), 0.88 (t, $J = 6.16$ Hz, 3H, H-16); ^{13}C NMR (75.6 MHz, $CDCl_3$): δ = 173.8 (CO_2), 137.1, 129.2, 128.3, 126.3, 110.0, 101.8, 100.4, 97.3, 80.0, 79.4, 75.2, 75.1, 73.0, 68.8, 68.7, 66.1, 35.1, 33.7, 31.9, 27.9, 26.8, 26.5, 26.3, 26.2, 26.1, 25.2, 23.8, 23.6, 22.6, 16.6; FAB-MS: *m/z*: 690 (M^+); C,H analysis calcd for $C_{38}H_{58}O_{11}$: C 66.07, H 8.46; found: C 66.22, H 8.76.

[13] D. R. Mootoo, P. Konradsson, U. Udodong, B. Fraser-Reid, *J. Am. Chem. Soc.* **1988**, *110*, 5583–5584.

[14] a) R. U. Lemieux, A. R. Morgan, *Can. J. Chem.* **1965**, *43*, 2190–2198; b) G. H. Veeneman, J. H. van Boom, *Tetrahedron Lett.* **1990**, *31*, 275–278; c) H. M. Zuurmond, P. H. van der Meer, P. A. M. van der Klein, G. A. van der Marel, J. H. van Boom, *J. Carbohydr. Chem.* **1993**, *12*, 1091–1103; d) K. Zegelaar-Jaarsveld, G. A. van der Marel, J. H. van Boom, *Tetrahedron* **1992**, *48*, 10133–10148.

[15] a) P. Konradsson, U. E. Udodong, B. Fraser-Reid, *Tetrahedron Lett.* **1990**, *31*, 4313–4316; b) K. Takeo, K. Nagayoshi, K. Nishimura, S. Kitamura, *J. Carbohydr. Chem.* **1994**, *13*, 1159–1177.

[16] For removal of an acetal or ketal by DDQ, see a) J. M. G. Fenandez, C. D. Mellet, A. M. Marin, J. Fuentes, *Carbohydr. Res.* **1995**, *274*, 263–268; b) A. Oku, M. Kinugasa, T. Kamada, *Chem. Lett.* **1993**, 165–168; c) K. Tanemura, T. Suzuki, T. Horaguchi, *J. Chem. Soc. Chem. Commun.* **1992**, 979–980.

[17] Selected spectroscopic data for tricolorin A (**1**): amorphous solid; $R_f = 0.56$ (CH_2Cl_2/CH_3OH, 17/3); $[\alpha]_D^{20} = -27.27$ ($c = 0.89$ in CH_3OH; $[\alpha]_D = -30.32$ ($c = 1.5$ in CH_3OH)[1]); IR (KBr): $\tilde{\nu}$ = 3429 (OH), 2934, 1739, 1463, 1384, 1249, 1137, 1070 cm^{-1}; ^1H NMR (600 MHz, C_5D_5N): δ = 5.82–5.76 (m, 3H), 5.69 (t, $J = 9.6$ Hz, 1H), 5.55 (br s, 1H), 5.50 (br s, 1H), 4.77 (m, 1H), 4.71 (m, 1H), 4.65 (m, 1H), 4.50 (br s, 1H), 4.40 (m, 1H), 4.34 (m, 1H), 4.23 (m, 3H), 4.12 (m, 2H), 4.01 (br s, 1H), 3.89 (m, 1H), 3.82 (m, 2H), 3.47 (m, 1H), 2.98 (m, 1H), 2.45 (m, 1H), 2.38 (m, 1H), 2.31 (m, 1H), 1.70 (d, $J = 5.4$ Hz, 3H, CH_3), 1.63 (d, $J = 5.4$ Hz, 3H, CH_3), 1.57 (d, $J = 6.6$ Hz, 3H, CH_3), 1.16 (d, $J = 7.8$ Hz, 3H, CH_3), 1.10 (d, $J = 7.2$ Hz, 3H, CH_3), 0.91 (t, $J = 6.6$ Hz, 3H, CH_3), 0.82 (m, 6H, 2CH_3); ^{13}C NMR (75.6 MHz, C_5D_5N): δ = 175.6, 175.5, 172.1, 104.5, 102.9, 99.7, 98.2, 80.8, 80.5, 78.8, 76.2, 76.1, 75.8, 74.5, 73.23, 73.18, 73.0, 72.6, 72.4, 72.2, 71.1, 70.4, 69.4, 67.1, 61.1, 41.7, 41.4, 41.3, 35.0, 34.3, 31.9, 31.6, 29.8, 29.4, 28.1, 27.8, 26.9, 26.7, 26.5, 25.5, 24.6, 23.5, 22.7, 18.4, 18.2, 17.2, 16.83, 16.78, 14.1, 11.7; ESI-MS: *m/z*: 1046 ($M + Na^+$), 1069 ($M + 2Na^+$).

Fluorous Biphasic Catalysis: Complexation of 1,4,7-[$C_8F_{17}(CH_2)_3$]$_3$-1,4,7-Triazacyclononane with [$M(C_8F_{17}(CH_2)_2CO_2)_2$] (M = Mn, Co) To Provide Perfluoroheptane-Soluble Catalysts for Alkane and Alkene Functionalization in the Presence of *t*-BuOOH and O_2**

Jean-Marc Vincent, Alain Rabion, Vittal K. Yachandra, and Richard H. Fish*

Recently, Horváth and Rábai published a seminal paper on a new homogeneous catalysis concept—Fluorous Biphasic Catalysis (FBC)—that entailed the use of a fluorocarbon as one phase containing a modified catalyst with polyfluorinated alkyl side chains (fluoroponytails), while the substrate and the product were soluble in a second hydrocarbon phase.[1] It is also important to note that low-boiling, perfluorinated solvents are immiscible both in water and many organic solvents.[2] Therefore, separation of the product from the catalyst occurred by solubility differences between the hydrocarbon and fluorocarbon phases; this process thus represents a potentially interesting new concept for the industrial synthesis of important chemicals.[1, 3, 4]

In this communication, we present the synthesis of a new fluoroponytailed ligand (**4**), namely, tris-*N*-(4,4,5,5,6,6,7,7,8,8,9,9,10,10,11,11,11-heptadecafluoroundecyl)-1,4,7-triazacy-

[*] Dr. R. H. Fish, Dr. J.-M. Vincent, Dr. V. Yachandra
Lawrence Berkeley National Laboratory
University of California
Berkeley, CA 94720 (USA)
Fax: Int. code +(510)486-7303
e-mail: rhfish@lbl.gov
Dr. A. Rabion
Groupement de recherche de Lacq, BP 34, F-64170 Artix (France)

[**] The studies at LBNL were generously supported by a gift grant (R. H. F.) and a postdoctoral fellowship to J.-M. V. from Elf Aquitaine Inc., and the Department of Energy (Contract No.DE-AC03-76SF00098). We thank Dr. István T. Horváth and Dr. Jozsef Rábai for helpful discussions concerning our FBC program. These studies were partially presented at the 10th International Symposium on Homogeneous Catalysis, August 11–16, 1996, Princeton University, Princeton, NJ, Abstract PP-A52.

 © WILEY-VCH Verlag GmbH, D-69451 Weinheim, 1997 0570-0833/97/3621-2346 $ 17.50+.50/0

clononane (R_fTACN), that is soluble in perfluoroalkanes, and new R_fMn^{2+} and R_fCo^{2+} fluoroponytailed carboxylate synthons **5** and **6**, as well as our initial results on the functionaliza-

$[Mn(O_2C(CH_2)_2C_8F_{17})_2]$ **5**

$[Co(O_2C(CH_2)_2C_8F_{17})_2]$ **6**

tion of alkanes and alkenes, using in situ generated $[R_fMn^{2+}(R_fTACN)]$ and $[R_fCo^{2+}(R_fTACN)]$ complexes (**7** and **8**, respectively) as catalysts that are totally soluble in the fluorous phase (Scheme 1). In contrast to the new FBC concept, the oxidation

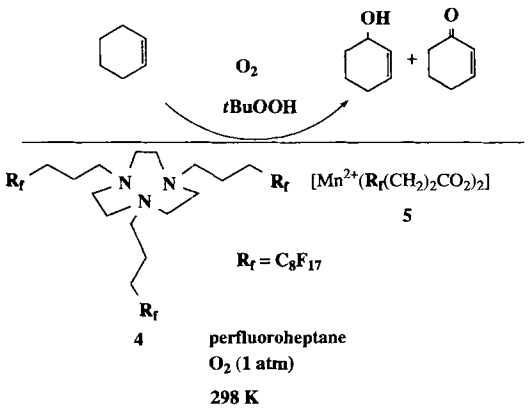

Scheme 1. Fluorous biphasic oxidation catalysis with cyclohexene as the substrate and complex **7** formed in situ with **4** and **5**.

of alkanes with *tert*-butyl hydroperoxide (TBHP) in acetonitrile and epoxidation of alkenes with H_2O_2 in acetone were previously achieved in one homogeneous phase by the in situ preparation of Mn^{2+} catalysts containing 2,2′-bipyridine and tris-N-methyl-TACN ligands, respectively, and separation of the Mn catalyst from the product is relatively difficult or impossible.[5] We will demonstrate that this novel FBC approach for separation of the catalyst from the substrate appears viable for oxidation of alkanes and alkenes in the presence of the necessary oxidants, TBHP and O_2 gas, and that these oxidation reactions occur by an autoxidation mechanism under our FBC conditions.[6, 7]

One key component of the FBC approach includes the new fluoroponytailed ligand **4**, synthesized by the sequence of reactions shown in Scheme 2. It is important to note that the three-methylene spacer in **3** is necessary, not only to insulate the amine from the powerful electron-withdrawing effect of the perfluoroalkyl group, but also to avoid a facile elimination reaction of HI that predominately occurs when a two-carbon spacer is used

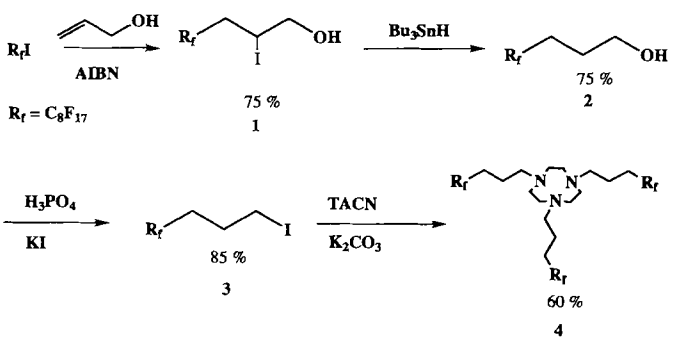

Scheme 2. Synthesis of **4**.

during the formation of **4**. The first step to the new perfluoroalkyl iodide **3** proceeds by a free radical addition of a perfluoroalkyl iodide (R_fI) to allyl alcohol that was initiated with AIBN to provide the perfluoroalkylated iodohydrin **1**.[8] Compound **1** was then reduced to the perfluoroalkyl alcohol **2** by using tributyltin hydride in dry benzotrifluoride.[9] Iodination of **2** to form **3** was achieved with 85% phosphoric acid in the presence of phosphorous pentaoxide and potassium iodide in 85% yield.[10] Finally, ligand **4** was obtained from TACN and **3** in $DMSO/K_2CO_3$ in 60% yield after recrystallization (Scheme 2; see Experimental Section). Compound **4** is soluble in cold perfluorohexane and perfluoromethylcyclohexane, and represents, to our knowledge, the first example of an R_f-amine ligand that is soluble in a perfluorocarbon solvent.

The other important components were the new R_fMn^{2+} and R_fCo^{2+} complexes **5** and **6** synthesized by reaction of $Mn(ClO_4)_2 \cdot 6H_2O$ or $Co(ClO_4)_2 \cdot 6H_2O$ in acetone with two equivalents of the triethylammonium salt of the 3-R_f-alkylpropanoic acid, $C_8F_{17}CH_2CH_2CO_2H$; elemental analysis of **5** and **6** provide a metal-to-carboxylate ligand ratio of 1:2, while **5** was found to be slightly soluble in perfluorocarbons, exhibits an intense and broad ESR signal at $g = 2$ (9 K), and displays the characteristic 6-line hyperfine structure ($J = 90$ G) of a mononuclear Mn^{2+} complex.[11] Interestingly, when one equivalent of **4** was added to a solution of **5** in perfluoroheptane, a UV absorption band appears at 320 nm, tentatively suggesting that a new $[R_fMn(R_fTACN)]^{2+}$ complex (**7**) was formed in situ. Similarly, when ligand **4** and complex **6** were combined the complex $[R_fCo(R_fTACN)]^{2+}$ (**8**) resulted.

The FBC oxidation results for several substrates are presented in Table 1. All the experiments were carried out under biphasic conditions, generating complexes **7** or **8** in situ in perfluoroheptane (Scheme 1), while the upper phase was the substrate itself. Importantly, the oxidation products were detected only in the colorless upper phase after decantation (GC), while the colored perfluoroheptane lower phase contains only traces (< 5%) of product. Clearly, a facile and rapid separation of the products from the catalyst was achieved with this FBC approach.

Table 1 demonstrates that the olefin with allylic hydrogens, cyclohexene, provides the highest yield of oxidation products (650% with TBHP in 3 h), while alkane oxidation was much lower (cyclohexane: 12% cyclohexanol (CyOH)/cyclohexanone (CyONE) with TBHP in 24 h; toluene: 65% $PhCH_2OH/PhCHO$ with TBHP in 24 h). In the presence of a vigorously stirred mixture of **7**, TBHP, and oxygen gas (1 atm), cyclohexene was converted into a product ratio of 2-cyclohexen-1-one (CyenONE, about 65%), 2-cyclohexen-1-ol (CyenOH, about

Table 1. Functionalization of alkenes and alkanes under fluorous biphasic catalysis conditions [a].

Cat.	Substrate	Oxidant	Product (μmol)	Yield [b] [%]	Time [h]
7	cyclohexene	$TBHP/O_2$	CyenOH (160), CyenONE (300)	650	3
7	cyclohexene	TBHP	CyenOH (<2), CyenONE (<2)		7
7	cyclohexene	O_2	CyenOH (<1), CyenONE (<1)		24
5	cyclohexene	$TBHP/O_2$	CyenOH (130), CyenONE (160)	360	12
7	styrene	$TBHP/O_2$	no epoxide		24
7	toluene	$TBHP/O_2$	PhCHO (15), $PhCH_2OH$ (30)	65	24
7	cyclohexane	$TBHP/O_2$	CyOH (5), CyONE (3.5)	12	24
8	cyclohexene	$TBHP/O_2$	CyenOH (185), CyenONE (360)	750	20
8	cyclohexane	$TBHP/O_2$	CyOH (7), CyONE (5.5)	17	24

[a] Conditions: **5** or **6** (3.5 μmol) and **4** (3.5 μmol) were dissolved in hot perfluoroheptane (3 mL) and then the substrate (2 mL) was added. The reaction starts after the addition of TBHP (90%, 72 μmol) under an O_2 atmosphere when required. [b] Total yield was based on TBHP added.

 © WILEY-VCH Verlag GmbH, D-69451 Weinheim, 1997 0570-0833/97/3621-2347 $ 17.50+.50/0

35%), and a small amount of cyclohexene oxide (<2%), while with complex **8** similar oxidation results were obtained. Styrene, with no allylic hydrogens, is not converted into styrene epoxide under these biphasic conditions. In the absence of O_2 or TBHP, only negligible amounts of 2-cyclohexen-1-ol and 2-cyclohexen-1-one were detected, indicative of an autoxidation reaction; that is, *both* were necessary for oxidation to proceed. At the end of the reaction the upper phase was removed, and new aliquots of cyclohexene and TBHP were added to provide a 400% yield after 5 h, showing that the catalyst, after decantation, was only present in the lower fluorocarbon phase.

These results were in agreement with an autoxidation mechanism involving alkoxy (RO$^\cdot$) or alkylperoxy (ROO$^\cdot$) radicals,[12] where the reaction was initiated by tBuO$^\cdot$ or tBuO$_2^\cdot$ radicals produced from redox reactions (Haber–Weiss Process, Equations 2 and 3 with Mn^{2+}/Mn^{3+}). In the case of the substrate

$$Mn^{2+} + RO\text{-}OH \xrightarrow{\text{Reduction}} RO^\cdot + Mn^{3+} + HO^- \quad (1)$$

$$Mn^{3+} + ROO\text{-}H \xrightarrow{\text{Oxidation}} RO_2^\cdot + Mn^{2+} + H^+ \quad (2)$$

cyclohexene, the allylic radical formed was then trapped by O_2 ($k > 10^9\,M^{-1}sec^{-1}$) to provide cyclohexenylperoxy radicals, which were able to homolytically remove a hydrogen (bond energy of RCOO–H 90 kcal mol^{-1}) from benzylic or allylic C–H bonds (85 kcal mol^{-1}), and hence, propagate the radical reactions. The secondary cyclohexenyl hydroperoxide that was formed then decomposes catalytically in the presence of the Mn catalyst to give the alcohol and the ketone products.[13]

The lower yields observed in the case of cyclohexane are consistent with the stronger C–H bond strength (95 kcal mol^{-1}),[12] which implicates the cyclohexylperoxy radical and thus causes a lowering of the rate of the propagation step. The chain termination step presumably comes mainly from the coupling of two cyclohexenylperoxy radicals to give alcohol, ketone, and O_2 (Russell-type mechanism).[12]

The R_fMn complex, formed during the oxidation of **7**, was plausibly a $R_fMn^{3+}Mn^{4+}$ dimer. Therefore, when TBHP was added to the reaction mixture, the solution turns brown and exhibits intense UV-Vis absorptions (ε per Mn atom is approximately 9000 and 1130 $M^{-1}cm^{-1}$ at 300 and 500 nm, respectively, after 1 h) characteristic of dinuclear $Mn^{3+}Mn^{3+}$, $Mn^{3+}Mn^{4+}$, or $Mn^{4+}Mn^{4+}$ complexes.[14] The occurrence of such a putative $R_fMn^{3+}Mn^{4+}$ dimer from starting complex **7**, under oxidation conditions, was unambiguously confirmed by ESR studies at 9 K. Thus, a strong, distinctive 16-line signal of an antiferromagnetically coupled $R_fMn^{3+}Mn^{4+}$ dimer complex at $g = 2$ was observed in the perfluoroheptane phase, after 1 h of reaction. Indeed, it has recently been shown that the decomposition of TBHP in the presence of a dinuclear Mn_2^{3+}(2-OHsalpn)$_2$ complex (salpn = bis(salicylidene)propylenediamine dianion) resulted in the formation of tBuO$^\cdot$ radicals and a dinuclear $Mn^{3+}(\mu\text{-}O)_2Mn^{4+}$ complex.[15]

Furthermore, reaction 2 was favored over reaction 3 with complex **7** for two important reasons: 1) It has been previously shown that in nonpolar solvents equation 3 was very slow,[16] and 2) the $R_fMn^{3+}Mn^{4+}$ dimeric species formed upon the addition of TBHP to complex **7** was not very efficient in the oxidation of TBHP. Interestingly, after three hours, the 16-line ESR signal had almost disappeared, which suggests that this $R_fMn^{3+}Mn^{4+}$ dinuclear mixed valent species might be involved in the catalytic decomposition of the cyclohexenyl hydroperoxide intermediate to provide the alcohol and ketone products.

Finally, as pointed out recently by Pozzi et al.,[17] despite the apparent simplicity of the FBC concept the concrete demonstration of this strategy is still a difficult challenge, since the solubilization of the fluoroponytailed metal complexes used in perfluorocarbons is one limiting step along with catalyst stability and the favorable recycling of the catalyst system. We now have been able to solubilize complexes **7** and **8** successfully in perfluoroheptane, using both the new R_fTACN ligand **4** and the new R_fMn^{2+} and R_fCo^{2+} complexes **5** and **6**, with fluoroponytailed carboxylate ligands. Moreover, we have been able to perform alkane and alkene oxidations under FBC conditions in the presence of TBHP and O_2 as oxidant, and hence, separate the products from the catalyst by a simple decantation process. The oxidation process occurs by an autoxidation mechanism, with formation of alkenyl or alkyl hydroperoxides as the key intermediates, which then are catalytically decomposed by the R_fMn- or R_fCoR_fTACN catalyst, probably at the solvent interface, to provide the alcohol and ketone products. Future studies will attempt to ascertain the unequivocal structures of complexes **5**–**8** by single-crystal X-ray crystallography, define the role of the dinuclear $R_fMn^{3+}Mn^{4+}$ complex in the decomposition of the alkyl and alkenyl hydroperoxide intermediates and determine its full structure, as well as further the scope of the FBC approach to oxidation chemistry.

Experimental Section

4: TACN (88.4 mg, 0.73 mmol), K_2CO_3 (423 mg, 3.1 mmol), and $R_fCH_2CH_2CH_2I$ (1.41 g, 2.41 mmol) were dissolved in DMSO (10 mL, distilled over CaH_2) and heated at 90 °C for 24 h. Then perfluoroheptane (20 mL) was added to the reaction mixture, and the brown fluorous lower phase was separated and then filtered. After removing the solvent, compound **4** was obtained as a brown oil. After crystallization from hot hexane, compound **4** was isolated as a yellowish powder in 60% yield. FAB/MS: m/z 1510 [$M+H^+$]. Elemental analysis calcd for $C_{39}H_{30}F_{51}N_3$: C 31.03, F 64.20, H 1.98, N 2.78; found: C 30.74, F 64.31, H 2.02, N 2.70. ^{1}H NMR (400 MHz, $CDCl_3$, 25 °C): $\delta = 2.71$ (s, 12H, NCH_2CH_2N), 2.55 (t, 6H, NCH_2CH_2), 2.17 (m, 6H, $CH_2CH_2CH_2$), 1.58 (m, 6H, $CH_2CH_2R_f$).

5: $CF_3(CF_2)_7CH_2CH_2CO_2H$ (1.35 g, 2.80 mmol) was dissolved in acetone (15 mL) and to this solution was added triethylamine (380 mL, 2.80 mmol). This resulting solution was added dropwise to $Mn(ClO_4)_2\cdot 6H_2O$ (500 mg, 1.37 mmol) dissolved in acetone (30 mL). The sticky precipitate that formed was vigorously stirred for 2 h. After filtration, **5** was obtained as a white powder in 75% yield. Elemental analysis calcd for $C_{22}F_{34}H_{12}O_6Mn$: C 24.61, F 60.19, H 1.12, Mn 5.12; found: C 25.37, F 59.77, H 0.94, Mn 5.50.

6: The same procedure as for complex **5** was used for the synthesis of **6**, except with $Co(ClO_4)_2\cdot 6H_2O$. A pink precipitate formed immediately, and after filtration, a pink powder was obtained in 100% yield. Elemental analysis calcd for $C_{22}H_{12}F_{34}CoO_6$: C 24.53, H 1.11, F 59.98, Co 5.46; found: C 25.05, H 1.27, F 60.15, Co 5.35.

Received: February 3, 1997
Revised version: May 12, 1997 [Z100701E]
German version: *Angew. Chem.* **1997**, *109*, 2438–2440

Keywords: biphasic catalysis · cobalt · fluorohydrocarbons · manganese · oxidations

[1] I. T. Horváth, J. Rábai, *Science* **1994**, *266*, 72, and references therein.
[2] M. Hudlicky, A. E. Pavlath, *Chemistry of Organic Compounds II*, Ellis Horwood, Chichester (UK), **1992**.
[3] M. Vogt, Dissertation, Technische Hochschule Aachen, **1991**.
[4] I. T. Horváth in *Applied Homogeneous Catalysis with Organometallic Compounds* (Eds.: B. Cornils, W. A. Herrmann), VCH, Weinheim, **1996**, pp. 601.
[5] a) S. Ménage, M.-N. Collomb-Dunand-Sauthier, C. Lambeaux, M. Fontecave, *J. Chem. Soc. Chem. Commun.* **1994**, 1885; b) D. De Vos, T. Vein, *ibid.* **1996**, 917.
[6] I. T. Horváth, J. Rábai, US-A 5,463,082. This patent noted the minor oxidation of cyclohexene under O_2 pressure (100 psi) with an in situ generated, and not fully identified, (perfluorodecyl)phthalocyaninato Co^{3+} complex that is soluble in a fluorocarbon. No details were given concerning the mechanism of this oxidation reaction.
[7] During the review process, alkene epoxidation under FBC conditions with a perfluorocarbon-soluble Co–porphyrin catalyst was reported: G. Pozzi, F. Montanari, S. Quici, *J. Chem. Soc. Chem. Commun.* **1997**, 69.

 © WILEY-VCH Verlag GmbH, D-69451 Weinheim, 1997 0570-0833/97/3621-2348 $ 17.50+.50/0

[8] This procedure was slightly different from the one described by Kotora et al., who synthesized 3-perfluorohexyl-1-propanol ($C_6F_{13}(CH_2)_3OH$) using copper powder as a free radical initiator in neat solution followed by tin hydride reduction: M. Kotora, M. Hajek, B. Ameduri, B. Boutevin, *J. Fluorine Chem.* **1994**, *68*, 85. Elemental analysis calcd for **1** ,($C_{11}H_6F_{17}IO$): C 21.87, H 1.00; found: C 22.06, H 0.97. EI-MS: *m/z*: 604 [*M* +]. ^{1}H NMR (400 MHz, $CDCl_3$, 25 °C): δ = 4.45 (m, 1H, C*H*I), 3.79 (m, 2H, CH_2OH), 2.9 (2m, 2H, R_f-CH_2), 2.04 (t, OH). M.p. 93–94 °C.

[9] Compound **2** was recrystallized from hexane. EI-MS: *m/z*: 477 [*M* +]. Elemental analysis calcd for $C_{11}H_7F_{17}O$: C 27.63, H 1.46; found: C 27.72, H 1.63. ^{1}H NMR (400 MHz, $CDCl_3$, 25 °C) δ = 3.75 (m, 2H, CH_2OH), 2.20 (m, 2H, Rf-CH_2), 1.88 (m, 2H, $CH_2CH_2CH_2$), 1.57 (s, OH).

[10] Compound **3** can be recrystallized from methanol. EI-MS: *m/z*: 588 [*M* +]. Elemental analysis calcd for $C_{11}F_{17}H_6I$: C 22.47, H 1.02; found: C 22.80, H 1.26. ^{1}H NMR (400 MHz, $CDCl_3$, 25 °C) δ = 3.26 (t, 2H, ICH_2), 2.16 (2m, 4H, $CH_2CH_2R_f$).

[11] P. Mathur, G. Dismukes, *J. Am. Chem. Soc.* **1983**, *105*, 7093.

[12] R. A. Sheldon, J. K. Kochi, *Metal-catalyzed Oxidations of Organic Compounds*, Academic Press, New York, **1981**.

[13] R. H. Fish, M. S. Konings, K. J. Oberhausen, R. H. Fong, W. M. Yu, G. Christou, J. B. Vincent, D. K. Coggin, R. M. Buchanan, *Inorg. Chem.* **1991**, *30*, 3002.

[14] Y.-M. Frappart, A. Boussac, R. Albach, E. Anxolabéhère-Malhart, M. Delroisse, J.-B. Verlhac, G. Blondin, J.-J. Girerd, J. Guilhem, M. Cesario, A. W. Rutherford, D. Lexa, *J. Am. Chem. Soc.* **1996**, *118*, 2669.

[15] M. T. Caudle, P. Riggs-Gelasco, A. K. Gelasco, J. E. Penner-Hahn, V. L. Pecoraro, *Inorg. Chem.* **1996**, *35*, 3577.

[16] R. A. Sheldon, J. K. Kochi, *Adv. Catal.* **1976**, *25*, 272.

[17] G. Pozzi, S. Banfi, A. Manfredi, F. Montanari, S. Quici, *Tetrahedron* **1996**, *52*, 36, 11879.

A 1,3,5-Triphosphinantriium Ion**

Ekaterina Gorbunowa, Gernot Heckmann, Ekkehard Fluck,* Matthias Westerhausen, and Rudolf Janoschek

Dedicated to Professor Hans Georg von Schnering

In 1976 we prepared the spherical, negatively charged $[P_{12}S_{12}N_{14}]^{6-}$ ion by reaction of P_4S_{10} with potassium cyanate.[1] In spite of the spatial proximity of the charge carriers, the anion is both thermally stable and stable to hydrolysis. The 1,1,3,3,5,5-hexakis(dimethylamino)-1λ^5,3λ^5,5λ^5-triphosphinantriium cation **2** has also proved to be thermally stable. The charge carriers in the six-membered ring are separated from one another by just a single CH_2 group. Cyclic phosphonium salts with two positively charged phosphorus atoms and symmetrically arranged phosphorus–carbon units have been described previously.[2–7] However, in the quadruply charged P–C heterocycles known to date, three or four methylene groups separate the individual phosphorus atoms and thus 16-membered or 20-membered rings are present.[4] A cyclic dication prepared by Karsch that contains two phosphonium centers and a phosphane center in the 1,3,5 positions could not be quaternized to the 1,3,5-trication; instead, ring-opening occurred.[8]

[*] Prof. Dr. E. Fluck
Gmelin-Institut für Anorganische Chemie der Max-Planck-Gesellschaft
Varrentrappstrasse 40/42, D-60486 Frankfurt am Main (Germany)
Fax: Int. code +(69)7917-391
Dr. E. Gorbunowa, Dr. G. Heckmann
Institut für Anorganische Chemie der Universität
Pfaffenwaldring 55, D-70569 Stuttgart (Germany)
Prof. Dr. M. Westerhausen
Institut für Anorganische Chemie der Universität
Meiserstrasse 1, D-80333 München (Germany)
Prof. Dr. R. Janoschek
Institut für Theoretische Chemie der Universität
Strassoldogasse 10, A-8010 Graz (Austria)

[**] This work was supported by the Fonds der Chemischen Industrie.

Compound **2** is formed by the reaction of 1,1,3,3,5,5-hexakis(dimethylamino)-1,3,5-triphosphinine (**1**) with $HBF_4 \cdot Et_2O$ in diethyl ether with a yield of 79.3 %. The colorless crystalline compound melts at 211–212 °C and is soluble in acetonitrile.

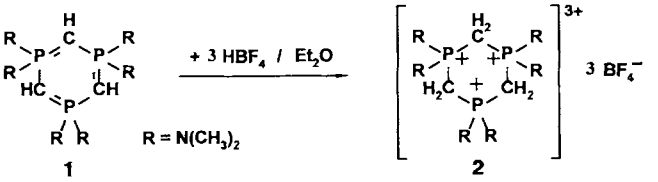

The singlet at δ = 45.21 in the $^{31}P\{^1H\}$ NMR spectrum of **2** indicates that a planar ring is present within the scope of the NMR time scale. The position of the singlet is—compared with the position of the signal of the ylidic PCP triad of the starting material **1**—shifted upfield by 20.2 ppm in the region of the λ^5-1,3-diphosphetes.[9] The base of the singlet has a narrow line width and is flanked by two pairs of ^{13}C satellites.[10] Together with the triplet observed in the $^{13}C\{^1H\}$ NMR spectrum at δ = 18.26, which displays individual lines with different structures, these four ^{13}C satellites permit the full evaluation of the A_2BX spin system of the [$^{13}C_1$] isotopomer of **2**. A ^{13}C-DEPT experiment confirmed unequivocally the presence of the endocyclic CH_2 groups. The small geminal P–P coupling constant of 4.0 Hz is characteristic for a P–CH_2–P group.[11] The ^2J(P,P) coupling constant of the P=C–P triad in the starting material **1** was determined to be 73 Hz. As is the case in **1**, a small negative vicinal P–C coupling constant is found in the ring (−1.8 Hz).[12]

The crystal structure analysis of **2** in the solid state revealed a six-membered heterocycle; the atoms P1, P3, C2, and C3 lie almost in a plane (Figure 1). P2 and C1 are both located above

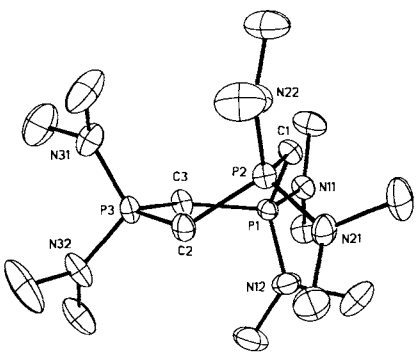

Figure. 1. Molecular structure of the cation **2** in the crystal (thermal ellipsoids at 50 % probability, H atoms not shown for clarity). Selected distances [pm] and angles [°]: P1–C1 178.9 (3), P1–C3 180.6(3), P2–C1 180.2(3), P2–C2 181.2(3), P3–C2 180.7(3), P3–C3 181.7(3); P1-C1-P2 114.3(2), P1-C3-P3 117.4(2), C1-P2-C2 108.32(13), P2-C2-P3 119.9(2), C2-P3-C3 108.90(14), C3-P1-C1 103.8(2).

this plane; their positions in the ring are characterized by greatly different bond angles (P2-C2-P3: 119.9°, C1-P1-C3: 103.8°) and by distances between 178.9 and 181.2 pm, which are typical for P–C single bonds.[13] The nitrogen atom environments are approximately planar. The P–N bond lengths (160.7–162.0 pm) are about 7 pm shorter than those found in the starting material **1** and in 1λ^5,3λ^5-diphosphinines.[14, 15] There are no interactions between the triply positively charged six-membered ring and the tetrafluoroborate ions, and there is no H···F bridging. The peaks of the singly and doubly charged cations

 © WILEY-VCH Verlag GmbH, D-69451 Weinheim, 1997 0570-0833/97/3621-2349 $ 17.50+.50/0

can be found in the positive-ion FAB mass spectrum of **2** with the corresponding ^{13}C peaks. The signal of the triply charged cation was not detected. Density function calculations (B3LYP/6-31G*) on the more simple ion $[\{P(NH_2)_2\}_3\{CH_2\}_3]^{3+}$ showed a puckered ring at the energy minimum for C_1 symmetry with an average P–C bond length of 185 pm.[16]

Experimental Section

A solution of $HBF_4 \cdot Et_2O$ (1.12 mL, 8.4 mmol, $\rho = 1.19\ g mL^{-1}$) in diethyl ether (10 mL) was slowly added to a cooled (−20 °C) solution of **1** (0.67 g, 1.69 mmol) in diethyl ether (10 mL). Compound **2** began to precipitate immediately. The pale pink colored reaction solution was warmed to room temperature and stirred for a further 12 h. After the mixture had been filtered, the resulting crystalline precipitate of **2** was analytically pure. Clear, colorless crystals were obtained by recrystallization from an acetonitrile/diethyl ether solution at room temperature. Yield: 0.91 g (79.3 %). $M = 659.8\ g mol^{-1}$. MS (positive-ion FAB, NBA) *m/z* (%): 398 (16) $[M^* - 2H^+, {}^{13}C]$, 397 (100) $[M^* - 2H^+]$, 199.6 (2) $[M^* - H^+, {}^{13}C]$, 199.1 (18) $[M^* - H^+]$; $M^* = M - 3BF_4^-$; ^1H NMR (250 MHz, CD_3CN, 300 K, TMS): δ = 4.06 (t, $^2J(H,P) = 17.7$ Hz, $^4J(H,P) < 0.3$ Hz, 6H; CH_2,), 2.97 (d, $^3J(H,P) = 12.2$ Hz, 36H; CH_3); $^{31}P\{^1H\}$ NMR (161.978 MHz, CD_3CN, 305 K, 85% H_3PO_4): $\delta = 45.21$ (s, $^2J(P,P) = 4.0$ Hz according to A_2BX simulation); ^{13}C NMR (100.614 MHz, CD_3CN, 305 K, TMS): $\delta = 18.26$ (A_2BX simulation: $^1J(P,C) = 80.0$ Hz, $^3J(P,C) = -1.8$ Hz, $^1J(C,H) = 130.2$ Hz; CH_2), 38.45 (s; CH_3); ^{19}F NMR (235.360 MHz, CD_3CN, 300 K, $CFCl_3$): $\delta = -149.31$ (s); IR (Nujol, CsBr plates): $\tilde{\nu}$ = 1301 (s), 1213 (m), 1168 (m), 1061 (vs), 1053 (sh), 998 (m), 991 (sh), 838 (m), 722 (vw), 521 (vw) cm^{-1}.

Received: April 14, 1997 [Z10347IE]
German version: *Angew. Chem.* **1997**, *109*, 2444–2445

Keywords: cations · heterocycles · phosphorus · ylides

[1] E. Fluck, M. Lang, F. Horn, E. Hädicke, G. M. Sheldrick, *Z. Naturforsch. B* **1976**, *31*, 419–426.
[2] S. O. Grim, R. Schaaf, *Angew. Chem.* **1963**, *75*, 669; *Angew. Chem. Int. Ed. Engl.* **1963**, *2*, 486.
[3] A. M. Aguiar, H. Aguiar, *J. Am. Chem. Soc.* **1966**, *88*, 4090–4091.
[4] L. Horner, P. Walach, H. Kunz, *Phosphorus Sulfur Relat. Elem.* **1978**, *5*, 171–184.
[5] H. Schmidbaur, T. Costa, B. Milewski-Mahrla, U. Schubert, *Angew. Chem.* **1980**, *92*, 557–558; *Angew. Chem. Int. Ed. Engl.* **1980**, *19*, 555–556.
[6] H. Schmidbaur, T. Costa, *Chem. Ber.* **1981**, *114*, 3063–3069.
[7] H.Schmidbaur, S. Strunk, C. E. Zybill, *Chem. Ber.* **1983**, *116*, 3559–3566.
[8] H. H. Karsch, *Z. Naturforsch. B* **1982**, *37*, 284–291.
[9] E. Fluck, G. Heckmann in *Phosphorus-31 NMR Spectral Properties in Compound Characterization and Structural Analysis* (Eds.: L. D. Quin, J. G. Verkade), VCH, New York, **1994**, pp. 69–80.
[10] Line width at the height of the ^{13}C satellite signals: 14 Hz.
[11] G. Heckmann, F. Rosche, F. Weller, E. Fluck, *Phosphorus Sulfur Silicon Relat. Elem.* **1996**, *115*, 3–18.
[12] G. Heckmann, E. Fluck, *Rev. Heteroatom Chem.* **1994**, *11*, 65–87.
[13] Crystal structure analysis: Single crystals obtained by recrystallization from acetonitrile/diethyl ether. $C_{15}H_{40}B_3F_{12}N_6P_3$, Siemens P2 diffractometer, $Mo_{K\alpha}$ radiation, −90 °C, programs: SHELXTL PLUS and SHELXL-93, monoclinic space group $P2_1/n$, $a = 984.3(2)$, $b = 2748.1(3)$, $c = 1105.2(2)$ pm, $\beta = 97.97(2)°$, $V = 2.9605(7)\ nm^3$, $Z = 4$, $\rho_{calcd} = 1.480\ g cm^{-3}$, crystal dimensions: $0.2 \times 0.4 \times 0.4\ mm^3$, ω scan, range $4° < 2\theta < 54°$, 6425 independent reflections, 4870 reflections with $I < 2\sigma(I)$, 520 parameters, $R1 = 0.0816$, $wR2 = 0.1617$ (all data), $R = 0.0580$, $wR2 = 0.1442$ (2σ data), max. residual electron density: $930\ e nm^{-3}$. Further details of the crystal structure investigation may be obtained from the Fachinformationszentrum Karlsruhe, D-76344 Eggenstein-Leopoldshafen (Germany), on quoting the depository number CSD-406834.
[14] E. Fluck, G. Heckmann, W. Plass, M. Spahn, H. Borrmann, *J. Chem. Soc. Perkin Trans. 1* **1990**, 1223–1224; W. Plass, Dissertation, Universität Stuttgart, **1989**.
[15] E. Fluck, B. Neumüller, G. Heckmann, W. Plass, P. G. Jones, *New J. Chem.* **1989**, *13*, 383–388; E. Fluck, W. Plass, G. Heckmann, H. Bögge, A. Müller, *Z. Naturforsch. B* **1991**, *46*, 202–208.
[16] E. Fluck, G. Heckmann, R. Janoschek , E. Gorbunowa, M. Westerhausen, unpublished results.

$[CH(Me)P(Et)_2NSiMe_3]^-$—A Carbanion That Functions as a Bridging Ligand**

Anita Müller, Bernhard Neumüller, and Kurt Dehnicke*

In the solid state the lithiation products of *N*-(trimethylsilyl)phosphanimines, for example the tetrameric methyl derivative **1**[1] and the dimeric compounds **2**[1] and **3**,[2] are aggregated to oligomers, in which the N atoms participate by internal solvation. Their preparative potential has scarcely been made use of to date. Compound **1** reacts with chlorotrimethylsilane under elimination of LiCl to form the corresponding silylation product,[3a] whereas the reaction of **1** with zinc chloride, in which the latter functions primarily as a catalyst, the carbadianionic Li_{14} cluster **4** is obtained.[4] Very recently the formation of trimethylsilyliminophosphoranylenamidolithium complexes by treatment of α-lithiated phosphanimines of type **1** with benzonitrile was reported.[3b]

$[\{LiCH_2P(Me)_2NSiMe_3\}_4]$ **1**

$[\{LiC(Me)_2P(iPr_2)NSiMe_3\}_2]$ **2**

$[\{Li(C_6H_4)P(Ph)_2NSiMe_3\}_2(Et_2O)]$ **3**

$[\{Li_7[CHP(Me)_2NSiMe_3]_3[OSi(Me)_2nBu]\}_2]$ **4**

We have now established that the ethyl derivative **5**, the crystal structure of which[5] is analogous to that of the tetrameric **1**, is an attractive reagent. Its carbanionic C atom is asymmetrically substituted and, as a consequence of the internal solvation of the Li atoms, it forms strained Li-C-P-N four-membered rings; thus, it is extraordinarily reactive. Compound **5** is readily obtained from $Me_3SiNPEt_3$ and *n*-butyllithium in *n*-hexane; it is a viscous oil, which crystallizes slowly at −30 °C. With copper(I) iodide and with zinc chloride, **5** reacts according to Equations (1) and (2) forming the well-defined metal derivatives **6** and **7**, respectively, with unusual structures.

$$\underset{\mathbf{5}}{[\{LiCH(Me)P(Et)_2NSiMe_3\}_4]} + 2\,CuI \longrightarrow \underset{\mathbf{6}}{2[CuLi\{CH(Me)P(Et)_2NSiMe_3\}_2]} + 2\,LiI \quad (1)$$

$$3\,\mathbf{5} + 12\,ZnCl_2 \rightarrow \underset{\mathbf{7}}{[\{ClZnCH(Me)P(Et)_2NSiMe_3\}_{12}]} + 12\,LiCl \quad (2)$$

Addition of **5** to suspensions of the metal halides in diethyl ether causes rapid dissolution of the solids; after a rather long crystallization period **6** and $7 \cdot 4Et_2O$ are obtained as colorless single crystals. According to the crystal structure analysis[6] **6** is a lithium cuprate whose carbanionic atoms C1 and C10 are asymmetrically substituted and in which both copper and lithium exhibit almost linear coordination (Figure 1). The two metal atoms link the two carbanions $[CH(Me)P(Et)_2NSiMe_3]^-$ to form an undulated eight-membered ring with approximate C_2 symmetry. The Li-N-P bond angles in **5** (94.6°) are smaller than in **6** (mean 112.3°), and the N-P-C angles of 108.8° in **5** are increased to 112.2° in **6**, indicating a practically unstrained eight-membered ring. A similar eight-membered ring structure to that in **6** occurs in the dimeric ylidic copper complex $[\{CuMe_2P(CH_2)_2\}_2]$ (**8**).[7]

[*] Prof. Dr. K. Dehnicke, Dr. A. Müller, Priv.-Doz. Dr. B. Neumüller
Fachbereich Chemie der Universität
Hans-Meerwein Strasse, D-35032 Marburg (Germany)
Fax: Int. code +(6421)288917

[**] This work was supported by the Fonds der Chemischen Industrie and the Deutsche Forschungsgemeinschaft.

 © WILEY-VCH Verlag GmbH, D-69451 Weinheim, 1997 0570-0833/97/3621-2350 $ 17.50+.50/0

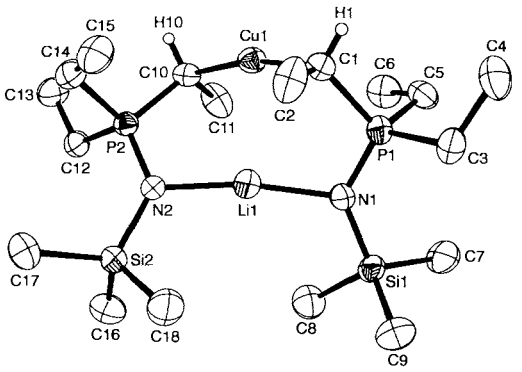

Figure 1. Molecular structure of **6** in the crystal. Selected (in some cases average) bond lengths [pm] and angles [°]: Cu–C 195.4(2), Li–N 194.2(4), P–C1,10 176.7(2), P–N 159.6(2); C1-Cu1-C10 167.2(1), N1-Li1-N2 169.9(3), Cu-C-P 108.5(2), Li-N-P 112.3(2), N-P-C1,10 112.2(1).

Figure 1 shows the (*S*,*S*) configurated molecule, which in the given centrosymmetric space group $P\bar{1}$ requires a (*R*,*R*) configurated molecule as counterpart. The Cu–C bond lengths of 195.1 and 195.6 pm agree well with those in other organocopper compounds in which the copper atom adopts a coordination number (CN) of 2.[8] In spite of the low coordination number at the lithium atom of **6** there is no tendency towards solvation with diethyl ether. This has recently been established for a series of lithium cuprates in THF solutions by accurate cryoscopic measurements, and leads to cleavage of higher aggregated structures.[9] We attribute this behavior of **6** to the shielding effect of the methyl groups of the $SiMe_3$ moieties. The two Li–N bonds in **6** are the same length within standard deviations; the average Li–N bond length of 194.2 pm in **6** is thus significantly shorter than that in trimeric lithium amides like $[\{LiN(SiMe_3)_2\}_3]$[10] and in the trimeric *N*-lithio-*N*-trimethylsilyl-9-amino-9-borabicyclo[3.3.1]nonane.[11] In these compounds, in which CN = 2 at Li and CN = 4 at the N atoms, the Li–N bond lengths range from 197 to 200 pm. Because of their ylidic character the P–C bonds of the carbanionic atoms C1 and C10 (176.7 pm) are, as in **5**, significantly shorter than the P–C(Et) bonds of 182.6 pm.

Likewise in the zinc compound **7**, the main feature of the structure[12] is the heterocyclic undulated eight-membered rings, in which pairs of zinc atoms are linked by the two carbanions $[CH(Me)P(Et)_2NSiMe_3]^-$ (Figure 2). Compared with simple dialkylzinc complexes that contain N-donor molecules, in which the Zn–C distances range between 197.5 and 200.0 pm and the Zn–N distances between 227 and 241 pm,[13] the average Zn–C bond lengths in **7** are slightly longer (204.9 pm), whereas the Zn–N distances of 203.2 pm are considerably shorter. Along with the relatively short P–C and P–N distances in the carbanionic bridging ligand this suggests electron delocalization within the CPN fragment. The eight-membered rings in **7** are additionally capped by a chlorine atom that bridges the two zinc atoms, forming acute Zn-Cl-Zn bond angles of 82.7°. The eight-memebered rings are organized to a cyclic dodecamer through the formation of μ_2-chloro bridges with obtuse Zn-Cl-Zn bond angles of 127.4° (Figure 3). Despite the different bond angles at the chlorine atoms all Zn–Cl distances are equal within standard deviations. The result is a 24-membered ring structure with an outer diameter of 2.5 nm, consisting of twelve Zn and twelve Cl atoms. The asymmetric unit contains six chiral centers at the zinc atoms and six at the carbanionic C atoms. Owing to the centrosymmetry of the dodecamer the entire molecule is a racemate. Considering the van der Waals radii the cavity in the interior of the ring has elliptic diameters of 140 and 430 pm, which is thus too narrow even for a H_2 molecule. Hence, a template effect similar to that considered responsible for the formation of some abiotic macrocycles[14] can be excluded for the synthesis of **7**.

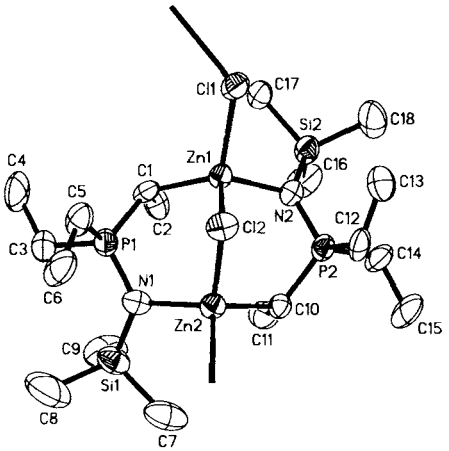

Figure 2. Section of the dodecameric structure of **7**. The average bond lengths [pm] and angles [°] refer to all atoms of the asymmetric unit: Zn–C 204.9(7), Zn–N 203.2(6), Zn–Cl 239.5(2), P–C(carbanion) 176.7(8), P–N 162.1(6); C-Zn-N 120.4(3), Cl-Zn-Cl 94.7(1), Zn-Cl[a]-Zn 82.7(1), Zn-Cl[b]-Zn 127.4(1), Zn-C-P 114.6(4), Zn-N-P 115.5(3), N-P-C 112.5(3). Cl[a]: inside dimeric units; Cl[b]: between dimeric units.

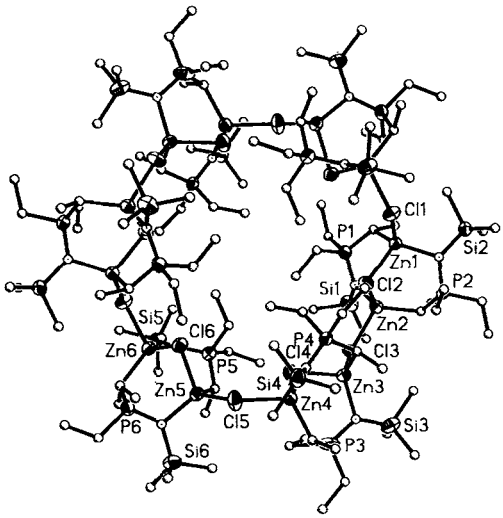

Figure 3. Dodecameric ring structure of **7** in the crystal; the atoms of the asymmetric unit are numbered.

Received: April 30, 1997 [Z10399IE]
German version: *Angew. Chem.* **1997**, *109*, 2447–2449

Keywords: carbanions · copper · phosphazenes · zinc

[1] A. Müller, B. Neumüller, K. Dehnicke, *Chem. Ber.* **1996**, *129*, 253.
[2] A. Steiner, D. Stalke, *Angew. Chem.* **1995**, *107*, 1908; *Angew. Chem. Int. Ed. Engl.* **1995**, *34*, 1752.
[3] a) H. Schmidbaur, G. Jonas, *Chem. Ber.* **1967**, *100*, 1120; b) P. B. Hitchcock, M. F. Lappert, Z.-X. Wang, *J. Chem. Soc. Dalton Trans.* **1997**, 1953.
[4] A. Müller, B. Neumüller, K. Dehnicke, J. Magull, D. Fenske, *Z. Anorg. Allg. Chem.* **1997**, *623*, 1306.
[5] Crystallographic data for **5**: four-circle diffractometer Enraf-Nonius CAD4, graphite-monochromated $Mo_{K\alpha}$ radiation, ω scans, direct methods, refined against F^2, empirical absorption correction, $\mu(Mo_{K\alpha}) = 2.6\ cm^{-1}$, H atoms freely refined; the calculations were performed with the programs SHELXTL, PLATON-94, ORTEP. Further details of the crystal structure investigations may be obtained from the Fachinformationszentrum Karlsruhe, 76344 Eggen-

 © WILEY-VCH Verlag GmbH, D-69451 Weinheim, 1997 0570-0833/97/3621-2351 $ 17.50+.50/0

stein-Leopoldshafen (Germany), on quoting the depository number CSD-406925. Space group $I4_1/acd$, $a = b = 1505.2(1)$, $c = 4747.4(6)$ pm, $V = 10756(2)$ Å^3, $Z = 8$, $\rho_{calcd} = 1.044$ g cm^{-3}, 193 K, 5173 measured reflections, 2363 unique reflections, [$R_{int} = 0.026$], 1855 with $F_o > 4\sigma(F_o)$, 210 parameters, $R_1 = 0.028$, wR_2 (all data) = 0.0813. Selected (in some cases average) bond lengths [pm] and angles [°]: Li–C 233.8(3), Li1a–N1 200.3(3), Li···Li 265.0(5), P1–C1 176.5(1), P1–N1 158.8(1); C-Li-C 106.9(1), Li-C-Li 69.07(9), Li-N-P 94.55(9), C1-P1-N1 108.77(6).

[6] Crystallographic data for **6**: IPDS system (Stoe), graphite monochromated MoKα radiation, Patterson technique, refined against F^2, numerical absorption correction, $\mu(Mo_{K\alpha}) = 10.1$ cm^{-1}, H atoms freely refined; the calculations were performed with the programs SHELXTL-Plus, SHELXTL, PLATON-94. Depository number CSD-406923. Space group $P\bar{1}$, $a = 1015.5(1)$, $b = 1166.6(1)$, $c = 1271.5(1)$ pm, $\alpha = 72.79(1)$, $\beta = 78.79(1)$, $\gamma = 73.98(1)°$, $V = 1372.5(3)$ Å^3, $Z = 2$, $\rho_{calcd} = 1.159$ g cm^{-3}, 193 K, 10812 measured reflections, 4956 unique reflections with [$R_{int} = 0.031$], 3283 reflections with $F_o > 4\sigma(F_o)$, 419 parameters, $R_1 = 0.027$, wR_2 (all data) = 0.0557.

[7] G. Nardin, L. Randaccio, E. Zangrando, *J. Organomet. Chem.* **1974**, *74*, C23.

[8] Reviews: a) G. van Koten, *J. Organomet. Chem.* **1990**, *400*, 283; b) P. P. Power, *Progr. Inorg. Chem.* **1991**, *39*, 75; c) G. van Koten, S. L. James, J. T. B. H. Jastrzebski, in *Comprehensive Organometallic Chemistry II, Vol. 3* (Eds.: E. W. Abel, F. G. A. Stone, G. Wilkinson), Pergamon/Elsevier, Oxford, **1995**, pp. 57–133; d) H. Lang, K. Köhler, S. Blau, *Coord. Chem. Rev.* **1995**, *143*, 113.

[9] A. Gerold, J. T. B. H. Jastrzebski, C. M. P. Kronenburg, N. Krause, G. van Koten, *Angew. Chem.* **1997**, *109*, 778; *Angew. Chem. Int. Ed. Engl.* **1997**, *36*, 755.

[10] R. D. Rogers, J. L. Atwood, R. Grüning, *J. Organomet. Chem.* **1978**, *157*, 229; D. Barr, W. Clegg, R. E. Mulvey, R. Snaith, *J. Chem. Soc. Chem. Commun.* **1984**, 285.

[11] B. Wrackmeyer, B. Schwarze, J. Weidinger, W. Milius, *Z. Naturforsch. B* **1997**, *52*, 431.

[12] Crystallographic data for $7 \cdot 4Et_2O$: IPDS system (Stoe), graphite-monochromated $Mo_{K\alpha}$ radiation, direct methods, refined against F^2, no absorption correction, $\mu(Mo_{K\alpha}) = 17.0$ cm^{-1}, H atoms in calculated positions; the calculations were performed with the programs SHELXTL-Plus, SHELXTL, ORTEP, PLATON-94. Depository number CSD-406924. Space group $P2_1/c$, $a = 1623.9(1)$, $b = 3386.1(2)$, $c = 1911.8(1)$ pm, $\beta = 91.69(1)°$, $V = 10508(1)$ Å^3, $Z = 2$, $\rho_{calcd} = 1.251$ g cm^{-3}, 190 K, 82457 measured reflections, 19919 unique reflections with [$R_{int} = 0.1761$], 5994 reflections with $F_o > 4\sigma(F_o)$, 818 parameters, $R_1 = 0.055$, wR_2 (all data) = 0.0955.

[13] Review: P. O'Brien, in *Comprehensive Organometallic Chemistry II, Vol. 3* (Eds.: E. W. Abel, F. G. A. Stone, G. Wilkinson), Pergamon/Elsevier, Oxford, **1995**, pp. 175–206.

[14] H. Plenio, *Angew.* Chem. **1997**, *109*, 358; *Angew. Chem. Int. Ed. Engl.* **1997**, *36*, 348.

Synthesis of Doubly Unsaturated Aldehydes and Ketones by a Novel β-Decarbopalladation**

Hiroto Harayama, Toshitsugu Kuroki, Masanari Kimura, Shuji Tanaka, and Yoshinao Tamaru*

Owing to their synthetic importance and mechanistic interest, transition metal catalyzed or promoted cyclizations of 1,ω isomers of enals,[1] enecarboxylic esters,[2] dienals,[3] dienes,[4] and enynes[5]—which provide vicinally difunctionalized cycloalkanes and heterocycles—have been rapidly developed and extensively studied. Interestingly, however, the reverse process, a ring-opening reaction, has received less attention. Here we report a novel Pd^0-catalyzed ring opening of 4-vinyl cyclic carbonates **1**, furnishing a variety of dienals and dienones **2** in excellent

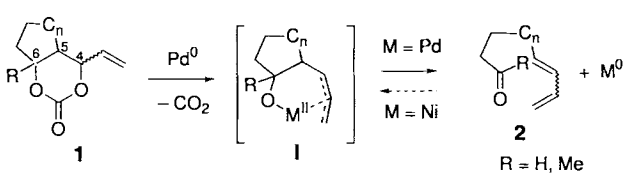

1 **I** **2**

yields. The reaction most likely proceeds by β-decarbopalladation of the π-allylpalladium intermediate **I** (M = Pd), which is formally the reverse process of the Ni^0-catalyzed cyclization of **2** to **I** (M = Ni) reported by Mori et al.[3]

We studied the Pd^0-catalyzed decarboxylative carbonylation (providing **4**, E = CO)[6] and the carbonate–carbamate transformation (providing **5**, E = TsNCO or ArNCO)[7] of monocyclic carbonates **3**. In the absence of electrophilic reagents E, **3** yielded aldehydes (e. g. benzaldehyde in 88% yield) and ketones **6** (e. g. dibenzyl ketone in 80% yield) upon treatment with $[Pd_2(dba)_3] \cdot CHCl_3$ (0.05 equiv, dba = dibenzylideneacetone) in dry acetonitrile at room temperature.

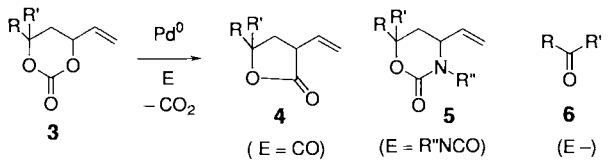

3 **4** **5** **6**

To test the generality of this fragmentation reaction, we examined tricyclic carbonate **1c** under various conditions (Scheme 1).

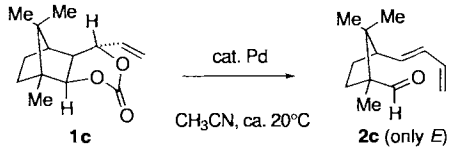

1c **2c** (only *E*)

1 $[Pd_2(dba)_3] \cdot CHCl_3$ / 72 h / 70%
2 $[Pd_2(dba)_3] \cdot CHCl_3$ + $P(OMe)_3$ (0.4 equiv) / 7 h / 82%
3 $[Pd(PPh)_4]$ / 72 h / 75%
4 $[PdCl_2\{P(o\text{-}Tol)_3\}_2]$ / 72 h / 0%
5 $Pd(OAc)_2$ / 120 h / 0%

Scheme 1. Yield of isolated **2c** depending on the reaction conditions. For each entry the palladium catalyst (0.1 equiv), reaction time, and yield of **2c** are given. In the case of entry 4 there was no reaction, and for entry 5 almost no reaction.

Irrespective of the presence or absence of phosphane and phosphite ligands, Pd^0 complexes cleanly promoted ring opening (entries 1–3). All reactions proceeded at room temperature and provided stereochemically homogeneous *cis*-1,2,2-trimethyl-3-(1,3-butadienyl)cyclopentanecarbaldehyde ((*E*)-**2c**) in good yields. The *E* isomer was identified from the coupling constant of the olefinic protons (J(H1,H2) = 15.4 Hz, 400-MHz ^{1}H NMR). Palladium(II) complexes were totally ineffective (entries 4 and 5).

Table 1 summarizes the results obtained for a variety of bi- and tricyclic carbonates **1**. It is apparent that the reaction tolerates a wide structural variety of **1**, and is independent of the length of the carbon chain between C5 and C6 ($n = 0, 1, 2, 4, 8$) and the substitution pattern of the olefinic portion. Furthermore, not only dienals, but also dienones (entries 5 and 9) were obtained in good yields.

[*] Prof. Dr. Y. Tamaru, Dr. H. Harayama, T. Kuroki, Dr. M. Kimura, Dr. S. Tanaka
Department of Applied Chemistry, Faculty of Engineering
Nagasaki University
Bunkyo-Machi 1-14, Nagasaki 852 (Japan)
Fax: Int. code +(958)47-9008
e-mail: tamaru@net.nagasaki-u.ac.jp

[**] We thank Mr. Y. Ohhama, NMR Facility, for his splendid technical assistance. Support by the Japanese Ministry of Education, Science, Sports and Culture is gratefully acknowledged.

Table 1. Synthesis of doubly unsaturated aldehydes and ketones **2** by Pd-catalyzed decarboxylative ring opening of cyclic carbonates **1**.

Entry	Carbonate **1**	*t*[h][a]	Product **2**[b]	Yield[%][c]	Isomers[d]
1	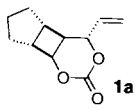 **1a**	0.5	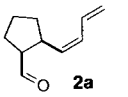 **2a**	81	*E*:*Z* = 1:6
2	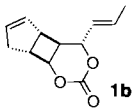 **1b**	0.2	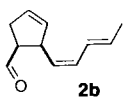 **2b**	75	only *Z*,*E*
3	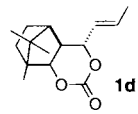 **1d**	55	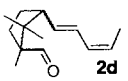 **2d**	73	only *E*,*Z*
4	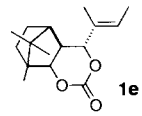 **1e**	30[e]	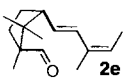 **2e**	58	only *E*,*Z*
5	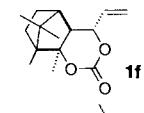 **1f**	6	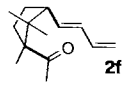 **2f**	91	only *E*
6	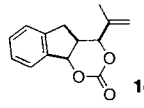 **1g**	52[f]	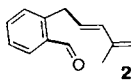 **2g**	82	only *E*
7	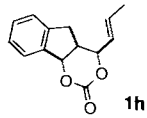 **1h**	12	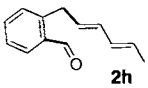 **2h**	93	only *E*,*E*
8	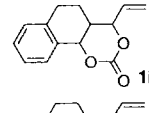 **1i**[g]	21	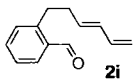 **2i**	77	*E*:*Z* = 10:1
9	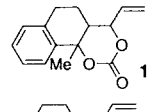 **1j**[g]	21	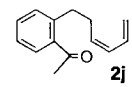 **2j**	81	*E*:*Z* = 1:1.3
10	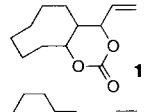 **1k**[g]	7	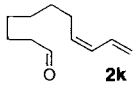 **2k**	54	*E*:*Z* = 1:4
11	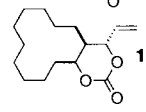 **1l**	5	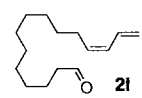 **2l**	85	*E*:*Z* = 1:3
12	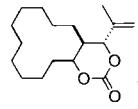 **1m**	24[h]	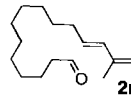 **2m**	63	only *E*

[a] Reaction conditions: **1** (1 mmol) and $[Pd_2(dba)_3]\cdot CHCl_3$ (0.05 mmol) in dry acetonitrile (5 mL) at ambient temperature under N_2. [b] Only the major isomer is shown. [c] Total yield of spectroscopically homogeneous **2** obtained after column chromatography over silica gel. [d] Ratios determined by ^1H NMR spectroscopy (400 MHz). [e] At room temperature for 30 h, then at 55 °C for 0.5 h. [f] At room temperature for 52 h, then at 55 °C for 1 h. [g] Complex diastereomeric mixture. [h] At room temperature for 24 h, then at 55 °C for 3 h.

The stereochemical outcome of the dienyl moiety of **2** may be rationalized according to Scheme 2. We postulate that *cis*-4,5-disubstituted 2-oxa-1-palladacyclopentane **II** is generated by oxidative addition of Pd^0 on the O3–C4 bond of **1** with inversion of configuration, and isomerizes to the corresponding *trans* isomer **III** via **IV** (a σ-π-σ interconversion that accompanies isomerization of the double bond (R ≠ H)). The thus formed

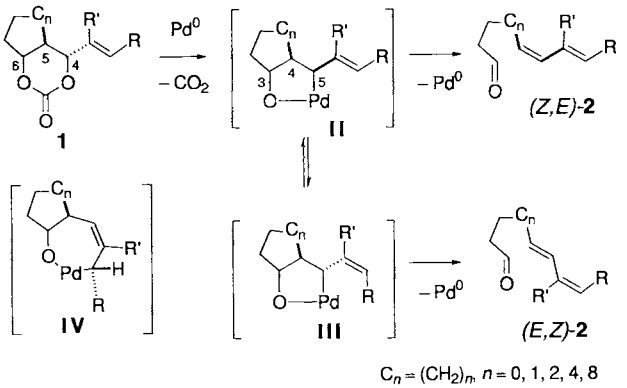

Scheme 2. Possible explanation for the stereochemical progress of reaction **1** → **2**.

intermediates **II** and **III** undergo C3–C4 bond fission (*cis*-β-decarbopalladation) to give (*Z*,*E*)-**2** and (*E*,*Z*)-**2**, respectively.

Intermediates **II**, generated from **1a** and **1b**, possess such strained cyclobutane C3–C4 bonds that they would readily fragment to provide (*Z*)-**2a** and (*Z*,*E*)-**2b** (entries 1 and 2 in Table 1). In the case of **1d** (entry 3), on the other hand, **II** possesses a less strained C3–C4 bond, but suffers from steric repulsion between *cis*-oriented C_n (= CH–CMe_2) and 1-propenyl groups (R = Me, R′ = H). Accordingly, it would rather isomerize to the thermodynamically more stable intermediate **III** to provide (*E*,*Z*)-**2** than fragment to (*Z*,*E*)-**2**. The exclusive formation of *E*-configurated double bonds in (*E*)-**2c**, (*E*,*Z*)-**2e**, and (*E*)-**2f** (Scheme 1 and entries 4 and 5 in Table 1) may be similarly rationalized. The *E*-selective formation of **2m** (entry 12), as opposed to the *Z*-selective formation of **2l** (entry 11), seems to be a natural consequence of steric repulsion between the C_n chain $(CH_2)_8$ and the isopropenyl groups in **II** (R = H, R′ = Me).

The clean and facile β-decarbopalladation[8] of **II** and **III** may primarily owe its origin to the C3–C4 bonds, which are weakened by the negatively charged O2,[9] and to their five-membered structures, which render an alternative β-dehydropalladation providing 2-alkenylidenecycloalkanols conformationally less favorable.[10] The ring opening of 2-oxa-1-palladacyclopentanes **II** and **III** to olefins and aldehydes contrasts the cyclization of some titanium–olefin complexes and aldehydes providing 2-oxa-1-titanacyclopentanes.[1, 11]

We have demonstrated that dienals and dienones **2** can be obtained from bi- and tricyclic carbonates **1** in excellent yields and stereoselectivities. Cyclic carbonates **1a**–**m** were prepared from cyclic ketones and α,β-unsaturated aldehydes.[12] Accordingly, as illustrated in Scheme 3, the overall transformation formally comprises aldol condensation of cyclic ketones with unsaturated aldehydes and hydrogenolysis of the C1–C2 bonds of thus formed α-alkenylidenecycloalkanones. The synthetic utility of this reaction may be augmented by the usefulness of **2** as synthetic intermediates, the ready availability of **1** with a wide structural variety,[12] and the mild reaction conditions under which the reaction can be easily performed.

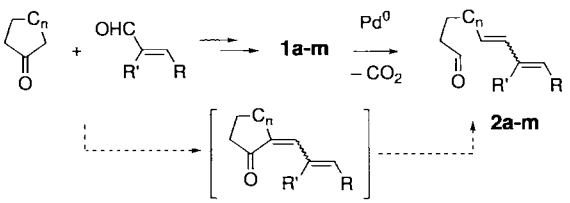

Scheme 3. Formal mechanism for the synthesis of **2** from cyclic ketones and α,β-unsaturated aldehydes.

 © WILEY-VCH Verlag GmbH, D-69451 Weinheim, 1997 0570-0833/97/3621-2353 $ 17.50+.50/0

Experimental Section

2d: A solution of **1d** (250 mg, 1 mmol: m. p. 79.0–80.0 °C (hexane)) [12] in dry acetonitrile (5 mL) was added with a syringe to a nitrogen-purged flask containing $[Pd_2(dba)_3]\cdot CHCl_3$ (51.8 mg, 0.05 mmol). After stirring for 55 h at room temperature, the reaction mixture was diluted with ether and filtered through a Celite pad with suction. The filtrate (30 mL) was washed with saturated $NaHCO_3$ (10 mL) and dried over magnesium sulfate. Removal of the solvent in vacuo followed by column chromatography over silica gel (hexane/ethyl acetate 64/1, v/v) gave **2d** as an oil (155 mg, 73% yield). IR (neat): $\tilde{\nu} = 1720$ (s) cm^{-1}; ^1H NMR (400 MHz, $CDCl_3$, TMS): $\delta = 0.79$ (s, 3H), 0.97 (s, 3H), 1.08 (s, 3H), 1.38 (ddd, $J = 5.5, 9.9, 13.9$ Hz, 1H), 1.68 (dddd, $J = 5.5, 9.9, 11.7, 13.9$ Hz, 1H), 1.75 (dd, $J = 1.8, 7.0$ Hz, 3H), 1.92 (ddt, $J = 4.7, 13.9, 9.9$ Hz, 1H), 2.42 (ddd, $J = 4.7, 11.7, 13.9$ Hz, 1H), 2.52 (dd, $J = 8.4, 9.9$ Hz, 1H), 5.42 (dq, $J = 11.0, 7.0$ Hz, 1H), 5.52 (dd, $J = 8.4, 15.0$ Hz, 1H), 6.00 (ddd, $J = 1.8, 11.0, 15.0$ Hz, 1H), 6.32 (dd, $J = 11.0, 15.0$ Hz, 1H), 9.65 (s, 1H); HR MS calcd for $C_{14}H_{22}O$: 206.1671; found (%): 206.1678 (75) [M^+], 191 (9), 122 (15), 95 (100).

Received: April 14, 1997 [Z10342IE]
German version: *Angew. Chem.* **1997**, *109*, 2449–2451

Keywords: aldehydes · dienes · palladium · ring opening · synthetic methods

[1] W. E. Crowe, A. T. Vu, *J. Am. Chem. Soc.* **1996**, *118*, 5508–5509; N. M. Kablaoui, S. L. Buchwald, *ibid.* **1996**, *118*, 3182–3191; N. M. Kablaoui, F. A. Hicks, S. L. Buchwald, *ibid.* **1996**, *118*, 5818–5819.

[2] J. Lee, C. H. Kang, H. Kim, J. K. Cha, *J. Am. Chem. Soc.* **1996**, *118*, 291–292; J. Lee, H. Kim, J. K. Cha, *ibid.* **1996**, *118*, 4198–4199.

[3] Y. Sato, M. Takimoto, K. Hayashi, T. Katsuhara, K. Takagi, M. Mori, *J. Am. Chem. Soc.* **1994**, *116*, 9771–9772.

[4] For Ti, see E. Negishi, M. D. Jensen, D. Y. Kondakov, S. Wang, *J. Am. Chem. Soc.* **1994**, *116*, 8404–8405. For Zr, see J. P. Morken, M. T. Didiuk, M. S. Visser, A. H. Hoveyda, *ibid.* **1994**, *116*, 3123–3124; E. Negishi, D. Choueiry, T. B. Nguyen, D. R. Swanson, *ibid.* **1994**, *116*, 9751–9752; D. F. Taber, J. P. Louey, Y. Wang, W. A. Nugent, D. A. Dixon, R. L. Harlow, *ibid.* **1994**, *116*, 9457–9463; K. H. Shaughnessy, R. M. Waymouth, *ibid.* **1995**, *117*, 5873–5874. For a review of Mo and Ru, see H.-G. Schmalz, *Angew. Chem.* **1995**, *107*, 1981–1984; *Angew. Chem. Int. Ed. Engl.* **1995**, *34*, 1833–1836.

[5] For Ti, see H. Urabe, T. Hata, F. Sato, *Tetrahedron Lett.* **1995**, *36*, 4261–4264; F. A. Hicks, N. M. Kablaoui, S. L. Buchwald, *J. Am. Chem. Soc.* **1996**, *118*, 9450–9451. For Fe, Co (Pauson–Khand reaction), and Ni, see X. Verdaguer, A. Moyano, M. Pericas, M. A. Riera, V. Bernardes, A. E. Greene, A. Alvarez-Larena, J. F. Piniella, *ibid.* **1994**, *116*, 2153–2154; N. Jeong, S. H. Hwang, Y. Lee, *ibid.* **1994**, *116*, 3159–3160. For Zr, see G. Angel, E. Negishi, *ibid.* **1991**, *113*, 7424–7426; G. J. Gordon, R. J. Whitby, *Synlett* **1995**, 77–78. For Ru, see N. Chatani, T. Morimoto, T. Muto, S. Murai, *J. Am. Chem. Soc.* **1994**, *116*, 6049–6050; S.-H. Kim, N. Bowden, R. H. Grubbs, *ibid.* **1994**, *116*, 10801–10802; W. J. Zuercher, M. Hashimoto, R. H. Grubbs, *ibid.* **1996**, *118*, 6634–6640. For Pd, see B. M. Trost, M. K. Trost, *ibid.* **1991**, *113*, 1850–1852; H. Yamada, S. Aoyagi, C. Kibayashi, *ibid.* **1996**, *118*, 1054–1059.

[6] a) Y. Tamaru, T. Bando, M. Hojo, Z. Yoshida, *Tetrahedron Lett.* **1987**, *28*, 3497–3500; b) T. Bando, S. Tanaka, K. Fugami, Z. Yoshida, Y. Tamaru, *Bull. Chem. Soc. Jpn.* **1992**, *65*, 97–110.

[7] Y. Tamaru, T. Bando, Y. Kawamura, K. Okamura, Z. Yoshida, *J. Chem. Soc. Chem. Commun.* **1992**, 1498–1500; T. Bando, H. Harayama, Y. Fukazawa, M. Shiro, K. Fugami, S. Tanaka, Y. Tamaru, *J. Org. Chem.* **1994**, *59*, 1465–1474.

[8] The reaction is reminiscent of the Pd^0-catalyzed decarboxylative diene syntheses of 3-acetoxy-4-pentenoic acids: B. M. Trost, J. M. Fortunak, *J. Am. Chem. Soc.* **1980**, *102*, 2841–2843.

[9] M. L. Steigerwald, W. A. Goddard, D. A. Evans, *J. Am. Chem. Soc.* **1979**, *101*, 1994–1997. For an anionic oxy-Cope rearrangement, see D. A. Evans, A. M. Golob, *ibid.* **1975**, *97*, 4765–4766; L. A. Paquette, C. F. Sturino, X. Wang, J. C. Prodger, D. Koh, *ibid.* **1996**, *118*, 5620–5633, and references therein. For the anionic oxygen accelerated ring-opening reactions, see M. Takayanagi, N. Umamori, K. Tanino, I. Kuwajima, *ibid.* **1993**, *115*, 12635–12636; C.-J. Li, D.-L. Chen, Y.-Q. Lu, J. X. Haberman, J. T. Mague, *ibid.* **1996**, *118*, 4216–4217.

[10] T. Fujinami, T. Suzuki, M. Kamiya, S. Fukuzawa, S. Sakai, *Chem. Lett.* **1985**, 199–200.

[11] K. Mashima, H. Haraguchi, A. Oyoshi, N. Sakai, H. Takaya, *Organometallics* **1991**, *10*, 2731–2736

[12] Precursors **1a–m** were obtained in the following yields (aldol addition, reduction with $LiAlH_4$ or addition of MeLi, cyclocarbonation with methyl chloroformate [6b]: **1a**: 98%, 25% (as a single diastereomer, column chromatography, silica gel, hexane/ethyl acetate gradient), 54%; **1b**: 95%, 25% (as a single diastereomer, column chromatography, silica gel, hexane/ethyl acetate gradient), 40%; **1c**: 98%, 98%, 37% (recrystallization from hexane); **1d**: 97%, 85%, 32% (recrystallization from hexane); **1e**: 98%, 98%, 20% (column chromatography, silica gel, hexane/ethyl acetate gradient); **1f**: 98%, 20%, 38% (recrystallization from hexane); **1g**: 95%, 12% (as a single diastereomer, column chromatography, silica gel, hexane/ethyl acetate gradient), 50% (recrystallization from benzene/hexane); **1h**: 70%, 98%, 14% (recrystallization from ethyl acetate/hexane); **1i**: 88%, 91%, 47% (recrystallization from benzene-hexane); **1j**: 88%, 74%, 61%; **1k**: 98%, 80%, 83%; **1l**: 95%, 80%, 20% (recrystallization from benzene/hexane; **1m**: 95%, 70%, 34% (recrystallization from benzene/hexane. All new compounds were characterized by NMR and IR spectrscopy as well as elemental analysis or high-resolution mass spectrometry.

Efficient Enzymatic Synthesis of the Core Trisaccharide of *N*-Glycans with a Recombinant β-Mannosyltransferase**

Gregory M. Watt, Leigh Revers, Matthew C. Webberley, Iain B. H. Wilson, and Sabine L. Flitsch*

The β-1,4-mannosidic linkage is common to most asparagine-linked oligosaccharides (*N*-glycans) in glycoproteins as part of their pentasaccharide core structure. Because of its importance and the difficulty of chemical synthesis, it has provided a challenge to organic chemists for some time and has resulted in a number of very elegant synthetic strategies.[1–10]

The β-mannosidic linkage is a good target for enzymatic methods. Unprotected chitobiosyl acceptor substrates can be used since regio- and stereoselectivity of the coupling reaction is ensured by the enzyme. Thus, glycosidases (β-mannosidases) have been used to catalyze the mannosylation,[11–13] but they suffer from low yields, especially where the chitobiosyl acceptor substrate is concerned, which has to be added in excess. As an alternative enzyme system, we therefore report the use of glycosyltransferases, in particular the β-1,4-mannosyltransferase from yeast, which catalyzes the mannosyl transfer from GDP-mannose to chitobiosyl-lipids **1** and **2** (Scheme 1).

The gene for the yeast enzyme *ALG1* (ALG = *A*sparagine-*L*inked *G*lycosylation) has been isolated and sequenced by Robbins and colleagues.[14, 15] The enzyme uses a complex, dolichol-linked acceptor substrate (**1**), which can be efficiently replaced by phytanol derivative **2**, obtainable in 70% yield from chitobiose octaacetate.[16–18] More simple chitobiosyl phosphate and alkyl chitobiosides were not accepted as substrates.[19] Expression of the mannosyltransferase in a heterologous host (*E. coli*) was possible,[14] but the yield was poor and purification proved difficult. Our aim was therefore to obtain a more practical biocatalyst by modifying *ALG1* and then inserting the modified gene into a suitable overexpression vector.

First the enzyme was made soluble by deleting a hydrophobic N-terminal sequence of amino acids 2–35 (generating AlgΔTM),[20] thus overcoming problems with expression, isolation, and stability of the enzyme. Second the highly immunogenic Myc polypeptide sequence (EQKLISEEDL) was fused to

[*] Dr. S. L. Flitsch, Dr. G. M. Watt, Dr. L. Revers, Dr. M. C. Webberley, Dr. I. B. H. Wilson
The Edinburgh Centre for Protein Technology
Department of Chemistry, King's Buildings
The University of Edinburgh
West Mains Road, Edinburgh EH93JJ (UK)
Fax: Int. code +(131)650-4737
e-mail: s.flitsch@ed.ac.uk

[**] This work was supported by the BBSRC, the British Council, and Zeneca Pharmaceuticals. We thank Dr Tony Merry, Oxford Glycosciences, Oxford (UK) for the ^1H NMR spectrum of Manβ1-4GlcNAcβ1-4GlcNAc derived from natural sources and Dr Chandralal Hewage, University of Edinburgh, for recording the NMR spectra.

 © WILEY-VCH Verlag GmbH, D-69451 Weinheim, 1997 0570-0833/97/3621-2354 $ 17.50+.50/0

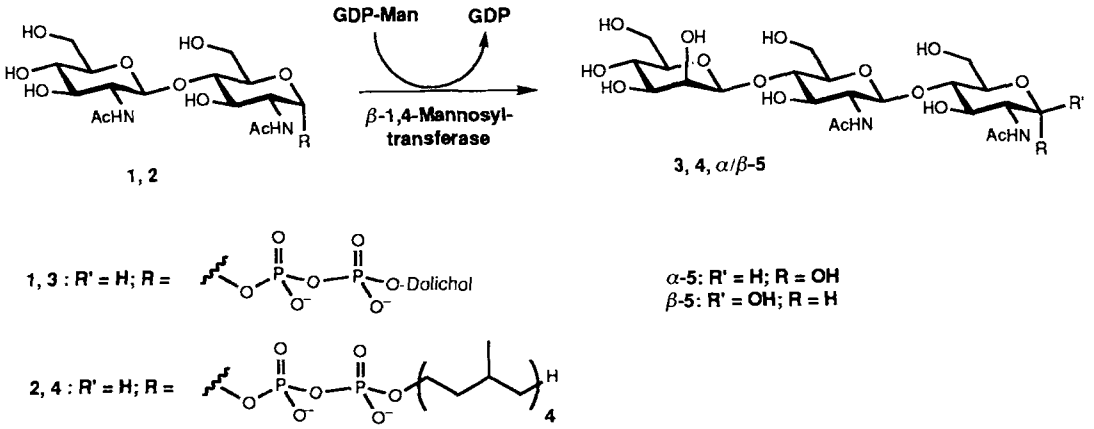

Scheme 1. Transferase-catalyzed mannosylation of **1** and **2** using GDP-mannose.

the N-terminus to aid detection of the enzyme by Western blotting with the commercially available anti-Myc monoclonal antibody.[21] Third a N-terminal decahistidine sequence (His_{10}) allows metal affinity chromatography of the protein.[22] The new *His10mycALG1ΔTM* gene was inserted into a variety of commercially available overexpression vectors, of which the pET-16b (AMS Biotechnology, Whitney, Oxon UK) proved to be the most successful. The new plasmid (pLR36) thus generated is shown in Figure 1.

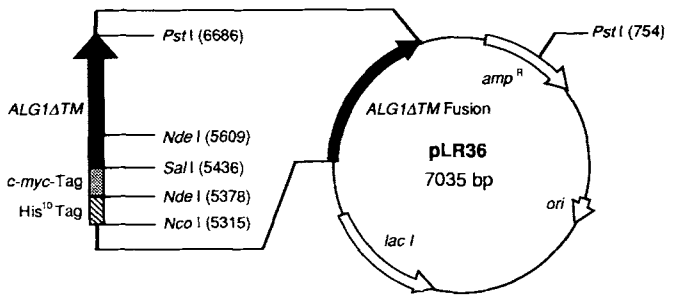

Figure 1. The new plasmid (pLR36).

Transformation of *E. coli* (BL21(DE3)pLysS) with the plasmid pLR36 yielded mannosyltransferase activity of about 0.2 U per gram of wet cells. Functionally pure, immobilized biocatalyst could be prepared by simply passing the crude cell lysate (obtained by a freeze–thaw cycle) through an affinity column charged with nickel(II) ions, followed by washing to remove impurities. This immobilization appeared to stabilize the enzyme, which can be stored at 4 °C for several days. Incubation with **2** and GDP-mannose yielded **4**, which after acid hydrolysis and purification by gel-permeation chromatography afforded the trisaccharide α/β-**5** as a mixture of C-1 anomers in 80% yield. Although alkaline phosphatase[23] was used in this reaction, assays showed that it provided no significant increase in GDP-mannose turnover. The ^{1}H NMR spectra showed that the trisaccharide was identical to that derived from a natural source.

In summary, the enzymatic formation of the β-1,4-mannosidic linkage was achieved both regio- and stereoselectively in good yield from the synthetic chitobiosyl phospholipid **2**. We are convinced that this approach will be particularly useful for providing biosynthetic intermediates for the studies of subsequent glycosyltransferases of the biosynthetic pathway of N-linked oligosaccharides[24] and for in vitro protein glycosylation.[25, 26] Further elongation of the Manβ1-4GlcNAcβ1-4GlcNAc lipid (**4**) with other transferases can also lead to short chemoenzymatic syntheses of the pentasaccharide core and of more complex *N*-glycans.[27]

Experimental Section

Enzymatic synthesis of Manβ1-4GlcNAcβ1-4GlcNAc (α/β-**5**): Phytanylpyrophosphoryl-α-*N*,*N*'-diacetylchitobioside **2**[18] (2.8 mg, 3.2 μmol) was incubated at 37 °C with GDP-mannose (2.4 mg, 4.0 μmol) with 50% (v/v) enzyme-charged resin (prepared from 5 g wet *E. coli* cells) in buffer (50 mM Tris-HCl, 5 mM $MgCl_2$, 0.25% Triton-X-100 (v/v), pH 7.5; 20 mL). Final concentrations were 160 μM **2** and 200 μM GDP-mannose. The reaction was shaken at 100 rpm for 30 min. and alkaline phosphatase (8 U) was added; shaking was continued for a further 1 h, whereafter the resin was filtered and washed exhaustively with chloroform/methanol/water (10/10/3). The combined organic and aqueous phases were evaporated to dryness, and the residue treated with 20 mM HCl (25 mL) at 100 °C for 1 h. The aqueous phase was subjected to Bio-Gel P4 gel-filtration chromatography, and fractions containing oligosaccharides corresponding to a hydrodynamic volume of 5 glucose units were pooled and lyophilized to give the target compound α/β-**5** as a mixture (α/β = 2/1) of anomers at the C-1 position (1.5 mg; yield 80% from **2**, 65% from GDP-mannose). Selected ^{1}H NMR data (600 MHz, D_2O): δ = 2.08, 2.10 (2 × s, 6H; 2 × $NHCOCH_3$), 3.44 (1H, m; H-5''), 4.08 (d, ^3J(H2'',H3'') = 3 Hz, 1H; H-2''), 4.62 (d, ^3J(H1',H2') = 8 Hz; H1'β), 4.63 (d, ^3J(H1',H2') = 8 Hz; H1'α), 4.72 (d, ^3J(H1,H2) = 8 Hz; H1β), 4.80 (s, 1H; H1''), 5.21 (d, ^3J(H1,H2) = 3 Hz; H1α).

Received: April 14, 1997 [Z10349IE]
German version: *Angew. Chem.* **1997**, *109*, 2445–2447

Keywords: enzyme catalysis · glycolipids · glycosylations · mannosyltransferases · oligosaccharides

[1] G. Ekborg, B. Lindberg, J. Lönngren, *Acta Chem. Scand.* **1972**, *26*, 3287–3292.
[2] M. A. E. Shaban, R. W. Jeanloz, *Carbohydr. Res.* **1976**, *52*, 103–114.
[3] H. Paulsen, O. Lockhoff, *Chem. Ber.* **1981**, *114*, 3102–3114.
[4] H. Kunz, W. Gunther, *Angew. Chem.* **1988**, *100*, 1118–1119; *Angew. Chem. Int. Ed. Engl.* **1988**, *27*, 1086–1087.
[5] S. David, A. Malleron, C. Dini, *Carbohydr. Res.* **1989**, *188*, 193–200.
[6] G. Stork, G. Kim, *J. Am. Chem. Soc.* **1992**, *114*, 1087–1088.
[7] F. Barresi, O. Hindsgaul, *Can. J. Chem.* **1994**, *72*, 1447–1465.
[8] Y. Ito, T. Ogawa, *Angew. Chem.* **1994**, *106*, 1843–1845; *Angew. Chem. Int. Ed. Engl.* **1994**, *33*, 1765–1767.
[9] F. Lichtenthaler, T. Schneider-Adams, *J. Org. Chem.* **1994**, *59*, 6728–6734.
[10] A. Dan, Y. Ito, T. Ogawa, *Tetrahedron Lett.* **1995**, *36*, 7487–7490.
[11] N. Taubken, J. Thiem, *Synthesis* **1992**, 517–518.
[12] N. Taubken, B. Sauerbrei, J. Thiem, *J. Carbohydr. Chem.* **1993**, *12*, 651–667.
[13] S. Singh, M. Scigelova, D. H. G. Crout, *Chem. Commun.* **1996**, 993–994.
[14] J. R. Couto, T. C. Huffaker, P. W. Robbins, *J. Biol. Chem.* **1984**, *259*, 378–382.
[15] C. F. Albright, P. W. Robbins, *J. Biol. Chem.* **1990**, *265*, 7042–7049.
[16] S. L. Flitsch, J. P. Taylor, N. J. Turner, *J. Chem. Soc. Chem. Commun.* **1991**, 380–381.
[17] S. L. Flitsch, J. P. Taylor, N. J. Turner, *J. Chem. Soc. Chem. Commun.* **1991**, 382–384.
[18] S. L. Flitsch, H. L. Pinches, J. P. Taylor, N. J. Turner, *J. Chem. Soc. Perkin Trans. 1* **1992**, 2087–2093.
[19] S. L. Flitsch, D. Goodridge, B. Guilbert, L. Revers, M. C. Webberley, I. B. H. Wilson, *Bioorg. Med. Chem.* **1994**, *2*, 1243–1250.

 © WILEY-VCH Verlag GmbH, D-69451 Weinheim, 1997 0570-0833/97/3621-2355 $ 17.50+.50/0

[20] L. Revers, I. B. H. Wilson, M. C. Webberley, S. L. Flitsch, *Biochem. J.* **1994**, *299*, 23–27.
[21] P. A. Kolodziej, R. A. Young, *Methods Enzymol.* **1991**, *194*, 508–519.
[22] A. Hoffmann, R. G. Roeder, *Nucleic Acids Res.* **1991**, *19*, 6337–6338.
[23] M. M. Palcic, *Methods Enzymol.* **1994**, *230*, 300–360.
[24] A. Herscovics, P. Orlean, *FASEB J.* **1993**, *7*, 540–550.
[25] B. Imperiali, T. L. Henrickson, *Bioorg. Med. Chem.* **1995**, *3*, 1565–1578.
[26] J. Lee, J. K. Coward, *Biochemistry* **1993**, *32*, 6794–6801.
[27] I. B. H. Wilson, M. C. Webberley, L. Revers, S. L. Flitsch, *Biochem. J.* **1995**, *310*, 909–916.

Artificial Phototropism: Reversible Photoseparation of Self-Assembled Interlocking Conjugates**

Andrew C. Benniston,* Anthony Harriman,* and Dimitri S. Yufit

Supramolecular structures, especially those constructed by interlocking redox-active host–guest species, offer the possibility for devising artificial phototropic systems.[1–4] The key feature of such units is the large light-induced conformational change along a preferred trajectory, which allows reversible cycling of the energy and information stored in the superstructure. Special interest should be given to systems in which the primary binding mode involves electron donor–acceptor interactions, since the association constant for self-assembly of the supramolecular structure can be modified dramatically and spontaneously by laser excitation.[1] In particular, interaction between a dicationic acceptor A^{2+} and a neutral donor D is often characterized by the development of a colored charge-transfer (CT) complex $D \cdot A^{2+}$. Direct excitation into the CT absorption band causes electron transfer from donor to acceptor and formation of a radical ion pair (RIP). Mutual electrostatic repulsion facilitates separation of the RIP into solvated radical cations,[4] provided charge recombination is not too fast (Figure 1).

Charge recombination is controlled by the amount of energy to be dissipated by vibrational modes, and the rate decreases with increasing energy of the RIP.[5] The energy-gap dependence is shallow, however, and, to benefit from such circumstances, donor–acceptor pairs displaying extreme redox potential difference must be used. A different strategy for stabilizing the RIP against rapid charge recombination involves extending the size of the overlapping π electron clouds.[6] This introduces additional CT states into the excited-state manifold and stabilizes the ground state of the CT complex by mixing with higher energy states.[6, 7] Indeed, the rate of charge recombination within RIPs decreases with increasing delocalization of HOMO or LUMO states.[8, 9] We now explored the idea that artificial phototropic systems can be devised by encapsulating a large dicationic electron acceptor inside the cavity of an electron-rich crown ether.[10]

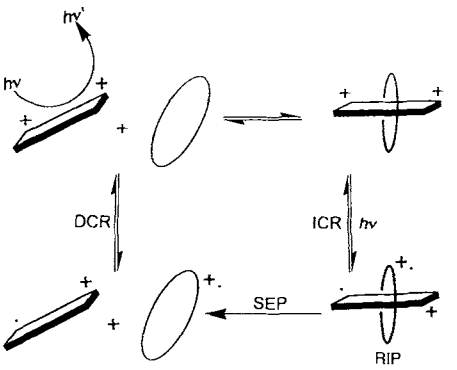

Figure 1. Pictorial representation of the events that follow from excitation of a CT complex formed by encapsulating a dicationic electron acceptor inside a macrocyclic receptor; ICR = intracomplex charge recombination, SEP = separation, DCR = diffusive charge recombination.

Mixing *N*,*N*′-dimethyl-2,7-diazapyrenium bis(hexafluorophosphate) ($DAP \cdot 2PF_6$) with dibenzo[34]crown-10 (CE10) in acetonitrile causes the appearance of a broad CT absorption band ($\lambda_{max} \approx 430$ nm) which is partially obscured on the high-energy side by local absorption bands. Progressive addition of CE10 to a solution of $DAP \cdot 2PF_6$ in acetonitrile is accompanied

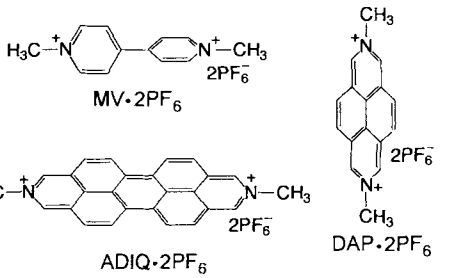

1 = $DAP \cdot 2PF_6$/CE10 1/1
2 = $MV \cdot 2PF_6$/CE10 1/1

by extinction of fluorescence from the pyrene derivative ($\Phi_F = 0.67$, $\tau_S = 10.1$ ns)[11] without formation of new fluorescent species. The fluorescence titration was consistent with the formation of a nonfluorescent 1:1 complex (**1**) with a binding constant K_A of $3900 \pm 360\,M^{-1}$ at 18 °C. Therefore, $DAP \cdot 2PF_6$ shows greater affinity for binding to CE10 than to the smaller dibenzo[24]crown-8 ($K_A = 840\,M^{-1}$).[12] *N*,*N*′-dimethyl-4,4′-bipyridinium bis(hexafluorophosphate) ($MV \cdot 2PF_6$) also binds to CE10 ($K_A = 50 \pm 10\,M^{-1}$),[10, 13] whereas a binding constant of $K_A = 425 \pm 40\,M^{-1}$ was found for the larger *N*,*N*′-dimethylanthra[2,1,9-*def*:6,5,10-*d*′*e*′*f*′]diisoquinoline bis(hexafluorophosphate) ($ADIQ \cdot 2PF_6$).

FAB mass spectra recorded for solutions containing different mole fractions of $DAP \cdot 2PF_6$ and CE10 in acetonitrile displayed a cluster of peaks at $m/z = 915$ ($[\mathbf{1} - PF_6]^+$) and $m/z = 770$ ($[\mathbf{1} - 2PF_6]^+$), which correspond uniquely to the 1:1 complex. Molecular ions attributable to 1:2, 2:1, or 2:2 supramolecular assemblies were not detected, even with a large molar excess of CE10. ^1H NMR spectroscopic titrations in which aliquots of CE10 were added to a solution of $DAP \cdot 2PF_6$ in [D_6]acetone showed pronounced upfield shifts for the α (− 0.34 ppm) and γ protons (− 0.36 ppm) on the $DAP \cdot 2PF_6$ moiety concomitant with the appearance of a resonance at $\delta = 5.57$ due to CE10.

[*] Dr. A. C. Benniston, Dr. D. S. Yufit
Chemistry Department
University of Glasgow
Glasgow G12 8QQ (UK)
Fax: Int. code +(0141)330-4888
e-mail: andrewb@chem.gla.ac.uk
Prof. A. Harriman
Laboratoire de Photochimie, E. C. P. M.
Université Louis Pasteur
1 rue Blaise Pascal, Strasbourg 67008 (France)
Fax: Int. code +(0388)601-213.
e-mail: harriman@chimie.u-strasbg.fr

[**] This work was supported by the University of Glasgow, the Nuffield Foundation (A. C. B.), the EPSRC (D. S. Y.), and The Royal Society of London (A. H.). A JWT Jones travel fellowship (A. C. B.) and the measurement of mass spectra by A. L. Ritchie (Glasgow) are also gratefully acknowledged.

 © WILEY-VCH Verlag GmbH, D-69451 Weinheim, 1997 0570-0833/97/3621-2356 $ 17.50+.50/0

The magnitude of the induced shifts are taken as firm evidence for the formation of an intimate CT complex in which there is strong overlap of π orbitals on donor and acceptor.[4] Analysis of the ^{1}H NMR spectral data with Job's method[14] indicates that the predominant species in acetone is the 1:1 complex, but there are hints that an unstable 1:2 complex might be formed at very high mole fractions of CE10.[15] Similar studies with MV·2PF$_6$ showed only the 1:1 complex, whereas ADIQ·2PF$_6$ formed both 1:1 and 1:2 complexes.[15]

According to X-ray diffraction studies of **1**, the dication is centered in the cavity of the crown and closely aligned with the two hydroquinol units. The separation between the parallel benzene rings of the crown host is 6.88 Å, but the rings are shifted so that each half of the guest interacts with only a single hydroquinol unit (Figure 2). The mean host–guest separation is

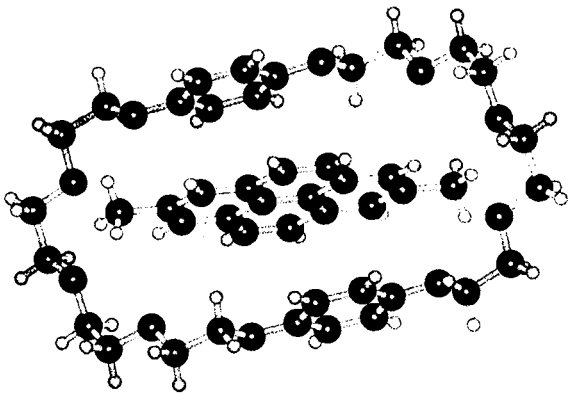

Figure 2. ORTEP representation of the crystal structure of the CT complex **1**. Hexafluorophosphate anions are omitted for clarity.

3.46 Å, and there is an angle of 3.9° between the planes of the benzene rings and the dication. The N(1)–N(1a) axis of the dication is tilted by about 21° with respect to the C(9)–C(12) axis of the macrocycle. Room-temperature NMR studies indicate fast rocking of the DAP·2PF$_6$ subunit about a perpendicular axis passing through the complex. Similar structural facets have been reported for complex **2** formed between MV·2PF$_6$ and CE10.[13]

Laser excitation of **1** in acetonitrile at 18 °C results in rapid establishment of the RIP, as detected by transient absorption spectroscopy.[5, 10] The RIP, which shows a similar differential absorption spectrum to that of the π radical cation formed upon one-electron reduction of DAP·2PF$_6$,[11] evolves from the initially formed Franck–Condon state on the timescale of a few picoseconds (Figure 3). Absorption due to the corresponding π radical cation of the crown ether is too weak to contribute appreciably to the observed signal. Deactivation of the RIP occurs by first-order kinetics with a rate constant k_{obs} of $7.7\times10^9\ s^{-1}$. This decay process partially (to 90%) restores the ground state of the complex; the approximately 10% of the initial signal that does not return to the prepulse baseline on the picosecond timescale is attributed to the formation of solvated π radical cations. On this basis it is possible to assign individual rate constants[5] for charge recombination ($k_{CR}\approx7\times10^9\ s^{-1}$) and separation ($k_{sep}\approx7\times10^8\ s^{-1}$). The solvated π radical cations recombine through diffusional contact over tens of microseconds. Under identical conditions, the RIP derived from **2** decays rapidly ($k_{obs}=1.82\times10^{10}\ s^{-1}$) without observable separation. Therefore, for **2** $k_{CR}\approx1.8\times10^{10}\ s^{-1}$ and $k_{sep}<1\times10^9\ s^{-1}$. It was not possible to excite selectively the

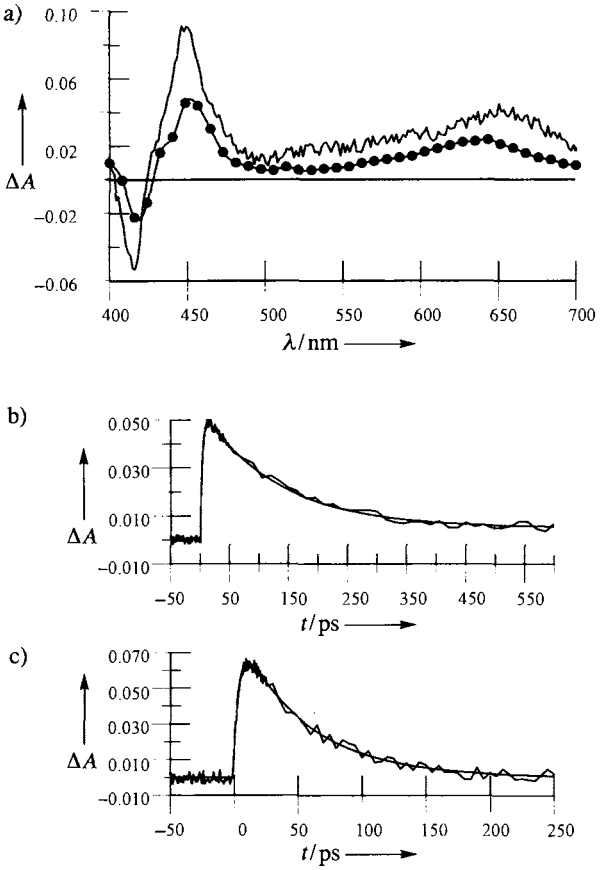

Figure 3. a) Transient differential absorption spectra recorded 25 ps (solid line) and 25 ns (-●-) after laser excitation of the CT complex **1**. b) Decay profile recorded at 630 nm for the CT complex **1**. c) Decay profile recorded at 610 nm for the CT complex **2**.

CT complex formed between ADIQ·2PF$_6$ and CE10 due to overlapping absorption bands localized on the acceptor.

Comparable amounts of vibrational energy have to be dissipated during charge recombination in the RIPs formed from **1** and **2**. This is evident by the similar maxima for CT absorption bands formed upon encapsulation of DAP·2PF$_6$ ($\lambda_{max}\approx430$ nm) and MV·2PF$_6$ ($\lambda_{max}\approx440$ nm) into CE10 and by the respective redox potentials. Cyclic voltammetry studies of **1** in butyronitrile showed two quasi-reversible one-electron reductions, with half-wave potentials of −0.60 and −1.30 V versus SCE, and an irreversible oxidation at +1.45 V versus SCE. Successive reductions occur at the diazapyrenium dication, first forming the π radical cation and then the neutral species, while oxidation takes place at the hydroquinol units. Complex **2** displayed one-electron reductions at −0.60 and −1.01 V versus SCE and an irreversible oxidation at +1.39 V versus SCE. Therefore, differences in the rates of charge recombination cannot be ascribed to either thermodynamic or stereochemical factors.

The main difference between diazapyrenium and viologen acceptors concerns the energy level of localized π–π* states. Indeed, the relatively low energy of π–π* states localized on the acceptor in **1**, compared to those in **2**,[16] facilitates mixing of these states with the CT state.[6, 7] Such an interaction, which introduces some π–π* character into the CT state, stabilizes the ground state of the complex[6] and decreases the rate of charge recombination in the RIP.[7, 8] It is this relatively slow rate of charge recombination (provided by interstate mixing), together with electrostatic repulsion between the partners within the RIP, that permits photoseparation of complex **1**.

 © WILEY-VCH Verlag GmbH, D-69451 Weinheim, 1997 0570-0833/97/3621-2357 $ 17.50+.50/0

Without interstate mixing the conjugate does not function as a phototropic assembly, and absorbed photons are converted into heat within about 50 ps. Interstate mixing extends the overall timescale for charge recombination to about 40 μs, but the phototropic process itself continues for milliseconds. This is because diffusional charge recombination occurs between separated π radical cations, and is followed by slower reinsertion of the dication into the receptor (see Figure 1). In contrast to the case with MV·2PF$_6$, where the acceptor is nonfluorescent and separation of the RIP is minimal, formation of free DAP·2PF$_6$ as a transitory species can be followed by fluorescence spectroscopy using two-color (or delayed pulse) excitation. Background fluorescence, being set by the amount of free DAP·2PF$_6$, can be suppressed with excess CE10, while the rate of reinsertion of DAP·2PF$_6$ into the cavity is solvent-dependent. Similar behavior is found for ADIQ·2PF$_6$, but the level of background fluorescence is too high for practical application. With complex **1**, however, laser-induced fluorescence selectively tracks the evolution and disappearance of free diazapyrenium dications.

Experimental Section

DAP·2PF$_6$ [11] and CE10 [17] were prepared by literature methods. ADIQ·2PF$_6$ was available from earlier work [11]. All compounds gave satisfactory analytical data that were consistent with their assigned structures. Fast kinetic measurements were made with nanosecond and sub-picosecond laser flash photolysis equipment, built for this purpose, similar to that described previously [11]. The excitation wavelength was 440 nm. Decay kinetics were obtained by collecting transient differential absorption spectral profiles at about 50 delay times. Binding constants were determined by fluorescence spectroscopy with about 50 different concentrations of crown ether being added to a solution of fluorophore in acetonitrile.

X-ray structure analysis of **1**: $C_{48}H_{54}F_{12}N_3O_{10}P_2$, $M_r = 1122.88$, yellow prisms, $0.15 \times 0.20 \times 0.45$ mm, measured at 293(2) K; triclinic, $P\bar{1}$, $a = 11.284(2)$, $b = 11.211(2)$, $c = 12.043(2)$ Å, $\alpha = 99.95(3)$, $\beta = 106.28(3)$, $\gamma = 107.15(3)°$, $V = 1342(4)$ Å^3, $\rho_{calcd} = 1.389$ mg m^{-3}, Enraf-Nonius CAD-4 diffractometer, $Mo_{K\alpha}$ radiation ($\lambda = 0.71069$ Å), $\mu = 0.179$ mm^{-1}, $\omega/2\theta$ scan, $2\theta \leq 60°$; of 7524 reflections measured, 6509 were independent; ψ-scan absorption correction, $T_{min} = 0.94$, $T_{max} = 1.00$. The structure was solved with direct methods (SHELXS-86), and refined on F^2 (SHELXL-93; non-hydrogen atoms, except disordered F atoms, were refined anisotropically, and H atoms at calculated positions in riding mode). $R_1 = 0.0959$ for 6494 reflections ($F_0 \geq 4\sigma(F)$), $wR_2 = 0.2949$ for all data, GOF = 1.0086, 330 parameters, $\Delta\rho_{max} = 1.042$ e Å^{-3} in the vicinity of a severely disordered solvent molecule. Crystallographic data (excluding structure factors) for the structures reported in this paper have been deposited with the Cambridge Crystallographic Data Centre as supplementary publication no. CCDC-100343. Copies of the data can be obtained free of charge on application to The Director, CCDC, 12 Union Road, Cambridge CB2 1EZ, UK (fax: int. code +(1223) 336-033; e-mail: deposit@chemcrys.cam.ac.uk).

Received: May 28, 1997 [Z10407IE]
German version: *Angew. Chem.* **1997**, *109*, 2451–2454

Keywords: charge transfer · crown compounds · fluorescence spectroscopy · photochemistry · polycycles

[1] a) A. C. Benniston, A. Harriman, *Angew. Chem.* **1993**, *105*, 1553–1555; *Angew. Chem. Int. Ed. Engl.* **1993**, *32*, 1459–1461; b) A. C. Benniston, *Chem. Soc. Rev.* **1996**, *25*, 427–435.
[2] M. Seiler, H. Dürr, *Liebigs Ann.* **1995**, 407–409.
[3] R. Ballardini, V. Balzani, M. T. Gandolfi, L. Prodi, M. Venturi, D. Philp, H. G. Ricketts, J. F. Stoddart, *Angew. Chem.* **1993**, *105*, 1362–1364; *Angew. Chem. Int. Ed. Engl.* **1993**, *32*, 1301–1304.
[4] A. C. Benniston, A. Harriman, V. M. Lynch, *J. Am. Chem. Soc.* **1995**, *117*, 5279–5291.
[5] a) A. C. Benniston, A. Harriman, D. Philp, J. F. Stoddart, *J. Am. Chem. Soc.* **1993**, *115*, 5298–5299; b) A. C. Benniston, A. Harriman, *ibid.* **1994**, *116*, 11531–11537.
[6] J. N. Murrell, *J. Am. Chem. Soc.* **1969**, *81*, 5037–5043.
[7] M. Bixon, J. Jortner, J. W. Verhoeven, *J. Am. Chem. Soc.* **1994**, *116*, 7349–7355.
[8] a) I. R. Gould, J. E. Moser, D. Ege, S. Farid, *J. Am. Chem. Soc.* **1988**, *110*, 1991–1993; b) A. M. Brun, A. Harriman, S. M. Hubig, *J. Phys. Chem.* **1992**, *96*, 254–257.
[9] A. C. Benniston, V. Grosshenny, A. Harriman, R. Ziessel, *Angew. Chem.* **1994**, *106*, 1956–1957; *Angew. Chem. Int. Ed. Engl.* **1994**, *33*, 1884–1885.
[10] A. C. Benniston, A. Harriman in *NATO ARW Physical Supramolecular Chemistry* (Eds.: A. E. Kaifer, L. Echegoyen), in press.
[11] A. M. Brun, A. Harriman, *J. Am. Chem. Soc.* **1991**, *113*, 8153–8159.
[12] P. R. Ashton, S. J. Langford, N. Spencer, J. F. Stoddart, A. J. P. White, D. J. Williams, *Chem. Commun.* **1996**, 1387–1388.
[13] B. L. Allwood, N. Spencer, H. Shahriari-Zavareh, J. F. Stoddart, D. J. Williams, *J. Chem. Soc. Chem. Commun.* **1987**, 1064–1066.
[14] S. Khazaeil, A. I. Popov, J. L. Dye, *J. Phys. Chem.* **1983**, *87*, 1832–1833.
[15] Complexation of higher order causes a slight curvature of the plateau region at high mole fractions of CE10. Such behavior is not seen in the mass-spectral studies. Formation of a 1:1 complex for ADIQ·2PF$_6$ in [D$_6$]acetone causes upfield shifts of −0.15, −0.13, and −0.022 ppm for the α, β, δ protons, respectively. Formation of a 1:2 complex causes further upfield shifts of −0.083 (α), −0.070 (β), and −0.012 ppm (δ). Both complexes are observed by FAB mass spectrometry in acetonitrile.
[16] These energy gaps, which are crudely estimated from absorption maxima of the lowest-energy π–π* transition localized on the acceptor and the CT transition are 1.6, 0.15, and −0.3 eV for MV·2PF$_6$, DAP·2PF$_6$, and ADIQ·2PF$_6$, respectively. For the latter, the CT band lies at higher energy than the lowest-energy π–π* transition.
[17] P. L. Anelli, P. R. Ashton, R. Ballardini, V. Balzani, M. Delgado, M. T. Gandolfi, T. T. Goodnow, A. E. Kaifer, D. Philp, M. Pietraszkiewicz, L. Prodi, M. V. Reddington, A. M. Z. Slawin, N. Spencer, J. F. Stoddart, C. Vicent, D. J. Williams, *J. Am. Chem. Soc.* **1992**, *114*, 193–218.

Novel Zwitterionic Diallylzirconium Complexes: Synthesis, Structure, Polymerization Activity, and Deactivation Pathways**

Gerardo Jiménez Pindado, Mark Thornton-Pett, Marco Bouwkamp, Auke Meetsma, Bart Hessen,* and Manfred Bochmann*

Group 4 metallocene complexes are becoming increasingly important as "single-site" catalysts for the polymerization of α-olefins,[1] and the number of industrial processes based on Cp complexes is growing rapidly.[2] The catalytically active species are electron-deficient complexes of the type $[Cp_2MR]^+$ (M = Ti, Zr, Hf), which are usually generated in situ by reacting a neutral metal alkyl complex with cation-generating activators such as methylaluminoxane (MAO) or, in aluminum-free systems, $M^+[B(C_6F_5)_4]^-$ ($M = HNMe_2Ph$, CPh_3), to give ion pairs $[Cp_2MR]^+X^-$ [X = Me-MAO, $B(C_6F_5)_4$].[1] Zwitterionic complexes such as $[Cp^*_2Zr(m\text{-}C_6H_3Et)B(C_6H_4Et)_3]$, $[Cp_2ZrMe(\mu\text{-}Me)B(C_6F_5)_3]$, $[Cp^*TiMe_2(\mu\text{-}Me)B(C_6F_5)_3]$ (Cp^* = tetramethylcyclopentadienyl), $[Zr(CH_2Ph)_3(\eta\text{-}Ph)BPh_3]$, and $[Zr(CH_2Ph)_3(\eta^6\text{-}PhCH_2)B(C_6F_5)_3]$ have proved to be useful catalyst precursors;[3–7] here the active species is generated by dissociation into ion pairs. More recently Erker et al. prepared zwitterionic allylic complexes $[Cp_2M(\eta^3\text{-}C_3H_4CH_2)B(C_6F_5)_3]$ by treating zirconocene and hafnocene butadiene complexes with $B(C_6F_5)_3$. These compounds are less electron-deficient than the alkyl complexes mentioned above and achieve an electron count of 18 through a weak Zr–F coordination.[8]

Structural and catalytic studies have so far mainly concentrated on the chemistry of highly reactive 14-electron alkyl complexes $[Cp_2MMe]^+$ (M = Ti, Zr, Hf). The isoelectronic cationic

[*] Prof. Dr. M. Bochmann, Dr. G. Jiménez Pindado, Dr. M. Thornton-Pett
School of Chemistry, University of Leeds
Leeds LS2 9JT (UK)
Fax: Int. code +(113) 233 6401
e-mail M.Bochmann@chem.leeds.ac.uk
Dr. B. Hessen, M. Bouwkamp, Dr. A. Meetsma
Department of Chemistry, University of Groningen
Nijenborgh 4, NL-9747 AG Groningen (The Netherlands)
e-mail hessen@chem.rug.nl

[**] This work was supported by the Engineering and Physical Sciences Research Council. G. J. P. thanks the Science and Education Ministry of Spain for a research fellowship.

 © WILEY-VCH Verlag GmbH, D-69451 Weinheim, 1997 0570-0833/97/3621-2358 $ 17.50+.50/0

diallyl complexes of the type $[CpM(\eta^3\text{-allyl})_2]^+$ should exhibit a similarly promising reactivity. We describe here the synthesis, catalytic activity, and structural characterization of the first zwitterionic diallylzirconium complexes. The ability of these species to undergo unusually facile C–H activation illustrates the remarkable difference in reactivity between mono-Cp $[CpM(allyl)_2]^+$ ions and the more familiar metallocene analogues $[Cp_2MR]^+$ (R = alkyl, allyl).

Treatment of a solution of $[Cp''Zr(\eta^3\text{-}C_3H_5)\{\eta^4\text{-}CH_2C(Me)C(Me)CH_2\}]$ (**1a**) [Cp'' = 1,3-$(SiMe_3)_2C_5H_3$] in toluene with $B(C_6F_5)_3$ at −78 °C leads to a color change from red to orange. Monitoring this reaction by NMR spectroscopy in CD_2Cl_2 between −70 and 20 °C reveals the formation of a single chiral complex; seven ^{1}H NMR resonances for allylic ligands (five from the η^3-C_3H_5 ligand, two from the η^3-dienyl unit) appear together with two broadened doublets for the -CH_2-B moiety at $\delta = -0.33$ and −1.78 (Table 1). These data are consistent with an attack by $B(C_6F_5)_3$ exclusively on one of the terminal carbon atoms of the diene ligand to give the zwitterionic diallyl complex **2a** [Eq. (a)]. The unusually high-field shifted ^{1}H NMR resonances for the CH_2–B moiety suggest possible C–H···Zr bonding.

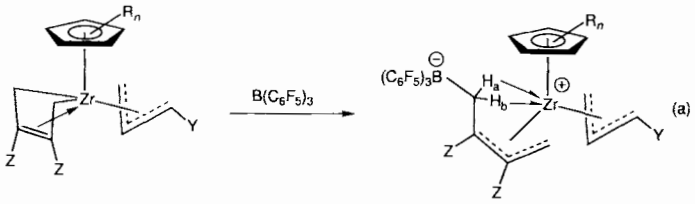

1a, R_n = 1,3-$(SiMe_3)_2$; Y = H, Z = Me
1b, R_n = 1,3-$(SiMe_3)_2$; Y = Me, Z = H
1c, R_n = Me_5; Y = Me, Z = H

2a - c

The ^{11}B NMR singlet of **2a** at $\delta = -12.0$ confirms the formation of a triarylborate. The ^{19}F NMR spectrum shows six resonances for the *ortho*-F atoms of three inequivalent C_6F_5 groups, whose rotation about the B–C_6 and B–CH_2 bonds is evidently highly hindered. All six *o*-F signals have chemical shifts between $\delta = -129$ and −135 and remain unchanged on cooling to −85 °C; a high-field shift of one of the *o*-F signals, which might indicate a metal–fluorine coordination,[9] is not observed.

Compound **2a** is isolated as air-sensitive orange crystals (83% yield) that are thermally stable at room temperature. Cooling solutions of **2a** in toluene to −16 °C afforded orange-yellow crystals of **2a**·toluene suitable for X-ray diffraction.[10] The sterically demanding ligands of the zwitterionic molecule (Figure 1) prevent any close intra- or intermolecular M···F interactions. The Zr–C distances in the $[Cp'Zr(allyl)_2]^+$ core correspond closely to the values of the neutral allyl precursor. The cationic 14-electron fragment is stabilized by two agostic interactions with the B–CH_2 group [Zr···H 2.29(5) and 2.30(5) Å].[11]

Compound **2a** crystallizes with one molecule of toluene, which in the crystal is associated with one of pentafluorophenyl rings; the distances between the plane of the six-membered ring of the toluene molecule and the best least-squares plane through the C_6F_5 group are relatively short (3.17–3.45 Å). This solvent binding is reminiscent of the well known 1:1 stacking phases formed between benzene and hexafluorobenzene.[12]

Mixtures of **1a** activated with one equivalent $B(C_6F_5)_3$ in toluene catalyze the polymerization of ethene under mild conditions (Table 2). While the M_w values are within the expected range, the broadening of the polydispersities with rising poly-

Table 1. Selected spectroscopic data.

2a: ^{1}H NMR (300 MHz, CD_2Cl_2, −40 °C; C atom numbering as in Figure 1): $\delta = -1.78$, −0.33 (br s, 1H each; H_2CB), 0.19, 0.36 (s, 9H each; SiMe), 1.41, 2.52 (d, $J = 8.3$ Hz, 1H each; CCH_2), 1.68, 1.76 (s, 3H each, diene-Me); 1.96 (m, 2H), 2.66 (br. d, 1H), 3.19 (d, $J = 15.3$ Hz 1H; 14 or 16-CH_2), 5.96 (m, 1H, 15-CH), 6.51, 6.96 (m, 1H, 4,5-C_5H_3), 6.44 (m, 1H, 2-C_5H_3); ^{13}C NMR (75.4 MHz, CD_2Cl_2, −40 °C): $\delta = -0.55$, −0.23 (q, $J = 119.1$, 119.6 Hz; SiMe), 16.93, 23.77 (q, $J = 129.5$, 127.8 Hz, diene-Me), 31.09 (vbr. t, CH_2B), 59.64 (t, $J = 150.1$ Hz, CCH_2), 67.12, 71.03 (t, $J = 155.9$, 158.6 Hz; CH_2 of C_3H_5), 112.91 (m, 8-C), 117.53 (d, $J = 170.5$ Hz; 2-C_5H_3), 124.0, 131.45 (d, $J = 169.8$, 172.0 Hz; 4,5-C_5H_3), 125.28, 129.26 (m, 1,3-C_5H_3), 138.06 (m, 7-C), 140.77 (d, $J = 153.2$ Hz, 11-CH); ^{11}B NMR (96.2 MHz, CD_2Cl_2, −40 °C): $\delta = -11.99$; ^{19}F NMR (CD_2Cl_2, −50 °C): $\delta = -129.6$, −132.2, −130.0, −132.6, −134.0, −134.7 (d, ^3J(F,F) = 19.6 Hz, 1F each; *o*-F), −159.9, −160.1, −160.6 (t, ^3J(F,F) = 19.7 Hz, 1F each; *p*-F); −164.2, −165.1, −165.6, −167.0 (m, 2F, 1F, 2F, 1F; *m*-F)

2b: ^{1}H NMR ([D$_8$]toluene, 300 MHz, −30 °C): $\delta = -1.68$ (s, br, 1H; BCH_2), −1.58 (d, $J = 14.4$ Hz, 1H; BCH_2), −0.22, 0.09 (s, 9H each; SiMe), 0.92 (d, $J = 5.61$ Hz, 3H; Me), 2.21, 1.98 (m, 1H; diene-CH_2), 1.65, 2.00 (dd, $J = 13.4$, 3 Hz, 1H; CH_2 of C_4H_7), 1.71 (m, 1H; C*H*Me of C_4H_7), 4.58 (dd, $J = 14.0$, 9.9 Hz, 1H; diene-CH), 5.01 (m, 1H; CH of C_4H_7), 5.17 (m, 1H; diene-CH), 5.87, 5.93, 6.63 (m, each 1H, C_5H_3); ^{13}C NMR ([D$_8$]toluene, −50 °C): $\delta = -0.91$, −0.71 (SiMe), 18.49 (Me), 28.0 (br., BCH_2), 57.58 (diene-CH_2), 61.18 (CH_2 of C_4H_7), 83.45 (diene-*C*HMe), 106.45 (diene-CH), 118.56, 124.43, 125.61 (2,4,5-C_5H_3), 126.35 (br., 1,3-C_5H_3), 133.09 (diene-CH), 137.37 (CH of C_4H_7), 137.23 (J(C,F) = 242.25 Hz, *m*-C, C_6F_5), 139.42 (J(C,F) = 235.0 Hz, *p*-C, C_6F_5), 148.23 (J(C,F) = 238.47 Hz, *o*-C, C_6F_5); ^{11}B{^{1}H} NMR ([D$_8$]toluene, −60 °C): $\delta = -12.58$; ^{19}F NMR ([D$_8$]toluene, −60 °C): $\delta = -131.2$, −132.9, −135.1 (br. s, 1F, 4F, and 1F; *o*-F); −158.9 (vbr. s, 3F; *p*-F); −164.3 (br. s, 6F, *m*-F)

3a: ^{1}H NMR (300 MHz, −20 °C): $\delta = -1.87$ (br. s, 1H; BCH_2); 0.12, 0.23 (s, 9H each; SiMe); 1.29 (d, $J = 5.4$ Hz; 1H, $=CH_2$ of diene), 1.49 (br. s, 1H, BCH_2), 1.67 (s, 9H; CMe_3), 1.80, 2.05 (s, 3H each; diene-Me), 2.06 (d, $J = 16.0$ Hz 1H; CH_2 of C_3H_5), 2.18 (m, 1H, $J = 16.0$ Hz; CH_2 of C_3H_5), 2.28 (d, $J = 5.4$ Hz, 1H; $=CH_2$ of diene), 3.66, 3.97 (m, 1H each; CH_2 of C_3H_5), 5.00, 5.01, 5.33 (m, 1H each; C_5H_3), 5.15 (m, 1H; CH of C_3H_5); ^{13}C NMR (CD_2Cl_2, −20 °C): $\delta = -0.27$, −0.03 (q, $J = 119.3$ Hz; SiMe), 21.83, 24.93 (q, $J = 125.0$, 126.3 Hz; diene-Me), 26.72 (br. s, BCH_2), 29.64 (q, $J = 129.5$ Hz; $C(CH_3)_3$), 47.1 (t, $J = 151.0$ Hz; diene-CH_2), 60.09 (s, CMe_3), 61.05, 68.25 (t, $J = 158.8$, 161.0 Hz; CH_2 of C_3H_5), 109.1 (d, $J = 170.0$ Hz; 2-C_5H_3), 117.71 (d, $J = 172.8$ Hz; 4,5-C_5H_3), 118.03, 118.81 (s, $=CMe$), 120.20 (m, 1,3-C_5H_3), 120.89 (t, $J = 150.1$ Hz; CH of C_3H_5), 124.6 (*ipso*-C, BC_6F_5), 136.54 (J(C,F) = 255.8 Hz; *m*-C, C_6F_5), 138.24 (J(C,F) = 249.7 Hz; *p*-C, C_6F_5), 147.97 (J(C,F) = 247.5 Hz; *o*-C, C_6F_5), 159.06 (s, CN); ^{11}B{^{1}H} NMR (CD_2Cl_2, −20 °C): $\delta = -14.02$; ^{19}F NMR (CD_2Cl_2, 10 °C): $\delta = -131.5$ (t, br, 6F; *o*-F), −163.1 (t, ^3J(F,F) = 19.8 Hz, 3F; *p*-F); −167.1 (br. 6F; *m*-F)

4b: ^{1}H NMR ([D$_8$]toluene, 300 MHz, 25 °C): $\delta = -0.14$, 0.05 (s, each 9H; SiMe), 0.59, 2.19 (t, br, $J = 8.9$ Hz, each 1H; CH_2), 2.21 (d, $J = 12.6$ Hz, 1H; BCH), 5.99 (t, br, 1H, C*H*=CB), 6.23 (q, $J = 9.2$ Hz, 1H; CH_2=CH), 6.48 (t, $J = 2.2$ Hz, 1H; 2-C_5H_3), 6.65, 7.59 (br. s, 1H each; 4.5-C_5H_3); ^{13}C NMR (CD_2Cl_2, −20 °C): $\delta = -0.95$, −0.73 (q, $J = 119.5$ Hz; SiMe), 67.62 (t, $J = 150.0$ Hz; CH_2), 93.64 (d, $J = 136.56$ Hz; BCH), 120.54, 129.53 (d, $J = 170.55$, 160.74 Hz; 4,5-C_5H_3), 124.65 (d, $J = 167.53$ Hz; *C*H=CB), 127.22 (d, $J = 169.04$ Hz; 2-C_5H_3), 135.64 (d, $J = 166.02$ Hz; H_2C=*C*H), 127.40, 134.56 (m; 1,3-C_5H_3); ^{11}B{^{1}H} NMR ([D$_8$]toluene, 15 °C): $\delta = 43$ (br. s); ^{19}F NMR ([D$_8$]toluene, −40 °C): *o*-F: $\delta = -114.1$ (br. s; 2F), −130.1 (d, J(F,F) = 19.7 Hz, 2F), −130.6 (br. s; 1F), −169.9 (br. s, 1F), *p*-F: $\delta = -149.3$ (br. s; 1F), −150.7 (t, 1F, J(F,F) = 21.1 Hz), −153.6 (t, 1F; J(F,F) = 19.7 Hz); *m*-F: $\delta = -156.2$, −156.5 (br. s, 1F each, overlaps with the *m*-F signal of **4b'**), −161.2 (m, 4F)

4b': ^{1}H NMR ([D$_8$]toluene, 300 MHz, 25 °C): $\delta = -0.15$, 0.03 (s, 9H, SiMe), 1.44 (m, 1H), 3.42 (dd, $J = 7.6$, 6.6 Hz, 1H; CH_2), 5.10 (m, 1H; H_2C=CH), 5.34 (d, $J = 12.0$ Hz; BCH), 5.82 (m, 1H; C*H*=CB), 5.97, 7.01 (m, 1H each; 4,5-C_5H_3), 7.71 (t, $J = 1.9$ Hz, 1H, 2-C_5H_3); ^{13}C NMR (CD_2Cl_2, −20 °C): $\delta = -1.39$, −0.47 (q, $J = 119.6$ Hz; SiMe), 82.31 (t, $J = 152.82$ Hz; CH_2), 97.17 (d, $J = 136.2$ Hz, BCH), 123.96, 134.05 (m, 1,3-C_5H_3), 125.68 (CH=CB); 125.9, 128.13 (4,5-C_5H_3); 129.68 (d, $J = 165.0$ Hz; H_2C=*C*H), 135.11 (d, $J = 172.06$ Hz; 2-C_5H_3); ^{11}B{^{1}H} NMR ([D$_8$]toluene, 15 °C): $\delta = 43$ (br. s); ^{19}F NMR ([D$_8$]toluene, −40 °C): *o*-F: $\delta = -118.7$ (d, J(F,F) = 25.4 Hz, 2F), −129.4 (br. s. 1F), −131.4 (d, J(F,F) = 16.9 Hz, 2F), −184.1 (br. s, 1F); *p*-F: $\delta = -151.6$, −155.3 (t, 1F each, J(F,F) = 19.7 Hz), −152.2 (t, 1F, J(F,F) = 21.1 Hz); *m*-F: $\delta = -156$ (1F, overlaps with the *m*-F signal of **4b**), −157.1 (br. s, 1F), −160.5, −162.2 (m, 2F each)

4c: ^{1}H NMR ([D$_8$]toluene, 500 MHz, −30 °C): $\delta = 1.53$ (s, 15H; Cp*), 2.38 (m, 1H; C*H*H), 2.63 (t, $J = 7.0$ Hz, 1H; CH*H*), 4.68 (br. m, 1H; C*H*=CB), 5.04 (m, 1H; CH_2=CH), 5.85 (d, $J = 12.7$ Hz, 1H; BCH); ^{13}C{^{1}H} NMR ([D$_8$]toluene, 125 MHz, −30 °C): $\delta = 10.96$ (Cp*-Me), 77.81 (CH_2), 95.94 (BCH), 124.08 (Cp* ring), 125.95 (*C*H=CB), 126.91 (H_2C=*C*H); ^{19}F NMR (C_6D_5Br, 282 MHz, −30 °C): *o*-F: $\delta = -120.3$ (1F), −130.5 (br., 1F), −130.55 (d, J(F,F) = 15 Hz; 2F), −136.5 (br., 1F), −180.0 (br., 1F); *p*-F: $\delta = -153.5$ (t, J(F,F) = 21 Hz, 1F), −154.2 (t, J(F,F) = 21 Hz, 1F), −156.0 (t, J(F,F) = 20 Hz, 1F); *m*-F: $\delta = -158.4$ (br, 1F), −159.2 (m, 1F), −160.2 (br, 1F), −161.9 (m, 1F), −163.7 (m, 2F).

 © WILEY-VCH Verlag GmbH, D-69451 Weinheim, 1997 0570-0833/97/3621-2359 $ 17.50+.50/0

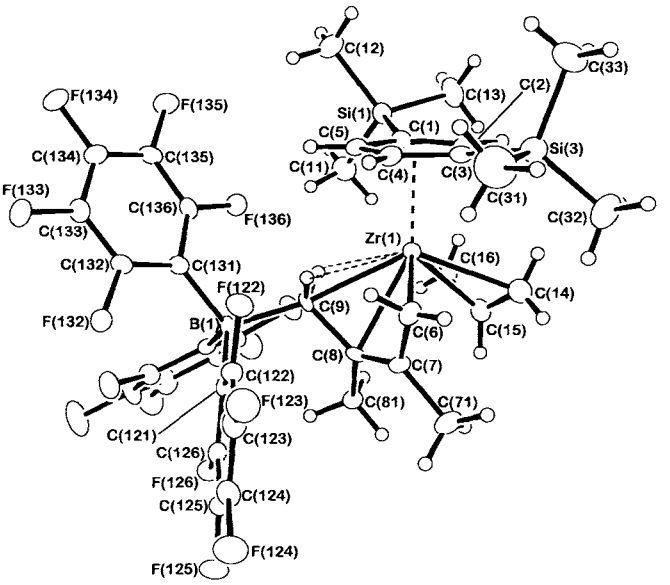

Figure 1. Structure of **2a** (ORTEX [22] diagram). Thermal ellipsoids are shown at the 40% probability level. Selected bond lengths [Å] and angles [°]: Zr(1)–C(6) 2.331(5), Zr(1)–C(7) 2.525(4), Zr(1)–C(8) 2.450(4), Zr(1)–C(9) 2.442(4), Zr(1)–C(14) 2.443(5), Zr(1)–C(15) 2.492(6), Zr(1)–C(16) 2.438(6), Zr(1)–C(1) 2.521(4), Zr(1)–C(2) 2.500(4), Zr(1)–C(3) 2.527(4), Zr(1)–C(4) 2.509(5), Zr(1)–C(5) 2.484(4), Zr(1)–H(9a) 2.30(5), Zr(1)–H(9b) 2.29(5), C(6)–C(7) 1.425(7), C(7)–C(8) 1.388(7), C(8)–C(9) 1.508(6), C(9)–B(1) 1.714(6), C(14)–C(15) 1.393(8), C(15)–C(16) 1.395(8); C(7)-C(6)-Zr(1) 80.6(3), C(8)-C(9)-B(1) 116.9(4), C(8)-C(9)-Zr(1) 72.3(2), B(1)-C(9)-Zr(1) 169.6(3).

Table 2. Ethene polymerizations with **1a**/$B(C_6F_5)_3$ [a].

Temperature [°C]	Time [min]	Polymer yield [g]	Productivity [b] $\times 10^{-3}$	M_w	M_w/M_n
0	3.5	0.144	98.7	201	3.5
20	5	0.132	63.3	181	4.7
44	10	0.180	43.2	107	5.2
60	10	0.190	45.6	77.3	7.6

[a] Conditions: **1a** (25 μmol), $B(C_6F_5)_3$ (25 μmol), toluene (20 mL), ethene 1 bar. [b] In 10^3 g PE (mol Zr)$^{-1}$ h^{-1}.

merization temperature to values significiantly higher than those typically obtained for metallocenes may suggest the loss of active site uniformity. Such behavior may offer advantages where the desired polymer properties or processing parameters favor broader polydispersities.[13, 14]

Treatment of **2a** with excess *tert*-butylisocyanide at 0 °C leads to the immediate formation of the adduct **3a** as yellow microcrystals. Rather unexpectedly, warming the reaction mixture did not lead to an isocyanide insertion product but to the quantitative regeneration of **1a**, together with *t*BuNC·$B(C_6F_5)_3$ ($\tilde{\nu}_{C\equiv N}$ = 2300 cm^{-1}), which, to our knowledge, is the first example of a fully reversible formation of a $[RB(C_6F_5)_3]^-$ borate unit. By contrast, di-Cp complexes such as $[Cp_2Zr\{C_3H_4CH_2{-}B(C_6F_5)_3\}]$ readily give the expected isocyanide insertion products.[8b]

The reaction of $B(C_6F_5)_3$ with the butadiene complexes **1b** and **1c** gives the corresponding zwitterionic complexes **2b** and **2c**, respectively. The spectroscopic data of these compounds are very similar to those of **2a**. Both catalyze the polymerization of ethene but are thermally less stable than the sterically more hindered **2a** and decompose by an unexpected C–H activation pathway, in which 2-butene is eliminated and a C_6F_5 group migrates from boron to zirconium to give **4** [Eq. (b)]. In the case

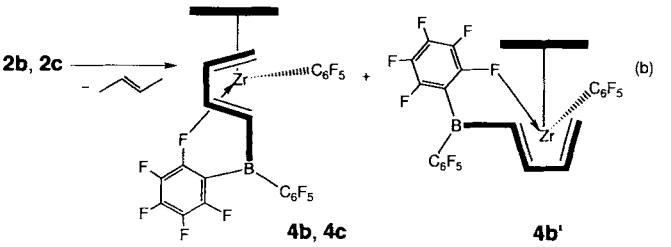

of **2b**, this reaction sequence is very facile even at −60 °C.[15] The transformation of the four-coordinate borate in **2b** into a three-coordinate boryl in **4b** is reflected in the change in the ^{11}B NMR signal from about $\delta = -12$ to $\delta = +43$. Compound **4b** is accompanied by a second, fluxional isomer **4b'**. The C_5Me_5 complex **2c** is more stable and rearranges to **4c** with $\tau_{1/2} \approx 20$ min in C_6D_6 and 2–3 min in C_6D_5Br at room temperature.

The X-ray structure analysis of **4c**·0.5 Et_2O (Figure 2)[16] shows a trigonal-planar $B(C_6F_5)_2$ unit; one *o*-F atom is coordinated to the metal center ($\delta(^{19}F) = -179.8$). The ZrC_4 core has the familiar metallacyclopentene envelope conformation.

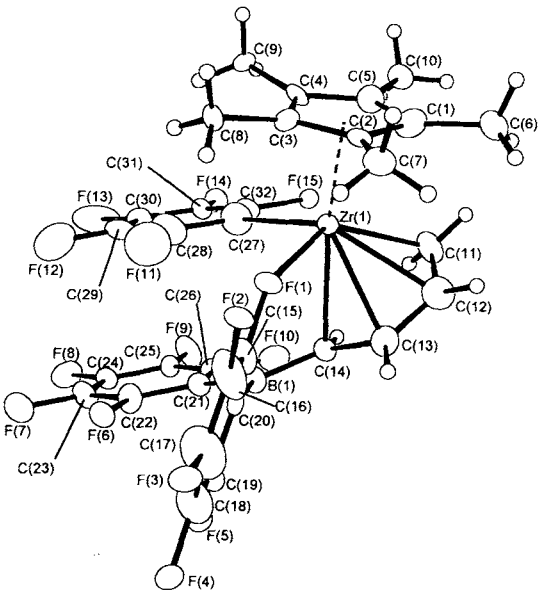

Figure 2. Structure of **4c**. Selected bond lengths [Å] and angles [°]: Zr(1)–C(11) 2.314(3), Zr(1)–C(12) 2.451(3), Zr(1)–C(13) 2.458(3), Zr(1)–C(14) 2.481(2), Zr(1)–C(27) 2.315(2), Zr(1)–F(1) 2.4292(15), C(11)–C(12) 1.414(4), C(12)–C(13) 1.375(4), C(13)–C(14) 1.454(3), B(1)–C(14) 1.488(3), B(1)–C(20) 1.582(4), B(1)–C(21) 1.590(3), C(15)–F(1) 1.380(3), C(19)–F(5) 1.351(3); F(1)-Zr(1)–C(27) 100.47(7), B(1)-C(14)-C(13) 126.3(2), C(11)-C(12)-C(13) 121.8(2), C(12)-C(13)-C(14) 120.5(2).

Surprisingly, the diene unit is oriented approximately orthogonal to the Cp ring and does not fall into either of the usual "prone" and "supine" categories.[17] The distribution of the bond lengths in the ZrC_4B unit, in particular the relatively short B–C(H) bond (1.485 Å), suggests that the zwitterionic resonance structure **B** may dominate over formulation **A**.[18]

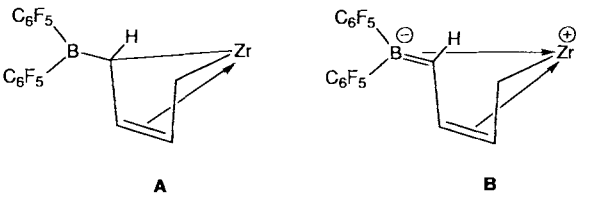

 © WILEY-VCH Verlag GmbH, D-69451 Weinheim, 1997 0570-0833/97/3621-2360 $ 17.50+.50/0

The results establish cationic 14-electron mono-Cp complexes as a new class of polymerization catalysts; their reactivity patterns, however, differ markedly from the behavior of the better-known di-Cp systems.

Experimental Section

All synthetic procedures were carried out under dry nitrogen using Schlenk techniques. NMR spectra were recorded on Bruker 300 and 500 MHz instruments. Compounds **1a**–**1c** were synthesized according to literature procedures [19].

2a: $B(C_6F_5)_3$ (0.89 g, 1.73 mmol) in toluene (20 mL) was added to a solution of **1a** (0.73 g, 1.72 mmol) in toluene (30 mL) at −78 °C. The mixture was stirred at this temperature for 30 min and then allowed to warm to room temperature. The color of the mixture changed instantaneously from red to dark orange. Concentration of the solution to 20 mL followed by cooling to −16 °C afforded orange crystals of **2a**·toluene (1.29 g, 1.38 mmol, 80%). Elemental analysis (%): Calcd for $C_{38}H_{36}BF_{15}Si_2Zr\cdot C_7H_8$: C 52.6, H 4.3; found: C 51.8, H 4.5.

3a: *t*BuNC (0.21 mL, 1.86 mmol) was added to a solution of **2a** (0.96 g, 0.93 mmol) in toluene (10 mL) at 0 °C. The resulting yellow mixture was concentrated and cooled to −16 °C to give yellow crystals of **3a** (0.79 g, 0.77 mmol, 83%). Elemental analysis (%): Calcd for $C_{43}H_{45}BF_{15}NSi_2Zr$: C 50.4, H 4.5, N 1.4; found: C 50.6, H 4.7, N 1.3. IR (Nujol): $\tilde{\nu}$ = 2179 cm^{-1} (C≡N).

2b: This compound is thermally sensitive and was therefore generated in solution and characterized spectroscopically. $B(C_6F_5)_3$ (52 mg, 0.1 mmol) in [D_8]toluene (0.2 mL) was added to a solution of **1b** (42 mg, 0.1 mmol) in [D_8]toluene (0.3 mL) at −60 °C. The orange solution contained **2b**, together with some **4b** and **4b′**.

4b: The compound was generated in situ from **1b** and $B(C_6F_5)_3$ (1 equiv) in [D_8]toluene at 0 °C; it slowly decomposed in solution at room temperature.

4c: A solution of $B(C_6F_5)_3$ (0.228 g, 0.44 mmol) in benzene (5 mL) was added to a solution of **1c** (0.148 g, 0.44 mmol) in benzene (5 mL) at room temperature. The resulting orange solution was stirred at ambient temperature for 40 min during which the solution turned red. The solvent was removed in vacuo and the residue was extracted with diethyl ether. Concentration and cooling of the solution to −70 °C yielded **4c**·0.5 Et_2O as a red crystalline solid (0.141 g, 0.20 mmol, 46%). Elemental analysis (%): Calcd for $C_{32}H_{20}BF_{15}Zr\cdot 0.5(C_2H_5)_2O$: C 48.8, H 3.0, Zr 10.9; found: C 48.5, H 3.0, Zr 10.8.

Received: April 14, 1997 [Z10339IE]
German version: *Angew. Chem.* **1997**, *109*, 2457–2460

Keywords: allyl complexes · C–H activation · diene complexes · homogeneous catalysis · zirconium

[1] M. Bochmann, *J. Chem. Soc. Dalton Trans.* **1996**, 255; H. H. Brintzinger, D. Fischer, R. Mülhaupt, B. Rieger, R. Waymouth, *Angew. Chem.* **1995**, *107*, 1255; *Angew. Chem. Int. Ed. Engl.* **1995**, *34*, 1143; M. Aulbach, F. Küber, *Chem. Unserer Zeit* **1994**, *28*, 197.

[2] A. M. Thayer, *Chem. Eng. News*, **1995**, Sept. 11, 15; *Chem. Br.* **1995**, 936; H. G. Hauthal, *Nachr. Chem. Tech. Lab.* **1995**, *43*, 822.

[3] G. G. Hlatky, H. W. Turner, R. R. Eckman, *J. Am. Chem. Soc.* **1989**, *111*, 2728.

[4] X. Yang, C. L. Stern, T. J. Marks, *J. Am. Chem. Soc.* **1991**, *113*, 3623; *ibid.* **1994**, *116*, 10015; M. Bochmann, S. J. Lancaster, M. B. Hursthouse, K. M. A. Malik, *Organometallics* **1994**, *13*, 2235.

[5] D. J. Gillis, M. J. Tudoret, M. C. Baird, *J. Am. Chem. Soc.* **1993**, *115*, 2543.

[6] M. Bochmann, G. Karger, A. J. Jaggar, *J. Chem. Soc. Chem. Commun.* **1990**, 1038.

[7] C. Pellecchia, A. Grassi, A. Immirzi, *J. Am. Chem. Soc.* **1993**, *115*, 1160; C. Pellecchia, A. Grassi, A. Zambelli, *J. Mol. Catal.* **1993**, *82*, 57.

[8] a) B. Temme, G. Erker, J. Karl, H. Luftmann, R. Fröhlich, S. Kotila, *Angew. Chem.* **1995**, *107*, 1867; *Angew. Chem. Int. Ed. Engl.* **1995**, *34*, 1755; b) B. Temme, J. Karl, G. Erker, *Chem. Eur. J.* **1996**, *2*, 919. For further examples for fluoroarylborate coordination see: X. Yang, C. L. Stern, T. J. Marks, *Organometallics* **1991**, *10*, 840; A. D. Horton, A. G. Orpen, *ibid.* **1991**, *10*, 3910; A. R. Siedle, R. A. Newmark, W. M. Lamanna, J. C. Huffman, *ibid.* **1993**, *12*, 1491; L. Lia, X. Yang, C. L. Stern, T. J. Marks, *ibid.* **1997**, *16*, 842.

[9] The coordinated *ortho*-F in [$Cp_2Zr\{C_3H_4CH_2B(C_6F_5)_3\}$] experiences an upfield shift of about 80 ppm to δ = −213.2 [8a].

[10] X-ray structure analysis of **2a**·toluene: An orange prism with dimensions 0.65 × 0.42 × 0.25 mm was grown from toluene and coated in perfluoropolyether RS3000 oil (Riedel De-Haën). $C_{38}H_{36}BF_{15}Si_2Zr\cdot C_7H_8$, M_r = 1028.01 (includes toluene molecule), triclinic, space group $P\bar{1}$, a = 10.4955(12), b = 13.538(2), c = 16.650(2) Å, α = 77.695(11), β = 83.542(10), γ = 78.945(14)°, Z = 2, V = 2262.2(5) Å^3, ρ_{calcd} = 1.509 Mg m^{-3}, μ = 3.344 mm^{-1}, $F(000)$ = 1044. Data collection was carried out at 160 K on a Stoe STADI4 four-circle diffractometer operating in the ω-θ scan mode using graphite-monochromated $Cu_{K\alpha}$ radiation (λ = 1.54184 Å). 7130 unique reflections were measured in the range 2.72 ≤ θ ≤ 64.54° (−12 ≤ h ≤ 12, −15 ≤ k ≤ 15, 0 ≤ l ≤ 18). The structure was solved by heavy atom methods using SHELXS-86 [20] and refined by full-matrix least-squares (against all the unique F^2 data) using SHELXL-93 [21]. Non-hydrogen atoms (including those of the toluene solvate molecule) were refined with anisotropic displacement parameters; hydrogen atoms were constrained to idealized positions by using a riding model with free rotation for methyl groups and fixed isotropic displacement parameters. Final $wR_2 = \{\sum[w(F_o^2 - F_c^2)^2]/\sum(F_o^2)^2]\}^{-1} = 0.1542$, conventional R = 0.0530 for F values of 6699 reflections with $F_o^2 > 2\sigma(F_o^2)$. Weighting scheme $w = [\sigma^2(F_o^2) + (0.0584P)^2 + 12.2995P]^{-1}$, where $P = (F_o^2 + 2F_c^2)/3$, goodness of fit = 1.069 for all F^2 values and 618 parameters. Maximum and minimum residual electron density 1.13 and −1.15 e Å^3, respectively [16b].

[11] Similar agostic interactions of two of the three methyl hydrogen atoms are found in $[(1,2\text{-}C_5H_3Me_2)_2ZrMe(\mu\text{-}Me)B(C_6F_5)_3]$ [Zr···H = 2.25(3) and 2.30(3) Å], while $[Cp_2ZrMe(\mu\text{-}Me)B(C_6F_5)_3]$ shows rather weaker agostic interactions [Zr···H 2.44(3) and 2.47(3) Å] [4].

[12] C. R. Patrick, G. S. Prosser, *Nature* **1966**, *187*, 1021; J. H. Williams, J. K. Cockcroft, A. N. Fitch, *Angew. Chem.* **1992**, *104*, 1666; *Angew. Chem. Int. Ed. Engl.* **1992**, *31*, 1655; J. H. Williams, *Acc. Chem. Res.* **1993**, *26*, 593.

[13] The "constraint geometry" complexes $[(C_5Me_4SiMe_2NtBu)Ti(C_4H_4R_2)]$ in the presence of $B(C_6F_5)_3$ are highly active for the copolymerization of ethene with 1-octene: D. D. Devore, F. J. Timmers, D. L. Hasha, R. K. Rosen, T. J. Marks, P. A. Deck, C. L. Stern, *Organometallics* **1995**, *14*, 3132. The living ethene oligomerization with activator-free $[(C_5Me_5)ZrR(2.3\text{-}Me_2C_4H_4)]$ has recently been reported: B. Hessen and H. van der Heijden, *J. Am. Chem. Soc.* **1996**, *118*, 11670.

[14] By contrast, propene polymerizations with $[Cp^*TiMe_3]/B(C_6F_8)_3$ give polymers with very narrow polydispersities and living characteristics: J. Sassmannshausen, M. Bochmann, J. Rösch, D. Lilge, *J. Organomet. Chem.*, in press.

[15] In contrast to the facile transfer of a C_6F_5 substituent from $B(C_6F_5)_3$ to a Zr atom, $B(C_6F_5)_3$ is inert towards electrophiles such as BBr_3 or Br_2. C_6F_5 transfer has been observed before at higher temperature and prolonged reaction times: R. Gomez, M. L. H. Green, J. L. Haggit, *J. Chem. Soc. Dalton Trans.* **1996**, 939.

[16] a) X-ray structure analysis of **4c**·0.5 Et_2O: an orange-red parallelepiped with dimensions 0.15 × 0.17 × 0.50 mm was grown from diethyl ether. Data were collected at 130 K. $C_{32}H_{20}BF_{15}Zr\cdot 0.5(C_2H_5)_2O$, M_r = 828.58, monoclinic $P2_1/n$, a = 12.903(1), b = 18.430(1), c = 13.389(1) Å, β = 96.08(1)°, V = 3166.0(4) Å^3, Z = 4, ρ_{calcd} = 1.738 Mg m^{-3}, μ = 4.64 cm^{-1}, 5128 reflections with $F_o \geq 4.0\sigma(F_o)$, 566 refined parameters. Data collection was carried out on an Enraf-Nonius CAD-4F^2 diffractometer using graphite-monochromated $Mo_{K\alpha}$ radiation (λ = 0.71073 Å; $\Delta\omega$ = 0.90 + 0.34tanθ). 6264 Unique reflections were measured in the range 2.2 ≤ 2θ ≤ 56.0° (−15 ≤ h ≤ 8, −1 ≤ k ≤ 20, 0 ≤ l ≤ 17). The structure was solved by Patterson methods and extension of the model was accomplished by direct methods applied to differene structure factors using the program DIRDIF [23]. The structure was refined by full-matrix least-squares (SHELXL93 [21]). Non-hydrogen atoms were refined with anisotropic displacement parameters. The diethyl ether solvent molecule was highly disordered over an inversion center. The programs PLATON [24] (calculation of geometric data) and PLUTO [25] (structure diagram) were used. Final $wR_2 = \{\sum[w(F_o^2 - F_c^2)^2]/\sum(F_o^2)^2]\}^{-1} = 0.0783$, conventional R = 0.0318 for F values of 5128 reflections with $F_o^2 > 2\sigma(F_o^2)$. Weighting scheme $w = [\sigma^2(F_o^2) + (0.0429P)^2 + 1.6097P]^{-1}$, where $P = (F_o^2 + 2F_c^2)/3$, goodness of fit = 1.066 for all F^2 values and 566 parameters. Maximum and minimum residual electron density 0.54 and −0.48 e Å^3, respectively. b) Crystallographic data (excluding structure factors) for the structures reported in this paper have been deposited with the Cambridge Crystallographic Data Centre as supplementary publication no. CCDC-100329. Copies of the data can be obtained free of charge on application to The Director, CCDC, 12 Union Road, Cambridge CB2 1EZ, UK (fax: Int. code +(1223) 336-033; e-mail: deposit@chemcrys.cam.ac.uk).

[17] H. Yamamoto, H. Yasuda, K. Tatsumi, K. Lee, A. Nakamura, J. Chen, Y. Kai, N. Kasai, *Organometallics* **1989**, *8*, 105.

[18] For a discussion of B–C bond lengths see: G. Herberich, A. Fischer, *Organometallics* **1996**, *15*, 58, and references therein.

[19] J. B. Blenkers, H. J. de Liefde Meijer, J. H. Teuben, *J. Organomet. Chem.* **1981**, *218*, 383; G. Erker, K. Berg, R. Benn, G. Schroth, *Chem. Ber.* **1985**, *118*, 1383; J. Blenkers, B. Hessen, F. van Bolhuis, A. J. Wagner, J. H. Teuben, *Organometallics*, **1987**, *6*, 459.

[20] G. M. Sheldrick, *Acta Crystallogr. Sect. A*, **1990**, *46*, 467.

[21] G. M. Sheldrick, SHELXL-93, Program for refinement of crystal structures, Universität Göttingen, **1993**.

[22] P. McArdle, *J. Appl. Crystallogr.* **1995**, *28*, 65.

[23] P. T. Beurskens, G. Beurskens, W. P. Bosman, R. de Gelder, S. Gracía-Granda, R. O. Gould, R. Israel, J. M. M. Smits, the DIRDIF-96 program system, University of Nijmegen, **1996**.

[24] A. L. Spek, PLATON, program for automated analysis of molecular geometry, University of Utrecht, **1996**.

[25] A. Meetsma, PLUTO, program for the display and analysis of crystal and molecular structures, University of Groningen, **1996**.

 © WILEY-VCH Verlag GmbH, D-69451 Weinheim, 1997 0570-0833/97/3621-2361 $ 17.50+.50/0

Regio- and Enantioselective Synthesis of α-Fluoroketones by Electrophilic Fluorination of α-Silylketone Enolates with *N*-Fluorobenzosulfonimide**

Dieter Enders,* Marcus Potthoff, Gerhard Raabe, and Jan Runsink

Dedicated to Professor Dieter Seebach on the ocassion of his 60th birthday

Over the last twenty years scientific and economic interest in organofluorine compounds has grown immensely due to their rapidly increasing practical use in plant protection, medicine, and other applications.[1, 2] The development of modern synthetic methods for electrophilic fluorination by substitution or addition with NF reagents has aided this advance, and various user-friendly NF fluorinating reagents are now available.[3] They provide a selective source of electrophilic fluorine that can be used in many ways. For this purpose *N*-fluorosulfonimides (**A**, **B**), *N*-fluorosulfonamides (**C**), and ammonium salts of type **D** were used. Davis et al.[4] reported the use of *N*-fluorobenzo-1,2-sulfonimide (**B**) for synthesizing fluorinated ketones, aldehydes, and esters. Differding et al. described the development and diverse application possibilities of *N*-fluoro-*N*,*N*-bis(phenyl)sulfonylamine (**A**, NFSI),[5] which was used for the electrophilic fluorinations presented here.

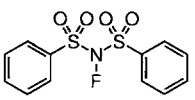

A (NFSI)

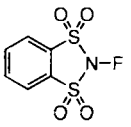

B

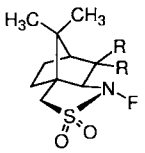

C (R=H,Cl)

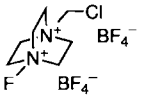

D

Until now the enantioselective synthesis of α-fluoroketones was only occasionally found in the literature. Differding et al.[5] reported the first enantioselective synthesis of α-fluorocarbonyl compounds using camphorsultam derivatives **C** (R = H, *ee* = 10–70%), and Davis et al.[4] described the fluorination of various carbonyl compounds with **C** (R = Cl, *ee* = 10–75% and R = H, *ee* = 25–70%). The enantiomeric excesses, however, reached no practical values. Kabat[6] recently published an enantioselective synthesis of α-fluoroketones by nucleophilic fluorination of allene oxides, which were synthesized by a Sharpless epoxidation. We have now, for the first time, obtained the title compounds in high yields, few steps, and very good enantiomeric excesses by a general synthetic route starting from simple ketones.

As shown in Scheme 1, α-silylketones (*R*)-**2a**, **b**, **d**, **e** and (*S*)-**2c** were converted with high enantiomeric purity (≥98%) in three

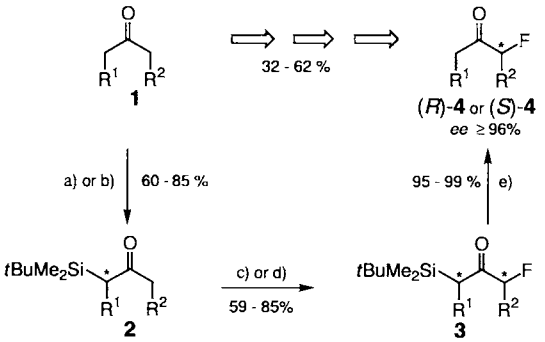

Scheme 1. Enantioselective synthesis of α-fluoroketones. a) Symmetrical ketones [(*R*)-**2**]: 1. SAMP, 12 h; 2. LDA, Et_2O, 0 °C, 4 h; 3. *t*$BuMe_2SiOTf$, −78 °C → RT; 4. O_3, CH_2Cl_2, −78 °C; b) unsymmetrical ketones (*S*)-**2** (R^1 = H): 1. SAMP, 12 h; 2. LDA, THF, 0 °C, 4 h; 3. *t*$BuMe_2SiCl$, −78 °C → RT; 4. *n*BuLi, Et_2O, 0 °C, 4 h; 5. diisopropylamine, EtBr, −78 °C → RT; 6. O_3, CH_2Cl_2, −78 °C; c) diastereoisomers **3c**–**e**: 1. LDA, THF, 0 °C, 4 h; 2. NFSI, −78 °C → RT, flash chromatography; d) diastereoisomers **3a**–**c**: 1. LHMDS, THF, 0 °C, 16 h; 2. NFSI, −78 °C → RT, flash chromatography; e) NH_4F (10 equiv), KH_2PO_4 (10 equiv), HF (aq, 1 equiv), nBu_4NF (1 equiv), THF, −78 °C → RT.

or four steps by the reaction of ketones **1a**–**e** with (*S*)-1-amino-2-methoxymethylpyrrolidine (SAMP) followed by silylation/α-alkylation and ozonolysis. Symmetric and unsymmetric (control of regiochemistry) as well as cyclic and acyclic ketones can be used as precursors.[7] After metalation with 1.1 equivalents of lithium diisopropylamide (LDA) in THF at 0 °C, electrophilic fluorination with NFSI at −78 °C led to α-fluoro-α′-silylketones (*S*,*S*)-**3c** or (*R*,*R*)-**3d**,**e** in good to very good diastereoselectivities (*de* from 67 to greater than 98%) and good yields (59–85%). After flash column chromatography the practically diastereomerically pure products (*de* greater than 98%) were obtained (Table 1). The *de* values of (*S*,*S*)-**3c** and (*R*,*R*)-**3d**,**e** were determined by ^{13}C NMR spectroscopy. For the synthesis of the product with the epimeric fluorinated center, the α-silylketones were converted into the enolates by treatment with 1.1 equivalents of lithium hexamethyldisilazide (LHMDS) at 0 °C in THF. The enolates were then fluorinated at −78 °C with NFSI to the appropriate α-fluoro-α′-silylketones (*S*,*R*)-**3a**,**b** and (*R*,*S*)-**3c** in good to high diastereoselectivities (*de* = 78–89%) and good yields (70–80%). Again, flash column chromatogra-

Table 1. Yields, base used, and diastereoisomeric excesses for the synthesis of α-fluoro-α′-silyl-ketones **3**.

3	R^1	R^2	Base [a]	Yield [%]	*de* [%] [b, c]
(*S*,*R*)-**3a**	Et	Et	LHMDS	80	89 (≥98)
(*S*,*R*)-**3b**	Pr	Pr	LHMDS	75	82 (≥98)
(*R*,*S*)-**3c**	Et	$PhCH_2$	LHMDS	70	78 (96)
(*S*,*S*)-**3c**	Et	$PhCH_2$	LDA	59	67 (≥98)
(*R*,*R*)-**3d**		$(CH_2)_3$	LDA	81	≥98
(*R*,*R*)-**3e**		$(CH_2)_4$	LDA	85	≥98

[a] Use of LHMDS leads to the (*Z*)-enolate of **2**, and use of LDA to the (*E*)-enolate of **2**. [b] In parentheses: diastereomeric excess after flash column chromatography (SiO_2, diethyl ether/pentane 1/100). [c] The *de* values were determined by ^{13}C NMR spectroscopy with a Varian Gemini 300 MHz (**3a**,**b**,**d**) or a Varian Unity 500 MHz spectrometer (**3c**,**e**).

[*] Prof. Dr. D. Enders, Dipl.-Chem. M. Potthoff, Dr. G. Raabe, Dr. J. Runsink
Institut für Organische Chemie der Technischen Hochschule
Professor-Pirlet-Strasse 1, D-52074 Aachen (Germany)
Fax: Int. code +(241) 888-8127
e-mail: enders@rwth-aachen.de

[**] This work was supported by the Deutsche Forschungsgemeinschaft (Leibniz-Preis and Sonderforschungsbereich 380) and the Fonds der Chemischen Industrie. We would like to thank the following companies for the donation of chemicals: Degussa, BASF, Hoechst, Bayer, and Wacker Chemie. We would particularly like to thank Allied Signal Inc., Buffalo, USA, for *N*-fluorobenzosulfonimide.

 © WILEY-VCH Verlag GmbH, D-69451 Weinheim, 1997 0570-0833/97/3621-2362 $ 17.50+.50/0

phy provided the practically diastereomerically pure products (*de* from 96 to greater than 98%, ^{13}C NMR). As for all acyclic ketones, alternative employment of lithium amide bases LDA and LHMDS allowed the formation of both α-fluorine epimers and finally both enantiomers, as shown for **3c**. This is rationalized by the differing enolate geometries [LDA (*E*), LHMDS (*Z*)]. This was confirmed by NMR spectroscopic analysis for the synthesis of the appropriate silylenol ether at both −78 and 0 °C according to Heathcock and Evans.[8]

Comparison of the ^1H NMR spectra of (*R*,*S*)-**3c**, (*S*,*S*)-**3c**, and (*R*,*R*)-**3e** (NOE measurements) supplied the preferred conformation in solution, with which the relative and absolute configuration of the newly generated stereocenter could be determined. This result was confirmed by an X-ray crystal structure analysis of (*R*,*R*)-**3e** (Figure 1);[9, 10] the fluorinating reagent approaches the enolate from the side opposite to that of the sterically demanding silyl group.

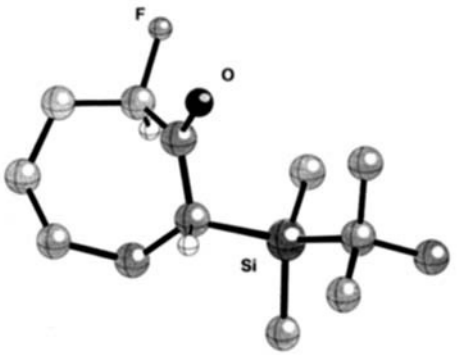

Figure 1. Crystal structure of α-fluoro-α′-silylketone **3e** [11].

For the racemization-free desilylation of α-fluoro-α′-silylketones **3a**–**e**, hydrofluoric acid and tetrabutylammonium fluoride were added to a suspension of ammonium fluoride and potassium dihydrogenphosphate in THF at −78 °C followed by the α-fluoro-α′-silylketone, and the reaction mixture was warmed.[12] Flash column chromatography provided α-fluoroketones **4a**–**e** in very good yields (95–99%) and high enantiomeric excesses (*ee* from 96 to greater than 98%), which were assigned by ^1H NMR spectroscopy with addition of a chiral co-solvent (Table 2).[13]

The regio- and enantioselective route described here presents the first general method for preparing practically enantiomerically pure α-fluoroketones from simple ketone precursors. By appropriate choice of base or starting ketone, both enantiomers of this important class of compounds can be obtained in good yield.[14]

Table 2. Yield, rotational value, and enantiomeric excesses of α-fluoroketones **4**.

4	R^1	R^2	Yield [%]	$[\alpha]_D^{25}$ (*c*, C_6H_6)	*ee* [%] [a]
(*S*)-**4a**	Et	Et	97	−47.88 (1.3)	≥96
(*S*)-**4b**	Pr	Pr	97	−59.63 (0.8)	≥96
(*R*)-**4c**	Et	$PhCH_2$	95	−68.59 (1.0)	≥96
(*S*)-**4c**	Et	$PhCH_2$	99	+66.42 (1.1)	≥96
(*R*)-**4d**	$(CH_2)_3$		99	+54.78 (1.0)	≥96
(*R*)-**4e**	$(CH_2)_4$		99	+72.87 (0.7)	≥96

[a] The *ee* values were determined by ^1H NMR spectroscopy (Varian Gemini 300 MHz spectrometer) with (−)-(*R*)-1-(9-anthryl)-2,2,2-trifluoroethanol as the co-solvent.

Experimental Section

Silylketones (*R*)-**2a**, **b**, **d**, **e** and (*S*)-**2c** were synthesized by the SAMP/RAMP-hydrazone method [7, 12].

Synthesis of **3a**–**e**: a) diastereoisomers (*S*,*S*)-**3c** and (*R*,*R*)-**3d**,**e**: To a solution of diisopropylamine (0.8 mL, 5.5 mmol) in THF (25 mL) at 0 °C was added *n*BuLi (3.7 mL, 1.5 N in *n*-hexane). After 30 min **2** (5 mmol) dissolved in THF (5 mL/mmol) was added. After 4 h the solution was cooled to −78 °C, and NFSI (1.58 g, 5 mmol) in THF (20 mL) was added dropwise. The reaction mixture was slowly warmed to room temperature, and the reaction quenched with an aqueous solution of NH_4Cl. The reaction mixture was then poured into water (10 mL), extracted three times with CH_2Cl_2 (15 mL), and dried over Na_2SO_4. The solvent was removed in vacuo. The crude oily solid was purified by distillation and then by column chromatography (SiO_2, ether/pentane 1/100), the remaining starting material was removed, and the diastereoisomers were separated to give (*S*,*S*)-**3c** and (*R*,*R*)-**3d** as colorless liquids and (*R*,*R*)-**3e** as a solid. b) Diastereoisomers (*S*,*R*)-**3a**,**b** and (*R*,*S*)-**3c**: To hexamethyldisilazane (1.15 mL, 5.5 mmol) in diethyl ether (10 mL) was added *n*BuLi (3.7 mL, 1.5 N in *n*-hexane) at 0 °C. The solution was warmed to room temperature, and the solvent removed under high vacuum. The remaining colorless solid was dissolved in THF (25 mL), cooled to 0 °C, and treated dropwise with **2** (5 mmol) dissolved in THF (5 mL/mmol). After 16 h the reaction mixture was cooled to −78 °C, and NFSI (1.58 g, 5 mmol) in THF (20 mL) was added. After the reaction mixture was slowly warmed to room temperature, it was quenched with an aqueous solution of NH_4Cl. The mixture was then poured into water (10 mL), extracted three times with CH_2Cl_2 (15 mL), and dried over Na_2SO_4. The solvent was removed in vacuo. The crude oily solid was purified by distillation and then by column chromatography (SiO_2, ether/pentane 1/100), the remaining starting material was removed, and the diastereoisomers were separated to give (*R*,*S*)-**3a**,**b** and (*R*,*S*)-**3c** as colorless liquids.

Desilylation of **3a**–**e**: NH_4F (10 equiv), KH_2PO_4 (10 equiv), Bu_4NF (1 mL, 1 M in THF), and HF (1 equiv of 40% solution in water) were added to THF (25 mL), and the solution was cooled to −78 °C. Then **3a**–**e** (1 mmol) in THF (10 mL) was added dropwise. After the mixture was slowly warmed to room temperature, it was quenched with a saturated solution of NH_4F. The reaction mixture was then poured into water (10 mL), extracted three times with of CH_2Cl_2 (10 mL), and dried over Na_2SO_4. The solvent was removed in vacuo. The crude brown-red products were purified by flash column chromatography (SiO_2, ether/pentane 1/40) to give **4a**–**e**. These colorless liquids can be stored at −20 °C under argon without racemization.

Received: July 15, 1997 [Z10683IE]
German version: *Angew. Chem.* **1997**, *109*, 2454–2456

Keywords: asymmetric synthesis · fluorinations · ketones · synthetic methods

[1] Reviews: a) S. Rozen, R. Filler, *Tetrahedron* **1985**, *41*, 1111–1153; b) S. Purrington, B. S. Kagan, T. B. Patrick, *Chem. Rev.* **1986**, *86*, 997–1018; c) J. Mann, *Chem. Soc. Rev.* **1987**, *16*, 381–436; d) J. T. Welch, *Tetrahedron* **1987**, *43*, 3123–3197; e) P. Bravo, G. Resnati, *Tetrahedron: Asymmetry* **1990**, *1*, 661–692; f) J. A. Wilkinson, *Chem. Rev.* **1992**, *92*, 505–519; g) O. A. Mascaretti, G. O. Danelon, *J. Fluorine Chem.* **1992**, *56*, 109–144; h) G. Resnati, *Tetrahedron* **1993**, *49*, 9385–9445; i) K. Iseki, Y. Kobayashi, *Rev. Heteroat. Chem.* **1995**, 211–237; j) J. M. Percy, *Contemp. Org. Synth.* **1995**, *2*, 251–268; k) J. T. Welch, R. Kawecki, *Stud. Nat. Prod. Chem.* **1995**, *16*, 727–744; l) S. Ozaki, *Med. Res. Rev.* **1996**, *16*, 51–86.

[2] Monographs: a) *Biomedical Aspects of Fluorine Chemistry* (Eds.: R. Filler, Y. Kobayashi), Elsevier Biomedical Press, Amsterdam, **1982**; b) *New Fluorinating Agents in Organic Synthesis* (Eds.: L. German, S. Zemskov), Springer, Berlin, **1989**; c) *Fluorine in Bioorganic Chemistry* (Eds.: J. T. Welch, S. Eswarakrishnan), Wiley, New York, **1991**; d) *Synthetic Fluorine Chemistry* (Eds.: G. A. Olah, R. D. Chambers, G. K. S. Prakash), Wiley, New York **1992**; e) *Organofluorine Chemistry: Principles and Commercial Applications* (Eds.: R. E. Banks, B. E. Smarts, J. C. Tatlow), Plenum, New York, **1994**; f) *Fluorine-containing Amino Acids* (Eds.: V. P. Kukhar, V. A. Soloshonok), Wiley, New York, **1995**; g) S. Rozen in *The Chemistry of Functional Groups, Supplement D2: The Chemistry of Halides, Pseudo-Halides and Azides* (Eds.: S. Patai, Z. Rappoport), Wiley, New York, **1995**.

[3] G. Sankar Lal, G. P. Pez, R. G. Syvret, *Chem. Rev.* **1996**, *96*, 1737–1755, and references therein.

[4] a) F. A. Davis, W. Han, *Tetrahedron Lett.* **1991**, *32*, 1631–1634; b) F. A. Davis, P. Zhou, C. K. Murphy, *ibid.* **1993**, *34*, 3971–3974; c) F. A. Davis, R. E. Reddy, *Tetrahedron: Asymmetry* **1994**, *5*, 955–960; d) F. A. Davis, C. K. Murphy, W. Han, V. Snieckus, F. Beaulieu, K. Mohri, *Tetrahedron Lett.* **1994**, *35*, 3465–3468; e) F. A. Davis, W. Han, C. K. Murphy, *J. Org. Chem.* **1995**, *60*, 4730–4737.

 © WILEY-VCH Verlag GmbH, D-69451 Weinheim, 1997 0570-0833/97/3621-2363 $ 17.50+.50/0

[5] a) E. Differding, R. W. Lang, *Tetrahedron Lett.* **1988**, *29*, 6087–6090; b) *Helv. Chim. Acta* **1989**, *72*, 1248–1252; c) E. Differding, G. M. Rüegg, *Tetrahedron Lett.* **1991**, *32*, 3815–3818; d) E. Differding, H. Ofner, *Synlett* **1991**, 187–189; e) E. Differding, R. O. Duthaler, G. M. Rüegg, C. Schmit, *ibid.* **1991**, 395–396; f) E. Differding, G. M. Rüegg, R. W. Lang, *Tetrahedron Lett.* **1991**, *32*, 1779–1782; g) E. Differding, M. Wehrli, *ibid.* **1991**, *32*, 3819–3822.
[6] M. M. Kabat, *Tetrahedron: Asymmetry* **1993**, *4*, 1417–1420.
[7] a) D. Enders, B. B. Lohray, *Angew. Chem.* **1987**, *99*, 359–360; *Angew. Chem. Int. Ed. Engl.* **1987**, *26*, 351–352; b) *ibid.* **1988**, *100*, 594-596 and **1988**, *27*, 581–583; c) B. B. Lohray, D. Enders, *Helv. Chim. Acta* **1989**, *72*, 980–984; d) D. Enders, B. B. Lohray, F. Burkamp, V. Bhushan, R. Hett, *Liebigs Ann.* **1996**, 189–200.
[8] a) D. A. Evans in *Asymmetric Synthesis, Vol. 3* (Ed.: J. D. Morrison), Academic Press, New York, **1984**, pp. 1–110; b) C. H. Heathcock in *Asymmetric Synthesis, Vol. 3* (Ed.: J. D. Morrison), Academic Press, New York, **1984**, pp. 111-212.
[9] Suitable crystals were obtained from pentane at −20 °C. $C_{13}H_{25}OFSi$, $M_r = 244.43$, crystal dimensions about $0.3 \times 0.3 \times 0.5$ mm, orthorhombic, $P2_12_12$ (no. 18), $a = 19.753(1)$, $b = 10.916(6)$, $c = 7.0199(9)$ Å, $V = 1513.7$ Å^3, $Z = 4$, $\rho_{calcd} = 1.073$ g cm^{-3}. Data were collected with an Enraf–Nonius CAD4 four-circle diffractometer with graphite-monochromated $Cu_{K\alpha}$ radiation ($\lambda = 1.54179$ Å). The structure was solved with direct methods (Gensin, Gentan, from Xtal3.2) [10]. Some of the hydrogen positions could be localized, and the remainder were calculated. There were 1461 observed reflexions [$I > 2\sigma(I)$], and 145 parameters refined; $R = 0.095$, $R_w = 0.061$; min./max. residual electron density −1.7/ + 0.6e Å^{-3}. The configuration at CF was determined by using the well-known configuration at CSi. Crystallographic data (excluding structure factors) for the structures reported in this paper have been deposited with the Cambridge Crystallographic Data Centre as supplementary publication no. CCDC-100579. Copies of the data can be obtained free of charge on application to The Director, CCDC, 12 Union Road, Cambridge CB21EZ, UK (fax: int. code +(1223)336-033; e-mail: deposit@chemcrys.cam.ac.uk).
[10] S. R. Hall, H. D. Flack, J. M. Stewart, *XTAL3.2 Reference Manual*, Universities of West Australia, Genf, and Maryland, **1992**.
[11] For the preparation of the software used, see Ball & Stick Ver. 2.2: A. Falk, N. Müller, G. Schoppel, L. Webb, Linz (Austria), Stafford (UK).
[12] D. Enders, D. Ward, J. Adam, G. Raabe, *Angew. Chem.* **1996**, *108*, 1059–1062; *Angew. Chem. Int. Ed. Engl.* **1996**, *35*, 981–984.
[13] D. Parker, *Chem. Rev.* **1991**, *91*, 1441–1457.
[14] All compounds gave appropriate spectroscopic data (IR, MS, NMR) and elemental analyses.

The Use of a Ten-Membered Tetraphosphole Macrocycle to Increase the Lifetime of a Palladium Catalyst

François Mercier, Frank Laporte, Louis Ricard, François Mathey,* Marc Schröder, and Manfred Regitz

Transient [PdL_2] complexes (L = phosphane) are the active intermediates in a number of reactions and processes[1] such as the Heck reaction[2] and the Stille cross-coupling reaction.[3] In some cases, the catalyst is lost at the end of the process as an insoluble precipitate, especially when the reaction is performed at relatively high temperature as in the case of the Heck reaction.[4] Recently we described a series of readily accessible tetraphosphole macrocycles of variable ring sizes (9–16 atoms).[5] The phosphorus atoms in these macrocycles are characterized by a low inversion barrier (about 16 kcal mol^{-1}) because of their incorporation into phosphole rings.[6] This means that a mixture of the various stereoisomers of each macrocycle behaves as the single stereoisomer that is the best adapted to coordinate to any given transition metal center.

In view of the importance of palladium catalysts in organic synthesis, we decided to study the properties of the palladium complexes of one of the most accessible tetraphosphole macrocycles, the ten-membered tetraphosphane **1**. The reaction of **1** with [$PdCl_2(PhCN)_2$] in dichloromethane immediately affords the red 1:1 complex **2** (Scheme 1), which was characterized by X-ray crystal structure analysis (Figure 1).

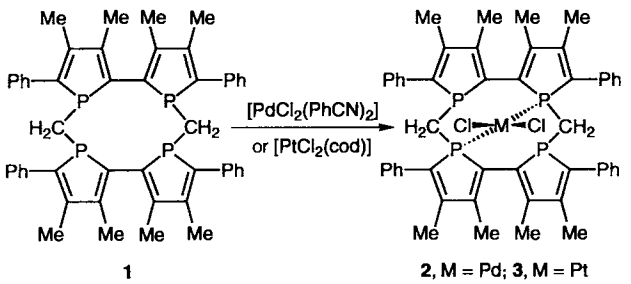

Scheme 1.

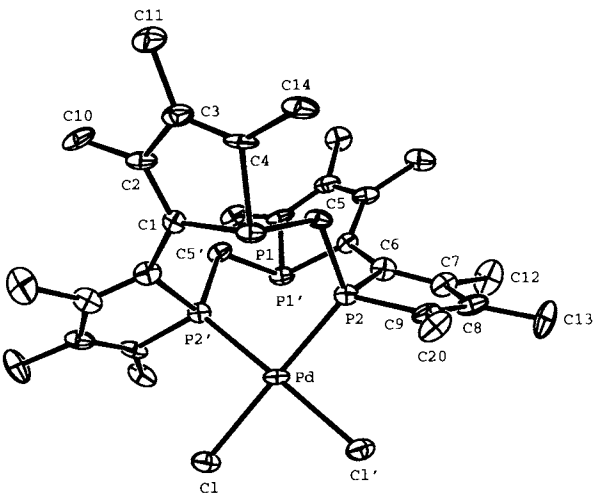

Figure 1. Crystal structure of **2**. Phenyl groups have been omitted for clarity. Important distances [Å] and angles [°]: Pd–Cl 2.344(2), Pd–Cl′ 2.346(2), Pd–P2 2.261(2), Pd–P2′ 2.264(2), Pd···P1 3.78; Cl-Pd-Cl′ 89.0(1), Cl-Pd-P2′ 89.18(6), Cl′-Pd-P2 89.16(6), P2-Pd-P2′ 93.2(1).

The structure shows a diagonal chelation of the palladium atom. The metal resides in a square-planar coordination environment with a *cis* arrangement of the phosphorus and chlorine atoms. The Pd···P1 separations are relatively short (3.79 Å). The angle between the lone pair at P1(P′1) and the P1(P′1)–Pd bond is calculated to lie around 72°. Thus, some through-space interaction probably exists between the noncoordinated phosphorus atoms and palladium. The ^{31}P NMR spectrum reveals the presence of two nonequivalent P atoms that show a large coupling (^2J(P,P) = 79 Hz). The analogous platinum complex **3** is similar (^2J(P,P) = 65 Hz), but additional Pt–P couplings are seen (^1J(Pt,P) = 3149 Hz). A simulation also indicates some coupling between the Pt and the noncoordinated P atoms (J(Pt,P) ≈ 127 Hz).

The structural characteristics of the Pd^{II} complex **2** suggested that some stabilization of a [Pd^0(**1**)] intermediate could be achieved because of the cradle conformation of **1** in the complex and because of the through-space interactions of the noncom-

[*] Prof. Dr. F. Mathey, Dr. F. Laporte, Dr. F. Mercier, Dr. L. Ricard
Laboratoire "Hétéroéléments et Coordination" URA 1499
DCPH Ecole Polytechnique
F-91128 Palaiseau Cedex (France)
Fax: Int. code +1 69 33 39 90
e-mail: francoismathey@polytechnique.fr
Prof. Dr. M. Regitz, Dipl.-Chem. M. Schröder
Fachbereich Chemie der Universität
Erwin-Schrödinger Strasse, D-67663 Kaiserslautern (Germany)

 © WILEY-VCH Verlag GmbH, D-69451 Weinheim, 1997 0570-0833/97/3621-2364 $ 17.50+.50/0

plexed lone pairs of electrons of **1** with the 14-electron palladium center. To test this hypothesis, we decided to compare the performance of **1** against the well-studied trifurylphosphane ligand Fu_3P in the palladium-catalyzed Stille cross-coupling reaction.[7, 8] Two types of catalytic systems were used for the comparison. The first, classical one used a mixture of one equivalent of $Pd(OAc)_2$ with four P donors (corresponding to one molar equivalent for **1**). In the second system, two equivalents of CuI were added.[8] The lifetime of the catalyst was evaluated by running the coupling of PhI with $CH_2=CHSnBu_3$ until the reaction stopped, then recharging the used catalyst with further batches of the same reagents. This process was repeated several times. The results are collected in Table 1. An inspection of these

Table 1. Stille coupling of iodobenzene with tributylvinyltin.

Entry	Phosphane	Catalyst (mol%)	T[°C]	t[h]	Conversion [%][a]
1	Fu_3P	Pd(5)	50	3	100
2	**1**	Pd(5)	50	3	85
3	Fu_3P	Pd(1)	80–90	3	100 [b]
4	**1**	Pd(1)	80–90	3	95
5a	Fu_3P	Pd/Cu(1)	80–90	3	100 [b]
5b	Fu_3P	Pd/Cu(1)	80–90	3	66
6	**1**	Pd/Cu(1)	80–90	3	100
7	Fu_3P	Pd/Cu(0.25)	60	5	85
	Fu_3P	Pd/Cu(0.25)	60	18	85
8a	**1**	Pd/Cu(0.25)	60	5	50
	1	Pd/Cu(0.25)	60	20	90
	1	Pd/Cu(0.25)	60	40	100
8b	**1**	Pd/Cu(0.25)	60	24	94
8c	**1**	Pd/Cu(0.25)	60	24	95

[a] Determined by gas chromatography. [b] Pd precipitate observed.

data clearly shows that the macrocycle **1** gives a slightly less active catalyst than with Fu_3P (compare entries 1 and 2 as well as 7 and 8a), which is consistent with the suspected higher stability of the [Pd(**1**)] system. In contrast, the lifetime of the [Pd(**1**)] catalyst is much longer than that of the $[Pd(Fu_3P)_2]$ species. Indeed, a precipitate is often observed at the end of the catalytic cycle with Fu_3P (entries 3 and 5a) and the activity of the catalyst drops sharply with time (entry 7). Recycling the catalyst is possible with **1**, even at low concentration (entries 8a–c) but this is not possible with Fu_3P (entries 5a, b). Consequently, the [Pd(**1**)] catalyst is much more cost-effective than $[Pd(Fu_3P)_2]$.

Similar results to those for the Stille coupling have been obtained in the Pd-catalyzed allylation of the malonate anion[9] (Table 2). In this case, the palladium complex of **1** is the best catalyst, especially at low concentration (entries 1 and 6). It is noteworthy that diagonal complexation of two of the four lone pairs of electrons of **1** by a $[Mo(CO)_4]$[5] fragment drastically decreases the efficiency of the catalyst (Table 2, entries 1 and 5).

Table 2. Palladium-catalyzed reaction of $PhCH=CHCH_2OAc$ with $NaCH(COOMe)_2$ [a].

Entry	Phosphane	Pd [mol%]	t[h]	Conversion [%][b]
1	**1**	0.5	3	95
2	Fu_3P	0.5	3	60
3	Ph_3P	0.5	3	10
4	$(Ph_2PCH_2)_2$	0.5	3	98
5	**1**·$Mo(CO)_4$	0.5	3	72
6	**1**	0.05	48	100
7	$(Ph_2PCH_2)_2$	0.05	48	93

[a] In THF at room temperature. [b] Traces of $(PhCH=CHCH_2)_2C(CO_2Me)_2$ are always formed.

This observation confirms the positive effect of the noncomplexed P atoms of **2** on the catalytic activity.

Finally, a comparison has been drawn with the palladacycles proposed by Herrmann et al.[4] for the Heck reaction (Scheme 2). After 48 h, we observed a 89% conversion; a 96%

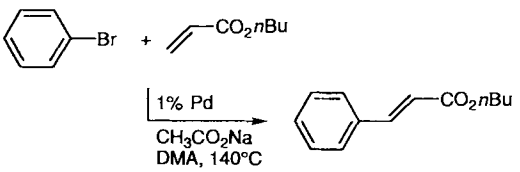

Scheme 2.

conversion was achieved with the catalyst from Herrmann et al.[4] However, our catalyst was still active, since quantitative conversion was observed after additional heating for 48 h. Thus, the extraordinary resistance of our system toward degradation is clearly established.

Experimental Section

2: **1** (0.39 g, 0.5 mmol) was dissolved under argon in CH_2Cl_2 (20 mL) and a solution of $[PdCl_2(PhCN)_2]$ (0.20 g, 0.5 mmol) in CH_2Cl_2 (5 mL) was added dropwise. After the mixture had been stirred at room temperature for 15 min, the solvent was evaporated under vacuum, and the residue was extracted with hot C_6H_6 (2 × 1 mL). The extracts were cooled to room temperature and allowed to stand to give dark red monocrystals of **2**. Yield: 0.43 g (90%). ^{31}P NMR (CD_2Cl_2): $\delta = -11.50$, 22.76 (AB system, $^2J(A,B) = 79.4$ Hz); ^1H NMR (CD_2Cl_2): $\delta = 1.82$ (s, 6H; CH_3), 1.94 (s, 6H; CH_3), 2.07 (d, $^4J(H,P) = 3.1$ Hz, 6H; CH_3), 2.11 (br., 4H; CH_2), 2.19 (d, $^4J(H,P) = 1.4$ Hz, 6H; CH_3), 6.60–7.90(m, 20H; Ph); ^{13}C NMR (CD_2Cl_2): $\delta = 13.3$, 15.52, 15.71, 17.64 (s; CH_3), 21.97 (pseudo-t; CH_2); elemental analysis (%): calcd for $\mathbf{2}\cdot 0.5\,C_6H_6$: C 64.35, H 5.20, P 12.53, Cl 10.76; found: C 64.47, H 5.35, P 13.20, Cl 10.67.

3: **1** (0.039 g, 0.05 mmol) was dissolved under argon in CH_2Cl_2 (2 mL) and a solution of $[PtCl_2(cod)]$ (0.020 g, 0.05 mmol) in CH_2Cl_2 (5 mL) was added dropwise. The mixture was heated for 15 min at 40 °C. After the solution had been allowed to cool, it was concentrated under vacuum, and Et_2O (5 mL) was added. The precipitate was washed with Et_2O and dried under vacuum. Yield 0.040 g (80%). ^{31}P NMR ([D$_6$]DMSO): $\delta = -8.50$, 9.17 (AB system, $^1J(P_A,Pt) = 3149$ Hz, $^1J(P_B,Pt) = 127$ Hz, $^2J(P_A,P_B) = 65.0$ Hz); ^1H NMR ([D$_6$]DMSO): $\delta = 1.34$ (s, 6H; CH_3), 1.46 (s, 6H; CH_3), 1.61 (s, 6H; CH_3), 1.73 (s, 6H; CH_3), 2.05 (d, $^2J(H,P) = 1.7$ Hz, 4H; CH_2), 6.11–7.40 (m, 20H; Ph); ^{13}C NMR ([D$_6$]DMSO): $\delta = 14.17$, 15.84, 16.04, 16.34 (s; CH_3), 20.0 (pseudo-t; CH_2).

Stille coupling: An appropriate amount of catalyst was preformed under argon in a dry schlenk flask equipped with a magnetic stirring bar in freshly degassed DMF (3 mL) at room temperature. It was prepared from either $Pd(OAc)_2$ (1 equiv) and tri-2-furylphosphane (4 equiv) or from $Pd(OAc)_2$ (1 equiv) and **1** (1 equiv) by stirring at 40 °C for 15 min. Iodobenzene (0.112 mL, 1 mmol) was added to the preformed catalyst and, after a period of 15 min at room temperature, tributylvinyltin (0.292 mL, 1 mmol) was introduced. Thereafter, in specific cases CuI (2 equiv) was added. The flask was then immersed in a thermostated bath, and the evolution of the crude reaction mixture was monitored by GC on a Varian 3400 apparatus equipped with a WCOT (25 m, 0.25 mm) capillary column, CP-SiP-SCB stationary phase between 40 °C and 220 °C.

Palladium catalyzed allylic substitution: A mineral oil dispersion of NaH (60% NaH, 1.25 mmol) was washed free of oil with dry *n*-pentane (2 × 5 mL). The oil-free NaH was suspended in THF (4 mL), stirred, cooled to 0 °C, and treated dropwise with a solution of dimethyl malonate (1.2 equiv). After the reaction was complete, the resulting solution of sodium dimethyl malonate was transferred by cannula under argon into a 50 mL flask containing 1-acetoxy-3-phenyl-2-propene (1.2 mmol), and the catalyst, which had been previously prepared by mixing solutions containing $[Pd(dba)_2]$ (1 equiv; dba = dibenzylidenacetone) in THF (1 mL) and the phosphane (4 equiv) in THF (1 mL,) and stirring under argon at room temperature (in the cases of **1** and **1**·$Mo(CO)_4$, the catalyst was prepared as above from tetraphosphole (1 equiv); the reaction was stirred for 15 min at 50 °C). The reaction mixture was stirred at room temperature and the degree of conversion was calculated from the crude reaction mixture by ^1H NMR spectroscopy. The work up involved dilution in glacial acetic acid, extraction with Et_2O, and washing with brine. Subsequent evaporation of the solvents gave the crude product as a yellow oil, which was purified by chromatography on alumina by using hexane/ethyl acetate (80/20).

Heck coupling: Aryl bromide (5 mmol), *N*,*N*-dimethyl acetamide (DMA) (5 mL), *n*-butyl acrylate (5.5 mmol), and anhydrous sodium acetate (0.5 g) were placed

 © WILEY-VCH Verlag GmbH, D-69451 Weinheim, 1997 0570-0833/97/3621-2365 $ 17.50+.50/0

under argon in a 50 mL double-necked flask equipped with a reflux condenser. The flask was heated at 140 °C and the solution of freshly prepared catalyst (1 equiv, 1 mL DMA) (see above), was added rapidly. The conversion of the aryl bromide was monitored by GC on 50 μL samples of the crude mixture dissolved in acetone (2 mL).

Received: March 11, 1997
Revised version: June 23, 1997 [Z10299IE]
German version: *Angew. Chem.* **1997**, *109*, 2460–2462

Keywords: homogeneous catalysis · P ligands · palladium · platinum

[1] J. Tsuji, *Palladium Reagents and Catalysts: Innovations in Organic Synthesis*, Wiley, Chichester, **1995**.
[2] A. de Meijere, F. E. Meyer, *Angew. Chem.* **1994**, *106*, 2473; *Angew. Chem. Int. Ed. Engl.* **1994**, *33*, 2379.
[3] J. K. Stille, *Angew. Chem.* **1986**, *98*, 504; *Angew. Chem. Int. Ed. Engl.* **1986**, *25*, 508.
[4] W. A. Herrmann, C. Brossmer, K. Öfele, C.-P. Reisinger, T. Priermeier, M. Beller, H. Fischer, *Angew. Chem.* **1995**, *107*, 1989; *Angew. Chem. Int. Ed. Engl.* **1995**, *34*, 1844.
[5] F. Laporte, F. Mercier, L. Ricard, F. Mathey, *J. Am. Chem. Soc.* **1994**, *116*, 3306.
[6] W. Egan, R. Tang, G. Zon, K. Mislow, *J. Am. Chem. Soc.* **1971**, *93*, 6205. Theoretical study: L. Nyulaszi, *J. Phys. Chem.* **1995**, *99*, 586.
[7] V. Farina, B. Krishnan, *J. Am. Chem. Soc.* **1991**, *113*, 9585.
[8] V. Farina, S. Kapadia, B. Krishnan, C. Wong, L. S. Liebeskind, *J. Org. Chem.* **1994**, *59*, 5905.
[9] For a recent review of this type of reaction, see ref.1, pp. 290–422.
[10] Crystallographic data (excluding structure factors) for the structures reported in this paper have been deposited with the Cambridge Crystallographic Data Centre as supplementary publication no. CCDC-100247. Copies of the data can be obtained free of charge on application to The Director, CCDC, 12 Union Road, Cambridge CB2 1EZ, UK (fax: int. code +(1223) 336-033; e-mail: deposit@chemcrys.cam.ac.uk).

Asymmetric Catalytic Protonation of Silyl Enol Ethers with Chiral Palladium Complexes**

Masaharu Sugiura and Takeshi Nakai*

The enantioselective protonation of prochiral enolates with a chiral proton source has attracted much attention as a general methodology for the asymmetric synthesis of α-substituted carbonyl compounds.[1] While most of the methods reported so far require the use of more than a stoichiometric amount of a chiral Brønsted acid, the catalytic use of a chiral acid, combined with a stoichiometric amount of an achiral proton source, has also been successful.[2] Disclosed here is a conceptually new approach to the asymmetric catalytic protonation of enol silyl ethers, which employs water as the proton source and a chiral palladium complex as the catalyst.

Scheme 1 illustrates our working hypothesis.[3] Chiral transition metal complex **A**, if coordinatively unsaturated, should activate silyl enol ether **1** and promote attack by water onto the silyl group to afford chiral metal enolate **B** and a silanol. Enolate **B** would then be diastereoselectively protonated by water to

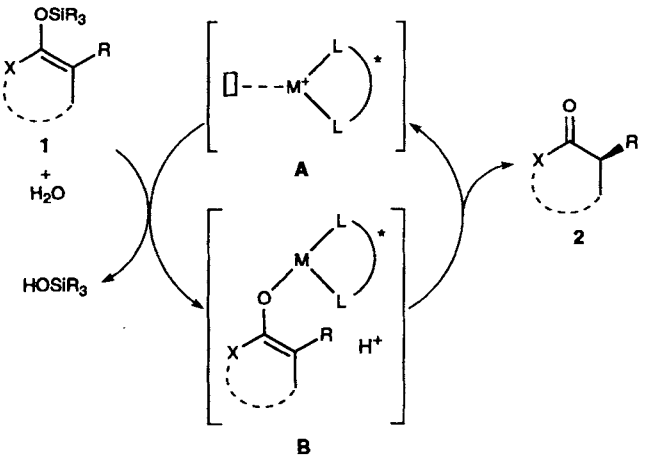

Scheme 1. The working hypothesis.

afford the enantiomerically enriched ketone **2** with regeneration of **A**. To realize this new concept, the chiral transition metal catalyst should be capable of preferentially activating the enol ether over the coexisting water and product ketone. Based on these considerations, we selected chiral cationic Pd complexes as the catalyst. Shibasaki et al. recently reported that the chiral cationic Pd complex prepared from [$PdCl_2$\{(*R*)-binap\}] (binap = 2,2′-bis(diphenylphosphanyl)-1,1′-binaphthyl) and AgOTf (1:1) in the presence of 4-Å molecular sieves (MS) in wet DMF serves as an efficient asymmetric catalyst for aldol reactions due to the intermediacy of a chiral Pd enolate.[4]

Therefore, we focused on the two chiral cationic Pd species generated from [$PdCl_2$\{(*R*)-binap\}] (**3a**) or [$PdCl_2$\{(*R*,*R*)-diop\}] (**3b**) and silver salts for the protonation of cyclic enol ether **1a** with water (Scheme 2). Whereas the Pd species generated by

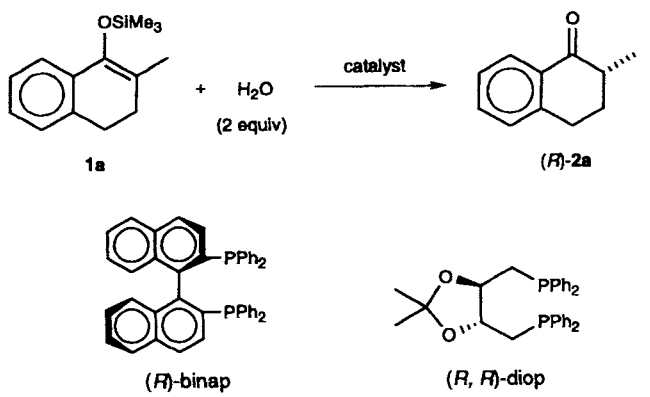

Scheme 2. Protonation of cyclic enol ether **1a** by water in the presence of chiral, cationic Pd complexes generated from [$PdCl_2$\{(*R*)-binap\}] (**3a**) or [$PdCl_2$\{(*R*)-diop\}] (**3b**) and silver salts.

mixing **3a** and two equivalents of $AgPF_6$ showed high catalytic activity but low enantioselectivity (Table 1, entry 1), that generated by the method of Shibasaki et al.[4] provided higher enantiomeric excesses; however, the reproducibility was very poor (entry 2). We therefore suspected that a contaminant plays a vital role in this reaction. Significantly enough, when a small amount of diisopropylamine—a possible contaminant of **1a**—was added to the catalyst solution, the enantioselectivity remarkably improved to 79% *ee*; the reproducibility was also very good (entry 3).[5] Analogous use of the diop complex **3b**

[*] Prof. T. Nakai, Dr. M. Sugiura
Department of Chemical Technology
Tokyo Institute of Technology
Meguro-ku, Tokyo 152 (Japan)
Fax: Int. code +(3)5734-2885
e-mail: takeshi@o.cc.titech.as.jp

[**] This work was supported by a JSPS Grant for the "Research for the Future" Program.

 © WILEY-VCH Verlag GmbH, D-69451 Weinheim, 1997 0570-0833/97/3621-2366 $ 17.50+.50/0

Table 1. Optimization of asymmetric catalysis for the protonation of **1a** with water [a].

Entry	Catalyst	Conditions	Yield [%][b]	*ee*[%][c] (Config.[d])
1	$[PdCl_2\{(R)$-binap$\}]$ (**3a**, 5 mol%) $AgPF_6$ (10 mol%) CH_2Cl_2/MeOH	RT 0.5 h	95	4–13 (*S*)
2	**3a** (5 mol%) AgOTf (5 mol%) 4-Å MS, DMF/H_2O	RT–30 °C 84–5 h	25–85	44–73 (*R*)
3	**3a** (5 mol%) AgOTf (5 mol%) 4-Å MS, DMF/H_2O then iPr_2NH (0.5 mol%)	50 °C 18 h	83	79 (*R*)
4	$[PdCl_2\{(R,R)$-diop$\}]$ (**3b**, 5 mol%) AgOTf (5 mol%) 4-Å MS, DMF/H_2O then iPr_2NH (0.5 mol%)	50 °C 5 h	78	3 (*S*)
5	$[PtCl_2\{(R)$-binap$\}]$ (5 mol%) AgOTf (5 mol%) 4-Å MS, DMF/H_2O then iPr_2NH (0.5 mol%)	50 °C 118 h	62	4 (*R*)

[a] All reactions were carried out with **1a** (0.5 mmol, see Experimental Section). [b] Yield of isolated product. [c] Determined by HPLC analysis on CHIRALCEL OD. [d] Assigned by comparing the optical rotation with literature values [6].

provided a lower enantiomeric excess (entry 4). A similar Pt–binap complex was also inferior to **3a** in both activity and enantioselectivity (entry 5). Furthermore, using $AgPF_6$ instead of AgOTf afforded **2a** in 81% yield and 76% *ee* (*R*), and using basic alumina instead of 4-Å molecular sieves resulted in 91% yield and 63% *ee*.

The question of what role the added diisopropylamine plays arises. Interestingly, addition of triethylamine gave essentially the same results (84% yield and 76% *ee*), indicating that the amine might act as a Lewis base, and not as a proton source. Moreover, ^{31}P NMR spectroscopic measurements of the catalyst solutions before and after addition of diisopropylamine[7] suggest that the amine might selectively deactivate one of the binap-bound Pd species initially formed. In other words, it appears that upon addition of the amine, the surviving Pd species act as the predominant catalyst(s), thus making the reaction slower but providing enhanced enantiomeric selectivity.

To gain further insight into the reaction mechanism, a labeling experiment with D_2O was carried out (Scheme 3).[8] Ketone **2a**, with 80% deuterium content at the α-position, was obtained together with traces of unexpected by-products,[9] implying that the reaction is more complicated than anticipated. More detailed studies must be awaited.

Finally, the present asymmetric catalysis was also applied to silyl enol ethers **1b–g**[5] under optimized conditions (Scheme 4).

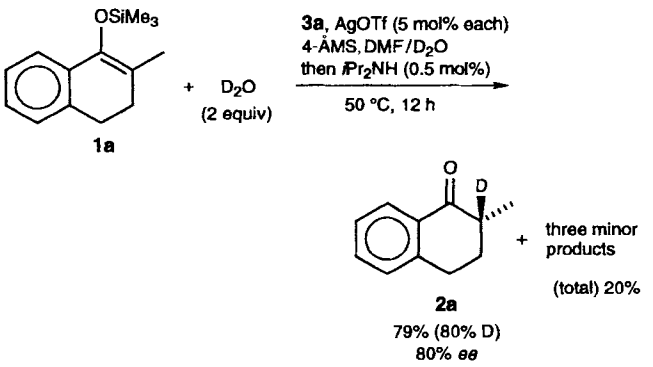

Scheme 3. Labeling experiments with D_2O.

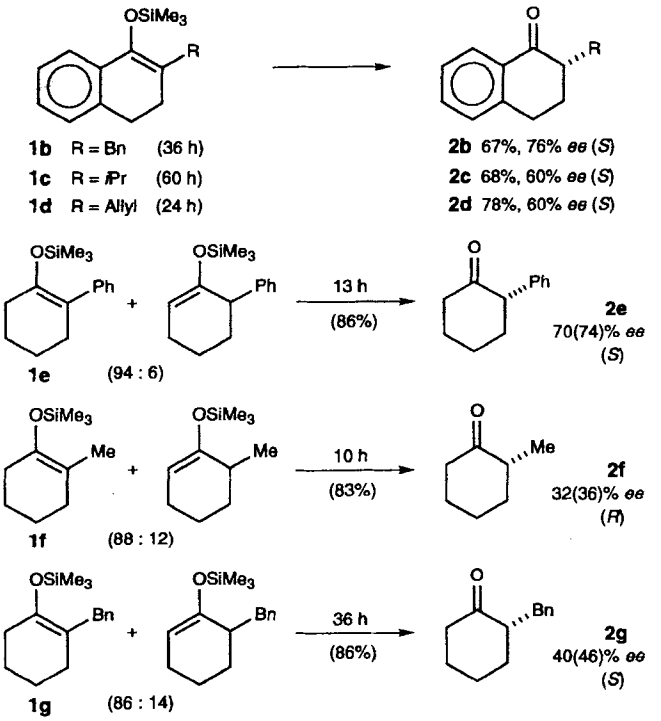

Scheme 4. Asymmetric catalytic protonation of various silyl enol ethers under optimal conditions. Values for **2e–g** that are corrected for the regioisomeric purity of the silyl enol ethers are given in parentheses.

While comparably high levels of enantiomeric selectivity were obtained with **2b–e**,[10] **1f** and **1g** gave moderate enantiomeric selectivity.

Experimental Section

In a typical reaction a mixture of **3a** (20 mg, 0.025 mmol), AgOTf (6.4 mg, 0.025 mmol), 4-Å MS powder (150 mg), DMF (1 mL), and water (36 μL) was stirred at room temperature for 2 h under an argon atmosphere. The resulting mixture was filtrated through a short Celite column to provide a red solution. An aliquot (10 μL) of a solution containing iPr_2NH (33 μL) and DMF (1 mL) was added along with water (18 μL), and the mixture stirred at room temperature for 30 min. Then, **1a** (116 mg, 0.5 mmol) was added, and the resulting solution stirred at 50 °C for 18 h. After dilution with ether (40 mL), addition of water (10 mL), and filtration through a Celite pad, the organic layer was washed with brine, dried over magnesium sulfate, and freed of solvent under reduced pressure. Purification by preparative thin-layer chromatography afforded **2a** (66 mg, 83%).

Received: March 19, 1997 [Z10280IE]
German version: *Angew. Chem.* **1997**, *109*, 2462–2464

Keywords: asymmetric catalysis · palladium · protonations

[1] Recent review: C. Fehr, *Angew. Chem.* **1996**, *108*, 2726–2748; *Angew. Chem. Int. Ed. Engl.* **1996**, *35*, 2566–2587.

[2] Asymmetric protonations of enolates using a catalytic amount of chiral proton sources: a) A. Yanagisawa, T. Kikuchi, T. Watanabe, T. Kuribayashi, H. Yamamoto, *Synlett* **1995**, 372–374; b) C. Fehr, J. Galindo, *Angew. Chem.* **1994**, *106*, 1967–1968; *Angew. Chem. Int. Ed. Engl.* **1994**, *33*, 1888–1889; c) C. Fehr, I. Stempf, J. Galindo, *ibid.* **1993**, *105*, 1093–1095 and **1993**, *32*, 1044–1046; d) Y. Nakamura, S. Takeuchi, A. Ohira, Y. Ohgo, *Tetrahedron Lett.* **1996**, *37*, 2805–2808; e) K. Ishihara, S. Nakamura, M. Kaneeda, H. Yamamoto, *J. Am. Chem. Soc.* **1996**, *118*, 12854–12855.

[3] For the conceptually different use of transition metal catalysts in the asymmetric protonation of enolates, see a) Pd/C coupled with a catalytic amount of a chiral Brønsted acid: J. Muzart, H. Hénin, S. J. Aboulhoda, *Tetrahedron: Asymmetry* **1997**, *8*, 381–389; b) $[Rh(binap)]^+$-catalyzed ketonization of an allylic alcohol: S. H. Bergens, B. Bosnich, *J. Am. Chem. Soc.* **1991**, *113*, 958–967.

[4] M. Sodeoka, K. Ohrai, M. Shibasaki, *J. Org. Chem.* **1995**, *60*, 2648–2649, and references therein.

 © WILEY-VCH Verlag GmbH, D-69451 Weinheim, 1997 0570-0833/97/3621-2367 $ 17.50+.50/0

[5] To prevent contamination by the amine, **1a** should be purified by column chromatography on neutral silica gel.
[6] G. Jaousen, A. Meyer, *J. Am. Chem. Soc.* **1975**, *97*, 4667–4672.
[7] ^{31}P NMR (109 MHz, [D$_6$]DMSO, H$_3$PO$_4$): the initial species: δ = 32.0–34.0, 27.5–29.5, 27.3 (s); after addition of *i*Pr$_2$NH (0.4 equiv based on Pd): δ = 27.5–29.5, 27.8 (s), 27.3 (s).
[8] For this experiment 4-Å MS powder was dried at 300 °C for 8 h under vacuum (< 0.05 Torr) to prevent contamination by water; otherwise, a lower deuterium content (55%) resulted. We thank Dr. Masahiro Terada for suggesting this procedure.
[9] The by-products were α-deuterated (to 70%) α-(trimethylsilylmethyl)tetralone (4%, 81% *ee*), α-hydroxy-α-methyltetralone (6%, 0% *ee*), and β-methyltetrahydro-α-naphthol (10%, 0% *ee*).
[10] Enantiomeric excesses were determined by HPLC on CHIRALCEL OD-H for **2b–e** and by capillary GLC on CP-chirasil-DEX CB for **2f** and **2g**. The configurations were assigned by comparing optical rotations with literature values: **2b**: M. Murata, M. Nakajima, K. Koga, *J. Chem. Soc. Chem. Commun.* **1990**, 1657–1658; **2c**: T. Yasukata, K. Koga, *Tetrahedron: Asymmetry* **1993**, *4*, 35–38; **2e**: G. Berti, B.Macchia, F. Macchia, L. Menti, *J. Chem. Soc. C* **1971**, 3371–3375; **2g**: A. I. Meyers, D. R. Williams, G. W. Erickson, S. White, M. Druelinger, *J. Am. Chem. Soc.* **1981**, *103*, 3081–3087. The configurations of **2d** and **2f**, though not yet determined, were assigned based on the similarity of the values.

Selective Enhancement of NMR Signals for α-Cyclodextrin with Laser-Polarized Xenon**

Yi-Qiao Song, Boyd M. Goodson, Rebecca E. Taylor, David D. Laws, Gil Navon, and Alexander Pines*

Xenon, hydrophobic and chemically inert, has been widely used as an NMR probe of chemical environments, both in solution and in the solid state.[1] With the application of optical pumping,[2] a large (> 10%) ^{129}Xe nuclear-spin polarization can be generated. This polarization has been used to increase the sensitivity of ^{129}Xe NMR spectroscopy[3, 4] and magnetic resonance imaging (MRI),[5] and to supply polarization to neighboring spins on surfaces.[6] It was recently shown that enhanced xenon polarization can also be transferred to molecules in solution[7] by cross-relaxation, a process dubbed the *s*pin *p*olarization *i*nduced *n*uclear *O*verhauser *e*ffect (SPINOE). Because the SPINOE depends on the proximity of ^{129}Xe atoms to neighboring spins, as well as their relative motion, more rapid transfer of polarization is expected when xenon is temporarily bound, thereby permitting selective enhancement of NMR signals of nuclear spins near xenon binding sites.

Here we report polarization transfer from laser-polarized ^{129}Xe to ^{1}H spins in two molecular systems in solution: *p*-nitrotoluene (*p*-NT), which couples mainly diffusively to xenon, and α-cyclodextrin (α-CD, Figure 1), a cyclic oligosaccharide with a hydrophobic pocket known to bind xenon[8, 9] and other guest species.[10] Binding of xenon to α-CD gives rise to cross-relaxation rates up to 150 times greater than those between xenon and *p*-NT; this results in more rapid transfer of polarization. Furthermore, enhancements of ^{1}H spins adjacent to the xenon binding site in α-CD are greater than those of ^{1}H spins further away.

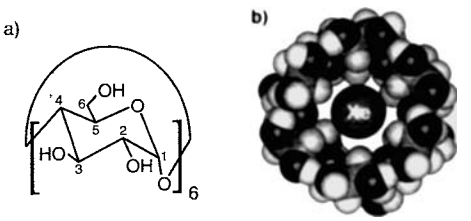

Figure 1. a) Structural formula of α-cyclodextrin. b) CPK model of α-cyclodextrin [16] in which a xenon atom is placed within the hydrophobic pocket containing the hydrogen atoms H3 and H5.

The change in the ^{1}H magnetization due to the presence of highly polarized xenon is well approximated by Equation (1).[7]

$$\frac{\Delta M^{H}}{M_{eq}^{H}} = -\sigma_n n^{Xe} T_1^{H} \frac{\gamma^{Xe}}{\gamma^{H}} \frac{\Delta M^{Xe}}{M_{eq}^{Xe}} (1-e^{-t/T_1^{H}}) \quad (1)$$

$$\sigma_n n^{Xe}, \quad \frac{1}{T_1^{Xe}} \ll \frac{1}{T_1^{H}} \quad (2)$$

Here, σ_n is the partial millimolar cross-relaxation rate, n^{Xe} is the concentration of ^{129}Xe in the solution, γ^{Xe}, γ^{H} are the magnetogyric ratios, M^{Xe}, M^{H} and M_{eq}^{Xe}, M_{eq}^{H} are the enhanced and equilibrium magnetization of ^{129}Xe and ^{1}H, respectively, T_1^{Xe}, T_1^{H} (under condition (2)) are the ^{129}Xe and ^{1}H spin-lattice relaxation times, and $\Delta M = M - M_{eq}$. In the absence of laser polarization, the ^{129}Xe–^{1}H NOE enhancement is minuscule ($\approx 10^{-5}$) due to low xenon concentration and weak ^{129}Xe–^{1}H coupling. In previous work[9, 11] ^{129}Xe–^{1}H interactions were indirectly observed by detecting changes in the xenon signal during proton saturation. With the use of laser-polarized xenon, however, the ^{129}Xe–^{1}H NOE enhancement ($\approx 10^{-2}$)[12] is detected directly in the resolved ^{1}H NMR spectrum.

The technique used for optically pumping xenon has been described elsewhere;[4] ^{129}Xe polarizations are typically 5–10%. To detect the SPINOE signals, we used a heteronuclear difference NOE pulse sequence (Figure 2), which suppresses the equilibrium ^{1}H magnetization and is therefore directly sensitive to the SPINOE. The ^{1}H SPINOE NMR spectra for 0.1 M *p*-NT in [D$_6$]benzene with laser-polarized xenon are shown in Figure 3. Equation (1) was used to determine values of σ_n for *p*-NT by assuming a linear dependence of the cross-relaxation rate on the concentration of polarized xenon (Table 1). The values are similar to that for the hydrogen atom of [D$_5$]benzene, which is in agreement with a rough theoretical

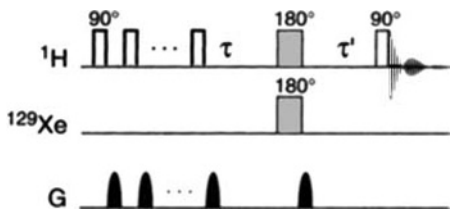

Figure 2. Heteronuclear difference NOE pulse sequence for ^{129}Xe–^{1}H SPINOE NMR spectroscopy based on sequences developed by Shaka [13]. The equilibrium ^{1}H NMR signal is saturated by 90° and gradient pulses (G); the saturation is maintained by a 180° pulse followed immediately by a gradient pulse. A xenon 180° pulse allows SPINOE signals to accumulate during the mixing periods τ and τ'. Each spectrum represents the difference of two scans.

[*] Prof. A. Pines, Y.-Q. Song, B. M. Goodson, R. E. Taylor, D. D. Laws
Materials Sciences Division, Lawrence Berkeley National Laboratory
and
Department of Chemistry
University of California
Berkeley, CA 94720 (USA)
Fax: Int. code +(510)486-5744
e-mail: pines@cchem.berkeley.edu
Prof. G. Navon
School of Chemistry, Tel Aviv University (Israel)

[**] We thank A. J. Shaka and M. Luhmer for helpful comments and suggestions. D. D. L. gratefully acknowledges the Howard Hughes Medical Institute for a pre-doctoral fellowship. G. N. is Visiting Miller Research Professor at the University of California, Berkeley. This work was supported by the Office of Basic Sciences, Materials Sciences Division of the U. S. Deptartment of Energy (contract no. DE AC03-76SF00098).

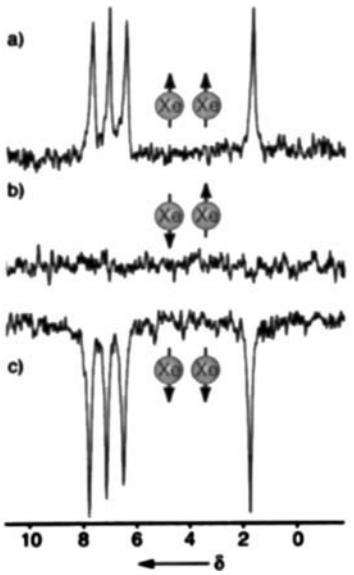

Figure 3. ^{1}H SPINOE NMR spectra of 0.1 M *p*-nitrotoluene in [D_6]benzene ($\tau = 4.5$ s and $\tau' = 3.5$ s). Chemical shifts are referenced to the signal for [D_5]benzene ($\delta = 7.16$). a) Spectrum acquired with the pulse sequence in Figure 2 after introduction of negatively polarized ^{129}Xe (with xenon spins "up", $\gamma^{Xe} < 0$); b) as in a), but in the absence of a xenon 180° pulse; c) spectrum acquired after introduction of positively polarized ^{129}Xe (prepared by inverting the magnetic field in which the ^{129}Xe is laser-polarized); this results in a sign change in the spectrum.

Table 1. ^{129}Xe–^{1}H cross-relaxation rates σ_n and ^{1}H spin-lattice relaxation times T_1

Molecule	Proton	σ_n [10^{-6} s^{-1} mM^{-1}]	T_1 [s] [a]
p-NT	CH_3	0.025 ± 0.007	6.8
	H3, H5	0.032 ± 0.006	35
	H2, H6	0.029 ± 0.005	23
[D_5]benzene [b]	H	0.028 ± 0.007	110
α-CD	H1	0.44 ± 0.14	1.1
	H2	1.3 ± 0.5	1.1
	H3	4.1 ± 0.8	1.2
	H4	1.6 ± 0.3	1.1
	H5	4.9 ± 1.2	0.87
	H6	1.2 ± 0.4	0.78
	OH(2)	0.70 ± 0.22	1.2
	OH(3)	0.86 ± 0.18	1.0
	OH(6)	0.36 ± 0.14	1.1

[a] The error range for the T_1 measurements is about ±5%. [b] Data for [D_5]benzene signals in the *p*-NT spectra.

estimate of the cross-relaxation rate based on dipolar coupling modulated by molecular diffusion.[7]

The first indication of stronger couplings for laser-polarized xenon in α-CD is the reduced ^{129}Xe relaxation time T_1 (≈20 s in 0.1 M α-CD/[D_6]DMSO), which is short compared to that for xenon in 0.1 M *p*-NT/[D_6]benzene (>500 s). The equilibrium ^{1}H NMR spectrum of α-CD is shown in Figure 4a; the chemical shifts were assigned by means of a 2D COSY spectrum. After introduction of laser-polarized ^{129}Xe into the solution, SPINOE NMR spectra (Figure 4b–d) were obtained by using the pulse sequence of Figure 2. Values of σ_n for the ^{1}H spins in α-CD were obtained by fitting the data to Equation (1) (Table 1). The increase in couplings between xenon and α-CD arising from xenon binding[14] demonstrates the sensitivity of σ_n to the binding of xenon with molecules in solution.

In the case of α-CD, variation of signal enhancements is observed in the ^{1}H NMR spectrum: The strongest SPINOEs are observed from the H3 and H5 atoms located inside the hydrophobic pocket. Differences in the xenon coupling to various protons is expected when binding occurs, because dipolar relaxation is sensitive to the distances between spins and varies as $\sigma_n \propto r^{-6}$.[15] For example, from this relationship a ratio of 1:1.5 can be estimated for the range of relative distances between Xe–H5 and Xe–H1, neglecting transferred NOEs.[17] According to the X-ray structure of α-CD,[16] a ratio between 1:1.2 and 1:2, corresponding to Xe–H5 distances of about 3 to 6 Å and Xe–H1 distances of about 6 to 8 Å, is consistent with a distribution of xenon locations within the hydrophobic pocket.

These results show the potential of ^{129}Xe–^{1}H SPINOE experiments for probing the structure and dynamics of molecules in solution. Furthermore, they may have implications for NMR studies of hydrophobic potentials in systems involved in hydrophobic binding, for example, inclusion compounds, membranes, and proteins.

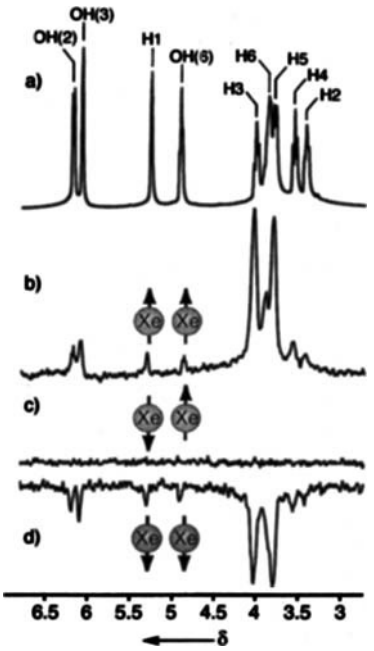

Figure 4. a) ^{1}H NMR spectrum of 0.05 M dehydrated α-cyclodextrin in [D_6]DMSO; b) ^{1}H SPINOE NMR spectrum of α-CD acquired with the pulse sequence in Figure 2 after introduction of negatively polarized ^{129}Xe; c) as in b), but in the absence of a xenon 180° pulse; d) ^{1}H SPINOE NMR spectrum acquired after introduction of positively polarized ^{129}Xe; b)–d) $\tau = 0.63$ s and $\tau' = 0.37$ s.

Received: June 16, 1997 [Z 19560 IE]
German version: *Angew. Chem.* **1997**, *109*, 2464–2466

Keywords: cyclodextrins · host–guest chemistry · laser polarization · NMR spectroscopy · xenon

[1] Reviews: a) J. Fraissard, T. Ito, *Zeolites* **1988**, *8*, 350–361; b) P. J. Barrie, J. Klinowski, *Prog. NMR Spectrosc.* **1992**, *24*, 91–108; c) J. Jokisaari, *ibid.* **1994**, *26*, 1–25; d) D. Raftery, B. Chmelka *NMR: Basic Princ. Prog* **1994**, *30*, 111–158; e) T. Pietrass, H. C. Gaede, *Adv. Mater.* **1995**, *7*, 826–838.

[2] a) A. Kastler, *J. Phys. Radium* **1950**, *11*, 255–265; b) M. A. Bouchiat, T. R. Carver, C. M. Varnum, *Phys. Rev. Lett.* **1960**, *5*, 373–375; c) T. G. Walker, W. Happer, *Rev. Mod. Phys.* **1997** *69*, 629–642.

[3] W. Happer, E. Miron, S. Schaefer, D. Schreiber, W. A. van Wijngaarden, X. Zeng, *Phys. Rev. A* **1984**, *29*, 3092–3110.

[4] D. Raftery, H. Long, T. Meersmann, P. J. Grandinetti, L. Reven, A. Pines, *Phys. Rev. Lett.* **1991**, *66*, 584–587.

[5] a) M. S. Albert, G. D. Cates, B. Driehuys, W. Happer, B. Saam, C. S. Springer Jr., A. Wishnia, *Nature* **1994**, *370*, 199–201; b) Y.-Q. Song, H. C. Gaede, T. Pietrass, G. A. Barrall, G. C. Chingas, M. R. Ayers, A. Pines, *J. Magn. Reson. A* **1995**, *115*, 127–130; c) J. R. Brookeman, J. P. Mugler III, B. Driehuys, C. D. Phillips, G. D. Cates, W. Happer, *Proc. RSNA, 82nd Annu.*

 © WILEY-VCH Verlag GmbH, D-69451 Weinheim, 1997 0570-0833/97/3621-2369 $ 17.50+.50/0

Meet. **1996**; d) S. D. Swanson, M. S. Rosen, B. W. Agranoff, K. P. Coulter, R. C. Welch, T. E. Chupp, 38th Experimental NMR Conference, Orlando (FL), **1997**.
[6] a) B. Driehuys, G. D. Cates, W. Happer, H. Mabuchi, B. Saam, M. S. Albert, A. Wishnia, *Phys. Lett. A* **1993**, *184*, 88–92; b) H. W. Long, H. C. Gaede, J. Shore, L. Reven, C. R. Bowers, J. Kritzenberger, T. Pietrass, A. Pines, P. Tang, J. A. Reimer, *J. Am. Chem. Soc.* **1993**, *115*, 8491–8492.
[7] G. Navon, Y.-Q. Song, T. Rõõm, S. Appelt, R. E. Taylor, A. Pines, *Science* **1996**, *271*, 1848–1851.
[8] J. A. Ripmeester, C. I. Ratcliffe, J. S. Tse, *J. Chem. Soc. Faraday Trans. 1* **1988**, *84*, 3731–3745.
[9] K. Bartik, M. Luhmer, S. J. Heyes, R. Ottinger, J. Reisse, *J. Magn. Reson. B* **1995**, *109*, 164–168.
[10] a) J. Szejtli, *Cyclodextrin Technology*, Kluwer, Dordrecht, **1988**; b) F. C. Cramer, F. M. Henglein, *Chem. Ber.* **1957**, *90*, 2561–2571, 2572–2575.
[11] Y. Xu, P. Tang, *Biochim. Biophys. Acta* **1997**, *1323*, 154–162.
[12] High xenon polarization should permit the observation of intermolecular scalar (*J*) couplings between xenon and molecules in solution. The SPINOE could also be significantly increased for dissolved molecules by using liquid or supercritical laser-polarized xenon as the solvent.
[13] A. J. Shaka, Royal Society of Chemistry NMR Meeting, Manchester, **1995**.
[14] For β-cyclodextrin, in which the pocket diameter is 37% larger, cross-relaxation rates are about 100 times smaller.
[15] I. Solomon, *Phys. Rev.* **1955**, *99*, 559–565.
[16] W. Saenger, M. Noltemeyer, *Angew. Chem.* **1974**, *86*, 594–595; *Angew. Chem. Int. Ed. Engl.* **1974**, *13*, 552–553.
[17] S. J. F. Vincent, C. Zwahlen, G. Bodenhausen, *Angew. Chem.* **1994**, *106*, 340–343; *Angew. Chem. Int. Ed. Engl.* **1994**, *33*, 343–346.

Reducible Nanoscale Molecular Rods Based on Diacetylene-Linked Poly(phenylthio)-Substituted Benzenes**

Marcel Mayor, Jean-Marie Lehn,*
Katharina M. Fromm, and Dieter Fenske

Structures of defined geometry and nanometric size containing electron-accepting subunits are of much interest as reducible molecular wires for the development of molecular and supramolecular electronic and photonic devices.[1–3] They may serve as connectors between components, and also possess marked nonlinear optical properties due to extended π conjugation.[4] Whereas the very actively studied entities built from conjugated electron-rich groups (such as thiophene, pyrrole[5]) lead to electronic conduction upon oxidation (p-doping), reducible wires are susceptible to n-doping through reduction and may show higher electronic mobility.

Molecular wires based on pyridinium end groups and carotenoid-type conjugated chains (termed caroviologens), which we investigated earlier, induce electron transport through lipid membranes.[5] Poly(phenylthio) aromatic systems such as **1** are well known for their host–guest chemistry in the solid state[6] and also display remarkably low reduction potentials.[7] They thus appeared to be promising candidates for incorporation into conjugated systems chosen for the development of novel types of reducible molecular wires.

We present here the synthesis, the structural characterization and some physicochemical properties of **2** and **3**, in which two

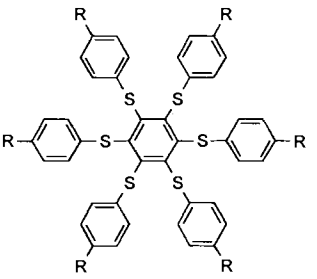

1a, R=H
1b, R=*t*Bu

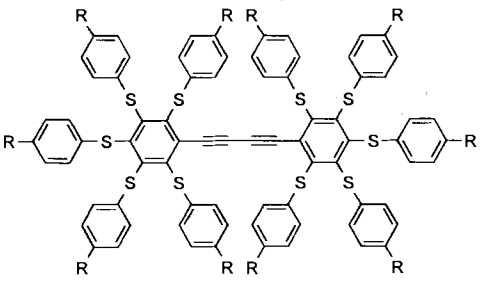

2a, R=H
2b, R=*t*Bu

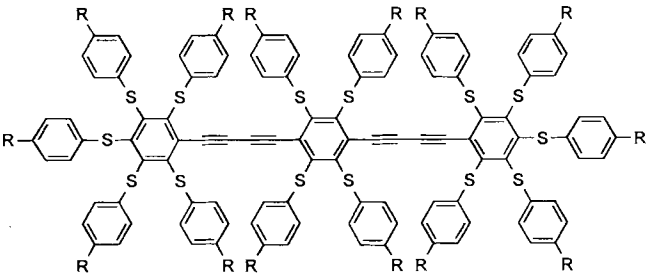

3, R=*t*Bu

and three poly(phenylthio)benzene subunits are linked by diacetylene bridges as efficient π-conjugation connectors. Starting from the corresponding halogenated benzaldehydes, the acetylene-functionalized phenylthio-substituted benzenes were synthesized in three steps (Scheme 1). Aromatic nucleophilic

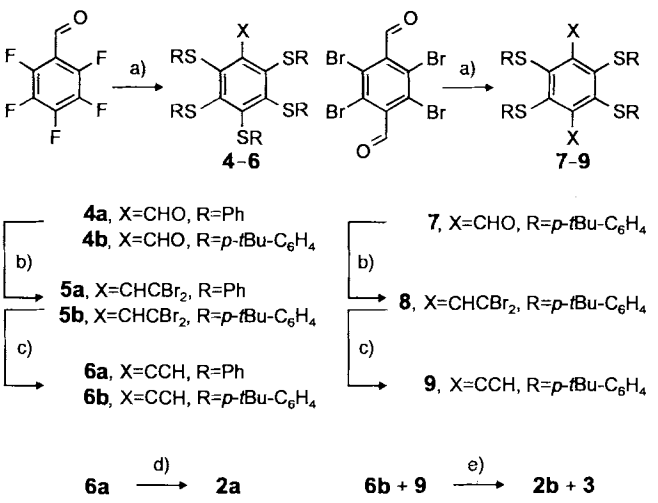

Scheme 1. Synthesis of **2** and **3**. a) DMI, NaSR, RT; b) CBr_4, PPh_3, CH_2Cl_2, RT; c) LDA, THF, −78 °C, H_2O; d) $Cu(OAc)_2$, pyridine, 45 °C; e) CuCl, TMEDA, O_2, $CHCl_3$, RT.

[*] Prof. Dr. J.-M. Lehn, Dr. M. Mayor
Laboratoire de Chimie Supramoléculaire
Institut Le Bel, Université Louis Pasteur
4, rue Blaise Pascal, F-67000 Strasbourg (France)
Fax: Int. code +(3)8841-1020.
Dr. K. M. Fromm, Prof. Dr. D. Fenske
Institut für Anorganische Chemie der Universität Karlsruhe (Germany)

[**] Supported by the CNRS (URA 422), the Swiss National Science Foundation, the Collège de France (postdoctoral fellowship to M. M.), and the Deutsche Forschungsgemeinschaft (postdoctoral fellowship to K. M. F.).

 © WILEY-VCH Verlag GmbH, D-69451 Weinheim, 1997 0570-0833/97/3621-2370 $ 17.50+.50/0

substitution of the halogens by thiophenyl anions in 1,3-dimethyl-2-imidazolidinone (DMI) yielded the phenylsulfanyl-substituted benzaldehydes **4** and **7** in yields of over 70%. Treatment with CBr_4/PPh_3 in CH_2Cl_2 gave the dibromoethylene derivatives **5** and **8** in good yields.[8] Reduction with excess lithium diisopropylamide (LDA) in THF led to acetylenes **6** and **9**, which were oxidatively coupled to provide poly(phenylthio)benzenes **2** and **3**.

Coupling[9] of pentakis(phenylthio)ethynyl benzene (**6a**) with copper acetate in pyridine at 45 °C gave **2a** as an orange crystalline solid in 65% yield.[10] Diacetylene **2a** is fairly soluble in organic solvents such as $CHCl_3$, CH_2Cl_2, toluene, or THF. Crystallization of **2a** from hot toluene gave single crystals suitable for X-ray analysis.[11] The solid-state structure shows that the molecule consists of two pentakis(phenylthio)benzene units linked by a diacetylene bridge, and presents a crystallographic inversion center at the middle of the C8–C8′ central bond (Figure 1) The two diacetylene-connected benzene rings lie in parallel planes and are separated by 0.75 Å. The bond lengths in the diacetylene bridge (C6C7≡C8C8′≡C7′C6′) are 1.436 (C6–C7),

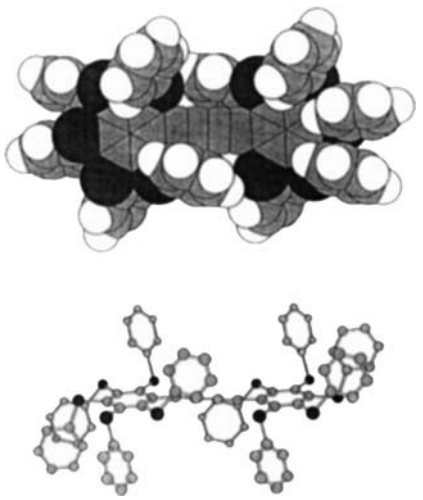

Figure 1. Crystal structure of **2a**. Top: plan view of the space-filling representation; bottom: side view of the ball-and-stick representation.

1.202 (C7–C8), and 1.372 Å (C8–C8′). The bridge angles of 175.5 (C6-C7-C8) and 178.2° (C7-C8-C8′) show slight deviation from linearity. The molecule is 15.8 Å long (distance between the two sulfur atoms that are *para* to the diacetylene linker). In analogy to the parent hexakis(phenylthio)benzene, an alternating up and down pattern (ababa) was expected for the phenylthio substituents.[14] In fact, **2a** presents a conformation in which the three phenylthio groups in *para* and *ortho* positions to the diacetylene bridge point to the same side of the benzene ring (abbba); the sulfur angles are, however, in the expected range (104–106°).

Oxidative coupling[15] of a mixture of **9** and nine equivalents of mono-acetylene **6b** in $CHCl_3$ with CuCl and *N,N,N′,N′*-tetramethyl 1,2-ethanediamine (TMEDA) under an oxygen atmosphere[16a] yielded diacetylenes **2b** and **3**, which were isolated in 45% and 16% yield, respectively, by size-exclusion chromatography. Both are intense dark orange solids and fairly soluble in organic solvents such as $CHCl_3$, CH_2Cl_2, or toluene; this allowed their characterization by ^1H and ^{13}C NMR spectroscopy as well as FAB mass spectrometry.[10, 16b]

Compounds **2** and **3** represent π-conjugated, rigid molecular rods of nanoscale dimensions with distances of 9.4 Å between the centers of the benzene cores and 15.8 Å and 25.2 Å, respectively, between the terminal sulfur atoms. The lateral phenyl groups may be considered to provide an insulating molecular sheath that protects the central functional component (see Figure 1).

UV/Vis spectra of **1b**, **2b**, and **3** (Figure 2) display an absorption maximum at about 255 nm, which may be attributed to the allowed π–π* transition in the peripheral *tert*-butylphenylthio moieties. Accordingly, the relative extinction coefficients of **1b**,

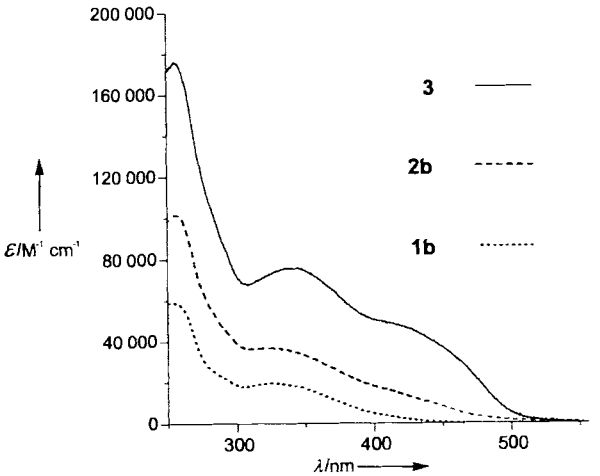

Figure 2. UV/Vis spectra of **1b**, **2b**, and **3** in CH_2Cl_2; $T = 298$ K.

2b, and **3** at 255 nm are proportional to the number of these substituents. Additional transitions are observed at 325–340 nm and, in the case of **2** and **3**, at about 430 nm. These longer wavelength transitions presumably arise from electronic interaction between poly(phenylthio)benzene and diacetylene units. Excitation of **1**–**3** in CH_2Cl_2 at 400 nm results in a moderately intense, structureless fluorescence which is not affected by oxygen. Whereas the presence of *tert*-butyl substituents in **1b** has little effect on the emission maximum (515 versus 520 nm for **1a** and **1b**, respectively), it produces a large hypsochromic shift in **2b** with respect to **2a** (560 versus 515 nm, respectively). This could reflect an alternative conformational preference that is induced by the steric requirements of the *tert*-butyl groups. Introduction of an additional dialkynephenylene unit results in further displacement of the emission to longer wavelengths in **3** ($\lambda_{max} = 600$ nm).

Of particular interest are the redox properties of **1**–**3**, which form a series with increasing conjugation. The cyclic voltammetry data are summarized in Table 1. None of the compounds **1**–**3** is oxidized up to +1.25 V. Monomeric **1a** and **1b** show a reversible one-electron reduction at −1.56 and −1.7 V, respectively. Dimeric **2a** and **2b** have two reversible one-electron re-

Table 1. Cyclic voltammetry data for **1**–**3** [a].

Compound	E_1^0 [V][b]	E_2^0 [V][b]
1a	−1.56	
1b	−1.7	
2a	−1.12	−1.38
2b	−1.17	−1.44
3	−0.98	−1.19[c]

[a] Platinum working electrode in 0.1 M $TBAPF_6$/DMF. [b] Versus ferrocene/ferrocenium, formal reduction potential $E^0 = (E_{pa} + E_{pc})/2$. [c] Two-electron reduction.

 © WILEY-VCH Verlag GmbH, D-69451 Weinheim, 1997 0570-0833/97/3621-2371 $ 17.50+.50/0

ductions at $-1.12/-1.38$ V and $-1.17/-1.44$ V, respectively; both processes are at less negative potential than the reduction of the corresponding monomeric units **1a** and **1b**. Trimeric **3** shows a reversible one-electron reduction at -0.98 V and a reversible two-electron reduction at -1.19 V.[17] The pronounced trend towards more positive reduction potentials with increasing molecular length (not only for addition of the first electron) confers the potential for very interesting electronic conductivity properties to this type of molecular wire.

The solubility and stability of the molecular rods **2** and **3** combined with their structural, optical, and electrochemical properties makes them promising candidates for the design of nanoscale molecular devices for molecular electronics and photonics.[1] The alkyne group allows connection of the rods with other alkyne-bearing components, and the peripheral phenylthio substituents can be functionalized to convey specific physical properties. We are currently investigating longer linear rods, *meta-* and *ortho-* dialkyne poly(phenylthio)benzene building blocks, and the corresponding cyclic structures.

Received: May 2, 1997 [Z 10411 IE]
German version: *Angew. Chem.* **1997**, *109*, 2468–2471

Keywords: alkynes · cyclic voltammetry · electrochemistry · nanostructures

[1] J.-M. Lehn, *Supramolecular Chemistry. Concepts and Perspectives*, VCH, Weinheim, **1995**, chap. 8.
[2] *Introduction to Molecular Electronics* (Eds.: M. C. Petty, M. R. Bryce, D. Bloor), Edward Arnold, London, **1995.**
[3] J. M. Tour, *Chem. Rev.* **1996**, *96*, 537–553.
[4] M. Schreiber, R. R. Tykwinski, F. Diederich, R. Spreiter, U. Gubler, C. Bosshard, I. Poberaj, P. Günter, C. Boudon, J.-P. Gisselbrecht, M. Gross, U. Jonas, H. Ringsdorf, *Adv. Mater.* **1997**, *9*, 339–343.
[5] T. S. Arrhenius, M. Blanchard-Desce, M. Dvolaitzky, J.-M. Lehn, J. Malthête, *Proc. Natl. Acad. Sci. USA* **1986**, *83*, 5355–5359; L. B. Å. Johansson, M. Blanchard-Desce, M. Almgren, J.-M. Lehn, *J. Phys. Chem.* **1989**, *93*, 6751–6754; S. I. Kugimiya, T. Lazrak, M. Blanchard-Desce, J.-M. Lehn, *J. Chem. Soc. Chem. Commun.* **1991**, 1179–1182.
[6] D. D. MacNicol, G. A. Downing in *Comprehensive Supramolecular Chemistry*, *Vol. 6* (Eds.: J. L. Atwood, J. E. D. Davies, D. D. MacNicol, F. Vögtle, J.-M. Lehn), Elsevier, Oxford, **1996**, pp. 421–464.
[7] J. H. R. Tucker, M. Gingras, H. Brand, J.-M. Lehn, *J. Chem. Soc. Perkin Trans. 2* **1997**, 1303–1307.
[8] E. J. Corey, P. L. Fuchs, *Tetrahedron Lett.* **1972**, 3769–3772.
[9] G. Eglinton, W. McCrea, *Adv. Org. Chem.* **1963**, *4*, 225–328.
[10] Melting points (uncorrected): **1b** (bright yellow, fluffy solid): 238 °C; **2a** (orange crystals): 186 °C; **2b** (dark orange solid): 137 °C; **3** (dark orange solid): 122 °C.
[11] Crystal data for **2a**: STOE-IPDS diffractometer, graphite-monochromated $Mo_{K\alpha}$ radiation ($\lambda = 0.71073$ Å), -70 °C; triclinic, space group $P\bar{1}$ (no. 2), $a = 8.148(2)$, $b = 10.663(2)$, $c = 18.453(4)$ Å, $\alpha = 85.62(3)$, $\beta = 77.89(3)$, $\gamma = 74.36(3)°$, $V = 1509.0(5)$ Å^3, $Z = 1$, $\mu = 0.413$ mm^{-1}, $F(000) = 666$, $\rho_{calcd} = 1.413$ Mg m^{-3}, $2\theta_{max} = 51.00°$. The primary structure was solved by direct methods (SHELXS-92) [11] and refined anisotropically for all non-hydrogen atoms with SHELXL-93[12]; of 11 837 reflections measured, 5438 were independent (R(int) = 0.0905), of which 5434 were used for refining 488 parameters. The structure was refined against F^2 with full-matrix least squares. $R1 = 0.0639$ (for 3584 reflections with $F_o > 4\sigma F_o$), $R1 = 0.1041$ (all data), and $wR2 = 0.1796$ (all data), GOF(F^2) = $S = 1.143$, max./min. residual electron density $+0.473/-0.512$ e Å^{-3}, $R1 = \sum||F_o| - |F_c||/\sum|F_o|$, $wR2 = [\sum w(F_o^2 - F_c^2)^2/\sum wF_o^4]^{1/2}$, GOF = $S = [\sum\{w(F_o^2 - F_c^2)^2\}/(n-p)]^{1/2}$ (n = number of reflections, p = number of parameters). Crystallographic data (excluding structure factors) for the structures reported in this paper have been deposited with the Cambridge Crystallographic Data Centre as supplementary publication no. CCDC-100421. Copies of the data can be obtained free of charge on application to The Director, CCDC, 12 Union Road, Cambridge CB21EZ, UK (fax: int. code +(1223)336-033; e-mail: deposit@chemcrys.cam.ac.uk).
[12] G. M. Sheldrick, *Acta Crystallogr. Sect. A* **1990**, *46*, 467–473.
[13] G. M. Sheldrick, SHELXL-93, Program for Crystal Structure Refinement, Universität Göttingen, **1993**.
[14] A. D. U. Hardy, D. D. MacNicol, D. R. Wilson, *J. Chem. Soc. Perkin Trans. 2* **1979**, 1011–1019.
[15] A. S. Hay, *J. Org. Chem.* **1960**, *25*, 1275–1276.
[16] a) No product was obtained under the coupling conditions used for **2a**. b) A small amount of the next member of the series **1b**, **2b**, **3** that incorporates one more *para*-C≡CC_6(tBuC_6H_4S)$_4$C≡C unit was also isolated and identified by mass spectrometry.
[17] The number of electrons was determined by measurements at the limiting current with a rotating disc electrode: C. M. A. Brett, A. M. Oliveira Brett, *Electrochemistry, Principles, Methods, and Applications*, Oxford University Press, Oxford, **1994**.

Synthesis, Structure, and Coordination Chemistry of Diisocyanomethane**

Jürgen Buschmann, Thilo Bartolmäs, Dieter Lentz,* Peter Luger, Ingo Neubert, and Matthias Röttger

About 30 years ago Neidlein reported the synthesis of diisocyanomethane (**1**).[1] However, its existence in solution could only be proved by derivatization. The isolation of this compound, which is isomeric with the long known malonodinitrile[2] and with isocyanoacetonitrile, which we recently synthesized in an analytically pure form and structurally characterized by X-ray crystal crystallography,[3] has thus far been unsuccessful. Although Neidlein reported that **1** is extremly unstable even in solution, we were able to isolate this first geminal diisocyanide by fractional condensation of a dichloromethane solution under high vacuum. Compound **1** was obtained as colorless crystals in a cooling trap at -55 °C; it melts at -15 °C and turning brown, and decomposes explosively at -10 °C to give a brown-black, virtually insoluble polymer. Since this polymer exhibits a strong fluorescence even in the NIR region, we were unable to record a Raman spectrum.

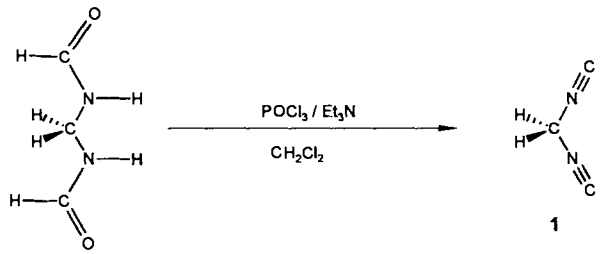

1

By using a gas IR cell that allowed **1** to be sublimed into a directly connected trap it was possible to record an IR spectrum of **1** in the gaseous state. The vibrational spectroscopic data were completed by a low-temperature FT Raman spectrum. In accord with the C_{2v} symmetry of **1**, two N≡C stretching modes were observed at 2173 and 2157 cm^{-1}. In the IR spectrum the symmetric stretching mode appears as a weak shoulder on the high frequency side in accordance with the results of an ab initio calculation.[4] The ^{1}H NMR ($\delta = 4.99$ (CH_2)), the ^{13}C {^{1}H} NMR ($\delta = 46.8$ (CH_2), 162.5 (NC)), and the ^{14}N NMR spectra ($\delta = -215.3$ (NC) ($\nu_{1/2} = 20$ Hz, due to the small electric field gradient at the nitrogen atom) exhibit chemical shift values typical for isocyanides.

[*] Priv.-Doz. Dr. D. Lentz, T. Bartolmäs, I. Neubert, M. Röttger
Institut für Anorganische und Analytische Chemie der Freien Universität
Fabeckstrasse 34–36, D-14195 Berlin (Germany)
Fax: Int. code +(30)838-2424
e-mail: lentz@chemie.fu-berlin.de
Dr. J. Buschmann, Prof. Dr. P. Luger
Institut für Kristallographie der Freien Universität Berlin (Germany)

[**] This work was supported by the Fonds der Chemischen Industrie and the Deutsche Forschungsgemeinschaft (DFG).

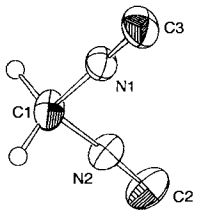

Figure 1. Molecular structure (ORTEP plot [7]) of diisocyanomethane **1** in the crystal.

Crystals suitable for an X-ray crystal structure analysis were obtained by slowly cooling a solution of **1** in diethyl ether/pentane from $-20\,^{\circ}C$ to $-90\,^{\circ}C$ in steps of 5 K per day (Figure 1). Although the studied crystal was nonmetrically twinned (2.22(2):1) the analysis of the orientation matrices showed a perfect superposition of the $0kl$ reflections, which could be scaled. A few superimposed $5kl$ and $7kl$ reflections were removed from the data file. The structure was solved by direct methods and refined in the monoclinic space group $P2_1/n$ (Table 1).[5] Interestingly, all three isomers crystallize in the monoclinic crystal system and show very similar lattice constants. Equivalent bond lengths are equal within 3σ. According to a comparison of the structure of **1** with the structures of isocyanides in the gas phase[6] and the structure obtained from the ab initio calculation, the N≡C bond length in **1** seems to be shortened due to libration effects.

Table 1. Bond lengths [pm] and angles [°] in **1** in comparison to those values obtained from an ab initio calculation.

Parameter	Crystal structure	MP2 6-31G**
C–N	142.7(1), 142.5(1)	142.2
C≡N	115.5(1), 115.1(1)	119.0
C–H	94.6(20), 97.7(19)	109.3
N-C-N	110.4(1)	110.5
C≡N-C	177.7(1), 175.9(1)	178.6

The stability of **1** increases considerably by coordination to a metal center. Reaction of **1** with $[Cr(CO)_5(thf)]$ or $[CpMn(CO)_2(thf)]$ results in the formation of monocoordinated products **2** and **4** and dicoordinated products **3** and **5**, in which **1** functions as a bridging ligand. The structures of **2** and **4** were elucidated by X-ray crystallography (Figure 2).[5] The striking differences in the C–N bond lengths of the free and coordinated isocyanide function in **2** and **4** might also be due to libration effects. The most significant differences are evident in the ^{13}C chemical shift values of the free ($\delta = 162.0$) and the coordinated

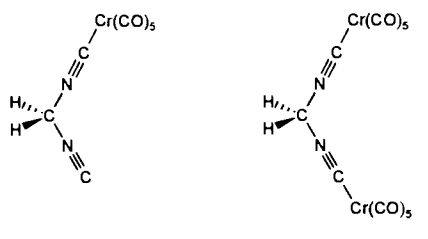

2 **3**

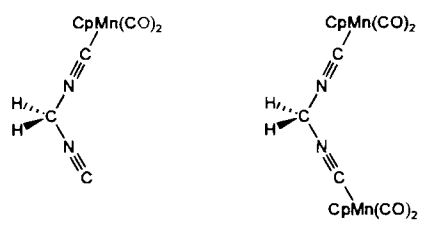

4 **5**

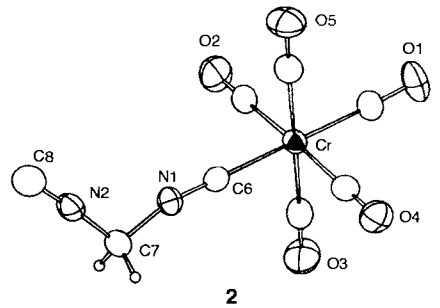

2

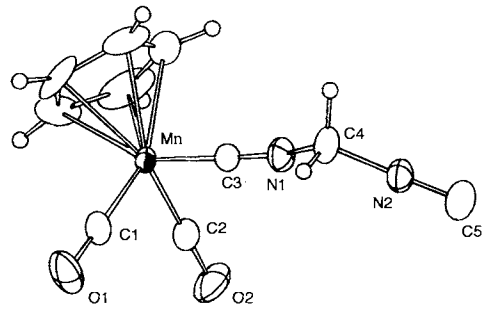

4

Figure 2. Molecular structure (ORTEP plot [7]) of **2** and **4** in the crystal. Selected bond lengths [pm] and angles [°]: **2**: Cr–CO_{trans} 188.6(4), Cr–CO_{cis} 188.7(4)–190.9(4), Cr–C6 197.4(4), C6–N1 115.8(4), N1–C7 142.9(5), C7–N2 139.8(5), N2–C8 114.2(6); N2-C7-N1 111.2(3), C6-N1-C7 166.8(4), C8-N2-C7 175.6(5); **4**: Mn–C3 1.835(3), C3–N1 1.172(4), C4–N1 1.418(4), C4–N2 1.436(4), C5–N2 1.155(4); N1-C4-N2 109.9(3), C3-N1-C4 159.2(3), C5-N2-C4 178.0(3).

($\delta = 210.5$) isocyanide function of the manganese complex **4**, which demonstrate the electronic differences resulting from coordination.

Experimental Section

1: Bis(formylamino)methane (1.02 g, 10 mmol) was suspended in dichloromethane (25 mL). Triethylamine (5.1 g, 50 mmol) was added and the mixture was cooled to $-60\,^{\circ}C$. Phosphoryl chloride (2 mL, 22 mmol) was added dropwise. After the mixture had been slowly warmed to $-20\,^{\circ}C$, it was stirred for an additional 30 min. After addition of saturated aqueous Na_2CO_3 solution the organic phase was washed twice with water (20 mL) and dried over KOH. Fractional condensation under vacuum (10^{-3} mbar) yielded **1** (500 mg, 75.8%) as colorless crystals in a trap maintained at $-55\,^{\circ}C$. M.p. $-15\,^{\circ}C$; ^1H NMR ($CDCl_3$, $-40\,^{\circ}C$): $\delta = 4.99$ (CH_2); $^{13}C\{^1H\}$ NMR ($CDCl_3$, $-40\,^{\circ}C$): $\delta = 46.8$ (CH_2), 162.5 (NC); ^{14}N NMR ($CDCl_3$, $-40\,^{\circ}C$, NH_4NO_3 ext. reference): $\delta = -215.3$ (NC); IR(g): $\tilde{\nu} = 2987$ (vw), 2170 (sh), 2132 (vs), 1380 (m), 996 (m), 941 (w), 712 (m) cm^{-1}. Raman: $\tilde{\nu} = 2997$ (m), 2956 (s), 2173 (s), 2157 (m), 1444 (m), 1361 (m), 1263 (m), 984 (w), 924 (m), 269 (m), 253 (w), 150 (w), 100 (w) cm^{-1}. MS (70 eV): *m/z*: 66 [M^+], 40 [CH_2NC^+], 28 [CH_2N^+].

2,3: $[Cr(CO)_6]$ (770 mg, 3.5 mmol) was dissolved in dry THF (50 mL) and irradiated for 6 h with a high-pressure Hg lamp. The CO that was released was removed under vacuum several times. Compound **1** (500 mg, 7.6 mmol) in dry THF (10 mL) was added to this solution at $-40\,^{\circ}C$. The reaction mixture was heated to ambient temperature, stirred for 30 min, and purified by column chromatography using dichloromethane/pentane 3:1 as eluent. Colorless crystals of **3** (200 mg, 12.7%) were obtained from the first fraction. M.p. 162 °C; ^1H NMR (CD_2Cl_2): $\delta = 5.28$ (CH_2); $^{13}C\{^1H\}$ NMR (CD_2Cl_2): $\delta = 51.2$ (CH_2), 177.6 (NC), 214.1 (CO_{cis}), 215.6 (CO_{trans}); IR (CH_2Cl_2): $\tilde{\nu} = 2160$ (w), 2132 (m), 2069 (m), 2042 (s), 1957 (vs) cm^{-1}; MS (70 eV): *m/z*: 450 [M^+], 422 [$M^+ - CO$], 394 [$M^+ - 2CO$], 366 [$M^+ - 3CO$], 338 [$M^+ - 4CO$], 310 [$M^+ - 5CO$], 282 [$M^+ - 6CO$], 254 [$M^+ - 7CO$], 232 [$[Cr(CO)_5(CNCH_2)]^+$], 226 [$M^+ - 8CO$], 204 [$[Cr(CO)_4(CNCH_2)]^+$], 198 [$M^+ - 9CO$], 176 [$[Cr(CO)_3(CNCH_2)]^+$], 170 [$M^+ - 10CO$], 148 [$[Cr(CO)_2(CNCH_2)]^+$], 130 ([$[Cr(CO)(CNCH_2)]^+$), 92 [$[Cr(CNCH_2)]^+$], 52 [Cr^+]; 28 [CO^+]. The second fraction yielded **2** (580 mg (64.2%) as pale yellow crystals. M.p. 101 °C; ^1H NMR (CD_2Cl_2): $\delta = 5.13$ (CH_2); IR (CH_2Cl_2): $\tilde{\nu} = 2160$ (w), 2136 (m), 2059 (m), 1962 (vs) cm^{-1}; MS (70 eV): *m/z* : 258 [M^+], 230 [$M^+ - CO$], 204 [$M^+ - 2CO$], 174 [$M^+ - 3CO$], 146 [$M^+ - 4CO$], 118 [$M^+ - 5CO$], 52 [Cr^+].

4,5: $[CpMn(CO)_3]$ (780 mg, 3.8 mmol) was dissolved in THF (80 mL) and irradiated for 6 h with a high-pressure Hg lamp. The CO that was released was removed under vacuum several times. Compound **1** (250 mg, 3.8 mmol) in dichloromethane

 © WILEY-VCH Verlag GmbH, D-69451 Weinheim, 1997 0570-0833/97/3621-2373 $ 17.50+.50/0

(10 mL) was added to this solution at −40 °C. The reaction mixture was allowed to warm to ambient temperature, stirred for 30 min, and the products were purified by chromatography on silica using dichloromethane/pentane 1:1 as eluent. Compound **5** (60 mg, 3.8%) was isolated from the first fraction as yellow crystals. M.p. 85 °C; IR (pentane): $\tilde{\nu}$ = 2028 (vs), 1942 (vs), 1919 (m) cm^{-1}; MS (70 eV): *m/z*: 418 [M^+], 362 [$M^+ - 2CO$] 216 [[$CpMn(CO)_2(CNCH_2)$]$^+$], 160 [[$CpMn(CNCH_2)$]$^+$], 120 [[CpMn]$^+$], 55 [Mn^+]. The second fraction gave **4** (180 mg, 19.6%) as yellow crystals. M.p. 76 °C; ^1H NMR (CD_2Cl_2): δ = 4.71 (C_5H_5, 5H), 5.01 (CH_2, 2H); $^{13}C\{^1H\}$ NMR (CD_2Cl_2): δ = 50.1 (CH_2), 83.4 (C_5H_5), 162.0 (NC), 210.5 (NC), 228.1 (CO); IR (CH_2Cl_2): $\tilde{\nu}$ = 2147 (m), 2086 (m), 2010 (m), 1903 (vs) cm^{-1}; MS (70 eV): *m/z*: 242 [M^+], 186 [$M^+ - 2CO$], 120 [[CpMn]$^+$], 55 [Mn^+].

Received: April 17, 1997 [Z10359IE]
German version: *Angew. Chem.* **1997**, *109*, 2466–2468

Keywords: C ligands · chromium · isocyanides · manganese · transition metals

[1] R. Neidlein, *Angew. Chem.* **1964**, *76*, 440; *Angew. Chem. Int. Ed. Engl.* **1964**, *3*, 382.

[2] *Beilsteins Handbuch der Organischen Chemie* **1920**, Bd. 2, p. 589; **1929**,; I Erg.-Werk, Bd. 2, p. 256; **1942**, II. Erg.-Werk, Bd. 2, p. 535; **1961**, III. Erg.-Werk, Bd. 2, p. 1634; **1976**, IV. Erg.-Werk, Bd. 2, p. 1892.

[3] J. Buschmann, D. Lentz, P. Luger, G. Perpetuo, D. Scharn, S. Willemsen, *Angew. Chem.* **1995**, *107*, 988; *Angew. Chem. Int. Ed. Engl.* **1995**, *34*, 914.

[4] Gaussian 92, Revision C: M. J. Frisch, G. W. Trucks, M. Head-Gordon, P. M. W. Gill, M. W. Wong, J. B. Foresman, B. G. Johnson, H. B. Schlegel, M. A. Robb, E. S. Replogle, R. Gomperts, J. L. Anders, K. Raghavachari, J. S. Binkley, C. Gonzalez, R. L. Martin, D. J. Fox, D. J. Defrees, J. Baker, J. J. P. Stewart, J. A. Pople, Gaussian, Pittsburgh, PA, **1992**.

[5] Crystal structure determinations: **1**: Monoclinic, $P2_1/n$, a = 631.0(3), b = 768.6(2), c = 799.3(2) pm, β = 99.81(3)°, $V = 3.820(2) \times 10^8$ pm^3, Z = 4, ρ_{calcd} = 1.149 $Mg\,m^{-3}$, 3479 measured reflections, 1606 crystallographically independent reflections, and 1224 reflections with $I > 2\sigma(I)$, $Mo_{K\alpha}$, λ = 71.069 pm, $2\theta_{max.}$ = 70°, ω-2θ scan, T = 126 K, no absorption correction (μ = 0.078 mm^{-1}), $R(F)_{obs.}$ = 0.0526, $wR(F^2)_{all}$ = 0.1571, $w = 1/[\sigma^2(F_o^2) + (0.0649P)^2 + 0.0747P]$, $P = [F_o^2 + 2F_c^2]/3$, anisotropic temperature factors for the C and N atoms, H atoms were refined isotropically. Starting coordinates by direct methodes (SHELXS-86 [8]), full-matrix least-squares refinement using F^2 (SHELXL-93 [9]), 54 refined parameters, max./min. residual electron density 0.325/ − 0.192 e $Å^{-3}$. A correction of libration effects with the program THMA11 [10] results in the following bond lengths: N1–C1 143.9, N2–C1 143.4, N1–C3 116.0, N2–C2 116.0, C1–H1 95.2, C1–H2 90.2 pm. **2:** Monoclinic, $C2/c$, a = 2499.6(7), b = 588.2(2), c = 2057.2(6) pm, β = 134.62(2)°, $V = 21.529(2) \times 10^8$ pm^3, Z = 4, ρ_{calcd} = 1.593 $Mg\,m^{-3}$, 4905 measured reflections, 3008 crystallographically independent reflections, and 1634 reflections with $I > 2\sigma(I)$, $Mo_{K\alpha}$, λ = 71.069 pm, $2\theta_{max}$ = 60°, ω scan, T = 293 K, no absorption correction (μ = 1.068 mm^{-1}), $R(F)_{obs}$ = 0.0582, $wR(F^2)_{all}$ = 0.1357, $w = 1/[\sigma^2(F_o^2) + (0.0497P)^2 + 0.0P]$, $P = [F_o^2 + 2F_c^2]/3$, anisotropic temperature factors for C, O, N, and Cr atoms, H atoms were refined isotropically. Starting coordinates by direct methodes (SHELXS-86 [8]), full-matrix least-squares refinement using F^2 (SHELXL-93 [9]), 145 refined parameters, max./min. residual electron density 0.325/ − 0.282 e $Å^{-3}$. **4:** Monoclinic, $P2_1/a$, a = 1214.3(4), b = 584.8(2), c = 1430.1(5) pm, β = 97.77(3)°, $V = 10.062(6) \times 10^8$ pm^3, Z = 4, ρ_{calcd} = 1.598 $Mg\,m^{-3}$, 1826 measured reflections, 1753 crystallographically independent reflections, and 1495 reflections with $I > 2\sigma(I)$, $Mo_{K\alpha}$, λ = 71.069 pm, $2\theta_{max}$ = 49°, ω-2θ scan, T = 113 K, no absorption correction (μ = 1.289 mm^{-1}), $R(F)_{obs}$ = 0.0355, $wR(F^2)_{all}$ = 0.0972, $w = 1/[\sigma^2(F_o^2) + (0.0538P)^2 + 0.9895P]$ with $P = [F_o^2 + 2F_c^2]/3$, anisotropic temperature factors for C, N, O, and Mn atoms, H atoms were refined isotropically. Starting coordinates by direct methodes (SHELXS-86 [8]), full-matrix least-squares refinement using F^2 (SHELXL-93 [9]), 136 refined parameters, max./min. residual electron density 0.695/ − 0.422 e $Å^{-3}$. Crystallographic data (excluding structure factors) for the structures reported in this paper have been deposited with the Cambridge Crystallographic Data Centre as supplementary publication no. CCDC-100304. Copies of the data can be obtained free of charge on application to The Director, CCDC, 12 Union Road, Cambridge CB2 1EZ, UK (fax: int. code +(1223) 336-033; e-mail deposit@chemcrys.cam.ac.uk).

[6] D. Christen, K. Ramme, B. Haas, H. Oberhammer, D. Lentz, *J. Chem. Phys.* **1984**, *80*, 4020; L. Halonen, I. M. Mills, *J. Mol. Spectrosc.* **1978**, *73*, 494.

[7] C. K. Johnson, ORTEP, A Fortran Thermal Ellipsoid Plot Program for Crystal Structure Illustrations, Report ORNL-3794. Oak Ridge National Laboratories, Oak Ridge, TN, **1970**. Modified Version XPMA, Zortep, L. Zsolnai, Universität Heidelberg, **1996**.

[8] G. M. Sheldrick, SHELXS-86, Program for Crystal Structure Solutions, *Acta Crystallogr. Sect. A* **1990**, 46, 467.

[9] G. M. Sheldrick, SHELXL-93, Program for Crystal Structure Determination, Universität Göttingen, **1993**.

[10] V. Schomaker, K. N. Trueblood, *Acta Crystallogr. Sect. B* 1968, 24, 63; K. N. Trueblood, W. B. Schweizer, THMA11, A Thermal Motion Analysis Program, ETH Zürich, **1987**.

Catalytic Conversion of Methane into Aromatic Hydrocarbons over Iron Oxide Loaded ZSM-5 Zeolites**

Bert M. Weckhuysen, Dingjun Wang, Michael P. Rosynek, and Jack H. Lunsford*

The catalytic conversion of methane to desirable commodity chemicals is a challenging approach to the utilization of natural gas resources; consequently, considerable effort has been devoted to the development of novel catalytic systems. Oxygen has generally been used to activate the methane, even at the expense of losing some of the feedstock as carbon dioxide. The most extensively studied processes are oxidative coupling of methane,[1, 2] partial oxidation of methane to synthesis gas,[3] and the formation of such oxygenated compounds as methanol.[4] Recent studies have demonstrated that methane can be selectively converted into benzene over Mo/H-ZSM-5 catalysts in the absence of an oxidant such as O_2.[5–10]

We report here on a stable and selective bifunctional catalyst for the conversion of methane into aromatic hydrocarbons such as benzene, toluene, and naphthalene in the absence of an oxidant. The catalyst consists of iron oxides dispersed on the surface of an acidic ZSM-5 zeolite. Methane activation occurs on supported iron oxide clusters, and the primary product, ethylene, undergoes subsequent oligomerization and cyclization reactions at Brønsted-acidic sites to form the aromatic products. The Fe/H-ZSM-5 catalyst is typically prepared by incipient wetness impregnation through addition of an aqueous iron(III) nitrate solution to the H-ZSM-5 zeolite, followed by drying at 90 °C and calcination in oxygen at 500 °C. The resulting orange material is characterized by a broad electron paramagnetic resonance (EPR) signal with a g-value of 2.47 and a peak-to-peak width (ppw) of 1515 G (Figure 1A). The signal broadens upon

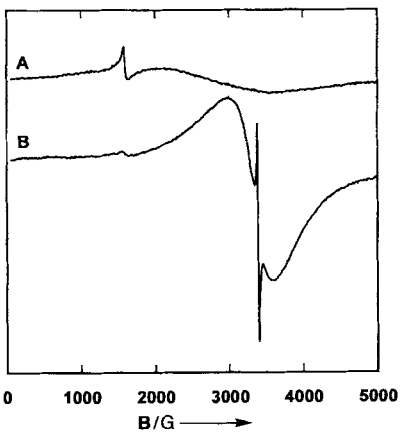

Figure 1. EPR spectra of A) a 0.6 wt% Fe/H-ZSM-5 catalyst calcined at 500 °C for 1 h, and B) an active 0.6 wt% Fe/H-ZSM-5 catalyst prereduced in CO and treated for 1 h in methane at 700 °C. The spectra were measured at 120 K, and the signal at g = 4.3 is due to distorted tetrahedral Fe^{3+} ions from the parent H-ZSM-5 material[12].

[*] Prof. J. H. Lunsford, Dr. B. M. Weckhuysen, Dr. D. Wang, Prof. M. P. Rosynek
Department of Chemistry
Texas A & M University
College Station, TX 77843(USA)
Fax: Int. code +(409)845-4719
e-mail: lunsford@chemvx.tamu.edu

[**] This work was sponsored by the National Science Foundation (CHE-9520806). B. M. W. is a postdoctoral research fellow of the Belgian National Fund of Scientific Research.

 © WILEY-VCH Verlag GmbH, D-69451 Weinheim, 1997 0570-0833/97/3621-2374 $ 17.50+.50/0

cooling and does not follow the Curie–Weiss law. Such behavior is typical for Fe_2O_3 clusters.[11, 12] The presence of iron(III) was further confirmed by X-ray photoelectron spectroscopy (XPS). The corresponding $2p_{3/2}$ and $2p_{1/2}$ binding energies (BE) of iron(III) were obtained at 710.7 eV and 724.5 eV, respectively. The spin-orbital splitting was 13.8 eV, and an accompanying weak 3d → 4s shake-up satellite peak was detected at 718.7 eV, all typical for iron(III).[13]

The calcined material was first reduced with CO at 500 °C for 6 h, heated to 700 °C in He, and then subjected to a continuous methane flow at 700 °C. Conversion and product formation were monitored by on-line gas chromatography. As an example, we will discuss the catalytic performance of a 2 wt% Fe/H-ZSM-5 catalyst in some detail (Figure 2). Similar results were

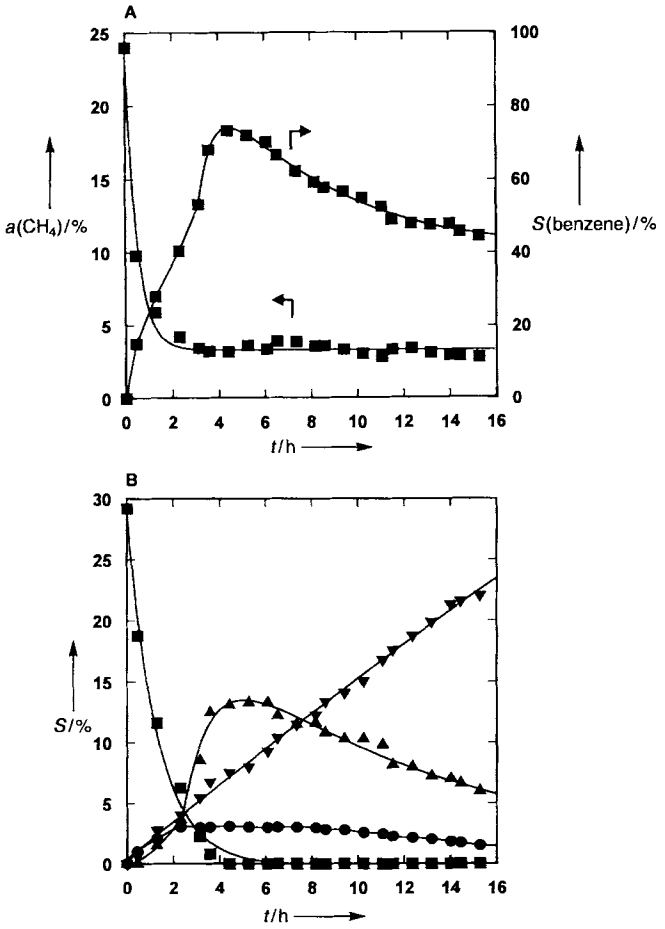

Figure 2. The catalytic performance of a Fe/H-ZSM-5 catalyst with 2 wt% iron: A) overall conversion $a(CH_4)$ [%] and benzene selectivity S(benzene) [%], and B) selectivities S [%] toward CO (■), napthalene(▲), toluene (●) and C2–C3 hydrocarbons (▼).

obtained for a 0.6 wt% Fe/H-ZSM-5 material. After an initial activation period of 4 h, a benzene selectivity of 74% was reached at a methane conversion of about 4%. During the first half-hour on stream, virtually no hydrocarbon products were formed, and the major gas-phase products were CO, CO_2, and H_2O. Because the catalyst was pretreated in He at high temperature before initiating the reaction, the only oxygen source for formation of oxygen-containing products is lattice oxygen from the catalyst. In addition to benzene, toluene and naphthalene were also formed, but with much lower selectivities. Naphthalene selectivity reached a value of 13% immediately following the initial activation period, but then declined slowly with increasing time on stream. For toluene, a maximum selectivity of 3% was observed. Thus, after a sufficiently long reaction time, mainly benzene was produced, along with some toluene and naphthalene, and the maximum selectivity toward aromatic hydrocarbons exceeded 85%. On the other hand, selectivity toward C_2 and C_3 hydrocarbons (mainly ethylene) increased continuously with increasing reaction time, as coke deposition gradually deactivated acidic sites in the zeolite where the ethylene undergoes secondary reaction. It is also remarkable that a stable conversion of 4% could be sustained even after 16 h on stream. The catalyst could be regenerated by heating the material in O_2 at 500 °C for 8 h; however, the resulting maximum methane conversion was only 3.5% at a benzene selectivity of 65%.

The black active catalyst had the typical EPR spectrum shown in Figure 1 B. Besides the sharp isotropic signal at $g \approx 2$ with ppw = 11.5 G, a broad EPR signal was observed with $g = 2.06$ and ppw = 600 G. The former signal followed the Curie–Weiss law, indicating the presence of organic radicals; that is, the formation of coke. This signal gradually increased in intensity during the course of reaction. The other EPR signal, centered at $g \approx 2.06$, broadened upon cooling and did not follow the Curie–Weiss law.[14] The nature of the species responsible for this signal was further analyzed by XPS. After passing methane gas over the catalyst, the Fe $2p_{3/2}$ and $2p_{1/2}$ BE values were determined to be 710.5 eV and 724.4 eV, respectively, and no other peaks were observed. In addition, no weak 3d → 4s shake-up satellite peak was detected at 718.7 eV. Thus, upon methane activation, the catalyst is partially reduced from Fe_2O_3 to Fe_3O_4.[13] Furthermore, the C 1s signal at 283.5 eV increased in intensity. This was due to coke formation during methane activation. Such coke may explain the decrease in selectivity toward aromatics.

By changing the CO prereduction time and temperature we were able to change the extent of the EPR-active Fe clusters. This resulted in materials with different catalytic activities, as shown in Figure 3. It is clear that an almost linear relationship exists between the level of EPR-active Fe clusters and methane-conversion activity of the catalyst at maximum benzene selectivity. This in turn suggests that such clusters may be involved in the activation of methane.

The primary products of methane activation, mainly ethylene, undergo further reaction at zeolitic acidic sites, result-

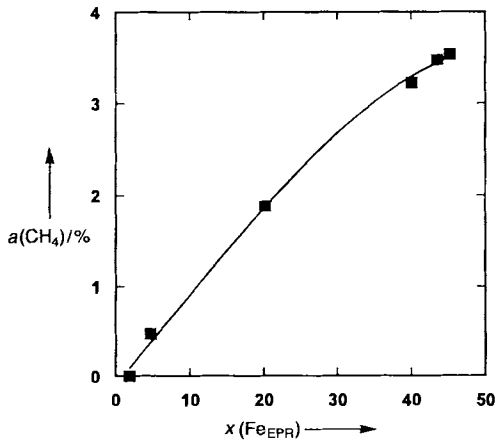

Figure 3. Methane activation behavior of Fe/H-ZSM-5 catalysts as a function of the extent of EPR-active Fe clusters, $x(Fe_{EPR})$ (in arbitrary units). The extent of such Fe clusters was determined by double integration of the recorded EPR spectra and subtraction of the contribution from a sharp isotropic signal at $g \approx 2$. Methane conversions refer to conversions at maximum benzene selectivity.

 © WILEY-VCH Verlag GmbH, D-69451 Weinheim, 1997 0570-0833/97/3621-2375 $ 17.50+.50/0

ing in the formation of benzene, toluene, and napthalene. The occurrence of such oligomerization and cyclization reactions has been demonstrated by partially and even fully exchanging the Brønsted acid sites of the starting H-ZSM-5 material with Na^+ ions. Treatment in this way resulted in a gradual decrease in the number of Brønsted acid sites, as evidenced by FT-IR spectroscopy, as well as a decrease in catalytic activity and selectivity of the catalyst. Thus, Brønsted acid sites play a crucial role in the catalytic performance of these materials. In another experiment we prepared solid-state, ion-exchanged Fe/H-ZSM-5 zeolites by using $Fe^{III}Cl_3$. The freshly prepared materials were totally inactive for methane activation. Only after CO treatment at relatively high temperatures was some activity detected. However, such materials were always catalytically inferior to those prepared by impregnation, and no naphthalene could be detected.

In conclusion, we have found that iron oxides supported on H-ZSM-5 zeolites are able to convert methane into aromatic hydrocarbons with a selectivity greater than 85%. The activity is based on a unique balance between formation of iron clusters on the surface of the zeolite and the presence of a sufficient number of Brønsted acid sites. It is also worth mentioning here that unsupported iron oxides are used industrially for the dehydrogenation of ethylbenzene to styrene under conditions similar to those applied in this study.[15] The XPS results confirm that neither metallic iron nor iron carbides are formed on this catalyst, which is significant in view of the fact that similar activation of CH_4 over an Mo/H-ZSM-5 catalyst has been proposed to involve Mo_2C, the presence of which was confirmed by XPS.[9, 10] Recently, Marczewski et al. have shown that methane can be converted into aromatics under nonoxidative conditions in a two-stage catalytic system.[16] Methane was converted into ethylene over a $Mn/Na/SiO_2$ catalyst (10% Mn, 3.4% Na) at 800 °C. The initially formed ethylene was then further converted into benzene and toluene over an H-ZSM-5 catalyst at 600 °C. Further studies on the mechanism of methane activation in the absence of oxygen, and extension to other transition metal oxides such as Cr_2O_3, V_2O_3, and WO_2 are in progress and should increase our understanding of these novel catalytic materials.

Experimental Section

Fe/H-ZSM-5 catalysts were prepared by impregnation with an aqueous solution of iron (III) nitrate onto commercial PQ Corp. H-ZSM-5 (CBU 5020E, with a Si/Al ratio of 25/1). The resulting materials were dried at 90 °C overnight (14 h) and calcined at 500 °C for 5 h. Reactions were carried out in a flow system, in reactors constructed from alumina tubes. The flow reactor had an internal diameter of 6.4 mm, and the amount of catalyst used was 1.0 g. To minimize contributions from possible gas-phase reactions, quartz chips filled the space above and below the catalyst beds in the flow reactors. A thermocouple in a smaller alumina tube was attached to the outside wall of each of the reactors. The gases, which included 10% N_2/CH_4 (UHP), O_2 (UHP), He (UHP), and CO (UHP) were obtained from Matheson and used without further purification. Gas flows were regulated by mass flow controllers (MKS Model 1159A). In the flow system the catalyst was heated in a 50 mL min^{-1} flow of O_2 to 500 °C, calcined for 1 h, and flushed in a 50 mL min^{-1} flow of He for 30 min. Reduction treatments were carried out at 500 or 700 °C for several hours in a 25 mL min^{-1} flow of CO. The total GHSV (gas hour space velocity) during methane conversion was 800 h^{-1}. The gas feed consisted of CH_4 that contained 10% N_2. The N_2 was used as an internal standard so that CH_4 conversion could be determined accurately. Coke formation during the reaction could be evaluated from a carbon mass balance. The mass balance indicated that about 5–10% of the CH_4 was converted into coke during methane activation. Reaction mixtures were analyzed by on-line gas chromatography (HP 5890A) using a 5% Bentone-34 on Chromosorb W-AW column and a HayeSep D column. All studies were carried out at atmospheric pressure. FT-IR spectra were obtained on a Perkin Elmer 2000 FT-IR spectrometer. Self-supporting wafers of 10–15 mg cm^{-2} were pressed from the powdered catalysts. Wafers were mounted on a fused-quartz bracket placed in an IR cell. The cell was equipped with KBr windows and a heated region into which the wafer could be raised and pretreated. For EPR spectroscopy, a Bruker ESP300 spectrometer at X-band (ca. 9.5 GHz) was used. EPR spectra of the active catalysts were obtained with a specially designed quartz reactor tube with a side-arm for EPR measurements. XPS spectra were acquired on a Perkin Elmer (PHI) model 5500 spectrometer. A quartz reactor system with in situ transfer capability made it possible to duplicate the conditions present in the catalytic reaction experiments.

Received: March 17, 1997 [Z10156IE]
German version: *Angew. Chem.* **1997**, *109*, 2471–2473

Keywords: arenes · heterogeneous catalysis · iron · methane activation · zeolites

[1] J. H. Lunsford, *Angew. Chem.* **1995**, *107*, 1059; *Angew. Chem. Int. Ed. Engl.* **1995**, *34*, 970.
[2] J. H. Lunsford, *Stud. Surf. Sci. Catal.* **1993**, *75*, 103.
[3] S. C. Tsang, J. B. Claridge, M. L. H. Green, *Catal. Today* **1995**, *23*, 3.
[4] M. Faraldos, M. Banares, J. A. Anderson, H. Hu, I. E. Wachs, J. L. G. Fierro, *J. Catal.* **1996**, *160*, 214; O. V. Krylov, *Catal. Today* **1993**, *18*, 209; N. D. Parkyns, C. I. Warburton, J. D. Wilson, *ibid.* **1993**, *18*, 385.
[5] L. Wang, L. Tao, M. Xie, G. Xu, J. Huang, Y. Xu, *Catal. Lett.* **1993**, *21*, 25.
[6] Y. Xu, S. Liu, L. Wang, M. Xie, X. Guo, *Catal. Lett.* **1995**, *30*, 135.
[7] F. Solymosi, A. Erdohelyi, A. Szöke, *Catal. Lett.* **1995**, *32*, 43.
[8] F. Solymosi, A. Szöke, J. Csere'nyi, *Catal. Lett.* **1996**, *39*, 157.
[9] D. Wang, J. H. Lunsford, M. P. Rosynek, *Top. Catal.* **1996**, *3*, 289.
[10] F. Solymosi, J. Csere'nyi, A. Szöke, T. Ba'nsa'gi, A. Oszko', *J. Catal.* **1997**, *165*, 150.
[11] F. E. Mabbs, D. Collison, *Electron Paramagnetic Resonance of d Transition Metal Compounds*, Elsevier, Amsterdam, **1992**.
[12] D. Goldfarb, M. Bernardo, K. G. Strohmaier, D. E. W. Vaughan, H. Thomann, *J. Am. Chem. Soc.* **1994**, *116*, 6344; B. D. McNicol, G. T. Pott, *J. Catal.* **1972**, *25*, 223; E. G. Derouane, M. Mestdagh, L. Vielvoye, *J. Catal.* **1974**, *33*, 169; P. Ratnasami, R. Kumar, *Catal. Today* **1991**, *9*, 328.
[13] *Practical Surface Analysis by Auger and X-ray Photoelectron Spectroscopy* (Eds.: D. Briggs, M. P. Seah), Wiley, New York, **1983**; C. D. Wagner, W. M. Riggs, L. E. Davis, J. F. Moulden, G. E. Muilenburg, *Handbook of X-ray Photoelectron Spectroscopy*, Perkin Elmer, Eden Prairie, MN, **1979**.
[14] Temperature-dependence EPR spectroscopy shows that the $g = 2.06$ and $g = 4.3$ signals correspond to different iron species. In addition, the two EPR signals respond differently toward different microwave powers, and the $g = 2.06$ signal saturates more readily at liquid N_2 temperature than the $g = 4.3$ signal. The behavior of the $g = 2.06$ signal must be due to cooperative magnetic phenomena (e.g., ferro-anti-ferromagnetism and dipole–dipole interaction).
[15] E. H. Lee, *Catal. Rev.* **1973**, *8*, 285.
[16] M. Marczewski, H. Marczewska, K. Mazowiecka, *React. Kinet. Catal. Lett.* 1995, **54**, 81.

Carbene Complex Modified Glycals: Synthesis and Reactivity**

Karl Heinz Dötz,* Richard Ehlenz, and Daphne Paetsch

Electrophilic carbene complexes are versatile reagents in stereoselective synthesis. They are applied in metal- and ligand-centered cycloaddition reactions[1] such as [3 + 2 + 1]benzannulation with alkynes[1a, b] and cyclopropanation,[1c, d] serve as precursors of photochemically generated ketene equivalents,[1e] and can be deprotonated to give organometallic analogues of enolates that are of interest in aldol and Michael addition reactions.[1f, g] The synthetic potential of organometallic compounds has been exploited only in rare occasions in carbohydrate chemistry. So far, reagents for the umpolung of the

[*] Prof. K. H. Dötz, Dr. R. Ehlenz, Dipl.-Chem. D. Paetsch
Kekulé-Institut für Organische Chemie und Biochemie der Universität
Gerhard-Domagk-Strasse 1, D-53121 Bonn (Germany)
Fax: Int. code +(228)735813
e-mail: doetz@snchemie1.chemie.uni-bonn.de

[**] Organotransition Metal Modified Sugars, Part. 7. This research was supported by the Volkswagenstiftung, the Fonds der Chemischen Industrie, and the Graduiertenkolleg "Spektroskopie isolierter und kondensierter Moleküle". Part 6: K. H. Dötz, W.-C. Haase, M. Klumpe, M. Nieger, *Chem. Commun.* **1997**, 1217.

 © WILEY-VCH Verlag GmbH, D-69451 Weinheim, 1997 0570-0833/97/3621-2376 $ 17.50+.50/0

anomeric center are restricted nearly exclusively to the main group metals lithium and tin. Glycosyl complexes are known for the transition metals manganese,[2a, b] iron,[2c] and cobalt.[2d] Synthetic applications, however, have been limited to manganese compounds, which, under high pressure conditions, have been applied occasionally to the synthesis of C-glycosides.[3] We set out to incorporate the anomeric center into an electrophilic metal carbene moiety,[4] which favors the addition of nucleophiles and as such may offer a novel approach to C- and heteroatom-glycosides. Recently, we reported on the synthesis of acyclic C-1 carbene complex functionalized sugars, which are accessible by a combination of a sugar electrophile and a carbonylmetalate nucleophile.[5] Subsequently, we applied a metal-assisted cycloisomerization of sugar alkynols to the preparation of spiroketal glycoside carbene complexes and their monocyclic

Herein we describe the synthesis of and first reactivity studies on two novel types of carbene complex modified carbohydrates derived from the lithioglucal **1**.[7] According to the classical Fischer route, **1** adds to a *carbonyl ligand* of the hexacarbonyl complexes of chromium, molybdenum, and tungsten to give pentacarbonyl acylmetalates, which undergo subsequent alkylation to give the glucal carbene complexes **2a–c** (Scheme 1). The

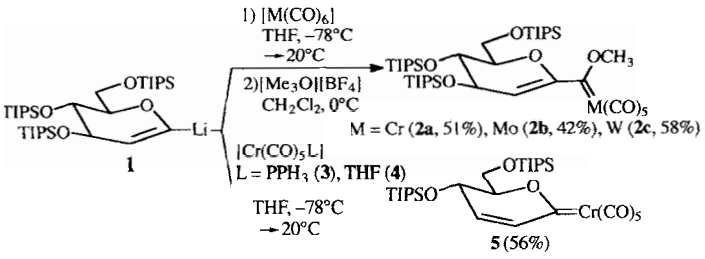

Scheme 1. Synthesis of complexes **2a–c** and **5**.

course of the reaction of the carbonyl complex with the glucal nucleophile is dependent on its substitution pattern. The presence of a good donor and leaving group ligand such as PPh_3 or THF in pentacarbonyl chromium complexes **3**[8] and **4**[9] favors the formation of the α,β-unsaturated glycosylidene complex **5**. This may be rationalized in terms of an addition/elimination sequence along which, with prior or concomitant elimination of the phosphane or THF ligand, the lithioglucal **1** first adds to the *metal* center to give an alkyl chromate intermediate,[10, 11] which subsequently, reminiscent of a Ferrier rearrangement,[12] undergoes elimination of the silyloxy group and generates the vinylcarbene complex **5**.

The synthetic potential of these carbene complexes is characterized by the vinyl carbene moiety and by the pronounced electrophilicity of the metal-coordinated carbene-carbon atom as evident from the ^{13}C NMR chemical shifts [δ = 338.0 (**2a**), 328.3 (**2b**), 310.9 (**2c**), and 325.7 (**5**)]. The glucal carbene complex **2a** undergoes a benzannulation reaction with 3-hexyne to give benzoglucals **6** and **7** (Scheme 2). After chromatographic work-up the hydroquinone complex **6** was obtained as a single diastereomer. However, this is not yet indicative of a diastereoselective carbene annulation since comparable yields of the uncoordinated hydroquinone derivative **7** were also isolated; thus, so far, it cannot be excluded that **7** is formed from the other diastereomer by decomplexation assisted by the bulky TIPS protecting groups.

The electrophilicity of the glycosylidene-carbon atom is evident from the ammonolysis of **5**. Ring-opening generates the

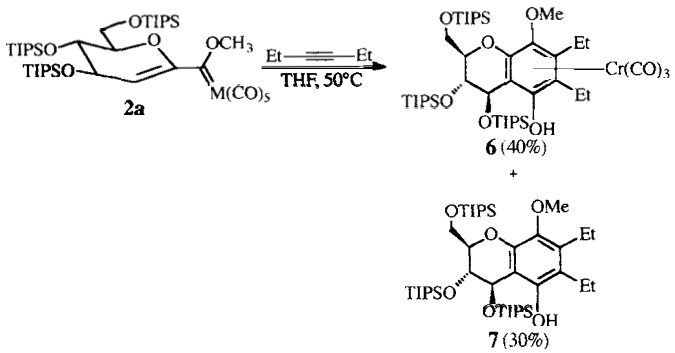

Scheme 2. Benzannulation of **2a**

α,β-unsaturated aminocarbene complex **8**, which is selectively deprotected in the 5-position. In comparison with its oxacyclic precursor **5**, complex **8** is distinctly less electrophilic (^{13}C NMR: δ = 268.9). Michael addition across the electron-deficient C=C bond, which generally occurs in vinyl carbene complexes as a competing pathway, is blocked by the adjacent sterically demanding silyl protecting group. The addition of nucleophiles can be exploited in the C_2-homologization of the glycosylidene ligand. This is demonstrated by the reaction with ethoxyethyne,[13, 14] which results in alkyne insertion, and stereoselectively affords the (*Z*)-isomer of **9** [15] (Scheme 3), whose dienyl

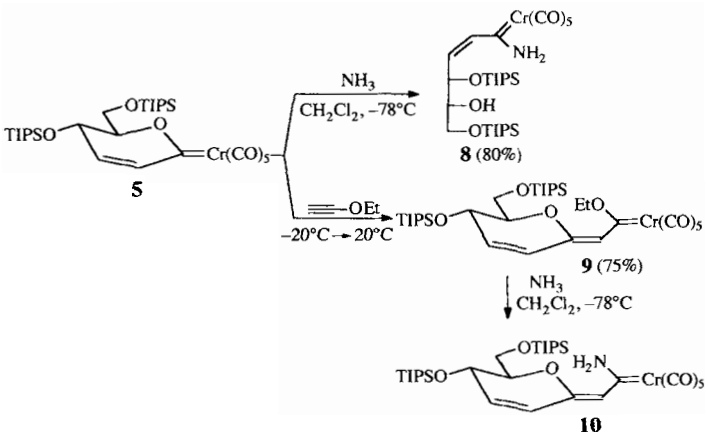

Scheme 3. Ammonolysis and C_2-homologization of **5**.

carbene ligand as a vinylogous Michael acceptor offers three alternatives for the addition of nucleophiles. A relatively hard nucleophile such as ammonia adds regioselectively to the carbene-carbon atom under the formation of the aminocarbene complex **10**.

The glycosylidene complexes described provide a novel strategy for modifying the anomeric center of carbohydrates by exploiting the metal carbene methodology. This approach offers a promising access to nonnatural sugar analogues as well as to unconventional synthetic routes to C- and heteroatom-glycosides.

Experimental Section

All operations were performed under argon. Solvents were dried by using standard methods. Yields reported refer to products purified by column chromatography.

2a: For the preparation of lithioglucal **1**, *n*BuLi (0.78 mL, 1.25 mmol, 1.6 M solution in hexane) was added slowly at −78 °C to a solution of 1,5-anhydro-3,4,6-tri-*O*-(triisopropylsilyl)-2-deoxy-1-tri-*n*-butyl-stannyl-D-arabino-hex-1-enitol (**11**) (0.94 g, 1.04 mmol) in THF (15 mL). The solution was stirred for 1 h at −78 °C. After

 © WILEY-VCH Verlag GmbH, D-69451 Weinheim, 1997 0570-0833/97/3621-2377 $ 17.50+.50/0

addition of hexacarbonylchromium (0.28 g, 1.25 mmol) the resulting suspension was allowed to warm to room temperature over a period of 4 h. The solvent was removed in vacuo, and the residue was dissolved in dichloromethane (50 mL). After addition of $[Me_3O][BF_4]$ (0.18 g, 1.25 mmol) at 0 °C, the mixture was stirred for 1 h. Yield: 0.45 g (0.52 mmol, 51%). ^{13}C NMR (100 MHz, $CDCl_3$): δ = 338.0 (C=Cr), 225.2 (*trans*-CO), 216.5 (*cis*-CO), 156.1 (C-1), 97.0 (C-2), 81.8 (C-3), 69.1 (C-4), 66.8 (C-5), 66.4 (OCH_3), 61.2 (C-6), 18.2–18.0 ($SiCH(CH_3)_2$), 12.5–12.0 ($SiCH(CH_3)_2$).

2b (42%) and **2c** (58%) were obtained similarly.

5: *n*BuLi (0.7 mL, 1.12 mmol) was added to a solution of **11** (0.92 g, 1.02 mmol) in THF (5 mL) at −78 °C. The solution was stirred at this temperature for 1 h and then added to a suspension of **3** (0.51 g, 1.12 mmol) in THF precooled to −78 °C or, alternatively, to a solution of **4** (18.6 mL, 1.12 mmol, 0.06 M in THF). The solution was stirred for 14 h and allowed to warm to room temperature. Yield: 0.36 g (0.57 mmol, 56%) from the reaction with **3**; 0.26 g (0.41 mmol, 40%) from **4**. ^{13}C NMR (62.5 MHz, $CDCl_3$): δ = 325.7 (C-1), 225.7 (*trans*-CO), 216.5 (*cis*-CO), 136.0 (C-2), 125.5 (C-3), 86.3 (C-4), 62.1 (C-5), 61.7 (C-6), 18.3–18.1 ($SiCH(CH_3)_2$), 12.7–12.0 ($SiCH(CH_3)_2$). HR-MS: Calcd. for $C_{29}H_{48}CrO_8Si_2$: 632.2293; found: 632.2284.

6: A solution of **2a** (0.32 g, 0.32 mmol) and 3-hexyne (0.5 mL, 4.0 mmol) in THF (4 mL) was degassed (three cycles "pump, freeze, thaw") and then warmed to 50 °C for 6 h. Work-up by column chromatography afforded **6** (0.14 g, 0.16 mmol, 40%) and **7** (0.09 g, 0.11 mmol, 30%). ^{13}C NMR (100 MHz, $CDCl_3$): δ = 234.4 ($Cr(CO)_3$), 134.1, 132.7, 118.6, 112.0, 90.14, 86.9 (C-5–C-10), 83.4, 67.7, 65.6, 64.8, 62.2 (C-2, C-3, C-4, C-1, OCH_3), 21.8 ($ArCH_2CH_3$), 19.6 ($ArCH_2CH_3$), 18.3–17.7 ($SiCH(CH_3)_2$), 16.0 ($ArCH_2CH_3$), 14.8 ($ArCH_2CH_3$), 13.0–11.8 ($SiCH(CH_3)_2$).

8: A 10 s flow of ammonia was condensed at −78 °C into a solution of **5** (0.29 g, 0.46 mmol) in dichloromethane (20 mL). The solution was stirred at this temperature for 1 min. Work-up by column chromatography afforded **8** (0.24 g, 0.37 mmol, 80%). ^{13}C NMR (100 MHz, $CDCl_3$): δ = 276.6 (C=Cr), 223.0 (*trans*-CO), 217.4 (*cis*-CO), 141.0 (C-2), 126.5 (C-3), 73.8, 70.5 (C-4, C-5), 65.7 (C-6), 18.1-17.8 ($SiCH(CH_3)_2$), 12.5, 11.8 ($SiCH(CH_3)_2$). HR-MS: Calcd. for $C_{24}H_{51}NCrO_3Si_2$ (M^+ − 5CO): 509.2825; found: 509.2819.

9: A solution of ethoxyethyne (0.59 mmol) in petroleum ether (1 mL, 40/60) was added to **5** (0.31 g, 0.49 mmol) in petroleum ether (20 mL, 40/60) at −20 °C. The solution was stirred for 24 h at room temperature, (0.26 g, 0.37 mmol, 75%). ^{13}C NMR (100 MHz, C_6D_6): δ = 322.9 (C=Cr), 224.6 (*trans*-CO), 217.8 (*cis*-CO), 148.6 (C-1), 143.5, 125.0, 121.4 (alkene-C), 81.6 (C-4), 76.2 (OCH_2CH_3) , 63.23 (C-5), 61.8 (C-6), 18.2–18.0 ($SiCH(CH_3)_2$), 14.9 (OCH_2CH_3), 12.8, 12.3 ($SiCH(CH_3)_2$). HR-MS: Calcd. for $C_{28}H_{54}O_4Si_2Cr$ (M^+ − 5CO): 562.2933; found: 562.2949.

Ammonolysis of **9** was carried out similarly to that of **5**.

Received: March 24, 1997 [Z10273IE]
German version: *Angew. Chem.* **1997**, *109*, 2473–2475

Keywords: alkyne complexes · carbene complexes · carbohydrates · glycals

[1] Reviews: a) K. H. Dötz, *Angew. Chem.* **1984**, *96*, 573; *Angew. Chem. Int. Ed. Engl.* **1984**, *23*, 587; W. D. Wulff, in *Comprehensive Organic Synthesis, Vol. 5*, (Eds.: B. M. Trost, I. Fleming), Pergamon, New York, **1991**, p. 1065; c) H.-U. Reissig, in *Organometallics in Organic Synthesis 2* (Eds.: H. Werner, G. Erker), Springer, Berlin, **1989**, 311; d) D. F. Harvey, D. M. Sigano, *Chem Rev.* **1996**, *96*, 271; e) L. S. Hegedus, in *Comprehensive Organometallic Chemistry II, Vol. 12*, (Eds.: E. W. Abel, F. G. Stone, G. Wilkinson), Pergamon Press, Oxford, **1995**, p. 549; f) W. D. Wulff, in *Comprehensive Organometallic Chemistry II, Vol. 12*, (Eds. E. W. Abel, F. G. Stone, G. Wilkinson), Pergamon Press, Oxford, **1995**, p. 469, g) A. de Meijere, *Pure Appl. Chem.* **1996**, *68*, 61.

[2] a) P. DeShong, G. A. Slough, V. Elango, G. L. Trainor, *J. Am. Chem. Soc.* **1985**, *107*, 7788; b) P. DeShong, G. A. Slough, V. Elango, *Carbohydr. Res.* **1987**, *171*, 342; c) G. L. Trainor, B. E. Smart, *J. Org. Chem.* **1983**, *48*, 2447; d) A. Rosenthal, H. J. Koch, *Tetrahedron Lett.* **1967**, 871.

[3] Reviews: a) M. H. D. Postema, *Tetrahedron* **1992**, *48*, 8545; b) M. H. D. Postema, *C-Glycoside Synthesis*, CRC, Boca Raton, FL, **1995**.

[4] The modification of protecting groups in the periphery of carbohydrate skeletons into carbene ligands is known: a) T. Pill, K. Polborn, U. Beck, *Chem. Ber.* **1990**, *123*, 11; b) R. Aumann, *Chem. Ber.* **1992**, *125*, 2773; *ibid.* **1994**, *127*, 725; c) H. Fischer, J. Schleu, G. Roth, *ibid.* **1995**, *128*, 373.

[5] K. H. Dötz, W. Straub, R. Ehlenz, K. Peseke, R. Meisel, *Angew. Chem.* **1995**, *107*, 2023; *Angew. Chem. Int. Ed. Engl.* **1995**, *34*, 1856.

[6] a) K. H. Dötz, O. Neuß, M. Nieger, *Synlett* **1996**, 995; b) K. H. Dötz, R. Ehlenz, O. Neuss, M. Teckenbrock, *Tetrahedron* **1997**, *53*, 5143.

[7] R. W. Friesen, C. F. Sturino, A. K. Daljeet, A. Kolaczewska, *J. Org. Chem.* **1990**, *55*, 2572.

[8] T. A. Magee, C. N. Methews, T. S. Wang, J. H. Wotiz, *J. Am. Chem. Soc.* **1961**, *83*, 3200.

[9] W. Strohmeier, *Angew. Chem.* **1964**, *76*, 873; *Angew. Chem. Int. Ed. Engl.* **1964**, *3*, 730.

[10] I. Lee, N. J. Cooper, *J. Am. Chem. Soc.* **1993**, *115*, 4389.

[11] H. Stadtmüller, P. Knochel, *Organometallics* **1995**, *14*, 3136.

[12] R. J. Ferrier, R. J. Prascadi, *J. Chem. Soc. Chem. Commun.* **1969**, 570.

[13] L. Brandsma, *Preparative Acetylenic Chemistry*, 2nd ed., Elsevier, Amsterdam, **1988**, p. 174.

[14] C. P. Casey, S. W. Polichnowsky, A. J. Shusterman, C. R. Jonas, *J. Am. Chem. Soc.* **1979**, *101*, 7282.

[15] The (*Z*)-configuration of the exocyclic C=C bond in **10** has been established by NOE experiments (NOE between H-2 and exocyclic = CH).

Stabilization of the (π-Indenyl)–Lead Bond: The First Structurally Authenticated Bis(η^5-indenyl) Complex of a Post-Transition Element, $[Pb\{1,3\text{-}(SiMe_3)_2C_9H_5\}_2]$**

Jason S. Overby, Timothy P. Hanusa,* and Paul D. Boyle

Although they are often considered as analogues of metallocenes, bis(π-indenyl) metal complexes, particularly those of main group elements, are not documented as well.[1] In complexes of post-transition metals, for example, the indenyl ligand is almost always σ-bonded (e. g., $M(\sigma\text{-}C_9H_7)_3$, M = B, Tl and $M(\sigma\text{-}C_9H_7)_nX_{4-n}$, M = Ge, Sn, Pb).[2–7] Two divalent Group 14 metal complexes of indenyl have been reported, $[Ge\{(SiMe_3)_2C_9H_5\}_2]$ and $[Ge(C_5Me_5)\{(SiMe_3)_2C_9H_5\}]$,[8] but only the latter was crystallographically characterized and shown to contain a π-bound indenyl ligand. We now report the synthesis of the first lead(II) indenyl complex, which highlights the sensitivity of such complexes to the steric and electron-donor properties of the indenyl group. The X-ray crystal structure is the first for a complex between a post-transition metal and two π-bound indenyl ligands.

Not all indenyl ligands are equally compatible with the redox-sensitive Pb^{II} center. For example, the reaction of potassium indenide, $K(C_9H_7)$, with PbI_2 in THF leads to deposition of elemental lead after several minutes. The more sterically demanding 1,3-diisopropylindenyl (Ind^{2i}) ligand was successfully used to prepare heavy alkaline earth derivatives.[1] Rapid workup (< 5 min) of the reaction between $K(Ind^{2i})$ and PbI_2 in THF or DME permits isolation of a red–orange solid that is tentatively identified as $[Pb(Ind^{2i})_2]$ (^1H NMR singlet at δ = 5.54 with $^2J(Pb,H)$ = 38.4 Hz).[9] However, even in the solid state, substantial decomposition to lead and the coupled ligand $(Ind^{2i})_2$ is apparent after several minutes at room temperature.

In contrast, the reaction of two equivalents of $K(Ind^{2Si})$ (Ind^{2Si} = 1,3-bis(trimethylsilyl)indenyl) with PbI_2 in DME provides the deep-red bis(indenyl) complex in moderate yield. Rapid workup of the reaction mixture is nevertheless required, as decomposition products (the coupled ligand and metallic lead) form if the reaction is stirred for more than 30 min at room temperature. Solid samples of $[Pb(Ind^{2Si})_2]$ are reasonably stable at room temperature, although slow decomposition oc-

[*] Prof. T. P. Hanusa, J. S. Overby
Department of Chemistry
Vanderbilt University
Nashville, TN 37235 (USA)
Fax: Int. code +(615)322-4936
e-mail: hanusat@ctrvax.vanderbilt.edu
Dr. P. D. Boyle
Department of Chemistry, North Carolina State University (USA)

[**] This work was supported by the U. S. National Science Foundation.

 © WILEY-VCH Verlag GmbH, D-69451 Weinheim, 1997 0570-0833/97/3621-2378 $ 17.50+.50/0

curs over several months. Immediate decomposition takes place upon heating the complex to 160 °C under high vacuum. The complex disintegrates within one minute upon exposure to air or moisture, and displays high solubility in both polar and nonpolar solvents (including alkanes).

$[Pb(Ind^{2Si})_2]$ was spectroscopically characterized by ^1H and ^{13}C NMR as well as IR spectroscopy. In the ^1H NMR spectrum, there is a substantial downfield shift of the C_5-ring proton to $\delta = 6.28$, which is consistent with a highly delocalized ring system. This shift is comparable to those observed for Ge^{II} complexes of Ind^{2Si} ($\delta = 6.42, 6.32$)[8] and for related Ca^{II}, Sr^{II}, and Ba^{II} complexes.[9] Furthermore, the ^{13}C spectrum of $[Pb(Ind^{2Si})_2]$ is nearly identical to that of the Ge^{II} complexes, which is another indication of π-bound indenyl ligands. Although the molecular ion is not observed in the mass spectrum (EI, CI, or FAB techniques), fragments corresponding to the loss of methyl groups and lead could be identified.

$[Pb(Ind^{2Si})_2]$ crystallizes with two independent enantiomeric molecules in the unit cell; one of them is shown in Figure 1.[10]

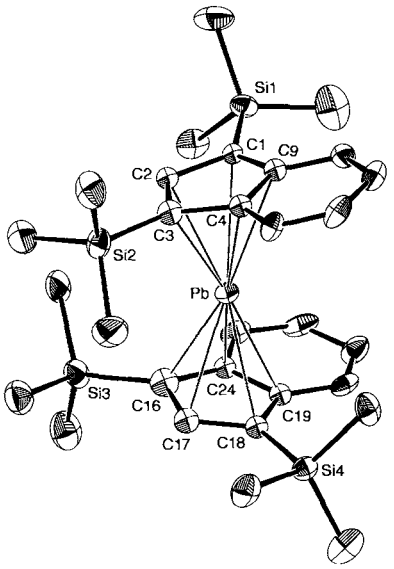

Figure 1. ORTEP plot of $[Pb\{1,3\text{-}(SiMe_3)_2C_9H_5\}_2]$; only non-hydrogen atoms are shown. Selected bond lengths [Å]: Pb–C1 2.793(11), Pb–C2 2.653(11), Pb–C3 2.669(12). Pb–C4 2.828(11), Pb–C9 2.910(12), Pb–C16 2.720(14), Pb–C17 2.736(13), Pb–C18 2.798(11), Pb–C19 2.813(11), Pb–C24 2.772(11).

The C_5 ring of each indenyl ligand is η^5-bound to the metal center; the average Pb–C distance in both complexes is 2.77(4) Å. The relevance of this value is lessened in view of the wide spread in individual bond distances [2.693(11)–2.873(12), 2.653(11)—2.910(12) Å]. Similarly broad ranges of metal—carbon distances were found in structurally characterized plumbocenes, for example, 2.69–2.90 Å in $[Pb(C_5Me_5)_2]$,[11] 2.680–2.871 Å in $[Pb\{C_5(PhCH_2)_5\}_2]$,[12] and 2.73—3.03 Å in $[Pb(C_5H_5)_2]$.[13] This demonstrates that somewhat asymmetric bonding is typical for η^5-bound rings on lead centers.

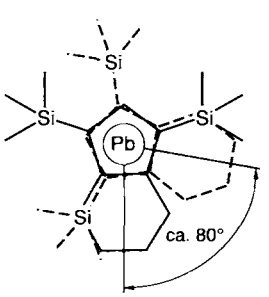

Figure 2. Gauche-eclipsed orientation of the indenyl ligands in $[Pb\{1,3\text{-}(SiMe_3)_2C_9H_5\}_2]$. Two of the C–$SiMe_3$ bonds of one indenyl ligand are aligned along the edges of the C_6 ring of the other ligand.

Interestingly, the structures display ring centroid–Pb–ring centroid angles of 173.3 and 172.9°, which represent only slight deviations from linearity. The two indenyl ligands are rotated by 83.3 and 78.7° relative to each other (Figure 2); this places the closest interligand methyl–methyl contacts at over 3.9 Å. The observed ligand orientations may serve to minimize unfavorable nonbonding interactions between the indenyl substituents. There is little evidence for stereochemical activity on the part of the metal-centered pair of valence electrons.

The synthetic restrictions detailed here concerning the isolation of bis(indenyl) complexes of Pb^{II} substantially limit the number of complexes that can be successfully prepared. Careful consideration must be given to the electronic and steric nature of the substituents on the indenyl ligand if other complexes of this nature are to be isolated. Our search for suitable ligands for use with lead and other Group 14 metals continues.

Experimental Section

Lead(II) iodide (0.24 g, 0.52 mmol) was dissolved in DME (50 mL). $K(Ind^{2Si})$ [14] (0.50 g, 0.83 mmol) was added in one portion to the orange–yellow solution; the mixture immediately turned red–orange. After the reaction mixture was stirred for 15 min, the solvent was removed under vacuum, and the residue extracted with hexane (50 mL). Filtration through a medium-porosity glass frit to remove KI followed by removal of the solvent from the filtrate provided dark red–orange $[Pb(Ind^{2Si})_2]$ in 63% yield (0.14 g, 0.19 mmol). ^1H NMR (300 MHz, C_6D_6, 20 °C): $\delta = 0.33$ (br s, 36H, $Si(CH_3)_3$), 6.28 (s, 2H, C_5-ring H; $^2J(Pb,H) = 13.0$ Hz), 7.01–6.98 (m, 4H, C_6-ring H), 7.49–7.46 (m, 4H, C_6-ring H); ^{13}C NMR (75.5 MHz, C_6D_6, 20 °C): $\delta = 1.3$ ($Si(CH_3)_3$), 114.2 ($CSiMe_3$), 122.3 (bridgehead C), 123.0 (C_5-ring CH), 130.3 (C_6-ring CH), 138.8 (C_6-ring CH); IR (KBr): $\tilde{\nu} = 3064$ (m), 2955 (s), 2895 (m), 1447 (m), 1407 (w), 1253 (vs), 1023 (m), 974 (w), 901 (vs), 838 (vs), 757 (s), 689 (m), 449 (m) cm^{-1}; MS (CI) $m/z = 561$ ($M^+ - 11$ Me), 518 ($M_+ - Pb$).

Received: April 23, 1997 [Z10378IE]
German version: *Angew. Chem.* **1997**, *109*, 2475–2476

Keywords: indenyl complexes · lead · sandwich complexes · structure elucidation

[1] J. S. Overby, T. P. Hanusa, *Organometallics* **1996**, *15*, 2205–2212.
[2] A. D. McMaster, S. R. Stobart, *J. Am. Chem. Soc.* **1982**, *104*, 2109–2112.
[3] J. L. Atwood, A. D. McMaster, R. D. Rogers, S. R. Stobart, *Organometallics* **1984**, *3*, 1500–1504.
[4] B. M. Milchailov, T. K. Baryshnikova, V. S. Bogdanovic, *Zh. Obshch. Khim.* **1973**, *43*, 1949–1955.
[5] N. Kumar, B. L. Kalostra, R. K. Multani, *J. Inorg. Nucl. Chem.* **1973**, *35*, 3019–3021.
[6] N. Kumar, B. L. Kalostra, R. K. Multani, *Curr. Sci.* **1973**, *42*, 58–59.
[7] A. K. Sharma, B. Bhushan, N. K. Kaushik, *Acta Chim. Hung.* **1983**, *113*, 29–33 [*Chem. Abstr.* **1983**, *99*, 212561].
[8] A. H. Cowley, M. A. Mardones, S. Avendano, E. Roman, J. M. Manriquez, C. Carrano, *Polyhedron* **1993**, *12*, 125–127.
[9] J. S. Overby, T. P. Hanusa, unpublished results.
[10] Crystal structure analysis: $C_{30}H_{46}PbSi_4$, $M = 726.24$, triclinic, space group $P\bar{1}$, $a = 11.444(2)$, $b = 17.275(3)$, $c = 18.634(6)$ Å, $\alpha = 103.480(16)$, $\beta = 105.53(2)$, $\gamma = 91.094(16)°$, $V = 3438.4(14)$ Å^3, $Z = 4$, $\rho_{calcd} = 1.403$ g cm^{-3}, $F(000) = 1443.47$, $\lambda = 0.71073$ Å, $T = -125$ °C, $\mu(Mo_{K\alpha}) = 51.0$ cm^{-1}, crystal size $0.28 \times 0.20 \times 0.03$ mm^3; of 11 970 unique reflections collected ($0 \le 2\theta \le 50°$), 7518 with $I > 2.5\sigma(I)$ were used for refinement; no decay correction; absorption correction with DIFABS (min./max. transmission 0.436/1.000). The structure was solved with SIR92 and Fourier techniques. All non-hydrogen atoms, with the exception of those in the C_5 rings were refined anisotropically; hydrogen atoms were inserted in calculated positions and included in the structure factor calculation as "riding" on the parent carbon atom. A secondary extinction correction was included late in the refinement. The highest peak on the final difference map was 2.6 e Å^{-3}, and was located 1.08 Å from the Pb position; $R = 0.054$, $R_w = 0.059$. Crystallographic data (excluding structure factors) for the structures reported in this paper have been deposited with the Cambridge Crystallographic Data Centre as supplementary publication no. CCDC-100348. Copies of the data can be obtained free of charge on application to The Director, CCDC, 12 Union Road, Cambridge CB21EZ, UK (fax: int. code +(1223)336-033; e-mail: deposit@chemcrys.cam.ac.uk).
[11] J. L. Atwood, W. E. Hunter, A. H. Cowley, R. A. Jones, C. A. Stewart, *J. Chem. Soc. Chem. Commun.* **1981**, 925–927.
[12] H. Schumann, C. Janiak, E. Hahn, C. Kolax, J. Loebel, M. D. Rausch, J. J. Zuckerman, M. J. Heeg, *Chem. Ber.* **1986**, *119*, 2656–2667.
[13] M. A. Beswick, C. Lopez-Casideo, M. A. Paver, P. R. Raithby, C. A. Russell, A. Steiner, D. S. Wright, *Chem. Commun.* **1997**, *1997*, 109–110.
[14] T. E. Ready, J. C. W. Chien, M. D. Rausch, *J. Organomet. Chem.* **1996**, *519*, 21–28.

 © WILEY-VCH Verlag GmbH, D-69451 Weinheim, 1997 0570-0833/97/3621-2379 $ 17.50+.50/0

New Insights into the Mechanism of the McMurry Reaction

Claude Villiers* and Michel Ephritikhine*

Reductive coupling of ketones to form alkenes, an extremely useful synthetic process in organic chemistry, is most often achieved with the aid of low-valent titanium reagents, according to the procedure developed by McMurry.[1] It is generally accepted that this reaction involves the intermediacy of a titanium pinacolate, which is subsequently deoxygenated to the corresponding alkene in the rate-determining step (Scheme 1). The

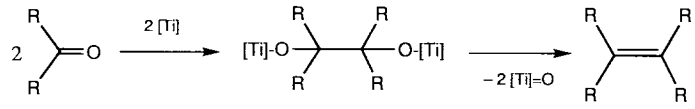

Scheme 1. Reductive coupling of ketones via a metallopinacol intermediate.

pinacolate could be formed by dimerization of two ketyl radicals or nucleophilic attack of the carbonyl dianion on a free ketone. In a number of instances, pinacols were indeed isolated by carrying out the reaction at low temperature; they were converted into the alkenes when resubmitted to the more forcing experimental conditions.

There are also a few examples of reductive coupling of ketones in which metallopinacols are clearly not the precursors of the alkene products. These transformations involve carbenoid species.[2, 3] In particular, reactions of ketones with W^{II} or W^{III} compounds proceed by initial cleavage of the ketonic C—O bond to give an alkylidene complex which further reacts with another ketone to afford the alkene, presumably via a metallaoxetane intermediate (Scheme 2).[2]

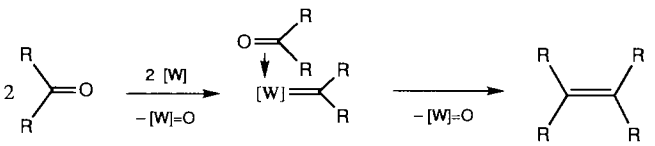

Scheme 2. Reductive coupling of ketones via a carbenoid species.

A clear mechanistic distinction is now recognized between these coupling reactions of ketones, depending on whether tungsten or titanium compounds are utilized. Although the possible involvement of carbenoid species in McMurry type reactions has been considered,[4] definite proof for their existence is lacking. In the course of our studies on the reductive coupling of ketones with uranium or titanium tetrachloride in the presence of alkali metal amalgam,[5] we undertook a careful analysis of the products and made observations that are not in agreement with the above ideas. We now put forward the dualistic aspects of the mechanism of these McMurry-type reactions.

Acetone reacted in tetrahydrofuran (THF) with one equivalent of $TiCl_4$ and excess Li(Hg) to give, after hydrolysis, a mixture of **1a** and **2a** as the major products; isopropanol and other

[*] Dr. C. Villiers, Dr. M. Ephritikhine
Service de Chimie Moléculaire
DSM, DRECAM, CNRS URA 331
CEA Saclay, F-91191 Gif sur Yvette (France)
Fax: Int. code +(1)6908-6640
e-mail: ephri@nanga.saclay.cea.fr

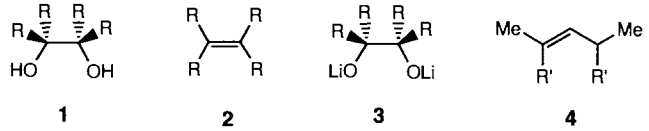

a, R = Me; **b**, R = Et; **c**, R = *i*Pr

a, R' = H; **b**, R' = Me

unidentified compounds, presumably products of aldol reactions, were also formed in lower yields. Total conversion of the carbonyl substrate was achieved in 10 h with three equivalents of lithium amalgam (Table 1). The formation of **2a** at 20 °C was

Table 1. Relative yields (in %) for the reaction of ketone R_2CO (R = Me, Et, *i*Pr) with MCl_4 (M = Ti, U) and Li(Hg) [a].

R, M	$HOCR_2CR_2OH$ **1**	$R_2C{=}CR_2$ **2**	R_2CHOH	$MeCR'{=}CHCHR'Me$ **4a** or **4b**	RCH_2R
Me, Ti	50	26	13	[b]	[b]
Me, U	87	0	8	[b]	[b]
Et, Ti	17	32	29	7	4
Et, U	56	5	11	21	0
*i*Pr, Ti[c]	0	23	38	10	4
*i*Pr, U[c]	0	27	23	29	1

[a] Molar ratio 1:1:3 (M = Ti) or 1:1:2 (M = U); all reactions were carried out in THF at 20 °C followed by hydrolysis; the organic products were identified by NMR spectroscopy, GC, and GC-MS. [b] Propene and propane were not detected. [c] About 10% of the ketone was recovered.

most intriguing, since the McMurry alkene synthesis supposedly requires higher temperatures for the deoxygenation step. In fact, a very small amount of **2a**, if any, appeared to have been produced by reduction and deoxygenation of a pinacolate intermediate, as shown by control experiments. The quantity of **2a** was not significantly increased after further addition of Li(Hg) to the reaction mixture, and only 5% of the alkene was obtained after 10 h at 20 °C upon treatment of the lithium pinacolate **3a** with $TiCl_4$ (or $TiCl_3$) and Li(Hg). The results of the reactions with **3** are summarized in Table 2.

Table 2. Relative yields (in %) for the successive treatment of **3** with MCl_4 and Li(Hg) [a].

R, M	$HOCR_2CR_2OH$ **1**	$R_2C{=}CR_2$ **2**	R_2CHOH	$MeCR'{=}CHCHR'Me$ **4a** or **4b**	RCH_2R
Me, Ti	92	5	0	[b]	[b]
Me, U	98	0	0	[b]	[b]
Et, Ti	35	52	0	5	1
Et, U	90	0	0	5	0
*i*Pr, Ti[c]	3	21	39	15	7
*i*Pr, U	90	1	5	0	0

[a], [b] See footnotes in Table 1; the molar ratios are here 1:2:4 (M = Ti) or 1:2:3 (M = U). [c] Treatment of **3c** with $TiCl_4$ gave iPr_2CO quantitatively (see text).

Similar treatment of diethylketone with $TiCl_4$ and Li(Hg) afforded **1b** and **2b**, but, in contrast to the reaction of acetone, the quantity of the alkene exceeded that of the diol. Most striking, however, was the formation of 2-pentene (**4a**) and *n*-pentane, which apparently resulted from deoxygenation of the ketone. Successive treatment of **3b** with $TiCl_4$ and Li(Hg) gave **2b**, indicating that the latter could be obtained by reduction of a pinacolate intermediate; however, **4a** was also formed, showing that the pinacolic C—C bond was cleaved under these conditions.

 © WILEY-VCH Verlag GmbH, D-69451 Weinheim, 1997 0570-0833/97/3621-2380 $ 17.50+.50/0

The trend observed in the product distribution was greatly amplified in the case of diisopropylketone. At room temperature, no **1c** but only **2c** resulted from the reductive coupling of $i\mathrm{Pr_2CO}$, whereas 2,4-dimethyl-2-pentene (**4b**) and 2,4-dimethylpentane were formed by deoxygenation of the carbonyl substrate. The titanium pinacolate $\mathrm{Cl_3TiOC}i\mathrm{Pr_2C}i\mathrm{Pr_2OTiCl_3}$, prepared by treating **3c** with $TiCl_4$, was not stable and transformed within 5 min into a mixture of $TiCl_3$ and $i\mathrm{Pr_2CO}$. Treatment of **3c** with $TiCl_3$ also gave $i\mathrm{Pr_2CO}$ as the major product (60%) along with $i\mathrm{Pr_2CHOH}$ (12%) and **4b** (2%). It was then doubtful that alkene **2c** resulted directly from deoxygenation of a metallopinacol; the facile cleavage of the titanium pinacolates, as well as the absence of pinacol in the product mixture, indicated that reductive coupling of diisopropylketone with the $TiCl_4$/Li(Hg) system does not proceed by dimerization of ketyl radicals.

Of course, such McMurry reactions of $i\mathrm{Pr_2CO}$ were previously performed with a number of titanium reagents, and, in agreement with our results, the corresponding pinacol was never detected among the coupling products. It is nevertheless very surprising that the formation of **4b** was overlooked so far. For example, it was reported that $i\mathrm{Pr_2CO}$ reacted with $TiCl_3$ in the presence of potassium to give **2c** in 37% yield;[6] we confirmed this result but also found that **4b** was the major product of the reaction (45%). More generally, deoxygenation of a ketone $\mathrm{RCOCH_2R'}$ to form the alkene $\mathrm{RCH{=}CHR'}$ was never noticed in a McMurry reaction, while the transformation $\mathrm{RCOCH_2R'} \rightarrow \mathrm{RCH_2CH_2R'}$ was observed with several hindered ketones;[7] the origin of the alkane has not been clarified.

Reductive coupling of ketones R_2CO (R = Me, Et, *i*Pr) was achieved by using UCl_4 in place of $TiCl_4$. We already reported that acetone reacted with UCl_4 and Li(Hg) in a molar ratio of 1:1:1 to give the bimetallic pinacolate dianion $[\mathrm{Cl_4U{-}OCMe_2CMe_2O{-}UCl_4}]^{2-}$ in almost quantitative yield;[5] with two equivalents of Li(Hg), formation of tetramethylethylene could be observed only upon heating the mixture at 60 °C. These results are in accordance with the postulated mechanism of the McMurry reaction. However, reactions of Et_2CO and $i\mathrm{Pr_2CO}$ with the UCl_4/Li(Hg) system afforded the same products as those obtained with $TiCl_4$: **4a** and **4b** were formed along with alkenes **2b** and **2c**, and pinacol **1c** was not detected. Complete conversion of these ketones required two equivalents of Li(Hg), which is in agreement with the fact that U^{III} instead of Ti^{II} species were the active species in the reduction process.[8] Most interestingly, the uranium pinacolates $\mathrm{Cl_3UOCR_2CR_2OUCl_3}$ (R = Me, Et, *i*Pr) were much more stable than their titanium counterparts. Treatment with Li(Hg) led essentially to the corresponding U^{III} complexes, which in no case could be further deoxygenated at 20 °C to alkenes **2** (Table 2).

The above results indicate that reactions of aliphatic ketones R_2CO (R = Me, Et, *i*Pr) with the MCl_4/Li(Hg) system (M = Ti or U) followed two distinct routes to lead to the metallopinacol or the tetraalkylethylene, respectively (Scheme 3). The former would be formed by dimerization of two ketyl radicals; this mechanism is generally accepted for the McMurry reaction (Scheme 1). The alkene $R_2C{=}CR_2$ would come from the reaction of the ketone with a carbenoid species (**A** in Scheme 3) that results from reduction and deoxygenation of the ketyl radical; this mechanism should be similar to that represented in Scheme 2. Rearrangement of the carbenoid intermediate **A** (R = Et or *i*Pr) would give alkenes **4a** and **4b** by migration of H (it is possible that propene, which could be formed from acetone, was not detected by GLC because it escaped into the vapor phase). Formation of **4a** and **4b**, which did not result from Li(Hg) reduction of the alkoxide derivatives $\mathrm{Cl_3TiOCHR_2}$ (R = Et, *i*Pr), was reminiscent of the synthesis of alkenes by

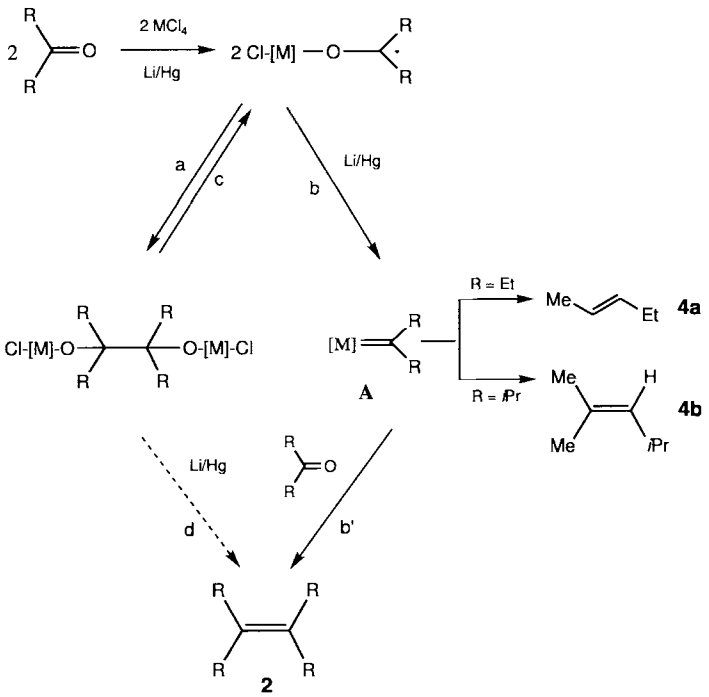

Scheme 3. Reductive coupling of R_2CO (R = Me, Et, *i*Pr) with the MCl_4/Li(Hg) system. ([M] = UCl_2 or TiCl). a) M = Ti, U; R = Me, Et; b), b') M = Ti; R = Me, Et, *i*Pr; M = U; R = Et, *i*Pr; c) M = Ti, U; R = Et, *i*Pr; d) M = Ti; R = Et.

treatment of alicyclic ketones with chlorotrimethyl silane and zinc, a reaction which likely involves organozinc carbenoid species.[9] The Me_3SiCl/Zn system also reductively coupled aryl and α,β-unsaturated carbonyl compounds; this transformation did not proceed via pinacol-type intermediates but presumably by a carbenoid.[3]

Currently, the actual carbenoid species **A** have not been characterized; they could not be detected by NMR spectroscopy. Except for the reaction of Et_2CO with the $TiCl_4$/Li(Hg) system, the two routes in Scheme 3 would be well separated, since the metallopinacols were not the precursors of alkenes $R_2C{=}CR_2$, at least at room temperature. Acetone underwent pinacolization exclusively (M = U) or preferentially (M = Ti), whereas diisopropyl ketone reacted solely by the alternative carbenoid route regardless of the system. This great difference in reactivity between Me_2CO and $i\mathrm{Pr_2CO}$ can be accounted for by steric factors; the more sterically hindered the ketyl radicals are, the more difficult they are to dimerize. Steric hindrance would also destabilize the pinacolate intermediates with respect to rupture of their C–C bond and reverse conversion into the ketyl radicals. Such reversible cleavage of metallopinacols was already assessed in the production of the unsymmetric alkene $\mathrm{Ph_2C{=}CTol_2}$ (Tol = *p*-Me-C_6H_4) by treating a mixture of pinacols $\mathrm{HOCPh_2CPh_2OH}$ and $\mathrm{HOCTol_2CTol_2OH}$ with uranium powder,[10] and in the reactions of benzophenone[11] or acetophenone[8] with titanium compounds.

The data reported here indicate that, contrary to the generally accepted mechanism, metallopinacols are not the sole precursors to the alkene products of the McMurry reactions. If the ketyl radicals—initially formed by electron transfer from the low-valent metal complex to the carbonyl substrate—can be effectively coupled into pinacolate intermediates, they can also be reduced and deoxygenated into carbenoid species; the latter provide the alkene after further reaction with the ketone. The course of the reaction, via the metallopinacol or the carbenoid intermediates, is largely determined by the steric hindrance of

 © WILEY-VCH Verlag GmbH, D-69451 Weinheim, 1997 0570-0833/97/3621-2381 $ 17.50+.50/0

the ketone; the less hindered ketones follow the pinacolization route. Even if they are formed, metallopinacols are not necessarily the precursors of the corresponding alkene, especially at room temperature, since they can be transformed back into the ketyl radicals by reversible cleavage of the pinacolic C–C bond.

Received: April 28, 1997 [Z10391IE]
German version: *Angew. Chem.* **1997**, *109*, 2477–2479

Keywords: carbenoids · C–C coupling · McMurry reactions · pinacol · titanium · uranium

[1] A. Fürstner, B. Bogdanović, *Angew. Chem.* **1996**, *108*, 2582; *Angew. Chem. Int. Ed. Engl.* **1996**, *35*, 2443; T. Wirth, *ibid.* **1996**, *108*, 65 and **1996**, *35*, 61; T. Lectka in *Active Metals: Preparation, Characterization, Applications* (Ed.: A. Fürstner), VCH, Weinheim, **1995**, p. 85; G. M. Robertson in *Comprehensive Organic Chemistry, Vol. 3* (Eds.: B. M. Trost, I. Fleming, G. Pattenden), Pergamon, Oxford, **1991**, p. 563; J. E. McMurry, *Chem. Rev.* **1989**, *89*, 1513.

[2] J. C. Bryan, J. M. Mayer, *J. Am. Chem. Soc.* **1990**, *112*, 2298; M. H. Chisholm, K. Folting, J. A. Klang, *Organometallics* **1990**, *9*, 602, 607; Y. Fujiwara, R. Ishikawa, F. Akiyama, S. Teranishi, *J. Org. Chem.* **1978**, *43*, 2477.

[3] A. K. Banerjee, M. C. Sulbaran de Carrasco, C. S. V. Frydrych-Houge, W. B. Motherwell, *J. Chem. Soc. Chem. Commun.* **1986**, 1803.

[4] A. Fürstner, A. Hupperts, A. Ptock, E. Janssen, *J. Org. Chem.* **1994**, *59*, 5215.

[5] O. Maury, C. Villiers, M. Ephritikhine, *New J. Chem.* **1997**, *21*, 137; *Angew. Chem.* **1996**, *108*, 1215; *Angew. Chem. Int. Ed. Engl.* **1996**, *35*, 1129; C. Villiers, R. Adam, M. Lance, M. Nierlich, J. Vigner, M. Ephritikhine, *J. Chem. Soc. Chem. Commun.* **1991**, 1144.

[6] J. E. McMurry, M. P. Fleming, K. L. Keese, L. R. Krepski, *J. Org. Chem.* **1978**, *43*, 3255.

[7] D. Lenoir, H. Burghard, *J. Chem. Res.* **1980**, 4715.

[8] B. Bogdanović, A. Bolte, *J. Organomet. Chem.* **1995**, *502*, 109.

[9] W. B. Motherwell, *J. Chem. Soc. Chem. Commun.* **1973**, 935.

[10] B. E. Kahn, R. D. Rieke, *Organometallics* **1988**, *7*, 463.

[11] R. S. P. Coutts, P. C. Wailes, R. L. Martin, *J. Organomet. Chem.* **1973**, *50*, 145.

Chemistry at the crossroads

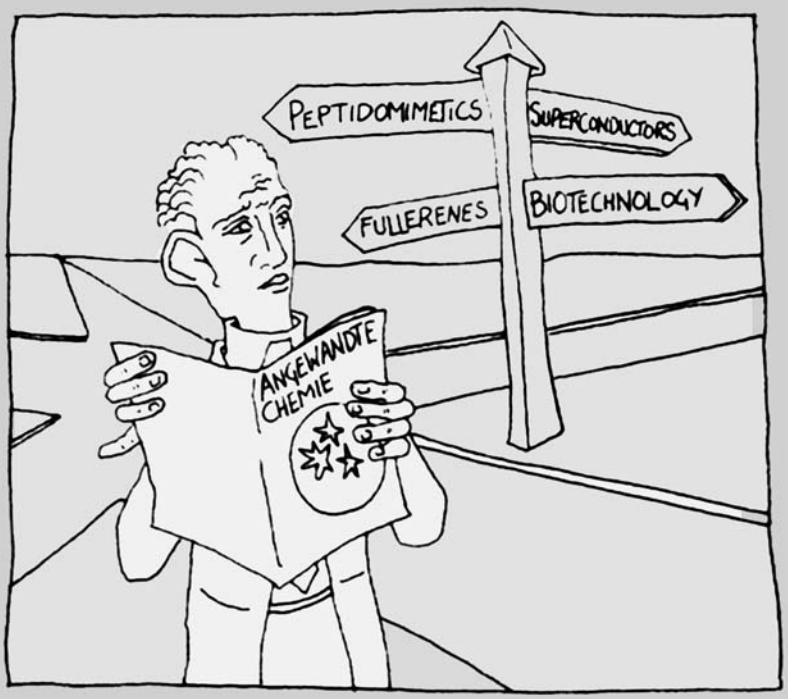

Pioneering scientists guide your way through newly charted territory with their topical reviews and discriminating highlights in **Angewandte Chemie.**

To start your own personal subscription, just fax.

An order form is provided on the last page for your convenience.

WILEY-VCH

 © WILEY-VCH Verlag GmbH, D-69451 Weinheim, 1997 0570-0833/97/3621-2382 $ 17.50+.50/0

Period Pieces!

Episodes from the History of the Rare Earth Elements. (Series: Chemists and Chemistry.) Edited by *C. H. Evans*. Kluwer, Dordrecht, 1996. 240 pp., hardcover £ 89.00.—ISBN 0-7923-4101-5

"I am willing to venture the opinion that the history of the rare earths is more fascinating, and illuminates more areas of chemical progress, than the history of any other group of elements." This view by C. H. Evans, the editor and a coauthor of this book, will be endorsed by many others besides rare earth enthusiasts and historians of science and technology. This 15th book in the series *Chemists and Chemistry* can also be regarded as forging links between chemistry and other sciences such as physics, medicine, biology, and geology. Eleven "episodes" from the history of the rare earth elements are described here by a team of well-chosen experts, mainly by examining the original literature and accounts of events. In the preface and in the introduction the editor gives a concise and informative explanation of the background to the two-part structure of the book (Part 1: Discovery, and Part 2: Applications). The story begins in 1787 with the discovery by the amateur mineralogist Lieutenant C. A. Arrhenius of the black mineral ytterbite (later called gadolinite). The 160-year history of the further discoveries that followed gives an impressive insight into the many technological innovations and advances in theory during that period.

As I read in Part 1 the history of how the dogged persistence and impatience of the experimental chemists were finally rewarded, I felt both pleasure and admiration. The authors of Chapters 1–5 (mostly Scandinavian) give a detailed, skillful, and sensitive account of the work leading to the discovery of the various elements. These discoveries were achieved largely without the guidance of Mendeleev's Periodic System, and were justly described by G. de Hevesy in 1926 as "one of the most brilliant accomplishments that experimental chemistry has ever produced". We learn that the fascinating history of the discoveries of cerium and of element 71 (lutecium) included fierce disputes about claims of priority. The articles include such interesting items as exchanges of letters, portraits of the chemists involved, and personal anecdotes relating to people such as C. G. Mosander, known affectionately to his friends as "Pater Moses", who was much more than a dedicated chemist. The introduction of spectrochemical analysis in 1859 not only gave a considerable new impetus to the discovery of new elements but also increased the opportunities for confusion, as the samples were seldom pure enough for the purpose. It was not until 1922 that Bohr's revolutionary theory of the atom paved the way for H. G. Moseley's development of the method of X-ray spectroscopy, eventually bringing order out of the chaos that had existed with regard to the number of rare earth elements and their structure. Although 16 of the 17 rare earth elements had already been discovered at that time, the skepticism of traditional experimental chemists towards the growing community of ambitious atomic physicists was such that the search for new rare earth elements went on regardless. However, we now read that "the new physics has changed the basis of rare earth research and stripped it of its chemical romance." The high point of this first part is undoubtedly the story of the discovery of the last (radioactive) rare earth element promethium in 1947 at the Clinton Laboratories, Oak Ridge, Tennessee, described in a lively style by its discoverer, J. A. Marinsky. The element was isolated by the ion-exchange technique that had recently been developed for separating radioactive fission products.

The second part of the book begins with a tribute to C. Auer von Welsbach who, true to his lifetime motto "plus lucis", invented the thorium–cerium incandescent mantle, and thus, in the forecourt of the café at the Viennese Opera, "illuminated" the birth of the rare earth industry. His life's work is analyzed by E. Baumgartner, a former employee of the Treibacher Chemical Works founded by von Auer. The account deals with the discovery of the elements neodymium, praseodymium, and lutecium, and the inventions of the oxide incandescent mantle, of the (osmium) metal filament lamp, and of the pyrophoric misch-metal alloys ("Auermetal" for lighter flints). In Chapter 8 two scientists from the Baotou Rare Earth Metals Research Institute report on work carried out in China to exploit 75% of the world's reserves of rare earth ores (the Baiyunebo mine in Inner Mongolia). As well as describing the raw material extraction processes and the separation and refinement of the metals by solvent extraction, the authors discuss potential areas of use. They give tables of data on production, consumption, and export quantities extending up to 1990. Unfortunately we learn nothing about the six-year plan which was mapped out by the Chinese government for the years 1990–1995. The last three "episodes" are concerned with geology, biology, and medicine, and as one with no special knowledge of these fields I found the discussions very interesting. Trace analytical methods such as neutron activation, yield reliable data about the occurrence and distribution of rare earths in nature, and thus give valuable clues concerning the formation of the earth's crust and the mantle. The cell biologist A. Weiss, one of the pioneers of this interdisciplinary field, describes the "lanthanum method", whereby the "spectroscopically inert" calcium(II) is replaced isomorphically by lanthanum(III), in order to study the biological role of calcium. In this example the method is used to investigate calcium mobilization patterns in smooth muscle. In the last chapter the editor reviews the medical applications of rare earths. These include the use of cerium nitrate for the control of vomiting and coughing, and of rare earth sulfates to treat infectious diseases such as tuberculosis. Two other compounds that are now used clinically are the anti-inflammatory

This section contains book reviews and a list of new books received by the editor. Book reviews are written by invitation from the editor. Suggestions for books to be reviewed and for book reviewers are welcome. Publishers should send brochures or (better) books to the Redaktion Angewandte Chemie, Postfach 101161, D-69451 Weinheim, Federal Republic of Germany. The editor reserves the right of selecting which books will be reviewed. Uninvited books not chosen for review will not be returned.

 © WILEY-VCH Verlag GmbH, D-69451 Weinheim, 1997 0570-0833/97/3621-2383 $ 17.50+.50/0

agent Phlogosol (sodium disulfosalicylatosamarium anhydride) and GdDTPA, which is a contrast agent for magnetic resonance imaging.

As a collection of episodes from the history of the rare earth elements, the book makes no claim to completeness, especially in the area of applications. Although the chapters are presented as separate stories in the individual style of their authors, sometimes with overlapping of the subject matter, the overall effect is quite well-integrated. The articles emphasize the interpretation of historical connections. Thus the work can be regarded as an excellent complement to the more technologically and scientifically orientated review by K. A. Gschneidner and C. R. Eyring ("Two Hundred Year Impact of Rare Earths on Science", *Handbook on the Physics and Chemistry of Rare Earths*, Elsevier, Amsterdam, 1988). But who is likely to be willing to buy it at this rather high price?

Reiner Anwander
Institut für Technische Chemie
der Universität Stuttgart (Germany)

The History of the Faraday Society. By *L. E. Sutton* and *M. M. Davies*. Royal Society, Cambridge, 1996. XV+414 pp., hardcover £ 20.00.—ISBN 0-85404-863-4

Because of the effect the Faraday Society has had on me it is difficult for me to give a dispassionate review of this book. As an undergraduate I was frequently recommended to read papers published in that Society's *Transactions* and *Discussions* and my own first research was published in the former just 60 years ago. But it was the debates, recorded *verbatim* in the *Discussions*, which really captured my attention and stimulated my imagination. The cut and thrust of the arguments of the proponents and opponents brought into sharp focus not only the scientific issues but also the personalities of some of the leading physical chemists of the time who spoke in the discussion. As I pointed out in the paper I was asked to give at celebratory 100th Faraday Discussion held at the Royal Institution on 24 April 1995, the effect on me of reading the comments in the general discussion which took place in 1921 and was published as Volume 17 of the *Transactions* "was a turning point for me because chemical kinetics came alive, the comments ... had all the excitement of a good novel, particularly when F. A. Lindemann demolished the idea separately propounded by Professor Lewis of Liverpool and Professor Perrin of Paris that "first order (gaseous) reactions were really photochemical" and "later in the discussion predicted that as the pressure was lowered such reactions would display second order kinetics" as later researchers were to verify". Thus it was I became an enthusiastic supporter of the Society and all its works and have remained so ever since; others have told me of similar experiences.

The recipe for such success was simple; circulate the page proofs of all the papers to all participants well before the meeting at which each author would be allowed only about 5–10 minutes to highlight the salient points, thereby leaving three or four times that time for discussion, and create an atmosphere and ample opportunity for informal conversations. The *Discussion* meetings have continued to flourish, to such a degree that physical chemists from other countries have not only flocked to them but invited the Society to hold their meetings overseas which is the greatest compliment they could pay. The *Transactions* have likewise prospered because they have changed to meet differing needs. Thus *Special Issues* have been published which concentrate on a particular topic and *Faraday Research Articles* have been incorporated in the *Transactions* which survey developments in a special area of current interest. Such innovations have doubtless contributed to the outstanding success of the *Transactions* as a highly regarded and popular international journal so that by 1996 an average of between four and five manuscripts were submitted each working day.

Who were the people who were influential in the society and made success possible? This book tells the story of the growth of the Faraday Society from its very modest beginnings in 1902 when a group of friends, some old and distinguished like Dr. (later Sir Joseph) Swan FRS, and C. V. Boys FRS, some young and later to become distinguished like F. G. Donnan, met and set up a committee to consider the desirability and feasibility of establishing an Electrochemical Society for which Germany in 1894 had already set an example. The first meeting of the Council of the new society which had appropriated the name "Faraday" doubtless as a means of gaining respect, as may also have been the case two years earlier when the *Elektrochemische Gesellschaft* became the *Deutsche Bunsen Gesellschaft für angewandte Chemie*, took place on 11 February 1903. For many years the Faraday Society had no rooms of its own, very few paid staff, and was administered by G. S. W. Marlow and Miss Beatrice Kornitzer who were completely devoted to its service, as I know from experience.

For me this book also has a special significance because it has two authors both of whom died before its publication. When I was an undergraduate Dr. Leslie Sutton was a young don, i.e. a lecturer, in Oxford making his name as an early skilled measurer of dipole moments and when I arrived in Cambridge Mansel Davies was a research student working on infrared spectroscopy under the supervision of G. B. B. M. Sutherland. Mansel became a life long friend and Leslie Sutton was later in life a colleague of mine at Oxford. Sutton covers the period 1903–1945 and Davies from 1945 to January 1972 when the Faraday Society became the Faraday Division of the Royal Society of Chemistry, a fusion which has been beneficial to both. The literary styles of the two authors are very different; so too are the matters they chose to emphasize. In my opinion these differences add to rather than detract from the interest of the book, and they give an enlarged and more diversified picture of the Society than either of them could have produced alone. The readers of the book will gain a fascinating insight into the way in which a society founded by a few enthusiasts became influential in the maturation of the subject of physical chemistry, how that subject interacted beneficially with biological and material sciences and was applied. I commend the book unreservedly as a vignette of social history of part of twentieth century science.

Lord Dainton
Oxford (UK)

Table of Isotopes. 8th Edition, Volumes 1 and 2. Edited by *R. B. Firestone* and *V. S. Shirley*. John Wiley & Sons Ltd, New York, 1996. XXIV, 2970 pp. with 9 appendices and CD-ROM, hardcover £ 190.00.—ISBN 0-471-14918-7 (text volumes)/0-471-16405-4 (CD-ROM)

The eighth edition of this standard work has now appeared, despite the fact that in 1978 the seventh edition was announced, in its preface, as being probably the last, to be replaced in the future by other forms of data compilation. That was not good news for those who had become used to looking up data in the *Table of Isotopes*, the "Blue Bible", but the thinking behind it was understandable when one compared the still handy sixth edition with the massive seventh—where would this growth finally end?

Now we have before us the latest version of the work: two volumes in a colorful binding, grown to 3100 pages listing

 © WILEY-VCH Verlag GmbH, D-69451 Weinheim, 1997 0570-0833/97/3621-2384 $ 17.50+.50/0

the nuclear properties of about 3200 isotopes and isomers of 111 elements. It is based on the combined efforts of more than 100 scientists from various countries, who have critically evaluated some 24000 publications and contributed their results to form the Evaluated Nuclear Structure Data Files (ENSDF) at the Brookhaven National Laboratory.

Despite the even greater quantity of data contained in the eighth edition, one is immediately at ease with using it, as the well proven structure has been retained. The data are arranged in mass chains with increasing mass number. Then within a given mass number the nuclear charge numbers increase, with radioactive decay schemes providing a system for quick optical orientation.

However, the details have undergone some considerable changes. Thus, only one set of data is given for each nuclide, namely that which the compilers regard as representing the current state of knowledge, instead of data from different authors being listed alongside each other. Many users will certainly regard this as an improvement. Where one wishes to consult the original sources, the well-chosen literature references given here are a useful starting point; alternatively one can obtain information from the *Nuclear Data Sheets*, from mass chains published in *Nuclear Physics*, or lastly from the actual ENSD files. In this edition greater attention has been paid to data on nuclear reactions. The excited nuclear states that they generate are now listed instead of being shown diagrammatically. Also the states that belong together within rotation bands are indicated by suitable schematic diagrams, leading to useful information about one important aspect of nuclear structure.

The appendices too have been considerably enlarged. In these, data that are scattered throughout the entire tabulation are systematically collected together under various properties headings. For example, the characteristic gamma-emissions of radioactive nuclides are arranged according to their energies, which is useful when one wishes to identify an unexpected gamma line. Various other properties of atoms, nuclei, and radiations, which users of the *Table of Isotopes* are likely to need frequently, are summarized in the form of diagrams or tables. There is even a short section on nuclear structure.

Furthermore, when you buy the *Table of Isotopes* you also receive a second copy in the form of an interactive CD-ROM edited by Frank Chu, which can be used with Windows, Macintosh, or UNIX systems. You can either load it into your desktop PC at home or carry the data around in your laptop computer. The data are exactly the same as in the printed volumes, but they are displayed in a much more spacious style and arranged in a clearly ordered manner, rather than in continuous lines as in the book version. This increases the number of pages to about 14000. Finding one's way around is helped by color codes and by "bookmarks". Data with common features can be quickly called up with a mouse click. Thus, starting from the mass chain one can easily find the radioactive decay data for a particular isotope, and proceeed from there to the decay scheme, and finally to the bibliography. There one can click on the abbreviated codes to read names of authors, titles, and short abstracts. Any details that are not sufficiently well resolved on the screen for easy reading, such as a complex decay scheme, can be magnified up to eightfold if necessary. On the whole, however, the hardcopies are beautifully sharp, even at normal size. Lastly, the CD-ROM also contains some additional information not provided in the book version, for example about the ENSDF system.

Although many users will continue to prefer the familiar printed version of the *Table of Isotopes*, especially for quickly looking up some item of information such as the half-life of a nuclide or a characteristic gamma line, the CD-ROM is undeniably the form that will prevail in the future. One quickly gets accustomed to using it. In the preface Richard Firestone assures us that there is still plenty of space on the CD-ROM, and points out that it can easily be updated from the database. For this reason he promises that updated editions will appear more frequently than in the past—the eighth edition will certainly not be the last. Users will look forward to that.

Günter Herrmann
Institut für Kernchemie
der Universität Mainz (Germany)

 © WILEY-VCH Verlag GmbH, D-69451 Weinheim, 1997 0570-0833/97/3621-2385 $ 17.50+.50/0

Schematic Binding Model for...

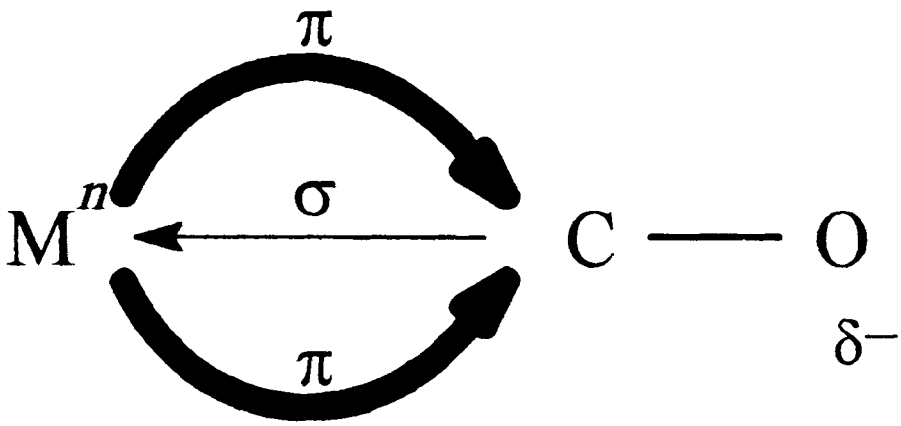

predominantly
π-bonded
highly reduced
carbonylmetalates,...

$n = -2, -3, -4$
$\tilde{\nu}(CO) < 2080\ cm^{-1}$

typical
metal
carbonyls,
and...

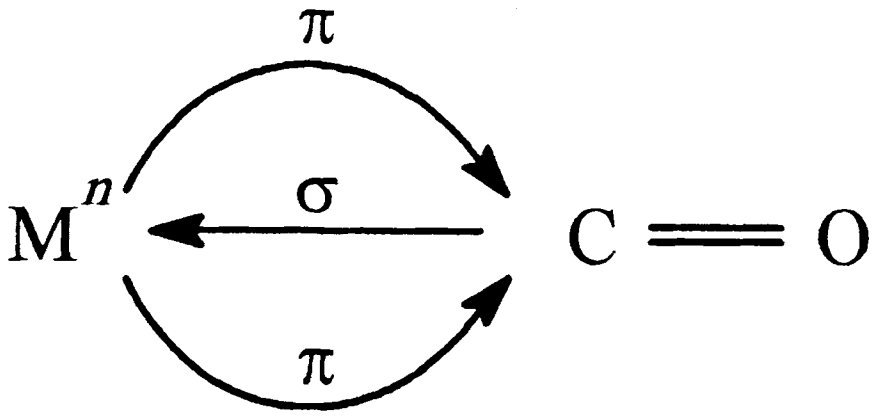

$n = -1, 0, +1$
$2080\ cm^{-1} < \tilde{\nu}\ (CO) < 2180\ cm^{-1}$

predominantly
δ-bonded metal
carbonyl cations.

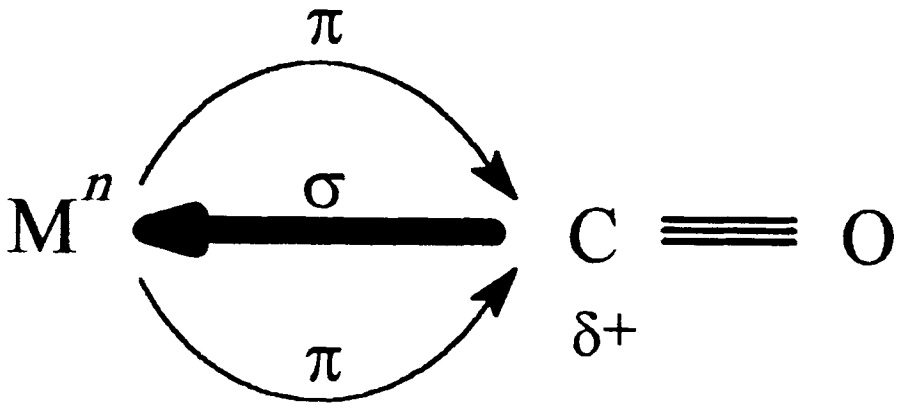

$n = +1, +2, +3$
$\tilde{\nu}\ (CO) > 2180\ cm^{-1}$

ANGEWANDTE CHEMIE © WILEY-VCH

Homoleptic Metal Carbonyl Cations of the Electron-Rich Metals: Their Generation in Superacid Media Together with Their Spectroscopic and Structural Characterization**

Helge Willner* and Friedhelm Aubke*

Homoleptic carbonyl cations of the electron-rich metals in Groups 8 through 12 are the newest members of the large family of transition metal carbonyls. They can be distinguished from typical metal carbonyl complexes in several respects. Their synthesis entails carbonylation of metal salts in such superacids as fluorosulfuric acid and "magic acid" HSO_3F–SbF_5. Thermally stable salts with $[Sb_2F_{11}]^-$ as counterion are obtained with antimony pentafluoride as reaction medium. Both the $[Sb_2F_{11}]^-$ anion and superacid reaction media have previously found little application in the organometallic chemistry of d-block elements. Also unprecedented in metal carbonyl chemistry are the coordination geometries with coordination numbers 4 (square-planar coordination) and 2 (linear coordination) for the cation. Formal oxidation states of the metals, and the charges of the complex cations, extend from +1 to +3: thus CO is largely σ-bonded to the metal, and the CO bond is strongly polarized. Minimal metal → CO π-backbonding and a positive partial charge on carbon are manifested in long M–C bonds, short C–O bonds, high frequencies for C–O stretching vibrations (up to 2300 cm^{-1}), and small ^{13}C NMR chemical shifts (up to $\delta_c = 121$). Prominent examples of these unusual homoleptic carbonyl cations, which were recently the subject of a Highlight in this journal, include the first carbonyl cation of a p-block metal $[Hg(CO)_2]^{2+}$, the first trivalent carbonyl cation $[Ir(CO)_6]^{3+}$, and the first multiply charged carbonyl cation of a 3d metal $[Fe(CO)_6]^{2+}$. In this overview we propose to a) outline the historical origins of cationic metal carbonyls and their methods of synthesis; b) present a summary of the general field of carbonyl cations, which has developed over a very short period of time; c) discuss the structural and spectroscopic characteristics of metal–CO bonding; d) discuss the special significance associated with reaction media and the $[Sb_2F_{11}]^-$ anion; and e) point to the most recent results and anticipated future developments.

Keywords: carbonyl complexes · cations · superacidic systems · synthetic methods · transition metals

1. Introduction

Carbon monoxide, CO, is the most important and versatile ligand in the organometallic chemistry of transition metals.[1] This simple diatomic molecule can bind in monodentate or multidentate fashion to a host of charged and uncharged metal atoms, clusters, organometallic fragments, and surfaces of metals or ionic crystals. The products range from diverse molecular complexes, through adsorbates, to matrix-isolated molecules. The origin of this multifaceted bonding potential is to be found in a synergistic interaction between σ-donor bonding of the 5σ molecular orbital of CO to a suitable atomic orbital on the metal atom with σ symmetry, and π-backbonding of the metal atom into the π* molecular orbitals of CO. In the case of typical mononuclear homoleptic metal carbonyls, several simplifications occur as a result of: a) the bonding nature of CO, which is in this case only monodentate; b) nearly strict observance of the 18-electron rule [the 17e molecule $V(CO)_6$ constitutes an exception], which permits the prediction of molecular structures and reactivity characteristics; and c) the need for optimization of the synergistic bonding, whereby the formal charge on the metal remains low (normally 0 or ±1). Especially π-backbonding serves to stabilize the M–CO bond in the presence of a low formal charge.

As a consequence of these conditions typical carbonyl complexes are formed in the middle of the d series (Groups 5 through 9). Their molecular geometries are predictable from VSEPR theory.[2] The geometries are mainly limited to three

[*] Prof. Dr. H. Willner
Institut für Anorganische Chemie der Universität
Callinstrasse 9, D-30167 Hannover (Germany)
Fax: Int. code +(511)762-3006
e-mail: willner@mbox.acc.uni-hannover.de
Prof. Dr. F. Aubke
Department of Chemistry, The University of British Columbia
Vancouver B. C. V6T1Z1 (Canada)
Fax: Int. code +(604)822-2847
e-mail: aubke@chem.ubc.ca

[**] Editorial note: In this review the recommendations of IUPAC Nomenclature have not been followed. The formulas of the neutral coordination compounds have not been enclosed by square brackets in order to distinguish more clearly the neutral compounds from ionic complexes and polyanions.

 © WILEY-VCH Verlag GmbH, D-69451 Weinheim, 1997 0570-0833/97/3622-2403 $ 17.50+.50/0

simple types: a) octahedral coordination, $[M(CO)_6]^m$, $m = -1$, 0, +1; b) trigonal-bipyramidal coordination, $M(CO)_5$; and c) tetrahedral coordination, $M(CO)_4$.

Thermally stable, isolable compounds do not exist for all these structural types. Until 1990, only carbonyl cations of the type $[M(CO)_6]^+$ (M = Mn, Tc, Re) were known.[3, 4] Among the neutral complexes $M(CO)_4$, only $Ni(CO)_4$, the oldest compound in the group,[5] is stable at room temperature, whereas the homologous complexes $Pd(CO)_4$ and $Pt(CO)_4$ exist exclusively at low temperature in the matrix.[6]

Very recently there have been two further developments reaching beyond the typical carbonyls:

1. Many new "highly reduced" metal carbonyl anions have been obtained through chemical reduction in basic solvents.[7] These are of the general type $[M(CO)_n]^{m-}$, where M is an element from Groups 4 through 9, the oxidation states/ionic charges m fall between -2 and -4, and the coordination numbers n are between 3 and 6. The molecular geometries are comparable to those of typical carbonyls (octahedral, trigonal bipyramidal, and tetrahedral). In addition, trigonal-planar anions of the type $[M(CO)_3]^{3-}$ (M = Co, Rh, Ir) have been described.[7] All these highly reduced carbonyl metalates obey the 18e rule, and form, together with the typical carbonyl metalates $[M(CO)_n]^-$ (M = an element of the Groups 5, 7, 9; $n = 6, 5, 4$) and $[M(CO)_4]^{2-}$ (M = Fe, Ru, Os), the largest group of mononuclear homoleptic carbonyl complexes.

2. Completely new homoleptic carbonyl cations, the subject of a recent highlight in this journal,[8] can be prepared[9] in superacid medium.[10] They are of the type $[M(CO)_n]^{m+}$, with M = an element of the Groups 8 through 11, $n = 6$ (octahedral),[11-13] $n = 4$ (square planar),[14] and $n = 2$ (linear),[15, 16] where $m = 1, 2, 3$. These cations form isolable, thermally stable salts with $[Sb_2F_{11}]^-$ as the anion. The boundary of the transition metals was crossed for the first time with $[Hg_n(CO)_2]^{2+}$, $n = 1, 2$.[15]

Metal carbonyl cations display two unique features: a) Cations with the electronic configurations d^8 and d^{10} are square planar or linear, respectively. These geometries are unprecedented in metal carbonyl chemistry. b) The number of valence electrons (16 or 14) violates the noble gas rule.

To this group can also be added the typical carbonyl cations $[M(CO)_6]^+$, M = Mn, Tc, Re, which have been known since 1961. All known mononuclear metal carbonyl complexes are listed in Table 1. They are divided into typical metal carbonyls, highly reduced carbonyl metalates,[7] and homoleptic metal carbonyl cations.[9] If one includes the carbonyl complexes with copper and silver, all the d-block metals except those in Group 3 (Sc, Y, La) form at least one type of carbonyl derivative. In addition to these mononuclear cases, two binuclear cations have so far been isolated from SbF_5 suspension or HSO_3F solution: linear $[Hg_2(CO)_2]^{2+}$ [15] and cyclic $[Pd_2(\mu\text{-}CO)_2]^{2+}$.[17] Whereas all the homoleptic carbonyl cations exist in magic acid (HSO_3F–SbF_5) the autoionization ion SO_3F^- is sufficiently

H. Willner

F. Aubke

Helge Willner, born in 1947 in Hamm, Westphalia, pursued an apprenticeship as laboratory assistant and studies at the Engineering School in Essen before embarking upon and completing in 1971 a chemistry degree at the University of Münster. In 1974 he presented a dissertation under the supervision of H. J. Becher on the subject of vibrational spectra of doped ionic crystals. He subsequently went to the University of Bochum to work on matrix-isolation spectroscopy and fluorine chemistry with A. Haas. He also acquired knowledge of special matrix techniques during 1977 in the laboratory of L. Andrews, Charlottesville, VA (USA). He then completed his habilitation in Bochum in 1981 with an investigation of binary sulfur and selenium fluorides, and in 1982 was called to a professorship in inorganic chemistry at the University of Hannover. During a sabbatical semester in 1989 with F. Aubke in Vancouver, Canada, he became interested in superacids, and there laid the groundwork for this article with the discovery of the $[Au(CO)_2]^+$ cation. His principal areas of activity are matrix-isolation spectroscopy of small, reactive molecules, especially in the fields of atmospheric and fluorine chemistry, as well as—in the past eight years—coordination chemistry in superacid media.

Friedhelm (Felix) Aubke was born in 1932 in Herne (Westphalia). He studied chemistry at the Technische Hochschule Aachen, where he received his doctorate under M. Schmeisser in 1962. After postdoctoral research in Seattle, Washington (G. H. Cady), and Hamilton, Ontario (R. J. Gillespie), he started his academic career in 1966 at the University of British Columbia, Vancouver, Canada, where he has been a full professor since 1978. His research in physical inorganic chemistry has been concerned with the development of new superacid systems, their application in the generation of unusual, highly electrophilic nonmetallic, metallic, and organometallic cations, and their subsequent spectroscopic and structural studies. Felix Aubke is the recipient of the Killam Senior Faculty Research Fellowship (1987) and the Alexander von Humboldt Research Prize (1995). He has been very active in fluorine chemistry, and has hosted in Vancouver both the 10th (1982) and the 15th (1997) International Symposia on Fluorine Chemistry

Table 1. Mononuclear homoleptic metal carbonyl species that are stable under ordinary conditions.

Group 4	5	6	7	8	9	10	11	12
typical metal carbonyl complexes								
	$[V(CO)_6]^-$	$Cr(CO)_6$	$[Mn(CO)_5]^-$	$[Fe(CO)_4]^{2-}$	$[Co(CO)_4]^-$	$Ni(CO)_4$		
	$V(CO)_6$		$[Mn(CO)_6]^+$	$Fe(CO)_5$				
	$[Nb(CO)_6]^-$	$Mo(CO)_6$	$[Tc(CO)_5]^-$	$[Ru(CO)_4]^{2-}$	$[Rh(CO)_4]^-$			
			$[Tc(CO)_6]^+$	$Ru(CO)_5$				
	$[Ta(CO)_6]^-$	$W(CO)_6$	$[Re(CO)_5]^-$	$[Os(CO)_4]^{2-}$	$[Ir(CO)_4]^-$			
			$[Re(CO)_6]^+$	$Os(CO)_5$				
highly reduced carbonylates [7]								
$[Ti(CO)_4]^{2-}$	$[V(CO)_5]^{3-}$	$[Cr(CO)_4]^{4-}$	$[Mn(CO)_4]^{3-}$	[a]	$[Co(CO)_3]^{3-}$			
$[Zr(CO)_4]^{2-}$	$[Nb(CO)_5]^{3-}$	$[Mo(CO)_4]^{4-}$		[a]	$[Rh(CO)_3]^{3-}$			
$[Hf(CO)_4]^{2-}$	$[Ta(CO)_5]^{3-}$	$[W(CO)_4]^{4-}$	$[Re(CO)_4]^{3-}$	[a]	$[Ir(CO)_3]^{3-}$			
metal carbonyl cations								
				$[Fe(CO)_6]^{2+}$			$[Cu(CO)_n]^+$ [b]	
				$[Ru(CO)_6]^{2+}$		$[Pd(CO)_4]^{2+}$	$[Ag(CO)_m]^+$ [c]	
				$[Os(CO)_6]^{2+}$	$[Ir(CO)_6]^{3+}$	$[Pt(CO)_4]^{2+}$	$[Au(CO)_2]^+$	$[Hg(CO)_2]^{2+}$

[a] $[M(CO)_4]^{2-}$ complexes with M = Fe, Ru, or Os are considered typical; $[M(CO)_3]^{4-}$ are anticipated. [b] $n = 1-4$, thermally unstable. [c] $m = 1-3$, thermally unstable.

nucleophilic in the protic acid HSO_3F to partially displace CO from the carbonyl cations. In this manner cationic derivatives of the general type $[M(CO)_n(SO_3F)_n]$, $n = 1, 2, 3$, are formed, in which fluorosulfate groups are covalently bonded through an oxygen atom to M. Examples include $Au(CO)SO_3F$,[16a] $M(CO)_2(SO_3F)_2$ in which M = Pd or Pt,[18] and $Ir(CO)_3(SO_3F)_3$.[19] They have been included in this overview for three reasons:

1. Their spectroscopic and bonding characteristics are similar to those of the corresponding homoleptic metal carbonyl cations.
2. The molecular structures of *cis*-$Pd(CO)_2(SO_3F)_2$,[18b] *mer*-$Ir(CO)_3(SO_3F)_3$,[19] and *cyclo*-$[Pd_2(\mu\text{-}CO)_2](SO_3F)_2$ [17] are known and provide useful structural information.
3. Most metal carbonyl fluorosulfates are easily converted by solvolysis in liquid SbF_5 under a CO atmosphere into the corresponding $[Sb_2F_{11}]^-$ salts.[14, 16b] The example of the pair $Au(CO)SO_3F$–$[Au(CO)_2][Sb_2F_{11}]$ [Eq. (a)] illustrates the relationship between the two groups.

$$Au(CO)SO_3F \underset{\text{in } HSO_3F:\ +SO_3F^-,\ -[Sb_2F_{11}]^-}{\overset{\text{in } SbF_5:\ +CO,\ -Sb_2F_9(SO_3F)}{\rightleftharpoons}} [Au(CO)_2][Sb_2F_{11}] \qquad (a)$$

Antimony pentafluoride as sole reaction medium for carbonylation,[20] and the use of binary metal fluorosulfates and halides as starting materials,[21] has in the meantime diminished the significance of metal carbonyl fluorosulfates as precursors in the synthesis of salts with metal carbonyl cations.

In certain cases, anhydrous hydrofluoric acid is used as a reaction medium for the preparation of metal carbonyl fluorides. Some of those considered here, such as $Ir(CO)_3F_3$,[22] possess fluorosulfate analogues, in this case $Ir(CO)_3(SO_3F)_3$.[19]

1.1. The History of Homoleptic Carbonyl Cations of Electron-Rich Metals

Many authors are of the opinion that the accidental discovery of $Ni(CO)_4$ by Mond, Langer, and Quincke in 1890[5] marks the beginning of metal carbonyl chemistry.[23] The organometallic chemistry of carbon monoxide was thereafter intensively developed through the contributions of W. Hieber and co-workers,[24, 25] and today constitutes an important component of modern transition metal chemistry.[1, 26, 27] Less well known is an earlier, equally fortuitous discovery in the year 1868 by Paul Schützenberger.[28, 29] During an attempt to catalyze the reaction of CO with Cl_2 to give $COCl_2$ with heated platinum Schützenberger succeeded in isolating and identifying three carbonyl chlorides of divalent platinum with the compositions $Pt(CO)_2Cl_2$, $Pt_2(CO)_4Cl_4$, and $Pt_2(CO)_3Cl_4$.[29] The compound *cis*-$[Pt(CO)_2Cl_2]$ has since been very thoroughly investigated, and it has been shown that CO is primarily σ-bonded to the Pt^{II} center.[30] Subsequent systematic studies of these compounds, which were regarded as CO adducts to transition metal chlorides, led to three important contributions by W. Manchot and co-workers:

1. Confirmation[31a] of the existence of the platinum carbonyl chlorides described by Schützenberger,[28, 29] and discovery of the first carbonyl derivative of palladium, with the composition $Pd(CO)Cl_2$.[31b]
2. The synthesis of Au(CO)Cl, the first carbonyl derivative of gold,[32] whose structure is also now known[33]—this simple four-atom molecule remained the only mononuclear gold(I) carbonyl complex for 65 years.
3. The first use of a strong protic acid (concentrated H_2SO_4) in the attempted preparation of carbonyl cations of silver.[34]

Much of this early work has been summarized by M. I. Bruce,[35] S. C. Tripathi et al.,[36a] and M. N. Vargaftik et al.[36b] More recent studies in the area of these noble metal carbonyl halides have been carried out by P. L. Goggin et al.[30] and F. Calderazzo et al.[37–39]

It has since become clear that a formal relationship[40] exists between Schützenberger's $Pt(CO)_2Cl_2$[28, 29] and the homoleptic cation $[Pt(CO)_4]^{2+}$.[14] The first thermally stable homoleptic carbonyl cations of the type $[M(CO)_6]^+$ (M = Mn,[41] Tc,[42] Re,[43]) were discovered, however, by E. O. Fischer, W. Hieber, and their co-workers in 1961. The syntheses were accomplished starting from $M(CO)_5X$, X = Cl or Br, through halide abstraction with Lewis acids at high temperature and high CO pressure [Eq. (b)].

$$M(CO)_5X + AlCl_3 + CO \xrightarrow[90°C]{\text{ca. 300 bar CO}} [M(CO)_6][AlCl_3X] \quad (b)$$

X = Cl, Br; M = Mn, Tc, Re

Detailed studies of vibrational spectra have shown that these cations have octahedral geometries.[44, 45] Subsequent attempts to extend the same synthetic methods to metal carbonyl halides of Group 8 ($M(CO)_4X_2$ where M = Fe, Os and X = Cl, Br), appeared to lead to the doubly charged cations $[M(CO)_6]^{2+}$ (M = Fe, Os) with $[AlX_4]^-$ (X = Cl, Br) as counterion.[43a] However, these as well as other reports of the synthesis of $[Fe(CO)_6]^{2+}$ [48] were repudiated within a few years.[49]

Not until 35 years later[43a] did it prove possible to obtain not only $[Os(CO)_6]^{2+}$ and $[Ru(CO)_6]^{2+}$,[11] but also $[Fe(CO)_6]^{2+}$,[12] as thermally stable $[Sb_2F_{11}]^-$ salts ($T_{decomp.} > 100\,°C$). Their synthesis required the development of a new carbonylation method in superacid media.[8] Again, as with the discovery of $Ni(CO)_4$ and the first synthesis of $Pt(CO)_2Cl_2$, the beginning was marked by an accidental discovery. Attempts to prepare the $[HCO]^+$ ion—previously discovered in interstellar space[50, 51]—by protonation of CO in the conjugated superacid HSO_3F–$Au(SO_3F)_3$[52] resulted instead in the reductive carbonylation of $Au(SO_3F)_3$ to form the first homoleptic noble metal carbonyl cation $[Au(CO)_2]^+$,[16a] initially in solution and later as the thermally stable salt $[Au(CO)_2][Sb_2F_{11}]$.[16b] The advances achieved in homoleptic metal carbonyl chemistry since that time are discussed below. The molecular ion $[HCO]^+$ has, interestingly, acquired great significance with respect to the discussion of bonding in metal carbonyl cations. Its CO force constant of $21.3 \times 10^2\ N\,m^{-1}$ [50c] can be regarded as a limiting value for the strongest C–O bond in carbonyl cations in the complete absence of π-back-bonding. The change from the ionizing protic acid HSO_3F and the magic acid HSO_3F–SbF_5 to liquid SbF_5 as sole reaction medium finally has permitted the facile preparation of such multiply charged carbonyl cations as $[M(CO)_6]^{2+}$, M = Fe,[12] Ru,[11] Os,[15] or $[Ir(CO)_6]^{3+}$,[13] none of which exist in HSO_3F.

1.2. Recent Developments in Cationic Carbonyl Complexes, and the Goal of this Article

Apart from the carbonyl cations mentioned above, the cationic carbonyl complexes of silver and copper, which display low thermal stability, are relevant to this article. The silver(I) carbonyls $[Ag(CO)_n]^+$, $n = 1-3$[53–56] exist with complex teflato counterions (teflate = $OTeF_5$) such as $[B(OTeF_5)_4]^-$ or $[Nb(OTeF_5)_6]^-$. They are formed by CO addition to the corresponding silver(I) salts, but under normal conditions are unstable and release CO spontaneously.[56] Nevertheless, it has been possible to determine two molecular structures by X-ray diffraction on single crystals at −125 °C: those of $Ag(CO)[B(OTeF_5)_4]$ and $[Ag(CO)_2][B(OTeF_5)_4]$.[53, 56]

Cationic complexes of copper(I), which are discussed elsewhere,[9b, 35] have a long history and important applications as carbonylation catalysts. It is interesting that cations such as $[Cu(CO)_n]^+$, $n = 1-4$, or $[Ag(CO)_2]^+$ are generated in strong protic acids like HSO_3F and HSO_3CF_3.[57] According to a recent study the isolable salt $[Cu(CO)][AsF_6]$,[58] which forms with the fluoro anion $[AsF_6]^-$, is capable at 0.3 bar CO pressure of accepting additional carbon monoxide up to a composition $[Cu(CO)_n]^+$, $n = 2, 3$.[59] Structural characterization in this case is so far limited to Cu(CO)Cl.[60] A comparison of the molecular structures of CO adducts for all three metals of Group 11 is possible for a series of tris(pyrazolyl)borate complexes of the type $[HB(3,5\text{-}(CF_3)_2Pz)_3]MCO$, M = Cu,[61] Ag,[62] and Au.[63] Structural comparisons with similar species from the Cambridge Data Index[64] are also useful. Observed bond lengths, for example, can be correlated with bond orders.[65, 66] Interionic and intermolecular secondary bond lengths, as defined by Alcock,[67] can also be compared with the sums of van der Waals radii.[68]

Among the homoleptic carbonyl cations, the largest group consists of the octahedral species $[M(CO)_6]^{n+}$ in which $n = 1$, (M = Mn, Tc, Re[41–43]), 2 (M = Fe,[12] Ru, Os[11]), and 3 (M = Ir[13] and Fe[12]). Both the neutral species $M(CO)_6$ (M = Cr, Mo, W) and the carbonyl metalates $[M(CO)_6]^-$ (M = V, Nb, Ta,[69, 70]) and $[M(CO)_6]^{2-}$ (M = Ti, Zr, Hf[71]) are known.

A comparison of the spectroscopic properties of these isosteric complexes is planned in this review. Since CO and the CN^- ion are isoelectronic, it is also reasonable to compare the metal carbonyl cations and the corresponding cyanometalate anions. Cyano complexes are known for almost all, but especially for the late transition metals.[72, 73] Corresponding isoelectronic and isosteric anionic cyano complexes exist for all the mononuclear homoleptic metal carbonyl cations characterized to date. Only $Hg(CN)_2$,[74] which corresponds to $[Hg(CO)_2]^{2+}$,[15] is neutral. Spectroscopic properties of the cyano complexes have been thoroughly investigated.[75]

The formation of thermally stable salts with $[M(CN)_n]^{(m-n)-}$ anions, where m is the oxidation state of the metal, is possible in numerous solvents and with many different countercations. On the other hand, it has so far been possible to stabilize homoleptic carbonyl cations only with the $[Sb_2F_{11}]^-$ anion, which is formed in SbF_5. The reasons for the special role of the $[Sb_2F_{11}]^-$ anion will be discussed in Section 2.1. There are of course many more known cyanometalate anions[72, 73] than homoleptic metal carbonyl cations. The chemical behavior of the established metal cyanide complexes has already been intensively investigated, whereas the chemistry of the new $[M(CO)_n]^{m+}$ species requires further research. Thus, the yellow ferrocyanide salt $K_4[Fe(CN)_6]\cdot 3H_2O$ has been known since 1752,[76] whereas the first successful synthesis of $[Fe(CO)_6][Sb_2F_{11}]_2$ did not occur until 1996.[12]

The common features of the two types of complexes with opposite charges relate to structural and spectroscopic characteristics. These are in turn a consequence of the similar bonding relationships of CN^- and CO to the metal ions M^{n+} ($n = 1-3$), including a largely σ-donor contribution and minimal π-back-bonding from ligand to metal ion. This is revealed especially clearly in the ν(CX) stretching frequencies (X = O, N) or in force constants, which will be compared and discussed in subsequent sections.

An overwhelmingly σ-bonded CO type of bonding is not exclusive to the metal carbonyl cations. Others have been discussed in a previous overview,[9b] including $BH_3\cdot CO$[77] and $[HCO^+]$,[50, 51] in which CO is coordinated to a main group

element. In recent years there have been numerous reports regarding CO adducts on the surface of ionic crystals and on zeolites doped with transition metal ions, in which chemisorbed CO functions as a surface probe.[78] Equally well documented is the use for carbonylation reactions of solvated Cu^I and Ag^I carbonyl cations in strong protic acids, including HSO_3F.[57] All these aspects have already been summarized,[9b] and will not be further examined here.

Recent reports concerning CO adducts with several organometallic Lewis acids should be mentioned as well: systems of the general type L_nM ($n = 2, 3$; L = Cp (η^5-C_5H_5) or Cp* (η^5-C_5Me_5); and M = d^0-metal ions, actinoides, or main group metals).[79] Among these carbonyls, $[Cp_2^*Zr(\eta^3\text{-}C_3H_5)(CO)][B(C_6H_5)_4]$[79a] is stable at room temperature. The species $[R_2Zr(\eta\text{-}COMe)(CO)][MeB(C_6F_5)_3]$ (R = Cp, Cp*)[79b] display absorption maxima in wavenumbers for CO stretching vibrations at 2105 and 2176 cm^{-1}, respectively. Based on Fenske–Hall molecular orbital calculations,[80] these metal–CO bonds are found to consist overwhelmingly of σ-donor contributions, with little π-backbonding despite the d^0 electron configurations. Noteworthy also are adducts of the type $Cp_2^*M(CO)$ (M = Si,[81] Ca[82]) and $(C_5Me_4H)_3U(CO)$, the first uranium carbonyl to be isolated.[83] These examples point to fascinating developments in metal carbonyl chemistry, and underscore the great versatility of CO as a ligand.

In contrast to the homoleptic carbonyl cations, such carbonyls are frequently of low thermal stability, the CO addition is reversible, and the M–CO bond is stabilized by other, ancillary ligands, especially Cp*. The development that has led to these new complexes[79, 81–83] began with the use of Cp*[84, 85] and followed the classical approaches and methods of organometallic chemistry. The synthesis of homoleptic carbonyl cations, on the other hand, has become possible only through the introduction of superacid media (Section 2).

2. Discussion

2.1. Superacid Reaction Media

Acidic reaction media have rarely been employed in transition metal carbonyl chemistry, with three exceptions:

1. Strong protic acids such as H_2SO_4 and CF_3SO_3H are occasionally utilized for the preparation of organometallic cations by protonation of suitable substrates.[3, 4, 86]
2. Selected Lewis acids like BF_3(g) and AlX_3 (X = Cl, Br) can serve as halide-abstracting agents.[3, 4, 41–43] Anions of stronger acids, or superacids of the type $[EF_6]^-$ (E = P, As, Sb, and others) are introduced in metathesis reactions to stabilize organometallic cations. Their use has previously been discussed.[3, 4]
3. The use of superacids as reaction media in synthetic chemistry has previously been the domain of inorganic main group chemistry and organic chemistry.[10] Superacids have been employed in metal carbonyl chemistry only occasionally in the generation of reactive cations of Ag^I and Cu^I intended as catalysts.[9b, 57] The first successful synthesis of a homoleptic metal carbonyl cation, $[Au(CO)_2]^+$,[16] became possible with use of the classical Brønsted superacid HSO_3F[10] and the molecular superacid SbF_5. This pair of superacids and the combination of the two, the conjugated superacid HSO_3F–SbF_5 or magic acid,[10a] are the only superacids we have utilized in the generation of homoleptic metal carbonyl cations.

2.1.1. *Fluorosulfuric acid, HSO_3F*

The acid–base characteristics of HSO_3F are best described by the autoionization equilibrium in Equation (c). The specific

$$2HSO_3F \rightleftharpoons H_2SO_3F^+ + SO_3F^- \quad (c)$$

conductivity of HSO_3F at 25 °C is $1.08 \times 10^{-4}\ \Omega^{-1}\,cm^{-1}$,[87a] and the limits of its application are defined by the protonation potential of the acidic ion $H_2SO_3F^+$ and the nucleophilicity of SO_3F^-. Electrophilic cations exist in HSO_3F as long as they are not further protonated by $H_2SO_3F^+$ or attacked by SO_3F^-. Fluorosulfuric acid is a very useful solvent for carbonylation reactions from both practical and chemical standpoints. Of practical importance for low-temperature studies and reactions at high temperature is the wide liquid range of the substance (f.p. −89, b.p. 163 °C). HSO_3F does not react with glass at room temperature and below. However, at elevated temperature a dissociation occurs [Eq. (d)], one consequence of which is an

$$HSO_3F \rightleftharpoons HF + SO_3 \quad (d)$$

attack on glass apparatus. The substance's high dielectric constant ε^{25} of about 120[87] causes it to be an excellent ionizing solvent. Although HSO_3F is commercially available, it must be purified before use.[87d] HSO_3F also displays certain unique features from a chemical viewpoint. For example, it is completely miscible with bis(fluorosulfuryl) peroxide, $S_2O_6F_2$. The latter reagent, first prepared in 1957 by Dudley and Cady,[88] can be obtained easily and safely by catalytic fluorination of SO_3.[89] Solutions of $S_2O_6F_2$ in HSO_3F are both strongly oxidizing and ionizing,[90] and they permit the facile synthesis of many binary fluorosulfates of the late transition metals,[91] such as that of $[Au(SO_3F)_3]_2$ [Eq. (e)].

$$2Au + 3S_2O_6F_2 \xrightarrow{HSO_3F} [Au(SO_3F)_3]_2 \quad (e)$$

The relevance to homoleptic metal carbonyl cations becomes clear when one considers that the carbonyl cations of Hg^{II},[15] Au^I,[16] and M^{II} (M = Ru, Os,[11] Pd, Pt[14]) have all been synthesized from the corresponding metal fluorosulfate precursors. These in turn arise by oxidation of the appropriate powdered metal with $HSO_3F/S_2O_6F_2$.[91] Apparently HSO_3F is also an excellent solvent for the growth of single crystals. A recently reported single-crystal study of the polymeric compounds $[SbF_2(SO_3F)]_x$, $[SbF(SO_3F)_2]_x$, and $[Sb(SO_3F)_3]_x$ underscores this point.[92] Thus, it is very convenient to use the same solvent (HSO_3F) both for the synthesis of the metal fluorosulfate as well as for its subsequent conversion into a homoleptic carbonyl cation and crystal growth. Excess $S_2O_6F_2$ is easily removed under vacuum, and remaining traces react with CO[16a] [Eq. (f)].

$$CO + S_2O_6F_2 \longrightarrow CO_2 + S_2O_5F_2 \quad (f)$$

CO_2 and $S_2O_5F_2$ arise also in the reductive carbonylation of metal fluorosulfates as a consequence of thermal decomposition of the phosgene analogue $OC(SO_3F)_2$.[93]

Although the solubility of CO in HSO_3F is low (less than 0.01 M at 1 bar CO and 25 °C[16a]), carbonylation reactions take place in superacids at 25–60 °C and CO pressures around 1 bar, usually within a few hours. These reaction conditions represent a remarkable contrast to the formation of $[M(CO)_6][AlX_4]$ (M = Mn,[41] Tc,[42] Re;[43] X = Cl, Br), which require 300–320 bar CO and temperatures around 90 °C.

In contrast to fluorosulfuric acid, the equally strong anhydrous hydrofluoric acid has found little application in synthetic transition metal carbonyl chemistry, probably for practical reasons. Two examples of synthetic applications are the oxidative carbonylation of gold with UF_6 in HF to give $[Au(CO)_2][UF_6]$[94a] and the fluorination of $Ir_4(CO)_{12}$ with XeF_2 in HF producing $Ir(CO)_3F_3$.[22]

Also of importance to this work are IR matrix studies on the isomeric molecular complexes FH···CO (**1**) and FH···OC (**2**).[94b] The observed shifts $\Delta\tilde{\nu}$(CO) of $+24\,cm^{-1}$ for **1** and $-9\,cm^{-1}$ for **2** relative to matrix-isolated CO, and the low frequency for the vibration of HF relative to that of CO (about $100\,cm^{-1}$ for both isomers) show that the hydrogen bonds are weak. This in turn makes the low solubility of CO in strong protic acids understandable. The different shifts $\Delta\tilde{\nu}$(CO) can be attributed to the different polarization of the CO bonds in **1** and **2**,[94c] analogous to HCO^+ and COH^+.[94d] The unusually high CO frequencies found for metal carbonyl cations point definitively to C-coordinated CO ligands, an interpretation also consistent with recently established structures and quantum mechanical calculations (see Section 2.5.4).

2.1.2. *Antimony Pentafluoride, SbF_5*

Among the known Lewis acidic fluorides, liquid SbF_5 is particularly favored as a reaction medium. Other Lewis acids such as BF_3, SiF_4, PF_5, and AsF_5 are gaseous under normal conditions, whereas oligomers such as TaF_5, NbF_5, and BiF_5 are solids.[95] SbF_5 displays a liquid region extending from 8 to 141 °C,[95] a range in which it is oligomeric and associated through F-bridges in a helical fashion,[96a] and hence extremely viscous.[85b] As a result of its low electrical conductivity of less than $7\times10^{-9}\,\Omega^{-1}cm^{-1}$, there is no evidence for autoionization. Consequently, nucleophiles such as $[SbF_6]^-$, like SO_3F^- in HSO_3F, are present only in very low concentration. Viewed overall, SbF_5 is a poor, exceptionally weakly ionizing solvent, and in many carbonylation reactions the starting materials and products are merely suspended rather than dissolved. Consequently, such heterogeneous reactions are frequently very time-consuming.

Whereas pure SbF_5 is seldom used as a reaction medium, it finds broad application in conjugated superacids such as $HF-SbF_5$[97] and HSO_3F-SbF_5 (magic acid),[10] in which SbF_5 is regarded as the strongest of the molecular Lewis acids.[10, 98] Many carbocations[10a, 99] and cations of the p-block elements[10b] are prepared in these systems. Earlier attempts at transforming various fluorosulfates into fluoroantimonates with SbF_5, as well as the first carbonylation reactions in SbF_5, have already been summarized.[20] A change from HSO_3F to SbF_5 as reaction medium was necessitated by the fact that many homoleptic carbonyl cations, including $[Au(CO)_2]^+$[16a] and $[M(CO)_4]^{2+}$ (M = Pd, Pt)[14] cannot be isolated from HSO_3F solution. In contrast to $[Au(CO)_2]^+$ and $[M(CO)_4]^{2+}$ (M = Pd, Pt), other homoleptic carbonyl cations such as $[Hg(CO)_2]^{2+}$,[15] $[M(CO)_6]^{2+}$ (M = Fe,[12] Ru, Os,[11] and $[Ir(CO)_6]^{3+}$[13]) do not exist in HSO_3F and can therefore be prepared only in SbF_5. Consequently, SbF_5 has been elevated to the position of sole reaction medium. An apparent disadvantage of SbF_5 consists in the difficulty of growing single crystals in this environment. The products are usually polycrystalline powders, which must then be recrystallized. The only medium that is suitable in this case is magic acid (HSO_3F-SbF_5) which will be discussed next.

2.1.3. *Magic Acid (HSO_3F-SbF_5) and the Undecafluorodiantimonate(V) Ion $[Sb_2F_{11}]^-$*

Addition of SbF_5 to HSO_3F causes the acidity to be increased by up to seven orders of magnitude as a result of the formation of a conjugated superacid.[10, 100] Simultaneously the basicity is decreased because of complexation of the fluorosulfate ion by SbF_5. This process can initially be visualized as a reaction between a Lewis acid and a Lewis base, namely SbF_5 and SO_3F^-, which shifts the autoionization equilibrium to the right [Eq. (g)].

$$2HSO_3F + SbF_5 \rightleftharpoons [H_2SO_3F]^+ + [SbF_5(SO_3F)]^- \qquad (g)$$

However, ^{19}F NMR studies on the system HSO_3F-SbF_5 show considerably greater complexity than Equation (g) suggests, and the presence of up to 15 different anions including $[Sb_2F_{11}]^-$ has subsequently been confirmed spectroscopically.[101–105] Although even at high SbF_5 concentrations (greater than 30 mol%) $[Sb_2F_{11}]^-$ is present in HSO_3F only in concentrations of a few mol%, its salts are only slightly soluble. This becomes apparent from the unexpected isolation of the oxonium salt $[H_3O][Sb_2F_{11}]$ from HSO_3F-SbF_5 and its single-crystal X-ray structure.[106] $[H_3O][Sb_2F_{11}]$ arises through a reaction between magic acid and glass. It is thus not surprising that two $[Sb_2F_{11}]^-$ salts with metal carbonyl cations, $[Hg(CO)_2][Sb_2F_{11}]$[15b] and $[Ir(CO)_5Cl][Sb_2F_{11}]_2$,[13] have been obtained as single crystals from magic acid and subsequently characterized by X-ray diffraction.

The geometry of the $[Sb_2F_{11}]^-$ anion in $[H_3O][Sb_2F_{11}]$ permits certain conclusions to be drawn about secondary interionic contacts. In $[H_3O][Sb_2F_{11}]$ three crystallographically distinct $[Sb_2F_{11}]^-$ anions are present, and they deviate in very similar ways from ideal D_{4h} symmetry (Figure 1). The three most impor-

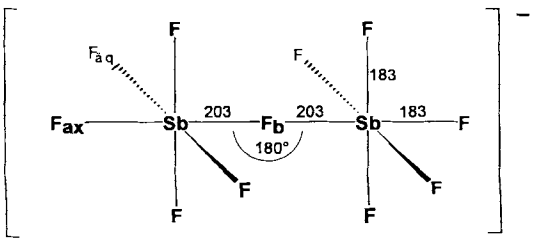

Figure 1. Geometric parameters [pm] for an undistorted $[Sb_2F_{11}]^-$ ion with D_{4h} symmetry.

tant deviations in the anion are 1) deformation of the $Sb-F_{(b)}-Sb$ bond angle from 180 through 149.4 to 145.9° in the $[H_3O]^+$ salt,[106] 2) torsion of the two planar $SbF_{4(eq)}$ groups from an eclipsed to a staggered conformation, and 3) slight changes in the $SbF_{(eq)}$ or the $SbF_{(ax)}$ bond lengths.

In addition to asymmetric hydrogen bonds of the type $O-H\cdots F$ in $[H_3O][Sb_2F_{11}]$,[106] which generate interionic contacts, similar contacts are known in compounds between $[Sb_2F_{11}]^-$ and nonmetal cations. Molecular structures have been described for a number of these salts with the cations $[I_2]^+$,[107] $[TeF_3]^+$,[108] $[IF_4]^+$,[109] $[XeF]^+$,[110] $[XeF_3]^+$,[111] $[SbCl_4]^+$,[112] and $[Se_2I_4]^{2+}$.[113]

In all cases, the $[Sb_2F_{11}]^-$ anion is distorted in a way similar to that in $[H_3O][Sb_2F_{11}]$. In $[H_3F_2][Sb_2F_{11}]$ and $[H_2F][Sb_2F_{11}]$ the $[Sb_2F_{11}]^-$ is regular.[114] A related structure is also encountered in $[Br_2][Sb_3F_{16}]$,[115] with significant $Br\cdots F$ contacts. A comparative overview of various structures containing $[Sb_2F_{11}]^-$ anions has been published.[45] Interionic contacts in these molecular structures[106-113] are manifested in two ways. First, many $F\cdots E$ distances are shorter than the sum of the corresponding van der Waal's radii.[68] In the examples presented,[106-115] acceptors in the interactions (apart from hydrogen) are the elements I, Br, Te, Xe, Sb, or Se in low oxidation states. Both Se and I function as acceptors in $[Se_2I_4]^{2+}$, the only doubly charged cation.[113] Second, the anion $[Sb_2F_{11}]^-$, or in one case $[Sb_3F_{16}]^-$,[115] is distorted relative to Figure 1. A reduced $Sb-F_b-Sb$ angle and changes in the dihedral angle $F_t-S_b-F_b-Sb$[45] are a good measure of interionic contacts in most of the structures.

The flexibility of the $[Sb_2F_{11}]^-$ anion result from weak bonding within the $(Sb-F_b-Sb)$ bridge. Since almost all thermally stable homoleptic carbonyl cations exist as $[Sb_2F_{11}]^-$ salts, the formation of significant interionic contacts is a further important characteristic of the $[Sb_2F_{11}]^-$ ion in addition to its low nucleophilicity. The extent and nature of these contacts will be discussed in detail in Section 2.4.2 for the cases $[Hg(CO)_2][Sb_2F_{11}]_2$[15b] and $[Ir(CO)_5Cl][Sb_2F_{11}]_2$.[13]

Apart from $[Sb_2F_{11}]^-$, another superacidic anion, $[Pt(SO_3F)_6]^{2-}$,[116] also exists and forms a thermally stable salt with $[Pt(CO)_4]^{2+}$ of the composition $[Pt(CO)_4][Pt(SO_3F)_6]$.[117] From ^{119}Sn Mössbauer parameters of various dimethyltin(IV) salts[118] it has been ascertained that $[Pt(SO_3F)_6]^{2-}$ is a weak nucleophile very similar in this respect to $[Sb_2F_{11}]^-$. Moreover, the $[Pt(SO_3F)_6]^{2-}$ anion is trigonally distorted as a consequence of secondary contacts between $Cs^+\cdots O$ and $Cs^+\cdots F$ in $Cs_2[Pt(SO_3F)_6]$,[106] in contrast to the regular octahedral form of the $[Sb(SO_3F)_6]^-$ anion[106,119] in $Cs[Sb(SO_3F)_6]$.

2.1.4. Alternative Solvents and Reaction Media

Apart from the superacid media, only a few other solvents find application in the synthesis and characterization of transition metal carbonyl cations. $[Au(CO)_2][Sb_2F_{11}]$ is very soluble in liquid SO_2,[16b] which is also utilized in the synthesis of $[Cu(CO)][AsF_6]$.[58] Nevertheless, $[M(CO)_4][Sb_2F_{11}]_2$ (M = Pd, Pt) are insoluble in SO_2,[14] and $[Hg(CO)_2][Sb_2F_{11}]$ decomposes in SO_2 with evolution of CO.[15] Perfluoroalkyl sulfonylfluorides, R_fSO_2F ($R_f = C_4F_9$, and higher homologues) are inert to metal carbonyl salts, but dissolve SbF_5 very well. They find limited application in purification processes.[15] Donor solvents easily displace CO, as the transformation of $[Au(CO)_2][Sb_2F_{11}]$ into $[Au(NCCH_3)_2][SbF_6]$ in acetonitrile demonstrates.[16b] The claimed formation of cations of the type $[Ag(CO)_n]^+$ ($n = 1, 2$) in the aprotic solvent 1,1,2-$C_2Cl_3F_3$ is difficult to reconcile with a postulated ionic structure for the silver carbonyl cation in the teflato complexes.[56]

2.2. Syntheses

2.2.1. General Aspects

The generation of homoleptic metal carbonyl cations and the synthesis of cationic metal carbonyl fluorosulfates and fluorides in superacid media is accomplished either by direct CO addition to highly reactive, naked metal cations, or by oxidation of neutral mono- or multinuclear metal carbonyls in the presence of CO.

Since homoleptic metal carbonyl cations of the general type $[M(CO)_n]^{m+}$ ($n = 2, 4, 6$; $m = 1, 2, 3$) exist almost exclusively with $[Sb_2F_{11}]^-$ as counterion, liquid SbF_5 is the reaction medium of choice. Similarly, metal carbonyl fluorosulfates or fluorides are best synthesized in HSO_3F or anhydrous hydrofluoric acid. Details of the most important syntheses are discussed below.

2.2.2. Carbonylations in Liquid SbF_5

Details of carbonylations in SbF_5 are summarized in Table 2. The syntheses are divided into three groups.

Table 2. Syntheses of homoleptic carbonyl cations as $[Sb_2F_{11}]^-$ salts.

Cation	[a]	Reagents	Conditions[b] $p(CO)$ [bar]	T [°C]	t	Ref.
$[Hg(CO)_2]^{2+}$	a	$Hg(SO_3F)_2$, CO, SbF_5	1	80	1 d	[11]
$[Hg_2(CO)_2]^{2+}$	a	$Hg_2(SO_3F)_2$, CO, SbF_5	0.5	60	1 d	[11]
$[Au(CO)_2]^+$	a	$Au(CO)SO_3F$, CO, SbF_5	1	60	2 h	[16b]
	b	$Au(SO_3F)_3$, CO, SbF_5	1	60	1 h	[21]
	b	$AuCl_3$, CO, SbF_5	1	60	3 d	[21]
	b	AuF_3, CO, SbF_5	1	25	3 d	[16b]
$[Pd(CO)_4]^{2+}$	a	$Pd(CO)_2(SO_3F)_2$, CO, SbF_5	1	60	5 h	[15]
	b	$Pd[Pd(SO_3F)_6]$, CO, SbF_5	0.5	80	1 d	[21]
	a	$PdCl_2$, CO, SbF_5	2	60	10 d	[21]
$[Pd_2(\mu\text{-}CO)_2]^{2+}$	d	$[Pd_2(\mu\text{-}CO)_2](SO_3F)_2$, SbF_5	–	20	20 d	[21]
$[Pt(CO)_4]^{2+}$	a	$Pt(CO)_2(SO_3F)_2$, CO, SbF_5	1	60	2 d	[15]
	b	$Pt(SO_3F)_4$, CO, SbF_5	0.5	80	2 d	[21]
	b	$PtCl_2$, CO, SbF_5	2	60	14 d	[21]
$[Ir(CO)_6]^{3+}$	b	IrF_6, CO, SbF_5	1	60	10 h	[14]
$[Fe(CO)_6]^{2+}$	c	$Fe(CO)_5$, CO, SbF_5, AsF_5 oder Cl_2	1	40	1 d	[13]
$[Ru(CO)_6]^{2+}$	b	$Ru(SO_3F)_3$, CO, SbF_5	1	80	3 d	[12]
$[Os(CO)_6]^{2+}$	b	$Os(SO_3F)_3$, CO, SbF_5	1	80	3 d	[12]
$[Mn(CO)_6]^+$	c	$Mn_2(CO)_{10}$, CO, SbF_5	2	40	7 d	[21]
$[Re(CO)_6]^+$	a	$Re(CO)_5Cl$, CO, SbF_5	1	60	8 h	[21]

[a] Synthetic methods: a: Carbonylation with retention of oxidation state, in some cases with simultaneous solvolysis; b: reductive carbonylation; c: oxidative carbonylation; d: metathesis. [b] Applicable to millimolar scale preparations. SbF_5 and CO in excess.

2.2.2.1. Solvolysis and Carbonylation

In the course of such a synthesis, the oxidation state of the metal in the starting compound remains unchanged. The synthesis of $[Hg(CO)_2][Sb_2F_{11}]_2$ serves as an example [Eq. (h)].[15]

$$Hg(SO_3F)_2 + 2CO + 8SbF_5 \longrightarrow [Hg(CO)_2][Sb_2F_{11}]_2 + 2Sb_2F_9(SO_3F) \quad (h)$$

The anion $[Sb_2F_{11}]^-$ forms in the course of the solvolysis. $Sb_2F_9(SO_3F)$, the most volatile of the known fluoride–fluorosulfates of antimony(v),[120] is easily separated. In the case of the starting material $Re(CO)_5Cl$, a volatile by-product has been formulated as SbF_4Cl. It corresponds approximately to a compound described by O. Ruff et al.[121] as $3SbF_5 \cdot SbCl_5$, the structure of which is unknown.[122]

2.2.2.2. Reductive Carbonylation

Reductive carbonylation is a simple, elegant process in which solvolysis is accompanied by reduction of the metal salt. In a single synthetic step CO functions as a reducing agent and ligand, while SbF_5 plays the dual role of reaction medium and source of the counterion $[Sb_2F_{11}]^-$. As the synthesis of $[Pt(CO)_4][Sb_2F_{11}]_2$ shows, all the by-products are volatile [Eq. (i)].[21] An interesting variant is the recently reported reductive carbonylation of IrF_6 [Eq. (j)],[13] in which octahedral

$$Pt(SO_3F)_4 + 5CO + 8SbF_5 \longrightarrow [Pt(CO)_4][Sb_2F_{11}]_2 + CO_2 + S_2O_5F_2 + 2Sb_2F_9(SO_3F) \quad (i)$$

$$2IrF_6 + 15CO + 12SbF_5 \longrightarrow 2[Ir(CO)_6][Sb_2F_{11}]_3 + 3COF_2 \quad (j)$$

coordination geometry at iridium is retained, fluoride is exchanged for CO, and the positive oxidation state of iridium changes from 6 to 3. The reductive carbonylation of $AuCl_3$ in SbF_5 leads to COF_2 as by-product, since the initially formed $COCl_2$ is fluorinated by the excess SbF_5.[123]

2.2.2.3. Oxidative Carbonylation

An example in this case is the synthesis of $[Fe(CO)_6][Sb_2F_{11}]_2$ by oxidation of $Fe(CO)_5$ with AsF_5 or Cl_2 [Eq. (k)].[12] The

$$Fe(CO)_5 + AsF_5 + 5SbF_5 + CO \longrightarrow [Fe(CO)_6][Sb_2F_{11}]_2 + AsF_3 \cdot SbF_5 \quad (k)$$

solid by-product $AsF_3 \cdot SbF_5$[124] is removed by repeated washing with SO_2. In the transformation of $Mn_2(CO)_{10}$ with SbF_5 and CO into $[Mn(CO)_6][Sb_2F_{11}]$, SbF_5 serves simultaneously as oxidizing agent and reaction medium.

2.2.3. Comments Regarding Reactions in Liquid SbF_5

As can be seen from Table 2, all the homoleptic metal carbonyl cations that form thermally stable $[Sb_2F_{11}]^-$ salts can be prepared by one of the three synthetic methods described. This also includes the binuclear cations $[Hg_2(CO)_2]^{2+}$[15] and *cyclo*-$[Pd_2(\mu\text{-}CO)_2]^{2+}$.[21] Limitations of the methods are encountered where reaction of the metal salt in SbF_5 proceeds in a different way, or where the resulting metal carbonyl cations are of limited thermal stability, which interferes with their isolation. An example of a different reaction pathway is the reductive carbonylation of FeX_3 (X = Cl, SO_3F), which leads to the known $Fe[SbF_6]_2$.[125a] This product belongs to a group of compounds of the type $M[SbF_6]_2$ (M = Cr, Mn, Fe, Co, Ni, Cu, Zn, Ag, Cd, Sn),[91, 125] all of which display layered structures. The M^{2+} cations occupy every second octahedral vacancy in the $Li[SbF_6]$-analogous structure. As would be expected, no salt in this category has so far been successfully carbonylated with CO in SbF_5.

Thermally unstable cations of the type $[Ag(CO)_n]^+$ ($n = 1$ or 2) are formed through the reductive carbonylation of $Ag(SO_3F)_2$.[126] Removal of excess SbF_5 under vacuum at room temperature produces solid $Ag[Sb_2F_{11}]$. Despite this limitation, a great many new homoleptic metal carbonyl cations were prepared in liquid SbF_5 within a short period of time as thermally stable salts with $[Sb_2F_{11}]^-$ counterions. The synthesis of multiply charged cations of the type $[M(CO)_n]^{m+}$ ($n = 2, 4, 6$; $m = 2, 3$) can be accomplished in a very simple manner. This is only rarely the case with the use of traditional methods.[3, 4] Among the singly charged cations in Group 11, only $[Au(CO)_2]^+$[16b] is sufficiently stable to be separated as an $[Sb_2F_{11}]^-$ salt from SbF_5.

2.2.4. Carbonylations in Brønsted Superacids

The two protic superacids HSO_3F[86] and anhydrous hydrogen fluoride[127] are very well suited to the preparation of metal carbonyl fluorosulfates and fluorides. A report has recently appeared concerning fluorine-containing organometallic compounds of the d-block elements.[128] Selected examples relevant to homoleptic carbonyl cations are discussed below.

2.2.4.1. Carbonylations in Fluorosulfuric Acid

Reactions leading to metal carbonyl fluorosulfates are summarized in Table 3. Most of the syntheses are reductive carbonylations, with the exception of the synthesis of $Ir(CO)_3(SO_3F)_3$,[19] which occurs by the addition of CO to $Ir(SO_3F)_3$[129] in HSO_3F. In contrast to the formation of $Ir(CO)_3(SO_3F)_3$, reductive carbonylations in HSO_3F occur rapidly, often within hours. The presentation in Table 3 is limited to fully characterized metal carbonyl fluorosulfates. There are indications of a mixture of isomeric species of the type

Table 3. Syntheses of metal carbonyl fluorosulfates.

Compound	[a]	Reagents	Conditions[b] p(CO) [bar]	T [°C]	t	Ref.
$Au(CO)SO_3F$	b	$Au(SO_3F)_3$, CO, HSO_3F	1	60	12 h	[16a]
$Pd(CO)_2(SO_3F)_2$	b	$Pd[Pd(SO_3F)_6]$, CO	1	20	5 h	[18a, b]
$[Pd_2(\mu\text{-}CO)_2](SO_3F)_2$	b	$Pd(CO)_2(SO_3F)_2$, HSO_3F	–	20	1 d	[17]
$Pt(CO)_2(SO_3F)_2$	b	$Pt(SO_3F)_4$, CO, HSO_3F	2	80	2 d	[18a]
$Ir(CO)_3(SO_3F)_3$	a	$Ir(SO_3F)_{3/4}$, CO, HSO_3F	2	60	7 d	[19]
$Mn(CO)_5(SO_3F)$	c	$Mn(CO)_5Cl$, $AgSO_3F$	[c]	25	5 d	[134]
$Re(CO)_5(SO_3F)$	c	$Re(CO)_5Cl$, $AgSO_3F$	[c]	25	5 d	[134]

[a] Synthetic methods: a: Carbonylation with retention of oxidation state; b: reductive carbonylation; c: metathesis. [b] Applicable to millimolar scale preparations, HSO_3F and CO in excess. [c] In CH_2Cl_2.

$M(CO)_4(SO_3F)_2$ (M = Ru, Os), but separation of these isomers has not yet proven possible. Isomer separation has succeeded, however, for $Ir(CO)_3(SO_3F)_3$ through recrystallization from HSO_3F. In this case the *mer* isomer is the preferred form, and only about 15% of *fac*-$Ir(CO)_3(SO_3F)_3$ is present in solution.[19] The compounds $M(CO)_2(SO_3F)_2$ (M = Pt, Pd)[18] arise through nucleophilic substitution starting from $[M(CO)_4]^{2+}$, and are present exclusively in the *cis* form.

2.2.4.2. *Syntheses in Anhydrous Hydrogen Fluoride*

The synthesis of mononuclear metal carbonyl fluorides of the type $M(CO)_nF_m$ (*m*, *n* = 2–4; M = Mo, Mn, Re, Ru, Os, Ir) is possible through fluorination of binary mono- or multinuclear metal carbonyls with MF_6, XeF_2, or F_2, either in HF or in fluorochlorocarbons such as 1,1,2-$C_2Cl_3F_3$.[128] Reaction of $Re_2(CO)_{10}$ with ReF_6 in HF[130] leads to a cationic carbonyl derivative $Re(CO)_5(\mu\text{-}F)ReF_5$ that has been characterized structurally.[131] Subsequent carbonylation in HF produces $[Re(CO)_6][ReF_6]$,[132] and the cation $[Re(CO)_6]^+$ permits comparisons with earlier vibrational spectroscopic studies.[43] An additional structurally characterized product from the reaction of $Re_2(CO)_{10}$ with ReF_6 in HF is $[Re(CO)_6][Re_2F_{11}]$.[45] The anion $[Re_2F_{11}]^-$ is very similar structurally to the $[Sb_2F_{11}]^-$ ion. $[Re(CO)_6]^+$ is the only octahedral homoleptic carbonyl cation whose structure is so far known. The molecular structure of *fac*-$Ir(CO)_3F_3$,[22] obtained from an analysis of EXAFS data, permits limited comparisons with *mer*-$Ir(CO)_3(SO_3F)_3$.[19] *Fac*-$Ir(CO)_3F_3$ is formed from $Ir_4(CO)_{12}$ by fluorination with XeF_2 in HF.[22] Finally, carbonylation of RuF_5 at 200 °C leads to a product with the composition $Ru(CO)_3F_2 \cdot RuF_5$,[133] which also arises from treatment of $Ru_3(CO)_{12}$ with XeF_2 in HF.

In both Brønsted superacids, HSO_3F and HF, the formation of covalently bonded metal carbonyl fluorosulfates and fluorides is to be expected. Only occasionally are homoleptic metal carbonyl cations like $[Re(CO)_6]^+_{solv}$[45,132] and $[Au(CO)_2]^+_{solv}$[16a] observed. In many cases, HF can be replaced for the preparation of metal carbonyl fluorides by the aprotic solvent 1,1,2-$C_2Cl_3F_3$, which displays sufficient resistance to powerful fluorinating reagents such as F_2 and XeF_2.

2.2.5. *Alternative Synthetic Methods*

Two alternative synthetic pathways have found limited application: metathesis reactions and CO addition to metal salts with weak coordinating anions. Metatheses with $AgSO_3F$ have been used for the preparation of $M(CO)_5SO_3F$ (M = Mn, Re).[134] Both compounds are included in Table 3. Tris(pyrazolyl)borate complexes of the type $[HB(3,5\text{-}(CF_3)_2Pz)_3]MCO$ (M = Cu, Ag, Au)[61–63] can be prepared by metathesis and subsequent CO addition with the appropriate metal complexes.[61,62] For metatheses of this sort there are numerous precedents,[3,4] but also certain limitations: Suitable precursors must be available, and separation of the solid products can be difficult. Advantage is often taken of solubility differences in coordinating solvents, and yields are generally low. Nevertheless, in the case of the above-mentioned investigations single crystals can be isolated, and three useful molecular structures have been determined.[61–63] The fundamental principle is reversible CO addition to coordinatively unsaturated metal salts with large, weakly coordinating anions.[135] This concept is based on the notion that the metal ions are present as strong Lewis acids that can also bind weak donor ligands. Relevant examples are $Cu[AsF_6]$,[136] which forms CO adducts of the type $[Cu(CO)_n][AsF_6]$ ($n = 1$,[58] 2, 3[59]), and $Ag[B(OTeF_5)_4]$, which accepts up to 3 molar equivalents of CO.[53–56] Either high CO pressure or low temperature is required to prevent a reversible loss of CO. Molecular structures are known for $Ag(CO)[B(OTeF_5)_4]$[53,56] and $[Ag(CO)_2][B(OTeF_5)_4]$.[54,56] Useful starting materials have so far been limited to Cu^I [58,59] and Ag^I [53–56] salts. For Cu^I and Ag^I the existence of multiple CO-containing compounds with very similar physical and spectroscopic properties[56,59] prevents a clean separation of the thermally unstable products. Synthesis of individual homogeneous compounds on a preparative scale can be assured only by temperature and pressure control during CO addition. In cases in which the preparation of homoleptic metal carbonyl cations in SbF_5 and their subsequent isolation as $[Sb_2F_{11}]^-$ salts fails, CO addition to coordinatively unsaturated salts with weak coordinating ligands is the method of choice. Reported structures[53,54,56] and the pyrazolylborate complexes of Cu, Ag, and Au[61–63] provide insight into the nature of the M–CO bond in these thermally unstable complexes.

2.2.6. *Syntheses of Cationic Metal Carbonyl Complexes: Comparisons and an Overview*

The principle underlying all the syntheses discussed here consists of creating metal ions that function as Lewis acids and are thus in a position to bind weak Lewis bases. In the case of Cu^I and Ag^I salts with weak coordinating anions,[53–56,58,59] the Lewis acid strength of the metallic centers is noticeably reduced by significant cation–anion contacts, and CO addition is reversible. Such contacts exist in any salt. Indeed, so-called noncoordinating anions[135,137] are known to be a myth. In salts with doubly and triply charged cations, lattice energies and secondary anion–cation contacts increase in strength, so reversible CO addition to MX_2 salts is possible only under matrix-isolation conditions.[138] In pyrazolylborate complexes[61–63] the Lewis acid strength of the metal ions is reduced through contact with N atoms of the ligands, whose basicity is in turn reduced by the electron-attracting CF_3 groups. Nevertheless, weak, overwhelmingly σ-bonded CO adducts can still be synthesized with these complexes.[61–63] The synthetic method (reversible CO addition at electrophilic M^I centers for M = Cu, Ag, Au[53,54,59,62,63]), solubility in aprotic solvents like 1,1,2-$C_2Cl_3F_3$,[56] CH_2Cl_2,[63] or THF[61,62], and low thermal stability of the products is more consistent with the behavior of molecular adducts than with that of salts containing metal carbonyl cations.

In contrast, reduction or solvolysis in superacid media can be used to achieve intermediate naked metal cations of the type M^{n+} ($n = 1-3$). These highly reactive cations are present in an acidic matrix and function as strong Lewis acids with respect to CO. The acceptor strength of M^{n+} increases with increasing *n*, and carbonyl cations with classical coordination geometries

(linear, square planar, octahedral; see Table 1) are formed as a function of the d-electron configuration. Thermally stable salts arise in liquid SbF_5 exclusively with the $[Sb_2F_{11}]^-$ anion. In the superacids HF[127] and HSO_3F[87] CO and the weakly nucleophilic autoprotolysis ions F^- and SO_3F^- compete, so in most cases metal carbonyl fluorides or fluorosulfates are formed. Oxidation of mono- and multinuclear metal carbonyls in superacids[12, 128] leads to coordinatively unsaturated metal carbonyl cations, which behave as Lewis acids relative to F^-[128] or CO[12] and lead either to metal carbonyl fluorides or, in the presence of CO, to homoleptic carbonyl cations like $[Fe(CO)_6]^{2+}$.[12]

Carbonylation reactions in superacid media have in the meantime found broad application (Tables 2 and 3). CO addition to metal complexes is only sensible to apply in the case of metals that form no thermally stable carbonyl cations.

The concept presented here—preparation of naked, uncoordinated metal ions in a superacidic matrix and their subsequent reaction with CO—is analogous to the formation of binary metal carbonyls through cocondensation of naked metal atoms with CO in an inert gas matrix,[6, 139, 140] or the reaction of metal vapors with CO in the gaseous phase at high temperature.[26, 27]

2.3. Physical and Chemical Properties of Cationic Metal Carbonyl Complexes

Most of the cationic metal carbonyl complexes have been synthesized and described within the past seven years. Although an impressive number of molecular structures has been elucidated, and the thermally stable species have been largely characterized by vibrational and ^{13}C NMR spectroscopy, little else is known apart from the development of alternative synthetic pathways. In a few cases characterization of the products has remained incomplete, as with two teflate complexes, formulated as $[M(CO)][OTeF_5]$ (M = Ag, Au),[56] for which ionic structures have been suggested and $\tilde{\nu}(CO)$ values below 2200 cm^{-1} have been observed. Equally questionable and unproven is an ionic formulation for $Au(CO)SO_3F$, suggested in the same paper on account of the known physical and spectroscopic characteristics.[16]

All the cationic metal carbonyl complexes discussed here are very sensitive to hydrolysis. Their reactivities and thermal stabilities vary within a wide range. The salts of such multiply charged cations as $[Ir(CO)_6][Sb_2F_{11}]_3$[13] and $[M(CO)_6][Sb_2F_{11}]_2$ (M = Ru, Os)[11] react with HSO_3F or HSO_3F–SbF_5 with release of CO, whereas $[Hg(CO)_2][Sb_2F_{11}]_2$ can be recrystallized only from magic acid. On the other hand, compounds in the series $[M(CO)_6][Sb_2F_{11}]_2$ (M = Fe, Ru, Os) possess extraordinarily high thermal stability,[11, 12] which suggests stabilization through high lattice energies. By contrast, CO adducts of the coinage metal salts are thermally unstable, but stable to aprotic solvents.[61–63] A remarkable exception is $[Au(CO)_2][Sb_2F_{11}]$[16b] with a decomposition point of 130 °C, compared with $[Ag(CO)_2][Sb_2F_{11}]$ that is not isolable, and $[Ag(CO)_2][B(OTeT_5)_4]$[54, 56] that under normal conditions releases CO. This is not entirely unexpected, because the stability constant of $[Au(CN)_2]^-$, isoelectronic with $[Au(CO)_2]^+$, is 15 orders of magnitude higher than that for $[Ag(CN)_2]^-$.[73] The capacity of gold to form strong covalent bonds in primarily linear complexes is well documented[141] and probably a consequence of relativistic effects,[142] which are especially pronounced for gold.[142a] Expansion of the coordination from 2 to 3 and 4 for Cu^I and Ag^I is most readily recognized in the case of the cyano complexes.[72, 73] The only such complex that exists for Au^I is $[Au(CN)_2]^-$, whereas for Ag^I and Cu^I not only $[M(CN)_2]^-$ but also complexes of the type $[M(CN)_3]^{2-}$ and $[M(CN)_4]^{3-}$ are known.

A limited number of chemical reactions has been reported in which so far only Au^I takes part. A ligand-exchange reaction [Eq. (l)] was discovered in the course of attempts at recrystallization and leads to an interesting molecular structure.[16b] Exchange of PF_3 for CO[143] [Eq. (m)] makes it clear that PF_3 is a better σ-donor than CO towards Au^I. The $[Au(PF_3)_2]^+$ cation, which can also be generated in situ [Eq. (n)], is the first thermally stable cation with PF_3 as ligand.[144]

$$[Au(CO)_2][Sb_2F_{11}] + 2CH_3CN \xrightarrow{CH_3CN} [Au(NCCH_3)_2][SbF_6] + 2CO + SbF_5 \quad (l)$$

$$[Au(CO)_2][Sb_2F_{11}](s) + 2PF_3(g) \longrightarrow [Au(PF_3)_2][Sb_2F_{11}](s) + 2CO(g) \quad (m)$$

$$Au(SO_3F)_3 + 3PF_3 \xrightarrow{HSO_3F} [Au(PF_3)_2]^+ + S_2O_5F_2 + POF_3 + SO_3F^- \quad (n)$$

These reactions illustrate the synthetic potential of homoleptic metal carbonyl cations. Finally, a kinetic study involving ^{13}C NMR spectroscopy of the CO exchange between $[Au(CO)]^+_{solv}$ and $[Au(CO)_2]^+_{solv}$ in HSO_3F and HSO_3F/SbF_5 led to the suggestion of a dissociative mechanism.[145]

Because CO complexes of Cu^I and Ag^I show low thermal stability, they are more reactive and serve as carbonylation catalysts in strong protic acid solution.[9b, 53, 56, 59]

In summary, it can be concluded that the synthetic routes as well as the chemical and physical properties of the two sets of compounds (that is, the salts of homoleptic metal carbonyl cations and CO adducts of Ag^I and Cu^I complexes) differ significantly. Because in both sets a series of molecular structures is now known, it has become possible to make comparisons in order to understand the origins of these differences better. Moreover, many vibrational spectroscopic studies of CO complexes[146–149] offer good opportunities for comparisons between the two groups of cationic complexes (see Section 2.5.1).

2.4. Molecular Structures of Cationic Metal Carbonyl Complexes

The discussion in this section is limited to two structural aspects: The internal bonding parameters of cationic metal carbonyl derivatives that reflect the nature of bonding between the metal and carbon monoxide, and external secondary contacts between differently charged ions, molecular species, or adjacent layers in the case of layered structures.

2.4.1. Internal Bonding Parameters

Structural data that are the subject of this section are presented in Table 4. The entries themselves can be divided into two

Table 4. Structural data for cationic metal carbonyl species and related carbonyl derivatives.

Compound	d(M-C) [pm]	$\bar{d}$(M-C) [pm][a]	d(C-O) [pm]	$\tilde{\nu}(CO)_{IR}$ [cm^{-1}][b]	d(M-X) [pm][c]	Ref.
$[Nb(CO)_6]^-$	208.9(5)	207.3	116.0(7)	1857	–	[70c]
$[Ta(CO)_6]^-$	208.3(6)	204.2	114.9(8)	1852	–	[70c]
$Mo(CO)_6$[d]	206.3(3)	197.3	114.5(3)	2003	–	[150]
$W(CO)_6$[d]	205.8(3)	200.7	114.8(3)	1998	–	[150]
$[Re(CO)_6][Re_2F_{11}]$	201.0(4)	193.3	113.0(3)	2084	–	[130b, 131]
$Re(CO)_5(\mu\text{-}F)ReF_5$	198.(4)	193.3	115.(5)	2099	220.(2) (X = μ-F)	[130b]
$[Ir(CO)_5Cl][Sb_2F_{11}]_2$	202.(2)	187.6	108.(2)	2254[e]	232.1(3) (X = Cl)	[14]
mer-$Ir(CO)_3(SO_3F)_3$	198.1(5)	187.6	110.5(8)	2218	204.4(5) (X = O)	[19]
fac-$Ir(CO)_3F_3$[f]	203.0(8)	187.6	–	2189	192.0(6) (X = F)	[22b]
cis-$Pd(CO)_2(SO_3F)_2$	193.2(3)	185.4[g]	110.8(6)	2218	201.1(3) (X = O)	[18]
$[Pd_2(\mu CO)_2](SO_3F)_2$	197.5(6)	200.4[h]	113.3(6)	1977	215.6(4) (X = O)	[17]
Cu(CO)Cl	186.(2)	200.3[i]	111.(2)	2127	236.4(3) (X = Cl)	[60]
$Cu(CO)L_F$[i]	180.8(4)	200.3	111.0(5)	2137	205.2 (X = N)	[61]
$Ag(CO)L_F$[j]	203.7(5)	209.3[i]	111.6(7)	2178	238.8 (X = N)	[62]
$Ag(CO)[B(OTeF_5)_4]$	210.(1)	209.3[i]	108.(2)	2204	238.0(7) (X = O)	[53, 56]
$[Ag(CO)_2][B(OTeF_5)_4]$	214.(4)	209.3[i]	107.(5)	2198	–	[54, 56]
Au(CO)Cl	193.(2)	200.3[i]	111.(3)	2170	226.1(6) (X = Cl)	[30, 33]
$Au(CO)L_F$[j]	186.2(9)	200.3[i]	113.(1)	2144	233.8(6) (X = N)	[63]
$[Hg(CO)_2][Sb_2F_{11}]_2$	208.(1)	201.5[j]	110.(1)	2279	–	[11b, 74b]

[a] $\bar{d}$(M–C) = average M–C distance according to ref. [64]. [b] $\tilde{\nu}(CO)_{IR}$: frequency of the IR-active CO vibration or its numerical mean value. [c] d(M–X): average M–X distance. [d] Electron diffraction data. [e] $\tilde{\nu}(F_{1u})$ for $[Ir(CO)_6]^{3+}$. [f] EXAFS data; d(C–O) not precisely determined. [g] $\bar{d}$(M–C) data for M = Pt. [h] $\bar{d}$(M–C) for μ^2CO. [i] $\bar{d}$(M–C) data for M–CN complexes; ref. [64]. [j] L_F signifies $[HB(3,5(CF_3)_2Pz)]^-$ (Pz = pyrazolyl). [k] Ref. [74b]: $Hg(CN)_2$.

groups: 1) cationic metal carbonyl derivatives drawn from element Groups 7 through 12, and 2) octahedral metal carbonyl complexes $[M(CO)_6]^-$ (M = Nb, Ta)[70c] and $M(CO)_6$ (M = Mo, W)[150] from the 4d and 5d series. These structures constitute the basis for a correlation of the spectroscopic properties of octahedral metal carbonyls of the 5d transition metal series, as discussed in the next section.

Table 4 also contains, for comparative purposes, average covalent bond lengths d(M–C), d(CM–O), and d(MM–X). Because the C–O bond lengths show little variation at higher bond orders (between 2 and 3),[1] the more informative mean vibrational frequencies $\nu(CO)_{avg}$ expressed in wavenumbers have also been tabulated from IR data. Difficulties associated with the interpretation of CO bond lengths become more apparent through an examination of data from the Cambridge Data Collection.[64] For the 10022 CO bond lengths registered for metal carbonyl complexes in that source, the mean value is 114.3, whereas the lower quartile mean value (q_l) is 113.2 and the upper quartile value (q_u) is 115.6. This means that 50%, or 5011 sets of data, fall in a narrow range of 2.4 pm, and are in fact identical within experimental error. Additional uncertainties arise in comparisons among the data in Table 4, because different measurement temperatures have been utilized, and corrections for thermal motion have not been applied uniformly. A good example is the linear cation $[Hg(CO)_2]^{2+}$ [15b] The mean vibrational frequency $\nu(CO)_{avg}$ for this cation is 2279 cm^{-1}, the highest yet reported for a metal carbonyl cation. One would therefore expect a very short CO bond. X-ray diffraction data at 195 K lead to a CO bond length of 110.4(12) pm. After correction for thermal motion, however, this becomes 112.6 pm, virtually identical with the 112.81 pm CO bond distance for gaseous CO.[151] Also problematic are structure determinations of low precision. A very short CO bond length of 107 pm is listed in Table 4 for $[Ag(CO)_2][B(OTeF_5)_4]$.[54, 56] However, the standard deviation of ± 5 makes a more detailed discussion meaningless. The data in Table 4 do support the conclusion that CO bond lengths for cationic metal carbonyl derivatives lie at the lower end of the scale, frequently below q_l,[64] whereas the ν(CO) data are comparable to or somewhat higher than the value for free CO itself (2143 cm^{-1}[149]).

If one assumes reduced π-backbonding as the cause of the short, strong CO bonds, this should be reflected in an increase in the metal–carbon bond length. It is difficult to find a solid basis for a sensible evaluation of M–C distances in Table 4, since eleven different metals are involved, and the oxidation states range from -1 to $+3$. Both metallic radii[152] and Shannon radii[153, 154] are of little help, because the latter are to some extent tabulated for other oxidation states or coordination numbers than those appearing here. We base our considerations therefore on the median $\bar{d}$(M–C) values for carbonyl compounds of known structure.[64] Unfortunately, in 1989 (date of the most recent edition of the Cambridge Data Collection[64]) distances were still missing for terminal Pd^{II}–CO bonds. In such cases we use for comparison $\bar{d}(Pt^{II}\text{–}CO)$ values in view of the similar metallic radii of 134 pm for Pd and 135 pm for Pt[152] and Shannon radii of 78 pm for Pd^{2+} and 74 pm for Pt^{2+} in a square-planar configuration.[153, 154] For the metal carbonyl derivatives of the coinage metals (Cu, Ag, Au) as well as mercury there exist in most cases more recent structural data, although these have not yet been tabulated. Recourse is therefore taken to the bond lengths in M–CN complexes,[64] although due to the greater σ-donor capacity of CN^-[72, 73] these are shorter (e.g., for $[Hg(CO)_2]^{2+}$ 208.3(10) pm,[15b] and for the isoelectronic $Hg(CN)_2$ 201.5(3) pm[74b]).

Two comments of a technical nature seem appropriate. Most of the structural data in Table 4 were obtained from X-ray diffraction on single crystals. The structure of $Hg(CN)_2$ was derived from a neutron diffraction study,[74b] and the structures of $M(CO)_6$ (M = Mo, W) from electron diffraction.[150] The molecular structure of *fac*-$Ir(CO)_3F_3$[22b] was obtained by analysis of EXAFS data. In this particular case the method permitted no reliable conclusions to be drawn about the CO distance. Moreover, the known difficulties in position determination for light atoms adjacent to heavier atoms often leads to large standard deviations.

The M–C distances for the 19 metal carbonyl derivatives in Table 4 fall between 180 and 210 pm. With the anionic and neutral octahedral species $[M(CO)_6]^-$ (M = Nb, Ta)[70b] and $M(CO)_6$ (M = Mo, W), the M–C distances are rather large relative to the average values $\bar{d}$(M–C). Similarly, long M–C bonds are also found for carbonyls in positive oxidation states. This observation appears at first unexpected, since positive charges usually cause adjacent bonds to be strengthened and shortened. The effect is particularly clear with iridium(III)

derivatives,[13, 19, 22b] where the measured M–C bonds are about 10 to 15 pm longer than the tabulated average $\bar{d}$(M–C) based on 148 structures. Even the q_1 value of 189.8 pm[64] is significantly smaller. Less pronounced differences exist for the M–C bonds in *cis*-$Pd(CO)_2(SO_3F)_2$[18b] and $[Hg(CO)_2]^{2+}$.[15b]

In all cases the ν(CO) values lie between 2200 cm^{-1} and 2279 cm^{-1}, which is consistent with a strong σ-bond and very little π-backbonding between metal and C.

For complexes with a singly positively charged metallic center only small deviations are observed from the mean $\bar{d}$(M–C) values. The M–C bond lengths for Re or Ag are greater than the tabulated mean values, and the values for Cu and Au are somewhat smaller. In complexes with a common ligand, $[HB(3,5(CF_3)_2Pz_3]^-$,[61–63] d(M–C) and $\tilde{\nu}$(CO) conform to the sequence Ag > Au > Cu. In the latter case $\tilde{\nu}$(CO) is only slightly greater than 2143 cm^{-1} (free CO[149]), which indicates only weak σ-donor bonding and π-backbonding. Even for $[Pd_2(\mu\text{-}CO)_2](SO_3F)_2$,[17] with bidentate, symmetrical bridging CO groups, the CO bond length of 113.3(6) pm is noticeably smaller than the mean length of 117.1 pm or the q_u value of 115.9 pm for this bond type.[64] In this arrangement there also appears to be reduced π-backbonding. For this compound d(Pd–C) is somewhat smaller than the $\bar{d}$(M–C) of 200.4 pm and nearly identical to the q_u value of 197.9 pm.[64]

The data presented in Table 4 support the conclusion that, in cationic metal carbonyls, the (M–C) bond length increases and the (C–O) bond becomes stronger with increasing oxidation state, as is also easily seen from vibrational frequencies. The observed, significant covalent (M–X) distances in cationic metal carbonyl complexes make it clear that homoleptic carbonyl cations are present in Table 4 in only three structurally characterized salts: $[Re(CO)_6][Re_2F_{11}]$,[130b] $[Ag(CO)_2][B(OTeF_5)_4]$,[54, 56] and $[Hg(CO)_2][Sb_2F_{11}]_2$.[15b] An ionic structure has also been established for $[Ir(CO)_5Cl][Sb_2F_{11}]_2$.[13] $Ag(CO)[B(OTeF_5)_4]$, on the other hand, contains no discrete $[Ag(CO)]^+$ cation, and is better formulated as a covalent complex.[53] The two Ag···O bonds to the teflate group ($OTeF_5$) of 232.4(6) and 243.6(7) pm[53, 54] are comparable to the two Ag···O contacts of 235.7(5) to 244.8(5) pm in Ag^I–succinimide complexes[155] as well as to the average value of 257.5 pm for Ag^I–ether complexes.[64] The coordination number of three for silver in $Ag(CO)[B(OTeF_5)_4]$ is normal,[156] as for example in $[Ag(CN)_3]^{2-}$.[72, 73] Convincing proof for the existence of the isolated cations $[Ag(CO)]^+$ and $[Au(CO)]^+$ is thus lacking.

Molecular structures for the two metal carbonyl fluorosulfates *cis*- $Pd(CO)_2(SO_3F)_2$[18b] and *mer*-$Ir(CO)_3(SO_3F)_3$[19] are reproduced in Figures 2 and 3. The noteworthy differences in stereochemistry are a consequence of the syntheses. *cis*-$Pd(CO)_2(SO_3F)_2$ arises through nucleophilic substitution of CO by SO_3F^- in the initially formed $[Pd(CO)_4]^{2+}$ [18] in HSO_3F solution. By contrast, *mer*-$Ir(CO)_3(SO_3F)_3$ is formed together with about 15% of the *fac* isomer by slow CO addition to $Ir(SO_3F)_3$[129] in HSO_3F. Both geometries are thus attributable to the *trans*-directing effects of the CO ligands.[157]

As can be seen from the two figures and the tables in publications [18b] and [19], the majority of the structural parameters, bond lengths, and bond angles for the two compounds are nearly identical. There are differences, however. Whereas the metal–oxygen bond lengths of about 200 pm in both compounds are similar, the metal–CO bond lengths differ in an interesting way. The Ir–C distance of 193.7(7) pm when the CO group is *trans* to SO_3F is very similar to the Pd–C distances of 194.5(5) and 191.9(5) pm. The Ir–C distances of 199.9(6) and 200.6(6) pm for a linear $Ir(CO)_2$ group are significantly larger. This points to less metal-to-CO π-backbonding in such groups. The FSO_2O ligands appear rather to function as weak π-electron donors. One should therefore expect a difference in the CO bond lengths: smaller CO distances are anticipated in the linear $Ir(CO)_2$ group. However, this is not the case. All five CO bond lengths are identical within experimental error. Moreover, the mean vibrational frequencies $\tilde{\nu}(CO)_{avg}$ of 2218 cm^{-1} for the two compounds are also identical.[18, 19] For this reason, other effects must influence the electron density in the π* orbitals of the CO ligands. These effects will be discussed in the following section.

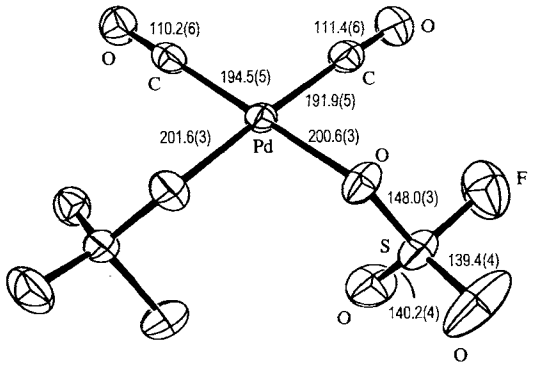

Figure 2. The molecular structure of *cis*-$Pd(CO)_2(SO_3F)_2$[18].

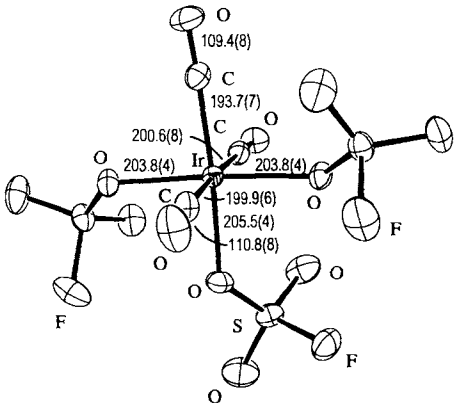

Figure 3. The molecular structure of *mer*-$Ir(CO)_3(SO_3F)_3$[19].

2.4.2. *External Bonding Parameters*

As was first established during the structure determination of *cis*-$Pd(CO)_2(SO_3F)_2$,[18b] weak but significant secondary contacts exist especially between the C atoms of the CO groups and noncoordinated terminal O atoms of FSO_2O groups, which lead apparently to small changes in the π*-electron density of the CO group. Based on a suggestion of Alcock,[67] secondary bonds can be recognized by distances that are larger than the sum of the covalent radii,[65, 152] but significantly smaller than the sum

of the van der Waal's radii.[68] In the case of the C···O and C···F contacts under consideration here, the sums of the covalent radii are 143.1 and 141.1 pm,[152] and those of the van der Waal's radii are 322 and 317 pm, respectively.[68] The observed C···O and C···F contacts fall in the approximate range of 260 to 300 pm (Table 5). In the above structures, the C atom of the carbonyl group functions as an acceptor and the O atom of the fluorosulfate group as a donor for secondary interactions. There are five such contacts per C atom for *cis*-$Pd(CO)_2(SO_3F)_2$,[18b] and an average of about four for *mer*-$Ir(CO)_3(SO_3F)_3$.[19] Details regarding the number and extent of secondary contacts can be extracted from Table 5.

Table 5. Secondary interactions in cationic metal carbonyl derivatives.

Geometry, Compound [c]	Secondary interactions			Ref.
		Type (number)	Distance [pm]	
linear				
$Ag(CO)[B(OTeF_5)_4]$	Ag-F	intra- and intermolecular (4)	295.9(6)–307.6(8)	[56]
$[Ag(CO)_2][B(OTeF_5)_4]$	Ag(1)-F	interionic (7)	275(1)–319(1)	[56]
(d_w(Ag-F) 319 pm)	Ag(2)-F	interionic (2)	302(1) (2x)	
	Ag(3)-F	interionic (4)	296(1) (2x), 309(1) (2x)	
$[Hg(CO)]_2[Sb_2F_{11}]_2$	Hg-F	interionic (4)	259.5(5) (2x), 269.1(4) (2x)	[11]
(d_w(Hg-F) 302 pm)	C-F	interionic (4)	265(1)–300(1)	
	C-F	between layers (1)	275(1)	
square-planar				
cis-$Pd(CO)_2(SO_3F)_2$	C(1)-O	intermolecular (4)	283.9(6)–317.2(6)	[18]
(d_w(Pd-O) 315 pm)	C(1)-F	intramolecular (1)	305.1(6)	
	C(2)-O	intermolecular (4)	283.9(6)–317.2(6)	
	C(2)-O	intramolecular (1)	284.3(6)	
	Pd-O	intermolecular (1)	300.7(4)	
	O-O	intermolecular (1)	286.1(5)	
octahedral				
mer-$Ir(CO)_3(SO_3F)_3$	C(1)-O[a]	inter- (3) and intramolecular (1)	277(1)–307(1)	[19]
	C(2)-O	inter- (2) and intramolecular (2)		
	C(3)-O	inter- (1) and intramolecular (1)		
	C(3)-F	intramolecular (1)	306(1)	
$[Ir(CO)_5Cl][Sb_2F_{11}]_2$	C(1)-F[b]	interionic (2)	284(2), 290(2)	[14]
	C(2)-F	interionic (3)	278(2)–300(2)	
	C(3)-F	interionic (3)		
	C(5)-F	interionic (3)		
	C(4)-F	interionic (4)	277(2)–298(2)	

[a] –O group *trans* to SO_3F. [b] C–O group *trans* to Cl. [c] d_w = sum of the van der Waals radii.

Only very weak interactions to the central metal atom are observed, as in the case of *cis*-$Pd(CO)_2(SO_3F)_2$ with a 300.7 pm Pd···O contact, which in view of the sum of van der Waals radii of 322 pm[68] must be regarded as weak. A weak CO···OS interaction of 286.1 pm in *cis*-$Pd(CO)_2(SO_3F)_2$ makes the distinct preference for C as acceptor quite obvious. With *mer*-$Ir(CO)_3(SO_3F)_3$[19] there are no contacts with Ir, since the central metal atom is less accessible than in square-planar *cis*-$Pd(CO)_2(SO_3F)_2$.

Secondary contacts also exist for the complexes of Group 11, as, for example, in $Ag(CO)[B(OTeF_5)_4]$,[53, 56] $[Ag(CO)_2][B(OTeF_5)_4]$,[54, 56] and even in the parent $Ag[B(OTeF_5)_4]$.[158] In the case of the two $[Sb_2F_{11}]^-$ salts of $[Hg(CO)_2]^{2+}$ [15b] and $[Ir(CO)_5Cl]^{2+}$ [13] several significant contacts are listed in Table 5. Here the interactions are largely interionic, and fluorine from the $[Sb_2F_{11}]^-$ anion functions as donor atom.

A further indication of interionic interactions exists for $[Sb_2F_{11}]^-$ salts as well. As in $[H_3O][Sb_2F_{11}]$,[106] the anion deviates from ideal D_{4h} symmetry. This is especially clear from the Sb-F_b-Sb angle, which is between 145.9(2) and 149.4(3)° in $[H_3O][Sb_2F_{11}]$[106] and 147.6(3)° in $[Hg(CO)_2][Sb_2F_{11}]_2$.[15b] In $[Ir(CO)_5Cl][Sb_2F_{11}]$[13] the deviation from linearity is less severe, and two Sb-F_b-Sb angles of 153.2(6) and 156.5(6)° are found.

On the other hand, in the structure of $[Re(CO)_6][Re_2F_{11}]$ there are no observable interionic contacts.[130b] Consequently, the $[Re_2F_{11}]^-$ anion displays D_{4h} symmetry. In $Re(CO)_5$-μ-F–ReF_5[130c] the shortest interionic C···F distance of 317.0 pm is almost identical with the sum of the van der Waals radii. Thus, in both rhenium carbonyl compounds the C atom is either less electrophilic or less accessible for secondary contacts.

In *fac*-$Ir(CO)_3F_3$,[22] two long Ir···F contacts of 339.0(7) and 356.0(8) pm have been described on the basis of EXAFS analyses.[22b] However, it is unclear whether these fluorine atoms also form intermolecular contacts to carbon. In Au(CO)Cl[33] the linear molecules are arranged antiparallel in the crystal lattice, which results in C···Cl contacts of 335 pm, slightly less than the sum of the van der Waals radii (345 pm).[68]

The contacts presented in Table 5 can be divided into four groups: 1) In molecular carbonyl derivatives one finds inter- and intramolecular interactions. 2) Mostly interionic contacts are observed for ionic derivatives. 3) Very rarely, contacts are observed between layers, as in $[Hg(CO)_2][Sb_2F_{11}]_2$.[15b] 4) Equally seldom are there C···F contacts in fluorosulfates, since in SO_3F the oxygen atom is more basic than the fluorine atom.

This observation is in good agreement with the coordination behavior of the FSO_2O group in metal fluorosulfates, in which coupling occurs over one, two, or three O atoms of the FSO_2O group, whereas coordination with the F atom is extremely rare.[159]

In most of the examples in Table 5, C atoms of the CO groups are the preferred acceptors for secondary contacts, because in cationic metal carbonyls, in which π-backbonding is significantly reduced, the carbon atom is exceptionally electrophilic. An ab initio study on carbonyl cations and isoelectronic cyano anions of the type $[M(CX)_n]^{+/-}$ (M = Ag, Au; X = O, N; n = 1–3), taking relativistic nuclear potentials into account,[160] has shown that the positive ionic charge of the cation distributes itself over the metal atoms and the carbon atoms, whereas the O atoms are negatively charged. Adjacent partial positive charges on M and C make the rather large M–C bond distances understandable, especially with metal formal charges of +2 and +3 (see Table 4). This charge distribution also explains why, apart from C, the metal center can also function as an acceptor for secondary contacts. Both centers are quite accessible in the case of linear cations. The structure of $[Hg(CO)_2][Sb_2F_{11}]_2$ offers an illustration.[15b] In a linear cation [the Hg–C–O angle is 177.7(7)°], mercury and the two C atoms all have four

interionic contacts with F atoms from the bent $[Sb_2F_{11}]^-$ anion. For the C atom there is also a supplementary C···F contact between layers. All the interionic contacts are of similar strength. Details of the very regular spatial arrangement of the fluorine atoms around Hg and C are illustrated in Figure 4.

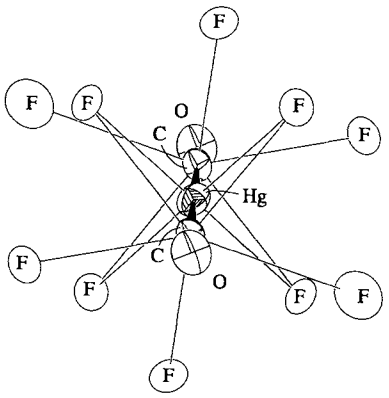

Figure 4. Excerpt from the crystal structure of $[Hg(CO)_2][Sb_2F_{11}]$[15b], in which nearest interionic contacts to the $[Hg(CO)_2]^{2+}$ cation are depicted.

Whereas the environment of Hg is distorted octahedral, the C atoms display a coordination number of 7. The resulting geometry can be approximately described as a compressed pentagonal bipyramid, with Hg and O in axial positions. All interionic contacts in $[Hg(CO)_2][Sb_2F_{11}]_2$ participate in the formation of a three-dimensional network, which includes the carbonyl groups.[15b] They further contribute significantly to the stability of the metal carbonyl cation in the solid state. Interestingly, there are similar intermolecular contacts in the isoelectronic $Hg(CN)_2$,[74b, 161] as well as in $HgCl_2$,[162] in which mercury is coordinated to N or Cl.

In contrast to $[Hg(CO)_2][Sb_2F_{11}]_2$, the structures of $[Ag(CO)_2][B(OTeF_5)_4]$[54, 56] and $Ag(CO)[B(OTeF_5)_4]$[53, 56] display interionic contacts exclusively between Ag and the O or F atoms of the anions. These Ag···O or Ag···F contacts are comparable in strength with those in the starting compound $Ag[B(OTeF_5)_4]$,[158] where they are somewhat more numerous (six Ag···F and three Ag···O contacts) than in $Ag(CO)[B(OTeF_5)_4]$[54] (four Ag···F and two covalent Ag–O distances) or $[Ag(CO)_2][B(OTeF_5)_4]$[56] (three, four, or seven Ag···F distances are found for the three $[Ag(CO)_2]$ groups). Secondary interionic contacts to the carbons of the CO groups are absent in the silver(I) carbonyl derivatives,[163] as seen in Table 5. Consequently, in the silver(I) carbonyl compounds the CO ligands do not participate in the formation of three-dimensional networks. The observed ready loss of CO thus leads to an increase in lattice energy with the formation of $Ag[B(OTeF_5)_4]$[158] or also $Ag(OTeF_5)$ and $B(OTeF_5)_3$.[56] The preferred coordination to Ag^I is explained by the fact that the positive charge of the cationic Ag(CO) complex seems to be localized primarily on Ag^I, consistent with the calculations of Veldkamp and Frenking.[160] For example, charge distributions for the linear cations $[M(CO)_2]^+$ (M = Ag, Au) have been calculated to be $Ag^{+0.82}-C^{+0.54}$ and $Au^{+0.61}-C^{+0.60}$.

As soon as the coordination number rises from 2 to 4 and 6 and the geometry is altered from linear to square planar and then octahedral, secondary contacts to the metal atom virtually disappear, whereas the carbon atom establishes an increased number of contacts. Moreover, and this is especially apparent in the molecular structure of $[Ir(CO)_5Cl][Sb_2F_{11}]_2$,[15] there is also a limited number of O···F and interanionic F···F contacts. Interionic O···F contacts up to 282 pm are significantly less than the 299 pm sum of van der Waals radii.[68] These and also the Cl···F interactions, with distances between 322 and 356 pm relative to a sum of van der Waals radii of 322 pm, are probably repulsive in nature, caused by C···F interactions. In octahedral carbonyl complexes, C···F contacts are imposed and possible only with simultaneous formation of O···F contacts. However, it is also possible that the positive partial charges in the highly charged cations (+2 or +3) distribute themselves additionally over oxygen, which should lead to weak, bonding O···F contacts.

The many weak secondary contacts exert a stabilizing effect on these molecular structures. The formation of extended three-dimensional networks is best demonstrated in $[H_3O][Sb_2F_{11}]$.[106] By contrast, $[H_3O][SbF_6]$[164] reveals an "ionic" cubic structure. These examples point to a unique role that the dioctahedral $[Sb_2F_{11}]^-$ ion plays. The absence of secondary F···C or O···C contacts in Ag^I-carbonyl complexes[53–56] is surely only one reason for their observed thermal instability. Significant also is both the Ag–C bond energy, which is actually low relative to that of Au–C,[160] and the relatively low lattice energies for salts with large, singly charged ions.[165]

In two areas the secondary contacts described here permit important conclusions to be drawn:

1) The preference for C in the CO group as acceptor for contacts shows clearly that in cationic metal carbonyls the CO group is polarized in the sense $C^{\delta+}-O^{\delta-}$. This polarization was recently confirmed through ab initio calculations as well, which provided an explanation for the high CO stretching frequencies and force constants.[166]

2) Both experiment[9b, 15b, 19] and theoretical calculations[80] suggest a low electron density in the $2\pi^*$ orbitals of CO in all carbonyl cations. For $[Hg(CO)_2][Sb_2F_{11}]_2$[15b] or $[Ir(CO)_5Cl][Sb_2F_{11}]_3$,[13] where secondary contacts are present, it is unclear whether the residual electron density originates with the metal (through π-backbonding) or with the anion (through secondary contacts).

Secondary interionic contacts are also observed with carbonyl metalates. In this case they are referred to as ion-pair effects[167] and involve the oxygen of the carbonyl group as donor and the cation as acceptor. In weakly ionizing solvents this leads to the formation of ion pairs.

2.5. Spectroscopic Properties and Bonding Relationships of Cationic Metal Carbonyl Complexes

The existing structural data, based mainly on X-ray diffraction, are of limited use for developing an intensive discussion of the bonding relationships in homoleptic metal carbonyl cations, since they are imprecise and so far available only for a small number of relevant compounds. Spectroscopic data are therefore especially important and highly informative for this class of compounds.

Table 6. Spectroscopic properties of homoleptic metal carbonyl cations, metal carbonyl fluorosulfates, and related species.

Compound [a]	$\tilde{\nu}(CO)_{IR}$ [cm^{-1}]	$\tilde{\nu}(CO)_{Raman}$ [cm^{-1}]	f_{CO} [10^2 N m^{-1}]	δ_C	$^1J_{MC}$ [Hz]	Ref.
$[Hg(CO)_2]^{2+}$	2278	2281	21.0	169	5220	[11]
$[Hg_2(CO)_2]^{2+}$	2247	2248	20.4	189	3350	[11]
$[Ag(CO)_2]^+$ [b]	2196	2220	19.7	172	232	[56]
$[Au(CO)_2]^+$	2217	2254	20.1	174		[16b]
$Au(CO)SO_3F$ [c]	2195	2198	19.5	162		[16]
$[Pd(CO)_4]^{2+}$	2248	2278, 2263	20.6	144		[15]
cis-$Pd(CO)_2(SO_3F)_2$	2227, 2208	2228, 2207	19.9	145		[18a]
$[Pd_2(\mu\text{-}CO)_2]^{2+}$	2006	2048	16.6			[21]
$[Pd_2(\mu\text{-}CO)_2](SO_3F)_2$	1977	2027	16.2	162[c]		[17]
$[Pt(CO)_4]^{2+}$	2244	2289, 2267	20.6	137	1550	[15]
$Pt(CO)_2(SO_3F)_2$	2219, 2185	2218, 2181	19.6	131	2011	[18a]
$[Ir(CO)_6]^{3+}$	2254	2295, 2276	20.8	121		[14]
mer-$Ir(CO)_3(SO_3F)_3$	2249, 2208, 2198	2249, 2206, 2196	20.0, 19.5			[19]
fac-$Ir(CO)_3(SO_3F)_3$	2232, 2156	2233, 2157	19.3			[19]
$[Fe(CO)_6]^{2+}$	2204	2241, 2220	19.8	179		[13]
$[Ru(CO)_6]^{2+}$	2199	2254, 2222	19.8	166		[12]
$[Os(CO)_6]^{2+}$	2190	2259, 2218	19.8	147		[12]
$[Mn(CO)_6]^+$	2100	2185, 2128	18.2	195		[e][44]
$[Re(CO)_6]^+$	2084	2197, 2122	18.1	171		[e][45]
$W(CO)_6$	1998	2126, 2021	16.4	192	125	[75, 168]
CO [d]	2143		18.6	184		[84, 16b]
$CO^+(X\,^2\Sigma^+)$ [d]	2184		19.3			[151]
$[HCO]^+$ [d]	2184		21.3			[50c]

[a] All cations as $[Sb_2F_{11}]^-$ salts. [b] As $[Nb(OTeF_6)_6]^-$ salt. [c] In HSO_3F. [d] Gas phase. [e] This paper; f(CO) calculated according to the CK method, ref. [169]

Vibrational spectroscopic data not only permit statements regarding the symmetry of the metal carbonyl fragments, but also allow calculations of CO bond strengths. ^{13}C NMR shifts and $^1J_{M,C}$ coupling constants are helpful for characterizing the M–CO bonds. The many sets of published vibrational[146–149] and ^{13}C NMR data[168] permit a comprehensive comparison with corresponding data for cationic metal carbonyl derivatives (Table 6).

2.5.1. *Vibrational Spectra*

Three elementary conditions should apply to the assignment and interpretation of vibrational data:

1) The composition and identity of the metal carbonyl complexes should be unambiguous, and the spectroscopic data must be reproducible.
2) Because of the high symmetry of the cations (O_h, D_{4h}, $D_{\infty h}$), both IR and Raman data must be available.
3) Vibrational analyses should, where possible, extend over the entire fundamental vibration region, and isotopic data should be included for the computation of reliable force constants.

The data presented in Table 6 generally fulfill the above criteria, and the resulting CO force constants permit comparisons with other carbonyl and isoelectronic cyanide species. All f_{CO} values have been calculated according to the method of Cotton and Kraihanzel (CK).[169] The fundamental assumption of isolated CO stretching is completely valid for homoleptic metal carbonyl cations whose $\tilde{\nu}(CO)_{avg}$ values fall between 2200 and 2300 cm^{-1}, whereas the remaining fundamental vibrations of the cations lie below 600 cm^{-1}. Moreover, a normal-coordinate analysis for $[Au(CO)_2]^+$ utilizing ^{13}C and ^{18}O isotopic data, together with the G and F matrix elements of the general valence force field proposed by Jones,[75] shows that calculated CO force constants obtained in this way do not differ significantly from those determined according to the CK method.[169]

To keep the discussion within bounds, we consider below in detail only the homoleptic metal carbonyl cations. Almost all the metal carbonyl fluorosulfates have been structurally characterized. They show fundamentally lower CO force constants than the corresponding homoleptic carbonyl cations, and these vary only slightly within the group: 19.3 for *fac*-$Ir(CO)_3(SO_3F)_3$,[19] 19.5 for $Au(CO)SO_3F$,[16a] 19.6 for *cis*-$Pt(CO)_2(SO_3F)_2$,[18a] 19.9 for *cis*-$Pd(CO)_2(SO_3F)_2$,[18a] and 20.0/19.5 $\times 10^2$ N m^{-1} for *mer*-$IR(CO)_3(SO_3F)_3$.[19] The two geometric isomers of $Ir(CO)_3(SO_3F)_3$ make it clear that a CO bond *trans* to an SO_3F group is weakened.

The isoelectronic pairs CO/CN^-, CO^+/CN, and HCO^+/HCN shown in Table 7 provide a basis for our discussion. For most of these, very precise bond lengths are available from analyses of microwave[51b, 170, 171] and electronic spectra,[151, 172] and data also exist for the latter for ν(CO) and ν(NO). In the linear species HCO^+ and HCN, ν(CX) is strongly coupled with ν(CH), which means CX force constants can be calculated only with the aid of a normal-coordinate analysis

Table 7. Bond lengths d(C–X) (X = O, N), stretching vibrational frequencies $\tilde{\nu}$(CX), and force constants f_{CX} for selected CO and CN species.

Compound	d(C-X) [pm]	$\tilde{\nu}$(CX) [cm^{-1}]	f_{CX} [10^2 N m^{-1}]	d(C-X)	Ref. $\tilde{\nu}$(CX)	f_{CX}
CO	112.8	2143	18.6	[151]	[149]	[16b]
CN^-	110(4)[a]	2038	15.8	[173]	[174]	[b]
CO^+	111.5	2184	19.3	[151]	[151]	[16b]
CN	117.18	2042	15.9	[151]	[151]	[75]
HCO^+	110.71	2184	21.3	[51b]	[176]	[16b]
HCN	115.51	2097	18.3	[171, 172]	[75]	[75]

[a] See text. [b] This paper.

based on the general valence force model.[75] In contrast to CO, the choice of the available data is problematic in the case of the cyanide ion. Examination of many X-ray structures has led to an approximate bond length of 110 ± 4 pm.[173] The origin of the extreme inaccuracy associated with ionic cyanides is to be found in the corrections for thermal motion and in problems due to disorder. Moreover, the corresponding CN bond lengths in cyano complexes are insensitive to electronic influences. This is reflected in a mean CN distance of 114.6 pm, derived from 168 structures of CN complexes, for which 50% of the data lie between 113.8 and 115.4 pm.[64] Of course, the vibrational frequency $\tilde{\nu}(CN^-)$ for the cyanide ion is also influenced by the environment. We have selected a value of 2038 cm^{-1} for the "free ion", established in a detailed study by Field and Sherman,[174] and from that we have calculated f_{CN}. Slightly larger values for f_{CN} (up to 16.5×10^2 $N m^{-1}$) have been reported elsewhere.[75, 175]

If one ignores the imprecision in the bond length for the cyanide ion, all CO bond lengths in Table 8 appear to be about 5 pm shorter than those of the corresponding CN species. This may be due in part to differences in the atomic radii of O and N.

Table 8. Comparison of bonding force constants for isoelectronic pairs of metal carbonyl cations and cyano complexes.

Metal carbonyl cations			Cyano complexes		
Complex	f_{CX} [10^2 $N m^{-1}$]	Ref.	Complex	f_{CX} [10^2 $N m^{-1}$]	Ref.
d^{10}-linear					
$[Hg(CO)_2]^{2+}$	21.0	[11a, b]	$Hg(CN)_2$	18.1	[75]
$[Hg_2(CO)_2]^{2+}$	20.4	[11a]			
$[Au(CO)_2]^+$	20.1	[16b]	$[Au(CN)_2]^-$	17.6	[75]
$[Ag(CO)_2]^+$	19.7	[a][56]	$[Ag(CN)_2]^-$	16.9	[75]
d^8-square-planar					
$[Pt(CO)_4]^{2+}$	20.6	[a][21]	$[Pt(CN)_4]^{2-}$	17.5	[a][75]
$[Pd(CO)_4]^{2+}$	20.6	[a][21]	$[Pd(CN)_4]^{2-}$	17.5	[a][75]
d^6-octahedral					
$[Ir(CO)_6]^{3+}$	20.8	[14]	$[Ir(CN)_6]^{3-}$	16.9	[75]
$[Fe(CO)_6]^{2+}$	19.8	[13]	$[Fe(CN)_6]^{4-}$	16.0	[75]
$[Ru(CO)_6]^{2+}$	19.8	[12]	$[Ru(CN)_6]^{4-}$	16.0	[a][178]
$[Os(CO)_6]^{2+}$	19.8	[12]	$[Os(CN)_6]^{4-}$	16.0	[a][179]

[a] This paper; calculated according to the CK method, ref. [169]; vibrational data from the cited literature.

The sums of the covalent radii for single, double, and triple bonds[152] are all about 4–5 pm shorter for C–O than for C–N. A relatively large difference of $2.8-3.4 \times 10^2$ $N m^{-1}$ can be established between force constants for the carbonyl and cyanide species.

Figure 5 depicts a correlation between f_{CO} and bond lengths for gaseous CO derivatives, for which precise bond lengths and force constants are known.[176, 177] The exponential function used to describe the correlation is suitable for estimating CO bond strengths or lengths in carbonyl complexes, as is demonstrated, for example, with $[Au(CO)_2]^+$.[16b] The introduction of average CO bond lengths and the previously mentioned q_l and q_u values[64] for metal carbonyl compounds in Figure 5 permits a further conclusion. Exactly 50% of all the CO bond lengths in the Cambridge Index fall within a narrow range of 2.4 pm, and are virtually identical within the usual limits of error.

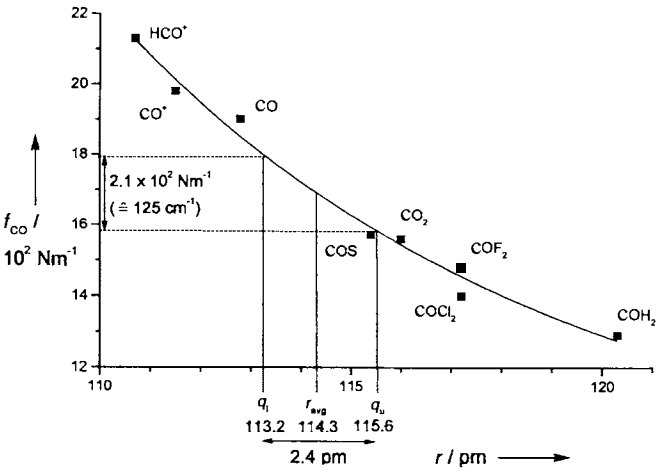

Figure 5. CO force constants as a function of CO bond lengths [$\bar{r}_{avg}$ = average CO bond length, established on the basis of 10022 sets of data (Cambridge Index)]. References for f(CO)/r(CO): HCO^+ [50c]/[51b], CO^+ ($X^2\Sigma^+$) and CO[151]/[151], COS[176a]/[176b], CO_2[176a]/[176c], COF_2[177a]/[176b], $COCl_2$[177b]/[176b], COH_2[177c]/[176c]

The extrapolated vibrational spectroscopic data extend over 2.1×10^2 $N m^{-1}$ (f_{CO}), or approximately 125 cm^{-1} (ν_{CO}), which permits a much more exact differentiation.

The usefulness of valence force constants becomes clear in Table 8 when comparing homoleptic metal carbonyl cations with the corresponding isoelectronic and isostructural cyano complexes. For both groups of compounds the force constants f_{CO} and f_{CN} are larger than those of the free ligands CO and CN^- (see Table 7). This means that in both cases the ligand-to-metal σ-bond is dominant, whereas π-backbonding in the examples presented is weak. For the protonated ligands HCO^+ and HCN, force constants of 21.3×10^2 and 18.3×10^2 $N m^{-1}$, respectively, represent limiting values for both series. The ligands are exclusively σ-bonded to H^+, since π-backbonding is impossible. Among the metal complexes cited, $[Hg(CO)_2]^{2+}$ and $Hg(CN)_2$ come closest to being *purely* σ-bonded, since the corresponding force constants of 21.0 and 18.1×10^2 $N m^{-1}$ are nearly identical to those of HCO^+ and HCN within the limits of error. The slightly smaller force constant in $[Hg(CO)_2][Sb_2F_{11}]$ relative to that of HCO^+ might be attributed to significant interionic F···C contacts (see Table 5 and Figure 4), which increase the electron density in the π* orbitals of CO and thus weaken the CO bond.

If the coordination number increases from 2 through 4 to 6 in CO and CN^- complexes, with the metal atom in the +2 oxidation state, the bond strength for CX (X = O, N) gradually decreases in both series. The decrease in f_{CX} is more pronounced for cyanometalates than for carbonyl cations.

The observed trend is a good illustration of the synergistic nature of the bonds between the metal ion and CO or CN^-. With an increasing number of ligands, the negative charge on the central atom is raised as a result of the σ-bond, and consequently π-backbonding increases. This is more prominent with CN^- than with CO, because cyanide is a better σ-donor.[1, 72, 73] In effect, bonds of the type CX (X = O, N) are weakened by increasing M-to-C π-backbonding. A second example of the synergistic nature of the metal–ligand bond in CO and CN^- complexes is found in the three pairs of isosteric complexes in

the 5d series: linear $[Au(CX)_2]^{\pm 1}$, square-planar $[Pt(CX)_4]^{\pm 2}$, and octahedral $[Ir(CX)_6]^{\pm 3}$ (X = O, N). In this series, the oxidation state of the metal increases at each step by 1, and the coordination number by 2. The values for f_{CN} decrease and those for f_{CO} increase with increasing coordination number. It appears that, for carbonyl cations, π-backbonding decreases with increasing oxidation state, whereas in the isoelectronic cyano ions it increases. Within the series of isostructural metal carbonyls and cyanometalates[178,179] in Groups 10 (Pd, Pt) and 8 (Fe, Ru, Os), all the force constants are nearly identical. This is no longer the case in Group 11, in which CX bonds in the silver complexes are clearly weaker than in the gold complexes. The f_{CO} value of 19.7×10^2 N m^{-1} for $[Ag(CO)_2]^+$ is the lowest for all the metal carbonyl cations in Table 8. Since no secondary contacts between the anions and the C atom are observed,[162] a smaller polarization of CO could be responsible for the weak CO bond in $[Ag(CO)_2]^+$.

Indications of the significance of polar components to the strength of the CN bond stem from two cationic derivatives of $Hg(CN)_2$.[180] Solvolysis of $Hg(CN)_2$ in anhydrous HF in the presence of AsF_5 or BF_3 leads to solids described as $[Hg(CN)][AsF_6]$ or $[Hg(CN)][BF_4]$ with IR bands at 2290 and 2270 cm^{-1}, respectively. This means that in the first compound the CN force constant is 19.9×10^2 N m^{-1}. As far as we know, this is the highest reported value for an isolable CN compound. In the cation $[Hg(CN)]^+$ the positive ionic charge is distributed between Hg and C, leading to a charge distribution $C^{\delta+}-N^{\delta-}$ for the ligand. Interestingly, the isoelectronic cation $[Hg(CO)]^{2+}$ remains unknown.

An additional informative correlation relates exclusively to metal hexacarbonyl complexes. Vibrational spectra in the CO stretching region for $W(CO)_6$,[75,149,168,181] $[Re(CO)_6]^+$,[44,130,132] $[Os(CO)_6]^{2+}$,[11-13] and $[Ir(CO)_6]^{3+}$[13] are reproduced in Figure 6. All three fundamental vibrations are shifted to higher frequency with increasing oxidation state of the metal. Moreover, the separation between the two Raman-active bands $\nu_1(A_{1g})$ and $\nu_3(E_g)$ becomes progressively smaller from 105 cm^{-1} for $W(CO)_6$ to 19 cm^{-1} for $[Ir(CO)_6]^{3+}$. The intensity of the totally symmetric A_{1g} band increases steadily relative to that of the E_g band. The origin of this trend is to be found in decreasing electronic vibrational coupling of the CO ligands in $W(CO)_6$ through $[Ir(CO)_6]^{3+}$.

The series of isoelectronic metal hexacarbonyl complexes is completed by the anions $[Ta(CO)_6]^-$[70c,149] and $[Hf(CO)_6]^{2-}$.[7,71b] Figure 7 shows two relationships between the force constants f_{CO} or ^{13}C chemical shifts (to be discussed in Section 3.5.2) and the nuclear charge number or oxidation state of the metal centers. Since Raman spectra for the two carbonyl metalates $[Hf(CO)_6]^{2-}$ and $[Ta(CO)_6]^-$ have apparently not been reported, the appropriate force constants were estimated to be 12.8×10^2 and 14.2×10^2 N m^{-1}, respectively, based on an extrapolation from the linear relationship between $\tilde{\nu}^2(F_{1u})$ and the f_{CO} values for the remaining four $[M(CO)_6]$ species. As can be seen in Figure 7, CO bond strength increases steadily with increasing oxidation state of the metallic center. The overall change in f_{CO} within the series amounts to 8×10^2 N m^{-1}. Since the increase in f_{CO} is only 1×10^2 N m^{-1} between $[Os(CO)_6]^{2+}$ and $[Ir(CO)_6]^{3+}$, the otherwise linear relationship becomes curved. Force constants for the osmium(II) and iridium(III) car-

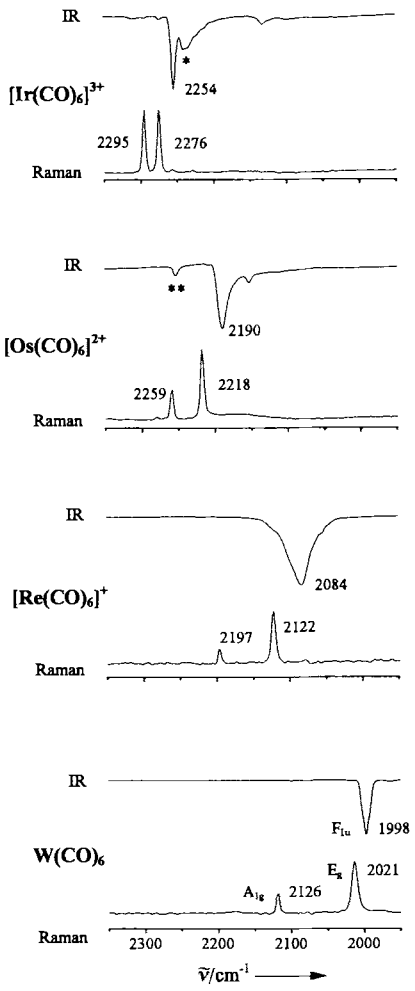

Figure 6. Vibrational spectra [ν(CO) region] for isosteric octahedral hexacarbonyl species $[M(CO)_6]^{n+}$ ($n = 0-3$) of the 5d metals (the IR band of the hydrolysis product of $[Ir(CO_6)]^{3+}$ is labeled with one asterisk, that of the cation $[Os(CO)_6]^{3+}$ at 2252 cm^{-1} with two).

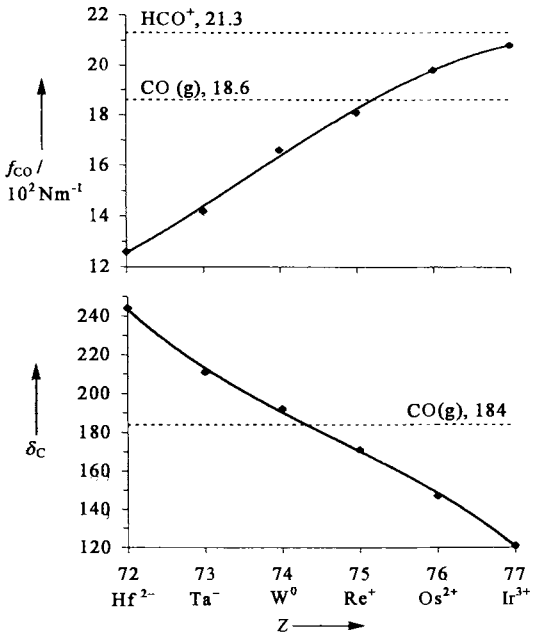

Figure 7. Relationship between CO force constants and ^{13}C NMR chemical shifts for the isosteric octahedral hexacarbonyl species $[M(CO)_6]^n$ ($n = -2$ to $+3$; M = Hf, Ta, W, Re, Os, Ir) with nuclear charges Z. The data for CO and HCO^+ define boundaries for the relevant bonding types (see text).

bonyls fall in a region defined by the f_{CO} values for CO ($f_{CO} = 18.6 \times 10^2\ N\,m^{-1}$) and HCO^+ ($f_{CO} = 21.3 \times 10^2\ N\,m^{-1}$) as upper and lower limits. The f_{CO} values for the remaining metal hexacarbonyl complexes lie outside this region. Similar relationships can also be established for other hexacarbonyls of the 4d and 3d metals, as shown in Table 9. With the exception of $[Tc(CO)_6]^+$, all the IR-active F_{1u} fundamental vibrations have been listed. Table 9 also contains ^{13}C NMR chemical shifts,

Table 9. Spectroscopic data for hexacarbonyl compounds derived from transition metals in Groups 4 through 9.

$\tilde{\nu}$ [cm^{-1}]	Group					
δ_C	4	5	6	7	8	9
	$[Ti(CO)_6]^{2-}$	$[V(CO)_6]^-$	$Cr(CO)_6$	$[Mn(CO)_6]^+$	$[Fe(CO)_6]^{2+}$	
F_{1u}	1748	1859	2000	2100	2203	
δ_C	246	224	212	195	179	
	$[Zr(CO)_6]^{2-}$	$[Nb(CO)_6]^-$	$Mo(CO)_6$	$[Tc(CO)_6]^+$	$[Ru(CO)_6]^{2+}$	
F_{1u}	1757	1860	2004	–	2198	
δ_C	245	217	204	–	166	
	$[Hf(CO)_6]^{2-}$	$[Ta(CO)_6]^-$	$W(CO)_6$	$[Re(CO)_6]^+$	$[Os(CO)_6]^{2+}$	$[Ir(CO)_6]^{3+}$
F_{1u}	1757	1850	1998	2084	2190	2254
δ_C	244	211	192	171	147	121

which will be discussed in Section 2.5.2. The 500 cm^{-1} range covered by $\tilde{\nu}$(CO) is much larger than usual for terminally bonded CO (1850 to 2125 cm^{-1}).[1, 75, 146–149] F_{1u} values for $[M(CO)_6]^{2+}$ (M = Fe, Ru, Os) and for $[Ir(CO)_6]^{3+}$ lie significantly above the limit of 2143 cm^{-1} for free CO.[149]

Comparatively high wavenumbers for the F_{1u} vibration have also recently been observed for $[Fe(CO)_6]^{3+}$ (2256 cm^{-1})[12] and $[Os(CO_6)]^{3+}$ (2252 cm^{-1}) and are currently being further investigated[181a] and subjected to theoretical calculation.[181b] As in the case of the f_{CO} and f_{CN} values for Groups 8 and 10 (see Table 8), all F_{1u} wave-number values within a group are independent (< 10 cm^{-1}) of the metal in question. In the case of all 15 species in Table 9, for identical octahedral geometry the charge on the complex is the only variable that establishes the relative proportions of σ-donor and π-acceptor contributions to the M–CO bond.

Starting from the carbonyl metalates of the early transition metals, with extensive π-backbonding, the σ bond becomes stronger with increasing oxidation state of the metal. When the charge rises to +2 and +3, the π contribution becomes smaller, whereas the σ-bonding fraction increases. This trend can be extended to Groups 10 and 11, although species such as $[Pt(CO)_6]^{4+}$ and $[Au(CO)_6]^{5+}$ appear not to exist. Instead, these metals form planar $[Pt(CO)_4]^{2+}$ (d^8) and linear $[Au(CO)_2]^+$ (d^{10}) as cations with the highest CO content.

2.5.2. ^{13}C NMR Spectra

Two sets of data are available from the ^{13}C NMR spectra of metal carbonyl complexes: chemical shifts δ_c and, in the case of metallic centers with a nuclear spin of 1/2, the coupling constants $^1J_{M,C}$. The chemical shift, which consists of a diamagnetic and a paramagnetic term, is sensitive to the σ, π, and polar contributions to bonding—as is the CO force constant, but in a different way. The coupling constant depends largely on the Fermi contact term and indicates the strength of MC σ-bonding.

As can be seen in Figure 7 for 5d $M(CO)_6$ complexes and in Tables 6 and 9 for additional metal carbonyl derivatives, trends similar to those discussed can also be established on the basis of ^{13}C chemical shifts. The chemical shift of free ^{13}CO at $\delta = 184$[16b, 168] relative to $(CH_3)_4Si$ (TMS) can be regarded as a limit for cationic carbonyl derivatives with smaller values, as well as typical of carbonyls and highly reduced carbonyl metalates with higher resonance frequencies and correspondingly higher δ values. Two exceptions to this rule are so far known. The chemical shift of $[Hg_2(CO)_2]^{2+}$ is $\delta = 189$, and the cations $[M(CO)_6]^+$ show resonances at $\delta = 195$ for M = Mn and $\delta = 171$ for M = Re, which fall on either side of ^{13}CO.

As can be seen in Table 9 for octahedral homoleptic $M(CO)_6$ complexes, the ^{13}C chemical shifts in the three *n*d series ($n = 3-5$) are dependent upon the oxidation state of the metal. With increasing charge from −2 to +3 the δ_C values decline, while the force constants rise simultaneously, as is also apparent from Figure 7 for the 5d metals. In addition, the resonance frequencies decrease with increasing atomic mass, although f_{CO} apparently does not change. Differences in the chemical shifts within Group 4 are very small, but they are larger for the remaining groups. It appears that increasing Lewis acid strength and the accompanying decrease in metal → CO π-backbonding is responsible for the "horizontal" trend, which influences δ_c and f_{CO} in similar ways. The "vertical" trend of δ_c is caused by increased shielding of the C atom with increasing atomic mass of the metal. As a consequence of the two trends, the smallest chemical shift of $\delta = 121$ is observed for $[Ir(CO)_6]^{3+}$.[13] It was shown through a recently completed density functional theory (DFT) study on 18 $[M(CO)_6]^n$ species that the paramagnetic contribution largely determines chemical shifts.[181c] The paramagnetic contribution is in turn dependent on the energy difference between the dπ orbitals of the metal and the π* orbitals of CO.

The δ_c values for $[Fe(CO)_6]^{3+}$ [12] and $[Os(CO)_6]^{3+}$ [181] are of interest in this context, but they have not yet been ascertained. For both complexes a paramagnetic ground state term is expected, which should affect the chemical shifts and cause broad resonance in the ^{13}C NMR spectrum.

A dependence is anticipated between ^{13}C chemical shift and coordination number in the 5d series $[Ir(CO)_6]^{3+}$, $[Pt(CO)_4]^{2+}$, and $[Au(CO)_2]^+$, with a common ratio (2:1) of number of CO ligands to ionic charge. The δ_C values increase from 121 through 137 to 174, whereas the f_{CO} values decrease only slightly from 20.8 through 20.6 to $20.1 \times 10^2\ N\,m^{-1}$. Substitution of CO in $[Au(CO)_2]^+$ [16] and $[M(CO)_4]^{2+}$ (M = Pd, Pt)[14] by SO_3F^- to give the metal carbonyl fluorosulfates $Au(CO)SO_3F$[16a] and *cis*-$M(CO)_2(SO_3F)_2$ (M = Pd, Pt)[18] strengthens the M → CO π-backbonding. Both f_{CO} and δ_C decrease. Interestingly, for the two Pd^{II} species $[Pd(CO)_4]^{2+}$ and *cis*-$Pd(CO)_2(SO_3F)_2$ the chemical shifts are very similar ($\delta = 144$ and 145). Much the same is true in Group 11. The ^{13}C chemical shifts for $[Ag(CO)_2]^+$ and $[Ag(CO)]^+$ are nearly identical at $\delta = 172.3$ and 171.4,[156] and slightly smaller than in the case of $[Au(CO)_2]^+$ [16b] ($\delta = 174$).

The currently known $^1J_{M,C}$ coupling constants are listed in Table 6. These include the nuclei ^{199}Hg,[15] ^{195}Pt,[181] and $^{109}Ag/^{107}Ag$.[56] All the J values are unusually large, often larger than those previously reported.[15, 56] The increase in Pt–CO bond strength is clearly evident in the transition from $[Pt(CO)_4]^{2+}$ with $^1J_{Pt,C} = 1550$ Hz to $Pt(CO)_2(SO_3F)_2$ with $^1J_{Pt,C} = 2011$ Hz. The same applies to the pair $[Hg(CO)_2]^{2+}$/$[Hg_2(CO)_2]^{2+}$ with $^1J_{Hg,C}$ values of 5220/3350 Hz. This correlates very well with thermal stabilities: $[Hg(CO)_2][Sb_2F_{11}]_2$ is thermally stable well above 100 °C, whereas $[Hg_2(CO)_2][Sb_2F_{11}]_2$ loses CO even at room temperature.

A detailed discussion of NMR data is envisioned for a later date, and appears inappropriate as part of this overview. The limited number of ^{13}C NMR data available for cyanometalates[75, 149] also eliminates the immediate possibility of a comprehensive comparison with the corresponding isoelectronic metal carbonyl cations.

2.5.3. Summary of Observed Trends in Spectroscopic Properties

The observed trends in spectroscopic properties for isosteric homoleptic metal carbonyl and cyano complexes can be summarized as follows: 1) Parameters such as the CX force constants f_{CO} or f_{CN}, selected CO vibrational frequencies, and ^{13}C chemical shifts are dependent upon the oxidation state, nuclear charge, and coordination geometry of the metal ion. 2) All spectroscopic properties change consistently and gradually with these parameters and can be extrapolated from correlations like the one shown in Figure 7. 3) The nearly constant differences in CO and CN bond strength apparent between CO/CN^-, HCO^+/HCN, and isoelectronic carbonyl/cyano complexes are a consequence of the differing bond polarities $C^{\delta+}-O^{\delta-}$ versus $C^{\delta-}-N^{\delta+}$, which strengthens the CO bond and weakens the CN bond.

2.5.4. Discussion of the Characteristics of the (M–C–O) Bond

The metal–CO bond in all metal carbonyl complexes can be described by a modified synergistic bonding model. For purposes of clarification Figure 8 has been devised to provide a schematic representation of orbital overlap in the individual (M–CO) segments with terminally bonded CO. The σ-donor bond from the 5σ molecular orbital of CO is shown as an arrow pointing in the direction of the metal atom. One component of the π-backbonding from the nd_{xz} or nd_{xy} metal orbital into the π* molecular orbitals of CO is symbolized by two curved arrows in the direction of CO. Thin lines indicate a weak bond, whereas thick lines depict the dominant bond type. Apart from these covalent bonding contributions, electrostatic effects in particular influence the CO bond, as shown by the most recent theoretical studies.[166, 181c] These electronic effects cause the indicated charges on the CO ligands (Figure 8a and c). In an analogous way, interionic contacts are directed toward the O atom in carbonyl metalates (a) and toward the C atom in carbonyl cations (c). The approximate wavelength regions for CO vibrations and oxidation states of the metal atoms are also indicated. Figures 8a and 8c represent limiting situations. In (a) π-backbonding dominates in a highly reduced carbonyl metalate, whereas in (c) a metal carbonyl cation, σ-bonding is overriding. Figure 8b

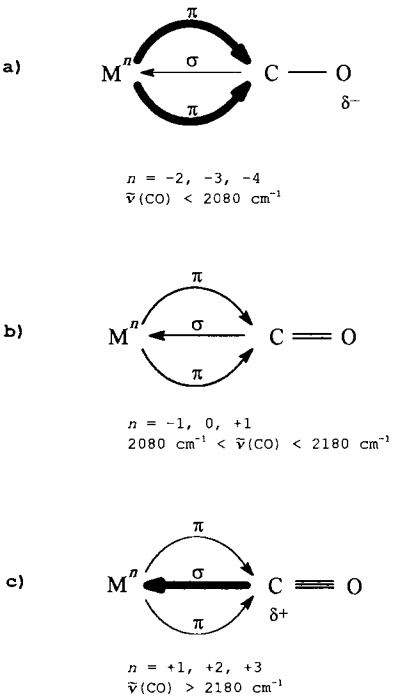

Figure 8. Schematic synergistic bonding model for a) predominantly π-bonded, highly reduced carbonyl metalates, b) typical metal carbonyls, and c) largely σ-bonded metal carbonyl cations.

characterizes the synergistic bonding in typical metal carbonyls, which may overlap with bond types (a) and (c) depending upon the oxidation state of the metal. So far, iridium is the only metal found to form a typical carbonyl complex $[Ir(CO)_4]^-$,[26, 27] a highly reduced complex $[Ir(CO)_3]^{3-}$,[7] and a homoleptic, mononuclear carbonyl complex $[Ir(CO)_6]^{3+}$,[13] where the oxidation states range from −3 to +3.

In this modified bonding model (Figure 8) that also takes into account electrostatic influences, σ- and π-bonding are regarded as complementary. Hence neither a "π-only" nor a pure "σ-only" situation exists. Although alternative bonding descriptions have been proposed,[182] the simple synergistic model according to Dewar, Chatt, and Duncanson[183–185] has not lost its appeal, thanks to its broad applicability also to a host of complexes with other π-acceptor ligands.[1, 26, 27] Many theoretical studies, only a few of which are cited here,[186–193] are based on the synergistic concept. Using various nuclear potentials and basis sets, structural parameters [d(M–C) and d(C–O)], spectroscopic properties [$\tilde{\nu}$(CO), δ_C, and electronic transitions], as well as M–CO bond energies and total energies for typical metal carbonyls have been well reproduced or predicted. There have also been many attempts to calculate relative σ- and π-contributions to overall bonding, and to compare various π-acceptor ligands. This does not apply in equal measure to the highly reduced carbonyl metalates and metal carbonyl cations. Ionic metal carbonyl species with charges of 2 or greater are to some extent stabilized by counterions through lattice energies, interionic interactions, or solvation in solution. In any case, theoretical calculations, which generally are based on gaseous free ions, become very complex if one attempts to extend them to the solid state or to solution conditions.

A comparative study of the homoleptic metal carbonyl cations $[M(CO)_n]^+$ ($n = 1, 2$) for all the 3d and 4d metals in the gaseous phase[194] apparently involves no overlap with our own work. More relevant in this context is a theoretical study taking into account relativistic nuclear potentials for metal carbonyl cations and cyano anions of the type $[M(CO)_n]^+$ and $[M(CN)_n]^{(n-1)-}$ (M = Cu, Ag, Au; $n = 1-3$)[160] and an experimental report of the determination of bond energies by mass spectrometry for the gaseous ions $[M(CO)_n]^+$ (M = Cu, Ag; $n = 1-4$).[195] There are three results in particular that coincide with our observations and conclusions: 1) linear species of the type ML_2 (M = Cu, Ag, Au; L = CO, CN^-) are more stable than species of the types ML, ML_3, ML_4;[160, 194] 2) for ML_n complexes ($n = 1-3$), stability decreases in the order $Au^I > Cu^I > Ag^I$;[160] 3) calculated partial charges for $[Au(CO)_2]^+$ and $[Ag(CN)_2]^-$ suggest differing bond polarities for the ligands.

Based on Fenske–Hall MO calculations,[80] it has been established that d^0 $[Cp_2Zr(CO)$[78, 79]] and d^{10} $[Ag(CO)$[53–56]] complexes involve significant π-backbonding. Also very promising is the most recent DFT study on octahedral $[M(CO)_6]^n$ species (M = metals of the 3d–5d series; $n = -2$ to $+3$).[181c] Apart from the frequencies of the CO vibrations and the ^{13}C NMR chemical shifts, which agree well with the experimental data in Tables 6 and 9, $(CO)_5M-CO$ dissociation energies were also calculated. The work of Ehlers, Ziegler, et al.,[181c] as well as that of Szilagyi and Frenking,[181d] suggests for $W(CO)_6$ the lowest M–CO dissociation energy of about 50 kcal mol^{-1}, and for $[Ir(CO)_6]^{3+}$ the highest of about 80 kcal mol^{-1}.

There is reason to hope that further calculations taking advantage of modern theoretical methods will permit ever deeper insights into the bonding relationships in all metal carbonyls. Moreover, the electronic spectra of certain $[M(CO)_n]^{m+}$ species are of interest as a way of ordering CO and CN^- with respect to their ligand field strengths in isoelectronic carbonyl and cyano complexes through ligand field analysis.[196]

The modified synergistic bonding model (Figure 8) suggested above permits several simple conclusions to be drawn:

1. CO is a far more versatile ligand than originally assumed.[1, 26, 27] The molecule forms thermally stable complexes with most metals apart from those of Group 3 (Sc, Y, La)[40] and a few main group metals.
2. The oxidation states of the metallic centers extend from −4 to +3. CO accommodates itself to this wide range through variation in both the σ- and π-components of overall bonding as well as through bond polarization. This variation is reflected in an enormous range for $\tilde{\nu}$(CO) for terminally bonded CO, extending from approximately 1400 to 2300 cm^{-1}, roughly three times as wide a range as previously assumed (1850 to 2125 cm^{-1} [1]).
3. Figure 8 illustrates qualitatively the synergistic M–CO bonding both in organometallic derivatives and in coordination compounds with classical linear and square-planar geometries.
4. Whereas one of the bond types (a) or (c) may dominate, the M–CO bond nevertheless remains synergistic. Strong σ-donor bonding leads to π-backbonding, and vice versa. Interpretations such as "σ-only" in cationic metal carbonyls[39, 56] are not consistent with the model, and not scientifically tenable, as the previous discussion of CO force constants demonstrates. The interpretation by Pearson,[198a] which classifies CO as a Lewis acid and M as a Lewis base, is limited to typical uncharged metal carbonyls. Extension of his interpretation (which is based on absolute electronegativities[198b]) to all three groups of carbonyl derivatives has not yet been accomplished. The dimensions of metal carbonyl chemistry have been considerably broadened with the discovery of highly reduced carbonyl metalates[7] and homoleptic metal carbonyl cations. Consequently, any description of the M–CO bond must now be seen in a wider perspective.

Strauss et al.[56] have proposed for the silver(I) CO adducts the vague, simplistic description "nonclassical" metal carbonyls,[56] and unfortunately we have also applied this designation to the $[Hg(CO)_2]^{2+}$ cation.[15b] In view of the results presented and discussed in the present publication, we are of the opinion that a distinction between classical and nonclassical carbonyls is nebulous, misleading, and unnecessary. Instead, we have adopted the terminology originally suggested by W. Hieber,[24] which combines the term "metal carbonyl cation" with the adjective "homoleptic". The designations "classical" and "nonclassical" are unfortunate from another standpoint as well: In the related field of carbocation chemistry[10a, 99] this terminology is no longer accepted by IUPAC.[199] Finally, a quotation from George Olah's Nobel Prize Lecture[200] makes the point well:

"The terms classical and nonclassical are expected, however, to fade away gradually as the general nature of bonding becomes recognized."

3. Summary and Conclusions

Superacids,[10] which were earlier used for the synthesis and investigation of very reactive cations, especially carbocations[10, 99, 200] and hetero- and homonuclear polycations of main group elements,[10b, 87c, 201, 202] have proven to be useful reaction media for the preparation of homoleptic metal carbonyl cations. In the context of the studies described here it has been observed that the Lewis superacid SbF_5[98] is an ideal reaction medium. Liquid SbF_5[20] allows preparation of highly reactive naked metal cations that are carbonylated under very mild conditions and can be isolated in the form of thermally stable salts of metal carbonyl cations with $[Sb_2F_{11}]^-$ as counterion. The ability of $[Sb_2F_{11}]^-$ to stabilize electrophilic cations is well documented,[107–115] and also becomes apparent through the three recently accomplished structure determinations of $[H_3O][Sb_2F_{11}]$,[106] $[Hg(CO)_2][Sb_2F_{11}]_2$,[15b] and $[Ir(CO)_5Cl]$-$[Sb_2F_{11}]_2$.[13] Significant secondary interionic and intermolecular contacts exist in *cis*-$Pd(CO)_2(SO_3F)_2$[18b] and *mer*-$Ir(CO)_3$-$(SO_3F)_3$[19] between the C atom of the CO group and an F[13, 15b] or O atom[18b, 19] of $[Sb_2F_{11}]^-$ or the SO_3F^- group. These contacts increase the lattice energies in salts with metal carbonyl cations,[11–16] and transform the molecular structures into three-dimensional networks.[17–19]

Species with linear[15, 16] and square-planar[14, 18] coordination geometries violate the 18e rule, and are without precedent

in metal carbonyl chemistry.[1, 26, 17] Equally unprecedented are the observed spectroscopic properties [$\tilde{\nu}$(CO), f_{CO}, δ_C, and $^1J_{M,C}$), with $\tilde{\nu}$(CO) values of up to 2300 cm^{-1}, greatly exceeding the 2143-cm^{-1} value for free CO.[84] These observations, together with closely related structural and spectroscopic properties of the isoelectronic cyanometalates,[72-75] point to a dominant OC → M σ-bond in the homoleptic metal carbonyl cations. The more the oxidation state of the metallic center decreases, the more π-backbonding of the typical metal carbonyls increases, until with the carbonyl metalates it becomes dominant. The gradual, charge-dependent change in σ/π bonding components and the CO charge polarization is reflected in gradual trends in spectroscopic properties.

With the carbonyl derivatives now known for transition metals from Groups 4 through 11, together with those of mercury and a number of main group metals,[40, 81-85] some of limited thermal stability, it becomes clear that the CO ligand, known for 130 years, is still capable of producing surprises.

The developments and results described in this review have occurred rapidly and unexpectedly. So unexpectedly, in fact, that in a future-oriented summary of metal carbonyl chemistry projected into the next century and published in 1990 in honor of the 100th anniversary of the discovery of $Ni(CO)_4$,[5] there is no mention of homoleptic metal carbonyl cations. It may therefore seem somewhat inappropriate for us now also to engage in prognoses for the future, although these are limited to homoleptic metal carbonyl cations. In the next few years we can expect:

1. The complete characterization of homoleptic metal carbonyl cations with paramagnetic ground states, so far a rarity in metal carbonyl chemistry.[1, 7, 26, 27] The most promising candidates are octahedral cations of the type $[M(CO)_6]^{3+}$ (M = Fe, Ru, Os). As previously noted, prospects are less bright for the formation of highly charged cations such as $[Pt(CO)_6]^{4+}$ and $[Au(CO)_6]^{5+}$ in the form of thermally stable salts.
2. At rhodium there still is a gap in the 4d series, although such cations as $[Ru(CO)_6]^{2+}$,[11] $[Pd(CO)_4]^{2+}$,[14] and $[Ir(CO)_6]^{3+}$[13] are known for the neighboring metals. We hope to close this gap with the square-planar $[Rh(CO)_4]^+$. A number of preliminary investigations indicate its existence (synthesis, IR, Raman, ^{13}C NMR spectra).[203] Together with the potentially analogous cations $[Ir(CO)_4]^+$ and $[Au(CO)_4]^{3+}$, as well as the known $[M(CO)_4]^{2+}$ (M = Pd, Pt),[14] comparisons within a systematic study would be possible.
3. Chemical properties of the $[M(CO)_n]^{m+}$ species have so far not been studied systematically. Attempted substitution of CO by other small molecular Lewis bases such as NO, N_2, or PF_3 would appear to be a worthwhile undertaking. A start has already been made with $[Au(PF_3)_2][Sb_2F_{11}]$.[143]
4. General opinion in the inorganic literature, as well as the modes of thought of teachers and students, is likely to change. The excessive importance previously attributed to π-backbonding and the 18-electron rule in metal carbonyl chemistry has been called into question. The homoleptic metal carbonyl cations described here make it clear that, in addition to the undoubtedly important organometallic chemistry, there exists also a much older coordination chemistry of carbon monoxide. It will be more difficult in the future to classify Schützenberger's[28, 29] pioneering efforts as laboratory curiosities. Our field of observation has been considerably widened.

We wish to express our deepest appreciation to our diplom, masters, and doctoral students for their engaged efforts over the course of many years, which constitute the basis for the developments described here. Equally important has been a collaboration with crystallographers from Simon Fraser University and the University of British Columbia, as well as discussions with numerous colleagues. All those who have participated in this work are acknowledged by name in the cited literature. We have received financial support from various sources: the Deutsche Forschungsgemeinschaft, The Fond der Chemischen Industrie (H. W.), the Natural Science and Engineering Research Council of Canada (F. A.), and the North Atlantic Treaty Organization in the form of a joint research grant. F. A. expresses his thanks to the Alexander von Humboldt Stiftung for a research prize 1995/96 and H. W. to the Degussa AG for gifts in the form of noble metal powders.

Received: January 22, 1997 [A202IE]
German version: *Angew. Chem.* **1997**, *109*, 2506-2530
Translated by Dr. W. E. Russey, Huntingdon, PA

[1] F. A. Cotton, G. Wilkinson, *Advanced Inorganic Chemistry*, 5th ed., Wiley, New York, **1988**, pp. 58, 1021.
[2] a) R. J. Gillespie, *Molecular Geometry*, van Nostrand, London, **1972**; b) R. J. Gillespie, I. Hargittai, *The VSEPR Model of Molecular Geometry*, Allyn and Bacon, Boston, **1991**; c) R. J. Gillespie, *Chem. Soc. Rev.* **1992**, *22*, 59-69; d) R. J. Gillespie, E. A. Robinson, *Angew. Chem.* **1996**, *108*, 539-560; *Angew. Chem. Int. Ed. Engl.* **1996**, *35*, 495-514.
[3] E. W. Abel, S. P. Tyfield, *Adv. Organomet. Chem.* **1970**, *8*. 117-165.
[4] W. Beck, K. Sünkel, *Chem. Rev.* **1988**, *88*, 1405-1421.
[5] L. Mond, C. Langer, F. Quincke, *J. Chem. Soc.* **1890**, 749-753.
[6] M. Moskovits, G. A. Ozin, *Cryochemistry*, Wiley, New York, **1976**, p. 261.
[7] J. E. Ellis, *Adv. Organomet. Chem.* **1990**, *31*, 1-51.
[8] L. Weber, *Angew. Chem.* **1994**, *106*, 1131-1132; *Angew. Chem. Int. Ed. Engl.* **1994**, *33*, 1077-1078.
[9] a) F. Aubke, *J. Fluorine Chem.* **1995**, *72*, 195-201; b) F. Aubke, C. Wang, *Coord. Chem. Rev.* **1994**, *137*, 483-524.
[10] a) G. A. Olah, G. K. S. Prakash, J. Sommer, *Superacids*, Wiley, New York, **1985**; b) T. A. O'Donnel, *Superacids and Acidic Melts as Inorganic Chemical Reaction Media*, VCH, Weinheim, **1993**.
[11] C. Wang, B. Bley, G. Balzer-Jöllenbeck, A. R. Lewis, S. C. Sui, H. Willner, F. Aubke, *J. Chem. Soc. Chem. Commun.* **1995**, 2071-2072.
[12] B. Bley, H. Willner, F. Aubke, *Inorg. Chem.* **1997**, *36*, 158-160.
[13] C. Bach, H. Willner, C. Wang, S. J. Rettig, J. Trotter, F. Aubke, *Angew. Chem.* **1996**, *108*, 2104-2106; *Angew. Chem. Int. Ed. Engl.* **1996**, *35*, 1974-1976.
[14] G. Hwang, C. Wang, F. Aubke, H. Willner, M. Bodenbinder, *Can. J. Chem.* **1993**, *71*, 1532-1536.
[15] a) H. Willner, M. Bodenbinder, C. Wang, F. Aubke, *J. Chem. Soc. Chem. Commun.* **1994**, 1189-1190; b) M. Bodenbinder, G. Balzer-Jöllenbeck, H. Willner, R. J. Batchelor, F. W. B. Einstein, C. Wang, F. Aubke, *Inorg. Chem.* **1996**, *35*, 82-92.
[16] a) H. Willner, F. Aubke, *Inorg. Chem.* **1990**, *29*, 2195-2200; b) H. Willner, J. Schaebs, G. Hwang, F. Mistry, R. Jones, J. Trotter, F. Aubke, *J. Am. Chem. Soc.* **1992**, *114*, 8972-8980.
[17] C. Wang, M. Bodenbinder, H. Willner, S. J. Rettig, J. Trotter, F. Aubke, *Inorg. Chem.* **1994**, *33*, 779-786.
[18] a) G. Hwang, C. Wang, M. Bodenbinder, H. Willner, F. Aubke, *J. Fluorine Chem.* **1994**, *66*, 159-166; b) C. Wang, H. Willner, M. Bodenbinder, R. J. Batchelor, F. W. B. Einstein, F. Aubke, *Inorg. Chem.* **1994**, *33*, 3521-3525.
[19] C. Wang, A. R. Lewis, R. J. Batchelor, F. W. B. Einstein, H. Willner, F. Aubke, *Inorg. Chem.* **1996**, *35*, 1279-1285.
[20] C. Wang, G. Hwang, S. C. Siu, B. Bley, M. Bodenbinder, C. Bach, H. Willner, F. Aubke, *Eur. J. Solid State Inorg. Chem.* **1996**, *33*, 917-930.
[21] C. Wang, S. C. Siu, G. Hwang, C. Bach, B. Bley, M. Bodenbinder, H. Willner, F. Aubke, *Can. J. Chem.* **1996**, *74*, 1952-1958.
[22] a) S. A. Brewer, J. H. Holloway, E. G. Hope, P. G. Watson, *J. Chem. Soc. Chem. Commun.* **1992**, 1577-1578; b) S. A. Brewer, A. K. Brisdon, J. H. Holloway, E. G. Hope, L. A. Peck, P. G. Watson, *J. Chem. Soc. Dalton Trans.* **1995**, 2945-2948.
[23] a) H. Werner, *Angew. Chem.* **1990**, *102*, 1109-1121; *Angew. Chem. Int. Ed. Engl.* **1990**, *29*, 1077-1089; b) W. A. Herrmann, *Chemie Unserer Zeit* **1988**, *22*, 113-122.

[24] W. Hieber, *Adv. Organomet. Chem.* **1970**, *8*, 1–28.
[25] W. Hieber, W. Beck, G. Braun, *Angew. Chem.* **1960**, *72*, 795–801.
[26] F. P. Pruchnick, *Organometallic Chemistry of Transition Elements*, Plenum, New York, **1990**.
[27] R. H. Crabtree, *The Organometallic Chemistry of The Transition Metals*, 2nd ed., Wiley, New York, **1994**.
[28] P. Schützenberger, *Bull. Soc. Chim. Fr.* **1868**, *10*, 188–192.
[29] P. Schützenberger, *C. R. Hebd. Sceances Acad. Sci.* **1870**, *70*, 1134–1136.
[30] J. Browning, P. L. Goggin, R. J. Goodfellow, M. G. Norton, A. J. M. Rattray, B. F. Taylor, J. Mink, *J. Chem. Soc. Dalton Trans.* **1977**, 2061–2067.
[31] a) W. Manchot, *Chem. Ber.* **1925**, *58*, 2518–2521; b) W. Manchot, J. König, *Chem. Ber.* **1926**, *59*, 883–886.
[32] W. Manchot, H. Gall, *Chem. Ber.* **1925**, *58*, 2175–2178.
[33] P. G. Jones, *Z. Naturforsch. B* **1982**, *37*, 823–824.
[34] W. Manchot, J. König, *Chem. Ber.* **1927**, *60*, 2183–2184.
[35] M. I. Bruce, *J. Organomet. Chem.* **1972**, *44*, 209–226.
[36] a) S. C. Thripathy, S. C. Srivastava, R. P. Mani, A. K. Shrimal, *Inorg. Chim. Acta* **1976**, *17*, 257–290; b) M. N. Vargaftik, T. A. Stromnova, I. I. Moiseev, *Russ. J. Inorg. Chem.* **1980**, *25*, 127–132.
[37] F. Calderazzo, *Pure Appl. Chem.* **1978**, *50*, 49–53.
[38] F. Calderazzo, D. Belli Dell'Amico, *Pure Appl. Chem.* **1986**, *58*, 561–566.
[39] F. Calderazzo, *J. Organomet. Chem.* **1990**, *400*, 303–320.
[40] J. E. Ellis, W. Beck, *Angew. Chem.* **1995**, *107*, 2695–2697; *Angew. Chem. Int. Ed. Engl.* **1995**, *34*, 2489–2491.
[41] a) E. O. Fischer, K. Fichtel, K. Öfele, *Chem. Ber.* **1961**, *94*, 1200–1204; b) *ibid.* **1962**, *95*, 249–252.
[42] W. Hieber, F. Lux, C. Herget, *Z. Naturforsch. B* **1965**, *20*, 1159–1165.
[43] a) W. Hieber, T. Kruck, *Angew. Chem.* **1961**, *73*, 580; b) *Z. Naturforsch. B* **1961**, *16*, 709–713.
[44] a) E. W. Abel, R. A. N. McLean, S. P. Tyfield, P. S. Braterman, A. P. Walker, P. J. Hendra, *J. Mol. Spectrosc.* **1969**, *30*, 29–50; b) R. A. N. McLean, *Can. J. Chem.* **1974**, *52*, 213–215.
[45] D. M. Bruce, J. E. Holloway, D. R. Russel, *J. Chem. Soc. Dalton Trans.* **1978**, 1627–1631.
[46] a) W. Hieber, G. Bader, *Chem. Ber.* **1928**, *61*, 1717–1722; b) W. Hieber, G. Bader, K. Ries, *Z. Anorg. Allg. Chem.* **1930**, *190*, 193–214; c) W. Hieber, G. Bader, K. Ries, *ibid.* **1931**, *201*, 329–336; d) W. Hieber, A. Wirsching, *ibid.* **1940**, *245*, 35–58.
[47] W. Hieber, H. Stallmann, *Chem. Ber.* **1942**, *75*, 1472–1480.
[48] H. W. Sternberg, A. R. Friedel, S. L. Shufler, I. J. Wender, *J. Am. Chem. Soc.* **1955**, *77*, 2675–2677.
[49] W. Hieber, V. Frey, P. John, *Chem. Ber.* **1967**, *100*, 1961–1974.
[50] a) D. Buhl, L. E. Snyder, *Nature* **1970**, *228*, 267–269; b) W. Klemperer, *ibid.* **1970**, *227*, 1230; c) E. Hirota, Y. Endo, *J. Mol. Spectrosc.* **1988**, *127*, 527–534.
[51] a) R. C. Woods, T. A. Dixon, R. J. Saykally, P. G. Szanto, *Phys. Rev. Lett.* **1975**, *35*, 1269–1272; b) R. C. Woods, R. J. Saykally, T. G. Anderson, T. A. Dixon, P. G. Szanto, *J. Chem. Phys.* **1981**, *75*, 4256–4260; c) R. C. Woods, *Philos. Trans. R. Soc. London A* **1988**, *324*, 141–146.
[52] a) K. C. Lee, F. Aubke, *Inorg. Chem.* **1979**, *18*, 389–393; b) *ibid.* **1980**, *19*, 119–122.
[53] P. K. Hurlburt, O. P. Anderson, S. H. Strauss, *J. Am. Chem. Soc.* **1991**, *113*, 6277–6278.
[54] P. K. Hurlburt, J. J. Rack, S. F. Dec, O. P. Anderson, S. H. Strauss, *Inorg. Chem.* **1993**, *32*, 373–374.
[55] J. J. Rack, B. Moasser, J. D. Gargulak, W. L. Gladfelter, H. D. Hochheimer, S. H. Strauss, *J. Chem. Soc. Chem. Commun.* **1994**, 685–686.
[56] P. K. Hurlburt, J. J. Rack, J. S. Luck, S. F. Dec, J. D. Webb, O. P. Anderson, S. H. Strauss, *J. Am. Chem. Soc.* **1994**, *116*, 10003–10014.
[57] Y. Souma, J. Iyoda, H. Sano, *Inorg. Chem.* **1976**, *15*, 968–970.
[58] C. D. Desjardins, D. B. Edwards, J. Passmore, *Can. J. Chem.* **1979**, *57*, 2714–2715.
[59] J. J. Rack, J. D. Webb, S. H. Strauss, *Inorg. Chem.* **1996**, *35*, 277–278.
[60] M. Håkansson, S. Jagner, *Inorg. Chem.* **1990**, *29*, 5241–5243.
[61] H. V. R. Dias, H.-L. Lu, *Inorg. Chem.* **1995**, *34*, 5380–5382.
[62] H. V. R. Dias, W. Jin, *J. Am. Chem. Soc.* **1995**, *117*, 11381–11382.
[63] H. V. R. Dias, W. Jin, *Inorg. Chem.* **1996**, *35*, 3694–3698.
[64] A. G. Orpen, L. Brammer, F. H. Allen, O. Kennard, D. G. Watson, R. Taylor, *J. Chem. Soc. Dalton Trans.* **1989**, pp. 1–83.
[65] a) I. D. Brown, *Structure and Bonding in Crystals, Vol. 2* (Eds.: M. O'Keeffe, A. Navrotsky), Academic Press, New York, **1981**; b) I. D. Brown, D. Altermatt, *Acta Crystallogr. Sect. B* **1985**, *41*, 244–247.
[66] M. O'Keeffe, N. E. Brese, *J. Am. Chem. Soc.* **1991**, *113*, 3226–3229.
[67] N. W. Alcock, *Adv. Inorg. Chem. Radiochem.* **1972**, *15*, 1–58.
[68] A. Bondi, *J. Phys. Chem.* **1964**, *68*, 441–451.
[69] R. Ercoli, F. Calderazzo, A. Alberola, *J. Am. Chem. Soc.* **1960**, *82*, 2966–2967.
[70] a) R. P. M. Werner, H. E. Podall, *Chem. Ind. (London)* **1961**, 144–145; b) R. P. M. Werner, A. H. Filbey, S. A. Manastyrskyi, *Inorg. Chem.* **1964**, *3*, 298–300; c) F. Calderazzo, U. Englert, G. Pampaloni, G. Pellizzi, R. Zamboni, *ibid.* **1983**, *22*, 1865–1867.
[71] a) K. M. Chi, S. R. Frerichs, S. B. Philson, J. E. Ellis, *J. Am. Chem. Soc.* **1988**, *110*, 303–304; b) J. E. Ellis, K. M. Chi, *ibid.* **1990**, *112*, 6022–6025.
[72] B. M. Chadwick, A. G. Sharpe, *Adv. Inorg. Chem. Radiochem.* **1966**, *8*, 83–176.
[73] A. G. Sharpe, *The Chemistry of the Cyano Complexes of the Transition Metals*, Academic Press, London, **1976**, and references therein.
[74] a) J. Hvoslef, *Acta Chem. Scand.* **1958**, *12*, 1568–1574; b) R. C. Seccombe, C. H. L. Kennard, *J. Organomet. Chem.* **1969**, *18*, 243–247.
[75] L. H. Jones, *Inorganic Vibrational Spectroscopy, Vol. 1*, Marcel Dekker, New York, **1971**.
[76] P. J. Macquer, *Mem. Math. Phys.* **1752**, *2*, 87.
[77] a) A. B. Burg, H. J. Schlesinger, *J. Am. Chem. Soc.* **1937**, *59*, 780–787; b) S. H. Bauer, *ibid.* **1937**, *59*, 1804–1812.
[78] a) L. H. Little, *Infrared Spectra of Adsorbed Species*, Academic Press, London, **1966**, p. 67; b) N. Sheppard in *Vibrational Spectra of Adsorbates* (Ed.: R. F. Willis), Springer, **1979**, p. 169.
[79] a) D. M. Antonelli, B. B. Tjaden, J. M. Stryker, *Organometallics* **1994**, *13*, 763–765; b) Z. Guo, D. C. Swenson, A. S. Guram, R. F. Jordan, *ibid.* **1994**, *13*, 766–773; c) W. A. Howard, T. M. Trnka, G. Parkin, *ibid.* **1995**, *14*, 4037–4039, and references therein.
[80] M. A. Lynn, B. E. Bursten, *Inorg. Chim. Acta* **1995**, *229*, 437–443.
[81] M. Tacke, Ch. Klein, D. J. Stufkens, A. Oskam, P. Jutzi, E. A. Bunte, *Z. Anorg. Allg. Chem.* **1993**, *619*, 865–868.
[82] P. Selg, H. H. Brintzinger, R. A. Anderson, I. T. Horvath, *Angew. Chem.* **1995**, *107*, 877–879; *Angew. Chem. Int. Ed. Engl.* **1995**, *34*, 791–793.
[83] J. Parry, E. Carmona, S. Coles, M. Hursthouse, *J. Am. Chem. Soc.* **1995**, *117*, 2649–2650.
[84] R. B. King, M. B. Bisnette, *J. Organomet. Chem.* **1967**, *8*, 287–297.
[85] J. E. Bercaw, H. H. Brintzinger, *J. Am. Chem. Soc.* **1971**, *93*, 2045–2046.
[86] a) J. Knight, M. J. Mays, *J. Chem. Soc. A* **1970**, 711–714; b) A. J. Deeming, B. F. G. Johnson, J. Lewis, *ibid.* **1970**, 2967–2971; c) A. A. Koridze, O. A. Kizas, N. M. Astakhowa, P. V. Petrovskii, Y. K. Grishin, *J. Chem. Soc. Chem. Commun.* **1981**, 853–855; d) P. Yarrow, P. C. Ford, *J. Organomet. Chem.* **1981**, *214*, 115–118; e) S. A. Brewer, J. H. Holloway, E. G. Hope, *J. Fluorine Chem.* **1995**, *70*, 167–169.
[87] a) R. C. Thompson in *Inorganic Sulphur Chemistry* (Ed.: G. Nickless), Elsevier, Amsterdam, **1978**, p. 587–606; b) A. W. Jache, *Adv. Inorg. Chem. Radiochem.* **1974**, *16*, 177–200; c) R. C. Gillespie, *Acc. Chem. Res.* **1968**, *1*, 202–209; d) J. Barr, R. J. Gillespie, R. C. Thompson, *Inorg. Chem.* **1964**, *3*, 1149–1156.
[88] F. B. Dudley, G. H. Cady, *J. Am. Chem. Soc.* **1957**, *79*, 513–515.
[89] D. Zhang, C. Wang, F. Mistry, B. Powell, F. Aubke, *J. Fluorine Chem.* **1996**, *76*, 83–89.
[90] W. V. Cicha, F. G. Herring, F. Aubke, *Can. J. Chem.* **1990**, *68*, 102–108.
[91] F. Aubke, M. S. R. Cader, F. Mistry in *Synthetic Fluorine Chemistry* (Eds.: G. A. Olah, R. D. Chamber, G. K. S. Prakash), Wiley, **1992**, pp. 43–86.
[92] D. Zhang, S. J. Rettig, J. Trotter, F. Aubke, *Inorg. Chem.* **1995**, *34*, 3153–3164.
[93] M. Lustig, *Inorg. Chem.* **1965**, *4*, 1828–1830.
[94] a) M. Adelhelm, W. Bacher, E. G. Höhn, E. Jacob, *Chem. Ber.* **1991**, *124*, 1559–1561; b) G. Schatte, H. Willner, D. Hoge, E. Knözinger, O. Schrems, *J. Phys. Chem.* **1989**, *93*, 6025–6028; c) W. Thiel, personal communication; d) A. Lupinetti, S. Fau, G. Frenking, S. H. Strauss, *J. Phys. Chem.*, in press.
[95] R. D. Kemmit, D. W. A. Sharp, in *Advances in Fluorine Chemistry, Vol. 4* (Eds.: M. Stacey, J. C. Tatlow, A. G. Sharpe), Butterworths, London, **1965**, pp. 210–211.
[96] a) C. J. Hoffman, W. L. Jolly, *J. Phys. Chem.* **1951**, *61*, 1574–1575; b) A. A. Woolf, N. N. Greenwood, *J. Chem. Soc.* **1950**, 2200–2204.
[97] a) H. H. Hyman, L. Quarterman, M. Kilpatrick, J. J. Katz, *J. Phys. Chem.* **1961**, *65*, 123–127; b) R. J. Gillespie, K. C. Moss, *J. Chem. Soc. A* **1966**, 1170–1175.
[98] P. L. Fabré, J. Devynk, B. Tremillon, *Chem. Rev.* **1982**, *82*, 591–614.
[99] *Carbonium Ions, Vol. I–V* (Eds.: G. A. Olah, P. von R. Schleyer), Wiley-Interscience, New York, **1968**, **1970**, **1972**, **1973**, and **1976**.
[100] R. Jost, J. Sommer, *Rev. Chem. Intermed.* **1988**, *9*, 171–199.
[101] R. C. Thompson, J. Barr, R. J. Gillespie, J. B. Milne, R. A. Rothenbury, *Inorg. Chem.* **1965**, *4*, 1641–1649.
[102] P. A. W. Dean, R. J. Gillespie, *J. Am. Chem. Soc.* **1970**, *92*, 2362–2364.
[103] G. A. Olah, A. Commeyras, *J. Am. Chem. Soc.* **1969**, *91*, 2929–2942.
[104] D. Brunel, A. Germain, A. Commeyras, *Nouv. J. Chim.* **1978**, *2*, 275–283.
[105] D. Zhang, M. Heubes, G. Hägele, F. Aubke, submitted.
[106] D. Zhang, S. J. Rettig, J. Trotter, F. Aubke, *Inorg. Chem.* **1996**, *35*, 6113–6130.
[107] C. G. Davies, R. J. Gillespie, P. R. Ireland, J. M. Sowa, *Can. J. Chem.* **1974**, *52*, 2048–2052.
[108] A. J. Edwards, P. Taylor, *J. Chem. Soc. Dalton Trans.* **1973**, 2150–2153.
[109] A. J. Edwards, P. Taylor, *J. Chem. Soc. Dalton Trans.* **1975**, 2174–2177.
[110] D. E. McKee, C. J. Adams, A. Zalkin, N. Bartlett, *J. Chem. Soc. Chem. Commun.* **1973**, 26–28.
[111] V. M. McRae, R. D. Peacock, D. R. Russel, *Chem. Commun.* **1969**, 62–63.
[112] H. B. Miller, H. W. Baird, C. L. Bramlett, W. K. Templeton, *J. Chem. Soc. Chem. Commun.* **1972**, 262–264.

[113] W. A. S. Nandana, J. Passmore, P. S. White, C.-M. Wong, *Inorg. Chem.* **1990**, *29*, 3529–3538.
[114] D. Mootz, K. Bartmann, *Angew. Chem.* **1988**, *100*, 424–425; *Angew. Chem. Int. Ed. Engl.* **1988**, *27*, 391–392.
[115] a) A. J. Edwards, G. R. Jones, R. J. C. Sills, *Chem. Commun.* **1968**, 1527–1528; b) A. J. Edwards, G. R. Jones, *J. Chem. Soc. A* **1971**, 2318–2320.
[116] K. C. Lee, F. Aubke, *Inorg. Chem.* **1984**, *23*, 2124–2130.
[117] G. Hwang, M. Bodenbinder, H. Willner, F. Aubke, *Inorg. Chem.* **1993**, *32*, 4667–4669.
[118] S. P. Mallela, S. Yap, J. R. Sams, F. Aubke, *Inorg. Chem.* **1986**, *25*, 4327–4328.
[119] D. Zhang, S. J. Rettig, J. Trotter, F. Aubke, *Inorg. Chem.* **1995**, *34*, 2269–2270.
[120] W. W. Wilson, F. Aubke, *J. Fluorine Chem.* **1979**, *13*, 431–445.
[121] O. Ruff, J. Zedner, H. Knoch, H. Graf, *Chem. Ber.* **1909**, *42*, 4021–4044.
[122] L. Kolditz in *Halogen Chemistry* (Ed.: V. Gutman), Academic Press, **1967**, p. 665.
[123] H. J. Emeléus, J. F. Wood, *J. Chem. Soc.* **1948**, 2183–2188.
[124] T. Birchall, P. A. W. Dean, B. D. Valle, R. J. Gillespie, *Can. J. Chem.* **1973**, *51*, 667–673.
[125] a) D. Gantar, I. Leban, B. Frlec, J. H. Holloway, *J. Chem. Soc. Dalton Trans.* **1987**, 2379–2383; b) M. S. R. Cader, F. Aubke, *Can. J. Chem.* **1989**, *67*, 1700–1707.
[126] P. C. Leung, F. Aubke, *Inorg. Chem.* **1978**, *17*, 1765–1772.
[127] M. F. A. Dove, A. F. Clifford in *Chemistry in Non-Aqueous Ionizing Solvents, Vol. 1, 2* (Eds.: J. Jander, H. Spandau, C. C. Addison), Vieweg, Wiesbaden, **1971**.
[128] N. M. Doherty, N. W. Hoffman, *Chem. Rev.* **1991**, *91*, 553–573.
[129] K. C. Lee, F. Aubke, *J. Fluorine Chem.* **1982**, *19*, 501–516.
[130] a) D. M. Bruce, J. H. Holloway, D. R. Russel, *J. Chem. Soc. Chem. Commun.* **1973**, 321; b) D. M. Bruce, J. H. Holloway, D. R. Russel, *J. Chem. Soc. Dalton Trans.* **1978**, 1627–1631.
[131] D. M. Bruce, J. H. Holloway, D. R. Russel, *J. Chem. Soc. Dalton Trans.* **1978**, 64–68.
[132] J. H. Holloway, J. B. Senior, A. C. Szary, *J. Chem. Soc. Dalton Trans.* **1987**, 741–745.
[133] A. J. Hewitt, J. H. Holloway, R. D. Peacock, J. B. Raynor, I. L. Wilson, *J. Chem. Soc. Dalton Trans.* **1976**, 579–583.
[134] S. P. Mallela, F. Aubke, *Inorg. Chem.* **1985**, *24*, 2969–2975.
[135] S. H. Strauss, *Chem. Rev.* **1993**, *93*, 927–942.
[136] C. D. Desjardins, J. Passmore, *J. Fluorine Chem.* **1975**, *6*, 379–388.
[137] M. R. Rosenthal, *J. Chem. Educ.* **1973**, *50*, 331–335.
[138] D. A. Van Leirsburg, C. W. De Kock, *J. Phys. Chem.* **1974**, *78*, 134–142.
[139] P. L. Timms, *Adv. Inorg. Chem. Radiochem.* **1972**, *14*, 121–171.
[140] G. A. Ozin, A. Van der Voet, *Acc. Chem. Res.* **1973**, *6*, 313–318.
[141] a) R. J. Puddephatt, *The Chemistry of Gold*, Elsevier, Amsterdam, **1980**; b) R. J. Puddephatt in *Comprehensive Coordination Chemistry, Vol. 7* (Ed.: G. Wilkinson), Pergamon, Oxford, **1987**, p. 861.
[142] a) P. Pyykkö, *Chem. Rev.* **1988**, *88*, 563–594, and references therein; b) P. Pyykkö, J. P. Desclaux, *Acc. Chem. Res.* **1979**, *12*, 276–281; c) K. S. Pitzer, *ibid.* **1979**, *12*, 271–276; d) P. Schwerdtfeger, *J. Am. Chem. Soc.* **1989**, *111*, 7261–7262.
[143] B. Bley, M. Bodenbinder, G. Balzer, H. Willner, G. Hägele, F. Mistry, F. Aubke, *Can. J. Chem.* **1996**, *74*, 2392–2394.
[144] J. F. Nixon, *Adv. Inorg. Chem. Radiochem.* **1985**, *29*, 41–141.
[145] M. Bodenbinder, B. Bley, G. Balzer, F. Mistry, G. Haegele, H. Willner, F. Aubke, unpublished.
[146] P. S. Braterman, *Metal Carbonyl Spectra*, Academic Press, New York, **1975**.
[147] a) S. F. A. Kettle, *Top. Curr. Chem.* **1977**, *71*, 111–148; b) L. M. Haines, M. H. B. Stiddard, *Adv. Inorg. Chem. Radiochem.* **1969**, *12*, 83–133; c) C. De La Cruce, N. Sheppard, *J. Mol. Struct.* **1990**, *224*, 141–161.
[148] D. M. Adams in *Metal-Ligand and Related Vibrations*, Arnold, London, **1967**, pp. 84–181.
[149] K. Nakamoto, *Infrared and Raman Spectra of Inorganic and Coordination Compounds*, 4th ed., Wiley, New York, **1986**, pp. 291–308.
[150] S. P. Arnesen, H. M. Seip, *Acta Chem. Scand.* **1966**, *20*, 2711–2727.
[151] K. P. Huber, G. Herzberg, *Molecular Spectra and Molecular Structure. Constants of Diatomic Molecules*, van Nostrand, New York, **1979**.
[152] L. Pauling, *The Nature of the Chemical Bond*, 2nd ed., Cornell University Press, Ithaca, **1948**, p. 410.
[153] R. D. Shannon, C. T. Prewitt, *Acta Crystallogr. Sect. B* **1969**, *25*, 925–946.
[154] R. Shannon, *Acta Crystallogr. Sect. A* **1976**, *32*, 751–767.
[155] J. Perron, A. L. Beauchamp, *Inorg. Chem.* **1984**, *23*, 2853–2859.
[156] R. J. Lancashire, *Comprehensive Coordination Chemistry, Vol. 7* (Ed.: G. Wilkinson), Pergamon, Oxford, **1987**, pp. 775–851.
[157] R. G. Wilkins, *Kinetics and Mechanism of Reactions of Transition Metal Complexes*, 2nd ed., VCH, Weinheim, **1991**, Chapter 4, and references therein.
[158] D. M. Van Seggen, P. K. Hurlburt, M. D. Noirot, O. P. Anderson, S. H. Strauss, *Inorg. Chem.* **1993**, *31*, 1423–1430.
[159] G. A. Lawrance, *Chem. Rev.* **1986**, *86*, 17–33.
[160] A. Veldkamp, G. Frenking, *Organometallics* **1993**, *12*, 4613–4622.
[161] R. J. Batchelor, F. W. B. Einstein, I. D. Gay, J.-H. Gu, M. B. Pinto, *J. Organomet. Chem.* **1991**, *411*, 147–157.
[162] V. Subramanian, K. Seff, *Acta Crystallogr. Sect. B* **1980**, *36*, 2132–2135.
[163] S. H. Strauss, personal communication.
[164] a) K. O. Christe, P. Charpin, E. Soulie, R. Bougon, J. Fawcett, D. R. Russel, *Inorg. Chem.* **1984**, *23*, 3756–3766; b) E. M. Larson, K. D. Abney, A. C. Larson, G. P. Eller, *Acta Crystallogr. Sect. B* **1991**, *47*, 206–209.
[165] D. A. Johnson, *Some Thermodynamic Aspects of Inorganic Chemistry*, Cambridge University Press, Cambridge, **1968**, pp. 17–36.
[166] A. S. Goldman, K. Krogh-Jespersen, *J. Am. Chem. Soc.* **1996**, *118*, 12159–12166.
[167] M. Y. Darrensbourg, *Prog. Inorg. Chem.* **1985**, *33*, 221–274.
[168] a) H. O. Kalinowski, S. Berger, S. Braun, *^{13}C NMR Spectroscopy*, Wiley-Interscience, New York, **1988**; b) B. E. Mann, *J. Chem. Soc. Dalton Trans.* **1973**, 1973–2012; c) B. E. Mann, *Adv. Organomet. Chem.* **1974**, *12*, 135–213.
[169] a) F. A. Cotton, C. S. Kraihanzel, *J. Am. Chem. Soc.* **1962**, *84*, 4432–4438; b) C. S. Kraihanzel, F. A. Cotton, *Inorg. Chem.* **1963**, *2*, 533–540.
[170] G. Winnewisser, A. G. Maki, D. R. Johnson, *J. Mol. Spectrosc.* **1971**, *39*, 149–158.
[171] E. F. Pearson, R. A. Creswell, M. Winnewisser, G. Winnewisser, *Z. Naturforsch. A* **1976**, *31*, 1394–1397.
[172] G. Herzberg, *Spectra of Diatomic Molecules*, 2nd ed., van Nostrand, New York, **1950**.
[173] A. F. Wells, *Structural Inorganic Chemistry*, Oxford University Press, London, **1962**, p. 733.
[174] G. R. Field, W. F. Sherman, *J. Chem. Phys.* **1967**, *47*, 2378–2389.
[175] K. F. Purcell, *J. Am. Chem. Soc.* **1967**, *89*, 247–250.
[176] a) H. Siebert, *Anwendungen der Schwingungsspektroskopie in der Anorganischen Chemie*, Springer, Berlin, **1966**; b) *Landolt-Börnstein, Structure Data of Free Polyatomic Molecules, Vol. 7*, Springer, Berlin, **1976**; c) *Landolt-Börnstein, Structure Data of Free Polyatomic Molecules. Vol. 15*, Springer, Berlin, **1987**.
[177] a) P. D. Mallison, D. C. McKean, J. H. Holloway, I. A. Oxton, *Spectrochim. Acta Part A* **1975**, *31*, 143–159; b) H. G. Schnöckel, *J. Mol. Struct.* **1975**, *29*, 123–131; c) J. S. Kwiatkowski, J. Leszczynski, *J. Mol. Spectrosc.* **1993**, *157*, 540–543.
[178] W. P. Griffith, G. T. Turner, *J. Chem. Soc. A* **1970**, 858–862.
[179] J. P. Mathieu, H. Poulet, *Spectrochim. Acta* **1963**, *19*, 1966.
[180] R. J. Gillespie, R. Hulme, D. A. Humphreys, *J. Chem. Soc. A* **1971**, 3574–3578.
[181] a) B. Bley, W. Thiel, K. Wieghardt, H. Willner, F. Aubke, unpublished; b) V. Jonas, W. Thiel, unpublished; c) A. W. Ehlers, Y. Ruiz-Motales, E. J. Baerends, T. Ziegler, *J. Am. Chem. Soc.*, submitted; d) R. K. Szilagyi, G. Frenking, *Organometallics*, in press.
[182] E. R. Davidson, K. L. Kunze, F. B. C. Machado, S. J. Chakravorty, *Acc. Chem. Res.* **1993**, *26*, 628–635, and references therein.
[183] J. S. Dewar, *Bull. Soc. Chim. Fr.* **1951**, *18*, C71–C79.
[184] J. Chatt, L. A. Duncanson, *J. Chem. Soc.* **1953**, 2939–2947.
[185] J. Chatt, R. G. Wilkins, *J. Chem. Soc.* **1952**, 2622–2626.
[186] S. Yamamoto, H. Kashiwagi, *Chem. Phys. Lett.* **1993**, *205*, 306–312.
[187] M. R. A. Blomberg, P. E. M. Siegbahn, T. J. Lee, A. P. Rendell, J. E. Rice, *J. Chem. Phys.* **1991**, *95*, 5898–5905.
[188] S. Smith, I. H. Hillier, W. von Niessen, M. F. Guest, *Chem. Phys.* **1989**, *135*, 357–361.
[189] T. Ziegler, V. Tschinke, C. Ursenbach, *J. Am. Chem. Soc.* **1987**, *109*, 4825–4837.
[190] R. L. Williamson, M. B. Hall, *Int. J. Quantum Chem.* **1987**, *21*, 503–512.
[191] M. B. Hall, R. F. Fenske, *Inorg. Chem.* **1972**, *11*, 1619–1624.
[192] N. A. Beach, M. B. Gray, *J. Am. Chem. Soc.* **1968**, *90*, 5713–5721.
[193] K. Pierlot, J. Verhulst, P. Verbeke, L. G. Vanquickenborn, *Inorg. Chem.* **1989**, *28*, 3059–3063.
[194] L. A. Barnes, M. Rosi, C. W. Bauschlicher, Jr., *J. Chem. Phys.* **1990**, *93*, 609–624.
[195] F. Meyer, Y.-M. Chen, P. B. Armentrout, *J. Am. Chem. Soc.* **1995**, *117*, 4071–4081.
[196] C. J. Ballhausen, *Introduction to Ligand Field Theory*, McGraw-Hill, New York, **1962**.
[197] B. N. Figgis, *Introduction to Ligand Fields*, Wiley, New York, **1966**.
[198] a) R. G. Pearson, *Inorg. Chem.* **1984**, *23*, 4675–4679; b) R. G. Parr, R. A. Donelly, M. Levy, W. E. Palke, *J. Chem. Phys.* **1978**, *68*, 3801–3807.
[199] *Compendium of Chemical Terminology, IUPAC Recommendations*, Blackwell, Oxford, **1987**.
[200] G. A. Olah, *Angew. Chem.* **1995**, *107*, 1519–1532; *Angew. Chem. Int. Ed. Engl.* **1995**, *34*, 1393–1405.
[201] T. A. O'Donnell, *Chem. Soc. Rev.* **1987**, *16*, 1–43.
[202] a) R. J. Gillespie, J. Passmore, *Adv. Inorg. Chem. Radiochem.* **1975**, *17*, 49–87; b) R. J. Gillespie, J. Passmore, *Int. Rev. Sci. Inorg. Chem. Ser. Two* **1975**, 121–136.
[203] C. Bach, C. Wang, H. Willner, F. Aubke, unpublished.

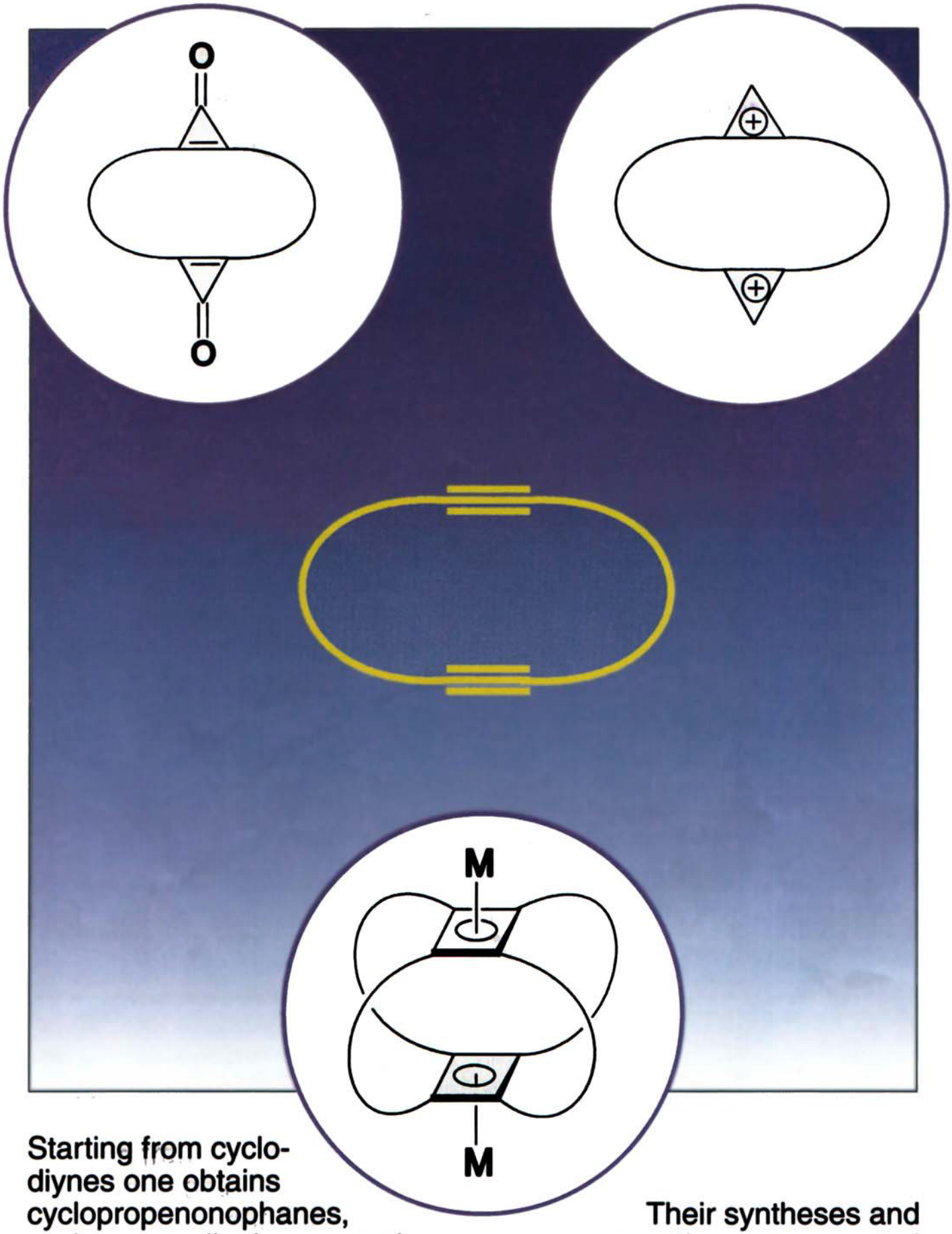

Starting from cyclodiynes one obtains cyclopropenonophanes, cyclopropenyliophanes, and cyclobutadienosuperphanes.

Their syntheses and properties are presented in the following review.

Phanes with Three- and Four-Membered Rings as Building Elements

Rolf Gleiter* and Martin Merger

Dedicated to Professor Roald Hoffmann on the occasion of his 60th birthday

The systematic integration of the small 2π- and 4π-electron systems cyclopropenylium ion, cyclopropenone, oxocyclobutenylium ion, and cyclobutadiene into phane chemistry was initiated only a few years ago. $[n_2]$Cyclopropenyliophanes, $[n_2]$cyclopropenonophanes, metal-capped $[n_4]$cyclobutadienosuperphanes, and other new families of double-decker phane species became available from cycloalkydiynes through special methods of double [2+1]cycloaddition with carbenes and metal complex induced dimerization by double [2+2]-cycloaddition. Phane-specific structural features were elucidated by X-ray structural analyses. Cyclic voltammetry and PE spectroscopy as well as MO calculations revealed considerable interactions between closely spaced π-electron systems. Decapping cyclobutadienosuperphanes formally extended the synthetic principle to threefold [2+2]cycloadditions resulting in $[n_4]$-bridged tricyclo[4.2.0.0^{3,5}]octa-3,7-dienes, which represent a new type of cage compounds. Moreover, completion to fourfold [2+2]addition was achieved with the photoinduced transformation of $[3_4]$-bridged tricyclo[4.2.0.0^{3,5}]octa-3,7-diene into propella$[3_4]$cubane.

Keywords: carbenes · cycloalkadiynes · cyclophanes · small ring systems · transition metals

1. Introduction

Phane chemistry has grown to an important discipline that attracts both synthetic and physical chemists. Bridged arenes such as [*n*]cyclophanes furnish information about the sensitivity of aromatic character with respect to deformation of the planar conjugated π system. $[n_m]$Phanes in which two or more π moieties are stacked onto each other at a fixed distance provide structures that are well suited for studying interactions between the functional groups. Furthermore, they are excellent host molecules and models for enzyme reactions.[1, 2]

Successful strategies were developed for constructing theoretically as well as aesthetically attractive target molecules to enrich our repertoire of synthetic methods and to increase our understanding of chemical bonds.[1, 2] Therefore, the original meaning of the term "phanes" was extended by several groups. It now comprises not only arenes but also nonaromatic π systems and even cycloaliphatic molecules ("aliphanes")[1] which are cyclically combined with the same or other functions, for example tricyclo[4.2.2.2^{2,5}]dodeca-1,5-diene[3] and cycloocta-1,5-diyne[4] (which are viewed as etheno- and acetylenosuperphanes)[5, 6] as well as $[2_2]$cyclooctatetraenophanes[7] and adamantanophanes.[8, 9]

However, this does not mean that the exploratory potential of phane chemistry in the area of arenes principally ebbs. Besides numerous fascinating contributions on phanes of benzenoid arenes, there has been little work done on the non-benzenoid 6π-electron arenes[1] cyclopentadienide ion, tropylium ion, and tropone, although they offer additional chances for studying charge–charge and dipole–dipole interactions when incorporated into $[n_2]$phanes.

It is even more remarkable that for decades the aromatic units used were limited to 6π and higher systems; the smallest are cyclopentadienide and five-membered heterocycles[1] such as thiophene, pyrrole, and furan. The 2π-electron species cyclopropenylium ion, an outstanding representative for Hückel aromaticity $[(4n+2)\pi, n = 0]$, was not introduced into phane chemistry until recently. Likewise, the related cyclopropenone and four-membered metal-stabilized systems oxocyclobutenyl cation and cyclobutadiene were widely neglected.

Now, however, we are able to present a first review on methods which were developed for synthesizing double-decker phanes of all these small π systems from cycloalkadiynes as well as on results of structural studies and investigations of intramolecular interactions between the π moieties. Moreover, we report some synthetically attractive transformations of cyclobutadienosuperphanes.

[*] Prof. Dr. R. Gleiter, Dr. M. Merger
Organisch-chemisches Institut der Universität
Im Neuenheimer Feld 270, D-69120 Heidelberg (Germany)
Fax: Int. code +(6221) 54-4205

 © WILEY-VCH Verlag GmbH, D-69451 Weinheim, 1997 0570-0833/97/3622-2427 $ 17.50+.50/0

2. $[n_2]$Phanes with C_3 Cycles

2.1. Cyclopropenonophanes

At a first glance the syntheses of $[n_2]$cyclopropenono-acetyleno-phanes and $[n_2]$cyclopropenonophanes may appear feasible by simple addition of dichlorocarbene to cyclic diynes and hydrolysis. This procedure was described by Breslow et al.[10-12] and Dehmlow[13,14] for preparing monofunctional cyclopropenones from alkynes. Although this method allowed ready access to a series of dialkylcyclopropenones, it was judged as preparatively "weak"[15] until 1992. The precursors used for generating dichlorocarbene (sodium trichloroacetate in dimethoxyethane at 80 °C[10-12] or ethyl trichloroacetate/sodium methoxide,[10,16] chloroform/sodium hydroxide under phase transfer conditions,[17,18] chloroform/potassium *tert*-butoxide[13,14,19] in petroleum ether or benzene and bromotrichloromethane/methyl lithium in diethyl ether at −95 °C[20,21]) afford the desired 3,3-dichlorocyclopropenes with only low selectivity. Particularly with alkynes **1**, in which there are CH_2 groups next to the triple bond, the yields of cyclopropenones **2** obtained after hydrolysis are on average a few percent.[10-12,15] Among the numerous side products α-chloroalkenylcyclopropenones **3**[13,22] and dichlorocyclobutenones **4**,[11,14] which result from insertion of a second dichlorocarbene, were identified.

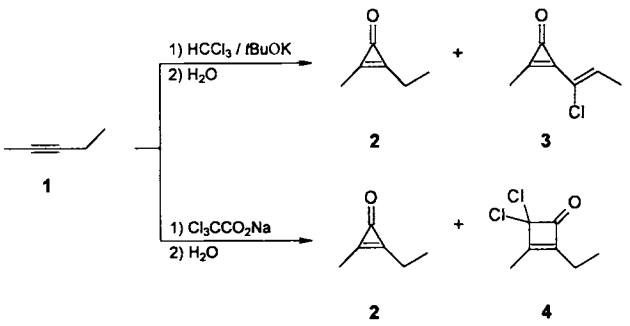

For the essentially more demanding cyclopropenation of difunctional acetylenic substrates, we turned our attention to complexes **5** ($n \leq 3$),[23-25] which are prepared from $HCCl_3$ and BuLi in THF [Eq. (1)], as an alternative source of dichlorocarbene. According to Köbrich et al.[26] and Hoeg et al.,[27] complexes **5** are considerably more stable than $LiCCl_3$ in diethyl ether.[20] They exhibit markedly reduced reactivity in alkene cyclopropanations, and, to our knowledge, have not been used in alkyne cyclopropenations. In our experiments with monoalkynes, the dichlorocarbenoid species **5** proved to be an effective cyclopropenation agent; side reactions were excluded to a large extent, and, thus, the selectivity raised in general to over 70%.[28]

$$HCCl_3 + BuLi \xrightarrow[-78\,^\circ C]{THF} Cl-\overset{Cl}{\underset{Cl}{C}}-Li \cdot 3\,THF \quad (1)$$

5

2.1.1. $[n_2]$Cyclopropenono-acetyleno-phanes

Treatment of cyclodeca-1,6-diyne (**6**), cyclododeca-1,7-diyne (**7**), and cyclotetradeca-1,8-diyne (**8**) with an equimolar amount of $LiCCl_3$ in THF at −78 to −10 °C allowed mono-dichlorocyclopropenation in about 80% yield, based on 80% conversion. Hydrolysis of the resulting dichlorobicycloalkenynes **9**–**11** in THF at −10 °C led, presumably via ambident chlorocyclopropenylium intermediates,[28] not only to the target compounds $[3_2]$-, $[4_2]$-, and $[5_2]$cyclopropenono-acetyleno-phanes **12**–**14**, but also to cycloalkadiynones **15**–**17** under ring expansion. In no case could a $[n_2]$cyclopropenonophane be detected as a by-product.

Rolf Gleiter, born in 1936 in Stuttgart, Germany, studied chemistry at the Universität Stuttgart and completed his doctoral thesis in 1964 with F. Effenberger. After postdoctoral stays in the U. S. A. with P. von R. Schleyer at Princeton University (1966) and R. Hoffmann at Cornell University (1967–1968), he went to Basel, Switzerland, and completed his habilitation in 1972. In the following year he accepted the position of professor of theoretical organic chemistry at the Technische Hochschule Darmstadt, Germany. Since 1979 he has been professor of organic chemistry at the Universität Heidelberg, Germany. His areas of interests include the interactions in nonconjugated π systems, the syntheses of model compounds, and quantum-chemical calculations.

R. Gleiter

M. Merger

Martin Merger, born in 1965 in Ludwigshafen/Rhein, Germany, studied chemistry at the Universität Heidelberg and, in addition, music (violin, concert exams) at the Hochschule Mannheim. In the group of Rolf Gleiter he completed his doctoral thesis on phanes of small π ring systems. He received a graduate fellowship from the Studienstiftung des deutschen Volkes and was a member of the Graduiertenkolleg "Selektivität und Katalyse in der organischen und metallorganischen Chemie". Since 1996 he has been working in the research department of the BASF AG.

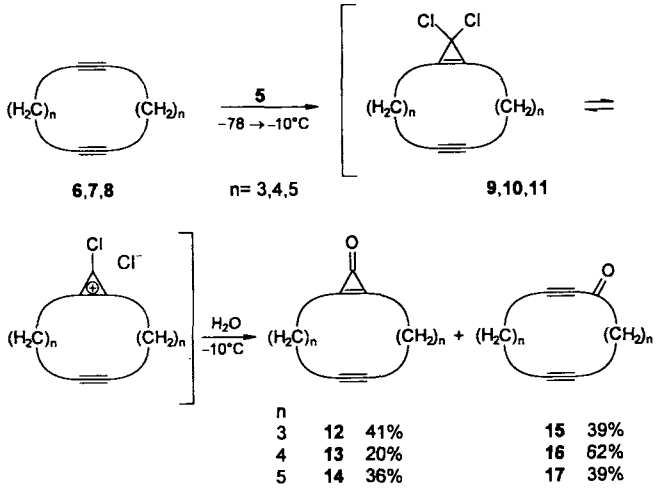

Phanes **12**–**14** enabled us to study the mutual influence of a triple bond and a cyclopropenone moiety (which have similar basis orbital energies) as a function of their intramolecular arrangement for the first time. We recorded the PE spectra of **12**–**14**;[29] the first PE bands of **12** and **13** are shown in Figure 1. In **12** a considerable interaction between the π orbital of

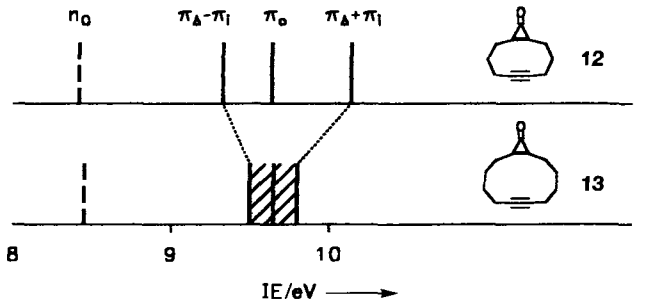

Figure 1. The first PE bands of **12** and **13**.

the cyclopropenone ring (π_A) and the in-plane π orbital of the triple bond (π_i) is observed with a split in π-bond energies of 0.81 eV. According to the corresponding wave functions (Figure 2), theinteraction occurs partly through space and partly

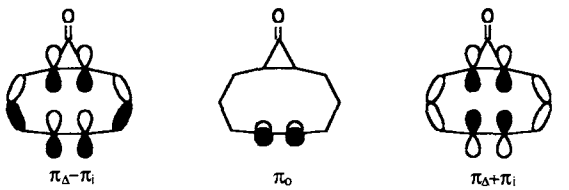

Figure 2. Schematic representation of the π wave functions of **12**.

through bonds. In **13** the distance between the π systems is considerably larger than in **12**, and hence the splitting of the π bands amounts to only 0.3 eV (Figure 1). In **14** there is no interaction, and both functional groups appear to be independent.

We successfully grew single crystals of **12**, and eludicated its molecular structure by X-ray analysis. As shown in Figure 3, **12** exists in a boat conformation in which the central CH_2 groups

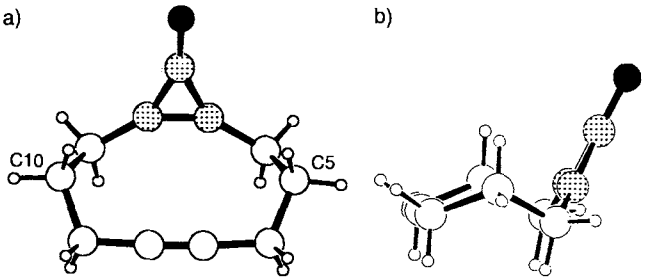

Figure 3. Molecular structure of **12** in the crystal; a) top view, b) side view. The stippled circles represent the carbon atoms of the three-membered rings, and the black circle represents the oxygen atom.

of both C_3H_6 bridges are oriented *syn* to the cyclopropenone moiety.[29] In contrast, the starting material **6** adopts a chair conformation.[30] However, molecular-mechanics calculations on **12** give evidence that a chair and an *anti*-boat conformation are close in energy to the *syn*-boat conformation found in the crystal. The transannular distance between the triple bond and the C–C double bond in **12** is 3.11 Å, which is only slightly larger than the transannular distance between the triple bonds in **6** (2.99 Å). The bond angles at the triple bond in **12** (175°) are larger than in **6** (171.7°). However, enough strain remains to pyramidalize the bridgehead carbons by 3 and 4.3°.

2.1.2. *[n_2]Cyclopropenonophanes*

Our efforts to prepare [n_2]cyclopropenonophanes directly from the cycloalkadiynes **6**–**8** failed, even with a large excess of **5**. After hydrolysis, only **12**–**14** were found in drastically reduced yields. The dichlorocyclopropene unit in intermediates **9**–**11** apparently shields the triple bond against attack by **5** and preferably reacts with additional carbenoid. This problem could be successfully overcome by cyclopropenating the second triple bond of **12**–**14** [see Section 2.1.1; Eq. (2)]. Conventional treat-

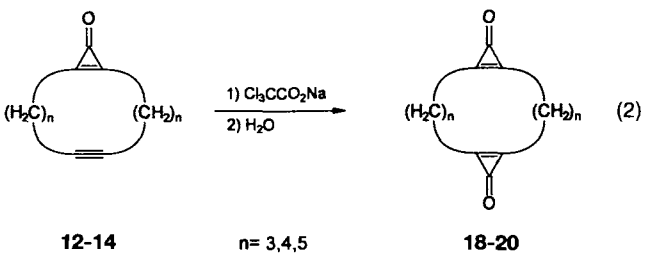

(2)

ment of **12**–**14** with one equivalent of sodium trichloroacetate followed by hydrolysis afforded [n_2]cyclopropenonophanes **18**–**20**[31] in 3–5% yields, which are within the usual range for known syntheses of monofunctional cyclopropenones.[10, 11]

To improve the preparative productivity, we designed an alternative synthesis[31] that is also based on cyclic diynes but does not involve dichlorocyclopropene intermediates. The key step consisted of hydride abstraction from dichlorotricyclodienes such as **21** and **22** to give dichloro[n_2]cyclopropenyliophanes (**23**, **24**), which were converted without isolation into [n_2]cyclopropenonophanes (**18**, **20**) by hydrolysis.

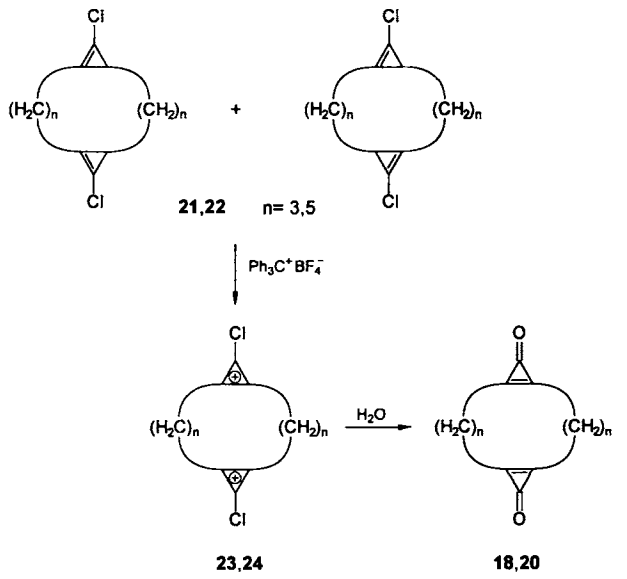

As the first representatives of a dichlorotricycloalkadiene, **21** ($n = 3$) and **22** ($n = 5$) could be prepared in a four-step sequence (Scheme 1) by applying a modified form of methods developed in the chemistry of monofunctional chlorocyclopropenes.[32]

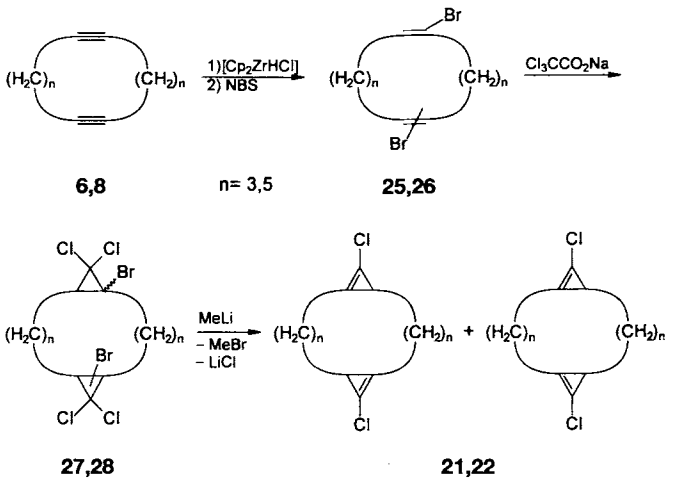

Scheme 1. Synthesis of dichlorotricycloalkadienes **21** and **22**.

Cyclodiynes **6** and **8** were treated with Schwartz's reagent and *N*-bromosuccinimide (NBS) to provide dibromides **25** and **26** (mixtures of isomers), which were submitted to dichlorocyclopropanation with a large excess of sodium trichloroacetate in dimethoxyethane at 80 °C to afford dibromotetrachlorotricycloalkanes **27** and **28** in about 50% yield. Dehalogenation of **27** and **28** with methyl lithium gave **21** and **22** in yields exceeding 90%. Finally, hydride abstraction from **21** and **22** with triphenylmethyl tetrafluoroborate[33] (not optimized) and subsequent hydrolysis resulted in conversion into **18** (13%) and **20** (78%).

The $[n_2]$cyclopropenonophanes **18**–**20** are crystalline, fairly stable compounds that melt at 215 (**18**), 191–193 (**19**), and 131 °C (**20**). The X-ray structure analysis[31] of **18** revealed that there is an interplanar angle of 95.5° between the cyclopropenone moieties (Figure 4). The ten-membered ring adopts

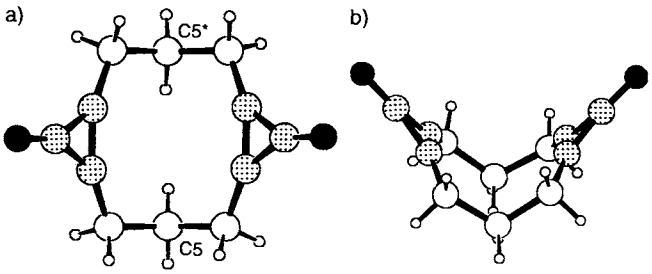

Figure 4. Molecular structure of **18** in the crystal, a) top view, b) side view. The stippled circles represent the carbon atoms of the three-membered rings, and the blacks circles the oxygen atoms.

a boat conformation, in which C5 and C5* are on the same side of the ring and opposite to the cyclopropenone moiety. In this respect **18** differs from the starting compound **12**, in which the carbon atoms C5, C10 and the cyclopropenone unit are on the same side (see Figure 3). The bridgehead atoms of **18** are pyramidalized by 8 and 9°, which indicates considerable strain and is probably partially induced by dipole–dipole interactions. The transannular distance between the bridgehead carbon atoms is 0.4 Å larger than in **12**. Nevertheless, splits of π-orbital energies from 0.53 to 0.83 eV for the low-energy conformers are indicated by ab initio calculations with a 6-31G* basis set (which reproduced remarkably well the interactions in **12** found by PE spectroscopy).[29] The interactions occur mainly through-space and only slightly through-bond (Figure 5). Preliminary MINDO/3 calculations do not indicate significant π–π interactions in **19** and **20**.

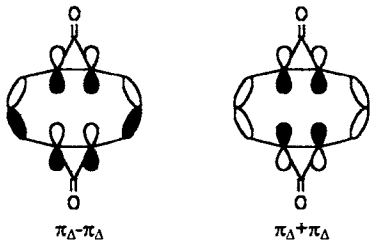

Figure 5. Schematic representation of the wave functions $\pi_\Delta - \pi_\Delta$ and $\pi_\Delta + \pi_\Delta$ of **18**.

2.1.3. *[n_2]Cyclopropenyliophanes*

Although dialkylcyclopropenylium salts (tetrafluoroborates, perchlorates) and their precursors dialkylcyclopropenecarboxylic acids, derived from alkynes, have been known since the 1960s,[34] no difunctional compounds of these types were reported before 1992. Hence, to synthesize $[n_2]$cyclopropenyliophanes on the basis of cycloalkadiynes via tricycloalkadiene dicarboxylic esters and acids, new methodical requirements arose (see Scheme 2).

In the standard method of Rh-catalyzed preparation of monofunctional dialkylcyclopropene-3-ethylcarboxylates from alkynes and diazoethyl acetate,[35–43] low alkyne conversion (<50%), low temperature (0–25 °C), and long reaction times (20 h) are essential for supressing a number of undesired side reactions—such as dimerization of ethoxycarbonylcarbene,[44–46] addition of a second ethoxycarbonylcarbene,[35, 36, 44, 47–51] and ring opening to ethoxycarbonylvinylcarbenes[43, 52]—which compete with the ethoxycarbonylcar-

bene. Evidently, the restriction of conversions to low levels by using high ratios of alkyne functionality to diazoethylacetate (2:1–20:1) cannot be held in the desired double cyclopropenation of cycloalkadiynes to the tricycloalkadiene dicarboxylic esters.

Our investigations with **6–8** showed rate and selectivity of cycloaddition to be strongly dependent on the reaction medium.[53] In ethers (diethyl ether, THF) carbene dimerization predominates, whereas cycloaddition proceeds very slowly and does not exceed the stage of mono-addition.[53, 88b] Both acceleration and increase in efficiency were achieved by initiating the cyclopropenation with small amounts of CH_2Cl_2 (needed to dissolve the solid substrates **6–8**) and performing it at 50–60 °C with continuous addition of diazo ethylacetate. While the "medium" rapidly adopted ester quality, conversion of cyclodiynes approached 100% within half an hour. The *cis*- and *trans*-tricycloalkadienedicarboxylic esters **32–34** were obtained in yields of about 45% along with up to 40% of recycleable mono-adducts **29–31** (bicycloalkenynecarboxylic esters; Scheme 2).[54] Saponification of **32–34** in methanolic KOH[55]

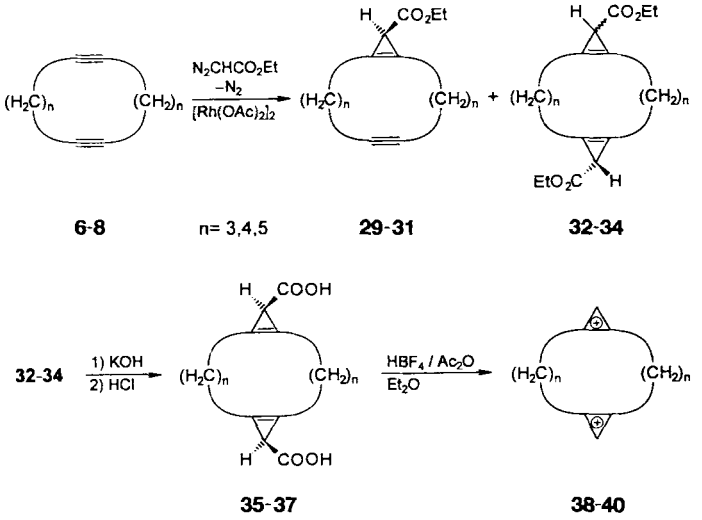

Scheme 2. Synthesis of $[n_2]$cyclopropenyliophanes.

and acidification led to dicarboxylic acids **35–37** without difficulties. It should be pointed out that **29–37**, the "intermediates" on the way to $[n_2]$cyclopropenyliophanes, may themselves be conceived as $[n_2]$phanes, **29–31** as $[n_2]$cyclopropeno-acetylenophanes, and **32–37** as $[n_2]$cyclopropenophanes.

Our attempts to transform **35–37** into cyclopropenyliophanes **38–40** by decarbonylation with aqueous HBF_4 (48%) and acetic anhydride (analogous to the synthesis of dipropylcyclopropenylium tetrafluoroborate)[34] failed. However, the extensive decomposition observed could be decisively suppressed by replacing aqueous HBF_4 with anhydrous HBF_4 in diethylether; this reduces the amount of acetic acid in the reaction mixture.[53, 54] Crystallization from acetonitrile/diethyl ether afforded $[3_2]$-, $[4_2]$-, and $[5_2]$cyclopropenyliophanes **38–40** (tetrafluoroborates) as colorless needles in 60–70% yield. They decompose rapidly upon heating with a color change to dark brown. They may be stored in the solid state at −30 °C without decomposition, but in solution they can be handled for only a short time. Compared to dipropylcyclopropenylium tetrafluoroborate, which melts at 70 °C without decomposition,[34] **38–40** appear to be considerably destabilized phane-specifically due to intramolecular charge–charge interaction.

The ^{1}H NMR signal for the protons of the three-membered rings appears at $\delta \approx 10.4$–10.5, which is characteristic of cyclopropenylio ions.[56] The structure of $[5_2]$cyclopropenylophane **40** could be eludicated by X-ray analysis (Figure 6).[57] Like the cyclopropenone units in **18**, the cyclopropenylium moieties face each other. The angle between the rings is 41.3°.

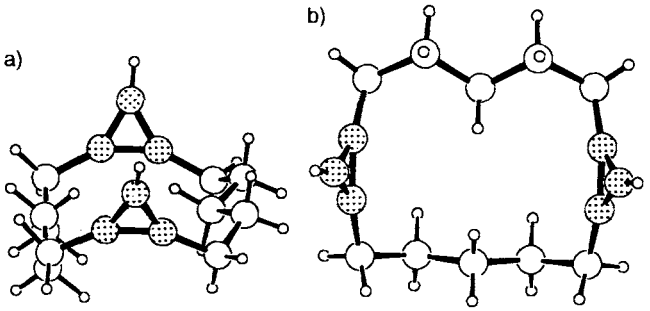

Figure 6. Molecular structure of **40** in the crystal; a) side view, b) top view. The stippled circles represent the carbon atoms of the three-membered rings.

3. $[n_2]$Phanes of C_4 Cycles

3.1. $[n_2]$Oxocyclobutenyl-tricarbonylcobalt-phanes

As outlined by Hughes et al,[58] complexation of disubstituted cyclopropenylium salts **41** with $[Co(CO)_4]^-$ involves selective CO insertion at a position vicinal to the nonsubstituted carbon atom to give 2,3-disubstituted (η^3-1-oxocyclobutenyl)tricarbonylcobalt (**42**). Having made the difunctional $[n_2]$cyclo-

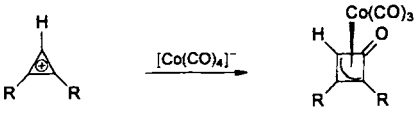

propenyliophanes **38–40** (see 2.1.3), we saw chances for preparing metal-complexed oxocyclobutenylphanes for the first time. This may attract attention also with regard to metal-stabilized cyclobutadienophanes (see Section 3.2), particularly as η^3-oxocyclobutenyl complexes are reported to be useful precursors for cyclobutadiene complexes.[59–61]

We succeeded in synthesizing cobalt complexes of this type from **39** and **40**, but so far not from the $[3_2]$-species **38**[57] (Scheme 3). Differing from single symmetrically disubstituted cyclopropenylium ions, $[n_2]$cyclopropenyliophanes give rise to four isomers, since CO may insert in either of the two C–C single bonds and, thus, somewhat complicate the preparation. Nevertheless, all isomers of $[5_2]$oxocyclobutenyl-tricarbonylcobalt-phane (**43a–d**) were isolable from the product mixture resulting from the reaction of **40** with $[Co(CO)_4]^-$ in acetoni-

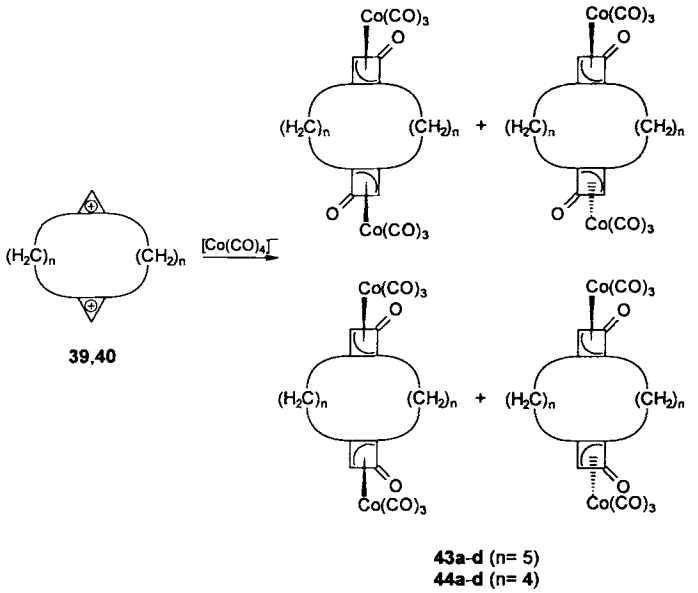

Scheme 3. Synthesis of metal-complexed oxocyclobutenylphanes.

trile. The yellow solids were obtained in an overall yield of 55%. Their IR and ^{1}H NMR data corresponded very well with those reported for the dipropyloxocyclobutenyl complex.[62]

The less stable [4$_2$]cyclopropenyliophane **39** could be complexed in an analogous fashion to yield a mixture of four isomeric [4$_2$]oxocyclobutenyl-tricarbonylcobalt-phanes (**44a–d**) in minor yield (20%). Predominating decomposition of **38** under complexation conditions inhibits transformation to [3$_2$]oxocyclobutenyl-tricarbonylcobalt-phanes in isolable amounts.

3.2. Metal-Capped Cyclobutadienophanes

The simplest single- and double-decker compounds of this type are [6]cyclobutadieno-tricarbonyliron-phane (**46**,[63] a single cyclobutadiene-complex unit 1,3-bridged with an oxohexamethylene chain, Scheme 4) and [2$_2$]1,3-cyclobutadieno-tri-

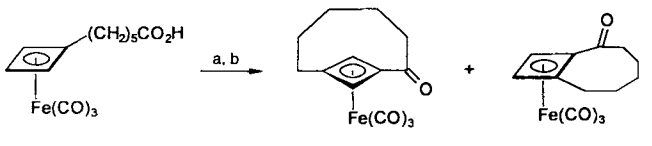

Scheme 4. a) $(COCl)_2$; b) $AlCl_3/CS_2$.

carbonyliron-phane (**54**, Scheme 5).[64] Their syntheses make use of the aromatic properties of the cyclobutadienetricarbonyliron moiety (**48**).[65] Phane **46** was obtained with its isomer **47** upon intramolecular acylation of **45**. Double bridging of two units of **48** to **54** was achieved in a multistep procedure:[64] Chloromethylation of **48** gave **49**, which was coupled directly with Zn or via sulfide **50** with [$Fe_2(CO)_9$] to yield **51**. Diformylation of **51** by the Vilsmeier procedure and coupling of the resulting **52** with Ti^0 led to phane **53**, which could be readily hydrogenated to **54**.

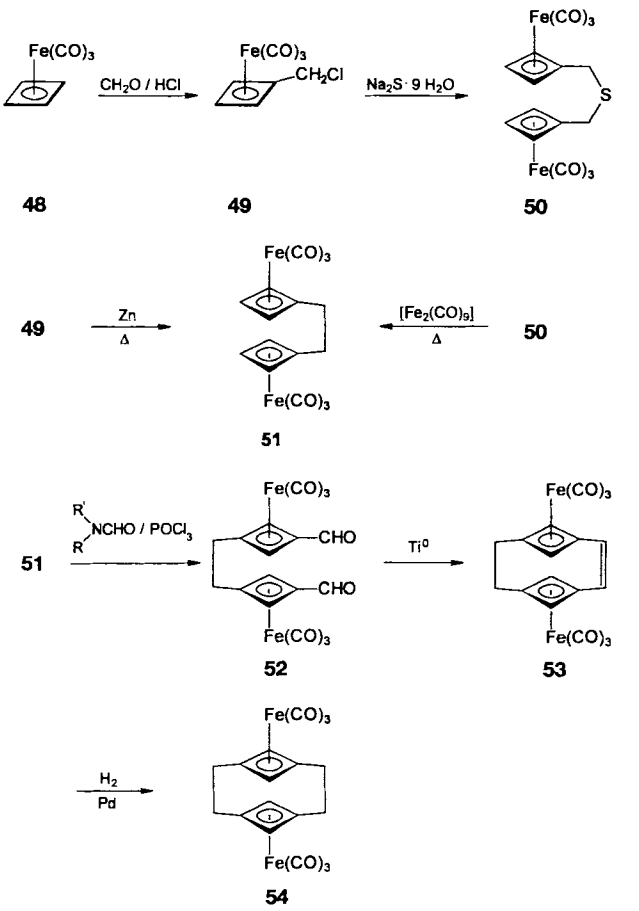

Scheme 5. Synthesis of cyclobutadieno-tricarbonyliron-phane **54**.

An X-ray investigation of **54** revealed that the two parallel metal-capped cyclobutadiene units are separated by 2.70 Å.[64] The methylene groups of the bridges are bent out of the cyclobutadiene planes by 20.6° away from the iron fragments.

3.2.1. Metal-Capped Cyclobutadienosuperphanes

3.2.1.1. One-Pot Synthesis

Our group entered the field of metal-capped cyclobutadienophanes "through the back door".[66] While investigating the electronic structure of cyclodeca-1,6-diyne (**6**),[30] we found that the highest occupied MO is the in-plane orbital $6a_u$. We concluded that side-on attack of an electrophilic metal fragment should be favored over a perpendicular approach. Hence, in the presence of [CpCo(CO)$_2$] (Cp = C_5H_5) **6** might undergo intermolecular reactions to yield oligomers rather than intramolecular [2+2]cycloaddition to give tricyclic metal-capped cyclobutadienes, a species which was discovered earlier by King and co-workers upon transforming higher cyclodiynes such as **7** and **8** with [CpCoL$_2$].[67–69]

Indeed, the main product isolated (12%) from the reaction mixture of **6** and [CpCo(CO)$_2$] in octane was CpCo-stabilized [3$_4$]cyclobutadienosuperphane (**55**)—which apperently results from dimerization of **6** by double [2+2]cycloaddition (Scheme 6, pathway b)—whereas the product of intramolecular [2+2]cycloaddition **57** was formed only to a minor extent (6%, Scheme 6, pathway a).[70,71] As a side product (0.7%) the

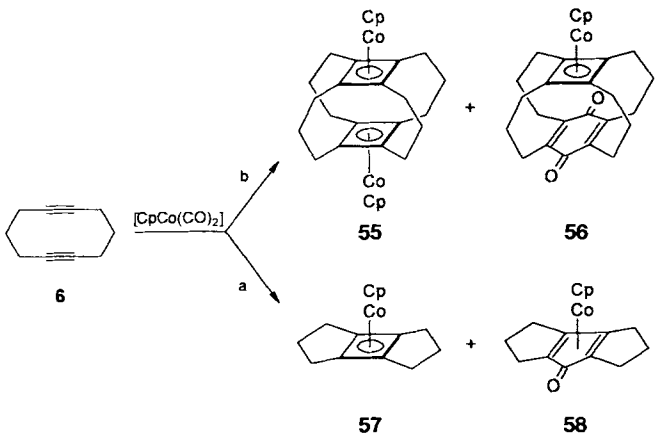

Scheme 6. Products resulting from the reaction of **6** with $[CpCo(CO)_2]$.

mixed superphane **56** was found, which is also generated by dimerization but requires additional CO insertions. On the other hand, when the reaction was carried out in toluene, ketone **58** was formed as well by intramolecular cycloaddition of **6** and CO insertion.[71]

The amazing one-pot synthesis of cyclobutadienosuperphanes inspired us to clarify the scope of its applicability and the essential features as well as to differentiate it from intramolecular reactions. With this goal set, one has to consider that superphane formation has a minor part within a complex system of cycloaddition reactions, and hence single correlations found do not allow general interpretations or definite predictions. Nevertheless, some determining features concerning structures, steric orientations, reactivity, and mechanisms could be outlined.

In principal, the formation of Co-complexed cyclobutadienes of general type **61** from diacetylene complexes **59**, which are made from two acetylene molecules and $[CpCoL_2]$ (similarly with $[Fe(CO)_5]$), is postulated to occur by [2+2+1]cycloaddition to metallacycle **60** and subsequent rearrangement thereof [Eq. (3)].[72] Direct transformation of **59** into **61** does not seem

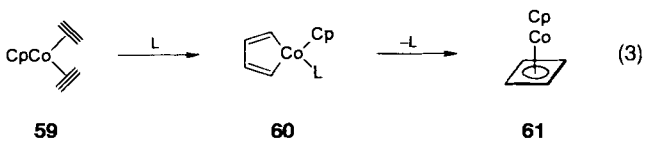

(3)

likely, since molecular orbital calculations predict a high activation energy for this symmetry-forbidden process.[73] The sequence **59** → **60** → **61** is supported by the work of Wakatsuki, Yamazaki et al.,[74] who were able to isolate phosphane-stabilized cobaltoles of type **60** (L = phosphane).

Transferring this sequence to cyclic diynes, one easily recognizes two product-determining alternatives (Scheme 7) for the [2+2+1]cycloaddition: the intramolecular pathway a or the intermolecular pathway b. Along pathway b further transformation of monocyclobutadienediyne intermediates may branch into pathways c (intramolecular) and d (intermolecular) to give cyclobutadienosuperphanes and higher molecular products, respectively. In summary, superphane formation from **6** is interpreted as a result of combining an intermolecular (pathway b) and an intramolecular [2+2]cycloaddition (pathway c; see also Section 3.2.1.2).

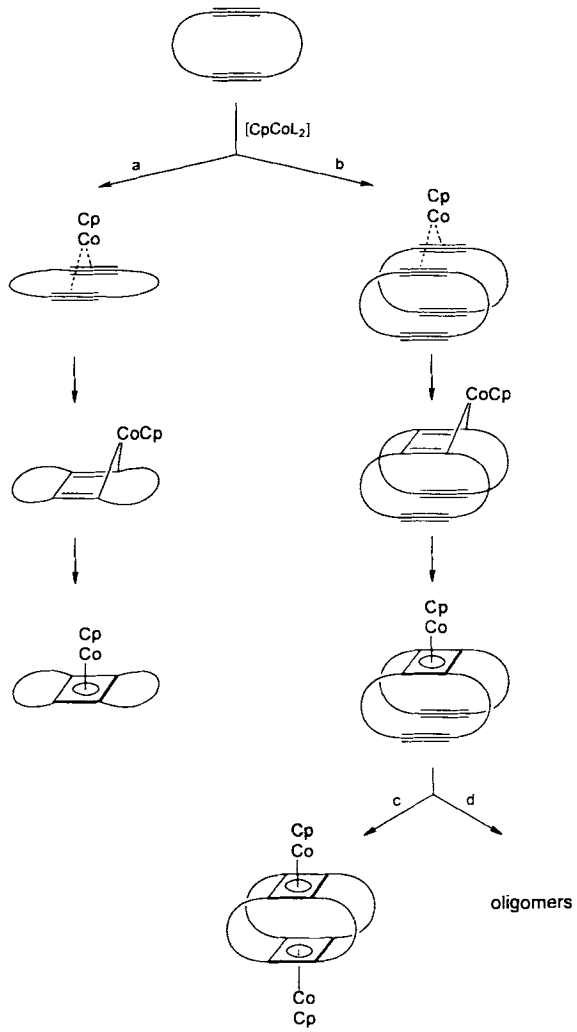

Scheme 7. In analogy to reaction (3), possible progess of the reaction of cyclodiynes with $[CpCoL_2]$.

The structures of **55** and **56** determined by X-ray analysis are shown in Figure 7. The central carbon skeleton in **55** (Figure 7, top)[70] shows C_{4h} symmetry. The two complexed cyclobutadiene units are separated by 2.94 Å. As seen in the top view, the propano bridges adopt a pin-wheel conformation. The mixed superphane **56** (Figure 7, bottom)[71] shows a deformation of the quinone ring, in which the carbonyl groups are twisted out of the plane of the double bonds by 27°. The four propano bridges adopt C_{2v} symmetry.

The preference of pathway b/c in Scheme 7 over pathway a by **6** might not only be due to the relatively high π_i-orbital energy, which favors a side-on approach, but also to the higher activation energy of pathway a (formation of a strained cobaltol species with a double anti-Bredt structure) and to an entropically convenient orientation of the two triple bonds in the intermediate monocyclobutadienediyne of the pathway b/c. These considerations led us to study the ratio of intramolecular versus intermolecular reactions (a/b, c/d) as a function of ring size by allowing 10- to 18-membered cyclodiynes to react with $[CpCoL_2]$ (L_2 = 2CO, cod). However, the investigation of the symmetric cyclodiynes **7**,[67] **8**,[75] **65**,[76] and **67**[76] in addition to **6** (Scheme 8) did not result in a continuous but in an alternating function, which apparently indicates that the conformations of

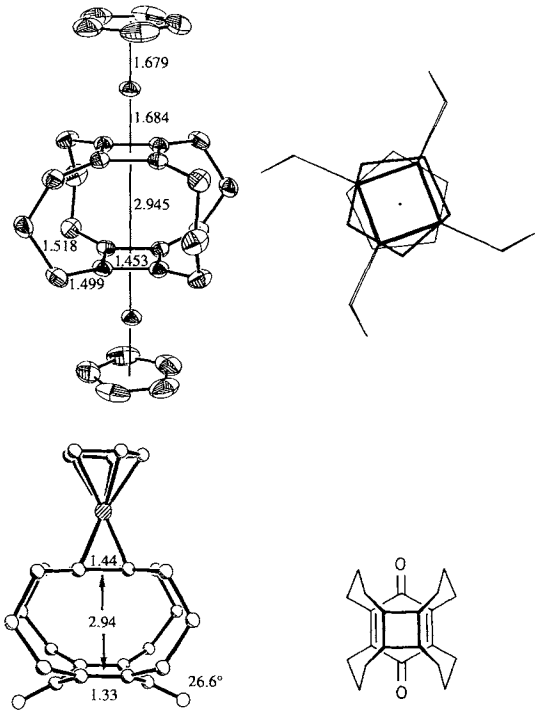

Figure 7. Molecular structure of **55** (top; side and top views) as well as of **56** (bottom; side view and the central skeleton as viewed from the top).

the bridges are predestinational factors. Only those symmetric diynes with an odd number of CH_2 units in the bridges (**6**, **8**, and **67**) gave cyclobutadienosuperphanes (**55**, **63**, and **68**, respectively), the yields of which decreased in the same order. In contrast, from cyclodiynes with an even number of CH_2 bridges (**7**, **65**), no superphanes were obtained. By intramolecular [2+2]cycloaddition (pathway a in Scheme 7) **7** was converted into **62** in strikingly high yield (86%), and **65** afforded tricycle **66** (70%).[75] The unsymmetric cycloundecadiyne **69** (with one odd and one even-numbered bridge)[76] behaved just like **7**, and gave no superphane in addition to the products of intramolecular [2+2]cycloaddition, **70** (32%) and **71**.

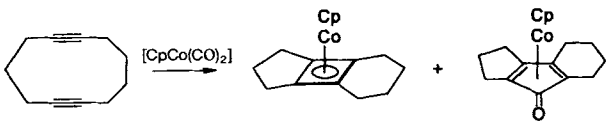

69 **70** **71**

The isomeric cycloundeca-1,5-diyne (**72**), however, follows neither pathway a nor pathway b/c.[77] It is outstanding in two respects: The complexed dimer **73** formed by intermolecular [2+2]cycloaddition (pathway b) could be readily isolated, and trimer **74** was identified as by-product. The mixed phane **74**

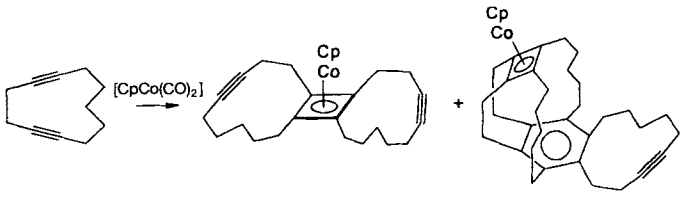

72 **73** **74**

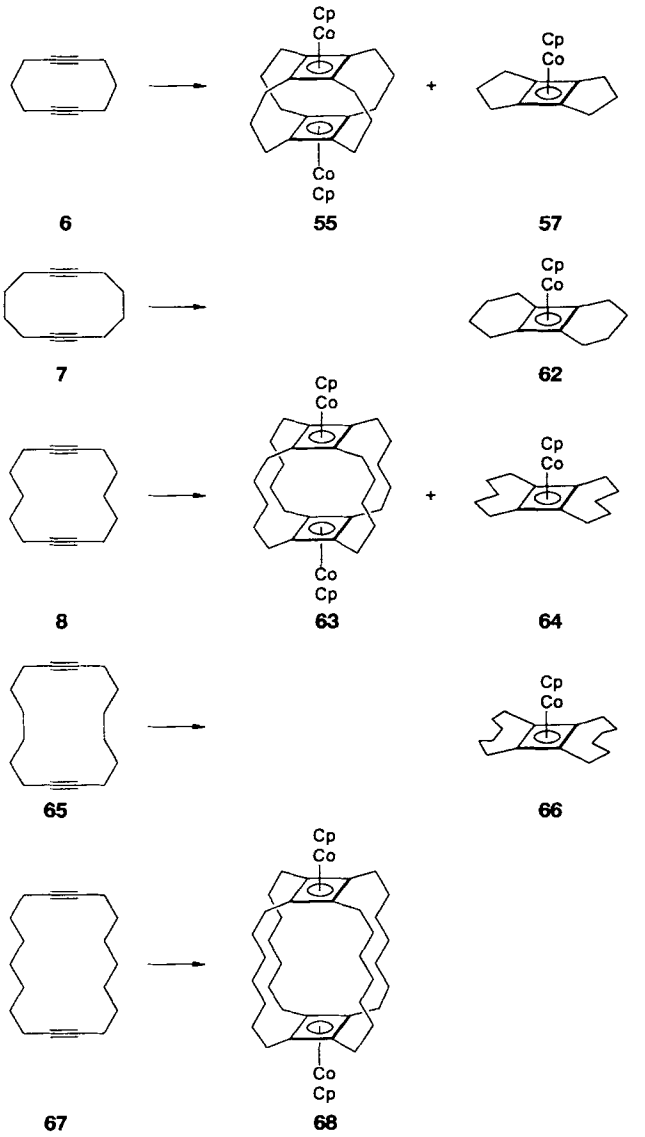

Scheme 8. Progress of the [$CpCoL_2$]-initiated [2+2]cycloadditions of cyclodiynes as a function of their ring size.

presumably results from [2+2+2]cycloaddition (pathway b/d) of **73** and **72**. In view of the strongly steric effects of bulky α substituents in asymmetric monoalkynes which are reported to give mainly C_{2v}-symmetric cyclobutadienes,[74] we synthesized a number of analogously structured, congested cyclic diynes[78] and treated them with [$CpCoL_2$]. In the cases of **75**, **76**, and **79** we obtained superphanes **77**, **78**, and **80** in unusually high yields (40–60%).[79] Clearly, the sila bridges display extensive directing effects and not only entirely block intramolecular [2+2]cycloaddition (pathway a in Scheme 7) but also strongly suppress oligomerization (pathway b/d) in favor of dimerization (pathway b/c). Moreover, the course of CpCo-induced double [2+2]cycloaddition (pathway b/c), leading exclusively to the C_{2v}-symmetric **79**, **78**, **80**, appears to be confined to cobaltol intermediates of type **A**, which apparently are sterically favored over cobaltols of type **B** already in the first stage. If any cobaltol of type **B** is formed, it further reacts selectively along pathway b/d. In contrast to **75**, **76**, and **79**, the less rigid systems **81**–**84** and **89**–**91** react with [CpCo(cod)] along the intramolecular pathway a and yield tricycles **85**–**88** and **92**–**94**[80].

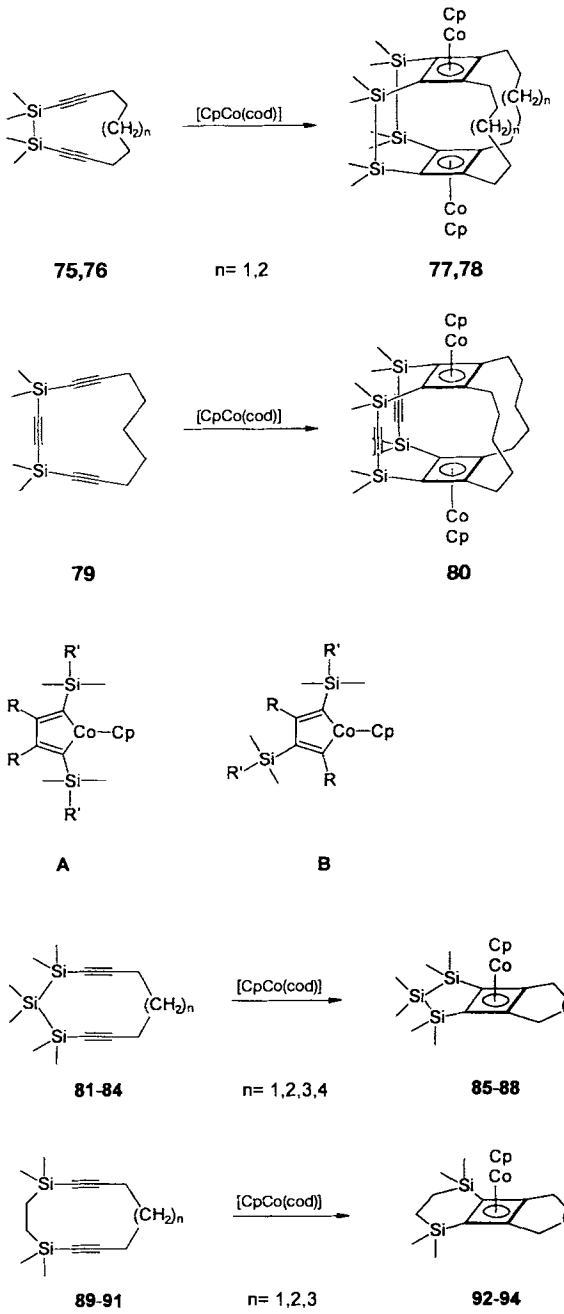

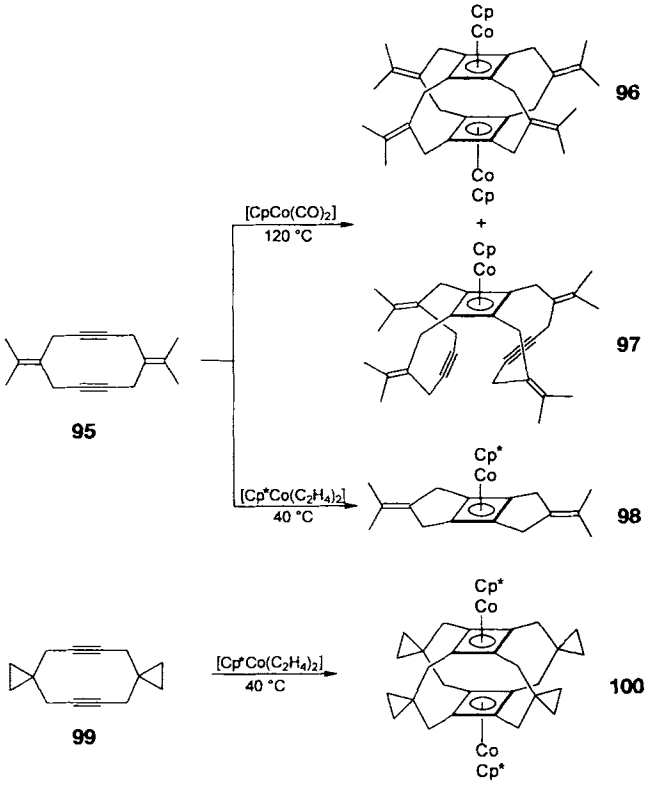

Scheme 9. Comparison of the cyclization behavior of **95** and **99**.

To obtain more information on sterical influences, we studied the 4,9-disubstituted cyclodeca-1,6-diynes **95**[81] and **99**[82] for comparison with the unsubstituted **6** under the assumption that in **95** the side-on approach of the complexing agent (inducing dimerization by pathway b) and in **99** the perpendicular attack (inducing intramolecular cyclization by pathway a) are disfavored. This rationalization seemed to be principally confirmed by the reactions of **99** and **95** with $[Cp^*Co(C_2H_4)_2]$ under mild conditions (40 °C, $Cp^* = C_5Me_5$, Scheme 9). Diyne **99** gave superphane **100** (10%) but no tricyclic product,[82] whereas **95** afforded the tricyclic complex **98** in nearly quantitative yield.[81] However, the reactivity of **95** proved to be strongly dependent on the properties of the complexing agent and the reaction conditions: With $[CpCo(CO)_2]$ and at 120 °C the reaction appeared to be totally reversed from pathway a to pathway b; superphane **96** (10%) and additionally **97** (2%), which is apparently the intermediate for pathway b/c[81] to **96**, were isolated.

Concerning the complexing agents, we found that the yield of superphanes of type **55** can be improved considerably by introducing electron-withdrawing substituents (formyl and carboxylic ester groups) into the Cp units of either $[CpCo(CO)_2]$ or [CpCo(cod)], thus raising the electrophilic character of the agents.[83] In summary, our investigations teach us that not only structural and electronic properties of the cycloalkadiynes as well of as the cyclobutadienediyne intermediates (pathway b in Scheme 7) but also the reactivity of the complexing agents and the reaction conditions are determining factors for cyclobutadienosuperphane synthesis.

3.2.1.2. Stepwise Synthesis of Cyclobutadienosuperphanes

Although the one-pot dimerization of cyclodiynes allows access to cyclobutadienosuperphanes and has proven to be applicable to a series of different substrates, an additional challenge arose to break its limitations, especially a) to exclude the competing intramolecular cycloadditions, b) to prepare cyclobutadienosuperphanes with even-numbered or different bridges, and c) to cap the phanes with two different metal fragments. Assuming that complexed tricyclic cyclobutadienediynes such as **97** are superphane precursors (see Section 3.2.1.1, Scheme 7, pathway b) and, furthermore, that the conformational influence of bridges is of less importance for pathways c and d than for pathways a and b, we focussed on replacing one of the triple bonds in cyclodiynes with a functional group, which after dimerization according pathway b should allow generation of this triple bond.

This concept proved to be feasible with cyclic ynols.[84] The first stepwise synthesis of a cyclobutadienosuperphane, incorporating different alkylene bridges, is briefly outlined in Scheme 10. 6-Cycloundecynol **101** was heated with [CpCo(cod)]

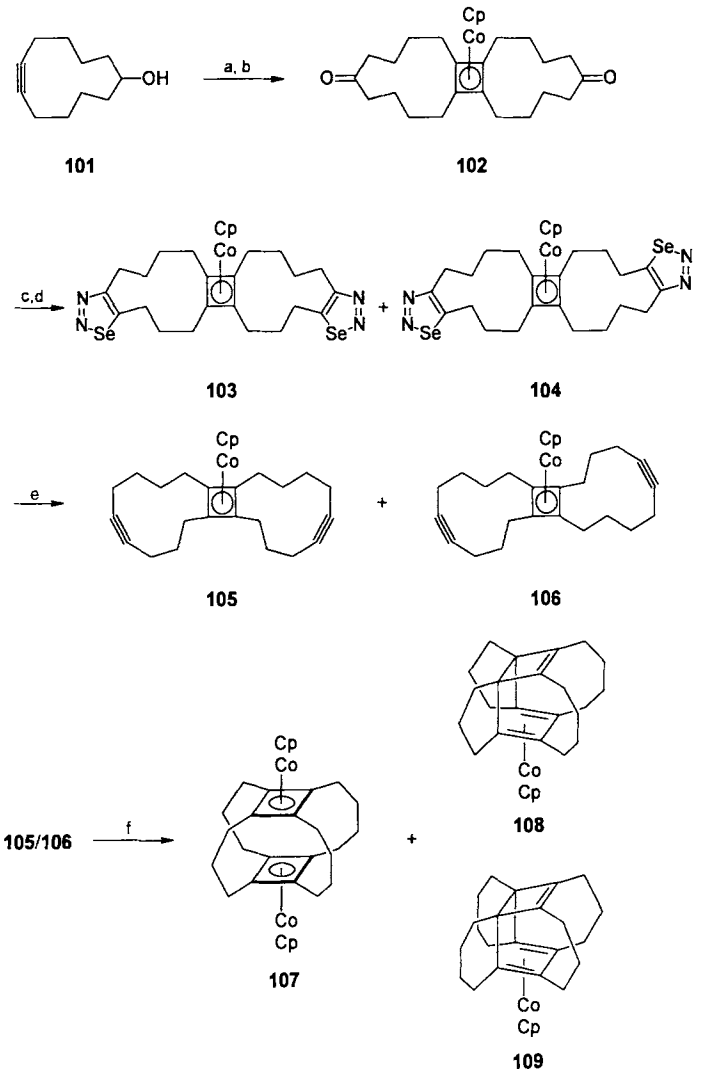

Scheme 10. Synthesis of the first cyclobutadienosuperphane **107** with various alkandiyl bridges. a) [CpCo(cod)], b) Oppenauer oxidation, c) semicarbazide acetate, d) SeO_2/HOAc, e) *n*BuLi/THF, f) $[CpCo(CO)_2]$.

and subsequently oxidized to ketone **102**. Reaction of **102** with semicarbazide followed by oxidation with SeO_2 provided an unseparable mixture of two regioisomeric bis(selenadiazoles) **103** and **104**, which were treated with *n*BuLi in THF at $-40\,^{\circ}C$ to yield a 1:1 mixture of diynes **105** and **106**. Finally, transformation of **105** and **106** with $[CpCo(CO)_2]$ gave superphane **107** and the bridged bicyclo[4.2.0]octa-2,4,7-triene complexes **108** and **109** in a 2:1:1 ratio. The unexpected formation of **108** and **109** is interpreted as resulting from a [4+2]cycloaddition of a cobaltole and a CpCo-bound cyclobutadiene unit. The structures of **107** and **109** were confirmed by X-ray investigations of single crystals. Due to the different lengths of the propano and butano bridges in **107**, the cyclobutadiene units are not parallel; their separation ranges from 3.0 to 3.4 Å.

Apparently, in the mixture **105/106**, only **105** reacts to form a phane. We ascribe this to the parallel orientation of the triple bonds in this molecule; in **106** both triple bonds are probably inclined towards each other.

Similarly to **105** and **106**, tricyclic diyne **110** was synthesized from 5-cyclodecynol.[84] According to X-ray studies of **110**, the acetylene units are parallel to each other at a distance of 6.3 Å. Its reactions are summarized in Scheme 11. Heating **110** and

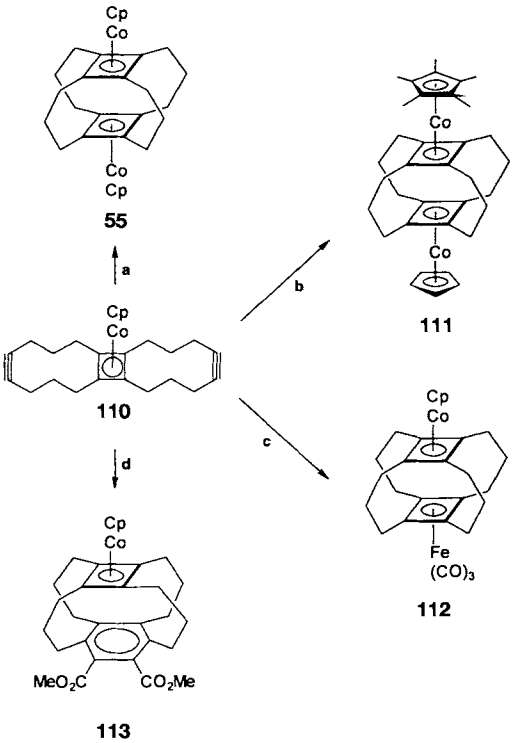

Scheme 11. Reactions of diyne **110**. a) $[CpCo(CO)_2]$, b) $[Cp^*Co(CO)_2]$, c) $[Fe(CO)_5]$, d) $MeO_2C-C\equiv C-CO_2Me$, $[CpCo(CO)_2]$.

$[CpCo(CO)_2]$ for 2 h in toluene gave superphane **55** in high yield (80%) and traces (1%) of **56** (see Scheme 6). With $[Cp^*Co(CO)_2]$ (in decalin) instead of $[CpCo(CO)_2]$, **111** was obtained in 80% yield. From **110** and $[Fe(CO)_5]$ in toluene at reflux, the mixed-capped superphane **112** was formed in only 8% yield.[84] Finally, heating **110** in the presence of dimethylacetylene dicarboxylate and $[CpCo(CO)_2]$ yielded the mixed cyclophane **113** as the minor product besides **55**. The quick formation of **55** supports our assumption that **110** is an intermediate in the synthesis of **55** from **6** (Scheme 6) according to Scheme 7, pathway b/c.

Another method that is suitable for the stepwise synthesis of (long-chain) cyclobutadienosuperphanes is the intermolecular McMurry coupling[85] of tricyclic diketocyclobutadiene complexes. In this way **114** (from **102**) and **115**, which represent cyclobutadieno- as well as ethenosuperphanes, were prepared.

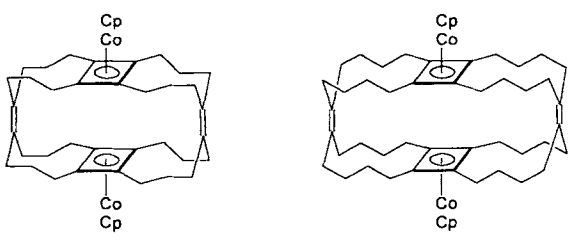

3.2.1.3. Properties and Reactions of Metal-Stabilized Cyclobutadienophanes

Superphanes **55**, **63**, and **68** are ideal models for studying interactions between two CpCo-capped cyclobutadiene units stacked onto each other at different well-defined distances. Cyclic voltammetry (CV) proved to be the method of choice for establishing such interactions. Figure 8 shows the CV data[86]

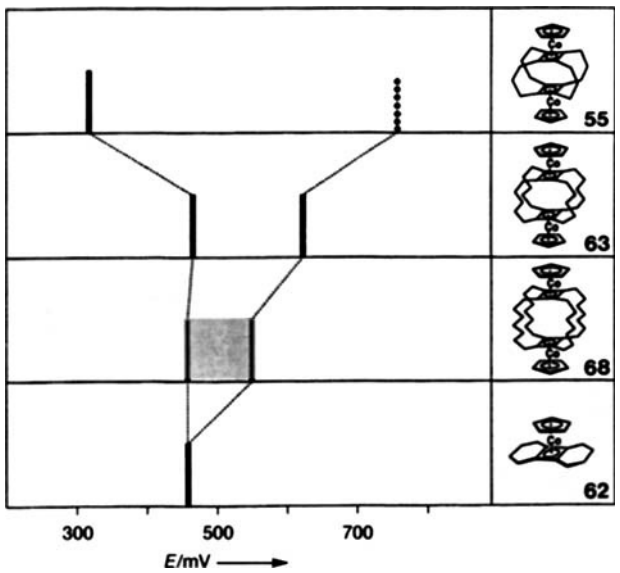

Figure 8. CV oxidation potentials of **55**, **63**, **68**, and **62**.

obtained for **55**, **63**, **68**, and the reference complex **62**. The first (reversible) oxidation step in **55** (E_{Ox1} = 0.31 eV), leading to a radical cation, proceedes more easily than that of **62** (E_{Ox1} = 0.46 eV); this indicates a considerable increase of the HOMO energy in the ground state of **55**. On the other hand, presumably due to delocalization of the positive charge over both π units, the second (irreversible) oxidation step in **55** needs considerably higher energy (E_{Ox2} = 0.76 eV). In the neutral compounds **63** and **68**, the less closely arranged π units appear to be independent, like that of **62**; concerning the first oxidation potentials, no significant differences are found. Nevertheless, the potentials required for the second oxidation step reveal marked interactions in the radical cation state of **63** and even of **68**, although it decreases with chain length.

Complex **56** (see Scheme 6) can be conceived as a donor–acceptor phane with the metal-stabilized cyclobutadiene unit as the donor and the quinone unit as the acceptor. This view is supported by a long wave length absorption band at 424 nm.[71]

The view of cyclobutadienosuperphanes as dimers of cyclodiynes and as products of double [2+2]cycloaddition involving all four triple bonds prompted us to investigate further synthetic application of [2+2]cycloaddition involving the four "double bonds" as well. The hypothetical, unstabilized cyclobutadienosuperphanes should provide chances for extending the coupling sequences to three- and fourfold [2+2]cycloadditions and thus make accessible fourfold-bridged *syn*-tricyclo[4.2.0.0^{2,5}]octa-3,7-dienes, a new species of cage compounds, and new representatives of propella[n_m]cubanes.

We succeeded in removing the CpCo fragments of the superphanes **55**, **96**, and **107** by oxidation with Ce^{IV} and in case of **55** (less efficiently) by irradiation.[87] The main product (80%) starting from **55** was the [3$_4$]-bridged *syn*-tricyclo[4.2.0.0^{2,5}]octa-3,7-diene **116**, as postulated according to the concept of threefold [2+2]cycloaddition (Scheme 12). The corresponding bridged *syn*-tricyclo[4.2.0.0^{2,5}]octa-3,7-dienes were obtained from **96** and **107**.[81,88a] The intramolecular cycloaddition of two cyclobutadiene moieties seems to be limited to cyclobutadienosuperphanes with up to four-membered bridges. Superphanes with longer chains, such as **63** and **68**, are not transformed to the corresponding cage compounds by oxidation or irradiation.

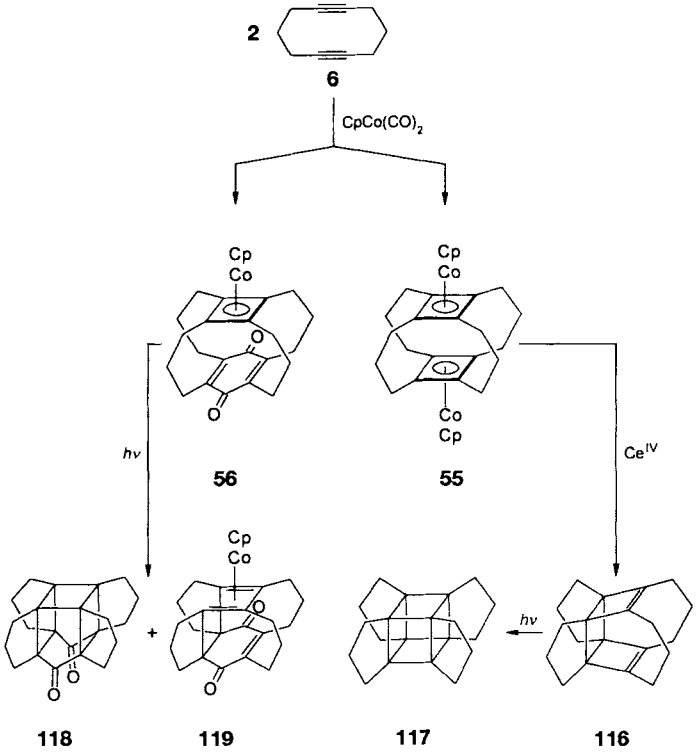

Scheme 12. Products of multiple cycloadditions starting from cyclodiyne **6**.

Finally, the last step of fourfold [2+2]cycloaddition could be achieved as well in two cases so far (Scheme 12).[87,89] Irradiation of **116** afforded the fourfold-bridged propella[3$_4$]cubane **117**, another dimer of cyclodecadiyne. Analogously, the photoinduced transformation of the mixed superphane **56** underwent two cycloaddition steps to lead to **118** accompanied by **119**.

4. Outlook

The availability of [n_2]cyclopropenyliophanes (**38**–**40**), [n_2]cyclopropenonophanes (**18**–**20**), and difunctional intermediates (**12**–**14**, **21**, **22**, **32**–**34**) provides new synthetic perspectives, especially with respect to applying known transformations of monofunctional systems (cyclopropenylium ions, cyclopropenones, 3-carboxycyclopropenes, 1-chlorocyclopropenes).

Foremost, we envision further bridging for construction of $[n_3]$cyclopropenyliosuperphanes **120**, counterparts of cyclobutadienosuperphanes that are still lacking.

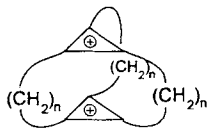

120

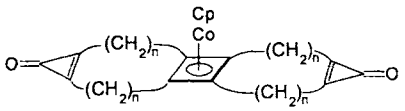

121

$[n_2]$Cyclopropenono-acetyleno-phanes such as **12**–**14**, which were successfully used for the synthesis of $[n_2]$cyclopropenone-superphanes **18**–**20** (see Section 2.1.2), and bicycloalkenyne carboxylic esters like **29**–**31** may generally serve as functionalized alkyne substrates. Thus, CpCo-induced dimerization of **12**–**14** by [2+2]cycloaddition could afford mixed phanes **121**.

In the area of cyclobutadienosuperphanes, variation of the complexing agent appears to be synthetically promising. As mentioned above, ester groups in the CpCo fragment markedly increase the selectivity of cyclodiyne dimerization by double [2+2]cycloaddition. Systematically fitting the complex ligand with substituents may not only allow an extention of the scope of superphane synthesis but also provide functionalities that are suitable for further transformations in the outer sphere. For example, the metal-stabilized dication species **122** might be derived from diester **105**.

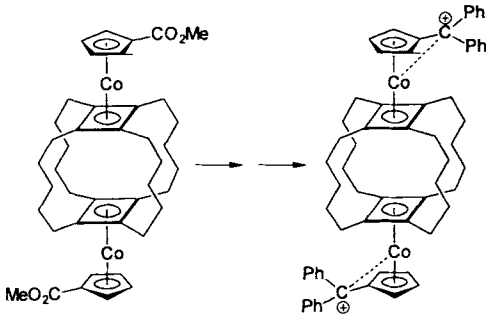

124 **122**

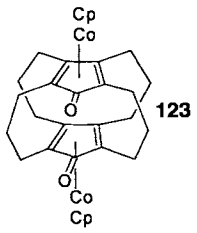

123

On the other hand, side products formed by insertion (**56**, **58**, **113**) indicate variability with respect to the π centers as well. Consequently, new attractive goals such as $[3_4]$cyclopentadienonosuperphane **123** can be specifically approached.

Financial support by the Deutsche Forschungsgemeinschaft (SFB 247), the Volkswagen-Stiftung, the Fonds der Chemischen Industrie, and the BASF AG, Ludwigshafen, is gratefully acknowledged. M. M. thanks the Studienstiftung des Deutschen Volkes for a graduate fellowship. We thank all members of the group mentioned in the references for their experimental and intellectual contributions. Thanks are also due to our colleagues H. Irngartinger, B. Nuber, and M. L. Ziegler for numerous X-ray structures analyses.

Received: October 21, 1996
Supplemented version: May 5, 1997 [A 194 IE]
German version: *Angew. Chem.* **1997**, *109*, 2532–2546

[1] F. Vögtle, *Cyclophane Chemistry: Synthesis, Structures and Reactions*, Wiley, Chichester, **1993**; P. M. Keehn, S. M. Rosenfeld, *Cyclophanes*, Academic Press, New York, **1983**.
[2] F. Diederich, *Cyclophanes*, The Royal Society of Chemistry, London, **1991**; D. J. Cram, J. M. Cram, *Container Molecules and Their Guests*, The Royal Society of Chemistry, London, **1994**.
[3] K. B. Wiberg, M. Matturro, R. Adams, *J. Am. Chem. Soc.* **1981**, *103*, 1600–1602.
[4] E. Kloster-Jensen, J. Wirz, *Angew. Chem.* **1973**, *85*, 723; *Angew. Chem. Int. Ed. Engl.* **1973**, *12*, 671.
[5] E. Heilbronner, Z. Yang, *Top. Curr. Chem.* **1983**, *115*, 1–55.
[6] R. Gleiter, D. Kratz, *Acc. Chem. Res.* **1993**, *26*, 311–318.
[7] L. A. Paquette, M. A. Kesselmayer, *J. Am. Chem. Soc.* **1990**, *112*, 1258–1259.
[8] F. Vögtle, J. Dohm, K. Rissanen, *Angew. Chem.* **1990**, *102*, 943–945; *Angew. Chem. Int. Ed. Engl.* **1990**, *29*, 902–904.
[9] R. Lemmerz, M. Nieger, F. Vögtle, *Chem. Ber.* **1994**, *127*, 1147–1156; S. Grimme, R. Lemmerz, F. Vögtle, *ibid.* **1994**, *127*, 2081–2088.
[10] R. Breslow, R. Peterson, *J. Am. Chem. Soc.* **1960**, *82*, 4426–4427.
[11] R. Breslow, L. J. Altman, A. Krebs, E. Mohacsi, I. Murata, R. A. Peterson, J. Posner, *J. Am. Chem. Soc.* **1965**, *87*, 1326–1331.
[12] R. Breslow, T. Eicher, A. Krebs, R. A. Peterson, J. Posner, *J. Am. Chem. Soc.* **1965**, *87*, 1320–1325.
[13] E. V. Dehmlow, *Tetrahedron Lett.* **1965**, 4003–4006.
[14] E. V. Dehmlow, *Chem. Ber.* **1967**, *100*, 3829–3834.
[15] M. Isaka, S. Ejiri, E. Nakamura, *Tetrahedron* **1992**, *48*, 2045–2057.
[16] W. E. Parham, E. E. Schweizer, *J. Org. Chem.* **1959**, *24*, 1733–1735.
[17] E. V. Dehmlow, *Methoden Org. Chem. (Houben-Weyl) 4th ed. 1952–*, Vol. E19b, **1989**, pp. 1461–1627.
[18] E. V. Dehmlow, S. S. Dehmlow, F. Marschner, *Chem. Ber.* **1977**, *110*, 154–164.
[19] W. von E. Doering, A. K. Hoffmann, *J. Am. Chem. Soc.* **1954**, *76*, 6162–6165.
[20] W. T. Miller Jr., D. M. Whalen, *J. Am. Chem. Soc.* **1964**, *86*, 2089–2090.
[21] R. Breslow, L. J. Altman, *J. Am. Chem. Soc.* **1966**, *88*, 504–509.
[22] E. V. Dehmlow, *Chem. Ber.* **1968**, *101*, 410–426.
[23] D. Seebach, H. Siegel, J. Gabriel, R. Hässig, *Helv. Chim. Acta* **1980**, *63*, 2046–2053.
[24] D. Seebach, R. Hässig, J. Gabriel, *Helv. Chim. Acta* **1983**, *66*, 308–337.
[25] J. Heinzer, J. F. M. Oth, D. Seebach, *Helv. Chim. Acta* **1985**, *68*, 1848–1862.
[26] G. Köbrich, K. Flory, R. H. Fischer, *Chem. Ber.* **1966**, *99*, 1793–1804; G. Köbrich, *Angew. Chem.* **1967**, *79*, 15–27; *Angew. Chem. Int. Ed. Engl.* **1967**, *6*, 41–52
[27] D. F. Hoeg, D. I. Lusk, A. L. Crumbliss, *J. Am. Chem. Soc.* **1965**, *87*, 4147–4155.
[28] R. Gleiter, M. Merger, *Synthesis* **1995**, 969–972.
[29] R. Gleiter, M. Merger, A. Altreuther, H. Irngartinger, *J. Org. Chem.* **1995**, *60*, 4692–4696.
[30] R. Gleiter, M. Karcher, R. Jahn, H. Irngartinger, *Chem. Ber.* **1988**, *121*, 735–740.
[31] R. Gleiter, M. Merger, A. Altreuther, H. Irngartinger, *J. Org. Chem.* **1996**, *61*, 1946–1953.
[32] M. S. Baird in *Advances in Strain in Organic Chemistry, Vol. 1* (Ed.: B. Halton), JAI Press, Greenwich, **1991**, pp. 65–116; B. Halton, M. G. Banwell in *The Chemistry of the Cyclopropyl Group, Vol. 2* (Ed.: Z. Rappoport), Wiley, Chichester, **1987**, pp. 1223–1339.
[33] J. M. White, M. K. Bromley, *Tetrahedron Lett.* **1993**, *34*, 4091–4094.
[34] R. Breslow, H. Höver, H. W. Chang, *J. Am. Chem. Soc.* **1962**, *84*, 3168–3174.
[35] M. N. Protopopova, E. A. Shapiro, *Usp. Khim.* **1989**, *58*, 1145–1174.
[36] G. Maas, *Top. Curr. Chem.* **1987**, *137*, 75–253.
[37] P. J. Pérez, M. Brookhart, J. L. Templeton, *Organometallics* **1993**, *12*, 261–262.
[38] N. Petiniot, A. J. Anciaux, A. F. Noels, A. J. Hubert, P. Teyssié, *Tetrahedron Lett.* **1978**, 1239–1242.
[39] I. N. Domnin, E. F. Zhuravleva, N. V. Pronina, *Zh. Org. Khim.* **1978**, *14*, 2323–2327 (English translation: 2144–2148).
[40] E. A. Shapiro, I. E. Dolgii, D. N. Nefedov, *Izv. Akad. Nauk SSSR, Ser. Khim* **1980**, *9*, 2096–2102 (English translation: 1493–1499).
[41] N. S. Zefirov, N. V. Averina, A. M. Boganev, A. S. Koz'min, V. S. Anufriev, V. M. Tatevskii, S. S. Yarovoi, R. N. Shchelokov, I. B. Baranovskii (Mosow State University) USSR, SU 825, 502, **1981** [*Chem. Abstr.* **1982**, *96*, 6244m].
[42] P. Dowd, P. Garner, R. Schappert, H. Irngartinger, A. Goldman, *J. Org. Chem.* **1982**, *47*, 4240–4246.
[43] P. Müller, C. Gränicher, *Helv. Chim. Acta* **1995**, *78*, 129–144.
[44] G. Maas, *Methoden Org. Chem. (Houben-Weyl) 4th ed. 1952–*, Vol. E19b, Part 2, **1989**, pp. 1022–1135.
[45] A. Nakamura, T. Koyama, S. Otsuka, *Bull. Chem. Soc. Jpn.* **1978**, *51*, 593–595.
[46] D. S. Wulfman, B. W. Peace, R. S. McDaniel, Jr., *Tetrahedron* **1976**, *32*, 1251–1255.
[47] N. Conde-Petiniot, A. J. Hubert, A. F. Noels, R. Warin, P. J. Teyssié, *Bull. Soc. Chim. Belg.* **1986**, *95*, 649–654.
[48] D. Wendisch, *Methoden Org. Chem. (Houben-Weyl), 4th ed. 1952–*, Vol. 4/3, **1971**, pp. 693–698.
[49] I. A. D'yakonov, M. I. Komendantov, *Zh. Obshch. Khim.* **1963**, *33*, 2448–2456.

[50] I. A. D'yakonov, V. V. Razin, M. I. Komendantov, *Tetrahedron Lett.* **1966**, 1127–1134.
[51] I. A. D'yakonov, V. V. Razin, M. I. Komendantov, *Dokl. Akad. Nauk SSSR* **1967**, *177*, 354–357.
[52] M. N. Protopopova, M. P. Doyle, P. Müller, D. Ene, *J. Am. Chem. Soc.* **1992**, *114*, 2755–2757.
[53] M. Merger, Dissertation, Universität Heidelberg, **1995**.
[54] R. Gleiter, M. Merger, *Tetrahedron Lett.* **1992**, *33*, 3473–3476.
[55] M. Vidal, M. Vincens, P. Arnaud, *Bull. Soc. Chim. Fr.* **1972**, 665–675.
[56] R. A. Moss, S. Shen, K. Krogh-Jespersen, J. A. Potenza, H. J. Schugar, R. C. Munjal, *J. Am. Chem. Soc.* **1986**, *108*, 134–140; S. Fliszár, G. Cardinal, M.-T. Béraldin, *ibid.* **1982**, *104*, 5287–5292.
[57] R. Gleiter, M. Merger, T. Oeser, H. Irngartinger, *Tetrahedron Lett.* **1995**, *36*, 6425–6428.
[58] R. P. Hughes, J. M. J. Lambert, J. L. Hubbard, *Organometallics* **1986**, *5*, 797–804.
[59] R. P. Hughes, W. Kläui, J. W. Reisch, A. Müller, *Organometallics* **1985**, *4*, 1761–1766.
[60] W. A. Donaldson, R. P. Hughes, R. E. Davis, S. M. Gadol, *Organometallics* **1982**, *1*, 812–819.
[61] R. P. Hughes, J. W. Reisch, A. L. Rheingold, *Organometallics* **1984**, *3*, 1761–1763.
[62] W. A. Donaldson, R. P. Hughes, *J. Am. Chem. Soc.* **1982**, *104*, 4846–4859.
[63] C. M. Adams, E. S. Crawford, E. Salim, *Tetrahedron Lett.* **1992**, *33*, 3963–3966.
[64] C. M. Adams, E. M. Holt, *Organometallics* **1990**, *9*, 980–986.
[65] J. D. Fitzpatrick, L. Watts, G. F. Emerson, R. Pettit, *J. Am. Chem. Soc.* **1965**, *87*, 3254–3255.
[66] R. Gleiter, *Angew. Chem.* **1992**, *104*, 29–46; *Angew. Chem. Int. Ed. Engl.* **1992**, *31*, 27–44.
[67] R. B. King, A. Efraty, *J. Am. Chem. Soc.* **1970**, *92*, 6071–6073; *ibid.* **1972**, *94*, 3021–3025.
[68] R. B. King, M. N. Ackermann, *J. Organomet. Chem.* **1974**, *67*, 431–441.
[69] A. Efraty, *Chem. Rev.* **1977**, *77*, 691–744.
[70] R. Gleiter, M. Karcher, M. L. Ziegler, B. Nuber, *Tetrahedron Lett.* **1987**, *28*, 195–198.
[71] R. Gleiter, D. Kratz, *Tetrahedron Lett.* **1990**, *31*, 5893–5896.
[72] J. P. Collman, L. S. Hegedus, J. R. Norton, R. G. Finke, *Principles and Applications of Organotransition Metal Chemistry*, University Science Books, Mill Valley, CA, USA, **1987**; L. P. McDonnell Bushnell, E. R. Evitt, R. G. Bergman, *J. Organomet. Chem.* **1978**, *157*, 445–456; G. A. Ville, K. P. C. Vollhardt, M. J. Winter, *Organometallics* **1984**, *3*, 1177–1187.
[73] F. D. Mango, J. H. Schachtschneider, *J. Am. Chem. Soc.* **1969**, *91*, 1030–1031.
[74] Y. Wakatsuki, O. Nomura, K. Kitaura, K. Morokuma, H. Yamazaki, *J. Am. Chem. Soc.* **1983**, *105*, 1907–1912.
[75] R. Gleiter, B. Treptow, D. Kratz, B. Nuber, *Tetrahedron Lett.* **1992**, *33*, 1733–1736.
[76] R. Gleiter, G. Pflästerer, B. Nuber, *J. Chem. Soc. Chem. Commun.* **1993**, 454–456.
[77] R. Gleiter, D. Kratz, M. L. Ziegler, B. Nuber, *Tetrahedron Lett.* **1990**, *31*, 6175–6178.
[78] R. Gleiter, H. Stahr, F. Stadtmüller, H. Irngartinger, H. Pritzkow, *Tetrahedron Lett.* **1995**, *36*, 4603–4606.
[79] R. Gleiter, H. Stahr, B. Nuber, *Tetrahedron Lett.* **1995**, *36*, 4607–4610.
[80] R. Gleiter, H. Stahr, B. Nuber, *Organometallics* **1997**, *16*, 646–650.
[81] R. Gleiter, R. Merger, B. Nuber, *J. Am. Chem. Soc.* **1992**, *114*, 8921–8927.
[82] R. Gleiter, R. Merger, H. Irngartinger, B. Nuber, *J. Org. Chem.* **1993**, *58*, 2025–2028.
[83] R. Gleiter, G. Pflästerer, *Organometallics* **1993**, *12*, 1886–1889.
[84] R. Gleiter, H. Langer, V. Schehlmann, B. Nuber, *Organometallics* **1995**, *14*, 975–986.
[85] R. Gleiter, H. Langer, B. Nuber, *Angew. Chem.* **1994**, *106*, 1350–1352; *Angew. Chem. Int. Ed. Engl.* **1994**, *33*, 1272–1274.
[86] R. Gleiter, H. Röckel, G. Pflästerer, B. Treptow, D. Kratz, *Tetrahedron Lett.* **1993**, *34*, 8075–8078.
[87] R. Gleiter, M. Karcher, *Angew. Chem.* **1988**, *100*, 851–852; *Angew. Chem. Int. Ed. Engl.* **1988**, *27*, 840–841.
[88] H. Langer, Dissertation, Universität Heidelberg, **1995**; D. Kratz, Dissertation, Universität Heidelberg, **1991**.
[89] S. Brand, R. Gleiter, *Tetrahedron Lett.* **1997**, *38*, 2939–2942.

Boryl Metal Complexes, Boron Complexes, and Catalytic (Hydro)boration

Hubert Wadepohl*

Boryl metal complexes had had a long run-up, and are now moving from the confines of boron chemistry into the spotlight of a much broader range of chemical interest. Their story began in the early 1960s, when Nöth and Schmid reported the first complexes in which a boryl group (BR_2) is directly bonded to a transition metal (M) through the boron atom.[1] In 1970 Schmid deduced that "Covalent bonds between boron and metals and boron and nonmetals are similar in character", and consequently derived a description of boryl metal complexes as simple borane derivatives $[R_2BML_n]$ (**1**).[2] Analogous to the (p → p) π contributions characteristic of many nonmetal–boron bonds (Scheme 1a), (d → p) π contributions are possible for transition metal–boron bonds (Scheme 1b), and, therefore, the BR_2 group can also be regarded as a complex-stabilized "pseudo-carbene".[3] The extent of such a π interaction between a metal and a boron atom is still disputed today, and of course it depends on the remaining ligands on the metal atom and on the substituents on the boron atom, all of which must compete with the electrophilic boron center for the π electrons.[4]

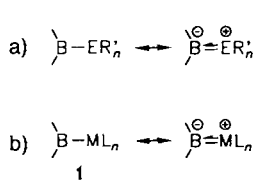

Scheme 1. a) Nonmetal–boron bonds and b) transition metal–boron bonds.

Early work soon fell into oblivion, perhaps because none of the boryl metal complexes could be crystallized and analyzed by X-ray crystallography, and because the spectroscopic methods of the time could not always characterize them to present standards.[5] It was not until 1985 that interest in boryl metal complexes was reawakened, this time as postulated intermediates, and they were reported once again by Nöth's research group.[6] Described in their contribution, a milestone of boron chemistry, is the first use of rhodium-complex catalysts to mediate the hydroboration of olefins by benzo-1,3,2-dioxaborolane (catecholborane, *H*Bcat, **2**) which otherwise reacts very sluggishly. There is no question about the importance of hydroboration in organic syntheses; the value of the catalytic variant lies not only in the activation of less reactive boranes, which are therefore easy to handle and store, but also in the controlling of the selectivity of the reaction. Already in this initial work, chemoselectivity was found: In unsaturated ketones, it is the C–C double bond and not the keto group which undergoes catalytic hydroboration. This is in contrast to the situation for the noncatalytic variant. Enantio-, regio-, and diastereoselective hydroborations are also known today.[7, 8]

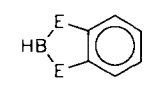

HBcat **2**, E = O
HBOp **19**, E = NH

Among the catalysts, complexes of late transition metals form the major group. Of these, hydridoboryl metal complexes, formed by oxidative addition of the borane to a coordinatively unsaturated metal center, play a key role. There are extensive high-level theoretical investigations of the reactions catalyzed by Rh^I. However, there still remain some differences in opinion over certain details of the mechanism. These boil down to the question of whether the olefin inserts into the M–H or the M–B bond in the key step. Schleyer et al.[9] favor a dissociative reaction pathway (Scheme 2), with an initial transfer of a hydrogen

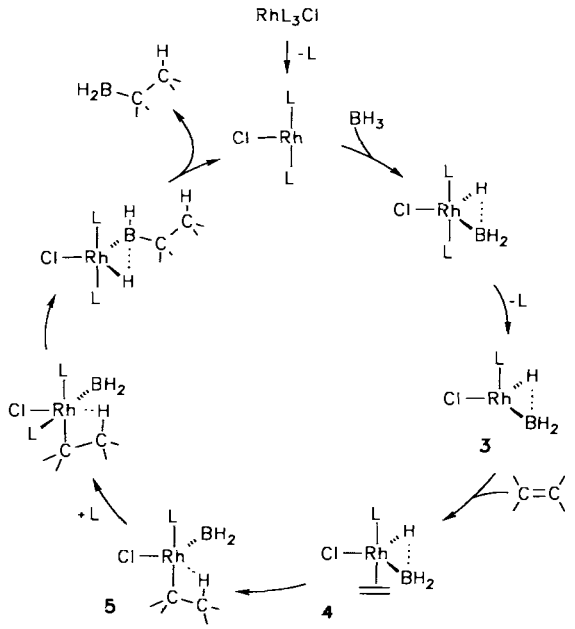

Scheme 2. Simplified catalytic cycle for hydroboration with the Rh^I catalyst according to calculations by Schleyer et al. [9].

atom onto the olefin (**4** → **5**). It is possible that there is an intermediate **3** with 14 valence electrons. On the other hand, Morokuma et al.[8] favor the migration of a boryl group (Scheme 3, **6** → **7**). Experimental (kinetic) results appear to be more in line with the first possibility.[10]

[*] Priv.-Doz. Dr. H. Wadepohl
Anorganisch-chemisches Institut der Universität
Im Neuenheimer Feld 270, D-69120 Heidelberg (Germany)
Fax: Int. code +(6221)54-4197
e-mail: bu9@ix.urz.uni-heidelberg.de

 © WILEY-VCH Verlag GmbH, D-69451 Weinheim, 1997 0570-0833/97/3622-2441 $ 17.50+.50/0

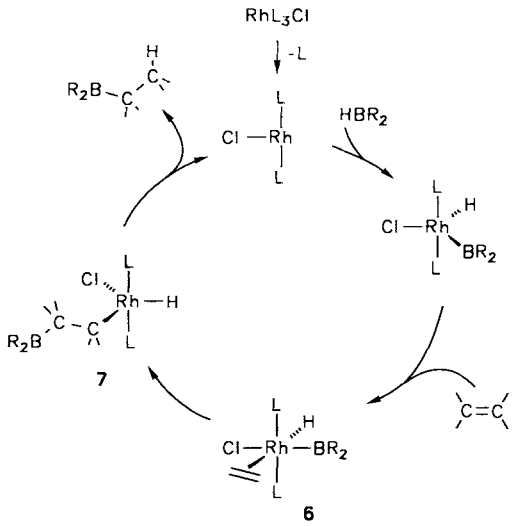

Scheme 3. Simplified catalytic cycle for hydroboration with the Rh^I catalyst according to calculations by Morokuma et al.[8].

The great potential of catalytic (hydro)boration of unsaturated C–C bonds has led to intensive research in the synthesis and, above all, the chemistry of boryl metal complexes in recent years.[11] Some reactions have been discovered in which even saturated hydrocarbons can become functionalized! This was found upon irradiation of the complexes $[(C_5Me_5)M(Bcat')(CO)_2]$ (**8**, M = Fe; **9**, M = Ru), and $[(C_5Me_5)W(Bcat')(CO)_3]$ (**10**) in alkanes (Bcat' = 3,5-dimethylcatecholboryl):[12] In highly selective stoichiometric reactions with alkanes, esters of boronic acid (alkyl-Bcat') are formed in which the catecholboryl group (Bcat') has replaced a hydrogen atom in the sterically least hindered, primary position of the alkane (Scheme 4). These

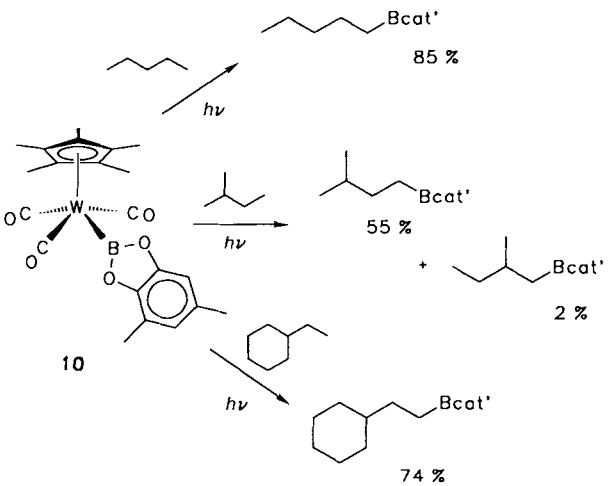

Scheme 4. Functionalization of saturated hydrocarbons with complex **10**.

reactions probably proceed via coordinatively unsaturated intermediates $[(C_5Me_5)M(Bcat')(CO)_{n-1}]$ (M = Fe, Ru, $n = 2$; M = W, $n = 3$), which can undergo either M–B/C–H σ-bond metathesis or oxidative addition of the alkane with subsequent reductive elimination of the borylated alkane. The major primary organometallic products are the photolabile hydrido complexes $[(C_5Me_5)MH(CO)_n]$, which then react further to give the binuclear complexes $[\{(C_5Me_5)M(CO)_n\}_2]$. It is not surprising that the high selectivity of the reaction towards sp^3 C–H bonds only then occurs if, as found for the Bcat'-complexes, no sp^2 C–H bonds are sterically accessible. Therefore, with $[(C_5H_5)Fe(Bcat)(CO)_2]$ and similar complexes, the more reactive C–H bonds of arenes can be functionalized, but not those of alkanes (in the absence of other arenes the phenylene ring of the catecholboryl ligand of a second molecule is probably attacked).[13]

Upon addition of diborane(4) derivatives (R_2BBR_2) C–C multiple bonds can be diborylated. Although this reaction, also known as boraborylation, has been known for a long time,[14] its usefulness in organic synthesis is severely limited by the fact that reactive tetrahalodiboranes(4) are rather unstable and hard to come by; the more readily obtainable tetraalkoxydiboranes(4) ($(RO)_2BB(OR)_2$) do not react. Again, a transition metal center can induce the desired activation, in the form of complexes with two boryl ligands. Indeed, *cis*-diboryl metal complexes such as **11** react stoichiometrically with alkynes to give *cis*-1,2-diborylalkenes [Eq. (1)].[15] The diborylation of

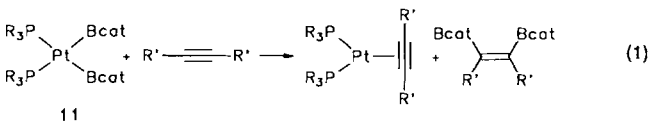

(1)

alkynes, for example catBBcat also proceeds under catalytic conditions; here, **11** shows greater activity[15b,16] than $[Pt(PPh_3)_4]$,[17] from which the precatalyst **11** is formed during the reaction. The experimental results show that, in contrast to the originally proposed mechanism,[17] the dissociation of phosphane from $[Pt(BR_2)_2L_2]$ (e. g. **11**) is a critical reaction step (Scheme 5).[15,16] Initially, monoolefins could not be diborylat-

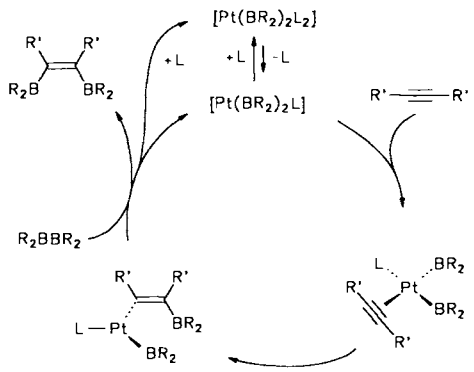

Scheme 5. Postulated catalytic cycle for the diboration of alkynes with Pt complexes.

ed with platinum catalysts. With typical Rh hydroboration catalysts, such as $[RhCl(PPh_3)_3]$, only a mixture of products was obtained in which products of β-hydrogen elimination dominated.[18] The β-elimination could be suppressed with an electron-rich Au^I catalyst (obtained in situ from $[AuCl(PEt_3)]$ and two equivalents of $(cHex_2PCH_2)_2$. However, this system only functioned with a few activated alkenes, such as vinyl- or allylbenzene, as the substrates.[18] If the dissociation of a phosphane ligand from **11** is decisive for the activation of the catalyst, then phosphane-free catalyst systems should be much more active. This was confirmed for the diborylation of 1,3-dienes with Pt

 © WILEY-VCH Verlag GmbH, D-69451 Weinheim, 1997 0570-0833/97/3622-2442 $ 17.50+.50/0

complexes as the catalysts:[19] $[Pt(dba)_2]$,[20] $[Pt(cod)_2]$,[21] and $[Pt(norbornene)_3]$[21] indeed catalyzed the diborylation of α-alkenes and some strained cycloalkenes (dba = dibenzylideneacetone, cod = (*Z*,*Z*)-1,5-cyclooctadiene)!

The use of organolanthanide complexes[22] and some complexes of the early transition metals[23–25] as hydroboration catalysts provide interesting perspectives for controlling selectivity. Several recent publications illustrate the particular features of the interaction of boranes with electron-poor transition metals: Whereas the oxidative addition of the B–H bond onto the metal center is characteristic of the late transition metals, in the complexes of early transition metals the type of bond between the borane and the metal center is very variable. Thus, the tantalum complexes **12** are genuine hydridoboryl complexes (structure type **A**);[26] this is also valid for tungsten complex **13**.[27] On the other hand, the NMR spectra and their changes upon deuteration of the niobium complex **14** were interpreted in terms of an equilibrium between two isomers in solution: structure type **A** (hydridoboryl complex) and **B** (hydridoborate). The crystal structure tends towards type **A**, whereas the structure of the 9-BBN derivative **15** is closer to **B** in the solid state.[27]

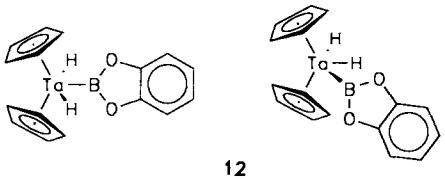

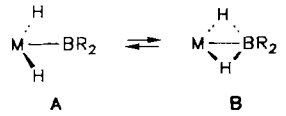

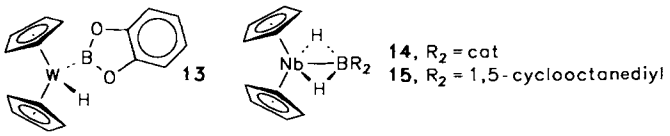

In complexes **16**[28] and **17**,[29] synthesized by Hartwig et al., the ligands are coordinated to the metal atom in a "side-on" fashion by their B–H bonds. This is shown by the spectroscopic

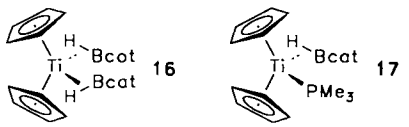

data measured in solution (high-field position and coupling to boron of the bridging hydrogen atoms in the ^1H NMR spectrum, low-frequency shift of the B–H stretching mode in the IR spectrum). The bridging hydrogens atoms were localized in X-ray crystal structure analyses: They are bound to both B and Ti. Acute B-Ti-H angles and large Ti–B distances indicate the presence of a (weakened) B–H bond. Until now, such σ complexes[30] were known only with η^2-H–H[31] and η^2-Si–H bonds.[32] With alkanes, there is only indirect evidence for this type of bonding, for which a role in C–H activation is ascribed.[33] However, its "intramolecular" variant, agostic C–H coordination, is wide-spread.

Based on MO calculations, the authors give a reason for the (relative) stability of the borane σ complexes: In addition to the donor function of the B–H σ bond there is the acceptor function of a p orbital on the boron atom (or better, of the LUMO of the borane, which is bonding with respect to B–H, but π-antibonding with respect to B–O).[28] The LUMO of the borane fits much better energetically than a σ* orbital of an alkane to the HOMO of the metal fragment, and allows therefore greater backbonding. This should also be valid for the (so far unknown) σ complexes with η^2-C–H(aromatic) coordination; this could be the reason for the easier activation of such bonds on the metal center. Addition of H_2SiPh_2 to **17** gives rise to an equilibrium between **17** and $[(C_5H_5)_2Ti(PMe_3)\{\eta^2\text{-}(HSi)HPh_2\}]$, which lies more on the side of the borane complex. The σ borane complex is therefore more stable than the σ silane complex, which is understandable in terms of the above-mentioned bonding mechanism and the greater Lewis acidity of boron. Likewise, it is not surprising that the borane ligands in **16** and **17** are much more active than in the free state; they stoichiometrically hydroborate alkynes and imines under very mild conditions.

In the rhodium-catalyzed hydroboration of alkenes to alkylboranes, "dehydrogenating borylation" often occurs as a side reaction, in which alkenyl boranes are formed (formal B–H/C–H bond metathesis).[34] Recently, Smith et al. succeeded in performing this reaction selectively with ethylene as the substrate and a titanium catalyst.[35] The same research group had already found that $[(C_5Me_5)_2Ti(\eta^2\text{-}CH_2{=}CH_2)]$ (**18**) reacts with catecholborane to produce **19a** with an η^2-vinyl-

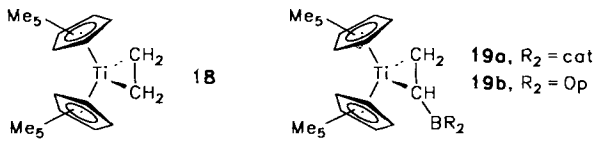

borane as a ligand.[36] Apparently, β-hydrogen elimination from the postulated primary product (**20** → **21**, Scheme 6) is more favorable than reductive elimination of an alkylborane. Additional products were ethane and $[(C_5Me_5)_2Ti]$. The latter is known to react with ethylene to give **18**, so that a closed cycle of stoichiometric reactions is formed. Under catalytic conditions, however, the catalyst decomposed to give a mixture of various Ti species, which led finally to only the usual hydroboration product CH_3CH_2Bcat. Therefore, the problem was to decrease the rate of the unproductive catalyst decomposition relative to that of regeneration of the ethylene complex **18** (**19** → **18** in Scheme 6). A simple modification of the borane—exchanging the dialkoxyborane (HBcat, **2**) for the isoelectronic diaminoborane benzo-1,3,2-diazaborolane (HBOp **22**)—already gave the desired results.[35] Owing to the stronger B–N bonds and the lower B–H activity, the stability of the catalytic species should be increased and its decomposition, for example by borylation of the vinylborane ligand in **19**, should be retarded. However, along with this effect, modification of the borane caused an unexpected, drastic acceleration of the reaction of **19** with ethylene (>90% turnover in <5 min at −80 °C for **19b**

 © WILEY-VCH Verlag GmbH, D-69451 Weinheim, 1997 0570-0833/97/3622-2443 $ 17.50+.50/0

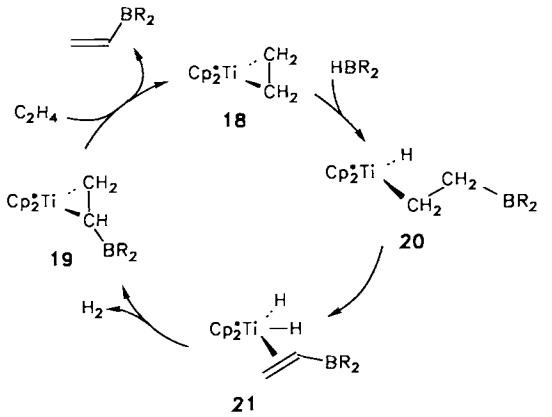

Scheme 6. Postulated catalytic cycle for the "dehydrogenative borylation" of ethene with a titanocene complex (Cp* = tetramethylcyclopentadienyl). The dihydrogen produced in step **21** → **19** reacts selectively with **18** to give ethane and "[Cp*$_2$Ti]", which reacts with ethylene to regenerate the catalyst **18**.

versus 40% turnover in 72 h at 25 °C in the case of **19a**). This very ligand exchange, in which the vinylborane is liberated and **18** regenerated, is the "bottle neck" of the catalytic cycle (Scheme 6).

These examples show, that even established reactions such as hydroboration can provide new facets if transition metals are brought into play. The end is not yet in sight. For example, Gladysz, Horváth et al. recently reported in this journal a new "environmental friendly" variation of Rh-catalyzed hydroboration, in which very high turnovers and excellent recovery of the catalyst was achieved by fluoric two-phase catalysis (with Wilkinson's catalyst modified by fluoroalkyl groups in a fluorinated solvent).[37] Numerous other novel types of reaction, related to those described here, are not usable without a catalyst. Silyl-,[38] stannyl-,[39,40] and sulfanylborations[41] as well as boron cross-couplings[42]—all of which yield valuable building blocks for organic and organometallic synthesis—may be named as examples. Boryl metal complexes play an important role as intermediates in all of them. With regard to new types of structures, the combination metal complex/borane continues to produce novelties, so that one can look forward to further developments.

German version: *Angew. Chem.* **1997**, *109*, 2547–2550

Keywords: boron · homogeneous catalysis · hydroborations · transition metals

[1] H. Nöth, G. Schmid, *Angew. Chem.* **1963**, *75*, 861; *Angew. Chem. Int. Ed. Engl.* **1963**, *2*, 623.
[2] G. Schmid, *Angew. Chem.* **1970**, *82*, 920; *Angew. Chem. Int. Ed. Engl.* **1970**, *9*, 819.
[3] a) G. Schmid, H. Nöth, *Chem. Ber.* **1967**, *100*, 2899; b) M. Fishwick, H. Nöth, W. Petz, M. G. H. Wallbridge, *Inorg. Chem.* **1976**, *15*, 490.
[4] H. Wadepohl, U. Arnold, H. Pritzkow, *Angew. Chem.* **1997**, *109*, 1009; *Angew. Chem. Int. Ed. Engl.* **1997**, *36*, 974.
[5] The first crystal structure analyses of borylmetal complexes were not published until 1990: R. T. Baker, D. W. Ovenall, J. C. Calabrese, S. A. Westcott, N. J. Taylor, I. D. Williams, T. B. Marder, *J. Am. Chem. Soc.* **1990**, *112*, 9399; J. R. Knorr, J. S. Merola, *Organometallics* **1990**, *9*, 3008.
[6] D. Männig, H. Nöth, *Angew. Chem.* **1985**, *97*, 854; *Angew. Chem. Int. Ed. Engl.* **1985**, *24*, 878.
[7] K. Burgess, M. J. Ohlmeyer, *Chem. Rev.* **1991**, *91*, 1179, and references therein.
[8] D. G. Musaev, A. M. Mebel, K. Morokuma, *J. Am. Chem. Soc.* **1994**, *116*, 10963.
[9] A. E. Dorigo, P. von R. Schleyer, *Angew. Chem.* **1995**, *107*, 108; *Angew. Chem. Int. Ed. Engl.* **1995**, *34*, 115.
[10] D. A. Evans, G. C. Fu, B. A. Anderson, *J. Am. Chem. Soc.* **1992**, *114*, 6679; see also ref. [34].
[11] For a good review of current work, see J. F. Hartwig, K. M. Waltz, C. N. Muhoro, Xiaoming He, O. Eisenstein, R. Bosque, F. Maseras in *Advances in Boron Chemistry* (Ed.: W. Siebert), Special Publication No. 201, The Royal Society of Chemistry, Cambridge, **1997**, pp. 373–396.
[12] K. M. Waltz, J. F. Hartwig, *Science* **1997**, *277*, 211.
[13] K. M. Waltz, Xiaoming He, C. Muhoro, J. F. Hartwig, *J. Am. Chem. Soc.* **1995**, *117*, 11357.
[14] G. Urry, J. Kerrigan, T. D. Parsons, H. I. Schlesinger, *J. Am. Chem. Soc.* **1954**, *76*, 5299.
[15] a) C. N. Iverson, M. R. Smith III, *J. Am. Chem. Soc.* **1995**, *117*, 4403; b) *Organometallics* **1996**, *15*, 5155.
[16] G. Lesley, P. Nguyen, N. J. Taylor, T. B. Marder, A. J. Scott, W. Clegg, N. C. Norman, *Organometallics* **1996**, *15*, 5137.
[17] a) T. Ishiyama, N. Matsuda, N. Miyaura, A. Suzuki, *J. Am. Chem. Soc.* **1993**, *115*, 11018; b) T. Ishiyama, N. Matsuda, M. Murata, F. Ozawa, A. Suzuki, N. Miyaura, *Organometallics* **1996**, *15*, 713.
[18] R. T. Baker, P. Nguyen, T. B. Marder, S. A. Westcott, *Angew. Chem.* **1995**, *107*, 1451; *Angew. Chem. Int. Ed. Engl.* **1995**, *34*, 1336.
[19] T. Ishiyama, M. Yamamoto, N. Miyaura, *Chem. Commun.* **1996**, 2073.
[20] T. Ishiyama, M. Yamamoto, N. Miyaura, *Chem. Commun.* **1997**, 689.
[21] C. N. Iverson, M. R. Smith III, *Organometallics* **1997**, *16*, 2757.
[22] K. M. Harrison, T. J. Marks, *J. Am. Chem. Soc.* **1992**, *11*, 9220.
[23] a) G. Erker, R. Noe, D. Wingbermühle, J. L. Petersen, *Angew. Chem.* **1993**, *105*, 1216; *Angew. Chem. Int. Ed. Engl.* **1993**, *32*, 1213; b) R. Noe, D. Wingbermühle, G. Erker, C. Krüger, J. Bruckmann, *Organometallics* **1993**, *12*, 4993.
[24] a) L. Deloux, E. Skrzypczak-Jankun, B. V. Cheesman, M. Srebnik, *J. Am. Chem. Soc.* **1994**, *116*, 10302; b) S. Pereira, M. Srebnik, *Organometallics* **1995**, *14*, 3127; c) *J. Am. Chem. Soc.* **1996**, *118*, 909.
[25] Xiaoming He, J. F. Hartwig, *J. Am. Chem. Soc.* **1996**, *118*, 1696, and references therein.
[26] D. R. Lantero, D. H. Motry, D. L. Ward, M. R. Smith III, *J. Am. Chem. Soc.* **1994**, *116*, 10811.
[27] J. F. Hartwig, S. R. De Gala, *J. Am. Chem. Soc.* **1994**, *116*, 3661.
[28] J. F. Hartwig, C. N. Muhoro, Xiaoming He, O. Eisenstein, R. Bosque, F. Maseras, *J. Am. Chem. Soc.* **1996**, *118*, 10936.
[29] C. N. Muhoro, J. F. Hartwig, *Angew. Chem.* **1997**, *109*, 1536; *Angew. Chem. Int. Ed. Engl.* **1997**, *36*, 1510.
[30] R. H. Crabtree, *Angew. Chem.* **1993**, *105*, 828; *Angew. Chem. Int. Ed. Engl.* **1993**, *32*, 789.
[31] D. M. Heinekey, W. J. Oldham, *Chem. Rev.* **1993**, *93*, 913, and references therein.
[32] U. Schubert, *Adv. Organomet. Chem.* **1990**, *30*, 151, and references therein.
[33] C. Hall, R. N. Perutz, *Chem. Rev.* **1996**, *96*, 3125, and references therein.
[34] K. Burgess, W. A. van der Donk, S. A. Westcott, T. B. Marder, R. T. Baker, J. C. Calabrese, *J. Am. Chem. Soc.* **1992**, *114*, 9350.
[35] D. H. Motry, A. G. Brazil, M. R. Smith III, *J. Am. Chem. Soc.* **1997**, *119*, 2743.
[36] D. H. Motry, M. R. Smith III, *J. Am. Chem. Soc.* **1995**, *117*, 6615.
[37] J. J. J. Juliette, I. T. Horváth, J. A. Gladysz, *Angew. Chem.* **1997**, *109*, 1682; *Angew. Chem. Int. Ed. Engl.* **1997**, *36*, 1610.
[38] K. Nozaki, K. Wakamatsu, T. Nonaka, W. Tückmantel, K. Oshima, K. Utimoto, *Tetrahedron Lett.* **1986**, *27*, 2007.
[39] S. Sharma, A. C. Oehlschlager, *Tetrahedron Lett.* **1988**, *29*, 261.
[40] M. Tanaka, S.-Y. Onozawa, T. Sakakura, Y. Hatanaka, *Contribution CB-16*, IXth International Meeting on Boron Chemistry (IMEBORON IX), Heidelberg, Germany, **1996**.
[41] T. Ishiyama, K. Nishijima, N. Miyaura, A. Suzuki, *J. Am. Chem. Soc.* **1993**, *115*, 7219.
[42] N. Miyaura, A. Suzuki, *Chem. Rev.* **1995**, *95*, 2457, and references therein.

 © WILEY-VCH Verlag GmbH, D-69451 Weinheim, 1997 0570-0833/97/3622-2444 $ 17.50+.50/0

Organic Tri- and Tetraradicals with High-Spin or Low-Spin States

Werner M. Nau*

When carbon, nitrogen, or oxygen atoms carrying an unpaired electron ("spin carriers") are linked through a coupling unit (CU) and incorporated into an organic molecular framework, polyradicals result. After the appearance of the most recent reviews on polyradicals and related structures with unpaired electrons, for example polycarbenes,[1] the design of novel tri- and tetraradicals, the lowest homologues, has been actively continued.[2–11] The fascination arises not only from the idea of using them as building blocks for larger polyradicals with potential practical applications[1, 7] and the interest of ESR spectroscopists in such model systems, but also from the structural and synthetic challenges as well as the aesthetic appeal they present. The possible topologies of tri- and tetraradicals are shown in Scheme 1. The introduction of three or four spin carriers into a molecular framework allows two- or three-dimensional spin–spin interactions, which are required for desirable bulk properties such as ferromagnetism.[1]

Scheme 1 represents the spin coupler's toolbox, since the building blocks **A**–**F** contain all the relevant topological information for constructing higher polyradicals. Although the jury is still out as to which of the candidates **A**–**F** will first be a practically applicable magnetic material, examples for all but one type are known to date: Triradicals **1**[1a] and **2**[2] correspond to type **A**, triradicals **3**–**5**[3, 4a, 5] to type **B**, tetraradicals **6**–**11**[6, 7, 8a, 9–11] to type **C**, and tetraradicals **12**[1e] and **13**[1b] to types **E** and **F**, respectively. No example has been reported for **D**, the type of lowest symmetry, but it is contained as a substructure in higher polyradicals.[10] Interestingly, the simplest derivative of type **F**, the tetramethylenemethane tetraradical $C(R_2C^{\bullet})_4$, has remained elusive.

Types **A** and **C** are chain-like homologues. Open chains lead to linear structures such as **6**–**9**, whereas linking the ends of the chain results in cyclic structures (for example **10** and **11**), which display distinct properties.[1e, 2] In contrast, **B**, **D**, and **F** are derived from branching at a coupling unit. In tetraradicals there is also the possibility for branching at a spin carrier (**E**) rather than at a coupling unit (**D** and **F**). Valence considerations for type **E** restrict the maximum connectivity at a carbon or nitrogen radical center to three (one unpaired electron and three free valences for branching), whereas no branching is possible for an oxygen atom as the spin carrier. However, the use of complexing metal centers as coupling units, akin to that in compound **11**, could be employed to bypass such valence limitations.[4b, 11] On the other hand, the connectivity at the coupling units is not restricted to structures like **B** and **F** but limited only by the fantasy of the synthetically inclined polyradical engineer, who may employ higher conjugated cyclic polyenes or even fullerenes. Types **B**, **E**, and **F** constitute the core of "dendritic" polyradicals.[1e]

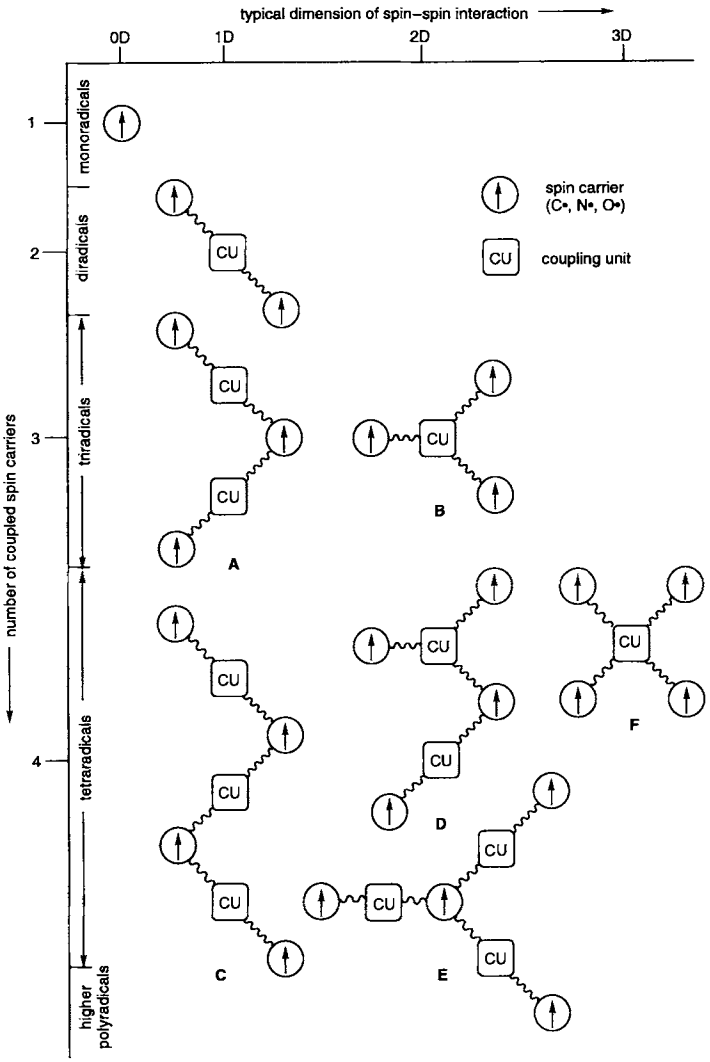

Scheme 1. Possible topologies of tri- and tetraradicals.

Generally speaking, the formation of structures **A**–**F** requires homolytic cleavage of three or four chemical bonds, or three or four one-electron oxidation or reduction steps. Experimentally, there appear to be four basic strategies for achieving this goal, the choice of which depends on the type of spin carrier and the coupling unit. First, oxidation of carbanions,[2, 5, 10] or amines[3] [Eqs. (1a) and (1b)] was used to access structures **2**, **3**,

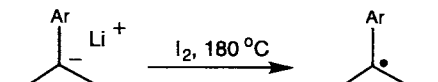

(1a)

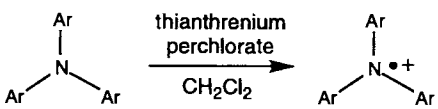

(1b)

[*] Dr. W. M. Nau
Institut für Physikalische Chemie der Universität
Klingelbergstrasse 80, CH-4056 Basel (Switzerland)
Fax: Int. code +(61)267-3855
e-mail: nau@ubaclu.unibas.ch

 © WILEY-VCH Verlag GmbH, D-69451 Weinheim, 1997 0570-0833/97/3622-2445 $ 17.50+.50/0

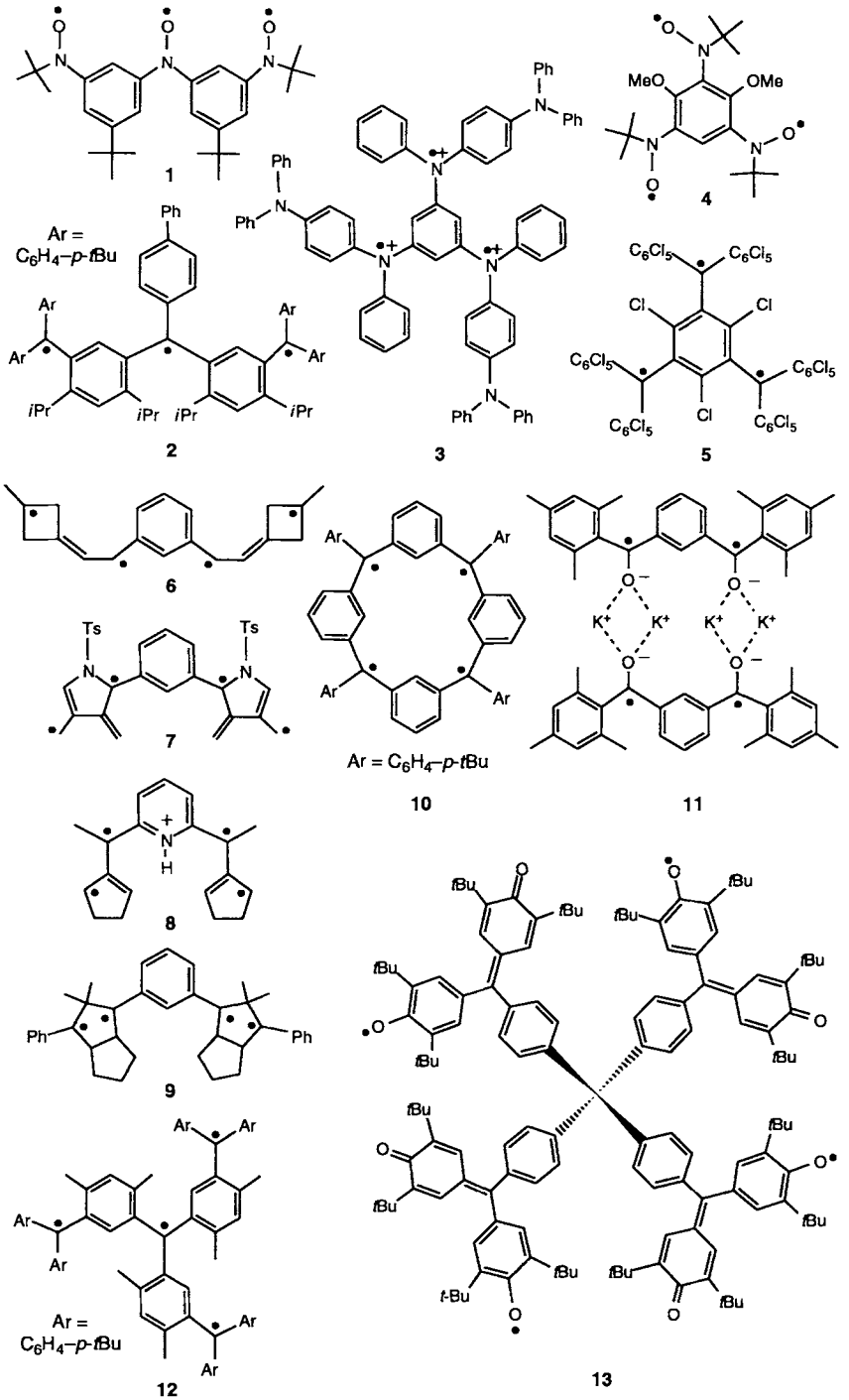

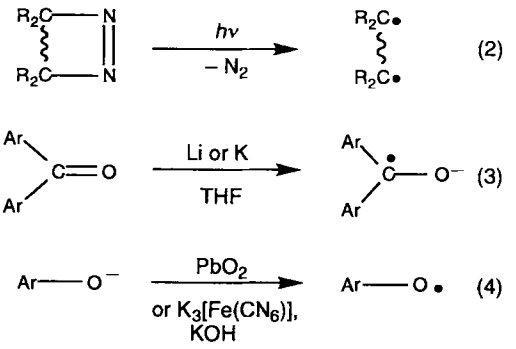

analogously for introducing more than one oxygen spin carrier (structures **1**, **4**, and **13**).[1, 4] The resulting "stable free tri- and tetraradicals",[1h] like some of the Gomberg-type derivatives with triaryl-substituted spin sites,[2, 3, 5, 10] are chemically stable at ambient temperature and relatively insensitive towards oxygen, an important aspect for potential practical use.

Coupling units may promote parallel or antiparallel spin alignment by a variety of electronic mechanisms (orthogonal orbitals, superexchange, and spin-polarization).[1] A parallel alignment leads to "ferromagnetic" or "high-spin" coupling, whereas an antiparallel orientation results in "antiferromagnetic" or "low-spin" behavior. From the application point of view, high-spin polyradicals could be useful as organic ferromagnets,[1] and most of the tri- and tetraradicals **1**–**13** have been studied in this context. Conversely, some low-spin polyradicals, for example those derived from the singlet tetraradical **14**, have recently been suggested to support electric conductivity.[7]

In open-chain tri- or tetraradicals the exclusive use of ferromagnetic coupling units gives rise to quartet ($S = 3/2$) or quintet spin states ($S = 2$) as ground states, as is the case for **1** and **2** (type **A**) or **6** and **9** (type **C**). In contrast, not all coupling units need to be antiferromagnetic to produce low-spin states. For example, to construct singlet ($S = 0$) tetraradicals of type **C** (three coupling units), it is sufficient to confer antiferromagnetic character either to the two outer coupling units (**14**)[8b] or only to the central unit (**15**).[7] Analogously, in triradicals of type **A** already a single antiferromagnetic coupling unit favors low-spin doublet states ($S = 1/2$). When all three electron spins in triradicals of the *cyclic* type **A** (or of type **B**) are antiferromagnetically coupled, an interesting situation arises. At least two electrons must be aligned in a parallel fashion—despite the antiferromagnetic interaction between them— such that a "spin-frustrated" system with two virtually degenerate low-spin (doublet) ground states may result. This exceptional phenomenon was recently described for structure **4**.[4a]

Experimental and theoretical studies[8, 12] demonstrated that the ferromagnetic or antiferromagnetic properties of various coupling units do not always follow intuitive or readily pre-

5, **10**, and **12**; the required intermediate carbanions are obtained by deprotonation of triarylmethanes,[5] or by reduction of triarylmethyl ethers with lithium in tetrahydrofuran.[2, 10] Since this procedure appears to be restricted to triaryl-substituted spin carriers, the second method, which employs photolysis of bisazoalkanes, is complementary [Eq. (2)]; the resulting hydrocarbon tetraradicals **6**–**9**,[6–9] however, are persistent only in low-temperature glasses. Third, reduction of aromatic ketones to produce ketyl radical anions [Eq. (3)] can be extended to generate tetraradicals such as **11**.[11] Of course, the well-established synthetic sequences for preparing "stable free radical" units such as nitroxide and galvinoxyl [Eq. (4)] can be used

 © WILEY-VCH Verlag GmbH, D-69451 Weinheim, 1997 0570-0833/97/3622-2446 $ 17.50+.50/0

dictable trends. The methylene group is the simplest coupling unit and, depending on the conformation, may give rise to ferromagnetic or antiferromagnetic coupling;[8b] difluoro substitution of the methylene group promotes the latter.[12b] The *m*-phenylene coupling unit has been most extensively employed (see **1**–**12**) due to its robust ferromagnetic coupling properties, synthetic compatibility, and the possibility of 2D spin–spin interaction through the 1,3,5-substitution pattern (Mataga polymer).[1] Moreover, the ferromagnetic coupling of *m*-phenylene can be modified by conformational constraints,[8c] aryl substituents,[4a, 12a] and the use of heteroaromatic analogues or ionic derivatives.[8a] Such magnetic fine-tuning promises some interesting twists in the design of more sophisticated structures. While the selection of the coupling unit is crucial for controlling spin multiplicity in tri- and tetraradicals, the type of spin carrier (C˙, N˙, O˙) appears to be less important, at least for *m*-phenylene as the coupling unit. Hence, even the hetero-substituted triradical cation **3** and the tetraradical anion **11** exhibit high-spin ground states, just as their neutral analogues **5** and **10**.

Tri- and tetraradicals can be conveniently observed and identified by ESR spectroscopy, with the exception of ESR-silent singlet tetraradicals such as **14** and **15** (here, the absence of ESR signals was taken as evidence for their singlet multiplicity).[7, 8b]

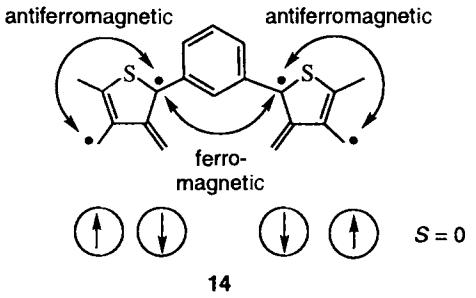

14

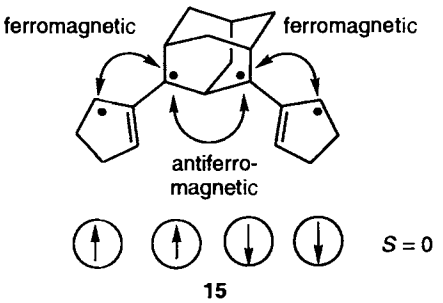

15

Quartet and quintet states produce very distinct ESR spectra, which yield the zero-field splitting parameters characteristic of tri- and tetraradicals, and provide a sensitive probe for their detection. In addition, the temperature dependence of the intensity of the ESR signal (Curie plot) can be employed to establish the quartet or quintet state as the ground state, and, in some cases, to estimate the energy gaps to the lower spin states (that is, the doublet of a triradical or the triplet and singlet of a tetraradical).[3, 8b]

The assignment of ESR spectra to high-spin tri- and tetraradicals is nowadays facilitated by computer simulations. Conversely, experimental high-spin ESR spectra were crucial for refining theoretical models of spin–spin interactions and accurately predicting the resulting ESR features.[6–10] The ESR spectra produced upon photolysis of bisazoalkanes[6–9] are particularly instructive, because stepwise nitrogen extrusion—that is, pairwise formation of spin carriers—produces first the triplet diradical ESR spectra [Eq. (5)], unless the diradicals have

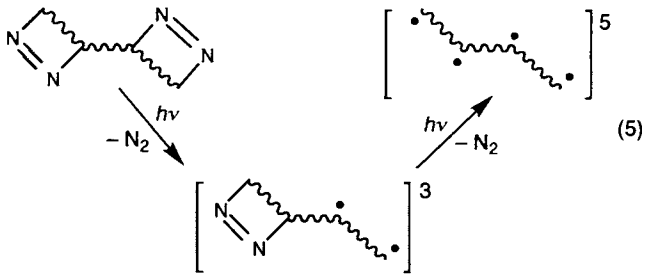

(5)

singlet ground states.[7, 8b] Discernible spectral changes are observed upon prolonged irradiation, which can be convincingly assigned to the quintet tetraradicals; ideally, all of the intermediate triplet diradicals are converted into the tetraradicals, leaving behind the pure quintet ESR spectra.

Magnetization studies offer another means of characterizing the high-spin character of tri- and tetraradicals, and constitute the greatest hurdle for any polyradical as far as potential applications as an organic ferromagnet are concerned. Depending on the applied magnetic field, the amount and magnetic moment of paramagnetic molecules, and the temperature, the spins in a sample align and the degree of alignment can be measured as magnetization or magnetic susceptibility.[1] Plotting the data according to theoretical functional relationships allows one to extract the spin multiplicity of a tri-, tetra-, or higher polyradical. Deviations from the expected magnetization functions were interpreted in terms of 1) molecular defects, 2) thermal equilibration between different spin states, and 3) concomitant *intermolecular* coupling between the paramagnetic molecules.[1, 10] This last effect is the stumbling block for many organic tri- or tetraradicals, since intermolecular coupling is often antiferromagnetic in nature,[1a, 11] which makes their practical use as organic ferromagnets questionable. This limitation necessitates the design of higher and truly 3D polyradicals, or, as alternative, warrants suitable crystal packing[1c, 13] and metal-coordinating strategies[4b, 11] to ensure ferromagnetic coupling even in the absence of covalent molecular connectivity.

German version: *Angew. Chem.* **1997**, *109*, 2551–2554

Keywords: EPR spectroscopy · magnetic properties · polyradicals · radicals · spin states

[1] a) H. Iwamura, N. Koga, *Acc. Chem. Res.* **1993**, *26*, 346–351; b) H. Kurreck, *Angew. Chem.* **1993**, *105*, 1472–1474; *Angew. Chem. Int. Ed. Engl.* **1993**, *32*, 1409–1411; c) O. Kahn, *Molecular Magnetism*, VCH, New York, **1993**; d) J. S. Miller, A. J. Epstein, *Angew. Chem.* **1994**, *106*, 399–432; *Angew. Chem. Int. Ed. Engl.* **1994**, *33*, 385–415; e) A. Rajca, *Chem. Rev.* **1994**, *94*, 871–893; f) J. A. Crayston, A. Iraqi, J. C. Walton, *Chem. Soc. Rev.* **1994**, 147–153; g) M. Baumgarten, K. Müllen, *Top. Curr. Chem.* **1994**, *169*, 1–104; h) M.-E. Brik, *Heterocycles* **1995**, *41*, 2827–2873.

[2] A. Rajca, S. Rajca, *J. Am. Chem. Soc.* **1995**, *117*, 9172–9179; *ibid.* **1996**, *118*, 8121–8126.

[3] a) K. R. Stickley, T. D. Selby, S. C. Blackstock, *J. Org. Chem.* **1997**, *62*, 448–449; b) M. M. Wienk, R. A. Janssen, *J. Am. Chem. Soc.* **1997**, *119*, 4492–4501.

 © WILEY-VCH Verlag GmbH, D-69451 Weinheim, 1997 0570-0833/97/3622-2447 $ 17.50+.50/0

[4] a) J. Fujita, M. Tanaka, H. Suemune, N. Koga, K. Matsuda, H. Iwamura, *J. Am. Chem. Soc.* **1996**, *118*, 9347–9351; b) K. Inoue, T. Hayamizu, H. Iwamura, D. Hashizume, Y. Ohashi, *ibid.* **1996**, *118*, 1803–1804.
[5] J. Veciana, C. Rovira, N. Ventosa, M. I. Crespo, F. Palacio, *J. Am. Chem. Soc.* **1993**, *115*, 57–64.
[6] S. J. Jacobs, D. A. Dougherty, *Angew. Chem.* **1994**, *106*, 1155–1157; *Angew. Chem. Int. Ed. Engl.* **1994**, *33*, 1104–1106.
[7] a) H. S. M. Lu, J. A. Berson, *J. Am. Chem. Soc.* **1996**, *118*, 265–266; *ibid.* **1997**, *119*, 1428–1438; b) J. A. Berson, *Acc. Chem. Res.* **1997**, *30*, 238–244.
[8] a) A. P. West, Jr., S. K. Silverman, D. A. Dougherty, *J. Am. Chem. Soc.* **1996**, *118*, 1452–1463; b) S. J. Jacobs, D. A. Shultz, R. Jain, J. Novak, D. A. Dougherty, *ibid.* **1993**, *115*, 1744–1753; c) S. K. Silverman, D. A. Dougherty, *J. Phys. Chem.* **1993**, *97*, 13273–13283.
[9] W. Adam, C. van Barneveld, S. E. Bottle, H. Engert, G. R. Hanson, H. M. Harrer, C. Heim, W. M. Nau, D. Wang, *J. Am. Chem. Soc.* **1996**, *118*, 3974–3975.
[10] A. Rajca, S. Rajca, S. R. Desai, *J. Am. Chem. Soc.* **1995**, *117*, 806–816.
[11] M. Baumgarten, L. Gherghel, T. Wehrmeister, *Chem. Phys. Lett.* **1997**, *267*, 175–178.
[12] a) S. Fang, M.-S. Lee, D. A. Hrovat, W. T. Borden, *J. Am. Chem. Soc.* **1995**, *117*, 6727–6731; b) S. J. Getty, D. A. Hrovat, W. T. Borden, *ibid.* **1994**, *116*, 1521–1527.
[13] a) R. Chiarelli, M. A. Novak, A. Rassat, J. L. Tholence, *Nature* **1993**, *363*, 147–149; b) M. M. Matsushita, A. Izuoka, T. Sugawara, T. Kobayashi, N. Wada, N. Takeda, M. Ishikawa, *J. Am. Chem. Soc.* **1997**, *119*, 4369–4379.

EVENTS

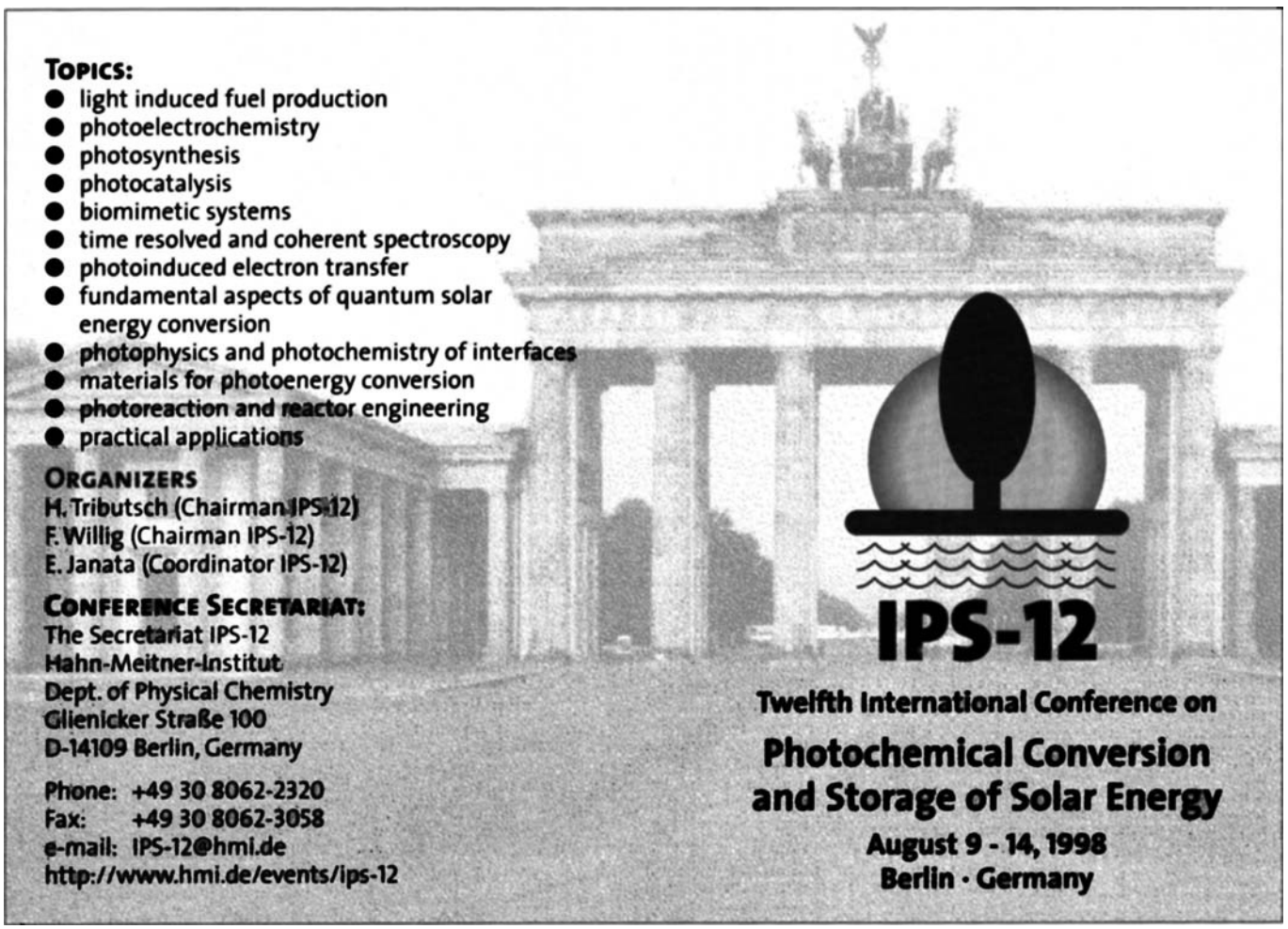

 © WILEY-VCH Verlag GmbH, D-69451 Weinheim, 1997 0570-0833/97/3622-2448 $ 17.50+.50/0

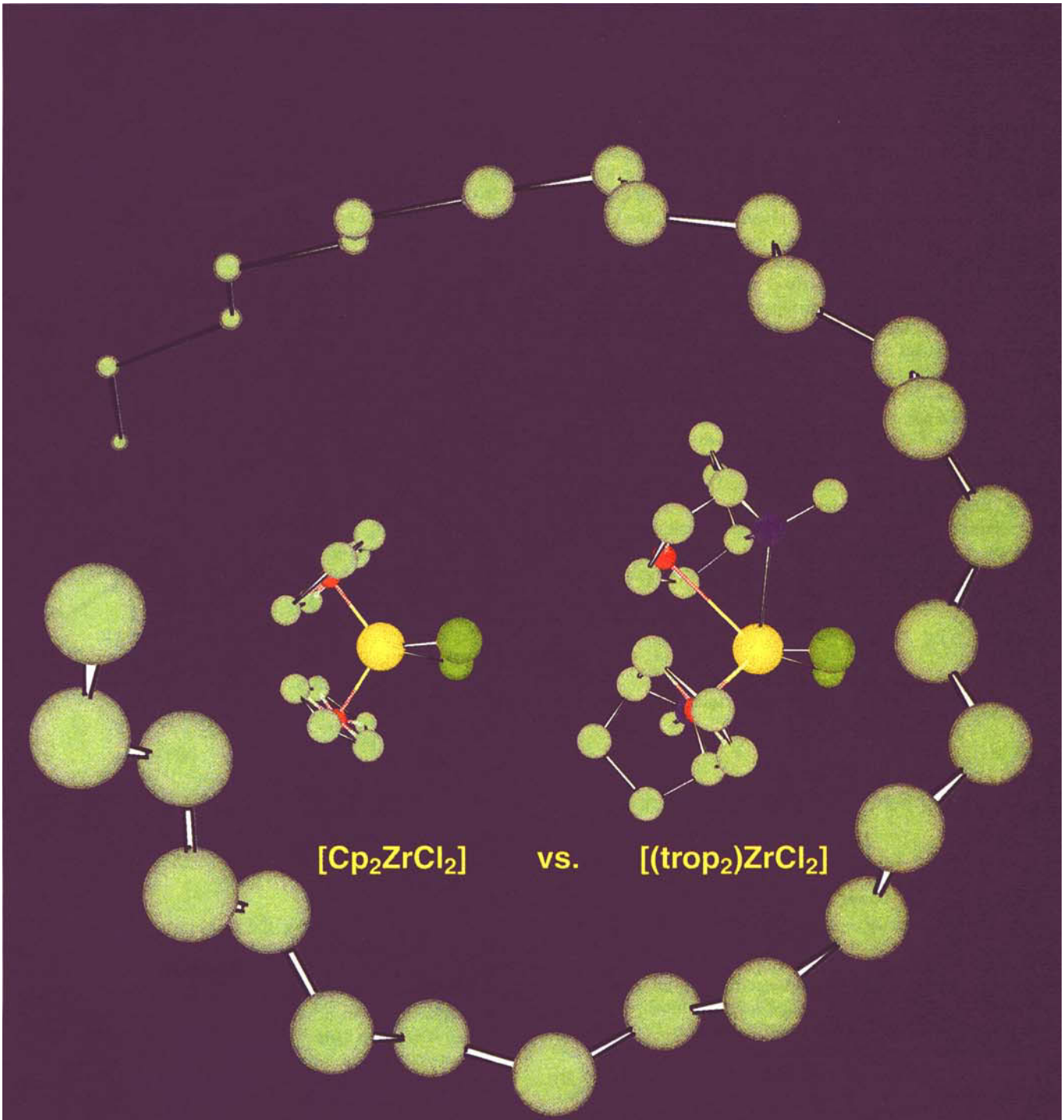

The tropidinyl (trop) group is a novel ligand that is isoelectronic with cyclopentadienyl (Cp), and is derived from a readily available natural product. It can be used to synthesize zirconium complexes that are analogous to metallocenes. When activated with methylalumoxanes they function as catalysts for ethylene polymerization. More about the synthesis and properties of this new class of complexes is reported by R. G. Bergman and G. G. Lavoie on p. 2450ff.

 © WILEY-VCH Verlag GmbH, D-69451 Weinheim, 1997 0570-0833/97/3622-2449 $ 17.50+.50/0

Synthesis, Structural Characterization, and Reactivity of Novel Zirconium(IV) Complexes Containing the Tropidinyl Ligand**

Gino G. Lavoie and Robert G. Bergman*

Cyclopentadienyl (Cp) and bis(cyclopentadienyl) complexes have played an enormous role in the development of fundamental and practical organometallic chemistry.[1] The use of metallocene catalysts for Ziegler–Natta polymerization of alkenes,[2] one of the most important recent advances in the latter area, has generated interest in the synthesis of ligands that are isoelectronic with Cp but might confer different properties (e. g., different rates or selectivities) on the derived metal complexes.

The conception of the Cp group as a delocalized three-electron anionic allyl ligand combined with a two-electron neutral alkene ligand raises the possibility of combining the allyl group with other two-electron donors to give complexes that would be isoelectronic with, but less symmetrical than, Cp complexes. However, allyl complexes of early transition metals often have low thermal stability.[3,4] We therefore sought a system in which an anionic allyl ligand is connected by two bridges to a neutral two-electron donor,[5] in the hope that this would make the derived organometallic materials more robust. We now report the execution of this idea in the synthesis of complexes derived from the readily available bicyclic molecule tropidine (**1**-H, Scheme 1). The advantages of **1** are that 1) the ligand derived

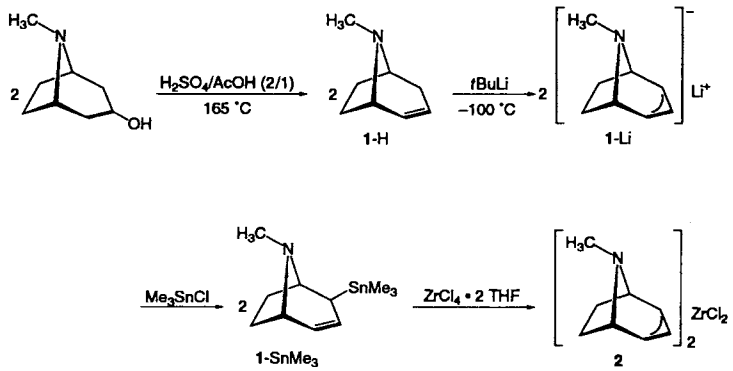

Scheme 1. Synthesis of **2** from tropine.

from it has separate 2σ- and 4π-electron donor sites, 2) the presence of the two-carbon bridge helps to localize the allyl functionality in a specific part of the molecule and prevents loss of the ligand by β-hydride elimination (Bredt's rule),[6–8] and 3) the ligand lacks groups that allow easy deactivation by cyclometallation (intramolecular C–H activation). To our knowledge, this is the first report of coordination of this ligand to a transition metal center.

Tropidine (**1**-H) can be readily obtained by dehydration of tropine under strongly acidic conditions (Scheme 1).[9] The allylic position was deprotonated by treating the bicyclic compound with a strong base such as *tert*-butyllithium at low temperature.[10] Subsequent addition of trimethyltin chloride to the lithium salt of the tropidinyl (trop) anion (**1**-Li) yields the stannylated compound **1**-$SnMe_3$ in good yield. Addition of two equivalents of **1**-$SnMe_3$ to a solution of $ZrCl_4 \cdot 2THF$ in dichloromethane gave the desired disubstituted zirconium complex $[(trop)_2ZrCl_2]$ (**2**) in 59% yield (Scheme 1). Other methods involving reaction of **1**-H or the corresponding silylated derivative with Zr^{IV} precursors such as $[Zr(NMe_2)_4]$, $[Zr(OtBu)_4]$, or $[Zr(CH_2Ph)_4]$ did not give the expected product, even at elevated temperature. Similarly, addition of the trop anion to Zr^{IV} starting materials led only to mixtures of unidentified complexes.

The ^1H NMR spectrum of **2** in CD_2Cl_2 shows a very simple pattern, which suggests that the complex may have C_2 symmetry. The solid-state structure was solved on a single crystal by direct methods[11] and expanded with Fourier techniques[12] (Figure 1).[13] Surprisingly, the complex has a C_1-symmetric structure in which the trop ligands are rotated by 76.86° with respect to one other. The trop ligand labeled C1, C2, C3, C8, N1 is bound symmetrically to the metal center. In contrast, the other trop ligand is unsymmetrically bound to zirconium, as evidenced by different bond lengths for Zr1–C9 and Zr1–C11. The Cl1-Zr1-Cl2 bond angle of 100.89(3)° is slightly more obtuse than the corresponding angle of 97.1° in $[Cp_2ZrCl_2]$.[14] The Zr1–Cl1 and Zr1–Cl2 bond lengths of 2.5051(8) and 2.5089(8) Å, respectively, are somewhat longer than that of 2.44 Å in zirconocene dichloride.[14]

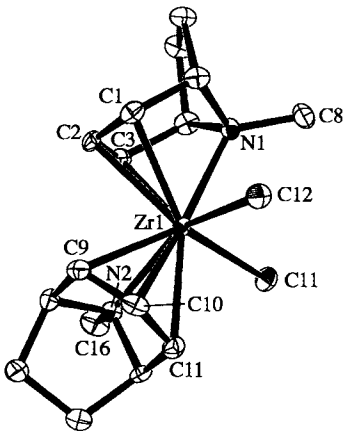

Figure 1. ORTEP plot of **2**. Selected bond lengths [Å] and angle [°]: Zr1–Cl1 2.5051(8), Zr1–Cl2 2.5089(8), Zr1–C1 2.537(3), Zr1–C2 2.518(3), Zr1–C3 2.523(3), Zr1–C9 2.493(3), Zr1–C10 2.595(3), Zr1–C11 2.595(3), Zr1–N1 2.353(3), Zr1–N2 2.369(3); Cl1-Zr1-Cl2 100.89(3).

The discrepancy between the solid-state structure and the observed ^1H NMR spectrum led us to investigate the fluxional behavior of **2**. A series of variable-temperature ^1H NMR (300 MHz) spectra were collected. These revealed strongly fluxional behavior, which resolved into a spectrum exhibiting nonequivalent trop ligands at −90 °C. The spectrum at −90 °C is consistent with the X-ray structure. The decoalescence of the central allylic protons at −48 °C indicates a free energy barrier for rotation of the trop ligands of 19 kcal mol^{-1}.

We carried out some preliminary reactivity studies on **2**. Addition of two equivalents of methyllithium gave the yellow dimethylzirconium complex $[(trop)_2ZrMe_2]$ (**3**, Scheme 2). As in the dichloride **2**, a simple pattern was observed in the room-temperature ^1H NMR spectrum of **3**. In contrast to **2**, however, no decoalescence of the signals was observed when **3** was cooled to the freezing point of dichloromethane.

Complex **3** was characterized by X-ray crystallography.[13] As in **2**, the trop ligands are related by no symmetry element, but are rotated with respect to one another by 87.71°, more than 10° greater than in **2**. We are unsure why the energy barrier for rotation of the trop ligands in **3** is substantially lower than that in the corresponding dichloride **2**. The Zr–trop bonds are also longer than those in **2**. The Zr–Me bond lengths and the Me-Zr-

[*] Prof. R. G. Bergman, Dr. G. G. Lavoie
Department of Chemistry
University of California
Berkeley, CA 94620 (USA)
Fax: Int. code +(510)642-7714
e-mail: bergman@cchem.berkeley.edu

[**] We thank Drs. P. A. Goodson, R. E. Powers, and F. Hollander for solving the crystal structures. We are also grateful to the U. S. National Science Foundation (grant no. CHE-9633374), the Union Carbide Co., and the Arthur C. Cope Fund of the American Chemical Society for funding this project.

 © WILEY-VCH Verlag GmbH, D-69451 Weinheim, 1997 0570-0833/97/3622-2450 $ 17.50+.50/0

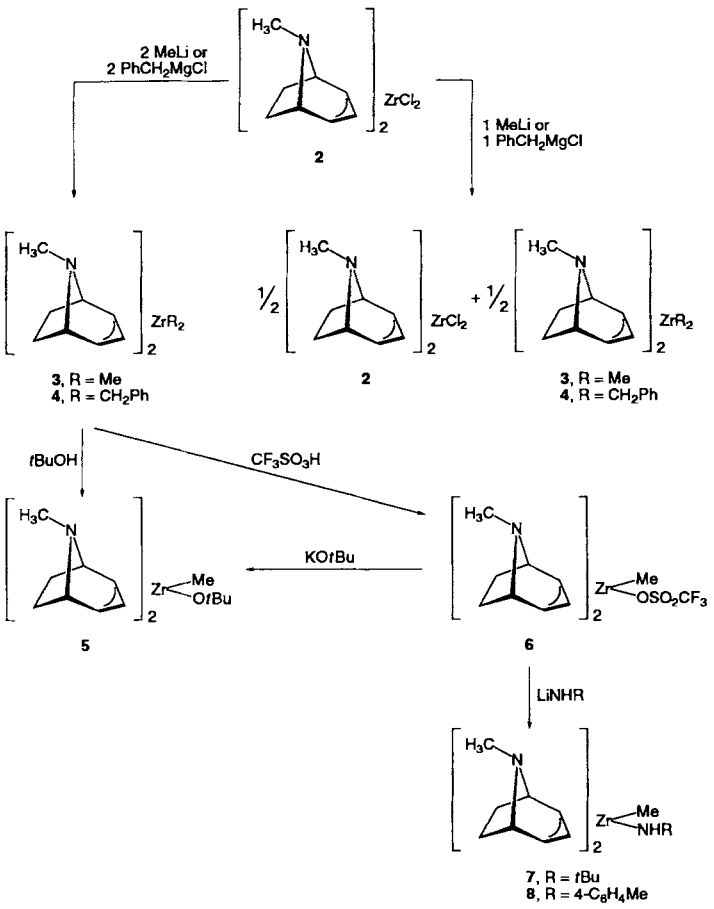

Scheme 2. Ligand-substitution reactions of **2**.

Me bond angle are 2.316(2) and 2.315(2) Å, and 95.75(9)°. These values are similar to those reported for dimethylzirconocene [2.280(5) Å and 2.275(5) Å, 95.6(12)°].[15] Complex **3** was unstable when placed under prolonged dynamic vacuum, and an uncharacterized white powder formed.

Addition of two equivalents of benzylmagnesium chloride to **2** gave the expected bis(benzyl)zirconium derivative **4**. The NMR spectrum shows apparent C_2 symmetry, but a recently determined X-ray structure of **4**[13] shows nonequivalent trop ligands analogous to those in **2** and **3**. When only one equivalent of methyllithium or benzylmagnesium chloride was added to **2**, a 1:1 mixture of **2** and the corresponding bis(alkyl)zirconium derivative was obtained.

Protonolysis of **3** with *tert*-butyl alcohol at room temperature gave the yellow complex **5** in quantitative yield. Treatment of **3** with *tert*-butylamine did not yield the corresponding *tert*-butylamido complex. Heating the reaction mixture to 77 °C led to decomposition of **3** prior to formation of the desired product **7**. The latter could, however, be prepared in 95% purity (92% yield) by protonation of **3** with one equivalent of trifluoromethanesulfonic acid to give **6** and subsequent addition of one equivalent of LiNH*t*Bu. Similarly, **8** and **5** can be synthesized by addition of the corresponding nucleophile to **6**. As was observed for **3**, placing **8** under vacuum for one hour led to decomposition to an uncharacterized white powder.

Preliminary experiments were carried out on the use of $[(trop)_2ZrX_2]$ complexes as polymerization catalysts. Addition of a large excess of methylaluminoxane (MAO) to a solution of **2** in toluene under an ethylene atmosphere gave a purple solution that was active for the polymerization of this alkene. The measured polyethylene productivity of 17 $kg\,mol^{-1}\,h^{-1}$, as determined by comparative studies, was roughly 14 times slower than ethylene polymerization by $[Cp_2ZrCl_2]$/MAO under the same conditions.[16] Further studies will be required to determine whether the trop ligands remain attached to the metal during polymerization, although the fact that $[(trop)_2ZrMe_2]$ retains these ligands on treatment with trifluoromethylsulfonic acid suggests that the trop—Zr bond is robust.

Straightforward synthetic routes can be devised for attaching substituents to the trop rings and for linking two trop ligands together to produce *ansa* analogues of the materials described here. Such studies are under way, as is the development of methods for attaching trop ligands to other metal centers.

Experimental Section

Synthesis and analytical data on complexes **1**-$SnMe_3$, **2**, **3**, and **4** are given here. Data on complexes **5**–**8** will be provided elsewhere.

Safety note: Because of the high toxicity of tin compounds and the high neurological activity of tropidine derivatives, all work must be performed in a well-ventilated working area and skin contact prevented with protective clothing and gloves.

1-$SnMe_3$: *tert*-Butyllithium (1.7 M in pentane, 52 mL, 88 mmol) was added dropwise over 15 min to tropine [9] (10.7 g, 88.9 mmol) in pentane (500 mL) at −100 °C. Deprotonation was allowed to proceed at −80 °C for 3 d. The resulting mixture was then cooled to −100 °C, and trimethyltin chloride (1 M in hexane, 104 mL, 104 mmol) was added over 15 min. The pale yellow solution immediately turned white with concomitant precipitation of white solid. The flask was warmed to room temperature over 1 h, and the mixture stirred for an additional 30 min. Water (100 mL) was carefully added, and the organic materials were extracted with pentane. The combined organic extracts were washed with brine and dried over sodium sulfate. The solvents were removed under water aspirator pressure, and the residue was distilled under vacuum (3 mtorr) at 50 °C to give 11.2 g (45%) of **1**-$SnMe_3$. ^1H NMR (C_6D_6): δ = 5.52 (m, 2H, olefinic), 3.13 (m, 1H, bridgehead), 3.04 (br s, 1H, bridgehead), 2.42 (s, 4H, N*Me* and C*H*$SnMe_3$), 2.07 (m, 2H, CH_2), 1.81 (m, 1H, CH_2), 1.46 (m, 1H, CH_2), 0.06 (s, 9H, $SnMe_3$; further split by 8.7 and 7.7% of ^{119}Sn and ^{117}Sn, respectively; J = 25.5 Hz); $^{13}C\{^1H\}$ NMR (C_6D_6): δ = 127.3, 127.1 (olefinic), 60.1, 58.7 (bridgehead), 36.7 (C7 or C8), 34.8 (NMe), 33.1 (C7 or C8), 30.5 (*C*H$SnMe_3$), −10.1 ($SnMe_3$); HRMS: *m/z* calcd for $C_{11}H_{21}N_1Sn$: 287.0696; found: 287.0702.

2: A Schlenk flask was charged with a solution of $ZrCl_4 \cdot 2THF$ (758 mg, 2.01 mmol) in dichloromethane (25 mL). **1**-$SnMe_3$ (1.16 g, 4.02 mmol) was added over 5 min with stirring. The solution immediately turned orange and was stirred for 4 d at room temperature. The reaction mixture was filtered, and the solid washed with dichloromethane. The volatile materials were removed in vacuo, and the residue was washed thoroughly with pentane and then extracted with toluene. The solvent was removed in vacuo to give 478 mg (59%) of an analytically pure, fine orange powder. ^1H NMR (CD_2Cl_2): δ = 5.72 (dd, J = 7 Hz, 2H, central allylic), 4.31 (d, J = 7 Hz, 2H, terminal allylic), 4.29 (d, J = 7 Hz, 2H, terminal allylic), 3.73 (br s, 4H, bridgehead), 2.48 (s, 6H, NMe), 2.23 (s, 8H, CH_2); ^1H NMR (C_6D_6): δ = 5.38 (dd, J = 7.3 Hz, 2H, central allylic), 4.26 (br s, 4H, terminal allylic), 3.54 (br s, 4H, bridgehead), 2.29 (s, 6H, NMe), 1.84 (s, 4H, CH_2), 1.68 (m, 4H, CH_2); $^{13}C\{^1H\}$ NMR (CD_2Cl_2): δ = 132.0 (C3) 87.6 (C2 and C4), 67.0 (C1 and C5), 41.2 (NMe), 38.9 (CH_2); elemental analysis calcd for $C_{156}H_{24}N_2Cl_2Zr_1$: C 47.28, H 5.95, N 6.89; found: C 46.78, H 5.85, N 6.60; HRMS: *m/z* calcd: 404.0364; found: 404.0361.

3: Complex **2** (118 mg, 0.290 mmol) was dissolved in 10 mL of THF and cooled to −30 °C. Methyllithium (1.4 M in ether, 414 mL, 0.580 mmol) was added, and the reaction mixture stirred at room temperature for an additional 3.5 h. The solvent was evaporated under reduced pressure, and the residue extracted with pentane. The combined pentane extracts were filtered. The filtrate was recovered, and the volatile components were removed in vacuo to yield 94.6 mg (89%) of analytically pure, yellow solid. ^1H NMR (C_6D_6): δ = 4.86 (dd, J = 7.4 Hz, 2H, central allylic), 3.87 (d, J = 7.3 Hz, 2H, terminal allylic), 3.86 (d, J = 7.3 Hz, 2H, terminal allylic), 3.31 (m, 4H, bridgehead), 2.12 (m, 4H, CH_2), 2.02 (s, 6H, NMe), 1.90 (m, 4H, CH_2), 0.22 (s, 6H, $ZrMe_2$); ^1H NMR (CD_2Cl_2): δ = 4.85 (dd, J = 7.2 Hz, 2H, central allylic), 3.87 (d, J = 7.2 Hz, terminal allylic), 3.51 (br s, 4H, bridgehead), 2.30 (s, 6H, NMe), 2.23 (s, 8H, CH_2), −0.30 (s, 6H, $ZrMe_2$); $^{13}C\{^1H\}$ NMR (C_6D_6): δ = 126.3 (central allylic), 80.4 (terminal allylic), 66.8 (bridgehead), 40.4 (NMe), 39.9 (CH_2), 25.8 ($ZrMe_2$); $^{13}C\{^1H\}$ NMR (CD_2Cl_2): δ = 149.7 (central allylic),

[(trop)$_2$Zr(Me)O*t*Bu] **5**

[(trop)$_2$Zr(Me)OSO$_2$CF$_3$] **6**

[(trop)$_2$Zr(Me)NH*t*Bu] **7**

[(trop)$_2$Zr(Me)NH-4-C$_6$H$_4$Me] **8**

 © WILEY-VCH Verlag GmbH, D-69451 Weinheim, 1997 0570-0833/97/3622-2451 $ 17.50+.50/0

103.9 (terminal allylic), 90.1 (bridgehead), 63.9 (NMe), 63.2 (CH_2), 47.6 ($ZrMe_2$); elemental analysis calcd for $C_{18}H_{30}N_2Zr_1$: C 59.12, H 8.27, N 7.66; found: C 59.43, H 8.38, N 7.60; LRMS (EI): *m/z* calcd: 364; found: 364.

4: Complex **2** (103 mg, 0.254 mmol) was dissolved in 10 mL THF and cooled to $-30\,^{\circ}C$. Benzylmagnesium chloride (1 M in ether, 481 mL, 0.481 mmol) was added, and the solution stirred at room temperature for 2 h. The solvents were removed in vacuo. Complex **4** was recovered by extraction of the residue with toluene. The volatile materials were removed to give 110 mg (88%) of an orange solid. Analytically pure crystals of **4** can be obtained by vapor diffusion of pentane into a toluene solution of this solid at $-30\,^{\circ}C$. ^1H NMR (C_6D_6): $\delta = 7.27$ (t, $J = 7.7$ Hz, 4H, Ar), 7.12 (t, $J = 7.7$ Hz, 4H, Ar), 6.90 (t, $J = 7.2$ Hz, 2H, Ar), 5.14 (dd, $J = 7.4$ Hz, 2H, central allylic), 3.80 (d, $J = 7.3$ Hz, 2H, terminal allylic), 3.78 (d, $J = 7.3$ Hz, 2H, terminal allylic), 2.85 (br s, 4H, bridgehead), 2.05 (s, 6H, NMe), 1.95 (m, 4H, CH_2Ph), 1.72 (s, 8H, CH_2); $^{13}C\{^1H\}$ NMR (C_6D_6): $\delta = 155.8$ (C_{ipso}), 128.9 (central allylic), 128.0 (Ar), 125.7 (Ar), 119.4 (C_{para}), 83.8 (terminal allylic), 66.4 (bridgehead), 58.6 (CH_2Ph), 40.2 (NMe), 39.5 (CH_2); elemental analysis calcd for $C_{30}H_{38}N_2Zr$: C 69.58, H 7.40, N 5.41; found: C 69.56, H 7.60, N 5.21.

Polymerization of C_2H_4 by **2** and MAO: A Schlenk flask was charged with **2** (5.3 mg, 13 mmol) and 8 mL toluene and placed under 1 atm ethylene. MAO (Akzo, type 4; 3.4 mL, 13 mmol) was added over 1 min at room temperature. The yellow solution immediately turned dark orange, then blue and violet. The color vanished within 15–20 min. The solution was stirred under 1 atm ethylene for 45 min, and then the polymerization was stopped by careful addition of an acidified methanol solution (5% HCl). The mixture was filtered, and the polymer thoroughly dried in vacuo. Yield: 102 mg (17 $kg\,mol^{-1}\,h^{-1}$). Similar conditions were used for the control experiment with Cp_2ZrCl_2 (240 $kg\,mol^{-1}\,h^{-1}$).

Received: May 20, 1997 [Z10450IE]
German version: *Angew. Chem.* **1997**, *109*, 2555–2558

Keywords: polymers · sandwich complexes · tropidine · zirconium

[1] J. P. Collman, L. S. Hegedus, J. R. Norton, R. G. Finke, *Principles and Applications of Organotransition Metal Chemistry*, University Science Books, Mill Valley, **1987**.
[2] H. H. Brintzinger, D. Fischer, R. Mülhaupt, B. Rieger, R. M. Waymouth, *Angew. Chem.* **1995**, *107*, 1255; *Angew. Chem. Int. Ed. Engl.* **1995**, *34*, 1143.
[3] G. Wilke, B. Bogdanovic, P. Hardt, P. Heimbach, W. Keim, M. Kröner, W. Oberkirch, K. Tanaka, E. Steinrücke, D. Walter, H. Zimmermann, *Angew. Chem.* **1966**, *78*, 157; *Angew. Chem. Int. Ed. Engl.* **1966**, *5*, 151.
[4] *Comprehensive Organometallic Chemistry II, Vol. 12* (Eds.: E. W. Abel, F. G. A. Stone, G. Wilkinson), Elsevier, **1995**.
[5] J. Blümel, N. Hertkorn, B. Kanellakopulos, F. H. Köhler, J. Lachmann, G. Müller, F. E. Wagner, *Organometallics* **1993**, *12*, 3896.
[6] K. J. Shea, *Tetrahedron* **1980**, *30*, 1683.
[7] G. L. Buchanan, *Chem. Soc. Rev.* **1974**, *3*, 41.
[8] G. Köbrich, *Angew. Chem.* **1973**, 85, 494; *Angew. Chem. Int. Ed. Engl.* **1973**, 464.
[9] A. Ladenburg, *Justus Liebigs Ann. Chem.* **1888**, *217*, 118.
[10] Deprotonation must be performed at low temperature to prevent decomposition of the product to an unidentified mixture of compounds.
[11] SIR92: A. Altomare, M. Cascarano, C. Giacovazzo, A. Guagliardi, *J. Appl. Cryst.* **1993**, *26*, 343.
[12] DIRDIF92: P. T. Beurskens, G. Admiraal, G. Beurskens, W. P. Bosman, S. Garcia-Granda, R. O. Gould, J. M. M. Smits, C. Smykalla, *The DIRDIF Program System, Technical Report of the Crystallography Laboratory*, University of Nijmegen, The Netherlands.
[13] X-ray quality crystals of **2** were obtained by slow diffusion of pentane into a solution of the complex in toluene at $-30\,^{\circ}C$. The structure was solved by direct methods with a full matrix least-squares refinement. Details of the X-ray structures of **3** and **4** will be reported in a full paper. Crystal data for **2**: $C_{16}H_{24}C_{12}N_2Zr$. Orange plate-like crystals ($0.08 \times 0.14 \times 0.35$ mm), monoclinic, space group $P2_1/n$ (no. 14), $a = 7.0931(2)$, $b = 18.2744(2)$, $c = 12.8139(3)$ Å; $\beta = 85.777(1)^{\circ}$, $V = 1652.53(5)$ Å^3. Number of observed reflections [$I > 3.00\sigma(I)$] 2193; 190 variables; $R = 0.028$, $R_w = 0.035$, $R_{all} = 0.042$, GOF = 1.33. Crystallographic data (excluding structure factors) for the structure reported in this paper have been deposited with the Cambridge Crystallographic Data Centre as supplementary publication no. CCDC-100489. Copies of the data can be obtained free of charge on application to The Director, CCDC, 12 Union Road, Cambridge CB21EZ, UK (Fax: Int. code +(1223)336-033; e-mail: deposit@chemcrys.cam.ac.uk).
[14] K. Prout, T. S. Cameron, R. A. Forder, S. R. Critchley, B. Denton, G. V. Rees, *Acta Crystallogr. Sect. B* **1974**, *30*, 2290.
[15] W. E. Hunter, D. C. Hrncir, R. V. Bynum, R. A. Penttila, J. L. Atwood, *Organometallics* **1983**, *2*, 750.
[16] Preliminary measurements showed that the polyethylene exhibits a relatively high molecular weight but a rather broad polydispersity ($M_w = 628045$; $M_n = 14267$). We are grateful to Drs. Timothy Wenzel and Thomas Peterson, Union Carbide Co., for arranging to have these measurements made.

High La^{III} Affinity of a Bis(spirobenzopyran) Azacrown Ether and Photoinduced Switching of its Ion Selectivity between Multivalent and Monovalent Metal Ions**

Keiichi Kimura,* Tomohito Utsumi, Takashi Teranishi, Masaaki Yokoyama, Hidefumi Sakamoto, Masanori Okamoto, Ryuichi Arakawa, Hiroshi Moriguchi, and Yoko Miyaji

The photochromicity of spirobenzopyran derivatives is due to photoisomerization between their electrically neutral spiropyran and zwitterionic merocyanine forms.[1] The photochromism can often be used for controlling physical properties.[2] We are interested in macrocyclic ligands that can switch their metal ion complexing ability and/or their ion selectivity photochemically, as well as their application in materials science and analytical chemistry. We therefore designed 1,3,3-trimethylindolino-6′-nitrobenzopyrylospiran derivatives with a crown ether moiety at the 8′-position, in which the phenolate oxygen atom of the merocyanine form plays an important role in metal ion complexation by forming a six-membered ring chelate with a nitrogen atom of the azacrown ether.[3] The spirobenzopyran azacrown ethers can undergo photochemical switching upon complexing monovalent metal ions, and have been successfully applied in photoresponsive ion-conducting systems.[4]

Recently the crown ether derivative **1**, which has two spirobenzopyran moieties, was designed for photocontrol of the complexation of divalent metal ions.[5] In our studies, we found that, even in the dark, **1** binds multivalent metal ions much more strongly than its corresponding parent azacrown ether **2** (Scheme 1). Here we report the remarkably high affinity of **1** for La^{3+} and the photochemical switching of its ion selectivity between trivalent and monovalent metal ions.

Absorption spectra of solutions containing equimolar amounts of **1** and a metal ion in acetonitrile recorded in the dark showed a significant peak between 500 and 600 nm, which were assigned to the merocyanine form of the photochromic moiety; isomerization into this form was induced by complexation of the cation by the crown ether moiety. In general, the merocyanine absorption was much more intense for mulitivalent metal ions such as Ca^{2+} and La^{3+} than for monovalent ions such as Na^+ and K^+. This suggests a higher affinity of **1** for multivalent metal ions than for monovalent ones. Clear evidence for this was given by ESI mass spectrometry. Figure 1 shows a mass spectrum of **1** and **2** in acetonitrile in the presence of the nitrates of Li^+, Na^+, K^+, Mg^{2+}, Ca^{2+}, Cd^{2+}, Pb^{2+}, La^{3+}, and Eu^{3+}. With **2**, medium-intensity peaks were observed for the Na^+ and K^+ complexes and a very small peak was seen for the Ca^{2+}

[*] Prof. Dr. K. Kimura, T. Utsumi, T. Teranishi, Prof. Dr. M. Yokoyama
Chemical Process Engineering, Faculty of Engineering
Osaka University
Yamada-oka, Suita, Osaka 565 (Japan)
Fax: Int. code +(6)879-7935
e-mail: kimura@chem.eng.osaka-u.ac.jp
Dr. H. Sakamoto
Department of Applied Chemistry, Faculty of Systems Engineering
Wakayama University (Japan)
M. Okamoto, Prof. Dr. R. Arakawa, H. Moriguchi, Y. Miyaji
Department of Applied Chemistry, Faculty of Engineering
Osaka University (Japan)

[**] This work was supported by a Grant-in-Aid for Scientific Research from the Japanese Ministry of Education, Science, Sports, and Culture. Financial support from Nagase Science and Technology Foundation is also acknowledged.

 © WILEY-VCH Verlag GmbH, D-69451 Weinheim, 1997 0570-0833/97/3622-2452 $ 17.50+.50/0

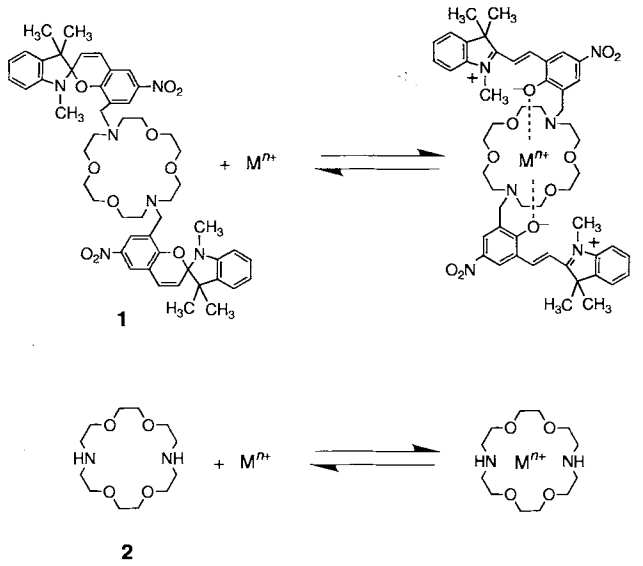

Scheme 1. Complexation of metal ions by **1** and **2**.

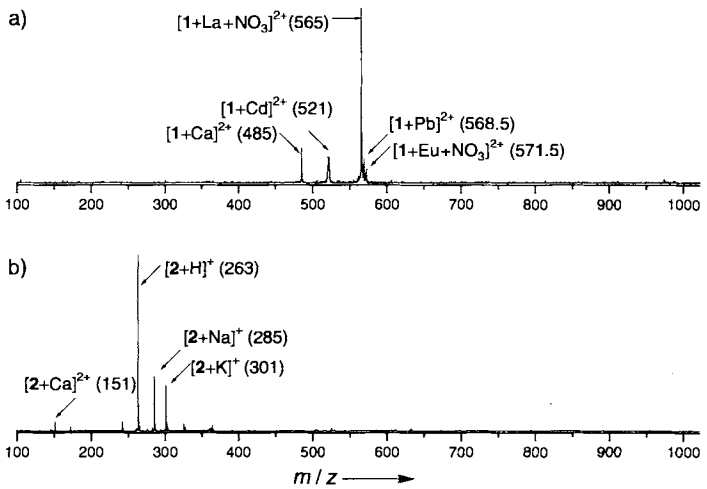

Figure 1. Mass spectra of solutions of **1** (a) and **2** (b) in acetonitrile in the presence of the nitrates of Li^+, Na^+, K^+, Mg^{2+}, Ca^{2+}, Cd^{2+}, Pb^{2+}, La^{3+}, and Eu^{3+} in the dark. $c(\mathbf{1}) = c(\mathbf{2}) = c$(metal nitrate) $= 1 \times 10^{-4}$ mol dm^{-3}.

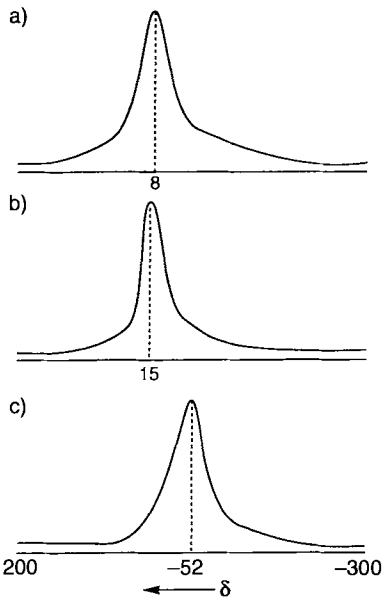

Figure 2. ^{139}La NMR spectra of a solution of $La(NO_3)_3$ in CD_3CN (a) and in the presence of **1** (b) and **2** (c) in the dark. $c[La(NO_3)_3] = 2 \times 10^{-2}$, $c(\mathbf{1}) = 1.5 \times 10^{-2}$, $c(\mathbf{2}) = 3 \times 10^{-1}$ mol dm^{-3}.

complex. There was no indication of complexation of other metal ions, especially trivalent ions, by **2**. This observation is in good accord with the general ion selectivity of the diaza-18-crown-6 ring.[6] Surprisingly, no significant peaks for the complexes of the monovalent metal ions with **1** were seen. Instead, medium-intensity peaks were observed for the complexes of divalent ions Ca^{2+}, Cd^{2+}, and Pb^{2+}. Most interestingly, the most intense peak corresponds to a complex of **1** with the trivalent ion La^{3+}.

Thus, with a preference for mulitivalent rather than monovalent metal ions, the complexation properties of **1** differ greatly from those of its parent crown ether. This suggests a strong ionic interaction of the phenolate anion of the merocyanine moiety with a metal ion in the crown ether component. Since the small cations Mg^{2+} and Eu^{3+} give no peak and a relatively small peak, respectively, for the complex with **1**, a size fit of the crown ether moiety to the metal ion is also crucial for formation of stable complexes with **1**.

^{139}La NMR spectroscopy provided important information on the strong interaction between La^{3+} and the phenolate anion in the complex **1**-La^{3+} (Figure 2). A ^{1}H NMR experiment indicated that both of the spirobenzopyran moieties in the **1**-La^{3+} complex are isomerized to the corresponding merocyanine form, even in the dark. Addition of **2** in high concentration to a solution of La^{3+} in acetonitrile led to broadening and a downfield shift of the ^{139}La NMR signal. This means that La^{3+} is complexed by the crown ether by an ion–dipole interaction, and that the complex is quite unsymmetrical. In contrast, addition of **1** gave a sharper peak and an upfield shift, indicating that the phenolate oxygen atoms of the merocyanine form of **1** act as axial ligands that interact strongly with an La^{3+} ion in the crown ether moiety. Since the La^{3+} complex of **1** gives a single peak in the mass spectrum, assigned to [**1**-$La(NO_3)$]$^{2+}$, the positive charge of La^{3+} in the crown ether moiety may be balanced not only by two phenolate anions but also by a nitrate anion. The peak sharpness also suggests that the asymmetry of the **2**-La^{3+} complex is alleviated by axial interaction with the phenolate oxygen atoms. Presumably, such strong ionic or coordinative interactions with the phenolate anions is responsible for the remarkable selectivity of **1** for multivalent metal ions, especially La^{3+}, over monovalent ones.

Since **1** and **2** differ so greatly in their selectivity for mono- and multivalent metal ions, photoisomerization of the merocyanine moiety of **1** back to its electrically neutral spiropyran form should switch the ion selectivity from multivalent to monovalent metal ions. We attempted to observe photoinduced ion selectivity switching of **1** by ESI-MS with an on-line photoirradiation apparatus.[7] As already mentioned, **1** has a much higher affinity for multivalent metal ions than for monovalent ones. However, with 100 molar equivalents of K^+ and one molar equivalent of La^{3+}, the ion peak of **1**-K^+ complex can be seen together with that of **1**-La^{3+} (Figure 3a). Mass spectra were recorded immediately after irradiation of the solution of **1** in acetonitrile with visible light (> 500 nm) in a glass capillary in the ESI interface. The peak ratio **1**-La^{3+}:**1**-K^+ was significantly lower after photoirradiation (Figure 3b). Clearly the ion selectivity of **1** can be switched from La^{3+} to K^+. When irradiation was ended, the high La^{3+} selectivity of **1** was restored.

Thus, crowned bis(spirobenzopyran) **1** has realized the extremely high affinity for La^{3+} by the powerful interaction with

 © WILEY-VCH Verlag GmbH, D-69451 Weinheim, 1997 0570-0833/97/3622-2453 $ 17.50+.50/0

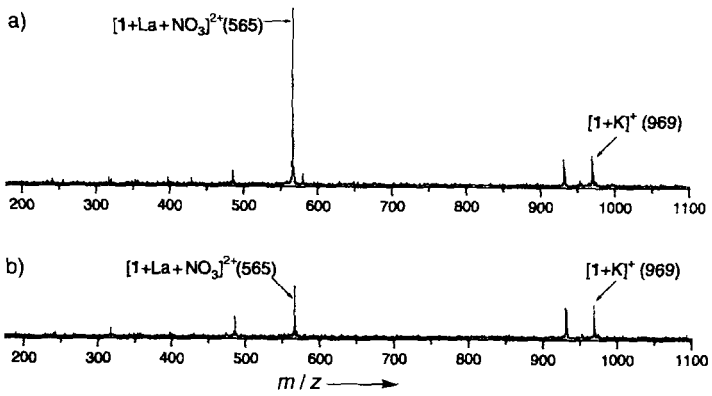

Figure 3. Mass spectra of a solution of **1** in acetonitrile containing La^{3+} and K^+ in the dark (a) and after irradiation with visible light ($\lambda > 500$ nm) for 20 min (b). $c(\mathbf{1}) = 1 \times 10^{-5}$, $c[La(NO_3)_3] = 1 \times 10^{-5}$, $c[KNO_3]$: 1×10^{-3} mol dm^{-3}.

two phenolate anions of its merocyanine moiety and the visible-light-induced selectivity switching from La^{3+} to K^+.

Received: May 14, 1997 [Z104361E]
German version: *Angew. Chem.* **1997**, *109*, 2558–2560

Keywords: crown compounds · host–guest chemistry · lanthanum · selectivity control · spiro compounds

[1] R. C. Bertelson, in *Photochromism* (Ed.: G. H. Brown), Wiley Interscience, New York, **1971**, pp. 45–431.

[2] J. Sunamoto, K. Iwamoto, Y. Mohri, T. Kominato, *J. Am. Chem. Soc.* **1982**, *104*, 5502–5504; J. D, Winkler, K. Deshayes, B. Shao, *ibid.* **1989**, *111*, 769–770; S. Kato, M. Aizawa, S. Suzuki, *J. Membr. Sci.* **1976**, *1*, 289–300; J. Anzai, A. Ueno, T. Osa, *J. Chem. Soc. Chem. Commun.* **1984**, 688–689; M. Irie, A. Menju, K. Hayashi, *Nippon Kagaku Kaishi* **1984**, 227–232; O. Ryba, J. Petranek, *Makromol. Chem. Rapid Commun.* **1988**, *9*, 125–128; M. Irie, T. Iwayanagi, Y. Taniguchi, *Macromolecules* **1985**, *18*, 2418–2422; F. Ciardelli, D. Fabbri, O. Pieroni, A. Fissi, *J. Am. Chem. Soc.* **1989**, *111*, 3470–3472.

[3] a) K. Kimura, T. Yamashita, M. Yokoyama, *J. Chem. Soc. Perkin Trans. 2* **1992**, 613-619; b) for similar spirobenzopyran crown ether derivatives, see M. Inouye, M. Ueno, T. Kitao, K. Tsuchiya, *J. Am. Chem. Soc.* **1990**, *112*, 8977–8979; S. Akabori, Y. Fujimine, *59th National Meeting of the Chemical Society of Japan*, **1990**, abstract 1E315.

[4] K. Kimura, T. Yamashita, M. Yokoyama, *J. Phys. Chem.* **1992**, *96*, 5614–5617.

[5] K. Kimura, T. Teranishi, M. Yokoyama, *Supramol. Chem.* **1996**, *7*, 11–13.

[6] R. M. Izatt, K. Pawlak, J. S. Bradshaw, R. L.Bruening, *Chem. Rev.* **1991**, *91*, 1721–2085.

[7] The sample solution was sprayed with a flow rate of 0.15 cm^3 h^{-1} from the tip of a quartz glass capillary needle to which a voltage 3.5 kV higher than that of the counterelectrode was applied.

Ion-Exchange Resins for Combinatorial Synthesis: 2,4-Pyrrolidinediones by Dieckmann Condensation**

Bheemashankar A. Kulkarni and Arasu Ganesan*

Dedicated to V. R. Mamdapur on the occasion of his 60th birthday

Combinatorial organic synthesis has tremendous potential in areas which benefit from high-throughput screening of compounds for a desired property. Thus far, the emphasis has been on drug discovery,[1] although applications[2] such as molecular recognition, catalysis, and materials science are likely to increase in importance. It is now clear that few, if any, organic reactions are incompatible with library synthesis. However, as most transformations are not quantitative, the major challenge lies in purifying products from unchanged starting materials, undesired by-products, as well as catalysts and other reagents.

Current library-purification methods rely on phase separation.[3] In the solid-phase procedure, the compound is covalently attached to a resin, while reagents are removed by simple filtration. This enables the use of large excesses of reagent to drive reactions forward. However, solid-phase synthesis has a number of limitations, including the need for translation of reaction conditions optimized in solution. Recently, solution-phase methods for library generation have gained in popularity, accompanied by protocols for achieving phase separation such as acid–base extraction,[4] resin-bound scavengers,[5] and fluorous three-phase partitioning.[6] Here we report a combinatorial synthesis in which an ion-exchange resin serves as a reagent and a purification agent.

We were interested in a modular synthesis of 2,4-pyrrolidinediones (tetramic acids) as a scaffold for novel biologically active compounds. These heterocycles were envisaged to arise by the following sequence (Scheme 1): 1) reductive alkylation[7] of an

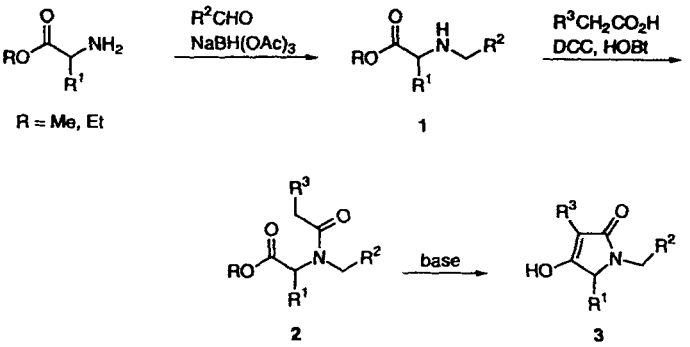

Scheme 1. Combinatorial synthesis of 2,4-pyrrolidinediones; DCC = dicyclohexyl carbodiimide, HOBt = 1-hydroxy 1*H*-benzotriazole hydrate.

α-amino acid ester, 2) acylation of product **1** with a substituted acetic acid, and 3) Dieckmann condensation[8] of amide ester **2** to yield 2,4-pyrrolidinedione **3**. The final products are thus assembled from three building blocks (amino acids, aldehydes, carboxylic acids) that are available with a high degree of diversity.

First we performed a model study: *N*-benzylglycine ethyl ester was coupled[9] with cyanoacetic acid to give amide **2a** (R^1 = H, R^2 = Ph, R^3 = CN). The desired Dieckmann condensation[10] occurred in 70–80% yield with various bases.[11] We also found that Amberlyst A-26 resin (OH^- form) promotes the cyclization. The simplicity of handling makes this the reagent of choice, and we believe this to be the first use of an ion-exchange resin for this venerable reaction.[12]

The pyrrolidinedione remains tightly bound to the resin until it is released by acid treatment (Scheme 2).[13] Only successfully cyclized material is resin-bound, whereas other components are washed away. This represents a new paradigm for solution-phase library purification. Previous applications of ion-exchange resins in combinatorial synthesis emphasized their use as activating agents[14] or scavengers.[15, 16] In this respect, our

[*] Dr. A. Ganesan, Dr. B. A. Kulkarni
Institute of Molecular and Cell Biology
National University of Singapore
15 Lower Kent Ridge Road, 119076 (Singapore)
Fax: Int. code +779-1117
e-mail: mcbgane@nus.sg

[**] This work was supported by funds from the National Science and Technology Board, Singapore.

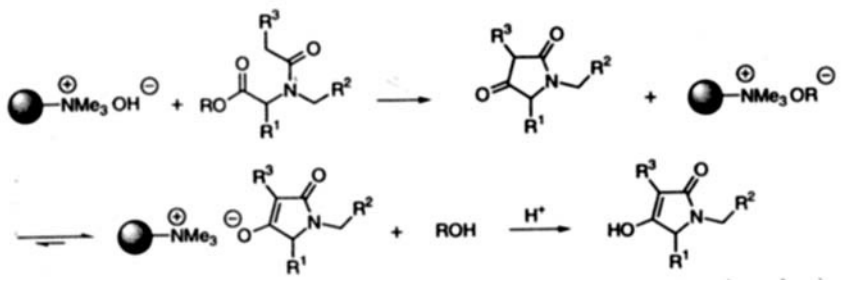

Scheme 2. A quaternary ammonium resin (OH^- form) catalyzes the Dieckmann condensation and purifies the reaction products.

positive selection of the desired product is analogous to Armstrong's[17] solid-phase resin capture.

The ion-exchange resin protocol is applicable to a variety of Dieckmann substrates (Table 1). A reasonably strong electron-withdrawing group (R^3) is required; when R^3 = Ph, no reaction was observed under the usual conditions. Upon prolonged stirring with resin, hydrolysis of the ester to the free carboxylic acid (**2**, R = H) occurred; this was also detected as a minor pathway when R^3 = SPh (**2d**).

Table 1. Yield and purity of representative examples of the Dieckmann condensation in the presence of the quaternary ammonium resin Amberlyst A-26 [a].

Amide	R^1	R^2	R^3	Product	Yield [%]	Purity [%]
2a	H	Ph	CN	**3a**	72	92
2b	H	Ph	o-$O_2NC_6H_4$	**3b**	73	89
2c	H	Ph	$P(O)(OEt)_2$	**3c**	86	87
2d	H	Ph	SPh	**3d**	87	71 [b]
2e	*i*Pr	Ph	CN	**3e**	80	94
2f	$CH_2CH_2SCH_3$	Ph	CN	**3f**	79	83
2g	CH_2Ph	Ph	CN	**3g**	77	85
2h	CH_2Ph	p-$MeOC_6H_4$	CN	**3h**	75	86
2i	CH_2Ph	p-$O_2NC_6H_4$	CN	**3i**	70	92
2j	CH_2Ph	p-*t*BuC_6H_4	CN	**3j**	71	88

[a] The yields reported are for the crude material and uncorrected for the possibility of hydrate formation. All compounds were fully characterized by NMR spectroscopy and MS. The purity was assessed by HPLC (UV detection at 254 nm). [b] The product is accompanied by the hydrolyzed ester (17%).

The selectivity of the resin-bound purification method has enabled us to carry out the overall process (**1** to **3**) with minimal purification. For example, crude **2g** was prepared from L-phenylalanine methyl ester by reductive alkylation and acylation with only aqueous washes in between, and cyclized to afford **3g** in 64% overall yield (comparable to the 68% obtained when chromatographically purified intermediates were used). We are presently adapting this methodology to the preparation of 2,4-pyrrolidinedione libraries by discrete parallel synthesis.

Experimental Section

2g: To a solution of L-*N*-benzylphenylalanine methyl ester [18] (330 mg, 1.23 mmol) in CH_2Cl_2 (10 mL) was added cyanoacetic acid (125 mg, 1.47 mmol) and 1-hydroxy 1*H*-benzotriazole hydrate (HOBt, 199 mg, 1.47 mmol). The solution was cooled to 0 °C, followed by slow addition of dicyclohexyl carbodiimide (DCC, 355 mg, 1.72 mmol). The reaction mixture was warmed to room temperature, stirred for 6 h, filtered, washed (water, saturated $NaHCO_3$, and brine), dried ($MgSO_4$), and concentrated. Flash chromatography (silica, 0–40% ethyl acetate/hexanes) yielded the amide (380 mg), which recrystallized (EtOAc/hexanes) as a white solid (360 mg, 87% yield); m.p. 90–92 °C; IR (Nujol): $\tilde{\nu}$ = 2258, 1733, 1645 cm^{-1}; ^1H NMR (300 MHz, $CDCl_3$): δ = 3.23–3.42 (m, 4H), 3.70 (s, 3H), 3.88 (d, J = 17.1 Hz, 1H), 4.34 (d, J = 17.0 Hz, 1H), 4.45 (dd, J = 5.6, 9.9 Hz, 1H), 7.09–7.16 (m, 5H), 7.25–7.32 (m, 5H); ^{13}C NMR (75 MHz, $CDCl_3$): δ = 25.62, 34.99, 52.45, 53.01, 62.11, 113.44, 126.97, 127.07, 128.25, 128.88, 129.05, 129.16, 134.63, 137.17, 162.74, 169.89; $[\alpha]_D^{22} = -132.4°$ (c = 0.5, $CHCl_3$); elemental analysis calcd for $C_{20}H_{20}N_2O_3$: C 71.41, H 5.99, N 8.32; found: C 71.22, H 6.11, N 8.23.

3g: To a stirred solution of **2g** (330 mg, 0.98 mmol) in MeOH (10 mL) was added Amberlyst A-26 resin [19] (450 mg, OH^- form). After 16 h the resin was filtered and washed three times with MeOH. The resin was then stirred for 30 min with MeOH (10 mL) and trifluoroacetic acid (TFA, 0.4 mL), filtered, and washed three times with MeOH. Concentration of the filtrate afforded the 2,4-pyrrolidinedione hydrate (241 mg), which recrystallized (MeOH/acetone/hexanes) as a white solid (215 mg, 68% yield); m.p. 234–237 °C; IR (Nujol): $\tilde{\nu}$ = 2214, 1678 (br), 1595 (br) cm^{-1}; ^1H NMR (300 MHz, [D_6]DMSO): δ = 2.94 (dd, J = 4.5, 14.2 Hz, 1H), 3.15 (dd, J = 4.4, 14.2 Hz, 1H), 3.89 (t, J = 4.4 Hz, 1H), 4.00 (d, J = 15.3 Hz, 1H), 4.86 (d, J = 15.3 Hz, 1H), 7.09–7.22 (m, 5H), 7.25–7.31 (m, 5H); ^{13}C NMR (75 MHz, [D_6]DMSO): δ = 34.12, 43.08, 60.95, 77.14, 115.01, 126.56, 127.12, 127.63, 128.00, 128.47, 129.36, 135.54, 137.58, 168.74, 185.63; $[\alpha]_D^{22} = -127.3°$ (c = 0.15, MeOH); HRMS (calcd/found): 304.1212/304.1234 [M^+]; elemental analysis calcd for $C_{19}H_{16}N_2O_2 \cdot H_2O$: C 70.79, H 5.62, N 8.68; found: C 70.64, H 5.49, N 8.55.

Received: May 20, 1997 [Z10456IE]
German version: *Angew. Chem.* **1997**, *109*, 2565–2567

Keywords: amino acids · combinatorial chemistry · cyclizations · heterocycles · ion-exchange resins

[1] Two recent reviews: a) F. Balkenhohl, C. von dem Bussche-Hünnefeld, A. Lansky, C. Zechel, *Angew. Chem.* **1996**, *108*, 2436–2487; *Angew. Chem. Int. Ed. Engl.* **1996**, *35*, 2288–2337; b) L. A. Thompson, J. A. Ellman, *Chem. Rev.* **1996**, *96*, 555–600.
[2] Review of this aspect of combinatorial chemistry: C. Gennari, H. P. Nestler, U. Piarulli, B. Salom, *Liebigs Ann.* **1997**, 637–647.
[3] D. P. Curran, *Chemtracts: Org. Chem.* **1996**, *9*, 75–87.
[4] S. Cheng, C. M. Tarby, D. D. Comer, J. P. Williams, L. H. Caporale, P. L. Myers, D. L. Boger, *Bioorg. Med. Chem.* **1996**, *4*, 727–737.
[5] S. W. Kaldor, M. G. Siegel, J. E. Fritz, B. A. Dressman, P. J. Hahn, *Tetrahedron Lett.* **1996**, *37*, 7193–7196.
[6] A. Studer, S. Hadida, R. Ferrito, S.-Y. Kim, P. Jeger, P. Wipf, D. P. Curran, *Science* **1997**, *275*, 823–826.
[7] A. K. Szardenings, T. S. Burkoth, G. C. Look, D. A. Campbell, *J. Org. Chem.* **1996**, *61*, 6720–6722.
[8] Review: B. R. Davies, P. J. Garratt in *Comprehensive Organic Synthesis, Vol. 2* (Eds.: B. M. Trost, I. Fleming), Pergamon, Oxford, **1991**, pp. 806–829.
[9] I. P. Piskunova, A. V. Eremeev, A. F. Mishnev, I. A. Vosekalna, *Tetrahedron* **1993**, *49*, 4671–4676.
[10] 3-Acyltetramic acids, found in a number of natural products, have been prepared similarly: B. J. L. Royles, *Chem. Rev.* **1995**, *95*, 1981–2001, and references therein.
[11] We tried lithium bis(trimethylsilyl)amide and potassium *tert*-butoxide.
[12] Quaternary ammonium resins have been used for other base-catalysed condensations, for example aldol, Henry, and Knoevenagel condensations.
[13] For example, **3a** (45 mg) was stirred overnight with resin (100 mg) in MeOH (10 mL). The resin was washed repeatedly (10 × 5 mL MeOH) without leakage of compound, as determined by thin-layer chromatography and a negative $FeCl_3$ reaction. After acidification (0.1 mL TFA in 10 mL MeOH), stirring for 30 min, filtration, and washing (3 × 10 mL MeOH), 42 mg (93%) of **3a** were recovered.
[14] J. J. Parlow, *Tetrahedron Lett.* **1996**, *37*, 5257–5260.
[15] a) D. L. Flynn, J. Z. Crich, R. V. Devraj, S. L. Hockerman, J. J. Parlow, M. S. South, S. Woodard, *J. Am. Chem. Soc.* **1997**, *119*, 4874–4881; b) L. M. Gayo, M. J. Suto, *Tetrahedron Lett.* **1997**, *38*, 513–516; c) M. G. Siegel, P. J. Hahn, B. A. Dressman, J. E. Fritz, J. R. Grunwell, S. W. Kaldor, *ibid.* **1997**, *38*, 3357–3360.
[16] Recently, amines containing an additional tertiary amine group were acylated, and the amides purified by cation exchange: R. M. Lawrence, S. A. Biller, O. M. Fryszman, M. A. Poss *Synthesis* **1997**, 553–558. In this case, the starting amine has to be completely consumed as it is also retained by the resin.
[17] a) T. A. Keating, R. W. Armstrong, *J. Am. Chem. Soc.* **1996**, *118*, 2574–2583; b) S. D. Brown, R. W. Armstrong, *ibid.* **1996**, *118*, 6331–6332.
[18] Obtained in 93% yield by reductive alkylation of L-phenylalanine methyl ester. For the enantiomer, see F. Effenberger, U. Burkard, J. Willfahrt, *Liebigs Ann.* **1986**, 314–333.
[19] This resin was obtained from Fluka (loading of 4.4 mmol OH^- per gram resin), prewashed with dry methanol, and dried under vacuum prior to use.

 © WILEY-VCH Verlag GmbH, D-69451 Weinheim, 1997 0570-0833/97/3622-2455 $ 17.50+.50/0

Insertion of Carbenoids into Cp–H Bonds of Ferrocenes: An Enantioselective-Catalytic Entry to Planar-Chiral Ferrocenes**

Stephan Siegel and Hans-Günther Schmalz*

Since the epoch-making discovery of ferrocene in 1951,[1] the chemistry of this organometallic compound has been intensely investigated. Even recently, the ferrocene substructure enjoys a keen scientific interest—especially as a sound construction element for developing new catalysts and materials.[2]

In the course of our work on the preparation and synthetic application of chiral transition metal π complexes,[3] we considered whether cyclization reactions of the type shown in Equation (1) are possible, or, more generally, if ferrocenes can be

(1)

functionalized (by C–H insertion) upon reaction with carbenes. We assumed that the comparably electron-rich cyclopentadienyl rings of ferrocene could react with electron-poor carbenes (or carbenoids). We report here the success of such reactions and, thus, the first examples of carbene insertion into Cp–H bonds of ferrocene derivatives.[4] Furthermore, we show that this chemistry can be used for the enantioselective-catalytic preparation of planar-chiral ferrocenes.[5]

We employed the metal-catalyzed decomposition of α-diazo carbonyl compounds, since it is a reliable method for generating carbenoid species.[6] The (nonstabilized) electrophilic metal–carbene intermediates show a chemical behavior similar to that of free carbenes, and are well suited for insertions into aryl C–H bonds.[6, 7] As substrates we chose the diazoketones **1**–**3**.

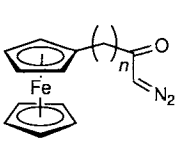

1: $n = 1$
2: $n = 2$

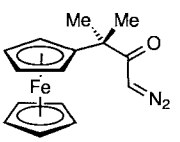

3

The synthesis of **1** (Scheme 1) started with acetylferrocene (**4**), which was subjected to a Willgerodt reaction to provide ferrocenyl acetic acid (**5**),[8, 9] which in turn was converted into diazoketone **1** in 95% yield by the one-pot procedure described in the Experimental Section.[10] To prepare the homologous substrate **2**, formylferrocene (**6**)[11] was first transformed by decarboxylative Knoevenagel condensation and catalytic hydrogenation into acid **7**,[11, 12] which was further converted into diazoketone **2** in high yield. Substrate **3** was synthesized by esterification of **5** to **8** (MeOH, $SOCl_2$, 83%). Two deprotonation/methylation cycles then afforded the dimethylated compound **9** in almost quantitative yields, from which diazoketone **3** was obtained after hydrolysis by the standard one-pot protocol.[9]

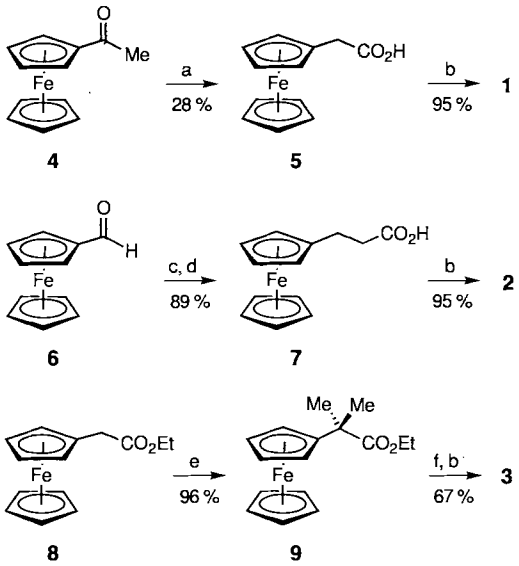

Scheme 1. Preparation of the cyclization precursors **1**–**3**. a) S_8, morpholine, 130 °C, 17 h, then 4N NaOH, reflux, 4 h; b) NaH, C_6H_6, room temperature (RT), then $(COCl)_2$, pyridine, 0 → 55 °C, 2 h, removal of solvent, then CH_2N_2, Et_2O, 0 °C, 30 min; c) $H_2C(CO_2H)_2$, cat. piperidine, pyridine, 100 °C, 2 h; d) H_2, Pd/C, EtOH, RT, 48 h; e) LDA, THF, −60 °C → RT, then aqueous work-up; repetition of the sequence; f) 10% NaOH, MeOH, reflux, 3 h.

We then investigated the projected cyclizations with the well-known (achiral) catalysts $[Rh_2(OAc)_4]$ and $[Rh_2(OCOCF_3)_4]$, and found suitable reaction conditions for all three substrates that allowed the preparation of the desired cyclization products (**10**, *rac*-**12**, and *rac*-**14**) in reasonable yields. The most important results are summarized in Table 1; however, here we emphasize some observations explicitly: A bridged ferrocene derivative (**11**) was obtained (as a side product) only in the case of **1**. In all reactions with $[Rh_2(OAc)_4]$ in halogenated solvents (Table 1, entries 1, 3, 6, and 7), ferrocene was isolated as a by-product in considerable amounts (10–20%).[13] Compared to reactions with $[Rh_2(OAc)_4]$, those of **1** and **2** with $[Rh_2(OCOCF_3)_4]$ proceeded much more cleanly (entries 2 and 4), and only 1 mol% of the catalyst was required to provide *rac*-**12** in acceptable yields (47% based on converted starting material). An attempt to carry out the $[Rh_2(OAc)_4]$-catalyzed reaction of **2** in benzene resulted in the formation of significant amounts of the (intermolecular) Buchner product **13**.[14] Preliminary cyclization experiments with **3**, which were carried out in an NMR tube with $[Rh_2(OAc)_4]$ or $[Rh_2(CF_3CO_2)_4]$ in C_6D_6 or

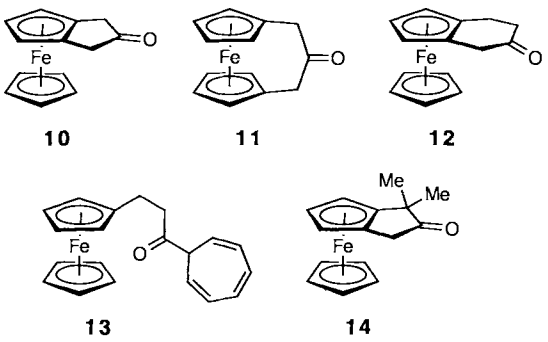

[*] Prof. Dr. H.-G. Schmalz, Dipl.-chem. S. Siegel
Institut für Organische Chemie der Technischen Universität
Strasse des 17. Juni 135, D-10623 Berlin (Germany)
Fax: Int. code +(30)314-21105
e-mail: schmalz@wap0109.chem.tu-berlin.de

[**] We thank the Volkswagen-Stiftung, the Fonds der Chemischen Industrie, and the BASF AG (graduate scholarship award to S. S.) for financial support.

 © WILEY-VCH Verlag GmbH, D-69451 Weinheim, 1997 0570-0833/97/3622-2456 $ 17.50+.50/0

Table 1. Results of the cyclization experiments carried out with substrates **1**–**3** in the presence of achiral catalysts [a].

Entry	Substrate	Catalyst	Amount [mol%]	Solvent	Products (yield[%][b])
1	**1**	$[Rh_2(OAc)_4]$	13	CH_2Cl_2	**10** (4), **11** (2)
2	**1**	$[Rh_2(CF_3CO_2)_4]$	8	CH_2Cl_2	**10** (35), **11** (4)
3	**2**	$[Rh_2(OAc)_4]$	5	CH_2Cl_2	*rac*-**12** (36)
4	**2**	$[Rh_2(CF_3CO_2)_4]$	1	CH_2Cl_2	*rac*-**12** (35)[c]
5	**2**	$[Rh_2(OAc)_4]$	5	benzene	*rac*-**12** (50), **13** (9)
6	**3**	$[Rh_2(OAc)_4]$	5	C_6H_5F	*rac*-**14** (28)
7	**3**	$[Rh_2(OAc)_4]$	5	$C_6H_5CF_3$	*rac*-**14** (35)
8	**2**	$Cu(hfacac)_2$	5	CH_2Cl_2	*rac*-**12** (38)
9	**3**	$Cu(hfacac)_2$	5	CH_2Cl_2	*rac*-**14** (66)

[a] See Experimental Section. [b] Yields of isolated products after chromatographic separation. [c] In this case, 24% of the starting material **2** was recovered.

$CDCl_3$, showed that the cyclization product *rac*-**14** formed only in traces when the latter was used as the solvent. In contrast, dichloromethane proved to be a more appropriate solvent, and was also better than fluorobenzene and trifluoromethylbenzene.[15] It is known that (in addition to rhodium salts) copper compounds are especially well suited as catalysts for the generation of carbenoids from diazo compounds.[6b] Therefore, we tested the cyclization of substrates **2** and **3** with $Cu(hfacac)_2$ (hfacac = hexafluoroacetylacetonate), which has proven useful for C–H insertions into electron-rich aromatic compounds (e. g. *N*-methyl pyrrol).[16] Indeed, we obtained good results with this catalyst—especially in the case of **3**, which in the presence of $Cu(hfacac)_2$ (5 mol%) afforded *rac*-**14** in 66% yield.

Table 2. Selected spectroscopic data for **1**–**3**, **10**, **11**, *rac*-**12**, and *rac*-**14**. IR (CCl_4); ^1H NMR (400 MHz, $CDCl_3$); ^{13}C NMR (67.7 or 100.64 MHz, $CDCl_3$, additional DEPT).

1: IR: $\tilde{\nu}$ = 3057, 3047, 2099, 1645, 1631, 1362, 1297, 1105, 1077, 822 cm^{-1}; ^1H NMR: δ = 3.34 (s, 2H), 4.12 (s, 5H), 4.14 (s, 4H), 5.14 (s, 1H); ^{13}C NMR: δ = 42.3 (CH_2), 64.0 (CH), 68.3 (CH), 68.7 (CH), 69.1 (CH), 80.8, 193.1; HR-MS: calcd for $C_{13}H_{12}FeN_2O$: 268.0299, found: 268.0297.

2: IR: $\tilde{\nu}$ = 3093, 2958, 2102, 1639, 1371, 1371, 1362 cm^{-1}; ^1H NMR: δ = 2.46–2.58 (m, 2H), 2.64–2.72 (pseudo t, 2H), 4.06 (s, 4H), 4.12 (s, 5H), 5.22 (s, 1H); ^{13}C NMR: δ = 24.9 (CH_2), 42.4 (CH_2), 54.5 (CH), 67.3 (CH), 68.0 (CH), 68.5 (CH), 87.4, 194.2; HR-MS: calcd for $C_{14}H_{14}FeN_2O$: 282.0455, found: 282.0463.

3: IR: $\tilde{\nu}$ = 3096, 2975, 2097, 1626, 1333, 819 cm^{-1}; ^1H NMR: δ = 1.56 (s, 6H), 4.15 (pseudo t, 2H), 4.2 (s, 5H), 4.22 (m, 2H), 5.02 (s, 1H); ^{13}C NMR: δ = 25.6 (CH_3), 45.5, 52.3 (CH), 66.6 (CH), 68.0 (CH), 68.6 (CH), 95.2, 199.2; HR-MS: calcd for $C_{15}H_{16}FeN_2O$: 296.0612, found: 296.0617.

10: IR: $\tilde{\nu}$ = 3095, 2887, 1858, 1760, 1408, 1401, 1241, 1169, 1154, 1104, 832, 805 cm^{-1}; ^1H NMR: δ = 3.14 (dd, J = 21, 1.5 Hz, 2H), 3.32 (dd, J = 21, 1.5 Hz, 2H), 4.03 (s, 5H), 4.13 (t, J = 2 Hz, 1H), 4.27 (d, J = 2 Hz, 2H); ^{13}C NMR: δ = 41.0 (CH_2), 62.7 (CH), 67.5 (CH), 69.8 (CH), 87.2, 215.3; HR-MS: calcd for $C_{13}H_{12}FeO$: 240.0238, found: 240.0249.

11: IR: $\tilde{\nu}$ = 3089, 2920, 1746, 1695, 1666, 1194, 809 cm^{-1}; ^1H NMR: δ = 3.04 (s, 4H), 4.04 (s, 4H), 4.17 (s, 4H); ^{13}C NMR: δ = 38.6 (CH_2), 70.0 (CH), 70.4 (CH), 76.4, 216.7; HR-MS: calcd for $C_{13}H_{12}FeO$: 240.0238, found: 240.0248.

rac-**12**: IR: $\tilde{\nu}$ = 3090, 2931, 2851, 1709, 1410, 1338, 1296, 1105, 1000, 822 cm^{-1}; ^1H NMR: δ = 2.6–2.84 (m, 3H), 2.88–3.0 (m, 1H), 3.18 (d, J = 20 Hz, 1H), 3.38 (d, J = 20 Hz, 1H), 4.07 (m, 1H), 4.08 (s, 5H), 4.11 (t, J = 2.5 Hz, 1H), 4.18 (m, 1H); ^{13}C NMR: δ = 22.5 (CH_2), 39.5 (CH_2), 40.1 (CH_2), 65.3 (CH), 65.7 (CH), 66.6 (CH), 69.2 (CH), 81.1, 84.1, 209.8; HR-MS: calcd for $C_{14}H_{14}FeO$: 254.0394, found: 254.0397.

rac-**14**: IR: $\tilde{\nu}$ = 3094, 2965, 2928, 1745, 1106, 820 cm^{-1}; ^1H NMR: δ = 1.12 (s, 3H), 1.56 (s, 3H), 3.18 (d, J = 20 Hz, 1H), 3.26 (d, J = 20 Hz, 1H), 4.04 (s, 5H), 4.16 (t, J = 2 Hz, 1H), 4.22 (d, J = 2 Hz, 1H), 4.3 (d, J = 2 Hz, 1H); ^{13}C NMR: δ = 23.0 (CH_3), 27.9 (CH_3), 38.5 (CH_2), 46.9, 59.9 (CH), 62.2 (CH), 67.0 (CH), 83.0, 100.3, 218.6; HR-MS: calcd for $C_{15}H_{16}FeO$: 268.0551, found: 268.0553.

rac-**15**: IR: $\tilde{\nu}$ = 3102, 2966, 2931, 2863, 1751, 1699, 1480, 1455 cm^{-1}; ^1H NMR: δ = 1.23 (s, 3H), 1.63 (s, 3H), 4.27 (s, 5H), 4.70 (pseudo d, J = 2.5 Hz, 1H), 5.03 (pseudo t, 1H, J = 2.5 Hz), 5.15 (d, J = 2.5 Hz, 1H); ^{13}C NMR: δ = 23.1 (CH_3), 30.1 (CH_3), 42.7, 65.0 (CH), 67.8 (CH), 76.0 (CH), 76.1 (CH), 77.2, 79.8, 175.9, 204.8; HR-MS: calcd for $C_{15}H_{14}FeO_2$: 282.0343, found: 282.0347

The cyclization products **10**, *rac*-**12**, and *rac*-**14** (spectroscopic data are given in Table 2) are surprisingly sensitive towards oxidation; they decompose upon exposure to air under formation of polar, intensely colored by-products. For instance, violet 1,2-diketone *rac*-**15** was isolated from a solution of *rac*-**14** with a catalytic amount of $Cu(hfacac)_2$ in dichloromethane that was exposed to the air for several hours. Furthermore, aerobic workup of the reaction mixture from the treatment of **1** with $Cu(hfacac)_2$ in dichloromethane provided a product of constitution **16**[17] in 19% yield as a 1:1 mixture of diastereomers. This was apparently formed by oxidative dimerization of **10**.

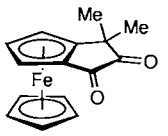

15

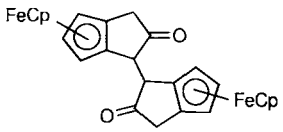

16

Because the cyclizations **2** → *rac*-**12** and **3** → *rac*-**14** represent chirogenic reactions[18] that can in general be conducted enantioselectively, it was straightforward to test these reactions with chiral catalysts.[19] Our first attempt with the prominent mepy-rhodium(II) complex[20] furnished disappointing results.[21] In contrast, cyclization experiments with the catalyst (5 mol%) prepared in situ from copper(I) triflate and **17**[22] in dichloromethane at reflux were successful. In the case of **2**, we obtained the cylization product **12**[23] in 72% yield with an enantiomeric excess of 78% *ee* (Scheme 2). Cyclization of **3**, performed under the same

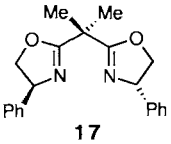

17

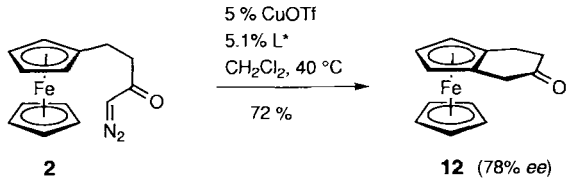

2 **12** (78% *ee*)

Scheme 2. Enantioselective cyclization of **2**. Tf = trifluoromethanesulfonyl, L* = chiral ligand.

conditions, also furnished an optically active product (**14**)[24] in good yield (89%) with an enantiomeric purity of 62% *ee* (Scheme 3). It is remarkable that these reactions not only proceeded with significant enantioselectivity but also gave higher chemical yields than those with the achiral catalysts. Further investigations must now show if the enantioselectivity can be increased by varying the catalyst systems.

The experiments described here show for the first time that carbene insertions into Cp–H bonds of ferrocene derivatives are possible and can be used (in a preparatively attractive man-

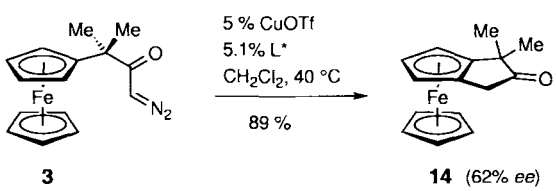

3 **14** (62% *ee*)

Scheme 3. Enantioselective cyclization of **3**.

 © WILEY-VCH Verlag GmbH, D-69451 Weinheim, 1997 0570-0833/97/3622-2457 $ 17.50+.50/0

ner) for synthesizing interesting new compounds. This extends the chemistry of ferrocene by a basic new variant, and also opens a unique opportunity for the enantioselective-catalytic synthesis of planar-chiral ferrocene derivatives.

Experimental Section

General procedure for preparing the cyclization precursors **1**–**3** from the corresponding ferrocenyl alkanoic acids: To a stirred suspension of the ferrocenyl alkanoic acid (4.1 mmol) in anhydrous benzene (60 mL) was added sodium hydride (4.18 mmol) under an argon atmosphere, and after 10 min pyridine (2.61 mmol). The mixture was cooled to 0 °C, and freshly distilled oxalyl chloride (26.5 mmol) added dropwise. After complete addition stirring was continued for 30 min at 0 °C, for 30 min at room temperature, and finally for 1 h at 55 °C. After filtration of the reaction mixture through a short pad of silica gel, the solvent and excess oxalyl chloride were completely removed in vacuo. The dark brown residue was dissolved in Et_2O (15 mL), and a solution of diazomethane (35 ml, ≈0.6 M in Et_2O) added at 0 °C. After the reaction mixture was stirred for 20 min at 0 °C excess diazomethane and solvent were completely removed in vacuo, and the residue was purified by flash chromatography (hexane/EtOAc).

General procedure for the cyclization experiments summarized in Table 1: To a solution of the catalyst (34 μmol; 5 mol%) in the anhydrous solvent (10 mL) was added dropwise at RT under an atmosphere of argon a solution of the diazoketone (0.68 mmol) in the solvent (5 mL) within about 30 min. Gas evolution (N_2) indicated the decomposition of the diazo compound. After complete addition stirring was continued until complete conversion was reached (usually about one hour). After rapid filtration of the dark brown reaction mixture through a short pad of silica gel under argon, the solvent was completely removed in vacuo. The products were separated and purified by flash chromatography or radial chromatography (using a chromatotron) under an argon atmosphere.

Enantioselective cyclizations: Ligand **17** (17.3 μmol) was added to a solution of $Cu^{I}OTf$ (17 μmol; weighed in a glove box) in CH_2Cl_2 (3 mL) under an argon atmosphere. After the reaction mixture was stirred for 2 h at RT, the green solution of the catalyst was heated to reflux, and a solution of the substrate (**2** or **3**; 0.34 mmol) in CH_2Cl_2 (10 mL) slowly added within 2 h with a syringe pump (all under argon). After complete addition the brownish solution was heated at reflux for 20 min before being subjected to work-up as described above. The enantiomeric excess of the product was determined with HPLC (Daicel, Chiralcel OJ).

Received: May 28, 1997 [Z 10490 IE]
German version: *Angew. Chem.* **1997**, *109*, 2569–2572

Keywords: asymmetric catalysis · C–H activation · carbene complexes · chirality · sandwich complexes

[1] T. J. Kealey, P. L. Pauson, *Nature* **1951**, *168*, 1039.
[2] *Ferrocenes. Homogeneous Catalysis – Organic Synthesis – Materials Science* (Eds.: A. Togni, T.Hayashi), VCH, Weinheim, **1995**.
[3] See for instance a) H.-G. Schmalz, A. Schwarz, G. Dürner, *Tetrahedron Lett.* **1994**, *35*, 6861; b) H.-G. Schmalz, E. Hessler, J. W. Bats, G. Dürner, *ibid.* **1994**, *35*, 4543; c) H.-G. Schmalz, S. Siegel, J. W. Bats, *Angew. Chem.* **1995**, *107*, 2597; *Angew. Chem. Int. Ed. Engl.* **1995**, *34*, 2383; d) H.-G. Schmalz, K. Schellhaas, *ibid.* **1996**, *108*, 2277 and **1996**, *35*, 2146.
[4] A literature search in Chemical Abstracts using the query [ferrocen# and (carben# or diazo#)] indicated that carbene chemistry [6], which has often proven its value for the functionalization of benzene derivatives, was never applied to ferrocenes. For intramolecular C–H insertions into allylic C–H bonds of butadiene-$Fe(CO)_3$ complexes, see T. A. Petrel, J. M. Stephan, K. F. McDaniel, M. C. McMills, A. L. Rheingold, G. P. A. Yap, *J. Org. Chem.* **1996**, *61*, 4188.
[5] Planar-chiral ferrocene derivatives are especially important in the field of enantioselective catalysis; see for instance a) T. Hayashi in ref. [2], pp. 105–142; b) Y. Butsugan, S. Araki, M. Watanabe in ref. [2], pp. 143–169; c) A. Togni, *Angew. Chem.* **1996**, *108*, 1581; *Angew. Chem. Int. Ed. Engl.* **1996**, *35*, 1475, and references therein.
[6] Reviews: a) T. Ye, M. A. McKervey, *Chem. Rev.* **1994**, *94*, 1091; b) A. Padwa, D. J. Austin, *Angew. Chem.* **1994**, *106*, 1881; *Angew. Chem. Int. Ed. Engl.* **1994**, *33*, 1797; c) A. Padwa, K. E. Krumpe, *Tetrahedron* **1992**, *48*, 5385; d) J. Adams, D. M. Spero, *ibid.* **1991**, *47*, 1765; e) H. Brunner, *Angew. Chem.* **1992**, *104*, 1208; *Angew. Chem. Int. Ed. Engl.* **1992**, *31*, 1183.
[7] a) M. Hrytsak, N. Etkin, T. Durst, *Tetrahedron Lett.* **1986**, *27*, 5679; b) M. Hrytsak, T. Durst, *J. Chem. Soc. Chem. Commun.* **1987**, 1150; c) S. D. Babu, M. Hrytsak, T. Durst, *Can. J. Chem.* **1989**, *67*, 1071; d) N. Etkin, S. D. Babu, J. C. Fooks, T. Durst, *J. Org. Chem.* **1990**, *55*, 1093.
[8] a) K. L. Rinehart, Jr., R. J. Curby, Jr., P. E. Sokol, *J. Am. Chem. Soc.* **1957**, *79*, 3420; b) M. Carmack, M. A. Spielman in *Organic Reactions, Vol. III* (Ed.: R. Adams), Wiley, New York, **1946**, p. 83.
[9] All new compounds were characterized by the usual spectroscopic methods (see Table 2) and gave correct elemental analysis and/or high-resolution mass spectra.
[10] This protocol is based on the procedure of C. Ray, B. Saha, U. R. Ghatak, *Synth. Commun.* **1991**, *21*, 1223.
[11] Compound **6** was prepared by formylation of ferrocene with *N*-methylformanilide/$POCl_3$ (74%) according to M. Rosenblum, A. K. Banerjee, N. Danieli, R. W. Fish, V. Schlatter, *J. Am. Chem. Soc.* **1963**, *85*, 316.
[12] K. Schlögel, *Monatsh. Chem.* **1957**, *88*, 601.
[13] We currently have no explanation for the formation of ferrocene from **1**, **2**, or **3** under these reaction conditions.
[14] For the reaction of diazo compounds with benzene derivatives leading to cycloheptatrienes (Buchner reaction), see ref. [6a], p. 1120, and references therein.
[15] Fluorinated solvents have been successfully used for catalytic transformations of metal carbenes: M. P. Doyle, *Chem. Rev.* **1986**, *86*, 919.
[16] B. E. Maryanoff, *J. Org. Chem.* **1982**, *47*, 3000.
[17] The formation of dimeric products of constitution **16** was evident from MS and NMR data: HR-MS: calcd for $C_{26}H_{22}Fe_2O_2$: 478.0319, found: 478.0315; MS (EI, 130 °C): 239 (100%; strongly stabilized radical cation of **10**); ^1H NMR: in addition to the Cp–H signals at $\delta = 3.9–4.25$, two pairs of coupled dubletts at $\delta = 2.75/3.16$ and 3.05/3.28 ($J_{gem} = 21$ Hz) were observed, which confirm the formation of only two diastereomers. A double set of signals also appeared in the ^{13}C NMR spectrum.
[18] S. Drenkard, J. Ferris, A. Eschenmoser, *Helv. Chim. Acta* **1990**, 1373.
[19] a) M. P. Doyle, Q.-L. Zhou, C. E. Raab, G. H. P. Roos, *Tetrahedron Lett.* **1995**, *36*, 4745; b) M. P. Doyle, M. N. Protopopova, C. D. Poulter, D. H. Rogers, *J. Am. Chem. Soc.* **1995**, *117*, 7281; c) H. Lim, G. A. Sulikowski, *J. Org. Chem.* **1995**, *60*, 2326; d) K. Burgess, H. Lim, A. M. Porte, G. A. Sulikowski, *Angew. Chem.* **1996**, *108*, 192; *Angew. Chem. Int. Ed. Engl.* **1996**, *35*, 220; e) N. Watanabe, T. Ogawa, Y. Ohtake, S. Ikegami, S. Hashimoto, *Synlett* **1996**, 85.
[20] M. P. Doyle, W. R. Winchester, M. N. Protapopova, A. P. Kazala, L. J. Westrum, *Org. Synth.* **1995**, *73*, 13, and references therein.
[21] The use of this catalyst resulted in an extremely slow conversion to give a complex mixture containing the desired cyclization product at best in traces.
[22] a) E. J. Corey, N. Imai, H.-Y. Zhang, *J. Am. Chem. Soc.* **1991**, *113*, 728; for the use of chiral bisoxazoline and semicorrin ligands, see b) A. Pfaltz, *Acc. Chem. Res.* **1993**, *26*, 339; c) A. Pfaltz in *Advances in Catalytic Processes, Vol. 1*, (Ed.: M. P. Doyle), JAI, Greenwich, CT, USA, **1995**, p. 61.
[23] $[\alpha]_D^{20} = -107.7$, $c = 0.115$ in $CHCl_3$. The absolute configuration of the cyclization product (**12** or *ent*-**12**) was not established; the enantiomeric excess was determined with HPLC using a Daicel Chiralcel OJ column.
[24] $[\alpha]_D^{20} = -68.8$, $c = 0.08$ in $CHCl_3$. The absolute configuration of the cyclization product (**14** oder *ent*-**14**) was not established; the enantiomeric excess was determined with HPLC using a Daicel Chiralcel OJ column.

Asymmetric Self-Replication of Chiral 1,2-Amino Alcohols by Highly Enantioselective Autoinductive Reduction**

Takanori Shibata, Tomohide Takahashi, Takashi Konishi, and Kenso Soai*

Dedicated to Professor Dieter Seebach on the occasion of his 60th birthday

Self-replication, like the chirality of the components, is one of the most characteristic features of living organisms. Therefore, self-replication of a chiral molecule is of much interest. The concept of self-replication, however, has not been applied in asymmetric synthesis; almost all conventional asymmetric syntheses require chiral auxiliaries with structures which differ from

[*] Prof. Dr. K. Soai, Dr. T. Shibata, T. Takahashi, T. Konishi
Department of Applied Chemistry, Faculty of Science
Science University of Tokyo
Kagurazaka, Shinjuku-ku, Tokyo 162 (Japan)
Fax: Int. code +(3)3235-2214
e-mail: ksoai@ch.kagu.sut.ac.jp

[**] This work was supported by the Proposed-Based Advanced Industrial Technology R & D Program from the New Energy and Industrial Technology Development Organization (NEDO) of Japan and by a Grant-in-Aid for Scientific Research from the Japanese Ministry of Education, Science, Sports, and Culture.

 © WILEY-VCH Verlag GmbH, D-69451 Weinheim, 1997 0570-0833/97/3622-2458 $ 17.50+.50/0

those of the chiral products. The only exceptions are the diastereoselective process with self-regeneration of a stereocenter,[1] the asymmetric autoinduction,[2] and the asymmetric autocatalytic reaction.[3] Asymmetric autoinduction has been limited to the enantioselective alkylation of aldehydes.[2] We report here the first highly enantioselective self-replication in an asymmetric autoinductive reduction in which the structure and configuration of the chiral ligand and product are identical.

We examined the asymmetric autoinductive reduction of α-amino ketones with lithium aluminum hydride[4] modified with a chiral 1,2-amino alcohol and an achiral additive[5] (Scheme 1).

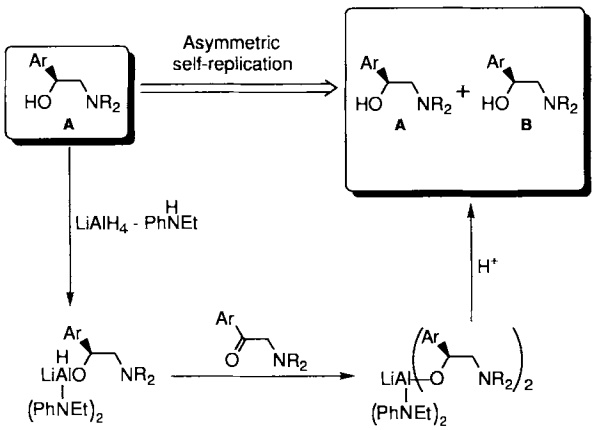

Scheme 1. Asymmetric self-replication of 1,2-amino alcohols; **A** = chiral ligand, **B** = reaction product. The ligand **A** recovered at the end of the reaction and the product **B** have the same structure and configuration.

2-Morpholinoacetophenone (**1a**) was reduced with chirally modified $LiAlH_4$, which was prepared in situ from $LiAlH_4$, chiral (*S*)-2-morpholino-1-phenylethanol (**2a**),[6] and *N*-ethylaniline[5a] in Et_2O at −78 °C. The 1,2-amino alcohol (*S*)-**2a** was obtained in 95.8% *ee* (Table 1, entry 1), which means that (*S*)-**2a** was newly formed in 78.8% yield with 82.4% *ee*.[7] This result implies that **1a** was enantioselectively reduced by chiral **2a** to give new **2a** with the same (*S*) configuration. Lowering the reaction temperature (from −78 to −100 °C) improved the chemical yield, and the enantioselectivity remained high (entry 3). When the chiral ligand (*R*)-**2a** was used instead of (*S*)-**2a**, (*R*)-**2a** was formed in 88.6% yield with 84.7% *ee* (entry 4). Entries 5–9 in Table 1 demonstrate that a variety of N-heterocycles can be used as amino substituents. The reactions of (*S*)-**2c** and **2d** at −78 °C[8] were also examined (entries 6 and 7); the enantioselectivity was very high in both cases (87.9 and 90.1% *ee*, respectively).[9] The *ee* values of products **2a**–**2d** (entries 4–7) were easily improved to greater than 99.5% *ee* by a single recrystallization. This means that, by the self-replication of amino alcohols used as chiral ligands, increased amounts of chiral amino alcohols were obtained with no loss of enantiomeric purity. With (*S*)-2-(*N*,*N*-dibenzylamino)-1-phenylethan-1-ol (**2e**) as the chiral ligand, product **2e** formed in moderate optical yields (72.2% *ee*, entry 8). Entry 9 shows the results of the reaction with (*S*)-1-(4-methylphenyl)-2-pyrrolidinoethan-1-ol (**2f**).[10]

The present method demonstrates the first highly enantioselective autoinductive reduction in which the product has the same structure and configuration as the chiral ligand; a separation of the product from the chiral ligand is therefore unnecessary. This system could introduce a new concept into asymmetric reduction.

Experimental Section

In the following, a typical experiment and the method used to calculate the yield and *ee* values of the newly formed 1,2-amino alcohol (Table 1, entry 3) are described. To a suspension (1 mL) of $LiAlH_4$ (47.4 mg, 1.25 mmol) in Et_2O was added a solution (14 mL) of (*S*)-**2a** (263.0 mg, 1.27 mmol, >99.5% *ee*) in Et_2O over a period of 10 min with vigorous stirring. The mixture was heated at reflux for 1 h, treated within 5 min with a solution (2 mL) of *N*-ethylaniline (309.0 mg, 2.55 mmol) in Et_2O, and heated again at reflux for an additional hour. After the reaction mixture was cooled to −100 °C, a solution (3 mL) of **1a** (102.7 mg, 0.50 mmol) in Et_2O was added dropwise. The reaction mixture was stirred at this temperature for 3–4 h, poured into 1 M hydrochloric acid (5 mL) to quench the reaction, and neutralized with a saturated aqueous solution of $NaHCO_3$ (15 mL) at 0 °C. The mixture was filtered over celite, the precipitate thoroughly washed with CH_2Cl_2 (30 mL), and the combined filtrate extracted with CH_2Cl_2. The extract was dried over anhydrous $MgSO_4$, and the solvent removed under reduced pressure. Purification of the crude product by flash column chromatography gave **2a** (355.5 mg) as a mixture of the newly formed product **2a** and the chiral ligand **2a** (263.0 mg). HPLC analysis of the mixture using a chiral column (DAICEL Chiralcel OD-H) provided an enantiomeric purity of 95.7% *ee*. Therefore, the mixture consisted of (*S*)-**2a** (347.9 mg) and (*R*)-**2a** (7.6 mg). The amount of newly formed **2a** was 355.5 − 263.0 = 92.5 mg (0.446 mmol, 89.2% yield), consisting of (*S*)-**2a** (347.9 − 263.0 = 84.9 mg) and (*R*)-**2a** (7.6 mg). The newly formed (*S*)-enriched amino alcohol **2a** had an enantiomeric purity of 83.6% *ee*.

Table 1. Asymmetric autoinductive reduction according to Equation (1) using 1,2-amino alcohols **2a**–**f** as chiral ligands [a].

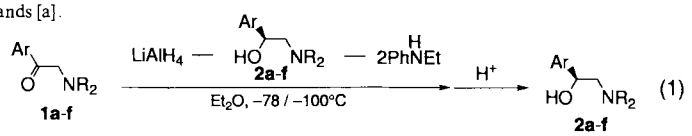

Entry	Ar	−NR2	Chiral ligand (*ee*/%) [b]	*T* [°C]	*ee*/% [b,c]	Product [d] Yield	*ee*/%
1	Ph	−N⟨⟩O	(*S*)-**2a** (>99.5)	−78	95.8 (*S*)	78.8	82.4 (*S*)
2	Ph	−N⟨⟩O	(*S*)-**2a** (>99.5)	−78	92.1 (*S*)	77.7	73.2 (*S*)
3	Ph	−N⟨⟩O	(*S*)-**2a** (>99.5)	−100	95.7 (*S*)	89.2	83.6 (*S*)
4	Ph	−N⟨⟩O	(*R*)-**2a** (>99.5)	−100	96.1 (*R*)	88.6	84.7 (*R*)
5	Ph	−N⟨⟩NBn	(*S*)-**2b** (>99.5)	−100	95.3 (*S*)	88.9	81.6 (*S*)
6	Ph	−N⟨⟩	(*S*)-**2c** (>99.5)	−78	97.7 (*S*)	73.0	87.9 (*S*)
7	Ph	−N⟨⟩	(*S*)-**2d** (>99.5)	−78	97.6 (*S*)	82.4	90.1 (*S*)
8	Ph	$-NBn_2$	(*S*)-**2e** (95.3)	−78	90.6 (*S*)	65.3	72.2 (*S*)
9	Tol	−N⟨⟩	(*S*)-**2f** (95.7)	−78	89.4 (*S*)	92.9	69.7 (*S*)

[a] Molar ratio **1**:$LiAlH_4$:**2**:*N*-ethylaniline for entries 1 and 3–9 1.0:2.5:2.5:5.0., for entry 2 1.0:1.8:1.8:3.6. [b] Enantiomeric purities were determined by HPLC analysis using a chiral column; >99.5% *ee* means that the minor peak was undetectable. [c] Enantiomeric purity of the total amount of isolated **2**. [d] The portion of **2** used at the beginning of the reaction as a chiral ligand was excluded in the calculation (see Experimental Section).

Received: June 2, 1997 [Z 10503 IE]
German version: *Angew. Chem.* **1997**, *109*, 2560–2562

Keywords: amino alcohols · asymmetric synthesis · hydrides · reductions

[1] D. Seebach, A. R. Sting, M. Hoffmann, *Angew. Chem.* **1996**, *108*, 2880–2921; *Angew. Chem. Int. Ed. Engl.* **1996**, *35*, 2708–2748.

[2] A. H. Alberts, H. Wynberg, *J. Am. Chem. Soc.* **1989**, *111*, 7265–7266; K. Soai, Y. Inoue, T. Takahashi, T. Shibata, *Tetrahedron* **1996**, *52*, 13355–13362; L. ShengJian, J. Yaozhong, M. Aiqiao, Y. Guishu, *J. Chem. Soc. Perkin Trans. 1* **1993**, 885–886.

 © WILEY-VCH Verlag GmbH, D-69451 Weinheim, 1997 0570-0833/97/3622-2459 $ 17.50+.50/0

[3] K. Soai, T. Shibata, H. Morioka, K. Choji, *Nature* **1995**, *378*, 767–777; T. Shibata, H. Morioka, T. Hayase, K. Choji, K. Soai, *J. Am. Chem. Soc.* **1996**, *118*, 471–472; T. Shibata, K. Choji, H. Morioka, T. Hayase, K. Soai, *Chem. Commun.* **1996**, 751–752; T. Shibata, K. Choji, T. Hayase, Y. Aizu, K. Soai, *ibid.* **1996**, 1235–1236; T. Shibata, H. Morioka, S. Tanji, T. Hayase, Y. Kodaka, K. Soai, *Tetrahedron Lett.* **1996**, *37*, 8783–8786; short review: C. Bolm, F. Bienewald, A. Seger, *Angew. Chem.* **1996**, *108*, 1767–1769; *Angew. Chem. Int. Ed. Engl.* **1996**, *35*, 1656–1658; K. Soai, T. Shibata, *Yuki Gosei Kagaku Kyokaishi* (*J. Synth. Org. Chem. Jpn.*), in press.

[4] E. R. Grandbois, S. I. Howard, J. D. Morrison, *Asymmetric Synthesis, Vol. 2* (Ed.: J. D. Morrison), Academic Press, New York, **1983**, pp. 71–90.

[5] a) S. Terashima, N. Tanno, K. Koga, *Chem. Lett.* **1980**, 981–984; N. Tanno, S. Terashima, *Chem. Pharm. Bull.* **1983**, *31*, 821–836, 837–851; b) J.-P. Vigneron, I. Jacquet, *Tetrahedron* **1976**, *32*, 939–944; J.-P. Vigneron, V. Bloy, *Tetrahedron Lett.* **1979**, 2683–2686; *ibid.* **1980**, *21*, 1735–1738.

[6] C. E. Harris, G. B. Fisher, D. Beardsley, L. Lee, C. T. Goralski, L. W. Nicholson, B. Singaram, *J. Org. Chem.* **1994**, *59*, 7746–7751.

[7] See the Experimental Section for details on how the amount of newly formed **2a** was calculated.

[8] In these reactions, lowering the reaction temperature had no significant effect on the yield or *ee* value.

[9] No distinct amplification of the *ee* value was observed for (*S*)-**2d** (51.7% *ee*) when (*S*)-**2d** with lower *ee* (51.4% *ee*) was used.

[10] Amino alcohol (*S*)-**2f** was prepared by asymmetric reduction of α-amino ketone **1f** with chirally modified lithium borohydride: K. Soai, S. Niwa, T. Kobayashi, *J. Chem. Soc. Chem. Commun.* **1987**, 801–802; recent examples of asymetric reduction of α-amino ketones for the preparation of chiral 1,2-amino alcohols: B. T. Chao, Y. S. Chun, *Tetrahedron: Asymmetry* **1992**, *3*, 341–342; G. J. Quallich, T. M. Woodall, *Tetrahedron Lett.* **1993**, *34*, 4145–4148.

Chiral Methyl-Branched Surfactants and Phospholipids: Synthesis and Properties

Michael Morr,* Jens Fortkamp, and Stefan Rühe

The recent publication of the synthesis and unusual properties of spiro-surfactants by Menger et al.[1] prompted us to report the results of our work on chiral methyl-branched surfactants and phospholipids which are obtained by formal opening of spiro-compounds. For some time we have been engaged in the isolation of chiral methyl-branched fatty acids, for example, (2*R*,4*R*,6*R*)-2,4,6-trimethyloctanoic acid (**1**)[2] from the preen gland of the musk duck *Cairina moschata* as well as (2*R*,4*R*,6*R*,8*R*)-2,4,6,8-tetramethyldecanoic acid (**2**) and (2*R*,4*R*,6*R*,8*R*)-2,4,6,8-tetramethylundecanoic acid (**3**)[3] from

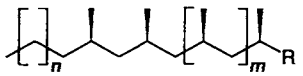

m	*n*	R	
1	0	0	COOH
2	1	0	COOH
3	1	1	COOH
lardolure	1	1	OCHO
norlardolure	1	0	OCHO

the preen gland of the domestic goose *Anser a.f. domesticus*. In addition to a number of new derivatives of these compounds—such as the mite pheromones lardolure and norlardolure[4, 5] as well as new, chiral ferro- and antiferroelectric liquid crystals with methyl side chains[6]—we were interested in the physical and chemical properties (such as critical micellization concentration (CMC)) of surfactants **4** and **5**, which are derived from

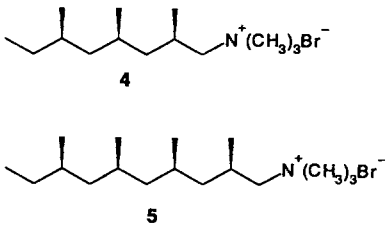

4

5

1 and **2**, respectively. We also focused our attention on the diacyl-*sn*-glcero-3-phosphatidylcholines **10**–**15**, which show high enantiomeric purity and a uniform chain length of ten carbon atoms, but varying numbers of methyl-substituted chiral

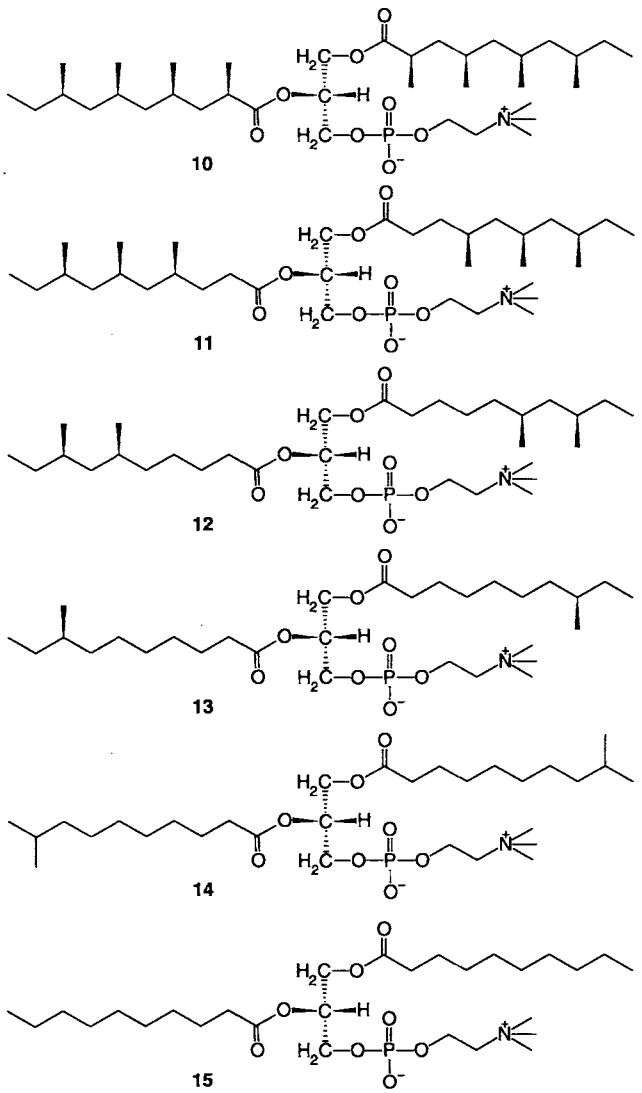

10

11

12

13

14

15

centers. Properties required for their useful applications (e. g. as membrane constituents) were analysed by differential scanning calorimetry (DSC) to determine the main phase-transition temperatures, and with a Langmuir film balance to record π-*A*-isotherms.

The methyl esters **6** of **1** and **2** were allowed to react with lithium aluminum hydride to give alcohols **7** ($n = 0, 1$; yield 95%), which were converted by tosylation (via **8**) into the bromides **9** with LiBr in acetone (85%). The reaction of **9** with trimethylamine in ethanol at 80 °C (in a pressure vessel) afforded **4** and **5** in quantitative yield.

[*] Dr. M. Morr, Dr. J. Fortkamp, S. Rühe
Gesellschaft für Biotechnologische Forschung mbH
Mascheroder Weg 1, D-38124 Braunschweig (Germany)
Fax: Int. code +(531)6181-444
e-mail: mmo@gbf-braunschweig.de

 © WILEY-VCH Verlag GmbH, D-69451 Weinheim, 1997 0570-0833/97/3622-2460 $ 17.50+.50/0

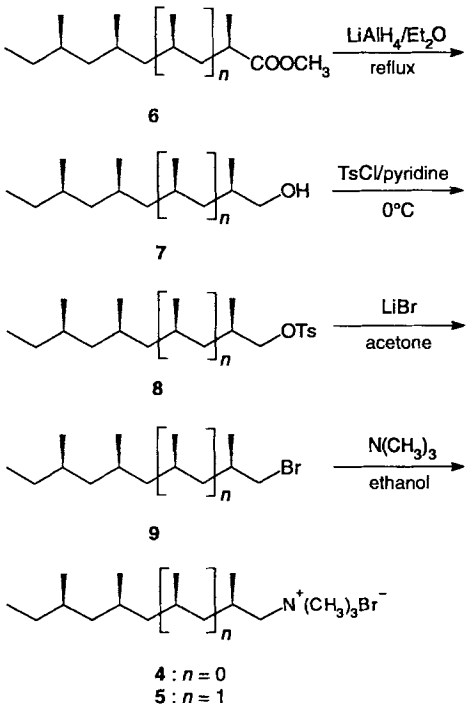

Aqueous solutions of **4** and **5** were analyzed tensiometrically at 25 °C. It is known that with common surfactants the surface tension decreases steadily until the CMC is reached. At higher surfactant concentrations surface tension does not decrease further, as there is a preferred invasion of surfactant molecules into the micelles instead of enrichment at the air–water interface. These characteristic properties were observed for **4**. The CMC is 9.12×10^{-2} M, which is comparable to that of 1.4×10^{-1} M (**A**) for the corresponding spiro-surfactant found by Menger et al.[1] Apparently, the tendency of **4** to form micelles is significantly lower than with common surfactants with the same total number of carbon atoms. Menger et al. also reported that formation of micelles seems to be inhibited by a certain rigidity of the methyl-branched aliphatic chain. They gave an estimated CMC for the spiro-compound of more than 4.4×10^{-3} M (**B**).[1] For

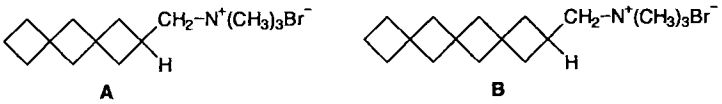

the corresponding compound **5** we observed a decrease in the surface tension to about 27 mN m^{-1} and a CMC of 1.5×10^{-2} M. As with the spiro-compound, the plot of the surface tension is anomalous since it is partially convex, and the surface tension changes only slightly at low concentrations.

Phospholipids **10**–**15** were synthesized according to Hermetter and Paltauf.[7, 8] When applied to the synthesis of **10**, the same method caused racemization at the 2-position of the carboxylic acid group; hence, an alternative approach had to be found. Using the method of Wood,[9] **2**, *sn*-glycero-3-phosphocholine (as the $CdCl_2$ complex), and dicyclohexyl carbodiimide (DCC)/4-dimethylamino pyridine (DMAP) in ethanol-free chloroform gave **10** in 66% yield after 10 d at room temperature. Gas-chromatographic analysis of an acidically methylated sample indicated that chirality was conserved to more than 95%. Compound **11** was synthesized by standard chain-elongation procedures (malonic ester method). (6*R*,8*R*)-6,8-Dimethyldecanoic acid, which was used to synthesize **12**, was obtained in a 16-step procedure, and (*R*)-8-methyldecanoic acid, required for **13**, required a 10-step synthesis.[2, 10]

The calorimetric analyses of the phospholipid suspensions **10**–**15** were performed on a "high-sensitivity" differential calorimeter (MC-2D, Micro Cal, Inc.), which functions according to the principle of dynamic performance differential calorimetry. No phase transitions were observed for **11**–**13** between −45 and 25 °C; Menger et al. found the same result with the spirophospholipids (Figure 1). This is in agreement with

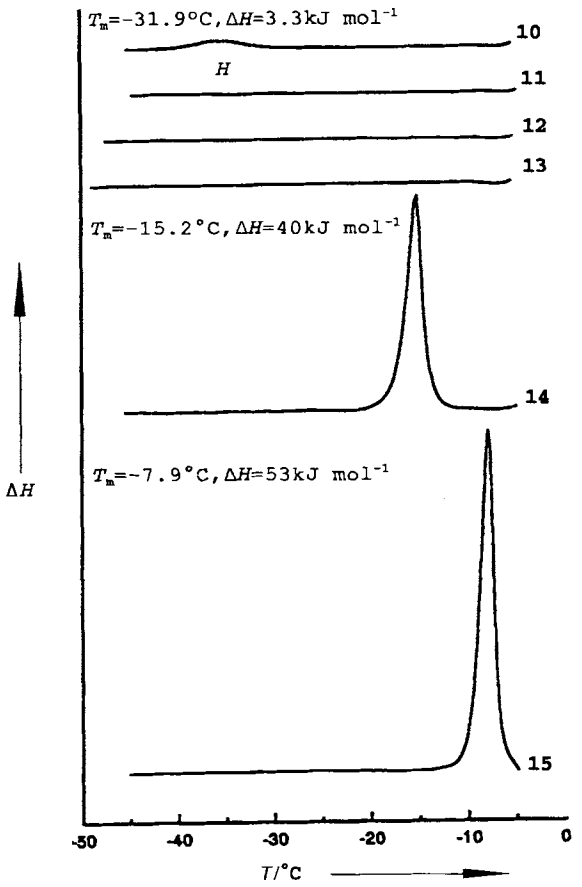

Figure 1. DSC heating thermograms of **10**–**15**, $c = 10$ mg mL^{-1} in water, heating rate = 20 °C h^{-1}.

expectations based on comparisons with the results of McElhaney et al.[11] Phospholipid **10** showed a main phase-transition temperature T_m of −31.9 °C. It is clear from the curve that it is a very broad phase transition with a relatively low transition enthalpy ΔH. Although DSC data do not provide information about processes at the molecular level, it is easy to imagine that—based on the three-dimensional structure derived from calculations of molecular dynamics[12] for **2**—the gel phase of such a compound is less ordered than that of the corresponding nonbranched compound. This is indicated by a lower transition enthalpy. The fact that **10**, in contrast to **11**–**13**, shows a phase transition within the temperature range used suggests that the acyl chains in **10** are more easily arranged, even if in a relatively unordered fashion. The chain is more bulky throughout the overall length of the molecule than the head group. This is different to the phosphatidylcholines, which show no phase transition, and is in accordance with the data from the film balance.

 © WILEY-VCH Verlag GmbH, D-69451 Weinheim, 1997 0570-0833/97/3622-2461 $ 17.50+.50/0

The data for **14** ($T_m = -15.2\,°C$, $\Delta H = 40\,kJ\,mol^{-1}$) are consistent with the results of McElhaney et al.[13] for other diacylphosphatidylcholines with longer chain lengths (e. g. $T_m = -18.8\,°C$ and $\Delta H = 32.6\,kJ\,mol^{-1}$ for bis(10-methylundecanoyl)phosphatidylcholine). Comparison of our data with that for the corresponding nonbranched didecanoylphosphatidylcholine (**15**; $T_m = -7.9\,°C$, $\Delta H = 53\,kJ\,mol^{-1}$) shows that, in contrast to compounds with linear chains, a slightly disturbed gel state can be assumed for the diisoacylphosphatidylcholines.

Diacylphosphatidylcholines **10**–**15** were analyzed with a film balance (Lauda FW 2) to ascertain their behavior at the water–air interface. The shapes of the π-A-isotherms at 0 and 20 °C are almost identical and characteristic of those from expanded films (Figure 2). An increase in the surface per molecule of 50 to

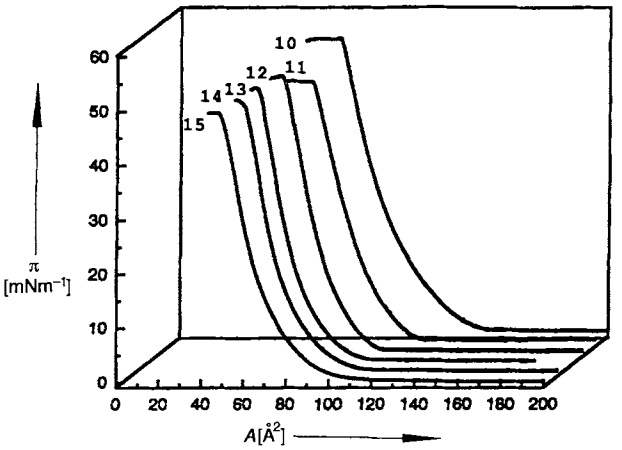

Figure 2. π-A-Isotherms of **10**–**15** on water at 0 °C, compression time = 30 min for 927 cm², A = molecule surface per molecule.

76 Å² is observed with an increasing number of methyl branches in the acyl chain. This is in accordance with the results for dipalmitoylphosphatidylcholine and the corresponding iso and anteiso compounds,[14] for which the maximum surface tensions differ only slightly (48–51 $mN\,m^{-1}$ for **11**–**14**). Surprisingly, the value for **10** is slightly higher (54 $mN\,m^{-1}$). An explanation for this could be the ratio of the steric requirements of the head group and the acyl chain. For the nonbranched compound the head group has a higher steric requirement than the acyl chains, whereas the methyl side chains in the other compounds disturb an optimized arrangement. For **10** the acyl chains are more bulky than the head group. This is supported by DSC data that show a phase transition within the investigated temperature range for **10**, but not for **11**–**13**. Further confirmation of this hypothesis is the absence of a condensed phase; phase transitions were found only for **10**, **14**, and **15**, and these were clearly below 0 °C. A pharmaceutically interesting application could be the modification of liposome properties with respect to their permeability by specific addition of branched phospholipids.

Received: June 2, 1997 [Z10500IE]
German version: *Angew. Chem.* **1997**, *109*, 2567–2569

Keywords: calorimetry · carboxylic acids · micelles · phospholipids · surfactants

[1] F. M. Menger, J. Ding, *Angew. Chem.* **1996**, *108*, 2266–2268; *Angew. Chem. Int. Ed. Engl.* **1996**, *35*, 2137–2139.
[2] J. Fortkamp, Dissertation, Technische Universität Braunschweig, **1994**.
[3] M. Morr, V. Wray, J. Fortkamp, R. D. Schmid, *Liebigs Ann. Chem.* **1992**, 433–439.
[4] M. Morr, C. Proppe, V. Wray, *Liebigs Ann.* **1995**, 2001–2004.
[5] Y. Kuwahara, N. Asami, M. Morr, S. Matsuyama, T. Suzuki, *Appl. Ent. Zool.* **1994**, *29*, 253–257.
[6] G. Heppke, D. Lötzsch, M. Morr, L. Ernst, *J. Mater. Chem.* **1997**, *7*, 1993–1999.
[7] A. Hermetter, F. Paltauf, *Chem. Phys. Lipids* **1981**, *28*, 111–115.
[8] All phosphatidylcholine derivatives were purified by preparative HPLC and obtained in the following yields: **10**:66%, **11**:34%, **12**:35%, **13**:18%, **14**:40%, **15**:24%.
[9] M. G. Wood, Dissertation, Emory University, Atlanta, **1988**.
[10] All new compounds were unequivocally characterized with ^1H and ^{13}C NMR spectroscopy and high-resolution FAB mass spectrometry.
[11] J. R. Silvius, R. N. McElhaney, *Chem. Phys. Lipids* **1980**, *26*, 67–77.
[12] J. Fortkamp, Diplomarbeit, Technische Universität Braunschweig, **1989**.
[13] R. N. A. H. Lewis, R. N. McElhaney, *Biochemistry* **1985**, *24*, 2431–2439.
[14] E. Kannenberg, A. Blume, R. N. McElhaney, K. Poralla, *Biochim. Biophys. Acta* **1983**, *733*, 111–118.

A Supercharged Anion with a Silyl-Substituted Eight-Center, Twelve-Electron π System: Synthesis and Characterization of the Tetralithium Salt of an Octasilyl-Substituted Trimethylenecyclopentene Tetraanion**

Akira Sekiguchi,* Tsukasa Matsuo, and Chizuko Kabuto

Supercharged anions with extended π-electron systems have attracted considerable interest owing to their unique structures and electronic properties.[1] The existence of a hexaanionic species in the solid state is inferred from the formation of K_6C_{60}, which was characterized by X-ray powder diffraction[2] and ^{13}C NMR spectroscopy.[3] Scott et al. recently reported on the tetralithium salt of the corannulene tetraanion ($C_{20}H_{10}$) and its derivatives.[4] The most recent, and, to our knowledge, only report on the molecular structure of a rubrene tetraanion (crystallized as a tetrasodium salt; rubrene = 5,6,11,12-tetraphenyltetracene, $C_{42}H_{28}$) that has been confirmed by X-ray crystallography was carried out by Bock et al.[5] We report here a tetraanion with a new silyl-substituted eight-center, twelve-electron π system, which was isolated as the tetralithium salt **2**.

As an appropriate precursor of the tetraanion, the octasilyl-substituted trimethylenecyclopentene **1** with an eight-electron π system was prepared as pale yellow crystals by the reaction of hexadecamethyl-3,5,8,10,13,15,18,20-octasilacycloicosa-1,6,11,16-tetrayne with $[(C_5H_4Me)Mn(CO)_3]$ under photochemical conditions. The molecular structure of **1** is shown in Figure 1.[6]

Reduction of **1** with lithium in dry, oxygen-free tetrahydrofuran at room temperature led to the formation of an orange solution of the tetraanion of **1** (Scheme 1). Crystallization from hexane afforded air- and moisture-sensitive pale orange crystals of the tetralithium salt **2**, which contains four molecules of THF.

[*] Prof. Dr. A. Sekiguchi, Dipl.-Chem. T. Matsuo
Department of Chemistry, University of Tsukuba
Tsukuba, Ibaraki 305 (Japan)
Fax: Int. code +(298)53-4314
e-mail: sekiguch@staff.chem.tsukuba.ac.jp
Dr. C. Kabuto
Graduate School of Science
Tohoku University
Aoba-ku, Sendai 980-77 (Japan)

[**] This work was supported by the Sumitomo Foundation (960548), Tokuyama Science Foundation, and a Grant-in-Aid for Scientific Research on Priority Areas (No. 09239101) from the Ministry of Education, Science, Sports, and Culture, Japan.

 © WILEY-VCH Verlag GmbH, D-69451 Weinheim, 1997 0570-0833/97/3622-2462 $ 17.50+.50/0

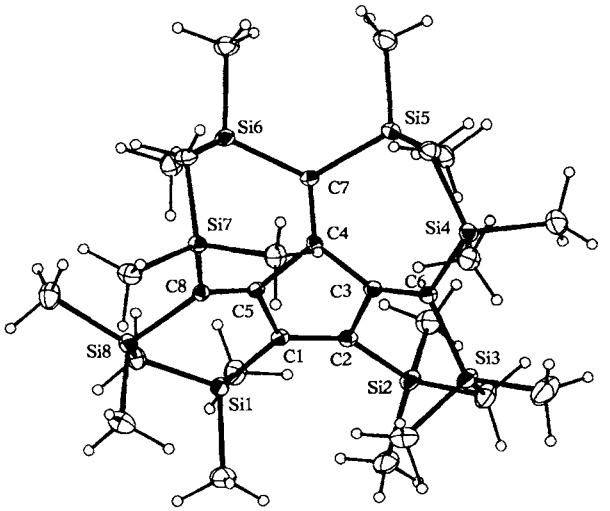

Figure 1. An ORTEP representation of the structure of **1** in the crystal. Selected bond lengths [Å] and angles [°]: C1–C2 1.372(8), C1–C5 1.506(7), C2–C3 1.520(8), C3–C4 1.512(8), C3–C6 1.354(8), C4–C5 1.523(7), C4–C7 1.358(8), C5–C8 1.348(7), C1–Si1 1.894(6), C2–Si2 1.897(6), C6–Si3 1.893(6), C6–Si4 1.889(6), C7–Si5 1.900(6), C7–Si6 1.899(6), C8–Si7 1.885(6), C8–Si8 1.884(6); C2-C1-C5 108.3(4), C1-C2-C3 109.3(4), C2-C3-C4 103.4(4), C2-C3-C6 125.2(5), C4-C3-C6 130.0(5), C3-C4-C5 101.4(4), C3-C4-C7 132.5(5), C5-C4-C7 124.9(4), C1-C5-C4 103.6(4), C1-C5-C8 128.3(4), C4-C5-C8 127.5(4).

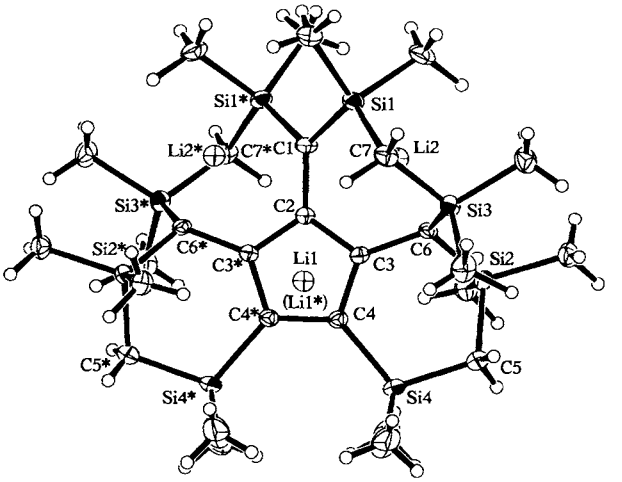

Figure 2. An ORTEP representation of the structure of **2** in the crystal (THF is omitted for the clarity). Selected bond lengths [Å] and angles [°]: C1–C2 1.537(7), C2–C3 1.443(5), C3–C4 1.464(5), C3–C6 1.534(5), C4–C4* 1.470(7), C1–Si1 1.832(3), C6–Si2 1.809 (4), C6–Si3 1.832(4), C4–Si4 1.878(4), Li1–C2 2.335(7), Li1–C3 2.248(7), Li1–C4 2.132(7), Li1–C3* 2.287(8), Li1–C4* 2.169(8), Li2–C1 2.255(7), Li2–C6 2.092(8), Li2–Si1 2.813(7), Li2–Si2 3.231(7), Li2–Si3 3.263(7); C1-C2-C3 125.6(2), C3-C2-C3* 108.8(4), C2-C3-C4 108.2(3), C2-C3-C6 123.3(3), C4-C3-C6 128.5(3), C3-C4-C4* 107.4(2).

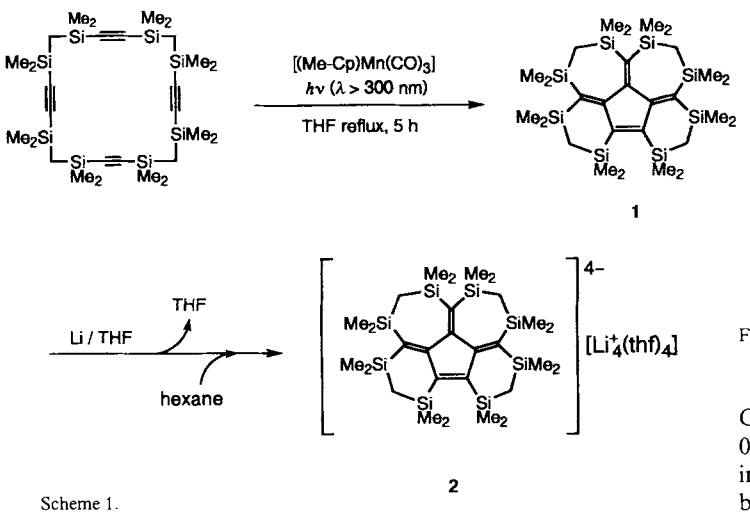

Scheme 1.

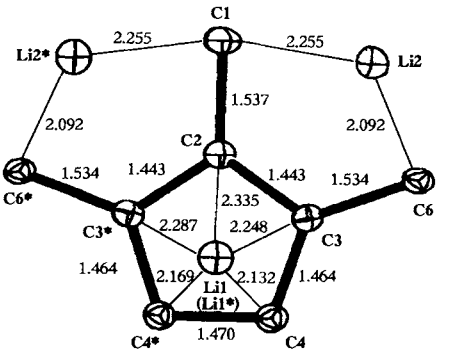

Figure 3. Section from the structure of **2** with selected distances [Å].

The molecular structure of **2** was determined by X-ray diffraction (Figure 2)[7] and shows that the molecule has C_2 symmetry and that the C1–C2 bond is a crystallographic twofold axis. The tetralithium salt **2** is monomeric and forms contact ion pairs in the crystals. One THF molecule is coordinated to each lithium atom. Li1 and Li1* are located near the center of the ring, above and below the plane of the five-membered ring. The distances between Li1 and the carbon atoms of the five-membered ring (C2, C3, C4, C4*, and C3*) range from 2.132 to 2.335 Å (av 2.234 Å). Li2 and Li2* are bonded to the two exocyclic carbon atoms (C1, C6 and C1, C6*) (Figure 3).

A comparison of the structural parameters of **1** and **2** is quite interesting. Eight carbon atoms of the π skeleton of **2** become completely coplanar by the four-electron reduction. The C3–C6, C3*–C6*, and C1–C2 distances in **2** are between 0.179 and 0.186 Å (av 0.182 Å) longer than the corresponding distances in **1**. In addition, the C4–C4* distance in **2** is elongated by 0.098 Å. By contrast, the C3–C4, C3*–C4*, C2–C3, and C2*–C3* distances in **2** are between 0.042 and 0.080 Å (av 0.062 Å) shorter than those in **1**. That is, the C–C double bonds in **1** are elongated, whereas the C–C single bonds are shortened by the reduction. The five-membered ring is planar and forms an almost equilateral pentagon, as determined by the internal bond angles of 107.4–108.8° (av 108.0°) and the sum of the bond angles (540.0°). The C–C distances in the five-membered ring range between 1.443 and 1.470 Å (av 1.457 Å). The Si–C bonds (C1–Si1, 1.832(3); C6–Si2, 1.809(4); C6–Si3, 1.832(4) Å) in **2** are considerably shorter than those in **1** (1.900(6), 1.893(6), and 1.889(6), respectively), because of the delocalization of the negative charge onto the silicon centers by pπ-σ* conjugation.

The structure of **2** in [D_6]benzene was characterized by ^{1}H, ^{13}C, ^{29}Si, and ^{6}Li NMR spectroscopy. The two methyl groups of $SiMe_2$ and the two hydrogen atoms of CH_2 are magnetically nonequivalent, which is attributed to the fixed six- or seven-membered ring and to the coordination by the lithium atoms. Thus, ^{1}H NMR spectrum of **2** in [D_6]benzene reveals the presence of eight signals for methyl groups and four doublets for methylene groups with geminal couplings of 13.2 and 13.7 Hz. In the ^{29}Si NMR spectrum, four signals are observed at $\delta = -16.1$, -15.1, -14.5, and -13.2, which are shifted to higher field in comparison to those of **1**. The ^{13}C NMR spectrum shows five signals for quaternary carbon atoms at

 © WILEY-VCH Verlag GmbH, D-69451 Weinheim, 1997 0570-0833/97/3622-2463 $ 17.50+.50/0

$\delta = 9.62$, 19.7, 107.0, 132.1, and 148.2. The signal at $\delta = 19.7$ splits into a triplet ($J(^{13}C,^{6}Li) = 6.2$ Hz) due to coupling with one ^{6}Li ($I = 1$), whereas the signal at $\delta = 9.62$ splits into a quintet ($J(^{13}C,^{6}Li) = 2.3$ Hz) due to coupling with two equivalent ^{6}Li centers. Thus, we assign the triplet to C6 and C6*, and the quintet to the C1 carbon atom. From the ^{13}C NMR spectral data, it is apparent that the negative charge is largely delocalized over the three exocyclic carbon atoms (C1, C6, and C6*) of the π-electron system of **2**. The signals of these carbon atoms in **2** are considerably shifted to higher field relative to those signals in **1** by $\Delta\delta = 169.3$ for C1 and $\Delta\delta = 152.9$ for C6 and C6*.

Interestingly, the ^{6}Li NMR spectrum of **2** yielded two signals of equal intensity at $\delta = -6.27$ and 2.47. The appreciable upfield shift at $\delta = -6.27$ is evidently caused by the strong shielding effect of the diamagnetic ring current resulting from the six π electron system. Thus, this ^{6}Li NMR signal is reasonably assigned to Li1 and Li1*, which are located above and below the five-membered ring, respectively.

On the basis of these spectroscopic data, the molecular structure of **2** in the crystal is maintained in solution. The results of the X-ray crystallographic and NMR studies presented here indicate that the tetraanion of **2** has a stable, closed-shell structure that is stabilized not only by the eight silicon atoms but also by the aromatic cyclopentadienyl anion.

Experimental Section

1: A mixture of 3,3,5,5,8,8,10,10,13,13,15,15,18,18,20,20-hexadecamethyl-3,5,8,10,13,15,18,20-octasilacycloicosa-1,6,11,16-tetrayne (201 mg, 0.33 mmol) and $[(C_5H_4Me)Mn(CO)_3]$ (93 mg, 0.43 mmol) in THF (30 mL) was irradiated with a 500 W high-pressure mercury lamp for 5 h through the cut off filter ($\lambda > 300$ nm) under the reflux in THF. After removal of the manganese complex, the reaction mixture was chromatographed on silica gel to produce pale yellow crystals of **1** in 17% yield. M.p. 229–230 °C; ^{1}H NMR ([D$_8$]toluene, TMS): $\delta = -0.28$ (d, $^{2}J(H,H) = 13.4$ Hz, 2H, CH_2), −0.16 (d, $^{2}J(H,H) = 13.4$ Hz, 2H, CH_2), 0.05 (s, 6 H, CH_3), 0.05 (d, $^{2}J(H,H) = 13.6$ Hz, 2H, CH_2), 0.18 (s, 6H, CH_3), 0.21 (s, 6H, CH_3), 0.23 (s, 6H, CH_3), 0.26 (s, 6H, CH_3), 0.29 (s, 6H, CH_3), 0.30 (s, 6H, CH_3), 0.31 (s, 6H, CH_3), 0.43 (d, $^{2}J(H,H) = 13.6$ Hz, 2H, CH_2); $^{13}C\{^{1}H\}$ NMR ([D$_1$]chloroform, TMS): $\delta = 1.00$, 1.13, 1.76, 2.54, 3.52, 3.69, 3.99, 4.77, 6.45, 12.0, 134.1, 135.7, 158.6, 172.6, 178.9; $^{29}Si\{^{1}H\}$ NMR ([D$_1$]chloroform, TMS): $\delta = -13.3$, −10.2, −10.0, −9.1.

2: Crystals of **1** (51 mg, 0.083 mmol) and lithium metal (30 mg, 4.3 mmol) were placed in a sealed tube with a magnetic stirrer. After the tube had been degassed, dry, oxygen-free THF (3 mL) was introduced by vacuum transfer, and the mixture was stirred at room temperature to give an orange solution of the tetraanion of **2** within 1 h. After the solvent had been removed in vacuo, degassed hexane was introduced by vacuum transfer. Then after the lithium had been removed, the solution was cooled to afford orange crystals of **2** in a quantitative yield. ^{1}H NMR ([D$_6$]benzene, TMS): $\delta = -0.72$ (d, $^{2}J(H,H) = 13.7$ Hz, 2H, CH_2), −0.20 (d, $^{2}J(H,H) = 13.7$ Hz, 2H, CH_2), 0.05 (s, 6H, CH_3), 0.08 (s, 6H, CH_3), 0.12 (d, $^{2}J(H,H) = 13.2$ Hz, 2H, CH_2), 0.29 (s, 6H, CH_3), 0.34 (d, $^{2}J(H,H) = 13.2$ Hz, 2H, CH_2), 0.54 (s, 6H, CH_3), 0.56 (s, 6H, CH_3), 0.61 (s, 6H, CH_3), 0.62 (s, 6H, CH_3), 0.63 (s, 6H, CH_3), 1.32 (m, 16H, THF), 3.56 (m, 16H, THF); $^{13}C\{^{1}H\}$ NMR ([D$_6$]benzene, TMS): $\delta = 5.37$, 5.67 (2CH_3), 6.65, 6.90, 6.96, 7.37, 7.53, 9.20, 9.62 (quint, $J(^{13}C,^{6}Li) = 2.3$ Hz), 11.6, 19.7 (t, $J(^{13}C,^{6}Li) = 6.2$ Hz), 25.4 (THF), 68.9 (THF), 107.0, 132.1, 148.2; $^{29}Si\{^{1}H\}$ NMR ([D$_6$]benzene, TMS): $\delta = -16.1$, −15.1, −14.5, −13.2; $^{6}Li\{^{1}H\}$ NMR ([D$_6$]benzene, LiCl in MeOH, external): $\delta = -6.27$, 2.47.

Received: May 22, 1997 [Z194671E]
German version: *Angew. Chem.* **1997**, *109*, 2572–2574

Keywords: carbanions · cyclopentadienes · lithium · silicon · reductions

[1] For reviews, see: a) K. Müllen, *Chem. Rev.* **1984**, *84*, 603; b) M. Rabinovitz, *Top. Curr. Chem.* **1988**, *14*, 99; c) A. M. Sapse, P. von. R. Schleyer, *Lithium Chemistry: A Theoretical and Experimental Overview*, Wiley, New York, **1995**.

[2] O. Zhou, J. E. Fischer, N. Coustel, S. Kycia, Q. Zhu, A. R. McGhie, W. J. Romanow, J. P. McCauley Jr, A. B. Smith III, D. E. Cox, *Nature* **1991**, *351*, 462.

[3] R. Tycko, G. Dabbagh, M. J. Rosseinsky, D. W. Murphy, R. M. Fleming, A. P. Ramirez, J. C. Tully, *Science* **1991**, *253*, 884.

[4] a) A. Ayalon, M. Rabinovitz, P. -C. Cheng, L. T. Scott, *Angew. Chem.* **1992**, *104*, 1691; *Angew. Chem. Int. Ed. Engl.* **1992**, *31*, 1636; b) A. Ayalon, A. Sygula, P. -C. Cheng, M. Rabinovitz, P. W. Rabideau, L. T. Scott, *Science* **1994**, *265*, 1065; c) M. Baumgarten, L. Gherghel, M. Wagner, A. Weitz, M. Rabinovitz, P. -C. Cheng, L. T. Scott, *J. Am. Chem. Soc.* **1995**, *117*, 6254.

[5] H. Bock, K. Gharagozloo-Hubmann, C. Näther, N. Nagel, Z. Havlas, *Angew. Chem.* **1996**, *108*, 720; *Angew. Chem. Int. Ed. Engl.* **1996**, *35*, 631.

[6] Crystal data for **1**: $C_{28}H_{56}Si_8$, $M_r = 617.43$; $a = 16.194(7)$, $b = 11.963(3)$, $c = 19.581(2)$ Å, $\beta = 97.94(2)°$, $V = 3757(2)$ Å^3, monoclinic, space group $P2_1/a$, $Z = 4$, $\rho_{calcd} = 1.091$ g cm^{-3} [7b]. The final R factor was 0.0799 ($Rw = 0.0914$) for 6229 reflections with $F_o > 3\sigma(F_o)$. The central five-membered ring has an envelope conformation; the angle formed by C3-C2-C1-C5 and C3-C4-C5 planes is 36.2° (see Figure 1). The internal bond angles of the five-membered ring are 101.4–109.3° (av 105.2°).

[7] a) A single crystal (0.20 × 0.20 × 0.20 mm) of **2** was sealed in capillary glass tube for the data collection. Diffraction data were collected at 13 °C on a Rigaku Denki AFC-5R diffractometer with a rotating anode (40 kV, 180 mA) employing graphite-monochromated $Cu_{K\alpha}$ radiation ($\lambda = 1.54718$ Å). A total of 4962 reflections ($3° < 2\theta < 120°$) was collected. Crystal data of **2**: $C_{44}H_{88}Li_4O_4Si_8$, $M_r = 933.62$: $a = 22.94(1)$, $b = 12.257(4)$, $c = 20.164(7)$ Å, $\beta = 106.49(3)°$, $V = 5435(3)$ Å^3, monoclinic, space group $C2/c$, $Z = 4$, $\rho_{calcd} = 1.141$ g cm^{-3}. The final R factor was 0.0574 ($R_w = 0.0650$) for 3546 reflections with $I > 3\sigma(I)$. b) Crystallographic data (excluding structure factors) for the structures reported in this paper have been deposited with the Cambridge Crystallographic Data Centre as supplementary publication no. CCDC-179175. Copies of the data can be obtained free of charge on application to The Director, CCDC, 12 Union Road, Cambridge CB2 1EZ, UK (fax: int. code +(1223) 336-033; e-mail: deposit@chemcrys.cam.ac.uk).

Tetradecanuclear Molybdenum (Tungsten)/Copper/Sulfur Heterobimetallic Clusters $[(n\mathrm{Bu})_4N]_4[M_4Cu_{10}S_{16}O_2E]\cdot H_2O$, (M = Mo, E = O; M = W, E = 1/2O + 1/2S)**

Jun Guo, Xintao Wu,* Wenjian Zhang, Tianlu Sheng, Qun Huang, Ping Lin, Quanming Wang, and Jiaxi Lu

The synthetic and structrual chemistry of heterometallic Mo(W)/Cu(Ag)/S clusters has developed rapidly.[1] Recently, certain clusters were found to exhibit strong nonlinear optical (NLO) properties,[2] which attracted many to synthesize more new structure types in this field. Starting from thiometalates we synthesized many Mo(W)/Cu(Ag)/S complexes such as the square-type octanuclear clusters $[Et_4N]_4[M_4Cu_4S_{12}O_4]$ (M = Mo, W),[3] the dodecanuclear clusters $[M_4Cu_4S_{12}O_4(Cu(tmen))_4]$ (tmen = tetramethylethylenediamine),[3] the eicosanuclear clusters $[Et_4N]_4[M_8Cu_{12}S_{28}O_4]\cdot DMF$ (DMF = *N*,*N*-dimethylformamide),[4] the linear-chain polymeric cluster $[WS_4Ag\cdot NH_3C(CH_2OH)\cdot 2DMF]_n$,[5] the double-chain polymeric cluster $[WS_4Ag\cdot NH_3C(CH_2OH)\cdot H_2O]_n$,[5] and the square-type octanuclear cyclic clusters $[W_4S_{16}Ag_5M(DMSO)_8]_n$ (M = Nd, La; DMSO = dimethyl sulfoxide).[6] The double incomplete cubane-like cluster compound $[Cu_6S_6W_2(SCMe_3)_2(O)_2(PPh_3)_4]$[7] is a structural model for the active center of nitrogenase.[8] Therefore, investigating the

[*] Prof. X.-T. Wu, J. Guo, W.-J. Zhang, T.-L. Sheng, Q. Huang, P. Lin, Q.-M. Wang, J.-X. Lu
State Key Laboratory of Structural Chemistry
Fujian Institute of Research on Structure of Matter
Chinese Academy of Sciences
Fuzhou, Fujian 350002 (China)
Fax: Int. code +(591)371-4946
e-mail: wxt@ms.fjirsm.ac.cn

[**] This research was supported by grants from the State Key Laboratory of Structure Chemistry, the Fujian Institute of Research on Structure of Matter, the Chinese Academy of Sciences, the National Science Foundations of China, and the Provincial Science Foundations of Fujian.

 © WILEY-VCH Verlag GmbH, D-69451 Weinheim, 1997 0570-0833/97/3622-2464 $ 17.50+.50/0

structural characteristics of Mo(W)/Cu(Ag)/S clusters may help us to understand the structure model of the active center of nitrogenase. We recently established a synthetic route in which sulfur is introduced into the systems $[MS_nO_{4-n}]^{2-}/Cu^+$ ($n = 3, 4$) by self-assembly, and obtained the novel tetradecanuclear clusters **1** and **2**. Here we report the syntheses and structures of these two complexes.

$[(n\text{Bu})_4\text{N}]_4[\text{Mo}_4\text{Cu}_{10}\text{S}_{16}\text{O}_3]\cdot\text{H}_2\text{O}$ **1**

$[(n\text{Bu})_4\text{N}]_4[\text{W}_4\text{Cu}_{10}\text{S}_{16.5}\text{O}_{2.5}]\cdot\text{H}_2\text{O}$ **2**

All syntheses were performed at room temperature under air.[9] Complex **1** was obtained by the reaction of K_2MoS_3O, CuBr, and $(n\text{Bu})_4\text{NBr}$ (1:2:1.5) in DMF for several hours with subsequent addition of an aqueous solution of Li_2S (excess). Complex **2** was synthesized in a similar manner except that $(NH_4)_2WS_3O$ was used instead of K_2MoS_3O. The S^{2-} ion in the reaction played an important role by substituting the ligands of the M/Cu/S compounds that show a weak affinity for copper(I). This is conducive to assembling larger clusters from smaller ones, and provides an attractive synthetic route to large clusters.

The two title complexes are isomorphous and crystallize in the orthorhombic space group $Pna2_1$ with four molecules in the unit cell.[10, 11] Therefore, only the structure of **1** will be described here (Figure 1). The anion of **1** has approximately *m*

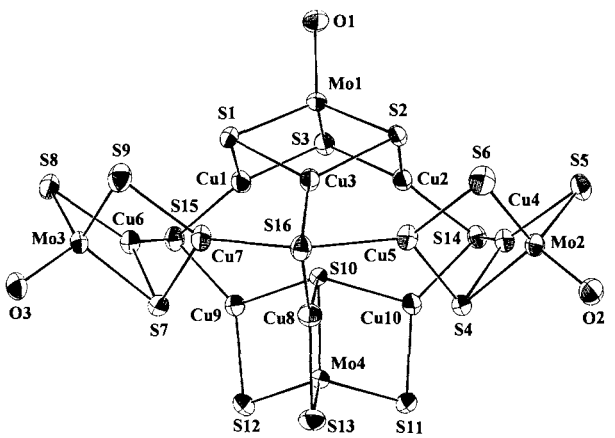

Figure 1. The structure of the anion of **1** (ORTEP representation, 20% displacement ellipsoids). Selected distances [Å] and angles [°] (range): Mo–Cu 2.660(2)–2.713(2), Cu–Cu 2.725(2)–2.953(2), Mo–O 1.697(9)–1.783(10), Mo–S 2.206(4)–2.278(3), Cu–S 2.202(4)–2.316(3); S-Mo-E (E = S, O) 106.90(11)–112.5(3), Cu-Mo-Cu 82.31(5)–94.04(6), Mo-Cu-Cu 122.03(7)–137.72(8), Mo-S-Cu 71.48(10)–75.10(12).

point group symmetry with a mirror plane through S3, O1, Mo1, Cu3, S16, Cu8, S10, S13, and Mo4 (mean deviation of 0.0073 Å). It can be viewed as consisting of one incomplete cubane-like Cu_3MoS_3O fragment, one trigonal-prism-type Cu_3MoS_4 fragment and two butterfly-type Cu_2MoOS_3 fragments that are bridged by one μ_4-S and two μ_3-S atoms. The "top" Cu_3MoS_3O subunits and the "bottom" Cu_3MoS_4 subunit are bridged by three S^{2-} ions (S14, S15, and S16); this shows some similarity to the structural characteristics of the Mo/Fe/S active center of nitrogenase,[8] whose M'_3MoS_3 and M'_4S_3 ($M' = Fe$) subunits are bridged by three S^{2-} ions. The two Cu_2MS_3O side groups (M = Mo, W) linked by the bridging sulfur atoms have a stable effect on the core (Figure 2). Apart from two Cu_2MS_3O side groups, the remaining six Cu atoms form a central trigonal prism which is capped by two M atoms;

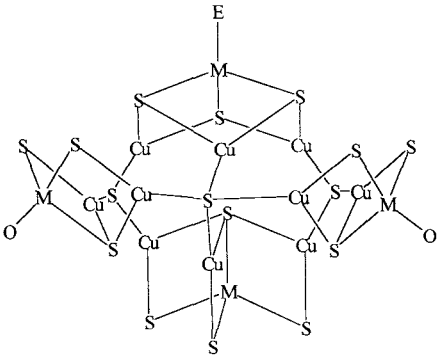

Figure 2. The framework of the anions of **1** and **2** (M = Mo. E = O; M = W, E = 1/2O + 1/2S).

the metal-connectivity pattern of $Cu_6M_2S_{10}$ core portion is similar to the structure model of the Mo/Fe/S active center of nitrogenase. We expected S10 to be outside the central unit, but it is indeed inside the core. This indicates that the present μ_4-S configuration is more stable. We reported another complex, $[Et_4N]_2[(\mu_6\text{-S})Cu_6S_6(S_2)_6Mo_6O_6]$, in which a μ_6-S atom is inside the metal core.[12] If S^{2-} ions exist, the six Fe atoms of the Mo/Fe/S active center of nitrogenase could coordinate with a μ_6-S atom.

The unconventional metal framework of the anion $[M_4Cu_{10}S_{16}O_2E]^{4-}$ (M = Mo, E = O; M = W, E = 1/2O + 1/2S) contains metal atoms in conventional trigonal-planar (Cu) and tetrahedral coordination enviroments (Mo, W). The Cu–Cu distances (2.725(2)–2.953(2) Å) in the anion of **1** are longer than 2.56 Å; Ahlrichs et al. consider this marginal covalent contribution, as a dispersion interaction of the d^{10} systems.[13] Because the Mo, Cu, and S atoms of the anion of **1** have several different coordination environments, their distances and angles vary. As is the case with Cu_2MoS_3O fragments, Mo–Cu distances in the Cu_3MoS_3E (E = O or S) fragments are 2.660(2)–2.677(2) Å and 2.682(2)–2.713(2) Å. The S14–Cu and S15–Cu bond lengths range from 2.202(4) to 2.214(4) Å, whereas the other S–Cu lengths are 2.218(4)–2.316(3) Å. With the exception of Cu-Mo4-Cu (87.66(6)–94.04(6)°), Cu-Mo-Cu angles range from 82.31(5) to 83.80(6)°. The S_M-Cu- S_M and S_M-Cu-S_b angles are 103.69(7)–107.20(13)° and 119.30(13)–136.03(15)°, respectively (S_b = S14, S15, S16; S_M represents the sulfur atoms of MoS_3O^{2-} and $MoS_4{}^{2-}$); these structureal parameters are consistent with those reported for $[Cu_6S_6W_2(SCMe_3)_2(O)_2(PPh_3)_4]$.[7]

The two title complexes crystallize in the noncentrosymmetric space group. Therefore, further research of their nonlinear optical properties is of interest.

Experimental Section

1: A solution of K_2MoS_3O (1.145 g, 4 mmol), CuBr (1.147 g, 8 mmol), and $(n\text{Bu})_4\text{NBr}$ (1.934 g, 6 mmol) in DMF (9 mL) was stirred for 12 h. A solution of Li_2S (0.45 g, 10 mmol) in water (1.5 mL) and DMF (3 mL) was then added. The reaction mixture was stirred for only one minute, the dark precipate removed by filtration, and *i*PrOH (3 mL) added. Dark crystals of **1** (0.90 g) were obtained by allowing the violet filtrate to stand at room temperature for one day.

2: A procedure similar to that used for the synthesis of **1** was employed except that $(NH_4)_2WS_3O$ (1.329 g,4 mmol) was used instead of K_2MoS_3O. Allowing the red filtrate to stand at room temperature for three days gave red crystals of **2** (0.85 g). Crystals of **2** were also obtained by allowing Et_2O to diffuse into the filtrate over four days.

Received: May 22, 1997
Revised version: June 23, 1997 [Z 10309 IE]
German version: *Angew. Chem.* **1997**, *109*, 2574–2576

Keywords: clusters · copper · molybdenum · sulfur · tungsten

 © WILEY-VCH Verlag GmbH, D-69451 Weinheim, 1997 0570-0833/97/3622-2465 $ 17.50+.50/0

[1] a) A. Müller, E. Diemann, R. Josters, H. Bogge, *Angew. Chem.* **1981**, *93*, 957; *Angew. Chem. Int. Ed. Engl.* **1981**, *20*, 934; b) X.-T. Wu, P.-C. Chen, S.-W. Du, N.-Y. Zhu, J.-X. Lu, *J. Clust. Sci.* **1994**, *5*, 265.
[2] a) S. Shi, W. Ji, S.-H. Tang, J.-P. Lang, X.-Q. Xin, *J. Am. Chem. Soc.* **1994**, *116*, 3615; b) X.-T. Wu, Q.-M. Wang, S. Shi, *Polyhedron* **1997**, 16, 945.
[3] Q. Huang, X.-T. Wu, Q.-M. Wang, T.-L. Sheng, J.-X. Lu, *Inorg. Chem.* **1996**, *35*, 893.
[4] Q. Huang, X.-T. Wu, T.-L. Sheng, Q.-M. Wang, *Polyhedron* **1996**, *15*, 3405.
[5] Q. Huang, X.-T. Wu, T.-L. Sheng, Q.-M. Wang, *Inorg. Chem.* **1995**, *27*, 4931.
[6] Q. Huang, X.-T. Wu, Q.-M. Wang, T.-L. Sheng, J.-X. Lu, *Angew. Chem.* **1996**, *108*, 985; *Angew. Chem. Int. Ed. Engl.* **1996**, *35*, 868.
[7] S.-W. Du, N.-Y. Zhu, P.-C. Chen, X.-T. Wu, *Angew. Chem.* **1992**, *104*, 1098; *Angew. Chem. Int. Ed. Engl.* **1992**, *31*, 1085.
[8] a) J. Kim, D. C. Rees, *Science* **1992**, *257*, 1677; b) M. K. Chan, J. Kim, D. C. Rees, *Science* **1993**, *260*, 792; c) J. T. Bolin, N. Campobasso, S. W. Muchmore, T. V. Morgan, L. E. Mortenson in *Molybdenum Enzymes, Cofactors and Model Systems* (Eds.: E. I. Stiefel, D. Ccoucouvanis, W. E. Newton), American Chemical Society, Washington, DC, **1993**, pp. 186–195.
[9] Complexes **1** and **2** are soluble in DMF, and slightly soluble in CH_3CN. Elemental analysis found for **1**: C 29.80, H 5.92, N 2.11, Br 0; calcd: C 29.93, H 5.73, N 2.18, Br 0; elemental analysis found for **2**: C 26.50, H 5.23, N 1.94, Br 0; calcd: C 26.26, H 5.03, N 1.91, Br 0; IR (KBr): $\tilde{\nu}$ [cm^{-1}] = Mo–O, 894.8 (vs), Mo–S 509.1 (w), 462.8 (s), 453.2 (s) for **1**; W–O, 914 (s); W–S 495.6 (m), 453.2 (s), 426.2 (m) for **2**; UV/Vis (in DMF): λ [nm] = 268, 325 (sh), 416, 536 (sh) for **1**; 278, 330 (sh), 440 (sh) for **2**.
[10] Crystal data for **1**: $[(n\mathrm{Bu})_4\mathrm{N}]_4[\mathrm{Mo_4Cu_{10}S_{16}O_3}]\cdot\mathrm{H_2O}$, $M = 2567.97$, orthorhombic, crystal dimensions $0.32\times0.32\times0.40$ mm; space group $Pna2_1$, $a = 26.6097(5)$, $b = 19.1527(3)$, $c = 21.3711(3)$ Å, $V = 10891.7(3)$ Å^3, $Z = 4$, $\rho_{calcd} = 1.566$ gcm^{-1}, $\lambda(\mathrm{Mo_{K\alpha}}) = 0.71073$ Å, $F(000) = 5216$. The raw data were collected at room temperature on a Siemens SMART-CCD area diffractometer. Of 15291 unique reflections, 13184 with $I > 2\sigma(I)$ were used to solve the structure with the SHELXTL program [14]. The atoms of the anion and nitrogen atoms of the cations were refined with anisotropic temperature factors. The positions of the hydrogen atoms were generated geometrically (C–H bond fixed at 0.96 Å); the hydrogen atoms were assigned isotropic thermal parameters and allowed to ride their respective parent C atoms until the final cycle of the least-squares refinement. The final cycle of full-matrix least-squares refinement converged with $R = \sum(||F_o| - |F_c||)/\sum|F_o| = 0.0560$ and $R_w = \{\sum w[(F_o^2 - F_c^2)^2]/\sum w[(F_o^2)^2]\}^{0.5} = 0.1393$, $w = [\sigma^2(F_o^2) + (0.0527\times P)^2 + 49.5023P]^{-1}$, $P = (F_o^2 + 2F_c^2)/3$ [11].
[11] Crystal data for **2**: $[(n\mathrm{Bu})_4\mathrm{N}]_4[\mathrm{W_4Cu_{10}S_{16.5}O_{2.5}}]\cdot\mathrm{H_2O}$, $M = 2927.64$, orthorhombic, crystal dimensions $0.20\times0.22\times0.40$ mm; space group $Pna2_1$, $a = 26.6045(4)$, $b = 19.1580(3)$, $c = 21.3875(3)$ Å, $V = 10901.0(2)$ Å^3, $Z = 4$, $\rho_{calcd} = 1.784$ gcm^{-1}, $\lambda(\mathrm{Mo_{K\alpha}}) = 0.71073$ Å, $F(000) = 5744$. The raw data were collected at room temperature on a Siemens SMART-CCD area diffractometer. Of 13949 unique reflections, 8926 reflections with $I > 2\sigma(I)$ were used to solve the structure with the SHELXTL program [14]. The atoms of the anion and the nitrogen atoms of the cations were refined with anisotropic temperature factors. The positions of the hydrogen atoms were generated geometrically (C–H bond fixed at 0.96 Å); the hydrogen atoms were assigned isotropic thermal parameters and allowed to ride their respective parent C atoms until the final cycle of least-squares refinement. The final cycle of full-matrix least-squares refinement converged with $R = \sum(||F_o| - |F_c||)/\sum|F_o| = 0.0821$ and $R_w = \{\sum w[(F_o^2 - F_c^2)^2]/\sum w[(F_o^2)^2]\}^{0.5} = 0.1536$, $w = [\sigma^2(F_o^2) + (0.0330\times P)^2 + 237.8371P]^{-1}$, $P = (F_o^2 + 2F_c^2)/3$. Further details of the crystal structure investigation may be obtained from the Fachinformationszentrum Karlsruhe, D-76344 Eggenstein-Leopoldshafen (Germany), on quoting the depository numbers CSD-407125 (**1**) and CSD-407149 (**2**).
[12] X.-T. Wu, B. Wang, Y.-F. Zheng, J.-X. Lu, *Jiegou Huaxue* (*Chin. J. Struct. Chem.*) **1988**, *71*, 47.
[13] S. Dehnen, A. Schäfer, D. Fenske, R. Ahlrichs, *Angew. Chem.* **1994**, *106*, 786; *Angew. Chem. Int. Ed. Engl.* **1994**, *33*, 746.
[14] G. M. Sheldrick, SHELXTL, Version 5. Siemens Analytical X-Ray Instrumentation Inc., Madison, WI, USA.

Olefin Metathesis in Compressed Carbon Dioxide**

Alois Fürstner,* Daniel Koch, Klaus Langemann, Walter Leitner,* and Christian Six

Numerous advantages are associated with the use of supercritical carbon dioxide ($scCO_2$) as an ecologically benign and economically feasible reaction medium for metal-catalyzed reactions.[1] Technical aspects like its nonflammability, the lack of virtually any toxicity, the absence of a gas/liquid phase boundary, and possible simplifications in work up favor $scCO_2$ as an alternative to conventional solvents. The utilization of $scCO_2$ as solvent *and* C_1-building block offers further opportunities for homogeneous catalysis.[2] Moreover, the physiochemical properties of a supercritical fluid can be tuned within a certain range by adjusting its density and the parameters pressure and temperature. Chemical interactions of $scCO_2$ with substrates and/or catalysts[3] offer additional potential for activity and selectivity control. Herein we report on transition metal catalyzed olefin metathesis in compressed CO_2. This reaction can be performed efficiently in this medium and, even more intriguingly, the properties of supercritical CO_2 remarkably increase the scope of this well-established transformation.

Olefin metathesis refers to the mutual alkylidene exchange reaction of alkenes.[4] This type of reaction became increasingly important as a synthetic tool during the last few years owing to the application of well-defined carbene complexes as catalysts or catalyst precursors.[5] Especially catalysts of type **1**[6a–c] and type **2**[6d] are distinguished by their high activity and by an excellent compatibility with a wide range of functional groups.

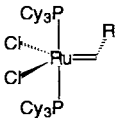

1a R = CH=CPh$_2$
1b R = Ph

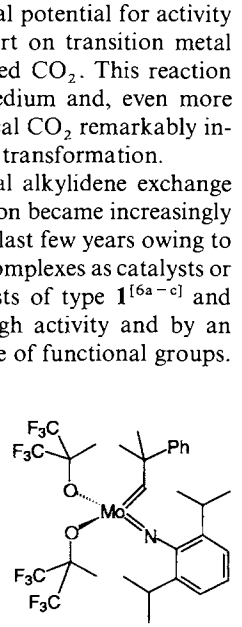

2

We found that both types of catalysts are suitable for ring opening metathesis polymerization (ROMP) of norbornene and cyclooctene in compressed carbon dioxide to form the technically important polymers Norsorex and Vestenamer (Table 1). The activities of these catalysts for ROMP of norbornene in compressed carbon dioxide are considerably higher than that observed with $[Ru(H_2O)_6(OTos)_2]$ in the same medium.[7] The desired polymers are obtained in excellent yields after short reaction times, both in liquid and in supercritical carbon dioxide.

[*] Priv.-Doz. Dr. A. Fürstner, Priv.-Doz. Dr. W. Leitner, D. Koch, K. Langemann, C. Six
Max-Planck-Institut für Kohlenforschung
Kaiser-Wilhelm-Platz 1, D-45470 Mülheim an der Ruhr (Germany)
Fax: Int. code +(208) 306 2980
e-mail: fuerstner@mpi-muelheim.mpg.de
: leitner@mpi-muelheim.mpg.de

[**] This work was supported by the Max-Planck-Gesellschaft and by the Gerhard-Hess-Program of the Deutsche Forschungsgemeinschaft (W. L.). K. L. thanks the Fonds der Chemischen Industrie for a Kekulé-Stipendium. We are especially indebted to Prof. Dr. G. Fink, Mülheim, for helpful suggestions and generous support concerning polymer analysis.

 © WILEY-VCH Verlag GmbH, D-69451 Weinheim, 1997 0570-0833/97/3622-2466 $ 17.50+.50/0

Table 1. Ring opening metathesis polymerization (ROMP) of norbornene and cyclooctene in compressed CO_2.

Entry	Monomer [a]	Cat.	Monomer/ Cat.	d [b] [g mL^{-1}]	p [c] [bar]	T [K]	t [h]	purified polymer [%]	*cis:trans* [d] [%]	M_n [e]	M_w/M_n	T_g [f] [K]
1	**A**	**1a**	845	0.44	95	329	0.1	40	23:77	62 500	26	315
2	**A**	**1b**	665	0.58	105	318	14	78	25:75	75 200	2.6	314
3	**A**	**1b**	580	0.55	56	296	1	94	25:75	206 100	3.2	314
4	**A**/Tol.	**1b**	625	0.54	102	318	1	97	22:78	[h]	[h]	315
5 [g]	**A**/Tol.	**1b**	100	–	–	298	1	88	25:75	28 800	2.3	305
6	**A**/Tol.	**2**	100	0.57	115	318	24	93	66:34	[h]	[h]	327
7	**A**	**2**	425	0.72	58	297	1	13	82:18	[h]	[h]	326
8	**B**	**1b**	195	0.56	100	318	6	47	28:72	10 900	2.0	298

[a] **A** = norbornene, **B** = *cis*-cyclooctene. **A**/Tol. = saturated solution of norbornene (85.1 %, GC) in toluene. [b] Density of reaction mixture (substrate + CO_2 + additives) based on the reactor volume V = 27 mL. [c] At reaction temperature, ± 5 bar. [d] From integration of the olefinic proton signals in the ^{1}H NMR. [e] From high-temperature GPC measurement in decalin at 423 K with polystyrene as reference. [f] Glass-temperature from DSC measurement. [g] Comparative experiment in CH_2Cl_2 (4.0 mL). [h] Not determined.

During the course of the reaction the polymers precipitate from the CO_2 phase and are readily isolated by simply venting the reactor. Under suitable reaction conditions and after removal of metallic residues by conventional methods, the products exhibit properties (molecular weight and microstructure) comparable to the materials prepared in CH_2Cl_2 by conventional means.[4] The catalyst should be injected as a solid or in dissolved form to the homogeneous solution of the monomer in CO_2 in order to avoid broad molecular weight distributions resulting from uncontrolled initiation of the polymerization reaction.

Catalysts of type **2** are known to initiate a "living" ROMP in organic solvents.[8] Complete conversion (yield 97%) of the monomer is observed if the amount of catalyst in $scCO_2$ is lowered to a ratio of norbornene/**2** of 625/1 under conditions otherwise identical to those given in Table 1, entry 6. The use of even lower catalyst loadings results in a sudden drop of the yield of polymer (norbornene/**2** 900/1: 19%; 1730/1: 6%). The reasons for this behavior are presently under investigation.

Even in the light of these very promising results on ROMP in $scCO_2$, the success of this methodology for ring-closing metathesis (RCM, Table 2) is remarkable. It may seem unfavorable at first sight to carry out a reaction that releases one equivalent of ethene at elevated pressure. However, since the total pressure in the reaction vessel is almost exclusively determined by the amount of CO_2 that does not participate in the reaction, it has little effect on the overall process.

During our investigations on the preparation of the 16-membered cyclic compound **10** by RCM of diene **9**[9a, b] in $scCO_2$ (Scheme 1), a remarkable influence of the density of the supercritical medium on product distribution was observed (Figure 1). Whereas the large ring was produced in excellent yields at densities of the compressed phase of $d \geq 0.65$ g mL^{-1}, mainly oligomers were obtained by ADMET[4] (acyclic diene metathesis) at lower densities.

This density effect on the reaction pathway may—at least in part—be attributed to the compressibility of the supercritical phase: Increasing the density at constant volume leads to an increasing number of inert solvent molecules and mimics the effect of dilution in conventional solvents ("Ziegler-Ruggli's dilution principle" [10]), favoring the intramolecular reaction pathway (Figure 2).[11] This effect has received little attention up to now and might be valid for other cyclization reactions as well.[12]

The scope of RCM in $scCO_2$ is evident from the examples for preparation of products of different ring sizes and functionalities compiled in Table 2. The five-membered ring **4** is obtained in almost quantitative yield from **3** in the form of colorless crystals after release of CO_2. The synthesis of karahanaenone **6**,

Table 2. Synthesis of carbo- and heterocyclic compounds by ring-closing metathesis (RCM) in compressed CO_2.

Entry	Substrate	Cat. [a]	Product	Yield [%] [b]
1	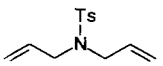 **3**	**1a**	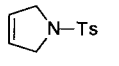 **4**	93
2	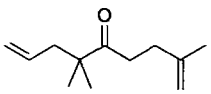 **5**	**2** [c]	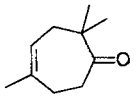 **6**	62
3	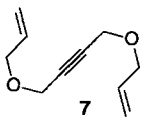 **7**	**1a**	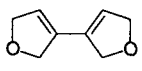 **8**	62
4	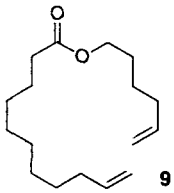 **9**	**1a** [d]	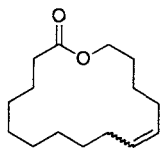 **10** (*Z* : *E* = 1 : 3.2)	88 [e]
5	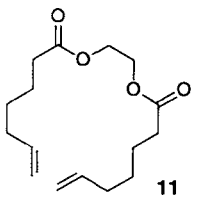 **11**	**1a** [f]	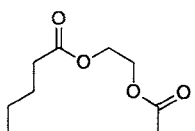 **12** (*Z* : *E* = 1 : 3.3)	30 [e]
6		**1a** [f,g]		67
7	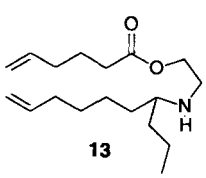 **13**	**1a**	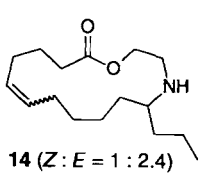 **14** (*Z* : *E* = 1 : 2.4)	74 [e]

[a] Reaction conditions: Catalyst (1 mol%), T = 313 K, d = 0.76 g mL^{-1}, t = 72 h. [b] Isolated yield. [c] 5 mol%. [d] d = 0.83 g mL^{-1}. [e] GC yield. [f] d = 0.62 g mL^{-1} [g] Using the remaining catalyst from entry 5, t = 170 h.

 © WILEY-VCH Verlag GmbH, D-69451 Weinheim, 1997 0570-0833/97/3622-2467 $ 17.50+.50/0

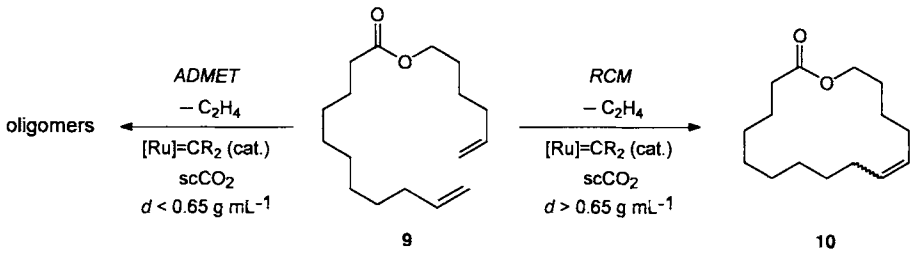

Scheme 1. Competition between RCM and ADMET during olefin metathesis of the acyclic diene **9** in compressed CO_2.

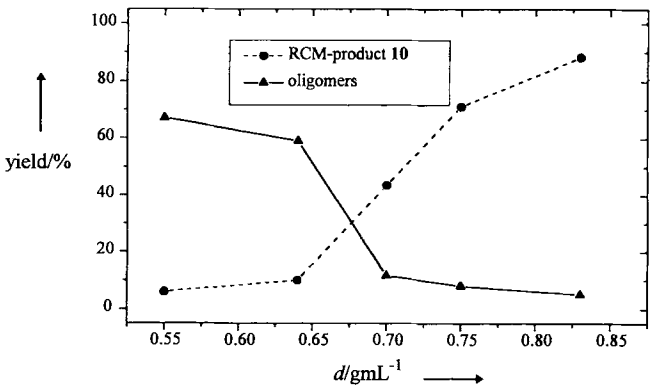

Figure 1. Effect of the density of the supercritical medium on the path of the metathesis of diene **9** leading to the formation of the macrocycle **10** or oligomeric products.

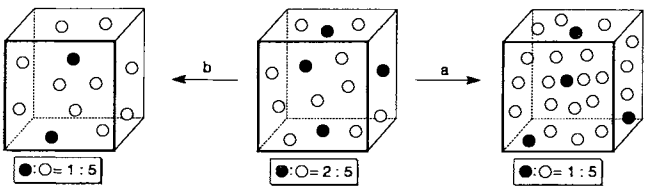

Figure 2. The dilution principle at constant volume: Increasing the density of a supercritical medium (a) or increasing the dilution in a conventional solvent (b) lead to a decreasing ratio of reactive particles (●) to inert solvent molecules (○) and thereby favor intramolecular pathways over intermolecular ones.

an olfactory substance contained in hops and cypress oil (*Cypressus sempervirens*),[13] is an example for the formation of a trisubstituted cycloalkene by using the alkylidene complex **2** in $scCO_2$. Entry 3 shows that enyne metathesis reactions[14] can also be successfully performed in $scCO_2$.

The remarkably simple syntheses of the macrocycles **10** and **12** are of special interest. These two compounds, which exhibit a strong musklike odor on their own, can be converted into the commercial perfume ingredients exaltolide and Arova 16 by hydrogenation of the C–C double bonds.[15] The products can be selectively removed from the reactor by virtue of the extractive properties of CO_2[16] and collected in cold traps. The metal residues in the autoclave are still active for RCM (entries 5 and 6) making this process potentially attractive for technical applications.

Metathesis catalysts of type **1** are deactivated by basic N–H groups; substrates containing this type of functionality can be cyclized only in protonated or otherwise protected form in conventional solvents.[17] In $scCO_2$, however, metathesis of diene **13** using catalyst **1a** forms epilachnene **14**[18] smoothly, showing that amines react without the need for protection. We attribute this to reversible formation of the corresponding carbamic acid under the reaction conditions. This example illustrates the possibility of using the reaction medium CO_2 as a "protecting group" in organic synthesis.

The results outlined above demonstrate for the first time the general applicability of olefin metathesis in compressed carbon dioxide and nicely illustrate some of the advantages related to this particular reaction medium. Although there is some experimental evidence that this transformation is homogeneously catalyzed,[19] no definite conclusion can be drawn at present. Our current efforts are directed to answering this question and to further broadening the scope of this methodology in organic synthesis.

Experimental Section

Ring opening metathesis polymerization in $scCO_2$: A stainless-steel high-pressure vessel ($V = 27$ mL) equipped with thick wall glass windows, PTFE-stirring bar, bore hole for a thermocouple, needle and ball valves was charged with norbornene (407 mg, 4.32 mmol) under argon. A dosing unit containing **1b** (5.50 mg, 0.67×10^{-2} mmol) was connected to the reactor through the ball valve. The reactor was filled through the needle valve with CO_2 (15.3 g, $d = 0.58$ gmL^{-1}) using a compressor. A colorless homogeneous supercritical phase was formed upon heating to 318 K under stirring. The dosing unit was pressurized with argon (150 bar), and by opening the ball valve the solid catalyst was introduced into the reaction vessel. After the mixture had been stirred for 14 h, the reactor was vented and the crude polymer (341 mg) was isolated. Purification of the polymer by conventional methods gave a white tacky material (316 mg, 78%). The analytical data are summarized in Table 1.

Macrocyclization by RCM in $scCO_2$: The unsaturated ester **9** (180 mg, 0.64 mmol) and the catalyst **1a** (7 mg, 7.55×10^{-3} mmol) were filled into separate compartments in a high-pressure vessel ($V = 225$ mL, equipment as above) under Ar. The reactor was pressurized with a certain amount of CO_2 using a compressor. The resulting reaction mixture was stirred for 72 h at 313 K. The volatiles were then passed through a cold trap at 233 K and the reactor was washed with acetone in order to quantitatively isolate any oligomers present. The fractions were combined and the solvent was evaporated. Low molecular weight compounds (unconverted **9** and cyclization product **10**) were separated from oligomers by column chromatography (silica gel, hexane/ethyl acetate). The results are represented graphically in Figure 1.

Received: May 20, 1997 [Z10455IE]
German version: *Angew. Chem.* **1997**, *109*, 2562–2565

Keywords: homogeneous catalysis · macrocycles · metathesis · polymers · supercritical fluids

[1] Reviews: a) G. Kaupp, *Angew. Chem.* **1994**, *106*, 1519; *Angew. Chem. Int. Ed. Engl.* **1994**, *33*, 1452; b) M. Poliakoff, S. M. Howdle, S. G. Kazarian, *ibid.* **1995**, *107*, 1409 and **1995**, *34*, 1275; c) P. G. Jessop, T. Ikariya, R. Noyori, *Science* **1995**, *269*, 1065; d) D. A. Morgenstern, R. M. LeLacheur, D. K. Morita, S. L. Borkowsky, S. Feng, G. H. Brown, L. Luan, M. F. Gross, M. J. Burk, W. Tumas in *Green Chemistry* (Eds.: P. T. Anastas, T. C. Williamson) (*ACS Symp. Ser.* **1996**, *626*, 132); e) E. Dinjus, R. Fornika, M. Scholz in *Chemistry under Extreme or Non-Classical Conditions* (Eds.: R. van Eldik, C. D. Hubbard), Wiley, New York, **1996**, p. 219 ff.

[2] a) P. G. Jessop, Y. Hsiao, T. Ikariya, R. Noyori, *J. Am. Chem. Soc.* **1996**, *118*, 344; b) M. T. Reetz, W. Könen, T. Strack, *Chimia* **1993**, *47*, 493.

[3] For the coordination chemistry of CO_2 and its relevance for catalysis see: a) W. Leitner, *Angew. Chem.* **1995**, *107*, 2391; *Angew. Chem. Int. Ed. Engl.* **1995**, *34*, 2207; b) *Coord. Chem. Rev.* **1996**, *153*, 257.

[4] K. J. Ivin, J. C. Mol, *Olefin Metathesis and Metathesis Polymerization*, Academic Press, New York, **1997**.

[5] R. H. Grubbs, S. J. Miller, G. C. Fu, *Acc. Chem. Res.* **1995**, *28*, 446.

[6] a) P. Schwab, R. H. Grubbs, J. W. Ziller, *J. Am. Chem. Soc.* **1996**, *118*, 100; b) P. Schwab, M. B. France, J. W. Ziller, R. H. Grubbs, *Angew. Chem.* **1995**, *107*, 2179; *Angew. Chem. Int. Ed. Engl.* **1995**, *34*, 2039; c) S. T. Nguyen, R. H. Grubbs, J. W. Ziller, *J. Am. Chem. Soc.* **1993**, *115*, 9858; d) R. R. Schrock, J. S. Murdzek, G. C. Bazan, J. Robbins, M. DiMare, M. O'Regan, *J. Am. Chem. Soc.* **1990**, *112*, 3875.

[7] a) C. D. Mistele, H. H. Thorp, J. M. DeSimone, *J. M. S.-Pure Appl. Chem.* **1996**, *33*, 953; b) for the application of $scCO_2$ as a reaction medium for other polymerization reactions see: J. M. DeSimone, E. E. Maury, Y. Z. Menceloglu, J. B. McClain, T. J. Romack, J. R. Combes, *Science* **1994**, *265*, 356.

 © WILEY-VCH Verlag GmbH, D-69451 Weinheim, 1997 0570-0833/97/3622-2468 $ 17.50+.50/0

[8] R. R. Schrock in *Ring-Opening Polymerization* (Ed.: D. J. Brunelle), Hanser Publishers, München, **1993**, p. 129.
[9] a) A. Fürstner, K. Langemann, *J. Org. Chem.* **1996**, *61*, 3942; b) *Synthesis*, **1997**, 792; c) A. Fürstner, N. Kindler, *Tetrahedron Lett.* **1996**, *37*, 7005; d) A. Fürstner, K. Langemann, *J. Org. Chem.* **1996**, *61*, 8746.
[10] a) K. Ziegler, *Methoden der Organischen Chemie (Houben-Weyl) 4th ed. 1952-, Vol. 4/II*, p. 72ff; b) a more accurate description refers to the effective molarity which considers the tendency for cyclization of a given substrate: L. Mandolini, *Adv. Phys. Chem.* 1986, *22*, 1.
[11] For a mathematical discussion of the specific solvent effects in supercritical fluids see: A. A. Clifford, K. Pople, W. J. Gaskill, K. D. Bartle, C. M. Rayner, *Chem. Commun.* **1997**, 595.
[12] a) This explanation does not take into account possible effects of negative reaction or activation volumes [12b] or of special "cage-effects" near the critical point [12c]; b) C. D. Hubbard, R. van Eldik in *Chemistry under Extreme or Non-Classical Conditions*, (Eds.: R. van Eldik, C. D. Hubbard), Wiley, New York, **1996**, p. 53 ff; c) J. M. Tanko, N. K. Suleman, B. Fletcher, *J. Am. Chem. Soc.* **1996**, *118*, 11958, and references therein.
[13] a) Y. Naya, M. Kotake, *Tetrahedron Lett.* **1968**, 1645; b) J. Garnero, P. Buil, R. Robertet, D. Joulain, R. Tabacchi, *Perfum. Flavor.* **1978**, *3*, 3.
[14] a) S.-H. Kim, W. J. Zuercher, N. B. Bowden, R. H. Grubbs, *J. Org. Chem.* **1996**, *61*, 1073; b) S.-H. Kim, N. Bowden, R. H. Grubbs, *J. Am. Chem. Soc.* **1994**, *116*,
[15] a) G. Ohloff, *Riechstoffe und Geruchssinn*, Springer, Berlin, **1990**. b) K. Bauer, D. Garbe, H. Surburg in *Ullmann's Encyclopedia of Industrial Chemistry, Vol. A 11*, VCH, Weinheim, 5th ed., **1988**, p. 141.
[16] K. Zosel, *Angew. Chem.* **1978**, *90*, 748; *Angew. Chem. Int. Ed. Engl.* **1978**, *17*, 702.
[17] G. C. Fu, S. T. Nguyen, R. H. Grubbs, *J. Am. Chem. Soc.* **1993**, *115*, 9856.
[18] a) Isolation: A. B. Attygalle, K. D. McCormick, C. L. Blankespoor, T. Eisner, J. Meinwald, *Proc. Natl. Acad. Sci. USA* **1993**, *90*, 5204; b) The synthesis of epilachnene and related azamacrolides by RCM of N-protected amine derivatives in solution is described in ref. [9b].
[19] The bulk amount of catalysts **1** remained undissolved during RCM as observed through the windows of the high-pressure reactor. Complex **2**, however, was at least partly soluble, giving rise to an intensively colored reaction mixture.

Unusual Regioselectivity in the Reductive Coupling of Alkynes and Allenes by Hydrozirconation and Zinca-Claisen Rearrangement

Keisuke Suzuki,* Takahiro Imai, Shigeo Yamanoi, Masao Chino, and Takashi Matsumoto

Dedicated to Prof. Dr. Dieter Seebach on the occasion of his 60th birthday

The allylmetalation of vinylmetal compounds is a new approach to C–C bond formation.[1, 2] Although the precise mechanism must still be elucidated, various features of the reaction are nicely summarized by the zinca-Claisen mechanism of Knochel and Normant and their co-workers[1d–h, 3a, 4] (Scheme 1): Coupling of vinylmetal compound **I** and allylmetal derivative **II** (M^1, M^2 = Li, MgX, ZnX, etc.) occurs by transmetalation with zinc to form **A** and/or **B**, which then undergoes bond reorganization.[4, 5] Substituted allyl–metal compounds (**II**: R′ ≠ H) tend to couple through **A** to form *gem*-bismetallic compounds **C** as the kinetically controlled products that give, upon hydrolysis, the γ-adducts **III**. Prolonged reaction results in equilibration of the organometallic species, leading to an increase in the fraction of isomeric *gem*-bismetallic compounds **D** that in turn produce the α-adducts **IV**. Unfortunately,

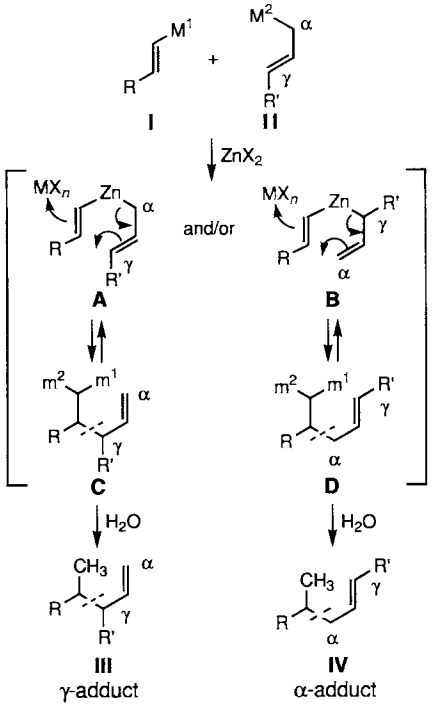

Scheme 1. Zinca-Claisen mechanism for the allylmetalation of vinylmetal compounds.

IV cannot be obtained selectively, because equilibration is slow and the α/γ ratio remains low even after extended reaction.[3] From an experimental standpoint, preparation of the starting organometallics **I** and **II** is sometimes troublesome as well.[6]

We report here an in situ approach to such precursors as **I** and **II** involving hydrozirconation[7, 8] [Eq. (1)], which facilitates the

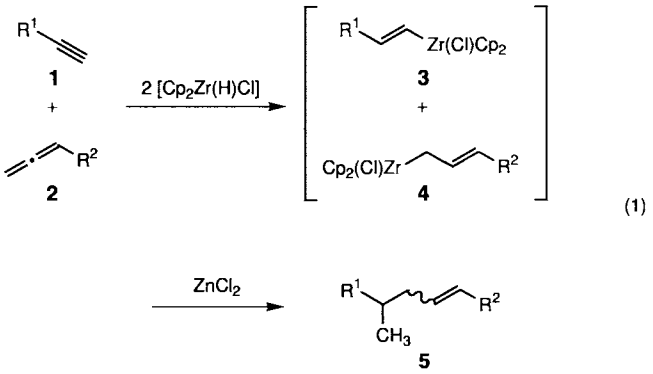

(1)

reductive coupling of a series of alkynes and allenes. A noteworthy feature of this method is that the α-adduct is obtained with high selectivity. We also discuss possible explanation for the unusual regioselectivity that is observed and examine the synthetic utility of the reaction in remote asymmetric induction for synthesis of the vitamin E side chain.

Treatment of alkyne **1a** (R^1 = TrOCH$_2$) and allene **2a** (R^2 = CH_2CH_2OMOM) with the Schwartz reagent[9] in CH_2Cl_2 (−78 → 25 °C) led to a red solution that was subsequently treated with $ZnCl_2$ at 0 °C. Stirring at 25 °C for 2 h gave the α-adduct **5a** (see Table 1) as the sole product; none of the γ-adduct was detected (α:γ > 98:2).[10, 11] Under the same conditions this unusual regioselectivity proved applicable to a wide range of starting allene/alkyne combinations (Tables 1 and 2).[11] The sole exception was reaction of methyl-

[*] Prof. Dr. K. Suzuki, Dr. T. Matsumoto
Department of Chemistry, Tokyo Institute of Technology
2-12-1, O-okayama, Meguro-ku, Tokyo 152 (Japan)
T. Imai, S. Yamanoi, M. Chino
Department of Chemistry, Keio University
3-14-1, Hiyoshi, Kohoku-ku, Yokohama 223 (Japan)

 © WILEY-VCH Verlag GmbH, D-69451 Weinheim, 1997 0570-0833/97/3622-2469 $ 17.50+.50/0

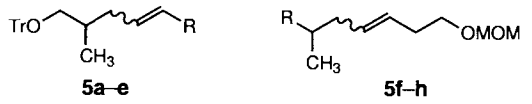

5a–e **5f–h**

Table 1. α-Adducts **5a–e** obtained by reaction of alkyne **1a** with various allenes (25 °C, 2 h)[a]. In no case could the presence of γ-product be verified[11].

	R	Yield[%]	*E*:*Z*
5a	CH_2CH_2OMOM	83	1:2.7
5b	$CH_2CH_2OTBDPS$	85	1.3:1
5c	*cyclo*-C_6H_{11}	76	ca. 1:1
5d	C_6H_5	60	49:1
5e	$CH_2CH(OC_2H_5)_2$	76	1:2.6

[a] Tr = triphenylmethyl, MOM = methoxymethyl, TBDPS = *tert*-butyldiphenylsilyl.

Table 2. Summary of α-adducts **5f–h** obtained by reaction of allene **2a** with various alkynes (25 °C, 2 h). In no case could the presence of γ-product be verified[11].

	R	Yield[%]	*E*:*Z*
5f	*n*-C_4H_9	82	1:4.9
5g	$C_6H_5(CH_3)_2Si$	83	1:2.7
5h	*cyclo*-C_6H_{11}	82	1:1.8

allene **6** with alkyne **1a**, which gave adduct **7** as an α/γ-mixture. This in turn provided a clue to the source of the unusual regioselectivity.

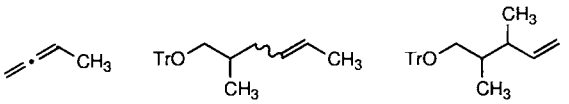

6 α-**7** γ-**7**

Figure 1 shows the time course for α-adduct content in the overall adduct mixture, which shows the existence here also of a $\gamma \rightarrow \alpha$ isomerization pathway (**C** → **D** in Scheme 1); however, in this case the isomerization is exceptionally rapid. Curve B describes the reaction of alkyne **1a** with **6**. After an initial γ-selective reaction,[12] the α/γ ratio steadily increases, reaching 83/17 after 9 h and 94/6 after 36 h (not shown). Such a rapid and complete $\gamma \rightarrow \alpha$ isomerization has not been observed previously

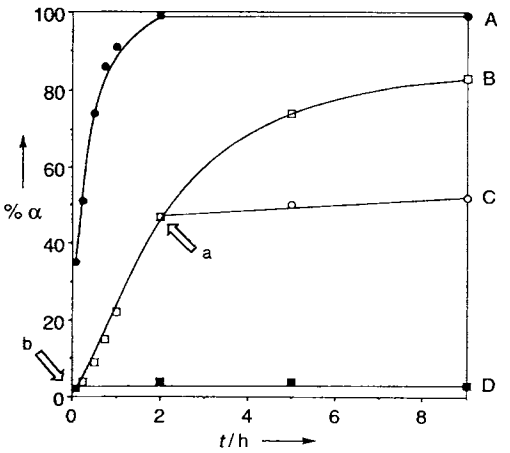

Figure 1. Time dependence of the fraction of α-adduct in the overall amount of adduct [α/(α+γ) × 100%]. A: Reaction of **1a** with **2a**. B: Reaction of **1a** with **6**. C: $MgBr_2$ addition 2 h after $ZnCl_2$ introduction (arrow a). D: $MgBr_2$ addition 5 min after $ZnCl_2$ introduction (arrow b).

in related reactions that involve organolithium and/or -magnesium reagents (vide supra).[3] The isomerization proceeds even more rapidly in reactions of other allenes, as exemplified by the reaction of allene **2a** (curve A): the $\gamma \rightarrow \alpha$ shift is so fast here that after 2 h at 25 °C only the α-adduct **5a** is observable.[12]

Why, then, does the present isomerization rate differ so markedly from that associated with the conventional protocol? A Mg^{II} salt plays a key role.[13] Thus, in the reaction of **1a** and **6**, the $\gamma \rightarrow \alpha$ isomerization virtually ceases upon addition of $MgBr_2$, as shown by curves C and D.[12, 14] Thus, the observed γ-selectivity in the previous examples[3] can be explained through inhibition of $\gamma \rightarrow \alpha$ isomerization by a Mg^{II} salt. In contrast, the present case is "magnesium-free," so the α-adduct is obtained selectively. Nevertheless, the precise nature of the inhibitory effect remains unknown.[14]

The process described here presented an opportunity for a new vitamin E synthesis involving remote stereocontrol.[15] Reaction of homochiral allene **8**[16] and alkyne **1a** as above gave the α-adduct **9** (Scheme 2). GC-Analysis of alcohol **10**, derived

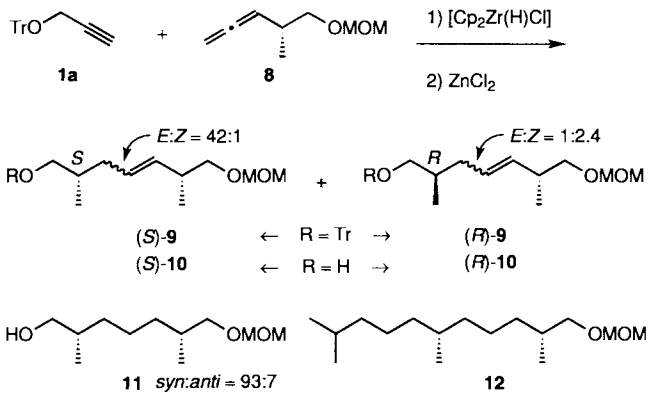

Scheme 2. Synthesis of an intermediate along the pathway to vitamin E (**12**) through the coupling of an alkyne with an allene. **9**: R = Tr; **10**: R = H.

from **9** [TsOH (cat.)/MeOH, quantitative], showed the ratio of the four isomers, (*S*,*Z*):(*S*,*E*):(*R*,*Z*):(*R*,*E*) to be 91:2:2:5, indicating a remarkable degree of selectivity *S*:*R* of 93:7 with respect to the newly formed chiral center.[17] Indeed, hydrogenation of **9** gave a 93:7 mixture of *syn*- and *anti*-**11**,[18] which could be converted (TsCl; $Me_2CH(CH_2)_2MgBr$, Cu^{2+}; H_3O^+) into **12**, a known intermediate in vitamin E synthesis.[15a] The origin of this high level of 1,5-asymmetric induction is currently under investigation.[19]

Experimental Section

In a typical experiment, a suspension of Schwartz reagent [9] was prepared by adding CH_2Cl_2 (1.0 mL) to $Cp_2Zr(H)Cl$ (603 mg, 2.34 mmol) at −78 °C [8c]. Then a mixture of alkyne **1a** (193 mg, 0.648 mmol) and allene **2a** (116 mg, 0.906 mmol) in CH_2Cl_2 (2.5 mL) was added. After gradual warming to 25 °C, the resulting red solution was chilled to 0 °C, and to this was added $ZnCl_2$ (0.69 M in ether, 1.3 mL). After 2 h at 25 °C the mixture was diluted with ether and poured into cooled, saturated aqueous $NaHCO_3$. The ether solution was extracted three times with EtOAc and the combined organic extracts were washed with saturated aqueous Na_2SO_4, dried over Na_2SO_4, and filtered through a Celite pad. Evaporation of volatile components and purification by preparative TLC (hexane/EtOAc = 9/1) gave **5a** (231 mg, 83%).

Received June 5, 1997 [Z105161E]
German version: *Angew. Chem.* **1997**, *109*, 2578–2580

Keywords: alkynes · allenes · asymmetric synthesis · C–C coupling · zirconium

 © WILEY-VCH Verlag GmbH, D-69451 Weinheim, 1997 0570-0833/97/3622-2470 $ 17.50+.50/0

[1] a) M. Gaudemar, *C. R. Acad. Sci. Paris (C)* **1971**, *273*, 1669; b) Y. Frangin, M. Gaudemar, *ibid.* **1974**, *278*, 885; c) *Synthesis* **1977**, 205; d) P. Knochel, J.-F. Normant, *Tetrahedron Lett.* **1986**, *27*, 1039, 1043, 4427, 4431, 5727.
[2] For a review of carbometalations see P. Knochel in *Comprehensive Organic Synthesis, Vol. 4* (Eds.: B. M. Trost, I. Fleming, M. F. Semmelhack), Pergamon, Oxford, **1991**, p. 865.
[3] a) I. Marek, J.-M. Lefrançois, J.-F. Normant, *J. Org. Chem.* **1994**, *59*, 4154; b) *Bull. Soc. Chim. Fr.* **1994**, *131*, 910.
[4] The term "metalla-Claisen mechanism" is used here simply as a means of describing the characteristics of the reaction. Other mechanisms such as the metallo-ene mechanism (see W. Oppolzer in *Comprehensive Organic Synthesis, Vol. 5* (Eds.: B. M. Trost, I. Fleming, L. A. Paquette), Pergamon, Oxford, **1991**, p. 29, and ref. [3a]) are also plausible. Nothing is known about either the nature of the incorporated metals (m^1, m^2 in Scheme 1) or the aggregation state of the dimetalated species. We wish to thank Dr. Ilane Marek for helpful discussions.
[5] No additional zinc salt is required if at least one of the starting materials is an organozinc derivative.
[6] For a review of allylmetal compounds see Y. Yamamoto, N. Asao, *Chem. Rev.* **1993**, *93*, 2207.
[7] J. Schwartz, J. A. Labinger, *Angew. Chem.* **1976**, *88*, 402; *Angew. Chem. Int. Ed. Engl.* **1976**, *15*, 333.
[8] Hydrozirconation of allenes: a) H. Maeta, T. Hasegawa, K. Suzuki, *Synlett* **1993**, 341; b) K. Suzuki, T. Hasegawa, T. Imai, H. Maeta, S. Ohba, *Tetrahedron* **1995**, *51*, 4482; c) M. Chino, T. Matsumoto, K. Suzuki, *Synlett* **1994**, 359.
[9] S. L. Buchwald, S. J. LaMaire, R. B. Nielsen, B. T. Watson, S. M. King, *Org. Synth.* **1992**, *71*, 77.
[10] Quenching the reaction with D_2O led to doubly deuterated **5a** (CHD_2 instead of CH_3).
[11] Absence of the γ-adduct was established by ^1H NMR, HPLC, and/or capillary GC. In each case, a comparison sample containing the γ-adduct was prepared by early quenching. Upon hydrogenation, each α-adduct gave a single saturated compound.
[12] The coupling reaction itself is complete within a few minutes after addition of $ZnCl_2$.
[13] Lithium salts (LiI, LiBr) also have a retarding effect, but much smaller. We originally thought that $[Cp_2ZrCl_2]$ present in the reaction mixture was responsible for the unusual regioselectivity, but this turned out not to be the case.
[14] Simple quenching by protic impurities that may have contained $MgBr_2$ was ruled out: Quenching with D_2O after addition of $MgBr_2$ produced a doubly deuterated product [10].
[15] For syntheses of the vitamin E side chain involving remote stereocontrol, see a) K.-K. Chan, N. Cohen, J. P. De Noble, A. C. Specian, Jr., G. Saucy, *J. Org. Chem.* **1976**, *41*, 3505; b) B. M. Trost, T. P. Klun, *ibid.* **1980**, *45*, 4256; c) W. C. Still, K. P. Darst, *J. Am. Chem. Soc.* **1980**, *102*, 7385; d) C. H. Heathcock, E. T. Jarvi, *Tetrahedron Lett.* **1982**, *23*, 2825; e) C. H. Heathcock, B. L. Finkelstein, E. T. Jarvi, P. A. Radel, C. R. Hadley, *J. Org. Chem.* **1988**, *53*, 1922.
[16] >98% *ee*. The synthesis of **8** will be described elsewhere.
[17] Analysis is based on a comparison with the authentic stereoisomers.
[18] Based on an MTPA(= α-methoxy-α-trifluoromethylphenylacetic acid) analysis of **11** by ^{19}F NMR spectroscopy.
[19] A chelating group in the allene is essential: Stereoselectivity fell to about 1:1:1:1 if the MOM substituent in **8** was replaced by a TBDPS group. On the other hand, the protective group of the alkyne is less influential, and *S*/*R* selectivity remains 9:1 irrespective of protection. The high (*Z*)-selectivity with (*S*)-**9** is noteworthy because of the contrast with lower selectivities with (*R*)-**9** or simpler, nonstereogenic substrates.

Copper Pnictogenides as Selective Reagents: A New Access to Functionalized Phosphanes and Arsanes**

Christian Meyer, Hansjörg Grützmacher,* and Hans Pritzkow

Dedicated to Professor Gottfried Huttner on occasion of his 60th birthday

Many catalytically effective transition metal complexes contain phosphane ligands, and increasing demands concerning the reactivity and selectivity of these catalysts require the synthesis of special ligands. Phosphanes are usually prepared by allowing either a halophosphane $R_{3-n}P(Hal)_n$ to react with carbanion equivalents M^+R^- or an alkali metal phosphide $(R_{3-n}P)^-M_n^+$ (M = Li, Na, K) to react with a carbocation equivalent R^1-Z (Z = leaving group).[1] Copper reagents proved to be versatile for the selective formation of C–X bonds (X = C, Si, Sn, S, Se, Te).[2] Recently we synthesized tris(telluro)carbenium ions $[(RTe)_3C]^+[CuBr_2]^-$ by treating the copper complex [(bpy)CuTeR] (bpy = 2,2′-bipyridyl) with CBr_4.[3] We now extended these investigations to the reaction of copper phosphides and arsanides with organohalides R–Hal, which, to our knowledge, has not been reported to date.

According to the method of Caulton et al.,[4] tetrameric copper(I) *tert*-butoxide (**1**) was allowed to react with diphenyl(element) hydrides **2**–**4** to provide the partially new copper pnictogenides **5**[5]–**7** as insoluble, red-brown coordination polymers of unknown structures (Scheme 1). In the presence of the nitrogen heterocycles bpy (**8**), phenanthroline (**9**, phen), or neocuproine (**10**, neocup), deeply colored complexes such as **11**–**14**, which are relatively soluble in aromatic hydrocarbons, are formed. In the copper phosphides, the R_2P group can take either a μ_2- (three-center four-electron bond) or a μ_3-bridging position (four-center four-electron bond) between the copper centers,[6a–e] as evidenced by ^{31}P NMR spectroscopy (significant shift towards low-resonance frequencies in the case of μ_3-PR_2 units: $\delta < -50$ versus 85% H_3PO_4). Accordingly, species with μ_2-bridging Ph_2P groups dominate in solutions of **12** and **13** (^{31}P NMR: $\delta = -25$; Table 1).

The X-ray structure analysis shows that in the solid state **12** consists of a six-membered Cu_3P_3 ring in a twist conformation with alternating Cu–P distances (2.24 and 2.30 Å, Scheme 1). The Cu–Cu distances (3.9–4.1 Å) preclude significant metal–metal bonding interactions.[7] The structure of the species

Table 1. Selected physical data for copper pnictogenide complexes **11**–**14**.

Compd	m.p. [°C]	$\delta(^{31}P\{^1H\}$ NMR) (121.5 MHz, C_6D_6)	$\lambda_{max}/\varepsilon$ [nm]/[L mol^{-1} cm^{-1}]
11	83–90	−15.3; −84.0	646.9/661
12	92 (decomp)	−24.0	651.7/3520
13	135 (decomp)	−25.2	556.1/3192
14	127 (decomp)	–	572.2/23980

[*] Prof. Dr. H. Grützmacher, Dipl.-Chem. C. Meyer
Laboratorium für Anorganische Chemie
ETH-Zürich
Universitätstrasse 6, CH-8092 Zürich (Switzerland)
Fax: Int. code +(1)632-1090
e-mail: gruetz@inorg.chem.ethz.ch
Dr. H. Pritzkow
Institut für Anorganische Chemie der Universität Heidelberg (Germany)

[**] We thank Prof. K. Caulton and Prof. S. R. Gilbertson for stimulating discussions, and the referees for critical comments.

 © WILEY-VCH Verlag GmbH, D-69451 Weinheim, 1997 0570-0833/97/3622-2471 $ 17.50+.50/0

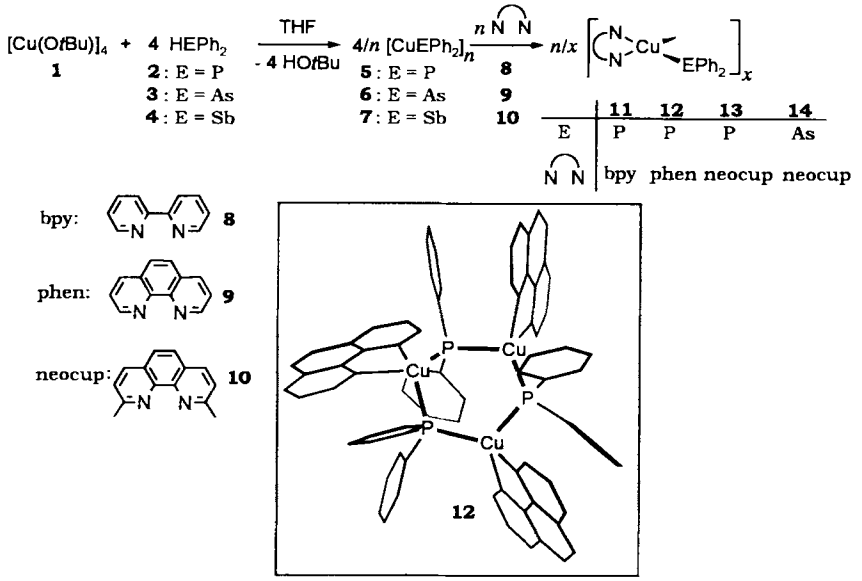

Scheme 1.

formed upon dissolving the bipyridine complex **11** is more complex: Resonances in the ^{31}P NMR spectrum are at $\delta = -15$ and -84; the latter is asigned to a μ_3-bridging Ph_2P unit.

We studied the reactivity of copper phosphide complexes **11**–**13** (E = P) and of arsanide complex **14** with respect to various organohalides containing further functional groups. Some examples are outlined in Scheme 2. The most remarkable result of this study is the selectivity and varying degrees of reactivity as a function of the nitrogen heterocycles $\widehat{NN}$, which control these reactions. Only activated chlorine or bromine centers in an allylic or benzylic position or situated α to an ester group are replaced by the Ph_2P group of **11**. The nitrile group in **15** or the ester group in **17** remain unaffected. The phosphanes **18** and **21** are thus obtained in good yields (Table 2).

Corresponding reactions employing lithium phosphide as the reagent lead to a mixture of compounds.[5c] Nonactivated alkyl halides react with the more reactive phenanthroline complex **12** to yield alkyl phosphanes. Neocuproine complexes **13** and **14** are the most reactive. In addition to all previously listed substrates, they also react with the protected brominated serine derivative **16** (which does not react with **11** or **12**). Using this method, chiral phosphanes *R,S*-**19**[8] and arsanes *R,S*-**20** are directly accessible, however, they are not enantiomerically pure. Starting with *S*-**16**, epimerization of the chiral center is observed in the course of the reaction. In addition to the products **19** or **20**, small amounts of phosphane **2** or arsane **3**, respectively, are detected.

To demonstrate the selectivity of the new reagents, we performed the sequential synthesis of the mixed (ω-phosphanyl)arsane **22** starting from 3-chloropropyl chloroacetate (**17**). In the first step the activated benzylic C–Cl functionality reacts with the less reactive copper phosphide **11** to give exclusively phosphane **21**. In the second step the more reactive neocuproine copper arsanide **14** reacts cleanly with substitution of the less reactive C–Cl unit to give **22** in good yields.

Certainly, simple phosphanes will continue to be synthesized by common methods. However, the use of copper pnictogenides $CuER_2$—whose reactivity can be fine-tuned by appropriate choice of a co-ligand—allows the relatively simple synthesis of phosphanes and, in particular, arsanes[9] bearing additional functional groups (CN, COOR, $CONR_2$). The reactions reported here are therefore a useful extension of established synthetic methods. Further optimization of the reaction conditions and variation of the nitrogen-containing ligands $\widehat{NN}$ should allow the synthesis of highly functionalized and even chiral ligands $ER^1R^2R^3$ (E = P, As, Sb).

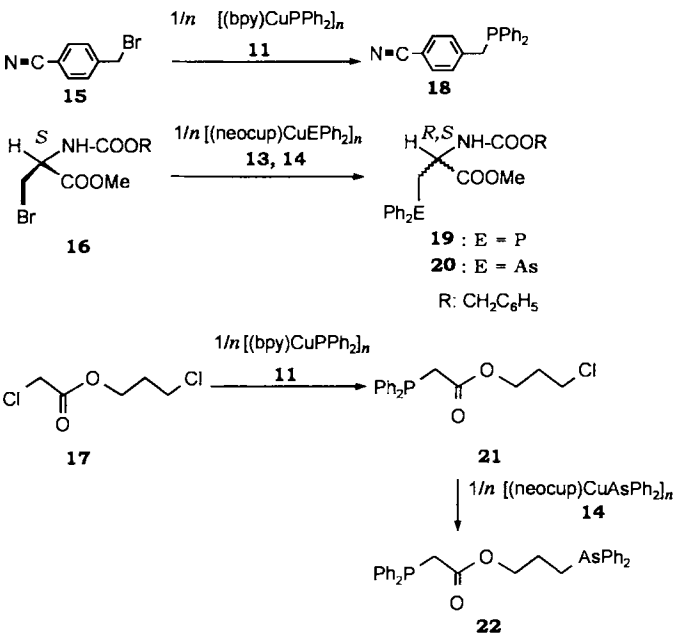

Scheme 2.

Table 2. Selected physical data for phosphanes **18**, **19**, and **21** as well as arsanes **20** and **22**.

Compd	b.p. [°C]	$\delta(^{31}P\{^1H\}$ NMR) (121.5 MHz, C_6D_6)	$\delta(^1H$ NMR) R_2E-CH_2 (300 MHz, C_6D_6)	$\delta(^{13}C$ NMR) R_2E-CH (75.5 MHz, C_6D_6)
18	119	−8.7	3.16 (s)	36.4 (d, ^1J(PC) = 36.4 Hz)
19	68 (m.p.)	−23.4	2.65 (dd, 1H, ^2J(HCH) = 14.1 Hz, P-CH_2)	^3J(HCCH) = 5.4 Hz, 31.8 (d, ^1J(PC) = 16.6 Hz)
			2.41 (dd, 1H, ^2J(HCH) = 14.1 Hz, P-CH_2)	^3J(HCCH) = 5.4 Hz
20	oil	–	2.48 (dd, 1H, ^2J(HCH) = 12.9 Hz, As-CH_2)	^3J(HCCH) = 5.9 Hz, 32.1 (s)
			2.50 (dd, 1H, ^2J(HCH) = 12.9 Hz, As-CH_2)	^3J(HCCH) = 5.9 Hz
21	oil	−16.5	2.98 (s)	35.1 (d, ^1J(PC) = 22.8 Hz)
22	oil	−16.7	1.83–1.78 (m, As-CH_2), 3.03 (s, P-CH_2)	25.6 (s, As-CH_2); 35.0 (d, ^1J(PC) = 22.5 Hz P-CH_2)

 © WILEY-VCH Verlag GmbH, D-69451 Weinheim, 1997 0570-0833/97/3622-2472 $ 17.50+.50/0

Experimental Section

5, **6**, and **7**: A solution of **2**, **3**, or **4** (11 mmol, 1.1 equiv) in THF (10 mL) was slowly added within 30 min to a vigorously stirred solution of **1** (10 mmol) in THF (40 mL). During addition **5**, **6**, and **7** precipitated as deeply colored powders, which were filtered, washed repeatedly with Et_2O, and finally dried under high vaccum; yields 79–98%.

11–14: Copper phosphanide **5** or copper arsanide **6** (1.2×10^{-3} mol, 1 equiv) was suspended in THF (50 mL). Under vigorous stirring a solution of the ligand (**8–10**; 1.3×10^{-3} mol, 1.1 equiv) in THF (20 mL) was slowly added. The reaction mixtures were filtered over silica and then concentrated to a few milliliters. The deeply colored, air-sensitive complexes **11–14** precipitated at −20 °C as microcrystalline materials; yields 53–70%.

18–22: Freshly prepared solutions of **11–14** in THF were allowed to react with one equivalent of the organohalide (**15–17**) dissolved in THF. After complete reaction (a deep red solution over a yellow precipitate formed) the solvent was removed under vaccum, and the residue suspended in Et_2O. A saturated solution of KCN in H_2O was added until two colorless, clear phases formed. The ether phase was seperated and washed with H_2O and then 2 N HCl/H_2O. After the organic phase was dried over Na_2SO_4, the volume of the solution was reduced under vacuum. The phosphanes (arsanes) **18–22** were obtained as colorless oils. The phosphanated amino acid derivative **19** could be recrystallized from EtOH. All compounds gave satisfactory elemental analyses.

Received: April 15, 1997
Revised version: June 24, 1997 [Z 10353 IE]
German version: *Angew. Chem.* **1997**, *109*, 2576–2578

Keywords: amino acids · As ligands · copper · P ligands

[1] a) D. G. Gilheany, C. M. Mitchell in *The Chemistry of Organophosphorus Compounds, Vol. 1*. (Ed.: F. R. Hartley), Wiley, Chichester, **1990**, p. 152; b) *Synthetic Methods of Organometallic and Inorganic Chemistry, Vol. 3*, (Eds.: W. A. Herrmann, G. Brauer, H. H. Karsch), Thieme, Stuttgart, **1996**.

[2] See contributions in *Organocopper Reagents, The Practical Approach in Chemistry Series* (Ed.: R. J. K. Taylor), University Press, Oxford, **1994**.

[3] D. Ohlmann, C. M. Marchand, H. Grützmacher, G. S. Chen, D. Framer, R. Glaser, A. Currao, R. Nesper, H. Pritzkow, *Angew. Chem.* **1996**, *108*, 317; *Angew. Chem. Int. Ed. Engl.* **1996**, *35*, 300.

[4] T. H. Lemmen, G. V. Goeden, J. C. Huffman, R. L. Geerts, K. G. Caulton, *Inorg. Chem.* **1990**, *29*, 3680.

[5] Pioneering work: a) K. Issleib, H.-O. Fröhlich, *Chem. Ber.* **1962**, *95*, 375; b) K. Issleib, E. Wenschuh, *Z. Naturforsch. B* **1964**, *19*, 199; c) synthesis of carboxyphosphanes from $NaPPh_2$ or $KPPh_2$ and $X-(CH_2)_n-COOR$: K. Issleib, G. Thomas, *Chem. Ber.* **1960**, *93*, 803, and references therein.

[6] a) A. Eichhöfer, D. Fenske, W. Holstein, *Angew. Chem.* **1993**, *105*, 257: *Angew. Int. Ed. Engl.* **1993**, *32*, 242; b) F. Gol, P. C. Knüppel, O. Stelzer, W. S. Sheldrick, *Angew. Chem.* **1988**, *100*, 1008; *Angew. Chem. Int. Engl.* **1988**, *27*, 956; c) D. J. Brauer, G. Hessler, P. C. Knüppel, O. Stelzer, *Inorg. Chem.* **1990**, *29*, 2370; d) A. H. Cowley, D. M. Giolando, R. A. Jones, C. M. Nunn, J. M. Power, *J. Chem. Soc. Chem. Commun.* **1988**, 208; e) S. F. Martin, J. F. Fishpaugh, J. M. Power, D. M. Giolando, R. A. Jones, C. M. Nunn, A. H. Cowley, *J. Am. Chem. Soc.* **1988**, *110*, 7226.

[7] **12**: monoclinic, space group $P2_1/n$, $V = 7188$ Å^3, $Z = 4$, $a = 13.469(5)$, $b = 25.082(10)$, $c = 21.304(9)$ Å, $\beta = 92.89(3)^\circ$, $2\theta_{max} = 48^\circ$, 11 369 reflections, 763 parameters. The structure was solved by direct methods (SHELXS-86) and refined (full matrix) against F_o^2 (SHELXL-93); R_1 $[F_o > 4\sigma(F_o)] = 0.086$, $R_w 2 = 0.193$. The compound crystallizes with disordered solvent molecules, which strongly affected the structure determination. Crystallographic data (excluding structure factors) for the structure reported in this paper have been deposited with the Cambridge Crystallographic Data Centre as supplementary publication no. CCDC-100508. Copies of the data can be obtained free of charge on application to The Director, CCDC, 12 Union Road, Cambridge CB2 1EZ, UK (fax: int. code + (1223) 336-033; e-mail: deposit@chemcrys.cam.ac.uk).

[8] Phosphanylated amino acids and peptides for combinatorial ligand design: a) S. R. Gilbertson, X. Wang, *Tetrahedron Lett.* **1996**, *37*, 6475; b) S. R. Gilbertson, X. Wang, G. S. Hoge, C. A. Klug, J. Schaefer, *Organometallics* **1996**, *15*, 4678; c) S. R. Gilbertson, R. V. Pawlick, *Angew. Chem.* **1996**, *108*, 963; *Angew. Chem. Int. Ed. Engl.* **1996**, *35*, 902, and references therein.

[9] Preliminary results show that stibanes may be synthesized using copper stibanide complexes as well.

Substrate Mimetic Mediated Peptide Synthesis: An Irreversible Ligation Strategy That Is Independent of Substrate Specificity**

Frank Bordusa, Dirk Ullmann, Christian Elsner, and Hans-Dieter Jakubke*

Chemical peptide synthesis requires large experimental efforts to protect the side chains of trifunctional amino acids, and the risk of racemization cannot be entirely eliminated. There is therefore a need to explore enzyme-based alternatives.[1] Despite the undisputed advantages of enzymatic syntheses, their application is limited by the restrictive substrate specificity of enzymes and by the risk of undesired proteolysis of the starting materials or the products of segment condensations.

As early as 1991 we reported the application of 4-guanidinophenyl esters of acylated amino acids (**1**) for trypsin-catalyzed peptide syntheses in collaboration with the research group of Mitin. We could show that even acylated donor esters containing proline, D-alanine, or β-alanine in the specificity-determining P_1 position could be coupled successfully.[2] The 4-guanidinophenyl ester (OGp) leaving group of these substrates binds to the active site of trypsin in a way that mimics trypsin-specific side chains (Arg, Lys). As a result, peptide coupling occurs irreversibly and independent of specificity. We therefore consider the term "substrate mimetics" more suitable than the older "inverse substrates".[3] Recent improvements in the chemical synthesis of guanidino- and amidinophenyl esters, especially in the lab of Tanizawa, and their utilization in trypsin-catalyzed synthesis[4] initiated more intensive investigation of this ligation strategy.

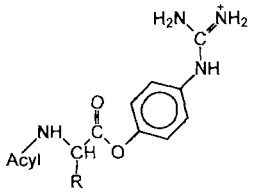

1

Here we describe studies on the utility of 4-guanidinophenyl esters for segment condensations catalyzed by trypsin in comparison to reactions catalyzed by thrombin and clostripain, which had not yet been exploited for this strategy. These enzymes have a primary specificity for basic side-chain functionalities. The OGp leaving group binds in place of the specificity-determining basic side-chain functionality, as demonstrated by the program Autodock (Figure 1).[5, 6] After formation of the acylated enzyme, deacylation by the added amino component occurs independent of the primary specificity of the protease. As a result, the newly formed peptide bond cannot be recognized by the enzyme and is not subject to secondary hydrolysis. Figure 2 shows the course of a (3 + 5) segment condensation of the simple model peptide Boc-Phe-Gly-Gly-Ala-Phe-Ala-Ala-Gly-OH (Boc = *tert*-butoxycarbonyl), and demonstrates the excellent utility of substrate mimetics for the clostripain-catalyzed ligation. The maximum product concentration is reached after a few minutes and remains unchanged after 72 hours; this clearly

[*] Prof. Dr. H.-D. Jakubke, F. Bordusa, Dr. D. Ullmann, C. Elsner
Fakultät für Biowissenschaften, Pharmazie und Psychologie
Institut für Biochemie der Universität
Talstrasse 33, D-04103 Leipzig (Germany)
Fax: Int. code + (341) 973-6998
e-mail: jakubke@rz.uni-leipzig.de

[**] This work was supported by the Deutsche Forschungsgemeinschaft (JA 559/9-1 and INK 23) and the Fonds der Chemischen Industrie. We wish to thank Prof. Dr. H.-J. Hofmann and Dipl.-Biochem. M. Thormann (Leipzig) for running the docking analyses, Dr. J. Stürzebecher (Erfurt) and Dr. R. Wohlgemuth (Fluka Chemie AG, Buchs) for providing samples of thrombin and clostripain, respectively, and ASTA Medica for special chemicals.

 © WILEY-VCH Verlag GmbH, D-69451 Weinheim, 1997 0570-0833/97/3622-2473 $ 17.50+.50/0

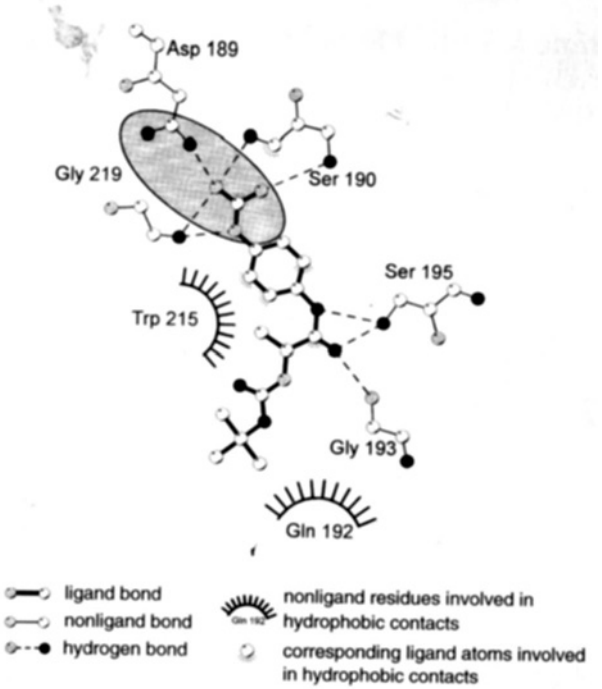

Figure 1. Ligplot drawing of the fit of Boc-Ala-OGp into the active site of the serine protease trypsin [6, 7].

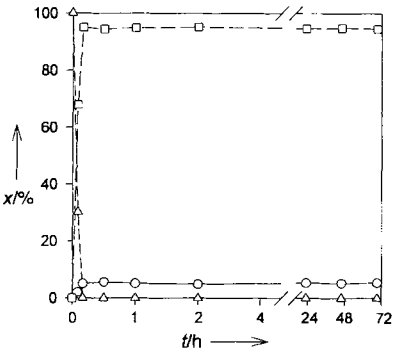

Figure 2. Course of the clostripain-catalyzed (3 + 5) segment condensation of Boc-Phe-Gly-Gly-OGp and H-Ala-Phe-Ala-Ala-Gly-OH (Boc-Phe-Gly-Gly-OGp (△); Boc-Phe-Gly-Gly-Ala-Phe-Ala-Ala-Gly-OH (□); Boc-Phe-Gly-Gly-OH (○)). Conditions were as described in ref. [8]; x = product yield.

proves the irreversibility of the ligation. In a preparative reaction with Boc-Phe-Gly-Gly-OGp (122 mg, 0.174 mmol) and H-Ala-Phe-Ala-Ala-Gly-OH (157 mg, 0.286 mmol), we obtained 177 mg (91% yield) of the Boc-protected octapeptide.[9]

Table 1 shows that all three enzymes are capable of catalyzing the (3 + 5) segment condensation, however, with largely varying yields. The highest yield was obtained with the cysteine protease clostripain, which also provided yields of over 90% for other 4-guanidinophenyl esters of acylated amino acids. Reactions of Boc-Xaa-OGp with H-Ala-Phe-Ala-Ala-Gly-OH under variation of the P_1 amino acid Xaa provided the yields given in parentheses: Gly (93%), Ala (95%), Leu (91%), Phe (91%), and Pro (90.5%).[8] A decisive advantage of clostripain in substrate mimetic mediated peptide syntheses results from its low P'_1 specificity for the N-terminal amino acid residue of the amino component. The results shown in Figure 3 clearly

Table 1. Product yield x of the thrombin-, trypsin-, and clostripain-catalyzed segment condensation of Boc-Phe-Gly-Gly-OGp (2 mM) and H-Ala-Phe-Ala-Ala-Gly-OH as a function of the concentration of the amino component [a].

AFAAG [mM]	x [%] thrombin	trypsin	clostripain
2.4	n.d. [b]	n.d. [b]	83
4	10	21	94
6	14	29	96
8	18	38	98

[a] Conditions were as described in ref. [8]. [b] n.d.: not determined.

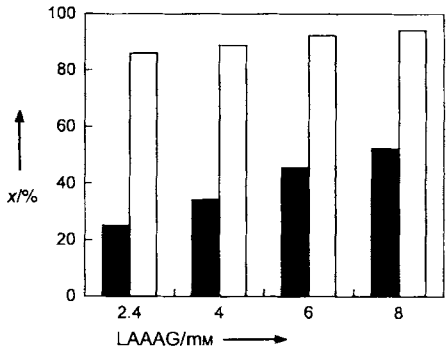

Figure 3. Product yield x for the segment condensation of Boc-Phe-Gly-Gly-OGp (2 mM) and H-Leu-Ala-Ala-Ala-Gly-OH catalyzed by clostripain (□) and trypsin (■) as a function of the concentration of amino component. Conditions were as described in ref. [8].

demonstrate that replacement of N-terminal Ala with Leu in the amino component has a less significant but positive influence on the yields of trypsin-catalyzed reactions; this is in accordance with the enzyme's known P'_1 specificity.[10] However, the high yields in clostripain-catalyzed segment condensations are nearly unaffected. A wide substrate specificity of the enzyme for the N-terminal amino acid of the amino component, which is desirable for segment condensations, can only be provided by clostipain, as demonstrated by acyl-transfer reactions with various amino components.[11]

Our results demonstrate that the serine protease thrombin can be utilized in substrate mimetic mediated segment condensations. However, the cysteine protease clostripain is of more general and practical importance for this new ligation strategy due to the high reaction yields and its low P'_1 specificity. Universal application of clostripain is only limited when using arginine-containing reagents. In these cases the residue should be placed at the N-terminus of the amino component. Alternatively, one can utilize the synthetic potential of zymogens, which are inactive in proteolysis reactions[12] and capable of accepting substrate mimetics during peptide synthesis. The current innovative method contributes to the development of practical enzymatic ligations for peptide and protein chemistry.

Received: May 14, 1997 [Z10400IE]
German version: *Angew. Chem.* **1997**, *109*, 2583–2585

Keywords: bioorganic chemistry · clostripain · enzyme catalysis · serine proteases · substrate mimetics

[1] H.-D. Jakubke, *Angew. Chem.* **1995**, *107*, 189–191; *Angew. Chem. Int. Ed. Engl.* **1995**, *34*, 175–177.
[2] V. Schellenberger, H.-D. Jakubke, N. P. Zapevalova, Y. V. Mitin, *Biotechnol. Bioeng.* **1991**, *38*, 104–108; *38*, 319–321; Y. V. Mitin, V. Schellenberger, U. Schellenberger, H.-D. Jakubke, N. P. Zapevalova, *Peptides 1990* (Eds.: E. Giralt, D. Andreu), ESCOM, Leiden, **1991**, pp. 287–288.
[3] The term "inverse ester" was introduced by G. Wagner and H. Horn (*Pharmazie* **1973**, *28*, 428–431) to describe 4-amidinophenyl esters of aromatic carboxylic acids as opposed to aryl esters of 4-amidinobenzoic acid in the

 © WILEY-VCH Verlag GmbH, D-69451 Weinheim, 1997 0570-0833/97/3622-2474 $ 17.50+.50/0

course of inhibition studies of trypsin and other serine proteases. This later led to the enzymological term "inverse substrates" (K. Tanizawa, Y. Kasaba, Y. Kanaoka, *J. Am. Chem. Soc.* **1977**, *99*, 4484–4488).

[4] H. Sekizaki, K. Itoh, E. Toyota, K. Tanizawa, *Chem. Pharm. Bull.* **1996**, *44*, 1577–1579, 1585–1587; *Tetrahedron Lett.* **1997**, *38*, 1777–1780.

[5] G. M. Morris, D. S. Goodsell, R. Huey, A. J. Olson, *J. Comput. Aided. Mol. Des.* **1996**, *10*, 293–303.

[6] The docking procedure was performed based on the crystal structure of trypsin 2TPN (J. Walter, W. Steigemann, T. P. Singh, H. Bartunik, W. Bode, R. Huber, *Acta Crystallogr. Sect. B* **1982**, *38*, 1462–1470) and the modeled structure of Boc-Ala-OGp. The 125 million enzyme-substrate conformations were generated in a $80 \times 72 \times 72$ Å^3 grid with a resolution of 1 Å. The conformation of lowest energy was used as the starting point for another docking procedure with 125 million enzyme-substrate conformations in a grid of $80 \times 80 \times 80$ Å^3 with a resolution of 0.35 Å. The CHARMm 23.1 template charges were used (F. A. Momany, R. Rone, H. Kunz, R. F. Frey, S. Q. Newton, L. Schäfer, *J. Mol. Strukt. (Theochem)* **1993**, *286*, 1–18). All torsion angles were allowed to rotate freely.

[7] A. C. Wallace, R. A. Laskowsy, J. M. Thornton, *Protein Eng.* **1995**, *8*, 127–132.

[8] The enzyme-catalyzed reactions were performed in 0.05 M 2-[4-(2-hydroxyethyl)]-1-piperazineethanesulfonic acid (HEPES, pH = 8.0), which was 0.1 M NaCl and 0.01 M $CaCl_2$. The concentration of Boc-Phe-Gly-Gly-OGp was 2 mM for all analytical reactions. The concentration of H-Ala-Phe-Ala-Ala-Gly-OH was 4 mM for reactions with Boc-Phe-Gly-Gly-OGp (Figure 2) and for reactions with Boc-Xaa-OGp. Enzyme concentrations used were [trypsin] = 9.6×10^{-6} M, [thrombin] = 2.2×10^{-5} M, and [clostripain] = 1.6×10^{-6} M in reactions with Boc-Phe-Gly-Gly-OGp. In the cases of Boc-Gly-OGp, Boc-Ala-OGp and Boc-Phe-OGp the same concentration of clostripain was used. In reactions with Boc-Leu-OGp or Boc-Pro-OGp the concentration of clostripain was 1.3×10^{-5} M. The reactions were analyzed under optimized conditions with reverse-phase HPLC using a RP-18 column (Vydac, 218TP54, 5 μM, 300 Å, 25×0.4 cm; The Separations Group), an SG-120 5 μm RP18 Grom Capcell column (Grom) of the same dimensions, and a 4.6×125 mm RP-4 column (Kromasil, EKA-NOBEL). Detection was carried out at 254 nm for the Phe-containing substrate mimetics Boc-Phe-Gly-Gly-OGp and Boc-Phe-OGp, and at 220 nm for all other mimetics Boc-Xaa-OGp. For the latter the yield was calibrated based on reactions in which the acylated donor ester was completely consumed.

[9] Boc-Phe-Gly-Gly-Ala-Phe-Ala-Ala-Gly-OH was synthesized in preparative amounts with 3 mM Boc-Phe-Gly-Gly-OGp and 4 mM H-Ala-Phe-Ala-Ala-Gly-OH. The total volume of the reaction mixture was 58 mL. Other reaction conditions were as described in ref. [8]. The enzymatic reaction was stopped by addition of trifluoroacetic acid (TFA, 1% solution); this led to precipitation of the desired peptide product, which was washed with water. Boc-Phe-Gly-Gly-Ala-Phe-Ala-Ala-Gly-OH·2.5 TFA·2 H_2O ($C_{43}H_{58.5}F_{7.5}N_8O_{18}$, 1117.98): calcd elemental analysis: C 46.20, H 5.27, N 10.02; found: C 45.22, H 5.80, N 10.81; MALDI-TOF: $m/z = 819.29$ $[M+Na]^+$.

[10] V. Schellenberger, C. W. Turck, L. Hedstrom, W. J. Rutter, *Biochemistry* **1993**, *32*, 4349–4353.

[11] D. Ullmann, H.-D. Jakubke, *Eur. J. Biochem.* **1994**, *223*, 865–872.

[12] H.-D. Jakubke, U. Eichhorn, M. Hänsler, D. Ullmann, *Biol. Chem.* **1996**, *377*, 455–464.

Stabilization of a C_{2v}-Distorted Methane Derivative in an Organometallic Framework**

Jörg Schottek, Gerhard Erker,* and Roland Fröhlich

Dedicated to Professor Dieter Seebach on the occasion of his 60th birthday

The molecular structure of tetrahedral methane can formally be distorted in different ways.[1] Opening both angles A^1-C-A^2 and A^3-C-A^4 from 109 to 180° in the same direction, to place the four substituents in one plane, leads to planar methane (D_{4h}, Scheme 1). In contrast to "natural" T_d methane, the D_{4h} species

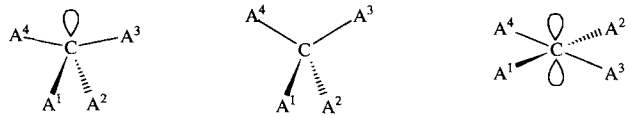

Scheme 1. Symmetries of methane derivatives.

has an electron-deficient σ system and two electrons in the 2p orbital perpendicular to the molecular plane. It is possible to stabilize this situation electronically,[2] and there are many examples of compounds that contain a planar-tetracoordinate carbon atom.[3] Opening only the A^3-C-A^4 angle of T_d methane leads to a series of C_{2v} methane derivatives; increasing this angle to greater than 180° provides an inverted tetracoordinate carbon atom.[4] Again, this deformation results in an electron-deficient σ system, now located at the A^3-C-A^4 moiety, and increased electron density at the opposite sides of the A^1–C and A^2–C vectors.[5] As with planar-tetracoordinate carbon, C_{2v} methane derivatives should be stabilized by electron-donor substituents that compensate for the electron deficiency in the σ system and by π-acceptor substituents that show conjugation of the resulting electron pair, but with a different spatial arrangement than in D_{4h} methane.

Here we report the preparation and the structural characterization of the stable organometallic C_{2v} methane derivative **2**, which contains an internal ion-pair interaction in a rigid organometallic framework that stabilizes the unusual geometry at carbon. The strong Lewis acid tris(pentafluorophenyl)borane adds regioselectively to the dinuclear bis(zirconocene) compound **1** to yield **2** in about 60% yield with formation of a B–C

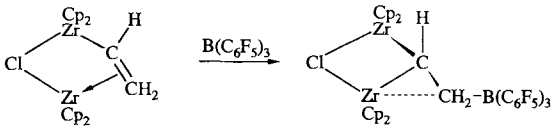

1 **2**

bond at the $=CH_2$ terminus of the bridging vinyl moiety. The starting material **1**[6] was obtained by hydrozirconation of acetylene followed by addition of the [Cp_2Zr] building block, which was generated photochemically from diphenylzirconocene.[7]

Single crystals of **2** that were suitable for X-ray structure analysis were obtained from toluene at −50 °C. The crystal structure of **2** (Figure 1) shows a dinuclear, chloro-bridged complex containing an asymmetric triangular Zr1-Cl-Zr2 framework. The Zr2–Cl bond is markedly shorter (2.5422(7) Å) than the rather long Zr1–Cl bond (2.6409(7) Å, angle Zr2-Cl-Zr1 86.05(2)°). The Zr1 ··· Zr2 separation of 3.5373(5) Å apparently precludes any direct metal–metal interaction. The two metallocene moieties are arranged in such a way (dihedral angles D1-Zr2-Cl-Zr1 117.0, D3-Zr1-Cl-Zr2 111.6°) that the Zr2-C1-Zr1 plane is the common σ-bonding plane.[8] Consequently, the carbon framework of the μ-$CHCH_2BR_3$ (R = C_6F_5) ligand is located in front of the Zr1 ··· Zr2 edge of the central Zr_2Cl triangle, as far as this is allowed by the bonding angles at the carbon atoms. The interaction of the μ-$CHCH_2$ moiety with both the transition metal centers is the main reason for the unusual and remarkable structural features of **2**. The quality of the X-ray analysis even allowed us to include the located hydrogen atoms at C1 and C2 into the structural description.

[*] Prof. Dr. G. Erker, Dipl.-Chem. J. Schottek, Dr. R. Fröhlich
Organisch-chemisches Institut der Universität
Corrensstrasse 40, D-48149 Münster (Germany)
Fax: Int. code +(251)83-39772
e-mail: erker@uni-muenster.de

[**] This work was supported by the Fonds der Chemischen Industrie, the Volkswagen-Stiftung, and the Ministerium für Wissenschaft und Forschung des Landes Nordrhein-Westfalen.

 © WILEY-VCH Verlag GmbH, D-69451 Weinheim, 1997 0570-0833/97/3622-2475 $ 17.50+.50/0

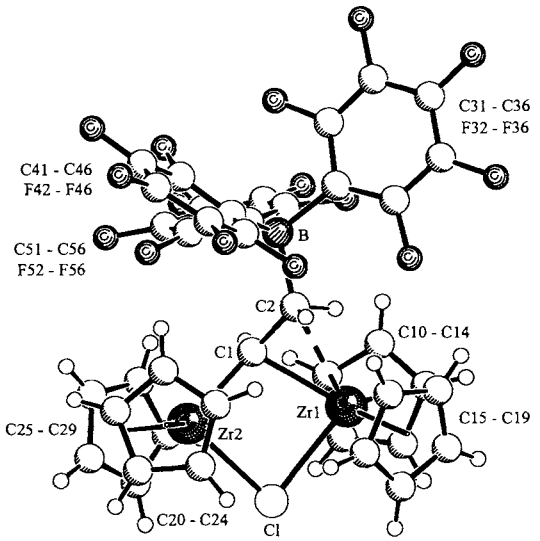

Figure 1. Molecular structure of **2**. Selected bond lengths [Å] and angles [°]: Zr1–Cl 2.6409(7), Zr2–Cl 2.5422(7), Zr1–Zr2 3.5373(5), Zr1–C1 2.396(3), Zr2–C1 2.156(3), Zr1–C2 2.600(3), C1–C2 1.502(3), C1–H1 0.98(3), C2–H2a 0.94(3), C2–H2b 0.99(3), C2–B 1.695(4), B–C31 1.669(4), B–C41 1.664(4), B–C51 1.647(4); Zr1-Cl-Zr2 86.05(2), Cl-Zr1-C1 81.89(6), Zr1-C1-Zr2 101.86(10), C1-Zr2-Cl 89.06(7), Zr2-C1-C2 145.9(2), Zr1-C1-C2 80.11(14), Zr1-C2-C1 65.22(13), Zr1-C2-B 155.0(2), C1-C2-B 119.2(2).

Carbon atom C1 is tetracoordinate and exhibits a strong distortion towards a C_{2v} structure (see Scheme 1). It is bonded to C2 (1.502(3) Å), H1 (0.98(3) Å), Zr1 (2.396(3) Å), and Zr2 (2.156(3) Å). The bonding angles of this moiety deviate considerably from tetrahedral angles. The Zr2-C1-C2 angle is 145.9(2)° (which corresponds to the increased A^3-C-A^4 angle in C_{2v} methane, Scheme 1). The angles Zr2-C1-H1 and C2-C1-H1 are 105.(2) and 109(2)°, respectively. In contrast, the remaining angles at C1 are much smaller (Zr2-C1-Zr1 101.86(10), Zr1-C1-C2 80.11(14)°); the Zr1-C1-H1 angle is 101(2)°. A noteworthy structural feature is the very short Zr2–C1 distance of 2.156(3) Å; to our knowledge, this is the shortest length for a bond from a zirconocene to a tetracoordinate carbon center.[9] This indicates the presence of an additional bonding interaction between the electron pair at the "backside" of carbon C1 in C_{2v} methane, which results from the severe distortion of the framework, and the coplanar acceptor orbital on the adjacent metallocene unit (see Figure 2). This carbon → metal donor interaction probably contributes substantially to the electronic stabilization of the distorted geometry of the tetracoordinate carbon center C1.

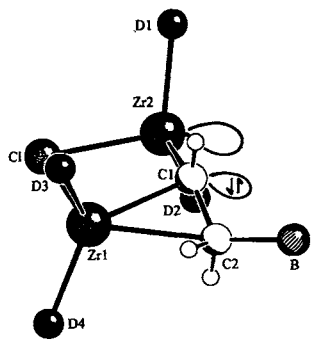

Figure 2. Partial structure of **2**. The orbitals depicted at C1 and Zr2 indicate a potential stabilizing interaction (D1—D4 denote the centroids of the Cp rings).

The bonding features at C2 are also unusual. Formally, C2 appears as a distorted trigonal bipyramidal pentacoordinate carbon atom.[10] However, there is only a minor distortion of the tetrahedral C1C2(H_2)BR_3 moiety (C1-C2-B 119.2(2), C1-C2-H2a 113.(2), C1-C2-H2b 110(2), B-C2-H2a 109(2), B-C2-H2b 102(2)°), which exhibits an additional bonding contact to Zr1 (C2–Zr1 2.600(3) Å). The C2–H2a and C2–H2b bonds are oriented toward Zr1, and the C2–B vector points in the opposite direction (Zr1-C2-B 155.0(2)°). The R_3B-C2 ··· Zr1 contact features properties typical of an electrostatic interaction. Complex **2** contains an internal ion-pair interaction between the cationic metallocene and the negatively polarized borate methylene group inside the dinuclear metallocene borate betaine structure.[11]

According to NMR spectroscopy, **2** shows a similar structure in solution. At 233 K **2** exhibits four resonances in both the ^{1}H and ^{13}C NMR spectra ([D_8]toluene) due to the two pairs of diastereotopic Cp ligands (δ = 5.44, 5.36, 5.26, 4.78 and 111.1, 110.2, 108.5, 107.1). There is an additional signal in each spectrum for C1H at δ = 7.12 and 174.7, respectively (^1J(C,H) = 122 Hz). The C2(H_2) signal at δ = 2.75 in the ^{1}H NMR spectrum is broad. Compound **2** shows temperature-dependent NMR spectra: Raising the temperature leads to a pairwise coalescence of the resonances for the Cp ligands. Therefore, at 298 K very simple ^{1}H and ^{13}C NMR spectra are observed, which each feature only two resonances for Cp (δ = 5.42, 5.18 and 111.6, 110.7). In the ^{13}C NMR spectrum the resonance for C2 appears at δ = 21.8.

The dynamic NMR spectra indicate an intramolecular enantiomerization process for **2**. It must be assumed that this proceeds with opening of the internal Zr1 ··· C2(H_2)BR_3 ion-pair bond. The rearrangement pathway probably passes through an intermediate structure that contains a normal tetrahedral carbon atom C1. From the temperature-dependent NMR spectra, a Gibbs activation energy for this thermally induced rearrangement was estimated to be $\Delta G^{\ddagger}_{enant} \approx 12.1 \pm 0.5$ kcal mol^{-1} for the temperature at which the signals for the Cp ligands coalesce (273 K).[12]

A qualitative estimate of the energetic properties at the C_{2v}-methane carbon atom C1 of **2** can be deduced from the dynamic behavior. In the course of the **2**⇌*ent*-**2** topomerization the inter-

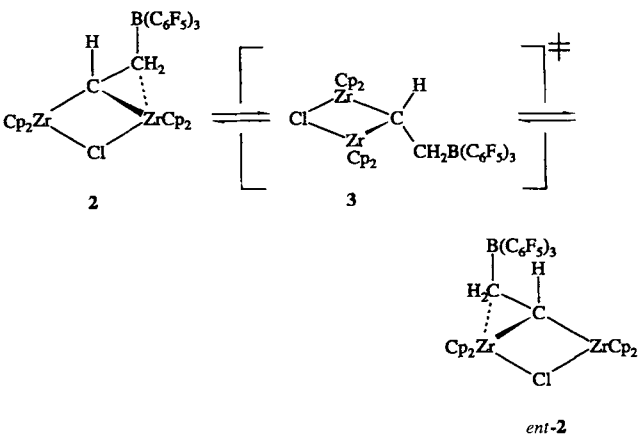

nal Zr1 ··· C2(H_2)BR_3 ion pair has to be cleaved. Assuming similar energetics as for the acyclic $[Cp_2ZrR]^+/[CH_3B(fluoroaryl)_3]^-$ ion pair,[11a] the bond dissociation energy for the Zr1 ··· C2(H_2)BR_3 group can be estimated to be about 16–18 kcal mol^{-1}. By comparing this value with the magnitude of $\Delta G^{\ddagger}_{enant}$ in **2**, it can be concluded that the distorted C_{2v} geometry at C1 of complex **2** is about 5 kcal mol^{-1} less favorable than the normal tetrahedral geometry, which is probably realized in the intermediate structure **3**. The unusual, distorted coordination geometry of C1 in **2** is therefore only observable because of the additional stabilization due to formation of the internal ion-pair interaction between Zr1 and the C2(H_2)BR_3 moiety. Thus, the otherwise disfavored system **2** gains so much stabiliza-

 © WILEY-VCH Verlag GmbH, D-69451 Weinheim, 1997 0570-0833/97/3622-2476 $ 17.50+.50/0

tion energy, compared to **3**, that it becomes the global minimum and is the only observed system.

This result emphasizes that the metal–ligand ion-pair bond is an important, but often unused, structural element for the composition of organometallic frameworks. The bonding strength of these ion-pair interactions is located between the weak noncovalent interactions and the covalent bonds of corresponding metal complexes. It is likely that such interactions will play an increasingly important role in the field of organometallic chemistry and catalysis.

Experimental Section

1: Vinylzirconocene chloride (0.70 g, 2.47 mmol) and diphenylzirconocene (0.93 g, 2.48 mmol) were dissolved in toluene (20 mL) and irradiated for 6 h at −78 °C (Philips HPK 125, Pyrex filter). The solvent was then removed in vacuo, and the residue washed with pentane to give **1** (660 mg, 53 %); m.p. 204 °C (decomp, determined by differential scanning calorimetry (DSC)). ^{1}H NMR (200 MHz, 300 K, [D$_6$]benzene): δ = 7.15, 3.92, 2.64 (ABX system, ^3J = 13.5, 17.8 Hz, ^2J = 1.8 Hz, each 1 H, vinyl), 5.61, 5.32, 5.25, 5.07 (s, each 5H, Cp); ^{13}C NMR (90 MHz, 300 K, [D$_6$]benzene): δ = 178.8, 63.1 (vinyl), 106.5, 105.2, 104.5, 103.6 (Cp).

2: Complex **1** (120 mg, 0.24 mmol) was mixed with B(C$_6$F$_5$)$_3$ (122 mg, 0.24 mmol). Toluene (30 mL) was added at 0 °C, and the reaction mixture stirred for 20 min at room temperature. The product was precipitated by adding pentane (20 mL). The solvent was decanted, and the residue stirred in pentane to give **2** (150 mg, 61 %); m.p. = 100 °C (DSC). Elemental analysis calcd for C$_{40}$H$_{23}$BF$_{15}$ClZr$_2$ (1018.9): C 47.23, H 2.28; found: C 47.01, H 2.74; ^{1}H NMR ([D$_8$]toluene, 600 MHz, 223 K): δ = 7.12 (m, 1H, C1H), 5.44, 5.36, 5.26, 4.78 (s, each 5H, Cp), 2.75 (br, 2H, C2(H$_2$)); ^{13}C NMR ([D$_8$]toluene, 150 MHz, 298 K): δ = 174.7 (^1J(C,H) = 122 Hz, C1), 148.3 (^1J (C,F) = 234 Hz), 139.4 (^1J(C,F) = 244 Hz), 136.8 (^1J(C,F) = 243 Hz, *o*-, *p*-, *m*-C$_6$F$_5$), 125.1 (*ipso*-C of C$_6$F$_5$), 111.6, 110.7 (Cp), 21.8 (br, C2); ^{19}F NMR ([D$_8$]toluene, 564 MHz, 213 K): δ = −130.7, −161.4, −166.0 (*o*-, *m*-, *p*-C$_6$F$_5$); ^{11}B NMR ([D$_8$]toluene, 64 MHz, 300 K): δ = −11.3.

X-ray crystal structure analysis of **2**: Single crystals were obtained from toluene, C$_{40}$H$_{23}$BClF$_{15}$Zr$_2$·2C$_7$H$_8$, M_r = 1201.55, crystal size 0.8 × 0.6 × 0.3 mm, a = 16.256(1), b = 18.248(1), c = 16.497(1) Å, β = 98.42(1)°, V = 4840.9(5) Å^3, ρ_{calcd} = 1.649 g cm^{-3}, μ = 0.582 mm^{-1}, Z = 4, monoclinic, space group $P2_1/n$ (no. 14), λ = 0.71073 Å, T = 223 K, $\omega/2\theta$ scans, 10176 measured reflections ($\pm h$, $-k$, $+l$), [(sin θ)/λ] = 0.62 Å^{-1}, 9828 independent and 7694 observed reflections [$I \geq 2\sigma(I)$], 669 refined parameters, R = 0.032, wR^2 = 0.078, max./min. residual electron density 0.62/ − 0.38 e Å^{-3}. Hydrogen atoms at C1 and C2 were taken from the difference Fourier analysis and isotropically refined; hydrogen atoms at the Cp rings and at both toluene solvent molecules were calculated and refined as riding. The data set was collected with an Enraf Nonius MACH3 diffractometer. The following programs were used: data reduction: MolEN, structure solution: SHELXS-86, structure refinement: SHELXL-93, graphics: SCHAKAL-92. Crystallographic data (excluding structure factors) for the structure reported in this paper have been deposited with the Cambridge Crystallographic Data Centre as supplementary publication no. CCDC-100458. Copies of the data can be obtained free of charge on application to The Director, CCDC, 12 Union Road, Cambridge CB21EZ, UK (fax: int. code +(1223)336-033; e-mail: deposit@chemcrys.cam.ac.uk).

Received: May 30, 1997 [Z10495IE]
German version: *Angew. Chem.* **1997**, *109*, 2585–2588

Keywords: anti-van't Hoff/LeBel compounds · betaines · ion pairs · sandwich complexes · zirconium

[1] H. J. Monkhorst, *J. Chem. Soc. Chem. Commun.* **1968**, 1111; S. Durmaz, J. N. Murrell, J. B. Pedley, *ibid.* **1972**, 933; W. Luef, R. Keese, *Adv. Strain Org. Chem.* **1993**, *3*, 229; M. S. Gordon, M. W. Schmidt, *J. Am. Chem. Soc.* **1993**, *115*, 7486; K. Sorger, P. von R. Schleyer, *J. Mol. Struct.* **1995**, *338*, 317.

[2] R. Hoffmann, R. W. Alder, C. F. Wilcox, *J. Am. Chem. Soc.* **1970**, *92*, 4992; R. Hoffmann, *Pure Appl. Chem.* **1971**, *28*, 181; J. B. Collins, J. D. Dill, E. D. Jemmis, Y. Apeloig, P. von R. Schleyer, R. Seeger, J. A. Pople, *J. Am. Chem. Soc.* **1976**, *98*, 5419.

[3] D. Röttger, G. Erker, *Angew. Chem.* **1997**, *109*, 840; *Angew. Chem. Int. Ed. Engl.* **1997**, *36*, 812.

[4] W. C. Agosta in *The Chemistry of Alkanes and Cycloalkanes* (Eds.: S. Patai, Z. Rappoport), Wiley, New York, **1992**, p. 928, and references therein.

[5] M. P. McGrath, L. Radom, H. F. Schaefer III, *J. Org. Chem.* **1992**, *57*, 4847; H. Dodziuk, *J. Mol. Struct.* **1990**, *239*, 167.

[6] G. Erker, K. Kropp, J. L. Atwood, W. E. Hunter, *Organometallics* **1983**, *2*, 1555; K. Kropp, Dissertation, Universität Bochum, **1981**.

[7] G. Erker, *J. Organomet. Chem.* **1977**, *134*, 189; G. Erker, J. Wicher, K. Engel, F. Rosenfeldt, W. Dietrich, C. Krüger, *J. Am. Chem. Soc.* **1980**, *102*, 6344; G. Erker, J. Wicher, K. Engel, C. Krüger, *Chem. Ber.* **1982**, *115*, 3300; G. Erker, C. Krüger, G. Müller, *Adv. Organomet. Chem.* **1985**, *24*, 1.

[8] H. H. Brintzinger, L. S. Bartell, *J. Am. Chem. Soc.* **1970**, *92*, 1105; J. W. Lauher, R. Hoffmann, *ibid.* **1976**, *98*, 1729.

[9] a) In zirconocene carbonyl complexes Cp$_2$Zr–C(sp) bonds can be as short as about 2.16 Å: D. J. Cardin, M. F. Lappert, C. L. Raston, *Chemistry of Organo-Zirconium and -Hafnium Compounds*, Wiley, New York, **1986**, and references therein; J. L. Atwood, R. D. Rodgers, W. E. Hunter, C. Floriani, G. Fachinetti, A. Chiesi-Villa, *Inorg. Chem.* **1980**, *19*, 3812; D. J. Sikora, M.-D. Rausch, R. D. Rodgers, J. L. Atwood, *J. Am. Chem. Soc.* **1981**, *103*, 1265; G. Erker, U. Dorf, C. Krüger, K. Angermund, *J. Organomet. Chem.* **1986**, *301*, 299; b) for unusually short {Cp$_2$Zr}–C(sp^2) bonds, see for example G. Erker, *Comments Inorg. Chem.* **1992**, *13*, 111, and references therein; c) for typical {Cp$_2$Zr}–C(sp^3) σ bond lengths, see J. L. Atwood, G. K. Barker, J. Holton, W. E. Hunter, M. F. Lappert, R. Pearce, *J. Am. Chem. Soc.* **1977**, *99*, 6645; J. Jeffrey, M. F. Lappert, N. T. Luong-Thi, M. Webb, J. L. Atwood, W. E. Hunter, *J. Chem. Soc. Dalton Trans.* **1981**, 1593; J. L. Atwood, W. E. Hunter, D. C. Hrncir, V. Bynum, R. A. Penttila, *Organometallics* **1983**, *2*, 750; C. Krüger, G. Müller, G. Erker, U. Dorf, K. Engel, *ibid.* **1985**, *4*, 215; A. G. Orpen, L. Brammer, F. H. Allen, O. Kennard, D. G. Watson, *J. Chem. Soc. Dalton Trans.* **1989**, S1; d) a complex related to **2** that also exhibits a rather short Zr–CH$_2$ bond (2.191(2) Å) was recently reported: G. J. Pindado, M. Thornton-Pett, M. Bochmann, *Chem. Commun.* **1997**, 609.

[10] G. A. Olah, G. K. S. Prakash, R. E. Williams, L. D. Field, K. Wade, *Hypercarbon Chemistry*, Wiley, New York, **1987**; selected examples: W. Kaminsky, J. Kopf, H. Sinn, H.-J. Vollmer, *Angew. Chem.* **1976**, *88*, 688; *Angew. Chem. Int. Ed. Engl.* **1976**, *15*, 629; C. McDade, V. C. Gibson, B. D. Santarsiero, J. E. Bercaw, *Organometallics* **1988**, *7*, 1; H. Yamamoto, H. Yasuda, K. Yokota, A. Nakamura, Y. Kai, N. Kasai, *Chem. Lett.* **1988**, 1963; S. L. Buchwald, E. A. Lucas, W. M. Davis, *J. Am. Chem. Soc.* **1989**, *111*, 397; R. W. Waymouth, K. S. Potter, W. P. Schaefer, R. H. Grubbs, *Organometallics* **1990**, *9*, 2843; A. R. Siedle, R. A. Newmark, J. N. Schroepfer, P. A. Lyon, *ibid.* **1991**, *10*, 400, and references therein; F. R. Lemke, D. J. Szalda, R. M. Bullock, *J. Am. Chem. Soc.* **1991**, *113*, 8466; F. R. Lemke, R. M. Bullock, *Organometallics* **1992**, *11*, 4261; T. Takahashi, K. Kasai, N. Suzuki, K. Nakajima, E. Negishi, *ibid.* **1994**, *13*, 3413; U. Radius, S. J. Silverio, R. Hoffmann, R. Gleiter, *ibid.* **1996**, *15*, 3737; Y. Sun, W. E. Piers, S. J. Rettig, *ibid.* **1996**, *15*, 4110; F. J. Fernández, P. Gómez-Sal, A. Manzanero, P. Royo, H. Jacobsen, H. Berke, *ibid.* **1997**, *16*, 1553; see also F. Scherbaum, A. Grohmann, G. Müller, H. Schmidbaur, *Angew. Chem.* **1989**, *101*, 464; *Angew. Chem. Int. Ed. Engl.* **1989**, *28*, 463.

[11] a) X. Yang, C. L. Stern, T. J. Marks, *J. Am. Chem. Soc.* **1994**, *116*, 10015; L. Jia, X. Yang, A. Ishihara, T. J. Marks, *Organometallics* **1995**, *14*, 3135; P. A. Deck, T. J. Marks, *J. Am. Chem. Soc.* **1995**, *117*, 6128; b) B. Temme, J. Karl, G. Erker, *Chem. Eur. J.* **1996**, *2*, 919; J. Karl, G. Erker, *J. Mol. Catal.*, in press; *Chem. Ber.* **1997**, *130*, 1261.

[12] M. L. H. Green, L.-L. Wong, A. Seela, *Organometallics* **1992**, *11*, 2660, and references therein.

[13] Reviews: R. J. Kulawiec, R. H. Crabtree, *Coord. Chem. Rev.* **1990**, *99*, 89; S. H. Strauss, *Chem. Rev.* **1993**, *93*, 927; J. L. Kiplinger, T. G. Richmond, C. E. Osterberg, *ibid.* **1994**, *94*, 373; M. Brookhart, M. L. H. Green, *J. Organomet. Chem.* **1983**, *250*, 395; M. Brookhart, M. L. H. Green, L.-L. Wong, *Prog. Inorg. Chem.* **1988**, *36*, 1.

[14] J. A. Connor, *Top. Curr. Chem.* **1977**, *71*, 71; J. K. Kochi, *Organometallic Mechanisms and Catalysis*, Academic Press, New York, **1978**, pp. 237–245; see also S. P. Nolan, D. Stern, T. J. Marks, *J. Am. Chem. Soc.* **1989**, *111*, 7844, and references therein.

Intramolecular Hydrocarbonation of ε-Alkynyl Malononitriles Catalyzed by Palladium Olefin Complexes

Naofumi Tsukada and Yoshinori Yamamoto*

Addition of a carbon nucleophile to a C–C multiple bond is one of the most important methods of C–C bond formation in organic synthesis. The Michael reaction is a classic and standard procedure for this purpose, in which an anionic organometallic species (NuM) adds to an activated alkene bearing an electron-

[*] Prof. Dr. Y. Yamamoto, Dr. N. Tsukada
Department of Chemistry, Graduate School of Science
Tohoku University
Sendai 980-77 (Japan)
Fax: Int. code +(22) 217-6784

 © WILEY-VCH Verlag GmbH, D-69451 Weinheim, 1997 0570-0833/97/3622-2477 $ 17.50+.50/0

withdrawing group (a Michael acceptor).[1] Addition of an NuM to a nonactivated alkene,[2] and the addition of pronucleophiles (NuH) to Michael acceptors,[3] takes place in the presence of certain transition metal catalysts. More recently it has been found that transition metal catalysts facilitate the "hydrocarbonation" of nonactivated C–C multiple bonds through activation of C–H bonds in active methylenes and methines,[4] terminal alkynes,[5] aldehydes,[6] or aromatic rings.[7] However, to the best of our knowledge, "hydrocarbonation" of simple alkynes with active methylenes and methines has not been reported, except for Gore–Balme's carbocyclization under basic conditions.[8] We wish to report that intramolecular hydrocarbonation of alkynes with an active methine proceeds very well under neutral and mild conditions in the presence of a 1,5-cyclooctadiene–Pd catalyst.[9]

Initially we investigated the palladium-catalyzed cyclization of internal alkyne **1a**, which bears a malononitrile group at the terminus of the carbon chain [Eq. (a); Tables 1 and 3]. The

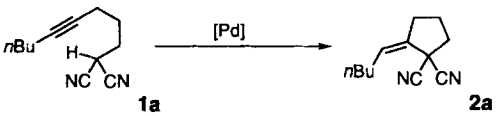

1a **2a** (a)

Table 1. Palladium-catalyzed cyclization of **1a** to **2a** [Eq. (a)][a].

Entry	Additive	T[°C]	Yield[%][b]
1	–	70	33
2	PPh_3	RT	35
3	1-octene	70	64[c]
4	1-octene	100	84
5	cod	RT	89
6	cod	RT	85[d]

[a] **1a** (0.3 mmol) was treated in 3 mL of ethanol over 12–36 h in the presence of $Pd(OAc)_2$ (0.06 mmol, 20 mol%) and an additive (PPh_3, 0.12 mmol, 1-octene 0.6 mmol, cod 0.12 mmol). [b] Determined by NMR spectroscopy with *p*-xylene as internal standard. [c] Significant amounts of **1a** were recovered. [d] With 5 mol% $Pd(OAc)_2$ and 20 mol% cod.

ε-alkynyl malononitrile **1a** indeed underwent cyclization in the presence of $Pd(OAc)_2$ in ethanol at 70 °C to afford alkylidenecyclopentane **2a** in 33% yield, together with unidentified products (entry 1). Use of ethanol as a solvent was essential; the reaction did not proceed at all in nonprotic solvents like toluene and THF. Cyclization of **1a** proceeded at room temperature in the presence of PPh_3, but the yield of **2a** was not improved (entry 2). Reaction at 70 °C decreased the yield to 25%. Use of 1-octene as an additive gave **2a** stereoselectively in 64% yield (entry 3). However, reaction was incomplete (entry 3), and palladium black appeared at an early stage.[10] Higher temperatures enhanced the yield of **2a** (entry 4), presumably because the reaction proceeded more rapidly and was complete before the "Pd^0" intermediate was converted into Pd-black. Finally, we discovered that use of 1,5-cyclooctadiene (cod) as an additive gave the best results (entry 5). The reaction proceeded very smoothly even at room temperature to give **2a** in 89% yield, and no Pd-black appeared during the process. The cod apparently acts as a chelate ligand for palladium(0).[11] Moreover, use of cod reduces the amount of catalyst required from 20 to 5 mol% (entry 6). The *Z*-isomer **2a** was obtained exclusively, and no *E*-isomer could be detected in any of the cases investigated. The olefin geometry was established unambiguously by NOE experiments. Use of $[Pd_2(dba)_3]\cdot CHCl_3$ and dppf gave **2a** in very low yield along with several unidentified compounds (dba = dibenzylideneacetone; dppf = 1,1-bis(diphenylphosphanyl)ferrocene). No reaction whatsoever was observed with $[Pd_2(dba)_3]\cdot CHCl_3$ and $Pd(PPh_3)_4$. Reaction of **1a** in toluene/ethanol (5/1) or THF/ethanol (5/1) in the presence of a mixture of $Pd(OAc)_2$ (5 mol%) and cod (20 mol%) also proceeded very smoothly, giving **2a** in 88 and 83% yield, respectively.

Cyclization reactions of various ε-alkynyl malononitriles **1** are summarized in Table 2 [Eq. (b)]. The reaction of **1b** which

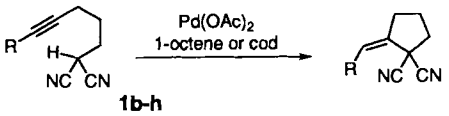

1b-h **2b-h** (b)

Table 2. Cyclization of ε-alkynyl malononitriles **1** to **2** [Eq. (b)][a].

Entry	1	R	Yield[%][b]
1	**1b**	H	39
2	**1c**	Me	70
3	**1d**	$HO(CH_2)_3$	76
4	**1e**	TBDMS-$O(CH_2)_3$	80
5	**1f**	TBDMS-OCH_2	80
6	**1g**	Ph	73[c]
7	**1h**	TMS	84[d]

[a] **1** (0.3 mol) in toluene/ethanol (5/1) was teated at room temperature over 30–96 h in the presence of 5 mol% $Pd(OAc)_2$ and 20 mol% cod. TBDMS = *tert*-butyldimethylsilyl, TMS = trimethylsilyl. [b] Isolated product. [c] Mixture of **2g** and **3** (93:7, determined by NMR spectroscopy). [d] Mixture of *Z*- and *E*-isomers (91:9, determined by NMR spectroscopy).

bears a terminal alkyne unit was sluggish and gave the methylenecyclopentane **2b** in 39% yield (entry 1); the low yield and slow reaction may be due to oxidative addition of Pd^0 into the C–H bond of the terminal alkyne.[5] Methylacetylene derivative **1c** gave **2c** in good yield (entry 2). The reaction of **1d** containing a hydroxy group gave **2d** in high yield without producing furan or pyran derivatives, which are major products in palladium-catalyzed cyclization of hydroxy acetylenes (entry 3).[12] It is interesting that hydroxy-free **1d** and hydroxy-protected **1e** gave similarly high yields (entries 3 and 4). Propargyl ether **1f** afforded **2f** in high yield (entry 5). Only **1g** resulted in both *exo*- and *endo*-cyclization, affording a 93:7 mixture of benzylidenecyclopentane **2g** and phenylcyclohexene **3** (entry 6). Cyclization of **1h** gave a 91:9 mixture of the *Z*- and *E*-isomers in 84% yield. It is worth noting that cyclization of **1h** using 1-octene rather than cod as an additive afforded primarily the *E*-isomer [13] [Eq. (c)],

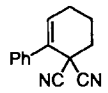

3

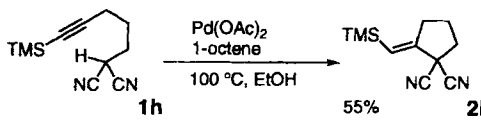

1h 55% **2h** (c)

E:*Z* = 76:24

whereas no *E*-isomer at all was obtained in the reactions of **1a** and **1c–g** under the same conditions (Table 1, entry 4). Reaction of other pronucleophiles, such as cyanoester **1i** and diester **1j**, produced no cyclization product.

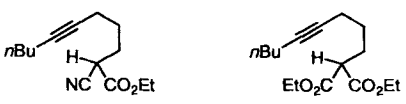

1i **1j**

 © WILEY-VCH Verlag GmbH, D-69451 Weinheim, 1997 0570-0833/97/3622-2478 $ 17.50+.50/0

Table 3. Spectroscopic data for the alkylidenecyclopentanes **2**, **8**, and **9**.

2a: IR (film): $\tilde{\nu}$ = 2959, 2934, 2874, 2245, 1452, 1381, 1192, 665 cm^{-1}; ^1H NMR (300 MHz, $CDCl_3$): δ = 0.94 (t, J = 7.1 Hz, 3H), 1.34–1.54 (m, 4H), 1.93 (m, 2H), 2.37 (m, 2H), 2.48–2.60 (m, 4H), 5.78 (tt, J = 2.0, 7.5 Hz, 1H); elemental analysis (%): calcd for $C_{12}H_{16}N_2$ (188.27): C 76.55, H 8.57, N 14.88; found: C 76.800, H 8.677, N 14.764

2b: IR (film): $\tilde{\nu}$ = 3000–2800, 2247, 1661, 1452, 1435, 1194, 918 cm^{-1}; ^1H NMR (300 MHz, $CDCl_3$): δ = 2.05 (m, 2H), 2.48 (t, J = 6.9 Hz, 2H), 2.62 (tq, J = 2.4, 7.5 Hz, 2H), 5.46 (m, 1H), 5.69 (m, 1H); ^{13}C NMR (75 MHz, $CDCl_3$): δ = 23.61, 30.24, 38.48, 39.75, 115.24, 144.94

2c: IR (film): $\tilde{\nu}$ = 3036, 3000–2800, 2247, 1450, 1382, 1194 cm^{-1}; ^1H NMR (300 MHz, $CDCl_3$): δ = 1.93 (m, 2H), 1.98 (dt, J = 2.2, 7.2 Hz, 3H), 2.52 (m, 2H), 2.57 (t, J = 7.2 Hz, 2H), 5.90 (tq, J = 2.0, 7.2 Hz, 1H); ^{13}C NMR (75 MHz, $CDCl_3$): δ = 14.79, 24.64, 32.98, 33.50, 41.23, 115.00, 126.79, 135.38; elemental analysis (%): calcd for $C_9H_{10}N_2$ (146.19): C 73.94, H 6.90, N 19.17; found: C 74.146, H 7.175, N, 18.827

2d: IR (film): $\tilde{\nu}$ = 3393, 3000–2800, 2245, 1724, 1450, 1192, 1057 cm^{-1}; ^1H NMR (300 MHz, $CDCl_3$): δ = 1.79 (m, 2H), 1.94 (m, 2H), 2.42–2.60 (m, 6H), 3.72 (t, J = 6.3 Hz, 2H), 5.81 (tt, J = 2.0, 7.7 Hz, 1H); ^{13}C NMR (75 MHz, $CDCl_3$): δ = 24.70, 26.20, 31.37, 33.12, 33.65, 41.29, 62.00, 115.45, 131.99, 135.05; HR-MS: m/z calcd for $C_{11}H_{14}N_2O$: 190.1107, found: 190.1111

2e: IR (film): $\tilde{\nu}$ = 3000–2800, 2245, 1472, 1256, 1107, 837, 777 cm^{-1}; ^1H NMR (300 MHz, $CDCl_3$): δ = 0.06 (s, 6H), 0.90 (s, 9H), 1.73 (m, 2H), 1.93 (m, 2H), 2.43 (m, 2H), 2.50–2.60 (m, 4H), 3.69 (t, J = 6.4 Hz, 2H), 5.83 (tt, J = 2.0, 7.5 Hz, 1H); elemental analysis (%): calcd for $C_{17}H_{28}N_2OSi$ (304.50): C 67.05, H 9.27, N 9.20; found: C 67.304, H 9.294, N 9.221

2f: IR (film): $\tilde{\nu}$ = 3028, 3000–2800, 2247, 1472, 1464, 1256, 1107, 839, 779 cm^{-1}; ^1H NMR (300 MHz, $CDCl_3$): δ = 0.14 (s, 6H), 0.93 (s, 9H), 1.94 (m, 2H), 2.56 (m, 4H), 4.52 (dt, J = 2.0, 5.5 Hz, 2H), 5.91 (tt, J = 2.0, 5.5 Hz, 1H); elemental analysis (%): calcd for $C_{15}H_{24}N_2OSi$ (276.45): C 65.17, H 8.75, N 10.14; found: C 65.435, H 8.720, N 10.003

2g: IR (KBr): ν = 3100–2800, 2243, 1495, 1437, 1192, 752, 700 cm^{-1}; ^1H NMR (300 MHz, $CDCl_3$): δ = 2.06 (m, 2H), 2.61 (t, J = 6.7 Hz, 2H), 2.78 (dt, J = 2.0, 7.2 Hz, 2H), 6.90 (s, 1H), 7.34–7.50 (m, 5H); ^{13}C NMR (75 MHz, $CDCl_3$): δ = 23.59, 33.39, 35.17, 42.55, 114.84, 128.57, 128.64, 128.78, 131.47, 134.34, 135.13

3: ^1H NMR (300 MHz, $CDCl_3$): δ = 2.03 (m, 2H), 2.39 (q, J = 5.5 Hz, 2H), 2.53 (m, 2H), 6.28 (t, J = 3.4 Hz, 1H), 7.36–7.54 (m, 5H)

(*E*)-**2h**: IR (film): $\tilde{\nu}$ = 3000–2800, 2247, 1626, 1250, 941, 843 cm^{-1}; ^1H NMR (300 MHz, $CDCl_3$): δ = 0.17 (s, 9H), 2.07 (m, 2H), 2.43 (t, J = 6.9 Hz, 2H), 2.57 (dt, J = 2.6, 7.5 Hz, 2H), 6.24 (t, J = 2.6 Hz, 1H); ^{13}C NMR (75 MHz): δ = −1.09, 24.11, 30.00, 38.78, 41.39, 115.64, 130.70, 150.57; HR-MS: m/z calcd for $C_{11}H_{16}N_2Si$: 204.1083, found: 204.1071

(*Z*)-**2h**: IR (film): $\tilde{\nu}$ = 3000–2800, 2247, 1730, 1630, 1252, 862, 843 cm^{-1}; ^1H NMR (300 MHz, $CDCl_3$): δ = 0.29 (s, 9H), 1.93 (m, 2H), 2.52–2.66 (m, 4H), 5.94 (s, 1H); ^{13}C NMR (75 MHz, $CDCl_3$): δ = −0.28, 23.84, 36.28, 36.58, 42.42, 116.10, 132.43, 150.43; HR-MS: m/z calcd for $C_{11}H_{16}N_2Si$: 204.1083, found: 204.1083

8: IR (film): $\tilde{\nu}$ = 3044, 3000–2800, 2247, 1450 cm^{-1}; ^1H NMR (300 MHz, $CDCl_3$): δ = 0.92 (t, J = 7.0 Hz, 3H), 1.28–1.48 (m, 4H), 1.83 (m, 2H), 2.02 (m, 2H), 2.14 (q, J = 6.8 Hz, 2H), 2.43 (m, 2H), 2.55 (t, J = 6.6 Hz, 2H), 2.64 (m, 2H), 2.74 (m, 2H), 5.64 (t, J = 7.2 Hz, 1H); ^{13}C NMR (75 MHz, $CDCl_3$): δ = 13.95, 22.43, 23.67, 25.46, 30.11, 30.49, 31.56, 32.87, 33.16, 37.83, 40.90, 115.23, 125.23, 129.99, 141.25, 143.20; elemental analysis (%): calcd for $C_{17}H_{22}N_2$ (254.38): C 80.27, H 8.72, N 11.02; found: C 80.217, H 8.724, N 10.950

9: IR (film): $\tilde{\nu}$ = 3000–2800, 2245, 1452, 1437, 1192 cm^{-1}; ^1H NMR (300 MHz, $CDCl_3$): δ = 0.91 (t, J = 7.1 Hz, 3H), 1.34–1.54 (m, 4H), 1.70 (m, 2H), 1.94 (m, 2H), 2.16 (m, 2H), 2.25 (m, 2H), 2.42–2.60 (m, 6H), 5.80 (t, J = 7.5 Hz, 1H); ^{13}C NMR (75 MHz, $CDCl_3$): δ = 13.60, 18.40, 18.51, 21.93, 24.68, 27.94, 28.87, 31.13, 33.15, 33.66, 41.44, 78.96, 81.17, 115.34, 131.88, 134.89; elemental analysis (%): calcd for $C_{17}H_{22}N_2$ (254.38): C 80.27, H 8.72, N 11.02; found: C 80.434, H 8.918, N 10.928

The addition of active methines and methylenes to 1,3-dienes or allenes probably proceeds by way of π-allyl palladium intermediates, which are generated by insertion of a double bond into a Pd–H bond, with subsequent addition of the pronucleophile.[4] However, the formation of **2** from **1** cannot be explained by hydride addition to the unsaturated C–C bond. A plausible mechanism is shown in Scheme 1. Cationic palladium hydride complex **4** and the carbanion **5** would be produced by abstraction of a proton from $HC(CN)_2R$ by Pd^0. Although the role of ethanol is not clear, it may assist in the formation of **4**.[14] Coordination of **4** to the triple bond of **5** would be followed by

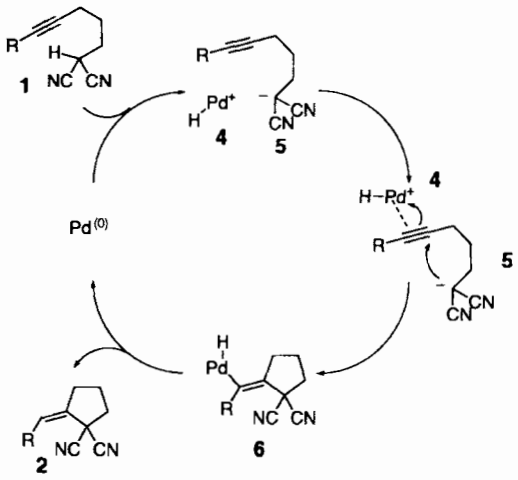

Scheme 1. Possible mechanism for the cyclization of **1**.

rapid intramolecular cyclization of **5** from the opposite side of Pd. This addition would be more rapid than migratory insertion of alkyne into the Pd–H bond (hydropalladation), and it affords the vinylpalladium compound **6**.[15] Reductive elimination of palladium(0) from **6** leads to cyclization product **2**. The observed *Z*-geometry of **2** is in accord with this mechanism.

Cyclization of diynyl malononitrile **7** afforded the tandem cyclization product **8** along with monocyclization compound **9** [Eq. (d)]. Treatment of **9** under the reaction conditions did not

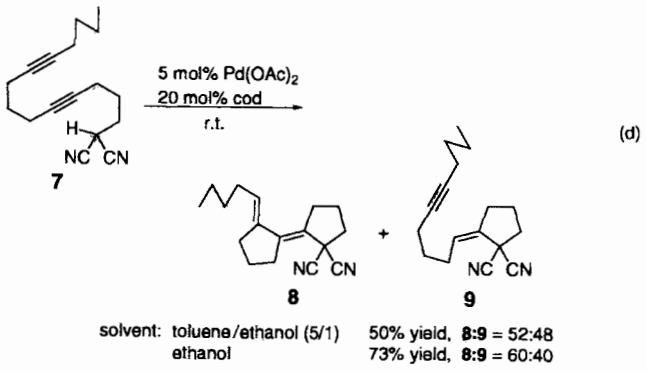

produce **8**.[14] These results support intervention of vinyl palladium species **6** in the catalytic cycle. The amount of ethanol present had no significant influence upon the ratio **8**:**9**.

Although the $[Ni(cod)_2]$ complex has been widely used as a catalyst or reagent in organic synthesis, use of a Pd^0–cod complex as a catalyst is unprecedented so far as we know.

Experimental Section

Representative procedure for the synthesis of **2e** from **1e**: To a solution of $Pd(OAc)_2$ (3.4 mg, 0.015 mmol) in toluene (1.0 mL) was added ethanol (0.5 mL) and 1,5-cyclooctadiene (7.4 mL, 0.06 mmol) under an argon atmosphere, and the mixture was stirred for 1 h at room temperature. A solution of **1e** (91 mg, 0.3 mmol) in 1.5 mL of toluene was then added. The mixture was stirred at room temperature, and the progress of the reaction was monitored by TLC. After 84 h, **1e** had been completely consumed. The reaction mixture was filtered through a short silica gel column (eluent: ethyl acetate). Concentration and purification by column chromatography over silica gel (hexane/ethyl acetate) afforded **2e** in 80% yield (73 mg).

Received: May 20, 1997 [Z 10453 IE]
German version: *Angew. Chem.* **1997**, *109*, 2588–2590

Keywords: alkene complexes · alkynes · C–H activation · cyclizations · palladium

 © WILEY-VCH Verlag GmbH, D-69451 Weinheim, 1997 0570-0833/97/3622-2479 $ 17.50+.50/0

[1] P. Perlmutter, *Conjugate Addition Reactions in Organic Synthesis*, Pergamon, Oxford, **1992**; M. E. Jung in *Comprehensive Organic Synthesis, Vol. 4* (Eds.: B. M. Trost, I. Fleming, M. F. Semmelhack), Pergamon, Oxford, **1991**, Chap. 1.1, pp. 1–67.

[2] a) L. S. Hegedus in ref. [2c], p. 571; b) For carbometalation, see: P. Knochel in ref. [2c], p. 865; c) *Comprehensive Organic Synthesis, Vol. 4* (Eds.: B. M. Trost, I. Fleming), Pergamon, Oxford, **1990**.

[3] a) S.-I. Murahashi, T. Naota, H. Taki, M. Mizuno, H. Takaya, S. Komiya, Y. Mizuho, N. Oyasato, M. Hiraoka, M. Hirano, A. Fukuoka, *J. Am. Chem. Soc.* **1995**, *117*, 12436, and citations therein; b) E. Gómez-Bengoa, J. M. Cuerva, C. Mateo, A. M. Echavarren, *ibid.* **1996**, *118*, 8553.

[4] 1,3-Dienes: a) K. Takahashi, A. Miyake, G. Hata, *Bull. Chem. Soc. Jpn.* **1972**, *45*, 1183; b) O. S. Andell, J.-E. Bäckvall, C. Moberg, *Acta. Chem. Scand. Ser. B* **1986**, *40*, 184; c) R. Baker, R. J. Popplestone, *Tetrahedron Lett.* **1978**, 3575; d) P. W. Jolly, N. Kokel, *Synthesis* **1990**, 771; e) B. M. Trost, L. Zhi, *Tetrahedron Lett.* **1992**, *33*, 1831; 1,3-enynes: f) M. M. Salter, V. Gevorgen, S. Saito, Y. Yamamoto, *J. Chem. Soc. Chem. Commun.* **1996**, 17; allenes: g) Y. Yamamoto, M. Al-Masum, N. Asao, *J. Am. Chem. Soc.* **1994**, *116*, 6019; h) B. M. Trost, V. J. Gerusz, *ibid.* **1995**, *117*, 5156; i) L. Besson, J. Goré, B. Cazes, *Tetrahedron Lett.* **1995**, *36*, 3853; j) Y. Yamamoto, M. Al-Masum, N. Fujiwara, N. Asao, *ibid.* **1995**, *36*, 2811; k) Y. Yamamoto, M. Al-Masum, *Synlett* **1995**, 969; l) Y. Yamamoto, M. Al-Masum, N. Fujiwara, *J. Chem. Soc. Chem. Commun.* **1996**, 381; m) Y. Yamamoto, M. Al-Masum, A. Takeda, *ibid.* **1996**, 831.

[5] a) B. M. Trost, C. Chan, C. Rühter, *J. Am. Chem. Soc.* **1987**, *109*, 3486; b) B. M. Trost, S. Matsubara, J. J. Caringi, *ibid.* **1989**, *111*, 8745; c) B. M. Trost, G. Kottirsch, *ibid.* **1990**, *112*, 2816; d) M. Yamaguchi, K. Omata, M. Hirama, *Tetrahedron Lett.* **1994**, *35*, 5689; e) M. Yamaguchi, Y. Kido, K. Omata, M. Hirama, *Synlett* **1995**, 1181.

[6] Intramolecular reactions: a) R. C. Larock, K. Oertle, G. F. Potter, *J. Am. Chem. Soc.* **1980**, *102*, 190; b) R. E. Campbell, C. F. Lochow, K. P. Vora, R. G. Miller, *ibid.* **1980**, *102*, 5824; c) K. P. Gable, G. A. Benz, *Tetrahedron Lett.* **1991**, *32*, 3473. Intermolecular reactions: d) T. Kondo, M. Akazome, Y. Tsuji, Y. Watanabe, *J. Org. Chem.* **1990**, *55*, 1286; e) T. Tsuda, T. Kujor, T. Saegusa, *ibid.* **1990**, *55*, 2554. Asymmetric additions: f) X. M. Wu, K. Funakoshi, K. Sakai, *Tetrahedron Lett.* **1993**, *34*, 5927; g) R. W. Banhart, X. Wang, P. Noheda, S. H. Bergens, J. Whelan, B. Bosnich, *Tetrahedron* **1994**, *50*, 4335.

[7] S. Murai, F. Kakiuchi, S. Sekine, Y. Tanaka, A. Kamatani, M. Sonoda, N. Chatani, *Nature (London)* **1993**, *336*, 529.

[8] a) N. Monteiro, G. Balme, J. Gore, *Tetrahedron Lett.* **1991**, *32*, 1645; b) N. Monteiro, J. Gore, G. Balme, *Tetrahedron* **1992**, 48, 10103.

[9] The cyclization of acetylenic carbonyl compounds proceeds by way of an ene reaction at high temperature or in the presence of Lewis acids or cobalt catalysts. Thermal cyclizations: a) J. M. Conia, P. Le Perchec, *Synthesis* **1975**, 1; Lewis acid catalyzed cyclizations: b) M. A. Boaventura, J. Drouin, J. M. Conia, *ibid.* **1983**, 801; c) W. P. Jackson, S. V. Ley, *J. Chem. Soc. Perkin Trans 1* **1981**, 1516; cobalt-catalyzed cyclizations: d) R. Stammler, M. Malacria, *Synlett* **1994**, 92; e) P. Cruciani, C. Aubert, M. Malacria, *Tetrahedron Lett.* **1994**, *35*, 6677; f) R. Stammler, C. Aubert, M. Malacria, *J. Org. Chem.* **1996**, *61*, 2699.

[10] It may be that $Pd(OAc)_2$ is reduced in situ by 1-octene to a very reactive Pd^0 species, which efficiently catalyzes the hydrocarbonation.

[11] M. Green, J. A. K. Howard, J. L. Spencer, F. G. A. Stone, *J. Chem. Soc. Dalton* **1977**, 271.

[12] K. Utimoto, *Pure Appl. Chem.* **1983**, *55*, 1845; M. Suzuki, A. Yanagisawa, R. Noyori, *J. Am. Chem. Soc.* **1988**, *110*, 4718.

[13] Since the *Z*-Isomer of **2h** is not isomerized under these drastic conditions (100 °C), and the reaction produces mainly the *E*-isomer at room temperature as well, *E*/*Z*-selectivity was a function of the additive (cod or 1-octene).

[14] In an attempt to prepare the Pd–H species in toluene/acetic acid (10/1) or THF/acetic acid (10/1), no **2** was obtained, but the starting material was recovered instead. B. M. Trost, D. L. Romero, F. Rise, *J. Am. Chem. Soc.* **1994**, *116*, 4268; see also B. M. Trost, F. D. Toste, *ibid.* **1996**, *118*, 6305.

[15] G. Fournet, G. Balme, J. Gore, *Tetrahedron*, **1991**, *47*, 6293; D. Bouyssi, G. Balme, J. Gore, *Tetrahedron Lett.* **1991**, *32*, 6541.

Ligand Effects in Diastereoselective Additions of Organocerium Reagents to Carbonyl Substrates**

Carmen Alcaraz and Ulrich Groth*

One of the most important contributions of lanthanide reagents to synthetic organic chemistry is the application of organocerium reagents in carbonyl addition reactions.[1] Owing to their low basicity and high nucleophilicity, organocerium reagents afford much higher yields of addition products with highly enolizable substrates than the corresponding organolithium or organomagnesium reagents from which they can be generated in situ. Furthermore, the steric bulk of organocerium reagents should make them suitable candidates for achieving high diastereoselectivity in additions to carbonyl derivatives.[2] The nature of the ligands determines the direction and extent of stereoselectivity in many carbonyl addition reactions,[3] but the sense and magnitude of diastereoselectivity achievable in the addition of organocerium reagents to chiral carbonyl substrates has to date not been explored in a systematic fashion.

We report here on the synthesis of new alkoxy- and amidocerium compounds of the general formula $ClCe(OR)_2$, $Ce(OR)_3$, and $Ce(NR_2)_3$. Cerium(III) trialkoxides were prepared by ligand exchange reactions of the known $Ce(OiPr)_3$[3c,4] with the appropriate alcohols[5] [Eq. (a)]; cerium(III) chloride dialkoxides were obtained by reaction of the relevant cerium(III) trialkoxides with one equivalent of acetyl chloride[6] [Eq. (b)]; amidocerium compounds were synthesized by reaction of the $CeCl_3 \cdot THF$ complex with three equivalents of lithium amides[7] [Eq. (c)]. All these alkoxy- and amidocerium compounds were

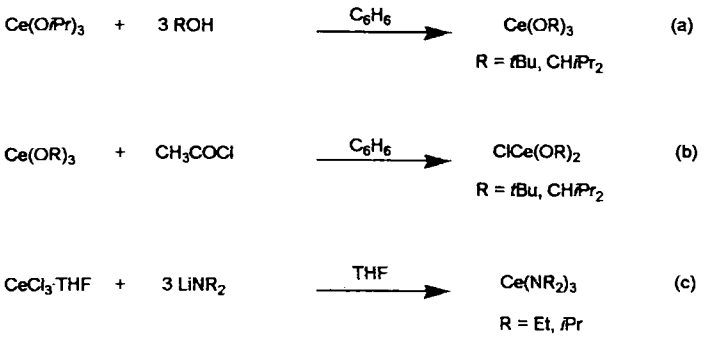

used without further purification; however, X-ray structures have not yet been obtained because of the low tendency of these compounds to form crystals.

For the addition reaction the cyclopentanone derivative *rac*-**1** was used as a substrate since it is well known that diastereoselectivities in the addition of organometallic reagents to cyclopentanones are lower than that to cyclohexanones. The yields are also lower because of the high tendency of cyclopentanone derivatives to undergo enolization. The organocerium reagents

[*] Prof. Dr. U. Groth, Dr. C. Alcaraz
Fakultät für Chemie der Universität
Universitätstrasse 10, D-78457 Konstanz (Germany)
Fax: Int code +(7531)884155
e-mail: Ulrich.Groth@uni-konstanz.de

[**] Lanthanoids in Organic Synthesis, Part 2. This work was supported by the EU Commission, Directorate General XII, and the Fonds der Chemischen Industrie. C. A. thanks the EU Commission for a fellowship (Contract-No. ERBCHBI-CT94-1465). Part 1: Ref. [4b].

 © WILEY-VCH Verlag GmbH, D-69451 Weinheim, 1997 0570-0833/97/3622-2480 $ 17.50+.50/0

were formed in situ by treatment of the cerium compounds (see [Eqs. (a)–(c)]) with organolithium reagents at −78 °C for 1 h. Then 2-methyl-3-vinylcyclopentanone (*rac*-**1**)[8] was added to afford the addition products *rac*-**2** and *rac*-**3**. The results are

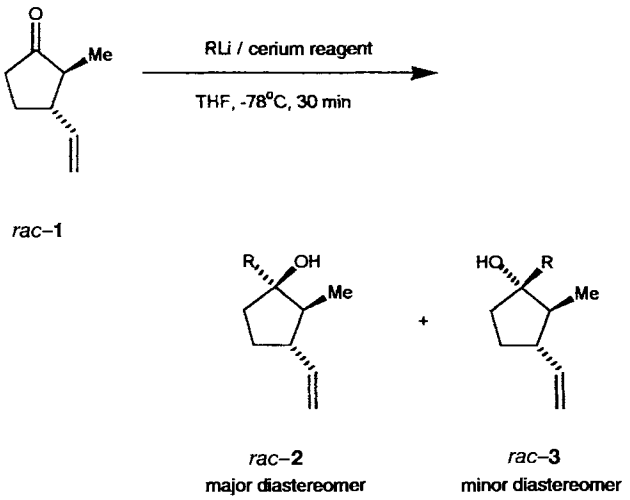

given in Table 1. The nature of these organocerium species is unknown and has proved resistant to study,[9] but most probably organocerium species derived from cerium chloride dialkoxides are neutral species of the type $RCe(OR')_2$ and those derived from cerium trialkoxides are ate-complexes of the type $Li[CeR(OR')_3]$.

Table 1. Stereoselective additions of organocerium reagents to 2-methyl-3-vinylcyclopentanone (*rac*-**1**)[12].

Entry	Reagent	*de*[%][a]	Yield[%]	Enolization[%]
1	MeLi	10	65	22
2	$MeLi/CeCl_3$	68	91	–
3	$MeLi/Ce(NEt_2)_3$	78	55	25
4	$MeLi/Ce(NiPr_2)_3$	79	50	36
5	$MeLi/Ce(OiPr)_3$	83	95	–
6	$MeLi/Ce(OiPr)_3$[b]	86	93	–
7	$MeLi/Ce(OiPr)_3$[c]	74	90	–
8	$MeLi/ClCe(OtBu)_2$	77	85	–
9	$MeLi/ClCe(OCHiPr_2)_2$	87	89	–
10	*n*BuLi	49	56	36
11	*n*BuLi/$ClCe(OCHiPr_2)_2$	89	90	–
12	*t*BuLi	77	35	57
13	*t*BuLi/$ClCe(OCHiPr_2)_2$	90	80	–
14	PhLi	85	70	24
15	PhLi/$ClCe(OCHiPr_2)_2$	94	95	–

[a] Determined by GC analysis. [b] Addition at −98 °C. [c] In Et_2O.

Enolization of the starting ketone was only observed with organocerium reagents derived from cerium triamides (Table 1, entries 3 and 4). The ligands have a pronounced influence on the stereoselectivity of the addition reactions. As expected, increasing steric hindrance led to increased diastereoselectivity. Unfortunately, no addition took place with the sterically most demanding compounds $Li[CeMe(OtBu)_3]$ and $Li[CeMe(OCHiPr_2)_3]$. Lowering the temperature (−98 °C) slighty improved the diastereoselectivity (entry 6) but carrying out the additions at −78 °C is more convenient. In Et_2O the diastereoselectivity obtained was lower than in THF (entry 7). The best results were achieved with $RCe(OCHiPr_2)_2$ in THF. Its addition to the cyclopentanone derivative *rac*-**1** (entries 9, 11, 13 and 15) proceeds with good to very good diastereoselectivities (87–94% *de*), which are among the best reported for the addition of organometallic reagents to simple cyclopentanones.[10, 11]

In order to establish the width of application of the new cerium derivatives in carbonyl addition reactions, the addition of organocerium reagents derived from $ClCe(OCHiPr_2)_2$ and $Ce(OCHiPr_2)_3$ to 2-methylcyclohexanone, 4-*tert*-butylcyclohexanone, and 2-phenylpropionaldehyde was investigated (Table 2).

Table 2. Stereoselective addition of organocerium reagents to selected carbonyl substrates.

Carbonyl derivative	Reagent	*de*[%][a]	Yield[%]
2-methylcyclohexanone	MeLi	63	74
2-methylcyclohexanone	$MeCeCl_2$	88	89
2-methylcyclohexanone	$MeCe(OCHiPr_2)_2$	97	91
2-methylcyclohexanone	$Li[CeMe(OCHiPr_2)_3]$	–	–[b]
2-methylcyclohexanone	*n*BuLi	78	80
2-methylcyclohexanone	$nBuCeCl_2$	94	92
2-methylcyclohexanone	$nBuCe(OCHiPr_2)_2$	98	88
4-*tert*-butylcyclohexanone	MeLi	24	50
4-*tert*-butylcyclohexanone	$MeCeCl_2$	36	93
4-*tert*-butylcyclohexanone	$Li[CeMe(OCHiPr_2)_3]$	68	88
2-phenylpropionaldehyde	MeLi	82	57
2-phenylpropionaldehyde	$MeCeCl_2$	84	85
2-phenylpropionaldehyde	$Li[CeMe(OCHiPr_2)_3]$	90	89

[a] Determined by GC analysis. [b] No addition took place, probably because of the bulky ligands.

As in the case of 2-methyl-3-vinylcyclopentanone (*rac*-**1**), no reaction took place in the addition of $Li[MeCe(OCHiPr_2)_3]$ to 2-methylcyclohexanone. In contrast, the addition of $MeCe(OCHiPr_2)_2$ and $nBuCe(OCHiPr_2)_2$ to 2-methylcyclohexanone gave the corresponding alcohols with diastereoselectivities of 97 and 98% *de*, by using the sterically less demanding organocerium compounds $MeCeCl_2$ and $nBuCeCl_2$ the selectivities dropped to 88 and 94% *de*, respectively. In the case of 4-*tert*-butylcyclohexanone and 2-phenylpropionaldehyde the addition reactions could be performed with the sterically most demanding compound $Li[MeCe(OCHiPr_2)_3]$ and gave yields between 88 and 89%. With 4-*tert*-butylcyclohexanone an increase of diastereoselectivity from 36% ($MeCeCl_2$) to 68% *de* ($Li[MeCe(OCHiPr_2)_3]$) was established. The addition of $Li[MeCe(OCHiPr_2)_3]$ to Cram's aldehyde (2-phenylpropionaldehyde) led to the corresponding alcohol with a diastereoselectivity of 90% *de*. In constrast the use of $MeCeCl_2$ (84% *de*) or MeLi (82% *de*) gave considerably lower selectivities. The application of these new organocerium reagents in natural product synthesis, for example for the enantioselective synthesis of the antifungal chokols,[10, 13] is currently under investigation.

Experimental Section

All reactions were performed with rigorous exclusion of oxygen and water under a dry nitrogen atmosphere, using Schlenk, vacuum-line, and glovebox techniques.

Preparation of cerium trialkoxides: To a solution of $Ce(OiPr)_3$ (6.0 mmol) in benzene (10 mL), the appropriate alcohol (20 mL) was added and the mixture was heated under reflux overnight. It was then cooled to room temperature and the solvent removed in vacuo (20 °C, 0.005 Torr) to afford the corresponding cerium trialkoxide in 90–95% yield.

Preparation of cerium chloride dialkoxides: Acetyl chloride (2.0 mmol) was added to a solution of the appropriate cerium trialkoxide (2.0 mmol) in benzene (20 mL), and a pale brown solid precipitated immediately. The mixture was heated to reflux for 2 h, cooled to room temperature, and the solvent removed by cannula. The solid was dried in vacuo (20 °C, 0.005 Torr) to afford the cerium chloride dialkoxide in 80–90% yield.

 © WILEY-VCH Verlag GmbH, D-69451 Weinheim, 1997 0570-0833/97/3622-2481 $ 17.50+.50/0

Carbonyl addition reactions: To a solution of the cerium compound (1.5 mmol) in THF (5 mL) cooled to −78 °C, methyllithium (1.2 mmol, 0.75 mL of a 1.6 N solution in diethyl ether) was added. After 1 h the appropriate carbonyl derivative (1.0 mmol) was added slowly and the mixture was stirred at −78 °C for 30 min. Then, a saturated aqueous NH_4Cl solution (10 mL) was added, solid material was removed through a short pad of Celite, the Celite was rinsed with diethyl ether, and the ethereal solution was dried with $MgSO_4$. The solvent was removed in vacuo and the residue purified by flash chromatography.

Received: May 5, 1997 [Z10422IE]
German version: *Angew. Chem.* **1997**, *109*, 2590–2592

Keywords: asymmetric synthesis · cerium · cycloalkanones ligand effects

[1] a) G. A. Molander, *Chem. Rev.* **1992**, *92*, 29–68; b) T. Imamoto in *Comprehensive Organic Synthesis, Vol. 1* (Eds.: B. M. Trost, I. Fleming, S. L. Schreiber), Pergamon, Oxford, **1991**, pp. 231–250.
[2] F. A. Cotton, G. Wilkinson, *Advanced Inorganic Chemistry*, 5th ed, Wiley, New York, **1980**.
[3] a) M. T. Reetz, *Organotitanium Reagents in Organic Synthesis*, Springer, Berlin, **1986**; b) M. T. Reetz, N. Harmat, R. Mahrwald, *Angew. Chem.* **1992**, 104, 333–334; Angew. *Chem. Int. Ed. Engl.* **1992**, *31*, 342–344; c) M. T. Reetz, H. Haning, S. Stanchev, *Tetrahedron Lett.* **1992**, *33*, 6963–6966; d) K. Chibale, N. Greeves, L. Lyford, J. E. Pease, *Tetrahedron: Asymmetry* **1993**, *4*, 2407–2410; e) N. Greeves, L. Lyford, J. E. Pease, *Tetrahedron Lett.* **1994**, *35*, 385–388; f) N. Greeves, J. E. Pease, M. C. Bowden, S. M. Brown, *ibid.* **1996**, *37*, 2675–2678; g) N. Greeves, J. E. Pease, *ibid.* **1996**, *37*, 5821–5824.
[4] a) A. Lebrun, J. L. Namy, H. B. Kagan, *Tetrahedron Lett.* **1991**, *32*, 2355–2358; b) improved synthesis of $Ce(OiPr)_3$: P. Eckenberg, U. Groth, T. Köhler, *Liebigs Ann. Chem.* **1994**, 673–677.
[5] In analogy to the preparation of $Gd(OR)_3$: R. C. Mehrotra, J. M. Batwara, *Inorg. Chem.* **1970**, *9*, 2505–2510.
[6] In analogy to the preparation of $ClSm(OR)_2$: B. S. Sankhla, R. N. Kapoor, *Can. J. Chem.* **1966**, *44*, 2131–2137.
[7] In analogy to the preparation of $Ce[N(SiMe_3)_2]_3$: D. C. Bradley, J. S. Ghorta, F. A. Hart, *J. Chem. Soc. Dalton Trans.* **1973**, 1021–1023.
[8] G. Quinkert, W.-D. Weber, U. Schwartz, H. Stark, H. Baier, G. Frank, G. Dürner, *Liebigs Ann. Chem.* **1981**, 2335–2371.
[9] a) S. E. Denmark, J. P. Edwards, O. Nicaise, *J. Org. Chem.* **1993**, *58*, 569–578; b) W. J. Evans, J. D. Feldman, J. W. Ziller, *J. Am. Chem. Soc.* **1996**, *118*, 4581–4584.
[10] a) E. A. Mash, *J. Org. Chem.* **1987**, *52*, 4143–4146; b) U. Groth, W. Halfbrodt, T. Köhler, P. Kreye, *Liebigs Ann. Chem.* **1994**, 885–890.
[11] G. A. Molander, E. R. Burkhardt, P. Weinig, *J. Org. Chem.* **1990**, *55*, 4990–4991.
[12] 2-Methyl-3-vinylcyclopentanone was obtained as a inseparable 93:7 mixture of *trans*/*cis* isomers. For this reason, in all the addition reactions 5–7% of the alcohol resulted from a β-attack of the organocerium reagent at the carbonyl group of ketone *cis*-**1**, see ref. [10].
[13] E. Urban, G. Knühl, G. Helmchen, *Tetrahedron* **1995**, *52*, 13031–13038.

Template-Mediated Self Assembly of Six- and Eight-Membered Iron Coronates **

Rolf W. Saalfrank,* Ingo Bernt, Eveline Uller, and Frank Hampel

Dedicated to Professor Gottfried Huttner on the occasion of his 60th birthday

The "synthesis of properties"[1] is a professed goal in supramolecular chemistry. There are a large number of naturally occurring iron oxide minerals with complex structures[2] that serve as model compounds. Additionally, the iron-storage protein ferritin, which is the biological prototype of these inorganic systems,[3, 4] has been investigated comprehensively. Furthermore, discrete clusters with up to nineteen oxygen-bridged iron atoms have been synthesized and unequivocally characterized.[3] For better understanding of electron transfer processes and of magnetic properties of polynuclear iron,[3, 5] manganese,[6] and nickel complexes[7] further studies on compounds of this type are necessary. The same is true for the recently described cyclic ferrocene heptamer[8] and for metallacrown ethers with an enclosed cation[9, 10] or anion.[11] With respect to potential applications, iron(III) compounds certainly play a central role.

Our investigations have revealed that parallel to the family of classical crown ethers, cryptands, and their complexes there exists a class of topomerically analogous metallacrown ethers,[10] metallacryptands,[12, 13] and their inclusion compounds. In all these cases, bisbidentate ligands act as ditopic bridges. In addition we have studied the formation of one- (1D), two- (2D), and three-dimensional (3D) coordination polymers using coordinatively unsaturated, effectively linear bidentate dinitrile monomers.[14] Through a combination of both methods, we planned to construct novel adamantanoid tetranuclear chelate complexes **1**. Following the strategy for the synthesis of the tetranuclear

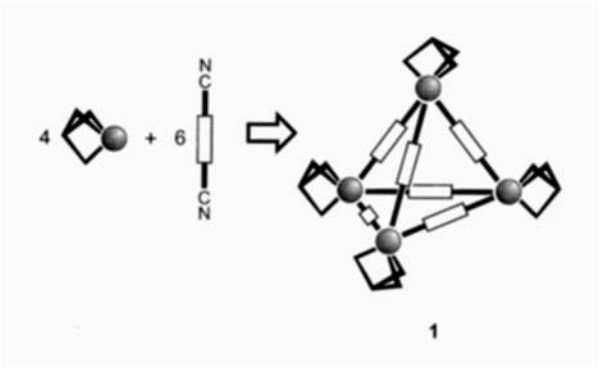

1

chelate complexes $[M \subset Fe_4L_6^1]$[12b] and of 1D coordination polymers $^1_\infty[NaL^2(pmedta)]$ (pmedta = pentamethyldiethylenetriamine),[14a] this objective should be accomplished by reaction of four equivalents of a tripodal metal template and six equivalents of a α,ω-dinitrile. Evidently, 1,1,1-tris(diphenylphosphinomethyl)ethane (triphos) used by Huttner et al.[15] was better suited for this purpose than the ligands triethanolamine **2** and *N*-methyldiethanolamine (**6**) that we have used.

Contrary to what was expected, treatment of triethanolamine **2** with sodium hydride, iron(III) chloride, and fumaric acid dinitrile in THF afforded the yellow solid **3**, in which the iron-to-ligand ratio was 1:1, instead of a tetranuclear chelate complex of type **1**. However, even when no dinitrile was used the same result was obtained. Since the ^1H and ^{13}C NMR spectra of product **3** do not allow an unequivocal characterization of its

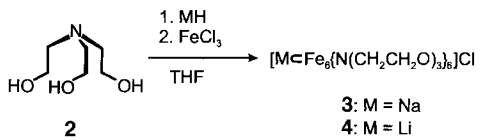

2

molecular structure, we carried out an X-ray crystallographic structure analysis.[16] According to this analysis, **3** is present in the crystal as a cyclic iron(III) complex with a [12]metallacrown-6 structure, in which a sodium ion is encapsulated in the center, and chloride is the counterion (Figure 1). The six crystallo-

[*] Prof. Dr. R. W. Saalfrank, Dipl.-Chem. I. Bernt, E. Uller, Dr. F. Hampel
Institut für Organische Chemie der Universität Erlangen-Nürnberg
Henkestrasse 42, D-91054 Erlangen (Germany)
Fax: Int. code +(9131)85-6864
e-mail: saalfrnk@organik.uni-erlangen.de

[**] Chelate complexes (metalla coronates), Part 9. This work was supported by the Deutsche Forschungsgemeinschaft, the Volkswagenstiftung and by the Fouds der Chemischen Industrie. We thank Prof. Dr. A. X. Trautwein and Dr. V. Schünemann, Universität Lübeck, for recording Mössbauer spectra. We also thank Prof. Dr. K.-P. Zeller, Universität Tübingen, and Prof. Dr. F. Vögtle, Universität Bonn, for recording numerous FAB-MS spectra. Part 8: Ref. [9].

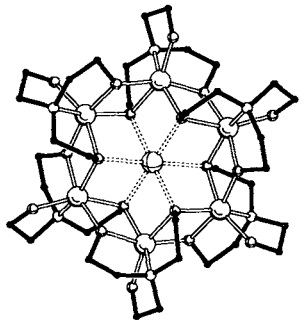

= Fe, = O, = N, • = CH_2

3: = Na **4**: = Li

Figure 1. Structures of the cations of **3** and **4** in the crystal (PLUTON representation; view along the crystallographic S_6 axis; H atoms excluded). For reasons of clarity the chloride ion and the crystal solvents were omitted. Selected bond lengths [Å] and angles [°] of **3**: Fe–N 2.215(3), Fe–μ_1O 1.872(3), Fe–μ_2O_{ipso} 2.030(3), Fe–$\mu_2O_{vic.}$ 1.984(3), Fe–μ_3O_{ipso} 2.082(3), Fe–$\mu_3O_{vic.}$ 2.017(3); μ_3O_{ipso}-Fe-$\mu_2O_{vic.}$ 74.81(10), $\mu_2O_{vic.}$-Fe-μ_1O 96.67(12), μ_1O-Fe-μ_2O_{ipso} 100.27(12), μ_2O_{ipso}-Fe-μ_3O_{ipso} 93.00(11). Selected bond lengths [Å] and angles [°] of **4**: Fe–N 2.195(6), Fe–μ_1O 1.882(5), Fe–μ_2O_{ipso} 2.030(5), Fe–$\mu_2O_{vic.}$ 1.969(5), Fe–μ_3O_{ipso} 2.082(5), Fe–$\mu_3O_{vic.}$ 2.027(5); μ_3O_{ipso}-Fe-$\mu_2O_{vic.}$ 76.2(2), $\mu_2O_{vic.}$-Fe-μ_1O 95.9(2), μ_1O-Fe-μ_2O_{ipso} 98.5(2), μ_2O_{ipso}-Fe-μ_3O_{ipso} 93.3(2).

graphically equivalent iron atoms of the centrosymmetric cation $[Na\subset Fe_6\{N(CH_2CH_2O)_3\}_6]^+$ of **3** are located in the corners of a regular hexagon. The Fe–Fe distance is 3.216 Å, the interior angles of the hexagon are 120°. The diameter of the hexagon, defined as the distance between two opposite iron atoms, is 6.431 Å. The distorted octahedral coordination sphere of the iron atoms is composed of one nitrogen donor, one μ_1-, and two μ_2- and μ_3-oxygen donors. Consequently, triethanolamine acts as a tritope tetradentate ligand and links three iron(III) ions.[11]

Three sets of six oxygen atoms are located at the corners of three pairs of regular triangles which are rotated 60° relative to each other (Figure 2, left). These trigonal faces are located parallel and equidistant in pairs, with one plane above and one below the hexagonal plane generated by the iron atoms. These six oxygen atoms are related by an S_6 axis. The sodium ion is located in the center of cation **3** and has a distorted octahedron coordination sphere from the six μ_3O atoms. The diameter (1.98 Å) of the cavity marked by opposite μ_3O atoms almost corresponds to double the ionic radius of sodium (2.04 Å). (Distances: Na–μ_3O: 2.372 = *a*;[17] Na–μ_2O: 3.504; Na–μ_1O: 4.998 Å).

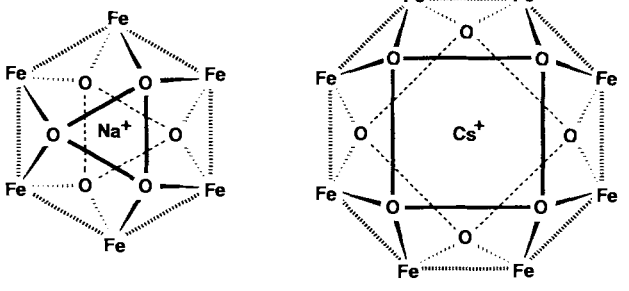

Figure 2. Left: Schematic representation of the central Fe_6O_6 backbone of **3**, showing the octahedral oxygen environment of sodium. Right: Schematic representation of the central Fe_8O_8 backbone of **5**, showing the quadratic antiprismatic oxygen environment of cesium. In both cases for reasons of clarity only the μ_3O atoms are displayed.

The different reactivity of the ligands triphos and triethanolamine (**2**) can be explained by the fact that the latter is a tetradentate ligand and moreover phosphorus generally does not bridge, whereas oxygen undergoes μ_2- and μ_3-linkages. According to Lehn et al.,[11a] in the case of the template-mediated self-assembly of a supramolecular system, amidst a set of possibilities the one combination of building blocks that leads to the best receptor for the substrate is realized. Therefore, *possibly* the six-membered cyclic structure **3** is exclusively selected from all the possible iron triethanolatamine oligomers when sodium ions are present. Thus, in the presence of cations with ionic radii that differ from that of sodium, variant structures are expected.

In order to test this hypothesis, we allowed triethanolamine **2** to react with lithium hydride and iron(III) chloride. The FAB-MS spectrum (FAB = fast atom bombardment) of the reaction product shows a peak at $m/z = 815$, which corresponds with the molecular ion $[Li\subset Fe_4\{N(CH_2CH_2O)_3\}_4]^+$ and indicates the formation of a tetranuclear complex.[18] The main product, however, is the hexanuclear complex $[Li\subset Fe_6\{N(CH_2CH_2O)_3\}_6]Cl$ **4** (distances: Li–μ_3O: 2.256; Li–μ_2O: 3.505; Li–μ_1O: 4.975 Å). The basic iron framework of the isostructural Li complex **4** and Na complex **3**[16] differs only slightly with respect to bond lengths and bond angles (see Figure 1).

We were more successful when we allowed triethanolamine **2** to react with cesium carbonate and iron(III) chloride. An X-ray structure analysis of the reaction product **5** revealed a cyclic

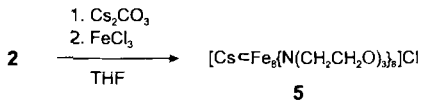

iron(III) complex with a [16]metallacrown-8 structure in which cesium was located in the center of the ring and chloride functioned as counterion (Figure 3). The eight iron atoms of the approximately centrosymmetric cation $[Cs\subset Fe_8\{N(CH_2CH_2O)_3\}_8]^+$ of **5** are located in the corners of a nearly regular octagon. The Fe–Fe distances range from 3.143 to 3.162 Å, and the interior angles of the octagon range from 135.17 to 133.33°.

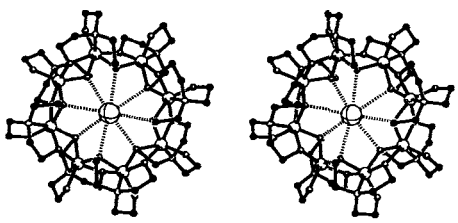

= Cs, = Fe, = O, = N, • = CH_2

Figure 3. Stereoview of the cation of **5** in the crystal (PLUTON representation; view along the crystallographic S_8 axis; H atoms excluded). For reasons of clarity the chloride ion and the crystal solvents were omitted. Selected bond lengths [Å] and angles [°] (mean values) of **5**: Fe–N 2.259, Fe–μ_1O 1.885, Fe–μ_2O_{ipso} 2.007, Fe–$\mu_2O_{vic.}$ 1.989, Fe–μ_3O_{ipso} 2.018, Fe–$\mu_3O_{vic.}$ 2.005; μ_3O_{ipso}-Fe-$\mu_2O_{vic.}$ 75.37, $\mu_2O_{vic.}$-Fe-μ_1O 93.29, μ_1O-Fe-μ_2O_{ipso} 98.49, μ_2O_{ipso}-Fe-μ_3O_{ipso} 100.06.

The diameter of the octagon, defined as the mean distance between opposite iron atoms, is 8.224 Å. The distorted octahedral coordination sphere of the iron atoms is composed of one nitrogen donor, one μ_1-, and two μ_2- and μ_3-oxygen donors. Three sets of eight of a total of twenty-four oxygen atoms are located in the corners of three pairs of square faces that are rotated 45°

 © WILEY-VCH Verlag GmbH, D-69451 Weinheim, 1997 0570-0833/97/3622-2483 $ 17.50+.50/0

relative to each other (Figure 2, right). The square faces are located parallel and almost equidistant in pairs, and one plane lies above and one plane lies below the octagon generated by the iron atoms; these structural elements share a common S_8 axis. The cesium ion lies directly above the center of the cation of **5**. It is shifted by about 0.5 Å towards the chloride counterion. The eight μ_3O atoms form a quadratic antiprism coordination sphere around the cesium center (mean distances: Cs–μ_3O: 3.291; Cs–μ_2O: 4.358; Cs-μ_1O 5.939). The distance between the cesium ion and the chloride ion is 3.446(9) Å.

Remarkably, the formation of the cations of **3** and **5** requires the spontaneous and correct assembly of 13 or 17 components (6/8 Fe^{3+}, 6/8 $[N(CH_2CH_2O)_3]^{3-}$ and 1 Na^+/Cs^+). Consequently, the two cations obey the three fundamental criteria, namely recognition, orientation, and termination, for the formation of supramolecular systems.

Furthermore, a common feature of complexes **3** and **5** is that the μ_1O atoms do not participate in the formation of the hexa- and octanuclear structures. They solely function as ligands for the coordinative saturation of the iron atoms. However, other donors such as chloride ions could also be candidates for this function. Therefore, we allowed *N*-methyldiethanolamine **6** to

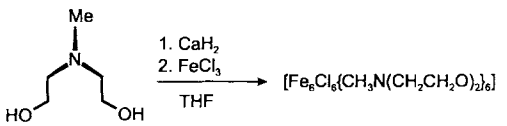

6 **7**

react with calcium hydride and iron(III) chloride and carried out an X-ray crystallographic structure analysis of the product formed.[16] According to this analysis, product **7** is present in the crystal as the unoccupied neutral iron(III) complex with [12]metallacrown-6 structure (Figure 4).

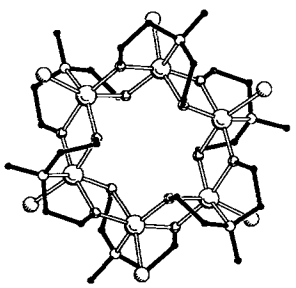

◯ = Fe, ◯ = Cl, ◎ = O, ○ = N, ● = CH_2, CH_3

Figure 4. Structure of **7** in the crystal (PLUTON representation; view along the crystallographic S_6 axis; H atoms excluded). For reasons of clarity the chloride ion and the crystal solvents are omitted. Selected bond lengths [Å] and angles [°] (mean values) of **7**: Fe–N 2.264, Fe–Cl 2.322, Fe–$\mu_2{}^i$O$_{ipso}$ 2.008, Fe–$\mu_2{}^i$O$_{vic.}$ 1.980, Fe–$\mu_2{}^a$O$_{ipso}$ 2.026, Fe–$\mu_2{}^a$O$_{vic.}$ 1.972; $\mu_2{}^i$O$_{ipso}$-Fe-$\mu_2{}^a$O$_{vic}$ 74.9, $\mu_2{}^a$O$_{vic}$-Fe-Cl 92.0, Cl-Fe-$\mu_2{}^a$O$_{ipso}$ 99.8, $\mu_2{}^a$O$_{ipso}$-Fe-$\mu_2{}^i$O$_{ipso}$ 94.9.

The six iron atoms of the centrosymmetric neutral molecule $[Fe_6\{H_3C\text{-}N(CH_2CH_2O)_2\}_6Cl_6]$ **7** are located in the corners of an almost regular hexagon. The Fe–Fe distances range from 3.167 to 3.185 Å, the interior angles of the hexagon range between 118.51 and 120.75°. The diameter of the hexagon, defined as the mean distance between two opposite iron atoms, is 6.361 Å. The distorted octahedral coordination sphere of the iron atoms comprises one nitrogen donor, one chloride ion, and four μ_2O donors.

Experimental Section

General method: To a suspension of sodium hydride (20 mmol, 0.48 g; for **3**), lithium hydride (20 mmol, 0.16 g; for **4**), cesium carbonate (15 mmol, 5.30 g; for **5**), or calcium hydride (7.5 mmol, 0.32 g; for **7**) in anhydrous THF (200 mL), triethanolamine **2** (5 mmol, 0.65 mL; for **3**, **4**, **5**) or *N*-methyldiethanolamine **6** (5 mmol, 0.60 mL; for **7**) was added. After the mixture had been stirred for 1 h at 20 °C, a solution of anhydrous iron trichloride (5 mmol, 0.81 g) was added dropwise. The reaction mixture was stirred for 4 days at 20 °C and the precipitate was subsequently collected on a glass frit. In the case of **3** and **4** the solid was extracted with dimethyl sulfoxide (150 mL). Chloroform (200 mL) and pentane (100 mL) were added, and the yellow microcrystalline precipitate was collected on a frit. In the case of **5** and **7** the solid was extracted with dichloromethane (300 mL) and upon evaporation of the solvent a yellow microcrystalline powder was isolated. Correct elemental analyses were obtained for all new compounds.

3·6$CHCl_3$: Yield: 0.94 g, (57%); amber-colored, cuboid crystals from chloroform/DMSO (1:1) by diffusion of pentane, m.p. >240 °C (decomp), IR (KBr): $\tilde{\nu}$ = 2860, 1462 cm^{-1}, Mössbauer spectrum of a powder sample, recorded at 77 K: ΔE_Q = 1.05 $mm\,s^{-1}$, δ = 0.47 $mm\,s^{-1}$, FAB-MS (3-nitrobenzyl alcohol matrix): *m/z*: 1235 $[Na\subset Fe_6\{N(CH_2CH_2O)_3\}_6]^+$.

4·6$CHCl_3$: Yield: 0.90 g (55%); amber-colored, cuboid crystals from chloroform/DMSO (1:1) by diffusion of pentane, m.p. >240 °C (decomp), IR (KBr): $\tilde{\nu}$ = 2857 cm^{-1}, 1467, FAB-MS (3-nitrobenzyl alcohol matrix): *m/z*: 1219 $[Li\subset Fe_6\{N(CH_2CH_2O)_3\}_6]^+$.

5·2CH_2Cl_2·2$CHCl_3$: Yield: 0.61 g (45%); amber-colored square plates from chloroform by diffusion of pentane, m.p. >220 °C (decomp), IR (KBr): $\tilde{\nu}$ = 2850, 1462 cm^{-1}, Mössbauer spectrum of a powder sample, recorded at 77 K: ΔE_Q = 0.91 $mm\,s^{-1}$, δ = 0.47 $mm\,s^{-1}$, FAB-MS (3-nitrobenzyl alcohol matrix): *m/z*: 1749 $[Cs\subset Fe_8\{N(CH_2CH_2O)_3\}_8]^+$.

7·2$CHCl_3$: Yield: 0.16 g (13%); greenish-yellow rhombic crystals from chloroform by diffusion of pentane, m.p. >240 °C (decomp), IR (KBr): $\tilde{\nu}$ = 2863, 1457 cm^{-1}, FAB-MS (3-nitrobenzyl alcohol matrix): *m/z*: 1215 $[Fe_6Cl_5\{H_3C\text{-}N(CH_2CH_2O)_2\}_6]^+$.

Received: May 16, 1997 [Z 10448 IE]
German version: *Angew. Chem.* **1997**, *109*, 2596–2599

Keywords: iron · crown compounds · metallacrown ethers · template synthesis

[1] E. Winterfeldt, *Nachr. Chem. Tech. Lab.* **1996**, *44*, 1217–1218.
[2] C. M. Flynn, Jr., *Chem. Rev.* **1984**, *84*, 31–41.
[3] K. L. Taft, C. D. Delfs, G. C. Papaefthymiou, S. Foner, D. Gatteschi, S. J. Lippard, *J. Am. Chem. Soc.* **1994**, *116*, 823–832, and references therein.
[4] R. R. Crichton, *Angew. Chem.* **1973**, *85*, 53–62; *Angew. Chem. Int. Ed. Engl.* **1973**, *12*, 57–65.
[5] C. Benelli, S. Parsons, G. A. Solan, R. E. P. Winpenny, *Angew. Chem.* **1996**, *108*, 1967–1970; *Angew. Chem. Int. Ed. Engl.* **1996**, *35*, 1825–1828; A.Caneschi, A. Cornia, A. C. Fabretti, D. Gatteschi, *ibid.* **1995**, *107*, 2862–2864 bzw. **1995**, *34*, 2716–2718.
[6] R. Sessoli, D. Gatteschi, A. Caneschi, N. A. Novak, *Nature* **1993**, *365*, 141–143; M. W. Wemple, D. Adams, K. S. Hagen, K. Folting, D. N. Hendrickson, G. Christou, *J. Chem. Soc. Chem. Commun.* **1995**, 1591–1593; H. J. Eppley, H.-L. Tsai, N. de Vries, K. Folting, G. Christou, D. N. Hendrickson, *J. Am. Chem. Soc.* **1995**, *117*, 301–317; D. P. Goldberg, A. Caneschi, S. J. Lippard, *ibid.* **1993**, *115*, 9299–9300; R. Cortés, L. Lezama, J. L. Pizarro, M. I. Arriortua, T. Rojo, *Angew. Chem.* **1996**, *108*, 1934–1936; *Angew. Chem. Int. Ed. Engl.* **1996**, *35*, 1810–1812.
[7] A. J. Blake, C. M. Grant, S. Parsons, J. M. Rawson, E. E. P. Winpenny, *J. Chem. Soc. Chem. Commun.* **1994**, 2363–2364.
[8] B. Grossmann, J. Heinze, E. Herdtweck, F. H. Köhler, H. Nöth, H. Schwenk, M. Spiegler, W. Wachter, B. Weber, *Angew. Chem.* **1997**, *109*, 384–386; *Angew. Chem. Int. Ed. Engl.* **1997**, *36*, 387–389; H. Plenio, *ibid.* **1997**, *109*, 358–360 bzw. **1997**, *36*, 348–351.
[9] R. W. Saalfrank, N. Löw, F. Hampel, H.-D. Stachel, *Angew. Chem.* **1996**, *108*, 2353–2354; *Angew. Chem. Int. Ed. Engl.* **1996**, *35*, 2209–2210.
[10] V. L. Pecoraro, A. J. Stemmler, B. R. Gibney, J. J. Bodwin, H. Wang, J. Kampf, A. Barwinski, *Prog. Inorg. Chem.* **1997**, *45*, 83–177; W. Hayes, J. F. Stoddart, *Large Ring Molecules* (Ed.: J. A. Semlyen), Wiley, New York, **1996**, p.433 ff; I. Haiduc, R. B. King, *ibid.* p.525 ff; A. J. Stemmler, J. W. Kampf, V. L. Pecoraro, *Angew. Chem.* **1996**, *108*, 3011–3013; *Angew. Chem. Int. Ed. Engl.* **1996**, *35*, 2841–2843; A. Caneschi, A. Cornia, S. J. Lippard, *ibid.* **1995**, *107*, 511–513 and **1995**, *34*, 467–469; A. J. Blake, R. O. Gould, C. M. Grant, P. E. Y. Milne, D. Reed, R. E. P. Winpenny, *ibid.* **1994**, *106*, 208–210 and **1994**, *33*, 195–197; A. J. Blake, R. O. Gould, P. E. Y. Milne, R. E. P. Winpenny, *J. Chem. Soc. Chem. Commun.* **1991**, 1453–1455; A. J. Blake, C. M. Grant, S. Parsons, J. M. Rawson, R. E. P. Winpenny, *ibid.* **1994**, 2363–2364; A. J. Stemmler, A. Barwinski, M. J. Baldwin, V. Young, V. L. Pecoraro, *J. Am. Chem. Soc.* **1996**, *118*, 11962–11963; A. Caneschi, A. Cornia, A. C. Fabretti, S. Foner, D. Gatteschi, R. Grandi, L. Schenetti, *Chem. Eur. J.* **1996**, *2*, 1379–1387.

[11] a) B. Hasenknopf, J.-M. Lehn, B. O. Kneisel, G. Braun, D. Fenske, *Angew. Chem.* **1996**, *108*, 1987–1990; *Angew. Chem. Int. Ed. Engl.* **1996**, *35*, 1838–1840; B. Hasenknopf, J.-M. Lehn, N. Boumediene, A. Dupont-Gervais, A. Van Dorsselaer, B. Kneisel, D. Fenske, *J. Am. Chem. Soc.* **1997**, *119*, in press; b) R. W. Saalfrank, S. Trummer, H. Krautscheid, V. Schünemann, A. X. Trautwein, S. Hien, C. Stadler, J. Daub, *Angew. Chem.* **1996**, *108*, 2350–2352; *Angew. Chem. Int. Ed. Engl.* **1996**, *35*, 2206–2208.

[12] a) R. W. Saalfrank, R. Burak, S. Reihs, N. Löw, F. Hampel, H.-D. Stachel, J. Lentmaier, K. Peters, E. M. Peters, H. G. von Schnering, *Angew. Chem.* **1995**, *107*, 1085–1087; *Angew. Chem. Int. Ed. Engl.* **1995**, *34*, 993–995; b) R. W. Saalfrank, R. Burak, A. Breit, D. Stalke, R. Herbst-Irmer, J. Daub, M. Porsch, E. Bill, M. Müther, A. X. Trautwein, *ibid.* **1994**, *106*, 1697–1699 and **1994**, *33*, 1621–1623; c) T. Beissel, R. E. Powers, K. N. Raymond, *ibid.* **1996**, *108*, 1166–1168 bzw. **1996**, *35*, 1084–1086.

[13] R. W. Saalfrank, A. Dresel, V. Seitz, F. Hampel, M. Teichert, D. Stalke, *Chem. Eur. J.* **1997**, *3*, no. 12.

[14] a) R. W. Saalfrank, O. Struck, M. G. Davidson, R. Snaith, *Chem Ber.* **1994**, *127*, 2489–2492; b) R. W. Saalfrank, O. Struck, K. Peters, H. G. von Schnering, *ibid.* **1993**, *126*, 837–840; c) R. W. Saalfrank, O. Struck, K. Nunn, C.-J. Lurz, R. Harbig, K. Peters, H. G. von Schnering, E. Bill, A. X. Trautwein, *ibid.* **1992**, *125*, 2331–2335; d) R. W. Saalfrank, O. Struck, K. Peters, H. G. von Schnering, *Inorg. Chim. Acta.* **1994**, *222*, 5–11.

[15] S. Mann, G. Huttner, L. Zsolnai, K. Heinze, *Angew. Chem.* **1996**, *108*, 2983–2984; *Angew. Chem. Int. Ed. Engl.* **1996**, *35*, 2808–2809. See also: D. Burdinski, F. Birkelbach, M. Gerdan, A. X. Trautwein, K. Wieghardt, P. Chaudhuri, *J. Chem. Soc. Chem. Commun.* **1995**, 963–964; P. Chaudhuri, M. Winter, P. Fleischhauer, W. Hasse, U. Flörke, H.-J. Haupt, *ibid.* **1990**, 1728–1730; C. Krebs, M. Winter, T. Weyhermüller, E. Bill, K. Wieghardt, P. Chaudhuri, *ibid.* **1995**, 1913–1915.

[16] X-ray crystal structure analyses: Nonius MACH3; $Mo_{K\alpha}$ radiation, $\lambda = 0.71073$ Å; the structures were solved by direct methods [19] and refined with full-matrix least-squares on F^2 [20]. Hydrogen atoms were fixed in idealized positions using a riding model. An absorption correction was carried out with Ψ scans. **3**: $C_{36}H_{72}ClFe_6N_6NaO_{18}\cdot 6CHCl_3$; $M_r = 1986.74$; trigonal, $R\bar{3}$; crystal dimensions $0.30\times0.30\times0.30$ mm^3; $a = b = 19.177(3)$, $c = 17.484(4)$ Å; $V = 5569(2)$ Å^3; $T = 173(2)$ K; $Z = 3$; $\rho_{calcd} = 1.777$ Mg m^{-3}; section of the reciprocal lattice $-20<h<0$, $-20<k<0$, $-21<l<21$; $\theta = 2.63-25.97°$; 2648 reflections observed, 2421 unique; reflections with $I>2\sigma(I)$: 1735, *R*1 [$I>2\sigma(I)$]: 0.0409, *wR*2: 0.0939; *R*1 (all data): 0.0748, *wR*2: 0.1102; largest difference peak and hole: 0.550/ -0.633 e Å^{-3}. **4**: $C_{36}H_{72}ClFe_6LiN_6O_{18}\cdot 6CHCl_3$; $M_r = 1970.69$; trigonal, $R\bar{3}$; crystal dimensions $0.30\times0.30\times0.25$ mm^3; $a = b = 19.103(2)$, $c = 17.453(4)$ Å; $V = 5516(2)$ Å^3; $T = 173(2)$ K; $Z = 3$; $\rho_{calcd} = 1.780$ Mg m^{-3} section of the reciprocal lattice $-22<h<0$, $0<k<19$, $0<l<20$; $\theta = 2.64-4.98°$; 1186 reflections observed, 1184 unique; reflections with $I>2\sigma(I)$: 988, *R*1 [$I>2\sigma(I)$]: 0.0493, *wR*2: 0.1641; *R*1 (all data): 0.0632, *wR*2: 0.1844; largest difference peak and hole: 0.830/ -0.664 e Å^{-3}. **5**: $C_{48}H_{96}ClFe_8N_8CsO_{24}\cdot 2CHCl_3\cdot 2CH_2Cl_2$; $M_r = 2193.08$; monoclinic, $P2/n$; crystal dimensions $0.30\times0.20\times0.20$ mm^3; $a = 17.684(4)$, $b = 13.034(3)$, $c = 19.359(4)$ Å; $b = 90.53(3)°$; $V = 4462(2)$ Å^3; $T = 173(2)$ K; $Z = 2$; $\rho_{calcd} = 1.632$ Mg m^{-3}; section of the reciprocal lattice $0<h<20$, $0<k<014$, $-22<l<22$; $\theta = 2.78-23.97°$; 6969 reflections observed, 6969 unique; reflections with $I>2\sigma(I)$: 3273, *R*1 [$I>2\sigma(I)$]: 0.1059, *wR*2: 0.2610; *R*1 (all data): 0.2219, *wR*2: 0.3120; largest difference peak and hole: 1.851/ -1.219 e Å^{-3}. In the asymmetric unit there is one molecule of chloroform and one molecule of dichloromethane that do not make contact with the iron complex. The chloroform is disordered on two positions with a probability of occupancy of 65:35%. The recorded data allowed only an isotropic refinement of the solvent molecules by using distance restrains for the C–Cl bond. **7**: $C_{30}H_{66}Cl_6Fe_6N_6O_{12}\cdot 2CHCl_3$; $M_r = 1489.42$; monoclinic, $P2(1)/c$; crystal dimensions $0.15\times0.15\times0.10$ mm^3; $a = 13.9130(9)$, $b = 18.701(5)$, $c = 11.305(4)$ Å; $\beta = 106.04(2)°$; $V = 2827.1(14)$ Å^3; $T = 173(2)$ K; $Z = 2$; $\rho_{calcd} = 1.750$ Mg m^{-3}; section of the reciprocal lattice $0<h<16$, $-22<k<0$, $-13<l<12$; $\theta = 2.33-24.97°$; 5172 reflections observed, 4960 unique; reflections with $I>2\sigma(I)$: 2664, *R*1 [$I>2\sigma(I)$]: 0.0731, *wR*2: 0.1849; *R*1 (all data): 0.1745, *wR*2: 0.2285; largest difference peak and hole: 1.234/ -1.320 e Å^{-3}. Crystallographic data (excluding structure factors) for the structures reported in this paper have been deposited with the Cambridge Crystallographic Data Centre as supplementary publications nos. CCDC-100097 (**3**) and CCDC-100472 (**4**, **5** and **7**). Copies of the data can be obtained free of charge on application to The Director, CCDC, 12 Union Road, Cambridge CB2 1EZ, UK (fax: int. code + (1223) 336-033; e-mail: deposit@chemcrys.cam.ac.uk). For green-red stereorepresentation of **3** see http://www.organik.uni-erlangen.de/saalfrank/.

[17] $d = 2a - 2r_O$.

[18] Hitherto it proved impossible to isolate the complex $[Li\subset Fe_4\{N(CH_2CH_2O)_3\}_4]Cl$.

[19] G. M. Sheldrick, SHELXS-96, *Acta Crystallogr. Sect. A*, **1990**, *46*, 467–473.

[20] G. M. Sheldrick, SHELXL-96, Program for crystal structure refinement, Universität Göttingen **1996**.

Specific Recognition of a Minimal Model of Aminoacylated tRNA by the Elongation Factor Tu of Bacterial Protein Biosynthesis**

Stefan Limmer,* Martin Vogtherr, Barbara Nawrot, Rainer Hillenbrand, and Mathias Sprinzl

In the course of protein biosynthesis the aminoacylated transfer RNA (aa-tRNA), which is correctly "charged" with its specific amino acid, has to be transported to the ribosome. In bacterial biosynthesis this function is carried out by the elongation factor Tu (EF-Tu), which must be able to recognize all aa-tRNAs as well as to reject uncharged elongator tRNAs and the initiator tRNA—in bacteria invariably fMet-tRNA (fMet = formylmethionyl), which is formylated and interacts with the initiation factor IF-2. Thus, the specific recognition of the aa-tRNAs may depend neither on variations in the sequences and the tertiary structures, nor on the nature of the attached amino acid itself.

The region common to all aa-tRNAs comprises the ubiquitous CCA terminus of the tRNA and the ester linkage at the 2′- or 3′-OH groups of the ribose of the terminal adenosine 76.[1] In solution the two isomers that have 2′- and 3′-ester bonds are in a dynamic equilibrium.[2] It was shown[3] that minihelices consisting of at least ten base pairs and an aminoacylated, single-stranded (A)CCA end are relatively tightly bound by EF-Tu·GTP. The smallest conceivable unit as a minimal model of aa-tRNA is made up of the terminal adenosine and an attached amino acid.[2] Indeed, such aminoacylated adenosines are able to compete sucessfully for the aa-tRNA binding site of a specific inhibitor of EF-Tu, namely *N*-tosyl-L-phenylalanylchloromethane.[4]

The stability of the ester bond between ribose and amino acid is rather low under conditions which are optimal for EF-Tu (pH = 7.5). Hence, we used anthranilic acid as an amino acid analogue, which has a higher stability with respect to hydrolysis of the ester bond. Its suitability for binding to EF-Tu was demonstrated for yeast $tRNA^{Phe}$ charged with anthranilic acid.[5] The transacylation rate of the anthranilic acid between the 2′ and 3′ ribose positions is drastically lower for anthraniloyladenosines **1**[6] than for corresponding aminoacylated adenosines; this

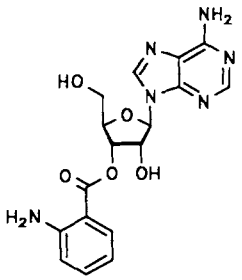

3′-1

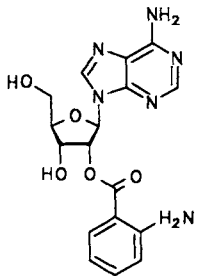

2′-1

[*] Priv.-Doz. Dr. S. Limmer, Dipl.-Chem. M. Vogtherr, Dipl.-Biol. R. Hillenbrand, Prof. Dr. M. Sprinzl
Laboratorium für Biochemie der Universität
D-95440 Bayreuth (Germany)

Dr. B. Nawrot
Centre of Molecular and Macromolecular Studies
Department of Bioorganic Chemistry
Polish Academy of Sciences, Lodz (Poland)

[**] This work was supported by the Deutsche Forschungsgemeinschaft. We wish to thank Norbert Grillenbeck for preparing EF-Tu, Karol Szkaradkiewicz for supplying IF-2, and Melissa Brown for helping with the translation.

 © WILEY-VCH Verlag GmbH, D-69451 Weinheim, 1997 0570-0833/97/3622-2485 $ 17.50+.50/0

correlates with the significantly increased stability of the ester bond towards hydrolysis. Due to the lack of important regions of the aa-tRNA—with which the EF-Tu interacts in its active, GTP-bound form[7]—only a drastically diminished affinity of **1** for EF-Tu can a priori be expected. This should give rise to an exchange of **1** between free and bound forms that is fast on the NMR time scale.[8, 9] In this case the observed values of chemical shift and linewidth represent the weighted averages of the corresponding quantities in the free and bound states. The linewidths of the signal for the small ligand molecule should continuously increase with rising protein concentration. Owing to the much larger molecular weight of the protein (ca. 45 kDa) and the therefore distinctly faster T_2 relaxation, the protein contributes merely a more or less pronounced, poorly resolved background to the ^{1}H NMR spectrum of the complex.

In Figure 1 the ^{1}H NMR spectra of the complexes of EF-Tu·GTP from the eubacterium *Thermus thermophilus* with **1** in varying molar ratios are displayed. As expected for fast exchange (that is, weak binding), the linewidth rises as the relative protein fraction increases from 1:20 to 1:2.5. The resonances for the 3′ isomer are broadened to a distictly greater extent than those for the 2′ isomer, suggesting a preferred binding of the former. This confirms earlier experiments[10] from which an almost exclusive binding of the 3′ isomer of aa-tRNA to EF-Tu was deduced. By contrast, a weakened interaction of both species with EF-Tu·GTP was found upon using aa-tRNA variants in which the terminal adenosine was replaced by 3′- or 2′-deoxyadenosine.[11]

All lines in the spectrum of **1** become broadened in the presence of EF-Tu (see Table 1 and Figure 1), although not to the same degree; the 2′ and 3′ ribose resonances of the 3′ isomer are particularly broadened. From these differences, conclusions concerning the contact sites of the ligand with the protein can be derived: For the molecular regions of the ligand with the closest contacts to the protein, the most significant alterations of the relaxation behavior are due to additional relaxation pathways involving protons of the protein. Such a difference in line broadening is often characteristic of a specific ligand–protein interaction.[14]

Table 1. Linewidths[Hz][a] and chemical shifts (in parentheses) in the ^{1}H NMR spectrum of free and EF-Tu·GTP-bound[b] **1**.

Proton	3′ Isomer free	3′ Isomer bound	2′ Isomer free	2′ Isomer bound
H8	2.6 (8.409)	28.0 (8.356)	2.6 (8.437)	13.0 (8.432)
H2	2.6 (8.292)	(8.240)[c]	2.5 (8.258)	(8.240)[c]
H1′	10.8 (6.257)	33.0 (6.207)	9.9 (6.442)	17.3 (6.446)
H2′	14.7 (5.156)	47.0 (5.121)	12.9 (5.870)	19.3 (5.848)
H3′	10.8 (5.598)	53.0 (5.598)	11.4 (4.817)	16.5 (4.812)

[a] Linewidths at half-height, measured over the multiplet structure. [b] 1 mM **1**, 0.18 mM EF-Tu·GTP in borate buffer, pH = 7.5, D_2O/[D_4]methanol 7/1, 281 K. [c] Strong overlap of the resonances for both isomers.

Remarkably, the integral ratio of the signals for 3′-**1** and 2′-**1** shifts from about 2:1 for free **1** towards 1:1 with rising protein concentration. This means that with an increasing fraction of bound **1**, which preferably binds as the 3′ isomer, the relative population of the 2′ isomer grows. The same effect is achieved when the binding equilibrium is shifted by varying the temperature while keeping the concentrations of protein and ligand constant. For 1 mM **1** and 0.18 mM EF-Tu·GTP, the ratio increases from about 1:1 (3′:2′) at 281 K to about 1.8:1 at 307 K. Preferred binding of the 3′ isomer alone is not sufficient to account for this behavior. One conceivable explanation is that,

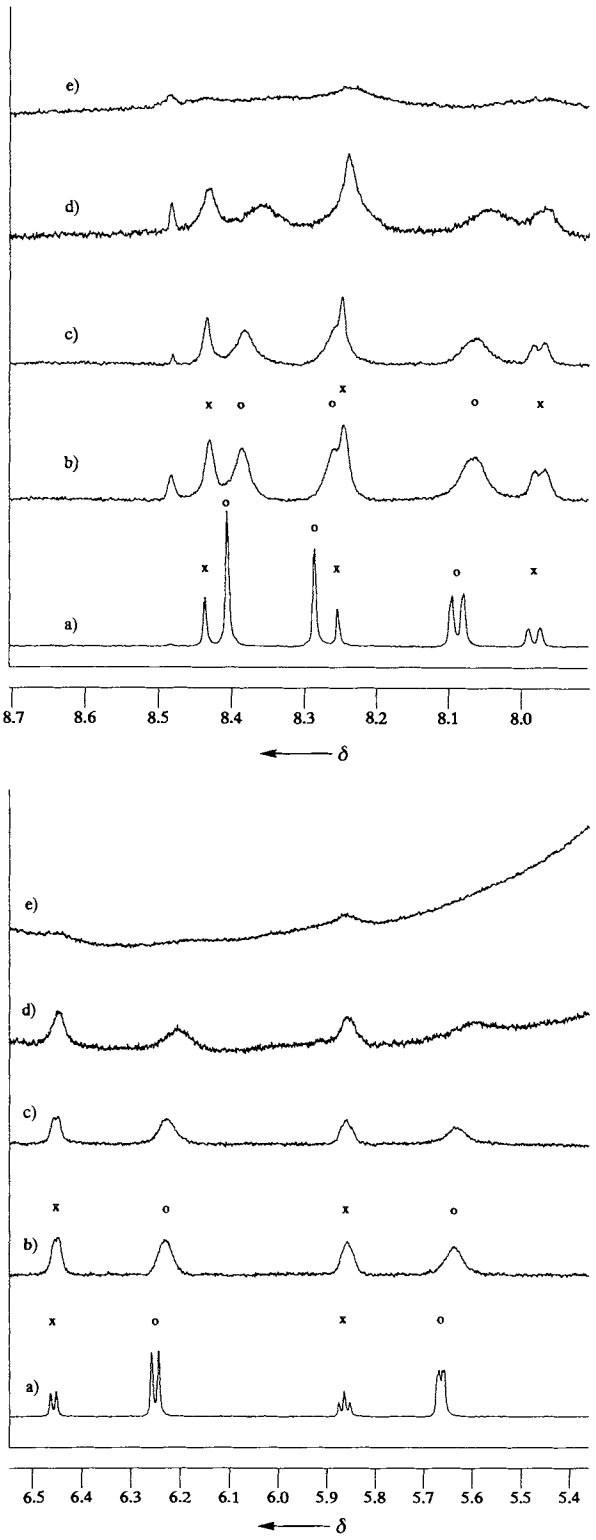

Figure 1. Portions of the ^{1}H NMR spectra with aromatic (top) and ribose 1′, 2′, and 3′ signals (bottom) of 3′(2′)-anthranyloyladenosine (**1**) in D_2O/[D_4]methanol (7/1) at 281 K. Concentration of **1** 1 mM, concentration of EF-Tu·GTP a) 0.00, b) 0.05, c) 0.08, d) 0.18, e) 0.4 mM. The signals of the 3′ and 2′ isomers are marked with o and x, respectively (for the assignment, see Table 1). The baseline distortion is due to the protein background spectrum.

 © WILEY-VCH Verlag GmbH, D-69451 Weinheim, 1997 0570-0833/97/3622-2486 $ 17.50+.50/0

compared to free **1**, transacylation of **1** is accelerated upon binding to EF-Tu. Since EF-Tu binds the two isomers with different strengths, an equilibrium is adjusted which reflects the different affinities for the protein and leads to an accumulation of the 2′ isomer.

The observed line broadening (and hence ligand binding) is independent of the guanosine nucleotide (GTP, GPPNHP, GDP) bound to EF-Tu, which is different than in the case of complete aa-tRNA.[12] The rearrangement of the EF-Tu structure[7, 16a, b] associated with GTP binding is a prerequisite for the binding of the tRNA in a cleft formed between domains I and II, in which stabilizing interactions between EF-Tu and tRNA are enabled. Naturally, these contacts cannot take place with the small ligand **1**, which may explain both the diminished affinity and the absence of any differences between the GTP/GPPNHP- or GDP-complexed forms with respect to binding to EF-Tu. For the specific interaction of the terminal A76, the relative orientation of the three EF-Tu domains—which is determined by the nature of the bound nucleotide—plays only a minor role.

To check the specificity of the complex formation, several control experiments with structurally related compounds of low molecular weight were carried out. In the case of the antibiotic puromycin (**2**) the ester bond between ribose and amino acid is replaced by an amide bond; in formylmethionyl-AMP (**3**) the amino group of the amino acid is formylated. In both cases only negligible increases in linewidth were measured under the conditions used for the **1**·EF-Tu complex (1 mM ligand, 0.08 mM EF-Tu·GTP, 281 K; Figure 2a and b). Evidently, these molecules are not bound by the protein; with **3**, neither of the two isomers is bound.

The higher affinity of 3′-**1** immediately suggests the question of whether only the esterified 3′-OH group is required for recognition and binding, or if the 2′-OH group is also necessary. The existence of the free 2′-OH group enables transacylation, which could also be possibly relevant in the recognition process. To check this, the binding of the 2′-deoxy derivative **4** was studied.

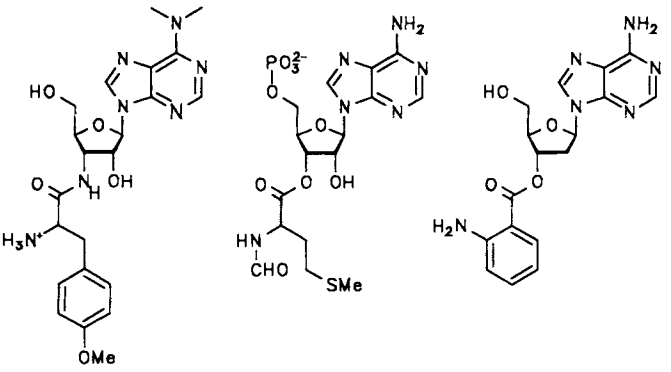

2 **3** **4**

Under the same conditions as before, the resonances become only slightly broadened yet again (Figure 2c), which indicates a distinctly reduced binding as compared to 3′-**1**. This hints at an important role of the 2′-OH group both in **1** and in the terminal adenosine of the aa-tRNA. This conclusion is corroborated by a crystal structure analysis,[7] according to which a hydrogen bond involving a conserved glutamate 271 can be formed. Indeed, a drastically diminished aa-tRNA binding strength is found for an EF-Tu variant, in which this glutamate was replaced by aspartate (E271D). The ^{1}H NMR signals of **1** (Figure 3) in the presence of the mutant protein E271D are broadened to a much lesser extent than with the wildtype potein, thus suggesting a distinctly reduced binding strength. This substanti-

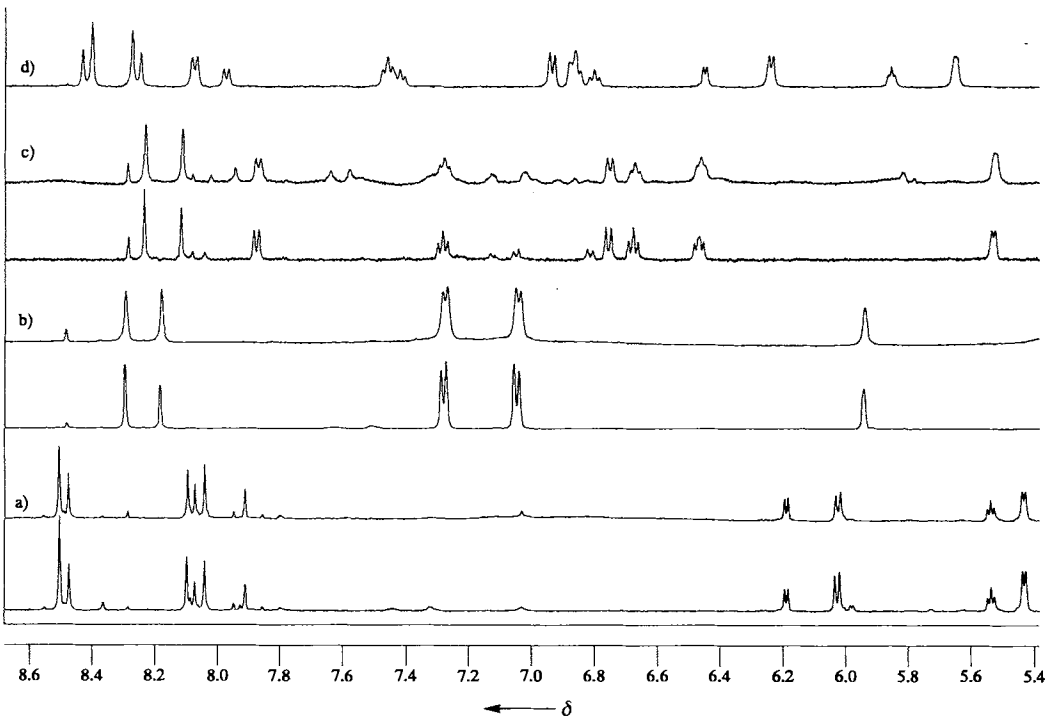

Figure 2. Portions of the ^{1}H NMR spectra with aromatic and ribose 1′, 2′, and 3′ signals at 281 K. a) fMet-AMP **3** free (bottom) and with 0.08 mM EF-Tu·GTP (top), both in D_2O; b) puromycin **2** free (bottom) and with 0.08 mM EF-Tu·GTP (top), both in D_2O/[D_4]methanol (7/1); c) 3′-anthranyloyl-2′-desoxyadenosin **4** free (bottom) and with 0.08 mM EF-Tu·GTP (top), both in D_2O/[D_6]DMSO (9/1); d) **1** with 0.08 mM IF-2 in D_2O/[D_4]methanol (7/1). The ligand concentration was always 1 mM.

 © WILEY-VCH Verlag GmbH, D-69451 Weinheim, 1997 0570-0833/97/3622-2487 $ 17.50+.50/0

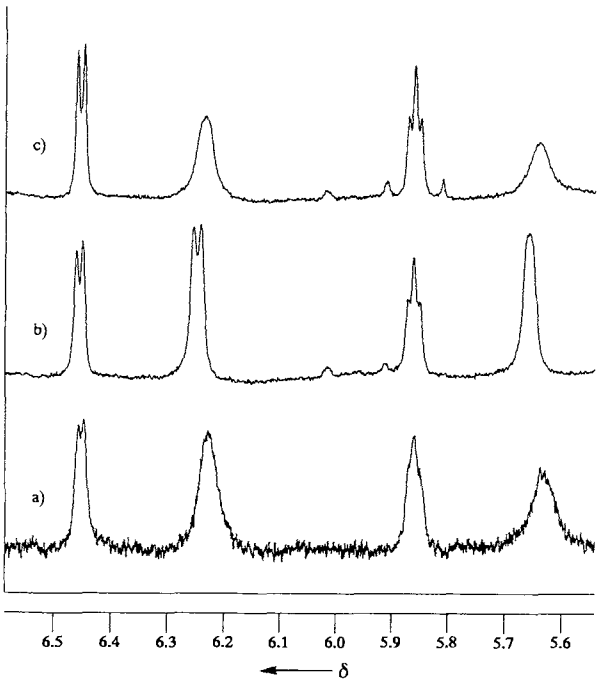

Figure 3. Ribose region of the ^{1}H NMR spectrum (281 K) of **1** with 0.08 mM a) EF-Tu·GTP wildtype, b) EF-Tu(E271D)·GTP, and c) EF-Tu(C82A/T394C)·GTP.

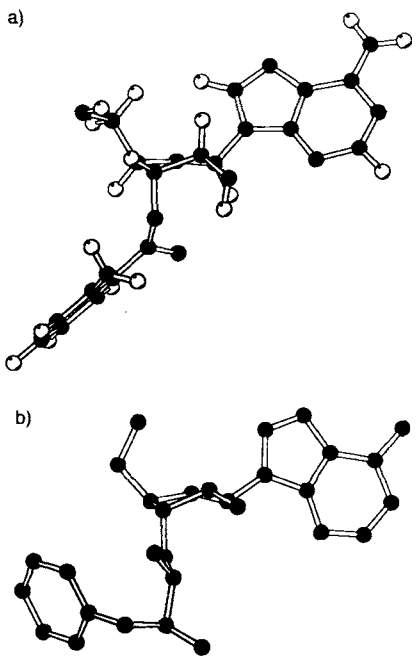

Figure 4. a) Structure in the EF-Tu·GTP bound state of **1** calculated from NMR data (MOLSCRIPT [22] representation). b) Conformation of the terminal adenosine in the aminoacylated tRNA^{Phe} from the crystal structure [7] of the ternary complex EF-Tu·GTP·Phe-tRNA^{Phe}.

ates the specificity of the interaction, also on the part of the protein, as the double mutant C82A/T394C gives rise to increases in linewidth that are comparable to those with the wildtype EF-Tu (Figure 3c). Since intact tRNA is able to make further contacts with EF-Tu,[7] aa-tRNA variants with terminal 2′- and 3′-deoxyadenosines are also bound by EF-Tu·GTP, however, with decreased affinity.[11] To rule out nonspecific interactions of **1** with proteins, in particular with those from the protein biosynthesis cycle, the interaction of **1** with the initiation factor IF-2 was investigated (again 1 mM ligand, 0.08 mM protein; Figure 2d). Here, too, no change in the spectrum as compared to that of free **1** (Figure 1a) was detected; this indicates a negligible interaction between **1** and IF-2.

The structure of free **1** was characterized recently.[6] The conformation of the EF-Tu-complexed molecule can be determined with transfer-NOE (TrNOE) measurements.[13, 14] This exploits the different signs and magnitudes of the NOE for a small molecule like **1** (slightly positive) and for a protein–ligand complex (strongly negative).[14] When the ligand (which is present in a large excess) exchanges rapidly between enzyme-bound and free forms, the NOE from the bound state is transferred into the free state and exceeds the NOE due to the free ligand by far. The measurement of the TrNOE thus permits a structure elucidation of the bound ligand. The complex of EF-Tu with the extremely slowly hydrolyzing GTP analogue GPPNHP was employed for the conformation analysis, in order to preclude any effects of the GTP hydrolysis and the concomitant conformational changes of EF-Tu[7, 16] during data acquisition. For technical reasons the spectra were measured at 298 K. In the NOESY spectrum (1 mM ligand, 0.05 mM EF-Tu) strong positive cross-peaks are observed,[8, 14] which are more intense for the 3′ isomer than for the 2′ isomer, due to the preferred binding of the former.

The structure of complexed **1** (Figure 4) was calculated using the full relaxation matrix. It differs only slightly from the structure postulated for free **1**.[6] In particular, the base is *anti* with respect to the ribose ring, and the sugar ring adopts a 2′-*endo* puckering. The structure thus obtained can be compared to that of the terminal adenosine of the aa-tRNA from the ternary complex EF-Tu·GTP·Phe-tRNA^{Phe} (Figure 4b).[7] The two structures are in fair agreement, in particular with reference to base orientation and ribose pucker. Moreover, since the amino groups of the amino acid of the aa-tRNA and of **1** are positioned similarly, they are able to interact with histidine 273 and asparagine 285 of EF-Tu.

The investigations presented here suggest that the specific recognition of EF-Tu by aminoacylated elongator tRNAs most likely occurs through contacts of the ribose of the terminal nucleotide of the tRNA, to which the amino acid is esterified. Clearly, the isomer with the amino acid attached to the 3′-OH position is bound much more strongly. The closest contact of the terminal aminoacylated adenosine with the protein is through the 2′-OH position of the ribose and the 3′-ester linkage. These findings could possibly serve as a starting point for the design of compounds based on **1**, which bind to EF-Tu even better and hence could act as specific inhibitors of the aa-tRNA–EF-Tu interaction and thus the whole bacterial protein biosynthesis.

Experimental Section

The synthesis of **1** followed the method in ref. [8]. The preparation and purification of EF-Tu [18] and IF-2 [20] from *Th. thermophilus* overproduced in *E. coli* were published previously. Compound **3** was synthesized according to ref. [19]. For solubility reasons, NMR samples of **1** and **2** were dissolved in a mixture of D_2O buffer (50 mM sodium borate pH = 7.5; 50 mM KCl) and [D_4]methanol (7/1). Methanol was not required for **3**, and [D_6]DMSO (9/1) was used instead of methanol for **4**. For final sample volumes of 500 μL, the protein was dissolved in 437.5 μL of the buffer and, after lyophilization, redissolved in the same volume of D_2O. A solution of **1** or **2** (8 mM, 62.5 μL) was subsequently added. Compounds **3** and **4** were treated in the respective solvents.

All NMR spectra were measured at 500 MHz on a Bruker DRX-500 spectrometer. The data was analyzed with the NDEE program package (Software Symbiose GmbH, Bayreuth, Germany). The NOESY spectra were recorded with 4 k data points in t_2 and 512 t_1 increments with mixing times of 70 or 150 ms. The HDO signal was suppressed by presaturation.

 © WILEY-VCH Verlag GmbH, D-69451 Weinheim, 1997 0570-0833/97/3622-2488 $ 17.50+.50/0

The XPlor program package [17] was employed to calculate the structure of protein-bound **1**. It cooled from 1200 to 50 K within 1 ps with both the geometric and a relaxation matrix (correlation time for the complex 20 ns) [21] energy terms turned on. The structures with the smallest *R* factor were selected.

Received: April 23, 1997
Revised version: July 14, 1997 [Z10376IE]
German version: *Angew. Chem.* **1997**, *109*, 2592–2596

Keywords: molecular recognition · NMR spectroscopy · nucleotides · proteins · RNA

[1] M. Sprinzl, C. Steegborn, F. Hübel, S. Steinberg, *Compilation of tRNA Sequences and Sequences of tRNA Genes, Nucleic Acids Res.* **1996**, *24*, 68–72.
[2] M. Taiji, S. Yokoyama, S. Higuchi, T. Miyazawa, *J. Biochem.* **1981**, *90*, 885–888.
[3] J. Rudinger, B. Blechschmidt, S. Ribeiro, M. Sprinzl, *Biochem.* **1994**, *33*, 5682–5688.
[4] a) J. Jonák, I. Rychlík, J. Smrt, A. Holý, *FEBS Lett.* **1979**, *98*, 329–332; b) J. Jonák, J. Smrt, A. Holý, I. Rychlík, *Eur. J. Biochem.* **1980**, *105*, 315–320.
[5] L. Servillo, C. Balestrieri, L. Quagliuolo, L. Iorio, A. Giovane, *Eur. J. Biochem.* **1993**, *213*, 583–589.
[6] B. Nawrot, W. Milius, A. Ejchart, S. Limmer, M. Sprinzl, *Nucleic Acids Res.* **1997**, *25*, 948–954.
[7] P. Nissen, M. Kjeldgaard, S. Thirup, G. Polekhina, L. Reshetnikova, B. F. C. Clark, J. Nyborg, *Science* **1995**, *270*, 1464–1472.
[8] O. Jardetzky, G. C. K. Roberts, *NMR in Molecular Biology*, Academic Press, Orlando, FL, USA, **1981**, pp. 115–142.
[9] L.-Y. Lian, G. C. Roberts in *NMR of Macromolecules* (Ed.: G. C. K. Roberts), IRL, Oxford, **1993**, pp. 153–182.
[10] M. Taiji, S. Yokoyama, T. Miyazawa, *J. Biochem.* **1985**, *98*, 1447–1453.
[11] M. Sprinzl, M. Kucharzewski, J. B. Hobbs, F. Cramer, *Eur. J. Biochem.* **1977**, *78*, 55–61.
[12] F. Janiak, V. A. Dell, J. K. Abrahamson, B. S. Watson, D. L. Miller, A. E. Johnson, *Biochem.* **1990**, *29*, 4268–4277.
[13] A. P. Campbell, B. D. Sykes, *Annu. Rev. Biophys. Biomol. Struct.* **1990**, *29*, 99–122.
[14] a) F. Ni, H. A. Scheraga, *Acc. Chem. Res.* **1994**, *27*, 257–264; b) F. Ni, *Prog. NMR Spectrosc.* **1994**, *26*, 517–606.
[15] D. Neuhaus, M. Williamson, *The Nuclear Overhauser Effect in Structural and Conformational Analysis*, VCH, New York, **1989**.
[16] a) H. Berchtold, L. Reshetnikova, C. O. A. Reiser, N. K. Schirmer, M. Sprinzl, R. Hilgenfeld, *Nature* **1993**, *365*, 126–132; b) M. Kjeldgaard, P. Nissen, S. Thirup, J. Nyborg, *Structure* **1993**, *1*, 35–50.
[17] A. T. Brünger, X-Plor, Version 3.843, **1996**.
[18] S. Limmer, C. O. A. Reiser, N. K. Schirmer, N. W. Grillenbeck, M. Sprinzl, *Biochem.* **1992**, *32*, 2970–2977.
[19] A. V. Azhayev, S. V. Popovkina, N. B. Tarussova, M. P. Kirpichnikov, V. L. Florentiev, A. A. Krayevsky, M. K. Kukhanova, B. P. Gottikh, *Nucleic Acids Res.* **1979**, *7*, 2223–2234.
[20] H.-P. Vornlocher, W.-R. Scheible, H. G. Faulhammer, M. Sprinzl, *Eur. J. Biochem.* **1997**, *243*, 66–71.
[21] C. R. Cantor, P. R. Schimmel, *Biophysical Chemistry, Part II*, W. H. Freeman, San Francisco, **1980**, p. 461.
[22] P. J. Kraulis, *J. Appl. Crystallogr.* **1991**, *24*, 946–950.

Electrostatic Layering of Giant Vesicles**

Fredric M. Menger* and Jason S. Keiper

In the Langmuir–Blodgett method, a vertical plate is dipped up and down through a water-supported monolayer, thereby depositing monolayers onto the plate one at a time.[1] Thus, the thickness and constitution of a multilayered assembly can be controlled. We report here experiments in which a giant vesicle, an object of considerable recent attention,[2–6] is successfully coated with lipid bilayers. The layering is electrostatically driven and detectable under phase-contrast microscopy. Controlled layering now joins growth, fusion, undulation, excretion, and healing[5, 6] as observable phenomena with giant vesicles.

Giant anionic vesicles (20–50 μm in diameter) were prepared from a mixture of 1-palmitoyl-2-oleoyl-*sn*-glycero-3-phosphocholine (POPC), the sodium salt of 1-palmitoyl-2-oleoyl-*sn*-glycero-3-[phospho-*rac*-(1-glycerol)] (POPG), and cholesterol in a molar ratio of 79:9:12. Giant cationic vesicles were prepared from POPC, didodecyldimethylammonium bromide (DDAB), and cholesterol (molar ratio also 79:9:12). Vesicle formation was carried out with the following protocol: Lipid mixtures in $CHCl_3$/MeOH were stripped of solvent, and the resulting films vortexed with deionized water. Lyophilization gave fluffy white powders. Afterwards, the powder (0.1 mg or less) was smeared onto the microscope slide (within the confines of a Teflon O-ring cemented onto the slide). The sample was hydrated with water (≈0.5 mL) for at least 30 min to give a polydisperse array of vesicular structures.

Giant vesicles of opposite charge were brought into contact according to the following procedure: A suitable anionic vesicle was grasped with a polished holding pipet (under slight suction provided by a picoinjector device) and guided into a vesicle-free region of the microscope field. Cationic vesicles from another preparation were then withdrawn into a capillary pipet with the aid of a hand-controlled microsyringe. This pipet was emptied of its contents adjacent to the lone anionic vesicle. Finally, the held anionic vesicle was brought into contact with a "free" cationic vesicle, and the interaction between the two membranes was observed as a function of time under 400-fold magnification. Others have shown that light defracted from even a single bilayer is visible by light microscopy,[7] and that vesicle adhesion is amenable to micromechanical testing.[8]

Neutral vesicles composed only of POPC and cholesterol failed to "stick" even when repeatedly pushed into contact; the free vesicle immediately diffused away from the one held stationary by the pipet. In contrast, two vesicles of opposite charge "snapped" together (Figure 1). The cationic vesicle formed a concavity on its surface in order to enhance its contact with the neighboring anionic vesicle. The configuration was, however, unstable. After approximately 90 s the cationic vesicle departed while concurrently "peeling" lipid away from the anionic vesicle, as evidenced by a decided thinning of the anionic membrane. When the same two vesicles were forced into contact following their separation, they were unable to adhere. Apparently, the transfer of lipid from anionic to cationic vesicle generated two multilamellar vesicles, both with outer anionic shells that repelled each other.

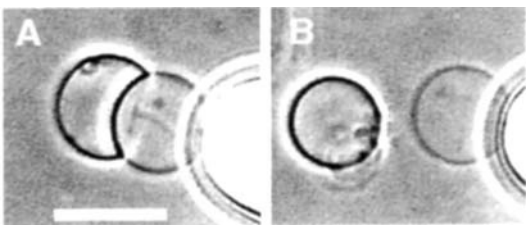

Figure 1. A) A "free" cationic vesicle that adheres to an anionic vesicle held by a micropipet. B) After about 90 s the cationic vesicle coats itself with anionic lipid from the stationary vesicle and diffuses away. Bar = 25 μm.

[*] Prof. F. M. Menger, J. S. Keiper
Department of Chemistry
Emory University
Atlanta, GA 30322 (USA)
Fax: Int. code +(404)727-6586

[**] This work was supported by the U. S. National Institutes of Health.

 © WILEY-VCH Verlag GmbH, D-69451 Weinheim, 1997 0570-0833/97/3622-2489 $ 17.50+.50/0

To confirm the above conclusions, the held vesicle from the preceding experiment was brought into contact with a new cationic vesicle. Adhesion occurred as with the first cationic vesicle (Figure 1). This is strong additional evidence that the anionic vesicle never lost its negative charge, and that lipid transfer was, therefore, unidirectional. The cationic vesicle must have thereby become coated with one or more of the anionic bilayers (the exact number is being now investigated by a newly designed Oxford Institute scanning transmission electron micropscope cryoprobe). If, instead, this receptor vesicle had actually incorporated anionic lipid within its outer cationic bilayer, its surface area would have greatly expanded; this was not observed. Moreover, such a direct transfer of lipid between bilayers should be slow as is "flip-flopping" between leaflets of a single bilayer.[9]

A cationic vesicle will frequently burst upon touching an anionic vesicle. Figures 2A and 2B show a small cationic vesicle that adhered to a larger anionic vesicle and then, upon bursting, coated only the "northern" hemisphere of the host vesicle (see the enhanced thickness of the coated region in Figure 2B). Subsequently, a second cationic vesicle fastened to an uncoated section of the anionic vesicle (Figure 2C). This cationic vesicle also burst to coat the remaining portion of the anionic vesicle (Figure 2D). When this anionic vesicle, now encapsulated with at least one cationic bilayer, was brought into contact with an anionic vesicle of nearly equal size, the latter adhered and burst (Figure 2E). The resulting lipid wrapped around the host membrane (Figure 2F), further thickening it. The twice-altered vesicle must have regained its negative charge because it could now no longer adhere to anionic vesicles.

The reproducible negative-positive-negative sequence in Figure 2 is reminiscent of the lamination possible with Langmuir–Blodgett films. The vesicle system has an operational advantage over films, however, in that films are blocked on one side by a solid support; this makes studies of diffusion through films more difficult. In any event, periodicity in vesicle membranes (as in solid films)[10] could lead to cooperative electronic effects and, thus, to systems with useful electrical, magnetic, and optical properties.

Servuss and Boroske[11] showed years ago that a membrane image can be scanned for intensity as a function of position as one passes through the membrane. We now applied this method to Figure 2 with the aid of an Image-Pro Plus processing routine. Figure 3A gives such an intensity distribution as the held vesicle (just prior to the adhesion shown in Figure 2A) is scanned along the indicated arrow. Intensities of 43 and 47 units correspond to the two points at which the arrow crosses a presumed single bilayer. After the small vesicle bursts and coats the northern hemisphere of the large vesicle (see Figure 2B), the scan changes to that in Figure 3B. The intensities are now 58 and 95 units, which correspond to single and double bilayers, respectively. The scan of Figure 2F (not shown) indicates that both crossover points are now triple bilayers (118 units).

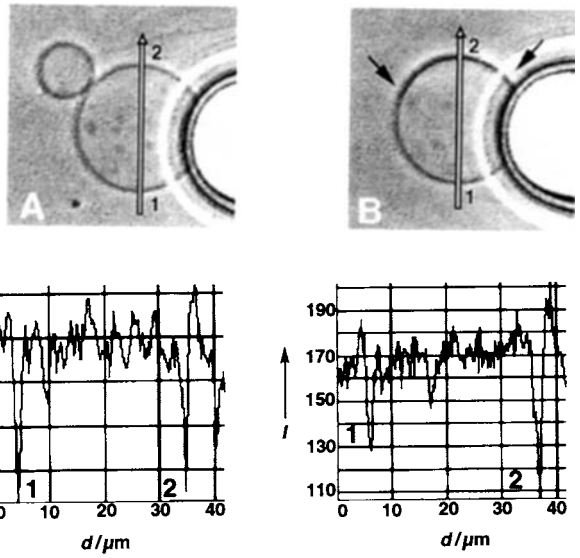

Figure 3. A) Intensity profile of the vesicle membrane prior to the adhesion shown in Figure 2A. The two minima represent the points where the white arrow in the micrograph crosses the bilayer. B) Intensity profile of the partially coated vesicle shown in Figure 2B. The intensity differences are measured from minima to adjacent maxima (representing the white "halo") and are in arbitrary units.

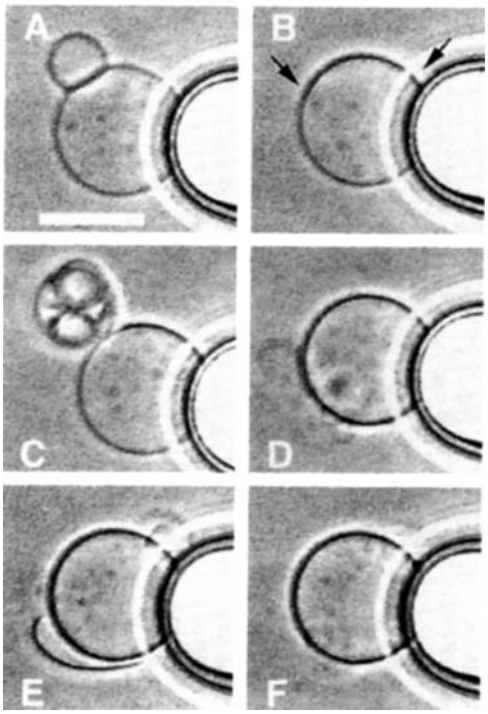

Figure 2. A) Adhesion of a small cationic vesicle to a large anionic vesicle. B) Within 10 s the cationic vesicle bursts and coats the northern region of the anionic vesicle (indicted by the arrows). C),D) A second cationic vesicle binds, bursts after 2 s, and coats the entire anionic vesicle. E),F) An anionic vesicle binds to the new cationic surface, bursts, and regenerates an anionic surface. Bar = 25 μm.

Electrostatic charge is an important feature of cell membranes,[12] and vesicles provide a useful means for evaluating this property. Most corresponding model studies in the past were carried out on submicroscopic vesicles (only 20–200 nm in diameter), for which information must be inferred spectroscopically.[13, 14] Giant vesicles, on the other hand, allow the surface charge to be controlled while the modifications are examined directly by optical methods.

Received: April 2, 1997 [Z10303IE]
German version: *Angew. Chem.* **1997**, *109*, 2602–2604

Keywords: cytomimetic chemistry · electrostatic interactions · microscopy · vesicles

[1] D. G. Zhu, M. C. Petty, H. Ancelin, J. Yarwood, *Langmuir* **1992**, *8*, 619.
[2] U. Seifert, *Adv. Phys.* **1997**, *46*, 13.
[3] K. Berndl, J. Käs, R. Lipowsky, E. Sackmann, U. Seifert, *Europhys. Lett.* **1990**, *13*, 659.
[4] H.-G. Döbereiner, E. Evans, M. Kraus, U. Seifert, M. Wortis, *Phys. Rev. E* **1997**, *55*, 4458.

 © WILEY-VCH Verlag GmbH, D-69451 Weinheim, 1997 0570-0833/97/3622-2490 $ 17.50+.50/0

[5] F. M. Menger, K. D. Gabrielson, *Angew. Chem.* **1995**, *107*, 2260; *Angew. Chem. Int. Ed. Engl.* **1995**, *34*, 2091.
[6] F. M. Menger, S. J. Lee, *Langmuir* **1995**, *11*, 3685.
[7] H. Ringsdorf, B. Scharb, J. Venzmer, *Angew. Chem.* **1988**, *100*, 117; *Angew. Chem. Int. Ed. Engl.* **1988**, *27*, 113.
[8] E. Evans, D. J. Klingenberg, W. Rawicz, F. Szoka, *Langmuir* **1996**, *12*, 3031.
[9] R. D. Kornberg, H. M. McConnell, *Biochemistry* **1971**, *10*, 1111.
[10] T. E. Mallouk, H. Lee, *J. Chem. Educ.* **1990**, *67*, 829.
[11] R.-M. Servuss, E. Boroske, *Chem. Phys. Lipids* **1980**, *27*, 57.
[12] G. Deng, T. Dewa, S. L. Regen, *J. Am. Chem. Soc.* **1996**, *118*, 8975.
[13] S. Ohki, S. Roy, H. Ohshima, K. Leonards, *Biochemistry* **1984**, *23*, 6126.
[14] L. Stamatatos, R. Leventis, M. J. Zuckermann, J. R. Silvius, *Biochemistry* **1988**, *27*, 3917.

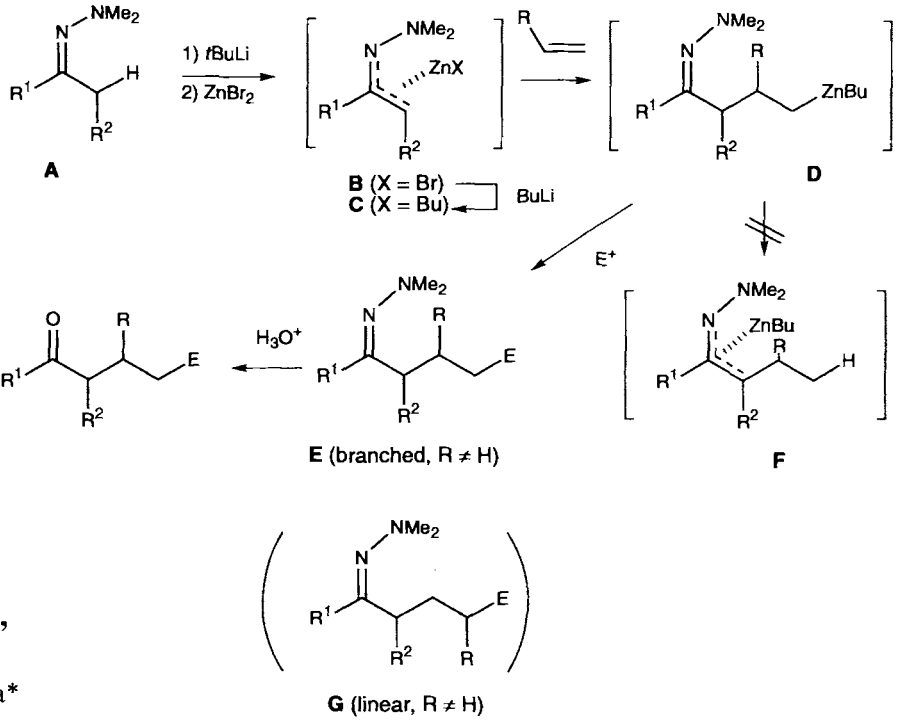

Scheme 1. Addition of a zinc hydrazone to a simple olefin; E = H, $H_2C{=}CHCH_2$, $H_2C{=}CHCH(Ph)$.

Addition of Azaenolates to Simple, Unactivated Olefins**

Katsumi Kubota and Eiichi Nakamura*

Whereas an enolate anion and its azaenolate congener readily add to a carbonyl compound,[1] they do not normally react with a simple, unactivated olefin;[2] little effort has been expended to effect such an "olefinic analogue" of the aldol reaction.[3, 4] We now found that addition of zinc hydrazone **C** to a simple olefin takes place at room temperature to afford the organozinc compound **D**, which then reacts with an added electrophile to give **E** in good yields (Scheme 1). The overall process represents a three-component synthesis of carbonyl derivatives. The key to a successful reaction is the use of the $BuZn^{II}$ species **C** instead of the $BrZn^{II}$ species **B**, with which the reaction was impractically slow.

N,*N*-Dimethylhydrazones **A** are ubiquitous synthetic substitutes of ketones, as they can be readily synthesized from and converted back into the corresponding ketones.[5] The addition reaction of the zinc hydrazone to an isolated olefin was carried out in the following manner for the *N*,*N*-dimethylhydrazone of 1,5-diphenylpentan-3-one (see Experimental Section for details): The hydrazone was treated in diethyl ether sequentially with one equivalent each of *t*BuLi, $ZnBr_2$ (to generate **B**), and BuLi (to generate **C**).[6] The solution of **C** was then placed under an ethylene atmosphere (5–10 atm) and stirred for four days at 20–35 °C. After the pressure had been released, water or D_2O was added to afford the ethylated product **E** in 88% yield (E = H or D, R = H; 100% deuterium incorporation at the terminal carbon atom; Table 1, entry 1). This indicates that the γ-zinc hydrazone **D** (a γ-enolate or "bis(homoenolate)")[7a] does not isomerize to a more stable isomer, such as **F**. We did not observe the formation of products due to addition of **D** to the C=N bond of **D** or **E**, or to further reaction of **D** with ethylene. There was no sign of butyl-group transfer from **C** in any of the reactions examined.[8] The use of the butylated species **C** is crucial, since **B** afforded **E** (E = H) in much lower yield (22%) under the same reaction conditions.[9]

Cyclic (entries 2 and 6) and acyclic ketone hydrazones (entries 1, 3–5, 7–13) reacted equally well. Deprotonation of an unsymmetrical ketone hydrazone (entry 5) took place at the less

1: R = H
2: R = C_6H_5
3: R = 4-$CH_3OC_6H_4$
4: R = 2-$CF_3C_6H_4$
5: R = $CH_3(CH_2)_5$
6: R = $(C_4H_9)_3SnCH_2$

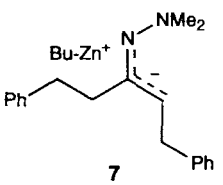

7

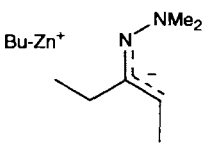

8

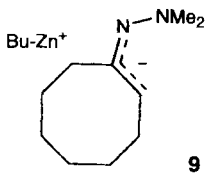

9

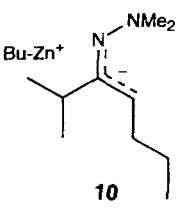

10

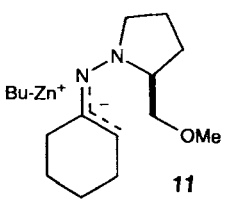

11

[*] Prof. E. Nakamura, Dr. K. Kubota
Department of Chemistry
The University of Tokyo
Bunkyo-ku, Tokyo 113 (Japan)
Fax: Int. code +(3)5800-6889
e-mail: nakamura@chem.s.u-tokyo.ac.jp

[**] We thank the Japanese Ministry of Education, Science, Sports, and Culture for financial support on the research. K. K. thanks the Japan Society for the Promotion of Science (JSPS) for a predoctoral fellowship.

 © WILEY-VCH Verlag GmbH, D-69451 Weinheim, 1997 0570-0833/97/3622-2491 $ 17.50+.50/0

hindered side, and the subsequent reaction with ethylene proceeded with retention of this regiochemistry.

Trapping **D** with carbon electrophiles provided a one-pot three-component coupling reaction; the results are summarized in entries 3–5 of Table 1. Allylation of **D** was achieved by an S_N2' reaction in the presence of a copper(I) salt.[10] Thus, **D** ($R^1 = PhCH_2CH_2$, $R^2 = PhCH_2$, R = H) reacts with CuCN and then with excess allyl bromide at 25 °C to afford an allylated product in 81% yield (entry 3). Reaction with cinnamyl bromide afforded exclusively an S_N2'-substituted product in 74% yield (entry 4).

Table 1. Hydrazone synthesis by a three-component coupling as an "olefinic analogue" of the aldol reaction [a].

Entry	Olefin	Zinc hydrazone[b]	Electrophile[c]	Product	Yield[%] [d]
1	**1**	**7**	$H_2O(D_2O)$	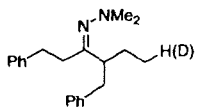	90
2	**1**	**9**	H_2O	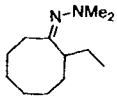	83
3	**1**	**7**	$H_2C{=}CHCH_2Br$, CuCN	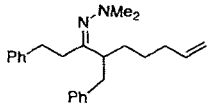	81
4	**1**	**8**	$PhCH{=}CHCH_2Br$, CuCN	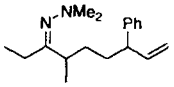	74[e]
5	**1**	**10**	$H_2C{=}CHCH_2Br$, CuCN	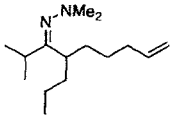	71
6	**1**	**11**	H_2O	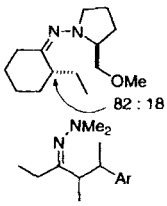	42
7	**2**	**8**	H_2O	Ar = C_6H_5	46[e,f]
8	**3**	**8**	H_2O	Ar = p-$CH_3OC_6H_4$	33[e,g]
9	**4**	**8**	H_2O	Ar = o-$CF_3OC_6H_4$	69[e,h]
10	**2**	**7**	H_2O	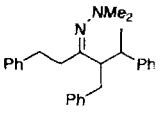	39[e,i]
11	**2**	**8**	$H_2C{=}CHCH_2Br$, CuCN	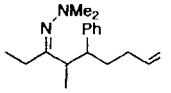	45[e]
12	**5**	**7**	H_2O	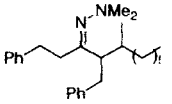	30[e,j]
13	**6**	**7**	H_2O	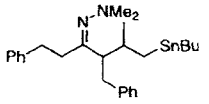	35[e,j]

[a] All reactions were carried out in diethyl ether at 25–35 °C for 4 (ethylene (**1**)) or 7–11 days (olefins **2**–**6**). The product consisted of a single stereoisomer (the stereochemistry was not determined). [b] See the Experimental Section for details of the metalation. [c] Excess H_2O (D_2O) was used for entries 1, 2, 6–10, 12, and 13. One equiv of CuCN, and three equiv of allyl bromide or cinnamyl chloride were used for entries 3–5 and 11. [d] Isolated product. [e] A 1:1 mixture of diastereomers. The ratio was determined by ^{13}C NMR spectropscopy. [f] The branched:linear ratio (**E**:**G**, Scheme 1) was 95:5. [g] **E**:**G** = 96:4. [h] **E**:**G** = 88:12. [i] **E**:**G** = 94:6. [j] The linear isomer was not detected.

Conversion of the alkylated *N*,*N*-dimethylhydrazones back into the corresponding ketones could be performed in high yield, for instance, with $CuCl_2$ catalysis (see Experimental Section).[5d] The SAMP hydrazone,[11] which was made from cyclohexanone and optically active hydrazine (S)-(−)-amino-2(methoxymethyl)pyrrolidine (SAMP), also reacted with excess ethylene to form the allylated product in 42% yield and a diastereomer ratio of 82:18 (entry 6).[12] These results suggest a new possibility for the asymmetric synthesis of carbonyl compounds.

The reaction with substituted olefins gave us some insight into the nature of the present reaction (Scheme 1; Table 1, entries 7–10). The zinc hydrazone reacted with a substituted styrene (6 equiv) at 20–25 °C to give mainly a "branched" adduct **E** (R = Ar) rather than a "linear" adduct **G**. Thus, *p*-methoxystyrene, styrene, and *o*-trifluoromethylstyrene reacted to provide the alkylated products in moderate yields (33–69%) with a ratio of branched to linear products (**E**:**G**) of 96:4, 95:5, and 82:18, respectively. The regioselectivity is hence opposite to that expected for conjugate addition of a free anionic species, in which the aryl group acts to stabilize the anion. There was however a small increase of the reaction rate in the given order, which suggests that there is some nucleophilic character to the reaction. The corresponding lithiated hydrazone is totally inert to styrene.[13] The styrene adduct could be utilized for further carbon-chain elongation (entry 11).

Aliphatic olefins such as 1-octene (entry 12) also took part, albeit slowly, in the reaction. It is noteworthy that allylstannane, which is normally regarded as a nucleophilic reagent, also reacted with a zinc hydrazone in 35% yield (entry 13).[14] Taken together with the styrene experiments, both the nucleophilicity of the azaenolate moiety and the electrophilicity of the zinc atom play equally important roles, as predicted for this type of reaction.[15] The product of the allylstannane reaction, **12**, possesses a novel assortment of functional groups: two organometallic groups of different reactivities and an electrophilic C–N double bond.

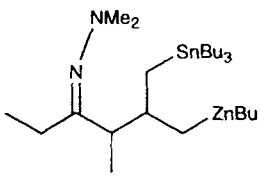

12

We have demonstrated that azaenolates add smoothly to simple, unactivated olefins to provide ketone derivatives by one-pot coupling of three components. Elucidation of the mechanism as well as development of enantioselective reactions[16] will be the subjects of further studies.

Experimental Section

1,5-Diphenyl-2-ethyl-3-pentanone *N*,*N*-dimethylhydrazone: To a solution of the *N*,*N*-dimethylhydrazone of 1,5-diphenylpentan-3-one (0.86 mL, 3.0 mmol) in Et_2O (3.0 mL) was added *t*BuLi in pentane (1.48 M, 2.0 mL, 3.0 mmol) at −70 °C, and the mixture warmed to 0 °C. After 4 h $ZnBr_2$ in Et_2O (0.33 M, 9.0 mL, 3.0 mmol) and, after another hour, BuLi in hexane (1.67 M, 1.8 mL, 3.0 mmol) were added, and the mixture was warmed to room temperature. After 1 h the prepared zinc hydrazone was transferred to an autoclave, and stirred under ethylene (8 atm) for four days. The resulting zinc hydrazone **D** was quenched with aq 30% potassium sodium tartrate, and the mixture extracted with ethyl acetate. After the organic extract was washed with aq sodium bicarbonate and aq sodium chloride, and dried over sodium sulfate, the solvent was removed in vacuo to provide 1.5 g of an oily crude product. Purification on silica gel (20 g, eluent Et_2O/hexane (5/95) and then Et_2O/hexane (15/85)) afforded a small amount of the starting hydrazone and the title compound (0.833 g, 90%). The product was fully characterized by IR, ^1H and ^{13}C NMR spectropscopy as well as elemental analysis.

 © WILEY-VCH Verlag GmbH, D-69451 Weinheim, 1997 0570-0833/97/3622-2492 $ 17.50+.50/0

Instead of treating **D** with water, **D** was allylated in situ (81% overall yield) by addition of $CuBr \cdot Me_2S$ (1.5 equiv) and then allyl bromide (3 equiv). The mixtrure was stirred for 3 h stirring and then subjected to aqueous workup as above (Table 1, entry 3). The hydrazone product was smoothly hydrolyzed (85% yield) according to a literature procedure [5d] by stirring a mixture of the hydrazone (1 mmol), $CuCl_2$ (1 mmol), 0.05 N phosphate buffer (3 mL), water (5 mL), and THF (15 mL) at 25–35 °C for 9 h.

Received: April 8, 1997
Revised version: July 14, 1997 [Z10326IE]
German version: *Angew. Chem.* **1997**, *109*, 2581–2583

Keywords: alkenes · hydrazones · ketones · zinc

[1] A. T. Nielsen, W. J. Houlihan, *Org. React.* **1968**, *16*, 1–438; T. Mukaiyama, *ibid.* **1982**, *28*, 203–331.
[2] The difficulty of this reaction is seen in the endothermicity of the reaction (26.5 kcal mol^{-1}, as calculated for free acetone enolate + ethylene, HF/3-21 + G).
[3] To improve the unfavorable thermodynamics a) the ring strain of a cyclic olefin was used (E. Nakamura, K. Kubota, *J. Org. Chem.* **1997**, *62*, 792–793) and b) an intramolecular reaction was carried out with an enolate bearing a $BrZn^{II}$ cation (P. Karoyan, G. Chassaing, *Tetrahedron Lett.* **1997**, *38*, 85–88; E. Lorthiois, I. Marek, J. F. Normant, *ibid.* **1997**, *38*, 89–92).
[4] Another recent (formally related) solution to the problem is the use of vinylmagnesium bromide as an "activated form" of ethylene (E. Nakamura, K. Kubota, G. Sakata, *J. Am. Chem. Soc.* **1997**, *119*, 5457–5458). This reaction, which takes place by a metalla-Claisen rearrangement, may be mechanistically unrelated to the present reaction.
[5] Utility of metalated hydrazones in the synthesis of carbonyl compounds is well documented: a) G. Stork, J. Benaim, *J. Am. Chem. Soc.* **1971**, *93*, 5938–5939; b) E. J. Corey, D. Enders, *Chem. Ber.* **1978**, *111*, 1337–1361 and **1978**, *111*, 1362–1383; c) D. E. Bergbreiter, M. Momongan, *Comprehensive Organic Synthesis, Vol. 2* (Eds.: B. M. Trost, I. Fleming), Pergamon, Oxford, **1991**, pp. 503–526; d) E. J. Corey, S. Knapp, *Tetrahedron Lett.* **1976**, *41*, 3667–3668.
[6] The structure of the zinc hydrazone is presently unknown. For the structures of lithium hydrazones, see D. B. Collum, D. Kahne, S. A. Gut, R. T. DePue, F. Mohamadi, R. A. Wanat, J. Clardy, G. V. Duyne, *J. Am. Chem. Soc.* **1984**, *106*, 4865–4869; R. A. Wanat, D. B. Collum, *ibid.* **1985**, *107*, 2078–2082; D. Enders, G. Bachstädter, K. A. M. Kremer, M. Marsch, K. Harms, G. Boche, *Angew. Chem.* **1988**, *100*, 1580–1581; *Angew. Chem. Int. Ed. Engl.* **1988**, *27*, 1522–1524.
[7] For a review of the related chemistry of homoenolates, see I. Kuwajima, E. Nakamura, *Comprehensive Organic Synthesis Vol. 2* (Eds.: B. M. Trost, I. Fleming), Pergamon, Oxford, **1991**, pp. 441–454.
[8] It is notable that the azaenolate moiety in **C**, and not the seemingly more reactive butyl group, reacts preferentially with the olefin. This lacking reactivity of the alkyl–zinc bond agrees with the fact that the product **E** does not react further with the starting olefin.
[9] The MeZn and *tert*-BuZn analogues of **C** are less reactive than **C**.
[10] See also K. Sekiya, E. Nakamura, *Tetrahedron Lett.* **1988**, *29*, 5155–5156; M. Arai, T. Kawasuji, E. Nakamura, *J. Org. Chem.* **1993**, *58*, 5121–5129, and references therein.
[11] D. Enders in *Asymmetric Synthesis, Vol. 3* (Ed.: J. M. Morrison), Academic Press, **1984**, pp. 275–339.
[12] The configuration of the new chiral center was assigned in anlogy to the reactions with SAMP hydrazones [11].
[13] Theory suggests that electrophilic activation of the olefin by the metal cation is important for the carbometalation of olefins: E. Nakamura, Y. Miyachi, N. Koga, K. Morokuma, *J. Am. Chem. Soc.* **1992**, *114*, 6686–6692; M. Nakamura, E. Nakamura, N. Koga, K. Morokuma, *J. Chem. Soc. Faraday Trans.* **1994**, *29*, 1789–1798; E. Nakamura, *Pure Appl. Chem.* **1996**, *68*, 123–130.
[14] Competition experiments indicated that 1-octene and the allylstannane react at roughly the same rate.
[15] The question still remains as to why the zinc hydrazone reacts much faster with olefins than with the polarized C=N bond.
[16] M. Nakamura, A. Hirai, E. Nakamura, *J. Am. Chem. Soc.* **1996**, *118*, 8489–8490; M. Nakamura, M. Arai, E. Nakamura, *ibid.* **1995**, *117*, 1179–1180.

Ligand-Mediated Coupling of Organometallic Reaction Centers**

Wolfgang Kaim,* Ralf Reinhardt, and Jan Fiedler

Dedicated to Professor Wolfgang Beck on the occasion of his 65th birthday

The electronic coupling of reversible single-electron transfer at individual redox centers as mediated by bridging molecules has played a pivotal role for the understanding of intra- and intermolecular electron transfer reactivity.[1] The mechanistic concepts of ligand-mediated "communication" between two or more electron-transfer-active metal sites have developed from simple systems, marked by the mixed-valent Creutz-Taube ion **1** as a molecular model for degenerate electron transfer between two separated metal ions,[1b, c, 2] to encompass a high degree of experimental and theoretical sophistication, and now extend from small molecules to large biological systems.[1a]

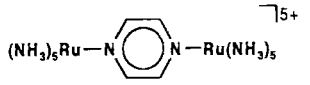

1

One common way[1c] to measure the metal–metal interaction in species like **1** is to determine the comproportionation constant K_c, which is defined in Equations (1) and (2) (Int: mixed-valent intermediate). However, for chemical purposes directed at synthetic transformations and eventual multielectron catalysis it would be more relevant to couple "redox reactivities" instead of mere electron transfer. Among the redox reactions beyond pure electron transfer processes, the EC-type "composite" mechanisms[3] represent the best understood examples: electron transfer (E) is followed by an elementary chemical step (C) such as a dissociation, and the thus created new species may eventually revert back to the starting compound through another set of EC steps. Composite processes such as EC or ECE (a two-electron variant) are crucial in organometallic chemistry and catalysis, for example, within reductive elimination/oxidative addition sequences.[3]

$$K_c = [Int]^2/[Ox] \times [Red] = 10^{\Delta E/59\ mV} \quad (1)$$

$$[Ox] + [Red] \rightleftharpoons 2[Int] \quad (2)$$

A well established reversible ECE process[4] involving Rh^{III} and coordinatively unsaturated Rh^{I} species has been used for some years for the catalysis of hydride transfer, for example, to H^+, NAD^+, or formate.[4a, 5] A single $\{Cp^*ClRh^+\}$ fragment ($Cp^* = C_5Me_5$) bound to an α-diimine ligand such as 2,2′-bipyridine or a 1,4-diaza-1,3-butadiene[4d, 6a] undergoes an ECE process in which the initial electron uptake is followed by a rapid dissociation of chloride as the chemical step and by a second electron acquisition. This reaction produces deeply colored neutral "Rh^{I}" compounds that are reoxidized at a significantly less

[*] Prof. Dr. W. Kaim, Dr. R. Reinhardt
Institut für Anorganische Chemie der Universität
Pfaffenwaldring 55, D-70550 Stuttgart (Germany)
Fax: Int code + (711) 685 4165
e-mail: kaim@anorg55.chemie.uni-stuttgart.de
Dr. J. Fiedler
J. Heyrovsky Institute for Physical Chemistry and Electrochemistry
Dolejskova 3, CZ-18223 Prague 8 (Czech Republic)
e-mail: jan.fiedler@jh-inst.cas.cz

[**] This work was supported through grants from the Deutsche Forschungsgemeinschaft (SFB 270, German–Czech Exchange Program), the Volkswagenstiftung, and the Fonds der Chemischen Industrie. Donations of $RhCl_3$ by Degussa AG are also gratefully acknowledged.

 © WILEY-VCH Verlag GmbH, D-69451 Weinheim, 1997 0570-0833/97/3622-2493 $ 17.50+.50/0

negative potential and then bind to the additional ligand.[4] In the catalytic cycle the active form Cp*Rh(α-diimine) can oxidatively add a proton to form the essential, reactive hydride intermediate [Cp*RhH(α-diimine)]$^+$.[4a, b, 5] The less reactive iridium analogues may be isolated and characterized.[6]

In a first systematic attempt to extend the coupling of electron transfer sites to the coupling of redox reaction centers through conjugated bridging ligands we have synthesized[7] the symmetrically dinuclear compounds [Cp*ClRh(μ-L)RhClCp*](PF$_6$)$_2$, L = bpip[8a] (**2**) and bptz[8b] (**3**) and studied their extended but

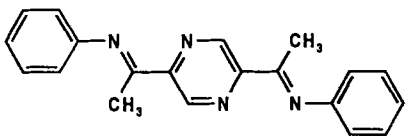

bpip

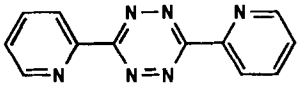

bptz

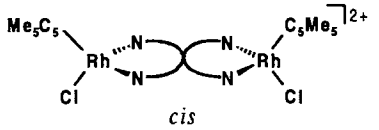

cis

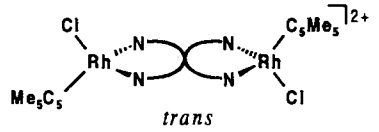

trans

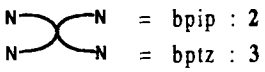

= bpip : **2**

= bptz : **3**

fully reversible electrochemistry by EPR and UV/Vis spectroscopic techniques. Whereas bpip resembles a bis-chelate modification of the familiar pyrazine ligand (see **1**), the bptz molecule was chosen because of its proven ability to promote very strong coupling between transition metal centers; for example, $K_c = 10^{15}$ for the bis(tetraammineruthenium) compound.[8b]

The results of the cyclic voltammetry of the dinuclear rhodium compounds reveal fully reversible cycles, including two separated halide dissociation/association processes and up to six electron transfer steps (Figure 1). Diagnostic criteria for the oxidation state formulation of the intermediates are the UV/Vis/NIR absorption spectra from OTTLE spectroelectrochemistry (Figure 2),[9] the release of chloride as studied by Hg polarography,[4e] and—in the case of paramagnetic compounds—the EPR signals. From this information we can derive the sequence summarized in Table 1.

In both cases (L = bpip and bptz), the first reduction is no longer an ECE process but an electrochemically reversible one-electron reduction. Absorption and EPR spectra clearly indicate L-centered spin (a radical anion ligand[10]). Chloride dissociation occurs only after the second one-electron reduction, indicating a decoupling of the ECE process[11] into an E and EC step. In other words, the ligand L acts as a remote electron storage or "reservoir"[3, 12] until the second electron triggers a

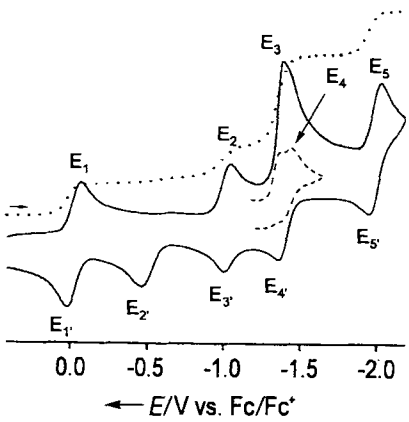

Figure 1. Cyclic voltammogram of [Cp*ClRh(μ-bptz)RhClCp*](PF$_6$)$_2$ in acetonitrile/0.1 M Bu_4NPF_6 at 100 mVs^{-1} (solid line) and 50 mVs^{-1} (broken line). Dotted line: response from rotating disk electrode (glassy carbon) at 20 mVs^{-1}, ω = 2000 rpm. Fc/Fc$^+$ = ferrocene/ferrocenium.

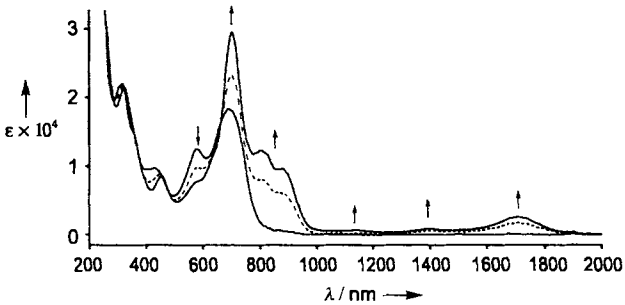

Figure 2. Spectroelectrochemical reduction of [Cp*Rh(μ-bpip)RhClCp*]$^+$ to [Cp*Rh(μ-bpip)RhCp*]$^+$ in acetonitrile/0.1 M Bu_4NPF_6.

Table 1. Electrochemical potentials [a], absorption maxima [b], and EPR data of dinuclear complexes with L = bpip (bptz).

	E_{pa}	E_{pc}	λ_{max} [nm]	
[Cp*ClRh(L)RhClCp*]$^{2+}$			456	(536)
	−0.43 (0.04)	−0.50 (−0.03)		
[Cp*ClRh(L)RhClCp*]$^{+}$			690[e]	(420,sh)[f]
+Cl$^-$ / −Cl$^-$	−0.43 (−0.46)	−0.76 (−1.06)		
[Cp*Rh(L)RhClCp*]$^+$			691	(614)
+Cl$^-$ / −Cl$^-$	−1.03 (−1.07)	−1.25 (−1.37)		
[Cp*Rh(L)RhCp*]$^{\cdot+}$ [c]			1708[c]	
	−1.33[c]	−1.39[c]		
[Cp*Rh(L)RhCp*]$^+$			1136	(792)
	−2.37 (−1.37)	−2.45 (−1.44)		
[Cp*Rh(L)RhCp*]$^{\cdot-}$				(866)[d, g]
	(−1.94)[d]	(−2.02)[d]		
[Cp*Rh(L)RhCp*]$^{2-}$				(691)[d]

[a] From cyclic voltammetry at 100 mVs^{-1} in acetonitrile/0.1 M Bu_4NPF_6, anodic and cathodic peak potentials E_{pa} and E_{pc} in V vs. Fc$^+$/Fc^0. [b] Long-wavelength absorption maxima λ_{max} in nm from spectroelectrochemistry. [c] Only for L = bpip. [d] Only for L = bptz. [e] g_{iso} = 1.9934 (270 K). [f] $g_\perp$ = 2.0019, $g_\parallel$ = 1.9914 (3.4 K). [g] g_1 = 2.151, g_2 = 2.035, g_3 = 1.960 (3.4 K).

combined metal-centered two-electron reduction of Rh^{III} to yield chloride-free Rh^I. The appearance of the {Cp*Rh^I} moiety bound to a π-acceptor ligand is evident from intense long-wavelength absorptions.[4c]

Interaction between the two organometallic reaction centers[11] is evident from the fact that the loss of chloride occurs stepwise, separated by significant potential differences of more than 300 mV. The class I[13] mixed-valent species [Cp*ClRh-

 © WILEY-VCH Verlag GmbH, D-69451 Weinheim, 1997 0570-0833/97/3622-2494 $ 17.50+.50/0

(μ-L)RhCp*]$^{\bullet+}$ formed in the first chloride-releasing process is reduced for L = bptz in an ECE step to neutral [Cp*Rh-(μ-bptz)RhCp*] at more negative potential; there are two more reversible one-electron steps with a paramagnetic intermediate that may be formulated[14] according to [Cp*Rh^{I}(μ-bptz^{-I})-Rh^{I}Cp*]$^{\bullet-}$ $\leftrightarrow$ [Cp*Rh^{I}(μ-bptz^{-II})Rh^{II}Cp*]$^{\bullet-}$ based on the significant g anisotropy[14] in comparison to that of [Cp*ClRh^{III}-(μ-bptz^{-I})Rh^{III}ClCp*]$^{\bullet+}$ (Table 1).

For L = bpip the second ECE step is once again decoupled but—unlike the first—in an EC process followed by an electron transfer E step. This sequence produces an unusual mixed-valent Rh^{II}/Rh^{I} intermediate with a comproportionation constant K_c of about $10^{2.4}$ and a series of fairly intense long-wavelength absorption bands in the near-infrared (NIR) region (Figure 2). This intermediate differs from the much investigated Creutz-Taube ion **1**[1c, 2] by being a d^7/d^8 [15] instead of a d^5/d^6 mixed-valent dimer. The higher reduced states of the bpip complex were too unstable for further characterization. In summary, the following general points can be made:

- The ECE processes observed for the mononuclear systems[4, 5] can be split in various ways (E + EC, EC + E).
- Acceptor ligands may act as passive electron storage sites until the necessary number of electrons is collected and then transferred to the potentially reactive site at the right potential for chemical reactivity.
- There is clearly a "communication" between the organometallic reaction sites in the dinuclear rhodium complexes bridged by bpip or bptz; the halide-releasing steps are separated by about 0.3 (L = bptz) and 0.5 V (L = bpip).

At this point the differences between the two systems are not immediately apparent, this first systematic study thus produces further questions related to the eventual construction of multielectron redox systems coupled with potentially catalytic chemical reactivity.

Received: April 24, 1997 [Z 10344 IE]
German version: *Angew. Chem.* **1997**, *109*, 2600–2602

Keywords: cyclic voltammetry · electrochemistry · electron transfer · reaction mechanisms · rhodium

[1] a) *Electron Transfer in Inorganic, Organic and Biological Systems* (Eds.: J. R. Bolton, N. Mataga, G. McLendon), *Adv. Chem. Ser. No. 228*, ACS, Washington, **1991**; see also chapter 1 in ref.[3]; b) H. Taube, *Angew. Chem.* **1984**, *96*, 315; *Angew. Chem. Int. Ed. Engl.* **1984**, *23*, 329; c) C. Creutz, *Prog. Inorg. Chem.* **1983**, *30*, 1.

[2] C. Creutz, H. Taube, *J. Am. Chem. Soc.* **1973**, *95*, 1086.

[3] D. Astruc, *Electron Transfer and Radical Processes in Transition-Metal Chemistry*, VCH, New York, **1995**.

[4] a) U. Kölle, M. Grätzel, *Angew. Chem.* **1987**, *99*, 572; *Angew. Chem. Int. Ed. Engl.* **1987**, *26*, 568; b) U. Kölle, B.-S. Kang, P. Infelta, P. Compte, M. Grätzel, *Chem. Ber.* **1989**, *122*, 1869; c) M. Ladwig, W. Kaim, *J. Organomet. Chem.* **1991**, *419*, 233; d) R. Reinhardt, W. Kaim, *Z. Anorg. Allg. Chem.* **1993**, *619*, 1998; e) W. Kaim, R. Reinhardt, E. Waldhör, J. Fiedler, *J. Organomet. Chem.* **1996**, *524*, 195; f) W. Kaim, R. Reinhardt, M. Sieger, *Inorg. Chem.* **1994**, *33*, 4453; g) R. Reinhardt, J. Fees, A. Klein, M. Sieger, W. Kaim in *Wasserstoff als Energieträger*, VDI-Verlag, Düsseldorf, **1994**, p. 133.

[5] a) D. Westerhausen, S. Herrmann, W. Hummel, E. Steckhan, *Angew. Chem.* **1992**, *104*, 1496; *Angew. Chem. Int. Ed. Engl.* **1992**, *31*, 1529; b) E. Steckhan, S. Herrmann, R. Ruppert, J. Thömmes, C. Wandrey, *ibid.* **1990**, *102*, 445 and **1990**, *29*, 388; c) C. Caix, S. Chardon-Noblat, A. Deronzier, R. Ziessel, *J. Electroanal. Chem.* **1993**, *362*, 301; d) R. Ziessel, *Angew. Chem.* **1991**, *103*, 863; *Angew. Chem. Int. Ed. Engl.* **1991**, *30*, 844; e) C. Caix, S. Chardon-Noblat, A. Deronzier, R. Ziessel, *J. Electroanal. Chem.* **1996**, *403*, 189.

[6] a) S. Greulich, W. Kaim, A. Stange, H. Stoll, J. Fiedler, S. Zalis, *Inorg. Chem.* **1996**, *35*, 3998; b) R. Ziessel, *J. Am. Chem. Soc.* **1993**, *115*, 118; c) M. Ladwig, W. Kaim, *J. Organomet. Chem.* **1992**, *439*, 79.

[7] a) General procedure: [{Cp*Cl$_2$Rh}$_2$] (250 mg, 0.4045 mmol) [4] was suspended in acetone (50 mL) and treated with $AgPF_6$ (204.5 mg, 0.809 mmol) and stirred for 30 min. The resulting AgCl was filtered off and Bu_4NPF_6 (620 mg, 1.6 mmol) was added to the filtrate. A solution of the bridging ligand (L = bpip or bptz, 0.32 mmol) in acetone (ca. 20 mL) was then added. After the mixture had been stirred for 6 h at room temperature the volume was reduced to about 20 mL and the light brown (L = bpip) or dark red (L = bptz) product was completely precipitated by addition of pentane. Filtration and washing with diethyl ether yielded about 70% of the product. Correct elemental analyses (C,H,N). b) The complexes are formed as mixtures of *cis* and *trans* isomers with respect to Cl and Cp* ligands. For L = bptz (ratio 4:1) the NMR signals of the minor component could not be completely identified due to partial overlap: ^{1}H NMR (250 MHz, CD_3NO_2, 298 K): δ = 1.98 (s, 30H; Cp*, major isomer), 1.99 (s, 30H; Cp*, minor isomer), 8.36 (ddd, 2H; H5,5'), 8.70 (td, 2H; H4,4'), 9.26 (m, 2H; H3,3'), 9.28 (m, 2H; H6,6'); J(H3,H4) 7.8, J(H4,H5) 7.8, J(H5,H6) 5.5, J(H3,H5) 1.2, J(H4,H6) 1.4 Hz. c) For L = bpip the *cis* and *trans* isomers are formed in a 1:1 ratio that can be shifted to 3:1 by fractional crystallization. As expected, cyclic voltammetry and spectroelectrochemistry are not perceptibly affected by the changing isomer ratio. ^{1}H NMR (250 MHz, CD_3NO_2, 298 K): δ = 1.65 (s, 30H; Cp*, isomer I), 1.63 (s, 30H; Cp*, isomer II), 2.94 (s, 6H; CH_3, isomer I), 2.98 (s, 6H; CH_3, isomer II), 7.65 (m, 4H; ^{o}-H,$^{o'}$-H, two isomers), 7.69 (m, 2H; ^{p}-H,$^{p'}$-H, two isomers), 7.83 (m, 4H; ^{m}-H,$^{m'}$-H, two isomers), 9.64 (s, 2H, ^{pz}-H; isomer I), 9.61 (s, 2H, ^{pz}-H; isomer II).

[8] a) T. Stahl, V. Kasack, W. Kaim, *J. Chem. Soc. Perkin Trans. 2* **1995**, 2127; b) J. Poppe, M. Moscherosch, W. Kaim, *Inorg. Chem.* **1993**, *32*, 2640.

[9] OTTLE cell (optically transparent thin-layer electrolytic cell): M. Krejcik, M. Danek, F. Hartl, *J. Electroanal. Chem.* **1991**, *317*, 179.

[10] W. Kaim, *Coord. Chem. Rev.* **1987**, *76*, 187.

[11] The mononuclear complex [Cp*RhCl(bptz)](PF$_6$) exhibits electrochemically irreversible reduction at E_{pc} = −0.59 V vs. Cp_2Fe^+/Fc^0.

[12] a) D. Astruc, *Chem. Rev.* **1988**, *88*, 1189; b) *Acc. Chem. Res.* **1986**, *19*, 377.

[13] M. B. Robin, P. Day, *Adv. Inorg. Chem. Radiochem.* **1967**, *10*, 247.

[14] For diruthenium analogues see V. Kasack, W. Kaim, H. Binder, J. Jordanov, E. Roth, *Inorg. Chem.* **1995**, *34*, 1924.

[15] A. Klein, W. Kaim, J. Fiedler, S. Zalis, *Inorg. Chim. Acta*, in press.

Isolation and X-ray Structural Determination of Both Folded and Twisted Conformers of Bis{4*H*,8*H*-4-(dicyanomethylene)-benzo[1,2-*c*:4,5-*c'*]bis[1,2,5]thiadiazol-8-ylidene}, an Overcrowded Ethylene with High Electron Affinity**

Takanori Suzuki,* Takanori Fukushima, Tsutomu Miyashi, and Takashi Tsuji

Recently much attention has been focused on optically responsive molecules, which are interesting as molecular devices or switches.[1] Overcrowded ethylenes are one of the promising candidates for this purpose,[2] because they exhibit a characteristic color change associated with their conformational isomerism. The leading compound in this area is bianthrone (**1**),[3] which adopts the doubly folded conformation **1A** in the ground state to reduce the steric repulsion in the fjord region.[4] Triggered by heating, photoexcitation, or pressure, this yellow conformer partly transforms into a green metastable form,[5] which is believed to be the twisted conformation **1B**.[6] Because the

[*] Prof. T. Suzuki, T. Fukushima,[*] Prof. T. Tsuji
Division of Chemistry, Graduate School of Science
Hokkaido University
Sapporo 060 (Japan)
Fax: Int. code +(11)746-2557
e-mail: tak@science.hokudai.ac.jp

[+] Permanent address: Tohoku University, Graduate School of Chemistry
Sendai (Japan)
Prof. T. Miyashi
Department of Chemistry, Tohoku University, Sendai (Japan)

[**] We thank Prof. Tamotsu Inabe (Hokkaido University) for the use of the X-ray structure analysis system and FT-IR microscope. T. F. thanks the Ministry of Education, Science, and Culture, Japan for a research grant (No. 0067) and JSPS Research Fellowships for Young Scientists.

 © WILEY-VCH Verlag GmbH, D-69451 Weinheim, 1997 0570-0833/97/3622-2495 $ 17.50+.50/0

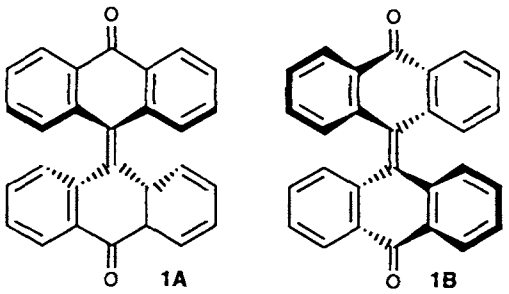

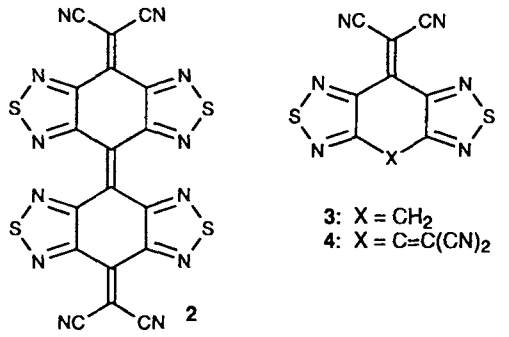

features of the analogous charged isomers are different from those of the corresponding neutral species, the conformational change can be also induced electrochemically.[7] Combination of the isomerism and electron transfer is expected to provide the multichannel response system depicted in Scheme 1, but none of

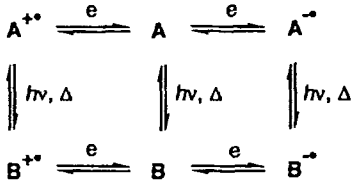

Scheme 1. Multichannel response system based on the conformational change of both the neutral and charged species.

the overcrowded ethylenes have yet afforded stable radical ion salts. We have designed and prepared the title electron acceptor **2**, whose radical anion is stable enough to be isolated. Neutral **2** exhibits the characteristic chromism involving the folded and twisted conformers. This compound is the first interconvertible overcrowded ethylene of which both conformers can be isolated and their geometries unambiguously determined by X-ray analyses.[8]

Ethylene **2** was obtained in 50% yield by oxidation of tricyclic compound **3**[9] with SeO_2 on heating under reflux in EtOH for 18 h and purification by successive recrystallization. The appearance of the crystalline sample differs in color significantly depending on the recrystallization solvents; yellow plates [m.p. 351–357 °C (decomp.)] were obtained from 1,2-dichloroethane, whereas deep violet needles [m.p. 110–112 °C (decomp.)] or cubes [m.p. 84–86 °C (decomp.)] were formed in CH_2Cl_2 or PhCN solution. Combustion analyses indicated that the latter two forms contain crystallization solvents (**2**·CH_2Cl_2 or **2**·2PhCN, respectively).[10]

X-ray analyses[11] clearly show that the molecule in the unsolvated yellow crystal adopts doubly folded geometry (**2A**) whereas the twisted conformer (**2B**) exists in the violet PhCN-solvated crystal (Figure 1). Both types of deformation are due to the

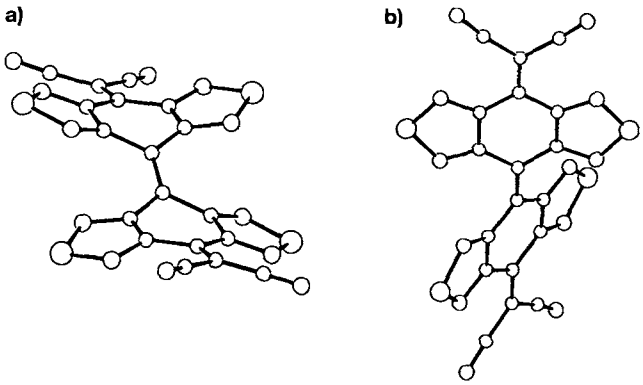

Figure 1. Two geometries of **2** determined by X-ray: a) the doubly folded conformer **2A** (in the unsolvated yellow crystal the molecule on the crystallographic center of symmetry); b) the twisted conformer **2B** in the violet PhCN-solvated crystal.

repulsive interaction through the short N···N contacts (2.67 Å in **2A**; 2.74 and 2.81 Å in **2B**) of less than the sum of van der Waals radii (3.0 Å). The central ethylene bond in **2A** [1.362(4) Å] is completely planar within only 0.01 Å deviation of six carbon atoms from the least-squares plane, yet the same bond in **2B** is twisted by 48.1° and much longer [1.388(7) Å] than in **2A**. On the other hand, the halves of the molecule containing the tricyclic moiety in violet **2B** are nearly planar (less than 0.11 Å deviation) as in **3** or **4**,[9] but the central six-membered ring in yellow **2A** deforms into the boat form with the dihedral angle of 149.8° between the fused heterocycles.

Upon heating, the solvated violet crystals turned yellow with loss of volatile CH_2Cl_2 or PhCN. The resulting solids as well as the yellow plates of **2A** did not show any indication of conformational isomerism to form violet **2B** up to the decomposition point of the **2A** crystal. These results indicate that in the solid state the doubly folded geometry is more stable at high temperature. The twisted conformer **2B** can be isolated as a solid only in the presence of suitable guest (solvent) molecules.[12] Inspection of the packing arrangement suggests that **2B**·2PhCN crystal is a clathrate complex, and the cavities formed by twisted conformers **2B** are filled with the solvent molecules (Figure 2). On the other hand, electrostatic S···N≡C interactions connect the folded conformers **2A** in the lateral direction to form an infinite "sheetlike" network, which is further stacked to form a layer structure as in **4**.[9] Such an attractive force is also at work, but less effectively, in **2B**·2PhCN; thus the stabilization by S···N≡C interaction may also contribute to the preference for the **2A** conformer in the crystalline state.

Upon grinding in a mortar, the yellow crystal of **2A** turned violet, illustrating its mechanochromic behavior. Under the FT-IR microscope a single crystal of **2A** showed a band at 1581 cm^{-1}, which is assigned to the C=C stretching mode of the dicyanomethylene groups. After grinding, this band remained at 1580 cm^{-1} in the spectrum (KBr disk) but a new and larger band appeared at 1553 cm^{-1}, a quite similar frequency to that of **2B**·CH_2Cl_2 (1551 cm^{-1}) and **2B**·2PhCN (1550 cm^{-1}) crystals. The new band disappeared concomitant with the fading of the violet color upon heating the KBr pellet at 220 °C for 5 h, and the original band grew in intensity. Such a phenomenon is best accounted for by the reversible mechano- and thermochromism involving the two conformers **2A** and **2B**.

In contrast to the solid state, in solution the twisted conformer **2B** seems to be more stable,[12] and both yellow and solvated violet crystals afforded identical violet solutions upon dissolution. The UV-Vis spectrum [λ_{max} (lg ε) = 313 (4.659), 400

 © WILEY-VCH Verlag GmbH, D-69451 Weinheim, 1997 0570-0833/97/3622-2496 $ 17.50+.50/0

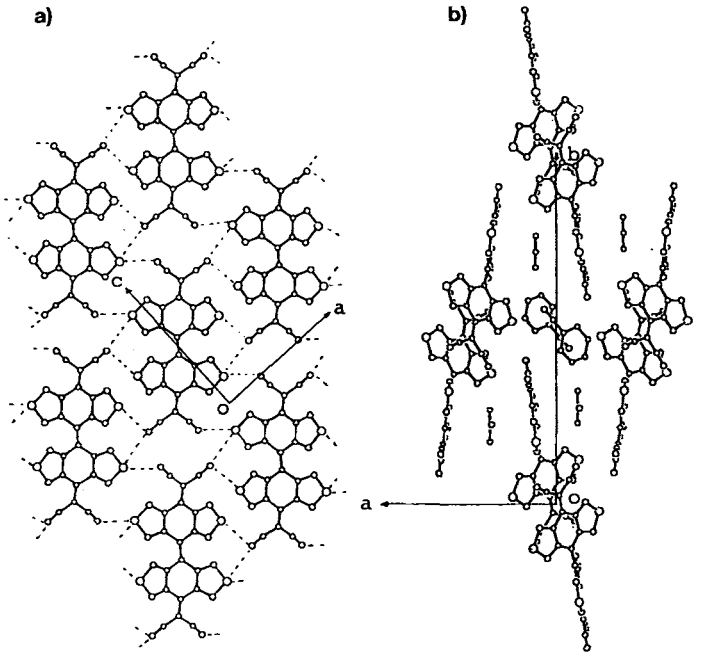

Figure 2. Arrangement of the molecules a) in the unsolvated yellow crystal (short S···N≡C contacts of 3.30, 3.32, and 3.36 Å are indicated by dotted lines) and b) in the violet PhCN-solvated crystal (two crystallographically independent PhCN molecules are included in the spatial cavity; short S···N≡C contacts (S···N = 3.01 Å) are observed along the *c* axis not shown in this view).

(4.165), 433 (sh, 4.096), 515 (sh, 4.470), 544 nm (4.513) in CH_2Cl_2 at 25 °C] closely resembles that of **2B**·CH_2Cl_2 crystal [KBr disk; λ_{max} (relative intensity) = 326 (1.00), 407 (0.28), 568 (sh, 0.84), 607 nm (0.87)]. Although the precise proportion of **2A** and **2B** in solution is not known, the cyclic voltammogram of **2** can be explained by assuming the presence of only one conformer (**2B**). Thus, four reversible, one-electron reduction waves were observed at +0.28, +0.06, −0.95, and −1.10 V vs the saturated calomel electrode (0.1 M nBu_4NBF_4 in CH_2Cl_2, Pt electrode, scan rate 100 mVs^{-1}, 25 °C). The electron affinity of **2** is similar to that of TCNQ (E_1^{red} = + 0.30 V) and much higher than those of **1** or its bis(dicyanomethylene) derivative[13] (E_p^{red} = −1.16 and −0.77 V, respectively, under the same conditions). Thus, by the reaction with iodide **2** was readily reduced to the radical anion, which could be isolated as stable salts.[14] Furthermore, **2** gave charge transfer complexes with some donors despite its severely deformed geometry. The moderate electrical conductivity ($\sigma = 3.4 \times 10^{-2}$ Scm^{-1}) of the 1:1:1 complex of **2**, tetrathiatetracene, and H_2O is noteworthy.

Received: April 8, 1997 [Z10325IE]
German version: *Angew. Chem.* **1997**, *109*, 2607–2609

Keywords: isomerizations · molecular devices · radical ions · redox chemistry · thermochromism

[1] Review: B. L. Feringa, W. F. Jager, B. de Lange, *Tetrahedron* **1993**, *49*, 8267.
[2] a) B. L. Feringa, W. F. Jager, B. de Lange, E. W. Meijer, *J. Am. Chem. Soc.* **1991**, *113*, 5468; b) M. Jørgensen, K. Lerstrup, P. Frederiksen, T. Bjørnholm, P. Sommer-Larsen, K. Schaumburg, K. Brunfeldt, K. Bechgaard, *J. Org. Chem.* **1993**, *58*, 2785.
[3] T. Bercovici, R. Korenstein, K. A. Muszkat, E. Fisher, *Pure Appl. Chem.* **1970**, *24*, 531.
[4] E. Harnik, G. M. J. Schmidt, *J. Chem. Soc.* **1954**, 3295; I. Agranat, Y. Tapuhi, *J. Org. Chem.* **1979**, *44*, 1941.
[5] H. Meyer, *Monatsh. Chem.* **1909**, *30*, 165; Y. Hirshberg, E. Fisher, *J. Chem. Soc.* **1953**, 629; D. L. Fanselow, H. G. Drickamer, *J. Chem. Phys.* **1974**, *61*, 4567.
[6] R. Korenstein, K. A. Muszkat, S. Sharafy-Ozeri, *J. Am. Chem. Soc.* **1973**, *95*, 6177.
[7] D. H. Evans, N. Xie, *J. Am. Chem. Soc.* **1983**, *105*, 315; D. H. Evans, R. W. Busch, *ibid.* **1982**, *104*, 5057; P. Neta, D. H. Evans, *ibid.* **1981**, *103*, 7041; B. A. Olsen, D. H. Evans, *ibid.* **1981**, *103*, 839.
[8] The folded isomer of bis[1,3-bis(dicyanomethylene)indan-2-ylidene] undergoes one-way isomerization to the severely twisted conformer, and X-ray analyses on both forms were successfully carried out: A. Beck, R. Gompper, K. Polborn, H.-U. Wagner, *Angew. Chem.* **1993**, *105*, 1424; *Angew. Chem. Int. Ed. Engl.* **1993**, *32*, 1352. Of the three structures of 2-(thioxanthen-9-ylidene)-indane-1,3-dione, the folded and folded-twisted conformers were determined by X-ray but the twisted one is missing: J. J. Stezowski, P. U. Biedermann, T. Hildenbrand, J. A. Dorsch, C. J. Eckhardt, I. Agranat, *J. Chem. Soc. Chem. Commun.* **1993**, 213.
[9] T. Suzuki, H. Fujii, Y. Yamashita, C. Kabuto, S. Tanaka, M. Harasawa, T. Mukai, T. Miyashi, *J. Am. Chem. Soc.* **1992**, *114*, 3034.
[10] Elemental analysis: Calcd for **2A** ($C_{18}N_{12}S_4$): C 42.18, N 32.79, S 25.02; found: C 42.25, N 32.99, S 24.82. Calcd for **2B**·2PhCN ($C_{32}H_{10}N_{14}S_4$): C 53.47, H 1.40, N 27.28; found: C 53.35, H 1.56, N 27.42. Calcd for **2B**·CH_2Cl_2 ($C_{19}H_2Cl_2N_{12}S_4$): C 38.20, H 0.34, N 28.13; found: C 38.80, H 0.66, N 28.26.
[11] Crystal structure analyses: **2A**: $C_{18}N_{12}S_4$, monoclinic, $P2_1/c$, $a = 10.226(2)$, $b = 7.820(1)$, $c = 11.725(1)$ Å, $\beta = 91.03(1)°$, $V = 937.5(3)$ Å^3, ρ_{calcd} ($Z = 2$) = 1.816 gcm^{-3}, $R = 0.039$. **2B**·2PhCN: $C_{32}H_{10}N_{14}S_4$, monoclinic, $P2_1/n$, $a = 13.554(2)$, $b = 26.348(5)$, $c = 8.929(1)$ Å, $\beta = 97.56(1)°$, $V = 3161.2(9)$ Å^3, ρ_{calcd} ($Z = 4$) = 1.511 gcm^{-3}, $R = 0.061$. Crystallographic data (excluding structure factors) for the structures reported in this paper have been deposited with the Cambridge Crystallographic Data Centre as supplementary publication no. CCDC-100324. Copies of the data can be obtained free of charge on application to The Director, CCDC, 12 Union Road, Cambridge CB2 1EZ, UK (fax: int. code +(1223)336-033; e-mail: deposit@chemcrys.cam.ac.uk).
[12] Calculated heats of formation (AM1) of **2A** and **2B** are 422.0 and 430.8 $kcal\,mol^{-1}$, respectively. The estimated atomic charges on heterocycles in **2B** (+ 0.61 on S; −0.29 on N) are marginally larger than those in **2A** (+ 0.58 on S; −0.26 on N), which might be related to the preference of **2B** in solution caused by effective solvation.
[13] S. Yamaguchi, T. Hanafusa, T. Tanaka, M. Sawada, K. Kondo, M. Irie, H. Tatemitsu, Y. Sakata, S. Misumi, *Tetrahedron Lett.* **1986**, *27*, 2411.
[14] The molar ratio present in both *N*-methylquinolinium and *N*-methylacridinium salts is 1:1 and the electrical conductivities are 3.2×10^{-3} Scm^{-1} and 6.2×10^{-4} Scm^{-1}, respectively.

A Calix[4]arenoporphyrin**

Richard G. Khoury, Laurent Jaquinod, Katsuhiro Aoyagi, Marilyn M. Olmstead, Andrew J. Fisher, and Kevin M. Smith*

Due to the potential biological or other catalytic activity of supramolecular arrays,[1, 2] much interest has been focused on the synthesis and chemistry of such assemblies. Recently, large cyclic structures were obtained based on porphyrin subunits as building blocks.[3] It was shown that supramolecular arrays of porphyrins with higher order structures act not only as unique molecular recognition species but also as enzyme-mimicking catalytic sites.[4]

Among the different building blocks that were studied for the synthesis of artificial receptor molecules, calixarenes,[5] cyclodextrins, and resorcinol-based cavitands are particularly useful.[6] Recently, considerable interest has been given to the use of calixarenes as platforms for the construction of supramolecular receptor assemblies.[7] Calixarenes are readily accessible cyclic polyphenols which are chemically transformable in a selective fashion, so that they are used as building blocks for larger

[*] Prof. Dr. K. M. Smith, R. G. Khoury, Dr. L. Jaquinod, Dr. K. Aoyagi, Dr. M. M. Olmstead, Dr. A. J. Fisher
Department of Chemistry, University of California
Davis, CA 95616 (USA)
Fax: Int. code +(916)752-8995
e-mail: smith@chem.ucdavis.edu

[**] This work was supported by the U. S. National Science Foundation (grant CHE-96-23117), the U. S. National Institutes of Health (grant HL-22252), and the Japanese Ministry of Education (Monbusho, grant 8-KO-271 to K.A.).

 © WILEY-VCH Verlag GmbH, D-69451 Weinheim, 1997 0570-0833/97/3622-2497 $ 17.50+.50/0

and more sophisticated molecular assemblies. Calixarenes have been very actively investigated, and a great number of derivatives of different types have been synthesized which display a variety of substrate binding and reactivity features.[8]

Aiming at the synthesis and elaboration of large systems based on both calixarene and porphyrin units, we utilized calixarenes as molecular platforms that allow the synthesis of supramolecular porphyrin assemblies with well-defined, conformationally fixed superstructures. Complexation of calix[4]-arenes, which possess strong ion-bonding properties, with porphyrins, which are pH-dependent photoactive chromophores, can potentially lead to new molecular receptors for the development of efficient sensing agents. Several porphyrin–calixarene complexes have been synthesized; however, the yields were usually less than one percent, or the complex contained only one porphyrin subunit.[9]

We adopted the Zinke–Cornforth procedure,[5b, 10] with some minor modifications, for synthesizing a calix[4]porphyrin. Two main issues addressed in the planning of our synthesis were solubility and steric congestion due to the large size of the porphyrin chromophore. By careful design and molecular modeling, we determined that a porphyrin with unsubstituted peripheral positions on its upper half would minimize any steric congestion among adjacent porphyrins, but that the resulting calixarene would probably have the $\alpha,\beta,\alpha,\beta$-atropisomeric conformation. On the lower half, ethyl groups were placed at the peripheral pyrrole subunit carbon atoms to increase solubility of the final product.

The upper half of the porphyrin was prepared by condensation of *p*-anisaldehyde and pyrrole in trifluoroacetic acid (TFA), resulting in methoxyphenyldipyrromethane (**1**) in 51% yield (Scheme 1).[11] Vilsmeier bisformylation of **1** gave **2** (86% yield), which reacted with 2,3,7,8-tetraethyldipyrromethane (**3**) to afford 4-(12,13,17,18-tetraethylporphyrinyl)anisole (**4**) in 49% yield. The methoxy group was then cleaved with BBr_3 to give 4-(12,13,17,18-tetraethylporphyrinyl)phenol (**5**) in quantitative yield. Nickel was then inserted (in 97% yield) to prevent any adverse interactions of the central nitrogen atoms of the porphyrin in the subsequent reactions. Heating the nickel(II) complex of **5** at reflux in dioxane containing NaOH gave a mixture of the monobenzylalchohol porphyrin **6** (major product, 61% yield), the starting porphyrin **5**-Ni, and the bis-(benzylalcohol)porphyrin **7** (9% yield). Heating the mixture at reflux in diphenyl ether containing NaOH followed by a workup with ethyl acetate gave a precipitate, which was dissolved in DMF and subjected to chromotography on Sephadex G-25-300. The fastest running band was collected to give calix[4]-arenoporphyrin **8** in 60% yield.

^{1}H NMR spectroscopy of **8** (in $(CD_3)_2SO$) showed broad signals, which were only marginally temperature dependent, at $\delta = 9.85$ (*meso*-H), 9.11 (β-H), 7.44 (OH), 7.34 (aromatic H), and 3.98 (methylene bridge). Peaks for the ethyl substituents appeared at $\delta = 4.13$ and 1.69. The methylene bridge carbon atoms were at $\delta = 29.8$ in the ^{13}C NMR spectrum. Spectrophotometry showed a broadened Soret band at $\lambda_{max} = 404$ nm (porphyrin monomer **5**-Ni: 399 nm). The calix[4]arenoporphyrin **8** was further characterized by mass spectrometry, elemental analysis, and X-ray diffraction studies. Figure 1 shows the molecular structure of **8**.[12] Surprisingly, the molecule adopts the cone $(\alpha,\alpha,\alpha,\alpha)$ conformation. Of the four configurations possible for the calix[4]arenoporphyrin (Figure 2), we anticipated, based on molecular modeling and other energetic considerations, that the molecule would adopt the $\alpha,\beta,\alpha,\beta$ configuration; we also expected that π-π stacking of the type shown in Figure 2 would be reasponsible for the broadening in the ^{1}H NMR spectrum. Fig-

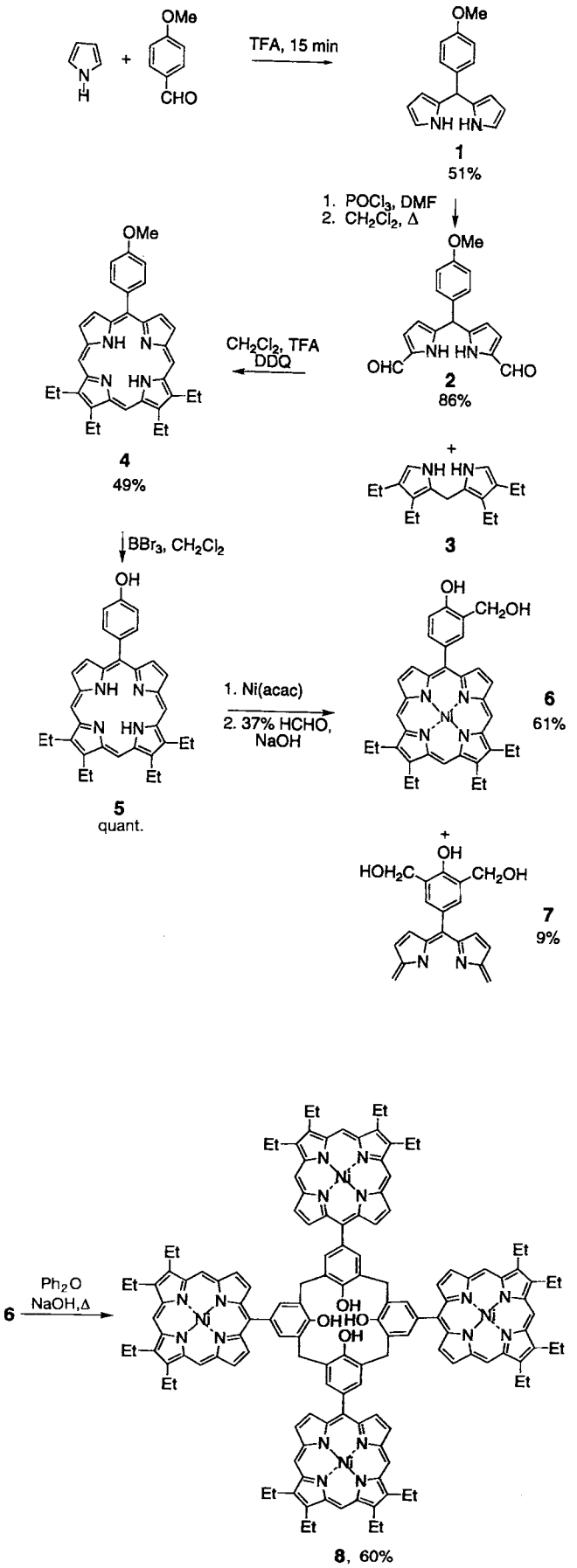

Scheme 1. Synthesis of calix[4]arenoporphyrin **8**.

 © WILEY-VCH Verlag GmbH, D-69451 Weinheim, 1997 0570-0833/97/3622-2498 $ 17.50+.50/0

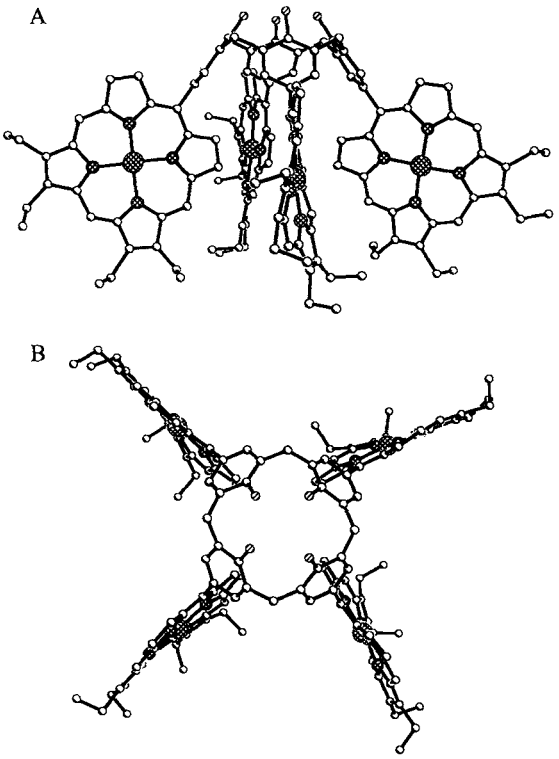

Figure 1. Molecular structure of calix[4]arenoporphyrin **8**; A: side view, B: top view. Hydrogen atoms have been omitted for clarity.

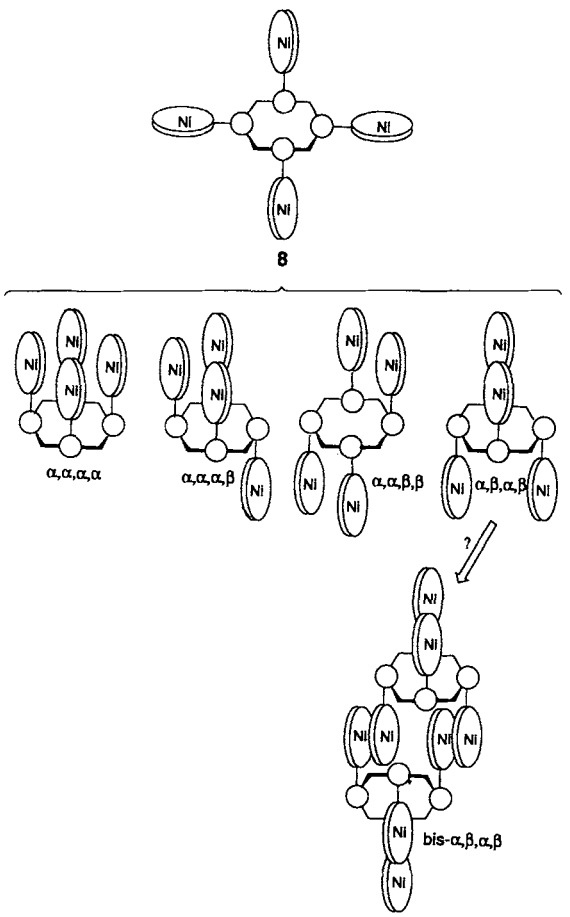

Figure 2. Schematic representation of the four major atropisomeric conformations of **8**, and the anticipated aggregation complex for the $\alpha,\beta,\alpha,\beta$ conformer (see text).

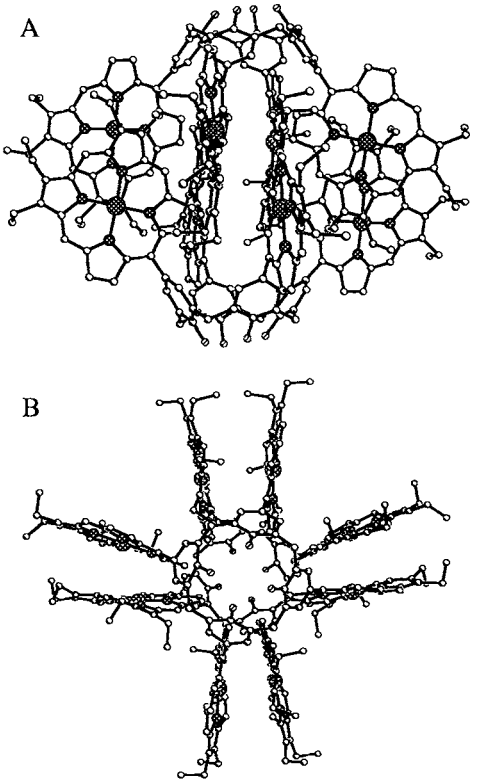

Figure 3. Molecular structure of the aggregated dimer of **8**; A: side view, B: top view. Hydrogen atoms have been omitted for clarity.

ure 3 shows the interactions which exist between two neighboring molecules of calix[4]arenoporphyrin, and fully explains the existence of the $\alpha,\alpha,\alpha,\alpha$ conformation. Aggregation between two molecules to give a cogwheel arrangement is clearly a dominating phenomenon, and this leads to a self-assembling supramolecular array which, as the nickel(II) complex, we have thus far been unable to uncog.

The unit cell in the crystal structure of **8** has the dimensions $a = b = 23.51$, $c = 100.61$ Å and a volume of 55609 Å^3. A large void exists in which methanol molecules of solvation partially occupy twelve sites; two more methanol sites exist within the cavity of each calix[4]arenoporphyrin. Inclination angles of the phenyl groups (with respect to the best plane of methylene groups) for the calixporphyrin complex are 130.1, 123.9, 118.5, and 126.2°; calix[4](*p-tert*-butylbenzene) has an inclination angle of 123°.[5b] Deviations from this value are usually caused by packing effects, or in this case, aggregation of the calix[4]-arenoporphyrin units. Another indicator of the strain placed on the calixarene by the porphyrin subunits are the larger O—O distances of 2.513, 2.872, 2.790, 2.479 Å; the average value in calix[4](*p-tert*-butylbenzene) is 2.650 Å.[5b] The asymmetric unit consists of two calix molecules, each of which forms an aggregate with its centrosymmetrically related pair. A fourfold screw axis along the *c* axis generates the packing system. Whereas one molecule occupies the space at the center of the cell, the other is positioned at the corners; this forms channels in the lattice packing model.

The structural features of **8** are unique. We consider the dimeric cogwheel compound derived from **8** to be a remarkable example of a robust, definitively structured, self-assembled supramolecular array of versatile chromophores. Further studies focus on the syntheses of calix[6]- and calix[8]arenoporphyrins, and formation of free base as well as other metal complexes. Based on the fact that the calix[8]arenoporphyrin might

 © WILEY-VCH Verlag GmbH, D-69451 Weinheim, 1997 0570-0833/97/3622-2499 $ 17.50+.50/0

afford a cyclic cogged dimer with sixteen π-stacked tetrapyrrole units, further studies are aimed at developing molecules which are potential models for systems such as the array of tetrapyrroles in the light-harvesting component of the bacterial light harvesting complex LH2.[14] Indeed, we note that the B800 and B850 components of the light-harvesting complex II in *Rhorospirillum molischianum* consist of eight and sixteen units of bacteriochlorophyll, respectively.[15]

Received: July 3, 1997 [Z 10632IE]
German version: *Angew. Chem.* **1997**, *109*, 2604–2607

Keywords: calixarenes · porphyrinoids · supramolecular chemistry

[1] See for example, a) D. E. Robertson, R. S. Farid, C. C. Moser, J. L. Urbauer, S. E. Mulholland, R. Pidikiti, J. D. Lear, A. J. Wand, W. F. DeGrado, P. L. Dutton, *Nature (London)* **1994**, *368*, 425; b) S. Anderson, H. L. Anderson, A. Bashall, M. McPartlin, J. K. M. Sanders, *Angew. Chem.* **1995**, *107*, 1196; *Angew. Chem. Int. Ed. Engl.* **1995**, *34*, 1096; D. W. J. McCallien, J. K. M. Sanders, *J. Am. Chem. Soc.* **1995**, *117*, 6611; c) K. M. Smith, L. A. Kehres, J. Fajer, *ibid.* **1983**, *105*, 1387; d) H. Tamiaki, T. Miyatake, R. Tanikaga, A. R. Holzwarth, K. Schaffner, *Angew. Chem.* **1996**, *108*, 810; *Angew. Chem. Int. Ed. Engl.* **1996**, *35*, 772; e) R. G. Khoury, L. Jaquinod, D. J. Nurco, R. K. Pandey, M. O. Senge, K. M. Smith, *ibid.* **1996**, *108*, 2657 and **1996**, *35*, 2496.

[2] For example, *Supramolecular Assemblies—New Developments in Biofunctional Chemistry* (Ed.: Y. Murakami), Mita Press, Tokyo, **1990**; J.-M. Lehn, *Supramolecular Chemistry*, VCH, Weinheim, **1995**; H. Kurreck, M. Huber, *Angew. Chem.* **1995**, *107*, 929; *Angew. Chem. Int. Ed. Engl.* **1995**, *34*, 849.

[3] C. M. Drain, K. C. Russell, J.-M. Lehn, *Chem. Commun.* **1996**, 337.

[4] a) C. J. Walfer, H. L. Anderson, J. K. M. Sanders, *J. Chem. Soc. Chem. Commun.* **1993**, 458; b) L. G. Mackay, R. S. Wylie, J. K. M. Sanders, *J. Am. Chem. Soc.* **1994**, *116*, 3142; c) D. M. Rudkevich, W. Verboom, D. N. Reinhoudt, *J. Org. Chem.* **1995**, *60*, 6585.

[5] a) Recent review: V. Böhmer, *Angew. Chem.* **1995**, *107*, 785; *Angew. Chem. Int. Ed. Engl.* **1995**, *34*, 713; b) J. Vicens, V. Böhmer, *Calixarenes: A Versatile Class of Macrocyclic Compounds*, Kluwer, Dordrecht, **1991**, p. 5.

[6] P. Timmerman, K. G. A. Nierop, E. A. Brinks, W. Verboom, F. C. J. M. van Veggel, W. P. van Hoorn, D. N. Reinhoudt, *Chem. Eur. J.* **1995**, *1*, 132.

[7] R. Perrin, R. Lamartine, M. Perrin, *Pure Appl. Chem.* **1993**, *65*, 1549.

[8] a) J. Bernard, R. de Vains, R. Lamartine, *Tetrahedron Lett.* **1996**, *37*, 6311; b) A. M. A. van Wageningen, P. Timmerman, J. P. M. van Duynhoven, W. Verboom, F. C. J. M. van Veggel, D. N. Reinhoudt, *Chem. Eur. J.* **1997**, *3*, 639; c) P. D. Beer, M. G. B. Drew, D. Hesek, K. C. Nam, *Chem. Commun.* **1997**, 107; d) K. Murayama, K. Aoki, *ibid.* **1997**, 119; e) T. Haino, M. Yanase, Y. Fukazawa, *Tetrahedron Lett.* **1997**, *38*, 3739; f) O. Struck, L. A. J. Chrisstoffels, R. J. W. Lugtenberg, W. Verboom, G. J. van Hummel, S. Harkema, D. N. Reinhoudt, *J. Org. Chem.* **1997**, *62*, 2487.

[9] a) Z. Asfari, J. Vicens, J. Weiss, *Tetrahedron Lett.* **1993**, *34*, 627; b) D. M. Rudkevich, W. Verboom, D. N. Reinhoudt, *J. Org. Chem.* **1995**, *60*, 6585; c) T. Nagasaki, H. Fujishima, M. Takeuchi, S. Shinkai, *J. Chem. Soc. Perkin Trans. 1* **1995**, 1883; d) T. Arimura, C. T. Brown, S. L. Springs, J. L. Sessler, *Chem. Commun.* **1996**, 2293.

[10] C. D. Gutsche, M. Iqbal, D. Stewart, *J. Org. Chem.* **1986**, *51*, 742.

[11] C.-H. Lee, J. S. Lindsey, *Tetrahedron* **1994**, *50*, 11427.

[12] Crystallographic details for **8**: $C_{141.75}H_{128}N_{16}Ni_4O_{5.75}$, dark green, octahedral crystal ($0.15 \times 0.10 \times 0.10$ mm), tetragonal space group $P4_122$ (no. 92); $a = b = 23.510(3)$, $c = 100.61(2)$ Å, $V = 55609(16)$ Å^3, $Z = 16$. Of 33061 reflections measured, 15009 were unique and 9740 observed ($R_{int} = 0.033$, $T_{min} = 0.90$, $T_{max} = 0.85$, $\mu = 1.047$ mm^{-1}, $\rho_{calcd} = 1.138$ g cm^{-3}); $R1 = 0.1142$ (observed data, $I > 2\sigma(I)$) and $wR2 = 0.3483$ (all data) for 2571 parameters. Data were collected at 113(2) K on a Siemens Hi Star multiwire proportional counter diffractometer mounted on a Rigaku RU300 rotating anode equipped with a 3.0×0.3 mm focal cup and Göbel mirrors ($Cu_{K\alpha}$ irradiation; $\lambda = 1.54178$ Å, ω scan mode, $2\theta_{max} = 90.2°$). The structure was solved by direct methods and refined (based on F^2 with all independent data) by full-matrix least-squares methods (Siemens SHELXTL Version 5.03). A total of fourteen methanol sites were found; twelve were located in regions of void, and the other two in the calixarene cavities. All sites showed only partial occupancy summing to a total of 1.75 methanol molecules. With the exception of the solvent molecules, non-hydrogen atoms were refined with anisotropic thermal parameters. Hydrogen atoms were generated by idealized geometry and treated as riding using isotropic thermal parameters (but not on the solvent molecules). The data were corrected for absorption [13]. Crystallographic data (excluding structure factors) for the structures reported in this paper have been deposited with the Cambridge Crystallographic Data Centre as supplementary publication no. CCDC-100523. Copies of the data can be obtained free of charge on application to The Director, CCDC, 12 Union Road, Cambridge CB2 1EZ, UK (fax: int. code +(1223)336-033; e-mail: deposit@chemcrys.cam.ac.uk).

[13] S. R. Parkin, B. Moezzi, H. Hope, *J. Appl. Crystallogr.* **1995**, *28*, 53.

[14] a) G. McDermott, S. M. Prince, A. A. Freer, A. M. Hawthornthwaite-Lawless, M. Z. Papiz, R. J. Cogdell, N. W. Isaacs, *Nature (London)* **1995**, *374*, 517; b) W. Kühlbrandt, *ibid.* **1995**, *374*, 497.

[15] J. Koepke, X. Hu, C. Muenke, K. Schulten, H. Michel, *Structure* **1996**, *4*, 581.

Synthesis, Structure, and Double Olefin Extrusion of All Three Diastereomers of 2,2,6,6-Tetrakis(4-chlorophenyl)-3,7-dimethyl-4-phenyl-1,5-dioxa-4λ^5-phosphaspiro[3.3]heptane**

Takayuki Kawashima,* Rei Okazaki, and Renji Okazaki*

In the course of our study on heterocyclobutanes **1**[1] bearing highly coordinated main group elements at the position adjacent to the heteroatom we have reported the syntheses and isolation of intermediates of the Wittig and Peterson-type reactions.[2] Recently we also achieved the synthesis of tetracoordinate and pentacoordinate 1,2-oxathietanes and their thermolysis to the oxirane with retention of configuration.[3] Our studies on the influence of ring size on the stability of 1,2-oxaphosphetanes led to the synthesis of **2**, the first stable pentacoordinate spirophosphorane with two 1,2-oxaphosphetane rings; the stability is attributed to the trifluoromethyl groups at the 4-position.[4, 5]

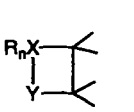

1

X= P, Si$^-$, Ge$^-$, Sn$^-$, S, Se
Y=O, NPh

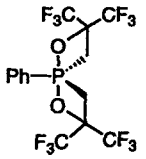

2

Unexpectedly, however, double olefin extrusion from **2** was unsuccessful, because of the electronic effect of the strong electron-withdrawing groups. Taking into consideration the bonding character of equatorial bonds in a trigonal-bipyramid (TBP) structure, an electron-releasing group such as an alkyl group at the 3-position is expected to stabilize a TBP structure sufficiently even in the absence of a strong electron-withdrawing group. The introduction of such a substituent at the 3-position may also lead to kinetic stabilization toward hydrolysis by steric protection, as observed in the tetracoordinate 1,2-oxathietanes.[3a] We now report the synthesis, crystal structures, and thermolysis of all three diastereomers of 2,2,6,6-tetrakis(4-chlorophenyl)-3,7-dimethyl derivatives **3**.

[*] Prof. Dr. T. Kawashima, Prof. Dr. Renji Okazaki, Rei Okazaki
Department of Chemistry, Graduate School of Science
The University of Tokyo
7-3-1 Hongo, Bunkyo-ku, Tokyo 113 (Japan)
Fax: Int. code +(3)5800-6899
e-mail: takayuki@chem.s.u-tokyo.ac.jp

[**] This work was partially supported by a Grant-in-Aid for Scientific Research on Priority Areas No. 09239101 (T.K.) from the Ministry of Education, Science, Sports, and Culture, Japan. We are grateful to Professor N. Tokitoh of the University of Tokyo for the determination of the X-ray structure of **3**. We also thank Tosoh Akzo Co. Ltd. for gifts of alkyllithium compounds.

 © WILEY-VCH Verlag GmbH, D-69451 Weinheim, 1997 0570-0833/97/3622-2500 $ 17.50+.50/0

Sequential treatment of diethylphenylphosphane oxide (**4**) with *n*BuLi, 4,4′-dichlorobenzophenone, and aqueous NH_4Cl gave a diastereomeric mixture of bis(β-hydroxyalkyl)phosphane oxides (**5a–c**) along with a diastereomeric mixture of monohydroxyalkyl derivatives **6** (35%). Cyclization and dehydration of **5a** or **5b** by Appel's method[6] gave the *cis-trans* isomer **3a**, while similar treatment of **5c** provided a mixture of the *cis-cis* isomer **3b** and the *trans-trans* isomer **3c** (Scheme 1). The two oxaphosphetane rings of the *cis-trans* isomer **3a** are different from each other, while those of the *cis-cis* and *trans-trans* isomers **3b** and **3c**, respectively, were equivalent.

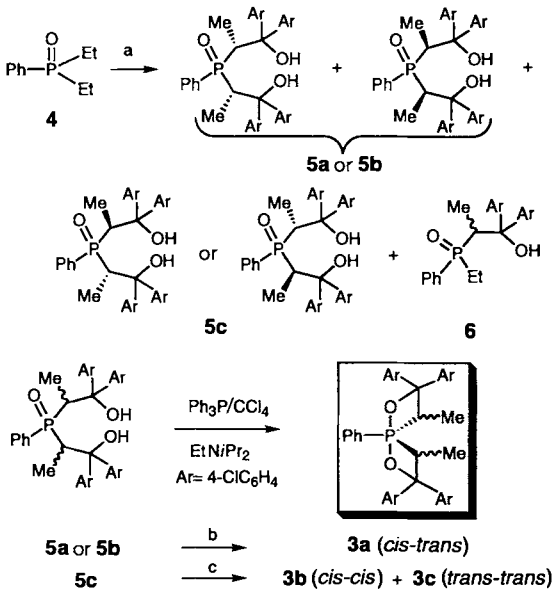

Scheme 1. a) 2.3 molar equiv *n*BuLi, THF, −78 → 25 °C, 10 min; 2.19 molar equiv 4,4′-dichlorobenzophenone, THF, −78 °C, 1 h; −78 → 25 °C; 25 °C, 2 h; aqueous NH_4Cl; b) **5a**: CH_3CN, 25 °C, 7 h; **5b**: CH_3CN, 40 °C, 8 h; c) CH_3CN, 25 °C, 6.5 h.

The X-ray crystallographic analysis of all three diastereomers showed that **3a** and **3b** have a distorted TBP structure with two oxygen atoms at apical positions, while **3c** has a distorted square-pyramidal (SP) structure with the phenyl carbon atom at apical and the other four atoms at basal positions, respectively (Figures 1 and 2).[7] In the crystal structure of the *cis-trans* isomer **3a** (TBP → SP[8] 19.0%) the apical bond angle deviates by 12.08(10)° from linearity. Deviations in the range between 10 and 20° are a common structural feature of hypervalent species containing a four-membered ring.[1a, b, 3b] On the other hand, in the *trans-trans* isomer **3c** (TBP → SP 73.7%) the apical P–C(Ph) bond length was 1.796(7) Å, while the basal P–C bond lengths were 1.835(7) and 1.829(7) Å, indicating that the apical bond is stronger than the basal bonds in an SP structure.

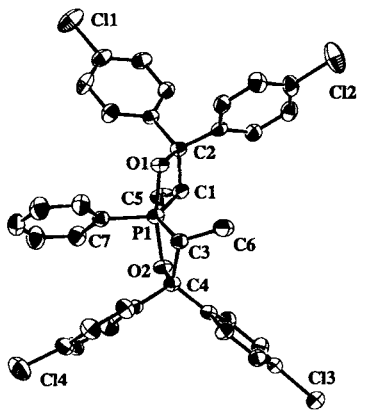

Figure 1. Structure of *cis-trans* **3a** (ORTEP drawing, thermal ellipsoid plots for 30% probability). Selected bond lengths [Å], bond angles [°], and torsion angles [°]: P1–O1 1.738(2), P1–O2 1.741(3), P1–C1 1.819(3), P1–C3 1.825(3), P1–C7 1.798(3); O1-P1-O2 167.92(10), C1-P1-C7 120.2(1), C1-P1-C3 128.0(1), C3-P1-C7 111.8(1), P1-C1-C2 89.4(2), C1-C2-O1 96.2(2), C2-O1-P1 96.4(1), O1-P1-C1 77.9(1), P1-C3-C4 87.9(2), C3-C4-O2 96.1(2), C4-O2-P1 95.1(2), O2-P1-C3 77.9(1), P1-C1-C2-O1 2.2(2), P1-C3-C4-O2 13.8(2).

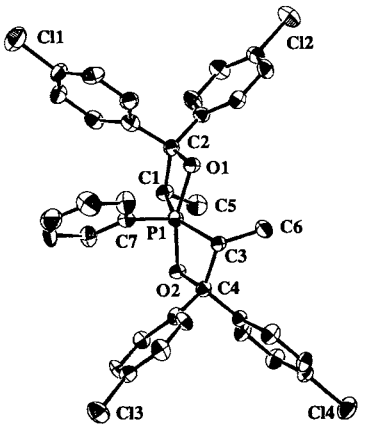

Figure 2. Structure of *trans-trans* **3c** (without Et_2O, ORTEP drawing with thermal ellipsoid plots for 30% probability). Selected bond lengths [Å], bond angles [°], and torsion angles [°]: P1–O1 1.719(4), P1–O2 1.715(4), P1–C1 1.835(7), P1–C3 1.829(7), P1–C7 1.796(7); O1-P1-O2 157.5(2), C1-P1-C7 108.8(4), C1-P1-C3 142.8(3), C3-P1-C7 108.4(4), P1-C1-C2 88.3(5), C1-C2-O1 95.6(5), C2-O1-P1 95.6(4), O1-P1-C1 76.7(3), P1-C3-C4 87.8(4), C3-C4-O2 95.6(5), C4-O2-P1 95.6(4), O2-P1-C3 77.4(3); P1-C1-C2-O1 15.2(4), P1-C3-C4-C2 14.6(4).

The ^{31}P NMR spectrum of **3c** in solution showed a peak at $\delta = -33.6$, which is similar to the values observed in the ^{31}P NMR spectra of **3a** ($\delta = -31.2$) and **3b** ($\delta = -32.7$), indicating that **3c** also has a TBP structure in solution.[9] Interestingly, the large difference in crystal structure between **3a,b** and **3c** is probably attributable to crystal packing forces, in other words, the energy difference between TBP and SP structures is quite small in this system as usual. Taking into consideration the high moisture sensitivity of a 3,7-unsubstituted derivative of **3**, it becomes clear that the electropositive substituents (CH_3) at the equatorial positions stabilize the TBP structure both thermodynamically and kinetically—evidently with support from the 4-chlorophenyl groups at the β-carbon atoms of the apical ligands.

Thermolysis of these compounds gave the corresponding olefin **7**, the ring-opened isomer of **3** (**8**), the dehydration product of **8** (**9**), and **5**. Interestingly, although the yields of the olefin are

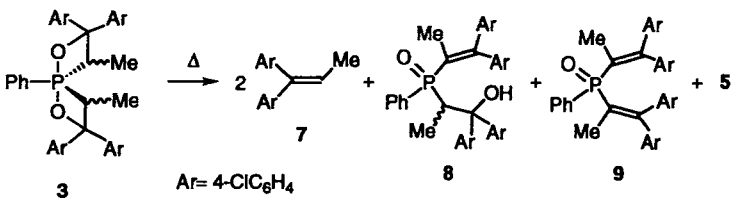

only moderate, they indicate that in sharp contrast to the thermolysis of **2**, one molecule of **3** afforded two molecules of the olefin by a double olefin extrusion (Table 1). Monitoring the reaction by NMR spectroscopy showed that there is an equilibrium between **3b** and **3c** during the reaction. Such an equilibrium has previously never been observed in pentacoordinate 1,2-oxaphosphetanes with two apical oxygen atoms.[10] Fur-

 © WILEY-VCH Verlag GmbH, D-69451 Weinheim, 1997 0570-0833/97/3622-2501 $ 17.50+.50/0

Table 1. Yields of products in the thermolysis of **3**. (Solvent C_6D_6, $T = 80\,^{\circ}C$.)

Entry	3	t	Additive	Yield[%][a] 7	8 [b]	9	5
1	**3a**	6 h	–	55	49(16:33)	23	traces
2	**3b**	6 h	–	29	62(51:11)	16	7
3	**3b**	6.5 d	$EtNiPr_2$	158	–	4	–
4	**3b**	20 h	$EtNiPr_2 \cdot HCl$	127	27(>100:1)	9	–
5	**3c**	5 h	–	67	36(>100:1)	10	20

[a] Based on **3** and determined by ^1H NMR spectroscopy. [b] The ratio of two diastereomers is shown in parentheses.

thermore, the thermolysis of **3b** in the presence of $Et(iPr)_2N$ and $Et(iPr)_2N \cdot HCl$ afforded the olefin in 158 and 127% yields, respectively (Table 1, entries 3 and 4). Judging from the longer reaction time of these reactions than that without an additive (entry 2), it is conceivable that the additives do not accelerate the olefin formation reaction, but retard the side reactions. Although we have no real evidence at present it is most likely that coordination of amine or chloride ion to the phosphorus center plays an important role in reducing the acidity of the methine proton. Further investigations on the effects of additives are in progress.

Experimental Section

*n*BuLi (1.64 M solution in hexane, 14.6 mL) was added to a solution of $PhP(O)Et_2$ (**4**) (1.89 g, 10.4 mmol) in dry THF (30 mL) at $-78\,^{\circ}C$ under argon. The reaction mixture was stirred at room temperature for 10 min, and cooled again to $-78\,^{\circ}C$. A solution of 4,4'-dichlorobenzophenone (5.73 g, 22.8 mmol) in THF (30 mL) was added to the cooled solution at $-78\,^{\circ}C$. After stirring at $-78\,^{\circ}C$ for 1 h, the reaction mixture was allowed to warm to 25 °C, stirred for 2 h, and then treated with aq NH_4Cl and extracted with CH_2Cl_2. The extracts were dried over anhydrous $MgSO_4$. After removal of the solvent under reduced pressure the residue was subjected to dry column chromatography to afford diastereomeric mixtures of **5** and **6** (1.25 g, 35%). These were purified by column chromatography (SiO_2, CH_2Cl_2), flash column chromatography (SiO_2, CH_2Cl_2/hexane, 3/2), and recrystallization (CH_2Cl_2). Yields based on ^1H NMR data: **5a**, 6.9%; **5b**, 19%; **5c**, 25%.

5a: Colorless crystals; m.p. 225.0–226.0 °C (decomp); elemental analysis calcd for $C_{36}H_{31}O_3Cl_4P$ (%): C 63.18, H 4.57, Cl 20.72; found: C 63.22, H 4.77, Cl 20.71; ^1H NMR (500 MHz, $CDCl_3$, 27 °C, TMS): $\delta = 1.44$ (dd, $^3J(H,P) = 15.0$ Hz, $^3J(H,H) = 7.3$ Hz, 6H, CH_3), 3.42 (quint, $^3J(H,H) = {}^2J(H,P) = 7.3$ Hz, 2H, CH), 5.35 (s, 2H, OH), 6.76–6.79 (m, 4H, 4-ClC_6H_4), 6.96–7.04 (m, 6H, Ar), 7.09–7.14 (m, 2H, Ph), 7.17–7.20 (m, 4H, 4-ClC_6H_4), 7.26–7.29 (m, 4H, 4-ClC_6H_4), 7.33–7.38 (m, 1H, Ph); $^{31}P\{^1H\}$ NMR (109 MHz, $CDCl_3$, 27 °C, 85% H_3PO_4): $\delta = 56.7$.

To a solution of phosphane oxide **5a** (59 mg, 0.087 mmol) and Ph_3P (228 mg, 0.87 mmol) in CH_3CN (6 mL), $Et(iPr)_2N$ (0.15 mL, 0.86 mmol) and CCl_4 (0.084 mL, 0.87 mmol) were syringed at 25 °C. After the mixture had been stirred for 7 h, *cis-trans* **3a** precipitated out (24 mg). The precipitates were filtered and the filtrate was subjected to column chromatography (SiO_2, CH_2Cl_2: hexane = 1:1) to afford *cis-trans* **3a** (23 mg, total yield was 81%). A similar reaction (40 °C, 8 h) using **5b** instead of **5a** gave **3a** (42%), while the reaction (25 °C, 6.5 h) using **5c** afforded a mixture of *cis-cis* **3b** (39%) and *trans-trans* **3**) (26%). Recrystallization from CH_2Cl_2/hexane gave an analytically pure sample, and single crystals suitable for X-ray crystallographic analysis were grown in ether/hexane.

cis-trans **3a**: Colorless crystals; m.p. 119.5–120.5 °C (decomp); elemental analysis calcd for $C_{36}H_{29}O_2PCl_4$ (%): C 64.88, H 4.38, Cl 21.27; found: C 64.81, H 4.57, Cl 20.88; ^1H NMR (500 MHz, $CDCl_3$, 27 °C, TMS): $\delta = 0.94$ (dd, $^3J(H,H) = 8.4$ Hz, $^3J(H,P) = 26.3$ Hz, 3H, CH_3), 1.35 (dd, $^3J(H,H) = 8.0$ Hz, $^3J(H,P) = 27.4$ Hz, 3H, CH_3), 4.24 (dq, $^2J(H,P) = 16.7$, $^3J(H,H) = 8.4$ Hz, 1H, CH), 4.58 (dq, $^2J(H,P) = 25.6$, $^3J(H,H) = 8.0$ Hz, 1H, CH), 6.96–7.09 (m, 9H, Ar), 7.20–7.35 (m, 10H, Ar), 7.87–7.96 (m, 2H, *o*-H of Ph); $^{31}P\{^1H\}$ NMR (109 MHz, $CDCl_3$, 27 °C, 85% H_3PO_4): $\delta = -31.2$.

Received: April 7, 1997 [Z103161E]
German version: *Angew. Chem.* **1997**, *109*, 2609–2612

Keywords: hypervalent compounds · olefinations · phosphorus heterocycles · spiro compounds · Wittig reactions

[1] a) T. Kawashima, R. Okazaki, *Synlett* **1996**, 600–608, and references therein; pentacoordinate 1,2λ^5-azaphosphetidine: b) T. Kawashima, T. Soda, R. Okazaki, *Angew. Chem.* **1996**, *108*, 1206–1208; *Angew. Chem. Int. Ed. Engl.* **1996**, *35*, 1096–1098; hexacoordinate 1,2-oxaphosphetanide: c) T. Kawashima, K. Watanabe, R. Okazaki, *Tetrahedron Lett.* **1997**, *38*, 551–554.

[2] For the Wittig reaction see: D. J. H. Smith in *Comprehensive Organic Chemistry*, *Vol. 2* (Eds.: D. H. R Barton, W. D. Ollis), Pergamon, Oxford, **1979**, pp. 1316–1329; I. Gosney, A. G. Rowley in *Organophosphorus Reagents in Organic Synthesis* (Ed.: J. I. G. Cadogan), Academic Press, New York, **1979**, pp. 17–153; B. E. Maryanoff, A. B. Reitz, *Chem. Rev.* **1989**, *89*, 863–927; for the Peterson-type reaction see: E. W. Colvin in *Silicon in Organic Synthesis*, Butterworths, London, **1981**, pp. 141–152; W. P. Weber, *Silicon Reagents for Organic Synthesis*, Springer, New York, **1983**; pp. 58–73; D. J. Ager, *Synthesis* **1984**, 384–398; *Org. React. NY* **1990**, *38*, 1–223; T. Kauffmann, *Top. Curr. Chem.* **1980**, *92*, 109–147; *Angew. Chem.* **1982**, *94*, 401–420; *Angew. Chem. Int. Ed. Engl.* **1982**, *21*, 410–429; M. Pereyre, J.-P. Quintard, A. Rahm, *Tin in Organic Synthesis*, Butterworths, London, **1987**, pp. 176–177.

[3] Tetracoordinate 1,2λ^4-oxathietane: a) T. Kawashima, F. Ohno, R. Okazaki, *Angew. Chem.* **1994**, *106*, 2188–2190; *Angew. Chem. Int. Ed. Engl.* **1994**, *33*, 2094–2095; pentacoordinate 1,2λ^6-oxathietane: b) F. Ohno, T. Kawashima, R. Okazaki, *J. Am. Chem. Soc.* **1996**, *118*, 697–698; c) T. Kawashima, F. Ohno, R. Okazaki, H. Ikeda, S. Inagaki, *ibid.* **1996**, *118*, 12455–12456.

[4] For compounds with phosphetane and oxaphosphetane rings: R. K. Oram, S. Trippett, *J. Chem. Soc. Perkin Trans. 1* **1973**, 1300–1310; H. A. E. Aly, J. H. Barlow, D. R. Russell, D. J. H. Smith, M. Swindes, S. Trippett, *J. Chem. Soc. Chem. Commun.* **1976**, 449–450; for compounds with two 1,3,2-diazaphosphetidine rings: M. Kubjacek, K. Utvary, *Monatsh. Chem.* **1978**, 587–595; H. W. Roesky, K. Ambrosius, M. Banek, W. S. Sheldrick, *Chem. Ber.* **1980**, *113*, 1847–1854; P. G. Jones, A. Meyer, R. Schmutzler, *Z. Naturforsch. B* **1990**, *45*, 175–183; L. Lamandé, *Tetrahedron* **1990**, *46*, 3527–3534.

[5] T. Kawashima, H. Takami, R. Okazaki, *J. Am. Chem. Soc.* **1994**, *116*, 4509–4510.

[6] Review: R. Appel, *Angew. Chem.* **1975**, *87*, 863–874; *Angew. Chem. Int. Ed. Engl.* **1975**, *14*, 801–811.

[7] Crystal data for **3a**; $C_{36}H_{29}O_2PCl_4$, $M_r = 666.41$, crystal dimensions $0.75 \times 0.50 \times 0.50$ mm, monoclinic, space group $C2/c$, $a = 26.95(3)$, $b = 16.32(1)$, $c = 19.94(2)$ Å, $\beta = 131.43(5)^{\circ}$, $V = 6578(13)$ Å^3, $Z = 8$, $\rho_{calcd} = 1.346$ g cm^{-3}, $\mu = 4.39$ cm^{-1}, $F(000) = 2832$. The intensity data ($2\theta < 55^{\circ}$) were collected at 296 K on a Rigaku AFC7R diffractometer with graphite-monochromated $Mo_{K\alpha}$ radiation ($\lambda = 0.71609$ Å) and the structure was solved by direct methods (SIR92). The non-hydrogen atoms were refined anisotropically. The final cycle of full-matrix least-squares refinement was based on 4357 observed reflections [$I > 3.00\sigma(I)$] and 388 variable parameters with $R(R_w) = 0.046(0.026)$. Crystal data for **3b**: $C_{36}H_{29}O_2PCl_4$, $M_r = 666.41$, crystal dimensions $0.30 \times 0.25 \times 0.15$ mm, monoclinic, space group $P2_1/c$, $a = 8.966(2)$, $b = 19.366(4)$, $c = 19.152(5)$ Å, $\beta = 96.70(2)^{\circ}$, $V = 3302(1)$ Å^3, $Z = 4$, $\rho_{calcd} = 1.340$ g cm^{-3}, $\mu = 4.38$ cm^{-1}, $F(000) = 1376$. The intensity data ($2\theta < 55^{\circ}$) were collected at 296 K on a Rigaku AFC5R diffractometer with graphite-monochromated $Mo_{K\alpha}$ radiation ($\lambda = 0.71609$ Å) and the structure was solved by direct methods (SHELXS86). The non-hydrogen atoms were refined anisotropically. The final cycle of full-matrix least-squares refinement was based on 1511 observed reflections [$I > 2.00\sigma(I)$] and 388 variable parameters with $R(R_w) = 0.075(0.034)$. Crystal data for **3c**: $C_{36}H_{29}O_2PCl_4 \cdot C_4H_{10}O$, $M_r = 740.53$, crystal dimensions $0.65 \times 0.50 \times 0.05$ mm, monoclinic, space group $C2/c$, $a = 36.852(9)$, $b = 10.001(8)$, $c = 21.495(4)$ Å, $\beta = 105.89(2)^{\circ}$, $V = 7619(6)$ Å^3, $Z = 8$, $\rho_{calcd} = 1.291$ g cm^{-3}, $\mu = 3.88$ cm^{-1}, $F(000) = 3088$. The intensity data ($2\theta > 55.1^{\circ}$) were collected at 296 K on a Rigaku AFC7R diffractometer with graphite-monochromated $Mo_{K\alpha}$ radiation ($\lambda = 0.71609$ Å) and the structure was solved by direct methods (SHELXS86). The non-hydrogen atoms were refined anisotropically. The final cycle of full-matrix least-squares refinement was based on 2424 observed reflections [$I > 3.00\sigma(I)$] and 433 variable parameters with $R(R_w) = 0.057(0.034)$. Crystallographic data (excluding structure factors) for the structures reported in this paper have been deposited with the Cambridge Crystallographic Data Centre as supplementary publication CCDC-100363. Copies of the data can be obtained free of charge on application to The Director, CCDC, 12 Union Road, Cambridge CB2 1EZ, UK (fax: int. code +(1223)336-033: e-mail:deposit@chemcrys.cam.ac.uk).

[8] R. R. Holmes, J. A. Deiters, *J. Am. Chem. Soc.* **1977**, *100*, 5130–5134.

[9] This is also supported by the following observation that although the $^1J(C,P)$ (P-Ph) and $^1J(C,P)$ (P-CH) values of **3c** were expected to be larger and smaller than those of **3a** or **3b**, respectively, judging from the bonding character of the square-pyramidal structure, the values observed were similar to those of **3a** and **3b**.

[10] Ramirez et al. reported that their 1,2-oxaphosphetanes with an alkoxy apical ligand undergo the Wittig olefination before isomerization takes place: F. Ramirez, C. P. Smith, J. F. Pilot, *J. Am. Chem. Soc.* **1968**, *90*, 6726–6732.

 © WILEY-VCH Verlag GmbH, D-69451 Weinheim, 1997 0570-0833/97/3622-2502 $ 17.50+.50/0

Hexaaryltetrasilabuta-1,3-diene: A Molecule with Conjugated Si–Si Double Bonds**

Manfred Weidenbruch,* Stefan Willms, Wolfgang Saak, and Gerald Henkel

Dedicated to Professor Hans Georg von Schnering

Since the isolation of the first molecular compound with an Si–Si double bond[1] the chemistry of disilenes has experienced an explosive development, which is reflected in numerous review articles.[2] However, molecules with conjugated Si–Si double bonds had not been reported previously. Recently, Kira et al. described the tetrasilacyclobutene **1**, the first compound to contain an endocyclic Si–Si double bond, which they obtained in very low yield.[3] Although **1** is thermally rather stable, on exposure to light it rearranges to the bicyclobutane derivative **2**, which, in turn, reverts back to **1** in the dark. A tetrasilabuta-1,3-diene was postulated as a feasible intermediate in the reaction sequence **1** ⇄ **2** but could not be isolated (Scheme 1).

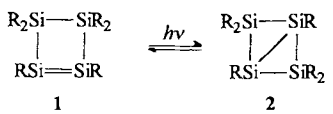

1 2

R = *t*BuMe$_2$Si

Scheme 1.

We now report on the synthesis and characterization of the tetrasilabuta-1,3-diene **6**, which is accessible in acceptable yield by a surprisingly simple process. In the course of the synthesis of the unsymmetrically substituted disilene Mes$_2$Si=SiTip$_2$ (Mes = 2,4,6-Me$_3$C$_6$H$_2$, Tip = 2,4,6-*i*PrC$_6$H$_2$) from Mes$_2$ClSiSiClTip$_2$ and lithium[4,5] we had observed that the yield of the disilene in the dehalogenation step passed through a maximum and then decreased again continuously. At the same time increasing amounts of 1,3,5-triisopropylbenzene were obtained, indicating that the cleavage of TipLi from already formed disilene with concomitant formation of the disilenyllithium compound Mes$_2$Si=SiTipLi proceeds as a competing reaction to the elimination of chlorine at the lithium surface (Scheme 2). A similar reaction mode had previously been observed by Masamune et al. in the reaction of naphthalene/lithium with a tetraaryldigermene.[6]

In order to keep the reaction process as simple as possible, we prepared the symmetrically substituted disilene **3**[7] according to the method of West et al.[8] and used this in the first step towards the postulated disilenyllithium compound **4**. The tendency for the formation of aryllithium compounds apparently present in this system was exploited in the second step of the reaction sequence in which half of **4** reacted with mesityl bromide to give the bromodisilene **5**. The resultant product **5** did indeed react with the remaining **4** smoothly to furnish the hexaaryltetrasilabuta-1,3-diene **6**, which was isolated in the form of reddish brown crystals.

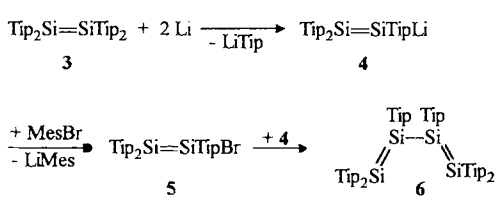

3 4 5 6

Tip = 2,4,6-*i*Pr$_3$C$_6$H$_2$; Mes = 2,4,6-Me$_3$C$_6$H$_2$

Scheme 2.

First indications on the constitution of **6** were provided by the ^{29}Si MMR spectrum, which revealed two signals shifted to low field. The singlet at $\delta = 52.3$ is typical for the Tip$_2$Si group of disilenes,[4,7,8] while the second signal at $\delta = 89.5$ is in the characteristic region for 1,2-diaryl-1,2-disilyldisilenes.[9] Additional information was furnished by the electron spectrum of **6** in which the absorption at longest wavelength at 518 nm is bathochromically shifted by about 100 nm in comparison to the signals of tetraaryldisilenes and even exceeds the absorption maxima of persilylated disilenes.[10] In a similar manner to that by which conjugation in buta-1,3-dienes effects a marked red shift of the bands in comparison to those of ethenes,[11] the lowering of the transition energy of **6** also supports a conjugation between the two double bonds in solution.

The X-ray crystallographic analysis (Figure 1)[12] not only confirmed the constitution of **6** but also revealed some noteworthy details. The conformation of the compound approaches the *cis* form; the dihedral angle between the two planes composed of the atoms Si1-Si2-Si2a and Si2-Si2a-Si1a is 51°. The molecules of **6** possess crystallographic C_2 symmetry; the C_2 axis passes through the middle of the central Si–Si bond and exactly bisects the dihedral angle. Compound **6** crystallizes with a molecule of diisopropyl ether, which merely serves to stabilize the lattice and does not interact with the silicon atoms. As in buta-1,3-dienes, the Si–Si double bonds in **6** are about 3 pm longer than those of tetraaryldisilenes such as, for example, **3**.[7] The reduction in length of the formal Si–Si single bond is more pronounced since it is markedly strained in view of the bulky substituents; it is even shorter than the Si–Si bonds lengths of 235 pm recorded for sterically inconspicuously substituted disilanes. Together with the electron spectrum, these values demonstrate that conjugation between the two double bonds of **6** exists both in solution and in the crystal.

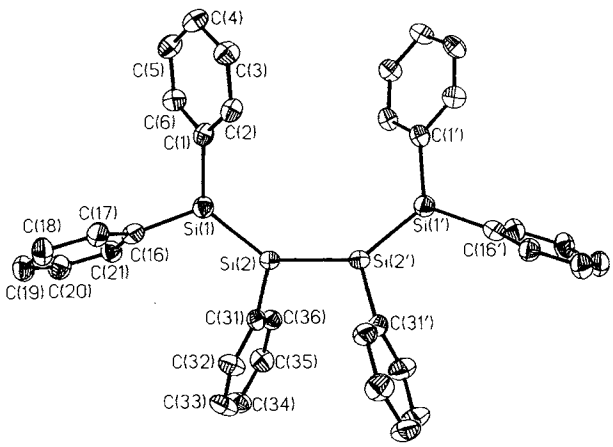

Figure 1. Structure of **6** in the crystal (50% probability, isopropyl groups and hydrogen atoms omitted). Selected bond lengths [pm] and angles [°]: Si1–Si2 217.5(2), Si2–Si2' 232.1(2), Si1–C1 189.4(4), Si1–C16 187.9(4) Si2–C31 190.4(4); Si1-Si2-Si2' 135.0(1), Si2-Si1-C1 128.9(1), Si2-Si1-C16 119.0(1), Si1-Si2-C31 117.0(1).

[*] Prof. Dr. M. Weidenbruch, Dipl.-Chem. S. Willms, Dipl.-Chem. W. Saak
Fachbereich Chemie der Universität
Carl-von-Ossietzky-Strasse 9–11, D-26111 Oldenburg (Germany)
Fax: Int. code +(441)798-3329
Prof. Dr. G. Henkel
Anorganische Chemie der Universität (GH)
Lotharstrasse 1, D-47048 Duisburg (Germany)

[**] Silicon compounds with strong intramolecular steric interactions. Part 64. This work was supported by the Deutsche Forschungsgemeinschaft and the Fonds der Chemischen Industrie. We thank Professor Marsmann, Paderborn, for the ^{29}Si NMR spectrum. Part 63: M. Weidenbruch, L. Kirmaier, E. Kroke, W. Saak, *Z. Anorg. Allg. Chem.* **1997**, *623*, 1277.

 © WILEY-VCH Verlag GmbH, D-69451 Weinheim, 1997 0570-0833/97/3622-2503 $ 17.50+.50/0

Even though compound **6** is extremely sensitive towards air it is thermally very stable and melts without decomposition at 237 °C. An irreversible rearrangement or decomposition reaction only occurs at above 267 °C and is indicated by a change in color from red to yellow. We will next investigate whether compound **6** can participate in typical reactions for 1,3-dienes, especially cycloadditions of the Diels–Alder type.

Experimental Section

Lithium (60 mg, 8.7 mmol) was added to a solution of **3** (700 mg, 0.81 mmol) in dimethoxyethane (30 mL) and the initially blue-green, later red, mixture was stirred for 2 h at room temperature. After separation of insoluble materials, the remaining solution was cooled to −30 °C and treated with mesityl bromide (80 mg, 0.40 mmol). After the solution had been allowed to warm to room temperature, it was stirred for 16 h. The precipitated solid was filtered off and recrystallized from toluene to furnish **6** (280 mg, 53% yield) as reddish brown crystals; m.p. 237–238 °C; ^{1}H NMR (Bruker AM 300, [D$_6$]benzene, 25 °C): $\delta = 0.16$ (d, 3H, $J = 6.6$ Hz), 0.24 (d, 3H, $J = 6.5$ Hz), 0.34 (d, 3H, $J = 6.5$ Hz), 0.45 (d, 3H, $J = 6.6$ Hz), 0.52 (d, 3H, $J = 6.5$ Hz), 0.85 (d, 3H, $J = 6.5$ Hz), 1.02 (d, 3H, $J = 7$ Hz), 1.08 (d, 3H, $J = 6.8$ Hz), 1.09 (d, 3H, $J = 6.8$ Hz), 1.14 (d, 3H, $J = 6.8$ Hz), 1.15 (d, 3H, $J = 6.8$ Hz), 1.34 (d, 3H, $J = 6.5$ Hz), 1.35 (d, 3H, $J = 6.5$ Hz), 1.37 (d, 3H, $J = 6.5$ Hz), 1.64 (d, 3H, $J = 6.5$ Hz), 1.69 (d, 3H, $J = 6.5$ Hz), 1.78 (d, 3H, $J = 6.6$ Hz), 1.88 (d, 3H, $J = 6.5$ Hz), 2.55 (sept., 1H, $J = 6.5$ Hz), 2.64 (sept., 1H, $J = 6.5$ Hz), 2.65 (sept., 1H, $J = 6.5$ Hz), 3.44 (sept., 2H, $J = 6.5$ Hz), 3,56 (sept., 1H, $J = 6.8$ Hz), 3.86 (sept., 1H, $J = 6.5$ Hz), 4.42 (sept., 1H, $J = 6.6$ Hz), 4.99 (sept., 1H, $J = 6.6$ Hz), 6.68 (d, 1H, $J = 1.5$ Hz), 6.84 (d, 1H, $J = 1.5$ Hz), 6.86 (d, 1H, $J = 1.5$ Hz), 6.94 (d, 1H, $J = 1.5$ Hz), 6.98 (d, 1H, $J = 1.5$ Hz), 7.20 (d, 1H, $J = 1.5$ Hz); ^{13}C NMR ([D$_6$]benzene, 25 °C): $\delta = 23.81$ (C$_p$), 23.90 (C$_p$), 24.09 (C$_p$), 24.22 (C$_p$), 24.48 (C$_p$), 24.66 (C$_p$), 24.79 (C$_p$), 25.12 (C$_p$), 25.31 (C$_p$), 25.50 (C$_p$), 31.12 (C$_t$), 34.21 (C$_t$), 34.47 (C$_t$), 34.85 (C$_t$), 37.46 (C$_t$), 37.79 (C$_t$), 38.08 (C$_t$), 38.31 (C$_t$), 39.41 (C$_t$), 121.74, 121.97, 122.50, 122.80, 123.69, 125.66, 129.29, 132.79, 135.64, 136.39, 150.44, 153.36, 153.84, 154.21, 154.44, 156.30; ^{29}Si NMR (Bruker AMX 300, [D$_6$]benzene, 25 °C): $\delta = 52.3$ (s), 89.5 (s); MS (CI, NH$_3$): m/z (%): 1349 (4, MNH$_4^+$), 1332 (9, MH$^+$); UV/Vis (THF): λ_{max} (lgε) = 392 (4.48), 518 (4.41) nm.

Received: June 12, 1997 [Z 10540 IE]
German version: *Angew. Chem.* **1997**, *109*, 2612–2613

Keywords: disilenes · silicon · tetrasilabutadienes

[1] R. West, M. J. Fink, J. Michl, *Science* **1981**, *214*, 1343.
[2] Reviews: R. West, *Angew. Chem.* **1987**, *99*, 1231; *Angew. Chem. Int. Ed. Engl.* **1987**, *26*, 1201; G. Raabe, J. Michl in *The Chemistry of Organic Silicon Compounds, Part 2* (Eds.: S. Patai, Z. Rappoport), Wiley, Chichester, **1989**, p. 1015; T. Tsumuraya, S. A. Batcheller, S. Masamune, *Angew. Chem.* **1991**, *103*, 916; *Angew. Chem. Int. Ed. Engl.* **1991**, *30*, 275; M. Weidenbruch, *Coord. Chem. Rev.* **1994**, *130*, 275; R. Okazaki, R. West in *Multiply Bonded Main Group Metals and Metalloids* (Eds.: R. West, F. G. A. Stone), Academic Press, San Diego, **1996**, p. 232.
[3] M. Kira, T. Iwamoto, C. Kabuto, *J. Am. Chem. Soc.* **1996**, *118*, 10303.
[4] M. Weidenbruch, A. Pellmann, Y. Pan, S. Pohl, W. Saak, H. Marsmann, *J. Organomet. Chem.* **1993**, *450*, 67.
[5] M. Weidenbruch, A. Pellmann, S. Pohl, W. Saak, H. Marsmann, *Chem. Ber.* **1995**, *128*, 935.
[6] S. Park, S. A. Batcheller, S. Masamune, *J. Organomet. Chem.* **1989**, *367*, 39.
[7] H. Watanabe, K. Takeuchi, N. Fukawa, M. Kato, M. Goto, Y. Nagai, *Chem. Lett.* **1987**, 1341.
[8] A. J. Millevolte, D. R. Powell, S. G. Johnson, R. West, *Organometallics* **1992**, *11*, 1091.
[9] R. S. Archibald, Y. van den Winkel, A. J. Millevolte, J. M. Desper, R. West, *Organometallics* **1992**, *11*, 3276.
[10] M. Kira, T. Murayama, C. Kabuto, K. Ebata, H. Sakurai, *Angew. Chem.* **1994**, *106*, 1575; *Angew. Chem. Int. Ed. Engl.* **1994**, *33*, 1489.
[11] J. March, *Advanced Organic Chemistry*, Wiley, New York, **1992**, p. 294.
[12] **6**: Single crystals from diisopropyl ether; diffractometer: Siemens P4RA, radiation Mo$_{K\alpha}$ (λ = 71.073 pm), graphite-monochromated, rotating anode, scintillation counter, T = 150 K, empirical absorption correction, SHELXTL-PLUS program system, direct methods, least-squares refinement, one scaling factor, one isotropic extinction parameter; **6**·$(C_3H_7)_2O$; formula $C_{96}H_{152}OSi_4$, formula weight 1434.54; monoclinic, space group $C2/c$, a = 2275.9(6), b = 2105.7(5), c = 2003.1(6) pm, β = 106.32(2)°, $V = 9212.8 \times 10^6$ pm^3, $Z = 4$, ρ_{calcd} = 1.034 g cm^{-3}, μ(Mo$_{K\alpha}$) = 0.11 mm^{-1}, transmission range 0.986–0.958, crystal dimensions 0.52 × 0.22 × 0.19 mm, ω scan, $2\theta_{max}$ = 48°, unique reflections 7217, $R(R_w)$ = 0.0629 (0.0547) for 4418 observed reflections [$I > 2\sigma(I)$], 480 parameters. Hydrogen atoms were placed in calculated positions, and all other atoms were refined anisotropically. Further details of the crystal structure determination may be obtained from the. Fachinformationsdienst Karlsruhe, D-76344 Eggenstein-Leopoldshafen (Germany), on quoting the depository number CSD-59437.

Synergism between the Guest Compound and the Host Framework in Zeolite CsNaY after Impregnation with Cesium Hydroxide**

Michael Hunger,* Udo Schenk, Beate Burger, and Jens Weitkamp

Over the past decades acid zeolites have found numerous applications as catalysts in industrial chemistry. In contrast, only scarce attention has been paid to basic zeolite catalysts, even though such materials show great potential for a number of industrially important reactions—such as dehydrogenation of alcohols, isomerization of olefins, side-chain alkylation of toluene, or the synthesis of 4-methylthiazol.[1] The chemical properties of basic zeolites are determined by the alkali metal cations, which act as weak Lewis acid sites, and the basic framework oxygen atoms. Exchanging sodium ions in the synthesized zeolites with rubidium or cesium ions brings about a decrease in the mean electronegativity of the framework, and the basicity of the oxygen atoms increases.[2] Strongly basic sites can be created by incorporating alkali metal oxides into the zeolite pores.[3, 4] Inside the zeolite host, such oxide guests can occur with a high dispersion. We have now applied multinuclear NMR spectroscopy to investigate the host–guest interactions of oxidic nanoparticles in a Y-type zeolite prepared by exchange with cesium cations followed by impregnation with cesium hydroxide and calcination (see Experimental Section).

According to Hathaway and Davis,[3] the selectivity for acetone formation in the conversion of propan-2-ol can be used as a measure of catalyst basicity. Propan-2-ol was converted at atmospheric pressure in a flow-type unit made of glass with a saturator, a fixed-bed reactor, and an on-line capillary gas chromatograph. All zeolites were first calcined in a flow of dry nitrogen for 12 h at 673 K. At this temperature and a modified residence time of $W/F_{P-2-ol} = 450$ g h mol^{-1}, conversions between 70 and 90% were achieved, and the acetone selectivities amounted to 0, 9, and 61% for NaY, CsNaY-70, and CsNaY-70/16CsOH, respectively. These figures clearly demonstrate the increase in catalyst basicity.

Prior to the NMR measurements the zeolites were heated in a glass tube at a rate of 10 K per hour and calcined for 12 h at 673 K and 10^{-2} Pa. Figure 1 shows the ^{27}Al NMR spectra of the dehydrated zeolites recorded with a spin-echo sequence.[5] The dominating solid-state interaction of the aluminum atoms in the framework of the dehydrated zeolites is that between the electric quadrupole moment Q and the z component of the electric field gradient V_{zz} at the sites of the resonating aluminum nuclei. The strength of this quadrupolar interaction is described by the quadrupole coupling constant $QCC = e\,Q\,V_{zz}/h$, where e is the elementary charge, and h Planck's constant. In a strained framework-AlO_4 tetrahedron, the charge distribution directly surrounding the resonating Al nucleus is unsymmetrical; hence, there is a high electric field gradient and a high ^{27}Al quadrupolar coupling constant. In other words, QCC furnishes information on the chemical bonds inside the zeolitic host framework, and the aluminum atoms represent internal probes for detecting changes in the framework bonds. Previous ^{27}Al NMR investiga-

[*] Priv.-Doz. Dr. M. Hunger, Dipl.-Phys. U. Schenk, Dr. B. Burger, Prof. Dr.-Ing. J. Weitkamp
Institut für Technische Chemie I der Universität
Pfaffenwaldring 55, D-70569 Stuttgart (Germany)
Fax: Int. code +(711)685-4065
e-mail: michael.hunger@po.uni-stuttgart.de

[**] This work was supported by the Deutsche Forschungsgemeinschaft, the Fonds der Chemischen Industrie, and the Max-Buchner-Forschungsstiftung.

 © WILEY-VCH Verlag GmbH, D-69451 Weinheim, 1997 0570-0833/97/3622-2504 $ 17.50+.50/0

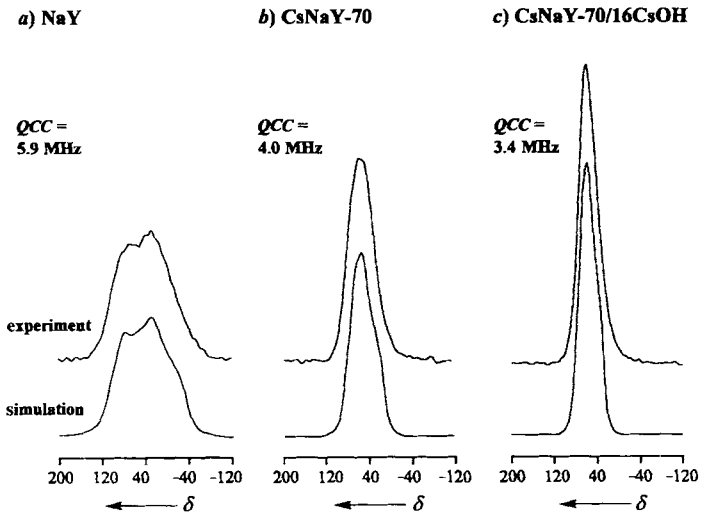

Figure 1. ^{27}Al NMR spectra (104.2 MHz) of dehydrated (673 K) zeolites a) NaY, b) CsNaY-70, and c) CsNaY-70/16CsOH. The quadrupole coupling constants QCC (see text) were determined by simulating the experimental spectra with the Bruker WINFIT software.

tions revealed a relationship between the chemical properties of dehydrated zeolites and the QCC values of the framework-AlO_4 tetrahedra.[5, 6] For acidic zeolites such as HZSM-5 ($n_{Si}/n_{Al} = 22.0$, $QCC = 15.5-16.0$ MHz),[5, 6] HMOR ($n_{Si}/n_{Al} = 8.0$, $QCC = 13.7$ MHz),[5] HY ($n_{Si}/n_{Al} = 3.1$, $QCC = 12.7-13.5$ MHz),[5, 6] and HNaX ($n_{Si}/n_{Al} = 1.4$, $QCC = 10.8$ MHz),[6] the ^{27}Al quadrupole coupling constant decreased with increasing aluminum content in the framework. Even more pronounced variations in QCC occur upon doing from an acidic form of zeolite Y ($QCC = 12.7-13.5$ MHz)[5, 6] to the basic sodium form ($QCC = 5.5$ MHz).[6] A simulation of the ^{27}Al spin-echo NMR spectra depicted in Figure 1 gives quadrupole coupling constants of 5.9 MHz, 4.0 MHz, and 3.4 MHz for zeolites NaY, CsNaY-70 and CsNaY-70/16CsOH, respectively. These values unambiguously show that the chemical bonds of the zeolite host are affected not only by ion exchange (NaY → CsNaY-70), but also by impregnation with cesium hydroxide.

The cesium oxide guest compound was directly investigated with ^{1}H and ^{133}Cs MAS NMR spectroscopy (MAS = magic angle spinning). The ^{1}H MAS NMR spectra of the three zeolites are shown in Figure 2. The concentrations of the hydroxyl groups were determined quantitatively by applying the absolute

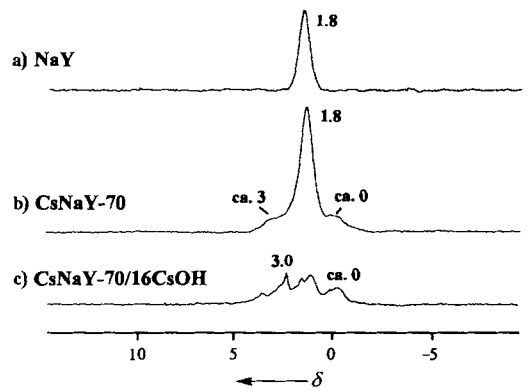

Figure 2. ^{1}H MAS NMR spectra (400.1 MHz) of dehydrated (673 K) zeolites a) NaY, b) CsNaY-70, and c) CsNaY-70/16CsOH; sample spinning rate about 10 kHz.

intensity mode with an external intensity standard (zeolite HNaY-35). The spectrum of zeolite NaY (Figure 2a) consists of one signal at $\delta = 1.8$ (referenced to TMS), which is caused by 1.4 ± 0.2 SiOH groups per unit cell (u.c.) at the framework defects and at the external surface of the zeolite crystallites.[7] Exchanging the sodium ions with cesium ions leads to an increase in the intensity of this signal (Figure 2b), corresponding now to 1.8 ± 0.2 SiOH/u.c. In addition, weak signals appear at $\delta \approx 0$ and 3, which can be assigned to undisturbed and hydrogen-bonded metal OH groups, respectively.[7] Upon impregnating zeolite CsNaY-70 with cesium hydroxide (Figure 2c), the concentration of the silanol groups drops to 0.4 ± 0.2 SiOH/u.c. However, there is no significant change in the signals at $\delta \approx 0$ and 3. Therefore, impregnation of CsNaY-70 does not result in the formation of hydroxyl groups bound to the alkali metal; that is, the guest compound exists as an oxide. On the other hand, the decrease in the concentration of the silanol groups indicates that the guest compound chemically interacts with the framework defect sites.

The ^{133}Cs MAS NMR spectra of the dehydrated zeolites CsNaY-70 and CsNaY-70/16CsOH are shown in Figure 3.

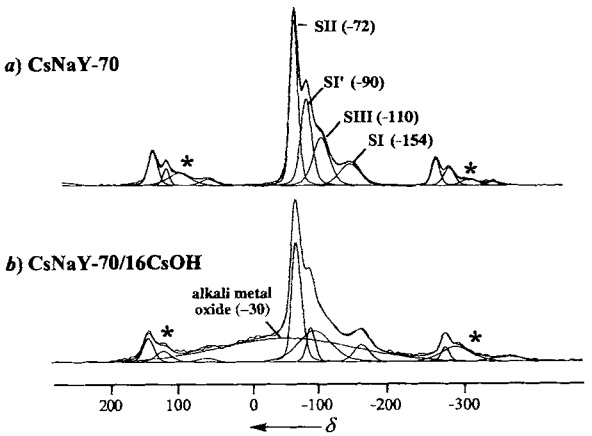

Figure 3. ^{133}Cs MAS NMR spectra (52.5 MHz) of dehydrated (673 K) zeolites a) CsNaY-70 and b) CsNaY-70/16CsOH; sample spinning rate about 10 kHz (*: MAS sidebands).

A modified 4-mm Bruker MAS NMR probe head was used. By applying a sample spinning rate of $\nu_{rot} \approx 10$ kHz ($\nu_{rot} \approx 4$ kHz was employed in earlier work),[8] the spectral resolution was significantly enhanced. This, in turn, was a prerequisite for investigating cesium oxide in zeolite CsNaY-70/16CsOH. The spectrum of dehydrated zeolite CsNaY-70 (Figure 3a) consists of signals at $\delta = -154$, -110, -90, and -72 (referenced to 1 M CsCl) due to cesium cations (37.3 Cs^+/u.c.) located at positions SI, SIII, SI', and SII, respectively.[8] For the impregnated zeolite (Figure 3b), an additional signal is observed with a linewidth of $\Delta\nu_{1/2} = 10 \pm 1$ kHz and a center of gravity at $\delta \approx -30 \pm 2$. Its intensity contribution of $30 \pm 5\%$ agrees well with the amount of cesium oxide introduced in the impregnation step (see below). To interpret the signal at $\delta = -30$, it is important to notice that pure cesium hydroxide (dehydrated for 12 h at 673 K) gives a narrow ^{133}Cs MAS NMR sideband pattern with an isotropic chemical shift of $\delta = 146$ (not shown). Consequently, the cesium oxide in CsNaY-70/16CsOH does not exist as pure isolated clusters. The strong broadening of the signal at $\delta = -30$ may originate in a distribution of chemical shifts for highly dispersed cesium oxide species bound in different ways to the framework.

 © WILEY-VCH Verlag GmbH, D-69451 Weinheim, 1997 0570-0833/97/3622-2505 $ 17.50+.50/0

Bosacek recently proposed a new method for characterizing the mean electronegativity and basicity of the zeolite lattice.[9] He found a correlation between the isotropic ^{13}C NMR shift of the methoxy groups formed upon adsorption of methyl iodide on dehydrated zeolites and the mean Sanderson electronegativity, S^m, of the lattice. Varying S^m from 3.04 for zeolite HZSM-5 ($n_{Si}/n_{Al} = 21.8$) to 2.26 for zeolite CsNaX-49 ($n_{Si}/n_{Al} = 1.2$) resulted in a change in the shift for the methoxy groups from $\delta(^{13}C) = 59.4$ to 54.1 ($\delta(^{13}C)/S^m \approx 6.8$).[9] Bosacek proposed ^{13}C cross-polarization (CP)/MAS NMR spectroscopy of the methoxy groups bound to the zeolite as a new method for determining the basicity of the framework oxygen atoms in zeolites. Figure 4 shows the ^{13}C CP/MAS NMR spectra of the dehydrated zeolites NaY, CsNaY-70, and CsNaY-70/16CsOH after adsorption of $16\,CH_3I$/u.c. The signals at $\delta = -20 \pm 0.5$ are due to physisorbed CH_3I.[9] The chemical shifts of the methoxy groups in zeolites NaY ($\delta = 56.7$, Figure 4a) and CsNaY-70 ($\delta = 56.1$, Figure 4b) correlate well with their mean Sanderson electronegativities ($S^m = 2.60$ and 2.46, respectively). The spectrum of zeolite CsNaY-70/16CsOH (Figure 4c) consists of signals at $\delta = 55.4$ and 50.3 due to methoxy groups and a narrow signal at $\delta = 61.0$. This latter signal has an intensity contribution of about 10% and is due to dimethyl ether.[9] Since there is no signal at $\delta = 56.1$ (for methoxy groups in zeolite CsNaY-70), the whole framework of zeolite CsNaY-70/16CsOH must have been uniformly affected by CsOH impregnation. The change in the ^{13}C shift from $\delta = 56.1$ for methoxy groups in zeolite CsNaY-70 to $\delta = 55.4$ for methoxy groups in zeolite CsNaY-70/16CsOH corresponds to an increased framework basicity of the latter. The high-field signal at $\delta = 50.3$ (Figure 4c), with MAS sidebands comparable to those of the signal at $\delta = 55.4$, indicates the existence of an additional strongly basic compound. Apparently, the methoxy groups responsible for this signal are bound to the alkali metal guest introduced upon impregnation. The high intensity of this signal ($32 \pm 5\%$ of the total intensity) points to a large surface and, hence, to a high dispersion of this alkali metal guest compound in CsNaY-70/16CsOH.

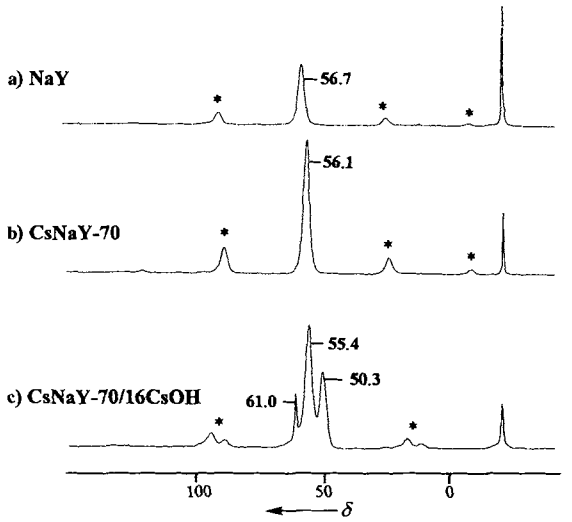

Figure 4. ^{13}C CP/MAS NMR spectra (100.6 MHz) of dehydrated (673 K) zeolites a) NaY, b) CsNaY-70, and c) CsNaY-70/16CsOH loaded with $16\,CH_3I$/u.c.; recorded with a contact time of 3 ms and a sample spinning rate of about 3 kHz (*: MAS sidebands).

In conclusion, impregnation and calcination of zeolite CsNaY-70 with cesium hydroxide not only creates a cesium oxide guest with a high dispersion, but it also affects the chemical properties of the zeolite framework. By using the methoxy groups as an NMR spectroscopic probe, a significant decrease in the mean electronegativity of the zeolite framework was detected upon impregnation with CsOH. Spin-echo NMR spectra of framework aluminum atoms functioning as internal probes revealed an impregnation-induced variation of the ^{27}Al quadrupole coupling constant and, hence, of the chemical bonding inside the dehydrated zeolite framework. A signal of the guest species was observed in the ^{133}Cs MAS NMR spectrum of the dehydrated zeolite CsNaY-70/16CsOH, which differs significantly from that of the pure dehydrated alkali metal hydroxide. The pronounced broadening of this signal points to a high dispersion of the guest inside the pores of zeolite CsNaY-70/16CsOH. The significant decrease in the intensity of the ^1H MAS NMR signal for defect SiOH groups accompanying impregnation is due to deprotonation of these sites by the alkali oxide, and possibly indicates that at least a part of the guest compound is bound to defect sites of the zeolite framework.

Experimental Section

The parent zeolite NaY (Union Carbide Corp., Tarrytown, NY, USA, $n_{Si}/n_{Al} = 2.6$) was ion-exchanged five times in a 0.4 M aqueous solution of CsCl at 353 K, which led to 70% exchange of sodium (zeolite CsNaY-70). Part of this material was then suspended in a 0.2 M solution of CsOH which contained exactly the amount of CsOH need for the final material. The suspension was stirred overnight to dryness at 353 K and calcined for 12 h at 673 K. The material coded CsNaY-70/16CsOH was impregnated with 16 CsOH/u.c. The chemical compositions of the samples were analyzed with inductively coupled plasma atomic emission spectrometry (ICPAES) and atomic absorption spectrometry (AAS). ^{27}Al and ^{29}Si MAS NMR spectroscopy (Bruker MSL 400) of the hydrated zeolites NaY, CsNaY-70 and CsNaY-70/16CsOH showed that no dealumination of the zeolite framework took place as a result of cesium exchange, impregnation with CsOH, and calcination.

Received: April 1, 1997 [Z10292IE]
German version: *Angew. Chem.* **1997**, *109*, 2613–2616

Keywords: heterogeneous catalysis · host–guest chemistry · NMR spectroscopy · solid-state bases · zeolites

[1] S. Feast, J. A. Lercher, *Stud. Surf. Sci. Catal.* **1996**, *102*, 363–412.
[2] M. Huang, S. Kaliaguine, *J. Chem. Soc. Faraday Trans.* **1992**, *88*, 751–758.
[3] P. E. Hathaway, M. E. Davis, *J. Catal.* **1989**, *116*, 263–278.
[4] D. Barthomeuf, *J. Phys. Chem.* **1984**, *88*, 42–45.
[5] M. Hunger, T. Horvath, *Ber. Bunsenges. Phys. Chem.* **1995**, *99*, 1316–1320.
[6] H. Ernst, D. Freude, I. Wolf, *Chem. Phys. Lett.* **1993**, *212*, 588–596.
[7] M. Hunger, *Solid State Nucl. Magn. Reson.* **1996**, *6*, 1–29.
[8] H. Koller, B. Burger, A. M. Schneider, G. Engelhardt, J. Weitkamp, *Microporous Mater.* **1995**, *5*, 219–232.
[9] V. Bosacek, *Z. Phys. Chem.* **1995**, *189*, 241–250.

 © WILEY-VCH Verlag GmbH, D-69451 Weinheim, 1997 0570-0833/97/3622-2506 $ 17.50+.50/0

1,8-Bis(allylstannyl)naphthalene Derivatives as Neutral Allylation Agents: Rate Acceleration by Chelation-Induced Lewis Acidity**

Naoki Asao, Pingli Liu, and Keiji Maruoka*

Allylation of aldehydes and ketones with trialkylallylstannanes to form homoallylic alcohols is one of the most powerful C–C bond forming reactions in organic synthesis, and a variety of procedures have been elaborated.[1] Most of the procedures developed so far involve the effective use of Lewis acids as activating agents under mild conditions, since noncatalyzed allylations do not occur or are exceedingly slow, even at elevated temperatures.[2] Brønsted acids and basic Bu_4NF can also be employed to promote this transformation.[3,4] Allylations that are induced photchemically or by high pressure can be executed under neutral conditions.[5,6] We here report a new type of noncatalyzed allylation of aldehydes and ketones using 1,8-bis(allylstannyl)naphthalene derivatives **1**, which is based on a chelation-induced Lewis acidity of neutral, bidentate organostannane reagents, as depicted in **A**.[7,8]

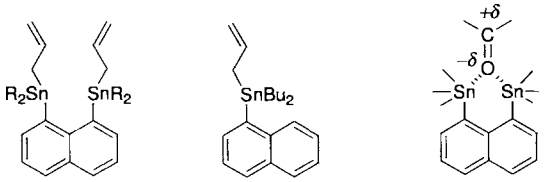

1a (R = Bu)
1b (R = Me)

2

A

The requisite 1,8-bis(allyldibutylstannyl)naphthalene (**1a**) can be prepared by treatment of 1,8-diiodonaphthalene[9] with BuLi (2 equiv), dibutyltin dichloride (2 equiv), and allylmagnesium bromide (2.2 equiv) in about 55% yield. The monostannyl compound **2** was also synthesized in analogy to **1a** from 1-bromonaphthalene. The reaction of **2** with cyclohexanone (**3**; $R^1 \cdot R^2 = -(CH_2)_5-$; 5 equiv) in toluene at 100 °C for four days proceeds very sluggishly to furnish 1-allylcyclohexanol (**4**;

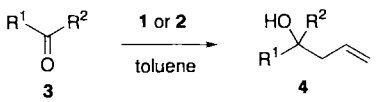

3 **4**

$R^1 \cdot R^2 = -(CH_2)_5-$) in only 4% yield. In contrast, **1a** afforded the allylation product in 80% yield upon reaction with cyclohexanone under similar conditions. This rate acceleration is ascribable to the appearance of the latent Lewis acidity, which is induced by the chelation effect of neutral, bidentate bis(stannane) **1** on the carbonyl group (structure **A**).[10] A similar tendency is also observed with 2-nonanone substrate **3** (R^1 = Me, $R^2 = C_7H_{15}$; see Table 1, entry 2).

[*] Prof. K. Maruoka, Dr. N. Asao, Dr. P. Liu
Department of Chemistry, Graduate School of Science
Hokkaido University
Sapporo, 060 (Japan)
Fax: Int. code +(11)746-2557

[**] We are grateful for an Inoue fellowship. This work was partially supported by the Asahi Glass Foundation, the Akiyama Foundation, the Ogasawara Foundation for the Promotion of Science and Engineering, and a Grant-in-Aid for Scientific Research from the Japanese Ministry of Education, Science, Sports and Culture.

Table 1. Allylation of various carbonyl substrates **3** with **1** under neutral conditions [a].

Entry	R^1	R^2	Reagent	Conditions	Yield [%] [b]
1	$-(CH_2)_5-$		**1a**	100 °C, 4 d	80 (4)
2	C_7H_{15}	CH_3	**1a**	100 °C, 3 d	44 (2)
3	Ph	H	**1a**	50 °C, 12 d	99 (5)
4	Ph	H	**1a**	70 °C, 82 h	98 (5)
5	Ph	H	**1b**	70 °C, 53 h	99 (4)
6	cyclohexyl	H	**1a**	50 °C, 12 d	99 (5)
7	cyclohexyl	H	**1a**	70 °C, 63 h	98 (3)
8	Ph	Cl	**1a**	100 °C, 1 h	64 [c] (<1)
9	C_7H_{15}	Cl	**1a**	100 °C, 1 h	57 [c] (<1)
10	Ph	OCH_3	**1a**	100 °C, 3 d	<1
11	PhCH=CH	CH_3	**1a**	100 °C, 7 d	40 [d]

[a] The reaction was carried out with 1 equiv of **1** and 5 equiv of **3** in toluene. [b] Yield of the isolated product. Yields obtained with monostannyl analogues **2** under similar reaction conditions are given in parentheses. [c] Yields of the corresponding ketones. [d] Yield of 1,2-addition product.

The selected allylations of carbonyl substrates listed in Table 1 provide the following conclusions: 1) Reactions of aldehydes proceed smoothly to give secondary homoallylic alcohols in almost quantitative yields (entries 3–7). 2) One characteristic feature is the smooth alkylation of acid chloride with **1a** (entries 8 and 9). Such a transformation is not realized with monostannane **2**, as reported earlier.[11] 3) Esters are inert under the standard reaction conditions (entry 10). 4) 1,8-Bis(allyldimethylstannyl)naphthalene (**1b**) showed reactivity similar to that of **1a** (entry 5). 5) Although the Lewis acid promoted allylation of α,β-unsaturated ketone with an allylstannane is reported to give a conjugate adduct selectively,[12] reaction with **1a** exclusively afforded a carbonyl allylation product (entry 11).

Another characteristic feature of the allylation is its applicability to more sensitive substrates, which normally provide side products in the existing acid-catalyzed allylations with monoallylstannanes. For example, α-bromo aldehyde **5**, *cis*-β,γ-unsaturated aldehyde **7**, and optically pure α-siloxyphenylacetaldehyde **9** afforded the corresponding bromohydrine **6** without epoxide formation, the bis(allylic) product **8** without olefin migration, and the 1,2-siloxy alcohol **10** without racemization, respectively.[13]

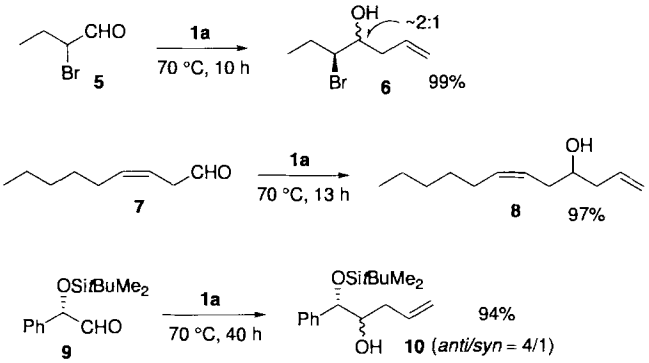

It is noteworthy that the present allylation can be utilized even in aqueous media. Highly reactive aldehydes such as α-keto aldehydes, trifluoroacetaldehyde, and α-halo aldehydes usually exist as hydrates, hemiacetals, or aqueous solutions. Our allylation works equally well in the presence of water with such commercially available aldehydes under mild conditions.[14] This provides a new, one-pot approach to allylated α-hydroxy esters from various tartrates via the intermediary glyoxylate hydrates (Scheme 1).

 © WILEY-VCH Verlag GmbH, D-69451 Weinheim, 1997 0570-0833/97/3622-2507 $ 17.50+.50/0

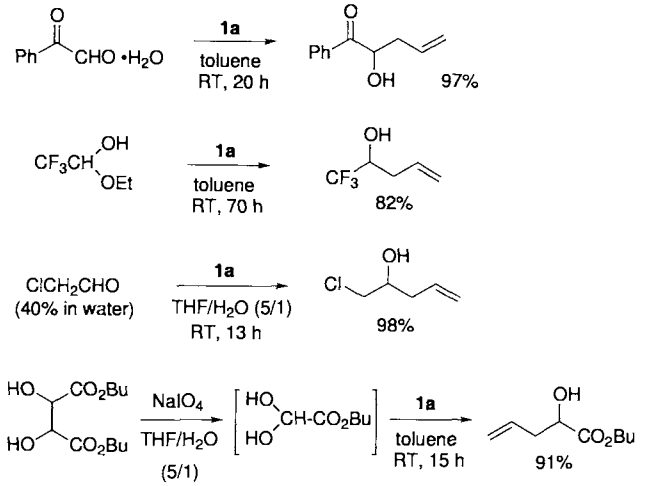

Scheme 1. Allylation with **1a** in the presence of water; RT = room temperature.

Allylation with bis(stannyl) derivatives **1** is highly chemoselective, and occurs exclusively at the less hindered carbonyl group, as demonstrated by the chemoselective allylation of dicarbonyl substrates **11** and **12**. Such ability to discrimate between two different carbonyl groups is far superior to that of conventional allylation agents (Scheme 2).[15]

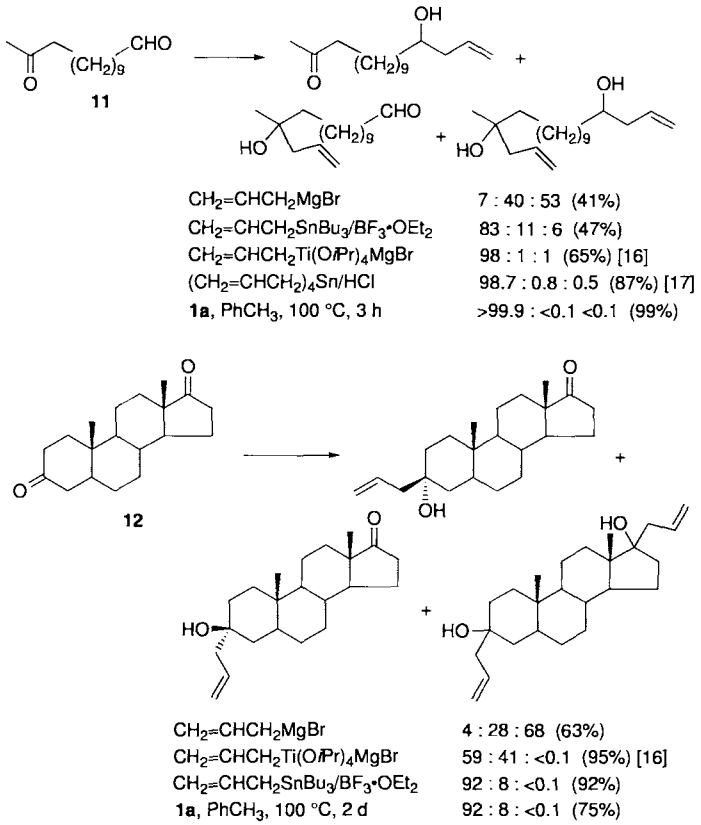

Scheme 2. Comparison of the chemoselectivity of the allylation with **1a** and other reagents [15].

The present allylation may proceed either intra- or intermolecularly. To explain the mechanism of the allylation, the cross-over reaction of **1a** and tributylprenyltin [1 equiv each, Eq. (1)] with benzaldehyde was carried out; allylation product **4**

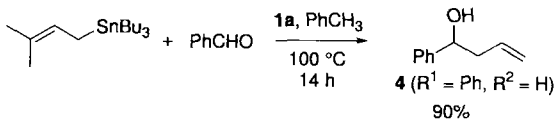

(1)

(R^1 = Ph, R^2 = H) was furnished solely in 90% yield without any prenylation product.[18, 19] This result and that of the reaction of 1,8-bis(dibutylprenylstannyl)naphthalene (**13**) with benzaldehyde, which afforded **14** exclusively in 56% yield [Eq. (2)],

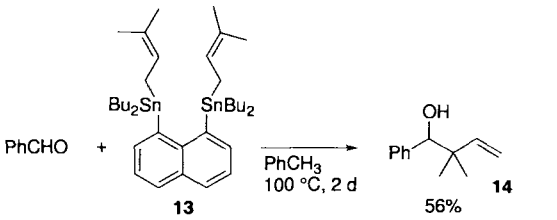

(2)

indicate that allylation with **1** takes place intramolecularly via a six-membered transition state with carbonyl substrates.

We have developed a new agent which is highly effective for the selective allylation of aldehydes and ketones under neutral conditions. The reaction proceeds without any catalyst by taking advantage of the chelation-induced Lewis acidity of bidentate bis(stannyl) compounds. More appropriate choice of metals and more sophisticated design of neutral, bidentate organometallic compounds possessing high latent Lewis acidity are the subjects of our ongoing studies.

Experimental Section

The allylation of cyclohexanecarboxaldehyde is representative: To a solution of **1a** (500 mg, 0.74 mmol) in toluene (3 mL) was added cyclohexanecarboxaldehyde (0.45 mL, 3.7 mmol) at room temperature under an argon atmosphere. The mixture was allowed to warm to 70 °C, and stirred for 63 h at this temperature. After the mixture cooled to room temperature the solvent was removed in vacuo, and the residue purified by column chromatography on basic silica gel with hexane/EtOAc (7/1) as eluent to give 1-cyclohexyl-3-buten-1-ol (110 mg, 98% yield) as a colorless oil.

Received: April 28, 1997 [Z10389IE]
German version: *Angew. Chem.* **1997**, *109*, 2616–2618

Keywords: allylations · chelates · chemoselectivity · Lewis acidity · tin

[1] Review: a) Y. Yamamoto, *Aldrichim. Acta* **1987**, *20*, 45–49; b) *Acc. Chem. Res.* **1987**, *20*, 243–249; c) C. Hull, S. V. Mortlock, E. J. Thomas, *Tetrahedron* **1989**, *45*, 1007–1015; d) Y. Nishigaichi, A. Takuwa, Y. Naruta, K. Maruyama, *ibid.* **1993**, *49*, 7395–7426.

[2] a) K. König, W. P. Neumann, *Tetrahedron Lett.* **1967**, 495–498; b) M. Pereyre, J.-P. Quintard, *Pure Appl. Chem.* **1981**, *53*, 2401–2417.

[3] Brønsted acid catalyzed allylation: a) S. E. Denmark, E. J. Weber, T. M. Wilson, T. M. Willson, *Tetrahedron* **1989**, *45*, 1053–1065; b) V. Gevorgyan, I. Kadota, Y. Yamamoto, *Tetrahedron Lett.* **1993**, *34*, 1313–1316.

[4] Bu_4NF-catalyzed allylation: Y. Yamamoto, S. Hatsuya, J. Yamada, *J. Chem. Soc. Chem. Commun.* **1987**, 561–562.

[5] High pressure induced allylation: a) Y. Yamamoto, K. Maruyama, K. Matsumoto, *J. Chem. Soc. Chem. Commun.* **1983**, 489–490; b) N. S. Isaacs, R. L. Marshall, D. J. Young, *Tetrahedron Lett.* **1992**, *33*, 3023–3024; c) Y. Yamamoto, K. Saito, *J. Chem. Soc. Chem. Commun.* **1989**, 1676–1678.

[6] Photochemically induced allylation: A. Takuwa, H. Tagawa, H. Iwamoto, O. Soga, K. Maruyama, *Chem. Lett.* **1987**, 1091–1094.

[7] 1,8-Bis(metal)naphthalene derivatives as chelating Lewis acids: M. Reilly, T. Oh, *Tetrahedron Lett.* **1995**, *36*, 221–224, and references therein.

[8] Behavior of chelating bis(halodiphenylstannyl) Lewis acids towards halide ions: D. Dakternieks, K. Jurkschat, H. Zhu, E. R. T. Tiekink, *Organometallics* **1995**, *14*, 2512–2521.

[9] H. O. House, D. G. Koepsell, W. J. Campbell, *J. Org. Chem.* **1972**, *37*, 1003–1011.

 © WILEY-VCH Verlag GmbH, D-69451 Weinheim, 1997 0570-0833/97/3622-2508 $ 17.50+.50/0

[10] ^{119}Sn NMR analysis of **1a** and a mixture of **1a** and a carbonyl substrate in C_6D_6 did not show any noticeable differences in the chemical shifts. The original Sn signals in **1a** appeared at $\delta = -49.15$ and, upon addition of DMF as a carbonyl substrate, the signal shifted slightly to $\delta = -49.07$ (Me_4Sn as external standard): a) P. J. Smith, A. P. Tupciauskas, *Annu. Rep. NMR Spectrosc.* **1978**, *8*, 291–370; b) T. Kawakami, T. Sugimoto, I. Shibata, A. Baba, H. Matsuda, N. Sonoda, *J. Org. Chem.* **1995**, *60*, 2677–2682, and references therein.
[11] M. Pereyre, J.-P. Quintard, A. Rahm, *Tin in Organic Synthesis*, Butterworths, London, **1987**, p. 200.
[12] A. Hosomi, H. Iguchi, M. Endo, H. Sakurai, *Chem. Lett.* **1979**, 977–980.
[13] I. Pri-Bar, P. S. Pearlman, J. K. Stille, *J. Org. Chem.* **1983**, *48*, 4629–4634.
[14] The allylation is somewhat accelerated in aqueous media. For example, the reaction of 3-phenylpropanal with **1a** in THF/H_2O (5/1) gave an allylation product in 82% yield; a yield of 62% was obtained in THF under similar reaction conditions.
[15] The ratio of the allylation products from keto aldehyde **11** was determined by gas chromatography.
[16] M. T. Reetz, B. Wenderoth, R. Peter, *J. Chem. Soc. Chem. Commun.* **1983**, 406–408; see also M. T. Reetz, *Organotitanium Reagents in Organic Synthesis*, Springer, Berlin, **1986**, p. 80.
[17] A. Yanagisawa, H. Inoue, M. Morodome, H. Yamamoto, *J. Am. Chem. Soc.* **1993**, *115*, 10356–10357.
[18] Use of excess prenyltributyltin (about 2–3 equiv) also gave none of the prenylation product.
[19] The Lewis acidity of 1,8-bis(stannyl)naphthalene derivatives was also examined for the allylation of monostannane **2** with benzaldehyde in the presence of 1,8-bis(tributylstannyl)naphthalene as a bidentate Lewis acid under reaction conditions similar to those described for entry 4 of Table 1. Since the allylated product was obtained in higher yield (14%) than that in entry 4, 1,8-bis(tributylstannyl)naphthalene seems to possess only weak Lewis acidity.

Copper(I) Helicates Containing Bridging But Nonchelating Polypyridine Fragments**

Raymond Ziessel,* Anthony Harriman,* Jean Suffert, Marie-Thérèse Youinou, André De Cian, and Jean Fischer

Polypyridine ligands can complex an inordinately wide range of cations and have numerous important analytical applications. These ligands have also found prominent use in supramolecular chemistry where, by virtue of their forming stable and well-defined complexes with metal cations, they have facilitated assembly of molecular (double and triple) helicates, knots, grids, ladders, catenates, rotaxanes,[1–4] and related exotic structures.[5, 6] Such elaborate molecular architectures are made possible by incorporating several polypyridine units into oligomeric or macrocyclic multitopic ligands. Subsequent coordination with copper(I), or similar metal centers, provides the impetus for self-organization into highly ordered structures. The resulting tetrahedral complexes are sufficiently stable for the copper(I), in general, to bind selectively to the polypyridine ligand, even if the molecule possesses additional coordination sites. Indeed, there are very few examples where a polypyridine unit is bypassed in favor of other coordination sites, and where this happens, these tend to be idealized stereospecific cavities.[7]

The ligands L^1 and L^2 possess two disparate binding sites in close proximity. They were synthesized by reaction of 2,2′-

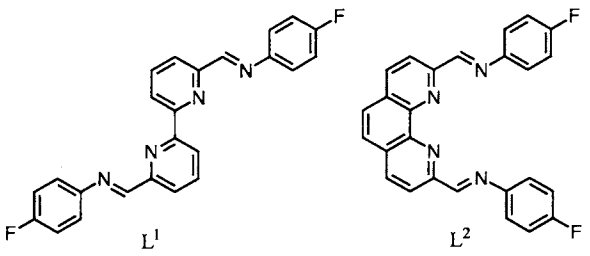

bipyridyl-6,6′-dicarbaldehyde[8] or 1,10-phenanthroline-2,9-dicarbaldehyde[9] with 4-fluoroaniline in the presence of catalytic amounts of *p*-TsOH. Both ligands react with $[Cu(CH_3CN)_4]ClO_4$[10] to afford *deep-green*, air-stable materials in almost quantitative yield. These products lack the metal-to-ligand charge-transfer (MLCT) absorption band considered to be characteristic of tetrahedral copper(I) polypyridine complexes. On the basis of FAB and ES mass spectrometry it was concluded that the isolated products were the corresponding binuclear copper(I) complexes, without contamination from mononuclear or polymeric structures. The products, therefore, may be assigned the general formula $[Cu_2L_2](ClO_4)_2$ ($L = L^1, L^2$). Direct involvement of the terminal imino groups in the coordination sphere was confirmed by solid-state and solution-phase FT-IR studies and by both ^1H and ^{13}C NMR spectroscopy. The NMR studies also indicated that the two ligands bound to each copper(I) cation were equivalent and that each ligand was symmetric about its center.

Indeed, the solid-state structures of $[Cu_2(L^1)_2](ClO_4)_2$ und $[Cu_2(L^2)_2](ClO_4)_2$ (Figure 1) are best described as double-stranded helicates with the two copper(I) cations lying at center-to-center separations of 2.885(2) and 2.748(1) Å, respectively. These separations are among the shortest metal–metal distances yet found in inorganic helicates,[11] being of the same order as observed in many copper-containing enzymes,[12] but there is no indication of a copper–copper bond. Each ligand wraps around the two copper(I) cations, and the polypyridine units become twisted (approximately 36° for $[Cu_2(L^1)_2](ClO_4)_2$) about the exocyclic central C–C bond. Interestingly, the copper(I) center is significantly closer to the imino N atom than to that of the adjacent pyridine unit, but there is no obvious indication of intramolecular π-stacking.

These crystallographic structures clearly indicate that, at least in the solid state, the two pyridine groups within a given ligand are complexed to different cations. Each copper(I) ion is coordinated to four nitrogen atoms, provided by the imine and pyridine groups of two distinct ligands, to give a distorted tetrahedron with a small angle of about 80°. It appears, therefore, that incorporation of imine groups at the α,α′ positions of a bipyridine or phenanthroline ligand causes the central unit to become nonchelating and, instead, to adopt a bridging role. This may not be too surprising for L^1, where individual pyridines can rotate freely, and is somewhat reminiscent of the double-helicates formed from sexipyridine ligands.[13] However, such behavior is unparalleled for a phenanthroline-based

[*] Dr. R. Ziessel
Ecole Chimie, Polymères, Matériaux (ECPM)
Université Louis Pasteur (ULP)
Laboratoire de Chimie, d'Electronique et de Photonique Moléculaires,
1 rue Blaise Pascal, F-67008 Strasbourg Cedex (France)
Fax: Int. code +388416-825
e-mail: ziessel@chimie.u-strasbg.fr
Prof. A. Harriman
ECPM, Laboratoire de Photochimie
Dr. M.-T. Youinou
ULP, Laboratoire de Chimie des Métaux de Transition et de Catalyse
Dr. J. Suffert
ULP, Centre de Neurochimie
Dr. A. DeCian, Prof. J. Fischer
ULP, Laboratoire de Cristallochimie et de Chimie Structurale

[**] This work was partially supported by the Centre National de la Recherche Scientifique and by the Engineering School of Chemistry (ECPM).

 © WILEY-VCH Verlag GmbH, D-69451 Weinheim, 1997 0570-0833/97/3622-2509 $ 17.50+.50/0

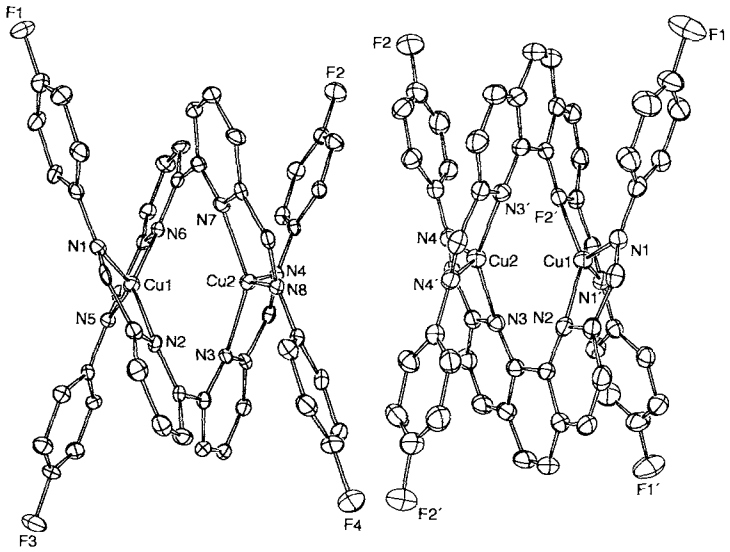

Figure 1. ORTEP drawing of $[Cu_2(L^1)_2](ClO_4)_2 \cdot CH_3CN$ (left) and $[Cu_2(L^2)_2](ClO_4)_2 \cdot H_2O$ (right); thermal ellipsoids are at 50% probability, and hydrogen atoms are omitted for clarity. Selected bond lengths [Å] and angles [°]: for the L^1 complex Cu1–N1 2.02(8), Cu1–N2 2.096(7), Cu1–N5 2.029(7), Cu1–N6 2.104(7), Cu2–N3 2.117(7), Cu2–N4 2.052(7), Cu2–N7 2.109(7), Cu2–N8 2.037(8), Cu1–Cu2 2.885(2); N1-Cu1-N2 81.6(3), N1-Cu1-N5 138.5(3), N1-Cu1-N6 110.8(3), N2-Cu1-N5 110.7(3), N2-Cu1-N6 146.3(3), N5-Cu1-N6 81.3(3), N3-Cu2-N4 81.0(3), N3-Cu2-N7 146.4(3), N3-Cu2-N8 112.0(3), N4-Cu2-N7 109.3(3), N4-Cu2-N8 140.1(3), N7-Cu2-N8 81.2(3); for the L^2 complex Cu1–N1 2.020(3), Cu1–N2 2.077(3), Cu2–N3 2.106(3), Cu2–N4 2.008(3), Cu1–Cu2 2.748(2); N1-Cu1-N2 80.1(1), N3-Cu2-N4 79.7(1).

ligand, and it is noteworthy that the pyridino N atoms in L^2 are well situated to form a chelate.

We were unable to isolate the mononuclear complex of L^1, and even in the presence of a 10-fold excess of ligand, $[Cu_2(L^1)_2]^{2+}$ was the only product observable by NMR spectroscopy. This was not the case with L^2 where the mononuclear complex $[Cu(L^2)_2]^+$ was isolated in low yield from reaction in the presence of excess ligand (ES-MS$^+$ in H_2O/CH_3CN: m/z 907.5). Although an X-ray structural determination remains elusive, it was firmly demonstrated by FT-IR as well as ^1H and ^{13}C NMR spectroscopy that the copper(I) cation is coordinated at the imino and adjacent pyridino binding sites. Again, the compound lacks the MLCT absorption band characteristic of a copper(I) bis(phenanthroline) complex.

Successive complexation of copper(I) with the multitopic ligands L^1 and L^2 was followed by spectrophotometric titration in deoxygenated acetonitrile/dichloromethane (4/1) containing tetraethylammonium perchlorate (0.1 M). The stability constants (K), as derived by global analysis of the titration data, are collected in Table 1. Evaluation of individual stability constants K_1, K_2, and K_3 is based on the mechanism for stepwise assembly of the metallohelicate described in Equations (1)–(3). Confidence in this model stems from our isolation of $[Cu(L^2)_2]^+$ and its subsequent conversion into $[Cu_2(L^2)_2]^{2+}$. In the case of L^2, it was possible to confirm the stability constant for the final step in helicate assembly by direct titration ($\lg K_3 = 6.08$). Furthermore, the overall stability constant (β_L) for each imino complex could be obtained by dissociative titration with 2,9-dimethyl-1,10-phenanthroline (neocuproine, L^3). This latter reaction (Eqs. 4 and 5) could be followed due to the development of the intense MLCT absorption band of $[Cu(L^3)_2]^+$. The corresponding β values can be expressed in terms of the overall stability constant for formation of copper(I) bis(neocuproine) ($\lg \beta_{L^3} = 14.2$) as follows: $\beta_4 = \beta_{L^3}^2/\beta$ where $\beta = K_1 K_2 K_3$ and $\beta_5 = \beta_{L^3}/K_1 K_2$.

$$Cu^+ + L \rightleftharpoons [CuL]^+ \quad (1)$$

$$[CuL]^+ + L \rightleftharpoons [CuL_2]^+ \quad (2)$$

$$Cu^+ + [CuL_2]^+ \rightleftharpoons [Cu_2L_2]^{2+} \quad (3)$$

Table 1. Stability constants (K) for individual steps in helicate assembly, overall association constants (β) for complex formation, and pK_A values for the free ligands L^1, L^2, and L^3. The numbers given in parentheses refer to values calculated from separate titrations.

Reaction	Ligand	$\lg K$	$\lg \beta$
Equation (1)	L^1	5.30	
	L^2	5.70	
	L^3	7.18	
Equation (2)	L^1	6.30	11.60
	L^2	3.74	9.44
	L^3	7.02	14.20
Equation (3)	L^1	14.87	26.47
	L^2	6.31 (6.08)	15.75
Equation (4)	L^1		1.82 (1.93)
	L^2		11.70 (12.65)
Equation (5)	L^2		4.83 (4.76)
$Cu^+ + 2L \rightleftharpoons [CuL_2]^+$	L^1		11.60
	L^2		9.44
	L^3		14.20
$2Cu^+ + 2L \rightleftharpoons [Cu_2L_2]^{2+}$	L^1		26.47
	L^2		15.75
$[Cu_2L_2]^{2+} + 2L \rightleftharpoons 2[CuL_2]^+$	L^2	3.56 (3.13)	

pK_a-values for the ligands L (reaction $L + H^+ \rightleftharpoons LH^+$): L^1: 5.52, L^2: 4.40, L^3: 5.35

$$[Cu_2L_2]^{2+} + 4L^3 \rightleftharpoons 2[Cu(L^3)_2]^+ + 2L \quad (4)$$

$$[CuL_2]^+ + 2L^3 \rightleftharpoons [Cu(L^3)_2]^+ + 2L \quad (5)$$

These stability constants contain information on both accumulation (i.e., collection) and organization (i.e., orientation).[1] The first step must involve attachment of a copper(I) fragment to a single N donor, but this species could not be isolated or resolved during titration. Molecular mechanics (MM2) simulations indicate that in the most stable conformations the free ligands are planar, due to charge transfer along the molecular axis, and have *trans* imino groups. For these conformations, SCF-MO calculations with PM3 parameters indicated that the imino N atoms possess slightly higher electron density than the pyridine N atoms. The terminal fluorine atoms do not influence the electronic properties of the ligands and are not essential for helicate formation. There appears to be little difference in the relative accessibility of these two sites towards a bulky cation such as $[Cu(CH_3CN)_4]^+$, but slight rotation of the terminal phenyl ring exposes the imino N atom to the approaching cation while, at least with L^2, blocking access to the pyridino N atoms. On this basis, we might expect the initial binding contact between copper(I) and a multitopic ligand to involve coordination at the imino function. Subsequent attachment to an adjacent pyridino N donor requires internal torsional motion, but may be driven by the chelate effect. The derived stability constants for this step (K_1) indicate that the ditopic ligands are somewhat inferior chelators than neocuproine, probably due to their increased stereochemical bulk and concomitant entropic factors. Interestingly, the order of K_1 values differs from the trend in pK_A values measured for the free ligands by potentiometric titration in a 1/1 mixture of dioxane and water (see Table 1).

Under the conditions used for the titrations (addition of copper(I) to excess ligand), coordination of a second ligand to the

 © WILEY-VCH Verlag GmbH, D-69451 Weinheim, 1997 0570-0833/97/3622-2510 $ 17.50+.50/0

mononuclear fragment [Eq. (2)] should be competitive with dimerization to form $[Cu_2L_2]^{2+}$. For neocuproine, this is a highly favorable process and is only slightly less propitious for L^1. Formation of the 1/2 complex is not so auspicious with L^2, presumably because of steric crowding, and there is a serious drop in stability constant for this step. Metallohelicate assembly, following coordination of a second copper(I) center [Eq. (3)], is considerably easier with the more flexible bipyridyl-based ligand than with its phenanthroline analogue. In part, this difference can be attributed to the relative capacity for internal rearrangement to provide a suitable binding geometry around the cation. It is during addition of the second copper(I) cation that the real differences emerge between the two multitopic ligands. It appears that L^1 exhibits positive cooperativity towards copper(I) in that $K_1 < K_2 < K_3$ and the overall stability constant for the metallohelicate ($\lg\beta_L = 26$) compares well with the only available published data for a somewhat comparable process.[14] In the case of L^2, helicate formation is not driven by positive cooperativity since $K_2 < K_1 < K_3$, and the overall stability constant ($\lg\beta_L = 16$) reflects the relative difficulty in attaining a suitable geometry. In fact, it is remarkable that this ligand supports helicate formation.

An important finding to emerge from this study is that positive cooperativity is not a prerequisite for helicate formation, although the noncooperativity found for L^2 causes the overall stability constant to decrease by ten orders of magnitude. A more remarkable aspect of this work, however, concerns our observation that the polypyridine units do not operate as single chelators for copper(I) but that individual N atoms act independently as secondary coordination sites. Self-organization into helicate structures is a multistep process, but in the case of L^2, we were able to isolate and characterize a crucial intermediary metallo fragment. In this latter system, helicate formation is restricted by thermodynamic considerations rather than kinetic factors as is the case in certain pentanuclear helicates.[15] These metallohelicates with copper(I) centers in unusually close proximity can be dismantled under mild conditions by a) oxidation, b) competitive complexation, or c) addition of excess ligand in the case of L^2. One clear advantage of these systems is that the terminal imino group is readily functionalized without disruption to the helicate structure. Thus such local molecular architectures can be readily included into organized macroscopic ensembles, such as calamitic mesophases.

Experimental Section

Synthesis and characterization of the free ligands and complexes used in this study will be reported elsewhere. All materials gave satisfactory elemental analyses and NMR, mass, and infrared spectra.

X-ray structure analyses: $[Cu_2(L^1)_2](ClO_4)_2 \cdot CH_3CN$, $M_r = 1163.9$; deep green crystals ($0.22 \times 0.18 \times 0.12$ mm^3); monoclinic space group $P2_1/c$ with $a = 13.667(5)$, $b = 25.617(8)$, $c = 15.195(6)$ Å, $\beta = 110.17(2)^\circ$, $V = 4993.6$ Å^3, $Z = 4$, $\rho_{calcd} = 1.548$ g cm^{-3}, $\mu = 27.086$ cm^{-1}. A total of 5651 reflections were collected on a Philips PW 1100/16 diffractometer at $-100\,^\circ$C with Ni-filtered $Cu_{K\alpha}$ radiation $\lambda = 1.5418$ Å. The systematic absences together with the E statistics and the NZ test suggested the space group $P2_1/c$. The structure was solved by a combination of Patterson, difference Fourier analysis, and full-matrix, least-squares methods. The final conventional residuals were $R = 0.050$ and $R_w = 0.070$ for 2820 reflections having $I > 3\sigma(I)$. $[Cu_2(L^2)_2](ClO_4)_2 \cdot H_2O$, $M_r = 1188.9$; dark green crystals ($0.32 \times 0.25 \times 0.12$ mm^3); monoclinic space group $C2/c$ with $a = 23.804(7)$, $b = 14.743(4)$, $c = 13.755(3)$ Å, $\beta = 90.68(2)^\circ$, $V = 4826.9$ Å^3, $Z = 4$, $\rho_{calcd} = 1.636$ g cm^{-3}, $\mu = 28.266$ cm^{-1}. Collected data: 2916; $R = 0.035$ and $R_w = 0.054$ for 2117 reflections having $I > 3\sigma(I)$. Crystallographic data (excluding structure factors) for the structures reported in this paper have been deposited with the Cambridge Crystallographic Data Centre as supplementary publication no. CCDC-100335. Copies of the data can be obtained free of charge on application to The Director, CCDC, 12 Union Road, Cambridge CB21EZ, UK (fax: int. code +(1223)336-033; e-mail: deposit@chemcrys.cam.ac.uk).

Titrations were made by adding successive aliquots of a solution of $[Cu(CH_3CN)_4](ClO_4)$ in deoxygenated acetonitrile to a solution of the ligand in deoxygenated CH_3CN/CH_2Cl_2 (4/1) containing tetraethylammonium perchlorate (0.1 M). Stability constants were calculated (30 concentrations analyzed at 60 different wavelengths) with the SPECFIT program and known spectra of the reactants and products. Similar titrations were made by addition of neocuproine to the copper(I) complexes in deoxygenated CH_3CN/CH_2Cl_2 4/1 containing tetraethylammonium perchlorate (0.1 M).

Received: March 17, 1997
Revised version: July 11, 1997 [Z10251IE]
German version: *Angew. Chem.* **1997**, *109*, 2621–2624

Keywords: coordination modes · copper · helical structures · N ligands · self-organization

[1] J.-M. Lehn, *Supramolecular Chemistry*, VCH, Weinheim, **1995**.
[2] J.-C. Chambron, C. O. Dietrich-Buchecker, J.-P. Sauvage, *Top. Curr. Chem.* **1993**, *165*, 131; J.-C. Chambron, C. O. Dietrich-Buchecker, V. Heitz, J.-F. Nierengarten, J.-P. Sauvage in *Transition Metals in Supramolecular Chemistry* (*Nato ASI Ser. Ser. C* **1993**, *448*), p. 371.
[3] D. S. Lawrence, T. Jiang, M. Levett, *Chem. Rev.* **1995**, *95*, 2229.
[4] B. Hasenknopf, J.-M. Lehn, B. O. Kneisel, G. Baum, D. Fenske, *Angew. Chem.* **1996**, *108*, 1987; *Angew. Chem. Int. Ed. Engl.* **1996**, *35*, 1838; M. Schwach, H. D. Hausen, W. Kaim, *Chem. Eur. J.* **1996**, *2*, 446; C. R. Woods, M. Benaglia, F. Cozzi, J. S. Siegel, *Angew. Chem.* **1996**, *108*, 1977; *Angew. Chem. Int. Ed. Engl.* **1996**, *35*, 1830.
[5] C. Piguet, G. Hopfgartner, B. Bocquet, O. Schaad, A. F. Williams, *J. Am. Chem. Soc.* **1994**, *116*, 9092; C. Piguet, G. Hopfgartner, A. F. Williams, J.-C. G. Bünzli, *J. Chem. Soc. Chem. Commun.* **1995**, 491.
[6] R. Ziessel, D. Matt, L. Toupet, *J. Chem. Soc. Chem. Commun.* **1995**, 2033; F. M. Romero, R. Ziessel, A. Dupont-Gervais, A. Van Dorsselaer, *Chem. Commun.* **1996**, 551.
[7] J. de Mendoza, E. Mesa, J.-C. Rodriguez-Ubis, P. Vazquez, F. Vögtle, P. M. Windscheif, K. Rissanen, J.-M. Lehn, D. Lilienbaum, R. Ziessel, *Angew. Chem.* **1991**, *103*, 1365; *Angew. Chem. Int. Ed. Engl.* **1991**, *30*, 1331.
[8] J. E. Parks, B. E. Wagner, R. H. Holm, *J. Organomet. Chem.* **1973**, *56*, 53.
[9] C. J. Chandler, L. W. Deady, J. A. Reiss, *J. Heterocycl. Chem.* **1981**, *18*, 599.
[10] B. J. Hathaway, D. G. Holah, J. D. Poslethwaite, *J. Chem. Soc.* **1961**, 3215.
[11] M. G. B. Drew, A. Lavery, V. McKee, S. M. Nelson, *J. Chem. Soc. Dalton Trans.* **1985**, 1771; C. Piguet, G. Bernardinelli, A. F. Williams, *Inorg. Chem.* **1989**, *28*, 2920; E. C. Constable, T. Kuke, M. Neuburger, M. Zehnder, *Chem. Commun.* **1997**, 489.
[12] W. Kaim, J. Rall, *Angew. Chem.* **1995**, *107*, 47; *Angew. Chem. Int. Ed. Engl.* **1996**, *35*, 43.
[13] E. C. Constable, M. D. Ward, D. A. Tocher, *J. Am. Chem. Soc.* **1990**, *112*, 1256.
[14] A. Pfeil, J.-M. Lehn, *J. Chem. Soc. Chem. Commun.* **1992**, 838.
[15] A. Marquis-Rigault, A. Dupont-Gervais, A. Van Dorsselaer, J.-M. Lehn, *Chem. Eur. J.* **1996**, *2*, 1395; A. Marquis-Rigault, A. Dupont-Gervais, P. N. W. Baxter, A. Van Dorsselaer, J.-M. Lehn *Inorg. Chem.* **1996**, *35*, 2307.

Photochemical Synthesis of Polyrotaxanes from Stilbene Polymers and Cyclodextrins**

Wolfgang Herrmann, Maria Schneider, and Gerhard Wenz*

Since the initial pioneering work the synthesis of rotaxanes[1] has been the subject of continuously increasing interest,[2] especially as it has been facilitated by supramolecular positioning of

[*] Prof. Dr. G. Wenz, W. Herrmann, Dr. M. Schneider
Polymer-Institut der Universität
Hertzstrasse 16, D-76187 Karlsruhe (Germany)
Fax: Int. code +(721)608-4421
e-mail: gerhard.wenz@chemie.uni-karlsruhe.de

[**] This work was supported by the Deutsche Forschungsgemeinschaft (Project WE 1092/2-1). We thank Wacker-Chemie (Burghausen, Germany) for the cyclodextrins.

 © WILEY-VCH Verlag GmbH, D-69451 Weinheim, 1997 0570-0833/97/3622-2511 $ 17.50+.50/0

the components (template synthesis[3]).[4] In particular the ability of cyclodextrins **1a–c** to include guest molecules was exploit-

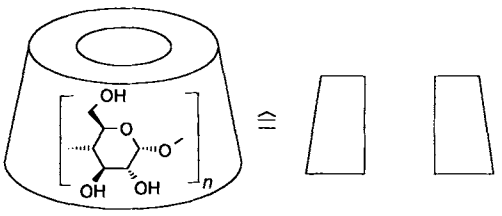

1a-c (n = 6-8)

ed for the synthesis of rotaxanes by covalent attachment of blocking groups.[5] The synthesis of polyrotaxanes by polymerization of monomeric cyclodextrin inclusion compounds[6] or by coupling of blocking groups to polymeric inclusion compounds was also described.[7] Often, choosing reaction conditions that allow both formation of the inclusion compound and attachment of blocking groups was difficult. Self organization of polymers with cyclodextrins takes place preferentially in aqueous solutions, whereas the reactions of blocking reagents with the polymers must usually be carried out in inert organic solvents.

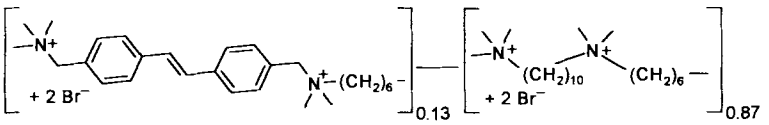

(*E*)-**2**

With the aim of forming polyrotaxanes photochemically[8] we synthesized the stilbene polymer (*E*)-**2**, whose decamethylene segments are well suited for threading cyclodextrins.[7b, 9] In addition, the polymer contains (*E*)-stilbene segments which are intended for the photosynthetic formation of blocking groups. The model compound (*E*)-**3** was converted into the (*Z*)-isomer upon irradiation with UV light in the presence of **1b**. In contrast, the inclusion of two guest molecules (*E*)-**3** in **1c** caused [2+2]cycloaddition leading to tetraphenylcyclobutanes.[10] When irradiated, an aqueous solution of (*Z*)-**2** isomerized, as expected, to the polymer (*Z*)-**2** (Scheme 1) without degradation of the polymer chain; this was confirmed by ^{1}H NMR and UV/Vis spectroscopy. The reduction of absorption in the UV region and the shift of the maximum to shorter wavelength, which are associated with the (*E*)/(*Z*) isomerization, were also observed for monomeric stilbenes (Figure 1a).[11, 12] There was no indication of the formation of [2+2]photoaddition products.

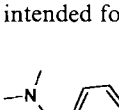

(*E*)-**3**

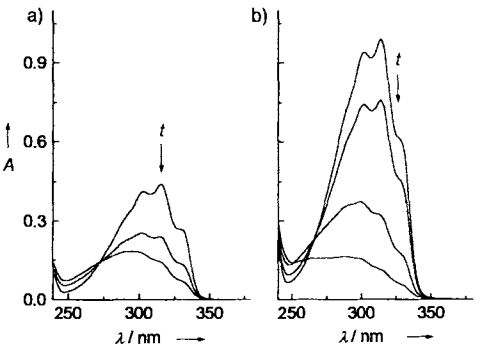

Figure 1. UV spectra of a) 0.18 mM (*E*)-**2** in water (not irradiated and after 30 and 120 min irradiation), b) 0.15 mM (*E*)-**2**·(*E*)-$\mathbf{3}_{0.13}$·$\mathbf{1b}_{0.87}$·$\mathbf{1c}_{0.13}$ in water (not irradiated, after 30 and 120 min and after 30 h irradiation). See Experimental Section for the reaction conditions.

We hoped that polyrotaxanes would form after inclusion of polymer (*E*)-**2** in cyclodextrin, and subsequent photoisomerization of (*E*)-**2** took place in the presence of **1b**. The polymeric inclusion compounds and the polyrotaxanes were distinguished by gel permeation chromatography (GPC) with detection of the optical rotation. For cyclodextrins, which are permanently bound to a polymer, a rotational signal in the polymer region (V_e = 4–7 mL) was expected, whereas for dissociated systems a rotational signal for free cyclodextrin at V_e = 9 mL was expected; the latter was found for (*Z*)-**2**·**1b** (Figure 2a). Therefore, (*Z*)-stilbene segments are not suitable blocking groups for **1b**.

To check whether photochemically formed tetraphenylcyclobutane groups are effective blocking groups for **1b**, the quaternary polymeric inclusion compound (*E*)-**2**·(*E*)-$\mathbf{3}_{0.13}$·$\mathbf{1b}_{0.87}$·$\mathbf{1c}_{0.13}$ was prepared by self organization in an aqueous solution. In this supramolecular complex each cyclodextrin ring **1c** encloses a polymer-bound (*E*)-**2** and a monomeric (*E*)-**3** stilbene unit (Scheme 2). According to the results of GPC, about 12% of the cyclodextrin remained bound to the polymer (Figure 2b). In an analogous test run without the addition of (*E*)-**3** no polymer-bound cyclodextrin was detected for the ternary inclusion compound (*E*)-**2**·$\mathbf{1b}_{0.87}$·$\mathbf{1c}_{0.13}$. Therefore, in the quaternary inclusion compound (*E*)-**2**·(*E*)-$\mathbf{3}_{0.13}$·$\mathbf{1b}_{0.87}$·$\mathbf{1c}_{0.13}$ the additionally included stilbene (*E*)-**3** acts as a stabilizing splint since the space inside **1c** is completely filled.

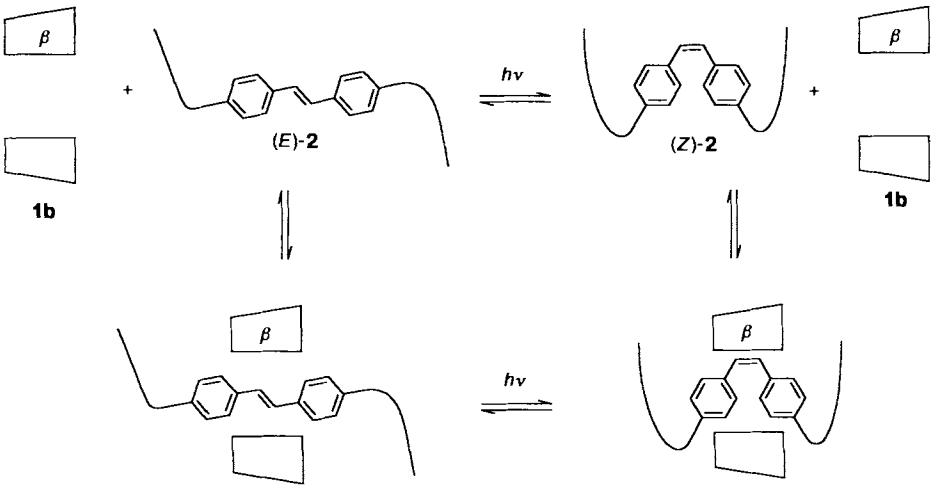

Scheme 1. Photochemical (*E*)/(*Z*) isomerization of polymer **2** and self-organization with cyclodextrin **1b**.

 © WILEY-VCH Verlag GmbH, D-69451 Weinheim, 1997 0570-0833/97/3622-2512 $ 17.50+.50/0

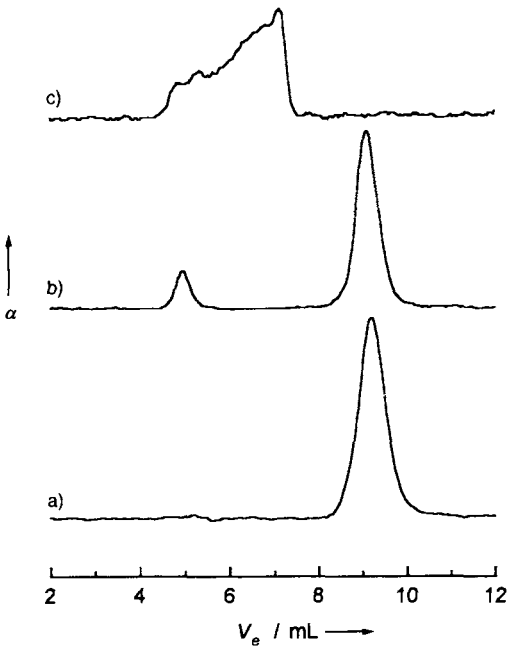

Figure 2. GPC elution curves of a) (*E*)-**2**·**1b**$_{0.87}$·**1c**$_{0.13}$, b) (*E*)-**2**·(*E*)-**3**$_{0.13}$·**1b**$_{0.87}$·**1c**$_{0.13}$, and c) **4**.

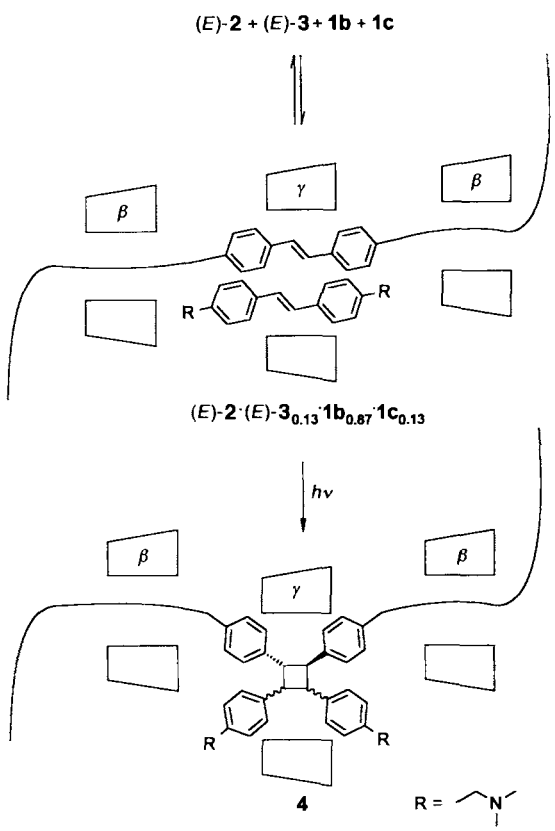

Scheme 2. Self-organization of the polymeric inclusion compounds (*E*)-**2**·(*E*)-**3**$_{0.13}$·**1b**$_{0.87}$·**1c**$_{0.13}$ and photochemical synthesis of polyrotaxane **4**.

The threaded rings and (*E*)-**3** can be completely separated from the polymer (*E*)-**2** by continuous ultrafiltration.

Irradiation of a saturated aqueous solution of (*E*)-**2**·(*E*)-**3**$_{0.13}$·**1b**$_{0.87}$·**1c**$_{0.13}$ with UV light at 312 nm for 30 h produced **4** (Scheme 2, Figure 1b). The increased absorption, especially at 250 nm, indicates isolated phenyl groups. In addition, the signals for the (*E*)- and (*Z*)-stilbene units in the ^{1}H NMR spectrum vanished. GPC of the raw product showed an increased amount (20%) of polymer-bound cyclodextrins. All free or not permanently bound cyclodextrin rings were removed by continuous ultrafiltration. In the residue **4** 20% of the repeating units remained included in cyclodextrin. GPC showed neither free cyclodextrin rings nor easily removable ones remaining in product **4** (Figure 2c). Therefore, **4** is a polyrotaxane, since unthreading of the cyclodextrin is hindered by the attached bulky tetraphenylcyclobutane groups.[13]

The additional inclusion of the monomeric stilbene (*E*)-**3** in the inclusion compound of the polymeric stilbene (*E*)-**2** not only stabilizes the supramolecular structure but makes possible further chemical modification. Therefore, to our knowledge, this is the first demonstration of the supramolecular catalysis of a polymer-analogous conversion; that is, a conversion of the repeating units without changing the chain length.

Experimental Section

GPC was performed on a HEMA-Bio column (Polymer Standards Service, Mainz, Germany, 1000 DEAE) with water/acetonitrile/glacial acetic acid 80/20/0.1. A continuous polarimeter (λ = 589 nm, Chiralyser, IBZ Messtechnik, Hannover, Germany) was used for detection. For the quantitative evaluation, equal specific-rotation values were assumed for polymer-bound and free cyclodextrins.

(*E*)-**2**: 1,10-Dibromodecane (35.100 g, 117.0 mmol) and *N*,*N*,*N*′,*N*′-tetramethyl-1,6-diaminohexane (22.400 g, 130.0 mmol) were dissolved in MeOH/*N*-methylformamide (1/1, 130 mL) and stirred at 50 °C. 4,4′-Bis(bromomethyl)-(*E*)-stilbene (4.759 g, 13.0 mmol, 0.1 equiv) was subsequently added. After two weeks at 50 °C the product was added dropwise to Et_2O (3 L) and thus precipitated. It was purified by dialysis in water with a hollow-fiber module (Allwall GFE 12, Gambro, Hechingen, Germany). The residual solution of (*E*)-**2** was freeze-dried (37.58 g, 60%). The ratio of the monomer units in the polymer (0.87:0.13) was determined from the integrals in the ^{1}H NMR spectrum. ^{1}H NMR (400 MHz, D_2O): δ = 1.33–1.45 (m, 14.4H; CH_2), 1.78 (br s, 7.5H; CH_2), 1.90 (m, 0.5H; CH_2), 3.05 (s, 12H; CH_3), 3.29 (m, 8.0H; NCH_2CH_2), 4.54 (s, 0.5H; $ArCH_2$), 7.44 (s, 0.5H; =CH), 7.61 (d, J = 7.9 Hz, 1.0H; ArH), 7.81 (d, J = 7.9 Hz, 1.0H; ArH); ^{13}C NMR (D_2O): δ = 24.64, 24.70, 27.97, 28.31, 31.01, 31.19 (CH_2), 52.41, 53.22 (CH_3), 66.64, 67.03 69.80 (NCH_2), 129.55, 130.01, 136.22, 141.87, 144.02 (=CH, Ar); UV/Vis (H_2O): λ (ε) = 304 (14600), 316 nm (16200).

(*Z*)-**2**: (*E*)-**2** (650 mg, 1.35 mmol) was dissolved in water and irradiated for 60 min with UV light (λ = 312 nm, Type-D89008 UV source, 6 W, Bioblock Scientific, Illkirch Cedex, France). (*Z*)-**2** was finally isolated in quantitative yield as a colorless powder by freeze-drying. ^{1}H NMR (400 MHz, D_2O): δ = 1.33–1.41 (m, 14.4H; CH_2), 1.74–1.88 (m, 8.0H; CH_2), 3.02 (s, 12H; CH_3), 3.26 (m, 8.0H; NCH_2), 4.43 (s, 0.5H; $ArCH_2$), 6.80 (s, 0.5H; =CH), 7.40 (s, 2.0H; ArH); UV/Vis (H_2O): λ (ε) = 293 nm (5500).

(*E*)-**2**·(*E*)-**3**$_{0.13}$·**1b**$_{0.87}$·**1c**$_{0.13}$: (*E*)-**2** (467.2 mg, 0.96 mmol), (*E*)-**3**·2HCl (46.0 mg, 0.13 mmol), **1b** (949.6 mg, 0.84 mmol), and **1c** (162.2 mg, 0.13 mmol) were dissolved in water (30 mL) and stirred for 7 d at room temperature. The product was obtained as a fine, colorless powder in quantitative yield by freeze-drying. ^{1}H NMR (400 MHz, D_2O): δ = 1.33–1.42 (*m*, 14.4H; (*E*)-**2**-CH_2), 1.76 (*m*, 8.0H; (*E*)-**2**-CH_2), 2.75 (s, 1.6H; (*E*)-**3**-CH_3), 3.04 (s, 12H; (*E*)-**2**-CH_3), 3.29 (m, 8.0H; (*E*)-**2**-CH_2), 3.58–3.70 (m, 14.3H; OH), 3.78–3.92 (m, 28.5H; OCH. OCH_2), 4.23 (br s, 0.5H; (*E*)-**3**-$ArCH_2$), 4.68 (br s, 0.5H; (*E*)-**2**-$ArCH_2$), 5.05–5.10 (m, 7.1H; OCH), 6.80 (m), 7.16 (br s), 7.34 (m), 7.53 (m), 7.61 (br s; ArH; =CH).

4: (*E*)-**2**·(*E*)-**3**$_{0.13}$·**1b**$_{0.87}$·**1c**$_{0.13}$ (150 mg, 0.089 mmol) was placed in water (2.5 mL) and irradiated for 6 h. The reaction mixture was finally diluted with water (100 mL) and purified by continuous ultrafiltration (Ultrafiltration cells Berghof, Eningen, Nadir-Polyethersulfone membrane 2000 Dalton, Hoechst, Frankfurt, Germany; 5 bar, 2.2 L water/18 h). Upon freeze-drying, **4** was obtained as a colorless powder (70 mg, 0.042 mmol). ^{1}H NMR (400 MHz, D_2O): δ = 1.33–1.41 (m, 14.4H; CH_2), 1.75 (m, 8.0H; CH_2), 2.57 (s, 1.6H; CH_3), 3.02 (s, 12H; CH_3), 3.27 (m, 8.0H; NCH_2), 3.56–3.70 (m, 2.9H; OCH), 3.79–3.86 (m, 5.7H; OCH, OCH_2), 3.98, 4.13, 4.33, 4.69 (1.6H; CH, $ArCH_2$), 5.01–5.08 (m; OCH), 7.21, 7.31, 7.41 (2.1H; ArH).

Received: May 21. 1997 [Z10463IE]
German version: *Angew. Chem.* **1997**, *109*, 2618–2621

Keywords: cyclodextrins · photochemistry · polymers · rotaxanes · supramolecular chemistry

 © WILEY-VCH Verlag GmbH, D-69451 Weinheim, 1997 0570-0833/97/3622-2513 $ 17.50+.50/0

[1] a) Rotaxanes are compounds in which a cyclic component encloses a linear component without covalent bonding between both components. Unthreading of the mechanically bound rings is prevented by sterically effective blocking groups attached to the linear component; b) I. T. Harrison, S. Harrison, *J. Am. Chem. Soc.* **1967**, *89*, 5723.

[2] a) C. O. Dietrich-Buchecker, J.-P. Sauvage, *Chem. Rev.* **1987**, *87*, 795; b) D. B. Amabilino, J. F. Stoddart, *ibid.* **1995**, *95*, 2725; c) H. W. Gibson, M. C. Bheda, P. T. Engen, *Prog. Polym. Sci.* **1994**, *19*, 843; d) R. Jäger, F. Vögtle, *Angew. Chem.* **1997**, *109*, 966; *Angew. Chem. Int. Ed. Engl.* **1997**, *36*, 930; e) N. Solladié, J.-C. Chambron, C. O. Dietrich-Buchecker, J.-P. Sauvage, *ibid.* **1996**, *108*, 957 and **1996**, *35*, 906; f) D. A. Leigh, A. Murphy, J. P. Smart, A. M. Z. Slawin, *ibid.* **1997**, *109*, 752 and **1997**, *36*, 728.

[3] W. H. Kruizinga, R. M. Kellog, *J. Chem. Soc. Chem. Commun.* **1979**, 286.

[4] a) D. Philp, J. F. Stoddart, *Synlett* **1991**, *7*, 445; b) J. C. Chambron, V. Heitz, J. P. Sauvage, *J. Chem. Soc. Chem. Commun.* **1992**, 1131; c) F. Vögtle, M. Händel, S. Meier, S. Ottens-Hildebrandt, F. Ott, T. Schmidt, *Liebigs. Ann.* **1995**, 739.

[5] a) G. Wenz, *Angew. Chem.* **1994**, *106*, 851; *Angew. Chem. Int. Ed. Engl.* **1994**, *33*, 803; b) H. Ogino, *J. Am. Chem. Soc.* **1981**, *103*, 1303; c) R. Isnin, A. E. Kaifer, *ibid.* **1991**, *113*, 8188; d) G. Wenz, F. Wolf, M. Wagner, S. Kubik, *New J. Chem.* **1993**, *17*, 729.

[6] a) N. Ogata, K. Sanui, J. Wada, *J. Polym. Sci. Polym. Lett. Ed.* **1976**, *14*, 459; b) I. Yamaguchi, K. Osakada, T. Yamamoto, *J. Am. Chem. Soc.* **1996**, *118*, 1811; c) M. B. Steinbrunn, G. Wenz, *Angew. Chem.* **1996**, *108*, 2274; *Angew. Chem. Int. Ed. Engl.* **1996**, *35*, 2139.

[7] a) A. Harada, J. L. M. Kamachi, *Nature* **1992**, *356*, 325; b) G. Wenz, B. Keller, *Angew. Chem.* **1992**, *104*, 201; *Angew. Chem. Int. Ed. Engl.* **1992**, *31*, 197; c) M. Born, H. Ritter, *ibid.* **1995**, *107*, 342 and **1995**, *34*, 309; d) *Makromol. Chem. Rapid Commun.* **1991**, *12*, 471; e) T. Ooya, H. Mori, M. Terano, N. Yui, *Macromol. Rapid Commun.* **1995**, *16*, 259.

[8] Supramolecular complexes are also interesting because they enable, for example, the investigation of electrochemical (L. Echegoyen, P. L. Boulas, M. Gomez-Kaifer, *Angew. Chem.* **1998**, *110*, in press; *Angew. Chem. Int. Ed. Engl.* **1998**, *37*, in press) or photochemical processes (V. Balzani, *Tetrahedron* **1992**, *48*, 10443; V. Ramamurthy, *ibid.* **1986**, *42*, 5753) in an environment with a defined geometry. Supramolecular structures can be fixed by irradiation with light (C. Mertesdorf, H. Ringsdorf, J. Stumpe, *Liq. Cryst.* **1991**, *9*, 337).

[9] a) G. Wenz, B. Keller, *Macromol. Symp.* **1994**, *87*, 11; b) W. Herrmann, B. Keller, G. Wenz, *Macromolecules*, **1997**, *30*, 4966.

[10] W. Herrmann, S. Wehrle, G. Wenz, *Chem. Commun.* **1997**, 1709.

[11] H. Meier, *Angew. Chem.* **1992**, *104*, 1425; *Angew. Chem. Int. Ed. Engl.* **1992**, *31*, 1399.

[12] The possibility of accomplishing the reverse reaction—that is, the (*Z*)/(*E*) isomerization—either photochemically or thermally was not investigated.

[13] The tetraphenylbutane groups probably prevent unthreading only of the **1b** rings, since monomeric tetraphenylcyclobutane is rapidly enclosed by **1c**[10]. The **1b** rings stop the **1c** rings from wandering.

New Reactions of a Silylene: Insertion into M–N Bonds of $M[N(SiMe_3)_2]_2$ (M = Ge, Sn, or Pb)**

Barbara Gehrhus, Peter B. Hitchcock, and Michael F. Lappert*

Transient silylenes SiX_2 (X^- = a monohapto ligand) are important synthons in organosilicon chemistry, being a source of unusual tetravalent silicon compounds. Typically this involves either a) reaction with an organic or inorganic unsaturated substrate,[1a] or b) insertion into a compound containing a M′–Hal (e.g. Hal = Cl and M′ = B, C, Si, or P) or M′–H (e.g. M′ = C, Si, or O) bond.[1b] In contrast, insertions into an M′–N bond are as yet unreported. We have recently shown that the thermally stable but reactive bis(amino)silylene **1**[2a] also undergoes both type a) (with a chalcogen[2a] or various C–C, C–O, and C–N multiply bonded compounds[2b]) and type b) (with CH_3–I or C_2H_5O-H[2a]) reactions. Thermally stable monomeric Group 14 metal(II) amides $M[N(SiMe_3)_2]_2$ (M = Ge, Sn, or Pb) have an extensive range of reactivity, but insertions into the M–N bonds giving rise to new divalent M(II) compounds has not previously been observed.

We now show that treatment of the pale yellow silylene **1**[2a] with the yellow-to-orange $M[N(SiMe_3)_2]_2$ compounds in *n*-hexane at ambient temperatures afforded after work-up the crystalline dark green (Sn) or black-green (Pb) bis(silyl)metal(II) compounds **2** or **3**, respectively, or the colorless azadisilagermole **4** (Scheme 1). The lead(II) compound **3** was appreciably more labile both in solution and in the solid than the isoleptic tin(II) compound **2**, and slowly deposited lead over a period of days.

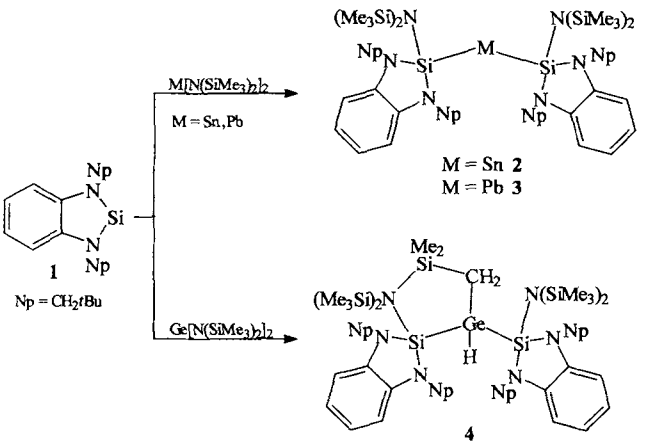

Scheme 1. Reactions of the cyclic silylene **1**, Np = neopentyl, with the metal amides $M[N(SiMe_3)_2]_2$, M = Ge, Sn, Pb.

Each of the compounds **2**–**4** gave satisfactory microanalysis, EI mass and multinuclear NMR spectra (see Experimental Section). In addition, single-crystal X-ray diffraction data revealed their molecular structures, illustrated for **2** or **3** in Figure 1;

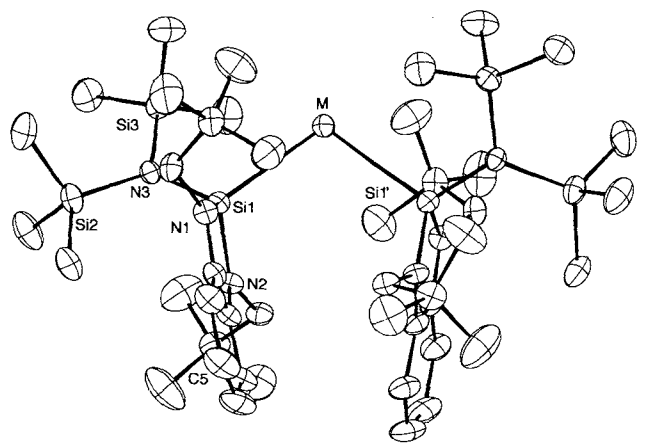

Figure 1. Crystal structures of **2** (M = Sn) and **3** [M = Pb; data shown in square brackets]. Selected bond lengths [Å] and angles [°]: M–Si1 2.712(1) [2.776(3)], Si1–N2 1.745(3) [1.751(9)], Si1–N3 1.768(3) [1.757(8)], Si1–N1 1.754(3) [1.755(8)]; Si1-M-Si1′ 106.77(5) [105.8(1)], N2-Si1-N3 115.1(2) [115.5(4)], N2-Si1-N1 92.0(2) [92.6(4)], N3-Si1-N1 111.5(2) [112.6(4)], N2-Si1-M 116.8(1) [116.1(3)], N3-Si1-M 112.5(1) [111.3(3)], N1-Si1-M 106.8(1) [107.1(3)].

[*] Prof. M. F. Lappert, Dr. B. Gehrhus, Dr. P. B. Hitchcock
The Chemistry Laboratory
University of Sussex
Brighton, BN1 9QJ (UK)
Fax: Int. code + (1273)677196
e-mail: M.F.Lappert@susx.ac.uk

[**] This work was supported by the Engineering and Physical Sciences Research Council and the European Union within the HCM Programme (Contact No. ERBCHBGCT 930264; Cat. 30 Fellowship for B. G.).

 © WILEY-VCH Verlag GmbH, D-69451 Weinheim, 1997 0570-0833/97/3622-2514 $ 17.50+.50/0

details for **4** will be published later. Compound **2** is to our knowledge the first two-coordinate tin(II) compound having the $SnSi_2$ framework, but for lead(II) there is a precedent for **3** in $Pb[Si(SiMe_3)_3]_2$.[3] The tin analogue of this lead compound is a Sn–Sn-bonded dimer, and the only other tin(II) silyl compound is $[Sn\{Si(SiMe_3)_3\}_2(\mu\text{-Cl})Li(thf)_3]$.[4]

We suggest that the reaction pathway for the conversion of **1** and $M[N(SiMe_3)_2]_2$ into the bis(silyl)metallene **2** or **3** proceeds via intermediates **5** and **6**. The cyclic transition state **7** may be

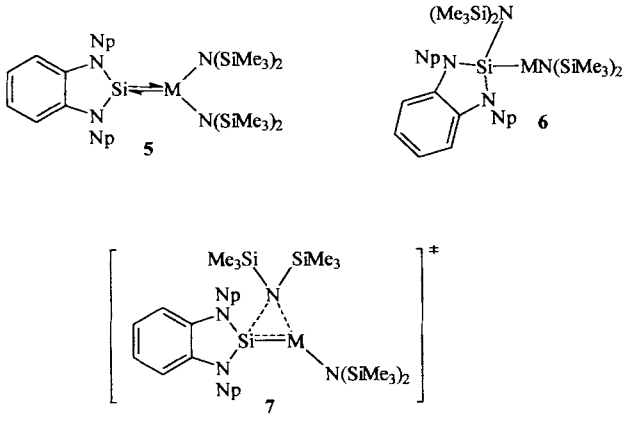

implicated in the transformation of **5** → **6** and a similar one also between **6** and the ultimate product **2** or **3**. The formation of **5** involves the notion that both **1** and $M[N(SiMe_3)_2]_2$ (M = Sn or Pb) are capable of behaving as a Lewis acid and a Lewis base. Precedents for compounds related to **5** in Group 14 element chemistry include the crystallographically characterized dinuclear M^{II}–M^{II} compounds $[M\{CH(SiMe_3)_2\}_2]_2$ (M = Ge or Sn),[5] $[Sn\{Si(SiMe_3)_3\}_2]_2$,[3] $[Sn\{2\text{-}t\text{Bu-}3,5,6\text{-}Me_3C_6H\}_2]_2$,[6] and $X_2SnSnCl_2$ [X = $CH(SiMe_3)(8\text{-}C_9H_6N)$].[7] As for **5** → **6**, 1,2-migration of a ligand from M → M′ is well documented, for example, for OMe from Si → Si (α-elimination),[8] for 2,4,6-$Me_3C_6H_2$ from Ge → Si,[9] for Cl from Sn → Sn,[7] and for C_6F_5 from B → Si [Eq. (1), Ar = C_6F_5[10]].

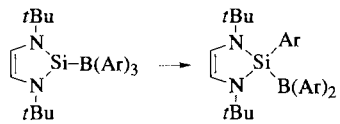

(1)

The synthesis of the germanium(IV) hydride **4** from **1** and $Ge[N(SiMe_3)_2]_2$ is believed to proceed through a similar pathway, except that steric acceleration caused the bis(silyl)-germylene **8** (the Ge analogue of **2** and **3**) to undergo cyclometalation. Thus **4** may be formed by insertion of the labile germylene **8** into a C–H bond of an $N(SiMe_3)_2$ group. Precedents for a related C–H activation have been described (Scheme 2), for example, the conversion of a) $Ge(2,4,6\text{-}tBu_3C_6H_2)_2$ into its Ge^{IV} isomer **A** in the presence of a Lewis acid such as $GeCl_2$,[11] b) $[Ti(\eta^5\text{-}C_5H_5)_2\{N(SiMe_3)_2\}_2]$ into **B** and $HN(SiMe_3)_2$,[12] and c) the formation of **C** from $[Ir(Cl)(CO)_3]$ generated in situ and $Ge[N(SiMe_3)_2]_2$.[13]

In the crystalline bis(silyl)tin(II) compound **2**, each molecule has a V-shaped skeletal structure and lies on a twofold rotation axis bisecting the Si1-Sn-Si1′ angle of 106.77(5)°. This value is at the upper end of the range of X-Sn-X′ angles for monomeric, crystalline Sn^{II} compounds (cf. 104.7(2)° in $Sn[N(SiMe_3)_2]_2$,[14] 109.7(2)° in $Sn[NC(Me_2)(CH_2)_3CMe_2]_2$,[15] 103.6(1)° in Sn-

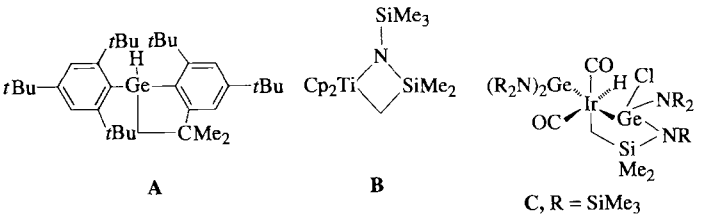

Scheme 2. Examples of products of C–H insertion reactions that could be formed analogously to **4**.

$(2,4,6\text{-}tBu_3C_6H_2)_2$,[16] 88.8(2)° in $Sn[O(2,6\text{-}tBu_3\text{-}4\text{-}Me\text{-}C_6H_2)]_2$,[17] 85.4(1)° in $Sn[S(2,4,6\text{-}tBu_3C_6H_2)]_2$,[18] or 98.8(4)° in $Sn[P\{Si(tBu)F(2,4,6\text{-}iPr_3C_6H_2)\}(SiiPr_3)]_2$[19]), but is similar to those in the Sn–Sn-bonded dinuclear compounds $[Sn\{CH(SiMe_3)_2\}_2]_2$[5] and $[Sn\{Si(SiMe_3)_3\}_2]_2$[3] of 109.2(2)° and 108.25(3)°, respectively. The very long Sn–Si bond of 2.712(2) Å in **2** is a noteworthy feature, particularly when this value is compared to the sum of the Sn and Si covalent radii of 2.58 Å or the Sn–Si distances of 2.666(7) Å in $[Sn\{Si(SiMe_3)_3\}_2]_2$[3] and of 2.681(2) Å in $[Sn\{Si(SiMe_3)_2\}_2(\mu\text{-Cl})Li(thf)_3]$.[4] The closest Sn···Sn contact for **2** is about 10 Å.

The lead(II) compound **3** is isostructural with **2**, and the molecular geometric parameters for the two are very similar, except that for M = Pb the M–Si bond is longer (2.776(3) Å) and the Si1-M-Si1′ angle is narrower (105.8(1)°). These observations are consistent with the pattern previously noted when comparing M–X bond lengths and X-M-X angles for pairs of MX_2 molecules (M = Sn or Pb). For example, the corresponding values in $Pb[N(SiMe_3)_2]_2$ are 2.24(2) Å and 103.6(7)°, respectively, and in the analogous tin(II) amide 2.09(1) Å and 104.7(2)°, respectively.[14] However, it is evident that the Pb–Si bond and Si1-Pb-Si1′ angle in **3** are significantly longer and narrower than in $Pb[Si(SiMe_3)_3]_2$ for which the values 2.702(3) Å and 113.56(10)°, respectively, were observed.[3] The torsion angle N1-Si1···Si1′-N2′ is 57° (Figure 2, Si1′ is masked by Si1) in the Sn compound **2** and 55° in the Pb compound **3**.

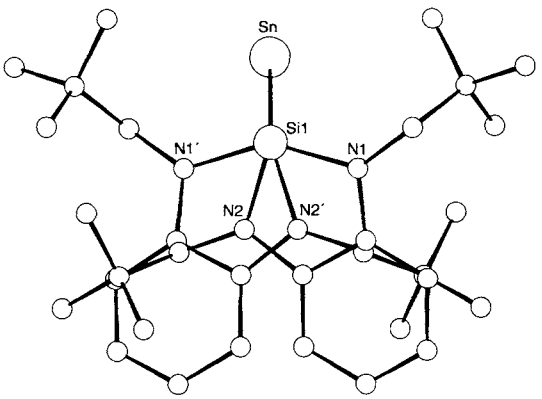

Figure 2. Side-on view of the framework of **2**, $N(SiMe_3)_2$ substituents omitted.

It is likely that in solution compounds **2** and **3** have similar structures to those in the solid; CP-MAS data, as well as UV/Vis spectra, will be discussed in a subsequent full paper.

The reactions in Scheme 1 may well be the first of a much wider series of transformations involving reactions between the stable **1** or a transient silylene and a carbene or carbene analogue (see, for instance, ref. [20]).

 © WILEY-VCH Verlag GmbH, D-69451 Weinheim, 1997 0570-0833/97/3622-2515 $ 17.50+.50/0

Experimental Section

2: A solution of **1** (0.3 g, 1.112 mmol) in *n*-hexane (10 mL) was added to a solution of $Sn[N(SiMe_3)_2]_2$ (0.49 g, 1.112 mmol) in *n*-hexane (10 mL), causing an immediate color change from orange to dark green-brown. The mixture was stirred for 4 h. The formed precipitate, which largely redissolved upon heating, was filtered hot, and the filtrate was slowly cooled to room temperature and then at −25 °C to afford compound **2** (0.48 g, 87%) as dark green crystals, m.p. 165–167 °C (decomp); correct elemental analysis; MS: *m/z* (%) 986 (4) $[M]^+$, 869 (57) $[M-119]^+$; ^{1}H NMR (300 MHz, [D$_6$][benzene], 298 K): δ = 0.16 and 0.47 ($SiMe_3$, 2s, 36H), 0.86 (CMe_3, s, 36H), 2.81, 2.86, 2.94 and 2.99 (CH_2, AB-type, broad, 8H), 6.58–6.62 and 6.82–6.86 (phenyl, m, 8H); $^{13}C\{^1H\}$ NMR (75.47 MHz, [D$_6$][benzene], 298 K): δ = 5.53 and 7.38 ($SiMe_3$), 29.31 (CMe_3), 32.52 (CMe_3), 56.88 (CH_2), 110.62, 117.76, and 142,94 (phenyl); $^{29}Si\{^1H\}$ NMR (99.33 MHz, [D$_8$][toluene], 298 K): δ = −2.00 and 9.74 ($SiMe_3$), no $^{119}Sn\{^1H\}$ signal was detected (cf. ref.[3]).

3: Compound **3** (0.45 g, 69%) was obtained as black-green crystals from $Pb[N(SiMe_3)_2]_2$ (0.32 g, 0.607 mmol) and **1** (0.33 g, 1.214 mmol) by a procedure as for **2**; m.p. 150–151 °C (decomp); correct elemental analysis; MS: *m/z* (%) 869 (7%) $[M-207]^+$; ^{1}H NMR (300 MHz, [D$_6$][benzene], 298 K): δ = 0.14 and 0.39 ($SiMe_3$, 2s, 36H), 0.89 (CMe_3, s, 36H), 2.95, 3.00, 3.34 and 3.38 (CH_2, AB-type, broad, 8H), 6.55–6.58 and 6.83–6.87 (phenyl, m, 8H); $^{13}C\{^1H\}$ NMR (75.47 MHz, [D$_6$][benzene], 298 K): δ = 5.78 and 9.37 ($SiMe_3$), 30.86 (CMe_3), 32.68 (CMe_3, broad), 57.35 (CH_2, broad), 112.60, 118.15 and 144.60 (phenyl); $^{29}Si\{^1H\}$ NMR (99.33 MHz, [D$_8$][toluene], 298 K): δ = 0.09 and 11.27 ($SiMe_3$).

4: A solution of **1** (0.68 g, 2.5 mmol) in *n*-hexane (10 mL) was added to a solution of $Ge[N(SiMe_3)_2]_2$ (0.58 g, 1.25 mmol) in *n*-hexane (20 mL). After the mixture had been stirred overnight, the solvent was removed in vacuo. The remaining white solid was recrystallized from *n*-pentane to afford **4** (0.85 g, 73%) as colorless crystals, m.p. 188–190 °C (decomp); correct elemental analysis; MS: *m/z* (%) 943 (50) $[M]^+$; ^{1}H NMR (500 MHz, [D$_6$][benzene], 298 K): δ = 0.11, 0.17 and 0.46 ($SiMe_3$, 3s, 27 H), 0.30 and 0.36 ($SiMe_2$, 2s, 12H), 0.82, 0.88, 1.09 and 1.17 (CMe_3, 4s, 36H), 0.53 (CH_2, dd, 2H, ^2J(H,H) 12.66 Hz, ^3J(H,H) 3.23 Hz), 4.00 (GeH, dd, 1H, ^3J(H,H) 3.22 and 11.94 Hz), 2.31, 2.36, 2.65, 2.68, 2.76, 2.79, 3.14, 3.17, 3.24, 3.26, 3.32, 3.35, 3.36, 3.38 (CH_2, AB type, 8H) and 6.56-6.88 (phenyl, m, 8H); $^{13}C\{^1H\}$ NMR (75.47 MHz, [D$_6$][benzene], 298 K): δ = 1.97 (CH_2), 2.90, 4.01, 5.91, 6.00 and 7.26 (SiMe), 29.25, 29.91 and 30.38 (CMe_3), 33.43, 33.92 and 34.41 (CMe_3), 57.51, 57.57, 58.31 and 58.72 (CH_2), 109.56, 110.37, 110.49, 110.68, 117.73, 118.07, 118.15, 118.29, 142.21, 142.71, 142.89 and 143.18 (phenyl); $^{29}Si\{^1H\}$ NMR (99.33 MHz, [D$_6$][benzene], 298 K): δ = 3.17, 3.71 and 4.78 ($SiMe_3$), 9.19 ($SiMe_2$), 2.06 and −10.18.

Crystal structure analysis for **2**: $C_{44}H_{88}N_6Si_6Sn$, a = 28.235(9), b = 10.856(4), c = 23.019(1) Å, β = 128.27(4)°, V = 5540(4) Å^3, Z = 4, monoclinic, space group $C2/c$ (no. 15), ρ_{calcd} = 1.19 mg m^{-1}, μ = 0.624 mm^{-1}, $R1$[for 3651 reflections with $I > 2\sigma(I)$] = 0.043, $wR2$[for all 4864 reflections] = 0.094, GOF on F^2 = 1.019. Crystal structure analysis for **3**: $C_{44}H_{88}N_6PbSi_6$, a = 28.274(12), b = 10.746(3), c = 22.784(9) Å, β = 127.96(4)°, V = 5458(4) Å^3, Z = 4, monoclinic, space group $C2/c$ (no. 15), ρ_{calcd} = 1.31 mg m^{-}, μ = 3.26 mm^{-1}, $R1$[for 3917 reflections with $I > 2\sigma(I)$] = 0.068, $wR2$[for all 4778 reflections] = 0.208, GOF on F^2 = 1.027. For both **2** and **3** the structure was solved by direct methods (SHELXS-86) and refined with full-matrix least-squares based on all F^2 (SHELXL-93). All non-H atoms were anisotropic, H atoms included in a riding mode. Further details of the crystal structure investigations may be obtained from the Fachinformationszentrum Karlsruhe, D-76344 Eggenstein-Leopoldshafen (Germany), on quoting the depository numbers CSD-407492 (**2**) and CSD-407493 (**3**).

Received: June 2, 1997 [Z10501IE]
German version: *Angew. Chem.* **1997**, *109*, 2624–2626

Keywords: bond activation · insertions · lead · silylene · tin

[1] a) See: M. Weidenbruch, *Coord. Chem. Rev.* **1994**, *130*, 275; b) C.-S. Liu, T.-L. Hwang, *Adv. Inorg. Chem.* **1985**, *29*, 1.
[2] a) B. Gehrhus, P. B. Hitchcock, M. F. Lappert, J. Heinicke, R. Boese, D. Bläser, *J. Organomet. Chem.* **1996**, *521*, 211; b) B. Gehrhus, M. F. Lappert, *Polyhedron* **1997**, in press.
[3] K. W. Klinkhammer, W. Schwarz, *Angew. Chem.* **1995**, *107*, 1448; *Angew. Chem. Int. Ed. Engl.* **1995**, *34*, 1334.
[4] A. M. Arif, A. H. Cowley, T. M. Elkins, *J. Organomet. Chem.* **1987**, *325*, C11.
[5] P. J. Davidson, D. H. Harris, M. F. Lappert, *J. Chem. Soc. Dalton Trans.* **1976**, 2268; D. E. Goldberg, P. B. Hitchcock, M. F. Lappert, K. M. Thomas, A. J. Thorne, T. Fjeldberg, A. Haaland, B. E. R. Schilling, *ibid.* **1986**, 2387.
[6] M. Weidenbruch, H. Kilian, K. Peters, H. G. von Schnering, H. Marsmann, *Chem. Ber.* **1995**, *128*, 983.
[7] W.-P. Leung, W.-H. Kwok, F. Xue, T. C. W. Mak, *J. Am. Chem. Soc.* **1997**, *119*, 1145.
[8] W. H. Atwell, D. R. Weyenberg, *Angew. Chem.* **1969**, *81*, 485; *Angew. Chem. Int. Ed. Engl.* **1969**, *8*, 469.
[9] K. M. Baines, J. A. Cooke, J. J. Vittal, *J. Chem. Soc. Chem. Commun.* **1992**, 1484; K. M. Baines, J. A. Cooke, C. E. Dixon, H. W. Liu, M. R. Netherton, *Organometallics* **1994**, *13*, 631.
[10] N. Metzler, M. Denk, *Chem. Commun.* **1996**, 2657.
[11] P. Jutzi, H. Schmidt, B. Neumann, H.-G. Stammler, *Organometallics* **1996**, *15*, 741.
[12] C. R. Bennett, D. C. Bradley, *J. Chem. Soc. Chem. Commun.* **1974**, 29.
[13] S. M. Hawkins, P. B. Hitchcock, M. F. Lappert, A. K. Rai, *J. Chem. Soc. Chem. Commun.* **1986**, 1689.
[14] T. Fjeldberg, H. Hope, M. F. Lappert, P. P. Power, A. J. Thorne, *J. Chem. Soc. Chem. Commun.* **1983**, 639.
[15] R. W. Chorley, P. B. Hitchcock, M. F. Lappert, W.-P. Leung, P. P. Power, M. M. Olmstead, *Inorg. Chim. Acta* **1992**, *198–200*, 203.
[16] M. Weidenbruch, J. Schlaefke, A. Schäfer, K. Peters, H. G. von Schnering, H. Marsmann, *Angew. Chem.* **1994**, *106*, 1938; *Angew. Chem. Int. Ed. Engl.* **1994**, *33*, 1846.
[17] B. Çetinkaya, I. Gümrükçü, M. F. Lappert, J. L. Atwood, R. D. Rogers, M. J. Zaworotko, *J. Am. Chem. Soc.* **1980**, *102*, 2088.
[18] P. B. Hitchcock, M. F. Lappert, B. J. Samways, E. L. Weinberg, *J. Chem. Soc. Chem. Commun.* **1983**, 1492.
[19] M. Driess, R. Janoschek, H. Pritzkow, S. Rell, U. Winkler, *Angew. Chem.* **1995**, *107*, 1746; *Angew. Chem. Int. Ed. Engl.* **1995**, *34*, 1614.
[20] C. Drost, B. Gehrhus, P. B. Hitchcock, M. F. Lappert, *Chem. Commun.* **1997**, 1845.

Platinum-Catalyzed Regioselective Silaboration of Alkenes**

Michinori Suginome, Hiroshi Nakamura, and Yoshihiko Ito*

Activation of thermally stable bonds between main-group elements such as boron, silicon, and tin has recently become the subject of growing interest. Addition of these intermetallic compounds to carbon–carbon multiple bonds (bis-metallation) has been achieved by using an appropriate transition metal catalyst; bis-metallated organic compounds are obtained that are otherwise difficult to synthesize. In addition to the homometallic compounds with B–B,[1] Si–Si,[2] and Sn–Sn bonds,[3] heterometallic compounds containing B–Si,[4] B–Sn,[5] and Si–Sn[6] bonds have been employed for the transition metal catalyzed bis-metallation of alkynes. Heterometallic bis-metallation is especially interesting, because the reactions proceed not only with high stereoselectivity but also high regioselectivity. However, to our knowledge, bis-metallation of alkenes with heterometallic compounds has not been reported, although addition of the homometallic compounds to C–C double bonds has been reported for diboron[7] and disilicon[2e, 8] compounds. Here we report that, in the presence of a platinum catalyst, addition of the B–Si bond to C–C double bonds takes place with regioselective bond formation between silicon and the terminal carbon atom. This result is interesting because silaboration of terminal alkynes proceeds with the opposite regiochemistry.[4]

Dimethylphenylsilyl(pinacol)borane (**1a**) and 1-octene (1.5 equiv) in dioxane were heated at reflux in the presence of transition metal catalysts (Scheme 1). As summarized in Table 1, platinum phosphane complex catalysts promoted the addition of the B–Si bond to the C–C double bond of 1-octene to give a silaboration product. It is noteworthy that silaboration to give 2-boryl-1-silyloctane **2a** is highly regioselective and that a small amount of 1-boryl-1-silyloctane **3a** is formed.

[*] Prof. Dr. Y. Ito, Dr. M. Suginome, H. Nakamura
Department of Synthetic Chemistry and Biological Chemistry
Graduate School of Engineering
Kyoto University
Kyoto 606-01 (Japan)
Fax: Int. code +(75)753-5668
e-mail: yoshi@sbchem.kyoto-u.ac.jp

[**] H. N. acknowledges fellowship support from the Japan Society for the Promotion of Science for Japanese Young Scientists.

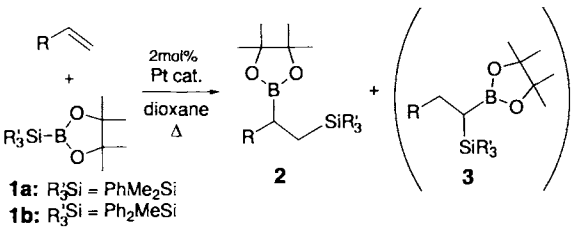

Scheme 1. Platinum-catalyzed silaboration of alkenes.

Table 1. Platinum-catalyzed silaboration of 1-octene [a].

Entry	1	Catalyst	Product	Yield[%]	Ratio 2:3
1	a	$[Pt(PPh_3)_4]$	2a	45	85:15
2	a	$[Pt(CH_2{=}CH_2)(PPh_3)_2]$	2a	53	87:13
3	b	$[Pt(CH_2{=}CH_2)(PPh_3)_2]$	2a′	65	93:7
4	a	$[Pt(PMePh_2)_4]$	2a	7	74:26

[a] Silylborane (1 equiv), 1-octene (1.5 equiv), and catalyst (0.02 equiv) were heated at reflux in dioxane for 2 h.

Triphenylphosphane (entries 1 and 2) was the ligand of choice with regard to catalytic activity and product selectivity (see entry 4). For the silaboration of 1-octene, methyldiphenylsilyl(pinacol)borane (**1b**) gave better yield and selectivity for 1,2-silaboration (entry 3), while catechol- and bis(diethylamino)borane derivatives did not afford silaboration products in the presence of the platinum catalysts.

The absence of 1-boryl-2-silyloctane **5**, the regioisomer of **2a**, in the reaction mixture of the silaboration of 1-octene was unambiguously confirmed by independent synthesis of **5** by palladium-catalyzed silaboration of 1-octyne,[4] followed by catalytic hydrogenation (Scheme 2).

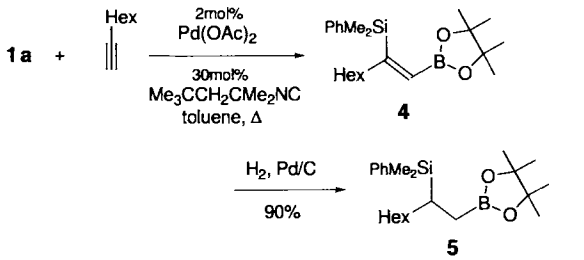

Scheme 2. Synthesis of 1-bora-2-silylalkane **5** by silaboration of 1-octene to give **4**, followed by hydrogenation.

Silaboration has successfully been applied to various alkenes, including functionalized alkenes and styrene derivatives (Table 2). Ester and ketone groups on the olefinic substrates were tolerated in the reaction with **1a** to give the corresponding silaboration products (entries 1 and 2). Styrene derivatives also underwent silaboration in moderate yield and high regioselectivity without formation of the 1,1-isomers (entries 3–5). Electronic effects of substituents on the aromatic ring of the styrene derivatives did not influence the yield. For these alkenes use of **1b** resulted in considerably lower yields. The silaboration of gaseous ethylene (60 atm) in the presence of $[Pt(CH_2{=}CH_2)(PPh_3)_2]$ as catalyst furnished 2-boryl-1-silylethane in 73% yield, accompanied by the formation of 1,2-bis(dimethylphenylsilyl)ethane in 10% yield (entry 6). Use of $[Pt(PPh_3)_4]$ as catalyst completely suppressed the by-product formation and gave exclusively the desired 2-boryl-1-silylethane **2g** (entry 7).

Table 2. Platinum-catalyzed silaboration of alkenes with **1a** [a].

Entry	R	Product	Yield[%]	Ratio 2:3
1	$AcOCH_2CH_2$	2b	46	84:16
2	$CH_3COCH_2CH_2$	2c	46	85:15
3	Ph	2d	51	>99:1
4	4-$MeOC_6H_4$	2e	53	>99:1
5	4-$CF_3C_6H_4$	2f	46	>99:1
6[b]	H	2g	73[c]	>99:1
7[b,d]	H	2g	74	>99:1

[a] Borane **1a** (1 equiv), alkene (1.5 equiv), and $[Pt(CH_2{=}CH_2)(PPh_3)_2]$ (0.02 equiv) were heated to reflux in dioxane for 2 h, unless otherwise noted. [b] Reaction under an ethylene pressure of 60 atm in toluene. [c] 1,2-Bis(dimethylphenylsilyl)ethane was also isolated (10%). [d] $[Pt(PPh_3)_4]$ (0.02 equiv) was used as a catalyst.

A catalyst prepared from $Pd(OAc)_2$ and 1,1,3,3-tetramethylbutyl isocyanide, which was the catalyst of choice in the silaboration of alkynes, as well as palladium phosphane catalysts such as $[Pd(PPh_3)_4]$, did not catalyze the silaboration reaction.

A possible mechanism of the silaboration of alkenes is depicted in Scheme 3. The catalytic cycle is initiated by oxidative addition of a B–Si bond of **1** to platinum to give **A**, followed by

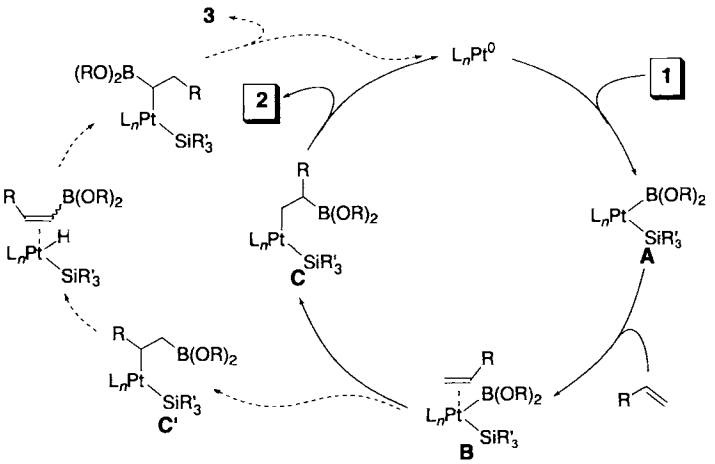

Scheme 3. Possible mechanism of the silaboration of alkenes.

alkene coordination to platinum (**B**) and then migratory insertion to give **C**. The platinum catalyst is regenerated by reductive elimination, with formation of the silaborated alkene **2**. Selective insertion of the C–C double bond into the Pt–B bond of **B**, which results in Pt–C bond formation at the terminal C atom, may be responsible for the high regioselectivity. Indeed, α-boryl-4-methoxystyrene, which may arise from β-hydride elimination from intermediate **C**, was isolated in 12% yield together with dimethylphenylsilane in the reaction of 4-methoxystyrene (Table 2, entry 4). The formation of the 1,1-isomer **3** as a by-product of the silaboration of aliphatic alkenes can be explained by another catalytic cycle, which splits from the main catalytic cycle with the regioisomeric insertion of the C–C double bond into the Pt–B bond of **B**. Intermediate **C′** thus generated produces **3** by β-hydride elimination and subsequent reinsertion of the resulting alkenylborane into the Pt–H bond, followed by reductive elimination.[9]

The formation of the bis-silylation product in the reaction of ethylene with $[Pt(CH_2{=}CH_2)(PPh_3)_2]$ as catalyst is suggestive of an intermediate bis(silyl)platinum complex **E**, which may be formed from Pt^{IV} complex **D**, which in turn is formed by double

 © WILEY-VCH Verlag GmbH, D-69451 Weinheim, 1997 0570-0833/97/3622-2517 $ 17.50+.50/0

oxidative addition of **1** to the Pt^0 complex,[10] followed by reductive elimination of diborane (Scheme 4). Formation of **D** could be suppressed by using $[Pt(PPh_3)_4]$ as a catalyst, that is, in the presence of excess PPh_3.

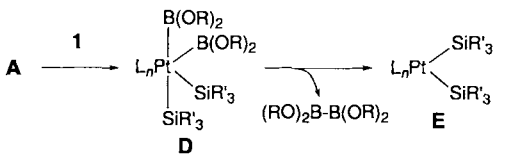

Scheme 4. Possible route of formation of a bis(silyl)platinum complex.

The silaboration reaction made possible a regioselective C–C bond formation at the boryl-substituted C atom. For example, one-carbon homologation of **2a** and **5**, prepared from 1-octene and 1-octyne, respectively, was carried out (Scheme 5). Treatment of **2a** and **5** with chloro(trimethylsilyl)methyllithium gave the corresponding homologation products **6** and **7**, respectively, after selective removal of the trimethylsilyl group by tetrabutylammonium fluoride (TBAF).[11]

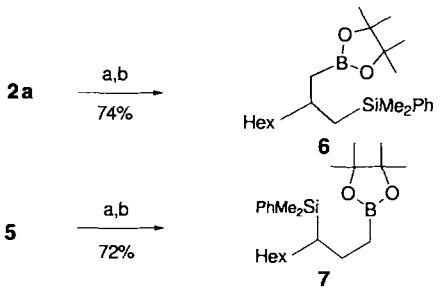

Scheme 5. Synthesis of **6** and **7**: a) Me_3SiCH_2Cl, *s*BuLi, *N,N,N',N'*-tetramethyl ethylene diamine, THF, −78 °C b) TBAF, THF, reflux.

Here we have presented preliminary results on the regioselective silaboration of simple alkenes. Optimization of the reaction conditions on the basis of the mechanism shown in Scheme 3 is currently underway.

Experimental Section

General procedure for silaboration of alkenes: To a solution of platinum catalyst (0.076 mmol) in dioxane (1 mL) were added silylborane **1** (3.9 mmol) and alkene (5.9 mmol). The mixture was heated at reflux for 2 h. Evaporation of volatile materials under reduced pressure was followed by column chromatography on silica gel to give **2** and **3** in the yields listed in Tables 1 and 2.

Received: May 6, 1997 [Z10419IE]
German version: *Angew. Chem.* **1997**, *109*, 2627–2628

Keywords: alkenes · boron · C–C coupling · silicon · platinum

[1] a) T. Ishiyama, N. Matsuda, N. Miyaura, A. Suzuki, *J. Am. Chem. Soc.* **1993**, *115*, 11018–11019; b) T. Ishiyama, N. Matsuda, M. Murata, F. Ozawa, A. Suzuki, N. Miyaura, *Organometallics* **1996**, *15*, 713–720.

[2] a) H. Okinoshima, K. Yamamoto, M. Kumada, *J. Organomet. Chem.* **1975**, *96*, C27–C30; b) H. Sakurai, Y. Kamiyama, Y. Nakadaira, *J. Am. Chem. Soc.* **1975**, *97*, 931–932; c) Y. Ito, M. Suginome, M. Murakami, *J. Org. Chem.* **1991**, *56*, 1948–1951; d) H. Yamashita, M. Catellani, M. Tanaka, *Chem. Lett.* **1991**, 241–244; e) F. Ozawa, M. Sugawara, T. Hayashi, *Organometallics* **1994**, *13*, 3237–3243; f) for a review on palladium-catalyzed bis-silylation, see K. A. Horn, *Chem. Rev.* **1995**, *95*, 1317–1350.

[3] T. N. Mitchell, K. Kwetkat, D. Rutschow, U. Schneider, *Tetrahedron* **1989**, *45*, 969–978.

[4] M. Suginome, H. Nakamura, Y. Ito, *Chem. Commun.* **1996**, 2777–2778.

[5] S. Onozawa, Y. Hatanaka, T. Sakakura, S. Shimada, M. Tanaka, *Organometallics* **1996**, *15*, 5450–5452.

[6] a) T. N. Mitchell, H. Killing, R. Dicke, R. Wickenkamp, *J. Chem. Soc. Chem. Commun.* **1985**, 354–355; b) B. L. Chenard, C. M. V. Zyl, *J. Org. Chem.* **1986**, *51*, 3561–3566; c) M. Murakami, H. Amii, N. Takizawa, Y. Ito, *Organometallics* **1993**, *12*, 4223–4227.

[7] a) R. T. Baker, P. Nguyen, T. B. Marder, S. A. Westcott, *Angew. Chem.* **1995**, *107*, 1451–1452; *Angew. Chem., Int. Ed. Engl.* **1995**, *34*, 1336–1337; b) T. Ishiyama, M. Yamamoto, N. Miyaura, *Chem. Commun.* **1997**, 689–690.

[8] a) T. Hayashi, T. Kobayashi, A. M. Kawamoto, H. Yamashita, M. Tanaka, *Organometallics* **1990**, *9*, 280–281; b) M. Murakami, P. G. Andersson, M. Suginome, Y. Ito, *J. Am. Chem. Soc.* **1991**, *113*, 3987–3988; c) M. Murakami, M. Suginome, K. Fujimoto, H. Nakamura, P. G. Andersson, Y. Ito, *ibid.* **1993**, *115*, 6487–6498; d) M. Suginome, Y. Yamamoto, K. Fujii, Y. Ito, *ibid.* **1995**, *117*, 9608–9609; e) M. Suginome, A. Matsumoto, Y. Ito, *ibid.* **1996**, *118*, 3061–3062.

[9] The reaction of (E)-$CH_3(CH_2)_5CH{=}CHB(OR)_2$, prepared independently by hydroboration, with $PhMe_2SiH$ in the presence of $[Pt(CH_2{=}CH_2)(PPh_3)_2]$ (2 mol%) at 110 °C for 10 h gave **3a** selectively, albeit in low yield (ca. 10%).

[10] M. Suginome, H. Oike, P. H. Shuff, Y. Ito, *J. Organomet. Chem.* **1996**, *521*, 405–408.

[11] D. S. Matteson, D. Majumdar, *Organometallics* **1983**, *2*, 230–236; D. J. S. Tsai, D. S. Matteson, *ibid.* **1983**, *2*, 236–241.

A Crossed Yne–Ene Metathesis Showing Atom Economy**

Roland Stragies, Matthias Schuster, and Siegfried Blechert*

Transition metal catalyzed olefin metathesis has recently acquired increasing significance in organic chemistry.[1] Ring-closing metatheses (RCM) have been shown especially reliable for the preparation of five- through eight-membered rings and larger systems.[2] Applications of RCM to the synthesis of fluvirucine,[3] epothilone,[4] and other natural products[5] verify the efficiency of this approach to carbon–carbon bond formation. To date, olefin metathesis has primarily been employed in organic chemistry as a synthetic method for cyclization. There are far fewer examples of the synthesis of acyclic alkenes by selective cross-metathesis of two different alkenes. In the cross-metathesis of two terminal alkenes **1** and **2** one must of necessity take into account the formation of homodimers **4** and **5** (Scheme 1a). Based on early results it is nonetheless possible to carry out highly selective couplings by the choice of suitable substituents.[6] To our knowledge, nothing has previously been

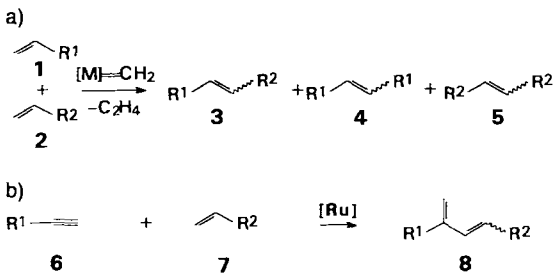

Scheme 1. a) Cross-metathesis of two terminal alkenes; b) crossed yne–ene metathesis.

[*] Prof. Dr. S. Blechert, Dr. M. Schuster, Dipl.-Chem. R. Stragies
Institut für Organische Chemie der Technischen Universität
Strasse des 17. Juni 135, D-10623 Berlin (Germany)
Fax: Int. code +(30)314-23619
e-mail: sibl@wap0105.chem.tu-berlin.de

[**] This work was supported by the Fonds der Chemischen Industrie.

 © WILEY-VCH Verlag GmbH, D-69451 Weinheim, 1997 0570-0833/97/3622-2518 $ 17.50+.50/0

reported with respect to the corresponding behavior of terminal alkynes. We describe here examples of atom economy[7] in selective cross couplings of monosubstituted alkynes with alkenes. Metatheses of alkynes are above all known from polymerizations and a few ring-closing metatheses. Thus, cyclizations of enynes to five- through seven-membered rings have been reported.[8a] This reaction principle found an elegant application in the synthesis of stemoamide.[8b] A double ring-closing metathesis to bicyclic systems has also been achieved by treatment of appropriate dienynes.[9] However, much more common than such intramolecular reactions is the intermolecular metathesis of alkynes, leading to polymers. Apart from the polymerization of simple alkynes,[10] the ring-closing metathesis polymerization of 1,6-heptadiynes has proven especially interesting.[11]

In the course of systematic studies on selective cross-metathesis we found that terminal alkynes **6** and terminal alkenes **7** were transformed selectively by ruthenium catalysis into disubstituted dienes **8** (Scheme 1b). In contrast to the cross-metathesis of two alkenes, no ethylene or other by-product is released in this case; that is, C–C bond formation occurs with atom economy. To date, catalysis of this reaction has been successful only with the Grubbs ruthenium catalyst[12] $[Cl_2(PCy_3)_2Ru{=}CHPh]$(**[Ru]**; Cy = cyclohexyl). Use of the more reactive Schrock molybdenum catalyst[13] $[PhMe_2CCH{=}Mo{=}N(2,6\text{-}iPr_2C_6H_3)\{OCMe(CF_3)_2\}_2]$ has polymerization of the alkyne component[9] as its only consequence under the same reaction conditions. Figure 1 illustrates several products of the new cross-metathesis process.[14] The reaction is carried out in dichloromethane at room temperature with 5–7 mol% **[Ru]**.

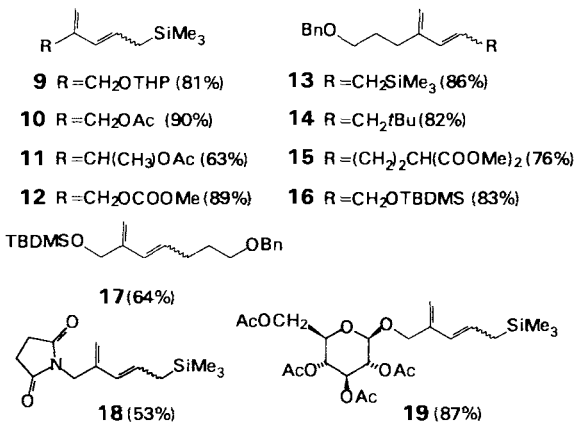

Figure 1. Products of the ruthenium-catalyzed crossed yne–ene metathesis. THP = tetrahydro-2*H*-pyran-2-yl, TBDMS = *tert*-butyldimethylsilyl.

Reported yields were achieved within 12–48 h using a two- to threefold excess of the alkene component; a greater excess leads to no increase in yield. With a 1:1 mixture one does indeed obtain dienes as the main products, but in lower yield. Dimerization of the alkenes occurs only to a very limited extent.

Because of the great synthetic potential of allylsilanes, we undertook initial experiments in the reaction of allyltrimethylsilane with alkynes. Once the alkene had been coupled with THP-protected propargyl alcohol highly selectively and in acceptable yield to give the 1,3-disubstituted diene **9**, we also examined the behavior of propargyl acetate and carbonate. Compounds **10**–**12** show that coupling occurs smoothly here as well. The resulting allyl acetate structural unit offers diverse possibilities for subsequent reactions. Allylic acetates as well as the usually more reactive allylic carbonates are of interest, for example, in π-allylpalladium chemistry.[15] Due to the combination of an allylsilane with an allylic acetate or carbonate, **10**–**12** can be regarded as vinylogous trimethylenemethane precursors.[16] We are currently investigating their Pd-catalyzed reactions. The facile, selective cross-coupling reactions with allylsilanes cannot be attributed to special electronic characteristics of this particular class of compounds: comparison of **13** and **14** shows that the carbon analogue of allyltrimethylsilane, 4,4-dimethyl-1-pentene, reacts in similarly high yield. Coupling product **15** from benzyl-protected 4-pentyne-1-ol and dimethyl (3-butenyl)-malonate demonstrates the applicability of strongly CH-acidic alkenes. However, no reaction occurs with the corresponding dimethyl allylmalonate, presumably due to steric effects.

The coupling of a TBDMS-protected allylic alcohol with an alkyne to give **16** is just as successful as the inverse combination of alkene and alkyne to **17**. It is apparent from the syntheses of **18** and **19** that nitrogen-containing and highly functionalized substrates are also applicable. Yields were considerably poorer with unprotected alcohols. Disubstituted alkynes or 1,2-substituted alkenes fail to react under the conditions employed. Coupling products **9**–**19** arise as isomeric mixtures; the (*Z*)/(*E*) ratios as determined by ^{1}H NMR spectroscopy lie in a range between 1:3 in the case of **11** and about 1:2 to 1:1 with the other compounds. Because of this lack of stereoselectivity we are currently investigating techniques for (*Z*)/(*E*) isomerization. One possibility is presented in Scheme 2 with the synthesis of α-triticene[17] (**21**), an antifungal compound isolated from cereal

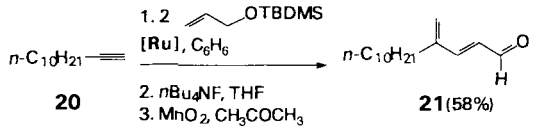

Scheme 2. Synthesis of α-triticene (**21**).

seeds. Because of the higher solubility of alkyne **20** this metathesis was carried out in benzene. The metathesis product was deprotected *in a one-pot reaction and oxidized* directly with MnO_2, in the course of which it was isomerized completely to the desired (*E*)-isomer, isolated in an overall yield of 58%.

Metallacyclobutenes are assumed to be intermediates in the reaction of alkynes with metathesis catalysts.[9, 11] Several mechanisms are possible for the ruthenium-catalyzed yne–ene metathesis. NMR studies have shown that the ruthenium catalyst reacts selectively with alkynes in the presence of alkenes. In the absence of alkene there occurs only a slow oligomerization, whereas in its presence a rapid subsequent reaction leads to product **8**. We therefore favor the reaction course illustrated in Scheme 3. We assume as the first step that the methylidene complex formed from the Grubbs catalyst undergoes a regioselective [2+2] cycloaddition with the triple bond of **6**. Subsequent cycloreversion leads to the stabilized, conjugated carbene complex **23**. This reacts through further [2+2] cycloaddition with alkene

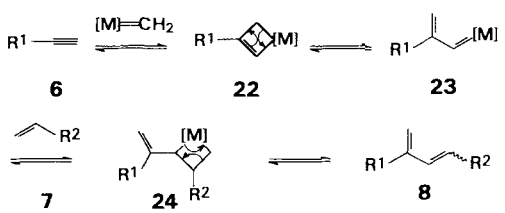

Scheme 3. Proposed mechanism for the yne–ene metathesis.

 © WILEY-VCH Verlag GmbH, D-69451 Weinheim, 1997 0570-0833/97/3622-2519 S 17.50+.50/0

component **7** to give **24**, and with subsequent cycloreversion to the conjugated diene **8**. The fact that coupling is limited to terminal alkynes may have a steric origin. Formation of the more stable and thus less reactive conjugated carbene complex **23** might explain why the yne–ene metathesis requires longer reaction times than conventional cross-metathesis between alkenes. Volatile ethylene is formed in the cross-metathesis of terminal alkenes, whereas the yne–ene metathesis takes place with atom economy. The driving force in yne–ene metathesis may be the formation of a conjugated diene.

The type of reaction described here is, to our knowledge, the first selective crossed yne–ene metathesis. Application of this cross-metathesis between terminal alkynes and alkenes has been demonstrated by the synthesis of variously functionalized dienes. The reaction opens the way to interesting structural elements: thus, conjugated allylsilanes have found a variety of applications, for example in Sakurai reactions.[18] The metathesis products are also of interest with respect to Diels–Alder reactions and cycloadditions. We are currently investigating the applications of yne–ene metathesis in natural product synthesis.

Received: May 15, 1997 [Z10444IE]
German version: *Angew. Chem.* **1997**, *109*, 2629–2630

Keywords: alkenes · alkynes · carbene complexes · metathesis · silanes

[1] Regarding olefin metathesis in organic synthesis: a) A. S. K. Hashmi, *J. Prakt. Chem.* **1997**, *339*, 195; b) M. Schuster, S. Blechert, *Angew. Chem.* **1997**, *109*, 2124; *Angew. Chem. Int. Ed. Engl.* **1997**, *35*, 2036.

[2] Reviews on ring-closing metathesis: a) H. G. Schmalz, *Angew. Chem.* **1995**, *107*, 1981; *Angew. Chem. Int. Ed. Engl.* **1995**, *34*, 1833; b) R. H. Grubbs, S. J. Miller, G. C. Fu, *Acc. Chem. Res.* **1995**, *28*, 446; selected recent examples of ring-closing metathesis: c) C. M. Huwe, S. Blechert, *Synthesis* **1997**, 61; d) A. B. Dyatkin, *Tetrahedron Lett.* **1997**, *38*, 2065; e) D. Meng, D.-S. Su, A. Balog, P. Bertinato, E. J. Sorensen, S. J. Danishefsky, Y.-H. Zheng, T.-C. Chou, L. He, S. B. Horwitz, *J. Am. Chem. Soc.* **1997**, *119*, 2733; f) K. Hammer, K. Undheim, *Tetrahedron* **1997**, *53*, 2309.

[3] A. F. Houri, Z. M. Xu, D. A. Cogan, A. H. Hoveyda, *J. Am. Chem. Soc.* **1995**, *117*, 2943.

[4] Z. Yang, Y. He, D. Vourloumis, H. Vallberg, K. C. Nicolaou, *Angew. Chem.* **1997**, *109*, 170; *Angew. Chem. Int. Ed. Engl.* **1997**, *36*, 166; D. Schinzer, A. Limberg, A. Bauer, O. M. Böhm, M. Cordes, *ibid.* **1997**, *109*, 543 and **1997**, *36*, 523.

[5] a) A. Fürstner, K. Langemann, *J. Org. Chem.* **1996**, *61*, 8746; b) A. Fürstner, N. Kindler, *Tetrahedron Lett.* **1996**, *37*, 7005; c) S. Hölder, S. Blechert, *Synlett* **1996**, 505; d) H. S. Overkleeft, U. K. Pandit, *Tetrahedron Lett.* **1996**, *37*, 547.

[6] Examples of cross-metatheses: a) O. Brümmer, A. Rückert, S. Blechert, *Chem. Eur. J.* **1997**, *3*, 441; b) J. Feng, M. Schuster, S. Blechert, *Synlett* **1997**, 129; c) A. G. M. Barrett, S. P. D. Baugh, V. C. Gibson, M. R. Giles, E. L. Marshall, P. A. Procopiou, *Chem. Commun.* **1997**, 155; d) W. E. Crowe, D. R. Goldberg, Z. J. Zhang, *Tetrahedron Lett.* **1996**, *37*, 2117; e) A. G. M. Barrett, J. C. Beall, V. C. Gibson, M. R. Giles, G. L. P. Walker, *Chem. Commun.* **1996**, 2229; f) W. E. Crowe, D. R. Goldberg, *J. Am. Chem. Soc.* **1995**, *117*, 5162; g) W. E. Crowe, Z. J. Zhang, *ibid.* **1993**, *115*, 10998; h) E. S. Finkelshtein, N. V. Ushakov, E. B. Portnykh, *J. Mol. Catal.* **1992**, *76*, 133.

[7] B. M. Trost, *Angew. Chem.* **1995**, *107*, 285; *Angew. Chem. Int. Ed. Engl.* **1995**, *34*, 259.

[8] a) A. Kinoshita, M. Mori, *Synlett* **1994**, 1020; b) *J. Org. Chem.* **1996**, *61*, 8356.

[9] S.-H. Kim, N. B. Bowden, R. H. Grubbs, *J. Am. Chem. Soc.* **1994**, *116*, 10801.

[10] a) R. Schlund, R. R. Schrock, W. E. Crowe, *J. Am. Chem. Soc.* **1989**, *111*, 8004; b) T. Masuda, T. Higashimura, *Acc. Chem. Res.* **1984**, *17*, 51.

[11] a) J. W. Park, J. H. Lee, H. N. Cho, S. K. Choi, *Macromolecules* **1993**, *26*, 1191; b) Review on metathesis polymerization: R. R. Schrock, *Pure Appl. Chem.* **1994**, *66*, 1447.

[12] P. Schwab, M. B. France, J. W. Ziller, R. H. Grubbs, *Angew. Chem.* **1995**, *107*, 2179; *Angew. Chem. Int. Ed. Engl.* **1995**, *34*, 2039.

[13] R. R. Schrock, J. S. Murdzek, G. C. Bazan, J. Robbins, M. DiMare, M. O'Regan, *J. Am. Chem. Soc.* **1990**, *112*, 3875.

[14] Representative experimental procedure for yne–ene cross-metathesis: propargyl acetate (280 mg, 2.85 mmol) and allyltrimethylsilane (980 mg, 8.57 mmol) were dissolved in dichloromethane (15 mL). After addition of **[Ru]** (165 mg, 0.19 mmol) the mixture was stirred for 24 h at room temperature. The reaction mixture was concentrated under vacuum and purified chromatographically with *tert*-butyl methyl ether/petroleum ether (1/9) on silica gel. There was obtained 543 mg (90%) of product **10**. (*E*)/(*Z*)-isomers were assigned on the basis of ^{1}H-^{1}H and ^{1}H-^{13}CNMR correlation measurements (400 MHz). Selected spectroscopic data: (E)-**10**: ^{1}H NMR (400 MHz, $CDCl_3$): δ = 5.91 (d, J = 16 Hz, 1H), 5.7 (dd, J = 16 Hz, 8 Hz, 1H), 5.03 (s, 1H), 5.00 (s, 1H), 4.70 (s, 2H), 2.07 (s, 3H), 1.54 (d, J = 8 Hz, 2H), −0.02 (s, 9H); ^{13}C NMR (67.9 MHz, $CDCl_3$): δ = 170.5 (C), 140.1 (C), 128.5 (CH), 127.3 (CH), 113.8 (CH_2), 64.1 (CH_2), 23.6 (CH_2), 20.7 (CH_3), −1.95 (CH_3); (*Z*)-**10**: ^{1}H NMR (400 MHz, $CDCl_3$): δ = 5.65 (d, J = 13 Hz, 1H), 5.63 (dd, J = 13 Hz, 8 Hz, 1H), 5.22 (d, J = 2 Hz, 1H), 5.10 (s, 1H), 4.66 (s, 2H), 2.07 (s, 3H), 1.73 (d, J = 8 Hz, 2H), 0.04 (s, 9H); ^{13}C NMR (67.9 MHz, $CDCl_3$): δ = 170.4 (C), 139.8 (C), 130.4 (CH), 123.7 (CH), 114.5 (CH_2), 66.8 (CH_2), 20.7 (CH_3), 20.0 (CH_2), −2.2 (CH_3); MS: m/z(%): 212 (5) [M^+], 197 (3), 169 (5) [$M^+ - C_2H_3O$], 117 (25), 79 (100), 73 (91), 43 (18); HR-MS: calcd for $C_{11}H_{20}O_2Si$ [M^+]: 212.1233, found: 212.122.

[15] J. Tsuji, *Tetrahedron* **1986**, *42*, 4361.

[16] a) B. M. Trost, *Angew. Chem.* **1986**, *98*, 1; *Angew. Chem. Int. Ed. Engl.* **1986**, *25*, 1; b) *Pure Appl. Chem.* **1988**, *60*, 1615.

[17] P. J. Spendley, P. M. Bird, J. P. Ride, D. P. Leworthy, *Phytochemistry* **1982**, *21*, 2403.

[18] D. Seyferth, J. Pornet, R. M. Weinstein, *Organometallics* **1982**, *12*, 1651.

Total Synthesis of Eleutherobin**

K. C. Nicolaou,* Floris van Delft, Takashi Ohshima, Dionisios Vourloumis, Jinyou Xu, Seijiro Hosokawa, Jeffrey Pfefferkorn, Sanghee Kim, and Tianhu Li

Eleutherobin[1, 2] **1** (Figure 1) is a newly discovered antitumor agent which has a mechanism of action[3] like Taxol (**2**) and a novel molecular architecture. Its structure was based on spectroscopic results,[1, 2] although no absolute configuration was assigned. Isolated from an *Eleutherobia* species of marine soft corals (possibly *E. albiflora* Alcynacea, Alcyoniidea) collected in the Indian Ocean near Bennett's Shoal in Western Australia, this substance is extremely scarce, and yet its tubulin polymerization and microtubule-stabilizing properties and 100-fold higher potency (over the mean cytotoxicity of an NIH cell line panel) against selected breast, renal, ovarian, and lung cancer cells[2] make it (along with epothilones[4–9] A (**3**) and B (**4**), Figure 1), one of the most promising antitumor agents isolated from nature in recent years. Here we report the first total synthesis of eleutherobin (**1**) which renders the natural product (**1**) and two biologically active analogues (**33** and **34**, see Scheme 3) readily available for further studies. Furthermore, the described chemical synthesis allows assignment of the absolute stereochemistry of eleutherobin (**1**) and opens an avenue for the generation of combinatorial libraries for biological screening purposes.

[*] Prof. Dr. K. C. Nicolaou, Dr. F. van Delft, Dr. T. Ohshima, Dr. D. Vourloumis, Dr. J. Xu, Dr. S. Hosokawa, J. Pfefferkorn, Dr. S. Kim, Dr. T. Li
Department of Chemistry and The Skaggs Institute for Chemical Biology
The Scripps Research Institute, 10550 North Torrey Pines Road
La Jolla, California 92037 (USA)
Fax: Int. code +(619)784-2469
e-mail: kcn@scripps.edu
and
Department of Chemistry and Biochemistry
University of California, San Diego
9500 Gilman Drive, La Jolla, California 92093 (USA)

[**] We thank Dr. W. Fenical for preprints of refs. [2, 25] as well as selected spectra of eleutherobin, and Dr. D. H. Huang and Dr. G. Siuzdak for NMR spectroscopic and mass spectrometric assistance, respectively. This work was supported by The Skaggs Institute for Chemical Biology, the National Institutes of Health USA, CaP CURE, Novartis, and by fellowships from the Netherlands Organization for Scientific Research (NWO) (to F. v. D.), Novartis (to D. V.), the Japanese Society for the Promotion of Science for Young Scientists (to S. H.), and the Department of Defense, USA (to J. P.). F. v. D., T. O., D. V., J. X., and S. H. contributed equally to this project.

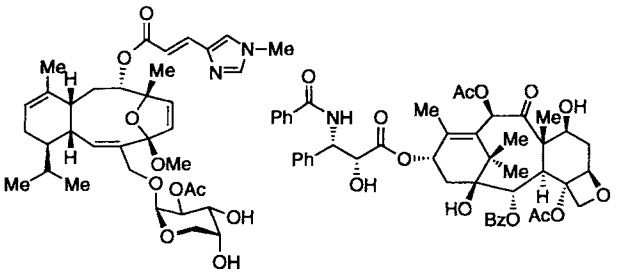

1: eleutherobin

2: Taxol

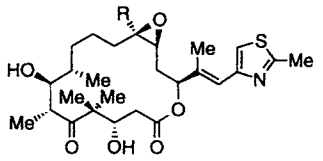

3: R = H : epothilone A
4: R = Me : epothilone B

Figure 1. Molecular structures of eleutherobin (**1**), Taxol (**2**), and epothilones A (**3**) and B (**4**) (Ac = acetyl, Bz = benzoyl).

The structure of eleutherobin (**1**), which is similar to those of eleuthosides[10] A and B, sarcodictyins[11–14] A and B, and valdivones[15], includes a synthetically challenging tricyclic skeleton (**ABC**, Figure 2) and two side chains, one containing an

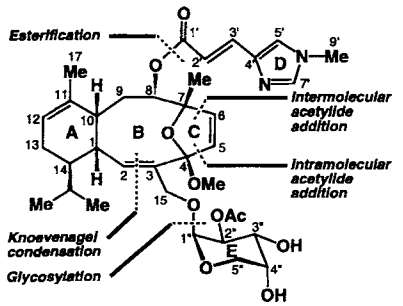

Figure 2. Numbering and strategic bond disconnections of eleutherobin (**1**) (Ac = acetyl).

(*E*)-*N*(6′)-methylurocanic acid residue (**D**) and the other a *β*-linked 2″-*O*-acetyl-D-arabinopyranose unit (**E**). The strategy for the total synthesis of this naturally occurring substance was designed based on a retrosynthetic analysis featuring the strategic bond disconnections highlighted in Figure 2. Thus, a properly functionalized ring **A** was to be derived from (+)-carvone and elaborated to a more advanced intermediate by an intermolecular acetylide addition to a ketone and a Knoevenagel condensation with an aldehyde functionality to form bonds C6–C7 and C2–C3, respectively. A glycosylation with a suitably functionalized D-arabinose derivative was then to follow, in order to introduce the carbohydrate moiety, whereas an intramolecular acetylide-aldehyde condensation was expected to form the 10-membered ring of the target molecule (bond C4–C5). Oxidation to an ynone and protecting group manipulations, followed by selective reduction of the triple bond (C5–C6) was expected to allow formation of the **BC** framework by intramolecular attack of the C7 hydroxyl function on the C4 carbonyl group. Finally, the (*E*)-*N*(6′)-methylurocanic acid moiety was to be introduced by esterification, following which eleutherobin (**1**) was expected to emerge upon deprotection.

Scheme 1 summarizes the construction of the initially targeted key ynal precursor **18**. Thus, the (+)-carvone-derived,[14, 16] TBS-protected (for abbreviations see legends) aldehyde **5** was converted to a C8 mixture (about 1.25:1) of hydroxyketones **6** by reaction with 1-ethoxyvinyllithium followed by acid hydrolysis (82% overall yield). Addition of ethynylmagnesium bromide to hydroxyketones **6** led, stereospecifically,[17] to a mixture of two acetylenic diols (C7, C8) **7** in 76% overall yield. Desilylation of **7** with TBAF afforded, after flash chromatography (silica gel, ether/hexane 3:1), pure triol **8** (52% yield) along with its C7, C8 diastereoisomer (40% yield). Triol **8** (identified by correlation with a previously synthesized sample)[14] was then converted to the primary alcohol **10** by persilylation (TES-OTf) and selective monodesilylation (PPTS-MeOH) in 98% overall yield. Oxidation of **10** with TPAP-NMO[18] then produced aldehyde **11** (98% yield) which underwent smooth Knoevenagel condensation with ethyl cyanoacetate in the presence of *β*-alanine[19] to afford, stereoselectively, the desired (*E*)-*α*,*β*-unsaturated cyanoester **12** in 95% yield. The reduction of **12** with DIBAL at −78 to −10 °C (hexanes) proceeded in high yield and with remarkable selectivity to afford the desired glycosylation acceptor, hydroxyaldehyde **13** in 75% yield.

The D-arabinose trichloroacetimidate derivative **17** required for coupling was prepared from the previously synthesized[20] phenyl thioglycoside **14**: The reaction of **14** with PMB-Cl in the presence of NaH afforded **15** (93% yield), and the acid-induced removal of the acetonide group gave the expected diol (84% yield). Subsequent silylation with TBS-OTf led to **16** (97% yield), whose reaction with NBS in acetone:H_2O (93:7) gave the corresponding lactol (80% yield), which underwent a reaction with CCl_3CN in the presence of NaH to give **17** (93% yield)[21].

Coupling of **13** with **17** (2.0 equiv) in ether proceeded smoothly in the presence of TMS-OTf at 0 °C to afford predominantly the *β*-glycoside **18** along with its *α*-anomer (**18′**) in high yield. Flash column chromatography (silica gel, Et_2O in hexanes, 1:20) led to pure *β*-glycoside **18** (54% yield) and *α*-glycoside **18′** (28% yield) (for spectroscopic data see Table 1).

The conversion of ynal **18** to eleutherobin (**1**) followed the path shown in Scheme 2. Ring closure of **18** was facilitated by the action of LiHMDS in THF at −20 °C, which furnished the 10-membered ring alcohol **19** (mixture of C4 diastereoisomers). Oxidation of **19** with Dess–Martin reagent[22] then led to the bis-conjugated ketone **20** (80% overall yield from **18**). At this stage, the acetyl group was installed on the carbohydrate ring of the molecule by removing the PMB group (DDQ, 90% yield) and acetylating the resulting secondary alcohol **21** (Ac_2O, Et_3N, 4-DMAP, 90% yield). The acetate **22** was then exposed to $Et_3N \cdot 3HF$ in THF at 25 °C, conditions which allowed the selective removal of both TES groups leading to diol **23** in 86% yield. Compound **23** was then subjected to Lindlar hydrogenation conditions, which gave crude lactol **25** in high yield. Although the postulated intermediate, bis-enone **24**, was not detected, its intermediacy in this sequence is logical and indeed required. Treatment of lactol **25** with PPTS in MeOH at 25 °C led to the isolation of its methoxy derivative **26** in 78% overall yield from **23**, as a single stereoisomer. The *β*-stereochemistry of the methoxy group in **26** was assumed on the basis of molecular models, and was confirmed by its conversion to eleutherobin (**1**).

For the purposes of esterification, the known[23] ethyl (*E*)-*N*(6′)-methylurocanate **27** (Scheme 2) was sequentially converted to sodium salt **28** (NaOH, THF, H_2O) and *tert*-butyl dride **29** [*t*BuC(O)Cl, THF, about 90% overall yield]. The at-

 © WILEY-VCH Verlag GmbH, D-69451 Weinheim, 1997 0570-0833/97/3622-2521 $ 17.50+.50/0

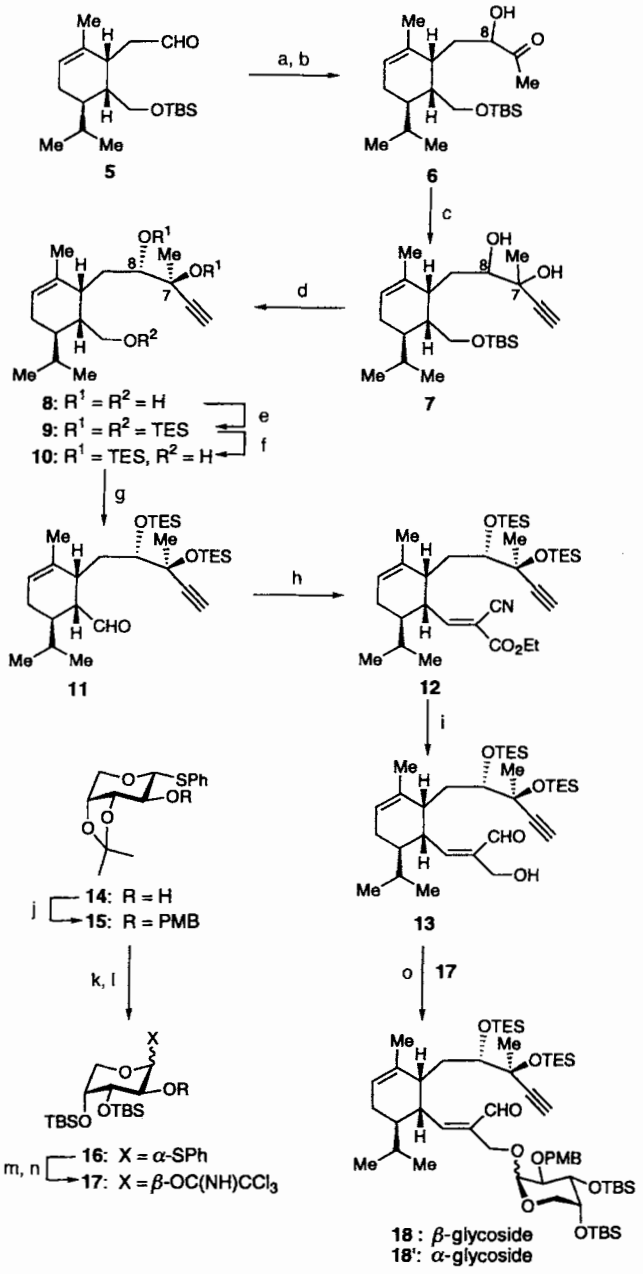

Scheme 1. Construction of the glycosylated ynal **18**: a) CH_2=CH(OEt) (2.0 equiv), *t*BuLi (1.8 equiv, 1.7 M in THF), THF, $-78 \rightarrow 0$ °C, 1 h; then cool to -78 °C and add **5** (1.0 equiv); then slowly warm to -40 °C; b) conc. H_2SO_4, Et_2O, 25 °C, 2 min, 82% for two steps; c) HC≡CMgBr (5.0 equiv, 0.5 M in THF), THF, $-78 \rightarrow -20$ °C, 14 h, 76% as an approximate 1.25:1 mixture of diastereoisomers; d) TBAF (2.0 equiv, 1 M in THF), THF, $0 \rightarrow 25$ °C, 1 h, **8** (52%), plus its C7–C8 diastereoisomer (40%); e) TES-OTf (5.0 equiv), Et_3N (10.0 equiv), CH_2Cl_2, 25 °C, 100%; f) PPTS (0.1 equiv), MeOH:CH_2Cl_2 (3:1), 25 °C, 45 min, 98%; g) TPAP (0.05 equiv), NMO (1.5 equiv), CH_2Cl_2, 4 Å MS, 1.5 h, 98%; h) $NCCH_2CO_2Et$ (30.0 equiv), β-alanine (4.0 equiv), 95% EtOH, 72 h, 50 °C, 95%; i) DIBAL (10.0 equiv), hexanes, $-78 \rightarrow -10$ °C, 75%; j) NaH (1.1 equiv), DMF, 0 °C, 30 min; then PMB-Cl (1.2 equiv), 2 h, 93%; k) TsOH·H_2O (0.1 equiv, 7.2 mM), ethylene glycol-MeOH (1:10), 25 °C, 6 h, 84%; l) TBDMS-OTf (4.0 equiv), Et_3N (10.0 equiv), CH_2Cl_2, 0 °C, 2 h, 97%; m) NBS (3.4 equiv), pyridine (11.0 equiv), acetone-H_2O (93:7), 80%; n) NaH (0.1 equiv), Cl_3CCN (5.0 equiv), CH_2Cl_2, 25 °C, 3.5 h, 93%; o) **17** (2.0 equiv), TMS-OTf (0.1 equiv), Et_2O, 0 °C **18** (54%), plus its α-anomer **18'** (28%). TBAF = tetra-*n*-butylammonium fluoride, TES-OTf = triethylsilyl trifluoromethanesulfonate, PPTS = pyridinium *p*-toluenesulfonate, TPAP = tetra-*n*-propylammonium perruthenate, NMO = 4-methylmorpholine *N*-oxide, DIBAL = diisobutylaluminum hydride, DMF = *N*,*N*-dimethylformamide, PMB-Cl = *p*-methoxybenzylchloride, TsOH·H_2O = *p*-toluenesulfonic acid monohydrate, TBDMS-OTf = *tert*-butyldimethylsilyl trifluoromethanesulfonate, NBS = *N*-bromosuccinimide, TMS-OTf = trimethylsilyl trifluoromethanesulfonate.

Table 1. Selected physical properties of compounds **18**, **30**, **33**, and **34**.

18: $R_f = 0.8$ [silica gel, hexane:ether (3:1)]; $[\alpha]_{25}^{D} = -28.3$ (c = 1.0 in chloroform). IR (film): $\tilde{\nu}_{max}$ 2954, 1676, 1612, 1512, 1461, 1364, 1250, 1114, 1038, 835, 740 cm^{-1}; ^1H NMR (500 MHz, $CDCl_3$, eleutherobin numbering): δ = 10.16 (s, 1H, H-4), 7.21 (d, J = 8.5 Hz, 2H), 6.94 (d, J = 11.5 Hz, H-2), 6.82 (d, J = 8.5 Hz, 2H), 5.38 (bs, 1H, H-12), 4.74 (d, J = 2.0 Hz, 1H), 4.62 (d, J = 11.9 Hz, 1H), 4.42 (d, J = 11.9 Hz, 1H), 4.21 (m, 2H), 3.92 (bs, 1H), 3.78 (s, 3H), 3.72 (m, 1H), 3.50 (m, 4H), 2.25 (m, 1H), 2.01 (m, 3H), 1.89 (m, 2H), 1.75 (m, 1H), 1.66 (s, 3H), 1.57 (m, 2H), 1.42 (m, 2H), 1.31 (s, 3H), 1.23 (m, 2H), 0.89 (m, 35H), 0.66 (m, 16H), −0.03 (m, 12H); ^{13}C NMR (125 MHz, $CDCl_3$): δ = 189.6, 159.1, 155.5, 136.3, 136.2, 130.8, 129.5, 121.0, 113.6, 99.3, 86.8, 78.8, 76.4, 75.5, 73.0, 72.7, 71.4, 67.1, 64.0, 55.2, 39.0, 37.2, 34.2, 29.7, 28.4, 26.0, 25.9, 24.4, 23.6, 21.9, 21.2, 18.2, 18.1, 17.0, 7.1, 7.0, 6.0, 5.6, −4.5, −4.6, −4.7, −4.9; HRMS (FAB): calcd for $C_{57}H_{102}O_9Si_4Na$ (M + Na^+): 1065.6499, found 1065.6543.

30: $R_f = 0.4$ [silica gel, ethyl acetate:hexane (4:1)]; $[\alpha]_{25}^{D} = -61.3$ (c = 0.6 in chloroform); IR (film): $\tilde{\nu}_{max}$ 2929, 2856, 2362, 2338, 1746, 1707, 1639, 1468, 1367, 1296, 1253, 1150, 1062, 1038, 1001, 886, 837, 775 cm^{-1}; UV(CH_2Cl_2) λ_{max} (log ε) 286 nm (0.924); ^1H NMR (600 MHz, $CDCl_3$, eleutherobin numbering): δ = 7.52 (d, J = 15.6 Hz, 1H, H-3'), 7.44 (s, 1H, H-7'), 7.07 (s, 1H, H-5), 6.55 (d, J = 15.6 Hz, 1H, H-2'), 6.08–6.05 (m, 2H, H-5, H-6), 5.55 (d, J = 9.5 Hz, 1H), 5.24 (bs, 1H, H-12), 4.99–4.96 (m, 1H), 4.88 (s, 1H), 4.79 (d, J = 7.4 Hz, 1H), 4.25 (d, J = 12.4 Hz, 1H), 3.97 (dd, J = 8.3, 2.3 Hz, 1H), 3.95–3.92 (m, 1H), 3.88–3.84 (m, 2H), 3.72–3.64 (m, 1H), 3.69 (s, 3H, H-21), 3.47 (dd, J = 11.6, 4.4 Hz, 1H), 2.58 (d, J = 11.2 Hz, 1H), 2.32–2.28 (m, 1H), 2.05–1.94 (m, 2H), 2.02 (s, 3H, C(O)CH_3), 1.61–1.51 (m, 5H), 1.51 (s, 3H, H-17), 1.42 (s, 3H), 1.25–1.22 (m, 4H), 0.95 (d, J = 6.6 Hz, 3H), 0.90 (d, J = 6.6 Hz, 3H), 0.87 (s, 9H), 0.86 (s, 9H), 0.08 (s, 3H), 0.05 (s, 3H), 0.04 (s, 3H), 0.04 (s, 3H); ^{13}C NMR (150 MHz, $CDCl_3$): δ = 170.2, 166.7, 139.2, 138.4, 136.3, 134.2, 133.9, 133.3, 130.8, 122.7, 121.2, 115.9, 95.0, 89.8, 81.5, 71.5, 69.5, 69.3, 64.0, 60.4, 49.6, 42.5, 38.6, 34.0, 33.6, 29.6, 29.0, 25.8, 24.4, 24.3, 22.2, 22.0, 21.1, 21.0, 20.6, 18.2, 18.1, 14.2, −4.2, −4.5, −4.7, −4.9; HRMS (FAB): calcd for $C_{47}H_{76}N_2O_{10}Si_2Cs$ (M + Cs^+): 1017.4093, found 1017.4139.

33: $R_f = 0.3$ [silica gel, ethyl acetate:hexane (2:1); $[\alpha]_{25}^{D} = -61.6$ (c = 0.3 in chloroform); IR (film): $\tilde{\nu}_{max}$ 3428, 2924, 2854, 1732, 1712, 1638, 1463, 1371, 1265, 1158, 1060, 997 cm^{-1}; ^1H NMR (600 MHz, $CDCl_3$, eleutherobin numbering): δ = 7.50 (d, J = 15.5 Hz, 1H, H-3'), 7.29 (s, 1H, H-5'), 6.65 (d, J = 15.5 Hz, 1H, H-2'), 6.09 (dd, J = 19.0, 5.9 Hz, 1H), 5.54 (d, J = 9.4 Hz, 1H), 5.26 (bs, 1H, H-12), 4.96 (dd, J = 9.8, 3.5 Hz, 1H), 4.90 (d, J = 3.6 Hz, 1H), 4.81 (d, J = 7.4 Hz, 1H), 4.28 (d, J = 12.2 Hz, 1H), 4.03–3.90 (m, 3H), 3.86 (d, J = 12.5 Hz, 1H), 3.81 (dd, J = 11.2, 2.0 Hz, 1H), 3.69 (dd, J = 12.6, 2.0 Hz, 1H), 3.20 (s, 3H, H-21), 2.72 (s, 3H, H-2''), 2.64–2.53 (m, 1H), 2.38–2.24 (m, 1H), 2.10 (s, 3H, C(O)CH_3), 1.55 (s, 3H, H-17), 1.50–0.70 (m, 8H), 1.50 (s, 3H, H-16), 0.97 (d, J = 6.5 Hz, 3H), 0.92 (d, J = 6.5 Hz, 3H); ^{13}C NMR (150 MHz, $CDCl_3$): δ = 171.2, 167.0, 166.3, 151.1, 137.2, 136.6, 133.9, 133.4, 132.6, 131.0, 121.8, 121.2, 119.9, 115.7, 93.4, 89.7, 81.7, 71.7, 69.3, 69.0, 68.0, 62.0, 49.6, 45.5, 42.3, 38.6, 34.1, 31.4, 29.6, 28.9, 24.4, 24.1, 22.1, 21.8, 20.9, 20.4, 19.3; HRMS (FAB): calcd for $C_{35}H_{47}NNaO_{10}S$ (M + Na^+) 696.2818, found 696.2802.

34: $R_f = 0.25$ [silica gel, methanol:dichloromethane (5%)]; IR (film): $\tilde{\nu}_{max}$ 3390, 2924, 2852, 2354, 1734, 1708, 1639, 1630, 1453, 1367, 1245, 1161, 1038, 999 cm^{-1}; UV(CH_2Cl_2) λ_{max} (log ε) 290 nm (0.828); ^1H NMR data (500 MHz, $CDCl_3$, eleutherobin numbering): δ 7.54 (d, J = 15.6 Hz, 1H, H-2'), 7.47 (s, 1H, H-7'), 7.11 (s, 1H, H-5'), 6.57 (d, J = 15.6 Hz, 1H, H-3'), 6.21 (d, J = 5.9 Hz, 1H, H-6), 6.00 (d, J = 5.9 Hz, 1H, H-5), 5.62 (d, J = 9.5 Hz, 1H), 5.30–5.26 (m, 1H), 4.97 (dd, J = 3.8, 2.0 Hz, 1H), 4.82 (d, J = 7.5 Hz, 1H), 4.72–4.69 (m, 1H), 4.17 (d, J = 10.8 Hz, 1H), 3.96 (d, J = 10.9 Hz, 1H), 3.72 (s, 3H, H-21), 3.65–3.62 (m, 2H), 3.55–3.43 (m, 5H), 3.23 (s, 3H, H-9'), 3.02–2.94 (m, 1H), 2.71–2.53 (m, 1H), 2.11 (s, 3H, C(O)CH_3), 2.01–1.96 (m, 9H), 1.56–1.21 (m, 3H), 1.53 (s, 3H, H-17), 1.46 (s, 3H, H-16), 1.00 (d, J = 6.6 Hz, 3H), 0.94 (d, J = 6.6 Hz, 3H); HRMS (FAB): calcd for $C_{35}H_{47}N_2O_{10}Cs$ (M + Cs^+): 789.2363, found 789.2334.

tachment of the (*E*)-*N*(6')-methylurocanic acid residue onto the main framework of eleutherobin was accomplished by reacting alcohol **26** with mixed anhydride **29** in the presence of Et_3N and 4-DMAP in CH_2Cl_2 at 25 °C, furnishing ester **30** in 75% yield (for spectroscopic data see Table 1). Finally, exposure of **30** to TBAF in THF generated eleutherobin (**1**) in 88% yield. Synthetic eleutherobin (**1**) exhibited identical properties to those reported[1, 2] for the natural substance (^1H and ^{13}C NMR, MS, $[\alpha]_{25}^{D}$, IR, and UV). The synthetic correlation of eleutherobin (**1**) ($[\alpha]_{25}^{D}$ = 67 (c = 0.2, MeOH)) to (+)-carvone and D-arabinose establishes its absolute stereochemistry as that shown in structure **1**.

In order to explore the structure–activity relationships of eleutherobin, two novel analogues were designed and targeted

 © WILEY-VCH Verlag GmbH, D-69451 Weinheim, 1997 0570-0833/97/3622-2522 $ 17.50+.50/0

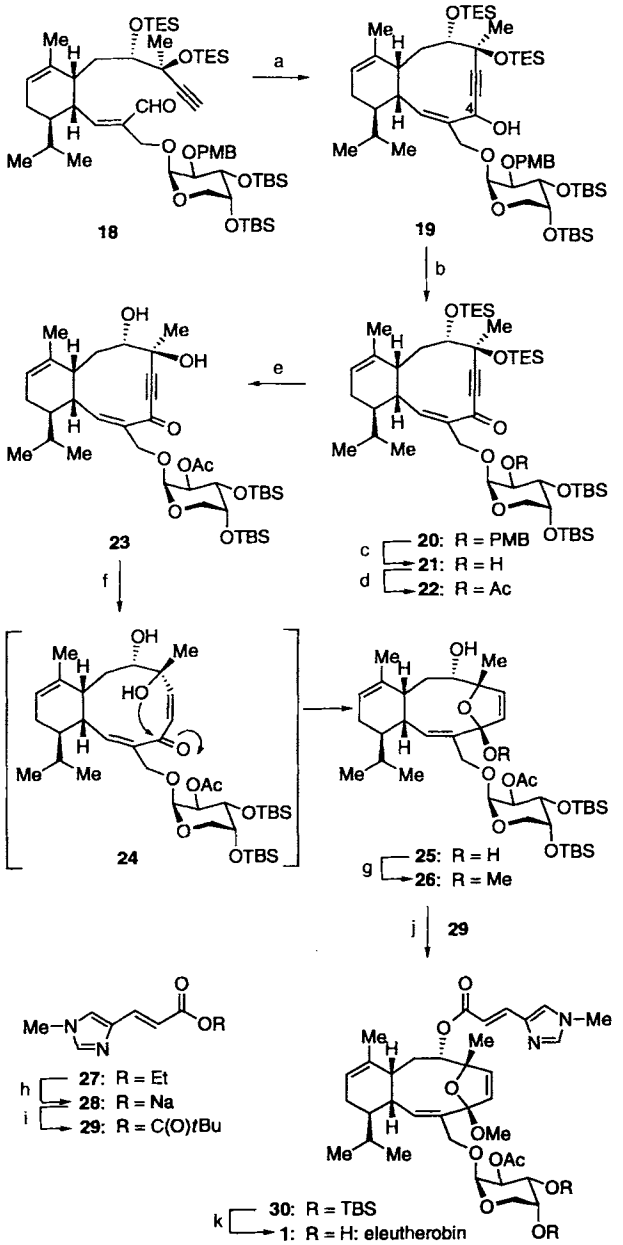

Scheme 2. Total synthesis of eleutherobin (**1**): a) LiHMDS (2.0 equiv), THF, −20 °C, 10 min; b) Dess-Martin periodinane (2.0 equiv), $NaHCO_3$ (10.0 equiv), pyridine (10.0 equiv), CH_2Cl_2, 0 °C, 20 min, 80% for two steps; c) DDQ (2.0 equiv), CH_2Cl_2:H_2O (19:1), 25 °C, 2 h, 90%; d) Ac_2O (10.0 equiv), Et_3N (10.0 equiv), 4-DMAP (3.0 equiv), 25 °C, 1.5 h, 90%; e) $Et_3N{\cdot}3HF$, THF (1:5), 0 → 25 °C, 3 h, 86%; f) Lindlar's catalyst (0.5 equiv), H_2, toluene, 25 °C, 30 min; g) PPTS (0.5 equiv), MeOH, 25 °C, 10 min, 78% for two steps; h) NaOH (1.05 equiv), THF:H_2O, 1:1, 25 °C, 8 h, 100%; i) *t*BuC(O)Cl (1.1 equiv), THF, 25 °C, 5 h; j) **29** (5.0 equiv), Et_3N (10.0 equiv), 4-DMAP (2.0 equiv), CH_2Cl_2, 25 °C, 30 h, 75%; k) TBAF (3.0 equiv), THF, 25 °C, 4 h, 88%. LiHMDS = lithium hexamethyldisilazide, DDQ = 2,3-dichloro-5,6-dicyano-1,4-benzoquinone, Ac = acetyl, 4-DMAP = 4-dimethylaminopyridine, PPTS = pyridinium *p*-toluenesulfonate, TBAF = tetra-*n*-butylammonium fluoride.

for synthesis (Scheme 3). The epothilone-inspired analogue **33**, which carries a thiazole-containing side chain instead of the *N*(6′)-methylurocanic acid residue, was constructed by esterification of alcohol **26** (DCC, 4-DMAP, 70% yield) with the corresponding carboxylic acid (**32**, prepared from aldehyde **31**[24] as shown in Scheme 3), followed by TBAF-induced desilylation (85% yield). The α-glycoside analogue of eleutherobin, compound **34**, was constructed from the α-glycoside **18′** (Scheme 3)

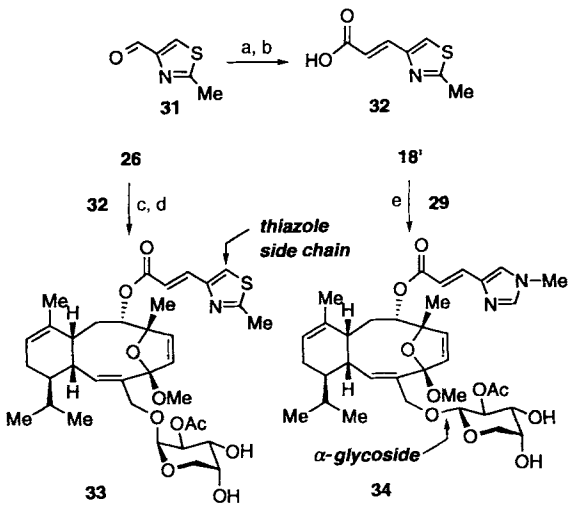

Scheme 3. Structure and synthesis of eleutherobin analogues **33** and **34**: a) $Ph_3P{=}CHCO_2Me$ (1.5 equiv), benzene, 80 °C, 85%; b) LiOH (3.0 equiv), THF:H_2O (1:1), 97%; c) DCC (1.8 equiv), 4-DMAP (0.5 equiv), **32** (2.0 equiv), CH_2Cl_2, 25 °C, 6 h, 70%; d) TBAF (5.0 equiv, 1 M in THF), THF, 25 °C, 3 h, 85% e) see legend to Scheme 2. DCC = 1,3-dicyclohexylcarbodiimide, 4-DMAP = 4-dimethylaminopyridine, TBAF = tetra-*n*-butylammonium fluoride.

by the same sequence and in similar yields as described for eleutherobin (**1**).

In the filtration-colorimetric tubulin polymerization assay[5] using MAP-rich tubulin, synthetic eleutherobin (**1**) and its analogues **33** and **34** exhibited activity comparable to that of Taxol (**2**) (**2**: 49%; **1**: 70%; **33**: 56%; **34**: 54%). The data for eleutherobin (**1**) are consistent with those obtained with the natural substance (**1**),[2, 25] whereas those for **33** and **34** establish the first important and path-pointing structure–activity relationships within the eleutherobin family.

The described chemistry opens a pathway for a practical synthesis of eleutherobin (**1**) and its analogues. Furthermore, the reported chemical synthesis allowed the assignment of the absolute stereochemistry of the natural product, and the preparation of its first biologically active analogues (**33** and **34**). Applications to the large-scale production of eleutherobin (**1**) and the generation of combinatorial libraries of this and related structures for chemical biology studies are now possible.

Received: October 10, 1997 [Z11024IE]
German version: *Angew. Chem.* **1997**, *109*, 2631–2634

Keywords: antitumor agents · eleutherobin · natural products · structure–activity relationships · total synthesis

[1] W. Fenical, P. R. Hensen, T. Lindel, US Patent No. 5473057, Dec. 5, **1995**.
[2] T. Lindel, P. R. Jensen, W. Fenical, B. H. Long, A. M. Casazza, J. Carboni, C. R. Fairchild, *J. Am. Chem. Soc.* **1997**, *119*, 8744–8745.
[3] P. B. Schiff, J. Fant, S. B. Horwitz, *Nature* **1979**, *277*, 665–667.
[4] G. Höfle, N. Bedorf, H. Steinmetz, D. Schomburg, K. Gerth, H. Reichenbach, *Angew. Chem.* **1996**, *108*, 1671–1673; *Angew. Chem. Int. Ed. Engl.* **1996**, *35*, 1567–1569.
[5] D. M. Bollag, P. A. McQueney, J. Zhu, O. Hensens, L. Koupal, J. Liesch, M. Goetz, E. Lazarides, C. M. Woods, *Cancer Res.* **1995**, *55*, 2325–2333.
[6] R. J. Kowalski, P. Giannakakou, E. Hamel, *J. Biol. Chem.* **1997**, *272*, 2534–2541.
[7] D.-S. Su, D. Meng, P. Bertinato, A. Balog, E. J. Sorensen, S. J. Danishefsky, Y.-H. Zheng, T.-C. Chou, L. He, S. B. Horwitz, *Angew. Chem.* **1997**, *109*, 775–777; *Angew. Chem. Int. Ed. Engl.* **1997**, *36*, 757–759.
[8] K. C. Nicolaou, N. Winssinger, J. A. Pastor, S. Ninkovic, F. Sarabia, Y. He, D. Vourloumis, Z. Yang, T. Li, P. Giannakakou, E. Hamel, *Nature* **1997**, *387*, 268–272.
[9] D. Schinzer, A. Limberg, A. Bauer, O. M. Böhm, M. Cordes, *Angew. Chem.* **1997**, *109*, 543–544; *Angew. Chem. Int. Ed. Engl.* **1997**, *36*, 523–524.

 © WILEY-VCH Verlag GmbH, D-69451 Weinheim, 1997 0570-0833/97/3622-2523 $ 17.50+.50/0

[10] S. Ketzinel, A. Rudi, M. Schleyer, Y. Benayahu, Y. Kashman, *J. Nat. Prod.* **1987**, *59*, 873–875.
[11] M. D'Ambrosio, A. Guerriero, F. Pietra, *Helv. Chim. Acta* **1987**, *70*, 2019–2027.
[12] M. D'Ambrosio, A. Guerriero, F. Pietra, *Helv. Chim. Acta* **1988**, *71*, 964–976.
[13] M. Ciomei, C. Albanese, W. Pastori, M. Grandi, F. Pietra, M. D'Ambrosio, A. Guerriero, C. Battistini, *Abstract 30, Proc. Am. Ass. Canc. Res.* **1997**, *38*, 5.
[14] K. C. Nicolaou, J. Y. Xu, S. Kim, T. Ohshima, S. Hosokawa, J. Pfefferkorn, *J. Am. Chem. Soc.*, in press.
[15] Y. Lin, C. A. Bewley, D. J. Faulkner, *Tetrahedron* **1993**, *49*, 7977–7984.
[16] B. M. Trost, A. S. Tasker, G. Ruther, A. Brands, *J. Am. Chem. Soc.* **1991**, *113*, 670–672.
[17] D. A. Evans, S. W. Kalder, T. K. Jones, J. Clardy, T. J. Stout, *J. Am. Chem. Soc.* **1990**, *112*, 7001–7031.
[18] W. P. Griffith, S. V. Ley, *Aldrichimica Acta* **1990**, *23*, 13–19.
[19] N. H. Anderson, F. A. Golec, Jr., *Tetrahedron Lett.* **1977**, 3783–3787.
[20] K. C. Nicolaou, J. I. Trujillo, K. Chibale, *Tetrahedron* **1997**, *53*, 8751.
[21] R. R. Schmidt, K.-H. Jung in *Preparative Carbohydrate Chemistry* (Ed.: S. Hanessian), Marcel Dekker Inc., New York, **1997**, pp. 283-312.
[22] D. B. Dess, J. C. Martin, *J. Org. Chem.* **1983**, *48*, 4155–4156.
[23] N. L. Viguerie, N. Sergueeva, M. Damiot, H. Mawlawi, M. Riviere, A. Lattes, *Heterocycles* **1994**, *37*, 1561–1576.
[24] K. C. Nicolaou, S. Ninkovic, F. Sarabia, D. Vourloumis, Y. He, H. Vallberg, M. V. R. Finlay, Z. Yang, *J. Am. Chem. Soc.* **1997**, *119*, 7974–7991.
[25] B. H. Long, A. M. Casazza, J. Carboni, C. R. Fairchild, T. Lindel, P. R. Jensen, W. Fenical, *Cancer Res*, submitted.

Chemistry at the crossroads

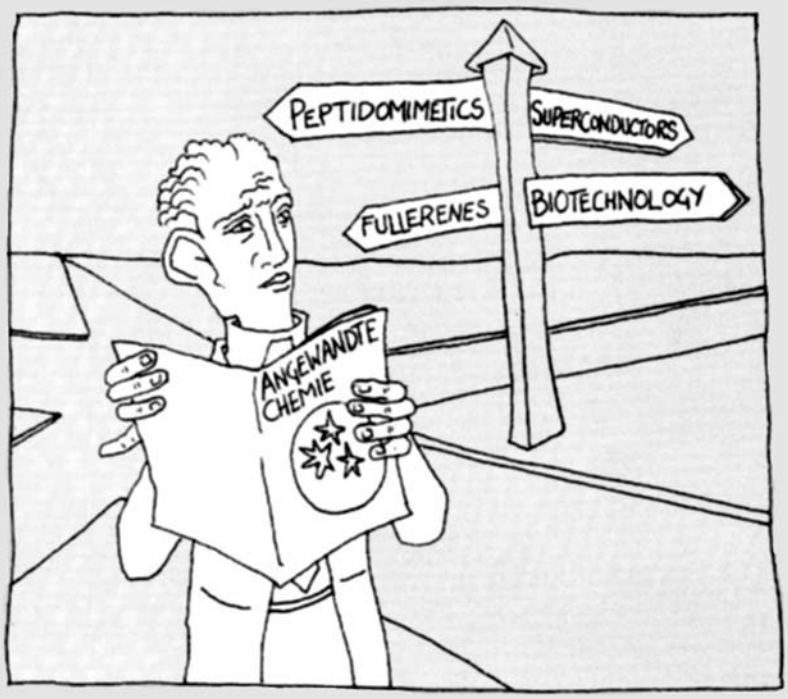

Pioneering scientists guide your way through newly charted territory with their topical reviews and discriminating highlights in **Angewandte Chemie.**

To start your own personal subscription, just fax.

An order form is provided on the last page for your convenience.

WILEY-VCH

 © WILEY-VCH Verlag GmbH, D-69451 Weinheim, 1997 0570-0833/97/3622-2524 $ 17.50+.50/0

Fuzzy Definitions

Concepts in Chemistry—A Contemporary Challenge. Edited by *D. H. Rouvray*. John Wiley & Sons, Chichester, 1997. xvi, 420 pp., hardcover £ 65.00.—ISBN 0-86380-200-1

The sixth in the series of Mathematical Chemistry Conferences was held on July 10–14, 1995, in Pitlochry, Scotland. The title of the conference was "Are the Concepts of Chemistry all Fuzzy?" Two books on mathematical chemistry have emerged from this meeting, both edited by one of the conference organizers, Professor Dennis H. Rouvray. One of them is under review here; the other is *Fuzzy Logic in Chemistry* (Academic Press, San Diego, 1997). Although the list of contributors is different in the two books, there is considerable overlap in the contents, with a very fuzzy dividing line between them. Thus it is curious that neither of the books makes explicit mention of the other.

The original stimulus for the editor's interest came from a dust jacket comment by Martin Gardner that "outside of mathematics and logic, all definitions are fuzzy." A statement by H. A. Kramers in 1946 is repeatedly quoted: "... in physical science in particular, the most important and fruitful concepts are those to which it is impossible to attach a well-defined meaning."

The 12 chapters of the book cover a wide range of topics and vary considerably in the depth of treatment of their subject matter. The introductory chapter by the editor, "Are the Concepts of Chemistry all Fuzzy?", is followed by one on the partnership between mathematics and chemistry (N. Trinajstic). This chapter goes back to such fundamentals as the definition of science and the roots of mathematics and of chemistry, and also covers such recent events as the discovery of buckminsterfullerene. It defines mathematical chemistry as "that part of theoretical chemistry which is concerned with the application of mathematical methods in the chemical world."

The next two chapters also deal with broad conceptual topics, one with periodicity (E. V. Babaev and R. Hefferlin) and the other with chemical structure (J. L. Villaveces C. and E. E. Daza C.). The remaining eight chapters focus on more specific areas such as allotropic structures, aromaticity, ring currents, porous delocalization of superconductors, chirality (two chapters), complexity, and immunological recognition.

Lest we judge the title of the book too pretentious, we must remember that the divergence of topics and depth of discussion derive from the conference program. There are conspicuous omissions from the point of view of the interplay between mathematics and chemistry, for example combinatorial chemistry and quasicrystals, both being recent hot topics. Nonetheless, what is presented here is a rich collection of interesting contributions.

One section in the chapter "The Concept of Chemical Structure" does not do justice to the rest of the volume. There are some trivial points that could easily be corrected, for example electron diffraction is called "electronic diffraction", and neutron diffraction is described as being performed on gases. Incidentally, electron diffraction is listed as a new experimental technique, quite a compliment for this 67-year-old tool, even if only gas-phase studies are considered. However, one aspect that could be conceptually damaging is the discussion of differences in the form of structural information originating from different techniques. The authors state that "this situation has created a profusion of geometrical parameters that greatly complicate the definition of molecular geometry." However, the complication may arise only from the lack of understanding of the physical origin of differences among these geometrical parameters. Decades ago, precision was generally too low to warrant concern about the differences in the physical meaning of the structural information originating from different techniques. Nowadays, however, a precise measurement or computation needs to be qualified by additional information as to its origin, so that one can assess its accuracy. To simply compare "experimental" and "computed" data, for example, is no longer acceptable because they may have a different physical basis. In addition to the difference in the physical phenomena utilized in various techniques, the extent of motion plays an important role in this, because of the very different ways in which the motional effects are averaged. The extent of motion also greatly influences the applicability of our model of chemical structure. We have to educate ourselves to an increased degree of rigor in these aspects, whether we are providers or users of structural information. This is a conceptual question, and this book missed an important opportunity to put it in proper perspective.

All in all, however, this book, along with its companion volume, discusses contemporary questions of mathematical chemistry at a high level. It has the potential of making its topics—which to many appear esoteric—accessible to a broad circle of chemists. Therefore, I recommend it to graduate students and researchers interested in aspects of their field beyond the confines of their research projects.

István Hargittai
Budapest Technical University
and Hungarian Academy of Sciences
Budapest (Hungary)

Fuzzy Logic in Chemistry. Edited by *D. H. Rouvray*. Academic Press, San Diego, 1997. 364 pp., hardcover $ 80.00.—ISBN 0-12-598910-6

The review articles collected together in this book are extended versions of papers presented during a conference held in 1995 on the subject of fuzzy logic in chemistry. The contributions can be roughly divided into three categories: introductory articles of a scientific/philosophical nature, articles concerned with the intrinsic problem of uncertainty and/or with the potential applications of fuzzy methods,

This section contains book reviews and a list of new books received by the editor. Book reviews are written by invitation from the editor. Suggestions for books to be reviewed and for book reviewers are welcome. Publishers should send brochures or (better) books to the editorial office: Redaktion Angewandte Chemie, Postfach 101161, D-69451 Weinheim, Germany. The editor reserves the right of selecting which books will be reviewed. Uninvited books not chosen for review will not be returned.

and lastly those in which the mathematical techniques based on the theory of fuzzysets are used to solve chemical problems. Rather surprisingly, there is no contribution on fuzzy control methods.

In the first article D. H. Rouvray explains how the motivation to develop a theory that can be applied to inexact quantities is a consequence of uncertainties that are inherent in the systems under investigation. Central to this is the philosophical question of the connection between knowledge, the degree of truth of that knowledge, and uncertainty. He gives a useful compilation of various definitions of uncertainty, emphasizing that there is no general agreement on this point.

The title chosen by G. Klir for his contribution already betrays the fact that he approaches the task of giving a mathematical introduction to the subject only in a half-hearted way. Instead, his article too consists largely of a discussion of philosophical aspects. It would have been more useful to put a greater emphasis on reporting the forum discussions between mathematicians and chemists, so as to clarify the issues and concepts; for example, compare the conflicting statements of Klir and Bangov about the relationship between fuzzy set theory and probability theory.

The next two articles belong to the second of the categories mentioned above. That by A. Amman sets out to provoke thought about the concept of chemical structure. Starting from quantum-mechanical considerations, he throws up a number of questions that can be expressed generally as follows: can deviations from classical behavior in chemistry be understood by treating strict classical behavior as a limiting case that corresponds to a crispset? According to this view, quantum-mechanical deviations from that situation, which result from a finite number of degrees of freedom or from finite masses, correspond instead to fuzzy sets. K. Mislow is thoroughly committed to the fuzzy concept in chemistry, and shows that in any case one does in fact think and express ideas in terms of fuzzy theories. In the main part of his article he gives a concise summary of his work on extending the concept of chirality.

All the following articles are concerned with applications of fuzzy set theory to the solution of chemical problems. The 86-page contribution by P. Mezey begins by discussing the relationship between fuzziness and resolution, and then deals with resolution-dependent chirality, symmetry, or measures of symmetry. In considering how to develop a fuzzy way of modeling electron density, Mezey uses the analogy between α-cuts and electron density levels, and also develops a generalization of the Hausdorff distance incorporating fuzziness. From this basis he then develops fuzzy generalizations of symmetry elements, measures of symmetry, and other classical concepts, which are used to describe the degree of correspondence of molecular form and size. He ends by describing various methods for calculating fuzzy electron density fragments, which are then stored in numerical databases and can be used as building blocks for constructing macromolecular electron density maps.

J. Brickmann discusses the use of mutual matching methods for molecular recognition. The starting point for this is the classification problem involved in the lock-and-key principle. One stage of this concerns the transformation of numerical data into diagrams, which allows one to visually inspect the system under investigation. To test the compatibility of numerical data with abstract categories of human thought processes, Brickmann uses the concept of linguistic variables. Finally he applies membership functions to a description of a soft surface, and develops strategies for fuzzy pattern recognition on surfaces.

The articles by J. Xu and I. Bangov are concerned with the use of fuzzy logic for interpreting spectra, with particular emphasis on applications involving 2D NMR techniques. Both authors set out to explain how fuzzy spectroscopic data can be correlated with fuzzy molecular graphs. Xu divides his method into two stages: first one evaluates the extent of agreement between the spin–spin couplings and the molecular topology, and secondly one evaluates the degree of similarity between the graphs by a fuzzy distance measurement. However, the explanation could have been improved by a better matching between the schematic examples that are given. The article ends by touching briefly on applications to IR spectroscopy and mass spectrometry. Bangov provides some well worked out examples of the use of fuzzy methods in computer-aided structure determination. However, Equation (5) contradicts Figure 1, and also appears to contain a printing error, as it implies that the number of spectral features available for determining the structure is equal to the number of atoms. Furthermore, on the basis of this equation the author derives some generalizations that are open to question. In the main part of the article Bangov gives a breadth-frist algorithm that can be used for generating structures, and allows the risk of a combinatorial explosion to be kept under control more effectively than in depth-first procedures.

The article by D.-D. Dumitrescu is concerned with the classification of unknown samples using fuzzy cluster analysis. In the mathematical part he proposes an extension of Bezdek's "fuzzy-c-means" algorithm. His approach to the "cluster validity" problem is based on proving the existence of a hierarchical structure within the data, and for this purpose he introduces the degree of polarization of a fuzzy partition. The algorithm makes use of binary partitions (divisive hierarchical clustering) based on procedures analogous to fuzzy-c-means. Furthermore, by using fuzzy cross-classification, the author classifies the objects according to their variables and the variables according to the objects, and investigates their interrelationship in the partitions. Some examples of analytical applications of these methods are described.

The fact that D. H. Rouvray has taken on the task of collecting together, for the first time, reports of work on the applications of fuzzy methods in chemistry-related research, is very much to be welcomed. Therefore, the uniqueness of this work—at least for the present—is in itself sufficient reason for recommending *Fuzzy Logic in Chemistry*. It will be useful not only for specialists in the particular fields concerned to study how classical concepts are being extended, but also for everyone interested in these methods, as an overview showing how far the theory of fuzzy sets has already entered chemical research.

Frank Ehrentreich
Institut für Analytische Chemie
der Technischen Universität Freiberg
(Germany)

Alkyl Polyglycosides. Technology, Properties and Applications. Edited by *K. Hill, W. von Rybinski* and *G. Stoll.* VCH Verlagsgesellschaft, Weinheim, 1996. ix, 242 pp., hardcover DM 148.00.—ISBN 3-527-29451-1

The appearance of a monograph on the properties and uses of alkyl polyglycosides (APGs), a new and interesting class of surfactants, is a welcome development. It will be especially useful for chemists who are active in the field of surfactants and are seeking new areas of application. The painstaking work of compiling the first complete picture of the technology, the physical and chemical properties, and the many applications of APGs has been undertaken by 36 scientists of the Henkel research group. This

 © WILEY-VCH Verlag GmbH, D-69451 Weinheim, 1997 0570-0833/97/3622-2526 $ 17.50+.50/0

was no easy task in view of the breadth of the subject and the enormously wide range of practical applications, and success was only made possible through the powerful research resources of the Henkel group.

The monograph consists of 14 chapters. Chapter 1 reviews the history of the industrial development of APGs and their place in surfactants chemistry, then Chapter 2 describes the technology of this class of compounds and the methods whereby they are synthesized, with clearly set out process schemes which help the reader's understanding. Chapter 3 describes the methods used for the analysis of APGs (HPLC, chromatography, etc.), enlivened by many instructive examples. Chapter 4 gives a very informative discussion of the physical and chemical properties of APGs, including mixtures of two or more compounds. Phase diagrams and related aspects are covered, thus providing the basis for understanding the later chapters. As well as treating binary and multicomponent systems, this chapter deals with the rheological properties of APGs, interfacial phenomena, and phase diagrams for microemulsions. This treatment provides the first comprehensive picture of the properties of APGs in their many aspects and variations, especially for multicomponent systems. Chapter 5 moves on from the basic knowledge covered in the previous chapters by describing the cosmetic and dermatological properties of APGs, and Chapter 6 discusses the cleansing effects of APGs on "hard" surfaces. Chapter 7 is concerned with the "formulation problems" involved in the agricultural uses of APGs. Chapters 8–10 then deal with synthetic aspects of the new nonionics and with their toxicological and dermatological properties. Chapters 11 and 12 are concerned with the environmental aspects of the use of APGs. Chapter 13 contains valuable information about the patent situation with regard to APGs, and lastly Chapter 14 gives a brief survey of the position regarding feedstocks for manufacturing APGs.

This monograph is unique in its treatment of a wide range of properties of APGs that are relevant to their applications, and thus it is extremely valuable for the laboratory scientist working in this field. As a consequence of the way in which the volume has been written, a certain amount of overlapping is unavoidable. The individual chapters make effective use of diagrams and schemes to aid the reader's understanding. There is a useful bibliography at the end of each chapter, although this often includes references to company research reports that are not easily accessible for ordinary readers. A possible improvement to the book would be to introduce each chapter with a short summary.

Hans-Dieter Dörfler
Fachrichtung Chemie/Kolloidchemie
der Technischen Universität Dresden
(Germany)

An Introduction to Polymer Science. By *H.-G. Elias*. WILEY-VCH, Weinheim, 1997. xxii, 470 pp., hardcover DM 88.00—ISBN 3-527-28790-6

This book is invaluable. It is well written, well organized, and captures the multidisciplinary nature of the field of polymer science. The book is organized into three sections with a total of fifteen chapters covering the various aspects of polymer chemistry, polymer physics, and polymer processing. It starts with a good introduction giving the reader a history lesson in the discovery/invention and subsequent development of polymer science. Then the author covers the basics of polymer structure and molecular weight distribution. Instead of separating the experimental determination of molecular weight distribution from the theoretical aspects (as commonly done in other textbooks), the author addresses both the theoretical aspect and experimental determination within the same chapter. This is an improvement over the way other authors present the subject. The remaining chapters in the "Chemistry" section cover the gamut of types of polymerization, including the usual anionic, cationic, free radical, and step growth. The chapter on free radical copolymerizations and the following appendix to Chapter 3 are especially well done. In addition, the chapter on biological polymerizations is helpful with respect to natural fiber production.

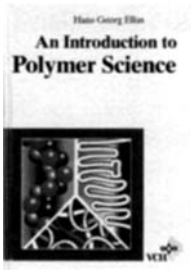

The next two sections of the book cover the physics and physical chemistry of polymers. The physical chemistry section concentrates on polymer packing, polymer chain motion, viscosity, and polymer thermodynamics. There is a strong emphasis on theoretical considerations within these sections. The section on polymer physics focuses on bulk properties of polymers. There is a particularly comprehensive chapter within this section on polymer transitions and relaxations. Finishing up this section is a chapter on solid state properties, which covers viscoelastic concepts, deformation of polymers, and failure modes of polymers. The last section of the book is entitled "Technology", meaning polymer technology. This section covers the pragmatic nuts and bolts of polymer processing, usage, disposal, and recycling.

Overall, the book is outstanding in a number of areas. The author is diligent and well organized with regard to the references at the end of every chapter, and general references for more in depth discussion of subject matter are always readily accessible. In addition, a comprehensive table of symbols and succinct appendices round off a truly excellent job of documentation. As an instructor, I found that some of the sections and some of the figures used as examples were more geared towards an intermediate audience rather than to beginning students in polymer science. As a reference source for technicians and scientists in industry who work in the polymer field, this is a "must have" book. However, most of the chapters are very well suited to instructing the novice polymer scientist, and I will use this book as a supplementary textbook for my next course.

Mark Soucek
Department of Polymers and Coatings
North Dakota State University
Fargo, ND (USA)

Enzymes. A Practical Introduction to Structure, Mechanism and Data Analysis. By *R. A. Copeland*. VCH Publishers, New York, 1996. 322 pp., hardcover DM 89.00.—ISBN 1-56081-903-0

This book is intended to serve as an introduction to working methods in enzymology for beginners. Seven of the eleven chapters are mainly devoted to a meticulous treatment of kinetic methods and the analysis of the data obtained.

Chapter 1 presents a short history of enzymology, which is unfortunately too brief and contains inaccuracies. Sanger published the complete sequence of insulin in 1953, not in 1957 as stated here, and his method did not involve the Edman breakdown reaction (p. 7). Chapter 2 contains a basic summary of the knowledge of general chemistry that should be familiar to every science student who has successfully reached the pre-degree year. Chapter 3, "Structural Components of Enzymes", summarizes the standard textbook knowledge concerning protein structure. The structures of five arbitrarily chosen cofactors are described; however,

 © WILEY-VCH Verlag GmbH, D-69451 Weinheim, 1997 0570-0833/97/3622-2527 $ 17.50+.50/0

the structure shown under the heading "nicotinamide" is that of the dihydro compound.

Chapter 5 is concerned with the chemical mechanism of enzyme catalysis, and explains the most commonly cited concepts and theories, which are associated with the names of Pauling, Koshland, Jencks, and Fersht. The "three-point attachment" concept is illustrated schematically using the example of alcohol dehydrogenase, but there is no mention here of the name of Ogston. The author fails to provide a geometrical explanation for the stereoselectivity. The serine proteases are discussed as an example of a detailed enzymatic mechanism. This chapter ends with sections on acid–base, nucleophilic, and electrophilic catalytic reactions.

The part of the book that is most useful for the experimentalist begins with Chapter 5, which deals with the stationary phase kinetics of single-substrate reactions. This concentrates mainly on the classical Michaelis–Menten kinetic model, with the usual mathematical, graphical, and linearized representations and analysis. The significance of the kinetic constants such as K_m, V_{max}, and k_{cat}/K_m, and various possible cases that can arise in measurements and calculations, are discussed in detail. Unfortunately, however, the running title throughout this chapter omits the important word "steady", so that it loses its intended meaning. Chapter 6 contains very detailed laboratory procedures for isolating enzymes and testing their activity. Sometimes aspects that are obvious are explained in minute detail. For example, the advice given on page 137 that turbid solutions can be cleared by filtration or centrifuging to remove particles (with a reference to the author's own report on this) is unnecessarily elaborate. The effects of pH, temperature, and isotopes on the enzyme activity are also discussed in this chapter.

The following three chapters deal with the various types of enzyme-inhibiting effects: reversible, tight-binding (practically irreversible), and time-dependent. The author's expertise is seen to good advantage in the treatment of this topic. He presents a rigorous and thorough discussion of competitive, noncompetitive, and uncompetitive inhibition processes, illustrated by examples. The practical importance of enzyme inhibitors in the pharmaceutical and agrochemical industries is emphasized by discussing examples such as Methotrexate, Flubriprofen, Mevinolin, and DuP697 (a prostaglandin G/H synthase inhibitor). The descriptions taken from the author's own research in this field are especially effective.

The last two chapters (10 and 11) are devoted to the kinetics of enzymatic reactions involving several substrates and to cooperative phenomena in enzyme catalysis. The book ends with two appendixes listing commercial suppliers of importance to enzymologists (with addresses) and computer software.

Enzymologists with a chemical bias will find that the book contains less on the structural aspects of enzyme catalysis than the title suggests. With regard to enzyme test methods the main emphasis in the book is on the UV spectroscopic assay, which is the method of choice for kinetic studies. For structure determination much more detailed information can be obtained by NMR spectroscopy, stereospecific isotopic labeling, and the use of substrate analogs, combined with site-directed mutagenesis. To sum up, Copeland has written a book that will be very useful for the enzyme kineticist, but will have only limited value outside this relatively narrow area of interest.

János Rétey
Institut für Organische Chemie
der Universität Karlsruhe (Germany)

Organic and Bio-organic Mechanisms. By *M. Page* and *A. Williams*. Addison-Wesley Longman, London, 1997. 298 pp., paperback £ 27.99.—ISBN 0-582-07484-3

The authors have written this book for advanced students, post-graduate students, and practicing scientists who are interested in mechanistic studies in organic and bioorganic chemistry, to provide these readers with an introduction to the subject. Some previous knowledge is assumed, and therefore the authors have not felt it necessary to include a long-winded introduction to the theory of transition states and kinetics; instead they deal with these aspects briefly and then quickly come to the main topic. The book is structured in such a way that individual readers have the choice of either going straight to the chapters that are most relevant for them, or working through the very readable chapters that explain the methodology of studying reaction mechanisms. The ease with which the authors are able to treat both conventional organic reactions and the enzymatic mechanisms of bioorganic chemistry using the same models and techniques is refreshing.

The book can be divided into three parts. The first two chapters deal with the fundamentals (transition states and kinetics). Then, in Chapters 3–6, the authors discuss the dependence of transition states on molecular structure, followed by isotope effects and solvent effects. Chapter 6, entitled "Transition State Structures—Anomalies", explains how certain situations can lead to incorrect conclusions about the mechanism. This chapter also serves to set the reader a sort of "on-line test", as the arguments are based on the fundamental principles explained earlier, allowing one to assess how well one has assimilated these ideas. In the third part, Chapters 7–10, some important aspects of enzymatic reactions and enzyme modeling systems are discussed.

The book begins, logically, with a chapter on the central idea of the transition state, factors that can stabilize it, and its importance in the progress of a reaction. Specific aspects of the transition state such as the stereoelectronic effect, energy transfer, and the principle of least movement are discussed. Chapter 2 deals with models for describing reaction kinetics, ranging from the simple rate equation to the Curtin–Hammett principle and labeling experiments. Here again the authors use examples from organic and bioorganic chemistry. The next three chapters may be grouped together under the heading of factors influencing the transition state and the reaction kinetics. Chapter 3 is concerned with the effects of structural factors on the reaction mechanism; here the important words "Hammett equation" give an indication of the chapter's contents. However, the text is not well matched to the diagrams, and as a result the reader is likely to be confused. Chapter 4 deals with the various aspects of isotope effects, then Chapter 5 describes how the reaction mechanism can be influenced by external factors such as different solvents, strongly basic or acidic media, temperature, and pressure. If this book had been a technical manual, Chapter 6 might well have been given the title "troubleshooting", as it deals with anomalies of the transition state, such as microscopic medium effects and Brönsted anomalies.

In Chapter 7 the authors consider the mechanisms by which functional groups of biological importance are transferred. Particular attention is given to the distinction between concerted and sequential mechanisms. Unfortunately, however, the treatment here is less thorough than in the previous chapters. For example, one might have expected that after explaining

 © WILEY-VCH Verlag GmbH, D-69451 Weinheim, 1997 0570-0833/97/3622-2528 $ 17.50+.50/0

(on page 13) the conclusions that can be drawn from the three-dimensional energy diagram, the authors would have cited this as evidence for a dissociative mechanism in the hydrolysis of phosphoric acid monoesters (S. J. Admiral, D. Herschlag, *Chemistry and Biology* **1995**, *2*, 729–739). In this chapter the possible reaction paths are described only in a general way, which is regrettable. Again, in Chapter 8, the important role of metal ions in the hydrolysis of acyl derivatives is not covered adequately, being limited to the Lewis acid activity and the increase in the acidity of coordinated water. Some important aspects, such as the suppression of pseudorotation in the hydrolysis of phosphates, are not mentioned.

Chapter 9 describes enzyme models, mainly involving a host–guest interaction followed by a reaction. Here the authors mention the important studies by Breslow using cyclodextrin as the guest molecule, as well as reactions involving micelles or macromolecules. Lastly, in Chapter 10, enzyme mechanisms are classified under five basic types—acyl group transfers, proton transfers, C–C bond-forming reactions, hydride transfers, and alkyl group transfers—and are discussed with the help of examples. The description of the mechanisms in this chapter gives a useful insight into enzymatic reactions, although the depth of treatment is scarcely more than one finds in a good organic chemistry textbook. Also the chapter fails to cover some important mechanisms, such as that of ribonucleotide reductase, or to discuss important techniques used to study enzymatic mechanisms, such as ESR spectroscopy.

The authors place special emphasis on the quantitative treatment of the reaction kinetics, and to this end they provide a useful appendix containing tables of various kinetic parameters, such as Hammett constants.

The book's main strength is in the descriptions of organic reactions. Although the authors cover the theoretical fundamentals for describing complex enzymatic reactions very thoroughly, the treatment of the mechanisms of such reactions in the second part of the book does not match up to the first part as regards depth and detail. As a further criticism of the book, some important methods that give only a semiquantitative or purely qualitative description of enzymatic processes are not mentioned, even though there exist many important and highly topical processes for which kinetic data alone are insufficent to determine the mechanism. The book can be recommended for readers who wish to brush up their knowledge about solvent effects and isotope effects, and about kinetic measurements for studying reaction mechanisms. However, for anyone seeking a comprehensive treatment of the details of biological reaction mechanisms, this is not a suitable book.

Markus Kalesse
Institut für Organische Chemie
der Universität Hannover (Germany)

Fundamental Toxicology for Chemists. Edited by *J. H. Duffus* and *H. G. J. Worth*. Royal Society, Cambridge, 1996. 329 pp., paperback £ 29.50.—ISBN 0-85404-529-5

Modern toxicology is an interdisciplinary subject involving chemistry, biology, medicine, and pharmacology, with the aim of understanding the dangers caused by chemicals and identifying areas of risk. These arise in the field of university teaching just as elsewhere, and lectures on the subject are provided for science students in German universities. Attendance at these is compulsory for chemistry students. The German Chemical Society (GDCh) recently set up a new working group on "Umweltchemie und Ökotoxikologie" (Environmental Chemistry and Ecotoxicology), a choice of name which underlines the importance attached to this subject. The main purpose of ecotoxicology is to investigate the risks of environmental damage from chemicals, and to suggest preventive measures.

This book has been sponsored by the International Union of Pure and Applied Chemistry (IUPAC), and is intended to serve mainly as an introductory textbook for chemistry undergraduates in British and American universities. The 21 chapters are the work of 16 authors. An introduction to the principles and methods of toxicology is followed by chapters dealing with the following aspects in the order given: toxicological kinetics and dynamics; the interpretation of data; risk assessment; risk management; exposure and monitoring; mutagenicity; carcinogenicity; reproductive toxicology; immunotoxicology; skin toxicity; inhalation toxicity; liver toxicology; renal toxicology; neurotoxicology; behavioral toxicology and cotoxicology; a chapter on radionuclides, biocides, and pesticides; safe handling of chemicals. Finally there are two appendices containing a curriculum on toxicology for chemists, and a glossary of commonly used terms. The topics covered correspond essentially to those that make up a typical lecture series on toxicology for students of natural sciences. The book could serve both as a useful accompaniment to such a lecture course for chemists, and as an introduction to toxicology for individual study.

As always with multiauthor textbooks, there is a danger that the chapters may show large differences in the quality of the writing. It is part of the editors' role to prevent this, but in this case they have not been very successful. In fact, a few of the chapters are of a poor standard. For example, the author of the chapter on mutagenicity gives a detailed description of the structure and function of DNA and of the genetic code, but fails to devote similar attention to commonly used toxicological procedures such as the Ames test or the HPRT/TK mutagenicity test using mammalian cell cultures (V79 etc.). Also the book does not include enough discussion of the relationship between chemical structures or compound classes and their toxicological properties, an aspect that is of particular interest to the chemist.

The value of this monograph must also be measured against the several German language textbooks on toxicology that have appeared in the last few years. If we compare it, for example, with the recently published book by Greim and Deml (*Toxikologie*), it fails to reach a similar standard. Also the new book by Dekant and Vamvakis (*Toxikologie*) is considerably better as an introduction for chemists, and is more soundly planned than this English-language textbook. Thus we can, at best, only recommend this book as supplementary reading to accompany a lecture course on toxicology.

Johannes Döhmer and *Dieter Lenoir*
GSF-Forschungszentrum für Umwelt
und Gesundheit
Neuherberg (Germany)

Handbook of Downstream Processing. Edited by *E. Goldberg*. Chapman & Hall, London, 1997. 720 pp., hardcover £ 149.00.—ISBN 0-7514-0364-4

One of the more complex, and at the same time fascinating, tasks of pharmaceutical biotechnology is that of isolating products from downstream processing, starting from biological sources, to provide new lead structures. There are no standard and universally applicable methodologies or strategies for isolating secondary metabolites or recombinant proteins produced by fermentation. The route from the culture solution to the pure isolated substance still depends to a large extent on the experimentalist's store of past experience and imaginative resources. Moreover, the procedure of finding new biologically active lead structures

 © WILEY-VCH Verlag GmbH, D-69451 Weinheim, 1997 0570-0833/97/3622-2529 $ 17.50+.50/0

from natural sources is made much more complicated when, in addition to the problems of isolating pure substances from fermentation products, one is constrained by the regulations and guidelines of "good manufacturing practice". One of the main aims of this book edited by E. Goldberg is to provide help with that task and to apply some systematic concepts to the complex subject of downstream processing.

The 720-page book contains 26 chapters by 33 different practitioners and experts, of whom all but two are from the USA and other parts of the English-speaking world. Many of these have a background in process technology. Thus the book is intended mainly for chemical and pharmaceutical process engineers who are involved in the design and construction of plant and buildings for biotechnology, and/or with the production and isolation of biologically active natural products, including the development and optimization of the relevant processes. Accordingly, therefore, most of the chapters deal with routine process stages such as cell disruption, filtration, solvent extraction, solid-phase extraction, membrane techniques, crystallization, and freeze-drying. However, it is unfortunate that chromatographic methods, which often serve as the key steps in work-up procedures, are not given enough space here, with no more than just a short chapter on affinity chromatography and one on the scale-up of column chromatography methods. In contrast, for example, the chapter on distillation processes is quite long. Thus the treatment of chromatographic processes is inadequate for a book with the above title.

Although the book's main emphasis is on practical aspects, some chapters also discuss the physical-chemical fundamentals of the methods concerned, and include the most important mathematical formulas that are essential for understanding the principles. Each chapter ends with a comprehensive and fairly up-to-date bibliography, covering publications up to 1992. Some chapters also include information about commercial manufacturers of equipment. However, it is regrettable that these are limited to suppliers in the USA, even in cases where the market leader in a particular field is based in Europe or Japan. Moreover, it is not very helpful that numerical data are often given in feet, inches, or gallons, so that one has to convert these to SI units. Admittedly there is a conversion table in the book, but American authors in engineering disciplines should by now be gradually becoming accustomed to internationally accepted units. Also, the usual practice internationally is to give temperatures in degrees Celsius or Kelvin rather than Fahrenheit. Also, not surprisingly, the biological safety levels used in the USA do not have quite the same meaning as those in European countries. Nevertheless, the importance of these criticisms should not be exaggerated.

Some notes and comments on a few of the chapters now follow. First there is an excellent description of the most important methods of mechanical cell disruption. The advantages and disadvantages of grinding and high-pressure homogenization are discussed. In a future revised edition it would be useful to also treat nonmechanical methods in more detail than here; such methods are becoming increasingly important, e.g. for isolating plasmid-DNA.

This is followed by chapters on filtration, extraction, and crystallization. These describe the current state of the art in these processes, although I found them too theoretically orientated. On the other hand, the chapters on drying and freeze-drying are highly informative, even for the specialist; the latter chapter is especially good. The contribution on membrane processes is also excellent, but that on electrodialysis is too long, especially since this method has only limited use in scaled-up versions.

The comprehensive treatment of methods for cleaning and sterilizing machinery, plants, and work areas is especially welcome. "Clean-in-place" and "sterilization-in-place" methods are described in detail, with examples showing how to set out protocols for these procedures. Water purification methods are also given due attention, and there is even a chapter devoted to waste treatment, an important aspect of any biotechnological process. I was especially impressed by the chapters on the planning and validation of biotechnological processes, which contain a wealth of useful information, even for the specialist. The manufacturing processes for bulk materials and for biologically active agents are compared in a chapter which makes interesting reading, even though this topic was not strictly necessary in a book on downstream processing.

The book is very attractively produced, with a clear typeface. The text is relieved by many figures and tables which contribute to the reader's understanding. These include flow charts showing biotechnological processes and plants in accurate detail.

To summarize, the book offers a great deal of useful information for readers from all disciplines concerned with the work-up of feedstocks produced by biological processes under cGMP conditions, even though the relative emphasis given to the individual topics does not always seem appropriate. For a handbook of this kind the treatment of chromatography is less than adequate. Apart from this criticism, the book will certainly be a valuable resource, especially for technologists involved in the design and setting up of biotechnological processes and plant. It also contains many useful ideas for everyone seeking mild techniques for the work-up of culture solutions, and it is a valuable addition to the literature on biotechnology.

Eberhard Ehlers
Hoechst Marion Roussel
Process Development, Frankfurt a. M.
(Germany)

Molecular Chemistry of the Transition Elements. An Introductory Course. By *F. Mathey* and *A. Sevin*. John Wiley & Sons, Chichester, 1996. 232 pp., paperback £ 18.99.—ISBN 0-471-95687-2

A growing demand for modern textbooks in transition metal chemistry recently has led to the publication of several new textbooks covering various aspects of this vast field. Whereas some emphasize classical coordination chemistry and its concepts based on the paradigm set by Alfred Werner and his successors (e.g., M. Gerloch and E. C. Constable, *Transition Metal Chemistry*, VCH Verlagsgesellschaft), others are primarily devoted to the area of organometallic complex chemistry (and explicitly say so in their title, e.g., C. Elschenbroich and A. Salzer, *Organometallics*, 2nd edition, VCH Verlagsgesellschaft). The book by Mathey and Sevin belongs to the latter category and the choice of the title may be traced to the "unconventional approach" that the authors announce in the preface. This textbook, which is based on lecture notes and the teaching experience of both authors, is intended as a guide to the different aspects of structure and reactivity in organometallics, emphasizing a conceptual approach, in particular the molecular orbital picture.

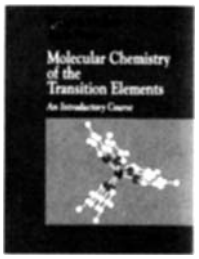

In a very short (possibly too short!) introductory chapter the authors give an overview of the history of organometallic

 © WILEY-VCH Verlag GmbH, D-69451 Weinheim, 1997 0570-0833/97/3622-2530 $ 17.50+.50/0

chemistry. Such historical chapters in textbooks tend to provoke criticism in reviews, since authors and reviewers have more or less subjective (usually disparate) views on how the history of a field of science should be presented. Nevertheless, the historical development of an area of science should be an integral part of a textbook, and the authors might consider expanding this section in a future edition of the book.

The second chapter, entitled "The fundamental concepts", aims to provide the basis of the whole didactic approach. The discussion covers formal electron counts of the most important ligands, some molecular orbital considerations, and the application of these to several important reactions, such as oxidative additions and reductive eliminations as well as nucleophilic attack at the CO ligand. My main criticism concerns the way in which molecular orbital theory is introduced. Although the students at the authors' universities may, at a very early stage of their course, have been taught the kind of fragment orbital approach to organometallic chemistry that was successfully introduced by R. Hoffmann and others, this is not generally so. Therefore an introduction to these methods, in particular the orbital perturbation approach, is absolutely necessary in a book which is explicitly aimed at the beginner in organometallic chemistry. However, this is not to deny that the fragment MO approach may be very effectively employed in the teaching of the concepts used to analyze structures and reaction pathways in organometallics.

Chapter 3 is a review of some of the most important chemical (especially structural) motifs in transition metal organometallic chemistry, introducing the basic features of metal hydrides, carbonyls and other compounds containing metal–carbon single and multiple bonds, π-coordination of olefins, and some important aspects of compounds containing metal–metal bonds. Unfortunately, several errors have crept into this section. For instance, the example given for a carbonylation on page 76 is actually a carboxylation, and the same reaction scheme is repeated one page later in the correct context. Another unnecessary duplication of reaction schemes has occurred with the reactions of Na[Mn(CO)5] on the same two pages. The section on phosphorus compounds (3.8) appears somewhat isolated and slightly misplaced in a book on transition metal chemistry.

Chapters 4 and 5 give a useful introduction to the applications of organometallic complexes in organic synthesis and homogeneous catalysis, covering both fundamental aspects and more recent developments. The authors succeed in developing the broad scope of present-day applications, and the examples they cite are well chosen.

In summary, I feel that the book could be a valuable addition to the existing introductory textbooks on transition metal organometallics if some of the theoretical fundamentals were introduced more coherently. Also some imprecise and occasionally confusing statements have crept in, although this may be due to the translation from the original French version. The book treats many aspects that have not been covered adequately by other textbooks. With some reservations as mentioned above, I can recommend it as a textbook for undergraduate chemistry students, not least because the paperback edition is very reasonably priced.

Lutz H. Gade
Institut für Anorganische Chemie
der Universität Würzburg (Germany)

 © WILEY-VCH Verlag GmbH, D-69451 Weinheim, 1997 0570-0833/97/3622-2531 $ 17.50+.50/0

different electrophore systems

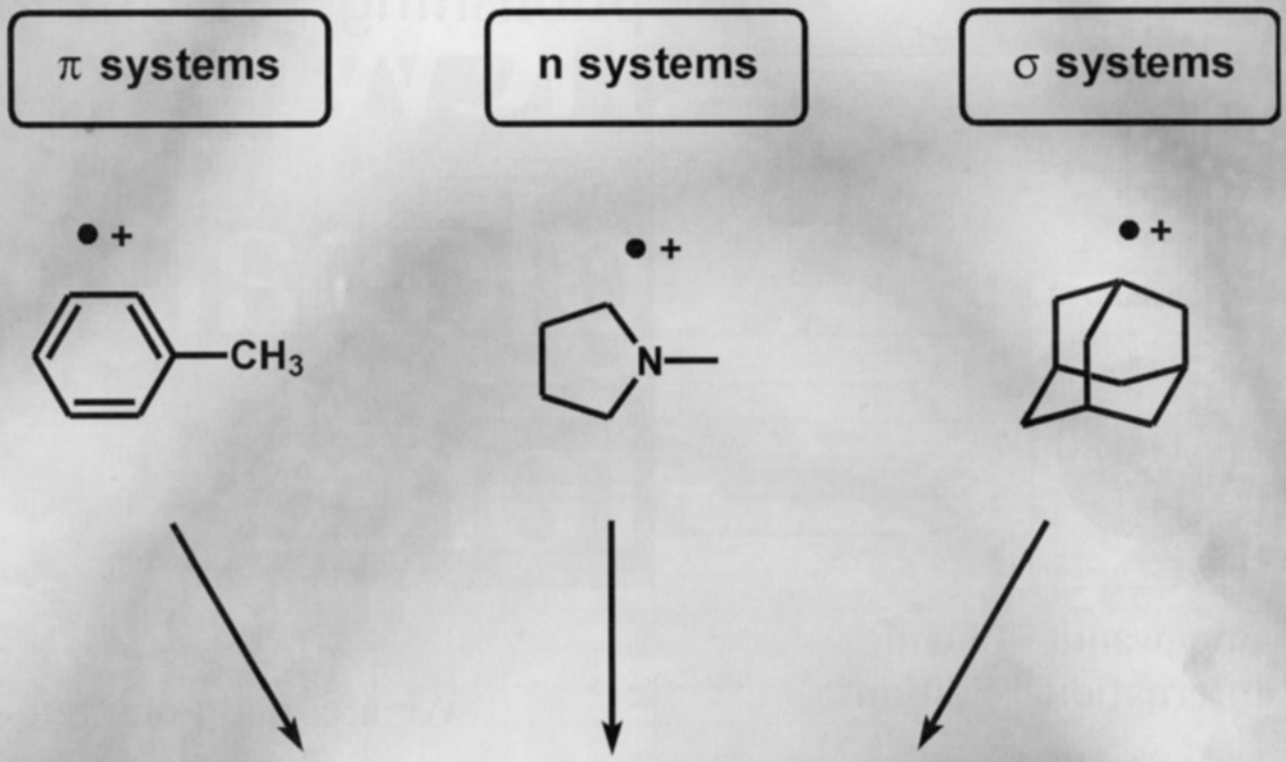

a unified reactivity scheme

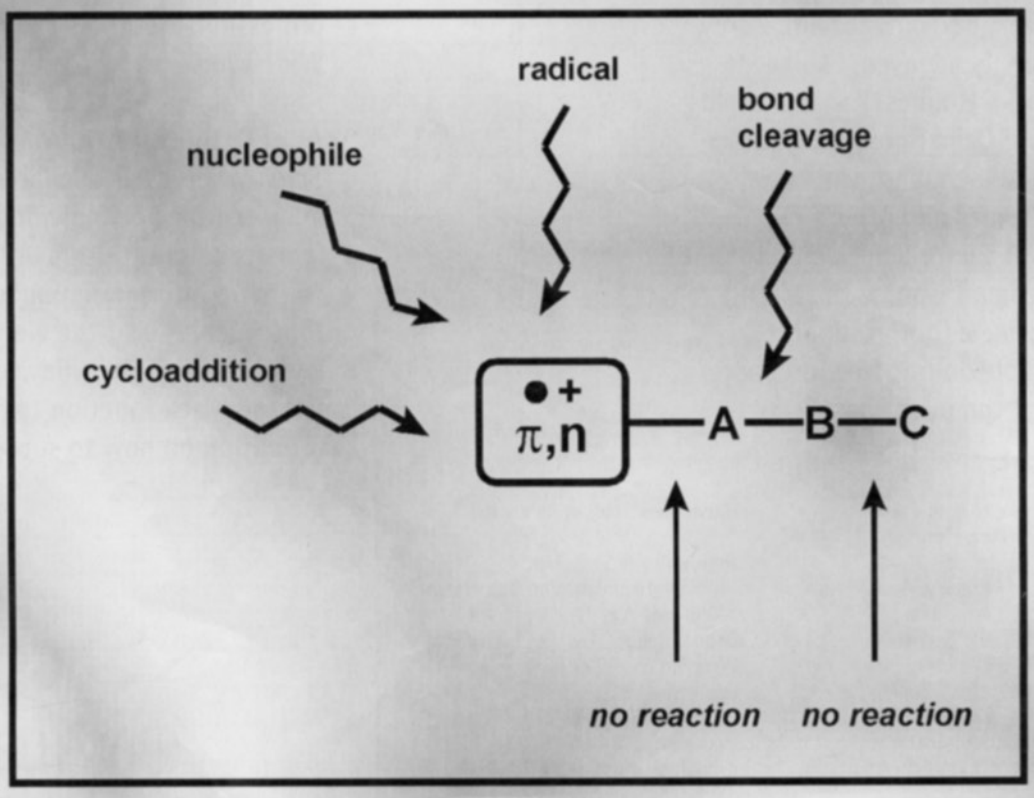

ANGEWANDTE CHEMIE ©WILEY-VCH

Understanding Reactivity Patterns of Radical Cations**

Michael Schmittel* and Armin Burghart

Dedicated to Professor Waldemar Adam on the occasion of his 60th birthday

Over the last 15 years electron transfer activation has emerged as a valuable concept for accomplishing novel reactions and has found widespread application in the selective transformation of increasingly complex molecules. This review presents in a conceptualized manner the vast number of radical cation reactions obtained after chemical, electrochemical, and photoinduced one-electron oxidation. To familiarize the reader with the concepts of electron transfer a simple and straightforward classification of radical cation reactions has been devised to allow the presentation of a manifold of reactions in a readily understandable manner. Whenever possible, thermochemical and kinetic data are provided.

Keywords: electron transfer · kinetics · radical ions · reaction mechanisms · thermodynamics

1. Introduction

While recent years have witnessed a steady increase in the use of complex reaction systems for accomplishing highly selective reactions, comparatively little attention has been devoted to exploiting the concepts of electron transfer in organic transformations. This is even more astounding in light of the fact that the transfer of one electron constitutes one of the simplest elemental reactions in chemistry, and is conceptually linked to photochemical activation. Although preparative photochemistry has adopted an important place in synthetic chemistry,[1] electron transfer chemistry[2] still awaits wide acceptance in the synthetic community in spite of the important merits of organic electrochemistry.[3]

Actually, only a small fraction of the plethora of preparative reactions is currently based on electron transfer processes.[4] Examples include the Birch reduction,[5] acyloin condensation,[6] Ullmann coupling,[7] formation of Grignard reagents,[8] and $S_{RN}1$ reactions.[9] Hence, most preparative chemists are still reluctant to use the concepts of electron transfer (ET) in a more general sense for designing new reactions. A reflection of this widespread neglect of ET concepts is the fact that we routinely investigate IR, NMR and UV spectroscopic data of compounds, but not their electrochemical data. A justification often quoted for this obvious neglect is the inherent complexity of ET-initiated processes and the lack of data available for making reliable predictions for new reactions. Consequently, this review was written in an attempt to provide a lucid perception of electron transfer activation concepts by, with the help of examples, juxtaposing results of preparative electron transfer chemistry and physical organic concepts.

Intriguingly, the last couple of years have shown a growing number of ET-promoted reactions that proceed with high selectivity and, in some cases, allow transformations that have never been realized before—for example Diels–Alder reactions of indoles[10] and ketenes[11] as dienophiles, or of vinylindoles as dienes[12] among others.[2] Nature also demonstrates the potential of ET activation in enzymatic processes,[13] such as in the monoamine oxidase[14] and the DNA-photolyase reaction.[15, 16] Selective ET processes and radical ion intermediates play an important role in coal chemistry,[17] photodegradation of polymers,[18] and DNA strand scission.[19] Hence, the recent progress in electron transfer chemistry prompts us to predict a much larger number of processes yet to be discovered.

Certainly one reason for the limited use of ET concepts in synthetic schemes is the aforementioned difficulty in controlling the various reaction events involving odd-electron species, regardless of whether a catalytic (Scheme 1a) or stoichiometric transformation is considered (Scheme 1b). To understand this problem better, let us have a closer look at a well-studied electron transfer process: the radical cation catalyzed Diels–Alder reaction, which has become a distinguished example for the potential of ET activation. After addition of 5–10 mol% of tris(*p*-bromophenyl)aminium hexachloroantimonate (CH_2Cl_2, room temperature, 15 min), the Diels–Alder cyclodimerization of cyclohexadiene can be

[*] Prof. Dr. M. Schmittel, Dipl.-Chem. A. Burghart
Institut für Organische Chemie der Universität
Am Hubland, D-97074 Würzburg (Germany)
Fax: Int. code + (931)888-4606
e-mail: mjls@chemie.uni-wuerzburg.de

[**] Abreviations used for one-electron oxidants: $NR_3^{+\cdot}$: triarylaminium salt; CAN: $Ce(NH_4)_2(NO_3)_6$; $Th^{+\cdot}$: thianthrenium perchlorate; DCB: 1,4-dicyanobenzene; 1-CN: 1-cyanonaphthalene; TCB: 1,2,4,5-tetracyanobenzene; DCN: 1,4-dicyanonaphthalene; DCA: 9,10-dicyanoanthracene; $TPP^{+\cdot}$: 2,4,6-triphenylpyrylium salt; CA: chloranil.

 © WILEY-VCH Verlag GmbH, D-69451 Weinheim, 1997 0570-0833/97/3623-2551 $ 17.50+.50/0

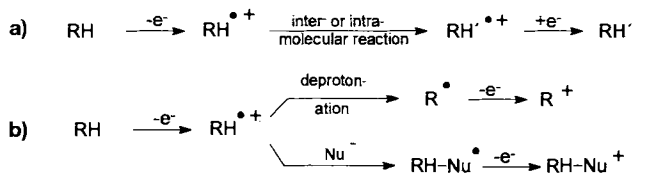

Scheme 1. Reaction of odd-radical species in catalytic (a) and stoichiometric amounts (b).

accelerated by a factor of 10^{15} with respect to the thermal reaction.[20] Based on the seminal mechanistic studies, mainly undertaken by Bauld[20] and Eberson,[21] the following mechanism may be proposed.[22] After an initiating one-electron oxidation (Scheme 2a; CHD = 1,3-cyclohexadiene, DA =

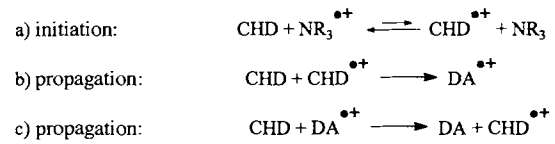

Scheme 2. Mechanism of the ET-induced Diels–Alder cyclodimerization of 1,3-cyclohexadiene (CHD); DA = Diels–Alder product.

Diels–Alder product), the endergonic equilibrium of which we can control on the basis of the redox potential data, the cycloaddition of $CHD^{\bullet+}$ with CHD to yield $DA^{\bullet+}$ takes place almost without an activation barrier ($\Delta H^{\neq} = 1.6$ kcal mol^{-1}).[22e] However, right after the cycloaddition step the highly reactive $DA^{\bullet+}$ has to be reduced in a controlled manner to make the desired overall reaction work; this can be achieved by reductive ET from either the diene or the triarylamine to the $DA^{\bullet+}$.[23] Recent work[11b] emphasized that the last reduction step may be pivotal in the reaction sequence, which underlines the importance of considering redox potentials and reorganization energies of both the reactants and the products.

In total, this cycloaddition and all following examples illustrate that we always have to control a whole series of events in order to obtain a successful reaction (Scheme 3): a) electron transfer (ET), b) primary reaction of the radical cation, c) reaction of the follow-up odd-electron species (secondary reaction), and d) trapping of the cationic intermediate.

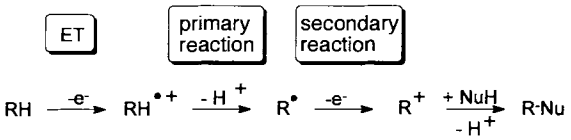

Scheme 3. Steps of an ET-induced reaction sequence.

Due to space limitations, we will only very briefly deal with the various ways of effecting electron transfer and instead concentrate on how the fate of the radical cation is predetermined by structural features (primary reactions). Likewise, it is of crucial importance to control the follow-up reactions (secondary reactions) of odd-electron intermediates and to trap finally closed-shell species for devising a clean, preparatively useful reaction.

Although we will restrict our discussion to the one-electron oxidation chemistry of neutral molecules in the following, a similar analysis of the chemistry of radical anions will be

A. Burghart M. Schmittel

Michael Schmittel was born in 1956 and studied chemistry at the Universität Freiburg. After receiving his Diplom in 1980 he briefly switched subjects and with a scholarship from the Studienstiftung des Deutschen Volkes studied French at the Sorbonne in Paris, where he finished the Diplôme de langue et civilisation française. After returning to Freiburg he received his doctorate in 1985 under the supervision of Christoph Rüchardt with a thesis on the cis → trans isomerization of azoalkanes that was recognized with the Gödecke-Preis. A NATO postdoctoral appointment brought him to Joseph P. Dinnocenzo at the University of Rochester, were his interest in electron transfer chemistry was ignited. He received a Liebig-Stipendium from the Fonds der Chemischen Industrie, returned to the Universität Freiburg in 1987, completed his habilitation in 1992, and was appointed Professor of Organic Chemistry at the Universität Würzburg in 1993. His research interests encompass electron transfer activation, radical cation catalysis, electroanalytical chemistry, stable simple enols, new trigger mechanisms for enediyne cycloaromatizations, novel thermal biradical cyclizations, electroactive protecting groups, activation of oxygen, radical dications, redox active materials for sensors, supramolecular coordination complexes, and topology in chemistry.

Armin Burghart was born in 1968 and studied chemistry at the Universität Freiburg. After completing his Diplom in 1993, he moved to Würzburg, where he in 1997 finished his doctoral thesis in the research group of Michael Schmittel in the field of stereoselective reactions of enol radical cations. His work was recognized by a scholarship from the Fonds der Chemischen Industrie.

reported in due course. The present treatment, however, also excludes distonic radical cations[24]—odd-electron species in which the charge and the radical cannot be localized on the same atom—that by their very nature act like uncharged electrophilic radicals. In addition, we will not treat the one-electron oxidation chemistry of carboxylic acids (the Kolbe reaction); this subject has been comprehensively described in recent reviews,[25] and in many cases it is not clear whether oxidation of the neutral molecules or the carboxylates is involved. This important reaction has now successfully been used in macrocyclizations[26] and in diastereoselective couplings as well.[27] Likewise, oxidations utilizing Mn^{III} salts, which have found extensive use in synthetic schemes,[28] will not be discussed here, since the radicals are formed from inner-sphere ET via manganese enolates with no involvement of radical cation species.

2. Generation of Radical Cations in Solution

First, two remarks: In contrast to neutral molecules, radicals are much easier to oxidize,[29] except for one distinguished case: the oxidation potentials of α-carbonyl radicals of electron-poor substrates are higher than those of the parent enol precursors.[30] Normally, under conditions of chemical and anodic oxidation, neutral radicals are, however, efficiently oxidized to cationic intermediates.

Radical cation processes do not always result under oxidative conditions. Irrespective of the method for generating radical cations in solution, one should always be aware that these highly acidic species may trigger acid-promoted reactions,[31, 32] which may be mistaken for ET-catalyzed processes.[33]

2.1. Chemical Oxidation

The generation of radical cations in solution can be accomplished by different methods; chemical oxidation of neutral molecules is one of the most important modi operandi. The thermochemistry of a simple ET reaction[34] (Scheme 4) is described by $\Delta G = -nF(E^0_{A/A^{\bullet-}} - E^0_{D/D^{\bullet+}})$. As a consequence, the Gibbs energy ΔG is negative only if E^0 for the couple $A/A^{\bullet-}$ is more positive than that for $D^{\bullet+}/D$. It should be noted that although redox potentials E^0 are strictly defined as reduction potentials,[34, 35] for organic substrates oxidation potentials of neutral compounds are conveniently used.[36] Because of the high reactivity of most organic radical cations, frequently only the potentials of the anodic peak are quoted; these are thermochemically not relevant but constitute acceptable approximations (± 0.2 V) if heterogeneous electron transfer is fast. Details have been described in several textbooks.[2, 3]

$$A + D \rightleftharpoons A^{\bullet-} + D^{\bullet+}$$

Scheme 4. Simple ET reaction between an acceptor A and a donor D.

In most synthetic schemes, one-electron transfer is set up in an endergonic preequilibrium that is rapidly depleted because of the fast follow-up reactions of radical cations. High concentrations of radical cations that generally lead to undesired reactions are thus avoided.

While many oxidants (such as transition metal oxides) react by inner-sphere electron transfer and do not generate free radical cationic intermediates, stable aminium salts[37a, b] and phenanthrolineiron(III) compounds[37c, d] have frequently been used as well-behaved one-electron oxidants. Oxidants[38] such as Ce^{IV}, Cu^{II}, and Ag^{II} constitute borderline cases that are difficult to classify.[2c] Despite some uncertainties, we have not excluded them from our analysis in Section 4.

2.2. Anodic Oxidation

Radical cations can also be produced electrochemically by means of heterogeneous ET between an electrode and a substrate in solution.[3a–e] Advantageously, electrochemical methods allow the application of exactly the electrode potential desired for transformation of the reactant (controlled-potential methods). When working under constant-current conditions the electrode potential is often not constant, and therefore selectivity problems may arise. Hence, to achieve high chemo- and regioselectivities, controlled-potential methods are often preferred.

One specialty of anodic oxidation is that radical cations are formed in much higher stationary concentrations than in homogeneous solution; this often has implications on follow-up reactions. For instance, radical cation catalyzed processes are less efficient and have a lower turnover under anodic oxidation conditions. Fortunately, the scope of electroorganic methods has been significantly enhanced, in particular through the work of Steckhan,[39] by using electrochemical mediators that work in homogeneous solution and thus provide conditions that are very similar to those of chemical oxidation.

2.3. Photoinduced Electron Transfer Oxidation

Photoinduced electron transfer (PET) is a rather novel oxidation technique with a great potential.[2b, 40] This method exploits the ability a) of electronically excited acceptors A to function as strong oxidants (Scheme 5a) and b) of electronically excited donors D to lose an electron rather easily (Scheme 5b). In the case of a) the oxidant is a short-lived intermediate, which will consequently not react with other short-lived intermediates such as radicals.[41] Hence, the substrate is oxidized under locally oxidative conditions; however, reductive conditions prevail after ET. There are many ways to avoid the energy-wasting back electron transfer through the proper choice of solvents and acceptors—in particular by addition of Li^+ ions,[42] cosensitizers, and sacrificial acceptors or by complexation of excited state acceptors to Mg^{2+}.[43] The special PET literature should be consulted for details.[2b, 40]

$$\text{a)}\quad D + A \xrightarrow{h\nu} D + A^{*} \longrightarrow D^{\bullet+} + A^{\bullet-}$$

$$\text{b)}\quad D + A \xrightarrow{h\nu} D^{\bullet} + A \longrightarrow D^{\bullet+} + A^{\bullet-}$$

Scheme 5. Photoinduced electron transfer after excitation of the acceptor A (a) or the donor D (b).

2.4. Special Methods for Generating Radical Cations

Although less convenient, some non-oxidative methods exist to generate radical cations (Scheme 6, [Eqs. (1)–(5)]), for example, according to Equation (5) in the Hofmann-Löffler-Freytag reaction.[44] The DNA strand scission in 4′-nucleotide radicals was explained by a heterolytic C–O bond cleavage yielding the corresponding radical cation[19c] [Eq. (4) and Scheme 7].

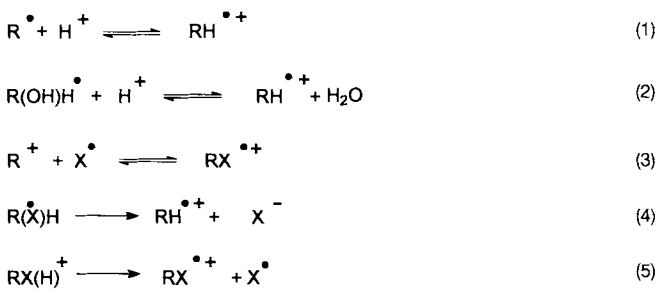

Scheme 6. Non-oxidative processes for the formation of radical cations.

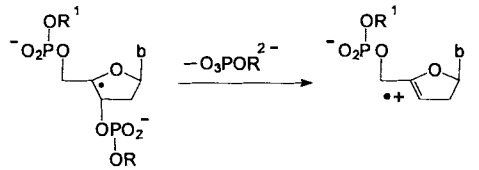

Scheme 7. Cleavage of the C–O bond of 4′-nucleotide radicals leading to DNA strand scission.

3. Our Classification Schemes—Primary and Secondary Reactions

Several monographies and reviews, in particular in electroorganic[3] and photoinduced electron transfer chemistry,[40] have conceptualized the inherent notions of electron transfer activation by using various classification schemes to arrange the manifold reactions available. In most cases the categorization illustrates the preparative aspects; for example, classification according to bond formation or the main functionality involved in the reaction was emphasized. While this approach is beneficial for selecting a suitable reaction, it does not convey the essential principles of radical cation chemistry in solution.

In contrast to earlier concepts we would like to present our analysis according to the primary reactions of the three main electrophoric systems involved in one-electron oxidation, hence conceptualizing the reactivity patterns in an insightful manner. The electrophore of the substrate to be oxidized is defined by the atom or group of atoms exhibiting the largest HOMO coefficient(s); this allows differentiation between π, n, and σ donors. Accordingly, toluene is a typical π donor, triethylamine an n donor, and cyclopropane a σ donor. To picture the bonds directly attached to the electrophore, we will use a special presentation. The benzylic hydrogens in a π donor such as toluene are therefore depicted as follows: ⓟ-C-H.

3.1. Molecular Orbital Picture of a Radical Cation

To understand some conceptual features of radical cation chemistry, a short interlude to the molecular orbital (MO) picture of toluene and the electron configuration of toluene•+ is very helpful (Scheme 8). An analysis of toluene•+ in light of

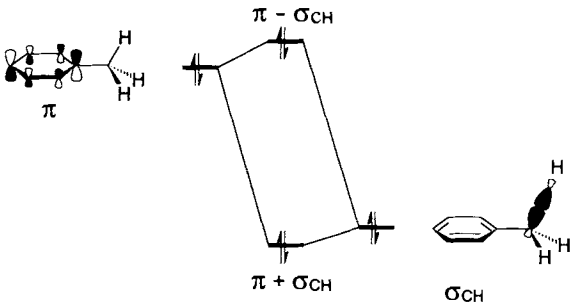

Scheme 8. Simplified orbital-interaction diagram for toluene.

the three-electron three-orbital three-configuration model[45] indicates that it possesses a Π ground state. Accordingly, one would expect that predominantly nucleophilic or radical attack at the aromatic nucleus should take place; however, deprotonation in the benzylic position is also an important reaction pathway. Clearly, excited electronic configurations, in which the C–H bond is severely weakened (Σ and Σ* configurations, Scheme 9), can mix with the Π ground state configuration to lead to an avoided crossing.

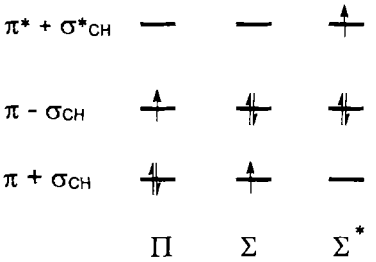

Scheme 9. Three-electron three-orbital three-configuration model[45].

With ⓞ•+ the chemistry is quite straightforward. Since the electron is removed from a scissile bond, the corresponding σ bond is cleaved basically exclusively.

3.2. Primary Reaction Pathways of π and n Radical Cations

The chemistry of a radical cation in solution is mainly determined by its primary reaction, which can be easily categorized as soon as we have identified the electrophore with the lowest oxidation potential. Importantly, however, the sort of radical cation reactions observed in solution does not depend on the nature of the electrophore (that is, ⓟ•+ or ⓝ•+) but rather on the structural motifs at the periphery of the electrophore. Only a limited number of reaction modes is usually observed that are equally present in ⓟ•+ or ⓝ•+ (Scheme 10, Table 1):

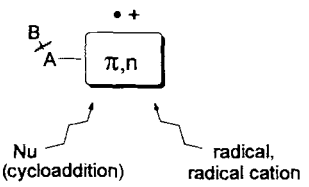

Scheme 10. Schematic representation of the most important primary reaction pathways for π and n radical cations (㊀•+ and ⓝ•+).

1) A–B bond cleavage at the periphery of the electrophore (A–B = C–H, A–H, C–X, C–C, X–Y; see Table 1),
2) reactions initiated by attack of nucleophiles (including rearrangements and cycloadditions), and
3) radical-based processes (ET, dimerization, reactions with radicals, and hydrogen transfer).

In contrast to A–B bond ruptures, ㊀-A•+ and ⓝ-A•+ bond cleavage directly at the electrophore is very rarely observed. The bond to be cleaved is orthogonal to the electrophore orbitals, whereas A–B may align with p orbitals of the electrophore (Scheme 11).

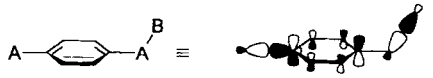

Scheme 11. Views of the orbital overlapping show why A–B bond cleavage is preferred over ㊀-A•+ cleavage.

While Scheme 10 gives a rough idea of the different primary reaction pathways available to π and n radical cations, Table 1 provides a more detailed list. It should be noted, however, that quite often a variation in the substituents at one electrophore site may entail a switch from ㊀•+ to ⓝ•+ within a series of related compounds (see Section 3.4).[46]

3.3. Secondary Reaction Pathways

An analysis of Table 1 indicates that the majority of the primary reaction products are odd-electron or other highly reactive species; their reactions should be carefully composed in the design of a successful reaction. The secondary reaction and, thus the fate of the primary intermediate may be controlled by the appropriate choice of the initial electron transfer oxidation system. In this context, it makes a tremendous difference whether we set up a reaction under PET or chemical oxidation conditions.

3.3.1. Radicals as Primary Intermediates

When using chemical or anodic oxidation, the radicals obtained after ㊀-C-H•+ deprotonation ([→CH], see below and Tables 1–3 for the classification system) are further oxidized in most cases ([R^{+}_{ox}]), so that products derived from cationic intermediates can be expected ([→CH, R^{+}_{ox}], Scheme 12). However, under conditions of photoinduced electron transfer the radicals and radical cations as primary intermediates are often reduced by the acceptor A•−. Hence, in the first case products are derived from anionic intermediates ([→CH, R^{-}_{red}], Scheme 13). In addition, radical intermediates can efficiently be trapped by addition to unsaturated compounds when their oxidation or reduction is slower than addition. Only the resulting secondary intermediates undergo subsequent oxidation or reduction ([→CH, $R^{+}_{add,ox}$] and [→CH, $R^{-}_{add,red}$], Scheme 14).

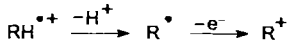

Scheme 12. Deprotonation of a radical cation and further oxidation of the formed radical: the [→CH, R^{+}_{ox}] reaction.

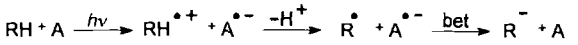

Scheme 13. Radical cations obtained by photoinduced electron transfer react after deprotonation to form radicals, which are reduced to the anion by an acceptor: the [→CH, R^{-}_{red}] reaction; bet = back electron transfer.

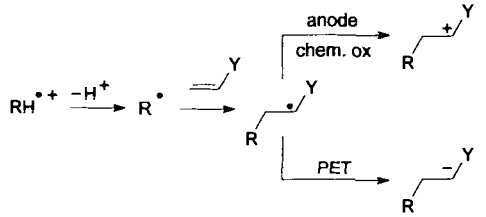

Scheme 14. Addition of radical intermediates on unsaturated compounds and subsequent oxidation or reduction: the [→CH, $R^{+}_{add,ox}$] and [→CH, $R^{-}_{add,red}$] reactions.

To indicate the mechanism operative for radical intermediates, we designed a simple code for abbreviating the primary (Table 1) and secondary reaction pathways (Table 2). It

Table 1. The most important primary reactions in radical cation chemistry of ㊀-A-B•+ and the symbols used. The same patterns are observed for ⓝ-A-B•+.

Symbol	Classification	Primary reaction	A	B
CH	C–H deprotonation	㊀-C-H•+ → ㊀-C• + H+	C	H
AH	*A–H deprotonation*	㊀-A-H•+ → ㊀-A• + H+	*O, N, S, X*	H
AB	A–B bond cleavage	㊀-A-B•+ → ㊀-A• + B+ or ㊀-A+ + B•	A	B
CC	C–C bond cleavage	㊀-C-C•+ → ㊀-C• + C+	C	C
CX	C–X bond cleavage	㊀-C-X•+ → ㊀-C• + X+	C	Si, Sn
Nu	attack of Nu	Nu + ㊀-A-B•+ → Nu-㊀-A-B•+	A	B
CA	cycloaddition	cycloaddition	A	B
R	rearrangement	rearrangement	A	B
ET	ET	㊀-A-B•+ ± e− → ㊀-A-B or ㊀-A-B2+	A	B
Rad	radical attack	R• + ㊀-A-B•+ → R-㊀-A-B+	A	B
RA	reaction with a radical anion	RA•− + ㊀•+ → •RA-㊀+	A	B
Dim	dimerization	2㊀-A-B•+ → (B-A-㊀)$_2^{2+}$	A	B
H	hydrogen transfer	H• + ㊀-A-B•+ → H-㊀-A-B+	A	B

Table 2. The most important secondary reactions in radical cation chemistry and the oxidation systems for setting up such reactions. Part 1: radicals ($R^{\bullet}$) as primary intermediates.

Code	Secondary reaction	Product	Oxidation system
$R^{\bullet}_{ox}$	$R^{\bullet} \rightarrow R^{+}$	cation	anode, chemical oxidation
$R^{\bullet}_{red}$	$R^{\bullet} \rightarrow R^{-}$	anion	PET
$R^{\bullet}_{rad}$	typical radical reactions	various	under all conditions
$R^{\bullet}_{add,ox}$	$R^{\bullet} + C{=}C \rightarrow R{-}C{-}C^{\bullet} \rightarrow R{-}C{-}C^{+}$ [a]	cation	anode, chemical oxidation
$R^{\bullet}_{add,red}$	$R^{\bullet} + C{=}C \rightarrow R{-}C{-}C^{\bullet} \rightarrow R{-}C{-}C^{-}$ [a]	anion	PET
$R^{\bullet}_{RA}$	reaction with radical anion	anion	PET

[a] Addition to a double or triple bond.

should be noted, however, that we omitted simple heteroatom deprotonation reaction as a secondary reaction in order to focus on the more relevant follow-up reactions. Hence, the code for the reaction shown in Scheme 15 is $[\rightarrow Nu, R^{\bullet}_{ox}]$.

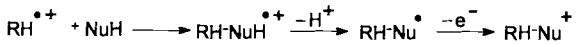

Scheme 15. The $[\rightarrow Nu, R^{\bullet}_{ox}]$ reaction.

Two examples (Scheme 16) shall illustrate how the outcome can be altered by controlling the secondary reaction. In both cases the primarily formed olefin radical cation is attacked intramolecularly by the carboxyl group to provide lactones **3** and **5**, respectively;[47, 48] however, in the first example the resulting radical is oxidized, and in the second it is reduced. To show the reaction steps involved in the primary and secondary processes we will use the classification system outlined in Tables 1–3. Hence, the primary reaction will be

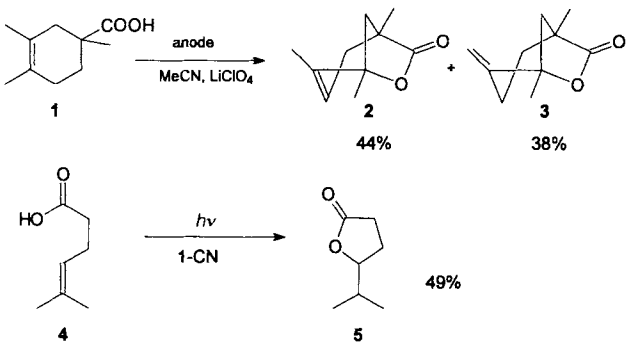

Scheme 16. The $[\rightarrow Nu, R^{\bullet}_{ox}]$ reaction according to Utley (1978, top) and the $[\rightarrow Nu, R^{\bullet}_{red}]$ reaction according to Gassman (1987, bottom).

termed $[\rightarrow Nu]$, corresponding to nucleophilic attack of the carboxyl group on the olefin radical cation. The secondary reactions are categorized as radical oxidation $[R^{\bullet}_{ox}]$[47] and radical reduction $[R^{\bullet}_{red}]$,[48] respectively.

3.3.2. *Radical Cations as Primary Intermediates*

Radical cations appear as primary intermediates in radical cation catalyzed processes, such as cycloadditions or rearrangements, or after intramolecular bond cleavage. The typical situation in a radical cation catalyzed process is depicted in the following. After rearrangement $[\rightarrow R]$ of the reactant radical cation $RH^{\bullet+}$ to $PH^{\bullet+}$, the chain is further propagated by ET reduction between RH and $PH^{\bullet+}$ ($[\rightarrow R, RC_{red}]$, Scheme 17).

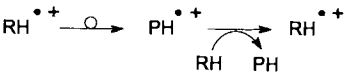

Scheme 17. Regeneration of the starting radical cation by radical cation catalyzed reaction with rearrangement and subsequent ET reduction.

Quite often after intramolecular bond cleavage a distonic radical cation is formed with a separated radical and cationic center. Whereas the radical center undergoes follow-up reactions similar to those of primary radicals (see Table 2), the cationic center usually reacts with added nucleophiles. The sequence of these events is for the most part not established by mechanistic investigations; the sequence chosen in the code is therefore purely arbitrary.

A simple example should demonstrate the classification. After C–C bond cleavage in the primary reaction $[\rightarrow CC]$, the distonic radical cation will be trapped by a nucleophile at the cationic center and also oxidized at the radical site (Scheme 18). The index used for trapping the nucleophile (Nu) is then combined with that for the radical oxidation: $[\rightarrow CC, RC_{Nu,ox}]$ (Table 3).

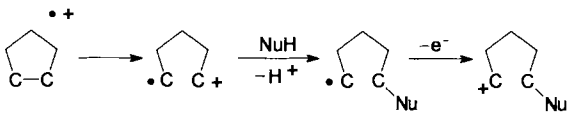

Scheme 18. Example of a $[\rightarrow CC, RC_{Nu,ox}]$ reaction.

The most important codes are provided in Table 3; the first index denominates the destiny of the cationic center, and the second the follow-up reaction of the radical site. Clearly, it will not always be possible to ascertain the sequence of events in complex reaction cascades without detailed mechanistic work. However, we consider this short classification according to primary and secondary reactions as a very helpful tool for explaining product formation without the need for detailed mechanistic discussions.

3.4. Electrophore Types

A particular difficulty in classifying the electrophoric system seems to arise when two different types of donors are linked together by a covalent bond, that is, ⓟ-ⓝ. The following procedure is therefore recommended. The bond between the two electrophore systems is cut, and hydrogen atoms are added to both fragments (ⓟ-H and ⓝ-H). The ⓟ–ⓝ system is now classified according to the isolated electrophore exhibiting the lower oxidation (or ionization) potential. Accordingly, aniline (**6**), for example, would be divided into the amine (n donor) and the phenyl part (π donor). As benzene (**7**) has the lower oxidation (or ionization) potential

(Scheme 19), aniline is classified as a π electrophore system, but *N*,*N*-dimethylaniline (**9**) as an n donor.

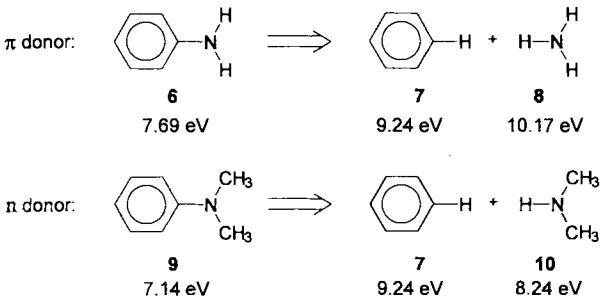

Scheme 19. Classification scheme for combined electrophore systems (see text for details); data for ionization potentials from ref. [49].

Interestingly, this simple classification scheme often allows a convincing explanation of the observed radical cation chemistry. For example, in the anodic oxidation of the n donor **9**,[50] the predominant product **14** mainly arises from side-chain functionalization, a reaction that is similar to anodic oxidations of simple aliphatic amines. In contrast, the π donor **6** affords **11**–**13** (Scheme 20) after one-electron oxidation,[51] which are coupling products typical of arene oxidations.

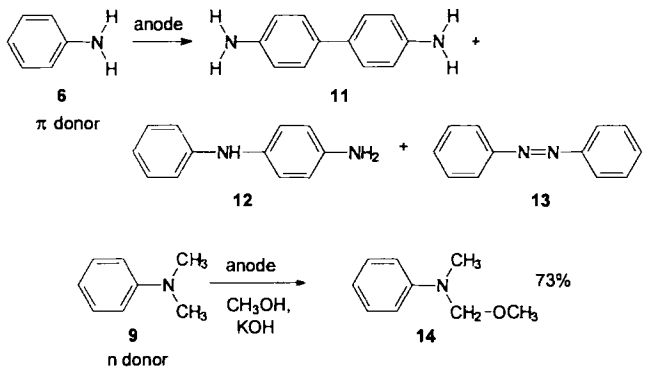

Scheme 20. The [→Nu,$R^{\bullet}_{ox}$] reaction according to Nelson (1974, top) and the [→CH,$R^{\bullet}_{ox}$] reaction according to Shono (1982, bottom).>

Clearly, this simple approach must have some limitations. For instance, there are some cases where the main reactivity patterns of the radical cation stem from the part of the electrophore with the higher oxidation potential, for example phenyl alkyl ethers. In line with the above considerations of ionization potentials, anisol (**15**) should be classified a π donor (Scheme 21). In the majority of anodic oxidation reactions of anisole under neutral conditions, typical reactions of $\textcircled{\pi}^{\bullet+}$ are indeed observed, for example coupling reactions[52] and nucleophilic attack at the aromatic nucleus.[53] However, upon changing to basic oxidation conditions, deprotonations at the position α to the oxygen atom are often encountered;[54] according to our classification that is typical for $\textcircled{n}^{\bullet+}$ (Scheme 22).

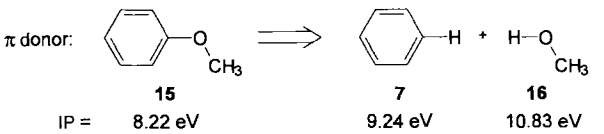

Scheme 21. Classification scheme for anisol (**15**); ionization potentials from ref. [49].

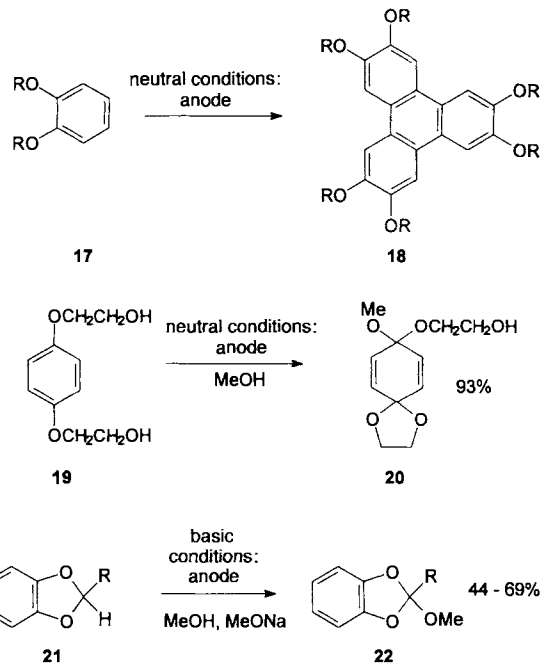

Scheme 22. The [→Nu,$R^{\bullet}_{ox}$] reactions according to Parker (1972, top) and Tissot (1975, middle) as well as the [→CH,$R^{\bullet}_{ox}$] reaction according to Thomas (1985, bottom).

Hence, the radical cation may sometimes show reactions typical for oxidation of the weaker donor; their portion in solution depends on the energy of the involved excited electronic configuration[45] and their relative reactivity. In

Table 3. The most important secondary reactions in radical cation chemistry and the oxidation systems for setting up such reactions. Part 2: Distonic and simple radical cations (RC) as primary intermediates[a].

Code	Secondary reaction	Product	Oxidation system
RC_{ox}	$RH^{\bullet+} \rightarrow RH^{2+}$	dication	anode, chemical oxidation
RC_{red}	$RH^{\bullet-} \rightarrow RH$	neutral	PET, radical cation chain
RC_{Nu}	cationic center reacts with nucleophile	radical	under all conditions
$RC_{Nu,ox}$	cationic center reacts with nucleophile, radical center will be oxidized	cation	anode, chemical oxidation
RC_{RA}	reaction with radical anion	neutral	PET
RC_{add}	radical center adds to unsaturated bond	radical cation	under all conditions
$RC_{CA,red}$	cycloaddition and reduction of reagent	neutral	under all conditions

[a] Distonic radical cations result mostly from intramolecular bond cleavage.

summary, the categorization in π or n donors will allow us to predict the reactivity mode by using the simple reactivity paradigms outlined in Section 4. However, we should always be aware of the limitations of this simplistic approach.

3.5. σ Radical Cations

Only a small selection of the molecules studied can be categorized as σ donors according to our classification. Nevertheless, σ radical cations ⓞ$^{\bullet+}$ have found wide recognition in synthetic schemes; most systems are derived from the very strong σ donors[55] of the C–Si and C–Sn type: ⓞ-C-Si$^{\bullet+}$ and ⓞ-C-Sn$^{\bullet+}$. In contrast, pure C–C electrophores show very high oxidation potentials, and they are usually not accessible with standard oxidation procedures.[56] Only strained carbocycles exhibit sufficiently low oxidation potentials, although in the meantime a PET protocol for functionalizing adamantane, cyclohexane, and 2,3-dimethylbutane has been set up as well.[57, 58] Adamantane is easier to oxidize than aliphatic ethers.[58]

Polysilanes and their radical cations have attracted much attention because of their potential utility as one-dimensional conductors.[59] According to ESR investigations, however, the unpaired electron in oligosilane radical cations is mostly confined to one elongated Si–Si bond.[60] Interestingly, the ionization potentials (IP) of allyltrimethylsilane (IP = 9.0 eV) and tetramethylsilane (IP = 9.5 eV) are even lower than that of propene (IP = 10 eV), which allows classification of both silanes as σ donors.[55] Indeed, considerations of ionization potential suggest that the donor capability of a C–Si σ bond is similar to that of a lone pair on oxygen.[55] Even stronger σ donors are germanes and stannanes, as indicated from the ionization potentials of $GeMe_4$ (IP = 9.2 eV) and $SnMe_4$ (IP = 8.76 eV).[49]

4. Reactivity Patterns in ⓟ$^{\bullet+}$, ⓝ$^{\bullet+}$, and ⓞ$^{\bullet+}$

The plethora of reactions hitherto realized after one-electron oxidation of neutral molecules has made it almost impossible to present an analysis in a sensible way. We will therefore restrict ourselves to the enumeration of a few selected examples of synthetic interest and instead try to present the typical reaction patterns operating in this chemistry. Furthermore, we will try to conceptualize structure–reactivity relationships on the basis of some recent data on the rates of reactions. There are also many possibilities for manipulating the primary reaction pathways of radical cations beyond the inherent reactivity patterns (Table 4).

Table 4. Some selected factors affecting the reactivity of radical cations.

Structural effects	External effects
delocalization of spin and charge	solvent [61]
distribution of spin and charge	anode material
release of strain	electrolytes, ions
stereoelectronic effects	(added nucleophiles)
steric factors	

4.1. C–H Deprotonation

4.1.1. A Physical Organic Prelude

Deprotonation at C–H is a typical reaction pathway for almost all radical cations of the type ⓟ-C-H$^{\bullet+}$ and ⓝ-C-H$^{\bullet+}$. Calculations using thermochemical cycles[62, 63] show that the acidity of a radical cation is inherently augmented, with respect to that of the neutral precursor, almost independent of the nature of the electrophore. This is a consequence of the fact that for essentially all cases R^- is more readily oxidized than RH ($E_{ox}(RH) > E_{ox}(R^-)$, Scheme 23a). The change in

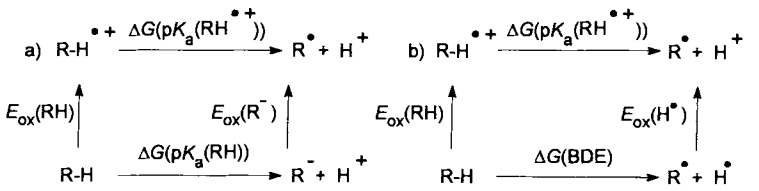

Scheme 23. Thermochemical cycle process for determining the acidity of radical cations.

pK_a (ΔpK_a) when switching from the neutral to the one-electron oxidized molecule can therefore be derived from $\Delta G = -nF[E_{ox}(RH) - E_{ox}(R^-)]$. Alternatively, if the pK_a of the neutral molecule is not known, that of the radical cation can nevertheless be determined through a different thermochemical cycle using the C–H homolytic bond dissociation energy and the oxidation potential of the neutral molecule (Scheme 23b). Within a series of related molecules exhibiting very similar values of ΔG(BDE) for the neutral compounds, one can expect the acidity of RH$^{\bullet+}$ to increase with the oxidation potential of RH. For instance, in the case of toluene$^{\bullet+}$, $\Delta G(pK_a^{\bullet+}) = -17$ kcal mol^{-1} in acetonitrile has been estimated, which corresponds to $pK_a = -13$.[62] Electron-donating substituents increase the stability of the arene radical cation and render the odd-electron species less acidic; for example, hexamethylbenzene$^{\bullet+}$ has a pK_a value of only 2.[64] Some representative thermodynamic acidities, mostly derived from calculations of thermochemical cycles and only rarely determined directly,[65] are listed in Table 5.

Table 5. Thermodynamic acidities of π radical cations for C–H deprotonation in DMSO.

R-H	$pK_a(RH^{\bullet+})$	$pK_a(RH)$	Ref.
$PhCH_2CN$	−32	21.9	[66]
$PhCH_2SO_2Ph$	−25	23.4	[67]
Ph_2CH_2	−25	32.2	[68]
$PhCH_3$	−20	43	[68]
indene (3-H)	−18	20.1	[69]
Cp*H*	−17	18.0	[68, 70]
fluorene (9-H)	−17	22.6	[71]
C_5Me_5H	−6.5	26.1	[70]

Fortunately, kinetic acidities of radical cations were investigated recently in some detail. From the seminal studies of Kochi,[64] Baciocchi,[72] Savéant,[73, 74] and others[75, 76] on the deprotonation rates of ⓟ-C-H$^{\bullet+}$, a linear relationship between

$\lg k_{dep}$ and pK_a is derived, which should allow rough predictions of kinetic acidities for alkyl arene radical cations (Figure 1). The Brønsted parameter $\alpha = 0.24$ suggests a reactant-like transition state with a low positive charge on the α carbon atom.[72]

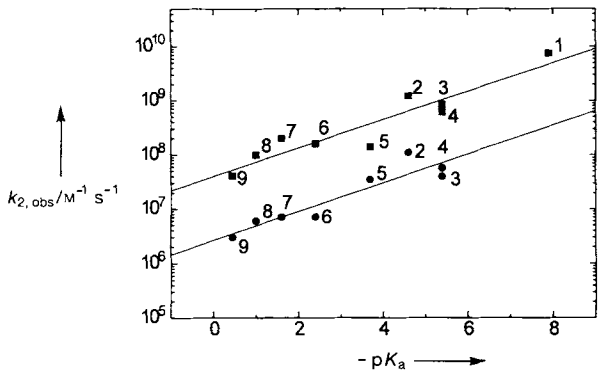

Figure 1. Brønsted plots for the deprotonation of 4-MeOPhCH$_2$X$^{\bullet+}$ by NO_3^- (■) und 2,6-lutidine (●)[72]. The numbers correspond to different compounds 4-MeOPhCH$_2$X$^{\bullet+}$:1: X = CN, 2: X = Cl, 3: X = OMe, 4: X = OH, 5: X = OAc, 6: X = Ph, 7: X = 4-MeOPh, 8: X = Me, 9: X = H.

However, this simple picture was questioned by the work of Savéant on NADH model compounds; the intrinsic barriers for deprotonation were found to correlate with homolytic bond dissociation energies but not with pK_a values.[73] Proton transfer from radical cations should therefore be viewed as concerted electron and hydrogen-atom transfer. While this controversy is far from being settled, the differences to the results presented above may be due to the fact that we are dealing with ⓝ-C=CCH$^{\bullet+}$ deprotonation in the latter case but ⓟ-C-H$^{\bullet+}$ in the former. These results on alkyl arene radical cations indicate that deprotonation at the benzylic position is often a rapid, and sometimes even a diffusion-controlled, process that depends on the acidity of the radical cation and the strength of the base used.

Somewhat less is known about the acidity of ⓝ-C-H$^{\bullet+}$; almost all data are for amine radical cations (Table 6) and only few for other systems (e. g. ether$^{\bullet+}$[77] and thioether$^{\bullet+}$[78]). In contrast to π radical cations, however, deprotonations directly at the electrophore are much better known for ⓝ-H$^{\bullet+}$ (e. g. $Me_2NH^{\bullet+}$: $pK_a = 6.5-7.5$).[79]

Table 6. C–H acidities of amine radical cations in DMSO[80].

ⓝ-C-H$^{\bullet+}$	pK_a(ⓝ-C-H$^{\bullet+}$)	pK_a(ⓝ-C-H)
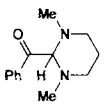	−13	27.9
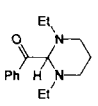	−11	27.0
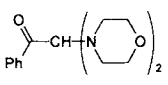	−11	24.4
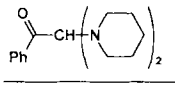	−9.4	25.6

The kinetics of proton transfer in amine radical cations is of wide interest because of the importance of such deprotonations in photochemical, electrochemical, and biochemical redox processes. Hence, their rates of α-deprotonation[81–88] and pK_a values[83–85] have been repeatedly reported. Although this complex issue is far from being settled, some major effects were identified that influence the kinetic acidity: steric and stereoelectronic effects,[87, 88] entropic factors,[84] base strength,[84] and late transition state.[84, 85]

A study of the substituent effects on C–H deprotonation in amine radical cations was recently undertaken by Mariano;[85b] this led to a scale of relative acidities. Absolute rate constants were reported for various substituents in $Ph_2NCHR^1R^{2\bullet+}$ (Table 7).[89] Importantly, the kinetic acidities parallel the thermodynamic pK_a values. It should, however, be noted that the observed substituent effects do not parallel those observed by Lewis.[88]

Table 7. Substituent effects on the deprotonation of $Ph_2NCHR^1R^{2\bullet+}$ (base: nBu$_4$NOAc in MeOH/MeCN (1/3) at 25 °C[89]).

R^1	R^2	k[M^{-1}s^{-1}]
Me	H	2.3×10^5
Me	Me	1.7×10^5
Ph	H	3.2×10^6
CH=CH$_2$	H	2.6×10^6
C≡CH	H	7.0×10^7

Very little is known about ⓞ:C-H$^{\bullet+}$ deprotonation. Recently, such processes were used in the arylation of alkanes in PET reactions with TCB or CA.[57, 58] All radical cations investigated exhibit a strongly negative Gibbs energy for deprotonation with strong preferences for the tertiary C–H bond over secondary or primary bonds (e. g. $\Delta G^0 = -11.5$ and -8.0 kcal mol^{-1} for the tertiary and secondary C–H bonds in adamantane$^{\bullet+}$).[57] Here, ⓞ:C-H$^{\bullet+}$ cleavage is observed although the HOMO of such compounds is mainly governed by C–C σ bonds.[90]

4.1.2. ⓟ-C-H$^{\bullet+}$ Deprotonation

Rapid ⓟ-C-H$^{\bullet+}$ deprotonation can often be utilized for highly selective functionalizations at allylic or benzylic positions. Interestingly, it was only in the late 1960s that these technically important reactions[91] were recognized as electron transfer processes.[92, 93] In the chemical or anodic oxidation of **23**[94] or **25**,[95] the radicals formed in the primary process are further oxidized to cationic intermediates ([$\rightarrow$CH, R$^+_{ox}$]) that are readily trapped with a variety of nucleophiles (Scheme 24). The analogous reaction sequence [$\rightarrow$CH, R$^+_{ox}$] has found widespread use in protecting-group chemistry, for example in the selective deprotection of alcohols[96] and carboxylic acids[97] from substituted benzyl ethers and esters,[39] respectively.

Screening the literature clearly indicates that most of the ⓟ-C-H$^{\bullet+}$ deprotonations are for aromatic or heteroaromatic[98] systems carrying alkyl side chains, whereas for simple olefinic systems,[99, 100] this is not such a dominant pathway with respect to nucleophilic attack and cycloaddition. Never-

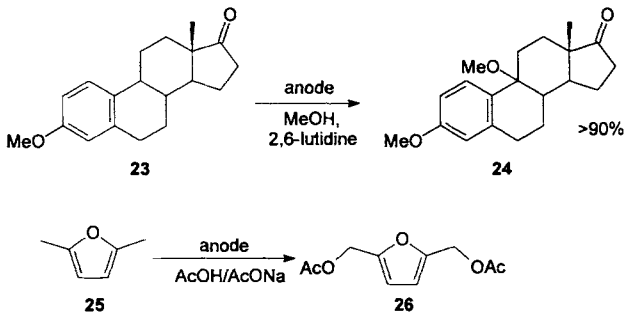

Scheme 24. The [→CH,R^{+}_{ox}] reactions according to Ponsold (1979, top) and Brettle (1966, bottom).

theless, deprotonation of various 1,4-cyclohexadiene radical cations[101] affords aromatized derivatives; this suggests that a similar mechanism may operate in the oxidation of arachidonic acid by lipoxygenase.[102]

A vast number of reactions could be listed here, which all show preferential deprotonation at the benzylic position. However, only a few examples exhibit deprotonation directly at the π electrophore, that is, involving the aromatic C–H protons. Although a pK_a of -4 was estimated for the benzene radical cation in acetonitrile,[63] deprotonation at the aromatic nucleus is in general a rare event. Since other reactions are much more preferred, for example nucleophilic attack on $ArH^{\bullet+}$, only sterically hindered bases such as di-*tert*-butyl pyridine were reported to induce deprotonation.[103]

Deprotonation of radical cations generated by PET is often too slow to compete with back electron transfer. However, when acceptors such as **27** give rise to strongly basic radical anions, deprotonation in the ion radical pair may become an efficient process (Scheme 25).[104]

Although stereoelectronic factors in π-C-H$^{\bullet+}$ deprotonation were recently studied in depth, their role remains obscure. Since deprotonation in π-C-H$^{\bullet+}$ should be accelerated by optimum overlap of the π-SOMO with the C–H bond, preferential deprotonation in *p*-methylcumene (*p*-cymene$^{\bullet+}$) at the methyl group rather than at the more acidic isopropyl group was originally rationalized in terms of

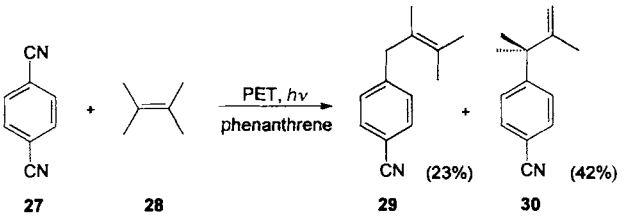

Scheme 25. The [→CH,R^{+}_{RA}] reaction according to Arnold (1984).

conformational restraints.[105, 106] Recent investigations on the same radical cation in solution[107] and in the gas phase[108] failed to observe significant stereoelectronic effects, which however showed up in the deprotonation of α-substituted *p*-xylene$^{\bullet+}$ at CH_3 instead of CH_2tBu.[109] This discrepancy, however, may be due to the fact that free radical cations were not always formed.[110] In a detailed study on the relative C–H deprotonation reactivity as a function of different electron transfer oxidants, the secondary C–H bond was the most reactive.[111] Such a reactivity pattern can be utilized for selective functionalizations,[112] in particular in rigid systems,[109] as recently illustrated by Arnold[113] in the PET-induced *cis* → *trans* isomerization of 1-methyl-2-phenylcyclopentane$^{\bullet+}$. The photostationary state (>99% *trans*) is controlled by the relative kinetic acidities of the isomers; both display the same thermodynamic acidity ($pK_a = -15$).

An insightful review on C–H deprotonations of alkyl arenes was provided by Baciocchi that illustrates that not only radical-stabilizing effects but also the charge distribution in the radical cation contribute to the positional selectivity.[114, 115] For example, electron-donating substituents increase the *para* to *meta* deprotonation selectivity in **31** (Scheme 26, Table 8).

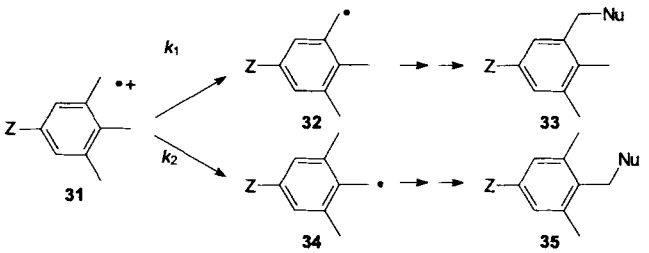

Scheme 26. Reaction pathways for the anodic functionalization of 5-Z-substituted 1,2,3-trimethylbenzenes according to Baciocchi (1986).

Table 8. Relative rates in the anodic functionalization of 5-Z-1,2,3-trimethylbenzenes (Scheme 26)[114].

Z	k_2/k_1	Z	k_2/k_1
CO_2Me	2.0	Br	42
H	3.4	Me	55
*t*Bu	24	OMe	>200

Electronic effects of α substituents on the deprotonation rates of alkylarene radical cations were also studied (see Figure 1); k_{dep} decreases with CN > Cl > OMe > OH > OAc > Ph > 4-MeOPh > Me > H.[72]

It is instructive to realize that deprotonation at the benzylic position in 1,2-diarylethane$^{\bullet+}$ is much faster than C–C bond cleavage, whereas with 2,3-dimethyl-2,3-diphenylbutane$^{\bullet+}$ C–C bond fragmentation is the predominanting process (Scheme 27). Similarly, substitution of an α-hydrogen

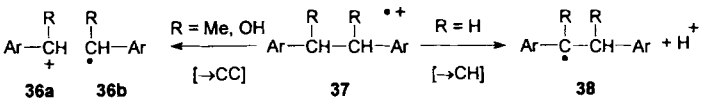

Scheme 27. Competition between deprotonation and C–C bond cleavage in 1,2-diarylethane$^{\bullet+}$.

atom by an α-hydroxy group accelerates C–C fragmentation. This is simply a consequence of the lower C–C bond dissociation energy; the acidity of the radical cations is changed less.[116]

4.1.3. ⓝ-C-H$^{\bullet+}$ and ⓝ-H$^{\bullet+}$ Deprotonation

In contrast to ⓟ-H$^{\bullet+}$ deprotonation, which is almost completely unknown, ⓝ-H$^{\bullet+}$ deprotonation directly at heteroatoms such as in RNH_2[117] or RSH[118] occurs quite frequently. For instance, it plays an important role in the oxidative N–H deprotonation[119, 120] triggered after intramolecular electron transfer in the linked donor–acceptor system **39** (Scheme 28).[121] Such reactions were successfully used in the construction of heterocyclic rings (including the benzomorphan skeleton)[122] and in the photo-Smiles rearrangement.[123, 124] The mechanism is, however, not undoubtedly established in all cases.

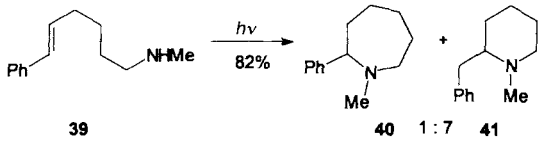

39 **40** 1 : 7 **41**

Scheme 28. The [→ ⓝH,R$^{\bullet}_{rad}$] reaction according to Lewis (1989).

Nevertheless, ⓝ-C-H$^{\bullet+}$ deprotonation at a position α to the heteroatom is by far the more important pathway, and it has received wide attention because of its occurrence in the biologically important monoamine oxidase reaction.[14] It is also the key step in the α functionalizations of amines,[125] hydroxylamines,[126] amides,[127] lactams,[128] carbamates,[129] amino acids,[130] dipeptides,[131] sulfides,[132] ethers,[77] phosphanes, and others.[2, 3, 40, 133] The plethora[134–140] is only poorly represented by the small selection (Scheme 29).[134, 135]

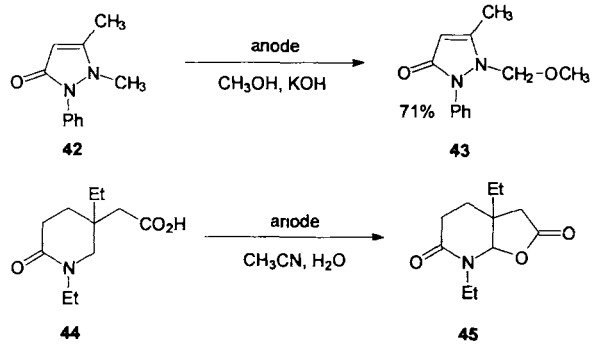

42 **43**

44 **45**

Scheme 29. The [→ CH,R$^{\bullet}_{ox}$] reactions according to Kaupp (1985, top) and Irie (1980, bottom).

Under chemical and anodic oxidative conditions, the resulting α-amino radicals are readily oxidized (e. g. $E^{ox}_{1/2}$ ($Me_2NCH^{\bullet}_2$) = −1.03 V versus SCE)[29] to give iminium ion intermediates. Interestingly, even PET conditions (when selected properly, as with **46**; Scheme 30)[137] allow access to cationic intermediates.[125] A special variant uses ⓝ-C-H$^{\bullet+}$ deprotonation after intramolecular ET, for example between the amine and the enone functionality of **48**, to effect cyclization at the stage of the α-amino radical and the radical anion of the enone (Scheme 31).[139]

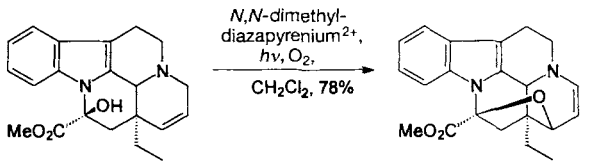

46 **47** (Criocerin)

Scheme 30. The [→ CH,R$^{\bullet}_{ox}$] reaction according to Santamaria (1995).

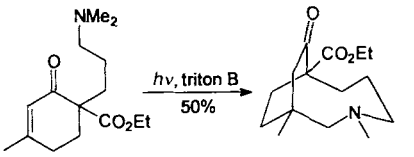

48 **49**

Scheme 31. The [→ CH,R$^{\bullet}_{add}$] reaction according to Kraus (1991); triton B = benzyltrimethylammonium hydroxide.

Such ⓝ-C-H$^{\bullet+}$ deprotonation reactions after intramolecular ET have found use in fascinating macrocyclizations, such as in **50** → **51** (Scheme 32),[141] and in the formation of

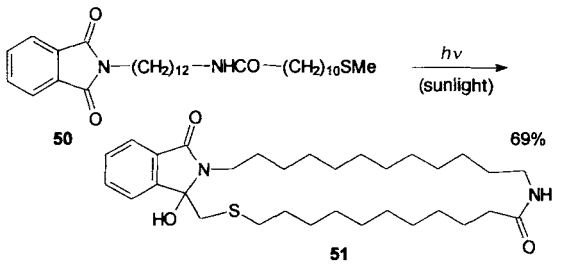

Scheme 32. The [→ CH,R$^{\bullet}_{rad}$] reaction according to Kanaoka (1992).

heterocyclic rings starting from amines[142] and thioethers,[143] as demonstrated through the elegant work by Kanaoka and Griesbeck. Furthermore, this strategy was used for the electrochemical preparation of the bicyclic, reverse-turn peptidomimetics **53** from dipeptide **52** (Scheme 33)[144] and in the synthesis of the berberine alkaloid chilinene.[145]

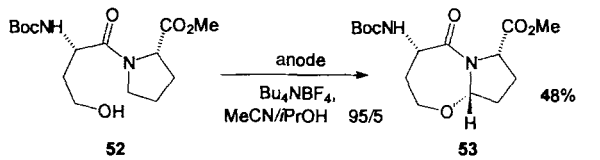

52 **53**

Scheme 33. The [→ CH,R$^{\bullet}_{ox}$] reaction according to Moeller (1995); Boc = *tert*-butoxycarbonyl.

In some cases the chemoselectivity can be steered by ingenious ways in anodic oxidations.[146] Direct anodic oxidation of **54** preferentially gives rise to ⓝ-C-H$^{\bullet+}$ deprotonation at the (ω − 1) position to yield **55** in 51% (Scheme 34); however, in the presence of NaCl anodically generated Cl^+ first produces N_α-chloroamine. Upon elimination of hydrogen chloride and addition of methanol, this methoxylation protocol afforded **56** in 70% yield.

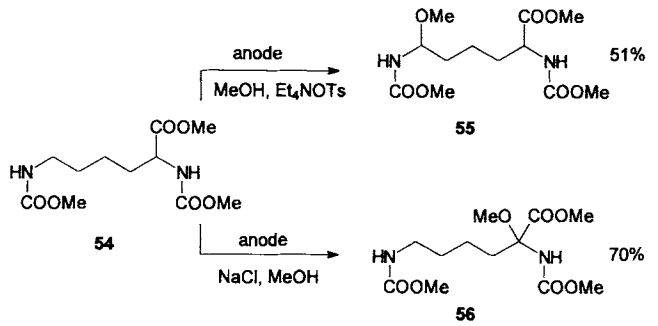

Scheme 34. Reaction **54** → **55**: the [→ CH,$R^{\bullet}_{ox}$] reaction according to Shono (1983); Ts = $H_3CC_6H_4SO_2$.

Very recently, the electrochemically mediated conversion of aspidofractinine-type alkaloids such as kopsingine to kopsidines A and B (**60**) was successfully realized (Scheme 35).[147] Likewise, anodic oxidation of 2,5-dihydro-*1H*-1-benzazepines provides a synthetic access to the rare *5H*-1-benzazepines.[148]

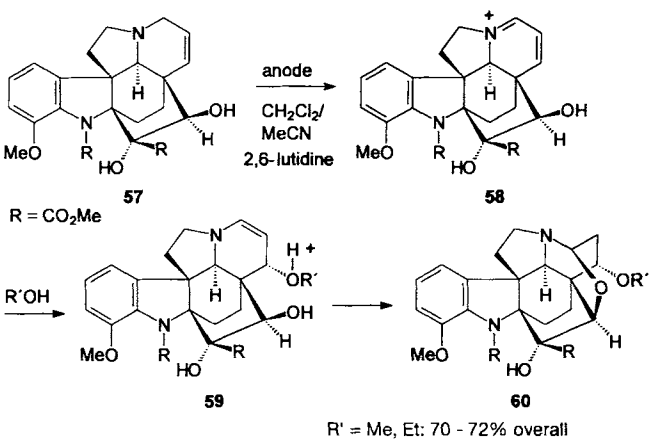

Scheme 35. The [→ CH,$R^{\bullet}_{ox}$] reaction according to Kam (1995).

Since the deprotonation step in ⓝ-C-$H^{\bullet+}$ requires the overlap of the half vacant p orbital with the incipient carbon radical orbital,[87, 88] stereoelectronic factors often give rise to preferential deprotonation at the less substituted side group, as in **61** (Scheme 36).[125] When overlap is impossible, as in triisopropylamine$^{\bullet+}$, deprotonation is almost perfectly inhibited.[149]

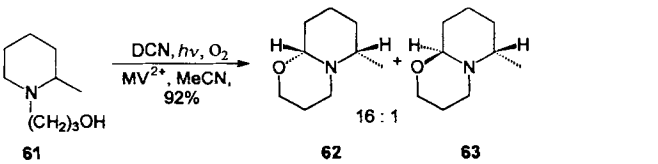

Scheme 36. The [→ CH,$R^{\bullet}_{ox}$] reaction according to Pandey (1991); MV^{2+} = methyl viologen.

4.1.4. ⓞ:C-H$^{\bullet+}$ Deprotonation

Evidence for ⓞ:C-$H^{\bullet+}$ cleavage was deduced from pulse-radiolysis studies.[150] From ESR investigations it was suggested that deprotonation preferentially occurs at the C–H bond with the highest unpaired electron density.[151] It was only recently that ⓞ:C-$H^{\bullet+}$ deprotonations were observed in the arylation of alkanes upon PET with TCB (**65**) or CA (Scheme 37).[57, 58] In **64**$^{\bullet+}$ deprotonation at the tertiary C atom is always strongly favored.

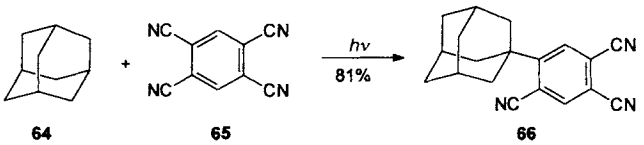

Scheme 37. The [→ CH,$R^{\bullet}_{RA}$] reaction according to Albini (1995).

In a series of substituted adamantanes, deprotonation was found to dominate over C–C bond cleavage in the *tert*-butyl- and methoxymethyl-substituted derivatives. Indeed, calculations of thermochemical cycles indicate C–H bond cleavage is exergonic, as opposed to endergonic C–C bond fragmentations (Table 9). A different behavior was found for *t*Bu-Ad after photoinduced and anodic oxidation; the first method provided mainly C–H,[58] and the latter C–C[58, 152] scission products. It was proposed that anodic oxidation may proceed via the corresponding dications as a result of the high stationary concentration at the electrode.[58]

Table 9. Gibbs energy for the bond dissociation of substituted adamantane radical cations in CH_3CN[58].

Reaction[a]	ΔG^0 [kcal mol^{-1}]
$AdH^{\bullet+} \rightarrow 1\text{-}Ad^{\bullet} + H^+$	−17.1
$AdH^{\bullet+} \rightarrow 2\text{-}Ad^{\bullet} + H^+$	−13.6
1-(*t*Bu)-$Ad^{\bullet+} \rightarrow$ 1-(3-*t*Bu)-$Ad^{\bullet} + H^+$	−15.3
1-(*t*Bu)-$Ad^{\bullet+} \rightarrow 1\text{-}Ad^{\bullet} + t\text{Bu}^+$	10.0
1-($MeOCH_2$)-$Ad^{\bullet+} \rightarrow$ 1-(3-$MeOCH_2$)-$Ad^{\bullet} + H^+$	−14.1
1-($MeOCH_2$)-$Ad^{\bullet+} \rightarrow 1\text{-}Ad^{\bullet} + MeOCH_2^+$	11.4

[a] Ad = adamantyl, AdH = adamantane.

4.2. A–H Deprotonation

When an AH (e. g. OH or NHR) and a CH_2R functionality are placed at the α-position of an electrophore, A–H deprotonation usually prevails over C–H deprotonation. The alternative bond cleavage—namely, formation of RA^+ and $H^{\bullet}$—is much more endergonic and does not play a role in solution.[153] For many substituted arenes the pK_a (ⓟ-A-$H^{\bullet+}$) values correlate with those for the gas phase[68] or with Brown substituent constants[157] when the solvation terms remain constant.

Unfortunately, only few kinetic data on deprotonation of ⓞ:A-$H^{\bullet+}$, ⓝ-A-$H^{\bullet+}$, and ⓟ-A-$H^{\bullet+}$ are available.[161, 162] The propensity of ⓟ-A-$H^{\bullet+}$ to undergo deprotonation may be directly related to their thermodynamic acidities (Table 10). From these data it becomes clear that ⓟ-O-$H^{\bullet+}$ species tend to be much more acidic than ⓟ-NH-$H^{\bullet+}$ species, which explains the occasionally observed reluctance of aniline radical cations to undergo deprotonations. However, this picture may be much more complex once reliable kinetic data

Table 10. Acidities of selected π-A-H$^{\bullet+}$ species.

R-A-H	$pK_a(RAH^{\bullet+})$	$pK_a(RAH)$	Solvent	Ref.
$PhNH_2$	+6.5	30.6	DMSO	[68]
$PhNH_2$	+7.05		H_2O	[154]
$4\text{-}MeOC_6H_4NH_2$	+10	32.5	DMSO	[155]
$4\text{-}MeOC_6H_4NH_2$	+9.6		H_2O	[156]
$2,4\text{-}Me_2C_6H_3NH_2$	8.0		H_2O	[157]
$PhNHCOCH_3$	−1.8	21.5	DMSO	[158]
$PhNHCOCF_3$	−14	12.6	DMSO	[158]
$4\text{-}Me_2NC_6H_4OH$	+6.2	19.8	DMSO	[159]
$4\text{-}NO_2C_6H_4OH$	−15	10.8	DMSO	[159]
Ph_2NH	+2.7	24.95	DMSO	[155]
carbazole	+1.5	19.9	DMSO	[155]
PhOH	−8.1	18.0	DMSO	[68]
$4\text{-}MeOC_6H_4OH$	−4.7	19.1	DMSO	[159]
PhSH	−12	10.3	DMSO	[68]
$Mes_2C{=}C(OH)H$	4.4	28	CH_3CN	[160]

are considered, which are unfortunately not available at present. Exceptions are data for enol[161] and phenol radical cations such as methoxyphenol$^{\bullet+}$ [163, 164] ($k = 2.2 \times 10^6\ s^{-1}$).[164]

Parker observed an unexpectedly fast rate for the endergonic π-N-H deprotonation of **68**$^{\bullet+}$ with various pyridines as bases (Table 10), which could be explained by taking hydrogen bonding between the radical cation and the base into account.[162] In contrast, the thermodynamically more feasible deprotonation of **67**$^{\bullet+}$ ($pK_a = 3.0$) is much slower (Table 11).

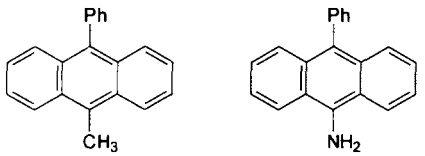

67 **68**

Table 11. π-C-H$^{\bullet+}$ versus π-N-H$^{\bullet+}$ deprotonation in CH_3CN in the presence of 2,6-di-*tert*-butylpyridine as base [162].

R-A-H	$pK_a(RAH^{\bullet+})$	k_{dep} [$M^{-1}s^{-1}$]
67	+3	27
68	+17	4.3×10^5

This indicates that charge distribution and the identity of the atom to which the proton is attached do play an important role in determining kinetic acidities. Thermochemical and kinetic data for deprotonation on π-A-H$^{\bullet+}$ are basically unkown with the exception of a few pK_a values for oxime radical cations (e. g. $CH_3CH{=}NOH^{\bullet+}$).[165]

4.2.1. π-A-H$^{\bullet+}$ Deprotonation

The π-A-H$^{\bullet+}$ deprotonation constitutes an extremely useful synthetic transformation, in particular for phenols,[166, 167] hydroquinones,[166] enols,[168] anilines,[169] and compounds with related functionalities.[170] In most cases, under anodic or chemical oxidation conditions the formed radicals are rapidly oxidized to intermediate cations ([$\rightarrow$AH, R^+_{ox}]), from which the observed chemistry is readily understood. The mechanistic scheme may end up being very complex when oxidation of the radicals is rather slow, since radical–neutral and radical–radical combination reactions may prevail (e. g. with phenoxyl radicals).[171]

The cations generated in a [$\rightarrow$AH, $R^{\bullet}_{ox}$] sequence were used for intriguing intramolecular reactions, for example in the synthesis of spiro compounds[172] and benzofurans,[168] the synthesis of natural products,[173] and other important transformations[166] (Scheme 38). Cations that are generated accordingly may also undergo fragmentation; this process is used in transacylation chemistry.[174]

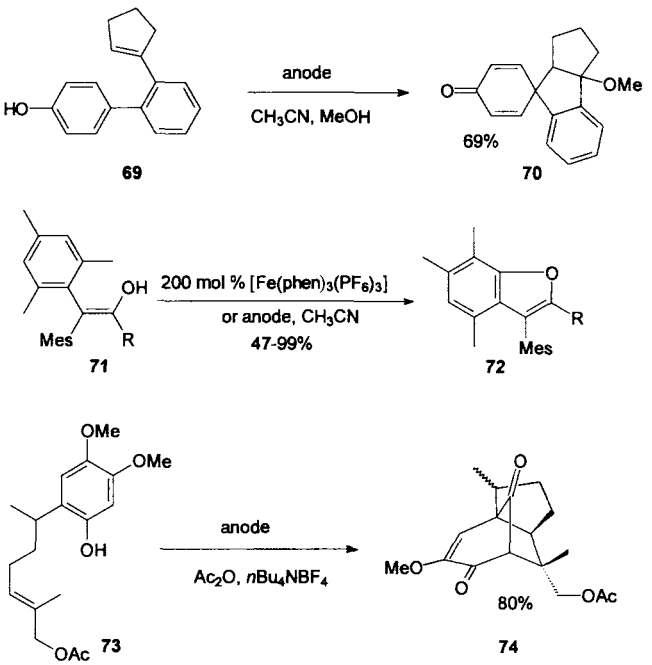

Scheme 38. The [$\rightarrow$AH, $R^{\bullet}_{ox}$] reactions according to Swenton (1991, top), Schmittel (1994, middle), and Yamamura (1991, bottom); phen = 1,10-phenanthroline; Mes = $2,4,6\text{-}Me_3C_6H_2$.

Importantly, the resulting cationic intermediates can also be trapped in intermolecular processes, such as in the synthesis of neolignan natural products.[175] The oxidation mechanism of phenols is of paramount interest in connection with biosynthetic coupling reactions,[176] with quinone and quinol[177] formation, and protecting-group chemistry.[178] Recently, this approach found intriguing use in the total synthesis of michellamines A, B, and C (Scheme 39), which are members of a biologically important class of quateraryls with outstanding activity against HIV.[179] Most importantly, such intermolecular coupling reactions can be conducted in a highly enantioselective way with chiral Cu^{II} complexes[180] or TEMPO-modified graphite electrodes in the presence of (−)-sparteine (Scheme 40).[181]

In most cases, α-carbonyl radicals are more difficult to oxidize than the parent enol precursors,[30] and mostly α-carbonyl radical chemistry is observed in such a protocol. For example, addition to unsaturated compounds led to inter-[182] and intramolecular bond formations; the latter has interesting applications in spiroannulation strategies.[183]

Whereas π-A-H$^{\bullet+}$ deprotonation reactions are often effected with π-O-H$^{\bullet+}$, they are rather rare with π-N-H$^{\bullet+}$. In the

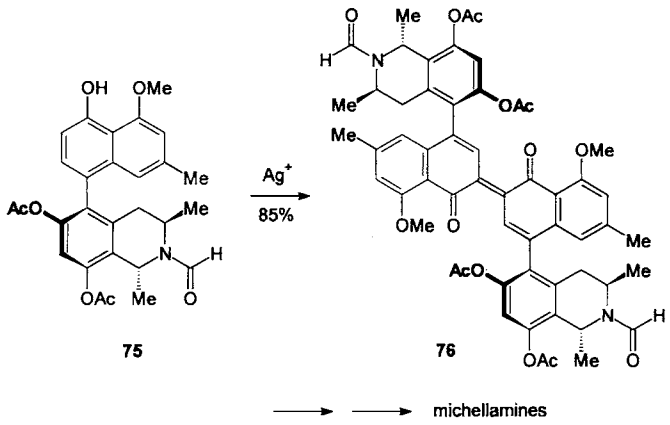

Scheme 39. The [→ AH, $R^{\bullet}_{ox}$] reaction according to Bringmann (1994).

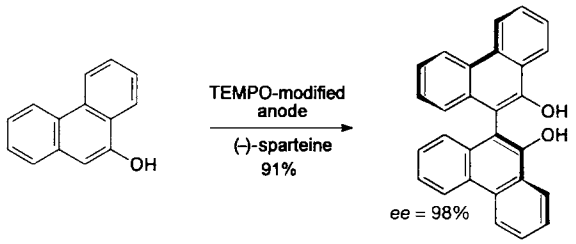

Scheme 40. The [→ AH, $R^{\bullet}_{rad}$] or the [→ AH, $R^{\bullet}_{ox}$] reaction according to Osa (1994); TEMPO = 2,2,6,6-tetramethylpiperidin-*N*-oxyl.

case of the latter ⓟ-C-H$^{\bullet+}$ deprotonation, if feasible, is often the dominant reaction pathway, as with the anodic dimerization of tetrahydrocarbazole.[184, 185] In contrast to the above-mentioned functionalities, enamines are most likely to be classified as ⓝ$^{\bullet+}$ [186] and will be treated in Section 4.2.2. However, the electron-deficient benzotriazole forms a π radical cation that can be arylated after ⓟ-N-H$^{\bullet+}$ deprotonation.[187]

The propensity to react via the cation formed after the secondary oxidation of the radical ([→ AH, $R^{\bullet}_{ox}$]) can be readily understood by comparing the oxidation potentials of neutral precursors and radicals. However, oxidation potentials of ⓟ-X$^{\bullet}$ are only scarcely known, except for phenols/phenoxyl radicals and enols/α-carbonyl radicals (Table 12). It is certainly helpful to recognize that the formal transformation (6) in Scheme 41 may be accessed as a function of the pH of the solution by reaction (7). This holds true in particular

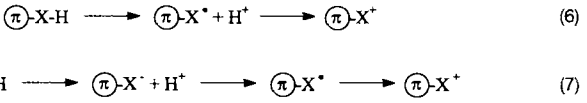

Scheme 41. The formal oxidation (6) can be realized as a function of the pH value as reaction (7).

for phenols and enols/ketones even at pH values well below the pK_a value,[190] as documented in the oxidation of teniposide,[191] the coupling of (+)-verbenone,[192] and in a new synthesis of hirsutene[193] (Scheme 42). Such an approach

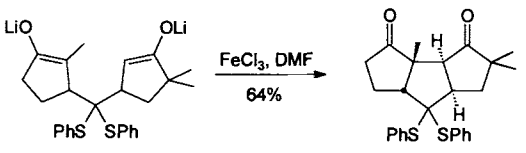

Scheme 42. Key step in the synthesis of hirsutene according to Cohen (1993).

allows additional control of the reaction: Radical or cationic intermediates can be generated in a defined manner, since oxidation potentials of phenolate/phenoxyl radical and enolate/α-carbonyl radical are neatly spaced.[160] Equally, such oxidative coupling can be performed with high simple and induced diastereoselectivity.[194]

4.2.2. ⓝ-A–H$^{\bullet+}$ Deprotonation

The ⓝ-A-H$^{\bullet+}$ deprotonations known at present are limited to a small number of functionalities derived from -N–OH, -N–NH_2, -S–SH, and -P–NH_2. Their synthetic potential is therefore still restricted to a few examples.[195] Nevertheless, ⓝ-A-H$^{\bullet+}$ deprotonation plays a dominant role in the oxidative formation of 1,2,4-triazoles from arylhydrazones such as **81** (Scheme 43),[196] azo compounds from hydrazines,[197] and pyrazoles from chalcones and benzalacetones[198] in the presence of nitriles. The mechanistic scenarios of these ⓝ-A-H$^{\bullet+}$ deprotonations are not fully settled. Hence, we assume, on the basis of the high acidity (see Table 10), that loss of a proton should always be much faster than nucleophilic attack. Follow-up radical oxidation should then provide intermediate cations, from which the reactions can be understood (Scheme 43). The same radical intermediates may be prepared from one-electron oxidation of the corresponding anions at rather low potential, as demonstrated for iminoxy radicals.[199]

The situation of hydrazine$^{\bullet+}$ is representative for all ⓝ-A-H$^{\bullet+}$ systems. While numerous reports deal with the chemistry and properties of fully alkylated hydrazine radical cations,[200] very little is known about the oxidation of mono-, di-, and trialkylated systems.[201] Equally little is known about the controlled one-electron oxidation of enamines for which N–H deprotonation could play a viable role,[202] presumably

Table 12. Oxidation potentials of ⓟ-A-H and ⓟ-A$^{\bullet}$ (versus SCE).

ⓟ-A-H	E_{ox}	Ref.	ⓟ-A$^{\bullet}$	E_{ox}	Ref.
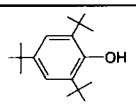	1.33	[188]	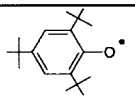	1.02	[188]
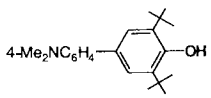	0.55	[189]	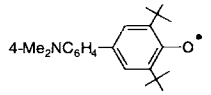	0.23	[189]
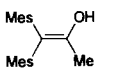	1.07	[160]	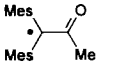	0.60	[160]
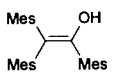	1.15	[160]	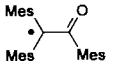	0.65	[160]

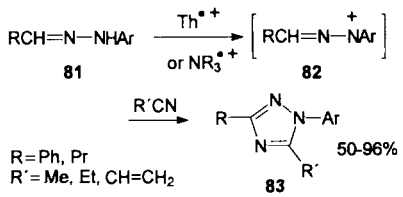

Scheme 43. The [→ AH, $R^{\bullet}_{ox}$] reaction according to Shine (1988).

because of their high reactivity with respect to oxygen.[203] Hence, such reactions have found only very limited use, for example in the formation of α,β-unsaturated imines.[204]

4.3. A–B Bond Dissociation

A thermochemical cycle similar to that in Scheme 23 is often used for predicting ㊀-A-B$^{\bullet+}$ or ⓝ-A-B$^{\bullet+}$ bond energies; however, two different cleavage modes are possible to yield either A or B as cationic fragments (Scheme 44). As expected, the fragment with the lower radical oxidation potential will always end up as the cation upon monomolecular bond scission. In reality, only a few combinations A–B have found use in synthesis (see below), since bond cleavage at the stage of the radical cation has to be fast to compete successfully with other pathways.

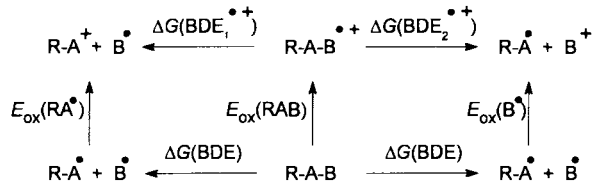

Scheme 44. Thermochemical cycle for determining the A–B bond dissociation energy (BDE) and cleavage selectivity.

Unfortunately, there is very little experimental data for the thermochemical driving force[205] and the kinetics of ㊀-A-B$^{\bullet+}$ cleavage. Fragmentations of ㊀-O-SiR$_3^{\bullet+}$ and ㊀-O-C$^{\bullet+}$ were investigated recently by Kochi[206a] and Schmittel.[206b, 207] From the few kinetic data available, it has become clear that ㊀-O-Si$^{\bullet+}$ bond cleavage is slower than that of ㊀-O-H$^{\bullet+}$, and that it can be induced by addition of nucleophiles such as alcohols and pyridines (Table 13). In accordance with the nucleophile-induced bond-cleavage mechanism,[208] the O–SiMe$_2$*t*Bu cleavage is significantly slower than that of O–SiMe$_3$.[206b]

Table 13. Kinetics of ㊀-O-Si$^{\bullet+}$ bond fragmentation in CH_3CN and CH_2Cl_2 [206b].

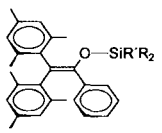

R′	R	k_{AB} [s^{-1}] (in CH_3CN)	k_{AB} [s^{-1}] (in CH_2Cl_2)	k_{AB} [$M^{-1}s^{-1}$], induced with MeOH (in CH_2Cl_2)
Me	Me	$> 10^4$	1.3×10^2	8.7×10^5
*t*Bu	Me	6.0×10^2	1.3×10^{-1}	1.1×10^2

4.3.1. ㊀-A-B$^{\bullet+}$ Bond Dissociation

Among the numerous combinations possible for ㊀-A-B, only A–B = O–SiR$_3$ (e. g. enol and phenol silyl ethers) were studied more extensively, whereas others with A–B = O–SnR$_3$,[209] O–COR,[207] O–P(OEt)$_2$,[210] O–PO(OEt)$_2$,[210] O–TiCp$_2$Cl,[211] O–AlCl$_2$,[212] S–CHR$_2$,[205] and Si–Si[213, 214] were only recently introduced. Bond cleavage of ㊀-A-B$^{\bullet+}$ was used in enone[215] formation and in the elegant chemoselective deprotection of silyl enol ethers in the presence of siloxy substituents (developed by Gassman).[216] Otherwise, ㊀-O-SiMe$_3^{\bullet+}$ bond cleavage was utilized in various intermolecular C–C bond formation processes.[217] After chemoselective oxidation of the trimethylsilyl dienol ether **85** the formed α-carbonyl radical is not further oxidized because of its high oxidation potential[30] but instead adds to **84** (Scheme 45). The resulting radical is only thereafter further oxidized ([→ AB, $R^{\bullet}_{add.ox}$]).[218] Similarly, ketene silyl acetals react under oxidative conditions in intermolecular C–C bond formations,[219] indicating that radical cations may play an important role in the Lewis acid mediated Mukaiyama–Michael reaction.[220]

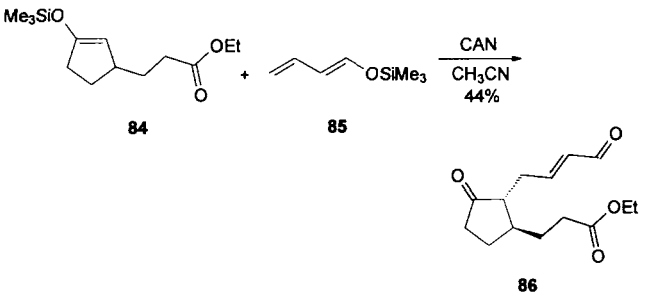

Scheme 45. The [→ AB, $R^{\bullet}_{add.ox}$] reaction according to Ruzziconi (1993).

Intermolecular reactions were accomplished with n nucleophiles, for example after desilylation of ㊀-O-SiMe$_3^{\bullet+}$ and further oxidation of the resulting radicals ([→ AB, $R^{\bullet}_{ox}$]),[221] as well as with anion radicals generated by PET.[222] Even ㊀-O-C$^{\bullet+}$ and ㊀-S-C$^{\bullet+}$ fragmentations are possible, as shown in the deprotection of aryl glycosides.[223]

4.3.2. ⓝ-A-B$^{\bullet+}$ Bond Dissociation

A particularly rich chemistry of ⓝ-A-B$^{\bullet+}$ fragmentations was reported for azoalkane radical cations. At first glance, one is led to classify such a process as bond cleavage directly at the electrophore. This, however, ought to be kinetically unfavorable in terms of the almost orthogonal arrangement of the two orbitals involved (n, σ).[224] Thus, we prefer to regard azoalkane radical cations as ⓝ=N-C$^{\bullet+}$ species in which the n electrophore is represented by the second nitrogen.

While little synthetic use has been made from acyclic azoalkane radical cations,[225] the corresponding cyclic systems give rise to distonic radical cations[226, 227] that undergo interesting rearrangements[228] with a remarkable stereochemical memory effect.[229] In addition, spiroethers were obtained after intramolecular cyclization (Scheme 46).[230]

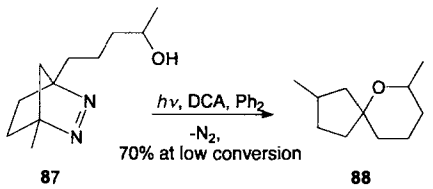

87 88

Scheme 46. The [→ AB, $RC_{Nu,red}$] reaction according to Adam (1993).

Predictions are difficult to make since only few kinetic data are available[231a] on the bond cleavage, but it seems that in bicyclic systems both strain[231b] and electronic effects[231a] are important. As expected, the efficiency of the fragmentation is determined by the stabilization of the resulting radical and cation.[224a, b] In acyclic *cis*-azoalkane radical cations, however, inversion at the nitrogen is more rapid than C–N bond cleavage.[232]

The ⓝ=N-N$^{\bullet+}$ bond cleavage that takes place in triazene radical cations with a rate constant k of about 0.01 s^{-1}[233] is much slower than the ⓝ=N-C$^{\bullet+}$ scission of azoalkane radical cations. It was indicated in several cases that clean N–N scission yielding a diazonium cation and a nitryl radical is the dominant reaction (Scheme 47);[234, 235] this may have important biochemical consequences, as triazenes are regarded as carcinogenic compounds.

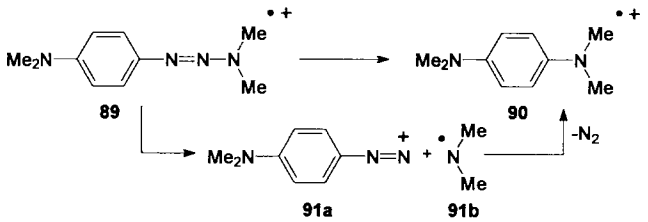

Scheme 47. The [→ AB, $R^{\bullet}_{rad}$] reaction according to Speiser (1992).

4.3.3. ⓢ:A-B$^{\bullet+}$ Bond Cleavage

Recently, major interest has focused on reactions of peralkylcyclopolysilanes which contain small and medium-sized rings and exhibit rather low oxidation potentials that decrease to 0.4 V versus SCE with decreasing ring size.[236] In line with our classification, the unpaired electron in hexamethyldisilane$^{\bullet+}$ and hexamethyldigermane$^{\bullet+}$ is localized in σ orbitals between the two metals.[237] Cleavage of the Si–Si bond in cyclopolysilane$^{\bullet+}$[238] to yield synthetically interesting α-alkoxypolysilanes[239] and in linear polysilane$^{\bullet+}$ was studied (Scheme 48).[240] In **94**$^{\bullet+}$[241] the Si–Si bond cleavage is an intramolecular nucleophile-assisted process, as deduced from mass spectrometry fragmentation profiles.[242]

Cleavage of the Si–Si bond was also observed upon PET of hexamethyldisilane and aromatic nitriles to provide silylation at the aromatic ring; unfortunately, it proceeded only in very moderate yields.[243] By the same token, Sn–Sn,[244] Sn–Ge,[244] Sn–Si,[244] and Ge–Ge[245] bond ruptures were documented at the stage of the radical cation. While kinetic data on these bond cleavages are lacking, a qualitative ranking was tentatively provided: Si–Si < Ge–Ge ≪ Sn–C.[245]

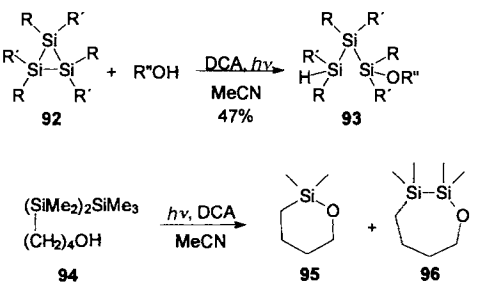

92 93

94 95 96

Scheme 48. The [→ AB, $RC_{Nu,red}$] reaction according to Hirai (1986, top) and the [→ AB] reaction according to Nakadaira (1991, bottom).

4.4. C–C Bond Dissociation

Although C–C bond fragmentations play an important role in synthetic radical cation chemistry, their special significance results from fundamental and industrial aspects, that is, the oxidative break down of softwood lignin[246] and new processes for converting coal into chemicals and fuels.[247] In numerous cases C–H deprotonation competes with C–C bond dissociation, and in order to prevail C–C bond fragmentations mostly need to be exergonic. As illustrated in Scheme 44, simple calculations of thermochemical cycles and semiempirical methods[248] can be used to estimate the two-center one-electron bond strengths.

Bibenzyl$^{\bullet+}$—the prototype of a coal model compound—preferentially reacts by deprotonation,[249, 250] since the estimated C–C bond strength of 29 kcal mol^{-1} in acetonitrile is too high.[251] In many investigations it became clear that upon adding alkyl,[113, 249] aryl,[252–255] hydroxy,[256–259] siloxy,[256] or alkoxy[251, 260–263] substituents to the CH_2CH_2 unit, the barrier for ⓟ-C-C$^{\bullet+}$ scission could be lowered because of the more favorable thermodynamics.[264] Such bond dissociation energies (Table 14) are helpful for devising fast cleavage reactions; for instance, a PET-induced fragmentation is only feasible if ΔG^0 is smaller than 10 kcal mol^{-1}, otherwise it may not compete with back electron transfer.[251]

Table 14. Calculated change in enthalpy for ⓟ-C-C$^{\bullet+}$ bond scission.

Reaction	ΔH_R(ⓟ-C-C$^{\bullet+}$) mesolyt. BDE [kcal mol^{-1}]	ΔH_R(ⓟ-C-C) homolyt. BDE [kcal mol^{-1}]	Ref.
CH_2=$CHCH_2$–$CH_3^{\bullet+}$ → Me$^{\bullet}$ + CH_2=$CHCH_2^+$	+41	+74	[265]
CH_2=$CHCH_2$–$CH_3^{\bullet+}$ → CH_2=$CHCH_3$ + Me^+	+80	+74	[265]
$PhCH_2$–$tBu^{\bullet+}$ → $PhCH_2^{\bullet}$ + tBu^+	+21	+73	[248]
$PhCH_2$–$CH_2OMe^{\bullet+}$ → $PhCH_2^{\bullet}$ + $MeOCH_2^+$	+10	+69	[77]
$PhCH_2$–$CH_2OH^{\bullet+}$ → $PhCH_2^{\bullet}$ + $HOCH_2^+$	+33	+70	[266]
$PhCH_2$–$CH_2Ph^{\bullet+}$ → $PhCH_2^{\bullet}$ + $PhCH_2^+$	+29	+64	[248]
Ph_2CH–$CHPh_2^{\bullet+}$ → $Ph_2CH^{\bullet}$ + Ph_2CH^+	+9	+48	[251]

Since C–C bond scissions most often proceed monomolecularly and only rarely in a nucleophile-assisted process,[267] it is possible to make reasonable predictions on the kinetics (based on the extensive work by Akaba,[268] Das,[269] and Maslak[270, 271]), as a linear correlation[272] between kinetic and thermodynamic data for ⓟ-C-C$^{\bullet+}$ rupture could be derived (Figure 2). Indeed, the activation barriers proved to be almost identical with experimental ΔG^0 values.[271] The activation data in Table 15 reveal strongly negative activation

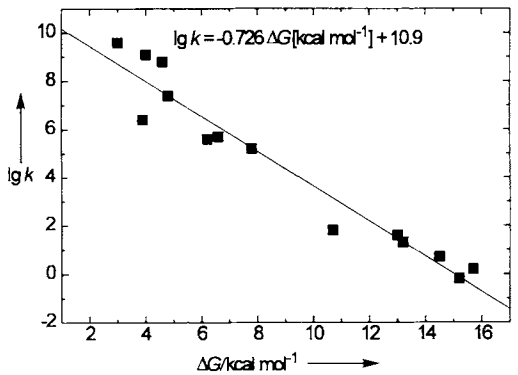

Figure 2. Linear correlation of $\lg k$ and the thermodynic driving force ΔG for the bond dissociation of substituted 1,2-biarylethanes [271].

entropies for all bicumyl$^{\bullet+}$ fragmentations, which demonstrates the importance of considering the charge localization and the concomitant changes in solvation in the transition state.[270] This charge localization in the scissile bond was verified in calculations as well,[45] whereas in the reactant radical cations (for example bibenzyl$^{\bullet+}$ [248] and aryl alkane$^{\bullet+}$ [45]) the charge and the spin density is only delocalized over one of the aromatic rings.[274] A lucid picture with regard to the role of stereoelectronic factors, charge delocalization, solvent effects etc. has been drawn in an insightful review.[275]

Table 15. Kinetic data for bicumyl$^{\bullet+}$ bond dissociation (X = *para* substituent).

X	k_{obs} at 253 K [s^{-1}]	$\Delta H^{\neq}$ [kcal mol^{-1}]	$\Delta S^{\neq}$ [e.u.]	Ref.
NO_2	3.5×10^{10} (300 K) 1.1×10^{3} (195 K)	7.0	−10	[273]
CN	3.3×10^{1}	11.8 ± 0.8	−27 ± 2	[270]
H	1.4×10^{2}	12.0 ± 0.8	−19 ± 3	[270]
OMe	7.9×10^{2}	12.8 ± 0.6	−12 ± 2	[270]
NMe_2	$> 5 \times 10^{4}$			[270]

An aspect of high synthetic consequence was recently disclosed through the work of Dinnocenzo,[267] who demonstrated that ⓝ-C-C$^{\bullet+}$ cleavage in **97** follows a nucleophile-induced cleavage pathway. Optically active (*R*)-**97** reacted with methanol under clean inversion to the optically active methyl ether **98** (Scheme 49).[267] The inversion of configuration at C2 was rationalized by attack of the nucleophile onto the ring-closed radical cation from the backside in a three-electron S_N2 reaction; the explicit mechanistic details could be construed with the valence-bond configuration-mixing model.[276] The observed bimolecular rate constants that are dominated by electronic rather than steric factors range around $10^6 - 10^8\,M^{-1}s^{-1}$, which points to rather fast induced C–C bond cleavage.[277] So far nucleophile-induced fragmentations are apparently restricted to strained systems.[278] In contrast, thermodynamic (Table 16) and kinetic data for ⓝ-C-C$^{\bullet+}$ fragmentation are only available for few systems: Ph(PhNH)CH–CHPh(OH)$^{\bullet+}$: $k_f = 3.7 \times 10^5\,s^{-1}$,[279] Ph(*N*-morpholinyl)HC–CHPh(*N*-morpholinyl)$^{\bullet+}$: $k_f = 9.6 \times 10^7\,s^{-1}$.[280]

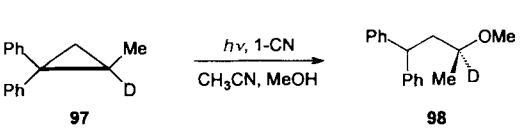

97 98

Scheme 49. The [→ Nu, $R^{\bullet}_{red}$] reaction according to Dinnocenzo (1990).

Table 16. Calculated change in enthalpy for ⓝ-C-C$^{\bullet+}$ bond cleavage [77,266].

Reaction	ΔH_R (ⓝ-C-C$^{\bullet+}$) mesolyt. BDE [kcal mol^{-1}]	ΔH_R (ⓝ-C-C) homolyt. BDE [kcal mol^{-1}]	Ref.
$tBu-CH_2OMe^{\bullet+} \rightarrow tBu^{\bullet} + MeOCH_2^+$	+1	+69.5	[77]
$H_2NCH_2-CH_2NH_2^{\bullet+} \rightarrow H_2NCH_2^{\bullet} + H_2NCH_2^+$	+22	+80	[248]
$H_2NCH_2-CH_2NH_2^{\bullet+} \rightarrow H_2NCH_2^{\bullet} + H_2NCH_2^+$	+16	+76	[266]
$Me_2NCH_2-CH_2NMe_2^{\bullet+} \rightarrow Me_2NCH_2^{\bullet} + Me_2NCH_2^+$	+13	+57	[266]
$HOCH_2-CH_2OH^{\bullet+} \rightarrow HOCH_2^{\bullet} + HOCH_2^+$	+20	+80	[248]
$HOCH_2-CH_2NH_2^{\bullet+} \rightarrow HOCH_2^{\bullet} + H_2NCH_2^+$	+8	+77	[266]

4.4.1. ⓟ-C-C$^{\bullet+}$ Bond Dissociation

The ⓟ-C-C$^{\bullet+}$ bond dissociation often has to compete with ⓟ-C-H$^{\bullet+}$ deprotonation, as long as the latter is feasible.[281] Hence, an extra driving force for ⓟ-C-C$^{\bullet+}$ bond scission may be desirable, and is often brought about in strained carbocyclic systems. A good part of the hitherto known examples stem indeed from strained cyclopropanes,[282] spiroalkanes,[283] cyclobutanes, or oxiranes.[284] Synthetically interesting reactions may subsequently be derived from trapping the ring-opened distonic radical cation with electron-rich double-bond systems,[285] oxygen,[286] NO,[287] or n nucleophiles (Scheme 50).[288, 289]

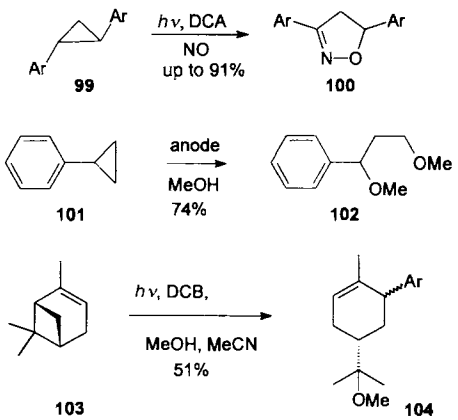

Scheme 50. The [→ CC, $RC_{Nu,rad}$] reaction according to Mizuno (1992, top), the [→ CC, $RC_{Nu,ox}$] reaction according to Shono (1970, middle), and the [→ CC, $RC_{Nu,RA}$] reaction according to Arnold (1989, bottom).

A high degree of stereo- and regioselectivity was disclosed in the PET oxidations of (1*R*,5*R*)-(+)-sabinene (**105**; Scheme 51), which emphasizes the importance of distribution

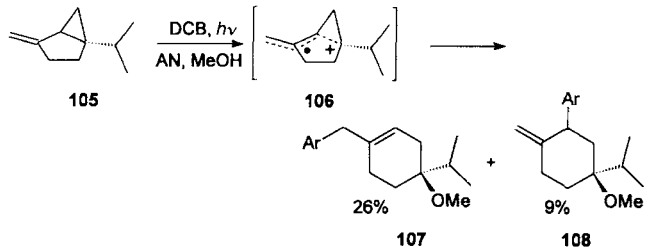

Scheme 51. The [→CC,$RC_{Nu,RA}$] reaction according to Roth (1994); AN = acetonitrile, Ar = 4-NCC_6H_4.

of spin and charge in the radical cation for the resulting chemistry[290] and points again to the occurrence of a nucleophile-assisted ⓟ-C-C$^{\bullet+}$ cleavage. Similarly, in the PET oxidation of (+)-carene, Arnold observed a stereo- and regioselective ⓟ-C-C$^{\bullet+}$ bond opening in the presence of methanol, whereas in acetonitrile (+)-carene$^{\bullet+}$ was partially racemized.[291] To rationalize the regioselective attack of methanol a simple rule was provided: The center with the lower oxidation potential will preferentially react as carbocation.[291]

One-electron oxidation of unstrained olefins and arenes equally leads to C–C bond cleavage if the bond dissociation energy can be lowered adequately (Scheme 52);[251, 292] the

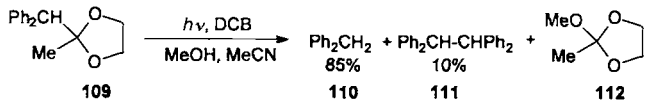

Scheme 52. The [→CC,$R^{\bullet}_{red}$] reaction according to Arnold (1989).

electron apportionment of the two cleavage fragments can be concluded by the thermodynamic stability of the two possible cations. The ⓟ-C-C$^{\bullet+}$ bond cleavage reactions of unstrained systems may also occur in a base- or nucleophile-induced mode, as demonstrated by Whitten and Baciocchi. However, only a few cases were reported so far (Scheme 53).[293]

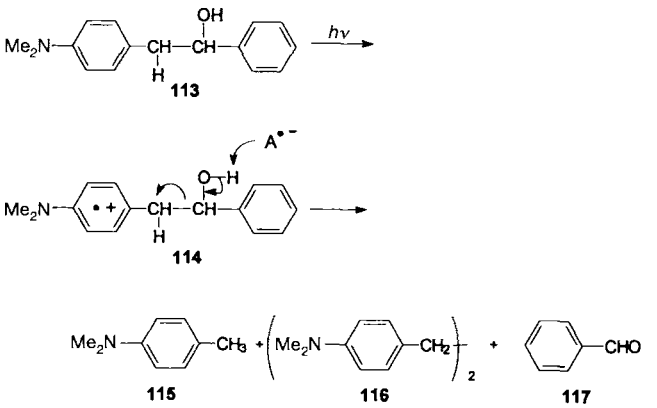

Scheme 53. The [→CC] reaction according to Whitten (1989); A = thioindigo.

Until now, only little attention has been devoted to stereoelectronic factors controlling ⓟ-C-C$^{\bullet+}$ bond scission. Clearly, the rate of fragmentation should be higher with increased overlap between the π electrophore and the scissile σ bond.[294] Conversely, a dihedral angle (defined by the plane of the π system and the C–C bond) of 90° ought to lead to slower cleavage, as demonstrated for the methyl 2-phenylcyclopentyl ether radical cation.[251, 261b] While *trans*-**118** readily underwent ⓟ-C-C$^{\bullet+}$ fragmentation, the *cis* compound **120** afforded **121** after oxidation, deprotonation, reduction, and reprotonation (Scheme 54). Similar stereoelectronic effects were detected for the ⓟ-C-C$^{\bullet+}$ cleavage of indane, 2,3-dihydrobenzofuran, and furan derivatives[262b] as well as for substituted cyclohexanes.[263]

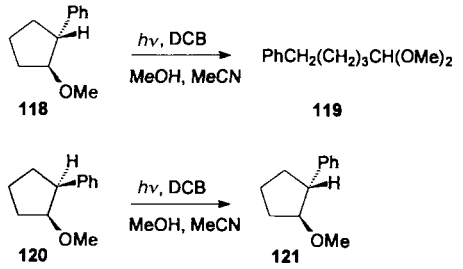

Scheme 54. The [→CC,$RC_{Nu,red}$] reaction according to Arnold (1989, top) and the [→CH,$R^{\bullet}_{red}$] reaction according to Arnold (1991, bottom).

In PET-initiated ⓟ-C-C$^{\bullet+}$ cleavages, the rate of back electron transfer may often surpass that of the desired reaction. An efficient strategy for avoiding back electron transfer in such schemes uses rapidly fragmentable acceptors in a cofragmentation protocol[295] or "cooperative C–C fragmentation". In the latter reaction the scissile bond is flanked by a radical cation and a radical anion substituent (see for example **123** in Scheme 55).[296]

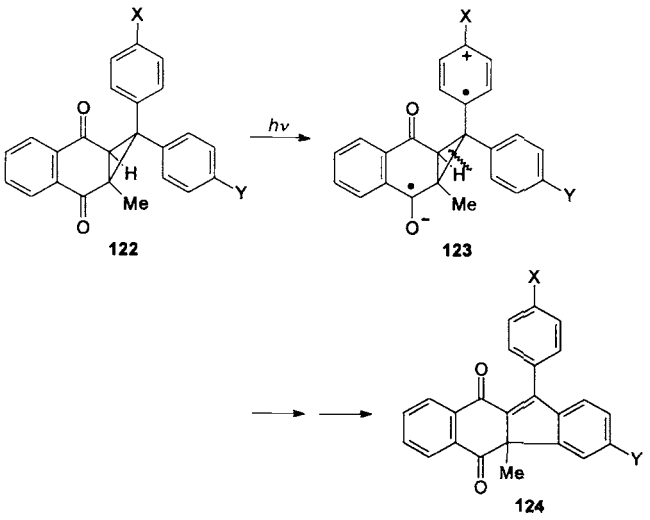

Scheme 55. The [→CC] reaction according to Oshima (1996); X = Y = H, Me, OMe.

4.4.2. ⓝ-C-C$^{\bullet+}$ Bond Dissociation

The controlled C–C bond rupture in ⓝ-C-C$^{\bullet+}$ has not been used as often as in ⓟ-C-C$^{\bullet+}$, but it was beautifully employed

in the synthesis of anhydrovinblastine.[297] Again, one has to provide the necessary thermochemical driving force, which can be accomplished by stabilizing the resulting cationic and/or radical fragments.[298, 299] Otherwise ⓝ-C-C$^{\bullet+}$ bond rupture may not compete successfully with deprotonation. As cation stabilization is the more important contributor, N, S, O, and aryl substituents are most helpful for inducing a ⓝ-C-C$^{\bullet+}$ cleavage mode, as demonstrated with amino ketones,[300] amino alcohols,[301] and β-phenylamines.[302] Fragmentations of amino alcohol radical cations may proceed by a base-assisted mechanism.[266] In addition, one finds ⓝ-C-C$^{\bullet+}$ bond scission is feasible in strained carbocyclic[303] or heterocyclic[304, 305] ring systems. In particular, substituted cyclopropyl sulfides such as **125**[303] and **129**[306c] were extensively exploited in intramolecular etherifications, spiroannulations, and diquinane synthesis (Scheme 56).[306]

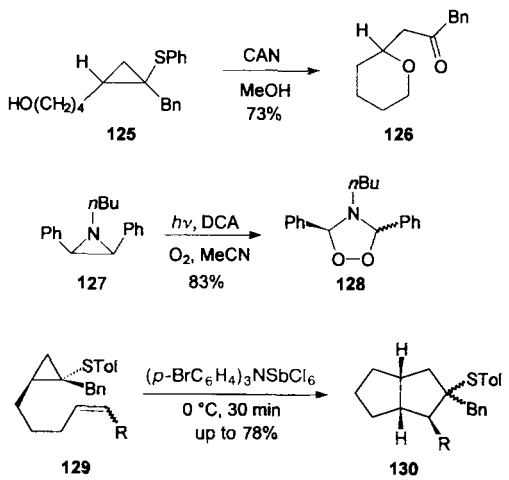

Scheme 56. The [→CC,RC$_{Nu,ox}$] reaction according to Iwata (1994, top) and the [→CC,RC$_{CA,red}$] reactions according to Schaap (1983, middle) and Iwata (1995, bottom); Tol = $H_3CC_6H_4$.

Depending on the structure ⓝ-C-C$^{\bullet+}$ cleavage can readily outrun ⓝ-C-H$^{\bullet+}$ deprotonation.[300b] Accordingly, deprotonation seems to be much less a problem with dioxolane$^{\bullet+}$, as C–C bond rupture is almost exclusively observed.[307] However, because of the high oxidation potentials of dialkyldioxolanes (> 2.7 V versus SCE), only very strong acceptors (such as excited TCB) provide enough driving force for the electron transfer. After ⓝ-C-C$^{\bullet+}$ bond cleavage in **131** the distonic radical cation couples to the TCB radical anion (Scheme 57).

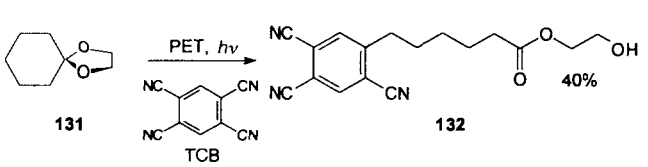

Scheme 57. The [→CC,RC$_{Nu,RA}$] reaction according to Albini (1992).

Through the proper choice of reaction conditions, radical–radical anion coupling can be avoided in such PET reactions; for example, **135** was obtained from **134** in the presence of thiols by hydrogen-atom abstraction (Scheme 58).[308] Likewise, aliphatic ethers readily undergo ⓝ-C-C$^{\bullet+}$ cleavage[309] after oxidation, since a portion of the driving force stems from their high oxidation potentials.[77]

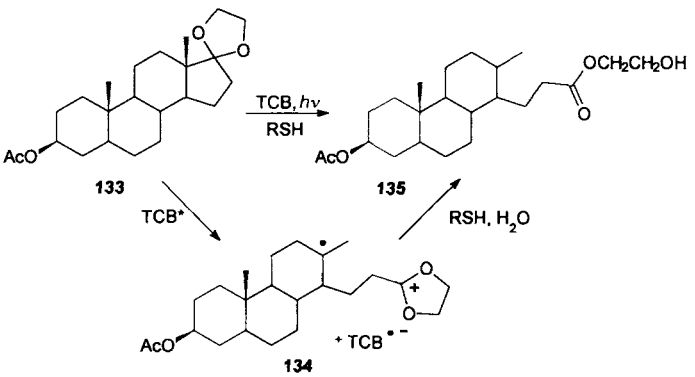

Scheme 58. The [→CC,RC$_{Nu,rad}$] reaction according to Albini (1994).

Steric and stereoelectronic effects in ⓝ-C-C$^{\bullet-}$ fragmentations were shown to be important in amino alcohols and diamines as well. The most favorable conformation for bond cleavage is that with the two heteroatomic functionalities in an antiperiplanar arrangement.[266]

4.4.3. ⓞ-C-C$^{\bullet+}$ Bond Dissociation

Important recent contributions to ⓞ:C-C$^{\bullet+}$ are derived from studies on strained carbocycles, for example cyclopropanes (Scheme 59),[310, 311] bicyclobutanes,[312] tetrahedranes,[313] and housanes.[229] ESR investigations on alkane radical cations show that in general inner C–C σ bonds are selectively weakened.[314] This is in line with cleavage selectivities observed in pulse-radiolysis experiments. Stereoelectronic factors are not expected to play an important role, as the unpaired electron is already removed directly from the scissile bond.

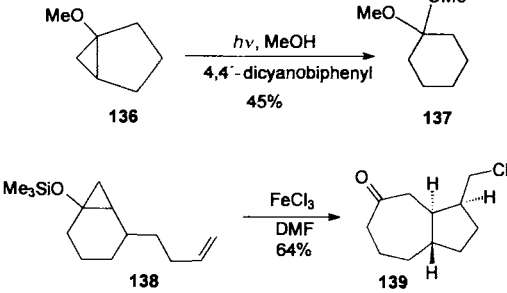

Scheme 59. The [→CC,RC$_{Nu,red}$] reaction according to Gassman (1988, top) and the [→CC,RC$_{-E,add}$] reaction according to Booker-Milburn (1992, bottom). RC$_{-E,add}$: radical cations result after loss of an electrofuge from a double bond.

4.5. C–X Dissociation

The C–X dissociation energies can be estimated according to the thermochemical cycle in Scheme 44 (Table 17). Unfortunately, their usefulness is not clear: Several examples of nucleophile-assisted ⓣ-C-Si$^{\bullet+}$ cleavages[208] were disclosed by Dinnocenzo, which were induced by addition of the appropriate nucleophiles. Only in light of such a mechanism can it

Table 17. Calculated change in enthalpy for π-C-X$^{\bullet+}$ bond cleavage.

Reaction	ΔH_R (π-C-X$^{\bullet+}$) BDE [kcal mol^{-1}]	ΔH_R (π-C-X) homolyt. BDE [kcal mol^{-1}]	Ref.
$PhCH_2$–$SiMe_3^{\bullet+}$ → $PhCH_2^{\bullet}$ + Me_3Si^+	+30	+77	[208]
$PhCH_2$–$Cl^{\bullet+}$ → $Cl^{\bullet}$ + $PhCH_2^+$	+40	+72	[318]
$PhCH_2$–$Br^{\bullet+}$ → $Br^{\bullet}$ + $PhCH_2^+$	+26	+58	[318]
$PhCH_2$–$OMe^{\bullet+}$ → $MeO^{\bullet}$ + $PhCH_2^+$	+43	+71	[318]
$PhCH_2$–$SMe^{\bullet+}$ → $MeS^{\bullet}$ + $PhCH_2^+$	+38	+61	[318]
PhS–Xan$^{\bullet+}$ → PhS$^{\bullet}$ + Xan$^+$ [a]	−11	+26.4	[319]
PhS–TPCP$^{\bullet+}$ → PhS$^{\bullet}$ + TPCP$^+$ [a]	−18.6	+40.3	[319]

[a] Xan: 9-xanthyl; TPCP: 1,2,3-triphenylcyclopropenyl.

be understood that a C–Si bond worth about 30 kcal mol^{-1} in the *p*-methoxybenzyltrimethylsilane$^{\bullet+}$ is selectively cleaved at about 1×10^6 s^{-1} at room temperature.[315-317] Consonant with this proposal, the rate of C–Si bond rupture increases with more nucleophilic partners and with less crowded SiR_3 fragments.

The kinetics of n-C-X$^{\bullet+}$ cleavages were only recently studied, however only for n-C-Si$^{\bullet+}$. In the case of $PhN(Me)CH_2$–$SiMe_3^{\bullet+}$ a clear dependence of k on the concentration of MeOH, H_2O, and nBu$_4$NF indicates a silophile-induced desilylation.[89] The second-order rate constants revealed the desilylation to be a rather rapid process: 8.9×10^5 (MeOH), 1.27×10^6 (H_2O), and 3.1×10^9 M^{-1}s^{-1} (nBu$_4$NF).

4.5.1. π-C-X$^{\bullet+}$ Bond Dissociation

Although π-C-X$^{\bullet+}$ have not been investigated as extensively as π-C-H$^{\bullet+}$ or π-C-C$^{\bullet+}$ scissions, they have some intriguing synthetic value insofar as they allow the predetermination of the scissile bond.[320] In particular, by using the trialkylsilyl or the trialkylstannyl group as a kind of "super proton" an interesting oxidative approach to the desired radicals can be set up (Scheme 60);[321] this works even better than π-C-H$^{\bullet+}$ deprotonation.[322] Such π-C-X$^{\bullet+}$ bond cleavage reactions with stannanes have some potential for unconventional imaging systems, an idea that was first exploited by Eaton.[323]

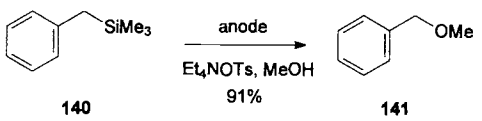

140 141

Scheme 60. The [→ CX, R$^{\bullet}_{ox}$] reaction according to Yoshida (1986).

The synthetic potential of π-C-SiR$_3^{\bullet+}$ and π-C-SnR$_3^{\bullet+}$ bond rupture was explored by Mariano in both intermolecular and intramolecular variants using iminium salts as photooxidants.[324] High yields could be realized through intramolecular radical–radical coupling reactions, for example **142** → **143** (Scheme 61). Alternatively, other processes can be triggered after π-C-X$^{\bullet+}$ bond scission (e. g. [→ CX, R$^{\bullet}_{RA}$]), as in the photobenzylation or allylation of aromatic or heteroaromatic compounds.[325-327]

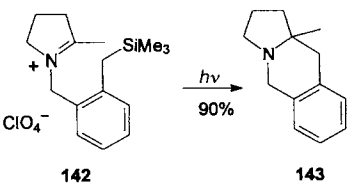

142 143

Scheme 61. The [→ CX, R$^{\bullet}_{rad}$] reaction according to Mariano (1984).

In particular, C–Si bond cleavage in benzyl and allyl silanes is so fast that substitution at the π system cannot compete.[328] As a consequence benzylsilanes were used as interesting mechanistic probes to differentiate between hydrogen-atom abstraction and electron transfer, for example in side-chain bromination.[329] Studies on silaindane$^{\bullet+}$ indicated that π-C-Si$^{\bullet+}$ bond cleavage is not dependent on stereoelectronic factors, presumably because of the strong Si–O bond formed in the nucleophile-assisted mode with ROH.[330]

4.5.2. n-C-X$^{\bullet+}$ Dissociation

Similar to the case of π-C-X$^{\bullet+}$, n-C-X$^{\bullet+}$ bond cleavage was exploited to cleave selectively a preconditioned bond (mostly in amines, sulfur, and other nitrogen-centered electrophores with X = SiR_3 and SnR_3 as superelectrofuges). For instance, α functionalization can readily be accomplished after n-C-X$^{\bullet+}$ bond scission of arylthiomethylsilane **144**[321a] as an alternative to n-C-H$^{\bullet+}$ deprotonation of sulfides (Scheme 62).[331] In some special cases the observed stereoselectivities indicate a n-C-X$^{\bullet+}$ fragmentation[332] induced by the intramolecular attack of a nucleophilic double bond. The

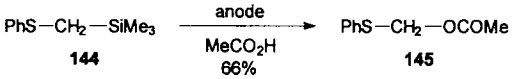

144 145

Scheme 62. The [→ CX, R$^{\bullet}_{ox}$] reaction according to Fuchigami (1989).

n-C-X$^{\bullet+}$ cleavages have efficiently been exploited in intramolecular cyclizations,[85, 332-334] for example in the synthesis of (−)-retronecanol,[332a] but only seldomly in intermolecular reactions, for example with α-silylthioethers[335] and with carbamates (Scheme 63).[336]

After intra- and intermolecular PET from α-silylamines onto enones, the follow-up reactions can be steered by the choice of solvent (Scheme 64). As proton transfer from the amine radical cation to the enone radical anion is fast in aprotic media (e. g. CH_3CN) almost no desilylation but mainly deprotonation is observed. In protic solvents, where a hydrogen bonding decreases the basicity, desilylation is preferred.[337] Intramolecular ET in **156** opened the way for a spiroannulation.[333] In continuation of the above strategy, a sequential double-desilylation methodology was recently devised for generating a nonstabilized azomethine ylide that could be employed in the synthesis of 1-azabicyclo[*m*.3.0]-alkanes.[338]

4.5.3. σ-C-X$^{\bullet+}$ Dissociation

Similar schemes as for π-C-X$^{\bullet+}$ and n-C-X$^{\bullet+}$ bond cleavages were set up in σ:C-X$^{\bullet+}$ reactions, in particular for silanes and stannanes such as silyl and stannyl[339] ethers as well as 2-silyl-[340] or 2-stannyl-1,3-dithianes.[341] After one-electron oxidation **158** cleaves to form the tributylstannyl

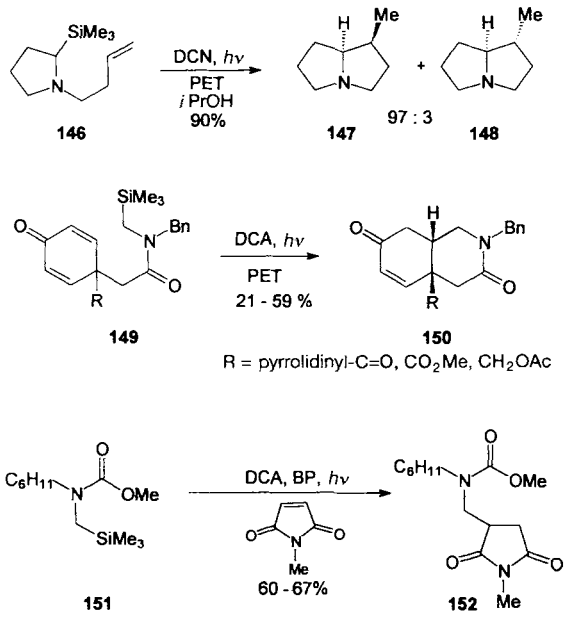

Scheme 63. The [→ CX, $R^{\bullet}_{add,red}$] reactions according to Pandey (1992, top), Mariano (1992, middle), and Steckhan (1995, bottom); BP = biphenyl.

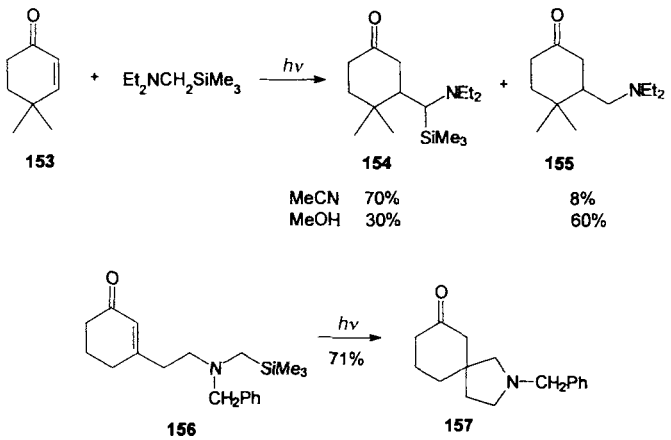

Scheme 64. The [→ CX, $R^{\bullet}_{RA}$] reactions according to Mariano (1988, top; 1989, bottom).

radical and the 1,3-dithian-2-yl cation;[342] the latter could be efficiently trapped with various unsaturated, electron-rich substrates such as olefins and silyl enol ethers (Scheme 65).

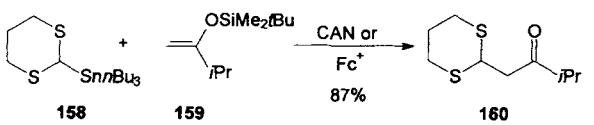

Scheme 65. The [→ CX, $R^{\bullet}_{ox}$] reaction according to Narasaka (1993); Fc^+ = ferrocenium ion.

The C–Sn unit as σ electrophore[343] and readily scissable element has found elegant use in the functionalization of stannyl ethers,[339] carbamates,[339] carboxamides,[344] benzil,[345] and carbamides.[344] Many C–X cleavages that take place after oxidation of simple allylsilanes and allylstannanes should also be categorized as ⓞ:C-$X^{\bullet+}$ reactions, for example **162** (+**161**) as [→ CX, $R^{\bullet}_{rad}$][346] and **162** (+**164**) as [→ CX, $R^{\bullet}_{RA}$] (Scheme 66).[347]

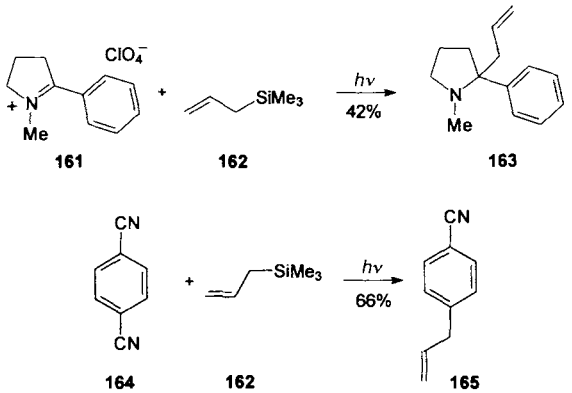

Scheme 66. The [→ CX, $R^{\bullet}_{rad}$] reaction according to Mariano (1982, top) and the [→ CX, $R^{\bullet}_{RA}$] reaction according to Otsuji (1985, bottom).

In a direct comparison it was found that ⓞ:C-$Sn^{\bullet+}$ bond cleavage is much more facile than ⓞ:C-$Si^{\bullet+}$ rupture,[342, 348] however, neither thermochemical nor absolute rate data are available.[349] In contrast to reports on π-C-$Si^{\bullet+}$ fragmentations[208], ⓞ:C-$Si^{\bullet+}$ do not undergo nucleophile-assisted cleavage.[348]

4.6. Attack of nucleophiles

In the preceeding sections, oxidative incorporation of a nucleophile was effected by trapping a cationic intermediate after cleavage (e. g. [→ CH, $R^{\bullet}_{ox}$] or [→ AB, $R^{\bullet}_{ox}$]). However, this is also possible by direct attack of a nucleophile onto a radical cation, for example in aromatic substitution.[350]

Although a large number of $RH^{\bullet+}$–Nu reactions were studied,[25] there are basically no general guidelines on how to set up an ideal system. Part of the problem arises from the complex mechanistic schemes that may be operative in seemingly identical reactions. Whereas mechanistic details were identified in singular cases, they are unknown for most reactions. Several mechanistic scenarios that depend on the nucleophile and $RH^{\bullet+}$ need to be discussed, as outlined in detail by Hammerich and Parker,[351] for example disproportionation,[352] complexation, and half-regeneration (Scheme 67). In addition, Okazaki stressed that deprotonation of the primary adduct is important for protic nucleophiles such as alcohols and water.[353]

While in the early 1980s the kinetics of radical cation–nucleophile combinations was intensely investigated, these studies were often hampered by the fact that complex mechanisms[354, 355] were operative as a consequence of using radical cations of low reactivity. A long-standing discussion on the reactivity of radical cations with nucleophiles[356–358] has taken place ever since. Although additional kinetic studies were undertaken with the advent of nanosecond and picosecond time resolved techniques, no consistent picture of this reaction mode has emerged so far.

disproportionation:

$$2\,RH^{\bullet+} \rightleftharpoons RH^{2+} + RH$$
$$RH^{2+} + Nu \longrightarrow \text{products}$$

complexation:

$$RH^{\bullet+} + Nu \rightleftharpoons (RH/Nu)^{\bullet+}$$
$$(RH/Nu)^{\bullet+} + RH^{\bullet+} \rightleftharpoons (RH/Nu)^{2+} + RH$$
$$(RH/Nu)^{2+} \longrightarrow \text{products}$$

half-regeneration

$$RH^{\bullet+} + Nu \rightleftharpoons RH^{\bullet}\text{-}Nu^{+}$$
$$RH^{\bullet}\text{-}Nu^{+} + RH^{\bullet+} \rightleftharpoons RH^{+}\text{-}Nu^{+} + RH$$
$$RH^{+}\text{-}Nu^{+} \longrightarrow \text{products}$$

deprotonation (for protic nudeophiles):

$$RH^{\bullet+} + HNu \rightleftharpoons RH^{\bullet}\text{-}NuH^{+}$$
$$RH^{\bullet}\text{-}NuH^{+} + HNu \longrightarrow RH^{\bullet}\text{-}Nu + H_2Nu^{+}$$
$$RH^{\bullet}\text{-}Nu - e^{-} \longrightarrow \text{products}$$

Scheme 67. Mechanistic scenario for the reaction of $RH^{\bullet+}$ with nucleophiles (Nu, HNu).

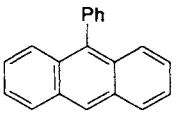

166

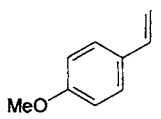

167

Table 18. Rate constants for the reaction of 9-phenylanthracene$^{\bullet+}$ (**166**$^{\bullet+}$) and *p*-methoxystyrene$^{\bullet+}$ (**167**$^{\bullet+}$) with various nucleophiles.

Nucleophile	k (**166**$^{\bullet+}$) [$M^{-1}s^{-1}$] (T[°C])	Ref.	k (**167**$^{\bullet+}$) [$M^{-1}s^{-1}$] (T[°C])	Ref.
anions				
azide			4.2×10^{10} (20)	[364]
acetate	3.4×10^{9} (25)	[361]	4.0×10^{10} (20)	[364]
trifluoroacetate	3.6×10^{6} (25)	[361]		
nitrate	1.5×10^{6} (25)	[361]	2.4×10^{9} (20)	[364]
amines				
NEt_3	3.0×10^{9} (23)	[360]	6.6×10^{9} (20)	[365]
sec-butylamine	7.7×10^{8} (23)	[360]		
tert-butylamine	3.3×10^{8} (23)	[360]	2.1×10^{9} (20)	[365]
trifluoroethylamine	8.1×10^{6} (23)	[360]		
pyridines				
pyridine	1.2×10^{7} (25)	[368]		
2-methylpyridine	1.1×10^{6} (25)	[368]		
4-cyanopyridine	7.2×10^{5} (25)	[368]		
2,6-dimethylpyridine	1.1×10^{3} (25)	[368]	3.9×10^{7} (20) [a]	[365]

[a] 2,4,6-trimethylpyridine.

A controversial message resulted from considerations of the valence-bond curve-crossing model,[358] which stated that the Ⓐ$^{\bullet+}$–Nu and Ⓝ$^{\bullet+}$–Nu reactions are formally forbidden, and therefore quite slow. The apparent failure of the curve-crossing model to predict correctly the barrier to the reaction of 9-phenylanthracene$^{\bullet+}$ with pyridine emphasized the necessity of taking additional parameters into consideration, that is, the association constants of ground and excited state reactants.[359]

A large body of kinetic data was published over the last decade, especially for substituted phenylanthracenes and styrenes by Parker[360-363] and Johnston,[364, 365] respectively (see Table 18). It was demonstrated that π radical cation–nucleophile combinations may be very rapid processes, and often approach the diffusion-controlled limit in the case of anionic nucleophiles. Despite the fact that many Ⓐ$^{\bullet+}$ compounds react rather rapidly, in particular with nitrogen nucleophiles, the situation is much more complex with oxygen nucleophiles[366] since examples exhibiting slow[367] and fast[364] attack have been documented. For example, primary amines react with the 9-phenylanthracene radical cation (**166**$^{\bullet+}$) by nucleophile addition at position 10 with second-order rate constants in the range 8×10^6 to $3 \times 10^9 M^{-1}s^{-1}$. The rates increased with increasing amine basicity and decreasing steric requirements.[360] In contrast, tertiary amines and anilines react with **166**$^{\bullet+}$ only by electron transfer (1.5×10^9 to $2 \times 10^{10} M^{-1}s^{-1}$), the rates of which correlate quite well with the oxidation potentials of the amine.[360] The reaction with substituted pyridines are markedly slower ($k = 10^3 - 10^7 M^{-1}s^{-1}$).[368]

Less studied are the kinetics with protic nucleophiles, which may react according to the deprotonation mechanism (see Scheme 67). In line with tabulated nucleophilicity data[369] the reaction rates with water and alcohols are much smaller than those with amines and pyridines.[353, 364] The Arrhenius activation energies determined for a series of substituted anthracene radical cations indicate the involvement of an initial π complex prior to bond formation (Scheme 68).[368]

$$A^{\bullet+} + Nu \longrightarrow (A/Nu)^{\bullet+}$$
$$(A/Nu)^{\bullet+} \longrightarrow A^{\bullet}\text{-}Nu^{+}$$

Scheme 68. Participation of a preliminary π complex in the reaction of substituted anthracene radical cations with nucleophiles.

Unfortunately, from a mechanistic point of view it is often very difficult to differentiate between Ⓐ$^{\bullet+}$+Ⓐ reactions (*r*adical *s*ubstrate *c*oupling, RSC) and Ⓐ$^{\bullet+}$/Ⓐ$^{\bullet+}$ combinations (*r*adical *r*adical *c*oupling, RRC). Clearly, the latter mode is often realized for anodic oxidations when the stationary concentration of the radical cations is as high as for the dimerization of triphenylamine.[370] Nevertheless, RSC mechanisms were established in the anodic dimerization of 4-methoxybiphenyl,[371] tetrahydrocarbazole,[354b] 4,4′-dimethoxystilbene,[372] and 9-methoxyanthracene radical cations.[373] It should be noted that under pulse-radiolysis conditions dimerization of triphenylamine proceeds preferentially by the rapid RSC mechanism ($k = 1 - 10 \times 10^7 M^{-1}s^{-1}$).[374]

Kinetic data on Ⓝ$^{\bullet+}$–Nu reactions are very scarce, but it was demonstrated recently that phosphane radical cations react with oxygen and sulfur nucleophiles[375] ($k = 10^5 - 10^7 M^{-1}s^{-1}$) following the same reactivity pattern as with styrene$^{\bullet+}$.[364] Moreover, a looser transition state for the reaction with thiols than with alcohols was indicated.[375]

Concerning intramolecular processes, cyclization rate constants for the attack of double bonds on dialkylamine radical cations[376] ($k = 2 \times 10^7 - 1 \times 10^{10} M^{-1}s^{-1}$) were four orders of magnitude faster than those of dialkylaminyl radicals.

4.6.1. *Attack of Nucleophiles on* Ⓐ$^{\bullet+}$

Part of the large interest in the Ⓐ$^{\bullet+}$–Nu reaction derives from the importance of radical cations as intermediates in the metabolic activation of polycyclic aromatic hydrocarbons.[377]

In addition, attack of nucleophiles on $\pi^{\bullet+}$ constitutes a reaction of large synthetic benefit and allows the formation of C–C, C–O, C–N, and other useful bonds.

Intramolecular reactions with π nucleophiles have attracted much attention because of their potential to construct synthetically useful five- and six-membered rings. In particular, arenes,[378, 379] alkyl enol ethers,[380, 381] enol thioethers,[381] silyl enol ethers,[378, 382–384] and enol esters[385] were used because of their low oxidation potentials (Scheme 69). According to Moeller,[386] enol ether cyclizations are best described as reversible; the outcome is controlled by the ease of oxidation of the intermediate distonic radical cation.

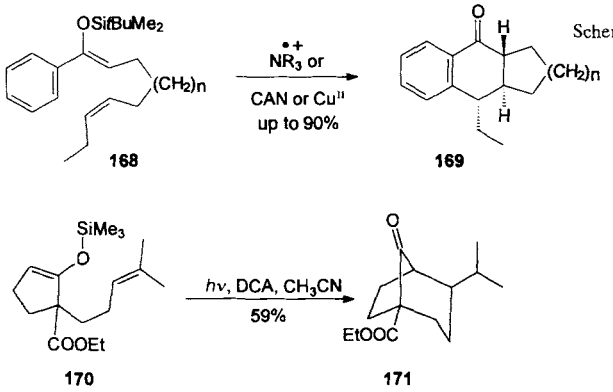

Scheme 69. The [→ Nu, $R^{\bullet}_{ox}$] reaction according to Snider (1990, top) and the [→ Nu, $R^{\bullet}_{red}$] reaction according to Mattay (1992, bottom).

The intramolecular variant with aromatic electrophores was often exploited for synthesis, for example in the transformation of the tetrahydroisoquinoline systems into alkaloids with the morphinane framework[387] and to kreysigine (**175**, Scheme 70).[388] Because of the electron-rich catechol unit, the π system of **172** and **174** is more readily oxidized

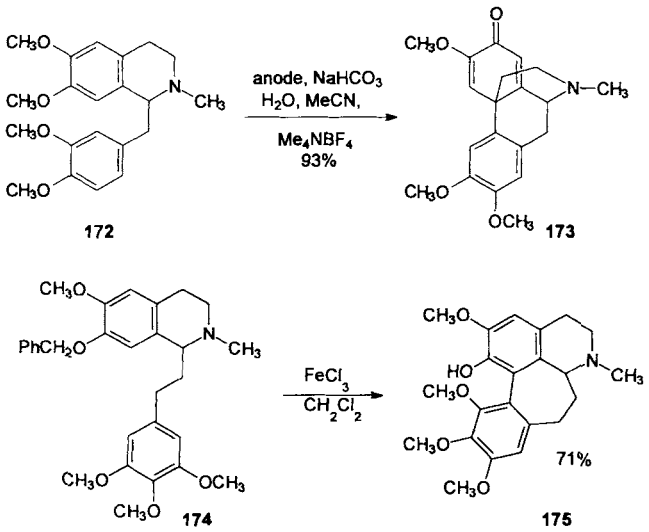

Scheme 70. The [→ Nu] reactions according to Miller (1978, top) and Herbert (1995, bottom).

than the amine functionality. Recent research focused on using this protocol for a biomimetic atropselective coupling to vancomycin antibiotics (**177**, Scheme 71),[389] as well as in the synthesis of isostegnan,[390] lignan lactones,[391] and deoxyschizandrins.[392]

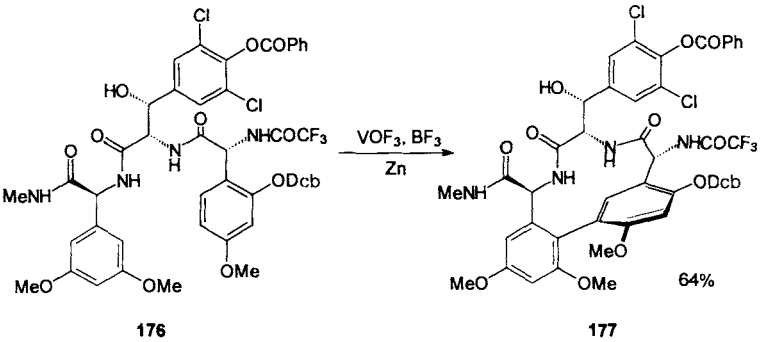

Scheme 71. The [→ Nu, $R^{\bullet}_{ox}$] reaction according to Evans (1993); Dcb = 3,4-dichlorobenzyl.

Likewise, n nucleophiles such as OH,[393, 394] COOH,[48, 395] and even NH_2[396, 397] can be applied in intramolecular cyclizations to trap olefin and arene radical cations, as demonstrated for the construction of **179** (Scheme 72).[396] Intramolecular attack of a hydroperoxy group onto an olefin radical cation is thought to constitute the key step in the synthesis of qinghaosu derivatives,[398] which makes use of the oxidant in only catalytic amounts (Scheme 72).

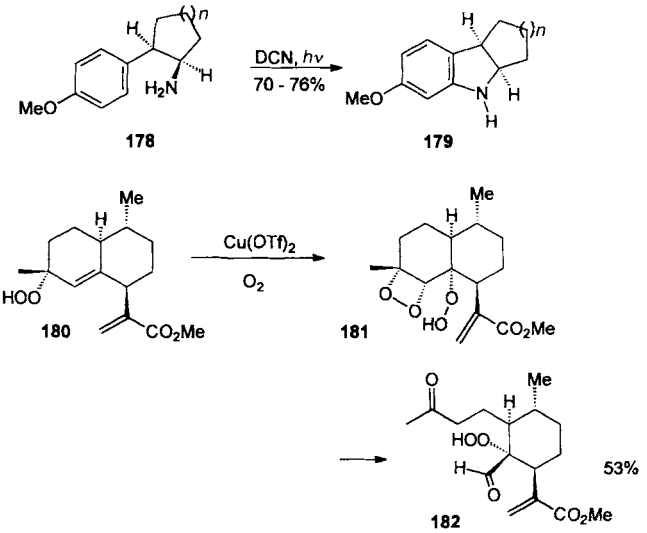

Scheme 72. The [→ Nu, $R^{\bullet}_{ox}$] reaction according to Pandey (1990, top) and the [→ Nu, $R^{\bullet}_{rad}$] reaction according to Haynes (1990, bottom); Tf = F_3CSO_2.

Synthetically useful intermolecular C–C bond formations were realized with π nucleophiles and cyanide, mostly under conditions of anodic oxidation (e. g. in dimerizations[399, 400] and cross couplings). As a special variant the photo-NOCAS (*n*ucleophile–*o*lefin *c*ombination *a*romatic *s*ubstitution) reaction after PET between an olefin and a cyanoaromatic acceptor was developed by Arnold (Scheme 73).[104, 401] First,

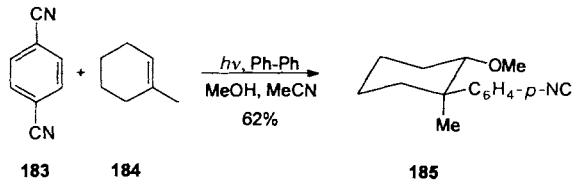

Scheme 73. The [→ Nu, $R^{\bullet}_{RA}$] reaction according to Arnold (1988).

184$^{\bullet+}$ is attacked by nucleophiles such as methanol or cyanide before the resulting radical reacts with the anion radical.

Transformations involving intermolecular attack of n nucleophiles at ⓟ$^{\bullet+}$ include reactions at olefins,[402] enol esters,[403] enol ethers (Scheme 74),[404] benzofurans,[400] dienes (Scheme 74),[405, 406] furans,[407] pyrrolidines,[408] and ketene imines.[409] In the cases where *cis* and *trans* adducts are formed, the diastereoselectivity depends on the solvent polarity and the bulkiness of the nucleophile.[402, 410] Importantly, the attack of n nucleophiles on ⓟ$^{\bullet+}$ proceeds by an *anti*-Markovnikov addition.[411]

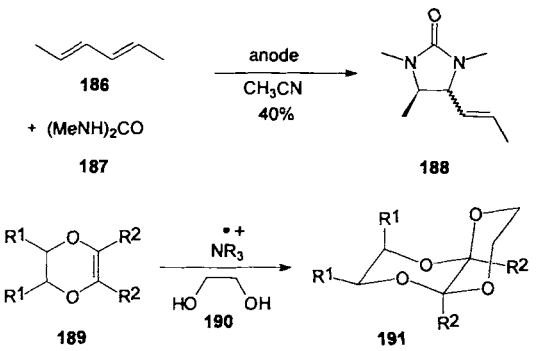

Scheme 74. The [→ Nu, $R^{\bullet}_{ox}$] reactions according to Schäfer (1979, top) and Lopez (1987, bottom).

In some instances interesting cyclizations of the resulting radical were triggered after attack by alcohols at the ⓟ$^{\bullet+}$ species.[412] Also the first enantioselective methanol addition under PET conditions was recently realized,[413] which required the enantiofacial-differentiating step to take place in a contact ion pair.[414] Further synthetic use of such ⓟ$^{\bullet+}$–Nu reactions was explored in intermolecular C–C bond formations starting from enamine[100, 415, 416] and silylated *aci*-nitroalkane radical cations.[417]

4.6.2. *Attack of Nucleophiles on* ⓝ$^{\bullet+}$

Attack of a nucleophile onto a ⓝ$^{\bullet+}$ species was observed mainly for nitrogen, phosphorous, and sulfur compounds. It plays an meaningful part in the formation of oxygenated derivatives (P,[418] S[419]) and in removing sulfur protecting groups.[420–422] In contrast to nitrogen-centered radical cations that undergo a rich chemistry with C–H and C–C bond cleavage, $R_3P^{\bullet+}$ and $R_2S^{\bullet+}$ suffer predominantly nucleophilic attack[423, 424] with only few exceptions.[425] Attack by carbon nucleophiles may also take place: For example, **192**$^{\bullet+}$ is attacked by a silyl enol ether to yield **195** by a Wittig rearrangement of the intermediate sulfonium salt (Scheme 75).[426]

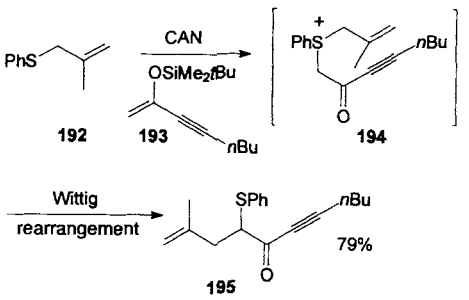

Scheme 75. The [→ Nu, $R^{\bullet}_{ox}$] reaction according to Narasaka (1991).

Intramolecular cyclizations of amine radical cations were exploited to furnish five-membered rings. In this protocol the distonic radical cation, formed after intramolecular cyclization to a π bond system, is further oxidized; this was demonstrated impressively in the anodic formation of **197** (Scheme 76).[427] A conceptually related cyclization protocol was devised by Newcomb that allows the synthesis of perhydroindoles, pyrrolizidines (for example **199**, Scheme 76), and other heterocyclic systems.[428] As an exception, the amine radical cation is generated by protonation of the neutral aminyl radical, which itself was formed from the PTOC carbamate **198**. As a pivotal point, the cyclization of the electrophilic radical cation has to be much more efficient than that of the neutral radical. The cyclized distonic radical cation is then deprotonated and trapped with RSH to afford product **199**. This strategy is related to the cyclization of *N*-chloroamines and nitrosamines in many ways.[429]

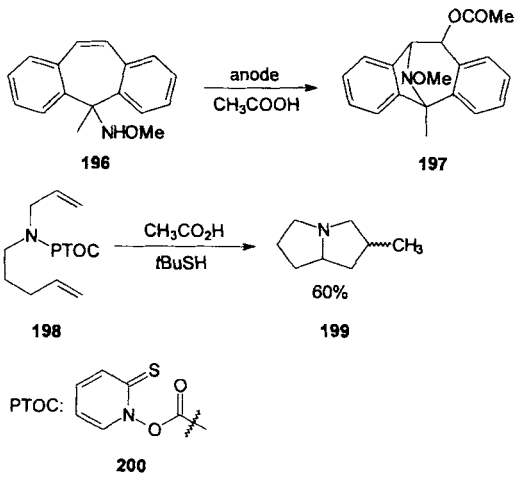

Scheme 76. The [→ Nu, $R^{\bullet}_{ox}$] reaction according to Karady (1989, top) and the [→ Nu, $R^{\bullet}_{add}$] reaction according to Newcomb (1987, bottom).

In very few cases the attack of a nucleophile can be stopped at the formation of a two-center three-electron bond.[430] An example is **201**$^{\bullet+}$, which exhibits a N–N distance of 216 pm that is shorter than in the neutral molecule (270 pm).[431]

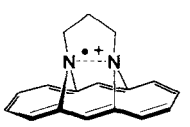

201

4.6.3. *Attack of Nucleophiles on* ⓞ$^{\bullet+}$

Although ⓞ$^{\bullet+}$–Nu combinations may be involved in the oxidative coupling of strained carbocyclic ring systems with inert nucleophiles,[310b, 432] mechanistically it is very difficult to decide if nucleophilic attack takes place prior to ⓞ:C-C$^{\bullet+}$ cleavage. A clear cut case, however, was detected for quadricyclane$^{\bullet+}$; its C–C bond was opened by *t*BuOH with $k = 2.0 \cdot 10^6\,M^{-1}s^{-1}$.[494]

4.7. Cycloadditions and Other Pericyclic Processes

4.7.1. *A Mechanistic Interlude*

Cycloadditions and other pericyclic processes[433] such as rearrangements and cheletropic reactions have mostly been observed for ⓟ$^{\bullet+}$. These transformations provide an attractive incentive to investigate radical cation chemistry, since in the majority of cases the observed activation barriers are extremely low, and even forbidden processes can quite often be initiated. For a radical cation catalyzed pericyclic reaction the product should exhibit a higher oxidation potential than the reactant (Figure 3). Follow-up oxidation reactions of the product are thus avoided.

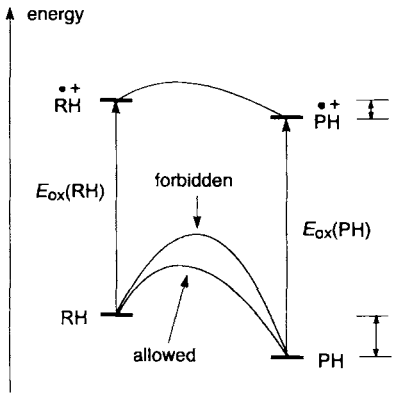

Figure 3. Energy diagramm of a radical cation catalyzed rearrangement RH → PH.

When selecting a chemical oxidant as catalyst (e. g. $NR_3^{\bullet+}$), it is advisable to generate the desired reactant radical cation in a moderately endergonic electron transfer preequilibrium with $\Delta E_{ox} = E_{ox}(RH) - E_{ox}(NR_3) \approx 0.3$–$0.6$ V (Scheme 77).

$$NR_3^{\bullet+} + RH \rightleftharpoons NR_3 + RH^{\bullet+} \qquad E_{ox}(NR_3) < E_{ox}(RH)$$

Scheme 77. The endergonic electron transfer equilibrium between RH and $NR_3^{\bullet+}$.

Since follow-up reactions of RH$^{\bullet+}$ are extremely rapid, the overall reaction rate is still reasonably fast despite the endergonic ET equilibrium. Larger differences in redox potential (ΔE_{ox}), however, slow down the overall reation too much. Kinetic studies of the Diels–Alder cycloaddition indeed revealed a curved Hammett–Brown plot, which is consistent with a mechanistic transition from reversible to rate-determining oxidation of RH.[434a] If ΔE_{ox} is too small, a very high concentration of the primary radical cations RH$^{\bullet+}$ results and leads to undesired radical cation–radical cation coupling reactions. Quite often the most critical step is the electron transfer reduction of PH$^{\bullet+}$ (Scheme 78, propagation

$$\begin{aligned}
&\text{initiation:} && NR_3^{\bullet+} + RH \rightleftharpoons NR_3 + RH^{\bullet+}\\
&\text{rearrangement:} && RH^{\bullet+} \longrightarrow PH^{\bullet+}\\
&\text{cycloaddition:} && RH^{\bullet+} + R^1H \longrightarrow PH^{\bullet+}\\
&\text{propagation 1:} && PH^{\bullet+} + NR_3 \longrightarrow PH + NR_3^{\bullet+}\\
&\text{or propagation 2:} && PH^{\bullet+} + RH \longrightarrow PH + RH^{\bullet+}
\end{aligned}$$

Scheme 78. Mechanism of pericyclic reactions initiated by chemical oxidation.

steps 1 and 2). Reduction can be more efficient when the neutral amine is added in excess,[435] and when neutral reductants are used instead of cationic reductants (e. g. $[Fe(phen)_3]^{2+}$).[11b] Chemical oxidation allows both modes of chain propagation, that is reduction of PH$^{\bullet+}$ by either the reduced oxidant (here NR_3) or by RH, whereas anodic initiation is limited to propagation step 2. In the case of chemical oxidation, propagation steps 1 and 2 are often parallel reactions; the former is strongly favored due to redox potential and reorganization considerations that render this mode much more efficient than anodic initiation.[436]

In PET-initiated pericyclic reactions the situation is quite different, since either an excited acceptor (Scheme 79) or—more rarely—an excited donor is used, which renders the initial ET process strongly exergonic. As reduction of PH$^{\bullet+}$ by A$^{\bullet-}$ is equally a strongly exergonic process, we usually do not see a chain process unless RH can compete as a reductant (Scheme 79). PET initiation allows for an array of additional

$$\begin{aligned}
&\text{initiation:} && A + h\nu \longrightarrow A^*\\
& && A^* + RH \longrightarrow A^{\bullet-} + RH^{\bullet+}\\
&\text{rearrangement} && RH^{\bullet+} \longrightarrow PH^{\bullet+}\\
&\text{cycloaddition:} && RH^{\bullet+} + R^1H \longrightarrow PH^{\bullet+}\\
&\text{termination:} && PH^{\bullet+} + A^{\bullet-} \longrightarrow PH + A\\
&\text{or propagation:} && PH^{\bullet+} + RH \longrightarrow PH + RH^{\bullet+}
\end{aligned}$$

Scheme 79. Mechanism of PET-initiated pericyclic reactions.

alterations to control the outcome of the reaction; the details of this[42] exceed the limits of this review.

Despite their synthetic value, very little is known about the thermodynamics and kinetics of radical cation cycloadditions. As the barriers for the individual cycloaddition steps should be very small, even slight variations in substituent may result in drastic changes. Clearly, cross-cycloadditions are synthetically more important than cyclodimerizations. Recent studies by Johnston, Takamuku, and Brede[437, 438] have for the first time

provided an insightful picture of the rate differences for cycloaddition of various alkenes or dienes to 4-methoxystyrene and 4-methoxy-β-methylstyrene radical cations (Table 19).

Table 19. Experimental kinetic (room temperature) and activation data for radical cation cycloadditions.

Reaction RH + R'H$^{\bullet+}$	k [$M^{-1}s^{-1}$]	$\Delta H^{\neq}$ [kcal mol^{-1}]	Remarks	Ref.
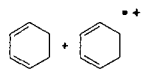	3×10^8	1.6		[22d,e]
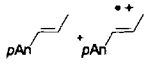	$< 6.7 \times 10^7$	0.8		[22e]
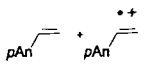	a) 1.4×10^9		a) evidence for a 1,4-radical cation as intermediate	[437c]
	b) 1.4×10^9		b) concerted cycloaddition assumed	[437b]
	c) 1×10^{10}		c) open distonic 1,4-radical cation as intermediate	
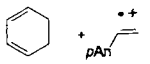	7×10^8		21% Diels–Alder adduct	[438]
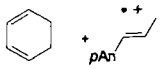	5.6×10^6		80% Diels–Alder adduct	[438]
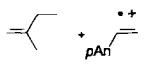	1.5×10^6		products unknown	[438]
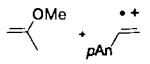	4.6×10^8		products unknown	[438]

Accordingly, steric effects at the electrophilic site as well as the ability of the added nucleophile RCH=CH_2 to stabilize radicals and cations play important roles; their importance is reflected in a rate decrease for R = Ph ≈ OR > vinyl > alkyl by a factor of 100–300.[437b] In principle, the observed trends follow those for the addition of carbocations to alkenes.[369]

Recently, a thorough study shed some light on the details of the dimerization of stilbene$^{\bullet+}$. The reaction of stilbene$^{\bullet+}$ with stilbene proceeds with $k = 3.4 - 3.9 \times 10^8\,M^{-1}s^{-1}$ to yield first a π dimer then a σ radical cation.[439] As the dimerization proved to be very susceptible to steric effects, but not to change in the configuration at the double bond of the stilbene, it was proposed to involve initial formation of a π complex with overlap of two benzene rings.[440] Likewise, the kinetics of intramolecular radical cation Diels–Alder reactions and cyclobutanations were investigated for their use as radical cation probes. Rate constants of 10^7 to $10^9\,s^{-1}$ were found.[434b]

4.7.2. Cycloadditions and Other Pericyclic Processes

Since we would like to restrict the discussion to deliberately triggered ET processes, we will not discuss here cycloaddi tion mechanisms in which radical ion pairs form upon mixing of strong donor dienes and acceptor dienophiles or vice versa.[441]

Cycloadditions and Cycloreversions

The paramount part of the literature is concerned with cycloadditions of olefins, whereas only very few contributions deal with cycloaddition on aromatic rings. After the pioneering work of Ledwith[442] and the seminal contributions of Bauld at the beginning of the 1980s,[443] numerous reports were published over the last 15 years that emphasize the synthetic value of this methodology.[444] This became particularly clear through the development of reactions that had not been realized by any other method before, for example Diels–Alder reactions of ketenes **202**[11] and indols **205**[10] as dienophiles and of vinylindoles[445] to carbazoles (such as **210**) and pyrido[1,2-*a*]indoles (Scheme 80). Since the richness of this chemistry is far beyond the scope of this article, the interested reader is refered to a recent review.[446]

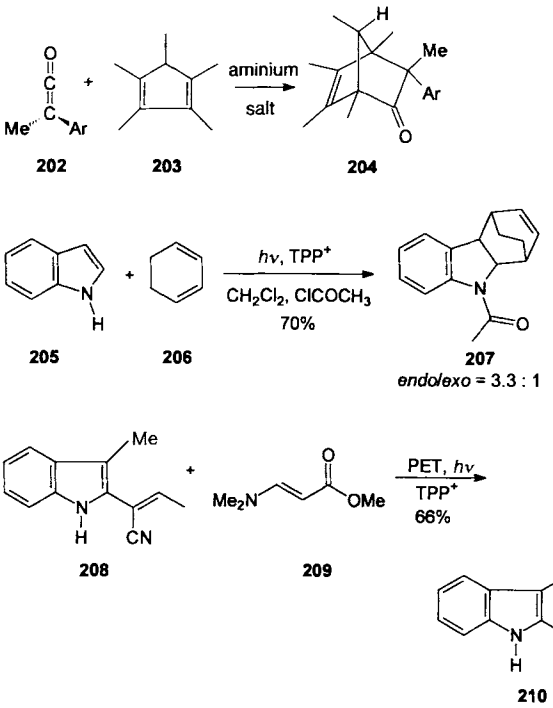

Scheme 80. The [→CA,RC_{red}] reactions according to Schmittel (1991, top), Steckhan (1990, middle) as well as Blechert and Steckhan (1994, bottom).

Although aromatic systems have a low propensity to take part in catalytic cycloadditions,[447] the driving force for the reaction of **211** and **212** is presumably due to the fact that *exo*-methylenecyclohexadiene$^{\bullet+}$ is more stable than toluene$^{\bullet+}$ (Scheme 81). Convincingly, the radical cation Diels–Alder cycloaddition was already tested in natural-product chemistry,[448] for example in the synthesis of β-selinene[449] and neolignan magnoshinin (**216**, Scheme 82).[450]

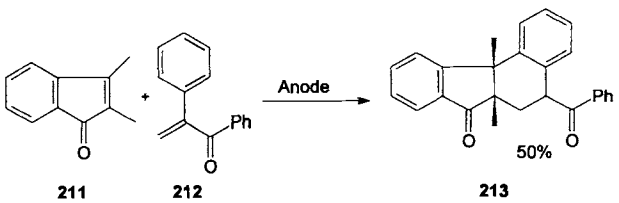

Scheme 81. The [→CA,RC_{red}] reaction according to Simonet (1986).

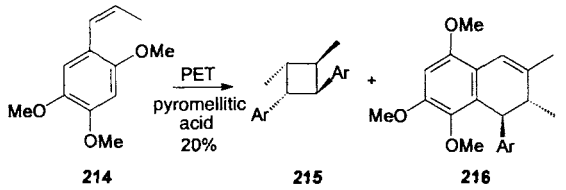

214 215 216

Scheme 82. The [→CA, RC_{red}] reaction according to Takeshita (1987).

The scope of radical cation catalysis was also extended to other cycloadditions, for example with diazomethane$^{\bullet+}$,[451] and to [2+2]cyclodimerizations of electron-rich alkenes.[452] Some of the PET-initiated [2+2]cycloadditions proceed stereoselectively, and others in a stepwise mode,[453] as in the case of 2,6-diarylocta-1,6-diene$^{\bullet+}$.[454]

From a mechanistic point of view, the Diels–Alder reaction can proceed via either a diene radical cation in a [3+2]cycloaddition or a dienophile radical cation in a [4+1]cycloaddition. Despite the fact that the [3+2] mechanism is formally forbidden[455] it proceeds as readily as the allowed [4+1] variant. In contrast to [4+1]cycloadditions, [3+2]cycloadditions, seem to occur by a stepwise mechanism, as recently disclosed for allene[456] and 2,3-diphenyl-1,3-butadiene[457] Diels–Alder reactions.

In other cases, radical cation catalysis was used to accelerate otherwise slow pericyclic processes. The most prominent example is the Diels–Alder cyclodimerization of cyclohexadiene,[22b] which was speeded up by a factor of 10^{15} with respect to the thermal reaction. Several other dienophiles and dienes were tested successfully as well.[446]

An exciting application was developed by Mattay.[458] Azirine$^{\bullet+}$ (generated by PET) can be opened to the 2-azaallenyl radical cations,[459] which readily add to various substrates such as imines and acetylenes to allow the synthesis of imidazoles,[458a, c] heterophanes,[458a, d] and even phorphyrines (Scheme 83).[458a, c] The intermediacy of an azaallene radical cation was demonstrated by an electron pulse radiolysis experiment, which indicated a lifetime in the microsecond range in the presence of imines.[458c]

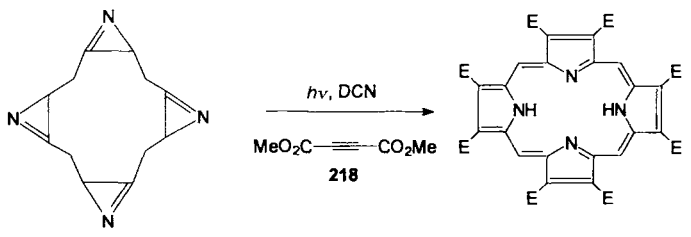

217 218 219

Scheme 83. The [→CC, $RC_{CA,red}$] reaction according to Mattay (1992).

A particularly promising variant of radical cation cycloadditions can be triggered by PET from charge-transfer complexes. By using this conceptually simple method, a potent procedure—for example in the *cis*-hydroxylation of benzene and substituted analogues—was developed that allowed synthetic access to inosite and condurite derivatives (Scheme 84).[460]

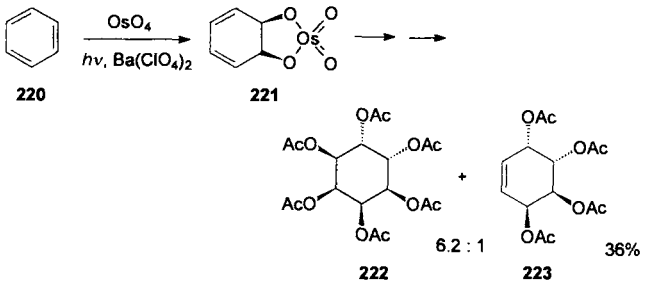

220 221 222 223

Scheme 84. The [→RA] reaction according to Motherwell (1995).

Although the data in Table 19 show that the cycloaddition is very rapid, realization of a ET reaction poses a substantial challenge, since cyclodimerization may effectively compete with the desired cross-cycloaddition. Fortunately, a thorough picture of the [2+1]cycloaddition of 4-methoxystyrene (**225**) became available very recently,[365] which emphasizes the importance of the rapid one-electron reduction of intermediate **226**$^{\bullet+}$ by **225** (Scheme 85). As a consequence, the dihydronaphthalene **229** is formed at low concentrations of **225**, cyclobutane **227** is the major product while at higher concentrations.

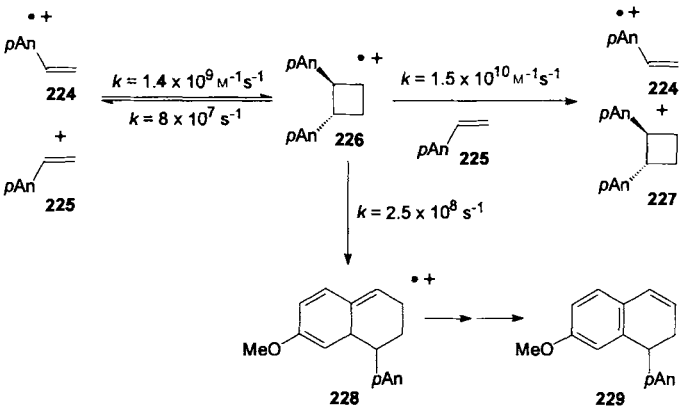

Scheme 85. [2+1]Cycloaddition of 4-methoxystyrene (**225**) according to Johnston (1995); pAn = 4-$MeOC_6H_4$.

Cheletropic Reactions

Cheletropic reactions constitute a recent addition to the realm of radical cation catalysis.[461] Two processes, namely hole-catalyzed epoxidation[462] and cyclopropanation,[463] exhibit different chemoselectivities when compared to other epoxidation and cyclopropanation strategies. In particular, the more highly substituted double bond is usually attacked.

Rearrangements, Cyclizations, and Isomerizations

Rearrangements of radical cations in matrices, in the gas phase, and/or at very low temperature[464] have received much interest. While these studies—for example on the rearrangements of benzvalene$^{\bullet+}$,[465] semibullvalene$^{\bullet+}$,[466] cyclooctatetraene$^{\bullet+}$,[467] dihydropentalene$^{\bullet+}$,[468] 1,5-hexadiene$^{\bullet+}$,[469] 1,5-hexadiyne$^{\bullet+}$,[470] and many others[471]—have greatly contributed to our understanding of the low activation barriers of radical cation chemistry, only few of these processes have been translated into synthetic solution chemistry.

In recent years, radical cation catalysis has found elegant use for the acceleration of many thermally allowed and forbidden processes. Examples include the Cope,[472] Claisen[473] (Scheme 86), epoxide → ketone,[474] vinylcyclo-

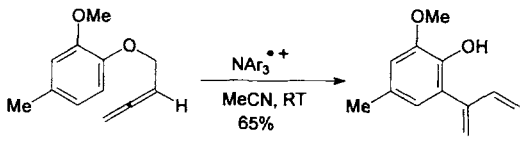

230 231

Scheme 86. The [→R,RC$_{red}$] reaction according to Venkatachalam (1994).

butane,[475] vinylcyclobutanone,[11b] and vinylcyclopropane[476] rearrangements as well as the 1,16-hydrogen shift in an A/D seco corrin radical cation.[477] The stereochemical course of these rearrangements is quite diverse, and is stereospecific in the vinylcyclobutane[475, 478] and the Cope[472b] rearrangement but proceeds with retention, inversion, or partial loss of the stereochemical integrity in the rearrangement of vinylcyclopropane[479] and vinylcyclobutanone[11b] radical cations.

Although *cis* ⇌ *trans* isomerizations[480] have seldom been used in synthetic schemes, they have attracted ample interest from a mechanistic point of view[481] because of their potential in petroleum formation.[482] For a long time it was believed that olefin radical cation isomerization—stilbene$^{\bullet+}$ is a particularly well-studied representative[483]—is quite fast; however, it proved to be rather slow ($k = 10^4\ s^{-1}$).[484] As a consequence of the fast dimerization of stilbene$^{\bullet+}$, an addition–elimination mechanism may be feasible for the isomerization.[481] In contrast, derivatives of *cis*-stilbene$^{\bullet+}$ containing a *p*-MeO group isomerize much more rapidly ($k = 4.5 \times 10^6 - 1.4 \times 10^7\ s^{-1}$) by a unimolecular pathway to provide an insightful picture of the importance of separation and localization of positive charge and spin.[440] In addition, the reduction of the electron density at the unsaturated linkage is thought to accelerate the *cis* → *trans* isomerization.[485] The thermal *cis* → *trans* isomerization of polyene$^{\bullet+}$ took place within about the same time, as indicated by lifetimes of 2 μs.[486]

Electrocyclic Processes

Several contributions have addressed the theory governing electrocyclic reactions of open-shell systems.[455, 487] Such reactions should be very facile,[488] and their stereochemical course should in general correspond to that of the neutral molecule. This picture was indeed confirmed through the observation of conrotatory ring-opening reactions for cyclobutene$^{\bullet+}$[489] and benzocyclobutene$^{\bullet+}$.[490] The stereoselective ring opening of oxaziridines to nitrones was similarly observed in PET reactions.[491] So far, photochemical electrocyclic processes[492] of radical cations have received little attention despite the often unexpected results.

4.7.3. Pericyclic Processes of ⓝ$^{\bullet+}$ and ⓞ$^{\bullet+}$

With the exception of quadricyclane$^{\bullet+}$,[493] pericyclic reactions of pure ⓝ$^{\bullet+}$ and ⓞ$^{\bullet+}$ have rarely been investigated so far. The rapid interconversion ($k = 10^6\ s^{-1}$)[494] of quadricyclane$^{\bullet+}$ to its valence isomer, norbornadiene$^{\bullet+}$, has been the target of ample attention for almost thirty years. This is due not only to its potential to store solar energy and optical data, but also since many endeavours to observe quadricyclane$^{\bullet+}$ directly originally failed.[495] CIDNP,[496] optical spectroscopy[497] and ESR[494] evidence only recently unambiguously established it as a minimum structure. Quadricyclane$^{\bullet+}$ is about 7 kcal mol^{-1} higher in energy than norbornadiene$^{\bullet+}$ and is separated from it by an activation energy of 11 kcal mol^{-1}.[493a]

Moreover, mechanistic investigation of pagodane$^{\bullet+}$ and isopagodane$^{\bullet+}$ revealed the extreme points of [2+1]cycloreversions.[498, 499] Oxidative rearrangements of other strained carbocyclic systems were observed,[310, 500] but only few lead to synthetically useful products, for example as in the radical cation catalyzed formation of diquinane (**233**, Scheme 87).[501]

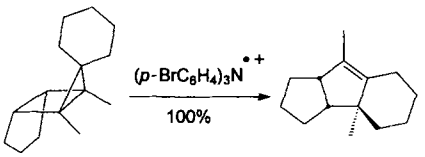

232 233

Scheme 87. The [→R,RC$_{red}$] reaction according to Adam (1995).

A rare event of a cycloaddition involving a σ radical cation was demonstrated for aryldiazomethanes **234**.[502] The radical cation chain cycloaddition ([→CA, RC$_{red}$]) could be triggered equally well by PET (DCA, *hν*) or chemical oxidation (Cu^{2+}, $NR_3^{\bullet+}$; Scheme 88).

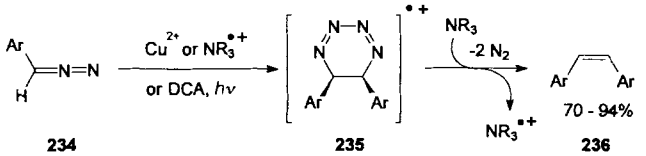

234 235 236

Scheme 88. The [→CA,RC$_{red}$] reaction according to Sawaki (1992).

4.8. Reactions with Radicals

Reactions with short-lived radicals are not only interesting from a mechanistic point of view, but have also found use in PET processes.[503, 504] However, we focus our attention on the reaction of radical cations with stable radicals.

4.8.1. Reaction of ⓟ$^{\bullet+}$, ⓝ$^{\bullet+}$, and ⓞ$^{\bullet+}$ with Oxygen

Ever since the seminal contribution by Barton[505] on the aminium salt catalyzed oxygenation of ergosteryl acetate, this mild synthetic access to dioxetanes has attracted widespread interest. It should be noted, however, that the radical cation chain mechanism of this reaction was only recognized years later.[506] Oxygenations of radical cations were also invoked in

biological systems, as in the metabolic conversion of phenothiazine-based drugs.[507] Importantly, direct evidence for the occurrence of a dioxetane radical cation could be obtained;[508] it results from the stepwise addition of $^3O_2$ to a olefin radical cation (Scheme 89). Under PET conditions

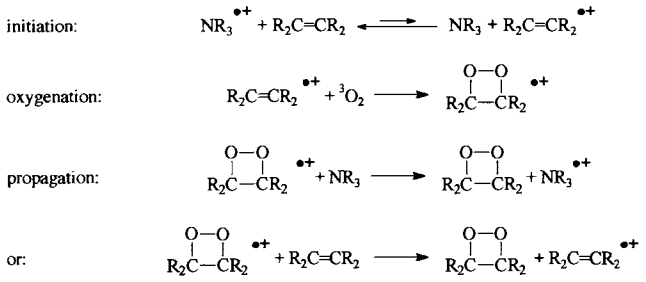

Scheme 89. Mechanism of the radical cation induced addition of $^3O_2$ to olefins.

oxygenation may also proceed by two other viable mechanisms: a) reaction of the olefin radical cation with superoxide formed by ET from the radical anion to oxygen[509] or b) by an exciplex oxygenation mechanism.[510]

Over the last couple of years several π electrophores were oxygenated by an ET strategy: olefins,[511] dienes (Scheme 90),[505, 506, 512, 513] enol ethers,[514] arenes,[515] and others.[516] Similar conditions were applied in the oxygenation of n donors, such as with aromatic sulfides,[507, 517] 1,3-dithianes,[518] aziridines,[519] and phosphorous compounds.[520]

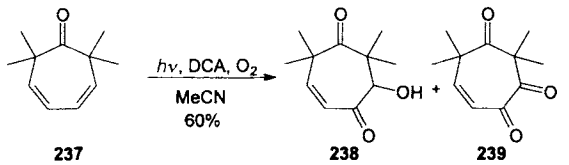

237 238 239

Scheme 90. The [→ Rad] reaction according to Schuster (1986).

Dioxanes and dioxolanes are accessible by oxygenation of distonic 1,4- or 1,3-radical cations. 1,2-Dioxanes, for instance, are formed after the photoinduced ET dimerization of diarylethenes[521] in the presence of oxygen via the intermediate 1,4-radical cation, which is attacked by $^3O_2$ at the radical site.[522] Furthermore, 1,4- and 1,3-radical cations obtained from C–C bond cleavage in cyclopropane$^{\bullet+}$, bicyclobutane$^{\bullet+}$ (Scheme 91),[523] and cyclobutane$^{\bullet+}$ equally react efficiently with molecular oxygen.[524, 525] Oxygenations can alternatively take place after ⓟ-C-H$^{\bullet+}$ or ⓝ-C-H$^{\bullet+}$ deprotonation to give rise to hydroperoxides[526] either with oxygen or superoxide.[527]

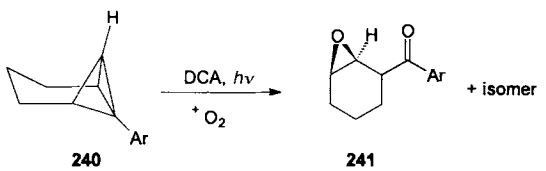

240 241

Scheme 91. The [→ CC,Rad] reaction according to Gollnick (1989).

Recently, oxygenation of radical cations was also accomplished with several other reagents, for example in the epoxidation of olefin$^{\bullet+}$ with NO_2,[528] NO_3,[528] and SeO_2[462] as well as in the formation of sulfoxides from PET oxidation of sulfides with tetranitromethane.[529] Interestingly, NO_2 seems to react more efficiently with radical cations than O_2;[528] however, detailed kinetic data are not available yet.

It was demonstrated that oxygenation rates of aryl olefin radical cations are on the order of $10^6 M^{-1}s^{-1}$.[530] Since two electron-deficient radicals are combined, the reaction rates are two or three orders of magnitude lower than those for neutral radicals with oxygen.[531] In contrast, *trans*-stilbene$^{\bullet+}$ exhibits little reactivity towards oxygen, whereas derivatives with a *p*-MeO group react on the order of $k = 1.2 \times 10^7 - 4.5 \times 10^7 M^{-1}s^{-1}$. The enhancement in reactivity is most certainly due to charge–spin separation.[440]

4.8.2. *Reaction of* ⓟ$^{\bullet+}$, ⓝ$^{\bullet+}$, *and* ⓞ$^{\bullet+}$ *with Neutral Radicals*

Unfortunately, limited use is still being made of radical cation–radical reactions.[503] This reaction mode was originally postulated to be the primary reaction in the charge-transfer nitration of aromatic systems with tetranitromethane.[64] However, Eberson later demonstrated that such radical cation–NO_2 combinations may be very slow.[532] Results from the anodic nitration starting from naphthalene/nitrite mixtures[533] and ^{15}N CIDNP investigations by Lehnig[534] into the nitration of dimethoxybenzenes confirmed the mechanism of charge-transfer nitration for electron-rich arenes.

Some synthetic applications of this reaction mode are derived from PET systems by using "self-destructive" electron acceptors that can generate radicals.[535] The scope of this approach is particularly well demonstrated in PET systems leading to an intra-[536] or intermolecular[537] radical ion pair. When the site of the anion radical is designed to loose a nucleofuge, it may provide a reactive radical that can combine with the site of the radical cation.[503] This protocol opened interesting synthetic approaches to cephalotaxine,[538] pyrrolobenzazocine,[539a] and indolactam (Scheme 92).[539b] Also ⓝ$^{\bullet+}$ may react with radicals, as illustrated in the arylation of trivalent phosphorous compounds in ET reaction with aryl diazonium salts.[540]

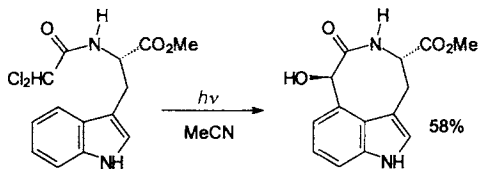

242 243

Scheme 92. The [→ Rad] reaction according to Moody (1988).

4.8.3. *Reaction of* ⓟ$^{\bullet+}$, ⓝ$^{\bullet+}$, *and* ⓞ$^{\bullet+}$ *with Anion Radicals*

Radical ion pairs may readily be generated from neutral precursors by PET. However, in most cases the only reaction

is unproductive back electron transfer of no synthetic value, except when one reactant is thus produced in the excited state. Nevertheless, there are two important reaction modes that have already found frequent use in synthetic schemes: deprotonations[503] and C–C bond formations.

In the context of deprotonation by radical anions, the reaction pathways may be controlled by choosing acceptors that produce highly basic radical anions after ET. However, in polar medium proton transfer may likewise involve the solvent as base, as elegantly demonstrated for 1,4-DCN–toluene.[154] While proton transfer within the ion radical pair provided the tetracyclic product **246** (Scheme 93), deprotonation of toluene$^{\bullet+}$ by the solvent resulted in the formation of *cis*-2-benzyl-1,2-dihydronaphthalene.[541]

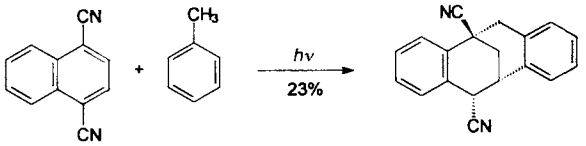

Scheme 93. The [→ CH, $R^{\bullet}_{RA}$] reaction according to Albini (1982, 1984).

Although direct bond formation between radical cations and radical anions is rare, it is thought to play an important role in PET Paterno–Büchi reactions, which were studied in detail by Mattay (Scheme 94).[542] A similar cycloaddition is triggered in the PET reaction of 1,4-naphthoquinones and 1,1-diarylethenes, which exhibits a distinctly different outcome depending on the ΔG^0 of the electron transfer.[543] Moreover, the photochemical reaction of aromatic nitro compounds[544] and alkenes[545] may proceed by combination of a radical anion and a radical cation.

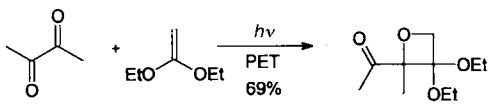

Scheme 94. The [→ RA] reaction according to Mattay (1987).

Combination of radical ions is a mechanistic borderline case in aromatic photonucleophile substitution (S_NAr^- versus S_NAr^*); it most likely takes place only in some limited cases.[546] A particular variant for combining radical ions is the reaction of ⓟ$^{\bullet+}$ with superoxide, which is generated by secondary ET from the acceptor radical anion to oxygen. Such combinations show rate constants near the diffusion limit,[530, 547] as in the case of stilbene$^{\bullet+}$ with $O_2^{\bullet-}$ ($k = 4.1 \times 10^{10}\,M^{-1}s^{-1}$).[530]

4.8.4. Dimerization of Radical Cations

As pointed out in Section 4.6, there is an unfortunate mechanistic uncertainty concerning as to whether a RSC or a RRC mechanism is operative[548] (Scheme 95) in oxidative dimerizations. Importantly, stable symmetric ⓟ$^{\bullet+}$ often undergo π dimer formation in the solid state[549] or in solution.[550]

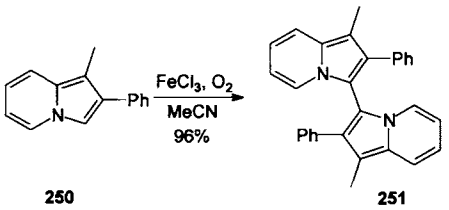

Scheme 95. The [→ Dim] reaction according to Greci (1988).

Nevertheless, dimerization of two radical cations[551] constitutes a process of utmost current interest, since it plays a key role in the industrially important electropolymerization of pyrroles and thiophenes.[552] It is, however, not clear whether the same mechanism that applies for the formation of bipyrrol is valid for the construction of a larger polymer backbone, as larger oligomers are expected to become less reactive.[553] For example, quinquethiophene radical cations[553] only dimerize with rate constants of $3 \times 10^3 - 5 \times 10^3\,M^{-1}s^{-1}$. Similarly, RRC of two Ph_2NH radical cations is the key process in the electrochemical formation of diphenylbenzidine[554] as well as with triphenylamine$^{\bullet+}$ and *N,N*-dimethylaniline$^{\bullet+}$ (Table 20).[555]

Table 20. Rates of the RRC coupling of selected aromatic amine radical cations at room temperature.

Substrate	$k\,[M^{-1}s^{-1}]$	Ref.
triphenylamine$^{\bullet+}$	3×10^3	[555]
diphenylamine$^{\bullet+}$	2.0×10^5	[554]
N,N-dimethylaniline$^{\bullet+}$	1.5×10^7	[555]

4.8.5. Atom Abstraction

Radical cations are by their very nature odd-electron species. However, atom-transfer reactions have not yet been extensively studied, although they are known to be of fundamental importance, for example in the Hofmann-Löffler-Freytag reaction,[556] and allow the synthesis of piperidine and pyrrolidine derivatives (Scheme 96). Whereas earlier data on relatively stable amine radical cations indicated that intermolecular hydrogen abstractions are very slow (1,3-cyclohexadiene and 9-anisylacridine$^{\bullet+}$: $k = 1.03 \times 10^3\,M^{-1}s^{-1}$ at

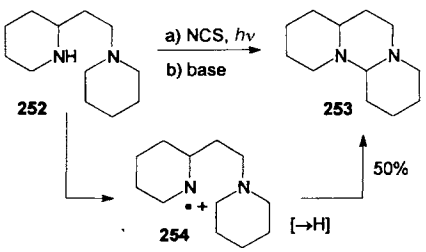

Schema 96. The [→ H, $R^{\bullet}_{rad}$] reaction according to Ban (1976); NCS = *N*-chlorosuccinimide.

298 K),[557] recent data on more reactive aminium systems led to much higher values ($k = 10^6 - 10^8\,M^{-1}s^{-1}$).[376]

5. Conclusion

This review was written to develop a conceptually simple rationalization of radical cation chemistry in solution, independent of whether these highly reactive species were formed by chemical, electrochemical, or photochemical oxidations. The pivotal step in our procedure is to identify the main electrophore in the molecule of interest, since the overwhelming amount of reactions will occur at the electrophore itself or at its periphery by fragmentation of the ⓟ-A-B, ⓝ-A-B, or ⓞ:A-B bond. Rewardingly, all types of radical cations—either π, n, or σ systems—show very similar reactivity patterns.

For the majority of substrates, the differentiation between π, n, and σ donors can be derived in a straightforward manner; nevertheless, numerous cases remain for which this distinction remains arbitrary. In particular, it is known for several functionalities that their HOMO energies are quite similar, so that a switch between π, n, and σ donor may occur after small variations in substituents.[451]

Beyond the simple reactivity paradigms provided above, distance[558] and stereoelectronic factors should find extensive use for controlling the outcome of the reaction. In the elegant construction of the harringtonine alkaloid skeleton,[559] Mariano demonstrated how these factors were advantageously combined (Scheme 97). In an intramolecular PET the less oxidizable electrophore (ⓟ-C-Si) is oxidized, as ET from the more electron-rich aryl functionality to the excited iminium acceptor is impeded by the perpendicular arrangement.

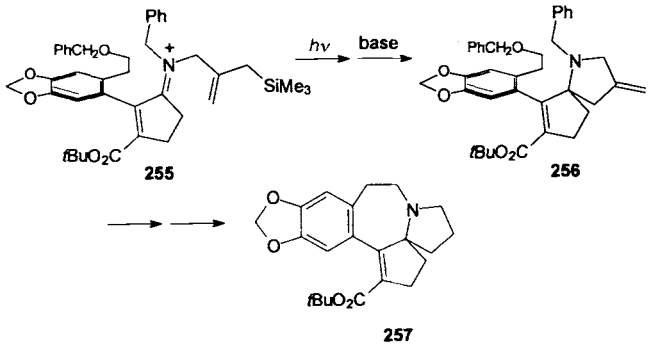

Scheme 97. The [→CX,$R^{\bullet}_{rad}$] reaction according to Mariano (1989).

Certainly, a vital aspect of our classification system is to make reliable predictions on the chemistry of complex molecules after one-electron oxidation, which is only possible at present with some limitations. In particular, there is lack of kinetic and thermochemical data and of investigations on steric as well as stereoelectronic factors. Extensive studies on how to induce high stereoselectivities in such processes are also urgently needed. In light of the multitude of highly stereoselective radical reactions that emerged over the last couple of years,[560] radical cation chemistry holds a great promise for synthetic transformations. A nearly unknown field of chemistry will additionally develop after one-electron oxidation of short-lived intermediates, for example, such as carbenes[561] and cations.[562] Unquestionably, with all the terra incognita yet to be discovered, the design of novel radical cation reactions will continue to present an intellectual challenge for experimental and theoretical chemists for years to come.

M.S. would like to thank all his co-workers whose commitment has made possible the joint contributions in the field of electron transfer activation: Ulrich Baumann, Ingo Bohn, Armin Burghart, Andreas Haeuseler, Susanne Kiau, Anja Langels, Michael Levis, Maik Röck, Barbara Rohwedder, Heinke von Seggern, Rolf Söllner, Holger Trenkle, and Clemens Wöhrle. Generous financial support over many years from the Deutsche Forschungsgemeinschaft, the Volkswagen-Stiftung, the Fonds der Chemischen Industrie, the Wissenschaftliche Gesellschaft Freiburg, and the BASF AG is gratefully acknowledged.

Received: April 9, 1996
Revised version: February 24, 1997 [A 162 IE]
German version: *Angew. Chem.* **1997**, *109*, 2658–2699

[1] a) *Photochemistry in Organic Synthesis* (Ed.: J. D. Doyle), The Royal Society of Chemistry, London, **1986**; b) *Photochemical Synthesis* (Eds.: I. Ninomiya, T. Naito), Academic Press, London, **1989**; c) *Photochemical Key Steps in Organic Synthesis* (Eds.: J. Mattay, A. Griesbeck), VCH, Weinheim, **1994**.

[2] a) D. Astruc, *Electron Transfer and Radical Processes in Transition-Metal Chemistry*, VCH, Weinheim, **1995**; b) G. J. Kavarnos, *Fundamentals of Photoinduced Electron Transfer*, VCH, New York, **1993**; c) L. Eberson, *Electron Transfer Reactions in Organic Chemistry*, Springer, Berlin, **1987**.

[3] a) A. J. Fry, *Synthetic Organic Electrochemistry*, Wiley, New York, **1989**; b) *Organic Electrochemistry* (Eds.: H. Lund, M. M. Baizer), Marcel Dekker, New York, **1991**; c) T. Shono, *Electroorganic Synthesis*, Academic Press, **1991**; d) J. Volke, F. Liška, *Electrochemistry in Organic Synthesis*, Springer, Berlin **1994**; e) D. Kyriacou, *Modern Electroorganic Chemistry*, Springer, Berlin, **1994**; f) "Electrochemistry I–VI": *Top. Curr. Chem.* **1997**, *185*; *ibid.* **1994**, *170*; *ibid.* **1990**, *152*; *ibid.* **1988**, *148*; *ibid.* **1988**, *143*; *ibid.* **1987**, *142*.

[4] Odd-electron intermediates were trapped in S_N2 reactions: P. Haberfield, *J. Am. Chem. Soc.* **1995**, *117*, 3314–3315; review: B. Speiser, *Angew. Chem.* **1996**, *108*, 2623–2626; *Angew. Chem. Int. Ed. Engl.* **1996**, *35*, 2471–2474.

[5] P. W. Rabideau, Z. Marcinow, *Org. React. (NY)* **1992**, *42*, 1–334.

[6] J. J. Bloomfield, D. C. Owsley, J. M. Nelke, *Org. React. (NY)* **1976**, *23*, 259–403.

[7] a) M. Xi, B. E. Bent, *J. Am. Chem. Soc.* **1993**, *115*, 7426–7433; b) J.-L. Lin, B. E. Bent, *ibid.* **1993**, *115*, 6943–6950.

[8] a) J. F. Garst, *Acc. Chem. Res.* **1991**, *24*, 95–97; b) H. M. Walborsky, *ibid.* **1990**, *23*, 286–293.

[9] a) G. A. Russell, *Adv. Phys. Org. Chem.* **1987**, *23*, 271–322; b) J. F. Bunnett, *Acc. Chem. Res.* **1978**, *11*, 413–420.

[10] a) A. Gieseler, E. Steckhan, O. Wiest, *Synlett* **1990**, 275–277; b) O. Wiest, E. Steckhan, F. Grein, *J. Org. Chem.* **1992**, *57*, 4034–4037.

[11] a) M. Schmittel, H. von Seggern, *Angew. Chem.* **1991**, *103*, 981–983; *Angew. Chem. Int. Ed. Engl.* **1991**, *30*, 999–1001; b) M. Schmittel, H. von Seggern, *J. Am. Chem. Soc.* **1993**, *115*, 2165–2177.

[12] C. F. Gürtler, S. Blechert, E. Steckhan, *Angew. Chem.* **1995**, *107*, 2025–2026; *Angew. Chem. Int. Ed. Engl.* **1995**, *34*, 1900–1901.

[13] Hemoprotein ligninase: K. E. Hammel, M. Tien, B. Kalyanaraman, T. K. Kirk, *J. Biol. Chem.* **1985**, *260*, 8348–8353; general acyl-CoA dehydrogenase: M. Lai, L. Liu, H. Liu, *J. Am. Chem. Soc.* **1991**, *113*, 7388–7397; extradiol catechol dioxygenase: J. Sanvoisin, G. J. Langley, T. D. H. Bugg, *ibid.* **1995**, *117*, 7836–7837.

[14] The originally proposed SET mechanism (R. B. Silverman, *Adv. Electr. Trans. Chem.* **1992**, *2*, 177–213) is not undebated, see J. R. Miller, D. E. Edmondson, C. B. Grissom, *J. Am. Chem. Soc.* **1995**, *117*, 7830–7831.

[15] a) H. W. Park, S. T. Kim, A. Sancar, J. A. Deisenhofer, *Science* **1995**, *268*, 1866–1872; b) J. E. Huyett, P. E. Doan, R. Gurbiel, A. L. P. Houseman, M. Sivaraja, D. B. Goodin, B. M. Hoffman, *J. Am. Chem. Soc.* **1995**, *117*, 9033–9041; c) J. A. Sancar, *Adv. Electr. Trans. Chem.* **1992**, *2*, 215–272; d) E. Cavalieri, E. Rogan, in *Polynuclear Aromatic Hydrocarbons: Formation,*

Metabolism and Measurements (Eds.: M. Cooke, A. J. Dennis), Batelle, Columbus, **1983**, pp. 1–26; e) C. Pac, J. Kubo, T. Majima, H. Sakurai, *Photochem. Photobiol.* **1982**, *36*, 273–282.
[16] The DNA-photolyase reaction most likely proceeds via a pyrimidine dimer radical anion. Such cycloreversions are known for simple cyclobutanes: M. Horner, S. Hünig, *Liebigs Ann. Chem.* **1982**, 1409–1422.
[17] J. H. Penn, J. H. Wang, *Energy Fuels* **1994**, *8*, 421–425.
[18] J. W. Leon, D. G. Whitten, *J. Am. Chem. Soc.* **1995**, *117*, 2226–2235.
[19] a) S. Peukert, B. Giese, *Tetrahedron Lett.* **1996**, *37*, 4365–4368; b) B. Giese, A. Dussy, C. Elie, P. Erdmann, U. Schwitter, *Angew. Chem.* **1994**, *106*, 1941–1944; *Angew. Chem. Int. Ed. Engl.* **1994**, *33*, 1861–1863; c) B. Giese, X. Beyrich-Graf, J. Burger, C. Kesselheim, M. Senn, T. Schäfer, *ibid.* **1993**, *105*, 1850–1852 and **1993**, *32*, 1742–1744; d) see also RNA model compounds: D. Crich, X.-S. Mo, *J. Am. Chem. Soc.* **1997**, *119*, 249–250.
[20] N. L. Bauld, *Tetrahedron* **1989**, *45*, 5307–5363; N. L. Bauld, R. Pabon, *J. Am. Chem. Soc.* **1983**, *105*, 633–634.
[21] L. Eberson, B. Olofsson, *Acta Chem. Scand.* **1991**, *45*, 316–326.
[22] There has been a dispute over the involvement of an electrophile-catalyzed mechanism in the aminium salt initiated Diels–Alder cyclodimerization of cyclohexa-1,3-diene, which, according to most experimental evidence, has been considered to constitute a typical radical cation reaction: a) L. Eberson, B. Olofsson, J.-O. Svensson, *Acta Chem. Scand.* **1992**, *46*, 1005–1015; b) W. Yueh, N. L. Bauld, *J. Chem. Soc. Perkin Trans. 2* **1995**, 871–873. Compelling experimental evidence and high-level ab initio calculation, however, support a concerted, almost activationless cycloaddition for this substrate at the stage of the radical cation: c) C. R. Jones, B. J. Allman, A. Mooring, B. Spahic, *J. Am. Chem. Soc.* **1983**, *105*, 652–654; d) G. C. Calhoun, G. B. Schuster, *ibid.* **1984**, *106*, 6870–6871; e) K. T. Lorenz, N. L. Bauld, *ibid.* **1987**, *109*, 1157–1160; f) N. L. Bauld, *ibid.* **1992**, *114*, 5800–5804.
[23] Reduction of $DA^{+\bullet}$ should be more favorable from NR_3 than from CHD considering the lower redox potential and the lower reorganization energy of the former.
[24] The term distonic (Latin distans = separate) was introduced (B. F. Yates, W. J. Bouma, L. Radom, *J. Am. Chem. Soc.* **1984**, *106*, 5805–5808) to describe a class of ions in which charge and radical center cannot be brought together on the same atom when using Lewis electronic structures. Often the charge and the radical are separated by at least one saturated atom.
[25] a) S. Torii, H. Tanaka in ref. [3b], chap. 16; b) H. J. Schäfer, *Top. Curr. Chem.* **1990**, *152*, 91–151.
[26] A. G. Griesbeck, A. Henz, K. Peters, E.-M. Peters, H. G. von Schnering, *Angew. Chem.* **1995**, *107*, 498–500; *Angew. Chem. Int. Ed. Engl.* **1995**, *34*, 474–476.
[27] B. Klotz-Berendes, H. J. Schäfer, M. Grehl, R. Fröhlich, *Angew. Chem.* **1995**, *107*, 218–220; *Angew. Chem. Int. Ed. Engl.* **1995**, *34*, 189–191.
[28] a) B. B. Snider, *Chem. Rev.* **1996**, *96*, 339–363; b) B. B. Snider, J. E. Merrit, *Tetrahedron* **1991**, *47*, 8663–8678.
[29] D. D. M. Wayner, D. J. McPhee, D. Griller, *J. Am. Chem. Soc.* **1988**, *110*, 132–137.
[30] M. Schmittel, *Top. Curr. Chem.* **1994**, *169*, 183–230.
[31] a) P. G. Gassman, D. A. Singleton, *J. Am. Chem. Soc.* **1984**, *106*, 6085–6086; b) *ibid.* **1984**, *106*, 7993–7994.
[32] F. Ciminale, L. Lopez, G. Mele, *Tetrahedron* **1994**, *50*, 12685–12696.
[33] a) L. Lopez, L. Troisi, *Tetrahedron* **1989**, *30*, 3097–3100; b) K. Uneyama, A. Isimura, K. Fujii, S. Torii, *Tetrahedron Lett.* **1983**, *24*, 2857–2860; c) J. Delaunay, A. Lebouc, A. Tallec, J. Simonet, *J. Chem. Soc. Chem. Commun.* **1982**, 387–388.
[34] J. Heinze, *Angew. Chem.* **1984**, *96*, 823–840; *Angew. Chem. Int. Ed. Engl.* **1984**, *23*, 831–847.
[35] a) D. R. Crow, *Principles and Applications of Electrochemistry*, Blackie Academic, London, **1994**; b) P. H. Rieger, *Electrochemistry*, Chapman & Hall, New York **1993**; c) A. J. Bard, L. R. Faulkner, *Electrochemical Methods*, Wiley, New York, **1980**.
[36] Often the half-wave potentials $E^{ox}_{1/2}(RH) = E^{red}_{1/2}(RH^{+\bullet})$ provided are not equivalent to the standard redox potentials, but they are acceptable approximations for most purposes.
[37] a) S. Dapperheld, E. Steckhan, K.-H. Grosse Brinkhaus, T. Esch, *Chem. Ber.* **1991**, *124*, 2557–2567; b) W. Schmidt, E. Steckhan, *ibid.* **1980**, *113*, 577–585; c) M. Schmittel, H. Ammon, C. Wöhrle, *ibid.* **1995**, *128*, 845–850; d) C. L. Wong, J. Kochi, *J. Am. Chem. Soc.* **1979**, *101*, 5593–5603.
[38] N. G. Connelly, W. E. Geiger, *Chem. Rev.* **1996**, *96*, 877–910.
[39] E. Steckhan, *Top. Curr. Chem.* **1987**, *142*, 1–69.
[40] M. Chanon, M.-A. Fox, *Photoinduced Electron Transfer, Parts A–D*, Elsevier, Amsterdam, **1988**.
[41] Since radicals are only oxidized when they exhibit extremely low E_{ox} values, they may already be oxidized by the ground-state acceptor or added oxidants.
[42] a) J. Mattay, *Angew. Chem.* **1987**, *99*, 849–870; *Angew. Chem. Int. Ed. Engl.* **1987**, *26*, 825; b) *Synthesis* **1989**, 233–252.
[43] S. Fukuzumi, T. Okamoto, J. Otera, *J. Am. Chem. Soc.* **1994**, *116*, 5503–5504.
[44] M. E. Weiss, *Chem. Rev.* **1963**, *63*, 55–64.
[45] For an insightful discussion on the three-electron three-orbital three-configuration approach to C–C dissociations, see O. Takahashi, O. Kikuchi, *Tetrahedron Lett.* **1991**, *32*, 4933–4936.
[46] T. Karatsu, H. Itoh, T. Kikunaga, Y. Ebashi, H. Hotta, A. Kitamura, *J. Org. Chem.* **1995**, *60*, 8270–8277.
[47] C. Adams, N. Jacobsen, J. H. P. Utley, *J. Chem. Soc. Perkin Trans. 1* **1978**, 1071–1076.
[48] a) P. G. Gassman, S. A. De Silva, *J. Am. Chem. Soc.* **1991**, *113*, 9870–9872; b) P. G. Gassman, K. J. Bottorf, *ibid.* **1987**, *109*, 7547–7548.
[49] "Energetics of Gaseous Ions": H. M. Rosenstock, K. Draxl, B. W. Steiner, J. T. Herron, *J. Phys. Chem. Ref. Data* **1977**, *6*, Suppl. 1.
[50] T. Shono, Y. Matsumura, K. Inoue, H. Ohmizu, S. Kashimura, *J. Am. Chem. Soc.* **1982**, *104*, 5753–5757.
[51] a) R. L. Hand, R. F. Nelson, *J. Electrochem. Soc.* **1978**, *125*, 1059–1969; b) *J. Am. Chem. Soc.* **1974**, *96*, 850–860.
[52] K. Bechgaard, V. D. Parker, *J. Am. Chem. Soc.* **1972**, *94*, 4749–4750; b) V. LeBerre, L. Angely, N. Simonet-Gueguen, J. Simonet, *J. Chem. Soc. Chem. Commun.* **1987**, 984–986.
[53] P. Margaretha, P. Tissot, *Helv. Chim. Acta* **1975**, *58*, 933–936.
[54] H. G. Thomas, A. Schmitz, *Synthesis* **1985**, 31–33; J. W. Scheren, H. J. M. Goossens, A. W. H. Top, *ibid.* **1978**, 283–284.
[55] J. M. White, *Aust. J. Chem.* **1995**, *48*, 1227–1251; H. Bock, B. Solouki, *Chem. Rev.* **1995**, *95*, 1161–1190.
[56] A. Hembrock, H. J. Schäfer, G. Zimmermann, *Angew. Chem.* **1985**, *97*, 1048–1049; *Angew. Chem. Int. Ed. Engl.* **1985**, *24*, 1055–1056.
[57] M. Mella, M. Freccero, A. Albini, *Tetrahedron* **1996**, *52*, 5533–5548; *J. Chem. Soc. Chem. Commun.* **1995**, 41–42.
[58] M. Mella, M. Freccero, T. Soldi, E. Fasani, A. Albini, *J. Org. Chem.* **1996**, *61*, 1413–1422.
[59] R. D. Miller, J. Michl, *Chem. Rev.* **1989**, *89*, 1359–1410.
[60] J. Kumagai, H. Yoshida, T. Ichikawa, *J. Phys. Chem.* **1995**, *99*, 7965–7969.
[61] L. Eberson, M. P. Hartshorn, O. Persson, *Angew. Chem.* **1995**, *107*, 2417–2418; *Angew. Chem. Int. Ed. Engl.* **1995**, *34*, 2268–2269.
[62] For a critical evaluation of thermochemical cycles, see D. D. M. Wayner, V. D. Parker, *Acc. Chem. Res.* **1993**, *26*, 287–294.
[63] A. M. de P. Nicholas, D. R. Arnold, *Can. J. Chem.* **1982**, *60*, 2165–2179.
[64] C. Amatore, J. K. Kochi, *Adv. Electron Transfer Chem.* **1991**, *1*, 55–148.
[65] S. Fukuzumi, Y. Tokuda, *Chem. Lett.* **1992**, 1721–1724.
[66] F. G. Bordwell, J.-P. Cheng, M. J. Bausch, J. E. Bares, *J. Phys. Org. Chem.* **1988**, *1*, 209–223.
[67] F. G. Bordwell, M. J. Bausch, J. C. Branca, J. A. Harrelson, Jr., *J. Phys. Org. Chem.* **1988**, *1*, 225–241.
[68] F. G. Bordwell, J.-P. Cheng, *J. Am. Chem. Soc.* **1989**, *111*, 1792–1795.
[69] F. G. Bordwell, A. V. Satish, *J. Am. Chem. Soc.* **1992**, *114*, 10173–10176.
[70] F. G. Bordwell, J.-P. Cheng, *J. Am. Chem. Soc.* **1988**, *110*, 2872–2877.
[71] F. G. Bordwell, J.-P. Cheng, M. J. Bausch, *J. Am. Chem. Soc.* **1988**, *110*, 2867–2872.
[72] E. Baciocchi, T. Del Giacco, F. Elisei, *J. Am. Chem. Soc.* **1993**, *115*, 12290–12295.
[73] A. Anne, P. Hapiot, J. Moiroux, P. Neta, J.-M. Savéant, *J. Am. Chem. Soc.* **1992**, *112*, 4694–4701.
[74] a) A. Anne, P. Hapiot, J. Moiroux, P. Neta, J.-M. Savéant, *J. Phys. Chem.* **1991**, *95*, 2370–2377; b) P. Hapiot, J. Moiroux, J.-M. Savéant, *J. Am. Chem. Soc.* **1990**, *112*, 1337–1343.
[75] G. N. R. Tripathi, *Chem. Phys. Lett.* **1992**, *199*, 409–416.
[76] a) D. T. Leeck, R. M. Li, L. J. Chyall, H. I. Kenttämaa, *J. Phys. Chem.* **1996**, *100*, 6608–6611; b) G. L. Hug, B. Marciniak, K. Bobrowski, *ibid.* **1996**, *100*, 14914–14921.
[77] E. Fasani, M. Mella, A. Albini, *J. Chem. Soc. Perkin Trans. 2* **1995**, 449–452.
[78] J. Monig, K. D. Asmus, R. Goslich, *Ber. Bunsen-Ges. Phys. Chem.* **1986**, *90*, 115–121.
[79] R. W. Fessenden, P. Neta, *J. Phys. Chem.* **1972**, *76*, 2857–2859.
[80] X. Zhang, F. G. Bordwell, *J. Org. Chem.* **1992**, *57*, 4163–4168.
[81] C. G. Shaefer, K. S. Peters, *J. Am. Chem. Soc.* **1980**, *102*, 7566–7567.
[82] A. Sinha, T. C. Bruice, *J. Am. Chem. Soc.* **1984**, *106*, 7291–7292.
[83] S. Das, C. von Sonntag, *Z. Naturforsch. B* **1986**, *41*, 505–513.
[84] J. P. Dinnocenzo, T. E. Banach, *J. Am. Chem. Soc.* **1989**, *111*, 8646–8653.
[85] a) W. Xu, X.-M. Zhang, P. S. Mariano, *J. Am. Chem. Soc.* **1991**, *113*, 8863–8878; b) W. Xu, P. S. Mariano, *ibid.* **1991**, *113*, 1431–1432.
[86] a) M. Goez, I. Sartorius, *Chem. Ber.* **1994**, *127*, 2273–2276; b) *J. Am. Chem. Soc.* **1993**, *115*, 11123–11133.
[87] F. D. Lewis, *Acc. Chem. Res.* **1986**, *19*, 401–405.
[88] F. D. Lewis, T.-I. Ho, J. T. Simpson, *J. Am. Chem. Soc.* **1982**, *104*, 1924–1929.
[89] X. Zhang, S.-R. Yeh, S. Hong, M. Freccero, A. Albini, D. E. Falvey, P. S. Mariano, *J. Am. Chem. Soc.* **1994**, *116*, 4211–4220.

[90] W. Schmidt, *Tetrahedron* **1973**, *29*, 2129–2134.
[91] K.-H. Grosse Brinkhaus, E. Steckhan, D. Degner, *Tetrahedron* **1986**, *42*, 553–560.
[92] P. J. Andrulis, Jr., M. J. S. Dewar, R. Dietz, R. L. Hunt, *J. Am. Chem. Soc.* **1966**, *88*, 5473–5478; T. Aratani, M. J. S. Dewar, *ibid.* **1966**, *88*, 5479–5482; P. J. Andrulis, Jr., M. J. S. Dewar, *ibid.* **1966**, *88*, 5483–5485.
[93] R. Landau, A. Saffer, *Chem. Eng. Prog.* **1968**, *64*, 20.
[94] K. Ponsold, H. Kasch, *Tetrahedron Lett.* **1979**, 4463–4464.
[95] A. J. Baggaley, R. Brettle, *J. Chem. Soc. Chem. Commun.* **1966**, 108.
[96] a) W. Schmidt, E. Steckhan, *Angew. Chem.* **1979**, *91*, 851–852; *Angew. Chem. Int. Ed. Engl.* **1979**, 18, 802–803; b) *ibid.* **1979**, *91*, 850–851 and **1979**, *18*, 801–802; c) *ibid.* **1978**, *90*, 717 and **1978**, *17*, 673–674.
[97] S. Dapperheld, E. Steckhan, *Angew. Chem.* **1982**, *94*, 785; *Angew. Chem. Int. Ed. Engl.* **1982**, *21*, 780–781.
[98] T. Thyrann, D. A. Lightner, *Tetrahedron Lett.* **1996**, *37*, 315–318.
[99] T. Shono, Y. Matsumura, Y. Nakagawa, *J. Am. Chem. Soc.* **1974**, *96*, 3532–3536.
[100] T. Chiba, M. Okimoto, H. Nagai, Y. Takata, *J. Org. Chem.* **1979**, *44*, 3519–3523.
[101] G. Giese, A. Heesing, *Chem. Ber.* **1991**, *124*, 2623–2628.
[102] T. J. Bill, S. Chen, R. A. Pascal, Jr., J. Schwartz, *J. Am. Chem. Soc.* **1990**, *112*, 9019–9020.
[103] B. Reitstöen, V. D. Parker, *J. Am. Chem. Soc.* **1990**, *112*, 4968–4969.
[104] R. M. Borg, D. R. Arnold, T. S. Cameron, *Can. J. Chem.* **1984**, *62*, 1785–1802.
[105] A. Onopchenko, J. G. D. Schulz, *J. Org. Chem.* **1972**, *37*, 2564–2566.
[106] A. Onopchenko, J. G. D. Schulz, R. Seekircher, *J. Org. Chem.* **1972**, *37*, 1414–1417.
[107] M. Fujita, S. Fukuzumi, *J. Chem. Soc. Chem. Commun.* **1993**, 1528–1529.
[108] E. Baciocchi, R. Gabrielli, C. Giancaspro, C. Rol, G. V. Sebastini, M. Speranza, *Tetrahedron Lett.* **1985**, *26*, 4269–4272.
[109] E. Baciocchi, M. Mattioli, R. Romano, R. Ruzziconi, *J. Org. Chem.* **1991**, *56*, 7154–7160.
[110] A. Albini, S. Sulpizio, *J. Org. Chem.* **1991**, *54*, 2147–2152.
[111] E. Baciocchi, F. D'Acunzo, C. Galli, O. Lanzalunga, *J. Chem. Soc. Perkin Trans. 2* **1996**, 133–140.
[112] L. M. Tolbert, R. K. Khanna, A. E. Popp, L. Gelbaum, L. A. Bottomley, *J. Am. Chem. Soc.* **1990**, *112*, 2373–2378.
[113] A. L. Perrott, D. R. Arnold, *Can. J. Chem.* **1992**, *70*, 272–279.
[114] E. Baciocchi, *Acta Chem. Scand.* **1990**, *44*, 645–652.
[115] E. Baciocchi, A. Dalla Cort, L. Eberson, L. Mandolini, C. Rol, *J. Org. Chem.* **1986**, *51*, 4544–4548.
[116] D. M. Camaioni, J. A. Franz, *J. Org. Chem.* **1984**, *49*, 1607–1613.
[117] E. Steckhan in ref. [3b], chap. 15.
[118] O. Hammerich, B. Svensmark in ref. [3b], chap. 17.
[119] a) F. D. Lewis, D. M. Bassani, G. D. Reddy, *J. Org. Chem.* **1993**, *58*, 6390–6393; b) F. D. Lewis, G. D. Reddy, S. Schneider, M. Gahr, *J. Am. Chem. Soc.* **1991**, *113*, 3498–3506; c) F. D. Lewis, *Tetrahedron Lett.* **1990**, *31*, 5293–5296.
[120] A. Sugimoto, K. Sumi, K. Urakawa, M. Ikemura, S. Sakamoto, S. Yoneda, Y. Otsuji, *Bull. Chem. Soc. Jpn.* **1983**, *56*, 3118–3122; A. Sugimoto, S. Yoneda, *J. Chem. Soc. Chem. Commun.* **1982**, 376–377.
[121] F. D. Lewis, G. D. Reddy, S. Schneider, M. Gahr, *J. Am. Chem. Soc.* **1989**, *111*, 6465–6466. The mechanism of this reaction could also be [→ RA].
[122] A. Sugimoto, R. Hiraoka, H. Inoue, T. Adachi, *J. Chem. Soc. Perkin Trans. 1* **1992**, 1559–1560.
[123] G. G. Wubbels, B. R. Sevetson, H. Sanders, *J. Am. Chem. Soc.* **1989**, *111*, 1018–1022. The cyclization may also be initiated by proton transfer between the radical cation and the radical anion site.
[124] K. Mutai, K. Kobayashi, K. Yokoyama, *Tetrahedron* **1984**, *40*, 1755–1759; K. Mutai, K. Yokoyama, S. Kanno, K. Kobayashi, *Bull. Chem. Soc. Jpn.* **1982**, 55, 1112–1115; K. Mutai, S. Kanno, K. Kobayashi, *Tetrahedron Lett.* **1978**, 1273–1276.
[125] G. Pandey, P. Y. Reddy, U. T. Bhalerao, *Tetrahedron Lett.* **1991**, *32*, 5147–5150.
[126] G. Pandey, G. Kumaraswamy, A. Krishna, *Tetrahedron Lett.* **1987**, *28*, 2649–2652.
[127] a) P. Brungs, K. Danielmeier, J. Jakobi, C. Nothelfer, A. Stahl, A. Zietlow, E. Steckhan, *J. Chim. Phys. Phys.-Chim. Biol.* **1996**, *93*, 575–590; b) K. D. Moeller, L. D. Rutledge, *J. Org. Chem.* **1992**, *57*, 6360–6363; c) T. Shono, Y. Matsumura, S. Katoh, K. Takeuchi, K. Sasaki, T. Kamada, R. Shimizu, *J. Am. Chem. Soc.* **1990**, *112*, 2368–2372; d) S. D. Ross, M. Finkelstein, R. C. Petersen, *ibid.* **1966**, *88*, 4657–4660.
[128] a) M. Mori, K. Kagechika, K. Tohjima, M. Shibasaki, *Tetrahedron Lett.* **1988**, *29*, 1409–1412; b) M. Okita, T. Wakamatsu, Y. Ban, *Heterocycles* **1983**, *20*, 401–404.
[129] T. Shono, H. Hamaguchi, Y. Matsumura, *J. Am. Chem. Soc.* **1975**, *97*, 4264–4268.
[130] a) A. G. M. Barrett, D. Pilipauskas, *J. Org. Chem.* **1991**, *56*, 2787–2800; b) K. D. Ginzel, P. Brungs, E. Steckhan, *Tetrahedron* **1989**, *45*, 1691–1701; c) T. Shono, Y. Matsumura, K. Inoue, *J. Org. Chem.* **1983**, *48*, 1388–1389.
[131] A. Papadopoulos, B. Lewall, E. Steckhan, K.-D. Ginzel, F. Knoch, M. Nieger, *Tetrahedron* **1991**, *47*, 563–572.
[132] a) T. Fuchigami, A. Konno, K. Nakagawa, M. Shimojo, *J. Org. Chem.* **1994**, *59*, 5937–5941; b) T. Fuchigami, K. Yamamoto, A. Konno, *Tetrahedron* **1991**, *47*, 625–634.
[133] G. Pandey, *Synlett* **1992**, 546–552.
[134] G. Kaupp, F. Köleli, E. Gründken, *Angew. Chem.* **1985**, *97*, 873–874; *Angew. Chem. Int. Ed. Engl.* **1985**, *24*, 864–865.
[135] K. Irie, M. Okita, T. Wakamatsu, Y. Ban, *Nouv. J. Chim.* **1980**, *4*, 275–277.
[136] T. Shono, Y. Matsumura, K. Inoue, H. Ohmizu, S. Kashimura, *J. Am. Chem. Soc.* **1982**, *104*, 5753–5757.
[137] J. Santamaria, *Pure Appl. Chem.* **1995**, *67*, 141–147.
[138] K. Irie, Y. Ban, *Heterocycles* **1982**, *18*, 255–258.
[139] G. A. Kraus, L. Chen, *Tetrahedron Lett.* **1991**, *32*, 7151–7154.
[140] T. Hasegawa, K. Mukai, K. Mizukoshi, M. Yoshioka, *Bull. Chem. Soc. Jpn.* **1990**, *63*, 3348–3350.
[141] Y. Sato, H. Nakai, M. Wada, T. Mizoguchi, Y. Hatanaka, H. Kanaoka, *Chem. Pharm. Bull.* **1992**, *40*, 3174–3180.
[142] a) H. Takechi, S. Tacheuchi, M. Machida, Y. Nishibata, K. Aoe, Y. Sato, Y. Kanaoka, *Chem. Pharm. Bull.* **1986**, *34*, 3142–3152; b) M. Machida, H. Kakecki, Y. Kanaoka, *Heterocycles* **1977**, *7*, 273–276.
[143] a) A. G. Griesbeck, J. Hirt, K. Peters, E.-M. Peters, H. G. von Schnering, *Chem. Eur. J.* **1996**, *2*, 1388–1394; b) Y. Hatanaka, Y. Sato, H. Nakai, M. Wada, T. Mizoguchi, Y. Kanaoka, *Liebigs Ann. Chem.* **1992**, 1113–1123; c) A. G. Griesbeck, H. Mauder, I. Müller, *Chem. Ber.* **1992**, *125*, 2467–2475; d) Y. Sato, H. Nakai, M. Wada, T. Mizoguchi, Y. Hatanaka, Y. Migita, H. Kanaoka, *Liebigs Ann. Chem.* **1985**, 1099–1118; e) Y. Sato, H. Nakai, T. Mizuguchi, Y. Hatanaka, H. Kanaoka, *J. Am. Chem. Soc.* **1976**, *98*, 2349–2351.
[144] F. Cornille, U. Slomczynska, M. L. Smythe, D. D. Beussen, K. D. Moeller, G. R. Marshall, *J. Am. Chem. Soc.* **1995**, *117*, 909–917.
[145] P. H. Mazzocchi, C. R. King, H. L. Ammon, *Tetrahedron Lett.* **1987**, *28*, 2473–2476.
[146] T. Shono, Y. Matsumara, K. Inoue, *J. Org. Chem.* **1983**, *48*, 1388–1389.
[147] G.-H. Tan, T.-M. Lim, T.-S. Kam, *Tetrahedron Lett.* **1995**, *36*, 1327–1330.
[148] B. Kharraz, P. Uriac, L. Toupet, J. P. Hurvois, C. Moinet, A. Tallec, *Tetrahedron* **1995**, *51*, 9611–9624.
[149] H. Bock, I. Göbel, Z. Havlas, S. Liedle, H. Oberhammer, *Angew. Chem.* **1991**, *103*, 193–196; *Angew. Chem. Int. Ed. Engl.* **1991**, *30*, 187.
[150] D. B. Clark, M. Fleischmann, D. Pletcher, *J. Chem. Soc. Perkin Trans. 2* **1973**, 1578–1581.
[151] a) K. Toriyama, K. Nunome, M. Iwasaki, *J. Phys. Chem.* **1986**, *90*, 6836–6842; b) M. Iwasaki, K. Toriyama, M. Fukaya, H. Muto, K. Nunome, *ibid.* **1985**, *89*, 5278–5284; c) K. Toriyama, K. Nunome, M. Iwasaki, *J. Chem. Phys.* **1982**, *77*, 5891–5912.
[152] G. J. Edwards, S. R. Jones, J. M. Mellor, *J. Chem. Soc. Perkin Trans. 2* **1977**, 505–510.
[153] X.-M. Zhang, F. G. Bordwell, *J. Am. Chem. Soc.* **1994**, *116*, 4251–4254.
[154] L. Qin, G. N. R. Tripathi, R. H. Schuler, *Z. Naturforsch. A* **1985**, *40*, 1026–1039.
[155] F. G. Bordwell, X.-M. Zhang, J.-P. Cheng, *J. Org. Chem.* **1993**, *58*, 6410–6416.
[156] M. Jonsson, J. Lind, T. E. Eriksen, G. Merényi, *J. Am. Chem. Soc.* **1994**, *116*, 1423–1427.
[157] M. Jonsson, J. Lind, G. Merényi, T. E. Eriksen, *J. Chem. Soc. Perkin Trans. 2* **1995**, 61–65.
[158] J.-P. Cheng, Y. Zhao, *Tetrahedron* **1993**, *49*, 5267–5276.
[159] F. G. Bordwell, J.-P. Cheng, *J. Am. Chem. Soc.* **1991**, *113*, 1736–1743.
[160] M. Röck, M. Schmittel, *J. Chem. Soc. Chem. Commun.* **1993**, 1739–1741.
[161] M. Schmittel, G. Gescheidt, M. Röck, *Angew. Chem.* **1994**, *106*, 2056–2058; *Angew. Chem. Int. Ed. Engl* **1994**, *33*, 1961–1963.
[162] V. D. Parker, Y. Chao, B. Reitstöen, *J. Am. Chem. Soc.* **1991**, *113*, 2336–2338.
[163] O. Hammerich, V. D. Parker, A. Ronlan, *Acta Chem. Scand. Ser. B* **1976**, *30*, 89–90. The rate constants of deprotonation were estimated based on shifts in kinetic potential; see also R. C. Nicholson, I. Shain, *Anal. Chem.* **1964**, *36*, 706–723.
[164] O. Brede, H. Orthner, V. Zubarev, R. Hermann, *J. Phys. Chem.* **1996**, *100*, 7097–7105.
[165] F. G. Bordwell, G.-Z. Ji, *J. Org. Chem.* **1992**, *57*, 3019–3025.
[166] O. Hammerich, B. Svensmark in ref. [3b], chap. 16.
[167] For chemical oxidations, see M. Hudlický, *Oxidations in Organic Chemistry*, ACS, Washington, **1990**, pp. 163–168.
[168] M. Röck, M. Schmittel, *J. Prakt. Chem.* **1994**, *336*, 325–329.
[169] K. Mutai, Y. Kajii, R. Nakagaki, K. Obi, *Tetrahedron Lett.* **1996**, *37*, 505–508; E. Steckhan in ref. [3b], chap. 15; R. L. Hand, R. F. Nelson, *J. Am. Chem. Soc.* **1974**, *96*, 850–860.
[170] M. Gullu, L. A. Razack, J. H. P. Utley, R. J. King, G. R. White, *Tetrahedron* **1991**, *47*, 675–684.
[171] E. T. Denisov, I. V. Khudyakov, *Chem. Rev.* **1987**, *87*, 1313–1357.

[172] G. W. Morrow, Y. Chen, J. S. Swenton, *Tetrahedron* **1991**, *47*, 655–664.
[173] S. Yamamura, Y. Shizuri, H. Shigemori, Y. Okuno, M. Ohkubo, *Tedrahedron* **1991**, *47*, 635–644.
[174] R. W. Johnson, M. D. Bednarski, B. F. O'Leary, E. R. Grover, *Tetrahedron Lett.* **1981**, *22*, 3715–3718.
[175] B. D. Gates, P. Dalidowicz, A. Tebben, S. Wang, J. S. Swenton, *J. Org. Chem.* **1992**, *57*, 2135–2143.
[176] *Oxidative Coupling of Phenols* (Eds.: W. I. Taylor, A. R. Battersby), Marcel Dekker, New York, **1967**.
[177] A. Rieker, E.-L. Dreher, H. Geisel, M. H. Khalifa, *Synthesis* **1978**, 851–855.
[178] A. Rieker, R. Beisswenger, K. Regier, *Tetrahedron* **1991**, *47*, 645–654.
[179] G. Bringmann, S. Harmsen, J. Holenz, T. Geuder, R. Götz, P. A. Keller, R. Walter, Y. F. Hallock, J. H. Cardellina II, M. R. Boyd, *Tetrahedron* **1994**, *50*, 9643–9648.
[180] a) M. Smrcina, J. Poláková, S. Vyskocil, P. Kocovský, *J. Org. Chem.* **1993**, *58*, 4534–4538; b) J. Brussee, J. L. C. Groenendijk, J. M. te Koppele, A. C. A. Jansen, *Tetrahedron* **1985**, *41*, 3313–3319.
[181] T. Osa, Y. Kashiwagi, Y. Yanagisawa, J. M. Bobbitt, *J. Chem. Soc. Chem. Commun.* **1994**, 2535–2537.
[182] J. Yoshida, K. Sakaguchi, S. Isoe, *J. Org. Chem.* **1988**, *53*, 2525–2533; E. I. Heiba, R. M. Dessau, P. G. Rodewald, *J. Am. Chem. Soc.* **1974**, *96*, 7977–7981; E. I. Heiba, R. M. Dessau, *ibid.* **1971**, *93*, 524–527, 995–999.
[183] V. Nair, J. Mathew, S. Alexander, *Synth. Commun.* **1995**, *25*, 3981–3991.
[184] C. L. Kulkarni, B. J. Scheer, J. F. Rusling, *J. Electroanal. Chem.* **1982**, *140*, 57–74.
[185] a) J. M. Bobbitt, J. P. Willis, *J. Org. Chem.* **1980**, *45*, 1978–1984; b) J. M. Bobbitt, J. P. Willis, *Heterocycles* **1977**, *6*, 899–903.
[186] An analysis of the electrophores involved is needed to classify enamines as $\textcircled{\pi}^{+\cdot}$ or $\textcircled{n}^{+\cdot}$, since the amino and unsaturated substituents have quite similar ionization potentials.
[187] J. Xu, J. He, Y. Qian, *J. Chem. Soc. Chem. Commun.* **1991**, 714–715.
[188] J. A. Richards, P. E. Whitson, D. H. Evans, *J. Electroanal. Chem.* **1975**, *63*, 311–327.
[189] B. Speiser, A. Rieker, *J. Electroanal. Chem.* **1979**, *102*, 373–395.
[190] P. Zuman, J. J. M. Holthuis, *Recl. Trav. Chim. Pays-Bas* **1988**, *107*, 403–406.
[191] J. J. M. Holthuis, D. E. M. M. Vendrig, W. J. Van Oort, P. Zuman, *J. Electroanal. Chem.* **1987**, *220*, 101–124.
[192] L. A. Paquette, E. I. Bzowej, B. M. Branan, K. J. Stanton, *J. Org. Chem.* **1995**, *60*, 7277–7283.
[193] T. Cohen, K. McNamara, M. A. Kuzemko, K. Ramig, J. J. Landi, Jr., Y. Dong, *Tetrahedron* **1993**, *49*, 7931–7942.
[194] T. Langer, M. Illich, G. Helmchen, *Tetrahedron Lett.* **1995**, *36*, 4409–4412.
[195] Cyclization of semicarbazide: O. Hammerich, V. D. Parker, *J. Chem. Soc. Perkin Trans. 1* **1972**, 1718–1720; cycloaddition of hyrazones: A. K. M. M. Hoque, A. C. Kovelesky, W.-K. Lee, H. J. Shine, *Tetrahedron Lett.* **1985**, *26*, 5655–5658.
[196] H. J. Shine, A. K. M. M. Hoque, *J. Org. Chem.* **1988**, *53*, 4349–4353.
[197] Y. H. Kim, D. W. Lee, W. K. Lee, *Bull. Korean. Chem. Soc.* **1995**, *16*, 1225–1227.
[198] A. C. Kovelesky, H. J. Shine, *J. Org. Chem.* **1988**, *53*, 1973–1979.
[199] F. G. Bordwell, S. Zhang, *J. Am. Chem. Soc.* **1995**, *117*, 4858–4861.
[200] a) S. F. Nelsen, L. J. Chen, P. A. Petillo, D. H. Evans, F. A. Neugebauer, *J. Am. Chem. Soc.* **1993**, *115*, 10611–10620; b) S. F. Nelsen, P. A. Petillo, J. Defelippis, Y. C. Wang, L. J. Chen, M. J. R. Yunta, F. A. Neugebauer, *ibid.* **1993**, *115*, 5608–5615; c) S. F. Nelsen, Y. Kim, T. B. Frigo, *ibid.* **1989**, *111*, 5387–5397; d) S. F. Nelsen, S. C. Blackstock, K. J. Haller, *Tetrahedron* **1986**, *42*, 6101–6109; e) S. F. Nelsen, T. B. Frigo, Y. Kim, J. A. Thompsoncolon, *J. Am. Chem. Soc.* **1986**, *108*, 7926–7934; f) M. Dietrich, H. Fischer, J. Heinze, F. A. Neugebauer, *Angew. Chem.* **1986**, *98*, 999–1000; *Angew. Chem. Int. Ed. Engl.* **1986**, *25*, 1021–1023; g) F. A. Neugebauer, M. Bock, S. Kuhnhauser, H. Kurreck, *Chem. Ber.* **1986**, *119*, 980–990.
[201] G. M. Abouelenien, *J. Electroanal. Chem.* **1993**, *346*, 367–375.
[202] P. Audebert, H. Bekolo, J. Cossy, A. Bouzide, *J. Electroanal. Chem.* **1995**, *389*, 215–218.
[203] a) K. Blau, V. Voerckel, *J. Prakt. Chem.* **1989**, *331*, 285–292; b) K. Blau, U. Kapst, V. Voerkel, *ibid.* **1988**, *330*, 671–676.
[204] J. Cossy, A. Bouzide, *Tetrahedron Lett.* **1993**, *34*, 5583–5586.
[205] E. Baciocchi, E. Fasella, O. Lanzalunga, M. Mattioli, *Angew. Chem.* **1993**, *105*, 1110–1112; *Angew. Chem. Int. Ed. Engl.* **1993**, *32*, 1071–1073.
[206] a) T. M. Bockman, J. K. Kochi, *J. Chem. Soc. Perkin Trans. 2* **1996**, 1633–1643; b) M. Schmittel, M. Keller, A. Burghart, *ibid.* **1995**, 2327–2333.
[207] M. Schmittel, J. Heinze, H. Trenkle, *J. Org. Chem.* **1995**, *60*, 2726–2733.
[208] J. P. Dinnocenzo, S. Farid, J. L. Goodman, I. R. Gould, W. P. Todd, S. L. Mattes, *J. Am. Chem. Soc.* **1989**, *111*, 8973–8975.
[209] Y. Kohno, K. Narasaka, *Bull. Chem. Soc. Jpn.* **1995**, *68*, 322–329.
[210] M. Schmittel, J.-P. Steffen, A. Burghart, *Chem. Commun.* **1996**, 2349–2350.
[211] M. Schmittel, R. Söllner, *Angew. Chem.* **1996**, 108, 2248–2250; *Angew. Chem. Int. Ed. Engl.* **1996**, *35*, 2107–2109.
[212] G. Sartori, R. Maggi, F. Bigi, A. Arienti, G. Casnati, G. Bocelli, G. Mori, *Tetrahedron* **1992**, *48*, 9483–9494.
[213] K. Mizuno, T. Tamai, I. Hashida, Y. Otsuji, *J. Org. Chem.* **1995**, *60*, 2935–2937.
[214] H. Sakurai, K. Sakamoto, M. Kira, *Chem. Lett.* **1984**, 1213–1214.
[215] A. Bhattacharya, L. M. DiMichele, U.-H. Dolling, E. J. J. Grabowski, V. J. Grenda, *J. Org. Chem.* **1989**, *54*, 6118–6120.
[216] P. G. Gassman, J. Bottorff, *J. Org. Chem.* **1988**, *53*, 1097–1100.
[217] a) A. B. Paolobelli, P. Ceccherelli, F. Pizzo, R. Ruzziconi, *J. Org. Chem.* **1995**, *60*, 4954–4958; b) T. Hirao, T. Fujii, Y. Ohshiro, *Tetrahedron* **1994**, *50*, 10207–10214; c) T. Fujii, T. Hirao, Y. Ohshiro, *Tetrahedron Lett.* **1992**, *33*, 5823–5826.
[218] a) A. B. Paolobelli, D. Latini, R. Ruzziconi, *Tetrahedron Lett.* **1993**, *34*, 721–724; b) E. Baciocchi, A. Casu, R. Ruzziconi, *ibid.* **1989**, *30*, 3707–3710.
[219] S. Fukuzumi, M. Fujita, J. Otera, *J. Org. Chem.* **1993**, *58*, 5405–5410.
[220] T. Sato, Y. Wakahara, J. Otera, H. Nozaki, *J. Am. Chem. Soc.* **1991**, *113*, 4028–4030.
[221] M. Schmittel, M. Levis, *Chem. Lett.* **1994**, 1939–1940.
[222] K. Maruyama, S. Tai, H. Imahori, *Bull. Chem. Soc. Jpn.* **1986**, *59*, 1777–1780.
[223] C. Amatore, A. Jutand, J.-M. Mallet, G. Meyer, P. Sinay, *J. Chem. Soc. Chem. Commun.* **1990**, 718–719; J. D. Timpa, M. G. Legendre, G. W. Griffin, P. K. Das, *Carbohydrate Res.* **1983**, *117*, 69–80.
[224] a) M. E. Mendicino, S. C. Blackstock, *J. Am. Chem. Soc.* **1991**, *113*, 713–715; b) G. Gescheidt, A. Lamprecht, C. Rüchardt, M. Schmittel, *Helv. Chim. Acta* **1991**, *74*, 2094–2099; c) F. Gerson, X.-Z. Qin, *ibid.* **1988**, *71*, 1498–1501; d) F. Williams, Q.-X. Guo, P. A. Petillo, S. F. Nelsen, *J. Am. Chem. Soc.* **1988**, *110*, 7887–7888.
[225] a) T. Karatsu, Y. Ichino, W. H. Owens, P. S. Engel, *J. Chem. Res. Syn.* **1995**, 440–441; b) P. S. Engel, D. M. Robertson, J. N. Scholz, H. J. Shine, *J. Org. Chem.* **1992**, *57*, 6178–6187; c) D. H. Bae, P. S. Engel, A. K. M. M. Hoque, D. E. Keys, W.-K. Lee, R. W. Shaw, H. J. Shine, *J. Am. Chem. Soc.* **1985**, *107*, 2561–2562.
[226] T. A. Zona, J. L. Goodman, *J. Am. Chem. Soc.* **1993**, *115*, 4925–4926.
[227] T. A. Zona, J. L. Goodman, *Tetrahedron Lett.* **1992**, *33*, 6093–6096.
[228] W. Adam, M. Dörr, *J. Am. Chem. Soc.* **1987**, *109*, 1570–1572.
[229] a) W. Adam, C. Sahin, J. Sendelbach, H. Walter, G.-F. Chen, F. Williams, *J. Am. Chem. Soc.* **1994**, *116*, 2576–2584; b) W. Adam, H. Walter, G.-F. Chen, F. Williams, *ibid.* **1992**, *114*, 3007–3014.
[230] W. Adam, J. Sendelbach, *J. Org. Chem.* **1993**, *58*, 5316–5322.
[231] a) H. Ikeda, T. Minegishi, Y. Takahashi, T. Miyashi, *Tetrahedron Lett.* **1996**, *37*, 4377–4380; b) W. Adam, C. Sahin, *ibid.* **1994**, *35*, 9027–9030.
[232] G. Gescheidt, A. Lamprecht, J. Heinze, B. Schuler, M. Schmittel, S. Kiau, C. Rüchardt, *Helv. Chim. Acta* **1992**, *75*, 1607–1612.
[233] B. Gollas, B. Speiser, *Angew. Chem.* **1992**, *104*, 336–338; *Angew. Chem. Int. Ed. Engl.* **1992**, *31*, 332–334.
[234] a) L. Dunsch, B. Gollas, A. Neudeck, A. Petr, B. Speiser, H. Stahl, *Chem. Ber.* **1994**, *127*, 2423–2429; b) B. Speiser, H. Stahl, *Tetrahedron Lett.* **1992**, *33*, 4429–4432.
[235] P. Rapta, L. Omelka, A. Staško, J. Dauth, B. Deubzer, J. Weis, *J. Chem. Soc. Perkin Trans. 2* **1996**, 255–261.
[236] H. Watanabe, K. Yoshizumi, T. Muraoka, M. Kato, Y. Nagai, T. Sato, *Chem. Lett.* **1985**, 1683–1686.
[237] J. T. Wang, F. Williams, *J. Chem. Soc. Chem. Commun.* **1981**, 666–668.
[238] Y. Nakadaira, N. Komatsu, H. Sakurai, *Chem. Lett.* **1985**, 1781–1782.
[239] H. Watanabe, M. Kato, E. Tabei, H. Kuwabara, N. Hirai, T. Sato, Y. Nagai, *J. Chem. Soc. Chem. Commun.* **1986**, 1662–1663.
[240] a) Y. Nakadaira, N. Komatsu, H. Sakurai, *Chem. Lett.* **1985**, 1781–1782; b) S. Kyushin, Y. Ehara, Y. Nakadaira, M. Ohashi, *J. Chem. Soc. Chem. Commun.* **1989**, 279–280.
[241] Y. Nakadaira, A. Sekiguchi, Y. Funada, H. Sakurai, *Chem. Lett.* **1991**, 327–330.
[242] Y. Nakadaira, S. Otani, S. Kyushin, M. Ohashi, H. Sakurai, Y. Funada, K. Sakamoto, A. Sekiguchi, *Chem. Lett.* **1991**, 601–602.
[243] S. Kyushin, Y. Ehara, Y. Nakadaira, M. Ohashi, *J. Chem. Soc. Chem. Commun.* **1989**, 279–280.
[244] S. Fukuzumi, T. Kitano, K. Mochida, *J. Am. Chem. Soc.* **1990**, *112*, 3246–3247.
[245] K. Mochida, C. Hodota, R. Hata, S. Fukuzumi, *Organometallics* **1993**, *12*, 586–588.
[246] T. H. Fisher, S. M. Dershem, *J. Org. Chem.* **1988**, *53*, 1504–1507.
[247] R. H. Schlosberg, *Chemistry of Coal Conversion*, Plenum, New York, **1985**.
[248] D. M. Camaioni, *J. Am. Chem. Soc.* **1990**, *112*, 9475–9483.
[249] D. M. Camaioni, J. A. Franz, *J. Org. Chem.* **1984**, *49*, 1607–1613.
[250] E. Bachiocci, D. Bartoli, C. Rol, R. Ruzziconi, G. V. Sebastiani, *J. Org. Chem.* **1986**, *51*, 3587–3593.
[251] D. R. Arnold, L. J. Lamont, *Can. J. Chem.* **1989**, *67*, 2119–2127.
[252] R. Popielarz, D. R. Arnold, *J. Am. Chem. Soc.* **1990**, *112*, 3068–3082.
[253] a) K. Ishiguro, T. Osaki, Y. Sawaki, *Chem. Lett.* **1992**, 743–746; b) S. Min, Y. Okamoto, S. Takamuku, *J. Chem. Res.* **1991**, 176–177.

[254] a) E. M. Arnett, R. A. Flowers II, *Chem. Soc. Rev.* **1993**, 9–15; b) E. M. Arnett, S. Venimadhavan, *J. Am. Chem. Soc.* **1991**, *113*, 6967–6975.

[255] K. Osoda, X. Pannecoucke, K. Narasaka, *Chem. Lett.* **1995**, 1119–1120.

[256] S. Perrier, S. Sankararaman, J. K. Kochi, *J. Chem. Soc. Perkin Trans. 2* **1993**, 825–837; S. Sankararaman, J. K. Kochi, *J. Chem. Soc. Chem. Commun.* **1989**, 1800–1802.

[257] J. H. Penn, J. H. Duncan, *J. Org. Chem.* **1993**, *58*, 2003–2008; J. H. Penn, Z. Lin, D.-L. Deng, *J. Am. Chem. Soc.* **1991**, *113*, 1001–1008; J. H. Penn, D.-L. Deng, K.-J. Chai, *Tetrahedron Lett.* **1988**, *29*, 3635–3638.

[258] D. S. Han, H. J. Shine, *J. Org. Chem.* **1996**, *61*, 3977–3982.

[259] A. Albini, S. Spreti, *J. Chem. Soc. Perkin Trans. 2* **1987**, 1175–1179.

[260] X. Ci, D. G. Whitten, *J. Am. Chem. Soc.* **1989**, *113*, 3459–3461.

[261] a) D. R. Arnold, X. Du, K. M. Henseleit, *Can. J. Chem.* **1991**, *69*, 839–852; b) D. R. Arnold, L. J. Lamont, A. L. Perrot, *ibid.* **1991**, *69*, 225–233.

[262] a) A. Okamoto, D. R. Arnold, *Can. J. Chem.* **1985**, *63*, 2340–2342; b) D. R. Arnold, B. J. Fahie, L. J. Lamont, J. Wierzchowski, K. M. Young, *ibid.* **1987**, *65*, 2734–2743.

[263] D. R. Arnold, L. J. Lamont, A. L. Perrott, *Can. J. Chem.* **1991**, *69*, 225–233.

[264] This trend can readily be understood based on calculations of thermochemical cycles, since the oxidation potentials of the 1,2-diarylethanes remain almost constant upon addition of the substituents at the ethylene moiety. However, the oxidation potentials of the radicals are significantly lowered, see ref. [261a].

[265] X. Du, D. R. Arnold, R. J. Boyd, Z. Shi, *Can. J. Chem.* **1991**, *69*, 1365–1375.

[266] M. A. Kellett, D. G. Whitten, *Res. Chem. Intermed.* **1995**, *21*, 587–611.

[267] J. P. Dinnocenzo, W. P. Todd, T. R. Simpson, I. R. Gould, *J. Am. Chem. Soc.* **1990**, *112*, 2462–2464. The rate constants reported by Dinnocenzo were later shown to be slightly too high: Y. Takahashi, N. Nishioka, F. Endoh, H. Ikeda, T. Miyashi, *Tetrahedron Lett.* **1996**, *37*, 1841–1844.

[268] a) R. Akaba, Y. Niimura, T. Fukushima, Y. Kawai, T. Tajima, T. Kuragami, A. Negishi, M. Kamata, H. Sakuragi, K. Tokumaru, *J. Am. Chem. Soc.* **1992**, *114*, 4460–4464; b) R. Akaba, M. Kamata, H. Sakuragi, K. Tokumaru, *Tetrahedron Lett.* **1992**, *33*, 8105–8108.

[269] H. F. Davis, B. B. Lohray, K. R. Gopidas, C. V. Kumar, P. K. Das, M. V. George, *J. Org. Chem.* **1985**, *50*, 3685–3692.

[270] P. Maslak, S. L. Asel, *J. Am. Chem. Soc.* **1988**, *110*, 8260–8261.

[271] P. Maslak, T. M. Vallombroso, W. H. Chapman, Jr., J. N. Narvaez, *Angew. Chem.* **1994**, *106*, 110–113; *Angew. Chem. Int. Ed. Engl.* **1994**, *33*, 73–75.

[272] Maslak et al. [271]) obtained a quadratic Marcus-type correlation for bond cleavages of radical cations and anion radicals; that is not detectable for radical cations only.

[273] P. Maslak, J. N. Narvaez, *Angew. Chem.* **1990**, *102*, 302–304; *Angew. Chem. Int. Ed. Engl.* **1990**, *29*, 283–285.

[274] Similarly, the unpaired electron in di(9-anthryl)methane$^{\bullet+}$ is only delocalized over one of the anthracene rings: A. Terahara, H. Ohya-Nishiguchi, N. Hirota, H. Higuchi, S. Misumi, *J. Phys. Chem.* **1986**, *90*, 4958–4961; for triptycene$^{\bullet-}$: H. Quast, H. L. Fuchsbauer, *Chem. Ber.* **1986**, *119*, 1016–1038.

[275] P. Maslak, *Top. Curr. Chem.* **1993**, *168*, 1–46.

[276] J. P. Dinnocenzo, S. S. Shaik, *J. Org. Chem.* **1990**, *55*, 3434–3436.

[277] J. P. Dinnocenzo, D. R. Lieberman, T. R. Simpson, *J. Am. Chem. Soc.* **1993**, *115*, 366–367.

[278] The rate of C–C bond fragmentation in the radical cations can in general be qualitatively predicted since it increases with increasing oxidation potential of the molecule, decreasing C–C bond strength, and decreasing oxidation potential of the fragment that ultimately appears as the carbocation. Since oxidation potentials for the starting compounds and the radicals are either available or can be estimated with reasonable accuracy, the bond dissociation energies of the radical cations can readily be calculated.

[279] R. D. Burton, M. D. Barthberger, Y. Zhang, J. R. Eyler, K. S. Schanze, *J. Am. Chem. Soc.* **1996**, *118*, 5655–5664; L. A. Lucia, R. D. Burton, K. S. Schanze, *J. Phys. Chem.* **1993**, *97*, 9078–9080.

[280] J. W. Leon, D. G. Whitten, *J. Am. Chem. Soc.* **1993**, *115*, 8038–8043.

[281] S. Fukuzumi, Y. Tokuda, T. Kitano, T. Okamoto, J. Otera, *J. Am. Chem. Soc.* **1993**, *115*, 8960–8968.

[282] G. Boche, H. M. Walborsky, *Cyclopropane Derived Reactive Intermediates, Updates from the Chemistry of Functional Groups* (Eds.: S. Patai, Z. Rappoport), Wiley, Chichester, **1990**.

[283] Y. Takahashi, H. Ohaku, S. Morishima, T. Suzuki, T. Miyashi, *Tetrahedron Lett.* **1995**, *36*, 5207–5210.

[284] A. P. Schaap, S. Siddiqui, G. Prasad, E. Palomino, L. Lopez, *J. Photochem.* **1984**, *25*, 167–181.

[285] H. Tomioka, D. Kobayashi, A. Hashimoto, S. Murata, *Tetrahedron Lett.* **1989**, *30*, 4685–4688.

[286] a) K. Mizuno, N. Kamiyama, Y. Otsuji, *Chem. Lett.* **1983**, 477–480; b) Y. Takahashi, T. Miyashi, T. Mukai, *J. Am. Chem. Soc.* **1983**, *105*, 6511–6513; c) K. Mizuno, N. Kamiyama, N. Ichinose, Y. Otsuji, *Tetrahedron* **1985**, *41*, 2207–2214.

[287] K. Mizuno, N. Ichinose, T. Tamai, Y. Otsuji, *J. Org. Chem.* **1992**, *57*, 4669–4675, and references therein.

[288] a) D. R. Arnold, X. Du, *J. Am. Chem. Soc.* **1989**, *111*, 7666–7667; b) K. Mizuno, J. Ogawa, Y. Otsuji, *Chem. Lett.* **1981**, 741–744.

[289] M. Klehr, H. J. Schäfer, *Angew. Chem.* **1975**, *87*, 173–174; *Angew. Chem. Int. Ed. Engl.* **1975**, *14*, 247–248; T. Shono, Y. Matsumura, *J. Org. Chem.* **1970**, *55*, 4157–4160.

[290] H. Weng, V. Sethuraman, H. D. Roth, *J. Am. Chem. Soc.* **1994**, *116*, 7021–7025.

[291] D. R. Arnold, X. Du, H. J. P. de Lijser, *Can. J. Chem.* **1995**, *73*, 522–530.

[292] a) A. Okamoto, M. S. Snow, D. R. Arnold, *Tetrahedron* **1986**, *42*, 6175–6187; b) D. R. A. M. Nicholas, R. J. Boyd, D. R. Arnold, *Can. J. Chem.* **1982**, *60*, 3011–3018; c) D. R. Arnold, A. J. Maroulis, *J. Am. Chem. Soc.* **1976**, *98*, 5931–5937.

[293] E. Baciocchi, M. Bietti, L. Putignani, S. Steenken, *J. Am. Chem. Soc.* **1996**, *118*, 5952–5960; X. Ci, D. G. Whitten, *ibid.* **1989**, *111*, 3459–3461.

[294] W. Adam, M. A. Miranda, F. Mojarrad, H. Sheikh, *Chem. Ber.* **1994**, *127*, 875–879.

[295] L. Chen, M. S. Farahat, H. Gan, S. Farid, D. G. Whitten, *J. Am. Chem. Soc.* **1995**, *117*, 6398–6399.

[296] H. Moriwaki, K. Fukushima, T. Nagai, T. Oshima, *Chem. Commun.* **1996**, 495–496.

[297] E. Gunic, I. Tabakovic, M. J. Gasic, *J. Chem. Soc. Chem. Commun.* **1993**, 1496–1497.

[298] M. A. Kellet, D. G. Whitten, *J. Am. Chem. Soc.* **1989**, *111*, 2314–2316.

[299] A. Albini, M. Mella, M. Freccero, *Tetrahedron* **1995**, *50*, 575–607.

[300] a) W. R. Bergmark, D. G. Whitten, *J. Am. Chem. Soc.* **1990**, *112*, 4042–4043; b) L. Y. C. Lee, X. Ci, C. Giannotti, D. G. Whitten, *ibid.* **1986**, *108*, 175–177.

[301] X. Ci, M. A. Kellett, D. G. Whitten, *J. Am. Chem. Soc.* **1991**, *113*, 3893–3904; X. Ci, D. G. Whitten, *ibid.* **1987**, *109*, 7215–7217.

[302] L. A. Lucia, D. G. Whitten, K. S. Schanze, *J. Am. Chem. Soc.* **1996**, *118*, 3057–3058.

[303] Y. Takemoto, T. Ohra, S. Furuse, H. Koike, C. Iwata, *J. Chem. Soc. Chem. Commun.* **1994**, 1529–1530.

[304] A. P. Schaap, *Tetrahedron Lett.* **1983**, *24*, 3047–3050.

[305] E. Hasegawa, S. Koshii, T. Horaguchi, T. Shimizu, *J. Org. Chem.* **1992**, *57*, 6342–6344.

[306] a) Y. Takemoto, T. Ohra, H. Koike, S. Furuse, C. Iwata, H. Ohishi, *J. Org. Chem.* **1994**, *59*, 4727–4729; b) Y. Takemoto, T. Ohra, S. Furuse, H. Koike, C. Iwata, *J. Chem. Soc. Chem. Commun.* **1994**, 1529–1530; c) Y. Takemoto, S. Furuse, H. Koike, T. Ohra, C. Iwata, H. Ohishi, *Tetrahedron Lett.* **1995**, *36*, 4085–4088.

[307] M. Mella, E. Fasani, A. Albini, *J. Org. Chem.* **1992**, *57*, 3051–3057.

[308] A. Albini, M. Mella, M. Freccero, *Tetrahedron* **1994**, *50*, 575–604.

[309] M. Mella, M. Fagnoni, A. Albini, *J. Org. Chem.* **1994**, *59*, 5614–5622.

[310] a) P. G. Gassman, S. J. Burns, *J. Org. Chem.* **1988**, *53*, 5576–5678; b) P. G. Gassman, B. A. Hay, *J. Am. Chem. Soc.* **1986**, *108*, 4227–4228; c) *ibid.* **1985**, *107*, 4075–4076.

[311] M. Abe, M. Nojima, A. Oku, *Tetrahedron Lett.* **1996**, *37*, 1833–1836; M. Abe, A. Oku, *J. Org. Chem.* **1995**, *60*, 3065–3073; *Tetrahedron Lett.* **1994**, *35*, 3551–3554; K. I. Booker-Milburn, *Synlett* **1992**, 809–810.

[312] C. J. Abelt, H. D. Roth, M. L. M. Schilling, *J. Am. Chem. Soc.* **1985**, *107*, 4148–4152; for homobenzvalene: E. Kim, M. Christl, J. K. Kochi, *Chem. Ber.* **1990**, *123*, 1209–1218.

[313] B. H. Hong, M. A. Fox, G. Maier, C. Hermann, *Tetrahedron Lett.* **1996**, *37*, 583–586; G. Maier, H. Rang, R. Emrich, S. Gries, H. Irngartinger, *Liebigs Ann.* **1995**, 161–167.

[314] K. Toriyama, M. Okazaki, *J. Phys. Chem.* **1992**, *96*, 6986–6991.

[315] J. P. Dinnocenzo, S. Farid, J. L. Goodman, I. R. Gould, W. P. Todd, S. L. Mattes, *J. Am. Chem. Soc.* **1989**, *111*, 8973–8975.

[316] W. P. Todd, J. P. Dinnocenzo, S. Farid, J. L. Goodman, I. R. Gould, *Tetrahedron Lett.* **1993**, *34*, 2863–2866.

[317] J. P. Dinnocenzo, S. Farid, J. L. Goodman, I. R. Gould, W. P. Todd, *Mol. Cryst. Liq. Cryst.* **1991**, *194*, 151–157.

[318] Derived from calculations of thermochemical cycles: J. P. Dinnocenzo, private communication (1987).

[319] S. Venimadhavan, K. Amarnath, N. G. Harvey, J.-P. Cheng, E. M. Arnett, *J. Am. Chem. Soc.* **1992**, *114*, 221–229.

[320] According to our classification, allyltrimethylsilane$^{\bullet-}$ is rather a ⓞ:C-Si$^{\bullet+}$ species, but substituted analogues are ⓟ-C-X$^{\bullet+}$.

[321] a) T. Koizumi, T. Fuchigami, T. Nonaka, *Bull. Chem. Soc. Jpn.* **1989**, *62*, 219–225; b) J. Yoshida, T. Murata, S. Isoe, *Tetrahedron Lett.* **1986**, *27*, 3373–3376.

[322] S. R. Sirimanne, Z. Li, D. R. VanderVeer, L. M. Tolbert, *J. Am. Chem. Soc.* **1991**, *113*, 1766–1769.

[323] D. F. Eaton, *J. Am. Chem. Soc.* **1980**, *102*, 3278–3280; *ibid.* **1980**, *102*, 3280–3281; *ibid.* **1981**, *103*, 7235–7239.

[324] P. S. Mariano, *Acc. Chem. Res.* **1983**, *16*, 130–137; A. J. Y. Lan, S. L. Quillen, R. O. Heuckeroth, P. S. Mariano, *J. Am. Chem. Soc.* **1984**, *106*, 6439–6440.

[325] M. Freccero, E. Fasani, A. Albini, *J. Org. Chem.* **1993**, *58*, 1740–1745.

[326] a) K. Mizuno, M. Ikeda, Y. Otsuji, *Tetrahedron Lett.* **1985**, *26*, 461–464; b) K. Mizuno, K. Terasaka, M. Ikeda, Y. Otsuji, *ibid.* **1985**, *26*, 5819–5822.

[327] K. Mizuno, G. Konishi, T. Nishiyama, H. Inoue, *Chem. Lett.* **1995**, 1077–1078.

[328] E. Baciocchi, M. Crescenzi, E. Fasella, M. Mattioli, *J. Org. Chem.* **1992**, *57*, 4684–4689.

[329] a) E. Baciocchi, M. Crescenzi, *Angew. Chem.* **1990**, *102*, 687–688; *Angew. Chem. Int. Ed. Engl.* **1990**, *29*, 658; b) E. Baciocchi, T. Del Giacco, F. Elisei, M. Ioele, *J. Org. Chem.* **1995**, *60*, 7974–7983.

[330] E. Baciocchi, R. Bernini, O. Lanzalunga, *J. Chem. Soc. Chem. Commun.* **1993**, 1691–1692.

[331] a) M. Kimura, K. Koie, S. Matsubara, Y. Sawaki, H. Iwamura, *J. Chem. Soc. Chem. Commun.* **1987**, 122–123; b) T. Fuchigami, Y. Nakagawa, T. Nonaka, *Tetrahedron Lett.* **1986**, *27*, 3869–3872.

[332] a) G. Pandey, D. Chakrabarti, *Tetrahedron Lett.* **1996**, *37*, 2285–2288; b) G. Pandey, G. D. Reddy, G. Kumaraswamy, *Tetrahedron* **1994**, *50*, 8185–8194; c) G. Pandey, G. D. Reddy, *Tetrahedron Lett.* **1992**, *33*, 6533–6536; d) G. Pandey, G. Kumaraswamy, U. T. Bhalerao, *ibid.* **1989**, *30*, 6059–6062.

[333] W. Xu, X. T. Jeon, E. Hasegawa, U. C. Yoon, P. S. Mariano, *J. Am. Chem. Soc.* **1989**, *111*, 406–408.

[334] Y. S. Jung, W. H. Swartz, W. Xu, P. S. Mariano, N. J. Green, A. G. Schultz, *J. Org. Chem.* **1992**, *56*, 6037–6047.

[335] E. Hasegawa, M. A. Brumfield, P. S. Mariano, U.-C. Yoon, *J. Org. Chem.* **1988**, *53*, 5435–5442.

[336] E. Meggers, E. Steckhan, S. Blechert, *Angew. Chem.* **1995**, *107*, 2317–2319; *Angew. Chem. Int. Ed. Engl.* **1995**, *34*, 2137–2139.

[337] E. Hasegawa, M. Brumfield, P. S. Mariano, U. C. Yoon, *J. Am. Chem. Soc.* **1988**, *110*, 8099–8111.

[338] G. Pandey, G. Lakshaiah, *Tetrahedron Lett.* **1993**, *34*, 4861–4864.

[339] J. Yoshida, Y. Ishichi, S. Isoe, *J. Am. Chem. Soc.* **1992**, *114*, 7594–7595.

[340] Based on our criteria, 2-silyl-1,3-dithianes have an n electrophore, see ref. [341a].

[341] Since both electrophores, the lone pair on sulfur and the σ C–Sn bond, have very similar ionization potentials, the choice of a ⓞ$^{+}$ species is arbitrary. Based on cyclic voltammetry measurements, however, we prefer to describe the 2-stannyl-1,3-dithianes as σ electrophores, see also a) R. S. Glass, A. M. Radspinner, W. P. Singh, *Pure Appl. Chem.* **1996**, *68*, 853–858; b) *J. Am. Chem. Soc.* **1992**, *114*, 4921–4923.

[342] a) K. Narasaka, N. Arai, T. Okauchi, *Bull. Chem. Soc. Jpn.* **1993**, *66*, 2995–3003; b) K. Narasaka, T. Okauchi, N. Arai, *Chem. Lett.* **1992**, 1229–1232.

[343] Even in the presence of an aromatic unit, it is the C–Sn electrophore that has a lower oxidation potential [344a].

[344] a) K. Narasaka, Y. Kohno, *Bull. Chem. Soc. Jpn.* **1993**, *66*, 3456–3463; b) K. Narasaka, Y. Kohno, S. Shimada, *Chem. Lett.* **1993**, 125–128.

[345] S. Kyushin, S. Otani, Y. Nakadaira, M. Ohashi, *Chem. Lett.* **1995**, 29–30.

[346] K. Ohga, P. S. Mariano, *J. Am. Chem. Soc.* **1982**, *104*, 617–619.

[347] a) T. Nishiyama, K. Mizuno, Y. Otsuji, H. Inoue, *Tetrahedron* **1995**, *51*, 6695–6706; b) K. Mizuno, M. Ikeda, Y. Otsuji, *Tetrahedron Lett.* **1985**, *26*, 461–464.

[348] M. Fagnoni, M. Mella, A. Albini, *Tetrahedron* **1994**, *50*, 6401–6410.

[349] A rate of 10^{7}–10^{8} s^{-1} was estimated for ⓞ:C-Sn^{+} bond cleavage [348].

[350] J. K. Kochi, R. T. Tang, T. Bernath, *J. Am. Chem. Soc.* **1973**, *95*, 7114–7123.

[351] O. Hammerich, V. D. Parker, *Adv. Phys. Org. Chem.* **1984**, *20*, 55–189.

[352] M. Fujita, S. Fukuzumi, *Chem. Lett.* **1993**, 1911–1914.

[353] a) M. Oyama, K. Nozaki, S. Okazaki, *J. Electroanal. Chem.* **1991**, *304*, 61–73; b) M. Oyama, K. Nozaki, T. Nagaoka, S. Okazaki, *Bull. Chem. Soc. Jpn.* **1990**, *63*, 33–41.

[354] Diagnostic criteria were proposed for differentiating 25 possible mechanisms for cathodic electrodimerization: a) L. Nadjo, J.-M. Savéant, *J. Electroanal. Chem.* **1973**, *44*, 327–360. These also apply to anodic electrodimerization processes: b) see ref. [184].

[355] V. D. Parker, *Acc. Chem. Res.* **1984**, *17*, 243–250.

[356] By comparing rate of nucleophile combination with those of radical cations and carbocations, Eberson concluded in 1978 that radical cation reactions are slow [357]. A little later, the inherent sluggishness of radical cation–nucleophile reactions was rationalized by the configuration-mixing model [358].

[357] L. Eberson, Z. Blum, B. Helgee, K. Nyberg, *Tetrahedron* **1978**, *34*, 731–739.

[358] a) A. Pross, *J. Am. Chem. Soc.* **1986**, *108*, 3537–3538; b) S. S. Shaik, A. Pross, *ibid.* **1989**, *111*, 4306–4312.

[359] V. D. Parker, K. L. Handoo, B. Reitstöen, *J. Am. Chem. Soc.* **1991**, *113*, 6218–6222.

[360] M. S. Workentin, L. J. Johnston, D. D. M. Wayner, V. D. Parker, *J. Am. Chem. Soc.* **1994**, *116*, 8279–8287.

[361] V. D. Parker, B. Reitstöen, M. Tilset, *J. Phys. Org. Chem.* **1989**, *2*, 580–584.

[362] H. Wang, G. Zheng, V. D. Parker, *Acta Chem. Scand.* **1995**, *49*, 311–312.

[363] F. Norrsell, K. L. Handoo, V. D. Parker, *J. Org. Chem.* **1993**, *58*, 4929–4932.

[364] L. J. Johnston, N. P. Schepp, *J. Am. Chem. Soc.* **1993**, *115*, 6564–6571.

[365] L. J. Johnston, N. P. Schepp, *Pure Appl. Chem.* **1995**, *67*, 71–78.

[366] H. Zipse, *J. Am. Chem. Soc.* **1995**, *117*, 11798–11806.

[367] M. Schmittel, M. Röck, *Chem. Ber.* **1992**, *125*, 1611–1620.

[368] B Reitstöen, V. D. Parker, *J. Am. Chem. Soc.* **1991**, *113*, 6954–6958.

[369] H. Mayr, M. Patz, *Angew. Chem.* **1994**, *106*, 990–1010; *Angew. Chem. Int. Ed. Engl.* **1994**, *33*, 938–955.

[370] a) R. F. Nelson, R. H. Philp, Jr., *J. Phys. Chem.* **1979**, *83*, 713–716; b) S. C. Creason, J. Wheeler, R. F. Nelson, *J. Org. Chem.* **1972**, *37*, 4440–4446.

[371] V. D. Parker, *Acta Chem. Scand. Ser. B* **1983**, *37*, 393–401.

[372] B. Aalstad, A. Ronlán, V. D. Parker, *Acta Chem. Scand. Ser. B* **1981**, *35*, 247–257.

[373] K. Nozaki, M. Oyama, H. Hatano, S. Okazaki, *J. Electroanal. Chem.* **1989**, *270*, 191–204.

[374] T. Sumiyoshi, *Chem. Lett.* **1995**, 645–646.

[375] S. Yasui, K. Shioji, M. Tsujimoto, A. Ohno, *Chem. Lett.* **1995**, 783–784.

[376] J. H. Horner, F. N. Martinez, O. M. Musa, M. Newcomb, H. E. Shahin, *J. Am. Chem. Soc.* **1995**, *117*, 11124–11133.

[377] P. Cremonesi, D. E. Stack, E. G. Rogan, E. L. Cavalieri, *J. Org. Chem.* **1994**, *59*, 7683–7687.

[378] H. E. Zimmerman, K. D. Hoffacker, *J. Org. Chem.* **1996**, *61*, 6526–6534; G. Pandey, A. Krishna, K. Girja, M. Karthikeyan, *Tetrahedron Lett.* **1993**, *34*, 6631–6634.

[379] W. Eilenberg, H. Schäfer, *Tetrahedron Lett.* **1984**, *25*, 5023–5026.

[380] K. D. Moeller, C. M. Hudson, L. V. Tinao-Wooldridge, *J. Org. Chem.* **1993**, *58*, 3478–3479; C. M. Hudson, M. R. Marzabadi, K. D. Moeller, D. G. New, *J. Am. Chem. Soc.* **1991**, *113*, 7372–7385; K. D. Moeller, M. R. Marzabadi, D. G. New, M. Y. Chiang, S. Keith, *ibid.* **1990**, *112*, 6123–6124.

[381] D. G. New, Z. Tesfai, K. D. Moeller, *J. Org. Chem.* **1996**, *61*, 1578–1598.

[382] K. D. Moeller, L. V. Tinao, *J. Am. Chem. Soc.* **1992**, *114*, 1033–1041.

[383] B. B. Snider, T. Kwon, *J. Org. Chem.* **1992**, *57*, 2399–2410; B. B. Snider, T. Kwon, *ibid.* **1990**, *55*, 4786–4788.

[384] A. Heidbreder, J. Mattay, *Tetrahedron Lett.* **1992**, *33*, 1973–1976.

[385] T. Shono, I. Nishiguchi, S. Kashimura, M. Okawa, *Bull. Chem. Soc. Jpn.* **1978**, *51*, 2181–2182.

[386] C. M. Hudson, K. D. Moeller, *J. Am. Chem. Soc.* **1994**, *116*, 3347–3356.

[387] L. L. Miller, R. F. Stewart, J. P. Gillespie, V. Ramachandran, Y. H. So, F. R. Stermitz, *J. Org. Chem.* **1978**, *43*, 1580–1586.

[388] R. B. Herbert, A. E. Kattah, A. J. Murtagh, P. W. Sheldrake, *Tetrahedron Lett.* **1995**, *36*, 5649–5650.

[389] D. A. Evans, C. J. Dinsmore, D. A. Evrard, K. M. DeVries, *J. Am. Chem. Soc.* **1993**, *115*, 6426–6427.

[390] R. C. Cambie, G. R. Clark, P. A. Craw, P. S. Rutledge, P. D. Woodgate, *Aust. J. Chem.* **1984**, *115*, 1775–1784.

[391] M. Tanaka, C. Mukaiyama, H. Mitsuhashi, T. Wakamatsu, *Tetrahedron Lett.* **1992**, *33*, 4165–4168.

[392] a) R. Dhal, Y. Landais, A. Lebrun, V. Lenain, J. P. Robin, *Tetrahedron* **1994**, *50*, 1153–1164; b) Y. Landais, J. P. Robin, A. Lebrun, *ibid.* **1991**, *47*, 3787–3804.

[393] A. K. Panfilov, G. V. Cherkaev, T. V. Magdesieva, N. M. Przhiyalgovskaya, *Zh. Org. Khim.* **1992**, *28*, 691–699; A. Clerici, F. Minisci, K. Ogawa, J. M. Surzur, *Tetrahedron Lett.* **1978**, *19*, 1149–1152.

[394] A. Goosen, C. W. McCleland, F. C. Rinaldi, *J. Chem. Soc. Perkin Trans. 2* **1993**, 279–281; B. C. Gilbert, C. W. McCleland, *ibid.* **1989**, 1545–1551.

[395] G. Pandey, A. Krishna, J. M. Rao, *Tetrahedron Lett.* **1986**, *27*, 4075–4076.

[396] G. Pandey, M. Sridar, U. T. Bhalerao, *Tetrahedron Lett.* **1990**, *31*, 5373–5376.

[397] F. D. Lewis, G. D. Reddy, B. E. Cohen, *Tetrahedron Lett.* **1994**, *35*, 535–538; F. D. Lewis, G. D. Reddy, *ibid.* **1992**, *33*, 4249–4252; F. D. Lewis, D. M. Bassani, G. D. Reddy, *Pure Appl. Chem.* **1992**, *64*, 1271–1277.

[398] R. K. Haynes, S. C. Vonwiller, *J. Chem. Soc. Chem. Commun.* **1990**, 451–453.

[399] M. Tanaka, H. Nakashima, M. Fujiwara, H. Ando, Y. Souma, *J. Org. Chem.* **1996**, *61*, 788–792; T. Douadi, M. Cariou, J. Simonet, *Tetrahedron* **1996**, *52*, 4449–4456; M.-A. Le Moing, G. Le Guillanton, J. Simonet, *Electrochim. Acta* **1981**, *26*, 139–144; H. Baltes, E. Steckhan, H. J. Schäfer, *Chem. Ber.* **1978**, *111*, 1294–1314; R. Engels, H. J. Schäfer, E. Steckhan, *Liebigs Ann. Chem.* **1977**, 204–224; D. Koch, H. Schäfer, E. Steckhan, *Chem. Ber.* **1974**, *107*, 3640–3657; D. Koch, H. Schäfer, *Angew. Chem.* **1973**, *85*, 264–265; *Angew. Chem. Int. Ed. Engl.* **1973**, *12*, 254–255.

[400] M. Cariou, J. Simonet, *Tetrahedron Lett.* **1991**, *32*, 4913–4916.

[401] a) D. R. Arnold, X. Du, H. J. P. de Lijser, *Can. J. Chem.* **1995**, *73*, 522–530; b) K. McMahon, D. R. Arnold, *ibid.* **1992**, *71*, 450–468; c) D. R. Arnold, X. Du, *J. Am. Chem. Soc.* **1989**, *111*, 7666–7667; d) D. R. Arnold, M. S. Snow, *Can. J. Chem.* **1988**, *66*, 3012–3026.

[402] M. Kojima, A. Ishida, S. Takamuku, Y. Wada, S. Yanagida, *Chem. Lett.* **1994**, 1897–1900.

[403] T. Shono, S. Kashimura, *J. Org. Chem.* **1983**, *48*, 1939–1940.
[404] L. Lopez, V. Calò, F. Stasi, *Synthesis* **1987**, 947–948.
[405] T. Shono, I. Nishiguchi, M. Okawa, *Chem. Lett.* **1976**, 573–576.
[406] H. Baltes, L. Stork, H. J. Schäfer, *Liebigs Ann. Chem.* **1979**, 318–327.
[407] Keysteps in the synthesis of a) maltol: T. Shono, Y. Matsumura, *Tetrahedron Lett.* **1976**, 1363–1364; b) rethrolones: T. Shono, Y. Matsumura, H. Hamaguchi, K. Nakamura, *Chem. Lett.* **1976**, 1249–1252; c) the flavoring agent cylotene: T. Shono, Y. Matsumura, H. Hamaguchi, *J. Chem. Soc. Chem. Commun.* **1977**, 712–713.
[408] T. Shono, Y. Matsumura, K. Tsubata, Y. Sugihara, S. Yamane, T. Kanazawa, T. Aoki, *J. Am. Chem. Soc.* **1982**, *104*, 6697–6703.
[409] J. Y. Becker, E. Shakkour, J. A. P. R. Sarma, *J. Org. Chem.* **1992**, *57*, 3716–3720; J. Y. Becker, E. Shakkour, J. A. P. R. Sarma, *J. Chem. Soc. Chem. Commun.* **1990**, 1016–1017.
[410] T. Yamashita, K. Shiomori, M. Yasuda, K. Shima, *Bull. Chem. Soc. Jpn.* **1991**, *64*, 366–374; K. Mizuno, I. Nakanishi, N. Ichinose, Y. Otsuji, *Chem. Lett.* **1989**, 1095–1098.
[411] R. A. Neunteufel, D. R. Arnold, *J. Am. Chem. Soc.* **1973**, *95*, 4080–4081.
[412] Y. Kubo, N. Asai, T. Araki, *J. Org. Chem.* **1985**, *50*, 5484–5487; K. Maruyama, Y. Kubo, *J. Am. Chem. Soc.* **1978**, *100*, 7772–7773.
[413] Y. Inoue, T. Okano, N. Yamasaki, A. Tai, *J. Chem. Soc. Chem. Commun.* **1993**, 718–720.
[414] The reaction may already proceed at the state of the exciplex.
[415] T. Shono, Y. Matsumura, H. Hamaguchi, *Bull. Chem. Soc. Jpn.* **1978**, *51*, 2179–2180.
[416] K. Narasaka, T. Okauchi, K. Tanaka, M. Murakami, *Chem. Lett.* **1992**, 2099–2101.
[417] K. Narasaka, K. Iwakura, T. Okauchi, *Chem. Lett.* **1991**, 423–426.
[418] S. Yasui, K. Shioji, A. Ohno, M. Yoshihara, *J. Org. Chem.* **1995**, *60*, 2099–2105.
[419] T.-L. Ho, *Synthesis* **1973**, 347–354.
[420] A. Lebouc, J. Simonet, J. Gelas, A. Debhi, *Synthesis* **1987**, 320–321; H. J. Cristau, B. Chabaud, C. Niangoran, *J. Org. Chem.* **1983**, *48*, 1527–1529.
[421] M. Kimura, S. Matsubara, Y. Sawaki, H. Iwamura, *Tetrahedron Lett.* **1986**, *27*, 4177–4178.
[422] T. Mandai, H. Yasunaga, M. Kawada, J. Otera, *Chem. Lett.* **1984**, 715–716; T. Mandai, H. Irei, M. Kawada, J. Otera, *Tetrahedron Lett.* **1984**, *25*, 2371–2374.
[423] G. Pandey, D. Pooranchand, U. T. Bhalerao, *Tetrahedron* **1991**, *47*, 1745–1752.
[424] H. J. Shine, *Phosporus Silicon Relat. Elem.* **1994**, *95–96*, 429–430.
[425] A cycloaddition of a sulfur radical cation is reported in ref. [449]. However, that system should be classified as a $\pi^{\cdot+}$ and not as $n^{\cdot+}$, which provides a rather simple rationalization for their different behavior.
[426] K. Narasaka, T. Okauchi, *Chem. Lett.* **1991**, 515–518.
[427] S. Karady, E. G. Corley, N. L. Abrahamson, J. S. Amato, L. M. Weinstock, *Tetrahedron* **1991**, *47*, 757–766; S. Karady, E. G. Corley, N. L. Abrahamson, L. M. Weinstock, *Tetrahedron Lett.* **1989**, *30*, 2191–2194. In this case, it cannot be excluded that a $\pi^{\cdot+}$ is attacked by the n nucleophile.
[428] M. Newcomb, K. A. Weber, *J. Org. Chem.* **1991**, *56*, 1309–1313; M. Newcomb, D. J. Marquadt, *Heterocycles* **1989**, *28*, 129–132; M. Newcomb, D. J. Marquardt, M. U. Kumar, *Tetrahedron* **1990**, *46*, 2345–2352; M. Newcomb, D. J. Marquardt, T. M. Deeb, *ibid.* **1990**, *46*, 2329–2344; M. Newcomb, T. M. Deeb, D. J. Marquardt, *ibid.* **1990**, *46*, 2317–2328; M. Newcomb, T. M. Deeb, *J. Am. Chem. Soc.* **1987**, *109*, 3163–3165.
[429] L. Stella, *Angew. Chem.* **1983**, *95*, 368–380; *Angew. Chem. Int. Ed. Engl.* **1983**, *22*, 337.
[430] Y. Deng, A. J. Illies, M. A. James, M. L. McKee, M. Peschke, *J. Am. Chem. Soc.* **1995**, *117*, 420–428; J. Rogowski, J. Adamus, J. Gebicki, S. F. Nelsen, *J. Chem. Soc. Perkin Trans. 2* **1994**, 779–783; H. Hungerbühler, S. N. Guha, K. D. Asmus, *J. Chem. Soc. Chem. Commun.* **1991**, 999–1001; J. P. Dinnocenzo, T. Banach, *J. Am. Chem. Soc.* **1988**, *110*, 971–973.
[431] F. Gerson, J. Knöbel, U. Buser, E. Vogel, M. Zehnder, *J. Am. Chem. Soc.* **1986**, *108*, 3781–3783.
[432] H. Weng, H. D. Roth, *J. Org. Chem.* **1995**, *60*, 4136–4145.
[433] We use the term "pericyclic process" to depict the overall reaction, although it was indicated that not all steps proceed in a concerted manner.
[434] a) W. Yueh, N. L. Bauld, *J. Chem. Soc. Perkin Trans. 2* **1996**, 1761–1766; b) G. A. Mirafzal, T. Kim, J. Liu, N. L. Bauld, *J. Am. Chem. Soc.* **1992**, *114*, 10968–10969.
[435] J. P. Dinnocenzo, M. Schmittel, *J. Org. Chem.* **1988**, *53*, 4145–4147.
[436] This is a consequence of the fact that, in most cases, not a pure radical cation chain mechanism, but a conventional catalytic mechanism is operative [21].
[437] a) O. Brede, F. David, *Radiat. Phys. Chem.* **1996**, *47*, 53–58; b) N. P. Schepp, L. J. Johnston, *J. Am. Chem. Soc.* **1994**, *116*, 6895–6903; c) S. Tojo, S. Toki, S. Takamuku, *J. Org. Chem.* **1991**, *56*, 6240–6243.
[438] N. P. Schepp, L. J. Johnston, *J. Am. Chem. Soc.* **1994**, *116*, 10330–10331.
[439] a) S. Tojo, K. Morishima, A. Ishida, T. Majima, S. Takamuku, *Bull. Chem. Soc. Jpn.* **1995**, *68*, 958–966; b) Y. Kuriyama, H. Sakuragi, K. Tokumaru, Y. Yoshida, S. Tagawa, *ibid.* **1993**, *66*, 1852–1855.
[440] S. Tojo, K. Morishima, A. Ishida, T. Majima, S. Takamuku, *J. Org. Chem.* **1995**, *60*, 4684–4685.
[441] a) M. Rese, M. Dern, K. Lücking, R. Sustmann, *Liebigs Ann.* **1995**, 1139–1152; b) K. Lücking, M. Rese, R. Sustmann, *ibid.* **1995**, 1129–1138; c) R. Sustmann, K. Lücking, G. Kopp, M. Rese, *Angew. Chem.* **1989**, *101*, 1701–1704; *Angew. Chem. Int. Ed. Engl.* **1989**, *28*, 1713; d) M. Dern, H.-G. Korth, G. Kopp, R. Sustmann, *ibid.* **1985**, *97*, 324–326; *and* **1985**, *24*, 337–339.
[442] F. A. Bell, R. A. Crellin, N. Fujii, A. Ledwith, *J. Chem. Soc. Chem. Commun.* **1969**, 251–252; A. Ledwith, *Acc. Chem. Res.* **1972**, *5*, 133–139.
[443] D. J. Bellville, D. A. Wirth, N. L. Bauld, *J. Am. Chem. Soc.* **1981**, *103*, 718–720; D. J. Bellville, N. L. Bauld, *ibid.* **1982**, *104*, 2665–2667; N. L. Bauld, R. A. Pabon, *ibid.* **1983**, *105*, 633–634; R. A. Pabon, D. J. Bellville, N. L. Bauld, *ibid.* **1983**, *105*, 5158–5159.
[444] J. Mattay, G. Trampe, J. Runsink, *Chem. Ber.* **1988**, *121*, 1991–2005. H. D. Roth, M. L. M. Schilling, C. J. Abelt, *J. Am. Chem. Soc.* **1986**, *108*, 6098–6099.
[445] C. F. Gürtler, E. Steckhan, S. Blechert, *J. Org. Chem.* **1996**, *61*, 4136–4143; C. F. Gürtler, S. Blechert, E. Steckhan, *Synlett* **1994**, 141–142; O. Wiest, E. Steckhan, *Angew. Chem.* **1993**, *105*, 932–934; *Angew. Chem. Int. Ed. Engl.* **1993**, *32*, 901.
[446] N. L. Bauld, *Adv. Electron Transfer Chem.* **1992**, *2*, 1–66.
[447] J. Delaunay, A. Orliac-Le Moing, J. Simonet, L. Toupet, *Tetrahedron Lett.* **1986**, *27*, 6205–6208.
[448] R. M. Wilson, J. G. Dietz, T. A. Shepherd, D. M. Ho, K. A. Schnapp, R. C. Elder, J. W. Watkins II, L. S. Geraci, C. F. Campana, *J. Am. Chem. Soc.* **1989**, *111*, 1749–1754.
[449] B. Harirchian, N. L. Bauld, *J. Am. Chem. Soc.* **1989**, *111*, 1826–1828.
[450] S. Kadota, K. Tsubono, K. Makino, M. Takeshita, T. Kibuchi, *Tetrahedron Lett.* **1987**, *28*, 2857–2860.
[451] K. Ishiguro, M. Ikeda, Y. Sawaki, *J. Org. Chem.* **1992**, *57*, 3057–3066.
[452] G. Jones II, W. G. Becker, S.-H. Chiang, *J. Am. Chem. Soc.* **1983**, *105*, 1269–1276.
[453] Acyclic 1,4-radical cations were observed directly [437a, c].
[454] Y. Takahashi, M. Ando, T. Miyashi, *J. Chem. Soc. Chem. Commun.* **1995**, 521–522.
[455] I. Dunkin, L. Andrews, *Tetrahedron* **1985**, *41*, 145–161.
[456] M. Schmittel, C. Wöhrle, I. Bohn, *Chem. Eur. J.* **1996**, *2*, 1031–1040; M. Schmittel, C. Wöhrle, *J. Org. Chem.* **1995**, *60*, 8223–8230.
[457] Y. Takahashi, R. Iida, T. Miyashi, *Res. Chem. Intermed.* **1995**, *21*, 765–775.
[458] a) F. Müller, J. Mattay, *Chem. Ber.* **1993**, *126*, 543–549; b) F. Müller, J. Mattay, S. Steenken, *J. Org. Chem.* **1993**, *58*, 4462–4464; c) F. Müller, A. Karwe, J. Mattay, *ibid.* **1992**, *57*, 6080–6082; d) F. Müller, J. Mattay, *Angew. Chem.* **1992**, *104*, 207–208; *Angew. Chem. Int. Ed. Engl.* **1992**, *31*, 209–210; e) *ibid.* **1991**, *103*, 1352–1353 and **1991**, *30*, 1336–1337.
[459] According to our classification the primary reaction of the radical cation is a π-C-C$^{\cdot+}$ bond cleavage.
[460] W. B. Motherwell, A. S. Williams, *Angew. Chem.* **1995**, *107*, 2207–2209; *Angew. Chem. Int. Ed. Engl.* **1995**, *34*, 2031–2033.
[461] W. Yueh, N. L. Bauld, *J. Am. Chem. Soc.* **1995**, *117*, 5671–5676; N. L. Bauld, W. Yueh, *ibid.* **1994**, *116*, 8845–8846.
[462] N. L. Bauld, G. A. Mirafzal, *J. Am. Chem. Soc.* **1991**, *113*, 3613–3614.
[463] N. L. Bauld, G. W. Stufflebeme, K. T. Lorenz, *J. Phys. Org. Chem.* **1989**, *2*, 585–601.
[464] T. Shida, E. Haselbach, T. Bally, *Acc. Chem. Res.* **1984**, *17*, 180–186.
[465] a) F. Gerson, A. Arnold, U. Burger, *J. Am. Chem. Soc.* **1991**, *113*, 4359–4360; b) C. J. Abelt, H. D. Roth, M. L. Schilling, *ibid.* **1985**, *107*, 4148–4152.
[466] S. Dai, J. T. Wang, F. Williams, *J. Am. Chem. Soc.* **1990**, *112*, 2835–2837.
[467] T. Bally, L. Truttmann, S. Dai, F. Williams, *J. Am. Chem. Soc.* **1995**, *117*, 7916–7922.
[468] T. Bally, L. Truttmann, J. T. Wang, F. Williams, *J. Am. Chem. Soc.* **1995**, *117*, 7923–7934.
[469] Q.-X. Guo, X.-Z. Qin, J. T. Wang, F. Williams, *J. Am. Chem. Soc.* **1988**, *110*, 1974–1976.
[470] S. Dai, R. S. Pappas, G.-F. Chen, Q.-Y. Guo, J. T. Wang, F. Williams, *J. Am. Chem. Soc.* **1989**, *111*, 8759–8760.
[471] Reviews: F. Gerson, *Acc. Chem. Res.* **1994**, *27*, 63–69; *Radical Ionic Systems* (Eds.: A. Lund, M. Shiotani), Kluwer, Amsterdam, **1991**.
[472] a) H. Ikeda, T. Oikawa, T. Miyashi, *Tetrahedron Lett.* **1993**, *34*, 2323–2326; b) T. Miyashi, A. Konno, Y. Takahashi, *J. Am. Chem. Soc.* **1988**, *110*, 3676–3677; c) K. Lorenz, N. L. Bauld, *Catalysis* **1985**, *95*, 613–616.
[473] S. Dhanalekshmi, C. S. Venkatachalam, K. K. Balasubramanian, *J. Chem. Soc. Chem. Commun.* **1994**, 511–512.
[474] a) L. Lopez, G. Mele, V. Fiandanese, C. Cardellicchio, A. Nacci, *Tetrahedron* **1994**, *50*, 9097–9106; b) L. Lopez, L. Troisi, *Tetrahedron Lett.* **1989**, *30*, 3097–3100.

[475] D. W. Reynolds, B. Harirchian, H.-S. Chiou, B. K. Marsh, N. L. Bauld, *J. Phys. Org. Chem.* **1989**, *2*, 57–88.
[476] J. P. Dinnocenzo, D. A. Conlon, *J. Am. Chem. Soc.* **1988**, *110*, 2324–2326.
[477] B. Kräutler, A. Pfaltz, R. Nordmann, K. O. Hodgson, J. D. Dunitz, A. Eschenmoser, *Helv. Chim. Acta* **1976**, *59*, 924–937.
[478] N. L. Bauld, *J. Comput. Chem.* **1990**, *11*, 896–898.
[479] J. P. Dinnocenzo, D. A. Conlon, *Tetrahedron Lett.* **1995**, *36*, 7415–7418.
[480] F. D. Lewis, M. Kojima, *J. Am. Chem. Soc.* **1988**, *110*, 8664–8670; H. D. Roth, M. L. M. Schilling, *ibid.* **1980**, *102*, 4303–4310.
[481] M. V. Vishnetskaya, B. V. Romanovskii, *Petroleum Chem.* **1993**, *33*, 299–302.
[482] Y. Kuriyama, H. Sakuragi, K. Tokumaru, Y. Yoshida, S. Tagawa, *Bull. Chem. Soc. Jpn.* **1993**, *66*, 1852–1855.
[483] F. D. Lewis, J. R. Petisce, J. O. Oxman, M. J. Nepras, *J. Am. Chem. Soc.* **1985**, *107*, 203–207.
[484] a) F. D. Lewis, A. M. Bedell, R. E. Dykstra, J. E. Ebert, I. R. Gould, S. Farid, *J. Am. Chem. Soc.* **1990**, *112*, 8055–8064; b) Y. Kuriyama, T. Arai, H. Sakuragi, K. Tokumaru, *Chem. Lett.* **1989**, 251–254.
[485] Y. Kuriyama, T. Arai, H. Sakuragi, K. Tokumaru, *Chem. Phys. Lett.* **1990**, *173*, 253–256.
[486] Z. Wang, W. G. McGimpsey, *J. Phys. Chem.* **1993**, *97*, 3324–3327.
[487] E. Haselbach, T. Bally, Z. Lanyiova, *Helv. Chim. Acta* **1979**, *62*, 577–592; N. L. Bauld, J. Cessac, *J. Am. Chem. Soc.* **1977**, *99*, 23–26.
[488] In the gas phase: C. Dass, M. L. Gross, *J. Am. Chem. Soc.* **1983**, *105*, 5724–5729; C. Dass, M. L. Gross, T. M. Sack, *ibid.* **1984**, *106*, 5780–5786; in a matrix: A. Faucitano, A. Buttafava, F. Martinotti, R. Sustmann, H.-G. Korth, *J. Chem. Soc. Perkin Trans. 2* **1992**, 865–869; A. Marcinek, J. Michalak, J. Rogowski, W. Tang, T. Bally, J. Gebicki, *ibid.* **1992**, 1353–1357; in solution: Y. Takahashi, K. Miyamoto, K. Sakai, H. Ikeda, T. Miyashi, Y. Ito, K. Tabohashi, *Tetrahedron Lett.* **1996**, *37*, 5547–5550, and references therein.
[489] T. Miyashi, K. Wakamatsu, T. Akiya, K. Kikuchi, T. Mukai, *J. Am. Chem. Soc.* **1987**, *109*, 5270–5271.
[490] Y. Takahashi, J. K. Kochi, *Chem. Ber.* **1988**, *121*, 253–269.
[491] Y. Iwano, Y. Kawamura, T. Horie, *Chem. Lett.* **1995**, 67–68.
[492] a) D. T. Breslin, M. A. Fox, *J. Org. Chem.* **1994**, *59*, 7557–7561; b) D. Sheng, J. T. Wang, F. Williams, *J. Am. Chem. Soc.* **1990**, *112*, 2837–2839; c) J. N. Aebischer, E. Haselbach, T. Bally, F. Gerson, K. Roth, X. Z. Qin, *ibid.* **1989**, *111*, 7909–7914.
[493] a) R. D. Bach, I. L. Schilke, H. B. Schlegel, *J. Org. Chem.* **1996**, *61*, 4845–4847; b) H. Weng, X.-M. Du, H. Roth, *J. Am. Chem. Soc.* **1995**, *117*, 135–140.
[494] K. Ishiguro, I. V. Khudyakov, P. F. McGarry, N. J. Turro, H. D. Roth, *J. Am. Chem. Soc.* **1994**, *116*, 6933–6934.
[495] E. Haselbach, T. Bally, Z. Lanyiova, P. Baertschi, *Helv. Chim. Acta* **1979**, *62*, 583–592.
[496] a) H. D. Roth, *Acc. Chem. Res.* **1987**, *20*, 343–350; b) H. D. Roth, M. L. M. Schilling, *J. Am. Chem. Soc.* **1981**, *103*, 7210–7217; c) H. D. Roth, M. L. M. Schilling, G. Jones II, *ibid.* **1981**, *103*, 1246–1248.
[497] J. L. Gebicki, J. Gebicki, J. Mayer, *Radiat. Phys. Chem.* **1987**, *30*, 165–167.
[498] H. Prinzbach, M. Wollenweber, R. Herges, H. Neumann, G. Gescheidt, R. Schmidlin, *J. Am. Chem. Soc.* **1995**, *117*, 1439–1440.
[499] G. Gescheidt, R. Herges, H. Neumann, J. Heinze, M. Wollenweber, M. Etzkorn, H. Prinzbach, *Angew. Chem.* **1995**, *107*, 1109–1112; *Angew. Chem. Int. Ed. Engl.* **1995**, *34*, 1016–1019.
[500] A. Arnold, U. Burger, F. Gerson, E. Kloster-Jensen, S. P. Schmidlin, *J. Am. Chem. Soc.* **1993**, *115*, 4271–4281.
[501] W. Adam, T. Heidenfelder, C. Sahin, *Synlett* **1995**, 1163–1170.
[502] High-level ab initio calculations and ESR evidence point to the occurrence of σ radical cations for aryldiazomethane$^{+\bullet}$ [451].
[503] A. Albini, E. Fasani, M. Mella, *Top. Curr. Chem.* **1993**, *168*, 143–173.
[504] a) F. D. Saeva, D. T. Breslin, H. R. Luss, *J. Am. Chem. Soc.* **1991**, *113*, 5333–5337; b) F. D. Saeva, D. T. Breslin, *J. Org. Chem.* **1989**, *54*, 712–714; c) J. L. Dektar, N. P. Hacker, *J. Photochem. Photobiol.* **1989**, *46*, 233–238.
[505] D. H. R. Barton, R. K. Haynes, G. Leclerc, P. D. Magnus, I. D. Menzies, *J. Chem. Soc. Perkin Trans. 1* **1975**, 2055–2065.
[506] R. Tang, H. J. Yue, J. F. Wolf, F. Mares, *J. Am. Chem. Soc.* **1978**, *100*, 5248–5249; R. K. Haynes, *Aust. J. Chem.* **1978**, *31*, 121–129, 131–138.
[507] E. Bosch, J. K. Kochi, *J. Chem. Soc. Perkin Trans. 2* **1990**, 451–453.
[508] S. F. Nelsen, D. L. Kapp, F. Gerson, J. Lopez, *J. Am. Chem. Soc.* **1986**, *108*, 1027–1032.
[509] A. P. Schaap, K. A. Zaklika, B. Kaskar, L. W.-M. Fung, *J. Am. Chem. Soc.* **1980**, *102*, 389–391; L. T. Spada, C. S. Foote, *ibid.* **1980**, *102*, 391–393.
[510] Y. Takahashi, K. Wakamatsu, K. Kikuchi, T. Miyashi, *J. Phys. Org. Chem.* **1990**, *3*, 509–518; Y. Araki, D. C. Dobrowolski, T. E. Goyne, D. C. Hanson, Z.-Q. Jiang, K. J. Lee, C. S. Foote, *J. Am. Chem. Soc.* **1984**, *106*, 4570–4575; D. C. Dobrowolski, P. R. Ogilby, C. S. Foote, *J. Phys. Chem.* **1983**, *87*, 2261–2263.
[511] S. F. Nelsen, M. F. Teasley, *J. Org. Chem.* **1986**, *51*, 3474–3479; S. F. Nelsen, R. Akaba, *J. Am. Chem. Soc.* **1981**, *103*, 2096–2097; E. L. Clennan, W. Simmons, C. W. Almgren, *ibid.* **1981**, *103*, 2098–2099.
[512] S. F. Nelsen, M. F. Teasley, D. L. Kapp, *J. Am. Chem. Soc.* **1986**, *108*, 5503–5509.
[513] W. A. Wilczak, D. I. Schuster, *Tetrahedron Lett.* **1986**, *27*, 5331–5334.
[514] L. Lopez, L. Troisi, *Tetrahedron* **1992**, *48*, 7321–7330.
[515] T. Yamashita, T. Tsurusako, N. Nakamura, M. Yasuda, K. Shima, *Bull. Chem. Soc. Jpn.* **1993**, *66*, 857–862.
[516] L. Lopez, *Top. Curr. Chem.* **1990**, *156*, 117–166.
[517] P. H. Sackett, J. S. Mayausky, T. Smith, S. Kalus, R. L. McCreery, *J. Med. Chem.* **1981**, *24*, 1342–1347.
[518] M. Kamata, M. Sato, E. Hasegawa, *Tetrahedron Lett.* **1992**, *35*, 5085–5088.
[519] a) A. P. Schaap, G. Prasad, S. Siddiqui, *Tetrahedron Lett.* **1984**, *25*, 3035–3038; b) A. P. Schaap, G. Prasad, S. D. Gagnon, *ibid.* **1983**, *24*, 3047–3050.
[520] S. Yasui, K. Shioji, M. Tsujimoto, A. Ohno, *Tetrahedron Lett.* **1996**, *37*, 1625–1628.
[521] a) M. Kojima, A. Ishida, S. Takamuku, *Chem. Lett.* **1993**, 979–982; b) S. L. Mattes, S. Farid, *J. Am. Chem. Soc.* **1986**, *108*, 7356–7361; c) K. Gollnick, A. Schnatterer, *Tetrahedron Lett.* **1984**, *25*, 185–188; d) R. K. Haynes, M. K. S. Probert, I. D. Wilmot, *Aust. J. Chem.* **1978**, *31*, 1737–1746.
[522] a) T. Tamai, K. Mizuno, I. Hashida, Y. Otsuji, A. Ishida, S. Takamuku, *Chem. Lett.* **1994**, 149–152; b) K. Mizuno, T. Tamai, I. Hashida, Y. Otsuji, Y. Kuriyama, K. Tokumaru, *J. Org. Chem.* **1994**, *59*, 7329–7334.
[523] K. Gollnick, M. Weber, *Tetrahedron Lett.* **1990**, *31*, 4585–4588; K. Gollnick, U. Paulmann, *ibid.* **1989**, *30*, 4481–4484.
[524] Cyclopropanes: A. P. Schaap, L. Lopez, S. D. Anderson, S. D. Gagnon, *Tetrahedron Lett.* **1982**, *23*, 5493–5496; K. Mizuno, N. Kamiyama, Y. Otsuji, *Chem. Lett.* **1983**, 477–480; T. Miyashi, M. Kamata, T. Mukai, *J. Am. Chem. Soc.* **1987**, *109*, 2780–2788.
[525] H. Ikeda, Y. Yamashita, C. Kabuto, T. Miyashi, *Chem. Lett.* **1988**, 1333–1336; K. Mizuno, K. Murakami, N. Kamiyama, Y. Otsuji, *J. Chem. Soc. Chem. Commun.* **1983**, 462–463.
[526] R. Akaba, M. Kamata, H. Itoh, A. Nakao, S. Goto, K. Saito, A. Negishi, H. Sakuragi, K. Tokumaru, *Tetrahedron Lett.* **1992**, *33*, 7011–7014; J. Santamaria, R. Jroundi, J. Rigaudy, *ibid.* **1989**, *30*, 4677–4680.
[527] S. Wu, J. Liu, Z. Jiang, *Chem. Commun.* **1996**, 493–494.
[528] E. Bosch, J. K. Kochi, *J. Am. Chem. Soc.* **1996**, *118*, 1319–1329.
[529] D. Ramkumar, S. Sankararaman, *Synthesis* **1993**, 1057–1058.
[530] M. Tsuchiya, T. W. Ebbesen, Y. Nishimura, H. Sakuragi, K. Tokumaru, *Chem. Lett.* **1987**, 2121–2124.
[531] Although the bimolecular rate constant of radical cations with superoxide anion is higher, this process most often results in electron transfer rather than oxygenation [530].
[532] L. Eberson, M. P. Hartshorn, F. Radner, J. O. Svensson, *J. Chem. Soc. Perkin Trans. 2* **1994**, 1719–1730.
[533] M. N. Cortona, N. Vettorazzi, J. J. Silber, L. Sereno, *J. Electroanal. Chem.* **1995**, *394*, 245–251.
[534] M. Lehnig, *J. Chem. Soc. Perkin Trans. 2* **1996**, 1943–1948.
[535] P. Maslak, J. Kula, J. E. Chateauneuf, *J. Am. Chem. Soc.* **1991**, *113*, 2304–2306.
[536] K. Mizuno, M. Ikeda, Y. Otsuji, *Tetrahedron Lett.* **1985**, *26*, 461–464.
[537] R. J. Sundberg in *Organic Photochemistry, Vol. 6* (Ed.: A. Padwa), Marcel Dekker, New York, **1983**, pp. 121–176.
[538] L. J. Dolby, S. J. Nelson, D. Senkovich, *J. Org. Chem.* **1972**, *37*, 3691–3695.
[539] a) M. Mascal, C. J. Moody, *J. Chem. Soc. Chem. Commun.* **1988**, 587–588; b) *ibid.* **1988**, 589–590.
[540] S. Yasui, M. Fujii, C. Kawano, Y. Nishimura, A. Ohno, *Tetrahedron Lett.* **1991**, *32*, 5601–5604; S. Yasui, M. Fujii, C. Kawano, Y. Nishimura, K. Shioji, A. Ohno, *J. Chem. Soc. Perkin Trans. 2* **1994**, 177–183; S. Yasui, K. Shioji, A. Ohno, *Tetrahedron Lett.* **1994**, *35*, 2695–2698.
[541] a) A. Albini, E. Fasani, A. Sulpizio, *J. Am. Chem. Soc.* **1984**, *106*, 3562–3566; b) A. Albini, E. Fasani, R. Oberti, *Tetrahedron* **1982**, *38*, 1027–1034.
[542] a) J. Mattay, J. Gersdorf, K. Buchkremer, *Chem. Ber.* **1987**, *120*, 307–318; b) J. Gersdorf, J. Mattay, H. Görner, *J. Am. Chem. Soc.* **1987**, *109*, 1203–1209.
[543] K. Maruyama, T. Otsuki, S. Tai, *J. Org. Chem.* **1985**, *50*, 52–60.
[544] D. Döpp, J. Heufer, *Tetrahedron Lett.* **1982**, *23*, 1553–1556.
[545] J. L. Charlton, C. C. Liao, P. de Mayo, *J. Am. Chem. Soc.* **1971**, *93*, 2463–2471.
[546] a) A. Cantos, J. Marquet, M. Moreno-Manas, *Tetrahedron Lett.* **1989**, *30*, 2423–2426; b) A. M. J. van Eijk, A. H. Huizer, C. A. G. O. Varma, J. Marquet, *J. Am. Chem. Soc.* **1989**, *111*, 88–95; c) N. J. Bunce, S. R. Cater, J. C. Scaiano, L. J. Johnston, *J. Org. Chem.* **1987**, *52*, 4214–4223.
[547] The reaction of a radical cation with $O_2^{-\bullet}$ most often results in electron transfer.
[548] R. Andruzzi, L. Cardellini, L. Greci, P. Stipa, M. Poloni, A. Trazza, *J. Chem. Soc. Perkin Trans. 2* **1988**, 3067–3070.
[549] H.-D. Hausen, W. Kaim, A. Schulz, M. Moscherosch, J. Jordanov, *Z. Naturforsch. B* **1993**, *48*, 1181–1186.
[550] F. Hilgers, W. Kaim, A. Schulz, S. Zális, *J. Chem. Soc. Perkin Trans. 2* **1994**, 135–138.

[551] I. Tabakovic, *Electrochim. Acta* **1995**, *40*, 2809–2813.
[552] A. F. Diaz in ref. [3b], chap. 33.
[553] P. Audebert, J.-M. Catel, G. Le Coustumer, V. Duchenet, P. Hapiot, *J. Phys. Chem.* **1995**, *99*, 11923–11929.
[554] H. G. Yang, A. J. Bard, *J. Electroanal. Chem.* **1991**, *306*, 87–109.
[555] D. Larumbe, I. Gallardo, C. P. Andrieux, *J. Electroanal. Chem.* **1991**, *304*, 241–247.
[556] M. Kimura, Y. Ban, *Synthesis*, **1976**, 201–202; M. W. Wolff, *Chem. Rev.* **1963**, *63*, 55–64.
[557] K. L. Handoo, J.-P. Cheng, V. D. Parker, *Acta Chem. Scand.* **1993**, *47*, 626–628.
[558] Y. Zhu, G. B. Schuster, *J. Am. Chem. Soc.* **1990**, *123*, 8583–8585.
[559] R. W. Kavash, P. S. Mariano, *Tetrahedron Lett.* **1989**, *30*, 4185–4188.
[560] D. P. Curran, N. A. Porter, B. Giese, *Stereochemistry of Radical Reactions*, VCH, Weinheim, **1996**.
[561] D. G. Stoub, K.-L. Cheng, J. L. Goodman, *Tetrahedron Lett.* **1996**, *37*, 4927–4930, and references therein.
[562] M. Schmittel, A. Langels, *Angew. Chem.* **1997**, *109*, 381–383; *Angew. Chem. Int. Ed. Engl.* **1997**, *36*, 392–395, and references therein.

Chemistry at the crossroads

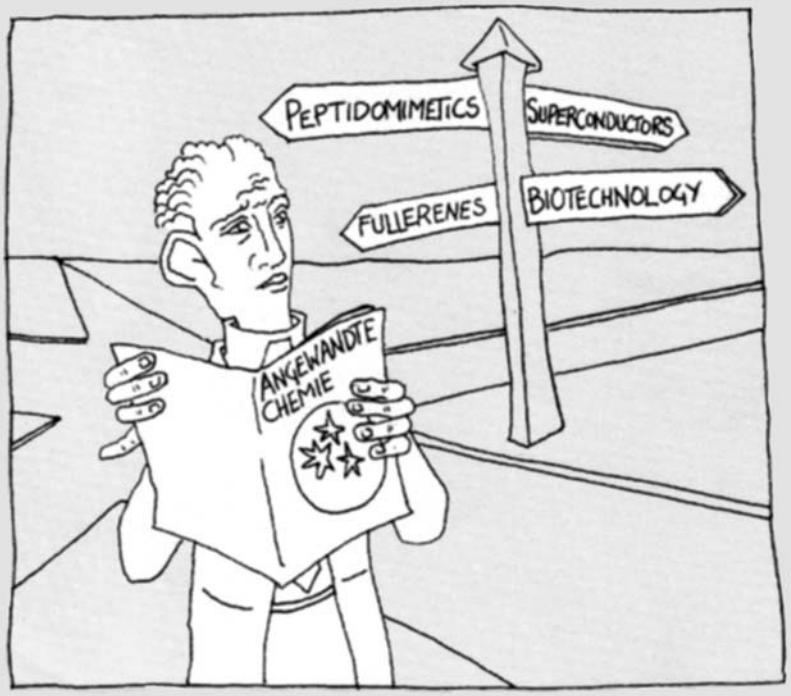

Pioneering scientists guide your way through newly charted territory with their topical reviews and discriminating highlights in **Angewandte Chemie.**

To start your own personal subscription, just fax.

An order form is provided on the last page for your convenience.

WILEY-VCH

A Novel Methyltrioxorhenium (MTO)-Catalyzed Epoxidation of Olefins: An Impressive Example of Simplicity, Selectivity, and Efficiency

Andreas Gansäuer*

One of the main goals of research in chemistry in recent years has been the development of new efficient catalytic reactions giving the desired products in high yield and selectivity under mild conditions without the formation of by-products and with low catalyst loading. In this context epoxidations are of great interest because epoxides can be readily transformed into a wide variety of useful compounds. Their sensitivity to ring opening, however, sets limits on the acidity and basicity of the reagents used.

The most widely used epoxidation reagent in research laboratories, *meta*-chloroperoxybenzoic acid (*m*-CPBA),[1] poses a number of problems that make the need for the development of efficient catalytic systems evident. Acid-sensitive epoxides are not tolerated under typical conditions because of the acidity of *m*-chlorobenzoic acid, and the reagent is not reactive enough in certain cases, for example for electron-deficient olefins. In a more general sense *m*-CPBA is not economical because hydrogen peroxide has first to be transformed into *m*-CPBA; thus, after the epoxidation *m*-chlorobenzoic acid has to be recovered and then recycled. Also the reagent cannot be stored in pure form because of the explosion hazards. Economically favorable are therefore reactions that employ cheap, readily available stoichiometric oxidants, such as oxygen, hydrogen peroxide, or bleach in a transition metal catalyzed reaction without the production of side products that are difficult to remove or to recycle.

Interesting reactions in this context are nickel-[2] and vanadium-catalyzed[3] epoxidations with oxygen, and manganese-catalyzed[4] reactions with bleach as stoichiometric oxidants. However, the former reaction usually requires the presence of stoichiometric amounts of aldehydes that are oxidized to acids, and the latter is limited to a certain degree by incomplete stereoselectivity. Both reactions therefore do not fully meet the demands of an efficient transformation.

A first breakthrough with rhenium compounds as catalysts was achieved by Herrmann et al.[5] The use of methyltrioxorhenium (MTO; 0.1–1.0 mol%) as powerful epoxidation catalyst is possible with anhydrous hydrogen peroxide in *tert*-butyl alcohol as stoichiometric oxidant. Most likely the catalytically active species is a bis(peroxo) complex of rhenium.[6] Although effective for numerous substrates, this method suffers somewhat from concomitant opening of the epoxide. To a ceratin degree this problem can be overcome by using amines and pyridines[7] as additives or by employing the urea hydrogen peroxide complex[8] as stoichiometric oxidant. However, catalyst turnover is decreased significantly and sensitive epoxides are still decomposed.

An effective system that avoids the above-mentioned disadvantages and preserves high catalyst activity and chemoselectivity has recently been developed by Sharpless et al.[9] By using aqueous hydrogen peroxide instead of anhydrous hydrogen peroxide as stoichiometric oxidant in combination with catalytic amounts of pyridine (12 mol%) and MTO (0.5 mol%) a variety of epoxides can be obtained with high chemoselectivity in good to excellent yields, as exemplified in Equation (a). The reaction is run at room temperature with high concentration of substrate (1–2 M) in dichloromethane. Product isolation is simple and convenient because the only by-product of the reaction is water. No products from ring opening of the epoxide are usually detected.

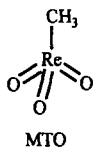

MTO

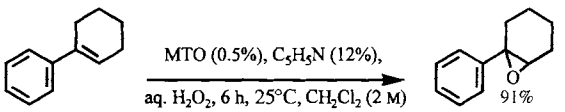

(a)

The crucial role of pyridine seems to be threefold: it increases catalytic activity, prevents product decomposition, and in sufficient concentration leads to an increase of catalyst lifetime. However, pyridine has to be used in excess with respect to MTO because of N-oxidation during the course of the reaction. In this respect the two-phase system has a unique advantage as demonstrated by Herrmann et al.[10] Pyridine-N-oxides, which are detrimental to catalyst activity, are mostly dissolved in the aqueous phase. Thus only pyridine, which is responsible for high catalyst activity and selectivity, remains in the organic phase ensuring efficient complexation of MTO. Sterically demanding pyridines, such as picoline, are ineffective in accelerating the reaction.

[*] Dr. A. Gansäuer
Institut für Organische Chemie der Universität
Tammannstrasse 2, D-37077 Göttingen (Germany)
Fax: Int. code + (551)392944
e-mail: agansae@gwdg.de

 © WILEY-VCH Verlag GmbH, D-69451 Weinheim, 1997 0570-0833/97/3623-2591 $ 17.50+.50/0

The epoxidation of terminal olefins still requires prolonged reaction times (usually longer than 92 h) under these conditions. A faster conversion of products can be achieved by ligand-tuning using sterically undemanding, electron-deficient pyridines like 3-cyanopyridine.[11] The epoxidation is usually complete in less than 30 h. Presumably, the electron deficiency of these pyridines facilitates the binding of the olefin substrate. For very acid-sensitive products, such as styrene oxide, pyridine is required additionally to prevent epoxide decomposition [Eq. (b)].

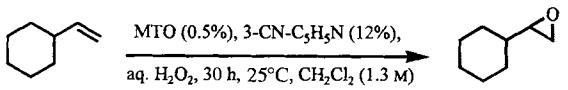

86 % (b)

In summary the novel ligand-accelerated catalytic system[12] described by the Sharpless et al. offers a simple, safe, economical, and easy to carry out epoxidation reaction that will undoubtedly find numerous applications in the synthesis of epoxides from olefins. With the recently devised efficient synthesis and recycling procedure for MTO by Herrmann et al.,[13] the reaction seems to be especially well-suited for large-scale applications and has the potential for enantioselective catalysis by using chiral pyridine derivatives as ligands.

German version: *Angew. Chem.* **1997**, *109*, 2701 – 2702

Keywords: chemoselectivity · epoxidations · homogeneous catalysis · rhenium

[1] A. S. Rao in *Comprehensive Organic Synthesis, Vol. 7* (Eds.: B. M. Trost, I. Fleming, G. Pattenden), Pergamon, Oxford, **1991**, pp. 358 – 375.
[2] T. Yamada, T. Takai, O. Rhode, T. Mukaiyama, *Bull. Chem. Soc. Jpn.* **1991**, 2109 – 2117.
[3] S. Inoki, T. Takai, T. Yamada, T. Mukaiyama, *Chem. Lett.* **1991**, 941 – 944.
[4] a) W. Zhang, N. H. Lee, E. N. Jacobsen, *J. Am. Chem.Soc.* **1994**, *116*, 425 – 426; b) H. Sasaki, R. Irie, T. Katsuki, *Synlett* **1994**, 356.
[5] W. A. Herrmann, R. W. Fischer, D. W. Marz, *Angew. Chem.* **1991**, *103*, 1706 – 1709; *Angew. Chem. Int. Ed. Engl.* **1991**, *30*, 1157 – 1160.
[6] W. A. Herrmann, R. W. Fischer, W. Scherer, M. U. Rauch, *Angew. Chem.* **1993**, *105*, 1209 – 1212; *Angew. Chem. Int. Ed. Engl.* **1991**, *30*, 1638 – 1641.
[7] W. A. Herrmann, R. W. Fischer, M. U. Rauch, W. Scherer, *J. Mol. Catal.* **1994**, *86*, 243 – 266.
[8] W. Adam, C. M. Mitchell, *Angew. Chem.* **1996**, *108*, 578 – 581, *Angew. Chem. Int. Ed. Engl.* **1996**, *35*, 533 – 535.
[9] J. Rudolph, K. L. Reddy, J. P. Chiang, K. B. Sharpless, *J. Am. Chem. Soc.* **1997**, *119*, 6189 – 6190.
[10] W. A. Herrmann, H. Ding, R. M. Kratzer, F. E. Kühn, J. J. Haider, R. W. Fischer, *J. Organomet. Chem.* **1997**, in press.
[11] C. Copéret, H. Adolfsson, K. B. Sharpless, *J. Chem. Soc. Chem. Commun.* **1997**, 1565 – 1566.
[12] D. J. Berrisford, C. Bolm, K. B. Sharpless, *Angew. Chem.* **1995**, *107*, 1159 – 1171, *Angew. Chem. Int. Ed. Engl.* **1995**, *34*, 1059 – 1070.
[13] W. A. Herrmann, R. M. Kratzer, R. W. Fischer, *Angew. Chem.* **1997**, *109*, 2767 – 2768, *Angew. Chem. Int. Ed. Engl.* **1997**, *36*, 2652 – 2654.

Polyamides as Artificial Regulators of Gene Expression

Klaus Weisz*

Numerous control mechanisms in the living cell are based on the sequence-specific recognition of nucleic acids. Thus, gene expression in organisms is controlled by proteins that selectively recognize and bind to nucleic acid sequences. In addition, a number of natural low molecular weight drugs are able to interact with DNA thereby interfering with genetic processes. The prospect of using DNA-specific ligands as novel tools in molecular biology or as drugs for a directed control of gene expression has greatly stimulated the rational development of artificial DNA-binding compounds. The major as well as minor groove of a DNA double helix may serve as a specific binding site for ligands. Each of the four base pairs has a characteristic pattern of available hydrogen bond donor and acceptor sites, which allows the recognition from both grooves under formation of specific hydrogen bonds (Scheme 1). However, the nearly symmetric arrangement of the thymine O2 and adenine N3 acceptor sites precludes a distinction of AT and TA base pairs in the minor groove at least by means of hydrogen bond interactions.

Netropsin and distamycin are two natural antibiotics that preferentially bind at A/T sequences in the minor groove of a DNA double helix (Scheme 2a,b).[1] The concave shape of these oligopeptides with their structural complementarity to the convex floor of the minor groove allows maximum interactions with the DNA, which are further enforced by the narrow groove of A/T-rich DNA tracts. In addition to electrostatic and van der Waals forces, hydrogen bonds between the amide protons of the oligopeptides and the adenine N3 as well as thymine O2 acceptor sites of the base pairs contribute to the stability and A/T preference of these drugs. The best-studied minor groove binding ligand is netropsin and it has frequently been taken as the paradigm for the rational design of synthetic drugs. The conversion of one or both of the pyrrole rings in netropsin to imidazole was a first attempt to extend the recognition code to G/C base pairs.[2] The resulting netropsin analogues were expected to allow specific hydrogen bonds between the imidazole ring nitrogen atom and the exocyclic amino group of the guanine bases. Although G/C base pairs were increasingly tolerated in the binding domain, there was an overall decrease in affinity

[*] Dr. K. Weisz
Institut für Organische Chemie der Freien Universität
Takustrasse 3, D-14195 Berlin (Germany)
Fax: Int. code + (30) 838-5310
e-mail: weisz@chemie.fu-berlin.de

 © WILEY-VCH Verlag GmbH, D-69451 Weinheim, 1997 0570-0833/97/3623-2592 $ 17.50+.50/0

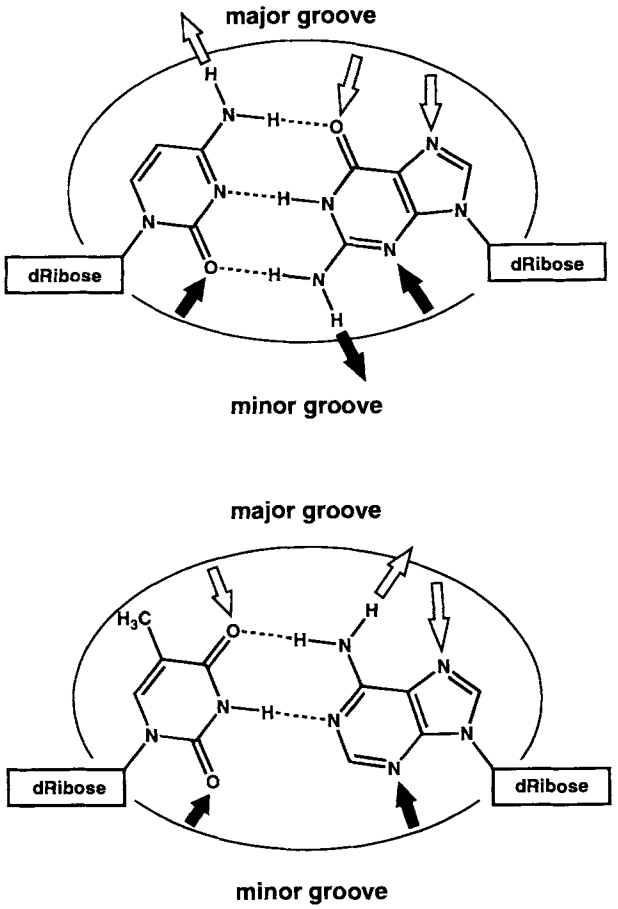

Scheme 1. GC (top) and AT base pair (bottom). Free hydrogen bond donor and acceptor sites in the major and minor groove of double-stranded DNA are indicated by white and gray arrows, respectively.

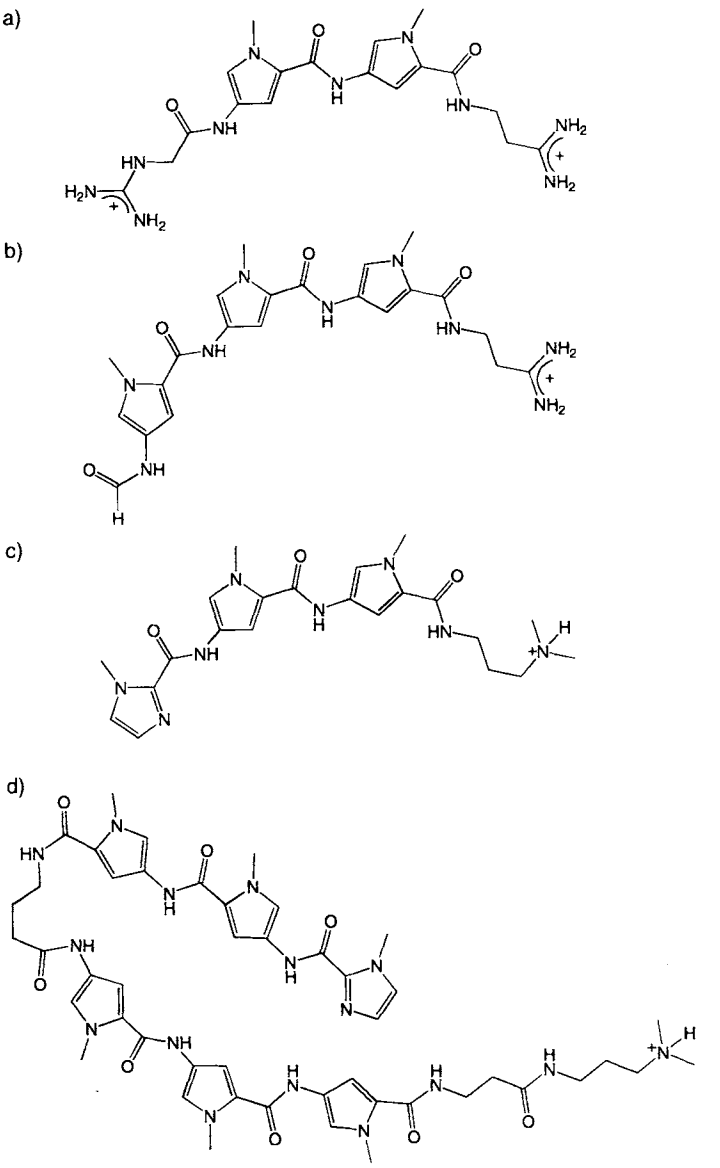

Scheme 2. Structure of DNA-binding natural and synthetic polyamides. a) Netropsin, b) distamycin, c) 1-methylimidazole-2-carboxamide-netropsin, d) hairpin polyamide ImPyPy-γ-PyPyPy-β-Dp (Im = *N*-methylimidazole, Py = *N*-methylpyrrole, γ = γ-aminobutyric acid, β = β-alanine, Dp = *N*,*N*-dimethylaminopropylamide).

and specificity of such ligands. Evidently, hydrogen bonds in these complexes are of minor importance and the decrease of other noncovalent interactions in the expanded minor groove of G/C segments impairs effective ligand binding.

Unexpected NMR results from Pelton and Wemmer on complexes of distamycin with double-helical DNA marked the turning point in the quest for netropsin derivatives with altered sequence specificity.[3] At higher concentrations of monocationic distamycin two molecules of the drug were found to be bound simultaneously in the minor groove of the central 5′-AAATT-3′ segment of a DNA double helix. Within these 2:1 complexes the two ligands are stacked antiparallel, side-by-side in the groove with each distamycin molecule preferentially forming hydrogen bonds with nucleobases of its adjacent DNA strand. Incorporation of a dimer results in the expansion of the groove favoring such a 2:1 motif in sequences with a wide minor groove.

The breakthrough in the development of netropsin analogues with an expanded recognition code was finally achieved by the groups of Dervan and Wemmer. 1-Methylimidazole-2-carboxamide-netropsin (Scheme 2c), a synthetic monocationic tripeptide with a N-terminal 1-methyl-2-carboxamide-imidazole residue and two *N*-methyl-2-carboxamide-pyrrole units recognized a 5′-TGACT-3′ sequence with high specificity.[4] Structural studies indicated the formation of a 2:1 complex with an antiparallel orientation of the two ligands in the DNA minor groove, as was found earlier for distamycin at high concentrations (Scheme 3a).[5] The specific recognition of GC and CG base pairs came as a surprise and can be attributed to the expected interaction between the N3 imidazole ring nitrogen atom and the 2-amino group of guanine protruding from the floor of the minor groove. Evidently, a binary code consisting of two polyamide units was required to distinguish GC, CG, and AT base pairs: an imidazole ring paired with a pyrrole ring of the second ligand in the dimeric motif recognizes a GC base pair; correspondingly, a pyrrole/imidazole combination targets a CG, and a pyrrole/pyrrole combination as well as N- and C-terminal alkyl residues target AT or TA base pairs. The latter are mostly degenerate. In contrast, the original netropsin ana-

 © WILEY-VCH Verlag GmbH, D-69451 Weinheim, 1997 0570-0833/97/3623-2593 $ 17.50+.50/0

logues failed to bind in a 2:1 motif because of their dicationic structure, which resulted in repulsive electrostatic forces on dimerization. The generality of this 2:1 recognition code was subsequently confirmed on various sequences.[6] Shortly thereafter further improvements in the design of pyrrole-imidazole polyamides were introduced by Dervan et al. By covalently connecting two polyamides with a γ-aminobutyric acid linker and by introducing a C-terminal β-alanine residue, both DNA affinity and specificity were significantly increased by the formation of a hairpin motif (Scheme 2d and 3b). Also, synthesis of the polyamides was greatly facilitated by using solid-phase methods.[7,8a-c]

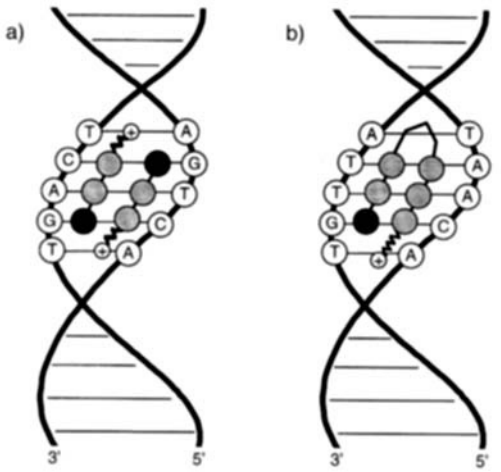

Scheme 3. Model of the sequence-specific binding of a) 1-methylimidazole-2-carboxamide-netropsin and b) ImPyPy-γ-PyPyPy-β-Dp in the minor groove of a DNA double helix. Gray and black circles represent pyrrole and imidazole units of the polyamide, respectively.

The recently published paper by Gottesfeld et al. adds one more chapter to the successful story of pyrrole-imidazole polyamides.[9] For the first time it was shown that polyamides are capable of selectively interfering with gene expression as artificial regulators in eukaryotic cells. An eight-ring polyamide targeted to the binding site of the transcription factor TFIIIA in the minor groove specifically inhibited transcription of the 5S RNA gene in *Xenopus* kidney cells. These experiments indicate that polyamides are capable of entering the cell and the nucleus and displacing transcription factors because of their higher affinity towards the target sequence.

However, despite these promising results the potential of synthetic polyamides to act as specific gene regulators cannot be definitely assessed yet. The majority of DNA-binding proteins interact with nucleobases in the DNA major groove. It remains to be seen whether and how minor groove binding ligands are capable of effectively modulating protein-DNA interactions and influencing the resulting regulatory mechanisms in a variety of cell types. Also, the question arises of how selectively genes are recognized by synthetic polyamides. Based on statistical arguments it can be shown that, depending on the base composition, approximately 17 base pairs must be read by a ligand to recognize a unique sequence in the human genome.[10] However, due to the degeneracy of AT and TA base pairs in the imidazole/pyrrole recognition code this number must be set even higher. Unfortunately, there are still some limitations with polyamide ligands. Polyamides having more than five rings, that is with binding sites longer than 7 base pairs, show a continuous decrease in their affinity and selectivity towards the target sequence.[11] This can be attributed to the nonperfect adjustment of the polyamide geometry to the double helix resulting in small irregularities, which, in turn, are amplified with increasing length of the binding site. By linking two three-ring polyamide subunits with a spacer like β-alanine, the recognition sequence of such an elongated ligand could be extended up to 13 base pairs.[12] However, in addition to the 2:1 binding motif with fully overlapping polyamides, "slipped" motifs with only partially overlapped monomers are formed as well. Thus, it will be important for the future to develop ligands that bind in a definite and predetermined manner also to longer base sequences with high affinity and specificity.

In contrast to polyamides, single-stranded "antigene" oligonucleotides bind in the major groove of a double helix forming a local triple helix. Recent studies on a covalently linked polyamide-oligonucleotide conjugate reveal that binding occurs simultaneously to the major and minor groove even at subnanomolar concentrations.[13] Since antigene oligonucleotides are modularly constructed from the same units as the double helix itself and are thus optimally adjusted to the target molecule, they have no limitations regarding the length of their binding site. On the other hand, only AT and GC base pairs in homopurine sequences are recognized, because an effective recognition code for TA and CG base pairs is still lacking. Combining both binding motifs in a chimeric ligand not only enhances binding affinity and specificity, but may also significantly expand the repertoire of possible target sequences. In view of this development in the design of artificial regulators of gene expression, DNA binding polyamides seem to be on their way to a promising future even with some questions still unresolved.

German version: *Angew. Chem.* **1997**, *109*, 2702–2705

Keywords: DNA recognition · gene expression · nucleic acids · polyamides

[1] S. Neidle, *Biopolymers* **1997**, *44*, 105–121.
[2] J. W. Lown, K. Krowicki, U. G. Bhat, A. Skorobogaty, B. Ward, J. C. Dabrowiak, *Biochemistry* **1986**, *25*, 7408–7416.
[3] J. G. Pelton, D. E. Wemmer, *Proc. Natl. Acad. Sci. USA* **1989**, *86*, 5723–5727.
[4] W. S. Wade, M. Mrksich, P. B. Dervan, *J. Am. Chem. Soc.* **1992**, *114*, 8783–8794.
[5] M. Mrksich, W. S. Wade, T. J. Dwyer, B. H. Geierstanger, D. E. Wemmer, P. B. Dervan, *Proc. Natl. Acad. Sci. USA* **1992**, *89*, 7586–7590.
[6] B. H. Geierstanger, M. Mrksich, P. B. Dervan, D. E. Wemmer, *Science* **1994**, *266*, 646–650.
[7] J. W. Trauger, E. E. Baird, P. B. Dervan, *Nature* **1996**, *382*, 559–561.
[8] a) E. E. Baird, P. B. Dervan, *J. Am. Chem. Soc.* **1996**, *118*, 6141–6146; b) M. E. Parks, E. E. Baird, P. B. Dervan, *ibid.* **1996**, *118*, 6147–6152; c) M. E. Parks, E. E. Baird, P. B. Dervan, *ibid.* **1996**, *118*, 6153–6159.
[9] J. M. Gottesfeld, L. Neely, J. W. Trauger, E. E. Baird, P. B. Dervan, *Nature* **1997**, *387*, 202–205.
[10] N. T. Thuong, C. Hélène, *Angew. Chem.* **1993**, *105*, 697–723; *Angew. Chem. Int. Ed. Engl.* **1993**, *32*, 666–690.
[11] J. J. Kelly, E. E. Baird, P. B. Dervan, *Proc. Natl. Acad. Sci. USA* **1996**, *93*, 6981–6985.
[12] J. W. Trauger, E. E. Baird, M. Mrksich, P. B. Dervan, *J. Am. Chem. Soc.* **1996**, *118*, 6160–6166.
[13] J. W. Szewczyk, E. E. Baird, P. B. Dervan, *Angew. Chem.* **1996**, *108*, 1596–1598; *Angew. Chem. Int. Ed. Engl.* **1996**, *35*, 1487–1489.

 © WILEY-VCH Verlag GmbH, D-69451 Weinheim, 1997 0570-0833/97/3623-2594 $ 17.50+.50/0

pH 6.3

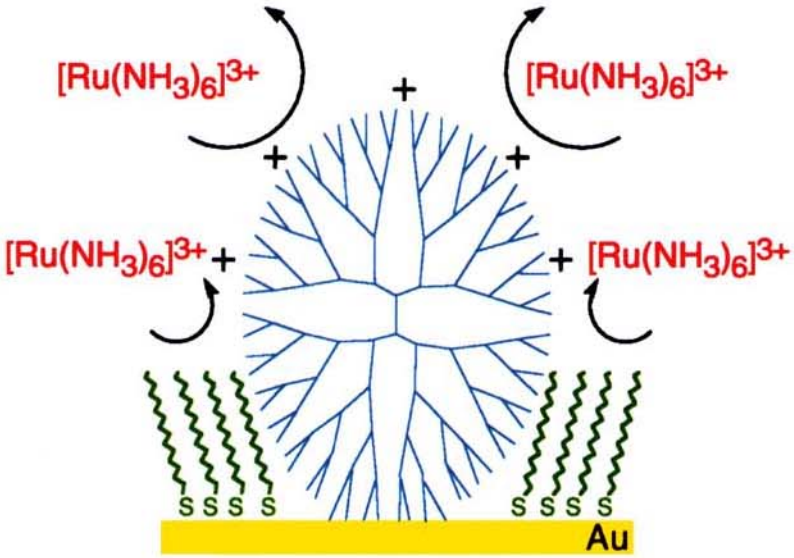

1. At low pH the terminal amine groups of the dendrimer are protonated, and the redox substrate cannot permeate the dendrimer interior.

A molecule-sized, gated electrode

(see the following pages)

pH 11.0

2. However, at high pH the terminal amine groups are deprotonated, and the substrate easily penetrates the dendrimer interior and is reduced.

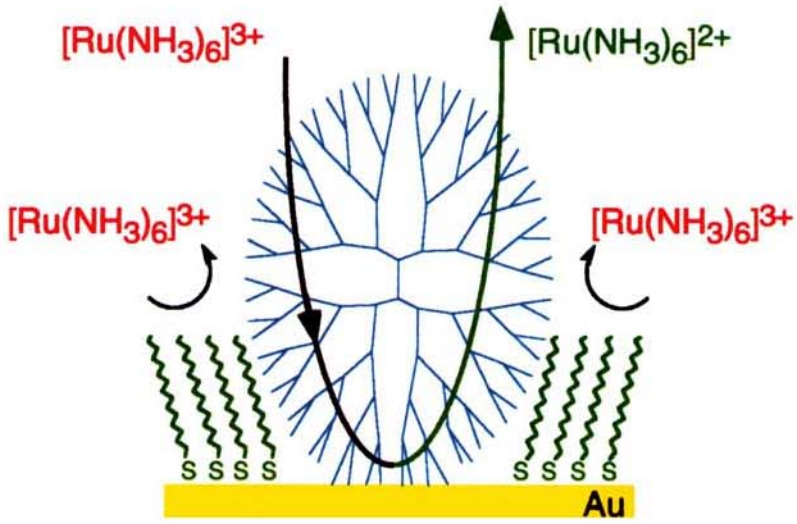

 © WILEY-VCH Verlag GmbH, D-69451 Weinheim, 1997 0570-0833/97/3623-2595 $ 17.50+.50/0

Molecule-Sized Gates Based on Surface-Confined Dendrimers**

Mingqi Zhao, Hideo Tokuhisa, and Richard M. Crooks*

In this report we demonstrate for the first time that surface-confined dendrimers[1-5] embedded within self-assembled monolayers (SAMs) of alkylthiols[6] can act as ion gates of molecular dimension.[7,8] These composite organic thin films are conceptually, structurally, and chemically very similar to the membrane/protein composites found in nature.[9] Molecular systems such as these are relevant for applications in electrocatalysis, chemical sensing, and separations.

Prior to the work described here, we showed that generation 0–8 (G0–G8) amine-terminated poly(amidoamine) (PAMAM) dendrimers[10] could be immobilized on surfaces by covalent attachment of the dendrimer amine groups to the acid terminus of a mercaptoundecanoic acid SAM.[1,11] Here we show that PAMAM dendrimers form high-density monolayers on Au surfaces, without the need for an intervening SAM adhesion layer, primarily as a consequence of multiple amine/Au interactions. This represents a major simplification of the previously described linking procedure. Additionally, we find evidence that single-component dendrimer monolayers result in a dendrimer conformation that is quite unlike the spherical form of G4 and higher generation PAMAM materials. In contrast, however, when a dendrimer monolayer is exposed to hexadecylthiol ($CH_3(CH_2)_{15}SH$, abbreviated C16SH), the dendrimer monolayer is compressed, and the molecule's conformation changes to that of an on-end oblate spheroid (see Scheme 1). Finally, and most significantly, of the redox probe molecules $[Ru(NH_3)_6]^{3+}$ and $[Fe(CN)_6]^{3-}$ at pH = 6.3, only the negatively charged $[Fe(CN)_6]^{3-}$ can penetrate a two-component monolayer composed of a G4 PAMAM dendrimer and C16SH and undergo electron exchange with the underlying electrode, whereas when the dendrimers are fully deprotonated at pH = 11, both redox probe molecules undergo electron transfer (Scheme 1). This effect is fully reversible as the pH is toggled between 6.3 and 11. Significantly, we provide unambiguous evidence for the first time that penetration by the redox probe molecules occurs *through* the interior of the dendrimers.[13-15]

Figure 1a shows an FTIR–external reflection (FTIR-ER) spectrum of a G4 PAMAM monolayer prepared by immersion of a Au/Ti/Si(100) substrate in a 0.1 mM ethanolic solution of the dendrimer for 20 h, followed by careful rinsing and drying in flowing N_2. The relevant peaks that confirm attachment of the dendrimer to the surface arise from the dendrimer framework: the amide I and amide II bands at 1661 and 1552 cm^{-1}, respectively, and bands resulting from the two kinds of methylene groups present in PAMAM dendrimers at 2926, 2852, and 2818 cm^{-1},[16] and the amide and amine N–H stretching modes centered around 3300 cm^{-1}. Mass titrations based on surface acoustic waves (SAWs)[17] indicate that about (88 ± 2)% of the Au surface is occupied by the dendrimers after this step. Figure 1b shows the effect of immersing the dendrimer-modified electrode in a 1 mM ethanolic solution of C16SH for 20 h: there is a dramatic increase of the band intensity in the hydrocarbon region, confirming adsorption of C16SH to the Au surface, and a slight increase in the amide bands, which probably results from the orientational change induced in the dendrimer structure by the C16SH SAM (see Scheme 1). The important point is that after exposure to C16SH, the dendrimer number density does not change significantly from its original value, but there is a shear force induced by the C16SH SAM that results in lateral compression of the dendrimers. On the basis of the mass titrations,

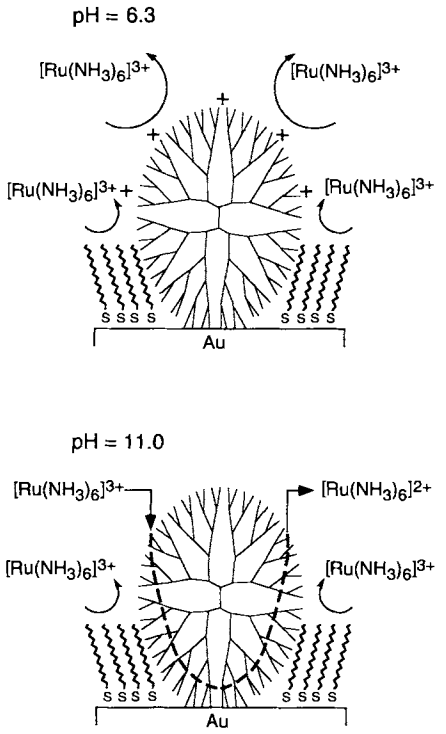

Scheme 1. Arrangement of PAMAM dendrimers on a gold surface in the presence of a long-chain thiol as a model to account for the observed results (for details see text).

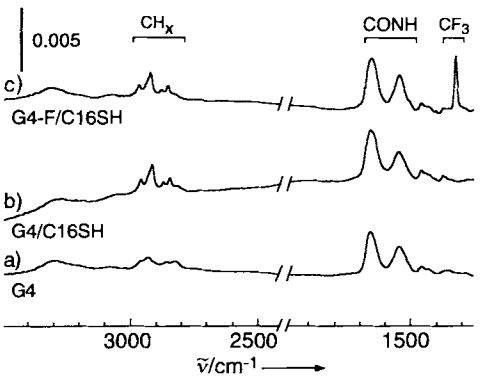

Figure 1. FTIR-ERS spectra of G4 dendrimer-modified Au substrates. a) G4 only; b) G4 after immersion in an ethanolic solution of C16SH; c) G4 followed by on-surface conversion of the primary amine groups to 4-(trifluoromethyl)benzamido groups and subsequent immersion in an ethanolic solution of C16SH.

[*] Prof. R. M. Crooks, M. Zhao, Dr. H. Tokuhisa
Department of Chemistry
Texas A&M University
College Station, TX 77843-3255 (USA)
Fax: Int. code + (409) 845-1399
e-mail: crooks@chemvx.tamu.edu

[**] Interactions Between Organized, Surface-Confined Monolayers and Liquid-Phase Probe Molecules, Part 5. We are grateful to the U.S. Office of Naval Research and the Robert A. Welch Foundation for support of this work. We also thank Dr. Antonio J. Ricco and Dr. Thomas M. Mayer (Sandia National Laboratories) for comments and suggestions, and Dendritech, Inc. (Midland, MI) for supplying samples of the Starburst PAMAM dendrimers used in this study. Part 4: O. Chailapakul, R. M. Crooks, *Langmuir*, **1995**, *11*, 1329.

 © WILEY-VCH Verlag GmbH, D-69451 Weinheim, 1997 0570-0833/97/3623-2596 $ 17.50+.50/0

FTIR-ERS, and ellipsometry[18] we estimate that the percentage of the surface accessible to the thiol increases from 12% to greater than 50% after exposure to C16SH.

Figure 2 shows cyclic voltammetric data obtained from the mixed G4/C16SH monolayer corresponding to Figure 1b. At low pH (Figure 2a) the terminal amine groups of the dendrimers are protonated (pK_a about 9.5)[12] and effectively block penetration, and hence electrochemical reduction, of $[Ru(NH_3)_6]^{3+}$. In contrast, the rate of reduction of negatively charged $[Fe(CN)_6]^{3-}$ is only slightly hindered relative to that at a naked Au electrode. Contrast these results with those obtained at high pH (Figure 2b) when the amine groups are in their neutral form. In this case, both the $[Fe(CN)_6]^{3-}$ and $[Ru(NH_3)_6]^{3+}$ penetrate the dendrimer portion of the mixed SAM. This result alone, however, does not definitely prove

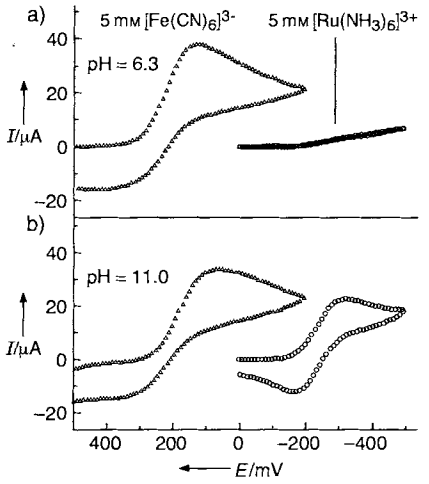

Figure 2. Cyclic voltammetry (E vs. Ag/AgCl, 3 M NaCl) of 5 mM $[Fe(CN)_6]^{3-}$ and 5 mM $[Ru(NH_3)_6]^{3+}$ in 0.5 M aqueous Na_2SO_4 electrolyte solutions at G4/C16SH-modified Au electrodes: a) pH = 6.3 (0.025 M Na_2HPO_4 + 0.025 M NaH_2PO_4), and b) pH = 11 (0.036 M NH_4Cl + 2.0 M "NH_4OH", prepared from a 28% solution of NH_3). Electrode area: 0.086 cm^2, scan rate: 50 $mV\,s^{-1}$.

intradendrimer mass transfer of the redox probes, since the observed effect could arise from probe penetration at the dendrimer/C16SH interface. Because of the strong shear force exerted on the dendrimers by C16SH, we view this as an unlikely scenario, but to show definitively that the dendrimers themselves, rather than dendrimer-induced defects in the monolayer, are acting as molecular gates we performed two additional experiments.

In the first experiment, we prepared a G4 monolayer as described previously, converted the terminal amine groups to 4-(trifluoromethyl)benzamido groups, soaked the resulting dendrimer surface in C16SH, and then examined the electrochemical response in the presence of $[Fe(CN)_6]^{3-}$ at pH 6.3. Conversion of the surface-confined dendrimer to the fluorinated derivative (G4-F), without loss of dendrimer from the surface, is confirmed by the appearance of the new CF_3 band in the FTIR-ERS spectrum at 1329 cm^{-1} and the slight increase in amide-band intensity resulting from coupling of the 4-(trifluoromethyl)benzoyl groups to the amine-terminated dendrimer (Figure 1c). Figure 3 compares the cyclic voltammetry that arises from G4/C16SH and G4-F/C16SH monolayers: the protonated amines pass $[Fe(CN)_6]^{3-}$, but the bulky and hydrophobic 4-(trifluoromethyl)benzamido groups prevent penetration. If penetration occurred primarily at defects in the G4/C16SH interface rather than through the dendrimer interior, then we might anticipate similar responses for the fluorinated and unfluorinated dendrimers.

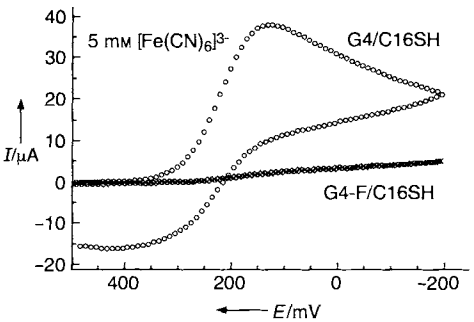

Figure 3. Cyclic voltammetry (E vs. Ag/AgCl, 3 M NaCl) of 5 mM $[Fe(CN)_6]^{3-}$ at a G4/C16SH-modified Au electrode and a G4-F/C16SH-modified Au electrode in a 0.5 M aqueous Na_2SO_4 electrolyte solution (conditions as in Figure 2a).

A second experiment provides additional evidence for intradendrimer mass transfer of the redox probes. Figure 4 shows results for cyclic voltammetric experiments obtained using electrodes prepared from mixed monolayers composed of G0, G4, or G8 dendrimers and C16SH for both positively and negatively charged redox probes at pH 6.3. Considering first the results obtained with the $[Fe(CN)_6]^{3-}$ probe (Figure 4a), we observe that the Faradaic current decreases as a

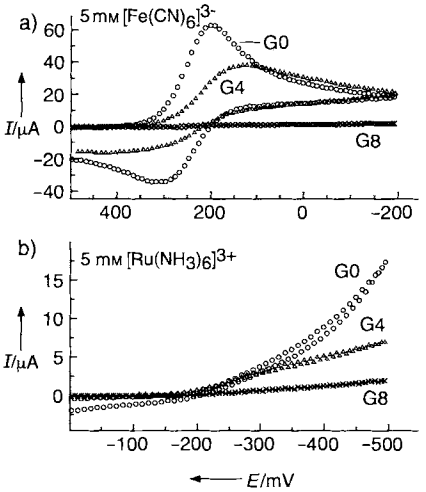

Figure 4. Cyclic voltammetry of 5 mM solutions of $[Fe(CN)_6]^{3-}$ (a) and $[Ru(NH_3)_6]^{3+}$ (b) at G0/C16SH-, G4/C16SH-, and G8/C16SH-modified Au electrodes in a 0.5 M aqueous Na_2SO_4 electrolyte solution (conditions as in Figure 2a).

function of increasing dendrimer generation. This result is a consequence of steric crowding on the exterior of the dendrimer as the number of terminal groups increases and a corresponding reduction in permeability. A similar trend is observed for $[Ru(NH_3)_6]^{3+}$ (Figure 4b), but the currents are much lower for all three dendrimer generations relative to that observed for $[Fe(CN)_6]^{3-}$, because of the electrostatic repulsion of the probe by the positively charged dendrimer surface.

In summary, we have reported four new findings. First, PAMAM dendrimers adsorb irreversibly onto Au at high

 © WILEY-VCH Verlag GmbH, D-69451 Weinheim, 1997 0570-0833/97/3623-2597 $ 17.50+.50/0

surface concentrations. Second, surface-confined dendrimers undergo a dramatic conformational change upon exposure to C16SH, resulting from shear compression. Third, and most significantly, the dendrimers act as molecular gates in that they can be tailored to permit selective intradendrimer mass transfer. Finally, we have shown that the primary amines of the surface-confined dendrimers can be easily functionalized without significant desorption of dendrimer. These four key results open the door to a new generation of dendrimer-modified surfaces suitable for a range of technologically important applications.

Received: May 20, 1997 [Z10459IE]
German version: *Angew. Chem.* **1997**, *109*, 2707–2710

Keywords: dendrimers · electrochemistry · molecular recognition · supramolecular chemistry · thin films

[1] M. Wells, R. M. Crooks, *J. Am. Chem. Soc.* **1996**, *118*, 3988.
[2] B. Alonso, M. Morán, C. M. Casado, F. Lobete, J. Losada, I. Cuadrado, *Chem. Mater.* **1995**, *7*, 1440.
[3] P. M. Saville, P. A. Reynolds, J. W. White, C. J. Hawker, J. M. J. Fréchet, K. L. Wooley, J. Penfold, J. R. P. Webster, *J. Phys. Chem.* **1995**, *99*, 8283.
[4] S. Watanabe, S. L. Regen, *J. Am. Chem. Soc.* **1994**, *116*, 8855.
[5] V. V. Tsukruk, F. Rinderspacher, V. N. Bliznyuk, *Langmuir* **1997**, *13*, 2171.
[6] L. H. Dubois, R. G. Nuzzo, *Annu. Rev. Phys. Chem.* **1992**, *43*, 437, and references therein.
[7] O. Chailapakul, R. M. Crooks, *Langmuir* **1995**, *11*, 1329.
[8] R. Bilewicz, M. Majda, *J. Am. Chem. Soc.* **1991**, *113*, 5464.
[9] H. Ringsdorf, B. Schlarb, J. Venzmer, *Angew. Chem.* **1988**, *100*, 117, *Angew. Chem. Int. Ed. Engl.* **1988**, *27*, 113.
[10] D. A. Tomalia, A. M. Naylor, W. A. Goddard III, *Angew. Chem.* **1990**, *102*, 119; *Angew. Chem. Int. Ed. Engl.* **1990**, *29*, 138, and references therein.
[11] L. Sun, R. M. Crooks, A. J. Ricco, *Langmuir* **1993**, *9*, 1775.
[12] Technical data supplied by Dendritech, Inc. (Midland, MI).
[13] J. F. G. A. Jansen, E. M. M. de Brabander-van den Berg, E. W. Meijer, *Science* **1994**, *266*, 1226.
[14] J. F. G. A. Jansen, E. W. Meijer, E. M. M. de Brabander-van den Berg, *J. Am. Chem. Soc.* **1995**, *117*, 4417.
[15] M. F. Ottaviani, S. Bossmann, N. J. Turro, D. A. Tomalia, *J. Am. Chem. Soc.* **1994**, *116*, 661.
[16] D. Lin-Vien, N. B. Colthup, W. G. Fateley, J. G. Grasselli, *Infrared and Raman Characteristic Frequencies of Organic Molecules* Academic, San Diego, **1991**, Chap. 2.
[17] D. L. Dermody, R. M. Crooks, T. Kim, *J. Am. Chem. Soc.* **1996**, *118*, 11912.
[18] Ellipsometric measurements indicate that a G4-modified surface changes in thickness from 1.9 ± 0.2 to 3.7 ± 0.2 nm after exposure to an ethanolic C16SH solution. Ellipsometric modeling results derived from the Bruggemann effective-medium approximation data suggest a change in the calculated, single-dendrimer height from 2.8 to 5.5 nm. H. Tompkins, *A Users Guide to Ellipsometry*, Academic, New York, **1993**, Apendix B.) Previously reported theoretical calculations (see ref. [10]) are consistent with this result.

Tetrathia- and Tetraoxarubyrins: Aromatic, Core-Modified, Expanded Porphyrins**

Alagar Srinivasan, VenkatRam M. Reddy, S. Jeyaprakash Narayanan, Bashyam Sridevi, Simi K. Pushpan, Murugaeson Ravikumar, and Tavarekere K. Chandrashekar*

Dedicated to Professor Varadachari Krishnan on the occasion of his 60th birthday

The current trend towards broadening the basis of porphyrin chemistry by developing novel polypyrrolic systems has stimulated an immense research effort in the area of "expanded porphyrins".[1] Synthetic work in this direction has led to several classes of expanded porphyrins including sapphyrin,[2] pentaphyrin,[3] hexaphyrin,[4] rosarin,[5] rubyrin,[6] and octaphyrin.[7] These generally have more than four pyrrole units linked through three or four *meso* carbon bridges. Many related studies have provided valuable information on ring size, aromaticity, macrocyclic stability, and the ability of the compounds to act as chelating receptors for the complexation of anions, cations, and neutral substrates.[8]

Replacement of one or more pyrrole rings by other heterocycles such as thiophene or furan rings leads to core-modified, expanded porphyrins that might have properties that are substantially different to those of well-studied nitrogen analogues[9] due to altered electronic structures. We have been interested in such core modification of porphyrin systems, and our efforts in this direction have revealed many similarities and differences in electrochemical, photochemical, and optical properties relative to the corresponding nitrogen analogues.[10] Here we report the first examples of expanded porphyrins containing either two bithiophene or two bifuran units covalently linked to two pyrrole rings through four methine bridges.[11] We refer to them as tetrathia- and tetraoxarubyrins **1** and **2**, which are analogous to the hexapyrrolic homologue rubyrin **3** reported by Sessler et al.[6]

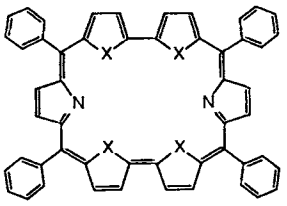

1 X = S
2 X = O

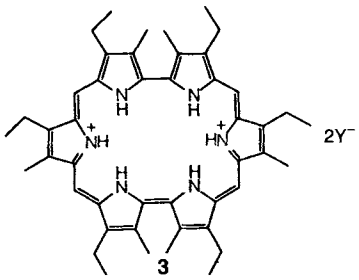

3

The synthetic method currently available for preparing five- or six-membered expanded porphyrins is based on an acid-catalyzed [3+2] or [4+2] MacDonald condensation between a dicarboxyl-substituted tripyrromethane or tetrapyrrolic unit with diformyl bipyrroles.[2b,c,6] The present method adopts a different approach based on the synthesis

[*] Prof. Dr. T. K. Chandrashekar, A. Srinivasan, Dr. V. M. Reddy, S. J. Narayanan, B. Sridevi, S. K. Pushpan, M. Ravikumar
Department of Chemistry
Indian Institute of Technology
Kanpur 208016 (India)
Fax: Int. code + (512) 590-007/597-436
e-mail: tkc@iitk.ernet.in

[**] This work was supported by the Department of Science and Technology (DST) of the government of India, New Delhi.

 © WILEY-VCH Verlag GmbH, D-69451 Weinheim, 1997 0570-0833/97/3623-2598 $ 17.50+.50/0

of core-modified mono- and dithiaporphyrins[9] (Scheme 1). Thus, the two key precursors bithiophenediol **5** and bifurandiol **7**—synthesized from thiophene via **4** or from furfual via

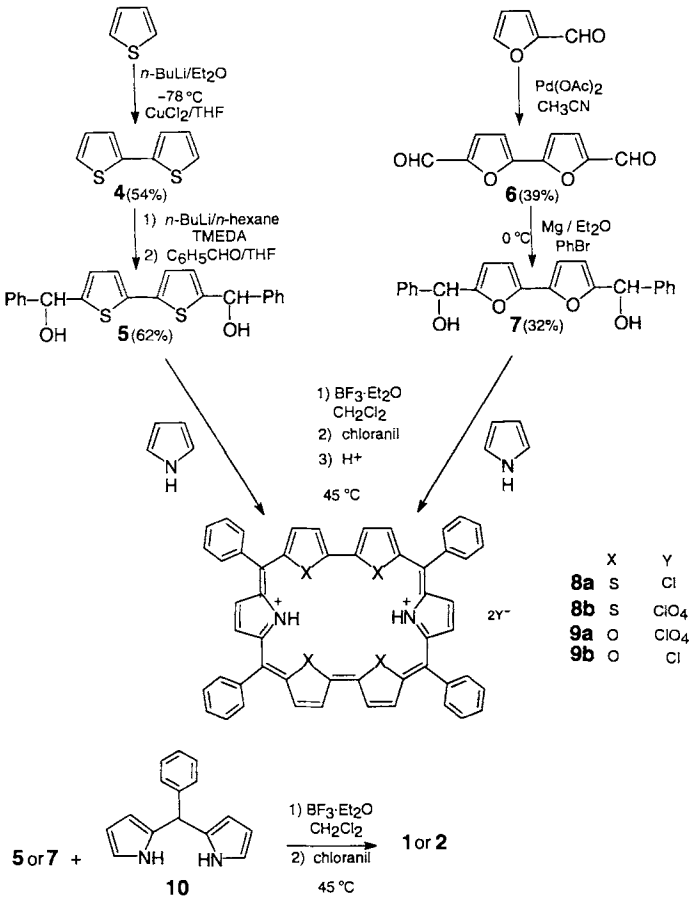

Scheme 1. Synthesis of tetraoxa- and tetrathiarubyrins **1** and **2**.

6, respectively—provide **1** and **2** as shiny green metallic solids in 28 and 15% yield, respectively, upon condensation with pyrrole under Lindsey conditions[12a] followed by oxidation with chloranil. Alternatively, reaction of **5** or **7** with dipyrromethane[12b] **10** under Lindsey conditions followed by oxidation afforded **1** or **2** in 20% yield. Treatment of **1** and **2** with HCl and $HClO_4$ gave **8a**, **8b** and **9a**, **9b**, respectively, in 85–90% yield.

The compositions of **1** and **2** were established from FAB mass spectra, which show peaks at 813 and 750, respectively, with 100% fragmentation. The electronic absorption spectra[13] of **1** and **2** in CH_2Cl_2 (Figure 1a) exhibit an intense Soret band and four Q bands. The electronic spectra generally resemble those of *meso*-tetraphenylporphyrins, but are significantly red-shifted; this is not surprising considering the larger aromatic systems (26 π electrons) in **1** and **2** relative to the 18 π electronic systems of *meso*-tetraphenylporphyrins.[14] Protonation of **1** and **2** by addition of a dilute solution of trifluoroacetic acid (TFA) in CH_2Cl_2 leads to further red shifting of both the Q and Soret bands (Figure 1b); this effect is typical of *meso*-tetraarylporphyrins. Changing the counterions in **8a** and **9a** produces only minor changes. Therefore, the similarity of the electronic absorption spectra of **1**, **2** and their protonated derivatives with that of *meso*-arylporphyrin and its protonated derivative confirms the aromatic nature of the former.

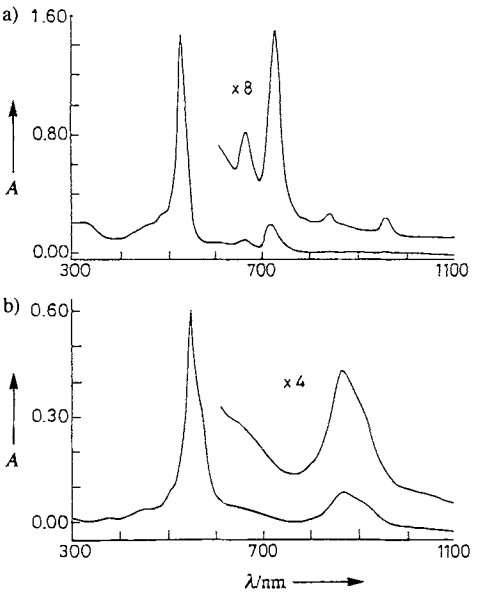

Figure 1. Electronic absorption spectra of **1** in CH_2Cl_2 (1.85×10^{-5} M) a) without TFA and b) with about 10^{-3} M TFA.

Energy-optimized structures for **1** and **2** are shown in Figure 2. It is clear from the structures of **1** and **2** that the two bithiophene/bifuran units, one containing a double bond and

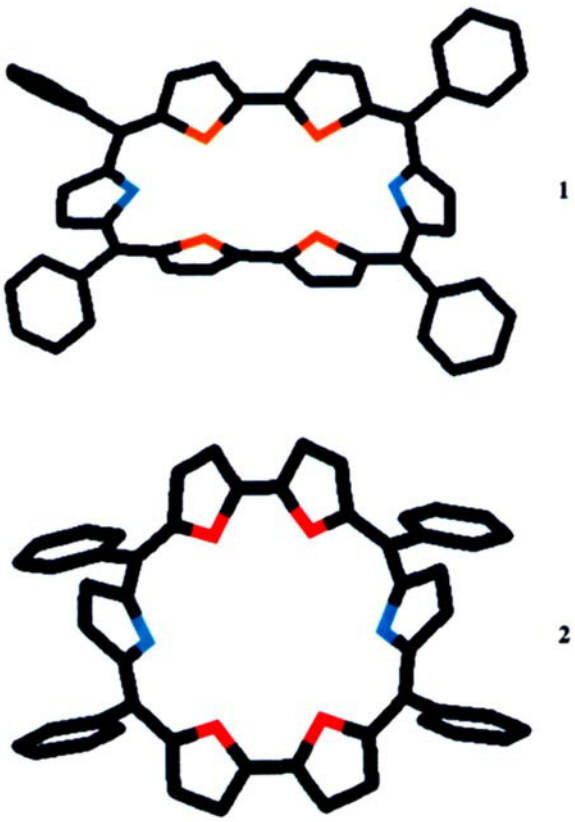

Figure 2. Geometry-optimized structures (Hyperchem 5.0 with AM1 basis set) of **1** and **2**; red: oxygen; yellow: sulfur; blue: nitrogen.

the other only a single bond, occupy different planes. This reflects their different magnetic environments. In fact, the observation of two doublets separated by 1.15 ppm for

 © WILEY-VCH Verlag GmbH, D-69451 Weinheim, 1997 0570-0833/97/3623-2599 $ 17.50+.50/0

bithiophene and by 1.00 ppm for bifuran protons in the ^{1}H NMR apectrum clearly reveals their magnetic inequivalence. Compound **3** also shows a difference in the chemical shift for the bipyrrole ethyl-methyl substituents of about 2 ppm .[6] The chemical shifts for the inner NH protons of $\delta = -5.15$ and -4.82 observed for **1** and **2**, respectively, in $CDCl_3$ containing deuterated TFA further establishes their aromatic character.

Additional evidence for the aromatic character of **1**, **8a**, and **8b** comes from preliminary cyclic voltammetric studies. The two quasi- reversible ring reductions observed for **1** in CH_2Cl_2 suggest stabilization of the corresponding LUMOs relative to the LUMOs of *meso*-tetraarylporphyrins by 370 mV. An estimated HOMO–LUMO gap of 1.64 V for **8b** in CH_3CN indicates a significant reduction relative to sapphyrin (1.88 V)[14] and *meso*-tetraphenyl porphyrin (2.26 V),[10] thus explaining the large red shifts for **1** and its protonated derivatives.

Spectral titrations of a methanolic solution of **8a** and **8b** with anions (F^-, N_3^-, and adenosine 5′-monophosphate (AMP)) results in a decrease in absorbance, a blue shift of the Soret bands in the absorption spectra by about 30 nm, and a blue shift of the emission bands by about 15 nm together with enhanced emission intensity (AMP shows the greatest increase of about 200%, probably due to charge neutralization); this suggests anion binding that is similar to that observed for sapphyrins[8] (Scheme 2). Binding constants

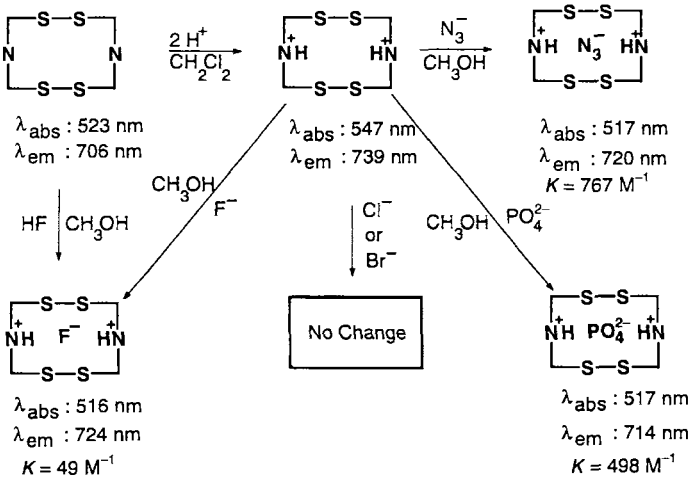

Scheme 2. Characteristics of anion binding of tetrathiarubyrin.

evaluated by an analysis of absorption data using the Nash equation[15] vary as $N_3^- > AMP > F^-$. Transport studies[16] in U tubes reveal the transport of F^- and AMP at lower rates than observed for sapphyrins and **3**.

In summary, we have synthesized two new core-modified, expanded porphyrins with 26 π electrons by a relatively easy method under mild conditions and demonstrated their anion-binding capabilities. This method avoids the difficult synthesis of sensitive precursors such as tripyrromethanes and tetrapyrrole units required for [3+2] and [4+2] condensations. The availability of gram quantities of these materials permits detailed spectroscopic and photochemical investigations that might in turn shed more light on the suitability of these materials for medicinal applications, including their use as sensitizers for photodynamic therapy and MRI contrasting agents.

Experimental Section

1: 5,5′-Bis(phenylhydroxymethyl)-2,2′-bithiophene (1 g, 2.65 mmol) and pyrrole (0.184 mL, 2.65 mmol) in dry CH_2Cl_2 (800 mL) were stirred under a nitrogen atmosphere for 15 min at room temperature. A freshly distilled solution of $BF_3 \cdot Et_2O$ (2.5 M, 10 mol%) in dry CH_2Cl_2 was added, and the reaction mixture stirred for one additional hour. The resulting solution was opened to air, chloranil (1 g, 4 mmol) was added, and the mixture was heated at reflux in a preheated oil bath at 45 °C. After removal of solvent, the crude product was purified by column chromatography. After an initial brown fraction was eluted with CH_2Cl_2/ethyl acetate (70/30), the second dark violet fraction was identified as **1** (28% yield). Alternatively, pyrrole was replaced by dipyrromethane **10** in the above procedure to generate **1** in 20% yield. A similar procedure was followed for the synthesis of **2** using bifurandiol.

1: ^{1}H NMR (300 MHz, $CDCl_3$): $\delta = 7.98$ (m, 12H), 8.55 (m, 8H), 9.06 (s, 4H), 10.49–10.50 (d, $J = 3.00$ Hz, 4H), 11.64–11.66 (d, $J = 6$ Hz, 4H); ^{1}H NMR (300 MHz, $CDCl_3$/TFA): $\delta = -5.15$ (s, 2H), 8.32–8.34 (m, 12H), 9.02–9.04 (m, 8H), 9.41 (s, 4H), 10.96–10.98 (d, $J = 3$ Hz), 11.74–11.76 (d, $J = 6$ Hz); UV/Vis (CH_2Cl_2/1% Et_3N): λ_{max} ($\varepsilon \times 10^{-3}$) = 523 (79.81), 659 (4.88), 717 (10.18), 837 (0.55), 958 nm (0.60); emission (CH_2Cl_2): $\lambda = 706$, 768 nm; MS (FAB): m/z (%) = 813 (100); CV (CH_2Cl_2/tetrabutyl ammonium perchlorate (TBAP, 1×10^{-2}‰M)): $E_{1/2}$(R1) = −0.86 V ($\Delta E_p = 150$ mV); $E_{1/2}$(R2) = −1.05 V ($\Delta E_p = 110$ mV); ΔE(red) = 190 mV; UV/Vis (CH_2Cl_2/TFA): λ_{max} ($\varepsilon \times 10^{-3}$) = 449 (3.3), 543 (44.0), 867 nm (6.2).

2: UV/Vis (CH_2Cl_2/1% Et_3N): λ_{max} ($\varepsilon \times 10^{-3}$) = 525 (5.97), 674 (1.04), 739 (1.86), 860 (0.70), 968 nm (0.93); MS (FAB): m/z (%) = 750 (100); ^{1}H NMR (300 MHz, $CDCl_3$/TFA) $\delta = -4.82$ (s, 2H), 8.13–8.15 (m, 12H), 8.27–8.29 (m, 8H), 9.00 (s, 4H), 10.71–10.72 (d, $J = 3$ Hz, 4H), 11.29–11.30 (d, $J = 3$ Hz, 4H); UV/Vis (CH_2Cl_2/TFA): λ_{max} ($\varepsilon \times 10^{-3}$) = 544 (15.7), 836 nm (3.96).

8a: UV/Vis (MeOH/1% HCl): λ_{max} ($\varepsilon \times 10^{-3}$) = 449 (3.50), 542 (29.95), 866 nm (6.53); emission (MeOH/1% HCl): $\lambda = 739$ nm; MS (FAB): m/z (%) = 815 (65).

8b: UV/Vis (MeOH/1% $HClO_4$): λ_{max} ($\varepsilon \times 10^{-3}$) = 448 (5.21), 542 (26.80), 863 nm (5.04); MS (FAB): m/z (%) = 815 (35); CV: (CH_2Cl_2/TBAP (1×10^{-2} M)): $E_{1/2}$(R1) = −0.78 V ($\Delta E_p = 130$ mV); $E_{1/2}$(R2) = −1.41 V ($\Delta E_p = 110$ mV); ΔE(red) = 630 mV; (CH_3CN/TBAP (1×10^{-2} M)): $E_{1/2}$(O1) = +0.86 V (irreversible); $E_{1/2}$(O2) = +1.12 V ($\Delta E_p = 170$ mV); $E_{1/2}$(O3) = +1.32 V ($\Delta E_p = 110$ mV).

9a: UV/Vis (MeOH/1% HCl): λ_{max} ($\varepsilon \times 10^{-3}$) = 533 (12.4), 830 nm (2.40).

9b: UV/Vis (MeOH/1% $HClO_4$): λ_{max} ($\varepsilon \times 10^{-3}$) = 532 (10.1), 829 nm (1.98).

Received: April 1, 1997
Supplemented version: July 25, 1997 [Z10297IE]
German version: *Angew. Chem.* **1997**, *109*, 2710–2713

Keywords: bithiophenes · porphyrinoids · rubyrin · sensitizers

[1] For a comprehensive review of expanded porphyrins, see J. L. Sessler, A. K. Burrel, *Top. Curr. Chem.* **1991**, *161*, 177–273.

[2] a) V. J. Bauer, L. J. Derrick Clive, D. Dolphin, J. B. Paine III, F. L. Harris, M. M. King, J. Lodger, S.-W. Chien Wang, R. B. Woodward, *J. Am. Chem. Soc.* **1983**, *105*, 6429–6436; b) J. L. Sessler, M. Cyr, A. K. Burrel, *Tetrahedron* **1992**, *48*, 9661–9672, and references therein; c) M. J. Broadhurst, R. Grigg, A. W. Johnson, *J. Chem. Soc. Perkin Trans. 1* **1972**, 2111–2116; d) P. J. Chmielewski, L. Latos-Grazynski, K. Rachlewicz, *Chem. Eur. J.* **1995**, *1*, 68–73.

[3] a) H. Rexhausen, A. Gossauer, *J. Chem. Soc. Chem. Commun.* **1983**, 275; b) A. Gossauer, *Bull. Soc. Chim. Belg.* **1983**, *92*, 793–795.

[4] J. L. Sessler, S. J. Weghorn, Y. Hiseada, V. Lynch, *Chem. Eur. J.* **1995**, *1*, 56–67.

[5] J. L. Sessler, S. J. Weghorn, T. Morishima, M. Rosingana, V. Lynch, V. Lee, *J. Am. Chem. Soc.* **1992**, *114*, 8306–8307.

[6] J. L.Sessler, T. Morishima, V. Lynch, *Angew. Chem.* **1991**, *103*, 1018–1021; *Angew. Chem. Int. Ed. Engl.* **1991**, *30*, 977–980.

[7] M. Broring, J. Jendrny, L. Zander, H. Schmickler, J. Lex, Y.-D. Wu, M. Nendel, J. Chen, D. A. Plattner, K. N. Houk, E. Vogel, *Angew. Chem.* **1995**, *107*, 2709–2711; *Angew. Chem. Int. Ed. Engl.* **1995**, *34*, 2515–2517.

[8] a) H. Furuta, M. J. Cyr, J. L. Sessler, *J. Am. Chem. Soc.* **1991**, *113*, 6677–6678; b) H. Furuta, K. Furuta, J. L. Sessler, *ibid.* **1991**, *113*, 4706–4707; c) H. Furuta, D. Magda, J. L. Sessler, *ibid.* **1991**, *113*, 978–985.

[9] a) L. Latos-Grazynski, J. Lisowski, M. M. Olmstead, A. L. Balch, *J. Am. Chem. Soc.* **1987**, *109*, 4428–4429; b) A. Ulman, J. Manassen, *ibid.* **1975**, *97*, 6540–6544; c) P. Chmielewski, M. Grazeszczuk, L. Latos-Grazynski, T. Lisowski, *Inorg. Chem.* **1989**, *28*, 3546–3552; d) A. Ulman, J. Manassen, F. Frolow, D. Rabinovich, *J. Am. Chem. Soc.* **1979**, *101*, 7055–7059.

[10] a) M. Ravikanth, T. K. Chandrashekar, *Struct. Bonding (Berlin)* **1995**, *82*, 105–188; b) R. P. Pandian, T. K. Chandrashekar, *Inorg. Chem.* **1994**, *33*, 3317–3324; c) R. P. Pandian, T. K. Chandrashekar, *J. Chem. Soc. Dalton*

 © WILEY-VCH Verlag GmbH, D-69451 Weinheim, 1997 0570-0833/97/3623-2600 $ 17.50+.50/0

Trans. **1993**, 119–125; d) M. Ravikanth, A. Mishra, T. K. Chandrashekar, S. Sathaiah, H. D. Bist, *Inorg. Chem.* **1994**, *33*, 392–394; e) R. P. Pandian, T. K. Chandrashekar, H. van Willigen, *Chem. Phys. Lett.* **1993**, *202*, 127–132.

[11] Two examples of core-modified expanded porphyrins that were previously reported are ozaphyrins and bronzaphyrin: a) D. C. Miller, M. R. Johnson, J. J. Becker, J. A. Ibers, *J. Heterocycl. Chem.* **1993**, *30*, 1485–1490; b) D. C. Miller, M. R. Johnson, J. A. Ibers, *J. Org. Chem.* **1994**, *59*, 2877–2879; c) M. R. Johnson, D. C. Miller, K. Bush, J. J. Becker, J. A. Ibers, *ibid.* **1992**, *57*, 4414–4417; d) H. Zhongying, C. Scordilis-Kelley, M. P. Cava, *Tetrahedron Lett.* **1993**, *34*, 1879–1882.

[12] a) J. S. Lindsey, I. C. Schreiman, H. C. Hsu, P. C. Kearney, A. M. Marguerettaz, *J. Org. Chem.* **1987**, *52*, 827–836; b) C.-H. Lee, J. S. Lindsey, *Tetrahedron* **1994**, *50*, 11427–11440.

[13] M. Gouterman in *The Porphyrins, Vol. III* (Ed.: D. Dolphin), Academic Press, New York, **1978**, pp. 1–165.

[14] M. Shionoya, H. Furuta, V. Lynch, A. Harriman, J. L. Sessler, *J. Am. Chem. Soc.* **1992**, *114*, 5714–5722.

[15] C. Nash, *J. Phys. Chem.* **1960**, *64*, 950–953.

[16] Transport experiments were carried out using a glass U tube with three compartments containing a solution of AMP (2 mL, 30 mM, sodium salt, Sigma, pH = 3), a solution of **8a** in CH_2Cl_2 (3×10^{-4} M), and water (2 mL, pH = 10).

Submolecularly Resolved Polymerization of Diacetylene Molecules on the Graphite Surface Observed with Scanning Tunneling Microscopy

Petrus C. M. Grim, Steven De Feyter, André Gesquière, Peter Vanoppen, Markus Rücker, Suresh Valiyaveettil, Georg Moessner, Klaus Müllen, and Frans C. De Schryver*

Polydiacetylenes (PDA) have become an important class of materials because of their interesting optical and electronic properties. Diacetylenes can in principle polymerize in the solid, liquid crystalline, or the molten state.[1] The solid-state topochemical 1,4-polymerization was first documented by Wegner in 1969.[2] The polymerization of thin films, such as Langmuir–Blodgett[3] and chemisorbed self-assembled monolayers on gold,[4] has been reported. A few studies dealt with physisorbed self-assembling monolayers on graphite. Ozaki et al. have shown evidence of polymerization in a vapor-deposited monolayer of diacetylene molecules with Penning ionization electron spectroscopy.[5] Rabe et al. have observed a physisorbed monolayer of a diacetylene compound at the liquid/graphite interface, with scanning tunneling microscopy (STM).[6] Since the first STM related publications of physisorbed monolayers on alkanes and long-chain alcohols,[7] such self-organized monomolecular adlayers have been studied with STM for a broad range of compounds.[8] Physisorbed monolayers of organic molecules at the liquid/graphite interface containing photoactive groups were recently reported,[9] and the light induced *cis–trans* isomerization could be imaged with submolecular resolution.[10,11] In this communication, we report the photopolymerization of a physisorbed monolayer containing diacetylene moieties, self-assembled from solution at the liquid/graphite interface. The monolayer structures before and after the polymerization have been imaged with submolecular resolution by means of STM. The visualization of the transformation from diacetylene to polydiacetylene in two dimensions might lead to a better understanding of the parametrization of such a polymerization.

When a drop of the solution of the isophthalic acid derivative **1** in 1-undecanol is applied to the graphite surface, a physisorbed monolayer is spontaneously formed at the liquid/graphite interface. Figure 1 (left) shows the image of the structure of such a monolayer observed with STM. A very clear image contrast is obtained due to an increased tunneling current over specific areas of the monolayer (e.g. aromatic moieties) and good stability of the monolayer. The structure

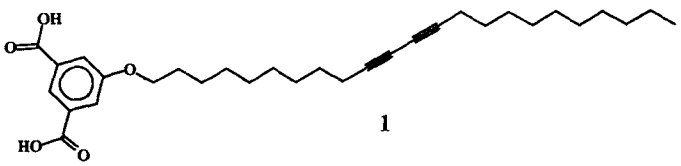

1

consists of lamellae of the molecules of **1** interspersed by alternate lamellae of solvent molecules. Such a solvent incorporation (or solvent codeposition) has recently been reported for isophthalic acid derivatives.[11] The carboxyl functions of the isophthalic acid (ISA) head groups can form hydrogen bonds between neighboring molecules of **1** or between molecules of **1** and solvent molecules. The latter possibility leads to the incorporation of the solvent molecules into the monolayer structure. One of the solvent lamellae is indicated in Figure 1 (left, arrow labeled SOLV). The

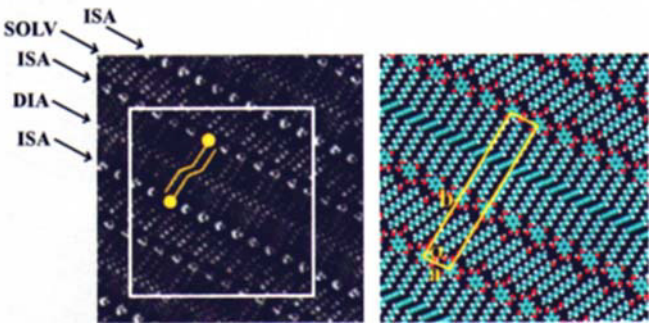

Figure 1. Left: STM image of a physisorbed monolayer of molecules of **1** from a solution in 1-undecanol (image size 12.7×12.7 nm^2). White corresponds to the highest and black to the lowest measured tunneling current in the image. Bias voltage and average tunneling current were -1.2 V and 1.0 nA, respectively. The isophthalic acid headgroups are labeled ISA, the diacetylene groups DIA and solvent molecules SOLV. Right: Model of the area indicated in the STM image, with superimposed unit cell.

undecanol molecules of the solvent lamellae are oriented at an angle of 68° relative to the direction of the lamellae. The lamellae of the molecules of **1** are characterized by the positions of the ISA headgroups and the diacetylene (DIA) moieties of the molecules. The diacetylene moieties, clearly visible in the STM image, appear as two bright spots in the

[*] Prof. F. C. De Schryver, Dr. P. C. M. Grim, S. De Feyter, A. Gesquière, P. Vanoppen, Dr. M. Rücker
University of Leuven
Department of Chemistry
Laboratory of Molecular Dynamics and Spectroscopy
Celestijnenlaan 200-F, B-3001 Heverlee (Belgium)
Fax: Int. code + (16) 327989
e-mail: Frans.DeSchryver@chem.kuleuven.ac.be
Prof. K. Müllen, Dr. S. Valiyaveettil, G. Moessner
Max-Planck-Institut für Polymerforschung, Mainz (Germany)

[**] The authors thank FKFO and DWTC for continuing financial support through IUAP-IV-11. S. De Feyter is a predoctoral fellow of the FWO and P. Vanoppen thanks the IWT for a predoctoral scholarship.

 © WILEY-VCH Verlag GmbH, D-69451 Weinheim, 1997 0570-0833/97/3623-2601 $ 17.50+.50/0

middle of the lamellae of **1**. It is possible to discern each molecule within the monolayer. For clarity, two molecules of **1** have been schematically drawn in the STM image. The headgroups of adjacent molecules of **1** point in opposite directions, thereby forming a close-packed, interdigitated lamella. The distance from one ISA headgroup to the next is 9.44 ± 0.09 Å. Comparison with the HOPG reference image (not shown), acquired immediately after the STM image of the physisorbed monolayer, shows that the alkyl chains of the molecules of **1** are lying in the direction of one of the main graphite axes. Based on these STM observations, a molecular model can be constructed for the physisorbed monolayer. Figure 1 (right) represents a model of the indicated area in Figure 1 (left), along with a unit cell of the observed structure. The unit cell parameters are $a = 9.44 \pm 0.09$, $b = 55.3 \pm 1.3$ Å and $\alpha = 82 \pm 4°$. The model suggests steric hindrance in the lamellae of **1** between the terminal methyl group of one molecule and a carboxyl function of the neighboring headgroup. In the adlayer this might be solved by a small tilt out of plane of one of these groups, but this can not be resolved in the STM image.

After the irradiation of the solution present on the graphite, the graphite surface was reexamined with the same scanning parameters as before. Monolayer structures are again observed. An example of such an image is shown in Figure 2A, where the ISA headgroups and solvent molecules can be easily recognized. The contrast in the middle of the lamellae of **1** can be described by a series of bright spots, whereas in Figure 1 (left) the direction of each diacetylene unit could easily be distinguished. The specific STM contrast in Figure 2A is more indicative of a polydiacetylene, characterized by a sequence of double, single, triple, and single bonds. This already suggests that the monolayer structure might be polymerized along the lamellar direction. An important change in the spacing between the ISA headgroups from the unpolymerized repeating distance of 9.44 ± 0.09 Å to 9.81 ± 0.05 Å is observed. The model of a polymerized monolayer also shows the unit cell (Figure 2B). The experimental value of 9.81 Å for the ISA headgroup distance is in perfect accord with the value of 9.82 Å obtained in a model optimized for the polymer chain. Consequently, the repeating distance in the polymer backbone is 4.91 Å (half of the headgroup spacing), which is in excellent agreement with the crystal structure data of polymerized diacetylenes.[12] From this it can be concluded that the monolayer structure has indeed polymerized. The unit cell parameters a', b', and α', as defined in the model for the polymerized monolayer, have been experimentally determined to be 9.81 ± 0.05, 54.8 ± 1.3 Å, and $82 \pm 4°$, respectively. These unit cell parameters are all in close agreement with the values determined from the model.

Since the polymerization is known to be topochemical,[2] it has to take place at the liquid/graphite interface, under well specified conditions. The analysis of a broad range of crystallized diacetylenes by X-ray crystallography[12] shows that topochemical polymerization can occur when the monomer stacking distance d is near 5 Å and the angle φ between the diacetylene rod and the stacking axis is around 45°. For our system, these values are 4.72 Å and 50°, respectively![12]

Scanning on a larger scale reveals the presence of domains. A domain boundary is depicted in Figure 2C: two domains are visible, pointing in slightly different directions. The domain in the lower left of the image represents an unpolymerized monolayer structure, since the ISA headgroup distance was determined to be 9.42 Å (mean value for three rows of ISA headgroups). In addition, no solvent codeposition was observed inside this domain. The other domain, rotated clockwise by 6° with respect to the first one, consists of a polymerized monolayer (ISA headgroup separation of approximately 9.81 Å). Polymerized lamellae without the incorporation of solvent are visible in the STM image in Figure 2C and are indicated by the arrows. Figure 2D shows an enlarged part of Figure 2C (as indicated) in more detail. Separated by a domain boundary, the upper, polymerized monolayer shows a bright contrast due to the polydiacetylene chains (as in Figure 2A), while in the lower, unpolymerized domain, the diacetylene groups of the individual molecules of **1** can again be distinguished. The average tunneling current at the positions of the diacetylene groups of the polymerized and the unpolymerized domain did not vary and was a factor of 1.5 higher than the average tunneling current at the positions of the alkyl chains. In principal, the diacetylene moieties can take two different orientations with respect to the lamellar direction. These two specific orientations are mirror images with respect to the lamellar direction. In the lamella in the lower left of the STM image in Figure 2D, the diacetylene groups are oriented almost horizontally, whereas in the next lamella they are oriented almost vertically. In the lamella in the lower right of the image, they are again oriented almost horizontally.

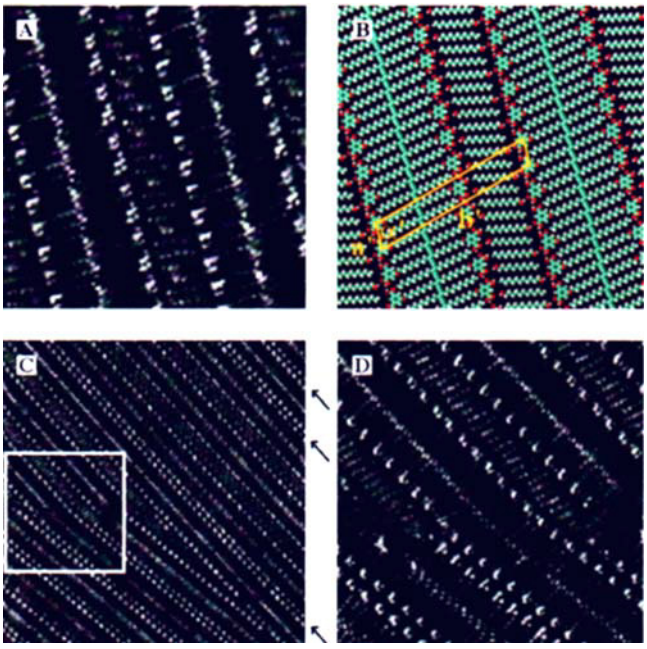

Figure 2. A) STM image of an irradiated monolayer. White corresponds to the highest and black to the lowest measured tunneling current in the image. Image size 10.8×10.8 nm^2; bias voltage -0.5 V and average tunneling current 1.0 nA. B) Model including unit cell of the imaged area in A. C) STM image of a domain boundary separating an unpolymerized (in the lower left) and a polymerized (rest of the image) region. Arrows indicate the absence of solvent codeposition inside the polymerized domain. Image size 38.5×38.5 nm^2; bias voltage -0.6 V and average tunneling current 1.0 nA. D) Zoom of the indicated area in C. Image size 15.3×15.3 nm^2; bias voltage -0.6 V and average tunneling current 1.0 nA.

Experimental Section

For the observation of the physisorbed monolayers, a commercial STM setup was used (Discoverer, Topometrix Inc., Santa Barbara, CA (USA)) operating under ambient conditions. STM tips were electrochemically etched from Pt/Ir wire (80%/20%, diameter 0.2 mm) with 6 N NaCN/2 N KOH in water as etching solution. The samples were prepared as follows: First **1** was dissolved in 1-undecanol (Aldrich, 99%), at a concentration of approximately 1 mg mL^{-1}.

 © WILEY-VCH Verlag GmbH, D-69451 Weinheim, 1997 0570-0833/97/3623-2602 $ 17.50+.50/0

One drop of this solution was applied to the basal plane of a piece of highly oriented pyrolytic graphite (HOPG, grade ZYB, Advanced Ceramics Inc., Cleveland, OH (USA)). The tip was immersed in the solution and brought close to the liquid/solid interface. During tip scanning the variations in the tunneling current were detected while keeping the average tunneling current at around 1 nA. Acquisition time for one image frame of 200 lines and 200 pixels per line was approximately 7 s (limits set by the Discoverer instrument). Tunneling voltages were between 0.5 and 1.5 V (sample negative). An image of the graphite surface could be obtained at low bias voltages. Immediately after each image a calibration image of the graphite surface was acquired at exactly the same position. This minimizes possible errors in the image analysis due to drift and scanner distortion effects, because these effects will appear to the same extent in the STM image of the monolayer structure as well as in the HOPG reference image. Lattice parameters of the observed monolayer can thus be determined with a high accuracy. The ISA headgroup separation was determined by averaging over a large number of repeating distances per row. The experimental values reported are mean values for many images, acquired during different experiments performed with different tips. After obtaining a HOPG reference image for calibration, the tunneling voltage could be increased to observe the physisorbed monolayer again. We have not seen any evidence that the monolayer was disturbed due to the calibration procedure described above. The STM data were not subjected to image processing. Irradiation was carried out as follows: first the tip was retracted and the STM head removed. Then the graphite, its surface still coated with solution, was irradiated by means of a CAMAG universal lamp (wavelength 254 nm) by putting it approximately 5 cm above the surface. The duration of the illumination was 20–30 minutes. After this time, the STM head was reinstalled and imaging resumed.

Received: April 7, 1997
Revised version: July 24, 1997 [Z10323IE]
German version: *Angew. Chem.* **1997**, *109*, 2713–2715

Keywords: alkynes · diacetylenes · monolayers · polymerizations · scanning tunneling microscopy

[1] T. Ogawa, *Prog. Polym. Sci.* **1995**, *20*, 943–985.
[2] G. Wegner, *Z. Naturforsch. B* **1969**, *24*, 824–832.
[3] a) A. Lio, A. Reichert, J. O. Nagy, M. Salmeron, D. H. Charych, *J. Vac. Sci. Technol.* **1996**, *B14*, 1481–1485; b) S. Nezu, J. B. Lando, *J. Polym. Sci.* **1995**, *A33*, 2455–2461.
[4] D. W. Batchelder, S. D. Evans, T. L. Freeman, L. Häussling, H. Ringsdorf, H. Wolf, *J. Am. Chem. Soc.* **1994**, *116*, 1050–1053.
[5] H. Ozaki, T. Funaki, Y. Mazaki, S. Masuda, Y. Harada, *J. Am. Chem. Soc.* **1995**, *117*, 5596–5597.
[6] J. P. Rabe, S. Buchholz, L. Askadskaya, *Synth. Met.* **1993**, *54*, 339–349.
[7] a) G. C. McGonical, R. H. Bernhardt, D. J. Thomson, *Appl. Phys. Lett.* **1990**, *57*, 28–30; b) J. P. Rabe, S. Buchholz, *Science* **1991**, *253*, 424–427.
[8] D. M. Cyr, B. Venkataraman, G. W. Flynn, *Chem. Mater.* **1996**, *8*, 1600–1615.
[9] R. Heinz, A. Stabel, J. P. Rabe, G. Wegner, F. C. De Schryver, D. Corens, W. Dehaen, C. Süling, *Angew. Chem.* **1994**, *106*, 2154–2157; *Angew. Chem. Int. Ed. Engl.* **1994**, *33*, 2080–2083.
[10] P. C. M. Grim, P. Vanoppen, M. Rücker, S. De Feyter, G. Moessner, S. Valiyaveettil, K. Müllen, F. C. De Schryver, *J. Vac. Sci. Technol. B* **1997**, *15*, 1419–1424.
[11] P. Vanoppen, P. C. M. Grim, M. Rücker, S. De Feyter, G. Moessner, S. Valiyaveettil, K. Müllen, F. C. De Schryver, *J. Phys. Chem.* **1996**, *100*, 19636–19641.
[12] V. Enkelmann, *Adv. Polym. Sci.* **1984**, *63*, 91–136.

Comparison of the Bioactive Conformations of Sialyl Lewis^X and a Potent Sialyl Lewis^X Mimic**

Wolfgang Jahnke,* Hartmuth C. Kolb, Marcel J. J. Blommers, John L. Magnani, and Beat Ernst

Interactions of glycopeptides and glycolipids bearing sialyl Lewis^X with a family of C-type lectins, the selectins, are responsible for the "rolling" event which is the initial step in leukocyte recruitment to sites of injury or inflammation.[1] This process plays a crucial role in a number of diseases and pathological situations, for example inflammation, reperfusion injury, rheumatoid arthritis, metastasis, and angiogenesis.

Currently, great research efforts are concentrated on developing carbohydrate-derived drugs which interfere with the rolling stage of the inflammatory response by blocking the selectin binding site.[2] To design sialyl Lewis^X mimics, a thorough understanding of the structure–activity relationship as well as the bioactive conformation (that is, the conformation of the mimic bound to the selectin) is required.

A powerful method for elucidating the bioactive conformation of selectin antagonists is offered by transfer NOE NMR spectroscopic techniques. This method is ideally suited for studying ligand–protein interactions with binding affinities in the micromolar to millimolar range,[3] affinities typical of selectin antagonists. Thus, the bioactive conformation of sialyl Lewis^X **1** was recently determined by transfer NOE NMR studies on the sialyl Lewis^X/E-selectin complex.[4] Here we describe the first bioactive conformation of a potent sialyl Lewis^X mimic (**2**, Scheme 1),[5] using the same technique. In

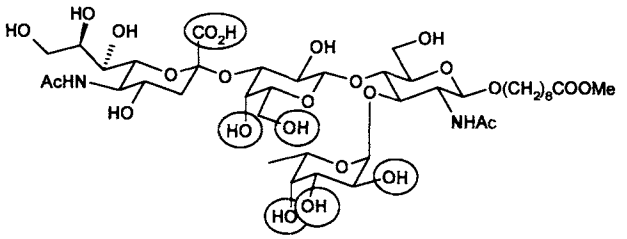

1

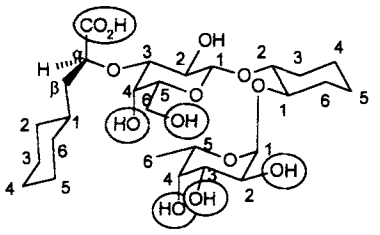

2

Scheme 1. Structures of sialyl Lewis^X **1** and the sialyl Lewis^X mimic **2** (with numbering schemes). Pharmacophores are highlighted with circles.

[*] Dr. W. Jahnke, Dr. H. C. Kolb, Dr. M. J. J. Blommers, Dr. B. Ernst
Novartis Pharma AG, CH-4002 Basel (Switzerland)
Fax: Int code + (61) 69-73704
e-mail: wolfgang.jahnke@pharma.novartis.com
Dr. J. L. Magnani
GlycoTech Corp., Rockville, MD 20850 (USA)

[**] We thank Prof. T. Peters (Medizinische Universität zu Lübeck, Germany) for valuable discussions and for the coordinates of bound sialyl Lewis^X, and Dr. T. Winkler (Novartis Agro) for stimulating discussions and expert advice.

 © WILEY-VCH Verlag GmbH, D-69451 Weinheim, 1997 0570-0833/97/3623-2603 $ 17.50+.50/0

our assays this mimic binds to E-selectin with an affinity that is more than ten times higher than that of sialyl Lewis^X (IC_{50} of **1**: 1.0–1.2 mM, of **2**: 0.10–0.11 mM).

The NMR resonances for the mimic **2** were assigned on the basis of two-dimensional ROESY, TOCSY, P.E.COSY, HSQC, and HSQC-TOCSY experiments. The latter two (involving the heteronucleus ^{13}C) were necessary for unambiguous assignment due to considerable overlap of resonances from the two cyclohexyl rings. The signals of the two diastereotopic exocyclic Hβ protons and (*S*)-cyclohexyllactic acid (Cyc-1) were individually assigned by analysis of homonuclear three-bond coupling constants from P.E.COSY, heteronuclear three-bond coupling constants from HMBC, and ROE intensities from ROESY. Table 1 lists the assignments for the ^1H and ^{13}C resonances for **2**.

Table 1. ^1H and ^{13}C chemical shifts of sialyl Lewis^X mimic **2** [a].

Position	Cyc-1	Gal	Cyc-2	Fuc
1	1.53 35.9	4.48 102.7	3.50 79.9	4.97 98.3
2	0.88(a) 1.77(e) 34.5	3.52 72.9	3.72 81.1	3.74 70.6
3	1.18(a) 1.66(e) 28.4	3.38 85.6	1.27(a) 2.09(e) 32.4	3.89 72.2
4	1.13(a) 1.58(e) 28.8	3.88 68.9	1.21(a) 1.68(e) 25.8	3.78 74.7
5	1.20(a) 1.63(e) 28.6	3.58 77.0	1.21(a) 1.67 25.8	4.60 69.2
6	0.93(a) 1.63(e) 31.8	3.71 64.2	1.24(a) 2.05(e) 31.8	1.18 18.0
COOH	– 185.5			
α	3.94 81.9			
β	1.51 (pro-*S*) 1.58 (pro-*R*) 43.9			

[a] At 25 °C in D_2O, 100 mM imidazole, pH = 7.4 (uncorrected). The upper numbers correspond to ^1H resonances, the lower numbers to ^{13}C resonances. All shifts are given relative to 3-(trimethylsilyl) 1-propanesulfonic acid (DSS). The symbol "a" refers to the axial protons, and "e" to the equatorial protons of the cyclohexyl rings of (*S*)-cyclohexyllactic acid (Cyc-1) or (1*R*,2*R*)-1,2-cyclohexanediol (Cyc-2).

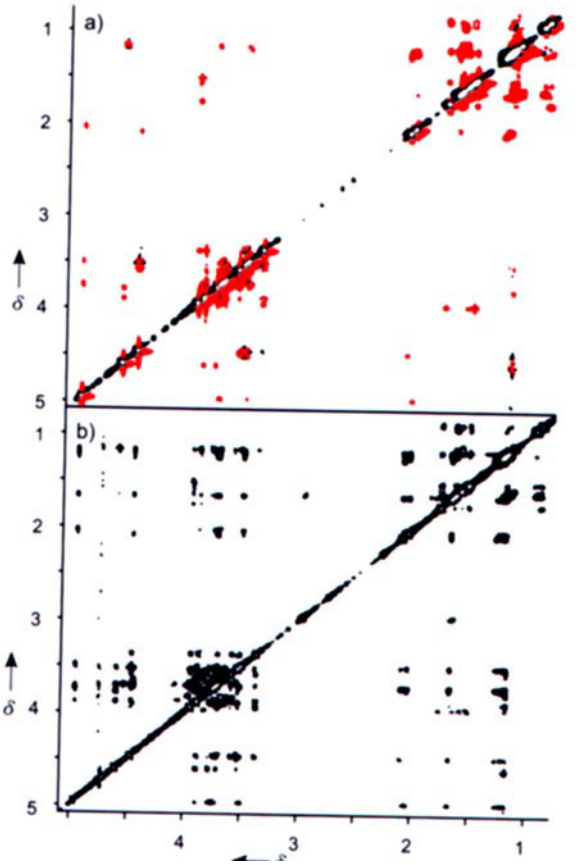

Figure 1. Two-dimensional NOESY spectra of a) free sialyl Lewis^X mimic **2** (17 mM) and b) **2** complexed to E-selectin (1.75 mM). Both spectra were acquired in the same buffer and at the same temperature (25 °C). The mixing time was 200 ms, and a $T_{1\rho}$ relaxation filter was used [6]. For experiment b) 35 μM E-selectin/IgG construct was added to yield an effective mixture of **2** to E-selectin in a ratio of 25:1.

The NOESY spectrum of unbound **2** shows weak positive NOEs (resulting in negative NOE cross-peaks, Figure 1a). When E-selectin is added, the NOESY spectrum measured with a $T_{1\rho}$ relaxation filter[6] displays intense negative NOEs. Therefore, all negative NOEs observed for the complexed mimic **2** can unambigously be attributed to transfer NOEs. This is in contrast to studies with sialyl Lewis^X **1**,[4c] for which negative NOEs were observed for both bound and unbound states. The opposite signs for NOEs measured for unbound **1** and **2** are caused by the different rates of molecular tumbling in solution, which results from their different molecular weights (**1**: M_r 991.0, **2**: M_r 578.6).

Transfer NOE spectra of the sialyl Lewis^X mimic **2** were recorded with mixing times of 25, 50, 80, 100, 150, 200, and 300 ms. In addition, a transfer ROESY spectrum was recorded with a mixing time of 80 ms. Transfer NOE intensities were extracted as cross-peak integrals and displayed as built-up curves. In total, built-up curves of 38 intramolecular distances were analyzed. On the basis of the built-up curves as well as the sign and intensities of the ROE, a total of 22 transfer NOEs were assigned as "direct NOEs", in which spin diffusion plays no dominant role. Those 22 NOEs were classified as strong, medium, or weak and translated into distances smaller than 3.5, 4.5, and 5.5 Å, respectively. Transfer NOEs that were clearly absent in transfer NOE spectra with mixing times shorter than 100 ms, and for which no NOE cross-peak was detected in the free ligand, were translated into distances larger than 4 Å. Table 2 lists the direct NOEs together with the corresponding distance constraints. These distance constraints are less rigorous than those resulting from the commonly used isolated spin pair approximation (ISPA).[7] Since the mimic **2** binds with an affinity that is more than ten times greater than that of the natural epitope sialyl Lewis^X **1**, ISPA-derived distance constraints would not give more accurate data. The large number of 22 distance constraints compensates for the lack of precision in the individual distance constraints and defines the resulting structures quite well. The structures were calculated with the distance geometry program DGII.

A superposition of 19 calculated structures of **2** bound to E-selectin is shown in Figure 2b. The position of the terminal cyclohexyl ring is not well defined, whereas the carboxylic acid clearly points out of the paper plane towards the observer. In the core the galactose and fucose ring systems,

 © WILEY-VCH Verlag GmbH, D-69451 Weinheim, 1997 0570-0833/97/3623-2604 $ 17.50+.50/0

Table 2. NOE distance constraints used for calculating structures of the bioactive conformation of sialyl Lewis^X mimic **2**[a].

	r_{min} [Å]	r_{max} [Å]
$H1^{Fuc}$-$He^{Cyc\text{-}2}$		3.5
$H1^{Fuc}$-$Ha^{Cyc\text{-}2}$		4.5
$H3^{Fuc}$-$H2^{Gal}$		4.5
$H4^{Fuc}$-$H2^{Gal}$		4.5
$H5^{Fuc}$-$H2^{Gal}$		3.5
$H5^{Fuc}$-$H6^{Gal}$		4.5
$H6^{Fuc}$-$H2^{Gal}$		4.5
$H2^{Cyc\text{-}2}$-$H1^{Gal}$		3.5
$He^{Cyc\text{-}2}$-$H1^{Gal}$		3.5
$Ha^{Cyc\text{-}2}$-$H1^{Gal}$		4.5
$H1^{Gal}$-$H\alpha^{Cyc\text{-}1}$		5.5
$H2^{Gal}$-$H\alpha^{Cyc\text{-}1}$		5.5
$H2^{Gal}$-$H1^{Cyc\text{-}1}$	4.0	
$H2^{Gal}$-$H\beta^{Cyc\text{-}1}$	4.0	
$H3^{Gal}$-$H\beta^{Cyc\text{-}1}$	4.0	
$H3^{Gal}$-$H\alpha^{Cyc\text{-}1}$		3.5
$H5^{Gal}$-$H\alpha^{Cyc\text{-}1}$		5.5
$He^{Cyc\text{-}1}$-$H\alpha^{Cyc\text{-}1}$		4.5
$Ha^{Cyc\text{-}1}$-$H4^{Gal}$	4.0	
$Ha^{Cyc\text{-}1}$-$H\alpha^{Cyc\text{-}1}$	4.0	

[a] Fuc = fucose, Gal = galactose; r_{min} = minimum distance, r_{max} = maximum distance. The two non-NOE constraints involving $H\beta^{Cyc\text{-}1}$ are applied to each of the β protons individually. If no lower limit is given, the limits are taken as the sum of the van der Waals radii.

which are linked by the (1*R*,2*R*)-1,2-cyclohexanediol spacer, are stacked. Figure 2c shows the same superposition from a slightly different angle. Here it can be seen that the Cα–C(O) bond vector of the (*S*)-cyclohexyllactic acid is rather well defined by the NMR data. Due to a lack of protons, however, the orientation of the oxygen atoms are not defined by the NMR data, and the carboxylic group appears to be freely rotatable.

A comparison of the bioactive conformations of **1** and **2** (Figures 2a and 2b) show that the core conformations of both bound sialyl Lewis^X **1**[4c] and bound mimic **2** are very similar. A characteristic feature of both compounds is the stacked arrangement of the core. The carboxylic group of *N*-acetylneuraminic acid and (*S*)-cyclohexyllactic acid also have the same orientation, whereas the residue of *N*-acetylneuraminic acid in **1** and the cyclohexyl ring in **2** clearly point in different directions.

The comparison of the bioactive conformations of **1** and **2** can be quantified by an internal coordinate plot (Figure 3). The core conformation, defined by the dihedral angle $C2^{NeuNAc}$-$O^{GlcNAc/Fuc}$-$C1^{Fuc}$-$C4^{Fuc}$, is plotted versus the orientation of the acid, defined by the dihedral angle $C1^{NeuNAc}$-$C2^{NeuNAc}$-$O^{GlcNAc/Fuc}$-$C1^{Fuc}$. In this internal coordinate system, the dihedral angle defining the core conformation of mimic **2** is $-36.4(5.8)^\circ$ and $-40.2(4.7)^\circ$ for **1**. The dihedral angle defining the acid orientation of mimic **2** is $120.5(16.1)^\circ$ and $110.7(9.0)^\circ$ for **1**. The bioactive conformations of both **1** and **2** thus occupy overlapping regions in the internal coordinate plots, and, consequently, are identical within experimental errors.

The presence of the carboxylic group is a prerequisite for biological activity.[8] Recent studies suggest that the bioactivity of a proposed mimic is related to its ability to present the carboxylic group in the required orientation.[5,8b] The results of this investigation clearly support this hypothesis by showing that the carboxylic group does indeed have the same orientation in the bioactive conformation of sialyl Lewis^X **1** and its mimic **2**. In summary, all the functional groups of **1** which are required for binding (see Scheme 1) are oriented very similarly in **2**. This suggests that both ligands have comparable binding modes.

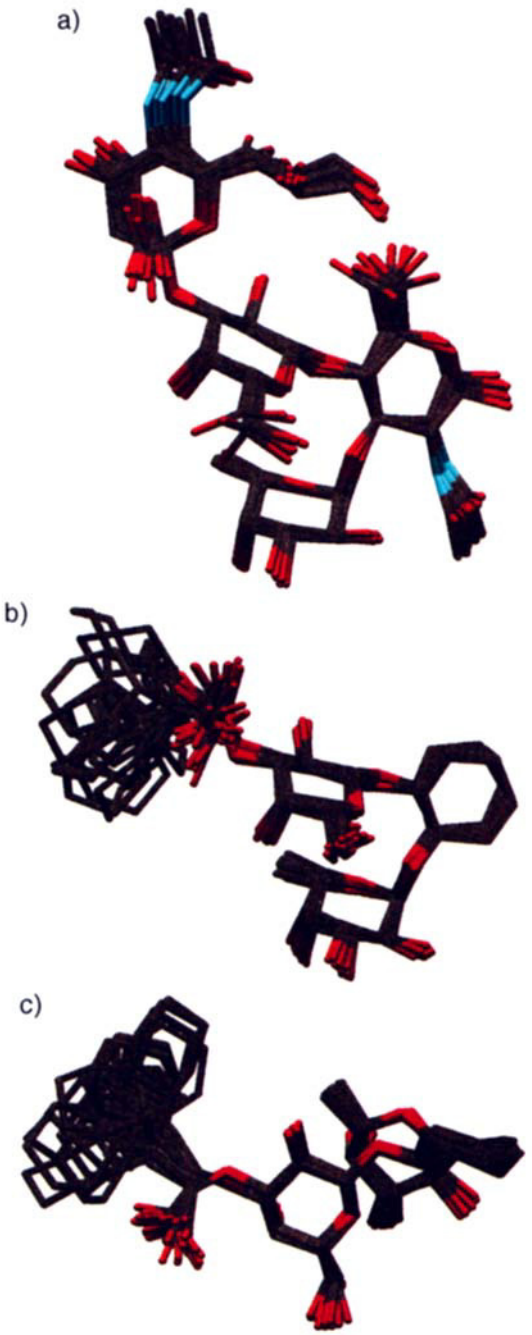

Figure 2. Bioactive conformations of E-selectin ligands: a) superposition of 10 structures of **1** bound to E-selectin [4c]; b) superposition of 19 distance geometry structures of **2** bound to E-selectin; c) portion b) viewed from a different angle.

Poorly defined parts of the structures determined by NMR spectroscopy, for example the orientation of the terminal cyclohexyl ring in the present study, can have two fundamentally different causes. First, "true" flexibility in the molecule and the corresponding decrease in correlation time of interproton vectors can lead to the absence of NOE cross-peaks, even if protons are close in space at least part of the time. Second, a lack of NOE cross-peaks simply caused by the absence of neighboring protons can produce apparent flexibility in structures calculated on the basis of NOE constraints, although the region may actually be rather rigid. In the case of mimic **2**, the observed lack of NOEs for the terminal ring would then simply result from the ring being extended,

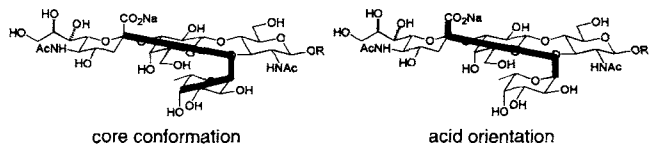

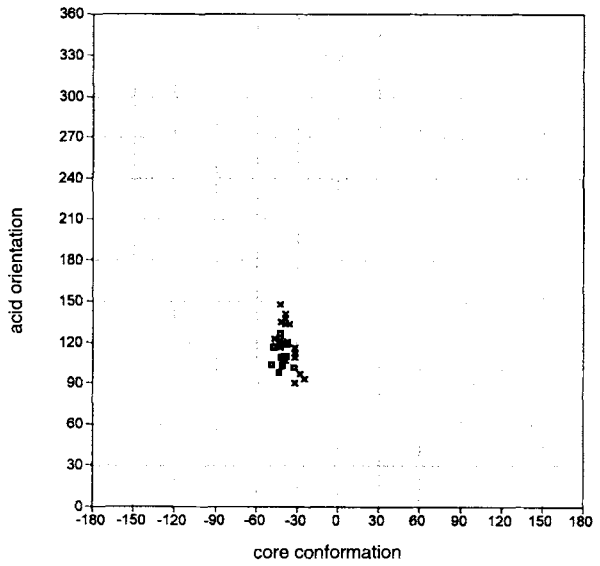

Figure 3. Internal coordinate plot [5] of the bioactive conformations of **1** (□) and **2** (×). See text for further details.

independent of flexibility. Thus, the two possibilities cannot be unequivocally distinguished for **2**. In principle the question could be resolved by measuring ^{13}C relaxation parameters and interpretating them in terms of motional models,[9] but such an analysis has not been carried out so far and seems rather challenging for *bound* sialyl Lewis^x. It should be emphasized that the disordered cyclohexyl ring does not necessarily reflect mobility in the bound form.

The rational design of sialyl Lewis^x mimics is crucially dependent on structural information of their complexes with E-selectin. Although no structure of an E-selectin/ligand complex has yet been reported, the X-ray structure of E-selectin[10] and the NMR structures of **1**[4] or **2** bound to E-selectin are now available. In addition, binding studies with sialyl Lewis^x analogues define functional groups involved in binding interactions with the receptor,[11] and point-mutation studies of E-selectin define the amino acid residues responsible for sialyl Lewis^x binding.[12] On the basis of these data, it is possible to develop a model for the E-selectin/sialyl Lewis^x complex which allows the rational design of more potent sialyl Lewis^x analogues.

Experimental Section

The ectodomains of human E-selectin were combined by means of the polymerase chain reaction (PCR) with the Fc region of human IgG1, and subcloned in the expression vector pcDNAI/neo (Invitrogen). Following transfection of CHO-K1 cells (ATCC CCL-61) and selection with G418 (Gibco), a stable cell line was obtained which secreted about 25 $\mu g\,mL^{-1}$ recombinant E-selectin/hIgG. To produce larger amounts, this cell line was cultivated in a hollow fiber bioreactor (1.1 m^2, 50 mL, Cellco) in Opti-MEM culture medium (Gibco) supplemented with 2% fetal-calf serum and 200 $mg\,mL^{-1}$ gentamycin. The supernatant of the conditioned cells was first purified by affinity chromatography on protein A/agarose (Sigma). The protein fraction obtained by elution with 20 mM glycine/HCl (pH = 3.0) was neutralized and purified by chromatography directly on an anti-human-E-selectin affinity column (2 mg monoclonal antibody 7A9 per milliliter affigel). Specifically bound E-selectin/IgG was eluted with 5 M urea in buffered salt solution and finally dialyzed against Dubeccos phosphate buffered saline (PBS) solution. The protein thus obtained showed, in sodium dodecyl sulfate (SDS) polyacrylamide gel electrophoresis under reducing conditions, a single band at about 140 kDa. For NMR spectroscopic analysis about 6 mg of E-selectin hIgG were dialysed against 100 mM perdeuterated imidazol (Sigma), 1 mM $CaCl_2$ (pH = 7.4) in D_2O and concentrated by means of Centricon YM-50 (Amicon) to a final volume of 0.5 mL.

IC_{50} values were determined with a standard ELISA assay using an E-selectin IgG and biotinylated polymer containing sLe^a. Wells in a microtiter plate (plate 1, Falcon probind) were coated with E-selectin/hIg chimera by incubation of 100 µL of the purified chimeric protein at a concentration of 200 ng/well in 50 mM Tris, 0.15 M NaCl, 2 mM $CaCl_2$ (pH = 7.4; Tris-Ca^{2+}). After 2 h 100 µL of a 1:1 mixture of 1% BSA in Tris-Ca^{2+} and Stabilcoat were added to each well and incubated at 22 °C to block nonspecific binding. During this incubation, inhibitory test compounds, diluted in Tris-Ca^{2+} and 1% BSA, were titrated by a twofold serial dilution in a second U-shaped bottom low-bind microtiter plate (plate 2, Costar). An equal volume of a preformed complex of a biotinylated sLe^a polymer and horseradish peroxidase labeled streptavidin (KPL, Gathersburg, MD, USA) at 1 $mg\,mL^{-1}$ in Tris-Ca^{2+} and 1% BSA was added to each well. After 2 h at 22 °C plate 1 was washed with Tris-Ca^{2+}, and 100 µL per well were transferred from plate 2 to plate 1. The binding reaction was allowed to proceed for 2 h at 22 °C while rocking. Plate 1 was then washed with Tris-Ca^{2+}, and 100 µL of 3,3′,5,5′-tetramethylbenzidine substrate (KPL, Gathersburg, MD, USA) was added to each well. After three minutes the colorimetric reaction was stopped by adding 100 µL of 1 M H_3PO_4 per well, and the optical density was determined at 450 nm.

All NMR experiments were carried out at 25 °C on a Varian UnityPlus 600 MHz spectrometer. Susceptibility-matched NMR tubes (Shigemi) were used with a sample volume of 220 µL. The sample contained 35 µM E-selectin construct and 1750 µM sialyl Lewis^x mimic **2** in 100 mM deuterated imidazole (pH = 7.4), 1 mM $CaCl_2$ in D_2O. Since each E-selectin/IgG molecule contains two binding sites for sialyl Lewis^x or mimics, the true ratio of protein to ligand was 1:25. NOESY spectra were acquired using a spin-lock filter [6] before t_1 of 20 ms duration and 9 kHz strength. A recycle time of 1.85 s was used. Spectra were acquired with 384 complex t_1 points and 32 transients per t_1 point.

Structures were calculated with the distance geometry program DGII (INSIGHTII, MSI) on a SGI workstation. As described in the text, 22 nontrivial distance constraints derived from NOE data were used. The sugar pucker of the four carbohydrate rings was determined by homonuclear and heteronuclear coupling constants for unbound **2**, and made plausible for bound **2** by analysis of NOE intensities in transfer NOE spectra. To fix the sugar puckers, 36 constraints between carbon atoms located within a distance of 3 Å in the same ring were used. Fifty structures were smoothed using triangle smoothing, and embedded in 4-D space. The structures were refined using 10000 steps of simulated annealing. During simulated annealing, the atomic mass was multiplied by a factor of 1000. The structures were finally minimized using 250 steps of conjugate gradient minimization. The sums of van der Waals radii were used as constraints. All other nonbonded interactions were excluded from the calculations to prevent possible bias induced by force-field parameters. Thus, the structural variations within the family of structures represents the measured data and is not simply a consequence of energy minimisation. A subset of 19 structures converged to conformations which satisfied all distance constraints as well as sugar pucker constraints within 0.05 Å. The average pairwise root mean square deviation (rmsd) was 0.25 Å for superposition of the fucose heavy atoms, galactose heavy atoms, (1*R*,2*R*)-1,2-cyclohexanediol (cyc-2) heavy atoms, and Cα–C(O) atoms of the (*S*)-cyclohexyllactic acid (cyc-1). For all heavy atoms, the average pairwise rmsd was 1.16 Å.

Received: May 20, 1997 [Z10449IE]
German version: *Angew. Chem.* **1997**, *109*, 2715–2719

Keywords: carbohydrates · NMR spectroscopy · sialyl Lewis^x

[1] a) S. R. Sharar, R. K. Winn, J. M. Harlan, *Springer Semin. Immunopathol.* **1995**, *16*, 359–378; b) F. Dasgupta, B. N. N. Rao, *Exp. Opin. Invest. Drugs* **1994**, *3*, 709–724; c) J. K. Welply, J. L. Keene, J. J. Schmuke, S. C. Howard, *Biochim. Biophys. Acta* **1994**, *1197*, 215–226; d) R. P. McEver, *Curr. Opin. Immunol.* **1994**, *6*, 75–84; e) S. D. Rosen, C. R. Bertozzi, *Curr. Opin. Cell Biol.* **1994**, *6*, 663–673.

[2] a) H. Ohmoto, K. Nakamura, T. Inoue, N. Kondo, Y. Inoue, K. Yoshino, H. Kondo, H. Ishida, M. Kiso, A. Hasegawa, *J. Med. Chem.* **1996**, *39*, 1339–1343; b) M. Yoshida, A. Uchimura, M. Kiso, A. Hasegawa, *Glycoconjugate J.* **1993**, *10*, 3–15; c) B. K. Brandley, M. Kiso, S. Abbas, P. Nikrad, O. Srivastava, C. Foxall, Y. Oda, A. Hasegawa, *Glycobiology* **1993**, *3*, 633–639; d) M. W. Cappi, W. J. Moree, L. Qiao, T. G. Marron, G. Weitz-Schmidt, C.-H. Wong, *Angew. Chem.* **1996**, *108*, 2501–2503; *Angew. Chem. Int. Ed. Engl.* **1996**, *35*, 2346–2348; e) G. Dekany, K. Wright, P. Ward, I. Toth, *J. Carbohydr. Chem.* **1996**, *15*, 383–398; f) C.-C. Lin, M. Shimazaki, M.-P.

 © WILEY-VCH Verlag GmbH, D-69451 Weinheim, 1997 0570-0833/97/3623-2606 $ 17.50+.50/0

Heck, S. Aoki, R. Wang, T. Kimura, H. Ritzèn, S. Takayama, S.-H. Wu, G. Weitz-Schmidt, C.-H. Wong, *J. Am. Chem. Soc.* **1996**, *118*, 6826–6840; g) J. C. Prodger, M. J. Bamford, M. I. Bird, P. M. Gore, D. S. Holmes, R. Priest, V. Saez, *Bioorg. Med. Chem.* **1996**, *4*, 793–801; h) S. Hanessian, H. Prabhanjan, *Synlett* **1994**, 868–870; i) B. Dupré, H. Bui, I. L. Scott, R. V. Market, K. M. Keller, P. J. Beck, T. P. Kogan, *Bioorg. Med. Chem. Lett.* **1996**, *6*, 569–572; k) J. Y. Ramphal, M. Hiroshige, B. Lou, J. J. Gaudino, M. Hayashi, S. M. Chen, L. C. Chiang, F. C. A. Gaeta, S. A. DeFrees, *J. Med. Chem.* **1996**, *39*, 1357–1360.

[3] a) G. M. Clore, A. M. Gronenborn, *J. Magn. Reson.* **1982**, *48*, 402–417; b) A. P. Campbell, B. D. Sykes, *Annu. Rev. Biophys. Biomol. Struct.* **1993**, *22*, 99–122; c) F. Ni, *Prog. Nucl. Magn. Reson. Spectrosc.* **1994**, *26*, 517–606.

[4] a) R. M. Cooke, R. S. Hale, S. G. Lister, G. Shah, M. P. Weir, *Biochemistry* **1994**, *33*, 10591–10596; b) P. Hensley, P. J. McDevitt, I. Brooks, J. J. Trill, J. A. Feild, D. E. McNulty, J. R. Connor, D. E. Griswold, N. V. Kumar, K. D. Kopple, S. A. Carr, B. J. Dalton, K. Johanson, *J. Biol. Chem.* **1994**, *269*, 23949–23958; c) K. Scheffler, B. Ernst, A. Katopodis, J. L. Magnani, W. T. Wang, R. Weisemann, T. Peters, *Angew. Chem.* **1995**, *107*, 2034–2037; *Angew. Chem. Int. Ed. Engl.* **1995**, *34*, 1841–1844.

[5] a) H. C. Kolb, B. Ernst, *Chem. Eur. J.* **1997**, *3*, 1571–1578; b) *Pure Appl. Chem.*, in press.

[6] T. Scherf, J. Anglister, *Biophys. J.* **1993**, *64*, 754–761.

[7] A. M. Gronenborn, G. M. Clore, *Prog. Nucl. Magn. Reson. Spectrosc.* **1985**, *17*, 1–32.

[8] a) C.-T. Yuen, A. M. Lawson, W. Chai, M. Larkin, M. S. Stoll, A. C. Stuart, F. X. Sullivan, T. J. Ahern, T. Feizi, *Biochemistry* **1992**, *31*, 9126–9131; b) G. Thoma, F. Schwarzenbach, R. O. Duthaler, *J. Org. Chem.* **1996**, *61*, 514–524.

[9] a) G. Lipari, A. Szabo, *J. Am. Chem. Soc.* **1982**, *104*, 4546–4559; b) R. Brüschweiler, D. Case, *Prog. Nucl. Magn. Reson. Spectrosc.* **1994**, *26*, 27–58.

[10] B. J. Graves, R. L. Crowther, C. Chandran, J. M. Rumberger, S. Li, K.-S. Huang, D. H. Presky, P. C. Familletti, B. A. Wolitzky, D. K. Burns, *Nature* **1994**, *367*, 532–538.

[11] a) J. Y. Ramphal, Z.-L. Zheng, C. Perez, L. E. Walker, S. A. DeFrees, F. C. A. Gaeta, *J. Med. Chem.* **1994**, *37*, 3459–3463; b) W. Stahl, U. Sprengard, G. Kretschmar, H. Kunz, *Angew. Chem.* **1994**, *106*, 2186–2188; *Angew. Chem. Int. Ed. Engl.* **1994**, *33*, 2096–2098; c) A. Hasegawa, M. Kato, T. Ando, H. Ishida, M. Kiso, *Carbohydr. Res.* **1995**, *274*, 165–181.

[12] a) D. V. Erbe, B. A. Wolitzy, L. G. Presta, C. R. Norton, R. J. Ramos, D. K. Burns, J. M. Rumberger, B. N. N. Rao, C. Foxall, B. K. Brandley, L. A. Lasky, *J. Cell Biol.* **1992**, *119*, 215–227; b) B. M. Revelle, D. Scott, T. P. Kogan, J. Zheng, P. J. Beck, *J. Biol. Chem.* **1996**, *271*, 4289–4297; c) B. M. Revelle, D. Scott, P. J. Beck, *ibid.* **1996**, *271*, 16160–16170.

Steric Stabilization of Nucleophilic Carbenes**

Michael K. Denk,* Avinash Thadani, Ken Hatano, and Alan J. Lough

After early studies by Wanzlick,[1] the chemistry of stable carbenes [1–7] underwent a revival in 1991 with the structural characterization of **1** (R = 1-adamantyl).[2] Stable carbenes such as **1** are now easily accessible and show a rich reaction chemistry.[2–4] Computational studies have confirmed that carbenes of type **1** possess aromatic stabilization.[5] The numerous aromatic carbenes **1** currently have only two nonaromatic counterparts, compounds **2**[6] and **3** (R = mesityl).[7] The isolation of the stable bis(diisopropylamino)carbene (**2**) by Alder et al.[6a] demonstrates for the first time that neither aromatic stabilization nor the constraints resulting from ring geometry are necessary to obtain stable diaminocarbenes. The dimerization of carbenes to olefins[8–11] can prevent their isolation but is thermodynamically unfavorable for carbenes **1**, as was shown by Taton and Chen.[11]

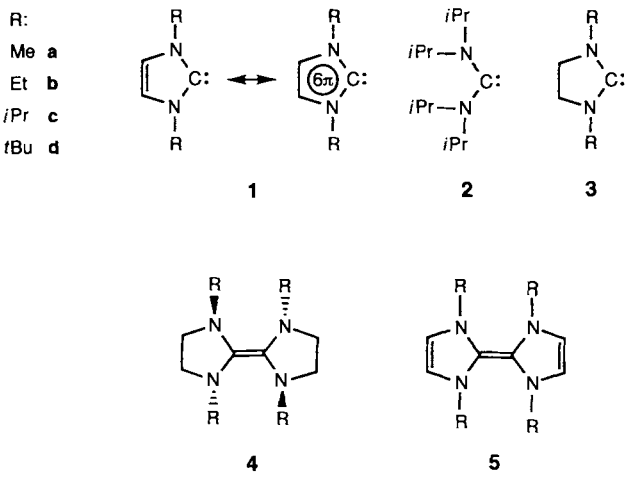

Following studies on stable silylenes,[12] germylenes,[13] and phosphenium cations[14] isostructural to **1** and **3**, we demonstrate herein that the successful isolation of carbenes **3** has kinetic reasons (in contrast with **1**) and is critically dependent on the bulk of the substituent R. The new carbenes **3a–3d**[6b] were obtained by reductive desulfurization from the corresponding thioureas[15] with potassium in boiling THF, a method used in the aromatic series (carbenes **1**) by Kuhn et al.[16] The analogous ureas are inert even after prolonged treatment with molten potassium. Carbene **3d**, the sterically most shielded carbene in this series, is a low-melting, colorless solid that distills without decomposition and is stable indefinitely under exclusion of air and moisture. For R = Me (**3a**), Et (**3b**), and *i*Pr (**3c**), the carbenes persist in solution but slowly dimerize to give the olefins **4a–4c**. Attempted distillation of the carbenes **3a–3c** (60 °C/0.1 Torr) yields the olefins as easily sublimable, air- and moisture-sensitive colorless solids. Compound **4a** was previously obtained by other methods[17,18] but has not been structurally characterized. The slow dimerization of **3a–3c** in solution suggests a substantial activation barrier. The dimerizations obey (^{1}H NMR) a second-order rate law and, accordingly, are concentration dependent.[19] The pure carbenes **3a–3c** dimerize within minutes, but frozen solutions of **3a–3c** in benzene can be stored indefinitely at −20 °C. Olefins of type **4** can fragment to give transition metal carbene complexes.[17] The dissociation of **4** to free carbenes **3** is of interest as a possible pathway for these reactions; however, high-temperature ^{1}H NMR spectra did not show any signs of this dissociation.[20]

The additional electronic stabilization in diaminocarbenes **1** is evident, for example, in that while **3c** dimerizes, the aromatic 4,5-dimethyl-substituted analogue of **1c** is stable.[21] Indeed, not a single carbene of type **1** has been observed to dimerize and olefins of type **5** require additional covalent bridging of the substituents R to be stable, as was shown by Taton and Chen.[11] The lack of aromatic stabilization in carbenes **3** is also shown by the deshiedling of the carbene-carbon atom ($\Delta\delta(^{13}C) \approx 30$ relative to those in **1**).[2–5,21]

A single-crystal X-ray structure analysis of **3d**[22] shows the two nitrogen atoms to be in nearly planar environments (sum of bond angles: N(1) 356°, N(2) 357°; see Figure 1). The valence angle at the carbene-carbon atom is significantly larger (106.44(9)°) than the N-Si-N and N-Ge-N angles of the

[*] Prof. Dr. M. K. Denk, A. Thadani, Dr. K. Hatano, Dr. A. Lough
University of Toronto, Department of Chemistry, Erindale College
3359 Mississauga Road North, Mississauga, Ontario L5L 1C6 (Canada)
Fax: Int. code +(905) 828-5335
e-mail: mdenk@credit.erin.utoronto.ca

[**] The authors thank Prof. Roger Alder (Bristol, UK) for important discussions and the communication of unpublished results [6b,19] and the Natural Sciences and Engineering Research Council of Canada (NSERC) and the Connaught Fund of the University of Toronto for support of this research.

 © WILEY-VCH Verlag GmbH, D-69451 Weinheim, 1997 0570-0833/97/3623-2607 $ 17.50+.50/0

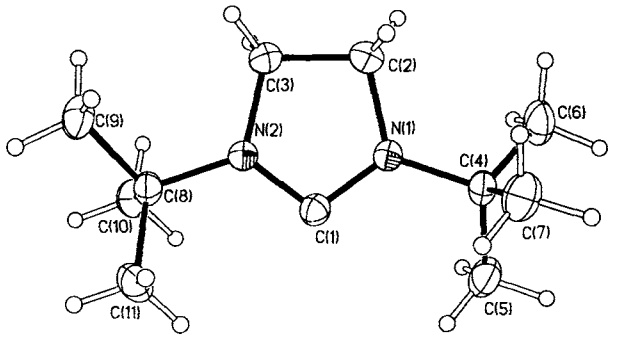

Figure 1. Molecular structure of **3d** in the solid state (ORTEP view, thermal ellipsoids are at the 50% probability level). Selected bond lengths [pm] and angles [°]: C(1)–N(1) 134.8(1), C(1)–N(2) 134.7(1), N(1)–C(2) 147.6(1), N(1)–C(4) 148.0(1), C(2)–C(3) 151.2(2), N(1)–C(1)-N(2) 106.44(9); C(1)-N(1)-C(2) 112.51(8), N(1)-C(2)-C(3) 101.34(9), C(4)-N(1)-C(2) 120.53(8), C(4)-N(1)-C(1) 123.10(8).

isostructural silylenes (95.4(1)[12] and germylenes 88.0(1).[13] The short C^{II}–N bond length (135 pm) indicates a partial double bond.

A comparison of the carbene **3d** with the olefin **4a** highlights characteristic changes in the five-membered C_2N_2C framework (Figure 1 and 2): the C–N bond lengths

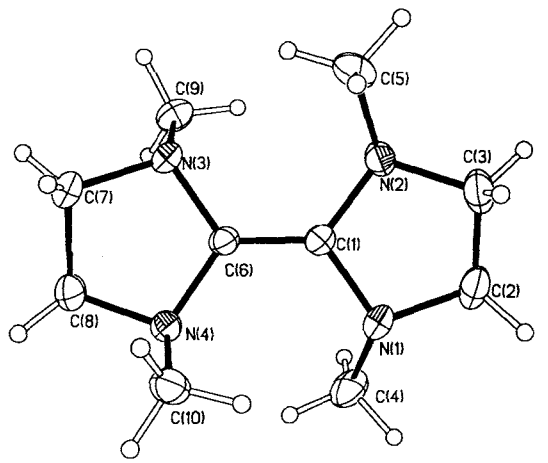

Figure 2. Molecular structure of **4a** (ORTEP view, thermal ellipsoids are at the 50% probability level). Selected bond lengths [pm], bond angles [°], and torsional angles [°]: C(1)–C(6) 134.94(11), N(1)–C(1) 142.05(11), N(2)–C(1) 141.77(11), N(3)–C(6) 143.63(11), N(4)–C(6) 144.30(10) N(2)–C(3) 146.34(12), C(3)–C(2) 150.7(2), N(4)–C(8) 147.20(11), C(8)–C(7) 152.54(14), C(7)–N(3) 147.02(12); N(1)-C(1)-N(2) 108.71(7), N(3)-C(6)-N(4) 111.29(7), N(3)-C(6)-C(1)-N(2) 5.94(13); N(3)-C(6)-C(1)-N(1) –173.57(7), N(4)-C(6)-C(1)-N(1) 8.01(13), N(4)-C(6)-C(1)-N(2) – 172.47(7).

increase from the carbene (**3d**: 135 pm) to the dimer (**4a**: 142–147 pm), and the nitrogen atoms pyramidalize (sum of the nitrogen bond angles in **4a**: 331–340°). The N-C-N bond angles of **3d** and **4a** are nearly identical. The twisting of the $N_2C{=}CN_2$ framework in **4a** (N-C-C-N torsional angles of 6 and 8°) is reproduced by calculations (AM1, MP4/6-31G*) both for **4a** and the unsubstituted derivative (R = H) and has, presumably, electronic rather than steric origins.

The structures of the open-chain carbene **2**[6] and the cyclic carbene **3d** show significant differences. The N-C-N bond angle in **3d** (106.44(9)°) is compressed compared to that in **2** (121.0(5)°) and the C^{II}–N bond length is shortened (134.8(3) pm in **3d**, 136.3(6) pm in **2**). The ^{13}C NMR shifts reflect the structural differences: the carbene–carbon atom in **3d** ($\delta = 238$) is strongly shielded compared to that in **2** ($\delta = 256$). We conclude that the ring geometry in carbenes **3** stabilizes the carbene (shortened C–N bond, shielded carbene signals) through an additional compression of the N-C-N valence angle. In support of our conclusion, diaminocarbenes and silylenes show decreased thermal stability if the ring size is increased from five (C_2N_2E:) to six (C_3N_2E:).[24]

Experimental Section

All operations were performed under argon (99.995%) with usual Schlenk techniques. The respective thiourea [15] (10 mmol), potassium (30 mmol), and THF (50 mL) were boiled under reflux for 30 min. After filtration and removal of the solvent under vacuum (–20 °C), the carbenes **3a**–**3c** were obtained as yellow, viscous oils. Distillation of **3d** (0.1 Torr, 120 °C oil bath) yielded the pure **3d** as a colorless, low-melting solid (m.p. 22–23 °C). Yields: quantitative for **3a**–**3c**, 85–95% for **3d**. Attempted distillation of **3a**–**3c** (0.1 Torr, 60 °C oilbath) led to sublimation of the olefins **4a**–**4c** as colorless, crystalline solids in quantitative yields. NMR data: C_6D_6, 20 °C,TMS.

3a: ^1H NMR: $\delta = 2.43$ (s, 2H; CH_2), 2.81 (s, 3H; CH_3); ^{13}C NMR: $\delta = 34.78$ (t, $^1J(C,H) = 145.7$ Hz; CH_2), 47.48 (q, $^1J(C,H) = 137.6$ Hz; CH_3), 239.8 (s; C:).

3b: ^1H NMR: $\delta = 1.06$ (t, $^3J(H,H) = 7.3$ Hz; CH_3), 2.93 (s; NCH_2), 3.41 (q, $^3J(H,H) = 7.3$ Hz; CH_2CH_3); ^{13}C NMR: $\delta = 12.05$ (q, $^1J(C,H) = 126.1$ Hz; CH_3), 42.17 (tq, $^1J(C,H) = 138.1$ Hz, $^2J(C,H) = 4.4$ Hz; CH_2CH_3), 45.00 (tt, $^1J(C,H) = 144.6$ Hz, $^2J(C,H) = 4.3$ Hz; NCH_2), 237.7 (s; C:).

3c: ^1H NMR: $\delta = 1.18$ (d, $^3J(H,H) = 6.6$ Hz; CH_3), 2.91 (s; CH_2), 3.92 (sept, $^3J(H,H) = 6.6$ Hz; CH); ^{13}C NMR: $\delta = 22.08$ (q, $^1J(C,H) = 124.9$ Hz; CH_3), 44.61 (t, $^1J(C,H) = 142.0$ Hz; CH_2), 50.53 (d, $^1J(C,H) = 136.7$ Hz; CH), 236.8 (s; C:).

3d: ^1H NMR: $\delta = 1.36$ (s; CH_3), 3.04 (s; CH_2); ^{13}C NMR: $\delta = 29.83$ (CH_3), 44.36 (CH_2), 55.68 ($C(CH_3)_3$), 238.25 (s; C:).

4a: ^1H NMR: $\delta = 2.62$ (s; CH_3), 2.76 (s; CH_2); ^{13}C NMR: $\delta = 40.21$ (q, $^1J(C,H) = 134.5$ Hz; CH_3), 52.70 (t, $^1J(C,H) = 139.7$ Hz; CH_2), 129.61 (C=).

4b: ^1H NMR: $\delta = 1.06$ (t, 7.5 Hz; CH_3), 2.80 (s; NCH_2), 3.05 (q, 7.5 Hz; CH_2CH_3); ^{13}C NMR: $\delta = 12.98$ (q, $^1J(C,H) = 124.8$ Hz; CH_3), 45.62 (t, $^1J(C,H) = 135.0$ Hz; CH_2), 49.08 (t, $^1J(C,H) = 139.2$ Hz; CH_2), 125.67 (s; C=).

4c: ^1H NMR: $\delta = 1.03$ (d, $^3J(H,H) = 6.6$ Hz; CH_3), 2.75 (s; CH_2), 4.12 (sept, $^3J(H,H) = 6.6$ Hz; CH); ^{13}C NMR: $\delta = 19.7$ (br.; CH_3), 46.4 (d, $^1J(C,H) = 139.9$ Hz; CH), 43.1 (t, $^1J(C,H) = 136.8$ Hz; CH_2), 124.3 (C=).

Received: May 13, 1997
Revised version: July 30, 1997 [Z10433IE]
German version: *Angew. Chem.* **1997**, *109*, 2719–2721

Keywords: carbenes · dimerizations · reductions · steric hindrance · thioureas

[1] a) H.-W. Wanzlick, E. Schikora, *Chem. Ber.* **1961**, *94*, 2389–2393; b) H.-W. Wanzlick, B. Lachmann, E. Schikora, *ibid.* **1965**, *98*, 3170–3177; c) H.-W. Wanzlick, H. J. Schönherr, *Angew. Chem.* **1968**, *80*, 153–154; *Angew. Chem. Int. Ed. Engl.* **1968**, *7*, 142. d) M. Regitz, *Methoden Org. Chem. (Houben-Weyl), 4th ed. 1952-, Vol. E19b.*

[2] a) A. J. Arduengo, R. L. Harlow, M. Kline, *J. Am. Chem. Soc.* **1991**, *113*, 361–363; b) A. J. Arduengo, H. V. Rasika-Dias, R. L. Harlow, M. Kline, *ibid.* **1992**, *114*, 5530–5534; c) A. J. Arduengo, H. V. Rasika-Dias, D. A. Dixon, R. L. Harlow, W. T. Klooster, T. F. Koetzle, *ibid.* **1994**, *116*, 6812–6822.

[3] W. A. Herrmann, L. J. Goossen, C. Köcher, G. J. Artus, *Angew. Chem.* **1996**, *108*, 2980–2982; *Angew. Chem. Int. Ed. Engl.* **1996**, *35*, 2805–2807.

[4] a) M. Regitz, *Angew. Chem.* **1991**, *103*, 691–693; *Angew. Chem. Int. Ed. Engl.* **1991**, *30*, 674–676; b) M. Regitz, *ibid.* **1996**, *108*, 791–794 and **1996**, *35*, 725–728.

[5] a) C. Boehme, G. Frenking, *J. Am. Chem. Soc.* **1996**, *118*, 2039–2046; b) C. Heinemann, T. Müller, Y. Apeloig, H. Schwartz, *ibid.* **1996**, *118*, 2023–2038.

[6] a) R. W. Alder, P. R. Allen, M. Murray, A. G. Orpen, *Angew. Chem.* **1996**, *108*, 1211–1213; *Angew. Chem. Int. Ed. Engl.* **1996**, *35*, 1121–1122. b) Carbene **3d** can also be obtained by deprotonation of the corresponding formamidinium salt (R. W. Alder, unpublished results).

[7] A. J. Arduengo, J. R. Goerlich, W. J. Marshall, *J. Am. Chem. Soc.* **1996**, *118*, 11027–11028.

[8] a) R. Hoffmann, R. Gleiter, F. B. Mallory, *J. Am. Chem. Soc.* **1970**, *92*, 1460–1466. b) K. Ohta, E. R. Davidson, K. Morokuma, *ibid.* **1985**, *107*, 3466–3471. See ref. [20].

 © WILEY-VCH Verlag GmbH, D-69451 Weinheim, 1997 0570-0833/97/3623-2608 $ 17.50+.50/0

[9] M. Driess, H. Grützmacher, *Angew. Chem.* **1996**, *108*, 900–929; *Angew. Chem. Int. Ed. Engl.* **1996**, *35*, 828–856.
[10] a) Z. Shi, V. Goulle, R. G. Thummel, *Tetrahedron Lett.* **1996**, *37*, 2357–2360; b) G. V. Tormos, M. G. Bakker, P. Wang, M. V. Lakshmikantham, M. P. Cava, R. M. Metzger, *J. Am. Chem. Soc.* **1995**, *117*, 8528–8535.
[11] T. A. Taton, P. Chen, *Angew. Chem.* **1996**, *108*, 1098–1100; *Angew. Chem. Int. Ed. Engl.* **1996**, *35*, 1011–1013.
[12] a) M. Denk, R. Lennon, R. Hayashi, R. West, A. V. Belyakov, H. P. Verne, A. Haaland, M. Wagner, N. Metzler, *J. Am. Chem. Soc.* **1994**, *116*, 2691–2692; b) M. Denk, R. K. Hayashi, R. West, *J. Chem. Soc. Chem. Commun.* **1994**, 33–34; c) M. Denk, J. Green, N. Metzler, M. Wagner, *J. Chem. Soc. Dalton Trans.* **1994**, 2405–2410; d) N. Metzler, M. Denk, *J. Chem. Soc. Chem. Commun.* **1996**, 2657–2658.
[13] W. A. Herrmann, M. Denk, J. Behm, W. Scherer, F.-R. Klingan, H. Bock, B. Solouki, M. Wagner, *Angew. Chem.* **1992**, *104*, 1489–1492; *Angew. Chem. Int. Ed. Engl.* **1992**, *31*, 1485–1488.
[14] M. K. Denk, S. Gupta, R. Ramachandran, *Tetrahedron Lett.* **1996**, *37*, 9025–9028.
[15] a) R. A. Donia, J. A. Shotton, L. O. Bentz, G. E. P. Smith, *J. Org. Chem.* **1949**, *14*, 946–951; b) C. Li, S. L. Mella, A. C. Sartorelli, *J. Med. Chem.* **1981**, *24*, 1089–1092.
[16] N. Kuhn, T. Kratz, *Synthesis* **1993**, 561–562.
[17] a) B. Çetinkaya, P. B. Hitchcock, M. F. Lappert, D. B. Shaw, K. Spyropoulos, N. J. W. Warhurst, *J. Organomet. Chem.* **1993**, *459*, 311–317; b) M. F. Lappert, *J. Organomet. Chem.* **1988**, *358*, 185–214.
[18] Reviews on enetetramines: N. Wiberg, *Angew. Chem.* **1968**, *80*, 809–833; *Angew. Chem. Int. Ed. Engl.* **1968**, *7*, 766–779; J. Hocker, R. Merten, *ibid.* **1972**, *84*, 1022; *Angew. Chem. Int. Ed. Engl.* **1972**, *11*, 964.
[19] Details will be published elsewhere. Different rate laws can be observed in the presence of protic impurities (R. W. Alder, personal communication).
[20] Earlier studies have ruled out the dissociation of olefins **4** into free carbenes: a) D. M. Lemal, R. A. Lovald, K. I. Kawano, *J. Am. Chem. Soc.* **1964**, *86*, 2518–2519. b) H. E. Winberg, J. E. Carnahan, D. D. Coffman, M. Brown, *ibid.* **1965**, *87*, 2055–2056.
[21] a) R. W. Alder, P. R. Allen, S. J. Williams, *J. Chem. Soc. Chem. Commun.* **1995**, 1267–1268; b) X.-W. Li, J. Su, G. H. Robinson, *J. Chem. Soc. Chem. Commun.* **1996**, 2683–2684.
[22] Crystal data for **3d**: $M_r = 182.31$, monoclinic, space group $P2_1/n$, $a = 6.2116(5)$, $b = 18.510(2)$, $c = 10.1210(9)$ Å, $\beta = 92.732(7)°$, $V = 1162.3(2)$ Å^3, $\rho_{calcd} = 1.042$ g cm^{-3}, $\mu(Mo_{K\alpha}) = 0.62$ cm^{-1}, $T = 173$ K, 3651 reflections collected ($3.0 < \theta < 30.0°$) and no absorption correction. Structure refined on F^2 and hydrogen atoms were refined with isotropic thermal parameters. Final $R1$ [$I > 2\sigma(I)$] = 0.0447 for 2698 observed reflections and w$R2$ (all data) = 0.1166 for 3383 independent reflections. Maximum and minimum peaks in final ΔF map were 0.31 and -0.26 e Å^{-3}. **4a**: $M_r = 196.30$, monoclinic, space group $P1$,$a = 7.731(3)$, $b = 8.100(2)$, $c = 9.912(2)$ Å, $\alpha = 96.74(2)$, $\beta = 99.37(2)$, $\gamma = 113.21(2)°$, $V = 551.5(2)$ Å^3, $\rho_{calcd} = 1.182$ g cm^{-3}, $\mu(Mo_{K\alpha}) = 0.75$ cm^{-1}, $T = 173$ K, 3395 reflections collected ($3.0 < \theta < 30.0°$) and no absorption correction. Structure refined on F^2 and hydrogen atoms in calculated positions. Final R_1 [$I > 2\sigma(I)$] = 0.0411 for 2342 observed reflections and wR_2 (all data) = 0.1209 for 3178 independent reflections. Maximum and minimum peaks in final ΔF map were 0.48 and -0.18 e Å^{-3}. Both structures were solved and refined by using SHELXTL/PC [23]. Crystallographic data (excluding structure factors) for **3d** and **4a** have been deposited with the Cambridge Crystallographic Data Centre as supplementary publication no. CCDC-100576. Copies of the data can be obtained free of charge on application to the Director, CCDC, 12 Union Road, Cambridge CB2 1EZ, UK (Fax: Int. Code +(1223) 336-033; e-mail: deposit@chemcrys.cam.ac.uk).
[23] G. M. Sheldrick, SHELXTL/PC V5.0, Program for Structure Solution and Refinement, Siemens Analytical X-ray Systems Inc. Madison, Wisconsin, USA, **1994**.
[24] M. Denk, results presented at the 80th Canadian Society for Chemistry Conference, Windsor, Ontario, June 1–4, **1997**.

Octaethyltetraselenaporphyrin Dication**

Emanuel Vogel,* Christoph Fröde, Andreas Breihan, Hans Schmickler, and Johann Lex

Dedicated to Professor Marianne Baudler on the occasion of her 75th birthday

The oxygen analogue of porphyrin, the D_{4h} symmetrical dication **1** (as its perchlorate),[1,2] constitutes a key compound in the chemistry of nonnatural porphyrins. There exists a close relationship between **1** and porphyrin, both in terms of their synthesis and their aromaticity, as evident from spectra and molecular structure. However, the two macrocycles differ markedly in their chemical properties. Unlike porphyrin and the neutral monooxa- and dioxaporphyrins,[3] **1** is no longer able to form complexes with metal ions because of its positive charge. Central to the chemistry of **1** are nucleophilic additions (and subsequent transformations) and the tetraoxaporphyrin redox system, which is derived from the dication and is interesting from many viewpoints.[4]

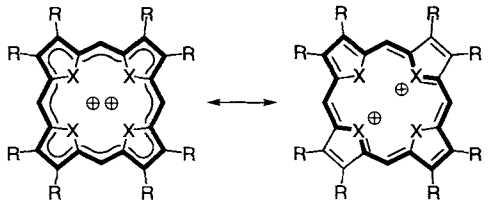

1–6

R=H **1**: X=O, **2**: X=S, **3**: X=Se (in solution only)
R=C_2H_5 **4**: X=O, **5**: X=S, **6**: X=Se

The recently synthesized tetrathiaporphyrin dication **2** (as its perchlorate)[5,6] and the tetraselenaporphyrin dication **3**,[5] which has until now only been obtained in solution, both resemble **1** in terms of their reactivity and spectral characteristics, even though the ring system deviates significantly from planarity because of the steric interactions of the heteroatoms. Since the study of **1**–**3** is adversely affected by problems associated with solubility and/or crystallization, it is sensible to follow the lead of porphyrin chemistry and turn to the octaethyl compounds **4**–**6**. After the syntheses of **4**[7] and **5**,[8] that of **6**, presented here, has also been achieved, and with it the set of chalcogenaporphyrins—with the exception of the tellura compound[9]—is now complete.

The 2-(hydroxymethyl)-3,4-diethylselenophene (**7**)[10] was chosen as the starting material in the synthesis of the octaethyltetraselenaporphyrin dication **6** (as its perchlorate). This would allow use of the route already proven in the synthesis of **1**, **4**, and **5**—the tetracyclocondensation to "porphyrinogen" and its oxidation with 2,3-dichloro-5,6-dicyano-1,4-benzoquinone (DDQ) with addition of $HClO_4$.

Treatment of **7** with one equivalent of *p*-toluene sulfonic acid in nitromethane at 80 °C (10 min) gave the expected octaethyltetraselenaporphyrinogen **8**, albeit only in small amounts. Analogous to the cyclocondensation of 2-(hydroxymethyl)-

[*] Prof. Dr. E. Vogel, Dr. C. Fröde, Dr. A. Breihan, Dr. H. Schmickler, Dr. J. Lex
Institut für Organische Chemie der Universität
Greinstrasse 4, D-50939 Köln (Germany)
Fax: Int. code +(221)470-5057

[**] We thank Prof. Dr. J. Hahn and Bruker Analytische Messtechnik GmbH, Karlsruhe for measuring the ^{77}Se NMR spectra.

 © WILEY-VCH Verlag GmbH, D-69451 Weinheim, 1997 0570-0833/97/3623-2609 $ 17.50+.50/0

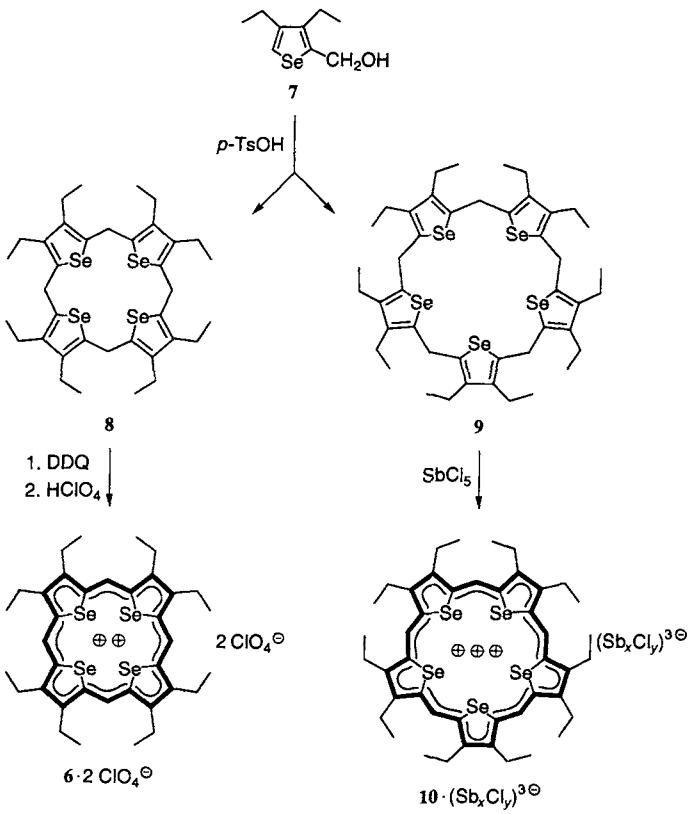

3,4-diethylthiophene,[8] the macrocycle **9**, which contains five selenophene units, was also formed. The complex reaction mixture was worked up conventionally in order to isolate the cyclocondensation products **8** and **9**. These were then further purified by chromatography using silica gel and *n*-hexane/dichloromethane (3/1). The first fraction contained several open-chain condensation products (all in less than 1% yield), after which **8** and **9** were eluted together.[11] It proved expedient to treat this fraction, after removal of the eluent, with *n*-hexane. This treatment left the major amount of **8** undissolved, and it could be filtered off. Chromatography of the filtrate with *n*-hexane/toluene (4/1), again on silica gel, finally allowed the remainder of **8** (first fraction) to be separated from **9**. Recrystallization of both compounds from ethanol yielded **8** as colorless needles (m.p. 220–222 °C) and **9** as an amorphous colorless powder (m.p. 130–132 °C, yield in each case 3%). The homologous compounds **8** and **9** could not be differentiated by NMR spectroscopy, and were thus assigned structurally on the basis of their mass spectra.

The tendency of **8** to form is very noticeably lower than that of its oxygen and sulfur analogues, which is probably due to the large increase in the angle between the exocyclic bonds at the α positions of the heterocycle (from 147° to 156°)[12] on going from thiophene to selenophene; such a change favors the formation of open-chain compounds. The helical effect[13] of the ethyl groups, to which the relatively high yields of porphyrinogens from 2-(hydroxymethyl)-3,4-diethylfuran and -thiophene is ascribed, evidently plays a negligible role in the case of **7**.

Oxidation of octaethyltetraselenaporphyrinogen (**8**) to give the octaethyltetraselenaporphyrin dication **6** (as its perchlorate) proceeded smoothly: **8** was heated to 80 °C in glacial acetic acid with DDQ (3 mol equiv) for 30 min and the reaction mixture was then treated with 70% perchloric acid (1:10 in HOAc; 5 mol equiv). Compound **6** was formed and separated upon cooling of the solution as a microcrystalline green powder. This was taken up in a small amount of trifluoroacetic acid, layered with three times the volume of acetic acid, and left to crystallize. After two days **6** had precipitated in the form of metallic green needles, which contained two equivalents of trifluoroacetic acid (material used for X-ray structure analysis). Heating the crystals to 50 °C under vacuum (0.01 Torr, 2 d) gave analytically pure **6** as a stable, very hydrolytically sensitive compound in 58% yield.

The ^{1}H NMR spectrum (CD_3NO_2) of **6** is very similar to the spectra of the oxygen and sulfur analogues **4** and **5**. In accord with the presence of an aromatic dicationic porphyrin, the singlet for the *meso*-protons (H_m) occurs at very low field (δ = 12.10, see Table 2). The slight high-field shift of the H_m signal in **6** compared to that in **5** ($\Delta\delta = 0.43$) most likely arises from the fact that the ring system in **6**, due to the larger van der Waals radius of the heteroatoms (S: 1.85 Å, Se: 2.0 Å), is more deformed than that in **5**. The ^{13}C NMR spectrum of **6**, which as expected contains five signals, corresponds well to that of the sulfur analogue. On the basis of Se–H coupling (^3J(Se,H_m) = 10.8 Hz), an inverse ^{1}H–^{77}Se NMR spectrum could be obtained, which indicated a chemical shift for the ^{77}Se nucleus of $\delta = 747$ (standard: $(CH_3)_2Se$). The UV/Vis spectrum of **6** in formic acid has a flattened maximum at 483 nm ($\varepsilon = 61\,800$), which can be interpreted as a bathochromically shifted Sôret band, but displays relatively high absorption ($\lambda = 700-800$ nm, $\varepsilon \approx 9000$) at longer wavelengths (in the Q band region); however, defined energy transitions cannot be recognized.

An X-ray crystallographic analysis of the octaethyltetraselenaporphyrin dication (**6**, as its perchlorate)[14] reveals that the molecule has a nonplanar ring conformation, as shown in Figure 1. In accordance with the established centrosymmetry of the dication, the four selenophene rings are twisted from the molecular plane (defined by the four *meso*-carbon atoms) in the sense of a *syn,syn,anti,anti* arrangement. The twist angles of the selenophene rings are 24.3° and 30.5°, respec-

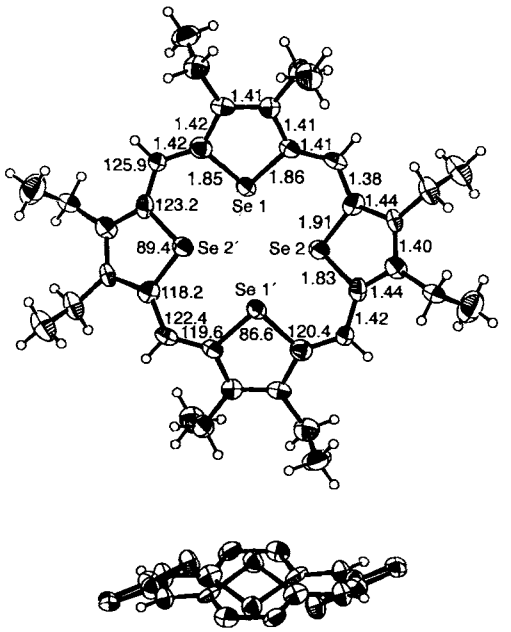

Figure 1. Structure of **6** in the crystal (top: plan view; bottom: side view; ethyl groups are omitted for clarity). Selected bond lengths [Å] and bond angles [°]; the vibrational ellipsoids represent 40% probability.

 © WILEY-VCH Verlag GmbH, D-69451 Weinheim, 1997 0570-0833/97/3623-2610 $ 17.50+.50/0

tively, and thus are significantly greater than those of the thiophene rings in the corresponding sulfur compound **5** (19°), which likewise exhibits centrosymmetry. The shortest Se···Se distance in **6** is 2.9 Å, that is more than 1 Å less than double the van der Waals radius of the selenium atom. The simplicity of the NMR spectra indicates that in solution **6** (like **5**) is a dynamic molecule, in which the hetero five-membered rings exchange sites rapidly by conformational processes.

The most remarkable chemical transformation of the dication **6** is its exhaustive reduction to the dianion **11**,[15] achieved by a potassium mirror in deuterated THF at −78 °C (complete conversion after two days with formation of a brown-red solution).[16] Whereas the sulfur compound **5** reacts under these conditions to give predominantly polymeric products, **6** amazingly accepts four electrons smoothly to give the aromatic dianion **11** with 22 π electrons. This was clearly identified by the ^{1}H NMR spectrum (analogous to that of **6**), the ^{13}C NMR spectrum (five signals), and the inverse ^{1}H–^{77}Se NMR spectrum (singlet, Table 1). That the signal of the *meso* protons of **11** is only shifted by $\Delta\delta = 1$ to higher field

Table 1. Characteristic NMR data for **6**[a] and **11**[b].

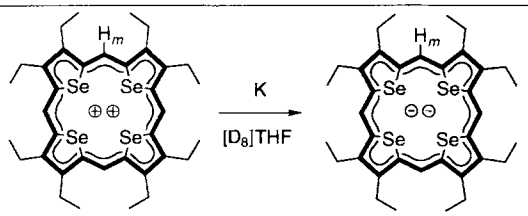

6 **11**

	6	**11**
δ H$_m$	12.10	11.03
δ C$_m$	138.21	107.45
δ Se	747 (^3J(Se,H$_m$) = 10.8 Hz)	586 (^3J(Se,H$_m$) = 14.9 Hz)

[a] ^{1}H-NMR 300 MHz, ^{13}C-NMR 75.5 MHz, ^{77}Se-NMR 57.2 MHz, CD_3NO_2. [b] ^{1}H-NMR 300 MHz, ^{13}C-NMR 75.5 MHz, ^{77}Se-NMR 76.3 MHz, [D$_8$]THF.

with respect to that of **6**, indicates that despite the negative charge on **11** strong deshielding is still prevalent. Thus the dianion maintains a pronounced diamagnetic ring current. On going from dication **6** to dianion **11** the center of ^{13}C resonances of the twenty perimeter carbon atoms is shifted to higher field by $\Delta\delta = 36$. This corresponds roughly to the value of 32, which is the value expected for **6** as derived from the empirical Spiesecke–Schneider correlation[17] between charge density and chemical shift in $(4n+2)\pi$-electron systems.[18]

The cyclocondensation product **9**, which contains five selenophene rings, should be capable of being oxidized[8] to the potentially aromatic 22π-electron decaethylpentaselenapentaphyrin trication (**10**). Thus **9** was treated with antimony(v) chloride in dichloromethane. A saltlike product was obtained (green needles with a metallic luster), whose cationic component was unambiguously shown to be the desired trication by NMR spectroscopy (Table 2). Isolation of **10** with a uniform counterion remains to be accomplished, since the anionic component of the oxidation product is a mixture of different chloroantimonate ions.

After the successful synthesis of cationic oxygen, sulfur, and selenium analogues of the porphyrins (the chalcogenaporphyrins with the exception of the tellurium compound), attention is now focussed on the fascinating neutral tetraphosphaporphyrins as the remaining synthetic challenge in the field of porphyrin derivatives, which are derived from the parent tetrapyrrolic macrocycle by substitution of the nitrogen atoms for other heteroatoms.

Table 2. Selected physical data for **6**–**14**[a].

6: ^{1}H NMR (CD_3NO_2): $\delta = 12.10$ (s, 4H; H$_m$), 4.16 (q, 16H; CH_2), 1.79 (t, 24H; CH_3); ^{13}C NMR (CD_3NO_2): $\delta = 173.39, 160.72, 138.21, 25.44, 17.74$; ^{77}Se NMR ($CD_3NO_2$): $\delta = 747$; MS (FAB): *m/z* (%): 793 (100) [$M^+ - 2\,ClO_4$]; IR (CsI): $\tilde{\nu}$= 2969, 2933, 2873, 1452, 1399, 1369, 1350, 1213, 1173, 1130, 1105, 1083, 625 cm^{-1}; UV/Vis (HCOOH): λ_{max} (ε) = 483 nm (61800), 700–800 (9000)

7: ^{1}H NMR ($CDCl_3$): $\delta = 7.45$ (s, 1H; H-5), 4.74 (s, 2H; H-2a), 2.90 (s, 1H; OH), 2.50 (q, 2H; H-3a), 2.48 (q, 2H; H-4a), 1.24 (t, 3H; H-4b), 1.07 (t, 3H; H-3b); ^{13}C-NMR ($CDCl_3$): $\delta = 146.10, 143.89, 141.25, 121.85, 59.86, 23.75, 21.10, 15.00, 13.44$; MS (GC-MS, EI, 70 eV): *m/z* (%): 218 (65) [M^+], 189 (45), 137 (100); IR (film): $\tilde{\nu}$= 3334, 2964, 2931, 2872, 1460, 1375, 1305, 1185, 1143, 1100, 1004, 924, 798, 782, 728 cm^{-1}; UV/Vis (CH_2Cl_2): λ_{max} (ε) = 257 nm (7400)

8: ^{1}H NMR ($CDCl_3$): $\delta = 4.05$ (s, 8H; H$_m$), 2.42 (q, 16H; CH_2), 1.06 (t, 24H; CH_3); ^{13}C NMR ($CDCl_3$): $\delta = 143.69, 140.50, 30.40, 21.61, 15.19$; ^{77}Se-NMR ($CH_2Cl_2$): $\delta = 600$; MS (FAB): *m/z* (%): 796 (5) [M^+], 307 (30). 154 (100), 137 (60); IR (KBr): $\tilde{\nu}$= 2959, 2928, 2899, 2868, 2822, 1462, 1445, 1374, 1307, 1280, 1115, 1047, 937 cm^{-1}; UV/Vis (CH_2Cl_2): λ_{max} (ε) = 258 nm (25400)

9: ^{1}H NMR ($CDCl_3$): $\delta = 4.14$ (s, 10H; H$_m$), 2.45 (q, 20H; CH_2), 1.08 (t, 30H; CH_3); ^{13}C NMR ($CDCl_3$): $\delta = 141.71, 140.60, 30.61, 21.68, 15.16$; MS (EI, 70 eV): *m/z* (%): 996 (60) [M^+], 967 (70), 201 (100); IR (KBr): $\tilde{\nu}$= 2962, 2928, 2869, 1451, 1375, 1311, 1293, 1119, 1048, 930 cm^{-1}; UV/Vis (CH_2Cl_2): λ_{max} (ε) = 257 nm (38900)

10: ^{1}H NMR (CD_3NO_2): $\delta = 14.78$ (s, 5H; H$_m$), 5.71 (q, 20H; CH_2), 2.56 (t, 30H; CH_3); ^{13}C NMR (CD_3NO_2): $\delta = 170.43, 162.93, 136.07, 28.37, 20.07$; MS (FAB): *m/z* (%): 991 (100) [M^+]; IR (CsI): $\tilde{\nu}$= 3526, 2968, 2930, 2870, 1521, 1473, 1448, 1419, 1373, 1308, 1256, 1183, 1110, 1052, 983, 925, 838 cm^{-1}; UV/Vis (CH_2Cl_2, 0.2% $SbCl_5$): λ_{max} = 551, 778, 856 nm (ε on the basis of mixed counterions, not exactly defined)

11: ^{1}H NMR ([D$_8$]THF): $\delta = 11.03$ (s, 4H; H$_m$), 4.01 (q, 16H; CH_2), 1.98 (t, 24H; CH_3); ^{13}C NMR ([D$_8$]THF): $\delta = 131.12, 126.08, 107.45, 24.48, 18.21$; ^{77}Se-NMR ([D$_8$]THF): $\delta = 586$

12[10]: ^{1}H NMR ($CDCl_3$): $\delta = 3.64$ (s, 6H; CH_3), 3.29 (s, 4H; CH_2); ^{13}C NMR ($CDCl_3$): $\delta = 171.07, 52.24, 23.14$; MS (EI, 70 eV): *m/z* (%): 226 (15) [M^+], 194 (35), 167 (15), 152 (10), 94 (15), 74 (20), 45 (100); IR (Film): $\tilde{\nu}$= 3003, 2953, 1733, 1437, 1409, 1270, 1109, 1010, 878, 770, 669 cm^{-1}; UV/Vis (CH_2Cl_2): λ_{max} (ε) = 242 nm (900)

13[10]: ^{1}H NMR (C_6D_6): $\delta = 3.30$ (s, 3H; $COOCH_3$), 2.90 (q, 2H; H-4a), 2.81 (q, 2H; H-3a), 1.15 (t, 3H; H-4b), 1.13 (t, 3H; H-3b); ^{13}C-NMR (C_6D_6): $\delta = 169.18, 163.25, 156.74, 155.29, 137.15, 134.84, 51.73, 22.75, 22.64, 14.92, 14.85$; MS (EI, 70 eV): *m/z* (%): 290 (100) [M^+], 275 (80), 257 (95), 91 (65); IR (KBr): $\tilde{\nu}$= 2982, 2875, 1715, 1680, 1653, 1541, 1277, 1264, 1249, 1229, 1153 cm^{-1}; UV/Vis (CH_2Cl_2): λ_{max} (ε) = 294 nm (13700)

14[10]: ^{1}H NMR ($CDCl_3$): $\delta = 7.72$ (s, 1H; H-5), 3.80 (s, 3H; $COOCH_3$), 2.93 (q, 2H; H-3a), 2.50 (q, 2H; H-4a), 1.23 (t, 3H; H-4b), 1.13 (t, 3H; H-3b); ^{13}C NMR ($CDCl_3$): $\delta = 163.96, 154.08, 147.40, 130.32, 129.79, 51.65, 23.63, 22.28, 14.17, 13.59$; MS (EI, 70 eV): *m/z* (%): 246 (100) [M^+], 231 (80), 215 (90), 91 (80); IR (film): $\tilde{\nu}$= 2968, 2874, 2837, 1709, 1547, 1452, 1383, 1309, 1233, 1189, 1167, 1112, 1088, 1059, 1023 cm^{-1}; UV/Vis (CH_2Cl_2): λ_{max} (ε) = 270 nm (10800)

[a] ^{1}H NMR 300 MHz, ^{13}C NMR 75.5 MHz, ^{77}Se NMR 57.2 or 76.3 MHz. Apart from **10** (mixture of chloroantimonate counterions) and **11** (generated in an NMR experiment), correct elemental analyses were obtained for all compounds.

Received: May 13, 1997 [Z10434IE]
German version: *Angew. Chem.* **1997**, *109*, 2722–2725

Keywords: aromaticity · heterocycles · macrocycles · porphyrinoids · selenium

[1] E. Vogel, W. Haas, B. Knipp, J. Lex, H. Schmickler, *Angew. Chem.* **1988**, *100*, 445; *Angew. Chem. Int. Ed. Engl.* **1988**, *27*, 406; W. Haas, B. Knipp, M. Sicken, J. Lex, E. Vogel, *ibid.* **1988**, *100*, 448 and **1988**, *27*, 409; for expanded tetraoxaporphyrin dications see: G. Märkl, H. Sauer, P. Kreitmeier, T. Burgemeister, F. Kastner, G. Adolin, H. Nöth, K. Polborn, *ibid.* **1994**, *106*, 1211 and **1994**, *33*, 1151; R. Bachmann, F. Gerson, C. Pütz, E. Vogel, *J. Chem. Soc. Perkin Trans. 2*, **1996**, 541.

[2] a) For mono- and dioxaporphyrins see: A. W. Johnson in *Porphyrins and Metalloporphyrins* (Ed.: K. M. Smith), Elsevier, Amsterdam, **1975**, p. 729; b) L. Latos-Grażyński, E. Pacholska, P. J. Chmielewski, M. M. Olmstead, A. L. Balch, *Angew. Chem.* **1995**, *107*, 2467; *Angew. Chem. Int. Ed. Engl.*

 © WILEY-VCH Verlag GmbH, D-69451 Weinheim, 1997 0570-0833/97/3623-2611 $ 17.50+.50/0

1995, *34*, 2252; c) dioxa-5-oxophlorins are described by T. D. Lash, Y. L. S.-T. Armiger, *J. Heterocycl. Chem.* **1991**, *28*, 965; T. D. Lash, *J. Org. Chem.* **1992**, *57*, 4312.

[3] Monooxa- and 21,23-dioxaporphyrins can form paramagnetic $Ni^{II}Cl$- and $Ni^{II}Cl_2$ complexes, respectively, with nickel chloride (the latter with pseudooctahedral coordination geometry): P. J. Chmielewski, L. Latos-Grażyński, M. M. Olmstead, A. L. Balch, *Chem. Eur. J.* **1997**, *3*, 268; Z. Gross, Technion, Haifa (Israel), personal communication.

[4] R. Bachmann, F. Gerson, G. Gescheidt, E. Vogel, *J. Am. Chem. Soc.* **1992**, *114*, 10855; E. Vogel, *Pure Appl. Chem.* **1993**, *65*, 143.

[5] E. Vogel, P. Röhrig, M. Sicken, B. Knipp, A. Herrmann, M. Pohl, H. Schmickler, J. Lex, *Angew. Chem.* **1989**, *101*, 1683; *Angew. Chem. Int. Ed. Engl.* **1989**, *28*, 1651.

[6] There are a number of reports on mono- and dithiaporphyrins as well as diselenaporphyrins: a) M. J. Broadhurst, R. Grigg, A. W. Johnson, *J. Chem. Soc. C* **1971**, 3681; b) A. Ulman, J. Manassen, *J. Am. Chem. Soc.* **1975**, *97*, 6540; c) A. Ulman, J. Manassen, F. Frolow, D. Rabinovich, *ibid.* **1979**, *101*, 7055; d) R. L. Hill, M. Gouterman, A. Ulman, *Inorg. Chem.* **1982**, *21*, 1450. For the coordination chemistry of monothia- and monoselenaporphyrins see: e) L. Latos-Grażyński, J. Lisowski, M. M. Olmstead, A. L. Balch, *J. Am. Chem. Soc.* **1987**, *109*, 4428; f) *Inorg. Chem.* **1989**, *28*, 1183; g) R. P. Pandian, T. K. Chandrashekar, *J. Chem. Soc. Dalton Trans.* **1993**, 119; h) M. Ravikanth, T. K. Chandrashekar, *Struct. Bonding (Berlin)* **1995**, *82*, 105; i) L. Latos-Grażyński, E. Pacholska, P. J. Chmielewski, M. M. Olmstead, A. L. Balch, *Inorg. Chem.* **1996**, *35*, 566; j) a monoselenasapphyrin was reported by J. Lisowski, J. L. Sessler, V. Lynch, *Inorg. Chem.* **1995**, *34*, 3567.

[7] E. Vogel, J. Dörr, A. Herrmann, J. Lex, H. Schmickler, P. Walgenbach, J. P. Gisselbrecht, M. Gross, *Angew. Chem.* **1993**, *105*, 1667; *Angew. Chem. Int. Ed. Engl.* **1993**, *32*, 1597.

[8] E. Vogel, M. Pohl, A. Herrmann, T. Wiß, C. König, J. Lex, M. Gross, J. P. Gisselbrecht, *Angew. Chem.* **1996**, *108*, 1677; *Angew. Chem. Int. Ed. Engl.* **1996**, *35*, 1520.

[9] Monotelluraporphyrins are already known, see refs. [2b] and [6c,i]. There should be no doubt as to the viability of the octaethyltetratelluraporphyrin dication, since octaethyl-*N,N',N'',N'''*-tetramethylporphyrin dication is both stable and aromatic, even though its ring skeleton is very strongly nonplanar.[5] Despite the advances in the chemistry of tellurium (see N. Petragnani, *Tellurium in Organic Syntheses*, Academic Press, London, **1994**), the synthetic route to the tellurium analogue of **4**, **5**, and **6** still appears to be strewn with difficulties.

[10] The new compound **7** can be obtained according to the following reaction scheme (in analogy to the corresponding thiophene [8]). For the preparation of the required **12** from Na_2Se and methyl chloroacetate see: H. Rheinboldt in *Methoden Org. Chem. (Houben-Weyl), 4th. ed. vol 9, p.* 976:

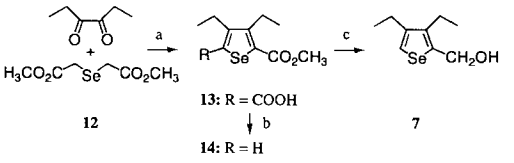

a) *t*BuOK in *t*BuOH, 1 h, 25 °C; crude **13** is sufficiently pure and is used directly; analytical sample: colorless crystals, m.p. 158 °C (*n*-hexane). b) Cu/ca. 300 °C, 0.5 h; **14** was purified by chromatography on silica gel, first with *n*-hexane (separation of diethylselenophene) then with *n*-hexane/ethyl acetate (5/1), and isolated in 38% yield; colorless crystals, m.p. 18 °C (from *n*-hexane). c) $LiAlH_4$ in THF, 1 h, 25 °C; **7** precipitated from *n*-hexane as a colorless, mother-of-pearl-like solid, m.p. 21 °C (yield 94%).

[11] The compounds **8** and **9** were identified on the basis of their characteristic violet color, which appeared on the thin layer chromatograms [*n*-hexane/toluene (4/1)] after treatment with nitric acid vapor (the color of the first fraction disappeared after a short time).

[12] Calculated from the relevant bond angles for thiophene and selenophene given in C. W. Bird, G. W. H. Cheeseman in *Comprehensive Heterocyclic Chemistry, Vol. 4, Part 3* (Eds.: A. R. Katritzky, C. W. Rees), Pergamon, Oxford, **1984**, p. 3.

[13] B. Franck, A. Nonn, K. Fuchs, M. Gosmann, *Liebigs Ann. Chem.* **1994**, 503; G. Bringmann, B. Franck, *ibid.* **1982**, 1272; see also L. F. Tietze, H. Geissler, *Angew. Chem.* **1993**, *105*, 1087; *Angew. Chem. Int. Ed. Engl.* **1993**, *32*, 1038.

[14] Crystal structure data for $\mathbf{6}\cdot 2\,CF_3COOH$: $C_{36}H_{44}Cl_2O_8Se_4\cdot 2\,CF_3COOH$, $M_r = 1219.51$, crystals from CH_3COOH/CF_3COOH (3/1); crystal dimensions $0.25\times0.18\times0.15$ mm^3, monoclinic, space group $P2_1/n$, $a = 7.9260(10)$, $b = 22.651(6)$, $c = 13.146(3)$ Å, $\beta = 98.12(2)^\circ$, $V = 2336.5(9)$ Å^3, $Z = 2$, $\rho_{calcd} = 1.733$ g cm^{-3}; $F(000) = 1212$; $\mu_{Mo} = 3.337$ mm^{-1}; 4536 measured reflections, 3854 independent, 2038 observed reflections ($F_o^2 > 2\sigma F_o^2$); $\theta_{max} = 25^\circ$; $R1 = 0.0940$, $wR2 = 0.1868$. Enraf-Nonius CAD4 diffractometer (room temperature, $Mo_{K\alpha}$ irradiation, $\lambda = 0.71069$ Å). The structure was solved by direct methods and refined with F^2 for all independent reflections (heavy atoms with anisotropic temperature factors, the positions of the H atoms were calculated); $wR2 = \{\sigma w(F_o^2 - F_c^2)^2/\sigma w(F_o^2)^2\}^{1/2}$. Programs used: MolEN (Enraf-Nonius) for structure determination and SHELXL-93 (G. M. Sheldrick, University of Göttingen) for refinement. Calculations were carried out at the Regionales Rechenzentrum der Universität Köln. The crystallographic data (excluding structure factors) for the structures reported in this paper have been deposited with the Cambridge Crystallographic Data Centre as supplementary publication no. CCDC-100418. Copies of the data can be obtained free of charge on application to The Director, CCDC, 12 Union Road, Cambridge, CB21EZ, UK (fax: Int code +(1223)336-033; e-mail: deposit@chemcrys.cam.ac.uk).

[15] Cyclovoltammetric studies on **6** indicate two reduction waves, which in terms of the electron transitions cannot be interpreted unambiguously because of the strong broadening.

[16] The reduction took place under an inert atmosphere in a reaction flask that was connected through a frit to a NMR tube.

[17] H. Spiesecke, W. G. Schneider, *Tetrahedron Lett.* **1961**, 468; B. Eliasson, U. Edlund, K. Müllen, *J. Chem. Soc. Perkin Trans. 2* **1986**, 937; G. A. Olah, G. D. Mateescu, *J. Am. Chem. Soc.* **1970**, *92*, 1430.

[18] The fairly good correlation of experimental and calculated $\Delta\delta$ values is astonishing, because the possibility that the heteroatoms in both **6** and **11** could carry charge was not taken into consideration.

Contracted Porphyrins: Octaethylisocorrole**

Emanuel Vogel,* Beate Binsack, Yvonne Hellwig, Christoph Erben, Andreas Heger, Johann Lex, and Yun-Dong Wu*

Dedicated to Sir Alan Battersby

The tetrapyrrolic aromatic macrocycle corrole **1**, pioneered in the 1960s by A. W. Johnson[1] (and related structurally to vitamin B_{12}[2] through corrin), is the prototype of the "contracted porphyrins". In analogy to porphyrin, compound **1** is distinguished by an 18 π main conjugation pathway, but has three internal NH hydrogen atoms, making it a potential trianionic ligand. As has been documented by publications from a series of research groups, **1** readily undergoes complexation to yield corrolates with numerous metal ions, in particular those of trivalent metals.[3] The ability of the corrole ligand to stabilize metal ions in higher oxidation states has recently been established.[4] This, along with the most recent synthesis of bis-corroles,[5] corrole heterodimers,[5] and *meso*-phenyl-substituted metallocorrolates[6] have all played a part in bringing the chemistry of corroles out of the shadows of porphyrin chemistry.

Starting from the conceptualization of structural isomers of porphyrin with N_4 coordination, four of which—porphycene, hemiporphycene, corrphycene, and isoporphycene—have already been synthesized,[7] it is a logical step to consider the possible existence of isomers of corrole. While porphyrin has no fewer than seven isomers, the absence of one *meso* unit reduces the possible number of isomers under discussion in the case of **1** to three: compounds **2**–**4**. These are given in Table 1 in order of their relative energies (with respect to **1**), calculated by the PM3 and BLYP/6-31G**//3-21G methods; the relative energies listed refer to the most stable NH tautomer.[7,8]

[*] Prof. Dr. E. Vogel, Dr. B. Binsack, Dr. Y. Hellwig, Dr. C. Erben, A. Heger, Dr. J. Lex
Institut für Organische Chemie der Universität
Greinstrasse 4, D-50939 Köln (Germany)
Fax: Int code + (221)470-5057
Prof. Dr. Y.-D. Wu
Department of Chemistry
The Hong Kong University of Science and Technology
Clear Water Bay, Kowloon, Hong Kong (China)
Fax: Int code + (2358)1594

[**] This work was funded by the Deutsche Forschungsgemeinschaft and the Fonds der Chemischen Industrie.

Table 1. Corrole **1** and its structural isomers **2**–**4**[a], arranged according to increasing relative energy [kcal mol^{-1}] with respect to **1**.

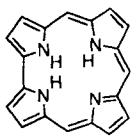	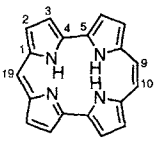	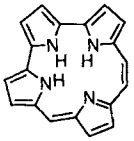	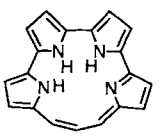
[18]Corrole-(1.1.1.0)	Corrole-(2.0.1.0)	Corrole-(2.1.0.0)	Corrole-(3.0.0.0)
Corrole	**Isocorrole**		
1	**2**	**3**	**4**
0.0	3.8	15.3	35.1
0.0	3.5	15.1	39.8

[a] In each case the most stable NH tautomer is shown. Top line: PM3, bottom line: BLYP/6-31G**//3-21G.

Amongst the corrole isomers, the most likely synthetic candidate appears to be the [18]corrole-(2.0.1.0) (**2**), which will be termed as isocorrole henceforth, since this has the advantage over the other possible isomers of being only 3.5–4 kcal mol^{-1} higher in energy than **1**. Having already obtained the isocorrole derivatives 19-formyl-3,6,13,16-tetrabromo-2,7,12,17-tetrapropylisocorrole[9] and 19-formyl-2,3,6,7,12,13,16,17-octaethylisocorrole[7] (unexpectedly), we are now able to report a rational synthesis of the 2,3,6,7,12,13,16,17-octaethylisocorrole (**8**), which can be considered as a model compound for isocorrole, and the 9-formyl derivative of **8**, that is, compound **11**. An entry to **8** on a preparative scale was offered by the McMurry reductive coupling of the tetrapyrrolic α,ω-dialdehyde **6**. Compound **6** was obtained by allowing the recently described tetrapyrrole **5**[10] to react with the Vilsmeier reagent dimethylformamide/phosphoryl trichloride (in a tenfold excess) in dichloromethane at room temperature (2 h). It was purified by column chromatography on aluminum oxide (activity III) with dichloromethane/ethyl acetate and recrystallized from toluene to give a green, microcrystalline powder with a metallic luster (m.p. 130–132 °C, yield 80%). As can be shown by 2D-NMR experiments, both **5** and **6**—analogous to the simple pyrromethenes[11]—are (*Z*) configured. Reductive coupling of **6** with low-valent titanium to afford **8** was performed similiarly to the method described for the preparation of porphycene from 5,5′-diformyl-2,2′-bipyrrole (see Experimental Section).[12] Since **8** thus formed was accompanied by a dihydroisocorrole, most likely compound **7**, the coupling product which, after conventional work-up, was present in ether, was treated with a solution of iron(III) chloride. Subsequent chromatography on neutral aluminum oxide with *n*-hexane/dichloromethane, followed by recrystallization from *n*-hexane/dichloromethane, gave the desired octaethylisocorrole **8** as violet rectangles with a metallic luster (m.p. 182–183 °C, yield 23%).

The tetrapyrrole **5** is similarly well suited as a starting material for the synthesis of a useful functionalized isocorrole, the 9-formyl-2,3,6,7,12,13,16,17-octaethylisocorrole (**11**), which is a regioisomer of the above-mentioned 19-formyl octaethylisocorrole. The route to **11** involves the conversion of **5** with a slight excess (1.5 equiv) of the vinylogous Vilsmeier reagent 3-(dimethylamino)acrolein (DMAA) and phosphoryl trichloride in dichloromethane, which leads predominantly to the amorphous monoaldehyde **9** (purity ca. 95%).[10] If the crude aldehyde is allowed to react with copper(II) acetate in methanol at room temperature, an unprecedented, probably template-controlled cyclization takes place, leading to the copper complex **10** (crystals of m.p. 174–176 °C, yield 52%),

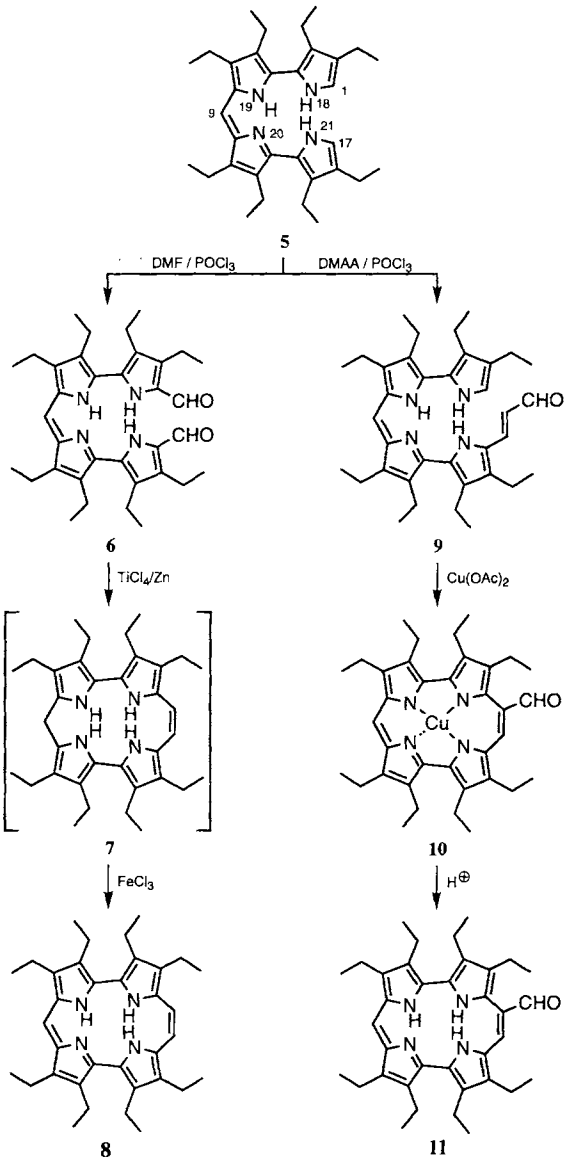

in which the metal ion is formally in the +3 oxidation state.[13] The complex was demetalated by reaction with concentrated sulfuric acid at room temperature, which liberated the free 9-formyl octaethylisocorrole **11** as a stable compound (m.p. 209–210 °C, yield 42%).

Octaethylisocorrole (**8**) is characterized by its spectra and molecular structure as an aromatic tetrapyrrolic macrocycle, closely related to its octaethylcorrole pendant. The ^{1}H NMR spectrum ($CDCl_3$, room temperature) of **8** displays the simple pattern (Table 2), expected on the basis of a rapid NH tautomerism, which increases the effective molecular symmetry: two singlets at $\delta = 8.76$ and 8.43 (for the perimeter protons H-19 and H-9,10 that are deshielded by the diamagnetic ring current), and four quartets and four triplets at $\delta =$ 3.63–3.49 and 1.61–1.47, respectively (methylene and methyl protons of the pairwise equivalent eight ethyl groups). The resonance of the NH protons required the temperature to be lowered to −50 °C before sufficiently sharp signals (singlets) were obtained; these lie at $\delta = 6.18$ (1H, shifted to low field by hydrogen bonding) and at $\delta = -1.20$ (2H). The assignments of the three NH protons to the four nitrogen atoms, along the lines of structural formula **8**—and therefore inverse in

 © WILEY-VCH Verlag GmbH, D-69451 Weinheim, 1997 0570-0833/97/3623-2613 $ 17.50+.50/0

comparison to the 19-formyl isocorrole[7,9]—were deduced from the ^{13}C resonances of rings A and D, which display low-field shifts typical of pyrrolenine units.

The UV/Vis spectrum of **8** is, like that of the octaethylcorrole, similar to those observed for the porphyrins (Figure 1, Table 2). It displays a Sôret band at $\lambda(\varepsilon) = 384$ nm (104900),

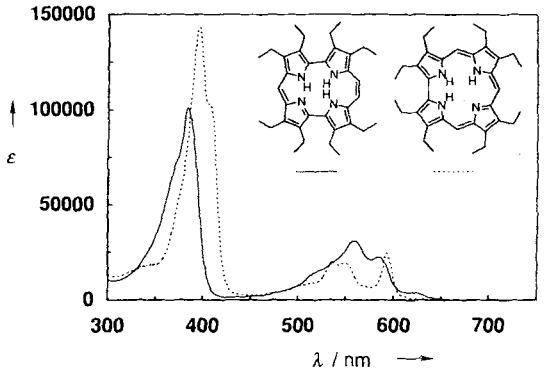

Figure 1. UV/Vis spectra of octaethylisocorrole (**8**) and octaethylcorrole (both in CH_2Cl_2).

Table 2. Selected physical data for the compounds **6**, **8**, **10**, and **11**[a].

6: M.p. 130–132 °C (toluene); ^1H NMR ($CDCl_3/Al_2O_3$, room temperature): $\delta =$ 11.80 (br. s, 1H; NH-19), 9.64 (s, 2H; CHO), 8.89 (br. s, 2H; NH-18,21), 6.83 (s, 1H; H-9), 2.75 (q, 4H; H-2a,16a), 2.64 (q, 4H; H-7a,11a), 2.60 (q, 4H; H-3a,15a), 2.54 (q, 4H; H-6a,12a), 1.25 (t, 6H; H-2b,16b), 1.22 (t, 6H; H-7b,11b), 1.10 (t, 6H; H-6b,12b), 0.92 (t, 6H; H-3b,15b); ^{13}C NMR ($CDCl_3$): $\delta = 177.10$ (CHO, $^1J(C,H) = 174$ Hz), 143.80, 141.79, 138.87, 137.52, 131.09, 130.04, 128.89, 127.88, 117.09 (C-9, $^1J(C,H) = 154$ Hz), 18.29, 17.88, 17.80, 17.53, 17.12, 16.96, 15.52, 15.34; MS (EI, 70 eV): *m/z* (%): 554 (100) $[M^+]$, 277 (54) $[M^{2+}]$; IR: $\tilde{\nu} = 3317$, 2966, 2932, 2871, 1628, 1599, 1459, 1413, 1374, 1317, 1281, 1227, 1197, 1010, 816, 770 cm^{-1}; UV/Vis: λ_{max} (ε) = 241 (18200), 284 (15900), 353 (25000), 532 nm (34000)

8: M.p. 182–183 °C (*n*-hexane/dichloromethane); ^1H NMR ($CDCl_3$, room temperature): $\delta = 8.76$ (s, 1H; H-19), 8.43 (s, 2H; H-9,10, $^3J(9,10) = 12.9$ Hz), 3.63 (q, 4H; H-6a,13a), 3.61 (q, 4H; H-3a,16a), 3.53 (q, 4H; H-2a,17a), 3.49 (q, 4H; H-7a,12a), 1.61 (t, 6H; H-2b,17b), 1.56 (t, 6H; H-3b,16b), 1.49 (t, 6H; H-6b,13b), 1.47 (t, 6H; H-7b,12b); ^1H NMR ($CDCl_3$, 223 K): 6.18 (br. s, 1H; NH-20), –1.20 (br. s, 2H; NH-21,22); ^{13}C NMR ($CDCl_3$): $\delta = 141.80$, 136.12, 131.02, 130.26, 128.80, 127.82, 124.08, 105.29 (C-9,10, $^1J(C,H) = 154$ Hz), 104.69 (C-19, $^1J(C,H) = 157$ Hz), 20.12, 19.92, 19.39, 19.02, 18.20, 17.53, 17.46, 17.30; MS (EI, 70 eV): *m/z* (%): 522 (100) $[M^+]$, 261 (43) $[M^{2+}]$; IR: $\tilde{\nu} = 3432$, 3364, 2964, 2930, 2869, 1521, 1463, 1375, 1343, 1276, 1181, 1108, 954 cm^{-1}; UV/Vis: λ_{max} (ε) = 250 nm (15700), 278 (16100), 372 sh (71600), 384 (104900), 523 sh (15400), 560 (30600), 585 (22300), 618 nm sh (4000)

10: M.p. 174–176 °C (dichloromethane/methanol); ^1H NMR ($CDCl_3$, 216 K): $\delta = 10.51$ (br. s, 1H; CHO), 7.47 (br. s, 1H; *meso*-CH, not assigned), 6.09 (br. s, 1H; *meso*-CH), 3.25 ($CH_2'CH_3$), 2.94 (CH_2CH_3), 1.31–1.22 (CH_2CH_3); ^1H NMR ($CDCl_3$, 309 K): $\delta = 10.49$ (br. s, 1H; CHO), 6.05 ($CH_2'CH_3$), 5.60 (br. s, 1H; *meso*-CH), 5.42–3.03 (CH_2CH_3), 1.59–0.84 (CH_2CH_3), –2.55 (br. s, 1H; *meso*-CH); MS (EI, 70 eV): *m/z* (%): 611 (8) $[(M+1)^+]$, 610 (6) $[M^+]$, 582 (35) $[(M-CO)^+]$; IR: $\tilde{\nu} = 2966$, 2931, 2871, 1662, 1565, 1471, 1372, 1280, 1195, 1145, 1129, 1055, 1019, 954 cm^{-1}; UV/Vis: λ_{max} (ε) = 286 (27500), 416 (54700), 557 nm (9800)

11: M.p. 209–210 °C (dichloromethane/*n*-hexane); ^1H NMR ($CDCl_3$): $\delta = 10.77$ (s, 1H; CHO), 8.78 (s, 1H; H-10), 8.72 (br. s, 1H; NH-20), 8.35 (s, 1H; H-19), 3.48 (q, 2H; H-13a), 3.45 (q, 2H; H-12a), 3.40 (q, 2H; H-3a), 3.36 (q, 2H; H-16a), 3.34 (q, 2H; H-2a), 3.28 (q, 2H; H-17a), 3.15 (q, 2H; H-6a), 2.97 (q, 2H; H-7a), 1.65 (br. s, 1H; NH-22), 1.55 (t, 3H; H-3b), 1.54 (t, 6H; H-2b,12b), 1.50 (t, 3H; H-17b), 1.48 (t, 3H; H-13b), 1.40 (t, 3H; H-16b), 1.26 (t, 3H; H-6b), 1.05 (t, 3H; H-7b), 0.61 (br. s, 1H; NH-21); ^{13}C NMR ($CDCl_3$): $\delta = 193.49$ (CHO, $^1J(C,H) = 175$ Hz), 143.50, 143.14, 139.51, 139.11, 139.04, 138.85, 136.36, 131.17, 130.49, 130.11, 128.44, 127.92, 126.24, 125.66, 124.70, 124.28, 116.01 (C-10, $^1J(C,H) = 150$ Hz), 115.81, 109.17 (C-19, $^1J(C,H) = 156$ Hz), 20.15, 19.78, 19.74, 19.50, 19.45, 19.22, 19.02, 18.77, 18.01, 17.92, 17.81, 17.32, 17.23, 16.77, 16.00, 15.94; MS (FAB): *m/z* (%): 551 (100) $[(M+1)^+]$; IR: $\tilde{\nu} = 3456$, 3198, 2967, 2930, 2869, 1649, 1559, 1540, 1468, 1429, 1272, 1207, 1182, 1130, 1112, 1051, 1015 cm^{-1}; UV/Vis: λ_{max} (ε) = 271 (14600), 295 (18300), 358 (17600), 413 (90000), 503 (5500), 541 (10700), 575 (16000), 614 nm (17100)

[a] ^1H NMR 300 MHz, ^{13}C NMR 75.5 MHz; IR: CsI; UV/Vis: CH_2Cl_2.

which, compared with that of the analogous corrole [396 nm (146000)], is slightly hypsochromically shifted, and also a series of Q bands at 520–620 nm. An X-ray crystallographic analysis[14] of **8** (Figure 2) indicates that the ring framework, as a consequence of the steric interactions of the imino-hydrogen atoms, deviates slightly more from planarity (maximum distance of the C and N atoms from the mean plane of the ring structure: ±0.38 Å) than that in 8,12-diethyl-2,3,7,13,17,18-hexamethylcorrole.[15] While the pyrrole rings

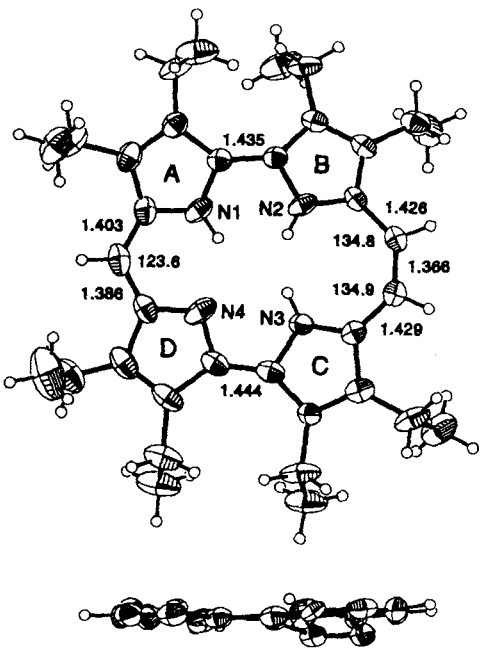

Figure 2. Structure of **8** in the crystal (top: plan view; bottom: side view, ethyl groups omitted for clarity). Vibrational ellipsoids (40% probability) and selected bond lengths [Å] and angles [°] (standard deviation ca. 0.008 Å and 0.5°, respectively). Selected distances [Å]: N1···N2 2.566, N1···N4 2.544, N2···N3 2.998, N3···N4 2.63.

A, C, and D, of which the rings A and D belong to a pyrromethene unit, are tilted from the mean plane by only 5–9°, ring B has a tilt angle of 18°. Interestingly, the imino-hydrogen atoms in **8** are not distributed, due to disorder, over the four nitrogen atoms, as is the case in the octaalkylcorroles mentioned earlier, but are localized on N1, N2, and N3, according to the molecular structure shown.

Isocorrole **2** has a coordination site, which—in a planar arrangement—is very similar to that of the parent compound **1**. In accordance with this, octaethylisocorrole (**8**) is capable of forming stable complexes with most of the metal ions that are known to give corrole complexes.[3] As is shown, particularly by the isolation of Co^{III}, Cu^{III}, Fe^{IV}, and Mn^{IV} isocorrolates[16,17] (these are still being investigated in part), **8** is a ligand that supplements the porphyrins, porphyrin isomers, and corroles as complex-forming tetrapyrrolic macrocyles.

Experimental Section

6: Anhydrous dimethylformamide (2.4 mL, 30 mmol) and freshly distilled phosphoryl trichloride (3.0 mL, 5.01 g, 33 mmol) in dichloromethane (15 mL) were added dropwise to a solution of tetrapyrrole **5** (1.5 g, 3 mmol) in dichloromethane (75 mL) at 0 °C, which caused the initially violet solution to gradually turn blue. This solution was stirred for a further 2 h, after which time the reaction

 © WILEY-VCH Verlag GmbH, D-69451 Weinheim, 1997 0570-0833/97/3623-2614 $ 17.50+.50/0 *Angew. Chem. Int. Ed. Engl.* **1997**, *36*, No. 23

mixture was carefully poured onto saturated potassium carbonate solution (300 mL)(with ice cooling), and worked-up conventionally. Subsequent chromatography of the product on aluminum oxide (activity grade III) (column: 25 × 3.5 cm) with dichloromethane/ethyl acetate (1/1) delivered a magenta major fraction, which contained the dialdehyde **6**. This precipitated from toluene as a green microcrystalline powder with a metallic luster; m.p. 130–132 °C; yield 1.33 g (80 %).

8: Zinc (7.8 g, 120 mmol) and copper(I) chloride (1.2 g, 12 mmol) were added to tetrahydrofuran (160 mL). This mixture was then treated with titanium tetrachloride (6.6 mL, 60 mmol) and heated to reflux for 2 h. Over the course of 20 min a solution of dialdehyde **6** (1.1 g, 2 mmol) in tetrahydrofuran (150 mL) was added dropwise and the reaction mixture was stirred at reflux for a further 5 min. Finally, the reaction mixture was hydrolyzed by pouring it into a 10 % aqueous ammonia solution (150 mL) at 0 °C, the product extracted into ether (multiple extraction of the residue with ether was necessary) and the washed ether solution was treated with 5 % iron(III) chloride solution. After chromatography on neutral alumina (activity grade III) (column: 25 × 3 cm) with *n*-hexane/dichloromethane (2/1), **8** was obtained as an intense red-orange fluorescent main fraction. Crystallization from *n*-hexane/dichloromethane gave **8** as violet, rectangular crystals with a metallic luster; m.p. 182–183 °C; yield 240 mg (23 %).

10: A solution of **9** (552 mg, 1 mmol) in methanol (100 mL) was treated with copper(II) acetate hydrate (1.0 g, 5 mmol) and the reaction mixture was stirred at room temperature for 1 h. After removal of the solvent in vacuum, the residue was purified by chromatography on silica gel (20 × 4 cm) with dichloromethane/*n*-hexane (2/1), from which minor (violet and brown) fractions were obtained. Change of the eluent to dichloromethane yielded the major fraction (brown), which contained the copper complex **10**. Crystallization from methanol/dichloromethane (6/1) delivered **10** as black needles; m.p. 174–176 °C; yield 318 mg (52 %).

11: Copper complex **10** (611 mg, 1 mmol) was treated, with stirring, with concentrated sulfuric acid (50 mL) at room temperature. Subsequently, the reaction mixture was poured onto ice (200 g), the product was extracted into dichloromethane, and the organic phase was washed with dilute ammonia solution. The residue formed after the usual work-up was purified by chromatography on silica gel (20 × 4 cm) with dichloromethane/*n*-hexane (2/1). The first fraction to elute was the unchanged copper complex. After changing the eluent to dichloromethane a second fraction was obtained, which was blue and contained **11**. Crystallization from *n*-hexane/dichloromethane (5/1) yielded **11** as red needles; m.p. 209–210 °C; yield 231 mg (42 %).

Received: May 13, 1997 [Z10435IE]
German version: *Angew. Chem.* **1997**, *109*, 2725–2728

Keywords: copper · isocorrole · McMurry reaction · N ligands · porphyrinoids

[1] A. W. Johnson, *Pure Appl. Chem.* **1971**, *28*, 195; R. Grigg in *The Porphyrins*, *Vol. II* (Ed.: D. Dolphin), Academic Press, New York, **1978**, p. 327.

[2] a) A. Eschenmoser, *Angew. Chem.* **1988**, *100*, 5; *Angew. Chem. Int. Ed. Engl.* **1988**, *27*, 5; b) A. I. Scott, *ibid.* **1993**, *105*, 1281 and **1993**, *32*, 1223; c) F. Blanche, B. Cameron, J. Crouzet, L. Debussche, D. Thibaut, M. Vuilhorgne, F. J. Leeper, A. R. Battersby, *ibid.* **1995**, *107*, 421 and **1995**, *34*, 383; d) B. Kräutler, C. Kratky, *ibid.* **1996**, *108*, 179 and **1996**, *35*, 167.

[3] For metal complexes of corroles see the excellent review by S. Licoccia, R. Paolesse, *Struct. Bonding (Berlin)* **1995**, *84*, 71.

[4] a) E. Vogel, S. Will, A. Schulze Tilling, L. Neumann, J. Lex, E. Bill, A. X. Trautwein, K. Wieghardt, *Angew. Chem.* **1994**, *106*, 771; *Angew. Chem. Int. Ed. Engl.* **1994**, *33*, 731; b) E. Van Caemelbecke, S. Will, M. Autret, V. A. Adamian, J. Lex, J.-P. Gisselbrecht, M. Gross, E. Vogel, K. M. Kadish, *Inorg.Chem.* **1996**, *35*, 184; c) S. Will, J. Lex, E. Vogel, H. Schmickler, J.-P. Gisselbrecht, C. Haubtmann, M. Bernard, M. Gross, *Angew. Chem.* **1997**, *109*, 367; *Angew. Chem. Int. Ed. Engl.* **1997**, *36*, 357.

[5] R. Paolesse, R. K. Pandey, T. P. Forsyth, L. Jaquinod, K. R. Gerzevske, D. J. Nurco, M. O. Senge, S. Licoccia, T. Boschi, K. M. Smith, *J. Am. Chem. Soc.* **1996**, *118*, 3869.

[6] R. Paolesse, S. Licoccia, G. Bandoli, A. Dolmella, T. Boschi, *Inorg. Chem.* **1994**, *33*, 1171.

[7] Review on porphyrin isomers and their metal complexes: E. Vogel, *J. Heterocycl. Chem.* **1996**, *33*, 1461. The [18]porphyrin-(3.0.1.0), designated as isoporphycene, was recently synthesized, as the octaethyl compound, via the corresponding nickel complex. While Ni^{II}-octaethylporphycenate displays the (*Z*) configuration, the free octaethylisoporphycene ligand has an (*E*) configuration both in solution and in the crystal: E. Vogel, M. Bröring, R. Demuth, C. Erben, P. Scholz, unpublished results.

[8] Calculations of the corrole isomers were carried out independently of ourselves by A. Ghosh and K. Jynge. The method used by these authors (LDF) produced relative stabilities for the isomers that correspond qualitatively with those reported here. We thank Prof. A. Ghosh, University of Tromsø (Norway) for sending us his manuscript.

[9] S. Will, A. Rahbar, H. Schmickler, J. Lex, E. Vogel, *Angew. Chem.* **1990**, *102*, 1434; *Angew. Chem. Int. Ed. Engl.* **1990**, *29*, 1390.

[10] E. Vogel, M. Bröring, C. Erben, R. Demuth, J. Lex, M. Nendel, K. N. Houk, *Angew. Chem.* **1997**, *109*, 363; *Angew. Chem. Int. Ed. Engl.* **1997**, *36*, 353.

[11] H. Falk, *The Chemistry of Linear Oligopyrroles and Bile Pigments*, Springer, Vienna, **1989**, p. 115.

[12] E. Vogel, P. Koch, X.-L. Hou, J. Lex, M. Lausmann, M. Kisters, M. A. Aukauloo, P. Richard, R. Guilard, *Angew. Chem.* **1993**, *105*, 1670; *Angew. Chem. Int. Ed. Engl.* **1993**, *32*, 1600.

[13] The copper complex **10**, which, in agreement with the presence of Cu^{III}, is diamagnetic, has a reasonably well resolved ^1H NMR spectrum at −57 °C. At higher temperatures, line broadening occurs—an indication of developing paramagnetism. Simultaneously the signals for the peripheral vinylic protons shift to higher field, and that of the protons of a CH_2 group shift to lower field (Table 2). Such a temperature dependence of the ^1H NMR spectrum may be due to a rapid equilibrium (on the NMR time scale) between molecules in the diamagnetic Cu^{III} ground state and others in a higher, excited, triplet (paramagnetic) state [4c]. A crystal structure analysis of **10** shows that the aldehyde group is disordered, but it can be definitely stated that the copper isocorrolate ring system is almost planar.

[14] Crystal structure data for **8**: $C_{35}H_{46}N_4 \cdot 0.5\ C_6H_6$, $M_r = 561.81$; crystals from benzene; crystal dimensions 0.35 × 0.30 × 0.30 mm; triclinic, space group $P\bar{1}$, $a = 12.117(3)$, $b = 12.961(3)$, $c = 13.373(3)$ Å, $\alpha = 64.71(2)$, $\beta = 63.02(2)$, $\gamma = 66.79(2)°$, $V = 1525.0(7)$ Å^3, $Z = 2$, $\rho_{calcd} = 1.138$ g cm^{-3}; $F(000) = 610$; $\mu_{Mo} = 0.67$ cm^{-1}; 5712 measured reflections; 4380 observed reflections. ($F_o^2 > 2\sigma F_o^2$); $\theta_{max} = 27°$; $R = 0.044$, $R_w = 0.052$. Enraf-Nonius CAD4 diffractometer (room temperature, $Mo_{K\alpha}$ radiation $\lambda = 0.71069$ Å). The structure was solved by using direct methods and subsequently refined (heavy atoms with anisotropic, H atoms with isotropic temperature factors). The calculations were carried out on a pdp-11/23-plus microcalculator using MolEN (Enraf-Nonius). The crystallographic data (excluding structure factors) for the structures reported in this paper have been deposited with the Cambridge Crystallographic Data Centre as supplementary publication no. CCDC-100426. Copies of the data can be obtained free of charge on application to The Director, CCDC, 12 Union road, Cambridge, CB2 1EZ, UK (fax: Int code + (1223)336-033; e-mail deposit@chemcrys.cam.ac.uk).

[15] H. R. Harrison, O. J. R. Hodder, D. Crowfoot Hodgkin, *J. Chem. Soc. B* **1971**, 640.

[16] Unpublished experiments with B. Binsack, S. Will, and C. Erben.

[17] The properties of the mono- and dinuclear Fe^{IV} isocorrolates correspond generally to those of the related Fe^{IV} corrolate pendants [4a]. However, due to disordered crystals more precise X-ray crystallographic data on these complexes are not available presently.

Twofold C–C Single Bond Activation and Cleavage in the Reaction of Octatetraynes with Titanocene and Zirconocene Complexes**

Paul-Michael Pellny, Normen Peulecke, Vladimir V. Burlakov, Annegret Tillack, Wolfgang Baumann, Anke Spannenberg, Rhett Kempe, and Uwe Rosenthal*

Dedicated to Professor Jörg Lorberth on the occasion of his 60th birthday

The synthesis of novel carbon modifications is an intensely researched area in modern acetylene chemistry.[1] Organometallic derivatives of carbon-rich polymers with conjugated π systems[2] have gained particular significance since they have facilitated the synthesis of various carbon networks, which form the basis for high-grade materials in the field of material science. We were interested in the interaction of

[*] Prof. Dr. U. Rosenthal, Dipl.-Ing. P.-M. Pellny, Dipl.-Chem. N. Peulecke, Dr. A. Tillack, Dr. W. Baumann, Dr. A. Spannenberg, Dr. R. Kempe
Abteilung Komplexkatalyse, Institut für Organische Katalyseforschung an der Universität Rostock e. V.
Buchbinderstrasse 5–6, D-18055 Rostock (Germany)
Fax: Int. code + (381) 4669386
e-mail: urosen@chemie1.uni-rostock.de

Dr. V. V. Burlakov
Institute for Organoelement Compounds of the Russian Academy of Sciences, Moscow

[**] This work was suported by the Max-Planck-Gesellschaft and the Fonds der Chemischen Industrie.

"carbyne" $(-C\equiv C-)_n$, the simplest carbon modification, with selected transition metal complexes. Since these polyalkyne carbon rods are difficult to investigate,[3] we turned our attention to the "smaller homologues", namely the butadiynes $R(-C\equiv C-)_2R$[4] and the octatetraynes $R(-C\equiv C-)_4R$, and herein report on the results of reactions of the latter with titanocene and zirconocene sources. The products obtained are highly dependent on the substituents R attached to the tetrayne and on the stoichiometry of the reaction.

The reaction of bis(trimethylsilyl)octatetrayne (**1**) with two equivalents of the $[Cp_2Ti]$ complex **2**, which readily releases bis(trimethylsilyl)acetylene and thus is a superb preparative source for the unstable titanocene "$[Cp_2Ti]$",[4] gave the dark

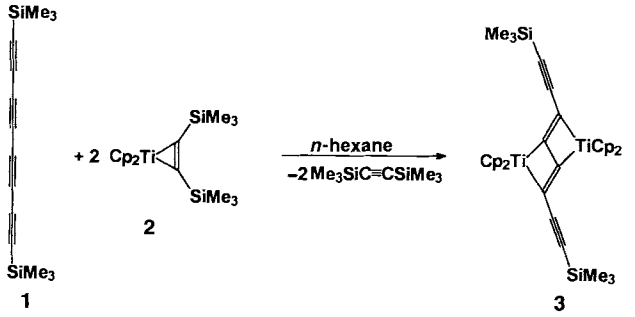

green complex **3** by complexation at the two middle triple bonds of **1**. According to its spectroscopic data, this complex is identical to the compound that Teuben and co-workers obtained previously from the reaction of $[Cp_2TiCl]_2$ with $Li-C\equiv C-C\equiv C-SiMe_3$, and which they then investigated with regard to reactions at the free triple bonds.[5]

Treatment of **1** with four equivalents of **2**, or reaction of **3** with two further equivalents of **2** led, under cleavage of the two outer C–C single bonds, to the dark red complex **5** in

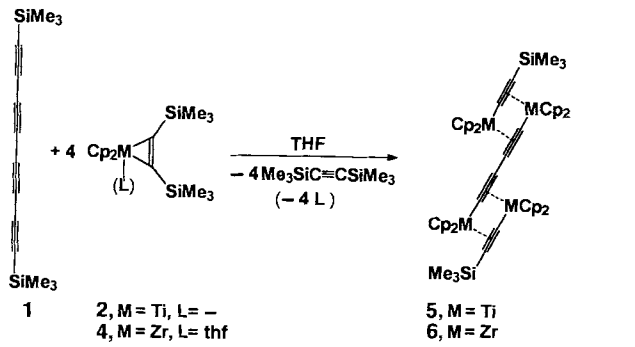

good yields (84%). Complex **5** is soluble in THF, slightly less soluble in benzene, and only sparingly soluble in *n*-hexane. The IR spectrum of **5** shows two bands in the expected range for complexed C–C triple bonds at 1816 and 1784 cm^{-1}. The ^1H [$\delta = 5.34$ (s, 40H; Cp), 0.31 (s, 18H; $SiMe_3$)] and ^{13}C NMR spectra [$\delta = 132.7$, 140.4, 208.5, 236.6 (C≡C)] confirm a symmetrical coordination. The crystal structure analysis[6] of **5** (Figure 1) provided clear evidence for the twofold bond cleavage at the outer C–C single bonds of **1**.

The golden yellow zirconium compound **6** was synthesized from **1** and four equivalents of the zirconocene source **4**;[4] compound **6** is analogous to **5** and shows very similar spectroscopic and structural properties.[7]

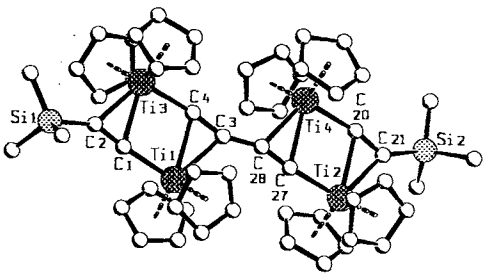

Figure 1. Molecular structure of **5** in the crystal (the structure of **6** is analogous).

The three C–C distances in **1** that correspond to single bonds are 1.39(1), 1.33(1), and 1.38(1) Å;[8a] in **5** two of these are significantly longer: C1···C4 3.02(7) and C20···C27 3.05(7) Å; this confirms the lack of a bond between these C atoms in **5**. The C–C distances in the inner C_4 chain [**5**: C4–C3 1.26(2), C3–C28 1.41(2), C28–C27 1.29(2); **6**: C4–C3 1.30(2), C3–C28 1.43(2), C28–C27 1.25(2) Å] and the short metal–C distances strongly indicate a diacetylene structure $M-C\equiv C-C\equiv C-M$, are less supportive of a cumulene structure $M=C=C=C=C=M$,[9] and virtually rule out the bis(carbyne) form $M\equiv C-C\equiv C-C\equiv M$.[10] Nevertheless, for example, the Ti–C σ bonds in **5** [Ti3–C4 2.06(2), Ti2–C27 2.06(2), Ti1–C1 2.09(2), Ti4–C20 2.07(2) Å] are significantly shorter than usual Ti–C single bonds, which lie within the range of 2.27 to 2.16 Å. The four associated Ti-C-C angles are nearly 180°; thus, a description of the Ti–C bonds as double bonds seems justified. All distances between Ti centers and the C atoms of the triple bonds to which they coordinate are almost identical. The description of the Zr compound **6** is analogous. The Zr–C σ bonds in **6** [Zr3–C4 2.18(2), Zr2–C27 2.17(2), Zr1–C1 2.20(2), Zr4–C20 2.17(2) Å] are all about 0.1 Å longer than the corresponding Ti–C bonds in **5**.

When the bis(*tert*-butyl)octatetrayne **7** was used instead of **1**, the subsequent reaction with four equivalents of the titanium complex **2** gave compound **8**; that is, in this case there are no C–C bond activations and bond cleavages, but an almost symmetrical complexation of a total of four titanocene cores to the octatetrayne occurs. Compound **8** is soluble in

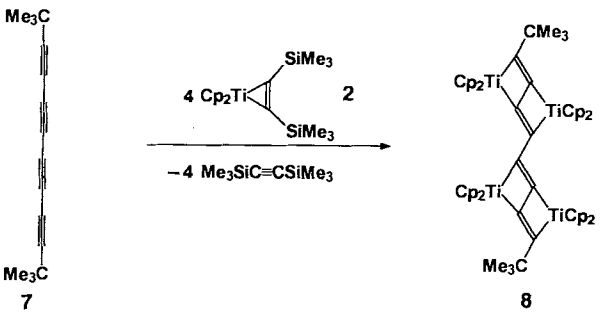

THF but only slightly soluble in *n*-hexane. The IR spectrum shows no band in the range expected for a complexed C–C triple bond; that is between 1900 and 1600 cm^{-1}. The ^1H [$\delta =$ 5.61 (s, 40H; Cp), 1.40 (s, 18H; CMe_3)] and ^{13}C NMR spectra [$\delta = 133.9$, 135.3, 210.2, 230.7 (C≡C)] confirm a symmetrical coordination of the octatetrayne.

Crystallization of **8** revealed that it occurs in two modifications. In addition to needlelike crystals (triclinic, space group $P\bar{1}$), rhombs (monoclinic, space group $C2/c$) were

 © WILEY-VCH Verlag GmbH, D-69451 Weinheim, 1997 0570-0833/97/3623-2616 $ 17.50+.50/0

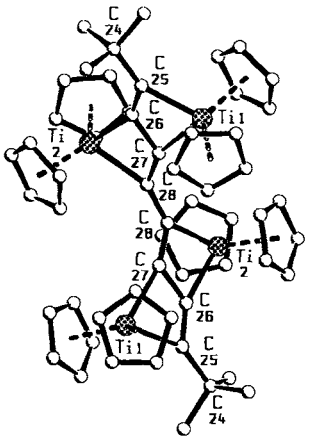

Figure 2. Molecular structure of **8** in the crystal.

observed. The crystal structure analysis[11] of the monoclinic modification of **8** (Figure 2) showed an arrangement with two intact μ-(1,3-η:2,4-η)-*trans*,-*trans*-tetradehydrobutadiene units between two titanocene cores that are both almost planar and that are connected by a C–C single bond [C28–C28 1.424(6) Å]. The angle between the two planes is about 68.6°. The ligand can be described as follows: two "zigzag butadienes" form the substituted and intact "zigzag octatetraene" with alternating C–C single and double bonds [for the two tetradehydrobutadiene units: C24–C25 1.515(5), C25–C26 1.313(5), C26–C27 1.503(5), C27–C28 1.315(4) Å]. In addition the angles correspond to those of conjugated alkenes [C24-C25-C26 130.6(4), C25-C26-C27 128.6(3), C26-C27-C28 128.2(3), C27-C28-C28 134.8(3)°]. It is remarkable that the C atoms in the middle and at the ends of the C chain show wider angles.

Investigations into the application of the reactivity pattern to other compounds such as substituted bis(σ-butadiynyl) metal complexes as well as tris- and hexakis(butadiynyl)benzene are currently in progress.

Experimental Section

All research was carried out under the exclusion of oxygen and moisture. Compound **1** was prepared according to method given in reference [8b], **7** according to that in reference [12]. The ^{1}H and ^{13}C NMR spectra of **3**, **5**, and **8** were recorded in [D$_8$]THF and those of **6** in [D$_6$]benzene on a Bruker-ARX-400 spectrometer at $T = 297$ K.

3: **1** (55 mg, 0.23 mmol) was added to a solution of **2** (161 mg, 0.46 mmol) in *n*-hexane (10 mL) at −40°C. The solution turned green and was left at −30°C. After 12 h the resulting yellow-brown solution gave compound **3** (120 mg, 87%), whose data correspond closely with those given in reference [5]: m.p. >250°C; C,H analysis for $C_{34}H_{38}Si_2Ti_2$ (598.62): calcd.: C 68.22, H 6.40; found: C 67.65, H 6.50; ^{1}H NMR: $\delta = 0.28$ (s, 18H; SiMe$_3$), 5.53 (s, 20H; Cp); ^{13}C NMR: $\delta = 108.2$ (Cp), 110.1, 113.8 (CSi), 146.0, 198.6 (C≡C); IR (Nujol): $\tilde{\nu} = 2077$ cm^{-1} (non-complexed C≡C); MS (70 eV): *m/z* 227 ([**1**−Me]$^+$), 178 ([Cp$_2$Ti]$^+$).

5: **1** (60 mg, 0.25 mmol) was added to a solution of **2** (345 mg, 0.99 mmol) in THF (20 mL). The mixture immediately turned yellow-brown, then green, and after stirring for 24 h at 40°C was red-brown. After all volatile components had been removed under vacuum, the residue was taken up in THF (5 mL) and layered with *n*-hexane (10 mL). After a few days at 0°C dark red needles precipitated, which were washed with cold *n*-hexane and dried under vacuum. Yield: 200 mg (85%). M.p. >250 C; C,H analysis for $C_{54}H_{58}Si_2Ti_4$ (954.75): calcd.: C 67.9, H 6.12; found: C 66.65, H 6.15; ^{1}H NMR: $\delta = 0.31$ (s, 18H, SiMe$_3$), 5.34 (s, 40H; Cp); ^{13}C NMR: $\delta = 1.8$ (SiMe$_3$), 104.6 (Cp), 132.7, 140.4, 208.5, 236.6 (C≡C); IR (Nujol): $\tilde{\nu} = 1816$, 1784 (coordinated C≡C), 1242 cm^{-1} (δ(SiCH$_3$)); MS (70 eV): *m/z* 275 ([Cp$_2$Ti−C$_2$SiMe$_3$]$^+$), 178 ([Cp$_2$Ti]$^+$).

6: Compound **6** was prepared analogously to **5** from **4** (461 mg, 0.99 mmol) and **1** (60 mg, 0.25 mmol) in THF. Golden yellow crystals, yield: 220 mg (79%); m.p. >250°C; C,H analysis for $C_{54}H_{58}Si_2Zr_4$ (1128.11): calcd.: C 57.49, H 5.18; found: C 57.51, H 5.28; ^{1}H NMR: $\delta = 0.44$ (s, 18H; SiMe$_3$), 5.42, 5.50 (s, each 20H; Cp); ^{13}C NMR: $\delta = 1.8$ (SiMe$_3$), 102.9, 103.6 (Cp), 143.6, 151.0, 216.8, 240.1 (C≡C); IR (Nujol): $\tilde{\nu} = 1797$, 1731 (coordinated C≡C), 1242 cm^{-1} (δ(SiCH$_3$)); MS (70 eV): *m/z* 318 ([Cp$_2$Zr−C$_2$SiMe$_3$]$^+$), 221 ([Cp$_2$Zr]$^+$).

8: A solution of **2** (697 mg, 2.00 mmol) in THF (10 mL) was allowed to react at room temperature with a solution of **7** (107 mg, 0.51 mmol) in THF (10 mL). The resulting mixture was left for a few days at room temperature, and then concentrated to 5 mL and layered with *n*-hexane (10 mL). After three days at room temperature dark green needles precipitated, which were washed with *n*-hexane and dried under vacuum. Yield: 328 mg (71%). M.p. >250°C; C,H analysis for $C_{56}H_{58}Ti_4$ (922.60): calcd.: C 72.90, H 6.34; found: C 72.13, H 6.42; ^{1}H NMR: $\delta = 1.40$ (s, 18H; CMe$_3$), 5.61 (s, 40H; Cp); ^{13}C NMR: $\delta = 33.4$ (*C*Me$_3$), 43.0 (*C*Me$_3$), 107.4 (Cp), 133.9, 135.3, 210.2, 230.7 (C≡C); MS (70 eV): *m/z* 259 ([Cp$_2$Ti−C$_2$CMe$_3$]$^+$), 178 ([Cp$_2$Ti]$^+$).

Received: June 25, 1997 [Z10599IE]
German version: *Angew. Chem.* **1997**, *109*, 2728–2730

Keywords: alkyne complexes · C–C activation · octatetraynes · titanium · zirconium

[1] a) "Oligoacetylenes": F. Diederich in *Modern Acetylene Chemistry* (Eds.: P. J. Stang, F. Diederich) VCH, Weinheim, **1995**, p. 43; b) F. Diederich, Y. Rubin, *Angew. Chem.* **1992**, *104*, 1123; *Angew. Chem. Int. Ed. Engl.* **1992**, *31*, 1101; c) R. Gleiter, D. Kratz, *ibid.* **1993**, *105*, 884 and **1993**, *32*, 842.

[2] a) W. Beck, B. Niemer, M. Wieser, *Angew. Chem.* **1993**, *105*, 969; *Angew. Chem. Int. Ed. Engl.* **1993**, *32*, 923; b) U. Bunz, *ibid.* **1996**, *108*, 1047 and **1996**, *35*, 969; c) H. Lang, *ibid.* **1994**, *106*, 569 and **1994**, *33*, 547; d) N. Pirio, D. Touchard, P. H. Dixneuf, M. Fettouhi, L. Ouahab, *ibid.* **1992**, *104*, 664 and **1992**, *31*, 651; e) W. Weng, T. Bartik, M. Brady, B. Bartik, A. M. A. Ramsden, J. A. Gladysz, *J. Am. Chem. Soc.* **1995**, *117*, 7129; f) H. Werner, *Nachr. Chem. Tech. Lab.* **1992**, *40*, 435.

[3] U. Bunz, *Angew. Chem.* **1994**, *106*, 1127; *Angew. Chem. Int. Ed. Engl.* **1994**, *33*, 1073.

[4] a) A. Ohff, S. Pulst, C. Lefeber, N. Peulecke, P. Arndt, V. V. Burlakov, U. Rosenthal, *Synlett* **1996**, 111; b) E. D. Jemmis, K. T. Giju, *Angew. Chem.* **1997**, *109*, 633; *Angew. Chem. Int. Ed. Engl.* **1997**, *36*, 606.

[5] J. Teuben, Groningen, personal communication.

[6] Crystal data of **5**: $C_{54}H_{58}Si_2Ti_4$ (954.75), $P2_1$, $a = 8.683(1)$, $b = 17.574(3)$, $c = 17.503(3)$ Å, $\beta = 91.13(1)°$, $V = 2670.4(8)$ Å^3, $Z = 2$, $\rho_{calcd} = 1.232$ g cm^{-3}, 7999 measured reflections, 7880 symmetry-independent reflections, 3183 of which were considered as observed ($I > 2\sigma(I)$), 561 refined parameters, $R1 = 0.063$, $wR2 = 0.176$ (all data), residual electron density 0.503 e Å^{-3} [13].

[7] Crystal data of **6**: $C_{54}H_{58}Si_2Zr_4$ (1128.11), $P2_1$, $a = 8.883(1)$, $b = 17.872(2)$, $c = 17.808(2)$ Å, $\beta = 91.35(1)°$, $V = 2826(3)$ Å^3, $Z = 2$, $\rho_{calcd} = 1.368$ g cm^{-3}, 8507 measured reflections, 8411 symmetry-independent reflections, 4009 of which were considered as observed ($I > 2\sigma(I)$), 561 refined parameters, $R1 = 0.062$, $wR2 = 0.160$ (all data), residual electron density 0.667 e Å^{-3} [13].

[8] a) B. F. Coles, P. B. Hitchcock, D. R. M. Walton, *J. Chem. Soc. Dalton Trans.* **1974**, 442; b) F. Waugh, D. R. M. Walton, *J. Organomet. Chem.* **1972**, *37*, 45.

[9] M. Brady, W. Weng, Y. Zhou, J. W. Seyler, A. J. Amoroso, A. M. Arif, M. Böhme, G. Frenking, J. A. Gladysz, *J. Am. Chem. Soc.* **1997**, *119*, 775.

[10] B. E. Woodworth, P. S. White, J. L. Templeton, *J. Am. Chem. Soc.* **1997**, *119*, 829.

[11] Crystal data of **8**: $C_{56}H_{58}Ti_4$ (922.60), $C2/c$, $a = 27.380(5)$, $b = 9.291(2)$, $c = 19.012(4)$ Å, $\beta = 109.23(3)°$, $V = 4566.6(16)$ Å^3, $Z = 4$, $\rho_{ber} = 1.342$ g cm^{-3}, 6654 measured reflections, 3678 symmetry-independent reflections, 2277 of which were considered as observed ($I > 2\sigma(I)$), 271 refined parameters, $R1 = 0.050$, $wR2 = 0.137$ (all data), residual electron density 0.272 e Å^{-3} [13].

[12] F. Bohlmann, *Chem. Ber.* **1953**, *86*, 657.

[13] Crystallographic data (excluding structure factors) for the structures reported in this paper have been deposited with the Cambridge Crystallographic Data Centre as supplementary publication no. CCDC-100516. Copies of the data can be obtained free of charge on application to The Director, CCDC, 12 Union Road, Cambridge CB2 1EZ, UK (fax: int. code +(1223) 336-033; e-mail: deposit@chemcrys.cam.ac.uk).

 © WILEY-VCH Verlag GmbH, D-69451 Weinheim, 1997 0570-0833/97/3623-2617 $ 17.50+.50/0

Synthetic, Structural, and Bonding Studies of Indacene Dianions**

Douglas R. Cary, Jennifer C. Green, and Dermot O'Hare*

The subject of aromaticity has been of fundamental importance to organic chemists since the early days of chemistry.[1] While numerous benzenoid compounds are known and have been studied over the years, the search for new highly conjugated molecules continues. Inorganic chemists have also been attracted to extended conjugated systems because of the potential for these ligands to promote metal–metal interaction, giving rise to materials with useful electronic properties.[2,3] It is for these reasons that the synthesis of 1,3,5,7-tetra-*tert*-butyl-*s*-indacene(**2**) by Hafner et al. has received a great deal of attention.[4] As an unusual example

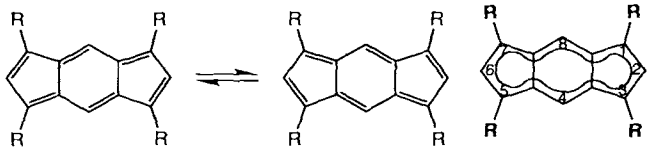

1A R = H
2A R = *t*Bu

1B R = H
2B R = *t*Bu

of a stable nonalternant antiaromatic compound,[5] **2** has been carefully studied by spectroscopy and most of the data presented suggest that it can be regarded as a delocalized structure (**2B**).[4,6–11] Several theoreticians have performed calculations on *s*-indacene (**1**) and most suggest the ground-state structure consists of two interconverting isomers **1A** with C_{2h} symmetry.[8,10,12,13] More recently, some higher level ab initio and density functional theory (DFT) calculations have indicated **1B** as the favored structure.[14,15] Various substituent effects have been examined for *s*-indacene and most results agree that the interconversion barrier is quite low in the case of 1,3,5,7-*tetra*-alkyl-*s*-indacenes (≤ 8 kJ mol^{-1}); *tert*-butyl substituents give rise to structures closer to the experimentally observed D_{2h} structure than those obtained with methyl substituents.

In the course of our investigations of bimetallic transition metal complexes with indacene ligands, which are expected to facilitate interaction between metal centers,[16–18] we have been surprised by the difficulty in preparing dianions of heavily alkylated *s*-indacenes.[17,18] Prior routes to transition metal indacene complexes have generally involved the double deprotonation of dihydroindacenes and subsequent salt metathesis with metal halide sources.[19–22] Syntheses with **2** differ in that a neutral ligand is available, which can then be treated with low-valent metal sources to give bimetallic species. We have been able to prepare bis(cyclopentadienylcobalt) compounds in this manner by using $[CpCo(C_2H_4)_2]$ as the metal source.[23] Based on Jonas's work on preparing [CpFe(diene)]$^-$-species, we have attempted to extend this chemistry to the iron analogues by the reduction of ferrocene with lithium in the presence of **2**.[24] Surprisingly, this reaction did not give an iron-containing product but rather dark orange crystals of $[(Li^+)_2(\mathbf{2}^{2-})(thf)_4]$. In the same manner, reduction of **2** with potassium in the presence of [18]crown-6 gives red crystals of $[(K^+)_2(\mathbf{2}^{2-})([18]crown\text{-}6)_2]$.

The isolation of these indacene dianions is unusual in that the parent compound $[(Li^+)_2(\mathbf{1}^{2-})]$ has always been used in situ, presumably due to its insolubility and sensitivity to air and moisture. Furthermore, previous work has indicated only the spectroscopic observation of the radical anion obtained from the in situ reduction of **2** with K, without evidence for a second reduction.[11] Reduction with $LiAlH_4$ under standard organic reaction conditions results in the formation of dihydro-**2**.[4] Using inert atmosphere techniques has enabled the isolation and study of these extremely sensitive species, which can be classified as the aromatic analogues of **2** (14 π electrons).

The spectroscopic and structural properties of $[(Li^+)_2(\mathbf{2}^{2-})(thf)_4]$ and $[(K^+)_2(\mathbf{2}^{2-})([18]crown\text{-}6)_2]$ are most easily examined in comparision to **2**. In each case, the NMR data indicate a delocalized structure on the NMR timescale. The ^{1}H NMR chemical shifts for the methine protons of $[(Li^+)_2(\mathbf{2}^{2-})(thf)_4]$ are $\delta = 6.77$ and 8.28 for the *C*-2,6 and *C*-4,8 positions, respectively. Thus these protons are significantly deshielded in comparison to the corresponding shifts in **2** ($\delta =$ 5.29 and 6.90, respectively), presumably due to an increase in the ring current. This effect is also observed for the *tert*-butyl groups, but to a lesser extent ($\delta = 1.90$ for the Li complex vs. 1.18 for **2**). As expected, the $^{13}C\{^1H\}$ NMR signals for the reduced species are significantly shielded ($\delta = 103.7$, 108.4, 111.7, 122.8) with respect to those of the neutral compound ($\delta = 124.9$, 129.1, 132.0, 164.3) due to increased electron density. The NMR data for $[(K^+)_2(\mathbf{2}^{2-})([18]crown\text{-}6)_2]$ are less informative due to its poor solubility, even in $[D_8]$THF.

The crystal structures of $[(Li^+)_2(\mathbf{2}^{2-})(OEt_2)_2(thf)_2]$ and $[(K^+)_2(\mathbf{2}^{2-})([18]crown\text{-}6)_2]$ are shown in Figure 1 These are the first structural reports on the indacene dianion. Recrystallization of $[(Li^+)_2(\mathbf{2}^{2-})(thf)_4]$ from diethyl ether resulted in the formation of $[(Li^+)_2(\mathbf{2}^{2-})(OEt_2)_2(thf)_2]$, which consists of discrete molecules of $[(Li^+)_2(\mathbf{2}^{2-})(OEt_2)_4]$ and $[(Li^+)_2(\mathbf{2}^{2-})(thf)_4]$. The most important features of each molecule are the geometric parameters for the indacendiide fragment, which are very nearly the same in each case; therefore, the molecular structure of $[(Li^+)_2(\mathbf{2}^{2-})(OEt_2)_4]$ will be used as an example for the discussion. As with **2**, each $\mathbf{2}^{2-}$ fragment is planar and lies on a crystallographic inversion center. In addition, the alkali metals are bonded fairly symmetrically to all five carbon atoms of the terminal indacene rings ($Li-C_{av} = 2.34$ Å for the diethyl ether adduct). This is in contrast to nearly all previous transition metal *s*-indacene structures, in which the metal has slipped off the centroid of the five-membered ring.[16,19,20,25] This is most likely the result of the metal–ligand bonding being predominantly electrostatic in nature, although previous structures of polycyclic hydrocarbon dianions have generally shown less symmetric coordination.[26–29] The observed *trans* arrangement is to be expected because of the electrostatic repulsions between lithium cations.

A comparison of the structural data for **2** and $\mathbf{2}^{2-}$ is given in Figure 2. Perhaps the most striking feature in this comparision is the similarity between the structures of the two fragments. The most signficant difference is in the C3–C5 distances (see, for example, Figure 1b), which are approximately 0.02 Å longer in the dianion. The remaining C–C distances are slightly lengthened in $\mathbf{2}^{2-}$, but to a lesser extent; the C-C-C angles are only slightly affected. These features are in sharp

[*] Dr. D. O'Hare, Dr. D. R. Cary, Dr. J. C. Green
Inorganic Chemistry Laboratory, University of Oxford
South Parks Road, Oxford OX1 3QR (UK)
Fax: Int. code +(1865) 272690
e-mail: Dermot.Ohare@icl.ox.ac.uk

[**] We gratefully acknowledge financial support from EPSRC.

 © WILEY-VCH Verlag GmbH, D-69451 Weinheim, 1997 0570-0833/97/3623-2618 $ 17.50+.50/0

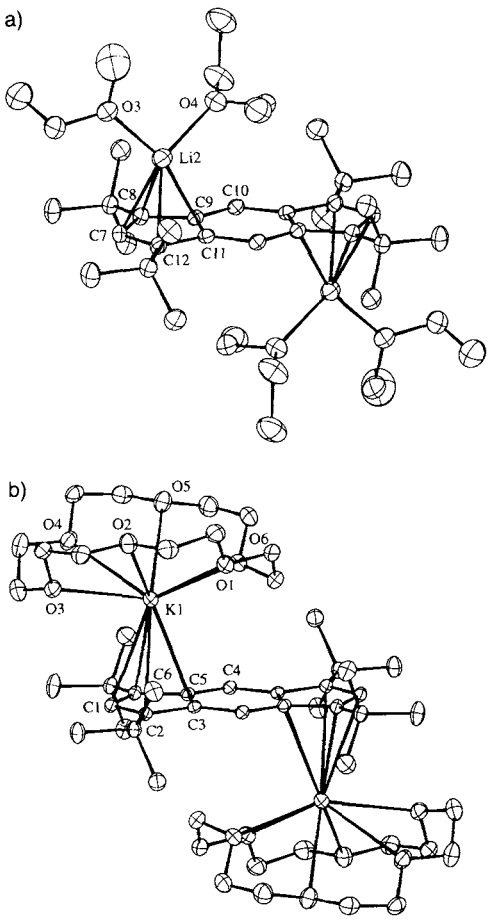

Figure 1. a) Crystal structure of $[(Li^+)_2(2^{2-})(OEt_2)_2(thf)_2]$. Selected interatomic distances [Å] and angles [°] for $[(Li^+)_2(2^{2-})(OEt_2)_4]$: Li2–O3 2.033(4), Li2–O4 2.057(4), Li2–C7 2.333(4), Li2–C8 2.337(4), Li2–C9 2.356(4), Li2–C11 2.352(4), Li2–C12 2.336(4); and for $[(Li^+)_2(2^{2-})(thf)_4]$ (not shown): Li1–O1 1.962(4), Li1–O2 1.979(4), Li1–C1 2.259(4), Li1–C2 2.269(4), Li1–C3 2.323(4), Li1–C5 2.338(4), Li1–C6 2.288(4), O1-Li1-O2 96.1(2). b) Molecular structure of $[(K^+)_2(2^{2-})([18]crown\text{-}6)_2]$. Selected interatomic distances [Å]: K1–O1 2.8836(9), K1–O2 3.1054(9), K1–O3 2.8937(9), K1–O4 3.0045(9), K1–O5 3.2372(9), K1–O6 2.7455(9), K1–C1 3.092(1), K1–C2 3.107(1), K1–C3 3.111(1), K1–C5 3.108(1), K1–C6 3.093(1).

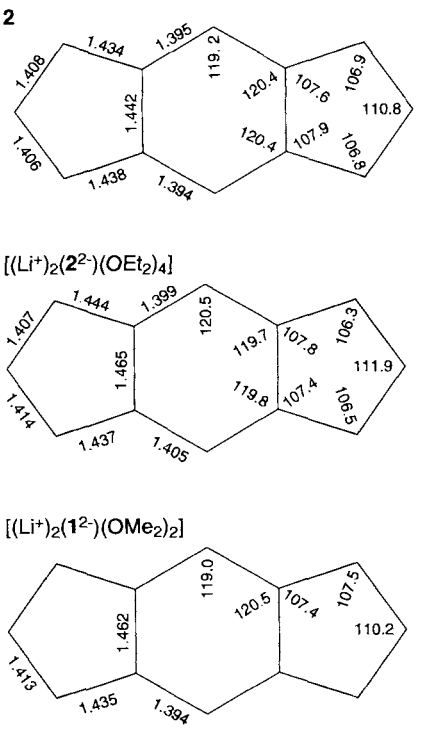

Figure 2. Selected structural data (bond lengths in Å and angles in °) for **2** (T = 100 K)[6], the indacendiide fragment of $[(Li^+)_2(2^{2-})(OEt_2)_4]$ (T = 150 K), and the calculated structure of $[(Li^+)_2(1^{2-})(OMe_2)_2]$ the estimated standard deviations for the last decimal place for bond lengths and angles of $[(Li^+)_2(2^{2-})(OEt_2)_4]$ are 3 and 2, respectively.

contrast to the transition metal structures solved in our laboratory thus far, which have invariably shown significant ring expansion (in terms of the size of the angles) as well as bending of the ligand in many cases.[16,23] The overall geometries are both essentially D_{2h}; the bond lengths are clearly not assignable to either single or double bonds. However, we cannot rule out the possibility of disorder effects.

In order to understand these surprising results, DFT calculations were carried out on $[(Li^+)_2(1^{2-})]$ and $[(Li^+)_2(1^{2-})(OMe_2)_2]$ using a generalized gradient approximation as implemented in the Amsterdam density functional code.[30] Initially, $[(Li^+)_2(1^{2-})]$ was constrained to have C_i symmetry, but the final geometry approximated C_{2h} and thus both $[(Li^+)_2(1^{2-})]$ and $[(Li^+)_2(1^{2-})(OMe_2)_2]$ were optimized with the constraint of C_{2h} symmetry. This is equivalent to D_{2h} symmetry for the 1^{2-} fragment of each molecule, indicating a delocalized ligand. Selected distances and angles obtained for $[(Li^+)_2(1^{2-})(OMe_2)_2]$ are included in Figure 2; they are in good agreement with the experimental data for 2^{2-}. Both model compounds give nearly the same geometries for the 1^{2-} fragment; the inclusion of ether groups primarily affects the metal–carbon distances (2.178 Å without OMe_2 vs. 2.305 Å with). Calculations on isolated 1^{2-} give bond lengths longer than for either molecular species. The frontier orbitals obtained are in agreement with previous extended Hückel, semiempirical, ab initio, and DFT calculations on *s*-indacene.[12,14,25] The HOMO contains π-electron density on C-1,3,4,5,7,8; the nodal planes pass through the bridgehead carbons as well as along the long axis through C-2 and C-6. The result is an almost nonbonding orbital with elongation in the direction of the short symmetry axis.

Experimental Section

$[(Li^+)_2(2^{2-})(thf)_4]$: Addition of THF (30 mL) to **2** (520 mg, 1.38 mmol) and small Li pieces (298 mg, 42.9 mmol) gave a orange solution and orange powder within 24 h. After the mixture had been stirred for 48 h, the solvent was removed under vacuum. *All of the orange solid was extracted from unconverted Li with toluene*, the mixture was concentrated, and cooled to −45 °C. Dark black-orange crystals were collected by filtration (271 mg, 29%). Satisfactory analytical data could not be obtained because of extreme air and moisture sensitivity. ^{1}H NMR (C_6D_6, 300 MHz): δ = 8.28 (s, 2H), 6.77 (s, 2H), 2.95 (m, 16H), 1.90 (s, 36H), 0.99 (s, 16H); $^{13}C\{^1H\}$ NMR (75 MHz, C_6D_6): δ = 122.8 (C-1,3,5,7 or C-3a,4a,7a,8a), 111.7 (C-2,6 or C-4,8), 108.4 (C-2,6 or C-4,8), 103.7 (C-3a,4a,7a,8a or C-1,3,5,7), 68.2 (THF), 33.4 (-C(CH_3)$_3$), 32.6 (-C(CH$_3$)$_3$), 25.3 (THF); IR (KBr/Nujol) [cm^{-1}]: $\tilde{\nu}$ = 1311 w, 1294 w, 1262 w, 1248 w, 1221 m, 1191 m, 1175 s, 1074 m, 1049 m, 1029 m, 999 m, 945 w, 917 w, 889 m, 825 s, 727 s.

$[(Li^+)_2(2^{2-})(OEt_2)_2(thf)_2]$: Dissolution of $[(Li^+)_2(2^{2-})(thf)_4]$ in diethyl ether, followed by crystallization from toluene yielded $[(Li^+)_2(2^{2-})(OEt_2)_2(thf)_2]$. ^{1}H NMR (300 MHz, C_6D_6): δ = 8.28 (s, 2H), 6.78 (s, 2H), 2.89 (m, 16H), 1.90 (s, 36H), 0.96 (m, 8H), 0.77 (t, 12H).

$[(K^+)_2(2^{2-})([18]crown\text{-}6)_2]$: Addition of THF (30 mL) to **2** (482 mg, 1.28 mmol), small K pieces (100 mg, 2.56 mmol), and [18]crown-6 (675 mg, 2.55 mmol) gave a dark red solution within 2 h. After the mixture had been stirred for 3 h, the solution was filtered and pentane was layered on top. Slow solvent diffusion resulted in the formation of dark red crystals (495 mg, 39%). Satisfactory analytical data could not be obtained because of extreme air and moisture sensitivity. ^{1}H NMR (300 Mhz, [D$_8$]THF): δ = 1.73 (s, 36H), 3.24 (s, 48H), 6.00 (s, 2H), 7.13 (s, 2H). IR (KBr/Nujol) [cm^{-1}]: $\tilde{\nu}$ = 1582 w, 1322 w, 1298 w, 1251 m, 1222 w, 1187 w, 1110 s, 960 s, 862 w, 831 m, 803 w, 723 m.

 © WILEY-VCH Verlag GmbH, D-69451 Weinheim, 1997 0570-0833/97/3623-2619 $ 17.50+.50/0

X-ray crystal structure analysis of $[(Li^+)_2(2^{2-})(OEt_2)_2(thf)_2]$: $C_{44}H_{76}Li_2O_4$, $P\bar{1}$, $a = 9.782(1)$, $b = 14.594(1)$, $c = 15.640(1)$ Å, $\alpha = 74.999(2)$, $\beta = 81.977(2)$, $\gamma = 83.417(2)°$, $V = 2128.34$ Å^3, $Z = 2$, $\rho_{calcd} = 1.07$ g cm^{-3}, $\mu = 0.060$ mm^{-1}, $T = 150$ K, crystal dimensions ca. $0.25 \times 0.50 \times 0.50$ mm^3, 90 frames, 26428 measured (8101 unique) reflections, $R = 0.0472$ and $R_w = 0.0475$ for 5823 reflections with $I > 6\sigma(I)$, maximum and minimum peak in final Fourier difference synthesis 0.58 and -0.42 e Å^{-3}. Unit weights were used in the refinements. The asymmetric unit consists of half of a molecule of $[(Li^+)_2(2^{2-})(OEt_2)_4]$ and half a molecule $[(Li^+)_2(2^{2-})(thf)_4]$, each located about an inversion center.

X-ray crystal structure analysis of $[(K^+)_2(2^{2-})([18]crown\text{-}6)_2]$: $C_{76}H_{88}K_2O_{12}$, $P2_1/n$, $a = 13.959(1)$, $b = 10.403(1)$, $c = 19.733(1)$ Å, $\beta = 107.376(1)°$, $V = 2740.31$ Å^3, $Z = 2$, $\rho_{calcd} = 1.19$ g cm^{-3}, $\mu = 0.22$ mm^{-1}, $T = 150$ K, crystal dimensions ca. $0.20 \times 0.25 \times 0.40$ mm^3, 90 frames, 29555 measured (6266 unique) reflections, $R = 0.0422$ and $R_w = 0.0464$ for 5403 reflections with $I > 3\sigma(I)$, maximum and minimum peak in final Fourier difference synthesis 0.36 and -0.23 e Å^{-3}. A weighting scheme based on an optimized three-coefficient Chebyshev polynomial was used in the refinements [31]. General crystallographic information: Data were collected on an Enraf-Nonius DIP 2000 image plate diffractometer using graphite-monochromated $Mo_{K\alpha}$ radiation (step of 2° between frames, $\theta_{max} = 26°$). Corrections were made for Lorentz and polarization effects [32]. The structures were solved by direct methods using SIR92 [33] and refined by using full-matrix least-squares. Hydrogen atoms were fixed in geometrically idealized positions and allowed to ride on their attached carbon atoms. Corrections for the effects of anomalous dispersion and isotropic extinction (through an overall extinction coefficient) [34] but not for absorption, were made in the final stages of refinement. All crystallographic calculations were performed by using the Oxford CRYSTALS system [35] running on a Silicon Graphics Indigo R4000 computer. Crystallographic data (excluding structure factors) for the structures reported in this paper have been deposited with the Cambridge Crystallographic Data Centre as supplementary publication no. CCDC-100693. Copies of the data can be obtained free of charge on application to The Director, CCDC, 12 Union Road, Cambridge CB2 1EZ, UK (fax: int. code + (1223) 336-033; e-mail: deposit@chemcrys.cam. ac.uk).

Received: June 10, 1997 [Z105301E]
German version: *Angew. Chem.* **1997**, *109*, 2730–2733

Keywords: alkali metals · aromaticity · density functional calculations · indacene · solid-state structures

[1] See P. von R. Schleyer, H. Jiao, *Pure Appl. Chem.* **1996**, *68*, 209–218.
[2] S. Barlow, D. O'Hare, *Chem. Rev.* **1997**,*97* 637–670.
[3] a) *Inorganic Materials*, (Eds.: D. L. Bruce, D. O'Hare), 2nd ed., Wiley, New York, **1997**; b) P. Cassoux, L. Valade in ref. [3a], Chapter 1; c) O. Kahn, Y. Pei, Y. Journaux in ref. [3a], Chapter 2; d) G. E. Kellogg, J. G. Gaudiello in ref. [3a], Chapter 7.
[4] K. Hafner, B. Stowasser, H. P. Krimmer, S. Fischer, M. C. Bohm, H. J. Lindner, *Angew. Chem.* **1986**,*98*, 646–648; *Angew. Chem. Int. Ed. Engl.* **1986**, *25*, 630–632.
[5] K. Hafner, *Angew. Chem.* **1963**, *75*, 1041–1059; *Angew. Chem. Int. Ed. Engl.* **1964**, *3*, 165–173.
[6] J. D. Dunitz, C. Kruger, H. Irngartinger, Y. Wang, M. Nixdorf, *Angew. Chem.* **1988**, *100*, 415–418; *Angew. Chem. Int. Ed. Engl.* **1988**, *27*, 387–389.
[7] R. Klann, R. J. Bäuerle, F. Laermer, T. Elsaesser, M. Niemeyer, W. Luttke, *Chem. Phys. Lett.* **1990**, *169*, 172–178.
[8] C. Gellini, G. Cardini, P. R. Salvi, G. Marconi, K. Hafner, *J. Phys. Chem.* **1993**, *97*, 1286–1293.
[9] C. Gellini, P. R. Salvi, K. Hafner, *J. Phys. Chem.* **1993** *97*, 8152–8157.
[10] C. Gellini, L. Angeloni, P. R. Salvi, G. Marconi, *J. Phys. Chem.* **1995**, *99*, 85–93.
[11] R. Bachmann, F. Gerson, G. Gescheidt, K. Hafner, *Magn. Reson. Chem.* **1995**,*33*, S60–S65.
[12] E. Heilbronner, Z.-Z. Yang, *Angew. Chem.* **1987**, *99*, 369–371; *Angew. Chem., Int. Ed. Engl.* **1987**, *26*, 360–362.
[13] M. Kataoka, *J. Chem. Res. Synop.* **1993**, 104–105.
[14] R. H. Hertwig, M. C. Holthausen, W. Koch, Z. B. Maksić, *Int. J. Quantum Chem.* **1995**, *54*, 147–159.
[15] R. H. Hertwig, M. C. Holthausen, W. Koch, Z. B. Maksić, *Angew. Chem.* **1994**, *106*, 1252–1254; *Angew. Chem., Int. Ed. Engl.* **1994**, *33*, 1192–1194.
[16] D. R. Cary, C. G. Webster, M. J. Drewitt, S. Barlow, J. C. Green, D. O'Hare, *Chem. Commun.* **1997**, 953–954.
[17] S. Barlow, M. J. Drewitt, D. R. Cary, D. O'Hare, *J. Organomet. Chem.* submitted.
[18] S. Barlow, D. O'Hare, *Organometallics* **1996**, *15*, 3483–3485.
[19] J. M. Manriquez, M. D. Ward, W. M. Reiff, J. C. Calabrese, N. L. Jones, P. J. Carroll, E. E. Bunel, J. S. Miller, *J. Am. Chem. Soc.* **1995**, *117*, 6182–6193.
[20] W. L. Bell, C. J. Curtis, C. W. Eigenbrot, Jr., C. G. Pierpont, J. L. Robbins, J. C. Smart, *Organometallics* **1987**, *6*, 266–273.
[21] S. Iijima, I. Motoyama, H. Sano, *Bull. Chem. Soc. Jpn.* **1980**, *53*, 3180–3183.
[22] T. J. Katz, V. Balough, J. Schulmann, *J. Am. Chem. Soc.* **1968**, *90*, 734–739.
[23] D. R. Cary, C. G. Webster, M. J. Drewitt, D. O'Hare, unpublished results.
[24] K. Jonas, *Adv. Organomet. Chem.* **1981**, *19*, 97–122.
[25] M. T. Garland, J.-Y. Saillard, I. Chávez, B. O'lckers, J.-M. Manríquez, *J. Mol. Struct. (Theochem)* **1997**, *390*, 199–208.
[26] J. J. Stezowski, H. Hoier, D. Wilhelm, T. Clark, P. von R. Schleyer, *J. Chem. Soc., Chem. Commun.* **1985**, 1263–1264.
[27] W. E. Rhine, J. H. Davis, G. Stucky, *J. Organomet. Chem.* **1977**, *134*, 139–149.
[28] W. E. Rhine, J. Davis, G. Stucky, *J. Am. Chem. Soc.* **1975**, *97*, 2079–2085.
[29] J. J. Brooks, W. Rhine, G. D. Stucky, *J. Am. Chem. Soc.* **1972**, *94*, 7346–7351.
[30] The calculations were performed with the density functional methods of the Amsterdam Density Functional (ADF) code, Version 2.0.1 (B. te Veide, E. J. Baerends, Vrije Universiteit, Amsterdam, **1995**). The basis set used double-zeta sets of Slater orbitals with an additional single polarization function (2 p on H, 3 d on Li, C, and O). The cores of the atoms were frozen (1 s of Li, C, and O). A local exchange correlation potential was employed (S. H. Vosko, L. Wilk, M. Nusair, *Can. J. Phys.* **1980**, *58*, 1200) with nonlocal exchange corrections according to Becke (A. D. Becke, *Phys. Rev. A* **1988**, *38*, 2398) and nonlocal correlation corrections according to Perdew (J. P. Perdew, *Phys. Rev. B* **1986**, *33*, 8822; *ibid.* **1986**, *34*, 7046).
[31] J. R. Carruthers, D. J. Watkin, *Acta Crystallogr. Sect. A* **1979**, *A35*, 698–699.
[32] A. C. T. North, D. C. Phillips, F. S. Matthews, *Acta Crystallogr. Sect. A* **1968**, *24*, 351–359.
[33] A. Altomare, G. Cascarano, C. Giacovazzo, A. Guagliardi, *J. Appl. Crystallogr.*. **1993**, *26*, 343–350.
[34] A. C. Larson, *Acta Crystallogr.* **1967**, *23*, 664–665.
[35] J. R. Carruthers, D. J. Watkin, *CRYSTALS User Manual*, Oxford University Computing Centre, Oxford 1975.

Highly Enantioselective Catalytic Conjugate Addition and Tandem Conjugate Addition–Aldol Reactions of Organozinc Reagents**

Ben L. Feringa,* Mauro Pineschi, Leggy A. Arnold, Rosalinde Imbos, and André H. M. de Vries

Dedicated to Professor D. Seebach on the occasion of his 60th birthday

Although efficient catalysts for a number of asymmetric carbon–carbon formations are known to date,[1] a highly enantioselective catalytic version of the conjugate addition of organometallic reagents to enones is lacking.[2] Recently chiral catalysts based on Cu^I, Ni^{II}, Zn^{II}, or Co^{II} complexes of a variety of ligands have shown enantioselectivities up to 90% in 1,4-additions of Grignard, organolithium, or dialkylzinc reagents.[3] The results so far have not revealed, however, the key elements for realization of complete stereocontrol but do reveal the rather complex nature of some of these chiral catalytic systems.[4] Previously we have demonstrated that copper complexes of chiral phosphorus amidites show relatively high *ee* values for the 1,4-adducts of R_2Zn reagents and acyclic as well as cyclic enones.[5]

In this communication both the first catalytic asymmetric 1,4-addition reactions of organometallic reagents with complete

[*] Prof. Dr. B. L. Feringa, Dr. M. Pineschi,[+] L. A. Arnold, R. Imbos, A. H. M. de Vries
Department of Organic and Molecular Inorganic Chemistry
University of Groningen
Nijenborgh 4, NL-9747 AG Groningen (The Netherlands)
Fax: Int. code + (50) 363-4296
e-mail: Feringa@chem.rug.nl

[+] Current address: Dipartimento di Chimica Bioorganica, Università di Pisa (Italy)

[**] We are grateful to Prof. Dr. P. Knochel, University of Marburg, for valuable discussions and suggestions on the preparation of organozinc reagents and to Dr. J. van Esch for the creation of the artwork. Financial support (TMR postdoctoral fellow for M. P.) from the European Community (EU contract no.: ERBFMBICT961635) is gratefully acknowledged.

 © WILEY-VCH Verlag GmbH, D-69451 Weinheim, 1997 0570-0833/97/3623-2620 $ 17.50+.50/0

stereocontrol and highly enantioselective tandem conjugate addition-aldol reactions are reported. In our design of a catalytic asymmetric 1,4-addition the following aspects were considered: a) Can very efficient ligand-accelerated catalysis [6] be achieved? b) Is it possible to use an enone and an olefin [Eq. (a)] as starting material? c) Are functional groups tolerated?

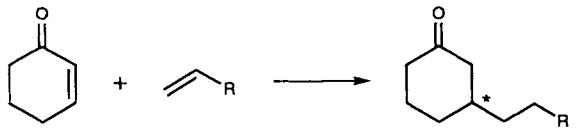

(a)

The remarkable ligand effect of binaphthol-derived phosphorus amidites on the copper-catalyzed 1,4-addition of Et_2Zn to enones[5] was explored by a modular variation of the binaphthyl and amine moieties in these ligands. Much to our delight the incorporation of two chiral structural units, that is, the sterically demanding (*R,R*)-bis(1-phenylethyl)amine and unsubstituted (*S*)-2,2′-binaphthol (as present in C_2 symmetric ligand **1**), resulted in a *matched* combination[7] and a highly selective catalyst for the addition of Et_2Zn to cyclohexenone (Scheme 1). Thus the catalyst prepared from $Cu(OTf)_2$

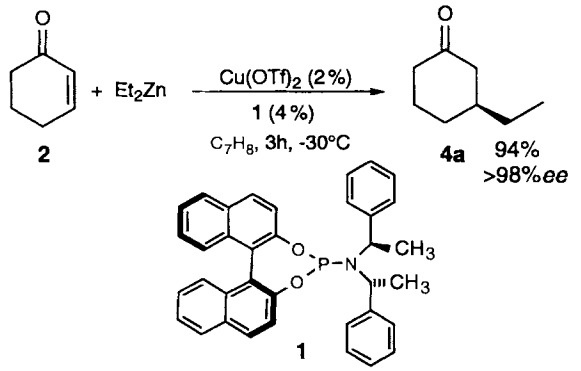

Scheme 1. Enantioselective 1,4-addition of Et_2Zn to **2**, catalyzed by $Cu(OTf)_2$/**1**. Tf = trifluoromethane sulfonate.

(2 mol%) and **1** (4 mol%) provided (*S*)-**4a** in 94% yield and an *ee* value greater than 98%. Excellent yields and enantiomeric excesses ranging from 94 to greater than 98% are obtained for cyclohexenone and substituted cyclohexenones with a variety of zinc reagents (Table 1).[8] Having realized complete stereocontrol in the formation of a number of 3-substituted cyclohexanones **4** (Table 1, entries 1, 4–7),

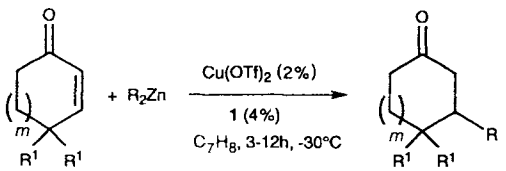

2a: R^1=H, *m*=1
2b: R^1=H, *m*=0
2c: R^1=H, *m*=2
2d: R^1=Me, *m*=1
2e: R^1=Ph, *m*=1

3a: R=Et
3b: R=Me
3c: R=Hep
3d: R=*i*Pr
3e: R=$(CH_2)_3$Ph
3f: R=$(CH_2)_5$OAc
3g: R=$(CH_2)_3CH(OEt)_2$
3h: R=$(CH_2)_6$OPiv

4a: R^1=H, R=Et, *m*=1
4b: R^1=H, R=Et, *m*=0
4c: R^1=H, R=Et, *m*=2
4d: R^1=H, R=Me, *m*=1
4e: R^1=H, R=Hep, *m*=1
4f: R^1=Me, R=Et, *m*=1
4g: R^1=Me, R=Me, *m*=1
4h: R^1=Ph, R=Et, *m*=1
4i: R^1=H, R=*i*Pr, *m*=1
4j: R^1=H, R=$(CH_2)_3$Ph, *m*=1
4k: R^1=H, R=$(CH_2)_5$OAc, *m*=1
4l: R^1=H, R=$(CH_2)_3CH(OEt)_2$, *m*=1
4m: R^1=H, R=$(CH_2)_6$OPiv, *m*=1

Table 1. Enantioselective 1,4-additions of dialkylzinc compounds to enones, catalyzed by $Cu(OTf)_2$/**1**[a].

Entry	Enone	R_2Zn	1,4-Adduct	Yield[%][b]	*ee*[%][c]
1	**2a**	**3a**	**4a**	94	>98[d]
2	**2b**	**3a**	**4b**	75	10
3	**2c**	**3a**	**4c**	82	53
4	**2d**	**3a**	**4f**	74	>98[d]
5	**2e**	**3a**	**4h**	93	>98[d]
6	**2a**	**3b**	**4d**	72	>98[d]
7	**2d**	**3b**	**4g**	68	>98[d]
8	**2a**	**3c**	**4e**	95	95
9	**2a**	**3d**	**4i**	95	94
10	**2a**	**3e**	**4j**	53	95
11	**2a**	**3f**	**4k**	77	95
12	**2a**	**3g**	**4l**	91	97
13	**2a**	**3h**	**4m**	87	93

[a] Reaction conditions as in ref. [5]. [b] Yields of isolated products. [c] Determined by ^{13}C NMR spectroscopy after derivatization with 1,2-diphenyl ethylenediamine [5, 16]. [d] (*S*)-**4** could not be detected.

we examined catalytic 1,4-additions of diheptyl zinc (**3c**) and functionalized dialkylzinc reagents (**3e**–**3h**).[9] The R_2Zn reagents were prepared from the corresponding alkenes by hydroboration and subsequent zinc exchange according to Knochel[10,11] or with the corresponding Grignard reagent (Table 1, entry 9). Again excellent enantioselectivities were achieved (Table 1, entries 8–13). It is particular noteworthy that the new catalyst tolerates ester and acetal functionalities. So far the catalyst based on $Cu(OTf)_2$/ligand **1** does not show satisfactory enantioselectivities for five- and seven-membered cyclic enones (Table 1, entries 2,3). For these substrates further ligand tuning is required.

A possible pathway for the 1,4-addition could involve transfer of an alkyl fragment from R_2Zn to the copper complex,[11] followed by π-complexation of the resulting copper alkyl species to the double bond of the enone[12] and of the alkylzinc ion to the enone carbonyl (Scheme 2). Next alkyl transfer to the β-position of the enone generates alkylzinc enolate **5**, which upon protonation provides cyclohexanone **4**.

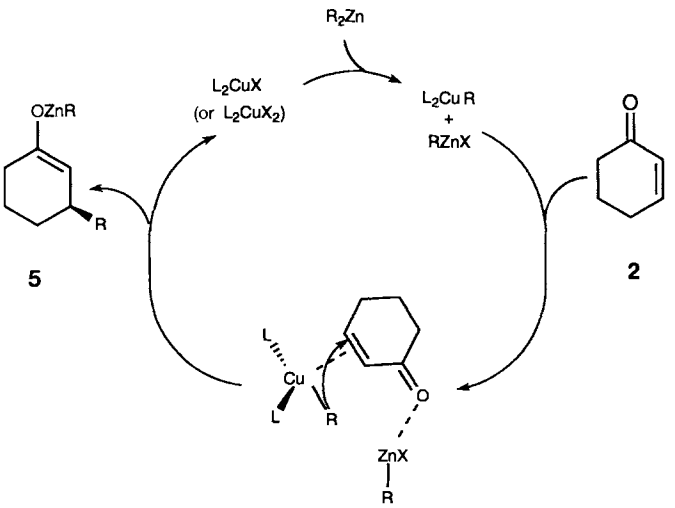

Scheme 2. Postulated catalytic cycle of the 1,4-addition.

It is anticipated that the zinc enolate **5**, resulting from the conjugate addition, might be trapped by an aldehyde in a subsequent aldol reaction.[13] The regio- and enantioselective catalytic three-component coupling was indeed achieved with

 © WILEY-VCH Verlag GmbH, D-69451 Weinheim, 1997 0570-0833/97/3623-2621 $ 17.50+.50/0

Table 2. 1,4-Additions of dialkylzinc compounds and subsequent aldol reactions of the zinc enolates **5**.

Entry	Lewis acid [a]	t[min] (T[°C])	Products	*erythro*:*threo* **6a–h**:**7a–h**	Yield [%] [b]	*ee* [%] [c]
1		10 (−30)	**6a/7a**	31:69	88	95
2		10 (−30)	**6b/7b**	38:62	85	93
3	$BF_3 \cdot Et_2O$	3 (−30)	**6b/7b**	46:54	78	92
4	$ZnCl_2 \cdot Et_2O$	3 (−20)	**6e/7e**	54:46	64	91
5		10 (−20)	**6e/7e**	38:62	67	91
6	$BF_3 \cdot Et_2O$	3 (−20)	**6f/7f**	52:48	82	> 99
7	$ZnCl_2 \cdot Et_2O$	10 (−30)	**6c/7c**	32:68 [d,e]	88	91
8		10 (−30)	**6d/7d**	44:56 [e]	92	95
9	$ZnCl_2 \cdot Et_2O$	30 (−30)	**6g/7g**	65:35 [e]	81	97
10	$ZnCl_2 \cdot Et_2O$	10 (−30)	**6h/7h**	48:52 [d,e]	75	97

[a] 1.0 equiv of Lewis acid added. [b] Yields of isolated, pure aldols. [c] See *Experimental Section* for the determination of the *ee* values. [d] An unseparable mixture of aldols was obtained. [e] The relative configuration (*erythro*:*threo*) has not been established.

in situ generated enolate (Table 2). For example, when enolate **5**, formed from **2** and diethylzinc in the presence of $Cu(OTf)_2$ (1.2 mol%) and ligand **1** (2.4 mol%), was treated with benzaldehyde at −30°C for 10 min, an approximately 3:7 mixture of *trans,erythro*-**6a** and *trans,threo*-**7a** was obtained in 88% isolated yield (Table 2, No. 1). The aldol products were readily separated by flash chromatography (SiO_2, 30% ethyl acetate, 70% hexanes) and oxidized to a single isomer of diketone **8a** with 95% ee. The results shown in Table 2

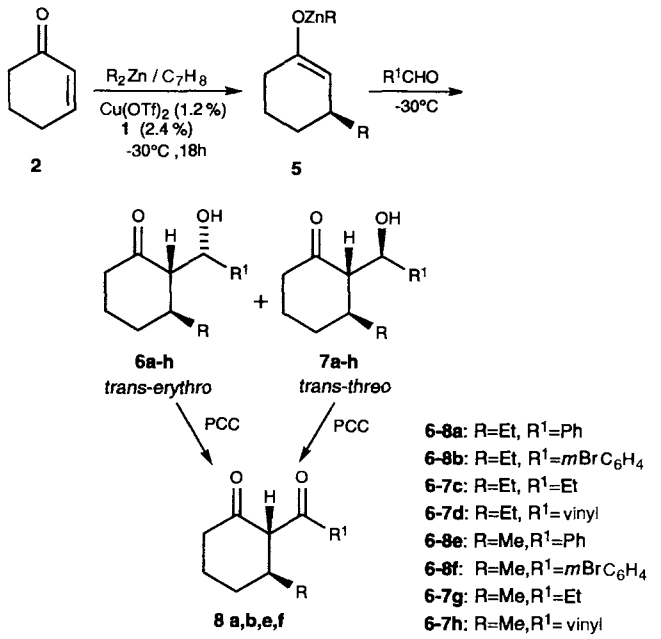

indicate that other representative aldehydes undergo the tandem 1,4-addition–aldol reactions (in the presence or absence of Lewis acids) affording the corresponding *trans*-2,3-disubstituted cyclohexanones with enantioselectivities always exceeding 90%. In all cases small amounts of copper catalyst (1.2 mol%) lead to clean zinc enolate formation, fast and regioselective aldol reactions and *trans*-vicinal disubstituted cyclohexanones are exclusively obtained. The relative and absolute stereochemistry of (−)-*trans-erythro*-**6b** was established to be 2*S*,3*S*,1′*S* on the basis of single crystal X-ray analysis.[14] As far as we know this represents the first catalytic one-pot organozinc conjugate addition–enolate-trapping reaction that proceeds with high enantioselectivity.

The synthetic versatility of the new catalytic enantioselective C–C bond formation is further illustrated by the 1,4-addition of Et_2Zn to highly symmetrical dienone **10** readily obtained by oxidation of hydroquinone **9** (Scheme 3).[15] In

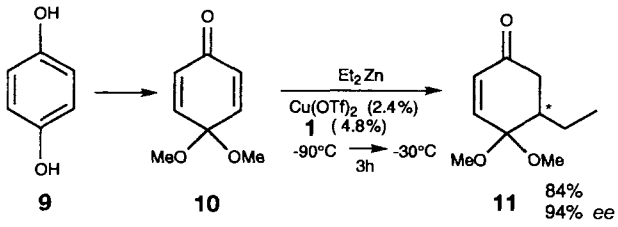

Scheme 3. Catalytic enantioselective 1,4-addition of Et_2Zn to the dienone **10**[15].

view of the potential to use various zinc reagents, the multifunctional nature of **11**, and the short, highly selective, and efficient route from hydroquinone, this new method may allow a versatile entry to a variety of optically active cyclohexenones.

Experimental Section

1: The procedure for related phosphorus amidites [5] was followed except that *n*BuLi/THF was used instead of Et_3N/toluene in the second step: chromatography (SiO_2, hexane:CH_2Cl_2 3:1), yield 40%, $[\alpha]_D = +456.0$ ($c = 0.79$, $CHCl_3$). ^1H NMR: $\delta = 7.98-8.08$ (m, 4H), 7.17–7.74 (m, 18H), 4.63 (q, $J = 7.2$ Hz, 2H), 1.85 (d, $J = 7.2$ Hz, 6H); ^{13}C NMR ($CDCl_3$): $\delta = 150.2$, 150.0, 149.6, 142.8, 132.8, 131.4, 130.5, 130.3, 129.4, 128.3, 128.1, 128.0, 127.9, 127.8, 127.2, 127.1, 126.7, 126.0, 124.7, 124.5, 122.4, 52.3, 51.1, 21.8; ^{31}P NMR: $\delta = 145.3$.

6b/7b,8b: Typical procedure for the conjugate addition–enolate-trapping reactions with **2**: A solution of $Cu(OTf)_2$ (0.0045 g, 0.012 mmol) and **1** (0.013 g, 0.024 mmol) in toluene (5.0 mL) was stirred for 1 h at room temperature under nitrogen. The colorless solution was cooled at −30°C and **2** (0.097 g, 1.0 mmol) and $ZnEt_2$ (1.0 mL of a 1.1 M solution in toluene) were added. After 18 h at −30°C *m*-bromobenzaldehyde (0.277 g, 1.5 mmol, freshly distilled) in toluene (1.0 mL) was added, and the reaction mixture was stirred for 10 min, quenched with saturated aqueous NH_4Cl (5.0 mL) and extracted with diethyl ether (2 × 30 mL). The combined organic layers were washed with brine (5.0 mL), dried over $Mg(SO_4)_2$, filtered, and evaporated to give a crude reaction product that was purified by flash chromatography (SiO_2, mixture of 20% ethyl acetate and 80% hexanes) to afford **6b** and **7b**. Yield of **6b**: 0.10 g, 32%; solid with m.p. 81.4–82.8°C; $[\alpha]_D = -50.0$ ($c = 1.52$, CH_2Cl_2); ^1H NMR (200 MHz, $CDCl_3$) δ 7.35–7.51 (m, 1H), 7.14–7.29 (m, 3H), 5.12 (t, $J = 6.1$ Hz, 1H), 3.31 (d, $J = 6.3$ Hz, OH), 2.63 (dd, $J = 6.8$ and 4.9 Hz, 1H), 2.31–2.40 (m, 2H), 1.18–1.96 (m, 7H), 0.76 (t, $J = 7.3$ Hz, 3H). ^{13}C NMR: $\delta = 214.8$, 145.0, 130.3, 129.7, 129.5, 124.9, 71.9, 60.5, 41.5, 39.3, 27.5, 26.0, 23.0, 10.4. HRMS calcd for $C_{15}H_{20}O_2$ 232.1463; found 232.1464. Yield of **7b**: 0.164 g, 53%; oil, $[\alpha]_D = -23.0$ ($c = 1.14$, CH_2Cl_2); ^1H NMR (200 MHz, $CDCl_3$): $\delta = 7.47$ (br.s, 1H), 7.14–7.37 (m, 3H), 4.83–4.89 (m, 1H), 2.61 (dd, $J = 7.8$ und 4.64 Hz, 1H), 1.20–2.38 (m, 9H), 0.88 (t, $J = 7.8$ Hz, 3H); ^{13}C NMR: $\delta = 215.0$, 145.9, 130.1, 129.7, 128.9, 124.3, 71.1, 60.9, 41.8, 41.7, 27.9, 25.5, 25.2, 10.2; HR-MS calcd for $C_{15}H_{20}O_2$ 232.1463; found 232.1467.

To a mixture of **6b/7b** (0.031 g, 0.1 mmol) in CH_2Cl_2 (2.0 mL) were added molecular sieves (4 Å, 0.10 g) and PCC (0.043 g, 0.2 mmol) at 0°C. After 2 h stirring at room temperature, the reaction mixture was diluted with diethyl ether, filtered over Celite, and evaporated to dryness. Purification by chromatography (SiO_2, mixture of 10% ethyl acetate and 90% hexanes) provided pure **8b** (0.025 g, 81%). The enantiomeric excess (93% *ee*) was determined by chiral HPLC [Regis (*R*, *R*)-Whelk-01 column, flow rate 0.5 mL min^{-1}, 5% *i*PrOH, 95% hexane, T_{ret} 34.5 min (3*S*, 2*R*), T_{ret} 37.2 min (3*R*, 2*S*)]. HPLC analysis of the recrystallized product (hexane) gave an *ee* value of > 98%. M.p. 82.5–83.2°C. $[\alpha]_D = -26.4$ ($c = 0.25$, CH_2Cl_2). ^1H NMR (200 MHz, $CDCl_3$): δ 7.98–8.00 (m, 1H), 7.65–7.77 (m, 2H), 7.29–7.37 (m, 1H), 4.09 (d, $J = 9.5$ Hz, 1H), 2.35–2.55 (m, 3H), 2.09–2.14 (m, 2H), 1.22–1.82 (m, 4H), 0.90 (t, $J = 7.3$ Hz, 3H). ^{13}C NMR: $\delta = 208.2$, 196.7, 138.9, 135.6, 130.9, 129.9, 126.4, 63.5, 41.9, 41.4, 27.7, 27.0, 23.9, 10.6. HRMS calcd for $C_{15}H_{17}O_2Br$ 308.0411; found 308.0418.

Received: August 1, 1997 [Z10770IE]
German version: *Angew. Chem.* **1997**, *109*, 2733–2736

Keywords: 1,4-additions · aldol reactions · asymmetric synthesis · C–C coupling · homogeneous catalysis · zinc

 © WILEY-VCH Verlag GmbH, D-69451 Weinheim, 1997 0570-0833/97/3623-2622 $ 17.50+.50/0

[1] a) *Catalytic Asymmetric Synthesis* (Ed.: I. Ojima), VCH, Weinheim, **1993**; b) R. Noyori, *Asymmetric Catalysis in Organic Synthesis*, Wiley, New York, **1994**; c) H.-U. Blaser, B. Pugin, F. Spindler in *Applied Homogeneous Catalysis with Organometallic Compounds, Vol. 2* (Eds.: B. Cornils, W. A. Herrmann), VCH, Weinheim, **1996**, p. 992.
[2] Recent review: B. L. Feringa, A. H. M. de Vries in *Advances in Catalytic Processes, Vol. 1* (Ed: M. D. Doyle), JAI, CT, USA, **1995**, p. 151.
[3] a) Q.-L. Zhou, A. Pfaltz, *Tetrahedron* **1994**, *50*, 4467; b) M. van Klaveren, F. Lambert, D. J. F. M. Eijkelkamp, D. M. Grove, G. van Koten, *Tetrahedron Lett.* **1994**, *35*, 6135; c) M. Spescha, G. Rihs, *Helv. Chim. Acta* **1993**, *76*, 1219; d) M. Kanai, K. Tomioka, *Tetrahedron Lett.* **1995**, *36*, 4275; e) K. Soai, T. Hayasaka, S. Ugajin, S. Yokoyama, *Chem. Lett.* **1988**, 1571; f) C. Bolm, M. Ewald, *Tetrahedron Lett.* **1990**, *31*, 5011; g) A. H. M. de Vries, J. F. G. A. Jansen, B. L. Feringa, *Tetrahedron* **1994**, *50*, 4479; h) A. H. M. de Vries, B. L. Feringa, *Tetrahedron: Asymmetry* **1997**, *8*, 1377.
[4] An excellent review on recent progress in organocopper chemistry: N. Krause, A. Gerold, *Angew. Chem.* **1997**, *109*, 194; *Angew. Chem. Int. Ed. Engl.* **1997**, *36*, 187.
[5] a) A. H. M. de Vries, A. Meetsma, B. L. Feringa, *Angew. Chem.* **1996**, *108*, 2526; *Angew. Chem. Int. Ed. Engl.* **1996**, *35*, 2374; b) one other example of an enantioselective copper-catalyzed addition of Et_2Zn to cyclohexenone (*ee* 30%) has been reported: A. Alexakis, J. Frutos, P. Mangeney, *Tetrahedron: Asymmetry* **1993**, *4*, 2427.
[6] D. J. Berrisford, C. Bolm, K. B. Sharpless, *Angew. Chem.* **1995**, *107*, 1159; *Angew. Chem. Int. Ed Engl.* **1995**, *34*, 1059.
[7] a) Mismatched ligand *S,S,S*-**1** afforded **4a** with 82% yield and 75% *ee*; b) the introduction of substituents at the 3,3'-positions of the binaphthol moiety only marginally affected the enantioselectivities.
[8] The spectral and analytical data for all new compounds were in agreement with the indicated structures.
[9] Cu^I-catalyzed addition of functionalized organozinc reagents; B. H. Lipshutz, M. R. Wood, R. Tirado, *J. Am. Chem. Soc.* **1995**, *117*, 6126.
[10] F. Langer, A. Devasagayaraj, P.-Y. Chavant, P. Knochel, *Synlett* **1994**, 410.
[11] P. Knochel, R. D. Singer, *Chem. Rev.* **1993**, *93*, 2117.
[12] a) C. Ullenius, B. Christenson, *Pure Appl. Chem.* **1988**, *60*, 57; b) E. J. Corey, N. W. Boaz, *Tetrahedron Lett.* **1985**, *26*, 6015; c) N. Krause, R. Wagner, A. Gerold, *J. Am. Chem. Soc.* **1994**, *116*, 381; d) J. P. Snyder, *Angew. Chem.* **1995**, *107*, 80; *Angew. Chem. Int. Ed. Engl.* **1995**, *34*, 80.
[13] a) For a catalytic asymmetric tandem Michael–aldol reaction, see T. Arai, H. Sasai, K. Aoe, K. Okamura, T. Date, M. Shibasaki, *Angew. Chem.* **1996**, *108*, 103; *Angew. Chem. Int. Ed. Engl.* **1996**, *35*, 104; b) M. Kitamura, T. Miki, K. Nakano, R. Noyori, *Tetrahedron Lett.* **1996**, *37*, 5141.
[14] The X-ray structural analysis of compound **6b** was performed by Dr. A. L. Spek (Utrecht University). Details will be reported separately.
[15] Synthesis of **10**: G. L. Buchanan, R. A. Raphael, R. Taylor *J. Chem. Soc. Perkin 1* **1972**, 373, and references therein.
[16] A. Alexakis, J. C. Frutos, P. Mangeney, *Tetrahedron: Asymmetry* **1993**, *4*, 2431.

Palladium-Catalyzed Cross-Coupling of Organozinc Bromides with Aryl Iodides in Perfluorinated Solvents**

Bodo Betzemeier and Paul Knochel*

The formation of new carbon–carbon bonds by palladium-catalyzed cross-coupling has experienced a spectacular development over the past ten years.[1] Most of these reactions require relatively large quantities of a costly palladium catalyst (1–5 mol%)[2] and removal of traces of palladium compounds from the reaction products; this has hampered applications of this methodology to large-scale syntheses. Recently we showed that perfluorinated solvents are a convenient medium for transition metal catalyzed oxidations with a perfluorinated metal complex as the catalyst.[3,4] At high temperatures (ca. 60 °C) many organic solvents and reagents are soluble in perfluorinated solvents, but at room temperature organic compounds are insoluble; this leads to a two-phase system at room temperature. Fluorous biphasic catalysis, popularized by Horvárth,[5] has the advantage of easy phase separation and avoids pollution of the reaction product with the transition metal catalyst, which is only soluble in the fluorous phase and can be reused several times after simple phase separation. Here we report that palladium(0)-catalyzed cross-coupling[6] between arylzinc bromides (Ar^1ZnBr, **1**) and aryl iodides (Ar^2I, **2**) proceeds smoothly in the presence of the perfluorinated phosphane **3** (0.6 mol%) and bis(dibenzylideneacetone)palladium(0) ([Pd(dba)$_2$], 0.15 mol%)[7] with 1-bromoperfluorooctane ($C_8F_{17}Br$) and toluene as the solvent system to provide polyfunctional biphenyls of type **4** in high yields (Table 1).

Table 1. Palladium-catalyzed cross-coupling between arylzinc bromides **1** and aryl iodides **2** in a toluene/1-bromoperfluorooctane biphasic system.

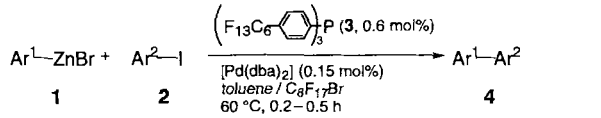

1 **2** **4**

Entry	Ar^1	Ar^2	Product **4**	Yield [%] [a]
1	Ph	4-$AcOC_6H_4$	**4a**	93
2	4-ClC_6H_4	4-$NO_2C_6H_4$	**4b**	93
3	4-ClC_6H_4	3-$EtO_2CC_6H_4$	**4c**	97
4	3-$CF_3C_6H_4$	4-$MeOC_6H_4$	**4d**	89
5	3-$CF_3C_6H_4$	4-BrC_6H_4	**4e**	92
6	2-thienyl	3-$MeOC_6H_4$	**4f**	98
7	2-thienyl	4-$NO_2C_6H_4$	**4g**	87
8	4-TIPS-OC_6H_4 [b]	3-$EtO_2CC_6H_4$	**4h**	97
9	4-TIPS-OC_6H_4	4-BrC_6H_4	**4i**	99

[a] Yield of isolated product. [b] TIPS = iPr_3Si.

Arylzinc bromides **1** were prepared from the corresponding aryl bromides by bromine–lithium exchange followed by lithium–zinc transmetalation with zinc bromide.[8] 2-Thienyllithium used to prepare 2-thienylzinc bromide was obtained by deprotonation of thiophene with *n*-butyllithium.[9] The use of triarylphosphane **3**, which bears long perfluorinated chains, is essential for the success of the reaction. No activity of the palladium catalyst was observed with the previously known $(C_6F_{13}C_2H_4)_3P$.[5,10] The new phosphane **3** was prepared in three steps from 4-iodoaniline. Treatment of **3** with copper and $C_6F_{13}I$ in DMSO (120 °C, 2 h) gave the substituted aniline **5** in 86% yield.[11] Sandmeyer reaction of **5** [a) $NaNO_2$, HBr; b) CuBr] provided the corresponding aryl bromide **6** in 76% yield. Bromine–lithium exchange with *n*BuLi in THF followed by addition of PCl_3 afforded the phosphane–borane complex **7** in 37% yield after protection with borane (Scheme 1). After **7** was purified, the borane protecting group was removed with diethylamine.[12]

The free phosphane **3** was treated with [Pd(dba)$_2$] in $C_8F_{17}Br$ to afford an orange solution of [Pd{P(C_6H_4-C_6F_{13})$_3$}$_4$] (**8**). With this catalyst (0.15 mol%), the reaction between an arylzinc bromide and an aryl iodide is complete within 0.5 h at 60 °C. At this temperature, the reaction mixture is homogeneous and a two-phase system is again obtained upon cooling to room temperature. The cross-coupling product **4** is easily

[*] Prof. Dr. P. Knochel, Dipl.-Chem. B. Betzemeier
Fachbereich Chemie der Universität
Hans-Meerwein-Strasse, D-35032 Marburg (Germany)
Fax: Int. code + (6421) 282-189
e-mail: knochel@ps1515.chemie.uni-marburg.de

[**] We thank the Deutsche Forschungsgemeinschaft (Schwerpunktprogramm "Peroxidchemie" and Leibniz-Preis) and the Fonds der Chemischen Industrie for generous financial support. We thank Elf-Atochem (France), Witco AG, BASF AG, Bayer AG, Chemetall GmbH, and SIPSY S.A. (France) for the generous gift of chemicals.

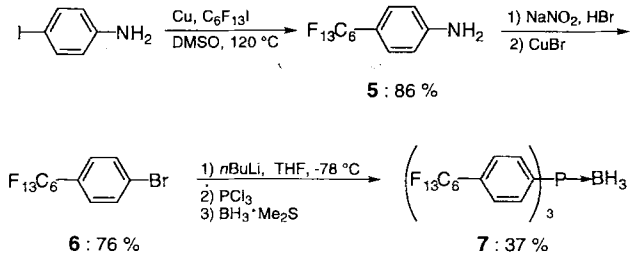

Scheme 1. Synthesis of perfluorinated phosphane **7**.

recovered from the toluene phase, whereas the palladium catalyst remains in the fluorous phase. The latter can be reused several times without significant changes in reaction yields. Thus, cross-coupling between phenylzinc bromide and 4-iodophenyl acetate in the presence of **8** (1.5 mol%) provides the biphenyl **4a** in 93% yield. Repeating the reaction four times with the same catalyst solution gave yields of 91, 90, 86, and 89%. Furthermore, **8** displays higher activity than $[Pd(PPh_3)_4]$, which may be due to the presence of the fluorinated carbon chain. It removes electron density from the phenyl ring to lead to an electron-deficient phosphane, and favors reductive elimination in these cross-couplings. The high activity of **8** allows the use of only 0.15 mol% of the catalyst under standard conditions. Upon further reducing the catalyst quantity to 0.07 mol%, a decrease in yield was observed (**4a** was obtained in only 76% yield, as opposed to 93%; Table 1, entry 1). Interestingly, these cross-coupling reactions tolerate several functional groups such as Cl, NO_2, CO_2R, CF_3, and iPr_3SiO. Furthermore, in the case of 4-bromoiodobenzene, only substitution of the iodide atom is observed; the C–Br bond is unaffected (entries 5 and 9). Cross-coupling can also be extended to alkenylzinc bromides[8] and benzylzinc bromides[13] to provide the styrene derivative **9** (76%) and diarylmethane **10** (92%), respectively (Scheme 2).

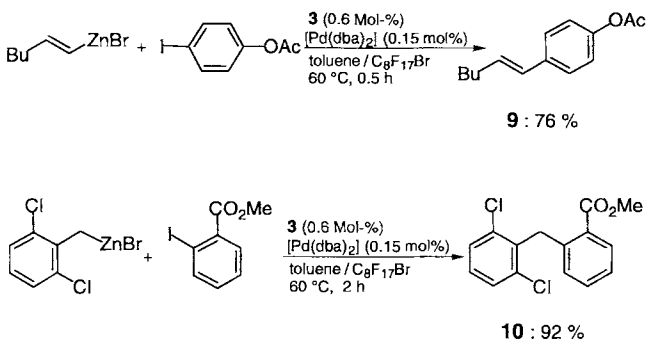

Scheme 2. Cross-coupling with an alkenyl- and a benzylzinc bromide.

We have prepared a new triarylphosphane **3** bearing perfluorinated substituents which allows efficient palladium-catalyzed cross-coupling between organozinc bromides and aryl iodides in biphasic catalysis. The simple work-up conditions and the possibility of reusing the catalyst for several reactions have been demonstrated. The performance of other transition metal catalyzed reactions of interest for organic synthesis with the new fluorous phosphane **3** is currently underway.

Experimental Section

Typical procedure: 4-acetoxybiphenyl (**4a**). A 10 mL Schlenk flask was charged with a solution of **8** (1.2 μmol, 0.15 mol%, prepared in situ) in $C_8F_{17}Br$ (2 mL). 4-Iodophenyl acetate (210 mg, 0.8 mmol) in toluene (2 mL) was added at 0°C followed by a solution of phenylzinc bromide (0.88 mmol, 1.1 equiv) in toluene (1 mL). The reaction mixture was stirred at 60°C for 0.5 h to provide a homogeneous solution. Upon cooling to 0°C, phase separation occured immediatly. The orange perfluorinated phase containing the catalyst **8** was recovered and could be used for further experiments. The organic phase was diluted with Et_2O and washed with a saturated aqueous solution of NH_4Cl. The crude product obtained after evaporation of the solvent was purified by flash chromatography (hexanes/ether 19/1) to yield pure **4a** (158 mg, 0.74 mmol, 93% yield).

Received: June 24, 1997 [Z105901E]
German version: *Angew. Chem.* **1997**, *109*, 2736–2738

Keywords: cross-coupling · fluorine · homogeneous catalysis · palladium · P ligands

[1] a) J. K. Stille, *Angew. Chem.* **1986**, *98*, 504; *Angew. Chem. Int. Ed. Engl.* **1986**, *25*, 508; b) N. Miyaura, A. Suzuki, *Chem. Rev.* **1995**, *95*, 2457; V. Farina, B. Krishnan, *J. Am. Chem. Soc.* **1991**, *113*, 9585; c) V. Farina, S. Kapadia, B. Krishnan, C. Wang, L. S. Liebeskind, *J. Org. Chem.* **1994**, *59*, 5905; d) I. Klement, M. Rottländer, C. E. Tucker, T. N. Majid, P. Knochel, *Tetrahedron* **1996**, *52*, 7201.

[2] For the use of highly efficient catalytic systems, see a) W. A. Herrmann, C. Brossmer, K. Öfele, C.-P. Reisinger, T. Priermeier, M. Beller, H. Fischer, *Angew. Chem.* **1995**, *107*, 1989; *Angew. Chem. Int. Ed. Engl.* **1995**, *35*, 1844; b) M. Beller, H. Fischer, W. A. Herrmann, K. Öfele, C. Brossmer, *ibid.* **1995**, *107*, 1992 and **1995**, *35*, 1848; c) J. Lourie, J. F. Hartwig, *ibid.* **1996**, *108*, 2531 and **1996**, *36*, 2359.

[3] I. Klement, H. Lütjens, P. Knochel, *Angew. Chem.* **1997**, *109*, 1605; *Angew. Chem. Int. Ed. Engl.* **1997**, *36*, 1496.

[4] I. Klement, P. Knochel, *Synlett* **1995**, 1113; *ibid.* **1996**, 1004.

[5] a) I. T. Horvárth, J. Rábai, *Science* **1994**, *266*, 72; b) S. M. Pereira, G. P. Savage, G. W. Simpson, *Synth. Commun.* **1995**, *25*, 1023; c) R. P. Hughes, H. A. Trujillo, *Organometallics* **1996**, *15*, 286; d) D. P. Curran, S. Hadida, *J. Am. Chem. Soc.* **1996**, *118*, 2531; e) D. P. Curran, M. Hoshino, *J. Org. Chem.* **1996**, *61*, 6480; f) D. P. Curran, *Chemtracts. Org. Chem.* **1996**, *9*, 75.

[6] a) E. Negishi, L. F. Valente, M. Kobayashi, *J. Am. Chem. Soc.* **1980**, *102*, 3298; b) M. Kobayashi, E. Negishi, *J. Org. Chem.* **1980**, *45*, 5223; c) E. Negishi, *Acc. Chem. Res.* **1982**, *15*, 340; Y. Tamaru, H. Ochiai, T. Nakamura, Z. Yoshida, *Tetrahedron Lett.* **1986**, *27*, 955.

[7] M. F. Rettig, P. M. Maitlis, *Inorg. Synth.* **1977**, *17*, 134.

[8] C. E. Tucker, T. N. Majid, P. Knochel, *J. Am. Chem. Soc.* **1992**, *114*, 3983.

[9] L. Brandsma, H. Verkruijsse, *Preparative Polar Organometallic Chemistry 1*, Springer, Heidelberg, **1987**, p. 125.

[10] F. Langer, K. Püntener, R. Stürmer, P. Knochel, *Tetrahedron: Asymmetry* **1997**, *8*, 715.

[11] a) Q. Y. Chen, Z. Y. Yang, Y. B. He, *J. Fluorine Chem.* **1987**, *37*, 171; b) N. Yoshino, M. Kitamura, T. Seto, Y. Shibata, M. Abe, K. Ogino, *Bull. Chem. Soc. Jpn.* **1992**, *65*, 2141.

[12] a) T. Imamoto, T. Kusomoto, N. Suzuki, K. Sato, *J. Am. Chem. Soc.* **1985**, *107*, 5301; b) A. Börner, J. Ward, W. Ruth, J. Holz, A. Kless, D. Heller, H. B. Kagan, *Tetrahedron Lett.* **1994**, *50*, 10419.

[13] S. C. Berk, M. C. P. Yeh, N. Jeong, P. Knochel, *Organometallics* **1990**, *9*, 3053.

 © WILEY-VCH Verlag GmbH, D-69451 Weinheim, 1997 0570-0833/97/3623-2624 $ 17.50+.50/0

Synthesis and Structure of Aluminum-Fluorine-Oxygen Clusters**

Said D. Waezsada, Feng-Quan Liu, Craig E. Barnes, Herbert W. Roesky,* Mavis L. Montero, and Isabel Usón

Dedicated to Professor Heribert Offermanns on the occasion of his 60th birthday

AlF_3 and cryolite (Na_3AlF_6) are of great importance in the exploitation of aluminum[1] and belong along with hydrogen fluoride to the most important technical inorganic fluorine products. In contrast, organic compounds with the composition $RAlF_2$ are virtually unknown. K. Ziegler mentioned the reaction of $EtAlCl_2$ with sodium fluoride; however the reaction product was not fully characterized.[2] We recently showed that $(R)(R')NAlMe_2$ compounds react with Me_3SnF under formation of Me_4Sn to give $(R)(R')NAlF_2$.[3] Structure analyses have shown that these compounds exist as trimers in the absence of donor solvents. On treatment with anhydrous THF, the trimers react as expected to give adducts with the composition $(R)(R')NAlF_2 \cdot THF$. We have now established that, depending on the substituents R and R', successive reactions can occur on recrystallizing the THF adducts from *n*-hexane. In the case of the compounds $(2,6\text{-}i\text{Pr}_2C_6H_3)[Si(i\text{Pr})Me_2]NAlF_2 \cdot THF$ (**1**) and $(2,6\text{-}i\text{Pr}_2C_6H_3)[Si(t\text{Bu})Me_2]NAlF_2 \cdot THF$ (**2**), the adducts are regenerated quantitatively. Compounds in which the substituents in the *ortho* position of the phenyl ring (group R) or the substituents on the silicon atom (group R') are smaller behave in a completely different manner; the compounds $(2,6\text{-}Me_2C_6H_3)[Si(t\text{Bu})Me_2]NAlF_2 \cdot THF$ (**3**) and $(2,6\text{-}i\text{Pr}_2C_6H_3)(SiMe_3)NAlF_2 \cdot THF$ (**4**) are converted into the aluminum clusters **3a** and **4a**, respectively, which both contain an oxygen atom in the center of the Al_6F_{12} tetrakishexahedron [Eq. (1)].

$$\underset{\mathbf{3,4}}{6\,(R)(R')NAlF_2 \cdot THF} \xrightarrow[-2\,(R)(R')NH]{n\text{-hexane}} \underset{\mathbf{3a,4a}}{[(R)(R')NAlF_2]_4[AlF_2(thf)]_2O} \qquad (1)$$

The basic framework of **1** corresponds to that of **2**, and that of **3a** corresponds to that of **4a**. It was therefore decided to dispense with a detailed discussion of the geometrical crystallographic data of **2** and **3a**. Compound **1** crystallized in the monoclinic space group $P2_1/c$.[4] Al(1) in **1** (Figure 1) is coordinated in a slightly distorted tetrahedral fashion with bond angles of between 98.6° and 118.1°. The average Al–F bond length (165.7 pm) is comparable with the terminal Al–F bond lengths in $[(2,6\text{-}i\text{Pr}_2C_6H_3)(SiMe_3)NAlF_2]_3$.[3] Compound **4a** also crystallized in the monoclinic space group $P2_1/c$.[4] Each Al atom in **4a** is six-coordinate (Figure 2). The aluminum atoms are each bonded to four fluorine atoms and to the central oxygen atom. In addition, amino groups are coordinated to Al(1) and Al(2), and a THF molecule to Al(3); the coordination sphere of these Al atoms can be described as distorted *trans*-octahedral (AlF_4ON and AlF_4O_2). The fluorine atoms each bridge two aluminum atoms; the average Al–F bond length is 182.8 pm. This value is significantly larger than the average terminal Al–F distance in **1**. The *trans*- and *cis*- F-Al-F angles at Al(3) (average value 172.0° and 89.9°, respectively) are larger than the angles at Al(1) and Al(2) (average values 150.2° and 86.5°, respectively). The O(3) atom in the center of the cage is coordinated in a distorted octahedral fashion to six aluminum atoms. The Al–O distance is shorter for Al(3) (1.903 pm) than for Al(1) and Al(2) (average value 2.267 pm).

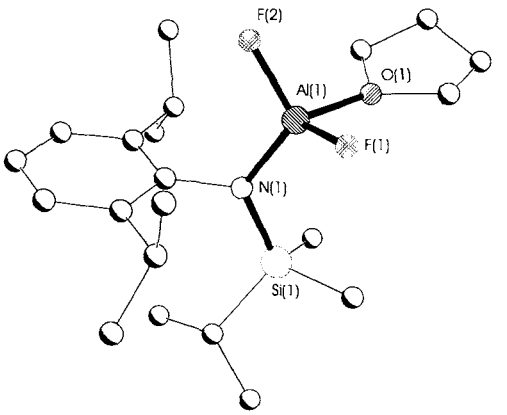

Figure 1. Structure of **1** in the crystal. Selected bond lengths [pm] and angles [°]: Al(1)–F(2) 165.3(2), Al(1)–F(1) 166.0(2), Al(1)–N(1) 180.9(2), Al(1)–O(1) 185.6(2); F(2)-Al(1)-F(1) 112.0(1), F(2)-Al(1)-N(1) 112.3(1), F(1)-Al(1)-N(1) 118.1(1), F(2)-Al(1)-O(1) 104.4(1), F(1)-Al(1)-O(1) 98.6(1), N(1)-Al(1)-O(1) 109.6(1).

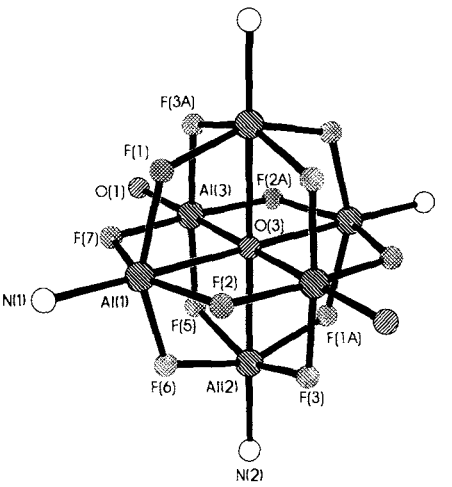

Figure 2. Structure of **4a** in the crystal. For clarity, only the atoms of the THF solvent molecules and the ligands bonding to aluminum are shown. Selected bond lengths [pm] and angles [°]: Al(2)–F(1A) 184.0(2), Al(3)–F(3A) 179.9(2), Al(3)–F(2A) 179.9(2); F(7)-Al(1)-F(1) 86.1(1), F(2)-Al(1)-F(6) 86.4(1), F(2)-Al(1)-F(1) 85.7(1), F(7)-Al(1)-F(6) 86.6(1), F(1)-Al(1)-F(6) 150.1(1), N(1)-Al(1)-O(3) 179.2(1), F(7)-Al(1)-F(2) 150.1(1), F(5)-Al(2)-F(6) 86.0(1), N(1)-Al(1)-F(6) 105.5(1), F(1)-Al(1)-O(3) 75.1(1), F(7)-Al(3)-F(5) 89.9(1), F(7)-Al(3)-O(1) 93.6(1).

The insertion of oxygen under elimination of two amine molecules could be caused by water or THF. In order to clarify this, temperature-dependent ^1H NMR and ^{19}F NMR spectra were made from solutions of **1** and **3** in $[D_8]$toluene (−90 to 0 °C). As expected, a singlet occurs in the ^{19}F NMR spectrum of **1** down to −90 °C. In contrast, the singlet in the ^{19}F NMR spectrum of **3** ($\delta = -174.3$ at room temperature) splits into three signals ($\delta = -134.2, -165.6, 172.7$) in the ratio 1:1:1 at −90 °C. Moreover, traces of the eliminated amine are evident in the ^1H NMR spectrum of **3**. The ^{19}F NMR spectrum of **3a**

[*] Prof. Dr. H. W. Roesky, Dipl.-Chem. S. D. Waezsada, Dr. F.-Q. Liu, Prof. C. E. Barnes, Dr. M. L. Montero, Dr. I. Usón
Institut für Anorganische Chemie der Universität
Tammannstrasse 4, D-37077 Göttingen (Germany)
Fax: Int. code + (551) 39-3373
e-mail: hroesky@gwdg.de

[**] This work was supported by the Deutsche Forschungsgemeinschaft.

([D$_6$]benzene) shows a number of resonance signals at room temperature that split into two signals in the ratio 1:2 at 70 °C. This spectrum can be unequivocally attributed to the cluster structure. The ^{1}H NMR spectra of the (R)(R′)NAlF$_2$ · THF compounds have both the expected resonance signals. No differentiation between coordinated THF and free THF is observed at −90 °C on addition of further amounts of THF to the samples. This confirms the rapid exchange of the THF molecules.

The possibility of a partial hydrolysis was ruled out by the controlled hydrolysis of a sample of **4**; the Me_3SiF signal in the ^{19}F NMR spectrum was of greater intensity after the hydrolysis. Thus, only the reaction with THF needs to be taken into consideration. Indeed, reactions of aliphatic ethers with halides of Group 13 have often been reported.[7] The reaction of R_2O with BCl_3 leads to the formation of RCl and $ROBCl_2$. In contrast, the corresponding reaction with BF_3 leads to alcohols (or water) and olefins.[8] Investigations into analogous reactions of THF with BF_3[9] and $AlCl_3$[10] have also been reported; these always led to cleavage of the THF and opening of the ring. Thus, the aluminum-fluorine-oxygen clusters obtained are dependent on the substituents R and R′ of (R)(R′)NAlF$_2$ · THF. A molecular compound of oxygen in which the oxygen atom is surrounded by six main group elements was thus obtained for the first time. This type of structure was, until now, only known for the d- and f-block elements.[1]

Received: July 10, 1997 [Z10667IE]
German version: *Angew. Chem.* **1997**, *109*, 2738–2739

Keywords: aluminum · clusters · fluorine · O ligands

[1] A. F. Holleman, E. Wiberg, *Lehrbuch der Anorganischen Chemie*, 101 st ed., de Gruyter, Berlin, **1995**.
[2] K. Ziegler, Max-Planck-Institut für Kohlenforschung, Mülheim, GB-B 779.873, **1957** [*Chem. Abstr.* **1957**, *51*, 17981 a].
[3] S. D. Waezsada, F.-Q. Liu, E. F. Murphy, H. W. Roesky, M. Teichert, I. Usón, H.-G. Schmidt, T. Albers, E. Parisini, M. Noltemeyer, *Organometallics* **1997**, *16*, 1260.
[4] Crystal structure analyses: **1**: $C_{21}H_{38}AlF_2NOSi$, $M_r = 413.59$, monoclinic space group $P2_1/c$, $a = 954.7(2)$, $b = 1324.6(3)$, $c = 1951.7(4)$ pm, $\beta = 90.54(3)°$, $V = 2.468(1)$ nm^3, $Z = 4$, $\rho_{calcd} = 1.113$ g cm^{-3}, $F(000) = 896$, $\lambda = 71.073$ pm, $T = 243$ K, $\mu(Mo_{K\alpha}) = 0.155$ mm^{-1}. Crystal dimensions: $0.4 \times 0.4 \times 0.2$ mm^3. $6 \le 2\theta \le 44°$. Of the 5216 reflections collected, 3226 were independent and used for the structure refinement of 252 parameters with the aid of 0 restraints. $R1 = 0.0572$ ($I > 2\sigma(I)$), $wR2 = 0.1722$ (all data), min./max. residual electron density: −332/226 e nm^{-3}. **2**: $C_{22}H_{41}AlF_2NOSi$, $M_r = 428.64$, triclinic space group $P\bar{1}$, $a = 1445.9(7)$, $b = 1638(1)$, $c = 2345.7(9)$ pm, $\alpha = 90.23(2)$, $\beta = 101.83(2)$, $\gamma = 110.54(2)°$, $V = 5.074(4)$ nm^3, $Z = 8$, $\rho_{calcd} = 1.122$ g cm^{-3}, $F(000) = 1864$, $\lambda = 71.073$ pm, $T = 193$ K, $\mu(Mo_{K\alpha}) = 0.153$ mm^{-1}. Crystal dimensions: $0.4 \times 0.3 \times 0.3$ mm^3. $4 \le 2\theta \le 52°$. Of the 78028 reflections collected, 20680 were independent and used for the structure refinement of 1225 parameters with the aid of 1204 restraints. $R1 = \Sigma||F_o| - |F_c||/|\Sigma F_o| = 0.0558$ ($I > 2\sigma(I)$), $wR2 = [\Sigma w(F_o^2 - F_c^2)^2/\Sigma wF_o^4]^{1/2} = 0.1244$ (all data), min./max. residual electron density: −250/563 e nm^{-3}. **3a**: $C_{64}H_{112}Al_6F_{12}N_4O_3Si_4$, $M_r = 1487.84$, monoclinic space group $P2_1/c$, $a = 3180.8(4)$, $b = 1569.4(3)$, $c = 2692.2(4)$ pm, $\beta = 113.11(1)°$, $V = 12.361(3)$ nm^3, $Z = 6$, $\rho_{calcd} = 1.261$ g cm^{-3}, $F(000) = 5004$, $\lambda = 71.073$ pm, $T = 133$ K, $\mu(Mo_{K\alpha}) = 0.209$ mm^{-1}. Crystal dimensions: $0.4 \times 0.4 \times 0.2$ mm^3. $4 \le 2\theta \le 52°$. Of the 41945 reflections collected, 22119 were independent and used for the structure refinement of 1525 parameters with the aid of 664 restraints. $R1 = 0.0725$ ($I > 2\sigma(I)$), $wR2 = 0.1702$ (all data), min./max. residual electron density: −613/696 e nm^{-3}. **4a**: $C_{68}H_{120}Al_6F_{12}N_4O_3Si_4$, $M_r = 1543.95$, monoclinic space group $P2_1/c$, $a = 1338.7(3)$, $b = 2468.3(8)$, $c = 1509.8(7)$ pm, $\beta = 115.82(2)°$, $V = 4.491(3)$ nm^3, $Z = 2$, $\rho_{calcd} = 1.248$ g cm^{-3}, $F(000) = 1804$, $\lambda = 71.073$ pm, $T = 193$ K, $\mu(Mo_{K\alpha}) = 0.197$ mm^{-1}. Crystal dimensions: $0.7 \times 0.6 \times 0.6$ mm^3. $6 \le 2\theta \le 48°$. Of the 8978 reflections collected, 7803 were independent and used for the structure refinement of 579 parameters with the aid of 338 restraints. $R1 = 0.0609$ ($I > 2\sigma(I)$), $wR2 = 0.1845$ (all data); min./max. residual electron density: −487/360 e nm^{-3}. The data from **1** and **3a** were collected by using a Stoe-Siemens-Huber four-circle diffractometer with a Siemens CCD surface detector. The intensities were recorded with and ω scans. The integration of the data was performed with the program SAINT. The data from **2** and **4a** were collected on a Stoe-Siemens-AED four-circle diffractometer. The structures were solved by direct methods (SHELXS-90/96) [5] and refined by the least-squares method against F^2. All non-hydrogen atoms were refined anisotropically [6]. All hydrogen atoms were positioned at the ideal geometric sites and included in the refinement. All disorders were resolved by means of distance restraints and *ADP*-restraints and refined anisotropically. The crystallographic data (excluding structure factors) for the structures reported in this paper have been deposited with the Cambridge Crystallographic Data Centre as supplementary publication no. CCDC-100624. Copies of the data can be obtained free of charge on application to the Director, CCDC, 12 Union Road, Cambridge CB21EZ (fax: int. code + (1223)336-033; e-mail: deposit@chemcrys.cam.ac.uk).
[5] G. M. Sheldrick, *Acta Crystallogr. Sect. A* **1990**, *46*, 467.
[6] G. M. Sheldrick, SHELXL-93/96, Programm für die Kristallstrukturverfeinerung, Universität Göttingen, **1993**.
[7] V. Bhatt, S. U. Kulkarni, *Synthesis* **1983**, 249.
[8] F. Mooney, M. A. Qaseem, *J. Chem. Soc. Chem. Commun.* **1967**, 230.
[9] C. Eaborn, N. Retta, J. D. Smith, P. B. Hitchcock, *J. Organomet. Chem.* **1982**, *235*, 265.
[10] L. Smith, *Organometallics* **1995**, *14*, 3098.

A Sequential Photoinduced Electron Relay Accelerated by Fullerene in a Porphyrin-Pyromellitimide-C_{60} Triad**

Hiroshi Imahori,* Koji Yamada, Masato Hasegawa, Seiji Taniguchi, Tadashi Okada,* and Yoshiteru Sakata*

Dedicated to Professor Emanuel Vogel on the occasion of his 70th birthday

In addition to displaying a variety of unique properties such as superconductivity, biological activity, and ferromagnetism,[1] C_{60} is a good electron acceptor as well as a sensitizer when employed in photophysical and photochemical processes.[2,3] We[3,4] and others[5–7] demonstrated that C_{60} can accelerate photoinduced charge separation (CS) and decelerate charge recombination (CR) in donor-linked fullerenes. Utilization of such a building block in more elaborate molecular systems seems to be promising for the construction of solar energy conversion systems. In photosynthesis the fundamental principle for converting light into chemical potential energy is photodriven CS and subsequent fast electron relay between well-arranged pigments within the reaction center.[8] Although there have been numerous attempts to mimic vectorial electron transport across the

[*] Dr. H. Imahori, Prof. Y. Sakata, K. Yamada
Institute of Scientific and Industrial Research
Osaka University
Mihoga-oka, Ibaraki, Osaka 567 (Japan)
Fax: Int. code + (6) 879-8479
e-mail: imahori@sanken.osaka-u.ac.jp
sakata@sanken.osaka-u.ac.jp
Prof. T. Okada, M. Hasegawa, S. Taniguchi
Department of Chemistry, Faculty of Engineering Science and
Research Center for Materials Science at Extreme Conditions
Osaka University
Toyonaka, Osaka 560 (Japan)
Fax: Int. code + (6) 850-6244
e-mail: okada@chem.es.osaka-u.ac.jp

[**] This work was supported by the Ministry of Education, Science, Sports and Culture, Japan (grants-in-aid 07213220, 07454166 (Y.S.), 05NP0301 (T.O.), 08740495 (H.I.)).

 © WILEY-VCH Verlag GmbH, D-69451 Weinheim, 1997 0570-0833/97/3623-2626 $ 17.50+.50/0

membrane using synthetic molecular arrays, it is still difficult to achieve a long-lived CS state with a high quantum yield without loss of a large amount of the input energy by the light.[9]

Here we report the synthesis and photophysical properties of the porphyrin-pyromellitimide-C_{60} triad **1** (P-Im-C_{60}; P = porphyrin, Im = imide). The energy gradients of each state are in the order P^*-Im-C_{60} > $P^{\bullet+}$-$Im^{\bullet-}$-C_{60} > $P^{\bullet+}$-Im-$C_{60}^{\bullet-}$. Accordingly, **1** will display a sequential electron transfer (ET) that is quite similar to primary ET events at reaction centers of photosynthesis. In addition, it is expected that the unique properties of C_{60} in ET will increase the yield of the CS state and prolong the lifetime[3,4] by storing a substantial amount of the excitation energy. The characteristic intense absorption band due to the imide anion radical as well as the conformational rigidity will be helpful for analyzing the dynamics of ET.[10]

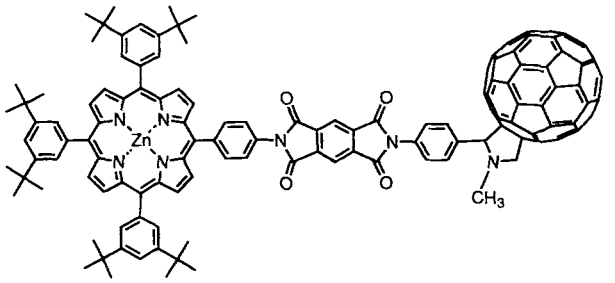

1

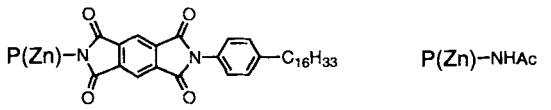

2 **3**

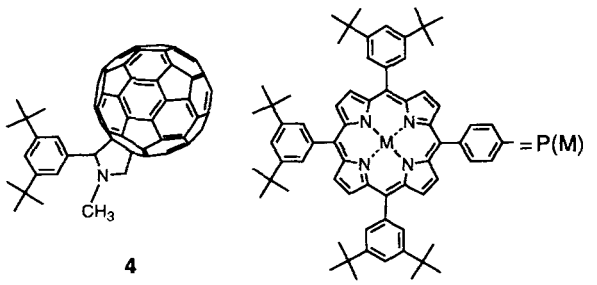

4

The synthesis of **1** is shown in Scheme 1. Cross-condensation of aminoporphyrin **5**, pyromellitic dianhydride, and protected formyl aniline in dimethylformamide (DMF) followed by deprotection of the formyl group gave pyromellitimide-substituted porphyrin **6** in 19% yield. The zincporphyrin-pyromellitimide-C_{60} triad **1** was obtained in 33% yield by 1,3-dipolar cycloaddition with **6**, *N*-methylglycine, and C_{60} in toluene and subsequent treatment with $Zn(OAc)_2$.[11] C_{60}-free dyads **2** as well as single-chromophore compounds **3** and **4** were also synthesized as references. Their structures were verified by analytical methods including ^1H and ^{13}C NMR spectroscopy and MALDI-TOF (matrix-assisted laser desorption/ionization time-of-flight) mass spectrometry.

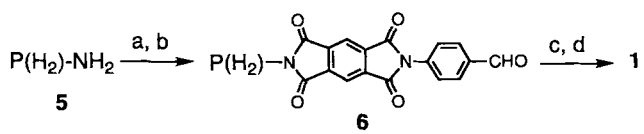

5 **6**

Scheme 1. Synthesis of **1**; a) pyromellitic dianhydride, 4-(5,5-dimethyl-1,3-dioxan-2-yl)aniline, DMF, reflux, overnight; b) trifluoroacetic acid (TFA), H_2SO_4, $CHCl_3$, room temperature, overnight; c) C_{60}, *N*-methylglycine, toluene, reflux, 6 h; d) $Zn(OAc)_2$, $CHCl_3$, reflux, 30 min.

The absorption spectra of **1** in dioxane and THF are essentially a linear combination of the absorption spectra of **2** and **4**, and give no indication for strong interactions between these chromophores. The absorption due to the C_{60} unit is much weaker and broader than that of the porphyrin, whereas discernible absorption of the imide moiety appears around 250–300 nm. The redox potentials of **1** (in CH_2Cl_2 with 0.1M nBu_4NPF_6 as a supporting electrolyte and quoted relative to the ferrocene/ferrocenium potential: −1.50, −1.21, −1.13, +0.31, +0.67 V) correspond roughly to the sum of **2** (−1.22, +0.31, +0.67 V) and **4** (−1.54, −1.15 V).

The fluorescence spectra of **1** and **2** are quenched more strongly than those of **3** when excited at the Soret band at the same concentration (0.06 for **1**, 0.08 for **2** in dioxane). These results show rapid quenching of the excited singlet state of the porphyrin by the imide, because the porphyrin is excited selectively.

Before discussing the photodynamics of **1**, those of **2** are described as a simple model. The transient spectrum of **2** in dioxane 20 ps after excitation with a pulse at 590 nm shows the immediate rise of bands at 650 and 720 nm, which are assigned to the zinc porphyrin radical cation ($ZnP^{\bullet+}$)[4] and imide radical anion ($Im^{\bullet-}$), respectively. The time profile of the absorbance at 456 nm, which corresponds to the $S_n \leftarrow S_1$ absorption of the porphyrin ($^1ZnP^*$) and $ZnP^{\bullet+}$, was analyzed by a single exponential decay with a time constant of 180 ps (Figure 1). Measurement of the fluorescence lifetime of **2** was carried out by a picosecond single photon counting technique with excitation at 400 nm and monitoring at 650 nm, the wavelength at which fluorescence is due only to the porphyrin. The decay curve at 650 nm was fitted by one major exponential decay with a time constant of 160 ps, which is in good agreement with that of the absorbance decay at 456 nm.

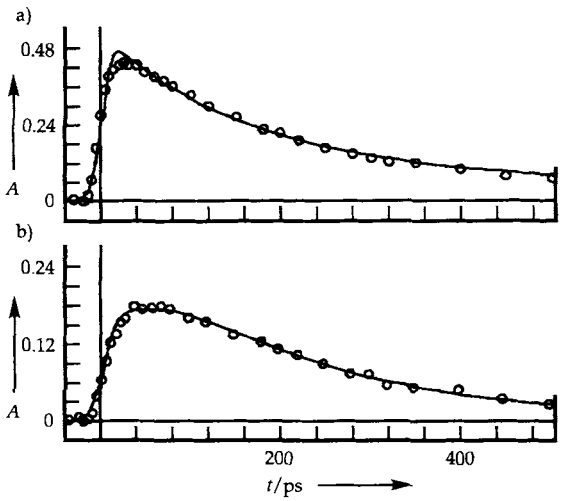

Figure 1. Time profiles of transient absorbances *A* of **2** in dioxane at a) 456 and b) 720 nm after excitation at 590 nm. The time constants for the exponential decrease in intensity is 180 ps in both cases; for b) the intensity of the absorption initially increases with a time constant of 60 ps.

 © WILEY-VCH Verlag GmbH, D-69451 Weinheim, 1997 0570-0833/97/3623-2627 $ 17.50+.50/0

On the other hand, the transient absorbance at 720 nm arises with a time constant of 60 ps and decays with that of 180 ps. These results indicate that CR is faster than CS, even in a nonpolar solvent like dioxane; the lifetime of the ion pair is considered to be 60 ps ($= \tau_1$).[4,10] The time-resolved transient absorption spectra for **1** in dioxane are shown in Figure 2. Immediately after excitation of **1** with a pulse at

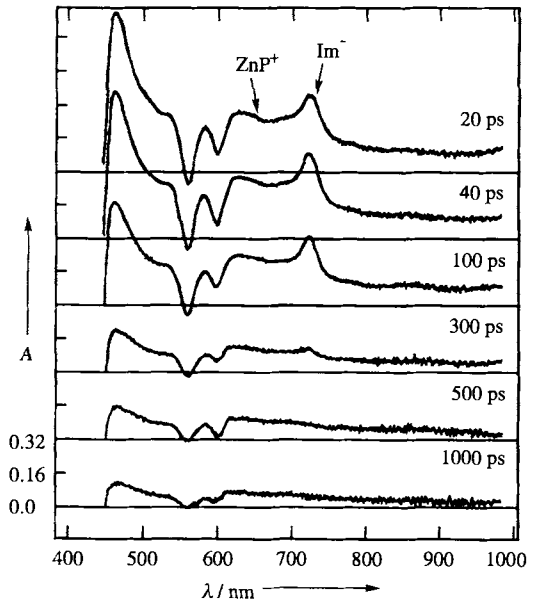

Figure 2. Absorption spectra of **1** in dioxane at different times (resolution in picosecond range) after excitation at 590 nm. The delay times between excitation and measurement are indicated on the right. A = Absorbance.

590 nm—the wavelength at which the porphyrin and the C_{60} unit absorb in a ratio of 14:1—bleaching of the ground-state porphyrin absorption of the Q bands at 560 and 600 nm, intense absorption with a maximum near 470 nm, and characteristic bands at 650 and 720 nm (attributable to $ZnP^{\bullet+}$ and $Im^{\bullet-}$, respectively) were observed. The absorbances at 460, 650, and 720 nm show biphasic decays with time constants of 120 ps and 1.3 ns; those at 650 and 720 nm display an additional rise with a time constant of 30 ps. However, the band for $Im^{\bullet-}$ decays much faster (120 ps) than that for $ZnP^{\bullet+}$. This shows the sole broad absorption due to ZnP^+, which eventually decays with a time constant of 1.3 ns. These results clearly demonstrate the initial formation of $ZnP^{\bullet+}$-$Im^{\bullet-}$-C_{60} followed by a charge shift (CSH) to produce $ZnP^{\bullet+}$-Im-$C_{60}^{\bullet-}$.[12] The photodynamic behavior of **1** in dioxane is summarized in Scheme 2.[13] The fluorescence decay of **1** at 650 nm was analyzed by one major exponential decay with a time constant of 100 ps, which is consistent with that of 120 ps for absorbance decays at 460, 650, and 720 nm. This implies that the rate constant k_{CR1} for charge recombination in **1** is larger than that for charge seperation (k_{CS}), which is similar to the situation with **2**; the lifetime of $ZnP^{\bullet+}$-$Im^{\bullet-}$-C_{60} is considered to be 30 ps ($= \tau_2$). Therefore, the rate constant for charge shift (k_{CSH}) is estimated to be $1.6 \times 10^{10}\ s^{-1}$ according to Equation (a).

$$k_{CSH} = (k_{CSH}+k_{CR1}) - k_{CR1} = 1/\tau_2 - 1/\tau_1 \qquad \text{(a)}$$

In spite of the small difference (0.08 V) in electron-accepting abilities between the imide and the C_{60} moieties, the rate

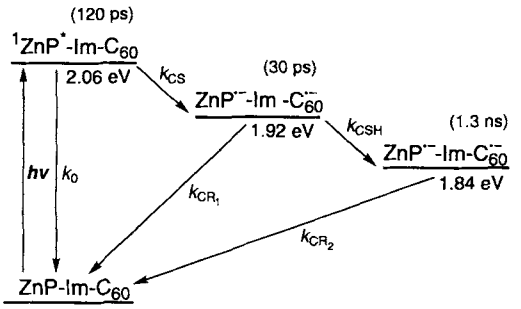

Scheme 2. Reaction scheme and energy diagram for **1** in dioxane [13]. The lifetime of each state is given in parentheses. $k_0 = 5.0 \times 10^8$, $k_{CS} = 7.8 \times 10^9$, $k_{CR1} = 1.7 \times 10^{10}$, $k_{CSH} = 1.6 \times 10^{10}$, and $k_{CR2} = 7.7 \times 10^8\ s^{-1}$.

of CSH competes well with that of CR ($k_{CR1} = 1.7 \times 10^{10}\ s^{-1}$), resulting in the formation of $ZnP^{\bullet+}$-Im-$C_{60}^{\bullet-}$ with a total quantum yield of 0.46.[10] It is remarkable that the lifetimes of the S_1 state due to the porphyrin are quite different for **1** and **2**; the lifetime of **1** is about 30% shorter than that of **2**. This may be explained by the acceleration effect of C_{60} on imide moiety mediated ET through the spacer[3,4,6] or the direct through-space ET from $^1ZnP^*$ to C_{60} concomitant with sequential ET. In the more polar solvent such as THF, excitation of **1** leads to the formation of $ZnP^{\bullet+}$-$Im^{\bullet-}$-C_{60} within 20 ps, but CR is much faster than CS, which makes formation of $ZnP^{\bullet+}$-Im-$C_{60}^{\bullet-}$ quite difficult.[10,13]

A sequential ET relay that mimicks the reaction center of photosynthesis and the resulting fairly long-lived CS state with moderate quantum yield have been realized in the triad system involving fullerene. These results show that C_{60} is a suitable building block for systems showing artificial photosynthesis. We are currently applying this strategy for the construction of solar energy conversion systems.[14]

Experimental Section

1: ^1H NMR (270 MHz, $CDCl_3$): $\delta = 9.05$ (d, 2H, $J = 5$ Hz), 9.03 (d, 2H, $J = 5$ Hz), 9.01 (d, 2H, $J = 5$ Hz), 8.97 (d, 2H, $J = 5$ Hz), 8.40 (s, 2H), 8.33 (d, 2H, $J = 8$ Hz), 8.12 (d, 4H, $J = 2$ Hz), 8.04 (d, 2H, $J = 2$ Hz), 7.92 (d, 2H, $J = 8$ Hz), 7.81 (t, 2H, $J = 2$ Hz), 7.76 (t, 1H, $J = 2$ Hz), 7.72 (m, 2H), 7.62 (d, 2H, $J = 8$ Hz), 4.42 (d, 1H, $J = 10$ Hz), 4.25 (s, 1H), 3.63 (d, 1H, $J = 10$ Hz), 2.66 (s, 3H), 1.56 (s, 54H); MALDI-TOF MS: $m/z = 2077$ $[M+H]^+$; UV/Vis (dioxane): $\lambda_{max} = 255$, 318, 405, 426, 518, 556, 596 nm.

Received: April 16, 1997 [Z10358IE]
German version: *Angew. Chem.* **1997**, *109*, 2740–2742

Keywords: donor–acceptor systems · electron transfer · fullerenes · photosynthesis · porphyrinoids

[1] A. Hirsch, *The Chemistry of the Fullerenes*, Thieme, Stuttgart, **1994**.
[2] C. S. Foote, *Top. Curr. Chem.* **1994**, *169*, 347; N. S. Sariciftci, *Prog. Quantum Electron.* **1995**, *19*, 131; A. W. Jensen, S. R. Wilson, D. I. Schuster, *Bioorg. Med. Chem.* **1996**, *4*, 767.
[3] H. Imahori, Y. Sakata, *Adv. Mater.* **1997**, *9*, 537.
[4] H. Imahori, K. Hagiwara, T. Akiyama, S. Taniguchi, T. Okada, Y. Sakata, *Chem. Lett.* **1995**, 265; H. Imahori, S. Cardoso, D. Tatman, S. Lin, L. Noss, G. R. Seely, L. Sereno, J. Chessa de Silber, T. A. Moore, A. L. Moore, D. Gust, *Photochem. Photobiol.* **1995**, *62*, 1009; H. Imahori, Y. Sakata, *Chem. Lett.* **1996**, 199; H. Imahori, K. Hagiwara, M. Aoki, T. Akiyama, S. Taniguchi, T. Okada, M. Shirakawa, Y. Sakata, *J. Am. Chem. Soc.* **1996**, *118*, 11771; H. Imahori, K. Hagiwara, T. Akiyama, M. Aoki, S. Taniguchi, T. Okada, M. Shirakawa, Y. Sakata, *Chem. Phys. Lett.* **1996**, *263*, 545; Y. Sakata, H. Imahori, H. Tsue, S. Higashida, T. Akiyama, E. Yoshizawa, M. Aoki, K. Yamada, K. Hagiwara, S. Taniguchi, T. Okada, *Pure Appl. Chem.* **1997**, *69*, 1951.
[5] P. A. Liddell, J. P. Sumida, A. N. Macpherson, L. Noss, G. R. Seely, K. N. Clark, A. L. Moore, T. A. Moore, D. Gust, *Photochem. Photobiol.* **1994**, *60*,

 © WILEY-VCH Verlag GmbH, D-69451 Weinheim, 1997 0570-0833/97/3623-2628 $ 17.50+.50/0

537; D. Kuciauskas, S. Lin, G. R. Seely, A. L. Moore, T. A. Moore, D. Gust, T. Drovetskaya, C. A. Reed, P. D. W. Boyd, *J. Phys. Chem.* **1996**, *100*, 15926; P. A. Liddell, D. Kuciauskas, J. P. Sumida, B. Nash, D. Nguyen, A. L. Moore, T. A. Moore, D. Gust, *J. Am. Chem. Soc.* **1997**, *119*, 1400.

[6] R. M. Williams, J. M. Zwier, J. W. Verhoeven, *J. Am. Chem. Soc.* **1995**, *117*, 4093; J. M. Lawson, A. M. Oliver, D. F. Rothenfluh, Y.-Z. An, G. A. Ellis, M. G. Ranasinghe, S. I. Khan, A. G. Franz, P. S. Ganapathi, M. J. Shephard, M. N. Paddon-Row, Y. Rubin, *J. Org. Chem.* **1996**, *61*, 5032; R. M. Williams, M. Koeberg, J. M. Lawson, Y.-Z. An, Y. Rubin, M. N. Paddon-Row, J. W. Verhoeven, *ibid.* **1996**, *61*, 5055.

[7] N. S. Sariciftci, F. Wudl, A. J. Heeger, M. Maggini, G. Scorrano, M. Prato, J. Bourassa, P. C. Ford, *Chem. Phys. Lett.* **1995**, *247*, 510; D. M. Guldi, M. Maggini, G. Scorrano, M. Prato, *J. Am. Chem. Soc.* **1997**, *119*, 974.

[8] *The Photosynthetic Reaction Center, Vol. 1,2* (Eds.: J. Deisenhofer, J. R. Norris), Academic Press, San Diego, **1993**.

[9] J. S. Connolly, J. R. Bolton in *Photoinduced Electron Transfer, Part D* (Eds.: M. A. Fox, M. Chanon), Elsevier, Amsterdam, **1988**, p. 303; M. R. Wasielewski in *Photoinduced Electron Transfer, Part A* (Eds.: M. A. Fox, M. Chanon), Elsevier, Amsterdam, **1988**, p. 161; *Chem. Rev.* **1992**, *92*, 435.

[10] M. Ohkohchi, A. Takahashi, N. Mataga, T. Okada, A. Osuka, H. Yamada, K. Maruyama, *J. Am. Chem. Soc.* **1993**, *115*, 12137; A. Osuka, S. Marumo, N. Mataga, S. Taniguchi, T. Okada, I. Yamazaki, Y. Nishimura, T. Ohno, K. Nozaki, *ibid.* **1996**, *118*, 155.

[11] M. Maggini, G. Scorrano, M. Prato, *J. Am. Chem. Soc.* **1993**, *115*, 9798.

[12] The characteristic band of C_{60}^{-} at 900–1100 nm lies outside the limits of the detector: T. Kato, T. Kodama, T. Shida, T. Nakagawa, Y. Matsui, S. Suzuki, H. Shiromaru, K. Yamauchi, Y. Achiba, *Chem. Phys. Lett.* **1991**, *180*, 446.

[13] The Gibbs energy for CR and CS, $-\Delta G_{CR}$ and $-\Delta G_{CS}$, are given by Equations (b)–(d); where $\Delta E_{0\text{-}0}$ is energy of the 0–0 transition between the

$$-\Delta G_{CR} = E_{ox} - E_{red} + \Delta G_s \quad \text{(b)}$$

$$-\Delta G_{CS} = \Delta E_{0\text{-}0} - (-\Delta G_{CR}) \quad \text{(c)}$$

$$\Delta G_s = \varepsilon^2/(4\pi\varepsilon_0)[\{1/(2R^+) + 1/(2R^-) - 1/R_{CC}\}(1/\varepsilon_s) - \{1/(2R^+) + 1/(2R^-)\}(1/\varepsilon_r)] \quad \text{(d)}$$

S_1 and S_0 states for the porphyrin, E_{ox} and E_{red} are the first oxidation potential of the donor and the first reduction potential of the acceptor in CH_2Cl_2, R^+ and R^- are the radii of D and A ($R^+(P) = 5.0$, $R^-(Im) = 3.5$, $R^-(C_{60}) = 4.4$ Å). R_{cc} is the distance between the centers of the two moieties ($R_{CC}(P{-}Im) = 12.3$, $R_{CC}(P{-}C_{60}) = 23.5$ Å), and ε_s and ε_r are static dielectric constants of solvent used and, when measured, the redox potentials ($\varepsilon_s = 7.4$ in THF and $\varepsilon_r = 8.9$ in CH_2Cl_2). In dioxane the Born equation does not give correct values for ΔG_s because of an overestimation of the polarity. Therefore, the value of $\Delta G_s = 0.40$ eV in dioxane is used tentatively, assuming that the value of ΔG_s for this system is identical to that of porphyrin-linked quinones: T. Asahi, M. Ohkohchi, R. Matsusaka, N. Mataga, R. P. Zhang, A. Osuka, K. Maruyama, *J. Am. Chem. Soc.* **1993**, *115*, 5665.

[14] T. Akiyama, H. Imahori, Y. Sakata, *Chem. Lett.* **1994**, 1447; T. Akiyama, H. Imahori, A. Ajavakom, Y. Sakata, *ibid.* **1996**, 907.

Detection of Scalar $^6Li,^{15}N$ Coupling across Coordinative Li–N Bonds**

Dietmar Hüls, Harald Günther,* Gerard van Koten, P. Wijkens, and J. T. B. H. Jastrzebski

Dedicated to Professor Reiner Radeglia on the occasion of his 60th birthday

Scalar NMR spin–spin coupling constants are structural parameters characteristic for the bonding and the connectivity in molecular systems. They also play an essential part in the structural elucidation of organolithium compounds.[1] In particular $^6Li,^{13}C$ and $^6Li,^{15}N$ couplings are important indicators of aggregate size, since their magnitude depends on the aggregation state of the metalated species.[1,2]

A typical phenomenon in organolithium chemistry is the stabilization of organometallic clusters through coordination with donor ligands like ethereal solvents or amines.[3] In particular *N,N,N′,N′*-tetramethylethylenediamine (TMEDA) finds broad application. These ligands can be detected quite frequently by NMR spectroscopy through signal integration or heteronuclear Overhauser (HOESY) experiments.[4] However, scalar coupling between lithium and ligand atoms is usually not observed. An exception are scalar $^6Li,^{15}N$ couplings for Li–N chelate bonds in a chiral bidendate lithium amide,[5a] for lithium hexamethylsilazide,[5b] and in 2-(dimethylaminomethyl)phenyllithium,[6] as well as $^7Li,^{31}P$ interactions in complexes between lithium cations and hexamethylphosphoric triamide (HMPTA).[7] We report here the detection of $^6Li,^{15}N$ coupling across coordinative Li–N bonds in a 2:2 benzyl/butyllithium aggregate.

Reaction of 1,3-bis(dimethylaminomethyl)-2,4,6-trimethylbenzene (**1**) with *n*-BuLi in a 1:1 molar ratio leads to the

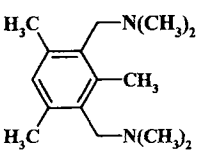

1

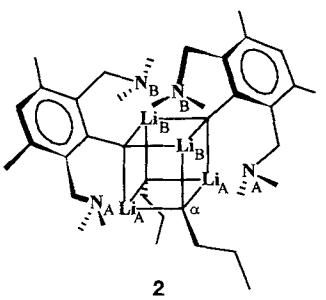

2

mixed aggregate **2**,[8] for which X-ray analysis yields relatively short Li–N distances of 212.3(6) pm for Li_A-N_A and 204.5(7) pm for Li_B-N_B.[8] A detailed NMR investigation of [^{6}Li]-**2**[9] confirms the tetrameric structure also for the compound in solution. Thus, in the region of slow exchange at 231 K, where inter- as well as intra-aggregate dynamics are "frozen" on the NMR time scale, we find two ^6Li resonances at $\delta = 0.68$ and 0.77 (relative to 0.1 M LiBr as external standard in THF, Figure 1a), which show in the $^6Li,^6Li$ INADEQUATE

[*] Dipl.-Chem. D. Hüls, Prof. Dr. H. Günther
Organische Chemie II, Fachbereich 8 der Universität
D-57068 Siegen (Germany)
Fax: Int. code + (271) 740-2512
Prof. Dr. G. van Koten, P. Wijkens, Dr. J. T. B. H. Jastrzebski
Debye Institute, Department of Metal-Mediated Synthesis
Utrecht University
Padualaan 8, NL-3584 CH Utrecht (The Netherlands)
Fax: Int. code + (2) 523-615

[**] NMR Spectroscopy of Organolithium Compounds, Part 21; Part 20: B. Böhler, H. Günther, *Tetrahedron Lett.* **1996**, *37*, 8723–8724.

 © WILEY-VCH Verlag GmbH, D-69451 Weinheim, 1997 0570-0833/97/3623-2629 $ 17.50+.50/0

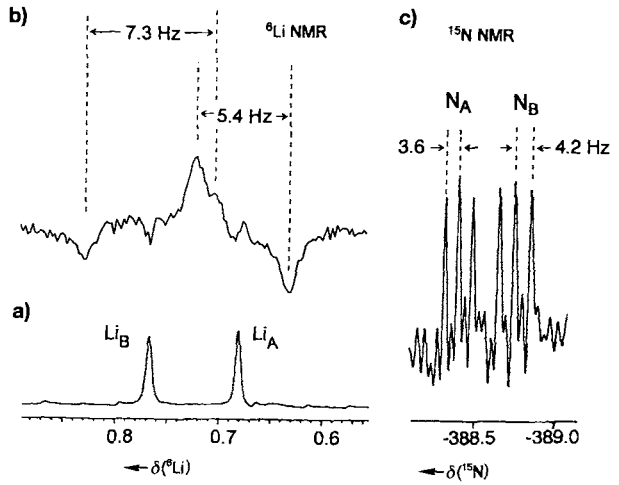

Figure 1. a) One-dimensional ^{6}Li NMR spectrum (58.88 MHz) of [^{6}Li]-**2**; δ scale relative to 0.1 M LiBr in THF. b) One-dimensional ^{6}Li,^{13}C HMQC experiment (58.88/100.13 MHz) for [^{6}Li]-**2** (0.24 M in [D_8]toluene); $T = 230$ K; $1/2J = 68.5$ ms, sweepwidth 35.3 Hz, relaxation delay 1 s; number of experiments 4 K; time for measurement 5.3 h; c) ^{15}N{^{1}H} NMR spectrum (40.54 Hz) of [^{6}Li]-**2** with ^{15}N in natural abundance (0.36%); sweepwidth 6.67 kHz; number of experiments 16 K; relaxation delay 2 s; δ scale relative to $CH_3{}^{15}NO_2$; time for measurement 11.3 h. All spectra were recorded on a Bruker AMX-400 spectrometer.

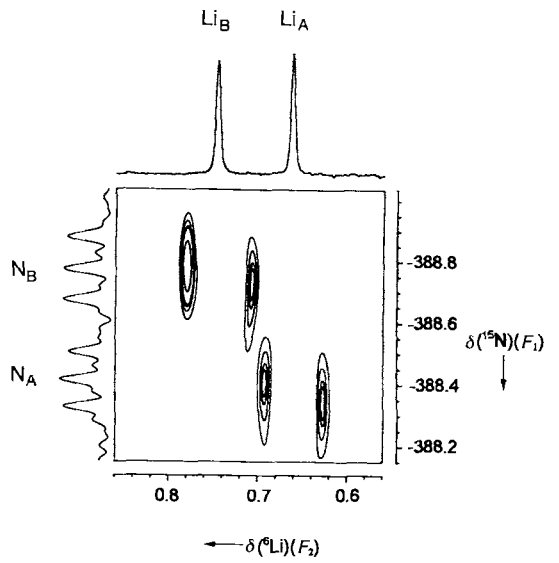

Figure 2. Two-dimensional ^{6}Li,^{15}N HMQC spectrum (55.88/40.54 MHz) of [^{6}Li]-**2** (0.24 M in [D_8]toluene) with ^{15}N in natural abundance (0.36%); $1/2J = 129.9$ ms, sweepwidths 65.9 Hz in F_1 (^{15}N) and 96 Hz in F_2 (^{6}Li); 12 t_1 experiments, 256 data points in F_2; digital resolution 5.49/0.38 Hz (F_1/F_2); 768 transients; time for measurement 6.5 h [19].

experiment[10] a homonuclear scalar ^{6}Li,^{6}Li coupling of 0.1 Hz. In the ^{13}C NMR spectrum only the lithiated carbon of the *n*-butyl residue, C_α, shows splitting by scalar ^{6}Li,^{13}C coupling. As in the majority of other benzyl lithium systems, the ^{6}Li,^{13}C coupling to the benzylic carbon is not resolved.[11]

The assignment of the two ^{6}Li resonances, which is important for the discussion below, follows from the different intensity of the ^{6}Li,$^{13}C_\alpha$ correlation signals found in the 2D ^{6}Li,^{13}C HMQC experiment[12] and of the ^{13}C satellites in the 1D ^{6}Li,^{13}C HMQC spectrum[1b] (Figure 1b). In both cases the high-field ^{6}Li signal shows the higher intensity and can thus be assigned to the Li_A positions, which are adjacent to *two* butyl residues and thus belong to a spin system with twice the ^{13}C natural abundance. From the satellite spectra as well as by line-shape analysis of the ^{13}C signal we obtained $J(^6Li_A,{}^{13}C_\alpha) = 5.4$ Hz and $J(^6Li_B,{}^{13}C_\alpha) = 7.3$ Hz.

To our surprise, the ^{15}N NMR spectrum then showed a 1:1:1 triplet splitting (Figure 1c) for the two ^{15}N resonances, expected on the basis of the C_2 symmetry of the aggregate, at $\delta = -388.4$ and -388.7 (relative to $CH_3{}^{15}NO_2$ as external standard). The coupling constants are 3.6 and 4.2 Hz for $J(Li_A,N_A)$ and $J(Li_B,N_B)$, respectively. The observed 1:1:1 multiplicity as well as the 2D ^{6}Li,^{15}N HMQC experiment[13] (Figure 2) performed in order to assign the ^{15}N resonances identify both splittings beyond doubt as ^{6}Li,^{15}N interactions. The assignment of the ^{15}N resonances and consequently also that of the observed couplings by the 2D ^{6}Li,^{15}N HMQC experiment rest on the ^{6}Li assignment discussed above.

Scalar coupling of this type has been detected so far nearly exclusively for lithium amides.[14] The scalar coupling across a coordinative bond found here can be explained by the short Li–N distances found in the solid, which are apparently maintained in solution. Remarkably, the magnitude of the coupling constants correlates with Li–N distances more typical for Li–N bonds in lithium amides[15] than for coordinative bonds of amine ligands (around 212–230 pm).[15] A correspondence between the distance of coupled nuclei and the magnitude of a scalar spin–spin interaction was also found in the case of a ^{15}N,^{107,109}Ag coupling in a bidentate silver(I) complex with amine/imine ligands.[16,17] A possible explanation of the unusual spin–spin interaction comes from the "through-space" mechanism, which is well established for ^{19}F,^{19}F and ^{1}H,^{1}H interactions in cases of steric compression.[18] Dynamic processes could be responsible for the fact that no ^{6}Li,^{15}N coupling has yet been found for TMEDA ligands.[20]

Received: May 6, 1997 [Z10414IE]
German version: *Angew. Chem.* **1997**, *109*, 2743–2744

Keywords: ligand effects · lithium · NMR spectroscopy

[1] Reviews: a) H. Günther in *Encyclopedia of NMR, Vol. 5* (Eds.: D. M. Grant, R. K. Harris), Wiley, Chichester, **1996**, pp. 2807–2828; b) in *Advanced Applications of NMR to Organometallic Chemistry* (Eds.: M. Gielen, R. Willem, B. Wrackmeyer), Wiley, Chichester, **1996**, pp. 247–290; c) D. B. Collum, *Acc. Chem. Res.* **1993**, *26*, 227–234; d) L. M. Jackman, J. Bortiatynski in *Advances in Carbanion Chemistry* (Ed.: V. Snieckus), Jai, Greenwich, CT (USA), **1992**, pp. 45–87; e) W. Bauer, P. von R. Schleyer in *Advances in Carbanion Chemistry* (Ed.: V. Snieckus), Jai, Greenwich, CT, **1992**, pp. 89–175; f) R. D. Thomas in *Isotopes in the Physical and Biomedical Sciences* (Eds.: E. Buncel, J. R. Jones), Elsevier, Amsterdam, **1991**, pp. 367–410.

[2] a) G. Fraenkel, M. Henrichs, J. M. Hewitt, B. M. Su, M. J. Geckle, *J. Am. Chem. Soc.* **1980**, *102*, 3345–3350; b) D. Seebach, H. Siegel, J. Gabriel, R. Hässig, *Helv. Chim. Acta* **1980**, *63*, 2046–2053; c) D. Seebach, R. Hässig, J. Gabriel, *ibid.* **1983**, *66*, 308–337; d) W. Bauer, W. R. Winchester, P. von R. Schleyer, *Organometallics* **1987**, *6*, 2371–2379; e) H. Günther, D. Moskau, D. Schmalz, Angew. Chem. **1987**, *99*, 1242–1250; *Angew. Chem. Int. Ed. Engl.* **1987**, *26*, 1212–1220.

[3] a) E. Weiss, *Angew. Chem.* **1993**, *105*, 1565–1587; *Angew. Chem. Int. Ed. Engl.* **1993**, *32*, 1501–1523; b) W. N. Setzer, P. von R. Schleyer, *Adv. Organomet. Chem.* **1985**, *24*, 353–451.

[4] Review: W. Bauer in *Lithium Chemistry—A Theoretical and Experimental Overview* (Eds.: A.-M. Saspe, P. von R. Schleyer), Wiley, Chichester, **1995**, pp. 125–172.

[5] a) D. Sato, H. Kawasaki, I. Shimada, Y. Arata, K. Okamura, T. Date, K. Koga, *J. Am. Chem. Soc.* **1992**, *114*, 761–763; b) B. L. Lucht, D. B. Collum, *ibid.* **1996**, *118*, 3529–3530.

[6] H. J. Reich, B. Ö. Gudmundsson, *J. Am. Chem. Soc.* **1996**, *118*, 6074–6075.

[7] a) D. Barr, W. Clegg, R. E. Mulvey, R. J. Snaith, *J. Chem. Soc. Chem. Commun.* **1984**, 79–80; b) H. J. Reich, D. P. Green, N. H. Phillips, *J. Am. Chem. Soc.* **1989**, *111*, 3444–3445; c) H. J. Reich, J. P. Borst, R. J. Dykstra, D. P. Green, *ibid.* **1993**, *115*, 8728–8741.

[8] P. Wijkens, E. M. van Koten, M. D. Janssen, J. T. B. H. Jastrzebski, A. L. Spek, G. van Koten, *Angew. Chem.* **1995**, *107*, 239–242; *Angew. Chem. Int. Ed. Engl.* **1995**, *34*, 219–222.

 © WILEY-VCH Verlag GmbH, D-69451 Weinheim, 1997 0570-0833/97/3623-2630 $ 17.50+.50/0

[9] H. Günther, D. Hüls, unpublished results.
[10] a) O. Eppers, H. Günther, K.-D. Klein, A. Maercker, *Magn. Reson. Chem.* **1991**, *29*, 1065–1067; b) O. Eppers, T. Fox, H. Günther, *Helv. Chim. Acta* **1992**, *75*, 883–891; c) N. Chandrakumar, H.-E. Mons, D. Hüls, H. Günther, *Magn. Reson. Chem.* **1996**, *34*, 715–718; see also ref. [1].
[11] a) W. Zarges, M. Marsch, W. Koch, G. Frenking, G. Boche, *Chem. Ber.* **1991**, *124*, 543–549; b) G. Fraenkel, K. V. Martin, *J. Am. Chem. Soc.* **1995**, *117*, 10336–10344.
[12] a) D. Moskau, F. Brauers, H. Günther, A. Maercker, *J. Am. Chem. Soc.* **1987**, *109*, 5532–5534; b) H.-J. Gais, J. Vollhardt, H. Günther, D. Moskau, H. J. Lindner, S. Braun, *ibid.* **1988**, *110*, 978–980.
[13] J. H. Gilchrist, A. T. Harrison, D. J. Fuller, D. B. Collum, *Magn. Reson. Chem.* **1992**, *30*, 855–859; we were able for the first time to perform the experiment on a sample with ^{15}N in natural abundance.
[14] K. B. Aubrecht, D. B. Collum, *J. Org. Chem.* **1996**, *61*, 8674, and references therein; see also ref. [1c].
[15] K. Gregory, P. von R. Schleyer, R. Snaith, *Adv. Inorg. Chem.* **1991**, *37*, 47–142.
[16] a) G. C. van Stein, G. van Koten, K. Vrieze, C. Brevard, A. L. Spek, *J. Am. Chem. Soc.* **1984**, *106*, 1003–1010; b) G. C. van Stein, G. van Koten, K. Vrieze, C. Brevard, *Inorg. Chem.* **1984**, *23*, 4269–4278; c) G. van Koten, *NATO ASI Ser., Ser. C* **1990**, *322*, 1–142.
[17] For the systems described by Reich et al. [6] no X-ray data are available; the coupling constants of 2.5–2.7 Hz here are slightly smaller than in our case.
[18] a) J. Hilton, L. H. Sutcliffe, *Prog. NMR. Spectrosc.* **1975**, *10*, 27–39; b) L. Ernst, K. Ibrom, *Angew. Chem.* **1995**, *107*, 2010–2012; *Angew. Chem. Int. Ed. Engl.* **1995**, *34*, 1881–1882.
[19] We point out that the software for Bruker AMX spectrometers contains an error which may lead to mirror-image spectra and thus to erroneous signal assignments for X,Y correlations that employ the third frequency channel.
[20] **Note added in proof** (October 21, 1997): The detection of a $^{6}Li,^{15}N$ coupling (2 Hz) for the $[(\{[^{6}Li]BuLi\}_2\{[^{15}N](tmeda)_2\}]$ complex ($[D_8]$toluene, −110 °C) was recently reported: D. Waldmüller, B. J. Kotsatos, M. A. Nichols, P. G. Williard, *J. Am. Chem. Soc.* **1997**, *119*, 5479–5480.

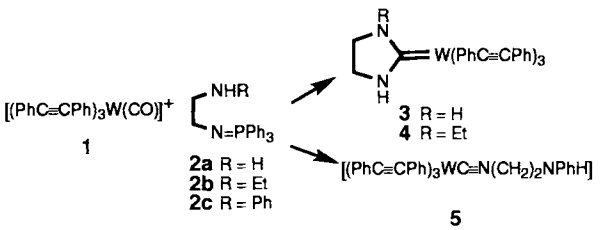

The crystal structure of **3** confirms the presence of a carbene moiety. Figure 1 shows the molecular structure of **3**, the first tungsten complex that contains only carbene and alkyne ligands. Comparing the bond lengths and angles of **3** and **1** shows the coordination geometry at the metal center to be essentially unchanged.[7] Apparently, changing from a π-acidic carbonyl ligand to a nucleophilic carbene ligand[8] has little influence on the structure. The W–C7 bond length (2.167(8) Å) lies within the normal range for metal carbene complexes and is only slightly shorter than that reported by Dötz et al. for $[(CO)_4W{=}C(OMe)(o\text{-}C_6H_4C{\equiv}CPh)]$ [2.181(5)Å].[2a]

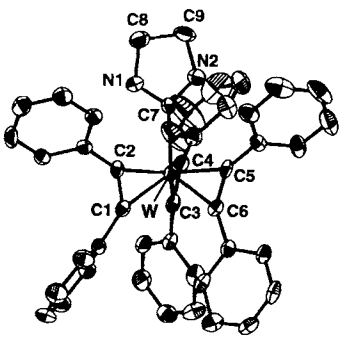

Figure 1. Molecular structure of **3** (numbering of aromatic carbon atoms omitted for clarity). Selected bond lengths [Å] and angles [°]: W–C7 2.167(8), W–C1 2.049(9), W–C2 2.064(8), W–C3 2.062(9), W–C4 2.067(9), W–C5 2.098(8), W–C6 2.053(8), C1–C2 1.32(1), C3–C4 1.31(1), C5–C6 1.30(1); W-C7-N1 124.4(6), W-C7-N2 132.9(6).

Novel Alkyne Carbene Tungsten Complexes**

Rong-Zhi Ku, Der-Yi Chen, Gene-Hsiang Lee, Shie-Ming Peng, and Shiuh-Tzung Liu*

Since the discovery of Fischer carbene complexes,[1a] numerous transition metal carbene complexes have been synthesized.[1] Among them, a few carbene complexes with coordinated alkyne ligands are known.[2–3] Such complexes are believed to be important intermediates for metal-mediated metathesis of alkynes.[2–4] Pioneering work by Dötz et al. has shown this reaction to be a versatile tool in organic synthesis.[4–5] All of these carbene complexes contain carbonyl ligands and transition metals in low oxidation states. We now report the synthesis of the first carbonyl-free alkyne carbene tungsten complexes **3** and **4**.

Treatment of **1** with an equimolar quantity of the amino-substituted iminophosphorane **2a** in dichloromethane gave the diaminocarbene complex **3** in 53% yield. The carbene group is presumably formed by deoxygenation of the carbonyl ligand by the iminophosphorane to give an isocyanide complex, which subsequently undergoes intramolecular attack by the amino group.[6] Complex **3** is stable in air and dissolves in most organic solvents. The ^{13}C NMR resonance of the carbene carbon atom at $\delta = 220.2$ is shifted downfield relative to that of $[(CO)_5W{=}C(NHCH_2)_2]$ ($\delta = 204.0$).[6]

[*] Prof. S.-T. Liu, R.-Z. Ku, D.-Y. Chen, G.-H. Lee, Prof. S.-M. Peng
Department of Chemistry, National Taiwan University
1, Roosevelt Road, Sec. 4, Taipeh, Taiwan 106 (Taiwan)
Fax: Int. code + (8862) 363-6359
e-mail: stliu@mail.ch.ntu.edu.tw

[**] This work was supported by the National Science Council of the Republic of China (Grant No. NSC86-2113-M002-21). We thank Professor Gwo-Rong Her for help in the mass determination of polymers.

The *N*-ethyl compound **4** was prepared analogously from **1** and **2b**, but the phenyl-substituted iminophosphorane **2c** did not give the corresponding cyclic carbene species. Instead, the isocyanide complex **5** was obtained, presumably for steric reasons and because of the lower nucleophilicity of the aromatic amine. The substituents on the alkyne ligands also influenced the formation of carbene complexes. Neither $[(PhC{\equiv}CEt)_3W(CO)]$ nor $[(EtC{\equiv}CEt)_3W(CO)]$ reacted with **2a** to give the desired complex, and tungsten starting material was recovered. This illustrates the limitations of iminophosphorane in extracting the oxygen atom from coordinated carbonyl ligands.[6] Nevertheless, this approach provides another synthetic route to diaminocarbenes.[9]

Complex **3** catalyzes the polymerization of diphenylacetylene. In a typical experiment, a mixture of **3** (10 mol%) and PhC≡CPh in chlorobenzene was heated to reflux for 48 h. Polydiphenylacetylene was obtained as a yellow precipitate in 66% yield (based on the amount of diphenylacetylene consumed). The reaction solution contained pentaphenylbenzene (1.3%), pentaphenylcyclopentadiene (2.3%), and hexaphenylbenzene (3.7%). The benzene derivatives are the result of trimerization, while the pentaphenylcyclopentadiene

is believed to be formed in a manner similar to that reported by Green et al. for the reaction of $[(PhC{\equiv}CPh)_3W(NCMe)]$ with *o*-diphenylphosphanylstyrene.[10] Polydiphenylacetylene is a yellow solid, insoluble in most organic solvents, even boiling dichlorobenzene. It was characterized by solid-state ^{13}C NMR and mass spectrometry. The parent peak at $m/z = 3402$ corresponds to 19 diphenylacetylene units. The ^{13}C NMR spectrum shows signals at $\delta = 125$ and 144 for the aromatic and olefinic carbon atoms, respectively. Possible applications of this polydiphenylacetylene are currently being investigated.

Experimental Section

3: A solution of **1** [7] (300 mg, 0.4 mmol) and iminophosphorane **2a** (141 mg, 0.44 mmol) in dichloromethane (20 mL) was stirred at 25 °C for 16 h. The solvents were removed and the residue was chromatographed on silica gel (15 g) with dichloromethane/hexane (2/5, v/v) as eluent. The eluate was collected and concentrated to give **3** as a white solid. M.p. 178–180 °C (decomp); ^1H NMR (300 MHz, $CDCl_3$): $\delta = 7.48-7.13$ (m, 30H, ArH), 6.50 (s, 2H, NH), 3.47(s, 4H, CH_2); ^{13}C NMR (75 MHz, $CDCl_3$): $\delta = 220.2$ (W=C), 198.9 (PhC), 181.7 (PhC), 143.9–125.5 (Ph), 45.8 (CH_2). Analysis: calcd for $C_{45}H_{36}N_2W$: C 68.53, H 4.60, N 3.55; found C 68.38, H 4.62, N 3.39.

Colorless single crystals of **3** were obtained by recrystallization from dichloromethane/hexane. Crystal data for **3**: $C_{45}H_{36}N_2W$, $M_r = 788.63$, orthorhombic, space group *Pbca*, $a = 20.589(5)$, $b = 20.463(6)$, $c = 16.503(6)$ Å, $V = 6953(4)$ Å^3, $Z = 8$, $\rho_{calcd} = 1.507$ g cm^{-3}, $\lambda = 0.7107$ Å, $\mu = 34.246$ cm^{-1}, $F(000) = 3144$, $T = 298$ K, crystal dimensions $0.30 \times 0.35 \times 0.70$ mm. All measurements were performed on a Nonius CAD-4 diffractometer and refined by a least-squares treatment. $R_F = 0.039$, $R_w = 0.040$ for 3344 reflections with $I_0 > 2.0\sigma(I_0)$ and 434 variables. The NRCVAX program was used for the computation.[11] Crystallographic data (excluding structure factors) for the structure reported in this paper have been deposited with the Cambridge Crystallographic Data Centre as supplementary publication no. CCDC-100570. Copies of the data can be obtained free of charge on application to The Director, CCDC, 12 Union Road, Cambridge CB21EZ, UK (Fax: Int. code + (1223)336-033; e-mail: deposit@chemcrys.cam.ac.uk).

4: White solid, m.p. 182–183 °C (decomp); ^1H NMR (300 MHz, $CDCl_3$): $\delta = 7.48-7.16$ (m, 30H), 3.81 (t, $^3J(H,H) = 9.3$ Hz, 2H), 3.26 (t, $^3J(H,H) = 9.3$ Hz, 2H), 2.27 (q, $^3J(H,H) = 7.4$ Hz, 2H), 0.03 (t, $^3J(H,H) = 7.4$ Hz, 3H); ^{13}C NMR (75 MHz, $CDCl_3$): $\delta = 219.9$, 198.5, 181.6, 143.8–125.5 (PhC), 47.4, 45.4, 43.2, 11.9; analysis: calcd for $C_{47}H_{40}N_2W$: C 69.12, H 4.94, N 3.43; found C 69.10, H 4.91, N 3.38.

5: White solid, m.p. 163–164 °C (decomp); ^1H NMR (300 MHz, $CDCl_3$): $\delta = 7.53-6.35$ (m, 35H), 4.07 (t, $^3J(H,H) = 5.3$ Hz, 2H), 3.43 (t, $^3J(H,H) = 5.3$ Hz, 2H); ^{13}C NMR (75 MHz, $CDCl_3$): $\delta = 193.7$, 177.9, 145.8, 142.2–112.8 (PhC), 44.2, 42.4; analysis: calcd for $C_{51}H_{40}N_2W$: C 70.84, H 4.66, N 3.24; found C 70.77, H 4.73, N 3.33.

Polydiphenylacetylene: Diphenylacetylene (225 mg) and **3** (100 mg, 0.126 mmol) in chlorobenzene were heated to reflux for 48 h. A yellow precipatate (149 mg, 66%) was collected by centrifugation with recovery of starting material (108 mg). ^{13}C NMR (solid state, 75 MHz): $\delta = 144$, 125; IR (KBr) $\tilde{\nu} = 1598$, 1578, 1492, 1441 cm^{-1}; MS (DCI): m/z 3402 ($[M+NH_4]^+$), 3224 ($[M+NH_4-178]^+$), 3046 ($[M+NH_4-2\times178]^+$), etc.

Received: May 2, 1997 [Z10409IE]
German version: *Angew. Chem.* **1997**, *109*, 2744–2746

Keywords: alkyne complexes · carbene complexes · polymerizations · tungsten

[1] a) E. O. Fischer, A. Maasböl, *Angew. Chem.* **1964**, *76*, 645; *Angew. Chem. Int. Ed. Engl.* **1964**, *3*, 580–581; b) P. Quayle in *Comprehensive Organic Functional Group Transformations, Vol. 5* (Eds.: A. L. Katritzky, O. Meth-Cohn, C. W. Rees), Pergamon, Oxford, **1995**, pp. 931–959.

[2] a) K. H. Dötz, T. Schäfer, F. Kroll, K. Harms, *Angew. Chem.* **1992**, *104*, 1257–1259; *Angew. Chem. Int. Ed. Engl.* **1992**, *31*, 1236–1238; b) S. G. Feng, P. S. White, J. L. Templeton, *Organometallics* **1993**, *12*, 2131–2139; c) N. M. Agh-Atabay, J. L. Davidson, G. Douglas, K. W. Muir, *J. Chem. Soc. Chem. Commun.* **1989**, 549–551; d) E. M. Carnahan, J. D. Protasiewicz, S. J. Lippard, *Acc. Chem. Res.* **1993**, *26*, 90–97; e) G. A. McDermott, A. Mayr, *J. Am. Chem. Soc.* **1987**, *109*, 580–582; f) J. D. Protasiewicz, A. Masschelein, S. J. Lippard, *ibid.* **1993**, *115*, 808–810 and references therein..

[3] a) J. Bao, W. D. Wulff, J. B. Dominy, M. J. Fumo, E. B. Grant, A. C. Rob, M. C. Whitcomb, S.-M. Yeung, R. L. Ostrander, A. L. Rheingold, *J. Am. Chem. Soc.* **1996**, *118*, 3392–3405; b) H. Rudler, A. E. Chelain, D. R. Goumont, A. Massound, A. Parlier, P. M. Rudler, R. Yefsah, C. Alvarez, F. Delgado-Reyes, *Chem. Soc. Rev.* **1991**, *20*, 503–531.

[4] K. H. Dötz in *Organometallics in Organic Synthesis* (Eds.: H. tom Dieck, A. de Meijere), Springer, Berlin, **1988**.

[5] a) K. H. Dötz, *Angew. Chem.* **1984**, *96*, 573–594; *Angew. Chem. Int. Ed. Engl.* **1984**, *23*, 587–608; b) *ibid.* **1975**, *87*, 672–673;. **1975**, *14*, 644–645.

[6] C.-Y. Liu, D.-Y. Chen, M.-C. Cheng, S.-M. Peng, S.-T. Liu, *Organometallics* **1996**, *15*, 1055–1061.

[7] R. M. Laine, R. E. Moriarty, R. Bau, *J. Am. Chem. Soc.* **1972**, *94*, 1402–1403.

[8] M. Regitz, *Angew. Chem.* **1996**, *108*, 791–794; *Angew. Chem. Int. Ed. Engl.* **1996**, *35*, 725—728 and references therein.

[9] a) W. A. Herrmann, M. Elison, J. Fischer, C. Köcher, G. R. J. Artus, *Chem. Eur. J.* **1996**, *2*, 772–780; b) K. Öfele, M. Herberhold, *Angew. Chem.* **1970**, *82*, 775–776; *Angew. Chem. Int. Ed. Engl.* **1970**, *9*, 739–740; c) B. Cetinkaya, E. Cetinkaya, M. F. Lappert, *J. Chem. Soc. Dalton Trans.* **1973**, 906–912.

[10] G. A. Cairns, N. Carr, M. Green, M. F. Mahon, *Chem. Commun.* **1996**, 2431–2432.

[11] F. E. Gabe, F. L. Lee, *Acta Crystallogr. Sect. A* **1981**, *37*, S339.

A Convergent Synthesis of (+)-Parviflorin, (+)-Squamocin K, and (+)-5*S*-Hydroxyparviflorin**

Barry M. Trost,* Trevor L. Calkins, and Christian G. Bochet

The diverse bioactivities of the annonaceous acetogenins as antitumor, immunosuppressive, pesticidal, antiprotozoal, anthelmintic, and antimicrobial agents have resulted in considerable attention being focused upon them.[1,2] The acetogenins almost invariably have the butenolide fragment **A** as a head group. Frequently, the most biologically active ones possess a hydroxyl group at C-4 of **A** and a dihydroxy bis(tetrahydrofuran) unit **B** somewhere in the chain.

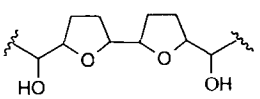

B

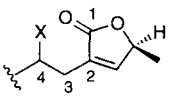

A

Special interest accrues to those members that show remarkable differential cell cytotoxicity. For example, parviflorin (squamocin E, **1**)[3] shows ED_{50} values against human lung, breast, and colon carcinoma of 1.3×10^{-15}, 1.7, and 0.5 respectively. In trying to devise a convenient convergent general strategy to these bioactive acetogenins, we chose parviflorin as a target because of its partially hidden symmetry revealed by our retrosynthetic analysis outlined in Scheme 1. Regio- and diastereoselective introduction of the C-4 hydroxyl

[*] Prof. Dr. B. M. Trost, Dr. T. L. Calkins, Dr. C. G. Bochet
Department of Chemistry, Stanford University
Stanford, CA 94305-5080 (USA)
Fax: Int. code + (650) 725-0259
e-mail: bmtrost@leland.stanford.edu

[**] We thank the National Institutes of Health, General Medical Sciences, and the National Science Foundation for their generous support of our programs. T.L.C. was supported in part by an NIH postdoctoral fellowship and C.G.B. was supported by a Swiss National Science Foundation fellowship. Mass spectra were provided by the Mass Spectrometry Facility, University of California-San Francisco, supported by the NIH Division of Research Resources.

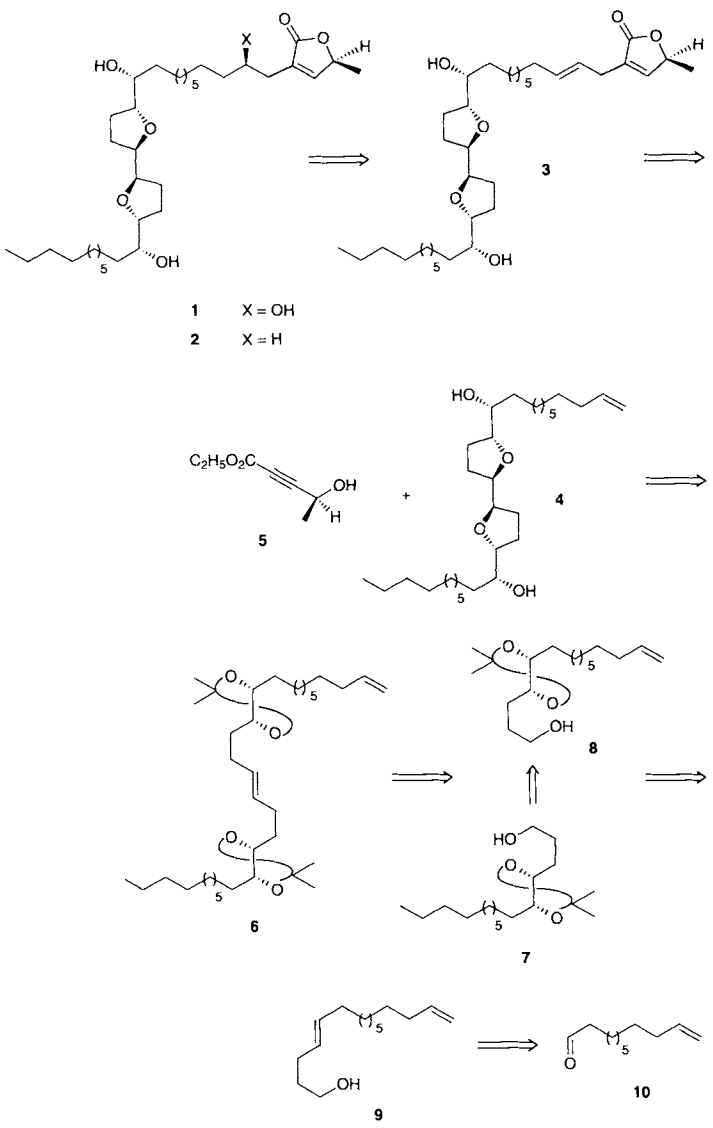

Scheme 1. Retrosynthesis of parviflorin (**1**).

group from an alkene precursor suggests that **3** may be a viable option. Such a precursor is particularly useful, since the double bond can serve as a focal point to diverge to other acetogenins such as squamocin K (**2**) or analogues by chemoselective oxidation at or adjacent to this alkene. The availability of our recently developed Ru-catalyzed Alder–ene type reaction[4] suggests as precursors the alkene **4** and alkyne **5**, which is already readily available from *S*-lactic ester.[4] The bis(tetrahydrofuran) **4** nearly possesses a C_2 symmetry axis; the presence of the terminal double bond is the only feature destroying this symmetry element. Envisioning the *trans*-alkene **6** as the precursor to **4** suggests an olefination to join **7** and **8** to create **6**. It is now obvious that since hydrogenation of **8** creates **7**, the former then becomes both halves of **4** and should readily derive from commercially available 10-undecenal (**10**) via the known **9**.[5] Thus, two units of **8** and one unit of **5** converge to create parviflorin and squamocin K.[6,7] In this paper, we report the realization of Scheme 1.

The first two nearly identical blocks **7**[8] and **8**[8] were synthesized as shown in Scheme 2 from **9**, which was prepared in three steps from **10** as previously described.[5] Dihydroxylation by the Sharpless protocol[9] required monitoring to avoid overoxidation. Stopping the reaction at approximately 2/3 conversion gave diol **11**[8] in 71% yield and 94% *ee*.[10] Protection of the diol gave the first half (**8**)[8] and subsequent catalytic hydrogenation produced the second half (**7**).[8]

The desire for the (*E*)-alkene **6** led us to choose the Julia olefination[11] for the coupling (Scheme 3). To this end, the alkene half **8** was converted straightforwardly into the sulfone **12**[8,12,13] and the alkane **7** into the aldehyde **13**.[8,14] The aldehyde **13** was added to a solution of the lithiated sulfone in THF, and the cold reaction quenched with benzoyl chloride to give adduct **14**[8] reproducibly in 74% yield. Control of the metalation time (30 min) and direct acylation were required to obtain these results. The benzoate **14** was particulary prone to undergo base-catalyzed eliminations under the reductive cleavage conditions even in the presence of numerous buffers. The best in minimizing the simple elimination proved to be boric acid. The alkene **6** was isolated in a 61% overall yield from **12** and **13** as a 3:1 *E*/*Z* mixture. It proved unnecessary to separate the *E*/*Z* mixture, since only the *E* isomer undergoes subsequent dihydroxylation.

The alkene **6** becomes a pivotal intermediate to approach a variety of diastereomeric acetogenins by both the choice of dihydroxylation protocol and hydroxyl group differentiation (in terms of which oxygen becomes the nucleophile and which oxygen the electrophile for formation of the tetrahydrofuran). For the synthesis of parviflorin, **6** was subjected to the Sharpless protocol using $(DHQ)_2PHAL$ to give diol **15**[8] (DHQ–H = dihydroquinine, PHAL = 1,3-phthalazinediyl; Scheme 4) as a single diastereomer, which formed the corresponding mesylate **16**[8] virtually quantitatively. Because hydrolysis of the acetonides was accompanied by partial cyclization, the crude hydrolysate was directly treated with base to give the bis(tetrahydrofuran) **4**. The stage is now set for the butenolide annulation: heating a 1:1 to 1:1.6 ratio of **4**:**5** in methanol at 60°C in the presence of 5 mol% [CpRu(COD)Cl][4] gave 71–98% yields of the butenolide **3**.[8] It is important to note that no protecting groups are required in this reaction. The synthesis of (+)-squamocin K (**2**) only required hydrogenation of the double bond, which proceeded quantitatively with Wilkinson's catalyst[15]

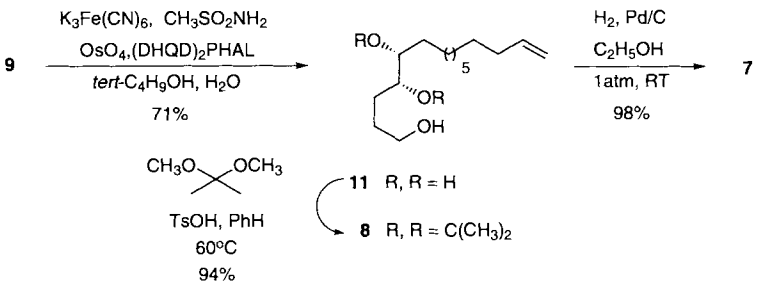

Scheme 2. Synthesis of the building blocks **7** and **8**. Ts = *p*-$CH_3C_6H_4SO_2$.

(C_2H_5OH/PhH (1/1.2), room temperature, 1 atm H_2). Comparison of the infrared and ^1H and ^{13}C NMR spectra of the synthetic and the natural product as well as rotation identified the product.

For parviflorin, we must install the C-5 hydroxyl group. The protocol began with a diastereoselective dihydroxylation to (5*S*)-hydroxyparviflorin (**17**,[8] Scheme 5).[16] Chemoselective deoxygenation of the C-5 hydroxyl group takes advantage of

the regioselective opening of an intermediate acetoxonium ion upon treatment with acetyl bromide to give bromoacetate **18**, which simultaneously acetylates the additional two hydroxyl groups. Radical debromination gave parviflorin triacetate **19**, which was readily hydrolyzed under acid conditions to give parviflorin, identical spectroscopically to the natural product.

This convergent sequence offers a flexible approach to the bis(tetrahydrofuran) acetogenins. For example, various diastereomers are easily accessed by the method of elaborating the alkene **6**. In addition to the *threo-trans-threo-trans-threo* series, the *threo-cis-threo-cis-threo*, *erythro-trans-threo-trans-*

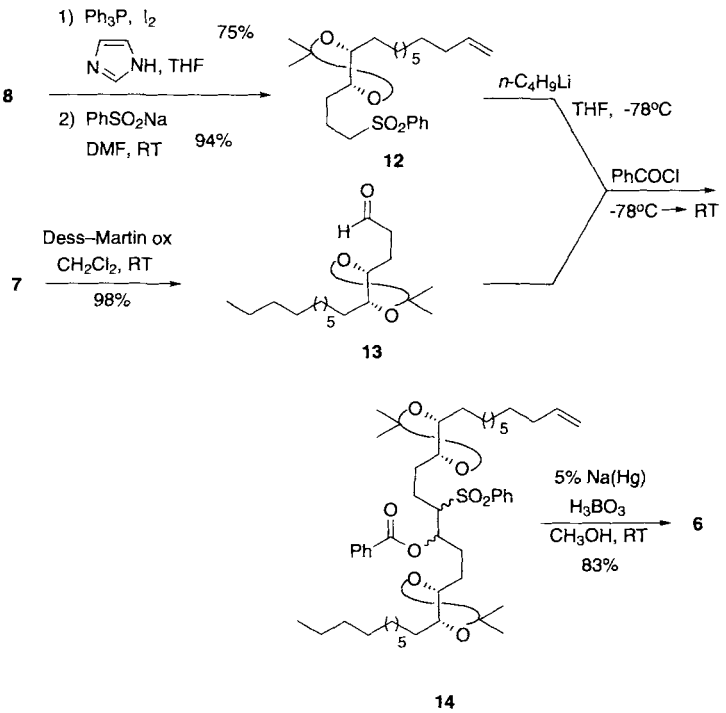

Scheme 3. Synthesis of alkene **6**.

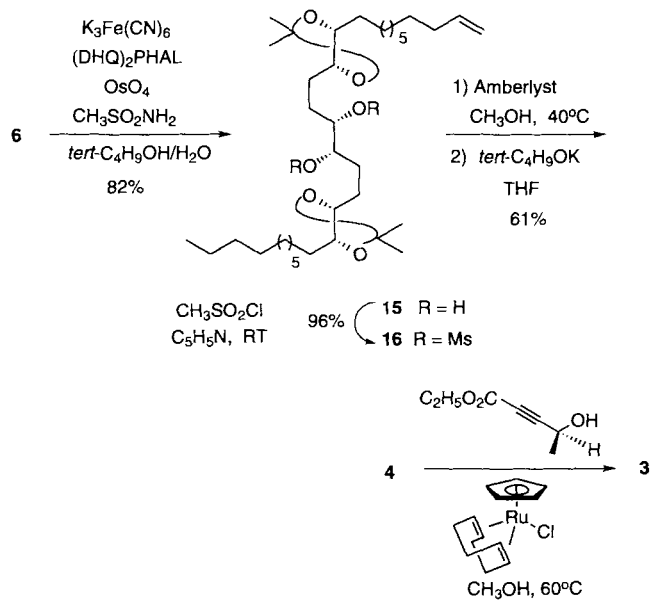

Scheme 4. Synthesis of butenolide **3**. Ms = CH_3SO_2.

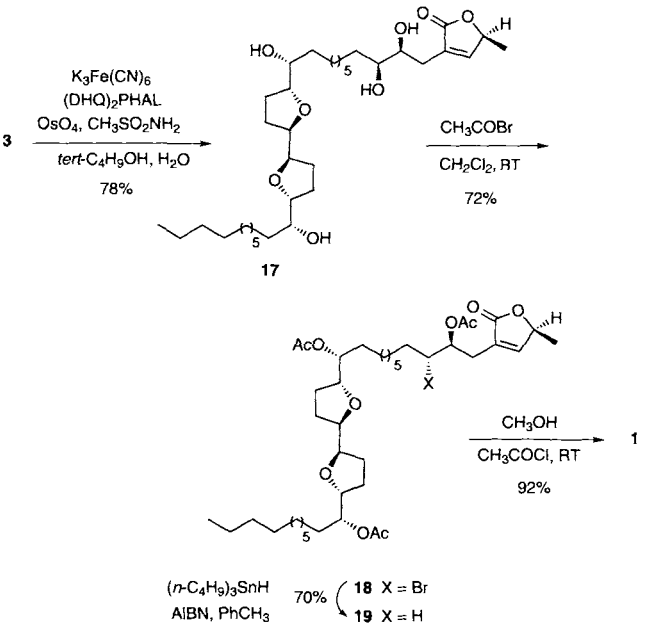

Scheme 5. Synthesis of parviflorin (**1**) from **3**. AIBN = α,α'-azobisisobutyronitrile.

erythro, *erythro-cis-threo-cis-erythro*, *threo-trans-erythro-trans-erythro*, and *erythro-trans-erythro-trans-threo* isomers should be available by manipulation of the oxygen pattern. To demonstrate this principle, *cis*-dihydroxylation of **6** with AD-mix β followed by the same protocol led to the *threo-cis-threo-cis-threo* isomer of **3**. The particular case of parviflorin illustrates the effectiveness of the strategy, since thirty of the carbon atoms and four stereogenic centers derive from a common building block, while the remaining five carbons and an additional stereogenic center are installed by the Ru-catalyzed Alder–ene reaction. Thus, this route should be a versatile approach to the bis(tetrahydrofuran) acetogenins.

Received: July 3, 1997 [Z10505IE]
German version: *Angew. Chem.* **1997**, *109*, 2746–2748

Keywords: acetogenins · asymmetric synthesis · butenolides · ene reactions · ruthenium

[1] Reviews: L. Zheng, Q. Ye, N. H. Oberlies, G. Shi, Z.-M. Gu, K. He, J. L. McLaughlin, *Nat. Prod. Rep.* **1996**, 275–306 and references cited therein; E. A. Ramirez, T. R. Hoye, *Studies in Natural Products Chemistry, Vol. 17, Structure and Chemistry, Part D* (Ed.: Atta-ur-Rahman), Elsevier, New York, **1995**, pp. 251–282; A. Cavé, D. Cortes, B. Figadère, R. Hocquemiller, O. Laprévote, A. Laurens, M. Leboeuf in *Phytochemical Potential of Tropical Plants* (Eds.: K. R. Downum, J. T. Romeo, H. E. Stafford), Plenum, New York, **1993**, pp. 167–202.

[2] Reviews on syntheses: R. Hoppe, H. D. Scharf, *Synthesis* **1995**, 1447–1464; B. Figadère, *Acc. Chem. Res.* **1995**, *28*, 359–365; U. Koert, *Synthesis* **1995**, 115–132.

[3] S. Ratnayake, Z.-M. Gu, L. R. Miesbauer, D. L. Smith, K. V. Wood, D. R. Evert, J. L. McLaughlin, *Can. J. Chem.* **1994**, *72*, 287–293; Z. Gu, X. Fang, L. Zeng, K. V. Wood, J. L. McLaughlin, *Heterocycles* **1993**, *36*, 2221–2228; M. Sahai, S. Singh, M. Singh, Y. K. Gupta, S. Akashi, R. Yuji, K. Hirayama, H. Asaki, H. Araya, N. Hara, T. Eguchi, K. Kakinuma, Y. Fujimoto, *Chem. Pharm. Bull.* **1994**, *42*, 1163–1174.

[4] B. M. Trost, T. J. J. Müller, J. Martinez, *J. Am. Chem. Soc.* **1995**, *117*, 1888–1899; B. M. Trost, Z. Shi, *ibid.* **1994**, *116*, 7459–7460.

[5] V. G. DeVries, D. B. Moran, G. R. Allen, S. J. Riggi, *J. Med. Chem.* **1976**, *19*, 946–957.

[6] For an elegant synthesis published during the course of this work, see: T. R. Hoye, Z. Ye, *J. Am. Chem. Soc.* **1996**, *118*, 1801–1802.

[7] For other recent work directed towards the bis(tetrahydrofuran) type acetogenins, see ref. [2] and E. Keinan, A. Sinha, A. Yazbak, S. C. Sinha, *Pure Appl. Chem.* **1997**, *69*, 423–430; S. C. Sinha, A. Sinha, A. Yazbak, E.

 © WILEY-VCH Verlag GmbH, D-69451 Weinheim, 1997 0570-0833/97/3623-2634 $ 17.50+.50/0

Keinan, *J. Org. Chem.* **1996**, *61*, 7640–7641; I. Wöhrle, A. Classen, M. Peterek, H.-D. Scharf, *Tetrahedron Lett.* **1996**, *37*, 7001–7004; H. Naito, E. Kawahara, K. Maruta, M. Maeda, S. Sasaki, *J. Org. Chem.* **1995**, *60*, 4419–4427; T. R. Hoye, L. Tan, *Tetrahedron Lett.* **1995**, *36*, 1981–1984. For efforts directed towards the bis(tetrahydrofuran) core, see: H. Wagner, U. Koert, *Angew. Chem.* **1994**, *106*, 1939–1941; *Angew. Chem. Int. Ed. Eng.* **1994**, *33*, 1873–1875; U. Koert, M. Stein, H. Wagner, *Liebig's Ann.* **1995**, 1415–1426; Z. Ruan, P. Wilson, D. R. Mootoo, *Tetrahedron Lett.* **1996**, *37*, 3619–3622; J. A. Marshall, K. W. Hinkle, *J. Org. Chem.* **1996**, *61*, 4247–4251.

[8] Spectroscopic data fully confirm the assigned structure.

[9] Review: H. C. Kolb, M. S. Van Nieuwenhze, K. B. Sharpless, *Chem. Rev.* **1994**, *94*, 2483–2547. Also see: H. Becker, M. A. Soler, K. B. Sharpless, *Tetrahedron* **1995**, *51*, 1345–1376; E. Keinan, S. C. Sinha, A. Sinha-Bagchi, Z.-M. Wang, X.-L. Zhang, K. B. Sharpless, *Tetrahedron Lett.* **1992**, *33*, 6411–6414.

[10] The enantiomeric ratio of sulfone **12** was determined by chiral HPLC on a Chiralcel OD column (heptanes:ethyl acetate, 95:5).

[11] S. E. Kelly, *Comprehensive Organic Synthesis, Vol. 1* (Eds.: B. M. Trost, I. Fleming, S. L. Schreiber), Pergamon, Oxford, **1991**, pp. 792–806; P. Kocienski, *Comprehensive Organic Synthesis, Vol. 6* (Eds.: B. M. Trost, I. Fleming, E. Winterfeldt), Pergamon, Oxford, **1991**, pp. 987–1000. Also see: G. E. Keck, K. A. Savin, M. A. Weglarz, *J. Org. Chem.* **1995**, *60*, 3194–3204.

[12] For the iodide, see: P. J. Garegg, R. Johansson, C. Ortega, B. Samuelsson, *J. Chem. Soc. Perkin 1* **1982**, 681–683.

[13] P. S. Manchand, H. S. Wong, J. F. Blount, *J. Org. Chem.* **1978**, *43*, 4769–4774.

[14] D. B. Dess, J. C. Martin, *J. Am. Chem. Soc.* **1991**, *113*, 7277–7287.

[15] J. A. Osborn, G. Wilkinson, *Inorg. Synth.* **1967**, *10*, 67–71.

[16] B. M. Trost, T. L. Calkins, *Tetrahedron Lett.* **1995**, *36*, 6021–6024.

Catalytic Asymmetric Alkylation of Nucleophiles: Asymmetric Synthesis of α-Alkylated Amino Acids**

Barry M. Trost* and Xavier Ariza

Modified peptides not only open a major avenue to understanding biological phenomena, but also offer opportunities for drug discovery.[1] Incorporating conformational constraints probes the molecular structure of receptors. By preorganizing the optimum conformation for binding, significant enhancements of biological activity can be expected. Introduction of alkyl groups at the α-carbon of amino acids introduces such conformational constraints and, furthermore, enhances metabolic stability. As a result, the synthesis of α-alkylated amino acids has attracted considerable attention.[2–6] Virtually all methods involve controlling diastereoselectivity—either by use of a chiral auxiliary[3] or by involving what is termed self-reproduction of chirality (also termed self-regeneration of stereocenters).[4] Methods in which the asymmetric inducing unit is required only catalytically are lacking. The major method for catalytic asymmetric synthesis of simple amino acids,[7a] hydrogenation of dehydroamino acids, is not applicable. We report a new strategy for the synthesis of α-alkylated amino acids, which are important building blocks for peptide synthesis.

[*] Prof. Dr. B. M. Trost, Dr. X. Ariza
Department of Chemistry, Stanford University
Stanford, CA 94305-5080 (USA)
Fax: Int. code + (650) 725-0259
e-mail: bmtrost@leland.stanford.edu

[**] We thank the National Science Foundation and the National Institutes of Health, General Medical Sciences Institute, for their generous support of our programs and the Ministerio de Educación y Ciencia (postdoctoral fellowship for X.A.). Mass spectra were provided by the Mass Spectrometry Facility, University of California-San Francisco, supported by the NIH Division of Research Resources.

The question relates to the broader one of inducing absolute stereochemistry at an enolate carbon. No reaction is as ubiquitous as alkylations of enolates and related intermediates. The major current approach to effect such reactions asymmetrically involves use of stoichiometric amounts of chiral auxiliaries.[3] Catalytic processes, outside of aldol-like reactions, are rare.[7b,8] An approach based upon palladium-catalyzed allylic alkylations faces the difficult obstacle, illustrated in Scheme 1, that the attacking nucleophile is very remote from the chiral inducing units L*—in fact, the nucleophile is insulated from these chiral ligands by the allyl moiety. It is not surprising that examination of such

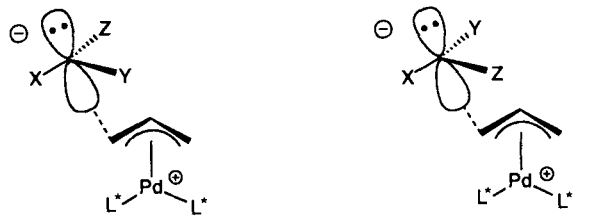

Scheme 1. Two competing arrangements for the approach in the asymmetric allylic alkylation at a nucleophilic carbon atom.

reactions to date have been disappointing.[9] Modest success stems from ligands with functional arms that appear to reach beyond the allyl barrier to help direct an incoming nucleophile. We have been exploring a different concept borrowed from the basic principles of an active site of an enzyme.[10] In this model, primary chirality in terms of structural units that contain stereogenic centers induces conformational chirality, which, in turn, creates chiral space. The ability of the reactants to "fit" into the "active site" then defines the molecular recognition and, consequently, the asymmetric induction.

One way to apply this concept to the asymmetric synthesis of α-alkylated amino acids invokes the allylation of the readily available azlactones.[11] The initial studies examined the reaction of the alanine-derived azlactone **1** (R = CH_3) and 3-acetoxycyclohexene (**2**) by using ligand **3** and a palladium complex **4** as a precatalyst (Scheme 2). On use of cesium

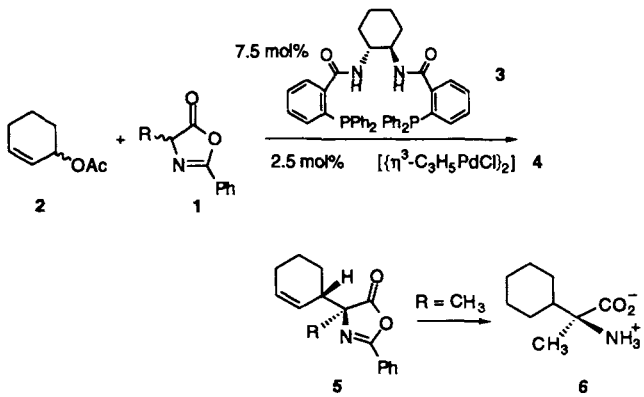

Scheme 2. Asymmetric alkylation of azlactones **1** with 3-acetoxycyclohexene **2**.

carbonate as base in dichloromethane at room temperature, a 2.5:1 diastereomeric ratio (d.r.) of alkylation product was obtained in 96% yield. Gratifyingly, the enantiomeric ex-

 © WILEY-VCH Verlag GmbH, D-69451 Weinheim, 1997 0570-0833/97/3623-2635 $ 17.50+.50/0

cesses (*ee*) were 94% and 92% for the major and minor diastereomers, respectively.[12] The major diastereomer is assigned as depicted in **5**, based on chemical correlation with the known amino acid **6**[13] and analogy to asymmetric alkylations of the allylic ester.[14] Variation to less polar (e.g., benzene) or more polar solvents (e.g., THF or DMSO) failed to improve the diastereomeric ratio or affect the *ee*. With dichloromethane as the standard solvent, the base was varied. Other inorganic or organometallic bases did not prove beneficial. Employing triethylamine, however, did enhance the d.r. to 2.8:1 and the *ee* to 99%. This result prompted our re-examination of the solvent effect with this base. In DMSO or DMF the diastereomeric ratio increased to greater than 4:1. The best diastereoselectivity was observed in acetonitrile. In this case a 90% yield of alkylated product with 8.7:1 d.r. and 99% *ee* of the major diastereomer was obtained. Since the minor diastereomer can be removed by column chromatography, **5** ($R = CH_3$) can be isolated diastereomerically and enantiomerically pure. Table 1 summarizes the alkylation for

Table 1. Results of the asymmetric alkylation of **1** with 3-acetoxycyclohexene (**2**).

Entry	R	Yield[%]	d.r.[a]	*ee*[%][a]
1	CH_3	90	8.7:1	99
2	CH_2Ph	74	12.4:1	99
3	$CH_2CH(CH_3)_2$	77[b]	13.3:1[c]	99[d]
4	$CH(CH_3)_2$	91	>19:1	95

[a] Determined by HPLC on a Chiralcel OD column with heptane/2-propanol mixtures unless stated otherwise. [b] Yield of pure major isomer only. [c] Determined by HPLC on a Microsorb Si 80-125-C5 column with a heptane/ethyl acetate mixture. [d] Determined by HPLC on a Chiralpak AD column.

a range of azlactones. Expectedly, as the size of the R group of the azlactone increased, the diastereoselectivity increased. 3-Acetoxycyclopentene behaved similarly. The tentative assignment of configuration is based upon analogy to that for **5** ($R = CH_3$).

An interesting approach to serine analogues is illustrated in Scheme 3. Palladium-catalyzed allylic alkylation of geminal dicarboxylates serves as a synthetic equivalent to an aldol

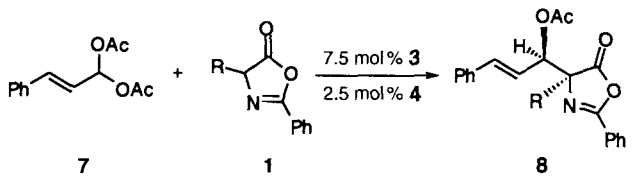

7 1 8

Scheme 3. Asymmetric alkylation of azlactones **1** with *gem*-dicarboxylate **7**.

reaction but for stablized pronucleophiles that do not normally provide stable adducts.[15] Thus, asymmetric desymmetrizations of such compounds function as the equivalent of an asymmetric addition of stabilized nucleophiles to carbonyl groups.[16] In this case the chiral recognition with respect to the allyl unit differs from that of Scheme 2, in which the attack of the nucleophile on the π-allylpalladium intermediate is the enantiodiscriminating step with respect to both partners. In Scheme 3 the configuration with respect to the allyl fragment is established in the ionization step, whereas that with respect to the nucleophiles is obviously fixed in the alkylation step. As shown in Table 2, entry 1, our standard conditions gave reasonable d.r. and *ee* values but not as high as those of Scheme 2. In our studies of desymmetrization of the geminal dicarboxylates with achiral nucleophiles, sodium hydride in DME proved to be effective.[16] Indeed, application of these conditions improved both the d.r. and *ee* value (Table 2,

Table 2. Conditions and results of the asymmetric alkylation of **1** with the *gem*-dicarboxylate **7**[a].

Entry	R	*T*	Yield[%][b]	d.r.[c]	*ee*[%][d]
1[e]	CH_3	RT[f]	73 (16)	4.4:1	83 (40)
2	CH_3	RT[f]	60 (9)	6.6:1	99 (96)
3	CH_2Ph	RT[f]	67 (7)	7.8:1	98 (94)[g]
4	CH_2Ph	0–5°C	75 (6)	9.7:1	99 (96)
5	$CH_2CH(CH_3)_2$	0–5°C	91 (6)	15:1	99 (95)[g]
6	$CH(CH_3)_2$	0–5°C	88 (4)	>19:1	99 (–)

[a] All reactions were performed with sodium hydride in DME unless stated otherwise. [b] Yields of isolated products for the major and minor (in parentheses) diastereomers. [c] Determined by ^1H NMR on the crude mixture. [d] Determined by HPLC on a Chiralcel OD column with heptane/2-propanol mixtures unless stated otherwise. Numbers in parentheses correspond to *ee* values for the minor diastereomer. [e] Performed with triethylamine in dichloromethane. [f] RT = room temperature. [g] Determined by HPLC on a Chiralpak AD column with heptane/2-propanol mixtures.

entry 2). Temperature also has an effect. In the case of the phenylalanine derivative (Table 2, entries 3 and 4), simply lowering temperature from room temperature to 0°C increases the diastereomeric ratio; the *ee* value also increased. Expectedly, increasing the size of the R group increases the diastereomeric ratio (entries 4–6). The configuration of these serine analogues is assigned based upon precedent in the desymmetrization reaction with achiral nucleophiles and the established configuration on alkylation of the azlactones **1** with **2**, and an X-ray crystal structure of **8** ($R = CH_2Ph$).

This new method for synthesis of α-alkylated amino acids is the first catalytic asymmetric reaction to yield members of this important family of compounds. Hydrolysis provides the amino acids (cf. Scheme 2) without danger of racemization. Furthermore, the azlactones can be used to construct constrained peptides by directly coupling them with a second amino acid unit.[11] By making available greater diversity in such novel amino acids, generation of libraries of peptidomimetics by combinatorial chemistry is facilitated. More generally, inducing chirality at a prochiral nucleophilic center by this mechanism may have broader applications. An important question to address is: why does the family of catalysts employing ligands like **3** function so well? Although detailed structural information is still lacking despite significant effort, the model in which a chiral pocket is envisioned as depicted in the cartoon of Scheme 4 does rationalize the result.[17]

Experimental Section

Alkylation of **2**: 3-Acetoxycyclohexene (**2**, 28 μg, 200 μmol) was added to a solution of Et_3N (56 μL, 400 μmol) and 4-alkyl-2-phenyl-2-oxazolin-5-one (450 μmol) in acetonitrile (1 mL, dry and oxygen free). A prepared solution of **4** (1.8 mg, 4.9 μmol) and chiral ligand **3** (10.4 mg, 15.1 μmol) in acetonitrile (1 mL) was added by cannula under N_2. The reaction mixture was quenched (2–6 h) with aqueous phosphate buffer (pH 7, 40 mL) and extracted with CH_2Cl_2 (3 × 30 mL). The combined organic layer was dried over Na_2SO_4 and concentrated in vacuo. The residue was purified by flash chromatography on silica gel (eluent: petroleum ether/EtOAc).

Alkylation of **7**: A solution of **1** (450 μmol) in DME (1 mL, dry and oxygen free) was added to NaH (95% in oil, 10.1 mg, 400 μmol) at –78°C and allowed to warm to room temperature. When gas evolution stopped, a solution of **4** (1.8 mg, 4.9 μmol) and ligand **3** (10.4 mg, 15.1 μmol) in DME (0.5 mL) was added. Finally a solution of **7** (46.9 mg, 200 μmol) in DME (1 mL) was added at the desired

 © WILEY-VCH Verlag GmbH, D-69451 Weinheim, 1997 0570-0833/97/3623-2636 $ 17.50+.50/0

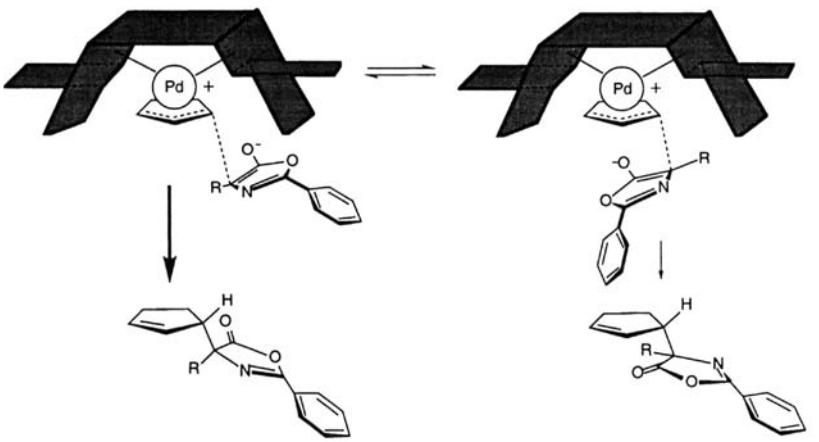

Scheme 4. Cartoon depicting the sense of asymmetric induction at an azlactone-derived nucleophile.

temperature (see Table 2). The reaction mixture was quenched (2–24 h) with aqueous phosphate buffer (pH 7, 40 mL) and extracted with CH_2Cl_2 (3 × 30 mL). The combined organic layer was dried over Na_2SO_4 and concentrated in vacuo. The residue was purified by flash chromatography on silica gel (eluent: petroleum ether/EtOAc).

Received: July 2, 1997 [Z10628IE]
German version: *Angew. Chem.* **1997**, *109*, 2749–2751

Keywords: alkylations · amino acids · asymmetric catalysis · palladium · peptidomimetics

[1] Selected reviews: a) D. F. Veber, R. M. Freidinger, *Trends Neurosci.* **1995**, *8*, 392; b) *A Textbook of Drug Design and Development* (Eds.: P. Krosgaard-Larsen, H. Bundgaard), Harwood Academic Publishers, Chur, **1991**; c) G. Jung, A. G. Beck-Sickinger, *Angew. Chem.* **1992**, *104*, 375; *Angew. Chem. Int. Ed. Engl.* **1992**, *31*, 367–383; d) P. Balaram, *Curr. Opin. Struct. Biol.* **1992**, *2*, 845–851; e) P. W. Schiller in *Medicinal Chemistry for the 21st Century* (Ed.: C. G. Wermuth), Oxford Blackwell Scientific Publications, Oxford, **1992**, Chapter 15; f) A. Giannis, T. Kolter, *Angew. Chem.* **1993**, *105*, 1303; *Angew. Chem. Int. Ed. Engl.* **1993**, *32*, 1244–1267; g) V. J. Hruby in *Peptides Chemistry, Structure and Biology, Proceedings of the 13th American Peptide Symposium* (Eds.: R. S. Hudges, J. A. Smith), Escom Science, **1993**, pp. 3–17; h) *Burger's Medicinal Chemistry and Drug Discovery*, 5th ed. (Ed.: M. E. Wolff), Wiley, New York, **1995**; i) M. Goodman, S. Ro in ref. [1h], Chapter 20, pp. 803–861; j) J. G. Cannon in ref. [1h], Chapter 19, pp. 783–801; k) A. Muscate, G. L. Kenyon in ref. [1h], Chapter 18, pp. 733–782; l) G. R. Marshall in ref. [1h], Chapter 15, pp. 573–660; m) B. Veerapandian in ref. [1h], Chapter 10, pp. 303–348.

[2] Selected reviews: R. M. Williams, *Synthesis of Optically Active α-Amino Acids*, Pergamon, Oxford, **1989**; H. Heimgartner, *Angew. Chem.* **1991**, *103*, 271; *Angew. Chem. Int. Ed. Engl.* **1991**, *30*, 238–264; I. Ojima, *Acc. Chem. Res.* **1995**, *28*, 383–389; Y. Ohfune, S.-H. Moon, M. Horikawa, *Pure Appl. Chem.* **1996**, *68*, 645–648; T. Wirth, *Angew. Chem.* **1997**, *109*, 235–237; *Angew. Chem. Int. Ed. Engl.* **1997**, *36*, 225–227.

[3] J. Seyden-Penne, *Chiral Auxiliaries and Ligands in Asymmetric Synthesis*, Wiley, New York, **1995**.

[4] D. Seebach, A. R. Sting, M. Hoffmann, *Angew. Chem.* **1996**, *108*, 2880–2921; *Angew. Chem. Int. Ed. Engl.* **1996**, *35*, 2708–2748.

[5] For recent reports, see U. Kazmaier, S. Maier, *Tetrahedron* **1996**, *52*, 941–954; U. Kazmaier, *J. Org. Chem.* **1996**, *61*, 3694–3699; V. Ferey, L. Toupet, T. Le Gall, C. Mioskowski, *Angew. Chem.* **1996**, *103*, 475–477; *Angew. Chem. Int. Ed. Engl.* **1996**, *35*, 430–432; D. Obrecht, M. Altorfer, C. Lehmann, P. Schönholzer, K. Müller, *J. Org. Chem.* **1996**, *61*, 4080–4086; B. Westermann, I. Gedrath, *Synlett* **1996**, 665–666; L. M. Harwood, K. J. Vines, M. G. B. Drew, *ibid.* **1996**, 1051–1053; D. Obrecht, C. Abrecht, M. Altorfer, U. Bohdal, A. Grieder, M. Kleber, P. Pfyffer, K. Müller, *Helv. Chim. Acta* **1996**, *79*, 1315–1337; B. G. M. Burgaud, D. C. Horwell, A. Padova, M. C. Pritchard, *Tetrahedron* **1996**, *52*, 13035–13050; C. Cativiela, M. D. Diaz-de-Villegas, J. A. Gálvez, Y. Lapeña, *ibid.* **1997**, *53*, 5891–5898.

[6] Allylated derivatives: T. M. Zydowsky, J. F. Dellaria, H. N. Nellans, *J. Org. Chem.* **1988**, *53*, 5607–5616; S. Thaisrivongs, D. T. Pals, S. R. Turner, L. T. Kroll, *J. Med. Chem.* **1988**, *31*, 1369–1376; M. W. Holladay, A. M. Nadzan, *J. Org. Chem.* **1991**, *56*, 3900–3905; A. B. Smith III; T. P. Keenan, R. C. Holcomb, P. A. Sprengeler, M. C. Guzman, J. L. Wood, P. J. Carroll, R. Hirschmann, *J. Am. Chem. Soc.* **1992**, *114*, 10672–10674; C. Bisang, C. Weber, J. Inglis, C. A. Schiffer, W. F. van Gunsteren, I. Jelesarov, H. R. Bosshard, J. A. Robinson, *ibid.* **1995**, *117*, 7904–7915; R. Badorrey, C. Cativiela, M. D. Diaz-de-Villegas, J. A. Gálvez, Y. Lapeña, *Tetrahedron: Asymmetry* **1997**, *8*, 331–317.

[7] a) Ref. [7c], Chapter 2, and references therein; b) ref. [7c], Chapter 4, pp. 207–212, Chapter 7, pp. 333–342; c) R. Noyori, *Asymmetric Catalysis in Organic Synthesis*, Wiley, New York, **1994**.

[8] M. Sawamura, M. Sudoh, Y. Ito, *J. Am. Chem. Soc.* **1996**, *118*, 3309–3310.

[9] J. C. Fiaud, A. H. De Gournay, M. Larchvéque, H. B. Kagan, *J. Organomet. Chem.* **1978**, *154*, 175–185; Y. Ito, M. Sawamura, M. Matsuoka, Y. Matsumoto, T. Hayashi, *Tetrahedron Lett.* **1987**, *28*, 4849–4852; J.-P. Genêt, S. Juge, S. Achi, S. Mallart, J. R. Montes, G. Levif, *Tetrahedron* **1988**, *44*, 5263–5275; T. Hayashi, K. Kanehira, T. Hagihara, M. Kumada, *J. Org. Chem.* **1988**, *53*, 113–120; M. Sawamura, Y. Nakayama, W.-M. Tang, Y. Ito, *ibid.* **1996**, *61*, 9090–9096.

[10] B. M. Trost, *Acc. Chem. Res.* **1996**, *29*, 355–364.

[11] Review on azlactones: A. K. Mukerjee, *Heterocycles* **1987**, *26*, 1077–1097; Y. S. Rao in *Oxazoles (The Chemistry of Heterocyclic Compounds), Vol. 45* (Ed.: I. J. Turchi), Wiley, **1986**, Chapter 3, pp. 361–615.

[12] The d.r. and *ee* values were established by means of HPLC with a Chiralcel OD column with heptane/2-propanol mixtures as eluent.

[13] H. Dahn, J. A. Garbarino, C. O'Murchu, *Helv. Chim. Acta.* **1970**, *53*, 1370–1378.

[14] B. M. Trost, R. C. Bunt, *J. Am. Chem. Soc.* **1994**, 116, 4089–4090.

[15] B. M. Trost, J. Vercauteren, *Tetrahedron Lett.* **1985**, *26*, 131–134.

[16] B. M. Trost, C.-B. Lee, J. M. Weiss, *J. Am. Chem. Soc.* **1995**, *117*, 7247–7248.

A Highly Efficient Aminohydroxylation Process**

A. Erik Rubin and K. Barry Sharpless*

Dedicated to Professor Dieter Seebach on the occasion of his 60th birthday

Stereospecific transformations of olefins to 1,2-diols[1,2] and β-amino alcohols[3,4] are very important due to the ready availability of the starting materials and the significance of the products as building blocks in the syntheses of drugs and natural products, ligands for asymmetric catalysis, and chiral auxiliaries.[1–5] The recently discovered catalytic asymmetric aminohydroxylation (AA) of olefins,[4] a close "relative" of the highly reliable catalytic asymmetric dihydroxylation (AD),[1] stereospecifically provides N-protected β-amino alcohols with the added benefit of good to excellent regio- and enantioselectivities. However, in the absence of cinchona alkaloid ligands (i.e., in the achiral mode, which yields racemic products if the olefin is prochiral), the reaction is plagued by the formation of large amounts of diol and suffers from a significant decrease in regioselectivity.[4,6]

[*] Prof. K. B. Sharpless, A. E. Rubin
Department of Chemistry
and
Skaggs Institute for Chemical Biology
The Scripps Research Institute
10550 N. Torrey Pines Road, La Jolla, CA 92037 (USA)
Fax: Int. code + (619) 784-7562
e-mail: sharples@scripps.edu

[**] We are grateful to the National Institute of General Medical Sciences, National Institutes of Health (GM-28384), the National Science Foundation (CHE-9531152), and the W. M. Keck Foundation for providing financial support. We thank Professors SonBinh T. Nguyen (Northwestern University), Derek W. Nelson (Loyola University of Chicago) and Dr. Pui Tong Ho for many helpful discussions. A.E.R. thanks NSERC (Canada) for a 1967 Science and Engineering Scholarship. Supporting information for this contribution is available on the WWW under www/wiley-vch.de/home/angewandte.

In our continuing effort to develop the AA further and to expand its scope, α,β-unsaturated amides were examined as potential substrates. Remarkably, they gave only racemic products in the AA with chloramine T.[7] On the other hand, they exhibited excellent reactivity and afforded very high yields of the hydroxysulfonamide products, whether or not ligand was added. A more detailed study of the "ligand-independent" aminohydroxylation of α,β-unsaturated amides was then undertaken (Scheme 1).

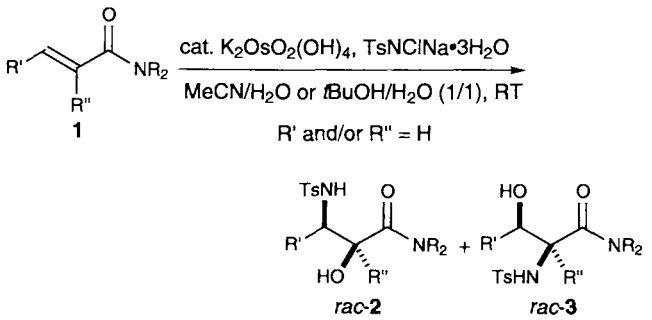

Scheme 1. Osmium-catalyzed aminohydroxylation of α,β-unsaturated amides with chloramine T; Ts = p-$MeC_6H_4SO_2$.

Aminohydroxylation of the differently N-substituted cinnamamides **1a**–**1f** gave excellent results, even though much lower amounts of the osmate catalyst, chloramine salt, and solvent were employed than are optimal for the standard AA (Table 1).[8] In all cases, the major regioisomer was **2**, in which the newly added nitrogen atom was in the benzylic position (see Scheme 1, R' = Ph).[9] This is the same, albeit weaker, regioselectivity observed for cinnamate *esters* in AA.[4] However, under otherwise identical experimental conditions, the nature of the substituents on the amide nitrogen atom had a significant effect on the extent to which **2** predominanted over **3** as well as on the reaction rates. The Weinreb methoxymethyl cinnamamide (**1a**)[10] proved to be the best substrate; it gave the highest regioselectivity and required the shortest reaction time. However, indicating that rapid turnover and high regioselectivity are not necessarily directly related, *N-tert*-butylcinnamamide (**1f**) was almost as reactive as **1a**, yet gave the poorest regioselectivity of the cinnamamides examined.

Table 1. Effect of N-substituents on the aminohydroxylation of cinnamamides [a].

Entry	Substrate	t[h][b]	**2**:**3**[c]	Yield of *rac*-**2**[%] (M.p.[°C])[d]
1	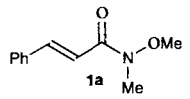 **1a**	1	7.3:1	82 (180–181)
2	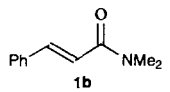 **1b**	4	5.0:1	75 (176–177)
3	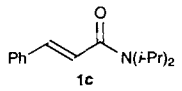 **1c**	20	3.3:1	65 (223–225)
4	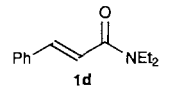 **1d**	6	2.8:1	65 (170–171)
5	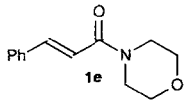 **1e**	2	2.6:1	51 (185–186)
6	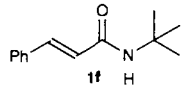 **1f**	2	1.6:1	[e]

[a] Reaction conditions: 1.0 mol% $K_2OsO_2(OH)_4$, 1.2 equiv of TsNClNa·$3H_2O$, $MeCN/H_2O$ (1/1), RT, 0.2 M olefin. [b] Approximate reaction time required for the disappearance of the starting olefin, as determined by TLC. [c] Determined by ^1H NMR spectroscopy. [d] Yield and melting point of the pure major regioisomer (**2**) after recrystallization of the crude product (which consisted of **2**, **3**, and excess $TsNH_2$) from *i*PrOH. [e] Recrystallization from *i*PrOH afforded **2f** and **3f** (2:1) in 72% yield.

Further studies with **1b** demonstrated that higher initial concentrations of the olefin as well as much lower loadings of the catalyst could be employed without compromising either the yield or the regioselectivity of the aminohydroxylation.[11] In addition, at olefin concentrations of 0.5 M or greater and with *t*BuOH in place of MeCN as the co-solvent, the hydroxysulfonamide products derived from cinnamamides precipitated directly from the reaction solution in high yield and could be conveniently isolated by filtration. This led to the development of two procedures for aminohydroxylation of α,β-unsaturated amides: method A when the products are insoluble in the reaction mixture, and method B when they are soluble. These procedures differ only in that the former calls for a 25% excess of the chloramine salt and *t*BuOH as the co-solvent, whereas the latter requires one equivalent of the co-oxidant and MeCN as the co-solvent. The excess chloramine T used in procedure A supports better turnover near the end of the reaction. However, elimination of the necessity of removing excess *p*-toluenesulfonamide (produced in the reductive workup) from the product far outweighs the inconvenience of the slightly longer reaction times needed in procedure B because no excess chloramine salt is used. Table 2 lists the results from the aminohydroxylation of different cinnamamides, alkyl-substituted acrylamides, and a parent acrylamide (**1i**) using procedures A and B.

As can be seen in Table 2, excellent yields of the hydroxysulfonamide products were obtained from each of the olefins examined. Most importantly, these high yields and short reaction times were achieved at high substrate concentrations and at room temperature with as little as 0.10 mol% of the catalyst. In the old racemic aminohydroxylation of olefins with on chloramine T,[3a–c] 1 mol% of OsO_4, reaction times in excess of 12 h, and temperatures of 60 °C were required to obtain moderate to good yields of the hydroxysulfonamide products. The poor turnover rates in the old system are now largely attributed to the small amount of water present in the original recipes. However, as mentioned earlier, in the absence of ligands the presence of more water does lead to greater intrusion of the competing dihydroxylation cycle. With olefins other than α,β-unsaturated amides, diol can be expected to constitute up to 70% of the product mixture in some cases.[6] It is the unique ability of α,β-unsaturated amides (e. g. **1a**–**1k**) to benefit from the rapid turnover rates associated with high concentrations of water while somehow avoiding the paths leading to a diol by-product, which accounts for their unprecedented efficiency in the aminohydroxylation.

The hydroxysulfonamide products are in general highly crystalline, and, due to the regioselectivity of the aminohydroxylation, the major regioisomer is usually obtained in pure form following a single recrystallization of the mixture of isomers. However, for cases in which separation is difficult or in order to fully exploit the high combined yields in which the products are obtained, reactions which transform both regioisomers into the same product are of interest. One such

 © WILEY-VCH Verlag GmbH, D-69451 Weinheim, 1997 0570-0833/97/3623-2638 $ 17.50+.50/0 *Angew. Chem. Int. Ed. Engl.* **1997**, *36*, No. 23

Table 2. Aminohydroxylation of α,β-unsaturated amides.

Entry	Substrate	Procedure [a] (Os [mol %]) [b]	t [h] [c]	2:3 [d]	Yield [%]
1	**1a**	A (0.10)* [e]	4	6.5:1	93
2	**1b**	A (0.25)	12	5.0:1	94
3	**1b**	A (0.20) [e]	12	3.0:1	94
4	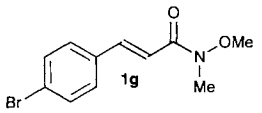 **1g**	A (0.25)*	2.5	3.7:1	95
5	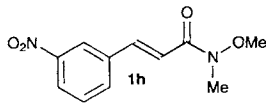 **1h**	A (0.50)*	4	5.8:1	95
6	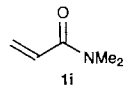 **1i**	B (0.50)	10	10:1	99
7	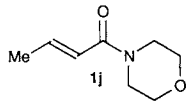 **1j**	B (0.50)	10	1:1.4	97
8	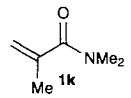 **1k**	B (1.0)	23	>20:1 [f]	90
9	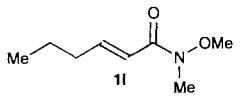 **1l**	B (0.50)* [g]	24	3.0:1	99

[a] Procedure A (for products that are *insoluble* in the reaction medium): 1. cat. $K_2OsO_2(OH)_4$ or OsO_4, 1.25 equiv of $TsNClNa \cdot 3H_2O$, tBuOH/H_2O (1/1), RT, olefin concentration: 0.5 M; 2. filtration; procedure B (for products that are *soluble* in the reaction medium): 1. cat. $K_2OsO_2(OH)_4$ or OsO_4, 1.0 equiv of $TsNClNa \cdot 3H_2O$, MeCN/H_2O (1/1), RT, olefin concentration: 0.5 M, 2. Na_2SO_3, 1 h. [b] An asterisk indicates that OsO_4 (0.1 M solution in MeCN) was used in place of $K_2OsO_2(OH)_4$. [c] Approximate reaction time required for the disappearance of the starting olefin, as determined by TLC. [d] Determined by ^1H NMR spectroscopy. [e] The concentration of the olefin was 0.8 M. [f] The presence of **3k** was not detected by ^1H NMR spectroscopy. [g] tBuOH was used as the co-solvent.

Table 3. Preparation of aziridines from regioisomeric mixtures of hydroxysulfonamides **2** and **3**.

Entry	Substrates (ratio)	Product	M.p. [°C]	Yield [%] [a]
1	**2b/3b** (5.0:1)	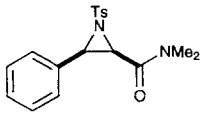 *rac*-**4b**	130–131	95
2	**2g/3g** (3.7:1)	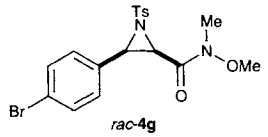 *rac*-**4g**	50–53	97
3	**2h/3h** (5.8:1)	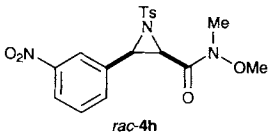 *rac*-**4h**	127–128	94
4	**2i/3i** (10:1)	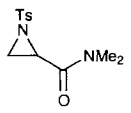 **4i**	(oil)	81
5	**2j/3j** (1:1.4)	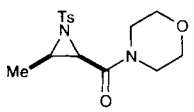 *rac*-**4j**	151–152	92
6	**2l/3l** (3.0:1)	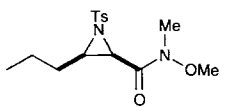 *rac*-**4l**	(oil)	87

[a] Yield of the pure aziridine after flash chromatography.

example is cyclodehydration of hydroxysulfonamides to give the corresponding aziridines (Scheme 2).[12] "Activated aziridines" such as **4** are versatile synthetic intermediates and have found wide use in the synthesis of biologically active compounds.[13]

The crude mixtures of hydroxysulfonamides **2** and **3**, obtained directly from the aminohydroxylation of olefins **1**, were cyclized to the aziridines **4** in a one-pot procedure (Scheme 2). The yields of the ring closure for several pairs of regioisomers are listed in Table 3. Thus, a highly efficient two-step synthesis of aziridines **4** from readily available

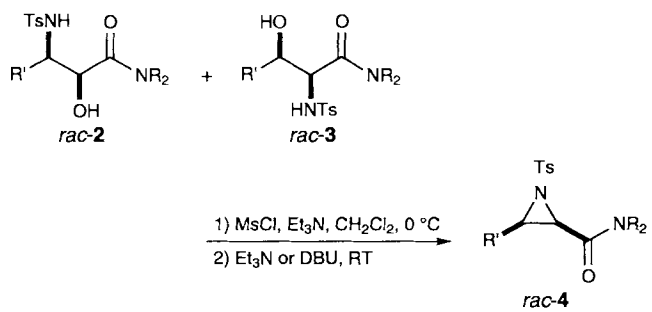

Scheme 2. Conversion of regioisomeric aminohydroxylation products **2** and **3** into the same aziridine **4**; Ms = $MeSO_2$.

olefins and without the need for purification of the intermediates is now available.

α,β-Unsaturated amides represent one of the few olefin classes for which the osmium-catalyzed aminohydroxylation is highly efficient in the absence of added ligands. The principal advantages of the method are excellent chemical yields, rapid turnover rates (enabling the use of very low loads of catalyst), the ability to use high concentrations of substrate, and the necessity for only one equivalent or a small excess of chloramine salt. The latter consideration along with the favorable "crystallinity factor" greatly simplifies product isolation and makes these processes ideal for large-scale applications. In addition, the rapid emergence of diversity chemistry[14] makes such powerful transformations, especially those yielding racemates,[15] more important than ever.

Experimental Section

Aminohydroxylation procedure A (when the products are insoluble in the reaction mixture), as described for the aminohydroxylation of *N,N*-dimethylcinnamamide (**1b**): To a mechanically stirred solution of **1b** (17.52 g, 100 mmol) and chloramine T trihydrate (35.2 g, 125 mmol) in tBuOH/water (130 mL, 1/1) was added $K_2OsO_2(OH)_4$ (73.7 mg, 0.20 mmol, 0.20 mol %). As the catalyst dissolved (20–30 min) the supernatant became orange and then darkened to deep orange-red once the solution was homogeneous. The reaction was stirred overnight at room temperature, during which time a fine precipitate appeared.

 © WILEY-VCH Verlag GmbH, D-69451 Weinheim, 1997 0570-0833/97/3623-2639 $ 17.50+.50/0

Subsequent thin-layer chromatography (TLC; silica, R_f(**1b**) = 0.20, R_f(products) = 0.15, EtOAc/hexane (1/1), two developments) indicated that the olefin had been completely consumed. The endpoint of the reaction was accompanied by a change in the color of the reaction solution back to yellow-orange. Water (50 mL) was added, and the reaction slurry cooled with stirring in an ice/water bath for 1 h. The solid product was collected by filtration, washed with water (2 × 50 mL), and dried under a stream of air overnight to afford the product (34.0 g, 94%) as a mixture of **2b** and **3b** (3.0:1). Recrystallization of a portion of this mixture from MeOH afforded analytically pure **2b** as colorless blocks: m.p. 176–177 °C (sealed tube); ^{1}H NMR (400 MHz, $CDCl_3$, TMS): δ = 7.56–7.53 (m, 2H), 7.24–7.20 (m, 5H), 7.16–7.13 (m, 2H), 5.52 (d, J = 6.1 Hz, 1H), 4.46 (dd, J = 6.9, 4.4 Hz, 1H), 4.42 (dd, J = 6.1, 4.4 Hz, 1H), 4.02 (d, J = 6.9 Hz, 1H), 2.84 (s, 3H), 2.67 (s, 3H), 2.36 (s, 3H); elemental analysis calcd for $C_{18}H_{22}N_2O_4S$: C 59.65, H 6.12, N 7.73; found: C 59.68, H 5.99, N 7.76.

Aminohydroxylation procedure B (when the products are soluble in the reaction mixture), as described for the aminohydroxylation of *N,N*-dimethylacrylamide (**1i**): To a magnetically stirred solution of **1i** (5.0 mL, 4.81 g, 48.5 mmol) and chloramine T trihydrate (14.0 g, 49.7 mmol) in MeCN (50 mL) and water (50 mL) was added $K_2OsO_2(OH)_4$ (89.3 mg, 0.24 mmol, 0.50 mol%). The color changes described for procedure A were noted, and the reaction mixture was stirred overnight at room temperature. TLC (silica, R_f(**1i**) = 0.27, R_f(products) = 0.40, EtOAc) revealed that the olefin had been completely consumed. Na_2SO_3 (10 g) and ethyl acetate (50 mL) were added and the triphasic mixture was vigorously stirred for a further hour, during which time the solids completely dissolved. After separating the phases and extracting the aqueous phase with ethyl acetate (2 × 50 mL), the combined organic phases were shaken with brine (50 mL), dried over Na_2SO_4, filtered, and concentrated under reduced pressure to yield an oil. Trituration of the oil with diethyl ether (ca. 30 mL) followed by filtration afforded the solid product (13.8 g, 99%) as a mixture of **2i** and **3i** (10:1). Recrystallization of a portion of this mixture from MeOH afforded analytically pure **2i** as colorless needles: m.p. 123–124 °C (sealed tube); ^{1}H NMR (400 MHz, $CDCl_3$, TMS): δ = 7.76–7.72 (m, 2H), 7.33–7.30 (m, 2H), 5.24–5.21 (m, 1H), 4.47–4.42 (m, 1H), 3.84 (d, J = 7.4 Hz, 1H), 3.28 (ddd, J = 13.2, 8.2, 3.2 Hz, 1H), 3.00 (s, 3H), 2.97 (s, 3H), 2.89 (ddd, J = 13.2, 7.4, 4.4 Hz, 1H), 2.43 (s, 3H); elemental analysis calcd for $C_{12}H_{18}N_2O_4S$: C 50.34, H 6.34, N 9.78; found: C 50.34, H 6.25, N 9.79.

Preparation of aziridines **4**, as described for *rac*-**4b**: A magnetically stirred solution of a mixture of **2b** and **3b** (5.0:1, 2.10 g, 5.8 mmol) and Et_3N (1.1 mL, 7.9 mmol) in CH_2Cl_2 (30 mL) under N_2 was cooled in an ice/H_2O bath, and methanesulfonyl chloride (0.58 mL, 7.5 mmol) was added dropwise over 30 min. After the addition was complete, stirring was continued at 0 °C for 30 min, before 1,8-diazabicyclo[5.4.0]undec-7-ene (DBU, 2.6 mL, 17.4 mmol) was added and the ice/water bath removed. After 15 min TLC (silica, R_f(**4b**) = 0.44, EtOAc/hexane 4/1) indicated that aziridine formation was complete. The reaction mixture was extracted with 2 N aqueous HCl (30 mL) followed by saturated aqueous $NaHCO_3$ (30 mL). The organic layer was dried over anhydrous Na_2SO_4, filtered, and concentrated under reduced pressure. Flash column chromatography on silica gel with EtOAc/hexane (3/1) as the eluent and subsequent removal of solvent provided **4b** (1.90 g, 95%) as a colorless solid: m.p. 130–131 °C (sealed tube); ^{1}H NMR (400 MHz, $CDCl_3$, TMS): δ = 7.98–7.95 (m, 2H), 7.35–7.33 (m, 2H), 7.30–7.26 (m, 5H), 4.14 (d, J = 7.5 Hz, 1H), 3.79 (d, J = 7.5 Hz, 1H), 2.90 (s, 3H), 2.70 (s, 3H), 2.42 (s, 3H); elemental analysis calcd for $C_{18}H_{20}N_2O_3S$: C 62.77, H 5.85, N 8.13; found: C 62.61, H 5.69, N 8.24.

Received: May 20, 1997 [Z10458IE]
German version: *Angew. Chem.* **1997**, *109*, 2751–2754

Keywords: amino alcohols · aziridines · chloramine T · homogeneous catalysis · osmium

[1] a) H. C. Kolb, M. S. VanNieuwenhze, K. B. Sharpless, *Chem. Rev.* **1994**, *94*, 2483–2547; b) H. Becker, K. B. Sharpless, *Angew. Chem.* **1996**, *108*, 447–449; *Angew. Chem. Int. Ed. Engl.* **1996**, *35*, 448–451.

[2] a) J. K. Cha, N.-S. Kim, *Chem. Rev.* **1995**, *95*, 1761–1795; b) T. K. M. Shing, E. K. W. Tam, V. W.-F. Tai, I. H. F. Chung, Q. Jiang, *Chem. Eur. J.* **1996**, *2*, 50–57.

[3] a) K. B. Sharpless, A. O. Chong, K. Oshima, *J. Org. Chem.* **1976**, *41*, 177–179; b) E. Herranz, K. B. Sharpless, *ibid.* **1978**, *43*, 2544–2548; c) *Org. Synth.* **1983**, *61*, 85–93; d) E. Herranz, S. A. Biller, K. B. Sharpless, *J. Am. Chem. Soc.* **1978**, *100*, 3596–3598; e) E. Herranz, K. B. Sharpless, *J. Org. Chem.* **1980**, *45*, 2710–2713; f) *Org. Synth.* **1983**, *61*, 93–97.

[4] a) G. Li, H.-T. Chang, K. B. Sharpless, *Angew. Chem.* **1996**, *108*, 449–452; *Angew. Chem. Int. Ed. Engl.* **1996**, *35*, 451–454; b) G. Li, K. B. Sharpless, *Acta Chem. Scand.* **1996**, *50*, 649–651; c) J. Rudolph, P. C. Sennhenn, C. P. Vlaar, K. B. Sharpless, *Angew. Chem.* **1996**, *108*, 2991–2995; *Angew. Chem. Int. Ed. Engl.* **1996**, *35*, 2810–2813; d) G. Li, H. H. Angert, K. B. Sharpless, *ibid.* **1996**, *108*, 2995–2999 and **1996**, *35*, 2813–2817; e) M. Bruncko, G. Schlingloff, K. B. Sharpless, *ibid.* **1997**, *109*, 1580–1583 and **1997**, *36*, 1483–1486.

[5] a) D. J. Ager, I. Prakash, D. R. Schaad, *Chem. Rev.* **1996**, *96*, 835–875; b) A. Studer, *Synthesis* **1996**, 793–815; c) G. Cardillo, C. Tomasini, *Chem. Soc. Rev.* **1996**, *25*, 117–128.

[6] H.-T. Chang, Dissertation, The Scripps Research Institute, La Jolla, CA (USA), **1996**.

[7] The absence of asymmetric induction in the AA of tertiary α,β-unsaturated amides is particularly surprising since these olefins are excellent substrates for the AD: Y. L. Bennani, K. B. Sharpless, *Tetrahedron Lett.* **1993**, *34*, 2079–2082.

[8] The standard conditions for the AA are 4 mol% $K_2OsO_2(OH)_4$, 5 mol% alkaloid ligand, three equiv of chloramine salt, and 0.07 M olefin in MeCN/H_2O (1/1) or *n*PrOH/H_2O (1/1) [4a–d]. Acetamide-based AA uses the same standard conditions but with 1.1 equiv of AcNLiBr in place of the chloramine salt [4e].

[9] A sample of the pure major product from the aminohydroxylation of **1b** was converted into its methyl ester analogue—1) 3 N HCl (aq), Δ, 93%; 2) 2.2 equiv of TMSCl, MeOH, RT, 91% (M. A. Brook, T. H. Chan, *Synthesis* **1983**, 201–203)—and shown to be identical (^{1}H and ^{13}C NMR) to an authentic sample of methyl (*R*,S**)-2-hydroxy-3-phenyl-3-(*p*-toluenesulfonamido)propanoate [3a].

[10] Review of the chemistry of Weinreb (*N*-methoxy-*N*-methyl) amides: M. P. Sibi, *Org. Prep. Proc. Intl.* **1993**, *25*, 15-40.

[11] The regioselectivities observed for the aminohydroxylation of olefins **1a**, **1b**, and **1i**–**1k** under the conditions of procedures A and B (see Table 2) were the same as those observed under the conditions described in Table 1. In one case, however, when the concentration of **1b** was raised from 0.5 to 0.8 M and the catalyst load was decreased from 0.25 to 0.20 mol%, there was a slight deterioration of the regioselectivity from 5.0:1 to 3.0:1 (see Table 2, entries 2 and 3).

[12] J.-E. Bäckvall, K. Oshima, R. E. Palermo, K. B. Sharpless, *J. Org. Chem.* **1979**, *44*, 1953–1957.

[13] a) D. Tanner, *Angew. Chem.* **1994**, *106*, 625–646; *Angew. Chem. Int. Ed. Engl.* **1994**, *33*, 599–619; b) W. H. Pearson, B. W. Lian, S. C. Bergmeier in *Comprehensive Hetyerocyclic Chemistry II, Vol. 1A* (Ed.: A. Padwa), Pergamon, New York, **1996**, pp. 1–60; c) H. M. I. Osborn, J. Sweeney, *Tetrahedron: Asymmetry* **1997**, *8*, 1693–1715.

[14] F. Balkenhohl, C. von dem Bussche-Hünnefeld, A. Lansky, C. Zechel, *Angew. Chem.* **1996**, *108*, 2436–2487; *Angew. Chem. Int. Ed. Engl.* **1996**, *35*, 2288–2337.

[15] Another advantage of racemates, pointed out by a reviewer, is that modern preparative chiral HPLC often enables access to both enantiomers. The pharmaceutical industry now favors this approach for quick "enantiodeconvolutiuon" of biological activity.

Di-, Tri-, and Tetranuclear Alkoxyaluminum Hydrides

Heinrich Nöth,* Andreas Schlegel, Jörg Knizek, and Holger Schwenk

Little is known about the degree of association of alkoxyalanes in the solid state or in solution. Seminal papers published in the 1960s describe reactions of short-chain alcohols with aluminum hydride.[1] Determination of the molecular mass proved that tBuOAlH$_2$ and (tBuO)$_2$AlH are dimeric in benzene. Recent X-ray structure analysis ascertained that the association occurs via an Al_2O_2 four-membered ring.[2] The syntheses of alkoxyalanes are described by Equations (1) and (2).

$$AlH_3 + HOR \longrightarrow H_2Al(OR) + H_2 \quad (1)$$

$$AlH_3 + 2\,HOR \longrightarrow HAl(OR)_2 + 2\,H_2 \quad (2)$$

Although it was demonstrated that the amount of hydrogen liberated during the reaction is equivalent to the molar amount of the alcohol, the composition of the product is dependent on the size and the branching of the alkyl

[*] Prof. Dr. H. Nöth, Dipl.-Chem. A. Schlegel, Dipl.-Chem. J. Knizek, Dr. H. Schwenk
Institut für Anorganische Chemie der Universität
Meiserstrasse 1, D-80333 München (Germany)
Fax: Int. code + (89) 590-2451

group R.[1] Mono- and disubstituted alkoxyalanes containing sterically less demanding *n*-alkyl groups disproportionate according to Equations (3) and (4). In addition, association to units of higher molecular order rises as the alkyl group becomes smaller.[1]

$$2(RO)AlH_2 \xrightleftharpoons{Et_2O} AlH_3 + (RO)_2AlH \quad (3)$$

$$2(RO)_2AlH \xrightleftharpoons{Et_2O} Al(OR)_3 + (RO)AlH_2 \quad (4)$$

The electron-deficient alkoxyalanes $(RO)_{3-n}AlH_n$ are intermolecularly stabilized by dimerization, oligomerization, or polymerization with formation of oxo or hydride bridges, thus increasing the coordination at the Al centers to four or five. Mixed polymers may be formed, as suggested but not structurally proven.[1] Disproportionation and association are at first sight two independent phenomena. However, they might cooperate and, as a consequence, make the isolation of analytically pure, well-defined compounds more difficult. The use of sterically demanding alcohols reduces the tendency of the alkoxyalanes to disproportionate and to oligomerize, as demonstrated for tBuOAlH$_2$ and (tBuO)$_2$AlH.[2] Nevertheless, ROAlH$_2$ with R = 2,6-di-*tert*-butyl-4-methylphenol can be obtained as an Me$_3$N adduct which is present both as a monomer and a hydride-bridged dimer in the crystal lattice.[3]

We now demonstrate that additional structural patterns emerge depending on the steric requirement of the alkyl group R. This is documented by compounds **1**–**4**, which are obtained by allowing the corresponding alcohols to react with AlH$_3$ in diethyl ether [Eqs. (1) and (2)].

[{(tBu)$_2$(Me)COAlH$_2$}$_2$] **1** [{(tBu)(Me)(H)COAlH$_2$}$_4$] **2**

[(iPrO)$_2$AlH{(iPrO)AlH$_2$}$_2$] **3a** Li[(tBuCH$_2$O)$_5$Al$_3$H$_5$]·Et$_2$O **4**

The reaction of tBu$_2$(Me)COH with AlH$_3$ in diethyl ether [Eq. (1)] yields the respective monoalkoxyalane, which is a dimer according to its mass spectrum and X-ray structure (Figure 1). Although the product of the 1:1 reaction of

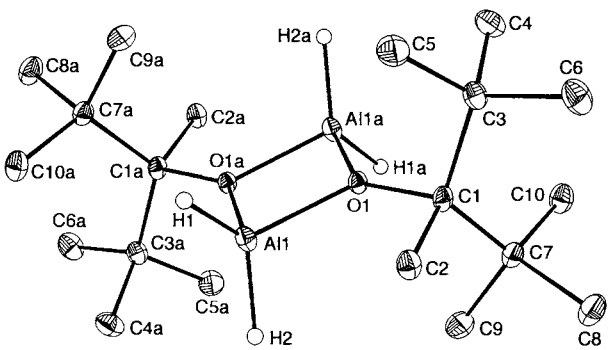

Figure 1. ORTEP representation of the molecular structure of **1**. Selected atomic distances [Å]: Al1–H1 1.49(2), Al1–H2 1.45(2), Al1 ··· Al1a 2.774(1), Al1–O1a 1.841(1), Al1a–O1 1.841(1), Al1–O1 1.854(1). Selected bond angles [°]: O1a-Al1-O1 82.73(6), Al1a-O1-Al1 97.27(6), H1-Al1-H2 119(1), Al1a-O1-C1 138.6(1), Al1-O1-C1 123.7(1).

tBuMeCHOH with AlH$_3$ is dimeric in the gas phase, as ascertained from its mass spectrum, the X-ray structure analysis reveals that in **2** two dimers are associated through two hydride bridges to form a tetranuclear alkoxyalane in the solid state (see Figure 2).

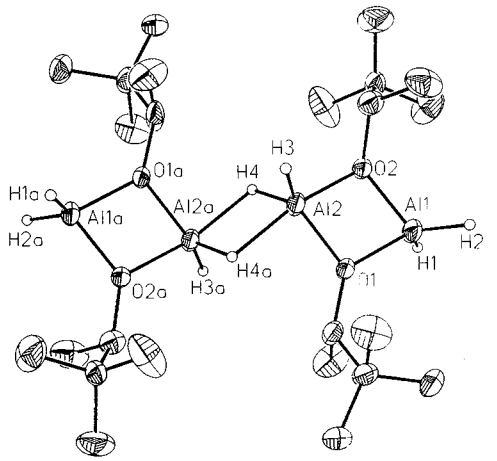

Figure 2. ORTEP representation of the molecular structure of **2**. Selected atomic distances [Å]: Al1–H1 1.38(7), Al1–H2 1.57(5), Al2–H3 1.49(5), Al2–H4 1.60(4), Al2–H4a 1.85(4), Al2 ··· Al2a 2.731(3), Al1–O1 1.837(3), Al2–O1 1.819(3), Al1–O2 1.808(3), Al2–O2 1.864(3). Selected bond angles [°]: O1-Al1-O2 80.9(1), O1-Al2-O2 79.9(1), Al1-O1-Al2 99.7(2), Al1-O2-Al2 99.1(2), H1-Al1-H2 123(2), H3-Al2-H4 116(2), H4-Al2-O2 97(2), H4-Al2-O1 120(2), H3-Al2-O1 123(2), H4a-Al2-O2 161(2).

In contrast, the analogous reaction with isopropyl alcohol does not lead to dimeric isopropoxyalane. Only part of the product can be sublimed under vacuum, and the most volatile component turned out to be the trinuclear complex **3a** (see Figure 3), which can be looked at as a mixed oligomer of two molecules of iPrOAlH$_2$ with one molecule of (iPrO)$_2$AlH. Complex **3a** is formed by partial disproportionation of iPrOAlH$_2$ in solution [Eq. (3)]. However, the sublimate not only furnishes single crystals of **3a** but also its chain polymer **3b**, in which the Al$_3$(OiPr)$_4$H$_5$ units are connected through hydride bridges (see Figure 4). Both species exhibit two identical ^{27}Al NMR signals in a 2:1 ratio for tetra- and pentacoordinated aluminum atoms. Therefore, there is only one trinuclear species present in solution. The IR spectrum shows bands for both terminal (1845 and 1824 cm^{-1}) and bridging hydrogen atoms (1785 and 1665 cm^{-1}). Complex **3a** is obtained in yields of over 90% by allowing 3 mol of AlH$_3$ to react with 4 mol of isopropyl alcohol.[4]

The solubility of ROAlH$_2$ and (RO)$_2$AlH increases when a slight excess of LiAlH$_4$ is applied in the preparation of AlH$_3$. This is particularly noticeable for the reaction of neopentyl alcohol with AlH$_3$ in diethyl ether [Eq. (2)]. Under these conditions—formally depicted in Equation (5)—compound **4** is produced, which can be formulated as Li[AlH$_3$(OCH$_2$ tBu)]·[(tBuCH$_2$O)$_2$AlH]$_2$·Et$_2$O.

$$LiAlH_4 + 2\,AlH_3 + 5\,t\text{BuCH}_2\text{OH} \longrightarrow \mathbf{4} + 5\,H_2 \quad (5)$$

The structures of the new alkoxyalanes were determined by X-ray crystallography. The structure of **1** (see Figure 1) is similar to that of *tert*-butoxyalane.[2] The molecule posesses a crystallographic center of inversion and an acute O-Al-O angle of 82.73(6)°, which corresponds to 81.0(2)° for *tert*-butoxyalane.[2] The sum of bond angles at the oxygen atoms is 359.6°, suggesting sp^2 hybridization for the oxygen atoms. Steric effects are most likely responsible for the large Al(1a)-O1-C1 bond angle of 138.6(1)°, because both *tert*-butyl groups at C1 point in the direction of Al(1a), whereas the sterically less demanding CH$_3$ group at C1 is associated with the much smaller Al1-O1-C1 bond angle of 123.7(1)°. While there are no intermolecular interactions in the lattice of **1** which exceed

those of van der Waals contacts, in the case of **2** two molecules of $[\{(t\mathrm{Bu})(\mathrm{Me})(\mathrm{H})\mathrm{COAlH_2}\}_2]$ associate through Al–H bridges to form "twin molecules" (see Figure 2). An analogous structure was recently reported by Raston et al. for $[\{t\mathrm{Bu_2}(\mathrm{H})\text{-}\mathrm{COAlH_2}\}_4]$.[5]

There are two Al atoms of coordination number 4 and two of coordination number 5 in **2**. The bonding parameters of the Al_2O_2 four-membered rings correspond closely to those of **1**; in particular, there is no noticeable elongation of the Al–O bond to the pentacoordinated Al centers. These feature a distorted trigonal-bipyramidal environment. Atoms H3, H4, and O1 are in the equatorial positions with bond angles close to 120°, while O2 and H4a occupy the axial positions. The hydrogen-brides are weak and asymmetric, similar to those in dimeric $AlH_3 \cdot THF$.[6] Consequently, for **2** only one signal for tetracoordinated Al ($\delta(^{27}\mathrm{Al}) = 121$) is observed in benzene and diethyl ether. The *tert*-butyl groups are in an anti-periplanar orientation with respect to the plane of the Al_2O_2 ring. Within the dimeric units, each asymmetrically substituted C atom posesses the same absolute stereoconfiguration: (*S*) in one unit, and (*R*) in the other. Consequently, there are double sets of ^1H and ^{13}C resonances.

$Al_3(O\mathit{i}\mathrm{Pr})_4H_5$ was isolated in two different modifications **3a** and **3b** (Figures 3 and 4, respectively). In **3a** the sum of angles for bonds from Al1 to O1, O4, and H2 is 360°, and the O2-Al1-O3 bond angle is 168°. This indicates the presence of a distorted trigonal-bipyramidal Al center. Accordingly, the Al–O bonds to the apical O atoms are longer. The Al_2O_2 four-membered rings are asymmetric inspite of their planarity. Due to the open H-Al-H bond angles (av 118.4°), there is considerable deviation from a tetrahedral geometry of the ligands. The hydrogen-bridged species **3b** (Figure 4) shows almost the same bonding parameters for the central Al1 atom as **3a**. The bond angles of Al2 and Al3, which show trigonal-bipyramidal configuration, compare well with the related coordination sphere of Al2 in **2**.

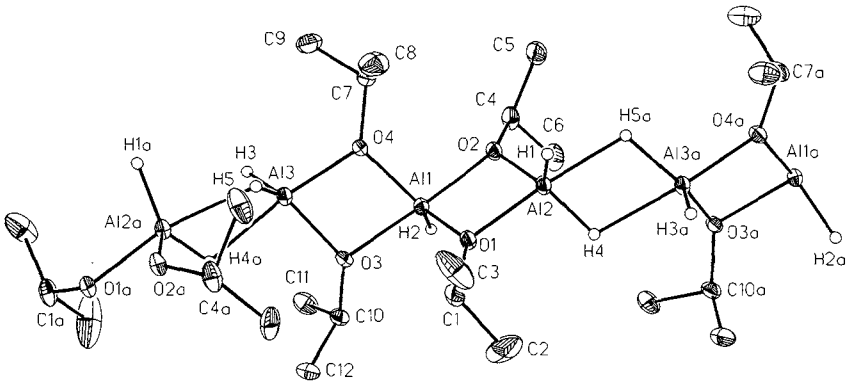

Figure 4. ORTEP representation of the molecular structure of **3b**. Selected atomic distances [Å]: Al1–H2 1.52(4), Al2–H1 1.47(4), Al2–H4 1.51(5), Al2–H5a 2.04(4), Al3–H3 1.50(4), Al3–H5 1.55(4), Al3–H4a 2.04(4), Al1–O1 1.830(3), Al2–O1 1.885(3), Al1–O4 1.827(3), Al3–O4 1.877(3), Al1–O2 1.938(3), Al2–O2 1.808(3), Al1–O3 1.952(3), Al3–O3 1.815(3), Al1 ··· Al2 2.885(1), Al1 ··· Al3 2.885(2). Selected bond angles [°]: Al1-O1-Al2 101.9(1), Al1-O2-Al2 100.7(1), Al1-O3-Al3 99.7(1), Al1-O4-Al3 102.1(1), O1-Al1-O2 77.7(1), O1-Al2-O2 79.7(1), O3-Al1-O4 77.8(1), O3-Al3-O4 80.0(1), O1-Al1-O3 97.8(1), O1-Al1-O4 114.7(1), O2-Al1-O3 171.0(1), O2-Al1-O4 96.8(1), H1-Al2-H4 119(2), H3-Al3-H5 117(2), H2-Al1-O1 122(2), H2-Al1-O2 97(1), H2-Al1-O3 92(1), H2-Al1-O4 124(2), H5a-Al2-O1 168(1), H4-Al2-O2 118(2), H1-Al2-O2 121(2), H5-Al3-H4a 72(2), H5a-Al2-H4 73(2), Al3-H5-Al2a 103(2), Al2-H4-Al3a 103(2).

The composition and the two ^{27}Al NMR signals at $\delta = 125$ and 81 indicate that **4** is an unusual compound (Figure 5). In contrast to the situation in the alkoxyalanes discussed so far, all Al atoms in **4** are pentacoordinated. This compound can be looked at as being built from one molecule of H_2AlOR with two molecules of $HAl(OR)_2$ by Al–O coordination to result

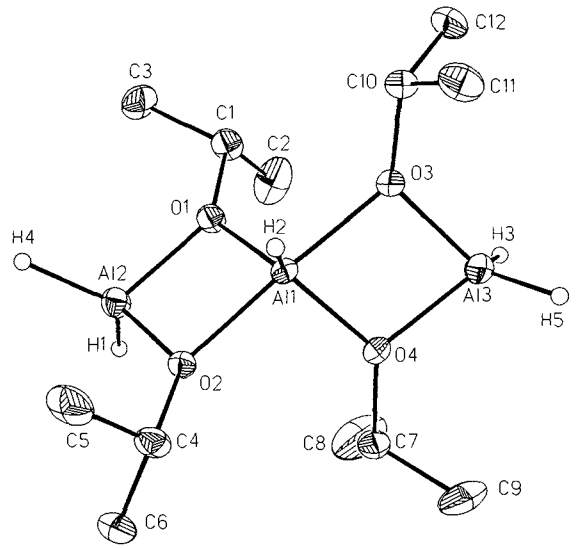

Figure 3. ORTEP representation of the molecular structure of **3a**. Selected atomic distances [Å]: Al1–H2 1.52(4), Al2–H1 1.54(4), Al2–H4 1.50(4), Al3–H3 1.52(5), Al3–H5 1.44(5), Al1–O1 1.832(3), Al2–O1 1.832(3), Al1–O4 1.839(3), Al3–O4 1.833(3), Al1–O2 1.918(3), Al2–O2 1.802(3), Al1–O3 1.925(3), Al3–O3 1.801(3), Al1 ··· Al2 2.842(2), Al1 ··· Al3 2.846(2). Selected bond angles [°]: Al1-O1-Al2 101.7(1), Al1-O2-Al2 99.5(1), Al1-O3-Al3 99.6(1), Al1-O4-Al3 101.6(1), O1-Al1-O4 115.4(1), O1-Al1-O2 77.8(1), O1-Al2-O2 80.8(1), O3-Al1-O4 77.6(1), O3-Al3-O4 81.0(1), O1-Al1-O3 96.2(1), O2-Al1-O3 168.1(1), O2-Al1-O4 95.6(1), H1-Al2-H4 118(2), H3-Al3-H5 119(3), H2-Al1-O1 124(2), H2-Al1-O2 99(2), H2-Al1-O3 93(2), H2-Al1-O4 121(2).

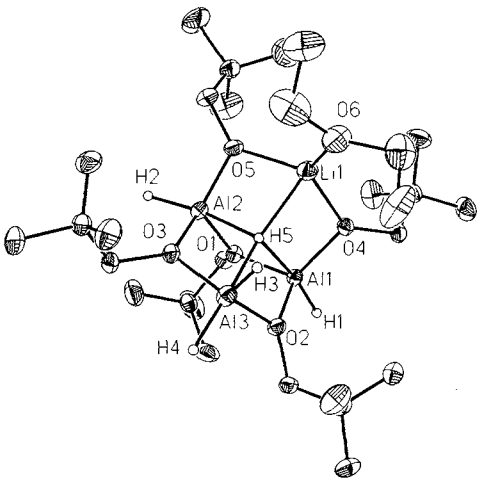

Figure 5. ORTEP representation of the molecular structure of **4**. Selected atomic distances [Å]: Al1–H1 1.48(3), Al2–H2 1.53(3), Al3–H3 1.48(3), Al3–H4 1.51(4), Al1–H5 1.83(3), Al2–H5 1.85(3), Al3–H5 2.02(3), Li1–H5 2.00(3), Al1–O1 1.841(2), Al2–O1 1.840(2), Al1–O2 1.841(2), Al2–O3 1.844(2), Al3–O2 1.859(2), Al3–O3 1.855(2), Al1–O4 1.774(2), Al2–O5 1.777(2). Selected bond angles [°]: Al1-O1-Al2 105.5(1), Al1-O2-Al3 111.2(1), Al2-O3-Al3 112.9(1), O1-Al1-O2 108.8(1), O1-Al2-O3 107.9(1), O2-Al3-O3 114.5(1), O4-Li1-O5 120.5(3), O4-Li1-O6 122.2(3), O5-Li1-O6 117.1(3), Al1-H5-Al2 106(1), Al1-H5-Al3 105(1), Al2-H5-Al3 106(1), Al2-H5-Li1 99(1), Al1-H5-Li1 98(1), Al3-H5-Li1 140(1).

 © WILEY-VCH Verlag GmbH, D-69451 Weinheim, 1997 0570-0833/97/3623-2642 $ 17.50+.50/0

in a six-membered ring with chair configuration. All Al–O bridges are of almost the same length. The endocyclic O-Al-O bond angles approach that of a tetrahedron. In addition, two exocyclic OR groups coordinate through their oxygen atoms to the lithium center of a "lithium hydride molecule".

The hydride ion of the "LiH component" lies above the Al atoms of the Al_3O_3 chair. It coordinates not only to the Li center but also to all three Al atoms. As far as we are aware, this is the first molecular compound with a tetracoordinated hydridic hydrogen atom. The distortion from a tetrahedral environment is small. Since the Al–H distances are about 0.5 Å longer than those for the terminal Al–H units, these bonds are weak. Moreover, we conclude that the $H_2Al(OR)_2$ group is a weaker hydride acceptor than the $HAl(OR)_3$ group, because the Al–H distance to the central hydride is longer (2.02 Å) than that of the $HAl(OR)_3$ groups (av 1.84 Å). The ^{27}Al NMR signal at $\delta = 81$ is assigned to the latter.

The examples presented here demonstrate that the chemistry and structural chemistry of alkoxyalanes is much more variable than hitherto assumed. Mixed oligomers $Al_n(OR)_{3n-m}H_m$ may form which can bind LiH with formation of alkoxyhydrido aluminates. We assume that alkoxyalanes can be developed into useful reagents for selectively reducing functional organic groups.

Experimental Section

All reactions were performed in an atmosphere of nitrogen using dry solvents. ^{27}Al NMR spectra: 70 MHz, 25 °C, C_6D_6; IR spectra: Nujol/Hostaflon; all compounds gave correct elemental analyses.

1: A solution of $AlCl_3$ (0.57 g, 4.3 mmol) in Et_2O (10 mL) was added to a stirred solution of $LiAlH_4$ (0.49 g, 12.9 mmol) in Et_2O (10 mL) at 0 °C[7]. A solution of tBu_2MeCOH (2.71 g, 17.1 mmol) in Et_2O (15 mL) was then added dropwise to the suspension. Hydrogen gas formed. After the suspension was stirred for 2 h, the insoluble material (LiCl) was removed by filtration (G4 glass frit). Et_2O was removed from the filtrate, and the residue dried in vacuo. Compound **1** crystallized from Et_2O/pentane (4/1) at −20 °C as colorless prisms [8]; yield 2.38 g (74.3 %), m.p. 160 °C (decomp). ^{27}Al NMR: $\delta = 117$ ($h_{1/2} = 3834$ Hz); IR: $\tilde{\nu} = 1872$ (vs), 1849 cm^{-1} (vs, $\nu_{as,s}(AlH_2)$); MS (70 ev): $m/z = 372$ [M^+], 315 [$M^+ - t$Bu].

2: A solution of $AlCl_3$ (1.66 g, 12.5 mmol) in Et_2O (40 mL) was added to a stirred solution of $LiAlH_4$ (1.42 g, 37.4 mmol) in Et_2O (20 mL) at 0 °C[7]. The resulting suspension was then treated with a solution of *t*BuMeCHOH (5.09 g, 6.2 mL, 49.8 mmol) in Et_2O (20 mL). Hydrogen gas was liberated. The suspension was stirred for 5 h, the insoluble material removed by filtration (G4 glass frit), the solvent removed from the filtrate, and the colorless residue dried in vacuo. Sublimation at 45 °C (bath temperature) and $3 \cdot 10^{-9}$ bar yielded colorless crystals of **2** [8]; yield 5.12 g (78.6 %); m.p. 72–75 °C. ^{27}Al NMR: $\delta = 121$ ($h_{1/2} = 3695$ Hz); IR: $\tilde{\nu} = 1854$ (sh), 1841 (vs; $\nu_{as,s}(AlH_2)$), 1645 (w, br), 1578 (w, br), 1531 cm^{-1} (w, br; ν(AlH bridge)]; MS (70 eV): $m/z = 260$ [M^+] for the dinuclear species, 259 [$M^+ - H$], 203 [$M^+ - t$Bu], 175 [$M^+ - t$BuCHCH$_3$], 159 [203 − CH_3CHO], 117 [161 − CH_3CHO].

3a and **3b**: A solution of $AlCl_3$ (1.62 g, 12.2 mmol) in Et_2O (30 mL) was added to a stirred solution of $LiAlH_4$ (1.39 g, 36.5 mmol) in Et_2O (20 mL) at 0 °C[7]. The resulting suspension wsa treated with *i*PrOH (2.92 g, 3.72 mL, 48.6 mmol) in Et_2O (20 mL) at 10 °C. Hydrogen was liberated. After the reaction mixture was stirred for 3 h, the insoluble material was removed by filtration (G4 glass frit), and the solvent removed from the filtrate under vacuum. Product **3a** was obtained from the colorless solid residue by sublimation at 35 °C (bath temperature) and at $1 \cdot 10^{-3}$ bar [8]. Product **3b** appeared as a second fraction subliming at 40 °C and 5×10^{-3} bar [8]; total yield 1.22 g (15.5 %). Softening range of **3a** and **3b**: 49–61 °C. ^{27}Al NMR: $\delta = 126$ ($h_{1/2} = 2118$ Hz), 60 ($h_{1/2} = 1283$ Hz); IR: $\tilde{\nu} = 1842$ (vs), 1825 (vs), 1785 (s, br; $\nu_{as,s}(AlH_a)$); 1665 cm^{-1} (m, br; $\nu(AlH_b)$).

4: A solution of $AlCl_3$ (1.59 g, 11.9 mmol) in Et_2O (25 mL) was added to a stirred solution of $LiAlH_4$ (1.57 g, 41.4 mmol) in Et_2O (20 mL) at 10 °C[7], followed by $tBuCH_2OH$ (8.41 g, 95.4 mmol) in Et_2O (30 mL). Hydrogen was liberated. Stirring was continued for 4 h at ambient temperature. Then the insoluble material was separated by filtration (G4 glass frit), and extracted twice with pentane (2 × 20 mL). Fractional crystallization at 2 °C yielded colorless needles of **4** [8]; yield 2.48 g (72.5 %); m.p. 104 °C (decomp). ^{27}Al NMR: $\delta = 125$ (br), 81 (br); ^7Li NMR (105 MHz, 25 °C, C_6D_6): $\delta = 1.09$: IR: $\tilde{\nu} = 1839$ (sh), 1821 (vs; $\nu_{as,s}(AlH_t)$), 1797 (m), 1739 cm^{-1} (w; $\nu_{as,s}(AlH_b)$).

Received: April 9, 1997 [Z103271E]
German version: *Angew. Chem.* **1997**, *109*, 2754–2758

Keywords: alcohols · aluminum · hydrides · multinuclear complexes · structure elucidation

[1] H. Nöth, H. Suchy, *Z. Anorg. Allg. Chem.* **1968**, *358*, 44.
[2] M. Veith, S. Faber, H. Wolfanger, V. Huch, *Chem. Ber.* **1996**, *129*, 381.
[3] M. D. Healy, M. R. Mason, P. W. Gravelle, S. G. Bott, A. R. Barron, *J. Chem Soc. Dalton Trans.* **1993**, 441.
[4] H. Nöth, D. Hauk, P. Rittmeyer, U. Wietelmann, A. Schlegel, patent submitted.
[5] G. A. Koutsantonis, F. C. Lee, C. L. Raston, *Main Group Chem.* **1995**, *1*, 21. We succeded in verifying the structure of [{tBu_2(H)COAlH$_2$}$_4$].
[6] I. B. Gorrell, P. B. Hitchcock, J. D. Smith, *J. Chem. Soc. Chem. Comm.* **1993**, 189.
[7] D. L. Schmidt, C. B. Roberts, P. F. Reigler, M. F. Lemanski, Jr., E. P. Schram, *Inorg. Synth.* **1973**, *14*, 47.
[8] Data for the X-ray structure determinations were collected with a Siemens P4 diffractometer equipped with a CCD area detector ($Mo_{K\alpha}$, $\lambda = 0.71073$ Å). The reflections were recorded in a total of 1200 frames with $\Delta\varphi = 0.3°$ at two different χ settings. The structures were solved with direct methods using the program XS (Siemens). The structure was refined with the least-squares method (program SHELXL93, G. M. Sheldrick, Göttingen, Germany, **1993**). Carbon-bound hydrogen atoms were included in the refinement with a riding model with fixed isotropic temperature parameter U, and the positions of the Al- and Li-bound hydrogen atoms were freely refined. The thermal ellipsoides in the Figures are depicted at a probability level of 25 %. Carbon-bound hydrogen atoms are omitted for clarity. Crystallographic data (excluding structure factors) for the structures reported in this paper have been deposited with the Cambridge Crystallographic Data Centre as supplementary publication no. CCDC-100400. Copies of the data can be obtained free of charge on application to The Director, CCDC, 12 Union Road, Cambridge CB2 1EZ, UK (fax: int. code + (1223) 336-033; e-mail: deposit@chemcrys.cam.ac.uk). **1**: $C_{20}H_{46}Al_2O_2$, colorless prism, $0.5 \times 0.4 \times 0.4$ mm^3, monoclinic, space group $P2_1/c$, $a = 8.3389(2)$, $b = 12.1377(2)$, $c = 11.7629(2)$ Å, $\beta = 106.908(1)°$, $Z = 4$, $V = 1139.12(4)$ Å^3, $\rho_{calcd} = 1.086$ g cm^{-3}, $\mu = 0.137$ mm^{-1}, $F(000) = 416$, $T = 193(2)$ K, $2\theta = 4.94 - 58.40°$; of 6394 reflections recorded, 2233 were unique (R(int) = 0.0585) and 1242 observed with $F > 4\sigma(F)$; 124 parameters were refined. $R = 0.0372$, $R2 = 0.0858$, GOF = 1.125; $\Delta\rho = 0.201$ e Å^{-3}. **2**: $C_{24}H_{60}Al_4O_4$, colorless block, $0.45 \times 0.35 \times 0.3$ mm^3, monoclinic, space group $P2_1/n$, $a = 11.6718(4)$, $b = 12.2962(4)$, $c = 12.1433(4)$ Å, $\beta = 101.291(1)°$, $Z = 4$, $V = 1709.1(1)$ Å^3, $\rho_{calcd} = 1.012$ Mg m^{-3}, $\mu = 0.159$ mm^{-1}, $F(000) = 576$, $T = 233$ K, $2\theta = 4.42 - 57.76°$; of 8992 reflections recorded, 3185 were unique (R(int) = 0.0767) and 1495 observed with $F > 4\sigma(F)$; 169 parameters were refined. $R = 0.0811$, $R2 = 0.1842$, GOF = 1.099; $\Delta\rho = 0.391$ e Å^{-3}. **3a**: $C_{12}H_{33}Al_3O_4$, colorless block, $0.37 \times 0.22 \times 0.2$ mm^3, orthorhombic, space group $P2_12_12_1$, $a = 9.405(1)$, $b = 11.492(1)$, $c = 18.845(1)$ Å, $Z = 4$, $V = 2036.8(2)$ Å^3, $\rho_{calcd} = 1.051$ Mg m^{-3}, $\mu = 0.192$ mm^{-1}, $F(000) = 704$, $T = 213(3)$ K, $2\theta = 4.16 - 54.76°$; of 6858 reflections, 3788 were unique (R(int) = 0.0518) and 3391 observed with $F > 4\sigma(F)$; 200 parameters were refined. $R = 0.0537$, $R2 = 0.1144$, GOF = 1.180; $\Delta\rho = 0.317$ e Å^{-3}. **3b**: $C_{12}H_{33}Al_3O_4$, colorless prism, $0.4 \times 0.27 \times 0.25$ mm^3, monoclinic, space group $P2_1/c$, $a = 16.7180(7)$, $b = 8.3793(4)$, $c = 15.0832(6)$ Å, $\beta = 110.625(1)°$, $Z = 4$, $V = 1977.5(2)$ Å^3, $\rho_{calcd} = 1.083$ Mg m^{-3}, $\mu = 0.197$ mm^{-1}, $F(000) = 704$, $T = 193$ K, $2\theta = 2.60 - 54.94°$; of 10011 reflections recorded, 3625 were unique (R(int) = 0.1147) and 2296 observed with $F > 4\sigma(F)$; 199 parameters refined. $R = 0.0723$, $R2 = 0.1267$, GOF = 1.203; $\Delta\rho = 0.382$ e Å^{-3}. **4**: $C_{29}H_{70}Al_3LiO_6$, colorless needles, $0.4 \times 0.24 \times 0.2$ mm^3, orthorhombic, space group $Pbca$, $a = 20.447(3)$, $b = 18.1972(1)$, $c = 21.833(6)$ Å, $Z = 8$, $V = 8123(2)$ Å^3, $\rho_{calcd} = 0.986$ Mg m^{-3}, $\mu = 0.124$ mm^{-1}, $F(000) = 2672$, $T = 203(3)$ K, $2\theta = 3.52 - 58.28°$; of 38008 reflections recorded, 8395 were unique (R(int) = 0.0765) and 4558 observed with $F > 4\sigma(F)$; 400 parameters were refined. $R = 0.0655$, $R2 = 0.1399$, GOF = 1.143; $\Delta\rho = 0.543$ e Å^{-3}.

 © WILEY-VCH Verlag GmbH, D-69451 Weinheim, 1997 0570-0833/97/3623-2643 $ 17.50+.50/0

Synthesis and Structure of a Tetragallane $[R_4Ga_4I_3]^-$ and a Polyhedral Nonagallane $[R_6Ga_9]^-$**

Wolfgang Köstler and Gerald Linti*

Dedicated to Professor Gottfried Huttner on the occasion of his 60th birthday

Compounds with metal–metal bonds have a special fascination and with a growing number of atoms, they provide an insight into the transition from molecules to metals. The digallanes(4) R_4Ga_2,[1] a cyclotrigallane $R_3Ga_3M_2$ ($R = 2,6\text{-}Mes_2C_6H_3$, M = Na, K),[2] a pentagallane $[Cl_2Ga(OEt_2)]_3[Cl\text{-}Ga(OEt_2)_2]Ga$,[3] and a cyclooctagallane $Ga_8I_8(PEt_3)_6$[4] represent structurally investigated electron-precise oligogallanes. The tetragallanes(4) $(RGa)_4$ [**1a**: $R = C(SiMe_3)_3$, **1b**: $R = Si(SiMe_3)_3$[5]] with a tetrahedral framework of gallium atoms are the only polyhedral molecular compounds of gallium that are considered electron deficient. The mixture (neopentyl-Ga)$_n$ ($n = 8.9-10.5$) obtained by reduction of (neopentyl)$_2$GaCl may also be classified in this group.[6]

Compounds **1a** and **1b** were prepared by reaction of gallium(II) halides $Ga_2X_4 \cdot 2$dioxane with three equivalents RLi; however, at best one third of R and half of the gallium used is found in the desired products. A more economical synthesis should be possible from gallium(I) derivatives. We describe herein the reaction of "GaI"—available from gallium and iodine in a simple manner[7]—with tris(trimethylsilyl)silyllithium (= hypersilyllithium).[8] The former has already been employed as the gallium(I) source in the preparation of $[Tp^{tBu2}]Ga$ (Tp^{tBu2} = tris(3,5-di-*tert*-butylpyrazolyl)hydroborate.[9]

Freshly prepared "GaI" was treated at −78 °C in toluene with $Li(thf)_3Si(SiMe_3)_3$ (Scheme 1), affording a dark red solution. After the reaction mixture had been concentrated to

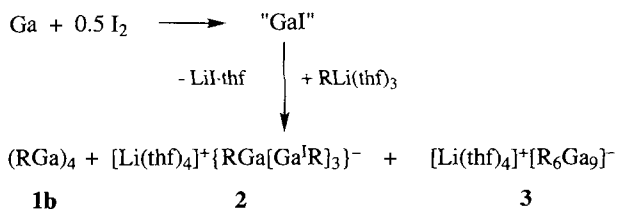

Scheme 1. R = $Si(SiMe_3)_3$.

dryness, **1b** crystallized from a violet-colored pentane extract. Prior to that, yellow crystals of **2** can be isolated. This compound forms preferentially if the Ga:I:hypersilyl ratio is changed from 1:1:1 to 2:1:0.7. This reproducible variation in the product distribution gives a clear indication of the problem associated with the "GaI" used. Evidently, it is a mixture of gallium subiodides, the composition of which requires further study. First indications are delivered by a detailed analysis of the reaction products. If the black residue left over after filtration is washed with toluene after the extraction with pentane, a dark red solution results, from which after separation of colorless crystals of lithium iodide · thf, black crystals of diamagnetic **3** can be obtained. The X-ray crystal structure analysis of the tetragallane derivative **2**[10] shows that it crystallizes in the monoclinic space group $P2_1/c$, and exhibits a cubane-type arrangement of four Ga atoms and three iodine atoms (Figure 1). One corner of the cube

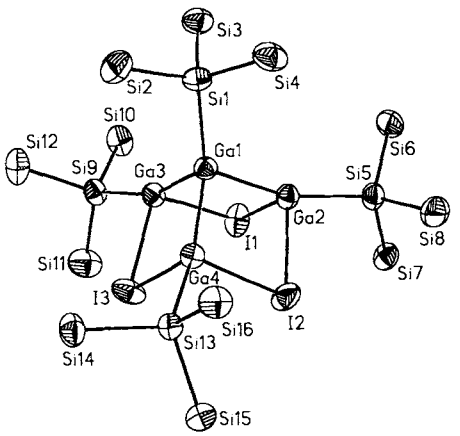

Figure 1. Crystal structure of the anion in **2**. The methyl groups have been omitted for clarity. Selected bond lengths [pm] and angles [°]: Ga1–Ga2 253.51(7), Ga1–Ga3 253.56(7), Ga1–Ga4 252.88(8), I1–Ga2 285.70(7), I1–Ga3 287.35(7), I2–Ga4 283.23(7), I2–Ga2 285.99(8), I3–Ga3 285.43(8), I3–Ga4 285.94(7), Ga1–Si1 242.23(14), Ga2–Si5 246.83(14), Ga3–Si9 246.90(14), Ga4-Si13 245.70(13), Si–Si 232.8–236.0; Ga4-Ga1-Ga2 94.05(3), Ga4-Ga1-Ga3 94.28(2), Ga2-Ga1-Ga3 94.52(2), Ga-I-Ga 81.04(2)–81.22(2), Ga1-Ga-I 91.90(2)–92.75(2), I-Ga-I 96.85(2)–99.39(3).

remains unoccupied. The three Ga–Ga edges are of equal length within the standard deviation criteria (av Ga–Ga: 253.3 pm). This value is in the typical range for Ga–Ga bonds in digallanes, for example, $[Ga_2Cl_2(hypersilyl)_2]_2$ (d_{Ga-Ga} = 250.5 pm).[11] The iodine bridges are nearly symmetric [$d_{Ga-I} = 283.2(1)-287.4(1)$ pm]. The Ga–I distances are about 30 pm longer than the terminal Ga–I bonds in $[GaI_4]^-$,[12] but are similar to the bridging ones in $Ga_8I_8(PEt_3)_6$.[4] The Ga1–Si1 distance [242.4(1) pm] is shorter than the other Ga–Si bonds (av 246.6 pm). This difference, which is accompanied by a slight reduction in the Si-Si-Si angles from 108.1° (on an average) at Si1 to 106.4° at Si5, Si9, and Si13, may be explained in part by the steric demand of the iodine atoms; however, it should not be overemphasized, because Ga–Si bond lengths are known to vary considerably.[13]

The X-ray crystal structure analysis of **3**[10] shows that it crystallizes in the monoclinic space group *C*2/*c* and verifies the composition as $[Li(thf)_4]^+$ $[(hypersilyl)_6Ga_9]^-$. The anions form channels in which the counterions are intercalated in a highly disordered manner. The C_2-symmetric cluster anion (Figure 2) is described as a slightly distorted pentagonal bipyramid of Ga atoms, two equatorial edges of which are bridged by further Ga atoms. Six of the Ga atoms, namely the apical ones, two equatorial, and the bridging ones, bear hypersilyl groups. Ga2, Ga3, and Ga4 form together with the Ga atoms at their symmetry-equivalent positions a five-membered ring, which deviates only marginally from planarity. Thus, Ga2 resides only 22 pm above the Ga3-Ga4-Ga3A plane. The bridging Ga atoms Ga5 and Ga5A also lie only slightly (11 pm) outside this plane. The distances (Figure 3) of

[*] Dr. G. Linti, Dipl.-Chem. W. Köstler
Institut für Anorganische Chemie der Universität
Engesserstrasse, Geb. 30.45, D-76128 Karlsruhe (Germany)
Fax: Int. code + (721) 608-4854
e-mail: linti@achpc9.chemie.uni-karlsruhe.de

[**] The Chemistry of Gallium, Part 11. We thank Prof. D. Fenske and Prof. P. Klüfers for their help with the crystal structure investigations, and the Deutsche Forschungsgemeinschaft for its financial support. Part 10: G. Linti, R. Frey, *Z. Anorg. Allg. Chem.* **1997**, *623*, 531–538.

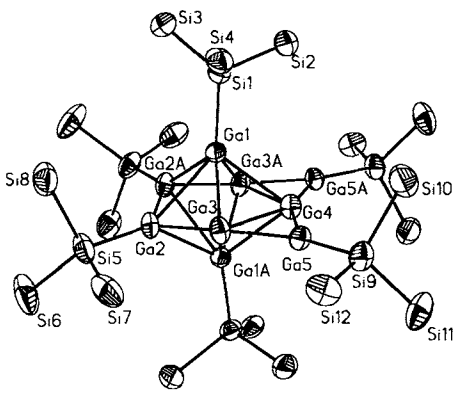

Figure 2. Crystal structure of the cluster anion in **3**. The methyl groups have been omitted for clarity.

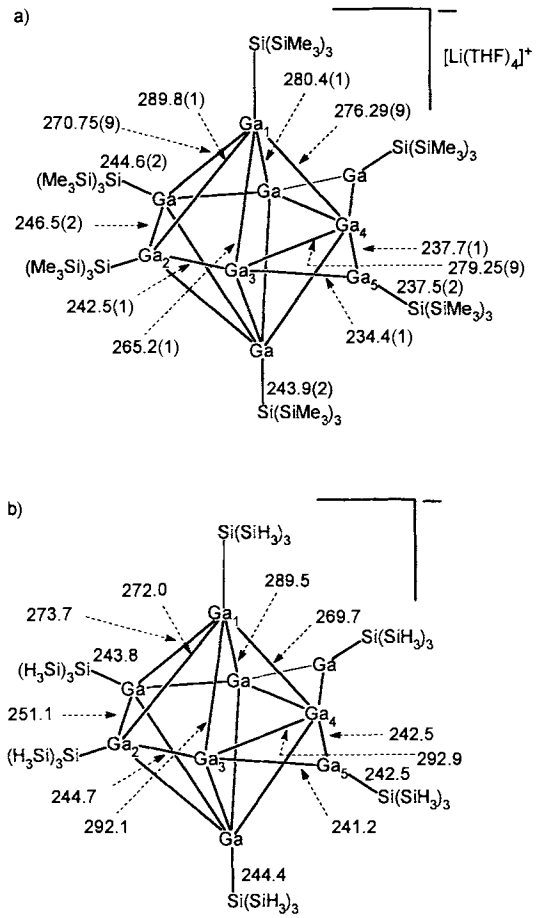

Figure 3. a) Selected distances [pm] in **3** determined by X-ray crystallography [pm]; b) results of the DFT calculation on $[\{(H_3Si)_3Si\}_6Ga_9]^-$

the apical Ga atoms to the basal ones range between 265 and 290 pm. The average distance (276.5 pm) is equivalent to the longer distances in elemental gallium. Within the five-membered ring four short distances (242.5, 246.5 pm) are found together with the long Ga3–Ga4 distance (279.2 pm). In contrast, the Ga3–Ga5 and Ga4–Ga5 distances (234.4 and 237.7 pm, respectively) to the edge-bridging gallium centers are very short. Comparatively speaking, the Ga–Ga distances in the electron-precise **2** are shorter by 16 and 6 pm, respectively, than those in the electron-deficient clusters **1a**[5a] and **1b**,[5b] which accounts for the transition from two-center, two-electron (2c–2e) bonds in **2** to multicenter bonds. The Ga–Ga distances in the nonclassical **3** (234.4–290 pm) cover a wide range, which is dependent on the varying coordination numbers 3 to 6 and the different surroundings of the gallium centers. In the Ga_{12} icosahedra present in the three-dimensional network of $Na_xMg_{5-x}Ga_9$ the Ga–Ga distances range between 269 and 273 pm.[14]

For cluster **3** ($n-1=8$) pairs of framework bonding electrons are available, if RGa is considered to contribute two electrons and the gallium atoms not bearing silyl substituents are considered to contribute one electron; thus, according to Wade–Rudolph–Mingos rules, a bicapped pentagonal bipyramid would be expected. Density functional theory (DFT) calculations[15] on $[Ga_9R_6]^-$ (R = H, SiH_3, $Si(SiH_3)_3$) show, in spite of the drastic reduction of the steric demand of the substituents, a good agreement of the structure of the Ga_9 framework with that of **3**. In Figure 3 the results of the crystal structure analysis are compared with the results of the quantum-chemical calculations. Consideration of the bonding properties with the aid of Roby–Davidson population analyses reveals that large three-center bond contributions are found on the polyhedral faces and the attached "ears". This is in accord with a description, adapted from borane clusters, with eight 2c–2e bonds and six 3c–2e bonds for the Ga_9Si_6 framework.

The synthesis of compound **3** has afforded a cluster with an unprecedented structure, in which the average oxidation state of gallium is 0.56. This shows—bearing in mind the still unknown constitution of the used "GaI"—the fine line between disproportionation to gallium and gallanes in higher oxidation states on the one hand and stabilization of lower oxidation states on the other hand. Compound **2**, which is isoelectronic to a trigallylarsane[16] $As[Ga(R)X]_3$, is a promising building block for further gallium cluster compounds with heteroatoms.

Experimental Section

a) A solution of $Li(thf)_3Si(SiMe_3)_3$ (1.42 g, 3.0 mmol) in toluene (20 mL) was added dropwise to an intensively stirred suspension of freshly prepared "GaI" (0.59 g, 3.0 mmol) in toluene (15 mL) at −78 °C. The mixture was allowed to warm to ambient temperature over a period of 3 h and was then stirred for a further 12 h. After evaporation of the reaction solution to dryness the residue was extracted with pentane (30 mL) and then with toluene (20 mL). Fractional crystallization from pentane at 0 °C afforded **1b** (0.38 g, 40%) and **2** (0.18 g, 12%). Compound 3 (0.09 g, 11%) crystallized after LiI·THF from the concentrated toluene fraction.

b) In the analogous reaction of "GaI" (0.77 g, 2.9 mmol with respect to GaI)—in the preparation of which a 100% excess of gallium was used—with $Li(thf)_3Si(SiMe_3)_3$ (0.96 g, 2.0 mmol) **1b** (0.07 g, 8%), **2** (0.55 g, 39%), and **3** (0.07 g, 9%) were isolated.

2: ^{1}H NMR (250 MHz, [D$_8$]THF, 300 K): $\delta = 0.282$, 0.276 (s each, 1:2, 81H, $SiMe_3$), 0.24 (s, 27H, $SiMe_3$); ^{1}H NMR (250 MHz, [D$_8$]THF, 323 K): $\delta = 0.297$, 0.290 (s each, 1:1, 81H, $SiMe_3$), 0.26 (s, 27H, $SiMe_3$) [This hints at an attack of THF on the Ga–I bridges]; ^{13}C NMR ([D$_8$]THF, 300 K): $\delta = 5.0$, 4.5, 3.9 ($SiMe_3$); ^{29}Si NMR ([D$_8$]THF, 300 K): $\delta = -7.5$ (3 $SiMe_3$), −9.0 (1 $SiMe_3$), −114.0 (3 Si), −121.5 (1 Si); MS(70 eV): selected, characteristic peaks: *m/z* (%): 1322 (1) [Ga_4(hypersilyl)$_4I^+$ − $SiMe_3$], 1085 (12) [Ga_3(hypersilyl)$_2I_3^+$], 73 (100) [$SiMe_3^+$].

3: ^{1}H NMR ([D$_8$]toluene, 300 K): $\delta = 3.49$ (OCH_2), 1.70 (CH_2), 0.49 ($SiMe_3$); MS(70 eV): selected, characteristic peaks: *m/z* (%): 843 (0.5) [Ga_5(hypersilyl)$_2^+$], 565 (7) [Ga(hypersilyl)$_2^+$], 232 (100) [hypersilyl$^+$ − Me].

Received: June 20, 1997 [Z10572IE]
German version: *Angew. Chem.* **1997**, *109*, 2758–2760

Keywords: density functional calculations · electron deficiency · gallium · main group elements · silicon

[1] a) W. Uhl, *Angew. Chem.* **1993**, *105*, 1449; *Angew. Chem. Int. Ed. Engl.* **1993**, *32*, 1386; b) C. Dohmeier, D. Loos, H. Schnöckel, *ibid.* **1996**, *108*, 141 and **1996**, *35*, 129; c) N. Wiberg, K. Amelunxen, H. Nöth, H. Schwenk, W. Kaim, A. Klein, T. Scheiring, *ibid.* **1997**, *109*, 1258 and **1997**, *36*, 1213.

[2] a) X.-W. Li, W. T. Pennington, G. H. Robinson, *J. Am. Chem. Soc.* **1995**, *117*, 7578; b) X.-W. Li, Y. Xie, P. R. Schreiner, K. D. Gripper, R. C. Crittendon, C. F. Campana, H. F. Schaefer, G. H. Robinson, *Organometallics* **1996**, *15*, 3798.

[3] D. Loos, H. Schnöckel, D. Fenske, *Angew. Chem.* **1993**, *105*, 1124; *Angew. Chem. Int. Ed. Engl.* **1993**, *32*, 1059.

[4] C. U. Doriat, E. Baum, A. Ecker, H. Schnöckel, *Angew. Chem.* **1997**, *109*, 2057; Angew. Chem. Int. Ed. Engl. **1997**, *36*, 1969.

[5] a) W. Uhl, W. Hiller, M. Layh, W. Schwarz, *Angew. Chem.* **1992**, *104*, 1378; *Angew. Chem. Int. Ed. Engl.* **1992**, *31*, 1364; b) G. Linti, *J. Organomet. Chem.* **1996**, *520*, 107.

[6] O. T. Beachley, Jr., J. C. Pazik, M. J. Noble, *Organometallics* **1994**, *13*, 2885.

[7] M. L. H. Green, P. Mountford, G. J. Smout, S. R. Speel, *Polyhedron* **1990**, *9*, 2763.

[8] a) H. Gilman, C. L. Smith, *J. Organomet. Chem.* **1968**, *14*, 91; b) G. Gutekunst, A. G. Brook, *ibid.* **1982**, *225*, 1; c) A. Heine, R. Herbst-Irmer, G. M. Sheldrick, D. Stalke, *Inorg. Chem.* **1993**, *32*, 2694.

[9] M. C. Kuchta, J. B. Bonnano, G. Parkin, *J. Am. Chem. Soc.* **1996**, *118*, 10914.

[10] X-ray crystal structure analysis: STOE IPDS, $Mo_{K\alpha}$ radiation. Structure solution with direct methods, full-matrix least-squares refinement against F^2, hydrogen atoms as riding model. Program used: Siemens SHELXTL 5.0 (PC). **2**: $C_{52}H_{140}Ga_4I_3LiO_4Si_{16}\cdot 0.25C_4H_{10}O$, crystal dimensions: $0.20\times 0.15\times 0.15$ mm^3, monoclinic, space group $P2_1/c$, $a=1763.3(2)$, $b=2377.3(3)$, $c=2517.4(5)$ pm, $\beta=99.91(2)^\circ$, $V=10.395(3)$ nm^3, $Z=4$, $\rho_{calcd}=1.255$ g cm^{-3}, $\mu=2.13$ mm^{-1}, 41561 measured reflections in $2\theta=4-50^\circ$, 16324 [13847 with $F>4\sigma(F)$] independent reflections, 945 parameters. $R_1=0.043$, $wR_2=0.135$ (all data), max. residual electron density 0.82 e Å^{-3}. Two hypersilyl groups are disordered in a manner, that for each of the three trimethylsilyl groups two silicon positions are observed, but 2/3 of the carbon atoms do not have split positions. **3**: $C_{70}H_{194}Ga_9LiO_4Si_{24}$, crystal dimensions: $0.20\times 0.20\times 0.15$ mm^3, monoclinic, space group $C2/c$, $a=2060.0(4)$, $b=2280.4(5)$, $c=2929.0(6)$ pm, $\beta=108.25(3)^\circ$, $V=13.067(5)$ nm^3, $Z=4$, $\rho_{calcd}=1.224$ g cm^{-3}, $\mu=2.078$ mm^{-1}, $F(000)=5056$, 38397 measured reflections in $2\theta=4-48^\circ$, 10081 (6456 with $F>4\sigma(F)$) independent reflections, 830 parameters. $R_1=0.044$, $wR_2=0.127$ (all data), max. residual electron density 0.82 e Å^{-3}. The extreme disorder of Li(thf)$_4^+$ is described only inadequately by a split model. The Ga_9 framework shows also slight disorder (96:4), which equals a rotation around a C_2 axis orthogonal to the Ga_7 plane. Further details of the crystal structure investigations are available on request from the Fachinformationszentrum Karlsruhe, D-76344 Eggenstein-Leopoldshafen, on quoting the depository numbers CSD-407072 (**2**) and CSD-407017 (**3**).

[11] G. Linti, W. Köstler, *Angew. Chem.* **1996**, *108*, 593; *Angew. Chem. Int. Ed. Engl.* **1996**, *35*, 550.

[12] a) J. C. Beamish, M. Wilkinson, I. J. Worrall, *Inorg. Chem.* **1978**, *17*, 2026; b) G. Gerlach, W. Hönle, A. Simon, *Z. Anorg. Allg. Chem.* **1982**, *486*, 7.

[13] G. Linti, R. Frey, A. Appel, *Chem Ber.* **1996**, *129*, 561.

[14] R. Nesper, *Angew. Chem.* **1989**, *101*, 99; *Angew. Chem. Int. Ed. Engl.* **1989**, *28*, 58.

[15] DFT calculations with RI-approximation using the program package TURBOMOLE; B-P86 functional, SV(P)-basis, R. Ahlrichs, **1996**.

[16] R. L. Wells, S. Shafieezad, A. T. McPhail, C. G. Pitt, *J. Chem. Soc. Chem. Commun.* **1987**, 1823.

Atomically Resolved Structure of Fracture Surfaces of a Ba/Si/O/C Glass with Atomic Force Microscopy**

Wolfgang Raberg, Volker Lansmann, Martin Jansen,* and Klaus Wandelt*

As sharp discrepancy with the importance of amorphous solids[1]—which include on one hand the oxide glasses as one of the largest and most versatile material classes and on the other the amorphous semiconductors[2] or the amorphous high performance ceramics[3] as materials of the future—the knowledge about their structures is far from complete.[4] Indeed, the highly developed repertoire of methods for structural analysis of molecules and crystalline solids fails when applied to samples which do not exhibit any translational symmetry.

Spectroscopic methods yield quite reliable information on the nearest neighbors (first coordination sphere) of a given atomic species.[5] Despite the enormous progress, for instance in nuclear magnetic resonance techniques (spin-echo and double-resonance techniques)[6] or in diffraction methods (determination of partial structure factors),[7] only averaged information about the medium- and long-range order is obtainable. For this reason only in specific cases (e.g., in the amorphous modification of elements)[8] has it been possible to develop concrete and detailed structural models that explain all experimental data.

A potential alternative to structurally sensitive probes, which reach their limits in applications on amorphous substances and therefore cannot give definite information on this topic, is the use of as many different methods as possible in order to obtain complementary as well as overlapping structural information. By combining this data with theoretical simulations concrete structural models may be developed. But again such a model gives the amorphous structure only indirectly. The better approach would be a direct imaging of the structure, which has recently become possible with scanning probe methods. In this paper we present the first image of the fracture surface of a glass with atomic resolution obtained with the atomic force microscope (AFM);[9] this image gives direct insight into the glass structure.

A barium silicate glass was chosen as test system for this investigation, since a good contrast and differentiated distance spectrum was expected from this material. Furthermore, the crystalline structures of several barium silicates are well known,[10] which may facilitate classification of the observed structural units. In order to strengthen the glass network, carbon was introduced in the melting process. That the carbon indeed was inserted into the silicate network was proved by ^{29}Si MAS-NMR spectroscopy.[11] The concomitant increase of the glass transition temperature indicates a higher degree of crosslinking in the oxycarbide glass than in the oxide glass. A

[*] Prof. Dr. M. Jansen, Dipl.-Chem. V. Lansmann
Institut für Anorganische Chemie der Universität
Gerhard-Domagk-Strasse 1, 53121 Bonn (Germany)
Fax: Int. code + (228) 73-5660
e-mail: une419@ibm.rhrz.uni-bonn.de
Prof. Dr. K. Wandelt, Dipl. Phys. W. Raberg
Physikalische Chemie der Universität
Wegelerstrasse 12, 53115 Bonn (Germany)
Fax: Int. code + (228) 73-2551

[**] This work was supported by the Deutsche Forschungsgemeinschaft (DFG) through Sonderforschungsbereich 408 (Inorganic solids without translational symmetry).

 © WILEY-VCH Verlag GmbH, D-69451 Weinheim, 1997 0570-0833/97/3623-2646 $ 17.50+.50/0

fragment of this oxycarbide glass was introduced into an ultra high vacuum chamber (UHV). The fracture surface of the sample was cleaned in an outgassing procedure and then investigated with the atomic force microscope in the contact mode.

On a 1000 nm × 1000 nm scale (Figure 1) of the untreated fracture surface one can clearly recognize a distinct granular structure comprising grains 150 nm to 200 nm in diameter.

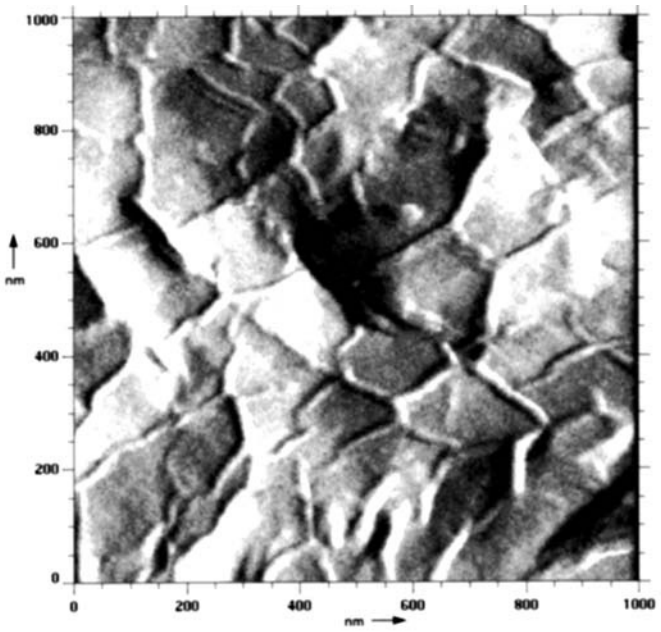

Figure 1. AFM image of the unprepared glass surface (contact force mode; maximum height difference about 50 nm).

These structures could not be observed in an earlier investigation with a conventional scanning electron microscope (usual lateral resolution in the range of 200 nm). The reason for the development of the grain boundaries and their composition is not known yet. An obvious possibility is a beginning phase separation.

Since the surface roughness between the domain walls is very small, the atomic structure of the fracture surface can be imaged. Figure 2 shows a topographic image of a 3.9 nm × 3.9 nm section after an outgasing procedure of several hours at around 400 K. The distances between the brighter regions, which correspond to elevations on the surface, are of the order of the expected interatomic distances and suggest that in this case atomic resolution was indeed obtained. There are no hints of periodic structures, only several more regular units like rings or chains.

In Figure 3 the pair distribution function corresponding to Figure 2 is shown, which in the following section is compared with the structural properties of a crystalline barium silicate, with experimental data (X-ray and neutron-scattering measurements[12]) on a barium disilicate glass, and with results from electron diffraction experiments[13] on the identical oxycarbide glass. The pair distribution function in Figure 3 is representative for the pair distribution functions corresponding to images of other areas of the fracture surface.

In the case of a totally disordered distance distribution one would expect a linear increase in the pair distribution function. This is indeed observed in Figure 3. In addition, several intensity peaks are superimposed upon the linearly

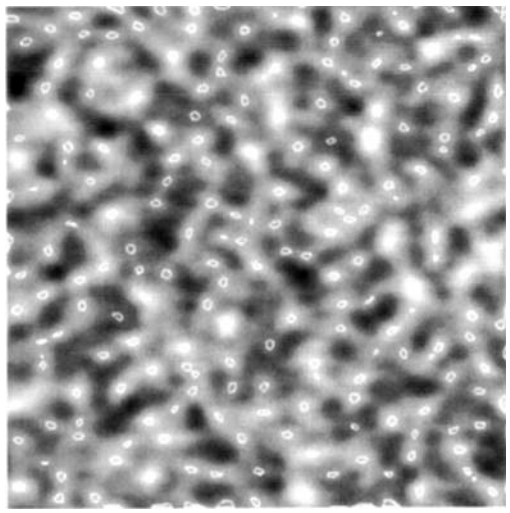

Figure 2. Topographic AFM image (constant force mode, $F = 25$ nN) of a 3.9 nm × 3.9 nm section of the Ba/Si/O/C glass after an outgasing procedure of several hours at around 400 K. The white circles indicate the atomic positions used for the calculation of the pair distance distribution. The grey scale corresponds to a height difference of 0.3 nm.

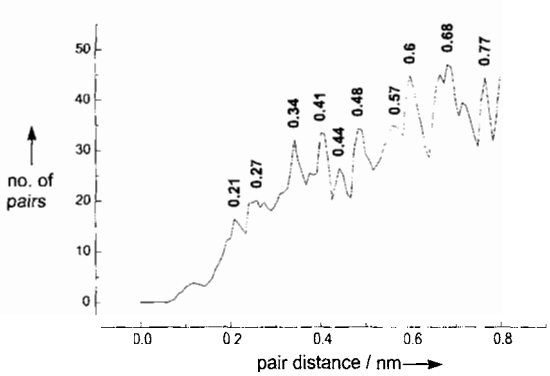

Figure 3. Interatomic pair distribution function determined from Figure 2

rising background, which indicates increased occurence of characteristic pair distances.

The shortest distance of 0.16 nm in the crystalline reference material is also observed in electron diffraction experiments with this glass, and in the X-ray and neutron scattering measurements of the barium disilicate glass, but does not appear in the AFM measurements (Table 1). Since this distance is attributed to Si–O bonding, this observation suggests that no Si atoms are on the surface and that the SiO_4 tetrahedra are intact. This is supported by the absence of a peak at 0.3 nm, corresponding to a Si–Si distance in the crystalline reference material.

The distance of 0.27 nm can be attributed to the Ba–O and the O–O distance (tetrahedral edge), in full agreement with the results from the crystalline barium disilicate and from the diffraction measurements with glasses. In contrast, the peak at 0.21 nm is not found in the reference data; this peak might represent an O–C distance (edge of an SiO_3C tetrahedron). In the same way the other distances (0.34 nm, 0.41 nm, and 0.44 nm) can be attributed to particular atomic pairs. The distance of 0.34 nm seems to be assignable only if Si atoms are considered. This is, however, not in contradiction to the interpretation that no silicon is at the surface, since this distance might result from a bond between an oxygen atom

 © WILEY-VCH Verlag GmbH, D-69451 Weinheim, 1997 0570-0833/97/3623-2647 $ 17.50+.50/0

Table 1. Comparison of interatomic distances [nm] and their assignment extracted from pair distribution functions of the Ba/Si/O/C glass with those in crystalline $BaSi_2O_5$ and amorphous barium disilicate.

From AFM of Ba/Si/O/C glass	From electron diffraction of Ba/Si/O/C glass [13]	From neutron and X-ray diffraction of a $BaSi_2O_5$ glass [12]	In crystalline $BaSi_2O_5$ [14]	Assignment
–	0.165	0.16	0.16	Si–O
0.21	–	–	–	C–O (?)
0.27	0.28	0.27	0.26	O–O
			0.27	Ba–O
–	–	–	0.30	Si–Si
0.34	–	0.34	0.35	Ba–Si
			0.35	Si–O
0.41	0.424	0.415	0.4	Ba–O
			0.4	Ba–Si
			0.4	O–O
			0.41	Si–O
0.44	–	–	0.45	Ba–Ba
0.48	0.50	0.494	0.48	mro
0.57		0.53		mro
0.6				mro
0.68				mro
0.77	0.78	0.78	0.77	mro

[a] Distances above 0.45 nm are not assigned to a certain atomic distance pair and are attributed to medium range order effects (mro).

situated perpendicular (with respect to the surface) to a Si atom and a neighboring atom.

At larger distances further peaks clearly indicate a medium-range order in the investigated glass. However, a definite assignment has yet to be done. The appearance of the 0.77 nm peak both in AFM and diffraction measurements is particularly remarkable, since this is a lattice constant of crystalline barium disilicate.

Two possible problems arise with the direct imaging of fracture surfaces of amorphous solids by atomic force microscopy, if one wants to resolve the bulk structure of glasses. First, the structures on the fracture surface might undergo a relaxation and therefore not correspond exactly to the position of the atoms in the bulk. Second, as the fracture will take place predominantly at the weaker bonds in the glass, these areas will dominate the images. However, since the relaxation in glasses with a highly developed network and low crystallization tendency will only result in displacements and not in reconstructions one can expect that the principles (repetition of structures, ring dimension, residues of translational symmetry) of medium- and long-range order will be preserved and reproduced in the image. In the case of the Ba/Si/O/C glass the justification for this assumption is proved by the good agreement of the AFM results with data obtained from completely independent measurements.

Atomic force microscopy is superior to all other methods of studying solids without translational symmetry in that it allows direct imaging of the atomic structure and therefore can be used to develop a reliable model of the structure of glasses. In the present case the classical controversy concerning the structure of glass between the hypothesis of Zachariasen ("network hypothesis")[15] and that of Lebedew ("crystallite theory")[16] can be settled. The AFM images show unambiguously that the barium silicate glass consists of a tetrahedral network.

Experimental Section

The Ba/Si/O/C glass was made under argon atmosphere by melting a mixture of $BaCO_3$, SiO_2, and SiC in a high frequency furnace in a BN crucible placed in a carbon crucible to ensure inductive coupling. The melt was held at 1650°C for 30 min and after switching off the furnace cooled down in a strong stream of argon. The average cooling rate from maximum temperature to around 700°C was about 10 $K s^{-1}$. The cation ratio Ba:Si in the starting mixture was 37:63 with 3 atom% carbon in form of SiC.

A fragment of this sample was clamped to the sample holder with a small vice. The images were obtained under ultrahigh vacuum after an outgassing procedure of several hours at about 400 K with a combined atomic force/scanning tunneling microscope (Omicron Vakuumphysik GmbH). The AFM measurements were carried out in the contact mode immediately after transfer with single crystal silicon cantilevers (Nanosensors) and constant loading forces in the range 25 nN—50 nN [17].

Received: June 5, 1997 [Z10511IE]
German version: *Angew. Chem.* **1997**, *109*, 2760–2762

Keywords: amorphous materials · atomic force microscopy · glasses · structure elucidation

[1] "Glasses and Amorphous Materials", *Materials Science and Technology Vol. 9* (Eds.: J. Zarzycki), VCH, Weinheim, **1991**.
[2] P. G. Le Comber, *J. Non-Cryst. Solids* **1989**, *115*, 1.
[3] a) H. P. Baldus, M. Jansen, *Angew. Chem.* **1997**, *109*, 339; *Angew. Chem. Int. Ed. Engl.* **1997**, *36*, 328; b) M. Jansen, *Solid State Ionics* **1996**, in press.
[4] S. R. Elliot, *Physics of Amorphous Materials, 2nd ed.*, Longman Scientific & Technical, Harlow, Essex, **1990**.
[5] *Experimental Techniques of Glass Science* (Eds.: C. J. Simmons, O. H. El-Bayoumi), The American Ceramic Society, Westerville, Ohio, **1993**.
[6] H. Eckert in *NMR Basic Principles and Progress, Vol. 33* (Eds.: P. Diehl, E. Fluck, H. Günther, R. Kosfeld, J. Seelig), Springer, Berlin, **1994**, 127.
[7] P. Lamparter, S. Steeb in *Materials Science and Technology, Vol. 1* (Eds.: Y. von Gerold), VCH, Weinheim, **1993**, 217.
[8] D. R. McKenzie, *Rep. Prog. Phys.* **1996**, *59*, 1611.
[9] a) G. Binnig, C. F. Quate, C. Gerber, *Phys. Rev. Lett.* **1986**, *56*, 930; b) K. Ichikawa, *J. Phys. I* **1995**, *7*, L135; c) T. M. Schaub, D. E. Bürgler, C. M. Schmidt, H.-J. Güntherodt, *J. Non-Cryst. Solids* **1996**, *205–207*, 748
[10] F. Liebau, *Structural Chemistry of Silicates*, Springer, Berlin, **1985**.
[11] V. Lansmann, W. Hoffbauer, N. Wartner, W. Mader, M. Jansen, *Ber. Bunsen-Ges. Phys. Chem.* **1996**, *100*, 1635.
[12] H. Hasegawa, I. Yasui, *J. Non-Cryst. Solids* **1987**, *95–96*, 201.
[13] N. Wartner, V. Lansmann, M. Jansen, W. Mader, unpublished.
[14] K. F. Hesse, F. Liebau, *Z. Kristallogr.* **1980**, *153*, 33.
[15] W. H. Zachariasen, *J. Am. Chem. Soc.* **1932**, *54*, 3841.
[16] A. A. Lebedew, *Arb. Staatl. Opt. Inst. Leningrad* **1921**, *2 No. 10*, 1
[17] W. Raberg, K. Wandelt, *Phys. Rev. B: Condens. Matter*, submitted.

Sergeants-and-Soldiers Principle in Chiral Columnar Stacks of Disc-Shaped Molecules with C_3 Symmetry**

Anja R. A. Palmans, Jef A. J. M. Vekemans, Edsko E. Havinga, and E. W. Meijer*

Seminal studies by Green and co-workers to understand the underlying principles of chirality in stiff helical polymers such as the polyisocyanates have led to observations referred to as the "Majority Rule" and the "Sergeants-and-Soldiers Principle".[1] Poly(*n*-alkyl isocyanates) adopt an extended helical conformation in which long stretches of one helical sense, *P* or *M*, are separated by high-energy reversals. To favor one

[*] Prof. Dr. E. W. Meijer, A. R. A. Palmans, Dr. J. A. J. M. Vekemans, Dr. E. E. Havinga
Laboratory of Organic Chemistry
Eindhoven University of Technology
P.O. Box 513, NL-5600 MB Eindhoven (The Netherlands)
Fax: Int. code + (40) 245-1036
e-mail: tgtobm@chem.tue.nl

[**] We would like to thank Dr. H. Fischer and Dr. R. Hikmet for stimulating discussions. Unrestricted research grants from Philips Research and DSM Research are gratefully acknowledged.

 © WILEY-VCH Verlag GmbH, D-69451 Weinheim, 1997 0570-0833/97/3623-2648 $ 17.50+.50/0

helical sense, it is only required to add a small portion of chiral units (sergeants) to the achiral units (soldiers) or to have a slight majority of *R* over *S* units in the polymer. Recently, it was shown that these effects are operative in other polymers with stiff helical backbones.[2] This is in sharp contrast to the behavior in small molecules where, for example, the optical rotation of a mixture of two enantiomers varies linearly with their ratio. Also in liquid crystals the induction of chirality is complex but seems to be predominantly linear or additive:[3] the more chiral molecules added to a nematic liquid crystal, the shorter the helical pitch of the induced cholesteric phase.[3b] In this communication we describe our results on the stereochemical issues of the associates of disc-shaped molecules **1** in diluted alkane solutions ($10^{-4}-10^{-6}$ mol L^{-1}). The molecules are stacked in highly ordered chiral columns, with a strong, cooperative response to chiral information. This amplification in chirality furnishes the first example in which the sergeants-and-soldiers principle is operative in dynamic structures of molecular aggregates.

Extended-core disc-shaped molecules are of interest, because they show liquid-crystalline properties within a broad temperature regime, and the stability of the molecular stacks is guaranteed by many secondary interactions.[4] We have studied in detail the synthesis and properties of achiral compounds **1**, in which the extended core is based on a concerted conformational preference owing to intramolecular H-bonding in the three acylated 3,3′-diamino-2,2′-bipyridine moieties.[5] Chiral analogue **1a** is synthesized starting from (*S*)-citronellol, which was successively hydrogenated, brominated, coupled to methyl 3,4,5-trihydroxybenzoate and transformed by established procedures[5] into the desired disc-shaped compound **1a**. Both **1a** and **1b** show a thermotropic

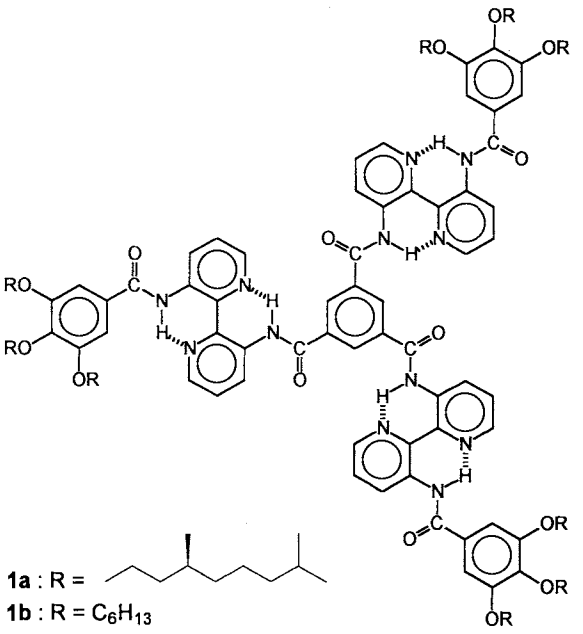

liquid crystalline D_{ho} phase, and X-ray diffraction suggests the presence of a helical superstructure. In concentrations greater than or equal to 7% w/w in apolar solvents like hexane, dodecane, and cyclohexane, molecules **1b** are organized in a columnar phase in which the 3.5 Å disc–disc distance within the columns is preserved.[6]

UV spectra of **1a,b** in different solvents show distinct differences in the $\pi-\pi^*$ transition of the bipyridine moiety (Figure 1). In $CHCl_3$ λ_{max} amounts to 351 nm ($\varepsilon = 5.3 \times 10^4$ L mol^{-1} cm^{-1}), whereas in dodecane a significant red shift of 13 nm is observed for λ_{max} to 364 nm ($\varepsilon = 3.2 \times 10^4$ L mol^{-1} cm^{-1}), and a shoulder in the spectrum in $CHCl_3$ has developed into a peak at 384 nm ($\varepsilon = 2.3 \times 10^4$ L mol^{-1} cm^{-1}) in dodecane. The spectrum in dodecane resembles the UV spectrum of a sheared film of pure **1a**, which is in a D_{ho} phase at room temperature. Heating the dodecane solution to 100°C leads to a blue shift of the λ_{max} to 357 nm and the disappearance of the fine structure. These results imply that **1a** is dissolved in $CHCl_3$ as individual molecules (and in dodecane at 100°C), while aggregation occurs in dodecane (and related alkane solvents) at room temperature in which the packing of the molecules in columns is similar to that in neat **1a**.

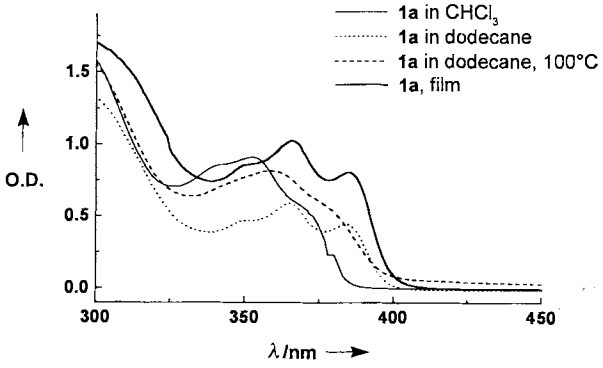

Figure 1. UV spectra of **1a** in $CHCl_3$ ($c = 1.7 \times 10^{-5}$ mol L^{-1}, $l = 1$ cm), in dodecane ($c = 1.8 \times 10^{-5}$ mol L^{-1}, $l = 1$ cm), and as a neat, sheared film.

In $CHCl_3$ compounds **1a,b** do not exhibit Cotton effects in the UV/Vis range of the circular dichroism (CD) spectrum. In dodecane, however, **1a** shows a very strong, negative Cotton effect associated with the $\pi-\pi^*$ absorption band of the bipyridine moiety at $\lambda = 387$ ($\Delta\varepsilon = -35.6$ L mol^{-1} cm^{-1}) and 369 nm ($\Delta\varepsilon = -23.6$ L mol^{-1} cm^{-1}) with chiral anisotropy factors[7] g of -1.5×10^{-3} and -7.4×10^{-4}, respectively. Heating the sample leads to a gradual decrease of the Cotton effects and a complete loss at 100°C. Subsequent cooling to room temperature restores the original Cotton effects. Most remarkably, the UV and CD spectra of the achiral compound **1b** in optically active (*R*)-(−)-2,6-dimethyloctane[8] as solvent are almost identical to the spectra of chiral compound **1a** in dodecane in the $\pi-\pi^*$ absorption band of the bipyridine moiety (Figure 2). The anisotropy factors g, however, are slightly lower (-8.5×10^{-4} at $\lambda = 386$ nm and -5.3×10^{-4} at $\lambda = 367$ nm). Again, heating of this sample leads to a decrease of the Cotton effects, showing the dynamics in chiral solvation.[9]

These results on chiral solvation indicate strong cooperative effects, suggesting a tendency of the stacks to take on a helical arrangement. We therefore attempted to apply the sergeants-and-soldiers principle to mixtures of **1a** and **1b** in hexane. As expected **1b** does not show any Cotton effect in hexane. However, addition of only 2.5% of chiral **1a** to achiral **1b** in hexane generates a strong Cotton effect, especially in the bipyridine transition band, which was similar in magnitude as for pure **1a** in hexane. The remarkable observation that the

 © WILEY-VCH Verlag GmbH, D-69451 Weinheim, 1997 0570-0833/97/3623-2649 $ 17.50+.50/0

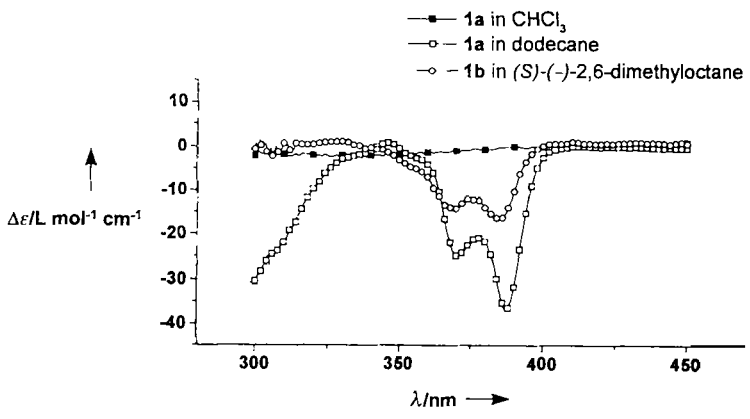

Cotton effects of the mixtures of about 10% **1a** and 90% **1b** are larger than for pure **1a** is tentatively explained by a more effective packing between achiral molecules **1b** than between chiral molecules **1a**.

The mixing experiment was repeated with solutions of different concentrations of compounds **1a** and **1b** in hexane. The dependence of the g values on the amount of chiral **1a** added to a solution of achiral **1b** is depicted in Figure 3. The curves show the same trend, although the effect is smaller for the lowest concentration (1.9×10^{-6} mol L^{-1}). We also found that the Cotton effect in the bipyridine band is almost independent of the concentration of pure **1a** in hexane within the range 10^{-6} - 10^{-3} mol L^{-1}, with a slight deviation at the low concentration end (Figure 3, inset).

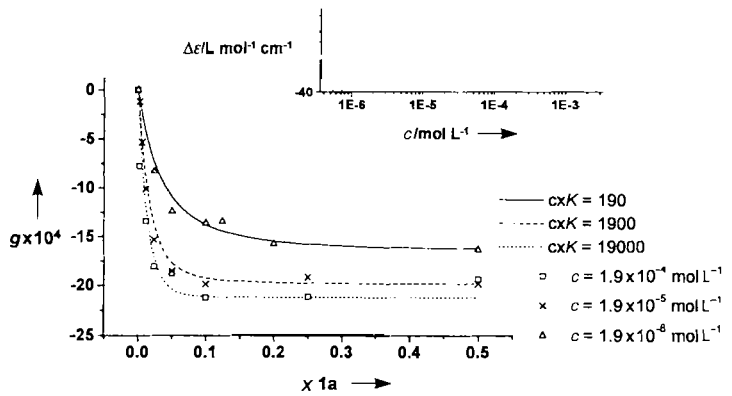

Figure 3. The anisotropy factor g as a function of the amount of **1a** (x in mol fraction) added to the achiral solution of **1b** in hexane in 1 mm (□), 1 cm (×), and 10 cm (△) cells. The fitted lines represent the theoretically predicted development of g as a function of the mol fraction of chiral compound **1a** present in the mixture (an association constant K of approximately 10^8 M and a cooperative length L_c of 81 gave the optimal fit). The inset gives

The results given above are in full agreement with the strong cooperative effect of the sergeants-and-soldiers principle, but now in a dynamic system. To quantify the experimental results presented in Figure 3, we developed a theoretical model to fit these data. In this model the association constant K and the cooperative length L_c—which is the length of that part of the stack with only one helical sense between the helix reversals—can be varied. We assume that the contributions to the Cotton effect in the bipyridine band of a stack is proportional to the number of monomeric units in the stack, and remaining nonassociated species do not contribute to the Cotton effect. Furthermore, the association constants K of chiral and achiral monomers are equal, and if a stack contains a chiral monomer, the latter will induce chirality in other molecules in the stack not further away than s units. For mixed stacks in equilibrium we can then deduce an equation to fit the experimental data points with K and s as variables.[10] A fit of this model to the experimental data leads to $K = (1 \pm 0.5) \times 10^8$ L mol^{-1} and $s = (40 \pm 2)$ which yields $L_c = 2s+1 \approx 80$.

We propose the following hypothesis to explain the cooperative response of compound **1** on external chiral information. The C_3-symmetrical molecules of type **1** adopt a propellerlike conformation in which the bipyridine wedges are tilted with respect to the central trimesic core.[11] In hexane molecules **1** are aggregated in columnar stacks, and the packing between subsequent molecules will be optimal when all bipyridine wedges are tilted in the same direction, which results in a preferred stable chiral conformation of each disc-shaped molecule.[12] This can be compared with propellers piled on top of each other. Rotating the first with respect to the second will improve the packing but will also give rise to a helix. Equal amounts of P and M helices are present within the stacks of achiral **1b**. The stack length is concentration-dependent and corresponds with $K \approx 10^8$ L mol^{-1}, while the cooperative length L_c of one helical sense between helical reversals is not concentration-dependent and has the value $L_c \approx 80$. On the other hand, the stacks of **1a** are assumed to have only one helical sense P or M. The instantaneous Cotton effect in the bipyridine band upon addition of chiral **1a** to a solution of achiral **1b** points to dynamic processes and an exchange of the molecules between different columns. By introducing on average one molecule of chiral **1a** per 80 molecules of **1b** into the stacks of **1b**, the chiral component (the sergeants) will dictate the helical sense of the total stack (of soldiers) for steric reasons. That a chiral alkane solvent can also dictate the sense of helicity of a stack of achiral molecules presumably means that the first layer of solvent organizes itself along the peripheral alkoxy chains of the molecules with precision. Again, steric factors will dictate which helical sense will lead to the most favorable interactions between subsequent molecules.

In conclusion, it is shown that the sergeants-and-soldiers principle and chiral solvation are operative in dynamic, columnar stacks of molecules **1** in alkane solvents.

Received: July 10, 1997 [Z 10675 IE]
German version: *Angew. Chem.* **1997**, *109*, 2763 - 2765

Keywords: chirality · circular dichroism · helical structures · stacking interactions · supramolecular

[1] M. M. Green, N. C. Peterson, T. Sato, A. Teramoto, R Cook, S. Lifson, *Science* **1995**, *268*, 1860,and references herein.
[2] a) D. S. Schlitzer, B. M. Novak, *Polym. Prep. Symp.* **1997**, *38*, 296; b) Q. S. Hu, D. Vitharana, G.-Y. Liu, V. Jain, M. W. Wagaman, L. Zhang, T. Randall Lee, L. Pu, *Macromolecules* **1996**, *29*, 1082.
[3] a) T. Nakagiri, H. Kodama, K. K. Kobayashi, *Phys. Rev. Lett.* **1971**, *27*, 564; b) J. Partyka, K. Hiltrop, *Liq. Cryst.* **1996**, *20*, 611.
[4] a) P. Herwig, L. W. Kayser, K. Müllen, H. W. Spiess *Adv. mater.* **1996**, *8*, 511; b) B. Mohr, G. Wegner, K. Ohta, *J. Chem. Soc. Chem. Commun.* **1995**, 995;

 © WILEY-VCH Verlag GmbH, D-69451 Weinheim, 1997 0570-0833/97/3623-2650 $ 17.50+.50/0

c) J. Zhang, J. S. Moore, *J. Am. Chem. Soc.* **1994**, *116*, 2655; d) C. Metsendorf, H. Ringsdorf, *Mol. Eng.* **1992**, *2*, 189; e) C. F. van Nostrum, S. J. Picken, A.-J. Schouten, R. J. M. Nolte, *J. Am. Chem. Soc.* **1995**, *117*, 9957.
[5] A. R. A. Palmans, J. A. J. M. Vekemans, H. Fischer, R. A. M. Hikmet, E. W. Meijer, *Chem. Eur. J.* **1997**, *3*, 300.
[6] Details will be published elsewhere.
[7] A measure for the chirality is given by the chiral anisotropy factor g ($= \Delta\varepsilon/\varepsilon$).
[8] (*R*)-(−)-2,6-Dimethyloctane was synthesized by catalytic hydrogenation of (*S*)-(+)-citronellyl bromide. ^{13}C NMR ($CDCl_3$): $\delta = 39.4, 36.9, 34.5, 29.5, 28.0, 24.9, 22.7, 22.6, 19.2, 11.4$; GLC-EI-MS: m/z 142 (M^+), 127 ($M^+ - CH_3$), 113 ($M^+ - CH_2CH_3$), 85, 71, 57, 43, 29; $[\alpha]_{20}^{D} = -5.5°$ (neat).
[9] M. M. Green, N. C. Peterson, C. Khatri, *J. Am. Chem. Soc.* **1993**, *115*, 4941.
[10] For mixed stacks in equilibrium we can deduce the following equation:

$$\frac{g}{g_0} = \frac{\sum_{n=2}^{\infty}[M_n]n(1-q^n)+\sum_{n=s+1}^{2s}[M_n]\left(n-\sum_{i=1}^{n/2}2q^{i+i}\right)+\sum_{n=2s+1}^{\infty}[M_n]\left(n-\sum_{i=1}^{s}2q^{n-s}-\sum_{i=s+1}^{n-s}q^{2s+1}\right)}{\sum_{n=2}^{\infty}[M_n]n}$$

in which g is the anisotropy factor for a mixture with mol fraction x of chiral **1a** in a solution of **1b**, g_0 is the anisotropy factor for the solution of pure **1a** [11], $a = K[M] = 1 + [(1 - \sqrt{1 + 4Kc})/2Kc]$ (M. B. Martin, *Chem. Rev.* **1996**, *696*, 3043), $q = 1 - x$, $t = aq$, $r = a\sqrt{q}$ and s is the number of molecules for which chirality is controlled in one direction. Evaluation gives:

$$\frac{g}{g_0} = 1 - \frac{(2-t)\left(\frac{t}{1-t}\right)^2 - \frac{s(1-t)+1}{(1-t)^2}t^{s+1} + \frac{2(t^{s+1}-t^{2s+1})}{(1-a)(1-q)} + \frac{t^{2s+1}}{(1-a)^2} - \frac{2(qr)^{s+1}(1-r)}{(1-q)(1-r)}}{(2-a)\left(\frac{a}{1-a}\right)^2}$$

[11] For the constant g_0, the g value of the 10/90 mixture **1a/1b** was used in the fit to compensate for packing effects.
[12] In (−)- and (+)-3,3′-di(camphanoylamino)-2,2′-bipyridine in MeOH and $CHCl_3$, weak Cotton effects are found in the bipyridine band, which are attributed to a small deviation from coplanarity of the bipyridine system.
[13] This packing of the molecules in columns could be stabilized by intermolecular H-bonding. See a) Y. Yasuda, E. Iishu, H. Inada, Y. Shirota, *Chem. Lett.* **1996**, 575; b) Y. Yasuda, Y. Takebe, M. Fukumoto, H. Inada, Y. Shirota, *Adv. Mater.* **1996**, *8*, 740.

$Ba_2Nd_7Si_{11}N_{23}$—A Nitridosilicate with a Zeolite-Analogous Si–N Structure**

Hubert Huppertz and Wolfgang Schnick*

In the past few decades zeolites and aluminosilicates have found important technological applications as microporous solids.[1] For the specific modification of their catalytic properties the tetrahedral centers aluminum and silicon were substituted by a large number of electropositive elements.[1,2] Recently, the replacement of the bridging atoms O by different atoms or building units in the network structures was successful.[3] For example, $Zn_6[P_{12}N_{24}]Cl_2$ with a sodalite-analogous structure of corner-sharing PN_4 tetrahedra was synthesized in our group.[4] Host–guest behavior by reversible encapsulation of molecular hydrogen was established for the analogous halogen-free nitridosodalite $Zn_6[P_{12}N_{24}]$.[5]

With regard to the material properties and the high stability of nitridosilicates, it seemed challenging to build up zeolite-analogous microporous network structures from SiN_4 tetrahedra. Typical for nearly all oxidic zeolites is a molar ratio of tetrahedral centers (T) to bridging atoms (X) of T:X = 1:2 (T = Al, Si; X = O).[6] This ratio should also hold for zeolite-analogous nitridosilicates. All nitridosilicates obtained so far by high-temperature synthesis possess Si–N substructures in the range $0.5 \leq T:X \leq 0.75$ having no open channels or large cavities.[7]

The synthesis of $Ba_2Nd_7Si_{11}N_{23}$ produced the first nitridosilicate with a zeolite-analogous Si–N network structure. The new nitridosilicate was synthesized in a high-frequency furnace[8] by reaction of stoichiometric amounts[9] of barium and neodymium with silicon diimide[10] under nitrogen atmosphere [Eq. (a)]. By this procedure $Ba_2Nd_7Si_{11}N_{23}$ is formed as a coarse crystalline, dark blue solid.[11] Like all other nitridosilicates synthesized in our group, $Ba_2Nd_7Si_{11}N_{23}$ is stable up to 1600°C and insensitive to hydrolysis.

$$2\,Ba + 7\,Nd + 11\,Si(NH)_2 + {}^1/_2\,N_2 \xrightarrow[\text{HF furnace}]{900-1650\,^\circ C,\,40\,h} Ba_2Nd_7Si_{11}N_{23} + 11\,H_2 \qquad \text{(a)}$$

The X-ray structure analysis[12] on single crystals of $Ba_2Nd_7Si_{11}N_{23}$ shows a three-dimensional network structure of corner-sharing SiN_4 tetrahedra according to $^3_\infty[(Si^{[4]}_{11}N^{[1]}_2N^{[2]}_{21})^{25-}]$. With a molar ratio of Si:N = 11:23, the degree of condensation is smaller than in most of the oxidic zeolites (Al/Si:O = 1:2).[13] Accordingly besides bridging atoms $N^{[2]}$, terminal atoms are connected to Si ($N^{[1]}$). (The superscript in square brackets in $N^{[x]}$ defines the number of Si atoms covalently bound to N, and vice versa for $Si^{[x]}$). The ratio of Q^4 and Q^2 tetrahedra in the Si–N network structure is 10:1. Thus $Ba_2Nd_7Si_{11}N_{23}$ shows the lowest degree of condensation amongst the Si–N network structures obtained so far. The network of corner-sharing SiN_4 tetrahedra in $Ba_2Nd_7Si_{11}N_{23}$ can be characterized by the specific distribution of Si_nN_n ring sizes.[14] In $Ba_2Nd_7Si_{11}N_{23}$ all ring sizes appear with the exception of $n = 2$ and 5.

Characteristic for the structure of $Ba_2Nd_7Si_{11}N_{23}$ (Figure 1) are channels along [001]. The Ba^{2+} ions are centered in the Si_8N_8 ring channels and in the Si_6N_6 ring channels along [100]. The Nd^{3+} ions are positioned in the smaller voids. The metal ions are coordinated by seven and eight nitrogen atoms of the Si–N network (Ba^{2+}–N: 273(1)–316(2) pm; Nd^{3+}–N: 229(2)–312(1) pm). The Ba^{2+} ions in the wide Si_8N_8 ring channels (Figure 2) have a markedly higher coordination number of 16 and corresponding longer distances to the nitrogen atoms (Ba^{2+}–N: 337(1)–441(2) pm).

The bond distances $Si–N^{[2]}$ in the network structure (167(1)–175.5(5) pm) are typical for simple bridging $N^{[2]}$ atoms in nitridosilicates.[7] The distances $Si–N^{[1]}$ (175.4(12) pm) correspond to the values of terminal N atoms in $Ba_5Si_2N_6$ (174–176 pm).[15]

A measure for the microporousity of a zeolite-analogous structure is the framework density (FD), which indicates the number of tetrahedral centers (T) in a volume of 1000 Å^3. With a FD of 18.5, $Ba_2Nd_7Si_{11}N_{23}$ is similar to typical zeolites (framework densities of some zeolites in T/(1000 Å^3): 17.5 ($AlPO_4$-5), 17.9 (ZSM-5), 19.3 (Nonasil)).[6]

The successful synthesis of $Ba_2Nd_7Si_{11}N_{23}$ is the first proof that not only highly condensed Si–N network structures but also open, zeolite-like networks of corner-sharing SiN_4 tetrahedra can be realized. In contrast to conventional zeolites, which are synthesized by solvothermal procedures using templates, the nitridosilicates are only accessible by high-temperature synthesis. The next aim of our efforts will be the exchange of the bulky metal ions for hydrogen atoms

[*] Prof. Dr. W. Schnick, Dipl.-Chem. H. Huppertz
Laboratorium für Anorganische Chemie der Universität
D-95440 Bayreuth (Germany)
Fax: Int. code + (921) 55-2788
e-mail: wolfgang.schnick@uni-bayreuth.de

[**] This work was supported by the Fonds der Chemischen Industrie and the Deutsche Forschungsgemeinschaft (Projekt "Nitridozeolithe" SCHN 377/6-1 and in the Gottfried-Wilhelm-Leibniz program).

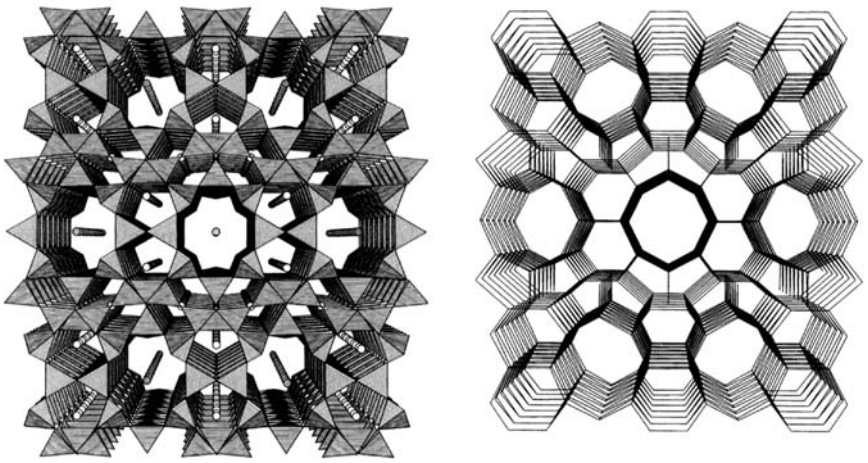

Figure 1. Crystal structure of $Ba_2Nd_7Si_{11}N_{23}$, viewed along [001]. Left: the SiN_4 tetrahedra are shown as closed polyhedra, Ba^{2+} as gray spheres, and Nd^{3+} as white spheres. Right: topology of the Si–N network; only the Si tetrahedral centers are directly connected.

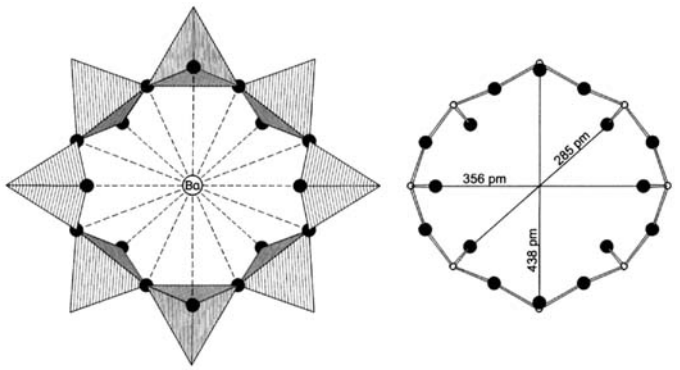

Figure 2. Sectional view of the wide Si_8N_8 ring channels ([001] **8** 285 × 438 pm²) in $Ba_2Nd_7Si_{11}N_{23}$. Left: coordination of the Ba^{2+} ions (coordination number 16). Right: the free diameter of the channels is calculated from the atomic coordinates considering the ionic radius of N^{3-} (146 pm); cf. also ref. [6].

bound to the nitrogen atoms of the Si–N network structures. The Ba^{2+} ions in the open channels of $Ba_2Nd_7Si_{11}N_{23}$ seem to be predestined for this procedure.

Received: June 27, 1997 [Z10606IE]
German version: *Angew. Chem.* **1997**, *109*, 2765–2767

Keywords: nitridosilicates · solid-state structures · structure elucidation · zeolite analogues

[1] a) J. V. Smith, *Chem. Rev.* **1988**, *88*, 149; b) D. W. Breck, *Zeolite Molecular Sieves*, Wiley, New York, **1974**.
[2] W. Hölderich, M. Hesse, F. Näumann, *Angew. Chem.* **1988**, *100*, 232; *Angew. Chem. Int. Ed. Engl.* **1988**, *27*, 226.
[3] C. L. Bowes, G. A. Ozin, *Adv. Mater.* **1996**, *8*, 13.
[4] W. Schnick, J. Lücke, *Angew. Chem.* **1992**, *104*, 208; *Angew. Chem. Int. Ed. Engl.* **1992**, *31*, 213.
[5] J. Weitkamp, S. Ernst, F. Cubero, F. Wester, W. Schnick, *Adv. Mater.* **1997**, *9*, 247.
[6] W. M. Meier, D. H. Olson, *Atlas of Zeolite Structure Types*, Butterworths, London **1987**.
[7] W. Schnick, H. Huppertz, *Chem. Eur. J.* **1997**, *3*, 679.
[8] T. Schlieper, W. Schnick, *Z. Anorg. Allg. Chem.* **1995**, *621*, 1037.
[9] In a typical batch 0.4 mmol Ba, 1.3 mmol Nd, and 2 mmol $Si(NH)_2$ were thoroughly mixed under inert gas atmosphere in a glove box and transferred in a tungsten crucible into the high-frequency furnace. Under nitrogen atmosphere the reaction mixture was heated to 900°C in 7 h and over a further 18 h to 1650°C followed by a cooling over 15 h to 1400°C and in another 15 min to room temperature.
[10] The X-ray amorphous product obtained by ammonolysis of $SiCl_4$ has the approximate composition $Si(NH)_2$. Despite its undefined character, silicon diimide is an important precursor for the technical production of Si_3N_4. Cf. H. Lange, G. Wötting, G. Winter, *Angew. Chem.* **1991**, *103*, 1606; *Angew. Chem. Int. Ed. Engl.* **1991**, *30*, 1579.
[11] The composition of $Ba_2Nd_7Si_{11}N_{23}$ determined by structural analysis was confirmed by energy dispersive X-ray microanalysis (Ba, Nd, Si). The absence of hydrogen (NH) was checked by IR spectroscopy.
[12] $Ba_2Nd_7Si_{11}N_{23}$: *Cmmm*, $a = 1096.20(6)$, $b = 2304.60(14)$, $c = 964.85(5)$ pm, $Z = 4$, Siemens P4 diffractometer, $Mo_{K\alpha}$ radiation, graphite monochromator, $F(000) = 3388.0$, $\mu(Mo_{K\alpha}) = 18.39\ mm^{-1}$, ω scan, 14287 measured reflections in the range $2° \le 2\theta \le 60°$, 2021 unique reflections with $F_o^2 \ge 0\sigma(F_o^2)$, empirical absorption correction (ψ scans), $R_{int} = 0.0472$; the crystal structure was solved by direct methods (SHELXTL, Vers. 5.03) and anisotropically refined by a least-squares procedure against F^2 with all data, 32 refined parameters, $R1 = 0.0440$, $wR2 = 0.0884$, GOF = 0.973. Further details of the crystal structure investigation may be obtained from the Fachinformationszentrum Karlsruhe, D-76344 Eggenstein-Leopoldshafen, on quoting the depository number CSD-407202.
[13] Most of the oxidic zeolites have a molar ratio T:O = 1:2. Nevertheless, there are exceptions like the zeolites -CHI, -CLO, -PAR, -RON, and -WEN with T:O < 1:2. Accordingly, terminal $O^{[1]}$ atoms were found as well as simple bridging $O^{[2]}$ atoms, cf. ref. [6].
[14] Network structures of connected SiN_4 can be characterized topologically by the cycle–class sequence. It specifies the relative abundance of Si_nN_n ring sizes (for $n = 1, 2, 3\ldots$) per unit cell. Cycle–class sequence of $Ba_2Nd_7Si_{11}N_{23}$: {–,0,6,1,0,12,24,30…}. Cf. also: a) W. E. Klee, *Z. Kristallogr.* **1987**, *179*, 67; b) A. Beukemann, W. E. Klee, *ibid.* **1994**, *209*, 709.
[15] H. Yamane, F. J. DiSalvo, *J. Alloys Comp.*, **1996**, *240*, 33.

Alkylrhenium Oxides from Perrhenates: A New, Economical Access to Organometallic Oxide Catalysts**

Wolfgang A. Herrmann,* Roland M. Kratzer, and Richard W. Fischer

Organometallic oxides have been thoroughly investigated, particularly because some representatives of this ever-growing class of compounds exhibit a variety of catalytic properties.[1] One of the main reasons behind our interest in rhenium is the diverse catalytic successes of methyltrioxorhenium (MTO).[2] This has recently been reported to catalyze different oxidation processes.[2–4] Twenty years after MTO was first observed,[5] two synthetic pathways have become established for access to organorhenium(VII) oxides:

[*] Prof. Dr. W. A. Herrmann, R. M. Kratzer
Anorganisch-chemisches Institut der Technischen Universität München
Lichtenbergstrasse 4, D-85747 Garching (Germany)
Fax: Int. code + (89) 289-13473
e-mail: herrmann@zaphod.anorg.chemie.tu-muenchen.de
Dr. R. W. Fischer
Corporate Research & Technology, Hoechst AG, Frankfurt am Main (Germany)

[**] Multiple Bonds between Transition Metals and Main Group Elements, Part 169. This work was generously supported by the Bayerische Forschungsverbund Katalyse. Part 168: W. A. Herrmann, H. Ding, R. M. Kratzer, F. E. Kühn, J. J. Haider, R. W. Fischer, *J. Organomet. Chem.*, in press.

1) Direct alkylation of dirhenium heptoxide (Re_2O_7) with tetraalkyltin or dialkylzinc. However, in this case 50% of the rhenium is lost in the form of unreactive trialkylstannyl- and zinc perrhenate.[6] 2) Alkylation of Re_2O_7 in the presence of trifluoroacetic anhydride. Here, the formation of rhenium-containing by-products is suppressed, but the anhydride used is expensive and rather sensitive.[7]

The disadvantage of both these methods is that the Re_2O_7 starting material is extremely moisture sensitive. Now for the first time, a simple one-pot reaction facilitates the use of a wide variety of easily accessible perrhenates as starting compounds. MTO **1**, for example, can be synthesized in excellent yields without the rigorous exclusion of air and moisture (Table 1). The perrhenates ($M[ReO_4]_n$, $n = 1$, 2 and

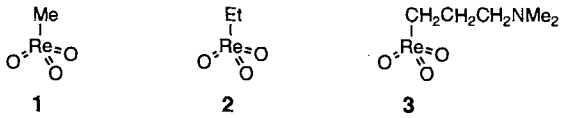

Table 1. Direct synthesis of organorhenium(VII) oxides from perrhenates (solvent: acetonitrile).

	Perrhenate	Alkylation reagent	Conditions t (h)	T (°C)	Yield $RReO_3$ (%)[a]
1	$Ag[ReO_4]$	$(CH_3)_4Sn$	12	25	76
2	$Ca[ReO_4]_2$	$(CH_3)_4Sn$	4	81	78
3	$Na[ReO_4]$	$(CH_3)_4Sn$	4	81	70
4	$K[ReO_4]$	$(CH_3)_4Sn$	24	25	63
5	$NH_4[ReO_4]$	$(CH_3)_4Sn$	24	25	56
6	$Zn[ReO_4]_2$	$(CH_3)_4Sn$	12	25	86[b]
7	$(CH_3)_3SnReO_4$	$(CH_3)_4Sn$	24	25	77[b]
8	$Na[ReO_4]$	Bu_3SnCH_3	4	81	46
9	$Ag[ReO_4]$	$Zn(C_2H_5)_2$	12	0	36
10	$Na[ReO_4]$	$Zn[(CH_3)_2NC_3H_6]_2$	12	0	25

[a] Isolated yield except the marked examples 6 and 7. [b] GC yield (±5%).

$M = Ag^+$, K^+, Na^+, Zn^{2+}, Ca^{2+}, NH_4^+; $(CH_3)_3SnReO_4$) are then treated with chlorotrimethylsilane and tetramethyltin. The addition of one equivalent of H_2SO_4 is recommended if only scarcely soluble perrhenates are used. With alkylzinc compounds this new synthetic route can be extended to the preparation of homologues of **1** and to alkyl-functionalized derivatives. For instance, ethyltrioxorhenium(VII) (**2**) is produced in 36% yield.[8] In addition, the oxidation catalyst [3-(dimethylamino)propyl]trioxorhenium(VII) (**3**) could be prepared by using this new method.[9]

A key advantage of this new route is the possibility of catalyst recycling in MTO-catalyzed oxidation processes; the perrhenates can be separated from exhausted catalyst solutions through simple precipitation of the perrhenic acid from the solution. This new aspect sets the industrial application of rhenium catalysts in a realistic context.

The synthesis proceeds as exemplified for MTO **1** (Scheme 1): First perrhenate is converted to trimethylsilyl perrhenate (**4**) and the respective metal chloride (1).[10,11] The next step is a condensation of two activated perrhenates **4** (2). The resulting dirhenium heptoxide is then cleaved with (the second equivalent of) chlorotrimethylsilane to give chlorotrioxorhenium (**5**) and **4** (3); the final alkylation of **5** (4) affords MTO **1**.

This new synthetic strategy represents an economical and simple access to organorhenium oxides from a plethora of readily available, rather cheap perrhenates. An extension of this concept to the neighboring elements of the periodic table seems feasible. One of our future goals is the activation of simple oxo salts (Cr, Mo, W, Mn) with chlorotrimethylsilane[11] with the aim of synthesizing novel organometallic oxides.

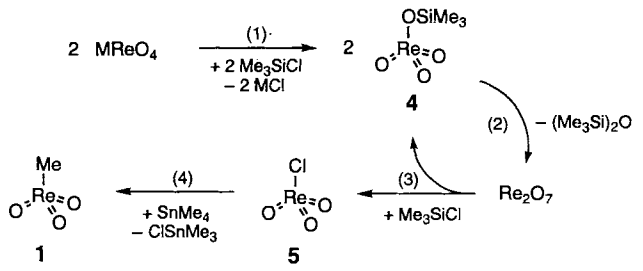

Scheme 1. Synthetic steps in the formation of methyltrioxorhenium from perrhenates.

Experimental Section

The perrhenates were prepared by oxidation of rhenium with H_2O_2 (30%) and precipitation (KCl, $AgNO_3$) or neutralization (e.g., NaOH, $Ca(OH)_2$). $Zn[ReO_4]_2$ and $(CH_3)_3SnReO_4$ were formed as by-products in the synthesis of organorhenium oxides[6,8]. Unless mentioned otherwise, acetonitrile (Merck, p. A.) was used without further purification or drying procedures. Chlorotrimethylsilane (98%, Aldrich) was distilled prior to use.

CH_3ReO_3 **1**: *Attention! Tetramethyltin and trimethyltin chloride are very toxic and volatile. All transformations are therefore to be performed in a hood.* $Ag[ReO_4]$ (1.00 g, 2.79 mmol) was dissolved in CH_3CN (20 mL) in a sealable 50-mL Erlenmeyer flask. After the addition of $ClSi(CH_3)_3$ (0.78 mL, 6.14 mol), a white precipitate was formed immediately. To the suspension $Sn(CH_3)_4$ (0.43 mL, 3.07 mol) was added and the mixture was stirred for 12 h at 25 °C. It was then filtered and the resulting yellow solution was evaporated in a Schlenk tube under reduced pressure (20 mbar). Due to the volatility of the tin compounds it is recommended that a trap cooled with nitrogen is installed between the Schlenk tube and the pump. The residue was sublimed at ambient temperature under high vacuum (10^{-2} mbar). Compound **1** was obtained in 76% yield (696 mg, m.p. 108 °C).

$Na[ReO_4]$ (1.00 g, 3.66 mmol) was suspended in CH_3CN (20 mL) in a 50-mL round-bottomed flask. After the addition of $ClSi(CH_3)_3$ (1.02 mL, 8.05 mol) and $Sn(CH_3)_4$ (0.56 mL, 4.03 mol) the reaction mixture was heated to reflux for 4 h. Then the cooled mixture was filtered and the yellow-orange solution was evaporated to dryness in a Schlenk tube under reduced pressure (20 mbar). The residue was sublimed at ambient temperature under high vacuum (10^{-2} mbar). Compound **1** was obtained in 70% yield (639 mg, m.p. 108 °C).

$K[ReO_4]$ (8.70 g, 0.03 mol) was suspended in CH_3CN (150 mL) in a 250-mL flask with a faucet. Concentrated H_2SO_4 (1.6 mL, 0.03 mol), $ClSi(CH_3)_3$ (8.30 mL, 0.066 mol), and $Sn(CH_3)_4$ (4.2 mL, 0.03 mol) were added and the reaction mixture was stirred at 25 °C for 24 h. Then the solution was evaporated to dryness without filtration at 20 mbar and the black residue was extracted with *n*-pentane (4 × 50 mL) for several hours each time. The combined extracts were evaporated to about 30 mL and maintained at −35 °C for 24 h. The precipitating MTO still contained Me_3SnCl and was therefore purified by sublimation (25 °C, 10^{-2} mbar). Yield: 63% (4.71 g). If the melting point of this MTO fraction is still below 100 °C, a second sublimation must follow.

$(CH_3)_2NCH_2CH_2CH_2ReO_3$ **3**: $Na[ReO_4]$ (0.50 g, 1.83 mmol) was suspended in dry CH_3CN (10 mL) under the exclusion of air and treated at −40 °C with $ClSi(CH_3)_3$ (0.46 mL, 3.66 mmol) and $Zn[(CH_3)_2NC_3H_6]_2$ (0.43 g, 1.83 mmol). The mixture was stirred at 0 °C for 12 h. Then the solution was evaporated to dryness and the residue was extracted with *n*-pentane (3 × 5 mL). The combined extracts were evaporated and kept in a cool place. Compound **3** precipitated from the solution in 25% yield. Elemental analysis for $C_5H_{12}NO_3Re$ (320.4): calcd. C 18.69, H 3.77, N 4.36; found C 18.76, H 4.00, N 4.08; IR (KBr): $\tilde{\nu} = 960\ cm^{-1}$ (Re=O), 917 (Re=O); ^1H NMR (200 MHz, CD_3CN, 20 °C): $\delta = 2.20$ (s, 6H, NCH_3), 2.85 (t, 2H, NCH_2), 3.02 (m, 2H, $CH_2CH_2CH_2$), 3.50 (t, 2H, $ReCH_2$); $^{13}C\{^1H\}$ NMR (200 MHz, CD_3CN, 20 °C): $\delta = 57.3$ (NCH_3), 80.2 (NCH_2), 47.2 ($CH_2CH_2CH_2$), 28.4 ($ReCH_2$).

$CH_3CH_2ReO_3$ **2**: The preparation of **2** was performed with $Zn(CH_2CH_3)_2$ under analogous conditions to those employed for **3**. Yield: 36%.

Received: July 11, 1997 [Z10677IE]
German version: *Angew. Chem.* **1997**, *109*, 2767–2768

 © WILEY-VCH Verlag GmbH, D-69451 Weinheim, 1997 0570-0833/97/3623-2653 $ 17.50+.50/0

Keywords: alkylations · homogeneous catalysis · oxidations · rhenium · synthetic methods

[1] Recent examples: a) L. L. Biosch, K. Abboud, J. M. Boncella, *J. Am. Chem. Soc.* **1991**, *113*, 7066–7068; b) J. H. Wengrovius, R. R. Schrock, *Organometallics* **1982**, *1*, 148–155; c) J. Kress, M. Wesolek, J. P. Le Ny, J. A. Osborn, *J. Chem. Soc. Chem. Commun.* **1981**, 1039–1040.

[2] Reviews: a) W. A. Herrmann, F. E. Kühn, *Acc. Chem. Res.* **1997**, *30*, 169-180; b) W. A. Herrmann, *J. Organomet. Chem.* **1995**, *500*, 149–174.

[3] a) J. Rudolph, K. L. Reddy, J. P. Chiang, K. B. Sharpless, *J. Am. Chem. Soc.* **1997**, *119*, 6189–6190; b) C. Copéret, H. Adolfsson, K. B. Sharpless, *Chem. Commun.* **1997**, 1565–1566; c) Z. Zhu, J. H. Espenson, *Organometallics* **1997**, *16*, 3658–3663; d) A. Goti, L. Nannelli, *Tetrahedron Lett.* **1996**, *37*, 6025–6028; e) R. W. Murray, K. Iyanar, *ibid.* **1997**, *38*, 335–338.

[4] The "base effect" [3a,b] in MTO-catalyzed olefin epoxidations has already been known for some time and provides an enormous extension of this catalyst's variety of application: a) W. A. Herrmann, R. W. Fischer, D. W. Marz, *Angew. Chem.* **1991**, *103*, 1706–1709; *Angew. Chem. Int. Ed. Engl.* **1991**, *30*, 1638–1641; b) W. A. Herrmann, R. W. Fischer, M. U. Rauch, W. Scherer, *J. Mol. Catal.* **1994**, *86*, 243–266; c) W. A. Herrmann, J. D. G. Correia, M. U. Rauch, G. R. J. Artus, F. E. Kühn, *ibid.* **1997**, *118*, 33–45.

[5] I. A. Beattie, P. J. Jones, *Inorg. Chem.* **1979**, *18*, 2318–2319.

[6] W. A. Herrmann, J. G. Kuchler, J. K. Felixberger, E. Herdtweck, W. Wagner, *Angew. Chem.* **1988**, *100*, 420–422; *Angew. Chem. Int. Ed. Engl.* **1988**, *27*, 394–396.

[7] W. A. Herrmann, F. E. Kühn, R. W. Fischer, W. R. Thiel, C. C. Romão, *Inorg. Chem.* **1992**, *31*, 4431–4432.

[8] W. A. Herrmann, C. C. Romão, R. W. Fischer, P. Kiprof, C. de Méric de Bellefon, *Angew. Chem.* **1991**, *103*, 183–185; *Angew. Chem. Int. Ed. Engl.* **1991**, *30*, 185–187.

[9] [3-(Diethylamino)propyl]trioxorhenium cf. ref. [4b].

[10] H. Schmidbaur, M. Schmidt, *Chem. Ber.* **1959**, *92*, 2667–2670.

[11] Reactions with chlorotrimethylsilane have been described for some metal oxides and alkoxides (e.g., of Ti, Cr, Sm), cf. a) R. Nomura, T. Matsuno, T. Endo, *J. Am. Chem. Soc.* **1996**, *118*, 11666–11667; b) A. Fürstner, A. Hupperts, *ibid.* **1995**, *117*, 4468–4475; c) A. Fürstner, N. Shi, *ibid.* **1996**, *118*, 2533–2534.

Repetitive Construction of Macrocyclic Oligophenylenes**

Volker Hensel, Karola Lützow, Joel Jacob, Katrin Gessler, Wolfram Saenger, and Arnulf-Dieter Schlüter*

Cyclic oligophenylenes[1] and related compounds with conformationally rigid structures[2] have attracted the interest of chemists for issues including aromaticity, host–guest chemistry, aggregation behavior, and molecular constructions. Repetitive strategies are of importance in synthetic chemistry whenever structurally defined and monodispersive molecular objects in the nm range are targeted.[3] Recently Moore[4a] and Höger[4b] applied this concept to hexagonal macrocycles with phenylacetylene units. Stimulated by these studies and given the experience in our group with Suzuki cross-coupling reactions,[5] we decided to develop a repetitive synthesis of soluble, regular macrocyclic oligophenylenes.

Macrocycles **1** ($n = 0$, 1) were selected as initial targets because they are the smallest cyclic hexagonal oligophenylenes in which the unavoidable solubilizing groups can be attached at the sides and not the corners. This leaves the option of introducing substituents at the latter, for example, for the construction of further macrocycles. The synthesis of **1** was achieved by subjecting a variety of kinked oligophenylene telechelics (modules)[6] to Suzuki cross-coupling.[7] They may be classified as either AB-type modules consisting of six (**2**, **4**) and twelve phenylene units (**3**, **5**) or AA- and BB-type modules consisting of three (**6a**) [**6b**: five] and five phenylene units (**7a**) [**7b**: seven], respectively.[8] For each module the conditions such as solvent, kind of catalyst and its relative amount, dilution, kind of base, temperature, scale of reaction, and reaction time were systematically optimized in order to gain maximum insight into the factors which influence these ring-closing reactions.[9,10]

The optimized yields are given in Scheme 1. They allow a number of conclusion to be drawn: a) Each of the routes actually furnishes macrocycle **1**,[11] however, the yields vary considerably (13–85%); b) neither module **2** nor **3** gives satisfactory yields; c) bromide is apparently far inferior to iodide; d) yields are highest (85%) if iodo telechelics are used that already carry the required number of phenylene units (**5a,b**); e) coupling of smaller telechelics (**4a,b**) saves three steps but leads to a decrease in yield (35–40%), regardless of whether the AA/BB- or AB-type approach is chosen;[12] f) pinacole esters of boronic acids are somewhat superior to the corresponding free acids with regard to coupling efficiency (for example, see the reaction of **5b** versus that of **5a**); handling and spectroscopic characterization of esters is also more convenient; g) the best results are generally obtained under high dilution using a syringe pump.[10] Conclusion b) deserves further comment: The $Br/(BOR)_2$ substitution pattern more or less fails with regard to ring formation because deboronification is no longer a well-known side reation[5a,13] but a main reaction. For example, the attempted coupling of **3a** gave, besides a few percent of desired ring **1b**, the deboronified starting compound and a deboronified noncyclic dimer in yields of approximately 43% each (HPLC). Clearly, deboronifaction and linear growth overrides ring closure.[14]

To accumulate knowledge on conformational characteristics of these oligophenylenes, in particular with regard to the relative positioning of the corners, attempts were made to crystallize **1b**.[15] Unfortunately these failed; flexible chains introduced to enhance solubility often reduce the ability of the compound to crystallize. However, crystals of **1a** could be grown from a solution in chloroform/ethanol, and the crystal structure of **1a** was solved by X-ray diffraction.[16,17] Cycle **1a** crystallizes as a 1:1 complex with chloroform (Figure 1).[18] In contrast to inclusion complexes in which the chloroform molecule is stabilized through van der Waals interactions,[19] the guest in **1a** is fully ordered. The hydrogen atom of chloroform points to the middle of a benzene ring, which leads to an unusual chloroform–arene hydrogen bond (distances C–π: 3.53 and 3.48 Å; H–π: 2.45 and 2.44 Å; angle C-H-π: 171.2 and 159.2°, respectively, for the two molecules in the asymmetric units). This weak hydrogen bond is comparable to acetylenic CH hydrogen bonds.[20] The chloroform molecule is held in its position not only by this hydrogen bond but also by van der Waals interactions involving the chlorine atoms and the opposite benzene rings.

Suzuki cross-coupling is a feasible method for the gram-scale synthesis of cyclic oligophenylenes. With the $I/B(OH)_2$ substitution pattern, yields as high as 85% can be reproducibly obtained. In view of the considerable size of cycles **1**, it is not only the efficient coupling chemistry which is responsible for this high yield, but presumably also the rigid structure of

[*] Prof. Dr. A.-D. Schlüter, Dipl.-Chem. V. Hensel, Dipl.-Chem. K. Lützow
Institut für Organische Chemie der Freien Universität
Takustrasse 3, D-14195 Berlin (Germany)
Fax: Int. code + (030) 838-3357
e-mail: adschlue@chemie.fu-berlin.de
Dipl.-Krist. J. Jacob, Dr. K. Gessler, Prof. W. Saenger
Institut für Kristallographie der Freien Universität Berlin (Germany)

[**] This work was supported by the Fonds der Chemischen Industrie.

 © WILEY-VCH Verlag GmbH, D-69451 Weinheim, 1997 0570-0833/97/3623-2654 $ 17.50+.50/0

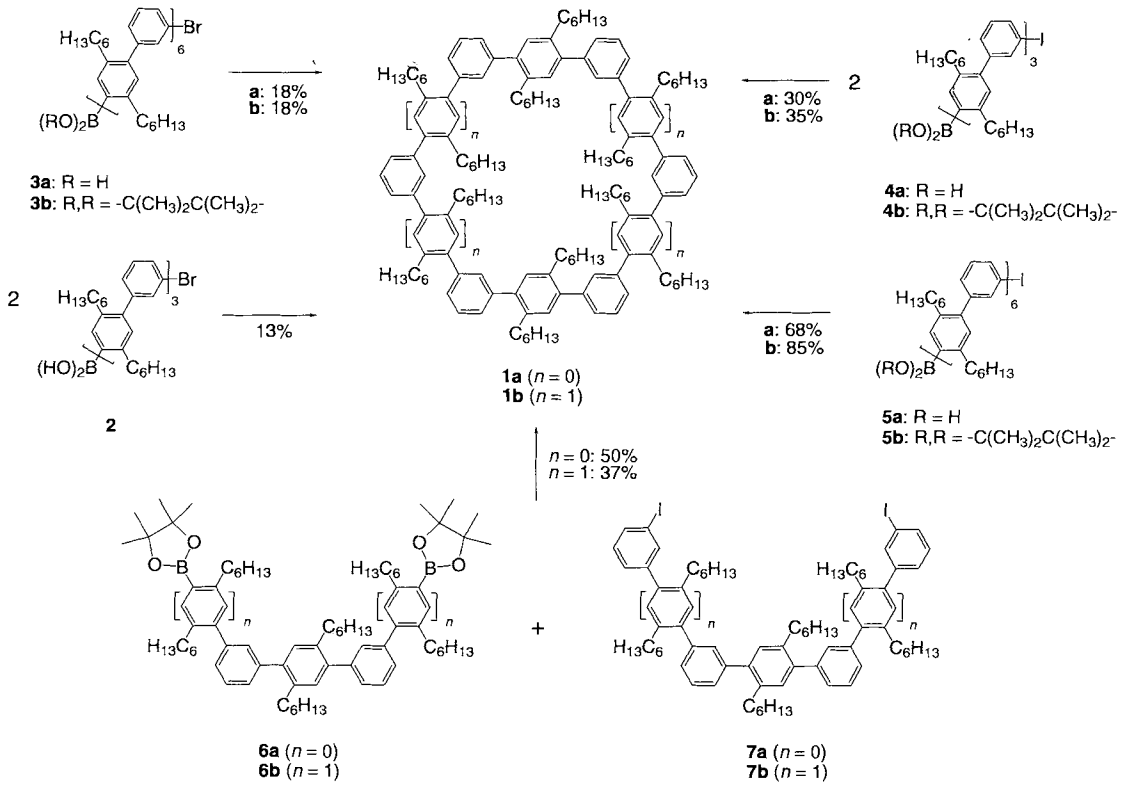

Scheme 1.

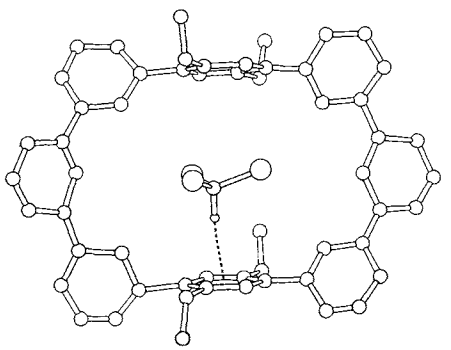

Figure 1. Molecular structure of the inclusion complex **1a**·$CHCl_3$ (one of the two molecules per unit cell). Chlorine, carbon, and hydrogen atoms are shown as big, medium, and small balls, respectively. Four carbon atoms per hexyl chain are omitted for clarity. The dashed line represents the CH–π hydrogen bond between the guest chloroform and the macrocyclic host.

the precursors to ring closure. This rigidity reduces their conformational space and, thus, the entropy costs associated with ring formation. We are now synthesizing cycles with chloride or trimethylsilyl groups at the corners in order to construct a second layer of hexagons.

Experimental Section

1b (typical procedure): A solution of **5b** (903 mg, 0.415 mmol) and [Pd{P(*o*-tol)$_3$}$_3$] (10 mg, 2.4 mol%) in dry toluene (25 mL) was added with a syringe pump within 54 h to a boiling mixture of [Pd{P(*o*-tol)$_3$}$_3$] (11 mg, 2.6 mol%) in 2N Na_2CO_3 (90 mL), dimethoxyethane (100 mL), and toluene (50 mL). The phases were then separated, and the organic phase was washed with water. Removal of the solvent in vacuo gave crude **1b** with a purity of 89% (analytical HPLC). Purification by preparative HPLC gave 678 mg of **1b** (85%).

Received: June 23, 1997 [Z10583IE]
German version: *Angew. Chem.* **1997**, *109*, 2768–2770

Keywords: cross-coupling · hydrocarbons · hydrogen bonds · macrocycles · repetitive synthesis

[1] H. Staab, F. Binnig, *Chem. Ber.* **1967**, *100*, 293; G. Wittig, K.-D. Rumpler, *Justus Liebigs Ann. Chem.* **1971**, *751*, 1; Y. Fujioka, *Bull. Chem. Soc. Jpn.* **1984**, *57*, 3494; D. J. Cram, T. Kaneda, R. C. Helgeson, S. B. Brown, C. B. Knobler, E. Maverick, K. N. Trueblood, *J. Am. Chem. Soc.* **1985**, *107*, 3645; V. Percec, S. Okita, *J. Polym. Sci. Polym. Chem. Ed.* **1993**, *31*, 877.

[2] For example, see F. Vögtle, K. Kadei, *Chem. Ber.* **1991**, *124*, 903; A. M. Boldi, F. Diederich, *Angew. Chem.* **1994**, *106*, 482, *Angew. Chem. Int. Ed. Engl.* **1994**, *33*, 486; A. de Meijere, S. Kozhushkov, C. Puls, T. Haumann, R. Boese, M. J. Cooney, L. T. Scott, *ibid.* **1994**, *106*, 934 *and* **1994**, *33*, 869; F. Diederich, *Nature* **1994**, *369*, 199; A. de Meijere, S. Kozhushkov, T. Haumann, R. Boese, C. Puls, M. J. Cooney, L. T. Scott, *Chem. Eur. J.* **1995**, *1*, 124; M. M. Haley, M. L. Bell, J. J. English, C. A. Johnson, T. J. R. Weakley, *J. Am. Chem. Soc.* **1997**, *119*, 2956; J. D. Tovar, N. Jux, T. Jarroson, S. I. Khan, Y. Rubin, *J. Org. Chem.* **1997**, *62*, 3432.

[3] For some representative examples, see E. Igner, O. I. Paynter, D. J. Simmonds, M. C. Whiting, *J. Chem. Soc. Perkin Trans. 1* **1987**, 2447; C. J. Hawker, J. M. J. Fréchet, *J. Am. Chem. Soc.* **1990**, *112*, 7638; J. S. Schumm, D. L. Pearson, J. M. Tour, *Angew. Chem.* **1994**, *106*, 1445, *Angew. Chem. Int. Ed. Engl.* **1994**, *33*, 1360.

[4] a) J. S. Moore, J. Zhang, *Angew. Chem.* **1992**, *104*, 873, *Angew. Chem. Int. Ed. Engl.* **1992**, *31*, 922; b) S. Höger, V. Enkelmann, *ibid.* **1995**, *107*, 2917 and **1995**, *34*, 2917.

[5] N. Miyaura, A. Suzuki, *Chem. Rev.* **1995**, *95*, 2457; A.-D. Schlüter, *Acta Polym.* **1993**, *59*, 44; P. Liess, V. Hensel, A.-D. Schlüter, *Liebigs Ann.* **1996**, 1037; V. Hensel, A.-D. Schlüter, *ibid.* **1997**, 303.

[6] For a definition of the term "module", see P. Kaszynski, A. C. Riedli, J. Michl, *J. Am. Chem. Soc.* **1992** *114*, 601; A.-D. Schlüter, V. Hensel, P. Liess, K. Lützow, "Towards Oligophenylene Cycles and Related Structures: A Repetitive Approach" in *Modular Chemistry* (Ed.: J. Michl), NATO Series, Kluwer, Dordrecht, The Netherlands, **1997**, in press.

[7] **1b**: ^{1}H NMR (500 MHz, CD_2Cl_2): $\delta = 0.89$ (t; 36H, CH_3), 1.32 (m; 72H), 1.60 (m; 24H, β-CH_2), 2.76 (t; 24H, α-CH_2), 7.30 (s; 12H, aromatic H), 7.45 (s; 6H, aromatic H), 7.48 (d; 12H; aromatic H), 7.59 (t; 6H, aromatic H); ^{13}C NMR (125 MHz, CD_2Cl_2): $\delta = 14.4$, 23.0, 29.8, 32.0, 32.1, 33.3, 128.1, 128.2, 131.0, 131.4, 138.1, 141.3, 142.3. The NMR spectra show no indication of conformational isomers at room temperature. MS (EI, 70 eV) $m/z = 1922$ (sample temperature 380°C).

[8] K. Lützow, V. Hensel, A.-D. Schlüter, unpublished results.

 © WILEY-VCH Verlag GmbH, D-69451 Weinheim, 1997 0570-0833/97/3623-2655 $ 17.50+.50/0

[9] For a discussion of factors influencing ring formation, see G. Illuminati, L. Mandolini, *Acc. Chem. Res.* **1981**, *14*, 95.
[10] Solvent systems: toluene/water, toluene/dimethoxyethane, xylene/dimethyl sulfoxide; catalyst precursors (and relative amounts): $[Pd(PPh_3)_4]$ (1–10 mol%, in some test series up to 70 mol%), $[Pd\{P(o\text{-tol})_3\}]$ (0.5–10 mol%); dilution: 0.01–0.0001M based on the organic phase after completion of additions with the syringe pump; base: Na_2CO_3 (2N), $Ba(OH)_2$ (conc); temperature: 85–150°C; scale: 50–1000 mg of module; reaction time: 12–96 h.
[11] Cycle **1a** was prepared only from **6a** and **7a**.
[12] Cycle **1a** was also prepared from commercially available 1,3-diiodobenzene and **6a** in 15% yield.
[13] H. G. Kuivila, J. F. Reuwer, Jr., J. A. Mangravite, *Can. J. Chem.* **1963**, *41*, 3081.
[14] This finding is not in contradiction to Suzuki polycondensation, for which the $Br/B(OH)_2$ substitution pattern gives rise to polymers of high molecular weight [5a]. These polycondensations are carried out in concentrated solutions in which deboronification cannot effectively compete with cross-coupling.
[15] Crystal structure of cyclic hexaphenylene: H. Irngartinger, L. Leiserowitz, G. M. J. Schmidt, *Chem. Ber.* **1970**, *103*, 1132.
[16] X-ray diffraction data were collected at room temperature with a CAD4 diffractometer on an FR571 rotating anode X-ray generator (Enraf-Nonius, Delft). A crystal of dimensions $0.4 \times 0.1 \times 0.1$ mm^3 was sealed in a quartz capillary. The space group and unit-cell parameters were determined from the diffraction angles of 25 reflections. The ccrystals belong to a monoclinic space group ($P2_1$, $Z = 4$), $a = 10.279(3)$, $b = 35.055(5)$, $c = 17.153(3)$, $\beta = 90.11(2)°$; two molecules in the asymmetric unit. Every molecule contains a chloroform molecule in its cavity (composition: $(C_{72}H_{80})_2 \cdot (CHCl_3)_2$). The structure was determined by direct methods (SIR92) using 4344 independent reflections and refined with full-matrix least squares. The relatively high final R value of 0.123 for 3698 data with $F \geq 2\sigma_F$ can be explained by the presence of eight hexyl chains. Two of these chains (one on every molecule) are not included in the model, since they have a high disorder which could not be resolved in the difference Fourier maps. A. Altomare, G. Cascarano, C. Giacovazzo, A. Guagliardi, M. C. Burla, G. Polidori, M. Camalli, *J. Appl. Crystallogr.* **1994**, *27*, 435. G. M. Sheldrick, *SHELXL76 Program for Crystal Structure Determination*, University of Cambridge, UK, **1976**.
[17] Crystallographic data (excluding structure factors) for the structure reported in this paper have been deposited with the Cambridge Crystallographic Data Center as supplementary publication no. CCDC-100529. Copies of the data can be obtained free of charge on application to The Director, CCDC, 12 Union Road, Cambridge CB21EZ (fax: int. code + (1223) 336-033; e-mail: deposit@chemcrys.cam.ac.uk).
[18] P. J. Kraulis, *J. Appl. Crystallogr.* **1991**, *24*, 946.
[19] J. Jazwinski, J.-M. Lehn, R. Méric, J.-P. Vigneron, M. Cesario, J. Guilhem, C. Pascard, *Tetrahedron Lett.* **1987**, *28*, 3489; G. Canceill, M. Cesario, A. Collet, J. Guilhem, L. Lacombe, B. Lozach, C. Pascard, *Angew. Chem.* **1989**, *101*, 1249; *Angew. Chem. Int. Ed. Engl.* **1989**, *28*, 1246; H. Nonoguchi, K. Yamamura, I. Tabushi, T. Higuchi, K. Hirotsu, *Bull. Chem. Soc. Jpn.* **1992**, *65*, 805.
[20] T. Steiner, E. Starikow, A. M. Amado, J. C. Teixeira-Dias, *J. Chem. Soc. Perkin Trans. 2* **1995**, 1321.

Solvation and the Synthesis of Self-Assembled Capsules**

Yuji Tokunaga, Dmitry M. Rudkevich, and Julius Rebek, Jr.*

Template effects appear frequently in biology and chemistry. Transcription and translation are among the earliest recognized examples in biology, whereas in chemistry the synthesis of macrocyclic crown ethers,[1] catenanes, rotaxanes,[2] and other ring systems[3] is most often associated with template effects. That solvents can act as templates was recognized by Cram et al.[4] and Sherman et al.[5] for the synthesis of carceplexes. Here we report that template effects involving solvents can be observed in the synthesis of hydrogen-bonded capsules, and suggest that this phenomenon may be a general feature in the synthesis of reversibly formed assemblies.

The capsules (softballs) have pseudo-spherical structures formed by dimerization of self-complementary subunits.[6] The synthesis concludes with the reaction of hydrazine derivative **1** with tetraesters **2a** or **2b** (Scheme 1). The reaction

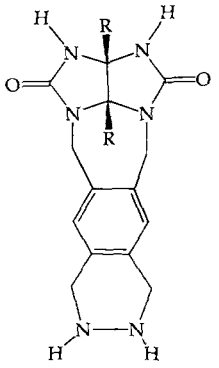

1, R = $CO_2CH_2CH_2CH(CH_3)_2$

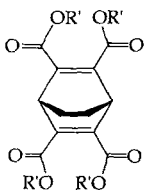

2a, R' = C_6F_5
2b, R' = 2,4,5-$Cl_3C_6H_2$

Scheme 1. Components for the final reaction in the synthesis of molecular softballs: hydrazine **1** and tetraesters **2a** and **2b**.

generally proceeds in high yield in a number of organic solvents and is complete within a few hours for **2a** or longer for the less reactive **2b**.[7] All three possible isomers are formed: C-shaped **3**, S-shaped **4**, and W-shaped **5** (Scheme 2 and Table 1); their distribution is dependent on the solvent. The C-isomer **3** is quite soluble in benzene or toluene, and forms the well-defined dimeric capsule **6** (Scheme 3), in which two solvent molecules are enclosed.[6,8] In $CDCl_3$, however, **3** behaves differently. At concentrations greater than 5mM the ^{1}H NMR spectrum of **3** contains broad signals and shows that the presence of other aggregates, which form and dissipate on the NMR time scale, is likely. In solvents such as dimethylsulfoxide (DMSO), which compete for hydrogen-bond donors, all three isomers **3**–**5** exist as monomers.

In those solvents that favor formation of the dimeric capsule **6**, the reaction between **1** and **2** gives a significant increase in the yield of **6** (Table 1). The expected statistical distribution of **3**, **4**, and **5** is 1:2:1. This distribution was, however, never realized. In "competitive" solvents such as THF and DMSO, the distribution came closest to the theoretical one. The yields of **3** in benzene, toluene, and *p*-xylene were 1.5 to 1.6 times higher; the product distribution of **3**, **4**, and **5** reaches 2.4:2.4:1.0 in toluene. On the other hand, in $CHCl_3$ and CH_2Cl_2 the yields of **3** were even lower than those expected statistically. Instead, these solvents favored the formation of S-shaped **4**.

The data suggest that solvent and hydrogen bonding play a role in the reaction, but what and when? The sequence of reactions leading to isomers **3**–**5** is straightforwarded: Four covalent bonds are formed (irreversibly), and processes

[*] Prof. J. Rebek, Jr., Dr. Y. Tokunaga, Dr. D. M. Rudkevich
The Skaggs Institute for Chemical Biology and
The Department of Chemistry
The Scripps Research Institute, MB-26
10550 North Torrey Pines Road, La Jolla, CA 92037 (USA)
Fax: Int. code + (619) 784-2876
e-mail: jrebek@scripps.edu

[**] We are grateful to the Skaggs Research Foundation and the U.S. National Institutes of Health for support of this research.

 © WILEY-VCH Verlag GmbH, D-69451 Weinheim, 1997 0570-0833/97/3623-2656 $ 17.50+.50/0

Table 1. Yields for the reactions of **1** with **2a** in different solvents [a–c].

Solvent	Yield [%]			3:4:5
	3	**4**	**5**	
calculated	25	50	25	1.0:2.0:1.0
DMSO	31	44	25	1.4:1.8:1.0
THF	25	46	29	0.9:1.6:1.0
benzene	36	43	20	1.8:2.2:1.0
toluene	41	41	17	2.4:2.4:1.0
p-xylene	39	48	13	3.0:3.7:1.0
$CHCl_3$	19	66	16	1.2:4.1:1.0
CH_2Cl_2	23	62	15	1.5:4.1:1.0

[a] Averaged value from at least two independent experiments (estimated error ±5%, total yield ca. 100%). [b] The concentration of **2a** was 5×10^{-3} M in all reactions. [c] Determined by ^{1}H NMR spectroscopy in [D_6]DMSO.

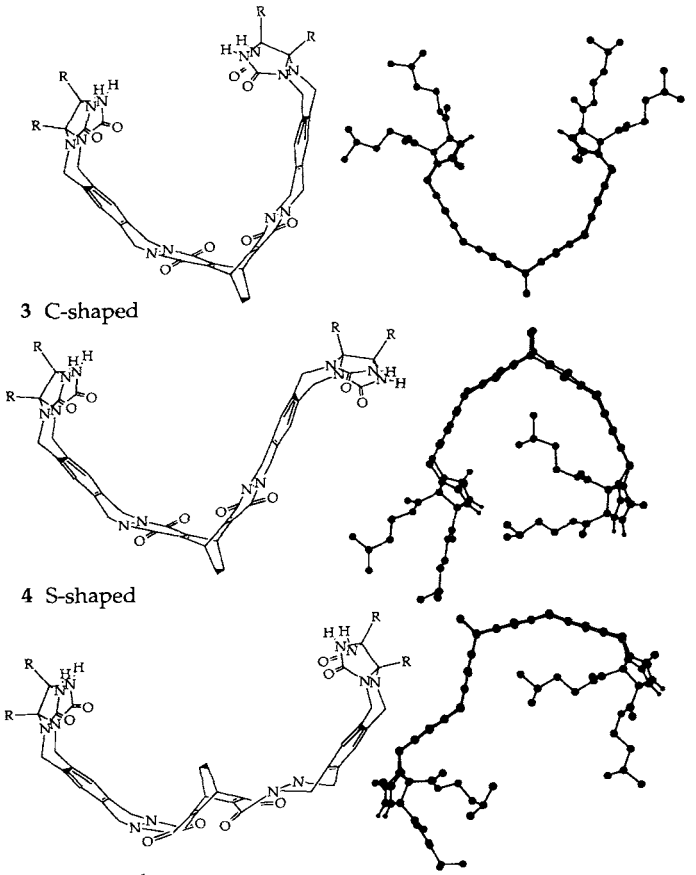

Scheme 2. Schematic representations of the three isomers **3**, **4**, and **5** (*left*) as well as their most compact energy-minimized [10] conformations (right). The carbon-bound hydrogen atoms are omitted for clarity

involving the preassociation of the reactive components should be considered.[9] Clearly, one amide bond forms slowly between **1** and, for example, **2a**. This is followed by a rapid cyclization that makes the second amide bond to produce intermediates **7** or **8**. Repitition of the sequence at the remaining two ester groups of the central unit completes the process. The first amide bond to be formed determines whether isomer **7** or **8** is the intermediate (i. e., whether the glycoluril substituents R are (*E*)- or (*Z*)-configured with respect to the bridge of the central unit). However, both isomers should form in equal amounts (Scheme 4). Indeed, the reaction of a truncated model system with **1** bears out this expectation: Equal amounts of the (*E*) isomer **9** and (*Z*) isomer **10** (Scheme 4) are formed, independent of solvent (benzene, $CHCl_3$, etc.). This places an upper limit of 50% on the yield of the C-shaped subunit **3**, since it can arise only

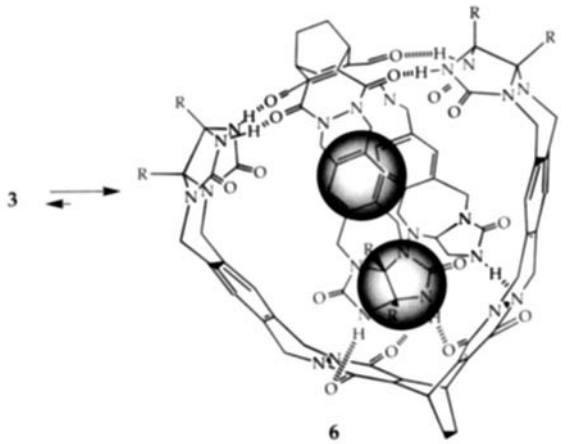

Scheme 3. Compound **3** forms the hydroden-bonded dimer **6** when two solvent molecules of appropriate size are encapsulated.

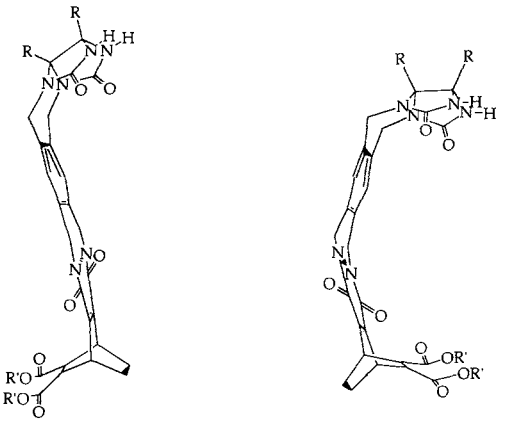

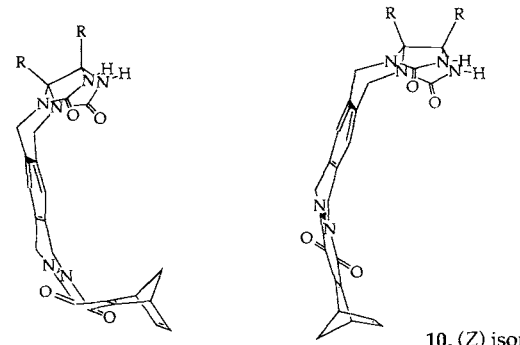

Scheme 4. Isolated intermediates: (*E*) isomer **7** and (*Z*) isomer **8** as well as the model compounds **9** and **10**.

from the (*Z*) isomer. Accordingly, the template effect of solvent, if any, must operate at the second stage of the reaction—namely, the partitioning of the (*E*) or (*Z*) isomers.

What accounts for the enhanced yield of **3** in aromatic solvents? Statistically, **8** is expected to give **3** and **4** in equal amounts. To test this, **7** and **8** were isolated from a preparative-scale synthesis and subjected to the second stage of the reaction in various media. When treated with one equivalent of **1** in DMSO, isomers **7** or **8** indeed gave **4** and **5** or **3** and **4**, respectively, in the expected 1:1 ratios (Table 2). This is in

 © WILEY-VCH Verlag GmbH, D-69451 Weinheim, 1997 0570-0833/97/3623-2657 $ 17.50+.50/0

Table 2. Yields for the reactions of **1** with **7** or **8** in different solvents[a–c].

Solvent	(1+7) Yield[%]		4:5	(1+8) Yield[%]		3:4
calculated	50	50	1.0:1.0	50	50	1.0:1.0
DMSO	50	50	1.0:1.0	51	49	1.04:1.0
benzene	62	38	1.6:1.0	64	36	1.8:1.0
$CHCl_3$	65	35	1.9:1.0	36	64	0.6:1.0

[a] Averaged value from at least two independent experiments (estimated error ±5%, total yield ca. 100%). [b] The concentration of **1** was 5×10^{-3} M in all reactions. [c] Determined by ^{1}H NMR spectroscopy in [D_6]DMSO.

good agreement with the distribution for the overall reaction in DMSO (Table 1). Unexpectedly, in $CHCl_3$, the (*E*) isomer **7** reacted with **1** to form **4** in yields of up to 65%. The same result holds for the reaction of the (*Z*) isomer **8** with **1**: 64% of S-shaped **4** was obtained. Whatever the reason, $CHCl_3$ disfavors the formation of C- or W-shaped products (Table 2). A factor that could be responsible is that $CHCl_3$ either fits into the transition state leading to the S-shaped product, or makes an inappropriate fit into the transition state leading to the other products. The S-shaped isomer may have a uniquely compact low-energy conformation (Scheme 2),[10] in which its internal cavity can be filled by the isopentyl esters of a glycoluril unit. In benzene the product distribution was reversed, and a yield of 64% was obtained for C-shaped **3**. This is the medium in which the solvent-occupied dimeric capsule enjoys the greatest stability.

It is possible to calculate the distributions of **3**–**5** in different solvents by using the data for the second stage and assuming that the first stage gives equal amounts of (*Z*) and (*E*) intermediates. The results (Table 3) compare well with the experimental observations summarized in Table 1, and clearly

Table 3. Estimated distribution of yield[%][a] for **3**–**5** in different solvents.

	3	4	5
DMSO			
total yield	31	44	25
(*E*) isomer	0	25	25
(*Z*) isomer	26	25	0
$CHCl_3$			
total yield	19	66	16
(*E*) isomer	0	33	18
(*Z*) isomer	18	32	0
benzene			
total yield	36	43	20
(*E*) isomer	0	31	19
(*Z*) isomer	32	18	0

[a] Calculated from the results of reactions **1**+**2a**, **1**+**7**, and **1**+**8**; [total yield] = [**3**]+[**4**]$_Z$+[**4**]$_E$+[**5**], where [**3**], [**4**]$_Z$, [**4**]$_E$, and [**5**] correspond to the concentrations of isomers **3**, **4**, and **5**, which are produced from both (*Z*) and (*E*) isomers.

justify the assumption that selection occurs in the second stage of the reaction.

It is hard to imagine that solvent plays a role in the first stage of the reaction, as the stereocenters are remote from each other and only connected by a single amide: No cavities are generated in the rate-determining step. However, the curvature and the concave shapes of the (*E*) and (*Z*) intermediates invite solvation. Benzene, toluene, or *p*-xylene can be recognized by and well fit within the (*Z*)-shaped intermediate. Subsequently, the remaining exposed surface of the solvent attracts reactant **1**, and lends stability to the reversibly formed zwitterionic, tetrahedral intermediate that leads to the C-shaped product (Scheme 5, left). One of these solvent molecules must fit well within the monomeric form of **3**, since

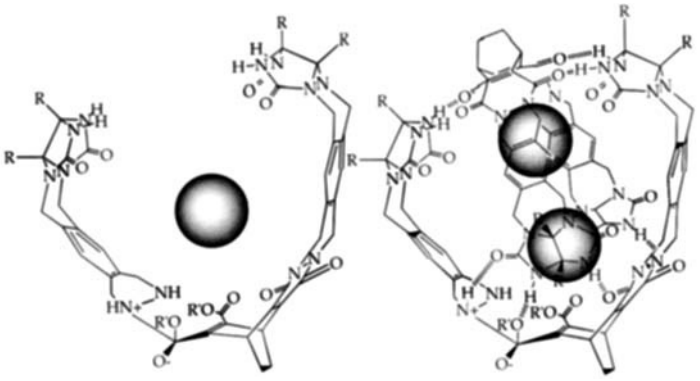

Scheme 5. Possible tetrahedral intermediates of the reaction between **1** and **2**: left: monomer A associated with one solvent molecule; right: templated complex B.

two of these molecules are accomodated inside the dimeric capsule.[6] Alternatively, or in addition, the templated pathway involving the hydrogen-bonded tetrahedral intermediate (Scheme 5, right) is possible.[11] Since the dimerization constant of **3** in benzene is high, the concentration of monomers **3** (template) and its complex (Scheme 5, right) must be very low. Such situations were encountered by von Kiedrowski[12] for templating hexadeoxynucleotides and Ghadiri et al. for templating peptides.[13] Autocatalysis in the case presented here has yet to be established. We are confident in this respect, as template effects of products during the synthesis of self-assembled dimeric capsules have already been observed.[9,14] Meanwhile, we propose that the most commonly encountered molecular recognition phenomenon—solvation—plays an active rather than a passive role in the formation of a covalent bond.

Received: May 26, 1997 [Z10475IE]
German version: *Angew. Chem.* **1997**, *109*, 2770–2773

Keywords: hydrogen bonds · self-assembly · solvent effects · supramolecular chemistry · template synthesis

[1] C. J. Pederson *J. Am. Chem. Soc.* **1967**, *89*, 7017–7036; *Angew. Chem.* **1988**, *100*, 1053–1059; *Angew. Chem. Int. Ed. Engl.* **1988**, *27*, 1021–1027.

[2] D. B. Amabilino, J. F. Stoddart, *Chem. Rev.* **1995**, *95*, 2725–2828; F. Vögtle, T. Dünnwald, T. Schmidt, *Acc. Chem. Res.* **1996**, *29*, 451–460; D. Philp, J. F. Stoddart, *Angew. Chem.* **1996**, *108*, 1242–1286; *Angew. Chem. Int. Ed. Engl.* **1996**, *35*, 1154–1196.

[3] Recent examples of template effects: S. Anderson, H. L. Anderson, J. K. M. Sanders, *Acc. Chem. Res.* **1993**, *26*, 469–475; R. Hoss, F. Vögtle, *Angew. Chem.* **1994**, *106*, 389–398; *Angew. Chem. Int. Ed. Engl.* **1994**, *33*, 375–384; B. Hasenknopf, J.-M. Lehn, B. O. Kneisel, G. Baum, D. Fenske, *ibid.* **1996**, *108*, 1987–1990 and **1996**, *35*, 1838–1840.

[4] J. A. Bryant, M. T. Blanda, M. Vincenti, D. J. Cram, *J. Am. Chem. Soc.* **1991**, *113*, 2167–2172; J. C. Sherman, C. B. Knobler, D. J. Cram, *ibid.* **1991**, *113*, 2194–2204.

[5] R. G. Chapman, N. Chopra, E. D. Cochien, J. C. Sherman, *J. Am. Chem. Soc.* **1994**, *116*, 369–370; R. G. Chapman, J. C. Sherman, *ibid.* **1995**, *117*, 9081–9082; K. Nakamura, C. Sheu, A. E. Keating, K. N. Houk, J. C. Sherman, R. G. Chapman, W. L. Jorgensen, *ibid.* **1997**, *119*, 4321–4322.

[6] R. S. Meissner, J. Rebek, Jr., J. de Mendoza, *Science* **1995**, *270*, 1485–11488; R. S. Meissner, X. Garcias, S. Mecozzi, J. Rebek, Jr., *J. Am. Chem. Soc.* **1997**, *119*, 77–85.

[7] In a typical experiment, a solution of **2a** or **2b** (10 mM, 5 equiv), **1** (10 equiv), and Et_3N (50 equiv) in dry solvent was stirred at room temperature until the reaction was complete. After removal of the volatile components in vacuo, the residue was redissolved in [D_6]DMSO and analyzed by ^{1}H NMR spectroscopy (600 MHz); integration of the signals in the CH_2N methylene region between $\delta = 6.0$ and 4.0 was used for determining product distributions. All new compounds were characterized by high-resolution NMR spectroscopy (600 MHz) and high-resolution mass spectrometry.

 © WILEY-VCH Verlag GmbH, D-69451 Weinheim, 1997 0570-0833/97/3623-2658 $ 17.50+.50/0

[8] For example, the ^{1}H NMR spectrum of **3** in [D$_6$]benzene contains sharp signals and, in particular, a downfield NH-singlet at $\delta = 8.83$ that is independent of concentration; the corresponding NH-singlet in model (nondimeric) glycolurils is at $\delta \approx 5.0$ in [D$_6$]benzene. The FT-IR spectrum of **3** (benzene, $2 \times 10^{-5} - 1 \times 10^{-3}$ M) showed only the NH stretching absorption at 3229 cm^{-1}, which is about 180 cm^{-1} lower than that observed for nonassembled glycolurils. From ^{1}H NMR dilution experiments ($5 \times 10^{-4} - 1.5 \times 10^{-2}$ M), a lower limit for the dimerization constant K_D of 10^7 M^{-1} was estimated. Solutions of **3** in benzene were analyzed by electrospray mass spectrometry (ESI-MS) and showed, in addition to the signal for monomer **3** at 1268 Da, a fairly strong (ca. 20%) signal for dimer **6** at 2535 Da.

[9] See, for example, D. M. Rudkevich, J. Rebek, Jr. *Angew. Chem.* **1997**, *109*, 877–879; *Angew. Chem. Int. Ed. Engl.* **1997**, *36*, 846–848.

[10] F. Mohamadi, N. G. Richards, W. C. Guida, R. Liskamp, M. Lipton, C. Caufield, G. Chang, T. Hendrickson, W. C. Still, *J. Comput. Chem.* **1990**, *11*, 440–467.

[11] The role of hydrogen bonding in the stabilization and/or destabilization of the tetrahedral zwitterionic intermediate has been discussed: C.-W. Su, J. Watson, *J. Am. Chem. Soc.* **1974**, *96*, 1854–1857; L. Wang, H. Zipse, *Liebigs Ann.* **1996**, 1501–1509; H. Zipse, L. Wang, K. N. Houk, *ibid.* **1996**, 1511–1522.

[12] G. von Kiedrowski, *Angew. Chem.* **1986**, *93*, 932–935; *Angew. Chem. Int. Ed. Engl.* **1986**, *25*, 932–935.

[13] D. H. Lee, J. R. Granja, J. A. Martinez, K. Severin, M. R. Ghadiri, *Nature (London)* **1996**, *382*, 525–528.

[14] 1-Adamantanecarboxyamide—known as a good guest for dimeric capsule **6** in benzene and *p*-xylene [6]—also enhanced the yields of **3** in these solvents but not in $CDCl_3$, in which the carboxamide is not encapsulated.

Synthesis and Structure of ITQ-3, the First Pure Silica Polymorph with a Two-Dimensional System of Straight Eight-Ring Channels**

Miguel A. Camblor,* Avelino Corma, Philip Lightfoot, Luis A. Villaescusa, and Paul A. Wright*

Silicon dioxide appears in nature in several crystalline forms of high density, like quartz, cristobalite, tridymite, moganite, and the high pressure polymorphs coesite, keatite, and stishovite.[1] The mineral melanophlogite also presents a framework of SiO_2, which contains cages in which gases are occluded. In the last two decades a number of new pure silica polymorphs, some of them with microporous frameworks, have been synthesized with the aid of organic structure-directing agents.[2] Microporous, pure silica polymorphs lacking Si–OH moieties arising from defects of connectivity between adjacent tetrahedra can have considerable technological interest in view of their hydrophobic properties.[3] For example, silica polymorphs with small channels (apertures formed by windows containing eight SiO_4 tetrahedra) would show shape-selectivity properties in adsorption and would find attractive potential applications in purification and separation processes. However, the only silica phases containing eight-ring (8MR) pores that are available so far, namely, decadodecasil-3R (with a two-dimensional (2D) system of sinusoidal 8MR channels) and RUB-3 (1D 8MR channels),[4] are relatively dense,[5] characterized by a framework density (*FD*, defined as the number of Si atoms per 1000 Å^3) of 17.7 and 17.4, respectively. These features limit their adsorption properties and are a clear drawback for this kind of application.

We report here on the synthesis and structure of ITQ-3,[6] the first pure silica polymorph containing a two-dimensional system of straight 8MR pores. This phase presents a very low density structure characterized by an *FD* of 16.3, which is the second lowest *FD* among silica polymorphs, the first one being that of the three-dimensional, large pore, 12-ring pure silica zeolite Beta ($FD = 15.6$).[7] Furthermore, ITQ-3 possesses the largest microporous volume as measured by N_2 adsorption (0.23 cm^{3}g^{-1}, relative to 0.22 cm^{3}g^{-1} measured for pure silica Beta).[7]

Calcined ITQ-3 consists of a three-dimensional framework of 4-connected SiO_4 tetrahedra with no Si-O-Si connectivity defects, as evidenced by its ^{29}Si MAS NMR spectrum (Figure 1), which shows no absorptions below $\delta = -105$ due to Si (3Si,1OH) species. Moreover, the spectrum shows a very high resolution of tetrahedral Si (4Si) sites, directly attributable to the crystallographically distinct Si environments in the structure. Such a high resolution is generally only observed when there is an essentially complete absence of Si–OH and Si-O-Al species.

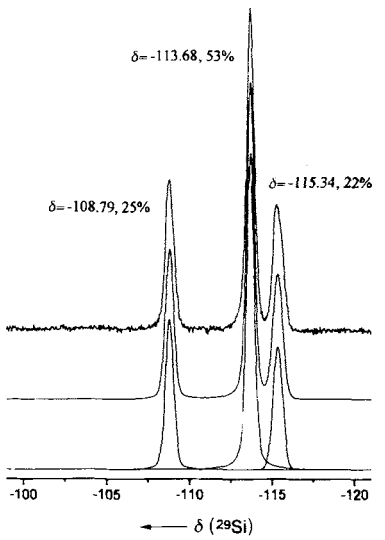

Figure 1. ^{29}Si MAS NMR spectrum of pure silica ITQ-3. From bottom to top: deconvoluted components, simulated, and experimental spectra.

The experimental synchrotron X-ray powder diffraction data of a calcined ITQ-3 sample was indexed as orthorhombic ($a = 20.622(1)$, $b = 9.7242(4)$, $c = 19.623(2)$ Å) and with symmetry *Cmcm*, *Cmc*2$_1$, or *C*2*cm* (determined by the examination of the systematic absences). These symmetries were consistent with the ^{29}Si MAS NMR spectrum of ITQ-3 (Figure 1), if the unit cell possessed four distinct crystallographic sites for silicon, each on general equivalent positions and two of the four having overlapping resonances.

The unit cell size and symmetry were observed to be consistent with a structural model that can be described as that produced by the unit cell twinning of the zeotype RUB-13

[*] Dr. M. A. Camblor, Prof. Dr. A. Corma, L. A. Villaescusa
Instituto de Tecnología Química
Universidad Politécnica de Valencia
Avda. Los Naranjos s/n, E-46022 Valencia (Spain)
Fax: Int. code + (346) 387-7809
e-mail: macamblo@itq.upv.es
Dr. P. A. Wright, Dr. P. Lightfoot
School of Chemistry
University of St. Andrews
The Purdie Building, North Haugh, St. Andrews, Fife KY16 9ST (UK)
Fax: Int. code + (01334) 463808
e-mail: paw2@st-andrews.ac.uk

[**] This work was supported in part by the Spanish DGICYT (MAT 94-0359-C02-01). P.L. and P.A.W. gratefully acknowledge the University of St. Andrews and the British Council for support. We also thank Dr. G. Bushnell-Wye (Daresbury) for his help in collecting the synchrotron data.

 © WILEY-VCH Verlag GmbH, D-69451 Weinheim, 1997 0570-0833/97/3623-2659 $ 17.50+.50/0

(structure code RTH).[8] A similar relationship is observed between the structure types TON and MTT.[9] To determine whether this proposed structure for ITQ-3 fits the experimental diffraction data, a model was obtained starting from the set of atomic coordinates for silicon atoms in RTH, applying *Cmcm* symmetry in the unit cell (with a doubled cell repeat along c^* relative to that in RTH, arising from the unit cell twinning), and placing oxygen atoms midway between the tetrahedral atoms. This model was refined against the diffraction data with the presence of constraints on the Si–O and Si–Si bond lengths and on the O-Si-O bond angles. Although the profile was reasonably well fitted, Bragg reflections related to the cell twinning exhibited broadening with respect to the other peaks. This broadening was matched empirically with the peak broadening options implemented within the GSAS program.[12] The fit was significantly improved if the low angle peaks (below 11°) were excluded, because the values of the peak broadening functions are largely determined by these intense peaks (if included), and these values are not accurately extrapolated over the rest of the profile. A more theoretical treatment of this peak broadening dependence on (*hkl*) is underway in terms of distances between stacking faults parallel to (001). The final fit to the diffraction profile is sufficiently close (Figure 2) to

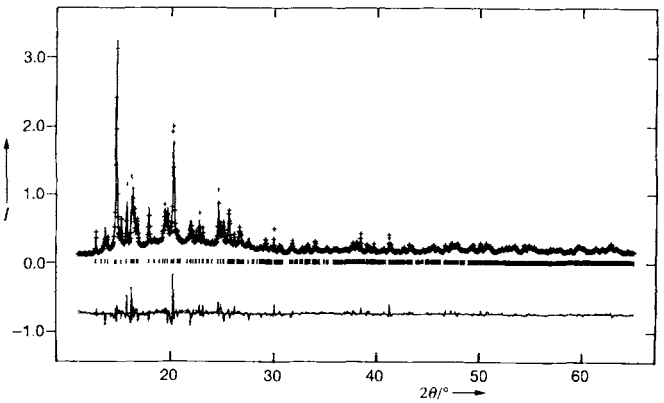

Figure 2. Observed (+) and calculated (bars) Rietveld refinement of ITQ-3, as well as the difference profile (bottom). The broad background hump arises from diffuse scattering from the silica glass capillary. I = intensity (in counts × 10^4).

indicate that the structural model is correct. No significant improvement in fit was obtained by lowering the symmetry. To demonstrate that ITQ-3 is indeed a distinct end-member of the structural series, Figure 3 compares the simulated diffraction patterns of ITQ-3 (this work) and RTH[8] with the experimental diffractogram measured on calcined ITQ-3 with a laboratory X-ray diffractometer.

A stereoplot of the ITQ-3 framework down [010] is given in Figure 4. The structure of ITQ-3 comprises a two-dimensional system of interconnected 8MR straight channels running along [010] and [001]. The intersection of both types of channels generates four large cavities per unit cell in which presumably the template cations are located (exactly one per cage, according to the chemical composition, see experimental section). These cavities, which can be denoted as $[4^65^86^48^4]$ (where n^i indicates that there are i faces of n sides in the polyhedral cage defining the cavity; Figure 5, right), are very similar to those found in the borosilicate RUB-13[8] (Figure 5, left) except for the presence of the mirror plane perpendicular to c, which RUB-13 lacks. This makes a significant difference in terms of shape of the cage (although not so in terms of

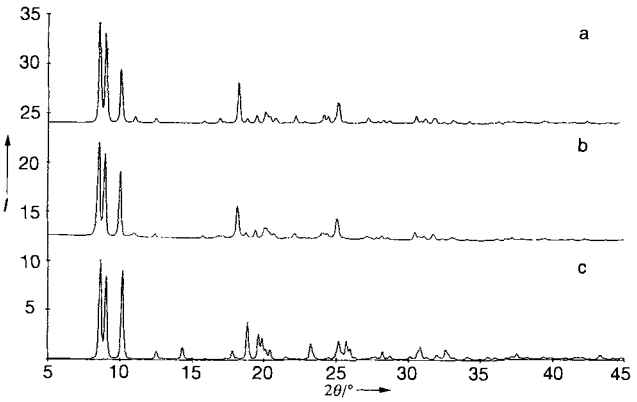

Figure 3. Comparison of the simulated X-ray diffraction pattern of ITQ-3 ($Cu_{K\alpha 1}$) (a) with experimental X-ray diffraction data (laboratory diffractometer) of calcined ITQ-3 (b). The pattern simulated from the atomic coordinates of RTH (c)[8] is also given. I = intensity (arbitary units).

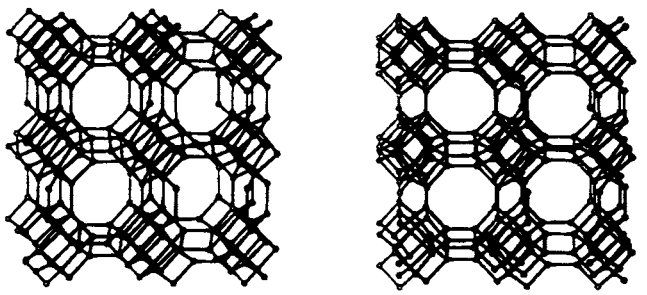

Figure 4. Stereo plot of the structure of ITQ-3 down [010]. Only tetrahedral atom connectivity is represented.

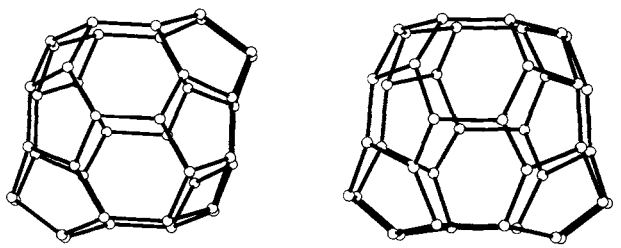

Figure 5. Comparison of the $[4^65^86^48^4]$ cages of RTH (left) and ITQ-3 (right).

volume), and presumably, the synthesis of ITQ-3 is made possible by a tight fit of the template cation in this cage. Further work to locate the exact position of the cation in as-made ITQ-3 is in progress to check this hypothesis, which would imply a true template effect in the synthesis of this new pure silica polymorph.

The incorporation of Al in framework positions of ITQ-3 is also easily achieved.[6] This allows the preparation of acid catalysts that, due to the small pore openings and the large cage present in the structure, show marked shape-selectivity properties. This catalyst can be advantageously used in several applications of high technological importance, like the selective cracking or hydrocracking of normal alkanes or alkenes, postreforming of gasoline, steam cracking, dewaxing by selective cracking of normal alkanes, and transformation of methanol to olefins.[6]

Finally, the synthetic procedure that led to the synthesis of ITQ-3 appears to show an outstanding ability to produce pure

 © WILEY-VCH Verlag GmbH, D-69451 Weinheim, 1997 0570-0833/97/3623-2660 $ 17.50+.50/0

silica polymorphs of remarkable low framework density. With different structure-directing agents the method has so far produced the spontaneous nucleation and growth of the Beta (BEA),[7] ITQ-4 (IFR),[10] and ITQ-3 pure silica polymorphs. These three phases share the notable characteristic of having the lowest framework densities ever reported for pure silica polymorphs (15.6, 17.0 and 16.3, respectively; compare with 17.4 for RTE and pure silica SOD). This synthetic methodology, based on the F^- method first introduced by Flanigen and Patton, and subsequently developed by others,[11] makes use of comparatively low temperatures (below 175°C, typically a maximum of 150°C) and low F^-/SiO_2 and H_2O/SiO_2 ratios (typically about 0.5 and ≤ 15, respectively) and appears to open a promising route to the synthesis of very open pure silica frameworks.

Experimental Procedure

Synthesis: Pure silica ITQ-3 was synthesized from 1,3,3,6,6-pentamethyl-6-azoniabicyclo[3.2.1.]octane ($C_{12}H_{24}N^+$) as structure-directing agent. This cation was prepared by reaction of the corresponding amine with an excess of CH_3I and was used in its hydroxide form after anion exchange of the iodide. The hydrothermal reaction (PTFE-lined stainless steel autoclaves, 150°C, rotation (60 rpm), 19 days, pH = 7.5, composition SiO_2:0.5 $C_{12}H_{24}NOH$:0.5 HF:7.7 H_2O) yielded a white highly crystalline solid (20.9 g per 100 g of initial mixture, amounting to about 90% of the silica recovered as ITQ-3). Chemical analysis of as-made ITQ-3 reveals that the sample contains no aluminum and that the organic cation is occluded intact within its pores (elemental analysis found: C 12.48, H 2.05, N 1.20, F 1.50%; the ideal unit cell composition of $(C_{12}H_{24}NF)_4(SiO_2)_{64}$ requires C 12.40, H 2.08, N 1.20, F 1.63%). The integrity of the organic cation in as-made ITQ-3 is also evidenced by ^{13}C CPMAS NMR spectroscopy. After calcination at 580°C the organics are removed from the material.

Structure determination: A synchrotron X-ray powder diffraction pattern was collected at room temperature over the range $3 \geq 2\theta \geq 66°$, with a 0.01° step size, over 12 hours on beamline 9.1 at the Daresbury synchrotron using X-rays of wavelength 1.2513(2) Å. No special precautions were taken to remove all of the water from the sample, which was packed in a 0.7 mm diameter silica glass capillary. X-ray diffraction data on the same sample was collected on a laboratory STOE powder diffractometer in transmission mode, with monochromated $Cu_{K\alpha 1}$ radiation ($\lambda = 1.54056$ Å). In this case the sample was prepared in a disc between thin mylar sheets.

Profile refinement of the structural model was performed with the Rietveld method within the GSAS program,[12] using bond length and bond angle constraints. In the final fit the profile was matched from $11 \geq 2\theta \geq 66°$. The final refinement used 59 variables and 57 constraints and had R_{wp} and R_p values of 8.6 and 6.2%, respectively. The average values and standard deviations of Si-O bond lengths were 1.60(4) Å and of O-Si-O angles were 109.4(3.5)°; the final atomic coordinates are given in Table 1. Further details of the crystal structure investigation may be obtained from the Fachinformationszentrum Karlsruhe, D-76344 Eggenstein-Leopoldshafen, on quoting the depository number CSD-407793.

Table 1. Atomic coordinates of ITQ-3 ($[SiO_2]_{64}$, orthorhombic, *Cmcm*, a = 20.622(1), b = 9.7242(4), c = 19.623(2) Å; standard deviations in parentheses).

Atom	x	y	z
Si(1)	0.32018(35)	−0.0430(10)	0.17011(35)
Si(2)	0.07561(30)	0.4067(10)	0.0561(5)
Si(3)	0.2641(5)	0.2255(10)	0.1121(5)
Si(4)	0.15302(35)	0.1551(10)	0.0036(5)
O(5)	0.3427(10)	−0.0581(20)	0.25
O(6)	0.2675(5)	−0.1485(15)	0.1491(10)
O(7)	0.0996(10)	0.5	0.0
O(8)	0.0978(5)	0.2516(10)	0.0287(10)
O(9)	0.0	0.4105(20)	0.0718(10)
O(10)	0.2148(5)	0.1587(15)	0.0569(10)
O(11)	0.3870(5)	−0.0628(15)	0.1288(5)
O(12)	0.2913(10)	0.1093(10)	0.1625(10)
O(13)	0.3275(5)	0.2871(15)	0.0695(5)
O(14)	0.1308(10)	0.0	0.0

Received: June 18, 1997 [Z10567IE]
German version: *Angew. Chem.* **1997**, *109*, 2774–2776

Keywords: heterogeneous catalysis · microporosity · silicon · structure elucidation · zeolite analogues

[1] a) A. F. Wells, *Structural Inorganic Chemistry*, 5th ed., Clarendon Press, Oxford, 1984, p. 1004–1008; b) G. Miehe, H. Graetsch, *Eur. J. Mineral.*, **1992**, *4*, 693–706.
[2] a) H. Gies, B. Marler, *Zeolites*, **1992**, *12*, 42–49; b) M. M. Helmkamp, M. E. Davis, *Annu. Rev. Mater. Sci.*, **1995**, *25*, 161–192.
[3] E. M. Flanigen, in *Zeolites: Science and Technology*, (Eds.: F. R. Ribeiro, A. E. Rodrigues, L. D. Rollmann, C. Naccache) (*NATO ASI Ser. Ser. E*, **1984**, *80*, pp. 3–34).
[4] a) H. Gies, *Z. Kristallogr.* **1986**, *175*, 93–104; b) B. Marler, A. Grünewald-Lüke, H. Gies, *Zeolites* **1995**, *15*, 388–399.
[5] W. M. Meier, D. H. Olson, C. Baerlocher, *Atlas of Zeolite Structure Types*, 4th ed., Elsevier, London, **1996**.
[6] L. A. Villaescusa, M. A. Camblor, A. Corma, (ITQ) ES-B P9701229, **1997**.
[7] M. A. Camblor, A. Corma, S. Valencia, *Chem. Commun.* **1996**, 2365–2366.
[8] S. Vortmann, B. Marler, H. Gies, P. Daniels, *Microporous Mater.* **1995**, *4*, 111-121.
[9] P. A. Wright, J. M. Thomas, G. R. Millward, S. Ramdas, S. A. Bari, *J. Chem. Soc., Chem. Commun.*, **1985**, 1117–1119.
[10] a) M. A. Camblor, A. Corma, L. A. Villaescusa, *Chem. Commun.* **1997**, 759–760; b) P. A. Barrett, M. A. Camblor, A. Corma, R. H. Jones, L. A. Villaescusa, *Chem. Mater.* **1997**, *9*, 1713–1715.
[11] a) E. M. Flanigen, R. L. Patton (Union Carbide) US-A 4073865, **1978**; b) J. L. Guth, H. Kessler, P. Caullet, J. Hazm, A. Merrouche, J. Patarin, *Proc. 9th Int. Zeolite Conf.*, (Eds.: R. von Ballmoos, J. B. Higgins, M. M. J. Treacy), Butterworth-Heinemann, London, **1993**, 215–222.
[12] A. C. Larson, R. B. von Dreele, *Generalised Crystal Structure Analysis System*, Los Alamos National Laboratory, USA, **1988**.

1,5,7-Triazabicyclo[4.4.0]dec-5-ene Immobilized in MCM-41: A Strongly Basic Porous Catalyst**

Yarlagadda V. Subba Rao, Dirk E. De Vos, and Pierre A. Jacobs*

Basic catalysis is in general an area that is less developed than acidic catalysis; this is particularly true for highly dispersed or porous materials.[1] Zeolites or mesoporous molecular sieves can acquire basicity by exchange or impregnation with Cs^+, but the limited strength of the resulting basic sites offers perspectives for only a small range of organic syntheses.[2] Similarly, aluminophosphate nitride catalysts show low basicity, and are relevant only in Knoevenagel additions.[3] As an alternative, highly reactive entities such as Na clusters have been introduced into zeolites. Although these materials can handle difficult reactions such as side-chain alkylations, they are extremely prone to deactivation by environmental CO_2 or water.[4] These examples illustrate the continuous interest in designing new solid, basic catalysts.[5–7] To facilitate handling these materials should have an inorganic backbone structure; however, classic oxides have the disadvantage of potentially releasing OH^- ions into solution. Here we present a novel heterogeneous, strongly basic catalyst, in which a guanidine base is covalently coupled to

[*] Prof. Dr. P. A. Jacobs, Dr. Y. V. Subba Rao, Dr. D. De Vos
Center for Surface Science and Catalysis
K. U. Leuven
Kardinaal Mercierlaan 92, 3001-Heverlee (Belgium)
Fax: Int. code + (16) 321-998
e-mail: pierre.jacobs@agr.kuleuven.ac.be.

[**] This work was supported by the Belgian Federal Government in the framework of an I.U.A.P. project. Y.V.S.R. and D.D.V. thank K. U. Leuven and FWO (Belgium) for post-doctoral stipends.

 © WILEY-VCH Verlag GmbH, D-69451 Weinheim, 1997 0570-0833/97/3623-2661 $ 17.50+.50/0

an inorganic siliceous mesoporous support. It is demonstrated that this material is truly catalytic for, for example, Michael additions under remarkably mild conditions. The pore structure influences the selectivity of the reaction, as shown by a comparison with a nonporous material. Reactions that are discussed include Michael additions, Robinson annulations, Knoevenagel condensations, and nucleophilic epoxidations.

1,5,7-Triazabicyclo[4.4.0]dec-5-ene (TBD, Scheme 1) is the prototype for a group of strong guanidine bases which can be used as stoichiometric reagents or as catalysts. The pK_B values

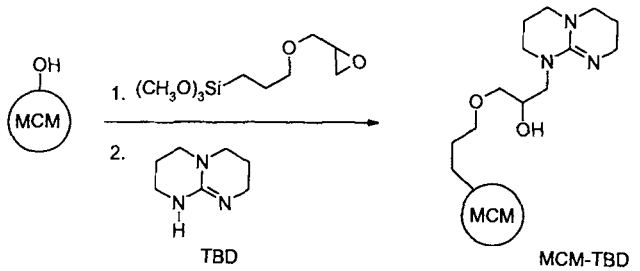

Scheme 1.

of these bases are about 25, ensuring a well-defined and strong basicity.[8] TBD contains a N–H group, which can be immobilized by nucleophilic attack on an immobilized electrophile. The traditional approach uses substitution of a chloro- or bromopropyl group with the amine. However, this requires harsh conditions, and the liberated acids (HCl, HBr) might poison the base sites. Furthermore, quaternization of the amine is a hardly avoidable side reaction.[5,6] Therefore, a route by surface glycidylation was designed. We previously applied this method successfully in the immobilization of an azacycloalkane epoxidation catalyst.[9] First, the mesoporous, siliceous MCM-41 support is obtained by the usual liquid crystal templated synthesis.[10] Next, its inner surface is covered with oxirane groups by reaction of the surface SiOH groups with 3-trimethoxylsilylpropoxymethyloxirane. Finally, TBD reacts under remarkably mild conditions with the epoxide group without formation of any by-products (Scheme 1).

The success of this reaction sequence was confirmed by IR and NMR spectroscopy as well as thermogravimetric analysis. For instance, the magic angle spinning solid-state NMR spectrum shows that the oxirane ring in the silane coupling agent is intact after the reaction with the surface hydroxyl groups. Measurement of the N_2-adsorption isotherm demonstrated that the pore volume with a radius smaller than 2 nm substantially decreases from 1.62 mL N_2 STP (standard temperature and pressure) to 1.2 mL per gram by the anchoring of the TBD unit. Moreover, the average pore diameter also shows a tendency to decrease, suggesting that the environment for organic reactions is spatially more constrained after surface modification.

The MCM-TBD material was used as a catalyst for Michael reactions (Scheme 2). It is critical that the catalyst accelerates only the desired 1,4-addition, and bypasses side reactions such as other condensations, dimerizations, or rearrangements. Some results are compiled in Table 1. Excellent selectivities were obtained for the reaction of typical Michael donors and enones. For instance, with ethylcyanoacetate (ECA) and cyclopentenone, the 1,4-adduct is obtained in 52% yield and

Table 1. MCM-TBD as a catalyst for Michael reactions of ethylcyano acetate (ECA) and diethyl malonate (DEM) [a].

Entry	Donor	Acceptor	T[K]	t[h]	Yield[%][b]
1	ECA	methyl vinyl ketone	338	0.5	98 (81)[c]
2	DEM	methyl vinyl ketone	338	0.5	34 (1)[c]
3	ECA	acrolein	313	0.5	100 (55)[c]
4	DEM	acrolein	313	0.5	100 (53)[d]
5	ECA	cyclopentenone	353	0.5	52
6	ECA	cyclohexenone	353	2	65 (5)[e]
7	ECA	acrylonitrile	338	1	84 (72)[c]
8	ECA	ethyl acrylate	338	1	75 (74)[c]
9	DEM	ethyl acrylate	338	5	49 (5)[c]
10	DEM	cyclohexenone	353	60	2.7
11	DEM	cyclohexenone	353	60	15
12	DEM	methyl vinyl ketone	338	0.5	7

[a] Conditions: 1 mmol of donor, 1 mmol of acceptor, 20 mg of catalyst (MCM-TBD for entries 1–10 and TBD-modified SiO_2 for entries 11 and 12), 2 mL of CH_3CN under N_2. [b] Yields are based on the Michael acceptor. [c] Molar yield of di-addition product in parentheses. [d] Cyclized product **1**. [e] Knoevenagel adduct.

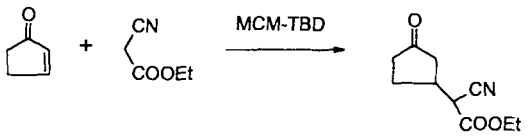

Scheme 2.

100% selectivity (Scheme 2). The well-defined strong basicity of the MCM-TBD catalyst ensures optimum selectivity for most reactions. Not only cyano-activated donors, but also the less acidic diethylmalonate (DEM) can be successfully used. Acrolein reacts with DEM to lead to double Michael addition of the acceptor on the donor and eventual cyclization to **1**. The preference for single or double addition can be controlled by reaction stoichiometry, time or, temperature. The previously reported Cs-MCM-41 materials only catalyze Michael reactions under much more drastic conditions (high concentrations, 24 h, 428 K).[26] In contrast, the present MCM-TBD catalyst requires 0.5–5 h at 293–353 K.

Ring formation to form **1** in the reaction of acrolein on DEM proves that the catalyst is also capable of performing the aldol condensation, which is the second stage in the

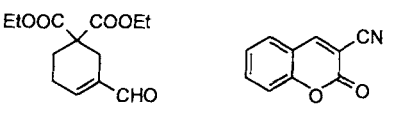

1 **2**

Robinson annulation. This was confirmed by reactions of indanedione or cyclohexan-1,3-dione with methyl vinyl ketone, in which both the primary adduct and the annulation product were obtained.

In most cases, the order of reactivity is as expected from electronic arguments. For acceptors in Michael additions the order is cyclopentenone ≈ cyclohexenone < acrylonitrile < ethyl acrylate ≈ methyl vinyl ketone < acrolein. However, anomalies are observed for the attempted formation of large Michael adducts with the MCM-TBD catalyst. This becomes most apparent when the MCM-TBD catalyst is compared with an amorphous silica on which TBD has been analogously

 © WILEY-VCH Verlag GmbH, D-69451 Weinheim, 1997 0570-0833/97/3623-2662 $ 17.50+.50/0

anchored (Table 1, entries 11 and 12). Differences in reactivity can therefore be traced directly back to the steric influence of the host structure. The MCM-TBD catalyst is more active for most reactions (e. g. methyl vinyl ketone + DEM, entries 2 and 12), which is presumably due to a higher surface loading of active groups. However, this activity order is reversed for the reaction of cyclohexenone and DEM (entries 10 and 11). The large size of the adduct and the reduced pore size in the modified MCM material suggest that this might be a case of transition state shape selectivity.

Whereas Michael reactions require a pronounced basicity, Knoevenagel condensations of aromatic aldehydes are a lot easier. With the MCM-TBD catalyst they proceed smoothly and even at room temperature (Table 2). The selectivity is excellent, usually over 90%, and in several cases yields approach 100%. In the reaction of salicylaldehyde and ECA, the 1,2-addition is followed by an intramolecular esterification, leading to 3-cyanocoumarin (**2**) in a 58% yield. The remarkable stability of the catalytic activity may well be due to the fact that the anchored TBD is a tertiary amine. This avoids the formation of Schiff bases, which is a major problem with the more familiar immobilized primary or secondary amines.[6]

Table 2. Knoevenagel condensations with MCM-TBD [a].

Donor	Acceptor	Yield [%] [b]
ethylcyano acetate	PhCHO	54
	PhCHO	41 [c]
	p-NO_2-PhCHO	95
	p-CH_3O-PhCHO	9
malononitrile	PhCHO	95
	p-NO_2-PhCHO	98
	p-CH_3O-PhCHO	48

[a] Conditions: 1 mmol of donor, 1 mmol of acceptor, 5 mg of catalyst, 2 mL of toluene, 1–2 h, 343 K, N_2 atmosphere. [b] Yields are based on the aldehyde. [c] 24 h, 293 K.

Even under the aqueous conditions of epoxidation with H_2O_2, the material still exhibits its basic properties. A heterogeneous catalyst for nucleophilic epoxidation of, for example, alkenones should selectively deprotonate H_2O_2, which is considerably more acidic than water. In case of MCM-TBD, the HOO^- anion forms a hydrophobic ion pair with the protonated catalyst. The lipophilicity of the MCM-TBD catalyst favors adsorption of the olefin substrate, which reacts via a 1,4-addition intermediate. While the yields for alkenals might be lowered by acetal formation, particularly alkenones are easily epoxidized with high selectivities (Table 3). Therefore, the use of the heterogeneous catalyst avoids the need for a liquid base and facilitates work-up of the product.

Our results prove that it is feasible to introduce strong, non-hydroxide basicity into a MCM-41 structure by the covalent bonding of the active centers on MCM carriers. The mechanical stability of the inorganic support materials ensures easy separation of the solid catalyst and the liquid phase, which is a serious problem for organic polymer supported catalysts.[5] The coupling procedure itself is highly convenient, and much more simple and general than an in situ synthesis approach.[7] Finally, the pool of available guanidine bases ensures optimum adaptability of the catalyst to specific reaction requirements.

Table 3. Epoxidations with MCM-TBD [a].

Substrate	TON	*S* [%]
methyl vinyl ketone	109	63 [b]
cyclopentenone	183	> 95
cyclohexenone	80	89
trans-2-hexenal	195	31 [c]

[a] Conditions: 1 mmol of substrate, 2 mmol of H_2O_2, 5 mg of catalyst, 1 mL of methanol, 273 K, 1–2 h. Turnover numbers TON were calculated as mole of product per mole of immobilized TBD. Selectivities *S* were calculated with respect to the enone or enal. [b] The remainder was the dimer of methyl vinyl ketone. [c] The remainder was the (hemi)acetal.

Experimental Section

Siliceous MCM-41 was obtained by the procedure of Beck et al. [10], and the residual template was removed by calcination. The vacuum-dried support (3 g) was allowed to react with trimethoxysilylpropoxymethyloxirane (4.5 mmol) in dry toluene at reflux for 24 h. IR spectroscopy shows that consumption of the surface silanol groups is almost complete. The glycidylated MCM-41 (1.0 g) was allowed to react with TBD (2.2 mmol) in toluene (15 mL) at 298 K for 10 h, and excess TBD was removed by lengthy soxhlet extraction with CH_2Cl_2. The resulting MCM-TBD catalyst was stored under vacuum. Thermogravimetric analysis provided a nitrogen content of 1.05 mmol per gram, which corresponds to 0.35 mmol of TBD per gram.

In a typical Michael addition the MCM-TBD catalyst (20 mg), the donor (1 mmol), CH_3CN (2 mL), and the acceptor (1 mmol) were placed successively in a Schlenk tube under nitrogen. The reaction was followed and quantified by gas chromatography, and products were identified with GC-MS and NMR spectroscopy.

Received: June 17, 1997 [Z10563IE]
German version: *Angew. Chem.* **1997**, *109*, 2776–2778

Keywords: basicity · C–C coupling · heterogeneous catalysis · MCM-41 · mesoporosity

[1] H. Hattori, *Chem. Rev.* **1995**, *95*, 537.
[2] a) A. Corma, R. M. Martin-Aranda, *J. Catal.* **1991**, *130*, 130; b) K. R. Kloetstra, H. van Bekkum, *J. Chem. Soc. Chem. Commun.* **1995**, 1005.
[3] M. J. Climent, A. Corma, V. Fornes, A. Frau, R. Guil-Lopez, S. Iborra, J. Primo, *J. Catal.* **1996**, *163*, 392.
[4] L. Martens, P. Grobet, P. A. Jacobs, *Nature* **1985**, *315*, 568.
[5] U. Schuchardt, R. M. Vargas, G. Gelbard, *J. Mol. Catal. A* **1996**, *109*, 37.
[6] A. Cauvel, G. Renard, D. Brunel, *J. Org. Chem.* **1997**, *62*, 749.
[7] R. Sercheli, A. Ferreira, M. Guerreiro, R. Vargas, R. Sheldon, U. Schuchardt, *Tetrahedron Lett.* **1997**, *38*, 1325.
[8] R. Schwesinger, J. Willaredt, H. Schlemper, M. Keller, D. Schmitt, H. Fritz, *Chem. Ber.* **1994**, *127*, 2435.
[9] Y. V. Subba Rao, D. E. De Vos, P. A. Jacobs, *Chem. Commun.* **1997**, 355.
[10] J. S. Beck, J. S. Vartuli, W. Roth, M. Leonowicz, C. Kresge, K. Schmitt, C. Chu, D. Olson, E. Sheppard, S. McCullen, J. Higgins, J. Schlenker, *J. Am. Chem. Soc.* **1992**, *114*, 10834.

 © WILEY-VCH Verlag GmbH, D-69451 Weinheim, 1997 0570-0833/97/3623-2663 $ 17.50+.50/0

Absorption/Electron Transfer/Absorption—An Efficient Pathway to Hydrated Electrons in Laser Flash Photolysis**

Valentin Zubarev and Martin Goez*

The solvated (hydrated) electron is a key intermediate in pulse radiolysis.[1] It can also be formed in laser flash photolysis by the absorption of a single photon[2] or, more frequently, by the successive absorption of two photons.[3] In all examples of the latter pathway reported so far, the intermediate that is ionized by the second photon has invariably been an excited state produced by absorption of the first photon. In this work, we present the first instances of photoionization by an absorption/electron transfer/absorption mechanism, that is, where the second photon is absorbed by a radical ion. As we will show, this pathway to hydrated electrons is quite efficient; moreover, it could be fairly common in laser flash photolysis and thus have consequences for mechanistic interpretations.

For detection we used Fourier Transform (FT) EPR spectroscopy.[4] Most of the investigations were carried out with the system anthraquinone-1,5-disulfonate/methionine (AS/Met). The experiments were performed in aqueous solution at pH $\approx$ 11, that is, well above pK_{a2} of the amino acid.[5]

Intersystem crossing of photoexcited ^{1}AS leads to the formation of a spin-polarized triplet state ^{3}AS,[6a] which is characterized by an electron spin relaxation time of 1 ns.[6b] From experiments with varying concentration of the amino acid, the rate constant for electron transfer quenching of ^{3}As by Met was estimated to be higher than 5×10^9 M^{-1}s^{-1}. Under our experimental conditions (typically, [Met] = 0.1 M) the life of ^{3}AS is thus decreased to well below 1 ns, and at least 30% of its spin polarization is transferred to the radical ions $AS^{\bullet-}$ and $Met^{\bullet+}$, which are the primary products of electron transfer quenching. Quinone concentrations below 5×10^{-4} M were chosen to avoid self-quenching of ^{3}AS and EPR line broadening due to spin-exchange, as well as to ensure homogeneous generation of the radicals (the optical density of the samples is smaller than 0.1 at the excitation wavelength of 308 nm). It was ascertained that the light is absorbed only by the quinone despite the disparately larger concentration of the quencher.

Figure 1 shows FT-EPR spectra of this system obtained at two different delay times between laser flash and acquisition pulse. The easily identifiable emission signal[6a] of the semiquinone radical anion $AS^{\bullet-}$ is found in all these measurements, whereas no signals of methionine-derived radicals are visible.[7] The most notable feature of the spectra in Figure 1 is the occurrence of an emissively polarized singlet EPR line. This peak is only observed at low quinone concentration ($\lesssim 5 \times 10^{-4}$ M); its intensity relative to the $AS^{\bullet-}$ signal increases with decreasing quinone concentration. Its g value of 2.00055 is indicative[3] of a hydrated electron. This assignment was rendered beyond doubt by experiments with

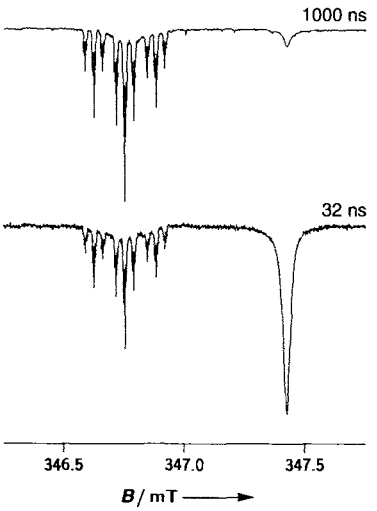

Figure 1. Spin-polarized FT-EPR signals (ν = 9.728 GHz) in the photoreaction of 1×10^{-4} M anthraquinone-1,5-disulfonate (AS) with 0.1 M methionine in H_2O at pH 11. Bottom trace: start of acquisition pulse 32 ns post flash, 100 transients; top trace: start 1000 ns post flash, 1000 transients. The intensities in both spectra are directly comparable. The multiplet is due to the semiquinone radical anion $AS^{\bullet-}$, the singlet to the hydrated electron e^-_{aq}.

the electron scavengers N_2O and $ClCH_2COO^-$, which do not undergo electron transfer with either ^{3}AS or $AS^{\bullet-}$. Saturation of the solution with N_2O completely suppressed the singlet EPR peak. The hydroxyl radical resulting from this scavenging process is unobservable owing to its fast reaction with Met.[9] When the photoreaction was carried out in the presence of 5×10^{-3} M of $ClCH_2COO^-$, the intensity of the emissive singlet was strongly reduced while the triplet of the $\cdot CH_2COO^-$ radical[10] appeared, also in emission. These experiments provide unequivocal evidence for the formation of the hydrated electron e^-_{aq} as an intermediate in the photoreaction of ^{3}AS with Met.

The FT-EPR signals of $AS^{\bullet-}$ and of e^-_{aq} exhibit an opposite time dependence (Fig. 1). From 32 ns post flash onwards (the shortest possible delay between the end of the laser flash and the start of the acquisition pulse with the spectrometer used), the polarization of e^-_{aq} decreases monotoneously to zero while the polarization of $AS^{\bullet-}$ increases by a comparable amount. By varying the reactant concentrations, it was established that these effects are due to the reaction of e^-_{aq} with ground state AS ($k \approx 2.5 \times 10^{10}$ M^{-1}s^{-1}),[11] which transfers emissive polarization from e^-_{aq} to $AS^{\bullet-}$; scavenging of e^-_{aq} by Met ($k < 1 \times 10^7$ M^{-1}s^{-1}),[12] and relaxation of e^-_{aq} ($T_1(e^-_{aq}) = 8$ μs)[3a] play only a secondary role under our experimental conditions.

The reaction of e^-_{aq} with AS provides the explanation why e^-_{aq} is not observed at quinone concentrations higher than about 5×10^{-4} M. First, in our experiments the linewidth of the e^-_{aq} singlet is determined by the chemical lifetime of this species. Hence, increasing the concentration of AS increases the linewidth of the e^-_{aq} signal and decreases its peak height proportionally. Second, the acquisition pulse (duration 48 ns) is not a δ-pulse (i.e., not infinitely short) on the timescale of the chemical decay. Sampling an exponentially decreasing magnetization with such a "long" pulse starting at a certain time after the laser flash is equivalent to sampling it with a δ-pulse that is delayed by an additional time τ;[14] under our experimental conditions, τ amounts to a constant 30 ns. Third, the rise time of the pulse (33 ns at a resonator frequency of 9.73 MHz and a Q value of 1000) acts like a further shift of the same magnitude.[14b] These delays cause a much stronger

[*] Prof. Dr. M. Goez, Dr. V. Zubarev
Fachbereich Chemie der Universität Halle-Wittenberg
Kurt-Mothes-Strasse 2, D-06120 Halle/Saale (Germany)
Fax: Int. code + (345) 55-27229
e-mail: goez@chemie.uni-halle.de

[**] Special gratitude is expressed to Dr. D. Beckert, Universität Leipzig, who generously provided measuring time on his EPR spectrometer and allowed us to use his software for processing the EPR spectra. V. Z. thanks Mrs. J. Geimer for training him on the spectrometer.

 © WILEY-VCH Verlag GmbH, D-69451 Weinheim, 1997 0570-0833/97/3623-2664 $ 17.50+.50/0

reduction of the e^-_{aq} signal with increasing quinone concentration than would be expected at the start of the observation pulse 32 ns post flash.

The polarization ratio $P(e^-_{aq})/P(AS^{\bullet-})$ depends on the intensity I_{exc} of the excitation light, a decrease of I_{exc} leading to a decrease of this ratio. After correction for the above-mentioned polarization transfer by the reaction of spin-polarized e^-_{aq} with ground-state AS, the relationship between I_{exc} and $P(e^-_{aq})/P(AS^{\bullet-})$ is approximately linear. This clearly shows that a second photon is involved in the production of e^-_{aq}. As virtually no EPR signals are observed in the absence of a quencher,[15] the hydrated electron must be generated by two successive monophotonic steps: first excitation of AS and then photoionization of an already spin-polarized intermediate.

$AS^{\bullet-}$ is the most likely candidate for this intermediate, photoionization of radical anions being a well-known process.[2a,b,16] It absorbs strongly at 308 nm ($\varepsilon \approx 1 \times 10^4\ M^{-1}cm^{-1}$).[18] The standard redox potential E^0 for the reaction (1) is calculated to be 2.27 V from E^0 for the half reactions (2) and (3)

$$AS^{\bullet} + nH_2O \rightleftharpoons AS + e^-_{aq} \quad (1)$$

$$e^-_{aq} \rightleftharpoons nH_2O + e \qquad E^0 = 2.77\ V\ [1] \quad (2)$$

$$AS + e^- \rightleftharpoons AS^{\bullet-} \qquad E^0 = -0.50\ V\ [17] \quad (3)$$

At 308 nm (i.e., 4.0 eV), photoionization of $AS^{\bullet-}$ is thus thermodynamically feasible.

An approximate expression for $P(e^-_{aq})/P(AS^{\bullet-})$ at the end of the laser pulse (duration $\tau_L = 20$ ns) can be derived by neglecting the secondary reaction of e^-_{aq} with AS. Assuming a rectangular laser pulse, the photoionization of $AS^{\bullet-}$ is described as a first-order process. This implies optically thin samples, which is fulfilled in our case. The corresponding rate constant k_{ion} is directly proportional to I_{exc}. Furthermore, the generation rate of $AS^{\bullet-}$ can be taken as constant because τ_L is much longer than the spin-polarized lifetime of excited ^3AS. For $P(e^-_{aq})/P(AS^{\bullet-})$ one obtains Equation (4) (cf. ref. [19]), the right-hand side of which is approximately equal to $k_{ion}\tau_L/2$, because in our experiments $k_{ion}\tau_L \lesssim 1$. This is in accordance with the experimentally observed dependence of $P(e^-_{aq})/P(AS^{\bullet-})$ on I_{exc}.

$$\frac{P(e^-_{aq})}{P(AS^{\bullet-})} = \frac{k_{ion}\tau_L}{1-\exp(-k_{ion}\tau_L)} - 1 \quad (4)$$

Hydrated electrons were also found in similar chemical systems. When ^3AS was quenched by triethylamine TEA ([TEA] = 0.03 M, pH = 9) instead of Met, the ratio $P(e^-_{aq})/P(AS^{\bullet-})$ at 32 ns post flash remained essentially the same. In this system, (emissive) polarizations were also observed for the quencher-based radicals $TEA^{\bullet+}$. Likewise, with SO_3^{2-} as quencher ($[SO_3^{2-}] = 0.1$ M, pH = 11) the three intermediates $AS^{\bullet-}$, $SO_3^{\bullet-}$, and e^-_{aq} were detected, all polarized in emission. Although in this case the yields of e^-_{aq} were rather low, which we ascribe to scavenging by an impurity (presumably hydrogen peroxide formed during preparation of the solutions), the intermediacy of much larger amounts of e^-_{aq} could be confirmed by adding the scavenger $ClCH_2COO^-$, which gave a strong signal of $\cdot CH_2COO^-$.

The all-emissive polarizations in the systems AS/TEA and AS/SO_3^{2-} show that the triplet mechanism is their only source. As no new polarizations are generated at the radical pair stage, the polarizations of e^-_{aq} and of $AS^{\bullet-}$ must thus be proportional to the respective concentrations, with identical constants of proportionality. Hence, it can be concluded from integration of the signals in Figure 1 that approximately equal amounts of e^-_{aq} and $AS^{\bullet-}$ are formed under the experimental conditions (maximum light intensity about 5×10^{16} photons per cm^2, which seems to be fairly representative for other laser flash photolysis experiments as well). The absorption/electron transfer/absorption pathway to e^-_{aq} is thus quite efficient. Despite this fact, it does not seem to have been observed before in laser flash photolysis, although reported routes to solvated electrons such as pulse radiolysis/absorption[2a] or chemical reduction/absorption[2b] bear resemblance to it.[19] The reasons why e^-_{aq} could be detected in the present work are, first, that its life was increased by the use of small sensitizer concentrations, and second, that a very specific detection method, EPR spectroscopy, was employed in its much more sensitive pulsed and FT variant.

It is expected that the described pathway to solvated (hydrated) electrons by two-photon ionization via radical ions is not confined to these few examples but is a general mechanistic possibility in photoinduced electron transfer reactions studied by laser flash photolysis, especially in strongly quenched samples. While e^-_{aq} might not be observable under normal experimental conditions—namely, higher sensitizer concentrations—because it is immediately scavenged, its intermediacy would nevertheless exert an influence on the quantum yields and, owing to its high reactivity, very likely also on product distributions and rate constants.

Received: May 23, 1997 [Z10468IE]
German version: *Angew. Chem.* **1997**, *109*, 2779–2781

Keywords: EPR spectroscopy · flash photolysis · photochemistry · radical ions · solvated electrons

[1] J. W. T. Spinks, R. J. Woods, *An Introduction to Radiation Chemistry*, 2nd ed., Wiley, New York, **1976**.

[2] See for instance, a) R. A. Holroyd, *J. Phys. Chem.* **1982**, *86*, 3541–3547; b) V. Rozenshtein, G. Zilber, H. Levanon, *ibid.* **1994**, *98*, 4236–4242; c) N. J. Turro, I. V. Khudyakov, H. van Willigen, *J. Am. Chem. Soc.* **1995**, *117*, 12273–12280; d) K. Nakagawa, A. Katsuki, S. Tero-Kubota, N. Tsuchihashi, T. Fujita, *ibid.* **1996**, *118*, 5778–5782.

[3] See for example: a) A. S. Jeevarajan, R. W. Fessenden, *J. Am. Chem. Soc.* **1992**, *96*, 1520–1523; b) N. Ishiwata, H. Murai, K. Kuwata, *J. Phys. Chem.* **1993**, *97*, 7129–7131; c) J. Säuberlich, D. Beckert, *ibid.* **1995**, *99*, 12520–12524; d) N. I. Avdievich, A. S. Jeevarajan, M. D. E. Forbes, *ibid.* **1996**, *100*, 5334–5342.

[4] The measurements were carried out with the laser flash photolysis/FT-EPR equipment described in ref. [3c].

[5] Solutions were deoxygenated with argon. High-quality Millipor water (18.2 $M\Omega\,cm^{-1}$) was used, and the pH was adjusted with KOH.

[6] a) D. Beckert, R. W. Fessenden, *J. Phys. Chem.* **1996**, *100*, 1622–1629; b) D. Beckert, G. Schneider, *Chem. Phys.* **1987**, *116*, 421–428.

[7] There are two likely reasons for the failure to detect these intermediates. On the one hand, their polarizations are distributed over several species: the initial open-chain, sulfur-centered radical cations **1** stabilize within nanoseconds or faster by formation of cyclic structures **2** with an intramolecular two-center, three-electron bond between sulfur and nitrogen, as well as of intermolecular adducts **3** with Met molecules [8, 9]; furthermore, fast deprotonation and decarboxylation of **2** (lifetime 220 ns) lead to α-thioalkyl and α-aminoalkyl radicals [9]. On the other hand, the line widths of these

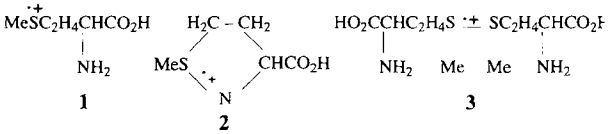

intermediates are expected to be much larger than those of $AS^{\bullet-}$ (3–5 μT), and their peak heights will thus be reduced proportionally.

[8] K. Bobrowski, G. L. Hug, B. Marciniak, H. Kozubek, *J. Phys. Chem.* **1994**, *98*, 537–544.

[9] K.-D. Asmus, M. Göbl, K.-O. Hiller, S. Mahling, J. Mönig, *J. Chem. Soc. Perkin Trans. 2* **1985**, 641–646.
[10] A. D. Trifunac, D. J. Nelson, *J. Am. Chem. Soc.* **1978**, *100*, 5244–5246.
[11] Pulse radiolysis experiments gave $k = 1.7 \times 10^{10}\ M^{-1}s^{-1}$ for this reaction (H. Pal, D. K. Palit, T. Mulherjee, J. P. Mittal, *Radiat. Phys. Chem.* **1991**, *37*, 227–235). We explain the difference by the higher ionic strength in our measurements.
[12] The rate constant in the literature ($k = 3.5 \times 10^7\ M^{-1}s^{-1}$ at pH 6.0) [13] is larger, because in our experiments Met is present in its deprotonated (anionic) form. For other amino acids, this deprotonation slowed down the reaction with e^-_{aq} by up to an order of magnitude [13].
[13] R. Braams, *Radiat. Res.* **1966**, *27*, 319–329.
[14] a) M. Goez, *Chem. Phys. Lett.* **1990**, *165*, 11–14; b) *J. Magn. Reson. A* **1996**, *123*, 161–167.
[15] Met alone or AS alone gave only minute EPR signals of e^-_{aq} (intensities lessthan 2% of those in the system AS/Met).
[16] M. A. Fox, *Chem. Rev.* **1979**, *79*, 253–273, and references therein.
[17] Value for anthraquinone (S. A. Carlson, D. M. Hercules, *Photochem. Photobiol.* **1973**, *17*, 123–131); the published spectrum of $AS^{\bullet-}$ in the range 360–490 nm [6a] is virtually identical.
[18] N. H. Furman, K. G. Stone, *J. Am. Chem. Soc.* **1948**, *70*, 3055–3061.
[19] Also related are two-photon processes in ketone photochemistry (absorption/fragmentation/absorption by the resulting radicals to give secondary fragmentation) under laser flash photolysis conditions; see, for example, F. Jent, H. Paul, H. Fischer, *Chem. Phys. Letters* **1988**, *146*, 315–319.

The Organic Chemistry of Coordination Compounds: Unprecedented Substitution Reactions of Functionalized Polypyridine Complexes

Dimitrios Tzalis and Yitzhak Tor*

The organic chemistry of coordination complexes is largely unexplored.[1] Despite a vast interest in utilizing polypyridine-containing coordination compounds for the study of energy and electron transfer, the construction of nanostructured materials, and the fabrication of molecular devices,[2] their full potential as synthetic building blocks remains unutilized. A better understanding of the effects of the coordinated metal ion on the reactivity and reaction pathways of the bound ligands should result in the prudent and targeted use of coordination compounds in various synthetic transformations.[3]

Early examples indicated that metal ion coordination can substantially alter aromatic electrophilic substitutions of coordinated phenanthrolines.[1,4] Much less is known, however, on nucleophilic substitution reactions of coordinated polypyridine ligands.[5,6] Nucleophilic displacements of 4-halopyridines have been found to be accelerated by metal coordination[1] and have been extended to Ru^{II}-coordinated 4,4′-dichloro-2,2′-bipyridines[7] and 4′-chloro-2,2′:6′,2″-terpyridines.[8] While the 4-position of an uncoordinated pyridine ring is inherently electrophilic, the 3-position is not.[9] Metal coordination might have been expected to sufficiently activate 3-halopyridines to enable nucleophilic substitutions. Yet, $[(bpy)_2Ru(3\text{-chloropyridine})_2]^{2+}$ (bpy = 2,2′-bipyridine) failed to react with a powerful nucleophile such as methanethiolate.[1]

We report here on the efficient nucleophilic substitution reactions of Ru^{II} and Os^{II} complexes of 3-bromo-1,10-phenanthroline. Reactions with fluoride, methoxide, and methanethiolate ions as representative nucleophiles provide novel coordination compounds of hitherto unknown phenanthroline derivatives. Under identical reaction conditions, the free ligand, 3-bromo-1,10-phenanthroline, completely fails to react. Our results illustrate an unprecedented reactivity of these polypyridyl complexes and establish the activating role of the coordinated metal ion. We demonstrate that these reactions proceed with retention of configuration at the metal center and discuss mechanistic implications.

The starting materials, $[(bpy)_2M(3\text{-bromo-1,10-phenanthroline})][PF_6]_2$ (**1a**, M = Ru; **1b**, M = Os) are conveniently prepared from $[(bpy)_2MCl_2]$ and 3-bromo-1,10-phenanthroline.[10] Treating these metal complexes with sodium methanethiolate in DMF (or methanol) at room temperature, sodium methoxide in methanol at 50°C, and anhydrous potassium fluoride in DMF at 130°C readily provided the substitution products **2a,b**, **3a,b**, and **4a,b**, respectively (Scheme 1).[11] The free 3-bromo-1,10-phenanthroline is unsusceptible to these nucleophiles even under forcing conditions. Effort has been invested to confirm the identity of the substitution products in order to exclude the possible formation of isomeric complexes. The one- and two-dimensional ^1H NMR spectra of **2a,b** and **3a,b** confirm the expected *meta*-substitution pattern, showing a typical 1,3 long-range coupling ($J \approx 1.5$ Hz) for H2 and H4 of the phenanthroline ligand. The proton-coupled ^{19}F NMR spectrum of **4a,b** shows a doublet of doublets at $\delta = -65$ ($^3J = 8.5$ and 8.0 Hz) verifying the presence of a 3-fluoro substituent.[12]

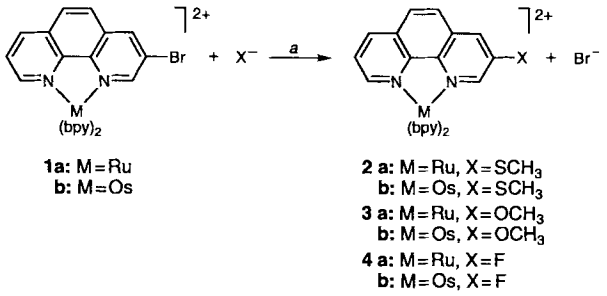

1a: M = Ru
b: M = Os

2 a: M = Ru, X = SCH_3
b: M = Os, X = SCH_3
3 a: M = Ru, X = OCH_3
b: M = Os, X = OCH_3
4 a: M = Ru, X = F
b: M = Os, X = F

Scheme 1. Displacement reactions of metal-coordinated 3-bromo-1,10-phenanthroline. a) Reaction conditions: for **2**: $NaSCH_3$ in DMF (or methanol) at room temperature (2–18 h); for **3**: $NaOCH_3$ in methanol, 50°C (2–6 h); for **4**: anhydrous KF in DMF, 130°C (6–24 h).

To investigate whether the coordinated metal ion is directly involved in these substitution reactions, the enantiomerically pure Λ-**1a** was treated with the same nucleophiles.[13] The CD spectrum of the product **3a** shows the expected minor shifts in the Cotton effects and $\Delta\varepsilon$ values very similar to those in the spectrum of the starting material Λ-**1a** (Figure 1).[14] These observations confirm the retention of configuration at the metal center. Following the course of the reactions by ^1H NMR spectroscopy showed a clean conversion of the starting material into the product. Taken together, these results exclude the possible interruption of the octahedral coordination geometry and the formation of associative intermediates as a major reaction pathway. To facilitate a nucleophilic attack at the unreactive 3-bromo-1,10-phenanthroline ring system, the coordinated metal ion has to alter the electronic properties of the ligand.

Two major mechanisms may be operative in these nucleophilic displacement reactions: the elimination–addition pathway (EA) or the addition–elimination pathway

[*] Prof. Dr. Y. Tor, D. Tzalis
Department of Chemistry and Biochemistry
University of California at San Diego
La Jolla, CA 92093-0358 (USA)
Fax: Int. code + (619) 534-5383
e-mail: ytor@ucsd.edu

 © WILEY-VCH Verlag GmbH, D-69451 Weinheim, 1997 0570-0833/97/3623-2666 $ 17.50+.50/0

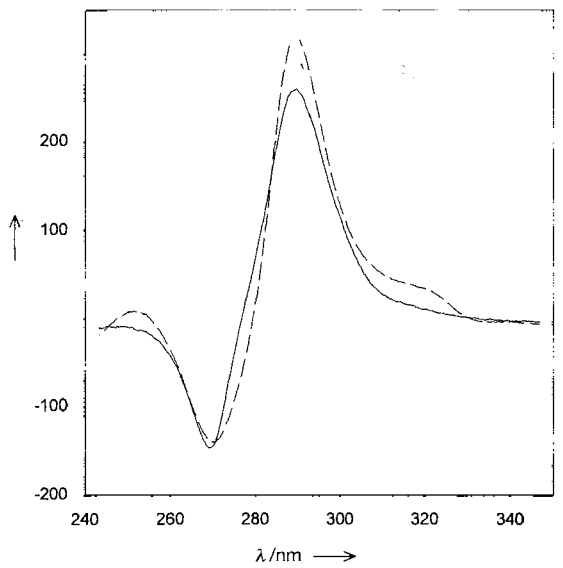

Figure 1. CD spectra of Λ-**1a** (solid line) and the displacement product (dashed line) obtained with sodium methoxide showing that the product has the same absolute configuration (i.e. Λ-**3a**). Spectra were recorded in acetonitrile.

(AE).[15] The EA mechanism should involve the highly reactive (and previously unobserved) metal-coordinated dehydrophenanthroline intermediate and might lead to the formation of *cine*-substitution products. While our data cannot unequivocally exclude the EA pathway in the highly basic KF/DMF and NaOMe/MeOH media at elevated temperatures, the exclusive formation of *ipso*-substitution products and the efficient reactions observed under very mild conditions with the soft and weakly basic CH_3S^- ion strongly support the AE mechanism.

How can metal coordination facilitate the nucleophilic addition to the funtionalized phenanthroline? Metal coordination is expected to decrease the electron density on the heterocyclic ligand by induction through the σ framework, making it more susceptible to nucleophilic attack, while π backbonding may diminish this polarization.[16] In general, this metal-induced polarization enhances the reactivity at positions 2 and 4 to the nitrogen in the electron-deficient pyridines, leaving the 3-position largely unaffected.[1,9] How can the high reactivity of the complexed 3-bromo-1,10-phenanthroline then be explained? We propose to view the complexed phenanthroline ring as composed of two components: 1) the reacting ring bearing N1 and the 3-bromo substituent, and 2) the activating unsubstituted ring bearing N10 (Scheme 2). A nucleophilic attack at the *ipso* position of substrate **A** would generate the "classical" addition intermediate **B**. This "anionic" σ-complex is stabilized by delocalization of the additional charge over the neighboring ring as well as the metal ion. As shown in **C** and **D**, this delocalization is facilitated by an electron-withdrawing group, the metal-coordinated N10 pyridine ring, at position 1a, which is *para* to the attacked *ipso* position. Elimination of bromide provides the substitution product **E**.

In many respects the efficient displacement reactions observed with the soft MeS^- ion have striking similarities to typical S_NAr substitution reactions of highly electron-deficient aromatic compounds (e.g. 2,4-dinitrohalobenzenes).[17] Specifically, the reaction of the fluoro-containing complex $[(bpy)_2Ru(3\text{-fluoro-}1,10\text{-phenanthroline})][PF_6]_2$ **4a** with sodium methanethiolate in methanol was found to proceed at least ten times faster than the corresponding reactions of the bromo-containing complex **1a**.[18] In addition, the reaction of the Os^{II}-containing complex **1b** with sodium methanethiolate was found to be four times slower than the corresponding reaction of the Ru^{II}-containing complex **1a**.[19] These observations suggest that the substitution reactions are subject to both Coulombic and frontier orbital controls.[20] Assuming that the elimination step is not rate-determining, the higher reactivity of the fluoro vs. the bromo derivative is consistent with a Coulombic contribution to rate enhancement. Furthermore, better π backbonding of Os^{II} relative to that of Ru^{II} is expected to increase the electron density of the complexed phenanthroline's LUMO, decreasing its interaction with the nucleophile's HOMO, thus leading to a slower reaction as observed.

We have established a novel and powerful approach for the efficient modification of coordination compounds at a position previously assumed to be unreactive. We have demonstrated, for the first time, that metal coordination activates the position *meta* to the nitrogen atom in 1,10-phenanthroline, leading to efficient nucleophilic substitutions. This unprecedented reactivity is attributed to the increased electrophilicity of the complexed ring upon metal coordination and the effective resonance stabilization of the "anionic" addition intermediate. This simple methodology opens new routes for the fabrication of previously inaccessible complexes and provides insight into the organic chemistry of coordination compounds.

Experimental Section

All reactions were carried out in the dark under Ar atmosphere, using anhydrous solvents and salts. All complexes were isolated as their PF_6^- salts. A representative procedure and spectroscopic data: **2a**: A mixture of **1a** (23.6 mg, 2.45×10^{-5} mol) and sodium methanethiolate (7.2 mg, 1.04×10^{-4} mol) was stirred in DMF (5 mL) at room temperature for 18 h. The crude reaction mixture was evaporated to dryness. The orange solid obtained was suspended in 3 mL water and filtered to yield 19.3 mg (85% yield) of the pure product **2a**. ESI/MS: *m/z*: 785.2 [M^+]; UV/Vis (CH_3CN): λ_{max} (ε) = 246 (4.4×10^4), 286 ($7.6 \times$

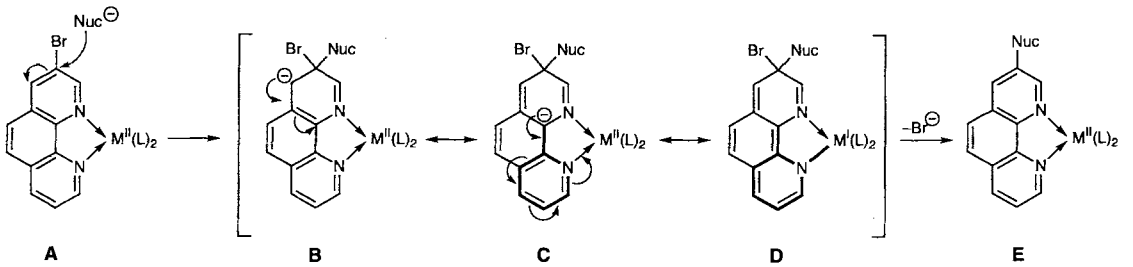

Scheme 2. The proposed mechanism for the nucleophilic substitution reactions of metal-coordinated 3-bromo-1,10-phenanthroline. The novel electron-withdrawing group, the metal-coordinated N10 pyridine ring, which is *para* to the attacked *ipso* position, is in bold.

10^4), 344 (2.0×10^4), 448 nm (1.5×10^4); ^{1}H NMR (500 MHz, CD_3CN): $\delta = 8.57$ (d, 1H), 8.51 (m, 4H), 8.37 (d, 1H), 8.20 (d, 1H), 8.13 (d, 1H), 8.10 (m, 2H), 8.00 (m, 3H), 7.85 (d, 1H), 7.80 (m, 2H), 7.67 (dd, 1H), 7.63 (d, 1H), 7.53 (d, 1H), 7.44 (t, 2H), 7.24 (m, 2H); ^{13}C NMR (125 MHz, CD_3CN): $\delta = 158.24$, 158.23, 157.98, 157.84, 153.33, 153.16, 153.07, 152.86, 152.78, 150.37, 148.57, 145.08, 141.38, 138.63, 138.45, 137.69, 131.74, 131.71, 131.12, 129.61, 128.42, 128.36, 128.31, 128.22, 128.15, 126.35, 125.22, 125.15, 125.11, 125.02, 14.80.

Received: May 30, 1997 [Z10498IE]
German version: *Angew. Chem.* **1997**, *109*, 2781–2783

Keywords: N ligands · nucleophilic aromatic substitutions · osmium · reaction mechanisms · ruthenium

[1] E. C. Constable, *Metals and Ligand Reactivity, An Introduction to the Organic Chemistry of Metal Complexes*, VCH, Weinheim, **1996**.
[2] A. Juris, V. Balzani, F. Barigelletti, S. Campagna, P. Belser, A. Von Zelewsky, *Coord. Chem. Rev.* **1988**, *84*, 85–277; J.-P. Sauvage, J.-P. Collin, J.-C. Chambron, S. Guillerez, C. Coudret, V. Balzani, F. Barigelletti, L. De Cola, L. Flamigni, *Chem. Rev.* **1994**, *94*, 993–1019; V. Balzani, A. Credi, F. Scandola, *Transition Metals in Supramolecular Chemistry* (Eds.: L. Fabbrizzi, A. Poggi), Kluwer, Dodrecht, **1994**, pp. 1–32; V. Balzani, A. Juris, M. Venturi, S. Campagna, S. Serroni, *Chem. Rev.* **1996**, *96*, 659–833, and references therein.
[3] For early reviews, see: R. D. Gillard, *Coord. Chem. Rev.* **1975**, *16*, 67–94; H. Taube, *Pure Appl. Chem.* **1979**, *51*, 901–912; N. Serpone, G. Ponterini, M. A. Jameson, F. Bolletta, M. Maestri, *Coord. Chem. Rev.* **1983**, *50*, 209–302; A. Blackman, *Adv. Heterocycl. Chem.* **1993**, *58*, 123–170.
[4] A. F. Richard, J. H. Ridd, M. L. Tobe, *Chem. Ind.* **1963**, 1727; R. D. Gillard, R. E. E. Hill, R. Maskill, *J. Chem. Soc. A* **1970**, 1447–1451; M. M. Jones, *Ligand Reactivity and Catalysis*, Academic Press, New York, **1968**.
[5] For an early review, see: E. C. Constable, *Polyhedron* **1983**, *2*, 551–572.
[6] K. Jackson, J. H. Ridd, M. L. Tobe, *J. Chem. Soc. Perkin. Trans. 2* **1979**, 611–617.
[7] E. C. Constable, *Inorg. Chim. Acta.* **1984**, *82*, 53–57; E. C. Constable, T. A. Leese, *ibid*, **1988**, *146*, 55–58.
[8] E. C. Constable, A. M. W. Cargill Thompson, P. Harveson, L. Macko, M. Zehnder, *Chem. Eur. J.* **1995**, *1*, 360–367.
[9] E. C. Constable, *Inorg. Chim. Acta* **1986**, *117*, L33–L34. See also: E. C. Constable, D. Phillips, *Chem. Commun.* **1997**, 827–828.
[10] D. Tzalis, Y. Tor, *Chem. Commun.* **1996**, 1043–1044; D. Tzalis, Y. Tor, S. Failla, J. S. Siegel, *Tetrahedron Lett.* **1995**, *36*, 3489–3490.
[11] The displacement reactions proceed in very good yields (83–95%). In most cases the products can be isolated in pure form by a simple precipitation or crystallization from acetonitrile/water.
[12] The ^{19}F NMR chemical shift is reported with reference to the PF_6^- internal standard.
[13] For the preparation of the enantiomerically pure Λ-**1a**, see: D. Tzalis, Y. Tor, *J. Am. Chem. Soc.* **1997**, *119*, 852–853.
[14] All other nucleophiles yielded enantiomerically pure products when reacted with Λ-**1a**.
[15] Another mechanism that can, in principle, be considered is the $S_{RN}1$ mechanism with free radicals.
[16] P. A. Lay, *Inorg. Chem.* **1984**, *23*, 4775–4777.
[17] J. Miller, *Aromatic Nucleophilic Substitutions*, Elsevier, New York, **1968**.
[18] At 2.5 mM in CD_3OD at 25°C, the reaction of **4a** and ten equivalents of sodium methanethiolate is complete within two minutes (estimated $t_{1/2} \leq 60$ s). In contrast, the half-life of the reaction of **1a** under the same conditions is 1×10^3 s.
[19] The pseudo-first-order rate constants were determined by ^{1}H NMR spectroscopy (at 25°C) by treating a 2.5 mM solution of the starting materials in CD_3OD with a tenfold molar excess of sodium methanethiolate. The rate constant for **1a**: 6.8×10^{-4} s^{-1}; for **1b**: 1.8×10^{-4} s^{-1}.
[20] I. Fleming, *Frontier Orbitals and Organic Chemical Reactions*, Wiley, New York, **1976**, pp. 66–69.

The Linking of Two Acetylide Units through a Plane of Four Iron Atoms**

John E. Davies, Martin J. Mays,* Paul R. Raithby, and Koshala Sarveswaran

There has been considerable interest in the nature of the bonding within octahedral organometallic clusters of the type *trans*-$E_2(ML_n)_4$, where M is a transition metal and E is a main group atom or conical fragment such as BH, CR, GeR, NR, PR, S, or Se.[1–4] A notable feature of the structures is that the E···E separation is short, and often lies in a range only 12–25% longer than that corresponding to a single E–E bond. Thus, for example, in $[Co_4(\mu_4\text{-}PPh)_2(\mu_2\text{-}CO)_2(CO)_8]$[5] the P···P distance of 2.537(6) Å is only 0.3 Å greater than an accepted P–P single bond length,[6] and in $[Co_5(CO)_{13}(\mu\text{-}CO)B_2H]$, which contains a Co_4B_2 core,[7] the B–B distance of 1.85 (4) Å is within the range observed for polyhedral boranes with B–B bonding.[8] These short distances have been attributed to an attractive direct E···E interaction, although the need to optimize M–M and M–E distances is also acknowledged to be an important factor.[1,5]

We now report the synthesis of **1** by thermolysis of $[Fe_2(CO)_6(\mu_2\text{-}\eta^2\text{-}C{\equiv}CPh)(\mu\text{-}PPh_2)]$ in toluene at 100°C. An

$[Fe(\mu_4\text{-}PPh_2)_2(\mu_4\text{-}\eta^2\text{-}C{\equiv}CPh)_2(CO)_8]$ **1**

X-ray crystallographic study of **1**[9] shows that the C–C separation of the two μ_4-C atoms across the Fe_4 plane is only 1.610(8) Å, less than 5% longer than a normal C–C single bond (Figure 1).

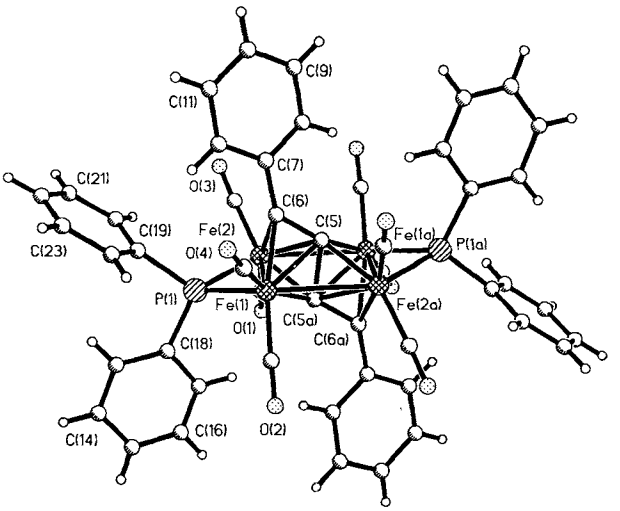

Figure 1. Molecular structure of **1**. Selected bond lengths [Å] and angles [°]: Fe(1)–C(6) 2.011(4), Fe(1)–C(5) 2.143(4), Fe(1)–Fe(2) 2.5334(9), Fe(2)–C(5A) 1.993(4), Fe(2)–C(5) 2.154(4), Fe(1)–Fe(1A) 2.8722(9), C(5)–C(5A) 1.610(8), C(5)–Fe(1A), 2.014(4), Fe(1)–C(5A) 2.014(4), Fe(1)–P(1) 2.2045(13), Fe(1)–Fe(2A) 2.8721(9), Fe(2)–C(6) 2.044(4), Fe(2)–P(1) 2.2037(13), C(5)–Fe(2A) 1.993(4), C(5)–C(6) 1.388(5); Fe(1)-Fe(2)-Fe(1A) 90.14(3), Fe(2)-P(1)-Fe(1) 70.16(4), Fe(2A)-C(5)-Fe(1A) 78.4(2), Fe(2A)-C(2)-Fe(1A) 87.9(2), Fe(1A)-C(5)-Fe(2) 87.1(2), Fe(1)-C(5)-Fe(2) 72.26(12), Fe(2)-Fe(1)-Fe(2A) 89.86(3).

[*] Dr. M. J. Mays, Dr. J. E. Davies, Dr. P. R. Raithby, K. Sarveswaran
Department of Chemistry
Lensfield Road
Cambridge CB2 1EW (UK)
Fax: Int. code + (1223) 336-362
e-mail: mjm14@cam.ac.uk

[**] We thank the Cambridge Commonwealth Trust and Professor B. F. G. Johnson for financial support (for K. S.).

 © WILEY-VCH Verlag GmbH, D-69451 Weinheim, 1997 0570-0833/97/3623-2668 $ 17.50+.50/0

The molecule is centrosymmetric and the four iron atoms form a rectangle. Each iron atom is terminally coordinated by two carbonyl groups. The opposing Fe–Fe edges bridged by the PR_2 groups are shorter (2.5534(9) Å) than the unbridged edges (2.8722(9) Å). The μ_4-η^2 acetylide ligands on each Fe_4 face are orientated *trans* to each other such that the C-Ph carbon atoms symmetrically bridge the two Fe–Fe edges, which are also bridged by the PPh_2 groups. The μ_4-C atoms and the four iron atoms may be regarded as a distorted octahedron that is face-capped by the two CPh groups on opposing faces. Viewed in this way the cluster has a polyhedral electron count of 68, with eight skeletal electron pairs rather than the seven required for conformity with Wade–Mingos rules.[10]

The short C–C distance across the Fe_4 plane must result in part from the need to optimize the Fe–Fe and Fe–C bond lengths. Such optimization in the related octahedral cluster $[Ru_5(CO)_{13}(\mu_4\text{-}\eta^2\text{-}C{\equiv}CPh)(\mu\text{-}PPh_2)]$ with an octahedral Ru_5C core results in the μ_4-C atom being only 0.841 Å above the Ru_4 plane that is capped on the other face by the fifth Ru atom.[11] There must, however, also be a direct interaction across the Fe_4 plane in **1** between orbitals on the two carbon atoms completing the distorted octahedral core; MO calculations on related μ_4-P and μ_4-B species suggest that this interaction is likely to be bonding in character.[1–5] Accordingly the two acetylide ligands in **1** can be regarded as being coupled together to form a ten-electron donor diyne ligand, which is threaded through and bonded to the Fe_4 plane. Similar coupling of two acetylide ligands on a Ru_4 butterfly framework in the complex **2** has recently been reported, but

$[Ru_4(CO)_8(C_4tBu_2)(\mu\text{-}PPh_2)_2]$ **2**

the resulting diyne ligand was bonded to one face only of the butterfly as shown in Scheme 1.[12] Complex **2** has the same

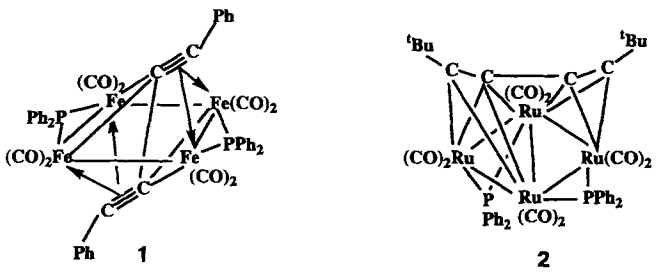

Scheme 1. Line drawings of the structures of **1** and **2**.

polyhedral electron count as **1** but there is an extra metal–metal bond and the diyne ligand acts as an eight- rather than a ten-electron donor to the metal framework.

The C–C distances within the C_4 diyne unit of **1** are 1.388(5) (outer) and 1.610(8) Å (inner); the corresponding distances in **2** are 1.332(7), 1.321(7) (outer) and 1.366(7) Å (inner). The fact that the inner, formally single, C–C bond in **1** is longer than that in **2** can be rationalized as being due to the need to accommodate the Fe_4 ring around the C–C axis. On the other hand the coupling of two acetylide ligands in dinuclear titanium and zirconium complexes to give C–C bonds longer than that in **1** is well known.[13] Long single C–C bonds have also been reported in a range of other molecules and have been the subject of theoretical investigations.[14]

The reactivity of **1** and the possibility of synthesizing related polycarbon ligands threaded through metal atom frameworks are under investigation.

Experimental Section

1: A stirred solution of $[Fe_2(CO)_6(\mu_2\text{-}\eta^2\text{-}C{\equiv}CPh)(\mu\text{-}PPh_2)]$ (0.80 g, 1.41 mmol) in toluene (50 mL) was heated at 100 °C for 24 h. The solvent was then removed on a rotary evaporator, the residue taken up in the minimum amount of CH_2Cl_2 and adsorbed onto silica. The silica was pumped dry and added to the top of a silica chromatography column. Elution with *n*-hexane/CH_2Cl_2 (4/1) and removal of solvent gave **1** as a brown powder (0.35 g, 21 %). Crystals suitable for the X-ray analysis were grown by slow evaporation of a 1/1 *n*-hexane/CH_2Cl_2 solution of the complex. Selected spectroscopic data for **1**: IR (CH_2Cl_2 solution) major bands: $\tilde{\nu}_{CO}$ = 2003 vs, 1976 s cm^{-1}; ^1H NMR (400.16 MHz, 25 °C, $CDCl_3$, $SiMe_4$): δ = 8.16(m, 3H; aryl C-H), 7.62(m, 6H; aryl C-H), 7.33(m, 3H; aryl C-H), 7.20(m, 3H; aryl C-H), 7.03(m, 6H; aryl C-H), 6.88(m, 3H; aryl C-H), 6.65(m, 6H; aryl C-H); ^{31}P NMR (162.000 MHz, 25 °C, $CDCl_3$, relative to $P(OMe)_3$ with upfield shifts negative): δ = 95.5 (μ-PPh_2); ^{13}C NMR (100.614 MHz, 20 °C, $CDCl_3$): δ = 212.4(s; FeCO), 211.0 (s; FeCO), 143.2 (d, $^2J(^{31}P^{13}C)$ = 22.4 Hz; -*C*CPh), 135.7–127.5 (m, 36C; aryl-C), 95.6 (s, 1C; C*C*Ph); MS (FAB): *m/z*: 1020 (M^+).

Received: May 28, 1997 [Z10485IE]
German version: *Angew. Chem.* **1997**, *109*, 2784–2785

Keywords: alkynes · C–C coupling · clusters · iron

[1] J.-F. Halet, R. Hoffmann, J.-Y. Saillard, *Inorg. Chem.* **1985**, *24*, 1695–1700.
[2] J.-F. Halet, J.-Y. Saillard, *New J. Chem.*, **1987**, *11*, 315-320.
[3] T. A. Albright, K. A. Yee, J.-Y. Saillard, S. Kahlal, J.-F. Halet, J. S. Leigh, K. H. Whitmire, *Inorg. Chem.* **1991**, *30*, 1179–1190.
[4] S. Kahlal, J. -F. Halet, J. -Y. Saillard, *Inorg. Chem.* **1991**, *30*, 2567–2569.
[5] R. C. Ryan, C. U. Pittman, Jr., J. P. O' Connor, L. F. Dahl, *J. Organomet. Chem.* **1980**, *193*, 247–269; R. C. Ryan, L. F. Dahl, *J.Am. Chem. Soc.* **1975**, *98*, 6904–6906.
[6] D. E. C. Corbridge in *Topics in Phosphorus Chemistry*, **1966**,*Vol.5* (Eds.: E. J. Griffith, M. Grayson), Interscience, New York, **1966**, pp. 57–394.
[7] C. S. Jun, T. P. Fehlner, A. L. Rheingold, *J. Am. Chem. Soc.* **1993**,*115*, 4393–4394; C. S. Jun, J.- F. Halet, A. L. Rheingold, T. P. Fehlner, *Inorg. Chem.* **1995**, *34*, 2101–2107.
[8] K. Wade, *Adv. Inorg. Chem. Radiochem.* **1976**, *18*, 1–66.
[9] Crystal data: **1**: $C_{48}H_{30}Fe_4O_8P_2$, M_r = 1020.06, triclinic, space group $P\bar{1}$ (no. 2), a = 11.3260(10), b = 12.173(2), c = 9.4010(10) Å, α = 101.68(2), β = 114.340(10), γ = 104.160(10)°, V = 1075.5(2) Å^3 (by least-squares refinement on diffractometer angles from 25 centered reflections, $30 < 2\theta < 40°$), T = 293 K, graphite-monochromated $Mo_{K\alpha}$ radiation, λ = 0.71073 Å, Z = 1, ρ_{calcd} = 1.575 Mg m^{-3}, $F(000)$ = 516, dark brown block, 0.30 × 0.20 × 0.18 mm, $\mu(Mo_{K\alpha})$ = 1.452 mm^{-1}, semi-empirical absorption correction based on φ scans, relative transmission 0.908–1.000, Rigaku AFC5R diffractometer, ω-2θ scans, data collection range $5.06 < 2\theta < 50.0°$, $+h$, $\pm k$, $\pm l$; three standard reflections showed no significant variation in intensity, 4006 reflections measured, 3796 unique (R_{int} = 0.034) used in all calculations. Solution by direct methods (SHELXTL PLUS) [15] and subsequent Fourier syntheses, anisotropic full- matrix least-squares refinement on F^2 (SHELXL93) [16], hydrogen atoms included by using a riding model. Final $wR(F^2)$ = 0.1855 on all data, conventional $R(F)$ = 0.0391 for 2632 observed reflections [$I > 2\sigma(I)$], weighting scheme $w = 1/[\sigma^2(F_o^2) + (0.0261P)^2 + 1.277P]$, where $P = (F_o^2 + 2F_c^2)/3$, 280 parameters, GOF = 1.012, maximum Δ/σ = 0.001, maximum $\Delta\rho$ = 0.366, minimum −0.413 e Å^{-3}. Crystallographic data (excluding structure factors) for the structure reported in this paper have been deposited with the Cambridge Crystallographic Data Centre (CCDC) as supplementary publication number CCDC-100483. Copies of the data can be obtained free of charge on application to The Director of the Cambridge Crystallographic Data Centre, 12 Union Road, Cambridge CB2 1EZ (UK) (fax: Int. code + (1223) 336033; e-mail: deposit@chemcrys.cam.ac.uk).
[10] D. M. P. Mingos, *Acc. Chem. Res.* **1984**, *17*, 311–319.
[11] S. A. Maclaughlin, N. J. Taylor, A. J. Carty, *Organometallics* **1983**, *2*, 1194–1202.
[12] Y. Chi, A. J. Carty, P. Blenkiron, E. Delgado, G. D. Enright, W. Wang, S-M. Peng, G-H. Lee, *Organometallics* **1996**, *15*, 5269–5271.
[13] E. D. Jemmis and K. T. Giju, Angew. Chem. **1997**, *109*, 633–635; *Angew. Chem. Int. Ed. Engl.* **1997**, *36*, 606–608 and references therein.
[14] G. Kaupp, J. Boy, *Angew. Chem.* **1997**, *109*, 48-50; *Angew. Chem. Int. Engl.* **1997**, *36*, 48–49 and references therein.
[15] G. M. Sheldrick, SHELXL PLUS, Siemens Analytical Instruments, Madison, WI, **1990**.
[16] G. M. Sheldrick, SHELXL93, University of Göttingen, **1993**.

 © WILEY-VCH Verlag GmbH, D-69451 Weinheim, 1997 0570-0833/97/3623-2669 $ 17.50+.50/0

Enantioselective Diels–Alder Cycloaddition by Preorganization on a Chiral Lewis Acid Template**

Hugues Bienaymé*

In memory of Wolfgang Oppolzer

Recent years have witnessed impressive advances in catalytic asymmetric [4+2]cycloadditions.[1] But tailoring an efficient chiral catalyst designed for a specific transformation is by no means an easy task: several parameters, such as the reactive conformation of the dienophile (s-*cis* or s-*trans*), the basic lone pair of the carbonyl to be coordinated, the degree of freedom, and the bonding mode of the Lewis acid/carbonyl complex,[2] just to mention a few, need to be carefully controlled. As a consequence of a potentially great number of thermally accessible reactive conformers, catalysts for enantioselective cycloadditions are always time-consuming to develop and often very substrate specific. Herein we disclose our preliminary results on "internally promoted" asymmetric Diels–Alder cycloadditions in connection with the synthesis of the potent, non-peptidic, NK1-selective, substance P antagonist RPR 107880.[3]

Preliminary work from our laboratory shows that dienes covalently connected to a Lewis acid, for example dimethylaluminum dienolates, are able to undergo extremely rapid and (regio/stereo)selective [4+2]cycloadditions with various dienophiles.[4] By virtue of their rigid bicyclic [6.6] transition states, these entropically favored cycloadditions were thought to overcome most of the impediments commonly associated with the design of an efficient chiral catalyst.

As depicted in Scheme 1, our plan for the industrial synthesis of RPR 107880 relies on a ligand-controlled asymmetric Diels–Alder cycloaddition between *N*-benzylmaleimide (NBM) and a chiral prenal enolate at an early stage. The *endo*-(3a*R*,4*S*,7a*R*) perhydroisoindole cycloadduct could then be easily manipulated by conventional chemistry to yield the target compound, (3a*S*,4*S*,6*R*,7a*R*)-4-(2-methoxyphenyl)-2-[(*S*)-2-(2-methoxyphenyl)propionyl]-6-methyl-perhydroisoindol-4-ol. Only the first key step of this synthesis will be reported here.

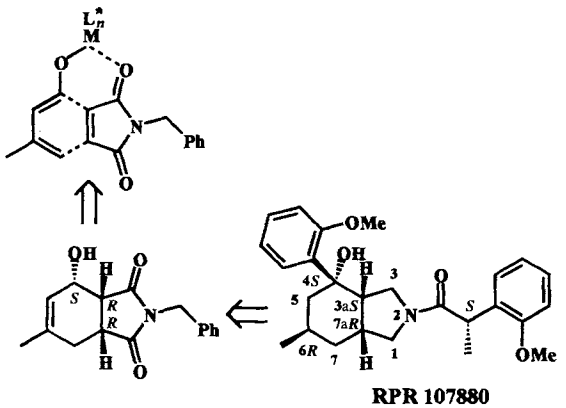

Scheme 1. Retrosynthesis of RPR 107880.

Titanium was identified as the best potential catalyst on the following considerations: a) Titanium dienolates can be prepared easily from available 1-acetoxybutadienes by an alkoxide transesterification reaction.[5] b) Chiral titanium alkoxide species are easily prepared by mixing chiral diols and titanium tetraalkoxides.[12b] c) Most of the chiral diol ligands known are reasonably accessible (derived from the natural pool or by short syntheses). d) Catalytic asymmetric cycloaddition is theoretically possible if the ligand exchange reaction is fast enough. e) Titanium tetraalkoxides are nontoxic, cheap, and nonpyrophoric.

To clarify the major kinetic parameters the nonasymmetric cycloaddition between 1-acetoxyisoprene and *N*-benzylmaleimide was first studied with titanium tetraisopropylate as the promoter (Scheme 2, Table 1). Two *endo* cycloadducts were isolated: alcohol *rac*-**1a** resulting from the expected titanium-catalyzed transesterification/cycloaddition process, and acetate *rac*-**2** from the thermal (or externally catalyzed) process. The product ratios varied with the amount of $Ti(OiPr)_4$ used; however, with a stoichiometric amount of $Ti(OiPr)_4$ the transesterification reaction (which is expected to be the rate-limiting step[4] in the process leading to *rac*-**1a**) was quite competitive with the easy thermal cycloaddition (entry 1). A marked temperature dependance was also noted: when 1.2 equiv $Ti(OiPr)_4$ was employed but the reaction was conducted at 0°C instead of 25°C, *rac*-**2** was formed as the major compound (240 min, *rac*-**2**/*rac*-**1a** $\approx$ 80/20). This is likely due to the occurrence of unreactive $Ti(OiPr)_4$ oligomers at lower temperatures.[6] Under these reaction conditions **1a** was not acylated to **2** or vice versa (however, on prolonged reaction time or heating at 60°C, **2** was partly transesterified to **1a**).

Various homochiral diols were then evaluated. Among commonly used ligands (+)-diisopropyltartrate and (+)-1,1-binaphthol either completely inhibited or slowed down the transesterification reaction, resulting in the formation of **2** as the exclusive or major product. The $\alpha,\alpha,\alpha',\alpha'$-tetraaryl-1,3-dioxolane-4,5-dimethanol (TADDOL)[7] ligands gave better results. They led to an overall substantial kinetic enhancement and a useful level of enantiocontrol (Table 1, entries 2–11). In a first set of experiments the isopropyl alcohol generated upon mixing $Ti(OiPr)_4$ and (−)-TADDOL ((*R*,*R*)-$\alpha,\alpha,\alpha',\alpha'$-tetraphenyl-1,3-dioxolane-4,5-dimethanol) was removed by distillation in vacuo as a toluene azeotrope. The expected oily (−)-TADDOL diisopropyltitanate was dissolved in a solvent and cooled before 1-acetoxyisoprene and NBM were added successively. Cycloadducts **1a** (and **2**) were purified by flash chromatography, and the enantiomer ratio (e.r.) of **1a** was determined by HPLC on a chiral stationary phase. Very interestingly, isopropropyl alcohol may not be removed from the reaction mixture, since cycloaddition is apparently faster than protonation of the dienolate. Furthermore, a slight increase in enantioselectivity was observed in that case (cf. entries 2 and 3). The main improvement came upon changing the $Ti(OiPr)_4$/(−)-TADDOL ratio. The optimum was found to be 2:1, whereas at higher ratios the selectivity dropped (entries 3–5). A marginal improvement was noted when the slightly more sterically demanding (−)-NpTADDOL ligand[8] was used (entry 6). Under optimized conditions an enantiomer ratio of 95:5 was reached, but the amount of **2** was also increased (entry 8). For the synthesis of RPR 107880 optically

[*] Dr. H. Bienaymé
Rhône-Poulenc Industrialization, CRIT
BP 62, F-69192 St-Fons (France)
Fax: Int. code + 472936721
e-mail: hugues.bienayme@rhone-poulenc.com

[**] We thank M. Lanson, L. Godde, J. L. Dumoulin, and J. Guillaud-Saumur for the analytical data and for helpful discussions, the X-Ray Structure Center of the Russian Academy of Science for the structure determination, and Rhône-Poulenc for permission to publish these results.

 © WILEY-VCH Verlag GmbH, D-69451 Weinheim, 1997 0570-0833/97/3623-2670 $ 17.50+.50/0

Table 1. Asymmetric, internally promoted Diels–Alder cycloadditions between *N*-alkylmaleimides and 1-acetoxybutadienes.

Entry	**1a–e** R^1	R^2	Solvent	$Ti(OiPr)_4$ (equiv)	Ligand (equiv)	T[°C]	t[min]	Yield(**1**+**2**) [%]	**1**:**2**	e.r.(**1a–e**) [a]
1	**1a** CH_3	$PhCH_2$	toluene	1.20	–	25	15	96	93:7	–
2	**1a**		–	1.20	(–)-TADDOL (1.2)	0	30	96	>95:5	75:25
3	**1a**		toluene/*i*PrOH[b]	1.20	(–)-TADDOL (1.2)	0	40	90	>95:5	80:20
4	**1a**		toluene/*i*PrOH[b]	2.25	(–)-TADDOL (1.12)	0	40	92	>95:5	91:9
5	**1a**		toluene/*i*PrOH[b]	4.50	(–)-TADDOL (1.12)	0	40	89	>95:5	81:19
6	**1a**		toluene/*i*PrOH[b]	2.20	(–)-NpTADDOL (1.10)	0	40	95	>95:5	93:7
7	**1a**		toluene/*i*PrOH[b]	2.00	(–)-NpTADDOL (0.20)	0	140	95	>95:5	65:35
8	**1a**		toluene/*i*PrOH[b]	2.06	(–)-NpTADDOL (1.03)	–15	240	96.5	90:10	95:5
9	**1b** CH_3	p-$BrC_6H_4CH_2$	toluene/*i*PrOH[b]	2.20	(–)-NpTADDOL (1.10)	–10	240	84[c]	[f]	93:7
10	**1c** CH_3	(*R*)-$PhCH_2(CH_3)$	toluene/*i*PrOH[b]	2.20	(–)-NpTADDOL (1.10)	–10	240	94[c]	[f]	93:7[d]
11	**1d** CH_3	CH_3	toluene/*i*PrOH[b]	2.20	(–)-NpTADDOL (1.10)	–10	240	58[c,e]	[f]	96:4
12	**1e** H	$PhCH_2$	toluene/*i*PrOH[b]	2.20	(–)-NpTADDOL (1.10)	–10	240	90[c]	[f]	92:8

[a] Determined by HPLC with a chiral column (Diacel Chiralpak AD, 250 × 4.6 mm; heptane/isopropyl alcohol 70/30). [b] Isopropyl alcohol generated from Ti(O*i*Pr)4 was left in the reaction mixture. [c] Yield for **1** only. [d] Diastereomer ratio. [e] 14% *exo* cycloadduct also present. [f] Not determined.

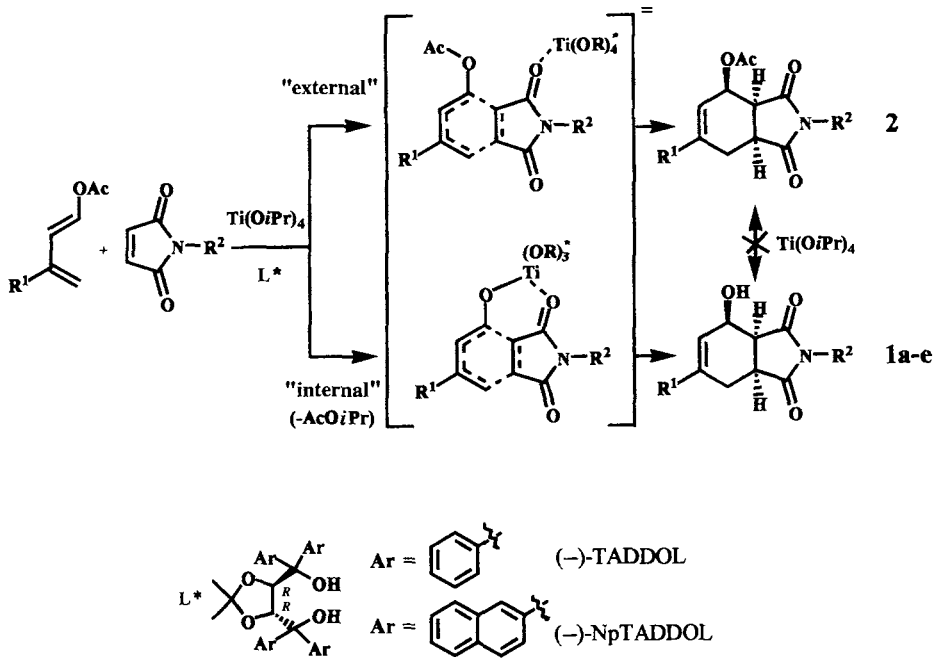

Scheme 2. Postulated transition states for the externally promoted (top) and internally promoted cycloadditions (bottom) of maleimides.

pure (–)-**1a** could be obtained from a single recrystallization (isopropanol, e.r. = 95:5 → 99:1; 75% overall isolated yield).

As we believed that internal coordination was key to the high enantioselectivity, the small amount of acetate **2** coproduced in optimized experiment 8 was isolated and saponified to **1a** (2 equiv $Ti(OiPr)_4$, *i*PrOH, 65°C, 10 h), which was found to be almost racemic (e.r. = 48:52). Apparently, neither of the two putative chiral species present, [(–)-TADDOL]$Ti(OiPr)_2$ and [(–)-TADDOL]Ti(O*i*Pr)-(O-isoprenyl), were efficient in promoting the asymmetric, externally catalyzed cycloaddition leading to **2**. This observation clearly illustrates the important role of reagent preorganization in this internally promoted cycloaddition.

Some experiments were also carried out to determine whether a catalytic amount of ligand would yield similar results (entry 7). Unfortunately, the enantiomer ratio of this cycloaddition dropped as the amount of ligand decreased. Apparently the (–)-TADDOL ligand remained strongly bound to the titanium nucleus and did not exchange with excess $Ti(OiPr)_4$ to regenerate the chiral catalyst.

We probed the scope and limitation of this reaction by changing the substituents on the diene and dienophile. Gratifyingly, the previously optimized protocol afforded high yields and enantiomer ratios in each case. These (limited) modifications to the diene and dienophile did not appear to alter the stereochemical outcome of the cycloaddition. This observation is important, since maleimides are monodentate C_{2v}-symmetric dienophiles (i.e. difficult dienophiles) and is also in sharp contrast with earlier results where low substrate diversity was the rule.[9]

The lack of published analytical data for enantiomerically pure structures of type **1** prompted us to obtain the X-ray crystal structure to ascertain the absolute configuration. We were not able to produce suitable crystals of either alcohol **1a**,

 © WILEY-VCH Verlag GmbH, D-69451 Weinheim, 1997 0570-0833/97/3623-2671 $ 17.50+.50/0

1b, or derivatized esters of **1a**. Only cycloadduct **1c** (from the cycloaddition with (*R*)-α-methylbenzylmaleimide) gave satisfactory crystals, the absolute stereochemistry of which proved to be (3a*S*,4*R*,7a*S*).[10,13] A favored ligand-controlled *endo-Si* approach (with (−)-TADDOLs) was thus postulated for all maleimides studied here.[11]

We propose the following model for the stereochemical outcome of the TADDOL–titanate internally promoted cycloadditions. TADDOL-based titanium catalysts have been used with success in various enantioselective transformations,[12] a certain amount of stereochemical information is thus available. Our rationale for the high enantioselectivities observed here is illustrated in Scheme 3 and parallels that proposed by Seebach et al. for the enantioselective *Si* addition of dialkylzinc reagents to aldehydes.[8] The well-documented

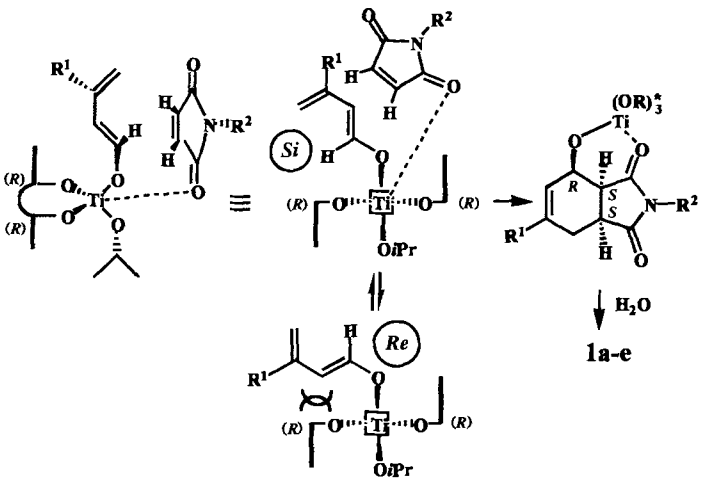

Scheme 3. Model for enantioface selection in internally promoted cycloadditions.

propeller-type arrangement of TADDOL titanates impose two quasi-axial aryl substituents to fill the top right and bottom left front octants around the titanium nucleus (this holds for the (−)-(*R*,*R*)-TADDOLs). These substituents are schematized by bold vertical bars in Scheme 3. The (substituted) butadienyloxy fragment will likely occupy the "free" octant in an extended conformation to minimize steric interactions with the ligand aryl rings, thus exposing its *Si* face to the dienophile. Another possible important feature in this cycloaddition, although not readily quantified, is a change in the coordination geometry of the metal center during the cycloaddition process (from tetrahedral in the starting titanium dienolate to trigonal-bipyramidal upon coordination with the dienophile). This change would push the butadienyl moiety further into the ligand sphere and thus reinforce potential nonbonding interactions. Lastly, our simplistic model does not account for the important role of the ligand/$Ti(OiPr)_4$ ratio, which still remains unclear.

We thus have developed a new potent coordination mode for the Diels–Alder cycloaddition, where cooperativity between enthalpic and entropic factors is likely responsible for the high enantioselectivities (and reactivities) observed. Though only stoichiometric for the moment, this method enables the reaction of difficult dienophiles such as maleimides with high selectivities and under very mild conditions. This type of catalysis, in which the Lewis acid and one of the reactants are chemically linked, should find new synthetic applications.

Experimental Section

Typical procedure for the internally promoted cycloaddition of 1-acetoxybutadienes with maleimides. (3a*S*,4*R*,7a*S*)-2-Benzyl-4-hydroxy-6-methyl-1,3,3a,4,7,7a-hexahydro-1*H*-isoindole (**1a**): (−)-NpTADDOL[7] (6.18 g, 9.27 mmol) was suspended in dry toluene (40 mL). The clear solution obtained upon addition of $Ti(OiPr)_4$ (5.50 mL, 18.5 mmol) was cooled to −15/−10°C, and freshly distilled 1-acetoxyisoprene (1.72 g, 13.6 mmol, Rhône-Poulenc Animal-Nutrition) and *N*-benzylmaleimide (1.68 g, 8.97 mmol) were added successively. After the dienophile had been consumed (TLC, Et_2O/pentane 70/30), 2N HCl (30 mL) and ice were added. The crude reaction mixture was extracted twice with Et_2O (60 mL) and the organic phase washed with saturated $NaHCO_3$ (50 mL). Flash chromatography (Et_2O/pentane (1/1) → Et_2O) furnished (in order): (−)-NpTADDOL (5.68 g after recrystallization, 92% recovered), acetate **2** (0.266 g, 9.5%) and alcohol **1a** (2.122 g, 87%, e.r. = 95:5). **1a** was recrystallized from isopropropyl alcohol (15 mL) to give 1.82 g of analytically and optically pure crystals (75% overall yield). **1a:** M_r = 271.31; m.p. 104.5–105°C; $[\alpha]_D$ = −27.4 (29°C, c = 1.7 in CH_2Cl_2); ^1H NMR (300 MHz, [D$_6$]DMSO, 25°C, HMDS): δ = 1.63 (br. s, 3H), 2.17 (dd, 1H, J = 16.4, 9.1 Hz), 2.33 (dd, 1H, J = 16.4, 5.5 Hz), 2.93 (dd, 1H, 9.1, 4.8 Hz), 3.18 (dt, 1H, J = 9.1, 5.5 Hz), 4.32 (m, 1H), 4.43–4.52 (m, 2H), 5.66 (m, 1H), 7.19 (m, 5H); IR (KBr): $\tilde{\nu}$ = 3512, 3091, 1772, 1698, 1606, 1586, 1497, 1401, 733, 704 cm^{-1}; HRMS: m/z calcd for $C_{16}H_{17}NO_3$: 271.1208; found: 271.1198. C,H,N analysis calcd for $C_{16}H_{17}NO_3$: C 70.83, H 6.31, N 5.16; found: C 71.60, H 6.30, N 5.30.

Received: May 30, 1997 [Z10492IE]
German version: *Angew. Chem.* **1997**, *109*, 2785–2789

Keywords: asymmetric synthesis · cycloadditions · TADDOL

[1] For recent reviews, see: a) T. Oh, M. Reilly, *Org. Prep. Proced. Int.* **1994**, *26*, 129–158; b) L. Deloux, M. Srebnik, *Chem. Rev.* **1993**, *93*, 763–784; c) H. B. Kagan, O. Riant, *ibid.* **1992**, *92*, 1007–1019; d) K. Narasaka, *Synthesis* **1991**, 1–11.

[2] On the bonding nature of Lewis acid/carbonyl complexes: a) S. E. Denmark, N. G. Almstead, *J. Am. Chem. Soc.* **1993**, *115*, 3133–3139; b) S. Shambayati, W. E. Crowe, S. L. Schreiber, *Angew. Chem.* **1990**, *102*, 273; *Angew. Chem. Int. Ed. Engl.* **1990**, *29*, 256–272; c) D. M. Birney, K. N. Houk, *J. Am. Chem. Soc.* **1990**, *112*, 4127–4133.

[3] S. Mutti, C. Daubié, F. Decalorgne, R. Fournier, P. Rossi, *Tetrahedron Lett.* **1996**, *37*, 3125–3128; see also: S. Mutti, C. Daubié, J. Malpart, X. Radisson, *ibid.* **1996**, *37*, 8743–8746; M. Tabart, J. F. Peyronel, *Bioorg. Med. Chem. Lett.* **1994**, *4*, 673–676.

[4] H. Bienaymé, A. Longeau, *Tetrahedron* **1997**, *53*, 9637–9646.

[5] This unusual dienolate preparation is likely favored by the relatively high reactivity of enol acetates in Ti-promoted transesterification reactions.

[6] J. A. Ibers, *Nature* **1963**, *197*, 686–687.

[7] A. K. Beck, B. Bastani, D. A. Plattner, W. Petter, D. Seebach, H. Braunschweiger, P. Gysi, L. La Vecchia, *Chimia* **1991**, *45*, 238–244.

[8] Np-TADDOL is a highly efficient ligand for the asymmetric addition of organozinc reagents to aldehydes: a) D. Seebach, D. A. Plattner, A. K. Beck, Y. M. Wang, D. Hunziker, W. Petter, *Helv. Chim. Acta* **1992**, *75*, 2171–2209; b) Y. N. Ito, X. Ariza, A. K. Beck, A. Bohac, C. Ganter, R. E. Gaw, Y. N. Ito, X. Ariza, A. K. Beck, A. Bohac, C. Ganter, R. E. Gawler, F. N. M. Kühnle, J. Tuleja, Y. M. Wang, D. Seebach, *Helv. Chim. Acta* **1994**, *77*, 2071–2110.

[9] The scope of the first efficient asymmetric cycloadditions involving N-substituted maleimides was narrow, and the maleimide N-substituents are not easily removed: E. J. Corey, S. Sarshar, D. H. Lee, *J. Am. Chem. Soc.* **1994**, *116*, 12089–12090.

[10] The absolute configuration was determined based on the known configuration of the side chain. Since the problem of double stereoinduction arises with this homochiral substrate (substrate and ligand-controlled Diels–Alder cycloaddition), several controls were performed with (*R*)-α-methylbenzylmaleimide and acetoxyisoprene under conditions for the nonasymmetric reaction with internal promotion ($Ti(OiPr)_4$ or $Ti(OiPr)_4$/*rac*-TADDOL). None of these controls exhibited a diastereomer ratio exceeding 60:40, a result indicating that (*R*)-α-methylbenzylmaleimide is not responsible for the enantiocontrol in cycloaddition leading to **4**. Furthermore, (*R*)-α-methylbenzylmaleimide is known to be a weakly diastereoselective dienophile in substrate-controlled Diels–Alder cycloadditions: S. W. Baldwin, P. Greenspan, C. Alaimo, A. T. McPhail, *Tetrahedron Lett.* **1991**, *32*, 5877–5880.

[11] The absolute stereochemistry shown in Scheme 2 is opposite to that required for the construction of the RPR 107880 core. However, this is of little concern, since both antipodal forms of TADDOL ligands are equally available from tartrate esters.

 © WILEY-VCH Verlag GmbH, D-69451 Weinheim, 1997 0570-0833/97/3623-2672 $ 17.50+.50/0

[12] For recent reviews on TADDOL-mediated reactions, see: a) M.Braun, *Angew. Chem.* **1996**, *108*, 565–568; *Angew. Chem. Int. Ed. Engl.* **1996**, *35*, 519–522; b) R. Dahinden, A. K. Beck, D. Seebach in *Encyclopedia of Reagents for Organic Synthesis, Vol. 3* (Ed.: L. Paquette), Wiley, Chichester, **1995**, pp. 2167–2170; c) R. O. Duthaler, A. Hafner, P. A. Alsters, P. Rothe-Streit, G. Ribs, *Pure Appl. Chem.* **1992**, *64*, 1897–1910; d) K. Narasaka, *ibid.* **1992**, *64*, 1889–1896.

[13] Crystallographic data (excluding structure factors) for the structure reported in this paper have been deposited with the Cambridge Crystallogrphic Data Centre as supplementary publication no. CCDC-100453. Copies of the data can be obtained free of charge on application to The Director, CCDC, 12 Union Road, Cambridge CB21EZ, UK (fax: Int. code + (1223) 336-033; e-mail: deposit@chemcrys.cam.ac.uk).

Cluster Assembly by Hydrogen Bonds: Channel Structure of Cu_4L_4 Cubanes

Hiroki Oshio,* Yuki Saito, and Tasuku Ito

Supramolecular chemistry of coordination compounds and organic solids is the subject of intense research.[1] It has been known for several years that self-assembly through hydrogen bonds leads to well-organized organic and inorganic supramolecular structures, and that channel structures, which are formed by self-assembly, can be applied in areas such as selective enclathration, microporosity, and catalysis.[2] On the other hand, transition metal complexes with a cubane structure, in which four metal ions are linked by hydroxo, alkoxo, azido, sulfido, or iminato bridges,[3] are a very important class of compounds (M_4L_4).[4] Among them, alkoxo-bridged copper(II) cubanes, many of which exhibit a quintet ground state because of weak intracluster ferromagnetic interactions, have been extensively studied from magneto-structural viewpoints.[5] We report here that introduction of a hydroxy group into the bridging ligand of a cubane core leads to the formation of a hydrogen-bond network with a channel structure.

The reaction of copper(II) acetate monohydrate with H_2hase (2-(4-hydroxysalicylideneamino)ethanol) in methanol followed by the recrystallization in acetonitrile gave dark blue crystals of **1**, , which crystallize in the monoclinic space group

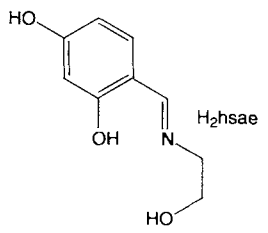

$[Cu_4(hsae)_4)] \cdot 2H_2O \cdot 4CH_3CN$ **1**

*C*2/*c*.[6] The structure of **1** contains a tetranuclear cubane core (Figure 1), which sits on a crystallographic twofold axis that passes through the middle of the Cu1 ··· Cu1′ and Cu2 ··· Cu2′ vectors. The asymmetric unit, thus, consists of half of the tetramer.

[*] Prof. H. Oshio, Y. Saito, Prof. T. Ito
Department of Chemistry
Graduate School of Science, Tohoku University
Aoba-ku, Sendai 980-77 (Japan)
Fax: Int. code + (22) 217-6548
e-mail: oshio@agnus.chem.tohoku.ac.jp

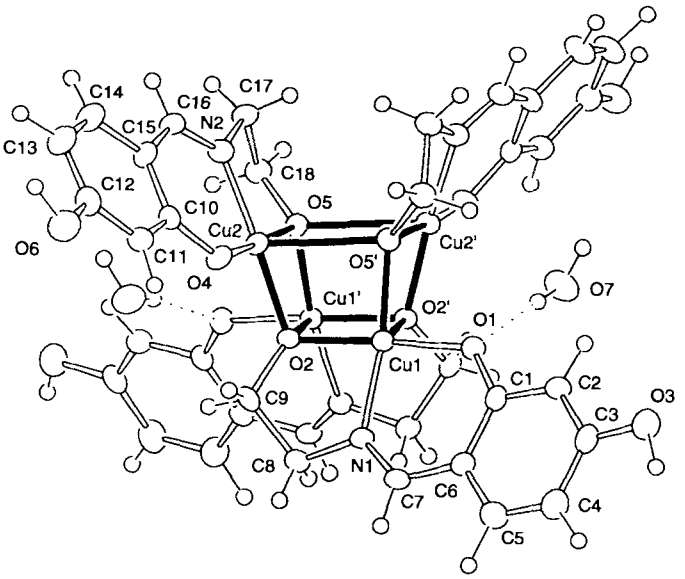

Figure 1. Crystal structure of **1** (ORTEP diagram; ellipsoids at the 50% probability level). Selected distances [Å] and angles with standard deviation in parentheses: Cu1–O1 1.894(3), Cu1–O2 1.959(3), Cu1–O2′ 2.467(3), Cu1–O5′ 1.956(3), Cu1–N1 1.925(4), Cu2–O2 1.930(3), Cu2–O4 1.939(3), Cu2–O5′ 2.562(3), Cu2–N2 1.914(4), Cu2–O5 2.000(3); Cu1-O2-Cu1′ 101.5(1), Cu1-O2-Cu2 106.1(1), Cu1′-O2-Cu2 90.1(1), Cu1-O5′-Cu2 85.8(1), Cu1-O5′-Cu2′ 104.8(1), Cu2-O5-Cu2′,104.2(1); key to symmetry operation for primed atoms: $1-x, y, 3/2-z$.

The cubane core of **1** is based on an approximately cubic array of alternating copper and oxygen atoms. The intracluster metal–metal separations are 3.108(1) (Cu1 ··· Cu2), 3.443(1) (Cu1 ··· Cu1′), 3.134(1) (Cu1 ··· Cu2′), and 3.6154(9) Å (Cu2 ··· Cu2′). Each copper atom resides in a square pyramidal coordination environment with one nitrogen and two oxygen atoms from the ligand and two oxygen atoms from neighboring units of the cubane. According to the four short and one long bond lengths (see Figure 1) between the copper and coordinating atoms, basal planes for Cu1 and Cu2 are O1-N1-O2-O5′ and O4-N2-O5-O2, in which the copper ions are displaced by 0.053(1) and 0.041(1) Å above the plane, respectively. The magnetic orbitals ($d_{x^2-y^2}$) of the Cu1 and Cu2 ions, which are perpendicular to each other, are parallel to the basal planes (Figure 2a).

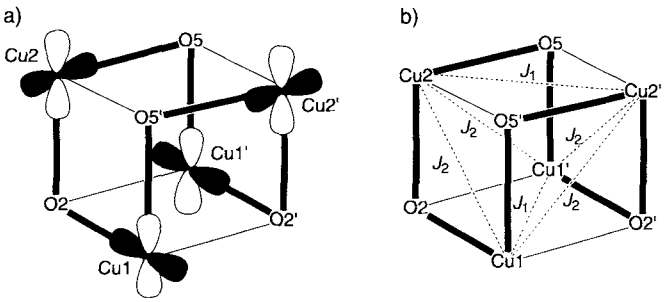

Figure 2. a) Arrangement of magnetic orbitals of **1**, b) magnetic interactions in **1**. Short bonds are represented by thick lines.

In **1**, water molecules (O7) and hydroxyl groups (O3 and O6) play an important role in constructing a network structure of hydrogen bonds; simple translations lead to the formation of a layer structure in the *ac* plane in which the hydrogen bonds are O(7)-H ··· O(1) 2.693(5) Å, O(3)-H ··· O(4) 2.710, and O(6)-H ··· O(7) 2.692 Å. The additional

 © WILEY-VCH Verlag GmbH, D-69451 Weinheim, 1997 0570-0833/97/3623-2673 $ 17.50+.50/0

hydrogen bond between the water molecule(O7) and the hydroxyl group (O6) requires an offset between successive layers that is generated by a twofold screw axis. Consequently, the hydrogen network forms a channel structure along the *b* axis (Figure 3).

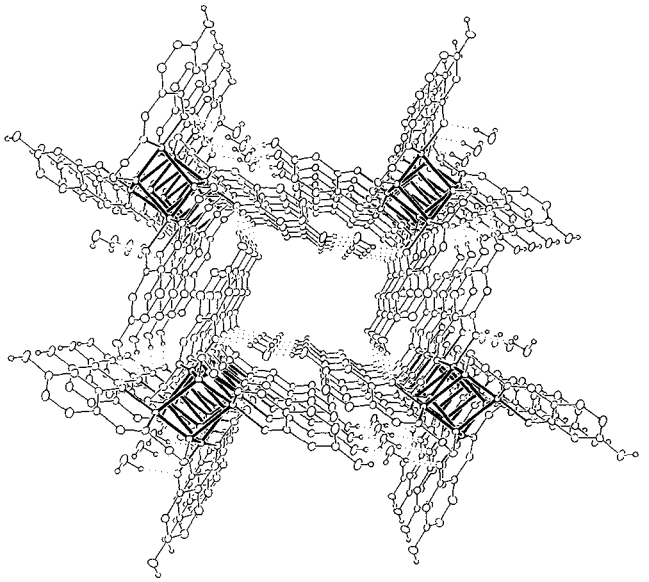

Figure 3. Channel structure of **1**.

The temperature dependence of the magnetic susceptibility of **1** was measured in the temperature range between 2.0 and 300 K (Figure 4). At room temperature the value of $\chi_m T$ is

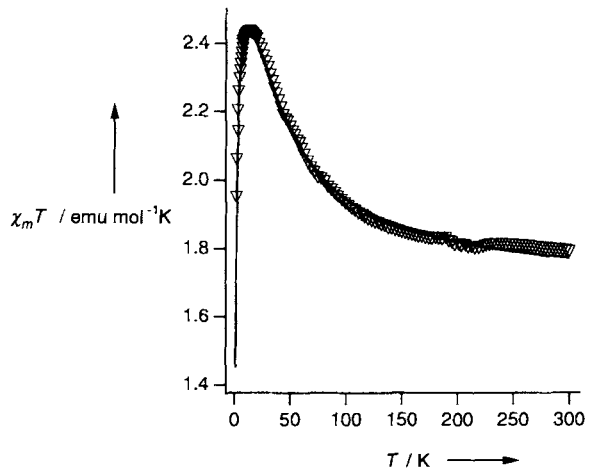

Figure 4. Plot of $\chi_m T$ as a function of T for **1**. The solid line was calculated with the parameters given in the text.

1.8 emu K mol^{-1} per molecule, as expected for four noncorrelated spins. Upon cooling the sample, $\chi_m T$ increases to a maximum value of 2.44 emu K mol^{-1} at 14 K, then decreases. This is indicative of an intracluster ferromagnetic interaction, since the intercluster metal–metal distances are over 7.0 Å these would only give rise to very weak magnetic interactions. The axial bonds Cu1–O2′ and Cu2–O5′ are elongated due to a pseudo Jahn–Teller effect, which leads to weaker magnetic interactions within the Cu2 ··· Cu2′ and Cu1 ··· Cu1′ pairs. The magnitudes of the magnetic interactions within the Cu1 ··· Cu2 and Cu1 ··· Cu2′ pairs are considered to be comparable, because the bridging angles and spacings for Cu1-O2-Cu2 and Cu1-O5′-Cu2′ are similar. The two exchange parameters J_1 and J_2 were, therefore, introduced for the analysis of the magnetic data and a schematic drawing of the magnetic pathways is depicted in Figure 2b. The experimental magnetic data were analyzed with the Hamiltonian operator $\mathscr{H}$ [Eq. (1)] and the intercluster interaction was

$$\mathscr{H} = -2J_1(S_{Cu1}S_{Cu1'} + S_{Cu2}S_{Cu2'}) - 2J_2(S_{Cu1}S_{Cu2} + S_{Cu1}S_{Cu2'} + S_{Cu1'}S_{Cu2} + S_{Cu1'}S_{Cu2'}) \quad (1)$$

included as a mean field correction θ. The least squares calculation yielded the best fit parameters of $g = 2.02(1)$, $J_1 = -17.6(1)$ cm^{-1}, $J_2 = +36.0(9)$ cm^{-1}, and $\theta = -1.0(1)$ K. The propagation of intracluster magnetic interactions occurs according to the known dependence of J versus bridging angles.[7] The magnetic orbital overlap through oxygen p-orbitals becomes nearly zero for the bridging angles Cu1-O2-Cu2 and Cu1-O5′-Cu2′ of 106.1(1) and 104.8(1)°, respectively.[8] Furthermore, the perpendicular arrangement of the magnetic metal orbitals (Figure 2a) results in zero orbital overlap leading to ferromagnetic interactions (J_2), while the parallel orientation results in antiferromagnetic interactions (J_1).

The present compound is an example of how the introduction of hydroxyl groups can be useful for assembling clusters. Furthermore, the compound is soluble not only in acetonitrile but also in water, which indicates that the compound has potential to clathrate organic molecules while still maintaining its hydrogen-bonding network.

Experimental Section

H_2hsae (0.138 g, 1 mmol), prepared by condensation of 2,4-dihydroxybenzaldehyde with 2-aminoethanol, was added to a solution of copper(II) acetate monohydrate (0. 199 g, 1 mmol) in methanol (80 mL). The resulting dark green pprecipitate was filtered, and recrystallization in acetonitrile gave dark blue tabletlike crystals, one of which was subjected to the X-ray structural analysis. Elemental analysis: found (calcd) C 45.25 (45.13), H 4.62 (4.48), N 9.40 (9.57).

Received: May 26, 1997 [Z10473IE]
German version: *Angew. Chem.* **1997**, *109*, 2789–2791

Keywords: copper · cubanes · self-assembly

[1] J.-M. Lehn, *Angew. Chem.* **1988**, *100*, 91; *Angew. Chem. Int. Ed. Engl.* **1988**, *27*, 89; V. Balzani, *Tetrahedron* **1992**, *48*, 10443; E. C. Constable, *Tetrahedron* **1992**, *48*, 10013; M. J. Zaworotko, *Chem. Rev.* **1994**, *23*, 283; Y. L. Chang, M. A. West, F. W. Fowler, J. W. Lauher, *J. Am. Chem. Soc.* **1993**, *115*, 5991; J. D. Wright, *Molecular Crystals*, 2nd ed., Cambridge University Press, Cambridge, **1994**; G. R. Desiraju, *Crystal Engineering. The Design of Organic Solids*, Elsevier, Amsterdam, **1989**; G. M. Frankenbach, M. C. Etter, *Chem. Mater.* **1992**, 4, 272.

[2] K. Endo, T. Sawaki, M. Koyanagi, K. Kobayashi, H. Masuda, Y. Aoyama, *J. Am. Chem. Soc.* **1995**, *117*, 8341; M. Simard, D. Su, J. D. Wuest, *ibid.* **1991**, *113*, 4696; X. Wang, M. Simard, J. D. Wuest, *ibid.* **1994**, *116*, 12119; B. F. Abraham, B. F. Hoskins, J. Liu, R. Robson, *ibid.* **1991**, *113*, 3045.

[3] M. A. Halcrow, J. C. Huffman, G. Christou, *Angew. Chem.* **1995**, *107*, 971; *Angew. Chem. Int. Ed. Engl.* **1995**, *34*, 889; H. -J. Mai, R. M. Köcker, S. Wocadlo, W. Massa, K. Dehnicke, *ibid.* **1995**, *107*, 1349 and **1995**, *34*, 1235; M. A. Halcrow, J.-S. Sun, J. C. Huffman, G. Christou, *Inorg. Chem.* **1995**, *34*, 4167.

[4] J. M. Berg, R. H. Holm in *Iron-Sulfur Proteins, Vol. 4* (Ed.: T. G. Spioro), Wiley-Interscience, New York, **1982**, Chapter. 1; R. H. Holm, S. Ciurli, J. A. Weigel, *Prog. Inorg. Chem.* **1990**, *38*, 1.

[5] L. Mertz, W. Haase, *J. Chem. Soc. Dalton Trans.* **1978**, 1594; L. Schawabe, W. Haase, *ibid.* **1985**, 1909; J. W. Hall, W. E. D. Estes, R. P. Scaringe, W. E. Williams, *Inorg. Chem.* **1977**, *16*, 1572; J. Sleten, A. Sorensen, M. Julve, Y. Journaux, *ibid.* **1990**, *29*, 5054.

 © WILEY-VCH Verlag GmbH, D-69451 Weinheim, 1997 0570-0833/97/3623-2674 $ 17.50+.50/0

[6] Crystal data of **1** ($C_{44}H_{52}Cu_4N_8O_{14}$): dark blue tablet ($0.2 \times 0.2 \times 0.3$ mm^3), $M_r = 1171.13$, monoclinic $C2/c$ with $a = 25.355(4)$, $b = 9.211(4)$, $c = 21.460(3)$ Å, $\beta = 98.23(1)°$, $V = 4960(2)$ Å^3 (by least-square refinement of 20 reflections ($25° < 2\theta < 30°$)), $Z = 4$, $\rho_{calcd} = 1.568$ g cm^{-3}, $F(000) = 2399$, $\mu(Mo_{K\alpha}) = 17.73$ cm^{-1}. Data collection: Rigaku AFC5S diffractometer, ω-2θ mode, scan width $1.45 + 0.40\tan\theta$, scan speed 4° min^{-1}, $Mo_{K\alpha}$ ($\lambda = 0.71073$ Å) radiation; $T = -120$ °C; 4325 reflections measured($3° < 2\theta < 55°$), 4325 unique reflections, of which 3519 ($I_0 > 3.0\sigma I_0$) were used for the calculation. Data were corrected for Lorentz and polarization and an empirical absorption correction (ψ-scan) was applied, which resulted in transmission factors ranging from 0.575 to 0.760. The structure was solved by a conventional heavy-atom method and refined by full-matrix least-squares by using Xtal 3.2 (*XTAL 3.2 User's Manual*, The University of Western Australia and Maryland). All non-hydrogen atoms were readily located and refined with anisotropic thermal parameters, and hydrogen atoms were located from difference Fourier maps and refined with isotropic thermal parameters. Final $R = 0.040$, $R_w = 0.032$ for 316 parameters. The final Fourier difference synthesis showed minimum and maximum peaks of -0.77 and $+0.67$ e Å^3.

[7] W. E. Hatfield in *Magneto-Structural Correlations in Exchange Coupled systems (NATO ASI Ser. Ser. C* **1985**, *140)*, p. 555.

[8] P. J. Hay, J. C. Thibeault, R. Hoffman, *J. Am. Chem. Soc.* **1975**, *97*, 4884.

Synthesis of a Small-Pore Microporous Material Using a Computationally Designed Template**

Dewi W. Lewis,* Gopinathan Sankar, Joanna K. Wyles, John Meurig Thomas,* C. Richard A. Catlow,* and David J. Willock

The ability to design and synthesize materials, with predetermined physical and catalytic properties is an oft-aspired goal of the chemist. Recent progress has demonstrated how this may well be viable in the field of microporous solids, particularly in the case of syntheses mediated by the use of structure-directing templates.[1–3] Here we demonstrate how we are able to design, using computational methods, an organic template suitable to form a targeted microporous material, which results not only in the formation of that crystalline structure, but also manifests a number of other predefined physical properties.

Microporous materials, both aluminosilicate and aluminophosphate based, with the Chabazite structure (IZA code CHA) act as catalysts for a number of important reactions. For example SAPO-34 is an effective catalyst for the conversion of methanol to light olefins.[4] However, there are a number of problems in the synthesis of such materials, which we believe arise from the choice of the organic species used as the structure-directing agent. These molecules facilitate the formation of the structure, being encapsulated in the resulting porous framework; the framework structure is a reflection, to varying degrees, of the size and shape of the organic species. Typically, small amines are used to form the chabazitic materials (for example, triethylamine, cyclohexylamine, and *N,N*-diethyl-2-aminoethanol).[5] Both experimentally[5] and computationally[6] it is generally noted that two such molecules can fit inside the CHA cage,[7] although full occupancy of all template sites is not a prerequisite of crystal formation. Such a templating regime requires first relatively high concentrations of aliovalent metal substituents (either M^{2+} on Al^{3+} sites or Si^{4+} on P^{5+} sites) as a result of the need to compensate for the 2+ charge of the protonated templates, per cage, and second the ordering of the templates in a close-packed configuration which requires relatively slow kinetics. The latter requirement results in the competitive formation of other microporous phases where template ordering is not as crucial—an effect particularly significant in aluminophosphate preparations where phases with the $AlPO_4$-5 (AFI) structure are readily formed.[8,9] Although the presence of aliovalent metal in the framework gives rise to catalytic centers, high concentrations can have a deleterious effect on the stability and performance of the material.

Our aim was therefore to synthesize an aluminophosphate-based material with the CHA structure which, by the use of a new template, would circumvent the above problems. Such a template would be designed computationally with our recently developed de novo design methodology.[3] We determined that the following properties would be crucial in our synthesis strategy: a) The selected template would form a CHA material quickly and in a phase pure form, with little or no extraneous microporous phases. b) The template would be present at a concentration of one molecule per unit cell and must fully occupy the CHA cage. c) The charge on the template would be able to be varied to accommodate a range of metal concentrations in the framework and thus allow a degree of control over the catalytic behavior arising from the presence of these substituents.

Once we had identified a suitable candidate template, a program of synthesis was undertaken, and the resulting products were characterized by a combination of XRD and EXAFS studies.

We applied de novo molecular design methods, as embodied in our ZEBEDDE code,[3] to computationally design a template to meet the above criteria. The method allows molecular entities to be grown from a so-called seed molecule, to which new molecular fragments are added from a library. A number of actions are possible, which under the control of a cost function based on van der Waals overlap, minimize the nonbonded contacts between the framework and the template.[3,10] Resulting species are subsequently ranked according to their binding energy (a measure of effective fit inside the pore), which can provide a guide to the likely efficacy of that molecule as a successful template for the structure in question.[11]

We performed a number of simulations, described in more detail elsewhere,[10] using seeds from C_1 (methane) to C_4 (*n*-butane). In each case the concentration of the resultant organic molecule was restricted to one per unit cell (or cage). Typical templates included branched hydrocarbons and amines (for example, 3,3,6-trimethyloctylamine and 6-ethyloctylamine) which are similar in structure and geometry to

[*] Dr. D. W. Lewis
Department of Materials Science and Metallurgy
University of Cambridge
Pembroke St, Cambridge CB2 3QZ (UK)
Fax: Int. code + (1223) 334567
e-mail: D. W.Lewis@msm.cam.ac.uk

Prof. C. R. A. Catlow, Dr. G. Sankar, J. K. Wyles, Prof. Sir J. M. Thomas
Davy Faraday Research Laboratory, The Royal Institution of Great Britain
21 Albemarle Street, London W1X 4BS (UK)

Dr. D. J. Willock
Department of Chemistry, University of Wales
Cardiff CF11XL, UK

[**] The EPSRC is thanked for general support of this work, especially a rolling grant to J.M.T., funding for C.R.A.C. and a CASE studentship to J. K. W. The Oppenheimer Trust of the University of Cambridge is acknowledged for a fellowship to D.W.L.

 © WILEY-VCH Verlag GmbH, D-69451 Weinheim, 1997 0570-0833/97/3623-2675 $ 17.50+.50/0

two triethylamine molecules—the common template used in Chabazitic MeAPO syntheses—linked across the cage.[10] However, although these may be suitable as templates from a space-filling point of view, their flexibility might lead to a large number of conformations, which will reduce the likelihood of the formation of a crystalline microporous material.

Another molecule generated by the code, bicyclohexane, is more rigid and therefore does not suffer this drawback. Furthermore, the symmetry of the molecule is such that any disorder of the molecule, both rotational and by inversion through the bridge between the cyclohexane rings, does not significantly alter the interactions between the template and the framework.

We therefore used this molecule as a basis for our synthetic strategy. Bicyclohexane is, however, incompatible with typical hydrothermal conditions, being insoluble in water. We therefore modified the molecule by introducing nitrogen centers: templates are typically amines. Although nitrogen can be included automatically by ZEBEDDE as part of a molecular fragment, its position is controlled by the order in which random actions occur, and therefore, post-growth modification is the most effective method of fine-tuning the suggested templates. Furthermore, there is little distinction between C and N in our cost function, since the function is based on van der Waals radii. However, with each modification, energy minimization calculations with the Discover code[12] were performed to ensure that the new template remained a suitable candidate. At the same time, we had to consider the availability and possible synthesis routes for the organic species. Bearing in mind that previous syntheses of CHA-structured cobalt aluminophosphate materials have proved most successful with Co concentrations equivalent to two Co atoms per unit cell, we identified 4-piperidinopiperidine as a suitable candidate for initial evaluation of templates based on the bicyclohexane motif; the commercial availability of this material is also important. The generation of 4-piperidinopiperidine from an ethane seed within the CHA structure is illustrated in Figure 1a, and Figure 1b depicts the energy-minimized geometry of the molecule in a siliceous unit cell of chabazite. We calculate the binding energy of 4-piperidinopiperidine to be $-54\ kJ\,mol^{-1}$, which compares favorably with that found for templates known to form CHA-structured materials,[6] for example, cyclohexylamine ($-61\ kJ\,mol^{-1}$).

Preparations with a typical gel composition of $0.2\,CoO:0.9\,Al_2O_3:1.5\,P_2O_5:30\,H_2O:2.0\,C_{10}H_{20}N_2$ yielded a single blue crystalline phase, which we designate DAF-5 (*D*avy *F*araday 5). Crystallization was carried out in a stainless steel autoclave in the temperature range 150–165°C, and DAF-5 was obtained after subjecting the gel to these hydrothermal conditions for about 4 hours. The resulting X-ray powder diffraction pattern (Figure 2a) can be readily indexed with the auto-indexing program TREOR[13] to a hexagonal cell (cell parameters: $a=b=13.537$ Å, $c=15.480$ Å; $\alpha=\beta=90.0$, $\gamma=120°$; cell volume $=2457$ Å^3) and is similar to that of the mineral chabazite and other related chabazitic materials (Figure 2).[14] The presence of the organic template, which is not ordered, makes a full structure determination from the powder pattern difficult, although a good model can be produced for the inorganic lattice, which results in a chabazitic cage structure. A more detailed structure determination is in progress from single crystal data. The influence of the template on the relative intensities of the diffraction patterns is illustrated in Figure 2b and c, demonstrating that the intensity differences between a typical calcined CHA-structured material[14] and the as-prepared

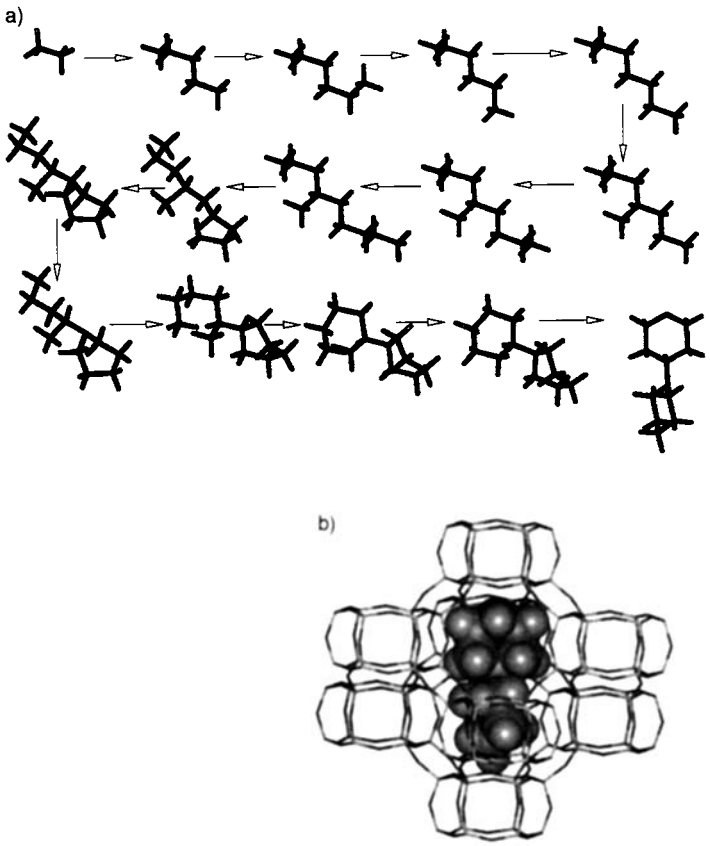

Figure 1. a) Generation of 4-piperidinopiperidine from an ethane seed in a siliceous CHA unit cell with the program ZEBEDDE [3]. Note that the molecule is oriented to best illustrate the growth process rather than its true position in the CHA cage. Further details are given elsewhere [10]. b) Energy-minimized location of 4-piperidinopiperidine in the CHA cage.

DAF-5 sample are consistent with the presence of the template. Elemental analysis gives a framework composition of $Co_{0.28}Al_{0.72}PO_4$, which is in close agreement with a theoretical composition of $Co_{0.25}Al_{0.75}PO_4$ for a material with 2 Co atoms per unit cell that compensate for the template's 2+ charge. Analysis of the Co K-edge EXAFS data (Figure 3) reveals that the cobalt is incorporated into the framework by substitution at tetrahedral sites. The Co–O and Co–P distances and the Co-O-P bond angle obtained from the analysis of the EXAFS data (multiple scattering methodology[15,16]) are given in Table 1 and are typical of many other Co-substituted aluminophosphate materials.[17]

The synthesis of DAF-5, a Chabazitic cobalt aluminophosphate has been achieved by the computational design of a new template. We have thereby again demonstrated that the computational method of de novo template design is viable as a tool for designing templates. Furthermore, the synthesis has achieved a number of other goals set out as objectives for the study and as such can be considered an example of a priori materials design. In particular, the disadvantages of small templates present at a concentration of two per unit cell—long preparation times and concomitant poor sample purity—were avoided with a larger template, which can only be present at a concentration of one per unit cell: the target structure was synthesized in less than 4 hours at reasonably low temperatures, and without interference from the formation of other microporous phases. A further goal was to provide control of the metal content of the framework by a

 © WILEY-VCH Verlag GmbH, D-69451 Weinheim, 1997 0570-0833/97/3623-2676 $ 17.50+.50/0

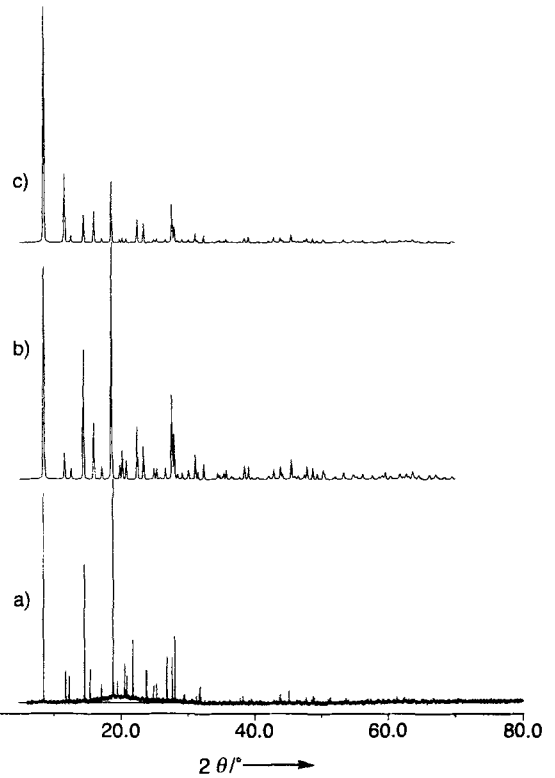

Figure 2. a) Experimental powder X-ray diffraction patterns for DAF-5, and for comparison the calculated diffraction patterns[19] for a CHA-structured aluminiumphosphate unit cell (space group $P1$) in the presence of (b) and in the absence of the template (c). The calculated pattern for the templated system is in excellent agreement with the peak positions and relative intensities of the experimental data, although only one unique template geometry was used to calculate the simulated pattern whereas other orientations are present in the experimental sample. Note that the peak width used in the simulated patterns is larger than that for the high-resolution powder pattern obtained from synchrotron radiation.

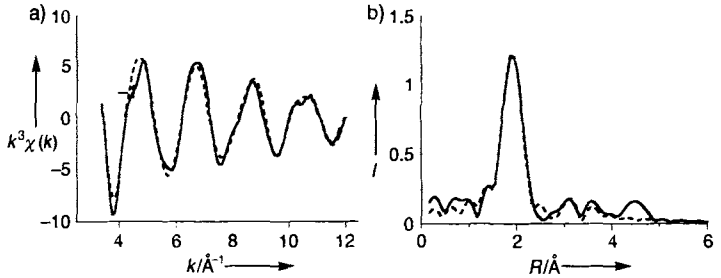

Figure 3. Co k-edge EXAFS (a) and the associated Fourier transform (I = FT magnitude) of the as-synthesized DAF-5 (b). In each case the solid line shows the experimental data and the dotted curve was calculated from the parameters given in Table 1.

template "tuneable" in terms of charge. Although we have considered only a 2+-charged template, given suitable synthesis conditions 4-cyclohexylpiperidine (which will have a charge of 1+ in the gel) is also likely to form a CHA-structured material. We should also note that if bicyclohexane could be incorporated into a nonpolar synthesis gel, such a gel may also be conducive to forming the siliceous or aluminophosphate end-members of this structural type. We note that gallophosphates (analogues of AlPOs) have been formed from such nonpolar gels, although with different templates to those used here.[18]

Table 1. Structural parameters DAF-5 obtained from Co K-edge EXAFS data; N is the coordination number, R the interatomic distance and σ^2 the Debye–Waller factor. The fit index is 14.18.

Atom pair	N	R[Å]	σ^2[Å]	Co-O-P bond angle
Co–O	4.1	1.94	0.0045	–
Co–P	2.6	3.17	0.006	133
Co–P	1.5	3.33	0.006	150

In this work we have demonstrated the successful application of computer-aided materials design, through the identification of critical parameters in the synthesis and the computational design of a suitable template, to the formation of a microporous material possessing predefined structural and physical properties. We believe that such an approach provides an effective route to the synthesis of novel microporous materials.

Experimental Section

DAF-5 was prepared from a gel with a typical composition of $0.2\,CoO : 0.9\,Al_2O_3 : 1.5\,P_2O_5 : 30\,H_2O : 2.0\,C_{10}H_{20}N_2$ in a Teflon lined stainless steel autoclave at between 150 and 165°C for a maximum of six hours. The gel was prepared from phosphoric acid, aluminium hydroxide, cobalt(II) acetate, and 4-piperidinopiperidine (all Aldrich). X-ray diffraction data were collected at room temperature on station 2.3 at the Daresbury Synchrotron source (operates at 2 GeV with typical currents between 120–250 mA) at $\lambda = 1.3999$ Å in capillary mode. Co K-edge EXAFS were collected at room temperature on station 7.1 at the Daresbury laboratory, and the data analyzed with the suite of programs available there (EXCALIB, EXBROOK, and EXCURV92).

Received: June 9, 1997 [Z10522IE]
German version: *Angew. Chem.* **1997**, *109*, 2791–2793

Keywords: aluminophosphates · materials science · molecular modeling · zeolite analogues

[1] J. M. Thomas, D. W. Lewis, *Z. Phys. Chemie* **1996**, *197* 37–48.
[2] M. E. Davis, *CHEMTECH* **1994**, *24*, 22–26.
[3] D. W. Lewis, D. J. Willock, C. R. A. Catlow, J. M. Thomas, G. J. Hutchings, *Nature (London)* **1996**, *382*, 604–606.
[4] a) J. A. Rabo, R. J. Pellet, P. K. Coughlin, E. S. Shamshoun in *Zeolites as Catalysts, Sorbents and Detergent Builders* (Eds.: H. G. Karge, J. Weitkamp), Elsevier, Amsterdam **1989**, pp. 1–17; b) J. Liang, H. Li, S. Zhao, W. Guo, R. Wang, M. Ying, *Appl. Catal.* **1990**, *64*, 31–40.
[5] S. T. Wilson, B. M. Lok, C. A. Messina, E. M. Flanigen, *Proc. Int. Conf. Zeolites 6th*, **1984**, pp. 97–109.
[6] D. W. Lewis, C. R. A. Catlow, J. M. Thomas, *Chem. Mater.* **1996**, *8*, 1112–1118.
[7] J. M. Bennett, B. K. Marcus in *Innovation in Zeolite Materials Science* (Eds.: P. J. Grobet, W. J. Mortier, E. F. Vansant, G. Schulzekloff), Elsevier, Amsterdam, **1988**, pp. 269–279.
[8] M. G. Uytterhoeven, R. A. Schoonheydt, *Proc. Int. Conf. Zeolites 9th*, **1992**, 329–336
[9] F. Rey, G. Sankar, J. M. Thomas, P. A. Barrett, D. W. Lewis, C. R. A. Catlow, S. M. Clark, G. N. Greaves, *Chem. Mater.* **1995**, *7*, 1435–1436.
[10] D. J. Willock, D. W. Lewis, C. R. A. Catlow, G. J. Hutchings, J. M. Thomas, *J. Mol. Catal. A* **1997**, *119*, 415–424.
[11] D. W. Lewis, C. M. Freeman, C. R. A. Catlow, *J. Phys. Chem.* **1995**, *99*, 11194–11202.
[12] Discover 94.0, Molecular Simulations Inc., San Diego, **1996**, using the cff 91 force field.
[13] P. W. Werner, L. Eriksson, M. Westdahl, *J. Appl. Cryst.* **1985**, *18*, 367–370
[14] M. M. J. Treacy, J. B. Higgins, R. von Ballmoos, *Collection of Simulated XRD Powder Patterns for Zeolites*, 3rd ed., Elsevier, Amsterdam, **1996**.
[15] G. Sankar, J. M. Thomas, G. N. Greaves, A. J. Dent, *J. Phys. IV* **1997**, *7*, 239–240.
[16] G. Sankar, D. W. Lewis, F. Rey, C. R. A. Catlow, J. M. Thomas, unpublished.
[17] P. A. Barrett, G. Sankar, C. R. A. Catlow, J. M. Thomas, *J. Phys. Chem.* **1996**, *100*, 8977–8985.
[18] A. M. Chippindale, A. R. Cowley, R. I. Walton, *J. Mater. Chem.* **1996**, *6*, 611–614.
[19] Calculated with the Solid Characterize module, Insight II 4.0.0, Molecular Simulations Inc., San Diego, **1996**.

Rapid and Highly Selective Cleavage of Ribonucleoside 2′,3′-Cyclic Monophosphates by Dinuclear Cu^{II} Complexes**

Shanghao Liu, Zhiyong Luo, and Andrew D. Hamilton*

Recently there has been increasing interest in the design of catalysts for the hydrolysis of phosphodiester groups in DNA and RNA.[1,2] These artificial nucleases have many potential applications as anticancer or antiviral drugs[2f-i,3-5] and as artificial restriction nucleases.[1,6] Since metal ions are found in the active sites of many natural nucleases,[6,7] it is not surprising that metal complexes constitute a major class of artificial catalysts for phosphodiester hydrolysis.[1,2] Inspired by natural nucleases that exploit two metal ions in their active sites, several research groups developed dinuclear metal complexes that show significantly higher activity than mononuclear metal complexes.[2a,b,d-g,8-11] We recently showed that dinuclear Cu^{II} complexes **1** and **2** are more active than mononuclear Cu^{II} complexes **3** and **4** in catalyzing transesterification of the RNA model compound 2-hydroxypropyl-*p*-nitrophenylphosphate (HPNPP).[12] Here we report that **1** and **2** are also more effective than **3** and **4** in promoting base- and regioselective hydrolysis of ribonucleoside 2′,3′-cyclic monophosphates **5**,[13] intermediates in the hydrolysis of RNA (Scheme 1).[14]

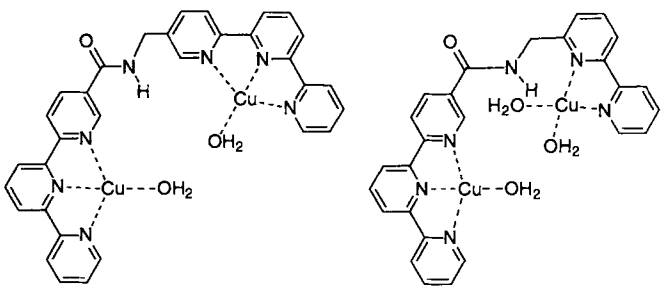

1 **2**

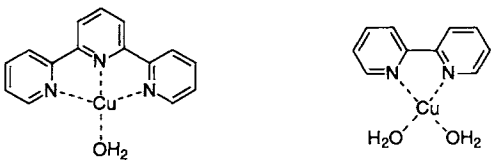

3 **4**

Hydrolysis of **5a–d** in the presence of excess **1–4** was conveniently monitored by HPLC; all reactions followed first-order kinetics. The pH–rate profiles for the hydrolysis of **5a** in the presence of **1** and **2** (Figure 1) show that maximal activities are reached at pH 7.5. Consequently, all other reactions were also carried out at pH 7.5. Table 1 summarizes rate constants and regioselectivities for the hydrolysis of **5a–d** catalyzed by **1–4**. Dinuclear complexes **1** and **2** are indeed more active than mononuclear complexes **3** and **4**. For example, **1** is almost 500 times more active than **3** in catalyzing the hydrolysis of **5b** (Table 1, entries 6 and 8). Similarly, although not as remarkably, **2** is about 35 times more active than **3** and about 22 times more active than **4** in catalyzing the

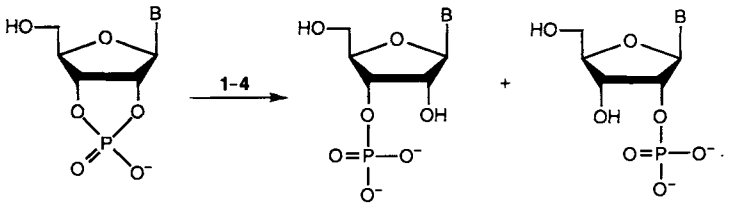

5 **6** **7**

Scheme 1. Cleavage of cyclic ribonucleoside 2′,3′-cyclic monphosphate (**5**) by copper complexes **1–4**; **a**: B = adenine, **b**: B = guanine, **c**: B = uracile, **d**: B = cytosine.

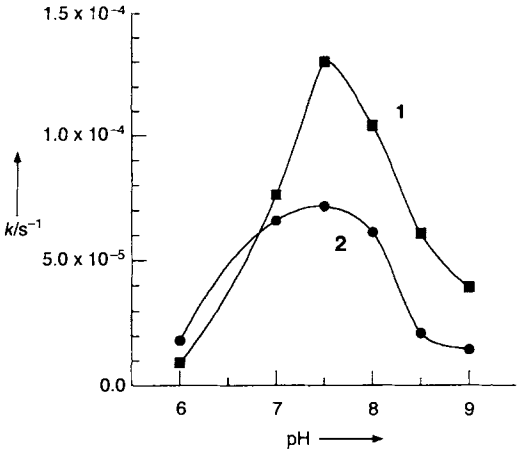

Figure 1. Interdependence of pH and rate (represented by k) for hydrolysis of **5a** (0.2 mM) at 20 °C in the presence of **1** and **2** (1.0 mM). The reaction media at pH 7.0, 7.5, and 8.0 are the HEPES buffers (0.05 M); those at pH 8.5 and 9.0 are the AMPSO buffers (0.05 M); and that at pH 6.0 is the MES buffer (0.05 M).

Table 1. Rate constants k and selectivities for hydrolysis of **5** catalyzed by **1–4**[a] under conditions for first-order kinetics (large excess of **1–4**).

Entry	Substrate	Catalyst	$k \times 10^6$ [s^{-1}]	Selectivity[b]
1	**5a**	**1**	130 ± 17	0.48 ± 0.01
2	**5a**	**2**	71.6 ± 7.7	1.92 ± 0.02
3	**5a**	**3**	2.03 ± 0.01	0.69 ± 0.01
4	**5a**	**4**	3.41 ± 0.11	2.97 ± 0.12
5	**5a**	–	0.0015[c]	1.2[c]
6	**5b**	**1**	713 ± 92	5.9 ± 0.1
7	**5b**	**2**	2.31 ± 0.15	0.73 ± 0.01
8	**5b**	**3**	1.56 ± 0.10	1.54 ± 0.05
9	**5b**	**4**	3.11 ± 0.43	3.45 ± 0.05
10	**5b**	–	0.0011[c]	1.1[c]
11	**5c**	**1**	360 ± 25	0.056 ± 0.002(17.7 ± 0.5[d])
12	**5c**	**2**	6.85 ± 0.35	0.62 ± 0.03
13	**5c**	**3**	1.26 ± 0.02	1.96 ± 0.02
14	**5c**	**4**	1.10 ± 0.05	2.01 ± 0.17
15	**5c**	–	0.00056[c]	1.0[c]
16	**5d**	**1**	84 ± 2	0.093 ± 0.003(10.7 ± 0.3[d])
17	**5d**	**2**	11.9 ± 0.9	1.20 ± 0.01
18	**5d**	**3**	0.84 ± 0.07	1.17 ± 0.02
19	**5d**	**4**	1.04 ± 0.22	1.86 ± 0.02
20	**5d**	–	0.00074[c]	0.9[c]

[a] At pH 7.5 (0.05 M HEPES buffer), 20 °C; [**1**, **2**] = 1.0 mM, [**3**, **4**] = 2.0 mM, [**5**] = 0.2 mM; all values of k and the selectivity are averages of two identical runs. [b] Ratio **6**:**7**. [C] Calculated from the data at pH 11.08 in ref. [15]. [d] Ratio **7**:**6**.

[*] Prof. A. D. Hamilton,[+] Dr. S. Liu, Z. Luo
Department of Chemistry, University of Pittsburgh
Pittsburgh, PA 15260 (USA)

[+] Current address: Department of Chemistry, Yale University
New Haven, CT 06520 (USA)
Fax: Int. code + (203)432-3221
e-mail: andrew.hamilton@yale.edu

[**] This work was supported by the U.S. National Institutes of Health (GM 53579).

 © WILEY-VCH Verlag GmbH, D-69451 Weinheim, 1997 0570-0833/97/3623-2678 $ 17.50+.50/0

hydrolysis of **5a** (Table 1, entries 2–4). These results demonstrate that the two Cu^{II} ions in **1** and **2** are highly cooperative in promoting hydrolysis of **5a–d**.

More interestingly, the dinuclear complexes show markedly higher, and in some cases opposite, base and regioselectivities relative to the mononuclear complexes. For example, **5b** is hydrolyzed about six times faster than **5a** when **1** is the catalyst but slightly *more slowly* than **5a** when **3** is the catalyst (Table 1, entries 1, 3, 6, and 8). Dinuclear complex **1** is not only the most active but also the most regioselective catalyst among the four complexes. For example, **1** cleaves the P–O (3′) bond in **5c** more than 17 times faster than the P–O (2′) bond (Figure 2 and Table 1, entry 11). In contrast, **2–4** cleave one P-O bond in **5c** no more than twice as fast as the other P–O bond (Figure 2 and Table 1, entry 12–14). Similarly, **1** is far more regioselective than **2–4** in hydrolyzing **5d** (Table 1, entries 16–19). Although not as active or regioselective as **1**, **2** is more base-selective than **1** and mononuclear complexes **3** and **4**. Dinuclear complex **2** hydrolyzes **5a** faster than the other three substrates with a maximun rate difference of 31-fold between **5a** and **5b** (Table 1, entries 2 and 7).

Natural ribonucleases hydrolyze RNA not only rapidly but also base-selectively. Furthermore, they hydrolyze **5a–d**, the intermediates in RNA hydrolysis, regiospecifically and produce only **6**.[14] Although a number of metal complexes were developed that cleave RNA and **5** rapidly,[1,2] few show significant base or regioselectivity.[2c,e,16] On the other hand, several catalysts, most having cyclodextrins as binding sites, show remarkable regioselectivities in catalyzing the hydrolysis of **5a–d**. However, the rate enhancements are usually less than ten times higher than the background rate of hydrolysis.[15,17,18] Dinuclear Cu^{II} complexes **1** and **2** cleave **5a–d** with both high activity (up to 10^6 rate enhancement over the background hydrolysis; Table 1, entries 6 and 10) and remarkable base and regioselectivities. In this regard, **1** and **2** resemble natural nucleases more closely than most nuclease mimics. Interestingly, the selectivity of **1** in cleaving **5c** and **5d** to produce more nucleoside 2′-monophosphate (**7c** and **7d**) than nucleoside 3′-monophosphate (**6c** and **6d**) is opposite to that of natural nucleases or the few nuclease mimics that show some regioselectivity. This reversed regioselectivity may be useful, since the 2′- and 3′-hydroxyl groups have quite different reactivities in enzymatic manipulation of RNA.

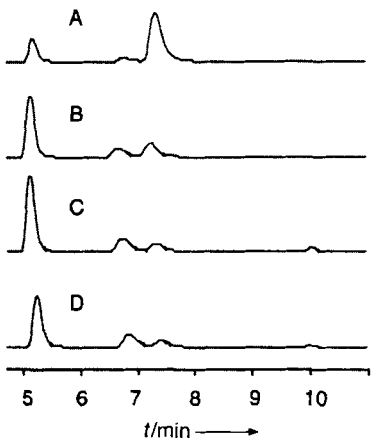

Figure 2. HPLC traces for the regioselective hydrolysis of **5c** (2′,3′-cUMP) in the presence of **1–4** in HEPES (0.05 M, pH 7.5) at 25 °C. [**5c**] = 0.2 mM; [**1**,**2**] = 1.0 mM; [**3**,**4**] = 2.0 mM. A: **1**, after 1.5 h; B: **2**, after 22.5 h; C: **3**, after 119 h; D: **4**, after 120 h. Retention times are as follows: 2′,3′-cUMP 5.2 min, 3′-UMP 6.8 min, 2′-UMP 7.4 min, uracil 10.1 min.

Natural nucleases achieve high base- and regioselectivities by recognizing and binding to nucleotide bases in the scissile region of RNA. We believe that **1** and **2** operate by similar mechanisms, based on an analysis of the data in Table 1. First, the high base and regioselectivities observed for **1** and **2** are likely due to active participation of the base groups in catalyst–substrate binding rather than steric effects, since the observed base- and regioselectivities do not correlate with the size or shape of the bases. For example, adenine and guanine in **5a** and **5b** are of similar size but show very different reactivities and regioselectivities. Second, the bases probably interact with the ligands instead of the Cu^{II} ions, since the observed base and regioselectivities do not correlate with known affinities of the nucleotide bases for metal ions.[19,20] For example, uracil and cytosine have very different affinities for metal ions, but both **5c** and **5d** show high regioselectivities with catalyst **1** (Table 1, entries 11 and 16).

Nucleotide bases can interact with the dinucleating ligands by hydrogen bonding to the amide linker or stacking to the π surface of the terpyridine or bipyridine subunits.[19,20] Scheme 2 shows two possible mechanisms by which **1** may hydrolyze **5**. Both mechanisms are consistent with a high degree of cooperativity between the two Cu^{II} ions in **1** (Table 1), which supports a double Lewis acid activation, and the bell-shaped pH–rate profile (Figure 1), which indicates both general base and general acid catalysis. The two mechanisms differ in the orientation of substrate with respect to the two Cu^{II} ions in **1**. As a result, the amide linker can potentially form a hydrogen bond in one but not the other orientation of the nucleotide base in the substrate–catalyst complex. Asymmetry of this type in substrate–catalyst interaction is required for there to be any difference in reactivity of the P–O (2′) and P–O (3′) bonds. Models show that the carbonyl group of uracil or cytosine in **5c** and **5d** is well positioned to form a hydrogen bond to the amide linker in **1** in only one catalyst–substrate complex. This suggests differential substrate–catalyst complex formation as a possible origin for the regioselectivities of **1**/**5c** and **1**/**5d**.

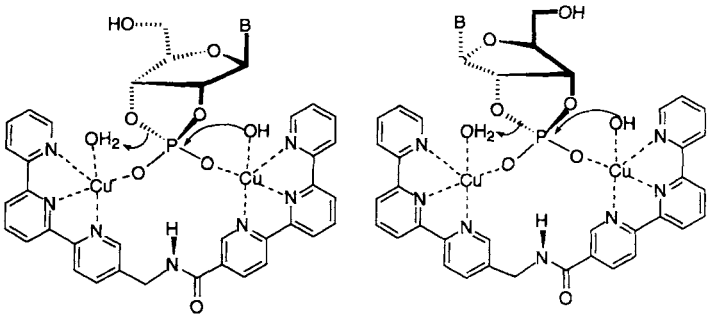

Scheme 2. Regioselective binding between the unsymmetric dinuclear metal complex **1** and **5a–d** as well as the resulting cleavage reactions. Since the two possible binding modes should have different binding energies, the left one is favored over the other and regioselective hydrolysis results.

Unlike **1**, the two Cu^{II} ions in **2** show only a moderate degree of cooperativity (Table 1), indicating a one Lewis acid–one general acid/base mechanism[12] and a reason for low regioselectivity. However, **2** shows higher selectivity for adenine relative to the other nucleotide bases. Sigel et al.

 © WILEY-VCH Verlag GmbH, D-69451 Weinheim, 1997 0570-0833/97/3623-2679 $ 17.50+.50/0

reported that the adenine group in 5′-AMP forms a stronger stacking interaction to bipyridinecopper(II) complexes than the uracil group in 5′-UMP.[19] Such a stacking interaction between adenine and bipyridine may account for the high selectivity of **2** for **5a** over **5b–d** (Table 1).

Dinuclear complexes **1** and **2** are highly active in promoting hydrolytic cleavage of nucleoside 2′,3′-cyclic monophosphates. Furthermore, **1** is highly regioselective and cleaves **5c** and **5d** predominantly to nucleoside 2′-monophosphates. On the other hand, **2** shows remarkable base selectivity and hydrolyzes **5a** much faster than **5b–d**. Presumably, **1** achieves high regioselectivity by regioselectively binding to the bases in the substrates, while **2** attains base selectivity by a preferential $\pi-\pi$ stacking interaction between the bipyridine unit in **2** and the bases in the substrates. More experiments are in progress to probe the exact nature of interactions that give rise to the high reactivities and base and regioselectivities shown by **1** and **2**.

Experimental Section

The preparation of **1–4** has been described previously [12]. Cleavage of **5** by **1–4** was followed by HPLC (Ranin). The following procedure is typical: **1** (1.1 mM, 4.5 mL) in a buffer was mixed with **5a** (2.0 mM, 0.5 mL) in the same buffer. Aliquots (200 μL) of the reaction mixture were quenched with ethylenediaminetetraacetate (EDTA, 20 mM, 200 μL). After any solid that formed was filtered, the quenched solution (20 μL) was injected onto a C-18 reversed-phase column and eluted for 10 min with 1–10% CH_3CN in H_2O containing 0.1% CF_3COOH (flow rate 1.0 mL min^{-1}). The eluent was monitored at λ_{max} of the nucleobase (260 nm for adenine and uracil, 252 nm for guanine, and 268 nm for cytosine) by a Rainin UV-C detector. The first-order rate constants k were obtained as slopes of plots of $\ln(A_0/A_t)$ versus t, where A_0 and A_t are integrations of the areas of the HPLC peaks for **5** at $t=0$ and t, respectively. Selectivities for the formation of 3′-monophosphate (**6**) with respect to 2′-monophosphate (**7**) were calculated from the ratios of integrations of the areas of the HPLC peaks for **6** and **7**. The identities of **6** and **7** were established with authetic samples (Sigma). The two isomers have nearly identical extinction coefficients at λ_{max} of the nucleobase. Therefore, the ratio of the HPLC peaks for **6** and **7** is equal to the ratio of the amounts of **6** and **7** produced (i. e., the regioselectivity). In all cases the ratios remained constant throughout the entire course of hydrolysis. For slow reactions ($k < 5\times10^{-6}$ s^{-1}), appreciable amounts of **6** and **7** were further hydrolyzed to give inorganic phosphate and the correponding nucleosides before **5** was completely hydrolyzed. However, the ratio of **6** to **7** in the reaction mixture remained unchanged. Duplicate runs showed measurement errors of less than ±15% for k and less than ±3% for the regioselectivity.

Received: June 9, 1997 [Z10523IE]
German version: *Angew. Chem.* **1997**, *109*, 2794–2796

Keywords: enzyme mimetics · hydrolyses · RNA

[1] Reviews: a) M. Komiyama, *J. Biochem.* **1995**, *118*, 665; b) J. R. Morrow, *Adv. Inorg. Biochem.* **1994**, *9*, 41; c) M. W. Gobel, *Angew. Chem.* **1994**, *106*, 1201; *Angew. Chem. Int. Ed. Engl.* **1994**, *33*, 1141; d) D. S. Sigman, A.Mazumder, D. M. Perrin, *Chem. Rev.* **1993**, *93*, 2295; e) J. Chin, *Acc. Chem. Res.* **1991**, *24*, 145.

[2] Recent examples: a) P.Hurst, B. K.Takasaki, J. Chin, *J. Am. Chem. Soc.* **1996**, *118*, 9982; b) M. J. Young, J. Chin, *ibid.* **1995**, *117*, 10577; c) B. Linkletter, J. Chin, *Angew. Chem.* **1995**, *107*; 529; *Angew. Chem. Int. Ed. Engl.* **1995**, *34*, 472; d) W. H. Chapman, Jr., R. Breslow, *J. Am. Chem. Soc.* **1995**, *117*, 5462; e) M. Yashiro, A. Ishikubu, M. Komoyama, *J. Chem. Soc. Chem. Commun.* **1997**, 83; f) M. Yashiro, A. Ishikubu, M. Komiyama, *ibid.* **1995**, 1793; g) M. Komiyama, N. Takeda, M. Irisawa, M. Yashiro in *DNA and RNA Cleavers and Chemotherapy of Cancer and Viral Diseases* (Ed.: B. Meunier), Kluwer, Boston, **1996**, p. 321; h) J. K. Bashkin, J. Xie, A. T. Daniher, L. A. Jenkins, G. C. Yeh, *ibid.* p. 355-366; i) R. Haner, J. Hall, D. Husken, H. E. Moser, *ibid.* p. 307; j) D. Magda, R. A. Miller, M. Wright, J. Rao, *ibid.* p. 337.

[3] C. A. Stein, J. S. Cohen, *Cancer Res.* **1988**, *48*, 2659.

[4] E. Uhlmann, A. Peyman, *Chem. Rev.* **1990**, *90*, 543.

[5] J. F. Milligan, M. D. Matteucci, J. C. Martin, *J. Med. Chem.* **1993**, 36, 1923.

[6] D. Pei, P. G. Schultz in *Nucleases* (Eds.: S. M. Linn, R. S. Lloyd, R. J. Roberts), 2nd ed., Cold Spring Harbor Laboratory Press, New York, **1993**, p. 317.

[7] N. Strater, W. N. Lipscomb, T. Klabunde, B. Krebs, *Angew. Chem.* **1996**, *108*, 2158; *Angew. Chem. Int. Ed. Engl.* **1996**, *35*, 2024.

[8] a) D. Wahnon, R. C. Hynes, J. Chin, *J. Chem. Soc. Chem. Commun.* **1994**, 1441; b) M. Wall, R. C. Hynes, J. Chin, *Angew. Chem.* **1993**, *105*, 1696; *Angew. Chem. Int. Ed. Engl.* **1993**, *32*, 1633; c) J. Chin, M. Banaszczyk, *J. Am. Chem. Soc.* **1989**, *111*, 4103.

[9] R. Breslow, S. Singh, *Bioorg. Chem.* **1988**, *16*, 408.

[10] a) D. H. Vance, A. W. Czarnik, *J. Am. Chem. Soc.* **1993**, *115*, 12165; b) Y. S. Chung, E. A. Akkaya, T. K. Venkatachalam, A. W. Czarnik, *Tetrahedron Lett.* **1990**, *31*, 5413.

[11] a) P. Hendry, A. M. Sargeson, *Prog. Inorg. Chem.* **1990**, *38*, 201; b) D. R. Jones, L. F. Lindoy, A. M. Sargeson, *J. Am. Chem. Soc.* **1984**, *106*, 7807; c) D. R. Jones, L. F. Lindoy, A. M. Sargeson, M. R. Snow, *Inorg. Chem.* **1982**, *21*. 4155.

[12] S. Liu, A. D. Hamilton, *Bioorg. Med. Chem. Lett.* **1997**, *7*, 1779.

[13] Hydrolysis of **5a** by **3** has been studied: J. K. Bashkin, L. A. Jenkins, *J. Chem. Soc. Dalton Trans.* **1993**, 3631.

[14] R. L. P. Adams, J. T. Knowler, D. P. Leader, *The Biochemistry of the Nucleic Acids*, 11th ed., Chapman and Hall, London, **1993**, p. 97.

[15] M. Komiyama, *J. Am. Chem. Soc.* **1989**, *111*, 3046.

[16] J. R. Morrow, V. M. Shelton, *New J. Chem.* **1994**, *18*, 371.

[17] a) M. Komiyama, Y. Takeshige, *J. Org. Chem.* **1989**, *54*, 4936; b) M. Komiyama, *Carbohydr. Res.* **1989**, *192*, 97; c) M. Komiyama, K. Isaka, S. Shinkai. *Chem. Lett.* **1991**, 937.

[18] For regioselective cleavage of a model compound for nucleoside 2′,3′-cyclic monophosphates, see R. Breslow, J. B. Doherty, G. Guillot, C. Lipsey, *J. Am. Chem. Soc.* **1978**, *100*, 3227; R. Breslow, P. Bovy, C. L. Hersh, *ibid.* **1980**, *102*, 2115.

[19] H. Sigel in *Metal–DNA Chemistry* (Ed.: T. D. Tullius), ACS, Washington, DC, **1989**, pp. 159.

[20] S. A. Kazakov in *Bioorganic Chemistry: Nucleic Acids* (Ed.: S. M. Hecht), Oxford University Press, New York, **1996**, 1244.

A Calixarene with Four Peptide Loops: An Antibody Mimic for Recognition of Protein Surfaces**

Yoshitomo Hamuro, Mercedes Crego Calama, Hyung Soon Park, and Andrew D. Hamilton*

The design of synthetic hosts that can recognize protein surfaces and disrupt biologically important protein–protein interactions remains a major unsolved problem in bioorganic chemistry.[1] In contrast, the immune system offers numerous antibodies that show high sequence and structural selectivity in binding to a wide range of protein surfaces.[2] This diversity of recognition is even more remarkable, because all antibody fragment antigen binding (FAB) regions share a common structural motif of six hypervariable loops held in place by the closely packed constant and variable regions of the light and heavy chains. Four of these loops (L2, L3, H2, and H3) generally take up a hairpin conformation and the remaining two form more extended loops.[2] X-ray analyses of protein–antibody complexes show that strong binding is achieved by the formation of a large and open interfacial surface (> 600 Å) composed primarily of residues that are capable of mutual hydrophobic, electrostatic, and hydrogen bonding interactions.[3–5] The majority of antibody complementary

[*] Prof. A. D. Hamilton,[+] Dr. Y. Hamuro, Dr. M. C. Calama, Dr. H. S. Park
Department of Chemistry, University of Pittsburgh
Pittsburgh, PA 15260 (USA)

[+] Current address: Department of Chemistry, Yale University
New Haven, CT 06520 (USA)
Fax: Int. code + (203) 432-3221
e-mail: andrew.hamilton@yale.edu

[**] This work was supported by the NIH (GM 53579) and post-doctoral fellowships to H.S.P. and M.C.C. from Korea Research Foundation (KRF) and NATO, respectively.

 © WILEY-VCH Verlag GmbH, D-69451 Weinheim, 1997 0570-0833/97/3623-2680 $ 17.50+.50/0

determining regions (CDRs) contact the antigen with four to six of the hypervariable loops.[4]

In recent years there has been considerable interest in the design of novel antibody-like recognition motifs.[6] Approaches have included the randomization of known CDR loops[7] or of two interhelix loops in a protein with four-helix bundles,[8] de novo protein design of loops based on a protein template,[9] or non-peptide artificial receptors.[10] However, the search for antibody mimics has not yet yielded compact and robust frameworks that reproduce the essential features of the CDRs.[11] Our strategy is to use a macrocyclic scaffold to which multiple peptide loops in stable hairpin-turn conformations can be attached. In this paper we report the synthesis of an antibody mimic based on calix[4]arene linked to four constrained peptide loops (Figure 1). The resulting host binds to the surface of cytochrome c in a manner similar to the natural protein partners.

Calix[4]arene was chosen as the core scaffold, as it is readily available[12,13] and can be locked into the semirigid cone conformation by alkylation of the phenol groups. This results in a projection of the *para*-substituents onto the same side of the ring to form a potential binding domain.[14] The required tetracarboxylic acid **1** was prepared by alkylation of calix[4]-arene[12c] (*n*-butyl bromide, NaH) followed by formylation (Cl_2CHOCH_3, $TiCl_4$) and oxidation ($NaClO_2$, H_2NSO_3H).[15]

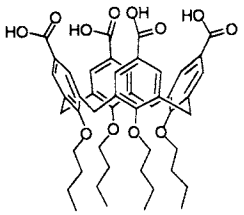

1

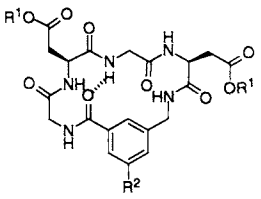

2: $R^1 = t$Bu, $R^2 = NH_2$,
4: $R^1 = H$, $R^2 = NO_2$,

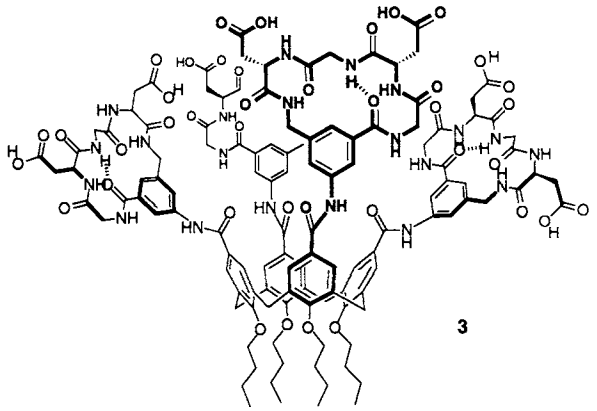

3

The peptide loop was based on a cyclic hexapeptide in which two residues were replaced by a 3-aminomethylbenzoyl (3amb) dipeptide analogue[16] containing a 5-amino substituent for facile linkage to the scaffold. Von Itzstein et al. and DeGrado et al. had previously shown that cyclic peptides of this type take up intramolecularly hydrogen-bonded β-turn conformations.[17] The 5-nitro substituted dipeptide analogue was formed by selective reduction (BH_3) of methyl 3-amidocarbonyl-5-nitrobenzoate, followed by deesterification (LiOH in THF) and reaction sequentially with Fmoc-Asp-(*t*Bu)-OH and H-Gly-Asp(*t*Bu)-Gly-OH (dicyclohexyl carbodiimide (DCC), *N*-hydroxysuccinimide) to yield Fmoc-Asp(*t*Bu)-5$NO_2$3amb-Gly-Asp(*t*Bu)-GlyOH. Cyclization with 4-dimethylaminopyridine (DMAP) and 2-(1*H*-benzotriazole-1-yl-1,1,3,3,-tetramethyluronium tetrafluoroborate (TBTU) was achieved in 70% yield, followed by reduction (H_2, Pd/C) to give the amino-substituted peptide loop **2**. Amine **2** was coupled to the tetraacid chloride derivative of **1** ($(COCl)_2$, DMF) and deprotected with trifluoroacetic acid (TFA) to give the tetraloop structure **3**. The molecular structure of this host (Figure 1) resembles that of the antigen

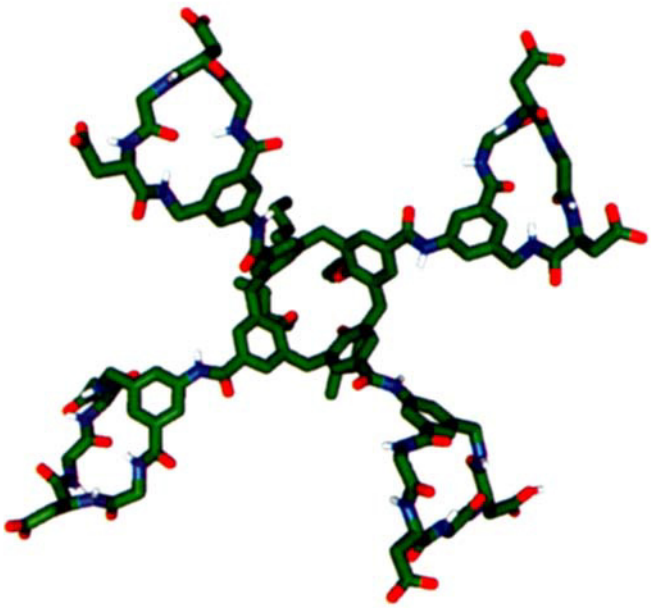

Figure 1. Representation of the structure of host **3** with four peptide loops [24].

binding region of an antibody but is based on four loops rather than six.[3] We chose cytochrome c as the initial protein target, since it is structurally well-characterized and contains a positively charged surface made up of several lysine and arginine residues.[18] In this study the negatively charged GlyAspGlyAsp sequence was used in the loops of **3**[19] to complement the charge distribution on the protein. However, the synthetic strategy permits the use of other sequences to generate antibody mimics with different recognition characteristics.

The special binding affinity afforded by the multiloop structure in **3** for cytochrome c (cyt c) was clearly seen by affinity chromatography. A mixture of **3** and single peptide loop diacid **4** in tris(hydroxylmethyl)aminomethane (Tris) buffer was added to a column containing agarose-linked cyt c followed by increasing concentrations of NaCl.[20] The monoloop derivative **4** eluted without NaCl, whereas the tetraloop receptor **3** required NaCl concentrations of 2 M before it passed through the column. This affinity compares well with cytochrome oxidase which was reported to elute from a similar column at NaCl concentrations of 100 mM.[21] Further support for a strong and discreet interaction came from gel permeation chromatography on Sephadex G-50 in 5 mM phosphate buffer at pH 7.4. A 2:1 mixture of **3** and cyt c gave a sharp band with a shorter retention time (reflecting larger

 © WILEY-VCH Verlag GmbH, D-69451 Weinheim, 1997 0570-0833/97/3623-2681 $ 17.50+.50/0

molecular size) than pure cyt c (Figure 2). Furthermore, a corresponding 1:2 mixture showed both bands in the chromatogram, confirming the presence of both complexed and free cytochrome c in solution.

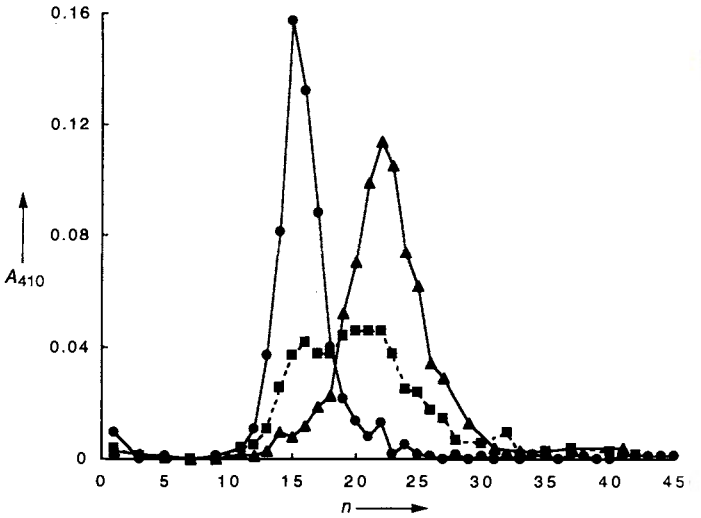

Figure 2. Gel permeation chromatography on Sephadex G-50 with phosphate buffer (5 mM, pH = 7.4) of cytochrome c (▲), 1:2 cytochrome c:**3** (●), and 2:1 cytochrome c:**3** (■). A_{410} is the absorbance at 410 nm; n is the fraction number.

The exact site on the surface of cytochrome that binds **3** has not yet been established. One likely possibility is the region close to the heme edge surrounded by the group of positively charged residues (Lys-17, 18, 21, 77, and 88),[22] which forms the primary interaction surface with electron transfer partners such as cytochrome c peroxidase and cytochrome oxidase.[23] Support for this binding arrangement came from ^{1}H NMR titration experiments: changes in the position of the hyperfine shifted heme-CH_3 resonances were followed as a function of increasing concentration of **3**.[25] The heme 8-CH_3 and 3-CH_3 resonances shifted upfield ($\Delta\delta = -0.27$) and downfield ($\Delta\delta = +0.25$), respectively, broadened, and reached saturation at approximately one equivalent of added **3**. The direction and the size of the shifts (-0.5 and $+0.5$) are similar to those seen in the equivalent titration between cyt c and cytochrome c peroxidase.[26] Docking a calculated structure for **3** with this region on the X-ray structure of cyt c[18] (Figure 3) confirms that the four peptide loops can contact four of the five lysine residues and cover a large area of the protein surface.[24]

A key goal in this work is to use our antibody mimics to disrupt the normal function of the protein. We have investigated the effect of complexation with **3** on the interaction of Fe^{III}-cyt c with reducing agents.[27,28] In phosphate buffer Fe^{III}-cyt c (1.57×10^{-5} M) is rapidly reduced by excess ascorbate (2.0×10^{-3} M) with a pseudo-first-order rate constant 0.1090 ± 0.001 (Figure 4). In the presence of **3** (1.91×10^{-5} M) the rate of cyt c reduction is diminished tenfold ($k_{obs} = 0.010 \pm 0.001\ s^{-1}$), consistent with the calixarene derivative's binding to the protein surface and inhibiting approach of ascorbate to the heme edge (Figure 3). A very similar inhibition of ascorbate reduction is seen with the cytochrome c/cytochrome c peroxidase complex,[27] further suggesting that **3** binds to a similar region of cyt c as its natural protein partners. A plot of k_{obs} vs. [**3**] shows a saturation curve that fits well to a 1:1 binding model and from which an association

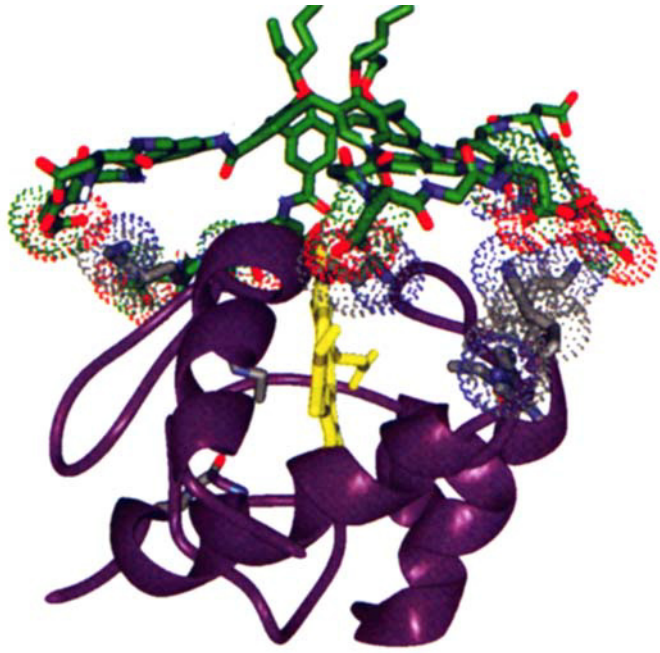

Figure 3. Proposed structure for the complex between cytochrome c and **3** [24].

constant of $(3.05 \pm 0.20) \times 10^6\ M^{-1}$ was calculated. The importance of the four loops in the design of **3** is seen by the minimal effect that even large concentrations of single loop **4** (5.36×10^{-4} M) had on the ascorbate reduction. Also, the interaction between **3** and cyt c is not simply a polyanion effect as excess concentrations of inositol hexaphosphate (Figure 4) or polyglutamate (at glutamate concentrations of 2.60×10^{-3} M) had only modest effect on the rate of ascorbate reduction.[28]

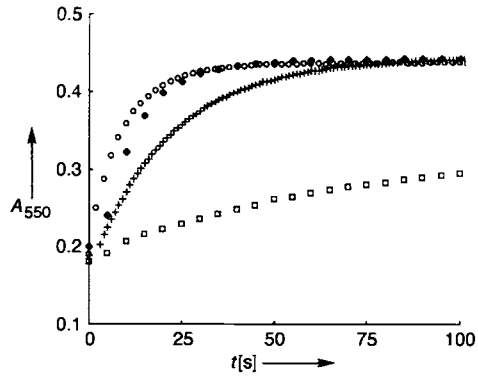

Figure 4. Kinetics of reduction of Fe^{III}-cyt c (1.57×10^{-5} M) by ascorbate in the presence of no receptor (○), **3** (1.91×10^{-5} M, □), **4** (5.36×10^{-4} M, ◆), and inositol hexaphosphate (2.55×10^{-4} M, +). A_{550} is the absorbance at 550 nm.

The new type of synthetic host **3** thus mimics antibody combining sites in having several peptide loops arrayed around a central binding region. The large surface area in the molecule allows strong binding to a complementary surface on cytochrome c and disrupts, in a similar way to cytochrome c peroxidase, the approach of reducing agents to the active site of the protein. We are currently preparing libraries of antibody mimics from different peptide loop sequences and screening their binding to a range of protein targets.

 © WILEY-VCH Verlag GmbH, D-69451 Weinheim, 1997 0570-0833/97/3623-2682 $ 17.50+.50/0

Experimental Section

3: To a solution of **1** [14,15] (86 mg, 0.10 mmol) and oxalyl chloride (254 mg, 2.0 mmol) in dry CH_2Cl_2 (10 mL) was added DMF (0.025 mL) through a silica gel filter, and the mixture was stirred at room temperature for 8 h. The reaction mixture was evaporated in vacuo to obtain the acid chloride (102 mg). A solution of **2** [17] (266 mg, 0.44 mmol) and diisopropylethylamine (DIEA, 80 mg, 0.60 mmol) in dry CH_2Cl_2 (10 mL) was added to the evaporated residue. The mixture was stirred at room temperature for 14 h. The reaction mixture was purified by preparative thin-layer chromatography (SiO_2; eluted with MeOH/CH_2Cl_2, first 1/9 and later 1/4) to afford the octa-*tert*-butyl ester derivative of **3** as a yellow powder (281 mg, 89%): m.p. > 350°C; ^{1}H NMR (300 MHz, [D$_6$]DMSO): $\delta = 10.10$ (br. s, 4H), 8.95 (br., 4H), 8.49 (br., 4H), 8.25 (d, $J = 8.7$ Hz, 4H), 8.09 (br., 4H), 7.99 (m, 8H), 7.67 (s, 4H), 7.60 (s, 8H), 7.37 (s, 4H), 4.81 (m, 8H), 4.51 (m, 8H), 3.99 (m, 20H), 3.63 (m, 8H), 3.46 (m, 4H), 2.79 (m, 4H), 2.62 (m, 4H), 2.31 (m, 8H), 1.97 (m, 8H), 1.47 (m, 8H), 1.35 (m, 72H), 1.02 (t, $J = 8.4$ Hz, 12H); ^{13}C NMR (75 MHz, [D$_6$]DMSO): $\delta = 120.1$, 117.8, 80.0 (2C), 75.0, 49.1, 48.8, 44.2, 42.3, 41.4, 37.5, 36.9, 31.9, 30.5, 27.6 (2C), 18.9, 14.0.

The octaester (298 mg, 0.093 mmol) was added to TFA (3 mL) and dry CH_2Cl_2 (3 mL), and the mixture was stirred at room temperature for 1 h. The mixture was evaporated under reduced pressure. The crude product was passed through anion exchange resin (Amberlite IRA-400(OH), water) and cation exchange resin (Amberlite IR 120 (plus), water) to remove ions. Water was lyophilized to give **3** (229 mg, 90%): m.p. > 350°C; ^{1}H NMR (300 MHz, [D$_6$]DMSO): $\delta = 10.02$ (s, 4H), 8.81 (s, 4H), 8.48 (s, 4H), 8.31 (d, $J = 8.7$ Hz, 4H), 7.97 (m, 12H), 7.64 (s, 4H), 7.55 (s, 8H), 7.30 (s, 4H), 4.76 (m, 8H), 4.52 (m, 8H), 4.0–3.4 (m, 32H), 2.8–2.6 (m, 8H), 2.5–2.3 (m, 8H), 1.97 (m, 8H), 1.50 (m, 8H), 1.01 (t, 8H); ^{13}C NMR (75 MHz, [D$_6$]DMSO): $\delta = 172.2$, 171.7, 170.9, 170.4, 169.3, 168.5 (2C), 165.1, 159.0, 140.2, 138.8, 134.4, 134.2, 128.7, 128.3, 121.4, 119.9, 117.7, 75.0, 49.1 (2C), 44.3, 42.2, 41.3, 36.1 (2C), 31.9, 30.5, 18.9, 14.0; high-resolution fast-atom-bombardment mass spectrometry (matrix: 3-nitrobenzyl alcohol): *m/z* calcd for $C_{128}H_{145}N_{24}O_{44}$ (M+H$^+$) 2721.9767; found 2721.985.

Received: June 12, 1997 [Z10543IE]
German version: *Angew. Chem.* **1997**, *109*, 2797–2799

Keywords: calixarenes · cytochrome c · molecular recognition · peptidomimetics · proteins

[1] For a general discussion of protein–protein recognition sites, see J. Janin, C. Chothia, *J. Biol. Chem.* **1990**, *265*, 16027–16030.
[2] C. Branden, J. Tooze, *Introduction to Protein Structure*, Garland, New York, **1991**, p. 187.
[3] I. A. Wilson, R. L. Stanfield, J. M. Rini, J. H. Arevalo, U. Schulze-Gahmen, D. H. Fremont, E. A. Stura, *Ciba Found. Symp.* **1991**, *159*, 13–39.
[4] D. R. Davies, S. Chacko, *Acc. Chem. Res.* **1993**, *26*, 421–427.
[5] a) C. Chothia, A. M. Lesk, A. Tramontano, M. Levitt, S. J. Smith-Gill, G. Air, S. Sheriff, E. A. Padlan, D. Davies, W. R. Tulip, P. M. Colman, S. Spinelle, P. M. Alzari, R. J. Pojak, *Nature* **1989**, *342*, 877–883; b) C. Chothia, A. M. Lesk, *J. Mol. Biol.* **1987**, *196*, 901–917.
[6] See P. Hollinger, H. R. Hoogenboom, *Trends Biotech.* **1995**, *13*, 7–9.
[7] C. F. Barbas, J. D. Bain, D. M. Hoekstra, R. A. Lerner, *Proc. Natl. Acad. Sci. USA* **1992**, *89*, 4457–4461.
[8] J. Ku, P. G. Schultz, *Proc. Natl. Acad. Sci. USA* **1995**, *92*, 6552.
[9] M. Mutter, P. Dumy, P. Garrouste, C. Lehmann, M. Mathieu, C. Peggion, S. Peluso, A. Razaname, G. Tucherer, *Angew. Chem.* **1996**, *108*, 1588–1591; *Angew. Chem. Int. Ed. Engl.* **1996**, *35*, 1482–1485.
[10] J. O. Magrans, A. R. Ortiz, M. Antonia Molins, P. H. P. Lebouille, J. Sanchez-Quesada, P. Prados, M. Pons, F. Gago, J. de Mendoza, *Angew. Chem.* **1996**, *108*, 1816–1819; *Angew. Chem. Int. Ed. Engl.* **1996**, *35*, 1712–1715.
[11] L. C. Hsieh-Wilson, X-D, Xiang, P. G. Schultz, *Acc. Chem. Res.* **1996**, *29*, 164–170.
[12] a) C. D. Gutsche, M. Iqbal, D. Stewart, *J. Org. Chem.* **1986**, *51*, 742–745; b) C. D. Gutsche, L-G. Lin, *Tetrahedron* **1986**, *42*, 1633–1640; c) M. Conner, V. Janout, S. L. Regen, *J. Org. Chem.* **1992**, *57*, 3744–3746.
[13] Calix[5]arene and calix[6]arene are also available and offer the potential for extending this approach to analogues with 5- and 6-loops.
[14] A related example: A. Casnati, M. Fabbi, N. Pelizzi, A. Pochini, F. Sansone, R. Ungaro, E. Modugno, G. Tarzia, *Bioorg. Med. Chem. Lett.* **1996**, *6*, 2699–2704; A. Marra, A. Dondoni, F. Sansone, *J. Org. Chem.* **1996**, *61*, 5155–5158.
[15] The syntheses of analogous compounds were described in R. H. Vreekamp, Thesis, University of Twente (The Netherlands), **1995**.
[16] M. Nigam, C. M. Seong, Y. Qian, M. A. Blaskovich, A. D. Hamilton, S. M. Sebti, *J. Biol. Chem.* **1993**, *268*, 20695–20698.
[17] a) M. L. Smythe, M. von Itzstein, *J. Am. Chem. Soc.* **1994**, *116*, 2725–2733; b) A. C. Bach, C. J. Eyerman, J. D. Gross, M. J. Bower, R. L. Harlow, P. C. Weber, W. F. DeGrado, *ibid.* **1994**, *116*, 3207–3219.
[18] G. W. Bushnell, G. V. Lourie, G. D. Brayer, *J. Mol. Biol.* **1990**, *214*, 585–595.
[19] NMR analysis shows that **2** takes up an intramolecularly hydrogen-bonded conformation similar to that seen in the cyclo-(Ala-Arg-Gly-Asp-Mamb) loop [17b].
[20] Cytochrome c linked to agarose was purchased from Sigma and packed in a 5 × 125 mm column. A mixture of 1.2 mmol of **3** and 2.5 mmol of **4** in Tris buffer (10 mM, pH = 7.4) was applied and eluted with the same buffer solution with stepwise increase in NaCl concentrations (20 mL each of 0, 0.5, 2, and 4 M).
[21] T. Ozawa, M. Tanaka, T. Wakabayashi, *Proc. Natl. Acad. Sci. USA* **1982**, *79*, 7175–7179.
[22] G. Mclendon in *Control of Biological Electron Transport via Molecular Recognition and Binding: The "Velcro" Model*; (Eds.: M. J. Clark, J. B. Goodenough, J. A. Ibers, C. K. Jorgensen, D. M. P. Mingos, J. B. Neilands, G. A. Palmer, D. Reinen, P. J. Sadler, R. Weiss, R. J. P. Williams), Springer, Heidelberg, **1991**, p 165.
[23] Crystal structure of the complex between cytochrome c and cytochrome c peroxidase: H. Pelletier, J. Kraut, J. *Science* **1992**, *258*, 1748–1755.
[24] Calculated with the program MacroModel of W. C. Still, Columbia University, New York (USA).
[25] ^{1}H NMR titration conditions: [Cyt c] = 3.0 mM in 12 mM KNO_3, pD = 9.3, [**3**] = 0–9 mM.
[26] NMR titration of cytochrome c with cytochrome c peroxidase: J. D. Satterlee, S. J. Moench, J. E. Erman, *Biochim. Biophys. Acta* **1987**, *912*, 87–97.
[27] E. Mochan, P. Nicholls, *Biochim. Biophys. Acta*, **1972**, *267*, 309–319.
[28] L. C. Petersen, R. P. Cox, *Biochem. J.* **1980**, *192*, 687–693.

$BaSn_3$: A Superconductor at the Border of Zintl Phases and Intermetallic Compounds. Real-Space Analysis of Band Structures**

Thomas F. Fässler* and Christian Kronseder

In memory of Jeremy Burdett

Superconducting intermetallic compounds that are rich in main group elements, especially the alloys that crystallize in the Cu_3Au structure type, have been a focus of research owing to the interesting dependence of their critical temperature T_c on their valence electron counts.[1] In the course of our investigations on phases rich in germanium, tin, and lead, we discovered superconducting compounds in the latter two systems. We report here the pure-phase synthesis, magnetic properties, and electronic structure of $BaSn_3$, which crystallizes in the Ni_3Sn structure type (hexagonal variant of Cu_3Au). Results of band-structure calculations on $BaSn_3$ that predict anisotropic conductivity and show very flat bands at the Fermi edge E_F were the impetus for our magnetic studies. The coincident appearance of quasi-molecular states (localization)—and therefore a high density of states at E_F—with steep, disperse bands crossing the Fermi level (delocalization) may be viewed as a "fingerprint" in the search for new superconductors.[2] The hypothesis that pairing localization of conducting electrons occurs in superconductors[3] was successfully tested with several model systems, for example $(RE)_2X_2C_2$ (RE = rare earth metal, X = halogen) and $La_9Br_5(CBC)_3$.[2,4] Note that even in the case of the superconducting cuprates, the maximum transition temperature corresponds to a high density of states at E_F (van Hove singularity).[5]

[*] Dr. T. F. Fässler, C. Kronseder
Laboratorium für Anorganische Chemie der
Eidgenössischen Technischen Hochschule
Universitätstrasse 6, CH-8092 Zürich (Switzerland)
Fax: Int. code + (1) 632-1149
e-mail: faessler@inorg.chem.ethz.ch

[**] This work was supported by the Eidgenössischen Technischen Hochschule Zürich. We thank D. von Arx and M. Spahr for performing the magnetic-susceptibility measurements and Prof. R. Nesper for friendly support.

$BaSn_3$ is a model superconducting compound, as it is the first material discovered at the border of intermetallic compounds and Zintl phases that exhibits these characteristics. In this work the electronic properties of $BaSn_3$ are rationalized using calculations of band structure and the electron localization function (ELF).[6] A real-space analysis of the band structure is accomplished with the aid of direction-dependent partial electron density (PED).[7] Such a depiction of the crystal-orbital densities allows an analysis of the band structure in real space that is unachievable with other methods,[11] and provides intuitive pictures for solid-state compounds that are similar to those provided by the popular orbital concept for molecular systems.

$BaSn_3$ was synthesized as a pure phase by the stoichiometric combination of the elements.[14–16] $BaSn_3$ crystallizes in the primitive hexagonal Ni_3Sn structure type (space group $P6_3/mmc$, $a=b=7.253(2)$, $c=5.496(2)$ Å) with the tin atoms at the nickel positions.[16] This structure type, which is common for intermetallic compounds, occurs by a 1:3 distribution of the Sn and Ba atoms within hexagonal layers (small and large circles in Figure 1a) that stack in an ABAB sequence (Figures 1a and 1b). The distortion within the layers of Sn atoms (Wyckoff site: $(6h)\,x$, $2x$, 1/4; $x=0.8594$) with respect to the corresponding sites in the aristotype structure ($x=0.8333$) leads to shorter contacts between Sn atoms within a layer (Sn–Sn 3.058 Å)[17] and longer distances between Sn and Ba centers (Sn–Ba 3.663 Å). The compression along the c axis ($c/a=0.758$) manifests itself in short interlayer distances between Ba and Sn atoms (Ba–Sn 3.641 Å); however, the Sn–Sn interlayer contacts (3.266 Å) are longer than the intralayer contacts.

The topology of the tin framework (Figure 1g) emphasizes the relationship to the hexagonal perovskite structure ($BaNiO_3$) and a description according to the concept of Zintl, Klemm, and Busmann. $BaSn_3$ may be described as a defect structure in which tin atoms are at the oxygen positions, and the centers of the octahedra are unoccupied ($Ba\square Sn_3$). The one-dimensional chains running along the c axis are constructed from elongated face-sharing octahedra and may be described as $^1_\infty[Sn_6^{4-}]$, a formula that invokes the transfer of Ba valence electrons to the Sn polyanion. If only the shortest Sn–Sn contacts are considered to be bonding, the tin atoms may be viewed as forming triangular Sn_3^{2-} ions (Scheme 1).[17] Such units are isoelectronic with aromatic 2π-electron cyclopropanyl cations ($C_3R_3^+$). Therefore, the chains of face-sharing octahedra may also be viewed as a stacking of triangular units with strong interactions between the component π systems.

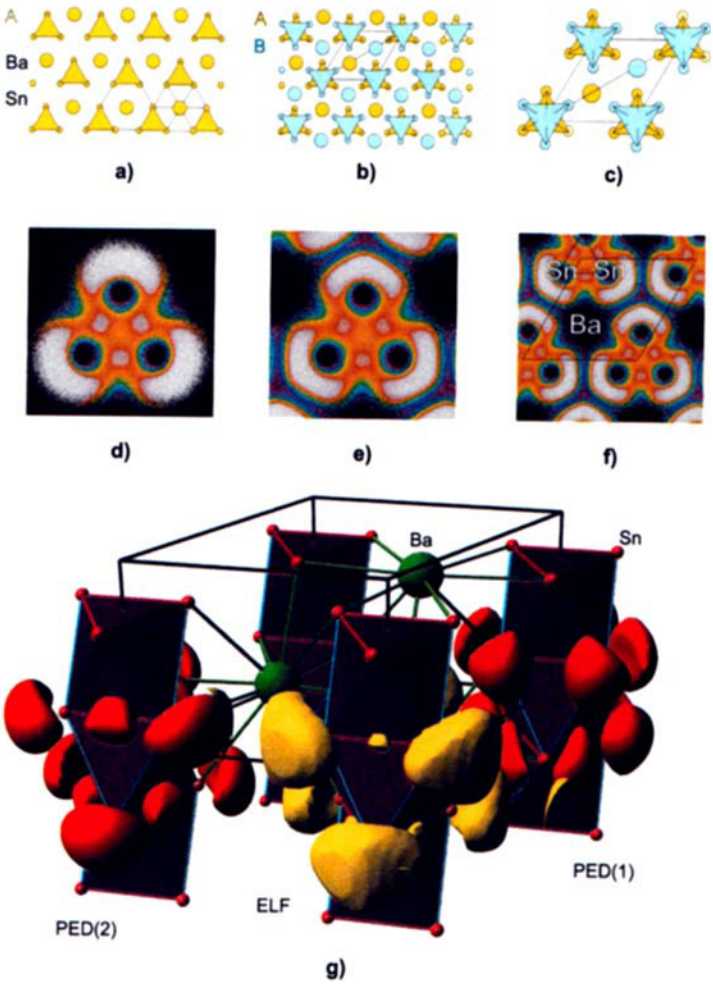

Figure 1. Structure and graphical analysis of the electronic structure of $BaSn_3$. a) A hexagonal layer with a 1:3 distribution of the atoms, b) AB stacking of two such layers ($z=1/4$ and 3/4), c) distortion from ideal hexagonal packing, d) the ELF in a plane through the atoms of an isolated one-dimensional $^1_\infty[Sn_6^{4-}]$ chain of octahedra, e) the ELF in $BaSn_3$ (same plane as in d)), f) a larger cross-section from the $BaSn_3$ structure, g) 3D representation of the face-sharing tin octahedra. ELF = 0.80 (yellow); the PED (red) isosurfaces of the band sections **1** (right) and **2** (left) have been added. The PED was calculated for the thick part of the flat bands near the Fermi level (between M and Γ) in Figure 3.

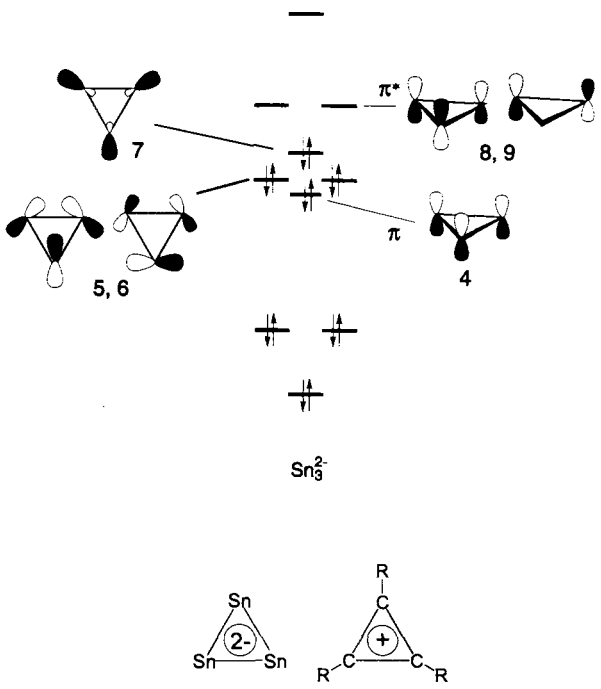

Scheme 1. MO scheme of a Sn_3^{2-} Zintl anion.

Measurements of the magnetic suseptibility at low field and at various temperatures showed the typical curves for diamagnetic shielding and the Meissner effect ($T_c=4.3$ K, Figure 2).[18] The transition temperature of $BaSn_3$ can be clearly differentiated from that of tin (3.7 K), as proven by similar measurements on elemental Sn and a simultaneous measurement of a mixture of Sn and $BaSn_3$ (inset of Figure 2).

The density of states and a section of the band structure obtained from LMTO calculations are shown in Figure 3.[19] The band structure of $BaSn_3$ (Figure 3a) features a large

 © WILEY-VCH Verlag GmbH, D-69451 Weinheim, 1997 0570-0833/97/3623-2684 $ 17.50+.50/0 *Angew. Chem. Int. Ed. Engl.* **1997**, *36*, No. 23

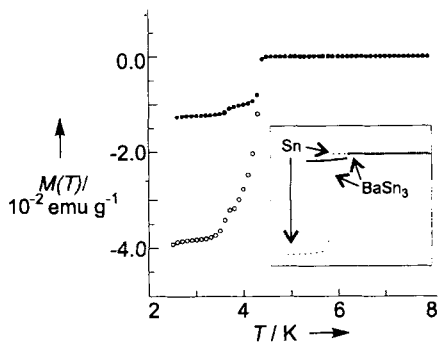

Figure 2. Diamagnetic shielding (○) and Meissner effect (●) in $BaSn_3$ as a function of temperature. The inset shows the results of a similar measurement on elemental tin.

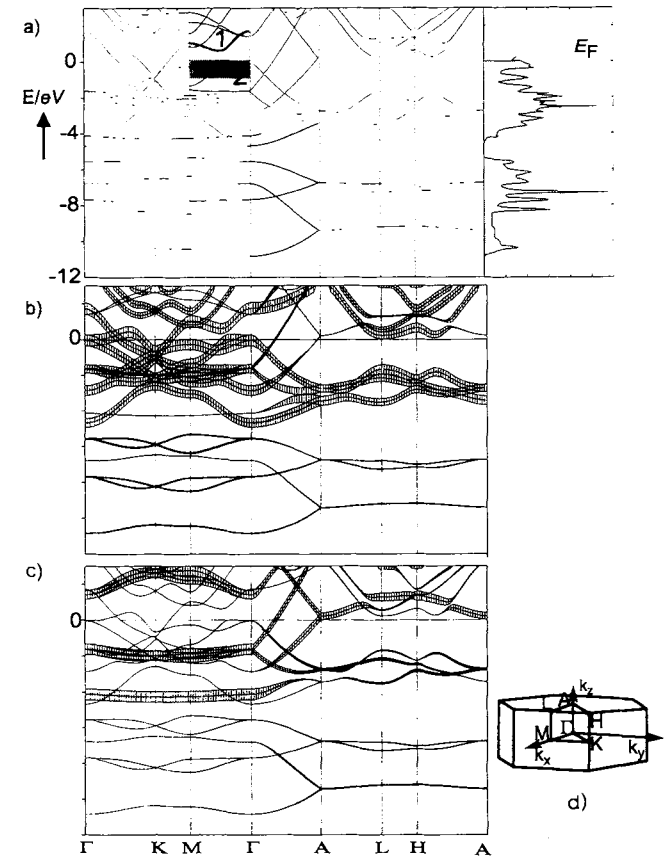

Figure 3. Band structure and density of states of $BaSn_3$. The contributions of the b) p_x, p_y and c) p_z orbitals the tin atom are plotted. The Fermi level is taken as the point of zero energy. The Brillouin zone is shown in d).

dispersion in the bands along the symmetry lines perpendicular to the distorted hexagonal layers; the bands parallel to the layers are comparatively flat. An anisotropic metallic conductivity is apparent in $BaSn_3$ with the special situation that flat bands and a degeneracy (in the zone center Γ) appear at the Fermi level. This leads to an increased density of states at E_F (Figure 3a, right). A "fat-band" analysis, in which the thickness of the band represents the corresponding orbital contribution, shows that the flat portions of the bands in the vicinity of E_F originate from p_x and p_y orbitals of the Sn atom (Figure 3b). Conversely, in the sections featuring steep bands, such as from Γ to A (i. e. parallel to the octahedral chains, z direction), increased mixing with the p_z orbital is observed (Figure 3c). From real-space PED plots, sections **1** and **2** of the band structure depicted in Figure 3a may be assigned to the molecular orbitals of the triangular Sn_3 unit shown in Scheme 1.

The result of the graphical analysis[20] of an extended-Hückel calculation,[21] which enables a qualitative analysis of the LMTO band structure, is shown in Figure 1g. Here the PED isosurface of the flat band from section **1** (along the M – Γ line) is shown on the right octahedral chain, and that of section **2** on the left.[22] The analysis shows that the bands below E_F arise from the lone electron pairs (MO 7, Scheme 1) with mixing of the "tangential orbitals" of the tin triangle (see MOs 5 and 6); above E_F, only the tangential orbitals are apparent. It is remarkable that the "MO-like" pictures in Figure 1g were obtained from calculations of band structures with the underlying symmetry of the k points in reciprocal space, and not calculated from points of higher symmetry (e. g. only at Γ), which is the usual method for depicting the wave function.[23] This enables consideration of anisotropic properties in real space.

To pinpoint the interaction between the free electron pairs at the Fermi level,[24] ELF analyses were performed.[20] Figure 1d shows the ELF of a layer parallel to the xy plane through three tin atoms of an isolated $^1_\infty[Sn_6^{4-}]$ octahedral chain. One can clearly discern three small bright areas, which are consistent with the Sn–Sn bond lengths that are about 0.2 Å shorter; this supports the formulation as a Sn_3^{2-} Zintl ion.[17] Three outer areas with half-moon shapes correspond to the free electron lone pairs of the tin atoms. The same cross-section from the full $BaSn_3$ structure is shown in Figure 1e, and a magnification of a unit in Figure 1f. The lone pairs are clearly flattened owing to interactions with neighboring electron pairs. This correlates with the strong lowering of the bands at the Fermi level (section **2**) that is observed in calculations for which a larger separation of the octahedral chains is effected by increasing the unit-cell parameters but retaining the same Sn–Sn bond lengths. The "compression" of the lone pairs in $BaSn_3$ may also be seen in three-dimensional ELF plots (yellow isosurface in Figure 1g).

The results obtained with PED and ELF demonstrate that the interaction of the lone pairs parallel to the layers are responsible for the band dispersion and for the elevation of certain bands at the Fermi level. The following qualitative picture of the electron – phonon interactions may be deduced: Lattice vibrations have a strong effect on the interactions between the lone pairs. Raising the states of the free electron pairs above the Fermi level results in electron transfer to the conduction band (and vice versa), that is, transitions between localized and conducting electrons may be dependent on lattice vibrations.

$BaSn_3$ may certainly be viewed as a borderline Zintl phase. Strong "interanionic" interactions between the π systems of the anionic units and weak interactions between the lone pairs must be considered. Similar situations were also found in other compounds. Interactions leading to 1D metallic properties were seen between the π systems of the central Si_6 rings in the stacked planar $[Si_{12}]^{20.5-}$ anions of $Ca_7Mg_{7.25}Si_4$.[25] Parabolic arrangements of lone pairs were observed in the intermetallic compound $RhBi_4$[26] and in the caverns of the lead substructure of K_5Pb_{24}.[8] Both $RhBi_4$[27] and K_5Pb_{24}[8] exhibit superconductivity. Superconductivity is also observed in the silicides $(Na,Ba)_xSi_{46}$.[28] The silicon atoms are tetravalent in the basic clathrate(I) structure type A_4Si_{23} where A = K, Na.[29] Assigning the composition of some compounds of this structure type as $A_4E_{22}\square_1$ (A = alkali metal, E = Si, Ge)

requires that one of the sites in the 3D network of E atoms is vacant.[30] Since sites adjacent to the empty position contain three-bonded atoms (that are isosteric to the Group 15 elements), these compounds may also be described as Zintl phases with interacting electron pairs. A strong interdependent influence of neighboring electron pairs of three-bonded atoms can also be found in the Zintl phase $K_6Sn_{23}Bi_2$.[8,31]

These observations can be interpreted as evidence for a correlation between the presence of localized states in the form of lone pairs in metallic conductors and superconductivity. Further examples and analyses may lend support to this theory. For $BaSn_3$, which resides on the border of intermetallic compounds, it appears that a balanced interplay of interactions between localized and delocalized structural components leads to the development of specific metallic properties.

Received: June 19, 1997 [Z10569IE]
German version: *Angew. Chem.* **1997**, *109*, 2800–2803

Keywords: electron localization function · intermetallic phases · superconductors · Zintl phases

[1] E. E. Havinga, *Phys. Lett. A* **1968**, *28*, 350; E. E. Havinga, H. Damsma, M. H. van Maaren, *Phys. Chem. Solids* **1970**, *31*, 2653.
[2] H. Mattausch, A. Simon, C. Felser, R. Dronskowski, *Angew. Chem.* **1996**, *108*, 1805; *Angew. Chem. Int. Ed. Engl.* **1996**, *35*, 1685.
[3] A. Simon, *Chem. Unserer Zeit* **1988**, *22*, 1; *Angew. Chem.* **1987**, *99*, 602; *Angew. Chem. Int. Ed. Engl.* **1987**, *26*, 579; *ibid.* **1997**, *109*, 1872 and **1997**, *36*, 1788.
[4] a) A. Simon, H. Mattausch, R. Eger, R. K. Kremer, *Angew. Chem.* **1991**, *103*, 1210; *Angew. Chem. Int. Ed. Engl.* **1991**, *30*, 1188; b) M. Bäcker, A. Simon, R. K. Kremer, H.-J. Mattausch, R. Dronskowski, J. Rouxel, *ibid.* **1996**, *108*, 837 and **1996**, *35*, 752; c) A. Simon, A. Yoshiasa, M. Bäcker, R. W. Henn, C. Felser, R. K. Kremer, H. Mattausch, *Z. Anorg. Allg. Chem.* **1996**, *622*, 123.
[5] D. M. Newns, H. R. Krishnamurthy, P. C. Pattnaik, C. C. Tsuei, C. C. Chi, C. L. Kane, *Physica B* **1993**, *186*, 801; O. K. Andersen, O. Jepsen, A. I. Liechtenstein, I. I. Mazin, *Phys. Rev. B* **1994**, *49*, 4145.
[6] A. D. Becke, E. Edgecombe, *J. Chem. Phys.* **1990**, *92*, 5397; A. Savin, A. D. Becke, J. Flad, R. Nesper, H. G. von Schnering, *Angew. Chem.* **1991**, *103*, 421; *Angew. Chem. Int. Ed. Engl.* **1991**, *30*, 185; T. F. Fässler, A. Savin, *Chem. Unserer Zeit* **1997**, *31*, 110; A. Savin, R. Nesper, S. Wengert, T. F. Fässler, *Angew. Chem.* **1997**, *109*, 1892; *Angew. Chem. Int. Ed. Engl.* **1997**, *36*, 1808.
[7] The PED was calculated by summing the square of the wave function at respective k points lying inside a selected energy window. This can be accomplished using a k point set standardized over the first Brillouin zone [9] or, as done here, by choosing k points along selected symmetry lines. Using the former method to calculate the PED over an energy window either above or below E_F leads to a density of states around the Fermi level that may be used to simulate tunneling electron microscope images [8–10].
[8] T. F. Fässler, Habilitation thesis, ETH Zürich, **1997**.
[9] T. F. Fässler, U. Häussermann, R. Nesper, *Chem. Eur. J.* **1995**, *1*, 625.
[10] M.-H. Whangbo, S. N. Magonov, *Adv. Mater.* **1994**, *6*, 355.
[11] See, for example, the fat band analyses in ref. [12] or the use of localized band orbitals with the aid of Wannier functions [13].
[12] Program TB-LMTO-ASA: M. van Schilfgarde, T. A. Paxton, O. Jepsen, O. K. Andersen, G. Krier, Max-Planck-Institut für Festkörperforschung, Stuttgart, **1994**; U. Barth, L. Hedin, *J. Phys. Chem.* **1972**, *5*, 1629; O. Jepsen, O. K. Andersen, *Z. Phys. B* **1995**, *97*, 35.
[13] K. A. Yee, T. Hughbanks, *Inorg. Chem.* **1991**, *30*, 2321; *ibid.* **1992**, *31*, 1620; Y. Tian, T. Hughbanks, *ibid.* **1993**, *32*, 400.
[14] Stoichiometric amounts of barium (0.538 g, surface impurities were removed immediately before loading) and tin powder (1.512 g) were heated in niobium ampoules at 150 degress per hour to 720 °C. The ampoules were held at 720 °C for 48 h and then cooled at 50 degrees per hour to 640 °C. They where then held at this temperature for 16 d. $BaSn_3$ was isolated as a microcrystalline, shiny silver powder. Resistivity measurements on pressed pellets show a linear increase with temperature in the region from −200 to 25 °C. A stable phase with this composition was identified in 1930 from thermal studies on the Ba/Sn system [15], and a single crystal isolated from investigations in a ternary system (Ba/Al/Sn) was structurally characterized [16]. We obtained single crystals of $BaSn_3$ in the investigation of the ternary K/Ba/Sn system.
[15] K. W. Ray, R. G. Thompson, *Met. Alloys* **1930**, *1*, 314.
[16] R. Kröner, Dissertation, Universität Stuttgart, **1989**.
[17] Typical Sn–Sn bond lengths: 2.78 Å in $(Ph_2Sn)_6$: D. H. Olson, R. E. Rundle, *Inorg. Chem.* **1963**, *2*, 1310; 2.77 Å in Ph_6Sn_2: H. Preut, H.-J. Haupt, F. Huber, *Z. Anorg. Allg. Chem.* **1973**, *396*, 81; 2.85–2.87 Å in $(Ar_2Sn)_3$ (Ar = 2,6-diethylphenyl): S. Masamune, L. R. Sita, *J. Am Chem. Soc.* **1983**, *105*, 630; 2.98 Å in K_4Sn_4: I. F. Hewaidy, E. Busmann, W. Klemm, *Z. Anorg. Allg. Chem.* **1964**, *328*, 283; further examples: D. E. Goldberg, P. B. Hitchcock, M. F. Lappert, K. M. Thomas, A. J. Thorne, T. Fjeldberg, A. Haarland, B. E. R. Schilling, *J. Chem. Soc. Dalton Trans.* **1986**, 2387.
[18] The magnetic susceptibility was measured with a SQUID magnetometer (MPMS 5, Quantum Design). The samples were cooled in the absence of a magnetic field. After introducing a field of 10 G, the sample was warmed ("shielding") and then cooled ("Meissner"). Suprasil quartz capillaries (5 mm diameter) served as sample holders. The shoulder at 3.7 K in the plot in Figure 2 can be assigned to trace amounts of elemental tin. As no lines characteristic of tin can be seen in an X-ray powder pattern, an impurity level of less than 5% tin can be estimated.
[19] Calculations were performed with the program TB-LMTO-ASA[12] without the addition of interstitial spheres with s-, p-, and ("down-folded") d-partial waves for Ba and Sn.
[20] The analyses were carried out with the program MEHMACC (U. Häusermann, S. Wengert, R. Nesper, T. F. Fässler, ETH Zürich, **1993**); the pictures were created with the program COLTURE for the isosurfaces (P. Hofmann, R. Nesper, ETH Zürich, **1993**) and GRAPA for the cross-sections (J. Flad, F.-X. Fraschio, B. Miehlich, Institut für Theoretische Chemie der Universität, Stuttgart, **1989**). The programs are available under mehmacc@inorg.chem.ethz.ch. MEHMACC is based on the QCPE extended-Hückel program EHMACC [21].
[21] Program EHMACC: M.-H. Whangbo, M. Evain, T. Hughbanks, M. Kertes, S. Wijeyesekera, C. Wilker, C. Zheng, R. Hoffmann, **1990**; relevant parameters (H_{ii}, ξ): Sn 5s −16.16 eV, 2.12, 6p −8.32 eV, 1.82; Ba 6s −4.76 eV, 1.263, 6p −2.64, 1.263.
[22] In the extended-Hückel band structures of band section **1**, no crossing of the next-highest band is observed between M and Γ.
[23] R. Hoffmann, *Solids and Surfaces. A Chemist's View of Bonding on Extended Surfaces*, VCH, Weinheim, **1988**.
[24] The possibility of nonbonding electron pairs participating in the pairing localization of electrons in superconductors is also mentioned in ref. [4a].
[25] A. Currao, S. Wengert, R. Nesper, J. Curda, H. Hillebrecht, *Z. Anorg. Allg. Chem.* **1996**, *622*, 501.
[26] Y. Grin, U. Wedig, H. G. von Schnering, *Angew. Chem.* **1995**, *107*, 1318; *Angew. Chem. Int. Ed. Engl.* **1995**, *34*, 1204.
[27] N. E. Alekseevskii, G. S. Zhandov, N. N. Zhuravlev, *Zh. Eksp. Teor. Fiz.* **1955**, *28*, 237.
[28] H. Kawaji, H. Horie, S. Yamanaka, M. Ishikawa, *Phys. Rev. Lett.* **1995**, *8*, 1427.
[29] J. S. Kaspar, P. Hagenmüller, M. Pouchard, C. Cros, *Science* **1965**, 1713; J. Gallmeier, H. Schäfer, A. Weiss, *Z. Naturforsch. B* **1967**, *22*, 1080.
[30] H. G. von Schnering, *Nova Acta Leopold.* **1985**, *59*, 168.
[31] T. F. Fässler, C. Kronseder, *Z. Anorg. Allg. Chem.*, in press; T. F. Fässler, *ibid.*, in press.

Carbohydrates Coordinated to Platinum(IV) through Hydroxyl Groups: A New Class of Platinum Complexes with Bioactive Ligands**

Dirk Steinborn,* Henrik Junicke, and Clemens Bruhn

The discovery of the carcinostatic effect of *cis*-$[PtCl_2(NH_3)_2]$ by Rosenberg et al.[1] and investigations on the mechanism of action of platinum compounds in chemotherapy[2] promoted the developement of the coordination chemistry of platinum(II) with biologically important ligands.[3–5] Nowadays attention is focused on platinum(IV) complexes with bioactive ligands, because of the lower toxicity of platinum(IV) and the possibility of oral administration of some potent platinum(IV) compounds as well as the

[*] Prof. Dr. D. Steinborn, Dipl.-Chem. H. Junicke, Dr. C. Bruhn
Institut für Anorganische Chemie der Universität Halle-Wittenberg
Kurt-Mothes-Strasse 2, D-06120 Halle (Germany)
Fax: Int. code + (345) 552-7028
e-mail: steinborn@chemie.uni-halle.de

[**] This work was promoted by the Deutsche Forschungsgemeinschaft and the Fonds der Chemischen Industrie, and supported by gifts of chemicals from Degussa and Merck.

fact that they can coordinate to DNA without prior reduction to platinum(II) compounds.[3,6,7] In general, they have been less thoroughly investigated than platinum(II) complexes. Although binding of metal ions to carbohydrates is essential in numerous biological processes,[8] complexes of platinum(IV) with carbohydrates have not yet been described, probably due to the reducing properties of the latter. Here we report on the coordination of 1,2-*O*-isopropylidene-protected α-D-gluco- and α-D-allofuranose to a trimethylplatinum cation to give the first carbohydrate platinum(IV) complexes.

$[(PtMe_3I)_4]$[9] reacts with $AgBF_4$ in acetone to give *fac*-$[PtMe_3(Me_2CO)_3]BF_4$ (**1**),[10] which is monomeric and highly moisture-sensitive in the solid state. Solutions of **1** in acetone react with stoichiometric amounts of 1,2:5,6-di-*O*-isopropylidene-α-D-glucofuranose (**2a**) and -α-D-allofuranose (**2b**) within a few hours to give trimethylplatinum(IV)-*O*-isopropylidene-α-D-glucofuranose (**3a**) and -α-D-allofuranose (**3b**) complexes (conversion 60–65%, yield ca. 40%; Scheme 1).

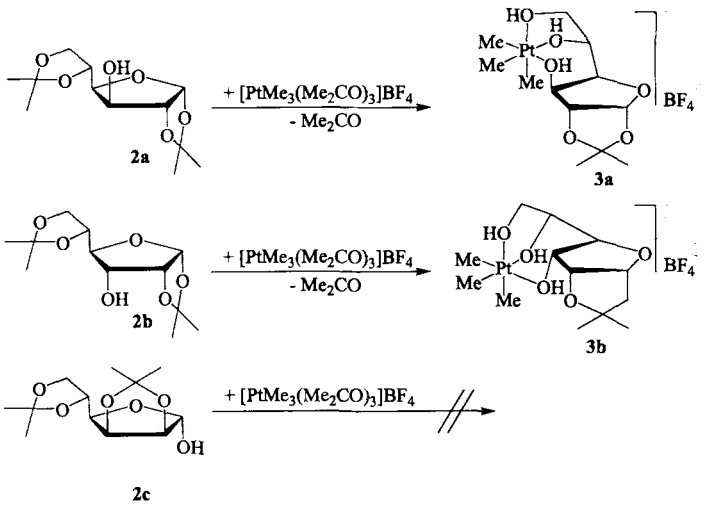

Scheme 1. Synthesis of complexes **3a** and **3b**.

One of the two isopropylidene protecting groups is removed as acetone by traces of water. With an excess of **2** (n(**1**):n(**2**) = 1:2), the protecting group of the surplus sugar is not cleaved, even if the reaction mixture is treated with 3–10 equivalents of water. This proves that the elimination of a protecting group is assisted by platinum. The higher (Brønsted) acidity of the aqua platinum complex (formed by H_2O–Me_2CO exchange in **1**) and/or coordination of a ketal oxygen atom to the platinum center could be decisive.

2,3:5,6-Di-*O*-isopropylidene-α-D-mannofuranose (**2c**) neither reacts with **1** to give a platinum complex according to Scheme 1 nor does it lose a protecting group. The first steps in the formation of **3a** and **3b** are probably coordination of the unprotected hydroxyl group (C3–OH) to platinum and formation of a chelate complex, followed by (platinum-assisted) elimination of an isopropylidene protecting group. Complex **3a** is also obtained in a reaction analogous to Scheme 1, with the singly protected sugar 1,2-*O*-isopropylidene-α-D-glucofuranose (**2a′**) instead of the doubly isopropylidene protected carbohydrate (yield 95%). However, using a small excess of **2a′** (n(**1**):n(**2a′**) = 1:1.1) led to decomposition.

Complexes **3a** and **3b** were fully characterized by ^1H, ^{13}C, and ^{195}Pt NMR spectroscopy.[11] The ^1H and ^{13}C NMR resonances were assigned on the basis of HETCOR experiments. In [D$_6$]acetone differences in the chemical shifts of up to $\Delta\delta = 3.0$ (**3a**) and 11.0 (**3b**) occur for the carbon atoms of the coordinated and noncoordinated ligands. Relative to the starting material **1**, the ^1H resonances for methyl ligands in **3a** and **3b** are shifted to higher field by $\Delta\delta = 0.11$, and the ^{195}Pt NMR resonances by 364 and 176, respectively. These results confirm complex formation in acetone. Since this is not observed in [D$_4$]methanol, it must be concluded that the complexes are largely dissociated in this solvent.

The single-crystal X-ray structure of **3a**[12] is shown in Figure 1. 1,2-*O*-Isopropylidene-α-D-glucofuranose acts as neutral tridentate ligand which is coordinated only through three hydroxyl groups ($\kappa^3O^{3,5,6}$ coordination). The five-, six-, and seven-membered 1,3,2-dioxaplatina rings exhibit envelope, distorted chair, and twist-boat conformations, respectively. The cyclic system is not free of angle strain, as revealed by the O-Pt-O angles in particular, two of which are distinctly smaller than 90° (O5-Pt-O6 75.7(6), O3-Pt-O5 78.6(4)°). The three Pt–O bonds are equal within the limits of error (223 pm). They are among the longest Pt–O bonds[13] being a consequence of the strong *trans* influence of the methyl groups.[14]

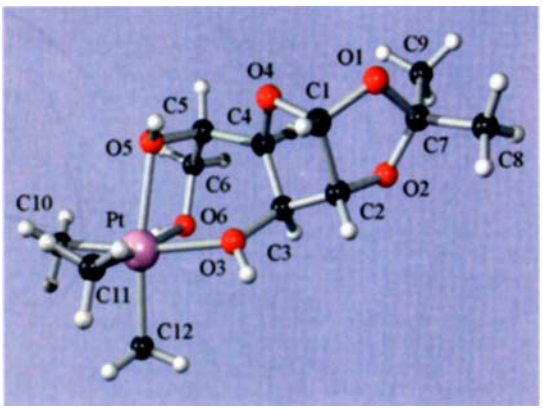

Figure 1. Molecular structure of the cation in **3a**. Selected bond lengths [pm] and angles [°]: Pt–C10 202(1), Pt–C11 202(2), Pt–C12 207(2), Pt–O3 222.7(7), Pt–O5 224(1), Pt–O6 223(1), O3–C3 147(2), O5–C5 147(3), O6–C6 145(2), C3–C4 147(2), C4–C5 153(2), C5–C6 149(3); C10-Pt-C11 91(1), C10-Pt-C12 90.5(9), C11-Pt-C12 89.3(7), O3-Pt-O5 78.6(4), O3-Pt-O6 87.5(6), O5-Pt-O6 75.7(6), C10-Pt-O3 172.5(8), C10-Pt-O5 93.9(7), C10-Pt-O6 91.2(8), C11-Pt-O3 90.0(8), C11-Pt-O5 99.1(6), C11-Pt-O6 174.6(7), C12-Pt-O3 97.0(7), C12-Pt-O5 170.4(6), C12-Pt-O6 95.7(7), Pt-O3-C3 123.5(8), Pt-O5-C5 107(1), Pt-O6-C6 113.0(9), O3-C3-C4 110(1), O5-C5-C6 108(1), O5-C5-C4 113(1), O6-C6-C5 110(1), C3-C4-C5 123.4(9), C4-C5-C6 115(2).

Complexes **3a** and **3b** belong to the less investigated transition metal complexes with "pure" polyalcohol ligands (i. e., coordinated only through hydroxyl groups).[15] They are not only the first carbohydrate complexes of platinum(IV) but also the only complexes of platinum that contain neutral carbohydrate ligands without anchor groups. Since these ligands play an important role under physiological conditions, **3a** and **3b** open a new class of platinum(IV) complexes with bioactive ligands, which are not only important for coordination chemistry but might also be of pharmacological interest.

Experimental Section

3a,b: [$(PtMe_3I)_4$] [9] (230 mg, 0.14 mmol) was added to a stirred solution of $AgBF_4$ (100 mg, 0.51 mmol) in dry acetone (20 mL) in the dark. After 30 min AgI was removed by filtration, and the colorless solution of **1** was added to a solution of **2a** or **2b** (141 mg, 0.54 mmol) in acetone (5 mL) and stirred for 12 h. The solvent was then removed, and the white residue extracted with chloroform (2 mL). The filtered extract was freed of solvent to give **3a** and **3b** as colorless

 © WILEY-VCH Verlag GmbH, D-69451 Weinheim, 1997 0570-0833/97/3623-2687 $ 17.50+.50/0

powders. Recrystallization from methanol at room temperature yielded single crystals of **3a**.

3a: Colorless powder, yield 116 mg (39%), m.p. 60°C, decomp above 145°C; elemental analysis calcd for $C_{12}H_{25}BF_4O_6Pt$: C 26.34, H 4.61; found: C 26.11, H 4.93. **3b**: Colorless powder, yield: 128 mg (42%), m.p. 85°C, decomp above 155°C; elemental analysis calcd for $C_{12}H_{25}BF_4O_6Pt$: C 26.34, H 4.61; found: C 26.52, H 4.43.

Received: July 14, 1997 [Z10680IE]
German version: *Angew. Chem.* **1997**, *109*, 2803–2805

Keywords: bioinorganic chemistry · carbohydrates · O ligands · platinum

[1] B. Rosenberg, L. VanCamp, J. E. Trosko, V. H. Mansour, *Nature (London)* **1969**, *222*, 385–386.

[2] a) *Metal Complexes in Cancer Chemotherapy* (Ed.: B. K. Keppler), VCH, Weinheim, **1993**; b) *Molecular Aspects of Anticancer Drug–DNA Interactions, Vol. 1* (Eds.: S. Neidle, M. Waring), Macmillan, Basingstoke, **1993**; c) K. M. Comess, S. J. Lippard in ref. [2b], pp. 134–168; d) M. J. McKeage, L. R. Kelland. in ref. [2b], pp. 169–212.

[3] a) J. Reedijk, *Inorg. Chim Acta* **1992**, *198–200*, 873–881, and references therein; b) A. Iakovidis, N. Hadjiliadis, *Coord. Chem. Rev.* **1994**, *135/136*, 17–63, and references therein; c) K. F. Morris, L. E. Erickson, B. V. Panajotova, D. W. Jiang, F. Ding, *Inorg. Chem.* **1997**, *36*, 601–607.

[4] Platinum(II) complexes of functionalized carbohydrates (coordination through the functional group): a) Y. Nagel, W. Beck, *Z. Naturforsch. B* **1985**, *40*, 1181–1187; b) T. Tsubomura, S. Yano, K. Kobayashi, T. Sakurai, S. Yoshikawa, *J. Chem. Soc. Chem. Commun.* **1986**, 459–460; c) T. Pill, W. Beck, *Z. Naturforsch. B* **1993**, *48*, 1461–1469; d) Y. Zhou, B. Wagner, K. Polborn, K. Sünkel, W. Beck, *ibid.* **1994**, *49*, 1193–1202; e) J. Kuduk-Jaworska, *Transition Met. Chem. (London)* **1994**, *19*, 296–298; f) T. V. RajanBabu, T. A. Ayers, *Tetrahedron Lett.* **1994**, *35*, 4295–4298.

[5] Platinum(II) complexes of nonfunctionalized carbohydrates: a) carbohydrate carbanions as ligands: ref. [4a]; b) carbohydrate dianions (diolates) as ligands: A. Appelt, A. C. Willis, S. B. Wild, *J. Chem. Soc. Chem. Commun.* **1988**, 938–940; M. A. Andrews, G. L. Gould, *Organometallics* **1991**, *10*, 387–389; M. A. Andrews, E. J. Voss, G. L. Gould, W. T. Klooster, T. F. Koetzle, *J. Am. Chem. Soc.* **1994**, *116*, 5730–5740.

[6] a) O. Nováková, O. Vrána, V. I. Kiseleva, V. Brabec, *Eur. J. Biochem.* **1995**, *228*, 616–624; b) R. M. Roat, J. Reedijk, *J. Inorg. Biochem.* **1993**, *52*, 263–274; c) L. T. Ellis, H. M. Er, T. W. Hambley, *Aust. J. Chem.* **1995**, *48*, 793–806.

[7] a) H. Bissinger, W. Beck, *Z. Naturforsch. B* **1985**, *40*, 507–511; b) H. O. Davies, D. A. Brown, A. I. Yanovsky, K. B. Nolan, *Inorg. Chim. Acta* **1995**, *237*, 71–77; c) T. G. Appleton, J. R. Hall, T. G. Jones, J. A. Sinkinson, *Polyhedron* **1995**, *14*, 2613–2622; d) B. Kayser, H. Nöth, M. Schmidt, W. Steglich, W. Beck, *Chem. Ber.* **1996**, *129*, 1617–1620; e) D. Steinborn, H. Junicke, F. W. Heinemann, *Inorg. Chim. Acta* **1997**, *256*, 87–92.

[8] a) S. Yano, *Coord. Chem. Rev.* **1988**, *92*, 113–156; b) S. J. Angyal, *Adv. Carbohydr. Chem. Biochem.* **1989**, *47*, 1–43; c) D. M. Whitfield, S. Stojkovski, B. Sarkar, *Coord. Chem. Rev.* **1993**, *122*, 171–225.

[9] J. C. Baldwin, W. C. Kaska, *Inorg. Chem.* **1975**, *14*, 2020.

[10] **1**: ^{1}H NMR ($(CD_3)_2CO$)/CD_3OD): $\delta = 1.37/1.06$ (s + d, $^2J(Pt,H) = 79.5/77.7$ Hz, 9H, $PtCH_3$), 2.09/2.15 (s, 18H, CH_3); ^{13}C NMR (CD_2Cl_2): $\delta = -11.1$ (s + d, $^1J(Pt,C) = 804$ Hz, $PtCH_3$), 31.1 (s, CH_3), 219.1 (s, CO); ^{195}Pt NMR: $\delta = 2672$ (CD_2Cl_2), 2614 (CD_3OD), 2696 ($(CD_3)_2CO$); elemental analysis calcd for $C_{12}H_{27}BF_4O_3Pt$: C 28.76, H 5.43; found: C 28.41, H 5.08; single crystal X-ray structure analysis: orthorhombic, *Pcab*, $Z = 8$, $a = 15.599(3)$, $b = 15.685(3)$, $c = 15.763(3)$ Å.

[11] **3a**: ^{1}H NMR [400 MHz, $(CD_3)_2CO$]: $\delta = 1.25$ (s, 3H, CCH_3), 1.26 [br s, 9H, $Pt(CH_3)_3$], 1.40 (s, 3H, CCH_3), 3.88 (dd, 1H, H6), 4.04 (m, 2H, H5/H6′), 4.15 (m, 1H, H4), 4.31 (dd, 1H, H3), 4.49 (d, 1H, H2), 5.84 (d, 1H, H1); ^{13}C{^{1}H} NMR (100 MHz; $(CD_3)_2CO$): $\delta = -11.58$ ($Pt(CH_3)_3$), 26.4 (CH_3), 27.2 (CH_3), 67.6 (C6), 73.7 (C5), 75.2 (C3), 82.5 (C4), 86.6 (C2), 106.2 (C1), 112.7 (OCO); ^{195}Pt{^{1}H} NMR (107 MHz; relative to $Na_2[PtCl_6]$ ($\delta = 4521$)): $\delta = 2350$ ($(CD_3)_2CO$); 2608 (CD_3OD). **3b**: ^{1}H NMR (400 MHz, $(CD_3)_2CO$): $\delta = 1.26$ (br s, 9H, $Pt(CH_3)_3$), 1.38 (s, 3H, CCH_3), 1.43 (s, 3H, CCH_3), 3.81 (dd, 1H, H6), 3.91 (dd, 2H, H5/H6′), 4.02 (dd, 1H, H4), 4.12 (m, 1H, H3), 4.55 (d, 1H, H2), 5.26 (d, 1H, H1); ^{13}C{^{1}H} NMR (100 MHz; $(CD_3)_2CO$): $\delta = -11.40$ (s + d, $^1J(Pt,C) = 814$ Hz, $Pt(CH_3)_3$), 26.6 (CH_3), 26.9 (CH_3), 67.8 (C6), 76.8 (C3), 83.2 (C5), 87.2 (C2), 88.5 (C4), 103.7 (C1), 110.9 (OCO); ^{195}Pt{^{1}H} NMR (107 MHz): $\delta = 2520$ ($(CD_3)_2CO$); 2607 (CD_3OD).

[12] Crystal structure data (STOE-IPDS diffractometer) for **3a**: $C_{12}H_{25}BF_4O_6Pt$, $M_r = 547.22$, crystal dimensions $0.2 \times 0.1 \times 0.05$ mm^3, $T = 220$ K, monoclinic, space group $P2_1$, $a = 1020.1(2)$, $b = 916.9(2)$, $c = 1085.5(2)$ pm, $\beta = 108.95(2)°$, $Z = 2$, $V = 0.9603(3)$ nm^3, $\rho_{calcd} = 1.893$ g cm^{-3}, $Mo_{K\alpha}$ radiation ($\lambda_0 = 0.71073$ Å), $\mu = 7.365$ mm^{-1}, $2\theta = 5–50°$; of 7763 reflections collected, 3361 were independent (R(int) = 0.0767) and 2700 observed ($I > 2\sigma(I)$); 226 refined parameters, numerical absorption correction ($T_{min.}$ 0.35 /$T_{max.}$ 0.41], GOF (based on F^2) = 0.968, $R1 = 0.0394$ (for observed reflections based on F), $wR2 = 0.0889$ (all reflections based on F^2), absolute structure parameter 0.01(2), residual electron density −0.654/0.859 e Å^{-3}. The structure was solved and refined with the programs SHELXS-86 and SHELXL-93. The H atoms were placed in their geometric positions (riding model). Crystallographic data (excluding structure factors) for the structure reported in this paper have been deposited with the Cambridge Crystallographic Data Centre as supplementary publication no. CCDC-100521. Copies of the data can be obtained free of charge on application to The Director, CCDC, 12 Union Road, Cambridge CB21EZ, UK (fax: int. code + (1223) 336-033; e-mail: deposit@chemcrys.cam.ac.uk).

[13] For comparison d(Pt–O): ligand L = H_2O: 202–218 pm (number of data $n = 14$); L = ROR′: 214–223 pm ($n = 9$); L = ROH: 211 pm ($n = 2$); L = RO^-: 197–215 pm ($n = 25$). Cambridge Structural Database (CSD), Cambridge Crystallographic Data Centre, University Chemical Laboratory, Cambridge (UK).

[14] a) M. M. Gofman, V. I. Nefedov, *Inorg. Chim. Acta* **1978**, *28*, 1–17; b) D. Steinborn, *Angew. Chem.* **1992**, *104*, 392–412; *Angew. Chem. Int. Ed. Engl.* **1992**, *31*, 401–421.

[15] Inosit complexes: K. Hegetschweiler, T. Kradolfer, V. Gramlich, R. D. Hancock, *Chem. Eur. J.* **1995**, *1*, 74–88; K. Hegetschweiler, M. Ghisletta, L. Hausherr-Primo, T. Kradolfer, *Inorg. Chem.* **1995**, *34*, 1950–1953; K. Hegetschweiler, T. Raber, G. J. Reiss, W. Frank, M. Wörle, A. Currao, R. Nesper, T. Kradolfer, *Angew. Chem.* **1997**, *109*, 2052–2054; *Angew. Chem. Int. Ed. Engl.* **1997**, *36*, 1964–1966; cyclotetrachromotropylene complexes: B. L. Poh, L. H. Seah, C. S. Lim, *Tetrahedron* **1990**, *46*, 4379–4386; camamycine complexes: A. Mashaly, *Polyhedron* **1993**, *12*, 745–748.

 © WILEY-VCH Verlag GmbH, D-69451 Weinheim, 1997 0570-0833/97/3623-2688 $ 17.50+.50/0

For a Heterogeneous Readership

Principles and Practice of Heterogeneous Catalysis. By *J. M. Thomas* and *W. J. Thomas*. WILEY-VCH, Weinheim, 1997. 669 pp., hardcover 128.00 DM—ISBN 3-527-29288-8

In their preface to this impressive book, the authors remark that "catalysis occupies a pivotal position in the physical and biological sciences" and that it is also "the mainstay of the chemical industry". The truth of these statements is itself sufficient justification as to why, in the absence of contemporary competitors, a book dealing with the "Principles and Practice of Heterogeneous Catalysis" should be warmly welcomed by all who work in the field of catalytic science. Yet, although the title of this book refers explicity to heterogeneous catalysis, and much of what the authors have to say concerns the nature, structure, and use of solid catalysts and the molecular mechanisms driving catalytic cycles, the book will nevertheless be of value to those whose main aim is to learn about the nature and behavior of catalysts in general. The authors of the present book correctly point out that the recent two or three decades have seen a revolution in our detailed understanding of the surface structure of solid materials, especially large single crystals with adsorbed layers. Such progress has been made through the use of sophisticated physical techniques, a number of which have also allowed the surface of catalysts to be studied in the working state.

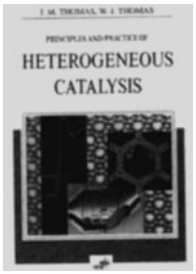

This is a substantial book covering some 669 pages of text in eight chapters, which are: 1. "Setting the Scene" (perhaps best described by the title of one of the sections, "Perspectives in Catalysis: Past, Present, Future"); 2. "The Fundamentals of Adsorption: Structural and Dynamic Considerations, Isotherms, and Energetics"; 3. Characterizing Catalysts and Their Surfaces"; 4. "The Significance of Pore Structure and Surface Area in Heterogeneous Catalysis"; 5. "The Solid-State and Surface Chemistry of Catalysts"; 6. "Poisoning, Promotion, Deactivation and Selectivity of Catalysts"; 7. "Catalytic Process Engineering"; 8. "Heterogeneous Catalysis: Examples and Case Histories".

In broad terms, these eight chapters cover the topic in adequate detail, but we particularly commend the authors for the inclusion of a chapter on "Catalytic Process Engineering" (Chapter 7) together with related material in Chapter 4 on diffusional effects in porous catalysts. These matters are so often ignored by chemists, yet even in laboratory-scale catalytic work, failure to appreciate heat- and mass-transport factors can lead to grossly misleading conclusions. Chapter 7 also describes a number of experimental and industrial reactors in a clear and instructive manner.

Each of the eight chapters is provided with a set of problem questions (typically 10–25 or so in number) with which readers may test their understanding of the material presented. These problems are seldom trivial, and any reader who is able to provide satisfactory answers to most of them would indeed be knowledgeable in the subject. Despite the authors' comments attached to the problems of Chapters 1 and 2, we suggest that a problem-solving reader would be best advised to use the entire book as source material, rather than relying only on the content of an individual chapter.

It is probably quite unreasonable to expect any book of the size and complexity of the present one to be without sins of commission and omission. We only draw attention to the following points in the hope that our comments may be of assistance to the readers.

In general, the authors have gone to a great deal of trouble to provide some historical background to the various topics which are then discussed in detail. This is certainly to be welcomed, and it will be of considerable value to readers whose main aim is to gain an overall view of the subject. Nevertheless, their historical approach needs to be used with caution. Thus (cf. Chapter 1) the emphasis of Balandin and others on the matching between the geometry of benzene and that of certain planes of transition metals should now be treated only as an interesting historical anecdote rather than a matter of real relevance to a reaction mechanism for, for example, benzene hydrogenation.

On page 27 there is some confusion in the definition of turnover frequency (TOF). This ought to be unambiguously defined as the reaction rate (i.e., dn/dt) per active site, as recommended by IUPAC and as is given on page 27 in eqn. (3). However, except in special circumstances (e.g., degree of conversion $\rightarrow 0$ or a zero-order reaction), dn/dt is not the same as the number of molecules reacting in time t as given in the text immediately preceding eqn. (3): this is not a TOF but a site–time yield. As the authors correctly point out, it is generally quite difficult to know the number of active sites per unit quantity of a heterogeneous catalyst: even so, we do not believe it is reasonable to recommend the use of a sort of TOF expressed per unit area or per unit volume of catalyst. The IUPAC definition for TOF is the number of times the catalytic cycle turns over per second. In fact, one of its main virtues is that it is expressed with only one unit—the second. In the discussion around this point on page 27, the authors correctly point out that chemisorption is a useful method by which, at least in some cases, the problem of estimating the active site concentration may be approached, and the text refers the reader to Chapter 3 for chemisorption methodology. In fact, Chapter 3 says almost nothing about this method (cf. a one-line entry in Table 3.1). The well-

This section contains book reviews and a list of new books received by the editor. Book reviews are written by invitation from the editor. Suggestions for books to be reviewed and for book reviewers are welcome. Publishers should send brochures or (better) books to the Redaktion Angewandte Chemie, Postfach 101161, D-69451 Weinheim, Federal Republic of Germany. The editor reserves the right of selecting which books will be reviewed. Uninvited books not chosen for reviews will not be returned.

known importance of chemisorption methods for catalyst characterization mandates more detail than is contained in a one-line-entry.

Chapter 8 ("Heterogeneous Catalysis: Examples and Case Histories") analyzes important and best-understood catalytic processes: Synthesis of Methanol, Fischer–Tropsch Catalysis, Synthesis of Ammonia, Oxidation of Ammonia, In-Situ Catalytic Reaction and Separation, Automobile Exhaust Catalysts, Photocatalytic Breakdown of Water and the Harnessing of Solar Energy, Catalysis Using Microporous or Mesoporous Solids and Modified Clays, Catalytic Processes in the Petroleum Industry, and The Role of Catalysis in Energy-Related Environmental Technology. In most instances, these topics are reasonably well treated, given the amount of space that could be made available and the huge quantity of technical detail which could be drawn upon. Chapter 8 also discusses reactor types for several large-scale processes, as well as some promising new multipurpose catalytic reactors involving simultaneous distillation, membrane permeation, or combustion. In two cases, the authors include a numerical example that is most instructive. Nevertheless, we have two critical comments. Firstly we believe it to be a pity that the authors did not deal with metal-catalyzed carbon–carbon bond rupture (i.e., hydrogenolysis) reactions since these are of considerable industrial significance and also provide some of the best available examples of catalytic selectivity control. Secondly we believe that in some aspects of their treatment of ammonia synthesis, the authors have done less than justice to what is known about this important catalytic process. In particular, it is now reasonably well established that the predominant active sites for this reaction are the so-called C_7 sites. Such sites occur on the (111) and (211) surface planes of iron. This is inadequately dealt with, and is not made clear that these active sites can be counted by the use of high-temperature nitrogen chemisorption.

When dealing with the book as a whole, we find we must take the authors to task over the matter of referencing for material in the text. Material (e.g., figures) taken unaltered from pre-existing literature is, of course, acknowledged in detail. However, in the text itself (i.e., as written by the authors), citations to the relevant literature are in general either not provided at all (e.g., an author's name may be cited but without *any* reference leading to the original literature), or else an author's name may be cited, together with a date, in which case the appropriate literature reference is likely to be found in the section "Further Reading" at the end of the chapter. The problem then is that the author's name which is cited in the text is not necessarily the name of the lead author in the reference, so that a frustrating search becomes necessary. Of course, the extent to which referencing to the literature is necessary in the text is dependent on who is going to read it. In our opinion, the usefulness of the book to researchers and advanced teachers is substantially diminished by the inadequate and idiosyncratic referencing to the relevant original literature. Furthermore, if the generally accepted practice had been followed, it would have been possible for appropriate credit to have been given to authors deserving of priority. As it now stands, these referencing deficiencies make it difficult for us fully to recommend the book as a reference work. In addition, the index is less than adequate.

Nevertheless, despite our reservations, the community in catalysis must be most grateful to the authors for writing a book which illustrates the vitality in the field in a readable manner. Anyone who has heard it said that catalysis is a mature field will be easily convinced, even after only a cursory perusal of this book, that scientists and engineers working in the theory and practice of catalysis are poised to discover, invent, and innovate. With this in mind, we suggest the book should be on the list of required reading for people such as university deans, industrial managers, foundation directors, and government officials in science policy. To this end, an executive summary would have been a valuable addition to each chapter. We also highly recommend the book as a "get acquainted" resource for senior chemistry and chemical engineering students and their advisors. The upbeat and inspirational style of the book will broaden the horizon of those looking for a challenging graduate program and an exciting professional career. Thank you, J. M. and W. J. Thomas, for your labor of love.

John R. Anderson
Monash University (USA)
and
Michel Boudart
Stanford University (USA)

Handbook of Heterogeneous Catalysis. By *G. Ertl, H. Knözinger,* and *J. Weitkamp.* WILEY-VCH, Weinheim, 1997. 2500 pp., 2030 fig., 500 tab., hardcover 2490.00 DM—ISBN 3-527-29212-8

This five-volume compendium follows in the spirit of those edited by Schwab in the 1940s and Emmett in the 1950s, and the editors state that this handbook is the first to describe comprehensively all facets of heterogeneous catalysis from scientific fundamentals to industrial processes. Although an ambitious undertaking involving more than 200 authors and requiring several years, as evidenced by the variation in the most recent references cited at the end of each chapter, the result is remarkably successful and coherent. In most cases, the editors have obtained some of the most knowledgeable and active scientists in each area to author or coauthor a review of that subject. At the very least, this handbook verifies the enormous impact heterogeneous catalysis has on our society through improvements in commercial processes.

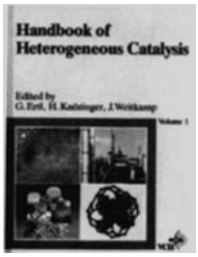

Volume 1 begins by stating general principles related to heterogeneous catalysis, then it provides historical perspectives of catalytic science as well as industrial catalysis. The remainder of the volume is devoted to describing the preparation of both unsupported and supported catalysts, with an emphasis on those catalysts, most important commercially, that is, metallic and bimetallic systems and zeolites. The chapters on zeolite acidity and basicity and on carbons are especially thorough (over 50 pages) with an excellent set of references provided in each case.

Volume 2 focuses on the characterization of both industrial-type high surface area catalysts as well as model systems. The standard methods for measuring physical properties are reviewed, and essentially all the various techniques that can provide information about chemical properties are discussed. Although a detailed introduction of the scientific fundamentals pertaining to each spectroscopic method could not be given due to space constraints, sufficient background is provided along with applications to allow the reader to understand the capability of the technique.

 © WILEY-VCH Verlag GmbH, D-69451 Weinheim, 1997 0570-0833/97/10923-2690 $ 17.50+.50/0

References to allow a more thorough understanding of the principles involved are invariably provided. The chapters on vibrational spectroscopy and the use of IR spectroscopy to characterize surface acidity and basicity are especially informative and contain extensive citations. The various UHV surface science technique are enumerated, and their applications to various single-crystal surfaces of metals, oxides, and bimetallic systems, as well as ultrathin oxide films, are described.

Volume 3 deals with core issues related to catalytic reactions and their economic industrial utilization. These include elementary steps, mechanisms and modeling, the effect of transport processes, deactivation and regeneration, types of laboratory reactors, and reaction engineering. Chemisorption in theory and practice is addressed initially. Fundamentals of catalytic rates are reviewed, theoretical modeling of surface reactions is discussed, and various approaches to kinetic modeling are then covered, as well as means to evaluate the validity of the model chosen. Although not lengthy, these treatises are sufficient when coupled with the references cited to provide guidance for those interested in kinetic modeling. Various experimental techniques for probing reaction mechanisms are reviewed, and the reader is also introduced to some of the conceptual aspects of heterogeneous catalysis such as structure sensitivity, promoters and poisons, and effects due to ensembles and ligands, spillover, and substituent groups. The importance of heat- and mass-transfer limitations on reaction rates is emphasized in a thorough mathematical approach, and criteria are provided to estimate the influence of these effects on experimental reaction rate data. The use of different laboratory test reactors is analyzed, and the utilization of commercial-type fixed-bed, fluidized-bed, and slurry reactors is described in some detail. Finally, special catalytic systems, including chemical sensors, electrocatalysis, and supercritical media, are discussed.

Volume 4 is devoted to processes of industrial interest and addresses environmental catalysis, inorganic reactions, and energy-related catalytic reactions. Consequently, the status of catalytic pollutant control from both gasoline and diesel engines as well as that related to stationary sources is summarized. The principal current problem of NO_x emissions is emphasized and one new technology applicable to the latter source—gas turbine catalytic combustion—is described. Up-to-date reviews are provided for six industrial inorganic reactions, the most important of which are NH_3 synthesis, NH_3 oxidation, SO_2 oxidation, and the Claus process to form sulfur. Reviews of the last group of reactions include those for steam and CO_2 reforming along with the water gas shift reaction and COS removal, CO and CO_2 hydrogenation, methanol synthesis, methanol to hydrocarbons, catalytic cracking, hydrocracking and dewaxing, catalytic reforming of gasoline, alkane isomerization, synthesis of gasoline additives (MTBE), hydrotreating reactions including demetalation, isobutane alkylation, alkane aromatization, coal gasification, and coal liquefaction. Reactions associated with fuel cells and photocatalysis are also addressed. The sections on methanol synthesis and catalytic cracking are particularly informative and the former has an especially good reference list.

Volume 5 concludes the series by giving detailed information about almost thirty types of catalytic organic reactions of industrial significance. Although all cannot be listed here, they encompass reactions dealing with hydrogenation/dehydrogenation, aromatic alkylation, hydroformylation, selective oxidation (including ammoxidation), amination, halogenation, metathesis, oligomerization, and polymerization. Enantioselective and immobilized enzyme catalyst systems are also covered. These chapters provide a summary of the chemistry involved as well as mentioning the principal catalysts used in each process.

In summary, the 2500 pages contained in these volumes provide a tremendous amount of information. The most recent citations at the end of each section range from 1992 to 1997 with most being 1994 or later; consequently, the reviews typically represent an up-to-date perspective on each topic. Unfortunately, a few of the chapters do not measure up to the high standards set by the remainder, and one chapter provides an inconvenience by listing references alphabetically, rather than numerically, as done in other chapters. Nevertheless, I consider this series to be a resource that will be invaluable to those in academia as well as to scientists in industrial and governmental laboratories and perhaps indispensable to researchers working in small industrial laboratories that have limited library facilities. The price of DM 2490 (or $1,740) is steep; however, when viewed relative to the annual subscription cost of a typical scientific journal, it is much more reasonable, particularly when the contents of this handbook will be valuable to scientists and students for years to come.

M. Albert Vannice
Dept. of Chemical Engineering
Pennsylvania State University
Pennsylvania (USA)

Encyclopedia of Molecular Biology and Molecular Medicine. Edited by *R. A. Meyers.* WILEY-VCH, Weinheim, 1996/97. 6 volumes, hardcover DM 2940.00, 6 Vol. Set—ISBN 3-527-28478-8—single volumes DM 590.00 each., Vol. 1: 462 pp., ISBN 3-527-28471-0; Vol. 2: 480 pp., ISBN 3-527-28472-9; Vol. 3: 522 pp., ISBN 3-527-28473-7; Vol. 4: 508 pp., ISBN 3-527-28474-5; Vol. 5: 516 pp., ISBN 3-527-28475-3; Vol. 6: 495 pp., ISBN 3-527-28476-1

The first volume of this six-volume encyclopedia appeared at the beginning of 1996, and only 18 months later, in early summer 1997, the work was completed with the publication of Volume 6. It is intended to serve as a comprehensive reference source on molecular aspects of biology and medicine. The complete work of 3000 pages (including the index) contains almost 300 articles on the molecular biology of living organisms.

The encyclopedia sets a new standard in the field of molecular biology, especially in the areas of genome research and the molecular basis of genetically caused diseases. Several articles are devoted to the human genome. Important analytical techniques used in biochemistry, molecular biology, and genetic engineering are described in detail, including the latest developments. Diagnostic techniques for diseases, and in some cases also therapeutic methods, are described. As well as purely scientific articles there are others dealing with important practical aspects, as for example in the contribution on "Transgenic Animal Patents". However, although the encyclopedia partly covers the molecular mechanisms of both well-established and modern drugs, such as enzyme inhibitors, receptor agonists and antagonists, transport blockers (uptake inhibitors), and ion channel ligands, the treatment of these aspects is rather brief and is limited to a few articles, such as the excellent but quite short contribution on "Medicinal Chemistry". Also the highly

 © WILEY-VCH Verlag GmbH, D-69451 Weinheim, 1997 0570-0833/97/10923-2691 $ 17.50+.50/0

topical subject of "Drug Targeting and Delivery" merited more than the mere two pages allowed here. However, the shortness of many of the articles is perhaps unavoidable in view of the broad conception of the work and the great variety of topics covered.

The first volume of this encyclopedia has already been reviewed in this journal (*Angew. Chem.* **1996,** *108,* 1218; *Angew. Chem. Int. Ed. Engl.* **1996**, *35*, 1578. The very favorable impression reported then is further reinforced on examining the complete work. The appearance of all six volumes within a short space of time has ensured that all the articles are similarly up-to-date. It is pleasing to find that the literature references extend up to 1996 in many cases. For example, the article on "Yeast Genetics" (Vol. 6, p. 305) mentions the complete sequencing of the yeast genome published in April 1996. The cross-references to related articles in the encyclopedia are especially useful; by following these through one can quickly find one's way around the available information on a particular area of interest. As an example, in the article on "Receptor Biochemistry" (although there is also an entry for "Other Receptors") we find that only membrane-bound receptors are mentioned there. However, information about soluble receptors can be found in the articles on "Endocrinology, Molecular" and "Steroid Hormones and Receptors", both of which are listed as cross-references. On the other hand, the articles "Vitamin Receptors" and "Zinc Finger DNA-Binding Motifs", which also contain information about important aspects of soluble receptors, are not mentioned.

Volume 6 contains a comprehensive index (127 three-column pages) listing all the subjects that are treated in more or less detail in the text but do not necessarily have a separate article devoted to them.

Much care has been devoted to the copy-editing, and the number of errors has been kept very low. To mention particular errors would probably convey a misleading impression of the whole. However, just one should be picked out because of its unintentional humor: on page 347 of Volume 2 the text refers throughout to "glucocerebrosidase" instead of distinguishing between this and "glucocerebroside", an error which is amusing rather than serious. As in Volume 1 reviewed earlier, the later volumes too contain a few incorrect structural formulas (e.g., those of estrone on p. 165 of Vol. 2 and of cyproterone acetate on p. 484 of Vol. 5).

There are a few omissions and other shortcomings that one would wish to see remedied in a revised edition, but their number is small. For example, there is no entry under the important heading "Proteome". Also there are a few minor weaknesses, which is almost inevitable in any multiauthor work. Thus, for example, combinatorial chemistry—perhaps as a result of its rapidly growing importance—appears in several different places, sometimes with identical figures (as in the illustration of the split-and-combine technique). However, a redundancy of this kind does no serious harm.

In agreement with the earlier verdict based on Volume 1, the *Encyclopedia of Molecular Biology and Molecular Medicine* is without a competitor in this field, and it is an important and valuable resource for one's daily work. Every chemist, biochemist, biologist, or medical scientist who is interested in a new topic in molecular biology or genome research will find this encyclopedia useful in providing a rapid overview of the subject of interest. It is an essential addition to the libraries of university departments, research institutes, and industry engaged in research in these areas. In most cases the high price will, of course, prevent individuals from buying their own copy. However, the publishers have devised an elegant solution to this problem, in the form of a shortened version entitled *Molecular Biology and Biotechnology. A Comprehensive Desk Reference* (VCH Publishers, New York, 1995. 1024 pp., hardcover DM 275.00; paperback DM 89.00.—ISBN 1-56081-569-8/1-56081-925-1). This should prove useful when the library copy that you so urgently need turns out (yet again) to have been lent out to a colleague.

Hugo Kubinyi
BASF AG, Ludwigshafen (Germany)

A Lifetime of Synergy with Theory and Experiment. (Series: Profiles, Pathways, and Dreams. Series editor: J. I. Seeman.) By *A. Streitwieser.* American Chemical Society, Washington, DC, 1996. 310 pp., hardcover $ 34.95—ISBN 0-8412-1836-6

In general, chemists have little inclination to study history, and the history of their own subject is no exception. Brought up to appreciate practical skills and used to learning by pictorial presentations, they often acquire a dislike of pure text ("when will there finally be a formula scheme"), which stands right at the heart of humanities, and therefore also of historical sciences. It is therefore not surprising that compared with the large number of biographical and historical works in the neighboring disciplines, there are only a few in the area of chemistry. Biographical material is likely to be found in obituaries, which naturally are meant to present the deceased from the most favorable point of view possible.

Several years ago, J. I. Seeman, himself active in the area of physical organic chemistry, asked a number of well-known chemists—the vast majority of whom come from the Anglo-American realm—to present essays on the development of organic chemistry over the past 30–40 years using their personal research work. The project, initially planned to be a terse one-volume compilation not including autobiographical material, has grown since 1990 to the proportions of 22 full-fledged autobiographies of prominent chemists. Andrew Streitwieser, one of the chosen authors, now presents his life's work. The external circumstances of this can be presented as a paradigm of the dynamics of American society: while his parents were not "dishwashers", they nevertheless were German immigrants struggling with the disaster of the Depression; so their son Andrew had to earn extra money to enable him to attend a science-oriented high school. He, like many others, had been won over to chemistry by his first chemistry set (which is no longer possible these days, as he deplores, because "all but the most innocuous chemicals are considered too dangerous—or perhaps too subject to lawsuits—for children to form part of their play and learning"). His career advanced steadily via the studies at Columbia and the post-doctorate at MIT to the tenured position at Berkeley, overshadowed only by the illness and death of his first wife. Accordingly, he does not report on any strife, let alone personal adversaries that might have impeded his progress. He only deplores the contemporary widespread disrespect for physical organic chemistry, and the problems that arise from ever fiercer competition for grant money, while funding through the department becomes ever more marginal—a situation that has become a threat to the freedom of research and teaching. Central to this book however is Streitwieser's chemical research, which began with solvolysis reactions, and

 © WILEY-VCH Verlag GmbH, D-69451 Weinheim, 1997 0570-0833/97/10923-2692 $ 17.50+.50/0

focused on CH-acidities, theoretical and organometallic (uranocene-)chemistry, and polycations. His commitments as the author of well-known textbooks and his role as an editor of *J. Org. Chem.* are also mentioned. Many references to the primary literature, a collection of short biographies of the chemists mentioned in the text, and an index are testimony of the author's diligent approach. The reader who expects a collection of "funny" anecdotes will therefore be disappointed, although there are references here and there to hobbies like fly fishing, and the author includes information about all of his students who are mentioned. Rather, Streitwieser endeavors to show how the mutual fertilization of theory and experiment have contributed to his scientific success. This book will therefore be of great value to those who wish to be informed about the research of Streitwieser's group and, moreover, about the development of physical organic chemistry in the USA over the past three to four decades.

Jens J. Wolff
Organisch-Chemisches Institut
der Universität Heidelberg (Germany)

Synthetic Methods of Organometallic and Inorganic Chemistry. Vol. 6. Lanthanides and Actinides. Edited by *F. T. Edelmann.* (Series editor: W. A. Herrmann). Georg Thieme Verlag, Stuttgart, 1997. 226 pp., hardcover DM 124.00.—ISBN 3-13-103071-2

This book is the best current source of preparative information on lanthanide and actinide complexes. It is an important resource for anyone involved in the chemistry of these metals.

The decision to update the classic *Handbook of Preparative Inorganic Chemistry* by G. Brauer, and to include organometallic as well as inorganic information, is an excellent one. In the past, "Brauer" has been extremely valuable as a concise source of detailed preparative information in the inorganic area. A single source of this type is useful not only to obtain specific information, but also to get an overview of an area, its techniques, and its potential applicability to a problem. The Herrmann/Brauer update of this series will be even more useful since it will extend the coverage to modern organometallic chemistry. This is a daunting task, however, and requires eight volumes!

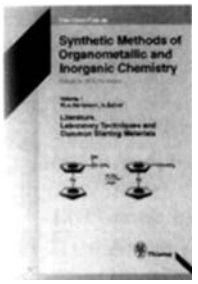

The decision to include in this series one volume on lanthanide and actinide chemistry was also an excellent choice. Lanthanide and actinide chemistry has been one of the most rapidly developing areas of inorganic and organometallic chemistry in recent years. Since this is a rather modern area, no single source of preparative information is available. Currently, this information must be obtained either from the primary literature or from review articles. As the field has grown, recent review articles must report only the latest results in order to maintain a manageable size. As a result, several sources must be examined sequentially to get synthetic information and to be to certain that it is up-to-date. The Edelmann volume of the Herrmann/Brauer series provides in a single book the information currently available on lanthanide and actinide synthesis.

Professor Edelmann did an excellent job in organizing this volume. Initially, he surveyed the lanthanide and actinide community for suggestions and contributions and used this input to select the specific syntheses to be included. All of the major types of compounds are represented in this volume, which is an outstanding achievement considering the space limitations. With the growth rate of this field, the volume could easily double in size in the next revision. Users of this volume should realize that the coverage is necessarily representative rather than comprehensive.

Professor Edelmann has also written introductions to each of the chapters, briefly surveying the synthetic aspects of each sub-category. These introductions are very valuable since this type of summary information on preparations is not readily available elsewhere. Occasionally, introductions to some of the specific syntheses have also been written to put the chemistry in context. These are stimulating since they sometimes include statements not universally accepted by the lanthanide and actinide community. For example, syntheses of some bimetallic compounds traditionally thought to have no metal–metal bonding are prefaced by comments that the distances suggest metal–metal interactions. Similarly, prefaces to some sections make statements about the relative sizes of cyclopentadienyl ligands for which there is not complete agreement among specialists.

The individual synthetic sections of the book are generally taken directly from the literature. As such, different syntheses have different levels of detail. For example, in some cases all of the infrared data on a series of analogous compounds is given, whereas in other cases no such information is included. Similarly, cell constants from X-ray crystallographic studies are sometimes, but not always, given when a structural study has been done. In the case of the syntheses taken from the older literature, some of the formulas for the starting materials are antiquated, particularly in terms of alkoxide precursors which have subsequently been found to have structures more complicated than $Ln(OR)_3$ or $Ln(OR)_4$. Hence, it must be remembered that this book is neither a critical review nor a publication such as *Inorganic Synthesis*, in which the preparations have been independently tested. In addition, since this field is moving quickly, the book already unavoidably contains some dated material. For example, it is stated in one section that the introduction of a third π ligand to a $(C_5Me_5)_2U$ unit is impossible.

The four chapters divide the book into lanthanide (inorganic and organometallic) and actinide (inorganic and organometallic) sections. The inorganic chapters are also valuable to organometallic researchers since they describe the preparation of starting materials. For example, since it is somewhat difficult to obtain truly anhydrous lanthanide starting materials, and the descriptions of the drying methods are in very early literature, it is particularly useful to have a modern analysis of this topic.

In summary, this lanthanide/actinide inorganic/organometallic volume is a unique resource in the field. This information has not previously been available in a single place and no modern compilation of these details is available. For someone interested in starting a project in lanthanide or actinide chemistry, this volume provides the information on how to begin experimentally. For any active lanthanide/actinide laboratory this book is an essential resource. It should be required reading for all new students in lanthanide/actinide laboratories, and I found that it can stimulate thought in the experienced researcher as well.

William J. Evans
Department of Chemistry,
University of California
Irvine, CA (USA)

 © WILEY-VCH Verlag GmbH, D-69451 Weinheim, 1997 0570-0833/97/10923-2693 $ 17.50+.50/0

Inorganic and Organometallic Reaction Mechanisms. Second Edition. By *J. D. Atwood.* WILEY-VCH, Weinheim, 1997. xiv, 312 pp., hardcover DM 98.00.—ISBN 0-471-18897-2

The material presented in this text (which is intended for students at the graduate level) encompasses kinetics and mechanisms of both "classical" inorganic reactions and organometallic transformations. While the book does cover the essentials of inorganic reaction mechanisms, the emphasis is clearly on organometallic reactions, which are treated in considerable detail. The material is arranged in eight chapters, each of which concludes with a list of references and a substantial collection of exercise problems. References have been included up to 1995, and about 40% of the problems have been taken from the primary literature.

Chapter 1 provides the grounding in chemical kinetics, discussing basic rate laws, activation parameters, the principle of microscopic reversibility, linear free energy relationships, a variety of techniques for following kinetic experiments, and schemes for the classification of reaction mechanisms. For more thorough coverage the reader is referred to a number of seminal texts in the references section, but will miss the recent work by R. B. Jordan (*Reaction Mechanisms of Inorganic and Organometallic Systems*, Oxford University Press, New York, 1991) which is not cited until Chapter 3. Chapters 2 and 3 deal with the stereochemistry, reactivity, and mechanisms of substitution of square-planar complexes and octahedral Werner-type complexes, respectively. Chapter 4 is the largest in the book, and discusses organometallic substitution reactions, the emphasis being on metal carbonyl complexes and hydride complexes. Oxidative addition/reductive elimination reactions, the centerpiece of organometallic synthesis, are covered in Chapter 5, which gives an overview of stereochemical and mechanistic investigations, including a brief section on free radical mechanisms. Chapter 6 provides further coverage of these reactions as applied in homogeneous catalysis (hydrogenation, hydroformylation, hydrocyanation, olefin metathesis, alkene polymerization, and methanol carbonylation). Chapter 7 is concerned with stereochemical nonrigidity of inorganic and organometallic systems, covering the topics of coordination number isomerization, migration of a metal around an unsaturated ring, and rearrangements in metal clusters. The final chapter deals with electron transfer reactions including long-range and multielectron transfer. A comparatively brief index concludes the book.

Most readers, in common with this reviewer, will probably compare *Inorganic and Organometallic Reaction Mechanisms* with Jordan's *Reaction Mechanisms of Inorganic and Organometallic Systems.* While both books nominally cover the same ground, there are considerable differences in emphasis. A strong point of the title under review is the detailed treatment of organometallic reactions which, amongst other aspects, emphasizes the importance of NMR techniques in mechanistic studies of fluxional systems and provides sample spectra. This emphasis comes at the expense of topics such as chelate formation, where the coverage is not nearly as comprehensive as in Jordan's work, or other subjects such as inorganic photochemistry and enzyme kinetics, which are not covered at all. Still, the book does provide a good introduction to the study of kinetics and reaction mechanisms and takes the reader with more "inorganic" leanings to a point where he or she can probe further with the aid of the excellent compilation of references. The problems are extensive and provide the reader with many an opportunity to practice newly acquired concepts on experimental data. While the book has generally been carefully produced, there are occasional inconsistencies in the labeling of figures (e.g., no units given in Fig. 1.18, and no specification of the "different mechanistic possibilities"), and minor errors in some of the derived functions (e.g., Eqs. 1.68–1.70, where the exponents are not recognizable as such). Also, phrases such as "Since NH_3 does not have an electron pair ..." (p. 85) are less than to the point. Overall, however, if it were not for the high list price, this book could be recommended as a worthy addition to the library of any graduate student with an interest in inorganic, and especially organometallic, reaction mechanisms.

Andreas Grohmann
Institut für Anorganische Chemie
der Universität Erlangen-Nürnberg
(Germany)

Handbook of Microscopy. Applications in Materials Science, Solid-State Physics and Chemistry. Edited by *S. Amelinckx, D. van Dyck, J. van Landuyt* and *G. van Tendeloo.* VCH Verlagsgesellschaft, Weinheim, 1996. Three volumes, hardcover DM 1197.00 (complete set); individual volumes DM 498.00 each. Vol. 1, 536 pp.—ISBN 3-527-29280-2; Vol. 2, 450 pp.—ISBN 3-527-29473-2; Vol. 3, 833 pp.—ISBN 3-527-29293-4

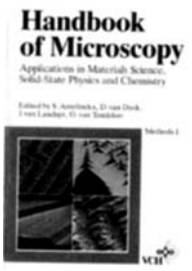

Editing a handbook of microscopy is a very ambitious project, even though its coverage is limited in this case to applications in materials science, solid state physics, and chemistry (thereby excluding the biological and medical sciences, two other major fields of application). Although it is not immediately obvious from the title whether "chemistry" here means chemistry in general or solid state chemistry in particular, one may assume the latter. The many authors of the individual chapters and sections of this three-volume handbook, who also include the editors themselves, are all well recognized experts in their fields.

The first two volumes ("Methods: I" and "Methods: II") are devoted to the various methods of microscopy, and form a single integrated unit. As explained in the preface, these volumes deal with all those methods that yield localized information about microstructure and/or composition. Their objektive is to enable the reader to choose the best method for a particular purpose and to understand its capabilities and limitations. The main topics covered in "Methods: I" are light microscopy (Raman, near-field optical, infrared, etc.), X-ray microscopy, acoustic microscopy, and the stationary beam methods of electron microscopy (transmission EM, high voltage EM, Lorentz microscopy, electron holography methods, and convergent beam electron diffraction—the latter being a departure from the handbook's main subject area). "Methods: II" begins with the scanning electron microscopy methods (SEM in the conventional reflection mode, scanning transmission EM, electron probe microanalysis, etc.). It continues with magnetic methods, emission methodes (photo-

 © WILEY-VCH Verlag GmbH, D-69451 Weinheim, 1997 0570-0833/97/10923-2694 $ 17.50+.50/0

electron emission, field emission and field ion microscopy), and scanning near-field probe methods (scanning tunneling, scanning force, and magnetic force microscopy). Finally there is a supplement which includes, along with other material, a very useful chapter on image recording and image processing.

It is already evident from the above (incomplete) list of topics that it is quite difficult to find suitable names for all the methods of interest, while avoiding creating verbal monstrosities. In striving to achieve a coherent system of nomenclature the editors have certainly been quite creative. For example, the chapter on scanning near-field probe methods is entitled "Scanning Point Probe Techniques", but this expression does not reappear thereafter.

The chapter on light microscopy begins with a historical outline, but a little more detail on this would have been welcome. In a handbook as comprehensive as this, it would have been desirable to include a separate short chapter on the history of microscopy as a whole.

The section on imaging by the scanning electron microscopy methods is agreeable to read, being clearly written and largely avoiding formulas and derivations, but one would have expected more than a mere 23 pages on this, which is probably the most widely used of the electron microscopy methods (including its use in the chemical industry). In contrast one finds, for example, that ballistic electron emission microscopy, a modern but comparatively exotic method, is treated in detail with 28 pages. It is surprising that scanning electron microscopy, a long-established and powerful method with some 20 thousand instruments installed worldwide, seems to deserve less space than that. Perhaps it is thought that exactly because it is so much more widely used than the other methods it involves less scientific depth.

Volume 3, "Applications", is divided according to areas of use, namely materials science, solid state physics, and chemistry. Its purpose is to explain which microscopy techniques are most appropriate for the various types of materials and problems, and thus this volume can be used independently. The following types of materials are discussed in turn: metals and alloys, rocks and minerals, semiconductors and semiconducting devices, optoelectronic materials, ferroic materials, structural ceramics, gemmological materials, superconducting ceramics, nonperiodic structures (amorphous materials and quasicrystals), medical and dental materials, carbon (graphite, diamond, buckminsterfullerene and related forms, nanotubes), engineering composites, polymers and their monomeric analogs, nuclear materials, and magnetic materials. There are special chapters on topics such as small particles, structural phase transformations, environmental problems, quantitative analysis from microscopic images, and (last but not least) the preparation of samples for transmission electron microscopy. Obviously the choice of types of materials to be included can never be completely exhaustive, and subjective preferences have certainly played a part. Moreover, there is undoubtedly a tendency, especially in this volume, to emphasize the authors' own publications or those in their own fields of research.

A single reviewer cannot, of course, pretend to be able to judge the scientific quality of the whole of such an extensive, wide-ranging, and detailed handbook with absolute reliability. I have carefully studied those chapters that deal with the areas most familiar to me, whereas other chapters were only skimmed through. Some random checks on the literature references revealed only trivial shortcomings, and although there were contradictions concerning the attribution of chapters or sections to the authors envolved, these too can be dismissed as unimportant. However, the work contains too many small inconsistencies and errors for my taste. One expects a handbook of microscopy to remain useful for a good number of years, and therefore it would have been worthwhile to devote more care to the editing. For example, very early on in the work ("Methods: I", p. 6) it is surprising to find that one of the pioneers of microscopy, Professor Henry F. W. Siedentopf of Jena (1872–1940), is credited with having received a Nobel Prize; although such an honor may well have been deserved, the world knows nothing of it. Many of the printing errors can be blamed on the computerized typesetting that is usual nowadays, but these ought to have been corrected by the publisher's copy editors (do such people still exist?). Just a few of these typos are listed below. "Silicium" instead of silicon and "Schockley" instead of Shockley ("Methods: I", pp. 353, 385, resp.) would hardly cause misunderstanding, but Ti_2O instead of NiO, and "stair red dislocations" for stair-rod dislocations (same volume, pp. 379, 384, resp.) could present difficulties. "Electromechanical" instead of electrochemical and "Heydenreich" instead of Heidenreich ("Applications", pp. 12, 5, resp.) will confuse. Surely it is already well known that the two important scientists with these rather similar names are unrelated. In the section on high-resolution transmission electron microscopy, which I read with special interest, the symbols ψ and φ for the object and image wave-functions are sometimes confused, in both the formulas and the figures (e.g., p. 358 of "Methods: I"), and the word "phase" is used quite loosely. In these cases experts will easily guess what was intended, but for other readers it is essential to be absolutely accurate to avoid misunderstandings.

However, although these shortcomings had to be mentioned in the interest of completeness, readers of *Angewandte Chemie* will be interested in other qualities of the handbook, insofar as it also aims to cover applications in chemistry and solid state chemistry. In this context, of course, we are not concerned with "Methods: I" and "Methods: II". But even in the "Applications" volume chemical aspects are only touched on in passing, and this applies to the chapters on superconductors, polymers, small particles, and medical and dental materials. This only serves to emphasize the general observation that microscopists working in the area of chemistry are not sufficiently assertive in bringing their achievements to the notice of the scientific world.

There is at present no other available work that is comparable to this *Handbook of Microscopy*, and for this reason alone it will certainly find buyers, especially libraries. In a limited sense it can be regarded as a successor to *Electron Microscopy in Solid State Physics*, by Bethge and Heydenreich, which was published ten years earlier. However, a more detailed comparison is not possible, as the present handbook covers a much wider range of subject matter, especially in the parts concerned with methods. Science libraries should certainly buy it. Prospective individual buyers should, in view of the high cost, try to take a look at a copy before deciding whether it meets their needs.

Reiner Ramlau
Max-Planck-Institut für
Festkörperforschung
Stuttgart (Germany)

 © WILEY-VCH Verlag GmbH, D-69451 Weinheim, 1997 0570-0833/97/10923-2695 $ 17.50+.50/0

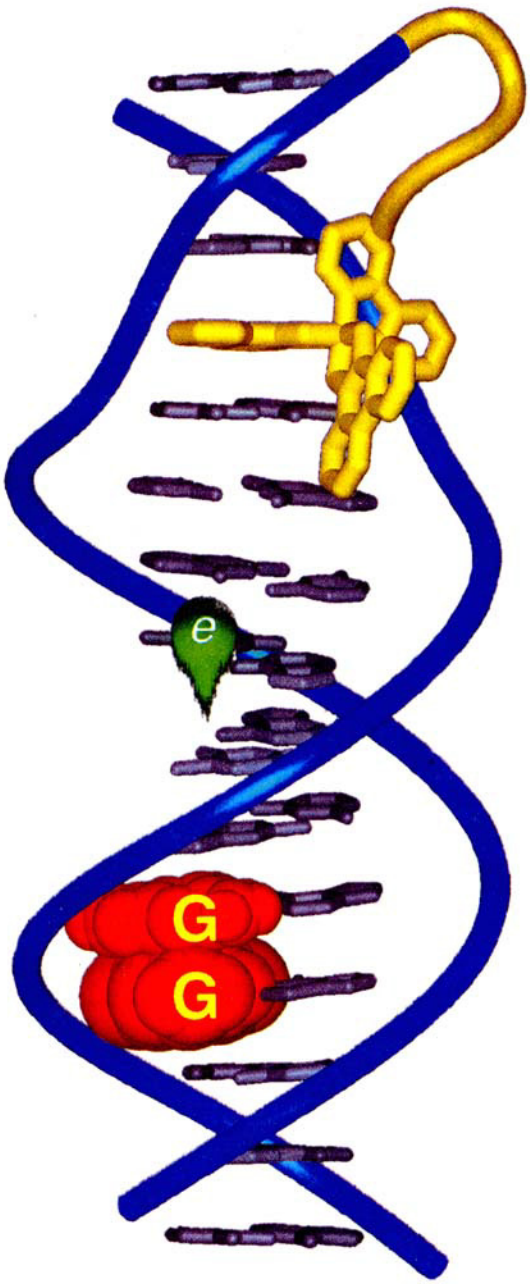

The major target of oxidative damage of nucleic acid within the cell is guanine (G). Metal intercalators which are strong photooxidants and attached to the DNA at a well-defined separation from a GG doublet can initiate selective oxidation of 5´-guanine from a distance.

Long-range charge transfer is mediated by the DNA base paired stack. Metal complexes whose ligands have an extended "aromatic surface" for intercalation in DNA can function as electron donors (red) and acceptors (yellow) to probe photoinduced electron transfer through the DNA base stack.

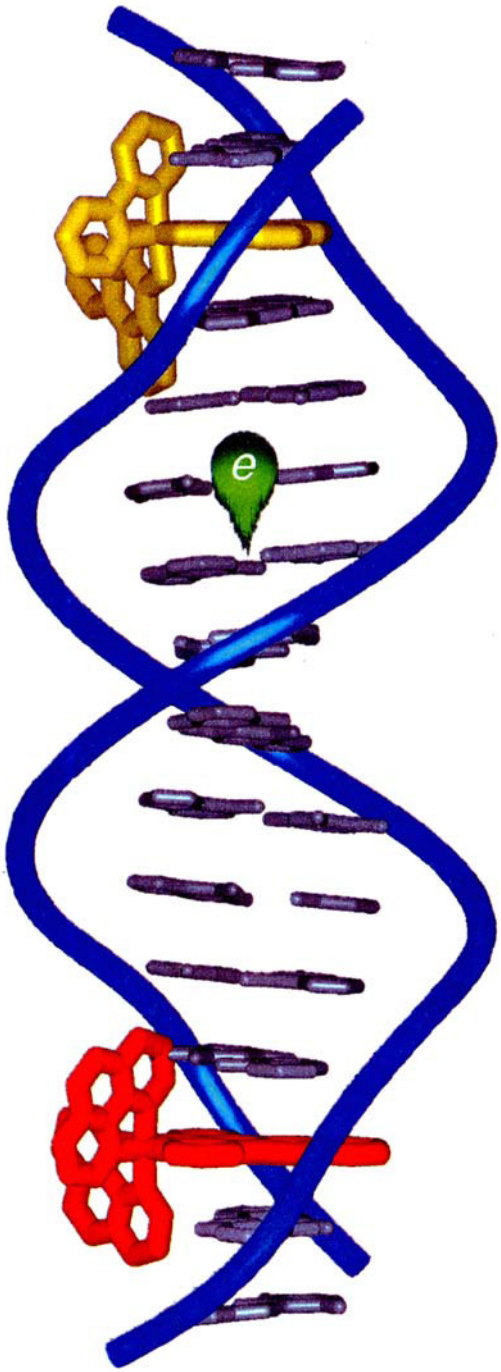

ANGEWANDTE CHEMIE ©WILEY-VCH

Charge Transfer through the DNA Base Stack

R. Erik Holmlin, Peter J. Dandliker, and Jacqueline K. Barton*

Whether the DNA base pair stack might serve as a medium for efficient, long-range charge transfer has been debated almost since the first proposal of the double-helical structure of DNA. The consequences of long-range radical migration through DNA are important with respect to understanding carcinogenesis and mutagenesis. Double-helical DNA has in its core a stacked array of aromatic heterocyclic base pairs, and this molecular π stack represents a unique system in which to explore the chemistry of electron transfer. We designed a family of metal complexes which bind to DNA by intercalative stacking within the helix; these metallointercalators may be usefully applied in probing DNA-mediated electron transfer. Here we describe a range of electron transfer reactions we carried out which are mediated by the DNA base paired stack. In some cases, DNA serves as a bridge, and spectroscopic analyses permit us to probe how the π stack couples DNA-bound donors and acceptors. These studies point to the sensitivity of coupling to DNA intercalation. However, if the DNA π stack effectively bridges donors and acceptors, the base-pair stack itself might serve not only as a conduit for electron transfer in DNA, but also in reactions initiated from a remote position. We carried out a series of reactions involving oxidative damage to DNA arising from the remotely positioned oxidant on the helix. The implications of long-range charge migration through DNA to effect damage are substantial. As in other DNA-mediated charge transfers, these reactions are highly dependent on DNA intercalation and the integrity of the intervening base-pair stack, but not on molecular distance. Furthermore, a physiologically important DNA lesion, the thymine dimers, can be reversed in a reaction initiated by electron transfer. This repair reaction can also be promoted from a distance as a result of long-range charge migration through the DNA base pair stack.

Keywords: base stacking · DNA oxidation · DNA repair · electron transfer · intercalations

1. Introduction

The biochemist perceives double-helical DNA primarily as a target for molecular recognition. As the molecular library of the cell, double-helical DNA must access genetic information and express it through an array of noncovalent interactions between proteins and nucleic acids.[1] The rational design of drugs targeted to DNA depends on determining general principles that govern the selective recognition of a nucleic acid site.[2] To understand in detail the remarkable variety of reactions involving the double helix within the cell, such as repair of DNA damage, coordination of the transcription of different genes, or screening of the fidelity of the DNA library, it becomes important to explore and consider the rich chemistry of DNA.[3]

Here we focused on the DNA double helix as a medium for charge transfer. From this perspective, the DNA polymer in its double-helical form may be viewed as an extended array of stacked, electronically coupled, aromatic heterocycles within a polyanionic sugar–phosphate backbone (Figure 1). Extended π systems in the solid state facilitate charge transport and are a major focus of study in materials research.[4, 5] The DNA double helix is a molecular π-stacked array, and may therefore represent a unique, structurally well-defined system to explore. We may ask, then, whether the DNA double helix facilitates charge transfer over long distances, and indeed, whether the base-pair stack can act as a conduit for chemistry at a distance.

Over the forty years since Watson and Crick first proposed the double-helical structure for DNA, scientists have considered the possibility of charge transfer through the base stack. Early theoretical models predicted that electron hopping from base to base might occur on the picosecond time scale.[6] Conductivity measurements on DNA fibers bracketed a "DNA band gap" of about 2 eV.[7] The question of whether radicals generated by high-energy irradiation of DNA migrate over distances of 2 or 200 base pairs has been the subject of intense debate amongst radiation biologists.[8] In the last decade, experimental studies by chemists of DNA as a

[*] Prof. J. K. Barton, R. E. Holmlin, Dr. P. J. Dandliker
Division of Chemistry and Chemical Engineering
California Institute of Technology
Pasadena, CA 91125 (USA)
Fax: Int. code + (818) 577-4976
e-mail: jkbarton@cco.caltech.edu

 © WILEY-VCH Verlag GmbH, D-69451 Weinheim, 1997 0570-0833/97/3624-2715 $ 17.50+.50/0

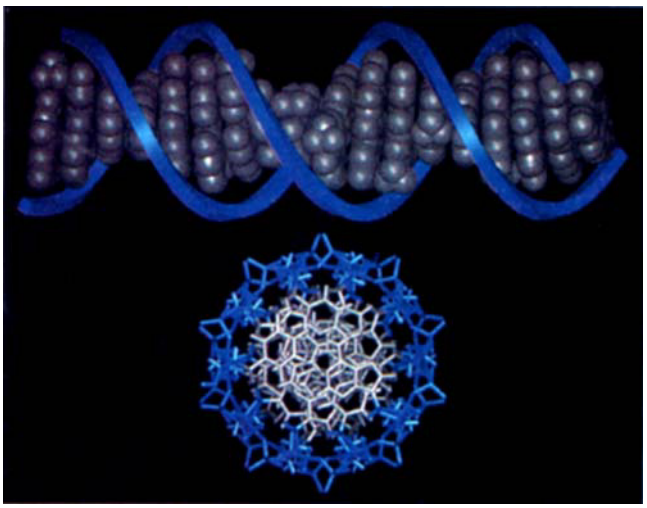

Figure 1. Schematic representation of double-helical DNA; the linear array of π-stacked aromatic heterocycles is gray, and the sugar–phosphate backbone blue. Top: view perpedicular to the helical axis; bottom: view down the helical axis.

medium for charge transfer have centered on photoinduced electron transfer between donors and acceptors bound to DNA in solution.[9, 10]

We designed small, coordinatively saturated transition metal complexes to interrogate the structure and function of nucleic acids.[11] To study DNA-mediated charge transfer, we exploited the well-characterized chemical and photophysical properties of polypyridyl metal complexes.[9, 12] Our first investigations revealed that the presence of the DNA polymer enhanced the efficiency of photoinduced electron transfer between complexes bound weakly to DNA;[13] the rate of luminescence quenching of photoexcited $[Ru(phen)_3]^{2+}$ by tris(phenanthroline) complexes of Co^{III} and Rh^{III} is enhanced by two orders of magnitude in the presence of DNA (phen = phenanthroline). Moreover, this electron transfer can be enantioselective. It is more efficient for Δ-$[Ru(phen)_3]^{2+}$, which binds to DNA somewhat more tightly, than for the Λ isomer. These studies demonstrated the utility of chiral, octahedral metal complexes in probing electron transfer through the DNA π stack. However, since DNA binding by tris(phenanthroline) metal complexes is not restricted to intercalation, several factors could contribute to the enhanced reactivity in the presence of DNA: a) the increased local concentration of reactants near the helix, b) the possibility of facilitated diffusion of species along the polymer, and, perhaps most intriguingly, c) the possibility that electron transfer may occur over a long range through the π stack.

Since these early studies, we have focused our attention on metallointercalators—complexes which bind to DNA by classical intercalation—to explore charge transfer through

R. E. Holmlin

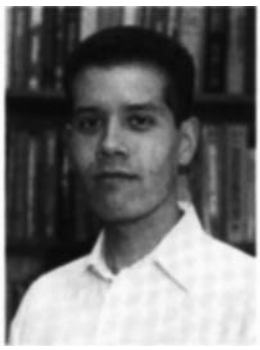

P. Dandliker

J. K. Barton

R. Erik Holmlin was born in 1967 and received a Bachelor of Arts degree in chemistry from Occidental College in Los Angeles. He began graduate studies as an National Science Foundation Graduate Research Fellow under Jacqueline Barton at the California Institute of Technology in 1993. His doctoral research has focused on applications of metallointercalators in DNA-mediated charge transfer.

Peter Dandliker was born in 1967 and received his Bachelor of Arts degree in chemistry at the University of California at Berkeley in 1990. In 1995 he earned his Ph.D. in organic chemistry with François Diederich at UCLA. He joined the research group of Jacqueline Barton as a Damon Runyon-Walter Winchell Cancer Fund Postdoctoral Fellow in 1995, where he has used intercalators to photochemically repair pyrimidine dimers in DNA. This past summer he joined Abbott Laboratories in Illinois as a research scientist.

Jacqueline K. Barton is the Hanisch Memorial Professor of Chemistry at the California Institute of Technology (Caltech). She received her Ph.D. in inorganic chemistry at Columbia University in 1979 with S. J. Lippard. After a postdoctoral fellowship at Bell Laboratories and Yale University, she became an assistant professor at Hunter College, City University of New York. In 1983 she returned to Columbia University, becoming an associate professor of chemistry and biological science in 1985 and professor in 1986. In the fall of 1989 she moved to Caltech. Barton has pioneered the application of transition metal complexes as tools to probe recognition and reactions of double-helical DNA. She has designed octahedral metal complexes which recognize nucleic acid sites with high affinities and specificities. These synthetic transition metal complexes have been useful in elucidating chemical principles which govern the recognition of nucleic acids, and in developing luminescent and photochemical reagents as new diagnostic tools. With these transition metal probes, studies to eludicate the chemistry of electron transfer mediated by the DNA double helix have also been carried out. Barton is the author of more than 100 publications and has received numerous awards, including the Paul Karrer Medal in 1996.

the π stack.[9] Tight binding and rigid association of the complexes with the helix restricts diffusion along the DNA polymer on the time scale of the reaction. Moreover, intercalative stacking of the donors and acceptors in the DNA helix provides a direct probe of the DNA π stack. In each system charge transfer mediated by the DNA is most affected by how the donors and acceptors are coupled into the DNA π stack. Therefore, DNA-mediated electron transfer depends strongly on π stacking.

Here we describe our recent investigations of DNA-mediated electron transfer with metallointercalators. We do not provide an exhaustive review of the literature, but instead present some of our experiments, which serve to illustrate principles we have learned and issues we need to understand better in delineating this chemistry. The study of DNA-mediated electron transfer is a challenging one, and requires a mix of bioinorganic chemistry, fast photophysics, and the chemistry of nucleic acid modification. The challenge, however, is worthwhile, since the DNA double helix is not simply a passive surface for reactions but instead a remarkable medium through which chemistry is carried out at a distance.

2. Metallointercalators as Probes for DNA-Mediated Electron Transfer

In probing DNA-mediated electron transfer, we focused on octahedral metal complexes which bind tightly to DNA by intercalation. NMR spectroscopy was useful for structurally characterizing the noncovalent association of these metal complexes with the DNA duplex, while photophysical and photochemical studies were exploited to determine the position and the factors affecting association of the complexes along the helical polymer. These companion experiments have proven to be powerful tools in defining the chemistry of charge transfer. Figures 2 and 3 schematically illustrate some of the complexes we may employ as donors and acceptors for photoinduced electron transfer.

2.1. Dipyridophenazine Complexes of Ruthenium and Osmium

The family of mixed-ligand complexes of type $[M(L)_2(dppz)]^{2+}$ (M = Ru, Os; L = phen, 2,2′-bipyridyl (bpy); dppz = dypyrido[3,2-*a*:2′,3′-*c*]phenazine) which contains the dppz ligand represents a straightforward extension of tris(phenanthroline) metal complexes; the "aromatic surface" of the dppz ligand provides an expansive platform for intercalation (Figure 2). The dppz complexes of ruthenium, osmium, and more recently cobalt, nickel, and rhenium, were shown to bind to DNA by preferential intercalation of the dppz ligand within the helical stack.[14–17] Binding affinities for duplex DNA are $\geq 10^7\ M^{-1}$, approximately three orders of magnitude higher than those of the simple tris(phenanthroline) metal complexes. NMR spectoscopic studies of selectively deuterated $[Ru(phen)_2(dppz)]^{2+}$ isomers bound to a DNA hexamer indicated intercalation from the major-groove side of the DNA helix with a family of orientations.[18] Although some sequence preferences are evident in the binding of the complexes to DNA, as determined from NMR spectroscopic studies, high sequence selectivity is not apparent; this is consistent with biophysical studies which indicate that classical intercalation occurs essentially randomly along a helical polymer. Because of the low sequence selectivity, however, a detailed structural determination of how these complexes stack in a helix is precluded.

The utility of the dppz complexes for our studies rests not only in the tight intercalative binding by the complexes but also in their unique photophysical properties. Irradiation of these complexes with visible light leads to efficient population of a metal-to-ligand charge-transfer (MLCT) excited state that is localized on the dppz ligand.[14, 19, 20] Although luminescence can be readily detected upon excitation in organic solvents, that in aqueous solution is quenched by proton transfer from solvent to the nitrogen atoms of phenazine.[19, 20] The DNA π stack provides protection from this quenching. Therefore, when the dppz ligand intercalates into the base-pair stack, the nitrogen atoms of phenazine are protected from water, and the complex is again emissive. This effect has proven to be a sensitive diagnostic for nucleic acids, and the term "molecular light switch" was adopted to describe this interesting luminescence property. Moreover, these molecules

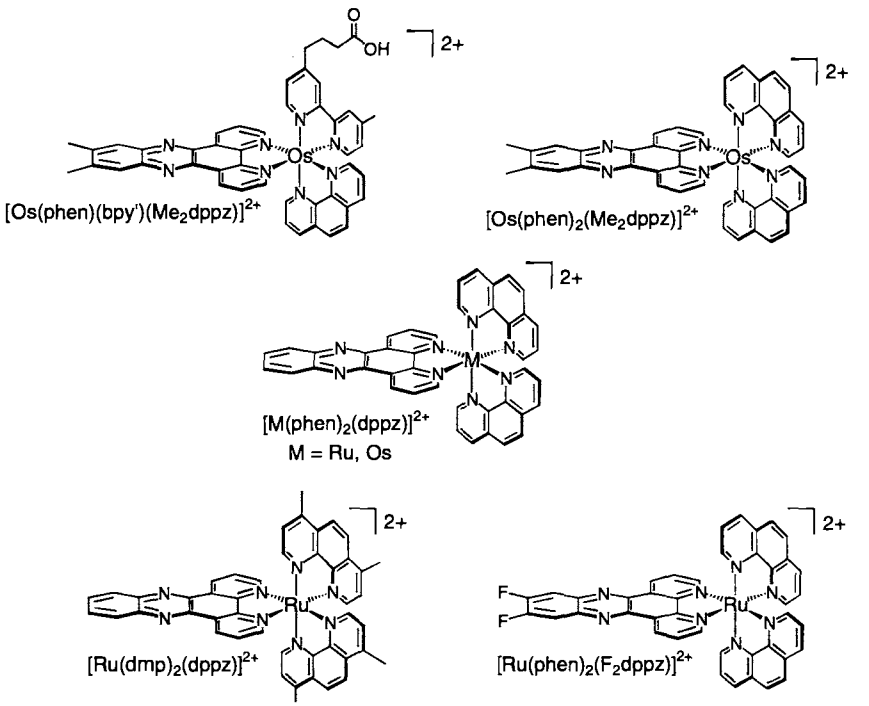

Figure 2. Derivatives of Δ-$[M(phen)_2(dppz)]^{2+}$ that bind DNA by preferential stacking of the dppz ligand between adjacent DNA base pairs (bpy′ = derivative of 2,2′-bipyridyl). In the MLCT excited state, these complexes direct an electron into the DNA π stack.

are generally useful for characterizing hydrophobic matrices, for example sodium dodecylsulfate (SDS) micelles[21] and Nafion films.[22]

Owing to the light-switch character of the $[Ru(L)_2(dppz)]^{2+}$ complexes, the steady-state and time-resolved emission profiles are particularly sensitive to the orientation of the metal complex within the DNA π stack.[14] For *rac*-$[Ru(phen)_2(dppz)]^{2+}$ bound to mixed-sequence *B*-form DNA (nucleotide:Ru = 100:1), the emission follows a biexponential decay with $\tau_1 = 130$ ns (80%) and $\tau_2 = 730$ ns (20%). Biexponential decays are also observed for the pure isomers Δ- and Λ-$[Ru(phen)_2(dppz)]^{2+}$ bound to DNA,[23] which likely reflects the population of binding orientations observed by NMR spectroscopy.[18] For Δ-$[Ru(phen)_2(dppz)]^{2+}$ bound to DNA, the emission decay is described by $\tau_1 = 150$ ns (80%) and $\tau_2 = 800$ ns (20%), whereas for Λ-$[Ru(phen)_2(dppz)]^{2+}$ bound to mixed-sequence DNA, the luminescence decays with $\tau_1 = 30$ ns (80%) and $\tau_2 = 160$ ns (20%). This difference in emission decay, manifested as an increase in the yield of steady-state emission for the DNA-bound Δ enantiomer, reflects greater protection of the intercalating ligand from the solvent. Such a propensity for intimate association between Δ-$[Ru(phen)_2(dppz)]^{2+}$ and double-helical DNA follows from the matching of symmetry between the right-handed DNA duplex and the right-handed metal complex.[24] The lifetimes and relative distributions of the excited state vary with the concentration of the bound species; this may reflect the sensitivity of these decay parameters to the rigidity of the helix, which increases with intercalator loading.

Substitution of ruthenium by osmium in $[M(phen)_2(dppz)]^{2+}$ does not alter the light-switch character or the DNA-binding properties of the complex, but provides an isostructural analogue for $[Ru(phen)_2(dppz)]^{2+}$ with distinct photophysical and electrochemical properties. Like the ruthenium analogue, no photoluminescence is detected upon irradiation of $[Os(phen)_2(dppz)]^{2+}$ in aqueous solution in the absence of DNA.[15, 25] In the presence of DNA, however, excitation of the complex affords significant, long-wavelength emission ($\lambda_{max} = 738$ nm). A biexponential decay in emission is observed for DNA-bound Δ-$[Os(phen)_2(dppz)]^{2+}$ with excited-state lifetimes below 10 ns. The osmium center stabilizes the 3+ oxidation state of the complex by about 500 mV relative to ruthenium, causing the oxidation of the osmium excited state ($E_{1/2}(*Os^{II}/Os^{III}) = 0.78$ V vs. NHE) to be about 200 mV more favorable than that of ruthenium ($E_{1/2}(*Ru^{II}/Ru^{III}) = 0.60$ V vs. NHE). We are also able to utilize phen or bpy analogues bearing electron-donating or electron-withdrawing substituents to tune further the electrochemical properties of these complexes over a range of potentials. Substitution of methyl groups onto positions 7 and 8 of the dppz ligand increases the excited-state lifetimes for both osmium and ruthenium derivatives bound to DNA (M = Ru: $\tau_1 = 370$ ns (65%), $\tau_2 = 1170$ ns (35%); M = Os: $\tau_1 = 2.18$ ns (50%), $\tau_2 = 10.1$ ns (50%)). This preferential charge transfer onto the dppz ligand is an important characteristic, which we exploited in our studies of DNA-mediated electron transfer, in that for the intercalated complex charge transfer upon excitation is directed into the π stack. These complexes are therefore particularly well-suited for probing DNA-mediated charge transfer.

2.2. Phenanthrenequinone Diimine Complexes of Rh^{III}

The rhodium intercalators we employed all contain the phenanthrenequinone diimine (phi) ligand. Several of the Rh^{III} complexes we constructed are schematically illustrated in Figure 3. For these complexes, too, one ligand provides an

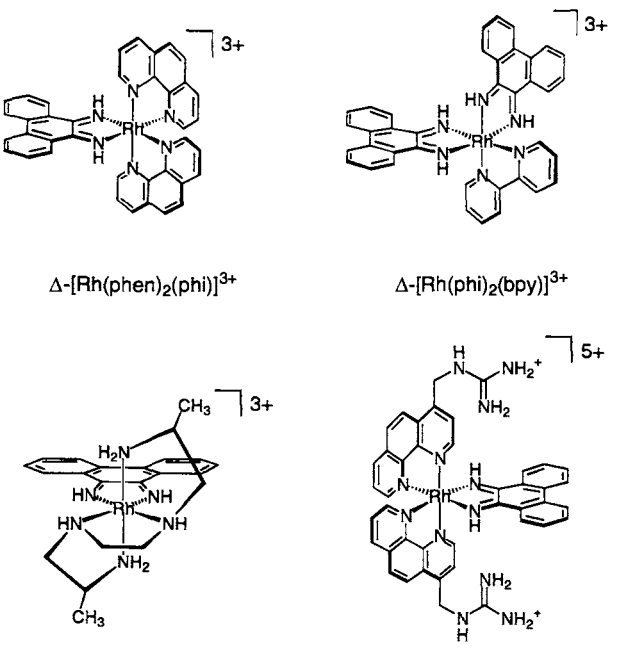

Δ-$[Rh(phen)_2(phi)]^{3+}$ Δ-$[Rh(phi)_2(bpy)]^{3+}$

Δ-α-$[Rh\{(R,R)\text{-}Me_2trien\}(phi)]^{3+}$ Λ-1-$[Rh(mgp)_2(phi)]^{5+}$

Figure 3. Illustrations of phi complexes of Rh^{III} which bind to DNA by intercalation (mgp = 4-guanidiummethyl-1,10-phenanthroline). The common feature in this family of metallointercalators is the phi ligand, which serves to anchor the complex in the major groove of DNA. Systematic variations in the ancillary ligands permit tuning of binding affinity and site selectivity.

extended aromatic surface for intercalation. Indeed, all the phi complexes of rhodium we prepared thus far bind tightly to DNA by preferential intercalation of the phi ligand. Affinities range from 10^6 to 10^8 M^{-1}, and the sites recognized may be tuned selectively by varying substitutents on the ancillary, nonintercalating ligands.[26, 27] Some of these complexes display DNA affinities and specificities rivaling those of DNA-binding proteins.[27]

NMR spectroscopy has been particularly valuable in determining how these complexes are associated with DNA.[28, 29] The complexes all appear to bind DNA from the major groove. When the complex is anchored by intercalation, functional groups incorporated on the ancillary ligands can interact with sites on the major groove to determine binding-site selectivity.[26, 27] Indeed, in the case of Δ-α-$[Rh\{(R,R)\text{-}Me_2(trien)\}(phi)]^{3+}$ (trien = triethylene tetraamine), we constructed the complex so as to specify an ensemble of noncovalent contacts in the major groove for predictive targeting of the sequence 5′-TGCA-3′. Recently, a high-

resolution structural model of this complex bound site specifically to a decamer was determined using NMR spectroscopy.[29] In this structure, the metal complex is well stacked and bound symmetrically to the double helix; the different noncovalent contacts between the ancillary ligand and major groove site 5′-TGCA-3′ are apparent. Importantly, the DNA helix is unwound to accomodate the intercalator, but otherwise little perturbation in the DNA base stack is evident.[29]

In studying DNA-mediated electron transfer between metallointercalators, we frequently employed $[Rh(phi)_2(L)]^{3+}$ complexes as ground-state electron acceptors. These complexes are primarily sequence neutral in association with DNA and therefore bind randomly to the duplex.[30] Characterization of the electrochemical properties of $[Rh(phi)_2(L)]^{3+}$ by cyclic voltammetry reveals that in DMF the formal $Rh^{III} \rightarrow Rh^{II}$ reduction occurs at about 0 V vs. NHE.[31] Hence, electron transfer from photoexcited $[M(phen)_2(dppz)]^{2+}$ to DNA-bound $[Rh(phi)_2(L)]^{3+}$ is thermodynamically favorable ($M = Ru$: $\Delta G^\circ = 0.56$ V; $M = Os$: $\Delta G^\circ = 0.73$ V).

The photochemistry of these phi complexes of rhodium has proven to be quite valuable first in determining where the metal complex is bound along the helical polymer in a given electron transfer reaction and in providing potent photooxidants which are intercalated in DNA. Therefore, given the rich photochemistry of these complexes, we are able to utilize light of different wavelengths to induce selectively different chemical reactions.[30, 32] Irradiation of the DNA-bound complexes with UV light ($\lambda = 313$ nm) leads to direct scission of the DNA sugar–phosphate backbone by a reaction consistent with hydrogen abstraction of the C3′-H atom from the deoxyribose moiety by the activated phi ligand at the intercalation site.[30] This strand scission marks the site of intercalation. This photochemical reaction has been used profitably for establishing the site selectivities of a range of complexes. If instead the $[Rh(phi)_2(L)]^{3+}$ complexes are excited with visible light ($\lambda \geq 365$ nm), a powerfully oxidizing intraligand excited state is populated.[32] Based on quenching studies in solution in the absence of DNA, the reduction potential of the excited state of $[Rh(phi)_2(phen)]^{3+}$ ($E_{1/2}(*Rh^{III}/Rh^{II})$) is estimated to be about 2 V vs. NHE. We can therefore exploit these rhodium intercalators not only as ground-state but also as excited-state electron acceptors.

3. DNA as a Bridge for Electron Transfer

Scheme 1 illustrates the cycle of electron transfer reactions between DNA-bound metallointercalators. Irradiation of the M^{II} complex with visible light leads to the formation of the photoexcited donor, which in the absence of acceptor may return to the ground state by emission of a photon. In the presence of an acceptor with the appropriate reduction potential, the photoexcited donor may transfer an electron to the ground-state acceptor (rate constant k_{et}), which results in quenching of the donor emission. The products of this forward electron transfer then undergo thermal recombination (rate constant k_{rec}) to regenerate the ground-state pair. We may therefore monitor electron transfer between metallointercalators with the DNA π stack as the intervening bridge.

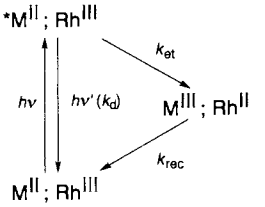

Scheme 1. Cycle of electron transfer reactions between DNA-bound metallointercalators.

3.1. Intercalative Coupling into the π Stack

We first compared the quenching of DNA-bound, photoexcited $[Ru(phen)_2(dppz)]^{2+}$ by two acceptors—namely, $[Rh(phi)_2(phen)]^{3+}$, which binds to DNA by intercalation, and $[Ru(NH_3)_6]^{3+}$, which binds to the surface of the double helix (Figure 4).[31] Since the $Rh^{III} \rightarrow Rh^{II}$ reduction potential of

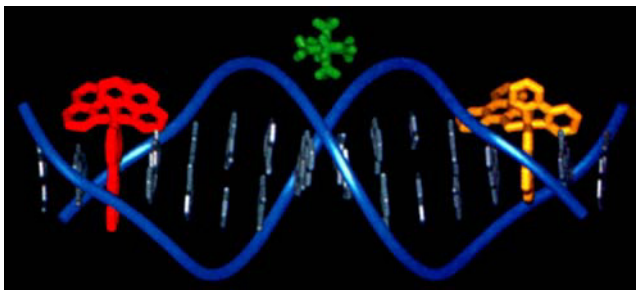

Figure 4. Schematic representation of transition metal complexes bound to DNA. Shown are Δ-$[Ru(phen)_2(dppz)]^{2+}$ (red), Δ-$[Rh(phi)_2(bpy)]^{3+}$ (yellow), and $[Ru(NH_3)_6]^{3+}$ (green). Δ-$[Ru(phen)_2(dppz)]^{2+}$ and Δ-$[Rh(phi)_2(bpy)]^{3+}$ are metallointercalators and probe the DNA base stack directly. $[Ru(NH_3)_6]^{3+}$, which does not have the ligand framework to support intercalation, binds only by surface association and therefore cannot access the π stack.

$[Rh(phi)_2(phen)]^{3+}$ ($E_{1/2}(Rh^{III}/Rh^{II}) = -0.03$ V vs. NHE) is nearly identical to that of $[Ru(NH_3)_6]^{3+}$ (0.01 V), the driving force for the reaction does not differ significantly between the two donor–acceptor pairs. When the intercalator $[Rh(phi)_2(phen)]^{3+}$ or $[Rh(phi)_2(bpy)]^{3+}$ is titrated into solutions of DNA-bound $[Ru(phen)_2(dppz)]^{2+}$, fast and efficient quenching of the ruthenium emission on the subnanosecond time scale is observed. Over a similar concentration range, $[Ru(NH_3)_6]^{3+}$ also quenches the luminescence of DNA-bound $[Ru(phen)_2(dppz)]^{2+}$. However, this quenching is less efficient and proceeds on the nanosecond time scale. In contrast to the intercalating acceptor, $[Ru(NH_3)_6]^{3+}$ exhibits a quenching profile that is consistent with a reaction which requires diffusion. Here, electron transfer does not proceed through the DNA, rather the DNA merely facilitates diffusion of the acceptor.

The distinction between electron transfer reactions involving intercalated donors and acceptors and those involving reactants bound in the groove is also evident in data emerging from other research groups.[10] For example, quenching of intercalated ethidium by *N*,*N*′-dimethyl-2,7-diazapyrenium dichloride (DAP) is enhanced compared to the reaction in the absence of DNA.[10] On the other hand, quenching of ethidium by groove-bound methyl viologen or palladium

porphyrins does not exhibit the remarkable efficiency and rate observed with the metallointercalators.[10] When methyl viologen is used to quench DNA-bound, photoexcited $[Ru(phen)_2(dppz)]^{2+}$, the quenching is also slow relative to reactions between molecules which access the π stack directly by intercalation.[10]

In fact, coupling into the π stack is so important, that even for molecules which intercalate in the DNA, the nature of the stacking interaction seems to affect the reactivity by electron transfer. For example, when $[Rh(phen)_2(phi)]^{3+}$ is titrated into solutions of DNA-bound $[Ru(phen)_2(dppz)]^{2+}$, we observe no quenching of the ruthenium photoluminescence, despite sufficient driving force for the reaction.[33] Based on photocleavage studies, $[Rh(phen)_2(phi)]^{3+}$ prefers to intercalate shape selectively at sites with an open major groove, and hence exhibits a greater sequence selectivity in binding to DNA than $[Rh(phi)_2(L)]^{3+}$.[33] Even though the complex binds by intercalation, the depth to which the complex intercalates is limited by steric clash between the ancillary phenanthroline ligands and the sugar–phosphate backbone of the DNA. Therefore, $[Rh(phen)_2(phi)]^{3+}$ appears unable to couple effectively into the DNA π stack and fails to quench the ruthenium emission.

The effect of stacking on quenching efficiency is also important for the electron donor. Owing to symmetry matching between the right-handed octahedral metal complexes and the right-handed DNA duplex,[24] the Δ enantimomer binds more deeply within the DNA base stack. It is not surprising then that Δ-$[Ru(phen)_2(dppz)]^{2+}$ is quenched more efficiently than Λ-$[Ru(phen)_2(dppz)]^{2+}$ by $[Rh(phi)_2(bpy)]^{3+}$.[33, 34] We also observed significant differences in quenching efficiency for photoinduced reactions with $[Ru(phen)_2(dppz)]^{2+}$ versus ethidium as donor when all donors and acceptors were fully bound. Here too we estimate no difference in the driving force for the two redox couples; yet, the intercalators appear to vary in how they stack in the DNA duplex, which affects the electron transfer. It is therefore clear that effective stacking is requisite for coupling into the DNA duplex. A challenge to us is to develop a good understanding of what characterizes this effective stacking and how we may develop quantitative parameters to assess this stacking and its effect on coupling into the helix.

Experiments with $[Os(phen)_2(dppz)]^{2+}$ as the photoexcited donor were valuable in characterizing the fast, static quenching, and have ruled out energy transfer and metal-complex diffusion as mechanisms for the efficient quenching between metallointercalators.[25] Just as with ruthenium, we observe efficient quenching of the osmium emission in reactions with $[Rh(phi)_2(bpy)]^{3+}$. In fact, over a range of acceptor concentrations, the osmium and ruthenium quenching profiles are remarkably similar. This is inconsistent with diffusional quenching. If molecular diffusion were important, one would predict a reduction in quenching efficiency for the osmium donor, since it has a significantly shorter excited-state lifetime than the ruthenium donor. Moreover, the red-shifted emission spectrum of the osmium complex does not overlap the acceptor absorption, which precludes energy transfer as the quenching mechanism. The correlation between the ruthenium and osmium reaction profiles also rules out participation of energy transfer in the quenching of either osmium or ruthenium by $[Rh(phi)_2(bpy)]^{3+}$.

A comparison of the quenching of ruthenium donors by DNA-bound rhodium acceptors bound to DNA and SDS micelles further illustrates the importance of the DNA π stack in mediating fast and efficient electron transfer (Figure 5).[33] The DNA double helix and the micelle both provide anionic

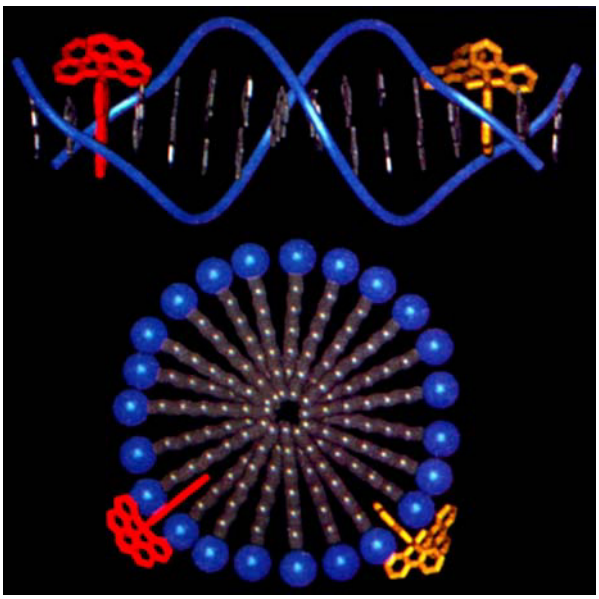

Figure 5. Illustration of the electron donor Δ-$[Ru(phen)_2(dppz)]^{2+}$ (red) and the electron acceptor Δ-$[Rh(phi)_2(bpy)]^{3+}$ (yellow) bound to double-helical DNA (top) and a SDS micelle (bottom).

surfaces to which the cationic donors and acceptors bind and a hydrophobic core region which accomodates their large, intercalating ligands. The primary difference between these two microheterogeneous environments is that the SDS micelle does not contain an organized pathway for electron transfer like the DNA. Accordingly, in the micellar system rhodium complexes do quench the ruthenium luminescence, but the electron transfer is much less efficient than the DNA-mediated reaction and proceeds on the nanosecond time scale. In fact, the quenching reaction in the micelle is diffusion-dependent and requires a collision between donor and acceptor. This in contrast to DNA-mediated electron transfer between metallointercalators, in which diffusion is clearly not required for quenching.

3.2. Rates of DNA-Mediated Electron Transfer

To deepen our understanding of electron transfer between metallointercalators, we sought to utilize ultrafast laser spectroscopy to monitor the reaction on the picosecond time scale, and, in so doing, hopefully determine the rates for these fast, photoinduced quenching processes.[34] To examine the rate of forward electron transfer (k_{et}, see Scheme 1), we employed time-correlated single-photon counting (TCSPC; resolution about 50 ps), with which the decay of the excited

state of the photoexcited $[M(phen)_2(dppz)]^{2+}$ donors could be monitored. Remarkably, when quenching of photoexcited $[Ru(phen)_2(dppz)]^{2+}$ by DNA-bound $[Rh(phi)_2(bpy)]^{3+}$ is followed by ultrafast TCSPC, no change in the kinetics of excited-state decay was detected as a function of quencher despite the significant intensity of the quenching. Instead, the quenching was manifested primarily as a loss of luminescence intensity at zero time; this intensity loss increased with increasing concentration of $[Rh(phi)_2(bpy)]^{3+}$. The same observation was made for the isostructural analogue $[Os(phen)_2(dppz)]^{2+}$. Such behavior implies that quenching by electron transfer proceeds faster than the time resolution of the instrument. Hence, we assigned a lower limit by $3 \times 10^{10}\ s^{-1}$ to the rate constant k_{et} describing this ultrafast reaction.

To monitor the back electron transfer we utilized ultrafast transient absorption spectroscopy. Following excitation of $[M(phen)_2(dppz)]^{2+}$ complexes at 390 nm, we monitored the change in the absorbance of the sample at 420 nm as a function of time. In the absence of acceptor, the kinetics of ground-state recovery match the luminescence lifetimes of the donors bound to DNA. As $[Rh(phi)_2(bpy)]^{3+}$ is titrated into solutions of DNA-bound donor, a new component is observed, which increases in intensity with increasing amounts of rhodium. Analysis of the transient absorption kinetics reveals that this fast phase is well described by $k_{rec} = 9.0 \times 10^{10}\ s^{-1}$ for M = Ru and $1.1 \times 10^{11}\ s^{-1}$ for M = Os. Since such a rate constant could not be detected in the kinetics of luminescence decay, we are confident in our assignment of this rate constant to the recombination reaction.

Transient absorption data for seven donor–acceptor pairs taken on the picosecond time scale are given in Table 1.[34]

Table 1. Rate constants for ground-state recombination following electron transfer from DNA-bound, photoexcited donors to Δ-$[Rh(phi)_2(bpy)]^{3+}$ [a, b].

Donor	DNA	k_{rec} [c] [$10^9\ s^{-1}$]	$-\Delta G°$ [d] [V]
Δ-$[Ru(phen)_2(dppz)]^{2+}$	calf thymus	9.2	1.66
rac-$[Ru(bpy)_2(dppz)]^{2+}$	calf thymus	7.1	1.69
Δ-$[Ru(dmp)_2(dppz)]^{2+}$	calf thymus	11	1.59
Δ-$[Ru(phen)_2(F_2dppz)]^{2+}$	calf thymus	7.7	1.68
rac-$[Ru(phen)_2(Me_2dppz)]^{2+}$	calf thymus	9.2	1.67
Δ-$[Os(phen)_2(dppz)]^{2+}$	calf thymus	11	1.21
Λ-$[Ru(phen)_2(dppz)]^{2+}$	calf thymus	4.5	
Δ-$[Ru(phen)_2(dppz)]^{2+}$	poly-d(AT)	7.4	
Δ-$[Ru(phen)_2(dppz)]^{2+}$	poly-d(GC)	0.21	

[a] Based on ref. [34]. The data were obtained by transient absorption spectroscopy. [b] Experimental conditions: [Ru], [Os] = 20 μM, [DNA] = 2 mM nucleotides (M:Nuc = 1:100), 5 mM tris(hydroxymethyl)aminomethane (Tris), 50 mM NaCl, pH = 8.5. [c] The error in k_{rec} was estimated to be ±10%. [d] $-\Delta G° = [E_{1/2}(M^{III}/M^{II}) - E_{1/2}(Rh^{III}/Rh^{II})]$. The error in $\Delta G°$ was estimated to be ± 50 mV.

Within this series, the reactants vary with respect to intercalating ligand, ancillary ligands, relative hydrophobicity, chirality, and metal center. Despite such a range of chemical properties, the rate observed for transient absorption is centered around $10^{10}\ s^{-1}$. Even for the osmium complex, in which the 3+ oxidation state is stabilized by about 500 mV relative to that of the ruthenium complex, the recombination rate is not significantly perturbed. A significant difference in rate is observed, however, when the absolute configuration of the donor is varied. For the right-handed Δ-$[Ru(phen)_2(dppz)]^{2+}$ $k_{rec} = 9.0 \times 10^{10}\ s^{-1}$, whereas for the left-handed enantiomer k_{rec} is diminished by a factor of 2.5. The faster electron transfer observed for Δ-$[Ru(phen)_2(dppz)]^{2+}$ is consistent with the deeper stacking of this enantiomer into the double helix.

Of particular interest is that these recombination reactions are relatively insensitive to the loading of acceptor on the helix. As the concentration of acceptor is increased throughout a titration, one expects (given random occupation of the helix) that the distribution of donor–acceptor separations should decrease. However, we observe in these experiments that, although the number of recombinations on the picosecond time scale increases with increasing amount of acceptor, the rate constant does not change as a function of acceptor concentration. This could indicate a reaction rate that exhibits a low dependence on distance.

These fast rates of reaction and insensitivity of fast recombination to loading could also be interpreted by a model in which the donor and acceptor bind cooperatively on the DNA helix.[34–36] With such a clustering model, the distances between metal complexes would be short, and, hence, the rates of reaction would be high and appear to be independent of loading. For the titration of DNA-bound $[Ru(phen)_2(dppz)]^{2+}$ with the rhodium quencher, such a clustering model can be fit but would require a cooperativity in binding of more than 1 kcal.[35] A perturbation in the circular dichroism (CD) spectrum of Δ-$[Ru(phen)_2(dppz)]^{2+}$ and Δ-$[Rh(phi)_2(bpy)]^{3+}$ bound to poly d(AT) at high loadings was interpreted as evidence for preferential binding of the rhodium complex near Δ-$[Ru(phen)_2(dppz)]^{2+}$.[36] It is difficult, however, to reconcile this clustering with several observations: a) the absence of fast quenching in the micelles where clustering should be encouraged, b) the presence of loading-independent kinetics for the full range of donors examined, and c) the random binding to DNA without conformational distortions of the donors and acceptors individually. In addition, there is no apparent structural basis for cooperative binding between ruthenium and rhodium to satisfy this model.

It is noteworthy that the largest change in electron transfer is observed as a function of the sequence of the DNA bridge.[34, 37] Evident in Table 1 are the rates of recombination k_{rec} from reduced acceptor to oxidized donor for poly d(AT) and poly d(GC): k_{rec} is 30 times higher with poly d(AT) than with poly d(GC). In addition, the yield of electron transfer from photoexcited $[M(phen)_2(dppz)]^{2+}$ to DNA-bound $[Rh(phi)_2(bpy)]^{3+}$ depends strongly on the nucleic acid sequence. For donors bound to poly d(AT) the fraction of excited states (M = Os or Ru) which undergo electron transfer resembles closely the yield of electron transfer for donors bound to mixed-sequence (calf-thymus) DNA. For the same donors bound to poly d(GC), however, the fraction quenched is significantly reduced. Nonetheless, while the yield of photoinduced electron transfer decreases for $[M(phen)_2(dppz)]^{2+}$ bound to poly d(GC) relative to mixed-sequence calf-thymus DNA and poly d(AT), the rate k_{et} of the forward reaction remains greater than $3 \times 10^{10}\ s^{-1}$.[34] These findings are also hard to reconcile with a clustering model, because both the

rate of recombination and yield of electron transfer appear to depend upon the DNA sequence between donor and acceptor.

Given these discrepancies, we reinvestigated the CD of Δ-$[Ru(phen)_2(dppz)]^{2+}$ and Δ-$[Rh(phi)_2(bpy)]^{3+}$ bound to different DNA polymers as a function of concentration to explore more fully the parameters affecting any possible clustering.[38] We found no systematic change in the CD as a function of loading on the helix nor as a function of polymer sequence. The induced CD observed with each intercalator upon addition of DNA arises whether they are bound together or separately. It is a function of binding to the chiral interbase pair site, and observed even with achiral intercalators. We also tested the clustering model more directly in an NMR experiment. Here, we examined the site selectivity of intercalation in DNA by monitoring perturbations in the signals for the exchangeable imino protons within each DNA base pair of a DNA decamer upon binding the ruthenium and rhodium intercalator separately or together. If anything, the NMR data indicate that the complexes bind anticooperatively to the decamer, and primarily at sites separated on the helix by four base pairs.

Nonetheless, this whole discussion of cooperative versus anticooperative binding on the helix teaches us some lessons. For all of these studies of electron transfer, a fundamental understanding of structure—that is, of how the donors and acceptors are associated with the helix—is essential. Moreover, to examine in detail the distance dependence of electron transfer, it is important to carry out such studies with donors and acceptors bound at a fixed separation and with a fixed intervening DNA sequence. With molecules bound noncovalently to DNA, a distribution of distances and sites occurs, and deconvoluting these different parameters becomes problematic.

3.3. Characterizing the Products of Electron Transfer

Can we provide more evidence that this fast quenching reaction is indeed electron transfer? The fraction of recombination reactions that occur on the picosecond time scale accounts for the majority of excited states which undergo electron transfer. However, a small fraction of reduced acceptor and oxidized donor appear to recombine on a longer time scale. To identify and characterize any long-lived intermediates of electron transfer between metallointercalators, we monitored the photoinduced electron transfer by transient absorption spectroscopy on the microsecond time scale. For $[Ru(dmp)_2(dppz)]^{2+}$ (dmp = 4,7-dimethyl-1,10-phenanthroline) and $[Os(phen)_2(dppz)]^{2+}$ donors, we actually observed rhodium-induced transients which persisted well into the microsecond regime.[25, 39] Owing to the stability of the osmium complex in the 3+ oxidation state, we were able to measure the wavelength dependence of the long-lived transient. The resulting difference spectrum ($Os^{III} - Os^{II}$) is nearly identical to those obtained either by chemical oxidation of $[Os(phen)_2(dppz)]^{2+}$ in solution or photochemical oxidation of DNA-bound, photoexcited $[Os(phen)_2(dppz)]^{2+}$. Thus, this long-lived intermediate was unambiguously identified as the oxidized donor, which establishes unequivocally that the reaction proceeds by electron transfer.

3.4. Electron Transfer over a Fixed Donor–Acceptor Separation

Experiments in which the donors and acceptors are bound noncovalently to the DNA duplex were all carried out at low reactant loadings in order to maximize donor–acceptor separation. In a typical experiment, a 1:1 ratio of donor to acceptor corresponds to an average separation of 25 base pairs. Remarkably, 50% of the Δ-$[M(phen)_2(dppz)]^{2+}$ excited states undergo electron transfer, indicating that the reaction is very efficient even at low loading. Under these conditions, however, a distribution of donor–acceptor separations is always present. Moreover, as discussed above, we cannot eliminate the possibility of clustering with metal complexes noncovalently bound to the helix. To establish definitively that photoinduced electron transfer may proceed over some distance, we needed to tether the donor and acceptor intercalators to opposite ends of a DNA duplex to provide an assembly in which the donor–acceptor separation might be fixed.

We constructed a DNA duplex in which $[Ru(phen)_2(dppz)]^{2+}$ and $[Rh(phi)_2phen]^{3+}$ derivatives were tethered by flexible linkers to opposite ends of a 15 base pair oligonucleotide (Figure 6).[40] The complexes were free to intercalate but

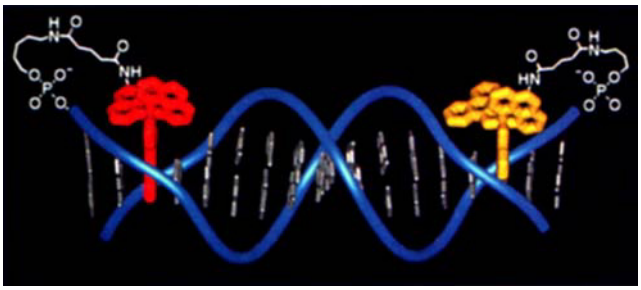

Figure 6. Schematic representation of a 15 base pair DNA duplex with Δ-$[Ru(phen)_2(dppz)]^{2+}$ as electron donor (red) and Δ-$[Rh(phi)_2(phen)]^{3+}$ as electron acceptor (yellow) tethered to opposite ends of the assembly; the complexes are intercalated but separated by a fixed distance. Shown is the most probable separation of 11 base pairs (41 Å).

separated by about 40 Å. Companion experiments with duplexes bearing either a tethered ruthenium or rhodium complex (but not both) allowed us to examine the integrity of the metal-modified DNA duplex and the intercalation sites. Owing to the sensitivity of the ruthenium luminescence to the local environment, we could characterize intercalation by the tethered ruthenium within the helix. In the conjugate assembly containing only a rhodium complex, a photocleavage experiment could be used to mark the site of intercalation.

In the 15 base pair assembly shown, intercalation of the metal complexes can occur either one or two base pairs from the end of the duplex, leading to a most probable separation of 41 Å between donor and acceptor.[40] Remarkably, no ruthenium luminescence was detected in the mixed-metal assembly upon excitation. Hence, as suggested by experiments with noncovalently bound donors and acceptors, photoinduced electron transfer through the double helix can proceed efficiently between metallointercalators over a long

molecular distance. A lower limit of $3 \times 10^9\ s^{-1}$ was set for the rate constant describing the photoinduced reaction. Therefore, the DNA double helix does indeed provide a bridge for long-range electron transfer.

Viewed in the context of classical studies of electron transfer through σ-bonded networks,[41] such long-range electron transfer through DNA was surprising. Chemists are now beginning to devote attention to developing a theoretical foundation for the consideration of charge transfer mediated by the DNA base stack.[42] Our studies point to stacking as a critical element in determining the efficiency of the reaction. An efficient reaction mediated by the DNA π stack requires full intercalation of donors and acceptors. Indeed significant differences in electron transfer are evident not only between groove-bound versus intercalated redox pairs, but also among intercalators which stack in the helix to differing extents. Our results highlight the importance of addressing this stacking parameter explicitly when constructing theoretical models of DNA-mediated charge transfer.

Other research groups have since constructed different DNA assemblies with covalently bound donors and acceptors. At first, the results with these different assemblies appear quite disparate. Meade and Kayyem developed a system in which a nonintercalating ruthenium complex is coordinated directly to amino-modified sugars at the terminal position of oligonucleotides.[43] They assert that electron transfer in this system is protein-like. Most recently, Lewis and co-workers[44] measured rates of photooxidation of a guanine base in a DNA hairpin by an associated stilbene unit bound at the top of the hairpin. By systematically varying the position of the guanine base within the hairpin and measuring the rate of electron transfer, a value for the electronic coupling parameter β could be estimated. Here, β was $0.64\ Å^{-1}$, which is intermediate between that for proteins with σ-bonded arrays and that expected for a highly coupled π-bonded array.

Most recently, we began to expand the scope of our studies to include organic intercalators such as ethidium.[45] With ethidium tethered and intercalated at one end of DNA oligonucleotides and a $[Rh(phi)_2(bpy)]^{3+}$ derivative covalently bound and intercalated at the opposite end, we also observed fast ($\geq 10^{10}\ s^{-1}$) photoinduced electron transfer. It is interesting that with excited ethidium as donor, either noncovalently or covalently bound, the efficiency of the reaction is reduced compared to that with ruthenium, despite similar driving forces. This difference in yield may reflect differences in intercalative stacking between the two donors. Importantly, systematic variation of the separation between donor and acceptor over distances ranging from 17–36 Å yields fluorescence quenching irrespective of distance, and the dependence of the quenching yield on distance is low. Although little sensitivity to distance is apparent, experiments carried out as a function of temperature and with intervening mismatches have underscored the remarkable dependence of these reactions on how the base pairs are stacked within the DNA duplex. Photoinduced quenching is apparent in an 11 base pair duplex containing tethered ethidium and rhodium (Table 2). However, if a single, intervening cytosine–adenine mismatch (C–A) is introduced, the long-range charge transfer is abolished. A guanine–adenine mismatch (G–A), which is known to be well stacked within *B*-form DNA, actually enhances quenching of electron transfer. These results certainly suggest the application of long-range electron transfer in developing new biosensors that sensitively report on the DNA bridge.

Table 2. Flourescence quenching in ethidium–Rh DNA duplexes with mismatched pairing [a].

Assembly	F_g[b]
Et'-5'-C-T-A-T-C-**T**A-T-C-G-T G-A-T-A-G-**A**-T-A-G-C-A-5'-Λ-Rh	0.21
Et'-5'-C-T-A-T-C-**C**A-T-C-G-T G-A-T-A-G-**A**-T-A-G-C-A-5'-Λ-Rh	0.04
Et'-5'-C-T-A-T-C-**G**A-T-C-G-T G-A-T-A-G-**A**-T-A-G-C-A-5'-Λ-Rh	0.26

[a] Based on ref. [45]. [b] F_g = fraction quenched: Fluorescence of duplexes containing ethidium (Et) and Rh compared to that of duplexes containing only ethidium.

Thus, we may begin to reconcile studies in our laboratory and elsewhere on DNA-mediated electron transfer in covalently bound assemblies by focusing on the issue of stacking. We find that electron transfer is most sensitive to the intervening base-pair stack. How the donor and acceptor are coupled into this stack varies in each system. In proteins for which the energetic differences in coupling depend upon σ-bonded interactions, small energetic differences between systems do not cause large differences in electronic coupling. In the DNA double helix, however, in which electronic coupling is mediated by π stacking, small energetic differences could lead to large differences in coupling efficiency. Hence, with donors and acceptors coordinated to sugar moieties, charge transfer first through a σ-bonded network could be rate-limiting. In the case of the stilbene-modified DNA hairpin, the stilbene group is closely associated but unstacked with the DNA base pairs, and hence, intermediate coupling might be expected. With well-intercalated donors and acceptors, coupling into the base-pair array should be optimum.

4. DNA-Mediated Electron Transfer Involving DNA Bases

In our studies of DNA as a bridge for electron transfer, we focused on the chemistry of DNA and put aside all considerations of the DNA helix as a biologically important entity. With metallointercalators as donor and acceptor, the DNA π stack can promote photoinduced electron transfer at long range. But can the DNA helix serve not only as a conduit for electron transfer but also as a reactant? Are there reactions within the cell in which radicals migrate through the DNA π stack to damage DNA? The chemistry of the DNA π stack could indeed be an issue in carcinogenesis and mutagenesis. Moreover, might this long-range chemistry be exploited by nature in sensing or repairing DNA damage, or even more generally in transmitting information over long molecular distances with modulation by the DNA π stack? These

intriguing questions were suggested by our studies on DNA as a bridge for electron transfer and some were ready to be investigated using chemistry we developed. Most importantly, it appeared that the sensitivity of electron transfer to the DNA π stack provided a route for exploring and exploiting DNA chemistry over large distances.

4.1. Oxidative DNA Damage by Long-Range Charge Transfer

The major target of oxidative damage of nucleic acid within the cell is guanine (G).[46] Experimental studies and calculations reveal guanine to be the most easily oxidized of the nucleic acid bases.[47,48] A variety of DNA-binding agents including riboflavin, anthraquinone derivatives, and napthalimides are known for inducing, with photoactivation, oxidative damage specifically at the 5′-G of 5′-GG-3′ doublets.[48] $[Rh(phi)_2(L)]^{3+}$ metallointercalators, which serve as potent photoxidants ($E_{1/2}(*Rh^{III}/Rh^{II}) > 2.0$ eV vs. NHE) upon irradiation with low-energy light ($\lambda \geq 365$ nm),[32] might be useful in the study of long-range, DNA-mediated oxidative damage to DNA.

We implemented the strategy outlined in Scheme 2 to investigate DNA damage by long-range oxidation.[49] We prepared DNA duplexes containing 5′-GG-3′ doublet sites and a rhodium intercalator, the oxidant, tethered to one end of the

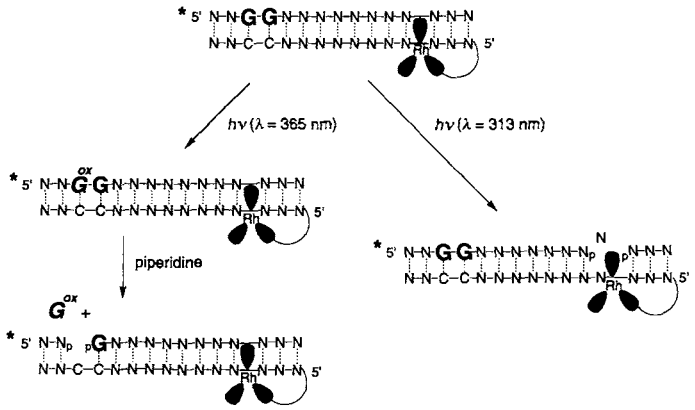

Scheme 2. Irradiation of a duplex DNA to which a rhodium complex is tethered with UV light permits determination of the site of intercalation (right) as well as the site and extent of long-range oxidation (left).

duplex. In this DNA assembly, the rhodium is separated in a well-defined manner from potential sites of oxidation. Direct strand cleavage of the DNA promoted by irradiation ($\lambda =$ 313 nm) of the rhodium-modified duplex marks the site of intercalation, and permits determination of the distance separating the rhodium complex from potential sites of damage. In contrast, irradiation of the assembly with low-energy light (365 nm) introduces a photoexcited site-specific hole into the DNA base stack and effects oxidation to yield a modified base site. The position and yield of damage is revealed subsequently by treatment of the modified DNA with piperidine, which promotes strand cleavage at the damaged site.

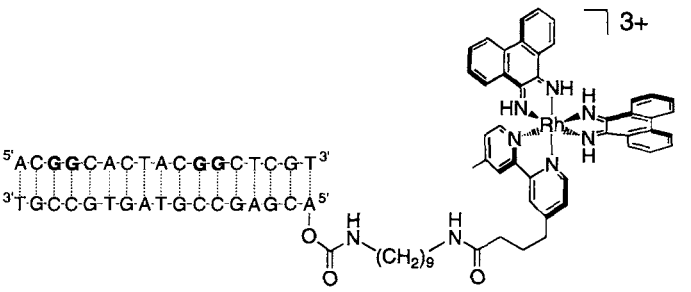

Figure 7. Rhodium-modified DNA duplex assembly constructed for investigating long-range oxidative DNA damage. The sequence shown contains two 5′-GG-3′ doublets (in bold face), potential oxidation sites, which are separated from the intercalated Rh complex by 17 Å and 34 Å [49]. For clarity the Rh complex is not shown intercalated.

An example of a rhodium-modified assembly containing 5′-GG-3′ doublets is illustrated in Figure 7.[49] In this modified duplex, there is significant oxidative DNA damage specifically at 5′-G of the 5′-GG-3′ sites upon irradiation at 365 nm. Remarkably, this oxidative damage must occur *from a distance*. With the rhodium intercalator tethered to the 5′ end, photocleavage ($\lambda = 313$ nm) indicates intercalation primarily three base pairs from the modified terminus. In fact, for the duplex shown in Figure 7, damage is observed at both 5′-GG-3′ sites located 17 and 34 Å from the rhodium intercalator. Moreover, the intensity of oxidative damage at the site distal to the rhodium complex is comparable to (or even higher than) that of the proximal 5′-GG-3′ doublet; this suggests that the yield of damage is not strongly dependent on distance. If we examine an assembly containing only the distal 5′-GG-3′ doublet, we still see comparable damage; this demonstrates that long-range oxidation of the 5′-GG-3′ doublet does not require the intervening oxidation site.

Although the yield of oxidative damage does not vary significantly with distance, it does depend strongly on sequence, which is known to modulate oxidation potential of the base.[48] A rhodium-modified duplex containing a 5′-GGG-3′ triplet was also constructed.[49] Molecular orbital calculations of the ionization potentials of the DNA bases indicated that 5′-G of the 5′-GGG-3′ triplet is even easier to oxidize than 5′-G of the 5′-GG-3′ doublet.[48b,e] In this assembly, oxidation was observed at the 5′- and central guanine bases of the triplet and, consistent with the calculated ionization potentials, was greatest at 5′-G.

Following enzymatic digestion of the damaged duplex, 8-oxo-G was isolated as the oxidative product. 8-Oxo-G is the primary lesion in cellular oxidative DNA damage. Formation of this product requires O_2. Therefore, while the oxidative reaction in our synthetic system employs rhodium photochemistry, one might consider alternative, perhaps more physiologically relevant means to introduce a hole into the π stack. Our results appear to indicate that, irrespective of the oxidant, once such a hole is introduced into the DNA π stack, it may migrate, leading effectively to oxidative DNA damage from a distance. This characteristic of double-helical DNA—the extended base-paired π stack which facilitates long-range charge transport—is therefore not simply one of chemical novelty. It is instead a characteristic with important implications for DNA mutagenesis and carcinogenesis within the cell.

In fact, many research groups have shown that a range of oxidants can be used to promote guanine damage in DNA; whether these oxidants can also promote damage at long range needs to be established.[48]

We recently found that ruthenium intercalators can also be employed to effect long-range oxidative DNA damage.[50] Scheme 3 illustrates the flash-quench experiment used to oxidize guanines in DNA with ground-state Ru^{III} generated in situ as oxidant. An analogous flash-quench method was employed in classic studies of protein-mediated electron transfer.[51]

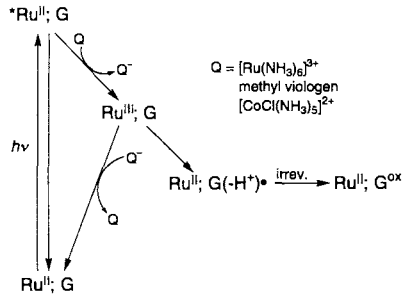

Scheme 3. Flash-quench experiment in which Ru^{III} prepared in situ oxidizes guanine in duplex DNA.

This flash-quench chemistry was exciting to us, since it offered another possibility for probing oxidative reactions on DNA from a distance. Moreover, the rhodium photochemistry is exceedingly inefficient and involves an excited-state oxidant. With ruthenium(III) generated in situ, more than a thousandfold increase in quantum yield occurs; the ruthenium complex represents a ground-state oxidant. Moreover, this methodology is particularly well suited for spectroscopic studies; for instance, the neutral guanine radical was identified within DNA by its characteristic transient absorption spectrum.[50a] Furthermore, with ruthenium tethered to a DNA duplex, we also find oxidative damage to DNA from a distance.[50b] Figure 8 illustrates a particularly interesting observation made using this chemistry. As with the rhodium photooxidant, reaction occurs preferentially at a 5′-GG-3′ doublet. But what if the 5′-GG-3′ doublet is removed by mutation? In that case we observed essentially equal oxidative damage distributed over all single G sites. This finding illustrates quite graphically that migration and equilibration of the oxidizing hole across the duplex must occur on a time scale which is fast compared to the trapping reaction. Our finding of damage at a distance with this system also highlights the likely generality of long-range oxidation through DNA. This chemistry may allow us to link the kinetics of these reactions (determined with spectroscopy) and the yield of products of the reaction (determined with biochemical methods) in a detailed mechanistic investigation.

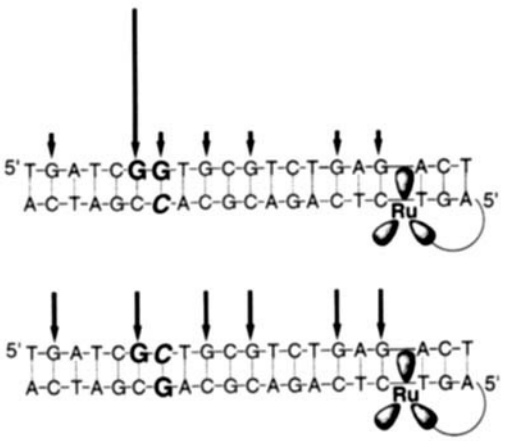

Figure 8. Long-range oxidative damage at guanine bases by tethered Ru^{III} in modified DNA duplexes with (top) and without a 5′-GG-3′ guanine doublet (bottom). With the 5′-GG-3′ site, oxidative damage is observed primarily at the 5′-G of the doublet. Without the 5′-GG-3′ site, oxidative damage is observed to an equivalent extent (indicated by the length of the arrows) at each guanine accross the duplex.

4.2. Sensitivity of Long-Range Oxidative DNA Damage to the Intervening Base-Paired Stack

Like electron transfer between metallointercalators, long-range oxidative damage is remarkably sensitive to stacking. For rhodium-modified oligonucleotides with tethered Δ-$[Rh(phi)_2(bpy)]^{3+}$, the yield of oxidized product is consistently higher than for conjugates with the rhodium center in the Λ configuration.[49] Hence, the deeper stacking of the right-handed metal complex in the DNA appears to enhance the efficiency of the damage.

We wanted to probe the sensitivity of the DNA-mediated reaction to stacking more generally by exploring whether perturbations in the intervening π stack between the donor and the acceptor also affect the oxidation.[52] The assemblies shown in Figure 9 are representative of a family of assemblies

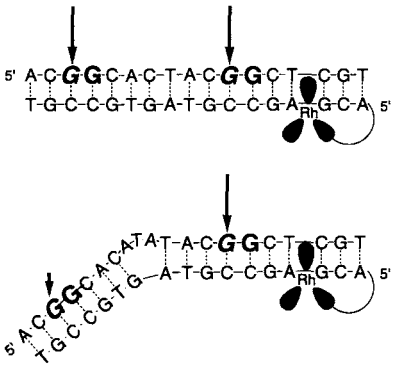

Figure 9. Long-range oxidative damage in rhodium-modified duplexes with a fully base-paired and stacked region (top) or a 5′-ATA-3′ bulged region (bottom) separating two 5′-GG-3′ potential oxidation sites. For the fully stacked duplex, the extent of damage (indicated by the length of the arrows) is nearly identical at both oxidation sites. With the 5′-ATA-3′ bulge, which disrupts the stacking between the distal 5′-GG-3′ site and the Rh intercalator but not the proximal, substantial diminution in the extent of damage at the distal site is observed [52].

prepared; each contains a rhodium oxidant and two 5′-GG-3′ doublets separated by a bulged base region. By comparing the extent of damage at the distal and proximal 5′-GG-3′ doublets in the presence and absence of the intervening bulged region, we could examine the effect of the intervening disruption in base stacking on long-range electron transfer.

Figure 9 shows the assembly containing the ATA bulge, one of the few bulges which has been characterized with high-resolution NMR spectroscopy.[53] From these structural studies it was apparent that the bulge leads to substantial but not complete disruption of the base stack: There is about 75% diminution in oxidation of the distal 5′-GG-3′ doublet compared to the proximal 5′-GG-3′ doublet. Hence, perturbations in the intervening π stack do indeed affect DNA-mediated electron transfer. In fact, these results indicate directly that the long-range hole transfer proceeds through the π stack.

These results also highlight a novel application of this chemistry. Long-range oxidation provides a means for probing the integrity of the base stack in solution. Base-pair stacking is not easily assayed by other techniques. What effects on long-range oxidation would be expected in the presence of covalent lesions to DNA, or if an intervening base were flipped out of the stack, or simply if a DNA-binding protein such as the TATA-box binding protein (which substantially distorts the duplex) were associated? Experiments that address these questions are currently underway.

Lastly, these results not only illustrate oxidative reactions on DNA from a remote site, but also suggest strategies for protecting DNA sequences within the cell from long-range damage by radicals. Oxidative damage to DNA from remote sites may be modulated by the intervening base-pair stack. For example, disruptions in the π stack, caused either by transient openings encoded by sequence or by protein binding, could actually provide a method for protecting DNA.

4.3. Remote Repair of the Thymine Dimer mediated by the DNA Base Stack

The chemistry of electron transfer may be exploited not only in effecting DNA damage but also in initiating the repair of a common light-induced DNA lesion, the thymine dimer.[54] Bacteria such as *E. coli* utilize photolyase enzymes to repair the thymine dimer photochemically.[55] In the key step of this process, visible light ($\lambda = 350-450$ nm) induces an electron transfer from an enzyme-bound flavin to the dimer, initiating repair. In model studies using photoexcited reductants, repair of the thymine dimer in duplex DNA was observed with high-energy irradiation ($\lambda \leq 300$ nm).[56] Excited-state oxidants which remove an electron from the dimer were shown to repair pyrimidine dimer model compounds when ultraviolet light (≤ 300 nm) was used to start the process.[57] Based on these results, we expected that excited-state rhodium metallointercalators, as powerful oxidants, might trigger repair of the thymine dimer in duplex DNA by injecting a photoexcited hole directly into the DNA base stack. Moreover, the thymine dimer and its repair, initiated simply by electron transfer, offered an attractive trapping reaction for characterizing parameters of DNA-mediated chemistry.

We found first that upon excitation with visible light ($\lambda = 400$ nm), $[Rh(phi)_2(dmb)]^{3+}$ (dmb = 4,4′-dimethyl-2,2′-bipyridine) initiated repair of a thymine dimer incorporated site-specifically in the center of a synthetic 16-mer oligonucleotide duplex ([duplex]:[$[Rh(phi)_2(dmb)]^{3+}$] = 1:1).[54] The repair mechanism is thought to proceed by oxidation of the dimer ($E_{1/2}(^{+}\widehat{TT}/\widehat{TT}) \approx 2.0$ V vs. NHE)[55] by the intraligand excited state of the rhodium complex, in which an electron deficiency (hole) is localized on the intercalated phi ligand.[32] Quantitative repair was also observed with concentrations of the rhodium complex as low as 500 nM and a 16-fold excess of DNA duplex (6.25 mol% $[Rh(phi)_2(dmb)]^{3+}$), indicating that the process is catalytic in rhodium. Treatment of damaged DNA with the rhodium catalyst and bright sunshine also removed the lesion completely. In these experiments, the noncovalently bound rhodium intercalator is free to sample all intercalation sites along the length of the duplex.

We next considered whether the DNA helix might facilitate oxidative repair over long ranges. We prepared dimer-containing duplexes possessing a Rh^{III} intercalator covalently tethered to one end to examine repair of the thymine dimer from a distance (Figure 10). Photocleavage of these rhodium-modified duplexes upon irradiation ($\lambda = 313$ nm) indicated

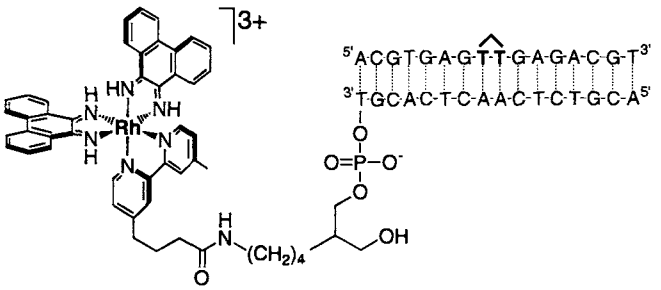

Figure 10. Rhodium-modified DNA duplex bearing a thymine dimer ($\widehat{TT}$) [54]. In the assembly shown, the Rh complex is tethered to the 3′-terminus of the modified oligonucleotide, which places the oxidant on 5′-side of the dimer. Application of oligonucleotides bearing the Rh photooxidant at either the 3′- or the 5′-terminus permits evaluation of the importance of directionality in the electron transfer.

intercalation up to four base steps from the end of the duplex, establishing that the metal center and the thymine dimer are separated by 19–26 Å through the DNA base stack. Irradiation with visible light ($\lambda = 400$ nm) also initiated dimer repair in these tethered assemblies (Table 3). Moreover, dilution and mixing experiments confirmed that the long-range repair reaction was intraduplex, and not catalyzed by rhodium tethered to a separate assembly.

How does repair efficiency vary as a function of distance and stacking? As seen in Table 3, increasing the separation between the thymine dimer from 19 to 26 Å produces only small changes in repair efficiency. As with guanine oxidation, the repair reaction is not very dependent on distance (over this range of distance), but is quite sensitive to stacking. In fact, repair efficiency is not only affected by the stacking of the catalyst but also that of the dimer and the intervening base pairs within the helix. We observed first the consistently greater repair efficiency with Δ than with Λ isomers, reflecting the deeper stacking of the right-handed metal complex into the right-handed DNA helix. We also see comparable repair efficiency in reactions with rhodium tethered to the 3′- or 5′-side of the dimer, and consequently infer that stacking on the 3′- and 5′-sides of the thymine dimer within the helix is not

Table 3. Long-range repair of thymine dimers in DNA duplexes modified with Δ-Rh [a].

Assembly	Distance [Å] [b]	Repair [%] [c]
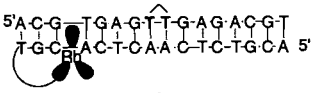	19	67
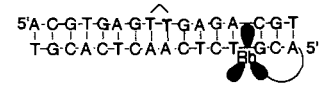	19	79
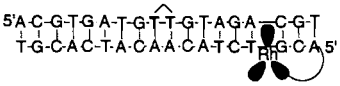	22	91
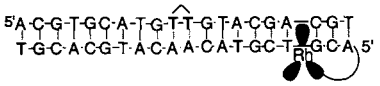	26	100
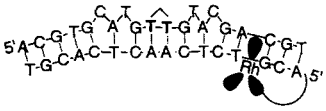		47

[a] Based on ref. [54]. [b] Distances between catalyst and thymine dimer were based on intercalation at the sites indicated. There is a separation of 3.4 Å adjacent base pairs as well as between the intercalated phi ligand and the first base step. [c] Expressed as the percentage of thymine dimer repaired after six hours of irradiation ($\lambda = 400$ nm).

substantially different. Importantly, as expected for a π stack mediated reaction, the repair is sensitive to the stacking of base pairs between the rhodium and the dimer. The decrease in repair efficiency caused by intervening bulges in the DNA illustrates this sensitivity dramatically and confirms that the DNA base stack mediates the reaction (Table 3).

Based on these data, it is interesting to compare repair efficiency by rhodium, tethered or bound noncovalently to DNA. Repair with the tethered complex is substantially (about 30-fold) reduced compared to the noncovalently bound catalyst. Given that the efficiency does not appear to be very sensitive to the distance separating the rhodium complex and dimer, the difference in efficiency may instead reflect features of how the thymine dimer is stacked within the duplex or perhaps also how the tethered rhodium is intercalated in the helix. The lower repair efficiency in rhodium-modified duplexes may indicate that the thymine dimer is not fully stacked in the helix to either its 3′- or 5′-side. Indeed, while our studies show that long-range oxidative repair through DNA is possible, the decreased efficiency of reactions with tethered rhodium (which are mediated by the helix) actually suggest that it may be advantageous in an enzymatic repair to project the thymine dimer fully out of the helix for efficient reaction. This was proposed based on the crystal structure of DNA photolyase.[55]

These results illustrate how a physiologically important reaction of DNA may be carried out using electron transfer, and, if mediated by the DNA base stack, how it may proceed upon activation from a distance. Reactions on DNA initiated from a remote site and modulated by base-pair stacking need to be considered in evaluating charge-transfer processes involving DNA within the cell and may actually be powerfully exploited.

5. Questions Concerning DNA-Mediated Charge Transfer

Although the concept of long-range charge transfer through DNA was recognized by many researchers, DNA is not seen as a remarkable electron transfer medium by all. The fact that studies of photoinduced electron transfer on DNA appear so different from analogous studies with proteins as a medium is surprising to some. On the other hand, given the chemical differences between the π-stacked DNA helix and largely σ-bonded network of a protein, such differences might be expected. Our understanding of DNA-mediated electron transfer is certainly less well developed at this point than that of proteins as a medium.

As in studies with proteins, experiments on DNA began with noncovalently bound donors and acceptors;[58] the results obtained here varied enormously depending upon the donors and acceptors employed. While with tightly bound metallointercalators we often saw fast, efficient luminescence quenching,[9, 25, 31, 33, 34, 38, 40] with some organic DNA-binding agents, notably with ethidium as photoinduced donor and DAP as acceptor, fast quenching was not observed.[10] We have attributed such variations in rates and efficiency to the efficacy of donor and acceptor coupling into the π stack. The comparison of photoinduced quenching of $[Ru(phen)_2(dppz)]^{2+}$ luminescence by $[Rh(phi)_2(bpy)]^{3+}$, an avid intercalator, with quenching by $[Ru(NH_3)_6]^{3+}$, a groove-binding agent, is a clear cut example.[31] With $[Rh(phi)_2(bpy)]^{3+}$ photoinduced quenching is faster than expected for a collisional mechanism, while dynamic quenching by $[Ru(NH_3)_6]^{3+}$ is consistent with such a mechanism. We also find differences in rates of electron transfer between enantiomeric metal complexes bound to the helix,[9, 34] which reveal that the reaction is sensitive to subtle variations in stacking. However, not all observations may be so neatly categorized. For example, we see no substantive quenching with $[Rh(phen)_2(phi)]^{3+}$, and we have ascribed the absence of fast quenching to poor overlap of the shape-selective DNA-binding agent with the π stack.[33] Using a metalloporphyrin as donor, Brun and Harriman also showed that the kinetics of electron transfer mediated by DNA need not be fast.[10h] Here too one may ascribe the lack of a fast reaction to poor overlap of the metal complex with the DNA base pair stack; the subsequent crystallographic analysis of a metalloporphyrin bound to DNA shows base displacement rather than stacking.[59] Certainly, based on the range of results obtained thus far, a clear quantitative parameter that one might use to gauge whether fast DNA-mediated electron transfer should arise has not yet emerged.

As noted earlier, some research groups have indicated that the fast quenching we observed might be explained more simply in terms of clustering.[35, 36] A straightforward explanation for static quenching on a time scale which is fast compared to diffusion is that no diffusion is necessary; if the metal complexes bind cooperatively on the helix, they would be placed in a manner to facilitate rapid electron transfer. Barbara and co-workers[35] offered an extensive analysis of the ultrafast quenching data for Δ-$[Ru(phen)_2(dppz)]^{2+}$ and Δ-$[Rh(phi)_2(bpy)]^{3+}$ bound to calf-thymus DNA, and show

that these data may be explained based on cooperative clustering. However, no analysis is provided for Λ-$[Ru(phen)_2(dppz)]^{2+}$, which shows a different, albeit fast, quenching profile. Nor are data provided for any of the other metal complexes, which differ with respect to hydrophobicity in the ancillary ligands and hence might be expected also to differ with respect to cooperativity.

There are many other questions raised by such a model, as noted earlier. Why should there be differences in rates of recombination with the same donor and acceptor but on different DNA sequences? Why is cooperative clustering supposed to occur between ruthenium and rhodium but not for each separately? What is the basis for clustering between ethidium (which lacks ancillary bulk) and rhodium, since such clustering must be invoked here as well to account for the fast quenching observed? What is the structural basis for this supposed cooperative association? In fact, the only experimental observation provided to support a clustering model is an ill-defined perturbation in the circular dichroism of Δ-$[Ru(phen)_2(dppz)]^{2+}$ and Δ-$[Rh(phi)_2(bpy)]^{3+}$ bound to poly d(AT) at high loadings.[36] Our more recent investigation of CD shows this earlier study to be incomplete. Both a more extensive CD study and an examination of DNA binding by NMR spectroscopy show that the metallointercalators bind noncooperatively, perhaps even anticooperatively, to the DNA duplex. Nonetheless, this whole issue underscores the importance of structural characterizations of DNA-bound donors and acceptors. Our results establish, at the very least, the striking sensitivity of DNA-mediated electron transfer to how donors and acceptors are bound to the helix.

Clearly, a clustering model can never be definitively ruled out for different species bound noncovalently to DNA, but it cannot be applied in reconciling data for systems in which electron donors and acceptors are tethered to DNA duplexes at known, fixed positions. With tethered intercalators, we examined electron transfer between metallointercalators tethered to a 15-mer DNA duplex,[40] and between ethidium and $[Rh(phi)_2(bpy)]^{3+}$ tethered to a series of DNA duplexes.[43] These results clearly support quenching of long-range electron transfer and are fully consistent with observations made with noncovalently bound complexes. However, in these studies we are able to measure only quenching (that is, the absence of luminescence), and therefore the interpretation of a striking long-range electron transfer rests primarily on a series of negative results. It is important to carry out ultrafast transient absorption experiments on these tethered DNA assemblies to measure rates of electron transfer. These studies will be challenging, however, since fast time resolution and low concentrations (to insure intramolecularity) are needed. In this context, experiments with noncovalently bound intercalators provide a valuable foundation.

In fact, it was because of the possible ambiguity in interpreting quenching studies that we first turned to studies with DNA as a reactant.[48–50, 52, 54] If we can measure a product of electron transfer at a distance away from the source of charge transport, then, irrespective of the time scale, one can document definitively a long-range effect. Hence, from this perspective, as well as in a biological context, our studies of oxidative damage to DNA over a long range using tethered oxidants have been important. Here, critics question the poor efficiency of the reaction. The quantum yield for oxidative damage is 10^{-7} for the rhodium oxidants; in fact, all photochemistry with these rhodium complexes is inefficient ((photoaquation) $= 10^{-4}$), owing in part to other overlapping transitions. With ruthenium(III) as oxidant, using the flash-quench methodology,[50] we found a quantum yield for damage over a distance of >30 Å of 0.002 with methyl viologen as quencher; this yield seems reasonably high considering the alternate reaction pathways available to ruthenium. Given this increased yield and the completely parallel observations made with the ruthenium and rhodium photochemistry, it becomes difficult to characterize these studies as merely the result of statistical fluctuations or "leakage". As shown by spectroscopic studies, these long-range reactions depend sensitively on stacking of the donor and the acceptor, and on structural perturbations in the intervening DNA helix. Moreover, in the case of long-range oxidative repair of thymine dimers in DNA,[54] conversion into repaired product is quantitative and triggered simply by electron transfer (requiring no additional, diffusing species). While it is still important to emphasize that these experiments do not provide a measurement of the rate of long-range electron transfer, they unambiguously establish chemistry over a distance.

Few theoretical treatments of DNA as a medium for electron transfer have been described, and here too there is much to debate. Beretan and co-workers[42c–d] described calculations which indicate that DNA is protein-like and serves as an insulator. These calculations show agreement with some kinetic data reported by Meade[39] and Harriman,[10] and show differerences of several orders of magnitude to our measurements of the quenching of electron transfer with covalently bound metallointercalators. The calculations, however, do not take into account any coupling that arises due to stacking, either of the bases or intercalators. Furthermore, no variations were made in sequence or base structure to establish a sensitivity in parameters to such changes, as was seen experimentally. Using calculations based upon Redfield theory, Friesner and co-workers[42a] suggested how base stacking could give rise to a delocalized "band", which might facilitate long-range charge transfer without a significant distance dependence. In fact, this work provides a prediction for experimentalists to pursue, namely that low temperatures should eliminate thermal access to this band and shut down the electron transfer. Calculations made more than twenty years ago[6] also led to substantial debate regarding both the energetics and mechanisms of long-range electron transfer. It is our view that more experimental data are needed to provide a firm foundation upon which theorists may build. At this stage hopping models, charge delocalization, and band theory all offer interesting perspectives from which our experiments may be interpreted, but experiments to distinguish between these models have not yet been established.

6. Summary and Outlook

Here we have described a range of charge-transfer reactions mediated by the DNA base pair stack. The reactions

proceed quickly and efficiently between donors and acceptors which are well coupled into the π stack. These reactions do not appear to depend sensitively upon the molecular distances between reactants but are exquisitely sensitive to stacking, the stacking of donor and acceptor, also the stacking of the bases which intervene.

These results provoke a host of questions and new experiments. Over what molecular distances can charge effectively be transported through DNA? We need to develop assays to examine reactions over 50–100 base pairs, not 10–20, as explored thus far. What are the rates of these reactions? Our instrumentation has allowed us only to place limits on rates for photoinduced quenching, and no systematic determination of how rates vary with distance and sequence was made. Such data are essential in developing a theoretical framework to describe this chemistry. We need also to understand how these reactions vary with temperature and with changes in nucleic acid conformation. Importantly, we need to develop quantitative parameters to describe stacking within the double helix and how such stacking affects electronic coupling in DNA.

Perhaps most intriguing are some of the biological consequences of this chemistry. Does radical damage to DNA arise from a distance within the cell? Are there cellular mechanisms which insulate sequences from such damage or through which the positioning of damage is controlled? Might such long range chemistry be exploited in new chemotherapeutic design or in the development of novel nucleic acid based sensors? Is long-range charge transport through DNA exploited within the cell for long range transmission of information across the DNA library? These questions are certainly provocative. They nonetheless represent important challenges for the future and, based upon future work, should become implicit to our understanding of the chemistry of DNA.

We are grateful to the National Institutes of Health (NIH) for their financial support of this work. We are also most grateful to our co-workers for their efforts in elucidating this chemistry. Their scientific contributions have been referenced throughout this review. This work began as a collaboration with C. V. Kumar and N. J. Turro, and it has been a most rewarding journey from those first experiments.

Received: February 27, 1997 [A213IE]
German version: *Angew. Chem.* **1997**, *109*, 2830–2848

[1] a) B. H. Geierstanger, D. E. Wemmer, *Annu. Rev. Biophys. Biomol. Struct.* **1995**, *24*, 463–493; b) R. Schleif, *Science* **1988**, *241*, 1182–1187; c) D. L. Ollis, S. W. White, *Chem. Rev.* **1987**, *87*, 981–995; d) A. A. Travers, *Annu. Rev. Biochem.* **1989**, *58*, 427–452; e) C. O. Pabo, R. T. Sauer, *ibid.* **1992**, *61*, 1053–1095; f) P. H. von Hippel, J. D. McGhee, *ibid.* **1972**, *41*, 231–300.

[2] a) T. W. Johann, J. K. Barton, *Philos Trans. R. Soc. London A* **1996**, *354*, 299–324; b) P. B. Dervan, *Science* **1986**, *232*, 464–471; c) J. C. Quada, Jr., M. J. Levy, S. M. Hecht, *J. Am. Chem. Soc.* **1993**, *115*, 12171–12172; d) D. S. Sigman, T. W. Bruice, A. Mazumder, C. L. Sutton, *Acc. Chem. Res.* **1993**, *26*, 98–104; e) K. C. Nicolaou, W.-M. Dai, *Angew. Chem .* **1991**, *103*, 1453–1481; *Angew. Chem. Int. Ed. Engl.* **1991**, *30*, 1387–1416.

[3] W. Saenger in *Principles of Nucleic Acid Structure* (Ed.: C. R. Cantor), Springer, New York, **1984**.

[4] a) J. S. Miller, A. J. Epstein, *Angew. Chem.* **1994**, *106*, 399–432; *Angew. Chem. Int. Ed. Engl.* **1994**, *33*, 385–415; b) M. A. Fox, *Acc. Chem. Res.* **1992** *25*, 569–574; c) T. J. Marks, *Science* **1985**, *227*, 881–889; d) M. Hanack, M. Lang, *Adv. Mater.* **1994**, *6*, 819–833.

[5] a) P. G. Schouten, J. M. Warman, M. P. de Haas, M. A. Fox, H.-L. Pan, *Nature* **1991**, *353*, 736–737; b) P. G. Schouten, J. M. Warman, M. P. de Haas, J. F. van der Pol, J. W. Zwikker, *J. Am. Chem. Soc.* **1992**, *114*, 9028–9034; c) P. G. Schouten, J. M. Warman, M. P. de Haas, C. F. van Nostrum, G. H. Gelinck, R. J. M. Nolte, M. J. Copyn, J. W. Zwikker, M. K. Engel, M. Hanack, Y. H. Chang, W. T. Ford, *ibid.* **1994**, *116*, 6880–6894.

[6] D. Dee, M. E. Baur, *J. Chem. Phys.* **1974**, *60*, 541–560.

[7] a) R. S. Snart, *Trans. Faraday Soc.* **1963**, *59*, 754–760; b) D. D. Eley, D. I. Spivey, *ibid.* **1962**, *58*, 411–415.

[8] P. O'Neill, E. M. Fielden, *Adv. Radiat. Biol.* **1993**, *17*, 53–120.

[9] a) E. D. A. Stemp, J. K. Barton in *Metal Ions in Biological Systems, Vol. 33* (Eds.: A. Sigel, H. Sigel), Marcel Dekker, New York, **1996**, p. 325; b) M. R. Arkin, Y. Jenkins, C. J. Murphy, N. J. Turro, J. K. Barton, *Adv. Chem. Ser.* **1995**, *246*, 449–469.

[10] a) T. J. Meade in *Metal Ions in Biological Systems, Vol. 32* (Eds.: A. Sigel, H. Sigel), Marcel Dekker, New York, **1996**, p. 453; b) B. Nordén, P. Lincoln, B. Akerman, E. Tuite, *ibid.* **1996**, p. 177; c) B. C. Baguley, M. Le Bret, *Biochemistry* **1984**, *23*, 937–943; d) L. M. Davis, J. D. Harvey, B. C. Baguley, *Chem. Biol. Interactions* **1987**, *62*, 45–58; e) S. J. Atherton, P. C. Beaumont, *J. Phys. Chem.* **1995**, *99*, 12025–12029; f) M. Manoharan, K. L. Tivel, M. Zhao, K. Nafisi, T. L. Netzel, *ibid.* **1995**, *99*, 17461–17472; g) P. Fromherz, B. Rieger, *J. Am. Chem. Soc.* **1986**, *108*, 5361–5362; h) A. M. Brun, A. Harriman, *ibid.* **1994**, *116*, 10383–10393; i) *ibid.* **1992**, *114*, 3656–3660; j) *ibid.* **1991**, *113*, 8153–8159; k) S. O. Kelley, G. Orellana, J. K. Barton, *J. Phys. Chem.*, submitted.

[11] a) C. Dupureur, J. K. Barton in *Comprehensive Supramolecular Chemistry, Vol. 5* (Ed.: J.-M. Lehn), Pergamon Press, **1996**, p. 295; b) A. Sitlani, J. K. Barton in *Handbook of Metal–Ligand Interactions in Biological Fluids, Vol. 1* (Ed.: G. Berthon), Marcel Dekker, New York, **1995**, p. 466; c) C. J. Murphy, J. K. Barton, *Methods Enzymol.* **1993**, *C226*, 576–594.

[12] a) T. J. Meyer, *Acc. Chem. Res.* **1989**, *22*, 163–170; b) A. Juris, V. Balzani, F. Barigelletti, S. Campagna, P. Belser, A. von Zelewsky, *Coord. Chem. Rev.* **1988**, *84*, 85–277; c) J.-P. Sauvage, J.-P. Collin, J.-C. Chambron, S. Guillerez, C. Coudret, *Chem. Rev.* **1994**, *94*, 993–1019; d) M. T. Indelli, C. A. Bignozzi, A. Harriman, J. R. Schoonover, F. Scandola, *J. Am. Chem. Soc.* **1994**, *116*, 3768–3779.

[13] a) J. K. Barton, C. V. Kumar, N. J. Turro, *J. Am. Chem. Soc.* **1986**, *108*, 6391–6393. b) M. D. Purugganan, C. V. Kumar, N. J. Turro, J. K. Barton, *Science* **1988**, *241*, 1645–1649.

[14] a) A. E. Friedman, J.-C. Chambron, J.-P. Sauvage, N. J. Turro, J. K. Barton, *J. Am. Chem. Soc.* **1990**, *112*, 4960–4962; b) A. E. Friedman, C. V. Kumar, N. J. Turro, J. K. Barton, *Nucleic Acid Res.* **1991**, *19*, 2595–2602; c) Y. Jenkins, A. E. Friedman, J. K. Barton, *Biochemistry* **1992**, *31*, 10809–10816.

[15] R. E. Holmlin, J. K. Barton, *Inorg. Chem.* **1995**, *34*, 7–8.

[16] S. Arounaguiri, B. G. Maiya, *Inorg. Chem.* **1996**, *35*, 4267–4270.

[17] a) H. D. Stoeffler, N. B. Thornton, S. L. Temkin, K. S. Schanze, *J. Am. Chem. Soc.* **1995**, *117*, 7119–7128; b) V. W.-W. Yam, K. K.-W. Lo, K.-K. Cheung, R. Y.-C. Kong, *J. Chem. Soc., Chem. Commun.* **1995**, 1191–1193.

[18] a) C. M. Dupureur, J. K. Barton, *Inorg. Chem.* **1997**, *36*, 33–43; b) *J. Am. Chem. Soc.* **1994**, *116*, 10286–10287; c) R. E. Holmlin, E. D. A. Stemp, J. K. Barton, *Inorg. Chem.* **1997**, in press.

[19] E. Amouyal, A. Homsi, J.-C. Chambron, J.-P. Sauvage, *J. Chem. Soc., Dalton Trans* **1990**, 1841–1845.

[20] C. Turro, S. H. Bossmann, Y. Jenkins, J. K. Barton, N. J. Turro, *J. Am. Chem. Soc.* **1995**, *117*, 9026–9032.

[21] J.–C. Chambron, J.-P. Sauvage, *Chem. Phys. Lett.* **1991**, *182*, 603–607.

[22] E. Sabatani, H. D. Nikol, H. B. Gray, F. C. Anson, *J. Am. Chem. Soc.* **1996**, *118*, 1158–1163.

[23] C. Hiort, P. Lincoln, B. Nordén, *J. Am. Chem. Soc.* **1993**, *115*, 3448–3454.

[24] J. K. Barton, *Science* **1986**, *233*, 727–734.

[25] R. E. Holmlin, E. D. A. Stemp, J. K. Barton, *J. Am. Chem. Soc.* **1996**, *118*, 5236–5244.

[26] a) A. Sitlani, C. M. Dupureur, J. K. Barton, *J. Am. Chem. Soc.* **1993**, *115*, 12589–12590; b) A. Sitlani, J. K. Barton, *Biochemistry* **1994**, *33*, 12100–12108; c) R. H. Terbrueggen, J. K. Barton, *ibid.* **1995**, *34*, 8227–8234.

[27] a) A. H. Krotz, L. Y. Kuo, T. P. Shields, J. K. Barton, *J. Am. Chem. Soc.* **1993**, *115*, 3877–3882; b) A. H. Krotz, B. P. Hudson, J. K. Barton, *ibid.* **1993**, *115*, 12577–12578.

[28] S. S. David, J. K. Barton, *J. Am. Chem. Soc.* **1993**, *115*, 2984–2985.

[29] B. P. Hudson, C. M. Dupureur, J. K. Barton, *J. Am. Chem. Soc.* **1995**, *117*, 9379–9380.

[30] A. Sitlani, E. C. Long, A. M. Pyle, J. K. Barton, *J. Am. Chem. Soc.* **1992**, *114*, 2303–2312.

[31] C. J. Murphy, M. R. Arkin, N. D. Ghatlia, S. H. Bossmann, N. J. Turro, J. K. Barton, *Proc. Natl. Acad. Sci. USA* **1994**, *91*, 5315–5319.

[32] C. Turro, A. Evenzahav, S. H. Bossmann, J. K. Barton, N. J. Turro, *Inorg. Chim. Acta* **1996**, *243*, 101–108.

[33] M. R. Arkin, E. D. A. Stemp, C. Turro, N. J. Turro, J. K. Barton, *J. Am. Chem. Soc.* **1996**, *118*, 2267–2274.

[34] M. R. Arkin, E. D. A. Stemp, R. E. Holmlin, J. K. Barton, A. Hörmann, E. J. C. Olson, P. F. Barbara, *Science* **1996**, *273*, 475–480.
[35] E. J. C. Olson, D. Hu, A. Hörmann, P. F. Barbara, *J. Phys. Chem.* **1997**, *101*, 299–303.
[36] P. Lincoln, E. Tuite, B. Nordén, *J. Am. Chem. Soc.* **1997**, *119*, 1454–1455.
[37] E. D. A. Stemp, R. E. Holmlin, M. R. Arkin, J. K. Barton, unpublished results.
[38] S. J. Franklin, C. R. Treadway, J. K. Barton, unpublished results.
[39] E. D. A. Stemp, M. R. Arkin, J. K. Barton, *J. Am. Chem. Soc.* **1995**, *117*, 2375–2376.
[40] C. J. Murphy, M. R. Arkin, Y. Jenkins, N. D. Ghatlia, S. H. Bossmann, N. J. Turro, J. K. Barton, *Science* **1993**, *262*, 1025–1029.
[41] a) R. A. Marcus, N. Sutin, *Biochim. Biophys. Acta* **1985**, *811*, 265–322; b) D. N. Beratan, J. N. Onuchic, J. R. Winkler, H. B. Gray, *Science* **1992**, *258*, 1740–1741; c) G. L. Closs, J. R. Miller, *ibid.* **1988**, *240*, 440–447.
[42] a) A. K. Felts, W. T. Pollard, R. A. Friesner, *J. Phys. Chem.* **1995**, *99*, 2929–2940; b) S. Priyadarshy, S. M. Risser, D. N. Beratan, *J. Phys. Chem.* **1996**, *100*, 17678–17682; c) S. M. Risser, D. N. Beratan, T. J. Meade, *J. Am. Chem. Soc.* **1993**, *115*, 2508–2510; d) D. N. Beratan, S. Priyadarshy, S. M. Risser, *Chem. Biol.* **1997**, *4*, 3–8.
[43] T. J. Meade, J. F. Kayyem, *Angew. Chem.* **1995**, *107*, 358–360; *Angew. Chem. Int. Ed. Engl.* **1995**, *34*, 352–354.
[44] F. D. Lewis, T. Wu, Y. Zhang, R. L. Letsinger, S. R. Greenfield, M. R. Wasielewski, *Science* **1997**, *277*,673–676.
[45] S. O. Kelley, R. E. Holmlin, E. D. A. Stemp, J. K. Barton, *J. Am. Chem. Soc.* **1997**, *119*, 9861–9870.
[46] J. Retèl, B. Hoebee, J. E. F. Braun, J. T. Lutgerink, E. van den Akker, A. H. Wanamarta, H. Joenje, M. V. M. Lafleur, *Mutation Res.* **1993**, *299*, 165–182.
[47] L. Kittler, G. Löber, F. A. Gollmick, H. Berg, *Bioelectrochem. Bioenerg.* **1980**, *7*, 503–511.
[48] a) D. T. Breslin, G. B. Schuster, *J. Am. Chem. Soc.* **1996**, *118*, 2311–2319; b) I. Saito, M. Takayama, H. Sugiyama, K. Nakatani, *ibid.* **1995**, *117*, 6406–6407; c) H. Kasai, Z. Yamaizumi, M. Berger, J. Cadet, *ibid.* **1992**, *114*, 9692–9694; d) K. Ito, S. Inoue, K. Yamamoto, S. Kawanishi, *J. Biol. Chem.* **1993**, *268*, 13221–13227; e) H. Sugiyama, I. Saito, *J. Am. Chem. Soc.* **1996**, *118*, 7063–7068.
[49] D. B. Hall, R. E. Holmlin, J. K. Barton, *Nature* **1996**, *382*, 731–735.
[50] a) E. D. A. Stemp, M. R. Arkin, J. K. Barton, *J. Am. Chem. Soc.* **1997**, *119*, 2921–2925; b) M. R. Arkin, E. D. A. Stemp, S. C. Pulver, J. K. Barton, *Chem. Biol.* **1997**, *4*, 389–400.
[51] a) I.-J. Chang, H. B. Gray, J. R. Winkler, *J. Am. Chem. Soc.* **1991**, *113*, 7056–7057; b) N. Liang, A. G. Mauk, G. J. Pielak, J. A. Johnson, M. Smith, B. M. Hoffman, *Science* **1988**, *240*, 311–313; c) D. A. Dunn, V. H. Lin, I. E. Kochevar, *Biochemistry* **1992**, *31*, 11620–11625.
[52] D. B. Hall, J. K. Barton, *J. Am. Chem. Soc.* **1997**, *119*, 5045–5046.
[53] M. A. Rosen, L. Shapiro, D. J. Patel, *Biochemistry* **1992**, *31*, 4015–4026.
[54] P. J. Dandliker, R. E. Holmlin, J. K. Barton, *Science* **1997**, *274*, 1465–1468.
[55] a) A. Sancar, *Biochemistry* **1994**, *33*, 2–9; b) S.-T. Kim, A. Sancar, *Photochem. Photobiol.* **1993**, *57*, 895–904; c) T. P. Begley, *Acc. Chem. Res.* **1994**, *27*, 394–401; d) J.-S. Taylor, *ibid.* **1994**, *27*, 76–82; e) P. F. Heelis, R. F. Hartman, S. D. Rose, *Chem. Soc. Rev.* **1995**, *24*, 289–297; f) P. F. Heelis, D. J. Deeble, S.-T. Kim, A. Sancar, *Int. J. Radiat. Biol.* **1992**, *62*, 137–143.
[56] C. Hélène, M. Charlier, *Photochem. Photobiol.* **1977**, *25*, 429–434.
[57] a) T. Young, R. Nieman, S. D. Rose, *Photochem. Photobiol.* **1990**, *52*, 661–668; b) C. Pac, I. Miyamoto, Y. Masaki, S. Furusho, S. Yanagida, T. Ohno, A. Yoshimura, *ibid.* **1990**, *52*, 973–979.
[58] B. E. Bowler, A. L. Raphael, H. B. Gray, *Prog. Inorg. Chem.* **1990**, *38*, 259–322.
[59] L. A. Lipscomb, F. X. Zhou, S. R. Presnell, R. J. Woo, M. E. Peek, R. R. Plaskon, L. D. Williams, *Biochemistry* **1996**, *35*, 2818–2823.

Nonenzymatic Kinetic Resolution of Secondary Alcohols

Peter Somfai*

Secondary alcohols are an important class of readily derivatizable compounds that can be incorporated into a variety of synthetic strategies. The kinetic resolution of these compounds, or more often of their corresponding acetates, has traditionally been achieved by using esterases and often with excellent results.[1] Recent developments of this approach, in which metal catalysts were used to racemize the substrate, led in combination with appropriate enzymes to efficient dynamic kinetic resolutions.[2] The nonenzymatic kinetic resolution of racemic alcohols has proven to be more difficult, the only prominent example being the Sharpless resolution of allylic alcohols;[3] recently, however, several impressive results have been documented. In principle, four strategies have been pursued with varying degrees of success. In the most straightforward one a preformed enantiomerically pure acylating agent, such as an acyl halide[4] or *N*-benzoyl oxazolidinone **1**,[5] is treated with a racemic secondary alcohol **2** to give the acylated product **3** and recovered starting material (Scheme 1). The inherent drawbacks with this

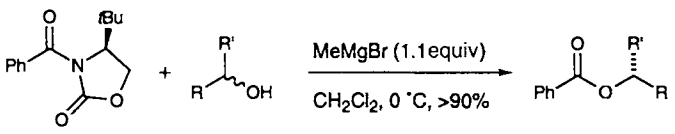

1 (1equiv) **2** (10equiv) **3a** *ee*=95%
a R=Ph, R'=Me **b** *ee*=65%
b R=Ph, R'=*i*Pr **c** *ee*=5%
c R, R'=*c*-C_6H_{11}, Me

Scheme 1. Kinetic resolution of **2** with oxazolidinone **1**[5].

method are that a stoichiometric amount of the chiral reagent is required and, in the case of the acyl halide, that the acylated product will be formed as a mixture of diastereomers unless the dynamic resolution reaction proceeds with complete selectivity.

Alternatively, advantage can be taken of the fact that the acylation of secondary alcohols is subjected to nucleophilic catalysis. In a pioneering study more than 60 years ago Wegler investigated the acylation of several racemic secondary alcohols mediated by brucine and strychnine.[6] For example, when racemic **2a** was treated with acetic anhydride in the presence of stoichiometric amounts of brucine, (*S*)-α-methylbenzyl acetate ((*S*)-**4**) was formed, although its optical purity cannot be ascertained from the data given. More recently the efficiency of other tertiary amines as acylation promoters have been investigated; the best result for the acylation of **2a** was obtained with amine **5** (**2a**:AcCl:**5**=2:1:1) and yielded (*S*)-**4** with an optical purity of 68%.[7]

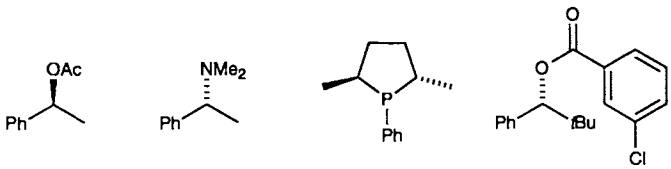

(*S*)-**4** **5** **6** **7**

The first example of a chiral nucleophilic promoter that is also capable of catalytic turnover was described by Vedejs et al.,[8] who showed that acylation of **2a** with Ac_2O in the presence of the C_2-symmetric phospholane **6** (**2a**:Ac_2O:**6**=1:2.5:0.16) gave **4** with an *ee* of 34% (44% conversion, $s=k_{fast}/k_{slow}=2.7$), while racemic 2,2-dimethyl-1-phenylpropanol was acylated with *m*-chlorobenzoic anhydride under the same reaction conditions to yield the corresponding ester **7** (*ee*=81%, 25% conversion, $s=12-15$).

In a continuation of these studies the enantiomerically pure DMAP analogue **8** (*ee*>99%, DMAP=4-dimethylaminopyridine) was prepared by the same group and converted into the pyridinium salt **9** (Scheme 2), which for steric reasons is not sufficiently reactive to promote acyl transfers to alcohol **2** by itself.[9] However, in the presence Lewis acids ($ZnBr_2$ or $MgBr_2$) and Et_3N, neither of which can be omitted, a slow acylation ensues to give the mixed carbonates **10** with high *ee* and impressively high *s* values.

The inherent problem with these resolutions is that the starting material becomes continuously enriched in the isomer that reacts more slowly as the reaction proceeds. Exceptionally large differences in rate between the enantiomers are thus required to obtain high *ee* values of the product, as well as of the enriched isomer in recovered starting material, together with high conversion (e.g. at 50% conversion, $s=200$, *ee*=96%; $s=500$, *ee*=98%). In an attempt to overcome this

[*] Dr. P. Somfai
Organic Chemistry 2, Center for Chemistry and Chemical Engineering
University of Lund, Lund Institute of Technology
P.O. Box 124, S-221 00 Lund (Sweden)
Fax: Int. code + (46)222-8209
e-mail: peter.somfai@orgk2.lth.se

 © WILEY-VCH Verlag GmbH, D-69451 Weinheim, 1997 0570-0833/97/3624-2731 $ 17.50+.50/0

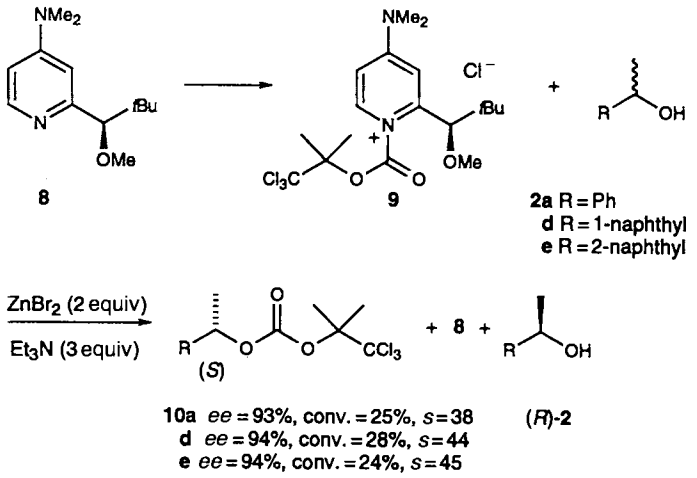

Scheme 2. Kinetic resolution of **2** with pyridinium salt **9**[9]. $s = k_{fast}/k_{slow}$.

difficulty, an ingenious protocol was developed by Vedejs and Chen in which two competing processes, with similar rates and selectivities but for opposite enantiomers, are run in parallel (parallel kinetic resolution, PKR), so that the optimal 1:1 ratio between the stereoisomers is maintained throughout the experiment.[10] The advantages can be appreciated by considering a PKR experiment in which two simultaneous reactions with selectivities for opposite isomers, each with $s = 49$ (100% conversion): ideally, this system would give both products with an *ee* value of 96%. In contrast, in order to equal this result a simple kinetic resolution would need to have $s = 200$ (50% conversion). Reagents **9** and **11** were selected as they were expected to behave as quasi-enantiomers and acylate opposite enantiomers of racemic secondary alcohols to give products that could be readily separated. In the event, when **9** and **11** were treated with three different aromatic secondary alcohols the corresponding carbonates were formed in high yield and *ee*, clearly demonstrating the potential of the method (Scheme 3).

In addition, two other research groups have described useful nucleophilic catalysts for the kinetic resolution of secondary alcohols. Ruble and Fu showed that azaferrocene **13**, which has a stereochemical environment in the proximity

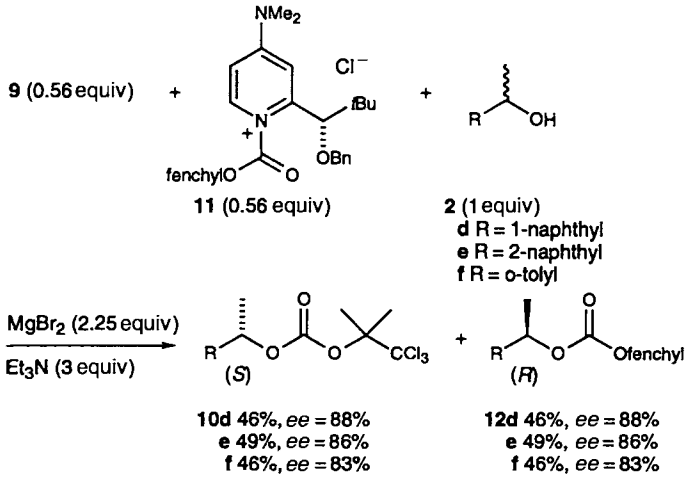

Scheme 3. Parallel kinetic resolution of **2**[10].

of the nitrogen atom quite different from that of **8**, catalyzes the acylation of **2d** with diketene (**2d**:diketene:**13** = 1:1.2:0.1) to give (*R*)-**2d** with *ee* = 87% (67% conversion, $s = 6.5$).[11] In

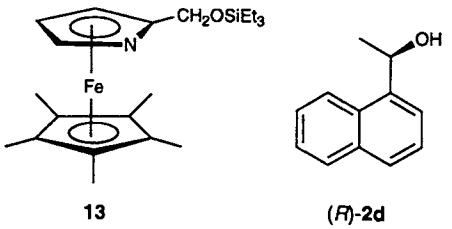

addition, compound **13** and derivatives thereof were shown to be promising catalysts for other transformations requiring nucleophilic promoters.

A completely different approach was pursued by Fuji and co-workers.[12] They prepared enantiomerically pure pyridine derivative **14**, reasoning that the reduced steric hindrance in the proximity of the nitrogen nucleus should result in efficient catalytic turnover and that chiral recognition might be possible by remote asymmetric induction in a process similar to the "induced fit" mechanism in enzymes. When **14** was treated with racemic **15b** and isobutyric anhydride, (1*R*,2*S*)-**15b** was recovered with *ee* = 81% (71% conversion, $s = 4.5$, Scheme 4). Interestingly, the optical purity of the recovered

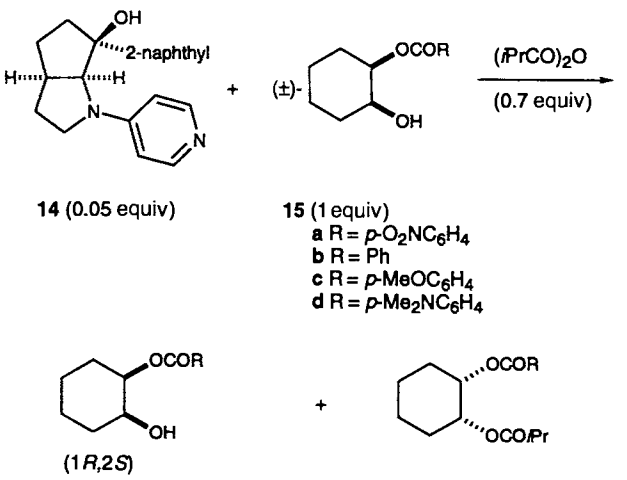

15a *ee* = 54%, conv. = 73%, $s = 2.4$
b *ee* = 81%, conv. = 71%, $s = 4.5$
c *ee* ≥ 85%, conv. = 70%, $s = 5.3$
d *ee* ≥ 99%, conv. = 72%, $s > 10.1$

Scheme 4. Kinetic resolution of **15** with pyridine derivative **14**[12].

alcohol is dependent on the electron-donating ability of the aromatic nuclei in the substrate, possibly indicating that $\pi-\pi$ stacking plays a pivotal role in the enantiodifferentiating event. It was also shown that the pyridinium ion derived from **14** and isobutyric anhydride adopts a "closed conformation", in contrast to **14** itself, in which the naphthyl moiety is situated over the pyridine ring, thus shielding the *si* face of the carbonyl group and supporting the "induced fit" concept.

The kinetic resolution of secondary alcohols is also subjected to asymmetric Lewis acid catalysis, as described in

 © WILEY-VCH Verlag GmbH, D-69451 Weinheim, 1997 0570-0833/97/3624-2732 $ 17.50+.50/0 *Angew. Chem. Int. Ed. Engl.* **1997**, *36*, No. 24

a recent elegant study by Oriyama et al.[13] The complex formed by mixing $SnBr_2$ and amine **16** derived from proline in the presence of molecular sieves catalyzed the benzoylation of racemic **17** to give benzoate **18** along with recovered (1*R*,2*R*)-**17** in exceptional yields and selectivities (Scheme 5). In the investigation with several other alcohols, the cyclic species generally performed better than the acyclic ones.

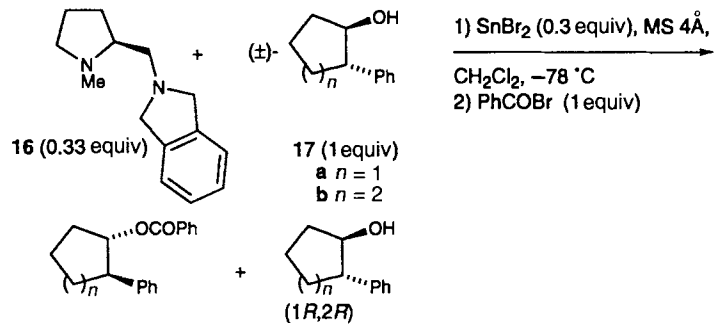

18a $n = 1$; 44%, $ee = 86\%$ **17a** 46%, $ee = 86\%$, $s = 27$
b $n = 2$; 44%, $ee = 97\%$ **b** 49%, $ee = 84\%$, $s > 100$

Scheme 5. Lewis acid catalyzed kinetic resolution of **17**[13].

Finally, Noyori and coworkers have shown that chiral Ru^{II}–diamine complexes are efficient catalysts for the enantioselective transfer hydrogenation of several prochiral ketones, using 2-propanol as the hydrogen source, to give the corresponding alcohols with high *ee* values.[14a] The reaction is microscopically reversible and the faster formed stereoisomer of the product is also the one that is most readily oxidized in the reverse process. Consequently, secondary alcohols with a high reduction potential should be eligible for kinetic resolution with these types of catalysts.[14a,b] That this is indeed the case was elegantly demonstrated with the Ru^{II} complex **19a**, or the mesitylene derivative **19b** (Scheme 6).

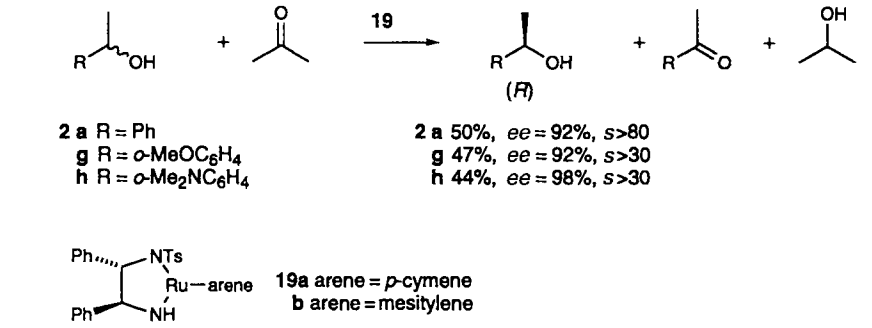

2a R = Ph **2a** 50%, $ee = 92\%$, $s > 80$
g R = o-MeOC$_6$H$_4$ **g** 47%, $ee = 92\%$, $s > 30$
h R = o-Me$_2$NC$_6$H$_4$ **h** 44%, $ee = 98\%$, $s > 30$

19a arene = *p*-cymene
b arene = mesitylene

Scheme 6. Ru^{II}-catalyzed kinetic resolution[14b].

Several alkyl aryl carbinols were successfully resolved by using **19** with excellent recovery of unchanged substrate with high *ee* values. Two cyclic allylic alcohols, 2-cyclohexen-1-ol and 3-methyl-2-cyclohexen-1-ol, were also suitable substrates in this resolution, both of which are particularly valuable substrates in organic synthesis. Although this transformation superficially bears resemblance to the Oppenauer oxidation it has unequivocally been shown that the Ru^{II}-catalyzed kinetic resolution proceeds by an 18-electron metal hydride species and not by a metal alkoxide intermediate, as is the case for the latter transformation.[14c]

In summary, scalemic secondary alcohols can be obtained by nonenzymatic kinetic resolution and in some cases with excellent selectivities. Although these results in general fall short when compared with those obtained with the esterase-promoted resolutions, it is expected that a more thorough understanding of the enantiodiscriminating event in these processes will result in the development of even more efficient catalysts.

German version: *Angew. Chem.* **1997**, *109*, 2849–2851

Keywords: alcohols · chiral recognition · enantiomeric resolution · enzyme catalysis

[1] Recent reviews on esterase-promoted resolutions: a) C. J. Sih, S.-H. Wu, *Top. Stereochem.* **1989**, *19*, 63; b) C.-S. Chen, C. J. Sih, *Angew. Chem.* **1989**, *101*, 711; *Angew. Chem. Int. Ed. Engl.* **1989**, *28*, 695; c) A. M. Klibanov, *Acc. Chem. Res.* **1990**, *23*, 114; d) S. C. Ward, *Chem. Rev.* **1990**, *90*, 1; e) D. G. Drueckhammer, W. J. Hennen, R. L. Pederson, C. F. Barbas III, C. M. Gautheron, T. Krach, C.-H. Wong, *Synthesis* **1991**, 499; f) S. M. Roberts, *Chimia* **1993**, *47*, 85.
[2] R. Stürmer, *Angew. Chem.* **1997**, *109*, 1221; *Angew. Chem. Int. Ed. Engl.* **1997**, *36*, 1173.
[3] Y. Gao, R. M. Hanson, J. M. Klunder, S. Y. Ko, H. Masamune, K. B. Sharpless, *J. Am. Chem. Soc.* **1987**, *109*, 5765.
[4] A. Mazón, C. Nájera, M. Yus, A. Heumann, *Tetrahedron: Asymmetry* **1992**, *3*, 1455; K. Ishihara, M. Kubota, H. Yamamoto, *Synlett* **1994**, 611.
[5] D. A. Evans, J. C. Anderson, M. K. Taylor, *Tetrahedron Lett.* **1993**, *34*, 5563.
[6] R. Wegler, *Liebigs Ann. Chem.* **1932**, *498*, 62; *ibid.* **1933**, *506*, 77; *ibid.* **1934**, *510*, 72.
[7] P. J. Weidert, E. Geyer, L. Horner, *Liebigs Ann. Chem.* **1989**, 533.
[8] E. Vedejs, O. Daugulis, S. T. Diver, *J. Org. Chem.* **1996**, *61*, 430.
[9] E. Vedejs, X. Chen, *J. Am. Chem. Soc.* **1996**, *118*, 1809.
[10] E. Vedejs, X. Chen, *J. Am. Chem. Soc.* **1997**, *119*, 2584.
[11] J. C. Ruble, G. C. Fu, *J. Org. Chem.* **1996**, *61*, 7230.
[12] T. Kawabata, M. Nagoto, K. Takasu, K. Fuji, *J. Am. Chem. Soc.* **1997**, *119*, 3169.
[13] T. Oriyama, Y. Hori, K. Imai, R. Sasaki, *Tetrahedron Lett.* **1996**, *37*, 8543.
[14] a) R. Noyori, S. Hashiguchi, *Acc. Chem Res.* **1997**, *30*, 97; b) S. Hashiguchi, A. Fujii, K.-J. Haack, K. Matsumura, T. Ikariya, R. Noyori, *Angew. Chem.* **1997**, *109*, 300; *Angew. Chem. Int. Ed. Engl.* **1997**, *36*, 288; c) K.-J. Haack, S. Hashiguchi, A. Fujii, T. Ikariya, R. Noyori, *ibid.* **1997**, *109*, 297 and **1997**, *36*, 285.

 © WILEY-VCH Verlag GmbH, D-69451 Weinheim, 1997 0570-0833/97/3624-2733 $ 17.50+.50/0

Valence Tautomeric Interconversion in Transition Metal 1,2-Benzoquinone Complexes

Philipp Gütlich* and Andrea Dei

Transition metal complexes with electronically labile ground states exhibiting interconversion between states of similar energy have been subject to extensive study in recent years. Mixed valency,[1] spin crossover,[2] and valence tautomerism[3,4] are some of the dynamic electronic processes that have attracted the attention of many research groups. One of their goals is to explore the factors inducing and affecting intramolecular electron transfer between metal centers in mixed-valence complexes, between different spin states in spin-crossover systems, or between the metal center and redox-active ligands in valence tautomers. There is, in fact, also hope that these electronic switching processes will provide the foundation for application in molecule-based devices.[5]

The concept of valence tautomerism was introduced to define the properties of a molecular adduct $A-D^+$ (A = acceptor, D = donor) whose electronic ground state is described by two or more isomers with different charge distributions. The interconversion between the different valence tautomers is accomplished by an intramolecular electron transfer according to Equation (a).

$$A-(D^+) \rightleftharpoons (A^+)-D \qquad (a)$$

To obtain molecular adducts characterized as valence tautomers, two conditions must be simultaneously satisfied: The degree of covalency in the interaction between A and D must be low, and the energy of the frontier orbitals of the two counterparts must be similar. The coexistence of both these conditions is hard to achieve, and, to our knowledge, only a few transition metal complexes of 1,2-benzoquinone exhibit this unusual property.[3,4] The behavior of this class of metal complexes originates from the small changes in free energy associated with the semiquinonato/catecholato (sq/cat) couples and from the fact that the electronic structures of the metal–1,2-benzoquinone complexes can often be described with localized electronic structures. Therefore, due to the low orbital mixing, there is a possibility for the existence of isomers differing in charge distribution. Consequently, when the energy difference between two electronic tautomers is small, intramolecular electron transfer between the metal and the ligand may occur to give rise to a valence tautomeric equilibrium.[6] From a phenomenological point of view the process is associated with large changes in structural, optical, and magnetic properties of the molecular systems.

[*] Prof. Dr. P. Gütlich
Institut für Anorganische Chemie der Universität
Staudinger Weg 9, D-55099 Mainz (Germany)
Fax: Int. code + (6131) 39-2990
e-mail: p.guetlich@uni-mainz.de
Prof. Dr. A. Dei
Dipartimento di Chimica, Università di Firenze (Italy)

The first report of this fascinating chemical phenomenon appeared in 1980.[7] The complex [Co(bpy)(dbsq)(dbcat)] (where bpy is 2,2′-bipyridine, and dbsq and dbcat are the semiquinonate and catecholate forms of 3,5-di-*tert*-butyl-1,2-benzoquinone) was shown to contain low-spin cobalt(III) in the solid state. However, the unusual temperature dependence of the magnetic and spectral properties of this complex in solution led to the postulation that the equilibrium shown in Scheme 1 exists.

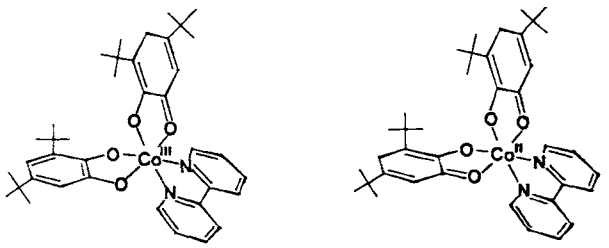

Scheme 1.

The two tautomers are related by an intramolecular one-electron transfer between the catecholate ligand and the cobalt(III) ion as well as a spin change $S=0 \rightarrow S=3/2$ at the cobalt center. This is in agreement with the change in the magnetic moment of the complex from 2.3 μ_B at low temperatures, at which the low-spin (ls) cobalt(III) tautomer with one unpaired electron at the sq ligand predominates, to 4.3 μ_B at higher temperatures, at which the complex is in the high-spin (hs) cobalt(II) form with one unpaired electron at each of the two sq ligands.

Following this first example, other metal–1,2-benzoquinone derivatives were found to undergo valence tautomerism. To date, however, the cobalt–1,2-benzoquinone complex is the only system involving valence tautomers whose electronic ground states are characterized by different spin multiplicities. For possible application it is necessary that the transition between two different electronic states is sharp and exhibits hysteresis effects. Therefore, attention has been focused on the molecular control of valence tautomerism of cobalt–1,2-benzoquinone complexes in the solid state.

The simple idea of controlling the interconversion equilibrium by systematically varying the redox potential of the cobalt acceptor offered the first significant breakthrough. In the family of $[Co(N-N)(diox)_2]$ complexes (N–N = diimine ligand, diox = 1,2-benzoquinone derivative) the solution critical temperature T_c (at 50% concentration of either tautomer) of the interconversion is systematically shifted depending on the donor ability of the N–N ligand.[8,9] Solid samples containing either pure $[Co^{III}(N-N)(dbcat)(dbsq)]$ or

 © WILEY-VCH Verlag GmbH, D-69451 Weinheim, 1997 0570-0833/97/3624-2734 $ 17.50+.50/0

$[Co^{II}(N-N)(dbsq)_2]$ at room temperature were isolated. Finally, it was established that valence tautomeric equilibrium can be thermally induced in the solid state. Data on magnetic susceptibility obtained at various temperatures showed that toluene-solvated $[Co(phen)(dbsq)_2]\cdot C_6H_5CH_3$ (phen = 1,10-phenanthroline) undergoes a reversible conversion between hs-Co^{II} and ls-Co^{III} tautomers, and that this interconversion occurs abruptly in the temperature range 220–260 K with a small hysteresis of 5 K. The X-ray structure analysis of this complex at 295, 238, and 137 K fully supports this hypothesis; the pattern of bond lengths indicates $[Co^{II}(phen)(dbsq)_2]$ at high temperatures and $[Co^{III}(phen)(dbcat)(dbsq)]$ at low temperatures.[9] The change in the average metal–ligand bond length is 0.18 Å as a consequence of the drastic change in the population of the antibonding e_g^* orbitals: $(t_{2g})^6$(ls-Co^{III}) $\rightarrow (t_{2g})^5(e_g^*)^2$(hs-$Co^{II}$). The presence of the toluene molecule is rather critical. The nonsolvated complex remains in the Co^{II} tautomeric form from 320 to 2 K. Studies on similar cobalt–1,2-benzoquinone complexes revealed the existence of valence tautomeric interconversion in the solid state.[10–12]

Very recently it was found that the interconversion can be driven by pressure as well as by changes in temperature.[13] Samples of both the nonsolvated and toluene-solvated complexes discussed above were subjected to increasing pressures at room temperature, and XANES (X-ray absorption near-edge spectroscopy) revealed the occurrence of valence tautomeric interconversion. This occurred at relatively low pressures for the toluene-solvated derivative, that is, in the range of 0.075 to 0.700 Gpa ($P_C\uparrow = 0.370$ Gpa; P_C is concentration of 50% of either tautomer). A much higher pressure was required for the conversion of the nonsolvated derivative ($P_C\uparrow = 1.1$ Gpa), which at ambient pressure exists in the Co^{II} form down to 2 K.

Further experiments showed that the interconversion may also be photoinduced. The photoelectron spectrum of solid $[Co^{III}(bpy)(dbsq)(dbcat)]$ was recorded during irradiation with a mercury lamp.[4] In the absence of light the expected Co^{III} spectrum was obtained. When the sample was irradiated, multiple satellites indicating the presence of the Co^{II} form were detected. Furthermore, a polymeric pyrazine-bridged $[Co^{III}(cat)(sq)]$ complex was prepared and characterized.[14] This compound exhibits, like all these Co^{III} complexes, an intense transition at 2500 nm, which was attributed to a ligand-to-metal charge transfer (LMCT); however, it is more likely due to a metal-mediated intervalence transition of the 1,2-benzoquinone ligands. When thin crystals of these compounds were irradiated with a tungsten lamp, rare photomechanical effects were observed. This behavior was attributed to cumulative structural changes associated with the valence interconversion, which propagate along the chain length of the polymer. Similar photomechanical effects were observed in crystals of [Co(bpy)(3,6-dbsq)(3,6-dbcat)].[10]

Picosecond laser flash photolysis studies on these cobalt complexes provided more detailed information on the nature of this interconversion.[15] A pump laser pulse into a LMCT band of the Co^{III} tautomer in the visible spectrum induces a transient absorption of a Co^{II} band and a corresponding transient bleaching of the Co^{III} band. Since the two transients are characterized by identical kinetics, it was suggested that the tautomerization is described by a first-order reaction. Apparently, there is no evidence for the existence of a ls-Co^{II} form, which in principle may be expected to be the reasonable intermediate species in the electron transfer.

All the available data indicate that the interconversion between the cobalt valence tautomers is similar to that associated with spin-crossover complexes.[2] The thermodynamic quantities ΔH and ΔS of the equilibrium involving [Co(bpy)(dbsq)(dbcat)] in the solid state are 32 kJ mol^{-1} and 98 J mol^{-1} K^{-1}, respectively.[16] These values, which were obtained from measurement of magnetic susceptibility, are in good agreement with those for the same equilibrium in toluene ($\Delta H = 33.9$ kJ mol^{-1} and $\delta S = 124$ J mol^{-1} K^{-1}). The process is characterized by a positive change in entropy due to the increase in spin multiplicity on passing from $[Co^{III}(cat)(sq)]$ to $[Co^{II}(sq)_2]$ and especially the increase in low-frequency vibrational activity according to the weakened metal–ligand bond in Co^{II} complexes.[9,11,16] The Co^{III} species lies at lower enthalpy with respect to the Co^{II} species and is therefore favored at low temperatures. However, if the entropy term is large, the Co^{II} species becomes stabilized at higher temperatures, similar to the high-spin state in spin-crossover systems.[17]

These considerations led to more sophisticated control of the phenomenon. It was convincingly demonstrated that the charge distribution depends on subtle co-ligand bonding effects. It was first established that the interconversion also occurs with pseudooctahedral complexes containing *trans* nitrogen donor atoms, for example pyridine ligands.[18] The change in geometry results in no substantial difference in behavior. The interconversion temperature in a series of $[Co(N-N)(diox)_2]$ complexes, where N–N is an aliphatic tertiary diamine, changes drastically upon varying the basicity of the bidentate ligand.[19] The T_c value of the propylene derivative is about 200 K lower than that of the corresponding ethylene complex. Furthermore, a large hysteresis effect ($T_c\uparrow = 340$ K vs. $T_c\downarrow = 100$ K) was observed in the bis(pyridine) ether derivative of the bis(1,2-benzoquinone)cobalt moiety.[20] Structural characterization of the two redox isomers at room temperature showed that the hysteresis effect is due to an alteration in the co-ligand structure as a consequence of the change in radius of the metal. At 273 K the metastable Co^{III} species can be converted into the Co^{II} isomer by optical excitation of the LMCT transition.

Valence tautomers were also observed for manganese–1,2-benzoquinone complexes. In this case three oxidation states of the metal ion (i.e., II, III, and IV) can be involved in the intramolecular electron transfer with the coordinated 1,2-benzoquinone ligand. However, since all the manganese ions have high-spin electronic ground states, and antiferromagnetic coupling occurs between the metal and the ligand spins,[4,21] the electronic ground states of a pair of valence tautomers (for example, Mn^{II}(sq) and Mn^{III}(cat) or Mn^{III}(sq) and Mn^{IV}(cat)) have the same spin multiplicity (quintet and quartet, respectively, for the two pairs considered). Therefore magnetic measurements fail to provide information on tautomeric equilibria. Nevertheless, $[Mn(N-N)(diox)_2]$ complexes show behavior similar to that of the cobalt complexes.

 © WILEY-VCH Verlag GmbH, D-69451 Weinheim, 1997 0570-0833/97/3624-2735 $ 17.50+.50/0

Shortly after the detection of the first valence tautomeric equilibrium, it was shown that the temperature-dependent solution electronic spectrum of the structurally characterized $[Mn^{IV}(py)_2(dbcat)_2]$complex was consistent with Equation (b).[22]

$$[Mn^{IV}(py)_2(dbcat)_2] \rightleftharpoons [Mn^{II}(py)_2(dbsq)_2] \quad (b)$$

This tautomeric equilibrium involves the simultaneous transfer of two electrons, but it probably proceeds via $[Mn^{III}(py)_2(dbcat)(dbsq)]$ as intermediate and in a stepwise fashion, as recently suggested.[23] Here manganese complexes of formula $[Mn(N-N)(diox)_2]$ were shown to contain the metal ion in the three oxidation states II, III, and IV depending on the donor ability of the ancillary ligand. In addition, the structural parameters of the *o*-phenanthroline complex were consistent with the presence of both the Mn^{III} and Mn^{IV} tautomers in the crystal lattice. As with the 1,2-benzoquinone complexes containing cobalt in different oxidation states, the presence of the Mn^{III} species is evidenced by a strong transition in the region of 2100–2200 nm. The intensity of the transition is temperature-dependent, which indicates the existence of interconversion equilibria between Mn^{IV} and Mn^{III} tautomers as well as between Mn^{III} and Mn^{II} tautomers. Again, in both equilibria the species with the metal in the higher oxidation state is stabilized at low temperature, therefore suggesting that both interconversions are driven by entropy.

On the basis of these results, one could reasonably expect that the conditions for the occurrence of valence tautomerism might also be achieved for bis(1,2-benzoquinone)iron analogues. Unfortunately, efforts in this regard were unsuccessful.[10,24] A series of $[Fe^{III}(N-N)(dbcat)(dbsq)]$ was prepared and characterized, but no evidence for interconversion to the corresponding $[Fe^{II}(N-N)(dbsq)_2]$ was found, although the latter was expected to be thermodynamically favored at high temperatures.

The different behavior of the three metal ions can be reasonably explained by taking into account the change in electronic configuration occurring during the intramolecular redox process. All these complexes are six-coordinate, and for the $Mn^{IV} \rightarrow Mn^{II}$ and $Co^{III} \rightarrow Co^{II}$ interconversions electrons are placed into e_g^* orbitals. Since these orbitals are σ-antibonding in character, a significant weakening of the metal–ligand bonds occurs and, thus, the intramolecular processes have large positive changes in enthalpy and entropy. This does not occur for the $Fe^{III} \rightarrow Fe^{II}$ system, since both are high or low spin and the change in electronic configuration does not involve a change in the population of the e_g^* orbitals. Hence the interconversion is expected to be characterized by a much smaller positive change in enthalpy with respect to those associated with the manganese and cobalt complexes. This is also reflected by the small differences (≈ 0.03 Å) in the metal–oxygen bond length in iron(III)– and iron(II)–1,2-benzoquinone complexes; the changess in bond lengths for the $Mn^{IV} \rightarrow Mn^{II}$ and $Co^{III} \rightarrow Co^{II}$ complexes are quite large (≈ 0.20 Å).[23,24]

Cobalt and manganese complexes 1,2-benzoquinones have provided the most fruitful examples for the investigation of this unusual phenomenon of electronic lability, and, as mentioned above, they are of relevant interest for the design of molecule-based switching devices. Nevertheless, there is evidence that other metal ions may be used to obtain 1,2-benzoquinone complexes characterized by valence tautomeric interconversion. The solution behavior of some nickel,[25] copper,[26] rhodium, and iridium[27] complexes can be correctly explained by valence tautomeric equilibria. Finally, the unusual photomechanical behavior exhibited by crystals of $[Rh(CO)_2(3,6\text{-dbsq})]$, which were reported to bend reversibly when exposed isothermally to low-energy light,[28] can likely be ascribed to an optically driven intramolecular electron transfer.[29]

German version: *Angew. Chem.* **1997**, *109*, 2852–2855

Keywords: cobalt · electron transfer · isomerism · manganese · redox chemistry

[1] a) P. Day, *Int. Rev. Phys. Chem.* **1981**, *1*, 149; b) C. Creutz, *Prog. Inorg. Chem.* **1983**, *30*, 1; c) D. E. Richardson, H. Taube, *Coord. Chem. Rev.* **1984**, *60*, 107; d) *Mixed Valence Systems: Applications in Chemistry, Physics, and Biology* (Ed.: K. Prassidis), *NATO ASI Ser. Ser. C* **1991**, *343*.
[2] a) P. Gütlich, *Struct. Bonding*, **1981**, *44*, 83; b) E. König, *Progr. Inorg. Chem.* **1987**, *35*, 527; c) J. K. Beattie, *Adv. Inorg. Chem.* **1988**, *32*, 1; d) H. Toftlund, *Coord. Chem. Rev.* **1989**, 94, 67; e) P. Gütlich, A. Hauser, H. Spiering, *Angew. Chem.* **1994**, *106*, 2109; *Angew. Chem. Int. Ed. Eng.* **1994**, *33*, 2024.
[3] C. G. Pierpont, R. M. Buchanan, *Coord. Chem. Rev.* **1981**, *38*, 45.
[4] C. G. Pierpont, C. W. Lange, *Progr. Coord. Chem.* **1993**, *41*, 381.
[5] a) O. Kahn, J. P. Launay, *Chemtronics*, **1988**, *3*, 140; b) O. Kahn, J. Kröber, C. Jay, *Adv. Mater.* **1992**, *4*, 718.
[6] A. Dei, *Inorg. Chem.* **1993**, *32*, 5730.
[7] R. M. Buchanan, C. G. Pierpont, *J. Am. Chem. Soc.* **1980**, *102*, 4951.
[8] D. M. Adams, A. Dei, A. L. Rheingold, D. N. Hendrickson, *Angew. Chem.* **1993**, *105*, 954; *Angew. Chem. Int. Ed. Engl.* **1993**, *32*, 880.
[9] D. M. Adams, A. Dei, A. L. Rheingold, D. N. Hendrickson, *J. Am. Chem. Soc.* **1993**, *115*, 8221.
[10] G. A. Abakumov, V. K. Cherkasov, M. P. Bubnov, O. G. Ellert, Z. B. Dobrokhotova, L. N. Zakharov, Y. T. Struchovkov, *Dokl. Akad. Nauk. USSR* **1993**, *328*, 12.
[11] O. S. Jung, C. G. Pierpont, *Inorg. Chem.* **1994**, *33*, 2227.
[12] O. S. Jung, C. G. Pierpont, *J. Am. Chem. Soc.* **1994**, *116*, 1127.
[13] C. Roux, D. M. Adams, J. P. Itiè, A. Polian, D. N. Hendrickson, M. Verdaguer, *Inorg. Chem.* **1996**, *35*, 2846.
[14] O. S. Jung, C. G. Pierpont, *J. Am. Chem. Soc.* **1994**, *116*, 2229.
[15] D. M. Adams, B. Li, J. D. Simon, D. N. Hendrickson, *Angew. Chem.* **1995**, *107*, 1580; *Angew. Chem. Int. Ed. Engl.* **1995**, *34*, 1481.
[16] C. G. Pierpont , O. S. Jung, *Inorg. Chem.* **1995**, *34*, 4281.
[17] D. M. Adams, D. N. Hendrickson, *J. Am. Chem. Soc.* **1996**, *118*, 11515.
[18] A. S. Attia, O. S. Jung, C. G. Pierpont, *Inorg. Chim. Acta*, **1994**, *226*, 91.
[19] O. S. Jung, D. H. Jo, Y. A. Lee, Y. S. Sohn, C. G. Pierpont, *Angew. Chem.* **1996**, *108*, 1796; *Angew. Chem. Int. Ed. Engl.* **1996**, *35*, 1694.
[20] O. S. Jung, D. H. Jo, Y. A. Lee, B. J. Conklin, C. G. Pierpont, *Inorg. Chem.* **1997**, *36*, 19.
[21] A. Dei, D. Gatteschi, *Inorg. Chim. Acta*, **1992**, *198-200*, 813.
[22] M. W. Lynch, D. N. Hendrickson, B. J. Fitzgerald, C. W. Pierpont, *J. Am. Chem. Soc.* **1984**, *106*, 2041.
[23] A. S. Attia, C. G. Pierpont, *Inorg. Chem.* **1995**, *34*, 1172.
[24] A. S. Attia, S. Bhattacharya, C. G. Pierpont, *Inorg. Chem.* **1995**, *34*, 4427.
[25] R. R. Rakhimov, P. M. Solozhenkin, N. N. Kopitaya, V. S. Pupkov, A. I. Prokof'ev, *Dokl. Akad. Nauk. SSSR*, **1988**, *300*, 1177.
[26] G. A. Abakumov, V. A. Garnov, V. I. Nevodchikov, V. K. Cherkasov, *Dokl. Akad. Nauk. SSSR*, **1989**, *304*, 107.
[27] G. A. Abakumov, G. A. Razuvaev, V. I. Nevodchikov, V. K. Cherkasov, *J. Organomet. Chem.* **1988**, *341*, 485.
[28] G. Abakumov, V. I. Nevodchikov, *Dokl. Akad. Nauk. SSSR*, **1982**, *266*, 1407.
[29] C. W. Lange, M. Foldeaki, V. I. Nevodchikov, V. K. Cherkasov, G. A. Abakumov, G. G. Pierpont, *J. Am. Chem. Soc.* **1992**, *114*, 4220.

 © WILEY-VCH Verlag GmbH, D-69451 Weinheim, 1997 0570-0833/97/3624-2736 $ 17.50+.50/0

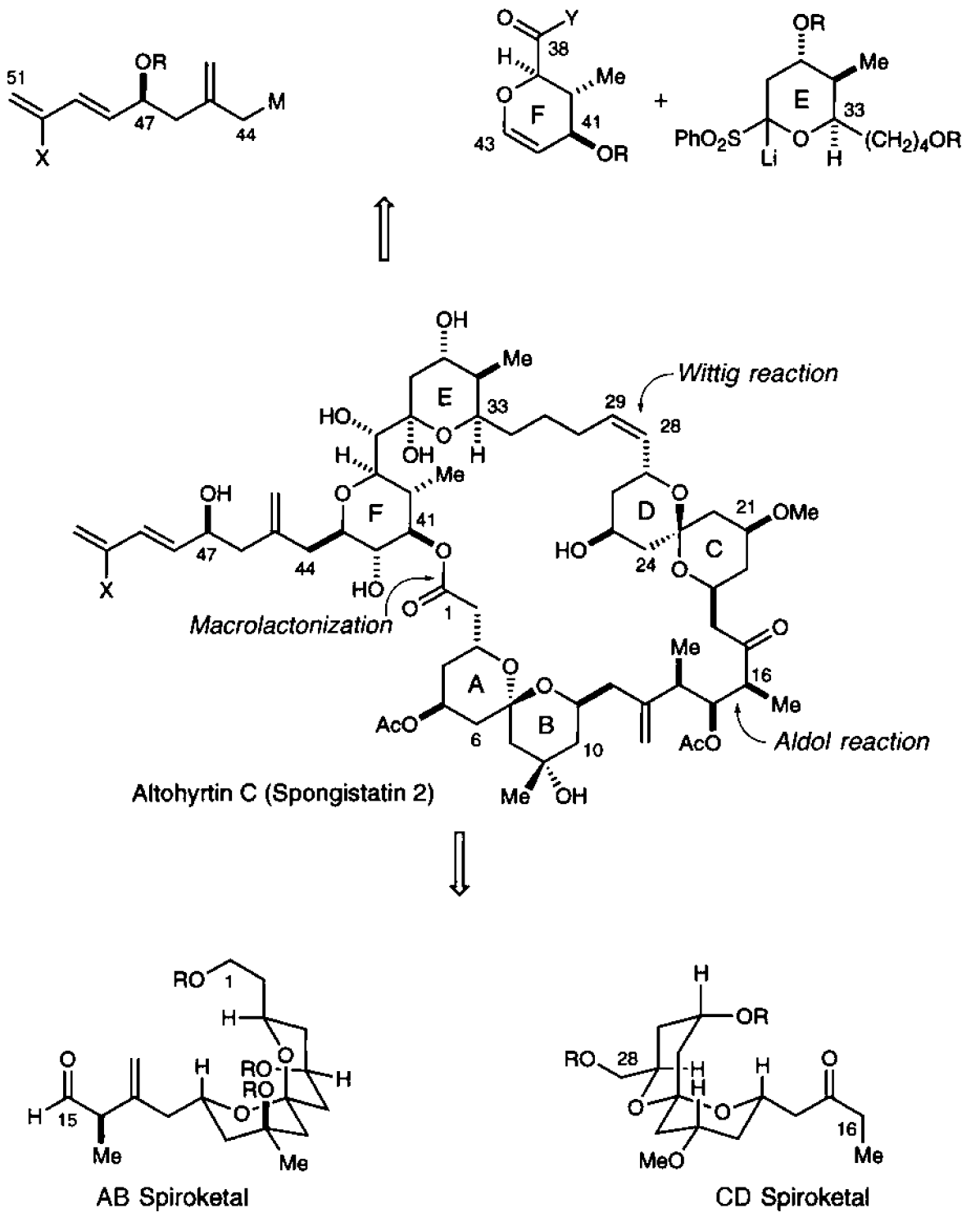

Altohyrtin C (spongistatin 2), whose total synthesis is described in the contributions of Evans et al. on the following pages, is one of a new class of marine natural products isolated at the beginning of the nineties from marine sponges. This class of compounds exhibits excellent antitumor activities.

 © WILEY-VCH Verlag GmbH, D-69451 Weinheim, 1997 0570-0833/97/3624-2737 $ 17.50+.50/0

Enantioselective Synthesis of Altohyrtin C (Spongistatin 2): Synthesis of the AB- and CD-Spiroketal Subunits**

David A. Evans,* Paul J. Coleman, and Luiz Carlos Dias

Dedicated to Professor Dieter Seebach and Professor Yoshito Kishi on the occasion of their 60th birthdays

The spongipyran macrolides, a new class of marine natural products, exhibit subnanomolar antitumor activities against a number of human cancer cell lines. Independent bioassay-guided isolation and structure elucidation efforts by the Pettit, Fusetani, and Kitagawa groups have recently identified the structurally related macrolides spongistatins (*Spongia* family),[1] cinachyrolide A (*Cinachyra* family),[2] and the altohyrtins (*Hyrtios* and *Spirastrella* families).[3] The structures of the major constituents in each study, spongistatin 1, cinachyrolide A, and altohyrtin A, were determined on the basis of NMR[4] spectroscopic investigations. While each of these structures has been assigned the same carbon skeleton, the proposed structures differ in the relative stereochemical relationships among the AB and CD spiroketals, rings E and F, and at the C_{15} and C_{16} stereocenters (Figure 1). Since only the Kitagawa altohyrtin structure elucidation included

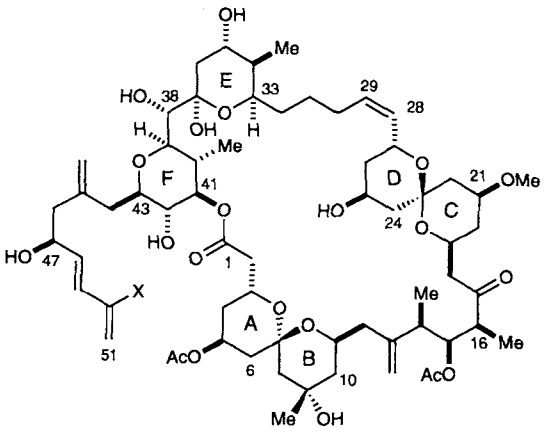

	X	IC_{50} (KB cell line)
Altohyrtin A	Cl	0.01 ng mL^{-1}
Altohyrtin B	Br	0.02 ng mL^{-1}
Altohyrtin C	H	0.40 ng mL^{-1}

Figure 1. Structures of altohyrtins A–C [3] and their antitumor activities.

an absolute configuration assignment,[3c,d] it is possible that, because of the lack of an adequate correlation of relative stereochemical assignments between subunits, the stereochemical configurations of some of the indicated skeletal subunits in both spongistatin 1 and cinachyrolide A could be antipodal. This raises the prospect that all three molecules could possess identical stereostructures. On the basis of the preceding discussion, we undertook an enantioselective synthesis of the proposed altohyrtin structure.

The total synthesis of altohyrtin C[3b] described in this and the following two communications verifies the Kitagawa altohyrtin structural assignment, and establishes the identity of altohyrtin C and the independently isolated spongistatin 2.[1b] In this communication, we describe the synthesis of the C_1-C_{15} AB-spiroketal and $C_{16}-C_{28}$ CD-spiroketal altohyrtin subunits, which will be joined through the illustrated aldol fragment coupling reaction (Scheme 1).

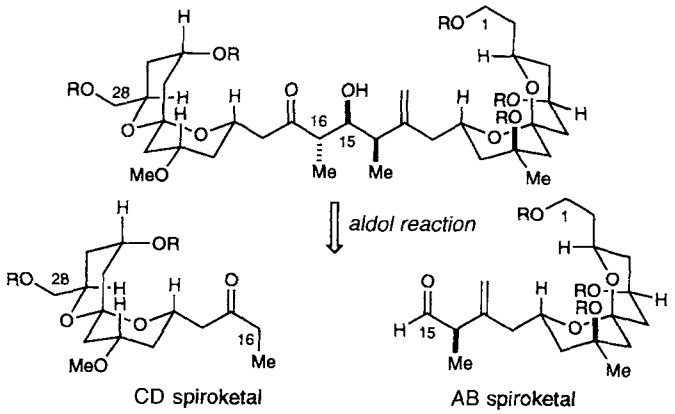

Scheme 1. Projected aldol coupling of the altohyrtin AB and CD spiroketals.

The synthesis plan for the C_1-C_{15} AB spiroketal[5] is outlined in Scheme 2. After the illustrated internal deketalization, disconnection of the simplified acyclic precursor at the C_7-C_8 bond affords two fragments of similar complexity, the synthesis and assembly of which is now described.

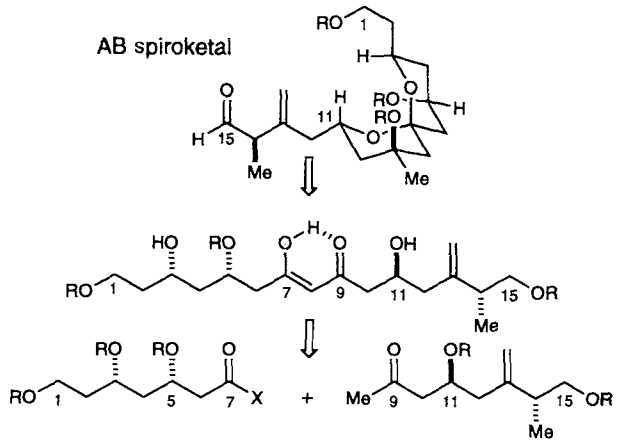

Scheme 2. Retrosynthesis of the AB spiroketal.

Synthesis of C_1-C_7 fragment **6** (Scheme 3) began from (*S*) alcohol **1**,[6] prepared from TBS-protected glutaric anhydride.[7] Successive trityl protection and DIBALH reduction afforded aldehyde **2** (81%) along with recovered (*S*)-2-naphthylethanol. Wittig homologation[8] and removal of the silyl protecting group afforded **4**, which was subjected to base-

[*] Prof. D. A. Evans, Dr. P. J. Coleman, Prof. L. C. Dias
Department of Chemistry & Chemical Biology
Harvard University
Cambridge, MA 02138 (USA)
Fax: Int. code + (617) 495-1460
e-mail: evans@chemistry.harvard.edu

[**] Financial support has been provided by the National Institutes of Health (NIH) and the National Science Foundation (NSF). The NIH BRS Shared Instrumentation Grant Program 1-S10-RR04870 and the NSF (CHE 88-14019) are acknowledged for providing NMR facilities.

 © WILEY-VCH Verlag GmbH, D-69451 Weinheim, 1997 0570-0833/97/3624-2738 $ 17.50+.50/0

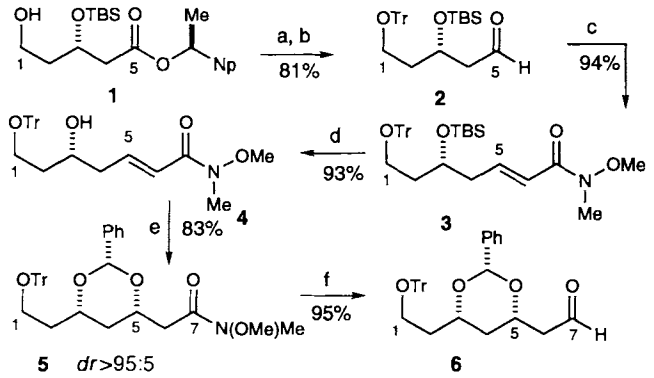

Scheme 3. Synthesis of C_1-C_7 fragment **6**. a) TrCl, Et_3N, CH_2Cl_2; b) DIBALH, toluene, −78°C; c) Ph_3P=CHCON(OMe)Me, CH_2Cl_2; d) TBAF, THF; e) 1. *t*BuOK, THF, 0°C; 2. PhCHO, 0°C; f) DIBALH, CH_2Cl_2, −78°C. (See ref. [4] for abbreviations.)

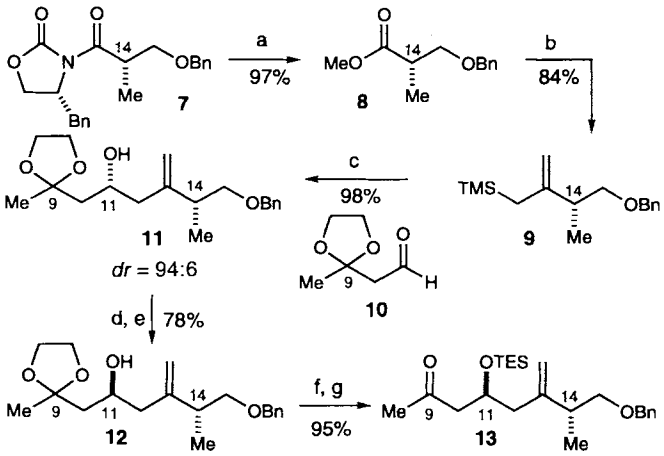

Scheme 4. Synthesis of C_8-C_{15} fragment **13**. a) $Sm(OTf)_3$ (10 mol%), MeOH; b) 1. $TMSCH_2MgCl$, $CeCl_3$, THF, −78 to +25°C; 2. silica gel, CH_2Cl_2, 25°C; c) 1. **9**, $SnCl_4$ (1.1 equiv), CH_2Cl_2, −78°C; 2. **10**, CH_2Cl_2, 3. Et_3N; d) *p*-$NO_2C_6H_4CO_2H$, PPh_3, di-*tert*-butyl azodicarboxylate, toluene/THF, 0°C; e) K_2CO_3, MeOH; f) PPTS, acetone, reflux; g) TESOTf, 2,6-lutidine, CH_2Cl_2, −78°C. (See ref. [4] for abbreviations.)

induced, intramolecular heteroconjugate 1,4-addition of the derived benzaldehyde hemiacetal to afford the 1,3-*syn* acetal **5** (83%, *dr* > 95:5).[9] DIBALH reduction provided aldehyde **6** in 56% overall yield for the six-step sequence.

The synthesis of the C_8-C_{15} fragment began with the chiral synthon **8**, readily derived from the oxazolidinone-mediated titanium enolate alkylation product **7** (Scheme 4).[10] Transformation of methyl ester **8** to the derived allylsilane **9** was achieved with (trimethylsilylmethyl)magnesium chloride and cerium(III) chloride, followed by elimination induced by acidic silica gel.[11] The optimal conditions for the allylsilane addition to aldehyde **10**[12] involved pretreatment of **9** with $SnCl_4$ followed by addition of **10**. This protocol provided **11** in 98% yield (*dr* = 94:6). Mitsunobu inversion of the C_{11} alcohol[13] (79%) and subsequent methanolysis (99%) provided **12** possessing the desired absolute stereochemical relationships at both C_{11} and C_{14}. Successive ketal hydrolysis and silyl protection afforded the C_8-C_{15} methyl ketone fragment **13** in 53% overall yield for the seven-step sequence.

Union of the C_1-C_7 and C_8-C_{15} fragments was initiated by treatment of methyl ketone **13** with dibutylboron triflate and iPr_2NEt[14] followed by addition of aldehyde **6** to provide aldol adduct **14** (79%) as a 1:1 mixture of C_7 diastereomers (Scheme 5). Oxidation of this mixture with chromium trioxide/pyridine/Celite[15] gave β-diketone **15** in 77% yield along with 12% recovered **14**. Multiple deprotection and spiroketalization of this substrate was achieved by treatment with $HF/H_2O/CH_3CN$. As anticipated, the only spiroketal diastereomer obtained (75%) from this transformation was the thermodynamically favored anomer **16**.[16]

With the AB-spiroketal framework in hand, the construction of the stereocenter at the tertiary atom C_9 was achieved by treatment of **17** with methyllithium/cerium trichloride in THF to provide axial alcohol **18** as a single diastereomer (Scheme 5; 86%; *dr* = > 95:5).[17] Silyl protection was followed by debenzylation (LDBB)[4,18] to afford the primary alcohol **19** in 61% yield (two steps). Oxidation (Dess–Martin periodinane, pyridine, 95%) to aldehyde **20** proceeded without epimerization of the C_{14} stereocenter. This oxidant is unique in its ability to execute this transformation without conjugating the proximal olefin. Aldehyde **20**, which is too labile for chromatographic purification, must be used immediately in the critical aldol coupling to the CD spiroketal.[19]

If the CD-spiroketal fragment is assembled from an acyclic precursor, the possibility exists for the formation of two diastereomeric structures, designated as CD_1 and CD_2 (Figure 2). Unlike the "axial–axial" AB spiroketal (analogous to CD_2, Figure 2), the CD spiroketal is disposed in an "axial–equatorial" configuration (CD_1, Figure 2), which is disfavored in isolated systems on stereoelectronic and steric grounds.[20] While the stabilization of diastereomer CD_1 in the altohyrtin

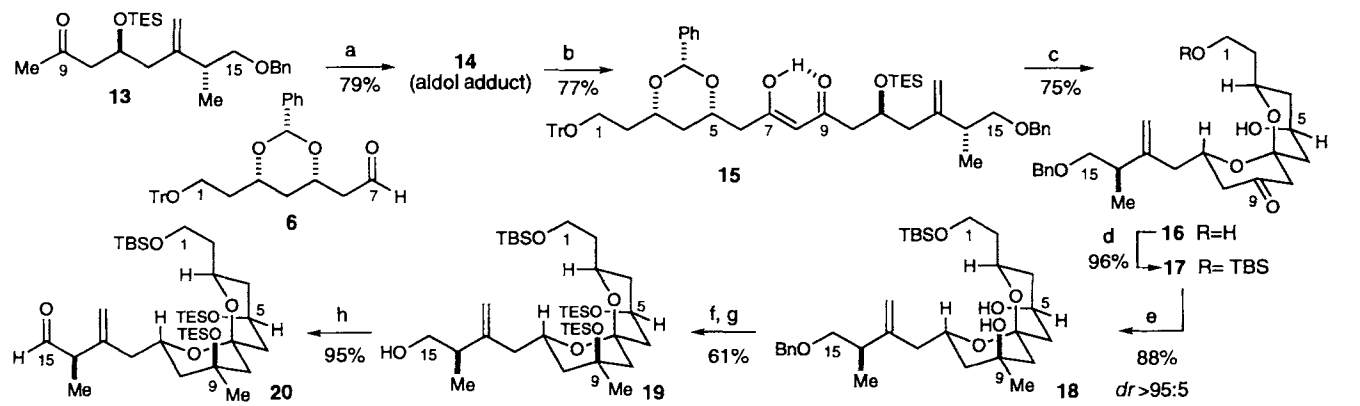

Scheme 5. Construction of the AB spiroketal **20**. a) 1. Bu_2BOTf, iPr_2NEt, CH_2Cl_2, −78°C; 2. **6**, CH_2Cl_2, −78°C; b) CrO_3, pyridine, Celite, CH_2Cl_2; c) $HF/CH_3CN/H_2O$; d) TBSCl, imidazole, CH_2Cl_2; e) MeLi, $CeCl_3$, THF, −78°C; f) TESOTf, 2,6-lutidine, CH_2Cl_2, −78°C; g) LDBB, THF, −78°C; h) Dess–Martin periodinane, pyridine, CH_2Cl_2. (See ref. [4] for abbreviations.)

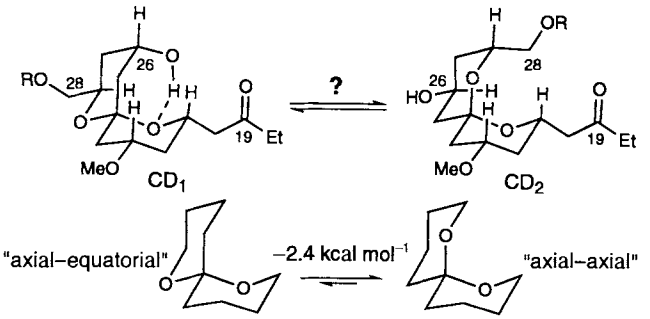

Figure 2. Possible CD-spiroketal configurations.

skeleton may be due to macrocyclic conformational constraints, structural features of the isolated CD system might also aid in enforcing this configuration. In this regard, the potential for an internal hydrogen bond between the C_{26} hydroxyl moiety and the ring-C skeletal oxygen (Figure 2) in spiroketal CD_1 was noted.

The synthesis of the CD spiroketal[21] was initiated by the regioselective opening of (*R*)-trityl glycidol[22] (**21**) with divinylcuprate (Scheme 6). The resulting alcohol (**22**) was transformed to methyl ketone **25** by a series of reactions presented in the preceding discussion (cf. Scheme 3). Aldol union of **25**, through its derived boron enolate,[14] with aldehyde **26**[6] afforded the adduct possessing the desired *S* configuration at C_{21} ($dr = 96{:}4$). Previous work from this laboratory has established that the dominant stereocontrol element in this reaction is the C_{25} alkoxy substituent on the enolate coupling partner and that the trend toward 1,5-*anti* induction is general.[23,24]

Several conventional refunctionalization steps were next carried out prior to spirocyclization. Methylation[25] of aldol adduct **27** afforded spirocyclization substrate **28**. The subsequent deprotection of the four oxygen protecting groups (at C_{19}, C_{25}, C_{27}, and C_{28}) and concomitant spirocyclization were achieved upon treatment of **28** with camphorsulfonic acid in a methanol/dichloromethane solution (1/15, 13 h, 25°C).[26] Two separable isomeric spiroketal products **29** and **30** (ratio 6:1) were isolated in 70% yield. A by-product that incorporated a second methyl ether at C_{25} was also identified (18%).[27] Diagnostic NOE experiments provided unequivocal stereochemical assignments for both spiroketal diastereomers.[28] The major isomer **29** possesses the undesired spirane ring fusion (CD_2, Figure 2). Equilibration[29] with three equivalents of $Mg(O_2CCF_3)_2$ in CF_3CO_2H/CH_2Cl_2 gave a 2.2:1 mixture of isomers **30** and **29**. We believe that the derived magnesium complexes of the two spiroketals are the species undergoing equilibration, thus altering the equilibrium ratio of spiroketal diastereomers.[30] Other conditions afforded higher ratios but lower yields of the isolated spiroketal ($ZnCl_2$, CH_2Cl_2, 22°C; **30**:**29** = 4.3:1).

Transformation of **30** to the desired CD-spiroketal ethyl ketone **33** (Scheme 7) was achieved by selective protection of the C_{28} hydroxyl group of **30** as its trityl ether, TBS-silylation

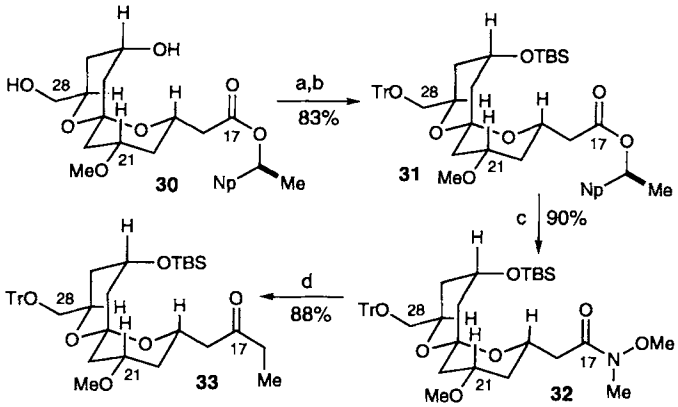

Scheme 7. Synthesis of CD-spiroketal ethyl ketone **33**. a) TrCl, pyridine, 60°C; b) TBSOTf, 2,6-lutidine; c) MeO(Me)NH·HCl, EtMgBr, THF, –10°C; d) EtMgBr, THF, 0°C. (See ref. [4] for abbreviations.)

at C_{25}, and transformation of the C_{17} ester functionality to an ethyl ketone through its corresponding Weinreb amide **32**.[31] Attempted transamidation of ester **31** under Lewis acidic conditions (MeONHMe·HCl, $AlMe_3$)[32] afforded none of the desired amide and led to appreciable epimerization of the spiroketal stereocenter.

The described syntheses of the AB- and CD-spiroketal subunits provide efficient routes to significant quantities of these portions of the spongipyran architecture. Realization of the aldol coupling of these fragments and further elaboration to altohyrtin C are discussed in a subsequent communication.[19]

Received: October 22, 1997 [Z11065IE]
German version: *Angew. Chem.* **1997**, *109*, 2951–2954

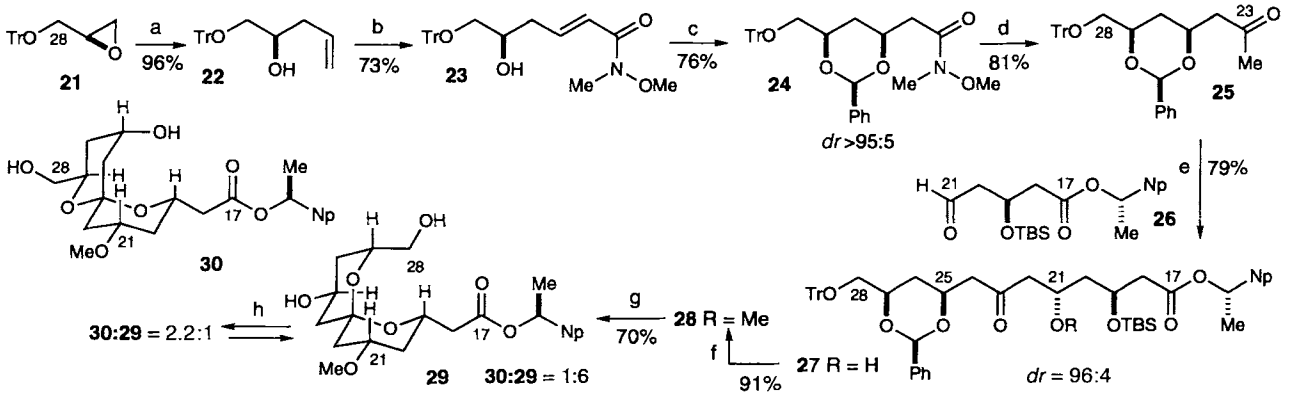

Scheme 6. Synthesis of CD spiroketal **30**. a) Vinylmagnesium bromide, CuI, THF, –78°C; b) O_3, CH_2Cl_2, Ph_3P, –78°C, then $Ph_3P{=}CHCON(OMe)Me$; c) *t*BuOK, PhCHO, 0°C; d) MeLi, THF, –78°C; e) Bu_2BOTf, *i*Pr_2NEt, Et_2O, –110°C, then **26**; f) Me_3OBF_4, 2,6-di-*tert*-butyl-4-methylpyridine; g) CSA, $MeOH/CH_2Cl_2$; h) 3 equiv of $Mg(O_2CCF_3)_2/CF_3CO_2H$, CH_2Cl_2: **30** (53%), recovered **29** (24%). (See ref. [4] for abbreviations.)

 © WILEY-VCH Verlag GmbH, D-69451 Weinheim, 1997 0570-0833/97/3624-2740 $ 17.50+.50/0

Keywords: altohyrtin · antitumor agents · natural products · spongistatin · total synthesis

[1] a) G. R. Pettit, Z. A. Cichacz, F. Gao, C. L. Herald, M. R. Boyd, J. M. Schmidt, J. N. A. Hooper, *J. Org. Chem.* **1993**, *58*, 1302–1304; b) G. R. Pettit, Z. A. Cichacz, F. Gao, C. L. Herald, M. R. Boyd, *J. Chem. Soc. Chem. Commun.* **1993**, 1166–1168; c) G. R. Pettit, Z. A. Cichacz, C. L. Herald, F. Gao, M. R. Boyd, J. M. Schmidt, E. Hamel, R. Bai, *ibid.* **1994**, 1605–1606.

[2] N. Fusetani, K. Shinoda, S. Matsunaga, *J. Am. Chem. Soc.* **1993**, *115*, 3977–3981.

[3] a) M. Kobayashi, S. Aoki, H. Sakai, K. Kawasoe, N. Kihara, T. Sasaki, I. Kitagawa, *Tetrahedron Lett.* **1993**, *34*, 2795–2798; b) M. Kobayashi, S. Aoki, H. Sakai, N. Kihara, T. Sasaki, I. Kitagawa, *Chem. Phar. Bull.* **1993**, *41*, 989–991; c) M. Kobayashi, S. Aoki, I. Kitagawa, *Tetrahedron Lett.* **1994**, *35*, 1243–1246; d) M. Kobayashi, S. Aoki, K. Gato, I. Kitagawa, *Chem. Phar. Bull.* **1996**, *44*, 2142–2149.

[4] Abbreviations: *dr* = diastereomer ratio; TBS = *tert*-butyldimethylsilyl; TES = triethylsilyl; TMS = trimethylsilyl; DIBALH = diisobutylaluminum hydride; Np = 2-naphthyl; TBAF = tetrabutylammonium fluoride; Tr = trityl = triphenylmethyl; Tf = trifluoromethanesulfonyl; Bn = benzyl; PPTS = pyridinium *p*-toluenesulfonate; CSA = camphorsulfonic acid; LDBB = di-*tert*-butylbiphenyllithium.

[5] Synthetic approaches to the AB spiroketal: a) M. M. Claffey, C. H. Heathcock, *J. Org. Chem.* **1996**, *61*, 7646–7647; b) I. Paterson, R. M. Oballa, R. D. Norcross, *Tetrahedron Lett.* **1996**, *37*, 8581–8584; (c) L. A. Paquette, D. Zuev, *ibid.* **1997**, *38*, 5115–5118.

[6] D. A. Evans, W. C. Black, *J. Am. Chem. Soc.* **1993**, *115*, 4497–4513.

[7] a) P. D. Theisen, C. H. Heathcock, *J. Org. Chem.* **1988**, *53*, 2374–2378; b) T. Rosen, C. H. Heathcock, *J. Am. Chem. Soc.* **1985**, *107*, 3731–3733.

[8] D. A. Evans, S. W. Kaldor, T. K. Jones, J. Clardy, T. J. Stout, *J. Am. Chem. Soc.* **1990**, *112*, 7001–7031.

[9] D. A. Evans, J. A. Gauchet-Prunet, *J. Org. Chem.* **1993**, *58*, 2446–2453.

[10] D. A. Evans, F. P. Urpi, T. C. Somers, J. S. Clark, M. T. Bilodeau, *J. Am. Chem. Soc.* **1990**, *112*, 8215–8216.

[11] B. A. Narayanan, W. H. Bunnele, *Tetrahedron Lett.* **1987**, *28*, 6261–6264.

[12] T. R. Kelly, L. Ananthasubramanian, K. Bovah, J. W. Gillard, R. N. Goerner, P. F. King, J. M. Lyding, W. G. Tsang, J. Vaya, *Tetrahedron* **1984**, *40*, 4569–4577.

[13] a) S. F. Martin, J. A. Dodge, *Tetrahedron Lett.* **1991**, *32*, 3017–3020; b) J. A. Dodge, J. I. Trujillo, M. Presnell, *J. Org. Chem.* **1994**, *59*, 234–236.

[14] a) T. Mukaiyama, T. Inoue, *Chem. Lett.* **1976**, 559–562; b) D. A. Evans, J. V. Nelson, E. Vogel, T. R. Taber, *J. Am. Chem. Soc.* **1981**, *103*, 3099–3111.

[15] a) A. B. Smith, P. A. Levemberg, *Synthesis* **1981**, 567–570; b) D. A. Evans, R. L. Dow, T. L. Shih, J. M. Takacs, R. Zahler, *J. Am. Chem. Soc.* **1990**, *112*, 5290–4313.

[16] The configuration of **16** was determined by NOESY experiments performed on the corresponding C_5 acetate.

[17] Similar alkylmetal additions to AB spiroketones have been documented; see reference 5.

[18] a) P. K. Freeman, L. L. Hutchinson, *J. Org. Chem.* **1980**, *45*, 1924–1930; (b) R. E. Ireland, M. G. Smith, *J. Am. Chem. Soc.* **1988**, *110*, 854–860.

[19] D. A. Evans, B. W. Trotter, B. Côté, P. J. Coleman, L. C. Dias, and A. Tyler, *Angew. Chem.* **1997**, *109*, 2957–2961; *Angew. Chem. Int. Ed. Engl.* **1997**, *36*, 2744–2747.

[20] P. Deslongchamps, D. D. Rowan, N. Pothier, T. Sauve, J. K. Saunders, *Can. J. Chem.* **1981**, *59*, 1105–1121.

[21] Synthetic approaches to the CD spiroketal: a) C. J. Hayes, C. H. Heathcock, *J. Org. Chem.* **1997**, *62*, 2678–2679; b) L. A. Paquette, A. Braun, *Tetrahedron Lett.* **1997**, *38*, 5119–5122.

[22] (*R*)-Trityl glycidol was prepared in 95% *ee* by Sharpless asymmetric epoxidation of allyl alcohol and in situ tritylation. Recrystallization provided the enantiomerically enriched compound: H. S. Hendrickson, E. K. Hendrickson, *Chemistry and Physics of Lipids*, **1990**, *53*, 115–120.

[23] Under these reaction conditions, aldehyde **26** has no preferred diastereoface. Coupling of methyl ketone **25** with the antipode of **26** under the same reaction conditions also gives a 1,5-*anti* product.

[24] The diastereoselectivity for this methyl ketone aldol coupling is 9.6:1 at −78°C. At −110°C, the diastereoselectivity increases to 22:1. a) D. A. Evans, P. J. Coleman, B. Cote, *J. Org. Chem.* **1997**, *62*, 788–789; b) I. Paterson, K. R. Gibson, R. M. Oballa, *Tetrahedron Lett.* **1996**, *37*, 8585–8588.

[25] a) D. A. Evans, A. M. Ratz, B. E. Huff, G. S. Sheppard, *Tetrahedron Lett.* **1994**, *35*, 7171–7172; b) H. Meerwein, G. Hinz, E. Kronig, E. Pfeil, *J. Prakt. Chem.* **1937**, 147, 257–285.

[26] Attempted spiroketalization of **28** in the absence of MeOH led to rapid β-elimination of the C_{21} methyl ether to give an α,β unsaturated ketone.

[27] Related case of methanol incorporation in a spirocyclization product: I. Paterson, S. Bower, M. D. McLeod, *Tetrahedron Lett.* **1995**, *36*, 175–178.

[28] Stereochemical assignments were supported by NOE experiments (1D and 2D) and ^{1}H NMR measurements. An NOE enhancement between H_{19} and H_{27} was observed in the axial–equatorial isomer **30**. The NMR signal for H_{25} was illuminating as well: **29**: $\delta = 3.9$ (m, $J(H_{25}, H_{26ax}) = 11$ Hz); **30**: $\delta = 3.9$ ppm (t, $J = 3.2$ Hz).

[29] Due to the sensitivity of spiroketal substrate **29** to acidic media, equilibration experiments were kept short (1–3 h). In dichloromethane/CSA, **29** equilibrated to a 1:1 (29:30) mixture of spiroisomers after 3 h.

[30] Presumably, the C_{25} hydroxyl is assisting in the equilibration to afford **30** by participating in an internal chelate with the metal cation and proximally positioned anomeric oxygen. For related cases see a) D. R. Williams, P. A. Jass, R. D. Gaston, *Tetrahedron Lett.* **1993**, *34*, 3231–3234; b) M. J. Kurth, E. G. Brown, E. Hendra, H. Hope, *J. Org. Chem.* **1985**, *50*, 1115–1117; c) S. L. Schreiber, T. L. Sommer, K. Satake, *Tetrahedron Lett.* **1985**, *26*, 17–20.

[31] J. M. Williams, R. B. Jobson, N. Yasuda, G. Marchesini, U. H. Dolling, E. J. Grabowski, *Tetrahedron Lett.* **1995**, *36*, 5461–5464.

[32] A. Basha, M. Lipton, S. M. Weinreb, *Tetrahedron Lett.* **1977**, *18*, 4171–4174.

Enantioselective Synthesis of Altohyrtin C (Spongistatin 2): Synthesis of the EF-Bis(pyran) Subunit**

David A. Evans,* B. Wesley Trotter, Bernard Côté, and Paul J. Coleman

Dedicated to Professor Dieter Seebach and Professor Yoshito Kishi on the occasion of their 60th birthdays

Concurrent with the syntheses of the AB- and CD-spiroketal subunits of the altohyrtin skeleton,[1] the synthesis of the altohyrtin C_{29}–C_{51} EF-bis(pyran) fragment was addressed. The principal subunits for this portion of the altohyrtin skeleton are illustrated in Figure 1. The retrosynthetic proposal focuses on the incorporation of the C_{44}–C_{51} side chains (X = H, Cl, Br) as allylmetal nucleophiles into the illustrated F-ring epoxide at a late stage in the synthesis. In turn, this bis(pyran) is assembled through acylation of the illustrated E-ring sulfonyl anion with an F-ring[2] carboxylic

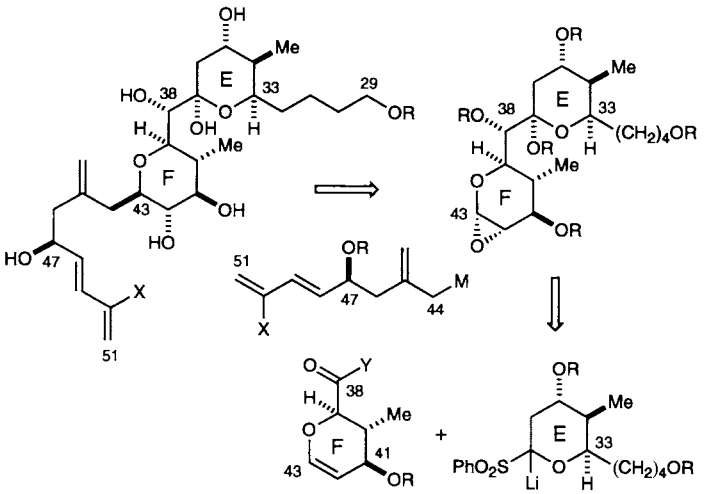

Figure 1. Retrosynthesis of the EF-bis(pyran) subunit.

[*] Prof. D. A. Evans, B. W. Trotter, Dr. B. Côté, Dr. P. J. Coleman
Department of Chemistry & Chemical Biology
Harvard University
Cambridge, MA 02138 (USA)
Fax: Int. code + (617)495-1460
e-mail: evans@chemistry.harvard.edu

[**] Financial support has been provided by the National Institutes of Health (NIH) and the National Science Foundation (NSF). The NIH BRS Shared Instrumentation Grant Program 1-S10-RR04870 and the NSF (CHE 88-14019) are acknowledged for providing NMR facilities.

 © WILEY-VCH Verlag GmbH, D-69451 Weinheim, 1997 0570-0833/97/3624-2741 $ 17.50+.50/0

acid derivative. This strategy accommodates the use of either antipode of the E- or F-ring subunits in the event of a stereochemical discrepancy in this portion of the structure.[3]

In conjunction with this plan, a practical solution for β-*C*-glycosidation through the allylstannane-mediated cleavage of glycal epoxides has been developed (Scheme 1).[4] Dihydropyran **1** was found to undergo highly stereoselective epoxidation by dimethyldioxirane in full accord with extensive precedent.[5] The resulting glycal epoxide **2**, when treated with tributylmethallylstannane and tributylstannyl triflate, was transformed to the F-ring analogue **3** with high diastereoselectivity. Tributylstannyl triflate was unique among the surveyed Lewis acid activators in providing exclusively the β isomer; other Lewis acids afforded significant amounts of diastereomeric addition products, presumably through the intervention of an oxocarbenium ion intermediate.

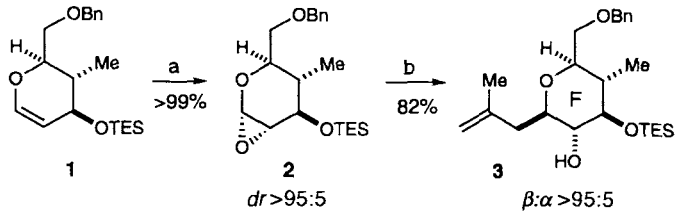

Scheme 1. β-*C*-glycosylation mediated by tributylstannyl triflate. a) Dimethyldioxirane, acetone, CH_2Cl_2, 0°C; b) 5 equiv of tributylmethallylstannane, 2 equiv of Bu_3SnOTf, CH_2Cl_2, −78°C. (See ref. [4] for abbreviations.)

Application of this methodology to a more highly functionalized system was next investigated. Synthesis of the $C_{29}-C_{37}$ E-ring fragment was initiated from the enantiomerically pure boron aldol adduct **4**[6] (Scheme 2). Sequential alcohol protection and amide reduction provided aldehyde **5**, which was subjected to a Felkin-selective Lewis acid catalyzed ($BF_3\cdot Et_2O$) aldol addition with thioketene acetal **6** to afford thioester **7** (87%; *dr* = 94:6). Fukuyama reduction to the derived aldehyde[7] and acid-catalyzed deprotection–acetalization followed by silyl protection of the remaining secondary alcohol afforded the E-ring methyl ketal **8** (81%, three steps).

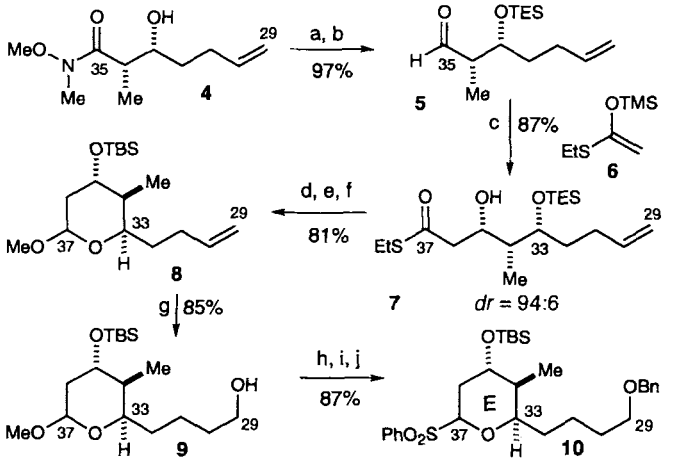

Scheme 2. Synthesis of E-ring phenylsulfone **10**. a) TESOTf, 2,6-lutidine; b) DIBALH, −78°C; c) **6**, $BF_3\cdot Et_2O$, CH_2Cl_2, −78°C; d) Lindlar catalyst, Et_3SiH, 1-hexene, acetone; e) CSA, MeOH; f) TBSCl, imidazole, DMF; g) 9-BBN, then H_2O_2; h) $TMSSPh$, ZnI_2; i) NaH, BnBr, Bu_4NI; j) *m*-CPBA, $NaHCO_3$. (See ref. [4] for abbreviations.)

Hydroboration of **8** with 9-BBN then afforded alcohol **9** (85%). Preparation of the E-ring phenylsulfone **10** was completed by anomeric sulfide formation ($TMSSPh$, ZnI_2),[8] C_{29} alcohol benzylation (NaH, BnBr, Bu_4NI, 90% from **9**), and sulfide oxidation (*m*-CPBA, $NaHCO_3$, 97%).

Synthesis of the F-ring dihydropyran began from our previously reported aldol adduct **11** (99% ee, *R* configuration; Scheme 3).[9] Fräter–Seebach alkylation (71% yield; *dr* = 5–8:1)[10] was followed by successive alcohol protection (TESCl, imidazole, 80%) and thioester reduction (DIBALH, 86%) to give aldehyde **13**. A Felkin-selective, 1,3-*anti* aldol reaction[11] with thioketene acetal **14** ($BF_3\cdot Et_2O$, toluene, −93°C) provided thioester **15** (88%; *dr* = 94:6). Silyl deprotection and Ag(I)-mediated lactonization (88%, two steps) followed by TES protection and DIBALH reduction (93%, two steps) afforded lactol **16**. $POCl_3$-mediated dehydration (81%), removal of the C_{38} benzyl group (LDBB, 99%), and Parikh–Doering oxidation (90%)[12] provided the F-ring dihydropyran aldehyde **17**. Buffered Kraus oxidation[13] of this intermediate provided a carboxylic acid that could be transformed to the activated benzotriazolyl amide **18** through the corresponding acid chloride.[14] In our subsequent sulfonyl carbanion acylation studies (vide infra), it was found that **18** is superior to the analogous acid chloride, which readily undergoes competitive carbanion-initiated proton transfer.

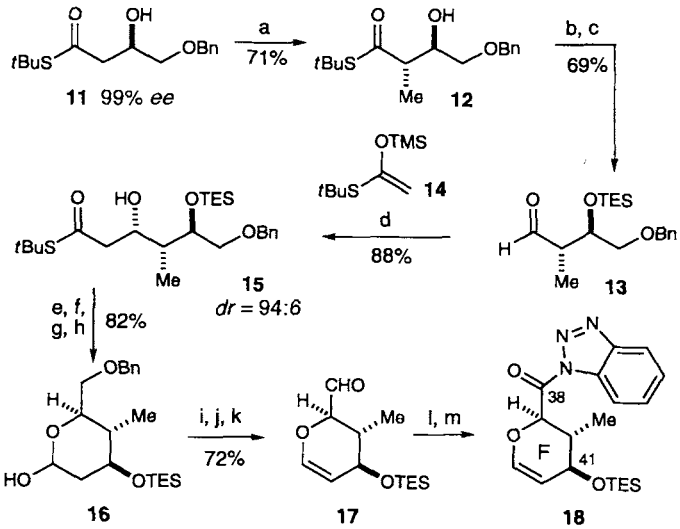

Scheme 3. Synthesis of the activated F-ring amide **18**. a) LDA, HMPA, MeI, THF, −55°C; b) TESCl, imidazole; c) DIBALH, −78°C; d) **14**, $BF_3\cdot Et_2O$, toluene, −93°C; e) PPTS, MeOH; f) AgO_2CCF_3, benzene; g)TESCl, imidazole; h) DIBALH, −78°C; i) $POCl_3$, pyridine, 80°C; j) LDBB, THF, −78°C; k) $SO_3\cdot$pyridine, DMSO, Et_3N; l) $NaClO_2$, 2-methyl-2-butene, ethyl-1-propenyl ether, *t*-BuOH, pH 5.5; m) 1. 1-chloro-*N*,*N*-trimethylpropenylamine; 2. benzotriazole, pyridine, DMAP. (See ref. [4] for abbreviations.)

Synthesis of the requisite allylstannane side chain began with the known (2*S*,3*E*)-hexa-3,5-diene-1,2-diol (**19**)[15] (Scheme 4). A three-step sequence provided monosilylated ether **20** in 90% overall yield without intervening purifications. Conversion of **20** into the corresponding alkyl triflate followed by treatment with the lithium enolate of methyl β-dimethylaminopropionate[16] provided **21** (80%). Quaternization and elimination of the dimethylamino group (MeI, Na_2CO_3, 94%) was followed by ester reduction (DIBALH, 95%) to give the corresponding allylic alcohol. In situ mesylation and displacement with tributylstannyllithium[17] gave TES-protected allylstannane **23** in 85% yield. Basic

 © WILEY-VCH Verlag GmbH, D-69451 Weinheim, 1997 0570-0833/97/3624-2742 $ 17.50+.50/0 *Angew. Chem. Int. Ed. Engl.* **1997**, *36*, No. 24

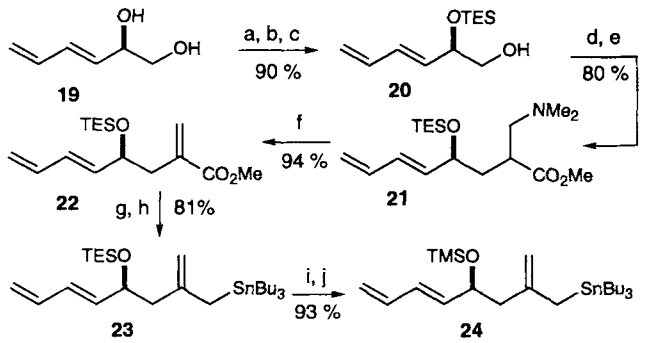

Scheme 4. Synthesis of altohyrtin C side chain **24**. a) AcCl, 2,6-lutidine, CH_2Cl_2, −78°C; b) TESCl, *imidazole*, CH_2Cl_2; c) DIBALH, toluene, −78°C; d) Tf_2O, pyridine, CH_2Cl_2, −10°C; e) methyl β-dimethylaminopropionate, LDA, THF, −78°C; f) MeI, Na_2CO_3, MeOH; g) DIBALH, CH_2Cl_2, −78°C; h) BuLi, MsCl, THF, −78°C, then Bu_3SnLi; i) NaOH, EtOH; j) *N,O*-bis(trimethylsilyl) acetamide. (See ref. [4] for abbreviations.)

deprotection and resilylation then provided TMS-protected allylstannane **24** in 93% yield.

At this stage, acylation of the E-ring phenylsulfone[18] with the activated F-ring amide was addressed (Scheme 5). While the use of F-ring derivatives including the C_{38} aldehyde **17**, activated esters, and acid chlorides engendered problems ranging from sulfone elimination to unwanted proton transfer, lithiation of 1.1 equivalents of sulfone **10** followed by addition of 1 equivalent of amide **18** provided the EF bis(pyran) **25** in 60% yield (four steps from **17**). Methanolysis of **25** provided ketone **26** isolated in 48% yield.[19] Of the hydride reducing agents surveyed, $KBHEt_3$ proved most effective in securing the desired configuration at C_{38} (90%; $dr > 99{:}1$). At this juncture, a single-crystal X-ray analysis of alcohol **27** unequivocally confirmed the structure of this advanced intermediate.[20]

After silylation of **27**, epoxidation of **28** with dimethyldioxirane again proceeded stereoselectively (100%; $dr > 95{:}5$) to afford **29**. Treatment of this epoxide with allylstannane **24** and tributylstannyl triflate provided the desired adduct **30** in 80% yield as a single diastereomer. The excess allylstannane from this experiment was recovered quantitatively after chromatography. The size of the C_{47} alcohol protecting group appears to play a significant role in this reaction; use of allylstannanes containing larger silyl protecting groups (e.g. **23**) resulted in lower yields of isolated **30** due to competitive decomposition of starting epoxide.

At this juncture, acidic catalysts were evaluated for the deprotection of the EF bis(pyran) **30**. Prior experience had revealed that ring-E Δ^{36} dihydropyran formation was to be avoided, since rehydration of this intermediate was problematic. Treatment of **30** with aqueous HF resulted in removal of all four silyl protecting groups as well as hydrolysis of the C_{37} methyl ether to the corresponding lactol [Eq. (1)]. This experiment allayed concerns that the unwanted elimination

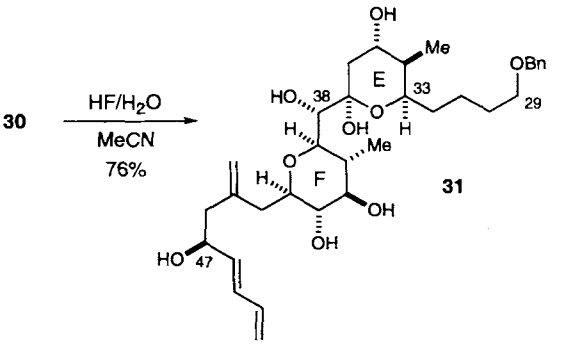

(1)

to the dihydropyran would complicate the projected final deprotection sequence leading to the target structure. In addition, ^1H NMR chemical shifts and coupling constants of **31** correlated very well with those reported for altohyrtin C (Table 1).[21] The union of the EF bis(pyran) **28** with the

Table 1. Chemical shifts (δ), multiplicities, and coupling constants [Hz] in [D6]DMSO.

Proton	Altohyrtin C[21]	**31**
$C_{38}H$	3.28 (d, 8)	3.16 (d, 8.2)
$C_{39}H$	3.60 (d-like, 10)	3.45 (d, 10.6)
$C_{41}H$	4.68 (t-like, 10)	2.91 (dt, 9.3, 5.5)
$C_{42}H$	3.04 (ddd, 10, 10, 6)	2.82 (dt, 8.7, 5.1)
$C_{43}H$	3.36 (t-like, 10)	3.21 (t-like, 9.7)
$C_{48}H$	5.72 (dd, 15, 6)	5.69 (dd, 15.2, 5.9)
$C_{49}H$	6.16 (dd, 15, 10)	6.14 (dd, 15.0, 10.7)
$C_{50}H$	6.30 (ddd, 17, 10, 10)	6.29 (ddd, 17, 10, 10)
$C_{51}H_2$	5.01 (d, 10)	5.00 (d, 10.8)
$C_{51}H_2$	5.14 (d, 17)	5.14 (dd, 17.0, 1.5)

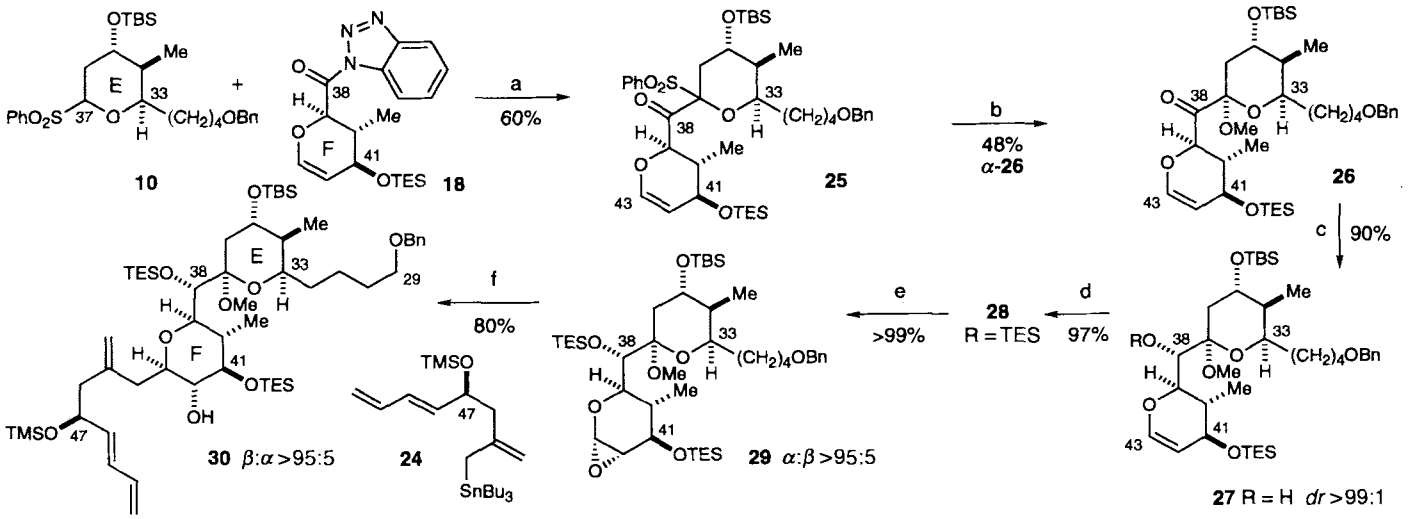

Scheme 5. Synthesis of the EF bicycle **30**. a) LDA, THF, −78°C, then **18**; b) 1. ZnI_2, MeOH; 2. $MgBr_2 \cdot Et_2O$, MeOH; c) $KBHEt_3$, THF, −78 to −40°C; d) TESCl, imidazole, DMF; e) dimethyldioxirane, acetone, CH_2Cl_2, 0°C; f) 16 equiv of **24**, 2 equiv of Bu_3SnOTf, CH_2Cl_2, −78°C. (See ref. [4] for abbreviations.)

 © WILEY-VCH Verlag GmbH, D-69451 Weinheim, 1997 0570-0833/97/3624-2743 $ 17.50+.50/0

ABCD bis(spiroketal) and the completion of the altohyrtin C synthesis is described in the following communication.[22]

Received: October 22, 1997 [Z110661E]
German version: *Angew. Chem.* **1997**, *109*, 2954–2957

Keywords: altohyrtin · antitumor agents · natural products · spongistatin · total synthesis

[1] D. A. Evans, P. J. Coleman, L. C. Dias, *Angew. Chem.* **1997**, *109*, 2951–2954; *Angew. Chem. Int. Ed. Engl.* **1997**, *36*, 2738–2741.
[2] Recent synthesis of the C_{36}–C_{46} (F ring) fragment: I. Paterson, L. Keown, *Tetrahedron Lett.* **1997**, *38*, 5727–5730.
[3] The relative stereochemical relationship between the C_{44}–C_{38} (F ring) and the C_{37}–C_{29} (E ring) segments has been assigned differently in the altohyrtin, spongistatin, and cinachyrolide series: a) M. Kobayashi, S. Aoki, K. Gato, I. Kitagawa, *Chem. Phar. Bull.* **1996**, *44*, 2142–2149; b) R. Bai, G. F. Taylor, Z. A. Cichacz, C. L. Herald, J. A. Kepler, G. R. Pettit, E. Hamel, *Biochemistry* **1995**, *34*, 9714–9721; c) N. Fusetani, K. Shinoda, S. Matsunaga, *J. Am. Chem. Soc.* **1993**, *115*, 3977–3981.
[4] Abbreviations: *dr* = diastereomer ratio; TBS = *tert*-butyldimethylsilyl; TES = triethylsilyl; TMS = trimethylsilyl; DIBALH = diisobutylaluminum hydride; Tr = trityl = triphenylmethyl; Tf = trifluoromethanesulfonyl; Bn = benzyl; PPTS = pyridinium *p*-toluenesulfonate; CSA = camphorsulfonic acid; LDBB = di-*tert*-butylbiphenyllithium; DMAP = 4-dimethylaminopyridine; 9-BBN = 9-borabicyclo[3.3.1]nonane; *m*-CPBA = *m*-chloroperbenzoic acid; LDA = lithium diisopropylamide HMPA = hexamethylphosphoric triamide.
[5] a) R. Halcomb, S. Danishefsky, *J. Am. Chem. Soc.* **1989**, *111*, 6661–6666; b) I. Kim, T. Park, S. Hu, K. Abrampah, S. Zhang, P. Livingston, S. Danishefsky, *J. Org. Chem.* **1995**, *60*, 7716–7717; c) T. Park, I. Kim, S. Hu, M. Bilodeau, J. Randolph, O. Kwon, S. Danishefsky, *J. Am. Chem. Soc.* **1996**, *118*, 11488–11500.
[6] D. A. Evans, W. C. Black, *J. Am. Chem. Soc.* **1993**, *115*, 4497–4513.
[7] T. Fukuyama, S. C. Lin, L. Li, *J. Am. Chem. Soc.* **1990**, *112*, 7050–7051.
[8] S. Hanessian, Y. Guindon, *Carbohydr. Res.* **1980**, *86*, C3–C6. Addition of Bu_4NI was found to be unnecessary for this transformation.
[9] D. A. Evans, J. A. Murry, M. C. Kozlowski, *J. Am. Chem. Soc.* **1996**, *118*, 5814–5815.
[10] a) M. Zuger, T. Weller, D. Seebach, *Helv. Chim. Acta* **1980**, *63*, 2005–2009; b) G. Frater, *Tetrahedron Lett.* **1981**, *22*, 425–428.
[11] D. A. Evans, M. J. Dart, J. L. Duffy, M. G. Yang, *J. Am. Chem. Soc.* **1996**, *118*, 4322–4343.
[12] J. R. Parikh, W. von E. Doering, *J. Am. Chem. Soc.* **1967**, *89*, 5505–5507.
[13] B. S. Bal, W. E. Childers, H. W. Pinnick, *Tetrahedron* **1981**, *37*, 2091–2096. The use of ethyl-1-propenyl ether prevented decomposition of the acid-sensitive dihydropyran.
[14] 1-chloro-*N*,*N*-trimethylpropenylamine: A. Devos, J. Rémion, A.-M. Frisque-Hesbain, A. Colens, L. Ghosez, *J. Chem. Soc. Chem. Commun.* **1979**, 1180–1181.
[15] A. Lubineau, J. Auge, N. Lubin, *J. Chem. Soc. Perkin Trans. 1* **1990**, 3011–3015. Diol **19** is prepared in three steps from (*S*)-glyceraldehyde acetonide.
[16] E. Rouvier, J.-C. Giacomoni, A. Cambon, *Bull. Soc. Chim. France*, **1971**, 1717–1723.
[17] a) L. E. Overman, P. A. Renhowe, *J. Org. Chem.* **1994**, *59*, 4138–4142; b) S. Weigand, R. Bruckner, *Synthesis* **1996**, 475–482.
[18] a) S. V. Ley, B. Lygo, A. Wonnacott, *Tetrahedron Lett.* **1985**, *26*, 535–538; b) C. Greck, P. Grice, S. V. Ley, A. Wonnacott, *ibid.* **1986**, *27*, 5277–5280; c) J.-M. Beau, P. Sinay, *ibid.* **1985**, *26*, 6185–6188; d) J.-M. Beau, P. Sinay, *ibid.* **1985**, *26*, 6189–6192; e) J.-M. Beau, P. Sinay, *ibid.* **1985**, *26*, 6193–6196.
[19] The two anomers of **25** underwent methanolysis at different rates. The mixture of anomers was subjected to ZnI_2/MeOH at room temperature, which converted the major anomer into **26** (> 95:5 α). The minor anomer of **25** was then separated and treated with $MgBr_2 \cdot Et_2O$ in refluxing MeOH to provide additional **26** (2:1 α). The major side product in these reactions was the enone product of sulfone elimination: D. S. Brown, S. V. Ley, S. Vile, M. Thompson, *Tetrahedron* **1991**, *47*, 1329–1342.
[20] The authors wish to thank Kevin R. Campos for performing the X-ray analysis of **27**.
[21] M. Kobayashi, S. Aoki, H. Sakai, N. Kihara, T. Sasaki, I. Kitagawa, *Chem. Phar. Bull.* **1993**, *41*, 989–991.
[22] D. A. Evans, B. W. Trotter, B. Côté, P. J. Coleman, L. C. Dias, and A. N. Tyler, *Angew. Chem.* **1997**, *109*, 2957–2961; *Angew. Chem. Int. Ed. Engl.* **1997**, *36*, 2744–2747.

Enantioselective Synthesis of Altohyrtin C (Spongistatin 2): Fragment Assembly and Revision of the Spongistatin 2 Stereochemical Assignment**

David A. Evans,* B. Wesley Trotter, Bernard Côté, Paul J. Coleman, Luiz Carlos Dias, and Andrew N. Tyler

Dedicated to Professor Dieter Seebach and Professor Yoshito Kishi on the occasion of their 60th birthdays

With convergent syntheses of the AB,[1] CD,[1] and EF[2] spongipyran fragments in hand, the assembly of these subunits to the altohyrtin C skeleton was addressed (Figure 1). While the C_{44}–C_{51} side chain had been successfully

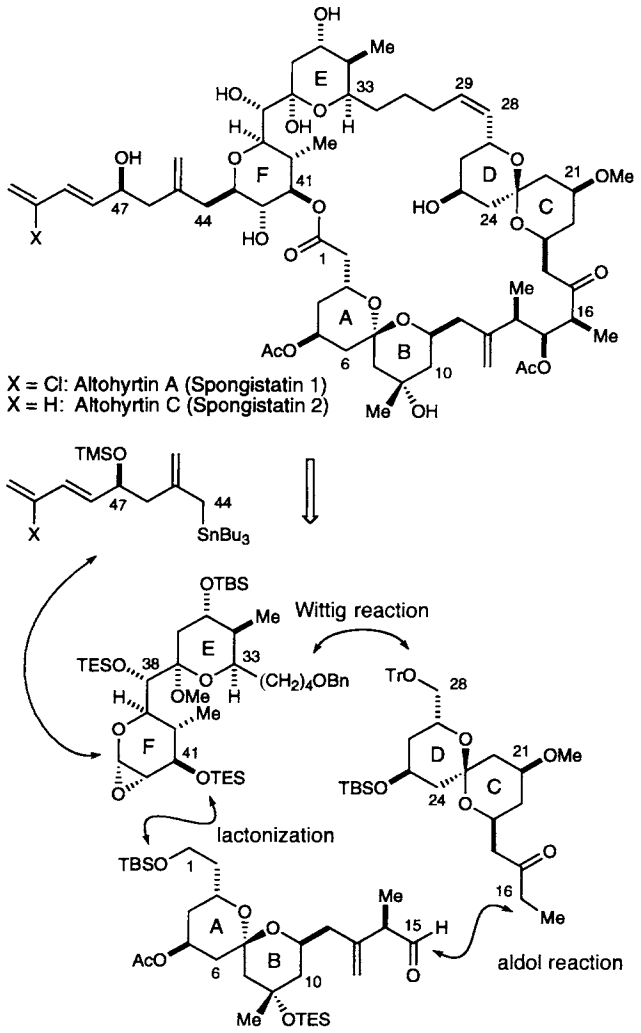

Figure 1. Assembly of the altohyrtin subunits. (See ref. [4] for abbreviations.)

[*] Prof. D. A. Evans, B. W. Trotter, Dr. B. Côté, Dr. P. J. Coleman, Prof. L. C. Dias, Dr. A. N. Tyler
Department of Chemistry & Chemical Biology
Harvard University
Cambridge, MA 02138 (USA)
Fax: Int. code + (617) 495-1460
e-mail: evans@chemistry.harvard.edu

[**] Financial support has been provided by the National Institutes of Health (NIH) and the National Science Foundation (NSF). The NIH BRS Shared Instrumentation Grant Program 1-S10-RR04870 and the NSF (CHE 88-14019) are acknowledged for providing NMR facilities.

 © WILEY-VCH Verlag GmbH, D-69451 Weinheim, 1997 0570-0833/97/3624-2744 $ 17.50+.50/0

incorporated into the isolated EF bis(pyran),[2] we planned to delay the introduction of this fragment until later in the assembly process. Since data obtained for the altohyrtins and spongistatins reveal that the identity of the side-chain substituent X exhibits a significant influence on the cytotoxic potency of these molecules,[3] we intend to develop syntheses of other side-chain analogues of these macrolides in forthcoming investigations. We report here the completion of the total synthesis of altohyrtin C (spongistatin 2), which employs a diastereoselective aldol union of the AB- and CD-spiroketal subunits, a Wittig coupling of the ABCD and EF fragments, a late-stage addition of the $C_{44}-C_{51}$ side chain to the fully elaborated ABCDEF system, and a regioselective macrolactonization, which exhibits fortuitous discrimination between the unprotected C_{41} and C_{42} diol functionalities of the F ring.

The aldol coupling of CD-spiroketal ethyl ketone **1**[1] with AB-spiroketal aldehyde **2**[1] was first addressed (Scheme 1).[4]

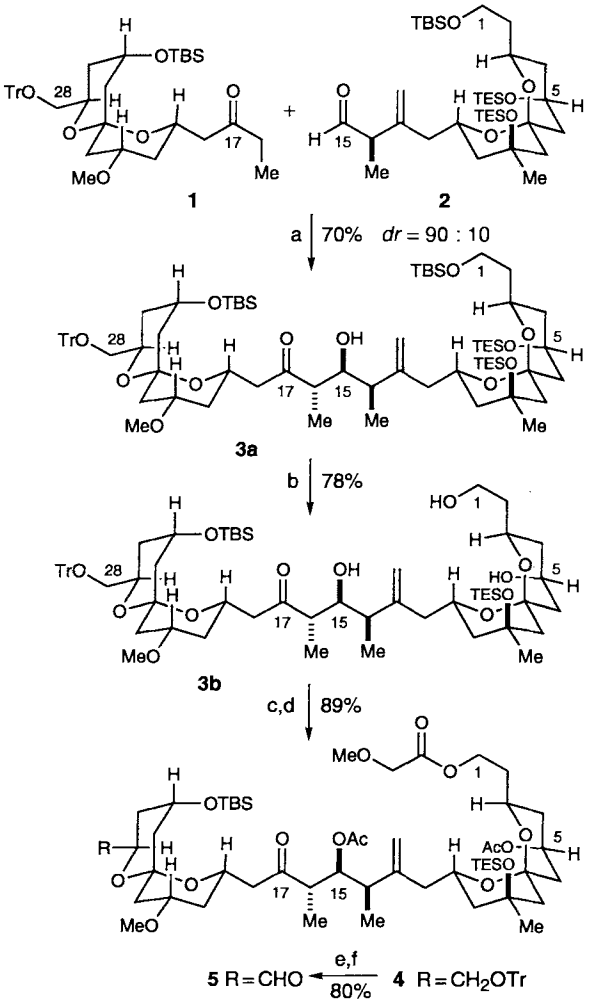

Scheme 1. AB/CD aldol fragment coupling. a) $(cHex)_2BCl$, Et_3N, pentane, 0°C, 90 min, then −78°C, addition of **2**; b) HF·pyridine, THF, 0°C; c) $(MeOCH_2CO)_2O$, iPr_2EtN, CH_2Cl_2; d) Ac_2O, DMAP, pyridine, 22°C; e) Me_2AlCl, CH_2Cl_2, −78°C; f) Dess–Martin periodinane, CH_2Cl_2. (See ref. [4] for abbreviations.)

Ample precedent exists for establishment of the 1,2-*anti* relationship between C_{15} and C_{16} through the use of *E* boron enolates;[5] however, control of the incipient C_{15}-hydroxyl configuration was a concern. Because each reacting partner in this proposed aldol reaction has stereocenters that can potentially influence the stereochemical outcome of the reaction, the stereochemical preferences of each fragment were separately examined.

An investigation of the intrinsic diastereofacial bias of the *E* boron enolate derived from **1** indicated that remote chirality on **1** would not significantly influence the stereochemical outcome of the proposed aldol union.[6] In contrast, treatment of model aldehyde **2a** with the *E* boron enolate of 3-pentanone gave the corresponding Felkin *anti* aldol adduct in 97:3 diastereoselectivity [Eq. (1); the *dr* value gives the ratio

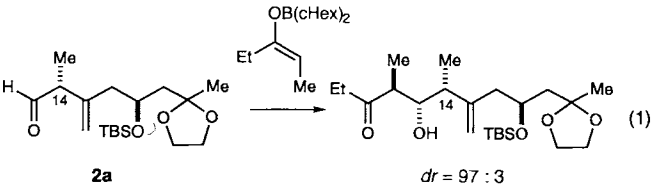

(1)

of the given isomer to all other isomers].[7] Control experiments demonstrate that *E* substituted boron enolates [Eq. (2)] exhibit enhanced Felkin selectivities in additions to chiral α-substituted aldehydes relative to their unsubstituted counterparts [Eq. (3)]. This increased selectivity can be

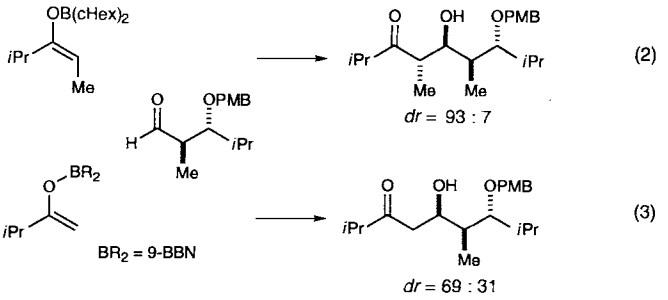

(2)

(3)

attributed to destabilization of the Felkin *anti* transition state by a developing *syn* pentane interaction [Eq. (4)].[8]

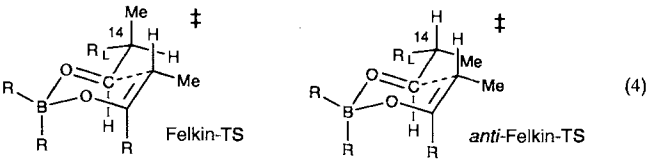

(4)

In the event, selective formation of the *E* boron enolate of ethyl ketone **1** with dicyclohexylchloroborane,[9] followed by the addition of aldehyde **2**[10] afforded a 9:1 mixture of product diastereomers (Scheme 1) favoring the desired Felkin adduct **3a** (70%). At this point in the synthesis, incorporation of the C_5 and C_{15} acetate residues present in the altohyrtin structure was addressed. Selective desilylation of **3a** at C_1 and C_5 with buffered HF·pyridine proceeded in good yield to give triol **3b** (78%).[11] Selective monoacetylation at the C_1-hydroxyl with methoxyacetic anhydride was followed by bis(acylation) at C_5 and C_{15} with acetic anhydride to afford **4** (89%). The selection of the methoxyacetyl residue for interim protection of the C_1 (carboxyl) terminus was made after difficulties were encountered in the selective hydrolysis of the corresponding C_1 acetate, which required extended reaction times. Under these conditions significant β-elimination of the C_{15} acetate residue was noted.

 © WILEY-VCH Verlag GmbH, D-69451 Weinheim, 1997 0570-0833/97/3624-2745 $ 17.50+.50/0

Refunctionalization of the C_1-C_{28} bis(spiroketal) **4** in preparation for the Wittig reaction was then undertaken. Removal of the C_{28} trityl ether with Me_2AlCl[12] under carefully controlled conditions afforded the corresponding alcohol,[13] which was oxidized with the Dess–Martin periodinane to give aldehyde **5**, the substrate required for the projected Wittig reaction. The requisite phosphonium salt **7** was prepared from EF-bis(pyran) benzyl ether **6**[2] (Scheme 2) by successive debenzylation (LDBB, 96%), mesylation (MsCl, Et_3N, 99%), sodium iodide displacement (NaI, acetone, 94%), and displacement by triphenylphosphane (PPh_3, MeCN, 91%). Deprotonation of **7** (1.26 equiv) with LiHMDS followed by addition of aldehyde **5** provided the desired Wittig product **8** in 64% yield (>95:5 *Z*:*E*).[14] Removal of the methoxyacetate C_1 protecting group was accomplished with NH_3/MeOH in 82% yield. While hydrolysis of the secondary acetates at C_5 and C_{15} was not observed, a minor by-product resulting from β-elimination of the C_{15}

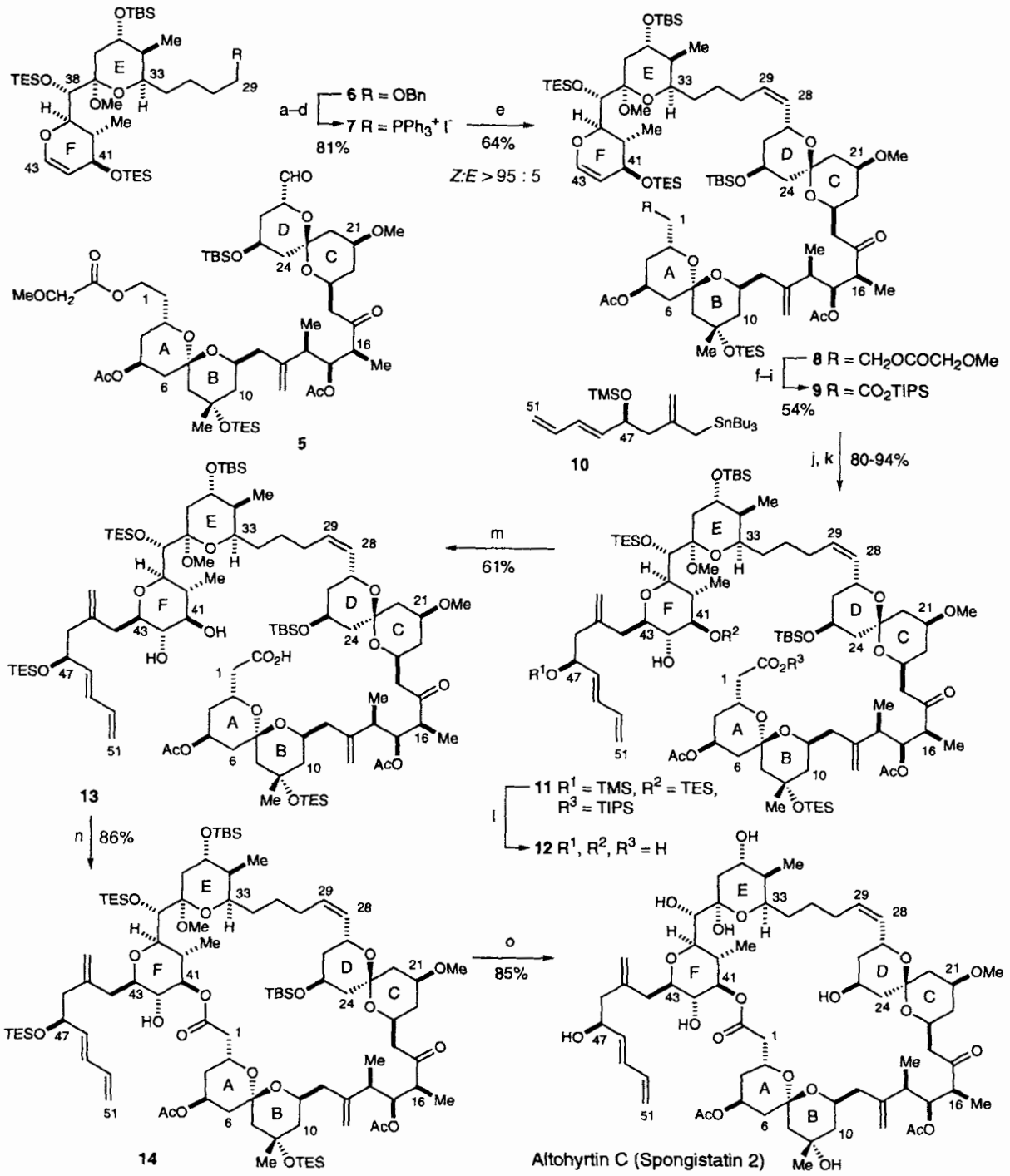

Scheme 2. Final assembly: a) LDBB, THF, −78°C; b) MsCl, Et_3N, CH_2Cl_2; c) NaI, $NaHCO_3$, Na_2SO_3, acetone; d) PPh_3, CH_3CN; e) LiHMDS, THF, −78°C, then **5**, −20°C; f) NH_3, MeOH; g) Dess–Martin periodinane, pyridine, CH_2Cl_2; h) $NaClO_2$, 2-methyl-2-butene, ethyl-1-propenyl ether, *t*BuOH, pH 5.5; i) TIPSCl, Et_3N, THF; j) dimethyldioxirane, acetone, CH_2Cl_2; k) 16 equiv of **10**, 2 equiv of Bu_3SnOTf, −78°C; l) HF·pyridine, pyridine, THF, 0°C; m) TESCl, imidazole, CH_2Cl_2, 0°C (61% from **11**); n) 2,4,6-trichlorobenzoyl chloride, iPr_2NEt, benzene, then DMAP, benzene, reflux; o) HF, H_2O, MeCN. (See ref. [4] for abbreviations.)

 © WILEY-VCH Verlag GmbH, D-69451 Weinheim, 1997 0570-0833/97/3624-2746 $ 17.50+.50/0

ester was isolated. Dess–Martin oxidation (92%) followed by buffered Kraus oxidation[2] and silyl protection (TIPSCl, Et_3N) provided TIPS ester **9** (72%, two steps).

At this stage, introduction of the $C_{44}-C_{51}$ side chain was undertaken. Epoxidation of the $C_{42}-C_{43}$ dihydropyran was accomplished with complete chemo- and stereoselectivity (as judged by ^1H NMR analysis) by addition of approximately 1.5 equivalents of dimethyldioxirane. Immediate treatment of the resulting epoxide with allylstannane **10**[2] (16 equiv) and tributylstannyl triflate (2 equiv) afforded the desired adduct **11**, comprising the full altohyrtin carbon skeleton, in 80–94% yield of isolated product as a single diastereomer. The excess allylstannane was recovered in quantitative yield after column chromatography.

As a prelude to macrocycle formation, a complex series of silyl deprotection operations on ester **11** was implemented. Treatment of this intermediate with buffered HF·pyridine (THF, 0°C), afforded selective deprotection of the TIPS ester at the C-terminus, the C_{47} TMS ether, and the C_{41} TES ether,[15] while retaining the four silyl protecting groups at C_9, C_{25}, C_{35}, and C_{38} (Scheme 2). Subjection of acid triol **12** to Yamaguchi macrolactonization conditions (2,4,6-trichlorobenzoyl chloride, iPr_2NEt, DMAP)[16] provided a product tentatively identified as the desired cyclization product bearing a trichlorobenzoyl group at the C_{47} oxygen. Accordingly, selective protection of acid triol **12** at the C_{47} hydroxyl was performed prior to macrolactonization to give TES ether **13** (TESCl, imidazole, 0°C, 61% from **11**).[17]

Exposure of **13** to Yamaguchi conditions provided a single regioisomeric lactone **14** in 86% yield. Deprotection (HF/H_2O/MeCN) provided the desired natural product, which was isolated in 85% yield after reverse phase HPLC. The regiochemical outcome of the macrocyclization was unambiguously established by observation of the coupling patterns among the $C_{40}-C_{44}$ protons in the COSY spectrum of the deprotected compound ([D_6]DMSO). This allowed an unambiguous assignment of resonances of hydrogen atoms at the C_{41} and C_{42} atoms; both the diagnostic downfield shift of the $C_{41}H$ resonance ($\delta = 4.68$ for $C_{41}H$, 3.04 for $C_{42}H$) and the presence of a $C_{42}H-C_{42}OH$ coupling verified that macrolactonization had occurred at the C_{41}-hydroxyl group. Our observation that the seco acid **13**, carrying an unprotected hydroxyl function at C_{42}, may be cyclized directly to the macrolactone **14** simplifies the later stages of the synthesis plan. The motivation for attempting this cyclization as part of the original plan was based on the conviction that any protecting group appended to the C_{42}-hydroxyl would add sufficient steric hindrance to the C_{41}-hydroxyl group to impair the macrolactonization process.

The synthetic material was identical to a sample of natural spongistatin 2[18] as judged by ^1H NMR (500 MHz, CD_3CN), HPLC, electrospray mass spectroscopy, and ultraviolet spectroscopy. Comparison of optical rotations confirmed that the synthetic and natural compounds possessed the same absolute stereochemistry (synthetic: $[\alpha]_D^{24}$ +21.3° ($c = 0.03$ in MeOH); natural: $[\alpha]_D^{24}$ +29.2° ($c = 0.12$ in MeOH)). Further, detailed comparison of one-dimensional ^1H NMR and two-dimensional COSY spectra (500 MHz, [D_6]DMSO) confirmed that our synthetic material was also identical to natural altohyrtin C.[19] We thus conclude that spongistatin 2 and altohyrtin C are identical compounds and speculate that the altohyrtin stereochemical assignment can be extended to the remaining members of the spongipyran family.

The route to altohyrtin C outlined here should be readily applicable to the side-chain congeners altohyrtin A (spongistatin 1) and altohyrtin B,[3] with dihydropyran **9** serving as a common intermediate for the synthesis of these compounds and additional unnatural analogues.[20]

Received: October 22, 1997 [Z11067IE]
German version: *Angew. Chem.* **1997**, *109*, 2957–2961

Keywords: altohyrtin · antitumor agents · natural products · spongistatin · total synthesis

[1] D. A. Evans, P. J. Coleman, L. C. Dias, *Angew. Chem.* **1997**, *109*, 2951–2954; *Angew. Chem. Int. Ed. Engl.* **1997**, *36*, 2738–2741.
[2] D. A. Evans, B. W. Trotter, B. Côté, P. J. Coleman, *Angew. Chem.* **1997**, *109*, 2954–2957; *Angew. Chem. Int. Ed. Engl.* **1997**, *36*, 2741–2744.
[3] Representative IC_{50} values against tumor cell lines: a) M. Kobayashi, S. Aoki, K. Gato, I. Kitagawa, *Chem. Phar. Bull.* **1996**, *44*, 2142–2149: altohyrtin A (X = Cl) 0.01 ng mL^{-1}, altohyrtin B (X = Br) 0.02 ng mL^{-1}, altohyrtin C (X = H) 0.40 ng mL^{-1}; b) R. Bai, G. F. Taylor, Z. A. Cichacz, C. L. Herald, J. A. Kepler, G. R. Pettit, E. Hamel, *Biochemistry* **1995**, *34*, 9714–9721: spongistatin 1 (X = Cl) 0.13 nM, spongistatin 2 (X = H) 0.85 nM.
[4] Abbreviations: dr = diastereomer ratio, 9-BBN = 9-borabicyclo[3.3.1]nonane, cHex = cyclohexyl, TIPS = triisopropylsilyl, TBS = *tert*-butyldimethylsilyl, TES = triethylsilyl, TMS = trimethylsilyl, Tr = trityl = triphenylmethyl, Tf = trifluoromethanesulfonyl, Bn = benzyl, LDBB = lithium di-*tert*-butylbiphenyl, DMAP = 4-dimethylaminopyridine, MsCl = methanesulfonyl chloride, LiHMDS = lithium hexamethyldisilazide.
[5] D. A. Evans, E. Vogel, J. V. Nelson, *J. Am Chem. Soc.* **1979**, *101*, 6120–6123.
[6] Reaction of the *E* boron enolate derived from **1** with isobutyraldehyde gave low stereoinduction (2:1).
[7] High levels of 1,2-diastereoselection in the addition of various nucleophiles to α-methyl-β-methylene substrates are precedented: a) F. Sato, Y. Takeda, H. Uchiyama, Y. Kobayashi, *J. Chem Soc. Chem. Commun.* **1984**, 1132–1134; b) F. Sato, M. Kusakabe, Y. Kobayashi, *ibid.* **1984**, 1130–1131; c) F. Sato, M. Kusakabe, T. Kato, Y. Kobayashi, *ibid.* **1984**, 1331–1332.
[8] a) D. A. Evans, J. L. Duffy, M. J. Dart, unpublished results; b) D. A. Evans, J. V. Nelson, T. Taber, in *Topics in Stereochem.* **1982**, *13*, pp. 1–115; c) W. R. Roush, *J. Org. Chem.* **1991**, *56*, 4151–4157.
[9] K. Ganesan, H. C. Brown, *J. Org. Chem.* **1993**, *58*, 7162–7169.
[10] Aldehyde **2** was used directly in these experiments without purification. Exposure of **2** to silica gel led to isomerization to the α,β-unsaturated aldehyde.
[11] The desilylation was interrupted before completion. Some monodesilylated material (hydroxy group at C_5) was recovered (15%).
[12] For removal of trityl ethers with Et_2AlCl see H. Köster, N. D. Sinha, *Tetrahedron Lett.* **1982**, *23*, 2641–2644.
[13] The use of aqueous Rochelle's salt in the isolation was essential for removing the organoaluminum salts prior to concentration; otherwise, residual aluminum-promoted spiroketal isomerization to the undesired diaxial anomer took place.
[14] Unchanged aldehyde **5** (11%) was also recovered in diastereomerically pure form.
[15] The moderate yield for this transformation may be partly due to difficulties in isolating the polar acid triol on small scale. TLC analysis of the reaction suggests a clean and selective transformation.
[16] J. Inanaga, K. Hirata, H. Saeki, T. Katsuki, M. Yamaguchi, *Bull. Chem. Soc. Jpn.* **1979**, *52*, 1989–1993.
[17] The initial product of the reaction is the corresponding C_1 TES ester, which is cleaved during purification on silica gel.
[18] We thank Professor G. R. Pettit for providing a natural sample of spongistatin 2.
[19] We thank Professor M. Kobayashi for providing copies of spectra of natural altohyrtin C.
[20] While addition of the side chain at an even later stage may be possible, preliminary investigations of an alternative route involving lactonization of the dihydropyran seco acid corresponding to **9** and subsequent side-chain addition suggest that the epoxidation/allylstannane addition sequence may be more difficult.

 © WILEY-VCH Verlag GmbH, D-69451 Weinheim, 1997 0570-0833/97/3624-2747 $ 17.50+.50/0

Artificial Anthraquinone–Carbohydrate Hybrids: Design, Synthesis, DNA Binding, and Cytotoxicity**

Kazunobu Toshima,* Hiromi Ouchi, Yoriko Okazaki, Takaaki Kano, Makoto Moriguchi, Akira Asai, and Shuichi Matsumura

Novel DNA-binding molecules, particularly those with high efficiency and sequence-specificity, are very interesting from the chemical and biological standpoint and offer considerable potential in medicine.[1-7] The design and synthesis of artificial molecules that exhibit such interactions with DNA is therefore an important goal in contemporary chemistry. Certain clinically important antitumor antibiotics such as anthracyclines,[8] aureolic acids,[9] and pluramycins,[10] which strongly bind to DNA in a sequence-selective manner, have already been found in nature (Scheme 1). Although these various agents have been regarded as belonging to distinct classes of antibiotics, from a chemical standpoint they are commonly found to contain arene and carbohydrate domains. In their DNA-binding activity the aromatic moieties function as DNA intercalators, whereas the carbohydrate residues bind to the DNA grooves. Even the active forms of enediyne antibiotics, which efficiently cleave DNA, can be viewed as aromatic–carbohydrate hybrids.[1] Based on these facts concerning compounds of natural origin, we considered the possibility of creating artificial DNA-binding molecules that consist of aromatic and carbohydrate domains. In this communication we discuss the molecular design, chemical synthesis, DNA-binding properties, and cytotoxicity of the novel and artificial anthraquinone–carbohydrate hybrids **1**–**4**.[11]

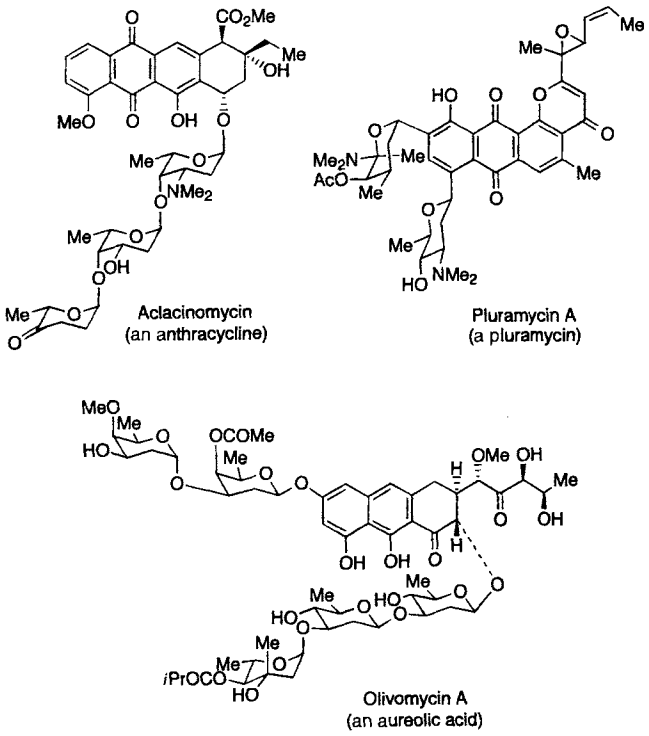

Scheme 1. Representative naturally occurring DNA-binding antitumor antibiotics constructed from arene and carbohydrate building blocks.

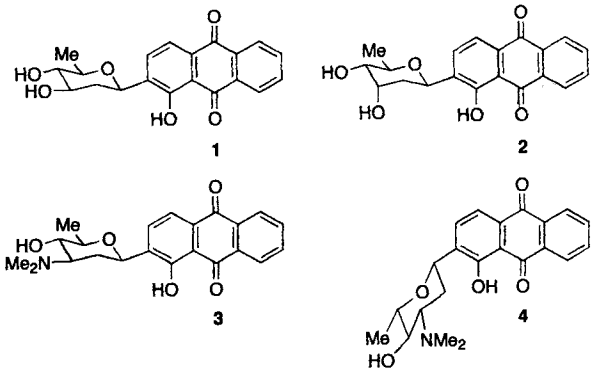

In our approach to DNA-binding hybrids we selected anthraquinone as the aromatic building block, because this is an aromatic skeleton present in many DNA-binding antitumor antibiotics. Certain 2,6-dideoxy sugars seemed appropriate as the carbohydrate source, since these are also found in many naturally occurring DNA-binding antitumor antibiotics, and the hydrophobicity[12-14] of 2,6-dideoxy sugars appeared advantageous for binding to the DNA groove.

The anthraquinone–carbohydrate hybrids **1**–**4** were synthesized by a short reaction sequence. The key step is an aryl C-glycosylation reaction with an unprotected sugar, recently developed in our laboratory (Scheme 2).[15] Aryl C-glycosylation of 9,10-dimethoxy-1-hydroxyanthracene (**5**) and the unprotected 2,6-dideoxy sugars D-olivose (**6**) and D-digitoxose (**7**) in the presence of a catalytic amount of trimethylsilyl trifluoromethanesulfonate (TMSOTf)/silver perchlorate in MeCN proceeded at room temperature to afford the unprotected aryl β-C-glycosides **10** and **11**, respectively, in a regio- and stereospecific fashion. Analogous transformations of **5** with **8** or its enantiomer **9** under TMSOTf catalysis in CH_2Cl_2 at 40 °C gave regio- and stereospecifically the unprotected aryl β-C-glycoside **12** and its enantiomer **13**, respectively. Subsequent oxidation of glycosides **10**–**13** with cerium(IV) ammonium nitrate (CAN) in MeCN/H_2O at −17 °C furnished the desired anthraquinone–carbohydrate hybrids **1**–**4**.

The DNA-binding characteristics of **1**–**4** were first assayed by the DNase I footprinting method with double-stranded M13mp18 DNA singly labeled with ^{32}P at the 5′ end. In the case of hybrids **1** and **2**, which both contain neutral sugars, no significant change from the cleavage pattern of the control was observed. By contrast, the cleavage patterns differ substantially from the control experiment with hybrids **3** and **4**, both of which contain an amino sugar, since cleavage in the 5′-TGC regions by DNase I is significantly diminished (Figure 1). This demonstrates convincingly that hybrids **3** and **4** bind to DNA in a sequence-selective fashion.[16] Interestingly, the DNA-binding ability of D-amino sugar hybrid **3** is stronger than that of L-amino sugar hybrid **4**. Furthermore, no

[*] Prof. Dr. K. Toshima, H. Ouchi, Y. Okazaki, T. Kano, M. Moriguchi, Prof. Dr. S. Matsumura
Department of Applied Chemistry, Faculty of Science and Technology
Keio University
3-14-1 Hiyoshi, Kohoku-ku, Yokohama 223 (Japan)
Fax: Int. code +(45)563-0446
e-mail: toshima@applc.keio.ac.jp
Dr. A. Asai
Tokyo Research Laboratories, Kyowa Hakko Kogyo Co., Ltd. Tokyo (Japan)

[**] This research was partially supported by a Grant-in-Aid for Scientific Research on Priority Area No. 08219236 from the Ministry of Education, Science, Sports, and Culture, Japan. We thank Mr. Naoyuki Hiraoka (Tokyo Research Laboratories, Kyowa Hakko Kogyo Co., Ltd.) for his skillful technical assistance.

 © WILEY-VCH Verlag GmbH, D-69451 Weinheim, 1997 0570-0833/97/3624-2748 $ 17.50+.50/0

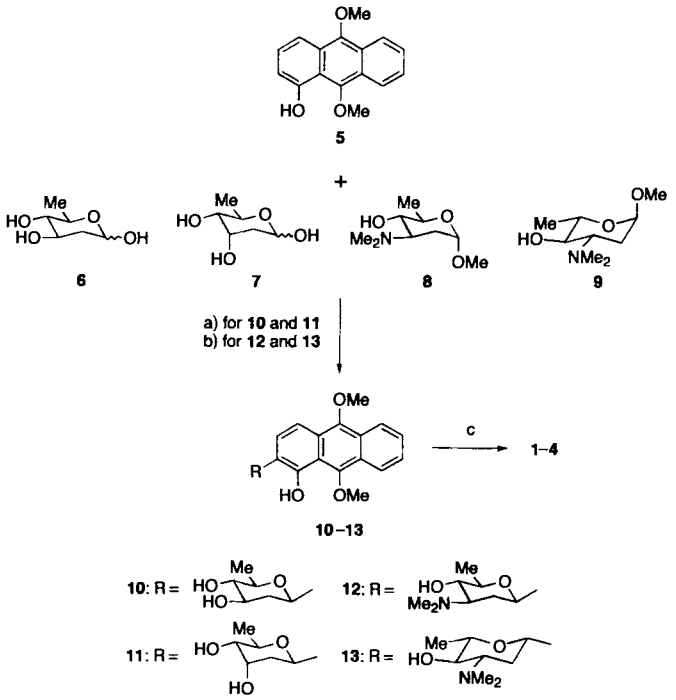

Scheme 2. Synthesis of **1**–**4**. a) TMSOTf (0.2 equiv), $AgClO_4$ (0.2 equiv), MeCN, 25 °C, 0.5 h, 75% (**10**), 25% (**11**); b) TMSOTf (1.2 equiv), CH_2Cl_2, 40 °C, 18 h, 63% (**12**), 64% (**13**); c) CAN (2.5 equiv), $MeCN/H_2O$, −17 °C, 0.5 h, 42% (**1**), 36% (**2**), 44% (**3**), 44% (**4**).

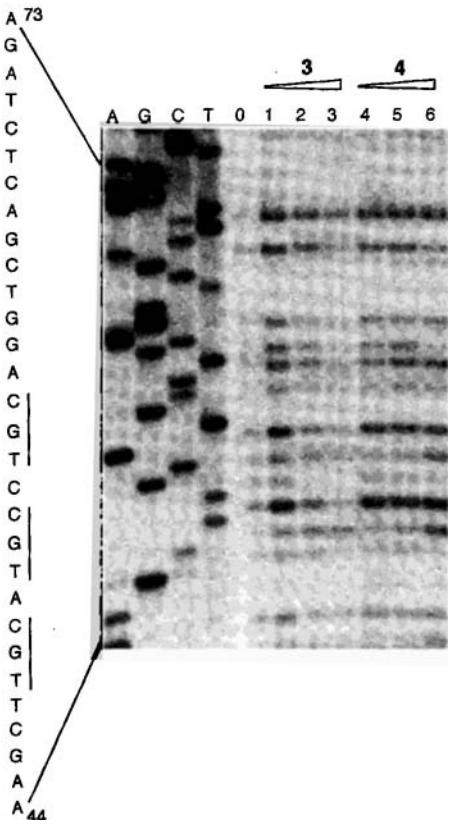

Figure 1. DNase I footprinting of 5'-end labeled M13mp18ds DNA bound to the hybrids **3** and **4**. DNase I digestion was carried out at room temperature for 1 min. Samples were assayed by electrophoresis on 15% polyacrylamide/8 M urea slab gel (bases 44–73 are shown). Lanes A, G, C and T: Sanger reactions of A, G, C and T, respectively; lane 0: control in the absence of added chemicals; lanes 1–6: **3** (20, 200, 2000 μM), **4** (20, 200, 2000 μM).

DNA binding could be demonstrated for the components of hybrid **3**, 1-hydroxyanthraquinone and amino sugar **8**, based on the DNase I footprinting assay. These results clearly indicate the importance of the hybrid structure constructed from anthraquinone and the amino sugar for DNA binding.

Confirmation that hybrids **3** and **4** bind to DNA with intercalation was obtained from a DNA unwinding assay with linearized pBR322 DNA and T4 DNA ligase.[17] The DNA intercalator first unwinds linearized DNA, which results in a change in the amount of twist in the double helix. Through formation by T4 ligase of a cyclic DNA from DNA bound to the intercalating compound, the linking number of the unwound DNA is frozen. Removal of the intercalating compound results in restoration of the normal degree of twist, while the linking number remains constant. This in turn leads to the introduction of negative superhelicity into the DNA. Figure 2 shows the product separation on an agarose gel for the DNA unwinding assay with DNA-binding hybrids **3** and **4**. Control DNA molecules appear as a lightly positively supercoiled population of topoisomers (lane 2). Upon ligation in the presence of an increasing concentration of intercalator, the molecular population becomes increasingly negatively supercoiled relative to the control. On the gel the topoisomers initially appear more relaxed and then progressively more negatively supercoiled. Under these assay conditions, **3** and **4** converted the topoisomers into more relaxed forms at low concentration and then to the completely negatively supercoiled form at high concentration. Furthermore, the intercalation potential of **3** is about five times greater than that of **4**. This result demonstrates that DNA intercalation activity is definitely dependent on the configuration of the sugar moiety in the hybrid.

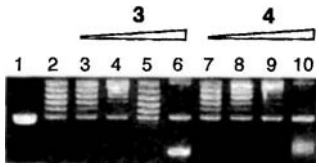

Figure 2. Effects of **3** and **4** on a DNA unwinding assay with T4 ligase. Unwinding mesurements were carried out as described in ref. [17]. Linearized plasmid DNA was incubated with T4 DNA ligase in the presence of the hybrids at various concentrations. Hybrid-induced DNA unwinding was detected on an agarose gel containing no ethidium bromide. Lane 1: linear DNA; lane 2: control in the absence of added chemicals; lanes 3–10: **3** (0.4, 2.0, 10, 50 μM), **4** (0.4, 2.0, 10, 50 μM).

The cytotoxicity of DNA-binding hybrids **3** and **4** was examined by using HeLa S3 cells exposed to each agent for 72 h.[18] The IC_{50} values of **3** and **4** were 9 and 58 μM, respectively. Hybrid **3** was about six times more cytotoxic than **4**, a result which is undoubtedly associated with the fivefold greater intercalation potential of **3** than of **4**. The cytotoxic activity of the anthraquinone–carbohydrate hybrids is thus correlated with their capacity to bind DNA.[19]

The present work demonstrates not only the molecular design and chemical synthesis of novel anthraquinone–carbohydrate hybrids, but also their DNA-binding profiles and cytotoxic activities. It has been shown that even a simple designed molecule can have strong DNA-binding properties in a sequence-selective fashion. The chemistry and biological evaluation presented provide significant information about the molecular design of novel and artificial DNA binding agents based on an intercalator–carbohydrate hybrid system.

Received: June 16, 1997
Revised version: August 11, 1997 [Z10548IE]
German version: *Angew. Chem.* **1997**, *109*, 2864–2866

Keywords: anthraquinones · carbohydrates · DNA hybrids · DNA recognition · intercalations

[1] a) K. C. Nicolaou, W.-M. Dai, *Angew. Chem.* **1991**, *103*, 1453–1481; *Angew. Chem. Int. Ed. Engl.* **1991**, *30*, 1387–1416; b) K. C. Nicolaou, A. L. Smith, E. W. Yue, *Proc. Natl. Acad. Sci. USA* **1993**, *90*, 5881–5888; c) K. C. Nicolaou, A. L. Smith, *Acc. Chem. Res.* **1992**, *25*, 497–503.

[2] a) P. B. Dervan in *Nucleic Acids and Molecular Biology, Vol. 2* (Eds.: F. Eckstein, D. M. J. Lilley), Springer, Heidelberg, **1988**, pp. 49–64; b) P. B. Dervan in *Oligodeoxynucleotides: Antisense of Gene Expression* (Ed.: J. S. Cohen), CRC, Boca Raton, FL, **1989**, pp. 197–210.

[3] J. W. Lown, *Chemtracts: Org. Chem.* **1993**, *6*, 205–237.

[4] a) P. E. Nielsen, *Bioconjugate Chem.* **1991**, *2*, 1–12; b) P. E. Nielsen, *Chem. Eur. J.* **1997**, *3*, 505–508.

[5] E. Uhlmann, A. Peyman, *Chem. Rev.* **1990**, *90*, 543–584.

[6] C. Helene, J.-J. Toulme in *Oligodeoxynucleotides: Antisense of Gene Expression* (Ed.: J. S. Cohen), CRC, Boca Raton, FL, **1989**, pp. 137–172.

[7] O. Kennard, *Pure Appl. Chem.* **1993**, *65*, 1213–1222.

[8] a) F. Arcamone in *Doxorubicin Anticancer Antibiotics. Medicinal Chemistry Series of Monographs, Vol. 17* (Ed.: G. Stevens), Academic Press, New York, **1981**; b) *Anthracycline and Anthracenedione Based Anticancer Agents* (Ed.: J. W. Lown), Elsevier, Amsterdam, **1988**.

[9] J. D. Skarbek, M. K. Speedie in *Antitumor Compounds of Natural Origin: Chemistry and Biochemistry* (Ed.: A. Aszalos), CRC, Boca Raton, FL, **1981**, pp. 191–235.

[10] M. R. Hansen, L. H. Hurley, *Acc. Chem. Res.* **1996**, *29*, 249–258.

[11] a) D. J. Mincher, G. Shaw, E. D. Clercq, *J. Chem. Soc. Perkin Trans. 1* **1983**, 613–618; b) D. J. Mincher, G. Shaw, *ibid.* **1984**, 1279–1282.

[12] S. Walker, K. G. Valentine, D. Kahne, *J. Am. Chem. Soc.* **1990**, *112*, 6428–6429.

[13] W. Ding, G. A. Ellestad, *J. Am. Chem. Soc.* **1991**, *113*, 6617–6620.

[14] M. Uesugi, Y. Sugiura, *Biochemistry* **1993**, *32*, 4622–4627.

[15] K. Toshima, G. Matsuo, M. Nakata, *J. Chem. Soc. Chem. Commun.* **1994**, 997–998.

[16] a) J. B. Chaires, W. Priebe, D. E. Graves, T. G. Burke, *J. Am. Chem. Soc.* **1993**, *115*, 5360–5364; b) J. B. Chaires, S. Satyanarayana, D. Suh, I. Fokt, T. Przewloka, W. Priebe, *Biochemistry* **1996**, *35*, 2047–2053.

[17] a) G. Camilloni, F. D. Seta, R. Negri, A. G. Ficca, E. D. Mauro, *EMBO J.* **1986**, *5*, 763–771; b) Y. Yamashita, S. Kawada, N. Fujii, H. Nakano, *Biochemistry* **1991**, *30*, 5838–5845.

[18] D. A. Scudiero, R. H. Shoemaker, K. D. Paull, A. Monks, S. Tierney, T. H. Nofziger, M. J. Currens, D. Seniff, M. R. Boyd, *Cancer Res.* **1988**, *48*, 4827–4833.

[19] *Anthracycline Antibiotics* (Ed.: W. Priebe), American Chemical Society, Washington DC, **1995** (*ACS Symp. Ser. 574*).

Synthesis of Optically Active Butenolides and γ-Lactones by the Sharpless Asymmetric Dihydroxylation of β,γ-Unsaturated Carboxylic Esters**

Christian Harcken and Reinhard Brückner*

The Sharpless asymmetric dihydroxylation ("AD") of olefins is an indispensable tool for contemporary organic synthesis.[1] Frequently, the obtained 1,2-diols are not yet the desired target molecules. Rather, they are so profoundly modified by follow-up reactions that it may no longer be clear from the structures of the final products how well an AD served in their construction. The present study reveals that enantiomerically pure or enantiomerically enriched γ-chiral butenolides and γ-chiral γ-lactones—for which many syntheses are known, but more efficient ones are continuously being sought[2,3]—must be considered interesting products of the AD, too (Scheme 1). Specifically, ADs of β,γ-unsaturated esters **4** provided (in accordance with the scarce literature precedence[4,5]) lactonized dihydroxylation products, that is,

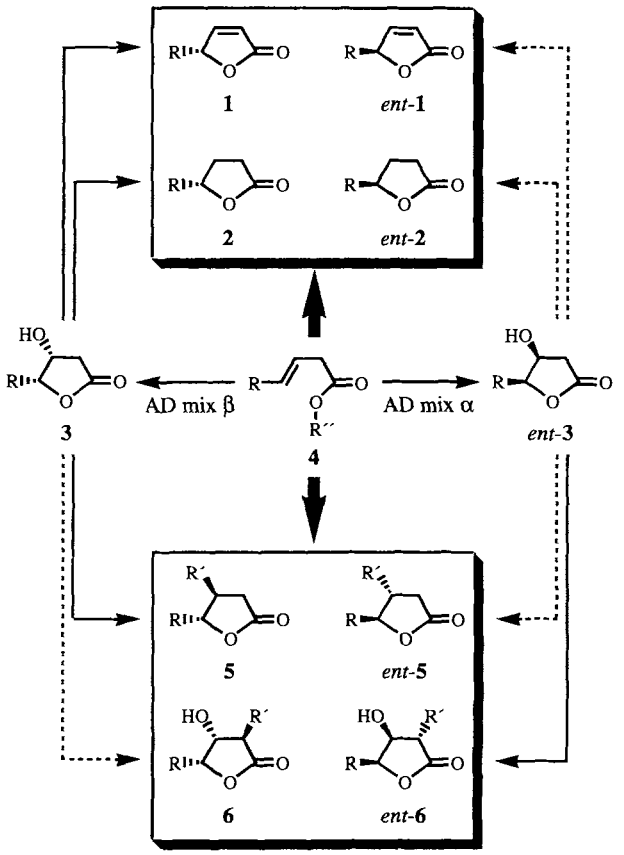

Scheme 1. Furanone derivatives accessible in two or three steps from **4**. Concrete examples for the reactions marked with solid arrows are given in Schemes 2–5. The dashed arrows refer to analogous transformations in the respective enantiomeric series that, however, have not yet been performed.

the compounds **3** or their enantiomers *ent*-**3** (78% ≤ *ee* ≤ 97%). From these, we have prepared to date chiral butenolides **1**/*ent*-**1**, monosubstituted γ-lactones **2**/*ent*-**2**, disubstituted γ-lactones **5**/*ent*-**5**, and trisubstituted γ-lactones **6**/*ent*-**6**. The transformations used are exemplified by enantioselective syntheses of the ranunculin aglycon (**11**; 92% *ee*; Scheme 2), the pheromone dodecanolide (**16**; 95% *ee*; Scheme 3), *trans* quercus lactone (**21**; 97% *ee*; Scheme 4), and one of the *epi*-blastmycinones (**25**; 78% *ee*; Scheme 5).

Our novel approach to γ-chiral butenolides **1** on the basis of the transformation type-**4**-ester → type-**3**-lactone is shown in Scheme 2. First, the known hydroxyester **7**[6] was O-silylated

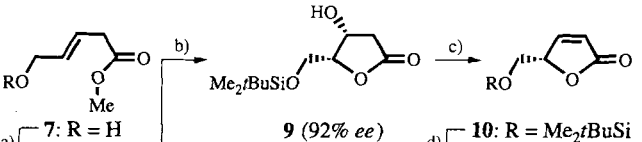

Scheme 2. a) *t*BuMe$_2$SiCl (1.5 equiv), imidazole (3.0 equiv), CH_2Cl_2, 0°C, 30 min; 84%. b) AD mix β (1.40 g per mmol of **8**), methanesulfonyl amide (1.0 equiv), *t*BuOH/H_2O (1/1), addition of **8**, 0°C, 36 h; 88%. c) NEt_3 (2.1 equiv), methanesulfonyl chloride (1.1 equiv), CH_2Cl_2, 0°C, 1 h; 72%. d) HF/pyridine complex (70%, 0.50 mL per mmol of **10**), THF, 0°C, 16 h; silica gel, 15 min; 85%.

[*] Prof. Dr. R. Brückner, Dipl.-Chem. C. Harcken
Institut für Organische Chemie der Universität
Tammannstrasse 2, D-37077 Göttingen (Germany)
Fax: Int. code + (551) 39-2944
e-mail: rbrueck@gwdg.de

[**] This work was supported by the Fonds der Chemischen Industrie, for which we are very grateful. In addition, we thank BASF AG for donating chemicals.

 © WILEY-VCH Verlag GmbH, D-69451 Weinheim, 1997 0570-0833/97/3624-2750 $ 17.50+.50/0

to form the β,γ-unsaturated ester **8**.[7] Then the compound was asymmetrically dihydroxylated by treatment with AD mix β to provide after purification by flash chromatography on silica gel[8] the *tert*-butyldimethylsilylated γ-lactone **9**[9] with 92% *ee*.[10] Mesylation with mesyl chloride/triethylamine followed by the spontaneous β-elimination of methanesulfonic acid introduced the C=C bond of the silylated butenolide **10**. Deprotection with HF/pyridine gave the ranunculin aglycon **11**.[11,12]

Our type-**4**-ester →type-**3**-lactone approach to chiral monosubstituted γ-lactones **2** is illustrated in Scheme 3 by an enantioselective synthesis of the rove beetle pheromone (+)-dodecanolide (**16**).[13] We started with a decarboxylative deconjugating Knoevenagel condensation between decanal and malonic acid; this provided the β,γ-unsaturated acid **12** predominantly as the desired *trans* isomer.[14] Four more steps (62% yield) led to the target structure **16**. They were: 1) esterification (→methyl ester **13**), 2) AD with AD mix β (→lactone **14**; 95% *ee*[10]), 3) mesylation/β-elimination (→butenolide **15**), and 4) Pd-catalyzed hydrogenation.[15]

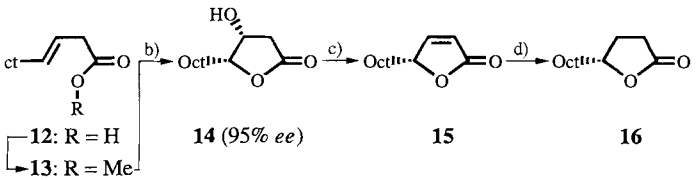

Scheme 3. a) MeOH (3.0 equiv), camphorsulfonic acid (1.0 mol%), $CHCl_3$, removal of water by azeotropic distillation, 12 h; 90%. b) AD mix β (1.40 g per mmol of **13**), methanesulfonyl amide (1.0 equiv), *t*BuOH/H_2O (1/1), addition of **13**, 0°C, 48 h; 81%. c) NEt_3 (2.1 equiv), methanesulfonyl chloride (1.1 equiv), CH_2Cl_2, 0°C, 15 min; 91%. d) Pd (10% on charcoal, 5 mol%), H_2 (3 bar), EtOAc, room temperature, 12 h; 94%.

Scheme 4 illustrates the AD-mediated type-**4**-ester →type-**3**-lactone approach to chiral disubstituted γ-lactones **5** by the hitherto shortest enantioselective synthesis[16] of *trans* quercus lactone (**21**).[17] This compound is formed in whisky barrels manufactured from oak-wood and contributes to the taste of the liquors stored therein. Acid **17**[14] was condensed with methanol and the resulting methyl ester **18** treated with AD mix β. Lactone **19** was obtained in 92% yield and with 97% *ee*.[18] Dehydration with the mesyl chloride/triethylamine mixture, which was also used in the **9**→**10** and **14**→**15** conversions, yielded butenolide **20**. Me_2CuLi added to this compound exclusively from the less hindered face, and we isolated the desired *trans*-configured 1,4-addition product **21** (the *trans* quercus lactone, also termed *trans* oak lactone or *trans* whisky lactone) and none of its *cis* isomer. The overall yield of this sequence was 47%.

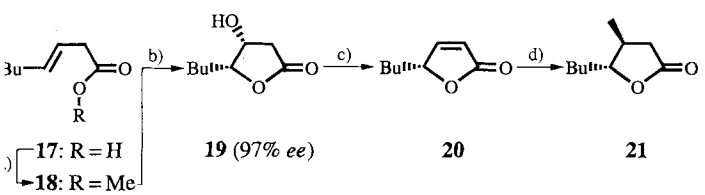

Scheme 4. a) MeOH (3.0 equiv), camphorsulfonic acid (1.0 mol%), $CHCl_3$, removal of water by azeotropic distillation, 6 h; 76%. b) AD mix β (1.40 g per mmol of **18**), methanesulfonyl amide (1.0 equiv), *t*BuOH/H_2O (1/1), addition of **18**, 0°C, 36 h; 92%. c) NEt_3 (2.1 equiv), methanesulfonyl chloride (1.1 equiv), CH_2Cl_2, 0°C, 15 min; 87%. d) CuI (1.5 equiv), Et_2O, 0°C; addition of MeLi (3.0 equiv); cooling to −78°C; addition of **20** in Et_2O, 1.5 h; 77% of **21**.

Scheme 5 shows how treatment of the commercially available methyl pentenoate **22** with AD mix α makes the type-**4**-ester →type-**3**-lactone conversion a remarkably efficient synthesis of chiral trisubstituted γ-lactones **6**. Not

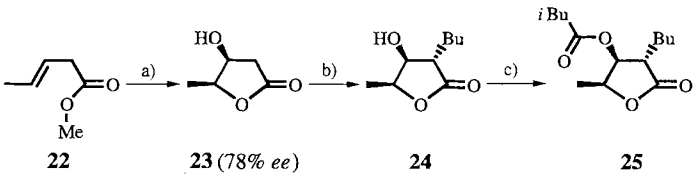

Scheme 5. a) AD mix α (1.40 g per mmol of **22**), *t*BuOH/H_2O (1/1), addition of **22**, 0°C, 5 d; 40%. b) LDA (3.0 equiv), THF, −78°C, 2 h; BuI (1.5 equiv) in THF/DMPU 1/1 (3 mL per mmol of BuI), −35°C, 20 h; 53% of **24**. c) 3-Methylbutanoyl chloride (1.5 equiv), CH_2Cl_2/pyridine 5/1, room temperature, 6 h; 83%.

unexpectedly,[19] the dihydroxylation product **23** exhibited only 78% *ee*.[10] With reference to the next step, it is known that in HMPA-containing THF (HMPA = hexamethyl phosphoric triamide) the α-alkylation of dilithiated β-hydroxy-γ-lactones akin to compound **23** occurs such that the α-substituent is oriented almost exclusively *trans* with respect to the β-OH group.[20] We were pleased to find that in 4:1 THF/DMPU[21] (DMPU = dimethylpropyleneurea) the butylation of the dilithiated β-hydroxylactone **23** itself also delivered only the *trans*-alkylated lactone **24** (53% yield) and no *cis* isomer at all. Acylation with isovaleroyl chloride led to the isovalerate **25**. As an epimer of blastmycinone, the antimycin A_3 degradation product, compound **25** had previously been synthesized several times, but with less rigorous stereocontrol.[22]

Several other AD-mediated butenolide and butyrolactone syntheses that exploit the ready availability of type-**4** esters[14] and employ type-**4**-ester →type-**3**-lactone conversions are under investigation in our laboratory.

Received: July 18, 1997 [Z10702IE]
German version: *Angew. Chem.* **1997**, *109*, 2866–2868

Keywords: asymmetric synthesis · butenolides · dihydroxylations · furanones · lactones

[1] Recent reviews: a) H. C. Kolb, M. S. VanNieuwenhze, K. B. Sharpless, *Chem. Rev.* **1994**, *94*, 2483–2547; b) G. Poli, C. Scolastico, *Methoden Org. Chem. (Houben-Weyl) 4th ed. 1952-*, Vol. E21e, pp. 4547–4598.

[2] Recent syntheses of nonracemic γ-chiral butenolides: a) B. Figadère, J.-F. Peyrat, A. Cavé, *J. Org. Chem.* **1997**, *62*, 3428–3429; b) J. A. Marshall, M. A. Wolf, E. M. Wallace, *ibid.* **1997**, *62*, 367–371; c) A. van Oeveren, B. L. Feringa, *ibid.* **1996**, *61*, 2920–2921.

[3] Recent syntheses of nonracemic γ-chiral γ-lactones: a) W.-Y. Yu, C. Bensimon, H. Alper, *Chem. Eur. J.* **1997**, *3*, 417–423; b) T. Chevtchouk, J. Ollivier, J. Salaün, *Tetrahedron: Asymmetry* **1997**, *8*, 1011–1014; c) A.-M. Fernandez, J.-C. Plaquevent, L. Duhamel, *J. Org. Chem.* **1997**, *62*, 4007–4014; d) S.-i. Fukuzawa, K. Seki, M. Tatsuzawa, K. Mutoh, *J. Am. Chem. Soc.* **1997**, *119*, 1482–1483.

[4] Z.-M. Wang, X.-L. Zhang, K. B. Sharpless, S. C. Sinha, A. Sinha-Bagchi, E. Keinan, *Tetrahedron Lett.* **1992**, *33*, 6407–6410 describe three examples each for the **4**→**3** and **4**→*ent*-**3** conversion (R = Et, Hex, Ph; *ee* 92% to >99%).

[5] Y. Miyazaki, H. Hotta, F. Sato, *Tetrahedron Lett.* **1994**, *35*, 4389–4392 effected a **4**→**3** conversion for R = $SiMe_3$ with 86% *ee*.

[6] C. S. Pak, E. Lee, G. H. Lee, *J. Org. Chem.* **1993**, *58*, 1523–1530.

[7] All new compounds gave satisfactory ^1H NMR spectra (300 MHz, $CDCl_3$), IR spectra (KBr), and combustion analyses.

[8] W. C. Still, M. Kahn, A. Mitra, *J. Org. Chem* **1978**, *43*, 2923–2925.

[9] Typical procedure for obtaining type-**3** γ-lactones from deconjugated esters **4**: [18].

 © WILEY-VCH Verlag GmbH, D-69451 Weinheim, 1997 0570-0833/97/3624-2751 $ 17.50+.50/0

[10] Optical purity determined by chiral capillary gas chromatography on heptakis-(2,6-di-*O*-methyl-3-*O*-pentyl-β-cyclodextrin/OV1701 (1/4, 25 m column); 70 kPa H_2, isothermal. R_T values of AD-based product (or the derived butenolide) and of its enantiomer (as observed in the corresponding racemic mixture): **10** 50.5 min (110°C; enantiomer 51.4 min); **15** 53.6 min (130°C; enantiomer 54.8 min); **23** 45.4 min (110°C; enantiomer 44.3 min).
[11] Stereostructure: R. Hill, R. van Heyningen, *Biochem. J.* **1951**, *49*, 332–335.
[12] Selected syntheses of levorotatory ranunculin aglycon: a) P. Camps, J. Cardellach, J. Font, R. M. Ortuño, O. Ponsati, *Tetrahedron* **1982**, *38*, 2395–2402 (from D-ribonolactone in two steps); b) B. Häfele, V. Jäger, *Liebigs Ann. Chem.* **1987**, 85–87, J. Mann, N. K. Partlett, A. Thomas, *J. Chem. Res. (S)* **1987**, 369 (from 1,2:5,6-di-*O*-isopropylidene-D-mannitol in three steps); c) K. Koseki, T. Ebata, H. Kawakami, H. Matsushita, Y. Naoi, K. Itoh, *Heterocycles* **1990**, *31*, 423–426 (from levoglucosenone in three steps); d) S. Takano, A. Kurotaki, M. Takahashi, K. Ogasawara, *Synthesis* **1986**, 403–406; G. A. Danilova, V. I. Mel'nikova, K. K. Pivnitsky, *Tetrahedron Lett.* **1986**, *27*, 2489–2490 (from 1,2:5,6-di-*O*-isopropylidene-D-mannitol in six steps); e) O. Yamada, K. Ogasawara, *Synthesis* **1995**, 1291–1294 (from *cis*-2-butene-1,2-diol in eleven steps); f) J. A. J. M. Vekemans, G. A. M. Franken, G. J. F. Chittenden, E. F. Godefroi, *Tetrahedron Lett.* **1987**, *28*, 2299–2300 (*O*-acetyl-**11**; from D-ribonolactone in two steps); g) S. Hanessian, P. J. Murray, S. P. Sahoo, *ibid.* **1985**, *26*, 5627–5630 (*O*-*tert*-BuPh$_2$Si-**11**; from L-glutamic acid in five steps).
[13] Stereostructure: J. W. Wheeler, G. M. Happ, J. Araujo, J. M. Pasteels, *Tetrahedron Lett.* **1972**, 4635–4638.
[14] Prepared in one step by the general procedure of N. Ragoussis, *Tetrahedron Lett.* **1987**, *28*, 93–96.
[15] Selected syntheses of (+)-dodecanolide: a) G. Tuynenburg Muys, B. van der Ven, A. P. de Jonge, *Nature* **1962**, *194*, 995–996; T. Ohkuma, M. Kitamura, R. Noyori, *Tetrahedron Lett.* **1990**, *31*, 5509–5512 (from commercially not available ethyl 4-oxododecanoate in two steps); b) Y. Naoshima, H. Hasegawa, T. Saeki, *Agric. Biol. Chem.* **1987**, *51*, 3417–3419 (from diethyl-3-oxoglutarate in four steps).; c) J. P. Vigneron, V. Bloy, *Tetrahedron Lett.* **1980**, *21*, 1735–1738 (from 1-undecyn-3-one in four steps); d) H. Kakeya, N. Sakai, T. Sugai, H. Ohta, *Agric. Biol. Chem.* **1991**, *55*, 1877–1881 (from 2-hydroxydecanenitril in six steps); e) C. Bonini, C. Federici, L. Rossi, G. Righi, *J. Org. Chem.* **1995**, *60*, 4803–4812 (from octanal in six steps); f) G. C. Paddon-Jones, C. J. Moore, D. J. Brecknell, W. A. König, W. Kitching, *Tetrahedron Lett.* **1997**, *38*, 3479–3482 (from L-glutamic acid in six steps); g) T. Ebata, H. Kawakami, K. Koseki, H. Matsushita, *Agric. Biol. Chem.* **1991**, *55*, 1685–1686 in continuation of steps described by M. P. Balfe, M. Irwin, J. Kenyon, *J. Chem. Soc.* **1941**, 313–316 (from tetrahydrofurfurol in seven steps); h) V. Cerè, C. Mazzini, C. Paolucci, S. Pollicino, A. Fava, *J. Org. Chem.* **1993**, *58*, 4567–4571 (from 1,4:3,6-dianhydro-D-mannitol in seven steps); i) T. Sugai, K. Mori, *Agric. Biol. Chem.* **1984**, *48*, 2497–2500 [from *N*-(chloroacetamidoyl)decanoic acid in eight steps]; j) S. Chattopadhyay, V. R. Mamdapur, M. S. Chadha, *Tetrahedron* **1990**, *46*, 3667–3672 (from 1,2:5,6-di-*O*-isopropylidene-D-mannitol in nine steps); k) H. Nemoto, H. Ishibashi, M. Mori, S. Fujita, K. Fukumoto, *J. Chem. Soc. Perkin Trans. 1* **1990**, 2835–2840 (from methyl 1-hydroxycyclopropanecarboxylate in ten steps).
[16] Selected syntheses of (−)-*trans* quercus lactone: a) D. Hoppe, O. Zschage, *Angew. Chem.* **1989**, *101*, 67–69; *Angew. Chem. Int. Ed. Engl.* **1989**, *28*, 69–71 (from crotyl alcohol in four steps); b) M. Beckmann, H. Hildebrandt, E. Winterfeldt, *Tetrahedron Asymmetry* **1990**, *1*, 335–345 in continuation of steps described by K. Matcheva, M. Beckmann, D. Schomburg, E. Winterfeldt, *Synthesis* **1989**, 814–817 (from maleic anhydride and an enantiopure diene in five steps); c) J. P. Marino, R. F. de la Pradilla, *Tetrahedron Lett.* **1985**, *26*, 5381–5384 (from *trans*-1-bromopropene in six steps); d) R. Bloch, L. Gilbert, *J. Org. Chem.* **1987**, *52*, 4603–4605 in continuation of steps described by R. Bloch, E. Guibé-Jampel, C. Girard, *Tetrahedron Lett.* **1985**, *26*, 4087–4090 (from the Diels–Alder adduct of maleic anhydride and furane in seven steps); e) R. M. Ortuño, R. Merce, J. Font, *Tetrahedron* **1987**, *43*, 4497–4506 (from D-ribonolactone in seven steps); f) C. Günter, A. Mosandl, *Liebigs Ann. Chem.* **1986**, 2112–2122 (from pentanal in eight steps); g) D. F. Taber, J. B. Houze, *J. Org. Chem.* **1994**, *59*, 4004–4006 (from geraniol in eleven steps). For another multistep synthesis see ref. [3b].
[17] Stereostructure: M. Masuda, K. Nishimura, *Phytochem.* **1971**, *10*, 1401–1402; M. Masuda, K. Nishimura, *Chem. Lett.* **1981**, 1333–1336.
[18] **19**: *trans*-octenoate **17** (2.66 mL, 2.34 g, 15.0 mmol) was added to a mixture of *t*BuOH (50 mL), H_2O (50 mL), AD-mix β (21.0 g), and methanesulfonyl amide (1.43 g, 15.0 mmol, 1.0 equiv). The solution was stirred for 36 h at 0°C. After the addition of saturated Na_2SO_3 solution (2 mL) the mixture was extracted with *t*BuOMe (3 × 100 mL). The extracts were dried over Na_2SO_4, and the solvent was removed. Flash-chromatography on silica gel (ref. [8]; 5 cm, petroleum ether/*t*BuOMe 1:1 → 1:3) yielded **19** (2.20 g, 92%) as a colorless liquid. $[\alpha]_D^{25} = 70.8°$ ($c = 1.36$ in MeOH). Chiral capillary gas chromatography (ref. [10]) at 130°C of **19** (R_T 75.6 min) vs. its enantiomer (R_T 77.3 min) revealed 97% *ee* in favor of **19**. IR (neat): $\tilde{\nu}$ = 3450, 2960, 2870, 1760, 1205, 1170, 1085, 1015, 975 cm^{-1}. ^{1}H NMR (300 MHz, $CDCl_3$): $\delta = 0.94$ (t, $J_{4',3'} = 7.0$, 4'-H_3), 1.32–1.56 (m, 2'-H_2, 3'-H_2), 1.66–1.94 (m, 1'-H_2), AB signal ($\delta_A = 2.55$, $\delta_B = 2.79$, $J_{AB} = 17.9$, additionally split by $J_{B,4} = 5.5$, 3-H_2), partially overlapped by 2.61 (br. s, OH), 4.37 (ddd, $J_{5,1'\text{-}H(1)} = 8.9$, $J_{5,1'\text{-}H(2)} = 5.8$, $J_{5,4} = 3.8$, 5-H), 4.48 (dd, $J_{4,3\text{-}H(B)} \approx J_{4,5} \approx 4.4$, 4-H). C,H analysis calcd for $C_8H_{14}O_3$ (158.2): C 60.74, H 8.92; found: C 60.59, H 9.15.
[19] ADs of disubstituted olefins *trans*-MeCH=CHR were reported to show 72% *ee* in the case of 2-butene ("unpublished results" in ref. [1a]), 73% *ee* in the case of 1-phenylpent-3-en-1-yne (K.-S. Jeong, P. Sjö, K. B. Sharpless, *Tetrahedron Lett.* **1992**, *33*, 3833–3836), and 95% *ee* in the cases of 1-chloro-2-butene (K. P. M. Vanhessche, Z.-M. Wang, K. B. Sharpless, *ibid.* **1994**, *35*, 3469–3472) or 4,4-dimethyl-2-pentene ("unpublished results" in ref. [1a]).
[20] Method: H.-M. Shieh, G. D. Prestwich, *J. Org. Chem.* **1981**, *46*, 4319–4321. *Methylations* of hydroxylactones analogous to **23** were possible in the absence of HMPA according to A. R. Chamberlin, M. Dezube, S. H. Reich, D. J. Sall, *J. Am. Chem. Soc.* **1989**, *111*, 6247–6256.
[21] a) D. Seebach, *Chimia* **1985**, *39*, 147–148; b) D. Seebach, A. K. Beck, A. Studer in *Modern Synthetic Methods 1995* (Eds.: B. Ernst, C. Leumann), VCH, Weinheim, **1995**, pp. 1–178.
[22] The enantiomer of *epi*-blastmycinone **25** was synthesized by J. Mulzer, T. Schulze, A. Strecker, W. Denzer, *J. Org. Chem.* **1988**, *53*, 4098–4103 and M. P. Sibi, J. Lu, C. L. Talbacka, *ibid.* **1996**, *61*, 7848–7855, while racemic **25** was synthesized by C. Mukai, O. Kataoka, M. Hanaoka, *ibid.* **1993**, *58*, 2946–2952.

A Hexaimidazole Ligand Binding Six Octahedral Metal Ions To Give an Infinite 3D α-Po-Like Network Through Which Two Independent 2D Hydrogen-Bonded Networks Interweave**

Bernard F. Hoskins, Richard Robson,* and Damian A. Slizys

The current intense activity in the area of crystal engineering can be traced back to a number of pioneering studies, an important one of which concerns the hexa-host clathrates introduced and elaborated by MacNicol et al. about twenty years ago.[1] This approach, which offered a very appealing element of deliberate design, led to the isolation and structural characterization of a wide range of new crystalline inclusion compounds by the use of host molecules based on benzene rings hexasubstituted by flexible but bulky side arms such as arylthio-, aryloxy-, and arylmethyl- groups. Weak van der Waals interactions were responsible in these cases for binding the hexa-host molecules together into a crystal lattice that left large cavities for guest molecules. Herein we make use of the hexa-host approach, but the six benzene substituents are terminated by outwardly directed imidazole donor ligands which can then, in principle, be bound together into a crystalline lattice by coordinate bonds to metal ions. Metal–ligand bonding in these systems may provide much better control and strength in assembling the hexa-hosts into lattices with larger cavities than could possibly be achieved by using the weaker and less predictable van der Waals interactions.

The ligand used here is hexakis(imidazol-1-ylmethyl)benzene (hkimb; **1**). Imidazole termini were deliberately chosen because they provide strong coordinate bonds and are small enough to allow six to assemble around an octahedrally coordinated metal ion (in contrast, for example, to pyridine donors).

[*] Dr. R. Robson, Dr. B. F. Hoskins, D. A. Slizys
School of Chemistry, University of Melbourne
Parkville, Victoria 3052 (Australia)
Fax: Int. code + (9)347-5180
e-mail: R.Robson@chemistry.unimelb.edu.au

[**] The authors gratefully acknowledge support from the Australian Research Council and the American Chemical Society Petroleum Research Fund.

 © WILEY-VCH Verlag GmbH, D-69451 Weinheim, 1997 0570-0833/97/3624-2752 $ 17.50+.50/0

Another fruitful approach introduced by MacNicol et al. was based on the so-called Piedfort concept, in which two centrosymmetrically related 1,3,5-trisubstituted six-membered aromatic systems bound together by face-to-face π interactions mimic a single hexa-host molecule.[2] The ligand **1**

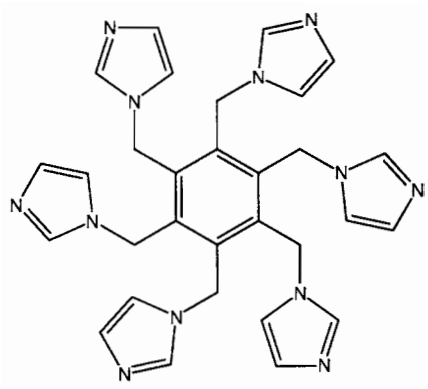

1

was arrived at, in part, by reverse Piedfort thinking as follows. The ligand 2,4,6-tri(4-pyridyl)-1,3,5-triazine (tpt) has recently been found to provide a number of highly symmetrical infinite coordination networks with unprecedented structures,[3–5] one in particular of which generates enormous sealed-off cavities.[3] The tpt ligands in these cases appear as closely associated centrosymmetrically related pairs that behave almost like single six-connecting units. A single hkimb ligand may be able to mimic these versatile $(tpt)_2$ pairs.

Compound **1** was synthesized by the reaction between hexakis(bromomethyl)benzene and sodium imidazolate and was structurally characterized as the hexahydrate by X-ray crystallography. To our surprise the molecule, in the crystal lattice, does not adopt the "1,3,5-up/2,4,6-down" conformation, but rather the "1,2,3-up/4,5,6-down" conformation (Figure 1). Hydrogen bonding of the exposed imidazole lone pairs to lattice water is responsible for this conformation. The closely related ligand hexakis(pyrazol-1-ylmethyl)benzene was reported recently and this does adopt the "1,3,5-up/2,4,6-down" conformation in the solid phase.[6]

The heavily hydrated $Cd(hkimb)F_2 \cdot 14H_2O$ was obtained by maintaining a hot aqueous solution containing CdF_2 and hkimb at 80 °C in an enclosed vessel for four days during which time colorless rhombohedral crystals separated. The structure was determined by X-ray crystallography, which revealed that every ligand, as intended, was attached to six cadmium centers and every cadmium was surrounded octahedrally by imidazole donors from six separate hkimb ligands (Figure 2). An infinite α-Po-related (or NaCl-related) coordination network is thereby formed in which alternating Cd center and benzene rings provide the six-connecting nodes (Figure 3). All ligands are equivalent as are all side arms

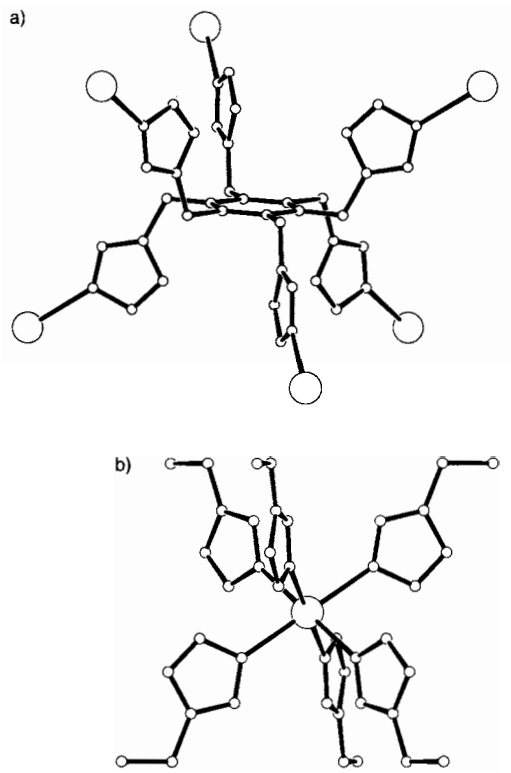

Figure. 2. Sections from the crystal structure of **2.** a) Six cadmium centers are attached to each imidazole ring of **1**. b) Each cadmium center is surrounded by six imidazole donors from six separate hkimb ligands. Cd – N, 2.350(3) Å.

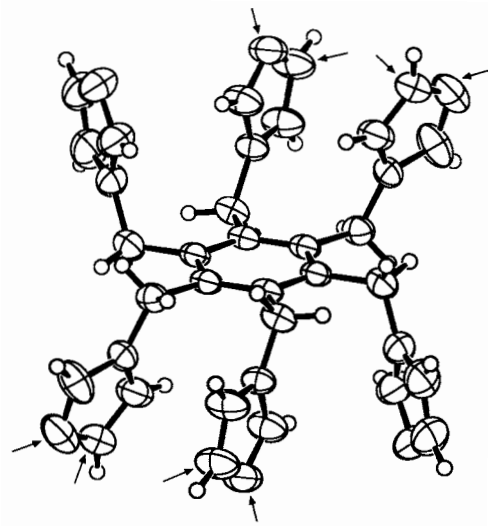

Figure 1. The structure of the centrosymmetric **1** in the $hkimb \cdot 6H_2O$ crystal. The symmetry-related imidazole residues at the top left and bottom right have the well-defined orientations shown, but the other two pairs show orientational disorder around the CH_2–N bond which interchanges N3 and C4–H.

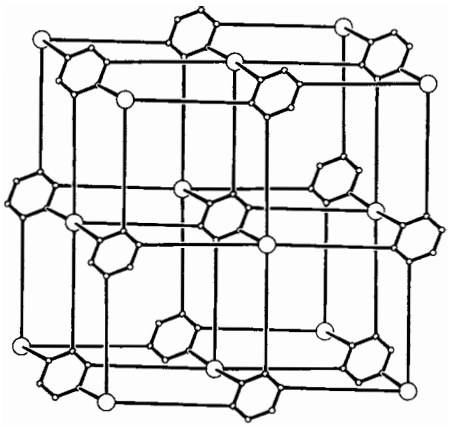

Figure. 3. Schematic representation of the infinite α-Po-related 3D net. The imidazolylmethyl links between Cd and the C_6 ring are represented by heavy lines.

 © WILEY-VCH Verlag GmbH, D-69451 Weinheim, 1997 0570-0833/97/3624-2753 $ 17.50+.50/0

within a ligand; all cadmium centers also are equivalent. The mean planes of all the benzene rings are parallel, the rhombohedral $\bar{3}$ axis passing perpendicularly through the center of the ring.

The fourteen molecules of water per cadmium arrange themselves into two independent undulating H-bonded 2D sheets. One of these, sheet A, includes the fluoride ion and the other, sheet B, consists entirely of water (Figure 4). The

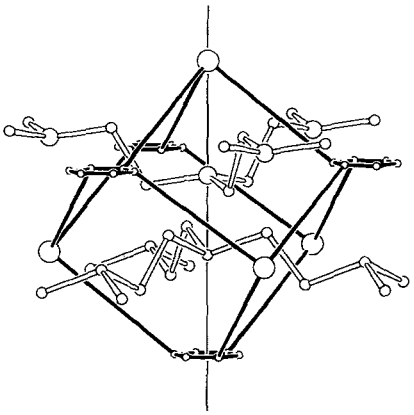

Figure. 4. Representation of the two independent H-bonded 2D sheets that weave through the 3D coordination polymer network of **2**. Circles in order of decreasing radius represent Cd, F, O, and C, respectively. "Open" connections represent H bonds. The fine vertical line passing through Cd, F, a water O atom, and the center of the C_6 ring represents the rhombohedral $\bar{3}$ axis. Sheet A is the upper one, sheet B the lower.

normals to the mean planes of the sheets are parallel with the $\bar{3}$ rhombohedral axis which is indicated in Figure 4 passing through a cadmium, a fluorine, and an oxygen center of one H_2O molecule belonging to sheet B and the center of the benzene ring. Within each cubelike rhomb of the sort represented by heavy lines in Figure 4 is found one F^- ion which is H-bonded to three symmetry-related water molecules of sheet A (F···O 2.634(9) Å). Each rhomb also contains an independent group of four water molecules of sheet B, consisting of a central water molecule located on the $\bar{3}$ axis, H-bonded to three symmetry-related water molecules (O···O 2.700(12) Å). These separate $F^-(H_2O)_3$ and $(H_2O)(H_2O)_3$ groups then connect to identical groups in adjacent rhombs by hydrogen bonds passing through the shared rhomb "windows" (Figure 4; O···O through the windows 2.99(2) Å for sheet A and 2.78(2) Å for sheet B). The closest oxygen-to-oxygen contact between the two sheets is 3.234(11) Å.

A large number of coordination networks have been generated recently by the use of two-, three-, and four-connecting ligands and the general area offers realistic promise of new materials with interesting and useful properties.[7] The easily synthesized six-connecting hkimb ligand reported here will undoubtedly afford many new types of framework materials.

Experimental Section

1: To a suspension under dinitrogen of NaH (3.159 g of a 60% dispersion in oil, 78.9 mmol) in THF (100 mL) was added a solution of imidazole (4,241 g, 62.3 mmol) in THF (200 mL). The resulting suspension was stirred for 30 minutes at which point hexakis(bromomethyl)benzene (5.815 g, 9.1 mmol) was added and washed into the suspension with THF (200 mL). The slurry was heated to 60 °C and was maintained at this temperature with stirring overnight. After the mixture had cooled the THF-insoluble solid was collected, washed with THF (20 mL), and then dissolved in water (30 mL). Aqueous HBr (2 M) was added dropwise until the pH had decreased to 6.5. A white precipitate formed during the addition. The solid was collected and recrystallized, with a hot filtration, from water to give the presumed the hexahydrobromide salt [3.723 g (39%)]. This was converted to the free base by passing an aqueous solution down an anion exchange column (Amberlite IRA 400) in the hydroxide form. The eluate was evaporated to dryness under reduced pressure and the residue was recrystallized from water to give hkimb·$6H_2O$ (2.168 g, 36%). ^{1}H NMR (CD_3OD) $\delta = 4.90$ (s, 2H; water), 5.48 (s, 2H; CH_2), 6.74 (1H, 4- or 5-imidazole), 6.86 (1H, 4- or 5-imidazole), 7.35 (1H, 2-imidazole); ^{13}C NMR (CD_3OD) $\delta = 45.82$, 120.06, 129.76, 137.93, 139.58. Elemental analysis for $C_{30}H_{30}N_{12}\cdot 5.7H_2O$: Calcd: C 54.5, H 6.3, N 25.4; found: C 54.5, H 6.1, N 25.5.

2: A solution of CdF_2 (22.1 mg, 0.147 mmol) in hot water (80 °C, 50 mL) was added to a solution of hkimb·$6H_2O$ (82.8 mg, 0.124 mmol) in hot water (80 °C, 50 mL). The initially clear solution was maintained at 80 °C in an enclosed vessel for four days during which time colorless rhombohedral crystals separated. The crystals of Cd(hkimb)$F_2\cdot 14H_2O$ (26.0 mg, 22%) were collected from the hot solution. Elemental analysis for $C_{30}H_{56}CdF_2N_{12}O_{13}$ (Cd(hkimb)$F_2\cdot 13H_2O$): Calcd: C 38.2, H 6.0, N 17.8, Cd 11.9, F 4.0; found: C 38.6, H 5.3, N 17.5, Cd 11.5, F 3.9.

Crystal data for hkimb·$6H_2O$. $M_r = 666.74$, monoclinic, space group $P2_1/c$ (No. 14), $a = 10.353(1)$, $b = 14.010(1)$, $c = 11.432(1)$ Å, $\beta = 97.32(1)°$, $V = 1644.6(2)$, $Z = 2$, $\rho_{calcd.} = 1.346$ g cm^{-3}, $\rho_{exp.} = 1.36(1)$ g cm^{-3}, $\mu(Cu_{K\alpha}) = 8.1$ cm^{-1}, $F(000) = 708$. Intensity data for 4133 reflections, yielding 3326 independent reflections ($R_{int} = 0.0227$), were measured at 295(2) K with $Cu_{K\alpha}$ radiation (graphite monochromator) using an Enraf-Nonius CAD-4 MachS diffractometer and employing the $\omega/2\theta$ method; absorption corrections were applied [8]. All non-hydrogen atoms were located by using direct methods [9]. Subsequent cycles of least-squares refinement and difference syntheses (SHELXL-93) [10] indicated disorder in the location of carbon and nitrogen atoms within the imidazole rings and in the position of the oxygen atoms of two of the water molecules; these features were incorporated in the model. All the hydrogen atoms of the hkimb molecule, including those associated with the partially occupied carbon/nitrogen sites, were revealed in difference syntheses during the final stages of refinement and they were included in the refinement at their geometrically constrained positions. Anisotropic displacement parameters were applied to all non-hydrogen atoms. Full-matrix least-squares refinement based on F^2 converged with $R1 = 0.0506$, $wR2 = 0.1445$ and GOF = 1.081; values of minimum and maximum residual electron density 0.376 and -0.210 e Å^{-3}. Crystal data for Cd(hkimb)$F_2\cdot 14H_2O$. $M_r = 961.29$, rhombohedral, space group $R\bar{3}m$ (hexagonal setting of No. 166), $a = 11.989(2)$, $c = 25.362(5)$, $V = 3157(1)$, $Z = 3$, $\rho_{calcd.} = 1.517$ g cm^{-3}, $\rho_{exp.} = 1.54(1)$ g cm^{-3}, $\mu(Cu_{K\alpha}) = 49.0$ cm^{-1}, $F(000) = 1500$. Intensity data for 1889 reflections, yielding 833 independent reflections ($R_{int} = 0.0340$), were measured at 295(2) K with $Cu_{K\alpha}$ radiation (graphite monochromator) using an Enraf-Nonius CAD-4 MachS diffractometer and employing the $\omega/2\theta$ method; absorption corrections were applied [8]. All non-hydrogen atoms were located by using the Patterson interpretation routine of SHELXS-86 program [9]. The ligand hydrogen atoms, all of which were revealed in the difference syntheses during the last stages of refinement [10], were included in the refinement at their geometrically constrained positions. Anisotropic displacement parameters were applied to all non-hydrogen atoms. Full-matrix least-squares refinement based on F^2 converged with $R1 = 0.0433$, $wR2 = 0.1184$ and GOF = 1.111; values of minimum and maximum residual electron density 0.905 and -0.989 e Å^{-3}. Crystallographic data (excluding structure factors) for the structures reported in this paper have been deposited with the Cambridge Crystallographic Data Center as supplementary publication no. CCDC-100665. Copies of the data can be obtained free of charge on application to The Director, CCDC, 12 Union Road, Cambridge CB2 1EZ (fax: Int. code + (1223) 336-033; e-mail: deposit@chemcrys.cam.ac.uk).

Received: May 26, 1997 [Z10476IE]
German version: *Angew. Chem.* **1997**, *109*, 2861–2863

Keywords: cadmium · coordination polymers · crystal engineering · hydrogen bonds · imidazole

[1] D. D. MacNicol, G. A. Downing, *Comprehensive Supramolecular Chemistry, Vol. 6*, Pergamon, Oxford, **1996**, Chap. 14, p. 421.
[2] A. S. Jessiman, D. D. MacNicol, P. R. Mallinson, I. Vallance, *J. Chem. Soc. Chem. Commun.* **1990**, 1619.
[3] S. R. Batten, B. F. Hoskins, R. Robson, *J. Am. Chem. Soc.* **1995**, *117*, 5385.
[4] B. F. Abrahams, S. R. Batten, H. Hamit, B. F. Hoskins, R. Robson, *Chem. Commun.* **1996**, 1313.
[5] B. F. Abrahams, S. R. Batten, H. Hamit, B. F. Hoskins, R. Robson, *Angew. Chem.* **1996**, *108*, 1795; *Angew. Chem. Int. Ed. Engl.* **1996**, *35*, 1691.
[6] C. M. Hartshorn, P. J. Steel, *Aust. J. Chem.* **1995**, *48*, 1587.
[7] C. L. Bowes, G. A. Ozin, *Adv. Mater.* **1996**, *8*, 13.

 © WILEY-VCH Verlag GmbH, D-69451 Weinheim, 1997 0570-0833/97/3624-2754 $ 17.50+.50/0

[8] G. M. Sheldrick, SHELX-76, Program for crystal structure determination, University of Cambridge, UK, **1976**.
[9] G. M. Sheldrick, SHELXS-86, Program for crystal structure determination, University of Cambridge in *Crystallographic Computing 3* (Eds.: G. M. Sheldrick, C. Kruger, R. Goddard), Oxford University Press, Oxford, **1985**, p. 175.
[10] G. M. Sheldrick, SHELXL-93, Program for crystal structure refinement, University of Göttingen, **1993**.

Periodic Structure of a Single Sheet of a Clothlike Macromolecule (Atomic Cloth) Studied by Scanning Tunneling Microscopy**

Tomohide Takami,* Hiroyuki Ozaki,* Mayumi Kasuga, Takao Tsuchiya, Yasuhiro Mazaki, Daiji Fukushi, Ayumi Ogawa, Masayuki Uda, and Masakazu Aono

Recently we prepared a single sheet of a sashlike or clothlike macromolecule (atomic sash or atomic cloth) by photopolymerization of alkadiyne or alkatetrayne molecules that were laid flat and closely packed in a vapor-deposited monolayer on a cooled graphite substrate. The process was monitored by Penning ionization electron spectroscopy (PIES).[1-3] Particularly the atomic cloth, which is composed of flatly lying alkyl chains cross-linked alternately by polydiacetylene (PD) and polyacetylene (PA) chains as shown in Figure 1, triggered our interest because of its molecular structure, electronic structure, and electrical properties. It is expected that the unit mesh of the atomic cloth is forced to have a parallelogram structure because of the peculiar clothlike configuration supported by the substrate. This is in spite of considerable strain mainly due to the overcrowding of hydrogen atoms at the crossing points of alkyl and PA chains.

[*] Dr. T. Takami[+]
Surface and Interface Laboratory
The Institute of Physical and Chemical Research (RIKEN)
Dr. H. Ozaki
Department of Material Systems Engineering, Faculty of Technology
Tokyo University of Agriculture and Technology
Koganei, Tokyo 184 (Japan)
Fax: Int. code + (423)85-7649
e-mail: hiroyuki@cc.tuat.ac.jp
M. Kasuga, T. Tsuchiya, A. Ogawa
Tokyo University of Agriculture and Technology
Dr. Y. Mazaki
Kitasato University
D. Fukushi, Prof. M. Uda
Waseda University
Dr. M. Aono
The Institute of Physical and Chemical Research (RIKEN) and
ERATO Aono Atomcraft Project
[+] Present address:
Research Institute for Scientific Measurements
Tohoku University
2-1-1 Katahira, Aoba-ku, Sendai 980-0812 (Japan)
Fax: Int. code + (22)217-5404
e-mail: takami@rism.tohoku.ac.jp

[**] We thank Dr. Naoaki Kanada and Mr. Takeharu Sekiguchi (The University of Tokyo), Dr. Toru Egawa (Hokkaido University), Prof. Toshimasa Ishida (University of Shizuoka), and Dr. Hideki Katagiri (Electrotechnical Laboratory) for helpful discussions. This work was partly supported by the Special Researchers' Basic Science Program in RIKEN, and a grant-in-aid for Scientific Research on Priority Areas "Molecular Superstructure—Design and Creation" (no. 262/08231219) from the Ministry of Education, Science, Sports, and Culture, Japan. For a definition of "atomic cloth", see ref. [2, 3] and Y. Harada, S. Masuda, H. Ozaki, *Chem. Rev.* **1997**, *97*, 1897–1952.

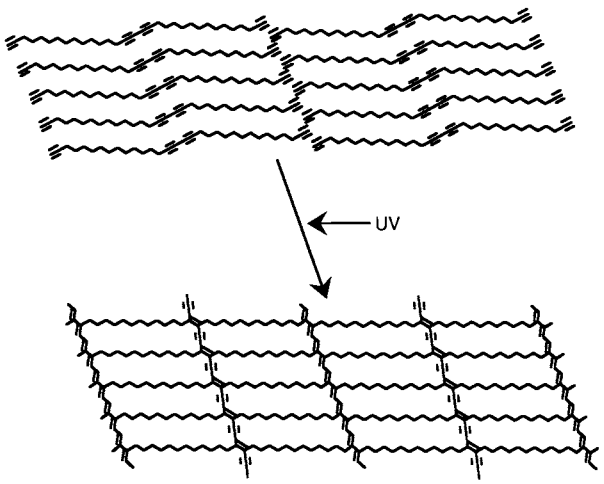

Figure 1. Schematic drawing of the atomic cloth prepared by photopolymerization of 1,15,17,31-dotriacontatetrayne molecules that were laid flat and closely packed in a monolayer.

The atomic cloth can also be regarded as a two-dimensional anisotropic sheet or an array of one-dimensional π-electron systems with fixed configuration, which cannot be easily obtained by ordinary preparative methods. Thus, it is of fundamental importance to prove and explain the periodic structure of the atomic cloth for studies on this fascinating material.

It was confirmed by PIES that 1) the graphite surface was just covered with the flatly lying alkyl chains, and the orientation was maintained throughout UV irradiation, 2) the π MOs of the diacetylene and acetylene units of the monomer (1,15,17,31-dotriacontatetrayne (DTTY)) were altered to the long conjugated systems of the PD and PA chains, and 3) unlike an unirradiated monolayer, the irradiated monolayer did not sublime under ultrahigh vacuum (UHV) upon heating to room temperature.[2] To obtain direct evidence for the formation of the clothlike structure, scanning tunneling microscopy (STM) was applied. We found the unit vectors of the atomic cloth by analyzing the periodic modulation of the STM image contrast due to the coincidence of the structure of the atomic cloth and that of the graphite substrate.

The specimen was prepared on a cleavage plane of highly oriented pyrolytic graphite (HOPG) in an UHV electron spectrometer, as previously described.[2,3] The atomic cloth did not show a different PIE spectrum after it was temporarily exposed to the air at room temperature and then returned to the spectrometer. The STM equipment (from WA Technology) was in another UHV chamber.[4] An STM tip made of tungsten wire (diameter 0.5 mm) was sharpened by electrochemical etching. STM images were obtained at room temperature in the constant-current topograph mode and calibrated with the images of HOPG and Si(111) 7×7 surfaces obtained immediately before and after the measurements of the atomic cloth. The scanning time was about 30 s for one image of 256×256 points.

The STM topograph of the atomic cloth is shown in Figure 2. This image was obtained at a sample bias voltage of +0.2 V, which corresponds to the unoccupied states. Sixteen bright lines running diagonally from the upper left to the lower right are observed; their brightness changes alternately.[5-7] The distance between the adjacent brighter and darker

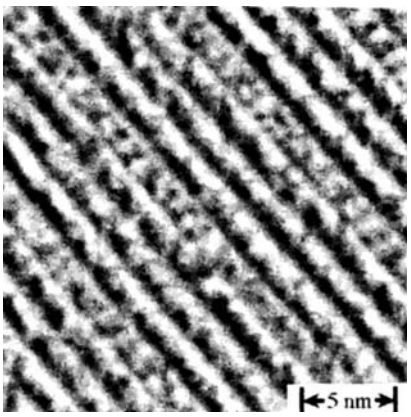

Figure 2. UHV-STM image of the atomic cloth on graphite. Sample bias voltage: +0.2 V, tunneling current: 0.1 nA, image sizes: 20.0 × 20.0 nm.

lines is 1.7 ± 0.1 nm. Taking into account the chemical structure of the atomic cloth, it is natural to ascribe this value to the distance between the neighboring PD and PA chains; this results in a distance D of 3.4 nm between two nearest PD or PA chains. It is noteworthy that there is a modulation in the STM image contrast at every fourth lines, that is, with a periodicity of $2D = 6.8$ nm. Moreover, an internal structure is observed between two of the four lines: runglike features are placed at an average rung–rung separation of $d = 1.4$ nm. This value is close to three times the width of an alkyl chain (0.47 nm). The peak–peak height of the topograph is about 0.4 nm, which is in agreement with the thickness of the atomic cloth. However, the real thickness cannot be estimated by STM.

Figures 3a and 3b show a Fourier-transformed power spectrum of the STM image (Figure 2) and its schematic interpretation, respectively. From the analysis of the Fourier transform we can make the following four findings: First, intense spots in Figure 3a (large spots in Figure 3b) result in the main interval in Figure 2 ($D/2 = 1.7$ nm), the distance between a PD chain and its neighboring PA chain. Second, additional spots in Figure 3a (small spots in Figure 3b) are

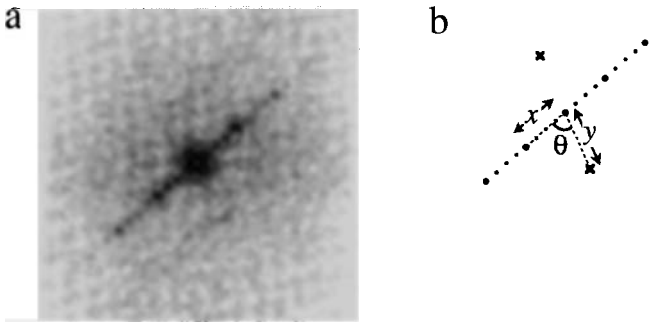

Figure 3. a) Fourier-transformed power spectrum of the STM image shown in Figure 2; b) schematic interpretation of the power spectrum.

lined up with the quartered interval of distance $2D = 6.8$ nm. This periodicity is observed as the four-line modulation pattern of the STM image contrast in Figure 2. Third, two diffuse spots (crosses in Figure 3b) are also observed in Figure 3a. Half of the distance between the diffuse spots corresponds to the spacing for the twisted features in Figure 2 ($d = 1.4$ nm), which is three times the width of the alkyl chain. Fourth, angle θ between the two lines drawn on the spots in Figure 3b is 71.7°, and ratio y/x is 1.18.

These results are explained by lattice matching between the atomic cloth and graphite according to Equation (a);

$$p \cdot \mathbf{a} = i \cdot \mathbf{a}_g + j \cdot \mathbf{b}_g,\ q \cdot \mathbf{b} = k \cdot \mathbf{a}_g + l \cdot \mathbf{b}_g \qquad \text{(a)}$$

$\mathbf{a}_g$ and $\mathbf{b}_g$ are the unit vectors of graphite, $\mathbf{a}$ and $\mathbf{b}$ vectors for the repeating units of the atomic cloth along a PD or PA chain and $-(\overset{|}{C}{=}\overset{|}{C}\text{-}C_{12}H_{24})_{2n}-$ chain, respectively, and $p\mathbf{a}$ and $q\mathbf{b}$ the unit vectors of the total system comprising the atomic cloth and graphite. Periodicities $2D$ and d (corresponding to $x/4$ and y in the Fourier transformation) imply $q = 2$ and $p = 3$. Using the values of $2D$, d, and θ, we can find the approximate commensuration $\begin{pmatrix} i & j \\ k & l \end{pmatrix} = \begin{pmatrix} 7 & -4 \\ 13 & -20 \end{pmatrix}$, as shown schematically in Figure 4. Furthermore, if the one-dimensional modulation of

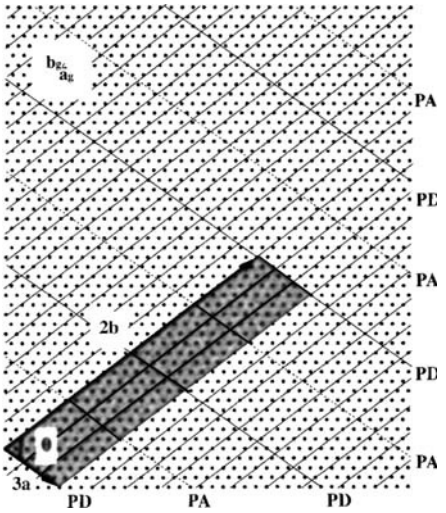

Figure 4. Proposed periodic structure of the atomic cloth on a graphite lattice (black circles). Solid and dashed lines show the PD and PA chains, respectively.

the STM image contrast with periodicity $2D$ is ascribed to the point-on-line coincidence,[8] which occurs when only j and l (or i and k) are integers and places all the lattice points of the organic layer on the (1,0) (or (0,1)) lines of graphite, values i and k are modified as 7.01 and 12.9 by introducing $m = |\mathbf{b}|/|\mathbf{a}| = (1/|\mathbf{a}|)/(1/|\mathbf{b}|) = (3y \sin\theta)/(x \sin\theta/2) = 6y/x = 7.07$ in Equation (b).

$$\begin{pmatrix} \frac{i}{p} \\ \frac{\sqrt{3}k}{2mq} \end{pmatrix} = \frac{1}{\sin\theta} \begin{pmatrix} -\sin\left(\theta + \frac{\pi}{3}\right) & 1 \\ -\frac{3}{4} & -\sin\left(\theta - \frac{\pi}{3}\right) \end{pmatrix} \begin{pmatrix} \frac{j}{p} \\ \frac{\sqrt{3}l}{2mq} \end{pmatrix} \qquad \text{(b)}$$

Equation (b) can be derived from the geometry of an adlayer whose structure on a hexagonal substrate is expressed by Equation (a). Thus, one obtains $|\mathbf{a}| = 0.499$ and $|\mathbf{b}| = 3.54$ nm; the former is comparable to the length of the repeating unit of various PDs (ca. 0.49 nm).[9]

Eichhorst-Gerner et al. prepared a one-dimensional hydrogen-bonded network with a donor–acceptor complex of 5-alkoxyisophthalic acid and 2,5-dimethylpyrazine at a liquid–graphite interface, and obtained the STM image with submolecular resolution.[10] In this network, the hydrogen bonds were introduced without altering the alkyl skeletons, and the methyl ends remained free. As a consequence, the direction of the zigzag coincides with that of vector $\mathbf{a}_g$, and the

 © WILEY-VCH Verlag GmbH, D-69451 Weinheim, 1997 0570-0833/97/3624-2756 $ 17.50+.50/0

length of the repeating unit nearly matches $|\mathbf{a}_g|$, which is responsible for the resolved STM pictures of the chains. This is usually the case for STM images of, for example, alkanes, alkanols, fatty acids, and dialkylbenzenes adsorbed on HOPG and observed with submolecular or atomic resolution.[11-13] In contrast, we introduced the new covalent bonds among molecules in a vapor-deposited monolayer and prepared a single sheet of a two-dimensional macromolecule: The centers and ends of chain molecules were transfixed with PD chains and stitched with PA chains, respectively, to afford condensed parallelograms without free methyl ends but with changes in the bond lengths and angles of the alkyl chains (see Figure 1). We consider that the drastic rearrangement of the covalent bonds detected by PIES[2] leads to the following results.

First, the atomic cloth is not commensurate with graphite in all directions. In fact, since i is very close to an integer (7)—to say nothing of j—the atomic cloth is almost point-on-point coincident with graphite along the **a** axis. On the other hand, since k is considerably different from an integer (13), there is no point-on-point but only point-on-line coincidence along the **b** axis. In other words, the periodicities of the PD and PA chains are approximately commensurate with that of graphite, while that of the $-(C{=}C_i-C_{12}H_{24})_{2n}-$ chains is not. It should be noted that neither the direction nor the periodicity of $-C_{12}H_{24}-$ matches that of graphite ($\mathbf{a}_g$ and $|\mathbf{a}_g|$). Second, the two-dimensionality of the atomic cloth may bring about slight local fluctuation or irregularity in the periodicity: The two-dimensional macromolecular network on a graphite lattice probably distorts the flexible portions in order to reduce the total energy of the system. Third, it is likely that these situations lead to the obviously observed periodicity $2D$ ($x/4$), but rather ambiguous periodicity d (y) in Figure 2 (Figure 3). It is surprising that the commensuration between PD/PA and graphite is present after such a drastic reaction. Studies on the structure of the DTTY monolayer are desired to elucidate the details. However, they are difficult, because the monomer monolayer is very liable to sublime under UHV at room temperature; furthermore, DTTY undergoes photopolymerization in the room light.

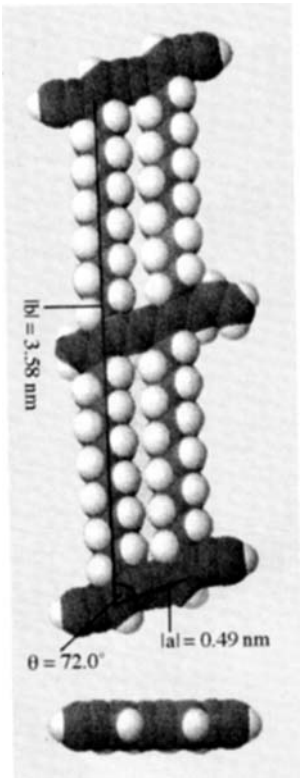

Figure 5. Structure of a model oligomer corresponding to the unit mesh of the atomic cloth obtained by MM2 calculation.

The periodic structure of the atomic cloth determined by STM can be supported by an MM2 calculation. Figure 5 shows the calculated structure of a model oligomer molecule corresponding to the unit mesh of the atomic cloth. The values of $|\mathbf{a}|$, $|\mathbf{b}|$, and θ are in good agreement with those observed.

We have observed the atomic cloth, a single sheet of a clothlike macromolecule, by STM. The periodic features and contrast modulation of the STM images are explained by lattice matching between the atomic cloth and graphite. The lengths of the unit vectors of the atomic cloth are 0.499 and 3.54 nm, and the angle between the vectors is 71.7°. These results show the great promise of STM in determining the structure of a two-dimensional macromolecule (organic monoatomic layer) prepared on a crystallographical surface.

Received: January 20, 1997
Revised version: June 30, 1997 [Z10008IE]
German version: *Angew. Chem.* **1997**, *109*, 2909–2912

Keywords: hydrocarbons · monolayers · polymers · scanning tunneling microscopy · surface chemistry

[1] H. Ozaki, T. Funaki, Y. Mazaki, S. Masuda, Y. Harada, *J. Am. Chem. Soc.* **1995**, *117*, 5596–5597.
[2] H. Ozaki, M. Kasuga, T. Tsuchiya, T. Funaki, Y. Mazaki, M. Aoki, S. Masuda, Y. Harada, *J. Chem. Phys.* **1995**, *103*, 1226–1228.
[3] H. Ozaki, *J. Electron Spectrosc. Relat. Phenom.* **1995**, *76*, 377–382.
[4] T. Takami, D. Fukushi, T. Nakayama, M. Uda, M. Aono, *Jpn. J. Appl. Phys.* **1994**, *33*, 3688–3695.
[5] We carried out ab initio calculations on some oligomeric models of the atomic cloth. The results showed that the LUMO is mainly distributed on the PD chains, whereas the HOMO is on the PA chains. If the picture presented in Figure 2 is assumed to be due to the LUMO, the brighter lines correspond to the PD chains, and the darker lines to the PA chains. However, this tentative assignment does not matter for the following discussion on the structure of the atomic cloth.
[6] We compared our STM images with the artifact images reported in C. R. Clemmer, T. P. Beebe, Jr., *Science* **1991**, *251*, 640–642 and H. Chang, A. J. Bard, Langmuir **1991**, *7*, 1143–1153, which were ascribed to the cleavage steps, strands, and small particles of HOPG. Our STM image, however, has a long periodicity and is different from the artifact images.
[7] Reversed STM images were observed upon changing the bias voltage; that is, PD and PA chains were dark, and alkyl chains bright. Nevertheless, there was no distinct feature corresponding to the latter chains but the undulation of contrast due to the former chains with periodicity $2D$. The image due to graphite was not observed either.
[8] A. Hoshino, S. Isoda, H. Kurata, T. Kobayashi, *J. Cryst. Growth* **1995**, *146*, 636–640.
[9] "Polydiacetylenes": V. Enkelmann in *Advances in Polymer Science, Vol. 63* (Ed.: H.-J. Cantow), Springer, Berlin, **1984**, pp. 91–136.
[10] K. Eichhorst-Gerner, A. Stabel, G. Moessner, D. Declerq, S. Valiyaveettil, V. Enkelmann, K. Müllen, J. P. Rabe, *Angew. Chem.* **1996**, *108*, 1599–1602; *Angew. Chem. Int. Ed. Engl.* **1996**, *35*, 1492–1495.
[11] G. C. McGonigal, R. H. Bernhardt, D. J. Thomson, *Appl. Phys. Lett.* **1990**, *57*, 28–30; G. C. McGonigal, R. H. Bernhardt, Y. H. Yeo, D. J. Thomson, *J. Vac. Sci. Technol. B* **1991**, *9*, 1107–1110.
[12] J. P. Rabe, S. Buchholz, *Science* **1991**, *253*, 424–427; S. Buchholz, J. P. Rabe, *Angew. Chem.* **1992**, *104*, 188-190; *Angew. Chem. Int. Ed. Engl.* **1992**, *31*, 189–191; J. P. Rabe, D. Buchholz, L. Askadskaya, *Synth. Met.* **1993**, *54*, 339–349, and references therein.
[13] M. Hibino, A. Sumi, I. Hatta, *Jpn. J. Appl. Phys.* **1995**, *34*, 3354–3359.

 © WILEY-VCH Verlag GmbH, D-69451 Weinheim, 1997 0570-0833/97/3624-2757 $ 17.50+.50/0

Conformation Control in Polymetallic Mesocycles by Metal–Metal Bonding: The First Example of an Hg–Cu Interaction**

Marc Bénard, Ulf Bodensieck, Pierre Braunstein,* Michael Knorr, Martin Strampfer, and Carsten Strohmann

Dedicated to Professor The Lord Lewis on the occasion of his 70th birthday

Seven- to ten-membered inorganic rings (mesocycles) in which two or more *consecutive* atoms are transition metals are relatively few, and heterometallic examples are even rarer.[1] By analogy with cyclic structures consisting of isolated metal centers connected by bridging ligands,[2] their structure, conformation, and topology should depend not only on the nature of the organic backbone, but also on the nature of the metal–ligand interactions. In addition, unique properties may result when metal–metal bonds are introduced,[3] and novel features can be anticipated when these interactions occur in directions different from those of the covalent bonding, as shown by the chemistry of gold.[4] Although this element exhibits the most pronounced relativistic effects, interactions involving other d^{10} closed-shell ions (such as Hg^{II}) are also expected to influence the structure and properties of complexes.[5] Here we report the first example of an attractive Cu–Hg interaction and show how its transannular orientation determines the conformation of an unprecedented cyclic polymetallic complex.

The central d^{10} ion in the heterotrinuclear complex **1** (dppm = $Ph_2PCH_2PPh_2$)[6] confers rigidity to the Fe-Hg-Fe chain and allows free rotation about the metal–metal bonds. We have now used this molecule as a large trimetallaphosphane ligand for the synthesis of unusual heterometallic ring and chain complexes. To our knowledge, only metallaphosphanes containing one[7] or two metal centers have been used previously.[8]

The reaction of **1** with two equivalents of [AuBr(tht)] (tht = tetrahydrothiophene) gave the yellow, air-stable chain complex **2**, whose spectroscopic data (see Experimental Section) are consistent with the structure shown in Scheme 1.

Upon mixing **1** with slightly more than two equivalents of $[Cu(NCMe)_4]PF_6$ in cold CH_2Cl_2, yellow complex **3** formed quantitatively. The ν(CO) region of its IR spectrum is very similar to that of **2**, and the presence of acetonitrile coordinated to copper is indicated by very weak bands at

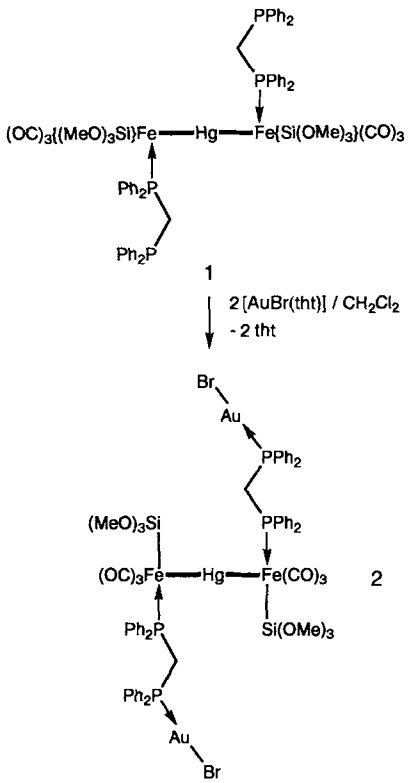

Scheme 1.

2314 and 2278 cm^{-1}. When crystals of **3** were dissolved in CH_2Cl_2/CD_2Cl_2 at room temperature, two sets of $^{31}P\{^1H\}$ NMR resonances were observed with approximately equal integral intensities. The first set comprised two broad signals at $\delta = 50.1$ and -13.1 for the open-chain complex **3**, while the second set consisted of a well-resolved multiplet at $\delta = 46.2$ and a broad multiplet at $\delta = -9.9$, which were assigned to the cyclic species **4**. On cooling to 223 K, the resonances assigned to **3** became two well-resolved doublets centered at $\delta = 48.0$ and -15.6 with $^2J(P,P) = 8$ Hz. The signals of **4** now appeared at $\delta = 46.2$ and -10.3, and their integral intensities were diminished to about 5–10% of those of **3**. No significant change was observed upon further cooling to 213 K. Orange **4** was independently synthesized in high yield by the reaction of **1** with only one equivalent of $[Cu(NCMe)_4]PF_6$ in CH_2Cl_2 (Scheme 2).

The structure of the cation of **4** is shown in Figure 1.[9] The Fe-Hg-Fe unit is linked to the Cu atom by dppm ligands. A C_2 axis passes through the Cu and Hg atoms. The geometry around Fe could be regarded as distorted octahedral, although the angle C2-Fe-C3 is only 162.2(3)°, as is observed in other complexes of the type $[MFe(SiR_3)(CO)_3(PR_3)]$.[10] The alternative description as trigonal bipyramidal, for which the Fe–Hg bond is neglected, is therefore more consistent with a formal d^8 Fe^0 center. The Fe–Hg distance of 2.611(4) Å is in the normal range.[6,11] The most unusual feature of this structure is the presence of an attractive Cu–Hg interaction, which results in a coordination number of three for both metal centers. The Cu–Hg bond appears to be the first of its kind, and the metal–metal distance of 2.689(2) Å can be compared to the sum of the Pauling covalent radii (1.17 (Cu) + 1.44 (Hg) = 2.61 Å). The P2-Cu-P2a angle of 160.16(9)° reflects the bonding interaction between the two d^{10} ions and illustrates the capacity of **1** to behave as a *trans* bridging

[*] Dr. P. Braunstein, Dr. U. Bodensieck, Dr. M. Knorr, Dr. M. Strampfer
Laboratoire de Chimie de Coordination, URA 416 CNRS
Université Louis Pasteur
4, rue Blaise Pascal, F-67070 Strasbourg Cédex (France)
Fax: Int. code + (3) 8841-6030
e-mail: braunst@chimie.u-strasbg.fr
Dr. M. Bénard
Laboratoire de Chimie Quantique, Université Louis Pasteur, Strasbourg
Dr. M. Knorr, Dr. C. Strohmann
Institut für Anorganische Chemie der Universität Saarbrücken (Germany)

[**] This work is based on the Ph.D. thesis of M.S. We are grateful to Dr. W. Deck and Prof. H. Vahrenkamp (Universität Freiburg, Germany) for the collection of preliminary X-ray data, and to Prof. M. Veith (Universität des Saarlandes, Germany) for access to X-ray facilities. We also acknowledge the Ministère de l'Enseignement Supérieur et de la Recherche (Paris, France) for a post-doctoral grant to U.B., the Centre National de la Recherche Scientifique and the Société des Amis des Sciences (Paris, M.K.), the Commission of the European Communities (contract CHRX-CT93-0277), and the Alexander-von-Humboldt Stiftung (award to P.B.) for financial support.

 © WILEY-VCH Verlag GmbH, D-69451 Weinheim, 1997 0570-0833/97/3624-2758 $ 17.50+.50/0

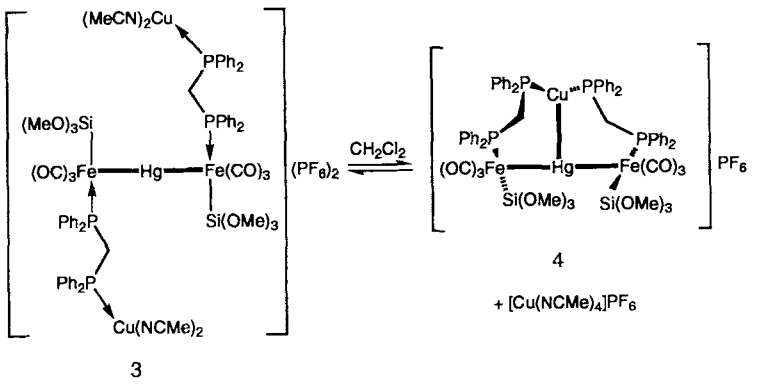

3 4

+ $[Cu(NCMe)_4]PF_6$

Scheme 2.

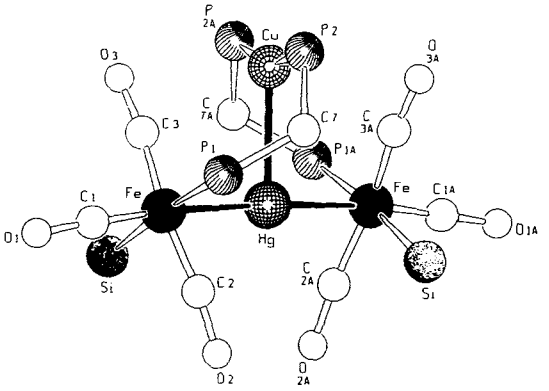

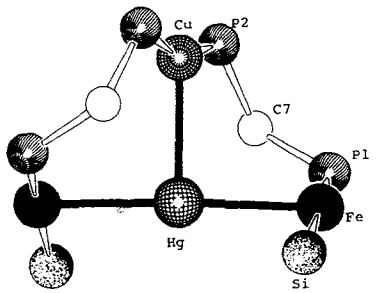

Figure 1. a) Top: Structure of the cation $[Hg\{Fe[Si(OMe)_3](CO)_3(\mu\text{-dppm})\}_2Cu]^+$ in $4\cdot 4CH_2Cl_2$ (SCHAKAL plot). Selected interatomic distances [Å] and angles [°]: Hg–Fe 2.613(2), Hg–Cu 2.689(2), Fe–Si 2.330(2), Fe–P1 2.260(2), Fe–C1 1.775(6), Fe–C2 1.794(7), Fe–C3 1.784(7), Cu–P2 2.228(2); Fe-Hg-Fe(a) 176.62(4), Fe-Hg-Cu 91.96(2), Hg-Fe-Si 82.97(6), Hg-Fe-P1 95.92(6), P1-Fe-Si 175.49(7), P2-Cu-P2a 160.16(9); b) Bottom: view of the heavy-atom core.

ligand. The linearity of the Fe-Hg-Fe chain is maintained in **4** and confers a T-shaped structure to the metal core.[12]

Extended Hückel calculations[13] on the model system **5** yielded the orbital interaction diagram shown in Figure 2.

$[Hg\{Fe[Si(OMe)_3](CO)_3(dppm\text{-}P)\}_2]$ **1**

$[Hg\{Fe[Si(OMe)_3](CO)_3(\mu\text{-dppm})AuBr\}_2]$ **2**

$[Hg\{Fe[Si(OMe)_3](CO)_3(\mu\text{-dppm})\}_2\{Cu(NCMe)_2\}_2][PF_6]_2$ **3**

$[Hg\{Fe[Si(OMe)_3](CO)_3(\mu\text{-dppm})\}_2Cu]PF_6$ **4**

On the left, the interaction diagram between the valence orbitals of an Hg atom and those of the $\{Fe[Si(OH)_3](CO)_3PR_3\}_2$ dimer (both fragments are assumed to be neutral) shows the origin of the Fe–Hg bonding interactions. The bonding orbital of lowest energy (−14.1 eV) is equally shared between the 6s orbital of mercury and an in-phase combination of the d_{z^2} orbitals of Fe (the z axis is parallel to the Fe-Hg-Fe direction). The antibonding counterpart of this interaction (−6.1 eV) is mainly centered on Fe, but still contains an important contribution (22%) from the s orbital of Hg. The second Fe-Hg-Fe bonding orbital (−12.1 eV) results from the favorable interaction between the out-of-phase combination of the d_{z^2} orbitals of iron with the p_z orbital of Hg. The latter orbital is not affected by the incoming $[Cu(PR_3)_2]^+$ cation and represents, practically unchanged, the HOMO of complex **5**. A cluster of eight orbitals with strongly dominant Fe character (−12.7 to −13.3 eV) also remains unperturbed by the approaching copper complex fragment.

$[Hg\{Fe[Si(OH)_3](CO)_3(\mu\text{-}H_2PCH_2PH_2)\}_2Cu]^+$ **5**

The Cu–Hg bonding orbital of lowest energy arises from the favorable overlap between the unoccupied p_x orbitals of both metal atoms, which point towards each other. However, the stabilized combination is too high in energy to be occupied (−9.3 eV). This orbital represents the LUMO of **5**. The only effective interaction between Cu and Hg involves the 6s orbital of Hg (stabilized by the d_{z^2} orbitals of Fe) and the d_{x^2} orbital of the copper fragment (the x axis is parallel to the Cu–Hg axis). The orbitals of both fragments are doubly occupied and generate a four-electron interaction, which is often considered to be unfavorable. However, the upper term of this interaction is only moderately destabilized due to contributions from energetically high-lying orbitals such as

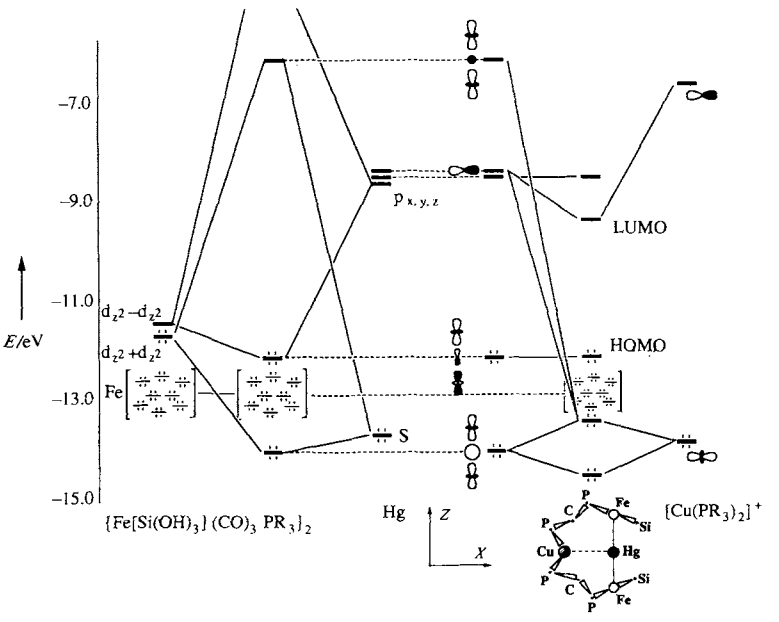

Figure 2. Simplified orbital interaction diagram between a $\{Fe[Si(OH)_3](CO)_3(PR_3)\}_2$ dimer and a Hg atom (left). Both fragments are assumed to be neutral. The orbitals of the resulting heterotrinuclear complex fragment are then allowed to interact with $[Cu(PR_3)_2]^+$, which yields $[Hg\{Fe[Si(OH)_3](CO)_3(\cdot\text{-}H_2PCH_2PH_2)\}_2Cu]^+$ (**5**; right).

 © WILEY-VCH Verlag GmbH, D-69451 Weinheim, 1997 0570-0833/97/3624-2759 $ 17.50+.50/0

the p_x orbital of Hg and the antibonding orbital of the trinuclear fragment referred to as $d_{z^2}(Fe_1) - s(Hg) + d_{z^2}(Fe_2)$. The four-electron interaction yields a moderate energy splitting of about 1 eV between the resulting orbitals, and should be considered as globally devoid of any repulsive character (Figure 2, right).

Although the short Cu–Hg distance cannot be ascribed to a definite metal–metal bond, the T shape of the complex allows the two metal atoms to approach each other to the limits of their covalent radii without developing the repulsion characteristic of pair–pair interactions. This is somewhat reminiscent of 1,6-transannular interactions in ten-membered organic rings. We believe the structure of complex **4** and the Cu–Hg distance to result, at least in part, from steric and strain factors that are expected to develop in the mesocycle constructed around the T-shaped metal framework, and from the van der Waals interactions between heavy-metal atoms with closed-shell configurations.[14]

The dynamic behavior observed for the PCH_2 protons of the dissymmetric molecule **4** (broad ^1H NMR signals at $\delta =$ 3.76 and 3.48), together with the successful simulation of the $^{31}P\{^1H\}$ NMR spectrum at 300 K as an AA′XX′ spin system, indicates the existence of an average plane of symmetry. This can be achieved by torsion along the Cu–Hg bond (Scheme 3), which can be compared to a "molecular torsion pendulum".

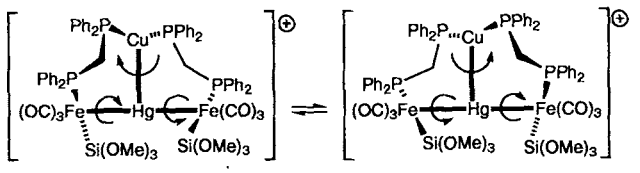

Scheme 3. The dynamic behavior of **4** in solution which accounts for the occurrence of an average mirror plane containing the four metal centers.

Owing to the lability of the P→Cu bond, the "locking/unlocking" equilibrium between the chain **3** and the ring **4** (Scheme 2) can be shifted towards **3** by lowering the temperature, which favors nitrile over phosphane coordination to Cu^I, and by increasing the MeCN and/or the Cu^+ concentration. The absence of MeCN ligand(s) on the copper atom of **4** supports the presence of a Cu–Hg bonding interaction, which decreases the coordinative unsaturation of the Cu atom.[15]

Experimental Section

All experiments were carried out under nitrogen by using Schlenk-tube techniques. Satisfactory elemental analyses were obtained for all complexes. NMR spectra were recorded on Bruker SY200 and AC300 instruments, and mass spectra were measured on a Fisons ZAB-HF spectrometer (Université Louis Pasteur, R. Hueber). Unless otherwise specified, the pure complexes are air-stable in the solid-state for prolonged periods of time.

2: Solid **1** (0.200 g, 0.134 mmol) and [AuBr(tht)] (0.050 g, 0.137 mmol) were mixed and cooled to −78 °C, and then CH_2Cl_2 (5 mL) was added. After the solution warmed to room temperature it was stirred for 1 h under exclusion of light. The resulting yellow solution was filtered, evaporated to 1 mL, and layered with 10 mL of hexane. The mixture was allowed to stand at 0 °C, and bright yellow crystals formed after one week (0.200 g, 75%). IR (KBr): ν(CO) = 2012 (vw), 1994 (s), 1943 (m), 1921 cm^{-1} (vs); FIR (polyethylene): ν(Au–Br) = 239 cm^{-1} (vs); ^1H NMR (200 MHz, $CDCl_3$, 323 K): $\delta = 3.54$ (s, 18H, OCH_3), 3.61 (br m, 4H, CH_2), 7.26–7.66 (m, 40H, C_6H_5); $^{31}P\{^1H\}$ NMR (81.02 MHz, CH_2Cl_2/C_6D_6, 303 K): $\delta = 48.3$ (br s, 2P, P(Fe), $^2J(P,^{199}Hg) \approx 170$ Hz), 21.8 (d, 2P, P(Au), $^2J(P,P) = 19$ Hz); (263 K): $\delta = 46.5$ (d, 2P, P(Fe), $^2J(P,P) = 19$, $^2J(P,^{199}Hg) = 180$ Hz), 21.0 (d, 2P, P(Au)).

3: Solid **1** (0.200 g, 0.134 mmol) was added at 0 °C to a solution of $[Cu(NCMe)_4]PF_6$ (0.100 g, 0.268 mmol) in CH_2Cl_2 (10 mL). The clear solution was stirred for 0.5 h, and then the volume reduced to about 5 mL. After layering the solution with hexane, yellow, air-stable crystals of **3** formed after a few days at 5 °C (0.26 g, 90%). IR (KBr): ν(CN) = 2314 (vw), 2278 (vw); ν(CO) = 1994 (s), 1935 (sh), 1929 (vs); ν(PF) = 840 cm^{-1} (vs); $^{31}P\{^1H\}$ NMR (81.02 MHz, CH_2Cl_2/CD_2Cl_2, 223 K): $\delta = 48.0$ (d, 2P, P(Fe), $^2J(P,P) = 8$ Hz), −15.6 (d, 2P, P(Cu)); (CH_2Cl_2/CD_3CN, 304 K): $\delta = 53.0$ (s, 2P, P(Fe), $^2J(P,^{199}Hg) \approx 170$ Hz), −13.5 (br s, 2P, P(Cu)).

4: Solid **1** (0.298 g, 0.200 mmol) was dissolved in CH_2Cl_2 (10 mL), and $[Cu(NCMe)_4]PF_6$ (0.075 g, 0.200 mmol) was added. The solution was stirred for 15 min and then layered with hexane. Large orange crystals of $4 \cdot 4CH_2Cl_2$ were isolated after one day. IR (KBr): 1999 (s), 1931 cm^{-1} (vs, br); $^{31}P\{^1H\}$ NMR (121.1 MHz, $CDCl_3$, 300 K): $\delta = 47.7$ (AA′XX′ spin system, 2P, P(Fe), $N =$ 51 Hz), −9.9 (br, 2P, P(Cu)).

Keywords: copper · mercury · metallacycles · metal–metal interactions · molecular dynamics

[1] *Comprehensive Organometallic Chemistry, Vol. 10*, 2nd ed. (Eds.: E. W. Abel, F. G. A. Stone, G. Wilkinson), Pergamon, Oxford, **1995**.

[2] See for example a) D. P. Funeriu, J.-M. Lehn, G. Baum, D. Fenske, *Chem. Eur. J.* **1997**, *3*, 99–104; b) A. F. Williams, *ibid.* **1997**, *3*, 15–19; c) J. A. Whiteford, C. V. Lu, P. J. Stang, *J. Am. Chem. Soc.* **1997**, *119*, 2524–2533; d) C. R. Woods, M. Benaglia, F. Cozzi, J. S. Siegel, *Angew. Chem.* **1996**, *108*, 1977–1980; *Angew. Chem. Int. Ed. Engl.* **1996**, *35*, 1830–1833; e) P. R. Ashton, S. Menzer, F. M. Raymo, G. K. H. Shimizu, J. F. Stoddart, D. J. Williams, *Chem. Commun.* **1996**, 487–490; f) M. Fujita, F. Ibukuro, K. Yamaguchi, K. Ogura, *J. Am. Chem. Soc.* **1995**, *117*, 4175–4176; g) P. J. Stang, D. H. Cao, S. Saito, A. M. Arif, *ibid.* **1995**, *117*, 6273; h) E. C. Constable, *Prog. Inorg. Chem.* **1994**, *42*, 67; i) *New J. Chem.* **1993**, *17*, 619–763, and references therein.

[3] P. Braunstein, B. Oswald, A. Tiripicchio, M. Tiripicchio Camellini, *Angew. Chem.* **1990**, *102*, 1206–1209; *Angew. Chem. Int. Ed. Engl.* **1990**, *29*, 1140–1143.

[4] See for example a) H. Schmidbaur, *Gold Bull.* **1990**, *23*, 11; b) H. Schmidbaur, *Pure Appl. Chem.* **1993**, *65*, 691; c) D. M. P. Mingos, *J. Chem. Soc. Dalton Trans.* **1996**, 561–566, and references therein.

[5] P. Pyykkö, *Chem. Rev.* **1988**, *88*, 563–594, and references therein.

[6] P. Braunstein, M. Knorr, A. Tiripicchio, M. Tiripicchio Camellini, *Inorg. Chem.* **1992**, *31*, 3685–3687.

[7] Review: J. T. Mague, *J. Cluster Sci.* **1995**, *6*, 217–269.

[8] N. Hadj-Bagheri, R. J. Puddephatt, *Inorg. Chem.* **1989**, *28*, 2384.

[9] a) Crystal structure determination of $4 \cdot 4CH_2Cl_2$: Crystallographic data: Siemens Stoe AED 2 diffractometer, $Mo_{K\alpha}$ radiation ($\lambda = 0.71073$ Å), graphite monochromator; intensity data were collected with the $\Omega/2\Theta$ scan mode at 293 K. $C_{66}H_{70}Cl_8CuF_6Fe_2HgO_{12}P_5Si_2$: orange crystals with approximate dimensions 0.5 × 0.4 × 0.4 mm, monoclinic, space group $P2/n$; $a =$ 15.663(6), $b = 12.120(5)$, $c = 22.620(7)$ Å, $\beta = 107.78(5)°$, $V = 4089(3)$ Å^3, $Z = 2$, $\rho_{calcd} = 1.6579$ g cm^{-3}, $F(000) = 2032$; 6997 independent reflections in the scan range $3.36 < 2\theta < 50.0°$, of which 6240 with $I > 2\sigma(I)$ were used in structure solution and refinement [9b] for 466 parameters; $R_1 = |F_o - F_c|/|F_o| = 0.0481 (I > 2\sigma(I))$, $wR_2 = [w(F_o^2 - F_c^2)^2/wF_o^4]^{1/2} = 0.1362$ (all data), GOF = 1.084; non-hydrogen atoms were refined anisotropically, and hydrogen atoms in idealized geometry; highest residual electron density 1.48 e Å^{-3}; b) SHELXL-93 (G. M. Sheldrick, Universität Göttingen, **1993**; c) The crystallographic data (excluding structure factors) for the structure reported in this paper have been deposited with the Cambridge Crystallographic Data Centre as supplementary publication no. CCDC-100337. Copies of the data can be obtained free of charge on application to The Director, CCDC, 12 Union Road, Cambridge CB2 1EZ, UK (fax: int. code + (1223) 336-033; e-mail: deposit@chemcrys.cam.ac.uk).

[10] a) P. Braunstein, M. Knorr, U. Schubert, M. Lanfranchi, A. Tiripicchio, *J. Chem. Soc. Dalton Trans.* **1991**, 1507–1514; b) P. Braunstein, T. Faure, M. Knorr, T. Stährfeldt, A. DeCian, J. Fischer, *Gazz. Chim. Ital.* **1995**, *125*, 35–50; c) M. Knorr, P. Braunstein, A. Tiripicchio, F. Ugozzoli, *Organometallics*, **1995**, *14*, 4910–4919; d) M. Knorr, P. Braunstein, A. Tiripicchio, F. Ugozzoli, *J. Organomet. Chem.* **1996**, *526*, 105–116.

[11] a) M. J. Chetcuti in ref. [1], pp. 23–84; b) E. Rosenberg, K. I. Hardcastle in ref. [1], pp. 323–350.

[12] P. Braunstein, U. Schubert, M. Burgard, *Inorg. Chem.* **1984**, *23*, 4057–4064, and references therein.

 © WILEY-VCH Verlag GmbH, D-69451 Weinheim, 1997 0570-0833/97/3624-2760 $ 17.50+.50/0

[13] a) R. Hoffmann, W. N. Lipscomb, *J. Chem. Phys.* **1962**, *36*, 2179–2189, 3489–3493; *ibid.* **1962**, *37*, 2872–2883; b) R. Hoffmann, *ibid.* **1963**, *39*, 1397–1412. Parameters were taken from the following references: Cu: P. J. Hay, J. C. Thibeault, R. Hoffmann, *J. Am. Chem. Soc.* **1975**, *97*, 4884–4899; Fe, P: R. H. Summerville, R. Hoffmann, *ibid.* **1976**, *98*, 7240–7254; Hg: D. J. Underwood, R. Hoffmann, K. Tatsumi, A. Nakamura, Y. Yamamoto, *ibid.* **1985**, *107*, 5968–5980; Si: N. Trong Anh, M. Elian, R. Hoffmann, *ibid.* **1978**, *100*, 110–116. The geometry used for the calculations was deduced from the X-ray structure of **4**.

[14] a) P. Pyykkö, N. Runeberg, F. Mendizabal, *Chem. Eur. J.* **1997**, *3*, 1451–1457; b) C. Hollatz, A. Schier, H. Schmidbaur, *J. Am. Chem. Soc.* **1997**, *119*, 8115–8116.

[15] J. Diez, M. P. Gamasa, J. Gimeno, A. Tiripicchio, M. Tiripicchio Camellini, *J. Chem. Soc. Dalton Trans.* **1987**, 1275.

Theoretical Studies of the Structure, Aromaticity, and Magnetic Properties of *o*-Benzyne**

Haijun Jiao, Paul von Ragué Schleyer,* Brett R. Beno, Kendall N. Houk,* and Ralf Warmuth*

In memory of Georg Wittig

o-Benzyne (1,2-didehydrobenzene, **1**) was postulated as an unstable intermediate by Wittig 57 years ago.[1] The distorted structure and the ability of **1** to participate in a wide variety of organic reactions have elicited intense interest in this reactive species.[2] The nature of **1** has been investigated extensively with both experimental[3–6] and theoretical methods.[7,8]

Warmuth recently reported the first ^{1}H and ^{13}C NMR spectra of **1** trapped within a hemicarcerand host.[9] Here we compare calculated ^{1}H and ^{13}C NMR chemical shifts as well as ^{13}C–^{13}C coupling constants to the experimental values, and report aromatic stabilization energies, magnetic susceptibilities, magnetic susceptibility exaltations, and nucleus-independent chemical shifts for **1**. These properties are used to probe the nature of **1**, and to address the possibility of bond localization induced by the in-plane π bond.

Benzene adopts its experimental geometry because the energetic preference for a σ bonding array with equal C–C bond lengths and D_{6h} symmetry is larger than the destabilization of the π system, which favors a bond-localized D_{3h} geometry.[10] Since the in-plane π bond in **1** distorts the molecule away from D_{6h} symmetry, reducing the σ stabilization, does bond localization of the π system result? If so, to what extent, and is **1** best described as a cyclohexadienyne (**1a**), a cyclic cumulene (**1b**), or a delocalized aryne (**1c**)?

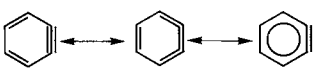

1a **1b** **1c**

[*] Prof. Dr. P. von R. Schleyer, Dr. H. Jiao
Computer-Chemie-Zentrum
Institut für Organische Chemie der Universität Erlangen-Nürnberg
Henkestrasse 42, D-91054 Erlangen (Germany)
Fax: Int. code + (9131) 85-9132
e-mail: pvrs@organik.uni-erlangen.de
Prof. K. N. Houk, Dr. R. Warmuth, Dr. B. R. Beno
Department of Chemistry and Biochemistry
University of California, Los Angeles
Los Angeles, CA 90095-1569 (USA)
Fax: Int. code + (310) 206-1843
e-mail: houk@chem.ucla.edu

[**] This work was supported by the Deutsche Forschungsgemeinschaft in Erlangen, and by the National Science Foundation and the Alexander von Humboldt Foundation (Feodor-Lynen fellowship for R.W.) in Los Angeles.

Recent experimental studies provided structural information for **1**. Radziszewski et al.[5d] measured a C≡C stretching vibration of 1846 cm^{-1} in a neon matrix. This is consistent with the value of (1860 ± 15) cm^{-1} given by an earlier laser photodetachment study.[6a] This frequency is closer to the C≡C stretching vibration in acetylene (1974 cm^{-1}) than to the C=C stretch in ethylene (1623 cm^{-1}).[11] Based on a dipolar ^{13}C NMR spectrum of 1,2-$^{13}C_2$-**1** in an argon matrix, Orendt et al.[12] deduced a C1–C2 length of (1.24 ± 0.02) Å, which is also indicative of partial triple bond character.

In the present study geometries were optimized with density functional theory (DFT) using the Becke3LYP[13] and BLYP[14] functionals and several basis sets with the Gaussian 94 program.[15] Magnetic susceptibilities (χ) were calculated at the Becke3LYP/6-31G* level with the CSGT method,[16] and nucleus-independent chemical shifts[17] at GIAO-SCF/6-31 + G*//Becke3LYP/6-31G*.[18] NBO analyses[19] provided the Wiberg bond indices (WBI) on the Becke3LYP/6-31G* geometries. The CSGT, GIAO, and NBO methods are implemented in Gaussian 94. The ^{1}H and ^{13}C NMR chemical shifts as well as the ^{13}C–^{13}C coupling constants were calculated using the PW91 (Perdew-Wang-91) exchange correlation potential and the IGLO-III basis set with the SOS-DFPT method (SOS-DFPT = *s*um *o*ver *s*tates *d*ensity *f*unctional *p*erturbation *t*heory)[20] in the deMon program.[21]

Table 1 summarizes the optimized C–C bond lengths of **1** at various computational levels. Most of the methods listed give C1–C2 bond lengths within 0.02 Å of the experimental value

Table 1. Optimized bond lengths [Å] for **1** at various computational levels.

Level	C1–C2	C2–C3	C3–C4	C4–C5
Becke3LYP/6-31G*	1.251	1.385	1.412	1.408
Becke3LYP/6-311 + G*	1.245	1.383	1.410	1.405
Becke3LYP/6-311G**	1.244	1.382	1.410	1.405
Becke3LYP/6-311 + G**	1.245	1.382	1.410	1.405
BLYP/D95**[12]	1.270	1.401	1.431	1.421
BLYP/6-31G*	1.264	1.394	1.424	1.415
BLYP/6-311 + G**	1.257	1.392	1.422	1.413
CASSCF(8,8)/DZ[8c]	1.274	1.412	1.406	1.432
CASSCF(8,8)/DZP[8a]	1.262	1.406	1.397	1.426
CASSCF(8,8)/cc-pVDZ[8b]	1.262	1.404	1.396	1.424
CASSCF(8,8)/(5s4p2d/3s2p)[8a]	1.251	1.399	1.390	1.420
GVB/6-31G*[7h]	1.260	1.383	1.389	1.404
GVB/6-31G**[7o]	1.260	1.383	1.389	1.404
MP2/6-31G**[7o]	1.268	1.389	1.405	1.410
MP2/DZ + P[7f]	1.275	1.398	1.413	1.417
MP2/TZ + 2P[7e]	1.259	1.385	1.404	1.406
MCSCF(2,2)/6-311G**[7n]	1.255	1.383	1.388	1.404
MCSCF(8,8)/3-21G[7n]	1.260	1.403	1.397	1.422
CCSD(T)/6-31G**[7o]	1.269	1.394	1.411	1.413
exptl[12]	1.24 ± 0.02			

of (1.24 ± 0.02) Å, but the Becke3LYP bond lengths are slightly closer.[12] The CASSCF structures have C2–C3, C3–C4, and C4–C5 bond lengths which alternate in the pattern long-short-long, while the those at the Becke3LYP level have bond lengths that follow the pattern short-long-short. On the basis of bond lengths alone, the CASSCF structures resemble **1a**, while the Becke3LYP geometries are closer to **1b**. Which more accurately describes the nature and electronic structure of **1**? To model the strain effects and bonding in **1** as closely as possible, we optimized the geometries of a set of reference molecules (**2**–**9**).

As shown in Figure 1, the bond length and the WBI of the triple bond in **1** are close to the mean of the corresponding values for 2-butyne (**2**) and the central C=C bond in

 © WILEY-VCH Verlag GmbH, D-69451 Weinheim, 1997 0570-0833/97/3624-2761 $ 17.50+.50/0

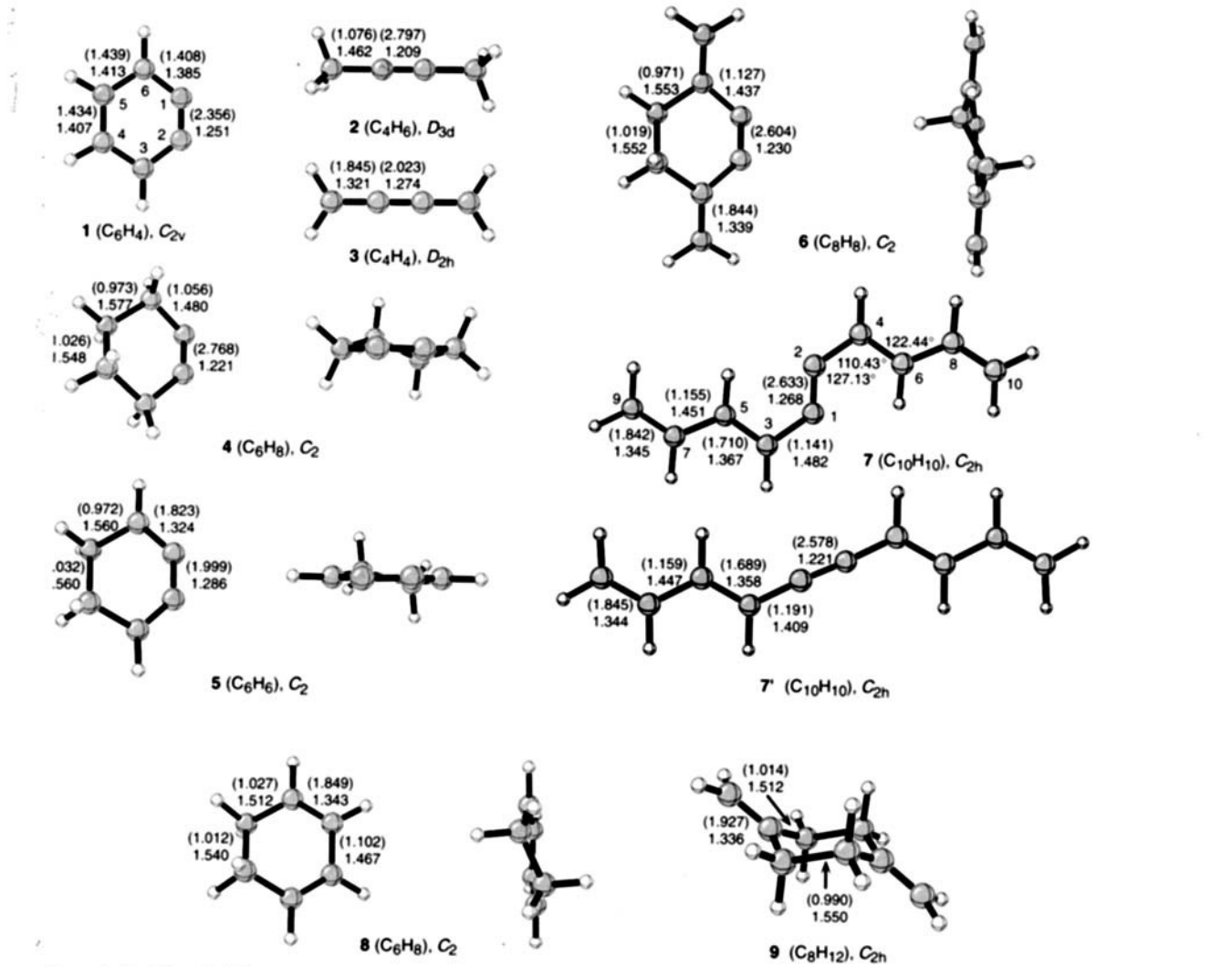

Figure 1. Bond lengths [Å] and corresponding Wiberg bond indices (in parentheses) for **1**–**9** optimized at the Becke3LYP/6-31G* level (**7** is partially optimized with bond angles fixed as in **1**).

butatriene (**3**). However, both **2** and **3** lack the strain present in **1**. Indeed, strain elongates the triple and cumulene bonds by 0.012 Å in both cyclohexyne (**4**) and 1,2,3-cyclohexatriene (**5**); the corresponding WBIs are smaller as well. However, neither **4** nor **5** are the best reference molecules. The triple bond in **1** is connected to two formally sp^2 carbon atoms, and this situation is not present in **4**. The most appropriate model compound, 1,4-dimethylene-2-cyclohexyne (**6**), has a longer C≡C bond length and a smaller WBI than **2**; both strain and conjugation effects are responsible. The strain effects were evaluated by comparing the distorted (partially optimized) reference molecule **7** (all-*trans*-1,3,7,9-decatetraene-5-yne) with the fully optimized **7′**, in which the bond angles are fixed as in **1**. The C≡C bond in **7** (1.268 Å) is longer than in **7′** (1.221 Å), and the corresponding WBI in **7** (2.633) is larger than in **7′** (2.578). Strain also elongates C1–C3 from 1.409 Å in **7′** to 1.482 Å in **7**.

At the Becke3LYP/6-31G* level, the WBI calculated for the triple bond in **1** (2.356) is smaller than that in **7** (2.633). The other WBIs are intermediate between those for the double and single bonds in **7**, and are close to the value for benzene (1.437). Although the geometry of **1** is distorted due to strain, the electron delocalization still resembles that of benzene. When the benzene WBI is subtracted, the net WBI of 0.919 for C1–C2 in **1** corresponds to a single bond (compare the difference in WBI (0.923) between the C1–C2 triple bond and the C3–C5 double bond in **7**. Thus, **1** is more acetylene-like (**1a**) than cumulene-like (**1b**).

Alternatively, the correct structure of **1** can be addressed by comparing the experimental and computed NMR chemical shifts based upon different (e. g. CASSCF(8,8), CCSD(T), and Becke3LYP) geometries. As shown in Table 2, the calculated ^{1}H NMR chemical shifts agree well with the experimental values.[9] However, discrepancies were found for the ^{13}C NMR chemical shifts, especially for C1 and C2. The best agreement with the experimental values is obtained using

Table 2. ^{1}H and ^{13}C NMR chemical shifts calculated at the SOS-DFPT-PW91/III level and determined experimentally; the differences $\delta_{calcd} - \delta_{exptl} = \Delta\delta$ are given in parentheses.

Nucleus	δ_{exptl} [9]	δ_{calcd} [a]	δ_{calcd} [b]	δ_{calcd} [c]
H(C3,C6)	7.6	7.9 (0.3)	7.8 (0.2)	7.9 (0.3)
H(C4,C5)	7.0	7.1 (0.1)	7.0 (0.1)	7.2 (0.2)
C1,C2	182.7	186.4 (3.7)	193.7 (11.0)	195.1 (12.4)
C3,C6	126.9	127.2 (0.3)	129.1 (2.2)	128.7 (1.8)
C4,C5	138.2	142.3 (4.1)	143.3 (5.1)	143.2 (5.0)

[a] With Becke3LYP/6-311 + G** geometry. [b] With CASSCF(8,8)/DZP geometry. [c] With CCSD(T)/6-31G** geometry.

 © WILEY-VCH Verlag GmbH, D-69451 Weinheim, 1997 0570-0833/97/3624-2762 $ 17.50+.50/0

the Becke3LYP/6-311 + G** geometry (C1–C2 1.245 Å; deviation of $\Delta\delta = 3.7$ for C1 and C2). The calculated ^{13}C NMR chemical shifts for C1 and C2 obtained using CASSCF(8,8)/DZP (C1–C2 1.262 Å) and CCSD(T)/6-31G** geometries (C1–C2 1.269 Å) are 11.0 and 12.4 ppm larger than the experimental value. The calculated $^{13}C-^{13}C$ coupling constants obtained using the Becke3LYP/6-311 + G** geometry agree well with the experimentally deduced values (Table 3). That the ^1H chemical shifts of **1** are close to that for benzene

Table 3. $^{13}C-^{13}C$ coupling constants [Hz] for **1** calculated at the SOS-DFPT-PW91/III//Becke3LYP/6-311 + G** level.

	C1–C2	C2–C3	C3–C4	C4–C5
^1J	191.9	72.8	49.8	69.0
$^1J_{expt}$ [9]	(177.9 ± 0.7)	(75.7 ± 0.9)	(50.9 ± 0.8)	(71.0 ± 0.8)
	C1–C3	C1–C5	C3–C5	
^2J	−10.9	3.4	−1.3	
	C1–C4	C3–C6		
^3J	10.8	2.1		

($\delta = 7.37$) also indicates a comparable degree of aromaticity. Hence, the geometry optimized for **1** at the Becke3LYP/6-311 + G** level should be reasonably accurate. We also predicted the ^2J and ^3J coupling constants to assist further experimental investigations (Table 3).

Does the in-plane π bond affect the aromaticity of **1**? The criteria of aromaticity—for example aromatic stabilization energy (ASE),[22] magnetic susceptibility exaltation (Λ),[23] and nucleus-independent chemical shifts (NICS)[17]—provide evidence for the degree of electron delocalization in **1**. The ASE of **1** can be estimated by using homodesmotic reactions [Eqs. (1) and (2)].[24] In Equation (1), angle strain corrected **7**

$$\mathbf{7} - \textit{trans}\text{-butadiene} = \mathbf{1} \quad (1)$$

$$\mathbf{6}+\mathbf{8} = \mathbf{9}+\mathbf{1} \quad (2)$$

and *trans*-butadiene are used as the reference molecules. Reference molecule **6**, 1,3-cyclohexadiene (**8**), and 1,4-dimethylene cyclohexane (**9**) are used in Equation (2); all molecules are the most stable isomers, and the strain contributions cancel to a large extent. The ASE of benzene, computed by using Equation (3), provides the most direct comparison.[25]

$$\text{all-}\textit{trans}\text{-decapentaene} - \textit{trans}\text{-butadiene} = \text{benzene} \quad (3)$$

The ASEs calculated for **1** using Equations (1) and (2) are larger than that obtained for benzene with Equation (3) (Table 4).[25] The considerable strain energy of **1** (53.6 kcal mol^{-1}), approximated by the energy difference between the partially optimized **7** and fully optimized **7'**, is responsible for its high reactivity. The aromaticity of **1** does not overcome the strain energy; the net destabilization of **1** is 35.0 kcal mol^{-1}. Despite the large strain, the singlet state of **1** is still 31.8 kcal mol^{-1} lower in energy than the triplet state (Becke3LYP/6-311 + G*). The value at this level is somewhat smaller than the experimental results based on photoelectron spectroscopy (e. g. 37.6 kcal mol^{-1} [6a] and (38.5 ± 2.4) kcal mol^{-1} [6b]) as well as high-level ab initio calculations (33.3 kcal mol^{-1} [7f] and (36 ± 2) kcal mol^{-1} [7n]). The Becke3-LYP/6-311 + G** C≡C stretching vibration at 1948 cm^{-1} (after scaling)[26] is larger than the value for the neon matrix (1846 cm^{-1}).[5d]

Table 4. Becke3LYP/6-31G* total energies E_{tot} in Hartree, ASE values in kcal mol^{-1}, and χ and Λ values in ppm cgs (at the CSGT-Becke3LYP/6-31G*// Becke3LYP/6-31G* level) for **1** and some important comparison compounds.

	E_{tot}	ASE [a]	χ	Λ [a]
1	−230.90996 [b]	−18.6 (1), −18.7 (2)	−46.4	−23.4 (1)
6	309.50726			
7 [c]	−386.87239		−45.8	
8	233.41892			
9	−312.04609			
trans-butadiene	−155.99216		−22.8	
all-*trans*-decapentaene	−388.21302		−51.7	
benzene	−232.24870	−17.5 (3)	−46.1	−16.7 (3)

[a] The homodesmotic Equation used for calculating the value is given in parentheses. [b] The Becke3LYP/6-311 + G* total energies for the singlet and triplet states of **1** are −230.96566 and −230.91499, respectively. [c] The total energy for fully optimized **7'** is −386.95777.

Like ASE, the magnetic susceptibility exaltation Λ[23] can also be estimated easily from homodesmotic equations, for example, from Equation (1). The calculated Λ value for **1** is greater than that for benzene (Table 4). The calculated NICS (which is proving to be a simple and efficient criterion of aromaticity)[17] of **1** is also much larger than that of benzene (Table 5). However, the local shielding of the in-plane π bond in **1** also contributes.

Table 5. The calculated NICS values for **1** and **6** as well as their difference (ΔNICS(**1** − **6**)) compared with those for benzene at the GIAO-SCF/6-31 + G*// Becke3LYP/6-31G* level.

R [Å] [a]	NICS(**1**)	NICS(**6**) [b]	NICS(**1**) − NICS(**6**)	NICS(benzene)
0.0	−20.8	−9.5	−11.3	−9.7
0.5	−19.1	−7.7	−11.4	−11.5
1.0	−14.3	−4.5	−9.8	−11.5
1.5	−9.1	−2.1	−7.0	−8.4
2.0	−5.4	−0.9	−4.5	−5.3
2.5	−3.3	−0.4	−2.9	−3.4
3.0	−2.1	−0.2	−1.9	−2.2

[a] Distance from the geometrical center and perpendicular to the ring plane. [b] Computed at the same distance (1.133 Å) as in **1** between the molecule center and the midpoint of the triple bond.

Reference molecule **6** was used to evaluate this in-plane contribution. The NICS value for **6** is −9.5 when computed at the same position in **6** as in **1** (i. e. using the same distance, (1.133 Å) between the center of the heavy atom and the midpoint of the triple bond). Taking this correction into account, the net NICS for **1** of −11.3 is still somewhat larger than that for benzene. Furthermore, the NICS values for the points perpendicular to the molecular plane of **1** are close to the corresponding values for benzene after correction (see Table 5).

The standard heat of formation ΔH_f(298 K) of **1** can be computed from Equation (4). From the Becke3LYP/6-311 + G** energy including the thermal correction at 298 K

$$\mathbf{1}+\textit{trans}\text{-2-butene} = \text{benzene} + \textit{trans}\text{-butadiene} \quad (4)$$

and the experimental heats of formation of the reference molecules in Equation (4),[27] ΔH_f(298 K) is 113.5 kcal mol^{-1}. This is higher than the experimental estimate of (106 ± 3) kcal mol^{-1} [3d, 7q] and the highest level ab initio result (106.0 kcal mol^{-1}).[7q]

In conclusion, *o*-benzyne is aromatic according to the geometric, energetic, and magnetic criteria. However, the in-

 © WILEY-VCH Verlag GmbH, D-69451 Weinheim, 1997 0570-0833/97/3624-2763 $ 17.50+.50/0

plane π bond induces a small amount of bond localization, resulting in a structure with more acetylenic (**1a**) than cumulenic (**1b**) character. The large angle strain in **1** is responsible for its high reactivity. Agreement between the computed and experimental ^{1}H and ^{13}C NMR chemical shifts as well as the $^1J(^{13}C,^{13}C)$ values supports the observation of **1** in a hemicarcerand strongly.[9] The Becke3LYP/6-311 + G** optimized structure of *o*-benzyne should be reasonably accurate.

Received: November 3, 1996
Revised version: August 7, 1997 [Z9783IE]
German version: *Angew. Chem.* **1997**, *109*, 2929 – 2933

Keywords: aromaticity · density functional calculations · 1,2-didehydrobenzene · NMR spectroscopy · strained molecules

[1] a) G. Wittig, G. Pieper, G. Fuhrmann, *Ber. Dtsch. Chem. Ges.* **1940**, *73*, 193 – 1218; b) G. Wittig, *Angew. Chem.* **1957**, *69*, 245 – 280.

[2] R. W. Hoffmann, *Dehydrobenzene and Cycloalkynes*, Academic Press, New York, **1967**, pp. 208 – 237.

[3] For example, the heat of formation ΔH_f(298 K) of **1** was measured: a) J. M. Riveros, S. Ingemann, N. M. M. Nibbering, *J. Am. Chem. Soc.* **1991**, *113*, 1053 [(105 ± 2.5) kcal mol^{-1}]; b) Y. Guo, J. J. Graboswki, *ibid.* **1991**, *113*, 5923 – 5931 [105 kcal mol^{-1}]; earlier determinations revised in this publication gave values of (118 ± 5) to (104 ± 5) kcal mol^{-1}; c) P. G. Wenthold, J. A. Paulino, R. R. Squires, *ibid.* **1991**, *113*, 7414 – 7415; d) P. G. Wenthold, R. R. Squires, *ibid.* **1994**, *116*, 6401 – 6412 [(106 ± 3) kcal mol^{-1}].

[4] UV spectrum: J. G. G. Simon, N. Münzel, A. Schweig, *Chem. Phys. Lett.* **1990**, *170*, 187 – 192; microwave spectrum: R. D. Brown, P. D. Godfrey, M. J. Rodler, *J. Am. Chem. Soc.* **1986**, *108*, 1296 – 1297.

[5] IR spectrum: a) C. Wentrup, R. Blanch, H. Briel, G. Gross, *J. Am. Chem. Soc.* **1988**, *110*, 1874 – 1880; b) O. L. Chapman, C. C. Chang, J. Kolc, N. R. Rosenquist, H. Tomioka, *ibid.* **1975**, *97*, 6586 – 6588; c) O. L. Chapman, K. Mattes, C. L. McIntosh, J. Pacansky, G. V. Calder, G. Orr, *ibid.* **1973**, *95*, 6134 – 6135; d) J. G. Radziszewski, B. A. Hess, Jr., R. Zahradnik, *ibid.* **1992**, *114*, 52 – 57.

[6] a) D. G. Leopold, A. E. S. Miller, W. C. Lineberger, *J. Am. Chem. Soc.* **1986**, *108*, 1379 – 1384; b) X. Zhang, P. Chen. *ibid.* **1992**, *114*, 3147 – 3148.

[7] a) J. O. Noell, M. D. Newton, *J. Am. Chem. Soc.* **1979**, *101*, 51 – 57; b) M. J. S. Dewar, G. P. Ford, C. H. Reynolds, *ibid.* **1983**, *105*, 3162 – 3167; c) S. Olivella, J. Salvador, *Int. J. Quantum Chem.* **1990**, *37*, 713 – 728; d) R. Liu, X. Zhao, P. Pulay, *J. Phys. Chem.* **1992**, *96*, 8336 – 8339; e) A. C. Scheiner, H. F. Schaefer III, *Chem. Phys. Lett.* **1991**, *177*, 471 – 476; f) A. C. Scheiner, H. F. Schaefer III, B. Liu, *J. Am. Chem. Soc.* **1989**, *111*, 3118 – 3124; g) I. Hiller, M. A. Vincent, F. M. Guest, W. von Niessen, *Chem. Phys. Lett.* **1987**, *134*, 403 – 406; h) K. Rigby, I. H. Hiller, M. Vincent, *J. Chem. Soc. Perkin Trans. 2* **1987**, 117 – 119; i) L. Radom, R. H. Nobes, D. J. Underwood, W.-K. Lee, *Pure Appl. Chem.* **1986**, *58*, 75 – 88; j) C. W. Bock, P. George, M. Trachtman, *J. Phys. Chem.* **1984**, *88*, 1467 – 1472; k) M. J. S. Dewar, T.-P. Tien, *J. Chem. Soc. Chem. Commun.* **1985**, 1243 – 1244; l) W. Thiel, *J. Am. Chem. Soc.* **1981**, *103*, 1420 – 1425; m) A. Nicolaides, W. T. Borden, *ibid.* **1993**, *115*, 11951 – 11957; n) S. G. Wierschke, J. J. Nash, R. R. Squires, *ibid.* **1993**, *115*, 11958 – 11967; o) E. Kraka, D. Cremer, *Chem. Phys. Lett.* **1993**, *216*, 333 – 340; we thank Prof. Dr. D. Cremer for providing the CCSD(T)/6-31G** *o*-benzyne geometry; p) E. Kraka, D. Cremer, *J. Am. Chem. Soc.* **1994**, *116*, 4929 – 4936; q) R. Lindh, M. Schütz, *Chem. Phys. Lett.* **1996**, *258*, 409 – 415; the experimental and theoretical thermochemical data are summarized in this paper; see also ref. [3b, d].

[8] a) R. Lindh, T. J. Lee, A. Bernhardsson, B. J. Persson, G. Karlström, *J. Am. Chem. Soc.* **1995**, *117*, 7186 – 7194; we thank Prof. Dr. R. Lindh for providing the CASSCF(8,8)/DZP *o*-benzyne geometry; b) O. Bludsky, V. Spirko, R. Kobayashi, P. Jørgensen, *Chem. Phys. Lett.* **1994**, *228*, 568 – 574; c) P. B. Karadakov, J. Gerratt, G. Raos, D. L. Cooper, M. Raimondi, *Isr. J. Chem.* **1993**, *33*, 253 – 264.

[9] R. Warmuth, *Angew. Chem.* **1997**, *109*, 1406 – 1409; *Angew. Chem. Int. Ed. Engl.* **1997**, *36*, 1347 – 1350.

[10] a) W. Kutzelnigg, *Einführung in die Theoretische Chemie*, 2nd ed., Verlag Chemie, Weinheim, New York, **1978**, p. 318; b) P. C. Hiberty, D. Danovich, A. Shurki, S. Shaik, *J. Am. Chem. Soc.* **1995**, *117*, 7760 – 7768, and references therein; c) A. Gobbi, Y. Yamguchi, G. Frenking, H. F. Schaefer III, *Chem. Phys. Lett.* **1995**, *244*, 27 – 31.

[11] W. J. Hehre, L. Radom, P. von R. Schleyer, J. A. Pople, *Ab Initio Molecular Orbital Theory*, Wiley-Interscience, New York, **1986**, p. 239.

[12] A. M. Orendt, J. C. Facelli, J. G. Radziszewski, W. J. Horton, D. M. Grant, J. Michl, *J. Am. Chem. Soc.* **1996**, *118*, 846 – 852.

[13] a) A. D. Becke, *J. Chem. Phys.* **1993**, *98*, 5648 – 5652; b) C. Lee, W. Yang, R. G. Parr, *Phys. Rev. B* **1988**, *37*, 785 – 789.

[14] A. D. Becke, *Phys. Rev. A* **1988**, *38*, 3098 – 3100.

[15] Gaussian 94, Revision D.2: M. J. Frisch, G. W. Trucks, H. B. Schlegel, P. M. W. Gill, B. G. Johnson, M. A. Robb, J. R. Cheeseman, T. A. Keith, G. A. Petersson, J. A. Montgomery, K. Raghavachari, M. A. Al-Latham, V. G. Zakrzewski, J. V. Ortiz, J. B. Foresman, J. Cioslowski, B. B. Stefanov, A. Nanayakkara, M. Challacombe, C. Y. Peng, P. Y. Ayala, W. Chen, M. W. Wong, J. L. Andres, E. S. Replogle, R. Gomperts, R. L. Martin, D. J. Fox, J. S. Binkley, D. J. Defrees, J. Baker, J. P. Stewart, M. Head-Gordon, C. Gonzalez, J. A. Pople, Gaussian, Inc., Pittsburgh, PA, **1995**.

[16] T. A. Keith, R. F. W. Bader, *Chem. Phys. Lett.* **1993**, *210*, 223 – 231.

[17] a) P. von R. Schleyer, C. Maerker, A. Dransfeld, H. Jiao, N. J. R. van Eikema Hommes, *J. Am. Chem. Soc.* **1996**, *118*, 6317 – 6318; b) H. Jiao, P. von R. Schleyer, *Angew. Chem.* **1996**, *108*, 2548 – 2551; *Angew. Chem. Int. Ed. Engl.* **1996**, *35*, 2383 – 2386; c) G. Subramanian, P. von R. Schleyer, H. Jiao, *ibid.* **1996**, *108*, 2824 – 2827 and **1996**, *35*, 2638 – 2641; d) H. Jiao, R. Nagelkerke, H. A. Kurtz, R. V. Williams, W. T. Borden, P. von R. Schleyer, *J. Am. Chem. Soc.* **1997**, *119*, 5921 – 5929; e) H. Jiao, P. von R. Schleyer, Y. Mo, M. A. McAllister, T. T. Tidwell, *ibid.* **1997**, *119*, 7075 – 7083; f) G. Subramanian, P. von R. Schleyer, H. Jiao, *Organometallics* **1997**, *16*, 2362 – 2369.

[18] a) R. Ditchfield, *Mol. Phys.* **1974**, *27*, 789 – 807; b) K. Wolinski, J. F. Hinton, P. Pulay, *J. Am. Chem. Soc.* **1990**, *112*, 8251 – 8260.

[19] A. E. Reed, L. A. Curtiss, F. Weinhold, *Chem. Rev.* **1988**, *88*, 899 – 926.

[20] For the calculation of chemical shifts, see V. G. Malkin, O. L. Malkina, M. E. Casida, D. R. Salahub, *J. Am. Chem. Soc.* **1994**, *116*, 5898 – 5908; for the calculation of coupling constants, see V. G. Malkin, O. L. Malkina, D. R. Salahub, *Chem. Phys. Lett.* **1994**, *221*, 91 – 99.

[21] Review: V. G. Malkin, O. L. Malkina, L. A. Eriksson, D. R. Salahub in *Modern Density Functional Theory* (Eds.: J. M. Seminario, P. Politzer), Elsevier, Amsterdam, **1995**, p. 273, and references therein.

[22] a) P. von R. Schleyer, P. K. Freeman, H. Jiao, B. Goldfuß, *Angew. Chem.* **1995**, *107*, 332 – 335; *Angew. Chem. Int. Ed. Engl.* **1995**, *34*, 337 – 340; b) P. von R. Schleyer, H. Jiao, *Pure Appl. Chem.* **1996**, *68*, 209 – 218; c) H. Jiao, N. J. R. van Eikema Hommes, P. von R. Schleyer, A. de Meijere, *J. Org. Chem.* **1996**, *61*, 2826 – 2828.

[23] H. J. Dauben, Jr., J. D. Wilson, J. L. Laity in *Non-Benzenoid Aromatics, Vol. 2* (Ed.: J. P. Snyder), Academic Press, New York, **1971**; for recent applications, see ref. [22].

[24] P. George, M. Trachtman, C. W. Bock, A. M. Bret, *J. Chem. Soc. Perkin Trans. 2* **1976**, 1222 – 1227.

[25] The computed ASE for benzene decreases when the length of the open-chain polyene used as the reference is increased. The ASE for benzene is −21.7 kcal mol^{-1} based on the homodesmotic equation: 3 × (*trans*-butadiene − ethylene) = benzene (see ref. [22c]).

[26] The correlation used for benzene was $y_{expt} = 19.9 + 0.96x$ (Becke3LYP/6-311 + G**).

[27] The standard heats of formation ΔH_f(298 K) are −(2.7 ± 0.2) kcal mol^{-1} for *trans*-2-butene, (19.8 ± 0.2) kcal mol^{-1} for benzene, and (26.3 ± 0.2) kcal mol^{-1} for *trans*-butadiene; see J. B. Pedley, R. D. Naylor, S. P. Kirby, *Thermochemical Data of Organic Compounds*, 2nd ed., Chapman and Hall, London, **1986**. The Becke3LYP/6-311 + G** total energies including thermal correction at 298 K are −230.89237 for **1**, −157.16078 for *trans*-2-butene, −232.20578 for benzene, and −155.95047 for *trans*-butadiene.

 © WILEY-VCH Verlag GmbH, D-69451 Weinheim, 1997 0570-0833/97/3624-2764 $ 17.50+.50/0

Merocyanine Dyes in the Cyanine Limit: A New Class of Chromophores for Photorefractive Materials**

Frank Würthner,* Rüdiger Wortmann,* Ralf Matschiner, Katarzyna Lukaszuk, Klaus Meerholz,* Yessika DeNardin, Reinhard Bittner, Christoph Bräuchle, and Rüdiger Sens

With the rapid progress in information and telecommunication technologies ("multimedia") faster methods for transmitting, storing, and processing data are required.[1] While fast optical data transmission through glass fibers is already well established, there is a need to develop high-speed storage and switching devices based on photons instead of electrons. A new promising method for reversible data storage is based on the photorefractive (PR) effect, whose "parallel character" allows optical processing of large amounts of data by holography.

Photorefractivity has been demonstrated only recently in amorphous organic materials.[2] Here, research is confronted with the difficult task of developing a complex functional material that provides photoconductivity and refractive-index modulation in films of high optical quality and stability against dielectric breakdown. The materials investigated so far are mostly composites consisting of a charge-transport agent (e. g. triarylamine or carbazole-based photoconductors[3]), an electrooptic (EO) chromophore with high second-order polarizability β,[4] small amounts of a sensitizer, and variable amounts of additives (plasticizer, polymeric binder).

Among the EO chromophores the azo dye 2,5-dimethyl-(4-nitrophenylazo)anisole (DMNPAA) dominates the scene

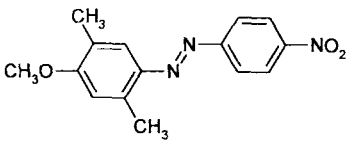

DMNPAA

because of its outstanding compatibility with carbazole charge-transport polymers.[5] With DMNPAA-doped polymers holographic gratings with almost 100% diffraction efficiency were achieved for the first time. To get such a strong PR effect, however, DMNPAA concentrations as high as 50 wt% and high electric fields of $50-100\ V\,\mu m^{-1}$ are required. For applications improved chromophores are needed to reduce the chromophore content and, thus, avoid problems with phase separation and to operate the devices at lower field strength. Here we introduce a conceptionally new class of dyes which represent a significant step towards this goal.

Our work was triggered by the fact that the refractive-index modulation in organic materials with a low glass-transition temperature is predominantly due to the Kerr and not the Pockels effect as in inorganic crystals.[7a] This difference is because in these composites the dipolar chromophores are able to reorient in the light-induced space-charge field.[6] As a result, a new figure-of-merit F_0 for photorefractive chromophores was derived which is approximated fairly well by Equation (1).[7a,8] Here M is the molecular weight, μ_g is the

$$F_0 = [9\mu_g\beta_0 + 2\mu_g^2\alpha_0/(kT)]/M \quad (1)$$

dipole moment, and α_0 and β_0 are two-level approximations for the static first- and second-order polarizabilities of the chromophore.[8] For "one-dimensional" chromophores consisting of a π system with donor and acceptor substitutents these polarizabilities can be reasonably approximated by considering the transition dipole μ_{ag}, the transition wavelength λ_{ag}, and the difference in dipole $\Delta\mu$ between the ground (g) and excited states (a) [Eqs. (2) and (3)].[7,8]

$$\alpha_0 = 2\mu_{ag}^2\lambda_{ag}/(hc) \quad (2)$$

$$\beta_0 = 6\mu_{ag}^2\Delta\mu\lambda_{ag}^2/(hc)^2 \quad (3)$$

Estimations for typical chromophores used in nonlinear optics (NLO) demonstrate that the main contribution in Equation (1) originates from the α term ("birefringence contribution"), whereas the β term ("electrooptical contribution") is only of minor importance.[7a,d] Therefore, design strategies should focus on the optimization of the α term, unlike in previously established concepts. According to a two-center charge-transfer model, the birefringence term is optimized when the ground and excited states display the same charge separation. For this *charge-resonance limit* the transition dipole μ_{ag} and therefore (according to Equation (2)) α_0 are maximized, whereas the change of dipole moment $\Delta\mu$ and therefore (according to Equation (3)) β_0 become zero.[7a] The first successful utilization of chromophores in the charge-resonance limit in PR polymers was demonstrated only recently.[7a-c]

According to Dähne et al.[9] and Marder et al.[10] merocyanines may be fine-tuned to become such a borderline case ("cyanine limit") with a 50% contribution each of the neutral and the zwitterionic resonance structures (Scheme 1). At this

Scheme 1.

point, the polymethine chain reaches the highest possible degree of conjugation with high values of μ_g and α, but a vanishing β.[9,10] Accordingly, we expected optimized neutrocyanines to be the best candidates for obtaining highly improved photorefractive materials.

[*] Dr. F. Würthner
Abteilung Organische Chemie II der Universität
Albert-Einstein-Allee 11, D-89081 Ulm (Germany)
Fax: Int. code + (731) 502-2840
e-mail: frank.wuerthner@chemie.uni-ulm.de

Priv.-Doz. Dr. R. Wortmann, Dipl.-Phys. R. Matschiner, Dipl.-Chem. K. Lukaszuk
Institut für Physikalische Chemie der Universität
Jakob Welder-Weg 11, D-55099 Mainz (Germany)
Fax: Int. code + (6131) 39-2980
e-mail: rwortmann@mzdmza.zdv.uni-mainz.de

Dr. K. Meerholz, Dipl.-Chem. Y. DeNardin, Dipl.-Chem. R. Bittner, Prof. Dr. C. Bräuchle
Institut für Physikalische Chemie der Universität
Sophienstrasse 11, D-80333 München (Germany)
Fax: Int. code + (89) 590-2290
e-mail: kmeerhol@olymp.phys.chemie.uni-muenchen.de

Dr. R. Sens
BASF, Farbenlaboratorium ZDT/N-C13, Ludwigshafen (Germany)

[**] This work was supported by BASF, the Volkswagen-Stiftung, and the German-Israeli Foundation. F.W. thanks the Fonds der Chemischen Industrie and the BMBF for a Liebig grant for "new materials". Y.D.N. thanks the Fondiatione "Ing. A. Gini" for a fellowship.

 © WILEY-VCH Verlag GmbH, D-69451 Weinheim, 1997 0570-0833/97/3624-2765 $ 17.50+.50/0

In contrast to the cationic cyanine and anionic oxonol dyes, little is known about the ideal charge-resonance state in uncharged merocyanines. Based on our experience with functional dyes for NLO[11] and thermal transfer printing,[12] monomethine dyes with electron-rich donor arenes and heterocyclic acceptors seemed most promising. Using 1-butyl-4-methyl-2,6-dioxo-1,2,5,6-tetrahydro-pyridine-3-carbonitrile (**2**)[13] as the acceptor unit, dyes **3** were synthesized in yields of over 80% (Scheme 2).[14]

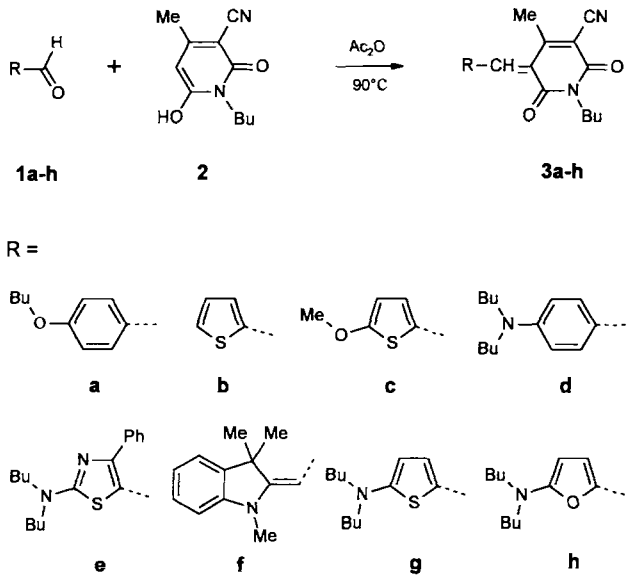

Scheme 2.

Based on the UV/Vis absorption spectra (Table 1 and Figure 1) a classification of merocyanines **3** in polyene-like and cyanine-like chromophores is possible. With increasing donor strength the absorption maximum is shifted to longer wavelengths, and the intensity of the transition increases. However, sharp and intense spectra which are typical for cyanine chromophores are observed only for the best donor units (**3f–h**).[15] In the *cyanine limit* both ground and excited states are characterized by equal contributions of the two resonance forms. As a consequence only small displacements of the nuclear coordinates occur upon excitation.

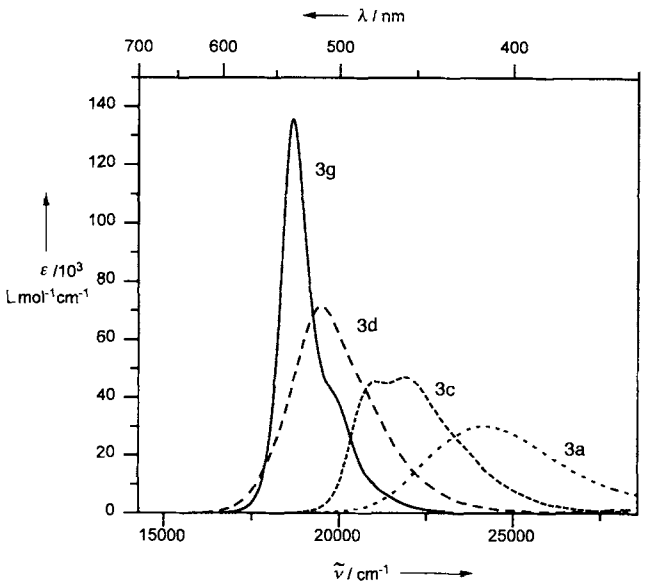

Figure 1. UV/Vis absorption spectra of the merocyanine dyes **3a**, **3c**, **3d**, and **3g** in dioxane.

To gain a more detailed insight into the electronic structure of these chromophores, we determined the dipole moments of the ground and excited states by means of electrooptic absorption measurements (EOAM; Table 1)[16] and estimated the values of α_0, β_0, and F_0 for the PR chromophores according to Equations (1)–(3). Based on these data the merocyanines **3a–d** are appropriately described as polyene-like compounds which are characterized by a large increase of their dipole moment upon excitation. Those compounds show also pronounced solvatochromism[17] and high β values, which are desired for applications in NLO.[11] The highest change in dipole moment (and also the highest β value) is observed for **3d.** From this it becomes clear that the cyanine limit is not accessible with benzene donor groups. This is due to the high aromaticity of the benzene ring, which counteracts the conjugation along the polymethine chain. Hence, the transition to cyanine-like chromophores is only possible with less aromatic heterocyclic donor groups. The series of five-membered heterocycles **3b**, **3c**, **3e**, **3g**, and **3h** illustrates this gradual change from a polyene-like to a cyanine-like dye system. Compounds **3f–h** exhibit negligible dipole changes of $\Delta\mu < 2$ D and thus represent cyanine dyes with optimized conjugation. Their PR figures-of-merit F_0 calculated accord-

Table 1. Optical[a] and electrical[b] properties of chromophores **3a–h** and DMNPAA, determined by UV/Vis and electrooptical absorption measurements in dioxane, and calculated PR figures-of merit F_0[c].

Compd	λ_{ag} [nm]	ε_{max} [L mol^{-1} cm^{-1}]	μ_{ag} [D]	μ_g [D]	$\Delta\mu$ [D]	α_0 [10^{-40} C V^{-1} m^2]	β_0 [10^{-50} C V^{-2} m^3]	F_0 [10^{-74} C^2 V^{-2} m^4 kg^{-1} mol]
3a	415	30100	7.4	6.9	9.7	26	52	0.21
3b	412	32700	7.5	6.6	6.0	26	32	0.22
3c	457	47100	8.4	8.4	5.0	36	42	0.49
3d	514	68000	9.5	10.8	9.1	52	122	0.87
3e	529	68900	8.9	10.0	4.0	47	51	0.54
3f	520	118000	10.2	12.8	1.9	61	31	1.38
3g	536	139000	9.6	14.0	1.8	55	27	1.40
3h	539	141000	9.7	14.6	1.1	57	17	1.62
DMNPAA	391	23000	7.0	6.4	13.0	22	56	0.20

[a] Absorption maximum λ_{ag}, extinction coefficient ε_{max}, and transition dipole μ_{ag}. [b] Ground-state dipole moment μ_g (1 D = 3.335 × 10^{-30} C m), difference between the dipole moments of the ground and the excited states $\Delta\mu = \mu_a - \mu_g$, and calculated static first- and second-order polarizabilities α_0 and β_0 according to Equations (2) and (3). With the same method β_0 values for *p*-nitroaniline and 5-dimethylamino-5′-nitro-2,2′-bithiophene [11] are 16 and 105 × 10^{-50} C V^{-2} m^3, respectively. [c] Calculated according to Equation (1).

 © WILEY-VCH Verlag GmbH, D-69451 Weinheim, 1997 0570-0833/97/3624-2766 $ 17.50+.50/0

ing to Equation (1) are almost ten times higher than those of DMNPAA, which raised our expectation of observing large photorefractive effects.

To demonstrate the validity of our concept and the utility of the new chromophores under conditions similar to those used for applications, we prepared PR composites consisting of the chromophores **3e** and **3g**, the charge-transport polymer poly(*N*-vinylcarbazole) (PVK), the IR sensitizer (2,4,7-trinitro-9-fluorenyliden)malononitrile (TNFM), and the plasticizer *N*-ethylcarbazole (ECZ). Despite their rather large dipole moments both chromophores exhibit excellent compatibility with the PVK matrix, allowing a chromophore content of up to 50% in the composite without problems of phase separation. The PR properties were investigated by two-beam coupling and four-wave mixing experiments at 790 nm (the samples were 105 μm thick). This yielded the gain coefficient Γ for the asymmetric energy transfer between the two beams writing the hologram and the diffraction efficiency η for the readout of the hologram by an independent probe beam.[5,7] These experiments revealed an additional advantage of the cyanine chromophores over traditional NLO chromophores: The shape of the absorption curve at the low energy side is rather steep (compare **3d** and **3g** in Figure 1), enabling the use of laser wavelengths closer to the wavelength of the absorption maximum and, thus, dispersive enhancement of the refractive-index modulation.

Figure 2 shows the results of our holographic investigation on the composite containing the thiophene chromophore **3g** (20 wt%). The field-dependent diffraction efficiency first

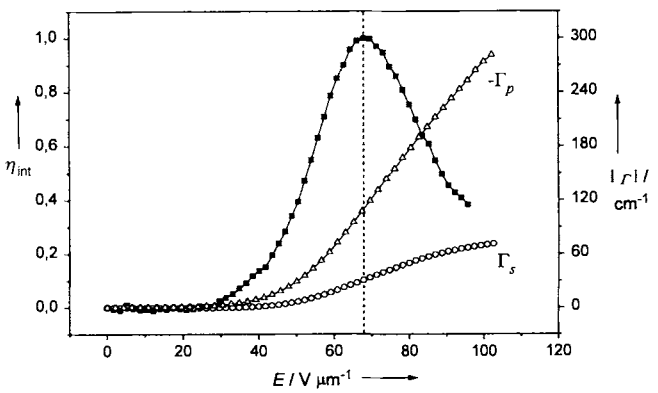

Figure 2. Dependence of the internal diffraction efficiency η_{int} for *s*-polarized writing beams ($I_1 \approx I_2 = 0.1$ W cm^{-2}) and *p*-polarized reading beam ($I_3 \ll I_1, I_2$) (■) as well as the absolute value of the gain coefficient Γ_s (○) and Γ_p (△) for *s*- or *p*-polarized writing beams ($I_1 = 100 \times I_2$) on the external applied electric field E. The composition of the material is **3g**:PVK:ECZ:TNFM = 20:45:33:2 (wt%). The experiments were performed with a tilted geometry (tilt angle $\Psi_{ext} = 60°$); the angle between the writing beams was $2\theta_{ext} = 20°$.

increases and reaches a maximum at $E_{max} = 68$ V μm^{-1}. This corresponds to complete internal diffraction of the readout beam ($\eta_{int} \approx 1$); externally, however, the achievable diffraction is limited to $\eta_{ext} \approx 0.3$ by the absorption of the material at the laser wavelength of 790 nm.[18] For even higher fields the diffraction efficiency decreases due to its $\sin^2$ dependency on the index-modulation amplitude Δn.[19] The maximum index-modulation amplitude achieved was $\Delta n \approx 5.2 \times 10^{-3}$ at 95 V μm^{-1}. The gain coefficient Γ increases monotonously with increasing field and finally reaches -280 cm^{-1} for *p*-polarized and $+70$ cm^{-1} for *s*-polarized beams. These values are among the largest ever reported for PR polymers, in particular in view of the long wavelength of 790 nm. The response time of the grating build-up was about 2800 ms at $E = 68$ V μm^{-1}.

For comparison, we also investigated a composite containing 50 wt% DMNPAA[5] under identical conditions. In this case complete internal diffraction was observed at slightly higher field ($E_{max} = 75$ V μm^{-1}). Assuming a quadratic dependence of Δn on the strength of the applied electric field,[6] this corresponds to a value for Δn that is 1.3 times larger in the composite using **3g**, even though the chromophore content is significantly lower.

Figure 3 shows the strengths of the electric fields which have to be applied to the device in order to achieve complete internal diffraction as a function of the chromophore content for **3e**, **3g**, and DMNPAA. The almost parallel shape of the

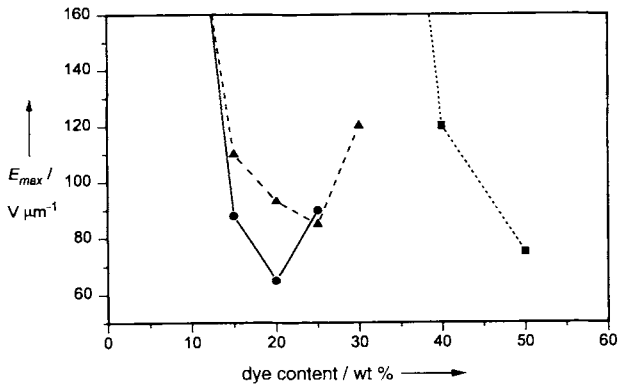

Figure 3. Dependence of the applied external field for achieving complete internal diffraction E_{max} on the chromophore content: **3g** (●), **3e** (▲), DMNPAA (■). By varying the ratio of PVK to ECZ the glass-transition temperature was adjusted to about 25 °C in all cases.

curves at low dye concentration agrees well with our expectations based on the electrooptic investigations. The thiophene chromophore **3g** was expected to show better photorefractive properties than **3e**, whereas both were considered to be much superior to the reference chromophore DMNPAA. However, by going to higher concentrations (≈ 50 wt%) an improvement in performance (reduction of E_{max}) is only observed for DMNPAA. By contrast, a significant drop in performance is observed already at a concentration of 25 wt% for the best chromophore of the series, the thiophene derivative **3g**. For loading above 40 wt%, no photorefractive effect could be observed.

To exploit the full potential of the new methine chromophores **3**, we are currently trying to solve the problems encountered at higher dye concentrations. These are possibly due to the formation of dye aggregates with antiparallel alignment of the dipoles which cannot be poled by the electric field. Therefore, we are attempting to reduce aggregation by attaching sterically demanding substituents to the chromophore core.

In conclusion, a material with excellent photorefractive performance was obtained with only 20% of **3g**. The new merocyanine dyes in the cyanine limit clearly demonstrate the benefit of optimizing chromophores according to Equation (1). The development of further new chromophores according to this design strategy will push forward the field of organic photorefractive materials.

Received: August 1, 1997 [Z10764IE]
German version: *Angew. Chem.* **1997**, *109*, 2933–2936

Keywords: chromophores · cyanines · donor–acceptor systems · holography · photorefractive materials

[1] a) M. Emmelius, G. Pawlowski, H. W. Vollmann, *Angew. Chem.* **1989**, *101*, 1475–1502; *Angew. Chem. Int. Ed. Engl.* **1989**, *28*, 1445–1471; b) W. A. Gambling, *Adv. Mater.* **1992**, *4*, 8–10.

[2] a) K. Meerholz, *Angew. Chem.* **1997**, *109*, 981–985; *Angew. Chem. Int. Ed. Engl.* **1997**, *36*, 945–948; b) O. Zobel, S. Schloter, D. Haarer, *Phys. Bl.* **1997**, *53*, 331–334; c) W. E. Moerner, S. M. Silence, *Chem. Rev.* **1994**, *94*, 127–155; d) Y. Zhang, R. Burzynski, S. Ghosal, M. K. Casstevens, *Adv. Mater.* **1996**, *8*, 111–124.

[3] a) H. Bässler, *Adv. Mater.* **1993**, *5*, 662–665; b) K.-Y. Law, *Chem. Rev.* **1993**, *93*, 449–486.

[4] Several reviews: *Chem. Rev.* **1994**, *94*, 1–278.

[5] a) K. Meerholz, B. L. Volodin, Sandalphon, B. Kippelen, N. Peyghambarian, *Nature* **1994**, *371*, 497–500; b) O. Zobel, M. Eckl, P. Strohriegl, D. Haarer, *Adv. Mater.* **1995**, *7*, 911–914.

[6] W. E. Moerner, S. M. Silence, F. Hache, G. C. Bjorklund, *J. Opt. Soc. Am. B* **1994**, *11*, 320–330.

[7] a) R. Wortmann, C. Poga, R. J. Twieg, C. Geletneky, C. R. Moylan, P. M. Lundquist, R. G. DeVoe, P. M. Cotts, H. Horn, J. E. Rice, D. M. Burland, *J. Chem. Phys.* **1996**, *105*, 10637–10647; b) D. M. Burland, R. G. Devoe, C. Geletneky, Y. Jia, V. Y. Lee, P. M. Lundquist, C. R. Moylan, C. Poga, R. J. Twieg, R. Wortmann, *Pure Appl. Opt.* **1996**, *5*, 513–520; c) P. M. Lundquist, R. Wortmann, C. Geletneky, R. J. Twieg, M. Jurich, V. Y. Lee, C. R. Moylan, D. M. Burland, *Science* **1996**, *274*, 1182–1185; d) B. Kippelen, F. Meyers, N. Peyghambarian, S. Marder, *J. Am. Chem. Soc.* **1997**, 119, 4559–4560.

[8] In a more refined treatment the dispersive enhancement of the first- and second-order polarizabilities at the laser frequency have to be taken into account. Moreover, the polarizability in the molecular dipole axis α_0 has to be replaced by the difference of the polarizabilities parallel and perpendicular to the molecular principal axis ($\Delta\alpha = \alpha_{\parallel} - \alpha_{\perp}$) [7a]. The letter h represents Planck's constant, and c the speed of light; β values are given in the Taylor-series convention. A survey of common β conventions is given in A. Willetts, J. E. Rice, D. M. Burland, D. P. Shelton, *J. Chem. Phys.* **1992**, *97*, 7590–7599.

[9] a) S. Dähne, *Chimia* **1991**, *45*, 288–296; b) S. Dähne, K.-D. Nolte, *J. Chem. Soc. Chem. Commun.* **1972**, 1056–1057.

[10] S. R. Marder, C. B. Gorman, F. Meyers, J. W. Perry, G. Bourhill, J.-L. Brédas, B. M. Pierce, *Science* **1994**, *263*, 511–514.

[11] a) F. Würthner, F. Effenberger, R. Wortmann, P. Krämer, *Chem. Phys.* **1993**, *173*, 305–314; b) F. Effenberger, F. Würthner, *Angew. Chem.* **1993**, *105*, 742–744; *Angew. Chem. Int. Ed. Engl.* **1993**, *32*, 719–721.

[12] G. Seybold, *J. Prakt. Chem.* **1996**, *338*, 392–396.

[13] J. Guareschi, *Ber. Dtsch. Chem. Ges. Bd. 4 (Referate, Patente, Nekrologe)* **1896**, *29*, 654–656.

[14] Methine dyes **3a–h** were characterized by ^{1}H NMR spectroscopy and correct elemental analysis; Bu = *n*-butyl.

[15] See for example C. Reichardt, H.-D. Engel, R. Allmann, D. Kucharczyk, M. Krestel, *Chem. Ber.* **1990**, *123*, 565–581.

[16] a) W. Liptay in *Excited States, Vol. 1* (Ed.: E. C. Lim), Academic Press, New York, **1974**, pp. 129–229; b) R. Wortmann, K. Elich, S. Lebus, W. Liptay, P. Borowicz, A. Grabowska, *J. Phys. Chem.* **1992**, *96*, 9724–9730.

[17] Solvatochromism (= displacement of the absorption bands under the influence of a solvent) is a direct consequence of the change in dipole upon excitation. Consequently, we observe a pronounced shift of the absorption maximum of 23 nm for **3d** ($\Delta\mu = 9$ D) in dimethylformamide compared to dioxane. On the other hand, **3g** has an absorption maximum at the same wavelength in both solvents.

[18] We assume that the somewhat high absorption is caused by complex formation between **3g** and TNFM. By reducing the amount of TNFM or by using a different sensitizer we hope to reduce the absorption losses.

[19] H. Kogelnik. *Bell System Tech. J.* **1969**, *48*, 2909–2947.

Self-Assembly of Several Components into a Highly Enantioselective Ti Catalyst for Carbonyl-Ene Reactions**

Koichi Mikami,* Satoru Matsukawa, Thorsten Volk, and Masahiro Terada

Dedicated to Professor Dieter Seebach on occasion of his 60th birthday

Asymmetric catalysis of organic reactions has become the focus of a great deal of research.[1] Berrisford, Bolm, and Sharpless recently emphasized the significance of "chiral ligand acceleration" in asymmetric catalysis.[2] Ligand-accelerated catalysis occurs when a more effective chiral catalyst for a particular reaction is obtained by the exchange of an achiral ligand for a chiral one [Reaction (1) in Scheme 1]; the reaction can thus proceed highly enantioselectively.[2] The combination of an achiral pre-catalyst with several chiral ligands or ligand components (L^{1*}, L^{2*},..) may selectively assemble into the most active and most enantioselective chiral catalyst among the possible catalysts derived from these ligand components in a quasi-combinatorial way [Reaction (2)].[3,4] Hill and Zhang recently reported the results of

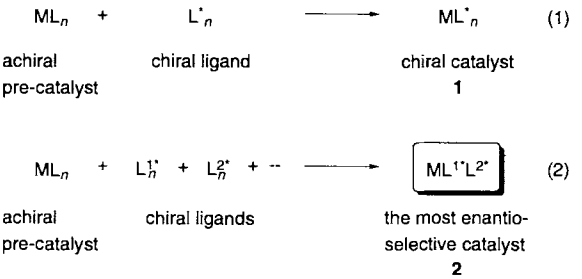

Scheme 1. General principle of the ligand exchange.

an elegant study in which such a "smart" self-assembly resulted in the creation of an achiral "immortal catalyst".[5] We here report on the first example of the formation of a chiral catalyst by virtue of the cooperation of several chiral ligands and an achiral complex by such a "smart" self-assembly. The application of this catalyst in the asymmetric catalysis of the carbonyl-ene reaction shows it to be not only the most enantioselective catalyst but also the most stable and therefore exclusively formed species. Thus, the present work can be considered in part as a "chiral evolution" of the studies by Hill and Zhang on an achiral system.

The self-assembly of a chiral titanium catalyst from an achiral precursor such as $Ti(OR)_4$ and two different chiral diol components is exemplified for two catalysts (Scheme 2), each of which was prepared by three routes. The combination of "acidic" (*R*)-binaphthol [(*R*)-BINOL][6] and the relatively basic diol (*R*)-$\alpha,\alpha,\alpha',\alpha'$-tetraphenyl-2,2-dimethyl-1,3-dioxo-

[*] Prof. Dr. K. Mikami, Dr. S. Matsukawa, Dr. T. Volk, Dr. M. Terada
Department of Chemical Technology
Faculty of Engineering
Tokyo Institute of Technology
2-12-1 Ookayama, Meguro-ku, Tokyo 152, (Japan)
Fax: Int. code + (3) 5734-2776
e-mail: kmikami@o.cc.titech.ac.jp

[**] This work was supported by the Alexander von Humboldt Foundation and the JSPS with a postdoctoral fellowship for T. V.

 © WILEY-VCH Verlag GmbH, D-69451 Weinheim, 1997 0570-0833/97/3624-2768 $ 17.50+.50/0

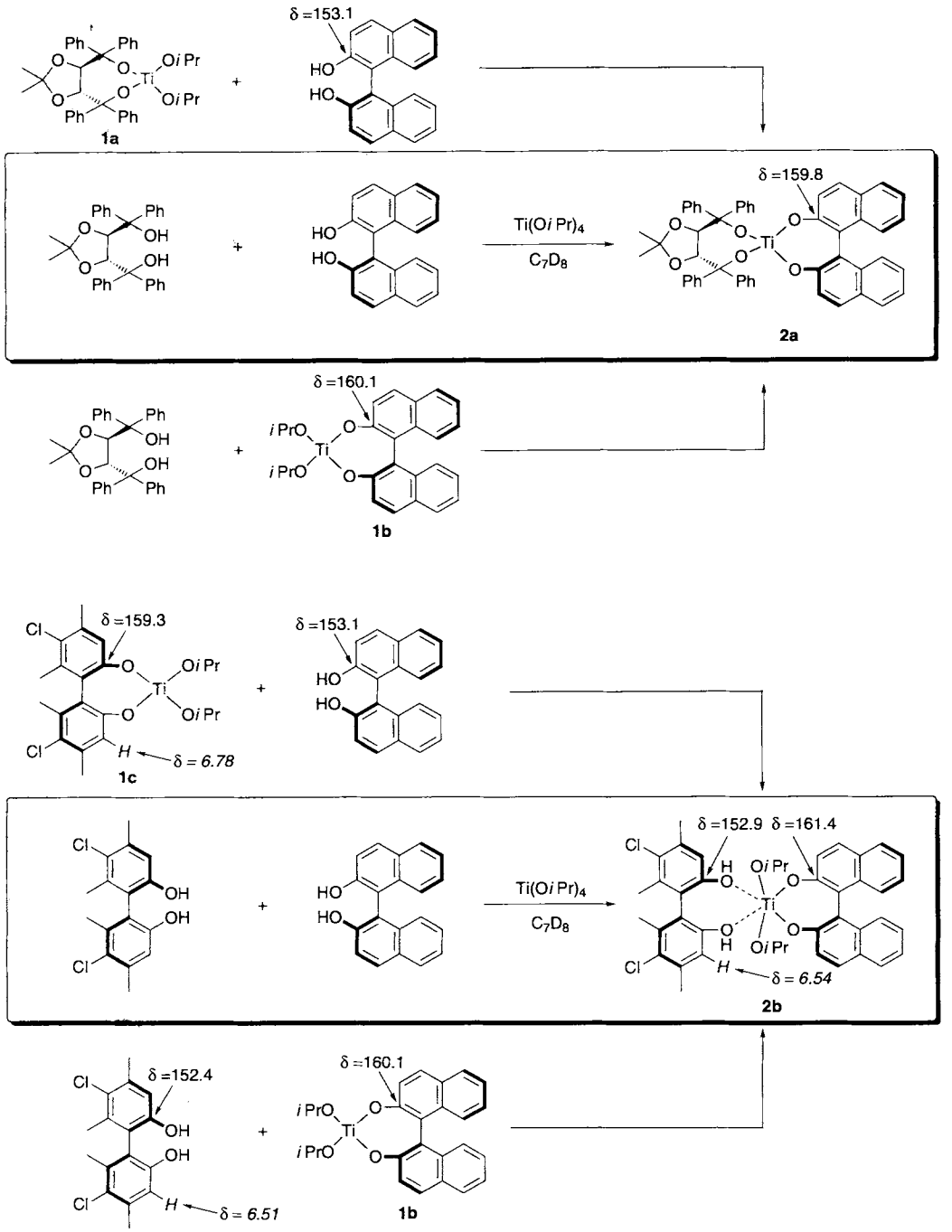

Scheme 2. "Smart" self-assembly of the highly active Ti catalysts **2a** and **2b**. The ^{1}H NMR spectrum of complex **2a** shows no *i*PrOH signals.

lane-4,5-dimethanol [(*R*)-TADDOL][7] with Ti(O*i*Pr)$_4$ in a molar ratio of 1:1:1 yielded a single chiral titanium complex by "push–pull" assembly of the TADDOL–BINOL combination. The [Ti{(*R*)-BINOLate}{(*R*)-TADDOLate}] complex (**2a**) was identified by ^{13}C and ^{1}H NMR spectroscopy in [D$_8$]toluene; these NMR spectroscopic studies also confirmed the absence of any other complexes, especially the symmetrically substituted [Ti{(*R*)-TADDOLate}$_2$] and [Ti{(*R*)-BINOLate}$_2$]. However, complex **2a** can also be obtained from [Ti{(*R*)-TADDOLate}(O*i*Pr)$_2$](**1a**)[8] by addition of (*R*)-BINOL and from [Ti{(*R*)-BINOLate}(O*i*Pr)$_2$](**1b**)[9] by addition of (*R*)-TADDOL as has been shown in separate sets of experiments.

Likewise, [{(*R*)-BINOLate}{(*R*)-5-Cl-BIPOL}(O*i*Pr)$_2$] (**2b**) (5-Cl-BIPOL = 5,5′-dichloro-4,4′,6,6′-tetramethyl-2,2′-biphenol) can be synthesized from Ti(O*i*Pr)$_4$ by reaction with (*R*)-BINOL and a more acidic diol such as (*R*)-5-Cl-BINOL.[10] Both the addition of (*R*)-5-Cl-BIPOL to [Ti{(*R*)-BIPOLate}(O*i*Pr)$_2$] (**1b**) and the addition of (*R*)-BINOL to [Ti{(*R*)-5-Cl-BIPOLate}(O*i*Pr)$_2$](**1c**)[11] afforded the complex **2b**, whose formation as the sole product of the reaction was confirmed by ^{13}C and ^{1}H NMR spectroscopy.

The importance of this selective multicomponent self-assembly is exemplified by attempts at the enantioselective catalysis of the carbonyl-ene reaction;[12,13] the results clearly show that a highly enantioselective catalyst is formed. The

catalyst was prepared in each case by mixing the components in a molar ratio of 1:1:1 (vide supra) and used in situ (10 mol% were employed with respect to olefin and glyoxylate) (Scheme 3 and Table 1).

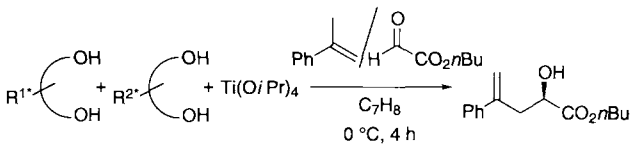

Scheme 3. General scheme for the Ti-catalyzed asymmetric glyoxylate-ene reaction.

Table 1. Asymmetric catalysis of the reaction of α-methylstyrene and *n*-butyl glyoxylate (Scheme 3), in which the catalysts are produced from $Ti(OiPr)_4$ and $R^{1*}(OH)_2$ and $R^{2*}(OH)_2$.

Entry	$R^{1*}(OH)_2$	$R^{2*}(OH)_2$	Yield [%] [a]	*ee* [%]
1	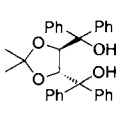	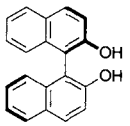	50	91
2	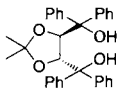	–	0	–
3	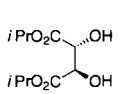	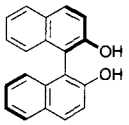	15	40
4	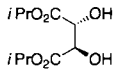	–	4	0
5	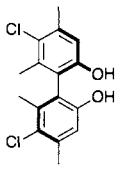	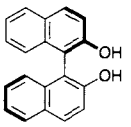	66	97
6	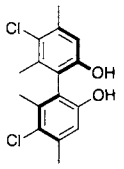	–	13	75
7	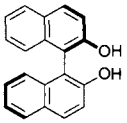	–	20	95

[a] The yield was determined by gas chromatography (OV-1701, benzophennone as internal standard).

The complex **1a** did not afford any of the carbonyl-ene product (Table 1, entry 2), in contrast, **2a** gave a yield of 50% with an enantiomeric excess (*ee*) of 91% [(*R*)-product; entry 1]. Similarly with $[Ti\{(R)\text{-}(OCHCO_2iPr)_2\}(OiPr)_2]$ virtually none of the product was obtained (entry 4),[14] whereas 15% of the coupling product was formed when $[Ti\{(R)\text{-}(OCHCO_2iPr)_2\}(OiPr)_2\{(R)\text{-BINOL}\}]$, with only 40% *ee* (entry 3). The use of (*R*)-5-Cl-BIPOL and (*R*)-BINOL proved to be the best combination for the self-assembly of a highly selective catalyst. The carbonyl-ene reaction proceeded quite smoothly to produce the highest enantioselectivity of 97% *ee* along with the highest yield (66%, entry 5). Significantly lower enantiomeric excesses and yields were obtained by using the catalyst **1c** (yield: 13%, 75% *ee*) or the catalyst **1b** (yield: 20%, 95% *ee*) (entries 6 and 7, respectively).

In summary, the "smart" self-assembly of a highly enantioselective catalyst from a pre-catalyst and *several* ligands has been achieved. The most effective and enatioselective catalyst among the possible combinations forms exclusively regardless of the starting conditions, thus facilitating a simple experimental procedure. The selective assembly of complexes to give systems containing several ligands might prove a powerful tool for the development of catalysts for asymmetric synthesis.

Experimental Section

The catalyst was prepared on a 0.1-mmol scale by mixing achiral $Ti(OiPr)_4$, (*R*)-BINOL, and a further chiral diol such as (*R*)-TADDOL or (*R*)-5-Cl-BIPOL in a molar ratio of 1:1:1 in toluene at 0°C under an argon atmosphere. The carbonyl-ene reaction was then carried out in situ by addition of α-methylstyrene (1 mmol) and *n*-butyl glyoxylate (1 mmol, freshly distilled prior to use) to the solution in toluene and was monitored by TLC. Standard workup (hydrolysis with H_2O, extraction with EtOAc, washing with 1N HCl, and drying over $MgSO_4$) followed by flash chromatography on silica afforded the carbonyl-ene product. Yields and enantiomeric excesses were determined by gas chromatography (OV-1701, standard: benzophenone) or with HPLC (Daicel CHIRALPAK AS column, hexane/2-propanol (3/1), 0.5 mL min^{-1}, $t_R = 9.48$ min (*S*), 12.60 min (*R*), respectively (Table 1).

Received: July 17, 1997 [Z10691IE]
German version: *Angew. Chem.* **1997**, *109*, 2936–2939

Keywords: asymmetric catalysis · biaryls · ene reactions · self-assembly · titanium

[1] *Advances in Catalytic Processes: Asymmetric Chemical Transformations, Vol. 1* (Ed.: M. P. Doyle), JAI Press, Greenwich, NJ, USA, **1995**; R. Noyori, *Asymmetric Catalysis in Organic Synthesis*, Wiley, New York, **1994**; *Catalytic Asymmetric Synthesis* (Ed.: I. Ojima), VCH, New York, **1993**; *Asymmetric Catalysis* (Ed.: B. Bosnich), Martinus Nijhoff Publishers, Dordrecht, Netherlands, **1986**; H. B. Kagen, *Comprehensive Organometallic Chemistry Vol. 8* (Eds.: G. Wilkinson, F. G. A. Stone), Permagon, Oxford, **1982**, pp. 463–498.

[2] Review on chiral ligand acceleration: D. J. Berrisford, C. Bolm, K. B. Sharpless, *Angew. Chem.* **1995**, *107*, 1159–1171; *Angew. Chem. Int. Ed. Engl.* **1995**, *34*, 1059–1070.

[3] Review on combinatorial catalysts: S. Borman, *Chem. Eng. News* **1996**, *74*, November 4, p. 37. Special issue on combinatorial libraries: *Acc. Chem. Res.* **1996**, *29*, No. 3; L. A. Thompson, J. A. Ellman, *Chem. Rev.* **1996**, *96*, 555–600. Review on combinatorial synthesis of small molecules: F. Balkenhohl, C. von dem Bussche-Hünnefeld, A. Lansky, C. Zechel, *Angew. Chem.* **1996**, *108*, 2436–2487; *Angew. Chem. Int. Ed. Engl.* **1996**, *35*, 2288–2337.

[4] For discovery of chiral catalysts and conditions identified by high-throughput screening, see: K. Burgess, H.-J. Lim, A. M. Porte, G. A. Sulikowski, *Angew. Chem.* **1996**, *108*, 192–194; *Angew. Chem. Int. Ed. Engl.* **1996**, *35*, 220-222. Combinatorial chemistry related to the ene reaction: L. F. Tietze, A. Steinmetz, *ibid.* **1996**, *108*, 682–683 and **1996**, *35*, 651–652. For discovery of chiral catalysts through ligand diversity, see: B. M. Cole, K. D. Shimizu, C. A. Krueger, J. P. A. Harrity, M. L. Snapper, A. H. Hoveyda, *ibid.* **1996**, *108*, 1776–1779 and **1996**, *35*, 1668–1671.

[5] C. L. Hill, X. Zhang, *Nature* **1995**, *373*, 324.

[6] Review: K. Mikami, Y. Motoyama in *Encyclopedia of Reagents for Organic Synthesis, Vol. 1* (Ed.: L. A. Paquette), Wiley, Chichester, UK, **1995**, p. 397.

[7] Reviews: M. Braun, *Angew. Chem.* **1996**, *108*, 565–568; *Angew. Chem. Int. Ed. Engl.* **1996**, *35*, 519–522; R. Dahinden, A. K. Beck, D. Seebach in *Encyclopedia of Reagents for Organic Synthesis, Vol. 3*, (Ed.: L. A. Paquette), Wiley, Chichester, UK, **1995**, p. 2167; K. Narasaka, N. Iwasawa, M. Inoue, T. Yamada, M. Nakashima, J. Sugimori, *J. Am. Chem. Soc.* **1989**, *111*, 5340–5345; A. K. Beck, B. Bastani, D. A. Plattner, W. Petter, D. Seebach, *Chimia* **1991**, *45*, 238–244; D. Seebach, R. Dahinden, R. E. Marti,

 © WILEY-VCH Verlag GmbH, D-69451 Weinheim, 1997 0570-0833/97/3624-2770 $ 17.50+.50/0

A. K. Beck, D. A. Plattner, F. N. M. Kuhnle, *J. Org. Chem.* **1995**, *60*, 1788–1799.
[8] D. Seebach, D. A. Plattner, A. K. Beck, Y. M. Yang, D. Hunziker, *Helv. Chim. Acta* **1992**, *75*, 2171–2209.
[9] Review: K. Mikami in *Encyclopedia of Reagents for Organic Synthesis, Vol. 1* (Ed.: L. A. Paquette), Wiley, Chichester, UK, **1995**, p. 407; C. A. Martin, Ph. D. Thesis, Massachusetts Institute of Technology, Cambridge, MA, USA, **1988**; J. T. Wang, X. Fan, X. Feng, Y. M. Qian, *Synthesis* **1989**, 291–292; G. E. Keck, K. H. Tarbet, L. S. Geraci, *J. Am. Chem. Soc.* **1993**, *115*, 8467–8468; K. Mikami, S. Matsukawa, *Tetrahedron: Asymmetry* **1995**, *6*, 2571–2574; J. W. Faller, D. W. Sams, X. Liu, *J. Am. Chem. Soc.* **1996**, *118*, 1217–1218; S. Weigand, R. Brückner, *Chem. Eur. J.* **1996**, *2*, 1077–1084.
[10] K. Mikami, S. Matsukawa, *Nature* **1997**, *385*, 613-615; M. Mori, H. Imma, N. Takai, *Tetrahedron Lett.* **1997**, *38*, 6229–6232.
[11] See Ref. [10] and for a similar (*R*)-3,3′,5,5′-tetrachloro-4,4′,6,6′-tetramethylbiphenol, see: E. J. Corey, M. A. Letavic, M. C. Noe, S. Sarshar, *Tetrahedron Lett.* **1994**, *35*, 7553–7556.
[12] Reviews on ene reactions: K. Mikami, M. Shimizu, *Chem. Rev.* **1992**, *92*, 1021–1050; B. B. Snider in *Comprehensive Organic Synthesis, Vol. 2 and 5B* (Eds.: M. Trost, I. Fleming), Pergamon, London, **1991**; H. M. R. Hoffmann, *Angew. Chem.* **1969**, *81*, 597–618; *Angew. Chem. Int. Ed. Engl.* **1969**, 8, 556–577.
[13] K. Mikami, M. Terada, T. Nakai, *J. Am. Chem. Soc.* **1989**, *111*, 1940–1941; *ibid.* **1990**, *112*, 3949–3954.
[14] M. G. Finn, K. B. Sharpless in *Asymmetric Synthesis, Vol. 5* (Ed.: J. D. Morrison), Academic Press, New York, **1985**, p. 247; M. G. Finn, K. B. Sharpless, *J. Am. Chem. Soc.* **1991**, *113*, 113–126.

Noncovalent Interactions in Organometallic Compounds: Formation of an Intramolecular Metal–Carbon Ion Pair in Zirconium Borate Betaines**

Jörn Karl, Gerhard Erker,* Roland Fröhlich, Frank Zippel, Friedrich Bickelhaupt, Marcel Schreuder Goedheijt, Otto S. Akkerman, Paul Binger, and Jörg Stannek

Noncovalent metal–ligand interactions and ion pairing will probably be of increasing importance as structural elements and latent functionalities in the organometallic chemistry of transition metals.[1] It will become necessary to learn about the factors that govern the formation of such bonding features. We now found that for a class of metallocene borate betaines geometric parameters of the allyl unit constitute the structural element that determines whether the electron-deficient metal center is stabilized by an intramolecular M···CH_2[B] ([B] = $B(C_6F_5)_3$) ion pair[2] or by M···F-C coordination.[3]

T. J. Marks et al. demonstrated that dimethylzirconocenes **1** (^{R}Cp = substituted cyclopentadienyl) are able to transfer a methyl anion to the strong Lewis acid tris(pentafluorophenyl)borane. The resulting products **2** favor structures with a rather stable ion pair in the solid state as well as in solution (Zr···CH_3[B] ≈ 2.55 Å, $\Delta G^{\neq}_{dis} \approx 16-18$ kcal mol^{-1}). Only the onset of polymerization upon treatment of these active Ziegler catalysts with α-olefins seems to cleave these ion pairs effectively.[4]

We recently found that (butadiene)zirconocene complexes **3**[5a] add $B(C_6F_5)_3$ at the terminal CH_2 group of the conjugated diene ligand to yield the metallocene borate betaines **4**.[6] The resulting substituted π-allyl moiety in **4** is *E*-configurated. This geometrically prohibits intramolecular Zr···CH_2[B] ion pairing in **4** analogous to the favorable Zr···CH_3[B] interaction in **2**. Instead, **4** is stabilized by

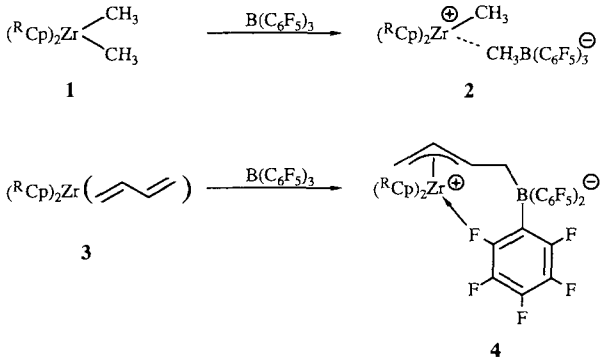

coordination of an *ortho*-F atom of a C_6F_5 substituent on boron to the electrophilic metal center. The strength of this Zr···F interaction was determined to be about 8.5 kcal mol^{-1}.[7] Addition of a reactive α-olefin again removes this "protecting group" from the catalytically active Zr^+ center, and complexes **4** serve as active single-component metallocene Ziegler catalysts.[6]

If the interpretation is correct that intramolecular Zr···CH_2[B] ion pairing in **4** is disfavored due to the geometrically prohibitive *E* position of the CH_2[B] substituent at the π-allyl ligand, then the intramolecular Zr–C ion pairs of the metallocene borate betaine system should be observed again in cases where the isomeric *Z*-allyl-CH_2[B] arrangements are favored. We have synthesized two such betaine systems, and characterized them stereochemically and with regard to the intramolecular interaction between allyl-CH_2[B] and Zr.

As a first substrate we employed (*ortho*-quinodimethane)-zirconocene (**5**).[5b] This complex marks the metallacyclic extreme of the (s-*cis*-diene)metallocene family of complexes: the π interaction between Zr and carbon atoms C2 and C3 is

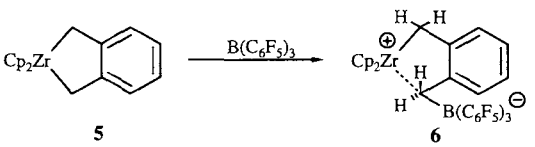

only marginally pronounced. Nevertheless, this complex, in which the cisoid arrangement of the C1–C2 and C3–C4 vectors has become fixed by the anellated phenylene moiety, exhibits a variety of chemical features typical of the (s-*cis*-1,3-diene)zirconium complexes.[5]

Complex **5** reacts instantaneously with one molar equivalent of $B(C_6F_5)_3$ at room temperature in toluene to form the 1:1 addition product **6**. Adding a layer of pentane above the solution of the product in toluene furnished single crystals of **6** within three days that were suited for an X-ray structure analysis. This confirmed that the $B(C_6F_5)_3$ moiety had added to the C4 atom. Compound **6** constitutes an internal ion pair that

[*] Prof. Dr. G. Erker, Dr. J. Karl, Dr. R. Fröhlich, Dr. F. Zippel
Organisch-chemisches Institut der Universität
Corrensstrasse 40, D-48149 Münster (Germany)
Fax: Int. code + (251) 83-39772
e-mail: erker@uni-muenster.de
Prof. Dr. F. Bickelhaupt, Dr. M. Schreuder Goedheijt, Dr. O. S. Akkerman
Fakulteit der Scheikunde, Vrije Universiteit Amsterdam (The Netherlands)
Prof. Dr. P. Binger, Dr. J. Stannek
Max-Planck-Institut für Kohlenforschung, Mülheim (Germany)

[**] Financial support by the Fonds der Chemischen Industrie, the Deutsche Forschungsgemeinschaft, and the Ministerium für Wissenschaft und Forschung des Landes Nordrhein-Westfalen is gratefully acknowledged. G.E. and F.B. thank the Alexander von Humboldt-Foundation for their support of this work with the Max-Planck-Forschungspreis.

contains a $[Cp_2ZrR]^+$ cation and a $[RB(C_6F_5)_3]^-$ anion in a single molecule (Figure 1). The Cp_2Zr moiety of **6** exhibits the usual structural parameters of Group 4 bent metallocenes.[8] The Zr–C1 bond is very short (2.264(3) as opposed to 2.776(3) for Zr–C2 and 2.898(3) Å for Zr–C3). It is the coordination

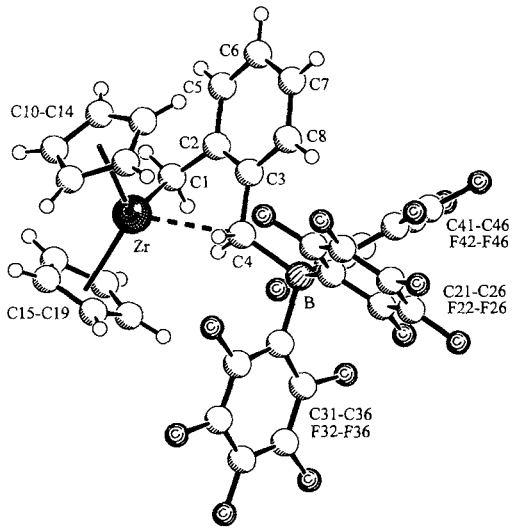

Figure 1. Molecular structure of betaine **6**. The ion-pair interaction between Zr and C4 is indicated by a dashed line. Selected bond lengths [Å] and angles [°]: Zr–C1 2.264(3), Zr–C4 2.595(3), Zr–C_{Cp} (av) 2.508(4), C1–C2 1.472(5), C2–C3 1.414(4), C2–C5 1.406(5), C5–C6 1.358(5), C6–C7 1.395(5), C7–C8 1.370(5), C3–C8 1.401(4), C3–C4 1.517(4), C4–B 1.682(3), B–21 1.655(4), B–C31 1.663(5), B–C41 1.646(5); C1-C2-C5 119.7(3), C2-C5-C6 122.3(3), C5-C6-C7 119.5(4), C6-C7-C8 119.9(4), C7-C8-C3 121.6(3), C8-C3-C4 119.8(3), C3-C4-B 119.1(3), C4-B-C21 117.4(2), C4-B-C31 108.1(3), C4-B-C41 103.3(2), C21-B-C31 102.3(2), C21-B-C41 112.1(3), C31-B-C41 114.0(2); see text for additional values.

pattern of the sp^3-hybridized carbon atom C4, which bears the $B(C_6F_5)_3$ substituent, that makes **6** structurally noteworthy. Atom C4 exhibits a rather short distance to the zirconium atom (2.595(3) Å), and the Zr-C4-B angle is 155.3(2)°. The C4–Zr vector points in a direction opposite to the C4–B vector. We regard the Zr–C4 bond as an electrostatic ion pair. Consequently, both C–H bonds at C4 are oriented toward the transition metal (C3-C4-B 119.1(3)°), which is different from the situation at the distorted-tetrahedrally tetracoordinated C1. The resulting "ion-paired five-membered metallacycle" is nonplanar and structurally resembles the "envelope" geometry of the starting material **5**; its folding angle (i. e., the angle between the Zr/C1/C4 and C2/C3/C5 – C8 planes in **6**) amounts to 68.6°.[9] Some of the bond angles inside the five-membered ring are quite different than normal (C1-Zr-C4 75.41(11), Zr-C1-C2 93.5(2), Zr-C4-C3 85.4(2), C1-C2-C3 121.7(3), C2-C3-C4 121.6(3)°). The heavy atoms at C4 (Zr, C3, B) are almost coplanar (sum of angles 359.8°). Thus, the C4–B vector attains an almost *gauche* orientation to its neighboring aromatic ring (dihedral angles C8-C3-C4-B −47.9(4), C2-C3-C4-B 135.0(3)°). The internal ion pair formed between Zr and C4 apparently leads to an optimal situation with regard to steric interaction and electrostatic stabilization of **6**.

In solution at 253 K **6** exhibits NMR signals for a pair of diastereotopic Cp ligands ($\delta(^1H/^{13}C) = 5.41/112.0$, 4.48/111.1 at 600/150 MHz) as well as C1 ($\delta(^1H) = 2.17$, 1.80) and C4 protons ($\delta(^1H) = 0.89$, 0.30).[9] The ^{13}C NMR resonance for C1 appears at $\delta = 57.6$; the signal for C4 is probably very broad due to the adjacent boron nucleus and could not be located. Complex **6** exhibits temperature-dependent ^{19}F NMR spectra. Already at 253 K 14 resonances are observed (two of the *ortho*-F resonances are accidentally isochronous). These spectra also clearly rule out the presence of any coordination of F to the electrophilic Zr center in solution. The observed characteristic splitting pattern originates from hindered rotation of the $B(C_6F_5)_3$ "propeller" on the NMR time scale, which is similar to the situation in several other $R\text{-}B(C_6F_5)_3$ systems.[10]

The formation of an internal ion pair in **6** is not unique, but apparently in general present as soon as the metallocene borate betaine features the sterically favorable *Z*-allyl arrangement.[11] Therefore, we treated the (η^4-butadiene)(η^8-cyclooctatetraene)zirconium complex **7**[12] with $B(C_6F_5)_3$. At ambient temperature the Lewis acidic borane adds instantaneously and with complete regioselectivity to the C4 atom of the butadiene ligand to form **8**. Again we obtained single

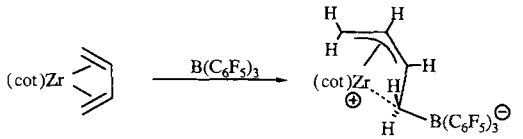

7 **8**

crystals from a solution in toluene within three days after cautiously adding a layer of pentane. The X-ray structure analysis of **8** shows the presence of a η^8-cot ligand (Zr–C(cot) 2.371(5) – 2.433(5) Å) and a *Z*-configured CH_2[B]-substituted allyl ligand at zirconium (Figure 2). The coordination of

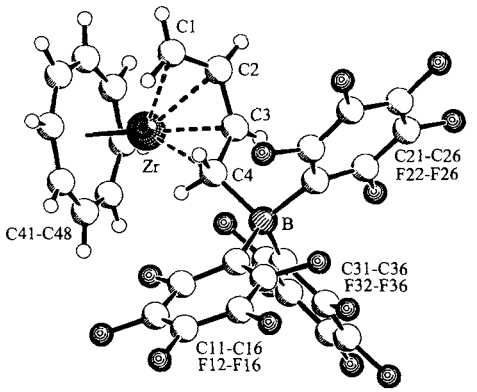

Figure 2. Molecular geometry of **8**. Selected bond lengths [Å] and angles [°]: Zr–C_{cot} (av) 2.403(3), B–C11 1.656(5), B–C21 1.645(5), B–C31 1.656(6); C1-Zr-C2 31.1(2), C1-Zr-C3 59.7(2), C1-Zr-C4 69.8(2), C2-Zr-C3 34.4(2), C2-Zr-C4 60.1(1), C3-Zr-C4 34.7(1), Zr-C1-C2 68.8(3), Zr-C2-C1 80.0(3), Zr-C2-C3 65.6(2), Zr-C3-C2 80.0(2), Zr-C3-C4 85.5(2), Zr-C4-C3 59.8(2), C1-C2-C3 123.2(4), C2-C3-C4 122.2(4), C3-C4-B 114.7(3); see text for additional values.

the allyl ligand to zirconium is rather unsymmetrical. The Zr–C3 bond is the shortest (2.266(4) Å), whereas the Zr–C2 and Zr–C1 bonds are markedly longer (2.450(4) and 2.588(5) Å, respectively). Accordingly, there is a short – long sequence of the C–C bond lengths in the allyl unit (C1–C2 1.359(8), C2–C3 1.407(6) Å). The C3–C4 bond length is 1.493(5) Å. Atom C4 again has distorted trigonal-bipyramidal coordination (C4–B 1.665(5), C4–Zr 2.614(4) Å; Zr-C4-B 148.8(3)°). The dihedral angle C2-C3-C4-B amounts to −139.6(4)°. The hydrogen atoms at C4 are apparently oriented in the direction of the metal atom. We conclude that **8** also forms an internal ion pair to give rise to a five-membered metallacycle. The essential structural features of the complexes **8** and **6** are closely related in this respect.

 © WILEY-VCH Verlag GmbH, D-69451 Weinheim, 1997 0570-0833/97/3624-2772 $ 17.50+.50/0

In solution **8** shows ^{1}H and ^{13}C NMR resonances for the η^8-cot ligand at $\delta = 5.94$ and 96.9, respectively ($^1J_{CH} = 169$ Hz). The ^{13}C NMR signals for the carbon atoms of the allyl ligand appear at $\delta = 79.9$ ($^1J_{CH} = 166$, 158 Hz), 127.1 (154 Hz), and 103.1 (172 Hz); the corresponding ^{1}H NMR resonances are at $\delta = 2.80$, 2.05 (*syn,anti*-1-H), 4.75 ("*meso*"-2-H), and 2.08 (*syn*-3-H).[13] The *gauche* orientation of the $B(C_6F_5)_3$ substituent at C4 (see above) together with the Zr–C4 ion pair make the hydrogen atoms 4-H and 4-H′ diastereotopic. Consequently two ^{1}H NMR resonances are found at $\delta = 0.07$ and -1.00. The ^{13}C NMR signal for C4 appears at $\delta = 14.1$ ($^1J_{CB} = 37$ Hz); this is typical for a CH_2[B] carbon atom that has a direct contact to zirconium. The ^{19}F NMR spectrum of **8** shows three sharp resonances for the *ortho*-, *meta*-, and *para*-F atoms of the $B(C_6F_5)_3$ substituent down to 193 K. There is no indication of C–F coordination in solution.

The results described here show that the intramolecular stabilization of Group 4 metallocene borate betaines is controlled by the geometrical features of their CH_2[B]-substituted allyl moiety. The *E* configuration leads to favored coordination of an *ortho*-C-F moiety to the zirconium center, whereas the respective *Z* orientation results in the formation of a stable ion pair interaction between the transition metal and the CH_2[B] unit.[14]

Experimental Section

All reactions were carried out under argon.

6: Complex **5** [5] (326 mg, 1.00 mmol) and $B(C_6F_5)_3$ (520 mg, 1.01 mmol) were suspended in toluene (2 mL), and a layer of pentane was carefully added. After three days the betaine was isolated as red crystals; yield 585 mg (70%); m.p. 104 °C (decomp). ^{1}H NMR (599.9 MHz, 253 K, [D$_8$]toluene): $\delta = 7.59$ (d, $^3J(H,H) = 8.1$ Hz, 1H, 5-H), 6.78 (pseudo t, 1H, 7-H), 6.73 (pseudo t, 1H, 6-H), 6.26 (d, $^3J(H,H) = 8.1$ Hz, 1H, 8-H), 5.41, 4.48 (each s, each 5H, Cp), 2.17 (d, $^2J(H,H) = 12.7$ Hz, 1H, 1-H′), 1.80 (d, $^2J(H,H) = 12.7$ Hz, 1H, 1-H), 0.89 (br, 1H, 4-H′), 0.30 (br, 1H, 4-H); ^{13}C NMR (150.8 MHz, 253 K, [D$_8$]toluene): $\delta = 148.3$ (d, $^1J(C,F) = 250$ Hz, *o*-$B(C_6F_5)_3$), 140.6, 140.3 (each C, C-2, C-3), 139.4 (d, $^1J(C,F) = 250$ Hz, *p*-$B(C_6F_5)_3$), 137.5 (d, $^1J(C,F) = 250$ Hz, *m*-$B(C_6F_5)_3$), 131.0 (CH, C-5), 130.6 (CH, C-7), 129.8 (CH, C-8), 126.3 (CH, C-6), 112.0, 111.1 (each CH, Cp), 57.6 (CH_2, C-1), signals for the *ipso*-C of C_6F_5 and C4 were not detected at 253 K (assignments were supported by the results of GCOSY, GHSQC, and GHMBC experiments [16]); ^{19}F NMR (564.3 MHz, 253 K, [D$_8$]toluene): $\delta = -167.3$, -166.1 (2 ×), -165.3, -164.7, -162.0 (br, 6F, *m*-F), -160.5, -159.6, -159.4 (br, 3F, *p*-F), -141.7, -137.3, -134.3, -130.6, -129.5, -128.8 (br, 6F, *o*-F); IR (KBr): $\tilde{\nu} = 3119$, 2963, 2921, 1642, 1513, 1458, 1382, 1281, 1085, 981, 825 cm^{-1}; elemental analysis calcd for $C_{36}H_{18}BF_{15}Zr$ (837.5): C 51.63, H 2.17; found: C 50.93, H 2.75.

8: Complex **7** [12] (250 mg, 1.00 mmol) and $B(C_6F_5)_3$ (520 mg, 1.02 mmol) were allowed to react in toluene (2 mL). The color of the solution changed from blue-green to red-brown. A layer of pentane (6 mL) was carefully added. After three days at ambient temperature the product was obtained as red crystals; yield 530 mg (70%); m.p. 54 °C (decomp). ^{1}H NMR (599.9 MHz, 298 K, [D$_8$]toluene): $\delta = 5.94$ (s, 8H, cot), 4.75 (m, 1H, 2-H), 2.80 (dd, $^{2/3}J(H,H) = 9.8$, 2.0 Hz, 1H, 1-H′), 2.08 (m, 1H, 3-H), 2.05 (d, $^2J(H,H) = 9.8$ Hz, 1H, 1-H), 0.07 (br, 1H, 4-H′), -1.00 (br, 1H, 4-H); ^{13}C NMR (150.8 MHz, 298 K, [D$_8$]toluene): $\delta = 148.4$ (d, $^1J(C,F) = 240$ Hz, *o*-$B(C_6F_5)_3$), 139.0 (d, $^1J(C,F) = 240$ Hz, *p*-$B(C_6F_5)_3$), 137.3 (d, $^1J(C,F) = 240$ Hz, *m*-$B(C_6F_5)_3$), 127.1 (CH, $^1J(C,H) = 154$ Hz, C-2), 103.1 (CH, $^1J(C,H) = 172$ Hz, C-3), 96.9 (CH, $^1J(C,H) = 169$ Hz, COT), 79.9 (CH_2, $^1J(C,H) = 166$, 158 Hz, $^3J(C,H) = 9$ Hz, C-1), 14.1 (CH_2, $^1J(C,B) = 37$ Hz, C-4), the signal for the *ipso*-C of C_6F_5 was not observed (the assignments were supported by GCOSY and GHSQC experiments [16]); ^{19}F NMR (564.3 MHz, 298 K, [D$_6$]benzene): $\delta = -165.7$ (t, $^3J(F,F) = 21$ Hz, 6F, *m*-F), -161.1 (t, $^3J(F,F) = 20$ Hz, 3F, *p*-F), -135.0 (d, $^3J(F,F) = 21$ Hz, 6F, *o*-F); IR (KBr): $\tilde{\nu} = 3086$, 2963, 2922, 1645, 1516, 1454, 1274, 1086, 976, 814, 757 cm^{-1}; elemental analysis calcd for $C_{30}H_{14}BF_{15}Zr$ (761.4): C 47.32, H 1.85; found: C 47.11, H 2.12.

X-ray crystal structure analysis of **6**: $0.60 \times 0.50 \times 0.08$ mm, $a = 27.026(2)$, $b = 12.785(1)$, $c = 20.425(1)$ Å, $\beta = 117.54(1)$, $V = 6256.7(7)$ Å^3, $\rho_{calcd} = 1.778$ g cm^{-3}, $\mu = 4.70$ cm^{-1}, empirical absorption correction with φ-scan data ($0.968 \le C \le 0.999$), $Z = 8$, monoclinic, space group $C2/c$ (no. 15), $\lambda = 0.71073$ Å, $T = 223$ K, $\omega/2\theta$ scans, 6543 measured reflections ($\pm h, -k, +l$), $[(\sin\theta)/\lambda] = 0.62$ Å^{-1}, 6357 independent and 3905 observed reflections [$I \ge 2\sigma(I)$], 478 refined parameters, $R = 0.038$, $wR^2 = 0.084$, max./min. residual electron density 0.69/−0.37 e Å^{-3}. Hydrogen atoms were calculated and refined as riding atoms.

X-ray crystal structure analysis of **8**: $0.60 \times 0.50 \times 0.40$ mm, $a = 11.365(1)$, $b = 17.676(1)$, $c = 14.047(3)$ Å, $\beta = 99.10(1)$, $V = 2786.4(7)$ Å^3, $\rho_{calcd} = 1.815$ g cm^{-3}, $\mu = 5.17$ cm^{-1}, empirical absorption correction with φ-scan data ($0.878 \le C \le 0.998$), $Z = 4$, monoclinic, space group $P2_1/n$ (no. 14), $\lambda = 0.71073$ Å, $T = 223$ K, $\omega/2\theta$ scans, 5889 measured reflections ($\pm h, -k, +l$), $[(\sin\theta)/\lambda] = 0.62$ Å^{-1}, 5661 independent and 4003 observed reflections [$I \ge 2\sigma(I)$], 424 refined parameter, $R = 0.046$, $wR^2 = 0.122$, max./min. residual electron density 0.83/−0.77 e Å^{-3}. Hydrogen atoms were calculated and refined as riding atoms.

Both data sets were measured on an Enraf Nonius MACH3-diffractometer. The following computer programs were used: MolEN for data reduction, SHELXS-86 for structure solution, SHELXL-93 for structure refinement, SCHAKAL-92 for graphics. Crystallographic data (excluding structure factors) for the structures reported in this paper have been deposited with the Cambridge Crystallographic Data Centre as supplementary publication no. CCDC-100478. Copies of the data can be obtained free of charge on application to The Director, CCDC, 12 Union Road, Cambridge CB21EZ, UK (fax: int. code + (1223) 336-033; e-mail: deposit@chemcrys.cam.ac.uk).

Received: June 11, 1997 [Z10534IE]
German version: *Angew. Chem.* **1997**, *109*, 2914–2917

Keywords: betaines · ion pairs · sandwich complexes · Ziegler catalysts · zirconium

[1] Electrostatically dominated bonding features are rather the rule with organometallic compounds of the electropositive main group metals; see for example A. M. Sapse, P. von R. Schleyer, *Lithium Chemistry*, Wiley, New York, **1995**, and references therein; *Comprehensive Organometallic Chemistry* II, *Vol. 1* (Eds.: E. W. Abel, F. G. A. Stone, G. Wilkinson), Pergamon, **1995**, and references therein.

[2] J. J. Eisch, K. R. Caldwell, S. Werner, C. Krüger, *Organometallics* **1991**, *10*, 3417; A. D. Horton, J. H. G. Frijns, *Angew. Chem.* **1991**, *103*, 1181; *Angew. Chem. Int. Ed. Engl.* **1991**, *30*, 1152; X. Yang, C. L. Stern, T. J. Marks, *J. Am. Chem. Soc.* **1991**, *113*, 3623; C. Sishta, R. M. Hathorn, T. J. Marks, *ibid.* **1992**, *114*, 1112; M. Bochmann, *Angew. Chem.* **1992**, *104*, 1206; *Angew. Chem. Int. Ed. Engl.* **1992**, *31*, 1181; M. Bochmann, S. J. Lancaster, M. B. Hursthouse, K. M. A. Malik, *Organometallics* **1994**, *13*, 2235; M. Bochmann, S. J. Lancaster, *Angew. Chem.* **1994**, *106*, 1715; *Angew. Chem. Int. Ed. Engl.* **1994**, *33*, 1634; P. A. Deck, T. J. Marks, *J. Am. Chem. Soc.* **1995**, *117*, 6128; M. A. Giardello, M. S. Eisen, C. L. Stern, T. J. Marks, *ibid.* **1995**, *117*, 12114; *J. Organomet. Chem.* **1995**, *497*, 55; A. Cano, T. Cuenca, P. Gómez-Sal, A. Manzanero, P. Royo, *ibid.* **1996**, *526*, 227; A. D. Horton, *Organometallics* **1996**, *15*, 2675; Y.-X. Chen, C. L. Stern, S. Yang, T. J. Marks, *J. Am. Chem. Soc.* **1996**, *118*, 12451; see also B. Temme, J. Karl, G. Erker, *Chem. Eur. J.* **1996**, *2*, 919; J. Karl, G. Erker, *J. Mol. Catal.*, in press; *Chem. Ber.* **1997**, *130*, 1261.

[3] a) A. D. Horton, A. G. Orpen, *Organometallics* **1991**, *10*, 3910; X. Yang, C. L. Stern, T. J. Marks, *ibid.* **1991**, *10*, 840; *Angew. Chem.* **1992**, *104*, 1406; *Angew. Chem. Int. Ed. Engl.* **1992**, *31*, 1375; J. Ruwwe, G. Erker, R. Fröhlich, *ibid.* **1996**, *108*, 108; bzw. **1996**, *35*, 80; b) A. R. Siedle, R. A. Newmark, W. M. Lamanna, J. C. Huffman, *Organometallics* **1993**, *12*, 1491. c) R. Uson, J. Forniés, M. Tomás, F. A. Cotton, L. R. Falvello, *J. Am. Chem. Soc.* **1984**, *106*, 2482; R. M. Catala, D. Cruz-Garritz, A. Hills, D. L. Hughes, R. L. Richards, P. Sosa, H. Torrens, *J. Chem. Soc. Chem. Commun.* **1987**, 261; H. Plenio, R. Diodone, *Chem. Ber.* **1996**, *129*, 1211; *J. Am. Chem. Soc.* **1996**, *118*, 356; H. Plenio, R. Diodone, D. Badura, *Angew. Chem.* **1997**, *109*, 130; *Angew. Chem. Int. Ed. Engl.* **1997**, *36*, 156; Reviews: R. J. Kulawiec, R. H. Crabtree, *Coord. Chem. Rev.* **1990**, *99*, 89; S. H. Strauss, *Chem. Rev.* **1993**, *93*, 927; J. L. Kiplinger, T. G. Richmond, C. E. Osterberg, *ibid.* **1994**, *94*, 373; R. J. Kulawiec, E. M. Holt, M. Lavin, R. H. Crabtree, *Inorg. Chem.* **1987**, *26*, 2559.

[4] X. Yang, C. L. Stern, T. J. Marks, *J. Am. Chem. Soc.* **1994**, *116*, 10015; L. Jia, X. Yang, A. Ishihara, T. J. Marks, *Organometallics* **1995**, *14*, 3135. $B(C_6F_5)_3$: A. G. Massey, A. J. Park, F. G. A. Stone, *Proceedings Chem. Soc.* **1963**, 212; A. G. Massey, A. J. Park, *J. Organomet. Chem.* **1964**, *2*, 245.

[5] a) G. Erker, C. Krüger, G. Müller, *Adv. Organomet. Chem.* **1985**, *24*, 1, and references therein. b) G. S. Bristow, M. F. Lappert, T. R. Martin, J. L. Atwood, W. E. Hunter, *J. Chem. Soc. Dalton Trans.* **1984**, 399.

[6] B. Temme, G. Erker, J. Karl, H. Luftmann, R. Fröhlich, S. Kotila, *Angew. Chem.* **1995**, *107*, 1867; *Angew. Chem. Int. Ed. Engl.* **1995**, *34*, 1755.

[7] J. Karl, G. Erker, R. Fröhlich, *J. Am. Chem. Soc.* **1997**, *119*, 11165; J. Karl, Dissertation, Universität Münster, **1997**. The remotely related complex $Cp_2^*ZrOB(C_6F_5)_3$ also features an internal Zr···F contact, whose bond dissociation energy was estimated to be about 10 kcal mol^{-1} from the temperature-dependent ^{19}F NMR spectra (see ref. [3b]).

[8] *Comprehensive Organometallic Chemistry, Vol. 4* (Eds.: E. Abel, F. G. A. Stone, G. Wilkinson), Pergamon, **1995**; D. J. Cardin, M. F. Lappert, C. L. Raston, *Chemistry of Organo-Zirconium and -Hafnium Compounds*, Wiley, New York, **1986**.

 © WILEY-VCH Verlag GmbH, D-69451 Weinheim, 1997 0570-0833/97/3624-2773 $ 17.50+.50/0

[9] Compound **5** is dynamic and shows a rapid flipping of the nonplanar metallacyclic five-membered ring, thereby interconverting the isoenergetic envelope conformations. The internal organometallic ion pair of **6** features an analogous automerization reaction, albeit with a substantially increased activation barrier ($T_{coalesence}$(Cp) ≈ room temperature).

[10] W. Ahlers, B. Temme, G. Erker, R. Fröhlich, T. Fox, *J. Organomet. Chem.* **1997**, *527*, 191; W. Ahlers, G. Erker, R. Fröhlich, F. Zippel, *Chem. Ber.*, **1997**, *130*, 1079.

[11] W. J. Highcock, R. M. Mills, J. L. Spencer, P. Woodward, *J. Chem. Soc. Chem. Commun.* **1982**, 128; D. J. Brauer, C. Krüger, *Organometallics* **1982**, *1*, 204, 207.

[12] a) G. Wilke, L. Stehling, unpublished results; b) G. Wilke in *Fundam. Res. Homogeneous Catal.* (Ed.: M. Tsutsui), Plenum Press, New York **1979**, *3*, p. 1; c) experimental procedure: J. Wicher, Dissertation, Universität Bochum, **1983**; d) ^{1}H NMR spectrum: R. Benn, G. Schroth, *J. Organomet. Chem.* **1982**, *228*, 71.

[13] E. G. Hoffmann, R. Kallweit, G. Schroth, K. Seevogel, W. Stempfle, G. Wilke, *J. Organomet. Chem.* **1975**, *97*, 183; A. D. Horton, *Organometallics* **1992**, *11*, 3271.

[14] The group in Amsterdam also added $B(C_6F_5)_3$ to 1,1-bis(cyclopentadienyl)-zirconaindane [15] with opening of the Zr–C(sp^3) bond. According to NMR spectroscopy we assume a specific product geometry that at the same time conformationally favors the interaction of the zirconium atom with the CH_2[B] moiety ($\delta(^{13}C) = 14.6$) and one of the *ortho*-fluorine substituents ($\delta(^{19}F) = -180.2$), which are both located in the major plane of the bent metallocene unit: M. Schreuder Goedheijt, dissertation, Vrije Universiteit Amsterdam, **1996**.

[15] G. Erker, K. Kropp, *J. Am. Chem. Soc.* **1979**, *101*, 3659.

[16] S. Braun, H. Kalinowski, S. Berger, *100 and More Basic NMR Experiments*, VCH, Weinheim, **1996**, and references therein.

A Cyclic Octadecairon(III) Complex, the Molecular 18-Wheeler**

Stephen P. Watton, Peter Fuhrmann, Laura E. Pence, Andrea Caneschi, Andrea Cornia, Gian Luca Abbati, and Stephen J. Lippard*

The development of strategies for the synthesis of high-nuclearity metal clusters has provided substantial impetus to in several different fields, including materials chemistry,[1] bioinorganic chemistry,[2] and solid-state physics.[3,4] The architecture of large transition metal clusters can often result in novel chemical and physical properties. For example, polyiron and polymanganese complexes of nanometer size and with high-spin ground states afford single-domain magnetic particles, which may display hysteresis effects of purely molecular origin.[1,3] It is of interest to investigate the properties of increasingly larger assemblies of interacting metal ions, because they are expected to evolve gradually towards those of bulk materials.[1a,1c] Furthermore, large cyclic polymetallic clusters are also valued for their ability to mimic the properties of linear coordination polymers.[5]

Previously we described a cyclic decairon(III) complex having the composition $[Fe(OCH_3)_2(O_2CCH_2Cl)]_{10}$, referred to as a molecular ferric wheel, the solid-state properties of which were thoroughly investigated.[5] A number of related circular clusters have been synthesized, the latest of which contains seven linked ferrocene rings and has been called a molecular scoop wheel.[6] In the present communication we report the synthesis, solid-state structure, and magnetic behavior of the compound **1** (where XDK is the dianion of *m*-xylylenediamine bis(Kemp's triacid imide)).[7] This complex, which we designate the "molecular 18-wheeler", is the largest cyclic ferric cluster reported so far, containing 18 iron(III) atoms in a ring.[8]

$[Fe(OH)(XDK)Fe_2(OCH_3)_4(O_2CCH_3)_2]_6$ **1**

The title compound was obtained in the presence of tetraalkylammonium carboxylate salts from slightly alkaline methanolic solutions of the diiron(III) complex **2** (see Experimental Section). This material was previously employed in

$[Fe_2O(XDK)(CH_3OH)_5(H_2O)](NO_3)_2 \cdot 4H_2O$ **2**

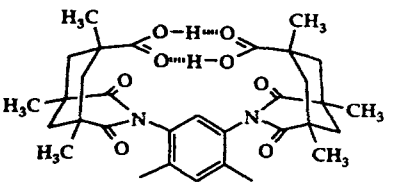

XDKH$_2$

our laboratories to prepare models of the carboxylate-bridged diiron cores present in a variety of non-heme proteins.[9] The composition of the crystalline compound, a double salt having the formula $\mathbf{1} \cdot 6Et_4N(NO_3) \cdot 15CH_3OH \cdot 6Et_2O \cdot 24H_2O$, was established by elemental analysis and a single-crystal X-ray diffraction investigation. Figure 1 displays the structure of the molecular 18-wheeler viewed perpendicular to the plane of the ring.

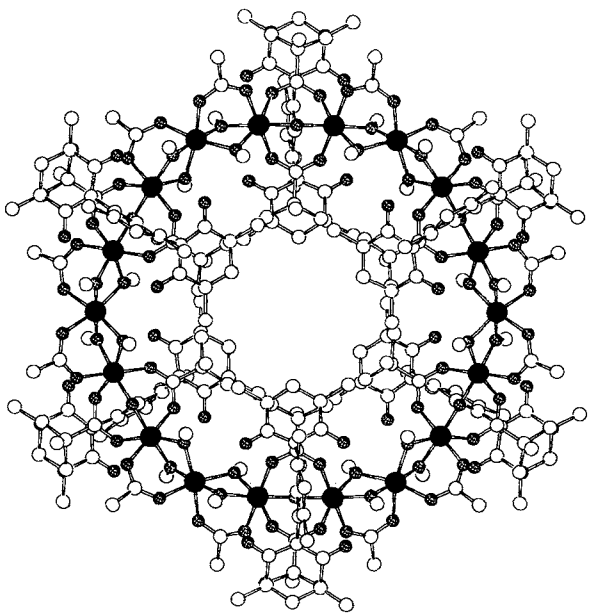

Figure 1. Ball-and-stick representation of **1**, viewed perpendicular to the plane of the ring. Iron atoms are drawn in black, oxygen atoms are shaded, carbon and nitrogen atoms are depicted as open circles, and hydrogen atoms are omitted for clarity.

[*] Prof. Dr. S. J. Lippard, Prof. Dr. S. P. Watton, Dr. P. Fuhrmann, Prof. Dr. L. E. Pence
Department of Chemistry
Massachusetts Institute of Technology
Cambridge, MA 02139 (USA)
Fax: Int. code + (617)258-8150
e-mail: lippard@lippard.mit.edu
Dr. A. Caneschi
Dipartimento di Chimica, Università degli Studi di Firenze (Italy)
Dr. A. Cornia, Dr. G. L. Abbati
Dipartimento di Chimica, Università degli Studi di Modena (Italy)

[**] This work was supported by grants from the National Science Foundation and the National Institute of General Medical Sciences (S.J.L.) and by a Coordinate Project of the Italian CNR (A.C.). L.E.P. thanks the National Institutes of Health for a postdoctoral fellowship.

 © WILEY-VCH Verlag GmbH, D-69451 Weinheim, 1997 0570-0833/97/3624-2774 $ 17.50+.50/0

The octadecairon cluster in **1** has idealized D_{3d} symmetry. The repeating unit comprises a (μ-hydroxo)bis(μ-carboxylato)-diiron(III) moiety linked by an acetate and two methoxide ions to a third iron atom (Figure 2). An acetate and two additional

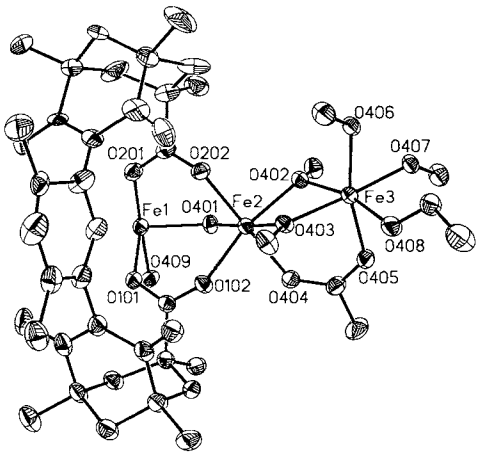

Figure 2. ORTEP view of the asymmetric unit of **1** showing 30% probability thermal ellipsoids and the labeling scheme for the iron and oxygen atoms. Hydrogen atoms are omitted for clarity. Selected bond lengths [Å]: Fe1–O401 1.975(3), Fe1–O407′ 1.977(3), Fe1–O406′ 1.985(3), Fe1–O201 2.011(4), Fe1–O101 2.031(3), Fe1–O409 2.054(4), Fe2–O403 1.968(3), Fe2–O401 1.971(3), Fe2–O402 1.989(3), Fe2–O202 2.025(3), Fe2–O102 2.037(3), Fe2–O404 2.060(3), Fe3–O403 1.965(3), Fe3–O407 1.967(3), Fe3–O406 1.999(3), Fe3–O402 2.005(3), Fe3–O405 2.050(3), Fe3–O408 2.063(4). Bond angles [°]: Fe2-O401-Fe1 123.7(2), Fe2-O402-Fe3 99.18(14), Fe3-O403-Fe2 101.29(14), Fe1′-O406-Fe3 99.50(14), Fe3-O407-Fe1′ 100.9(2). Nonbonded distances [Å]: Fe1···Fe2 3.479(1), Fe2···Fe3 3.041(1), Fe3···Fe1′ 3.041(1).

methoxide ligands on this iron center form bridges to the next trinuclear repeating unit in the cluster. The (μ-acetato)bis(μ-alkoxo)diiron(III) center in the cluster is relatively rare, appearing mainly in oligomeric structures such as the ferric wheel[5] and similar compounds.[10] A discrete complex having the related (μ-carboxylato)(μ-hydroxo)(μ-aqua)diiron(III) or (μ-carboxylato)bis(μ-hydroxo)diiron(III) core would be of great value, since this Fe_2 core occurs in the resting state of the hydroxylase enzyme of soluble methane monooxygenase.[11]

Each iron atom in **1** has distorted octahedral symmetry. The assignment of the bridging oxygen atom O401 (Figure 2) as a hydroxide ion is supported by the Fe–O bond distances of 1.971(3) and 1.975(1) Å, the charge neutrality, and the magnetic behavior of **1**. A plot of the magnetic susceptibility per iron atom, χ_{Fe}, versus temperature T measured on a microcrystalline sample at an applied field of 1 T in the range $2.2 < T < 260$ K displays a broad maximum at about 60 K (Figure 3). This behavior is indicative of antiferromagnetic interactions between the high-spin iron(III) ions ($S = 5/2$). In antiferromagnetically coupled rings containing an even number of equivalent metal ions, the position of the maximum and the corresponding value of the susceptibility per metal ion are expected to scale linearly with the isotropic coupling constant J between nearest neighbors. Comparison of the χ_{Fe} vs. T curves for **1** with those for related complexes containing six- or ten-membered rings (Figure 3)[5,12] suggests the presence of more than one kind of magnetic interaction in **1**. This result presumably reflects the presence of two different types of bridging units. In order to explore this issue in a more quantitative manner, we introduced a simplified six-sided

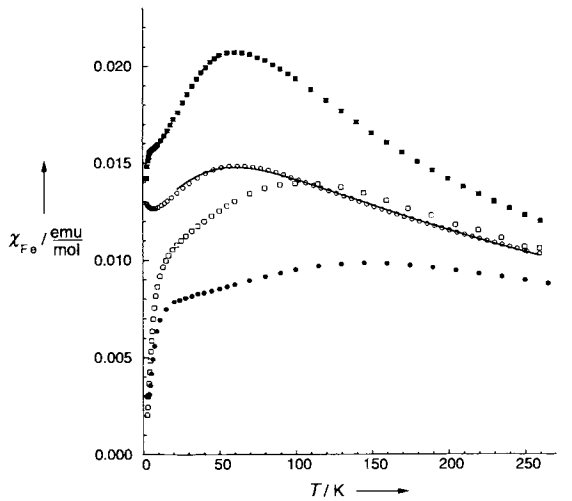

Figure 3. Observed magnetic susceptibility per iron atom versus temperature data for solid samples of **1** (○), $[NaFe_6(OCH_3)_{12}(dbm)_6]^+$ (●, $J = 20.4$ cm^{-1}), $[LiFe_6(OCH_3)_{12}(dbm)_6]^+$ (□, $J = 14.3$ cm^{-1}), and $[Fe_{10}(OCH_3)_{20}(O_2CCH_2Cl)_{10}]$ (■, $J = 9.6$ cm^{-1}) at 1 T. The solid line represents the curve calculated with the parameters given in the text for a solid sample of **1**. dbm = 1,3-diphenylpropane-1,3-dione.

polygon model to simulate the magnetic properties of **1**. The pattern of nearest-neighbor Heisenberg interactions was described by the Hamiltonian given in Equation (1), which matches the alternation of chemically different bridging units (Figures 1 and 2).

$$\mathcal{H} = \Sigma_i J_i (S_i \cdot S_{i+1}) \quad (1)$$

where $S_7 = S_1$, and J_i varies as $\ldots J_A, J_A, J_B, J_A, J_A, J_B \ldots$

The best fit parameters with a fixed g of 2.00 were $J_A = 19.9$ cm^{-1} and $J_B = 6.8$ cm^{-1}. The calculated susceptibility versus temperature plot (solid line in Figure 3) is in fairly good agreement with the experimental data. The values of the coupling constants are in the range expected for bis(methoxide) and mono(hydroxide)bis(carboxylate) bridging units[13,14] and eliminate the possibility of oxo bridges, which would lead to much stronger antiferromagnetic interactions ($J = 80 - 120$ cm^{-1}).[14] The magnetic properties of **1** render it an important addition to the class of antiferromagnetically coupled cyclic metal complexes.[4] Ferromagnetically coupled cyclic complexes containing metal ions other than iron(III) are available and illustrate the effect of metal d electron count on magnetic exchange.[15]

The self-assembly of an octadecanuclear iron(III) complex provides further evidence for the tendency of metal atoms linked by alkoxide or hydroxide ligands (monoatomic bridges) and *syn,syn* η^2-carboxylate bridges to form large cyclic structures. The bending module afforded by two one-atom and one η^2-carboxylate bridge leading to the decanuclear ferric wheel was discussed previously.[5] The repeating unit in the 18-wheeler consists of the XDK ligand attached to one of these bending modules at either end (Figures 1 and 2). The mean deviation of the 18 iron atoms from the calculated best plane through them is 0.388 Å. To compare the contributions of the different iron sites to the total bend of the molecule, the iron atoms were projected onto this plane and the bend angles determined. The main bend of 32.8° occurs at Fe3 and is more than twice those at Fe1 and Fe2 (12.4° and 14.8°, respectively). These values satisfy the relationship in

 © WILEY-VCH Verlag GmbH, D-69451 Weinheim, 1997 0570-0833/97/3624-2775 $ 17.50+.50/0

Equation (2). The two pairs of methoxide bridges at Fe3 allow

$$\begin{aligned} &6[180^\circ - \sphericalangle(\text{Fe1–Fe2–Fe3})] \\ &+6[180^\circ - \sphericalangle(\text{Fe2–Fe3–Fe1})] \\ &+6[180^\circ - \sphericalangle(\text{Fe2–Fe1–Fe3})] = 360^\circ \end{aligned} \quad (2)$$

a much higher bending modulus within the circle than the three carboxylate bridges for Fe1 and Fe2. Examination of a space-filling model of the structure reveals that it has a central hole with an approximate inside diameter of 4–5 Å. The hydrophobic environment afforded by the XDK ligand on the inner surface of the wheel is incompatible with occupancy by cations, as occurs in smaller metallocycles lacking this feature.[12]

In conclusion, the molecular architecture of **1** underscores the ability of chemical synthesis to enrich our visual world with objects of beauty.[16] Once again the tendency of complex molecules to form highly symmetrical structures is manifest.

Experimental Section

1: **2** (0.05 g, 0.046 mmol), synthesized as described in ref. [9], was mixed with solid $Et_4N(O_2CCH_3)\cdot 4H_2O$ (0.024 g, 0.093 mmol, 2 equiv). Methanol (1 mL) was added to afford a golden brown solution. Upon addition of 8 μL (0.100 mmol, 2 equiv) of 1-methylimidazole the solution turned a darker brown. Careful layering of diethyl ether on the resulting solution provided large golden-yellow, well-shaped cubic crystals of **1** in low yield (about 10%) within several days. The crystals are extremely sensitive to solvent loss, cracking immediately upon exposure to air. Elemental analysis found for a sample flushed extensively with Ar: C 45.15, H 6.28, N 4.38, Fe 13.25. Calcd. for $\mathbf{1}\cdot 6Et_4N(NO_3)\cdot 24H_2O$: C 45.40, H 6.75, N 4.41, Fe 13.19. IR (Nujol, NaCl): $\tilde{\nu}$ = 1732, 1694, 1537, 1364, 1335, 1195, 1047, 958, 850 cm^{-1}. Crystal structure data for **1**: $C_{327}H_{522}Fe_{18}N_{20}O_{142}$, M_r = 8010.95, trigonal, space group $R\bar{3}$ (hexagonal axes), $a = b = 29.841(2)$, c = 41.085(6) Å, $V = 31684(6)$ $Å^3$, $Z = 3$, $F(000) = 12684$, $\lambda = 0.71073$ Å, T = 188(2) K, $\mu(Mo_{K\alpha}) = 0.681$ mm^{-1}. The intensities were measured by a Siemens SMART-CCD system on a golden-yellow crystal with the dimensions 0.44 × 0.4 × 0.4 mm^3, which was mounted under a stream of nitrogen on the tip of a quartz glass capillary with Paratone N. The data were integrated to a resolution of 0.9 Å. Of 45106 reflections, 10145 were independent and 10141 were used in the structure refinement. The structure was solved by direct methods and refined by using the SHELXTL program package[17]. During subsequent refinement cycles all of the non-hydrogen atoms could be located. Hydrogen atoms were added in idealized positions. Twelve non-hydrogen atoms in the asymmetric unit for the XDK ligand were disordered, and an appropriate model was introduced and refined; restraints for the anisotropic thermal parameters were applied for these atoms. A tetraethylammonium ion was treated similarly. One molecule of diethyl ether was also located, and its non-hydrogen atoms were refined anisotropically. The values for $R1$ and $wR2$ were 0.0628 and 0.1893, respectively, and the maximum and minimum residual electron density was 0.622 and −0.451 e $Å^{-3}$. Crystallographic data (excluding structure factors) for the structure reported in this paper have been deposited with the Cambridge Crystallographic Data centre as supplementary publication no. CCDC-100663. Copies of the data can be obtained free of charge on application to The Director, CCDC, 12 Union Road, Cambridge CB21EZ, UK (fax: int. code + (1223)336-033; e-mail: deposit@chemcrys.cam.ac.uk).

Received: August 13, 1997 [Z10812IE]
German version: *Angew. Chem.* **1997**, *109*, 2917–2919

Keywords: clusters · iron · magnetic properties · solid-state structures · transition metals

[1] a) D. Gatteschi, A. Caneschi, L. Pardi, R. Sessoli, *Science* **1994**, *265*, 1054–1058; b) L. Thomas, F. Lionti, R. Ballou, D. Gatteschi, R. Sessoli, B. Barbara, *Nature* **1996**, *383*, 145–147; c) D. Gatteschi, A. Caneschi, R. Sessoli, A. Cornia, *Chem. Soc. Rev.* **1996**, *25*, 101–109.

[2] a) R. J. Debus, *Biochim. Biophys. Acta* **1992**, *1102*, 269–352; b) S. J. Lippard, *Angew. Chem.* **1988**, *100*, 353–371; *Angew. Chem. Int. Ed. Engl.* **1988**, *27*, 344–361.

[3] A.-L. Barra, P. Debrunner, D. Gatteschi, C. S. Schulz, R. Sessoli, *Europhys. Lett.* **1996**, *35*, 133–138.

[4] A. Lascialfari, D. Gatteschi, F. Borsa, A. Cornia, *Phys. Rev. B* **1997**, *55*, 14341–14349.

[5] K. L. Taft, C. D. Delfs, G. C. Papaefthymiou, S. Foner, D. Gatteschi, S. J. Lippard, *J. Am. Chem. Soc.* **1994**, *116*, 823–832.

[6] B. Grossmann, J. Heinze, E. Herdtweck, F. Köhler, H. Nöth, H. Schwenk, M. Spiegler, W. Wachter, B. Weber, *Angew. Chem.* **1997**, *109*, 384–386; *Angew. Chem. Int. Ed. Engl.* **1997**, *36*, 387–389.

[7] a) J. Rebek, Jr., L. Marshall, R. Wolak, K. Parris, M. Killoran, B. Askew, D. Nemeth, N. Islam, *J. Am. Chem. Soc.* **1985**, *107*, 7476–7481; b) L. Marshall, K. Parris, J. Rebek, Jr., S. V. Luis, M. I. Burguete, *ibid.* **1988**, *110*, 5192–5193.

[8] For cyclic, high-nuclearity, mixed-valent iron–sulfur clusters, see J.-F. You, G. C. Papaefthymiou, R. Holm, *J. Am. Chem. Soc.* **1992**, *114*, 2697–2710.

[9] S. P. Watton, A. Masschelein, J. Rebek, Jr., S. J. Lippard, *J. Am. Chem. Soc.* **1994**, *116*, 5196–5205.

[10] C. Benelli, S. Parsons, G. A. Solan, R. E. P. Winpenny, *Angew. Chem.* **1996**, *108*, 1967–1970; *Angew. Chem. Int. Ed. Engl.* **1996**, *35*, 1825–1828.

[11] A. C. Rosenzweig, P. Nordlund, P. M. Takahara, C. A. Frederick, S. J. Lippard, *Chem. Biol.* **1995**, *2*, 409–418.

[12] a) A. Caneschi, A. Cornia, S. J. Lippard, *Angew. Chem.* **1995**, *107*, 511–513; *Angew. Chem. Int. Ed. Engl.* **1995**, *34*, 467–469; b) A. Caneschi, A. Cornia, A. C. Fabretti, S. Foner, D. Gatteschi, R. Grandi, L. Schenetti, *Chem. Eur. J.* **1996**, *2*, 1379–1387; c) G. L. Abbati, A. Caneschi, A. Cornia, A. C. Fabretti, D. Gatteschi, W. Malavasi, L. Schenetti, *Inorg. Chem.*, in press.

[13] F. Le Gall, F. F. de Biani, A. Caneschi, P. Cinelli, A. Cornia, A. C. Fabretti, D. Gatteschi, *Inorg. Chim. Acta*, **1997**, *262*, 123–132.

[14] D. M. Kurtz, Jr., *Chem. Rev.* **1990**, *90*, 585–606.

[15] a) E. Rentschler, D. Gatteschi, A. Cornia, A. C. Fabretti, A.-L. Barra, O. I. Shchegolikhina, A. A. Zhdanov, *Inorg. Chem.* **1996**, *35*, 4427–4431; b) A. J. Blake, C. M. Grant, S. Parsons, J. M. Rawson, R. E. P. Winpenny, *J. Chem. Soc. Chem. Commun.* **1994**, 2363–2364.

[16] R. Hoffmann, *Sci. Am.* **1993**, *268* (2), 66–73.

[17] SHELXTL: Structure Analysis Program, 5th ed, Siemens Industrial Automation, Inc., Madison, WI (USA), **1995**.

Scission of DNA with Bis(1,10-phenanthroline)copper without Intramolecular Hydrogen Migration**

Ottilie Zelenko, James Gallagher, and David S. Sigman*

The principal products of the chemical cleavage of DNA by bis(1,10-phenanthroline)copper ($[Cu(phen)_2]^+$) and hydrogen peroxide are 5′- and 3′-phosphomonoesters, free purines and pyrimidines, and 5-methylene furanone (5-MF; Scheme 1).[1] Since 5-MF is a cyclic lactone whose carbonyl oxygen atom does not exchange with solvent once it is formed,[2] the source of this atom is solvent water.[3] The reaction proceeds rapidly under physiological conditions and does not require base to catalyze the elimination reactions which cause breaks in the phosphodiester backbone.[3] Isolation of 5-MF,[4] the 3′-displacement in the scission sites of the two strands of duplex DNA,[4–6] and the protection from scission by minor-groove ligands such as netropsin[7] strongly suggest that the reaction of the tetrahedral chelate complexes occurs from a binding site within the minor groove.

We initiated a series of studies using DNA with deuterium-substituted deoxyriboses to probe the detailed mechanism of the chemical cleavage.[8] The elegant studies by Sugiyama, Fujimoto, and Saito—who prepared C-2′ radicals by photo-

[*] Prof. D. S. Sigman, O. Zelenko, J. Gallagher
Department of Biological Chemistry, School of Medicine
Department of Chemistry and Biochemistry
and Molecular Biology Institute
University of California
Los Angeles, CA 90095-1570 (USA)
Fax: Int. code + (310) 206-7286
e-mail: sigman@mbi.ucla.edu

[**] This research was supported by U.S. Public Health Service (GM 21199). We would like to thank Ed Ruth of the Environmental Engineering Analytical Chemistry Laboratory, Department of Civil and Environmental Engineering, University of California, for assistance with the mass-spectrometry analyses.

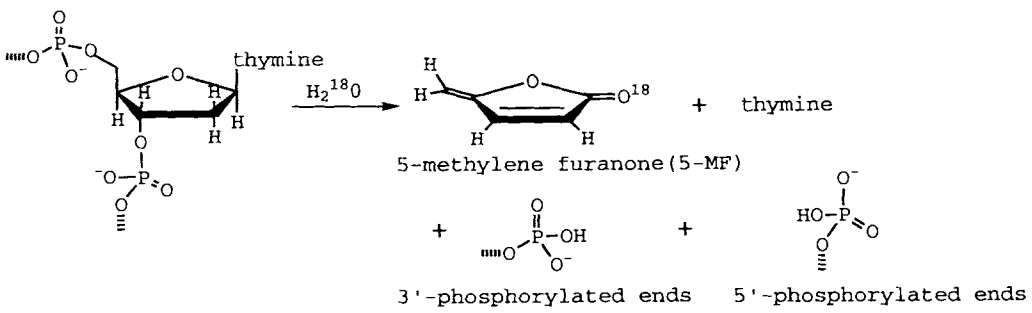

Scheme 1. SET = one-electron transfer

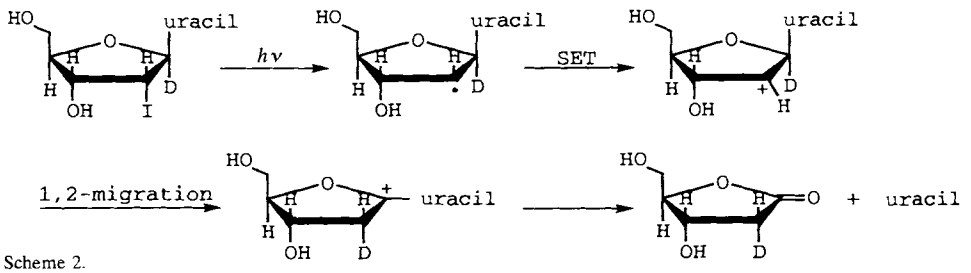

Scheme 2.

lysis of 5-iodouridine and 2'-deoxy-2-iodouridine—suggested a novel mechanism for initiating scission of the phosphodiester backbone[9] which we had not previously considered. Sugiyama et al demonstrated that photolysis of C-1'D-2'-deoxy-2-iodouridine yields the corresponding 2-deoxyribolactone with greater than 90% retention of deuterium at C-2' of the deoxyribose moiety (Scheme 2). The yield of 5-MF accompanying this reaction is variable and depends on solvent polarity.[9] The authors suggested that the presence of a 3'-phosphate group would facilitate heterolytic scission of the carbon–oxygen bond.[9]

Based on these studies, one possible pathway for the scission of DNA would be hydrogen-atom abstraction from C-2'H in the minor groove formed by oxidation of $[Cu(phen)_2]^+$ by hydrogen peroxide via an intermediate whose precise structure is under investigation (Scheme 3). Following hydrogen-atom abstraction the C-2' radical would be subjected to one-electron oxidation by the DNA-bound $[Cu(phen)_2]^{2+}$-OH leading to a C-2' carbocation. A 1,2-hydride shift would then generate a C-1' carbocation. A series of nonstereospecific elimination reactions could then proceed to give the anticipated products with oxygen atoms from water incorporated into 5-MF, as previously demonstrated.[3]

We tested the possibility of C-2' hydrogen abstraction and an intramolecular 1,2-hydrogen shift for scission by $[Cu(phen)_2]^+$ using DNA containing C-1'D-thymidine. This specifically labeled DNA, which corresponds to sequence positions from −40 to +40 of the *E. coli* lac UV-5 fragment, was synthesized with C-1'-deuterated thymidine in both strands. Following digestion by $[Cu(phen)_2]^+$, 5-MF was isolated and analyzed by mass spectrometry using the same methods previously employed to identify the source of the oxygen atom in 5-MF.[3] Analysis of 5-MF isolated from unlabeled DNA according to Grundmann and Kober[10] demonstrated that the isotopic ratio *m/z* 97:96 reflecting the natural occurrence of deuterium and ^{13}C was 4.5 ± 0.4% (5.6% was expected). The isotopic ratio of *m/z* 97:96 for 5-MF isolated from DNA prepared with C-1'-deuterated thymidine following cleavage was 5.3%. We conclude that 5-MF isolated is not enriched in deuterium under these experimental conditions.

These findings rule out initial C-2'H abstraction (first step in Scheme 3) but are consistent with the reaction mechanism that we postulated involving initial C-1'H abstraction (Scheme 4) followed by one-electron oxidation by $[Cu(phen)_2]^{2+}$-OH to give the C-1' carbocation. Since spontaneous scission of the DNA backbone occurs in the absence of heat and base, we proposed that this intermediate does not react to give a deoxyribonolactone. Rather, it loses a proton

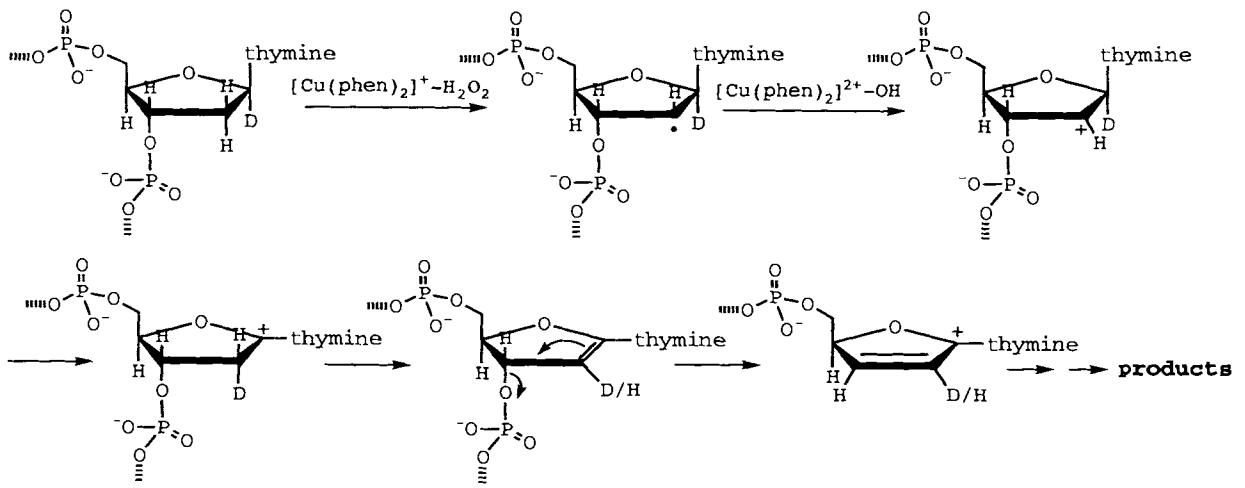

Scheme 3.

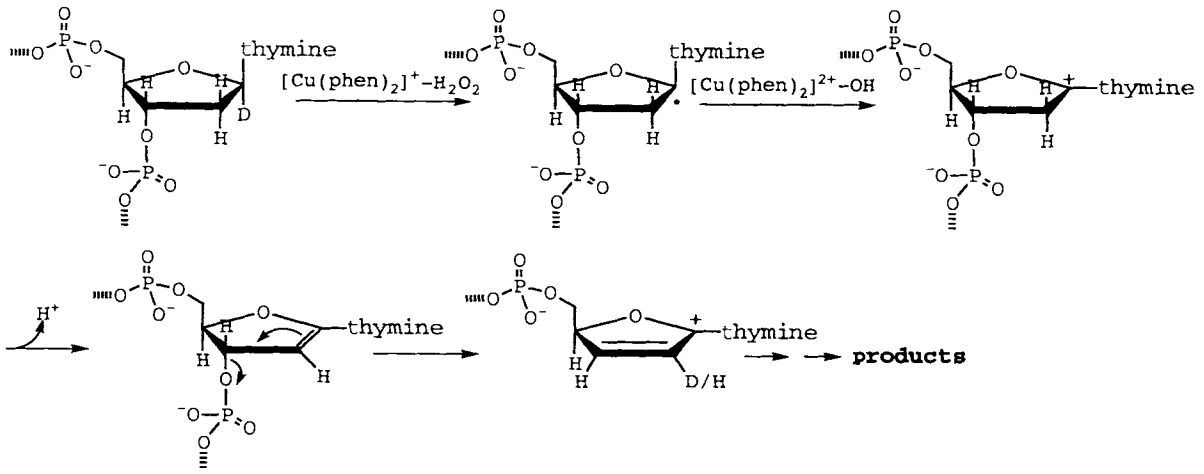

Scheme 4.

(Scheme 4) in a step which could be favored electrostatically by the neighboring 3′-phosphate. Elimination of the 3′phosphate ensues, resulting in the formation of the resonance-stabilized carbocation, which is then subjected to nucleophilic attack by water, the source of oxygen for 5-MF. Based on the studies of Sugiyama et al.[9] the intramolecular 1,2-hydride shift is stereospecific, but the loss of C-2′H should not exhibit a strong stereochemical preference. Since approximately 30% of the nucleotides cleaved in the DNA were thymidine groups, and the scission is effectively "nucleotide neutral" with a modest preference for guanine, a reduced preference for cytosine, and no preference for adenine and thymine,[5,6], the isotopic ratio of *m/z* 97:96 would have been an easily observable 19%.

The use of isotope scrambling in DNA prepared from nucleotides that are specifically deuterated in the deoxyribose moiety provides a method for studying intermediates not formed in a kinetically slow step. The formation of 5-MF as a result of the chemical cleavage of DNA by $[Cu(phen)_2]^+$ and H_2O_2 requires the loss of a C-2′ hydrogen atom. If there had been migration of C-1′D to the C-2 position, as expected from mechanistic studies on the photolysis of C-1′D-2′-deoxy-2-iodouridine, the *m/z* 97:96 of 5-MF should have been enhanced. Our inability to observe migration of the C-1′ deuterium atom strongly argues against initial oxidative attack of the pro *R* hydrogen atom of C-2′ by the DNA-bound oxidative species formed in the reaction of hydrogen peroxide and cuprous ion. Our data are consistent with the initial abstraction of the C-1′ hydrogen atom by the chemical nuclease that is reactive in the minor groove.

Experimental Section

All chemicals for the synthesis of organic products were obtained from Aldrich. The phosphoramidite building blocks for the synthesis of oligonucleotides were purchased from Glen Research. The thymidine phosphoramidite labeled with deuterium at the C-1′ position of the deoxyribose was synthesized according to published procedures [11,12]. The structure of the compound was verified by ^{1}H NMR and ^{31}P NMR spectroscopy (Bruker, 400 MHz). The deuterium content was determined to be $\geq 95\%$ by ^{1}H NMR spectroscopy. The single strands of the lac UV5 fragment (−40 to +40) were synthesized on a Pharmacia LKB Gene Assembler using standard methods for phosphoramidites. The oligonucleotide were purified by polyacrylamide gel electrophoresis (PAGE, 15%) under denaturing conditions.

In a typical cleavage experiment, $[Cu(phen)_2]^+$ (10:1 phen:$CuSO_4$) was added until a final concentration of 10 μM Cu^{2+} to the double-stranded lac UV5 fragment (250 μg, 15 μM) in 50 mM Tris/HCl (pH = 8.0) and 5 mM ascorbic acid. The reaction was performed at room temperature for 40 min. After heating the mixture at 90 °C for 40 min 5-MF was isolated by extraction into Et_2O. The concentrated ether extract was analyzed by GC-MS as previously described [3]. Under these conditions, DNA was complete cleaved, as shown by the analysis of reactions in which ^{33}P-labeled DNA was used. Using 20% PAGE, no parent band was left, and only one major band corresponding to a fragment ≤ 2 bases long was obtained.

Received: February 21, 1997
Revised version: August 18, 1997 [Z10147IE]
German version: *Angew. Chem.* **1997**, *109*, 2906–2908

Keywords: bioinorganic chemistry · copper · DNA cleavage · reaction mechanisms

[1] D. S. Sigman, A. Mazumder, D. M. Perrin, *Chem. Rev.* **1993**, *93*, 2295–2316.
[2] M. Pitie, J. Bernadou, B. Meunier, *J. Am. Chem. Soc.* **1995**, *117*, 2935–2936.
[3] M. Meijler, O. Zelenko, D. S. Sigman, *J. Am. Chem. Soc.* **1997**, *119*, 1135–1136.
[4] T. E. Goyne, D. S. Sigman, *J. Am. Chem. Soc.* **1987**, *109*, 2846–2848.
[5] C. Yoon, M. D. Kuwabara, R. Law, R. Wall, D. S. Sigman, *J. Biol. Chem.* **1988**, *263*, 8458–8463.
[6] C. Yoon, M. D. Kuwabara, A. Spassky, D. S. Sigman, *Biochemistry* **1990**, *29*, 2116–2121.
[7] M. Kuwabara, C. Yoon, T. E. Goyne, T. Thederahn, D. S. Sigman, *Biochemistry* **1986**, *25*, 7401–7408.
[8] a) L. Worth, Jr., B. L. Frank, D. F. Christner, M. J. Absalon, J. Stubbe, J. W. Kozarich, *Biochemistry* **1993**, *32*, 2601–2609; b) W. K. Pogozelski, T. J. McNeese, T. D. Tullius, *J. Am. Chem. Soc.* **1995**, *117*, 6428–6433; c) G. Pratviel, J. Bernadou, B. Meunier, *Angew. Chem.* **1995**, *107*, 819–845; *Angew. Chem. Int. Ed. Engl.* **1995**, *34*, 746–769.
[9] H. Sugiyama, K. Fujimoto, I. Saito, *J. Am. Chem. Soc.* **1995**, *117*, 2945–2946.
[10] C. Grundmann, E. Kober, *J. Am. Chem. Soc.* **1955**, *77*, 2332–2333.
[11] P. Kohn, R. H. Samaritano, L. M. Lerner, *J. Am. Chem. Soc.* **1965**, *87*, 5475–5480.
[12] M. D. Matteucci, M. H. Caruthers, *J. Am. Chem. Soc.* **1981**, *103*, 3185–3191.

 © WILEY-VCH Verlag GmbH, D-69451 Weinheim, 1997 0570-0833/97/3624-2778 $ 17.50+.50/0

Rhenium Complexes with a Photochemically Variable Anthracene Subunit: A Molecular Switch**

Andreas Beyeler, Peter Belser,* and Luisa De Cola

The outstanding feature of supramolecular systems, as compared to simple compounds, is their ability to perform more complex functions. As molecular devices they can, according to the type of system, also be used in practical applications. The molecular switches belong to a particularly interesting group, and can be used for data storage in computers.[1,2] In the case of a simple yes/no switch,[3] those triggered by light differ from redox and pH switches[4] in that they do not have to be in solution, but can also be used in a solid matrix.

The system described here is an example of such a photoswitch. It consists of two separate subunits: the switch and the detector. The latter is influenced by the switching subunit in that it indicates the state of the switch. For the molecular device reported here, a subunit has been chosen for the switch which has already been reported[5] and which consists of two parallel anthracenes linked by a C_3 bridge. On irradiation with visible light, intramolecular dimerization takes place (**1**→**2**). The back reaction (**2**→**1**) is triggered by irradiation with UV light (254 nm). Linkage of this switching unit to a 2,2′-bipyridine (bpy) ligand makes it accessible for complexation. The complexed metal center can then act as a detector, because the intensity of the emissions from the metal center differ according to the state of the switching unit.

Since alcohol **1** is rather inert towards chemical reactions for steric reasons, esterification was the only possible way to link the switching unit to the ligand. The choice of the acid employed was also decisive for the formation of the product. Diisopropylcarbodiimide was used for the esterification instead of the usual dicyclohexylcarbodiimide (DCC),[6] since the latter gives a 1:1 adduct with the resulting ester **4**. In order to investigate the separate switching processes, both types of ligand, **4** and **5**, were synthesized from the alcohols **1** and **2**, respectively. The rhenium complexes **6** and **7** were both synthesized by known methods (Scheme 1).[7]

The switching process **4**→**5** is triggered by irradiation with visible light, and the back reaction **5**→**4** with UV light. The change in the spectrum on irradiation is easily monitored by the changes in the absorption , for example, at 256 and 388 nm (see arrows in Figure 1). Since the anthracenes not only undergo the desired 4π+4π-cyclization, but also the irreversible photoaddition of singlet oxygen to give a 9,10-μ-peroxo bridge, the irradiation experiments had to be performed under the exclusion of oxygen. Therefore, all the investigated solutions were saturated with argon. In order to investigate the reversibility of the switch, a cyclohexane solution of the closed ligand **5** was irradiated (5 min) with a UV lamp, followed by irradiation (10 min) with visible light. After this cycle, the initial state was nearly reached (insert in Figure 1). For both the forward and backward reactions, the changes in the signals observed were constant. In order to investigate the reaction accurately, measurements were carried out in shorter intervals during the first cycle, but not for the subsequent cycles.

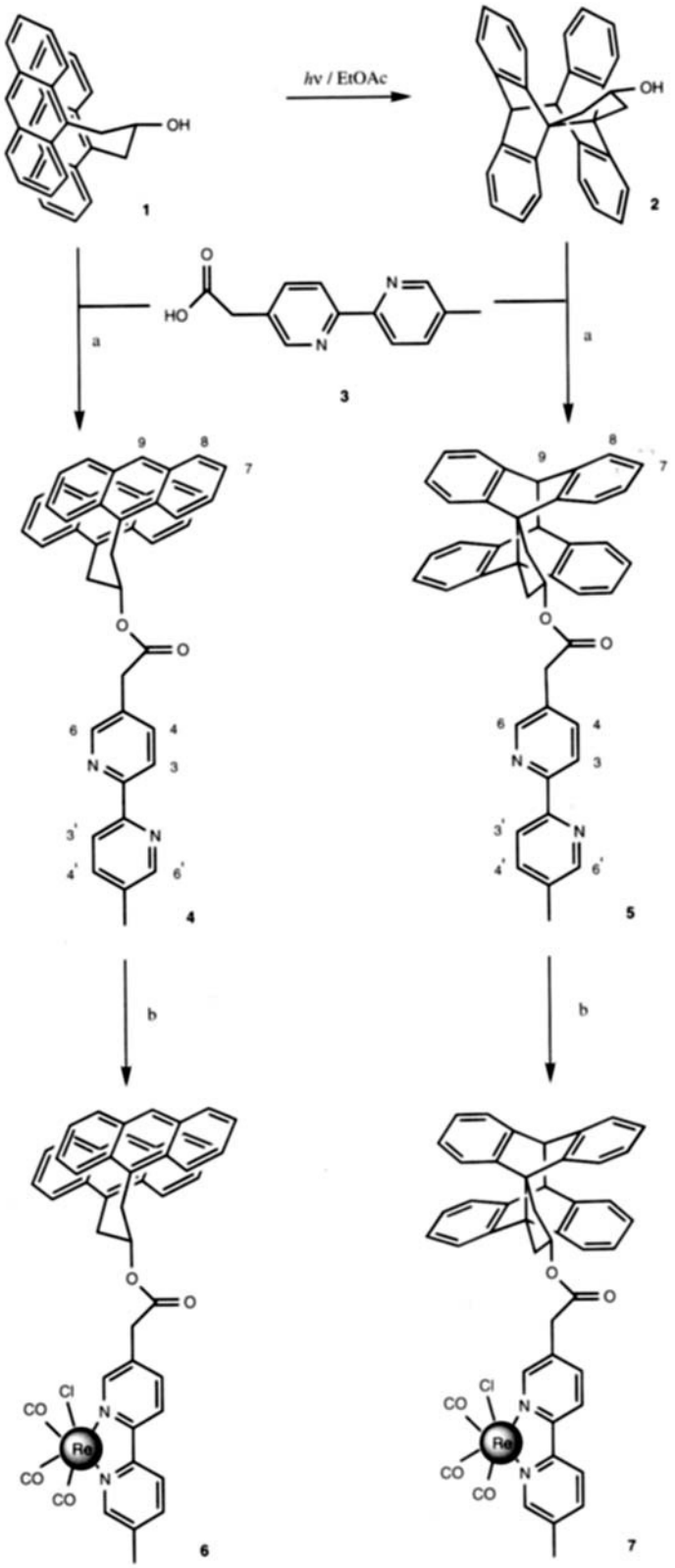

Scheme 1. Synthesis of the anthracene–rhenium complex switch: a) diisopropylcarbodiimide, DMAP, CH_2Cl_2; b) $[Re(CO)_5Cl]$, toluene.

[*] Prof. Dr. P. Belser, Dr. A. Beyeler
Institut für Anorganische und Analytische Chemie
Pérolles, CH-1700 Fribourg (Switzerland)
Fax : Int. code + (26)300-9738
e-mail: Peter.Belser@unifr.ch
Dr. L. De Cola
Dipartimento di Chimica, Università di Bologna
Via Selmi 2, I-40126 Bologna (Italy)

[**] This work was supported by the Swiss National Science Foundation.

 © WILEY-VCH Verlag GmbH, D-69451 Weinheim, 1997 0570-0833/97/3624-2779 $ 17.50+.50/0

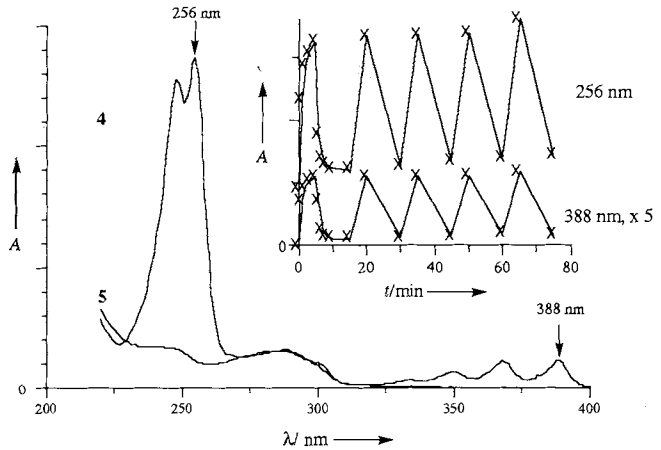

Figure 1. Absorption spectra of ligands **4** (open form) and **5** (closed form) as well as a diagram for the reversibility of the switching process (insert).

The separately synthesized rhenium complexes **6** and **7** exhibited markedly different emissions. While the emission of **7** was as expected, that of **6** was almost completely quenched (Figure 2). The two anthracenes quench the emission in the

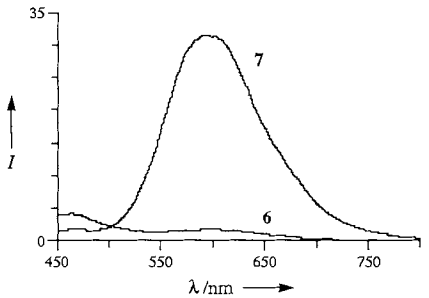

Figure 2. Emission spectra of the rhenium complexes **6** (open form) and **7** (closed form).

complexed subunit very effectively; this has also been observed in other complexes. In this case there is a fast transfer of energy from the metal complex unit to the anthracene unit.

The combination of a photochemically variable anthracene subunit with the observed emission from the rhenium subunit makes it possible for this switch to function. A further important condition is the reversibility of such systems, which is ensured in the investigated compounds.

Because of the photoinduced $4\pi+4\pi$-cyclization of the parallel anthracenes, the extended π systems are disrupted and can therefore no longer act as quenchers. On continuous irradiation of **6** with visible light, there should be a rhenium emission that increases with the irradiation time; this was confirmed experimentally. A corresponding decrease of the emission was observed for **7** as soon as its solution was irradiated with UV light. Preliminary experiments showed that solvation effects strongly influence the reaction rate of the switching process. Depending upon the choice of the solvent, side-reactions may appear.

This system provides a new, efficient photoswitch, which permits a reversible change in the emission of a spatially separated subunit of the molecule. Further experiments on the photophysical and photochemical properties of the rhenium complexes as well as the analogous ruthenium complexes are currently in progress.

Experimental Section

1: The synthesis was carried out according to the method applied by Becker and Amin[5]; however, the product was purified by Soxhlet extraction with hot *n*-hexane until no more anthracene could be detected in the tube (14 h) (SiO_2, hexane/ethyl acetate (8/2), $R_f = 0.82$). The residue in the Soxhlet tube was extracted with hot dichloromethane (100 mL). The mixture was cooled and the yellow crystals filtered off (41 % yield).

3: 5,5′-dimethyl-2,2′-bipyridine (3.68 g, 20 mmol) was dissolved in anhydrous THF (50 mL) and cooled to −78 °C under Ar. This solution was treated with LDA solution (13.3 mL, 20 mmol of a 1.5 M solution in cyclohexane) by slow dropwise addition through a septum, and the mixture was stirred for 2 h. Anhydrous gaseous CO_2 was bubbled through the black solution, which gave rise to an increase in the temperature and eventually a clear yellow solution was formed. The mixture was stirred for 1 h at −78 °C under a flow of CO_2 gas, then it was gradually allowed to warm to room temperature to produce a yellowish precipitate. After addition of several drops of water, the solvents were evaporated. The residue was taken up in 1 M NaOH (200 mL), extracted with hexane (200 mL), and the organic phase washed with 1 M NaOH (2 × 100 mL). The acidity of the combined aqueous phases was adjusted to pH = 5 by the addition of 3 M HCl, and the mixture was then concentrated until crystallization commenced. The crystals were dried at 50 °C and 200 mbar to give **3** (2.38 g, 10.4 mmol, 52 %). ^{1}H NMR (300 MHz, [D$_6$]DMSO, 25 °C, TMS): $\delta = 12.50$ (br. s, 1 H, COOH), 8.53 and 8.51 (both s, 1 H, CH(6 and 6′, respectively)), 8.29 and 8.25 (both d, 1 H, CH(3 and 3′, respectively)), 7.80 and 7.74 (both dd, 1 H, CH(4 and 4′, respectively)), 3.70 (s, 2 H, CH_2), 2.35 (s, 3 H, CH_3); MS (EI): *m/z*: 228 (M^+), 183 (M^+ − COOH), 155 (M^+ − CH_2COOH), 141 (bpy), 128, 115, 102, 92, 65, 51, 45; HR-MS: calcd. for $C_{13}H_{12}N_2O_2$: 228.0899, found: 228.0891.

4: **3** (133 mg, 0.58 mmol), **1** (240 mg, 0.58 mmol), and a spatula tip of 4-(dimethylamino)pyridine (DMAP) were dissolved in anhydrous dichloromethane (40 mL). After addition of diisopropylcarbodiimide (120 mg, 0.95 mmol), the apparatus was closed with a drying tube and the mixture was stirred at room temperature for 36 h. The reaction mixture was filtered through celite and washed with dichloromethane (40 mL). The filtrate was extracted with 1 M HCl (2 × 50 mL), 1 M NaOH (2 × 50 mL), and water (50 mL), then it was dried over $MgSO_4$, and evaporated to dryness. The crude yellow product was dissolved in THF, mixed with an equal amount of silica gel, and evaporated to dryness. The residue was applied to a silica gel column and eluted with hexane/ethyl acetate (8:2) until unconverted **1** had been completely removed. Subsequently, the column was eluted with THF. The powder obtained after evaporation was purified over a Sephadex column (LH-20, eluent THF), to remove the urea by-product. Yield: 200 mg (0.32 mmol, 55 %) **4**. M.p. 233–235 °C; ^{1}H NMR (300 MHz, $CDCl_3$, 25 °C, TMS): $\delta = 8.50$ (d, 1 H, CH(6′)), 8.36 (s, 2 H, CH(9)), 8.24 (d, 1 H, CH(3′)), 8.22 (d, 1 H, s, CH(6)), 8.08 (d, 1 H, CH(3)), 7.96 (d, 8 H, CH(8)),7.61 (dd, 1 H, CH(4′)), 7.40–7.25 (m, 8 H, CH(7)), 7.09 (dd, 1 H, CH(4)), 5.78 (quint., 1 H, CHO), 4.14 and 3.79 (both dd, 2 H, CH_2), 3.29 (s, 2 H, CH_2COO), 2.38 (s, 3 H, CH_3); MS (FAB): *m/z*: 623 (M^+), 530, 485, 438, 423, 394 (**1** − OH), 229 (**3**), 184 (**3** − COOH), 155 (Me-bpy); correct elemental analysis for $C_{44}H_{34}N_2O_2 \cdot 0.75\,H_2O$.

The ester **5** was synthesized analogously from **2**[5] and **3**. M.p. 226–227 °C; ^{1}H NMR (300 MHz, $CDCl_3$, 25 °C, TMS): $\delta = 8.72$ (d, 1 H, CH(6′)), 8.53 (d, 1 H, CH(6)), 8.46 (d, 1 H, CH(3′)), 8.34 (d, 1 H, CH(3)), 7.92 (dd, 1 H, CH(4′)), 7.66 (dd, 1 H, CH(4)), 7.22 (m, 2 H, CH(7,8)), 7.13 (m, 2 H, CH(7,8)), 6.94 (m, 2 H, CH(7,8)), 6.90–6.77 (m, 10 H, CH(7,8)), 5.98 (quint., 1 H, CHO), 4.53 (s, 2 H, CH(9)), 3.90 (s, 2 H, CH_2COO), 2.99 („t", 2 H, CH_2), 2.88 (dd, 2 H, CH_2), 2.41 (s, 3 H, CH_3); MS (FAB): *m/z*: 623 (M^+), 394 (**1** − OH), 329, 307, 289, 229 (**3**); correct elemental analysis for $C_{44}H_{34}N_2O_2 \cdot 0.5\,H_2O$.

Rhenium complex[7]: **6**: Under argon, [Re(CO)$_5$Cl] (27.3 mg, 0.075 mmol) was dissolved in anhydrous toluene (10 mL). At 60 °C **4** (47 mg, 0.075 mmol) was added in a countercurrent of argon. The reaction mixture was heated to 80 °C for 15 h to give a yellow precipitate. The cooled solution was filtered, and the solid washed with toluene (1 mL) and ether (15 mL). The crude product was taken up in chloroform (20 mL), mixed with silica gel (ca. 400 mg), and evaporated. The yellow granular powder was applied to a column (SiO_2, 11 × 1 cm) and eluted with ethyl acetate until the first contaminant was washed off. The mobile phase was washed with dichloromethane until the product was eluted. After evaporation of the solvent, **6** (50 mg, 0.054 mmol, 72 %) was obtained as a pale yellow powder. ^{1}H NMR (300 MHz, $CDCl_3$, 25 °C, TMS): $\delta = 8.84$ (d, 1 H, CH(6′)), 8.53 (d, 1 H, CH(6)), 8.40 and 9.37 (both s, 1 H, CH(9)), 7.97 (td, 8 H, CH(8)), 7.91 (d, 1 H, CH(3′)), 7.81 (dt, 1 H, CH(4′)), 7.60 (d, 1 H, CH(3)), 7.43–7.29 (m, 8 H, CH(7)), 7.00 (dd, 1 H, CH(4)), 5.87 (quint., 1 H, CHO), 4.20 (m, 2 H, CH_2), 3.91 (dm, 2 H, CH_2), 3.27 (s, 2 H, CH_2COO), 2.49 (s, 3 H, CH_3); MS (FAB): *m/z*:

 © WILEY-VCH Verlag GmbH, D-69451 Weinheim, 1997 0570-0833/97/3624-2780 $ 17.50+.50/0

928 (M^+), 893 ($M^+ - Cl$), 844 ($M^+ - 3CO$), 809 ($M^+ - 3CO - Cl$), 499, 454, 426, 307.

Rhenium complex **7**: Under argon, $[Re(CO)_5Cl]$ (27.3 mg, 0.075 mmol) was dissolved in anhydrous toluene (10 mL). At 60 °C, **5** (47 mg, 0.075 mmol) was added in a countercurrent of argon and the reaction mixture heated to 80 °C for 15 h. The cooled solution was filtered, washed with toluene (1 mL), suspended in ether, filtered, and dried in a high vacuum to give **7** (66 mg, 0.071 mmol, 94%) as a yellow powder. ^1H NMR (300 MHz, $CDCl_3$, 25 °C, TMS): $\delta = 9.04$ (s, 1H, CH(6')), 8.88 (d, 1H, CH(6)), 8.21 (dd, 1H, CH(4')), 8.17 (d, 1H, CH(3')), 8.08 (dd, 1H, CH(3)), 7.86 (dd, 1H, CH(4)), 7.22 (m, 2H, CH(7,8)), 7.12 (m, 2H, CH(7,8)), 6.96 (m, 2H, CH(7,8)), 6.90–6.78 (m, 10H, CH(7,8)), 6.00 (quint., 1H, CHO), 4.54 (s, 2H, CH(9)), 3.99 (s, 2H, CH_2COO), 3.06 („t"d, 2H, CH_2), 2.85 (dd, 2H, CH_2), 2.52 (s, 3H, CH_3); MS (FAB): *m/z*: 928 (M^+), 893 ($M^+ - Cl$), 844 ($M^+ - 3CO$), 499 ($M^+ - \mathbf{1}$), 471, 454, 307.

Received: May 15, 1997 [Z10442IE]
German version: *Angew. Chem.* **1997**, *109*, 2878–2881

Keywords: energy transfer · molecular switches · photochemistry · photoswitchable systems · rhenium

[1] V. Balzani, F. Scandola, *Supramolecular Photochemistry*, Horwood, Chichester, UK, **1991**.
[2] J.-M. Lehn, *Supramolecular Chemistry*, VCH, Weinheim, **1995**.
[3] A. P. de Silva, H. Q. N. Gunaratne, C. P. McCoy, *Nature* **1993**, *364*, 42.
[4] L. Fabbrizzi, A. Poggi, *Chem. Soc. Rev.* **1995**, *24*, 197.
[5] H. D. Becker, K. A. Amin, *J. Org. Chem.* **1989**, *54*, 3182.
[6] B. Neises, W. Steglich, *Angew. Chem.* **1978**, *90*, 556; *Angew. Chem. Int. Ed. Engl.* **1978**, *17*, 522.
[7] a) G. Tapolsky, R. Duesing, T. J. Meyer, *Inorg. Chem.* **1990**, *29*, 2285; b) L. A. Worl, R. Duesing, P. Chen, L. Delle Ciana, T. J. Meyer, *J. Chem. Soc. Dalton Trans.* **1991**, 849.

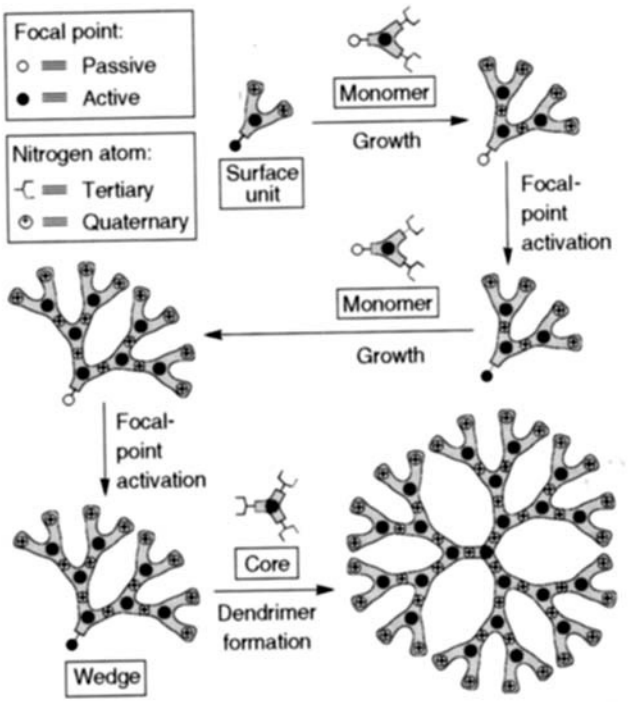

Scheme 1. Schematic representation of the convergent approach to the synthesis of a third-generation polycationic dendrimer with quaternary ammonium linkages.

Polycationic Dendrimers**

Peter R. Ashton, Kazusato Shibata, Andrew N. Shipway, and J. Fraser Stoddart*

Dedicated to Professor Achim Müller on the occasion of his 60th birthday

Dendritic molecules[1] carrying multiple cationic sites are—unlike their polyanionic counterparts[2]—still very rare.[3] The catalytic activity of a dendrimer coated with quaternary ammonium centers on its surface has been investigated,[4] and a series of dendrimers in which the core and branch points are either ammonium[5] or phosphonium sites[6] have been reported. However, the potential applications of dendrimers might be hindered by the low yields of their syntheses.

We are interested in creating dendritic microenvironments, in which a wide range of different chemical reactions can be carried out.[7] It is not unlikely that dendrimers with cavities that are splattered with positive charges and yet largely lipophilic should be able to bind simultaneously counterions—in the shape of reactive nucleophiles[8]—and organic substrates.[9]

Here we present a particularly attractive and efficient convergent approach (Scheme 1) to gram quantities of polycationic wedges and dendrimers.[10] The core and branching points are based on a mesitylene framework. Generation growth is achieved by using the high-yielding Menschutkin reaction, in which the growing dendritic wedge bearing a reactive benzylic CH_2Br group at the focal point is attached to the benzylic CH_2NEt_2 functionalities in a monomer unit, thereby producing new cationic sites.[11] The larger "passive" wedge is isolated, and the new benzylic CH_2OH group then converted into the reactive CH_2Br group to afford a larger "active" wedge. The series of first-, second-, and third-generation wedges are incorporated into the corresponding dendrimers by allowing the active wedges to react with the core, namely, 1,3,5-tris(diethylaminomethyl)benzene (**C**). To ensure that the Menschutkin reaction is high-yielding, the amines (i. e., the monomer **M** and the core **C**) must be of extremely high purity. As new cationic sites are created, the "soft" PF_6^- anion is introduced to aid the solubility of the positively charged macromolecules in organic solvents.

The synthesis[12] of the monomer **M**, the core **C**, the first-generation ($g = 1$) wedge **1GW**·$2PF_6$, and the zero-generation ($g = 0$) dendrimer **0GD**·$3PF_6$ are summarized in Scheme 2. 1,3,5-Tris(bromomethyl)benzene (**2**), which was obtained by bromination of 1,3,5-tris(hydroxymethyl)benzene[13] (**1**) with three equivalents of Ph_3P/CBr_4 in THF, was treated with an excess of Et_2NH to give the core **C** (97% yield). Reaction of **1** with two equivalents of Ph_3P/CBr_4 in THF afforded 3,5-bis(bromomethyl)phenylmethanol (**3**, 55% yield), which was converted into the monomer **M** (86% yield) by treatment with excess Et_2NH. Reaction of **3** with excess Et_3N yielded **4**·2Br quantitatively. After counterion exchange with NH_4PF_6/H_2O to produce **4**·$2PF_6$, the CH_2OH group in $\mathbf{4}^{2+}$ was converted into a CH_2Br group with HBr/HOAc to afford, after counterion exchange, the wedge **1GW**·$2PF_6$ ($g = 1$, 89% yield). Successive treatment of **2** with an excess of NEt_3 and NH_4PF_6 yielded the dendrimer

[*] Prof. J. F. Stoddart
Department of Chemistry and Biochemistry
University of California at Los Angeles
405 Hilgard Avenue, Los Angeles, CA 90095 (USA)
Fax: Int. code + (310) 206-1843
e-mail: Stoddart@chem.ucla.edu
P. R. Ashton, Dr. K. Shibata, Dr. A. N. Shipway
School of Chemistry, University of Birmingham (UK)

[**] This research was sponsored in the UK by the Engineering and Physical Sciences Research Council.

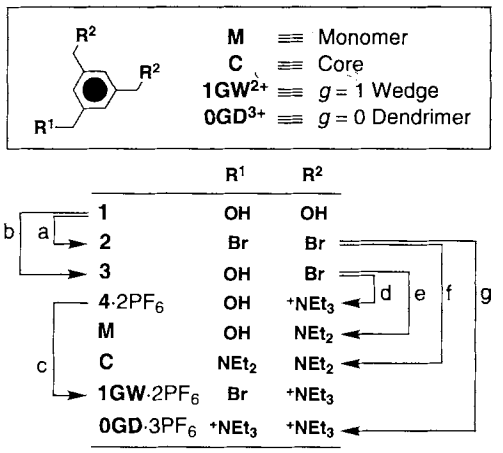

Scheme 2. Synthesis of the key building blocks—namely, the monomer **M**, the core **C**, the first-generation wedge **1GW**·2PF$_6$ ($g=1$), and the zero-generation dendrimer **0GD**·3PF$_6$ ($g=0$)—from 1,3,5-tris(hydroxymethyl)benzene (**1**). a) 45% HBr in AcOH, 20°C, 46 h, 98%; b) CBr_4/PPh_3/THF, 20°C, 2 h, 55%; c) 1. 45%. HBr in AcOH, 20°C, 20 h; 2. NH_4PF_6/H_2O, 100%; d) Et_3N/Me_2CO/MeOH, 20°C, 2 h, 100%; e) Et_2NH, 20°C, 4 h, 86%; f) Et_2NH/Et_2O, 20°C, 23 h, 97%; g) Et_3N/MeOH, 20°C, 2 h, 49%.

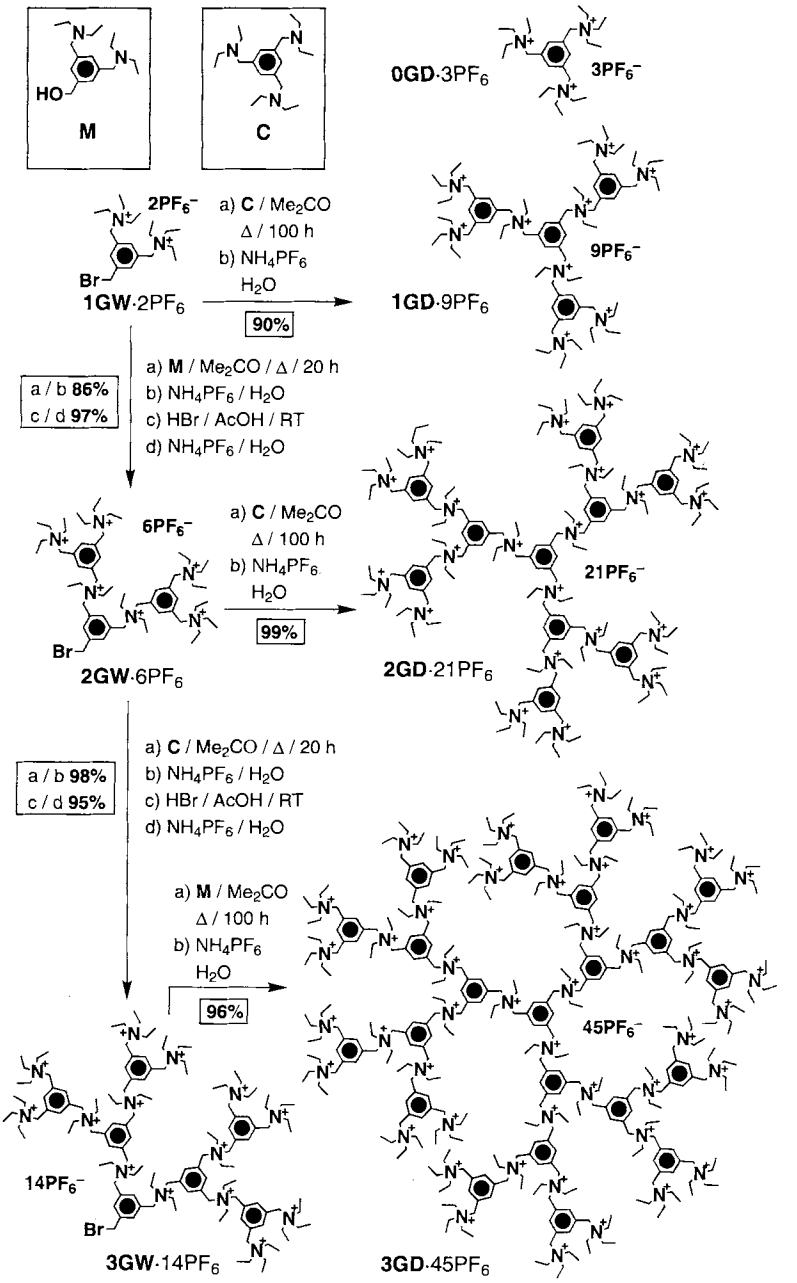

Scheme 3. Synthesis of up to third-generation dendrimers and wedges from the monomer **M**, the core **C**, and the first-generation wedge **1GW**·2PF$_6$.

0GD·3PF$_6$ ($g=0$, 67% yield), which is stable[14] upon heating in CD_3SOCD_3 at 100°C in the presence of about ten equivalents of NaOMe.

Wedge growth (Scheme 3) as far as the third-generation wedge ($g=3$, **3GW**$^{14+}$) was achieved by a repetitive sequence of steps: a) successive Menschutkin reactions between **M** and wedges **1GW**·2PF$_6$ ($g=1$) and **2GW**·6PF$_6$ ($g=2$) in Me_2CO, b) subsequent counterion exchange, c) treatment of the benzylic alcohol functionality with HBr/HOAc to give the benzylic bromide, and d) counterion exchange with aqueous NH_4PF_6. All the steps proceeded with better than 90% yields. Dendrimers **1GD**·9PF$_6$ ($g=1$), **2GD**·21PF$_6$ ($g=2$), and **3GD**·45PF$_6$ ($g=3$) with 9, 21, and 45 cationic sites, respectively, were synthesized in yields of 90, 99, and 96% by allowing the core **C** to react with the wedges **1GW**·2PF$_6$, **2GW**·6PF$_6$, and **3GW**·14PF$_6$ in turn in Me_2CO to effect the three necessary Menschutkin reactions followed by counterion exchange. They are all stable white solids which decompose without melting above 200°C; they are very soluble in organic solvents such as Me_2CO, DMF, DMSO, $MeNO_2$, and MeOH. The constitutions and purities of all the wedges and dendrimers were established by LSI mass spectrometry, ^1H and ^{13}C NMR spectroscopy, and elemental analysis. The LSI mass spectra of **1GW**·2PF$_6$, **2GW**·6PF$_6$, **3GW**·14PF$_6$, **0GD**·3PF$_6$, and **1GD**·9PF$_6$ display peaks at $m/z=543$, 1706, 4027, 710, and 2451, respectively, corresponding to $[M-PF_6]^+$. **2GD**·21PF$_6$ and **3GD**·45PF$_6$ do not exhibit $[M-PF_6]^+$ ions, possibly as a result of their highly charged character.

An extremely efficient synthetic route to polycationic dendrimers has been established. There is every reason to believe that further growth of the dendrimers beyond the third generation will be possible using, for example a "double-stage" approach.[15] This simple and very high-yielding synthetic methodology for constructing monodisperse macromolecular polyelectrolytes, whose solubility can be influenced by the nature of the counterions, has important implications when it comes, for example, to investigating interfacial phenomena and devising new analytical procedures[16] and catalytic processes.

Experimental Section

3: m.p. 94–95°C; MS(EI): $m/z=294$ [M^+], 213 [M^+-Br], 134 [M^+-2Br]; ^1H NMR ($CDCl_3$, 300 MHz): $\delta=1.80$ (br s, 1H), 4.45 (s, 4H), 4.68 (s, 2H), 7.32 (s, 3H); ^{13}C NMR ($CDCl_3$, 75 MHz): $\delta=32.7$, 64.4, 127.3, 128.7, 138.6, 142.2; elemental analysis calcd for $C_9H_{10}Br_2O$: C 36.77, H 3.43; found: C 36.85, H 3.32.

C: b.p. 129°C (0.40 torr); MS (EI): $m/z=333$ [M^+]; ^1H NMR ($CDCl_3$, 300 MHz): $\delta=1.02$ (t, 18H, $J=7$ Hz), 2.49 (q, 12H, $J=7$ Hz), 3.53 (s, 6H), 7.14 (s, 3H); ^{13}C NMR ($CDCl_3$, 75 MHz): $\delta=11.7$, 46.6, 57.4, 128.0, 139.3; elemental analysis calcd for $C_{21}H_{39}N_3$: C 75.62, H 11.78, N 12.60; found: C 75.50, H 11.86, N 12.86.

M: b.p. 129°C (0.10 torr); MS (EI): $m/z=278$ [M^+]; ^1H NMR ($CDCl_3$, 300 MHz): $\delta=1.02$ (t, 12H, $J=7$ Hz), 2.49 (q, 8H, $J=7$ Hz), 3.53 (s, 4H), 4.63 (s, 2H),

 © WILEY-VCH Verlag GmbH, D-69451 Weinheim, 1997 0570-0833/97/3624-2782 $ 17.50+.50/0

7.15–7.22 (m, 3H); ^{13}C NMR ($CDCl_3$, 75 MHz): δ = 11.4, 46.5, 57.3, 64.7, 126.1, 128.8, 139.5, 141.2; elemental analysis calcd for $C_{17}H_{30}N_2O$: C 73.33, H 10.86, N 10.06; found: C 73.40, H 10.86, N 9.92.

4·2 PF_6: m.p. 185–187 °C (decomp); MS (LSI): *m/z*: 481 [$M^+ - PF_6$]; ^{1}H NMR (CD_3SOCD_3, 300 MHz): δ = 1.31 (t, 18H, *J* = 7 Hz), 3.17 (q, 12H, *J* = 7 Hz), 4.49 (s, 4H), 4.60 (d, 2H, *J* = 6 Hz), 5.46 (t, 1H, *J* = 6 Hz), 7.40 (s, 1H), 7.56 (s, 2H); ^{13}C NMR (CD_3SOCD_3, 75 MHz): 7.4, 52.0, 58.9, 62.0, 128.4, 132.0, 134.5, 144.4; elemental analysis calcd for $C_{21}H_{40}F_{12}N_2OP_2$: C 40.26, H 6.44, N 4.47; found: C 40.32, H 6.39, N 4.34.

1GW·2 PF_6: **4**·2 PF_6 (14.1 g, 22.4 mmol) was added to 45%. HBr in HOAc (60 mL). The reaction mixture was stirred for 65 h before being concentrated under vacuum to yield a brown oil, which was treated with aqueous NH_4PF_6 to afford **1GW**·2 PF_6 as a white solid (13.8 g, 20.0 mmol, 89%); m.p. 183–185 °C (decomp); MS (LSI): *m/z* = 543 [$M^- - PF_6$]; ^{1}H NMR (CD_3SOCD_3, 300 MHz): δ = 1.31 (t, 18H, *J* = 7 Hz), 3.17 (q, 12H, *J* = 7 Hz), 4.50 (s, 4H), 4.83 (s, 2H), 7.48 (s, 1H), 7.72 (s, 2H); ^{13}C NMR (CD_3SOCD_3, 75 MHz): δ = 7.4, 32.9, 52.0, 58.5, 129.1, 135.0, 136.1, 139.9; elemental analysis calcd for $C_{21}H_{39}BrF_{12}N_2P_2$: C 36.59, H 5.70, N 4.06; found: C 36.33, H 5.50, N 3.88.

2GW·6 PF_6 and **3GW**·14 PF_6: Wedge **1GW**·2 PF_6 or **2GW**·6 PF_6 and the monomer **M** (0.45 mol%) were heated at reflux in Me_2CO. After removal of the solvent under vacuum, the residue was treated with an excess of NH_4PF_6 in aqueous Me_2CO. The precipitated PF_6^- salts were isolated by filtration, washed with H_2O, and dried before being stirred with 45% HBr in HOAc at room temperature for 65 h. Concentration of the solution under vacuum afforded a brown oil, which was treated with aqueous NH_4PF_6 to yield the appropriate second- or third-generation wedge

2GW·6 PF_6: white solid (97% yield); decomposition without melting above 130 °C; MS (LSI): *m/z* = 1706 [$M^- - PF_6$]; ^{1}H NMR (CD_3SOCD_3, 300 MHz): δ = 1.33 (t, 36H, *J* = 7 Hz), 1.45 (t, 12H, *J* = 7 Hz), 3.19 (m, 32H), 4.53 (s, 8H), 4.66 (br s, 8H), 4.80 (s, 2H), 7.69 (s, 3H), 7.76 (s, 4H), 7.82 (s, 2H); ^{13}C NMR (CD_3SOCD_3, 75 MHz): δ = 7.4, 8.4, 32.6, 52.0, 52.7, 58.2, 60.3, 129.2, 129.3, 129.4, 135.6, 136.5, 138.2, 138.6, 140.0; elemental analysis calcd for $C_{59}H_{107}BrF_{36}N_6P_6$: C 38.30, H 5.83, N 4.54; found: C 38.28, H 5.89, N 4.59.

3GW·14 PF_6: white solid (95% yield); decomposition without melting above 100 °C; MS (LSI): *m/z* = 4027 [$M^+ - PF_6$]; ^{1}H NMR (CD_3SOCD_3, 300 MHz): δ = 1.33 (br s, 72H), 1.50 (m, 36H), 3.20 (br s, 72H), 4.52 (br s, 16H), 4.68 (br s, 24H), 4.80 (s, 2H), 7.60–7.95 (m, 21H); ^{13}C NMR (CD_3SOCD_3, 75 MHz): δ = 7.4, 8.4, 52.0, 52.7, 58.2, 59.8, 129.2, 129.5, 138.5, 139.0; elemental analysis calcd for $C_{135}H_{243}BrF_{84}N_{14}P_{14}$: C 38.87, H 5.87, N 4.70; found: C 38.78, H 6.08, N 4.75.

0GD·3 PF_6: Et_3N (5 mL) was added with constant stirring to a solution of **2** (0.13 g, 0.39 mmol) and NH_4PF_6 (0.15 g, 1.3 mmol) in Me_2CO (5 mL), and then the reaction was stirred for 3 h. The solution was filtered and dried over K_2CO_3, and the solvent removed. The product was purified by recrystallization from Me_2CO/hexane to give **0GD**·3 PF_6 (white solid, 67% yield); MS(EI): *m/z* = 710 [$M^- - PF_6$]; ^{1}H NMR (CD_3COCD_3, 300 MHz): δ = 1.56 (t, 27H, *J* = 7 Hz), 3.51 (q, 18H, *J* = 7 Hz), 4.79 (s, 6H), 8.08 (s, 3H); ^{13}C NMR (CD_3COCD_3, 75 MHz): δ = 8.0, 53.5, 59.9, 130.8, 139.6.

1GD·9 PF_6, **2GD**·21 PF_6, and **3GD**·45 PF_6: Wedge **1GW**·2 PF_6, **2GW**·6 PF_6, or **3GW**·14 PF_6 (3.1 equiv) and the core **C** were heated at reflux in Me_2CO for 100 h. The solution was then added to an excess of aqueous NH_4PF_6, and the mixture stirred for 10 min. The resulting precipitate was filtered, washed with H_2O, and dried.

1GD·9 PF_6: white solid (90% yield); decomposition without melting above 200 °C; ^{1}H NMR (CD_3SOCD_3, 300 MHz): δ = 1.33 (br s, 54H), 1.50 (br s, 18H), 3.18 (br s, 48H), 4.51 (br s, 12H), 4.68 (brs, 12H), 7.60–8.00 (m, 12H); ^{13}C NMR (CD_3SOCD_3, 75 MHz): δ = 7.4, 8.4, 52.0, 52.7, 58.1, 59.8, 129.2, 129.5, 138.4; elemental analysis calcd for $C_{84}H_{156}F_{54}N_9P_9$: C 38.85, H 6.05, N 4.85; found: C 38.64, H 6.46, N 4.52.

2GD·21 PF_6: white solid (99% yield); decomposition without melting above 200 °C; ^{1}H NMR (CD_3SOCD_3, 300 MHz): δ = 1.33 (br s, 108H), 1.47 (m, 54H), 3.19 (m, 108H), 4.53 (br s, 24H), 4.65 (br s, 36H), 7.60–8.00 (m, 30H); ^{13}C NMR (CD_3SOCD_3, 75 MHz): δ = 7.4, 8.4, 52.0, 52.7, 58.2, 60.2, 129.2, 129.3, 129.4, 138.2, 138.3, 138.4, 138.5; elemental analysis calcd for $C_{198}H_{360}F_{126}N_{21}P_{21}$: C 39.12, H 5.97, N 4.84; found: C 39.12, H 5.84, N 4.92.

3GD·45 PF_6: white solid (96% yield); decomposition without melting above 200 °C; ^{1}H NMR (CD_3SOCD_3, 300 MHz): δ = 1.33 (br s, 216H), 1.51 (br s, 126H), 3.18 (br s, 228H), 4.52 (br s, 48H), 4.67 (br s, 84H), 7.70–7.90 (m, 66H); ^{13}C NMR (CD_3SOCD_3, 75 MHz): δ = 7.4, 8.4, 52.0, 52.7, 58.2, 59.8, 129.2, 129.5, 138.4; elemental analysis calcd for $C_{426}H_{768}F_{270}N_{45}P_{45}$: C 39.22, H 5.93, N 4.83; found: C 39.09, H 5.94, N 4.78.

Received: June 17, 1997 [Z10564IE]
German version: *Angew. Chem.* **1997**, *109*, 2902–2905

Keywords: dendrimers · Menschutkin reaction · polycations polyelectrolytes

[1] a) D. A. Tomalia, A. M. Naylor, W. A. Goddard III, *Angew. Chem.* **1990**, *102*, 119–157; *Angew. Chem. Int. Ed. Engl.* **1990**, *29*, 138–175; b) G. R. Newkome, C. N. Moorefield, F. Vögtle, *Dendritic Molecules*, VCH, Weinheim, **1996**; c) O. A. Matthews, A. N. Shipway, J. F. Stoddart, *Prog. Polym. Sci.*, **1998**, *23*, 1–56.

[2] Many dendrimers with polyanionic surfaces have been synthesized, see for example a) K. R. Gopidas, A. R. Leheny, G. Caminati, N. J. Turro, D. A. Tomalia, *J. Am. Chem. Soc.* **1991**, *113*, 7335–7342; b) C. J. Hawker, K. L. Wooley, J. M. J. Fréchet, *J. Chem. Soc. Perkin Trans. 1* **1993**, 1287–1297.

[3] Apart from cationic sites being introduced into an organic compound during its synthesis, polycationic dendrimers have been produced by a) modification of neutral dendrimers (see for example C. Larré, A.-M. Caminade, J.-P. Majoral, *Angew. Chem.* **1997**, *109*, 614–617; *Angew. Chem. Int. Ed. Engl.* **1997**, *36*, 596–599) and b) incorporating transition matals into the dendritic structure (see for example S. Campagna, G. Dendti, S. Serroni, A. Juris, M. Venturi, V. Ricevuto, V. Balzani, *Chem. Eur. J.* **1995** *1*, 211–221; S. Achar, J. Puddephatt, *J. Chem. Soc. Chem. Commun.* **1994**, 1895–1896).

[4] J.-J. Lee, W. T. Ford, J. A. Moore, Y. Li, *Macromolecules* **1994**, *27*, 4632–4634.

[5] a) K. Rengan, R. Engel, *J. Chem. Soc. Chem. Commun.* **1992**, 757–758; b) R. Engel, K. Rengan, C. S. Chan, *Heteroatom Chem.* **1993**, *4*, 181–184.

[6] K. Rengan, R. Engel, *J. Chem. Soc. Perkin Trans. 1* **1991**, 987–990.

[7] Although many diverse examples of catalytic dendrimers have been reported, they rely upon the incorporation of a known catalytic site inside or on the surface of the dendritic structure rather than upon the unique dendritic microenvironment itself, see for example a) J. W. J. Knapen, A. W. van der Made, J. C. de Wilde, P. W. N. M. van Leeuwen, P. Wijkens, D. M. Grove, G. van Koten, *Nature* **1994**, *372*, 659–663; b) A. Miedaner, C. J. Curtis, R. M. Barkley, D. L. DuBois, *Inorg. Chem.* **1994**, *33*, 5482–5490; c) P. J. Dandliker, F. Diederich, J.-P. Gisselbrecht, A. Louati, M. Gross, *Angew. Chem.* **1995**, *107*, 2906–2909; *Angew. Chem. Int. Ed. Engl.* **1995**, *34*, 2725–2727.

[8] For examples of the encapsulation of guest molecules inside dendritic structures, see a) A. M. Taylor, W. M. Goddard III, G. E. Keifer, D. A. Tomalia, *J. Am. Chem. Soc.* **1989**, *111*, 2339–2341; b) G. R. Newkome, C. N. Moorefield, G. R. Baker, M. J. Saunders, S. H. Grossman, *Angew. Chem.* **1991**, *103*, 1207–1209; *Angew. Chem. Int. Ed. Engl.* **1991**, *30*, 1178–1180; c) C. J. Hawker, K. L. Wooley, J. M. J. Fréchet, *J. Chem. Soc. Perkin Trans. 1* **1993**, 1287–1297; d) J. F. G. A. Jansen, E. M. M. de Brabander-van den Berg, E. W. Meijer, *Science* **1994**, *266*, 1226–1229; e) J. F. G. A. Jansen, E. W. Meijer, E. M. M. de Brabander-van den Berg, *J. Am. Chem. Soc.* **1995**, *117*, 4417–4418.

[9] Examples of catalyses have been observed in cationic micelles (F. M. Menger, L. G. Whitesell, *J. Am. Chem. Soc.* **1985**, *107*, 707–708) and in polymerized micelles (A. Kumar, G. Oehme, J. P. Roque, M. Schwarze, R. Selke, *Angew. Chem.* **1994**, *106*, 2272–2274; *Angew. Chem. Int. Ed. Engl.* **1994**, *33*, 2197–2199).

[10] C. J. Hawker, J. M. J. Fréchet, *J. Am. Chem. Soc.* **1990**, *112*, 7638–7647.

[11] The formation of this polycationic dendrimer is exactly analogous to that of the Fréchet dendrimers, except that the nucleophile in this case is an $ArCH_2NEt_2$ rather than a phenoxide group. For this reason, the two systems should be compatible in the construction of mixed-monomer dendritic architectures.

[12] The nomenclature employed for describing the wedges and dendrimers: a number (**0**, **1**, **2**, or **3**) denoting the generation followed by the letter **G** for generation, and thereafter by the letter **W** or **D** for a wedge or a dendrimer, respectively.

[13] Although **1** is commercially available, it is convenient and economical to make on a 100-g scale. Esterification of 1,3,5-tribenzenecarboxylic acid (trimesic acid) with $MeOH/H_2SO_4$ followed by reduction of the triester affords 1,3,5-tris(hydroxymethyl)benzene in quantitative yield.

[14] The ^{1}H NMR spectrum of a mixture of **0GD**·3 PF_6 (10 mg) and NaOMe (5 mg) in CD_3SOCD_3 (0.7 mL) was essentially unchanged after heating at 100 °C for 72 h.

[15] K. L. Wooley, C. J. Hawker, J. M. J. Fréchet, *J. Am. Chem. Soc.* **1991**, *113*, 4252–4261.

[16] S. A. Kuzdzal, C. A. Monnig, G. R. Newkome, C. N. Moorefield, *J. Am. Chem. Soc.* **1997**, *119*, 2255–2261.

 © WILEY-VCH Verlag GmbH, D-69451 Weinheim, 1997 0570-0833/97/3624-2783 $ 17.50+.50/0

A Highly Enantiomerically Enriched α-Thiobenzyl Derivative with Unusual Configurational Stability**

Dieter Hoppe,* Bernd Kaiser, Oliver Stratmann, and Roland Fröhlich

Dedicated to Professor Waldemar Adam on the occasion of his 60th birthday

α-Heterosubstituted, enantiomerically enriched alkyllithium compounds **1** have gained importance in the field of enantioselective synthesis.[1-4] Electrophilic reagents react with retention of configuration (R^1, R^2 = alkyl, H), whereas inversion of configuration takes place at the benzylic position.[2n-p,3h] The configurational stability reaches a synthetically useful level and provides the possibility of handling **1** or *ent*-**1** without racemization for only a few α-oxy-[2] or α-amino-substituted[3] species (**1a**–**1e**) and for lithiated alkyl trifluoromethyl sulfones[4] (**1f**) between −80 and −30 °C (Scheme 1).

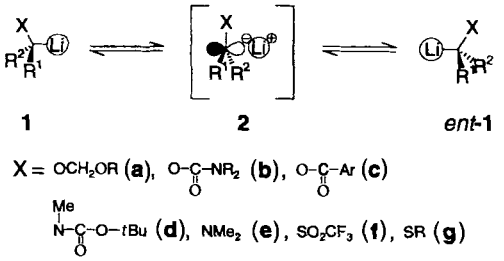

Scheme 1. Inversion of the configuration of alkyllithium compounds **1**.

However, α-thio-substituted alkyllithium derivatives **1g** are characterized by a notorious lability of configuration.[5] As far as we know, the only exception is the lithiated *S*-(α-trimethylsilylalkyl) thiocarbamate **3b**.[6] It can be kept in diethyl ether at −78 °C for several hours without noticeable racemization, whereas non-silylated **3a** shows configurational

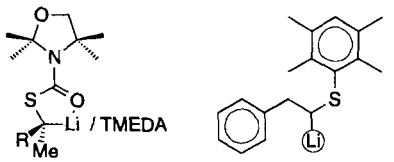

lability under these conditions (TMEDA = *N*,*N*,*N*′,*N*′-tetramethylethylenediamine).[7] Based on work by H. J. Reich et al.[5a-e] and R. W. Hoffmann et al.,[5f-l] this is caused by a different mechanism of racemization. Neither formation of a solvent-separated ion pair nor inversion of configuration at the carbanionic center but rotation of the hyperconjugated S–C bond seems to be the rate-determining step (Scheme 2). In this case the barrier of racemization should be enhanced by

Scheme 2. Proposed mechanism for the inversion of configuration in **2g**.

bulky substituents R at the sulfur atom (as for **4**)[5k-l] and by branching at the carbanionic center.

With respect to these results we investigated the lithium compound (*S*)-**8**, which can be expected to have a larger tendency to form solvent-separated ion pairs than **3a** because of the additional resonance stabilization of the anion. Thiocarbamate (*S*)-**7**[8] (>99% *ee*)[9] was synthesized from (*R*)-1-phenylethanol[10] [(*R*)-**6**, Scheme 3], which was ob-

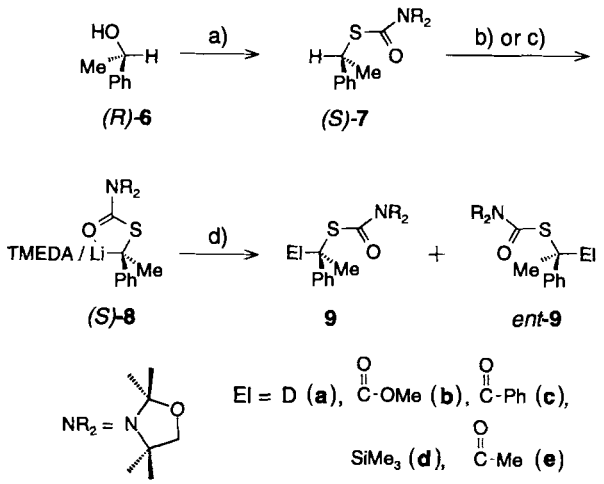

Scheme 3. Synthesis of (*S*)-**8**, **9**, and *ent*-**9**. a) 1. Diisopropyl azodicarboxylate (DIAD)/Ph_3P/MeCOSH (THF), 70%; 2. $LiAlH_4$ (Et_2O), 99%; 3. NaH/$ClCONR_2$ (THF) 92%; b) *sec*-BuLi/TMEDA (Et_2O, −78 °C; c) *sec*-BuLi/TMEDA (Et_2O, −78 °C–0 °C; d) ElX.

tained by the classical method of resolution. Deprotonation[11] was achieved by adding *sec*-butyllithium/TMEDA to a solution of (*S*)-**7** in diethyl ether at −78 °C. At this temperature the solution was quenched with several electrophilic reagents (method A). We obtained the substitution products (*S*)-**7** (reprotonation with MeOH or AcOH), **9a**, and *ent*-**9b**–*ent*-**9e** with 97% to greater than 99% *ee* (Table 1).

Table 1. Lithiation and substitution of (*S*)-**7**.

Electrophile (ElX)	Method	Product [a]	Yield [%]	*ee* [%]	$[\alpha]_D^T$ [b]
H*OMe*	A	(*S*)-**7**	95	99	−127.2
H*OMe*	B	(*S*)-**7**	91	≥99	−128.6
H*OAc*	A	(*S*)-**7**	98	≥99	−133.5
D*OMe*	A	**9a** [c]	94	98	−129.1
MeO(CO)*Cl*	A	*ent*-**9b**	98	≥99	−24.6
MeO(CO)*Cl*	B	*ent*-**9b**	98	≥99	−25.5
CO_2 [d]	A	*ent*-**9b**	90	99	−22.5
Ph(CO)*Cl*	A	*ent*-**9c**	82	99	+116.5
Me_3SiCl	A	*ent*-**9d**	93	≥97	−90.7
Me(CO)*Cl*	A	*ent*-**9e**	95	≥99	−22.5
Me(CO)*Cl*	B	*ent*-**9e**	98	≥99	−21.8
Ac*OAc*	A	**9e**	75	57	+12.3

[a] All products were obtained analytically pure (C ± 0.4%, H ± 0.3%, N 0.3%). [b] $T = 20-27$ °C, $c = 1.06-1.93$ g(100 mL)$^{-1}$ in CH_2Cl_2. [c] Degree of deuteration 86%. [d] Without deacidification, followed by esterification of the carboxylic acid with diazomethane.

[*] Prof. Dr. D. Hoppe, Dr. B. Kaiser, Dipl.-Chem. O. Stratmann, Dr. R. Fröhlich[+]
Organisch-chemisches Institut der Universität
Corrensstrasse 40, D-48149 Münster (Germany)
Fax: Int. code + (251) 83-39772

[+] X-ray structure analyses

[**] This work was supported by the Deutsche Forschungsgemeinschaft and by the Fonds der Chemischen Industrie.

 © WILEY-VCH Verlag GmbH, D-69451 Weinheim, 1997 0570-0833/97/3624-2784 $ 17.50+.50/0

The absolute configuration of compounds *ent*-**9b** to *ent*-**9d** was confirmed by single-crystal X-ray diffraction analysis with anomalous dispersion.[12]

In further experiments a solution of (*S*)-**8** was maintained at -2 to 0 °C for ten minutes and then cooled again to -78 °C before the electrophile was added (method B). The products (*S*)-**7**, *ent*-**9b**, and *ent*-**9e** still had the high enantiomeric purity of $\geq 99\%$ *ee*.[13] Therefore, the half-life of racemization of **8** can be extrapolated to several hours.[14] As observed for the corresponding benzylcarbamate (O instead of S in **8**), substitution mainly takes place with inversion of configuration.[2n-p] Only electrophilic reagents that tend to coordinate the lithium cation react suprafacially with retention of configuration; examples are protonic acids or acid anhydrides as shown for **9e** in Table 1. The combination of effective kinetic acidification of the optically active precursor **7** by an *S*-carbamoyl group with hindrance of rotation of the adjacent C–S bond in the ion pair provided the first, and probably generalizable, access to highly enantiomerically enriched α-thiocarbanions.

Experimental Section

Method A: Salt-free *sec*-butyllithium (1.25 mmol, $\approx$1.3 M in isopentane/cyclohexane) was added to a solution of TMEDA (174 mg, 1.50 mmol) and (*S*)-**7** (293 mg, 1.00 mmol) in diethyl ether (10.0 mL) at -78 °C. After 2 h of stirring the electrophile was injected, and the reaction mixture stirred for a further 2–5 h. The cool solution was poured into a mixture of diethyl ether (10 mL) and 2 N HCl (10 mL). The aqueous phase was extracted three times with diethyl ether. After the combined organic phases were dried and deacidified with Na_2SO_4/$NaHCO_3$, the crude product was purified by flash chromatography on silica gel.

Method B: After lithiation and 1 h of stirring at -78 °C the reaction mixture was warmed to -2 to 0 °C (internal thermometer) in an ice/water bath within 2–5 min, kept at this temperature for 10 min, and cooled to -78 °C with a dry ice/acetone bath within about 10 min. The electrophile was added, and the reaction mixture treated as described for method A.

Received: June 25, 1997 [Z10598IE]
German version: *Angew. Chem.* **1997**, *109*, 2872–2874

Keywords: carbanions · chirality · configuration inversion · ion pairs · lithium

[1] Reviews: a) V. Aggarwal, *Angew. Chem.* **1994**, *106*, 185–187; *Angew. Chem. Int. Ed. Engl.* **1994**, *33*, 175–177; b) P. Beak, A. Basu, D. J. Gallagher, Y. S. Park, S. Thayumanavan, *Acc. Chem. Res.* **1996**, *29*, 552–560; c) D. Hoppe, T. Hense, *Angew. Chem* **1997**, *109*, 2376–2410; *Angew. Chem. Int. Ed. Engl.* **1997**, *36*, 2282–2316.

[2] Examples of the preparation of enantiomerically enriched, configurationally stable and not mesomerically stabilized α-oxycarbanion equivalents: a) W. C. Still, C. Sreekumar, *J. Am. Chem. Soc.* **1980**, *102*, 1201–1202; b) P.-C.-M. Chan, J. M. Chong, *J. Org. Chem.* **1988**, *53*, 5584–5586; c) J. A. Marshall, W. Y. Gung, *Tetrahedron* **1989**, *45*, 1043–1052; d) D. S. Matteson, P. B. Tripathy, A. Sarkar, K. M. Sadhu, *J. Am. Chem. Soc.* **1989**, *111*, 4399–4402; e) D. Hoppe, F. Hintze, P. Tebben, *Angew. Chem.* **1990**, *102*, 1457–1459; *Angew. Chem. Int. Ed. Engl.* **1990**, *29*, 1424–1425; f) K. Tomooka, T. Igarashi, T. Nakai, *Tetrahedron* **1994**, *50*, 5927–5932; g) L. Colombo, M. Di Giacomo, G. Brusotti, G. Delogu, *Tetrahedron Lett.* **1994**, *35*, 2063–2066; h) M. Hoffmann, H. Kessler, *ibid.* **1995**, *36*, 6067–6070; i) S. D. Rychnovsky, *Chem. Rev.* **1995**, *95*, 2021–2040; k) N. S. Mani, C. A. Townsend, *J. Org. Chem.* **1997**, *62*, 636–640; resonance-stabilized α-oxycarbanion equivalents: l) O. Zschage, J.-R. Schwark, D. Hoppe, *Angew. Chem.* **1990**, *102*, 336–337; *Angew. Chem. Int. Ed. Engl.* **1990**, *29*, 296–298; m) O. Zschage, J.-R. Schwark, T. Krämer, D. Hoppe, *Tetrahedron* **1992**, *48*, 8377–8388; n) D. Hoppe, A. Carstens, T. Krämer, *Angew. Chem.* **1990**, *102*, 1455–1456; *Angew. Chem. Int. Ed. Engl.* **1990**, *29*, 1422–1424; o) A. Carstens, D. Hoppe, *Tetrahedron* **1994**, *50*, 6097–6108; p) C. Derwing, D. Hoppe, *Synthesis* **1996**, 149–154; q) F. Hammerschmidt, A. Hanninger, *Chem. Ber.* **1995**, *128*, 1069–1077.

[3] Examples of α-amino-substituted carbanion equivalents: a) S. T. Kerrick, P. Beak, *J. Am. Chem. Soc.* **1991**, *113*, 9708–9710; b) R. E. Gawley, Q. Zhang, *Tetrahedron* **1994**, *50*, 6077–6088; c) A. F. Burchat, J. M. Chong, S. B. Park, *Tetrahedron Lett.* **1993**, *34*, 51–54; d) W. H. Pearson, A. C. Lindbeck, J. W. Kampf, *J. Am. Chem. Soc.* **1993**, *115*, 2622–2636; e) T. R. Elworthy, A. I. Meyers, *Tetrahedron* **1994**, *50*, 6089–6096; f) M. E. Kopach, A. I. Meyers, *J. Org. Chem.* **1996**, *61*, 6764–6765; g) I. Coldham, R. Hufton, D. J. Snowden, *J. Am. Chem. Soc.* **1996**, *118*, 5322–5323; h) G. A. Weisenburger, P. Beak, *ibid.* **1996**, *118*, 12218–12219.

[4] a) H.-J. Gais, G. Hellmann, H. Günther, F. Lopez, H. J. Lindner, S. Braun, *Angew. Chem.* **1989**, *101*, 1061–1063; *Angew. Chem. Int. Ed. Engl.* **1989**, *28*, 1025–1027; b) G. Raabe, H.-J. Gais, J. Fleischhauer, *J. Am. Chem. Soc.* **1996**, *118*, 4622–4630.

[5] a) H. J. Reich, M. D. Bowe, *J. Am. Chem. Soc.* **1990**, *112*, 8994–8995; b) H. J. Reich, R. R. Dykstra, *Angew. Chem.* **1993**, *105*, 1489–1491; *Angew. Chem. Int. Ed. Engl.* **1993**, *32*, 1469–1471; c) *J. Am. Chem. Soc.* **1993**, *115*, 7041–7042; d) H. J. Reich, K. J. Kulicke, *ibid.* **1995**, *117*, 6621–6622; e) *ibid.* **1996**, *118*, 273–274; f) R. W. Hoffmann, T. Rühl, J. Harbach, *Liebigs Ann. Chem.* **1992**, 725–730; g) R. W. Hoffmann, M. Julius, F. Chemla, T. Ruhland, G. Frenzen, *Tetrahedron* **1994**, *50*, 6049–6060; h) H. Ahlbrecht, J. Harbach, R. W. Hoffmann, T. Ruhland, *Liebigs Ann.* **1995**, 211–216; i) R. W. Hoffmann, W. Klute, *Chem. Eur. J.* **1996**, *2*, 694–700; k) R. K. Dress, T. Rölle, R. W. Hoffmann, *Chem. Ber.* **1995**, *128*, 673–677; l) R. W. Hoffmann, R. K. Dress, T. Ruhland, A. Wenzel, *ibid.* **1995**, *128*, 861–870; m) K. Brickmann, F. Hambloch, E. Spolaore, R. Brückner, *ibid.* **1994**, *127*, 1949–1957.

[6] B. Kaiser, D. Hoppe, *Angew. Chem.* **1995**, *107*, 344–346; *Angew. Chem. Int. Ed. Engl.* **1995**, *34*, 323–325; b) see also: T. Shinozuka, Y. Kikori, M. Asaoka, H. Takei, *J. Chem. Soc. Perkin Trans. 1* **1996**, 119–120.

[7] An α-(phenylselenoalkyl)magnesium compound that is configurationally stable at -78 °C was prepared by kinetic resolution: W. Klute, M. Krüger, R. W. Hoffmann, *Chem. Ber.* **1996**, *129*, 633–638.

[8] (*S*)-**7**: M.p. 96 °C; ^{1}H NMR (300 MHz, $CDCl_3$): $\delta = 1.45-1.64$ (m, 12H), 1.70 (d, 3H), 3.72 (s, 2H), 4.79 (q, 1H), 7.20–7.40 (m, 5H); ^{13}C NMR (75 MHz, $CDCl_3$): $\delta = 23.0$ (CH_3), 24.8 (CH_3), 25.8 (CH_3), 44.0 (C), 60.9 (C), 76.7 (CH_2), 97.3 (C), 127.0 (CH), 127.4 (CH), 129.0 (CH), 143.0 (C), 163.2 (C); IR (KBr): $\tilde{\nu} = 1610\ cm^{-1}$ (C=O); $[\alpha]_D^{25} = -133.1$ ($c = 1.22$, CH_2Cl_2, >99% *ee*); addition of (+)-Eu(hfc)$_3$ (40 mol%) leads to splitting of the down field shifted singlet for the CH_2 group in the ^{1}H NMR spectrum (300 MHz) by $\Delta\delta = 0.03$.

[9] All experiments were also carried out with the racemic starting material *rac*-**7**. The enantiomeric excesses were determined with ^{1}H NMR spectroscopy (300 MHz) by addition of (+)-Eu(hfc)$_3$ or (+)-Pr(hfc)$_3$ (11–56 mol%) in $CDCl_3$ (0.8 mL) and comparison with corresponding spectra of the racemic compounds. Usually the highly enantiomerically enriched products showed only the signal for one enantiomer. In these cases the given enantiomeric excesses and detection limits were confirmed by addition of the racemic compounds.

[10] Preparation of (*R*)-**6** by enzyme-catalyzed hydrolysis of the racemic acetate with the lipase SAM II: K. Laumen, D. Breithoff, M. P. Schneider, *J. Chem. Soc. Chem. Commun.* **1988**, 1459–1461.

[11] Deprotonation of monothiocarbamates: a) *S*-alkyl: P. Beak, P. D. Becker, *J. Org. Chem.* **1982**, *47*, 3855–3861; b) *S*-1-alkenyl: D. Hoppe, L. Beckmann, R. Follmann, *Angew. Chem.* **1980**, *92*, 305–306; *Angew. Chem. Int. Ed. Engl.* **1980**, *19*, 303–304.

[12] X-ray structure analyses: a) *ent*-**9b**: $C_{18}H_{25}NO_4S$, $M_r = 351.45$, $0.5 \times 0.35 \times 0.25\ mm^3$, $a = 6.225(1)$, $b = 12.754(1)$, $c = 23.029(1)$ Å, $V = 1828.4(3)$ Å^3, $\rho_{calcd} = 1.277\ g\,cm^{-3}$, $\mu = 17.49\ cm^{-1}$, $Z = 4$, orthorhombic, space group $P2_12_12_1$ (no. 19), $\lambda = 1.54178$ Å, $T = 223$ K, $\omega/2\theta$ scans, 2220 reflections collected ($+h$, $-k$, $-l$), $(\sin\theta)/\lambda = 0.62$ Å^{-1}, 2220 independent and 2172 observed reflections with $I \geq 2\sigma(I)$, 224 refined parameters, $R = 0.043$, $wR^2 = 0.121$, max./min. residual electron density 0.57/$-$0.27 e Å^{-3}, Flack parameter $-0.03(3)$; hydrogen atoms were calculated and refined as riding. b) *ent*-**9c**: $C_{23}H_{27}NO_3S$, $M_r = 397.52$, $0.6 \times 0.3 \times 0.2$ mm, $a = 9.931(1)$, $c = 18.842(2)$ Å, $V = 1609.3(3)$ Å^3, $\rho_{calcd} = 1.231\ g\,cm^{-3}$, $\mu = 15.17\ cm^{-1}$, empirical absorption correction with φ-scan data ($0.895 \leq C \leq 0.999$), $Z = 3$, trigonal, space group $P3_1$ (no. 144), $\lambda = 1.54178$ Å, $T = 223$ K, $\omega/2\theta$ scans, 6770 reflections collected ($\pm h$, $\pm k$, $-l$), $(\sin\theta)/\lambda = 0.62$ Å^{-1}, 2263 independent and 2188 observed reflections with $I \geq 2\sigma(I)$, 259 refined parameters, $R = 0.041$, $wR^2 = 0.107$, max./min. residual electron density 0.34/$-$0.25 e Å^{-3}, Flack parameter 0.02(2); hydrogen atoms were calculated and refined as riding. c) *ent*-**9d**: $C_{19}H_{31}NO_2SSi$, $M_r = 365.60$, $0.70 \times 0.50 \times 0.20$ mm, $a = 11.501(2)$, $b = 7.914(2)$, $c = 11.599(2)$ Å, $\beta = 96.21(2)$, $V = 1045.9(4)$ Å^3, $\rho_{calcd} = 1.161\ g\,cm^{-3}$, $\mu = 19.98\ cm^{-1}$, empirical absorption correction with φ-scan data ($0.831 \leq C \leq 0.999$), $Z = 2$, monoclinic, space group $P2_1$ (no. 4), $\lambda = 1.54178$ Å, $T = 223$ K, $\omega/2\theta$ scans, 4574 reflections collected ($\pm h$, $-k$, $\pm l$), $(\sin\theta)/\lambda = 0.62$ Å^{-1}, 2294 independent and 1964 observed reflections with $I \geq 2\sigma(I)$, 225 refined parameters, $R = 0.065$, $wR^2 = 0.147$, max./min. residual electron density 0.60/$-$0.44 e Å^{-3}, Flack parameter $-0.01(3)$; hydrogen atoms were calculated and refined as riding. All data were collected on an Enraf Nonius CAD4 diffractometer. Programs used: data reduction MolEN, structure solution SHELXS-86, structure refinement SHELXL-93. Crystallographic data (excluding structure factors) for the structures reported in this paper have been deposited with the Cambridge Crystallographic Data Centre as supplementary publication no. CCDC-

 © WILEY-VCH Verlag GmbH, D-69451 Weinheim, 1997 0570-0833/97/3624-2785 $ 17.50+.50/0

100446. Copies of the data can be obtained free of charge on application to The Director, CCDC, 12 Union Road, Cambridge CB21EZ, UK (fax: int. code + (1223)336-033; e-mail: deposit@chemcrys.cam.ac.uk).
[13] Reproduction of these results requires salt-free *sec*-butyllithium and highly pure, and in particular disulfide-free, **7**; otherwise lower yields and enantiomeric excesses are registered.
[14] An experiment in which (*S*)-**8** is warmed to −2 to 0 °C for 1 h and quenching with methyl chloroformate leads to *ent*-**9b** in 58% yield with 73% *ee*. A longer reaction time at 0 °C causes severe decomposition.

A Highly Stable Silver(I) Complex of a Macrocycle Derived from Tetraazatetrathiacyclen**

Thomas Gyr, Helmut R. Mäcke,* and Michael Hennig

The chemistry of the coinage metals is of special interest in many diverse fields; one notable example is the medical application of gold(I) complexes for treating rheumatoid arthritis and as cytotoxic agents.[1] Another promising application is the use of the β-ray-emittig radionuclides ^{111}Ag[2] and ^{198}Au[3] in selective internal radiotherapy of tumors as radiometal-based bioconjugates. To reach their biological target intact, the radiometal is generally immobilized with a chelating ligand to withstand attack of the metal ions from body fluids and to avoid transfer of these metals to proteins. There has been great progress along these lines with other metallic radionuclides for radiotherapy, for example with ^{67}Cu[4] and ^{90}Y.[5] However, the considerable efforts expended in synthesizing complexes of silver(I) with sufficient stability to allow their use in vivo[2,6] have not been successful.

Here we describe the initial results of a study directed at synthesizing stable Ag(I) complexes. Preliminary results indicated that the macrocyclic chelating ligand 1,4,7,10-tetrakis[2-methylsulfanyl)ethyl]-1,4,7,10-tetraazacyclododecane (dotete, **1**; the letters A–E identify carbon atoms whose

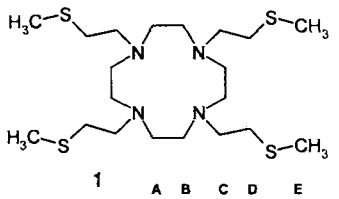

1 A B C D E

resonances appear in the ^{13}C NMR spectra in Figure 3) shows a very high affinity for Ag^+, which is strongly preferred over Pb^{2+}; the two ions are found together in nature.[7] Moreover, it was of interest to ascertain if the coordination number for Ag^+ could be extended to eight by a strong electronic interaction between Ag^+ and the thioether functional groups,[8] utilizing the conformational rigidity and potential preorganization of cyclen-like macrocycles with side chains (cyclen = 1,4,7,10-tetraazacyclododecane).[9] Despite the preference of Ag^+ for coordination numbers two and four,[10] the use of crown thioether ligands produced complexes with coordination number six.[11] We report here the synthesis, characterization, and X-ray crystal structure of a novel N4S4 macrocycle as well as the crystal and solution structures of its new extraordinarily stable Ag^+ complex. Its stability is also compared to that of the Pb^{2+} complex.

The reaction of cyclen with 2-chloroethyl methyl sulfide in CH_3CN and in the presence of K_2CO_3 as base readily yields dotete. A solution of dotete in CH_2CL_2 was mixed with an equimolar amount of silver nitrate in CH_3CN; addition of ammonium hexafluorophosphate gave colorless crystals of $[Ag(dotete)]PF_6$ (**2**). The effective encapsulation of Ag^+ by dotete was confirmed by two qualitative observations: 1) $[Ag(dotete)]^+$ is stable in phosphate-buffered saline for 24 h, and 2) a slight excess of dotete readily dissolves AgI.

By using pH titrations and argentometric methods the protonation constants for dotete and complexation constants with Ag^+ in MeOH/H_2O (1/1) were determined to $pK_{a1} = 11.26$ and $pK_{a2} = 6.02$; the complexation constant is $\lg K_{[Ag(dotete)^+]} = 19.63$. This is by far the highest binding constant reported for silver(I) ions.

The high stability is preserved at lower pH values; the protonated species $[Ag(Hdotete)]^{2+}$ was formed with $\lg K_{[Ag(Hdotete)^{2+}]} = 2.8$. Measurements on the concentration of free silver ion gave values of 0.3% at pH = 2.2, which is consistent with that obtained from pH titrations. The extraordinary stability of $[Ag(dotete)]^+$ was confirmed by a competition experiment with the strong Ag^+-chelating ligand [18]aneS6 ([18]aneS6 = 1,4,7,10,13,16-hexathiacyclooctadecane). An equimolar amount of Ag^+ with traces of $^{110m}Ag^+$ was added to a 90% methanolic, neutral, phosphate-buffered solution of [18]aneS6 and dotete [10:1, Eq. (a)]. The mixture was investigated with HPLC and TLC using radiometric detection methods.

$$^{110m}Ag^+ + \text{dotete (1 equiv)} + \text{[18]aneS6 (10 equiv)} \rightarrow [^{110m}Ag(dotete)]^+ + \text{[18]aneS6} \quad \text{(a)}$$

Both methods showed exclusive formation of $[^{110m}Ag(dotete)]^+$, indicating that this complex possesses a stability constant that is at least three orders of magnitude higher than that for $[Ag([18]aneS6)]^+$ under these conditions. For $[Pb(dotete)]^{2+}$ stability constants of $\lg K_{[Pb(dotete)^{2+}]} = 8.8$ and $\lg K_{[Pb(Hdotete)^{3+}]} = 3.0$ were found.

The X-ray structures were determined for the uncomplexed monoprotonated dotete (counter ion PF_6^-) and for $[Ag(dotete)]PF_6$ (**2**).[15] In the case of **2**, there are two molecules in the asymmetric unit. They possess similar conformations with the exception of a disordered side chain in one molecule, which was refined for two slightly different conformations. The molecule without disorder is shown in Figure 1. Both independent cations show the same coordination geometry: The Ag^+ ion is hexacoordinated to the four nitrogen and two of the four possible sulfur donor atoms. The molecules are chemically equivalent but differ in the orientation of the terminal methyl group on the coordinated sulfur atoms. The four nitrogen atoms are nearly coplanar (maximum deviation 0.018 Å), and the silver ion is located 1.346 and 1.329 Å above the best N_4 plane. The Ag–N (av 2.53(3) Å) and Ag–S bond lengths (av 2.72(3) Å) are not unusual. Two opposite noncoordinating sulfur atoms are more than 5.0 Å from Ag. The structure of the free protonated ligand is shown in Figure 2. Its preorganization is clear even in the solid state. The N4 plane is intact (maximum deviation 0.055 Å), and the side chains are all *syn* to the N4 plane.

[*] Prof. Dr. H. R. Mäcke, Dipl.-Chem. T. Gyr
Institut für Nuklearmedizin des Universitätsspitals
Petersgraben 4, CH-4031 Basel (Switzerland)
Fax: Int. code + (61)265-4897
e-mail: maecke@ubaclu.unibas.ch
Dr. M. Hennig
Hoffmann-La Roche, Basel

[**] This work was supported by the Swiss National Science Foundation (no. 31-42516/94). Karin Stalder and Pia Powell are acknowledged for expert technical help.

 © WILEY-VCH Verlag GmbH, D-69451 Weinheim, 1997 0570-0833/97/3624-2786 $ 17.50+.50/0

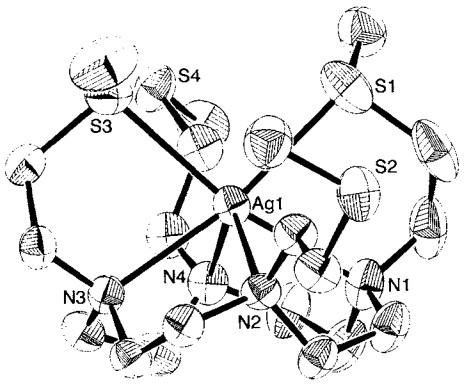

Figure 1. ORTEP representation of the crystal structure of [Ag(dotete)]$^+$ (ellipsoids at the 50% probability level). Selected bond lengths [Å] and angles [°]: Ag(1)–N(1) 2.562(8), Ag(1)–N(2) 2.547(7), Ag(1)–N(3) 2.553(7), Ag(1)–N(4) 2.470(7), Ag(1)–S(1) 2.704(3), Ag(1)–S(3) 2.744(3), Ag(1)···S(2) 5.91, Ag(1)···S(4) 5.10); N(1)-Ag(1)-N(2) 72.0(2), N(1)-Ag(1)-N(3) 115.4(3), N(1)-Ag(1)-S(1) 76.4(2), N(1)-Ag(1)-S(3) 168.7(2), S(1)-Ag(1)-S(3) 92.52(10).

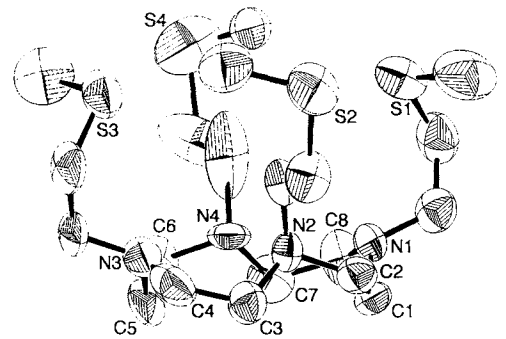

Figure 2. ORTEP representation of the crystal structure of Hdotete$^+$ (thermal ellipsoids at the 50% probability level). Selected bond lengths [Å] and angles [°]: N(1)–C(1) 1.428(13), N(1)–C(8) 1.450(2), N(4)–C(6) 1.540(2), N(4)–C(7) 1.478(14); C(1)-N(1)-C(8) 114.7(10), C(3)-N(2)-C(2) 111.1(9), C(5)-N(3)-C(4) 112.0(11), C(7)-N(4)-C(6) 109.5(9).

To probe the nature of Ag coordination in solution and to understand the high solution stability of **2**, $^{13}C\{^1H\}$ NMR spectra were measured at different temperatures in acetone. The room-temperature spectra in various solvents indicate the equivalence of the four side chains. The spectra consist of four resonances at $\delta = 53.69$ (C), 50.99 (A,B), 32.65 (D), and 16.32 (E; see formula drawing of **1** and Scheme 1). This is somewhat surprising considering the hexacoordination of Ag^+ in the solid state with binding to two transannular sulfur atoms. Therefore, in order for all four side chains to be equivalent in solution, either all S-donor atoms are bound to Ag^+, or there is rapid interchange between the different bound and unbound states at room temperature on the NMR time scale. The equivalence of ^{13}C NMR signals for carbon atoms C, D, and E (101 MHz) holds to 183 K, the lowest temperature we could achieve. However, the resonance for ring carbon atoms A and B, arising as a singlet around $\delta = 51$ at room temperature (Figure 3), broadens at lower temperatures and splits into a doublet below 253 K. This fluxionality indicates inequivalence of the ring carbon atoms at lower temperature, and was found with cyclen derivatives with side chains as ligand in octacoordinate complexes (i.e., $[M(dotam)]^{2+}$; dotam = 1,4,7,10-tetrakis(acetamido)-1,4,7,10-cyclododecane; M = Ca^{2+}, Cd^{2+}, Pb^{2+}, Zn^{2+}). These observations are attributed to rapid interconversion of the helical arrangement of the side chains in a square-antiprismatic complex as shown in Scheme 1.[9,12] The rate of interconversion and the Gibbs energy of activation for this process at the coalescence temperature (270 K) were estimated to be 240 s^{-1} and $\Delta G^{\ddagger} = 53.5$ kJ mol^{-1}, respectively.

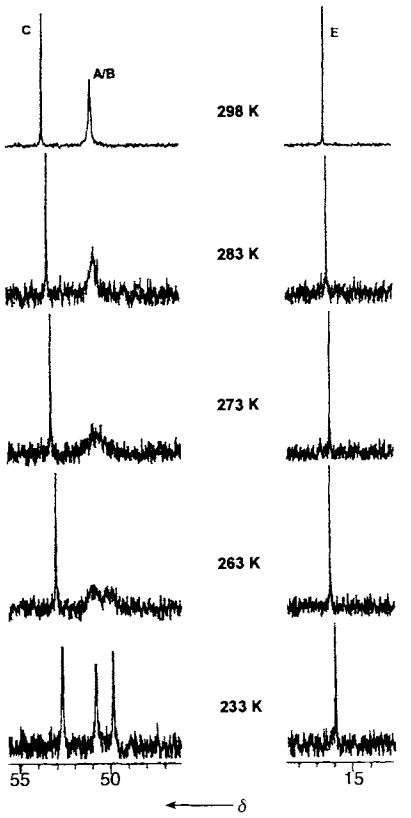

Figure 3. Sections of ^1H-decoupled ^{13}C NMR spectra (101 MHz) of 4×10^{-2} M [Ag(dotete)]PF_6 in acetone at different temperatures. See the formula drawing of **1** and Scheme 1 for assignment of the signals.

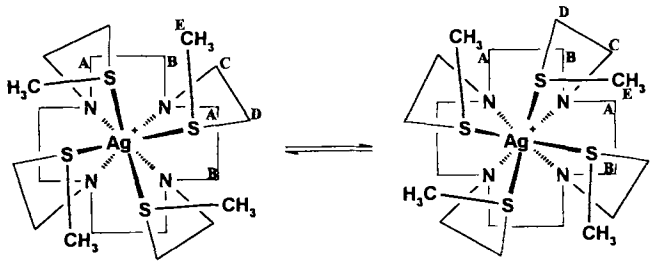

Scheme 1. Helicity reversal of the side chains in [Ag(dotete)]$^+$ leading to equivalence of the ring carbon atoms A and B on the NMR time scale.

Our results obtained with dotete serve as a useful guide for the design of bifunctional ligands by functionalizing the carbon backbone of the macrocycle along the lines already published.[4a,b,5a] It appears that, despite the high degree of preorganization of dotete, the soft Ag^+ ion prefers the tertiary amine donors over the soft S-donor atoms. Nevertheless, our data indicate that all four S-donor atoms contribute to the highest stability found for a silver(I) complex in solution. Finally, we achieved very high discrimination between silver(I) and lead(II), with the former being favored by more than a factor of $10^{10.8}$; this is the highest value reported.[13]

 © WILEY-VCH Verlag GmbH, D-69451 Weinheim, 1997 0570-0833/97/3624-2787 $ 17.50+.50/0

Experimental Section

1: The reaction of cyclen (1.00 g, 5.8 mmol) with 2-chloroethyl methyl sulfide (2.95 mL, 29.0 mmol, 5 equiv) in CH_3CN and excess K_2CO_3 at 40 °C for 24 h affords dotete (1.72 g, 72% yield). FAB-MS: $m/z = 469.0$ $[M+H]^+$; ^1H NMR (400 MHz, CD_3OD, 25 °C): $\delta = 2.12$ (s, 12H), 2.54–2.71 (m, 32H); $^{13}C\{^1H\}$ NMR (101 MHz, CD_3OD, 25 °C): $\delta = 15.80$, 32.48, 53.07, 56.47. Hdotete$^+BF_4^-$ was obtained by adding HBF_4 in Et_2O to dotete in $CHCl_3$. After 4 h at room temperature the mass was triturated, filtrated, and dried for 24 h under high vacuum; yield 94%. Elemental analysis calcd for $C_{20}H_{46}S_4F_8N_4B_2$: C 36.98, H 7.14, F 23.41, N 8.63, B 3.33; found: C 36.28, H 7.00, F 23.77, N 8.51, B 3.32. The PF_6 salt prooved to be more suitable for crystallization.

2: The dotete (149.2 mg, 0.318 mmol) was dissolved in CH_2Cl_2 (4 mL), and a solution of $AgNO_3$ (54 mg, 0.318 mmol) in CH_3CN (4 mL) added. The colorless mixture was stirred for 30 min at room temperature to afford a clear solution of the Ag^+ complex. Removal of the solvent under vacuum and redissolution of the residue in CH_3OH followed by the addition of NH_4PF_6 (51.8 mg, 0.317 mmol) produced colorless crystals of **2**; yield 54.2 mg (23.6%). EI-MS: $m/z = 575.3/577.3$ $[^{107,109}Ag(dotete)]^+$; ^1H NMR (400 MHz, CD_3OD, 25 °C): $\delta = 2.21$ (d, 12H), 2.48–2.85 (br m, 32H); $^{13}C\{^1H\}$ NMR (101 MHz, CD_3OD, 25 °C): $\delta = 15.80$, 32.48, 53.07, 56.47; elemental analysis calcd for $C_{20}H_{44}AgS_4PF_6N_4$: C 34.17, H 6.44, Ag 14.50, N 7.66, found: C 33.29, H 6.15, Ag 14.95, N 7.76.

pH and argentometric titration: Due to the low solubility of dotete in water at pH > 10, the titration was performed in 50% aqueous methanol ($I = 0.1$ (KNO_3), 2.1×10^{-3} M dotete, 2.05×10^{-3} M Ag^+, 0.5 M $(CH_3)_4NOH$). An automatic titration system consisting of a Metrohm-654 potentiometer and a Metrohm-665 dosimat with a pH electrode (Metrohm 6.0726.100; saturated KCl solution as the inner electrolyte, and 0.1 M KNO_3 in 50% aqueous methanol as the outer electrolyte) was used. Data was acquired with a 386 computer using TITFIT software [14]. The concentration of free Ag^+ ions was determined using a silver electrode with a Ag/AgCl reference electrode (Metrohm 6.0133.100) calibrated against six solutions of known Ag^+ concentrations (10^{-3}–10^{-6} M).

Received: July 3, 1997 [Z10631IE]
German version: *Angew. Chem.* **1997**, *109*, 2869–2871

Keywords: macrocycles · N ligands · radionuclides · silver · S ligands

[1] P. J. Sadler, R. E. Sue in *Handbook of Metal–Ligand Interactions in Biological Fluids, Vol. 2* (Ed: G. Berthon), Marcel Dekker, Basel, **1995**, pp. 1039–1051.
[2] R. Alberto, P. Bläuenstein, I. Novak-Hofer, A. Smith, P. A. Schubiger, *Appl. Radiat. Isot.* **1992**, *43*, 869–872.
[3] C. A. Hoefnagel, *Eur. J. Nucl. Med.* **1991**, 408–431.
[4] a) C. F. Meares, M. K. Moi, M. J. McCall, W. C. Cole, S. J. DeNardo, *Anal. Biochem.* **1985**, *148*, 249–253; b) J. R. Morphy, D. Parker, R. Kataky, A. Harrison, M. A. W. Eaton, A. Millican, A. Phipps, C. Walker, *J. Chem. Soc. Chem. Commun.* **1989**, 792–794; c) P. M. Smith-Jones, R. Fridrich, T. A. Kaden, I. Novak-Hofer, K. Siebold, D. Tschudin, H. R. Mäcke, *Bioconjugate Chem.* **1991**, *2*, 415–421.
[5] a) M. K. Moi, C. F. Meares, S. J. DeNardo, *J. Am. Chem. Soc.* **1988**, *110*, 6266–6267; b) R. W. Kozak, A. Raubitschek, S. Mirzadeh, M. W. Brechbiel, R. Junghaus, O. A. Gansow, T. A. Waldmann, *Cancer Res.* **1989**, *49*, 2639–2644.
[6] a) A. S. Craig, R. Kataky, D. Parker, H. Adams, N. Bailey, H. Schneider, *J. Chem. Soc. Chem. Commun.* **1989**, 1870–1872; b) P. C. Riesen, T. A. Kaden, *Helv. Chim. Acta* **1995**, *78*, 1325–1333; c) R. Alberto, W. Nef, A. Smith, P. A. Schubiger, T. A. Kaden, M. Neuburger, M. Zehnder, A. Frey, U. Abram, *Inorg. Chem.* **1996**, *35*, 3420–3427.
[7] K. R. Adam, D. S. Baldwin, A. Bashall, L. F. Lindoy, M. McPartlin, H. R. Powell, *J. Chem. Soc. Dalton Trans.* **1994**, 237–238.
[8] J. Clarkson, R. Yagbasan, P. J. Blower, S. C. Rawle, S. R. Cooper, *J. Chem. Soc. Chem. Commun.* **1987**, 950–951.
[9] H. Maumela, R. D. Hancock, L. Carlton, J. H. Reibenspies, K. P. Wainwright, *J. Am. Chem. Soc.* **1995**, *117*, 6698–6707.
[10] F. A. Cotton, G. Wilkinson, P. L. Gaus, *Grundlagen der Anorganischen Chemie*, VCH, Weinheim, **1990**, p. 582 f.
[11] a) A. J. Blake, R. O. Gould, G. Reid, M. Schröder, *Polyhedron* **1989**, 513–518; b) A. J. Blake, R. O. Gould, S. Parsons, C. Radek, M. Schröder, *Angew. Chem.* **1995**, *107*, 2563–2565; *Angew. Chem. Int. Ed. Engl.* **1995**, *34*, 2374–2376.
[12] A. K. W. Stephens, R. S. Dhillon, S. E. Madbak, S. L. Whitbread, S. F. Lincoln, *Inorg. Chem.* **1996**, *35*, 2019–2024.
[13] R. M. Izatt, K. Pawlak, J. S. Bradshaw, R. L. Bruening, *Chem. Rev.* **1991**, *91*, 1721–1735.
[14] A. D. Zuberbühler, T. A. Kaden, *Talanta* **1982**, *29*, 201–206.
[15] Crystal structure analyses. a) General: All measurements were made on a Nicolet P3 diffractometer with graphite-monochromated $Mo_{K\alpha}$ radiation. Crystallographic data (excluding structure factors) for the structures reported in this paper have been deposited with the Cambridge Crystallographic Data Centre as supplementary publication no. CCDC-100510. Copies of the data can be obtained free of charge on application to The Director, CCDC, 12 Union Road, Cambridge CB2 1EZ, UK (fax: int. code + (1223) 336-033; e-mail: deposit@chemcrys.cam.ac.uk). b) Hdotete$^+PF_6^-$: $C_{20}H_{45}F_6N_4PS_4$, monoclinic $P2_1/n$, $a = 14.487(3)$, $b = 14.225(3)$, $c = 14.848(3)$ Å, $\beta = 95.81(3)°$, $V = 3044.2(11)$ Å^3, $Z = 4$, $\rho_{calcd} = 1.339$ g cm^{-3}, $T = 293$ K. The structure was solved using direct methods, expanded by fourier techniques, and refined against F^2 by full-matrix least-squares methods using the Shelx 93 crystallographic software package [16]. Anisotropic temperature factors were refined with restraints because of the weak data. Of 2390 reflections collected (maximum $2\Theta = 35°$), 1886 were unique. The final residuals for 317 parameters and 93 restraints refined against 1457 unique data with $I > 2\sigma(I)$ were $R = 0.117$ and $R_w = 0.249$. c) **2**: $C_{40}H_{88}Ag_2N_8S_8P_2F_{12}$, monoclinic, $P2_1/a$, $a = 14.330(4)$, $b = 25.350(5)$, $c = 17.932(3)$ Å, $\beta = 107.66(3)°$, $V = 6207.1(24)$ Å^3, $Z = 8$, $\rho_{calcd} = 1.539$ g cm^{-3}, $T = 293$ K. The structure was solved using Patterson methods, expanded by fourier techniques, and refined against F^2 by full-matrix least-squares methods using the Shelx 93 crystallographic software package [16]. There are two molecular units in the asymmetric unit. The disordered side chain of one molecule was refined isotropically in two conformations. No hydrogen atoms were included for atoms involved in the disorder. All other atoms were refined anisotropically, and hydrogen atoms were included and refined using a riding model. Of 11351 reflections collected (maximum $2\Theta = 50°$), 10876 were unique. The final residuals for 649 parameters and 4 restraints refined against 7701 unique data with $I > 2\sigma(I)$ were $R = 0.0558$ and $R_w = 0.1467$.
[16] G. M. Sheldrick, *Acta Crystallogr. Sect. A* **1990**, *46*, 467–473.

A New Technique for Assembling Thin, Defined Multilayers**

André Laschewsky,* Bernd Mayer, Erik Wischerhoff, Xavier Arys, Alain Jonas, Martti Kauranen, and André Persoons

Three principal techniques are used presently to prepare ultrathin multilayer films by self-organization: the Langmuir–Blodgett technique,[1] chemical self-assembly with stepwise activation of the surface,[1,2] and alternating physisorption of oppositely charged polyelectrolytes.[3] All these techniques have their advantages and disadvantages.[4] Recently, we presented a new multilayer technique combining features of the "classical" methods, which has the potential to profit from their strong points and to avoid some of their drawbacks. The method is physisorption of a reactive polyion by electrostatic interactions (alike physisorption of oppositely charged polyelectrolytes), followed by chemical activation (alike chemical self-assembly) with a reagent of low molar mass in order to reverse the charge at the surface (*Co*atings by *M*ultiple *P*olyelectrolyte *A*dsorption/*S*urface Activation, CoMPAS, Figure 1).[5] The use of a polymeric adsorbate distinguishes CoMPAS from the related techniques of step-

[*] Prof. A. Laschewsky, Dr. B. Mayer, Dr. E. Wischerhoff
Département de Chimie
Université Catholique de Louvain
1, Place Louis Pasteur, B-1348 Louvain-la-Neuve (Belgium)
Fax: Int. code + (10) 47-28 36
e-mail: laschewsky@cico.ucl.ac.be
X. Arys, Prof. A. Jonas
Département des Sciences des matériaux et des procédés
Université Catholique de Louvain
Dr. M. Kauranen, Prof. A. Persoons
Departement Scheikunde, Katholieke Universiteit Leuven (Belgium)

[**] This work was financially supported by the DG Recherche Scientifique of the French Community of Belgium (convention 94/99-173) and by the Belgian State (Services du Premier Ministre—Services fédéraux des Affaires scientifiques, program PAI4/11).

 © WILEY-VCH Verlag GmbH, D-69451 Weinheim, 1997 0570-0833/97/3624-2788 $ 17.50+.50/0

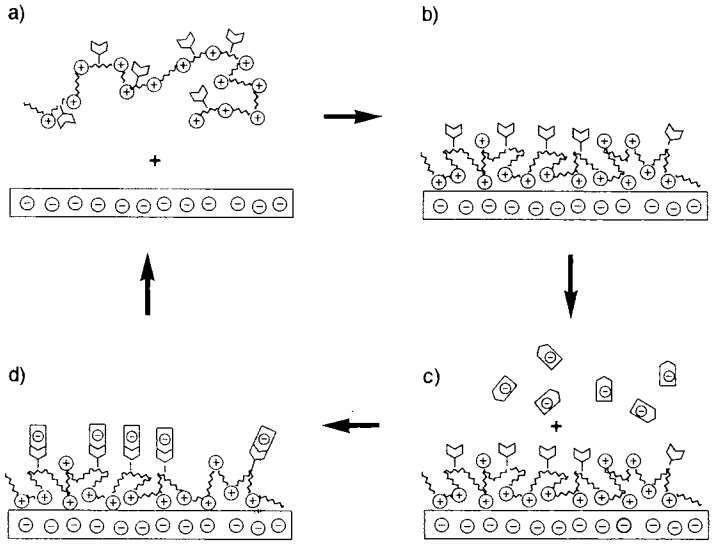

Figure 1. Schematic representation of the CoMPAS technique. a) Physisorption: A support having a negatively charged surface is dipped into a solution of a polycation containing reactive groups. b) Adsorption of the polycation; reactive groups are presented at the surface. c) Activation: The assembly is dipped into a solution of a negatively charged reagent. d) After the interfacial reaction the negative surface charge is restored, and the sample is ready for the next cycle.

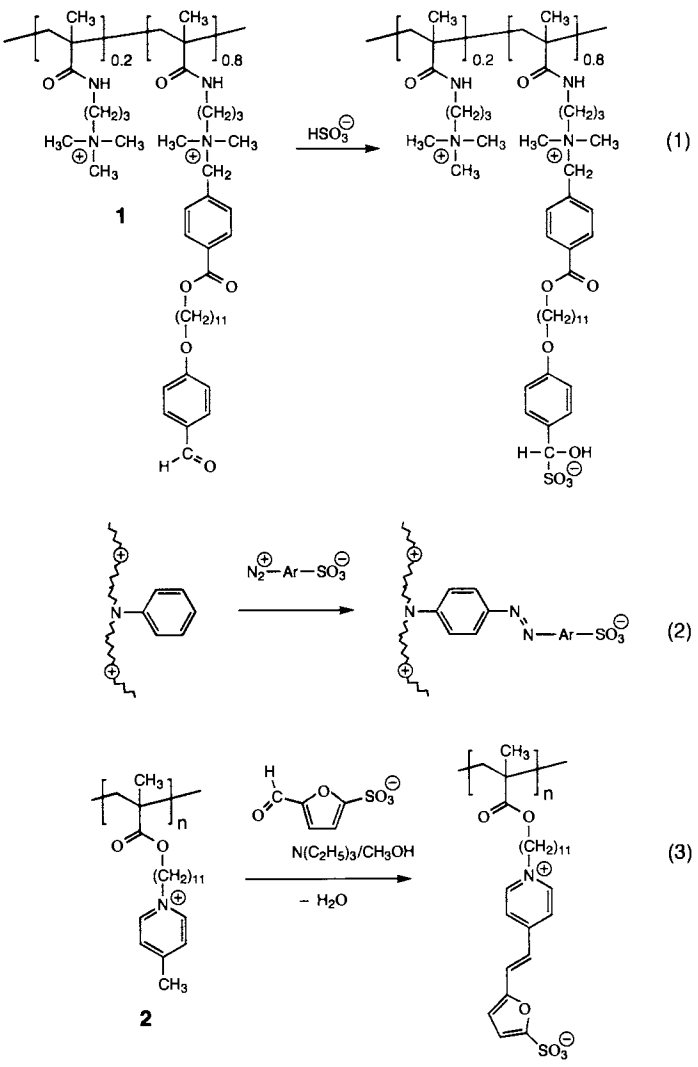

wise chemisorption/activation by H. Katz et al.[6] or chemisorption/polymerization by T. Marks et al.[7] The polymeric character of the adsorbate makes the method less prone to defect propagation in higher layers. Furthermore, CoMPAS requires only a minimum of equipment and is rather fast (< 1 h per layer).

The reactive polymers have to be designed properly for CoMPAS: besides the essential ionic fragments and polar reactive groups, spacer groups separating the two seem to be necessary.[8] Presumably, the spacers enable the reactive groups to accumulate at the film surface, as required for obtaining charge reversal at the surface.

A variety of reactive polyions and complementary reagents of low molar mass proved to be useful for CoMPAS. Under standard conditions[3,5] polycations bearing aldehyde groups can be activated by the bisulfite anion at ambient temperature in water [Eq. (1)].[9] Under similarly mild conditions, polycations with aniline residues can be activated by coupling with diazonium salts bearing negative charges [Eq. (2)].[9] However, the good stability and adhesion of the multilayers due to the electrostatic interactions also allow for activation under harsher conditions: Polymers with γ-picolinium residues (e. g. **2**) can be condensed with a negatively charged aldehyde by heating at reflux in methanol [Eq. (3)].[10]

The success of the activation step is evidenced by characteristic fragments of the coupling products seen in secondary ion mass spectrometry,[5] as well as by UV/Vis spectroscopy. The systems were chosen such that the activation step induces a change in the electronic spectra of the films. Therefore, the chemical reaction and the layer-by-layer growth are easily monitored (see Figure 2). As condensation of picolinium salts with aldehydes and azo coupling lead to strong chromophores, the evolution of color during the reaction allows verification of the macroscopic homogeneity of the assemblies, which often is a crucial point in the analysis of thin films. In fact, the multilayers obtained are homogeneous to the naked eye and the optical microscope.

Whereas the success of CoMPAS depended sensitively on the detailed systems for reactive polycations bearing aldehyde or picolinium moieties, generally good results were obtained so far with polycations bearing aniline residues activated by azo coupling. The aniline residue can be located in the side chains (**3**–**5**) as well as in the main chain (**6**, **7**) with different contents of hydrophobic groups. Also, a variety of diazonium salts could be used for the activation step, including bulky **9** and **10**.

UV/Vis spectroscopic studies on multilayer films are exemplified for polycation **2**, which is activated by 5-formyl-2-furanesulfonic acid [Eq. (3)], and for assemblies of polycations **4** or **6**, which are activated by the diazonium salt **8**. The plots of absorbance versus the number of deposition cycles are linear, pointing to a regular and reproducible assembly process (Figure 2).

However, several analytical techniques must be employed to judge unambiguosly the quality of the films. Though UV/Vis spectroscopy indicates a regular increase in deposited material with every cycle in assemblies of polymers **4** and **6** activated with **8**, X-ray reflectivity reveals that the average thickness of the assembly made up of **4** is as low as 0.6 nm. Furthermore, the roughness of the film increases with ongoing growth, suggesting incoherent layers. In contrast, rather smooth films with an average thickness of 1.32 nm per layer are obtained with polycation **6** (Figure 3).

The success of the CoMPAS technique implies a basic noncentrosymmetric film structure. Therefore, this process

 © WILEY-VCH Verlag GmbH, D-69451 Weinheim, 1997 0570-0833/97/3624-2789 $ 17.50+.50/0

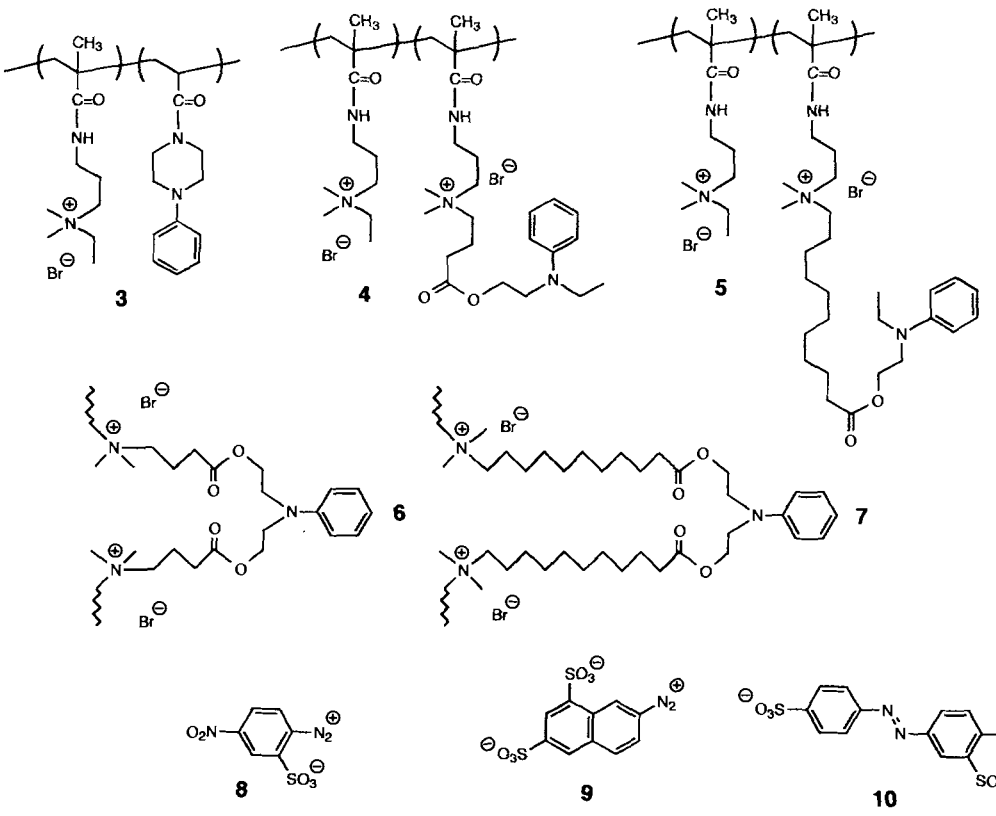

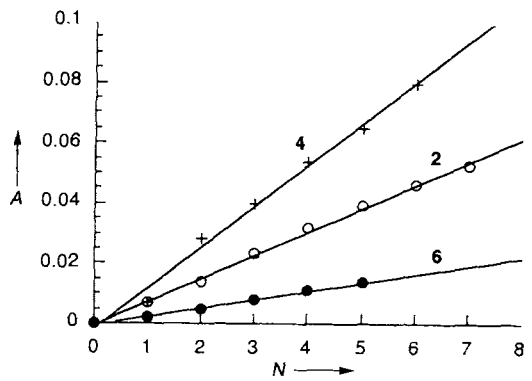

Figure 2. Plot of absorbance A versus the number of deposition cycles N for polymer **2** activated with 5-formyl-2-furansulfonic acid ($\lambda_{max} = 385$ nm) and for polymers **4** ($\lambda_{max} = 498$ nm) and **6** ($\lambda_{max} = 450$ nm) activated with diazonium salt **8**. The lines give the best linear fits.

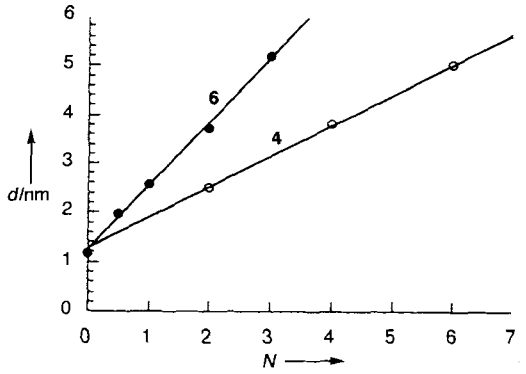

Figure 3. Dependence of thickness d, as determined by X-ray reflectivity, on the number of deposition cycles N for assemblies made from polycations **4** and **6** activated with diazonium salt **8**. The offset at zero is due to a primary layer pair of poly(ethyleneimine)/poly(vinylsulfate). The lines give the best fits to the data.

may allow the preparation of functional noncentrosymmetric films, which is notoriously difficult to achieve. A noncentrosymmetric orientation of the chromophores formed in the deposition process—alike the forced noncentrosymmetric orientation of chromophores in self-assembled multilayers[6,7]—is not compulsory, but should be possible. As activation of the aniline-bearing polycations and the polymeric picolinium salts yields chromophores with strong nonlinear optical properties, these assemblies were analyzed by second harmonic generation (SHG) experiments.

For coatings made up of the picolinium salt **2** activated with 5-formyl-2-furansulfonic acid, no second-harmonic signal could be detected. Possibly, the elevated temperatures of the activation reaction lead to a randomization of the orientations of the chromophores. In contrast, multilayer assemblies of polycations **4** and **7** activated with **8** showed significant SHG activity. It is important to notice that the SHG intensity of the signal increases with the number of layers (Figure 4); this demonstrates a noncentrosymmetric orientation of the chromophores not only in the first, but also in the subsequent layers. Nevertheless, the increase in intensity is not quadratic, as is expected for assemblies with the same orientation for each layer. Therefore, the degree of orientation must be lower for higher layers, but the noncentrosymmetric character still persists.

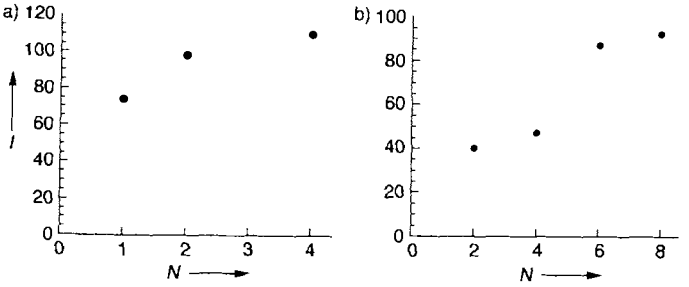

Figure 4. Second-harmonic intensity I (arbitrary units) in dependence of the number of deposition cycles N for polycations a) **4** and b) **7** activated with diazonium salt **8**.

The methodologies to fabricate thin, defined multilayers are enriched by the new CoMPAS technique. A particularly interesting feature is the possible access to noncentrosymmetric films. Still, the problem of reproducible orientation of the chromophores with ongoing film growth needs to be addressed in the future.

Received: June 23, 1997 [Z10584IE]
German version: *Angew. Chem.* **1997**, *109*, 2899–2902

 © WILEY-VCH Verlag GmbH, D-69451 Weinheim, 1997 0570-0833/97/3624-2790 $ 17.50+.50/0

Keywords: nonlinear optics · polyelectrolytes · self-assembly · surface chemistry · thin films

[1] A. Ulman, *An Introduction to Ultrathin Organic Films*, Academic Press, Boston, **1991**.
[2] L. Netzer, J. Sagiv, *J. Am. Chem. Soc.* **1983**, *105*, 674.
[3] G. Decher, J.-D. Hong, J. Schmitt, *Thin Solid Films* **1992**, *210/211*, 831.
[4] A. Laschewsky, *Eur. Chem. Chron.* **1997**, *2*, 13.
[5] A. Laschewsky, B. Mayer, E. Wischerhoff, X. Arys, P. Bertrand, A. Delcorte, A. Jonas, *Thin Solid Films* **1996**, *284/285*, 334.
[6] H. E. Katz, G. Scheller, T. M. Putvinsky, M. L. Schilling, W. L. Wilson, C. E. D. Chidsey, *Science* **1991**, *254*, 1485.
[7] Wenbin Lin, Weiping Lin, G. K. Wong, T. J. Marks, *J. Am. Chem. Soc.* **1996**, *118*, 8034.
[8] For example, the use of an analogue of **2** with only an ethylene spacer did not allow multilayer growth by CoMPAS.
[9] *Organikum*, 16th ed., VEB Deutscher Verlag der Wissenschaften, Berlin, **1986**, pp. 329 and 549.
[10] A. P. Phillips, *J. Org. Chem.* **1949**, *14*, 302.

Interchangeable Coordination Geometries: pH-Controlled Change of Trigonal-Prismatic to Octahedral Metal Coordination in a Dinuclear Cobalt(II) Complex**

Carsten Wendelstorf and Roland Krämer*

The coordination geometry of metal complexes has substantial influence on their physical and chemical properties. There is considerable interest both in a detailed understanding of the factors that determine the coordination geometry and in the control of complex structure by ligand design.[1] Transition metal ions with coordination number (CN) 6 are octahedrally coordinated in most cases. A trigonal-prismatic arrangement of donor atoms is less common. Intramolecular repulsion of donor atoms and ligand field stabilization are two important parameters which energetically favor an octahedral geometry.[2]

Although trigonal-prismatic structures are considered as intermediates of intramolecular rearrangement processes of octahedral complexes, it is usually not possible to isolate the two geometrical isomers ("allogons").[3] To our knowledge, switching the octahedral to the trigonal-prismatic structure of a metal complex in a controlled and reversible fashion has never been reported. We have now observed this feature for the first time on a macrocyclic dicobalt(II) complex, $[(\mathbf{L})Co_2]^{4+}$.

The novel decaaza macrocycle **L** was prepared by N-alkylation of a previously described hexaaza macrocycle[4] with 2-(chloromethyl)pyridine. Ligands that are structurally related to the pentadentate 2,6-bis(*N*-picolylaminomethyl)-pyridine subunit of **L** form octahedral transition metal complexes with coordination of, for example, a solvent molecule at the sixth coordination site.[5] In $[(\mathbf{L})Co_2(X)_2]^{n+}$ such a behavior would result in substantial steric repulsion of solvent ligands X according to molecular models.

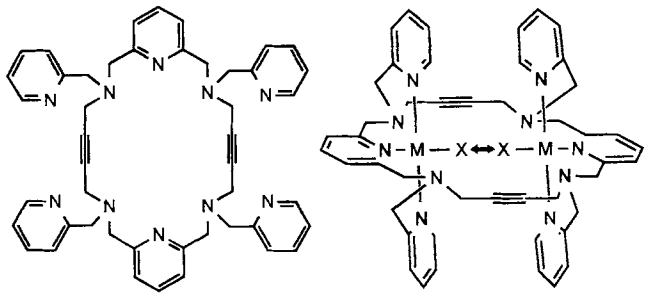

In the dicopper(II) complex of a related, bis(tetradentate) ligand such steric stress generates vacant coordination sites at the metal centers.[6] $[(\mathbf{L})Co_2(X)_2]^{n+}$ obviously finds another way out with retention of CN 6: the metal ions switch to trigonal-prismatic coordination! Usually cobalt(II) adopts the latter geometry only with rigid chelate ligands in which the donor atoms are more or less preorientated in a trigonal-prismatic fashion.[7] Figure 1 shows the crystal structure[8] of the purple complex $[(\mathbf{L})Co_2(CH_3CN)_2](ClO_4)_4$ (**1**), which was prepared by reaction of **L** with two equivalents of $Co(ClO_4)_2 \cdot 6H_2O$ in acetonitrile. The complex cation is located on a

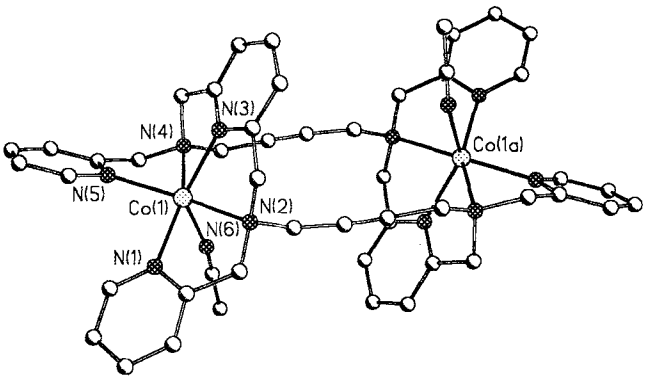

Figure 1. Structure of the $[(\mathbf{L})Co_2(CH_3CN)_2]^{4+}$ ion of **1**. Hydrogen atoms not shown. Selected distances [Å] and angles [°]:Co(1)–N(1) 2.184(5), Co(1)–N(2) 2.312(4), Co(1)–N(3) 2.082(5), Co(1)–N(4) 2.417(5), Co(1)–N(5) 2.138(4), Co(1)–N(6) 2.096(6), Co···Co 7.78; N(6)-Co(1)-N(1) 84.0(2), N(6)-Co(1)-N(2) 91.1(2), N(2)-Co(1)-N(1) 74.6(2), N(5)-Co(1)-N(3) 103.1(2), N(5)-Co(1)-N(4) 72.2(2), N(4)-Co(1)-N(3) 103.1(2), N(6)-Co(1)-N(4) 80.0(2), N(3)-Co(1)-N(2) 74.8(2), N(5)-Co(1)-N(1) 90.4(2), N(6)-Co(1)-N(5) 111.0(2), N(4)-Co(1)-N(2) 130.5(1), N(3)-Co(1)-N(1) 136.7(2).

crystallographic center of symmetry. The Co^{II} ion displays near trigonal-prismatic coordination. The triangles N(1)-N(2)-N(6) and N(3)-N(4)-N(5) (see Figure 3) are twisted along the axis defined by the triangle centers by an average angle of $\theta = 12°$ (perfect trigonal prism 0°; perfect octahedron = trigonal antiprism 60°). It is evident from Figure 1 that the trigonal prismatic coordination avoids any steric repulsion of acetonitrile ligands.

The color of an aqueous solution of $[(\mathbf{L})Co_2](NO_3)_4$, prepared in situ from **L** and $Co(NO_3)_2 \cdot 6H_2O$, immediately turns from purple to yellow-green on addition of one equivalent of NaOH. The reaction product was isolated by addition of $NaClO_4$. From acetonitrile/diethyl ether yellow-green single crystals of $[(\mathbf{L})Co_2(\mu\text{-}OH)](ClO_4)_3$ (**2**) were grown.[8] Both cobalt(II) ions display a distorted octahedral

[*] Dr. R. Krämer, Dipl.-Chem. C. Wendelstorf
Anorganisch-chemisches Institut der Universität
Wilhelm-Klemm-Strasse 8, D-48149 Münster (Germany)
Fax: Int. code + (251) 833-8366
e-mail: kramerr@nwz.uni-muenster.de

[**] This work was supported by the Deutsche Forschungsgemeinschaft and the Fonds der Chemischen Industrie. We thank Dipl.-Chem. O. Conrad and Dipl.-Chem. I. Jolk for the crystallographic data collection.

 © WILEY-VCH Verlag GmbH, D-69451 Weinheim, 1997 0570-0833/97/3624-2791 $ 17.50+.50/0

geometry. They are cristallographically nonequivalent, but bonding parameters within the coordination polyhedron are similar (Figure 2). Both in **2** and in **1** the Co–N distances are

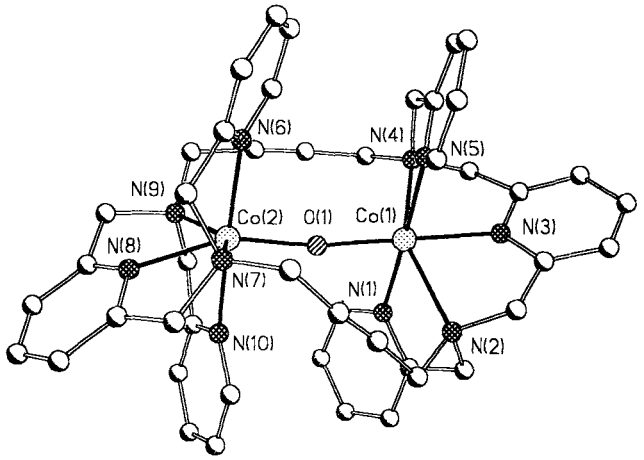

Figure 2. Structure of the $[(\mathbf{L})Co_2(\mu\text{-}OH)]^{3+}$ cation of **2**. Hydrogen atoms not shown. Selected distances [Å] and angles [°]: Co(1)–O(1) 1.951(2), Co(1)–N(1) 2.210(2), Co(1)–N(2) 2.335(2), Co(1)–N(3) 2.090(2), Co(1)–N(4) 2.276(2), Co(1)–N(5) 2.183(2), Co(2)–O(1) 1.975(2), Co(2)–N(6) 2.169(2), Co(2)–N(7) 2.322(2), Co(2)–N(8) 2.103(2), Co(2)–N(9) 2.257(2), Co(2)–N(10) 2.304(2), Co···Co 3.91; Co(2)-O(1)-Co(1) 170.7(2), O(1)-Co(1)-N(3) 168.6(1), N(5)-Co(1)-N(1) 177.46(9), N(4)-Co(1)-N(2) 148.26(8), O(1)-Co(2)-N(8) 157.9(1), N(10)-Co(2)-N(6) 175.6(1), N(9)-Co(2)-N(7) 147.15(8).

consistent with high-spin electron configuration, which is expected for Co^{II} complexes with CN 6.[9] Incorporation of a bridging hydroxide ligand enables the metals in **2** to switch to octahedral geometry. The hydroxo bridge is almost linear (Co-O-Co-angle of 170.8°). The average twist angles θ of the triangles N(1)-N(2)-O(1) and N(3)-N(4)-N(5) at Co(1) and of triangles N(6)-N(7)-O(1) and N(8)-N(9)-N(10) at Co(2), respectively, are 42° and 38° (Figure 2). Thus, cobalt coordination is not perfectly octahedral, but distorted towards a trigonal-prismatic geometry—as it is often observed for transition metal ions of CN 6. The change from the trigonal prism in **1** to the octahedron in **2** is not a simple twist of the triangles represented in Figure 3. Additionally, the configuration of one of the chiral nitrogen atoms is inverted. Consequently, the picolyl substituents of the mononuclear subunit are *trans*-oriented relative to the macrocyclic framework in **2** but *cis*-oriented in **1**.

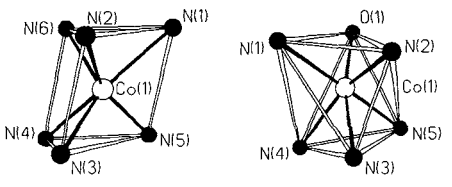

Figure 3. Cobalt(II) coordination polyhedra in **1** and **2**.

In solution the interconversion of the trigonal-prismatic and the octahedral complex was followed by spectrophotometric titration. An aqueous solution of $[(\mathbf{L})Co_2](NO_3)_4$ is acidic (pH 4.0), purple in color, and displays an optical band at $\lambda_{max} = 530$ nm, $\varepsilon = 39\,M^{-1}cm^{-1}$. A solution of a crystalline sample of **1** in acetonitrile has a comparable spectrum ($\lambda_{max} = 530$ nm, $\varepsilon = 59\,M^{-1}cm^{-1}$). It is obvious that $[(\mathbf{L})Co_2]$ is trigonal-prismatically coordinated in aqueous solution, with a H_2O molecule in the sixth site of each metal. On titration with NaOH the color of the solution turns yellow-green (Figure 4). After addition of 1.0 equivalent of NaOH (pH 6.5)

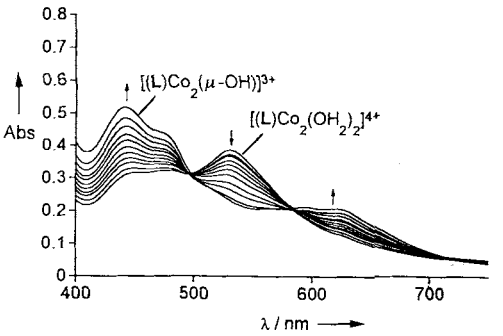

Figure 4. Spectrophotometric titration of $[(\mathbf{L})Co_2(OH_2)_2](NO_3)_4$ (10 mM in H_2O), prepared in situ from **L** and $2\,Co(NO_3)_2 \cdot 6H_2O$, with NaOH (0–1 equiv). Spectra correspond to NaOH addition in steps of 0.1 equiv.

the optical spectrum ($\lambda_{max} = 441$ nm, $\varepsilon = 60\,M^{-1}cm^{-1}$; $\lambda(sh) = 475$ nm; $\lambda_{max} = 595$ and 623 nm, $\varepsilon = 21$ and $22\,M^{-1}cm^{-1}$) corresponds to the spectrum of a solution of crystalline **2** in acetonitrile ($\lambda_{max} = 443$ nm, $\varepsilon = 57\,M^{-1}cm^{-1}$; $\lambda(sh) = 475$ nm; $\lambda_{max} = 597$ and 625 nm, $\varepsilon = 24$ and $24\,M^{-1}cm^{-1}$). Isosbestic points at 500 nm and 585 nm indicate smooth conversion of $[(\mathbf{L})Co_2(OH_2)_2]^{4+}$ into $[(\mathbf{L})Co_2(\mu\text{-}OH)]^{3+}$. Addition of one equivalent of HNO_3 to $[(\mathbf{L})Co_2(\mu\text{-}OH)]^{3+}$ regenerates the spectrum of $[(\mathbf{L})Co_2(OH_2)_2]^{4+}$, and titration with NaOH is reproducible. By addition of 0.5 equivalents of NaOH to $[(\mathbf{L})Co_2(OH_2)_2]^{4+}$ a 1:1 mixture of aqua and hydroxo complex is obtained at pH 4.5. This allows a rough estimate of the hydroxide binding constant of $[(\mathbf{L})Co_2]^{4+}$, which is rather large relative to that of other macrocyclic dicobalt(II) complexes.[10]

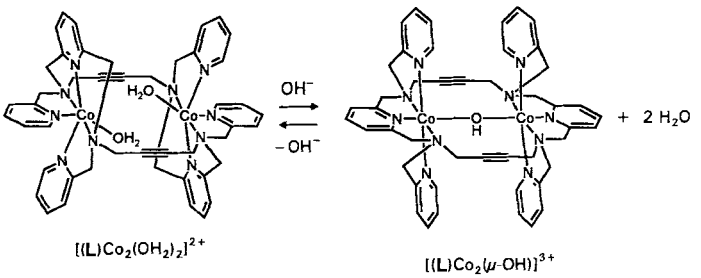

It is evident from the spectrophotometric titrations that a simple variation of pH effects reversible switching from trigonal-prismatic to octahedral state of the metal ions in $[(\mathbf{L})Co_2]^{4+}$. $[(\mathbf{L})Co_2(OH_2)_2]^{4+}$ and $[(\mathbf{L})Co_2(\mu\text{-}OH)]^{3+}$ are not isomeric, but the donor environments of the metal ions differ only marginally ($-OH_2$ ligand is replaced by "OHM ligand").

The observations described above are not specific for cobalt(II). Preliminary studies indicate that switching the coordination geometries of the Mn^{II}, Ni^{II}, and Zn^{II} complexes of **L** is possible in a similar fashion.

Received: August 21, 1997 [Z10836IE]
German version: *Angew. Chem.* **1997**, *109*, 2888–2890

 © WILEY-VCH Verlag GmbH, D-69451 Weinheim, 1997 0570-0833/97/3624-2792 $ 17.50+.50/0

Keywords: cobalt · coordination modes · dinuclear complexes · macrocyclic ligands

[1] A. von Zelewsky, *Stereochemistry of Coordination Compounds*, Wiley, Chichester (UK), **1996**; P. Comba, *Coord. Chem. Rev.* **1993**, *123*, 1–48; D. L. Kepert, *Inorganic Chemistry Concepts, Vol. 6*, Springer, Berlin, **1980**, p. 71–116.

[2] R. Hoffmann, J. M. Howell, A. R. Rossi, *J. Am. Chem. Soc.* **1976**, *98*, 2484; E. Larsen, G. N. La Mar, B. E. Wagner, J. E. Parks, R. H. Holm, *Inorg. Chem.* **1972**, *11*, 2652–2668; R. A. D. Wentworth, *Coord. Chem. Rev.* **1972**, *9*, 171; W. O. Gillum, R. A. D. Wentworth, R. F. Childers, *Inorg. Chem.* **1970**, *9*, 1825–1832; R. Eisenberg, *Prog. Inorg. Chem.* **1970**, *12*, 295.

[3] Very rare example for the presence of both octahedral and trigonal-prismatic environments for metal ions (Ca^{2+}) in the same crystal, but with a different set of donor atoms: V.-C. Arunasalam, I. Baxter, S. R. Drake, M. B. Hursthouse, K. M. Abdul-Malik, D. J. Otway, *Inorg. Chem.* **1995**, *34*, 5295–5306.

[4] S. Warzeska, R. Krämer, *Chem. Ber.* **1995**, *128*, 115.

[5] K. Bernauer, P. Pousaz, *Helv. Chim. Acta* **1984**, *67*, 796; H. Stoeckli-Evans, L. Brehm, P. Pousaz, K. Bernauer, *ibid.* **1985**, *68*, 185.

[6] S. Warzeska, R. Krämer, *J. Chem. Soc. Chem. Commun.* **1996**, 499–500.

[7] a) S. A. Kubow, K. J. Takeuchi, J. J. Grzybowski, A. J. Jircitano, V. L. Goedken, *Inorg. Chim. Acta* **1996**, *241*, 21–30; b) D. R. Boston, N. J. Rose, *J. Am. Chem. Soc.* **1973**, 95, 4163; c) G. A. Zakrzewski, C. A. Ghilardi, E. C. Lingafelter, *ibid.* **1971**, 93, 4411. See, however, H. Al-Sagher, I. Fallis, L. J. Farrugia, R. D. Peacock, *J. Chem. Soc. Chem. Commun.* **1993**, 1499–1500; J. A. Bertrand, J. A. Kelley, E. G. Vassian, *J. Am. Chem. Soc.* **1969**, 91, 2394.

[8] Crystallographic data of **1**: orthorhombic, *Pbca*, $a = 16.787(3)$, $b = 14.534(3)$, $c = 23.584(5)$ Å, $\beta = 94.71(3)^\circ$, $V = 5754.1(20)$ Å^3, $Z = 4$, $Mo_{K\alpha}$ radiation, no absorption correction, $T = 213(2)$ K, 38879 reflections measured, 3203 observed $I > 2\sigma(I)$, 522 parameters, $R(F_o) = 0.0674$, $R_w(F_o^2) = 0.1591$, min./max. residual electron density: $-0.41/0.37$ e Å^{-3}; strucutre solution: Patterson-method of SHELXS 86, structure refinement: SHELXL 93, full matrix least squares. H atoms: "riding model". Crystallographic data of **2**: monoclinic, $P2_1/n$, $a = 10.349(2)$, $b = 24.384(5)$, $c = 20.376(4)$ Å, $\beta = 94.71(3)^\circ$, $V = 5124.5(18)$ Å^3, $Z = 4$, $Mo_{K\alpha}$ radiation, no absorption correction, $T = 163(2)$ K, 11715 reflections measured, 7409 observed $I > 2\sigma(I)$, 840 parameters, $R(F_o) = 0.0399$, $R_w(F_o^2) = 0.0924$, min./max. residual electron density: $-0.43/0.68$ e Å^{-3}; structure solution: Patterson-method of SHELXS 86, structure refinement: SHELXL 93, full matrix least squares. H atoms: "riding model". Further crystallographic details are available on request from Fachinformationszentrum Karlsruhe, D-76344 Eggenstein-Leopoldshafen, on quoting the deposition numbers CSD 407716 (**1**) and CSD 407717 (**2**).

[9] Low-spin Co^{II} complexes of CN 6 are rare, the Co–N distances are about 0.1 Å shorter; see for example [7a].

[10] R. J. Motekaitis, A. E. Martell, J.-M. Lehn, E. I. Watanabe, *Inorg. Chem.* **1982**, *21*, 4253; R. Menif, J. Reibenspies, A. E. Martell, *ibid.* **1991**, *30*, 3446–3454; L. H. Tan, M. R. Taylor, K. P. Wainwright, P. A. Duckworth, *J. Chem. Soc. Dalton Trans.* **1993**, 2921–2928.

From D-Glucose to a New Chiral Cyclooctenone**

Barbara Werschkun and Joachim Thiem*

Eight-membered carbocycles have increasingly attracted the interest of natural product chemists in recent years. The discovery of a growing number of naturally occurring compounds with eight-membered rings as a structural feature especially among the diterpenes, of which particularly the highly functionalized taxane derivatives show exceptional biological activity, has led to a significant increase in synthetic efforts in this area. The formation of eight-membered rings is a special problem in organic chemistry: owing to the unfavorable energetic relations that are caused by Pitzer strain and transannular interactions, the usual ring-closing methods can often only be applied with low product yields, if at all.[1] Thus alternative synthetic routes such as fragmentations or ring enlargements are of great importance. An elegant variation of the latter reaction is the Claisen rearrangement of 2-methylene-6-vinyl-tetrahydropyrans to cyclooctenone derivatives used by Paquette et al. in the synthesis of several natural products.[2,3]

The tetrahydropyran structure of the starting material and the complex oxygen-rich chiral eight-membered rings that are difficult to obtain by other methods, which were expected as products of the rearrangement, made it seem reasonable to apply the reaction to carbohydrates. The Claisen rearrangement has been used in carbohydrate chemistry as an efficient C–C coupling method for a long time, but its application was restricted to the introduction of alkyl branches and the synthesis of C glycosides.[4] A skeletal rearrangement with loss of the sugar structure was hitherto unknown as was the synthesis of 5,6-unsaturated *C*-vinylglycosides such as **4**, which we have achieved by a simple sequence of well-known reactions (Scheme 1).

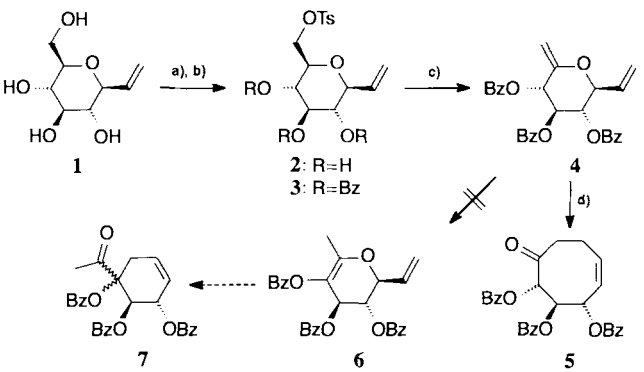

Scheme 1. Synthesis and rearrangement of **4**. a) TsCl, pyridine, 62%; b) BzCl, pyridine, 89%; c) DMSO, 80 °C, 1. NaI, Bu_4NI, 2. 1,8-diazabicyclo[5.4.0]undec-7-ene (DBU), 52%; d) xylene, reflux, 60%.

The β-*C*-vinylglycoside **1** is available as a pure anomer from the Grignard reaction of acetobromoglucose with vinylmagnesium bromide in approximately 30% yield.[5] The selective reaction of the primary hydroxy group with tosyl chloride (TsCl) to give **2**, and the subsequent perbenzoylation with benzoyl chloride (BzCl) to afford the protected tosylate **3** are standard methods. In a one-pot reaction introduced by Sato et al.,[6] the sulfonate moiety is first replaced by an iodine substituent, followed by base-catalyzed elimination of hydrogen iodide, during which the exocyclic double bond is formed. The allyl enol ether **4**, which is obtained in 50% yield, is stable enough to be purified on silica gel and kept for several weeks at -18 °C.

Simple heating of a solution of **4** in boiling xylene leads to the carbocycle **5** in 60% yield after 12 h, as the expected product of the sigmatropic rearrangement. In spite of the well-known tendency of 2-methylene-substituted tetrahydropyrans to isomerize under conversion of the exo- into an endocyclic double bond,[7] neither the derivative **6** nor its hypothetical reaction product **7** was found. It has to be emphasized that due to the β configuration of the C-glycosidic vinyl group a

[*] Prof. Dr. J. Thiem, Dipl.-Chem. B. Werschkun
Institut für Organische Chemie der Universität
Martin-Luther-King-Platz 6, D-20146 Hamburg (Germany)
Fax: Int. code + (40)4123-4325
e-mail: thiem@chemie.uni-hamburg.de

[**] This work was supported by the Fonds der Chemischen Industrie. We thank Dr. V. Sinnwell for the valuable help with the elucidation of the conformation by NMR spectroscopy.

 © WILEY-VCH Verlag GmbH, D-69451 Weinheim, 1997 0570-0833/97/3624-2793 $ 17.50+.50/0

sigmatropic rearrangement can only occur out of the $^1C_4$ conformation of the carbohydrate ring, and that this is the first example of a Claisen rearrangement of such a configured compound. The boat–chair conformation of **5** shown in Figure 1 can be deduced from the ^3J couplings in the ^{1}H NMR

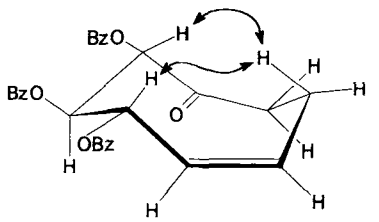

5

Figure 1. Boat–chair conformation of **5** deduced from NMR data. The arrows reproduce the observed NO effects.

spectrum and is supported by the transannular NOEs observed in the two-dimensional experiment. The very sharp signals point to the fact that the flexibility is strongly reduced by the three sp^2 carbon centers, which for less substituted systems has already led to remarkable stereoselectivity in follow-up reactions.[8]

This fact together with the three defined chiral centers from the original carbohydrate framework and the high density of oxygen-containing substituents, which can be readily modified synthetically, make compounds like **5** attractive as useful synthetic building blocks, particularly since they are now available from the simple and common starting material D-glucose in few steps.

Experimental Section

5: A solution of **4** (52 mg, 0.11 mmol) in dry xylene (5 mL) was heated to reflux for 12 h. After evaporation of the solvent the residue was purified by chromatography on silica gel with petroleum ether/ethyl acetate (5/1) as eluent. This afforded **5** (31 mg, 60%) as a colorless syrup. $[\alpha]_{20}^{D} = -49.5$ ($c = 1$, chloroform). ^{1}H NMR (400 MHz, $CDCl_3$): $\delta = 2.43-2.50$ (m, H-7eq), 2.60 (ddd, H-8ax, $J = 4.6$, 12.7, 13.2 Hz), 2.85–2.95 (m, H-7ax), 3.13 (ddd, H-8eq, $J = 4.1$, 12.7 Hz), 5.53 (d, H-2, $J = 8.6$ Hz), 5.62 (dd, H-5, $J = 7.1$, 11.2 Hz), 5.71 (dd, H-3, $J = 8.6$, 10.7 Hz), 5.92 (m, H-6), 6.22 (ddd, H-4, $J = 1.5$, 7.1, 10.2 Hz), 7.20–7.47, 7.79–7.85 (2 × m, 9H, 6 H, aryl). ^{13}C NMR (100 MHz, $CDCl_3$): $\delta = 22.01$ (C-7), 42.08 (C-8), 68.91 (C-4), 69.51 (C-3), 76.32 (C-2), 126.88–132.63 (C-5, C-6, aryl-C), 164.45, 164.48, 164.74 (3 × CO_2), 203.78 (C-1).

Received May 14, 1997 [Z10438IE]
German version: *Angew. Chem.* **1997**, *109*, 2905–2906

Keywords: carbocycles · carbohydrates · rearrangements

[1] a) N. A. Petasis, M. A. Patane, *Tetrahedron* **1992**, *48*, 5757–5821; b) M. Braun, *Nachr. Chem. Tech. Lab.* **1985**, *33*, 1066–1069; c) G. Illuminati, L. Mandolini, *Acc. Chem. Res.* **1981**, *14*, 95–102.

[2] a) L. A. Paquette, C. M. G. Philippo, N. H. Vo, *Can. J. Chem.* **1992**, *70*, 1356–1365; b) C. M. G. Philippo, N. H. Vo, L. A. Paquette, *J. Am. Chem. Soc.* **1991**, *113*, 2762–2764; c) L. A. Paquette, D. Friedrich, R. D. Rogers, *J. Org. Chem.* **1991**, *56*, 3841–3849; d) L. A. Paquette, H.-J. Kang, *J. Am. Chem. Soc.* **1991**, *113*, 2610–2621; e) H.-J. Kang, L. A. Paquette, *ibid.* **1990**, *112*, 3252–3253; f) J. Ezquerra, W. He, L. A. Paquette, *Tetrahedron Lett.* **1990**, *31*, 6979–6982; g) W. A. Kinney, M. J. Coghlan, L. A. Paquette, *J. Am. Chem. Soc.* **1985**, *107*, 7352–7360; h) W. A. Kinney, M. J. Coghlan, L. A. Paquette, *ibid.* **1984**, *106*, 6868–6870.

[3] See also: a) R. W. Carling, A. B. Holmes, *J. Chem. Soc. Chem. Commun.*, **1986**, 325–326; b) M. A. M. Fuhry, A. B. Holmes, D. R. Marshall, *J. Chem. Soc. Perkin Trans. 1* **1993**, 2743–2746.

[4] For example: a) R. W. Gable, L. M. McVinish, M. A. Rizzacasa, *Aust. J. Chem.* **1994**, *47*, 1537–1544; b) I. Pelyvás, T. K. Lindhorst, J. Thiem, *Liebigs Ann. Chem.* **1990**, 761–769; c) D. P. Curran, Y.-G. Suh, *Carbohydr. Res.* **1987**, *171*, 161–191; d) R. E. Ireland, D. W. Norbeck, *J. Am. Chem. Soc.* **1985**, *107*, 3279–3285; e) D. B. Tulshian, B. Fraser-Reid, *J. Org. Chem.* **1984**, *49*, 518–522; f) R. E. Ireland, J. P. Daub, *ibid.* **1981**, *46*, 479–485; g) R. E. Ireland, S. Thaisrivongs, N. Vanier, C. S. Wilcox, *ibid.* **1980**, *45*, 48–61; h) R. J. Ferrier, N. Vethaviyasar, *J. Chem. Soc. Perkin Trans. 1* **1973**, 1791–1793.

[5] a) M. L. Shulman, S. D. Shiyan, A. Y. Khorlin, *Carbohydr. Res.* **1974**, *33*, 229–235; b) S. D. Shiyan, M. L. Shulman, A. Y. Khorlin, *Izv. Akad. Nauk SSR, Ser. Khim.* **1973**, 2386–2387.

[6] a) K. Sato, N. Kubo, R. Takada, S. Sakuma, *Bull. Chem. Soc. Jpn.* **1993**, *66*, 1156–1165; b) K. Sato, S. Sakuma, Y. Nakamura, J. Yoshimura, H. Hashimoto, *Chem. Lett.* **1991**, 17–20; c) K. Sato, N. Kubo, R. Takada, A. Aqeel, H. Hashimoto, J. Yoshimura, *ibid.* **1988**, 1703–1704.

[7] a) R. E. Ireland, D. Häbich, *Chem. Ber.* **1981**, *114*, 1418–1427; b) *Tetrahedron Lett.* **1980**, 1389–1392.

[8] a) S. L. Schreiber, D. B. Smith, G. Schulte, *J. Org. Chem.* **1989**, *54*, 5994–5996; b) S. A. Hardinger, P. L. Fuchs, *ibid.* **1987**, *52*, 2739–2749; c) W. C. Still, I. Galynker, *Tetrahedron* **1981**, *37*, 3981–3996.

Synthesis of an ABC Ring Analogue of Kapurimycin A_3 as an Effective DNA Alkylating Agent**

Kazuhiko Nakatani,* Akimitsu Okamoto, and Isao Saito*

The antitumor antibiotic kapurimycin A_3 (**1**),[1] whose structure is closely related to that of pluramycins,[2] alkylates DNA by attacking the epoxide subunit on guanine at N7 to form a kapurimycin–DNA adduct.[3] The high efficiency of the selective alkylation of guanine at N7 implies that the epoxide subunit is placed in the major groove of DNA with an appropriate alignment to N7 of guanine through precovalent intercalation of the aromatic moiety, as previously suggested for aflatoxin B_1[4] and altromycin B.[5,6] To identify the factors responsible for such an efficient and selective guanine alkylation and to devise new DNA-alkylating agents possessing an epoxide subunit, we synthesized the truncated kapurimycin analogues **2** and **3** as well as their epoxy alcohol and

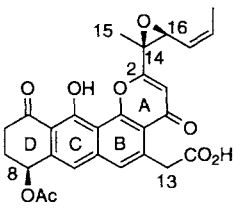

kapurimycin A_3 **1**

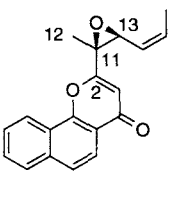

2

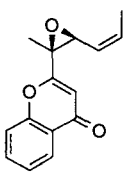

3

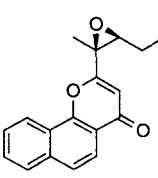

4

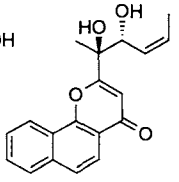

5

[*] Dr. K. Nakatani, Prof. I. Saito, A. Okamoto
Department of Synthetic Chemistry and Biological Chemistry
Faculty of Engineering, Kyoto University
Kyoto 606-01 (Japan)
CREST, Japan Science and Technology Corporation
Fax: Int. code. + (75)753-5676
e-mail: saito@sbchem.kyoto-u.ac.jp

[**] Special thanks are due to Drs. Y. Uosaki, M. Hara, and H. Saito (Kyowa Hakko Kogyo CO., LTD.) for valuable discussions and a generous gift of kapurimycin A_3.

diol derivatives **4** and **5**, respectively, and examined their activity toward DNA alkylation. We report here that the ABC ring analogue **2** of kapurimycin A_3 fulfills a minimal structural requirement for this antibiotic in terms of efficiency and sequence selectivity for guanine alkylation.

The ABC ring analogue **2**, which has the same absolute configuration as **1** (14*S*, 16*S*),[7] was synthesized by a highly convergent route that features coupling of 1-*tert*-butyldimethylsilyloxy-2-naphthoaldehyde (**9**) with the precursor for the chiral side chain **8** followed by efficient pyranone formation (ring A, Scheme 1). Asymmetric dihydroxylation of *p*-methoxybenzyl ether **6**, obtained from a commercially available alcohol with AD-mix-β,[8] produced the corresponding diol, which was converted into alcohol **7**. After recrystallization, **7** had an enantiomeric purity of 93% *ee*, as determined by ^{1}H NMR spectroscopy of the α-methoxy-α-(trifluoromethyl)-phenylacetic acid (MTPA) ester. Oxidation of **7** followed by Wittig olefination with ethylidene triphenylphosphorane provided the alkene (Z:E = 5:1),[9] which was desilylated to **8**. Addition of **9** to lithiated **8** provided the corresponding coupling product, which was subsequently oxidized with manganese dioxide to ketone **10**. Selective formation of the pyranone ring was achieved by treating **10** with KF and [18]crown-6 in anhydrous DMF[10] to give the tricyclic compound **11** in high yield.[11] Hydrolysis of the acetal produced diol **5**, which was further subjected to intramolecular Mitsunobu reaction[12] to furnish the desired (11*S*,13*S*)-**2**.[13] Kapurimycin analogues **3** and **4** were synthesized by similar routes.

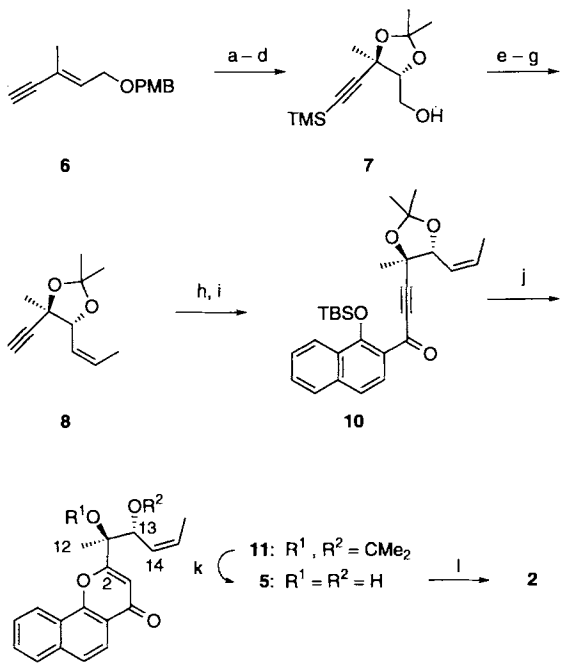

Scheme 1. Synthesis of the ABC ring analogue **2**. a) AD-mix-β, 76%; b) $Me_2C(OMe)_2$, 95%; c) lithium 1,1,1,3,3,3-hexamethyldisilazane (LiHMDS), Me_3SiCl, 89%; d) 2,3-dichloro-5,6-dicyano-1,4-benzoquinone (DDQ), 99%; e) Dess–Martin oxidation, 94%; f) $Ph_3P{=}CHCH_3$, 78%, Z:E = 5:1; g) NaOMe, 80%; h) LiHMDS, $CeCl_3$, 1-*tert*-butyldimethylsilyloxy-2-naphthoaldehyde (**9**), 47%; i) MnO_2, 76%; j) KF, [18]crown-6, DMF, 80%; k) cat. HCl, AcOH, 98%; l) diethylazodicarboxylate (DEAD), Ph_3P, 76%.

The activity of these kapurimycin analogues with respect to DNA cleavage was examined by a relaxation assay of supercoiled plasmid DNA (Figure 1). Supercoiled plasmid DNA was treated with the kapurimycin analogue (5 h, 37 °C) and then incubated for 24 h at 37 °C to complete heat-induced strand breaks at alkylated guanine residues. A distinct cleavage band was observed when DNA was treated with **2** and further incubated for 24 h at 37 °C (lane 3). Analysis of the nucleosides in calf-thymus DNA treated with **2** followed by enzymatic digestion showed that the content of 2′-deoxyguanosine decreased considerably (28%), while other nucleosides remained unchanged. These results strongly suggest that the ABC ring analogue **2** induced DNA cleavage by selective modification of the guanine base.

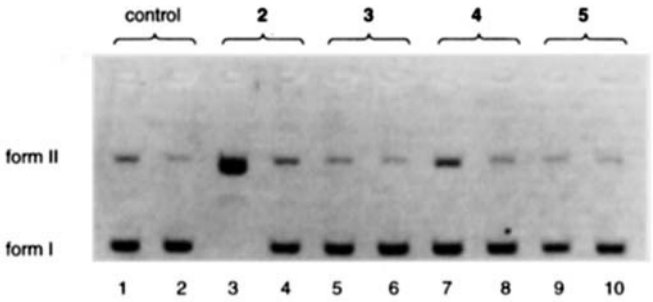

Figure 1. Cleavage of supercoiled circular pBR322 DNA (form I) by kapurimycin analogues **2**–**5** into nicked circular DNA (form II). Supercoiled pBR322 DNA (40 μM) in Tris/HCl buffer (5 mM, pH = 7.6) was incubated in the presence of **2**, **3**, **4**, or **5** (10 μM) for 5 h at 37 °C. Unbound drugs were removed by precipitation with ethanol, and the recovered DNA was dissolved in Tris/HCl buffer (condition A). To complete strand cleavage, the solution of DNA was further incubated for 24 h at 37 °C (condition B). DNA treated under condition A (even-numbered lanes) and condition B (odd-numbered lanes) were analyzed by electrophoresis on 1% agarose gel containing ethidium bromide (0.2 μg mL^{-1}). Lane 1, control for condition B; lane 2: control for condition A; lanes 3 and 4: **2**; lanes 5 and 6: **3**; lanes 7 and 8: **4**; lanes 9 and 10: **5**.

The complete lack of the DNA-cleavage activity of diol **5** (lanes 9 and 10) indicated that the epoxide subunit of **2** would be the site for DNA alkylation.[3b] A weak cleavage band detected for DNA treated with epoxy alcohol **4** (lane 7 in comparison with lane 3) suggested that the alkenyl group directly attached to the epoxide ring remarkably accelerates the rate of nucleophilic ring opening of the epoxide moiety. While the observed rates for hydrolytic cleavage of the epoxide moieties in tris(hydroxymethyl)aminomethane (Tris)/HCl buffer (pH = 7.5) at 37 °C were comparable for **1**, **2**, and **3** (half lives ($t_{1/2}$) of 3.5, 5.6, and 5.9 h, respectively) it was substantially longer for **4** under these conditions ($t_{1/2}$ > 150 h).[15] These observations may explain the extremely low DNA-cleavage activity of **4**. Of special interest is the large difference in activity between **2** and **3** (lanes 3 and 5), which is caused only by the presence or absence of ring C; this suggests stronger intercalation of the ABC rings of **2** into the DNA duplex. This assumption was proved by DNA-unwinding assays[16] with **12** and **13**; both lack an epoxide subunit for DNA alkylation. Figure 2 clearly indicates more enhanced DNA unwinding of supercoiled pBR322 DNA when treated with **13**.

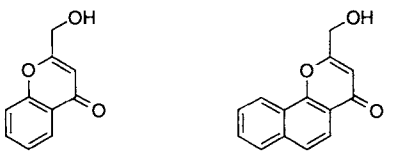

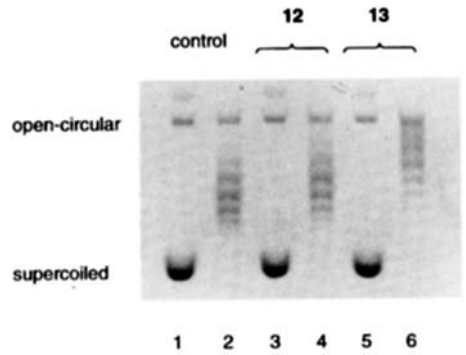

Figure 2. Unwinding of DNA by kapurimycin analogues **12** and **13**. Supercoiled pBR322 DNA (40 μM; lane 1) was first treated with topoisomerase I (topo I; 4 units) for 30 min in a buffer (10 mM Tris/HCl, pH = 7.9, 1 mM ethylenediaminetetraacetic acid (EDTA), 150 mM NaCl, 0.1 mM spermidine, 5% glycerol, 0.1% bovine serum albumin (BSA)), and further incubated for 30 min in the absence (lane 2) and presence of **12** and **13** (100 μM; lanes 4 and 6, respectively). In lanes 3 and 5 the DNA was incubated with **12** and **13**, respectively, in the absence of topo I. The resulting DNA sequences were analyzed by electrophoresis on 1% native agarose gel at 1.3 V cm^{-1} for 15 h. Lane 1: supercoiled DNA; lane 2: DNA treated with topo I; lane 3: **12**; lane 4: **12** plus topo I; lane 5: **13**; lane 6: **13** plus topo I.

DNA cleavage by the ABC ring analogue **2** was compared with that of natural kapurimycin A_3 (**1**) with respect to the efficiency and sequence selectivity for guanine alkylation (Figures 3 and 4). As shown in Figure 3, **1** cleaves DNA even

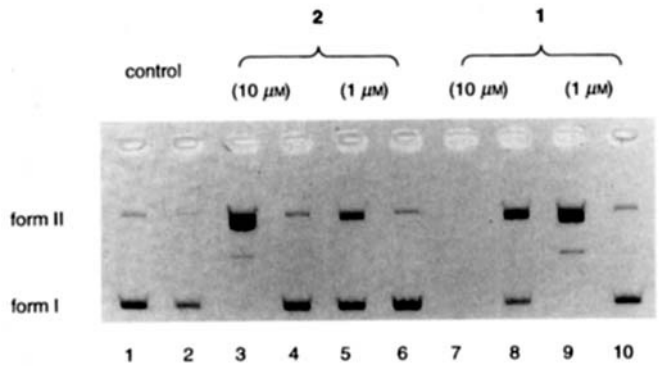

Figure 3. Cleavage of supercoiled circular pBR322 DNA by kapurimycin A_3 (**1**) and the ABC ring analogue **2**. The DNA was treated with the drugs for 5 h at 37 °C (even-numbered lanes) and further incubated for 24 h as described for Figure 1 (odd-numbered lanes). Lanes 1 and 2: controls; lanes 3 and 4: **2** (10 μM); lanes 5 and 6: **2** (1 μM); lanes 7 and 8: **1** (10 μM); lanes 9 and 10, **1** (1 μM). DNA bands in lane 7 disappeared due to the excessive cleavage by **1** under the given conditions.

at a concentration of 1 μM (lane 9), whereas **2** requires 10 μM for comparable cleavage (lanes 3 and 9). In contrast, the sequence selectivity for guanine alkylation observed for **2** shows a strong preference for the guanine group on the 5′-end of the 5′-GPu-3′ sequences, which was very similar to that observed for **1** (Figure 4).[17] These results suggest that despite the lack of ring D and other functional groups, the highly simplified analogue **2** could exhibit a very similar 5′-selectivity for guanine alkylation of duplex DNA.

We thus established a highly stereoselective and convergent synthetic route for a series of truncated analogues of kapurimycin A_3 of defined absolute configurations. We also demonstrated that the simplified analogue **2** with a minimal structure for kapurimycin A_3 can serve as an effective guanine alkylating agent for duplex DNA with a strong preference for 5′-GPu-3′.

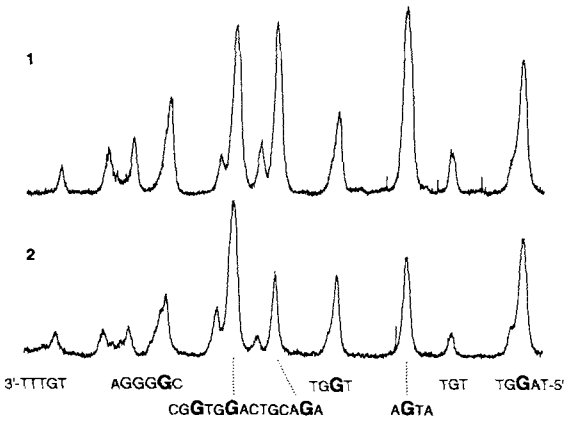

Figure 4. Sequence selectivity for guanine alkylation by natural kapurimycin A_3 (**1**, top) and the ABC ring analogue **2** (bottom). The DNA sequences including strong G-cleavage bands (bold face) are shown.

Experimental Section

Analysis of the nucleosides in calf-thymus DNA: Calf-thymus DNA (200 μM) was treated with **2** (1 mM) in Tris/HCl (pH = 7.5) for 24 h at 37 °C, and the mixture digested with snake-venom phosphodiesterase and alkaline phosphatase. The resulting mixture of nucleosides was analyzed by HPLC (Cosmosil C18-AR column, elution with 2 → 5% acetonitrile in 50 mM ammonium formate (linear gradient) over 30 min).

Rates of hydrolytic cleavage: Solutions of **1**–**4** (each 100 μM) in Tris/HCl buffer (50 mM, pH = 7.5) were incubated at 37 °C. The amounts of unchanged starting materials after a certain time interval were determined by HPLC.

Analysis of the sequence selectivity for guanine alkylation: A ^{32}P-5′-end-labeled DNA fragment (513 bp *Eco*R I-*Rsa* I fragment of pBR322 DNA) was incubated in the presence of **1** (1 μM) and **2** (10 μM) for 24 h at 37 °C in Tris/HCl buffer (pH = 7.6). DNA recovered by precipitation with ethanol was heated (90 °C, 30 min) in the presence of 10% piperidine and analyzed by electrophoresis with 8% polyacrylamide and 7 M urea (1900 v for 1.5 h). The gel was dried and exposed to a X-ray film with an intensifying sheet at −70 °C. The intensity of the cleavage bands was determined by densitometeric analysis. The DNA sequence shown in Figure 4 is as follows: 3′-TTTGT TTATC CCCAA GGCGC GTGTA AAGGG GCTTT TCACG GTGGA CTGCA GATTC TTTGG TAATA ATAGT ACTGT AATTG GTA-5′.

Received: June 5, 1997 [Z10512IE]
German version: *Angew. Chem.* **1997**, *109*, 2881–2883

Keywords: alkylations · antitumor agents · DNA cleavage · drug design · kapurimycin A_3

[1] a) M. Hara, T. Mokudai, E. Kobayashi, K. Gomi, H. Nakano, *J. Antibiot.* **1990**, *43*, 1513–1518; b) M. Yoshida, M. Hara, Y. Saitoh, H. Sano, *ibid.* **1990**, *43*, 1519–1523.

[2] Review of antibiotics in the pluramycin family: U. Séquin, *Fortschr. Chem. Naturst.* **1986**, *50*, 57–122.

[3] a) M. Hara, M. Yoshida, H. Nakano, *Biochemistry* **1990**, *29*, 10449–10455; b) K. L. Chan, H. Sugiyama, I. Saito, *Tetrahedron Lett.* **1991**, *52*, 7719–7722.

[4] a) M. P. Stone, S. Gopalakrishnan, T. M. Harris, D. E. Graves, *J. Biomol. Struct. Dyn.* **1988**, *5*, 1025–1041; b) S. Gopalakrishnan, S. Byrd, M. P. Stone, T. M. Harris, *Biochemistry* **1989**, *28*, 726–734; c) M. P. Stone, S. Gopalakrishnan, K. D. Raney, V. M. Raney, S. Byrd, T. M. Harris in *Molecular Basis of Specificity in Nucleic Acid–Drug Interactions* (Eds.: B. Pullman, J. Jortner), Kluwer, Dordrecht, **1990**, pp. 451–480; d) K. D. Raney, S. Gopalakrishnan, S. Byrd, M. P. Stone, T. M. Harris, *Chem. Res. Toxicol.* **1990**, *3*, 254–261; e) K. D. Raney, T. M. Harris, M. P. Stone, *ibid.* **1993**, *6*, 64–68.

[5] M. R. Hansen, L. H. Hurley, *Acc. Chem. Res.* **1996**, *29*, 249–258.

[6] a) D. Sun, M. Hansen, J. J. Clement, L. H. Hurely, *Biochemistry* **1993**, *32*, 8068–8074; b) M Hansen, H. Hurley, *J. Am. Chem. Soc.* **1995**, *117*, 2421–2429; c) D. Sun, M. Hansen, H. Hurley, *ibid.* **1995**, *117*, 2430–2440, and references therein.

 © WILEY-VCH Verlag GmbH, D-69451 Weinheim, 1997 0570-0833/97/3624-2796 $ 17.50+.50/0

[7] The absolute configuration of **1** was determined to be *8S*, *14S*, and 16*S*: Y. Uosaki, H. Saito, *Abstr. Pap. 69th Annu. Meeting Chem. Soc. Jpn.* **1995**, p. 1013.
[8] K. B. Sharpless, W. Amberg, Y. L. Bennani, G. A. Crispino, J. Hartung, K.-S. Jeong, H.-L. Kwong, K. Morikawa, Z.-M. Wand, D. Xu, K.-L. Zhang, *J. Org. Chem.* **1992**, *57*, 2768–2771.
[9] The *E* and *Z* isomers could not be separated throughout the synthesis.
[10] a) K. Nakatani, A. Okamoto, M. Yamanuki, I. Saito, *J. Org. Chem.* **1994**, *59*, 4360–4361; b) K. Nakatani, A. Okamoto, I. Saito, *Tetrahedron* **1996**, *52*, 9427–9446.
[11] The relative configuration of the two asymmetric centers in **11** was confirmed by the presence of an NOE between C12-Me and C14-H.
[12] O. Mitsunobu, *Synthesis* **1981**, 1–28.
[13] The absolute configuration of **5** was determined to be 11*S* and 13*R* by a modified Mosher method [14] applied for the MTPA ester of **5**.
[14] I. Ohtani, T. Kusumi, Y. Kashman, H. Kakisawa, *J. Am. Chem. Soc.* **1991**, *113*, 4092–4096.
[15] Hydrolysis of **2** produced diol **5** as a sole product with inversion of the configuration at C13; this indicates that the reaction proceeded by an S_N2 mechanism.
[16] R. Kuroda, E. Takahashi, C. A. Austin, L. M. Fisher, *FEBS Lett.* **1990**, *262*, 293–298.
[17] Further evidence for alkylation of guanine by **2** was obtained by sequencing analysis. Thus, smear cleavage bands obtained by heating DNA treated with **2** did not co-migrate with Maxam–Gilbert G bands, whereas the clear G bands in Figure 4 were obtained by heating the same samples with piperidine. The observed band shift is a typical indication for alkylation of guanine at N7.

Synthesis and Crystal Structure of $[Cd_{10}Se_4(SePh)_{12}(PPh_3)_4]$ and $[Cd_{16}(SePh)_{32}(PPh_3)_2]$**

Silke Behrens, Marco Bettenhausen, Andreas Eichhöfer, and Dieter Fenske*

The synthesis of nanoclusters and colloids of II/VI compounds is of interest with regard to their size-dependent optical and electronic properties. If the radius of the particles exceeds the excitonic Bohr radius of the bulk material, a size-quantization effect occurs, and the band gap increases relative to that of the bulk material.[1,2,3] Measurements on cluster molecules of defined size could therefore lead to an exact interpretation of the observed effects. Dance et al. have already prepared a number of cadmium chalcogenide clusters.[4] Recently we synthesized the largest structurally characterized cadmium chalcogenide cluster $[Cd_{32}Se_{14}(SePh)_{36}(PPh_3)_4]$ by reaction of $[CdCl_2(PPh_3)_2]$ with $PhSeSiMe_3$ with elimination of chlorosilane.[5] This compound is isostructural with the sulfur derivatives characterized by Herron and Weller.[6,7] Further application of this synthetic principle led to the synthesis and structural characterization of the clusters **1** and **2** (Figures 1 and 2).[8]

$[Cd_{10}Se_4(SePh)_{12}(PPh_3)_4]$ **1**

$[Cd_{16}(SePh)_{32}(PPh_3)_2]$ **2**

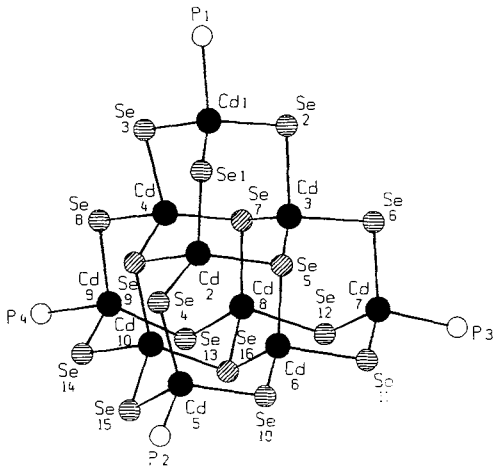

Figure 1. Molecular structure of **1**. The phenyl groups of the $SePh^-$ ligands (Se1–Se4, Se6, Se8, Se10–Se15 (●)) are omitted). Se5, Se7, Se9 and Se16 (◍) are Se^{2-} ligands.

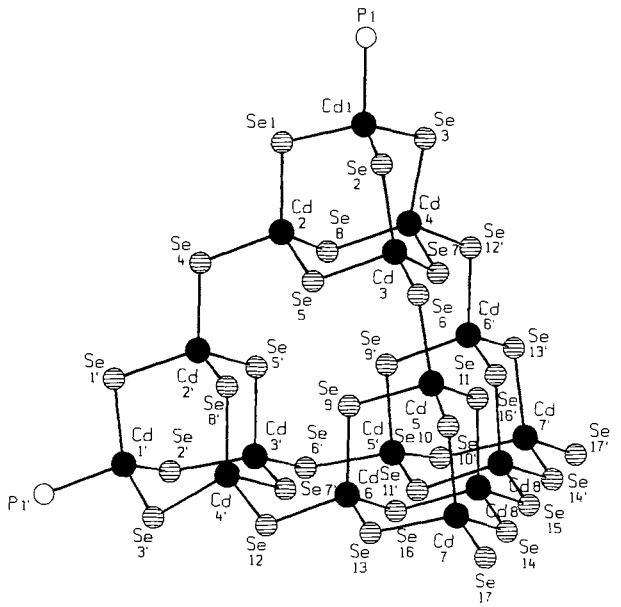

Figure 2. Molecular structure of **2** [12]. The phenyl groups of the $SePh^-$ ligands are omitted for clarity.

The reaction of $[CdCl_2(PPh_3)_2]$ with $PhSeSiMe_3$ in diethyl ether afforded colorless crystals of **1** [Eq. (a)], which crystal-

$$[CdCl_2(PPh_3)_2] \xrightarrow[Et_2O]{PhSeSiMe_3} [Cd_{10}Se_4(SePh)_{12}(PPh_3)_4] \quad \textbf{1} \qquad (a)$$

lizes in the triclinic space group $P\bar{1}$. The cluster core is composed of four fused adamantanoid cages. It is a section of the sphalerite structure, which is also found in CdSe.[9] The $[Cd_{10}Se_{16}P_4]$ cluster core forms a tetrahedron with an average edge length of 1.3 nm. The Cd atoms are coordinated in a distorted tetrahedral fashion by the Se atoms of the μ_2-$SePh^-$ (Se1–Se4, Se6, Se8, Se10–Se15) and μ_3-Se^{2-} ligands (Se5, Se7, Se9, Se16) and by the P atoms of the PPh_3 ligands [Se-Cd-Se 95.56(7)–130.23(7)°, Se-Cd-P 100.88(11)–115.70(12)°].

[*] Prof. Dr. D. Fenske, Dipl.-Chem. S. Behrens, Dipl.-Chem. M. Bettenhausen, Dr. A. Eichhöfer
Institut für Anorganische Chemie der Universität
Engesserstrasse, Geb.-Nr.30.45
D-76128 Karlsruhe (Germany)
Fax: Int. code + (721) 661-921
e-mail: behrens@achibm6.chemie.uni-karlsruhe.de

[**] We thank Dr. A. Deveson for correcting the English of this article. This work was supported by the Deutsche Forschungsgemeinschaft (SFB195) and the Bundesministerium für Bildung, Wissenschaft, Forschung und Technologie.

The Cd–Se bond lengths vary between 256.9(2) and 275.0(2) pm. In CdSe (zinc blende structure) the bond length is 262 pm.[7] Shorter distances [256.9(2)–261.3(2) pm] correspond to the bonds between the μ_3-Se^{2-} ligands and the Cd atoms. The four outer Cd atoms (Cd1, Cd5, Cd7, Cd9) are coordinated by the PPh_3 ligands. The structure is thus analogous to that of $[Cd_{10}Se_4(SePh)_{16}]^{4-}$, characterized by Dance et al.,[4] which contains terminal $SePh^-$ ligands in place of the PPh_3 ligands. Whereas this compound is a cluster anion, **1** is a neutral compound.

In diglyme $[CdCl_2(PPh_3)_2]$ reacts with $PhSeSiMe_3$ to give a colorless solution, from which colorless crystals of **2** are formed [Eq. (b)]. In contrast to **1**, the four adamantanoid

$$[CdCl_2(PPh_3)_2] \xrightarrow[\text{Diglyme}]{PhSeSiMe_3} \underset{\mathbf{2}}{[Cd_{16}(SePh)_{32}(PPh_3)_2]} \qquad \text{(b)}$$

$[Cd_4Se_6]$ cages of **2** are not directly fused together, but are linked by $SePh^-$ ligands to form a $[Cd_{16}Se_{30}]$ skeleton. The two phosphorus ligands (P1, P1′) are bound to Cd1 and Cd1′. In addition Cd7 and Cd7′ also form bonds to terminal $SePh^-$ ligands (Se17, Se17′). All Cd atoms have a distorted tetrahedral coordination geometry involving the Se atoms of the $SePh^-$ and the P atoms of the PPh_3 ligands [Se-Cd-Se 96.63(8)–122.83(6)°, Se-Cd-P 105.41(9)–106.62(9)°]. The Cd–Se bond lengths range between 249.4(3) and 279.6(4) pm.

Since the phenyl groups of the $SePh^-$ ligands all lie at the surface of the cluster, the center of the cluster contains a cavity of about 420 pm diameter. The space-filling model of **2** (Figure 3) shows that this cavity is completely shielded from

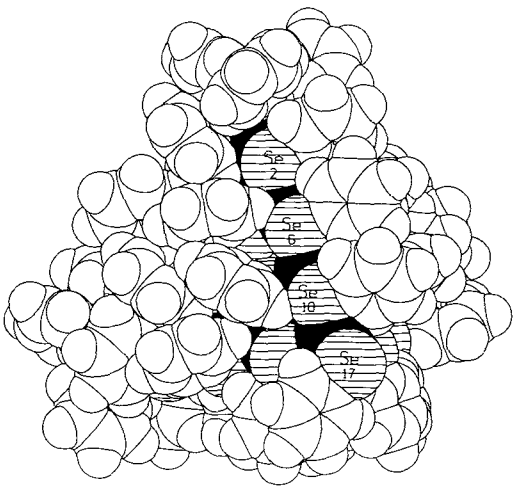

Figure 3. Space-filling model of **2**; the view corresponds to the orientation in Figure 2. Hydrogen atoms were generated by the program SCHAKAL92 [13].

the outside by the phenyl rings of the $SePh^-$ ligands. This cavity could be suitable for interstitial inclusion of other transition metal ions, but such experiments have not yet been successful. Elimination of twelve phenyl rings of the $SePh^-$ ligands and insertion of a further $[SeCd_4]$ tetrahedron into the cavity would lead to a $[Cd_{20}Se_{13}(SePh)_{20}(PPh_3)_2]^{6-}$ cluster consisting of ten fused adamantanoid cages. However, the formation of such a cluster might be unfavorable because of its high charge.

In **2** the $[Cd_{16}Se_{30}P_2]$ cluster forms a tetrahedron with an average edge length of 1.7 nm. This outer tetrahedron can be divided into four corner-sharing tetrahedra which contain the $[Cd_4Se_6]$ cages. Such corner-sharing tetrahedra also form the structural principle of nonmolecular compounds such as $Cd(SPh)_2$.[10] It is noteworthy that Dance et al. have already postulated the possible existence of a structurally analogous compound, namely, $[Cd_{16}(SPh)_{32}(dmf)_2]$, on the basis of ^{113}Cd and ^{13}C NMR data.[11]

The size-dependent optical absorption spectra of **1** and **2** are currently the subject of further investigations, and we are are extending the work presented here to the Hg/Te system. The reaction of $HgCl_2$ with $PtBu_3$ and $PhTeSiMe_3$ yields yellow crystals. Preliminary single crystal X-ray structure analysis indicates the formula $[Hg_{16}(TePh)_{32}(PtBu_3)_2]$, which is analogous to that of **2**.

Experimental Section

All steps were performed under a nitrogen atmosphere in absolute solvents.

1: $PhSeSiMe_3$ (0.96 mL, 3.8 mmol) was added to a suspension of $[CdCl_2(PPh_3)_2]$ (0.68 g, 0.96 mmol) in diethyl ether (50 mL). After a few hours colorless platelets of **1** and a yellow precipitate of unknown composition were obtained (yield 15%).

2: $PhSeSiMe_3$ (0.54 mL, 2.18 mmol) was added to a suspension of $[CdCl_2(PPh_3)_2]$ (0.77 g, 1.08 mmol) in diglyme (100 mL) to give a colorless solution, from which colorless needlelike crystals of **2** formed (yield 40%).

Received: July 14, 1997 [Z10679IE]
German version: *Angew. Chem.* **1997**, *109*, 2874–2876

Keywords: cadmium · clusters · nanostructures · selenium · structure elucidation

[1] C. J. Murphy, *J. Cluster Science* **1996**, *7*, 341.
[2] C. B. Murray, D. J. Norris, M. G. Bawendi, *J. Am. Chem. Soc.* **1993**, *115*, 8706.
[3] H. Weller, *Angew. Chem.* **1993**, *105*, 43; *Angew. Chem. Int. Ed. Engl.* **1993**, *32*, 41.
[4] I. G. Dance, K. Fisher in *Progress in Inorganic Chemistry*, vol. 41, (Ed.: K. D. Karlin), **1994**.
[5] S. Behrens, M. Bettenhausen, A. C. Deveson, A. Eichhöfer, D. Fenske, A. Lohde, U. Woggon, *Angew. Chem.* **1996**, *108*, 2361; *Angew. Chem. Int. Ed. Engl.* **1996**, *35*, 2215.
[6] N. Herron, J. C. Calabrese, W. E. Farneth, Y. Wang, *Science* **1993**, *259*, 1426.
[7] T. Vossmeier, G. Reck, B. Schulz, L. Katsikas, H. Weller, *J. Am. Chem. Soc.* **1995**, *117*, 12881.
[8] Crystal structure analysis data: STOE IPDS diffractometer with and without Siemens rotating anode, $Mo_{K\alpha}$, 200 K.
1: $a = 1940.4(6)$, $b = 2053.9(4)$, $c = 2327.1(6)$ pm, $\alpha = 75.42(2)$, $\beta = 65.63(2)$, $\gamma = 76.40(2)°$, $V = 8085(4) \times 10^6$ pm^3; space group $P\bar{1}$ (no. 2), $Z = 2$, $\mu(Mo_{K\alpha}) = 4.973$ mm^{-1}, $2\theta_{max} = 45°$; 35357 reflections measured, of which 19957 were independent, and 13395 observed with $I > 2\sigma(I)$, 867 parameters (Cd, Se, P anisotropically and C isotropically refined). Atomic coordinates for H atoms were calculated with an idealized geometry.), $R_1 = 0.0793$, $wR_2 = 0.2005$, max. residual electron density 1.502 e Å^{-3}. One solvent molecule (diethyl ether) was refined per asymmetric unit.
2: $a = 3009.5(6)$, $b = 3359.8$ (7), $c = 3151.5(6)$ pm, $\beta = 114.48(3)°$, $V = 29001(10) \times 10^6$ pm^3; space group *I2/a* (no. 15), $Z = 4$, $\mu(Mo_{K\alpha}) = 5.213$ mm^{-1}, $2\theta_{max} = 45°$; 41006 reflections measured, of which 18494 were independent, and 12239 observed with $I > 2\sigma(I)$, 520 parameters (Cd, Se, P anisotropically and C isotropically refined; phenyl rings defined as rigid groups.), $R_1 = 0.0773$, $wR_2 = 0.2310$, max. residual electron density 2.465 e Å^{-3}. Se4, Se14, Se15, and some of the phenyl groups are disordered over two sites. Refinement in *Ia* and *I2* did not lead to any improvement in terms of this disorder. Other crystals also showed this disorder. Crystallographic data (excluding structure factors) for the structures reported in this paper have been deposited with the Cambridge Crystallographic Data Center as supplementary publication no. CCDC-100535. Copies of the data can be obtained free of charge on application to The Director, CCDC, 12 Union Road, Cambridge CB2 1EZ, UK (fax: int. code + (1223) 336-033; e-mail: deposit@chemcrys.cam.ac.uk).

 © WILEY-VCH Verlag GmbH, D-69451 Weinheim, 1997 0570-0833/97/3624-2798 $ 17.50+.50/0

[9] V. M. Goldschmidt in *Geochemische Verteilungsgesetze der Elemente, Bd. 8, Untersuchungen über Bau und Eigenschaften von Krystallen* (Ed.: J. Dybwad), Oslo, **1927**.
[10] D. Craig, I. G. Dance, R. Garbutt, *Angew. Chem.* **1986**, *98*, 178; *Angew. Chem. Int. Ed. Engl.* **1986**, *25*,165; I. G. Dance, R. G. Garbutt, D. C. Craig, M. L. Scudder, *Inorg. Chem.* **1887**, *26*, 4057.
[11] I. G. Dance, R. G. Garbutt, T. D. Bailey, *Inorg. Chem.* **1990**, *29*, 603.
[12] Se4, Se14, Se14', and Se15 are disordered over two sites. For reasons of clarity only the coordinates of the center of gravity are shown.
[13] E. Keller, *SCHAKAL-A FORTRAN Program for Graphical Representation of Molecular and Crystallographic Models*, Universität Freiburg, **1992**.

Structural Evolution from the Solid State to the Molecule for BaI_2: Synthesis and Crystal Structures of $[BaI_2(\mu_2\text{-}OH_2)_2]_{3/\infty}$, $[BaI_2(\mu_2\text{-}OH_2)(OC_3H_6)]_{2/\infty}$, $[BaI_2(thf)_3]_{1/\infty}$, and $[BaI_2(thf)_5]\cdot THF$ **

Katharina M. Fromm*

For chemists in all disciplines it is becoming more and more important to study and understand the region between infinite, extended structures and molecules, and this area of research has become more significant in the last few years. However, surprisingly few results have been obtained for relatively simple binary compounds such as the alkaline and alkaline earth metal halides,[1] which can in part be attributed to the difficult handling of such products. We here report herein on the synthesis of a series of donor ligand stabilized structural units that can be derived from the solid-state structure of BaI_2.

Barium iodide dissolves better than most other alkaline and alkaline earth metal halides in organic N- and O-donor solvents. In most cases yellow solutions are obtained, which indicate that the solid state structure has decomposed. Solvation with water, acetone, and THF gave rise to different BaI_2 adducts, which were isolated and characterized. The structural features of these adducts can be derived from the solid-state structure of BaI_2. On the one hand, these adducts are structurally related, and on the other hand, they build up different aggregations such as three-dimensional nets, two-dimensional layers, one-dimensional strands, or even molecular species. On solvation with water, the compounds **1** and, with additional acetone, **2** can be isolated. Compounds **3** and **4** crystallize from THF.

$[BaI_2(\mu_2\text{-}OH_2)_2]_{3/\infty}$ **1**

$[BaI_2(\mu_2\text{-}OH_2)(OC_3H_6)]_{2/\infty}$ **2**

$[BaI_2(thf)_3]_{1/\infty}$ **3**

$[BaI_2(thf)_5]\cdot THF$ **4**

[*] Dr. K. M. Fromm
Institut für Anorganische Chemie der Universität Karlsruhe
Engesserstrasse, Geb. Nr. 30.45
D-76128 Karlsruhe (Germany)
Fax: Int. code + (721) 608-2718
e-mail: fromm@achibm6.chemie.uni-karlsruhe.de

[**] K. M. F. thanks Prof. Dr. D. Fenske and Prof. Dr. J. Strähle for their friendly support. This work was supported by the Deutsche Forschungsgemeinschaft.

Anhydrous, white barium iodide crystallises, as does $BaCl_2$ and $BaBr_2$, in the $PbCl_2$ structure type (Figure 1).[2] The barium center is surrounded by six iodine atoms in the form of a distorted trigonal prism. The rectangular faces of the prism

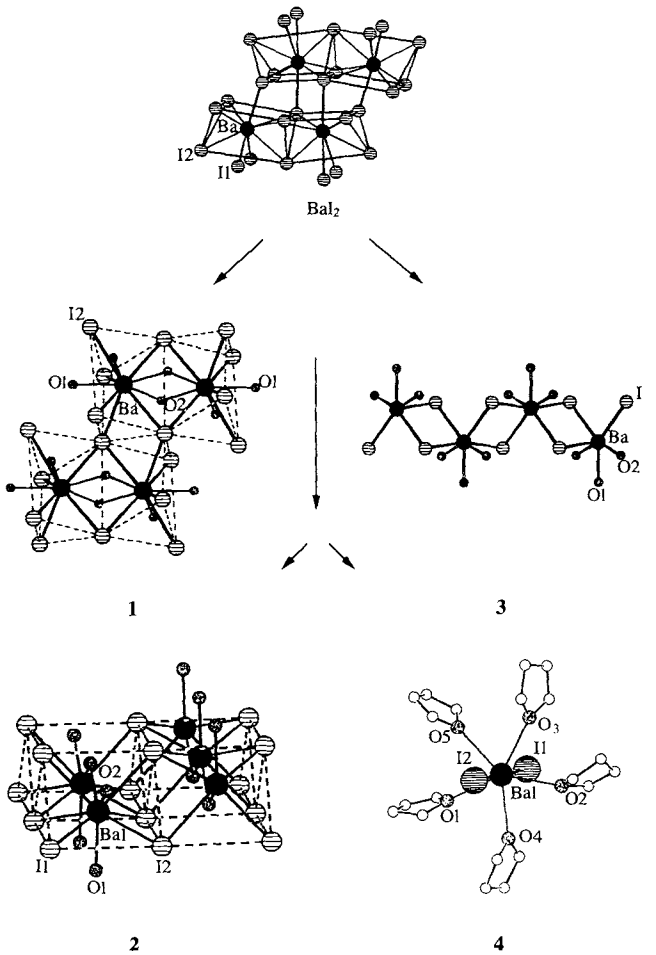

Figure 1. Sections of the crystal structures of BaI_2, **1**, **2**, and **3**, and the molecular structure of **4**. Important bond lengths [Å] and angles [°]: **1**: Ba–I 3.596, 3.715, 3.718; Ba–O 2.833, 2.894; Ba-O-Ba 104.95; **2**: Ba–O1 2.671; Ba–O2 2.868; Ba–I1 3.589, 3.635; Ba–I2 3.606, 3.667; Ba-I1-Ba 84.13, 105.12; Ba-I2-Ba 83.66, 104.12; Ba-O2-Ba 113.98; **3**: Ba–O1 2.757; Ba–O2 2.717; Ba–I 3.457, 3.524; O1-Ba-O2 70.05; Ba-I-Ba 97.28; **4**: Ba–I1 3.383; Ba–I2 3.375; Ba–O 2.696-2.738; O-Ba-O 70.87-74.30; I1-Ba-I2 178.61, I-Ba-O 86.10-93.12

are capped by three additional halide atoms. These three iodine atoms lie approximately in the same plane as the barium atom, which leads to approximate D_{3h} symmetry. The distortion of the structure is clearly evident from the different Ba–I bond lengths, which can be divided into seven shorter (3.38–3.63 Å) and two longer bonds (4.10 Å); the coordination number for iodine is four and five, respectively. BaI_2 is not air stable but reacts hygroscopically with water. This solvation process affords compound **1**, which can be isolated and structurally characterized.[3]

Compound **1** forms a three-dimensional structure that contains a structural unit of BaI_2, namely a trigonal prism of I atoms (Figure 1). The barium-centered prisms of I atoms share common edges, and two of the rectangular faces are each bridged by two μ_2-oxygen atoms. Since the third rectangular face is not bridged by oxygen atoms, cavities

 © WILEY-VCH Verlag GmbH, D-69451 Weinheim, 1997 0570-0833/97/3624-2799 $ 17.50+.50/0

Table 1. Important structural parameters for compounds **1**–**4** [a].

	BaI_2	**1**	**2**	**3**	**4**
dimensionality	3	3	2	1	0
CN for I	4, 5	3	3	2	1
CN for Ba	9	10	9	7	7
Ba–I	3.38–3.63, 4.10	3.5960–3.7182	3.5895–3.6671	3.4565, 3.5241	3.374, 3.3822
Ba–O	-	2.833–2.894	2.671, 2.868	2.717, 2.757	2.696–2.741

[a] Distances in [Å]; CN = coordination number.

occur here in the structure. The coordination number of barium increases from nine in BaI_2 to ten in **1**, whereas the coordination number for iodine decreases to three.

Compound **2**[4] is obtained in the form of pale yellow crystals from a solution of BaI_2 in acetone. The target compound **2** can be prepared by two synthetic pathways, one starting from **1** and absolute acetone, the other from dried BaI_2 and technical grade acetone. Compound **2** forms a two-dimensional layered structure that is unique for alkaline earth metal halides (Figure 1). As in the three-dimensional grid of BaI_2 and **1**, **2** also contains a trigonal prism of I atoms. The Ba-centered I prisms are condensed through two edges of the triangular faces as well as perpendicular to these through two parallel edges of one rectangular face to form a two-dimensional layered structure. In the direction of the rectangular faces, the barium centers are additionally linked through μ_2-bridging water molecules. The structure growth into the third dimension is inhibited by terminally bound acetone molecules. The Ba–I distances (3.5895(7)–3.6672(9) Å) are in the range found for the shorter Ba–I bonds in BaI_2. The coordination number for the barium atom remains the same as in BaI_2, whereas the I atoms act as μ_3-bridging ligands.

The Ba–O(H_2O) distances in **1** and **2** are 2.833–2.894 Å and 2.868 Å, respectively, and thereby shorter than those in comparable structures (2.948 Å in $[Ba(ClO_4)_2(OH_2)(py)]$ and 2.918 Å in $\{[(phen)_2BaCl(OH_2)_2(\mu\text{-}OH_2)_2(H_2O)_2ClBa(phen)_2]Cl_2 \cdot phen \cdot 4H_2O\}$[5]).

Compound **3** has a one-dimensional structure in which the barium atoms are each bridged by two μ_2-I atoms, leading to the formation of strands. The Ba_2I_2 rhombs are inclined by 74.35° toward each other and can be derived from compounds **1** and **2**; two Ba centers are bridged by two I atoms that belong to the triangular faces of the prisms. As in the solid-state structure of $[BaI_2]_\infty$, the Ba_2I_2 rings in **3** are arranged *cisoid* to the Ba center. The coordination sphere around the alkaline earth metal cation in **3** is completed by three terminally bound THF molecules. Thus, the barium center achieves a coordination number of seven and C_{2v} symmetry; the three O atoms and two of the I ligands occupy approximate equatorial positions and the other two I atoms occupy axial positions of a distorted pentagonal bipyramid.

$[BaI_2(bpy)_2]_{1/\infty}$(bpy = bipyridine) exhibits a similar one-dimensional infinite structure,[7] which is also based on Ba-vertex-linked Ba_2I_2 rhombs. The Ba–I distances in $[BaI_2(bpy)_2]_{1/\infty}$ and **3** are similar. In comparison to **3**, three THF donor molecules have formally been replaced by two bidentate N-donor ligands. Owing to the chelating effect $[BaI_2(bpy)_2]_{1/\infty}$ is thermodynamically more stable than **3**, and can easily be handled at room temperature, whereas **3** decomposes under elimination of THF molecules.

In addition to the three- (**1**), two- (**2**), and one-dimensional compounds (**3**), the zero-dimensional THF adduct **4**[8] was isolated and structurally characterized, thus completing the set of compounds based on BaI_2. In compound **4** molecular BaI_2 is stabilized by five THF molecules (Figure 1). The barium center is nearly linearly surrounded by two halide atoms, whereas in the gas phase free molecular BaI_2 has an I-Ba-I angle of between 102° and 105°.[9] The THF donor ligands complete the coordination sphere to form a pentagonal bipyramid; they occupy the equatorial positions. The coordination number for barium is seven and that for iodine is one.

These results reveal that the coordination number of iodine is influenced by the kind and number of O-donor ligands. Thus, the transition from the BaI_2 solid-state structure to **1** and **2** is accompanied by a decrease in the coordination number for iodine from four and five in BaI_2 to three in **1** and **2**, respectively. The distortion of the trigonal prisms disappears in **1** and **2**. Aggregation of the solid-state structure of $[BaI_2]_\infty$ seems to be stopped by breaking the longest Ba–I bonds. Formally, the iodine atoms capping the prism are replaced by O-donor ligands. The bridging to give a three-dimensional structure is suppressed in **2** and layers are formed by terminally bound O-donor molecules. The coordination number is three for all halogen atoms. The loss of a further dimension (as for **3**) results in a coordination number of two for all halogen atoms, and thus one-dimensional strands are observed. The series is completed by compound **4** with a zero-dimensional structure—molecular BaI_2 stabilized by donor ligands. In particular the Ba–I distances become shorter as the dimensionality decreases (Table 1), thus supporting the covalent character of the Ba–I bond.

In summary we have clearly shown the similarities of compounds **1**–**4** with the solid-state structure of BaI_2. Thus, a "genealogy tree" can be elaborated in which the influence of the number and size of donor ligands is given. The aim of future investigations will be to find out if this behavior can be extended to other ligand systems as well as other alkaline and alkaline earth metal compounds. Furthermore, studies are also required to determine whether the compounds can be combined to produce new structures.

Experimental Section

1: Anhydrous barium iodide reacted in air with water to yield colorless crystals of **1**.

2: $BaI_2(\mu_2\text{-}OH_2)_2$ (0.5 g, 1.17 mmol) was dissolved in dried and freshly distilled acetone (30 mL). After 48 h at −30 °C, pale yellow cubic crystals of **2** were isolated from the yellow solution. The crystals decomposed above −10 °C, and on contact with air they quickly lost solvent molecules.

Another synthetic pathway involved the use of dry BaI_2 with technical acetone. The desired product was isolated from this solution at −30 °C.

3: BaI_2 (0.5 g,1.28 mmol) (dried in high vacuum at 500 °C) was dissolved under nitrogen in dried and freshly distilled THF (50 mL). The yellow solution was concentrated to half the volume and layered with diethyl ether (10 mL). Pale yellow blocks of **3** crystallized at −30 °C. The compound is sensitive to air and reacts at room temperature under elimination of solvent molecules.

4: BaI_2 (0.4 g, 1 mmol; dried (see **3**)) was dissolved with heating in dried and freshly distilled THF (30 mL) under nitrogen. Pale yellow rhombs of **4** resulted after the solution was kept at −30 °C. The compound decomposed rapidly above this temperature.

Received: May 6, 1997
Revised version: July 25, 1997 [Z10417IE]
German version: *Angew. Chem.* **1997**, *109*, 2876–2878

 © WILEY-VCH Verlag GmbH, D-69451 Weinheim, 1997 0570-0833/97/3624-2800 $ 17.50+.50/0

Keywords: barium · ligand effects · polymers · solid-state structures · solvent effects

[1] a) T. P. Hanusa, *Polyhedron* **1990**, *9*, 11, 1345; b) D. Seebach, *Angew. Chem.* **1988**, *100*, 1685; *Angew. Chem. Int. Ed. Engl.* **1988**, *27*, 1624; c) C. Schade, P. von R. Schleyer, *Adv. Organomet. Chem.* **1987**, *27*, 169; d) S. Pohl, M. Peters, D. Haase, W. Saak, *Z. Naturforsch. B* **1992**, *47*, 741; e) W. S. Sheldrick, J. Kiefer, *ibid.* **1992**, *47*, 1079; f) K. Hyvärinen, M. Klinga, M. Leskelä, *Polyhedron* **1996**, *15*, 13, 2171; g) M. Driess, G. Huttner, N. Knopf, H. Pritzkow, L. Zsolnai, *Angew. Chem* **1995**, *107*, 354; *Angew. Chem. Int. Ed. Engl.* **1995**, *34*, 316; h) D. Hoffmann, A. Dorigo, P. von R. Schleyer, H. Reif, D. Stalke, W. S. Sheldrick, E. Weiss, M. Geissler, *Inorg. Chem.* **1995**, *34*, 262; i) H. Nöth, H. Sachdev, M. Schmidt, H. Schwenk, *Chem. Ber.* **1995**, *128*, 105; j) C. L. Raston, B. W. Skelton, C. R. Whitaker, A. H. White, *Aust. J. Chem.* **1988**, 41, 341 and 1925, and references therein; k) A. Simon, *Z. Anorg. Allg. Chem.* **1973**, *301*, 395; l) K. F. Tesh, D. J. Burkey, T. P. Hanusa, *J. Am. Chem. Soc.* **1994**, *116*, 2409; m) Y. H. Kim, J. Calabrese, C. McEwen, *ibid.* **1996**, *118*, 1545.

[2] E. B. Brackett, T. E Brackett, R. L. Sass, *J. Phys. Chem.* **1963**, *67*, 2132-2135.

[3] Crystal structure of **1**: $[BaI_2(\mu_2\text{-}OH_2)_2]_{3/\infty}$, $M_r = 427.17\ g\,mol^{-1}$, monoclinic, space group $C2/c$, $a = 11.042(2)$, $b = 7.574(2)$, $c = 8.622(2)$ Å, $\beta = 113.17(2)°$, $V = 662.9(3)$ Å^3, $Z = 4$, $\rho_{calcd} = 4.280\ Mg\,m^{-3}$, $F(000) = 728$, $\lambda(Mo_{K\alpha}) = 0.71069$ Å, $\mu = 14.292\ mm^{-1}$, 1921 reflections of which 800 are independent and 788 observed ($I > 2\sigma I$), 33 parameters, GooF = 1.272, $R1 = 0.0352$, $wR2 = 0.0866$ (against $|F^2|$), Ψ scan. The data for **1** were collected on a STOE four-circle diffractometer at $-70\,°C$ under a nitrogen atmosphere. The structure was solved by direct methods with the program SHELXS86 [10] and was refined anisotropically with SHELXL93 [11]. The H atoms of the water molecules were calculated on idealized positions [8b].

[4] Crystal structure of **2**: $[BaI_2(\mu_2)(OC_3H_6)]_{1/\infty}$, $M_r = 467.22\ g\,mol^{-1}$, orthorhombic, space group $Pnnm$, $a = 9.844(2)$, $b = 20.890(4)$, $c = 4.8100(10)$ Å, $V = 989.1$ Å^3, $Z = 4$, $\rho_{calcd} = 3.083\ Mg\,m^{-3}$, $F(000) = 784$, $\lambda(Mo_{K\alpha}) = 0.71069$ Å, $\mu = 9.981\ mm^{-1}$, 2608 reflections of which 1326 are independent and 1016 observed ($I > 2\sigma I$), 45 parameters, GooF = 1.137, $R1 = 0.0319$, $wR2 = 0.0759$ (against $|F^2|$), Ψ scan. The data for **2** were collected on an Enraf Nonius CAD4 diffractometer at $-70\,°C$ under a nitrogen atmosphere. The structure was solved by direct methods with the program SHELXS86 [10] and refined anisotropically with SHELXL93 [11]. The methyl group of acetone was disordered and the corresponding C atom was only refined isotropically. Thus, the H atoms were neither found nor calculated [8b].

[5] a) D. L. Kepert, A. F. Waters, A. H. White, *Aust. J. Chem.* **1996**, *49*, 117; b) D. L. Kepert, B. W. Skelton, A. F. Waters, A. H. White, *ibid.* **1996**, *49*, 47

[6] Crystal structure of **3**: $[BaI_2(thf)_3]_{1/\infty}$, $M_r = 607.45\ g\,mol^{-1}$, monoclinic, space group $C2/c$, $a = 13.451(3)$, $b = 15.603(3)$, $c = 9.426(2)$ Å, $\beta = 106.38(3)$, $V = 1897.9(7)$ Å^3, $Z = 4$, $\rho_{calcd} = 2.098\ Mg\,m^{-3}$, $F(000) = 1096$, $\mu(Mo_{K\alpha}) = 0.71069$ Å, $\mu = 5.030\ mm^{-1}$, 2228 reflections of which 2079 are independent and 2001 are observed ($I > 2\sigma I$), 110 parameters, GooF = 1.061, $R1 = 0.0840$, $wR2 = 0.2494$ (against $|F^2|$). The data for **3** were collected on an Enraf Nonius four-circle diffractometer under a nitrogen atmosphere at $-70\,°C$. The structure was solved by direct methods with the program SHELXS86 [10] and refined with SHELXL93 [11]. One THF molecule was disordered, and split positions were refined for the C atoms. They were described isotropically, the corresponding H atoms were not refined. The positions of the H atoms in the other THF molecule were calculated. This together with the slight dissociation of the crystal during data collection are the reasons for the rather high $R1$ value [8b].

[7] B. W. Skelton, A. F. Waters, A. H. White, *Aust. J. Chem.* **1996**, *49*, 99.

[8] a) Crystal structure of **4**: $[BaI_2(thf)_5][THF]$, $M_r = 1675.61\ g\,mol^{-1}$, monoclinic, space group $P2_1/c$, $a = 9.469(3)$, $b = 13.323(2)$, $c = 27.664(4)$ Å, $\beta = 92.04(2)°$, $V = 3487.8(13)$ Å^3, $Z = 2$, $\rho_{calcd} = 1.515\ Mg\,m^3$, $F(000) = 1528$, $\lambda(Mo_{K\alpha}) = 0.71069$ Å, $\mu = 2.934\ mm^{-1}$, 7118 reflections of which 6119 are independent and 6101 observed ($I > 2\sigma I$), 259 parameters, GooF = 1.189, $R1 = 0.0585$, $wR2 = 0.1307$ (against $|F^2|$), Ψ scan. The data for **4** were collected on a STOE four-circle diffractometer at $-70\,°C$ under a nitrogen atmosphere. The structure was solved by direct methods with the program SHELXS86 [10] and refined with SHELXL93 [11]. The positions of H atoms of the THF molecules were calculated. Two free THF molecules in the asymmetric unit were disordered and the atoms were refined on positions with occupation factors of 1/2. b) Further details of the crystal structure investigations may be obtained from the Fachinformationszentrum Karlsruhe, D-76344 Eggenstein-Leopoldshafen (Germany), on quoting the depository numbers CSD-407360 (**1**), CSD-380094 (**2**), CSD-404952 (**3**), and CSD-407359 (**4**).

[9] R. J. Gillespie, E. A. Robinson, *Angew. Chem.* **1996**, *108*, 539; *Angew. Chem. Int. Ed. Engl.* **1996**, *35*, 477.

[10] G. M. Sheldrick, *Acta Crystallogr. Sect. A* **1990**, *46*, 467.

[11] G. M. Sheldrick, *J. Appl. Crystallogr.*, in press.

Rate Enhancement of the Pauson–Khand Reaction by Primary Amines**

Takumichi Sugihara,* Mamiko Yamada, Hitoshi Ban, Masahiko Yamaguchi,* and Chikara Kaneko

The Pauson–Khand reaction is one of the most powerful methods for constructing cyclopentenones[1,2] and has been widely utilized for the synthesis of a variety of natural products.[3] "Hard" ligands, which usually contain an N or O atom, in metal-carbonyl complexes labilize the CO ligands and therefore facilitate the ligand substitution reaction.[4,5] If the "hard" ligands react with $Co_2(CO)_6$(alkyne) complexes in the presence of olefins, the substitution of CO ligands by the olefins might be facilitated. Since the coordinated alkyne is also made reactive by the labilizing effect of the "hard" ligands, the Pauson–Khand reaction might be promoted.[6] To confirm our hypothesis, we first investigated the use of "hard" ligands as solvents to study their effect on the Pauson–Khand reaction. The results are shown in Table 1. In the aprotic solvents usually used in the Pauson–Khand reaction, the desired cyclization did not proceed at 35°C even after three days (Nos. 1–4). Complex **1a** was also recovered almost quantitatively when ethanol or triethylamine, either of which might act as "hard" ligands, was used as solvent (No. 5 and 6). However, whereas the cyclization proceeded slowly in diethylamine (No. 7), it was complete within 5 min in cyclohexylamine to give **2a** in good yield (No. 10).[7,8] Comparison

Table 1. The Pauson–Khand reaction of **1a** in different solvents[a].

No.	Solvent	$CyNH_2$ [equiv][b]	T [°C]	t	Yield[%] **2a**	Yield[%] **1a**
1	*n*-hexane	–	35	3d	–	99
2	toluene	–	35	3d	–	98
3	1,2-dichloroethane	–	35	3d	–	99
4	1,4-dioxane	–	25	4d	–	98
5	EtOH	–	35	3d	–	99
6	Et_3N	–	35	3d	–	99
7	Et_2NH	–	35	3d	46[c]	23
8	$nPrNH_2$	–	35	5 min	52[c]	–
9	$iPrNH_2$	–	35	5 min	68[c]	–
10	$CyNH_2$[b]	–	35	5 min	72[c]	–
11	$tBuNH_2$	–	35	3d	54[c]	15
12	1,2-dichloroethane	10	25	10d	46[d]	13
13	1,2-dichloroethane	6	83	5 min	99	–
14	1,2-dichloroethane	3.5	83	5 min	99	–
15	1,2-dichloroethane	3	83	15 min	99	–
16	1,2-dichloroethane	1	83	90 min	94	–
17	1,2-dichloroethane	0	83	10 h	62[c]	–

[a] All reactions were carried out in 0.2 M solution under argon atmosphere. [b] Cy = cyclohexyl. [c] Unidentified polar by-products were also formed. [d] 1-phenyl-6-hepten-1-yne (**3a**) was also formed in 26% yield.

[*] Dr. T. Sugihara, Prof. Dr. M. Yamaguchi, M. Yamada, H. Ban, Prof. Dr. C. Kaneko
Faculty of Pharmaceutical Sciences, Tohoku University
Aobayama, Sendai 980-77 (Japan)
Fax: Int. code + (22)217-6811
e-mail: taku@mail.pharm.tohoku.ac.jp

[**] This work was supported in part by an Inoue Research Award for the Young Scientist and by grants from the Japan Society of Promotion of Science (Research for the Future Program) and the Ministry of Education, Science, Sports, and Culture, Japan (No. 08404050 and 09771890). T.S. gratefully thanks Dr. Christophe Coperét at the Scripps Research Institute, CA (USA), for his advice during the preparation of this manuscript.

 © WILEY-VCH Verlag GmbH, D-69451 Weinheim, 1997 0570-0833/97/3624-2801 $ 17.50+.50/0

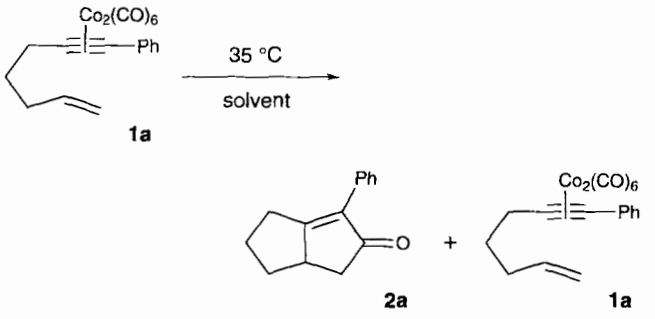

of Nos. 6–11 shows that the use of primary amines as solvents dramatically enhanced the rate of the reaction. The alkyl group on the primary amines also has a great influence on the course of the reaction. The moderately hindered primary amines, such as the ones containing secondary alkyl groups, seem to promote the Pauson–Khand reaction most effectively. The yield of **2a** reduced when an amine with a primary alkyl group was employed (No. 8). The tertiary alkyl substituted amine retarded the reaction (No. 11).

Since cyclohexylamine seemed to be the best promoter for the Pauson–Khand reaction, we varied the amount used to optimize the conditions. The results are also shown in Table 1. When the reaction of **1a** was carried out with 10 equivalents of the amine in 1,2-dichloroethane at 25°C, the desired cyclization was slow and decomplexation reduced the yield of **2a** (No. 12). In contrast, the cyclized product **2a** was produced in quantitative yield at 83°C (No. 13). No. 12–17 shows that more than three equivalents of the amine and the higher reaction temperature were both necessary to perform the desired cyclization in a short time as well as in quantitative yield. Various solvents were examined, such as *n*-hexane, toluene, 1,2-dimethoxyethane, THF, 1,4-dioxane, 2-propanol, acetonitrile, and *N*,*N*-dimethylformamide, but so far 1,2-dichloroethane remains the best solvent to obtain clean reactions and quantitative yields in this reaction system. The present conditions are a new and convenient method to promote the Pauson–Khand reaction without using oxidants.

Since primary amines were effective as promoter, we felt that ammonia should not be an exception. When **1a** was dissolved in 1,4-dioxane that was saturated with ammonia gas at 0°C and stirred in a sealed tube at 30°C for 4.5 days, the desired **2a** was produced along with **3a**. Since the use of a

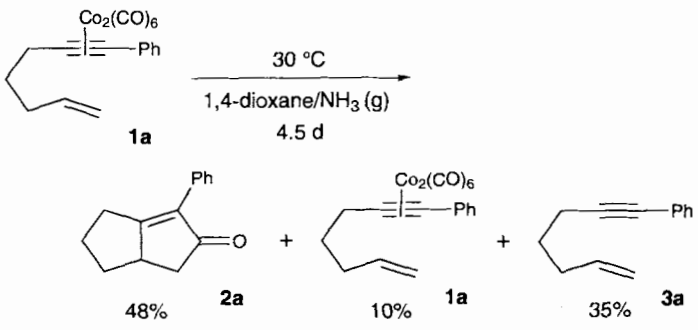

sealed tube is not convenient especially on a large scale, we decided to use a biphasic system[9] in which an aqueous solution of ammonium hydroxide would be the source of ammonia. The results under different conditions are summarized in Table 2. When 16M aqueous solution of ammonium hydroxide was used as cosolvent, the cyclization proceeded

Table 2. The Pauson–Khand reaction of **1a** in a biphasic system under different conditions[a].

No.	Aqueous solvent	T[°C]	t	Yield[%] **2a**	**1a**	**3a**
1	16M NH_4OH	25	2 d	72	–	25
2	H_2O	25	4 d	–	97	–
3	H_2O	100	30 min	–	91	–
4	16M NH_4OH	70	15 min	83	–	16
5	16M NH_4OH	100	15 min	95	–	4
6	4M NH_4OH	100	15 min	91	–	9
7	2M NH_4OH	100	15 min	93	–	7
8	1M NH_4OH	100	45 min	96	–	–
9	5M NaOH	100	15 min	38[b]	–	–
10	4.7M NH_4Cl	100	15 min	22	62	–

[a] All reactions were carried out in 0.1M solution of 1,4-dioxane/aqueous solvent (1:3 v/v). [b] Unidentified polar by-products were also formed.

even at 25°C (No. 1), although the enyne **3a** released from the complex was also produced. Comparison of No. 1 with the reaction of **1a** with gaseous ammonia in 1,4-dioxane suggests that water also affects the course of the reaction. Water itself, however, is not an effective promoter, since the reaction did not occur even at 100°C (No. 2 and 3). Moreover, higher temperatures favor cyclization over decomplexation (No. 1, 4, and 5). Even less concentrated solutions of ammonium hydroxide promoted the cyclization reaction (No. 6 and 7)

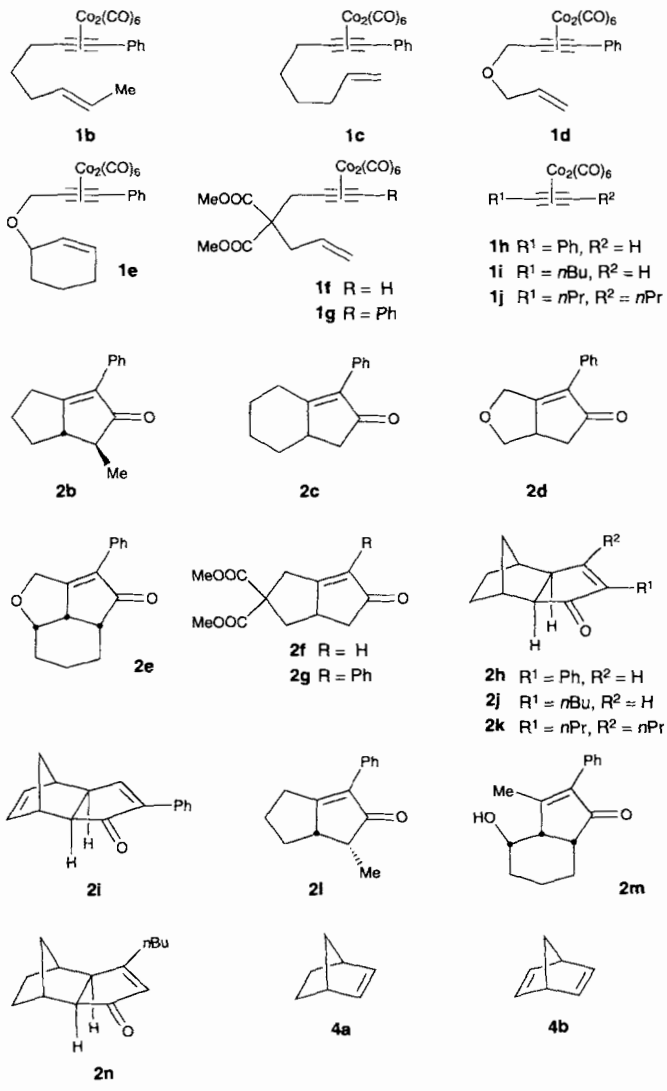

 © WILEY-VCH Verlag GmbH, D-69451 Weinheim, 1997 0570-0833/97/3624-2802 $ 17.50+.50/0

until a threshold dilution of about 1M at which the reaction slowed down (No. 8). Moderate concentrations of ammonium hydroxide are apparently important. In addition, when an aqueous solution of sodium hydroxide was used instead of ammonium hydroxide, the desired cyclization did not proceed cleanly but afforded a complex reaction mixture (No. 9). Furthermore, aqueous ammonium chloride slowed down the reaction (No. 10). Therefore, neither hydroxide anions nor ammonium cations but ammonia itself is essential to enhance the rate of the Pauson–Khand reaction in this biphasic system. It is worth pointing out that aqueous ammonium hydroxide is the cheapest and the most convenient promoter for the Pauson–Khand reaction and that a simple extraction workup gave the spectroscopically pure samples of the product in the present system.[10] To our knowledge, this method is the first report of the Pauson–Khand type cyclization[1,2,11] in the presence of water.[12]

Two sets of conditions to promote the Pauson–Khand reaction, namely, 3.5 equivalents of cyclohexylamine in 1,2-dichloroethane at 83°C (conditions A) and a 1:3 mixture (v/v) of 1,4-dioxane and 2M aqueous solution of ammonium hydroxide at 100°C (conditions B), were applied to various substrates. The results are summarized in Table 3. In all cases the reaction was complete in short times and afforded the desired cyclopentenones in good yield. The two methods gave comparable results in terms of the rates and yields.

Table 3. The Pauson–Khand reaction of **1b–j** under different conditions

No.	Starting material 1	4	Product 2	Conditions A [a] t[min]	Yield[%]	Conditions B [b] t[min]	Yield[%]
1	**b**		**b**	10	89[c]	30	92
2	**c**		**c**	30	90[d]	30	90
3	**d**		**d**	10	60	10	78
4	**e**		**e**	30	71[e]	45	75[f]
5	**f**		**f**	10	62	30	67
6	**g**		**g**	20	89	30	90
7	**h**	**a**[g]	**h**	10	98[h]	10	100[h]
8	**h**	**b**[g]	**i**	10	83[h]	30	50[h,i]
9	**i**	**a**[g]	**j**	15	94[h]	10	92[j]
10	**j**	**a**[g]	**k**	10	45[h]	135	42[h]

[a] Reactions were carried out in 0.2M solution of 1,2-dichloroethane at 83°C in the presence of 3.5 equiv of cyclohexylamine under argon atmosphere. [b] Reactions were carried out in 0.1M solution of 1,4-dioxane/2M aqueous solution of NH_4OH (1:3 v/v) at 100°C under argon atmosphere. [c] Cyclopentenones **2c** and **2l** were also produced in 5% and 5% yield, respectively. [d] Cyclopentenones **2b** and **2l** were also produced in 5% and 2% yield, respectively. [e] Cyclopentenone **2m** was also produced in 14% yield. [f] Cyclopentenones **2m** was also produced in 12% yield. [g] A 1.5 equiv of **4a** or **4b** was used. [h] No regio- or stereoisomer was detected. [i] The reaction of **1h** with **4b** (10 equiv) for 30 min under conditions B gave **2i** in 91% yield. [j] Cyclopentenone **2n** was also produced in 4% yield.

In conclusion, convenient and economical promoters for the Pauson–Khand reaction have been developed. We are now trying to clarify the reaction mechanism and studying the reaction of the $Co_2(CO)_6$(alkyne) complexes with primary amines in more detail.

Experimental Section

For conditions A: Synthesis of **2a**: Under an argon atmosphere, a solution of **1a** (456 mg, 1.00 mmol) and cyclohexylamine (0.395 mL, 3.49 mmol) in 1,2-dichloroethane (5 mL) was stirred at 83°C for 5 min. After cooling, Et_2O was added, and the resulting suspension was filtered. The filtrate was washed successively with 5% aqueous HCl, H_2O, and saturated aqueous $NaHCO_3$, dried over $MgSO_4$, and concentrated in vacuo. Purification by silica gel column chromatography (Et_2O/*n*-hexane 15/85) gave 197 mg (99%) of **2a**. M.p. 65°C (Et_2O/*n*-hexane); IR (neat): $\tilde{\nu}$ = 1693, 740, 700 cm^{-1}; ^1H NMR (300 MHz, $CDCl_3$, 25°C, TMS): δ = 1.0–1.25 (m, 1H), 2.0–2.15 (m, 2H), 2.15–2.35 (m, 2H), 2.55–2.75 (m, 1H), 2.75–3.0 (m, 3H), 7.2–7.35 (m, 1H), 7.35–7.45 (m, 2H), 7.55–7.65 (m, 2H); ^{13}C NMR (75 MHz, $CDCl_3$, 25°C): δ = 25.57, 26.98, 30.61, 42.61, 44.29, 127.50, 128.05, 128.08, 131.66, 134.14, 185.50, 208.58; C,H analysis (%) calcd. for $C_{14}H_{14}O$ (198.26): C 84.81, H 7.12; found: C 84.53, H 7.12.

For conditions B: Synthesis of **2h**: Under an argon atmosphere, a solution of **1h** (440 mg, 1.13 mmol) and norbornene (**4a**; 160 mg, 1.70 mmol) in 1,4-dioxane (3.0 mL) and 2M aqueous solution of NH_4OH (9.0 mL) was stirred at 100°C for 10 min. After cooling, Et_2O was added, and the resulting suspension was filtered. The filtrate was washed successively with H_2O, 5% aqueous HCl, and saturated aqueous $NaHCO_3$, dried over $MgSO_4$, and concentrated in vacuo. Purification by silica gel column chromatography (Et_2O/*n*-hexane 15/85) gave 253 mg (100%) of **2h**. M.p. 95°C (Et_2O/*n*-hexane); IR (neat): $\tilde{\nu}$ = 1693 cm^{-1}; ^1H NMR (300 MHz, $CDCl_3$, 25°C, TMS): δ = 0.95–1.05 (m, 1H), 1.05–1.2 (m, 1H), 1.25–1.45 (m, 2H), 1.55–1.8 (m, 2H), 2.28 (br. d, J = 3.8 Hz, 1H), 2.37 (d, J = 5.2 Hz, 1H), 2.50 (br. d, J = 3.8 Hz, 1H), 2.65–2.75 (m, 1H), 7.25–7.45 (m, 3H), 7.64 (d, J = 2.7 Hz, 1H), 7.65–7.75 (m, 2H); ^{13}C NMR (75 MHz, $CDCl_3$, 25°C): δ = 28.24, 28.99, 31.13, 38.22, 39.33, 39.52, 47.59, 54.83, 127.06, 128.40, 131.57, 146.07, 160.31, 209.12; C,H analysis (%) calcd. for $C_{16}H_{16}O$ (198.26): C 86.45, H 6.35; found: C 86.33, H 6.55.

Received: January 7, 1997
Revised version: August 22, 1997 [Z9965/9966IE]
German version: *Angew. Chem.* **1997**, *109*, 2884–2886

Keywords: alkyne complexes · amines · carbonyl complexes · cobalt · cyclization

[1] a) I. U. Khand, G. R. Knox, P. L. Pauson, W. E. Watts, *J. Chem. Soc. Chem. Commun.* **1971**, 36; b) I. U. Khand, G. R. Knox, P. L. Pauson, W. E. Watts, M. I. Foreman, *J. Chem. Soc. Perkin Trans. 1* **1973**, 977; c) P. L. Pauson, I. U. Khand, *Ann. NY Acad. Sci.* **1977**, 295, 2; d) P. L. Pauson, *Tetrahedron* **1985**, *41*, 5855.

[2] For recent reviews, see; a) P. L. Pauson in *Organometallics in Organic Synthesis* (Eds.: A. de Meijere, H. tom Dieck), Springer, Berlin, **1987**, p. 233; b) N. E. Shore, *Chem. Rev.* **1988**, *88*, 1081; c) N. E. Schore in *Organic Reactions, Vol. 40* (Ed.: L. A. Paquette), Wiley, New York, **1991**, p. 1; d) N. E. Schore in *Comprehensive Organic Synthesis, Vol. 5* (Eds.: B. M. Trost, I. Fleming, L. A. Paquette), Pergamon, Oxford, **1991**, p. 1037; e) N. E. Schore in *Comprehensive Organometallic Chemistry II, Vol. 12* (Ed.: E. W. Abel, F. G. Stone, G. Wilkinson), Elsevier, New York, **1995**, p. 703.

[3] Lading references for applications to the synthesis of natural products: a) D. C. Billington, P. L. Pauson, *Organometallics* **1982**, *1*, 5861; b) C. Exon, P. Magnus, *J. Am. Chem. Soc.* **1983**, *105*, 2477; c) N. E. Schore, E. G. Rowley, *ibid.* **1988**, *110*, 5224; d) S. Takano, K. Inomata, K. Ogasawara, *J. Chem. Soc. Chem. Commun.* **1992**, 169; e) S. Takano, K. Inomata, K. Ogasawara, *Chem. Lett.* **1992**, 443; f) S. Yoo, S.-H. Lee, N. Jeong, I. Cho, *Tetrahedron Lett.* **1993**, *34*, 3435; g) T. F. Jamison, S. Shambayati, W. E. Crowe, S. L. Schreiber, *J. Am. Chem. Soc.* **1994**, *116*, 5505.

[4] For instance, see C. M. Lukehart, *Fundamental Transition Metal Organometallic Chemistry*, Brooks/Cole, Monterey, **1985**.

[5] There is an example in which THF, a "hard" ligand, is used as a promoter for ligand substitution reactions in the synthesis of $[Cr(CO)_3$(arene)] complexes. C. A. L. Mahaffy, P. L. Pauson, *Inorg. Synth.* **1979**, *19*, 155.

[6] Other promoters for the Pauson–Khand reaction have been reported. Amine oxides: a) S. Shambayati, W. E. Crowe, S. L. Schreiber, *Tetrahedron Lett.* **1990**, *31*, 5289; b) N. Jeong, Y. K. Chung, B. Y. Lee, S. H. Lee, S.-E. Yoo, *Synlett* **1991**, 204; c) W. J. Kerr, G. G. Kirk, D. Middlemiss, *ibid.* **1995**, 1085. Phosphine oxides: d) D. C. Billington, I. M. Helps, P. L. Pauson, W. Thomson, D. Willson, *J. Organomet. Chem.* **1988**, *354*, 233. Sulfoxides: e) Y. K. Chung, B. Y. Lee, N. Jeong, M. Hudecek, P. L. Pauson, *Organometallics*, **1993**, *12*, 220.

[7] The rate enhancement in the Pauson–Khand reaction was observed with the substrates possessing tertiary amines or sulfides. M. E. Krafft, I. L. Scott, R. H. Romero, S. Feibelmann, C. E. Van Pelt, *J. Am. Chem. Soc.* **1993**, *115*, 7199.

[8] For a report that the amine could stabilize the coordinatively unsaturated Co intermediate, see ref. [6b,c].

[9] Recent reviews about reactions in a biphasic system: a) W. A. Herrmann, C. W. Kohlpaintner, *Angew. Chem.* **1993**, *105*, 1588; *Angew. Chem. Int. Ed. Engl.* **1993**, *32*, 1524; b) A. Lubineau, J. Augé, Y. Queneau, *Synthesis* **1994**, 741.

[10] Spectroscopically pure samples of cyclopentenones could not be obtained from the Pauson–Khand reaction under simple thermal conditions [1,2] in some cases without passing through silica gel pads.

 © WILEY-VCH Verlag GmbH, D-69451 Weinheim, 1997 0570-0833/97/3624-2803 $ 17.50+.50/0

[11] See also E. Negishi in *Comprehensive Organic Synthesis, Vol. 5* (Eds.: B. M. Trost, I. Fleming, L. A. Paquette), Pergamon, Oxford, **1991**, p. 1163.
[12] A couple of reports dealing with cobalt-mediated synthetic organic reactions in aqueous media deal mainly with hydroformylations and carbonylations mediated by the $Co(CO)_4^-$ ion produced by a reaction of $[Co_2(CO)_8]$ with H_2O or HO^-. a) F. Francalanci, M. Foá, *J. Organomet. Chem.* **1982**, *232*, 59; b) P. Eilbracht, E. Balb, M. Acker, *Tetrahedron Lett.* **1984**, *25*, 1131; c) M. Miura, F. Akase, M. Nomura, *J. Org. Chem.* **1987**, *52*, 2623; d) C. Zucchi, G. Pályi, V. Galamb, E. Sámpár-Szerencsés, L. Markó, P. Li, H. Alper, *Organometallics* **1996**, *15*, 3222.

Stepwise Reaction of Bis(iodozincio)methane with Two Different Electrophiles**

Kiitiro Utimoto,* Narihiro Toda, Takeshi Mizuno, Masami Kobata, and Seijiro Matsubara

Geminal dimetallic reagents have attracted considerable attention as versatile reagents in organic synthesis,[1] and consequently their preparation has been extensively studied.[2] Application of the reagents has focused on regioselective olefination of carbonyl compounds[3] and coupling with two different electrophilic building blocks.[4] We have developed a method for preparing *gem*-bis(halozincio)alkanes from the corresponding dihalides and have used the organozinc compounds for the olefination of aldehydes and ketones.[5] We have also observed that one of the two C–Zn bonds of bis(iodozincio)methane is much more reactive than the other in the reaction with water or iodine.[5b] These results suggested that the two C–Zn bonds could be used separately. We describe here a stepwise reaction of *gem*-dizinc compounds with two different electrophiles under palladium catalysis.

We initially examined the Pd-catalyzed coupling of bis(iodozincio)methane (**1**) with allyl chlorides. As shown in Equation (1), an allyl chloride **2** (1.0 mmol) was treated with

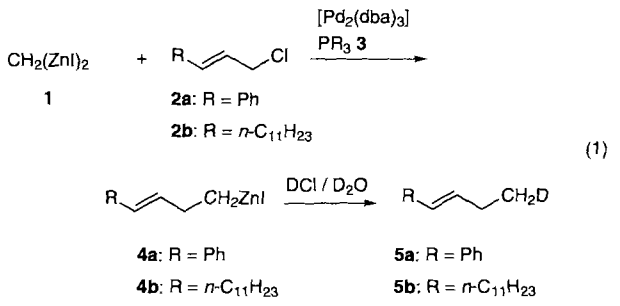

1 (1.0 mmol) in the presence of $[Pd_2(dba)_3]\cdot CHCl_3$ (0.025 mmol) and a phosphane **3** (0.1 mmol) as a ligand in THF (dba = dibenzylideneacetone). After 30 min the resulting mixture was quenched with DCl–D_2O to give the deuterated product **5**. Combinations of allyl chlorides and ligands, as well as yields of coupling products **5** are summarized in Table 1. Excellent results were obtained by ligand tuning; phosphane ligands with electron-withdrawing groups such as tris[3,5-bis(trifluoromethyl)phenyl]phosphane (**3c**) and tris(2-furanyl)phosphane (**3d**) afforded the coupling products in good-to-excellent yields. Quantitative formation of iodozinciomethylated products **4a** was confirmed by ^1H NMR spectroscopy in $[D_8]$THF; the spectra showed the

Table 1. Yields [%] of the products **5** obtained by Pd-catalyzed coupling of **1** with allyl chlorides **2** depending on the phosphane **3**.

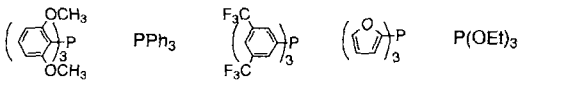

3a **3b** **3c** **3d** **3e**

	3a	3b	3c	3d	3e
2a[a]	< 1	16	88	97	14
2b[a]	< 1	< 1	82	91	< 1

[a] Reaction mixture was treated with DCl–D_2O. The D contents of the products were determined by ^1H NMR spectroscopy (> 95%).

exclusive formation of (*E*)-4-phenyl-3-butenylzinc iodide when **3d** is employed as a ligand.

The intermediary organozinc compounds **4a** and **4b** reacted with other electrophiles such as allyl or acyl halides under the same palladium catalysis as shown in Equation (1).[6,7] This reaction permits a sequential coupling of bis(iodozincio)methane with two different electrophiles [Eq. (2)]

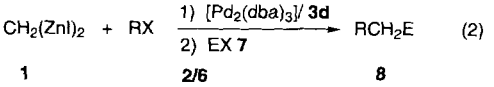

to give the three-component-coupling products in excellent yields. The results of such sequential reactions are shown in Table 2. The formation of **8d** and **8e** can be explained by Equation (3).

Table 2. Stepwise reaction of bis(iodozincio)methane with two electrophiles.

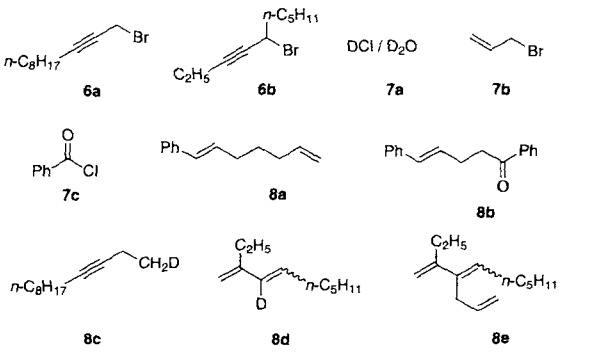

Entry	RX	EX	Product	Yield [%][a]
1	**2a**	**7b**	**8a**	87
2	**2a**	**7c**	**8b**	78
3	**6a**	**7a**	**8c**	55[b]
4	**6b**	**7a**	**8d**	80[b,c]
5	**6b**	**7b**	**8e**	70[c]

[a] Yield of isolated product. [b] > 95% D. [c] Isolated as a diastereomeric mixture.

[*] Prof. K. Utimoto, N. Toda, T. Mizuno, M. Kobata, Dr. S. Matsubara
Department of Material Chemistry, Graduate School of Engineering
Kyoto University
Yoshida, Sakyo, Kyoto, 606-01 (Japan)
Fax: Int. code + (75)753 4863
e-mail: utimoto@orgrx2.kuic.kyoto-u.ac.jp

[**] This work was supported by the Ministry of Education, Science and Culture (grant in Aid nos. 06403025, 09231223, and 09238221)

 © WILEY-VCH Verlag GmbH, D-69451 Weinheim, 1997 0570-0833/97/3624-2804 $ 17.50+.50/0

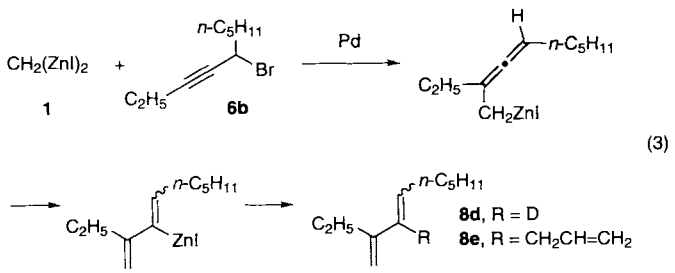

(3)

1,1-Bis(iodozincio)ethane (**9**) reacted with cinnamyl chloride (**2a**) to give the organozinc intermediate **10**, which yielded the deuteriodezincated product (**10**, D in place of ZnI) in 65% yield. The direct coupling of **10** with the allyl bromide **7b** did not occur. In this case, the copper-mediated reaction[8] gave the double coupled product **11** in 66% yield [Eq. (4)].

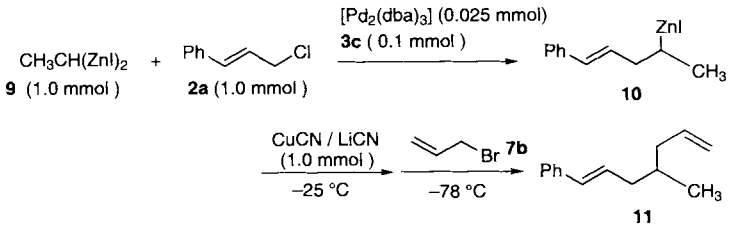

(4)

Experimental Section

THF (2 mL) was added to a mixture of $[Pd_2(dba)_3]\cdot CHCl_3$ (0.025 g, 0.025 mmol) and **3d** (0.023 g, 0.1 mmol) and the mixture was stirred for 5 min at 20°C. A solution of **2a** (0.15 g, 1.0 mmol) in THF (1 mL) was added to the mixture at 20°C, then a solution of **1a** (0.5 M, 2 mL, 1.0 mmol) in THF was added at 20°C and the resulting mixture was stirred for 30 min at 20°C. Thereafter a solution of **7b** (0.15 g, 1.2 mmol) in THF (1 mL) was added at 20°C, and the resulting mixture was stirred for 2 h and then poured into 1 M HCl (20 mL) and extracted with ether. The combined organic layers were washed with brine and dried over Na_2SO_4. Purification by column chromatography (silica gel) gave 1-phenyl-1,6-heptadiene (**8a**) in 87% yield.

Received: July 22, 1997 [Z10720IE]
German version: *Angew. Chem.* **1997**, *109*, 2886–2888

Keywords: C–C coupling · copper · palladium · zinc

[1] I. Marek, J.-F. Normant, *Chem. Rev.* **1996**, *96*, 3241–3267; F. Bickelhaupt, *Angew. Chem.* **1987**, *99*, 1020–1035; *Angew. Chem. Int. Ed. Engl.* **1987**, *26*, 990–1005; P. Knochel, J. F. Normant, *Tetrahedron Lett.* **1986**, *27*, 5727.

[2] B. J. J. Van de Heisteeg, G. Schat, M. A. G. M. Tinga, O. S. Akkerman, F. Bickelhaupt, *Tetrahedron Lett.* **1986**, *27*, 6123–6126; M. Hogenbirk, N. J. Van Eikema Hommes, G. Schat, O. S. Akkerman, F. Bickelhaupt, *ibid.* **1989**, *30*, 6195–6198.

[3] a) Cr: K. Takai, K. Nitta, K. Utimoto, *J. Am. Chem. Soc.* **1986**, *108*, 7408; T. Okazoe, K. Takai, K. Utimoto, *ibid.* **1987**, *109*, 951; D. M. Hodgson, *J. Organomet. Chem.* **1994**, *476*, 1; b) Cr–Sm: S. Matsubara, M. Horiuchi, K. Takai, K. Utimoto, *Chem. Lett.* **1995**, 259–260; c) Zn–$TiCl_4$: T. Okazoe, K. Takai, K. Oshima, K. Utimoto, *J. Org. Soc.* **1987**, *52*, 4410; K. Takai, Y. Kataoka, T. Okazoe, K. Utimoto, *Tetrahedron Lett.* **1988**, *29*, 1065–1068; K. Takai, Y. Kataoka, J. Miyai, T. Okazoe, K. Oshima, K. Utimoto, *Org. Synth.* **1996**, *73*, 73–84; L. Lombardo, *ibid.* **1987**, *65*, 81–89.

[4] P. Knochel, J. F. Normant, *Tetrahedron Lett.* **1986**, *27*, 4427–4430, 4431–4434; F. Chemla, I. Marek, J. F. Normant, *Synlett* **1993**, 665–668; E. Nakamura, K. Kubota, G. Sakata, *J. Am. Chem. Soc.* **1997**, *119*, 5457–5458.

[5] a) K. Takai, T. Kakiuchi, Y. Kataoka, K. Utimoto, *J. Org. Chem.* **1994**, *59*, 2668–2670; b) K. Utimoto, T. Mizuno, M. Kobata, S. Matsubara, K. Takai, unpublished results.

[6] Review on organozinc compounds under Pd catalysis: P. Knochel, R. D. Singer, *Chem. Rev.* **1993**, *93*, 2117–2188; P. Knochel, *Synlett* **1995**, 393–403.

[7] The palladium catalyst used in the first step is still active and catalyzes the reaction in the second step.

[8] Review on copper-mediated reaction of organozinc compounds with electrophiles: ref. [6].

Trisannelated Benzenes by Cyclotrimerization of Bromostannylalkenes**

Richard Durr, Sergio Cossu, Vittorio Lucchini, and Ottorino De Lucchi*

Trisannelated benzenes are enjoying growing interest both as aromatic molecules with alternating bond lengths [1] and as potential precursors of significant fullerene fragments.[2] Except for the simplest cases (triphenylene and tricycloalkyl derivatives),[3] trisannelated benzenes of polycyclic molecules are prepared by two routes: from chloroalkenes with a strong base[4] or from dibromoalkene derivatives by metal–halogen exchange reactions.[5] In both cases the yields are very low—usually 10% or less—and substantial amounts of polymers are formed. The use of metal templates such as nickel[6] also leads to unpredictable and erratic results. Because of poor yields, the real utility of these molecules as precursors to fullerene substructures and eventually to fullerenes themselves can be seriously questioned, and new reactions for the aromatic cyclotrimerization of suitable precursors have clearly become necessary for the development of routes to these molecules. Here we present a method that is readily carried out under very mild reaction conditions, and consistently and reproducibly affords high yields of trimers.

We planned to apply the Stille coupling[7] to olefins containing a suitable metal atom M at one carbon and a leaving group X at the other, in the hope that it would result in trimerization to a trisannelated aromatic product rather than uncontrolled polymerization. Eventually we found that olefins containing the trimethylstannyl group as "metal" along with bromine as a leaving group smoothly afford good yields of cyclotrimers upon reaction with $Cu(NO_3)_2\cdot 3H_2O$ (Scheme 1).

The starting materials for the cyclotrimerization reactions are bromo(trimethylstannyl)alkenes. We chose the norbornene derivatives **1a–c** because such five- and six-membered

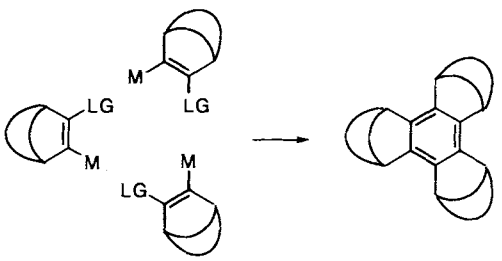

Scheme 1. Stille coupling of polycyclic olefins leading to trisannelated benzenes. M = metal, organometallic group; LG = leaving group.

[*] Prof. Dr. O. De Lucchi, Dr. R. Durr, Dr. S. Cossu
Dipartimento di Chimica,
Università Ca' Foscari di Venezia
Dorsoduro 2137, I-30123 Venezia (Italy)
Fax: Int. code + (41) 529-8517
e-mail: delucchi@unive.it
Prof. Dr. V. Lucchini
Dipartimento di Scienze Ambientali,
Università Ca' Foscari di Venezia

[**] Work supported by C.N.R. (Rome). We thank the Regione Veneto, Dipartimento per l'Industria e l'Energia, for financial support in purchasing a Varian Unity 400 NMR spectrometer and Prof. Dr. Metin Balci for a sample of dibromobenzonorbornadiene.

 © WILEY-VCH Verlag GmbH, D-69451 Weinheim, 1997 0570-0833/97/3624-2805 $ 17.50+.50/0

ring-containing compounds would be precursors for fullerene substructures if the cyclotrimers could be properly rearranged.

Bromo(stannyl) derivatives **1a–c**[8] were obtained in high yield under standard conditions from dibromo compounds **2a–c**[9] by metal–halogen exchange with *n*-butyllithium in THF followed by treatment with trimethyltin chloride. When

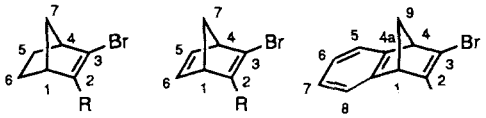

1, R = $SnMe_3$
2, R = Br
3, R = H
4, R = Cl

a THF solution of **1a–c** was added to an equimolar amount of $Cu(NO_3)_2 \cdot 3H_2O$ in THF, a rapid reaction occurred, as shown by a color change from blue to brown. Cyclotrimerized products **5a–c**[10] were obtained as a statistical (3:1) mixture of the *anti* and *syn* isomers in yields up to 80%.

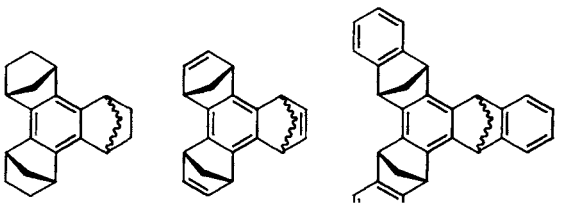

Minor differences were noticed in reactions leading to **5a–c**. Although **5a** and **5b** were obtained essentially pure from **1a** and **1b**, minor amounts of dimers **6c** and **6′c**[11] (15%) arose from **1c**. However, in contrast to other cyclotrimerization procedures, no polymeric material whatsoever was formed.[4,5]

Isomeric dimers **6c** and **6′c** form as an approximately 1:1 mixture. The centrosymmetric structure of **6c** and the C_2-symmetric structure of **6′c** prevented assignment of NMR signals by the usual methods (NOE differential spectroscopy). No crystals suitable for X-ray analysis could be grown. According to literature reports, the dimers were indeed the only products to be expected.[12]

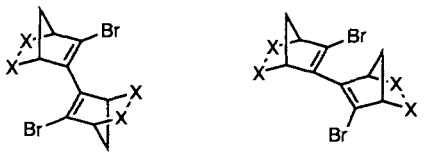

6a-c **6′a-c**

a, X-X = CH_2-CH_2
b, X-X = CH=CH
c, X-X = C_6H_4

Reaction conditions have some influence on the product composition. For example, in the case of **1c** high dilution affords predominantly the protodestannylated compounds **3c**[13] (0–10%) and a smaller amount of dimers **6c/6′c**, while high concentration favors dimers **6c/6′c** relative to the trimers. Higher temperature also favors the formation of dimers. Based on our experiments, the highest proportion of annelated compounds is obtained by adding copper(II) nitrate at room temperature to a roughly 0.1M solution of the appropriate bromo(stannyl) compound in THF.

It is also possible to carry out the reaction in a single pot starting from the dibromo compounds **2a–c**. Sequential addition of *n*BuLi, Me_3SnCl, and $Cu(NO_3)_2 \cdot 3H_2O$ affords a 50–60% yield of trimers **5a–c**, although the product is contaminated with small amounts of the chlorobromo derivatives **4a–c** (5–15%) and the protodestannylated compounds **3a–c** (0–15%). The formation of **3a–c** is not surprising because of the presence of water in the copper salt. Formation of the chlorine-containing derivative may be a result of chloride ion liberated from trimethyltin chloride.

The reaction with other copper salts takes other paths. For example, **1b** and **1c** under similar reaction conditions afford quantitatively with $CuCl_2$ the tin-chloride substitution products **4b** and **4c**, respectively.[14] No cyclotrimers or dimers could be detected in this case. Reaction of **1c** with copper(I) chloride in DMF[15] leads quantitatively to the corresponding substitution product **4c**.[14] Iron(III) chloride gives exclusively **3a–c**, whereas Pd^0[16] under standard Stille conditions is ineffective, since only starting material was recovered from the experiments in question.[7]

The mechanism of cyclotrimer formation under the catalytic influence of copper(II) nitrate is still unclear. Based on similar experiments and literature reports[13] it is possible to conjecture tin–copper transmetalation with formation of an organocopper species that evolves into a vinyl radical. At ambient temperature the intermediate radical is sufficiently reactive to displace bromine from another molecule repeatedly until the trisannelated product **5** is formed. At lower temperature it does not possess sufficient energy, so it can only react with water or dimerize. Dimerization is further encouraged by high concentration. For maximum cyclotrimerization efficiency, the concentration of radicals along the entire reaction path must not become too high (to avoid coupling). Therefore, C–Cu bond cleavage should not occur too rapidly. The formation of chloro derivatives with $CuCl_2$ might well be accounted for by internal nucleophilic substitution by a ligand coupling mechanism[17] of the hypervalent species formed by attack of chloride ion on the tin atom.

Received: June 27, 1997 [Z10610IE]
German version: *Angew. Chem.* **1997**, *109*, 2912–2914

Keywords: aromaticity · C–C coupling · cyclotrimerizations · synthetic methods · tin

[1] K. K. Baldridge, J. S. Siegel, *J. Am. Chem. Soc.* **1992**, *114*, 9583–9587; A. M. Rouhi, *Chem. Eng. News* **1996**, *74*(14), 27–31.
[2] R. Faust, *Angew. Chem.* **1995**, *107*, 1559–1562; *Angew. Chem. Int. Ed. Engl.* **1995**, *34*, 1429–1432.
[3] C. M. Buess, D. D. Lawson, *Chem. Rev.* **1960**, *60*, 313–330; S. Hagen, L. T. Scott, *J. Org. Chem.* **1996**, *61*, 7198–7199.
[4] For example: K. Shahlai, H. Hart, *J. Am. Chem. Soc.* **1988**, *110*, 7136–7140; S. B. Singh, H. Hart, *J. Org. Chem.* **1990**, *55*, 3412–3415; N. L. Frank, K. K. Baldridge, J. S. Siegel, *J. Am. Chem. Soc.* **1995**, *117*, 2102–2103.
[5] For example: M. A. Pericas, A. Riera, O. Rossell, F. Serratosa, M. Seco, *J. Chem. Soc. Chem. Commun.* **1988**, 942–943; K. Komatsu, S. Aonuma, Y. Jinbu, R. Tsuji, C. Hirosawa, K. Takeuchi, *J. Org. Chem.* **1991**, *56*, 195–203.

[8] **1a**: oil; ^1H NMR ($CDCl_3$, 400 MHz): $\delta = 2.95$ (1H, m, H1 or H4), 2.90 (1H, m, H4 or H1), 1.62 and 0.97 (2H, split AB system, $J(5,5') = 10.2$ Hz, H5), 1.61 and 1.17 (2H, split AB system, $J(6,6') = 11.0$ Hz, H6), 1.57 and 1.10 (2H, split AB system, $J(7,7') = 8.4$ Hz, H7), 0.22 (9H, s with tin satellites,

 © WILEY-VCH Verlag GmbH, D-69451 Weinheim, 1997 0570-0833/97/3624-2806 $ 17.50+.50/0

$J(H,^{117}Sn) = 54.0$ Hz, $J(H,^{119}Sn) = 56.6$ Hz, Me); ^{13}C NMR ($CDCl_3$, 100 MHz): $\delta = 147.46$ (C2, $J(C,^{117}Sn) = 408.8$, $J(C,^{119}Sn) = 427.8$ Hz), 146.16 (C3, $J(C,Sn) = 3.2$ Hz), 52.16 (C1 or C4, $J(C,Sn) = 30.5$ Hz), 49.06 (C4 or C1, $J(C,Sn) = 32.3$ Hz), 47.79 (C7, $J(C,Sn) = 19.8$ Hz), 25.72 (C5, $J(C,Sn) = 4.5$ Hz), 24.48 (C6, $J(C,Sn) = 9.7$ Hz), −9.33 (Me, $J(C,^{117}Sn) = 346.6$ Hz, $J(C,^{119}Sn) = 362.3$ Hz). **1b**: oil; ^1H NMR ($CDCl_3$, 400 MHz): $\delta = 6.86$ (1H, dd, $J = 5.2$, 3.1 Hz, H5 or H6), 6.68 (1H, dd, $J = 5.2$, 2.9 Hz, H6 or H5), 3.75 (1H, bs, H1 or H4), 3.52 (1H, br. s, H4 or H1), 2.20 (1H, dt, $J = 6.0$, 1.7 Hz, H7), 1.99 (1H. dt, $J = 6.0$, 1.7 Hz, H7), 0.22 (9H, s with tin satellites, $J(H,^{117}Sn) = 54.5$, $J(H,^{119}Sn) = 57.0$ Hz, Me); ^{13}C NMR ($CDCl_3$, 100 MHz): $\delta = 150.72$ (C3, $J(C,^{117}Sn) = 414.7$, $J(C,^{119}Sn) = 433.9$ Hz), 148.88 (C2, $J(C,Sn) = 12.5$ Hz), 142.57 (C5, $J(C,Sn) = 4.6$ Hz), 141.51 (C6, $J(C,Sn) = 7.2$ Hz), 73.20 (C6, $J(C,Sn) = 16.6$ Hz), 60.32 (C1 or C4, $J(C,Sn) = 31.2$ Hz), 56.99 (C4 or C1, $J(C,Sn) = 33.7$ Hz), −9.56 (Me, $J(C,^{117}Sn) = 349.5$, $J(C,^{119}Sn) = 365.8$ Hz). **1c**: oil; ^1H NMR ($CDCl_3$, 400 MHz): $\delta = 7.31$ (1H, m, H5 or H8), 7.14 (1H, m, H8 or H5), 6.96 (2H, m, H6 and H7), 4.00 (1H, m, H1 or H4), 3.84 (1H, m, H4 or H1), 2.52 (1H, dt, $J = 7.3$, 1.6 Hz, H9), 2.25 (1H, dt, $J = 7.3$, 1.5 Hz, H9), 0.21 (9H, s with tin satellites, $J(H,^{117}Sn) = 54.8$, $J(H,^{119}Sn) = 57.2$ Hz, Me); ^{13}C NMR ($CDCl_3$, 100 MHz): $\delta = 152.12$ (C3, $J(C,^{117}Sn) = 396.1$, $J(C,^{119}Sn) = 414.6$ Hz), 149.87 (C4a, $J(C,Sn) = 3.7$ Hz), 149.57 (C8a, $J(C,Sn) = 7.9$ Hz), 147.70 (C2, $J(C,Sn) = 9.2$ Hz), 124.98, 124.32, 121.93, 121.20 (C5, C6, C7, C8), 68.22 (C9, $J(C,Sn) = 16.8$ Hz), 60.28 (C1 or C4, $J(C,Sn) = 31.0$ Hz), 57.04 (C4 or C1, $J(C,Sn) = 33.0$ Hz), −9.30 (Me, $J(C,^{117}Sn) = 349.9$, $J(C,^{119}Sn) = 365.8$ Hz).

[9] a) **2a**: P. G. Gassman, I. Gennick, *J. Org. Chem.* **1980**, *45*, 5211–5213; b) **2b**: J. Kenndoff, K. Polborn, G. Szeimies, *J. Am. Chem. Soc.* **1990**, *112*, 6117–6119; c) **2c**: see citation in ref. [10c].

[10] **5a**: quantitative yield, identical to an authentic sample (mixture of the *syn* and *anti* isomers) obtained as in P. Gassman, I. Gennick, *J. Am. Chem. Soc.* **1980**, *102*, 6863–6864. **5b**: 78%, identical to an authentic sample (mixture of the *syn* and *anti* isomers) obtained as in R. Durr, O. De Lucchi, S. Cossu, V. Lucchini, *Chem. Commun.* **1996**, 2447–2448. **5c**: 81%, identical to an authentic sample obtained as in S. Cossu, O. De Lucchi, V. Lucchini, G. Valle, M. Balci, A. Dastan, B. Demirci, *Tetrahedron Lett.* **1997**, *38*, 5319–5322.

[11] For dimers **6c, 6′c**, see ref. [10c].

[12] S. Ghosal, G. P. Luke, K. S. Kyler, *J. Org. Chem.* **1987**, *52*, 4296–4298; R. L. Beddoes, T. Cheeseright, J. Wang, P. Quayle, *Tetrahedron Lett.* **1995**, *36*, 283–286.

[13] **3a** and **3b**: see ref. [9a,b]. **3c**: J. W. Wilt, P. J. Chenier, *J. Org. Chem.* **1970**, *35*, 1562–1570.

[14] **4b**: ^1H NMR ($CDCl_3$, 200 MHz): $\delta = 6.86$–6.93 (2H, m), 3.58–3.63 (1H, m), 3.50–3.55 (1H, m), 2.41–2.46 (1H, dt, $J = 6.3$, 1.6 Hz), 2.16–2.21 (1H, dt, $J = 6.3$, 1.6 Hz); ^{13}C NMR ($CDCl_3$, 50 MHz): $\delta \approx 144.00$, 141.64, 141.06, 128.30, 71.49, 57.86, 56.87; see also ref. [9b]. **4c**: oil; ^1H NMR ($CDCl_3$, 200 MHz): $\delta = 7.40$–7.34, 7.05–7.00 (4H, m), 3.90 (1H, bs), 3.85 (1H, s), 2.73 (1H, dt, $J = 7.6$, 1.6 Hz), 2.40 (1H, dt, $J = 7.6$, 1.6 Hz); ^{13}C NMR ($CDCl_3$, 50 MHz): $\delta = 148.16$, 147.71, 144.33, 129.16, 125.52, 125.48, 122.03 (2C), 66.74, 57.98, 56.98; GC-MS: $m/z = 256$, 254, 221, 219, 195, 177 (100), 175, 139, 115, 99, 87, 63.

[15] E. Piers, T. Wong, *J. Org. Chem.* **1993**, *58*, 3609–3610; E. Piers, M. A. Romero, *J. Am. Chem. Soc.* **1996**, *118*, 1215–1216; E. Piers, E. J. McEachern, M. A. Romero, *Tetrahedron Lett.* **1996**, *37*, 1173–1176.

[16] Dimers are often observed as by-products in Stille-type couplings; for example, L. S. Liebeskind, G. B. Stone, S. Zhang, *J. Org. Chem.* **1994**, *59*, 7917–7920.

[17] S. Oae, Y. Uchida, *Acc. Chem. Res.* **1991**, *24*, 202–208.

β-Donor Bonds in Compounds Containing SiON Fragments**

Norbert W. Mitzel* and Udo Losehand

Dedicated to Professor Evelyn A. V. Ebsworth

We investigated $H_3SiONMe_2$ and $H_2Si(ONMe_2)_2$, which unequivocally show the formation of Si–N β-donor bonds and are probably the simplest isolable compounds containing a SiON fragment. Recently we reported (4+4) coordination at the silicon center in $Si(ONMe_2)_4$.[1] This compound has an Si-O-N angle that is compressed by more than 16° with respect to the Si-O-C angle in the isoelectronic $Si(OCHMe_2)_4$. Ab initio calculations on $H_3SiONMe_2$ and $FH_2SiONMe_2$ predicted narrow Si-O-N angles (102.5 and 90°, respectively) and short Si–N distances.[1]. So far there has been no experimental evidence for these postulated extreme bonding situations in the SiON unit. The knowledge of the formation of Si–N β-donor interactions in SiON compounds is important for understanding the effect of *O*-silylated hydroxylamines and oximes as cross-linking agents[2] and cold-curing catalysts[3] in the synthesis of silicon polymers with low molecular weights, which can be used in electronics, construction, and medical applications. Acceleration of hydrolysis and alcoholysis of Si–H bonds in the presence of catalytic amounts of R_2NOH-type compounds was only recently established.[4] It can be explained by this interaction, which is unusual in the chemistry of p-block elements.

Numerous attempts to prepare $H_3SiONMe_2$ by condensation of H_3SiCl or H_3SiBr with $HONMe_2$ in the presence of auxiliary bases as well as reactions of $HONMe_2$ with silylamines failed. Despite the high reactivity of the agents, the reaction of H_3SiBr with $LiONMe_2$ proved to be the best synthetic method [Eq. (1)]. $H_2Si(ONMe_2)_2$ was prepared in a similar way from dichlorosilane [Eq. (2)]. Both products are

$$H_3SiBr + LiONMe_2 \longrightarrow H_3SiONMe_2 + LiBr \quad (1)$$

$$H_2SiCl_2 + 2\,LiONMe_2 \longrightarrow H_2Si(ONMe_2)_2 + 2\,LiBr \quad (2)$$

extremely sensitive to moisture, but are not pyrophoric. Although isomerization of $H_3SiONMe_2$ and $H_2Si(ONMe_2)_2$ to the aminosilanoles is thermodynamically favored, they can be heated to about 100 °C.

The identity of the compounds was proven by ^1H, ^{13}C, ^{15}N, ^{17}O, and ^{29}Si NMR spectroscopy, gas-phase IR spectroscopy, and mass spectrometry. Since $H_3SiONMe_2$ melts at low temperatures (≈ -60 °C), a single crystal for X-ray diffraction analysis had to be grown by in situ methods.[5] The molecules contain a crystallographically imposed mirror plane with an Si-O-N angle of only 102.63(5)° and short Si···N distances of 2.453(1) Å (Figure 1; the sum of the van der Waals radii of Si and N is 3.54 Å[6]). This is in excellent agreement with the

[*] Dr. N. W. Mitzel, Dipl.-Chem. U. Losehand
Anorganisch-chemisches Institut der Technischen Universität München
Lichtenbergstrasse 4, D-85747 Garching (Germany)
Fax: Int. code + (89) 289-13125
e-mail: n.mitzel@lrz.tu-muenchen.de

[**] This work was supported by the Bayrisches Staatsministerium für Unterricht, Kultus, Wissenschaft und Kunst (Bayerischer Habilitationsförderpreis 1996 for N.W.M.), the Deutsche Forschungsgemeinschaft, and the Leonhard Lorenz-Stiftung. We are grateful to Professor H. Schmidbaur for his generous support, and Mr. J. Riede for establishing the crystallographic data sets.

 © WILEY-VCH Verlag GmbH, D-69451 Weinheim, 1997 0570-0833/97/3624-2807 $ 17.50+.50/0

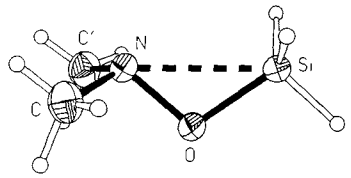

Figure 1. Molecular structure of $H_3SiONMe_2$. The Si–N β-donor bond is represented by the dashed line.

Table 1. Selected bond lengths [Å] and angles [°] of $H_3SiONMe_2$ and $H_2Si(ONMe_2)_2$ according to results of X-ray diffraction (XRD) studies and quantum-chemical calculations.

	$H_3SiONMe_2$		$H_2Si(ONMe_2)_2$	
	XRD	MP2/6-311G**[1]	XRD	MP2/6-31G*
Si–O	1.668(1)	1.682	1.656(1), 1.657(1)	1.699
O–N	1.471(1)	1.459	1.481(1), 1.477(1)	1.477
Si···N	2.453(1)	2.454	2.300(1), 2.336(1)	2.333
Si-O-N	102.63(5)	102.5	94.16(7), 96.19(7)	94.2
O-Si-O			100.95(5)	101.5
C-N-O	105.50(6)	105.3	105.6(1)–106.8(1)	105.2
O-Si-H(1)	110.4(6)	111.5	109.3(7)–110.5(7)	110.2
O-Si-H(2)	101.7(8)	104.4		

results of quantum-chemical calculations (Table 1). The aggregation of the molecules through O···Si contacts (2.92 Å) rather than N···Si contacts (Figure 2) indicates that

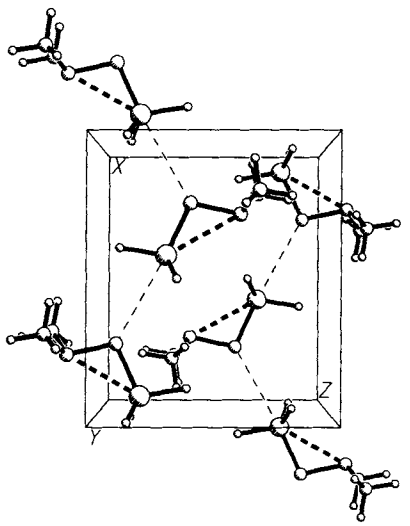

Figure 2. Intermolecular O···Si contacts between $H_3SiONMe_2$ molecules in the crystal.

the oxygen atoms are more basic than the nitrogen atoms. This implies the involvement of the electron lone pair on nitrogen in the β-donor bond to the silicon atom and the increase of basicity at the oxygen atom through a narrow Si-O-N angle. Taking the Si···O contacts into consideration, the coordination geometry at the oxygen atoms is crystallographically planar (similar to the case in $MeOSiH_3$,[7] $(H_3Si)_2O$,[8] and $(H_3Si)_2NOMe$[9]), and the electronic situation at the oxygen centers can neither be described properly with an sp^3 nor an sp^2 hybridization model (narrow Si-O-N angle).

To get an idea of the strength of a Si–N β-donor bond, several geometrical optimizations[10] at the MP2/6-31G* level of theory were peformed with successive alteration of fixed Si-O-N angles (Figure 3). Based on a comparison with

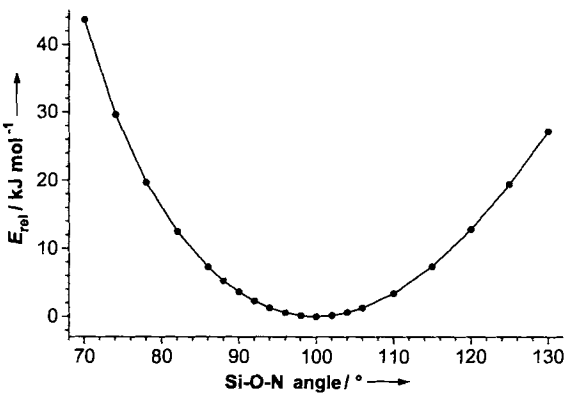

Figure 3. Relative energies (MP2/6-31G*) of $H_2SiONMe_2$ at different fixed Si-O-N bond angles.

Si-O-C angles of isoelectronic SiOCH compounds that are not capable of forming Si–N β-donor bonds (e. g. H_3SiOMe: 120.1,[7] $Si(OCHMe_2)_4$: 124.7°)[1] the Si-O-N angle can be estimated to be 120° in the hypothetical absence of a β-donor interaction. This results in an estimated bond energy of 15 kJ mol^{-1}.

The β-donor bond in $H_2Si(ONMe_2)_2$ is even stronger, as shown by an X-ray diffraction analysis of a single crystal prepared by in situ methods (Figure 4).[5] The Si-O-N angle is

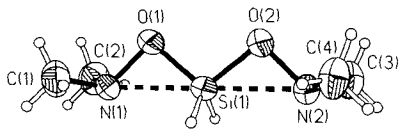

Figure 4. Molecular structure of $H_2Si(ONMe_2)_2$.

on average as small as 95.1°, and the Si···N distances of 2.300(1) and 2.336(1) Å are about 0.1 Å shorter than in $H_3SiONMe_2$. The increased coordination number at silicon (4+2) leads to a compressed O-Si-O angle of only 100.95(5)°. The N–O bonds in $H_3SiONMe_2$ and $H_2Si(ONMe_2)_2$ are more than 0.02 Å longer than that in $HONMe_2$. No intermolecular Si···O contacts were found in crystals of $H_2Si(ONMe_2)_2$.

These results show that the formation of relatively strong β-donor bonds are possible even between p-block elements. For a deeper understanding further investigations of this and related classes of compounds are necessary. Kinetic studies on $ClH_2SiONMe_2$, which we also isolated, will show to what extent the increased coordination number accelerates nucleophilic substitution.

Experimental Section

All NMR spectra were recorded at 21 °C with solutions in C_6D_6.

$H_3SiONMe_2$: *n*-Butyllithium (1.8 g, 28 mmol, 1.8 M in hexane) was added dropwise to a solution of Me_2NOH (1.7 g, 28 mmol) in pentane (50 mL). The mixture was stirred for 1 h at room temperature, and the solvent removed in vacuo. Dimethyl ether (5 mL) and bromosilane (3.1 g, 28 mmol) were added at −196 °C by condensation. The mixture was warmed to −30 °C and stirred for 2 h. All volatile products were condensed into a trap at −196 °C. Distillation through a series of traps (−50, −78, −100, and −196 °C) resulted in condensation of $H_3SiONMe_2$ in the −78 °C trap. ^1H NMR: $\delta = 2.32$ (s, 6H, H_3C), 4.58 (s, 3H, H_3Si); ^{13}C NMR: $\delta = 49.1$ (qq, $^1J(C,H) = 135.4$ Hz, $^3J(C,H) = 5.4$ Hz, CH_3); $^{15}N\{^1H\}$ NMR (DEPT): $\delta = -234.0$ (s); $^{17}O\{^1H\}$ NMR: $\delta = 112.1$ (s); ^{29}Si NMR (DEPT): $\delta = -49.5$ (q, $^1J(Si,H) = 219.3$ Hz); IR (gas): $\tilde{\nu} = 2177$ cm^{-1} (s, ν(Si–H)).

$H_2Si(ONMe_2)_2$: Methyllithium (2.5 g, 0.11 mol, 1.60 M in diethyl ether) was added dropwise to a solution of Me_2NOH (6.9 g, 0.11 mol) in diethyl ether (25 mL) at

 © WILEY-VCH Verlag GmbH, D-69451 Weinheim, 1997 0570-0833/97/3624-2808 $ 17.50+.50/0

0 °C and then stirred for 1 h at room temperature. At −196 °C dichlorosilane (5.7 g, 56 mmol) was condensed onto the mixture, which was then stirred for 1 h at −78 °C. After the mixture was warmed to room temperature all volatile components were separated from the salt by condensation. $H_2Si(ONMe_2)_2$ (4.2 g, 28 mmol, 50%) could be isolated at −35 °C as an air-sensitive, colorless liquid (m.p. 0 °C) by condensation through a series of traps (−35, −35, −78, and −196 °C). ^1H NMR: $\delta = 2.42$ (s, 12H, H_3C), 4.70 (s, 2H, H_2Si); ^{13}C NMR: $\delta = 49.7$ (qq, $^1J(C,H) = 135.4$ Hz, $^3J(C,H) = 5.4$ Hz, CH_3); $^{15}N\{^1H\}$ NMR (DEPT): $\delta = -249.2$ (s); $^{17}O\{^1H\}$ NMR: $\delta = 141.1$ (s); ^{29}Si NMR (DEPT): $\delta = -49.8$ (q, $^1J(Si,H) = 219.3$ Hz); IR (gas): $\tilde{\nu} = 2193$ cm^{-1} (s, ν(Si–H)); MS (CI): $m/z = 149$ [$M^+ - 1$].

Received: June 16, 1997 [Z.10547IE]
German version: *Angew. Chem.* **1997**, *109*, 2897–2899

Keywords: donor–acceptor bonds · hydrides · hydroxylamines · silicon · structure elucidation

[1] N. W. Mitzel, A. J. Blake, D. W. H. Rankin, *J. Am. Chem. Soc.* **1997**, *119*, 4143–4148.
[2] a) J. Patzke, E. Wohlfarth, *Chem.-Ztg.* **1973**, *97*, 176–180; b) H. Lücke, *Adhäsion* **1968**, *12*, 353–365.
[3] M. G. Voronkov, E. A. Maletina, V. K. Roman, *Heterosiloxanes: Derivatives of Nitrogen and Phosphorus, Vol. 2*, Harwood Academic Publishers, Chur, **1991**.
[4] Y. Hamada, S. Mori, *Proc. 29th Organosilicon Symp.*, Evanston, IL, USA, **1996**.
[5] X-ray structure analyses: a) General: Enraf–Nonius Turbo CAD 4 diffractometer, graphite-monochromated $Mo_{K\alpha}$ radiation, ω/θ scans. The structures were solved by direct methods and refined on F_o^2 with SHELXTL-PC [11]. Non-hydrogen atoms were refined with allowed anisotropic thermal motion, and all hydrogen atoms were localized and refined with isotropic thermal displacement parameters (SHELXL-93 [12]). Crystallographic data (excluding structure factors) for the structures reported in this paper have been deposited with the Cambridge Crystallographic Data Centre as supplementary publication no. CCDC-100491. Copies of the data can be obtained free of charge on application to The Director, CCDC, 12 Union Road, Cambridge CB2 1EZ, UK (fax: int. code +(1223)336-033; e-mail: deposit@chemcrys.cam.ac.uk). b) $H_3SiONMe_2$: orthorhombic, space group *Pnma*, $Z = 4$, $a = 8.134(1)$, $b = 7.025(1)$, $c = 9.690(1)$ Å, $V = 553.70(12)$ Å^3, $T = 133$ K, $2\theta_{max} = 72°$; of 1365 independent reflections ($R_{int} = 0.008$), 1151 had $F_0 > 4\sigma(F_0)$; 48 varied parameters, $R(F) = 0.033$ (measured), $wR(F^2) = 0.097$, max./min. residual electron density 0.46/−0.56 e Å^{-3}. c) $H_2Si(ONMe_2)_2$: monoclinic, space group *C2/c*, $Z = 8$, $a = 21{,}453(1)$, $b = 6.799(1)$, $c = 12.609(1)$ Å, $V = 1761.9(3)$ Å^3, $T = 223$ K, $2\theta_{max} = 52°$; of 1717 independent reflections ($R_{int} = 0.031$), 1451 had $F_0 > 4\sigma(F_0)$. An extinction-correction parameter refined to 0.027(2), 139 varied parameters, $R(F) = 0.035$ (measured), $wR(F^2) = 0.105$, max./min. residual electron density 0.36/−0.39 e Å^{-3}.
[6] J. Emsley, *The Elements*, Clarendon, Oxford, **1989**.
[7] M. J. Barrow, E. A. V. Ebsworth, M. M. Harding, *Acta Crystallogr. Sect. B* **1979**, *35*, 2093–2099.
[8] A. J. Blake, M. Dyrbush, E. A. V. Ebsworth, S. G. D. Henderson, *Acta Crystallogr. Sect. C* **1988**, *44*, 1–3.
[9] N. W. Mitzel, E. Breuning, A. J. Blake, H. E. Robertson, B. A. Smart, D. W. H. Rankin, *J. Am. Chem. Soc.* **1996**, *118*, 2664–2668.
[10] Calculations were performed using standard methods implemented in Gaussian 94: M. J. Frisch, G. W. Trucks, H. B. Schlegel, P. M. W. Gill, B. G. Johnson, M. A. Robb, J. R. Cheeseman, T. Keith, G. A. Petersson, J. A. Montgomery, K. Raghavachari, M. A. Al-Laham, V. G. Zakrzewski, J. V. Ortiz, J. B. Foresman, J. Cioslowski, B. B. Stefanov, A. Nanayakkara, M. Challacombe, C. Y. Peng, P. Y. Ayala, W. Chen, M. W. Wong, J. L. Andres, E. S. Replogle, R. Gomperts, R. L. Martin, D. J. Fox, J. S. Binkley, D. J. Defrees, J. Baker, J. P. Stewart, M. Head-Gordon, C. Gonzalez, J. A. Pople, Gaussian 94, Revision C.2, Gaussian, Pittsburgh, PA, USA, **1995**.
[11] G. M. Sheldrick, SHELXTL/PC, Version 5.03, Siemens Analytical X-Ray Instrumentation, Madison, WI, USA, **1995**.
[12] G. M. Sheldrick, SHELX93, Universität Göttingen, **1993**.

PHONA–PNA Co-Oligomers: Nucleic Acid Mimetics with Interesting Properties

Anusch Peyman,* Eugen Uhlmann, Konrad Wagner, Sascha Augustin, Caroline Weiser, David W. Will, and Gerhard Breipohl

Oligonucleotide analogues are of special interest in molecular biology and medicinal chemistry because of their use as diagnostic agents and their potential application as therapeutics.[1,2] PNAs are nucleic acid mimetics in which the sugar–phosphate backbone is completely replaced by an *N*-(2-aminoethyl)glycine scaffold. The nucleobases are attached to this backbone through methylenecarbonyl linkers (Scheme 1).[3–5] PNAs bind remarkably strongly to complementary DNA and RNA sequences.[5] This is partly due to the

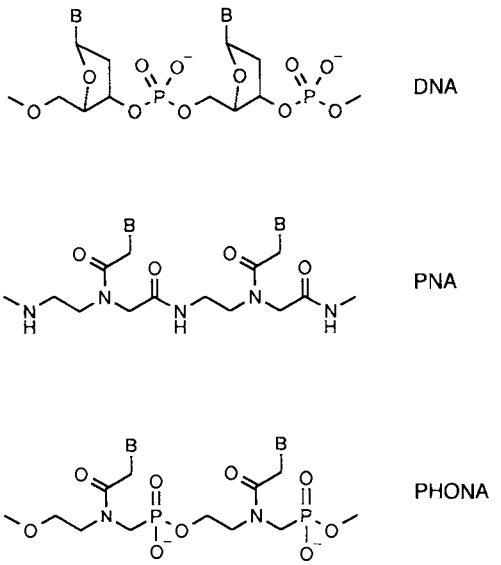

Scheme 1. Structures of DNA, PNA, and PHONA.

lack of negative charges on the PNA backbone, which, however, results in poor water solubility and inadequate cellular uptake.[5,6] The reintroduction of negative charges into PNAs is possible by, for example, the synthesis of PNA–DNA chimeras,[7] or by the synthesis of a further structural variant, the PHONAs (Scheme 1).[8] PHONAs are analogues of PNAs in which the peptide bond is replaced by a phosphonic acid ester bridge.

The abundance of available nucleic acid mimetic structures offers the organic chemist the possibility of combining appropriate building blocks to create oligomers with customized properties. On the other hand prediction of the binding properties of chimeric oligomers is fraught with uncertainty, as the structures of the complexes of different nucleic acid analogues with their complementary DNA can vary widely. This is illustrated by a comparison of the structures of DNA · DNA and PNA · DNA duplexes.[9] Here we report the synthesis and binding properties of alternating PHONA–PNA

[*] Dr. A. Peyman, Dr. E. Uhlmann, K. Wagner, S. Augustin, C. Weiser, Dr. D. W. Will, Dr. G. Breipohl
Hoechst Marion Roussel Deutschland GmbH
D-65926 Frankfurt (Germany)
Fax: Int. code + (69)33-1399
e-mail: anusch.peyman@hmrag.com

 © WILEY-VCH Verlag GmbH, D-69451 Weinheim, 1997 0570-0833/97/3624-2809 $ 17.50+.50/0

oligomers. The oligomers contain only the nucleobase thymine, as protection of exocyclic amino functions is unnecessary.

The central building block for the synthesis of PHONA–PNA oligomers is the dimer block **11** (see Scheme 3), which carries two orthogonal protecting groups: the acid-labile 4-methoxytriphenylmethyl (Mmt) protecting group for the amino function and the 4-nitrophenylethyl (NPE) phosphonic acid ester,[10] which can be cleaved by β-elimination. The synthesis of the amino-PHONA building block is shown in Scheme 2. The strategy is largely analogous to the previously

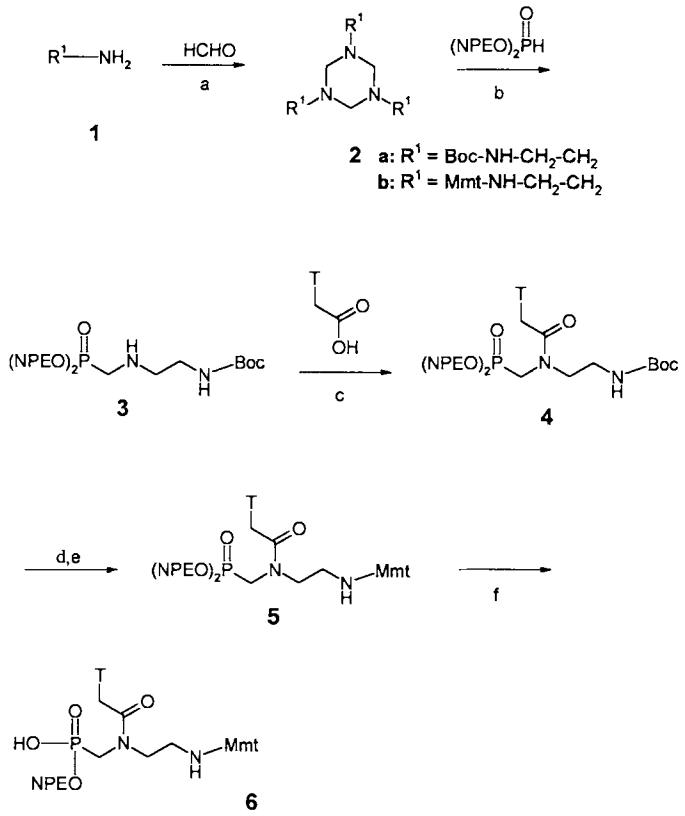

Scheme 2. Synthesis of the PHONA monomer; T = 1-thyminyl: a) 1.5 equiv HCHO, methanol, room temperature (RT), 1 h, 37%; b) 1 equiv phosphite, 2.5 h, 100°C, 23%; c) 1 equiv 1-thyminylacetic acid, 3 equiv *N*-ethylmorpholine, 1.1 equiv HATU, DMF, 24 h, RT, 66%; d) 100% trifluoroacetic acid, 0–10°C, 100%; e) 1.1 equiv MmtCl, 3 equiv diisopropylethylamine, 12 h, 0–5°C, 100%; f) 0.1M diazabicycloundecene (DBU) in acetonitrile, 24 h, 0°C, 77%.

described synthesis of the corresponding hydroxy-PHONA building block.[8] However, it was necessary to use the *tert*-butyloxycarbonyl (Boc) protecting group for the amino function. This could be exchanged for the Mmt group after attachment of the phosphonic acid. The addition of the phosphite to the corresponding Mmt-protected imine **2b** did not give the desired phosphonic acid, presumably because partially released formaldehyde reacted with both secondary amino functions. The hydroxyethylglycine-based building block **7** [7a,b] (Scheme 3) was converted into its allyl ester, and after cleavage of the Mmt protecting group, was coupled with PHONA monomer **6** by using the coupling reagent 3-nitro-1-(*p*-toluenesulfonyl)-1H-1,2,4-triazole (TSNT).[11] The allyl ester of dimer block **10** can be cleaved selectively[12] with Pd^0, which leaves the Mmt and NPE protecting groups intact.

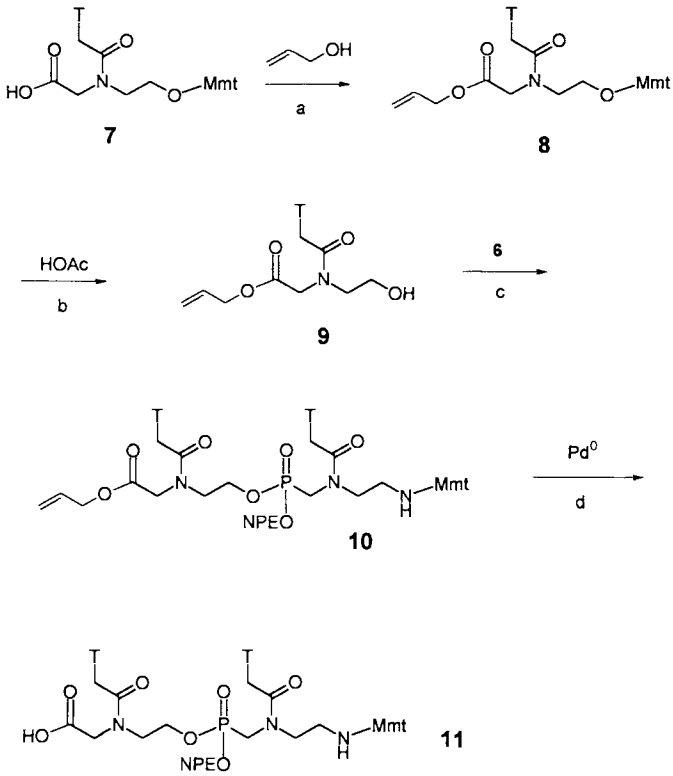

Scheme 3. Synthesis of mixed PHONA–PNA building block **11**: a) 2 equiv allyl alcohol, 3 equiv TSNT, pyridine, 24 h, 0°C, 86%; b) 80% acetic acid, 3 h, RT, 100%; c) 1 equiv **6**, pyridine, 4 equiv TSNT, 14 h, 0°C, 65%; d) $Pd[(PPh_3)]_4$, PPh_3, diethylammonium hydrogen carbonate, CH_2Cl_2, 1 h, 70%.

The assembly of the oligomer was carried out on aminohexylsuccinyl–CPG solid support analogously to PNA synthesis.[7f] The synthesis cycle (Scheme 4) consists of

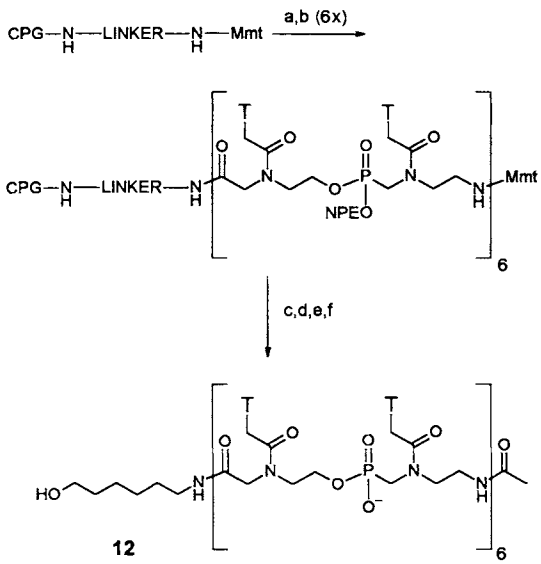

Scheme 4. Synthesis of alternating PHONA–PNA oligomer **12**: LINKER: $-C(O)CH_2CH_2C(O)O(CH_2)_6-$; a) 80% acetic acid, 3 h, 100%; b) double coupling with 4 equiv **11** (0.2M solution in DMF), 8 equiv *N*-ethylmorpholine, 4 equiv HOAt (1-hydroxy-7-azabenzotriazole), 4 equiv HATU [13], 5 h, RT; 90%; c) 80% acetic acid, 3 h, 100%; d) acetic anhydride, *N*-methylimidazole, 10 min, RT; e) 0.5M DBU in acetonitrile, 6 h, RT; f) conc. NH_4OH, 12 h, RT. MS (electrospray): M_{calcd} for $C_{134}H_{185}N_{43}O_{62}P$: 3576.04; M_{found}: 3575.71.

 © WILEY-VCH Verlag GmbH, D-69451 Weinheim, 1997 0570-0833/97/3624-2810 $ 17.50+.50/0

removal of the Mmt group with 80% acetic acid and coupling of the dimer block **11**. The use of a fourfold excess of **11** and HATU as the coupling reagent[13] resulted in coupling efficiencies of greater than 90%. After completion of oligomer assembly the N-terminus was acetylated with acetic anhydride, and the NPE groups were removed by treatment with 0.5 M DBU in acetonitrile. The oligomer **12** was then cleaved from the solid support by treatment with concentrated NH_4OH and purified by polyacrylamide gel electrophoresis. The highly water-soluble oligomer **12** was characterized by HPLC and electrospray-MS; its mass is 3575.7 (calculated: 3576.0).

The binding properties of alternating PHONA-PNA co-oligomer **12** were investigated by hybridization with complementary $(dA)_{12}$. On heating the hybrid gives a clear phase transition (Figure 1), with a melting temperature of 62.6°C.

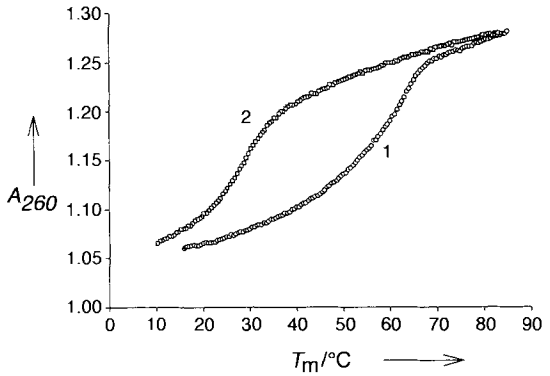

Figure 1. Determination of the melting temperature of the hybrid formed by $d(A)_{12}$ and **12** in the ratio 1:1 by UV spectroscopy at 270 nm. Buffer: 140 mM KCl, 10 mM NaH_2PO_4, 0.1 M EDTA, pH = 7.4; heating and cooling rate: 1 K min^{-1}.

As with PNAs, however, the cooling curve displays a marked hysteresis, with a melting temperature of 29.0°C. The sequence specificity of the binding is clearly demonstrated by the drastic drop in melting temperature on introduction of a mismatch in the complementary DNA strand. Replacement of just one (dA) by (dG) to give **14** results in a drop in T_m to 52.3°C. Replacement of two neighboring (dA)'s by $(dG)_2$ to give **15** gives twice as large a drop in T_m to 39.5°C, and replacement of two nonneighboring (dA)'s to give **16** reduces the T_m to 36.9°C. In this case no phase transition could be observed on cooling. Under the same conditions the corresponding DNA·DNA duplex had a melting temperature of 29.3°C (Table 1).

Comparison with the UV-melting properties of DNA·DNA and PNA·DNA complexes (the T_m of the complex of PNA-T_{10} with $(dA)_{10}$ is 73°C[14]) indicates that PHONA-PNA co-oligomers resemble the latter more closely. The prediction that in this case, as with PNAs, triple-helical structures are formed was confirmed by measurement of a Job plot.[15] (Figure 2; 2:1 ratio of **12** to $(dA)_{12}$). In addition the UV-melting behavior of a 1:1 and a 2:1 ratio of **12** to $(dA)_{12}$ are identical, the only difference being a doubling of the

Table 1. Melting temperatures T_m of **12** with completely or partially complementary DNA (ratio 1:1; buffer 140 mM KCl, 10 mM NaH_2PO_4, 0.1 M EDTA, pH = 7.4).

Strand 1	Strand 2	T_m[°C][a]	T_m[°C][b]
$(dA)_{12}$ **13**	**12**	62.6	29.0
$(dA)_6dG(dA)_5$ **14**	**12**	52.3	17.1
$(dA)_5(dG)_2(dA)_5$ **15**	**12**	39.5	15.0
$(dA)_3dG(dA)_3dG(dA)_4$ **16**	**12**	36.9	–
$(dA)_{12}$ **13**	$(dT)_{12}$	29.3	29.0

[a] On heating. [b] On cooling.

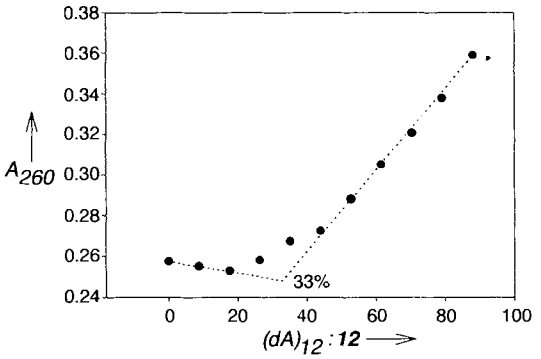

Figure 2. Job plot (continuous titration) of the interaction between **12** and $d(A)_{12}$: UV absorption at 260 nm versus mole ratio $d(A)_{12}$/**12** at 20°C, 500 mM NaCl, 10 mM HEPES, pH 7.5; 2 h equilibration before each measurement.

change in absorbance at the phase transition. Presumably half of the $(dA)_{12}$ present is bound in a $(\mathbf{12})_2 \cdot (dA)_{12}$ complex, and the other half is unbound. The hysteresis observed on cooling is possibly due to formation of the $\mathbf{12} \cdot (dA)_{12}$ duplex, which would suggest relatively slow kinetics for the formation of the triple helix.[16]

The high melting temperature of 62.6°C shows that the PHONA-PNA transitions cause very little structural perturbation in the triple helix. The somewhat lower melting temperature relative to that of $(PNA)_2 \cdot DNA$ triple helices is easily explained by the repulsion of the negative charges of the phosphate and phosphonate groups. These charges reverse the dependence of the melting temperature on salt concentration that is observed for PNAs. Changing the buffer salt concentration from 140 mM KCl to 500 mM NaCl had very little effect on the melting temperature (T_m = 64.7°C).

We have described the synthesis of new nucleic acid mimetics, the alternating PHONA-PNA co-oligomers. Their binding properties with complementary DNA are very similar to those of PNAs, but they have a much better water solubility. The synthesis and binding properties of mixed sequences, as well as the evaluation of cellular uptake and stability under biological conditions, will be reported separately.

Received: July 18, 1997 [Z10698IE]
German version: *Angew. Chem.* **1997**, *109*, 2919-2922

Keywords: helical structures · nucleic acids · oligonucleotides · PNA

[1] a) E. Uhlmann, A. Peyman, *Chem. Rev.* **1990**, *90*, 543-584; b) A. De Mesmaker, R. Häner, P. Martin, H. E. Moser, *Acc. Chem. Res.* **1995**, *28*, 366-374; c) *Methods in Molecular Medicine: Antisense Therapeutics* (Ed.: S. Agrawal), Humana Press, Totowa, NJ, USA, **1996**; d) E. Uhlmann, A. Peyman, D. W. Will in *Encyclopedia of Cancer* (Ed.: J. R. Bertino), Academic Press, New York, **1997**, pp. 64-81.

[2] a) U. Englisch, D. Gauss, *Angew. Chem.* **1991**, *103*, 629-646; *Angew. Chem. Int. Ed. Engl.* **1991**, *30*, 613-630; b) H. Shikata, N. Utsumi, H. Kuivaniemi, G. Tromp, *J. Lab. Clin. Med.* **1995**, *125*, 421-432.

[3] E. Uhlmann, A. Peyman in *Methods in Molecular Biology, Vol. 20: Protocols for Oligonucleotides and Analogs* (Ed.: S. Agrawal), Humana Press, Totowa, NJ, USA, **1993**, Chapter 16, pp. 355-389.

[4] P. E. Nielsen, *Annu. Rev. Biophys. Biomol. Struct.* **1995**, *24*, 167-183.

[5] B. Hyrup, P. E. Nielsen, *Bioorg. Med. Chem.* **1996**, *4*, 5-23.

 © WILEY-VCH Verlag GmbH, D-69451 Weinheim, 1997 0570-0833/97/3624-2811 $ 17.50+.50/0

[6] J. C. Hanvey, N. J. Peffer, J. E. Bisi, S. A. Thomson, R. Cadilla, J. A. Josey, D. J. Ricca, F. Hassman, M. A. Bonham, K. G. Au, S. G. Carter, D. A. Bruckenstein, A. L. Boyd, S. A. Noble, L. E. Babiss, *Science* **1992**, *258*, 1481–1485.
[7] a) F. Bergmann, W. Bannwarth, S. Tam, *Tetrahedron Lett.* **1995**, *36*, 6823–6826; b) E. Uhlmann, D. W. Will, G. Breipohl, D. Langner, A. Ryte, *Angew. Chem.* **1996**, *108*, 2793–2797; *Angew. Chem. Int. Ed. Engl.* **1996**, *35*, 2632–2635; c) P. J. Finn, N. J. Gibson, R. Fallon, A. Hamilton, T. Brown, *Nucl. Acids Res.* **1996**, *24*, 3357–3363; d) K. H. Petersen, D. K. Jensen, M. Egholm, P. E. Nielsen, O. Buchardt, *Bioorg. Med. Chem. Lett.* **1995**, *5*, 1119–1124; e) A. C. van der Laan, N. J. Meeuwenoord, E. Khyl-Yehesliely, R. S. Oosting, R. Brands, J. H. van Boom, *Recl. Trav. Chim. Pays-Bas* **1995**, *114*, 295–297; f) D. W. Will, G. Breipohl, D. Langner, J. Knolle, E. Uhlmann, *Tetrahedron* **1995**, *51*, 12069–12082.
[8] a) A. Peyman, E. Uhlmann, K. Wagner, S. Augustin, G. Breipohl, D. W. Will, A. Schäfer, H. Wallmeier, *Angew. Chem.* **1996**, *108*, 2797–2800; *Angew. Chem. Int. Ed. Engl.* **1996**, *35*, 2636–2638; b) A. Peyman, E. Uhlmann, G. Breipohl, H. Wallmeier (Hoechst AG), EP 0739898A2, **1996**; c) A. C. van der Laan, R. Strömberg, J. H. van Boom, E. Kuyl-Yeheskiely, V. A. Efimov, O. G. Chakhmakcheva, *Tetrahedron Lett.* **1996**, *37*, 7857–7860.
[9] M. Eriksson, P. E. Nielsen, *Nature Structural Biol.* **1996**, *3*, 410–413.
[10] E. Uhlmann, W. Pfleiderer, *Helv. Chim. Acta* **1981**, *64*, 1688–1703.
[11] C. B. Reese, *Tetrahedron* **1978**, *34*, 3143–3179.
[12] H. Kunz, C. Unverzagt, *Angew. Chem.* **1984**, *96*, 426–427; *Angew. Chem. Int. Ed. Engl.* **1984**, *23*, 436–437; Y. Hayakawa, M. Hirose, R. Noyori, *J. Org. Chem.* **1993**, *58*, 5551–5555.
[13] HATU: *O*-(7-azabenzotriazol-1-yl)-*N*,*N*,*N*',*N*'-tetramethyluronium hexafluorophosphate: L. A. Carpino, *J. Am. Chem. Soc.* **1993**, *115*, 4397–4398.
[14] M. Egholm, P. E. Nielsen, O. Buchardt, R. Berg, *J. Am. Chem. Soc.* **1992**, *114*, 9677–9678.
[15] T. L. Trapane, R. I. Hogrefe, M. A. Reynolds, L.-S. Kan, P. O. P. Ts'o, *Biochemistry* **1996**, *35*, 5495–5508; P. Job, *Ann. Chim. (Paris)* **1928**, *9*, 113–134.
[16] M. C. Griffith, L. M. Risen, M. J. Greig, E. A. Lesnik, K. G. Sprankle, R. H. Griffey, J. S. Kiley, S. M. Freier, *J. Am. Chem. Soc.* **1995**, *117*, 831–832.

Cylindrical Molecular Brushes**

Peter Dziezok, Sergei S. Sheiko, Karl Fischer, Manfred Schmidt,* and Martin Möller

Regular brush- or comblike macromolecules are principally accessible by homopolymerization of macromonomers. Until recently, however, the degree of polymerization of the main chain did not significantly exceed the length of the macromonomer itself, and almost spherical or starlike structures were obtained. The work presented here was initiated by a report from Tsukahara et al., who successfully polymerized methacryloyl end functionalized polystyrene macromonomers with extremely high degrees of polymerization ($P_w \approx 1000$).[1] The subsequent characterization clearly demonstrated that such molecules adopt the structure of a cylindrical brush with an extremely stiff main chain and a Kuhn statistical segment length of $l_k \approx 1000-2000$ Å.[2] The stiffness of the normally flexible polymethacrylic main chain originates from overcrowding of the side chains; a polystyrene chain with a molar mass of 2000–4000 g mol^{-1} is attached to the main chain every 2.5 Å.[3–5]

[*] Prof. Dr. M. Schmidt, Dipl.-Chem. P. Dziezok, Dr. K. Fischer
Institut für Physikalische Chemie der Universität
Jakob-Welder-Weg 11, D-55128 Mainz (Germany)
Fax: Int. code + (6131) 39-2970
e-mail: mschmidt@mzdmza.zdv.uni-mainz.de
Dr. S. S. Sheiko, Prof. Dr. M. Möller
Abteilung Organische Chemie III/Makromolekulare Chemie
der Universität Ulm (Germany)

[**] This work was supported by the Deutsche Forschungsgemeinschaft.

We report here on the synthesis and structure of a polymacromonomer consisting of poly-2-vinylpyridine (PVP). Compared to polystyrene (PS), polyvinylpyridine has many advantages: It is easily converted into a polyelectrolyte brush, complexed by heavy metal ions, and undergoes strong interactions with various polar substrates. The PVP macromonomer was prepared according to Scheme 1. The

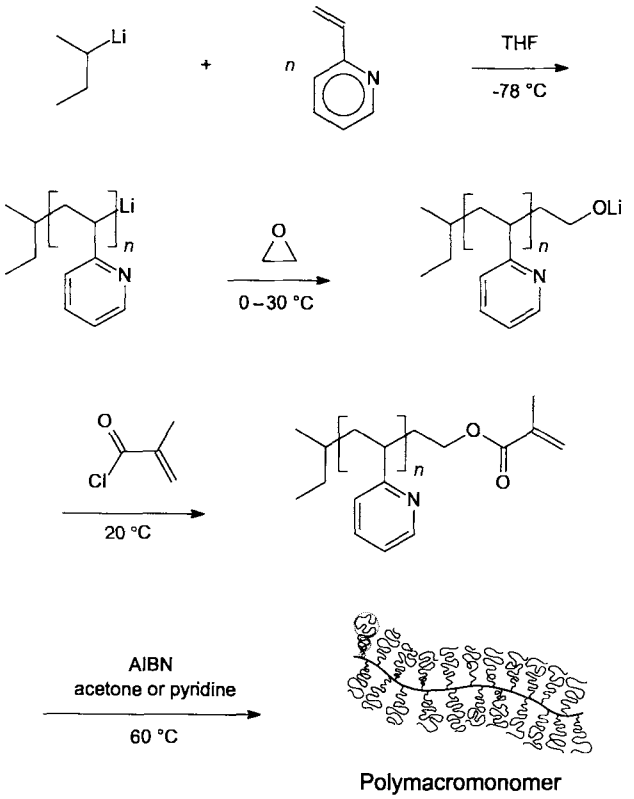

Scheme 1. Synthesis of the PVP polymacromonomer; AIBN = azobis(isobutyronitrile).

success of the synthesis was monitored by matrix-assisted laser-desorption/ionization time-of-flight (MALDI-TOF) mass spectrometry (Figure 1). Free radical polymerization

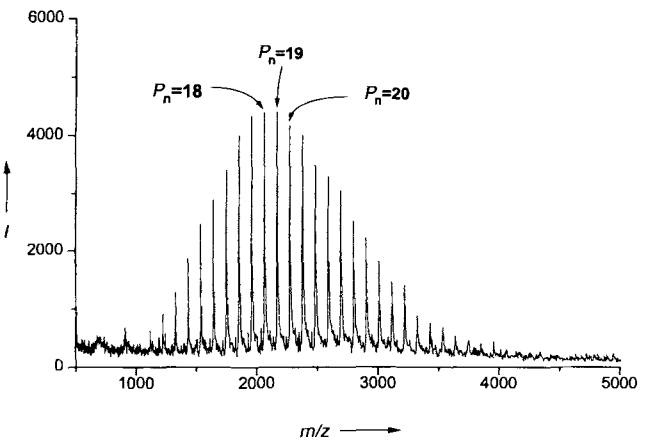

Figure 1. MALDI-TOF mass spectrum of a PVP macromonomer (intensity I in arbitrary units). The signals indicate different degrees of polymerization (P_n). The molar masses for the individual peaks are within ±0.5 Dalton of the expected molar masses of the end-functionalized PVP.

 © WILEY-VCH Verlag GmbH, D-69451 Weinheim, 1997 0570-0833/97/3624-2812 $ 17.50+.50/0

of the PVP macromonomers ($M_n = 2.350\,g\,mol^{-1}$, $M_w/M_n = 1.07$) yields the polymacromonomer with high degrees of polymerization (see Table 1). To achieve high molar masses the macromonomer has to be very clean, and the polymerization has to be conducted at high concentrations (i. e., 70% macromonomer in acetone or pyridine) to form a highly viscous solution which strongly decreases the diffusion of the growing chain even at low conversion. In contrast to PS polymacromonomers, PVP polymacromonomers could not yet be characterized by multi-angle light-scattering gel permeation chromatography (GPC), because of bleeding of particles (80–100 nm in size) from the column in DMF, the solvent of choice for PVP.

Table 1. Results of light-scattering experiments with cylindrical PVP brushes.

Sample	M_w [g mol^{-1}]	R_g [nm]	R_h [nm]	l_k [a]
PVP-PMA	2.7×10^6	70	34	900

[a] Calculated from R_g and R_h by assuming a Schulz–Flory distribution of the molar mass.

The PVP polymacromonomers were deposited from a dilute solution on freshly cleaved mica. To visualize single molecules a highly diluted solution ($c = 0.02\,g\,L^{-1}$) of PVP polymacromonomers in chloroform was sprayed onto mica (Figure 2). Owing to the strong interaction of PVP with mica the molecules are "squeezed" onto the surface, as their width $d = 10 \pm 1$ nm is significantly larger than their height $h = 2.3 \pm 0.1$ nm. The width was estimated by considering the radius of the AFM tip (AFM = atomic force micro), which was determined to be $r_a = 8-10$ nm as described before.[10] In addition, the width can be determined from the lateral periodicity in the condensed films (see Figures 4–6). Both values agree fairly well. Assuming an ellipsoidal cross section with $h = 2.3 \pm 0.1$ nm and $d = 10 \pm 1$ nm and taking into account the known ratio of mass to length, the density within a single macromolecule is determined to be $\rho = 0.87 \pm 0.2\,g\,cm^{-3}$. This value is consistent within experimental uncertainty with the bulk density of PVP. As shown in Figure 2b, the diameter of the molecules vary within one molecule to resemble a caterpillar. The periodicity along the contour line is roughly 20 nm. The uneven thickness of the molecules is consistent with laterally inhomogeneous structures observed for planar polymer brushes at intermediate grafting densities.[11–13]

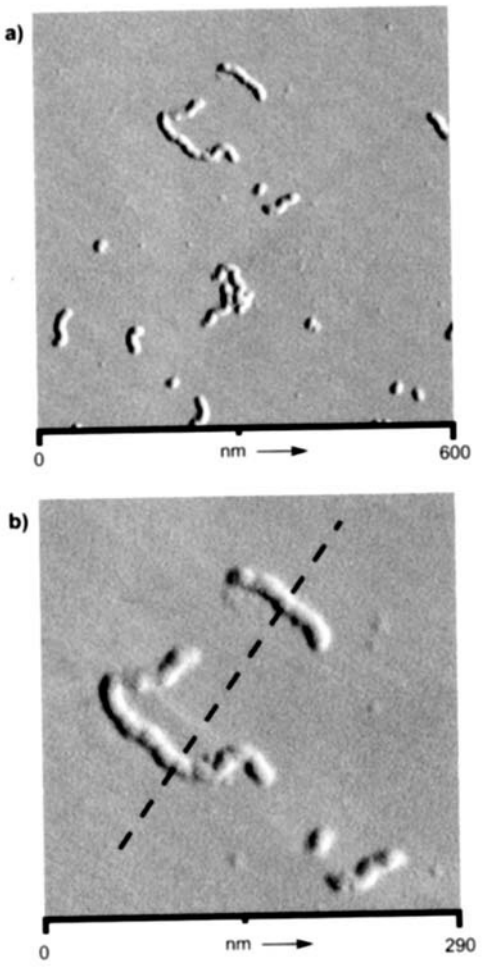

Figure 2. a), b) AFM images of cylindrical brushes of polyvinylpyridine prepared by spraying a solution in chloroform ($0.02\,g\,L^{-1}$) onto the surface of mica. b) The enlargement makes clear the caterpillarlike shape of the brushes. The thickness of the adsorbed molecules was determined to 2.2 nm from the cross-sectional profile recorded along the dashed line.

To exclude the possibility that the caterpillarlike structures consist of end-to-end aggregated short segments, we compared the mean length of the molecules with the absolute molar mass determined by static light-scattering experiments. The lengths of 278 molecules were averaged to yield a number average contour length of $L_n^{AFM} = 57$ nm and a weight average contour length of $L_w^{AFM} = 89$ nm. A histogram of the chain-length distribution is given in Figure 3. The value of L_w^{AFM} has

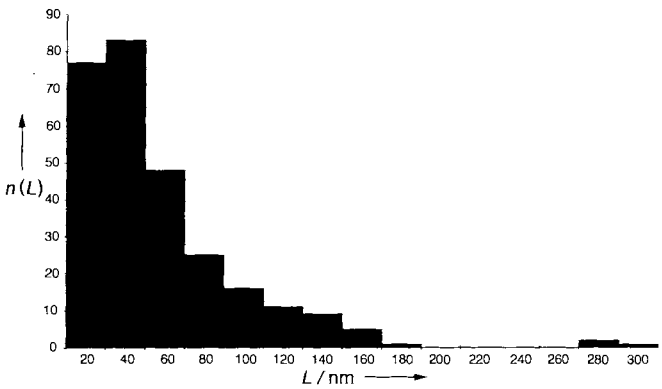

Figure 3. Histogram of the chain-length distribution measured by AFM.

to be related to the molar mass $M_w = 2.7 \pm 0.1 \times 10^6\,g\,mol^{-1}$, which was determined by light-scattering experiments in ethyl methyl ketone (MEK). Assuming an all-*trans* conformation for the main chain, a value of $L_w^{LS} = 287$ nm results, which is clearly larger. This comparison qualitatively demonstrates that the AFM technique provides images of "real" cylindrical brushes and not end-associated short fragments. However, the problem is to how to account quantitatively for the difference between L_w^{AFM} and L_w^{LS}; this seems to be beyond the experimental error of either technique.

Owing to the lack of good solvents for PVP, aggregation could falsely increase the molar mass determined by light-scattering experiments in MEK. Comparison with data on PS cylindrical brushes dissolved in the excellent solvent toluene render this possibility as extremely improbable, as both cylindrical brushes exhibit almost identical molecular characteristics (i. e., identical Kuhn statistical segment lengths). This

 © WILEY-VCH Verlag GmbH, D-69451 Weinheim, 1997 0570-0833/97/3624-2813 $ 17.50+.50/0

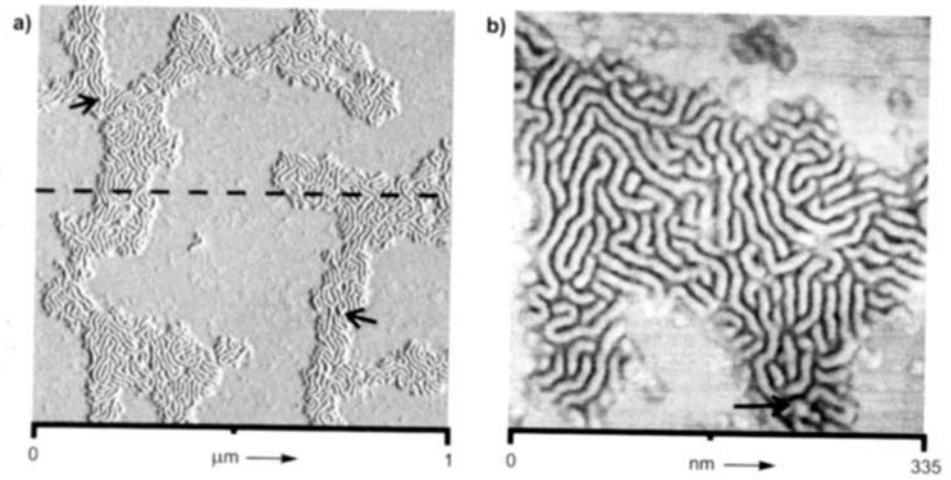

Figure 4. a) Amplitude and b) phase AFM images of a thin film prepared by spin-casting the polyvinylpyridine brushes onto the surface of mica from a solution in chloroform (0.07 $g L^{-1}$). The phase image of the enlarged area (bottom left in a) allows complete resolution of single molecules with clear discrimination of the chain ends. The cross-sectional profile recorded along the dashed line in a) yields a monolayer thickness of 2.2 ± 0.2 nm. The two arrows in a) indicate crossed molecules which are shown in detail in Figure 5.

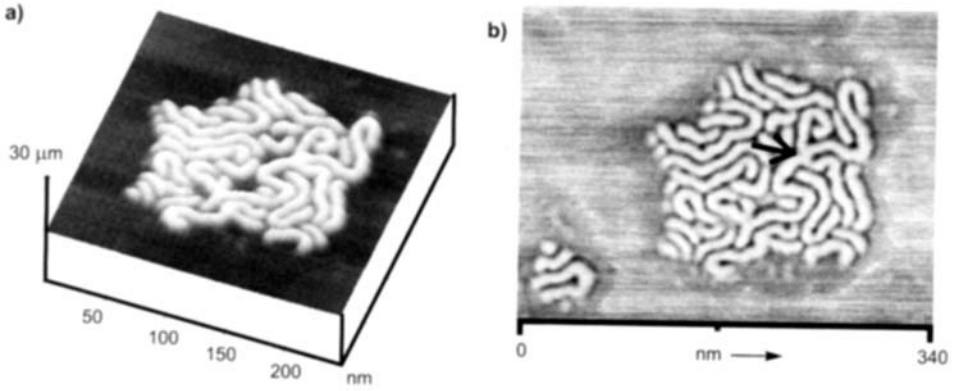

Figure 5. a) Three-dimensional and b) phase AFM images of a monolayer island obtained by spin-casting a solution in chloroform (0.04 $g L^{-1}$) onto mica. Two crossed molecules are marked by the arrow in b). The enlarged topographic image in a) clearly shows that one molecule lies above the other.

agreement is expected, because the chain stiffness should not depend on the chemical nature of the monomer units but rather on the degree of spatial overcrowding of the side chains, which is comparable for both samples. Alternatively, the contour length per monomer unit could be less than 2.5 Å (the value for an all-*trans* chain) due to a helical conformation of the main chain. This would yield the contour length per monomer unit to be only 0.8 Å, which seems to be too small. Even in the most extended rodlike conformation a radius of gyration of $R_g \approx 45$ nm would result; this is much smaller than the measured value of $R_g \approx 70$ nm. We are currently investigating this discrepancy.

To prepare monolayers a drop of a solution of polymer in chloroform (concentrations between 0.02 and 1 $g L^{-1}$) was typically spin-casted onto mica. Depending on the concentrations the polymer forms a more or less incomplete monolayer with an uniform thickness of about 2.2 nm (Figure 4, $c = 0.07\ g L^{-1}$). The small depositions in the dewetted areas of the substrate are attributed to a small fraction of unchanged PVP macromonomers. The topographic and phase images in Figure 4 demonstrate remarkable contrast and resolution of the densely packed brushes. Apparently, individual molecules do not overlap; that is, the side chains of adjacent molecules do not interdigitate. The formation of hairpins (tight backfolds) might be explained by the dewetting process in which capillary forces as well as adsorption are effective.[14]

At higher magnification it can be seen that some molecules in the monolayer lie across others (marked by arrows in Figure 4, 5). The height at the intersections shown in Figure 5a is about 3.2 nm, which is smaller than twice the thickness of the monolayer (4.4 nm). This might indicate either some deformation or molecular interdigitation of the side chains of the two polymers at the crossing point. Crossed and backfolded molecules are also depicted in Figure 6, which shows a fragment of a sample where the substrate was covered completely by a monolayer prepared by spin-casting a solution of concentration 0.14 $g L^{-1}$. Again, the irregularly but densely packed molecules hardly overlap with the exception of the crossed molecules, which are seen in the micrograph in Figure 6 as protrusions above the film surface. When the samples were annealed above the glass-transition temperature, the observed structures do not change.

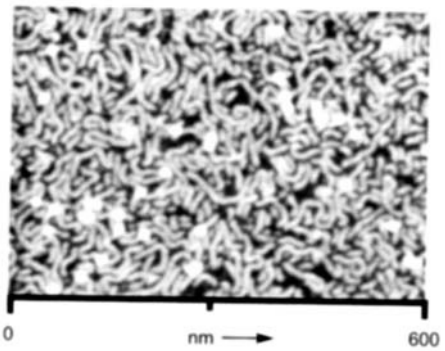

Figure 6. A height AFM image of a complete monolayer prepared by spin-casting a solution in chloroform (0.14 $g L^{-1}$). The white areas correspond to elevations due either to crossed molecules or protruding chain ends.

 © WILEY-VCH Verlag GmbH, D-69451 Weinheim, 1997 0570-0833/97/3624-2814 $ 17.50+.50/0

In conclusion, intersections and hairpins are rather typical defects in the regular packing or ordering of the brushes in monolayers. This documents the essential differences in the adsorption behavior of linear flexible macromolecules and stiff brushes;[15-17] the latter are more likely to form trains rather than loops on the surface. A more perfect order—that is, straightening and disentangling of the brushes—may be enforced by charging the vinylpyridine units chemically. Therefore, such polyelectrolyte brushes may constitute a unique system for preparing striped patterns whose periodicity is defined on a sub 10 nm scale.

Experimental Section

The PVP macromonomer with a methacrylate end group was prepared by anionic polymerization as shown in Scheme 1. Tetrahydrofuran was dried over $LiAlH_4$, degassed by three freeze–thaw cycles on a vacuum line, and then destilled directly into the reaction vessel. 2-Vinylpyridine (2-VP) was dried over calcium hydride for 24 h, degassed, and destilled under reduced pressure. 2-VP (20–25 g) was dissolved in THF (≈500 mL), and the polymerization started at about −90 °C by *sec*-BuLi. The solution was dark red. After completion of the polymerization the "living" anions were terminated with excess ethylene oxide. Subsequently, the chains with terminal hydroxy groups were esterified with excess methacryloyl chloride at room temperature for 12 h. The resulting macromonomer was purified three times by precipitation of a solution of 2-propanol with petroleum ether (40–60 °C) and then freeze-dried in benzene.

For the free radical polymerization AIBN (20 mg; purified by recrystallization from methanol), was dissolved in 20 mL of acetone or pyridine and carefully degassed. The macromonomer (5 g) was then dissolved in a solution of the initiator (2.5 mL) for 12 h to yield an extremely viscous solution, which was kept at 60 °C in a thermostate bath for one week. During polymerization a phase separation occured into a polymacromonomer rich gel phase and a liquid phase; towards the end of the reaction only the gel phase was present. Addition of more acetone or pyridine resulted in a homogeneous solution, from which the polymer was precipitated with petroleum ether. The maximum yield of polymer was on the order of 70%. The unchanged macromonomer was fractionated off by precipitation with 2-propanol/petroleum ether (1/2).

The atomic force micrographs were recorded at ambient conditions with a Nanoscope III instrument (Digital Instruments, St. Barbara, USA) operating in the tapping mode [6] at a resonance frequency of about 300 kHz. The Si probes had a spring constant of about 50 $N m^{-1}$. In this mode a cantilever with a sharp tip is oscillated by a piezo driver near its resonance frequency. As the tip taps the surface both the amplitude and the phase of the oscillation change, which allows recording of images with a topographic or viscoelastic contrast [7–9].

Received: June 13, 1997 [Z10544IE]
German version: *Angew. Chem.* **1997**, *109*, 2894–2897

Keywords: atomic force microscopy · nanostructures · polymacromonomers · polymers

[1] Y. Tsukahara, K. Tsutsumi, Y. Yamashita, S. Shimada, *Macromolecules* **1990**, *23*, 5201.
[2] M. Wintermantel, M. Schmidt, Y. Tsukahara, K. Kajiwara, S. Kohjiya, *Macromol. Rapid Commun.* **1994**, *15*, 279.
[3] G. H. Fredrickson, *Macromolecules* **1993**, *26*, 2825.
[4] E. B. Zhulina, O. V. Borisov, V. A. Pryamitsyn, *J. Colloid Interface Sci.* **1990**, *137*, 495.
[5] M. Wintermantel, K. Fischer, M. Gerle, R. Ries, M. Schmidt, K. Kajiwara, H. Urakawa, I. Wataoka, *Angew. Chem.* **1995**, *107*, 1606; *Angew. Chem. Int. Ed. Engl.* **1995**, *34*, 1472.
[6] Q. Zhong, D. Inniss, V. B. Elings, *Surf. Sci.* **1993**, *290*, L688.
[7] M. Radmacher, M. Fritz, C. M. Kacher, J. P. Cleveland, P. K. Hansma, *Biophys. J.* **1996**, *70*, 556.
[8] R. G. Winkler, J. P. Spatz, S. Sheiko, M. Möller, P. Reineker, O. Marti, *Phys. Rev. B* **1996**, *54*, 8908.
[9] N. A. Burnham, O. P. Behrend, F. Oulevey, G. Gremaud, P.-J. Gallo, D. Gourdon, E. Dupas, A. J. Kulik, H. M. Pollock, G. A. D. Briggs, *Nanotechnology* **1997**, 8 (2), 67.
[10] S. S. Sheiko, M. Möller, E. M. C. M. Reuvekamp, H. W. Zandbergen, *Phys. Rev. B* **1993**, *48*, 5675.
[11] K. G. Soga, H. Guo, M. J. Zuckermann, *Europhys. Lett.* **1995**, *29*, 531.
[12] D. F. Siqueira, K. Kohler, M. Stamm, *Langmuir* **1995**, *11*, 3092.
[13] P.-Y. Lai, K. Binder, *J. Chem. Phys.* **1992**, *97*, 586.
[14] A. S. Dimitrov, C. D. Dushkin, H. Yoshimura, K. Nagayama, *Langmuir* **1994**, *10*, 432.
[15] C. C. van der Linden, F. A. M. Leermakers, G. J. Fleer, *Macromolecules* **1996**, *29*, 1172.
[16] A. Matsuyama, K. Umemoto, T. Kato, *J. Chem. Phys.* **1996**, *105*, 1594.
[17] A. R. Khokhlov, F. F. Ternovsky, E. A. Zheligovskaya, *Makromol. Chem. Theory Simul.* **1993**, *2*, 151.

The First Structurally Authenticated σ-Bonded Organosamarium(II) Derivative and Its Reaction with Benzophenone

William Clegg, Colin Eaborn, Keith Izod,* Paul O'Shaughnessy, and J. David Smith

Until recently the organometallic chemistry of the three lanthanide elements stable in the +2 oxidation state (Sm, Eu, Yb) was confined to compounds containing cyclopentadienyl-type ligands.[1] Despite much progress in the synthesis of σ-alkyl derivatives of ytterbium(II) and europium(II),[1b] such as the dialkyl compounds $Yb\{C(SiMe_3)_3\}_2$ and $Eu\{C(SiMe_3)_3\}_2$,[2,3] the isolation of a σ-bonded organosamarium(II) complex has remained an elusive goal. We now describe the synthesis and molecular structure of **1**, which contains Sm–C σ bonds, and report its reaction with benzophenone to give the ketyl radical anion complex **2.** Compound **1** was obtained in high yield from the reaction of $[SmI_2(thf)_2]$ with two equivalents of $K\{C(SiMe_3)_2(SiMe_2OMe)\}$ in THF and isolated as air-sensitive, deep green-black crystals.

$[Sm\{C(SiMe_3)_2(SiMe_2OMe)\}_2(thf)]$ **1**

$[Sm\{C(SiMe_3)_2(SiMe_2OMe)\}_2(OCPh_2)]$ **2**

An X-ray diffraction study[4] of **1** revealed that the samarium atom lies in a distorted square pyramidal environment with each alkyl ligand bound through both its carbanion center and the oxygen atom of its methoxy substituent to give a four-membered chelate ring. The coordination sphere of samarium is completed by a molecule of THF at the apex of the pyramid (Figure 1). The Sm–C1 and Sm–C2 distances of 2.787(5) and 2.845(5) Å, respectively, are the first Sm^{II}–C σ bonds lengths to be measured. These values are about 0.3–0.5 Å larger than those found for the Sm^{III}–$C(sp^3)$ bonds in $Sm\{CH(SiMe_3)_2\}_3$ (2.33(2) Å)[5] and for the terminal alkyl group in $[(thf)Li(\mu\text{-}CH_2SiMe_3)(\mu\text{-}OAr)Sm(CH_2SiMe_3)(\mu\text{-}OAr)_2Li(thf)]$ (2.451(10) Å; Ar = 2,6-$iPrC_6H_3$).[6] A smaller difference of about 0.19 Å between the Sm^{II}–C and the Sm^{III}–C σ bonds would be expected from consideration of the reported ionic radii for Sm^{II} and Sm^{III}.[7] The Sm–O1, Sm–O2, and Sm–O(thf) distances in **1** are similar to several previously determined Sm^{II}–O(thf) distances.[8,9]

[*] Dr. K. Izod, Prof. W. Clegg, P. O'Shaughnessy
Department of Chemistry, University of Newcastle upon Tyne
Newcastle upon Tyne, NE1 7RU (UK)
fax: Int. code +(191)2226929
e-mail: k.j.izod@ncl.ac.uk
Prof. C. Eaborn, Dr. J. D. Smith
School of Chemistry, Physics and Environmental Science
University of Sussex
Falmer, Brighton, BN1 9QJ (UK)

 © WILEY-VCH Verlag GmbH, D-69451 Weinheim, 1997 0570-0833/97/3624-2815 $ 17.50+.50/0

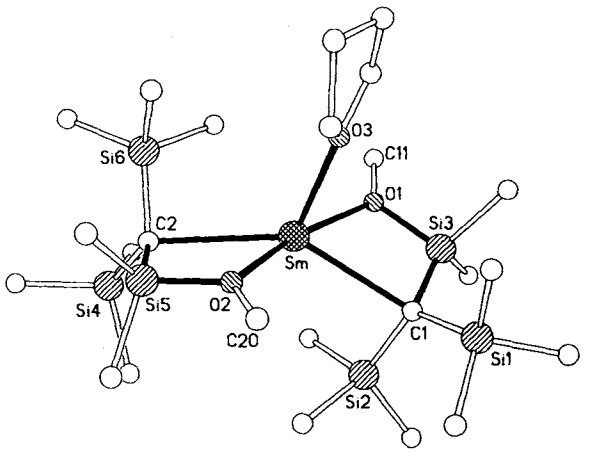

Figure. 1. Molecular structure of **1**. Selected bond lengths [Å] and angles [°]: Sm–C1 2.787(5), Sm–C2 2.845(5), Sm–O1 2.570(3), Sm–O2 2.520(3), Sm–O3 2.545(4); C1-Sm-O1 62.11(12), C1-Sm-C2 144.67(12), C1-Sm-O3 101.06(13), O3-Sm-O1 90.40(13), C2-Sm-O3 110.43(13), O2-Sm-O3 84.55(12).

Samarium diiodide is widely used as a reagent in organic synthesis and is believed to give organosamarium intermediates in Barbier-type SmI_2-mediated additions of alkyl halides to ketones.[10,11] We were interested to see whether ketones would undergo a Grignard-type reaction with **1** or give a ketyl radical anion complex similar to the recently described $[Sm^{III}(OC_6H_3\text{-}2,6\text{-}t\text{Bu-}4\text{-}Me)_2(OC_{13}H_8)(thf)_2]$ (**3**), isolated as an intermediate in the pinacol coupling of fluorenone.[12]

Reaction of **1** with one equivalent of benzophenone in light petroleum resulted in an immediate color change from dark green to deep purple. Crystallization of the resulting compound **2** from methylcyclohexane gave dark purple crystals, which exhibited broad peaks in their ^1H NMR spectrum that could be assigned to the alkyl ligands, but no signals for the benzophenone.

An X-ray crystallographic study revealed that **2** has a very similar molecular structure to **1**,[13] but with a molecule of benzophenone bound through its oxygen atom in place of the THF (Figure 2). The essentially isostructural nature and identical coordination numbers of **1** and **2** allow the bond lengths and angles within the two molecules to be compared directly and provide a method for determining whether the benzophenone is bound as a neutral ketone or as a ketyl radical anion. The Sm–C1 and Sm–C2 distances in **2** are 2.625(5) and 2.631(5) Å, respectively, approximately 0.19 Å shorter than the corresponding bond lengths in **1** (consistent with a change in oxidation state from Sm^{II} to Sm^{III}).[7] Similarly, the Sm–O1 and Sm–O2 distances of 2.367(3) and 2.387(3) Å in **2** are approximately 0.17 Å shorter than the corresponding distances in **1**. This strongly indicates that **2** is a Sm^{III} complex of a ketyl radical anion. In support of this, bond lengths and angles within the benzophenone fragment are very similar to those found for fluorenone in **3**.[12] The absence of signals due to benzophenone in the ^1H NMR spectrum of **2** is also consistent with its being bound as a delocalized ketyl radical anion.

In contrast to the behavior observed for **3**, we observed no change upon dissolution of **2** in noncoordinating solvents such as light petroleum or methylcyclohexane. This may be because the sterically demanding alkyl ligands in **2** impede further reaction.

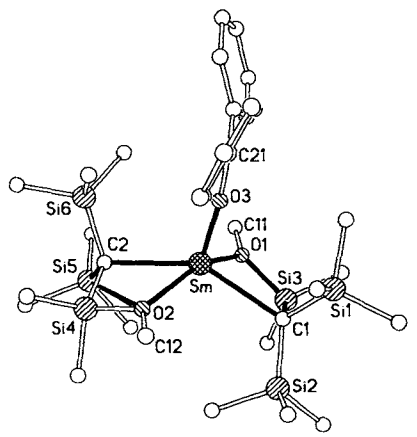

Figure. 2. Molecular structure of **2**. Selected bond lengths [Å] and angles [°]: Sm–C1 2.625(5), Sm–C2 2.631(5), Sm–O1 2.367(3), Sm–O2 2.387(3), Sm–O3 2.093(3), C21–O3 1.346(6); C1-Sm-O1 66.10(13), C1-Sm-C2 142.33(15), C1-Sm-O3 105.81(14), O3-Sm-O1 107.93(13), C2-Sm-O3 111.67(14), O2-Sm-O3 99.12(12).

Experimental Section

1: A solution of $[K\{C(SiMe_3)_2(SiMe_2OMe)\}]$ (0.99 g, 3.45 mmol) in THF (30 mL) was added to a solution of $[SmI_2(thf)_2]$ (0.97 g, 1.77 mmol) in THF (20 mL). The mixture was stirred at room temperature for three days, the solvent then removed under reduced pressure, and the residue extracted with methylcyclohexane (40 mL). The extract was filtered and the filtrate concentrated to 10 mL, then kept at −30 °C for 12 h to give dark green crystals of **1**. Yield 0.90 g (71 %), m.p. 120 °C (decomp); elemental analysis calcd. for $C_{24}H_{62}O_3Si_6Sm$: C 40.14, H 8.71;. found C 39.23, H 8.81; ^1H NMR (500 MHz, C_6D_6, 25 °C): $\delta = -9.22$ (s, 6H; $SiMe_3$), −7.06 (s, 3H; MeO), 4.28 (s, 18H; $SiMe_3$), 6.94 (s, br, 2H; THF), 19.29 (s, br, 2H, THF); EIMS (70 eV): *m/z* (%): 648 (18) $[M^+ - THF]$, 249 (20) $[C(SiMe_3)_2(SiMe_2OMe)$ (R)], 233 (100) [RH − Me], 217 (30) [RH − MeO], 73 (90) $[Me_3Si]$.

2: A solution of benzophenone (0.01 g, 0.2 mmol) in light petroleum (b.p. 40–60 °C, 5 mL) was added to a solution of **1** (0.15 g, 0.21 mmol) in the same solvent (15 mL). The mixture was stirred for 1 h and the solvent then removed under vacuum. The residue was crystallized from cold (−30 °C) methylcyclohexane (2 mL) to give deep purple crystals of **2**. Yield 0.08 g (69 %), m.p. 105 °C (decomp); ^1H NMR (500 MHz, C_6D_6, 25 °C): $\delta = -1.81$ (s, 3H; OMe), −0.12 (s, br, 18H; $SiMe_3$), 3.25 (s, br, 6H; $SiMe_2$).

Received: June 9, 1997 [Z 10525 IE]
German version: *Angew. Chem.* **1997**, *109*, 2925–2926

Keywords: alkyl compounds · ketones · radical ions · samarium · silicon

[1] a) W. J. Evans, *Polyhedron* **1987**, *6*, 803–835; b) F. T. Edelmann, *Angew. Chem.* **1995**, *107*, 2647–2669; *Angew. Chem. Int. Ed. Engl.* **1995**, *34*, 2466–2488.

[2] C. Eaborn, P. B. Hitchcock, K. Izod, J. D. Smith, *J. Am. Chem. Soc.* **1994**, *116*, 12071–12072.

[3] C. Eaborn, P. B. Hitchcock, K. Izod, Z.-R. Lu, J. D. Smith, *Organometallics* **1996**, *15*, 4783–4790.

[4] Crystal data for $C_{24}H_{62}O_3Si_6Sm$ **1**: $M_r = 717.6$, crystal dimensions $0.28 \times 0.16 \times 0.12$ mm^3, monoclinic, $P2_1$, $a = 9.4931(9)$, $b = 16.5417(16)$, $c = 12.3227(12)$ Å, $\beta = 106.773(3)°$, $V = 1852.7(3)$ Å^3, $Z = 2$, $\rho_{calcd.} = 1.286$ g cm^{-3}, $Mo_{K\alpha}$ radiation ($\lambda = 0.71073$ Å), $\mu = 1.80$ mm^{-1}, $T = 160$ K. 11830 data (6524 unique, $R_{int} = 0.0267$, $2\theta < 56.8°$) were collected on a Siemens SMART CCD area detector diffractometer using 0.3° steps in ω and were corrected semiempirically for absorption (transmission 0.621–0.789). The structure was solved by heavy-atom methods and refined on F^2 values for all data (G. M. Sheldrick, SHELXTL-manual, Siemens Analytical X-ray Instruments Inc., Madison, USA, **1994**) to give $R_w = \{\Sigma[w(F_o^2 - F_c^2)]/\Sigma[w(F_o^2)^2]\}^{1/2} = 0.0707$, conventional R value $R = 0.0312$ for F values of 5928 reflections with $F_o^2 > 2\sigma(F_o^2)$, $S = 1.007$ for 336 parameters. All non-H atoms were refined anisotropically, H atoms were constrained with a riding model. Twofold disorder was resolved for one CH_2 group of the THF molecule. The residual electron density extremes were +0.93/−0.67 e Å^{-3} [13b].

[5] P. B. Hitchcock, M. F. Lappert, R. G. Smith, R. A. Bartlett, P. P. Power, *J. Chem. Soc. Chem. Commun.* **1988**, 1007–1009.

 © WILEY-VCH Verlag GmbH, D-69451 Weinheim, 1997 0570-0833/97/3624-2816 $ 17.50+.50/0

[6] D. L. Clark, J. C. Gordon, J. C. Huffman, J. G. Watkin, B. D. Zwick, *Organometallics* **1994**, *13*, 4266–4270.
[7] R. D. Shannon, *Acta Crystallogr. Sect. A* **1976**, *32*, 751–767.
[8] W. J. Evans, D. K. Drummond, H. Zhang, J. L. Atwood, *Inorg. Chem.* **1988**, *27*, 575–579.
[9] W. J. Evans, T. S. Gummersheimer, J. W. Ziller, *J. Am. Chem. Soc.* **1995**, *117*, 8999–9002.
[10] a) G. A. Molander, *Chem. Rev.* **1992**, *92*, 29–68; b) *ibid.* **1996**, *96*, 307–338; c) T. Imamoto, *Lanthanides in Organic Synthesis*, Academic Press, London, **1994**.
[11] a) D. P. Curran, T. L. Fevig, M. J. Totleben, *Synlett* **1990**, 773–774; b) J. L. Namy, J. Collin, C. Bied, H. B. Kagan, *ibid.* **1992**, 733–734.
[12] Z. Hou, T. Miyano, H. Yamazaki, Y. Wakatsuki, *J. Am. Chem. Soc.* **1995**, *117*, 4421–4422.
[13] a) Crystal data for $C_{33}H_{64}O_3Si_6Sm$ **2**: $M_r = 827.7$, crystal dimensions $0.20 \times 0.10 \times 0.08$ mm^3, monoclinic, $P2_1/c$, $a = 14.8555(2)$, $b = 12.5108(2)$, $c = 23.9352(3)$ Å, $\beta = 105.960(2)^\circ$, $V = 4276.99(10)$ Å^3, $Z = 4$, $\rho_{calcd.} = 1.285$ g cm^{-3}, $\mu(Mo_{K\alpha}) = 1.57$ mm^{-1}. 25355 data (9695 unique, $R_{int} = 0.0826$, $2\theta < 56.7^\circ$), transmission 0.584–0.890. Methods were as for **1**. $R_w = 0.0951$, $R = 0.0551$ (5710 F values), $S = 0.984$ for 403 parameters, residual electron density extremes $+1.02/-1.56$ e Å^{-3}. b) Crystallographic data (excluding structure factors) for the structures reported in this paper have been deposited with the Cambridge Crystallographic Data Center as supplementary publication no. CCDC-100466. Copies of the data can be obtained free of charge on application to The Director, CCDC, 12 Union Road, Cambridge CB2 1EZ (fax: Int. code + (1223) 336-033; e-mail: deposit@chemcrys.cam.ac.uk).

Stuctural Reorganization of Anthracene-Bridged Stilbenoids by Oxidation and Reduction**

Andreas Knorr and Jörg Daub*

Compounds with conjugated extended π-electron systems are most promising for generating new optoelectronic materials and models for energy and electron transfer as well as for mimicking charge separation. Furthermore, there are additional conceivable applications in display and optical storage devices, electrochromic materials, and systems for optoelectronic switching.[1] Simple stilbenoid pyrenes and anthracenes were recently studied due to their electrochemically generated luminescence (ECL) and application in organic light-emitting diodes (OLEDs).[2] Here we report the oxidation and reduction properties of anthracene systems **5** and **6**, which are composed of electron transfer active stilbenoid subunits that are covalently linked through the 9,10-positions of anthracene. The investigations by cyclic voltammetry and spectroelectrochemical combination techniques were supplemented by semiempirical quantum mechanical calculations.

Derivatives **1**, **4**, and **5** was synthesized by a Wittig reaction of [2-(anthraquinone)methyl]triphenylphosphonium bromide with anthracene-9-carbaldehyde (formation of **1**) or from [3-(10-methyl-10*H*-phenothiazinyl)methyl]triphenylphosphonium bromide with 10-methyl-9-anthracenecarbaldehyde (formation of **4**) or anthracene-9,10-dicarbaldehyde (formation of **5**). Compound **2** was obtained by the reaction of 5,10-dihydro-5,10-dimethyl-2-phenazincarbaldehyde with (9-anthrylmethyl)triphenylphosphonium bromide, and **6** was synthesized by a random 1:1 Wittig reaction of anthracene-9,10-dicarbaldehyde with [11-(dibenzo[*a*,*c*]phenazinyl)methyl]triphenylphosphonium bromide followed by treatment of the formed monoaldehyde with [3-(10-methyl-10*H*-phenothiazinyl)methyl]triphenylphosphonium bromide. Compound **3** was obtained by the reaction of 10-methyl-9-anthracenecarbaldehyde with [11-(dibenzo[*a*,*c*]phenazinyl)methyl]triphenylphosphonium bromide. All reactions, except for the synthesis of **1** (in EtOH/NEt_3), were carried out in THF under an N_2 atmosphere with *n*BuLi as base,[3] and led exclusively to (*E*)-stilbenes; the analogous (*Z*)-stilbenes could never be detected.[4]

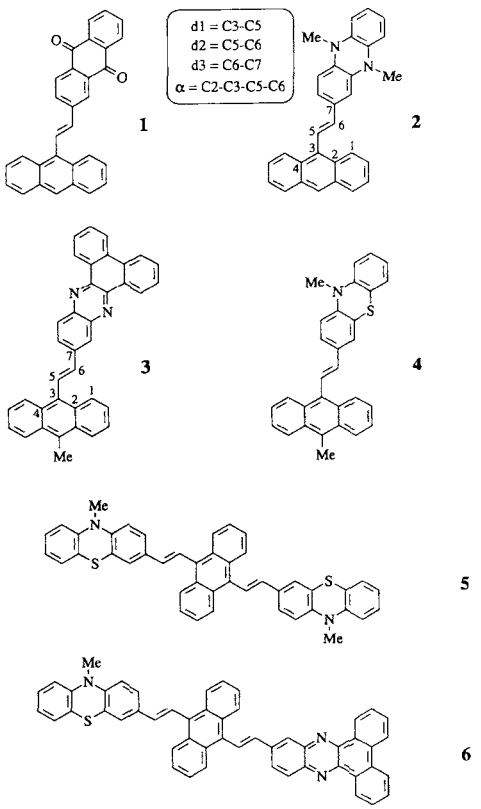

Investigations of **1**–**6** by cyclic voltammetry show reversible oxidations and/or reductions. With the exception of the two-electron wave for the oxidation of **5**, all redox reactions involve the transfer of one electron. The electrochemical processes take place at significantly lower potential than for the corresponding basis compounds (Table 1), which indicates an interaction between the functional groups and the anthracene unit. Even the comparison of the oxidations of **4** and **5** as well as of the second reduction steps of **3** and **6** demonstrates the effect of this interaction (Table 1).

Spectroelectrochemistry confirms the findings of cyclic voltammetry and provides insight into the absorption characteristics of the radical ions and respective dications and dianions. Compounds **1**–**6** show a significant red shift of the lowest energy absorption bands when compared with the corresponding absorption bands for radical ions of the basis compounds (Table 1). Doubly charged species such as dianions $\mathbf{1}^{2-}$, $\mathbf{3}^{2-}$, and $\mathbf{6}^{2-}$ or dications $\mathbf{2}^{2+}$ and $\mathbf{5}^{2+}$ exhibit strong absorptions in the near-infrared region, which is in agreement with the presence of a highly delocalized quinoid species (Table 1 as well as Figures 1 and 2).

[*] Prof. J. Daub, Dr. A. Knorr
Institut für Organische Chemie der Universität
Universitätsstrasse 31, D-93040 Regensburg (Germany)
Fax: Int. code + (941) 943-4984
e-mail: joerg.daub@chemie.uni-regensburg.de

[**] This work was supported by the Bundesministerium für Forschung und Technologie (BMBF, grant 03N1004C6). A.K. gratefully acknowledges a Doktoranden-Stipendium from the Fonds der Chemischen Industrie and a Forschungs-Stipendium from the Deutsche Forschungsgemeinschaft.

 © WILEY-VCH Verlag GmbH, D-69451 Weinheim, 1997 0570-0833/97/3624-2817 $ 17.50+.50/0

Table 1. Data from cyclic voltammetry [a] and spectroelectrochemistry of **1**–**6**.

Compound		$E_{1/2}$ [mV]	N(e^-) [b]	λ_{max} [nm] [c]	Solvent
1 [d]	red 1	−1260	1	1040	MeCN
	red 2	−1820	1	1040	MeCN
	red 3	−2285	1	–	MeCN
	ox	E_{pa} 820	irrev	–	MeCN
2 [d]	red	−2250	1	–	MeCN
	ox 1	−250	1		MeCN
	ox 2	435	1	1035	MeCN
3 [d]	red 1	−1825	1	1300 (sh)	THF
	red 2	−2260	1	1020	THF
4 [d]	red 1	−2255	1	–	MeCN
	red 2	E_{pc} −2620	irrev	–	MeCN
	ox	280	1	1190	MeCN
5 [d]	red	E_{pc} −2215	irrev	–	CH_2Cl_2
	ox 1	175	2	1015	CH_2Cl_2
	ox 2	680	1	–	CH_2Cl_2
6 [d]	red 1	−1810	1	1325	THF
	red 2	−1990	1	1031	THF
	ox	290	1	1365	THF

[a] A standard one-compartment, three-electrode arrangement was used with a platinium-disc working electrode and a pseudo Ag/AgCl reference. The reversible oxidation signal of ferrocene/ferrocenium (FOC) was used as an internal standard. Tetra-*n*-butylammonium hexafluorophosphate (TBAHFP) was the supporting electrolyte in all measurements, and the scan rates were 250 mV s^{-1}. All experiments were carried out under N_2. [b] The number of transferred electrons was obtained by referencing against ferrocene. [c] After cyclic voltammetry the solutions of substrate were transferred with a syringe into the previously described spectroelectrochemical cell [7]. [d] Reference compounds: anthraquinone red 1 −1320 mV/980 nm, red 2 −1920 mV/638 nm (MeCN); 9,10-dimethylphenazine ox 1 −245 mV/724 nm, ox 2 509 mV/538 nm (MeCN); phenothiazine ox 325 mV/846 nm (MeCN); 11-methyldibenzo[*a*,*c*]-phenazine red 1 −1920 mV/928 nm, red 2 /590 nm, anthracene red −2415 mV, ox E_{pa} 900.

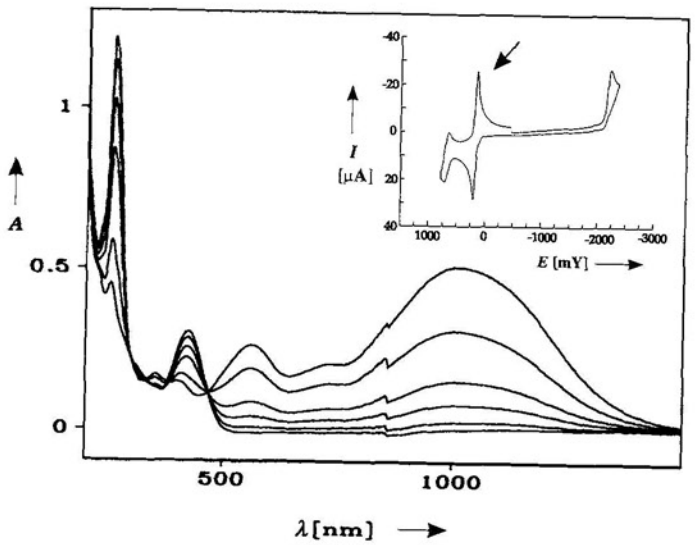

Figure 1. Spectroelectrochemistry of the oxidation of **5** to 5^{2+}; inset: the cyclovoltammogram.

To clarify the molecular and electronic structures of the species obtained by reduction and oxidation, semiempirical quantum mechanical calculations with the programs AM1 and PM3 were carried out for **2** and **3**.[5] The calculated bond lengths and dihedral angles (Table 2) allow the following conclusions: The neutral compounds show a basically decoupled set of chromophores, whereas the corresponding radical cations or anions exhibit increased interaction between the stilbenoid subunits. This is indicated by a decrease in the dihedral angles and by changes in the bond length (Table 2).

Table 2. Calculated bond lengths and dihedral angles for **2** and **3**.

	Compound	d1 [Å]	d2 [Å]	d3 [Å]	α [°]
AM1 calculations	**2**	1.460	1.342	1.453	61
	$2^{\bullet+}$	1.458	1.345	1.449	56
	2^{2+}	1.368	1.433	1.367	8
	3	1.461	1.341	1.455	64
	$3^{\bullet-}$	1.452	1.352	1.434	56
	3^{2-}	1.365	1.430	1.366	7
PM3 calculations	**2**	1.466	1.339	1.460	72
	$2^{\bullet+}$	1.463	1.343	1.455	65
	2^{2+}	1.371	1.430	1.369	5
	3	1.467	1.338	1.461	81
	$3^{\bullet-}$	1.461	1.344	1.449	66
	3^{2-}	1.367	1.432	1.366	7

The doubly charged ions of **2** and **3** have almost planar quinoid structures; comparable results were obtained for **1**, **5**, and **6** (Figure 2).[6] The lowest energy UV transitions for the

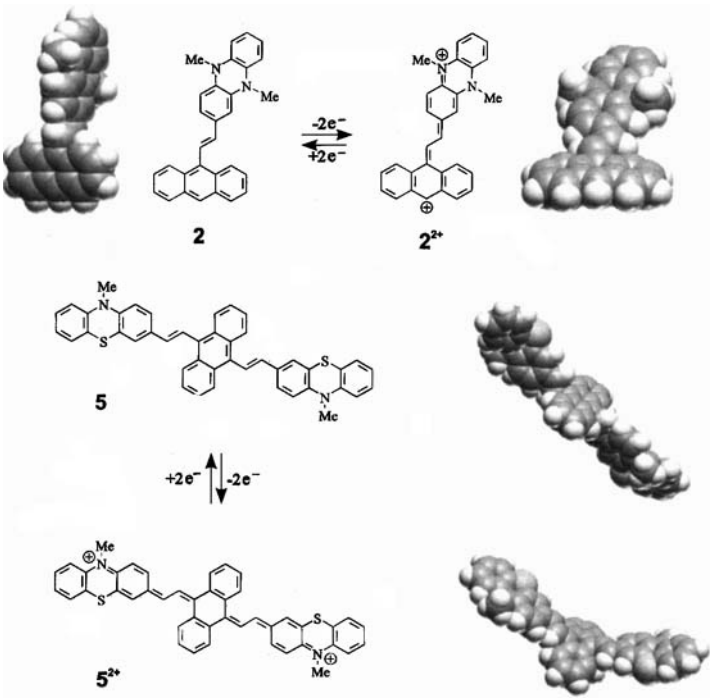

Figure 2. Calculated structures (AM1) of the neutral molecules as well as the dications of **2** and **5**.

dications and dianions of **2** and **3** evaluated by semiempirical limited-CI calculations using a continuum solvent model[8] and the predicted planar quinoid structure are in good agreement with the experimental data: For 2^{2+} the HOMO–LUMO-dominated allowed transitions at 854 (AM1, MeCN) and 1096 nm (PM3, MeCN) were obtained (experimental: 1035 nm, MeCN). For 3^{2-} the calculation yields HOMO–LUMO-dominated allowed transitions at 915 (AM1, CH_2Cl_2) and 1332 nm (PM3, CH_2Cl_2; experimental: 1020 nm, THF.)

The experimental and theoretical findings show that one-electron transfer results in increased coupling of the subunits which do not interact in the neutral forms. The formation of the doubly charged species is accompanied with even more

 © WILEY-VCH Verlag GmbH, D-69451 Weinheim, 1997 0570-0833/97/3624-2818 $ 17.50+.50/0

severe structural reorganization: The perpendicular benzoid system is transformed into a planar quinoid structure (Figure 2).

Received: May 14, 1997
Revised version: August 14, 1997 [Z10439IE]
German version: *Angew. Chem.* **1997**, *109*, 2926–2929

Keywords: arenes · cyclic voltammetry · electron transfer · radical ions · stilbenes

[1] J.-M. Lehn, *Supramolecular Chemistry*, VCH, Weinheim **1995**; H. Meier, *Angew. Chem.* **1992**, *104*, 1425; *Angew. Chem. Int. Ed. Engl.* **1992**, *31*, 199.

[2] A. Knorr, J. Daub, *Angew. Chem.* **1995**, *107*, 2925; *Angew. Chem. Int. Ed. Engl.* **1995**, *34*, 2664; J. Daub, M. Beck, A. Knorr, H. Spreitzer, *Pure Appl. Chem.* **1996**, *68*, 1399; K. Kelnhofer, A. Knorr, J. Daub, Y.-H. Tak, H. Bässler, *Acta Polym.* **1997**, *48*, 188.

[3] A. Knorr, Dissertation, Universität Regensburg, **1995**; F. Effenberger, C.-P. Niesert, *Synthesis* **1992**, 1137; G. Bartocci, U. Mazzucato, A. Spalletti, G. Orlandi, G. Poggi, J. *Chem Soc. Faraday Trans.* **1992**, 3139; T. Arai, T. Karatsu, H. Misawa, Y. Kuriyama, H. Okamoto, T. Hiresaki, H. Furuuchi, H. Zeng, H. Sakuragi, K. Tokumaru, *Pure Appl. Chem.* **1988**, *60*, 989.

[4] **1**: M.p. 281.5–282.5 °C, red needles, yield 27%, purification by column chromatography on SiO_2 with CH_2Cl_2; **2**: m.p. 208–209 °C, red crystals, yield 80%, purification by recrystallization from CH_2Cl_2/hexanes; **3**: m.p. 322 °C (decomp), microcrystalline orange solid, yield 28%, no purification necessary, filtration from the mother liquor; **4**: m.p. 195 °C, yellow needles, yield 100%, purification by column chromatography on SiO_2 with CH_2Cl_2/hexanes (1/1) and recystallization from CH_2Cl_2/hexanes; **5**: m.p. 317–319 °C, yellow microcrystalline solid, yield 62%, purification by column chromatography on SiO_2 with CH_2Cl_2/hexanes (1/1) and recystallization from $CHCl_3$; **6**: m.p. 235 °C (decomp), dark red solid, yield 67%, purification by column chromatography on SiO_2 with CH_2Cl_2/hexanes (1/1) and recrystallization from CH_2Cl_2/hexanes.

[5] a) AM1: M. J. S. Dewar, E. G. Zoebisch, E. F. Healy, J. J. P. Stewart, *J. Am. Chem. Soc.* **1985**, *107*, 3902; b) PM3: J. J. P. Stewart, *J. Comput. Chem.* **1989**, *10*, 209; c) G. Rauhut, A. Alex, J. Chandrasekhar, T. Steinke, T. Clark, VAMP5.01, Oxford Molecular Ltd., Oxford, **1993**. d) The geometries of closed-shell species were optimized using the RHF formalism, and those of open-shell species were treated with the AUHF formalism. All obtained structures were characterized as stationary points on the energy surface by vibrational analysis.

[6] The calculations of the neutral species showed that rotation about bond d1 leads to two transition states with dihedral angles α of 10° and 90°: **2** (10°): 8.80 (AM1), 4.20 kcal mol^{-1} (PM3); **3** (10°): 8.53 (AM1), 4.46 kcal mol^{-1} (PM3); **2**: (90°): 0.34 (AM1), 0.05 kcal mol^{-1} (PM3); **3** (90°): 0.25 (AM1), 0.03 kcal mol^{-1} (PM3). Activation enthalpies of 1.63 to 1.26 kcal mol^{-1} were found for rotation about bond d3 depending on the model system and the hamiltonian used. An analagous calculation for the correponding dication of **2** and dianion of **3** showed that rotation about bonds d1, d2, and d3 have activation barriers between 21.18 and 26.25 kcal mol^{-1}, again depending on the compound and the semiempirical method applied. It is remarkable that rotation about bond d2 (a formal single bond) leads to such high energy barriers. Furthermore, according to the semiempirical calculations the s-*cis* conformation of these doubly charged species represents a transition state and not a minimum on the energy surface of the rotation process (all transition states were characterized by vibrational analysis).

[7] H. Spreitzer, M. Scholz, G. Gescheidt, J. Daub, *Liebigs Ann.* **1996**, 2069.

[8] For the limited-CI calculation the four highest occupied and four lowest unoccupied orbitals using only single and pairwise double excitation microstates were considered. Implementation of a perpendicular geometry for 2^{2+} and 3^{2} in the calculation of the UV transitions yields numbers that significantly deviate from the experimental findings. For computational details, see ref. [5c].

Complexes with Sb_2 and *cyclo*-Sb_3 Ligands: The Tetrahedranes $[\{C_5H_5(CO)_2Mo\}_2Sb_2]$, $[C_5H_5(CO)_2MoSb_3]$, and $[C_5Me_5(CO)_2MoSb_3]$**

Hans Joachim Breunig,* Roland Rösler, and Enno Lork

Dedicated to Professor Ionel Haiduc on the occasion of his 60th birthday

Although complexes with organosubstituent-free *cyclo*-P_n or *cyclo*-As_n ligands ($n = 3-6$) have been investigated intensively,[1] analogous compounds with *cyclo*-Sb_n ligands have not yet been described. Known complexes contain Sb_1,[1] Sb_2,[2] Sb_3^{3-},[3] Sb_7^{3-}[4] or organoantimony rings[5] as ligands. An interesting example of an Sb_2 complex is the tetrahedrane derivative **1**,[2] described by Rheingold, which can be considered an analogue of Sb_4. We report here on a favorable synthesis of **1** and on the preparation and the structure of **2** and **3**, the first complexes with *cyclo*-Sb_n ligands.

$[\{C_5H_5(CO)_2Mo\}_2Sb_2]$ **1**

$[C_5H_5(CO)_2MoSb_3]$ **2**

$[C_5Me_5(CO)_2MoSb_3]$ **3**

Compounds **1** and **2** are formed by the reaction[6] of $(t\mathrm{BuSb})_4$[7] with $[\{C_5H_5Mo(CO)_3\}_2]$ in boiling toluene. Although the Sb:Mo molar ratio of approximately 3:1 should favor the formation of **2**, the main product is **1**. Complex **2** forms in 2.3% yield as dark red, crystal needles with a metallic luster. Solutions of **2** in toluene or benzene are yellow. The crystals decompose at 110 °C and turn black. The analogous reaction of $(t\mathrm{BuSb})_4$ with $[\{C_5Me_5Mo(CO)_3\}_2]$ produced red needles of **3** in 27% yield. All three compounds are air-sensitive. The identity of the compounds was confirmed by elemental analysis and by ^{1}H NMR, IR and mass spectra. The structures of **2** and **3** were determined by X-ray structure

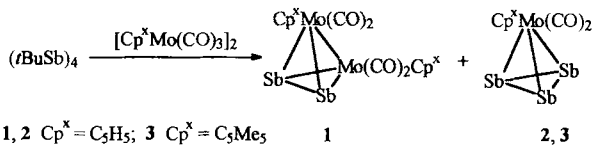

1, 2 $Cp^x = C_5H_5$; **3** $Cp^x = C_5Me_5$ **1** **2, 3**

analysis.[8] Complex **2** crystallizes with two independent molecules in the asymmetric unit. Both molecules contain slightly distorted tetraehedral $MoSb_3$ units in which the antimony atoms form an almost equilateral triangle. The average Sb–Sb bond length in **2** is 274.94(10) pm. This is considerably shorter than the Sb–Sb single bond lengths in $MeC(CH_2Sb)_3$ (280–282 pm),[9] $(t\mathrm{BuSb})_4$ (281.8(2) pm),[8b] or Sb_7^{3-} (287.6–290.6 pm),[3] but longer than Sb–Sb multiple bond lengths (double bond in $[\{C_5H_5Mo(CO)_2\}_2Sb_2]$

[*] Prof. Dr. H. J. Breunig, R. Rösler, Dr. E. Lork
Institut für Anorganische und Physikalische Chemie (FB 02)
der Universität
Postfach 330440, D-28334 Bremen (Germany)
Fax: Int. code + (421) 218-4042
e-mail: breunig@chemie.uni-bremen.de

[**] This work was supported by the Deutsche Forschungsgemeinschaft. We thank Prof. O. Scherer and his group at the Universität Kaiserslautern for the support given to R.R. during during a research visit.

267.8(1) pm,[2] triple bond in $[Sb_2\{W(CO)_5\}_3]$ 266.3(3) pm[10]). The average Mo–Sb bond length in **2** is 290.25(10) pm, which is longer than those in **1** (276.2(1), 285.4(1) pm).[2]

The molecular structure of **3** is shown in Figure 1. The distorted tetrahedral $MoSb_3$ unit resembles very closely the

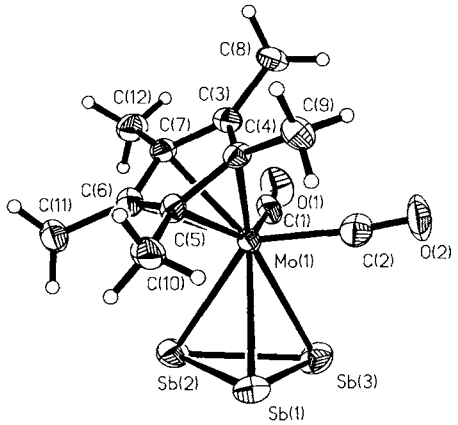

Figure 1. Molecular structure of **3** in the crystal. Selected bond lengths [pm] and mean angles [°]: Sb(1)–Sb(2) 276.82(8), Sb(1)–Sb(3) 274.25(10), Sb(2)–Sb(3) 273.97(9), Mo(1)–Sb(1) 285.12(8), Mo(1)–Sb(2) 286.00(9), Mo(1)–Sb(3) 292.52(9); Sb-Sb-Sb 60.00(2), Sb-Sb-Mo 61.47(2), Sb-Mo-Sb 56.06(2).

$MoSb_3$ unit in **2**. The crystal packing of **2** and **3** is, however, different (Figures 2 and 3). In both cases the molecules

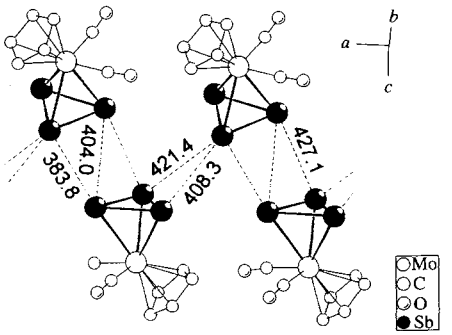

Figure 2. Selected contacts between the molecules in the crystal of **2** with Sb–Sb contact distances smaller than 440 pm.

associate through close intermolecular Sb···Sb contacts to form supramolecular units. In the case of **2** the relevant intermolecular contact distances range from 383.8–427.1 pm, within the van der Waals limit of 440 pm. Similar short Sb···Sb contact distances are also found in thermochromic organo distibanes Me_4Sb_2 (368 pm)[11] and $(Me_3Si)_4Sb_2$ (399 pm),[12] and the organo cyclostibanes $(2,4,6\text{-}Me_3C_6H_2Sb)_4$ (390 pm)[13] and $MeC(CH_2Sb)_3$ (397-401 pm).[9] The molecules in **2** associate to form to corrugated bands, which overlap like roofing tiles. The $[C_5H_5Mo(CO)_2]$ units lie above and below the antimony layers. In the crystal of **3** the molecules are associated through intermolecular Sb···Sb interactions with distances of 374.5 and 383.4 pm. The number of contacts between the molecules is smaller, because the pentamethylcyclopentadienyl groups shield the tetrahedrane molecules more thoroughly.

Experimental Section

1 and **2**: $(t\text{BuSb})_4$ (2.00 g) and $[\{C_5H_5(CO)_3Mo\}_2]$ (2.00 g) are stirred under reflux in 70 mL toluene for about 6 h. The dark red solution is decanted, and the black precipitate washed with 50 mL toluene. The solvent is removed from the combined extracts under reduced pressure, and the residue washed with 2 × 80 mL petroleum ether. The purple red powder that was not dissolved by petroleum ether was taken up in toluene (20 mL), combined with Al_2O_3 (10 g), dried to a flowing powder under reduced pressure, and placed on a chromatography column (3 × 10 cm neutral Al_2O_3 according to Brockmann, particle size 0.063–0.200 mm, degree of activity II). Compound **2** is eluted as a yellow fraction with petroleum ether/toluene (10/1) and crystallizes after concentration of the solution. Yield 50 mg (2.3%). ^1H NMR (360 MHz, C_6D_6, 25 °C): $\delta = 4.22$ (s, C_5H_5); IR (toluene): $\tilde{\nu} = 1962$, 1910 cm^{-1} (C≡O); MS (EI, 70 eV): *m/z*: 584 (90) $[M^+]$, 556 (50) $[M^+ - CO]$, 528 (100) $[M^+ - 2CO]$. Thereafter a broad red fraction is obtained with toluene giving crystals of **1** upon concentration. Yield 0.96 g, 76%. The ^1H NMR, IR and MS data are in accordance with the literature. [2]

3: The reaction of $(t\text{BuSb})_4$ (1.63 g) with $[\{C_5Me_5(CO)_3Mo\}_2]$ (0.85 g) and subsequent work-up are performed analogously. However, the crude material is not washed with petroleum ether. By successive chromatography with petroleum ether, petroleum ether/toluene (12/1), petroleum ether/toluene (8/1), and petroleum ether/toluene (2/1) four fractions are obtained. The first fraction contains 65 mg $(t\text{BuSb})_4$, the third (0.37 g $[\{C_5Me_5Mo(CO)_2\}_2]$). Concentration of the fourth fraction and cooling to −20 °C yields red needles of **3** (0.47 g, 27%). m.p. 198–199 °C (decomp.); ^1H NMR (360 MHz, C_6D_6, 25 °C) $\delta = 1.70$ (s, CH_3); IR (toluene): $\tilde{\nu} = 1951$, 1897 cm^{-1} (C≡O); MS (EI, 70 eV): *m/z*: 654 (40) $[M^+]$, 626 (20) $[M^+ - CO]$, 596 (100) $[M^+ - 2CO]$.

Received: July 8, 1997 [Z10651IE]
German version: *Angew. Chem.* **1997**, *109*, 2941–2942

Keywords: antimony · molybdenum · Sb ligands · structure elucidation

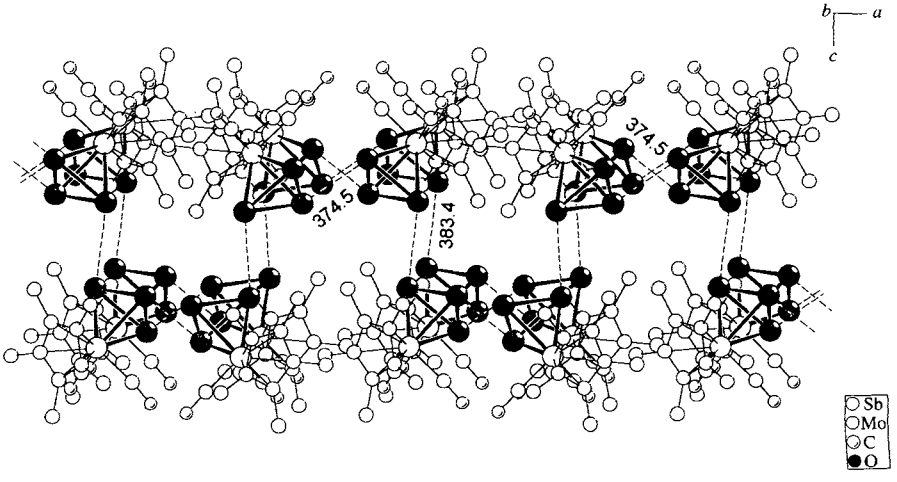

Figure 3. Side view of a layer of molecules in the crystal of **3**.

[1] O. J. Scherer, *Angew. Chem.* **1990**, *102*, 1137–1155; *Angew. Chem. Int. Ed. Engl.* **1990**, *29*, 1104–1122; M. Scheer, E. Herrmann, *Z. Chem.* **1990**, *30*, 41–55; A.-J. DiMaio, A. L. Rheingold, *Chem. Rev.* **1990**, *90*, 169–190.
[2] J. R. Harper, A. L. Rheingold, *J. Organometal. Chem.* **1990**, *390*, C36.
[3] W. J. Evans, S. L. Gonzales, J. W. Ziller, *J. Chem. Soc. Chem. Commun.* **1992**, 1138–1139.
[4] U. Bolle, W. Tremel, *J. Chem. Soc. Chem. Commun.* **1994**, 217–219; S. Charles, B. W. Eichhorn, A. L. Rheingold, S. G. Bott, *J. Am. Chem. Soc.* **1994**, *116*, 8077–8086.
[5] J. Ellermann, A. Veit, *J. Organomet. Chem.* **1985**, *290*, 307–319; H. J. Breunig, J. Pawlik, *Z. Anorg. Allg. Chem.* **1995**, *621*, 817–822.
[6] J. Queisser, H. Oesen, D. Fenske, B. Lehari, *Z. Anorg. Allg. Chem.* **1994**, *620*, 1821–1831; J. Queisser, H. Oesen, D. Fenske, H. Schottmüller, *ibid.* **1996**, *622*, 1731–1739; O. M. Kekia, R. L. Jones, Jr., A. L. Rheingold, *Organometallics* **1996**, *15*, 4104–4106.

 © WILEY-VCH Verlag GmbH, D-69451 Weinheim, 1997 0570-0833/97/3624-2820 $ 17.50+.50/0

[7] a) K. Issleib, B. Hamann, L. Schmidt, *Z. Anorg. Allg. Chem.* **1965**, *339*, 298–303; b) O. Mundt, G. Becker, H.-J. Wessely, H. J. Breunig, K. Kischkel, *ibid.* **1982**, *486*, 70–89.

[8] X-ray crystal structure analyses: Siemens P4 four-circle diffractometer, $Mo_{K\alpha}$ radiation, $\lambda = 71.073$ pm, scan mode ω^2/θ, $T = 173(2)$ K, absorption correction DIFABS, structure solution: direct methods with SHELXS-86, refinement: full-matrix least-squares against F^2, refinement program SHELXL-93, hydrogen atoms geometrically positioned and refined with a riding model. **2**: crystal dimensions $0.6 \times 0.5 \times 0.1$ mm^3, triclinic, space group $P\bar{1}$, $a = 715.60(10)$, $b = 1243.3(2)$, $c = 1387.7(2)$ pm, $\alpha = 105.490(10)$, $\beta = 96.330(10)$, $\gamma = 104.329(10)°$, $V = 1.1321(3)$ nm^3, $Z = 4$, $\rho_{calcd} = 3.416$ Mg m^{-3}, $\theta_{max.} = 27.50°$, 10436 measured reflections, 5137 unique ($R_{int} = 0.0752$), absorption coefficient 8.130 mm^{-1}, number of free parameters 237, final R value($I > 2\sigma I$), $R1 = 0.0600$, $wR2 = 0.1448$. **3**: crystal dimensions $0.7 \times 0.3 \times 0.3$ mm^3, orthorhombic, space group $Pbca$, $a = 1256.00(10)$, $b = 906.80(10)$, $c = 2874.4(3)$ pm, $V = 3.2738(6)$ nm^3, $Z = 8$, $\rho_{calcd} = 2.647$ Mg m^{-3}, $\theta_{max.} = 27.48°$, 4137 measured reflections, 3142 unique ($R_{int} = 0.0306$), absorption coefficient 5.638 mm^{-1}, number of free parameters 170, final R value ($I > 2\sigma I$), $R1 = 0.0387$, $wR2 = 0.0757$. The crystallographic data (excluding structural factors) for the structures reported in this publication have been deposited as supplementary publication no. CCDC-100534 at the Cambridge Crystallographic Data Centre. Copies of the data can be obtained free of charge on application to The Director, CCDC, 12 Union Road, Cambridge CB2 1EZ, UK (fax: int. code + (1223) 336-033; e-mail:deposit@chemcrys.cam.ac.uk).

[9] J. Ellermann, E. Köck, H. Burzlaff, *Acta Cryst. Sect. C* **1985**, *41*, 1437–1439.

[10] G. Huttner, U. Weber, B. Sigwarth, O. Scheidsteger, *Angew. Chem.* **1982**, *94*, 210–211; *Angew. Chem. Int. Ed. Engl.* **1982**, *21*, 215–216; *Angew. Chem. Suppl.* **1982**, 414–416.

[11] O. Mundt, H. Riffel, G. Becker, A. Simon, *Z. Naturforsch. B* **1984**, *39*, 317–322; A. J. Ashe III, E. G. Ludwig, J. Oleksyszyn, J. C. Huffman, *Organometallics* **1984**, *3*, 337–338.

[12] G. Becker, H. Freudenblum, C. Witthauer, *Z. Anorg. Allg. Chem.* **1982**, *492*, 37–51.

[13] M. Ates, H. J. Breunig, S. Gülec, W. Offermann, K. Häberle, M. Dräger, *Chem. Ber.* **1989**, *122*, 473–478.

A Novel Approach to the CP-225,917 and CP-263,114 Core**

K. C. Nicolaou,* Maarten H. D. Postema, Neil D. Miller, and Guang Yang

The naturally occurring substances CP-263,114 (**1**) and CP-225,917(**2**) possess intriguing molecular architecture,[1] important biological properties, and an interesting mechanism of action.[2] As inhibitors of squalene synthase and farnesyl transferase, these substances are attractive from the pharmaceutical point of view, particularly with regards to lowering cholesterol levels and to treating cancer. Isolated from an unidentified species of fungi, these compounds include within their structures a novel bicyclo[4.3.1]dec-1(9),4-dien-10-one framework onto which a variety of substituents are attached. We have previously reported on an approach to the central core of these molecules relying on an intramolecular Diels–Alder reaction.[3]

In preliminary studies designed to explore the feasibility of a strategy towards the total synthesis of the CP molecules involving a rhodium-catalyzed carbenoid generation and intramolecular trapping, followed by a divinylcyclopropane rearrangement[4] and a radical cyclization (Scheme 1) the core

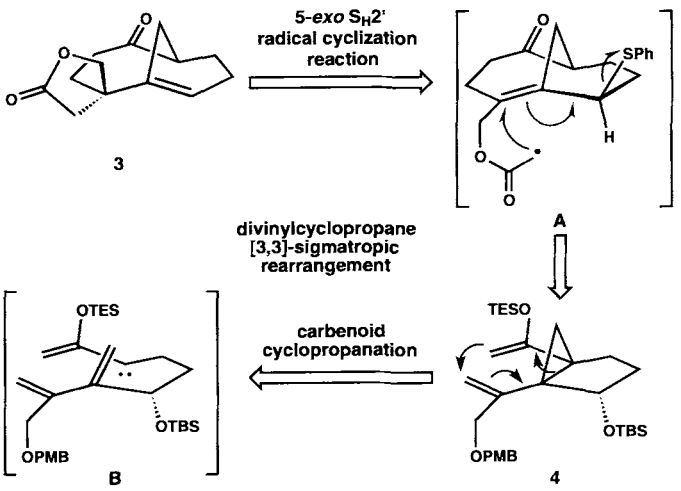

Scheme 1. Retrosynthetic analysis of the CP core model system **3**.

model system **3** was defined as a target. We wish to report here the execution of this strategy, which culminated in the construction of racemic **22** which has the opposite stereochemistry at the quaternary center.

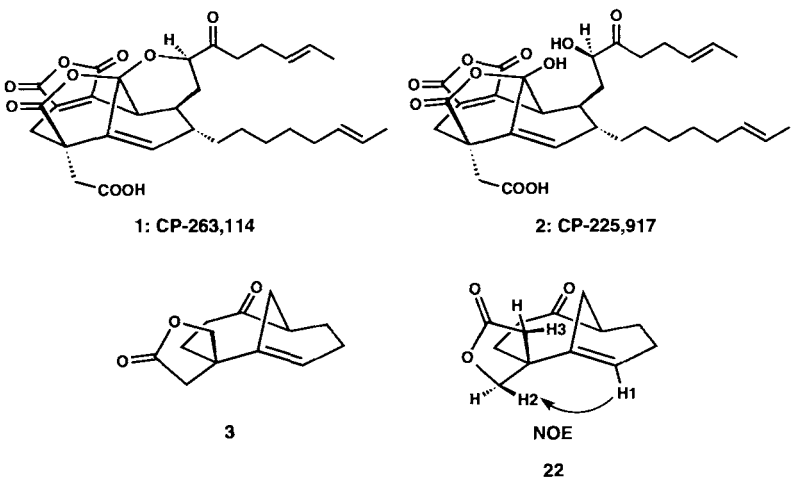

The synthesis of the requisite ketocyclopropane **15** proceeded as summarized in Scheme 2. Thus, methyl vinyl ketone (**5**) was treated with formaldehyde under Baylis–Hillman[5] conditions to afford, after *p*-methyoxybenzylation,[6] compound **6** in 25% overall yield. Formation of the enol triflate from **6** (60% yield), followed by palladium-catalyzed coupling with $Me_3SnSnMe_3$ resulted in the formation of vinyltin compound **7** (73% yield). Metal exchange followed by reaction with $TBSO(CH_2)_4CHO$ and silylation furnished bis(silyl)ether **8** in 80% overall yield. Sequential deprotection, Swern and $NaClO_2/NaH_2PO_4$/2-methyl-2-butene oxidations, followed by exposure of the resulting carboxylic acid to

[*] Prof. Dr. K. C. Nicolaou, Dr. M. H. D. Postema, Dr. N. D. Miller, Dr. G. Yang
Department of Chemistry and The Skaggs Institute for Chemical Biology
The Scripps Research Institute
10550 North Torrey Pines Road, La Jolla, CA 92037 (USA)
Fax: Int. code + (619) 784-2469
and
Department of Chemistry and Biochemistry
University of California, San Diego
9500 Gilman Drive, La Jolla, CA 92093 (USA)

[**] This work was financially supported by The Skaggs Institute for Chemical Biology and the National Institutes of Health (USA). We thank Dr. Dee H. Huang and Dr. Gary Siuzdak for help with NMR spectroscopy and mass spectrometry, respectively.

 © WILEY-VCH Verlag GmbH, D-69451 Weinheim, 1997 0570-0833/97/3624-2821 $ 17.50+.50/0

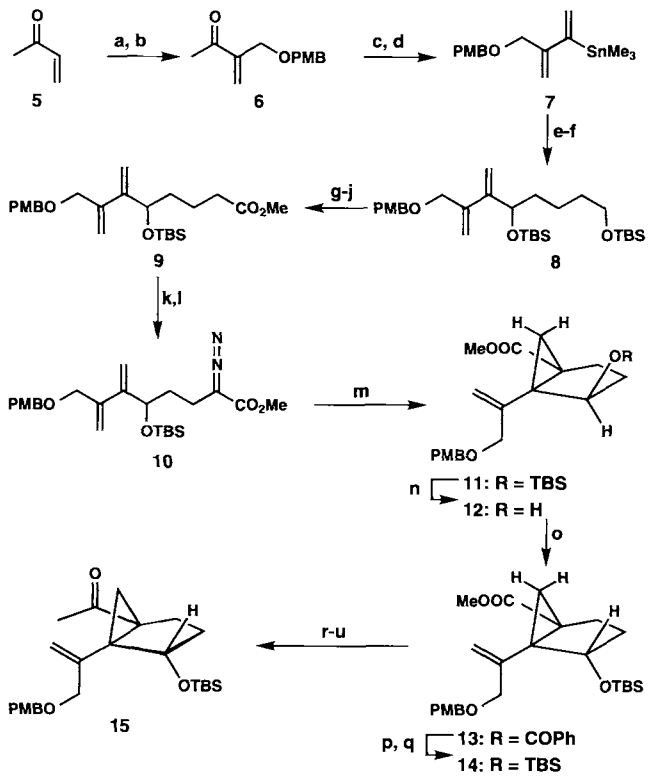

Scheme 2. Synthesis of ketocyclopropane **15**. a) DABCO (0.3 equiv), CH_2O (1.1 equiv), THF, 0→23°C, 48 h, 30%; b) $PMBOC(NH)CCl_3$ (2.0 equiv), CSA (0.1 equiv), CH_2Cl_2, 23°C, 3 h, 78%; c) NaHMDS (2.0 equiv), $PhNTf_2$ (2.0 equiv), THF, −40°C, 1 h, 60%; d) $Me_3SnSnMe_3$ (1.1 equiv), LiCl (10.0 equiv), $[(Ph_3P)_4Pd]$ (3 mol%), THF, 60°C, 8 h, 73%; e) *n*BuLi (1.1 equiv), THF, −78°C, 20 min; then $TBSO(CH_2)_4CHO$ (1.5 equiv), THF, −78→0°C, 1 h, 86% over two steps; f) TBSCl (2.0 equiv), imidazole (3.0 equiv), DMF, 50°C, 4 h, 94%; g) CSA (0.3 equiv), $MeOH/CH_2Cl_2$, 0°C, 20 min, 91%; h) DMSO (2.0 equiv), $(COCl)_2$ (1.8 equiv), Et_3N (4.0 equiv), CH_2Cl_2, −78°C, 30 min; i) $NaClO_2$ (2.0 equiv), NaH_2PO_4 (3.0 equiv), 2-methyl-2-butene (2.5 equiv), THF, H_2O, *t*BuOH, 0°C, 1 h; j) CH_2N_2, Et_2O, 23°C, 5 min, 87% over three steps; k) KHMDS (2.5 equiv), $PhCO_2Me$ (3.0 equiv), THF, −78→23°C, 4 h, 93%; l) 4-nitrobenzenesulfonyl azide (2.0 equiv), DBU (2.0 equiv), CH_2Cl_2, 0→23°C, 1 h, 95%; m) $Rh_2(OAc)_4$ (3 mol%), CH_2Cl_2, 0°C, 3 min, 87% (**11**:**14** ≈ 6.7:1, ^1H NMR); n) TBAF (1.5 equiv), THF, 0→23°C, 2 h, 95%; o) DEAD (1.5 equiv), Ph_3P (1.5 equiv), $PhCO_2H$ (1.5 equiv), THF, −20→23°C, 95%; p) NaOMe (10.0 equiv), MeOH, 23°C, 18 h, 93%; q) TBSOTf (1.5 equiv), 2,6-lutidine (2.0 equiv), CH_2Cl_2, −78→0°C, 2 h, 98%; r) DIBAL (2.2 equiv), CH_2Cl_2, −78→0°C, 2 h, 86%; s) TPAP (0.2 equiv), NMO (1.2 equiv), 4 Å molecular sieves, CH_2Cl_2, 23°C, 1 h; t) MeMgCl (3.0 equiv), THF, 0°C, 20 min; u) TPAP (0.2 equiv), NMO (1.2 equiv), 4 Å molecular sieves, CH_2Cl_2, 23°C, 1 h, 93% over three steps. CSA = (+)-camphorsulfonic acid; DABCO = 1,4-diazabicyclo[2.2.2]octane; DBU = 1,8-diazabicyclo[5.4.0]undec-7-ene; DEAD = diethyl azodicarboxylate; DIBAL = diisobutylaluminum hydride; DMSO = dimethyl sulfoxide; HMDS = hexamethyldisilazanide; NMO = *N*-methylmorpholine *N*-oxide; TBAF = tetrabutylammonium fluoride; Tf = trifluoromethanesulfonyl; TPAP = tetra-*n*-propylammonium perruthenate.

diazomethane led to methyl ester **9** in 87% overall yield. The diazo ester **10** (Table 1) was synthesized from **9** by a modified Taber procedure.[7] The crucial carbenoid generation and intramolecular trapping[8] was achieved by treatment of diazo compound **10** with catalytic amounts of $Rh_2(OAc)_4$ in CH_2Cl_2 at 0°C, and led predominantly to vinylcyclopropane **11** together with its C-2 diastereoisomer **14** (ca. 6.7:1 by ^1H NMR).[9] The configuration of **11** was inverted by: 1. desilylation (95% yield for **12** and its C-2 diastereoisomer) and 2 chromatographic separation, followed by Mitsunobu inversion[10] of **12** (DEAD-Ph_3P-PhCOOH, 95% yield), leading to benzoate **13**. The inversion was deemed necessary for the pending 5-*exo*-S_H2' radical cyclization, although the stereochemical requirement for this process has not been fully established. Removal of the benzoate group from **13** generated the corresponding alcohol, which was silylated by treatment with TBSOTf/2,6-lutidine to afford compound **14** (98% yield; the minor C-2 diastereoisomer corresponding to **12** was directly converted to **14** by silylation). Finally, the desired ketocyclopropane **15** (Table 1) was reached from **14** by the following sequence: 1. DIBAL reduction (86% yield), 2. NMO/TPAP oxidation,[11] 3. MeMgCl addition, and 4. a second NMO/TPAP oxidation (93% for three steps).

Treatment of **15** with an excess of KHMDS and Et_3N/TESCl at −78°C as prescribed by Ireland[12] gave the intermediate silyl enol ether **16**, which underwent divinylcyclopropane rearrangement[13] at 45°C to give, after removal of both silyl groups, alcohol **4** in 95% overall yield (Scheme 3,

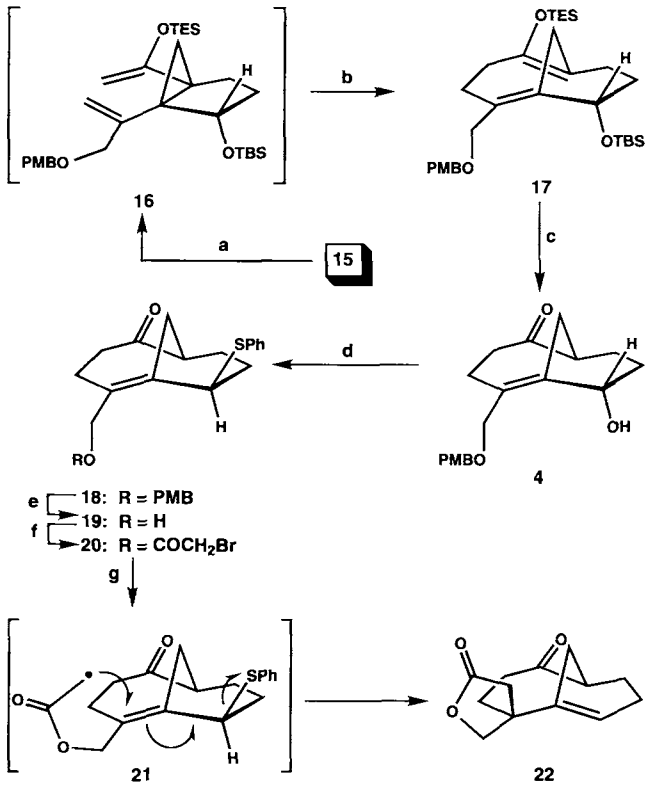

Scheme 3. Synthesis of **22**. a) KHMDS (3.1 equiv), TESCl:Et_3N:THF (3:1:1) (5.1 equiv), THF −78°C, 1 h; b) THF, −78→45°C, 4 h; c) TBAF (3.5 equiv), THF, 0→23°C, 2 h, 95% over two steps; d) PhSSPh (2.0 equiv), nBu_3P (2.0 equiv), C_6H_6, 23°C, 30 min, then **4**, 23°C, 12 h, 65% based on 50% conversion; e) DDQ (1.3 equiv), CH_2Cl_2:H_2O (10:1), 23°C, 6 h, 85%; f) $BrCH_2CO_2H$ (1.5 equiv), DCC (1.6 equiv), 4-DMAP, (0.1 equiv), CH_2Cl_2, 23°C, 1 h, 81%; g) $Me_3SnSnMe_3$ (5.0 equiv), C_6H_6, *hν*, 35°C, 8 h, 61%. DCC = dicyclohexylcarbodiimide; DDQ = 2,3-dichloro-5,6-dicyano-1,4-dibenzoquinone; 4-DMAP = 4-dimethylaminopyridine.

Table 1). The structure of **4** was rigorously assigned by a combination of 2D NMR experiments. Alcohol **4** was then converted to phenyl sulfide **18** (65% based on 50% conversion) by a modified Mitsunobu-type reaction,[14] and the PMB group was exchanged for an α-bromoacetate moiety, furnishing compound **20** via **19** (69% yield over two steps). Exposure of bromosulfide **20** to $Me_3SnSnMe_3$ and irradiation (hv) in degassed benzene led to lactone **22** (61%) by means of radical intermediates (e.g. **21**) and ring closure with concomitant expulsion of sulfenyl radical (see Scheme 3).[15] This last operation served admirably to simultaneously generate the required quaternary center (albeit

 © WILEY-VCH Verlag GmbH, D-69451 Weinheim, 1997 0570-0833/97/3624-2822 $ 17.50+.50/0

Table 1. Selected physical properties of compounds **4**, **10**, **15**, and **22**.

10: yellow oil; $R_f = 0.69$ (ethyl acetate/benzene 9/1); FT-IR (CH_2Cl_2 cast): $\tilde{\nu}$= 2953, 2359, 2081, 1696, 1612, 1514, 1438, 1249, 1188, 1085, 836, 777 cm^{-1}; ^1H NMR (600 MHz, C_6D_6): $\delta = 7.23$ (m, 2H, Ar*H*), 6.80 (m, 2H, Ar*H*), 5.36 (s, 1H, C=C*H*H), 5.28 (s, 1H, C=CH*H*), 5.24 (s, 1H, C=C*H*H), 5.23 (s, 1H, C=CH*H*), 4.54 (dd, $J = 5.2, 5.2$ Hz, 1H, TBSO-C*H*), 4.34 (d, $J = 11.5$ Hz, 1H, ArCH*H*), 4.31 (d, $J = 11.5$ Hz, 1H, ArC*H*H), 4.06 (d, $J = 12.5$ Hz, 1H, C=CCH*H*), 4.02 (d, $J = 12.5$ Hz, 1H, C=CC*H*H), 3.36 (s, 3H, C(O)OCH_3), 3.30 (s, 3H, ArOCH_3), 2.23–2.38 (m, 2H, CH_2), 1.74–1.84 (m, 2H, CH_2), 0.97 (s, 9H, $(CH_3)_3$CSi), 0.06 (s, 3H, CH_3Si), 0.04 (s, 3H, CH_3Si); ^{13}C NMR (150.9 MHz, C_6D_6): δ = 159.7, 148.7, 143.2, 130.8, 129.5, 114.1, 114.0, 112.9, 72.5, 71.9, 71.8, 54.7, 51.3, 35.1, 26.0, 19.4, 18.4, −4.5, −5.1 (the carbonyl and diazo carbons do not appear in this spectrum); HR-MS: calcd. for $C_{25}H_{38}O_5N_2Si$ [M+H$^+$]: 475.2628, found: 475.2644

15: clear oil; $R_f = 0.20$ (hexanes/diethyl ether 6/4); FT-IR (CH_2Cl_2 cast): $\tilde{\nu}$= 2954, 2856, 1688, 1613, 1513, 1464, 1362, 1302, 1250, 1174, 1093, 1038, 890, 836, 776 cm^{-1}; ^1H NMR (600 MHz, C_6D_6): $\delta = 7.25–7.22$ (m, 2H, Ar*H*), 6.86–6.83 (m, 2H, Ar*H*), 5.38 (br. s, 1H, C=CHH), 4.99 (br. s, 1H, C=CHH), 4.41 (d, J = 11.5 Hz, 1H, ArCHH), 4.38 (d, $J = 11.5$ Hz, 1H, ArCHH), 4.14 (d, $J = 5.0$, Hz, 1H, TBSO-CH), 4.06 (d, $J = 13.0$ Hz, 1H, C=CCH*H*), 3.78 (s, 3H, ArOCH_3), 3.70 (d, $J = 13$ Hz, 1H, C=CCHH), 2.61 (ddd, $J = 12.0, 12.0, 8.2$ Hz, 1H, CH*H*), 2.10 (s, 3H, O=CCH_3), 1.78 (dd, $J = 12.5, 7.5$ Hz, CHH), 1.61–1.55 (m, 3H, CHH, includes d ($\delta = 1.58$), $J = 5.0$ Hz, cyclopropyl-H), 1.44–1.40 (m, 2H, CHH), 0.90 (d, $J = 5.0$ Hz, 1H, cyclopropyl-H), 0.83 (s, 9H, $(CH_3)_3$CSi), −0.01 (s, 3H, CH_3Si), −0.05 (s, 3H, CH_3Si); ^{13}C NMR (150.9 MHz, C_6D_6): δ = 206.9, 159.1, 140.5, 130.7, 129.2, 118.4, 113.7, 76.9, 72.8, 72.0, 55.3, 50.0, 44.5, 31.4, 28.5, 26.8, 25.9, 20.0, 18.1, −4.6, −4.8; HR-MS: calcd. for $C_{25}H_{38}O_4Si$ [M+Na$^+$]: 453.2437, found: 453.2446

4: clear oil; $R_f = 0.26$ (diethyl ether/hexanes 8/2); FT-IR (CH_2Cl_2 cast): $\tilde{\nu}$= 3418 (OH), 2924, 2820, 2360, 1696, 1612, 1513, 1453, 1248, 1174, 1034, 820 cm^{-1}; ^1H NMR (600 MHz, C_6D_6): $\delta = 7.28–7.24$ (m, 2H, Ar*H*), 6.79–6.75 (m, 2H, Ar*H*), 4.37 (d, $J = 11.3$ Hz, 1H, C=CC*H*H), 4.31 (d, $J = 11.3$ Hz, 1H, ArC*H*H), 4.26 (d, $J = 11.3$ Hz, 1H, ArCH*H*), 4.10 (d, $J = 11.3$ Hz, C=CCH*H*), 4.04 (ddd, $J = 10.6, 6.0, 6.3$ Hz, 1H, HO-C*H*), 3.26 (s, 3H, ArOCH_3), 2.98 (d, $J = 6.0$ Hz, 1H, CHO*H*), 2.53 (ddd, $J = 16.0, 11.1, 6.4$ Hz, 1H, CH*H*), 2.42 (ddd, $J = 15.5, 2.9, 2.9$ Hz, 1H, CH*H*), 2.41–2.35 (m, 2H, CH*H*), 2.13 (ddd, $J = 13.7, 11.1, 2.2$ Hz, 1H, CH*H*), 2.08–2.07 (m, 1H, CHH), 2.00 (ddd, $J = 15.2, 10.7, 2.0$ Hz, 1H, CH*H*), 1.94–1.87 (m, 1H, CH*H*), 1.58–1.51 (m, 1H, CH*H*), 1.30 (dd, $J = 12.7, 2.6$ Hz, CH*H*), 1.17–1.10 (m, 1H, CH*H*); ^{13}C NMR (150.9 MHz, C_6D_6): δ = 209.1, 159.7, 145.4, 130.8, 129.6, 127.3, 114.1, 76.4, 71.8, 70.0, 54.7, 51.2, 39.6, 39.2, 33.9, 28.2, 27.0; HR-MS: calcd. for $C_{19}H_{24}O_4$ [M+Na$^+$]: 339.1572, found: 339.1565

22: beige oil; $R_f = 0.20$ (diethyl ether); FT-IR (CH_2Cl_2 cast): $\tilde{\nu}$= 2925, 2855, 1778, 1699, 1461, 1399, 1184, 1020 cm^{-1}; ^1H NMR (600 MHz, C_6D_6): $\delta = 4.66$ (m, 1H, C=C*H*), 3.73 (d, $J = 9.0$ Hz, 1H, O=COCH*H*), 3.38 (d, $J = 9.0$ Hz, 1H, O=COCH*H*), 2.04–1.95 (m, 3H, CH*H*), 1.93 (dd, $J = 18.2, 1.3$ Hz, CC(O)CH*H*), 1.86 (dd, $J = 18.2, 1.3$ Hz, CC(O)CH*H*), 1.77 (ddd, $J = 12.0, 6.0, 2.5$ Hz, 1H, CH*H*), 1.72–1.64 (m, 1H, CH*H*), 1.62–1.58 (m, 1H, CH*H*), 1.45–1.26 (m, 3H, CH*H*), 1.16 (d, $J = 13.6$ Hz, 1H, CH*H*), 0.95 (ddd, $J = 13.4, 3.9, 1.2$ Hz, 1H, CH*H*); ^{13}C NMR (150.9 MHz, C_6D_6): δ = 212.5, 174.3, 144.9, 122.8, 75.4, 47.7, 46.4, 42.7, 38.6, 37.4, 30.2, 28.6, 23.6, 21.0; HR-MS: calcd. for $C_{13}H_{16}O_3$ [M+H$^+$]: 221.1178, found: 221.1169

with the opposite stereochemistry to that of **3**) and the bridgehead olefin, two of the most challenging structural elements in **1** and **2**. The structure of this cyclization product was assigned by spectroscopic means (see also Table 1). Thus, ^1H NMR spectroscopy (1D-GOESY) showed NOE of the H2 signal upon irradiation of H1, whereas molecular dynamics and minimization calculations (CV Force Field)[16] revealed interatomic distances of 2.5 and 4.3 Å for H1–H2 and H1–H3, respectively, supporting structure **22** rather than **3**.

The described chemistry demonstrates an efficient entry into the unusual carbon skeleton found in the CP core by combining three powerful synthetic operations (intramolecular cyclopropanation, divinylcyclopropane rearrangement, and radical cyclization). Although modifications are required, this strategy should facilitate the chemical synthesis of both natural products and relatives thereof for chemical biology investigations.

Received: July 8, 1997 [Z10653IE]
German version: *Angew. Chem.* **1997**, *109*, 2922–2925

Keywords: cyclizations · cyclopropanations · natural products · rearrangements

[1] T. T. Dabrah, T. Kaneko, W. Massefski, Jr., E. B. Whipple, *J. Am. Chem. Soc.* **1997**, *119*, 1594.
[2] T. T. Dabrah, H. J. Harwood, Jr., L. H. Huang, N. D. Jankovich, T. Kaneko, J.-C. Li, S. Lindsey, P. M. Moshier, T. A. Subashi, M. Therrien, P. C. Watts, *J. Antibiot.* **1997**, *50*, 1.
[3] K. C. Nicolaou, M. W. Härter, L. Boulton, B. Jandeleit, *Angew. Chem.* **1997**, *109*, 1243; *Angew. Chem. Int. Ed. Engl.* **1997**, *36*, 1194.
[4] While this work was in progress a preliminary report appeared outlining a strategy for the preparation of the CP core using the divinylcyclopropane rearrangement: H. M. L. Davies, R. Calvo, G. Ahmed, *Tetrahedron Lett.* **1997**, *38*, 1737.
[5] For recent insights on this reaction see: a) L. J. Brzezinski, S. A. Rafel, J. W. Leahy, *J. Am. Chem. Soc.* **1997**, *119*, 4317; b) S. Rafel, J. W. Leahy, *J. Org. Chem.* **1997**, *62*, 1521, and references therein.
[6] N. Nakajima, K. Horita, R. Abe, O. Yonemitsu, *Tetrahedron Lett.* **1988**, *62*, 4139.
[7] D. F. Taber, K. You, Y. Song, *J. Org. Chem.* **1995**, *60*, 1093.
[8] For leading references to rhodium carbenoid chemistry, see: a) D. F. Taber, Y. Song, *J. Org. Chem.* **1996**, *61*, 6706; b) H. M. L. Davies in *Comprehensive Organic Synthesis, Vol. 4* (Ed.: B. M. Trost), Pergamon, New York, **1991**, p. 1031.
[9] The stereochemistry of compound **11** was assigned through the use of COSY, NOESY, ROESY, and HMQC NMR experiments on the corresponding primary alcohol obtained by reduction (DIBAL 2.2 equiv).
[10] D. L. Hughes, *Org. React.* **1992**, *42*, 335.
[11] S. V. Ley, J. Norman, W. P. Griffith, S. P. Marsden, *Synthesis* **1994**, 639.
[12] R. E. Ireland, M. D. Varney, *J. Org. Chem.* **1986**, *51*, 635.
[13] P. A. Wender, M. P. Filosa, *J. Org. Chem.* **1976**, *41*, 3490; for a review on this type of reaction see: E. Piers, *Comprehensive Organic Synthesis, Vol. 5* (Ed.: B. M. Trost), Pergamon, New York, **1991**, p. 971.
[14] J. A. Marshall, D. G. Clearly, *J. Org. Chem.* **1986**, *51*, 858.
[15] a) Y. Ueno, S. Aoki, M. Okawara, *J. Am. Chem. Soc.* **1979**, *101*, 5414; b) G. E. Keck, J. H. Byers, K. A. M. Walker, *J. Org. Chem.* **1985**, *50*, 5444; c) D. E. Ward, Y. Gai, B. F. Kaller, *ibid.* **1995**, *60*, 7830.
[16] These operations were performed on an SGI Indigo-2 workstation using the program Insight II (Biosym Technologies, Inc., San Diego, CA)

Five-Coordinate Silicon in Zeolites: Probing $SiO_{4/2}F^-$ Sites in Nonasil and ZSM-5 with ^{29}Si Solid-State NMR Spectroscopy**

Hubert Koller,* Axel Wölker, Hellmut Eckert, Christian Panz, and Peter Behrens

The primary building blocks in a wide variety of tectosilicates are corner-sharing $SiO_{4/2}$ tetrahedra.[1] Silicon typically has a coordination number of four in inorganic silicates, and only a few structures are known with other coordination numbers. Six-coordinate silicon has been found in a variety of minerals and silicon phosphates.[2] Recently, van de Goor et al. found a five-coordinate silicon site ($SiO_{4/2}F^-$) by single-crystal X-ray structure analysis of the clathrasil nonasil, which was hydrothermally crystallized from a silica gel in the presence of cobaltocenium cations and fluoride anions.[3] This nonasil will be designated as [Cp_2Co]-F-[Si-NON].[4]

Fluoride ions can be used as a substitute for OH^- in the syntheses of zeolites and clathrasils. Both F^- and OH^- are

[*] Dr. H. Koller, A. Wölker, Prof. H. Eckert
Institut für Physikalische Chemie der Universität
Schlossplatz 4/7, D-48149 Münster (Germany)
Fax: Int. code + (251) 83-29159
e-mail: hkoller@uni-muenster.de
C. Panz, Prof. P. Behrens
Institut für Anorganische Chemie der Universität München (Germany)

[**] We thank the Fonds der Chemischen Industrie, the German Bundesministerium für Bildung, Wissenschaft, Forschung und Technologie, and the Deutsche Forschungsgemeinschaft (KO 1817/1-1) for financial support.

 © WILEY-VCH Verlag GmbH, D-69451 Weinheim, 1997 0570-0833/97/3624-2823 $ 17.50+.50/0

called "mineralizing agents" since they solubilize the silica components in hydrothermal syntheses. The synthesis with fluoride results in zeolite structures containing only few defect sites;[5,6] however, the structural rationale for this phenomenon is not known. In contrast, high-silica zeolites (that is, those that have a high silicon content) made in the presence of OH^- have many defect sites which form $SiO^- \cdots HOSi$ hydrogen bonds.[6]

Since the first clathrasils and zeolites were crystallized by the fluoride route,[7] the range of structures that are synthesized in the presence of F^- (instead of OH^-) keeps increasing.[8] Aside from the aforementioned case of nonasil,[3] the structural role of fluoride was only clarified for the clathrasil octadecasil, in which F^- is located in double four ring units.[9] In the case of the high-silica zeolite ZSM-5, which is made with tetrapropylammonium cations and fluoride ions (designated as [TPA]-F-[Si-MFI]), the location of the fluoride ions was investigated by X-ray diffraction experiments on powders[10] and twinned crystals.[11] However, the results of the two studies provide different fluoride positions, and neither implies five-coordinate silicon. Apparently, the disorder of the tetrapropylammonium cations, the lack of good single crystals, and (as will be shown below) a motion of the fluoride ions caused some difficulties for the use of diffraction techniques. Here we show with ^{29}Si magic-angle spinning (MAS) NMR experiments that five-coordinate silicon in the form of $SiO_{4/2}F^-$ exists in [Cp_2Co]-F-[Si-NON] and [TPA]-F-[Si-MFI]. ^{29}Si NMR spectroscopy is a suitable method for distinguishing between four-, five- and six-coordinate silicon sites by considering their chemical shifts.[2]

Specifically, the cross-polarization (CP) technique, which relies on heteronuclear dipole–dipole interactions, allows one to probe the spatial proximity among spins. ^{29}Si NMR signals for silicon sites near fluorine can be selectively enhanced by polarization transfer from ^{19}F in $^{29}Si\{^{19}F\}$ CPMAS NMR experiments. Therefore, $SiO_{4/2}F^-$ sites will give a relatively strong signal due to the short Si–F distance.

Figure 1a shows the ^{29}Si NMR spectrum of [Cp_2Co]-F-[Si-NON]. There is partial overlapping of the resonances for ten distinct crystallographic silicon sites[3] between $\delta = -104$ and -116. Particularly interesting is a weak additional signal at $\delta = -145$, which we assign to the five-coordinate silicon in the structure of [Cp_2Co]-F-[Si-NON]. A similar chemical shift by

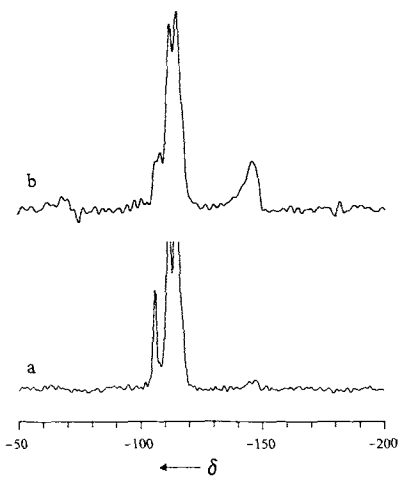

Figure 1. Nonasil sample [Cp_2Co]-F-[Si-NON]: a) $^{29}Si\{^1H\}$ CPMAS NMR spectrum, $B_0 = 7.05$ T, contact time 10 ms; b) $^{29}Si\{^{19}F\}$ CPMAS NMR spectrum, $B_0 = 4.7$ T, contact time 5 ms.

$\delta = -150$ for five-coordinate silicon was observed by solid-state ^{29}Si NMR spectroscopy in a quenched potassium silicate glass by Stebbins.[12] Figure 1b shows that the line at $\delta = -145$ in the $^{29}Si\{^{19}F\}$ CPMAS NMR spectrum is dramatically enhanced, hence confirming the assignment to a $SiO_{4/2}F^-$ species.

The $^{29}Si\{^1H\}$ CPMAS NMR spectrum of [TPA]-F-[Si-MFI] at 298 K is shown in Figure 2a. In the range of chemical shifts for four-coordinate silicon ($\delta = -107$ to -117) there are narrow signals for distinct crystallographic $SiO_{4/2}$ tetrahedra.

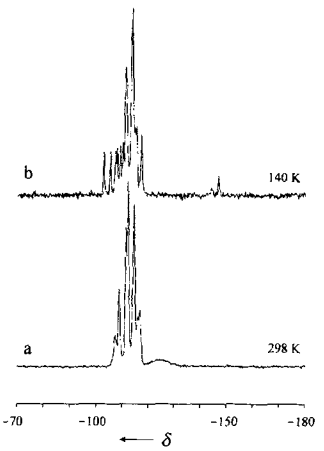

Figure 2. $^{29}Si\{^1H\}$ CPMAS NMR spectra of the ZSM-5 sample [TPA]-F-[Si-MFI], $B_0 = 7.05$ T, contact time 10 ms: a) $T = 298$ K, $\delta = -107.4, -108.9, -111.6, -112.3, -114.5, -116.2, -116.8, -125.0$; b) $T = 140$ K, $\delta = -103.0, -105.5, -107.5, -108.1, -109.3, -110.3, -111.4, -113.7, -114.8, -115.4, -117.3, -144.1, -147.0$.

However, not all of the expected signals are resolved due to overlapping of some lines. A significantly broader line is observed at $\delta \approx -125$. Although several groups obtained similar ^{29}Si NMR spectra of [TPA]-F-[Si-MFI], this broad signal at $\delta = -125$ has not been commented on before. The intensity of this signal is greatly enhanced in the $^{29}Si\{^{19}F\}$ CPMAS NMR spectrum of [TPA]-F-[Si-MFI]. Therefore, we conclude that this signal must be due to silicon sites that are in close proximity to fluorine. The chemical shift at $\delta = -125$ falls between that expected for a $SiO_{4/2}F^-$ site ($\delta \approx -145$) and the range for four-coordinate silicon ($\delta = -107$ to -117). In the following it will be shown that the line at $\delta = -125$ corresponds to an averaged signal due to dynamic exchange between four- and five-coordinate silicon.

[TPA]-F-[Si-MFI] has a phase transition at 175 K that is associated with a change in the space-group symmetry.[13] Figure 2b shows the $^{29}Si\{^1H\}$ CPMAS NMR spectrum of [TPA]-F-[Si-MFI] below this phase-transition temperature. In this spectrum the broad line at $\delta = -125$ is not observed, and instead two sharp lines for at least two distinct $SiO_{4/2}F^-$ sites are found at $\delta = -144.1$ and -147.0. The strong dipolar interaction between the ^{29}Si and ^{19}F nuclei, which would result in broader lines, is effectively averaged out by the MAS technique. Therefore, ^{19}F decoupling was not necessary to obtain the narrow lines in Figure 2b. At room temperature the fluoride ion exchanges between different $SiO_{4/2}$ tetrahedra of the MFI structure, which leads to the broad feature at $\delta = -125$. This motion is frozen out at 140 K, producing the sharp lines for the $SiO_{4/2}F^-$ sites. These observations clearly show that five-coordinate silicon exists in [TPA]-F-[Si-MFI], that is,

 © WILEY-VCH Verlag GmbH, D-69451 Weinheim, 1997 0570-0833/97/3624-2824 $ 17.50+.50/0

high-silica ZSM-5 made with fluoride as the mineralizing agent.

When crystals of [TPA]-F-[Si-MFI] are calcined, then tetrapropylammonium cations and fluoride anions are removed from the structure to leave behind a bare microporous SiO_2 framework of ZSM-5 without five-coordinate silicon. This calcined zeolite was studied in detail by others.[2,14] Work is now in progress to identify in more detail the fluoride binding sites, to characterize the motional process of the fluoride ions, and to measure the relevant ^{19}F–^{29}Si distances.

Received: July 10, 1997 [Z10668IE]
German version: *Angew. Chem.* **1997**, *109*, 2939–2940

Keywords: coordination modes · NMR spectroscopy · silicon · zeolites

[1] F. Liebau, *Structural Chemistry of Silicates—Structure, Bonding, and Classification*, Springer, Berlin, **1985.**
[2] a) G. Engelhardt, H. Koller, *NMR Basic Principles and Progress* **1994**, *31*, 1; b) G. Engelhardt, D. Michel, *High-Resolution Solid-State NMR of Silicates and Zeolites*, Wiley, Chichester, **1987.**
[3] G. van de Goor, C. C. Freyhardt, P. Behrens, *Z. Anorg. Allg. Chem.* **1995**, *621*, 311.
[4] "NON" is the three-letter code recommended by the International Zeolite Association for this framework structure: W. M. Meier, D. H. Olson, C. Baerlocher, *Atlas of Zeolite Structure Types*, Elsevier, New York, **1996.**
[5] J. M. Chézeau, L. Delmotte, J. L. Guth, M. Soulard, *Zeolites* **1989**, *9*, 78.
[6] H. Koller, R. F. Lobo, S. L. Burkett, M. E. Davis, *J. Phys. Chem.* **1995**, *99*, 12588.
[7] a) E. M. Flanigen, R. L. Patton, US-A 4073865, **1978**; b) J. L. Guth, H. Kessler, J. M. Higel, J. M. Lamblin, J. Patarin, A. Seive, J. M. Chézeau, R. Wey, *ACS Symp. Ser.* **1989**, 398, 176.
[8] a) J. L. Guth, H. Kessler, P. Caullet, J. Hazm, A. Merrouche, J. Patarin, *Proc. 9th Int. Zeolite Conf* (Eds.: R. von Ballmoos, J. B. Higgins, M. M. J. Treacy), Butterworth-Heinemann, Montreal, **1993**, p. 215; b) M. A. Camblor, C. Corell, A. Corma, M. J. Díaz-Cabañas, S. Nicolopoulos, J. M. González-Calbet, M. Vallet-Regí, *Chem. Mater.* **1996**, *8*, 2415; c) M. A. Camblor, A. Corma, L. A. Villaescusa, *Chem. Commun.* **1997**, 749; d) R. E. Morris, S. J. Weigel, N. J. Henson, L. M. Bull, M. T. Janicke, B. F. Chmelka, A. K. Cheetham, *J. Am. Chem. Soc.* **1994**, *116*, 11849; e) J. E. Lewis, C. C. Freyhardt, M. E. Davis, *J. Phys. Chem.* **1996**, *100*, 5039; f) A. Kuperman, S. Nadimi, S. Oliver, G. A. Ozin, J. M. Garcés, M. M. Olken, *Nature* **1993**, *365*, 239.
[9] P. Caullet, J. L. Guth, J. Hazm, J. M. Lamblin, H. Gies, *Eur. J. Solid State Inorg. Chem.* **1991**, *28*, 345.
[10] B. F. Mentzen, M. Sacerdote-Peronnet, J. L. Guth, H. Kessler, *C.R. Acad. Sci. Paris Ser. II* **1991**, *313*, 177.
[11] G. D. Price, J. J. Pluth, J. V. Smith, J. M. Bennet, R. L. Patton, *J. Am. Chem. Soc.* **1982**, *104*, 5971.
[12] J. F. Stebbins, *Nature* **1991**, *351*, 638.
[13] J. M. Chézeau, L. Delmotte, T. Hasebe, N. B. Chanh, *Zeolites* **1991**, *11*, 729.
[14] C. A. Fyfe, Y. Feng, H. Grondey, G. T. Kokotailo, H. Gies, *Chem. Rev.* **1991**, *91*, 1525.

Highly Precise Shape Mimicry by a Difluorotoluene Deoxynucleoside, a Replication-Competent Substitute for Thymidine**

Kevin M. Guckian and Eric T. Kool*

Until recently, the large majority of studies of the origins of DNA replication fidelity have concluded that complementarity of hydrogen bonding is the chief source of energetic selectivity between the four nucleotides at the transition state for initial insertion.[1,2] As part of this field of study, a wide number of modified nucleoside analogues have been incorporated into DNA in an effort to study the origins of mutagenesis and mechanisms for the fidelity of DNA replication.[3] Virtually all of these differed from natural nucleosides both in their hydrogen bonding arrangement and in their size and shape. While such approaches have led to valuable insights, with such analogues it is extremely difficult to distinguish between steric and hydrogen bonding effects as sources of observed differences in replication properties.[4,5]

To address this problem we proposed the structures of four nucleoside analogues designed to mimic as closely as possible the structure of natural nucleosides, but lacking standard polar hydrogen bonding functionality. For example, compound **1**, a difluorotoluene deoxynucleoside, was designed to

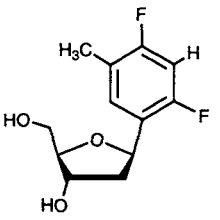

1

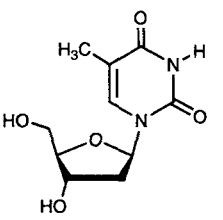

2

mimic the shape of the natural deoxynucleoside thymidine (**2**). Its difluorotoluene "base" is isoelectronic with thymine, and through the replacement of the carbonyl groups with C–F and the polar N–H group with C–H the two compounds are isosteric as well.[4]

Studies of the properties of nucleoside **1** have indicated that the compound is quite nonpolar and that the difluorotoluene moiety shows no measurable hydrogen bonding tendency in aqueous and organic solutions. For example, titration of **1** with adenine derivatives in chloroform does not lead to measurable complex formation. Further, replacement of thymine with difluorotoluene in the center of a DNA duplex 12 base pairs in length causes strong destabilization, and the difluorotoluene shows no preferential pairing with adenine over the other three bases; in contrast, thymine shows a 3–4 kcal mol^{-1} preference.[6,7] Based on the hydrogen bonding complementarity model of DNA replication fidelity, it was expected that during replication this analogue would serve as a very poor enzyme substrate and would show very little

[*] Prof. E. T. Kool, K. M. Guckian
Department of Chemistry, University of Rochester
Rochester, NY 14627 (USA)
Fax: Int. code + (716) 473-6889
e-mail: etk@etk.chem.rochester.edu

[**] This research was supported by the National Institutes of Health (GM52956). We thank Prof. T. R. Krugh for helpful discussions, Prof. W. D. Jones and Dr. R. Lachicotte for assistance with the crystallographic data, and Dr. J. Perlstein for assistance with the graphics.

 © WILEY-VCH Verlag GmbH, D-69451 Weinheim, 1997 0570-0833/97/3624-2825 $ 17.50+.50/0

selectivity for inserting any one of the natural bases over another.

Despite this expectation, a recent study, in which the difluorotoluene analogue replaces thymidine in template DNA strands, has shown that it serves as an excellent and highly specific template for replication. The Klenow fragment (KF) of *E. coli* DNA polymerase I accepts this compound in the template with efficiency nearly matching that of thymine, and the enzyme specifically inserts adenine opposite it.[5] Thus, despite the poor hydrogen bonding abilities of the nucleoside isostere, the enzyme treats it almost as if it were thymidine. If the size, shape, and conformation of the analogue are assumed to be the same as those of thymidine, then one is led to conclude that hydrogen bonding may be less important in the fidelity of replication than previously believed, and that steric effects may play a more direct role. This argument depends strongly, however, on the similarity of the size, shape, and conformation of **1** and thymidine. We now report the results of detailed structural studies of compound **1**, with comparison to natural thymidine. We have obtained X-ray structural data for **1** and have carried out solution studies of it and thymidine by ^{1}H NMR spectroscopy as well.

We were able to obtain X-ray quality crystals of deoxynucleoside **1** from ethanol. Analysis of the solid-state structure reveals that the nucleoside analogue is a remarkably good structural mimic of thymidine. The C-nucleoside crystallized in the $P2_1$ space group and has three molecules in the asymmetric unit. All three molecules have the *anti*-glycosidic conformation; two have *S*-type (C2′-*endo*) puckers in the sugar moiety; the third has an *N*/*S* intermediate conformation (C4′-*exo*). The average bond lengths for **1** and published structural data for thymidine are given in Figure 1.[8,9] In addition, dihedral torsion angles for one of the molecules in the asymmetric unit are given in Table 1 (C6-C(N)1-C1′-C2′ is referred to as C6-C2′), again along with the analogous angles for thymidine (C(N)1-C1′). Examination of the data shows that the conformations of the five-membered rings in the two compounds are essentially identical. The glycosidic torsion angles are also similar, only 18° apart. Bond lengths for the thymine base and difluorotoluene base mimic are nearly all within 0.07 Å of each other. The chief difference is the C=O bond lengths (1.23 and 1.21 Å) as compared to the analoguous C–F bond lengths (averaging 1.37 Å and 1.37 Å, respectively).

Table 1. Structural data for **1** and thymidine obtained by X-ray crystallographic analysis.

Nucleoside	Dihedral angles[°][d]					
	C6-C2′	O4′-C3′	C1′-C4′	C2′-C5′	C(N)1-C3′	C3′-C1′
1[a]	−97.6	+32.2	−36.7	−91.5	+153.2	−9.0
thymidine[b]	−79.5	+28.4	−37.2	−87.3	+147.8	−16.8
H1′-H2′	H1′-H2″	H2′-H3′	H2″-H3′	H3′-H4′	C(N)1-H2′	
1[c]	+157.2	+35.5	−73.4	+84.2	−93.9	+34.0
thymidine[c]	+149.2	+21.9	−41.7	+87.2	−88.5	+33.8

[a] Data for one of the three molecules in the asymmetric unit (see Figure 1). [b] Data from ref.[9]. [c] The H–H dihedral angles were obtained from the crystal structures with atoms added to give normal sp^3 and sp^2 geometries. [d] Only those atoms at the end of the sequence forming the dihedral angle are given. For example, C6-C2′ refers to C6-C(N)1-C1′-C2′.

Also of interest are the noncovalent interactions found in the crystal structure of difluorotoluene deoxynucleoside and those of thymidine (Figure 2). In both structures the 3′ and 5′ hydroxyl groups form intermolecular hydrogen bonds. For compound **1**, the sugar hydroxyls are hydrogen bonded to other sugar hydroxyl groups. For thymidine, the carbonyl and N–H groups, which undergo Watson–Crick hydrogen bonding in DNA, are found to be hydrogen bonded to the sugar hydroxyl groups of neighboring molecules.[9] For deoxynucleoside **1**, no hydrogen bonds or other close contacts[10] are observed with the fluorines on the aromatic ring (the nearest contacts are several F–H contacts of 2.49–2.79 Å).[10,11] In the crystal packing array, the nonpolar difluorotoluenes are segregated from the more polar, H-bonding furanose groups (Figure 2B). Finally, in the thymidine crystal structure the heterocyclic bases are stacked in a linear array; in contrast, the difluorotoluene rings do not form stacks.

To examine these structural details in solution we carried out a conformational analysis of the difluorotoluene deoxynucleoside and of thymidine in D_2O by measuring the furanose coupling constants (Table 2).[12,13] The sugar ring protons for both molecules were completely assigned, and the coupling constants were measured at 500 MHz. The chief difference in furanose resonances for the two compounds is found in the H1′ signals; that for thymidine is $\delta = 0.93$ downfield of that for **1**, consistent with the strong difference in glycosidic bond polarities.

Despite the large difference in polarity of the glycosidic bonds, the sugar ring conformations of **1** and **2** are very similar. Analysis using published methods[13] allowed us to assign the overall conformation of the two deoxynucleosides in both cases as *S* type; thymidine is classified as 70% *S*, while the difluorotoluene compound is 90–100% *S*. In addition, NOE studies carried out on the two structures provided evidence as to the preferred glycosidic conformations in solution. Selective irradiation at the frequency of the H6 signal led to qualitatively larger enhancements of the C-5 methyl signal than of the H1′ signal, and the ratios of these two enhancements were similar for compound **1** and thymidine. This is consistent with predominantly *anti*- glycosidic conformations for both compounds in solution. Thus, we

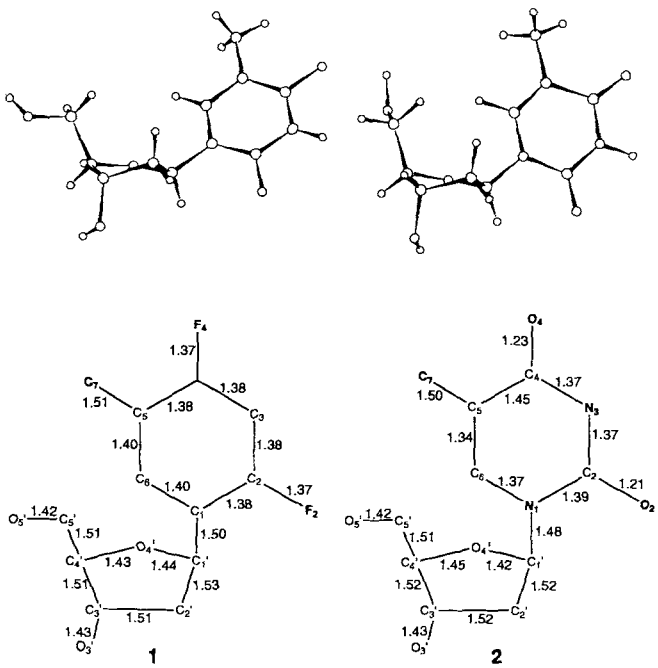

Figure 1. Single-crystal X-ray structure of difluorotoluene deoxynucleoside **1** compared to the published structure of thymidine **2**[8,9]. Top: Structures of the isolated nucleosides. Note that **1** has three different molecules in the asymmetric unit. Bottom: Bond lengths [Å] for **1** (averaged over the three molecules in the asymmetric unit) and thymidine.

 © WILEY-VCH Verlag GmbH, D-69451 Weinheim, 1997 0570-0833/97/3624-2826 $ 17.50+.50/0

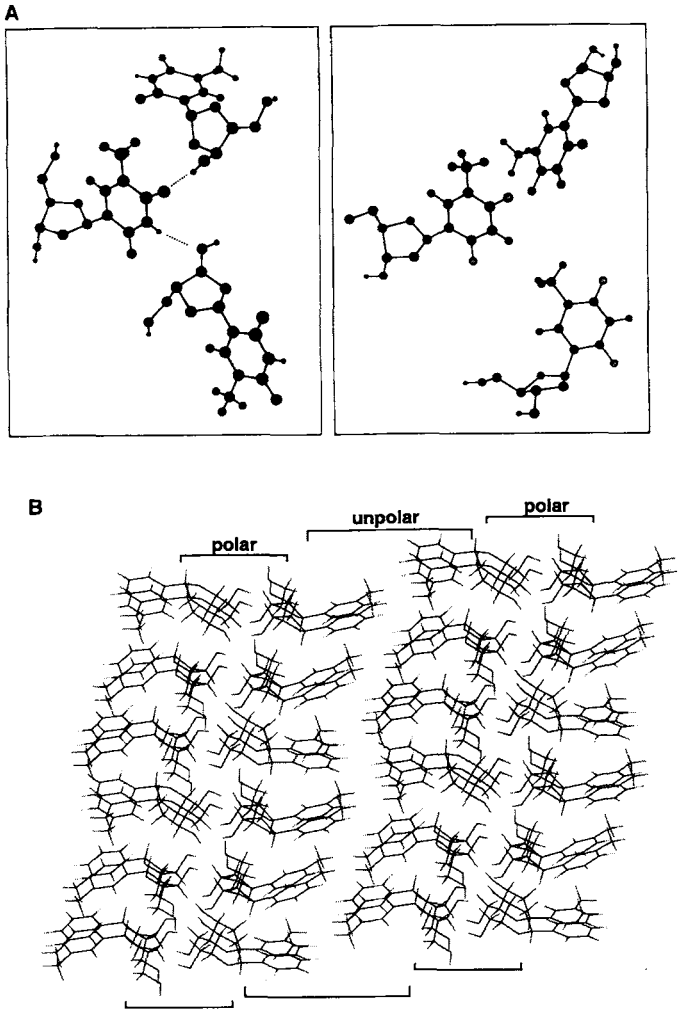

Figure 2. Intermolecular arrangement in the crystal structures of thymidine [9] and nucleoside **1**. A) Local environment surrounding the aromatic "bases" of the nucleosides. Note the presence of two hydrogen bonds between the thymine bases and lack of such contacts for difluorotoluene. B) Overall packing arrangement for **1** showing segregation of polar deoxyribose units from nonpolar difluorotoluene rings.

Table 2. ^{1}H NMR data for **1** and thymidine in D_2O.

Chemical shift	H1′	H2′	H2″	H3′	H4′	H5′
1 (δ)	5.42	2.21	2.33	4.48	4.08	3.75
thymidine (δ)	6.35	2.42	2.42	4.52	4.06	3.85
Coupling constants	H1′-H2′	H1′-H2″	H2′-H3′	H2″-H3′	H3′-H4′	H2′-H2″
1 J[Hz]	10.37	5.80	5.79	≈1.0	2.44	13.58
summed J values	Σ(23+23)-Σ(1′) 3′+2″3′)		Σ(2′)	Σ(2″)	Σ(3′)	
1 [Hz]	6.80	16.17	29.74	20.88	9.73	
thymidine [Hz]	10.68	13.74	[a]	[a]	14.65	

[a] Not determined.

conclude that in solution the difluorotoluene nucleoside adopts an overall conformation virtually the same as that of thymidine, despite the replacement of the natural (and more polarized) C–N glycosidic bond by a C–C bond.

These structural studies have relevance to the question of how DNA is synthesized with high specificity. We have shown that the difluorotoluene nucleoside is replicated by KF polymerase with efficiency and specificity almost identical to that with thymidine when placed in synthetic DNA templates.[5] It is clear that the fluorines in **1**, which replace carbonyl groups in thymidine, have very little (if any) tendency to form hydrogen bonds, especially in aqueous solution, and this is further supported by the lack of such noncovalent contacts in the crystal structure. Moreover, the thymine heterocycle and difluorotoluene have very different electrostatic charge localizations; octanol/water partioning studies showed **1** to be highly nonpolar while thymidine is very polar.[7] These data support the notion that the structural, rather than electrostatic, mimicry of **1** may lead to its specific replication.

As a result of these studies we are developing a new model for the physical origins of the fidelity of DNA synthesis. The KF enzyme initially selects an incorrect nucleotide in DNA synthesis only once in 10^3-10^4 times, and virtually the same selectivity is seen for insertion of A (rather than C, T, G) opposite compound **1**.[5] We propose that the primary factor in this selectivity is steric exclusion of incorrect nucleotides. In this model the active site is a tightly restricted pocket defined by the surrounding enzyme and the DNA base in the template strand. The presence of thymine (or an isosteric replacement) in a template excludes guanine, cytosine, and thymine nucleotides by steric clashes with their DNA bases or with the molecules of water solvating them. Adenine is allowed because its shape and size fit perfectly into the active site cavity. This shape-selection hypothesis is currently being examined further in a number of ongoing studies.

In summary, we have analyzed the steric shape and conformation of the C-nucleoside **1** both in solution and in the solid state. The findings indicate that the difluorotoluene nucleoside is a nearly perfect isostere of the natural compound, both in bond lengths and in overall conformation. This nonpolar isostere may be therefore generally useful in the study of molecular recognition and catalytic events that involve the natural structure thymidine, such as protein–DNA recognition and enzymatic synthesis of nucleic acids.

Experimental Section

Crystal structure analysis: Single crystals of the complex were grown from a concentrated ethanol solution. A colorless crystal of approximate dimensions 0.56 × 0.24 × 0.08 mm was mounted on a glass fiber with epoxy and placed on the X-ray diffractometer for data collection at room temperature. The X-ray intensity data were collected on a standard Siemens SMART CCD Area Detector System equipped with a normal focus molybdenum-target X-ray tube operated at 1.5 kW (50 kV, 30 mA). A total of 1321 frames of data (1.3 hemispheres) were collected using a narrow-frame method with scan widths of 0.3° in ω and exposure times of 10 s per frame; the detector-to-crystal distance was 5.094 cm ($2\theta_{max} = 56.52°$). Frames were integrated with the Siemens SAINT program to yield a total of 10400 reflections, of which 6606 were independent ($R_{int} = 0.0425$, $R_{sigma} = 0.0614$ with $R_{int} = \Sigma|F_o^2 - F_c^2(\text{mean})|/\Sigma[F_o^2]$ and $R_{sigma} = \Sigma[\sigma(F_o^2)]/\Sigma[F_o^2]$). Crystal structure data: monoclinic, $a = 13.9262(2)$, $b = 6.4932(0)$, and $c = 19.8156(5)$ Å, $\beta = 104.574(1)°$, and $V = 1753.18(5)$ Å^3 ($T = 23°C$); least-squares refinement of three-dimensional centroids of >1000 reflections. (The integration program SAINT produces unreasonably cell constant errors, since systematic error is not included.) The space group was assigned as $P2_1$ on the basis of systematic absences and intensity statistics by using the XPREP program (Siemens, *SHELXTL 5.04*). The structure was solved with direct methods included in the SHELXTL program package and refined by full-matrix least-squares on F^2. For $Z = 6$, there are three independent molecules in the asymmetric unit. Although the frames were integrated to a $2\theta_{max} = 56.52°$, there were essentially no observed data >45°. Therefore these data were omitted from the refinement yielding a total of 7118 reflections, of which 4101 were independent ($R_{int} = 0.0368$, $R_{sigma} = 0.0437$) and 3548 reflections had $>2\sigma(I)$. All non-hydrogen atoms were refined anisotropically with hydrogens included in idealized positions giving a data:parameter ratio of approximately 10:1. The structure refined to a goodness of fit (GOF) of 1.157 and final residuals of $R_1 =$

 © WILEY-VCH Verlag GmbH, D-69451 Weinheim, 1997 0570-0833/97/3624-2827 $ 17.50+.50/0

0.0498 ($I > 2\sigma(I)$), $wR_2 = 0.1073$ ($I > 2\sigma(I)$) (GOF = $[\Sigma[w(F_o^2 - F_c^2)^2]/(n-p)]^{1/2}$, where n and p denote the number of data and parameters; $R_1 = (\Sigma \| F_o| - |F_c \|)/\Sigma |F_o|$; $wR_2 = [\Sigma[w(F_o^2 - F_c^2)^2]/\Sigma[w(F_o^2)^2]]^{1/2}$ with $w = 1/[\sigma^2(F_o^2) + (a \cdot P)^2 + b \cdot P]$ and $P = [\max(F_o^2, 0) + 2(F_c^2)/3]$).

Received: June 11, 1997 [Z10533IE]
German version: *Angew. Chem.* **1997**, *109*, 2942–2945

Keywords: carbohydrates · conformation · hydrogen bonds · nucleosides · structure elucidation

[1] a) A. Kornberg, T. A. Baker, *DNA Replication*, 2nd ed., Freeman, New York, **1992**, p. 113; b) L. A. Loeb, T. A. Kunkel, *Ann. Rev. Biochem.* **1982**, *52*, 429; c) M. F. Goodman, S. Creighton, L. B. Bloom, J. Petruska, *Crit. Rev. Biochem. Mol. Biol.* **1993**, *28*, 83.
[2] See also discussions of replication fidelity in current textbooks: a) J. D. Watson, N. H. Hopkins, J. W. Roberts, J. A. Steitz, A. M. Weiner, *Molecular Biology of the Gene*, 4th ed., Benjamin/Cummings, Menlo Park, **1987**, p. 283; b) L. Stryer, *Biochemistry*, 4th ed., Freeman, New York, **1995**, p. 89.
[3] See, for example: a) E. Freese, *J. Mol. Biol.* **1959**, *1*, 87; b) L. C. Sowers, G. V. Fazakerley, R. Eritja, B. E. Kaplan, M. F. Goodman, *Proc. Natl. Acad. Sci. USA* **1986**, *83*, 5434; c) R. Eritja, D. M. Horowitz, P. A. Walker, J. P. Ziehler-Martin, M. S. Boosalis, M. F. Goodman, K. Itakura, B. E. Kaplan, *Nucleic Acids Res.* **1986**, *14*, 8135; d) B. Singer, S. Spengler, *Biochemistry* **1981**, *20*, 1127; e) P. Strazewski, C. Tamm, *Angew. Chem.* **1990**, *102*, 37; *Angew. Chem. Int. Ed. Engl.* **1990**, *29*, 36; f) S. Shibutani, M. Takeshita, A. P. Grollman, *Nature* **1991**, *349*, 431; g) D. C. Ward, E. Reich, *J. Biol. Chem.* **1972**, *247*, 705.
[4] B. A. Schweitzer, E. T. Kool, *J. Org. Chem.* **1994**, *59*, 7238.
[5] S. Moran, R. X.-F. Ren, S. Rumney, E. T. Kool, *J. Am. Chem. Soc.* **1997**, *119*, 2056.
[6] B. A. Schweitzer, E. T. Kool, *J. Am. Chem. Soc.* **1995**, *117*, 1863.
[7] S. Moran, R. X.-F. Ren, E. T. Kool, *Proc. Natl. Acad. Sci. USA* **1997**, *94*, 10506.
[8] D. W. Young, P. Tollin, H. R. Wilson, *Acta Crystallogr. Sect. B* **1969**, *25* 1423.
[9] A. N. Chekhlov, *J. Struct. Chem.* **1995**, *36*, 155.
[10] Close F–H contacts are defined here as contacts ≤ 2.35 Å [11].
[11] J. A. K. Howard, V. J. Hoy, D. O'Hagan, G. T. Smith, *Tetrahedron* **1996**, *52*, 12613.
[12] S. S. Wijmenga, M. M. W. Mooren, C. W. Hilbers in *NMR of Macromolecules: A Practical Approach* (Ed.: G. K. Roberts), Oxford University Press, Oxford, **1993**, p. 258.
[13] L. J. Rinkel, C. Altona, *J. Biomol. Struct. Dyn.* **1987**, *4*, 621.

[2+1] Cycloadditions of Diazoalkanes to Enol Ethers Catalyzed by Chromium Complexes—The First Direct Spectroscopic Observation of a Carbene Complex Intermediate**

Jürgen Pfeiffer and Karl Heinz Dötz*

Dedicated to Professor Dieter Seebach on the occasion of his 60th birthday

Reactions of aliphatic diazo compounds with alkenes catalyzed by transition metal complexes are among the most important methods for obtaining cyclopropanes.[1] The generally accepted mechanism involves the formation of a reactive carbene complex intermediate, resulting from electrophilic attack at the carbon atom of the diazo group and subsequent elimination of N_2. Transfer of the carbene fragment to the alkene regenerates the catalytically active species and the catalytic cycle starts again. Although a carbene complex intermediate has not yet been observed directly, convincing experimental results support this model:

1. The high asymmetric induction observed when chiral metal complexes are used requires strong steric interactions between alkene, metal complex, and carbene during the face-selective reaction step.[2]
2. Reactivity/selectivity correlations between reactions catalyzed by $[Rh_2(OAc)_4]$ and stoichiometric reactions with $[(CO)_5W{=}C(H)Ph]$ indicate a similar mechanism for the two types of reactions.[3]
3. The synthesis of stable carbene complexes from diazoalkanes[4,5] as well as that of cyclopropanes from carbene complexes support the mechanism outlined above.[1a,6] Furthermore, a chiral ruthenium complex that catalyzes the [2+1] cycloaddition of ethyl diazoacetate and styrene in high enantiomeric excess was obtained recently; the corresponding carbene complex, which also catalyzes the reaction, is isolable in the absence of styrene.[7]

The ability of chromium(0) complexes to catalyze [2+1] cycloadditions was hitherto studied in less detail.[8] During our research aimed at the synthesis of stable chromium carbene complexes from diazoalkanes and chromium complexes of the type $[(CO)_5CrL]$ (L = THF, *cis*-cyclooctene), we became interested in the utiliziation of these compounds for catalytic cyclopropanations of alkenes with diazoalkanes.

Reactions of ethyl diazoacetate **1** with electron-rich alkenes (5 equivalents) in the presence of pentacarbonyl(η^2-*cis*-cyclooctene)chromium(0) (**2**) (5 mol%; Scheme 1) afford the donor–acceptor substituted cyclopropanes **3**–**5** in good

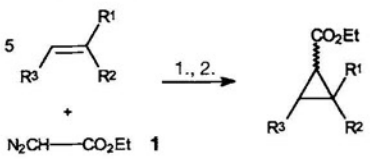

Scheme 1. Synthesis of the cyclopropanes **3**–**6**. 1: **2** (5 mol%), 5 °C, 4 h, CH_2Cl_2, $-N_2$, $-C_8H_{14}$; 2: 20 °C, 8 h, CH_2Cl_2; 28–79%.

[*] Prof. Dr. K. H. Dötz, Dipl.-Chem. J. Pfeiffer
Kekulé-Institut für Organische Chemie und Biochemie der Universität
Gerhard-Domagk-Strasse 1, D-53121 Bonn (Germany)
Fax: Int. code + (228)735813

[**] Reactions of Complex Ligands, Part 78. This work was supported by the Volkswagenstiftung, the Fonds der Chemischen Industrie, and the "Graduiertenkolleg Spektroskopie isolierter und kondensierter Moleküle". Part 77: K. H. Dötz, P. Tomuschat, M. Nieger, *Chem. Ber. Recueil* **1997**, *130*, 1605.

 © WILEY-VCH Verlag GmbH, D-69451 Weinheim, 1997 0570-0833/97/3624-2828 $ 17.50+.50/0

yields (Table 1).[10] Compound **6**, which is formed by the reaction with styrene, could only be obtained in poor yield, whereas alkyl- and acceptor-substituted alkenes gave no [2+1] cycloaddition products under these conditions.[11] Attempts to trap or provide evidence for a carbene complex

Table 1. Chromium-catalyzed cyclopropanations of electron-rich alkenes with ethyl diazoacetate **1** [a, b].

Product	R^1	R^2	R^3	Yield [%]	*cis*/*trans* [c]
3	OC_2H_5	H	H	79	1:1.8
4	OCH_3	CH_3	H	77	1:2.1
5	H	$-O-CH_2-CH_2-$		72	1:4.0 [d]
6	C_6H_5	H	H	28	1:2.0

[a] Reaction at 5 °C for 4 h in dichloromethane. [b] Elemental analyses and/or high-resolution mass spectra were obtained for **3**–**6**; the identification and assignment of the isomers were performed by comparison with data from the literature [12]. [c] Assigned by ^{1}H NMR spectroscopy and GC-MS. [d] *endo*/*exo*.

intermediate during these reactions have not been successful.

Reactions of equimolar amounts of 9-(9*H*)-diazofluorene (**7**) with enol ethers in the presence of **2** (2 mol%) also afford the corresponding spirocyclopropanes **8**[13]–**11** in good to very good yields (Scheme 2, Table 2).[14] Again, no [2+1] cycloaddition was observed with alkyl-substituted alkenes.[11] A control experiment with ethyl acrylate in the absence of **2** indicates that **12** is formed by an uncatalyzed [2+1] cycloaddition.[15] All catalyzed reactions occur with darkening of the reaction mixture; thin-layer chromatography (TLC) shows the typical violet spot for pentacarbonyl[9-(9*H*)-fluorenylidene]chromium(0) (**13**), which, in the absence of alkenes, is isolable from stoichiometric reactions of **2** with **7**.[9]

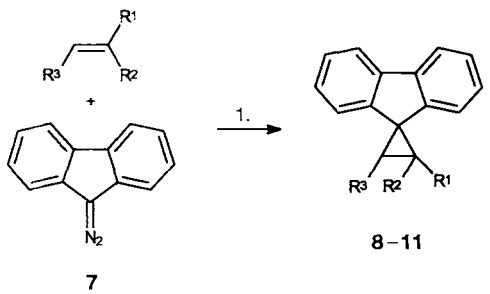

7 8–11

Scheme 2. Synthesis of the cyclopropanes **8**–**11**. 1: **2** (2 mol%), 20 °C, 16 h, CH_2Cl_2, $-N_2$, $-C_8H_{14}$; 25–93%.

Table 2. Chromium-catalyzed reactions of 9-(9*H*)-diazofluorene **7** with electron-rich alkenes [a].

Product	R^1	R^2	R^3	Yield [%]	Workup	Eluent [b]
8	OC_2H_5	H	H	93	A	PE/CH_2Cl_2 2:3
9	OCH_3	CH_3	H	87	A	PE/CH_2Cl_2 1:1
10	H	$-O-CH_2-CH_2-$		73	A	PE/CH_2Cl_2 1:2
11	C_6H_5	H	H	25	B	PE/Et_2O 5:1

[a] Reaction at 20 °C for 8 h in dichloromethane. [b] PE = petroleum ether (40/60).

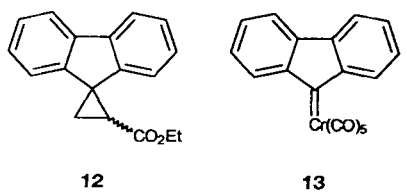

12 13

Direct evidence for **13** during the reaction of **7** with ethyl vinyl ether in the presence of **2** (5 mol%) by ^{13}C NMR spectroscopy is provided by "freezing" the reaction by cooling to -30 °C. In the range between $\delta = 200$ and 380, the ^{13}C NMR spectrum (Figure 1) exhibits the signals of **13** ($\delta =$ 217.58, 238.92, 361.32), **2** ($\delta = 216.04$, 224.31), and of hexacarbonylchromium(0). In addition, further signals are observed which could not be assigned.

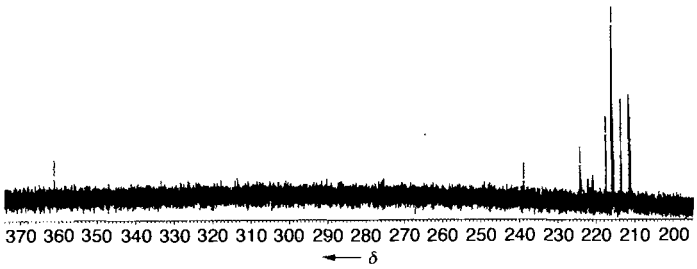

Figure 1. Section of the ^{13}C NMR spectrum (125.6 MHz, $CDCl_3$, 243 K) recorded during the reaction of **7** with ethyl vinyl ether catalyzed by **2**.

Scheme 3 presents a catalytic cycle that is consistent with the experimental results; however, the detailed mechanism of the carbene transfer from the carbene complex to the alkene remains unclear.

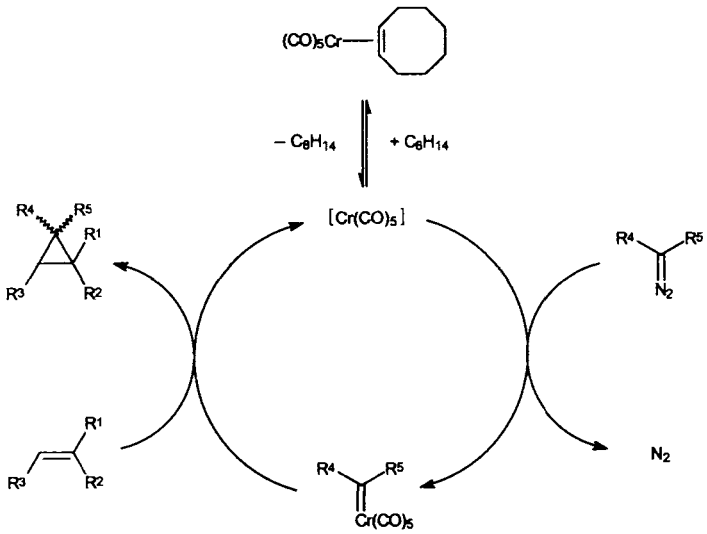

Scheme 3. Catalytic cycle of the chromium complex catalyzed [2+1] cycloadditions.

The chromium-catalyzed reactions of **1** and **7** with alkenes proceed with pronounced chemoselectivity with regard to the electronic properties of the olefin substituents. The preference of electron-rich C–C double bonds can be rationalized in terms of the electrophilic character of the postulated or detected intermediates $[(CO)_5Cr{=}C(H)CO_2Et]$ and **13**, respectively.

We have demonstrated that chromium(0) complexes can efficiently catalyze cyclopropanations. The presence of a weakly coordinated ligand such as *cis*-cyclooctene, which dissociates under mild conditions, generating the catalytically active species "$Cr(CO)_5$", is crucial. Furthermore, the observation of **13** by ^{13}C NMR spectroscopy represents the first

 © WILEY-VCH Verlag GmbH, D-69451 Weinheim, 1997 0570-0833/97/3624-2829 $ 17.50+.50/0

direct evidence for a carbene complex intermediate during a [2+1] cycloaddition catalyzed by a transition metal complex. Further studies on the mechanism and the stereochemical course of the reactions are in progress.

Experimental Section

General procedures: All reactions were performed under argon. Solvents were dried and degassed according to standard procedures. Yields refer to products isolated after column chromatography. Compounds **1** [16], **2** [17], and **7** [18] were synthesized according to literature methods.

3–6: A solution of **1** (1.14 g, 10 mmol) in CH_2Cl_2 (20 mL) was added dropwise over 4 h to a stirred solution of **2** (0.15 g, 0.5 mmol, 5 mol%) in the corresponding alkene (50 mmol), precooled to 5 °C. The reaction mixture changed color from yellow to green-brown under evolution of N_2. After the mixture had been stirred for a further 8 h at 20 °C and the solvent and excess alkene had been removed under reduced pressure, the residue was purified by column chromatography (petroleum ether (40/60)/Et_2O 2:1).

8–11: A solution of **7** (0.57 g, 3 mmol) in CH_2Cl_2 (30 mL) was added dropwise over 8 h to a stirred solution of the corresponding alkene (3 mmol) and **2** (0.02 g, 0.06 mmol, 2 mol%) in CH_2Cl_2 (10 mL). The reaction mixture changed color from yellow to brown-violet under the evolution of N_2. After the mixture had been stirred for a further 8 h at 20 °C and the solvent had been removed under reduced pressure, workup was performed according to one of the following procedures (see Table 2).

A: Workup by column chromatography.

B: The residue was washed several times with portions of petroleum ether(40/60) (10 mL) and filtered until only bis[9-(9*H*)-fluorenylidene]azine could be detected in the solution (TLC-control, petroleum ether (40/60)/CH_2Cl_2 1:1, $R_f = 0.35$). The combined filtrates were concentrated, and purified by column chromatographic workup.

9: ^{1}H NMR (500 MHz, $CDCl_3$): $\delta = 7.89$ (d, 1H), 7.88 (d, 1H), 7.52 (d, 1H), 7.41 (t, 1H), 7.39 (t, 1H), 7.34 (t, 1H), 7.32 (t, 1H), 7.18 (d, 1H), 3.04 (s, 3H), 2.27 (dd, $^2J = 6.15$ Hz, $^4J = 0.55$ Hz, 1H; H-3), 1.91 (d, $^2J = 6.15$ Hz, 1H; H-3), 1.82 (d, $^4J = 0.49$ Hz, 3H; CH_3); ^{13}C NMR (125.6 MHz, $CDCl_3$): $\delta = 144.9$, 144.7, 141.1, 139.9 (4quart. C), 126.5 (CH), 126.0 (CH), 125.82 (CH), 125.78 (CH), 122.7 (CH), 121.5 (CH), 119.9 (CH), 119.5 (CH), 70.3 (s, 1C; C-2), 54.8 (q, 1C; OCH_3), 41.5 (s, 1C; C-1), 30.4 (t, $^1J = 160.8$ Hz, 1C; C-3), 16.8 (q, 1C, CH_3); IR (KBr): $\tilde{\nu}$(cm^{-1}) = 3059 (m), 2962 (m), 1473 (s), 1442 (s), 1240 (vs), 1065 (vs), 813 (s), 736 (vs); MS (EI, 70 eV): *m/z* (%): 236 (95) [M^+], 221 (100) [$M^+ - CH_3$], 205 (35) [$M^+ - OCH_3$], 178 (50) [$C_{14}H_{10}^+$], 165 (44) [$C_{13}H_9^+$], 152 (25) [$C_{12}H_8^+$]; elemental analysis calcd for $C_{17}H_{16}O$ (236.31): C 86.41, H 6.82; found: C 86.11, H 6.82.

10: ^{1}H NMR (500 MHz, $CDCl_3$): $\delta = 7.87$ (d, 1H), 7.75 (d, 1H), 7.40 (t, 1H), 7.32 (t, 2H), 7.25 (d, 1H), 7.24 (t, 1H), 6.80 (d, 1H), 4.65 (d, $^3J = 5.76$ Hz, 1H; H-1), 4.48–4.39 (m, 2H; H-3), 2.62 (ddd, $^3J = 1.76$, 5.68, 7.37 Hz, 1H; H-5), 2.48–2.31 (m, 2H; H-4); ^{13}C NMR (125.6 MHz, $CDCl_3$): $\delta = 145.9$, 141.6, 141.4, 138.3 (4quart. C), 126.8 (CH), 126.2 (CH), 125.9 (CH), 125.8 (CH), 123.0 (CH), 120.2 (CH), 119.5 (CH), 118.4 (CH), 77.0 (t, 1C; C-3), 71.6 (d, $^1J = 199.43$ Hz, 1C; C-1), 43.8 (s, 1C; C-6), 33.6 (d, $^1J = 173.3$ Hz, 1C; C-5), 25.6 (t, 1C; C-4); IR (KBr): $\tilde{\nu}$(cm^{-1}) = 3032 (m), 2968 (m), 1438 (vs), 1340 (vs), 1039 (s), 927 (s), 744 (vs); MS (EI, 70 eV): *m/z* (%): 234 (78) [M^+], 205 (85) [$M^+ - C_2H_5$], 178 (100) [$C_{14}H_{10}^+$], 165 (25) [$C_{13}H_9^+$]; elemental analysis calcd for $C_{17}H_{14}O$ (234.30): C 87.15, H 6.02; found: C 86.73, H 6.05.

11: ^{1}H NMR (400 MHz, $CDCl_3$): $\delta = 7.85$ (d, 1H), 7.80 (d, 1H), 7.41 (t, 1H), 7.36 (t, 1H), 7.30–7.19 (m, 7H), 6.92 (t, 1H), 6.15 (d, 1H), 3.38 (t, $^3J = 8.41$ Hz, 1H; H-2), 2.22 (d, $^3J = 8.41$ Hz, 2H; H-3); ^{13}C NMR (100.6 MHz, $CDCl_3$): $\delta = 148.2$, 144.2, 140.4, 139.6, 137.1 (5quart. C), 130.1 (2CH), 128.1 (2CH), 126.8 (CH), 126.7 (CH), 126.0 (CH), 125.8 (CH), 125.7 (CH), 121.5 (CH), 119.7 (CH), 119.6 (CH), 118.5 (CH), 35.5 (s, 1C; C-1), 34.9 (d, $^1J = 160.6$ Hz, 1C; C-2), 22.3 (t, $^1J = 162.3$ Hz, 1C; C-3); IR (KBr): $\tilde{\nu}$(cm^{-1}) = 3055 (m), 3034 (m), 1496 (m), 1444 (s), 777 (vs), 748 (vs), 696 (vs); MS (EI, 70 eV): *m/z* (%): 268 (100) [M^+], 252 (40) [$M^+ - CH_2$], 165 (25) [$C_{13}H_9^+$], 91 (17) [$C_7H_7^+$]; MS-HR calcd for $C_{21}H_{16}$: 268.1252; found: 268.1249.

Two control experiments in the absence of **2** and in the presence of [$Cr(CO)_6$] (10 mol%), respectively, have been performed for each catalytic reaction under the reaction conditions described above. A [2+1] cycloaddition was observed in the absence of the chromium complexes [15] only in the reaction of ethyl acrylate with **7**.

Received: August 13, 1997 [Z10807IE]
German version: *Angew. Chem.* **1997**, *109*, 2948–2950

Keywords: carbene complexes · chromium · cyclopropanations · homogeneous catalysis

[1] Reviews: a) M. P. Doyle, in *Comprehensive Organometallic Chemistry 2, Vol. 12* (Eds.: E. W. Abel, F. G. A. Stone, G. Wilkinson), Pergamon, New York, **1995**, p. 387; b) S. D. Burke, P. A. Grieco, *Org. React. (NY)* **1979**, *26*, 361; c) M. P. Doyle, *Chem. Rev.* **1986**, *86*, 919; d) A. Padwa, K. E. Krumpe, *Tetrahedron* **1992**, *48*, 5385.
[2] Reviews: a) H.-U. Reissig, *Methoden Org. Chem. (Houben-Weyl)* 4th ed. *1952–*, Vol. E21c, p. 3179; b) A. Pfaltz, *Acc. Chem. Res.* **1993**, *26*, 339; c) M. P. Doyle in *Catalytic Asymmetric Synthesis* (Ed.: I. Ojima), VCH, New York, **1993**, 63; d) T. Aratani, *Pure Appl. Chem.* **1985**, *57*, 1839.
[3] a) M. P. Doyle, J. H. Griffin, V. Bagheri, R. L. Dorow, *Organometallics* **1984**, *3*, 53; b) M. P. Doyle, R. L. Dorow, W. E. Buhro, J. H. Griffin, W. H. Tamblyn, M. L. Trudell, *ibid.* **1984**, *3*, 44.
[4] a) W. A. Herrmann, *Angew. Chem.* **1978**, *90*, 855; *Angew. Chem. Int. Ed. Engl.* **1978**, *17*, 800; b) W. A. Herrmann, J. L. Hubbard, I. Bernal, J. D. Korp, B. L. Haymore, G. L. Hillhouse, *Inorg. Chem.* **1984**, *23*, 2978.
[5] a) P. Schwab, M. B. France, J. W. Ziller, R. H. Grubbs, *Angew. Chem.* **1995**, *107*, 2179; *Angew. Chem. Int. Ed. Engl.* **1995**, *34*, 2039; b) P. Schwab, J. W. Ziller, R. H. Grubbs, *J. Am. Chem. Soc.* **1996**, *118*, 100.
[6] Review: M. Brookhart, W. B. Studabaker, *Chem. Rev.* **1987**, *87*, 411.
[7] a) H. Nishiyama, Y. Itoh, H. Matsumoto, Y. Sugawara, K. Itoh, *Bull. Chem. Soc. Jpn.* **1995**, *68*, 1247; b) S.-B. Park, N. Sakata, H. Nishiyama, *Chem. Eur. J.* **1996**, *2*, 303.
[8] a) M. P. Doyle, R. L. Dorow, W. L. Tamblyn, *J. Org. Chem.* **1982**, *47*, 1538; b) M. P. Doyle, J. G. Davidson, *ibid.* **1980**, *45*, 1538.
[9] K. H. Dötz, J. Pfeiffer, *Chem. Commun.* **1996**, 895.
[10] The formal carbene dimers diethyl maleate and -fumarate were isolated as by-products.
[11] 1-Hexene, cyclohexene, cyclooctene, furan, and ethyl acrylate were examined.
[12] **3**, **4**: M. P. Doyle, D. van Leusen, W. H. Tamblyn, *Synthesis* **1981**, 787; **5**: I. Reichelt, H.-U. Reissig, *Chem. Ber.* **1983**, *116*, 3895; **6**: M. P. Doyle, K.-L. Loh, K. M. DeVries, M. S. Chinn, *Tetrahedron Lett.* **1987**, *28*, 833.
[13] T. W. Hanks, P. W. Jennings, *J. Am. Chem. Soc.* **1987**, *109*, 5023.
[14] The formal carbene dimer 9,9′-bisfluorenylidene and bis[9-(9*H*)-fluorenylidene]azine were isolated.
[15] The uncatalyzed [2+1] cycloaddition of **7** is known, for example, for reaction with methyl acrylate: L. Horner, E. Lingnau, *Liebigs Ann. Chem.* **1955**, *591*, 21.
[16] N. E. Searle, *Org. Synth. Coll. Vol. 4* **1963**, 424.
[17] F. W. Grevels, V. Skibbe, *J. Chem. Soc. Chem. Commun.* **1984**, 681.
[18] A. Schönberg, W. Awad, N. Latif, *J. Chem. Soc.* **1951**, 1368.

Creation of Enantioselective Biocatalysts for Organic Chemistry by In Vitro Evolution

Manfred T. Reetz,* Albin Zonta, Klaus Schimossek, Klaus Liebeton, and Karl-Erich Jaeger*

The development of chiral catalysts for the enantioselective synthesis of optically active compounds is of great academic[1] and industrial interest.[2] Inspite of worldwide intensive research in the area of homogeneous transition metal catalysis, the number of really efficient enantioselective catalysts is limited. Owing to a lack of general principles, the development of a single highly effective chiral catalyst requires laborious preparation and testing of many ligands. Alternatively, biocatalysts can be used, but by nature the problem of limited substrate specificity persists.[3] In some cases site-directed mutagenesis can be applied to improve enzyme activity and selectivity but not in a general way,

[*] Prof. M. T. Reetz, Dr. A. Zonta, Dipl.-Chem. K. Schimossek
Max-Planck-Institut für Kohlenforschung
Kaiser-Wilhelm-Platz 1, D-45470 Mülheim an der Ruhr (Germany)
Fax: Int. code + (208)306-2985
e-mail: reetz@mpi-muelheim.mpg.de
Priv.-Doz. Dr. K.-E. Jaeger, Dipl.-Biol. K. Liebeton
Lehrstuhl für Biologie der Mikroorganismen der Universität
D-44780 Bochum (Germany)
Fax: Int. code + (234)7094-425
e-mail: karl-erich.jaeger@ruhr-uni-bochum.de

 © WILEY-VCH Verlag GmbH, D-69451 Weinheim, 1997 0570-0833/97/3624-2830 $ 17.50+.50/0

because the process requires detailed knowledge of the three-dimensional structure of the enzyme and its catalytic mechanism as well as a certain degree of intuition concerning the choice of the amino acid to be substituted.[4] Here we describe a new approach to developing enantioselective catalysts, namely in vitro evolution as a method to increase stepwise the enantioselectivity of a given unselective biocatalyst.[5] The underlying principle—"evolution in the test tube"—does not require any knowledge of the enzyme structure or of its catalytic mechanism. In vitro evolution[6] was already used successfully in efforts directed towards increasing the thermal stability and activity of enzymes.[7,8] Proper molecular-biological methods for random mutagenesis and expression of genes coupled with an efficient screening system for the rapid identification of enantioselective mutants form the basis of our strategy.[5]

The enantioselective hydrolysis of racemic *p*-nitrophenyl 2-methyldecanoate (**1**) was chosen as the test reaction. The free (*S*)-configurated acid belongs to a class of chiral compounds which are useful as drugs, plant-protecting agents, and chiral building blocks in organic synthesis.[2] The lipase from the

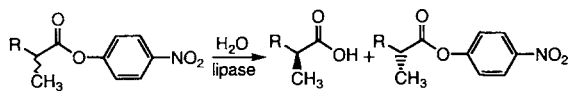

1, R = *n*-C_8H_{17} **2** (*R*)-**1**

bacterium *Pseudomonas aeruginosa* PAO1, which in its mature form is composed of 285 amino acids, was used as the biocatalyst.[9] The wild-type enzyme shows an enantioselectivity (*ee*) of only 2% in favor of the (*S*)-configurated acid **2**.

The number of mutants for a given enzyme in which one amino acid per enzyme molecule was substituted by one of the remaining 19 amino acids is given by Equation (a): N is the

$$N = 19^M X!/[(X-M)!M!] \quad \text{(a)}$$

number of mutants, M the number of substituted amino acids per enzyme (in this case 1), and X the total number of amino acids per enzyme. Therefore, the corresponding library of *P. aeruginosa* lipase mutants would contain 5415 members. Although such a library is already relatively small, our studies show that upon screening an even smaller number of mutants, catalysts with clearly improved enantioselectivity can be obtained.

Using the "error-prone polymerase chain reaction" (epPCR),[10] the lipase gene consisting of 933 base pairs was subjected to random mutagenesis.[11a] By changing the PCR reaction components and conditions, for example variation of the Mg^{2+} concentration, the mutation frequency was empirically adjusted so that statistically one to two base substitutions per lipase gene were introduced; this could lead to substitution of up to two amino acids per lipase molecule. This low number of mutations per lipase molecule was chosen on the assumption that the identification of the rarely occurring mutations with a positive effect would not be prevented by the more commonly occurring mutations with a negative effect. The mutated genes were ligated into a suitable expression vector, amplified in *E. coli*, and transformed into *P. aeruginosa*.[5,11b] The bacterial clones were then cultivated, each theoretically producing a mutant lipase.

About 1000 mutants isolated in this manner had to be screened for their enantioselectivity in the test reaction. To accomplish this difficult feat within a reasonable period of time, an efficient test system had to be developed; conventional separation based on liquid or gas chromatography was unsuitable due to the expected number of samples. Accordingly, the 96 wells of commercially available microtiter plates were loaded pairwise with the culture supernatants of the lipase mutants together with 0.01M Tris/HCl buffer (pH 7.5; Tris = tris(hydroxymethyl)aminomethane) followed by the addition of enantiomerically pure (*R*) and (*S*) substrates dissolved separately in DMF. Thus, up to 48 mutants per microtiter plate could be screened. The enzyme-catalyzed hydrolysis of each (*R*)/(*S*) hydrolysis pair was monitored by measuring the absorption of the *p*-nitrophenolate anion at 410 nm as a function of time. Figure 1 shows the effect of the

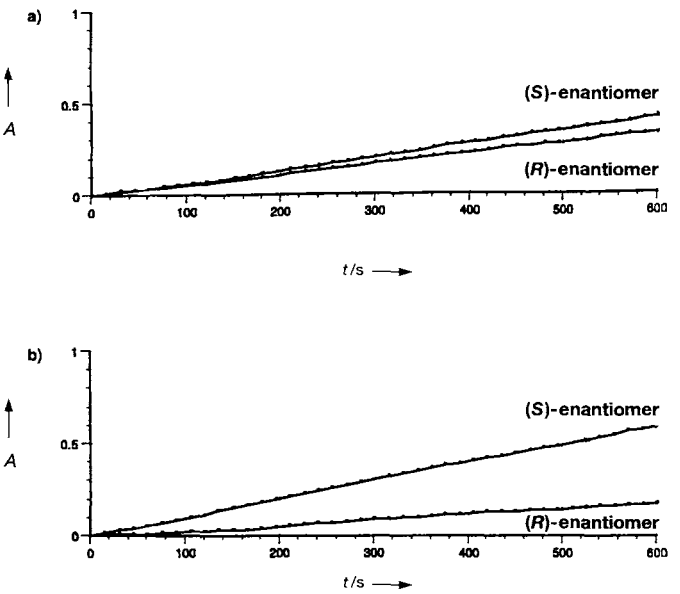

Figure 1. Course of the lipase-catalyzed hydrolysis of the *R*- and *S*-ester **1** as a function of time. a) Wild-type lipase from *P. aeruginosa*, b) improved mutant in the first generation.

original wild-type lipase as well as the typical reaction profile of an improved mutant. Although the relative slopes of the two straight lines can serve as a basis for calculating the corresponding enantioselectivity, we used them only to obtain a qualitative indication due to the possibility of various sources of error. Of 1000 mutants of the first generation tested, 12 showed an increase in enantioselectivity. The exact enantioselectivity was determined by hydrolyzing the racemate **1** in the presence of the corresponding mutant lipases and analyzing the reaction products by gas chromatography on chirally modified capillary columns. The best mutant, P1B01-E4, showed an enantioselecivity of 31% *ee*.

In each generation the clone with the highest enantioselectivity was chosen for the subsequent mutagenesis cycle (Table 1). Figure 2 shows that it was possible to increase the enantioselectivity from 2% *ee* (wild-type enzyme) to 81% *ee* in only four generations.

Table 1. Results of screening.

Generation	Number of clones tested	Number of positive clones	Designation of the chosen clone
1	1000	12	P1B01-E4
2	2200	10	P2B08-H3
3	2400	1	P3B13-D10
4	2000	6	P4B04-H3

 © WILEY-VCH Verlag GmbH, D-69451 Weinheim, 1997 0570-0833/97/3624-2831 $ 17.50+.50/0

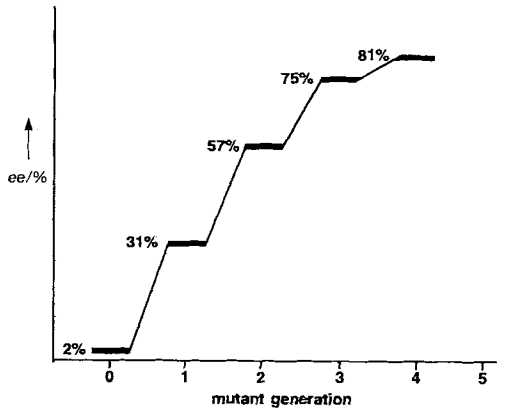

Figure 2. Sequential increase of enantioselectivity in the test reaction of **1** in the course of the mutagenesis experiments. (The *ee* values refer to the corresponding best mutant in a reaction with a conversion range of 20–30%; corresponding *E* values: 1.00, 2.10, 4.40, 9.40, and 11.3, respectively.)

In view of the fact that only four mutant generations were produced and only relatively few mutants were actually screened, the results obtained so far are remarkable. To increase the enantioselectivity even more we are currently exploring four possibilities: 1) more comprehensive screening, 2) production of further generations, 3) DNA-shuffling[6b,7] as an alternative mutagenesis method, and 4) saturation mutagenesis[12] (systematic substitution at the mutated positions with the remaining amino acids). At present it is not possible to predict which of the four strategies will lead most rapidly to an even further increase in enantioselectivity.[13] Investigations concerning sequence determination of the mutant genes as well as modelling the three-dimensional structure of the mutant proteins are also under way.

Lipases from different organisms serve routinely as catalysts in the enantioselective synthesis of chiral esters, alcohols, amines, diols, diesters, diamines, amino alcohols, α- and β-amino acid derivatives, and cyanohydrins, albeit not always with acceptable *ee* values.[3,14] Therefore, our method, which is presumably not restricted to lipases, opens up new perspectives in organic chemistry. The evolutive optimization of enantioselectivity described here can now be combined with the search for higher enzyme stability and activity.[15] All efforts in this new area depend upon the development of further screening methods.[5,16]

Received: October 30, 1997 [Z11106IE]
German version: *Angew. Chem.* **1997**, *109*, 2961–2963

Keywords: asymmetric catalysis · enzyme catalysis · lipases · mutagenesis · screening methods

[1] See for example a) D. J. Berrisford, C. Bolm, K. B. Sharpless, *Angew. Chem.* **1995**, *107*, 1159–1171; *Angew. Chem., Int. Ed. Engl.* **1995**, *34*, 1059–1070; b) R. Noyori, *Asymmetric Catalysis in Organic Synthesis*, Wiley, New York, **1994**; c) A. Pfaltz, *Acc. Chem. Res.* **1993**, *26*, 339–345.

[2] a) *Chirality in Industry: The Commercial Manufacture and Applications of Optically Active Compounds* (Eds.: A. N. Collins, G. N. Sheldrake, J. Crosby), Wiley, Chichester, **1992**; b) *Chirality in Industry II: Developments in the Commercial Manufacture and Applications of Optically Active Compounds* (Eds.: A. N. Collins, G. N. Sheldrake, J. Crosby), Wiley, Chichester, **1997**; c) A. Persidis, *Nat. Biotechnol.* **1997**, *15*, 594–595; d) R. A. Sheldon, *Chirotechnology: Industrial Synthesis of Optically Active Compounds*, Dekker, New York, **1993**; e) *Industrial Enzymology* (Eds.: T. Godfrey, S. West), 2nd ed., Macmillan Press, London, **1996**.

[3] a) H. G. Davies, R. H. Green, D. R. Kelly, S. M. Roberts, *Biotransformations in Preparative Organic Chemistry: The Use of Isolated Enzymes and Whole Cell Systems in Synthesis*, Academic Press, London, **1989**; b) C. H. Wong, G. M. Whitesides, *Enzymes in Synthetic Organic Chemistry*, Pergamon, Oxford, **1994**; c) *Enzyme Catalysis in Organic Synthesis* (Eds.: K. Drauz, H. Waldmann), VCH, Weinheim, **1995**; d) K. Faber, *Biotransformations in Organic Chemistry*, 3rd ed., Springer, Berlin, **1997**.

[4] a) A. J. Russell, A. R. Fersht, *Nature (London)* **1987**, *328*, 496–500; b) M. Holmquist, I. G. Clausen, S. Patkar, A. Svendsen, K. Hult, *J. Protein. Chem.* **1995**, *14*, 217–224; c) H. D. Beer, G. Wohlfahrt, J. E. G. McCarthy, D. Schomburg, R. D. Schmid, *Protein Eng.* **1996**, *9*, 507–517; d) Y. Hirose, K. Kariya, Y. Nakanishi, Y. Kurono, K. Achiwa, *Tetrahedron Lett.* **1995**, *36*, 1063–1066; e) M. J. Haas, R. D. Joerger, G. King, R. R. Klein, *Ann. N. Y. Acad. Sci.* **1996**, *799*, 115–128.

[5] M. T. Reetz, A. Zonta, K. Schimossek, K. Liebeton, K.-E. Jaeger, patent application DE A 19731990.4.

[6] a) K. Chen, F. H. Arnold, *Proc. Natl. Acad. Sci. USA* **1993**, *90*, 5618–5622; b) W. P. C. Stemmer, *Nature (London)* **1994**, *370*, 389–391.

[7] a) A. Crameri, G. Dawes, E. Rodriguez, Jr., S. Silver, W. P. C. Stemmer, *Nat. Biotechnol.* **1997**, *15*, 436–438; b) W. P. C. Stemmer, *Proc. Natl. Acad. Sci. USA* **1994**, *91*, 10747–10751; c) J.-H. Zhang, G. Dawes, W. P. C. Stemmer, *Proc. Natl. Acad. Sci USA* **1997**, *94*, 4504–4509.

[8] a) J. C. Moore, F. H. Arnold, F. H. *Nat. Biotechnol.* **1996**, *14*, 458–467; b) F. H. Arnold, *Chem. Eng. Sci.* **1996**, *51*, 5091–5102; c) Z. Shao, F. H. Arnold, *Curr. Opin. Struct. Biol.* **1996**, *6*, 513–518; d) L. You, F. H. Arnold, *Protein. Eng.* **1996**, *9*, 77–83; e) A. Shinkai, A. Hirano, K. Aisaka, *J. Biochem. (Tokyo)* **1995**, *120*, 915–921.

[9] a) K.-E. Jaeger, B. Schneidinger, K. Liebeton, D. Haas, M. T. Reetz, S. Philippou, G. Gerritse, S. Ransac, B. W. Dijkstra in *Molecular Biology of Pseudomonads* (Eds.: T. Nakazawa, K. Furukawa, D. Haas, S. Silver), ASM Press, Washington, **1996**, pp. 319–330; b) K.-E. Jaeger, K. Liebeton, A. Zonta, K. Schimossek, M. T. Reetz, *Appl. Microbiol. Biotechnol.* **1996**, *46*, 99–105.

[10] a) D. W. Leung, E. Chen, D. V. Goeddel, *Technique (Philadelphia)* **1989**, *1*, 11–15; b) K. A. Eckert, T. A. Kunkel, *PCR Methods Appl.* **1991**, *1*, 17–24; c) R. C. Cadwell, G. F. Joyce, *ibid* **1992**, *2*, 28–33.

[11] a) The lipase gene cloned into pBluescript II KS (Stratagene) was mutagenized by epPCR[6a,9] using the following primers: A: 5′-GCG CAA TTA ACC CTC ACT AAA GGG AAC AAA-3′ and B: 5′-GCG TAA TAC GAC TCA CTA TAG GGC GAA-3′. PCR was performed under the following conditions: 2 min at 98 °C (1 ×); 1 min at 94 °C, 2 min at 64 °C, 1 min at 72 °C (25 ×); 7 min 72 °C (1 ×); b) PCR products were ligated into plasmid pUCPL6A derived from pUCPKS (A. A. Watson, R. A. Alm, J. S. Mattick, *Gene* **1996**, *172*, 163–164). Plasmids were propagated in *E. coli* JM 109, isolated, and used to transform *P. aeruginosa* PABST7.1 (K.-E. Jaeger, B. Schneidinger, F. Rosenau, M. Werner, D. Lang, B. W. Dijkstra, K. Schimossek, A. Zonta, M. T. Reetz, *J. Mol. Catal. B: Enzym.* **1997**, *3*, 3–12). For each new cycle of mutagenesis the lipase gene of the best perfoming clone for a given mutant generation was isolated and recloned into pBluescript II KS.

[12] a) H. Flores, J. Osuna, J. Heitman, X. Soberon, *Gene* **1995**, *157*, 295-301; b) M. S. Warren, S. J. Benkovic, *Protein Eng.* **1997**, *10*, 63–68.

[13] Our current strategy of using the best mutant of a given generation is not necessarily optimal. It is conceivable that a less selective mutant may lead to a better result in the subsequent mutagenesis round.

[14] a) W. Boland, C. Frössl, M. Lorenz, *Synthesis* **1991**, 1049–1072; b) F. Theil, *Chem. Rev.* **1995**, *95*, 2203–2227; c) *Lipases, Part A: Biotechnology* (Eds.: B. Rubin, E. A. Dennis), Academic Press, San Diego, **1997** (*Methods Enzymol.* **1997**, *284*); d) *Lipases, Part B: Enzyme Characterization and Utilization* (Eds.: B. Rubin, E. A. Dennis), Academic Press, San Diego, **1997** (*Methods Enzymol.* **1997**, *286*); e) E. N. Vulfson in *Lipases* (Eds.: P. Woolley, S. B. Petersen), Cambridge University Press, Cambridge, **1994**, pp. 271–288; f) *Engineering of/with Lipases* (Ed.: F. X. Malcata), Kluwer, Dordrecht, **1996** (*NATO ASI Ser. Ser. E.* **1996**, *317*).

[15] In our studies this also occurred to some extent, since the mutants having a low activity (which in some cases may lead to higher enantioselectivities) are "sorted out" upon screening. Only those mutants are considered which induce a notable conversion within ten minutes under the reaction conditions. Indeed, many mutants show practically no activity, which is not surprising.

[16] L. E. Janes, R. J. Kazlauskas, *J. Org. Chem.* **1997**, *62*, 4560–4561.

 © WILEY-VCH Verlag GmbH, D-69451 Weinheim, 1997 0570-0833/97/3624-2832 $ 17.50+.50/0

Shape-Selective Hydrogenation and Oxidation over a Platinum-Containing Ultramicroporous Heteropolyoxometallic Compound**

Yusuke Yoshinaga, Kohei Seki, Teruyuki Nakato, and Toshio Okuhara*

Shape-selective catalysis like that typically demonstrated by zeolites is of great interest from a scientific as well as an industrial viewpoint.[1-6] However, certain factors restrict the general application of zeolites: their acid strength is not very great,[7] their pore sizes are not sufficiently variable, and the choice of constituent elements is limited. Various alternative microporous inorganic materials have been synthesized for possible use as catalysts. Thus, Toba et al.[8] prepared microporous SiO_2/Al_2O_3 by a sol–gel method, and Maier et al.[9,10] described a series of microporous oxides, including SiO_2, TiO_2, ZrO_2, Al_2O_3, and related mixed oxides.

Heteropolyacids can be regarded as cluster models for mixed oxides. They are also fascinating and important catalysts from a practical standpoint, because they and their acidic cesium salts are very acidic and much more active than such zeolites like H-ZSM-5 in various acid-catalyzed reactions.[7,11-13] It is known that ammonium and cesium salts of the Keggin heteropolyacid $H_3PW_{12}O_{40}$ have porous secondary structures.[14-17] Recently Hölderich and co-workers[18] claimed that an organic salt of a Dawson heteropolyacid ($H_6P_2W_{18}O_{62}$) with 1,6-hexanediyldiamine has pores in its crystal structure. In addition, Müller et al. synthesized a supramolecular molybdenum oxide cluster with the form of a ferris wheel and thus with an opening in the center.[19] More recently, it was found that the cesium salt $Cs_{2.2}H_{0.8}PW_{12}O_{40}$ is microporous.[20] We have now succeeded in synthesizing a novel platinum-containing compound (5 wt% Pt), $Pt/Cs_{2.1}H_{0.9}PW_{12}O_{40}$ (**1**), in which all of the ultramicropores have diameters smaller than benzene (5.9 Å). Ultramicropores are defined as pores with widths less than 7 Å.[21] Here we report that **1** is an efficient catalyst for shape-selective hydrogenation of alkenes and complete oxidation of alkanes.

The adsorption isotherms of **1** are Type I isotherms[22] characteristic of microporous materials (Figure 1). On the other hand, $Pt/Cs_{2.5}H_{0.5}PW_{12}O_{40}$ (**2**) gave a Type IV isotherm in which a hysteresis was observed. A Type IV isotherm is usually associated with mesoporous materials.[22] In addition, the steep increase in adsorbed amount of gas in the low-pressure region ($p/p_0 < 0.1$) of this isotherm indicates the presence of both micropores and mesopores. The inset of Figure 1 shows Horváth–Kawazoe plots for N_2 adsorption[23] that reveal sharp peaks for **1** and **2** at 5.5 Å and 5.9 Å, respectively. Thus, **1** is microporous, while **2** contains both micro- and mesopores. However, pore diameters estimated with the Horváth–Kawazoe method are not necessarily reliable, because the analysis is performed with parameters based on the interaction between N_2 and graphite,[23] not between N_2 and an oxide.

To determine the pore size for **1**, adsorption experiments were carried out for molecules of different sizes with the aid of a microbalance (Shimadzu TG-30) connected directly to a high-vacuum system (molecular probe method). The results are summarized in Table 1. It should be noted that N_2 adsorption was measured at 77 K, and the other adsorption experiments were carried out at room temperature at a relative pressure $p/p_0 = 0.2$ (exception: 2,2-dimethylpropane $p/p_0 = 0.1$). Benzene, 2,2-dimethylpropane, CCl_4, and 1,3,5-trimethylbenzene were adsorbed on **2**. On the other hand, **1** adsorbed only small amounts of these compounds, but large amounts of N_2. This demonstrates that **1** possesses only ultramicropores with a diameter of 3.6–5.9 Å. and that the external surface area is negligibly small. By contrast, **2** has pores with a diameter of at least 7.5 Å (Table 1).

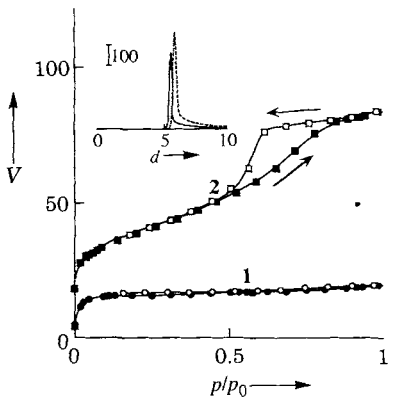

Figure 1. N_2 adsorption/desorption isotherms for **1** (black/white circles) and **2** (black/white squares) at 77 K. The samples were pretreated at 573 K in vacuum. Inset: Horváth–Kawazoe analysis [23] for **1** (solid line) and **2** (dotted line), calculated from the N_2 adsorption isotherms from standard parameters [23]. p/p_0 = relative pressure, V = adsorbed volume (in $cm^3 g^{-1}$ at standard temperature and pressure), d = pore diameter in Å; the ordinate of the inset represents $\Delta V/\Delta d$ in $mm^3 Å^{-1} g^{-1}$.

Table 1. Adsorption of various molecules on **1**, **2**, and Pt/SiO_2 (each with 0.5 wt% Pt).

Molecule	Diameter [Å]	Amount adsorbed [μmol g^{-1}] [a]		
		1 [57 $m^2 g^{-1}$]	**2** [130 $m^2 g^{-1}$]	Pt/SiO_2 [274 $m^2 g^{-1}$]
N_2	3.6	659 (64)	1679 (164)	3530 (344)
Benzene	5.9 [24]	10 (2)	507 (93)	845 (155)
2,2-DMP [b]	6.2 [24]	5 (1)	302 (68)	393 (88)
CCl_4	6.9 [24]	5 (1)	436 (85)	484 (94)
1,3,5-TMB [c]	7.5 [1]	6 (2)	566 (140)	1196 (296)

[a] Measurements were carried out at room temperature under a relative pressure (p/p_0) of 0.2 (exceptions: 77 K for N_2; $p/p_0 = 0.1$ for 2,2-dimethylpropane). Prior to measurement, samples were pretreated at 573 K in vacuum. The figures in square brackets are BET surface areas, and those in parentheses are adsorption areas [$m^2 g^{-1}$], calculated from the amount adsorbed and the molecular cross section. [b] 2,2-dimethylpropane. [c] 1,3,5-trimethylbenzene.

Figure 2 depicts the pore-size distribution for **1** and **2** in the range of mesopores, as derived from the desorption branch of the N_2 isotherm on use of the Dollimore–Heal method.[25] No mesopores are present in **1**, whereas **2** contains mesopores with a diameter of about 40 Å, consistent with the results presented in Table 1.

Catalytic activities of **1**, **2**, and a Pt/SiO_2 with respect to hydrogenation and oxidation are summarized in Table 2. In the case of hydrogenation of ethene, conversions decreased gradually with time; the conversions leveled off for all

[*] Prof. T. Okuhara, Y. Yoshinaga, K. Seki, Dr. T. Nakato
Graduate School of Environmental Earth Science,
Hokkaido University
Sapporo 060 (Japan)
Fax: Int. code + (11) 757-5995
e-mail: oku@ees.hokudai.ac.jp

[**] This study was supported in part by a Grant-in-Aid for Scientific Research on Priority Areas (No. 08232202) from the Ministry of Education, Science, Sports and Culture of Japan.

 © WILEY-VCH Verlag GmbH, D-69451 Weinheim, 1997 0570-0833/97/3624-2833 $ 17.50+.50/0

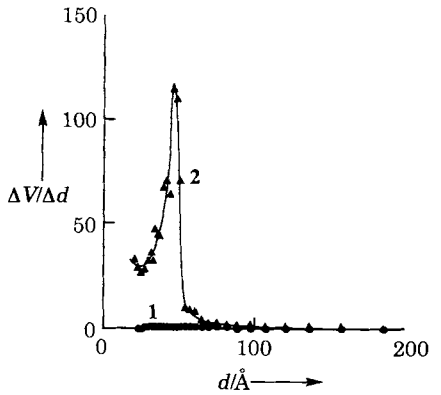

Figure 2. Pore-size distributions derived by the Dollimore–Heal method [25] for **1** (circles) and **2** (triangles) from the N_2 isotherms in Figure 1. The analysis was performed using the desorption data.

Table 2. Relative catalytic activities of **1**, **2**, and Pt/SiO_2 (each with 0.5 wt % Pt) toward hydrogenation and oxidation [a].

Reaction	T[K]	Catalytic activity [b]		
		1	**2**	Pt/SiO_2
Hydrogenation of				
ethene	320	0.9	1.9	12.7
		(7.1)	(15.0)	(100)
cyclohexene	273	0.1	18.8	52.1
		(0.2)	(36.1)	(100)
Oxidation of				
methane	573	22.5	34.5	23.0
		(97.8)	(150.0)	(100)
2,2-dimethylpropane	493	2.6	103.5	28.6
		(9.1)	(361.9)	(100)

[a] The activity is given in $mmol\,g^{-1}\,min^{-1}$ for ethene and in $\mu mol\,g^{-1}\,min^{-1}$ for the other compounds. [b] Numbers in parentheses are activities relative to those of the Pt/SiO_2 catalyst.

catalysts after about two hours under the reaction conditions employed (see Experimental Section). The activity of **1** for ethene hydrogenation (reported per unit catalyst weight) at this stationary conversion was about half that of **2**, while Pt/SiO_2 was more active than these heteropolyoxometallic catalysts. In contrast, the conversion for the hydrogenation of cyclohexene was 0.2% for **1** and 0.5% for both **2** and Pt/SiO_2. As a matter of fact, cyclohexene (which has a diameter of about 6 Å) was not adsorbed on **1** at room temperature (less than 5 $\mu mol\,g^{-1}$), whereas it was appreciably adsorbed on **2** (1300 $\mu mol\,g^{-1}$). These results indicate that **1** exhibits shape selectivity for the hydrogenation of alkenes. The amount of cyclohexene adsorbed on **2** was larger than the corresponding amounts of benzene or CCl_4. A probable explanation is that some dimerization of cyclohexene occurred on **2** as a result of superacidity [11,12] and the mesoporous structure. Another cause may be the conformational flexibility of cyclohexene.

Catalytic activities are also compared in Table 2 for oxidation of methane and 2,2-dimethylpropane; the collected data refer to the stationary states attained after about two hours. In these reactions, the decreases in conversion as a function of time were small. For methane oxidation, all the catalysts exhibited similar activities; the relative activities of Pt/SiO_2, **1**, and **2** were 1.0, 1.0, and 1.5, respectively. However, the activity of **1** for oxidation of 2,2-dimethylpropane was less than 3% that of **2** and 9% that of Pt/SiO_2. As can be seen in Table 1, 2,2-dimethylpropane was adsorbed on both **2** and Pt/SiO_2, but not on **1**. Therefore, the low activity of **1** in this reaction is due to limited adsorption and/or diffusion of the reactant molecules in the constrained pores of **1**. This is an example of shape-selective oxidation of alkanes, which is of interest for applications in catalysis and sensor materials for gas detection.

The line widths in X-ray diffractograms reveal that these cesium–hydrogen salts consist of primary crystallites with a size of about 120 Å. The primary crystallites, which are themselves nonporous,[12,15] aggregate to produce secondary particles. It is reasonable to assume that the close-packed aggregates resulting from the primary crystallites are responsible for the voids with diameters of about 40 Å. This represents a possible mechanism for the formation of mesopores in **2**. In the case of **1**, most of the mesopores might be filled with molecules of the acidic form ($H_3PW_{12}O_{40}$) during preparation. After heat treatment this salt is probably converted into a material with nearly uniform composition.[16] In both salts, pores are present between the primary crystallites. We currently speculate that micropores in **1** are generated by crystallographic mismatching of the facets.

An attempt was made to detect platinum particles in **1** and **2** by the use of transmission electron microscopy (TEM) and X-ray diffraction (XRD). TEM produced images of aggregates of fine primary crystallites of the Cs salts, but no platinum particles could be localized, even with a resolution of about 1 nm. XRD results also failed to show peaks attributable to platinum particles. These results suggest that the platinum centers are highly dispersed, with crystallite (particle) size less than 1 nm. While the surface area of **1** was about 50% that of **2**, the activity of **1** was only 0.6% and 2.5% that of **2** for cyclohexene hydrogenation and 2,2-dimethylpropane oxidation, respectively (Table 2). These results indicate that platinum particles are located exclusively within the pores of **1**.

In conclusion, a novel catalyst ($Cs_{2.1}H_{0.9}PW_{12}O_{40}$ containing 0.5 wt % platinum) exhibited shape-selective catalysis in the hydrogenation of alkenes and the oxidation of alkanes and preferentially catalyzed reactions of smaller molecules. This is the first example of shape selectivity by an ultramicroporous heteropolyoxometallic compound containing an additional metal, and it may lead to novel applications in the field of shape-selective catalysis.

Experimental Section

Both **1** and **2** were prepared by a titration method. For each an aqueous solution of $[Pt(NH_3)_4]\cdot(OH)_2$ ($0.03\,mol\,L^{-1}$) was added to an aqueous solution of $H_3PW_{12}O_{40}$ ($0.08\,mol\,L^{-1}$) at room temperature. An aqueous solution of Cs_2CO_3 ($0.10\,mol\,L^{-1}$) was then added dropwise at a rate of $1\,mL\,min^{-1}$ with vigorous stirring at room temperature. The cesium content was controlled by the amount of Cs_2CO_3 added. The platinum content was adjusted to 0.5 wt %. A pale yellow precipitate was obtained, the color of which was due to the presence of Pt. The solution was allowed to stand overnight at room temperature. The solid obtained by drying at 318 K was pretreated in a flow of O_2 at 573 K for 2 h. A Pt/SiO_2 catalyst (0.5 wt % Pt), prepared from $[Pt(NH_3)_4]\cdot(OH)_2$ and SiO_2 (AEROSIL 300, $274\,m^2\,g^{-1}$) by an impregnation method and then calcined at 773 K in air, was used as a reference. Nitrogen adsorption/desorption isotherms were measured with a BELSORP 28SA apparatus (BEL Japan, Inc.).

Catalytic reactions were carried out in a flow reactor (Pyrex, 12 mm inside diameter) at atmospheric pressure. Conditions for ethene hydrogenation: ethene 9%, H_2 91% (He diluent gas), flow rate $27.5\,mL\,min^{-1}$, 320 K, catalyst 20 mg (in powdered quartz, 200 mg); for cyclohexene hydrogenation: cyclohexene 1.5%, H_2 82% (He diluent gas 16.5%), flow rate $30.5\,mL\,min^{-1}$, 273 K, catalyst 200 mg (in powdered quartz, 200 mg); for methane oxidation: methane 30%, O_2 20% (He diluent gas 50%), flow rate $20\,mL\,min^{-1}$, 573 K, catalyst 100 mg (in powdered quartz, 300 mg); for 2,2-dimethylpropane oxidation: 2,2-dimethylpropane 4%, O_2 40% (He diluent gas 56%), flow rate $50\,mL\,min^{-1}$, 493 K, catalyst weight 20–100 mg (in powdered quartz, 100 mg). Prior to the reactions, catalysts were pretreated in a flow of O_2 at 573 K for 1 h, and then in a flow of H_2 at 573 K

 © WILEY-VCH Verlag GmbH, D-69451 Weinheim, 1997 0570-0833/97/3624-2834 $ 17.50+.50/0

for 1 h in the case of hydrogenation, or in a flow of He at 573 K for 1 h for oxidation. The catalytic test was conducted with fine powders (μm range) of the catalysts.

Received: March 7, 1997 [Z10213IE]
German version: *Angew. Chem.* **1997**, *109*, 2946–2948

Keywords: heterogeneous catalysis · heteropolyacids · hydrogenations · oxidations · platinum · shape-selectivity

[1] D. W. Breck, *Zeolite Molecular Sieves*, Wiley, New York, **1974**.
[2] N. Y. Chen, W. E. Garwood, F. G. Dwyer, *Shape Selective Catalysis in Industrial Applications*, Marcel Dekker, New York, **1989**.
[3] J. M. Thomas, *Sci. Am.* **1992**, *266(4)*, 82–88.
[4] S. M. Csicsery, *Pure Appl. Chem.* **1986**, *58*, 841–856.
[5] W. Hölderich, M. Hesse, F. Näumann, *Angew. Chem.* **1988**, *100*, 232–252; *Angew. Chem. Int. Ed. Engl.* **1988**, *27*, 226–246.
[6] J. Weitkamp, S. Ernst, C. Y. Chen, *Stud. Surf. Sci. Catal.* **1989**, *49B*, 1115–1123.
[7] T. Okuhara, T. Nishimura, M. Misono, *J. Mol. Catal.* **1992**, *14*, 247–256.
[8] M. Toba, F. Mizukami, S. Niwa, K. Maeda, *J. Chem. Soc. Chem. Commun.* **1990**, 1211–1212.
[9] W. F. Maier, J. A. Martens, S. Klein, J. Heilmann, R. Porton, K. Vercruysse, P. A. Jacobs, *Angew. Chem.* **1996**, *108*, 222–224; *Angew. Chem. Int. Ed. Engl.* **1996**, *35*, 180–182.
[10] S. Klein, W. F. Maier, *Angew. Chem.* **1996**, *108*, 2376–2379; *Angew. Chem. Int. Ed. Engl.* **1996**, *35*, 2230–2233.
[11] M. Misono, T. Okuhara, *CHEMTECH* **1993**, *23*, 23–29.
[12] T. Okuhara, N. Mizuno, M. Misono, *Adv. Catal.* **1995**, *41*, 113–252.
[13] T. Nishimura, T. Okuhara, M. Misono, *Appl. Catal.* **1991**, L7–L11.
[14] S. T. Gregg, M. M. Tayyab, *J. Chem. Soc. Faraday Trans. 1* **1978**, *74*, 348–358.
[15] N. Mizuno, M. Misono, *Chem. Lett.* **1987**, 961–964.
[16] T. Okuhara, T. Nishimura, H. Watanabe, K. Na, M. Misono, *Stud. Surf. Sci. Catal.* **1994**, *90*, 419–428.
[17] K. Inumaru, H. Nakajima, T. Ito, M. Misono, *Chem. Lett.* **1996**, 559–560.
[18] M. Hölscher, U. Englert, B. Zibrowius, W. F. Hölderich, *Angew. Chem.* **1994**, *106*, 2552–2554; *Angew. Chem. Int. Ed. Engl.* **1994**, *33*, 2491–2493.
[19] A. Müller, E. Kricemeyer, J. Meyer, H. Bögge, F. Peters, W. Plass, E. Diemann, S. Dillinger, F. Nonnenbruch, M. Randerath, C. Menke, *Angew. Chem.* **1995**, *107*, 2293–2295; *Angew. Chem. Int. Ed. Engl.* **1995**, *34*, 2122–2124.
[20] T. Okuhara, T. Nishimura, M. Misono, *Chem. Lett.* **1995**, 155–156.
[21] J. Rouquerol, D. Avnir, C. W. Fairbridge, D. H. Everett, J. H. Haynes, N. Pernicone, J. D. F. Ramsey, K. S. W. Sing, K. K. Unger, *Pure Appl. Chem.* **1994**, *66*, 1739–1758.
[22] S. J. Gregg, K. S. W. Sing, *Adsorption, Surface Area and Porosity*, 2nd ed., Academic Press, London, **1982**.
[23] G. Horváth, K. Kawazoe, *J. Chem. Eng. Jpn.* **1983**, *16*, 470–475.
[24] D. E. W. Vaugham, R. Lussier, *Proceedings of the 5th International Conference on Zeolites* (Ed.: L. V. Rees), pp. 94–101, Heyden, London, **1980**.
[25] D. Dollimore, G. R. Heal, *J. Colloid. Interface Sci.* **1970**, *33*, 508–519.

Stabilization of Atomic Nitrogen Inside C_{60}**

Harald Mauser, Nicolaas J. R. van Eikema Hommes, Timothy Clark, Andreas Hirsch,* Björn Pietzak, Alois Weidinger, and Lothar Dunsch

Until now only electropositive metal cations[1,2] or noble gas atoms[3,4] were incorporated into fullerenes. The first member of a new class of endohedral complexes in which the guest is a very reactive nonmetal is the recently described $N@C_{60}$.[5] ESR and electron nuclear double resonance (ENDOR) spectroscopic analyses of this system show an astonishing and unprecedented situation: Nitrogen is in its atomic ground state ($^4S_{3/2}$) and not covalently bound to the carbon atoms of the fullerene cage.[5] Therefore, the concave inner face of C_{60} must be extraordinarily inert. We now investigated the influence of the shape of a carbon network on its reactivity, and present here a topological explanation for this result. Moreover, we predict that the energy barrier for the penetration of nitrogen through the cage is comparatively low, and confirm this experimentally.

To prove that nitrogen is atomic in $N@C_{60}$ and not covalently bound to the cage atoms we performed semiempirical (PM3-UHF[6a,b]/RHF) and density functional calculations (UB3LYP/D95*//PM3[6c]) on the system N/C_{60} with the programs VAMP 6.1[7a] and Gaussian 94.[7b] The structure of $N@C_{60}$ with nitrogen in the center of the cage is the global minimum for endohedral complexation (Tables 1 and 2, Figure 1). The formation of $N@C_{60}$ from the free components is more or less thermoneutral. PM3-UHF calculations give a relative binding enthalpy of $+10.5$ kcal mol^{-1}; the UB3LYP/D95* value for the PM3-UHF geometry is -0.9 kcal mol^{-1} (Table 2). The Coulson and Mulliken charges on the nitrogen atom are both negligible according to PM3 and density functional calculations. The spin density is almost exclusively

Table 1. Geometries and dipole moments (according to PM3-UHF calculations) of exo- and endohedral N/C_{60} complexes.

Compound	Position of N	Dipole moment [D]	d(C–N) [Å]	d(C–C) [Å]
NC_{60} (*exo*)	[5,6] aza bridge [a] (open)	1.22	1.42	2.23
NC_{60} (*exo*)	[6,6] aza bridge [a] (open)	1.12	1.41	2.24
NC_{60} (*exo*)	[6,6] aza bridge [a] (closed)	1.46	1.46	1.54
$N@C_{60}$ (*endo*)	[5,6] aza bridge [a] (closed)	0.71	1.53	1.48
$N@C_{60}$ (*endo*)	[6,6] aza bridge [a] (closed)	0.91	1.52	1.46
$N@C_{60}$ (*endo*)	in center [a] (doublet)	0.0	3.33	–
$N@C_{60}$ (*endo*)	in center [a] (quartet)	0.0	3.33	–
$N@C_{60}$ (TS) [b]	center → *endo* bound ([5,6])	1.30	1.99	1.44
$N@C_{60}$ (TS) [b]	center → *endo* bound ([6,6])	1.28	2.06	1.39
$N@C_{60}$ (TS) [b]	[5,6]-endohedral → exohedral	0.39	1.36	1.75
$N@C_{60}$ (TS) [b]	[6,6]-endohedral → exohedral	0.53	1.35	1.75

[*] Prof. Dr. A. Hirsch, Dipl.-Chem. H. Mauser
Institut für Organische Chemie der Universität Erlangen-Nürnberg
Henkestrasse 42, D-91054 Erlangen (Germany)
Fax: Int. code + (9131) 85-6864
e-mail: hirsch@organik.uni-erlangen.de
Dr. N. J. R. van Eikema Hommes, Priv.-Doz. Dr. T. Clark
Computer-Chemie-Centrum, Universität Erlangen-Nürnberg (Germany)
Dipl.-Phys. B. Pietzak, Prof. Dr. A. Weidinger
Hahn-Meitner-Institut, Berlin (Germany)
Dr. L. Dunsch
Institut für Festkörper- und Werkstofforschung, Dresden (Germany)

[**] This work was supported by Bundesministerium für Bildung und Forschung (BMBF) and the Fonds der Chemischen Industrie.

 © WILEY-VCH Verlag GmbH, D-69451 Weinheim, 1997 0570-0833/97/3624-2835 $ 17.50+.50/0

for 1 h in the case of hydrogenation, or in a flow of He at 573 K for 1 h for oxidation. The catalytic test was conducted with fine powders (μm range) of the catalysts.

Received: March 7, 1997 [Z10213IE]
German version: *Angew. Chem.* **1997**, *109*, 2946–2948

Keywords: heterogeneous catalysis · heteropolyacids · hydrogenations · oxidations · platinum · shape-selectivity

[1] D. W. Breck, *Zeolite Molecular Sieves*, Wiley, New York, **1974**.
[2] N. Y. Chen, W. E. Garwood, F. G. Dwyer, *Shape Selective Catalysis in Industrial Applications*, Marcel Dekker, New York, **1989**.
[3] J. M. Thomas, *Sci. Am.* **1992**, *266(4)*, 82–88.
[4] S. M. Csicsery, *Pure Appl. Chem.* **1986**, *58*, 841–856.
[5] W. Hölderich, M. Hesse, F. Näumann, *Angew. Chem.* **1988**, *100*, 232–252; *Angew. Chem. Int. Ed. Engl.* **1988**, *27*, 226–246.
[6] J. Weitkamp, S. Ernst, C. Y. Chen, *Stud. Surf. Sci. Catal.* **1989**, *49B*, 1115–1123.
[7] T. Okuhara, T. Nishimura, M. Misono, *J. Mol. Catal.* **1992**, *14*, 247–256.
[8] M. Toba, F. Mizukami, S. Niwa, K. Maeda, *J. Chem. Soc. Chem. Commun.* **1990**, 1211–1212.
[9] W. F. Maier, J. A. Martens, S. Klein, J. Heilmann, R. Porton, K. Vercruysse, P. A. Jacobs, *Angew. Chem.* **1996**, *108*, 222–224; *Angew. Chem. Int. Ed. Engl.* **1996**, *35*, 180–182.
[10] S. Klein, W. F. Maier, *Angew. Chem.* **1996**, *108*, 2376–2379; *Angew. Chem. Int. Ed. Engl.* **1996**, *35*, 2230–2233.
[11] M. Misono, T. Okuhara, *CHEMTECH* **1993**, *23*, 23–29.
[12] T. Okuhara, N. Mizuno, M. Misono, *Adv. Catal.* **1995**, *41*, 113–252.
[13] T. Nishimura, T. Okuhara, M. Misono, *Appl. Catal.* **1991**, L7–L11.
[14] S. T. Gregg, M. M. Tayyab, *J. Chem. Soc. Faraday Trans. 1* **1978**, *74*, 348–358.
[15] N. Mizuno, M. Misono, *Chem. Lett.* **1987**, 961–964.
[16] T. Okuhara, T. Nishimura, H. Watanabe, K. Na, M. Misono, *Stud. Surf. Sci. Catal.* **1994**, *90*, 419–428.
[17] K. Inumaru, H. Nakajima, T. Ito, M. Misono, *Chem. Lett.* **1996**, 559–560.
[18] M. Hölscher, U. Englert, B. Zibrowius, W. F. Hölderich, *Angew. Chem.* **1994**, *106*, 2552–2554; *Angew. Chem. Int. Ed. Engl.* **1994**, *33*, 2491–2493.
[19] A. Müller, E. Kricemeyer, J. Meyer, H. Bögge, F. Peters, W. Plass, E. Diemann, S. Dillinger, F. Nonnenbruch, M. Randerath, C. Menke, *Angew. Chem.* **1995**, *107*, 2293–2295; *Angew. Chem. Int. Ed. Engl.* **1995**, *34*, 2122–2124.
[20] T. Okuhara, T. Nishimura, M. Misono, *Chem. Lett.* **1995**, 155–156.
[21] J. Rouquerol, D. Avnir, C. W. Fairbridge, D. H. Everett, J. H. Haynes, N. Pernicone, J. D. F. Ramsey, K. S. W. Sing, K. K. Unger, *Pure Appl. Chem.* **1994**, *66*, 1739–1758.
[22] S. J. Gregg, K. S. W. Sing, *Adsorption, Surface Area and Porosity*, 2nd ed., Academic Press, London, **1982**.
[23] G. Horváth, K. Kawazoe, *J. Chem. Eng. Jpn.* **1983**, *16*, 470–475.
[24] D. E. W. Vaugham, R. Lussier, *Proceedings of the 5th International Conference on Zeolites* (Ed.: L. V. Rees), pp. 94–101, Heyden, London, **1980**.
[25] D. Dollimore, G. R. Heal, *J. Colloid. Interface Sci.* **1970**, *33*, 508–519.

Stabilization of Atomic Nitrogen Inside C_{60}**

Harald Mauser, Nicolaas J. R. van Eikema Hommes, Timothy Clark, Andreas Hirsch,* Björn Pietzak, Alois Weidinger, and Lothar Dunsch

Until now only electropositive metal cations[1,2] or noble gas atoms[3,4] were incorporated into fullerenes. The first member of a new class of endohedral complexes in which the guest is a very reactive nonmetal is the recently described $N@C_{60}$.[5] ESR and electron nuclear double resonance (ENDOR) spectroscopic analyses of this system show an astonishing and unprecedented situation: Nitrogen is in its atomic ground state ($^4S_{3/2}$) and not covalently bound to the carbon atoms of the fullerene cage.[5] Therefore, the concave inner face of C_{60} must be extraordinarily inert. We now investigated the influence of the shape of a carbon network on its reactivity, and present here a topological explanation for this result. Moreover, we predict that the energy barrier for the penetration of nitrogen through the cage is comparatively low, and confirm this experimentally.

To prove that nitrogen is atomic in $N@C_{60}$ and not covalently bound to the cage atoms we performed semiempirical (PM3-UHF[6a,b]/RHF) and density functional calculations (UB3LYP/D95*//PM3[6c]) on the system N/C_{60} with the programs VAMP 6.1[7a] and Gaussian 94.[7b] The structure of $N@C_{60}$ with nitrogen in the center of the cage is the global minimum for endohedral complexation (Tables 1 and 2, Figure 1). The formation of $N@C_{60}$ from the free components is more or less thermoneutral. PM3-UHF calculations give a relative binding enthalpy of $+10.5$ kcal mol^{-1}; the UB3LYP/D95* value for the PM3-UHF geometry is -0.9 kcal mol^{-1} (Table 2). The Coulson and Mulliken charges on the nitrogen atom are both negligible according to PM3 and density functional calculations. The spin density is almost exclusively

Table 1. Geometries and dipole moments (according to PM3-UHF calculations) of exo- and endohedral N/C_{60} complexes.

Compound	Position of N	Dipole moment [D]	d(C–N) [Å]	d(C–C) [Å]
NC_{60} (*exo*)	[5,6] aza bridge [a] (open)	1.22	1.42	2.23
NC_{60} (*exo*)	[6,6] aza bridge [a] (open)	1.12	1.41	2.24
NC_{60} (*exo*)	[6,6] aza bridge [a] (closed)	1.46	1.46	1.54
$N@C_{60}$ (*endo*)	[5,6] aza bridge [a] (closed)	0.71	1.53	1.48
$N@C_{60}$ (*endo*)	[6,6] aza bridge [a] (closed)	0.91	1.52	1.46
$N@C_{60}$ (*endo*)	in center [a] (doublet)	0.0	3.33	–
$N@C_{60}$ (*endo*)	in center [a] (quartet)	0.0	3.33	–
$N@C_{60}$ (TS) [b]	center → *endo* bound ([5,6])	1.30	1.99	1.44
$N@C_{60}$ (TS) [b]	center → *endo* bound ([6,6])	1.28	2.06	1.39
$N@C_{60}$ (TS) [b]	[5,6]-endohedral → exohedral	0.39	1.36	1.75
$N@C_{60}$ (TS) [b]	[6,6]-endohedral → exohedral	0.53	1.35	1.75

[*] Prof. Dr. A. Hirsch, Dipl.-Chem. H. Mauser
Institut für Organische Chemie der Universität Erlangen-Nürnberg
Henkestrasse 42, D-91054 Erlangen (Germany)
Fax: Int. code + (9131) 85-6864
e-mail: hirsch@organik.uni-erlangen.de
Dr. N. J. R. van Eikema Hommes, Priv.-Doz. Dr. T. Clark
Computer-Chemie-Centrum, Universität Erlangen-Nürnberg (Germany)
Dipl.-Phys. B. Pietzak, Prof. Dr. A. Weidinger
Hahn-Meitner-Institut, Berlin (Germany)
Dr. L. Dunsch
Institut für Festkörper- und Werkstofforschung, Dresden (Germany)

[**] This work was supported by Bundesministerium für Bildung und Forschung (BMBF) and the Fonds der Chemischen Industrie.

 © WILEY-VCH Verlag GmbH, D-69451 Weinheim, 1997 0570-0833/97/3624-2835 $ 17.50+.50/0

Table 2. Enthalpies of formation, spin densitites $|S^2|$, and total and relative energies of the exo- and endohedral N/C_{60} complexes.

Compound	Position of N	PM3-UHF			PM3/RHF[c]			UB3LYB/D95*//PM3[d]	
		enthalpy of formation [kcal mol^{-1}]	relative enthalpy of formation [kcal mol^{-1}]	spin density $\|S^2\|$ [6b]	enthalpy of formation [kcal mol^{-1}]	relative enthalpy of formation [kcal mol^{-1}]	total energy[e]	relative energy[b] [kcal mol^{-1}]	spin density $\|S^2\|$
NC_{60} (*exo*)	[5,6] aza bridge[a] (open)	828.3	−83.9	6.12	875.6	−49.1	−2341.02492	−50.4	0.776
NC_{60} (*exo*)	[6,6] aza bridge[a] (open)	839.6	−72.6	5.74	891.1	−33.7	−2340.99040	−28.8	0.763
NC_{60} (*exo*)	[6,6] aza bridge[a] (closed)	844.3	−67.9	5.53	867.8	−57.0	−2341.02170	−48.4	0.754
N@C_{60} (*endo*)	[5,6] aza bridge[a] (closed)	954.6	42.5	6.50	1014.4	89.6	−2340.84762	60.8	0.776
N@C_{60} (*endo*)	[6,6] aza bridge[a] (closed)	944.8	32.6	6.22	1004.6	79.9	−2340.89144	33.3	0.760
N@C_{60} (*endo*)	in center[a] (doublet)	944.5	32.4	1.75	982.8	58.1			
N@C_{60} (*endo*)	in center[a] (quartet)	922.7	10.5	3.75	962.9	38.1	−2340.94597	−0.9	3.753
N@C_{60} (TS)[f]	center →*endo* bound ([5,6])	974.8	62.7	6.18	1017.3	92.6			
N@C_{60} (TS)[f]	center →*endo* bound ([6,6])	973.9	61.7	6.08	1011.1	86.4			
N@C_{60} (TS)[f]	[5,6]-endohedral →exohedral	993.7	81.5	6.70	1053.5	128.8	−2340.80645	86.7	1.549
N@C_{60} (TS)[f]	[6,6]-endohedral →exohedral	985.7	73.6	6.19	1028.3	103.6	−2340.83958	65.9	0.761

[a] Optimized geometry. [b] Based on free C_{60} and N in the ground state (ΔH_f^0). [c] Based on the PM3-UHF geometry. [d] To reach SCF convergence faster, we calculated with five instead of six d functions. [e] Atomic units a.u. [f] TS = transition state.

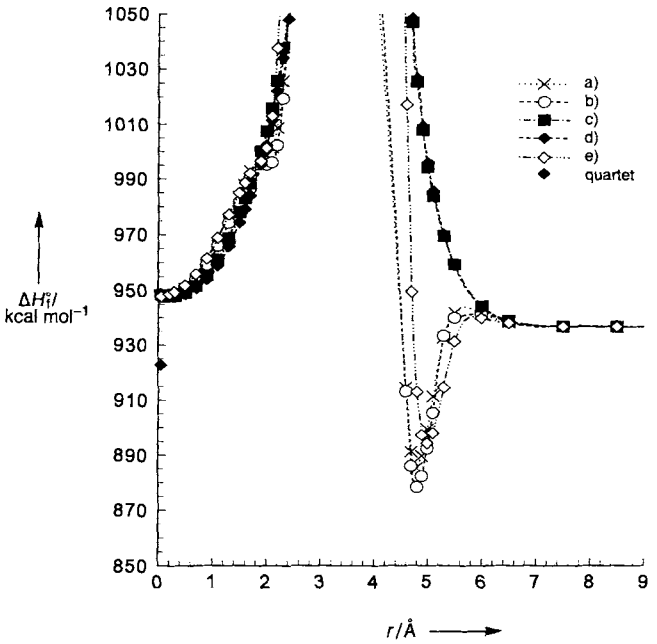

Figure 1. Enthalpies of formation ΔH_f^0 (according to PM3-UHF calculations) for N/C_{60} complexes as a function of the distance r from N to the cage center with retention of a rigid cage geometry. Displacement of the cage center towards a) a [5,6] bond, b) a [6,6] bond, c) the center of a pentagon, d) the center of a hexagon, and e) a C atom.

localized at the nitrogen atom. The fact that no charge transfer from the nitrogen atom to the fullerene takes place is due to the low, even slightly negative, electron affinity[8] of N (−0.32 eV), which is comparable with that of He (−0.59 eV). The transition from the quartet to the doublet state of the encapsulated N atom needs 22 kcal mol^{-1} (PM3-UHF). The endohedral complexation causes a lowering of the differences in energy between the doublet and the quartet state by about 20 kcal mol^{-1}.

The reaction coordinates for the endo- and exohedral approach of the N atom to a C atom, a [6,6] double bond, a [5,6] single bond, the center of a six-membered ring, and the center of a five-membered ring of fixed or optimized fullerene cage structures are shown in Figures 1 and 2. To obtain useful results, all calculations were performed for the doublet states to allow a comparison of the energies of the bound and unbound structures. With a fixed cage geometry the energy increases continuously when the N atom moves from the center to the cage, independent of the direction of approach (Figure 1). In contrast, there are strong attractive interactions if the N atom approaches a C atom, a [6,6] bond, or a [5,6] bond from the outside. This can be explained with the pyramidalization of the C atoms of C_{60}. Thus, the π orbitals do not have pure p character. The π orbital axis vector (POAV) analysis of Haddon[9] gives an average σ-bond hybridization of $sp^{2.278}$ for C_{60} and a fractional s character of the "p orbitals" of 0.085. Due to electron-pair repulsion the charge density on the outside of the fullerenes is higher than on the inside. This means that, in contrast to the reactive exterior, the orbital overlap between the fullerene and a N atom is essentially unfavorable inside C_{60}; at the same time there is a repulsion of the valence electron pairs (Figure 3).

If the fullerene cage is allowed to relax during the approach of the N atom to a C Atom, a [6,6] bond, or a [5,6] bond (Figure 2), there are local minima for the endohedral complexes corresponding to covalently bound structures with a C–N bond, an aza bridge over a closed [6,6] bond, and an aza bridge over a closed [5,6] bond (Figure 4). These local minima are about 20–50 kcal mol^{-1} higher in energy than the global minimum of N@C60 with N in the center of the cage (Table 2, Figure 3). In contrast to the corresponding exohedral complexes, no energy gain is accompanied with covalent endohedral binding and subsequent relaxation of the cage geometry (Table 2, Figure 2). This is because endohedral addition at the relatively rigid cage structure of C_{60} leads to very unfavorable geometries, such as distortion of the tetrahedral angles and untypical bond lengths near the bound addends (Figure 4b, Table 1). In the case of the corresponding exohedral adducts the opposite effect takes place. Here the cage geometry supports the formation of normal, less strained geometries in the region of the addend (Figure 4d, Table 1). For endohedral additions the considerable σ strain of the fullerene cage would be enlarged, but if the addition is exohedral the strain of the cage would decrease. The tendency of the outside surface of fullerenes to undergo addition reactions easily is confirmed by many experimental examples of exohedral adduct formation.[10,11]

The energy barriers for the penetration of nitrogen from the interior through a [5,6] or a [6,6] bond in the doublet state are 49 and 41 kcal mol^{-1}, respectively, according to PM3-UHF calculations (Figure 2), and therefore significantly lower than the most favorable value (225 kcal mol^{-1}) calculated for the penetration of He out of He@C_{60} by a one- or two-window mechanism.[3,12] Even the escape of N starting from the quartet state costs little more than 60 (PM3) or 67 kcal mol^{-1}

 © WILEY-VCH Verlag GmbH, D-69451 Weinheim, 1997 0570-0833/97/3624-2836 $ 17.50+.50/0 *Angew. Chem. Int. Ed. Engl.* **1997**, *36*, No. 24

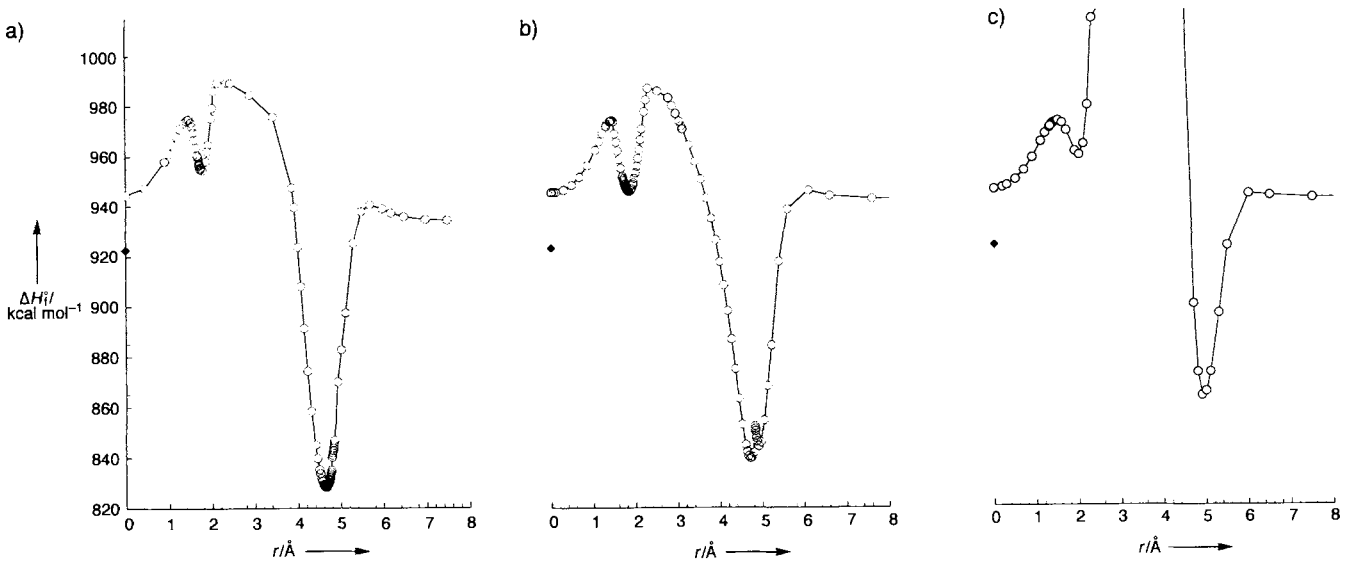

Figure 2. Enthalpies of formation ΔH_f^0 (PM3-UHF) of N/C_{60} complexes with relaxed (optimized) geometry as a function of the distance r from N to the cage center. Displacement of N from the cage center towards a) the center of a [5,6] bond, b) the center of a [6,6] bond, and c) a C atom; ◆ represents the quartet minimum. The calculations were performed for N in the doublet state. Analysis of the reaction coordinates with configuration-interaction (CI) calculations showed that the ground state is very close to the excited states of the same multiplicity. Thus, points of discontinuity of the reaction coordinates in a) and b) are due to internal crossing between different energy surfaces. The discontinuity of the reaction coordinate in b) next to the exohedral minima corresponds to the opening of the bridged [6,6] bond (Tables 1 and 2). As expected [10], this opening does not occur for the analogous bridged C_{60}NH compounds.

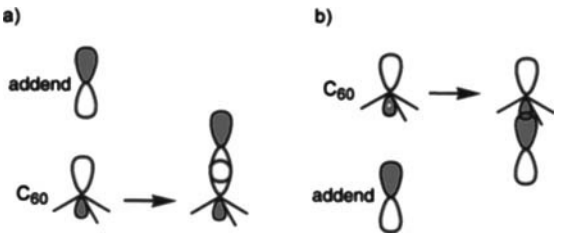

Figure 3. Schematic representation of a) exohedral and b) endohedral addition of the p orbital of the addend to the fullerene with fixed cage geometry.

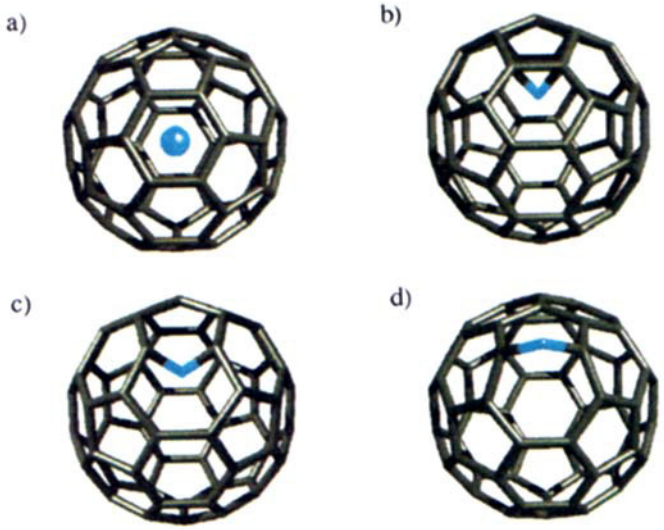

Figure 4. PM3-UHF geometries of the stationary points for the movement of an N atom from the cage center through a [5,6] bond (see also Figure 2). a) Structure of the global minimum of N@C_{60} with N in the center of the cage, b) structure of the local minimum of N@C_{60} with a covalent [5,6] aza bridge, c) transition structure for the penetration of N through a [5,6] bond, and d) structure of the minimum with an open [5,6] bond.

(UB3LYP). This is reasonable, because in the case of N@C_{60} nitrogen penetrates after formation of covalently bound adducts with endohedral [5,6] or [6,6] aza bridges (Figures 2 and 4). This bridging elongates the C–C bond (Table 1), and the penetration of the N atom through the cluster (Figure 4) and subsequent dissociation is favored. This autocatalytic bond breakage requires less energy than the considerable cage distortion needed for penetration by He. Experimentally He is able to leave C_{60} only after thermal treatment for hours at 600 to 850 °C; this process is accompanied by irreversible destruction of the fullerene cage.[3] In contrast, we showed in this study that N escapes from N@C_{60} under considerably milder conditions. In the ESR spectra of N@C_{60} at 260 °C (Figure 5) the intensity of the signals decreases continuously during the measurement. When the sample is then cooled to 220 °C, the spectrum shows the same symmetric triplet but with significantly decreased intensity. This indicates that under thermal treatment N@C_{60} leads to diamagnetic prod-

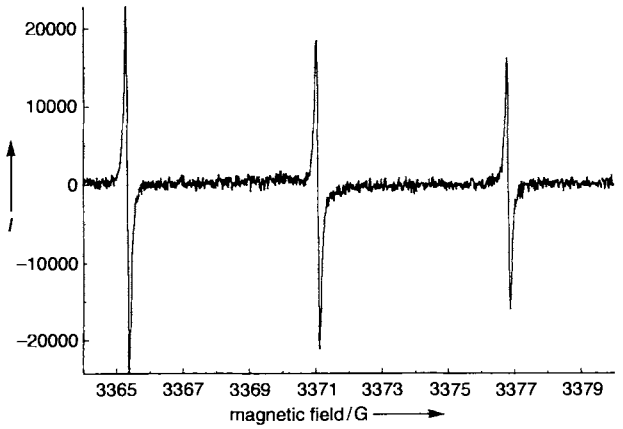

Figure 5. ESR spectra of N@C_{60} at 260 °C; sweep time 84 s for 16 G, intensity I in arbitrary units. The concentration of N@C_{60} decreased to 68% in the time between the first and the third peak (59.2 s).

 © WILEY-VCH Verlag GmbH, D-69451 Weinheim, 1997 0570-0833/97/3624-2837 $ 17.50+.50/0

ucts. Thus, the N atom must have penetrated the fullerene cage, because free or bound radicals can only be stabilized on the outside by subsequent reactions. According to the observed decrease in the intensity of the ESR peaks with time, it is possible to determine the lifetime of the N atoms in $N@C_{60}$ at 260 °C. With an attempt frequency of 10^{13} Hz the activation energy for N extrusion can be estimated with the Arrhenius equation to be about 40 kcal mol^{-1}.

We have now given evidence that the rigid concave shape of the interior of C_{60} is responsible for the astonishing inertness towards N atoms. The reactivity of a carbon network characteristically depends on its shape. In an upcoming theoretical study we will demonstrate that C_{60} is also a "chemical Faraday cage" for other reactive substances such as F and H atoms or the methyl radical.

Received: June 3, 1997 [Z10504IE]
German version: *Angew. Chem.* **1997**, *109*, 2858–2861

Keywords: density functional calculations · EPR spectroscopy · fullerenes · semiempirical calculations

[1] a) D. S. Bethune, R. D. Johnson, J. R. Salem, M. S. de Vries, C. S. Yannoni, *Nature* **1993**, *366*, 123; b) F. T. Edelmann, *Angew. Chem.* **1995**, *107*, 1071; *Angew. Chem. Int. Ed. Engl.* **1995**, *34*, 981.

[2] R. Tellgmann, N. Krawez, S.-H. Lin, I. V. Hertel, E. E. B. Campbell, *Nature* **1996**, *382*, 407.

[3] a) T. Weiske, D. K. Böhme, J. Hrusak, W. Krätschmer, H. Schwarz, *Angew. Chem.* **1991**, *103*, 898; *Angew. Chem. Int. Ed. Engl.* **1991**, *30*, 884; b) T. Weiske, J. Hrusak, D. K. Böhme, H. Schwarz, *Chem. Phys. Lett.* **1991**, *186*, 459; c) T. Weiske, D. K. Böhme, H. Schwarz, *J. Phys. Chem.* **1991**, *95*, 8451; d) T. Weiske, T. Wong, W. Krätschmer, J. K. Terlouv, H. Schwarz, *Angew. Chem.* **1992**, *104*, 242; *Angew. Chem. Int. Ed. Engl.* **1992**, *31*, 183; e) T. Weiske, H. Schwarz, A. Hirsch, T. Grösser, *Chem. Phys. Lett.* **1991**, *95*, 5720.

[4] M. Saunders, R. J. Jiménez-Vázquez, R. Shimshi, A. Khong, *Science* **1996**, *271*, 1693.

[5] a) T. Almeida Murphy, T. Pawlik, A. Weidinger, M. Höhne, R. Alcala, J.-M. Spaeth, *Phys. Rev. Lett.* **1996**, *77*, 1075; b) C. Knapp, K.-P. Dinse, B. Pietzak, M. Waiblinger, A. Weidinger, *Chem. Phys. Lett.* **1997**, *272*, 433–437.

[6] a) J. J. Stewart, *J. Comput. Chem.* **1989**, *10*, 209, 221. b) The PM3 method was used with standard parameters and the UHF formalism. Although the numerical value of S^2 is very high for adducts of fullerene radicals (and also for C_{60} itself), the energetic and geometric effects of spin contamination are small because of the very high multiplicities of the principal spin contaminants; c) B3LYP: P. J. Stephens, F. J. Devlin, C. F. Chabalowski, M. J. Frisch, *J. Phys. Chem.* **1994**, *98*, 11623.

[7] a) G. Rauhut, A. Alex, J. Chandrasekhar, T. Steinke, W. Sauer, B. Beck, M. Hutter, P. Gedeck, T. Clark, VAMP 6.1, Oxford Molecular, Madawar Centre, Oxford Science Park, Standford-on-Thames, Oxford OX44GA, UK, **1996**; b) M. J. Frisch, G. W. Trucks, H. B. Schlegel, P. M. Gill, B. G. Johnson, M. A. Robb, J. R. Cheeseman, T. Keith, G. A. Petersson, J. A. Montgomery, K. Raghavachari, M. A. Al-Laham, V. G. Zakrzewski, J. V. Ortiz, J. B. Foresman, J. Cioslowski, B. B. Stefanov, A. Nanayakkara, M. Challacombe, C. Y. Peng, P. Y. Ayala, W. Chen, M. W. Wong, J. L. Andres, E. S. Replogle, R. Gomberts, R. L. Martin, D. J. Fox, J. S. Binkley, D. J. Defrees, J. Baker, J. P. Stewart, M. Head-Gordon, C. Gonzales, J. A. Pople, Gaussian 94, *Revision* D.3, Gaussian, Pittsburgh (PA), USA, **1995**.

[8] A. F. Hollemann, E. Wiberg, *Lehrbuch der Anorganischen Chemie*, 81st–90th ed., Walter de Gruyter, Berlin, **1976**, p. 106.

[9] R. C. Haddon, *Acc. Chem. Res.* **1992**, *25*, 127.

[10] A. Hirsch, *The Chemistry of the Fullerenes*, Thieme, Stuttgart, **1994**.

[11] R. C. Haddon, *Science* **1993**, *261*, 1545.

[12] S. Patchkovskii, W. Thiel, *J. Am. Chem. Soc.* **1996**, *118*, 7164.

 © WILEY-VCH Verlag GmbH, D-69451 Weinheim, 1997 0570-0833/97/3624-2838 $ 17.50+.50/0

Author Index

The numbers in brackets indicate the corresponding page(s) on which the articles appear in the German version [*Angew. Chem.* **1997**, *109*]

Abbati, G. L. 2774–2776 [2917–2919]
Akkerman, O. S. 2771–2774 [2914–2917]
Aono, M. 2755–2757 [2909–2912]
A.Persoons 2788–2791 [2899–2902]
Arys, X. 2788–2791 [2899–2902]
Asai, A. 2748–2750 [2864–2866]
Ashton, P. R. 2781–2783 [2902–2905]
Augustin, S. 2809–2812 [2919–2922]
Ban, H. 2801–2804 [2884–2886]
Barton, J. K. 2715–2730 [2830–2848]
Behrens, P. 2823–2825 [2939–2940]
Behrens, S. 2797–2799 [2874–2876]
Belser, P. 2779–2781 [2878–2881]
Beno, B. R. 2761–2764 [2929–2933]
Bettenhausen, M. 2797–2799 [2874–2876]
Beyeler, A. 2779–2781 [2878–2881]
Beynard, M. 2758–2761 [2890–2893]
Bickelhaupt, F. 2771–2774 [2914–2917]
Binger, P. 2771–2774 [2914–2917]
Bittner, R. 2765–2768 [2933–2936]
Bodensieck, U. 2758–2761 [2890–2893]
Braunstein, P. 2758–2761 [2890–2893]
Bräuchle, C. 2765–2768 [2933–2936]
Breipohl, G. 2809–2812 [2919–2922]
Breunig, H. J. 2819–2821 [2941–2942]
Brückner, R. 2750–2752 [2866–2868]
Caneschi, A. 2774–2776 [2917–2919]
Clark, T. 2835–2838 [2858–2861]
Clegg, W. 2815–2817 [2925–2926]
Coleman, P. J. 2738–2741, 2741–2744, 2744–2747 [2951–2954, 2954–2957, 2957–2961]
Cornia, A. 2774–2776 [2917–2919]
Cossu, S. 2805–2807 [2912–2914]
Côté, B. 2741–2744, 2744–2747 [2954–2957, 2957–2961]
Dandliker, P. J. 2715–2730 [2830–2848]
Daub, J. 2817–2819 [2926–2929]
Dei, A. 2734–2736 [2852–2855]
DeLucchi, O. 2805–2807 [2912–2914]
DeNardin, Y. 2765–2768 [2933–2936]
Dias, L. C. 2738–2741, 2744–2747 [2951–2954, 2957–2961]
Dötz, K. H. 2828–2830 [2948–2950]
Dunsch, L. 2835–2838 [2858–2861]
Durr, R. 2805–2807 [2912–2914]
Dziezok, P. 2812–2815 [2894–2897]
Eaborn, C. 2815–2817 [2925–2926]
Eckert, H. 2823–2825 [2939–2940]
Eichhöfer, A. 2797–2799 [2874–2876]
Eikema Hommes, N. van 2835–2838 [2858–2861]
Erker, G. 2771–2774 [2914–2917]
Evans, D. A. 2738–2741, 2741–2744, 2744–2747 [2951–2954, 2954–2957, 2957–2961]
Fenske, D. 2797–2799 [2874–2876]
Fischer, K. 2812–2815 [2894–2897]
Fröhlich, R. 2771–2774, 2784–2786 [2914–2917, 2872–2874]
Fromm, K. M. 2799–2801 [2876–2878]
Fuhrmann, P. 2774–2776 [2917–2919]
Fukushi, D. 2755–2757 [2909–2912]
Gallagher, J. 2776–2778 [2906–2908]
Guckian, K. M. 2825–2828 [2942–2945]
Gütlich, P. 2734–2736 [2852–2855]
Gyr, T. 2786–2788 [2869–2871]
Harcken, C. 2750–2752 [2866–2868]
Hennig, M. 2786–2788 [2869–2871]
Hirsch, A. 2835–2838 [2858–2861]
Holmlin, R. E. 2715–2730 [2830–2848]
Hoppe, D. 2784–2786 [2872–2874]
Hoskins, B. F. 2752–2755 [2861–2863]
Houk, K. N. 2761–2764 [2929–2933]
Izod, K. 2815–2817 [2925–2926]
Jaeger, K. E. 2830–2832 [2961–2963]
Jiao, H. 2761–2764 [2929–2933]
Jonas, A. 2788–2791 [2899–2902]
Kaiser, B. 2784–2786 [2872–2874]
Kaneko, C. 2801–2804 [2884–2886]
Kano, T. 2748–2750 [2864–2866]
Karl, J. 2771–2774 [2914–2917]
Kasuga, M. 2755–2757 [2909–2912]
Kauranen, M. 2788–2791 [2899–2902]
Knorr, A. 2817–2819 [2926–2929]
Knorr, M. 2758–2761 [2890–2893]
Kobata, M. 2804–2805 [2886–2888]
Koller, H. 2823–2825 [2939–2940]
Kool, E. T. 2825–2828 [2942–2945]
Krämer, R. 2791–2793 [2888–2890]
L. DeCola 2779–2781 [2878–2881]
Laschewsky, A. 2788–2791 [2899–2902]
Liebeton, K. 2830–2832 [2961–2963]
Lippard, S. J. 2774–2776 [2917–2919]
Lork, E. 2819–2821 [2941–2942]
Losehand, U. 2807–2809 [2897–2899]
Lucchini, V. 2805–2807 [2912–2914]
Lukaszuk, K. 2765–2768 [2933–2936]
Mäcke, H. R. 2786–2788 [2869–2871]
Matschiner, R. 2765–2768 [2933–2936]
Matsubara, S. 2804–2805 [2886–2888]
Matsukawa, S. 2768–2771 [2936–2939]
Matsumura, S. 2748–2750 [2864–2866]
Mauser, H. 2835–2838 [2858–2861]
Mayer, B. 2788–2791 [2899–2902]
Mazaki, Y. 2755–2757 [2909–2912]
Meerholz, K. 2765–2768 [2933–2936]
Mikami, K. 2768–2771 [2936–2939]
Miller, N. D. 2821–2823 [2922–2925]
Mitzel, N. W. 2807–2809 [2897–2899]
Mizuno, T. 2804–2805 [2886–2888]
Moriguchi, M. 2748–2750 [2864–2866]
Müller, M. 2812–2815 [2894–2897]
Nakatani, K. 2794–2797 [2881–2883]
Nakato, T. 2833–2835 [2946–2948]
Nicolaou, K. C. 2821–2823 [2922–2925]
Ogawa, A. 2755–2757 [2909–2912]
Okamoto, A. 2794–2797 [2881–2883]
Okazaki, Y. 2748–2750 [2864–2866]
Okuhara, T. 2833–2835 [2946–2948]
O'Shaughnessy, P. N. 2815–2817 [2925–2926]
Ouchi, H. 2748–2750 [2864–2866]
Ozaki, H. 2755–2757 [2909–2912]
Panz, C. 2823–2825 [2939–2940]
Pence, L. E. 2774–2776 [2917–2919]
Peyman, A. 2809–2812 [2919–2922]
Pfeiffer, J. 2828–2830 [2948–2950]
Pietzak, B. 2835–2838 [2858–2861]
Postema, M. H. D. 2821–2823 [2922–2925]
Reetz, M. T. 2830–2832 [2961–2963]
Robson, R. 2752–2755 [2861–2863]
RÜsler, R. 2819–2821 [2941–2942]
Saito, I. 2794–2797 [2881–2883]
Schimossek, K. 2830–2832 [2961–2963]
Schleyer, P. von R. 2761–2764 [2929–2933]
Schmidt, M. 2812–2815 [2894–2897]
Schreuder Goedheijt, M. 2771–2774 [2914–2917]
Seki, K. 2833–2835 [2946–2948]
Sens, R. 2765–2768 [2933–2936]
Sheiko, S. S. 2812–2815 [2894–2897]
Shibata, K. 2781–2783 [2902–2905]
Shipway, A. N. 2781–2783 [2902–2905]
Sigman, D. S. 2776–2778 [2906–2908]
Slizys, D. A. 2752–2755 [2861–2863]
Smith, J. D. 2815–2817 [2925–2926]
Somfai, P. 2731–2733 [2849–2851]
Stannek, J. 2771–2774 [2914–2917]
Stoddart, J. F. 2781–2783 [2902–2905]
Strampfer, M. 2758–2761 [2890–2893]
Stratmann, O. 2784–2786 [2872–2874]
Strohmann, C. 2758–2761 [2890–2893]
Sugihara, T. 2801–2804 [2884–2886]
Takami, T. 2755–2757 [2909–2912]
Terada, M. 2768–2771 [2936–2939]
Thiem, J. 2793–2794 [2905–2906]
Toda, N. 2804–2805 [2886–2888]
Toshima, K. 2748–2750 [2864–2866]
Trotter, B. W. 2744–2747 [2957–2961]
Trotter, B. W. 2741–2744 [2954–2957]
Tsuchiya, T. 2755–2757 [2909–2912]
Tyler, A. N. 2744–2747 [2957–2961]
Uda, M. 2755–2757 [2909–2912]
Uhlmann, E. 2809–2812 [2919–2922]
Utimoto, K. 2804–2805 [2886–2888]
Volk, T. 2768–2771 [2936–2939]
Wagner, K. 2809–2812 [2919–2922]
Warmuth, R. 2761–2764 [2929–2933]
Watton, S. P. 2774–2776 [2917–2919]
Weidinger, A. 2835–2838 [2858–2861]
Weiser, C. 2809–2812 [2919–2922]
Wendelstorf, C. 2791–2793 [2888–2890]
Werschkun, B. 2793–2794 [2905–2906]
Will, D. W. 2809–2812 [2919–2922]
Wischerhoff, E. 2788–2791 [2899–2902]
Wölker, A. 2823–2825 [2939–2940]
Wortmann, R. 2765–2768 [2933–2936]
Würthner, F. 2765–2768 [2933–2936]
Yamada, M. 2801–2804 [2884–2886]
Yamaguchi, M. 2801–2804 [2884–2886]
Yang, G. 2821–2823 [2922–2925]
Yoshinaga, Y. 2833–2835 [2946–2948]
Zelenko, O. 2776–2778 [2906–2908]
Zippel, F. 2771–2774 [2914–2917]
Zonta, A. 2830–2832 [2961–2963]

 © WILEY-VCH Verlag GmbH, D-69451 Weinheim, 1997 0570-0833/97/03624-2841 $ 17.50+.50/0